

Toward a definition of colonic inertia

Gabrio Bassotti, Giuseppe de Roberto, Luca Sediari, Antonio Morelli

Gabrio Bassotti, Giuseppe de Roberto, Luca Sediari, Antonio Morelli, Gastroenterology and Hepatology Section, Department of Clinical and Experimental Medicine, University of Perugia Medical School, Perugia 06131, Italy

Correspondence to: Dr Gabrio Bassotti, Strada del Cimitero, 2/a, 06131 San Marco Perugia, Italy. gabassot@tin.it

Fax: +39-75-584-7570

Received: 2004-02-02 **Accepted:** 2004-02-24

Abstract

Chronic constipation is a relatively frequent symptom; among its subtypes, the so called-colonic inertia represents a disease condition that is often considered for surgery. However, to date, there has been no agreement on definition of colonic inertia, and a literature review showed that this definition was given to numerous entities that differ from each other. In this paper these concepts are reviewed and a more stringent definition of colonic inertia is proposed.

Bassotti G, de Roberto G, Sediari L, Morelli A. Toward a definition of colonic inertia. *World J Gastroenterol* 2004; 10 (17): 2465-2467

<http://www.wjgnet.com/1007-9327/10/2465.asp>

INTRODUCTION

Starting from the (interrupted) building of the Babylon Tower, human beings have been plagued by a difficulty in understanding each other, even for that concerns trivial concepts. This is especially true in the medical field, and the concept of functional gastrointestinal disorders appears to be a particularly fertile one. In fact, apparently simple complaints such as dyspepsia, diarrhea and constipation bear no single label and are still variously defined. A few years ago, a process was started that aimed at having at least a common discussion ground in defining functional gastrointestinal disorders. This process, through the work of several working teams, produced a series of documents to define the various functional gastrointestinal entities by means of the so-called Rome Criteria, now in their second version (Rome II Criteria)^[1].

Defining and diagnosing constipation

Chronic constipation is one of the most common gastrointestinal complaints^[2], and is usually defined by symptoms such as infrequent bowel movements, the presence of hard stools, an excessive time necessary to evacuate, straining, and the sense of incomplete evacuation of the bowel^[3].

The Rome II Criteria for constipation^[4] are shown in Table 1. Although these criteria represent a common ground to define constipation for research purposes, they do not take into consideration the various types of constipation, which may further be classified in to three main subgroups: normal transit constipation, disorders of defecatory or rectal evacuation (outlet obstruction), and slow transit constipation (STC)^[5].

Recent guidelines on constipation^[6] thoroughly summarize the current diagnostic approach to this symptom, obviously taking into account the fact that the suggested diagnostic tests still do not have their sensitivities established and the details

of their performances have not been well specified^[7]. Colonic transit studies with radiopaque markers are simple and reproducible tests^[8] that can be recommended for any patient undergoing evaluation for constipation. Other tests mainly focus on the anorectal and pelvic function: the balloon expulsion test (simple, inexpensive)^[9] is a useful screening one for major evacuatory dysfunctions; defecography (simple, minimal radiation exposure) can quantify defecatory function^[10]; anorectal manometry (variable methodologies, data from different centers not standardized) is useful to exclude Hirschsprung's disease and provide supportive data for a diagnosis of pelvic floor dysfunction^[11]. These tests are commonly employed in the diagnostic work-up of constipated patients, with further specific tests (rectal perception or distention or electrical stimuli, electromyography of the external sphincter or puborectalis, pudendal nerve terminal motor latency, pancolonic electromyography or manometry) usually being carried out only in clinical research or not generally applicable in common daily practice^[12].

Colonic inertia: a "smoky" entity

Among the above reported subtypes of constipation, the STC one (characterized by an abnormally delayed colonic transit time) represents approximately 15-30% of constipated patients^[13] and usually includes those with intractable constipation^[14]. The latter are usually those "refractory" to medical management, often labeled as "colonic inertia" patients, and frequently referred to the surgeon for a more drastic approach^[15]. However, it appears to be some semantic confusion concerning the term colonic inertia, which is often inappropriately used to define various types of constipation (see below).

How is colonic inertia perceived?

An internet-based search strategy of the Medline and Science Citation Index was performed using the keywords colon, colonic, inertia in various combinations with the Boolean operators AND, OR and NOT. Only articles related to human studies were used, and manual cross-referencing was also performed. Articles published in English between January 1965 and October 2003 were selected; however, a search in non-English languages and in older than 1965 journals was also performed in our library. Letters and case reports were excluded, and abstracts quoted only when the full papers were unavailable.

Table 2 summarizes the various definitions of colonic inertia found in literature, according to the method employed for diagnosis; however, although grouped together for practical purposes, it must be noted that even these subgroups have some internal differences which increase the simple definition of this entity to a number of twelve, and make difficult the interpretation of results.

According to the most frequently performed diagnostic study, radiopaque markers transit, colonic inertia patients have been classified as: (1) having a delayed transit with markers scattered throughout the viscus^[16-20], with exclusion of obstructed defecation on manometry or defecography^[21,22]; (2) synonymous of STC (without specification of markers' distribution)^[23-34]; (3) presenting markers' delay in the ascending^[35] or the right colon^[36]; (4) showing a delayed transit only in the left colon, or in both the left and right colon^[37]; or (5) displaying a delayed right and left colonic transit, but with normal transit in the sigmoid colon and rectum^[38].

Table 1 Rome II Criteria for constipation^[4]

Two or more of the following for at least 12 wk (not necessarily consecutive) in the preceding 12 mo:

- Straining during >25% of bowel movements;
- Lumpy or hard stools for >25% of bowel movements;
- Sensation of incomplete evacuation for >25% of bowel movements;
- Sensation of anorectal blockage for >25% of bowel movements;
- Manual maneuvers (digital evacuation, support of the pelvic floor) to facilitate >25% of bowel movements;
- Less than 3 bowel movements per week;

Loose stools are not present, and there are insufficient criteria for irritable bowel syndrome

Table 2 The various definitions of colonic inertia in literature*According to radiopaque transit studies:*

- Delayed colonic transit with markers distributed throughout the colon;
- Colonic inertia equates to slow transit constipation;
- Delayed transit in the right colon;
- Delayed transit in the left colon, or both in the left and right colon;
- Delayed transit in the right and left colon, with normal transit in the sigmoid and rectum

According to scintigraphic transit studies:

- Scintigraphic delay in the transverse and splenic flexure;
- Scintigraphic delay in the cecum, ascending colon, hepatic flexure, and transverse colon;
- Scintigraphic delay in the whole colon

According to manometric and/or electromyographic findings:

- Almost complete or complete absence of colonic motility

Miscellaneous:

- Decreased colonic motility;
 - Severe constipation and abdominal pain, abnormal transit study, normal anorectal manometry;
 - Refractory constipation and motility abnormalities only of the lower gastrointestinal tract
-

Analysis of these reports shows that, whereas patients in group 1 could indeed somewhat represent a homogeneous group, those in groups 2-5 are highly heterogeneous, and probably include subjects with specific abnormalities (particularly outlet obstruction).

As regards colonic inertia patients defined by scintigraphic transit, they have been classified as: (1) with delay limited to the transverse colon and the splenic flexure^[39]; (2) with delay limited to the cecum, ascending colon, hepatic flexure, and transverse colon^[40]; and (3) with delay in the whole colon^[41]. Once again, it may be noted that colonic inertia is differently defined by different authors, and the patients under investigation do not represent a homogeneous entity.

Things are not better when colonic inertia patients are classified on the basis of instrumental evaluations, which include: (1) a generic "decrease" of colonic motility^[42]; (2) disturbance of colonic motility, defined by severe constipation and abdominal pain, abnormal transit study, and normal anorectal manometry^[43]; (3) refractory constipation and motility abnormalities only of the lower gastrointestinal tract^[44]; and (4) complete or almost complete absence of colonic motility, documented by manometry or electromyography^[45-48]. Again, the great variability of definitions makes likely confusion between entities, as some of the patients in groups 1-3 could easily fit criteria for the irritable bowel syndrome.

The above considerations, far from the simple semantic misunderstanding, are important in that many of the reports described in these series came from surgical groups, and were pertinent to patients in whom a surgical operation was performed, or to patients evaluated for surgery. It is therefore intuitive that such a confusion in defining an entity with potential surgical implications also generates confusion on which patients should be referred for surgery, objective evidence indicates that severely constipated patients judged to be "intractable" might actually respond to colonic pharmacologic stimulation^[49,50], suggesting that they might be responsive to more aggressive forms of medical treatment.

Toward a definition of colonic inertia

On the above grounds, colonic inertia should be better defined, and it should not be synonymous of STC or other well-categorized subtypes of constipation. The Rome Criteria have already given us a common definition of functional constipation and pelvic floor dyssynergia^[51], and STC is well recognized by the delayed colonic transit with radiopaque markers scattered within the colon, there might be the possibility of an intermediate form combining the two entities.

Colonic inertia could be characterized as a distinct form: in fact, the term *inert* literally means "(1) *inactivity* or (2) *activity or motion modest or absent*"^[52]. Under these terms, this (actually rare) form might be defined by: (1) severe functional constipation (according to Rome Criteria); (2) absence of outlet obstruction; (3) delayed transit with markers distributed throughout the colon; (4) manometric and/or electromyographic documentation of absent or almost absent colonic motor activity (including responses to meals); and (5) no response to pharmacologic stimulation (bisacodyl, others) during colonic motility recording.

It remains to be shown, however, whether this definition could predict the success of surgery more accurately, help select more accurately those patients actually needing surgery, as their colon is beyond each possible therapeutic rescue, and better understand the basic mechanisms of constipation through selection of more homogeneous cohorts of patients.

REFERENCES

- 1 **Drossman DA**, Corazziari E, Talley NJ, Thompson WG, Whitehead WE. Rome II: The functional gastrointestinal disorders. *Degnon Associates McLean (Va)* 2000
- 2 **Stewart WF**, Liberman JN, Sandler RS, Woods MS, Stemhagen A, Chee E, Lipton RB, Farup CE. Epidemiology of constipation (EPOC) study in the United States: relation of clinical subtypes to sociodemographic features. *Am J Gastroenterol* 1999; **94**: 3530-3540
- 3 **Koch A**, Voderholzer WA, Klauser AG, Muller-Lissner S. Symp-

- toms in chronic constipation. *Dis Colon Rectum* 1997; **40**: 902-906
- 4 **Thompson WG**, Longstreth GF, Drossman DA, Heaton KW, Irvine EJ, Muller-Lissner SA. Functional bowel disorders and functional abdominal pain. *Gut* 1999; **45**(Suppl II): II43-II47
 - 5 **Leambo A**, Camilleri M. Chronic constipation. *N Engl J Med* 2003; **349**: 1360-1368
 - 6 **Locke GR**, Pemberton JH, Phillips SF. American Gastroenterological Association medical position statement: guidelines on constipation. *Gastroenterology* 2000; **119**: 1761-1766
 - 7 **Locke GR**, Pemberton JH, Phillips SF. AGA technical review on constipation. *Gastroenterology* 2000; **119**: 1766-1778
 - 8 **Degen LP**, Phillips SF. Variability of gastrointestinal transit in healthy women and men. *Gut* 1996; **39**: 299-305
 - 9 **Preston DM**, Lennard-Jones JE. Anismus in chronic constipation. *Dig Dis Sci* 1985; **30**: 413-418
 - 10 **Shorvon PJ**, McHugh S, Diamant NE, Somers S, Stevenson GW. Defecography in normal volunteers: results and implications. *Gut* 1989; **30**: 1737-1749
 - 11 **Diamant NE**, Kamm MA, Wald A, Whitehead WE. AGA technical review on anorectal testing techniques. *Gastroenterology* 1999; **116**: 735-754
 - 12 **Wald A**. Anorectum. In Schuster MM. Atlas of Gastrointestinal Motility in Health and Disease. Baltimore: *Williams Wilkins* 1993: 229-249
 - 13 **Knowles CH**, Martin JE. Slow transit constipation: a model of human gut dysmotility. Review of possible aetiologies. *Neurogastroenterol Mot* 2000; **12**: 181-196
 - 14 **Camilleri M**, Thompson WG, Fleshman JW, Pemberton JH. Clinical management of intractable constipation. *Ann Intern Med* 1994; **121**: 520-528
 - 15 **Schiller LR**. Review article: the therapy of constipation. *Aliment Pharmacol Ther* 2001; **15**: 749-763
 - 16 **Schang JC**, Devroede G, Duguay C, Hémond M, Hébert M. Constipation par inertie colique et obstruction distale: étude électromyographique. *Gastroenterol Clin Biol* 1985; **9**: 480-485
 - 17 **Wald A**. Colonic transit and anorectal manometry in chronic idiopathic constipation. *Arch Intern Med* 1986; **146**: 1713-1716
 - 18 **Berman IR**, Manning DH, Harris MS. Streamlining the management of defecation disorders. *Dis Colon Rectum* 1990; **33**: 778-785
 - 19 **Bergin AJ**, Read NW. The effect of preliminary bowel preparation on a simple test of colonic transit in constipated subjects. *Int J Colorect Dis* 1993; **8**: 75-77
 - 20 **Herman R**, Gregorczyk A, Walega P, Kawiorski W. Radiologic methods of evaluating colonic transit time in functional disorders of the large intestine. *Przegl Lek* 1994; **51**: 343-346
 - 21 **Wexner SD**, Daniel N, Jagelman DG. Colectomy for constipation: physiologic investigation is the key to success. *Dis Colon Rectum* 1991; **34**: 851-856
 - 22 **Costalat G**, Garrigues JM, Didelot JM, Yousfi A, Boccasanta P. Subtotal colectomy with ceco-rectal anastomosis (Deloyers) for severe idiopathic constipation: an alternative to total colectomy reducing risks of digestive sequelae. *Ann Chir* 1997; **51**: 248-255
 - 23 **Wilcox R**. Colonic inertia and rectal obstruction (Arbuthnot Lane disease). *Ann Gastroenterol Hepatol* 1986; **22**: 347-352
 - 24 **Wehrli H**, Akovbiantz A. Surgical therapy of severe idiopathic constipation. *Schweiz Med Wochenschr* 1990; **120**: 496-498
 - 25 **Meyer-Wyss B**. Motility of the large intestine: from irritable colon to obstipation. *Ther Umsch* 1991; **48**: 488-493
 - 26 **Fleshman JW**, Dreznik Z, Cohen E, Fry RD, Kodner IJ. Balloon expulsion facilitates diagnosis of pelvic floor outlet obstruction due to nonrelaxing puborectalis muscle. *Dis Colon Rectum* 1992; **35**: 1019-1025
 - 27 **Mollen RM**, Claassen AT, Kuijpers JH. The evaluation and treatment of functional constipation. *Scand J Gastroenterol* 1997; **223**(Suppl): 8-17
 - 28 **Bernini A**, Madoff RD, Lowry AC, Spencer MP, Gemlo BT, Jensen LL, Wang WD. Should patients with combined colonic inertia and nonrelaxing pelvic floor undergo subtotal colectomy? *Dis Colon Rectum* 1998; **41**: 1363-1366
 - 29 **Thiede A**, Kraemer M, Sailer M, Fuchs KH. Open surgical therapy of constipation. *Zentralbl Chir* 1999; **124**: 812-817
 - 30 **Fan CW**, Wang JY. Subtotal colectomy for colonic inertia. *Int Surg* 2000; **85**: 309-312
 - 31 **Santos SL**, Barcelos IK, Mesquita MA. Total and segmental colonic transit time in constipated patients with Chagas' disease without megaesophagus or megacolon. *Braz J Med Biol Res* 2000; **33**: 43-49
 - 32 **Thompson WG**. Constipation: a physiological approach. *Can J Gastroenterol* 2000; **14**(Suppl D): 155D-162D
 - 33 **Sarli L**, Costi R, Sarli D, Roncoroni L. Pilot study of subtotal colectomy with antiperistaltic cecoproctostomy for the treatment of chronic slow-transit constipation. *Dis Colon Rectum* 2001; **44**: 1514-1520
 - 34 **Zhao RH**, Baig MK, Thaler KJ, Mack J, Abramson S, Woodhouse S, Tamir H, Wexner SD. Reduced expression of serotonin receptor(s) in the left colon of patients with colonic inertia. *Dis Colon Rectum* 2003; **46**: 81-86
 - 35 **Watier A**, Devroede G, Duranceau A, Abdel-Rahman M, Duguay C, Forand MD, Tetreault L, Arhan P, Lamarche J, Elhiali M. Constipation with colonic inertia. A manifestation of systemic disease? *Dig Dis Sci* 1983; **28**: 1025-1033
 - 36 **Husni-Hag-Ali R**, Gomez Rodriguez BJ, Mendoza Olivares FJ, Garcia Montes JM, Sachez-Gey Venegas S, Herrerias Gutierrez JM. Measuring colic transit time in chronic idiopathic constipation. *Rev Esp Enferm Dig* 2003; **95**: 186-190
 - 37 **Verne GN**, Hocking MP, Davis RH, Howard RJ, Sabetai MM, Mathias JR, Schuffler MD, Sninsky CA. Long-term response to subtotal colectomy in colonic inertia. *J Gastrointest Surg* 2002; **6**: 738-744
 - 38 **You YT**, Wang JY, Changchien CR, Chen JS, Hsu KC, Tang R, Chiang JM, Chen HH. Segmental colectomy in the management of colonic inertia. *Am Surg* 1998; **64**: 775-777
 - 39 **Roberts JP**, Newell MS, Deeks JJ, Waldron DW, Garvie NW, Williams NS. Oral [¹¹¹In]DTPA scintigraphic assessment of colonic transit in constipated subjects. *Dig Dis Sci* 1993; **38**: 1032-1039
 - 40 **Krevsky B**, Maurer AH, Fisher RS. Patterns of colonic transit in chronic idiopathic constipation. *Gastroenterology* 1989; **84**: 127-132
 - 41 **Stivland T**, Camilleri M, Vassallo M, Proano M, Rath D, Brown M, Thomforde G, Pemberton J, Phillips S. Scintigraphic measurement of regional gut transit in idiopathic constipation. *Gastroenterology* 1991; **101**: 107-115
 - 42 **Smout AJ**, Brummer RJ. Gastrointestinal surgery and gastroenterology. IX. Obstipation: etiology and diagnosis. *Ned Tijdsch Geneesk* 2000; **144**: 878-884
 - 43 **Webster C**, Dayton M. Results after colectomy for colonic inertia: a sixteen-year experience. *Am J Surg* 2001; **182**: 639-644
 - 44 **Redmond JM**, Smith GW, Barofsky I, Ratych RE, Goldsborough DC, Schuster MM. Psychological tests to predict long-term outcome of total abdominal colectomy for intractable constipation. *Am J Gastroenterol* 1995; **90**: 748-753
 - 45 **Frexinos J**. Inertie colique primitive: mythe ou réalité? *Gastroenterol Clin Biol* 1987; **11**: 302-306
 - 46 **Bassotti G**, Betti C, Pelli MA, Morelli A. Extensive investigation on colonic motility with pharmacological testing is useful for selecting surgical options in patients with inertia colica. *Am J Gastroenterol* 1992; **87**: 143-147
 - 47 **Snape WJ**. Role of colonic motility in guiding therapy in patients with constipation. *Dig Dis* 1997; **15**(Suppl 1): 104-111
 - 48 **Shafik A**, Shafik AA, El-Sibai O, Mostafa RM. Electric activity of the colon in subjects with constipation due to total colonic inertia: an electrophysiological study. *Arch Surg* 2003; **138**: 1007-1011
 - 49 **Bassotti G**, Chiarioni G, Germani U, Battaglia E, Vantini I, Morelli A. Endoluminal instillation of bisacodyl in patients with severe (slow transity type) constipation is useful to test residual colonic propulsive activity. *Digestion* 1999; **60**: 69-73
 - 50 **De Schryver AM**, Samsom M, Smout AI. Effects of a meal and bisacodyl on colonic motility in healthy volunteers and patients with slow-transit constipation. *Dig Dis Sci* 2003; **48**: 1206-1212
 - 51 **Whitehead WE**, Wald A, Diamant NE, Enck P, Pemberton JH, Rao SS. Functional disorders of the anus and rectum. *Gut* 1999; **45**(Suppl II): II55-II59
 - 52 **Churchill's illustrated medical dictionary**. *Churchill Livingstone New York* 1994

Advantages of assaying telomerase activity in ascites for diagnosis of digestive tract malignancies

Chung-Pin Li, Tze-Sing Huang, Yee Chao, Full-Young Chang, Jacqueline Whang-Peng, Shou-Dong Lee

Chung-Pin Li, Full-Young Chang, Shou-Dong Lee, Division of Gastroenterology, Department of Medicine, Taipei Veterans General Hospital and Institute of Clinical Medicine, National Yang-Ming University School of Medicine, Taipei 11217, Taiwan, China

Tze-Sing Huang, Jacqueline Whang-Peng, Cancer Research Division, National Health Research Institutes and Institute of Clinical Medicine, National Yang-Ming University School of Medicine, Taipei 11217, Taiwan, China

Yee Chao, Cancer Center, Taipei Veterans General Hospital, Central Clinic Hospital, and National Yang-Ming University School of Medicine, Taipei 11217, Taiwan, China

Supported by the grant NSC89-2320-B-075-049 from the National Science Council, Taiwan

Correspondence to: Chung-Pin Li, M.D., Division of Gastroenterology, Department of Medicine, Taipei Veterans General Hospital, No. 201, Sec. 2, Shih-Pai Road, Taipei 11217, Taiwan, China. cpli@vghtpe.gov.tw

Telephone: +886-2-28757308 **Fax:** +886-2-28739318

Received: 2003-12-11 **Accepted:** 2004-02-24

Abstract

AIM: To evaluate the diagnostic value of assaying telomerase activity in ascites cells for the differential diagnosis of malignant and non-malignant ascites.

METHODS: Ascites from 40 patients with hepatocellular carcinoma (HCC), 31 with non-HCC gastrointestinal carcinoma (CA), and 24 with liver cirrhosis (LC) were analyzed for telomerase activity. The telomerase activities in cell pellets from ascites were measured according to the Telomeric Repeat Amplification Protocol (TRAP) and quantified with a densitometer.

RESULTS: Positive telomerase activity was detected in 16 of 31 (52%) CA patients, 10 of 40 (25%) HCC patients, and 1 of 24 (4%) LC patients ($P < 0.001$). The telomerase activity was higher in the ascites of CA patients than in the ascites of HCC or LC patients (CA: 22.9 ± 5.8 , HCC: 6.7 ± 2.5 , LC: 1.3 ± 1.3 , $P = 0.001$). Cytology was positive in 18 CA patients (58%) and 1 HCC patient (2.5%), respectively. The positive telomerase activity was not related to patients' age, gender, and ascitic protein concentration, but to white blood count ($r = 0.31$, $P = 0.002$), neutrophil count ($r = 0.29$, $P = 0.005$), and the C-reactive protein level ($r = 0.29$, $P = 0.018$). When the results of both cytological examination and telomerase assay were considered together, the sensitivity increased to 77% for CA patients, 25% for HCC patients, and 48% for all 71 gastrointestinal cancer patients.

CONCLUSION: Combining cytological examination of ascites with telomerase activity assay significantly improves the differential diagnosis between malignant and non-malignant ascites.

Li CP, Huang TS, Chao Y, Chang FY, Whang-Peng J, Lee SD. Advantages of assaying telomerase activity in ascites for diagnosis of digestive tract malignancies. *World J Gastroenterol* 2004; 10(17): 2468-2471

<http://www.wjgnet.com/1007-9327/10/2468.asp>

INTRODUCTION

Ascites is a common complication of malignancy. Carcinoma of any organ can metastasize to the peritoneum. Gastric, colon, pancreatic, ovarian, breast, and lung carcinomas, as well as lymphoma, are the most common tumors associated with malignant ascites^[1]. Hepatocellular carcinoma (HCC) is the leading cause of cancer mortality in Asia^[2]. Ascites is also commonly seen in HCC patients, especially in terminal stage or when complicated with liver cirrhosis (LC). The pathophysiological mechanisms for the ascites production in LC are quite distinct from those for malignancy-related ascites^[3]. The conventional diagnostic methods are sometimes inefficient and unsatisfactory to diagnose ascites as malignancy-related. For example, malignant ascites could be diagnosed by cytological examination of the ascitic fluids in only 50-70% of patients with ascites^[1].

Telomeres (special DNA structures that contain TTAGGG repeats at the ends of all eukaryotic chromosomes) have important functions in protecting genomic DNA from degradation and deleterious recombination events^[4]. Telomerase, an RNA-dependent DNA polymerase, can maintain the telomeric length by acting as a reverse transcriptase^[4]. In humans, tumor cells escape programmed cell senescence through reactivation of telomerase^[5]. These immortalized cells can compensate for telomeric shortening at each cell division, leading to progressive neoplastic evolution^[5,6]. Telomerase re-expression was found in 85% of human malignant tumors^[7-10]. The use of telomerase assay for cancer diagnosis might be possible because telomerase is thought to be re-expressed in malignant lesions but rarely in normal somatic cells^[7-10]. Some studies also suggested that the telomerase activity of ascites could be a sensitive marker for differentiating malignancy-related ascites from nonmalignant ascites^[11-13]. However, these studies included only small numbers of gastrointestinal tract cancer and HCC patients.

This study was to assess the diagnostic value of using telomerase activity assay to distinguish digestive tract cancer-derived ascites from benign ascites.

MATERIALS AND METHODS

Patients

Ninety-five patients with ascites undergoing a therapeutic or diagnostic paracentesis in Taipei Veterans General Hospital were enrolled prospectively into this study. These patients were divided into three groups on the basis of the cause of the ascites.

HCC Group consisted of 40 patients with HCC. The diagnoses were made by imaging studies (abdominal sonography and/or computed tomography and/or magnetic resonance imaging) and serum α -fetoprotein levels above 400 IU/mL in 34 patients, and were confirmed by liver biopsy in the remaining 6 patients.

CA Group consisted of 31 patients with non-HCC gastrointestinal carcinoma, including 10 gastric, 8 colon, 10 pancreatic cancers, and 3 cholangiocarcinomas (19 with liver metastasis and 12 without). All diagnoses were histologically confirmed.

LC Group comprised 24 patients with sterile uncomplicated cirrhotic ascites. Liver cirrhosis was diagnosed by typical clinical findings (splenomegaly, ascites and/or esophageal

varices), imaging studies (abdominal sonography and/or computed tomography and/or magnetic resonance imaging) and laboratory findings in 20 patients, and was confirmed by a liver biopsy in the remaining 4 patients. The serum α -fetoprotein level was <20 IU/mL, and an ultrasound showed no evidence of malignancy in each patient.

Ascitic fluids were subjected to routine assays, such as cell count and categorization, Gram's stain and culture, total proteins, albumin, and cytological examination. Blood samples for serum albumin determination were also taken at the same time as the above measurements to calculate the serum-ascites albumin gradient (SAAG). The ascites was also centrifuged and the sediment was detected with the Telomeric Repeat Amplification Protocol (TRAP). The samples were collected in heparinized containers and centrifuged at 2 000 r/min for 10 min at 4 °C. The supernatant was decanted. Cells were washed twice with ice-cold phosphate-buffered saline (PBS) and were stored in a 1.5-mL tube at -80 °C until assay. For bloody specimens, excessive RBCs were removed by Ficoll-Hypaque density-gradient centrifugation^[14]. All samples were coded so that technicians running the assays were blinded as to the source of the samples.

Telomeric repeat amplification protocol (TRAP)

The telomerase activity was assayed according to the protocol described previously^[15]. Cell lysates were prepared in 200 μ L of lysis buffer consisting of 10 mmol/L Tris-HCl (pH 7.5), 5 g/L CHAPS, 1 mmol/L MgCl₂, 1 mmol/L EGTA, 100 mL/L glycerol, 0.1 mmol/L benzamidine, and 5 mmol/L β -mercaptoethanol. Aliquots of extracts were treated with or without RNase A (Sigma, St. Louis, MO) in a final concentration of 0.05 mg/mL for 30 min at 37 °C. Then, each TRAP reaction was performed at 30 °C for 30 min in 50 μ L of reaction mixture containing 200 ng of cell lysates, 20 mmol/L Tris-HCl (pH 8.3), 0.5 g/L Tween-20, 1.5 mmol/L MgCl₂, 63 mmol/L KCl, 1 mmol/L EGTA, 250 μ mol/L dNTPs, Primer Mix (Intergen Co., Purchase, NY), and 2 units of Taq polymerase (Roche Molecular Biochemicals, Indianapolis, IN), and followed by 33 cycles of PCR: at 94 °C for 0.5 min and 59 °C for 0.5 min. One half of each reaction mixture was resolved in a 125 g/L polyacrylamide gel, and after staining with SYBR® Green (Molecular Probes, Eugene, OR), the image of the telomeric repeat pattern was printed and quantified within a range from 50 to 100 base pairs by Alpha-InnoTech IS500 Digital Imaging System (Avery Dennison, CA). All samples were run in duplicate and the reproducibility was confirmed. All extracts that produced 6-base-pair ladders were tested for sensitivity to RNase A pretreatment, which is indicative of real telomerase activity.

The positive telomerase activity in the ascites cell pellet was calculated according to TPG (Total Product Generated) = $(X - X_0) C_R / C (R - R_0) \times 100$, X: density of sample, X₀: density of heat- or

RNase-treated sample, C: density of internal standard of the sample, C_R: density of internal standard of the control template, R: density of control template, and R₀: density of lysis buffer.

Statistical analysis

Results were expressed as mean \pm SE. Unpaired Student's *t*-test or one-way analysis of variance (ANOVA) was used to analyze continuous variables between groups. Chi-square test or Fisher's exact test was used for comparison of categorical variables. Pearson's correlation was performed to determine whether a relationship between two parameters was significant. Sensitivities and specificities were calculated in accordance with standard methods. Statistical analyses were performed using the SPSS software (SPSS 10.0, SPSS Inc., Chicago, IL). Results were considered statistically significant at $P < 0.05$.

RESULTS

Patient characteristics

The composition of the patients' ascites is shown in Table 1. The ascites protein level was significantly higher in CA than in HCC and LC patients ($P < 0.001$). In addition, the SAAG of HCC and LC relative to CA patients was significantly elevated ($P < 0.01$). The white blood cells in the ascites consisted mainly of lymphocytes in all groups of patients (CA: 74 \pm 5%, HCC: 72 \pm 5%, LC: 86 \pm 4%). The high mean PMN count in HCC patients resulted from blood leakage due to tumor rupture in some HCC patients.

Cytological examination of ascites

Positive cytological examination of ascites was recorded in 18 of 31 (58%) CA patients and 1 of 40 (2.5%) HCC patients. As a control group, none of LC samples showed a positive cytological outcome (Table 2). For the totally 71 gastrointestinal cancer patients, the diagnostic specificity of our cytological examination reached 100%. Because a positive cytological result could make a diagnosis of malignancy, our data suggested that the conventional cytological examination had a sensitivity of 58% for diagnosing the ascites of CA patients, while the sensitivity was only 2.5% for the HCC ascites.

Telomerase activity in ascites

Ascitic telomerase activity was detected by TRAP assay. Representative examples of the results are shown in Figure 1. Positive telomerase activity was detected in 16 of 31 (52%) CA patients and 10 of 40 (25%) HCC patients (Table 2). Only one LC patient (4%) showed positive ascitic telomerase activity ($P < 0.001$). Among CA patients, 5 of 10 gastric cancers (50%), 3 of 8 colon cancers (38%), 7 of 10 pancreatic cancers (70%), and 1 of 3 cholangiocarcinomas (33%) were positive for ascitic telomerase activity (Table 2).

Table 1 Clinical characteristics and ascitic fluid analyses

	CA	HCC	LC
Number of patients	31	40	24
Age (yr)	65 \pm 2	65 \pm 2	67 \pm 2
Sex: Male/Female	21/10	35/5	18/6
Protein (g/dL)	2.9 \pm 0.2	1.5 \pm 0.1 ^d	1.5 \pm 0.2 ^d
SAAG (g/dL)	1.1 \pm 0.1	2.0 \pm 0.2 ^b	2.0 \pm 0.2 ^b
WBC (cells/mm ³)	481 \pm 107	847 \pm 590	149 \pm 27
RBC (cells/mm ³)	13 093 \pm 7 975	192 633 \pm 104 982	3 730 \pm 1 515
PMN (cells/mm ³)	177 \pm 78	698 \pm 550	20 \pm 8
Lymphocytes (cells/mm ³)	305 \pm 77	149 \pm 46 ^a	128 \pm 26 ^a

Data are expressed as mean \pm SE. CA: non-HCC gastrointestinal cancer, HCC: hepatocellular carcinoma, LC: liver cirrhosis, SAAG: serum-ascites albumin gradient, WBC: white blood count, PMN: polymorphonuclear cells. ^a $P < 0.05$, ^b $P < 0.01$, ^d $P < 0.001$ if compared with CA patients.

Table 2 Comparison of telomerase activity assay and cytological examination (n, %)

Group (n)	Underlying diseases (n)	Positive telomerase	Positive cytology
CA (31)		16 (52)	18 (58)
	Gastric cancer (10)	5 (50)	6 (60)
	Colon cancer (8)	3 (38)	4 (50)
	Pancreatic cancer (10)	7 (70)	8 (80)
	Cholangiocarcinoma (3)	1 (33)	0 (0)
HCC (40)		10 (25)	1 (2.5)
LC (24)		1 (4)	0 (0)

CA: non-HCC gastrointestinal carcinoma, HCC: hepatocellular carcinoma, LC: liver cirrhosis.

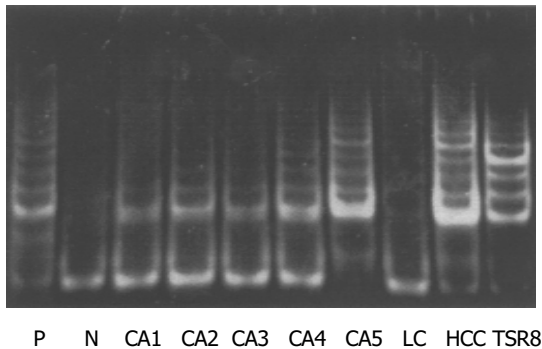


Figure 1 Representative results of ascitic telomerase activity assay. Lane P: positive control, Lane N: heat-inactivated sample, TSR8, quantitation control, CA: non-HCC gastrointestinal carcinoma, HCC: hepatocellular carcinoma, LC: liver cirrhosis.

It was noted that telomerase activity was higher in the ascites of CA patients than in the ascites of HCC and LC patients (CA: 22.9 ± 5.8 , HCC: 6.7 ± 2.5 , LC: 1.3 ± 1.3 , $P = 0.001$, Figure 2). In addition, as shown in Table 3, the telomerase activity was not related to patients' age, gender, serum albumin and ascitic protein amount, but to patients' white blood count ($r = 0.31$, $P = 0.002$), blood neutrophil count ($r = 0.29$, $P = 0.005$), and C-reactive protein level ($r = 0.29$, $P = 0.018$).

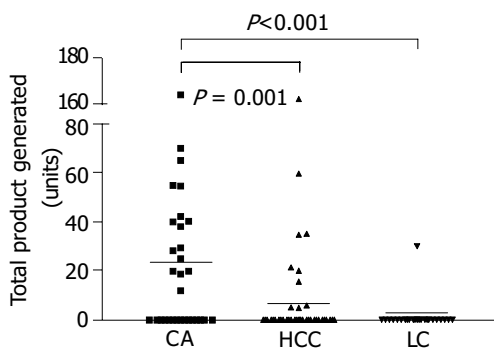


Figure 2 Individual and mean values of telomerase activities in CA, HCC and LC ascites.

When the results of both cytological examination and telomerase assay were combined together, the sensitivity increased to 77% (24/31) for CA patients, 25% (10/40) for HCC patients, and 48% (34/71) for the 71 gastrointestinal cancer patients. While cytological examination alone had a sensitivity of 27% (19/71) and telomerase assay alone had a sensitivity of 37% (26/71).

Table 3 Correlation between ascitic telomerase activity and clinical parameters

	<i>r</i>	<i>P</i>
Age (yr)	-0.05	0.65
Sex: Male/Female	-0.18	0.09
Serum albumin	-0.03	0.81
Ascites protein	0.08	0.44
Blood WBC	0.31	0.002
Blood neutrophil	0.29	0.005
Serum C-reactive protein	0.29	0.018

WBC: white blood count.

DISCUSSION

Diagnosis of cancer primarily depends on pathological examination. Ascites is a common complication of malignant neoplasms. The conventional cytological assessment of ascitic fluid can provide highly specific and accurate diagnoses of malignancies, but its unsatisfactory low sensitivity does not allow pathologists to early differentiate malignant ascites from non-malignant ascites^[16]. Some studies have suggested that assay of telomerase activity in ascites might be an alternative method to improve the diagnosis^[11,12]. However, only small numbers of patients with gastrointestinal tract cancers and HCC were included in those studies. The present study is the first one evaluating the value of telomerase activity assay in differential diagnosis of malignant and nonmalignant ascites of gastrointestinal cancers.

In our study, the sensitivity of telomerase activity assay of ascites from CA patients was 52%, comparable to that (58%) by cytological examination. This result is consistent with a previous report^[11]. However, our TRAP sensitivity seemed to be less than that reported in another paper about ovarian cancers^[17]. Although the average incidence of abnormal telomerase activity occurred in as high as 85% of human cancer patients, the incidence varied with different cancer types^[8,18]. Among these, kidney, ovarian, and breast cancers showed the highest mean values of quantitatively assessed telomerase activities^[19].

Ascites is commonly seen in HCC patients, especially in decompensated stages. Concomitant cirrhosis was present in more than 97% of HCC patients^[20]. Not only the tumor growth, but also the underlying liver cirrhosis, led to ascites^[20,21]. In analysis of our 24 LC and 40 HCC patients, only one HCC patient had a positive cytological diagnosis. This agrees with previously published data showing that malignant cells detected in ascites occurred in only 0-12% of the HCC patients^[20-24], suggesting cytological examination is not an efficient tool for distinguishing HCC ascites from non-HCC LC ascites. Assay of telomerase activity (which was positive in 25% of HCC ascites samples were positive) is obviously better than the conventional cytological assessment.

Moreover, we speculated combining the results of both cytological examination and telomerase activity assay might improve diagnosis. We were able to identify malignancy in 77% of CA patients and 25% of HCC patients. For all 71 gastrointestinal cancer patients, the sensitivity of diagnosis increased to 48% (by the combination of both techniques) from 27% (by the cytological examination alone). Our study results thus indicate that TRAP assay is a useful tool for detecting cancer cells in ascites from gastrointestinal cancer patients.

Noteworthy, ascitic telomerase activity of gastrointestinal cancers is correlated with the increase in blood leukocytes and C-reactive protein. Leukocytosis and C-reactive protein are major markers of inflammation and cancer^[25,26]. The source of

telomerase activity in ascitic cells could be cancer cells shed into the ascitic fluid or ascitic fluid leukocytes that were up-regulated by cancer-related cytokines^[27-35]. Whatever the mechanism(s), assay of telomerase activity in ascitic cells may provide an adjunct to cytological examination in the diagnosis of digestive tract cancers.

REFERENCES

- 1 **Parsons SL**, Watson SA, Steele RJ. Malignant ascites. *Br J Surg* 1996; **83**: 6-14
- 2 **Tang ZY**. Hepatocellular carcinoma-cause, treatment and metastasis. *World J Gastroenterol* 2001; **7**: 445-454
- 3 **Runyon BA**. Care of patients with ascites. *N Engl J Med* 1994; **330**: 337-342
- 4 **Blackburn EH**. Structure and function of telomeres. *Nature* 1991; **350**: 569-573
- 5 **Shay JW**. Telomerase in human development and cancer. *J Cell Physiol* 1997; **173**: 266-270
- 6 **Wright WE**, Piatyszek MA, Rainey WE, Byrd W, Shay JW. Telomerase activity in human germline and embryonic tissues and cells. *Dev Genet* 1996; **18**: 173-179
- 7 **Kim NW**, Piatyszek MA, Prowse KR, Harley CB, West MD, Ho PL, Coviello GM, Wright WE, Weinrich SL, Shay JW. Specific association of human telomerase activity with immortal cells and cancer. *Science* 1994; **266**: 2011-2015
- 8 **Shay JW**, Wright WE. Telomerase activity in human cancer. *Curr Opin Oncol* 1996; **8**: 66-71
- 9 **Shay JW**, Bacchetti S. A survey of telomerase activity in human cancer. *Eur J Cancer* 1997; **33**: 787-791
- 10 **Yakoob J**, Hu GL, Fan XG, Zhang Z. Telomere, telomerase and digestive cancer. *World J Gastroenterol* 1999; **5**: 334-337
- 11 **Toshima S**, Arai T, Yasuda Y, Takaya T, Ito Y, Hayakawa K, Shibuya C, Yoshimi N, Shibayama M, Kashiki Y. Cytological diagnosis and telomerase activity of cells in effusions of body cavities. *Oncol Rep* 1999; **6**: 199-203
- 12 **Tangkijvanich P**, Tresukosol D, Sampatanukul P, Sakdikul S, Voravud N, Mahachai V, Mutirangura A. Telomerase assay for differentiating between malignancy-related and nonmalignant ascites. *Clin Cancer Res* 1999; **5**: 2470-2475
- 13 **Braunschweig R**, Yan P, Guilleret I, Delacretaz F, Bosman FT, Mihaescu A, Benhattar J. Detection of malignant effusions: comparison of a telomerase assay and cytologic examination. *Diagn Cytopathol* 2001; **24**: 174-180
- 14 **Boyum A**. Isolation of mononuclear cells and granulocytes from human blood. Isolation of mononuclear cells by one centrifugation, and of granulocytes by combining centrifugation and sedimentation at 1 g. *Scand J Clin Lab Invest Suppl* 1968; **97**: 77-89
- 15 **Lee CC**, Huang TS. A novel topoisomerase II poison GL331 preferentially induces DNA cleavage at (C/G)T sites and can cause telomere DNA damage. *Pharm Res* 2001; **18**: 846-851
- 16 **Ehya H**. Effusion cytology. *Clin Lab Med* 1991; **11**: 443-467
- 17 **Duggan BD**, Wan M, Yu MC, Roman LD, Muderspach LI, Delgado E, Li WZ, Martin SE, Dubeau L. Detection of ovarian cancer cells: comparison of a telomerase assay and cytologic examination. *J Natl Cancer Inst* 1998; **90**: 238-242
- 18 **Kim NW**. Clinical implications of telomerase in cancer. *Eur J Cancer* 1997; **33**: 781-786
- 19 **Gelmini S**, Caldini A, Becherini L, Capaccioli S, Pazzagli M, Orlando C. Rapid, quantitative nonisotopic assay for telomerase activity in human tumors. *Clin Chem* 1998; **44**: 2133-2138
- 20 **Falconieri G**, Zancanati F, Colautti I, Dudine S, Bonifacio-Gori D, Di Bonito L. Effusion cytology of hepatocellular carcinoma. *Acta Cytol* 1995; **39**: 893-897
- 21 **Colli A**, Cocciolo M, Riva C, Marcassoli L, Pirola M, Di Gregorio P, Buccino G. Ascitic fluid analysis in hepatocellular carcinoma. *Cancer* 1993; **72**: 677-682
- 22 **Yuasa S**, Itoshima T, Nagashima H. Clinical studies of hepatocellular carcinoma with liver cirrhosis and ascites. *Acta Med Okayama* 1984; **38**: 291-299
- 23 **Runyon BA**, Hoefs JC, Morgan TR. Ascitic fluid analysis in malignancy-related ascites. *Hepatology* 1988; **8**: 1104-1109
- 24 **Nakashima T**, Okuda K, Kojiro M, Jimi A, Yamaguchi R, Sakamoto K, Ikari T. Pathology of hepatocellular carcinoma in Japan. 232 Consecutive cases autopsied in ten years. *Cancer* 1983; **51**: 863-877
- 25 **Toniatti C**, Arcone R, Majello B, Ganter U, Arpaia G, Ciliberto G. Regulation of the human C-reactive protein gene, a major marker of inflammation and cancer. *Mol Biol Med* 1990; **7**: 199-212
- 26 **Mahmoud FA**, Rivera NI. The role of C-reactive protein as a prognostic indicator in advanced cancer. *Curr Oncol Rep* 2002; **4**: 250-255
- 27 **Akiba J**, Yano H, Ogasawara S, Higaki K, Kojiro M. Expression and function of interleukin-8 in human hepatocellular carcinoma. *Int J Oncol* 2001; **18**: 257-264
- 28 **Chau GY**, Wu CW, Lui WY, Chang TJ, Kao HL, Wu LH, King KL, Loong CC, Hsia CY, Chi CW. Serum interleukin-10 but not interleukin-6 is related to clinical outcome in patients with resectable hepatocellular carcinoma. *Ann Surg* 2000; **231**: 552-558
- 29 **Price JA**, Kovach SJ, Johnson T, Koniaris LG, Cahill PA, Sitzmann JV, McKillop IH. Insulin-like growth factor I is a comitogen for hepatocyte growth factor in a rat model of hepatocellular carcinoma. *Hepatology* 2002; **36**: 1089-1097
- 30 **Su Q**, Liu YF, Zhang JF, Zhang SX, Li DF, Yang JJ. Expression of insulin-like growth factor II in hepatitis B, cirrhosis and hepatocellular carcinoma: its relationship with hepatitis B virus antigen expression. *Hepatology* 1994; **20**(4 Pt 1): 788-799
- 31 **Akiyama M**, Hideshima T, Hayashi T, Tai YT, Mitsiades CS, Mitsiades N, Chauhan D, Richardson P, Munshi NC, Anderson KC. Cytokines modulate telomerase activity in a human multiple myeloma cell line. *Cancer Res* 2002; **62**: 3876-3882
- 32 **Wilson J**, Balkwill F. The role of cytokines in the epithelial cancer microenvironment. *Semin Cancer Biol* 2002; **12**: 113-120
- 33 **Counter CM**, Gupta J, Harley CB, Leber B, Bacchetti S. Telomerase activity in normal leukocytes and in hematologic malignancies. *Blood* 1995; **85**: 2315-2320
- 34 **Hiyama K**, Hirai Y, Kyoizumi S, Akiyama M, Hiyama E, Piatyszek MA, Shay JW, Ishioka S, Yamakido M. Activation of telomerase in human lymphocytes and hematopoietic progenitor cells. *J Immunol* 1995; **155**: 3711-3715
- 35 **Weng NP**, Levine BL, June CH, Hodes RJ. Regulated expression of telomerase activity in human T lymphocyte development and activation. *J Exp Med* 1996; **183**: 2471-2479

Edited by Zhu LH and Xu FM

Thrombocytosis: A paraneoplastic syndrome in patients with hepatocellular carcinoma

Shinn-Jang Hwang, Jiing-Chyuan Luo, Chung-Pin Li, Cheng-Wei Chu, Jaw-Ching Wu, Chiung-Ru Lai, Jen-Huei Chiang, Gar-Yang Chau, Wing-Yiu Lui, Chun-Chung Lee, Full-Young Chang, Shou-Dong Lee

Shinn-Jang Hwang, Department of Family Medicine, Taipei Veterans General Hospital and National Yang-Ming University School of Medicine, Taiwan, China

Shinn-Jang Hwang, Jiing-Chyuan Luo, Chung-Pin Li, Cheng-Wei Chu, Jaw-Ching Wu, Full-Young Chang, Shou-Dong Lee, Division of Gastroenterology, Department of Medicine, Taipei Veterans General Hospital and National Yang-Ming University School of Medicine, Taiwan, China

Chiung-Ru Lai, Department of Pathology, Taipei Veterans General Hospital and National Yang-Ming University School of Medicine, Taiwan, China

Jen-Huei Chiang, Department of Radiology, Taipei Veterans General Hospital and National Yang-Ming University School of Medicine, Taiwan, China

Gar-Yang Chau, Wing-Yiu Lui, Department of Surgery, Taipei Veterans General Hospital and National Yang-Ming University School of Medicine, Taiwan, China

Chun-Chung Lee, Central Laboratory, Shin Kong Wu Ho-Su Memorial Hospital, Taiwan, China

Shinn-Jang Hwang, Taipei Municipal Yang-Ming Hospital, Taipei, Taiwan, China

Supported by a grant from Taipei Veterans General Hospital, Taiwan, No. VGH88-299

Correspondence to: Shinn-Jang Hwang, M.D., F.A.C.G., Superintendent Office, Taipei Municipal Yang-Ming Hospital, 105 Yu-Sheng Street, Shih-Lin, Taipei, 111, Taiwan, China. sjhwang@vghtpe.gov.tw

Telephone: +886-2-28353461 **Fax:** +886-2-28347528

Received: 2004-02-06 **Accepted:** 2004-02-24

Abstract

AIM: Hepatocellular carcinoma (HCC) patients manifest a variety of paraneoplastic syndromes. Thrombocytosis was reported in children with hepatoblastoma. The aims of this study were to evaluate the prevalence and clinical significance of thrombocytosis in HCC patients and its relationships with serum thrombopoietin (TPO).

METHODS: We retrospectively reviewed clinical, biochemical and image data of 1 154 HCC patients. In addition, we measured platelet count and serum TPO in HCC patients with and without thrombocytosis, in patients with cirrhosis, chronic hepatitis and healthy subjects in a cross-sectional study.

RESULTS: Thirty-one (2.7%) of 1 154 HCC patients had thrombocytosis (platelet count ≥ 400 K/mm³). HCC patients with thrombocytosis were significantly younger, had a higher serum α -fetoprotein, higher rate of main portal vein thrombosis, larger tumor volume, shorter survival, and were less likely to receive therapy than HCC patients without thrombocytosis. Multivariate logistic regression analyses showed that tumor volumes $\geq 30\%$ and serum α -fetoprotein ≥ 140 000 ng/mL could significantly predict thrombocytosis. HCC patients with thrombocytosis had a significantly higher mean serum TPO than those without, as well as patients with cirrhosis, chronic hepatitis and healthy subjects. Platelet count and serum TPO dropped significantly after tumor resection in HCC patients with thrombocytosis and re-elevated after tumor recurred.

Furthermore, the expression of TPO mRNA was found to be more in tumor tissues than in non-tumor tissues of liver in an HCC patient with thrombocytosis.

CONCLUSION: Thrombocytosis is a paraneoplastic syndrome of HCC patients due to the overproduction of TPO by HCC. It is frequently associated with a large tumor volume and high serum α -fetoprotein.

Hwang SJ, Luo JC, Li CP, Chu CW, Wu JC, Lai CR, Chiang JH, Chau GY, Lui WY, Lee CC, Chang FY, Lee SD. Thrombocytosis: A paraneoplastic syndrome in patients with hepatocellular carcinoma. *World J Gastroenterol* 2004; 10(17): 2472-2477 <http://www.wjgnet.com/1007-9327/10/2472.asp>

INTRODUCTION

Hepatocellular carcinoma (HCC) is the most common malignancy in Taiwan. During its clinical course, patients may manifest a variety of paraneoplastic syndromes, including hypercholesterolemia, hypoglycemia, hypercalcemia, and erythrocytosis^[1]. According to our previous reports, the prevalence of paraneoplastic syndromes was 11.4-12.1% for hypercholesterolemia, 2.8-5.3% for hypoglycemia, 1.8-4.1% for hypercalcemia, and 2.5-3.1% for erythrocytosis^[2-6]. Thrombocytosis has been found in children with hepatoblastoma and other malignancies^[7-9]. The prevalence and clinical significance of thrombocytosis in adult patients with HCC have not been previously reported.

Human thrombopoietin (TPO), also known as megakaryocyte growth factor, is known to play a key role in the development of megakaryocytes^[10,11]. TPO is secreted principally by hepatocytes and bone marrow stromal cells^[10-14]. In addition, the expression of TPO gene has been found in both rat and human hepatoma cell lines^[15,16]. The relationships between serum TPO levels and platelet counts in HCC patients, especially those associated with thrombocytosis, are of clinical interest. Our aim was to evaluate the prevalence of thrombocytosis in Chinese patients with HCC in a retrospective study. The clinical, biochemical and image characteristics of HCC patients with thrombocytosis were evaluated. Moreover, in order to evaluate the role of serum TPO in the manifestations of thrombocytosis in HCC patients, serum TPO levels were measured in HCC patients (with and without thrombocytosis), cirrhotic patients, chronic hepatitis patients, and normal subjects in a cross-sectional study.

MATERIALS AND METHODS

The clinical, laboratory and image data were retrospectively reviewed in 1 269 consecutive patients diagnosed with HCC at the Division of Gastroenterology, Taipei Veterans General Hospital, from January 1991 to December 1994^[6]. Of these patients, 1 253 were enrolled in this study who met the following criteria: (1) histological proof of HCC; or (2) at least two typical HCC image findings (ultrasonography, computerized tomography, celiac angiography or magnetic resonance imaging) along with a serum AFP of more than 20 ng/mL. Among

the 1 253 patients, data of 1 197 cases were analyzed after excluding the patients with incomplete examination and data for analysis. Finally, data of 1 154 patients were selected for analyses in this study after excluding 43 patients with an evidence of acute infections or gastrointestinal bleeding. Patients with polycythemia vera were also excluded.

We defined hypercholesterolemia in HCC patients as a serum cholesterol level greater than 250 mg/dL (two standard deviations above the mean value of age-and-sex-matched healthy controls); hypoglycemia as plasma glucose less than 60 mg/dL; hypercalcemia as corrected serum calcium level more than 11.0 mg/dL; and erythrocytosis as a hemoglobin level greater than 16.7 gm/dL or hematocrit greater than 50% as in our previous reports^[2-6]. Thrombocytosis was defined as having a platelet count greater than 400 K/mm³.

To compare the serum TPO level, 18 consecutive HCC patients with thrombocytosis and 72 age-sex-tumor volume matched HCC patients without thrombocytosis were consecutively collected in a cross-sectional study from January 1999 to December 2000. In addition, 42 age-sex-matched cirrhotic patients and 66 chronic hepatitis patients were randomly selected for comparison. The etiologies of chronic hepatitis and cirrhosis were either viral hepatitis B or hepatitis C, which were all confirmed by liver biopsies. None of the patients with chronic hepatitis or cirrhosis received interferon or other antiviral treatments before blood sampling. Alcoholic patients were not enrolled. Patients were also excluded if an acute infection or gastrointestinal bleeding was noted during enrollment. In addition, 62 healthy subjects who received their annual physical examinations at Taipei Veterans General Hospital, and whose age and sex were matched with the aforementioned 90 HCC patients, were randomly selected as healthy controls. Sera of the aforementioned subjects or patients were stored in aliquots at -70 °C until analyzed.

The underlying liver cirrhosis in HCC patients was diagnosed histologically or by characteristic image findings with the presence of ascites or esophageal varices. Patients with cirrhosis were given a score from 5-15 according to Child-Pugh's classification^[17]. Tumor volume was calculated from computerized tomographic films and was expressed as percentages of tumor volume in total liver volume. The grade of differentiation and arrangement of tumor cells were assessed by a liver pathologist according to the classification of Edmondson and Steiner^[18]. The pathologist was not given any clinical information pertaining to the biopsy specimens.

All clinical data of HCC patients including age, sex, Child-Pugh's scores, liver biochemistries (measured by a Hitachi Model 736 automatic analyzer, Tokyo, Japan), prothrombin time, and complete blood counts were recorded when an HCC was first diagnosed or at the time the thrombocytosis developed. Serum α -fetoprotein (AFP) was measured by a commercial kit (ELSA2-AFP, CIS bio-international, Cedex, France). Anti-HCV was measured by a second-generation enzyme immunoassay kit (Abbott Laboratories, Chicago, IL, USA). The serum markers of hepatitis B surface antigen (HBsAg) and antibody to hepatitis D virus (Abbott Laboratories) were recorded. Distant metastases to extrahepatic regional lymph nodes or other organs were evaluated by image studies. Methods of therapy for HCC, including surgical resection of tumors, transcatheter arterial chemoembolization (TACE), sono-guided percutaneous ethanol injection, or systemic chemotherapy and survival times were recorded in each patient. This study was approved by Taipei Veterans General Hospital, Taiwan.

Serum TPO levels were quantitatively measured by a solid phase enzyme immunoassay (Quantikine, R&D systems, Abingdon, UK). For the expression of TPO mRNA, an equal amount of fresh frozen tumors and non-tumor parts of the liver samples from a patient with thrombocytosis who received lobectomy

for HCC were homogenized with a pestle. Total RNA was purified by TRIZOL reagent (Invitrogen and Life Technologies, Rockville, MD, USA). Reverse transcription-polymerase chain reaction (RT-PCR) was carried out to amplify 1 μ g RNA using the First-strain cDNA Synthesis Kit (Amersham Pharmacia Biotech, Buckinghamshire, UK) according to the instruction manual. PCRs were carried out with 35 cycles at 94 °C for 1 min, at 60 °C for 1 min and at 72 °C for 1 min. Primer sequences were sense: 5'-TGCGTTTCCTGATGCTTGAG-3' and anti-sense: 5'-AACCTTACCCTTCCTGAGACA-3'^[12]. β -actin was used as an internal standard and diethyl pyrocarbonate-treated water was used as a negative control. The analysis of PCR products was performed by 20 g/L agarose gel electrophoresis. For quantitation of TPO mRNA, the PCR product was purified by the QIAquick Gel Extraction Kit (QIAGEN GmbH, Hilden, Germany) and $A_{260\text{ nm}}$ was measured to estimate the DNA contents. Serial dilutions of this standard were then included in the following real-time PCR along with samples to produce a standard curve. Quantitative PCR was performed in 20 μ L reaction capillaries using 1 \times DNA master SYBR Green I mix (Roche Diagnostics, Indianapolis, IN, USA), bovine serum albumin, 4 mmol/L MgCl₂, 200 μ mol/L dNTPs, 0.4 U InViTaq-polymerase (InViTec; Berlin, Germany), 1 μ L cDNA and 0.5 μ mol/L of the TPO-specific sense and antisense primers. DNA amplification, data collection and analyses were performed with LightCycler (Roche Diagnostics)^[19]. The program was optimized and performed finally as denaturation at 94 °C for 30 s followed by 40 cycles of amplification (at 94 °C for 0.1 s, 60 °C for 0.1 s, 72 °C for 20 s). The temperature ramp rate was 20 °C/s. At the end of each extension step, the fluorescence of each sample was measured to allow the quantification of the PCR product. After the PCR was completed, the melting curve of the product was measured by a temperature gradient from 60 °C to 96 °C at 0.2 °C/s with continuous fluorescence monitoring to produce a melting profile of the primers. For normalization, the amount of TPO amplicon was divided by the amount of β -actin amplicon of the respective sample.

All data are expressed as mean \pm SD. Results were compared between groups using the Chi-square test, Fisher's exact test, Student's *t*-test, Mann-Whitney test or cross tabulation depending on the type of data analyzed. Survival adjusted for therapy was analyzed using the Kaplan-Meier method and was compared using the log rank method. Univariate and multivariate logistic regression using SPSS software (SPSS Inc., Chicago, IL, USA) were performed to evaluate the predictive values of the patients' clinical, laboratory, and tumor features associated with thrombocytosis. For all tests, only the results with *P* values less than 0.05 (two-tail test) were considered to be statistically significant.

RESULTS

Among the 1 154 HCC patients (1 005 males, 149 females, mean age 62.0 \pm 12.0 years, with a range of 13 to 84 years), 735 (63.7%) patients were HBsAg positive, 180 (15.6%) were anti-HCV positive, 49 (4.3%) were positive for both HBsAg and anti-HCV and 19 (1.6%) were positive for HBsAg and antibody to hepatitis D virus. The mean serum AFP level was 43 983 \pm 163 097 ng/mL (median 268 ng/mL, range 3-1 892 500 ng/mL).

Totally, 243 (21.1%) of 1 154 patients had paraneoplastic syndromes during the clinical course of HCC, in which 175 had a single paraneoplastic manifestation and 68 had multiple paraneoplastic manifestations. Thirty-one (2.7%) of 1 154 HCC patients had thrombocytosis (mean platelet count 484 \pm 87 K/mm³, range 403-688 K/mm³). The prevalence of hypercholesterolemia was 12.6%, hypoglycemia was 5.4%, hypercalcemia was 4.4%, and erythrocytosis was 3.2%. Eighteen of 31 HCC patients with thrombocytosis had other paraneoplastic manifestations

(11 with hypercholesterolemia, 1 with hypoglycemia, 4 with hypercholesterolemia and hypoglycemia, 1 with hypercholesterolemia and hypercalcemia, and 1 with hypercholesterolemia, hypoglycemia and hypercalcemia). Nine hundred and eleven HCC patients were free of paraneoplastic manifestations.

In comparison of the clinical, laboratory data and tumor features between HCC patients with thrombocytosis and those without, HCC patients with thrombocytosis were significantly younger in age, had a higher mean serum AFP level, higher rate of main portal vein (MPV) thrombosis, bilobar tumor involvement, larger tumor volume, were less likely to receive or be suitable for HCC therapy, and had a shorter survival time than those without thrombocytosis (Table 1). HCC patients with thrombocytosis tended to have more extra-hepatic metastases than those without thrombocytosis (32% vs 19%, $P = 0.059$). There were no significant differences in sex distribution, viral etiologies, mean Child-Pugh's scores, and rates of cirrhosis between the two groups. Two hundred and fifty-eight (22%) of 1154 HCC patients and 10 (32%) of 31 patients with thrombocytosis had their HCC tissues for histological analyses. Among the 10 HCC patients with thrombocytosis, tumor cell arrangement showed a trabecular pattern in 7 patients, and a mixed trabecular and acinar pattern in 3. Tumor cell differentiation revealed grade I in 3 patients, grade II in 4 patients, and grade III in 3 patients. The tumor cell arrangement and differentiation showed no significant differences between patients with and without thrombocytosis.

Age, sex, viral hepatitis markers, serum AFP, MPV thrombosis, metastases, bilobar tumor involvement, and tumor volumes were

all selected as independent variables in logistic regression analyses, with the presence of thrombocytosis as the dependent variable. The continuous variables were transformed to categorical variables with the cut-off points determined by the Receiver Operating Characteristic Curve. In an univariate analysis, an age <60 years, serum AFP >140 000 ng/mL, tumor volume >30% of the total liver volume, bilobar tumor involvement, and MPV tumor thrombosis were significantly correlated with the presence of thrombocytosis (Table 2). In a stepwise multivariate analysis, a tumor volume >30% (odds ratio: 9.901, 95% confidence interval: 2.187-44.402, $P = 0.003$) and serum AFP >140 000 ng/mL (odds ratio: 2.660, 95% confidence interval: 1.090-6.487, $P = 0.031$) were significant predictive variables associated with the presence of thrombocytosis in HCC patients.

In the cross-sectional study, the mean platelet count was 440 ± 43 K/mm³ (range 401 to 540 K/mm³) in 18 HCC patients with thrombocytosis, 174 ± 100 K/mm³ (range 102 to 396 K/mm³) in 72 HCC patients without thrombocytosis, 72 ± 29 K/mm³ (range 18 to 154 K/mm³) in 41 patients with cirrhosis, 178 ± 48 K/mm³ (range 105 to 300 K/mm³) in 66 patients with chronic hepatitis, and 212 ± 35 K/mm³ (range 125 to 347 K/mm³) in 62 healthy controls. The mean serum TPO level was significantly higher in HCC patients with thrombocytosis (404 ± 196 pg/mL), when compared with HCC patients without thrombocytosis (181 ± 85 pg/mL), cirrhotic patients (103 ± 34 pg/mL), chronic hepatitis patients (113 ± 46 pg/mL), and healthy subjects (123 ± 53 pg/mL) (Figure 1). Serum TPO levels were positively correlated with platelet counts among 90 HCC patients ($r = 0.474$, $P < 0.001$). Among the 10 HCC patients with thrombocytosis, the

Table 1 Comparison of clinical and laboratory data, and tumor features between hepatocellular carcinoma (HCC) patients with and without thrombocytosis

	HCC patients with thrombocytosis (n = 31)	HCC patients without thrombocytosis (n = 1123)	P value
Age (yr)	52±19	62±12	<0.001
Sex (male: female)	25:6	980:143	0.201
HBV: HCV: HBV+HCV-related	24:1:0	711:179:49	0.114
Mean Child-Pugh's scores	7.2±2.1	6.8±2.2	0.336
Mean platelet counts (k/mm ³)	484±87	154±80	<0.001
Median (range)	441 (403-688)	133 (11-396)	
Mean α-fetoprotein (ng/mL)	251 042±458 734	57 879±212 788	<0.001
Median (range)	4 859 (4-1 892 500)	252 (3-1 621 700)	
Cirrhosis (+:-)	23:8	913:210	0.445
MPV tumor thrombosis (+:-)	11:20	171:952	0.005
Tumor metastases (+:-)	10:21	196:927	0.059
Tumor volumes %	63.5±21.2	30.7±26.9	<0.001
Both lobes with tumor involvements (+:-)	22:9	439:684	<0.001
Therapy for HCC (+:-)	10:21	583:540	0.048
Mean survival (d)	144±208	373±521	<0.001
Median (range)	77 (4-852)	147(2-3 666)	

Data were expressed as mean±SD. HBV: hepatitis B virus, HCV: hepatitis C virus, MPV: main portal vein.

Table 2 Significant predictive variables in association with thrombocytosis in hepatocellular carcinoma patients using univariate logistic analyses

Variables	Odds ratio	95% confidence interval	P value
Age <60 yr	2.905	1.415-5.967	0.004
α-fetoprotein >140 000 ng/mL ¹	6.802	3.515-14.663	<0.001
Tumor volume >30% ¹	16.1	3.757-68.333	<0.001
Both lobes with tumor involvements	3.788	1.732-8.306	<0.001
Main portal vein tumor thrombosis	3.408	1.435-6.467	0.004

¹Significantly predictive variables in multivariate analyses.

mean platelet count dropped significantly from 420 ± 48 K/mm³ to 278 ± 38 K/mm³ ($P < 0.001$) after a surgical tumor resection or TACE, while the mean platelet count for HCC patients with thrombocytosis, who did not receive any therapy, showed a progressive increase during follow up.

Figure 2 illustrates the relationship of platelet counts with the serum levels of cholesterol, AFP and TPO in a 36-year-old HCC male patient. The serum AFP level was 164 000 ng/mL and serum HBsAg was positive. Image studies revealed a large tumor mass over the right lobe of liver with an invasion to the left medial segment. Hypercholesterolemia (serum cholesterol level 602 mg/dL) and thrombocytosis (platelet count 403 K/mm³) were noted at the diagnosis of HCC. He received a surgical removal of tumors followed by chemotherapy with 5-fluorouracil for 12 wk. Platelet counts, serum levels of cholesterol and AFP dropped significantly after a surgical removal of the tumors. However, all re-elevated when the tumor recurred 18 wk after surgical treatment. Serum TPO level was 360 pg/mL before surgery (platelet count 403 K/mm³), and fell to 130 pg/mL one week after operation (platelet count 120 K/mm³). Figure 3 shows the qualitative expression of TPO mRNAs using RT-PCR in tumor and matched non-tumor tissues of the resected liver samples. The expression of TPO mRNAs was more intensive in tumor than in the non-tumor liver tissues. The results from the quantitative real-time PCR also revealed that the concentration of TPO mRNAs in tumors was 1.92 times greater than in matched non-tumor liver tissues.

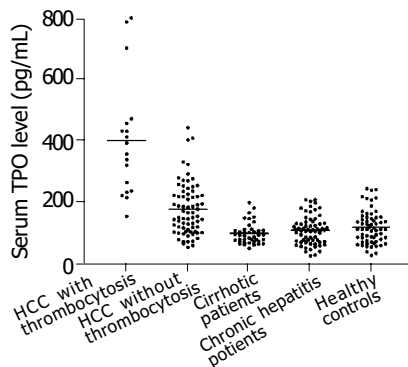


Figure 1 Distribution of serum thrombopoietin levels in hepatocellular carcinoma (HCC) patients with and without thrombocytosis, patients with cirrhosis, chronic hepatitis and healthy subjects. The mean serum thrombopoietin level in HCC patients with thrombocytosis was significantly higher than in HCC patients without thrombocytosis, patients with cirrhosis, chronic hepatitis and healthy subjects.

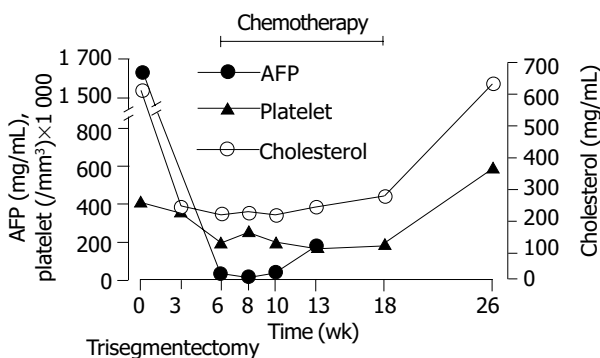


Figure 2 Clinical course of a hepatocellular carcinoma patient with thrombocytosis. The serum alpha-fetoprotein (AFP) level was 164 000 ng/mL before tumor resection. Hypercholesterolemia (serum cholesterol level: 602 mg/dL) and thrombocytosis (platelet count: 403 K/mm³) were noted before operations. The platelet counts, serum levels of cholesterol

and AFP fell significantly after a surgical removal of the tumors. However, all re-elevated when the tumor recurred 18 wk after surgical treatments.

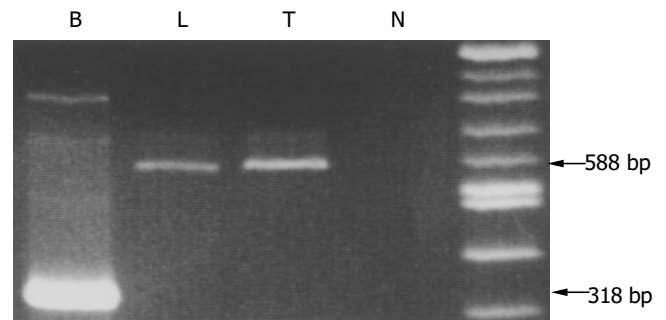


Figure 3 Analyses of thrombopoietin from tumor tissues (T) and non-tumor liver tissues (L) in a hepatocellular carcinoma patient with thrombocytosis using reverse-transcription polymerase chain reaction. β -actin was used as an internal standard (B). N: negative control. Results from an agarose gel electrophoresis showed a more intense density of thrombopoietin band from tumor tissues when compared with non-tumor liver tissues.

DISCUSSION

Common paraneoplastic syndromes seen in HCC patients include hypercholesterolemia, hypoglycemia, hypercalcemia, and erythrocytosis^[1]. Thrombocytosis has been reported in children with hepatoblastoma^[7-9]. The prevalence of thrombocytosis in HCC patients has not been previously reported. Our results showed that 2.7% of HCC patients had thrombocytosis which was defined as a platelet count >400 K/mm³. The prevalence of thrombocytosis might be underestimated because most HCC patients were associated with liver cirrhosis, and thrombocytopenia was frequently seen in these patients.

The clinical significance of thrombocytosis in HCC patients were similar to HCC patients with other paraneoplastic syndromes, including hypercholesterolemia, hypoglycemia, hypercalcemia, and erythrocytosis^[2-6]. Large tumor volumes, high serum AFP, high rates of MPV tumor thrombosis, low rates of receiving therapy and poor prognosis have been identified in HCC patients with thrombocytosis. According to the multivariate logistic regression analyses, HCC patients with thrombocytosis were characterized by a large tumor volume and high serum AFP. HCC patients with thrombocytosis seemed to have a similar life expectancy as HCC patients with erythrocytosis or hypercholesterolemia, and had a better prognosis than patients with hypoglycemia and hypercalcemia which were usually pre-terminal events^[6].

Before the cloning of TPO, the cause of thrombocytosis in children with hepatoblastoma and in other malignancies remains unclear. TPO, a glycoprotein hormone, is a potent stimulator of the growth and maturation of megakaryocytes and platelet production^[10,11]. The main sites of TPO production are the liver and, to a lesser degree, the kidneys, bone marrow and spleen. Messenger RNA transcripts of TPO have been found mainly in the liver and released into circulation^[14-16]. Most TPO is bound with and degraded by circulating platelets and megakaryocytes in the bone marrow, and the serum level is low. Circulating TPO levels are inversely correlated with the number of TPO receptors (c-Mpl-molecules) in regulating megakaryocytopoiesis and platelet production. When thrombocytopenia develops, binding receptors decrease and serum TPO levels increase. Elevated TPO levels stimulate megakaryocytopoiesis and result in increased platelet production^[20-25]. This reverse relationship of platelet counts and serum TPO levels has been found in patients

with hematological diseases^[26,27]. Patients with cirrhosis were frequently associated with low platelet counts. However, serum TPO levels in cirrhotic patients were found to be lower than chronic hepatitis patients or normal subjects due to inadequate TPO production by the diseased livers^[28-32]. Serum TPO of cirrhotic patients increased after orthotopic liver transplantation, which was followed by an increase in platelet counts^[14,33-35]. Our results revealed serum TPO levels were significantly lower in cirrhotic patients than in patients with chronic hepatitis or normal controls, and were consistent with previous reports.

Despite the fact that hepatoma cells have been found to express TPO *in vitro* and in animal models, the mechanisms by which thrombocytosis develops in HCC patients have not been studied. According to our results, HCC patients with thrombocytosis had a significantly higher mean serum TPO level than HCC patients without thrombocytosis. In addition, the platelet counts and serum TPO levels in HCC patients with thrombocytosis dropped after a surgical removal of the tumor or TACE, and re-elevated when a tumor recurred. Changes of platelet counts and serum TPO levels were parallel to the changes of serum AFP. Furthermore, by using the reverse transcription and real-time PCR methods, we demonstrated that the expression of TPO mRNA was more in tumor tissues than in matched non-tumor tissues in an HCC patient with thrombocytosis. Our results were consistent with the report that thrombocytosis in patients with hepatoblastoma was related to increased TPO production in tumors^[9]. Thus, we speculate that thrombocytosis in HCC patients is due to the overproduction of TPO by tumors, and mostly in patients with a large tumor burden. The mechanisms of thrombocytosis in HCC patients are similar to those for other paraneoplastic manifestations. Hypoglycemia has been related to the overproduction of insulin-growth-factor II with insulin-like activities^[2]. The cause of hypercalcemia has been related to overproduction of a parathyroid-related protein which interacts with parathyroid hormone receptors^[4,36]. Elevation of serum erythropoietin has been seen in HCC patients with erythrocytosis^[5,37].

In conclusion, thrombocytosis is one of the paraneoplastic syndromes in patients with HCC, due to the overproduction of TPO by HCC. HCC patients with thrombocytosis are associated with a large tumor volume and high serum AFP level.

REFERENCES

- Okuda K, Kondo Y. Primary carcinomas of the liver. In: Haubrich WS, Schaffner F, Berk JE, eds. *Gastroenterology Volume 3.5th ed.* Philadelphia: W. B. Saunders 1995: 2467-2468
- Wu JC, Daughaday WH, Lee SD, Hsiao TSY, Chou CK, Lin HD, Tsai YT, Chiang BN. Radioimmunoassay of serum IGF-I and IGF-II in patients with chronic liver diseases and hepatocellular carcinoma with or without hypoglycemia. *J Lab Clin Med* 1988; **112**: 589-594
- Hwang SJ, Lee SD, Chang CF, Wu JC, Tsay SH, Lui WY, Chiang JH, Lo KJ. Hypercholesterolemia in patients with hepatocellular carcinoma. *J Gastroenterol Hepatol* 1992; **7**: 491-496
- Yen TC, Hwang SJ, Wang CC, Lee SD, Yeh SH. Hypercalcemia and parathyroid hormone-related protein in hepatocellular carcinoma. *Liver* 1993; **13**: 311-315
- Hwang SJ, Lee SD, Wu JC, Chang CF, Lu CL, Tsay SH, Lo KJ. Clinical evaluation of erythrocytosis in patients with hepatocellular carcinoma. *Chin Med J* 1994; **53**: 262-269
- Luo JC, Hwang SJ, Li CP, Hsiao LT, Lai CR, Chiang JH, Lui WY, Chang FY, Lee SD. Paraneoplastic syndromes in patients with hepatocellular carcinoma in Taiwan. *Cancer* 1999; **86**: 799-804
- Nickerson HJ, Silberman TL, McDonald TP. Hepatoblastoma, thrombocytosis, and increased thrombopoietin. *Cancer* 1980; **45**: 315-317
- Shafford EA, Ritchard JP. Extreme thrombocytosis as a diagnostic clue to hepatoblastoma. *Arch Dis Child* 1993; **69**: 171-174
- Komura E, Matsumura T, Kato T, Tahara T, Tsunoda Y, Sawada T. Thrombopoietin in patients with hepatoblastoma. *Stem Cells* 1998; **16**: 329-333
- de Sauvage FJ, Hass PE, Spencer SD, Malloy BE, Gurney AL, Spencer SA, Darbonne WC, Henzel WJ, Wong SC, Kuang WJ, Oles KJ, Hultgren B Jr, Solberg LA, Goeddel DV, Eaton DL. Stimulation of megakaryocytopoiesis and thrombopoiesis by the c-Mpl ligand. *Nature* 1994; **369**: 533-538
- Lok S, Kaushansky K, Holly RD, Kuijper JL, Lofton-Day CE, Oort PJ, Grant FJ, Helpel MD, Burkhead SK, Kramer JM, Bell LA, Sprecher CA, Blumberg H, Johnson R, Prunkard D, Ching AFT, Mathewes SL, Bailey MC, Forstrom JW, Buddle MM, Osborn SG, Evans SJ, Sheppard PO, Presnell SR, O'hara PJ, Hagen FS, Roth GJ, Foster DC. Cloning and expression of murine thrombopoietin cDNA and stimulation of platelet production *in vivo*. *Nature* 1994; **369**: 565-568
- Sungaran R, Markovic B, Chong BH. Localization and regulation of thrombopoietin mRNA expression in human kidney, liver, bone marrow and spleen using *in situ* hybridization. *Blood* 1997; **89**: 101-107
- Nomura S, Ogami K, Kawamura K, Tsukamoto I, Kudo Y, Kanakura Y, Kitamura Y, Miyazaki H, Kato T. Cellular localization of thrombopoietin mRNA in the liver by *in situ* hybridization. *Exp Hematol* 1997; **25**: 565-572
- Martin TG, Somberg KA, Meng YG, Cohen RL, Heid CA, de Sauvage FJ, Shuman MA. Thrombopoietin levels in patients with cirrhosis before and after orthotopic liver transplantation. *Ann Intern Med* 1997; **127**: 285-288
- Shimada Y, Kato T, Ogami K, Horie K, Kokubo A, Kudo Y, Maeda E, Sohma Y, Akahori H, Kawamura K, Miyazaki H. Production of thrombopoietin (TPO) by rat hepatocytes and hepatoma cell lines. *Exp Hematol* 1995; **23**: 1388-1396
- Hino M, Nishizawa Y, Tagawa S, Yamane T, Morii H, Tatsumi N. Constitutive expression of the thrombopoietin gene in a human hepatoma cell line. *Biochem Biophys Res Commun* 1995; **217**: 475-481
- Pugh RN, Murray-Lyon M, Dawson JL, Pietroni MC, Williams R. Transection of esophagus for bleeding esophageal varices. *Br J Surg* 1973; **60**: 646-649
- Okuda K, Kondo Y. Primary carcinomas of the liver. In: Haubrich WS, Schaffner F, Berk JE, eds. *Gastroenterology Volume 3.5th ed.* Philadelphia: W. B. Saunders 1995: 2462-2463
- Wittwer CT, Ririe KM, Andrew RV, David DA, Gundry RA, Balis UJ. The LighCycler™ a microvolume multisample fluorimeter with rapid temperature control. *Biotechniques* 1997; **22**: 176-181
- McCarty JM, Sprugel KH, Fox NE, Sabath DE, Kaushansky K. Murine thrombopoietin mRNA levels are modulated by platelet count. *Blood* 1995; **86**: 3668-3675
- Nichol JL, Hekom MM, Hornkohl A, Sheridan WP, Ohashi H, Kato T, Li YS, Bartley TD, Choi E, Bogenberger J. Megakaryocyte growth and development factor. Analyses of *in vitro* effects on human megakaryopoiesis and endogenous serum levels during chemotherapy-induced thrombocytopenia. *J Clin Invest* 1995; **95**: 2973-2978
- Cohen-Solal K, Villeval JL, Titeux M, Lok S, Vainchenker W, Wendling F. Constitutive expression of Mpl ligand transcripts during thrombocytopenia or thrombocytosis. *Blood* 1996; **88**: 2578-2584
- Stoffel R, Wiestner A, Skoda RC. Thrombopoietin in thrombocytopenic mice: evidence against regulation at the mRNA level and for a direct regulatory role of platelets. *Blood* 1996; **87**: 567-573
- Emmons RV, Reid DM, Cohen RL, Meng G, Young NS, Dunbar CE, Shulman NR. Human thrombopoietin levels are high when thrombocytopenia is due to increased platelet destruction. *Blood* 1996; **87**: 4068-4071
- Eaton DL, de Sauvage FJ. Thrombopoietin: the primary regulator of megakaryocytopoiesis and thrombopoiesis. *Exp Hematol* 1997; **25**: 1-7
- Tahara T, Usuki K, Sato H, Ohashi H, Morita H, Tsumura H, Matsumoto A, Miyazaki H, Urabe A, Kato A. A sensitive sandwich ELISA for measuring thrombopoietin in human serum: serum thrombopoietin levels in healthy volunteers and in patients with haemopoietic disorders. *Br J Haematology* 1996;

- 93: 783-788
- 27 **Tomita N**, Motomura S, Sakai R, Fujimaki K, Tanabe J, Fukawa H, Harano H, Kanamori H, Ogawa K, Mohri H, Marata A, Kodama F, Ishigatsubo Y, Tahara T, Kato T. Strong inverse correlation between serum TPO level and platelet count in essential thrombocythemia. *Am J Hematol* 2000; **63**: 131-135
- 28 **Peck-Radosavljevic M**, Zacherl J, Meng YG, Pidlich J, Lipinski E, Langle F, Steininger R, Muhlbacher F, Gang A. Is inadequate thrombopoietin production a major cause of thrombocytopenia in cirrhosis of the liver? *J Hepatol* 1997; **27**: 127-131
- 29 **Sezai S**, Kamisaka K, Ikegami F, Usuki M, Urabe A, Tahara T, Kato T, Miyazaki H. Regulation of hepatic thrombopoietin production by portal hemodynamics in liver cirrhosis. *Am J Gastroenterol* 1998; **93**: 80-82
- 30 **Wolber EM**, Ganschow R, Burdelski M, Jelkmann W. Hepatic thrombopoietin mRNA levels in acute and chronic liver failure of childhood. *Hepatology* 1999; **29**: 1739-1742
- 31 **Giannini E**, Borro P, Botta F, Fumagalli A, Malfatti F, Podesta E, Romagnoli P, Testa E, Chiarbonello B, Polegato S, Mamone M, Testa R. Serum thrombopoietin levels are linked to liver function in untreated patients with hepatitis C virus related chronic hepatitis. *J Hepatol* 2002; **37**: 572-577
- 32 **Koruk M**, Onuk MD, Akcay F, Savas MC. Serum thrombopoietin levels in patients with chronic hepatitis and liver cirrhosis, and its relationship with circulating thrombocyte counts. *Hepatology* 2002; **49**: 1645-1648
- 33 **Goulis J**, Chau TN, Jordan S, Mehta AB, Watkinson A, Rolles K, Burroughs AK. Thrombopoietin concentrations are low in patients with cirrhosis and thrombocytopenia and are restored after orthotopic liver transplantation. *Gut* 1999; **44**: 754-758
- 34 **Faeh M**, Hauser SP, Nydegger UE. Transient thrombopoietin peak after liver transplantation for end stage liver disease. *Br J Haematol* 2001; **112**: 493-498
- 35 **Tsukahara A**, Sato Y, Yamamoto S, Szuki S, Nakatsuka H, Watanabe T, Kameyama H, Hatakeyama K. Thrombopoietin levels and peripheral platelet counts following living related donor liver transplantation. *Hepatology* 2003; **50**: 227-230
- 36 **Suva LJ**, Winslow GA, Weltenhall RE, Hammonds RG, Moseley JM, Difenbach-Jagger H, Rodda CP, Kemp BE, Rodriguez H, Chen EY. A parathyroid hormone-related protein implicated in malignant hypercalcemia: cloning and expression. *Science* 1987; **237**: 893-896
- 37 **Kew MC**, Fisher JW. Serum erythropoietin concentrations in patients with hepatocellular carcinoma. *Cancer* 1986; **58**: 2485-2488

Edited by Zhu LH and Xu FM

Potential involvement of leptin in carcinogenesis of hepatocellular carcinoma

Xiu-Jie Wang, Shu-Lan Yuan, Qing Lu, Yan-Rong Lu, Jie Zhang, Yan Liu, Wen-Dong Wang

Xiu-Jie Wang, Shu-Lan Yuan, Yan-Rong Lu, Jie Zhang, Division of Experimental Oncology, Key Laboratory of Biotherapy of Human Diseases of Ministry of Education, China, West China Hospital, Sichuan University, Chengdu 610041, Sichuan Province, China

Qing Lu, Yan Liu, Department of General Surgery, West China Hospital, Sichuan University, Chengdu 610041, Sichuan Province, China

Wen-Dong Wang, Pathology Department of West China Healthy College, Sichuan University, Chengdu 610041, Sichuan Province, China

Supported by the Grants From Sasakawa Medical Foundation of International Cooperation Department of Ministry of Public Health of China (054) and Science Foundation of West China University of Medical Sciences (L99016)

Correspondence to: Dr. Xiu-Jie Wang, Division of Experimental Oncology, Key Laboratory of Biotherapy of Human Diseases of Ministry of Education, China, West China Hospital, Sichuan University, Chengdu 610041, Sichuan Province, China. xiujiawang@yahoo.com

Telephone: +86-28-8423059 **Fax:** +86-28-85178772

Received: 2003-10-24 **Accepted:** 2003-12-29

Abstract

AIM: To investigate the potential involvement of leptin in carcinogenesis of hepatocellular carcinoma (HCC) and to elucidate the etiology, carcinogenesis and progress of HCC.

METHODS: Expressions of Ob gene product, leptin and its receptor, Ob-R were investigated in 36 cases of HCC specimens and corresponding adjacent non-tumorous liver tissues with immunohistochemical staining. The effect of leptin on proliferation of Chang liver cell line and liver cancer cell line SMMC-7721 was studied with cell proliferation assay (MTT).

RESULTS: Leptin expression was detected in 36 cases of adjacent non-tumorous liver tissues (36/36,100%) with moderate (++) to strong (+++) intensity; and in 72.22% (26/36) of HCC with weaker (+) intensity ($P<0.05$). Thirty of 36 (83.33%) cases of adjacent non-tumorous liver tissues were positive for Ob-R, with moderate (++) to strong (+++) intensity. In HCC, 11/36 (30.56%) cases were positive, with weak (+) intensity ($P<0.05$). In cell proliferation assay, leptin inhibited the proliferation of Chang liver cells. The cell survival rate was 10-13% lower than that of the untreated cells ($P>0.05$). Leptin had little effect on the proliferation of liver cancer cells ($P>0.05$).

CONCLUSION: High level expression and decreased or absent expression of leptin and its receptor in adjacent non-tumorous liver cells and HCC cells, inhibitory effect of leptin on the proliferation of normal Chang liver cells and no effect of leptin on proliferation of liver cancer cells, may provide new insights into the carcinogenesis and progression of human HCC. It could be assumed that leptin acting as an inhibitor and/or promoter, is involved in the process of carcinogenesis and progress of human HCC.

Wang XJ, Yuan SL, Lu Q, Lu YR, Zhang J, Liu Y, Wang WD. Potential involvement of leptin in carcinogenesis of hepatocellular carcinoma. *World J Gastroenterol* 2004; 10(17): 2478-2481 <http://www.wjgnet.com/1007-9327/10/2478.asp>

INTRODUCTION

Leptin, a circulating hormone secreted by adipocytes, is one of the major adipose cytokines acting as an important signaling molecule in energy regulation and food intake, and controls body weight homeostasis^[1-3]. It modulates various physiological and pathophysiological states, including lipid metabolism, hematopoiesis, thermogenesis, obesity, and polycystic ovary syndrome^[1,4]. Besides, leptin is also involved in obesity and carcinogenesis of some human cancers.

Recent studies suggested that leptin might play an important role in the process of initiation and progression of human cancers^[2,3,5-12], but there were a difference and discordance among the results. Circulating levels of leptin were higher in cases of breast cancer^[5], colorectal cancer^[8], prostate cancer^[6], eudiometrical cancer^[13], and lower in cases of uterine leiomyomas than the controls^[10], or had no difference in breast cancer^[14]. One study showed that leptin might play a role in the development of prostate cancer^[11]. Another study suggested plasma leptin was not associated with prostate cancer risk^[10]. On the other hand, studies suggested that leptin expression was associated with invasive potential of functioning pituitary adenomas^[15], and influenced cellular differentiation and the progression of prostate cancer^[11]. *In vitro* experimental studies, leptin not only stimulate proliferation of some human cancer cell lines, including breast cancer cell lines (ZR75-1, MCF-7, T-47D)^[2,7,9,16-18], esophageal cancer cell lines (KYSE410, 150), prostate cancer cell lines (DU145 and PC-3)^[2,3], acute myelogenous leukemia (AML)^[19] cell lines, but also inhibited the growth of some human cancer cell lines, such as pancreas cancer cell lines (PANC-1, Mia-PaCa)^[2]. The study results indicated that leptin had divergent effects on human cancer cell proliferation.

Hepatocellular carcinoma (HCC) is one of the most common malignancies in the world, and causes an estimated one million deaths annually. It has a poor prognosis due to its rapid infiltrating growth and complicating liver cirrhosis^[20,21]. Epidemiological studies suggested that obesity was a risk factor of HCC complicated with alcoholic liver disease and cryptogenic cirrhosis^[22,23]. Clinical investigations showed that serum leptin levels in alcoholic and post-hepatitis liver cirrhosis patients with or without HCC increased significantly compared with those in control subjects^[24-30], suggesting that leptin is involved in the etiogenesis of hepatocellular carcinoma (HCC) in cirrhotic patients. Therefore, we hypothesises that leptin might be associated with the growth of liver cells and HCC cells, and played a role in carcinogenesis of hepatocellular carcinoma, but such a study has been reported. In order to confirm this hypothesis, the expression of leptin in human HCC and adjacent non-tumorous liver tissues was analyzed by immunohistochemical staining, and the effect of leptin on proliferation of normal liver cells and HCC cells *in vitro* was studied in this study.

MATERIALS AND METHODS

Immunohistochemical analysis of leptin and Ob-R expressions in human HCC and adjacent non-tumorous liver tissues

Patients and samples HCC specimens and corresponding adjacent non-tumorous liver tissues were collected from 36

patients surgically treated in West China Hospital of Sichuan University in China in 2000, all the patients were informed and consented to use their samples for this study. Of the 36 patients, 29 (80.56%) were males, 7 (19.44%) were females, their age ranged from 27 to 68 years (mean, 49.4 years), Twenty patients (20/36, 55.56%) were infected with HBV, 32 (32/36, 88.89%) were complicated with liver dysfunction, and 10 (10/36, 27.78%) with liver cirrhosis. None had any treatment before the surgical operation. All patients were diagnosed as HCC. The tissue specimens were routinely processed, formalin-fixed, and paraffin- embedded. Paraffinized sections were made for hematoxylin and eosin (HE) and immunohistochemical staining.

Reagents Ob (A-20) and Ob-R (H-300) rabbit anti-human polyclonal antibodies were purchased from Santa Cruz Biotechnology, USA. S-P immunohistochemical staining kit (SP9001) was purchased from Beijing Zhongshan Biological Technology Ltd.

Method Leptin protein and Ob-R were detected immunohistochemically with S-P method. Briefly, tissue sections were deparaffinized and rehydrated through graded alcohols. Antigen retrieval was performed by heating in microwave oven in 0.1 mol/L citrate buffer (pH 6). Then, endogenous peroxidase activity was blocked with 30 mL/L H₂O₂, and after treatment with normal goat serum, the sections were incubated with Ob (A-20) or Ob-R (H-300) rabbit anti-human polyclonal antibodies at a dilution of 1:100, overnight at 4°C, with biotinylated second antibody for 20 min, and with streptavidin/peroxidase for 30 min at room temperature. Subsequently, the sections were subjected to color reaction with 0.2 g/L 3,3-diaminobenzidine tetrahydrochloride containing 0.05 mL/L H₂O₂ in PBS (pH 7.4), and counterstained with hematoxylin lightly. In each staining run, a known leptin positive sample of fat tissue was added as a positive control, and a section of the same fat tissue incubated in PBS instead of Ob or Ob-R was included as a negative control.

Semi-quantitative evaluation was used to determine positively expressed cells by viewing 10 vision fields at ×400. Negative (-) indicated cells were stained less than 10%, mildly positive (+) showed 11-25% cells were stained, moderately positive (++) demonstrated 26-50% cells were stained, strongly positive (+++) revealed over 50% cells were stained. The intensity of staining in positive cells was compared with the negative control and scored as follows: negative (-), weak (+), moderate (++), strong (+++), the last three grades were all regarded as positive.

Proliferation assay in vitro

Reagents Chang liver cell line (ATCC CCL13) and liver cancer cell line SMMC-7721 were obtained from Shanghai Cell Biology Institute of Chinese Academy of Sciences. Human recombinant leptin was a product from Signa-Aldrich, Inc. USA. RPMI-1640 was the product of Gibco/BRL (Invitrogen Corporation, USA). Fetal bovine serum (FBS) was purchased from Huaxi Biology Institute (Chengdu, China). Trypsin, 3-(4, 5-dimethylthiazol-2-yl)-2, 5-diphenyltetrazolium bromide (MTT), and DMSO were purchased from the Sino-American Biotechnology Company of Beijing.

Cell culture Both Chang liver cell line and SMMC-7721 cell line were cultured in RPMI-1640 medium supplemented with 100 mL/L FBS, 100 U/mL penicillin, and 100 µg/mL streptomycin, at 37°C in a humidified atmosphere containing 50 mL/L CO₂.

Proliferation assay (MTT) Chang liver cells and SMMC-7721 cells were suspended at a concentration of 5×10⁴/mL. Then 200 µL of the cell suspension was placed in each well of a replicate 96-well microtiter plate. The cells were allowed to adhere overnight. Then different concentrations (10, 20, 40, 80, 160, 320 ng/mL) of leptin were added to each kind of cells. MTT assay was performed after 1-, 3-, 5-d growth. A 20 µL of 5 mg/mL of MTT was added to each well followed by incubation for 4 h at 37 °C. Formazan products were solubilized with DMSO; A values were

read with an enzyme-linked immunosorbent assay reader (Bio-Tek, Houston, USA) at wavelength of 570 nm. All experiments were performed in triplicate. The effect of leptin on proliferation of Chang liver cells and SMMC-7721 cells were expressed as cell survival rates: A value of the treated group ÷ A value of control group × 100 %.

Statistics analysis

The data of immunohistochemical staining were analyzed with chi-square test. The data of cell proliferation assay were analyzed with variance analysis. *P* < 0.05 was considered statistically significant.

RESULTS

Leptin expression in human HCC and adjacent non-tumorous liver tissues

The expressed Ob gene product, leptin was detected in all 36 specimen from adjacent non-tumorous liver tissues (36/36, 100%), with moderate (++) to strong (+++) intensity. The expression rate in HCC was 72.22% (26/36), but the intensity was weaker (+) than that in adjacent non-tumorous liver tissues (Figure 1), a significant difference in leptin expression was found between adjacent non-tumorous liver tissues and HCC (*P* < 0.05). Ten of 36 specimens from HCC (10/36, 27.78%) even lost the expression of leptin, but Kupffer cells and vascular endothelial cells expressed high levels of leptin (Figure 2).

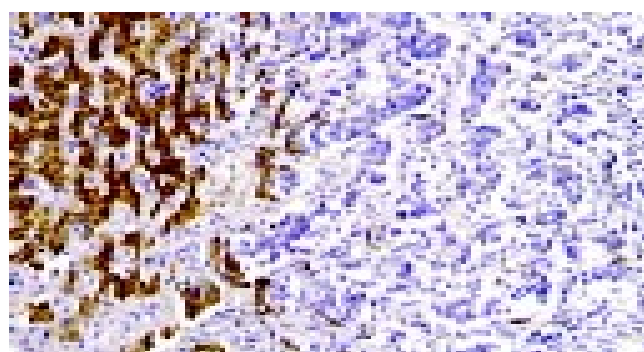


Figure 1 Expression of leptin in adjacent non-tumorous liver live cells (left) and absent expression in HCC cells (right). S-P immunohistochemical staining ×200.

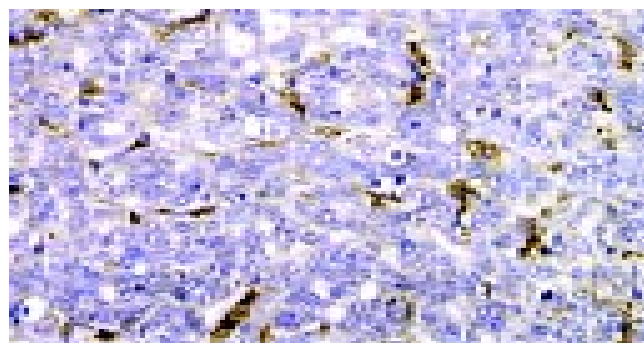


Figure 2 Absent expression of leptin in HCC cells, Kupffer cells and vascular endothelial cells expressed high levels of leptin. S-P immunohistochemical staining ×400.

Ob-R expression in human HCC and adjacent non-tumorous liver tissues

Thirty out of 36 specimens from adjacent non-tumorous liver tissues (30/36, 83.33%) were positive for Ob gene receptor product, with a moderate (++) to strong (+++) intensity. Only

11 of 36 specimens from HCC (11/36, 30.56%) were positive, with a weak (+) intensity. The expression of Ob-R was significantly lower than that of adjacent non-tumorous liver tissues ($P < 0.05$).

Effect of leptin on the proliferation of Chang liver cells *in vitro*

Leptin inhibited the proliferation of Chang liver cells on the 5th d after leptin treatment at various concentrations. The cell survival rate was 10-13% lower than that of the untreated cells (Figure 3A), although without statistical significance ($P > 0.05$).

Effect of leptin on proliferation of SMMC-7721 cells *in vitro*

Leptin had little effect on the proliferation of liver cancer cells (Figure 3B), the cell survival rate on each day after leptin treatment was lightly lower than that of the controls, but no statistical significance was found ($P > 0.05$).

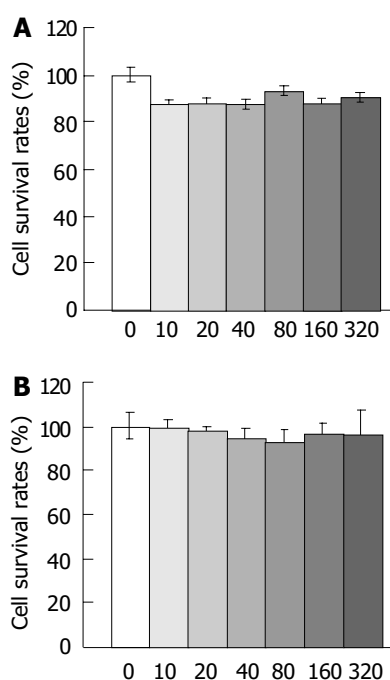


Figure 3 Effect of leptin at different concentrations (ng/mL) on proliferation of Chang liver cells and liver cancer cells on d 5 (MTT assay). A: Effect of leptin at different concentrations (ng/mL) on proliferation of Chang liver cells on d 5 (MTT assay), B: Effect of leptin at different concentrations (ng/mL) on proliferation of liver cancer cells on d 5 (MTT assay).

DISCUSSION

It has found that certain cancers are associated with obesity, including breast, prostate, colon, uterus, renal cell, pancreas carcinoma and esophagus adenocarcinoma^[2,22,31]. Leptin, an Ob gene product, could control body weight homeostasis through food intake and energy expenditure, and was closely associated with obesity^[1-3]. Although epidemiological observation showed that obesity was a risk factor of HCC complicated with alcoholic liver disease and cryptogenic cirrhosis^[22,23,32], clinical investigations have identified that serum leptin levels in alcoholic and post-hepatitis liver cirrhosis patients with or without HCC are increased significantly in comparison with those in control subjects^[22,24-30]. There was no study on the role of leptin in carcinogenesis of human hepatic cellular carcinoma^[2,22-30].

The present study investigated the expression of leptin and its receptor Ob-R in both adjacent non-tumorous liver tissues and HCC tissues with immunohistochemical staining, and found that adjacent non-tumorous liver cells expressed higher levels of leptin and its receptor than corresponding HCC cells, about one fourth of HCC tissues lost the expression of leptin, and

two thirds had no Ob-R expression (Figures 1, 2). These findings suggest that leptin could act *in vivo* as a paracrine/endocrine growth factor towards hepatocytes, and played a possible role in the process of initiation and progression of HCC, which could thus contribute to the explanation of the reasons why alcoholic and post-hepatitis liver cirrhosis patients with or without HCC had high levels of serum leptin^[24-30] and the reasons why obesity was a risk factor of developing HCC^[22,23].

In proliferation assay *in vitro*, leptin had differential effects on the proliferation of human cancer cells. It caused growth potentiation in breast, esophagus, and prostate cancer cells, but inhibited the proliferation of pancreatic cancer cells^[2,19,32]. In MCF-7 cells, leptin and high glucose stimulated cell proliferation as demonstrated by the increases in DNA synthesis and expression of cdk2 and cyclin D1. However, they had no significant effect on the proliferation of multidrug-resistant human breast cancer NCI/ADR-RES cells^[16]. In this study, leptin alone showed some inhibitory effect on the proliferation of normal Chang liver cells, and no effect on liver cancer SMMC-7721 cells. However, Chang liver cell line was originally thought to be derived from normal liver tissue, but was subsequently found on the basis of isoenzyme analysis, HeLa marker chromosomes, and DNA fingerprinting, to have HeLa cell contamination when it was established (www.atcc.org). Therefore, these findings *in vitro* might be associated with different biological characteristics of cancer cells to react to leptin treatment, and/or the organ derivation of cancer cell lines^[2]. In addition, Chang liver cell line was not a good control of normal liver cells.

In vivo animal experiments findings showed that Leptin was a growth factor that could stimulate proliferation of colonic epithelial cells in mice^[33]. It is also a profibrogenic cytokine and could play a key role in liver fibrosis^[34]. *ob/ob* mice having a naturally occurring mutation in the *ob* gene that prevents the synthesis of leptin had an increased incidence of HCC^[31]. This study showed that leptin had some inhibitory effect on the proliferation of normal Chang liver cells and no effect on the proliferating of liver cancer SMMC-7721 cells (Figures 3A,3B), and adjacent non-tumorous liver tissues could express higher levels of leptin and its receptor than the corresponding HCC cells (Figure 1). It could be assumed that leptin acting as an inhibitor and/or promoter, was involved in the process of carcinogenesis and progression of human HCC. In addition, the high levels of leptin expression in Kupffer cells and vascular endothelial cells might be associated with liver cirrhosis^[24,27,35,36] and angiogenesis of cancer tissues^[1,14,37], because these lesions might deteriorate HCC.

In summary, a preliminary investigation of the possible involvement of leptin in carcinogenesis of human hepatocellular carcinoma was performed in this study to elucidate the etiology and carcinogenesis of HCC. To the best of our knowledge^[2,20-30], this is the first report on involvement of leptin in HCC. The presence of leptin and its receptor in adjacent non-tumorous liver and HCC cells, and the effects of leptin on proliferation of normal Chang liver cells and liver cancer cells may provide new insights into the carcinogenesis and progression of human HCC.

REFERENCES

- 1 Sierra-Honigmann MR, Nath AK, Murakami C, Garcia-Cardena G, Papapetropoulos A, Sessa WC, Madge LA, Schechner JS, Schwabb MB, Polverini PJ, Flores-Riveros JR. Biological action of leptin as an angiogenic factor. *Science* 1998; **281**: 1683-1686
- 2 Somasundar P, Yu AK, Vona-Davis L, McFadden DW. Differential effects of leptin on cancer *in vitro*. *J Surg Res* 2003; **113**: 50-55
- 3 Onuma M, Bub JD, Rummel TL, Iwamoto Y. Prostate cancer cell-adipocyte interaction: Leptin mediates androgen-independent prostate cancer cell proliferation through c-Jun NH2-ter-

- minal kinase. *J Biol Chem* 2003; **278**: 42660-42667
- 4 **Janeckova R.** The role of leptin in human physiology and pathophysiology. *Physiol Res* 2001; **50**: 443-459
 - 5 **Stephenson GD, Rose DP.** Breast cancer and obesity: an update. *Nutr Cancer* 2003; **45**: 1-16
 - 6 **Stattin P, Kaaks R, Johansson R, Gislefoss R, Soderberg S, Alfthan H, Stenman UH, Jellum E, Olsson T.** Plasma leptin is not associated with prostate cancer risk. *Cancer Epidemiol Biomarkers Prev* 2003; **12**: 474-475
 - 7 **Catalano S, Marsico S, Giordano C, Mauro L, Rizza P, Panno ML, Ando S.** Leptin enhances, via AP-1, expression of aromatase in the MCF-7 cell line. *J Biol Chem* 2003; **278**: 28668-28676
 - 8 **Stattin P, Palmqvist R, Soderberg S, Biessy C, Ardnor B, Hallmans G, Kaaks R, Olsson T.** Plasma leptin and colorectal cancer risk: a prospective study in Northern Sweden. *Oncol Rep* 2003; **10**: 2015-2021
 - 9 **Hu X, Juneja SC, Maible NJ, Cleary MP.** Leptin-a growth factor in normal and malignant breast cells and for normal mammary gland development. *J Natl Cancer Inst* 2002; **94**: 1704-1711
 - 10 **Chan TF, Su JH, Chung YF, Chang HL, Yuan SS.** Decreased serum leptin levels in women with uterine leiomyomas. *Acta Obstet Gynecol Scand* 2003; **82**: 173-176
 - 11 **Saglam K, Aydur E, Yilmaz M, Goktas S.** Leptin influences cellular differentiation and progression in prostate cancer. *J Urol* 2003; **169**: 1308-1311
 - 12 **Kote-Jarai Z, Singh R, Durocher F, Easton D, Edwards SM, Ardern-Jones A, Dearnaley DP, Houlston R, Kirby R, Lees R.** Association between leptin receptor gene polymorphisms and early-onset prostate cancer. *BJU Int* 2003; **92**: 109-112
 - 13 **Petridou E, Belechri M, Dessypris N, Koukoulomatis P, Diakomanolis E, Spanos E, Trichopoulos D.** Leptin and body mass index in relation to endometrial cancer risk. *Ann Nutr Metab* 2002; **46**: 147-151
 - 14 **Coskun U, Gunel N, Toruner FB, Sancak B, Onuk E, Bayram O, Cengiz O, Yilmaz E, Elbeg S, Ozkan S.** Serum leptin, prolactin and vascular endothelial growth factor (VEGF) levels in patients with breast cancer. *Neoplasma* 2003; **50**: 41-46
 - 15 **Isono M, Inoue R, Kamida T, Kobayashi H, Matsuyama J.** Significance of leptin expression in invasive potential of pituitary adenomas. *Clin Neurol Neurosurg* 2003; **105**: 111-116
 - 16 **Okumura M, Yamamoto M, Sakuma H, Kojima T, Maruyama T, Jamali M, Cooper DR, Yasuda K.** Leptin and high glucose stimulate cell proliferation in MCF-7 human breast cancer cells: reciprocal involvement of PKC-alpha and PPAR expression. *Biochim Biophys Acta* 2002; **1592**: 107-116
 - 17 **Dieudonne MN, Machinal-Quelin F, Serazin-Leroy V, Leneveu MC, Pecquery R, Giudicelli Y.** Leptin mediates a proliferative response in human MCF7 breast cancer cells. *Biochem Biophys Res Commun* 2002; **293**: 622-628
 - 18 **Laud K, Gourdou I, Pessemeesse L, Peyrat JP, Djiane J.** Identification of leptin receptors in human breast cancer: functional activity in the T47-D breast cancer cell line. *Mol Cell Endocrinol* 2002; **188**: 219-226
 - 19 **Bruserud O, Huang TS, Glenjen N, Gjertsen BT, Foss B.** Leptin in human acute myelogenous leukemia: studies of *in vivo* levels and *in vitro* effects on native functional leukemia blasts. *Haematologica* 2002; **87**: 584-595
 - 20 **Qian J, Feng GS, Vogl T.** Combined interventional therapies of hepatocellular carcinoma. *World J Gastroenterol* 2003; **9**: 1885-1891
 - 21 **Zhu AX.** Hepatocellular carcinoma: are we making progress? *Cancer Invest* 2003; **21**: 418-428
 - 22 **Nair S, Mason A, Eason J, Loss G, Perrillo RP.** Is obesity an independent risk factor for hepatocellular carcinoma in cirrhosis? *Hepatology* 2002; **36**: 150-155
 - 23 **Roth MJ, Baer DJ, Albert PS, Castonguay TW, Dorgan JF, Dawsey SM, Brown ED, Hartman TJ, Campbell WS, Giffen CA, Judd JT, Taylor PR.** Relationship between serum leptin levels and alcohol consumption in a controlled feeding and alcohol ingestion study. *J Natl Cancer Inst* 2003; **95**: 1722-1725
 - 24 **Wang YY, Lin SY.** Leptin in relation to hepatocellular carcinoma in patients with liver cirrhosis. *Horm Res* 2003; **60**: 185-190
 - 25 **Lin SY, Wang YY, Sheu WH.** Increased serum leptin concentrations correlate with soluble tumour necrosis factor receptor levels in patients with cirrhosis. *Clin Endocrinol* 2002; **57**: 805-811
 - 26 **Testa R, Franceschini R, Giannini E, Cataldi A, Botta F, Fasoli A, Tenerelli P, Rolandi E, Barreca T.** Serum leptin levels in patients with viral chronic hepatitis or liver cirrhosis. *J Hepatol* 2000; **33**: 33-37
 - 27 **Comlekci A, Akpınar H, Yesil S, Okan I, Ellidokuz E, Okan A, Ersoz G, Tankurt E, Batur Y.** Serum leptin levels in patients with liver cirrhosis and chronic viral hepatitis. *Scand J Gastroenterol* 2003; **38**: 779-786
 - 28 **Greco AV, Mingrone G, Favuzzi A, Capristo E, Gniuli D, Addolorato G, Brunani A, Cavagnin F, Gasbarrini G.** Serum leptin levels in post-hepatitis liver cirrhosis. *J Hepatol* 2000; **33**: 38-42
 - 29 **Campillo B, Sherman E, Richardet JP, Bories PN.** Serum leptin levels in alcoholic liver cirrhosis: relationship with gender, nutritional status, liver function and energy metabolism. *Eur J Clin Nutr* 2001; **55**: 980-988
 - 30 **Serin E, Ozer B, Gumurdulu Y, Kayaselcuk F, Kul K, Boyacioglu S.** Serum leptin level can be a negative marker of hepatocyte damage in nonalcoholic fatty liver. *J Gastroenterol* 2003; **38**: 471-476
 - 31 **Somasundar P, Riggs D, Jackson B, Vona-Davis L, McFadden DW.** Leptin stimulates esophageal adenocarcinoma growth by nonapoptotic mechanisms. *Am J Surg* 2003; **186**: 575-578
 - 32 **Yang S, Lin HZ, Hwang J, Chacko VP, Diehl AM.** Hepatic hyperplasia in noncirrhotic fatty livers: is obesity-related hepatic steatosis a premalignant condition? *Cancer Res* 2001; **61**: 5016-5023
 - 33 **Hardwick JC, Van Den Brink GR, Offerhaus GJ, Van Deventer SJ, Peppelenbosch MP.** Leptin is a growth factor for colonic epithelial cells. *Gastroenterology* 2001; **121**: 79-90
 - 34 **Saxena NK, Saliba G, Floyd JJ, Anania FA.** Leptin induces increased alpha2(I) collagen gene expression in cultured rat hepatic stellate cells. *J Cell Biochem* 2003; **89**: 311-320
 - 35 **Leclercq IA, Farrell GC, Schriemer R, Robertson GR.** Leptin is essential for the hepatic fibrogenic response to chronic liver injury. *J Hepatol* 2002; **37**: 206-213
 - 36 **Shimizu H, Kakizaki S, Tsuchiya T, Nagamine T, Takagi H, Takayama H, Kobayashi I, Mori M.** An increase of circulating leptin in patients with liver cirrhosis. *Int J Obes Relat Metab Disord* 1998; **22**: 1234-1238
 - 37 **Iversen PO, Drevon CA, Reseland JE.** Prevention of leptin binding to its receptor suppresses rat leukemic cell growth by inhibiting angiogenesis. *Blood* 2002; **100**: 4123-4128

Function of oval cells in hepatocellular carcinoma in rats

Chi-Hua Fang, Jia-Qing Gong, Wei Zhang

Chi-Hua Fang, Jia-Qing Gong, Wei Zhang, Department of Hepatobiliary Surgery, Zhujiang Hospital, First Military Medical University, Guangzhou 510282, Guangdong Province, China

Supported by the Natural Science Foundation of Guangdong Province, No. 2001.010593, 2002.020097 and Key Science and Technology Research Project of Guangzhou, No. B012000-X-005-01-05

Correspondence to: Chi-Hua Fang, Department of Hepatobiliary Surgery, Zhujiang Hospital, First Military Medical University, Guangzhou 510282, Guangdong Province, China. fch58520@sina.com

Telephone: +86-20-84360607 Fax: +86-20-61643210

Received: 2003-06-05 Accepted: 2003-07-31

Abstract

AIM: To study oval cells' pathological characteristics and relationship with the occurrence of hepatocellular carcinoma (HCC); to observe the form and structural characteristics of oval cells; to explore the expression characteristics of C-kit, PCNA mRNA and *c-myc* gene during the occurrence and development of HCC and the effect of ulinastatin (UTI) on C-kit and PCNA expression.

METHODS: One hundred and twenty-five SD rats fed on 3,3'-diaminobenzidine (DAB) to construct HCC models were divided into control group, cancer-inducing group and UTI intervention group. In each group, rat liver samples were collected at weeks 2, 4, 6, 8, 10, 12, 14, 16, 18, 20, 22 and 24 respectively to study pathological distribution characteristics of oval cells in the process of carcinogenesis under optical microscope. Oval cells were separated by the methods of improved density gradient centrifugation and their structural characteristics were observed under optical microscope and electronic microscope respectively; the oval cells expressing C-kit and PCNA in the collected samples were observed by the methods of immunohistochemistry and image analysis and the expression of *c-myc* mRNA was also detected by reverse transcription polymerase chain reaction (RT-PCR).

RESULTS: Oval cells proliferated firstly in the portal area then gradually migrated into hepatic parenchyma in the inducing group and intervention group. The oval cells distributed inside and outside the carcinoma nodes. The oval cells presented the characteristics of undifferentiated cells: a high ratio of nucleolus and cellular plasm and obvious nucleoli, rare organelle in plasm. Only a few mitochondria and endoplasmic reticulum and some villus-like apophysis on surface of cells could be seen. Cells stained with C-kit and PCNA antibody were mainly oval cells distributed in the portal area. The expression of *c-myc* mRNA increased with the progression of HCC. However, in the intervention group, UTI could retard its increase.

CONCLUSION: Oval cells work throughout the development of HCC, and might play important roles in this process. *c-myc* gene may be a kind of promoter gene of HCC, and play a key role in hepatic injury and development of HCC. UTI could retard the occurrence of HCC.

Fang CH, Gong JQ, Zhang W. Function of oval cells in hepatocellular carcinoma in rats. *World J Gastroenterol* 2004; 10(17): 2482-2487

<http://www.wjgnet.com/1007-9327/10/2482.asp>

INTRODUCTION

HCC is one of the most common malignant carcinomas in China. Because of its high rate of metastasis and recurrence and lack of typical symptoms in early stage, HCC has the second mortality rate among all the malignant carcinomas^[1,2]. Up to now, obvious progress has been made in the study of cell origin of HCC. One is that HCC is originated from abnormally differentiated oval cells, the other is that it results from dedifferentiation of mature liver cells. In order to probe the relationship between oval cells and HCC, we explored the pathologic distribution characteristics, structural features of oval cells in the pathogenesis of HCC in experimental SD rats and the expression characteristics of C-kit, PCNA and *c-myc* genes in oval cells.

MATERIALS AND METHODS

Materials

One hundred and twenty-five clearing SD rats (100±20 g) (Experimental Center of Zhongshan University) were fed in the environment of 18-28 °C and 40-70% humidity in Animal Feeding Unit, Zhujiang Hospital, First Military Medical University. DAB (Dako, Japan) was used as inducing drug for HCC in rat; proline, asparagic acid, serine phenylalanine, tyrosine pyruvate sodium, transferrin, epidermal growth factor (EGF) (Sigma, USA) and F12, F12/DMEM (1:1) (Gibco, USA), and fetal bovine serum (Sijiqing Co, Hangzhou, China) were used for culture medium for oval cells. Collagenase VI and density gradient centrifugation (percoll) (Sigma) were used for separating oval cells. C-kit polyclonal antibody (Sigma), immunohistochemical kits (SABC methods) and poly-lysine for adhibiting section, neutral resin for envelop section (Boshide Co, Wuhan); PCNA immunohistochemical kits (SP methods), DAB dyeing reagent (Zhongshan Co, Beijing); *c-myc* mRNA kit, total RNA extraction kits, DNA marker (100 bp), primers for polymerase chain reaction (PCR) and RNasin (Huamei Bioengineering Co), M-MLV reverse transcriptase (Promega USA), *Taq* DNA polymerase (Gibco), 4×dNTP (Sigma), amplification primer for reverse transcription polymerase chain reaction (RT-PCR) were synthesized by Shanghai Biotech Co. according to the GenBank database.

Methods

HCC model The method of constructing HCC model in the cancer-inducing group and inter group was according to the references^[3,4]. After fed on DAB for 14 wk, rats were given normal drinking water, but in control group, the rats were fed on standard food. In the interference group, as soon as the DAB was administrated, UTI (2-10⁴ U/kg) was injected into abdominal cavity, twice a week until wk 14^[5,6]. One hundred and twenty-five clearing SD rats were divided into control group (24 rats), cancer-inducing group (48 rats) and UTI interference group (48 rats), the other 5 rats were used to construct the

model of oval cells proliferation. Each group was divided into 12 sub-groups, and there were 2 rats in sub-group of the control group and the cancer-inducing group, 4 rats in sub-group of interference group. Two pieces of 1 cm×1 cm×1 cm tissue taken from the right liver lobe of each rat in sub-group were fixed in 40 g/L formaldehyde and 2-4 pieces of soybean-sized tissue taken from the left liver lobe of each rat in sub-group were placed respectively in the 0.5 mL centrifuge tube and preserved in a refrigerator at -80 °C at wk 2, 4, 6, 8, 10, 12, 14, 16, 18, 20, 22 and 24 respectively during construction of HCC model. The samples of right liver lobes were sliced serially to count cancerous nodes under low power microscope. Nodes more than 0.05 mm² were measured by the gridding ocular micrometer.

Separation of oval cells When the rats have been fed DAB for 4 wk, a large number of oval cells proliferated from the hepatic portal area, which could be identified by HE dyeing section analysis. Firstly, D-Hanks' solution was perfused through portal vein until the liver color turned yellow, then 1 g/L collagenase IV was affused to digest liver. The digested liver was put in a beaker, washed 3 times with Hank's solution, and minced thoroughly at the same time, then 0.6 g/L collagenase IV was added to further digest liver for 30 min at 37 °C. The cell suspension was filtrated through 100 holes/cm² sieve, then centrifuged at 300 r/min at 4 °C for 5 min, the cell suspension was extracted and centrifuged again at 2 000 r/min at 4 °C for 10 min. The upper layer solution abandoned, then cells were suspended again with 10 mL F12 solution. The density gradient centrifugation solution (percoll) was blended with 100 g/L NaCl at a ratio of 9:1 and diluted with F12 into the solution of 90%, 70% and 50%, respectively. Ten mL of each solution was put in a high-speed centrifugation tube of 50 mL, according to the concentration gradient of 90%, 70% and 50%. A 10 mL cell suspension was placed on the top of each tube, then centrifuged for 30 min at 4 °C, 12 000 g so that the oval cells were located between the centrifugation solution of 70% and 50%, then the oval cell suspension was extracted carefully to another tube. Hanks' solution was added with 5 kU/L benzylpenicillin and streptomycin A, then centrifuged at 1 000 r/min for 5 min, the precipitate was retained. Culture medium F12/DMEM (1:1) solution was added to suspend cells. Then the suspension was inoculated into 25 cm³ plastic culture bottles, according to the density of 2×10⁸/L, placed into incubating cabin with 5 mL/L CO₂ at 37 °C. After 24 h the culture solution was replaced and oval cells could be seen adhering to the bottle wall.

Culture of oval cells The culture medium consisted of 200 mL/L fetal bovine serum which was diluted with the solution of DMEM/F12(1:1) containing epidermal growth factor (20 µg/L), transferring (20 µg/L) and some kinds of amino acid. The culture medium was replaced every 2 or 3 d. When cells overgrew in the bottles, some parts of cells were transferred into another culture bottle. The culture medium in the bottles was extracted; F12 solution was added to clean the cells three times, then mixed with 2.5 g/L pancreatin to digest. The cells were observed under the microscope for about 1 min, then oval cells could be seen floating and then the culture medium was added to terminate digestion. After the cells were separated completely, they were inoculated into another bottle.

C-kit immunohistochemistry Carry sheet glasses were treated by polylysine. Paraffin sections (5 µm thick) were dewaxed by dimethylbenzene and alcohol respectively. After washed by 0.01 mol/L PBS for 2 min 3 times, the sections were incubated in 3 mL/L H₂O₂ solution for 10 min to inactivate endogenous peroxides, heated in citric acid sodium solution in microwave oven at 100 °C to retrieve antigen for 10 min and then cooled for 25 min. After washed with 0.1 mol/L PBS for 2 min 3 times, they were incubated with normal goat serum to block nonspecific binding of antibodies for 10 min at room temperature. The sections were then incubated with IgG of rabbit antiserum

against mouse at 37 °C for 24 h or at 4 °C overnight, washed with 0.01 mol/L PBS for 3 times for 2 min each, then incubated with goat IgG anti-rabbit at 37 °C for 20 min, washed with 0.01 mol/L PBS for 2 min 3 times, Reagent SABC was added and incubated at 37 °C for 20 min, section were washed again with 0.01 mol/L PBS for 3 times. The immunoreacted cells were then visualized by using DAB kits as follows: a drop of reagent A, B and C was added into 1 mL distilled water, then they were blended completely and dripped on the sections. The sections were counterstained with hematoxylin for 50 s, then dehydrated and observed with light microscope.

PCNA immunohistochemistry (SP methods) The SABC reagent was replaced by the solution of streptavidin marked with horse-radish peroxidase in the first steps and the other steps were the same as C-kit immunohistochemistry. C-kit protein was stained brown yellow. The localization of C-kit protein and its change in quantity were observed when the rats' livers were injured. PCNA protein was stained as brown yellow. The localization of PCNA positive cells in the hepatic lobule was observed and PCNA labeling index (proliferating index) was calculated by randomly observing 5 fields under high microscope in each section. The positive cells among 100 cells were counted in each field and mean values were taken.

RNA extraction and assessment The preserved 50-100 mg liver tissues were mixed and grinded evenly with 1 mL cold denaturant. A 1 mL lysis liquid was added into a 2.0 mL centrifuge tube and then mixed with 0.1 mL sodium acetate (pH4.0). A 100 mL phenol/chloroform mixture was mixed with the above mentioned liquid and intensely vibrated for 10 s, then placed on ice for 10 min. The liquid was centrifuged at 4 °C. The top layer liquid was transferred into a 1.5-mL centrifuge tube and kept at -20 °C for 15 min after mixed with isopropanol of identical volume. White jelly-like precipitate after centrifugation at 10 000 g for 15 min at 4 °C was the total RNA. RNA was resolved completely by 1 mL lysis and RNA precipitate and wall of the tube liquid were washed with 250 mol/L alcohol. Resolved RNA in RNase-free water and preserved it at -20 °C. The absorbance (A) of total RNA was measured by ultraviolet spectrophotometer and the RNA concentration(g/L) was $A_{260} \times \text{nucleic acid dilution times} \times 40 / 1\ 000 (A_{260} / A_{280})$ (if A of RNA > 1.8, the RNA is pure enough to be used in the following experiment).

Agarose electrophoresis RNA solution 1 µL mixed with 2 µL bromphenol blue buffer was electrophored in the level electrophoresis chamber treated by RNase-free water at 100 V for 20 min then the gelatum was taken to be observed. Three RNA straps of 28 s, 18 s, and 5 s could be seen through gel electrophoresis.

cDNA synthesis and PCR reaction A 2 µL (1 µg) total RNA, 4 µL (20 pmol) of c-myc downstream primer and 8 µL of RNA-free water were mixed well at the room temperature, put in water bath at 70 °C to degenerate for 5 min. Then they were put on ice for 1 min, centrifuged at 200 g for 30 s. A 5 µL M-MLV reverse transcriptase 5×Buffer, 5 µL dNTP (2.5 mmol/L), 5 µL rRNasin (20 U) and 5 µL M-MLV RT were added and the total reaction volume was 34 µL. The mixture was treated at 42 °C for 60 min and at 95 °C for 5 min to inactivate reverse transcriptase, then maintained at -30 °C. Sixteen µL of cDNA, 5 µL 10×Buffer (no MgCl₂), 3 µL solutions MgCl₂ (25 mmol/L), 4 µL (2.5 mmol/L) dNTP, 3 µL (15 pmol) of sense including target gene and mark gene respectively, 3 µL (15 pmol) antisense including target gene and mark gene respectively, 1 µL (3U) *Taq* DNA enzyme and 9 µL RNA-free water were mixed totally at the room temperature, and the above total reactive volume was 50 µL. Then a drop of paraffin oil treated at high temperature was added onto the surface of mixture, and degenerated at 94 °C for 5 min. PCR cycle was at 94 °C, 50 °C and 72 °C respectively, for 1 min each. After 35 cycles, an extension at 72 °C was performed

for 5 min.

Agarose electrophoresis A 8 μ L product of c-myc DNA was taken for caraphoresis in 20 g/L sepharose (containing small quantity EB), and two straps of 228-bp and 120-bp (the product of mark gene) were found under light. The caraphoresis strap of PCR was scanned and quantitatively analyzed with gel image analysis system.

Statistical analysis

Experiment results were analyzed with SPSS10.0 software. Data were analyzed with single-side analysis of variance and with LSD methods for inter-group analysis. Chi-squared test was used to compare rates between two groups. $P < 0.05$ indicates significant difference.

RESULTS

Pathological characteristics

The rats' liver cells in the early period of cancer-inducing group showed balloon-like degeneration under light microscope (1-8 wk). Since the 2nd wk in the cancer-inducing group, the oval cells started to proliferate in portal area and gradually migrated into liver parenchyma (Figure 1). The pseudo-lobules formed in the liver and oval cells migrated into lobules in the middle period from the 15th to 24th wk. The cancer cell nucleus presented in different sizes and karyokinesis often occurred. Cancer cells infiltrated toward the periphery of liver tissue, and at the same time, focal bleeding and necrosis obviously occurred. Huge amounts of leucocytes infiltration could be seen in the peripheral area of nodes and portal area, and lots of oval cell proliferations were shown in portal area and in cancer nodes (Figure 2). Beginning from the 2nd wk of cancer induction, the proliferation of oval cells could be seen in portal area. Firstly oval cells appeared in the epithelial lining of bile duct of portal area and then gradually proliferated and migrated into liver parenchyma. In the fibrosis formation period, the proliferation of oval cells could be seen in portal area and in its peripheral area. The volume of oval cells was about as big as one third of normal liver cells, round or oval-shaped and its margin was unclear with scant cytoplasm and basophils. The cell nucleus was round or oval shaped, with slight stain, vague membrane and obvious nucleolus. Oval cells proliferated first in portal area and then in liver limiting plate, migrated along liver sinusoids and to the middle part of lobules. These cells often presented as two lines or branches, destroying the neighboring liver cord. The left lobe liver cells were scattered among the proliferated oval cells that distributed inside and mainly outside of the cancer nodes. Oval cells showed the characteristics of undifferentiated cells: a big ratio of nucleus and plasm and obvious nucleoi, rare organele in plasm, only a few mitochondria, endoplasmic reticulum and some villus-like apophysis on surface of cells could be seen under the electronic microscope (Figure 3).

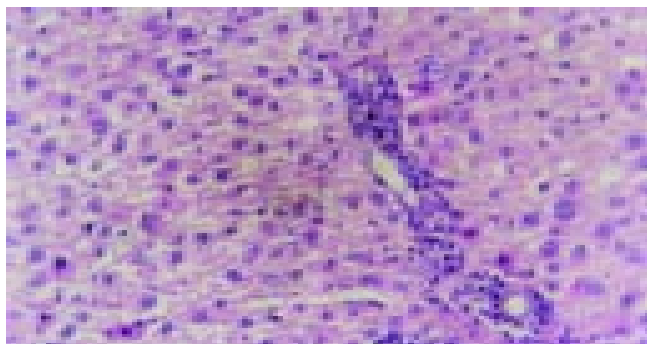


Figure 1 Early inflammatory liver tissues in cancer inducing group at the 2nd wk and the differentiation of oval cells in the portal area (HE staining, original magnification: $\times 200$).

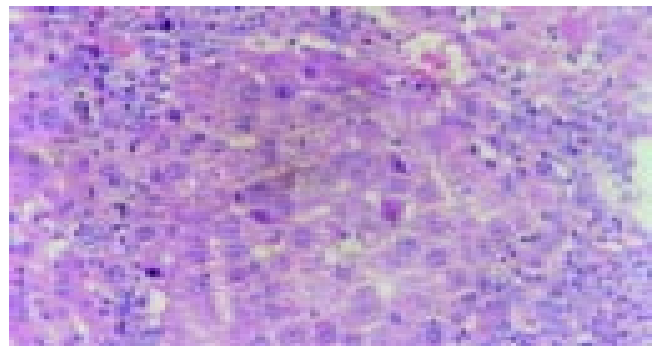


Figure 2 A large quantity of oval cells gathered around the cancer nodes in cancer inducing group at 20th wk (HE staining, original magnification: $\times 200$).

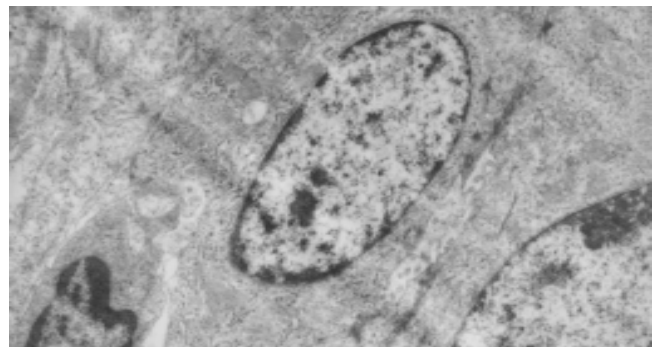


Figure 3 Electron microscopic observation showed: the volume of oval cell was about as big as one third of normal liver cell, round or oval shaped, scant cytoplasm with unclear cell margin.

The effect of UTI on cancer induction: in the early period, the balloon-like degeneration of liver cells was much milder than that of the liver cells in cancer-inducing group. The balloon-like degeneration of liver cells was obvious in the middle period and local liver cells became necrosis, liver lobes were destroyed and the liver fiber proliferated and the pseudo-lobules formed in the local area with a large amount of oval cell aggregating in the portal area and liver parenchyma could be seen. In the period of carcinoma formation, pseudo-lobules were seen apparently in large parts of liver parenchyma and a large number of oval cells aggregated to an extreme extent. Some liver cancer cells with column-like or glandular-like structure appeared in part of liver parenchyma and oval cells scattered among the cancer cells. The neoplasia nodes were counted as in Table 1.

Table 1 Number of cancerous nodes and cancer nodes' area in rat liver (mean \pm SD, $n=8$)

t/wk	Cases of hepatic cancer		Number of cancerous		Area of cancer nodes (mm ²)	
	A	B	A	B	A	B
2-4	0	0	0	0	0	0
6-8	0	0	0	0	0	0
10-12	2	0	4	0	9.5 \pm 8.2	0
14-16	6	2	15	5	10.7 \pm 8.7	5.8 \pm 4.5 ^a
18-20	8	4	17	9	11.4 \pm 8.9	8.5 \pm 7.6
22-24	8	4	16	10	11.2 \pm 9.3	8.6 \pm 7.3

^a $P < 0.05$ vs group A; A: cancer- induction group; B: intervention group.

Characteristics of c-kit positive stain cells

C-kit positive stain localized in cell plasm in normal liver showed brown-yellow and was mainly in the mitotic and proliferating

liver cells. At the 2nd wk in the cancer-inducing group, some c-kit positive stain cells, mainly oval cells, appeared in the portal area and punctated positive pigmentations could be seen in liver lobules as well. At the 8th wk, oval cells in the portal area in the cancer-inducing group were obviously positively stained, with some positive pigmentation forming patches and some punctating in the rim of portal area (Figure 4). At the 14th wk, the normal liver structure was replaced by a lot of pseudo-lobule and still a large number of c-kit positive stain cells could be seen which mainly gathered in portal area. In the 22nd wk in the cancer-inducing group, a large number of cancerous nodes formed and some positive cells scattered among them (Figure 5). The characteristics of c-kit positive staining cells in the samples of intervention group was almost identical with that in cancer-inducing group.

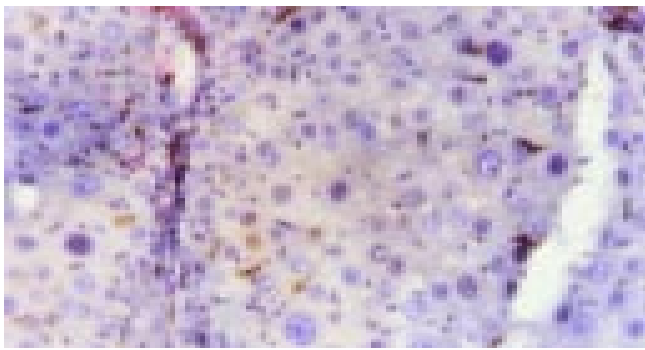


Figure 4 Expression of c-kit in liver tissue in cancer inducing group at the 8th wk. The oval cells were mainly stained in portal areas (Immunohistochemistry, $\times 200$).

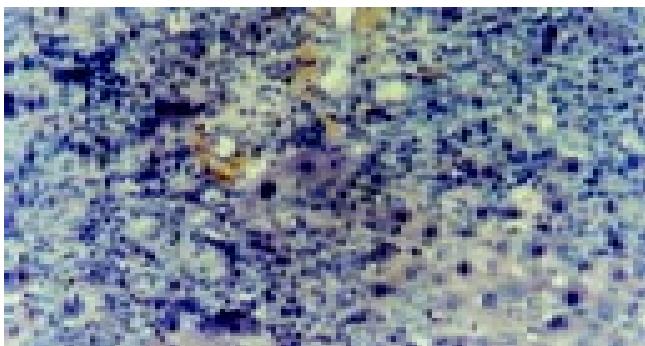


Figure 5 Expression of c-kit in the HCC tissue in cancer inducing group in the 24th wk (Immunohistochemistry, $\times 200$).

Characteristics of PCNA positive cells

PCNA positive staining located in the nucleus, as granules or diffusively. Occasionally positive stains were seen in normal liver tissue. At the 2nd wk of the cancer-induction, the PCNA positive cells firstly appeared among the oval cells in the portal area. At the 4th wk, a lot of hepatic cells were positively stained, especially in central vein area. At the 6th wk, also the middle stage of inflammatory process, PCNA positive cells were seen all over the lobules of liver. At the 8th wk, the number of PCNA cells was comparatively decreased and nuclei of positive cells around the portal area tended to become larger gradually. From the 10th to 14th wk, some of the proliferating hepatic fibers were lightly stained and the oval cells in portal area still over expressed PCNA. From the 16th to 24th wk, a large number of cancerous nodes formed and PCNA over expressed in some cancerous nodes (Figure 6), while the number of positive cells was relatively fewer in necrotic cancerous nodes than in other areas and the number of dotted positive stain cells adjacent to the carcinoma tissue was apparently fewer than inside the

carcinoma tissue. In the intervention group, PCNA positive stain cells firstly appeared among the oval cells in portal area, and then their number increased with the aggravation of hepatic intoxication by DAB. The PCNA positive stain rate and expression level reached the peak at the 10th wk in rat liver. The distribution characteristics of PCNA positive cells were similar to those in the cancer inducing group when HCC formed. The labeling index of PCNA positive stain cells is shown in Table 2.

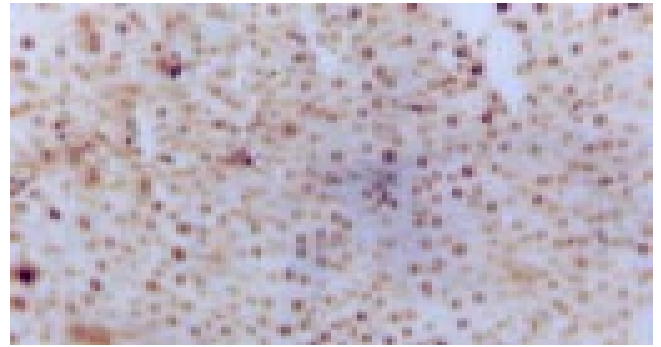


Figure 6 PCNA expression in HCC tissue in the cancer inducing group at the 24th wk (Immunohistochemistry, $\times 200$).

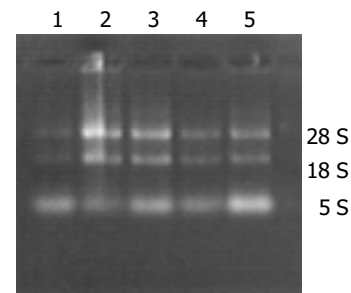


Figure 7 Electrophoresis image of total RNA in rat liver tissue.

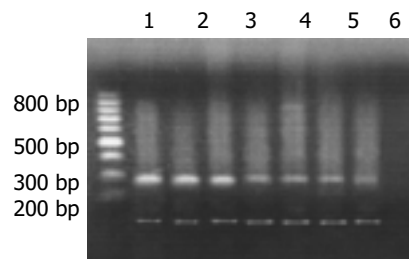


Figure 8 Products of RT-PCR of c-myc mRNA (up-strap: 228-bp c-myc; low-strap: 120-bp β -actin; Lanes 1 and 2: Hepatocarcinoma tissue; Lane 3: Hepatocirrhosis tissue; Lanes 4-6: Inflammation tissue; Lane 7: Normal tissue).

Table 2 PCNA positive index and c-myc relative gray value in liver (mean \pm SD)

t/wk	Cancer induction (n = 8)			Intervention (n = 8)		Control (n = 4)
	PCNA (%)	RGV	PCNA (%)	RGV	PCNA (%)	RGV
2-4	14.1 \pm 7.5 ^a	1.3 \pm 1.0	7.6 \pm 3.3	1.2 \pm 0.6	3.0 \pm 1.2	1.0 \pm 0.3
6-8	48.2 \pm 15.5 ^b	2.0 \pm 0.7	24.3 \pm 7.4 ^a	1.5 \pm 0.7	2.9 \pm 1.5	1.1 \pm 0.4
10-12	23.7 \pm 9.6 ^a	3.6 \pm 1.2 ^a	35.1 \pm 6.5 ^b	2.2 \pm 0.9	3.3 \pm 0.9	1.1 \pm 0.5
14-16	25.9 \pm 5.1 ^a	5.7 \pm 1.4 ^a	21.5 \pm 4.2 ^a	3.5 \pm 1.0 ^a	3.7 \pm 2.1	1.3 \pm 0.4
18-20	36.8 \pm 6.3 ^b	7.8 \pm 1.4 ^a	29.6 \pm 7.6 ^a	6.5 \pm 1.1 ^a	3.6 \pm 1.3	1.3 \pm 0.6
22-24	41.2 \pm 8.2 ^b	8.2 \pm 2.2 ^b	30.2 \pm 8.7 ^a	8.0 \pm 1.3 ^b	3.5 \pm 2.2	1.3 \pm 0.4

^aP<0.05, ^bP<0.01 vs group C; RGV: Relative gray value.

c-myc gene expression

Expression of *c-myc* gene existed in normal rat liver tissue, but the expression quantity is relatively small. The expression of *c-myc* mRNA increased as soon as liver was intoxicated with DAB and its expression quantity tended to gradually increase with the aggravation of liver injury. In the period of carcinoma formation, *c-myc* mRNA expression level also gradually rose with the development of HCC (Table 2, Figures 7, 8). The intervention of UTI could not stop but could retard the increase of expression level of *c-myc* mRNA.

DISCUSSION

Oval cells are round or oval shaped with scant and basophilic cytoplasm, and round or oval shaped nucleus, small and clear light stained nucleolus and clear nuclear membrane. Because they can differentiate towards hepatic cells or bile duct epithelial cells when hepatic cells are severely injured or the proliferation is inhibited, oval cells are considered as a kind of progenitor cells with potential bilateral differentiation^[7]. It is reported that the activation of Ito cells was probably a precondition for the activation of oval cells and stimulates oval cells in the portal areas to migrate towards the hepatic fibrosis area. Consequently, oval cells may participate in the formation of HCC^[8-11].

There is no doubt that there are hepatic stem cells in hepatic tissues, but where do the hepatic stem cells come from? Some researchers thought that they were originated from the terminal biliary duct of portal area^[12,13], but some insisted that they were from the canal of Hering^[14-16], and some even found authentic evidence that the oval cells came from bone marrow stem cells^[17-20]. In order to identify the origin of hepatic stem cells and the relationship between hepatic stem cells and the development of HCC, we carried out the study on the surface marker antigen *c-kit* with immunohistochemical methods, and found that: (1) In the early stage of hepatic injury, the *c-kit* positive stain cells firstly appeared among the oval cells in the portal area. (2) In the late stage of inflammatory lesion, *c-kit* was over expressed in the oval cells in the portal area and positive pigmentation presented as patches. (3) During the period of hepatic proliferation and fibrosis, positive expression of *c-kit* in portal area decreased compared with that in the late stage of inflammatory lesion. (4) In period of the formation of HCC, heteromorphisms of cancer cells were obvious and *c-kit* was still expressed in portal area. (5) At the beginning of inflammatory lesion, there were small quantities of *c-kit* positive cells in hepatic lobules with smaller nuclei and more were found near portal area. During the period of hepatic fibrosis, *c-kit* positive cells were rarely seen in hepatic lobules, but during the formation of HCC, *c-kit* positive cells appeared both inside and around the cancerous nodes. (6) In the normal hepatic tissues, *c-kit*-positive stain cells could be occasionally observed in the mitotic and proliferating hepatic cells. From these results, we can conclude that: (1) Oval cells had the highest expression level of *c-kit* in the portal area from hepatic injury to the occurrence and development of HCC. As it has been proved that the oval cells originate from bile duct epithelial cells in the portal area, we suggest that the terminal bile ducts are an important source of hepatic stem cells. (2) In the course of hepatic injury, *c-kit* positive cells could be found in hepatic lobules as well, especially near the portal area, which may be related to migration of oval cells along hepatic fibrosis into hepatic lobules. (3) *C-kit* was not only expressed in hepatic stem cells, but in the mitotic and proliferating hepatic cells, which indicated that *c-kit* might be a specific mark antigen for a type of juvenile cells, express only in a certain stage of mitotic and proliferation of hepatic cells. (4) *C-kit* positive stain cells played a role in the whole process of occurrence and development

of HCC and appeared in cancerous nodes, so we thought that hepatic stem cells, just as was reported in literature, were involved in the occurrence and development of HCC.

PCNA is a type of M_r 36 000 nuclear protein which is only synthesized and expressed in proliferating cells. Cyto-dynamics shows that PCNA begins to increase in the late G_1 phase in the cell cycle, reaches the peak in the S phase and begins to decrease in the G_2 -M phase, in this way it regulates the replication of DNA^[21-23]. Therefore, PCNA can effectively reflect the proliferation ability of cells. In this experiment we found that the high level expression of PCNA appeared firstly in the oval cells in portal area at the early stage of inflammation, significantly higher than adjacent tissue. When the mitosis and proliferation of hepatic cells were inhibited, oval cells presented firstly with active proliferation and DNA was synthesized in a large amount in nucleus. The farther they were away from the portal area, the more mature the oval cells differentiated and the larger the size of nucleus tended to be. Thus the expression of PCNA distributed radiatively and regionally around the portal area and the regional predominance was kept for a long time in the process of carcinoma induction. Oval cells took part in the whole process of development of HCC, we could speculate that there might be close relationship between the development of HCC and the PCNA overexpressing oval cells.

c-myc gene is a maintaining gene for malignant tissue, coding for a protein located in nucleolus, a type of DNA conjugated protein with the function of transcription regulation^[24-27]. This experiment suggested that the expression of *c-myc* gene increased slightly at the beginning of hepatic injury and the expression of *c-myc* mRNA increased progressively with the aggravation of hepatic injury. The expression of *c-myc* mRNA also tended to increase with the development of HCC. The above results indicated that: (1) As an oncogene, *c-myc* might be a promoter gene for HCC and played an important role in maintaining hepatic injury and hepatocyte carcinomatous change. (2) During the development of HCC, the expression level of *c-myc* continued to increase, indicating that *c-myc* was not only a maintaining gene for malignant carcinoma, but the quantity of its expression was a symbol for the degree of malignancy and progression of HCC.

UTI is a kind of broad-spectrum trypsin inhibitor extracted from human beings' urine. It has been found that UTI plays a prominent role in preventing cancer cells from spread. Some researchers pointed out that there were combination spots with UTI on the surface of nearly all kinds of cancer cells membrane and UTI could inhibit cancer cells to secrete granulocyte protein lyase, fibrinoclastase, matrix metalloproteinase and collagenase^[28,29], which can degrade peripheral matrix and lead tumor cells to spread, by combining with their receptors on the surface of cancer cell membrane. Some clinical reports showed that UTI could inhibit the cancer cells to combine with other anti-cancer drugs^[30]. In this experiment, the interference of UTI throughout development of HCC and its effect on HCC were observed. It was found that from the 14th to 16th wk, the occurrence rate of HCC in the interference group was 25% (2/8), which was significantly different ($P < 0.05$) from that of cancer induction group at the same time. During the 18th to 20th wk and the 22nd to 24th wk, the occurrence rate of HCC was both 50% (4/8), which was lower than that in the cancer inducing group at the same time. UTI's effect on inhibiting the occurrence of cancer was related to the following factors: (1) The occurrence of HCC needed certain micro-environment and UTI could inhibit some local cells from releasing inflammatory mediators by stabilizing lysosome membrane, then the inflammatory cells' chemotaxis was inhibited and local inflammation was relieved, thus it could inhibit the occurrence of tumor by stabilizing micro-environment. (2) Researches proved that UTI had fairly strong function to inhibit and clear away oxygen-derived free

radicals, while a lot of oxygen-derived free radical receptors existed on the surfaces of liver cells and oval cells, so possibly UTI could protect liver tissue from being damaged by oxygen-derived free radicals. Furthermore, during the whole process of cancer induction, the average cancer node area of liver rats in interference group was smaller than that of cancer inducing group at the same time points ($P < 0.05$), especially at the early stage of carcinogenesis, which indicated that UTI could partly inhibit the growth and local spreading of tumor cells.

The results that interference of UTI could not stop but could retard the increase of the expression of *c-myc* mRNA indicate two points: (1) UTI can prevent the occurrence of hepatic injury and HCC to some extent, but can not inhibit the expression of *c-myc* gene, which might be related with inhibitory effect on hepatic tissue inflammation and protective effect on hepatocytes of UTI. (2) The expression of *c-myc* gene closely relates to the severity of hepatic injury.

REFERENCES

- Dominguez-Malagon H, Gaytan-Graham S. Hepatocellular carcinoma: an update. *Ultrastruct Pathol* 2001; **25**: 497-516
- Hou L, Li Y, Jia YH, Wang B, Xin Y, Ling MY, Lü S. Molecular mechanism about lymphogenous metastasis of hepatocarcinoma cells in mice. *World J Gastroenterol* 2001; **7**: 532-536
- Liu H, Nobumoto K, Yamada Y, Higashi K, Hiai H. Modulation of genetic resistance to hepatocarcinogenesis in DRH rats by partial hepatectomy. *Cancer Lett* 2003; **196**: 13-16
- Karmakar R, Banik S, Chatterjee M. Inhibitory effect of vitamin D3 on 3'methyl-4-dimethyl-amino-azobenzene-induced rat hepatocarcinogenesis: a study on antioxidant defense enzymes. *J Exp Ther Oncol* 2002; **2**: 193-199
- Biswas SJ, Khuda-Bukhsh AR. Effect of a homeopathic drug, Chelidonium, in amelioration of p-DAB induced hepatocarcinogenesis in mice. *BMC Complement Altern Med* 2002; **2**: 4
- Koizumi R, Kanai H, Maezawa A, Kanda T, Nojima Y, Naruse T. Therapeutic effects of uLinastatin on experimental crescentic glomerulonephritis in rats. *Nephron* 2000; **84**: 347-353
- Freitas I, Fracchiolla S, Baronzio G, Griffini P, Bertone R, Sitar GM, Barni S, Gerzeli G, Sacco MG. Stem cell recruitment and liver de-differentiation in MMTV-neu (ErbB-2) transgenic mice. *Anticancer Res* 2003; **23**: 3783-3794
- Benedetti A, Di Sario A, Casini A, Ridolfi F, Bendia E, Pignini P, Tonnini C, D'Ambrosio L, Feliciangeli G, Macarri G, Svegliati-Baroni G. Inhibition of the NA(+)/H(+) exchanger reduces rat hepatic stellate cell activity and liver fibrosis: an *in vitro* and *in vivo* study. *Gastroenterology* 2001; **120**: 545-556
- Nakamura Y, Trosko JE, Chang CC, Upham BL. Psyllium extracts decreased neoplastic phenotypes induced by the Ha-Ras oncogene transfected into a rat liver oval cell line. *Cancer Lett* 2004; **203**: 13-24
- Martel M, Sarli D, Colecchia M, Coppa J, Romito R, Schiavo M, Mazzaferro V, Rosai J. Fibroblastic reticular cell tumor of the spleen: report of a case and review of the entity. *Hum Pathol* 2003; **34**: 954-957
- Shan CM, Li J. Study of apoptosis in human liver cancers. *World J Gastroenterol* 2002; **8**: 247-252
- Paku S, Schnur J, Nagy P, Thorgeirsson SS. Origin and structural evolution of the early proliferating oval cells in rat Liver. *Am J Pathol* 2001; **158**: 1313-1323
- Toshihior M. Hepatic stem cells: from bone marrow cells to hepatocytes. *Biochem Biophys Res Commun* 2001; **281**: 1-5
- Vessey CJ, de la Hall PM. Hepatic stem cells: a review. *Pathology* 2001; **33**: 130-141
- Badve S, Logdberg L, Lal A, de Davila MT, Greco MA, Mitsudo S, Saxena R. Small cells in hepatoblastoma lack "oval" cell phenotype. *Mod Pathol* 2003; **16**: 930-936
- Okano J, Shiota G, Matsumoto K, Yasui S, Kurimasa A, Hisatome I, Steinberg P, Murawaki Y. Hepatocyte growth factor exerts a proliferative effect on oval cells through the PI3K/AKT signaling pathway. *Biochem Biophys Res Commun* 2003; **309**: 298-304
- Laperche Y. Oval cells and liver regeneration. *Med Sci* 2003; **19**: 697-698
- Hsu HC, Ema H, Osawa M, Nakamura Y, Suda T, Nakauchi H. Hematopoietic stem cells express Tie-2 receptor in the murine fetal liver. *Blood* 2000; **96**: 3757-3762
- Crosbie OM, Reynolds M, McEntee G, Traynor O, Hegarty JE, O'Farrelly C. *In vitro* evidence for the presence of hematopoietic stem cells in the adult human liver. *Hepatology* 1999; **29**: 1193-1198
- Petersen BE, Bowen WC, Patrene KD, Mars WM, Sullivan AK, Murase N, Boggs SS, Greenberger JS, Goff JP. Bone marrow as a potential source of hepatic oval cells. *Science* 1999; **284**: 1168-1170
- Arroyo MP, Wang TS. Schizosaccharomyces pombe replication and repair proteins: proliferating cell nuclear antigen (PCNA). *Methods* 1999; **18**: 335-348
- Miura M. Detection of chromatin-bound PCNA in mammalian cells and its use to study DNA excision require. *J Radiat Res* 1999; **40**: 1-12
- Gong Y, Deng S, Zhang M, Wang G, Minuk GY, Burczynski F. A cyclin-dependent kinase inhibitor (p21(WAF1/CIP1)) affects thymidine incorporation in human liver cancer cells. *Br J Cancer* 2002; **86**: 625-629
- Jonas JC, Laybutt DR, Steil GM, Trivedi N, Pertusa JG, Van de Castele M, Weir GC, Henquin JC. High glucose stimulates early response gene c-Myc expression in rat pancreatic beta cells. *J Biol Chem* 2001; **276**: 35375-35381
- Deng CX, Brodie SG. Roles of BRCA1 and its interacting proteins. *Bioessays* 2000; **22**: 728-737
- Fields WR, Desiderio JG, Putnam KP, Bombick DW, Doolittle DJ. Quantification of changes in c-myc mRNA levels in normal human bronchial epithelial (NHBE) and lung adenocarcinoma (A549) cells following chemical treatment. *Toxicol Sci* 2001; **63**: 107-114
- Langa F, Lafon I, Vandormael-Pournin S, Vidaud M, Babinet C, Morello D. Healthy mice with an altered c-myc gene: role of the 3' untranslated region revisited. *Oncogene* 2001; **20**: 4344-4353
- Kobayashi H. Suppression of urokinase expression and tumor metastasis by bikunin overexpression (mini-review). *Hum Cell* 2001; **14**: 233-236
- Kobayashi H, Suzuki M, Tanaka Y, Hirashima Y, Terao T. Suppression of urokinase expression and invasiveness by urinary trypsin inhibitor is mediated through inhibition of protein kinase C- and MEK/ERK/c-Jun-dependent signaling pathways. *J Biol Chem* 2001; **276**: 2015-2022
- Noie T, Sugawara Y, Harihara Y, Takayama T, Kubota K, Ohashi Y, Makuuchi M. Kinetics of urinary trypsin inhibitor in patients undergoing partial hepatectomy. *Scand J Gastroenterol* 2001; **36**: 410-416

A candidate DNA vaccine elicits HCV specific humoral and cellular immune responses

Li-Xin Zhu, Jing Liu, Ye Ye, You-Hua Xie, Yu-Ying Kong, Guang-Di Li, Yuan Wang

Li-Xin Zhu, Jing Liu, Ye Ye, You-Hua Xie, Yu-Ying Kong, Guang-Di Li, Yuan Wang, State Key Laboratory of Molecular Biology, Institute of Biochemistry and Cell Biology, Shanghai Institutes for Biological Sciences, Chinese Academy of Sciences, Shanghai 200031, China

Supported by the National High Technology R&D Program of China, No. 2001AA215171

Correspondence to: Professor Yuan Wang, Institute of Biochemistry and Cell Biology, Shanghai Institutes for Biological Sciences, Chinese Academy of Sciences, Yue-Yang Road 320, Shanghai 200031, China. wangy@sibs.ac.cn

Telephone: +86-21-54921103 **Fax:** +86-21-54921011

Received: 2004-02-02 **Accepted:** 2004-02-21

Abstract

AIM: To investigate the immunogenicity of candidate DNA vaccine against hepatitis C virus (HCV) delivered by two plasmids expressing HCV envelope protein 1 (E1) and envelope protein 2 (E2) antigens respectively and to study the effect of CpG adjuvant on this candidate vaccine.

METHODS: Recombinant plasmids expressing HCV E1 and E2 antigens respectively were used to simultaneously inoculate mice with or without CpG adjuvant. Antisera were then collected and titers of anti-HCV antibodies were analyzed by ELISA. One month after the last injection, animals were sacrificed to prepare single-cell suspension of splenocytes. These cells were subjected to HCV antigen specific proliferation assays and cytokine secretion assays to evaluate the cellular immune responses of the vaccinated animals.

RESULTS: Antibody responses to HCV E1 and E2 antigens were detected in vaccinated animals. Animals receiving CpG adjuvant had slightly lower titers of anti-HCV antibodies in the sera, while the splenocytes from these animals showed higher HCV-antigen specific proliferation. Analysis of cytokine secretion from the splenocytes was consistent with the above results. While no antigen-specific IL-4 secretion was detected for all vaccinated animals, HCV antigen-specific INF- γ secretion was detected for the splenocytes of vaccinated animals. CpG adjuvant enhanced the secretion of INF- γ but did not change the profile of IL-4 secretion.

CONCLUSION: Vaccination of mice with plasmids encoding HCV E1 and E2 antigens induces humoral and cellular immune responses. CpG adjuvant significantly enhances the cellular immune response.

Zhu LX, Liu J, Ye Y, Xie YH, Kong YY, Li GD, Wang Y. A candidate DNA vaccine elicits HCV specific humoral and cellular immune responses. *World J Gastroenterol* 2004; 10(17): 2488-2492 <http://www.wjgnet.com/1007-9327/10/2488.asp>

INTRODUCTION

Hepatitis C virus (HCV) infection is a worldwide health problem^[1]. Up to now, no effective medical treatment is available for the majority

of HCV infected patients^[2,3], while new infections are continuously emerging from blood transfusion, needle sharing, unprotected sex, close contact of HCV infected patient and other unidentified sources^[4]. Thus to control the spread of HCV by vaccination becomes an urgent task, especially in developing countries including China, where there is a large infected population.

Various routes were taken to develop a vaccine against HCV infection. Recombinant HCV antigens purified from *E.coli*, yeast or insect cells could not protect the vaccinee from virus challenge^[5], possibly due to the fact that post-translational modification of the virus antigens in mammalian cells is greatly different from that in the bacterial or yeast cells. So the study on vaccine development has been focused on mammalian systems. Although many efforts have been made in vaccine development and some encouraging results have been obtained^[5-8], no effective vaccine is available.

The RNA genome of HCV has a high mutation rate, which explains the existence of many genotypes, subtypes and quasispecies^[9-10]. Although there is still a possibility to develop a universal vaccine against HCV of all genotypes, the use of local HCV strain in vaccine study is preferred. Our laboratory has been focusing on DNA vaccine development^[11] using an HCV strain isolated from a patient in northern China^[12], since DNA vaccine is effective in eliciting cellular immune responses^[13] which play key roles in viral clearance.

Envelope proteins were the first choice in the development of vaccines against virus infection. HCV envelope protein 2 has become the major target in HCV vaccine development not only because it is the putative major envelope protein^[14], but also because E2 could mediate the binding of HCV particle to host cells^[15] and is the ligand of the possible HCV receptor CD81 on the host cell surface^[16]. It makes E2 an attractive choice for vaccine development as it has been shown to be a major target of immune response in HCV infected patients^[17,18]. Previous studies also revealed multiple neutralizing epitopes in E2 proteins^[19-22]. Another envelope protein of HCV, E1, is also desirable for vaccine development, since its possible role in maintaining the natural conformation of E2 protein (through E1-E2 complex)^[23] and the possibility of its cooperation with E2 in mediating host cell binding and entry^[24]. However, low expression levels of both E1 and E2 proteins were observed when they were expressed in a single open reading frame (data not shown). In this study, we expressed HCV E1 and E2 proteins separately and analyzed the immune responses of DNA vaccination delivered by two plasmids encoding HCV E1 and E2 proteins respectively.

Recent studies showed that the immune system responded to CpG motifs by activating potent Th1-like immune responses^[25]. There have also been several reports demonstrating that CpG could enhance humoral immune responses elicited by DNA vaccination^[24,25], possibly due to indirect effect of enhanced cellular immune responses. The effect of CpG adjuvant on the immune response elicited by the candidate DNA vaccine was also investigated in this study.

MATERIALS AND METHODS

Plasmids, CpG oligodeoxynucleotide (ODN) and cells

For the construction of pSecTagB/sE2, the fragment of HCV

E2 (aa. 384–661) was amplified using plasmid pUC18/E^[12] as template with following primers: sense, 5' GGCGTTAAGCTTAA CACCTACGTG3' (HindIII site underlined); antisense, 5' CAG GAATTCTCACTCTGATCTATC3' (EcoRI site underlined). Insertion of the PCR product into pSecTagB (Invitrogen, California) resulted in pSecTagB/sE2, in which a secretion signal was provided at the N-terminal of E2 sequence. The recombinant plasmid was sequenced before further experiments.

HCV E1 encoding plasmid pSec-preS1-E1t340 (pSecTagB/sE1) was constructed as previously described^[26]. CpG ODN1826 with phosphorothioate backbone was synthesized in Promega (Shanghai) according to the published sequence 5' TCCATGA CGTTCCTGACGTT3'^[27]. The cell line used for transient expression of the recombinant plasmids, BHK-21, was maintained in DMEM supplemented with 50 mL/L FCS and antibiotics under 50 mL/L CO₂ in a humidified 37 °C incubator.

Transient expression

Transfection of BHK-21 cells with HCV-encoding plasmid or empty vector using lipofectAMINE (Invitrogen) was done according to the manuals of the manufacturer. Cells were harvested 48 h after transfection, lysed in SDS-PAGE loading buffer, and subjected to SDS-PAGE (10%). The resolved samples were then transferred onto nitrocellulose membrane and probed with polyclonal anti-E1 (Liu *et al.*, unpublished data) or polyclonal anti-E2 antisera^[28]. The signals were visualized with SuperSignal West Pico stable peroxide solution (Pierce, USA).

DNA immunization and sera preparation

Four groups of 5 female BALB/c mice (6–8 weeks old) purchased from the Shanghai Laboratory Animal Center were injected 3 times in quadriceps muscles: group 1, with 100 µg pSecTagB in 100 µL PBS; group 2, with 50 µg pSecTagB/sS1E1 and 50 µg pSecTagB/sE2 in a total volume of 100 µL PBS; group 3, with 100 µg pSecTagB together with 10 µg CpG in a total volume of 100 µL PBS; group 4, with 50 µg pSecTagB/sS1E1, 50 µg pSecTagB/sE2 and 10 µg CpG in a total volume of 100 µL PBS. Injections were performed at 0, 4 and 8 wk and blood samples were taken at -2, 2, 6 and 10 wk. Mice were bled under anesthesia through the retro-orbital plexus. Blood was incubated at room temperature for 4 h and centrifuged at 2 700 r/min at 4 °C for 10 min. Obtained sera were stored at -20 °C.

Anti-HCV antibody analysis

Enzyme-linked immunosorbent assay (ELISA) was used to determine the presence of antibodies against HCV E1 and E2 antigens in serum samples. *E. coli*-expressed HCV E1 (aa 192 to 315) or HCV E2 (aa 450 to 565^[31]) was used to coat 96-well plates (MaxiSorp Surface, Nunc) at the concentration of 1 µg/mL. The antigens were suspended in PBS with 0.2 g/L sodium azide and incubated overnight at 4 °C. After the plates were washed with PBS plus 0.5 g/L Tween 20 (PBS-T) and blocked in blocking buffer (50 g/L fat-free milk powder in PBS-T), twofold serial dilutions of serum samples in blocking buffer were added and incubated for 2 h at 37 °C. After three wash steps with PBS-T, horseradish peroxidase (HRP) conjugated goat-anti-mouse IgG (Dako, Denmark; 1 000-fold diluted in blocking buffer) was added and incubated for 1 h at 37 °C. The plate was then developed with substrate buffer (50 mmol/L Na₂HPO₄, 25 mmol/L citric acid, 75 µg/mL 3,3',5,5'-tetramethylbenzidine, 0.15 mL/L H₂O₂). After 30 min of incubation at room temperature, the reaction was stopped by adding 0.5 mol/L H₂SO₄, and absorbance was measured at 450 nm on a microplate reader (Model 450, Bio-Rad Laboratories). Antibody titers were calculated as the highest dilution which gave a positive reading. The cutoff value was set as mean absorbency (A) of sera from the control mice vaccinated with non-recombinant plasmid multiplied by 2.

Preparation of splenocytes

Mice were sacrificed by cervical dislocation. Spleens from these mice were ground on metal mesh to prepare single-cell suspension in grinding media (RPMI1640 supplemented with 100 mL/L FCS, 1 mmol/L Sodium pyruvate and 50 µmol/L β-ME). Red blood cells were lysed by incubating the splenocyte preparations with lysis buffer (0.15 mol/L NH₄Cl, 10 mmol/L KHCO₂, 0.1 mmol/L EDTA, pH7.2–7.4) briefly and then washed with grinding media. The cells were resuspended in a small volume of grinding media and counted in the presence of Trypan blue. Splenocytes were immediately used for further experiments.

Assay for HCV antigen specific splenocyte proliferation

Splenocytes from vaccinated mice or naïve mice were diluted to 4×10⁶/mL with grinding media and plated onto 24-well-plates at 2 mL/well. The cells were *in vitro* stimulated with 500 ng E2 (aa 450 to 565^[31]) or mock stimulated for 3 d. The media were collected for cytokine assay. Fresh grinding medium with 0.5 µCi/mL [³H] thymidine (Amersham Pharmacia Biotech) was added for another 24 h. Cells were then washed with PBS and 100 g/L trichloroacetic acid (TCA), incubated with 100 g/L TCA for 10 min at 37 °C. Afterwards, TCA was removed and cells were lysed with lysis buffer containing 0.33 mol/L NaOH and 10 g/L sodium dodecyl sulfate (SDS). [³H] thymidine incorporation in the cell lysates was measured by liquid scintillation counting. Antigen specific proliferation was presented by stimulation index (SI): SI = cpm of the cells stimulated by antigen/cpm of mock stimulated cells. Splenocytes from naïve mice were used to monitor the specificity of this assay.

Analysis of HCV antigen specific cytokine secretion

Media from the *in vitro* stimulated splenocytes were collected and precleared by centrifugation at 10 000 g and 4 °C for 10 min. Concentration of INF-γ and IL-4 in the media was determined by ELISA using the mouse cytokine assay kits (Jingmei Biotech, Shenzhen) according to the protocols provided by the manufacturer. HCV E2 specific cytokine secretion was represented by stimulation index (SI): SI = cytokine secreted upon E2 stimulation/cytokine secreted upon mock stimulation. Splenocytes from naïve mice were used to monitor the specificity of this assay.

Statistical analysis

Statistical analysis was performed with unpaired 2-sided Student *t* test. Differences with *P* values <0.05 were considered significant.

RESULTS

Transient expression of HCV antigens in mammalian cells

Because the expression level was low when E1 and E2 were expressed in one open reading frame (data not shown), we expressed HCV E1 and E2 genes in separate plasmids in this study. To achieve high-level expression and proper post-translational modification of HCV envelope proteins, the pSecTagB vector with an efficient secretion signal of IgG molecules was chosen. Plasmid expressing HCV E2 was constructed as described in Materials and Methods. C-terminal hydrophobic sequence of E2 was truncated to facilitate the secretion of E2 and to obtain complex-type glycosylation modification, which was presented on the surface of HCV particles^[29]. Secreted E2 protein was shown to have better antigenicity, possibly due to its proper modification by Golgi enzymes^[30]. Plasmid pSecTagB/sE1 was taken as another component of the candidate DNA vaccine since high-level expression of E1 with this plasmid was observed previously in transiently and stably transfected NIH3T3 cells^[26]. Before vaccination experiment, BHK-21 cells were transfected with pSecTagB/sE1 and pSecTagB/sE2, respectively, to check if they

would properly express the target HCV proteins in this cell line. By Western blot, both E1 and E2 were detected as glycosylated proteins with MW higher than those of polypeptide backbones, respectively (Figure 1). Secreted products were also detected for E1^[26] and E2 (data not shown).

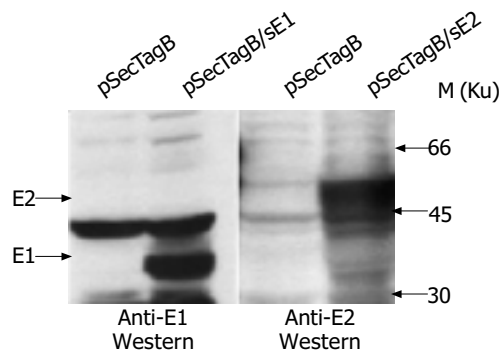


Figure 1 Transient expression with plasmids used in vaccination. Plasmids used for transfection are indicated at the top of each lanes. E1 and E2 products are indicated by arrowheads.

Humoral immune responses after DNA vaccination

DNA vaccination using the above characterized plasmids was carried out as described in Materials and Methods. After two injections, HCV E1 and E2 specific antibodies were detected in the sera of several mice. Without CpG adjuvant, the seroconversion rate was 2/5 for anti-E1 antibody, and 1/5 for anti-E2 antibody. When CpG was included as an adjuvant, the seroconversion rate was 3/4 for anti-E1 antibody and 2/4 for anti-E2 antibody. After the third injection, all animals became seroconverted to both anti-E1 and anti-E2 antibodies. The highest anti-E1 titer was 1:320 after the third injection for mice receiving plasmids only, while the highest titer for mice receiving plasmids with CpG was 80. The highest anti-E2 titers for both groups reached 1 280, but the average anti-E2 titer for mice receiving CpG was slightly lower than that for those receiving no CpG (Table 1).

E2 specific splenocyte proliferation

All the animals were sacrificed 30 d after the last injection to analyze cellular immune responses of the memory phase. Single-cell suspension of splenocytes was prepared for each individual animal. Splenocytes were immediately cultured in the presence of HCV E1 peptide or E2 protein. [³H] thymidine was then added to the cells to measure HCV antigen specific proliferation. In our experiments, HCV E1 specific proliferation was not observed, neither was E1 specific cytokine secretion (data not shown), possibly due to insufficient stimulation. For E2 specific splenocyte proliferation, as shown in Figure 2, animals vaccinated with pSecTagB only or pSecTagB plus CpG had stimulation indexes similar to that of naïve mice. Some of the animals vaccinated with

plasmids pSecTagB/sE1+pSecTagB/sE2 showed E2 specific splenocyte proliferation while the others did not. This gave an average SI slightly higher than that of pSecTagB vaccinated mice. Animals vaccinated with HCV gene encoding plasmids together with CpG all showed E2 specific splenocyte proliferation, which resulted in a significant difference ($P = 0.005$) of SI between animals injected with pSecTagB/sE1+pSecTagB/sE2+CpG and animals injected with pSecTagB+CpG.

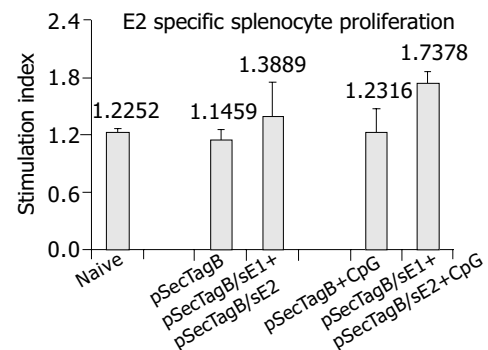


Figure 2 E2-specific splenocyte proliferation. Error bars represent the standard errors. Asterisk indicates the significant difference of the average SI between animals injected with (pSecTagB/sE1+pSecTagB/sE2+CpG) and animals injected with (pSecTagB+CpG) ($P = 0.005$).

E2 specific cytokine secretion

Cellular immune responses were also evaluated by cytokine secretion assay of the *in vitro* stimulated splenocytes from all vaccinated animals. INF- γ secretion is a marker of Th1 type antigen-specific cellular immune responses and plays key roles in fighting virus infection. Mice injected with pSecTagB/sE1+pSecTagB/sE2 showed heterogeneous cellular immune responses, some had E2 stimulated INF- γ secretion, while the rest did not. This resulted in a slightly higher average of SI compared to the control group injected with pSecTagB (Figure 3A). Mice injected with pSecTagB/sE1+pSecTagB/sE2+CpG all showed highly E2-specific INF- γ secretion, showing a SI higher than 3, while the control group injected with pSecTagB+CpG had an average SI similar to those of naïve mice and mice injected with pSecTagB alone. The difference of SI between the experiment group and its control group was very significant ($P = 0.0003$).

IL-4 secretion is a marker of Th2-like cellular immune responses. No significant difference in IL-4 secretion was detected between all groups receiving different inoculums (Figure 3B). IL-4 secretion of the vaccinated animals was similar to that of naïve mice, indicating that Th2-like cellular immune response was decreased to basal level, if there was ever a Th2-like response. In terms of IL-4 secretion, no effect of CpG was detected.

Table 1 Anti-HCV titers¹ after the third injection

Vaccine	Anti-E1 titers				
	1	2	3	4	5
pSecTagB/sE1+pSecTagB/sE2 ²	320	40	Dead animal	320	320
pSecTagB/sE1+pSecTagB/sE2+CpG ³	80	80	Dead animal	80	80
	Anti-E2 titers				
	1	2	3	4	5
pSecTagB/sE1+pSecTagB/sE2 ²	160	160	Dead animal	1 280	1 280
pSecTagB/sE1+pSecTagB/sE2+CpG ³	160	160	Dead animal	160	1 280

¹Titers were determined as described in Materials and Methods. Serial dilution of anti-sera started from 1:40, thus titers lower than 40 were not determined and considered 0. ²The cutoff value was established as mean A of sera from the control mice vaccinated with pSecTagB. ³The cutoff value was established as mean A of sera from the control mice vaccinated with pSecTagB+CpG.

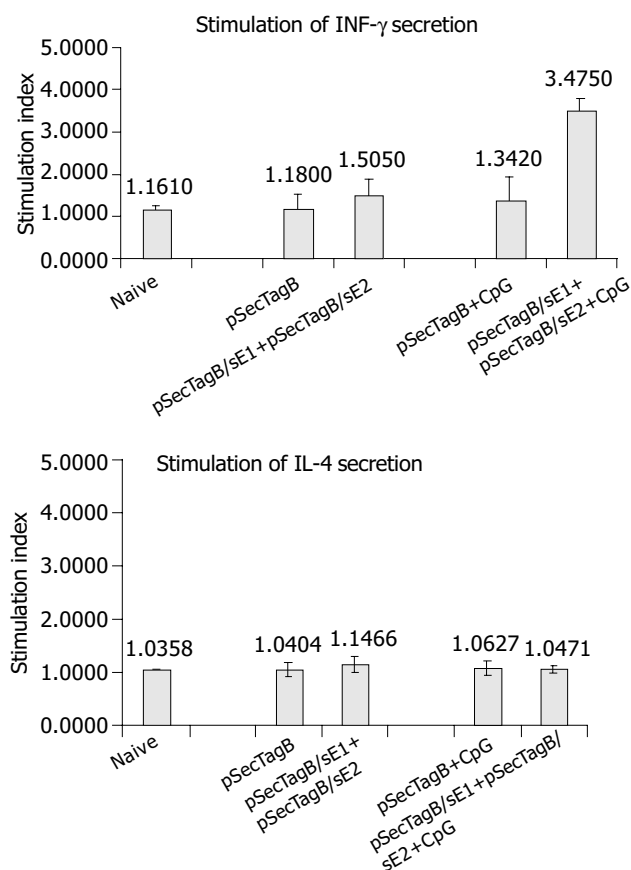


Figure 3 E2-specific cytokine secretion. Error bars represent the standard errors. Asterisk indicates the very significant difference of the average SI between animals injected with (pSecTagB/sE1+pSecTagB/sE2+CpG) and animals injected with (pSecTagB+CpG) in terms of INF- γ secretion ($P = 0.0003$).

DISCUSSION

In this study, target HCV antigens encoded by the DNA vaccine candidate, E1 and E2, were delivered by two separate plasmids that achieved higher-level expression and appropriate glycosylation of both antigens. DNA immunization results demonstrated that this DNA vaccine candidate could induce HCV specific humoral and cellular immune responses in mice. Anti-E2 titer obtained in this study was similar to our previous study^[11], which was also comparable to the results from other laboratories^[31-35]. We also detected comparable levels of anti-E1 antibodies in the sera of vaccinated mice, which together with anti-E2 antibodies, might be important in neutralizing the circulating HCV virus and preventing its spread in patients. HCV antigen specific splenocyte proliferation indicated that our candidate DNA vaccine was able to induce cellular immune response, which was critical in viral clearance. Cytokine secretion analysis revealed that the cellular immune response is Th1 type, which could activate CTL to remove cells with HCV antigen expression. Studies of HCV patients showed that protection against HCV infection was positively correlated with cellular immune responses^[36,37], indicating that cellular immune responses might be more important in evaluating a candidate vaccine. The ability of our candidate vaccine to induce HCV specific cellular immune responses makes it a favorable choice in the development of prophylactic and therapeutic vaccine against HCV.

CpG motif, that is, CpG dinucleotide in particular base context (XCGY, where X is any base but C, and Y is any base but G), was first found to be immunoinactive in activating B cells^[38]. These CpG motifs are prevalent in bacterial and many viral DNAs but are heavily methylated and suppressed in vertebrate genomes^[38,39]. Recent studies have shown that the immune

system could respond to CpG motifs by activating potent Th1-like immune responses^[23]. Several reports demonstrated that CpG could enhance humoral immune responses elicited by DNA vaccination^[24,25], possibly due to indirect effect of enhanced cellular immune responses. In our vaccination experiment, we observed that after the second injection, the seroconversion rate for mice receiving CpG adjuvant was higher than that for those not receiving CpG. This enhanced humoral immune response at the early stage was likely due to the indirect positive effect of CpG on antigen presentation (via activation of antigen presenting cells by Th1). However, after the third injection, when all animals became seroconverted, those who received CpG as an adjuvant showed lower titers of both anti-E1 and anti-E2. This was consistent with the notion that when Th1-like response is the major immune response, Th2-like response is usually inhibited, followed by decreased antibody production. Further analysis of antigen specific cytokine secretion was consistent with this explanation. E2 specific INF- γ secretion was enhanced in splenocytes from those animals receiving CpG in vaccination, while this adjuvant did not change the E2 specific IL-4 secretion profile. These results indicated that CpG enhanced the Th1-like cellular immune response.

Apart from DNA vaccine, live virus vaccine and peptide vaccine are also efficient in inducing cellular immune response. Live virus vaccine using several different viral vectors has been under investigation^[8,28,40], with continuous promising progresses. However, the interest in peptide vaccine is diminishing. The problem lies in the polymorphism of MHC molecules in the population. Certain individuals may have the MHC molecules necessary to bind a specific antigenic peptide, while others may not. Thus, the universality of a vaccine based on a specific peptide becomes a concern. Recently, combinational vaccination strategy with different species of vaccine components has been successful in laboratory in protecting against some elusive infectious reagents^[41,42]. Combinational vaccination could reduce host immune responses against the viral vector itself, thus enhancing the efficiency of delivery. More importantly, combinational vaccination with different components could activate different components of the host immune surveillance system and result in enhanced immune responses. Our next effort will be focused on combinational vaccination with DNA vaccine described above as one component.

ACKNOWLEDGEMENT

We thank Professor Yu Wang (Peking University) for providing HCV cDNA for this study.

REFERENCES

- 1 **Cohen JC.** The scientific challenge of hepatitis C. *Science* 1999; **285**: 26-30
- 2 **McHutchison JG,** Gordon SC, Schiff ER, Shiffman ML, Lee WM, Rustgi VK, Goodman ZD, Ling MH, Cort S, Albrecht JK. Interferon alfa-2b alone or in combination with ribavirin as initial treatment for chronic hepatitis C. Hepatitis International Therapy Group. *N Engl J Med* 1998; **339**: 1485-1492
- 3 **Zein CO,** Zein NN. Advances in therapy for hepatitis C infection. *Microbes Infect* 2002; **4**: 1237-1246
- 4 **Williams I.** Epidemiology of hepatitis C in the United States. *Am J Med* 1999; **107**: 2S-9S
- 5 **Choo QL,** Kuo G, Ralston R, Weiner A, Chien D, Van Nest G, Han J, Berger K, Thudium K, Kuo C. Vaccination of chimpanzees against infection by the hepatitis C virus. *Proc Natl Acad Sci U S A* 1994; **91**: 1294-1298
- 6 **Fournillier A,** Depla E, Karayiannis P, Vidalin O, Maertens G, Trepo C, Inchauspe G. Expression of noncovalent hepatitis C virus envelope E1-E2 complexes is not required for the induction of antibodies with neutralizing properties following DNA immunization. *J Virol* 1999; **73**: 7497-7504

- 7 **Gordon EJ**, Bhat R, Liu Q, Wang YF, Tackney C, Prince AM. Immune responses to hepatitis C virus structural and nonstructural proteins induced by plasmid DNA immunizations. *J Infect Dis* 2000; **181**: 42-50
- 8 **Makimura M**, Miyake S, Akino N, Takamori K, Matsuura Y, Miyamura T, Saito I. Induction of antibodies against structural proteins of hepatitis C virus in mice using recombinant adenovirus. *Vaccine* 1996; **14**: 28-36
- 9 **Davis GL**. Hepatitis C virus genotypes and quasispecies. *Am J Med* 1999; **107**: 21S-26S
- 10 **Chen S**, Wang YM. Genetic evolution of structural region of hepatitis C virus in primary infection. *World J Gastroenterol* 2002; **8**: 686-693
- 11 **Zhu J**, Wang CL, Zhu LX, Kong YY, Wang Y, Li GD. DNA immunization with recombinant HCV E2 expression plasmids. *Shengwu Huaxue Yu Shengwu Wuli Xuebao* 2002; **34**: 445-451
- 12 **Wang Y**, Okamoto H, Tsuda F, Nagayama R, Tao QM, Mishiho S. Prevalence, genotypes, and an isolate (HC-C2) of hepatitis C virus in Chinese patients with liver disease. *J Med Virol* 1993; **40**: 254-260
- 13 **Gurunathan S**, Wu CY, Freidag BL, Seder RA. DNA vaccines: a key for inducing long-term cellular immunity. *Curr Opin Immunol* 2000; **12**: 442-447
- 14 **Hijikata M**, Kato N, Ootsuyama Y, Nakagawa M, Shimotohno K. Gene mapping of the putative structural region of the hepatitis C virus genome by *in vitro* processing analysis. *Proc Natl Acad Sci U S A* 1991; **88**: 5547-5551
- 15 **Rosa D**, Campagnoli S, Moretto C, Guenzi E, Cousens L, Chin M, Dong C, Weiner AJ, Lau JY, Choo QL, Chien D, Pileri P, Houghton M, Abrignani S. A quantitative test to estimate neutralizing antibodies to the hepatitis C virus: cytofluorimetric assessment of envelope glycoprotein 2 binding to target cells. *Proc Natl Acad Sci U S A* 1996; **93**: 1759-1763
- 16 **Pileri P**, Uematsu Y, Campagnoli S, Galli G, Falugi F, Petracca R, Weiner AJ, Houghton M, Rosa D, Grandi G, Abrignani S. Binding of hepatitis C virus to CD81. *Science* 1998; **282**: 938-941
- 17 **Zonaro A**, Ravaggi A, Puoti M, Kremendorf D, Albertini A, Cariani E. Differential pattern of sequence heterogeneity in the hepatitis C virus E1 and E2/NS1 proteins. *J Hepatol* 1994; **21**: 858-865
- 18 **Shimizu YK**, Hijikata M, Iwamoto A, Alter HJ, Purcell RH, Yoshikura H. Neutralizing antibodies against hepatitis C virus and the emergence of neutralization escape mutant viruses. *J Virol* 1994; **68**: 1494-1500
- 19 **Zibert A**, Schreier E, Roggendorf M. Antibodies in human sera specific to hypervariable region 1 of hepatitis C virus can block viral attachment. *Virology* 1995; **208**: 653-661
- 20 **Lechner S**, Rispeter K, Meisel H, Kraas W, Jung G, Roggendorf M, Zibert A. Antibodies directed to envelope proteins of hepatitis C virus outside of hypervariable region 1. *Virology* 1998; **243**: 313-321
- 21 **Meunier JC**, Fournillier A, Choukhi A, Cahour A, Cocquerel L, Dubuisson J, Wychowski C. Analysis of the glycosylation sites of hepatitis C virus (HCV) glycoprotein E1 and the influence of E1 glycans on the formation of the HCV glycoprotein complex. *J Gen Virol* 1999; **80**(4 Pt 1): 887-896
- 22 **Meyer K**, Basu A, Ray R. Functional features of hepatitis C virus glycoproteins for pseudotype virus entry into mammalian cells. *Virology* 2000; **276**: 214-226
- 23 **Krieg AM**. CpG motifs in bacterial DNA and their immune effects. *Annu Rev Immunol* 2002; **20**: 709-760
- 24 **Moldoveanu Z**, Love-Homan L, Huang WQ, Krieg AM. CpG DNA, a novel immune enhancer for systemic and mucosal immunization with influenza virus. *Vaccine* 1998; **16**: 1216-1224
- 25 **Encke J**, zu Putnitz J, Stremmel W, Wands JR. CpG immunostimulatory motifs enhance humoral immune responses against hepatitis C virus core protein after DNA-based immunization. *Arch Virol* 2003; **148**: 435-448
- 26 **Zhu J**, Kong YY, Liu J, Zhang ZC, Wang Y, Li GD. Secretory expression of different C-terminal truncated HCV E1 proteins in mammalian cells and characterization of the expressed products. *Shengwu Huaxue Yu Shengwu Wuli Xuebao* 2001; **33**: 634-640
- 27 **Chu RS**, Targoni OS, Krieg AM, Lehmann PV, Harding CV. CpG oligodeoxynucleotides act as adjuvants that switch on T helper 1 (Th1) immunity. *J Exp Med* 1997; **186**: 1623-1631
- 28 **Liu J**, Zhu L, Zhang X, Lu M, Kong Y, Wang Y, Li G. Expression, purification, immunological characterization and application of *Escherichia coli*-derived hepatitis C virus E2 proteins. *Biotechnol Appl Biochem* 2001; **34**(Pt2): 109-119
- 29 **Sato K**, Okamoto H, Aihara S, Hoshi Y, Tanaka T, Mishiho S. Demonstration of sugar moiety on the surface of hepatitis C virions recovered from the circulation of infected humans. *Virology* 1993; **196**: 354-357
- 30 **Inudoh M**, Nyunoya H, Tanaka T, Hijikata M, Kato N, Shimotohno K. Antigenicity of hepatitis C virus envelope proteins expressed in Chinese hamster ovary cells. *Vaccine* 1996; **14**: 1590-1596
- 31 **Zucchelli S**, Capone S, Fattori E, Folgori A, Di Marco A, Casimiro D, Simon AJ, Laufer R, La Monica N, Cortese R, Nicosia A. Enhancing B- and T-cell immune response to a hepatitis C virus E2 DNA vaccine by intramuscular electrical gene transfer. *J Virol* 2000; **74**: 11598-11607
- 32 **Tedeschi V**, Akatsuka T, Shih JW, Battegay M, Feinstone SM. A specific antibody response to HCV E2 elicited in mice by intramuscular inoculation of plasmid DNA containing coding sequences for E2. *Hepatology* 1997; **25**: 459-462
- 33 **Ou-Yang P**, Hwang LH, Tao MH, Chiang BL, Chen DS. Co-delivery of GM-CSF gene enhances the immune responses of hepatitis C viral core protein-expressing DNA vaccine: role of dendritic cells. *J Med Virol* 2002; **66**: 320-328
- 34 **Encke J**, zu Putnitz J, Geissler M, Wands JR. Genetic immunization generates cellular and humoral immune responses against the nonstructural proteins of the hepatitis C virus in a murine model. *J Immunol* 1998; **161**: 4917-4923
- 35 **Dou J**, Liu K, Chen Z, Wo J, He N, Liu Y, Zhang M, Wang X, Xu C. Effect of immunization in mice with recombinant DNA encoding the hepatitis C virus structural protein. *Chin Med J* 1999; **112**: 1036-1039
- 36 **Cooper S**, Erickson AL, Adams EJ, Kansopon J, Weiner AJ, Chien DY, Houghton M, Parham P, Walker CM. Analysis of a successful immune response against hepatitis C virus. *Immunity* 1999; **10**: 439-449
- 37 **Lechner F**, Wong DK, Dunbar PR, Chapman R, Chung RT, Dohrenwend P, Robbins G, Phillips R, Klenerman P, Walker BD. Analysis of successful immune responses in persons infected with hepatitis C virus. *J Exp Med* 2000; **191**: 1499-1512
- 38 **Krieg AM**, Yi AK, Matson S, Waldschmidt TJ, Bishop GA, Teasdale R, Koretzky GA, Klinman DM. CpG motifs in bacterial DNA trigger direct B-cell activation. *Nature* 1995; **374**: 546-549
- 39 **Jones PA**. The DNA methylation paradox. *Trends Genet* 1999; **15**: 34-37
- 40 **Ezelle HJ**, Markovic D, Barber GN. Generation of hepatitis C virus-like particles by use of a recombinant vesicular stomatitis virus vector. *J Virol* 2002; **76**: 12325-12334
- 41 **Amara RR**, Villinger F, Altman JD, Lydy SL, O'Neil SP, Staprans SI, Montefiori DC, Xu Y, Herndon JG, Wyatt LS, Candido MA, Kozyr NL, Earl PL, Smith JM, Ma HL, Grimm BD, Hulsey ML, Miller J, McClure HM, McNicholl JM, Moss B, Robinson HL. Control of a mucosal challenge and prevention of AIDS by a multiprotein DNA/MVA vaccine. *Science* 2001; **292**: 69-74
- 42 **Haddad D**, Liljeqvist S, Stahl S, Hansson M, Perlmann P, Ahlborg N, Berzins K. Characterization of antibody responses to a Plasmodium falciparum blood-stage antigen induced by a DNA prime/protein boost immunization protocol. *Scand J Immunol* 1999; **49**: 506-514

• *H pylori* •

***Helicobacter pylori* cagA, iceA and vacA genotypes in patients with gastric cancer in Taiwan**

Hwai-Jeng Lin, Chin-Lin Perng, Wen-Ching Lo, Chew-Wun Wu, Guan-Ying Tseng, Anna Fen-Yau Li, I-Chen Sun, Yueh-Hsing Ou

Hwai-Jeng Lin, I-Chen Sun, Division of Gastroenterology, Department of Medicine, VGH-TAIPEI, Taiwan, China

Chin-Lin Perng, I-Lan Hospital, Department of health, Taiwan, China

Wen-Ching Lo, Zhongxiao Municipal Hospital, Taipei, Taiwan, China

Chew-Wun Wu, Division of General Surgery, Department of Surgery, VGH-TAIPEI, Taiwan, China

Guan-Ying Tseng, Ton-Yen General Hospital, Hsin-Chu, Taiwan, China

Anna Fen-Yau Li, Department of Pathology, VGH-TAIPEI, Taiwan, China

Yueh-Hsing Ou, Institute of Biotechnology in Medicine, School of Medical Technology and Engineering, and School of Medicine, National Yang-Ming University, Taiwan, China

Supported by VGH 91-274, NSC 91-2314-B075-127

Correspondence to: Professor Hwai-Jeng Lin, Division of Gastroenterology, Department of Medicine, VGH-TAIPEI, Shih-Pai Rd, Sec 2, Taipei, 11217, Taiwan, China. hjlin@vghtpe.gov.tw

Telephone: +886-2-28712121 Ext. 2015 **Fax:** +886-2-28739318

Received: 2003-11-12 **Accepted:** 2003-12-15

Ou YH. *Helicobacter pylori* cagA, iceA and vacA genotypes in patients with gastric cancer in Taiwan. *World J Gastroenterol* 2004; 10(17): 2493-2497

<http://www.wjgnet.com/1007-9327/10/2493.asp>

INTRODUCTION

Helicobacter pylori (*H pylori*) is one of the most common bacterial infections of humans^[1]. It has been closely linked to chronic gastritis, peptic ulcer, gastric cancer and MALT-lymphoma^[2,3]. It has heterogeneous genotypes and phenotypes^[4,5].

The International Agency for Research on Cancer of the World Health Organization recommends that *H pylori* be classified as a group I carcinogen^[6]. In a long-term follow-up study, gastric cancers developed in 36 (2.9%) of the 1 246 infected and none of the 280 uninfected patients ($P < 0.001$)^[7]. Enomoto *et al.* and Uemura *et al.* also confirmed that very few patients who had gastric cancer were not infected with *H pylori*^[7,8].

The clinical outcome of *H pylori* infection was supposed to be linked to certain strains, *e.g.* vacuolating cytotoxin (*vacA*) and the cytotoxin-associated gene (*cagA*)^[9,10]. However, controversy exists concerning the relationship between *H pylori* and gastric cancer. It is now evident that approximately 25-50% of the world's population is infected by *H pylori*. Why, then, did only a minority of them develop gastric cancer? A report of an epidemiological study in Africa suggested that *H pylori* infection did not always directly correlate with the risk for gastric cancer^[11]. The same phenomenon occurred in southern Asia^[12]. The prevalence of *H pylori* is high in India and Bangladesh, but low gastric cancer rates have been reported. In addition, Louw *et al.* did not find difference in the prevalence of *H pylori* infection when comparing gastric cancer cases with matched controls^[13].

How could the above phenomenon be explained? Although *H pylori* infection is very common, there is geographic distribution of different subtypes^[14]. Is it possible that different subtypes of *H pylori* cause different outcomes? In Taiwan, specific genotypes of *H pylori* have been found in patients with peptic ulcer or non-ulcer dyspepsia^[15,16]. There is no report concerning the genotype of gastric cancer in Taiwan so far. The aim of this study was to determine the *vacA*, *cagA*, and *iceA* genotypes of *H pylori* in patients with gastric cancer as compared with those in patients with peptic ulcer or chronic gastritis in Taiwan.

MATERIALS AND METHODS

Patients with gastric cancer, peptic ulcers (gastric ulcer or duodenal ulcer, at least 5 mm in diameter) or chronic gastritis were invited to enter the study. Patients with pregnancy, bleeding tendency (platelet count less than 50 000/mm³, prothrombin time less than 30%, or taking anti-coagulants), age under 10, or over 90 years, and inability to cooperate were excluded from the study. The study was approved by the Clinical Research Committee of the Veterans General Hospital, Taipei.

Endoscopic examination and biopsy were performed after informed consent was obtained. In patients with peptic ulcer or chronic gastritis, we took one specimen from the antrum of

Abstract

AIM: *Helicobacter pylori* (*H pylori*) has been linked to chronic gastritis, peptic ulcer, gastric cancer and MALT-lymphoma. The link of genotypes of *H pylori* to gastric cancer remains controversial. The aim of this study was to investigate the *H pylori* *vacA* alleles, *cagA* and *iceA* in patients with gastric cancer in Taiwan.

METHODS: Patients with gastric cancer, peptic ulcer and chronic gastritis were enrolled in this study. We obtained biopsy specimens from the stomach at least 2 cm away from the tumor margin in patients with gastric cancer, and from the antrum of stomach in patients with peptic ulcer or chronic gastritis. DNA extraction and polymerase chain reaction were used to detect the presence or absence of *cagA* and to assess the polymorphism of *vacA* and *iceA*.

RESULTS: A total of 168 patients (gastric ulcer: 77, duodenal ulcer: 66, and chronic gastritis: 25) were found to have positive PCR results of the biopsy specimens from patients with peptic ulcer and chronic gastritis. We found positive *cagA* (139/168, 83%), *m2* (84/168, 50%) and *iceA1* (125/168, 74%) strains in the majority of patients. In patients with gastric cancer, the *vacA* *s1a* and *s1c* subtypes were less commonly found than those in non-cancer patients (35/66 *vs* 127/168, $P = 0.0001$ for *s1a* and 13/66 *vs* 93/168, $P < 0.0001$ for *s1c*). In the middle region, the *m1T* strain in patients with gastric cancer was more than that of non-cancer patients (23/66 *vs* 33/168, $P = 0.02$).

CONCLUSION: In Taiwan, *H pylori* with positive *vacA* *s1a*, *cagA* and *iceA1* strains are found in the majority of patients with gastric cancer or non-cancer patients. In patients with gastric cancer, the *vacA* *s1a* and *s1c* subtypes are less and *m1T* is more than in patients with peptic ulcer and chronic gastritis.

Lin HJ, Perng CL, Lo WC, Wu CW, Tseng GY, Li AFY, Sun IC,

each patient for rapid urease test, one specimen from the gastric antrum for DNA extraction and PCR assay. In patients with gastric cancer, we took two specimens from the stomach at least 2 cm from the cancer part for rapid urease test and DNA extraction and PCR assay. Lysates of gastric mucosa biopsy specimens were used for PCR. DNA of gastric biopsy specimens was extracted according to the method described by Boom^[17]. Briefly, biopsy specimens were homogenized in guanidinium isothiocyanate, using a sterile micropestle. DNA was extracted, washed and eluted in 100 µL of 10 mmol/L Tris-HCL (pH 8.3). Two microliters of the eluted DNA were used for each PCR reaction.

All pathological samples from patients with gastric cancer were evaluated by a single experienced pathologist, and classified in accordance with the Lauren classification as diffuse, intestinal or mixed types^[18]. The description of advanced gastric cancer was based on Borrmann's classification^[19]. The morphological subtypes of early gastric cancer were classified according to the guidelines of Japanese Endoscopy Society^[20].

Oligonucleotide primers for PCR amplification of specific segments are shown in Table 1^[15,21,22]. For *vacA* evaluation, the PCR program comprised 35 cycles of denaturation (at 94 °C for 1 min), annealing (at 56 °C for 2 min, extension at 72 °C for 1 min), and one final extension (at 72 °C for 10 min). For *cagA*, amplification was performed with 35 cycles of denaturation (at 94 °C for 1 min, annealing at 56 °C for 2 min, extension at 72 °C for 1 min), and one final extension (at 72 °C for 5 min). For *iceA* amplification, amplifications were performed with 40 cycles of denaturation (at 95 °C for 30 s), annealing (at 50 °C for 45 s), extension (at 72 °C for 45 s) and one final extension (at 72 °C for 10 min).

The association between *H pylori* genotypes and clinical diseases was determined using the chi-square test with Yates' correction or Fisher's exact test when appropriate. A *P* value less than 0.05 was considered statistically significant.

RESULTS

Patients with peptic ulcer and chronic gastritis

Between January 2002 and February 2003, a total of 278 patients with peptic ulcer or chronic gastritis were included in this study. There were 200 males and 78 females with a mean age of 62.1 years, 95% C.I.: 61.1-64.3 years. One hundred and forty patients had gastric ulcers, 101 patients had duodenal ulcers, 37 patients

had chronic gastritis. Among these patients, 168 patients (65.9%) (comprising 25 patients with chronic gastritis, 77 patients with gastric ulcer, and 66 patients with duodenal ulcer) were found to have positive PCR (Table 2). Of them, the urease test was found to be positive in 152 patients (90.5%). There was no significant difference in age of the patients with chronic gastritis (mean: 51 years, 95% CI: 42.8-59.2 years), gastric ulcer (65.3 years, 62.3-68.9), duodenal ulcer (58.9 years, 54.7-63.1) and gastric cancer (69 years, 67-91).

In the s-region, *vacA* s1a was most frequently found (76%, 127/168, *P*<0.001 vs s1b, s1c and s2) followed by s1c (93/168, 55%), s1b (9/168, 5%), and s2 (2/168, 1%) (Table 3). In the m-region, m2 was most frequently found (84/168, 50%) (*P*<0.0001 vs m1T and m1), followed by m1T (33/168, 20%) and m1 (2/168, 2%). *CagA* was found in 139 patients (83%). *IceA1* was found most commonly in comparison with *iceA2* (125 vs 29, *P*<0.0001).

Patients with gastric cancer

A total of 167 patients with gastric cancers were enrolled in this study (mean age: 69 y/o, 95% CI: 67.0-91.0, sex M/F: 130/37). We obtained specimens through endoscopic biopsy from 66 patients and surgery from 101 patients. After PCR assessment of gastric specimens, a total of 66 patients (39.5%) were found to be positive (24 patients from endoscopic biopsy and 42 patients from surgical specimens) (Table 3). We found early gastric cancer in seven patients (type IIc: 2, IIc+III: 5) and advanced gastric cancer in 59 patients (Borrmann type I: 7, II: 28, III: 14, IV: 10) (Table 4).

Among these patients, 35 (53%) were found to have *vacA* s1a (*P*<0.001 vs s1c, s1b, and s2), followed by s1c (13 patients, 20%) (*P*<0.001 vs s1b and s2) and s1b (1 patient, 2%), s2 (1 patient, 2%) (Table 3). In the m-region, m2 was most commonly found (32 patients, 48%) (*P*<0.0001 vs m1) followed by m1T (23 patients, 35%) and m1 (1 patient, 2%). In the *iceA* subtypes, *iceA1* was most commonly found (39 patients, 59%) followed by *iceA2* (15 patients, 23%) (*P*<0.0001). *CagA* was found in 76% (50/66) of the patients.

The genotypes between early gastric cancer and advanced gastric cancer were similar (Table 4). There was no difference of genotypes according to Borrmann's classification (Table 5). Regarding the histological classification, there was no difference of genotypes among the diffuse type, intestinal type and mixed types (Table 6).

Table 1 Oligonucleotide primers used for *cagA*, *vacA* and *iceA* genotyping

Region detected	Primer designation	Primer sequence	Size of PCR product (bp)	References
s1 and s2	VA1-F	5'ATGGAATACAACAACACACC3'	259/286	14
	VA1-R	5'CTGCTTGAATGCGCCAAACTTTATC3'		
s1a	SS1-F	5'GTCAGCATCACACCGCAAC3'	190	20
s1b	SS3-F	5'AGCGCCATACCGCAAGAG3'	187	20
s1c	S1C-F	5'CTYGCTTTAGTRGGGYTA3'	213	26
M1	VA3-F	5'GGTCAAAATGCGGTCATGG3'	290	20
	VA3-R	5'CCATTGGTACCTGTAGAAAC3'		
M1T	m1T-F	5'GGTCAAAATGCGGTCATGG3'	290	14
	m1T-R	5'CTCTTAGTGCCATAAAGAAACA3'		
M2	VA4-F	5'GGAGCCCCAGGAAACATTG3'	352	20
	VA4-R	5'CATAACTAGCGCCTTGAC3'		
iceA1	iceA1F	5'GTGTTTTTAACCAAAGTATC3'	247	21
	iceA1R	5'CTATAGCCASTYTCTTTGCA3'		
iceA2	iceA2F	5'GTTGGGTATATCACAATTTAT3'	229	21
	iceA2R	5'TTRCCCTATTTTCTAGTAGGT3'		
lcagA	lcagAD008	5'ATAATGCTAAATTAGACAACCTTGAGCGA3'	297	8
	lcagAR008	5'TTAGAATAATCAACAACATCACGCCAT3'		

Table 2 Genotypes of *H. pylori* in patients with non-gastric cancer (chronic gastritis, gastric ulcer and duodenal ulcer) (%)

Diagnosis	No of Patients	s1a	s1b	s1c	s2	s1a+s1c	s1a+s1b	s1b+s1c	s1a+s1b+s1c	m1	m1T	m2	m1T+m2	cagA	iceA1	iceA2	iceA1+iceA2
Chronic gastritis	25	21 (84)	0 (0)	14 (56)	0 (0)	11 (44)	0 (0)	0 (0)	0 (0)	0 (0)	8 (32)	12 (48)	2 (8)	22 (88)	22 (88)	2 (8)	0 (0)
Gastritic ulcer	77	59 (77)	1 (1)	42 (55)	0 (0)	36 (47)	0 (0)	0 (0)	0 (0)	0 (0)	11 (14)	45 (58)	1 (1)	63 (82)	54 (70)	17 (22)	3 (4)
Duodenal ulcer	66	47 (71)	8 (12)	37 (56)	2 (3)	30 (45)	7 (11)	2 (3)	4 (6)	2 (3)	14 (21)	27 (41)	7 (11)	54 (82)	49 (74)	10 (15)	3 (5)

$P > 0.05$ for all genotypes among three groups.

Table 3 Genotypes of *H. pylori* in patients with gastric cancer (GC) and non-gastric cancer (non-GC) (%)

Diagnosis	No of Patients	s1a	s1b	s1c	s2	s1a+s1c	s1a+s1b+s1c	s1a+s1b	m1	m1T	m2	m1T+m2	cagA	iceA1	iceA2	iceA1+iceA2
GC	66	35 ^b (53)	1 (2)	13 ^l (20)	1 (2)	7 (11)	1 (2)	0 (0)	1 (2)	23 ^a (35)	32 ^h (48)	4 (6)	50 (76)	39 ^f (59)	15 (23)	2 (3)
Non-GC	168	127 ^d (76)	9 (5)	93 ⁱ (55)	2 (1)	77 (46)	2 (2)	4 (2)	2 (2)	33 ^a (20)	84 ^j (50)	10 (6)	139 (83)	125 ^f (74)	29 (17)	6 (4)

^b $P < 0.001$ vs s1b, s1c and s2 of non-GC, ^d $P < 0.0001$ vs m1T, m1 of non-GC, ^f $P < 0.0001$ vs ice A2 of non-GC, ^h $P < 0.001$ vs s1c, s1b and s2 of GC, ⁱ $P < 0.0001$ vs m1 of GC, ^j $P < 0.0001$, ^a $P = 0.02$.

Table 4 Genotypes of *H. pylori* in patients with early or advanced gastric cancer (%)

Diagnosis	No of Patients	s1a	s1b	s1c	s2	s1a+s1c	s1a+s1b+s1c	m1	m1T	m2	m1T+m2	cagA	iceA1	iceA2	iceA1+iceA2
EGC	7	4 (57)	0 (0)	2 (29)	0 (0)	1 (14)	0 (0)	0 (0)	1 (14)	3 (43)	0 (0)	6 (86)	4 (57)	1 (4)	0 (0)
AGC	59	31 (53)	1 (2)	11 (19)	1 (2)	6 (10)	1 (2)	1 (2)	22 (37)	29 (49)	4 (7)	44 (75)	35 (59)	14 (24)	2 (3)

Table 5 Genotypes of *H. pylori* in patients with advanced gastric cancer according to Borrmann's classification (%)

Diagnosis	No of Patients	s1a	s1b	s1c	s2	s1a+s1c	s1a+s1b+s1c	m1	m1T	m2	m1T+m2	cagA	iceA1	iceA2	iceA1+iceA2
I	7	4 (57)	0 (0)	2 (29)	0 (0)	1 (14)	0 (0)	0 (0)	5 (71)	1 (14)	0 (0)	5 (71)	5 (71)	1 (14)	0 (0)
II	28	15 (54)	1 (4)	3 (11)	1 (4)	3 (11)	1 (4)	1 (4)	8 (29)	13 (46)	1 (4)	20 (71)	17 (61)	6 (21)	1 (4)
III	13	6 (46)	0 (0)	5 (38)	0 (0)	2 (15)	0 (0)	0 (0)	3 (23)	8 (62)	1 (8)	11 (85)	8 (62)	3 (23)	0 (0)
IV	10	5 (50)	0 (0)	1 (10)	0 (0)	0 (0)	0 (0)	0 (0)	5 (50)	7 (70)	2 (20)	8 (80)	5 (50)	4 (40)	1 (10)

Table 6 Genotypes of *H. pylori* in patients with gastric cancer according to histological classification. (%)

Diagnosis	No of Patients	s1a	s1b	s1c	s2	s1a+s1c	s1a+s1b+s1c	m1	m1T	m2	m1T+m2	cagA	iceA1	iceA2	iceA1+iceA2
Intestinal	28	15 (54)	0 (0)	5 (18)	0 (0)	3 (5)	0 (0)	0 (0)	7 (25)	16 (57)	2 (7)	21 (75)	16 (57)	8 (29)	1 (4)
Diffuse	24	12 (50)	1 (4)	4 (17)	1 (4)	2 (8)	1 (4)	0 (0)	9 (38)	10 (42)	1 (4)	18 (75)	15 (63)	4 (17)	1 (4)
mixed	11	5 (45)	0 (0)	3 (27)	0 (0)	1 (9)	0 (0)	1 (9)	5 (45)	5 (45)	1 (9)	9 (82)	6 (55)	3 (27)	0 (0)

Comparison of gastric cancer patient with non-cancer (peptic ulcer and chronic gastritis) patients

In patients with gastric cancer, the *vacA* s1a and s1c subtypes were less commonly found than those in non-cancer patients (35/66 vs 127/168, $P < 0.001$ for s1a and 13/66 vs 93/168, $P < 0.0001$ for s1c) (Table 3). In the middle region, the m1T in patients with gastric cancer was more than that in non-cancer patients (23/66 vs 33/168, $P = 0.02$). There was no difference in *iceA* and *cagA* between patients with gastric cancer and non-cancer status.

DISCUSSION

This is the first study to investigate the allelic variations of *H. pylori vacA*, *cagA* and *iceA1* in gastric cancer patients in Taiwan. The results showed *vacA* s1a, m2, and *iceA1* predominated in patients with gastric cancer and those without.

H. pylori has become a world-wide infective agent ranging from 25% in developed countries to more than 80% in the developing world^[23]. Not all individuals infected with *H. pylori* developed gastric illness and this might be related to various factors such as environmental factors, host genetic factors, and bacterial virulent ability^[24]. Certain genotypes (*e.g.* *cagA*,

vacA s1a) have been closely related to severe clinical outcome and response to anti-*H. pylori* therapy^[25,26]. However, these findings were not supported by other studies^[27].

Different genotypes of *H. pylori* have been confirmed in patients with peptic ulcer or non-ulcer dyspepsia from diverse geographic areas^[14,23]. For example, in Northern and Eastern Europe, 89% strains were *vacA* s1a. *VacA* s1a and s1b were equally present in France and Italy. In Spain and Portugal, 89% of the strains were *vacA* s1b. While in north America, s1a and s1b were equally prevalent. *VacA* s1c was only found in East Asia. In Taiwan, *H. pylori* with *vacA* s1a was the major strain^[15,16]. Because of this diversity, it is interesting to analyze the genotypes in different areas.

In this study, predominance of *vacA* s1a was found in patients with gastric cancer (53%) and non-cancer status (76%). Our findings were similar to those reported by other authors in patients with peptic ulcer or non-ulcer dyspepsia^[15,16]. In Hong Kong and Korea, a low incidence of *vacA* s1a subtype was found^[28,29]. The previous Taiwan reports gave no data concerning *vacA* s1c^[6,15]. *VacA* s1c was frequently found (20% in gastric cancer and 55% in non-cancer) in this study. In contrast, *vacA* s1b and s2 were rare. Our findings were compatible with those

in mainland China^[30]. A high incidence of *vacA* s1c in this study was similar to the reports of Hong Kong^[28], Korea^[29], and Japan^[31], but different from those of the Western world^[14].

Concerning the m-region of *vacA*, m1 strains predominated in most Western reports^[14,23]. However, there were few m1 subtypes (2% in cancer and 2% in non-cancer) in this study. We used a modified primer (m1T)^[15] and found that some patients (35% in gastric cancer, 20% in non-cancer) with *H pylori* infection contained this genotype. M2 strains predominated (48% in gastric cancer and 50% in non-cancer) in this study. Our findings were consistent with reports from our previous experience^[32], other studies in Taiwan^[15,16], Hong Kong^[28], and mainland China^[30]. In contrast, Japan and Korea had a much lower incidence of m2 strain^[27,29]. We could not detect the m-region in some patients (15% in gastric cancer and 28% in non-cancer). This indicates a great variation in the *vacA* region in Taiwan, particularly in the mid-region locus. *H pylori* may have a different geographic evolution in Taiwan even compared with other East Asian countries.

IceA1 has been suggested to be related to peptic ulcer disease^[22,33]. But, like other authors, we doubted this finding^[27-29,32]. It has been found that *IceA1* is the predominant subtype of *ice* in the East Asia, while *iceA2* is the predominant subtype in the USA and Columbia^[27]. In this study, we found *iceA1* was the predominant subtype and showed no difference in patients with gastric cancer and non-cancer status.

The clinical relevance of putative virulence-associated genes of *H pylori* in patients with gastric cancer is a matter of controversy. Enomoto *et al.* found that 98% of patients with gastric cancer were *H pylori*-positive^[12]. Many studies suggested the strong association of certain genotypes of *H pylori* with gastric cancer^[34-38]. A significant association (o.r. 2.94) between *cagA* and gastric cancer was found in young Italian patients^[34]. Miehle *et al.* suggested a significant association between the *H pylori vacA* s1, m1, *cagA* and gastric cancer^[35]. Kidd *et al.* confirmed that the *vacA* s1b, m1 and *iceA1* were closely linked to gastric cancer in South Africa^[36]. van Doorn *et al.* found a significant association between the presence of ulcers or gastric cancer and the presence of *vacA* s1 and *cagA*^[37]. Basso *et al.* and Qiao *et al.* also concluded that *H pylori* infection caused by *cagA* positive/*vacA* s1 was a frequent finding in patients with gastric cancer^[38,39].

However, some authors have presented different observations. Mitchell *et al.* compared serum antibody to *cagA* antigen in patients with gastric cancer and normal subjects^[40]. They found no association between *cagA* and gastric cancer in Chinese subjects. Other authors also confirmed no relationship between *cagA* status and the risk of gastric cancer^[41]. Some Japanese studies did not support the link of *vacA* and *cagA* with gastric cancer^[42,43]. In these Japanese studies, the majority of the controls had positive *vacA* and *cagA*. Therefore, they obtained a different result as compared with those of the Western studies. In addition, the case number was small in their series. Increased number is needed to avoid bias. In this study, we found no difference in *cagA* between gastric cancer and non-cancer status. But, we found less *vacA* s1a, s1c and more m1T in patients with gastric cancer.

There is a paucity of *iceA* allele data in isolates from patients with gastric cancer. Gastric cancer isolates from Japan and Korea were distinguished by the prevalence of *iceA1* (67%) while 75% of isolates from the USA were *iceA2*^[27]. In this study, we found that *iceA1* predominated (59%) in patients with gastric cancer.

Patients with histologic findings of severe gastric atrophy, corpus-predominant gastritis or intestinal metaplasia are at an increased risk for gastric cancer. *H pylori* carrying the *cagA* gene might have promoted the atrophic metaplastic mucosal lesions that represent the pathway in multistep intestinal type gastric oncogenesis^[25,44]. Correa *et al.* and Uemura *et al.* found

that severe atrophic gastritis accompanying intestinal metaplasia caused by persistent *H pylori* infection was closely related to the development of intestinal type gastric cancer^[9,45]. But, some authors present different results. No significant relationship was found between *H pylori* and diffuse type gastric cancer because atrophic change was not evident in these patients^[46,47]. In addition, other authors did not support this finding due to epidemiological and pathological evidence^[48,49]. In this study, we found no difference in genotypes among diffuse, intestinal and mixed types of gastric cancer. In addition, there was no difference of genotypes in patients with early and advanced gastric cancer. However, the case number should be increased to avoid type II error.

In conclusion, *vacA* s1a, m2, and *iceA1* predominate in patients with gastric cancer. As compared with those of non-cancer patients, patients with gastric cancer have less *vacA* s1a, s1c and more m1T subtypes. Genotypes are similar according to morphological and pathological classification.

REFERENCES

- Blaser MJ. Ecology of *Helicobacter pylori* in the human stomach. *J Clin Invest* 1997; **100**: 759-762
- Dunn BE, Cohen H, Blaser MJ. *Helicobacter pylori*. *Clin Microbiol Rev* 1997; **10**: 720-741
- Wang RT, Wang T, Chen K, Wang JY, Zhang JP, Lin SR, Zhu YM, Zhang WM, Cao YX, Zhu CW, Yu H, Cong YJ, Zheng S, Wu BQ. *Helicobacter pylori* infection and gastric cancer: evidence from a retrospective cohort study and nested case-control study in China. *World J Gastroenterol* 2002; **8**: 1103-1107
- Akopyants N, Bukanov NO, Westblom TU, Kresovich S, Berg DE. DNA diversity among clinical isolates of *Helicobacter pylori* detected by PCR-based RAPD fingerprinting. *Nucleic Acids Res* 1992; **20**: 5137-5142
- Foxall PA, Hu LT, Mobley HL. Use of polymerase chain reaction-amplified *Helicobacter pylori* urease structural genes for differentiation of isolates. *J Clin Microbiol* 1992; **30**: 739-741
- International Agency for Research on Cancer. Schistosomes, liver flukes and *Helicobacter pylori* IARC Monographs on the Evaluation of Carcinogenic Risks to Humans. 61. Lyon, France: IARC 1994
- Uemura N, Okamoto S, Yamamoto S, Matsumura N, Yamaguchi S, Yamakido M, Taniyama K. *Helicobacter pylori* infection and the development of gastric cancer. *N Engl J Med* 2001; **345**: 784-789
- Enomoto H, Watanabe H, Nishikura K, Umezawa H, Asakura H. Topographic distribution of *Helicobacter pylori* in the resected stomach. *Eur J Gastroenterol Hepatol* 1998; **10**: 473-478
- Covacci A, Censini S, Bugnoli M, Petracca R, Burroni D, Macchia G, Massone A, Papini E, Xiang Z, Figura N. Molecular characterization of the 128-kDa immunodominant antigen of *Helicobacter pylori* associated with cytotoxicity and duodenal ulcer. *Proc Natl Acad Sci U S A* 1993; **90**: 5791-5795
- Cover TL. The vacuolating cytotoxin of *Helicobacter pylori*. *Mol Microbiol* 1996; **20**: 241-246
- Holcombe C. *Helicobacter pylori*: The African enigma. *Gut* 1992; **33**: 429-431
- Miwa H, Go MF, Sato N. *H pylori* and gastric cancer: The Asian enigma. *Am J Gastroenterol* 2002; **97**: 1106-1112
- Louw JA, Kidd MSG, Kummer AF, Taylor K, Kotze U, Hanslo D. The relationship between *Helicobacter pylori* infection, the virulence genotypes of the infecting strain and gastric cancer in the African setting. *Helicobacter* 2001; **6**: 268-273
- van Doorn LJ, Figueiredo C, Megráud F, Pena S, Midolo P, Queiroz DM, Carneiro F, Vanderborght B, Pegado MD, Sanna R, De Boer W, Schneeberger PM, Correa P, Ng EK, Atherton J, Blaser MJ, Quint WG. Geographic distribution of *vacA* allelic types of *Helicobacter pylori*. *Gastroenterology* 1999; **116**: 823-830
- Wang HJ, Kuo CH, Yeh AAM, Chang PCL, Wang WC. Vacuolating toxin production in clinical isolates of *Helicobacter pylori* with different *vacA* genotypes. *J Inf Dis* 1998; **178**: 207-212
- Lin CW, Wu SC, Lee SC, Cheng KS. Genetic analysis and

- clinical evaluation of vacuolating cytotoxin gene A and cytotoxin-associated gene A in Taiwanese *Helicobacter pylori* isolated from peptic ulcer patients. *Scand J Infect Dis* 2000; **32**: 51-57
- 17 **Boom R**, Sol CJ, Salimans MM, Jansen CL, Mertheim-van Dillen PM, van der Noordaa J. Rapid and simple method for purification of nucleic acids. *J Clin Microbiol* 1990; **28**: 495-503
 - 18 **Lauren P**. The two histological main types of gastric carcinoma: Diffuse and the so-called intestinal type carcinoma. *Acta Path Microbiol Scand* 1965; **64**: 31-49
 - 19 **Borrmann R**. (1926) Handbuch der speziellen Pathologisch Anatomie und Histologie, Vol 4/1, (ed) Henke F and Lubarsch O, ch C, pt5. *Berlin Springer*
 - 20 Japanese Research Society for Gastric Cancer. The general rules for the Gastric Cancer Study in Surgery and Pathology. Part I, clinical classification and Part II, histological classification of gastric cancer. *Jpn J Surg* 1981; **11**: 127-145
 - 21 **Atherton JC**, Cao P, Peek RM, Tumuru MKR, Blaser M, Cover TL. Mosaicism in vacuolating cytotoxin alleles of *Helicobacter pylori*. *J Biol Chem* 1995; **270**: 17771-17777
 - 22 **van Doorn LJ**, Figueiredo C, Sanna R, Plaisier A, Schneeberger P, de Boer W, Quint W. Clinical relevance of the *cagA*, *vacA* and *iceA* status of *Helicobacter pylori*. *Gastroenterology* 1998; **115**: 58-66
 - 23 **Pounder RE**. The prevalence of *Helicobacter pylori* in different countries. *Aliment Pharmacol Ther* 1995; **9**(Suppl 2): 33-40
 - 24 **Malaty HM**, Graham DY. Importance of childhood socioeconomic status on the current prevalence of *Helicobacter pylori* infection. *Gut* 1994; **35**: 742-745
 - 25 **Parsonnet J**, Friedman GD, Orentreich N, Vogelmann H. Risk for gastric cancer in people with *cagA* positive or *cagA* negative *Helicobacter pylori* infection. *Gut* 1997; **40**: 297-301
 - 26 **Atherton JC**. The clinical relevance of strain types of *Helicobacter pylori*. *Gut* 1997; **40**: 701
 - 27 **Yamaoka Y**, Kodama T, Gutierrez O, Kim JG, Kashima K, Graham DY. Relationship between *Helicobacter pylori* *iceA*, *cagA*, and *vacA* status and clinical outcome: studies in four different countries. *J Clin Microbiol* 1999; **37**: 2274-2279
 - 28 **Wong BC**, Yin Y, Berg DE, Xia HX, Zhang JZ, Wang WH, Wong WH, Huang XR, Tang VS, Lam SK. Distribution of distinct *vacA*, *aga* and *iceA* alleles in *Helicobacter pylori* in Hong Kong. *Helicobacter pylori* 2001; **6**: 317-324
 - 29 **Kim SY**, Woo CW, Lee YM, Son BR, Kim JW, Chae HB, Youn SJ, Park SM. Genotyping *cagA*, *vacA* subtype, *iceA1*, and *BabA* of *Helicobacter pylori* isolates from Korean patients, and their association with gastroduodenal diseases. *J Korean Med Sci* 2001; **16**: 579-584
 - 30 **Pan ZJ**, Berg DE, van der Hulst RWM, Su WW, Raudonikienė A, Xiao SD, Dankert J, Tytgat GN, van der Ende A. Prevalence of vacuolating cytotoxin production and distribution of distinct *vacA* alleles in *Helicobacter pylori* from China. *J Infect Dis* 1998; **178**: 220-226
 - 31 **Fukuta K**, Azuma T, Ito Y, Suto H, Keida Y, Wakabayashi H, Watamabe A, Kuriyama M. Clinical relevance of *caeE* gene from *Helicobacter pylori* strains in Japan. *Dig Dis Sci* 2002; **47**: 667-674
 - 32 **Perng CL**, Lin HJ, Sun IC, Tseng GY, Chang FY, Lee SD. *Helicobacter pylori* *cagA*, *iceA* and *vacA* status in Taiwan patients with peptic ulcer and gastritis. *J Gastroenterol Hepatol* 2003; **18**: 1244-1249
 - 33 **Figura N**, Vindigni C, Covacci A, Presenti L, Burrone D, Vernillo R, Banducci T, Roviello F, Marrelli D, Bicontri M, Kristodhullu S, Gennari C, Vaira D. *CagA* positive and negative *Helicobacter pylori* strains are simultaneously present in the stomach of most patients with non-ulcer dyspepsia: relevance to histological damage. *Gut* 1998; **42**: 772-778
 - 34 **Rugge M**, Busatto G, Cassaro M, Shiao YH, Russo V, Leandro G, Avellini C, Fabiano A, Sidoni A, Covacci A. Patients younger than 40 years with gastric carcinoma: *Helicobacter pylori* genotype and associated gastritis phenotype. *Cancer* 1999; **85**: 2506-2511
 - 35 **Miehlke S**, Kirsch C, Agha-Amiri K, Gunther T, Lehn N, Malfertheiner P, Stolte M, Ehninger G, Bayerdorffer E. The *Helicobacter pylori* *vacA* s1, m1 genotype and *cagA* are associated with gastric carcinoma in Germany. *Int J Cancer* 2000; **87**: 322-327
 - 36 **Kidd M**, Peek RM, Lastovica AJ, Israel DA, Kummer AF, Louw JA. Analysis of *iceA* genotypes in South African *Helicobacter pylori* strains and relationship to clinically significant disease. *Gut* 2001; **49**: 629-635
 - 37 **van Doorn LJ**, Figueiredo C, Rossau R, Jannes G, van Asbroeck M, Sousa JC, Carneiro F, Quint WG. Typing of *Helicobacter pylori* *vacA* gene and detection of *cagA* gene by PCR and reverse hybridization. *J Clin Microbiol* 1998; **36**: 1271-1276
 - 38 **Basso D**, Navaglia F, Brigate L, Piva MG, Toma A, Greco E, Di Mario F, Galeotti F, Roveroni G, Corsini A, Plebani M. Analysis of *Helicobacter pylori* *vacA* and *cagA* genotypes and serum antibody profile in benign and malignant gastroduodenal diseases. *Gut* 1998; **43**: 182-186
 - 39 **Qiao W**, Hu JL, Xiao B, Wu KC, Peng DR, Atherton JC, Xue H. *cagA* and *vacA* genotype of *Helicobacter pylori* associated with gastric disease in Xi'an area. *World J Gastroenterol* 2003; **9**: 1762-1766
 - 40 **Mitchell HM**, Hazell SL, Li YY, Hu PJ. Serological response to specific *Helicobacter pylori* antigens: antibody against *cagA* antigen is not predictive of gastric cancer in a developing country. *Am J Gastroenterol* 1996; **91**: 1785-1788
 - 41 **Kikuchi S**, Crabtree JE, Forman D, Kurosawa M. Association between infections with *cagA*-positive or -negative strains of *Helicobacter pylori* and risk for gastric cancer in young adults. *Am J Gastroenterol* 1999; **94**: 3455-3459
 - 42 **Shimoyama T**, Yoshimura T, Mikami T, Fukuda S, Crabtree JE, Munakata A. Evaluation of *Helicobacter pylori* *vacA* genotypes in Japanese patients with gastric cancer. *J Clin Pathol* 1998; **51**: 299-301
 - 43 **Maeda S**, Ogura K, Yoshida H, Kanai F, Ikenoue T, Kato N, Shiratori Y, Omata M. Major virulence factors, *vacA* and *cagA* are commonly positive in *Helicobacter pylori* isolates in Japan. *Gut* 1998; **42**: 338-343
 - 44 **Rugge M**, Cassaro M, Farinati F, Saggioro A, Di Mario F. *Helicobacter pylori* and atrophic gastritis: importance of *cagA* status. *J Natl Cancer Inst* 1996; **88**: 762-764
 - 45 **Correa P**. Human gastric carcinogenesis: a multistep and multifactorial process-First American Cancer Society Award Lecture on Cancer Epidemiology and Prevention. *Cancer Res* 1992; **52**: 6735-6740
 - 46 **Sipponen M**, Kosunen TU, Valle J, Riihela M, Seppala K. *Helicobacter pylori* infection and chronic gastritis in gastric cancer. *J Clin Pathol* 1992; **45**: 319-323
 - 47 **Solcia E**, Fiocca R, Luinetti O, Villani L, Padovan L, Calistri D, Ranzani GN, Chiaravalli A, Capella C. Intestinal and diffuse gastric cancers arise in a different background of *Helicobacter pylori* gastritis through different gene involvement. *Am J Surg Pathol* 1996; **20**(Suppl 1): 8-22
 - 48 **Kikuchi S**, Wada O, Nakajima T, Kobayashi O, Konishi T, Inaba Y. Serum anti-*Helicobacter pylori* antibody and gastric carcinoma among young adults. *Cancer* 1995; **75**: 2789-2793
 - 49 **Kokkola A**, Valle J, Haapiainen R, Sipponen P, Kivilaakso E, Puolakkainen P. *Helicobacter pylori* infection in young patients with gastric carcinoma. *Scand J Gastroenterol* 1996; **31**: 643-647

Construction of attenuated *Salmonella typhimurium* Strain expressing *Helicobacter pylori* conservative region of adhesin antigen and its immunogenicity

Yang Bai, Ya-Li Zhang, Ji-De Wang, Zhao-Shan Zhang, Dian-Yuan Zhou

Yang Bai, Ya-Li Zhang, Ji-De Wang, Dian-Yuan Zhou, PLA Institute for Digestive Medicine, Nanfang Hospital, the First Military Medical University, Guangzhou 510515, Guangdong Province, China

Zhao-Shan Zhang, Institute of Biotechnology, Academy of Military Medical Sciences, Beijing 100071, China

Supported by the National Natural Science Foundation of China, No. 30270078

Correspondence to: Dr. Yang Bai, PLA Institute for Digestive Medicine, Nanfang Hospital, the First Military Medical University, Guangzhou 510515, Guangdong Province, China. baiyang1030@hotmail.com

Telephone: +86-20-61641532

Received: 2003-11-04 **Accepted:** 2004-01-12

Abstract

AIM: To construct a non-resistant and attenuated *Salmonella typhimurium* (*S. typhimurium*) strain which expresses conservative region of adhesin AB of *Helicobacter pylori* (*H pylori*) and evaluate its immunogenicity.

METHODS: The AB gene amplified by PCR was inserted into the expression vector pYA248 containing *asd* gene and through two transformations introduced into the delta *Cya*, delta *Crp*, delta *Asd* attenuated *Salmonella typhimurium* strain, constructing balanced lethal attenuated *Salmonella typhimurium* strains X4072 (pYA248-AB). Bridged ELISA method was used to measure the expression of AB antigen in sonicate and culture supernatant. According to the method described by Meacock, stability of the recombinant was evaluated. Semi-lethal capacity test was used to evaluate the safety of recombinant. The immunogenicity of recombinant was evaluated with animal experiments.

RESULTS: The attenuated *S. typhimurium* X4072 (pYA248-AB) which expresses AB was successfully constructed. Furthermore, bridged ELISA assay showed that the content of AB in recombinant X4072 (pYA248-AB) culture supernatant was higher than that was in thallus lytic liquor. And after recombinant X4072 (pYA248-AB) was cultured for 100 generations without selection pressure, the entire recombinant bacteria selected randomly could grow, and the AB antigen was detected positive by ELISA. The growth curve of the recombinant bacteria showed that the growth states of X4072 (pYA248) and X4072 (pYA248-AB) were basically consistent. The survival rate of C57BL/6 was still 100%, at 30 d after mice taking X4072 (pYA248-AB) 1.0×10^{10} cfu orally. Oral immunization of mice with X4072 (pYA248-AB) induced a specific immune response.

CONCLUSION: *In vitro* recombinant plasmid appears to be stable and experiments on animals showed that the recombinant strains were safe and immunogenic *in vitro*, which providing a new live oral vaccine candidate for protection and care of *H pylori* infection.

Bai Y, Zhang YL, Wang JD, Zhang ZS, Zhou DY. Construction

of attenuated *Salmonella typhimurium* Strain expressing *Helicobacter pylori* conservative region of adhesin antigen and its immunogenicity. *World J Gastroenterol* 2004; 10 (17): 2498-2502

<http://www.wjgnet.com/1007-9327/10/2498.asp>

INTRODUCTION

The discovery of *Helicobacter pylori* (*H pylori*) has brought about a revolution in the research of etiological factor and prevention and cure of chronic gastritis, peptic ulcer and the associated diseases^[1,2]. It has been confirmed that *H pylori* is the main cause of chronic gastritis and peptic ulcer, and an important factor for the infection of gastric cancer and mucosa-associated lymphoid tissue (MALT) lymphoma and primary gastric non-Hodgkin's lymphoma^[3-7]. In 1994, the World Health Organization has defined it as a class I carcinogen, and direct evidence of its carcinogenesis has recently been demonstrated in an animal model and a retrospective cohort study and nested case-control study in China^[8,9]. Data of epidemiology showed that 50 percent of the population all over the world is infected with *H pylori*, and China has a high infection rate^[10]. Based on it, eradication of *H pylori* is one of the main methods for preventing and treating the above-mentioned diseases. At present, the widely used method for eradication of *H pylori* in clinical practice is the antibiotic treatment, though high the eradication rate is, such problems as high expenses, yearly reduced eradication rate resulting from gradually increasing drug-resistant strains, side effects of drugs and low patient compliance have still not been solved^[11-13]. Immunization against *H pylori* infection has been one of the most prospective treatments. In view of the fact that the conservative region of four confirmed adhesins is outer membrane protein and porin type component, outer membrane protein and porin are the excellent candidate components vaccination^[14-16]. In addition, the attenuated *Salmonella typhimurium* strain expressing foreign antigen is a very hopeful new-generation of vaccine. Experiments on human body indicated that the attenuated *Salmonella typhimurium* strain has very good endurance and immunogenicity, which can be used to transmit foreign antigen, therefore, the problem of adjuvant as well as the problem of high cost for taking subunit protein vaccine orally are solved. At present, the research of attenuated *Salmonella typhimurium* strain in application to *H pylori* vaccine has been done, but non-resistant and attenuated *Salmonella typhimurium* strain containing the balanced lethal system has not yet been applied to the research and production of *H pylori* vaccine. We attempted to construct the non-resistance and attenuated *Salmonella typhimurium* strain expressing AB, and to study its biological properties to pave the way for further research of biological treatment.

MATERIALS AND METHODS

Materials

The strains and plasmids used in the experimental processes are showed in Table 1.

Table 1 Strain (plasmid) and genotype

Strain (plasmid)	Genotype	Source
<i>E. coli</i> X6097	<i>Asd</i>	Dr. Roy Curtiss
Salmonella		
<i>typhimurium</i> X3181	Wild strain	Institute for the control of biological product, Ministry of Health
X3730	<i>GalE</i> , <i>hsd</i> , <i>asd</i>	Dr. Roy Curtiss
X4072	<i>Cya</i> , <i>Crp</i> , <i>Asd</i>	Dr. Roy Curtiss
pET-22b (+)-AB	<i>Amp^r</i> , AB	Construction in the previous research ^[17-20] , Dr. Roy Curtiss
pYA248	<i>Asd^r</i>	Construction in the research
pYA248-AB	AB	

Thirty specific-pathogen free male C57BL/6 mice, aged 4 wk, were purchased from Animal Center of our institute. Restriction enzymes, such as *EcoR* I, *Sal* I *etc.* and T4 DNA ligase, Vent DNA polymerase *etc.* were purchased from New England Biolabs corporation, Promega corporation and Sino-American Hua Mei Biotechnology Company, respectively. The goat anti-rabbit IgG-HRP and IgA-HRP were purchased from Sino-American Hua Mei Biotechnology Company. Our institute provided anti-AB antibody and AB antigen. DAP (50 mg/L) was purchased from Sigma corporation. Other reagents were analytically pure reagents produced in China.

Recombinant DNA techniques

The alkaline lysis method was chosen for rapid and large-scale preparations of plasmid DNA as described previously^[21]. In accordance with the the gene sequence in conservative region, we designed specific primers and added appropriate restriction enzyme sites on its 5' termini, which was synthesized by Shanghai Boya Co. The sequences of primers were as follows: conservative region 1: 5'-CCG GAA TTC AAC GCG CTC AAC AAT CAG-3'; conservative region 2, 5'-CAC GTC GAC CTA GAA TGA ATA CCC ATA AG-3'. Conservative region 1 and conservative region 2 contained *EcoR* I and *Sal* I sites, respectively. The template was pET-22b (+) -AB. PCR was performed by the hot start method. The PCR condition was that after initial denaturing at 95 °C for 30 s, each cycle of amplification consisted of denaturation at 95 °C for 30 s, annealing at 55 °C for 30 s and polymerization at 72 °C for 30 s, and a further polymerization for 10 min after 35 amplification cycles. PCR products were separated by electrophoresis analysis on a 8 g/L agarose gel. The PCR product was harvested from agarose gel, digested with *EcoR* I and *Sal* I, and inserted into the *EcoR* I and *Sal* I restriction fragments of the expression vector pYA248 using T4 DNA ligase. The resulting plasmids pYA248-AB were transformed into *E. coli* X6097, Salmonella typhimurium X3730 and X4072 one by one and positive clone was screened through assay of double restriction enzyme digestion. DNA sequence was performed with the DNA automatic sequencer.

Assay of AB protein expressed by recombinant strain

Recombinant strain *S. typhimurium* X4072 (pYA248-AB) cells, after being inoculated in the culture medium of LB liquids, were cultured with shaking at 37 °C for 15-16 h, and then centrifuged, to collect thallus and supernatant. Thallus, after being washed with saline once and centrifuged, suspended with deionized water. The suspension was sonicated on ice for three min, and centrifuged, to obtain the supernatant. Bridged ELISA was used to measure the expression of AB antigen in sonicate and culture supernatant.

Assay of stability of recombinant strain

The experiment testing stability of recombinant strain was performed according to the method described by Meacock^[37,38]. Ten percent of thallus, incubated with shaking at 37 °C overnight, was inoculated in LB culture medium containing DAP and was

further cultured for 12 h, from which the another 10 percent was inoculated in LB culture medium containing DAP and cultured for another 12 h, which was continued in the same way for up to 50 h. By this time, recombinant X4072 (pYA248-AB) cells had been cultured for 100 generations, and then it was diluted to 10⁶-fold. A total volume of 100 µL of the diluted solution was taken and paved on LB agar plate containing DAP. After being cultured overnight, 100 single thalluses were randomly selected and transferred on LB agar plate without containing DAP. Bacteria could not grow on agar plate without containing DAP liquids, means plasmid loss; through this method stability of recombinant plasmid was verified. Meanwhile, ELISA was used to measure the expression of AB antigen in the culture supernatant of these 100 thalluses.

Assay of growth curve of recombinant strain

Single clone *S. typhimurium* X4072 (pYA248) and *S. typhimurium* X4072 (pYA248-AB) were selected and inoculated in culture medium of LB liquid, respectively. After being cultured with shaking at 37 °C for 10 h, 50 µL of it was inoculated in 5 mL culture medium of LB liquid, followed by culture with shaking at 37 °C. The value of A₆₀ was measured once every other hour, from which growth curve was drawn.

Assay of immunology of recombinant strain

Three groups of 5 mice including controls were used as follows: (1) PBS control group was non-immunized mice that received PBS; (2) Salmonella control group was immunized with attenuated *S. typhimurium* X4072 (pYA248) strain; (3) The vaccine group was immunized with *S. typhimurium* X4072 (pYA248-AB) strain expressing AB. Prior to immunizations, the mice were left overnight without solid food and 4 h without water. A total volume of 100 µL of 30 g/L sodium bicarbonate were given orally using a stainless steel catheter tube to neutralize the stomach pH. Immediately after stomach neutralization, mice from PBS control group received 100 µL PBS, and mice from the Salmonella control group and Salmonella vaccine group, received 1.0×10⁹ colony forming units (c.f.u) of *S. typhimurium* strain X4072 (pYA248) and *S. typhimurium* strain X4072 (pYA248-AB), respectively, in a total volume of 100 µL. Water and food were returned to the mice after immunization. At 4 wk after immunization, mice were sacrificed by terminal cardiac puncture under metoxyfluorance anesthesia and the small intestines were taken from mice to prepare intestine fluid. Indirect ELISA was used to evaluate serum samples and intestine fluid from mice for AB-specific IgG or IgA. Purified *H. pylori* AB was used as the coating antigen in ELISA immunoassays.

RESULTS

Construction of recombinant plasmid containing *asd* gene and encoding AB gene

The size of plasmid pYA248 was 3.0 kb. Promotor was *P_{trc}* and multiclonal points included *EcoR* I *Hin* d III and *Sal* I *etc.* and pYA248 was digested with *EcoR* I and *Sal* I, and large E-S

sequences were recovered as vector. The same enzymes were used to completely digest AB PCR product and mixed with vector for connection after being recovered, and then transformed into *E. coli* X6097 by the means of CaCl_2 . Transformer could grow on LB agar plate without containing DAP and further extracted plasmid for verification. The results of double restriction enzyme digestion of recombinant plasmid pYA248-AB are showed in Figure 1.

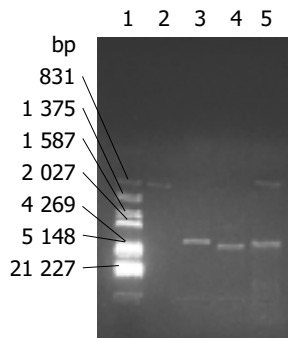


Figure 1 Double restriction enzyme digestion map of recombinant plasmid PYA248-AB. Lane1: DNA marker; Lane2: PCR product; lane3: pYA248/*EcoRI*; lane4: pYA248-AB/*EcoRI*; lane5: pYA248-AB/*EcoRI*+*Sall*.

Construction of recombinant strain

Recombinant plasmid extracted from *E. coli* X6097 (pYA248-AB) was transformed into *S. typhimurium* X3730 and X4072 by the transformation of electricity one by one. Owing to the difference between two kinds of *S. typhimurium*, the best transformational conditions were worked out. By adopting the first condition: cuvette gap 0.2 cm, voltage 2.5 kV, field strength 12.5 E, capacitor 25 μF , resistor 200 Ω , time constant 4.5-5.0 ms, recombinant plasmid was transformed into *S. typhimurium* X3730 and then separated from it. By adopting the second condition: cuvette gap 0.2 cm, voltage 2.4 kV, field strength 12.0 E, capacitor 25 μF , resistor 400 Ω , time constant 9-13 ms, recombinant plasmid was transformed into *S. typhimurium* X4072, from which recombinant strain *S. typhimurium* X4072 (pYA248-AB) was obtained.

Assay of AB protein expressed in recombinant strain

The results of AB expressed in X4072 (pYA248-AB) culture and sonicate supernatant assayed by bridged ELISA are shown in Table 2. The fact that the content of AB in recombinant germ X4072 (pYA248-AB) culture supernatant was higher than that in sonicate supernatant indicated that AB existed mainly in culture supernatant was expressed in the form of secretion.

Table 2 Expression of AB in X4072 (PYA248-AB) assayed by bridged ELISA

Sample	$A_{492\text{nm}}$	P/N
Negative control of X4072 (pYA248) culture supernatant	0.04	
Negative control of X4072 (pYA248) sonicate supernatant	0.04	
Positive control of BL21 (pET-AB) periplasm	1.08	27.0
X4072 (pYA248-AB) culture supernatant	0.96	24.0
X4072 (pYA248-AB) sonicate supernatant	0.78	19.5

Assay of stability of AB antigen expressed in recombinant strain

After recombinant germ pYA248-AB was cultured 100 generations, 100 bacteria were randomly selected and then transferred onto LB agar plate containing DAP. All of them could grow and the AB antigen was detected positive by ELISA. For the recombinant the mean of the value of $A_{492\text{nm}}$ plus or minus standard deviation

was 0.979 ± 0.052 , and the value of $A_{492\text{nm}}$ of negative control X4072 (pYA248) was 0.040, which indicated that recombinant germ, after seeing cultured for 100 generations, could stably exist in attenuated *S. typhimurium* strain.

Growth curve of recombinant strain

Single clone X4072 (pYA248) and X4072 (pYA248-AB) were selected and then inoculated in the culture medium of LB liquid. After being cultured at 37 °C overnight, 50 μL of it was inoculated in 5 mL culture medium of LB liquid and then cultured with shaking at 37 °C. The value of A_{600} was measured and recorded once every other hour, from which growth curve (Figure 2) was drawn. It can be discovered from Figure 2 that the growth states of all bacteria were basically consistent, that is, metabolism of the bacteria were basically unaffected by transforming recombinant plasmid into attenuated *S. typhimurium* strain.

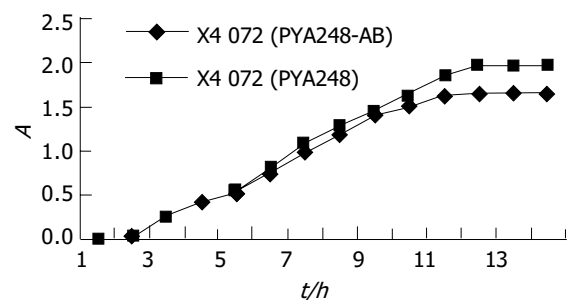


Figure 2 A growing curve of X4072 (PYA248) and X4072 (PYA248-AB).

Safety of recombinant strain

The results of experiments testing safety of C57BL/6 mice taking recombinant strain orally are shown in Table 3. After taking virulent strain $X3181 \times 10^7$ c.f.u, all the mice died within 5 d, but after taking recombinant strain X4072 (pYA248-AB) 1.0×10^{10} c.f.u, the survival rate was still 100 percent. It can be noticed from the table that the number of live bacteria of C57BL/6 mice taking recombinant strain orally was 10^3 fold more than that of the lethal dose of virulent strain X3181.

Table 3 Survival of mice after oral inoculation with virulent and recombinant *S. typhimurium* strains

Strain	Relevant phenotype	Inoculating dose (c.f.u)	Observation intervals (d)	Survival (live/total)
X3181	wild type	1.0×10^7	5	0/5
		2.6×10^5	30	2/5
X4072 (PYA248-AB)	Cya Crp-AB ⁺	1.0×10^{10}	30	5/5

Immunology of recombinant strain

The positive results detected by ELISA had colors, but the negative results had no colors, or weak colors. The five mice (group 3) serums and intestinal fluid immunized with vaccine *S. typhimurium* X4072 (pYA248-AB) showed positive results. In contrast, the mice serums and intestinal fluid of PBS control group and Salmonella control group showed negative results. It indicated *S. typhimurium* X4072 (pYA248-AB) could enable the organism to generate specific mucous membrane and humoral immunity.

DISCUSSION

S. typhimurium strain, through adhesion, invasion and inhabitation in intestine-associated lymph tissue, can be phagocytosed by macrophage and M cells in Peyer node and through mesentery

lymph node reaches liver and spleen, which further stimulate other organs and tissue to develop mucous membrane, cell and body fluid immunization responses effectively. In recent few years, the research and production of gastrointestinal tract vaccine with attenuated *S. typhimurium* strain as the release system have become a new trend in the research of a new-type recombinant live vaccine taken orally. In it, attenuated *S. typhimurium* strain as a kind of vaccine carrier carrying foreign antigen is, up to now, the most widely used strain. This is mainly due to the fact that the model of mice infected by *S. typhimurium* strain is basically consistent with the organism of man infected by typhoid, and the virulence factor of *S. typhimurium* strain has been deeply researched^[25,26]. The genes of virulence which have already been used in attenuated mutation of *S. typhimurium* strain include: *aro* gene controlling synthesis of aromatic compound^[22]; *gal E* gene affecting synthesis of lipopolysaccharide^[23]; *cya*, *crp* gene adjusting metabolic level of cyclic adenosine monophosphate(cAMP)^[24], *pur* gene controlling synthesis of purine organism^[25]; non-specific acid phosphoric acid enzyme *phoP* gene manipulating transcription of gene and *omp* gene adjusting porin expression *etc*^[26,27]. Many laboratories have successfully constructed attenuated and immunity *S. typhimurium* strain by mutating relative genes, which have been proved to be safe through experiments on animals, such as mice, cattle, and pig and even on human volunteers^[28-33]. But when these attenuated *S. typhimurium* strains are used to express foreign protective antigen, genes encoding protective antigen are usually cloned on a vector containing drug resistance gene. In order to make sure of the stability of plasmid, antibiotic must be used as selection pressure. According to the rules stipulated in American Food and Drug Administration, drug resistance plasmid can not exist in live vaccine and the stability of recombinant plasmid can not be maintained in human beings and animals by antibiotic^[28].

In order that foreign protective antigen can be stably expressed in attenuated *S. typhimurium* strain without antibiotic, a new type of plasmid vector system has been now developed, that is, the vector-host balanced lethal system. Host strain in the vector-host balanced lethal system is a type of chromosome mutant, and the mutated gene is housing keeping gene. Because the product of its encoding catalysed the genetic metabolic reaction of bacteria, the defects of the gene will certainly result in nutritious deficiency of bacteria, therefore, it can not grow in normal culture medium. Under this condition, plasmid must be necessary for the existence of bacteria. Once the transformed plasmid is lost, bacteria will not synthesize the essential substance so as not to grow in normal culture medium. Therefore, all bacteria that can grow in normal culture medium certainly contain recombinant plasmid, so as to construct the balanced lethal system. In this system, foreign protective antigen can be stably expressed without antibiotic in host strain. And the balanced lethal system constructed by *asd* gene has been widely used, for example, Redman *et al.*^[34] cloned the surface protein antigen gene of *streptococcus* to plasmid with *asd*, and then transformed it to $\Delta cya\Delta crp\Delta asd$ defective *S. typhimurium* strains which were taken by mice orally. The results showed that recombinant strain could induce mice to produce continuous reaction of antibody response^[34]. Scholars experimented $\Delta cya\Delta(crp\ cdt)\Delta asd$ expressing hepatitis B virus core pre S protein on adult women volunteers, showing that the strain could stimulate organism to develop system and mucous immunity response, and produce a unique secreted antibody (sIgA) in urinary and reproductive tract and intestinal tract^[35].

By adopting the system as described above, we successfully carried out the construction of attenuated *S. typhimurium* strain expressing AB. Because the cell wall of *S. typhimurium* strain is thick and so hard to be transformed, *E. coli* X6097 with

knocked out *asd* gene was used as host strain for screening recombinant clone. The screened recombinant plasmid was transformed electrically to host *S. typhimurium* X3730. X3730 with knocked out gene *asd* is the gene *galE* mutated strain of *S. typhimurium* strain LT-2 and loses the effect of restriction but possess the effect of modification, because of which plasmid transformed into *S. typhimurium* strain can obtain the methylated model of *S. typhimurium* strain and thus stably exists in *S. typhimurium* strain. Recombinant plasmid with methylated model extracted from X3730 was transformed into final *S. typhimurium* strain X4072 without restriction and so the construction work was finished.

Experiment on animals has proved that recombinant strain is safe. It was found by ELISA that AB protein was expressed mainly in the form of secretion, but the expression level was comparatively low. For recombinant strain with vaccine construction as the aim, however, a more important issue than high level expression is the stability of expressing foreign gene, because only when engineering bacteria can exist in body for a relatively long period and stably release antigen, it can effectively stimulate the immune system response of organism and expression with too high level may destroy the biological and chemical balance of strain as a complete organism which makes it hard for *S. typhimurium* strain to maintain the stable expression of foreign gene. The recombinant strain we constructed possessed a good stability, and under the condition without selection pressure, we recombinant plasmid could exist stably, and the foreign gene could also be expressed stably whose growth curve showed no obvious changes for expression of foreign gene. The main reason for it is probably that the expression level of foreign gene is suitable to *S. typhimurium* strain. In addition, according to Sutton *et al.*'s^[36] principle of immunization protection and cure of *H pylori* "less is best", that is, low dose of antigen has better immunization effect, and maybe this *S. typhimurium* strain live vaccine expressing *H pylori* antigen with a low but stable level can create better immunization effect. In this study, the serums and intestine fluid from the mice immunized with *S. typhimurium* X4072 (pYA248-AB) expressed specific antibody aimed to AB, but the serums and intestine fluid from the mice in the control group failed to express. These results suggest that *S. typhimurium* X4072 (pYA248-AB) might be a good candidate as a vaccine. However, whether it can be used as a vaccine or not need be researched further. To achieve his goal we are carrying out the associated experiments on animals now.

REFERENCES

- 1 Janowitz HD, Abittan CS, Fiedler LM. A gastroenterological list for the millennium. *J Clin Gastroenterol* 1999; **29**: 336-338
- 2 Kirsner JB. The origin of 20th century discoveries transforming clinical gastroenterology. *Am J Gastroenterol* 1998; **93**: 862-871
- 3 Bai Y, Zhang YL, Jin JF, Wang JD, Zhang ZS, Zhou DY. Recombinant *Helicobacter pylori* catalase. *World J Gastroenterol* 2003; **9**: 1119-1122
- 4 Blaser MJ. Polymorphic bacteria persisting in polymorphic hosts: assessing *Helicobacter pylori*-related risks for gastric cancer. *J Natl Cancer Inst* 2002; **94**: 1662-1663
- 5 Bai Y, Zhang YL, Wang JD, Zhang ZS, Zhou DY. Construction of the non-resistant attenuated Salmonella typhimurium strain expressing *Helicobacter pylori* catalase. *Diyi Junyi Daxue Xuebao* 2003; **23**: 101-105
- 6 Fireman Z, Trost L, Kopelman Y, Segal A, Sternberg A. *Helicobacter pylori*: seroprevalence and colorectal cancer. *Isr Med Assoc J* 2000; **2**: 6-9
- 7 Bai Y, Zhang YL, Wang JD, Yang YS, Chen Y, Zhang ZS, Zhou DY. Study on the cloning, expression and the immunogenicity of *Helicobacter pylori* heat shock protein 60 gene. *Diyi Junyi Daxue Xuebao* 2002; **22**: 3-5
- 8 Parsonnet J, Friedman GD, Vandersteen DP, Chang Y, Vogelstein JH, Orentreich N, Sibley RK. *Helicobacter pylori* infec-

- tion and the risk of gastric carcinoma. *N Engl J Med* 1991; **325**: 1127-1131
- 9 **Parsonnet J**, Hansen S, Rodriguez L, Gelb AB, Warnke RA, Jellum E, Orentreich N, Vogelmann JH, Friedman GD. *Helicobacter pylori* infection and gastric lymphoma. *N Engl J Med* 1994; **330**: 1267-1271
- 10 **Bai Y**, Chen Y, Lin HJ, Wang JD, Chang SH, Zhou DY, Zhang YL. *In vitro* evaluation of the safety and biological activity of recombinant *Helicobacter pylori* blood group antigen-binding adhesin. *Diyi Junyi Daxue Xuebao* 2003; **23**: 882-884
- 11 **Michetti P**. Vaccine against *Helicobacter pylori*: fact or fiction? *Gut* 1997; **41**: 728-730
- 12 **Lahaie RG**, Chiba N, Fallone C. Meeting review-*Helicobacter pylori*: basic mechanisms to clinical cure 2000. *Can J Gastroenterol* 2000; **14**: 856-861
- 13 **Bai Y**, Chang SH, Wang JD, Chen Y, Zhang ZS, Zhang YL. Construction of the *E.coli* clone expressing adhesin BabA of *Helicobacter pylori* and evaluation of the adherence activity of BabA. *Diyi Junyi Daxue Xuebao* 2003; **23**: 293-295
- 14 **Tomb JF**, White O, Kerlavage AR, Clayton RA, Sutton GG, Fleischmann RD, Ketchum KA, Klenk HP, Gill S, Dougherty BA, Nelson K, Quackenbush J, Zhou L, Kirkness EF, Peterson S, Loftus B, Richardson D, Dodson R, Khalak HG, Glodek A, McKenney K, Fitzgerald LM, Lee N, Adams MD, Venter JC. The complete genome sequence of the gastric pathogen *Helicobacter pylori*. *Nature* 1997; **388**: 539-547
- 15 **Doig P**, Trust TJ. Identification of surface-exposed outer membrane antigens of *Helicobacter pylori*. *Infect Immun* 1994; **62**: 4526-4533
- 16 **Rijpkema SG**. Prospects for therapeutic *Helicobacter pylori* vaccines. *J Med Microbiol* 1999; **48**: 1-3
- 17 **Bai Y**, Zhang YL, Wang JD, Lin HJ, Zhang ZS, Zhou DY. Conservative region of the genes encoding four adhesins of *Helicobacter pylori*: cloning, sequence analysis and biological information analysis. *Diyi Junyi Daxue Xuebao* 2002; **22**: 869-871
- 18 **Bai Y**, Dan HL, Wang JD, Zhang ZS, Odenbreit S, Zhou DY, Zhang YL. Cloning, expression, purification and identification of conservative region of four *Helicobacter pylori* adhesin genes in AlpA gene. *Prog Biochem Biophys* 2002; **29**: 922-926
- 19 **Bai Y**, Zhany YL, Chen Y, Wang JD, Zhou DY. Study of Immunogenicity and safety and adherence of conservative region of four *Helicobacter pylori* adhesin *in vitro*. *Prog Biochem Biophys* 2003; **30**: 422-426
- 20 **Bai Y**, Zhang YL, Wang JD, Zhang ZS, Zhou DY. Cloning and immunogenicity of conservative region of adhesin gene of *Helicobacter pylori*. *Zhonghua Yixue Zazhi* 2003; **83**: 736-739
- 21 **Sambrook J**, Fritsch EF, Maniatis T. Molecular cloning: a laboratory manual. New York: *Cold Spring Harbor Laboratory Press* 1989
- 22 **Stocker BA**. Auxotrophic *Salmonella typhi* as live vaccine. *Vaccine* 1988; **6**: 141-145
- 23 **Hone D**, Morona R, Attridge S, Hackett J. Construction of defined galE mutants of *Salmonella* for use as vaccines. *J Infect Dis* 1987; **156**: 167-174
- 24 **Curtiss R 3rd**, Kelly SM. *Salmonella typhimurium* deletion mutants lacking adenylate cyclase and cyclic AMP receptor protein are avirulent and immunogenic. *Infect Immun* 1987; **55**: 3035-3043
- 25 **McFarland WC**, Stocker BA. Effect of different purine auxotrophic mutations on mouse-virulence of a Vi-positive strain of *Salmonella dublin* and of two strains of *Salmonella typhimurium*. *Microb Pathog* 1987; **3**: 129-141
- 26 **Hohmann EL**, Oletta CA, Miller SI. Evaluation of a phoP/phoQ-deleted, aroA-deleted live oral *Salmonella typhi* vaccine strain in human volunteers. *Vaccine* 1996; **14**: 19-24
- 27 **Dorman CJ**, Chatfield S, Higgins CF, Hayward C, Dougan G. Characterization of porin and ompR mutants of a virulent strain of *Salmonella typhimurium*: ompR mutants are attenuated *in vivo*. *Infect Immun* 1989; **57**: 2136-2140
- 28 **Curtiss R 3rd**, Galan JE, Nakayama K, Kelly SM. Stabilization of recombinant avirulent vaccine strains *in vivo*. *Res Microbiol* 1990; **141**: 797-805
- 29 **Maskell DJ**, Sweeney KJ, O'Callaghan D, Hormaeche CE, Liew FY, Dougan G. *Salmonella typhimurium* aroA mutants as carriers of the *Escherichia coli* heat-labile enterotoxin B subunit to the murine secretory and systemic immune systems. *Microb Pathog* 1987; **2**: 211-221
- 30 **Clements JD**, El-Morshidy S. Construction of a potential live oral bivalent vaccine for typhoid fever and cholera-*Escherichia coli*-related diarrheas. *Infect Immun* 1984; **46**: 564-569
- 31 **Giron JA**, Xu JG, Gonzalez CR, Hone D, Kaper JB, Levine MM. Simultaneous expression of CFA/I and CS3 colonization factor antigens of enterotoxigenic *Escherichia coli* by delta aroC, delta aroD *Salmonella typhi* vaccine strain CVD 908. *Vaccine* 1995; **13**: 939-946
- 32 **Formal SB**, Baron LS, Kopecko DJ, Washington O, Powell C, Life CA. Construction of a potential bivalent vaccine strain: introduction of *Shigella sonnei* form I antigen genes into the galE *Salmonella typhi* Ty21a typhoid vaccine strain. *Infect Immun* 1981; **34**: 746-750
- 33 **Hone DM**, Harris AM, Chatfield S, Dougan G, Levine MM. Construction of genetically defined double aro mutants of *Salmonella typhi*. *Vaccine* 1991; **9**: 810-816
- 34 **Redman TK**, Harmon CC, Michalek SM. Oral immunization with recombinant *Salmonella typhimurium* expressing surface protein antigen A (SpaA) of *Streptococcus sobrinus*: effects of the *Salmonella* virulence plasmid on the induction of protective and sustained humoral responses in rats. *Vaccine* 1996; **14**: 868-878
- 35 **Nardelli-Haeffliger D**, Benyacoub J, Lemoine R, Hopkins-Donaldson S, Potts A, Hartman F, Kraehenbuhl JP, De Grandi P. Nasal vaccination with attenuated *Salmonella typhimurium* strains expressing the *Hepatitis B* nucleocapsid: dose response analysis. *Vaccine* 2001; **19**: 2854-2861
- 36 **Sutton P**, Wilson J, Lee A. Further development of the *Helicobacter pylori* mouse vaccination model. *Vaccine* 2000; **18**: 2677-2685
- 37 **Meacock PA**, Cohen SN. Partitioning of bacterial plasmids during cell division: a cis-acting locus that accomplishes stable plasmid inheritance. *Cell* 1980; **20**: 529-542
- 38 **Meacock PA**, Cohen SN. Genetic analysis of the inter-relationship between plasmid replication and incompatibility. *Mol Gen Genet* 1979; **174**: 135-147

Adaptive cytoprotection through modulation of nitric oxide in ethanol-evoked gastritis

Joshua Ka-Shun Ko, Chi-Hin Cho, Shiu-Kum Lam

Joshua Ka-Shun Ko, School of Chinese Medicine, Hong Kong Baptist University, Hong Kong, China

Chi-Hin Cho, Department of Pharmacology, Faculty of Medicine, The University of Hong Kong, Hong Kong, China

Shiu-Kum Lam, Department of Medicine, Faculty of Medicine, The University of Hong Kong, Hong Kong, China

Correspondence to: Dr. Joshua Ka-Shun Ko, 4/F, School of Chinese Medicine Building, 7 Hong Kong Baptist University Road, Hong Kong, China. jksko@hkbu.edu.hk

Telephone: +852-3411 2907 **Fax:** +852-3411 2461

Received: 2004-02-02 **Accepted:** 2004-03-24

Abstract

AIM: To assess the mechanisms of protective action by different mild irritants through maintenance of gastric mucosal integrity and modulation of mucosal nitric oxide (NO) in experimental gastritis rats.

METHODS: Either 200 mL/L ethanol, 50 g/L NaCl or 0.3 mol/L HCl was pretreated to normal or 800 mL/L ethanol-induced acute gastritis Sprague-Dawley rats before a subsequent challenge with 500 mL/L ethanol. Both macroscopic lesion areas and histological damage group were determined in the gastric mucosa of each group of animals. Besides, gastric mucosal activities of NO synthase isoforms and of superoxide dismutase, along with mucosal level of leukotriene (LT)₄ were measured.

RESULTS: Macroscopic mucosal damages were protected by 200 mL/L ethanol and 50 g/L NaCl in gastritis rats. However, although 200 mL/L ethanol could protect the surface layers of mucosal cells in normal animals (protection attenuated by N^G-nitro-L-arginine methyl ester), no cytoprotection against deeper histological damages was found in gastritis rats. Besides, inducible NO synthase activity was increased in the mucosa of gastritis animals and unaltered by mild irritants. Nevertheless, the elevation in mucosal LTC₄ level following 500 mL/L ethanol administration and under gastritis condition was significantly reduced by pretreatment of all three mild irritants in both normal and gastritis animals.

CONCLUSION: These findings suggest that the aggravated 500 mL/L ethanol-evoked mucosal damages under gastritis condition could be due to increased inducible NO and LTC₄ production in the gastric mucosa. Only 200 mL/L ethanol is truly "cytoprotective" at the surface glandular level of non-gastritis mucosa. Furthermore, the macroscopic protection of the three mild irritants involves reduction of LTC₄ level in both normal and gastritis mucosa, implicating preservation of the vasculature.

Ko JKS, Cho CH, Lam SK. Adaptive cytoprotection through modulation of nitric oxide in ethanol-evoked gastritis. *World J Gastroenterol* 2004; 10(17): 2503-2508
<http://www.wjgnet.com/1007-9327/10/2503.asp>

INTRODUCTION

Excessive ethanol ingestion can result in gastritis characterized by mucosal edema, subepithelial hemorrhages, cellular exfoliation and inflammatory cell infiltration^[1]. Alcohol has been shown to affect the mucosal barrier and histology^[2]. Morphologically, alcohol-induced gastric superficial injury involves mostly the inter-foveolar epithelium and gastric pits, and heals rapidly by restitution^[3]. On the other hand, the deeper lesions involve intramucosal hemorrhage and vascular engorgement^[4]. As a consequence of damage to microvessels, leakage of inflammatory mediators occurs, and vasoconstriction of submucosal arteries would result in ischemia. Eventually, these events would enhance the formation of more severe necrotic mucosal injury. Several products of arachidonate metabolism have been implicated to participate in the pathogenesis of ethanol-induced gastric mucosal damage^[5].

It is known that neuronal modulating processes such as the release of vasoactive mediators are crucial for the gastric mucosa to resist the continual onslaught of aggressive agents^[6]. Previous findings have suggested that there are interactions between the endothelium-derived vasodilator mediators, including that prostaglandins (PG), can regulate gastric mucosal microcirculation and integrity^[7]. Endothelial cells also release a highly labile humoral vasodilator substance, now known to be nitric oxide (NO), that mediates the vascular relaxation induced by vagal stimulation^[8]. Nonetheless, it should be noted that the production of NO from a calcium-independent (inducible) form of the enzyme could lead to cell injury in the endothelium^[9]. Thus, the induction of NO synthesis may not always be beneficial. For instance, formation and interaction between superoxide and NO radicals are the key elements of oxidative challenges in the gastric mucosa.

There are some endogenous proinflammatory mediators that could be activated during the aggressive attack of noxious agents or severe tissue trauma. Leukotriene (LT)₄ is one of these substances which would lead to microcirculatory disturbances and severe mucosal tissue injury^[10]. Such a detrimental action may somehow involve the generation of reactive oxygen free radicals. In other words, these effects could be modulated by enzyme systems of the oxygen-handling cells, such as superoxide dismutase (SOD), which are able to protect cells against the toxic effects caused by oxygen species^[11].

Acute hemorrhagic gastritis patients have underlying predisposing conditions such as alcohol abuse or use of NSAID. Besides endoscopic and surgical therapy, the focus on pharmacotherapy would be the enhancement of mucosal defense mechanisms so as to accelerate healing and prevent relapses^[12]. The present study attempted to illustrate that different mild irritants had differential modes of action in the adaptive cytoprotection against ethanol-induced gastric mucosal damage in animals under gastritis condition, whereas some of these involved modulation of eicosanoids and NO biosynthesis in the gastric mucosa. These data may also provide the explanation why gastritis can predispose the stomach to ulceration.

MATERIALS AND METHODS

Animals

Male Sprague-Dawley rats (240-260 g) were used after

acclimatization for at least three days in a controlled room with constant temperature (22 ± 1 °C) and humidity (65-70%). They were fed a standard diet of laboratory chow (Ralston Purina, USA) and had free access to tap water *ad libitum*. All experimental animals were deprived of food in individual wired cages 24 h beforehand.

Treatments and induction of gastritis

Animals in the "normal" (non-gastritis) groups received oral administration (10 mL/kg) of either distilled water or one of the three mild irritants, 200 mL/L ethanol, 50 g/L NaCl and 0.3 mol/L HCl via a stainless steel orogastric tube, 15 min before the administration of 500 mL/L ethanol (10 mL/kg). For animals that were used to demonstrate the action of mild irritants alone (basal), distilled water was given instead of 500 mL/L ethanol. All animals were sacrificed 30 min later.

To induce gastritis, 800 mL/L ethanol was given to the rats orally (10 mL/kg). The treated animals were returned to their home cages with provision of food and tap water. After 24 h, all the 800 mL/L ethanol-treated animals were deprived of food again, with tap water supply only. Similar experiments as those of the "normal" animals were performed using these gastritis rats 24 h following starvation (i.e. the experiments were carried out 48 h after the induction of gastritis). Our preliminary study showed that at this time point the gastritis animals were free from any gross macroscopic lesion or erosion, but the deeper mucosal cells comprising more than 800 mL/L of the total mucosal thickness were damaged or morphologically changed when observed microscopically.

In order to investigate the participation of the endogenous vasoactive mediator during the processes, N^G -nitro-L-arginine methyl ester (L-NAME, 12.5 mg/kg, i.v.) was pretreated 15 min before the administration of mild irritants to inhibit endogenous NO production^[13].

Macroscopic evaluation of gastric mucosal damage

The animals were sacrificed by a sharp blow behind the head and followed by cervical dislocation. Their stomachs were removed and opened along the greater curvature. After thoroughly rinsed in ice-cold saline solution and blotted dry, the area of macroscopic lesions on the mucosa was traced onto a glass slide, and measured by transparent 1-mm² grids^[14]. A section of each stomach tissue was removed and preserved for subsequent microscopic studies. Finally, the glandular mucosa of the rest of stomach tissue was scrapped by using a glass slide, weighed and immediately frozen in liquid nitrogen. The mucosal samples were stored at -70 °C until assayed for various endogenous mediators.

Histological evaluation of gastric mucosal damage

Within a week of formalin fixation, the gastric tissues were processed for paraffin embedding. A (1.0×0.5×0.3) cm³ block of gastric tissue was dehydrated by immersion in progressively increasing concentrations of ethanol. Slices of 6- μ m thick sections were stained by the periodic acid-Schiff technique, and counterstained by Harris' hematoxylin solution. The stained sections were then left in the fume-cupboard overnight.

An Olympus microscope (200×) with a scaled eyepiece was used for the morphometric study. Any histological damage in a section was quantified according to the method from O'Brien and coworkers^[15]. The criteria for damage were the absence of gastric mucosal cells or the presence of grossly disrupted cells. The standards for evaluation of the severity of microscopic mucosal damage were as follows: type I damage-length of luminal surface mucous cells damaged or vacuolated, type II damage-extensive luminal surface cell damage with disrupted and exfoliated cells lining the gastric pits, type III damage-disrupted cells of the gastric glands beneath the damaged surface and gastric pit cells. For each tissue sample, four

measurements of the total mucosal length as well as the length with damaged or disrupted mucosal cells were examined (in mm) and averaged. The final index for the degree of histological damage was represented by the percentage of the damaged mucosal length in terms of the total length of the gastric mucosa.

Determination of NO synthase activity in gastric mucosa

A mucosal sample was placed in a buffer solution (pH 7.2) containing 10 mmol/L HEPES, 0.32 mol/L sucrose, 0.1 mmol/L EDTA, 1 mmol/L DL-dithiothreitol, 10 μ g/mL of soybean trypsin inhibitor, 10 μ g/mL of leupeptin, 2 μ g/mL of aprotinin, and 1 mg/mL of phenyl-methanesulfonyl fluoride. The sample was homogenized for 20 s under ice-cold condition, and then centrifuged at 22 000 g for 30 min at 4 °C. An aliquot of 100 μ L from the supernatant was withdrawn for protein assay^[16].

The NO synthase activity was determined from the conversion of [³H] L-arginine to the NO co-product citrulline^[17]. The supernatant was passed over a 0.75-mL column containing Dowex AG50WX-8 resins to remove any endogenous arginine^[18]. The reaction mixture comprised 100 μ L of the supernatant and 150 μ L of buffered solution (pH 7.2) containing 10 mmol/L HEPES, 0.7 mmol/L NADPH, 150 μ mol/L CaCl₂, 7 mmol/L L-valine to inhibit any arginase^[19], and 1 μ Ci of [³H] L-arginine. The amount of [³H] L-citrulline formed in this reaction mixture represented the total NO synthase activity. A similar reaction mixture was also prepared, with the addition of 1 mmol/L EGTA, which removed Ca²⁺ ions from the system^[13]. Product formation that remained persistent in this system determined the inducible NO synthase activity. Incubation of the mixtures with or without EGTA was continued for 30 min at 37 °C. The reaction was terminated by adding 50 μ L of 200 mL/L perchloric acid, and the solution mixture was neutralized by 160 μ L of 1 mol/L NaOH^[20]. This was followed by the dilution with 540 μ L of deionized water containing 1 mmol/L L-arginine and 1 mmol/L citrulline. Subsequently, the resulting 1 mL mixture in each reaction tube was applied onto a chromatographic column containing 0.5 g of Dowex AG50WX-8 resins^[21]. Following the separation from unreacted [³H] L-arginine by cation-exchange chromatography, the product [³H] L-citrulline was eluted through the column by 1 mL of deionized water and collected into a scintillation vial. The samples were counted for the amount of radioactivity using a liquid scintillation counter (2 000 CA, Packard, USA). The data obtained were corrected for background counts obtained by a similar procedure but with heat-inactivated mucosal tissue. The final results were represented as cpm/min/mg protein. Constitutive NO synthase activity was obtained by subtracting the inducible NO synthase activity by the total NO synthase activity.

Determination of LTC₄ level in gastric mucosa

The pre-weighed mucosal samples were homogenized for 15 s under ice-cold condition in phosphate buffer (50 mmol/L, pH 7.4) with indomethacin (28 μ mol/L), to prevent any neof ormation of cyclooxygenase products during the extraction process. The homogenized samples were then centrifuged at 1 400 r/min for 15 min at 4 °C. An aliquot of 100 μ L from the supernatant was withdrawn for protein assay^[16]. The assay was carried out by using a LTC₄ [³H] RIA kit (NEN Dupont, USA.). A standard curve was constructed with a range of 0.025-1.6 ng/100 μ L. The final values of the samples obtained were represented as pg/mg protein.

Determination of SOD activity in gastric mucosa

The pre-weighed mucosal samples were homogenized for 20 s under ice-cold condition in phosphate buffer (50 mmol/L, pH 7.4). The homogenized samples were then centrifuged at 20 000 g for 15 min at 4 °C. An aliquot of 100 μ L from the supernatant was withdrawn for protein assay^[16].

The SOD activity in tissue homogenates was determined by the NBT reaction^[22]. A 10 μ L of the homogenates was added to a solution mixture containing 150 μ L each of 2 mmol/L xanthine, 2 mmol/L EDTA and 0.5 mmol/L NBT, 500 μ L of Na₂CO₃ and 75 μ g/mL of BSA. After being made up to a 2.85 mL solution with phosphate buffer, the mixture was incubated for 3 min in a 25 °C bath. Following that, 150 μ L of 0.12 μ mol/L xanthine oxidase was added to the mixture and 3 mL solution was incubated further at 25 °C for 20 min. The reaction was terminated by adding 1 mL of 0.8 mmol/L CuCl₂ solution to each tube. The inhibition of NBT reduction in each sample was determined spectrophotometrically at 560 nm and the final value of SOD activity was represented as units/mg protein.

Drugs

[³H] L-arginine (specific activity = 36.1 Ci/mmol) and the [³H] LTC₄ RIA kit were purchased from NEN DuPont (Boston, MA, USA.). L-NAME, DL-dithiothreitol, soybean trypsin inhibitor, leupeptin, aprotinin, phenylmethanesulfonyl fluoride, L-valine, L-arginine and DL-citrulline were all products of Sigma Chemicals (St. Louis, MO, USA.).

Statistical analysis

All the results were expressed as mean \pm SE of 6 animals per group. The means were compared by the analysis of variance followed by unpaired Student's *t* test. Differences were considered statistically significant if the *P* value was less than 0.05.

RESULTS

Adaptive cytoprotection of mild irritants against 50% ethanol-induced macroscopic lesion formation in gastritis rats (Table 1)

Under gastritis condition, there was a general aggravating effect on the macroscopic ethanol-evoked gastric mucosal damage in all experimental groups, when compared with the damaging effects of 500 mL/L ethanol in normal animals. The degree of

protection by 200 mL/L ethanol and 50 g/L NaCl in gastritis rats was lessened when compared to that in normal animals, while the gastroprotection of 0.3 mol/L HCl was completely relieved in gastritis animals. As in normal animals, L-NAME pretreatment alleviated the protective action of 200 mL/L ethanol in gastritis animals. Nonetheless, the protective action of 50 g/L NaCl was preserved under gastritis condition.

Table 1 Effect of mild irritants on 500 mL/L ethanol-induced macroscopic lesion formation in gastric mucosa of normal and gastritis rats, and modulation by pretreatment with L-NAME

Pretreatment	Macroscopic lesion areas (mm ²)	
	Normal	Gastritis
H ₂ O (Control)	41.17 \pm 7.85	134.17 \pm 19.23 ^d
200 mL/L EtOH	2.00 \pm 0.93 ^b	31.33 \pm 5.96 ^{b,f}
50 g/L NaCl	0 \pm 0 ^b	15.00 \pm 3.80 ^{b,f}
0.3 mol/L HCl	0 \pm 0 ^b	124.33 \pm 20.60 ^f
L-NAME+H ₂ O	42.50 \pm 10.65	125.40 \pm 17.75 ^f
L-NAME+200 mL/L EtOH	32.33 \pm 9.95 ^a	98.83 \pm 7.22 ^{b,f}
L-NAME+50 g/L NaCl	0 \pm 0 ^b	32.25 \pm 7.49 ^{b,f}
L-NAME+0.3 mol/L HCl	0 \pm 0 ^b	104.25 \pm 12.20 ^b

Values are mean \pm SE (*n* = 6), ^b*P*<0.001 vs corresponding H₂O group without mild irritant. ^a*P*<0.05, ^f*P*<0.001 vs corresponding group without drug pretreatment. ^d*P*<0.01, ^b*P*<0.001 vs corresponding group without gastritis (Normal).

Adaptive cytoprotection of mild irritants against 50% ethanol-induced histological damage in gastritis rats (Table 2)

The type II and type III histological damages induced by 500 mL/L ethanol were generally aggravated in the gastric mucosa of gastritis animals. In addition, the histological cytoprotection of 200 mL/L ethanol that could be observed in normal animals (the total, type I and type II histological damages, which was alleviated by the pretreatment with L-NAME) was completely

Table 2 Effect of mild irritants on 500 mL/L ethanol-induced histological damage in gastric mucosa of normal and gastritis rats, and modulation of protective action of 200 mL/L ethanol by pretreatment with L-NAME

Treatment	Histological damage (% total mucosal thickness)							
	Total	Normal			Gastritis			
		Type I	Type II	Type III	Total	Type I	Type II	Type III
H ₂ O (Control)	70.80 \pm 1.26	16.23 \pm 1.07	21.92 \pm 1.01	31.36 \pm 1.67	91.13 \pm 4.31 ^f	14.99 \pm 1.14	27.37 \pm 1.83 ^e	48.77 \pm 3.69 ^f
200 mL/L EtOH	59.61 \pm 2.04 ^b	11.12 \pm 0.97 ^b	15.27 \pm 1.10 ^b	33.20 \pm 1.80	92.23 \pm 3.89 ^g	14.17 \pm 1.26	25.06 \pm 1.77 ^g	53.00 \pm 3.16 ^g
50 g/L NaCl	73.16 \pm 1.82	15.37 \pm 1.26	22.64 \pm 1.54	35.15 \pm 2.07	90.73 \pm 3.15 ^f	12.11 \pm 1.02	28.33 \pm 1.60 ^e	50.29 \pm 3.40 ^f
0.3 mmol/L HCl	66.37 \pm 2.21	18.20 \pm 1.55	20.01 \pm 1.98	28.16 \pm 3.04	89.83 \pm 3.71 ^f	13.72 \pm 1.33	25.69 \pm 1.52 ^e	50.40 \pm 2.56 ^f
L-NAME+H ₂ O	74.2 \pm 1.96	16.41 \pm 1.72	21.19 \pm 1.70	36.62 \pm 3.21	94.27 \pm 3.06 ^f	15.21 \pm 1.31	29.61 \pm 1.97 ^f	49.42 \pm 3.90 ^e
L-NAME+200 mL/L EtOH	69.75 \pm 2.11 ^d	15.55 \pm 1.41 ^a	20.48 \pm 1.88 ^e	33.71 \pm 2.86	95.10 \pm 3.62 ^f	13.78 \pm 1.56	27.49 \pm 1.81 ^e	53.82 \pm 4.11 ^f

Values are mean \pm SE (*n* = 6), ^b*P*<0.01, ^c*P*<0.001 vs corresponding H₂O group without mild irritant. ^a*P*<0.05, ^d*P*<0.01 vs corresponding group without drug pretreatment. ^e*P*<0.05, ^f*P*<0.01, ^g*P*<0.001 vs corresponding group without gastritis (Normal).

Table 3 Effect of mild irritants and/or 500 mL/L ethanol on constitutive and inducible nitric oxide synthase activity in gastric mucosa of normal and gastritis rats

	Nitric oxide synthase activity (cpm/min/mg protein)							
	H ₂ O		200 mL/L EtOH		50 g/L NaCl		0.3 mol/L HCl	
	Constitutive	Inducible	Constitutive	Inducible	Constitutive	Inducible	Constitutive	Inducible
Basal normal	266.01 \pm 22.10	96.97 \pm 12.72	768.98 \pm 93.17 ^b	107.66 \pm 17.17	734.68 \pm 74.67 ^b	84.13 \pm 19.26	328.77 \pm 48.23	97.52 \pm 16.12
500 mL/L EtOH normal	132.18 \pm 16.49 ^d	106.55 \pm 13.19	326.54 \pm 33.43 ^{a,h}	143.51 \pm 15.71	282.67 \pm 23.86 ^{a,d}	109.67 \pm 12.32 ^a	160.86 \pm 25.07	137.24 \pm 16.13
Basal gastritis	31.56 \pm 7.20 ^f	856.58 \pm 93.82 ^f	31.13 \pm 10.47 ^f	746.05 \pm 94.07 ^f	41.26 \pm 11.64 ^f	649.89 \pm 81.83 ^f	22.27 \pm 8.01 ^f	949.87 \pm 106.22 ^f
500 mL/L EtOH gastritis	56.21 \pm 8.64 ^l	972.29 \pm 123.73 ^f	39.12 \pm 3.09 ^f	888.88 \pm 129.36 ^f	42.72 \pm 10.29 ^f	853.36 \pm 103.64 ^f	49.82 \pm 10.58 ^l	875.24 \pm 122.44 ^f

Values are mean \pm SE (*n* = 6), ^b*P*<0.001 vs corresponding H₂O group without mild irritant treatment. ^a*P*<0.05, ^b*P*<0.01, ^d*P*<0.001 vs corresponding group without 500 mL/L EtOH treatment (Basal). ^l*P*<0.01, ^f*P*<0.001 vs corresponding group without gastritis (Normal).

Table 4 Effect of mild irritants and/or 50% ethanol on superoxide dismutase (SOD) activity in gastric mucosa of normal and gastritis rats

	SOD activity (units/mg protein)			
	H ₂ O	200 mL/L EtOH	50 g/L NaCl	0.3 mol/L HCl
Basal normal	32.08±2.20	36.07±3.18	38.01±1.55	37.53±3.06
500 mL/L EtOH normal	37.20±2.51	41.14±1.82	40.48±0.99	41.33±3.78
Basal gastritis	41.92±2.42 ^a	47.51±3.27 ^a	48.03±2.06 ^b	50.56±3.88 ^a
500 mL/L EtOH gastritis	50.85±4.46 ^a	49.76±3.36 ^a	57.68±6.04 ^a	54.92±4.74 ^a

Values are mean±SE (n = 6), ^aP<0.05, ^bP<0.01 vs corresponding group without gastritis (Normal).

Table 5 Effect of mild irritants and/or 50% ethanol on leukotriene C₄ (LTC₄) level in gastric mucosa of normal and gastritis rats

	LTC ₄ level (pg/mg protein)			
	H ₂ O	200 mL/L EtOH	50 g/L NaCl	0.3 mol/L HCl
Basal normal	13.33±3.08	5.77±0.86 ^a	4.19±0.67 ^a	4.28±0.81 ^a
500 mL/L EtOH normal	29.28±5.46 ^c	10.01±1.87 ^b	9.15±3.05 ^b	8.17±2.42 ^b
Basal gastritis	35.08±6.28 ^e	17.05±4.22 ^{a,e}	12.88±3.68 ^{a,e}	14.86±3.60 ^{a,e}
500 mL/L EtOH gastritis	43.84±3.79	18.86±4.66 ^b	17.70±3.06 ^d	21.28±6.33 ^a

Values are mean±SE (n = 6), ^aP<0.05, ^bP<0.01, ^dP<0.001 vs corresponding H₂O group without mild irritant. ^cP<0.05 vs corresponding group without 500 mL/L EtOH treatment (Basal). ^eP<0.05 vs corresponding group without gastritis (Normal).

relieved. Five percent NaCl and 0.3 mol/L HCl did not exert any cytoprotective action in the histological level whatsoever.

Effects of mild irritants on NO synthase activity in gastric mucosa of gastritis rats, during basal condition or followed by 500 mL/L ethanol challenge (Table 3)

The condition of gastritis caused a profound elevation of inducible NO synthase activity as well as a reduction of constitutive NO synthase activity in all experimental groups. The elevation of constitutive NO synthase activity induced by 200 mL/L ethanol or 50 g/L NaCl was also alleviated in gastritis rats, with the inducible NO synthase activity remained unaltered by mild irritants. On the other hand, the overall inhibitory effect of 500 mL/L ethanol on mucosal constitutive NO synthase activity was relieved in gastritis animals, of which the activation of the constitutive isozyme by 200 mL/L ethanol and 50 g/L NaCl was also completely prevented.

Effects of mild irritants on SOD activity in gastric mucosa of gastritis rats, during basal condition or followed by 500 mL/L ethanol challenge (Table 4)

SOD activity was significantly increased in all gastritis animals, when compared to normal rats. On the other hand, neither the mild irritants nor 500 mL/L ethanol significantly altered SOD activity in the gastric mucosa.

Effects of mild irritants on LTC₄ level in gastric mucosa of gastritis rats, at basal condition or followed by 500 mL/L ethanol challenge (Table 5)

In general, there was a higher LTC₄ level in the gastric mucosa of all gastritis animals. Nevertheless, all three mild irritants significantly reduced the level of LTC₄ in the gastric mucosa of both normal and gastritis rats. Fifty percent ethanol significantly increased the amount of mucosal LTC₄ in normal animals, but not in gastritis animals. The ability of mild irritants to reduce mucosal LTC₄ level remained persistent in all 500 mL/L-ethanol-treated groups.

DISCUSSION

Previous studies investigating on the phenomenon of gastric

adaptive cytoprotection were conducted in normal animals. The present investigation demonstrated the adaptive cytoprotection of mild irritants in gastritis rats. It is known that after deep mucosal injury involving extensive hemorrhage and tissue destruction, as in the case of gastritis induced by 80% ethanol, epithelial restitution still occurred^[23]. The term "hemorrhagic gastritis" is a term used to describe the appearance of subepithelial hemorrhage in the stomach. Some patients with gastric subepithelial hemorrhage could be expected to have associated histologic gastritis. Hence, histological protection and the preservation of vascular integrity were the two main criteria of gastroprotection^[24]. Our findings indicated that the gross macroscopic protective actions of 200 mL/L ethanol and 50 g/L NaCl remained persistent in the gastritis stomach. The loss of protective effect of 0.3 mol/L HCl under gastritis condition implied that a normal functional mucosa could be essential for the protective mechanism of the mild acid. We previously reported that adaptive cytoprotection by 0.3 mol/L HCl was completely blocked by vagotomy, implicating that innervation of an intact vagus nerve was one of the prerequisites of this mild irritant to induce physiological responses in the mucosal oxyntic cells^[25]. Similarly, normal integrity of the mucosa that was interfered under gastritis condition may also be important for the protective action of HCl. Apart from that, 50 g/L NaCl and 0.3 mol/L HCl failed to preserve the mucosal cells histologically, even in non-gastritis normal animals, leaving 200 mL/L ethanol to be the only agent that could exert "true cytoprotection" at the surface glandular level. Nevertheless, the loss of histological protective ability of 200 mL/L ethanol during gastritis condition also suggests that the initiation of its histologic adaptive cytoprotection may also require an intact glandular mucosa to operate. Clinically, the histologic gastritis that attributed to ethanol was somehow related to the underlying presence of *H pylori*, although ethanol did not seem to initiate *H pylori*-associated histologic gastritis directly^[26]. Treatment of *H pylori* was associated with almost complete normalization of histologic findings^[27]. In other words, 200 mL/L ethanol may only be responsible for the improvement of macroscopic gastric mucosal lesion formation by surface epithelial restitution, while *H pylori* eradication is capable of restoring the deep subepithelial mucosa in histologic gastritis.

In general, inflammatory reactions were initiated and amplified by proinflammatory mediators from injured tissues as well as those being synthesized during the process^[28]. These substances could result in further local tissue injury by release and activation of destructive enzymes as well as production of oxygen-derived free radicals. Thus, removal of oxygen-derived free radicals could stimulate the healing of ethanol-induced acute gastric mucosal injury in rats^[29]. Increased superoxide generation was resulted from activation of polymorphonuclear leukocytes and macrophages, which were the stimuli that induced the production of NO by inducible NO synthase^[30]. NO produced in a relatively high concentration by this inducible enzyme might react with oxygen or superoxide to yield more reactive oxidants, such as the peroxynitrite^[31]. These secondary oxidants are believed to be responsible for most biological oxidative damages, and are often the targets of antioxidant defense. In the present study, inducible NO synthase activity was significantly increased for many folds in gastritis animals, which could be correlated with the aggravation in 500 mL/L ethanol-induced mucosal damage and the alleviation of the histological cytoprotection induced by 200 mL/L ethanol. Although the administration of 500 mL/L ethanol to normal rats did not cause any significant activation of inducible NO synthase activity, the activity of constitutive NO isozyme was inhibited. Production of NO from the calcium-dependent constitutive enzyme has been known to play a role in the modulation of gastric mucosal integrity^[32]. The general suppression of this constitutive isozyme in gastritis mucosa could be due to the loss of endothelial integrity. Alternatively, the gastroprotection caused by 200 mL/L ethanol and 50 g/L NaCl, which concurrently maintained the constitutive NO synthase activity following 500 mL/L ethanol challenge in normal animals, must be due to the preservation of endothelium and hence to maintain vascular integrity. However, L-NAME pretreatment only reversed the protective action of 200 mL/L ethanol but not that of 50 g/L NaCl, suggesting that the involvement of NO from the constitutive form in the anti-lesion action of NaCl is still uncertain. Nevertheless, the suppression of constitutive NO synthase activity and the loss of its activation by 200 mL/L ethanol in the gastritis mucosa may explain why gastritis provoked ethanol ulceration and attenuated the protective action of 200 mL/L ethanol, respectively^[33]. In addition, the damaged mucosa could activate the inducible NO isozyme and trigger the release of more free radicals, thus producing extensive tissue necrosis under gastritis condition.

Local SOD has been shown to abolish the gastric mucosal injury induced by the cytotoxic level of NO, possibly due to the prevention of peroxynitrite formation from interaction between superoxide and cytotoxic NO^[34]. Our results demonstrated that under gastritis condition, SOD activity was significantly elevated. This could be a defensive mechanism of the gastric mucosa that would be activated when a tremendous amount of superoxide and other free radicals was produced following severe tissue injury. Indeed, acute administration of either mild irritants or 500 mL/L ethanol did not induce a similar increase in SOD activity in the gastric mucosa. Hence, the acute protective action of mild irritants in both normal and gastritis rats did not seem to involve the modulation of mucosal SOD activity.

It was reported in a human study that the basal release of PGE₂ and LTC₄ in alcoholics was higher than that in healthy volunteers, and that alcohol administration could cause an increase in PGE₂ and LTC₄ in healthy volunteers^[35]. In addition, by using a rat model, the same group of investigators further proposed that the anti-lesion effect of some gastroprotective agents was related to the inhibition of LTC₄ formation and an increase in PGE₂ biosynthesis in the gastric mucosa^[36]. Our findings in fact indicated that LTC₄ level in the mucosa was significantly increased in gastritis rats, which was similar to the

state in alcoholics. Moreover, the challenge with 500 mL/L ethanol also stimulated an increase in LTC₄ level, as in the case of healthy volunteers. In fact, increased synthesis of mucosal PGE₂ in alcoholics could also indicate a defensive mechanism of the mucosa, mainly to counteract with the proinflammatory action of LTC₄ generated from the tissue. In the present study, mild irritants were able to induce a significant inhibition on the release of LTC₄ in both normal and gastritis mucosa. Reduction of this autacoid would attenuate vascular disturbances and decrease hemorrhagic lesions in the gastric mucosa^[37].

In summary, aggravation in 500 mL/L ethanol-induced gastric mucosal damages under gastritis condition can be due to increased mucosal biosynthesis of inducible NO and LTC₄. The protective action of 200 mL/L ethanol could be restricted to the surface mucosal cells, thus having no effect on deeper histologic lesions. In general, deep histologic protection by mild irritants could not be found in gastritis animals. On the other hand, mild irritants could also act by reducing gastric mucosal LTC₄ level, which can lessen gross vascular injury and subsequently reduce hemorrhagic lesion even in gastritis mucosa.

REFERENCES

- 1 **Guslandi M.** Effect of ethanol on the gastric mucosa. *Dig Dis Sci* 1987; **5**: 21-32
- 2 **Laine L, Weinattein WM.** Histology of alcoholic hemorrhagic "gastritis": a prospective evaluation. *Gastroenterology* 1988; **94**: 1254-1262
- 3 **Lacy ER, Morris GP, Cohen MM.** Rapid repair of the surface epithelium in human gastric mucosa after acute superficial injury. *J Clin Gastroenterol* 1993; **17**(Suppl 1): S125-S135
- 4 **Guth PH, Paulsen G, Nagata H.** Histologic and microcirculatory changes in alcohol-induced gastric lesions in the rat: effect of prostaglandin cytoprotection. *Gastroenterology* 1984; **87**: 1083-1090
- 5 **Peskar BM, Lange K, Hoppe U, Peskar BA.** Ethanol stimulates formation of leukotriene C₄ in rat gastric mucosa. *Prostaglandins* 1986; **31**: 283-293
- 6 **Yonei Y, Holzer P, Guth PH.** Laparotomy-induced gastric protection against ethanol injury is mediated by capsaicin-sensitive sensory neurons. *Gastroenterology* 1990; **99**: 3-9
- 7 **Whittle BJR, Lopez-Belmonte J, Moncada S.** Regulation of gastric mucosal integrity by endogenous nitric oxide: interaction with prostanoids and sensory neuropeptides in the rat. *Br J Pharmacol* 1990; **99**: 607-611
- 8 **Palmer RMJ, Ferrige AG, Moncada S.** Nitric oxide release accounts for the biological activity of endothelium-derived relaxing factor. *Nature* 1987; **327**: 524-526
- 9 **Palmer RMJ, Bridge L, Foxwell NA, Moncada S.** The role of nitric oxide in endothelial cell damage and its inhibition by glucocorticoids. *Br J Pharmacol* 1992; **105**: 11-12
- 10 **Tsuji S, Kawano S, Sato N, Kamada T.** Mucosal blood flow stasis and hypoxemia as the pathogenesis of acute gastric mucosal injury: role of endogenous leukotrienes and prostaglandins. *J Clin Gastroenterol* 1990; **12**(Suppl 1): S85-S91
- 11 **Szelenyi I, Brune K.** Possible role of oxygen free radicals in ethanol-induced gastric mucosal damage in rats. *Dig Dis Sci* 1988; **33**: 865-871
- 12 **Chamberlain CE.** Acute hemorrhagic gastritis. *Gastroenterol Clin North Am* 1993; **22**: 843-873
- 13 **Tepperman BL, Soper BD.** Interaction of nitric oxide and salivary gland epidermal growth factor in the modulation of rat gastric mucosal integrity. *Br J Pharmacol* 1993; **110**: 229-234
- 14 **Cho CH, Chen BW, Hui WM, Luk CT, Lam SK.** Endogenous prostaglandins: its role in gastric mucosal blood flow and ethanol ulceration in rats. *Prostaglandins* 1990; **40**: 397-403
- 15 **O'Brien P, Schultz C, Gannon B.** An evaluation of the phenomenon of cytoprotection using quantitative histological criteria. *J Gastroenterol Hepatol* 1987; **2**: 113-121
- 16 **Read SM, Northcote DH.** Minimization of variation in the response to different proteins of the Coomassie Blue G-binding assay for protein. *Anal Biochem* 1981; **116**: 53-58
- 17 **Knowles RG, Palacios M, Palmer RM, Moncada S.** Formation

- of nitric oxide from L-arginine in the central nervous system: a transduction mechanism for stimulation of the soluble guanylate cyclase. *Proc Natl Acad Sci U S A* 1989; **86**: 5159-5162
- 18 **Bredt DS**, Snyder SH. Nitric oxide mediates glutamate-linked enhancement of cGMP levels in the cerebellum. *Proc Natl Acad Sci U S A* 1989; **86**: 9030-9033
- 19 **Tepperman BL**, Vozzolo BL, Soper BD. Effect of neutropenia on gastric mucosal integrity and mucosal nitric oxide synthesis in the rat. *Dig Dis Sci* 1993; **38**: 2056-2061
- 20 **Rees DD**, Palmer RMJ, Schulz R, Hodson HF, Moncada S. Characterization of three inhibitors of endothelial nitric oxide synthase *in vitro* and *in vivo*. *Br J Pharmacol* 1990; **101**: 746-752
- 21 **Kostka P**, Jang E, Watson EG, Stewart JL, Daniel EE. Nitric oxide synthase in the autonomic nervous system of canine ileum. *J Pharmacol Exp Ther* 1993; **264**: 34-39
- 22 **Beauchamp C**, Fridovich I. Superoxide dismutase: improved assays and an assay applicable to acrylamide gels. *Anal Biochem* 1971; **44**: 276-287
- 23 **Lacy ER**. Epithelial restitution in the gastrointestinal tract. *J Clin Gastroenterol* 1988; **10**(Suppl 1): S72-S77
- 24 **Ko JKS**, Ching CK, Chow JYC, Zhang ST, Lam SK, Cho CH. The vascular and glandular organoprotective properties of metronidazole in the rodent stomach. *Aliment Pharmacol Ther* 1997; **11**: 811-819
- 25 **Ko JKS**, Cho CH. Adaptive gastric mucosal cytoprotection in rats: different modes of action by three mild irritants. *Digestion* 1996; **57**: 54-59
- 26 **Laine L**. *Helicobacter pylori*, gastric ulcer, and agents noxious to the gastric mucosa. *Gastroenterol Clin North Am* 1993; **22**: 117-125
- 27 **Uppal R**, Lateef SK, Korsten MA, Paronetto F, Lieber CS. Chronic alcoholic gastritis. Roles of alcohol and *Helicobacter pylori*. *Arch Intern Med* 1991; **151**: 760-764
- 28 **Kozol RA**, Downes RJ, Kreutzer DL, Wentzel S, Rossomando E, Elgebaly SA. Release of neutrophil chemotactic factors from gastric tissue. Initial biochemical characterization. *Dig Dis Sci* 1989; **34**: 681-687
- 29 **Salim AS**. Removing oxygen-derived free radicals stimulates healing of ethanol-induced erosive gastritis in the rat. *Digestion* 1990; **47**: 24-28
- 30 **Morris SM Jr**, Billiar TR. New insights into the regulation of inducible nitric oxide synthesis. *Am J Physiol* 1994; **266**: E829-E839
- 31 **Mannick EE**, Bravo LE, Zarama G, Realpe JL, Zhang XJ, Ruiz B, Fontham ET, Mera R, Miller MJ, Correa P. Inducible nitric oxide synthase, nitrotyrosine, and apoptosis in *Helicobacter pylori* gastritis: effect of antibiotics and antioxidants. *Cancer Res* 1996; **56**: 3238-3243
- 32 **Tepperman BL**, Whittle BJR. Endogenous nitric oxide and sensory neuropeptides interact in the modulation of the rat gastric microcirculation. *Br J Pharmacol* 1992; **105**: 171-175
- 33 **Palmer RMJ**, Reed DD, Ashton DS, Moncada S. L-Arginine is the physiological precursor for the formation of nitric oxide in endothelial-dependent relaxation. *Biochem Biophys Res Commun* 1988; **153**: 1251-1255
- 34 **Lamarque D**, Whittle BJR. Role of oxygen-derived metabolites in the rat gastric mucosal injury induced by nitric oxide donors. *Eur J Pharmacol* 1995; **277**: 187-194
- 35 **Franco L**, Cavallini G, Bovo P, Marcori M, Orlandi PG, Moltrè F, Vetturi B, Velo GP. Gastric eicosanoid synthesis in normal subjects and alcoholics after ethanol stimulation. *Ital J Gastroenterol* 1995; **27**: 244-247
- 36 **Franco L**, Velo GP. Eicosanoid and gastroprotection by copper derivatives and NDGA. *Inflamm Res* 1995; **44**: 139-142
- 37 **Ko JKS**, Ma JJ, Chow JYC, Ma L, Cho CH. The correlation of the weakening effect on gastric mucosal integrity by 5-HT with neutrophil activation. *Free Rad Biol Med* 1998; **24**: 1007-1014

Edited by Wang XL and Xu FM

Effects of motilin and ursodeoxycholic acid on gastrointestinal myoelectric activity of different origins in fasted rats

Ping Fang, Lei Dong, Jin-Yan Luo, Xiao-Long Wan, Ke-Xin Du, Ning-Li Chai

Ping Fang, Lei Dong, Jin-Yan Luo, Xiao-Long Wan, Ning-Li Chai, Department of Gastroenterology, Second Hospital of Xi'an Jiaotong University, Xi'an 710004, Shaanxi Province, China

Ke-Xin Du, Functional Center, Medical School, Xi'an Jiaotong University, Xi'an 710004, Shaanxi Province, China

Supported by the National Natural Science Foundation of China, No. 30170414

Correspondence to: Professor Lei Dong, Department of Gastroenterology, Second Hospital of Xi'an Jiaotong University, Xi'an 710004, Shaanxi Province, China. pingf7613@sina.com

Telephone: +86-29-83098317 **Fax:** +86-29-87231758

Received: 2003-10-27 **Accepted:** 2003-12-29

Abstract

AIM: To investigate gastrointestinal migrating myoelectric complex (MMC) and the effects of porcine motilin and ursodeoxycholic acid (UDCA) on MMC of gastrointestinal tract of different origins in fasted rats.

METHODS: Three bipolar silver electrodes were chronically implanted on the antrum, duodenum and jejunum. Seven days later 24 experimental rats were divided into 2 groups. One group was injected with porcine motilin *via* sublingual vein at a dose of 20 µg/kg, the other group was perfused into stomach with UDCA. The gastrointestinal myoelectric activity was recorded 1 h before and 2 h after the test substance infusions into the rats.

RESULTS: In all fasted rats a typical pattern of MMC was observed. Among the totally 68 activity fronts recorded in fasted rats under control, 67% started in duodenum, and 33% in antrum. MMC cycle duration and duration of phase III of antral origin were longer than those of duodenal origin. Administration of 20 µg/kg porcine motilin induced a premature antral phase III of antral origin. But perfusion into stomach with UDCA resulted in shorter MMC cycle duration, longer duration of phase III of duodenal origin, which were followed with shorter cycle duration and duration of antral phase III.

CONCLUSION: In fasted rats, MMC could originate from antrum and duodenum respectively. The characteristics of MMC of different origins may contribute to the large variations within subjects. The mechanisms of different origins of phase III may be different. Porcine motilin and UDCA could affect MMC of different origins of the gastrointestinal tract in fasted state, respectively.

Fang P, Dong L, Luo JY, Wan XL, Du KX, Chai NL. Effects of motilin and ursodeoxycholic acid on gastrointestinal myoelectric activity of different origins in fasted rats. *World J Gastroenterol* 2004; 10(17): 2509-2513

<http://www.wjgnet.com/1007-9327/10/2509.asp>

INTRODUCTION

The migrating myoelectric complex (MMC) is a distinct pattern

of electromechanical activity observed in gastrointestinal tract during fasting. It is thought to serve a housekeeping role and sweep undigested residual through the digestive tract. Phase III of MMC originates at variable sites in the gut from the esophagus (especially from antrum and duodenum) to proximal ileum. Large variations in MMC characteristics were described both within subjects and between subjects. The reason for the large variation in MMC characteristics is unknown. However, regarding the supposed differences in mechanisms that regulate the phase III of MMC of antral or duodenal origins, different origin of phase III within subject could be a basis for the differences in MMC characteristics^[1,2].

Motilin, a 22 amino acid peptide secreted by endocrinocytes in the mucosa of the proximal small intestine, participates in controlling the pattern of smooth muscle contractions in the upper gastrointestinal tract. These bursts of motilin secretion are temporarily related to the onset of housekeeping contractions, which sweep the undigested material of stomach and small intestine^[3]. Previous studies showed that the enterohepatic circulation of bile acids and interdigestive motility must somehow be associated with each other. Phase III of MMC played an important role in the transport of bile acids from the proximal duodenum to the distal small intestine, where bile acids were absorbed for transport back to the liver.

The purpose of the present study was to investigate the gastrointestinal MMC characteristics with respect to the different origin of phase III in fasted rats. Furthermore, the effects of exogenous porcine motilin and UDCA on the interdigestive myoelectric activity were investigated and the relationship between the above two drugs and the MMCs of different origin in conscious rats were studied.

MATERIALS AND METHODS

Animal preparation

Twenty-four healthy Sprague-Dawley rats (15 male and 9 female) weighing 200-250 g were fed with a dry rat food, and tap water for drinking *ad libitum*. After fasted for one night, the rats were intraperitoneally anesthetized with sodium pentobarbital 30 mg/kg. The hair on the skull and abdomen was shaved. The surgery was done with sterile instruments, and under strict aseptic conditions. The abdominal musculature and peritoneum were opened through the linea alba. Three bipolar insulated silver electrodes made by Teflon-coated wire (0.5 mm in outer diameter, 20 cm in length) were implanted into the muscular layer of the bowel with a needle as a trocar. One millimeter of the wire was exposed near the implanted end, and the interval between pairs of electrodes should be 2.0-3.0 mm. The electrodes were placed on the gastric antrum at 5 mm proximal to the pylorus, on the duodenum and jejunum respectively at 1 cm and 15 cm distal to the pylorus. The bundled electrode wires were grasped by the clamp through a silastic tube (2.4 mm in diameter), which then passed through the subcutaneous tunnel from the abdominal incision to the back of the shoulder exit. During operation the intestine was kept moist with sterile 9 g/L NaCl solution, and 4 mL of this solution was applied intraperitoneally before closure of the abdomen to compensate for intraoperative fluid loss. The abdominal wall was closed in three layers with

running Vicryl 4-0 sutures. The rats were kept in a humidified incubator at 37 °C for 2 to 4 h after operation. Following this, they were individually housed with free access to water and food. Housing conditions were kept constant with temperature at 22 °C, humidity of 60% and a 12-h light/dark cycle. The rats were allowed to adjust to these conditions for 1 wk before experiment.

Motility recordings

Rats were fasted for 16 h with free access to water. The experiments were performed in conscious rats. The gastrointestinal myoelectric activity recordings were monitored by using an electrical swivel mechanism to a computerized, multichannel recorder (RM-6280C, Chengdu, China). Myoelectric activity was sampled at a rate of 1 kHz. The signals were amplified and bandpass filtered (frequencies above 0.3 Hz and below 100 Hz were cut off). The amplitudes of contractions were recorded in μV .

Experimental procedures

A randomized, placebo-controlled experiment was performed. The rats were coded and divided into 2 groups, 12 in each group. On each experimental day, at the beginning of the experiments, the gastrointestinal myoelectric activity was recorded for 1 h for each rat, and during this period at least 2 or 3 MMCs appeared. The substances were dissolved immediately before use in normal saline. In each group, 4 rats were placed as control that received placebo (vehicle), 0.2 mL saline containing 250 μg bovine serum albumin (BSA, Sigma). One group was injected with porcine motilin (Sigma) *via* sublingual vein at a dose of 20 $\mu\text{g}/\text{kg}$, and the other group was perfused into stomach with UDCA (Pharmaceutical Factory of Changzhou City) respectively. After the substances were used, the gastrointestinal myoelectric activity of the rats was continuously recorded at least for 2 h. After the conversion from analog to digital, the signals were stored on optical disk for later analysis.

Statistical analysis

All variables followed a normal distribution and are expressed as mean \pm SD unless otherwise stated. The presented means are unweighted means, *i.e.*, means of all subjects after first calculating the mean within each subject separately. The MMC characteristics such as MMC cycle duration, duration of phase III, mean amplitude and frequency of phase III were examined by using the ANOVA model, both before and after discrimination for antral or duodenal phase III origin effects. The homogeneity of variance for each variable, after being divided into antral and duodenal phase III origin effects, was tested and appeared equal. Within-subject and between-subject effects were analyzed by the ANOVA model. For the MMC cycle duration, the corresponding variance components between and within individuals were used to calculate the variance between individuals as a percentage of the total variance. To explain the importance of the factor preceding phase III origin in the total variance, the sum of squares of the factor preceding phase III origin was calculated as a percentage of the total sum of squares in the ANOVA model. The effects of unfamiliarity with gastrointestinal catheter studies on MMC cycle duration was examined using the ANOVA model. Student's *t* test was used to compare the different paired values before and after the test substances administration in the above 2 groups. Statistical significance was defined as two-tailed $P < 0.05$.

RESULTS

MMC characteristics of different origin

In all fasted rats typical pattern of MMCs were observed. The total number of MMC cycles recorded was 68. The mean MMC cycle duration was 746 \pm 140 s. In total, phase III cycles were

observed with 23 (33%) of antral origin and 45 (67%) of duodenal origin. Fifty-nine percent of the total variance in MMC cycle duration was explained by the within-subject variance. The duration and the amplitude of phase III were significantly different between subjects ($P < 0.05$; Table 1). The large variation in MMC cycle duration is visible in Figure 1. The MMC cycle duration following a phase III of antral origin was significantly longer than those of duodenal origin ($P < 0.05$; Table 2). When the factor preceding phase III origin was included in our model, this factor contributed significantly to the total variation in MMC cycle duration; 31% of the total sum of squares was explained by the factor preceding phase III in comparison to 36% explained by the between-subject variance. The duration of phase III for duodenum was significantly longer when it started in the antrum than in the duodenum ($P < 0.05$). The other characteristics of MMC for duodenum were not significantly different between the phase III of the above two origins.

Table 1 MMC characteristics in 24 normal rats

MMC characteristics	mean \pm SD
MMC cycle duration/s	746 \pm 140 ^a
Duration of phase III/s	214 \pm 53 ^a
Amplitude of phase III/ μV	287 \pm 23 ^a
Frequency of phase III/(bursts/min)	11.4 \pm 0.3

Values are shown for duodenum. ^a $P < 0.05$ vs between subjects.

Table 2 MMC characteristics of different origin of ongoing phase III ($n = 24$, mean \pm SD)

MMC characteristics	After phase III of antral origin	After phase III of duodenal origin
MMC cycle duration/s	901 \pm 74	667 \pm 91 ^a
Duration of phase III/s	271 \pm 30	186 \pm 35 ^a
Amplitude of phase III/ μV	292 \pm 17	284 \pm 25
Frequency of phase III/(bursts/min)	11.2 \pm 0.5	11.6 \pm 0.2

Values are shown for duodenum. ^a $P < 0.05$ vs antral.

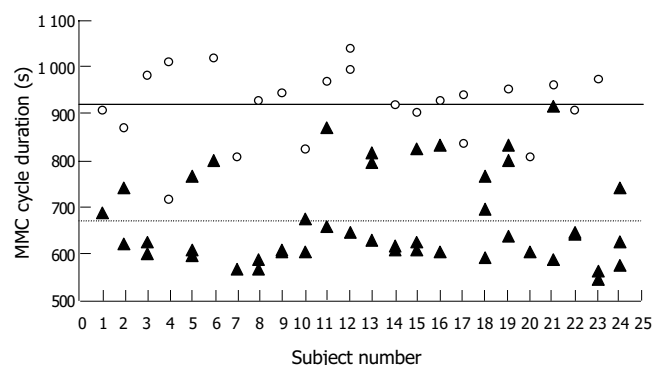


Figure 1 MMC cycle duration of all subjects following phase III. \circ , antral origin; \blacktriangle , duodenal origin; Solid line: antral mean MMC cycle duration (746.3); Dotted line: duodenal mean MMC cycle duration (667.0).

Effects of porcine motilin and UDCA

The effects of porcine motilin on the interdigestive gastrointestinal myoelectric activity were established within 1 to 2 min after the injection *via* sublingual vein at a dose of 20 $\mu\text{g}/\text{kg}$. A premature antral phase III which did not migrate caudad to the duodenum and jejunum was observed. And one injection only induced

one premature antral phase III. The characteristics of premature antral phase III were different significantly from those of normal antral phase III. The shorter duration and higher amplitude of premature antral phase III appeared (Figure 2). The effects of UDCA on the interdigestive gastrointestinal myoelectric activity were established within 3 to 4 min after the stomach was perfused of UDCA. The shorter MMC cycle duration, and the longer duration of phase III of duodenal origin, followed by the shorter cycle duration and duration of antral phase III were observed. There was no significant difference in the other parameters of MMC of antrum and duodenum before and after the treatment (Figure 3, Table 3). Furthermore, there was no significant difference in the MMC characteristics before and after placebo treatment in the above 2 experiments.

Table 3 Effects of UDCA on the interdigestive gastrointestinal myoelectric activity ($n = 8$, mean \pm SD)

MMC characteristics	Antrum		Duodenum	
	Before	After	Before	After
The number of MMC	7	11	11	21
MMC cycle duration/s	885 \pm 106	800 \pm 48 ^a	780 \pm 45	602 \pm 78 ^a
Duration of phase III/s	161 \pm 13	113 \pm 19 ^a	156 \pm 9	241 \pm 20 ^a
Amplitude of phase III/ μ V	297 \pm 11	284 \pm 20	288 \pm 22	285 \pm 19
Frequency of phase III/(bursts/min)	3.1 \pm 0.5	3.2 \pm 0.6	11.2 \pm 1.6	11.5 \pm 1.8

^a $P < 0.05$ vs before treatment.

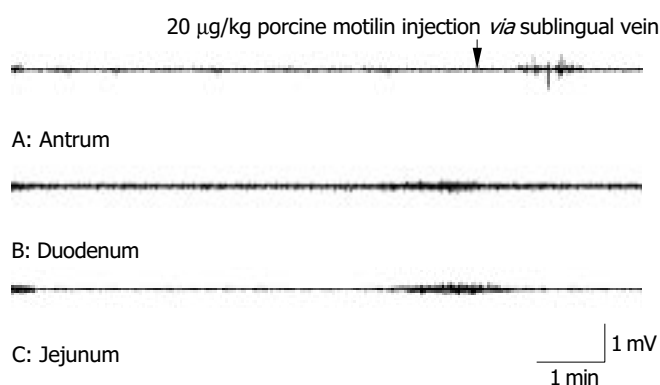


Figure 2 Effects of porcine motilin on the interdigestive gastrointestinal myoelectric activity in one case.

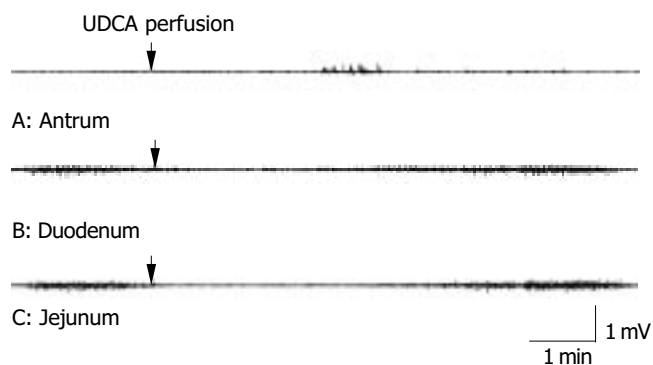


Figure 3 Effects of UDCA on the interdigestive gastrointestinal myoelectric activity in one case.

DISCUSSION

Gastrointestinal motility pattern could mainly be divided into the interdigestive and digestive states. The interdigestive state

is characterized by the cyclical occurrence of activity front, phase III contractions, which could occur in the antrum, duodenum and migrate to the small intestine. The digestive state is characterized by sustained contractions with different amplitude in the gastric antrum and small intestine. In our experiments, a typical pattern of MMC in interdigestive state was observed in all rats. The phases of the MMC can be distinguished: phase III, motor quiescence, phase III, a period of irregular contractile activity and phase III, a period of rhythmic contractions. The MMC pattern was disrupted by feeding, and irregular contractions with different amplitude were sustained in the antrum, duodenum and jejunum for at least 30 min after feeding. MMC was firstly described in the small intestine of fasting dogs and observed in the overall gastrointestinal tract of several species, including rats^[4-6]. In our study they have also been found in gastric antrum and small intestine. A method that could record the gastrointestinal myoelectrical activities in physiological conditions was established in our experiment. The model we have developed seemed to be suitable for studying the gastrointestinal myoelectric activities. The effects we obtained could be attributed to neither sedatives nor operative stress because of the method unable to record the gastrointestinal motility without the use of anesthesia. Furthermore, the surgical operations were well tolerated by the animals, especially by small animals. At present the method of stationary manometry was used in most of the experiments of this field^[7,8]. But it is not suitable for small animal experiments. Our method was simple, easy and successful. Few tissue was injured. Several pairs of electrodes could be implanted and work stably and repeatedly. The experimental techniques would be helpful for further studying the mechanisms of gastrointestinal motility.

A typical pattern of MMC was observed in all fasted rats. Among the totally 68 activity fronts recorded in them under control, 67% started in the duodenum, and 33% in the antrum. The MMC cycle duration and duration of phase III of antral origin were longer than those of duodenal origin. The MMCs were subject to large variations in its characteristics, both between subjects and within subjects. The reason for this wide variation is unknown. Our results contributed to a better understanding of this variation. Our study showed that MMC characteristics had close relationship with the origin of phase III. But Gregersen *et al.* described a positive correlation between the duration of phase III in the duodenum and the duration of the next MMC cycle^[9]. They could not attribute this to a difference in origin of phase III, most likely due to the limited number of observations within each subject. The percentages of antral and duodenal originated phase III observed within a subject would strongly affect the mean MMC cycle duration of this subject as well as the overall mean of a group of subjects^[10,11]. An explanation for the differences in MMC cycle duration and duration of phase III was that it might imply differences in the mechanism controlling interdigestive motility in antrum and small intestine. This may reflect functional differences existing in the hormonal mechanisms involved in the regulation of antral and duodenal phase III. It was thought that a difference might exist in the refractory period between the gastric antrum and small intestine, with a shorter refractory period in the duodenum compared with the antrum. Another possible reason may be the anatomic structure of rats. Because there is no gallbladder in rats, bile acids secreted to duodenum directly. In addition, our study could not explain why the density and the sensitivity of receptor in gastrointestinal tract changed^[12,13].

The mechanisms regulating MMC is not understood completely. Previous study showed that the area postrema of medulla oblongata, vagal innervation, enteric nervous system and gastrointestinal hormone could regulate the MMC. Among them motilin in plasma plays a very critical role in the initiation of MMC. Motilin is one of the gastrointestinal hormones. It

belongs to gut-brain peptide and distributes in the brain and gastrointestinal tract^[14-22]. Plasma levels of the motilin fluctuate in synchrony with the different phase of MMC. Motilin could stimulate the gastrointestinal motility of many animals, and there were species differences in its effects^[23]. After duodenectomy, no obvious phase III contractions were seen in the gastric antrum, but the contractile response of the stomach to exogenous motilin was similar to that of intact dogs^[24]. This experiment showed that endogenous motilin was released from duodenum. One research showed that the motilin could activate calcium current in human and canine jejunal circular smooth muscle. Furthermore, the density and sensitivity of motilin receptor of different parts of gastrointestinal tract were different. But recently the close relationship between motilin and MMC of antral but not duodenal origin was found^[25]. Porcine motilin could influence the MMC of antral origin in our experiment. Administration of 20 µg/kg porcine motilin could induce a premature antral phase III in rats. The characteristics of it were different significantly from those of normal antral phase III. But the results of our experiments were coincident with previous studies. Maybe the density and sensitivity of motilin receptor of antrum were higher than those of other parts of gastrointestinal tract^[12,13]. Some studies showed that duodenal pH governed interdigestive motility in humans. But neither duodenal acidification nor increases in motilin concentration were necessary to initiate MMC in man^[26]. Administration of a low dose of erythromycin induced an MMC that started from the gastric antrum, unaccompanied by a motilin peak. These findings showed that the activation of motilin receptor triggered the MMC.

Another important factor influencing MMC is enterohepatic cycle of bile acids. The enterohepatic cycle of bile acids had close relationship with MMC. The possible explanation was that the development of MMC of duodenal origin was not autonomous but dependent on the stimulation of bile acids to the local mucous of duodenum. Furthermore, duodenum, possibly by releasing endogenous motilin, might recruit and further augment the gastric response to initiation of the MMC of antral origin^[27-29]. So there are maybe two mechanisms for initiation of MMC in the stomach and duodenum. In our experiment perfusion into stomach of rats with UDCA could shorten the MMC cycle duration and elongate the duration of phase III of duodenal origin, which was followed by the contractions of antrum within a short time. We suggest that UDCA may drain into the duodenum influencing the MMC of duodenal origin and stimulate the release of endogenous motilin from the mucous of duodenum, because crushing the gallbladder of patient during operation could eject the bile acids and induce a higher level of plasma motilin. On the contrary, some researchers thought that bile acids in duodenum could not induce the release of motilin and affect the MMC^[30]. In the study of patients with gallstone, the motilin in plasma did not decrease obviously vs control group. But according to the above supposition, we could infer that the motilin in plasma should decrease obviously compared with control group because the motility of gallbladder decreased in most of the patients. The results obtained from this experiment did not coincident with those of previous experiments. Another research showed that the kinetics of duodenum did not change significantly after cholecystectomy. So these studies did not support the local stimulatory theory^[31,32]. But one study showed that the occurrence of MMC had close relationship with the increase of the plasma concentration of motilin and bile acids. Maybe it could explain the contradiction in this respect to some extent^[33]. But our study could not draw this conclusion.

Gastrointestinal motility disorder is common in clinical practice, and studying the mechanisms of it is very important to its diagnosis and therapy. Our study showed that the

mechanisms of different origin of phase III may be different and porcine motilin and UDCA could affect the MMC of different origin of the gastrointestinal tract in fasting state respectively. This may provide novel treatments for patients with disturbed gut motility.

REFERENCES

- 1 **Gielkens HA**, Nieuwenhuizen A, Biemond I, Lamers CB, Masclee AA. Interdigestive antroduodenal motility and gastric acid secretion. *Aliment Pharmacol Ther* 1998; **12**: 27-33
- 2 **Bush TG**, Spencer NJ, Watters N, Sanders KM, Smith TK. Spontaneous migrating motor complexes occur in both the terminal ileum and colon of the C57BL/6 mouse *in vitro*. *Auton Neurosci* 2000; **84**: 162-168
- 3 **Suzuki H**, Mochiki E, Haga N, Satoh M, Mizumoto A, Itoh Z. Motilin controls cyclic release of insulin through vagal cholinergic muscarinic pathways in fasted dogs. *Am J Physiol* 1998; **274**(1 Pt 1): G87-95
- 4 **Powell AK**, Fida R, Bywater RA. Motility in the isolated mouse colon: migrating motor complexes, myoelectric complexes and pressure waves. *Neurogastroenterol Motil* 2003; **15**: 257-266
- 5 **Kaji T**, Takamatsu H, Kajiya H. Motility of the gastrointestinal tract and gallbladder during long-term total parenteral nutrition in dogs. *J Parenter Enteral Nutr* 2002; **26**: 198-204
- 6 **Romanski KW**, Rudnicki J, Slawuta P. The myoelectric activity of ileum in fasted and fed young pigs. *J Physiol Pharmacol* 2001; **52**(4 Pt 2): 851-861
- 7 **Matsunaga H**, Tanaka M, Takahata S, Ogawa Y, Naritomi G, Yokohata K, Yamaguchi K, Chijiwa K. Manometric evidence of improved early gastric stasis by erythromycin after pylorus-preserving pancreatoduodenectomy. *World J Surg* 2000; **24**: 1236-1241
- 8 **Andrews JM**, O'donovan DG, Hebbard GS, Malbert CH, Doran SM, Dent J. Human duodenal phase III migrating motor complex activity is predominantly antegrade, as revealed by high-resolution manometry and colour pressure plots. *Neurogastroenterol Motil* 2002; **14**: 331-338
- 9 **Gregersen H**, Rittig S, Vinter-Jensen L, Kraglund K. The relation between antral contractile activity and the duodenal component of the migrating motility complex. *Scand J Gastroenterol Suppl* 1988; **152**: 36-41
- 10 **Qian LW**, Pasricha PJ, Chen JD. Origins and patterns of spontaneous and drug-induced canine gastric myoelectrical dysrhythmia. *Dig Dis Sci* 2003; **48**: 508-515
- 11 **Luiking YC**, Akkermans LM, van der Reijden AC, Peeters TL, van Berge-Henegouwen GP. Differential effects of motilin on interdigestive motility of the human gastric antrum, pylorus, small intestine and gallbladder. *Neurogastroenterol Motil* 2003; **15**: 103-111
- 12 **Koenig JB**, Cote N, LaMarre J, Harris WH, Trout DR, Kenney DG, Monteith G. Binding of radiolabeled porcine motilin and erythromycin lactobionate to smooth muscle membranes in various segments of the equine gastrointestinal tract. *Am J Vet Res* 2002; **63**: 1545-1550
- 13 **Depoortere I**. Motilin and motilin receptors: characterization and functional significance. *Verh K Acad Geneesk Belg* 2001; **63**: 511-529
- 14 **Wang L**, Zhou L, Tian R. Role of the area postrema of medulla oblongata in the regulation of canine interdigestive migrating motor complex. *Chin Med J* 2002; **115**: 384-388
- 15 **Wang L**, Zhou L, Tian R. Effect of electrical lesion of the area postrema on gastrointestinal interdigestive migrating motor complex in conscious dogs. *Zhonghua Yixue Zazhi* 2000; **80**: 764-768
- 16 **Hashmonai M**, Szurszewski JH. Effect of cerebroventricular perfusion of bombesin on gastrointestinal myoelectric activity. *Am J Physiol* 1998; **274**(4 Pt 1): G677-686
- 17 **Guan Y**, Tang M, Jiang Z, Peeters TL. Excitatory effects of motilin in the hippocampus on gastric motility in rats. *Brain Res* 2003; **984**: 33-41
- 18 **Tang M**, Zhang HY, Jiang ZY, Xu L, Peeters TL. Effect of central administration of motilin on the activity of gastric-related neurons in brain stem and gastric motility of rats. *Shengli*

- Xuebao* 2000; **52**: 416-420
- 19 **Romanski KW**. Influence of various feeding conditions, the migrating myoelectric complex and cholinergic drugs on antral slow waves in sheep. *Arch Tierernahr* 2002; **56**: 393-408
 - 20 **Tanaka T**, Kendrick ML, Zyromski NJ, Meile T, Sarr MG. Vagal innervation modulates motor pattern but not initiation of canine gastric migrating motor complex. *Am J Physiol Gastrointest Liver Physiol* 2001; **281**: G283-G292
 - 21 **Tanaka T**, VanKlompenberg LH, Sarr MG. Selective role of vagal and nonvagal innervation in initiation and coordination of gastric and small bowel patterns of interdigestive and postprandial motility. *J Gastrointest Surg* 2001; **5**: 418-433
 - 22 **Tanaka T**, Zyromski NJ, Libsch KD, Kendrick ML, Sarr MG. Canine ileal motor activity after a model of jejunoileal autotransplantation. *Ann Surg* 2003; **237**: 192-200
 - 23 **Sasaki N**, Yoshihara T. The effect of motilin on the regulation mechanism of intestinal motility in conscious horses. *J Vet Med Sci* 1999; **61**: 167-170
 - 24 **Suzuki H**, Mochiki E, Haga N, Shimura T, Itoh Z, Kuwano H. Effect of duodenectomy on gastric motility and gastric hormones in dogs. *Ann Surg* 2001; **233**: 353-359
 - 25 **Luiking YC**, Peeters TL, Stolk MF, Nieuwenhuijs VB, Portincasa P, Depoortere I, van Berge Henegouwen GP, Akkermans LM. Motilin induces gall bladder emptying and antral contractions in the fasted state in humans. *Gut* 1998; **42**: 830-835
 - 26 **Tomita R**, Fujisaki S, Tanjoh K, Fukuzawa M. Studies on gastrointestinal hormone and jejunal interdigestive migrating motor complex in patients with or without early dumping syndrome after total gastrectomy with Roux-en-Y reconstruction for early gastric cancer. *Am J Surg* 2003; **185**: 354-359
 - 27 **Kajiyama Y**, Irie M, Enjoji A, Ozeki K, Ura K, Kanematsu T. Role of bile acids in duodenal migrating motor complexes in dogs. *Dig Dis Sci* 1998; **43**: 2278-2283
 - 28 **Van Ooteghem NA**, Van Erpecum KJ, Van Berge-Henegouwen GP. Effects of ileal bile salts on fasting small intestinal and gallbladder motility. *Neurogastroenterol Motil* 2002; **14**: 527-533
 - 29 **Einarsson C**, Ellis E, Abrahamsson A, Ericzon BG, Bjorkhem I, Axelson M. Bile acid formation in primary human hepatocytes. *World J Gastroenterol* 2000; **6**: 522-525
 - 30 **van Ooteghem NA**, Moschetta A, Rehfeld JF, Samsom M, van Erpecum KJ, van Berge-Henegouwen GP. Intraduodenal conjugated bile salts exert negative feedback control on gallbladder emptying in the fasting state without affecting cholecystokinin release or antroduodenal motility. *Gut* 2002; **50**: 669-674
 - 31 **Stolk MF**, Van Erpecum KJ, Peeters TL, Samsom M, Smout AJ, Akkermans LM, Vanberge-Henegouwen GP. Interdigestive gallbladder emptying, antroduodenal motility, and motilin release patterns are altered in cholesterol gallstone patients. *Dig Dis Sci* 2001; **46**: 1328-1334
 - 32 **Andersen PV**, Mortensen J, Oster-Jorgensen E, Rasmussen L, Pedersen SA, Qvist N. Cholecystectomy in patients with normal gallbladder function did not alter characteristics in duodenal motility which was not correlated to size of bile acid pool. *Dig Dis Sci* 1999; **44**: 2443-2448
 - 33 **Portincasa P**, Peeters TL, van Berge-Henegouwen GP, van Solinge WW, Palasciano G, van Erpecum KJ. Acute intraduodenal bile salt depletion leads to strong gallbladder contraction, altered antroduodenal motility and high plasma motilin levels in humans. *Neurogastroenterol Motil* 2000; **12**: 421-430

Edited by Zhu LH and Chen WW Proofread by Xu FM

Improvement of barrier function and stimulation of colonic epithelial anion secretion by *Menoese Pills*

Jin-Xia Zhu, Ning Yang, Gui-Hong Zhang, Lai-Ling Tsang, Yu-Lin Gou, Hau-Yan Connie Wong, Yiu-Wa Chung, Hsiao-Chang Chan

Jin-Xia Zhu, Lai-Ling Tsang, Yu-Lin Gou, Hau-Yan Connie Wong, Yiu-Wa Chung, Hsiao-Chang Chan, Epithelial Cell Biology Research Center, Department of Physiology, Faculty of Medicine, The Chinese University of Hong Kong, Shatin, Hong Kong, China
Jin-Xia Zhu, Ning Yang, Gui-Hong Zhang, Department of Physiology, Medical School, Zhengzhou University, Zhengzhou 450052, Henan Province, China

Supported by a fund from the Innovation and Technology Commission of Hong Kong, SAR

Correspondence to: Professor Hsiao-Chang Chan, Epithelial Cell Biology Research Center, Department of Physiology, Faculty of Medicine, The Chinese University of Hong Kong, Shatin, NT, Hong Kong, China. hsiaocchan@cuhk.edu.hk

Telephone: +852-26096839 **Fax:** +852-26035022

Received: 2004-02-02 **Accepted:** 2004-03-04

Abstract

AIM: *Menoese Pills* (MP), a Chinese medicine-based new formula for postmenopausal women, has been shown to modulate the endocrine and immune systems^[1]. The present study investigated the effects of MP and one of its active ingredients, *ligustrazine*, on epithelial barrier and ion transport function in a human colonic cell line, T₈₄.

METHODS: Colonic transepithelial electrophysiological characteristics and colonic anion secretion were studied using the short circuit current (I_{sc}) technique. RT-PCR was used to examine the expression of cytoplasmic proteins associated with the tight junctions, *ZO-1* (zonula occludens-1) and *ZO-2* (zonula occludens-2).

RESULTS: Pretreatment of T₈₄ cells with MP (15 µg/mL) for 72 h significantly increased basal potential difference, transepithelial resistance and basal I_{sc}. RT-PCR results showed that the expressions of *ZO-1* and *ZO-2* were significantly increased after MP treatment, consistent with improved epithelial barrier function. Results of acute stimulation showed that apical addition of MP produced a concentration-dependent (10-5 000 µg/mL, EC₅₀ = 293.9 µg/mL) increase in I_{sc}. MP-induced I_{sc} was inhibited by basolateral treatment with bumetanide (100 µmol/L), an inhibitor of the Na⁺-K⁺-2Cl⁻ cotransporter, apical addition of Cl⁻ channel blockers, diphenylamine-2, 2'-dicarboxylic acid (1 mmol/L) or glibenclamide (1 mmol/L), but not 4, 4'-diisothiocyanostilbene-2, 2'-disulfonic acid or epithelial Na⁺ channel blocker, amiloride. The effect of MP on *ZO-1* and *ZO-2* was mimicked by *Ligustrazine* and the *ligustrazine*-induced I_{sc} was also blocked by basolateral application of bumetanide and apical addition of diphenylamine-2, 2'-dicarboxylic acid or glibenclamide, and reduced by a removal of extracellular Cl⁻.

CONCLUSION: The results of the present study suggest that MP and *ligustrazine* may improve epithelial barrier function and exert a stimulatory effect on colonic anion secretion, indicating the potential use of MP and its active ingredients for improvement of GI tract host defense and alleviation of constipation often seen in the elderly.

Zhu JX, Yang N, Zhang GH, Tsang LL, Gou YL, Wong HYC, Chung YW, Chan HC. Improvement of barrier function and stimulation of colonic epithelial anion secretion by *Menoese Pills*. *World J Gastroenterol* 2004; 10(17): 2514-2518
<http://www.wjgnet.com/1007-9327/10/2514.asp>

INTRODUCTION

It is well known that the gastrointestinal (GI) epithelium of the host, as the first defense line, plays an important role in protecting enteric epithelia from invasion of most pathogens. Intestinal epithelial barrier function regulates epithelial ions and nutrient transport as well as host defense mechanisms. Epithelial membrane pumps, ion channels and tight junctions tightly control epithelial transcellular and paracellular fluxes^[2,3]. Cl⁻ secretion also provides an essential driving force for lubrication of intestinal contents during regular bowel movements or flushing of microbial organisms or artificial irritants in host defense responses^[4,5]. Epithelial Cl⁻ channels play an important role in regulation and maintenance of normal GI physiological functions. Abnormal regulation of Cl⁻ channels may result in diarrhea^[6-8] or constipation^[9,10]. While the latter represents one of the frequently encountered conditions in aged people, few remedies are available for alleviation of the condition in the elderly.

Menoese Pills (Modified *Bak Foong Pills*, MP), a newly developed formula based on traditional Chinese medicine *Bak Foong Pills* (*BFP*, also known as *Baifeng Wan*)^[11-17], has been designed for the use of postmenopausal women. It has been demonstrated that MP can regulate hormonal profiles (Gou *et al*, unpublished data) and immune system in the elderly^[1], indicating its beneficial effects for postmenopausal or elderly women. Since our previous studies have demonstrated that *BFP* could increase colonic epithelial Cl⁻ and pancreatic duct epithelial HCO₃⁻ secretion^[11,15,16] and both *BFP* and MP have a common active ingredient, *ligustrazine*, we undertook the present study to examine whether MP and *ligustrazine* exerted any effect on Cl⁻ secretion and epithelial electrophysiological characteristics using human colonic T₈₄ cells in conjunction with the short-circuit current technique and RT-PCR.

MATERIALS AND METHODS

Chemicals and solutions

Dulbecco's Modified Eagle's medium (DMEM)/F12, Hank's balanced salt solution (HBSS), and fetal bovine serum were from Gibco Laboratories (New York, NY). 4, 4'-diisothiocyanostilbene-2, 2'-disulfonic acid (DIDS) and glibenclamide were from Sigma (St. Louis, MO). MP was obtained from Eu Yan Sang Ltd (Hong Kong). Diphenylamine-2, 2'-dicarboxylic acid (DPC) was purchased from Riedel-de Haen Chemicals (Hannover, Germany). Calbiochem (San Diego, CA) was the source for amiloride hydrochloride and bumetanide. Krebs-Henseit (K-H) solution had the following composition (mmol/L): NaCl, 117; KCl, 4.5; CaCl₂, 2.5; MgCl₂, 1.2; NaHCO₃, 24.8; KH₂PO₄, 1.2; glucose, 11.1. The solution was gassed with 950 mL/L O₂ and 50 mL/L CO₂, at pH 7.4.

MP extraction

Five hundred gram of MP powder in 700 mL/L ethanol at a ratio of 1 to 10 (g/mL) was put in round-bottomed flask and boiled under reflux for 2 h. The mixture was filtered and the residues of MP were subject to the same treatment for a second time. The filtrates from the two treatment procedures were collected and put in the vacuum rotary evaporator for concentration. The extracts were collected and lyophilized by a freeze dryer.

Cell culture

Human colonic T₈₄ cells were purchased from American Type Culture Collection (Rockville, MD). The cells were grown in DMEM/F12 with 100 mL/L fetal bovine serum. For I_{SC} recording the cells (2-3×10⁵/mL) were plated onto each floating permeable support, which was made of a Millipore filter with a silicone rubber ring attached on top of it for confining the cells (culture area 0.45 cm²). For the RT-PCR analysis, cells were seeded on the Millipore filter with a confined culture area of 4.5 cm². Cultures were incubated at 37 °C in 950 mL/L O₂ and 50 mL/L CO₂ for 6 d before experiments. For the experiments of MP and *ligustrazine* pretreatments, MP (15 µg/mL) or *ligustrazine* (100 µmol/L) was added into the culture medium at 72 h before experiments, when the cells became semi-confluent.

Short-circuit current measurement

The measurement of I_{SC} has been described previously^[18]. Monolayers grown on permeable supports were clamped vertically between two halves of the Ussing chamber. The monolayers were bathed in both sides with Krebs-Henseit solution, which was maintained at 37°C by a water jacket enclosing the reservoir. The Krebs-Henseit solution was bubbled with 950 mL/L O₂ and 50 mL/L CO₂ to maintain the pH of the solution at 7.4. Drugs could be added directly to apical or basal side of the epithelium. Usually, the epithelia exhibited a basal transepithelial potential difference for every monolayer examined, which was measured by the Ag/AgCl reference electrodes (World Precision Instruction) connected to a preamplifier which was in turn connected to a voltage-clamp amplifier (World Precision Instruction, DVC-1000). In most of the experiments, the change in I_{SC} was defined as the maximal rise in I_{SC} following agonist stimulation and it was normalized to current change per unit area of the epithelial monolayer (µA/cm²). The total charges transported for 15 min (the area under the curve of the agonist-induced I_{SC} responses) were also used to describe the agonist-induced responses (µC/cm²). In each experiment, a transepithelial potential difference was 0.1 mV. The change in current in response to the applied potential was used to calculate the transepithelial resistance (TER) of the monolayer using Ohm's Law. Experiments were normally repeated in different batches of culture to ensure that the data were reproducible.

Reverse transcription PCR (RT-PCR) analysis

Total RNA (15 µg) was extracted from the T₈₄ (control, MP and *ligustrazine* pretreated). Expressions of *ZO-1* and *ZO-2* were analyzed by competitive RT-PCR. The specific oligo nucleotide primers for *ZO-1* was CGGTCCTCTGAGCCTGTAAG for sense and GGA TCTACATGCGACGACAA for antisense corresponding to nucleotides 3 100-3 470 with an expected cDNA of 371 bp^[19], and for *ZO-2* was GCCAAAACCCAGAACAAAGA for sense and ACTGCTCTCTCCACCTCCT for antisense corresponding to nucleotides 3 018-3 283 with an expected cDNA of 212 bp^[19]. GAPDH was used as an internal marker for semi-quantitative analysis of expressions of *ZO-1* and *ZO-2* of T₈₄ cells. The specific oligonucleotide primers for GAPDH were TCC CAT CAC CAT CTT CCA G for sense and TCC ACC ACT GAC ACG TTG for antisense corresponding to nucleotides 249-764 bp with an expected cDNA of 515 bp^[20].

Data analysis

Results were expressed as mean±SD. The number of experiments represents independent measurements on separate monolayers. Comparisons between groups of data were made by Student's *t*-test. A *P* value less than 0.05 was considered statistically significant. EC₅₀ values were determined by nonlinear regression using GraphPad Prism software.

RESULTS

Effect of pretreatment with MP on electrophysiological characteristics

Pretreatment of T₈₄ cells with MP 15 µg/mL (*n* = 15) for 72 h significantly increased the basal transepithelial potential difference from 0.39±0.07 to 2.27±0.59 mV (Figure 1A, *P*<0.01), basal I_{SC} from 3.05±0.44 to 7.14±1.80 µA/cm² (Figure 1B, *P*<0.05) and transepithelial resistance (TER) from 0.14±0.01 to 0.37±0.04 µC/cm² (Figure 1C, *P*<0.001).

Effect of pretreatment with MP on expressions of ZO-1 and ZO-2

In order to see whether MP-induced TER increase was related to the cytoplasmic proteins associated with tight junctions, *ZO-1* (zonula occludens-1) and *ZO-2* (zonula occludens-2), we used RT-PCR analysis to examine the expression levels of *ZO-1* and *ZO-2* in T₈₄ cells (Figure 2A). Semi-quantitative analyses showed that the expression levels of both *ZO-1* and *ZO-2* after MP pretreatment were significantly elevated, the ratio of *ZO-1* to GAPDH was from 0.46±0.08 to 0.81±0.10 (*n*=6, *P*<0.05, Figure 2B), and the ratio of *ZO-2* to GAPDH was from 0.76±0.12 to 1.27±0.12 (*n* = 4, *P*<0.001, Figure 2C), indicating the enhancement of epithelial barrier function.

MP-induced I_{SC} response

As shown in Figure 3, apical addition of MP (10-5000 µg/mL) produced an I_{SC} increase which was concentration-dependent (Figure 3A) with an apparent EC₅₀ of about 293.9 µg/mL (Figure 3B). MP-induced changes in I_{SC} were calculated as total charges transported for 15 min (µC/cm², the area under the curve of the MP-induced I_{SC} responses for the given time period) since the current kinetics did not sustain. MP at 10, 50, 100, 500, 1 000 and 5 000 µg/mL produced I_{SC} increases of 306.7±25.5 (*n* = 4), 673.3±91.3 (*n* = 4), 1380.0±119.4 (*n* = 4), 7624.0±309.7 (*n* = 5), 9580.0±734.9 (*n* = 6) and 10053.3±979.1 µC/cm² (*n* = 4), respectively.

Anion dependence of MP-induced I_{SC}

In order to study the ion species involved in mediating MP-induced I_{SC}, a Na⁺ channel blocker, amiloride and a couple of Cl⁻ channel blockers, DPC, glibenclamide and DIDS were examined (Figure 4). The change in I_{SC} was defined as the maximal rise in I_{SC} following MP stimulation and it was normalized to current change per unit area of the epithelial monolayer (µA/cm²). DPC (1 mmol/L, *n* = 4, Figure 4A) or glibenclamide (1 mmol/L, *n* = 5) added to the apical side reduced MP (500 µg/mL)-induced responses from 10.0±0.97 µA/cm² to 1.78±0.18 µA/cm² (*P*<0.01) or from 9.44±0.49 µA/cm² to 1.39±0.5 µA/cm² (*P*<0.001) respectively, but apical addition of amiloride (10 µmol/L, *n* = 4) or DIDS (100 µmol/L, *n* = 4) had no significant effects (Figure 4B). Basolateral addition of bumetanide (100 µmol/L, *n* = 6), a strong inhibitor of the Na⁺-K⁺-2Cl⁻ cotransporter reduced the MP-induced I_{SC} from 9.33±0.64 to 2.31±0.74 µA/cm² (Figure 4B, *P*<0.01).

Mimicking effects of MP by *ligustrazine*

Similar to the effects of pretreatment with MP, treating T₈₄ cells with *ligustrazine*, one of the active ingredients of MP, for 72 h also increased the levels of *ZO-1* and *ZO-2*, the ratio of *ZO-1* to GAPDH was raised from 0.46±0.08 to 0.65±0.11 (*n* = 6, Figure 2B)

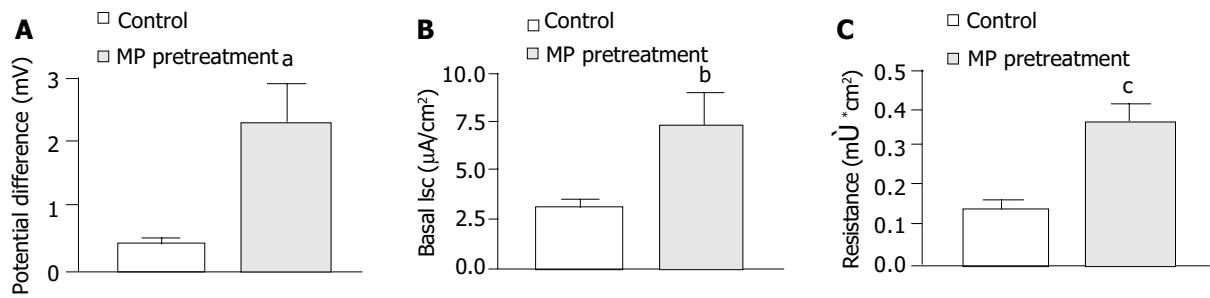


Figure 1 Effects of MP pretreatment on transepithelial electrophysiological characteristics. Comparison of potential difference (A) transepithelial I_{sc} (B) and transepithelial resistance (C) in T₈₄ cells with and without MP (15 µg/mL, 72 h) pretreatment. Values are mean±SE; ^{a(b)}P<0.01; ^{b(a)}P<0.05; ^{c(d)}P<0.001.

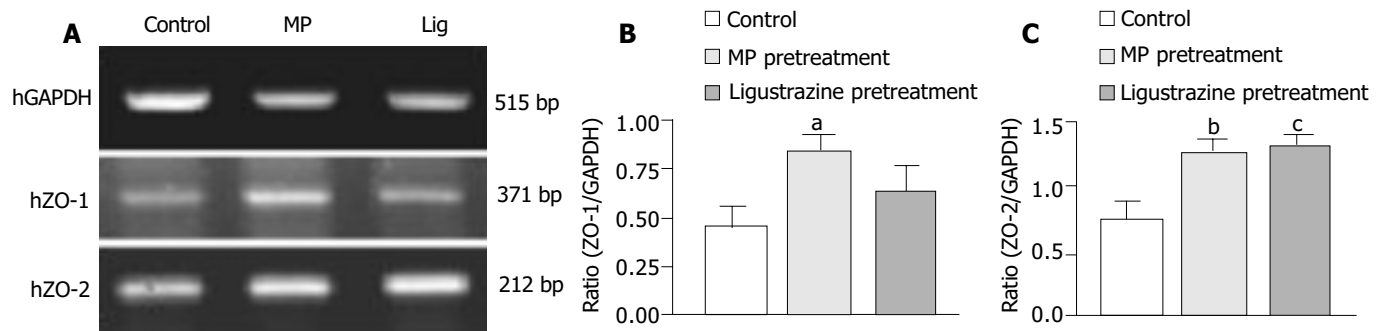


Figure 2 RT-PCR analyses of mRNA expressions of ZO-1 and ZO-2 in T₈₄ cells. (A) RT-PCR results with products as expected of ZO-1 and ZO-2 found in control, MP pretreatment and *ligustrazine* pretreatment. Semi-quantitative analyses of ZO-1 (B) and ZO-2 (C) expressions in T₈₄ cells without and with MP or *ligustrazine* pretreatment, which were shown in ratio of ZO-1 or ZO-2 to GAPDH (internal marker). Values are mean±SE; ^aP and ^{b(c)}P<0.05; ^{c(d)}P<0.001.

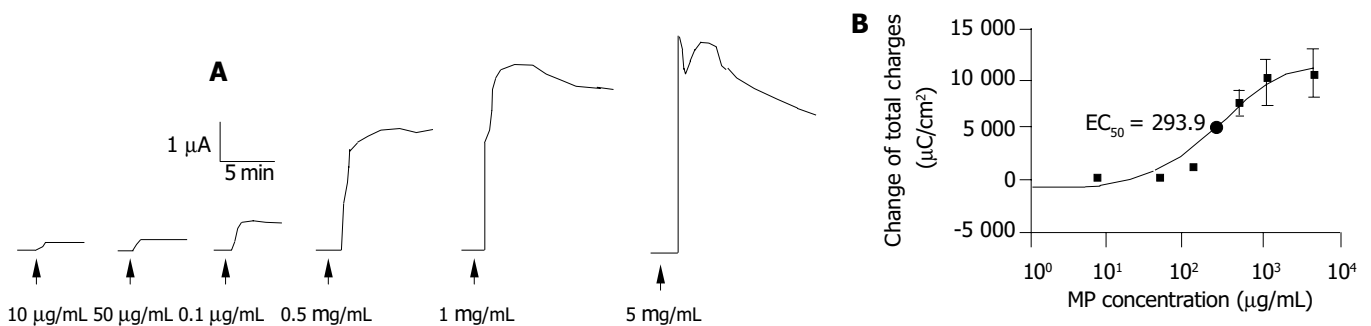


Figure 3 MP-induced I_{sc} in T₈₄ cell lines. A: Representative I_{sc} recordings in response to MP (10, 50, 100, 500, 1000 and 5000 µg/mL) added to the apical side. Arrowheads indicate the time of MP addition. B: The concentration-response curve for MP-induced responses. Different concentrations of MP were added to the apical side and each data was obtained from at least 3 individual experiments. Values are mean±SE of maximal I_{sc} increase.

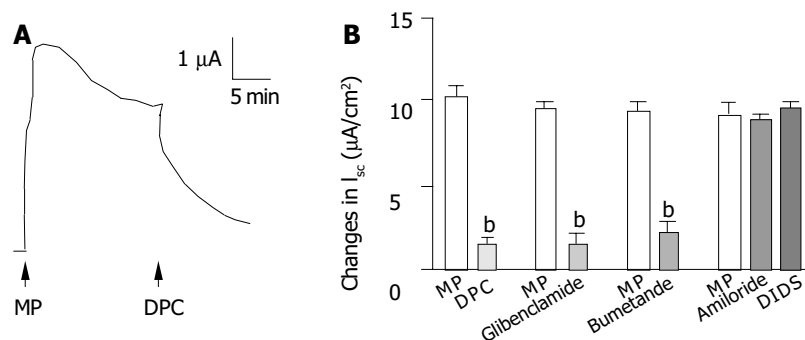


Figure 4 Anion dependence of MP-induced I_{sc}. A: Representative I_{sc} recording with arrows indicating the time for apical addition of MP (500 µg/mL) and DPC (1 mmol/L). B: Summary of the effects of DPC (1 mmol/L, apical), glibenclamide (1 mmol/L, apical), bumetanide (100 µmol/L, basolateral), amiloride (10 µmol/L, apical) and DIDS (100 µmol/L, apical) on MP-induced I_{sc}. Values are mean±SE; ^bP<0.01.

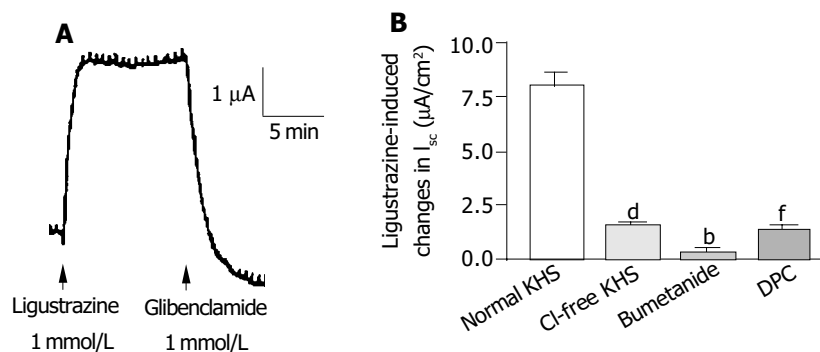


Figure 5 Anion dependence of *ligustrazine*-induced I_{sc} . **A**: Representative I_{sc} recording with arrows indicating the time for apical addition of *ligustrazine* (1 mmol/L) and glibenclamide (1 mmol/L). **B**: Summary of the effects of removal of extracellular Cl^- , basolateral addition of bumetanide (100 μ mol/L) and apical addition of DPC (1 mmol/L) on *ligustrazine*-induced I_{sc} . Values are mean \pm SE; ^d P , ^b P and ^f P <0.001.

and the ratio of ZO-2 to GAPDH was from 0.76 ± 0.12 to 1.33 ± 0.07 ($n=4$, $P<0.001$) (Figure 2C).

Acute stimulation with *ligustrazine* (1 mmol/L, apical side) produced a current increase which was similar to that induced by acute addition of MP (0.5 mg/mL, apical) ($n=6$, Figure 5A). Removal of Cl^- from KHS ($n=4$), apical addition of DPC or glibenclamide (1 mmol/L) ($n=3$) and basolateral administration of bumetanide (100 μ mol/L) ($n=3$) reduced *ligustrazine*-induced current increases by 79.9% ($P<0.001$), 82.4% ($P<0.001$) and 96.2% ($P<0.001$), respectively (Figure 5B).

DISCUSSION

The present study has provided scientific evidence for the pharmacological action of MP, a Chinese medicine-based formula for postmenopausal women, on the GI tract. The results demonstrated that MP could stimulate Cl^- secretion in human colonic epithelial cell line T_{84} . The supporting evidence includes: MP-induced responses were insensitive to Na^+ channel blockers; the response was inhibited by Cl^- channel blockers; and substantially inhibited by the $Na^+-K^+-2Cl^-$ cotransporter inhibitors. The stimulatory effects of MP on colonic anion secretion were mimicked by its active ingredient, *ligustrazine*. Since *ligustrazine* is an active ingredient common in both MP and *BFP*, a traditional formula previously shown to stimulate anion secretion by GI tract epithelia^[11,15,16], the present results suggest that *Ligustrazine* may be one of the responsible ingredients involved in mediating the secretory effects of both MP and *BFP*.

Apart from its acute stimulatory effects on colonic anion secretion, MP, by treating T_{84} cells for 72 h, was also demonstrated to significantly alter the electrophysiological characteristics of the colonic epithelia. Increases in transepithelial potential and basal I_{sc} may represent an increased driving force for anion secretion and basal secretion, respectively. These results indicate long-term treatment of MP can promote colonic anion secretion, consistent with its acute effects. On the other hand, pretreatment of T_{84} cells with MP also increased the transepithelial resistance, indicating its effect on improving epithelial barrier function. This was confirmed by RT-PCR results, which showed that pretreatment with MP significantly up-regulated gene expressions of tight junction related proteins, ZO-1 and ZO-2. Similar results were obtained using *Ligustrazine*, suggesting that *ligustrazine* was able to improve barrier function in addition to colonic secretion. It has been reported that an elevation of intracellular calcium could decrease the tight junction resistance in T_{84} monolayers^[21]. Since *Ligustrazine* has been shown to decrease intracellular Ca^{2+} by inhibiting Ca^{2+} entry and/or Ca^{2+} release^[22,23], *ligustrazine* as well as *ligustrazine*-containing MP may strengthen tight junctions, thereby enhancing transepithelial resistance. In fact, we have found that intracellular calcium

could also be reduced by an apical addition of MP (data not shown), indicating a possible mechanism for improving barrier function. Further studies may be required to understand the detailed mechanisms.

Taken together, the present results have demonstrated that MP and *Ligustrazine* exert a stimulatory effect on gastrointestinal Cl^- secretion and improvement of epithelial barrier function. Since MP is designed for postmenopausal or elderly women, its demonstrated effects on the colonic epithelia, in addition to its beneficial effect on endocrine (Gou *et al.*, unpublished data) and immune systems previously shown^[1], suggest that MP and its active ingredient, *ligustrazine*, may be used to alleviate some of the GI tract disorders, such as infection and constipation, often seen in the elderly.

REFERENCES

- 1 Ho AL, Gou YL, Rowlands DK, Chung YW, Chan HC. Effects of Bak Foong Pills and Menoease Pills on white blood cell distribution in old age female rats. *Biol Pharm Bull* 2003; **26**: 1748-1753
- 2 Baumgart DC, Dignass AU. Intestinal barrier function. *Curr Opin Clin Nutr Metab Care* 2002; **5**: 685-694
- 3 Balkovetz DF, Katz J. Bacterial invasion by a paracellular route: divide and conquer. *Microbes Infect* 2003; **5**: 613-619
- 4 Hosoda Y, Winarto A, Iwanaga T, Kuwahara A. Mode of action of ANG II on ion transport in guinea pig distal colon. *Am J Physiol Gastrointest Liver Physiol* 2000; **278**: G625-634
- 5 Albanese CT, Cardona M, Smith SD, Watkins S, Kurkchubasche AG, Ulman I, Simmons RL, Rowe MI. Role of intestinal mucus in transepithelial passage of bacteria across the intact ileum *in vitro*. *Surgery* 1994; **116**: 76-82
- 6 Forte LR, Thorne PK, Eber SL, Krause WJ, Freeman RH, Francis SH, Corbin JD. Stimulation of intestinal Cl^- transport by heat-stable enterotoxin: activation of cAMP-dependent protein kinase by cGMP. *Am J Physiol* 1992; **263**(3 Pt 1): C607-615
- 7 Grondahl ML, Jensen GM, Nielsen CG, Skadhauge E, Olsen JE, Hansen MB. Secretory pathways in Salmonella Typhimurium-induced fluid accumulation in the porcine small intestine. *J Med Microbiol* 1998; **47**: 151-157
- 8 Lencer WI, Delp C, Neutra MR, Madara JL. Mechanism of cholera toxin action on a polarized human intestinal epithelial cell line: role of vesicular traffic. *J Cell Biol* 1992; **117**: 1197-1209
- 9 Tenore A, Fasano A, Gasparini N, Sandomenico ML, Ferrara A, Di Carlo A, Guandalini S. Thyroxine effect on intestinal Cl^-/HCO_3^- exchange in hypo- and hyperthyroid rats. *J Endocrinol* 1996; **151**: 431-437
- 10 Ewe K. Intestinal transport in constipation and diarrhoea. *Pharmacology* 1988; **36**(Suppl 1): 73-84
- 11 Tang N, Zhu JX, Zhao WC, Xing Y, Gou YL, Rowlands DK, Chung YW, Chan HC. Effect of Bak Foong pills on exocrine pancreatic-bile secretion. *Biol Pharm Bull* 2003; **26**: 1384-1387
- 12 Zhou Q, Rowlands DK, Gou YL, Tsang LL, Chung YW, Chan HC. Cardiovascular protective effects of traditional Chinese

- medicine Bak Foong pills in spontaneously hypertensive rats. *Biol Pharm Bull* 2003; **26**: 1095-1099
- 13 **Liu B**, Dong XL, Xie JX, Gou YL, Rowlands DK, Chan HC. Effect of Bak Foong pills on enhancing dopamine release from the amygdala of female rats. *Biol Pharm Bull* 2003; **26**: 1028-1030
- 14 **Gou YL**, Ho AL, Rowlands DK, Chung YW, Chan HC. Effects of Bak Foong Pill on blood coagulation and platelet aggregation. *Biol Pharm Bull* 2003; **26**: 241-246
- 15 **Zhu JX**, Chan YM, Tsang LL, Chan LN, Zhou Q, Zhou CX, Chan HC. Cellular signaling mechanisms underlying pharmacological action of Bak Foong Pills on gastrointestinal secretion. *Jpn J Physiol* 2002; **52**: 129-134
- 16 **Zhu JX**, Lo PS, Zhao WC, Tang N, Zhou Q, Rowlands DK, Gou YL, Chung YW, Chan HC. Bak Foong Pills stimulate anion secretion across normal and cystic fibrosis pancreatic duct epithelia. *Cell Biol Int* 2002; **26**: 1011-1018
- 17 **Rowlands DK**, Tsang LL, Cui YG, Chung YW, Chan LN, Liu CQ, James T, Chan HC. Upregulation of cystic fibrosis transmembrane conductance regulator expression by oestrogen and Bak Foong Pill in mouse uteri. *Cell Biol Int* 2001; **25**: 1033-1035
- 18 **Ussing HH**, Zerahn K. Active transport of sodium as the source of electric current in the short-circuited isolated frog skin. Reprinted from *Acta. Physiol. Scand.* **23**: 110-127, 1951. *J Am Soc Nephrol* 1999; **10**: 2056-2065
- 19 **Youakim A**, Ahdieh M. Interferon-gamma decreases barrier function in T₈₄ cells by reducing *ZO-1* levels and disrupting apical actin. *Am J Physiol* 1999; **276**(5 Pt 1): G1279-1288
- 20 **Usui T**, Hara M, Satoh H, Moriyama N, Kagaya H, Amano S, Oshika T, Ishii Y, Ibaraki N, Hara C, Kunimi M, Noiri E, Tsukamoto K, Inatomi J, Kawakami H, Endou H, Igarashi T, Goto A, Fujita T, Araie M, Seki G. Molecular basis of ocular abnormalities associated with proximal renal tubular acidosis. *J Clin Invest* 2001; **108**: 107-115
- 21 **Tai YH**, Flick J, Levine SA, Madara JL, Sharp GW, Donowitz M. Regulation of tight junction resistance in T₈₄ monolayers by elevation in intracellular Ca²⁺: a protein kinase C effect. *J Membr Biol* 1996; **149**: 71-79
- 22 **Pang PK**, Shan JJ, Chiu KW. Tetramethylpyrazine, a calcium antagonist. *Planta Med* 1996; **62**: 431-435
- 23 **Liu SY**, Sylvester DM. Antiplatelet activity of tetramethylpyrazine. *Thromb Res* 1994; **75**: 51-62

Edited by Zhu LH and Xu FM

Morphologic and biomechanical changes of rat oesophagus in experimental diabetes

Yan-Jun Zeng, Jian Yang, Jing-Bo Zhao, Dong-Hua Liao, En-Ping Zhang, Hans Gregersen, Xiao-Hu Xu, Hong Xu, Chuan-Qing Xu

Yan-Jun Zeng, Xiao-Hu Xu, Hong Xu, Chuan-Qing Xu, Forensic Medicine Department, Medical College, Santou University, Santou 515031, Guangdong Province, China

Jian Yang, En-Ping Zhang, Beijing University of Technology, Beijing 100022, China

Jing-Bo Zhao, Dong-Hua Liao, Hans Gregersen, Department of Gastrointestinal Surgery, Aalborg University, Denmark

Correspondence to: Yan-Jun Zeng, Forensic Medicine Department, Medical College, Shantou University, Shantou 515031, Guangdong Province, China. yjzeng@bjut.edu.cn

Telephone: +86-10-67391685 **Fax:** +86-10-67391738

Received: 2003-8-26 **Accepted:** 2003-10-22

Abstract

AIM: To study morphologic and biomechanical changes of oesophagus in diabetes rats.

METHODS: Diabetes was induced by a single injection of streptozotocin (STZ). The type of diabetes mellitus induced by parenteral STZ administration in rats was insulin-dependent (type I). The samples were excised and studied *in vitro* using a self-developed biomaterial test machine.

RESULTS: The body mass was decreased after 4 d with STZ treatment. The length of esophagus shortened after 4, 7, 14 d. The opening angle increased after 14 d. The shear, longitudinal and circumferential stiffness were obviously raised after 28 d of STZ treatment.

CONCLUSION: The changes of passive biomechanical properties reflect intra-structural alteration of tissue to a certain extent. This alteration will lead to some dysfunction of movement. For example, tension of esophageal wall will change due to some obstructive disease.

Zeng YJ, Yang J, Zhao JB, Liao DH, Zhang EP, Gregersen H, Xu XH, Xu H, Xu CQ. Morphologic and biomechanical changes of rat oesophagus in experimental diabetes. *World J Gastroenterol* 2004; 10(17): 2519-2523

<http://www.wjgnet.com/1007-9327/10/2519.asp>

INTRODUCTION

Esophagus is a distensible muscular tube that connects pharynx and stomach. The function of the esophagus is to transport food by peristaltic movement, which is the result of the interaction of the tissue forces in the esophageal wall and the hydrodynamic forces in the food bolus. Esophagus has been studied by radiography^[1], concurrent videofluoroscopy and manometry^[2,3], high-frequency ultrasonography^[4-6], and endoscopic sclerotherapy^[7,8]. Motility disorders^[9], bolus transport^[10,11], systemic sclerosis^[12], pain^[13], wall distensibility^[8], impedance planimetric characterization^[14] and the effects of epidermal growth factor^[15] on esophagus have been reported

in many papers. Since the function of esophagus is mainly mechanical, our work was focused on providing quantitative measurement of passive biomechanical properties of esophagus. Many investigations on biomechanics of esophagus are available in the literature^[16,17]. Gregersen *et al.* studied strain distribution in the layered wall^[18,19], relation between pressure and cross-sectional area^[20] and other biomechanical properties^[21-23] of esophagus. A more recent work used a novel ultrasound technique to study the biomechanics of the human esophagus *in vivo*^[24]. Patel represented biomechanical and sensory parameters of the human esophagus at four levels^[25]. Researchers have done a lot of biomechanical studies on gastrointestinal tract such as intestine^[26,27], small intestine^[28-32], ileum^[33], duodenum^[34] and large intestine^[35,36].

Most previous studies have explained the relationship between the diabetes and gastrointestinal tract function^[37,38]. Some researches studied relationship between esophageal dysfunction and neuropathy^[39], oesophagus scintigraphy^[40] and the relationship between esophageal motility and transit^[41] in diabetic patients. More recently, Jorgensen reported tension-strain relations and morphometry of rat small intestine in experimental diabetes^[42]. Zhao introduced the remodeling of zero-stress state of small intestine in streptozotocin-induced diabetic rats^[43].

This paper presents the effect of experimental diabetes on the morphologic and biomechanical properties of the esophagus. The result of this study indicated that experimental type I diabetes caused significant changes in the passive biomechanical properties in the rat esophagus.

MATERIALS AND METHODS

Materials

Diabetes was induced by a single injection of streptozotocin (STZ). The form of diabetes mellitus induced by parenteral STZ administration in rats is insulin-dependent (type I). Twenty-seven rats were divided into 4 groups according to the survival time after STZ treatment: 4 d ($n = 7$), 7 d ($n = 7$), 14 d ($n = 7$), 28 d ($n = 6$). Another 8 rats were used as normal controls. The samples were taken from the middle part of esophagus. Two rings were cut from each end of the sample to measure the geometric parameters of the no-load state and the opening angle at zero-stress state. The remaining part was excised and studied *in vitro* using a self-developed biomaterial test machine.

Methods

Using this machine, the esophagus was stepwise elongated and inflated and continuously twisted in circumferential-longitudinal direction. In the normal controls and 28 d of diabetes group, after the intact esophagus was tested, the mucosa and muscle layers were separated using microsurgery and tested in the same loading procedure as mentioned above. The esophagus was treated as a membrane when the stress and strain were calculated, the longitudinal and circumferential stresses were considered to be evenly distributed along the wall thickness while the radial stress and other transverse shear stresses were

ignored. The torque vs twist-angle relation was approximately linear at a specified pressure and longitudinal stretch ratio. Thus, the shear modulus can be computed by the torque, twist angle and polar moment of inertial at this state. However, the shear modulus varied greatly with the changing inflation pressure and longitudinal stretch ratio.

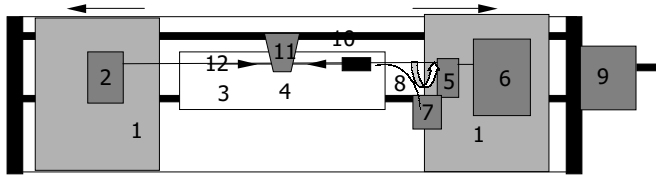


Figure 1 Simplified diagram of biomaterial test machine. 1: Linear stage, 2: Torque transducer, 3: Organ bath, 4: Specimen, 5: Force transducer, 6: Motor for axial rotation, 7: Pressure transducer, 8: Infusion channel, 9: Motor for linear stage, 10: Rails for linear stage, 11: CCD camera, 12: Plastic rod.

RESULTS

Type I diabetes could induce the following effect on the biomechanical and morphologic properties of esophagus: body weight and morphology, shear modulus, circumferential and longitudinal stress-strain relationship, stress-strain relationship of muscle layer and mucosa layer.

Body weight and morphology

The body mass kept a steady increase in the control rats. But it went down after 4 d in the diabetes rat (Figure 2A). The length of esophagus *in vivo* obviously declined after 4, 7, 14 d, but it would return to normal level after 28 d (Figure 2B). The mass per unit length *in vitro* changed little (Figure 2C). In the intact esophagus, the opening angle increased after 14 d of STZ treatment (Figure 2D).

Shear modulus

Changes of elastic shear moduli in the course of diabetes development at longitudinal stretch ratio $\lambda_{zz} = 1.5$ and various

transmural pressure are shown in Figure 3A. Elastic shear modulus would rise with increased transmural pressure. Especially when transmural pressure was more than 0.25 kPa, the shear moduli for various transmural pressure were remarkably different. And diabetes has notably affected the shear modulus. This effect showed that shear moduli are obviously increased after 28 d.

Changes of elastic shear modulus in the course of diabetes development at transmural pressure $P = 1$ kPa and various longitudinal stretch ratio are pictured in Figure 3B. Elastic shear modulus would rise with increased longitudinal stretch ratio. Shear moduli were remarkably different at various longitudinal stretch ratios. And diabetes has notably affected the shear modulus. This effect demonstrated that shear moduli were obviously increased after 28 d of STZ treatment.

Circumferential and longitudinal stress-strain relationship

Figure 4A shows the changes of circumferential stress-strain relationship in the course of diabetes development at longitudinal stretch ratio $\lambda_{zz} = 1.5$ and various transmural pressure. All curves of experimental group inclined to left side except that after 4 d. The curve after 28 d was on the most left side. The circumferential stiffness increased after 7, 14, 28 d of diabetes.

The changes of longitudinal stress-strain relationship in the course of diabetes development at transmural pressure $P = 0.25$ kPa and various longitudinal stretch ratio are pictured in Figure 4B. The stress-strain curve after 28 d was obviously inclined to left side. So the longitudinal stiffness notably increased after 28 d.

Stress-strain relationship of muscle layer and mucosa layer

The circumferential stress-strain relationship of muscle layer and mucosa layer in the process of inflation at a longitudinal stretch ratio of 1.5 is pictured in Figure 5A. And the experimental diabetes was after 28 d. For muscle layer, there was no obvious difference between the control and diabetes groups. For mucosa layer, the stress-strain curve moved to left side in parallel. So circumferential stiffness of mucosa layer with diabetes was larger than that of control.

Figure 5B shows longitudinal stress-strain relationship of muscle layer and mucosa layer in the process of elongation at a transmural pressure of 0.25 kPa. For muscle layer, there was no obvious difference between control and diabetes groups. There was no notable difference for mucosa layer either.

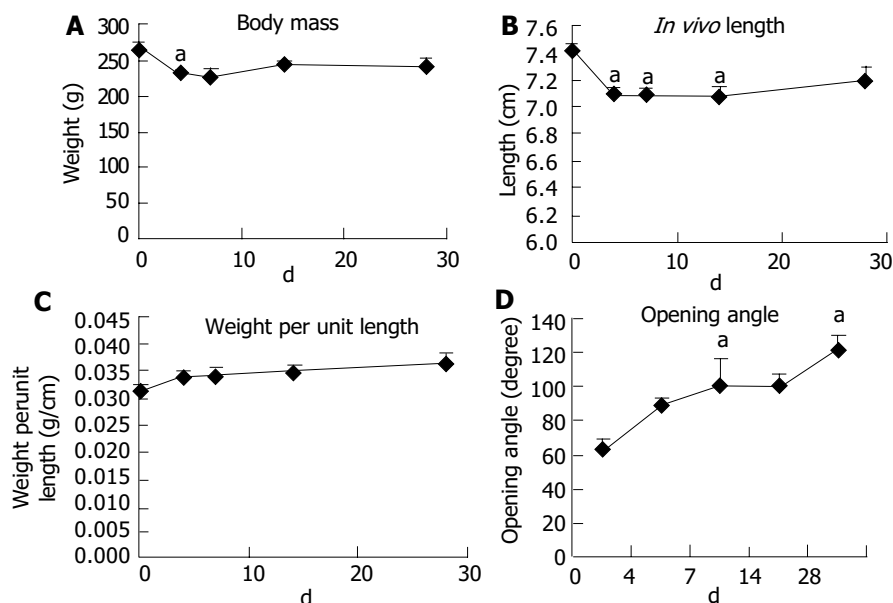


Figure 2 Changes of body mass and esophagus morphology and opening angle at zero-stress state in the process of diabetes development. Dunnett's test result: significant difference vs normal control ($*P < 0.05$). A: Change of body mass, B: Change of *in vivo* length, C: Change of mass per unit length, D: Change of opening angle.

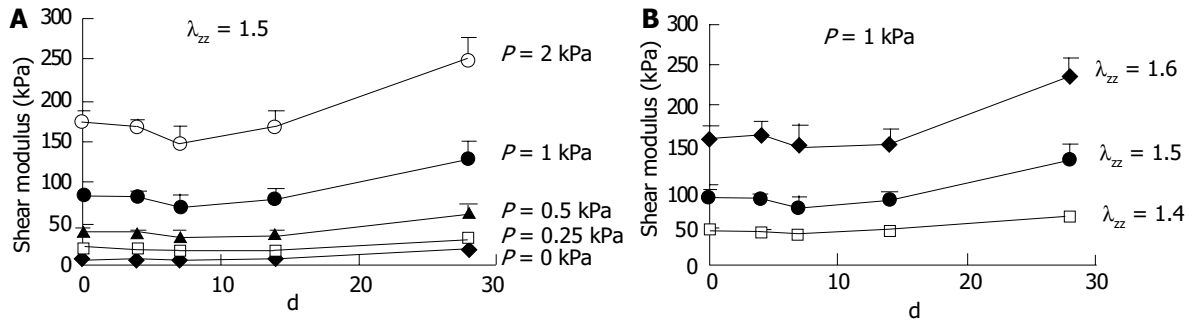


Figure 3 Change of elastic shear modulus in the process of diabetes development. A: Change at $\lambda_{zz} = 1.5$ and various transmural pressure, B: Change at $P = 1$ kPa and various longitudinal stretch ratio.

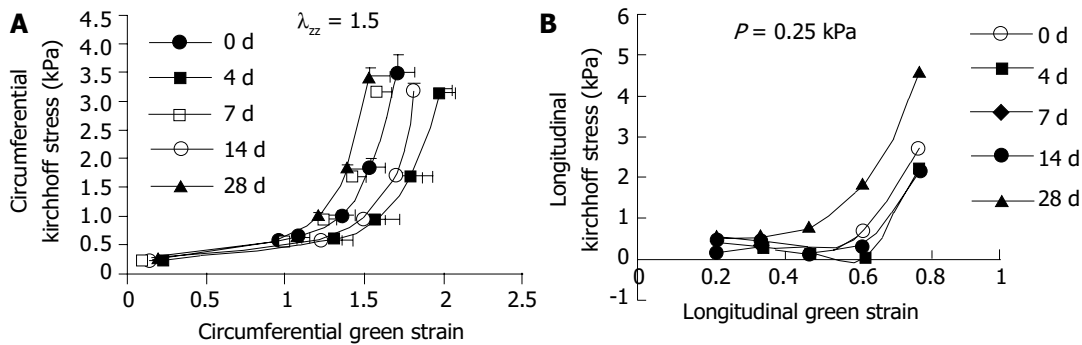


Figure 4 A: Change of circumferential stress-strain relation in the course of diabetes development at $\lambda_{zz} = 1.5$ and various transmural pressure. B: Change of longitudinal stress-strain relation in the course of diabetes development at $P = 0.25$ kPa and various longitudinal stretch ratio.

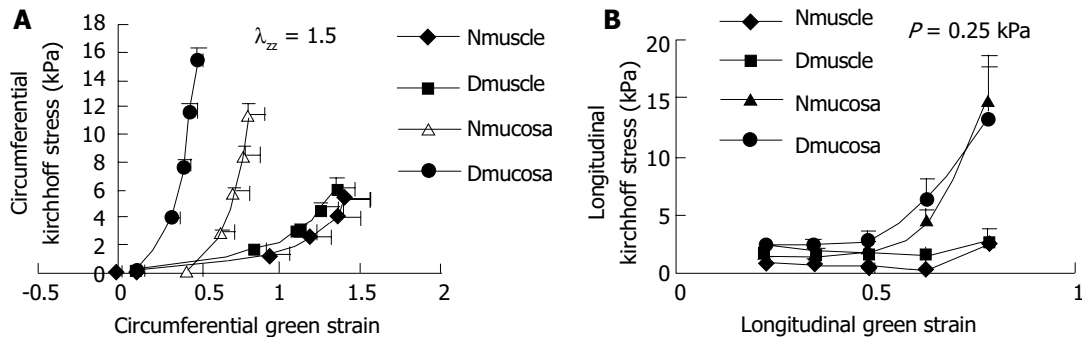


Figure 5 A: Circumferential stress-strain relation between muscle layer and mucosa layer in the process of inflation at a longitudinal stretch ratio of 1.5. N: Normal control, D: 28 d of diabetes. B: Longitudinal stress-strain relation between muscle layer and mucosa layer in the process of elongation at a transmural pressure of 0.25 kPa. N: Normal control, D: 28 d of diabetes.

DISCUSSION

A large number of studies have discovered that diabetes can affect the movement of oesophagus. Transportation of oesophagus may delay or slow down, and movement of esophagus can not coordinate.

This dysfunction of movement can be a result of muscle and nerve cooperative failure^[39-41,44-47]. Histologic research has proved that diabetes can destroy vagus nerve^[48]. Though there are many papers on movement and function of oesophagus in diabetes, few data on morphologic and passive biomechanical properties are seen. The change of passive biomechanical properties reflects intra-structural alteration of tissue to a certain extent. This alteration will result in some dysfunction of movement, for example, tension of esophageal wall will change due to some obstructive disease^[49,50], and therefore, it is necessary to study biomechanics and morphology together.

The body mass is decreased in rat with diabetes. This is

consistent with other studies^[43,51]. Diabetes will lead to hyperplasia of some organs. Hyperplasia of esophagus is less frequent than that of small intestine^[52,53]. Diabetes has caused rise of the opening angle of small intestine^[44], also it is seen for esophagus.

In this paper, the shear, longitudinal and circumferential stiffnesses were obviously elevated after 28 d with STZ treatment. Jorrensen^[42], Liu^[54] and Zhao^[51] have discovered that stiffness is raised in diabetes in small intestine, blood vessel and arterial wall.

We can draw a conclusion that the changes of passive biomechanical properties reflect intra-structural alteration of tissue to a certain extent. This alteration will lead to some dysfunction of movement.

REFERENCES

1 **Grishaw EK**, Ott DJ, Frederick MG, Gelfand DW, Chen MY. Functional abnormalities of the esophagus: a prospective analysis of radiographic findings relative to age and symptoms. *Am*

- J Roentgenol* 1996; **167**: 719-723
- 2 **Pouderoux P**, Shi G, Tatum RP, Kahrilas PJ. Esophageal solid bolus transit: studies using concurrent videofluoroscopy and manometry. *Am J Gastroenterol* 1999; **94**: 1457-1463
 - 3 **Narawane NM**, Bhatia SJ, Mistry FP, Abraham P, Dherai AJ. Manometric mapping of normal esophagus and definition of the transition zone. *Indian J Gastroenterol* 1998; **17**: 55-57
 - 4 **Nicosia MA**, Brasseur JG, Liu JB, Miller LS. Local longitudinal muscle shortening of the human esophagus from high-frequency ultrasonography. *Am J Physiol Gastrointest Liver Physiol* 2001; **281**: G1022-1033
 - 5 **Pehlivanov N**, Liu J, Kassab GS, Puckett JL, Mittal RK. Relationship between esophageal muscle thickness and intraluminal pressure: an ultrasonographic study. *Am J Physiol Gastrointest Liver Physiol* 2001; **280**: G1093-1098
 - 6 **Assentoft JE**, Gregersen H, O'Brien WD Jr. Determination of biomechanical properties in guinea pig esophagus by means of high frequency ultrasound and impedance planimetry. *Dig Dis Sci* 2000; **45**: 1260-1266
 - 7 **Juhl CO**, Vinter-Jensen L, Djurhuus JC, Gregersen H, Dajani EZ. Biomechanical properties of the oesophagus damaged by endoscopic sclerotherapy. An impedance planimetric study in minipigs. *Scand J Gastroenterol* 1994; **29**: 867-873
 - 8 **Petersen JA**, Djurhuus C, Koff J, Vinter-Jensen L, Gregersen H. Endoscopic sclerotherapy in porcine esophagus changes luminal cross-sectional area and wall distensibility dose- and time-dependently. *Dig Dis Sci* 1998; **43**: 521-528
 - 9 **Hewson EG**, Ott DJ, Dalton CB, Chen YM, Wu WC, Richter JE. Manometry and radiology. Complementary studies in the assessment of esophageal motility disorders. *Gastroenterology* 1990; **98**: 626-632
 - 10 **Nicosia MA**, Brasseur JG. A mathematical model for estimating muscle tension *in vivo* during esophageal bolus transport. *J Theor Biol* 2002; **219**: 235-255
 - 11 **Ren J**, Massey BT, Dodds WJ, Kern MK, Brasseur JG, Shaker R, Harrington SS, Hogan WJ, Arndorfer RC. Determinants of intrabolus pressure during esophageal peristaltic bolus transport. *Am J Physiol* 1993; **264**(3 Pt 1): G407-413
 - 12 **Villadsen GE**, Storkholm J, Zachariae H, Hendel L, Bendtsen F, Gregersen H. Oesophageal pressure-cross-sectional area distributions and secondary peristalsis in relation to subclassification of systemic sclerosis. *Neurogastroenterol Motil* 2001; **13**: 199-210
 - 13 **Drewes AM**, Schipper KP, Dimcevski G, Petersen P, Andersen OK, Gregersen H, Arendt-Nielsen L. Multimodal assessment of pain in the esophagus: a new experimental model. *Am J Physiol Gastrointest Liver Physiol* 2002; **283**: G95-103
 - 14 **Gregersen H**, Vinter-Jensen L, Juhl CO, Dajani EZ. Impedance planimetric characterization of the distal oesophagus in the goettingen minipig. *J Biomech* 1996; **29**: 63-68
 - 15 **Vinter-Jensen L**, Juhl CO, Eika B, Gregersen H, Dajani EZ. Epidermal growth factor attenuates the sclerotherapy-induced biomechanical properties of the oesophagus. An experimental study in minipigs. *Scand J Gastroenterol* 1995; **30**: 614-619
 - 16 **Gregersen H**, Weis SM, McCulloch AD. Oesophageal morphometry and residual strain in a mouse model of osteogenesis imperfecta. *Neurogastroenterol Motil* 2001; **13**: 457-464
 - 17 **Gregersen H**, Lee TC, Chien S, Skalak R, Fung YC. Strain distribution in the layered wall of the esophagus. *J Biomech Eng* 1999; **121**: 442-448
 - 18 **Lu X**, Gregersen H. Regional distribution of axial strain and circumferential residual strain in the layered rabbit oesophagus. *J Biomech* 2001; **34**: 225-233
 - 19 **Liao D**, Fan Y, Zeng Y, Gregersen H. Stress distribution in the layered wall of the rat oesophagus. *Med Eng Phys* 2003; **25**: 731-738
 - 20 **Gregersen H**, Christensen LL. Pressure-cross-sectional area relations and elasticity in the rabbit oesophagus *in vivo*. *Digestion* 1996; **57**: 174-179
 - 21 **Orvar KB**, Gregersen H, Christensen J. Biomechanical characteristics of the human esophagus. *Dig Dis Sci* 1993; **38**: 197-205
 - 22 **Barlow JD**, Gregersen H, Thompson DG. Identification of the biomechanical factors associated with the perception of distension in the human esophagus. *Am J Physiol Gastrointest Liver Physiol* 2002; **282**: G683-689
 - 23 **Drewes AM**, Pedersen J, Liu W, Arendt-Nielsen L, Gregersen H. Controlled mechanical distension of the human oesophagus: sensory and biomechanical findings. *Scand J Gastroenterol* 2003; **38**: 27-35
 - 24 **Takeda T**, Kassab G, Liu J, Puckett JL, Mittal RR, Mittal RK. A novel ultrasound technique to study the biomechanics of the human esophagus *in vivo*. *Am J Physiol Gastrointest Liver Physiol* 2002; **282**: G785-793
 - 25 **Patel RS**, Rao SS. Biomechanical and sensory parameters of the human esophagus at four levels. *Am J Physiol* 1998; **275**(2 Pt 1): G187-191
 - 26 **Dou Y**, Lu X, Zhao J, Gregersen H. Morphometric and biomechanical remodelling in the intestine after small bowel resection in the rat. *Neurogastroenterol Motil* 2002; **14**: 43-53
 - 27 **Dou Y**, Gregersen S, Zhao J, Zhuang F, Gregersen H. Morphometric and biomechanical intestinal remodeling induced by fasting in rats. *Dig Dis Sci* 2002; **47**: 1158-1168
 - 28 **Dou Y**, Gregersen S, Zhao J, Zhuang F, Gregersen H. Effect of re-feeding after starvation on biomechanical properties in rat small intestine. *Med Eng Phys* 2001; **23**: 557-566
 - 29 **Zhao J**, Yang J, Vinter-Jensen L, Zhuang F, Gregersen H. The morphometry and biomechanical properties of the rat small intestine after systemic treatment with epidermal growth factor. *Biorheology* 2002; **39**: 719-733
 - 30 **Liao D**, Yang J, Zhao J, Zeng Y, Vinter-Jensen L, Gregersen H. The effect of epidermal growth factor on the incremental Young's moduli in the rat small intestine. *Med Eng Phys* 2003; **25**: 413-418
 - 31 **Zhao J**, Yang J, Vinter-Jensen L, Zhuang F, Gregersen H. Biomechanical properties of esophagus during systemic treatment with epidermal growth factor in rats. *Ann Biomed Eng* 2003; **31**: 700-709
 - 32 **Zeng YJ**, Qiao AK, Yu JD, Zhao JB, Liao DH, Xu XH, Hans G. Collagen fiber angle in the submucosa of small intestine and its application in Gastroenterology. *World J Gastroenterol* 2003; **9**: 804-807
 - 33 **Yang J**, Zhao JB, Zeng YJ, Gregersen H. Biomechanical properties of ileum after systemic treatment with epithelial growth factor. *World J Gastroenterol* 2003; **9**: 2278-2283
 - 34 **Gao C**, Zhao J, Gregersen H. Histomorphometry and strain distribution in pig duodenum with reference to zero-stress state. *Dig Dis Sci* 2000; **45**: 1500-1508
 - 35 **Gao C**, Gregersen H. Biomechanical and morphological properties in rat large intestine. *J Biomech* 2000; **33**: 1089-1097
 - 36 **Yang J**, Zhao J, Zeng Y, Vinter-Jensen L, Gregersen H. Morphological properties of zero-stress state in large intestine during systemic EGF treatment. *Dig Dis Sci* 2003; **48**: 442-448
 - 37 **Murtagh JE**. Diabetes mellitus: the general practitioner's perspective. *Clin Exp Optom* 1999; **82**: 74-79
 - 38 **Verne GN**, Sninsky CA. Diabetes and the gastrointestinal tract. *Gastroenterol Clin North Am* 1998; **27**: 861-874
 - 39 **Kinekawa F**, Kubo F, Matsuda K, Fujita Y, Tomita T, Uchida Y, Nishioka M. Relationship between esophageal dysfunction and neuropathy in diabetic patients. *Am J Gastroenterol* 2001; **96**: 2026-2032
 - 40 **Westin L**, Lilja B, Sundkvist G. Oesophagus scintigraphy in patients with diabetes mellitus. *Scand J Gastroenterol* 1986; **21**: 1200-1204
 - 41 **Holloway RH**, Tippet MD, Horowitz M, Maddox AF, Moten J, Russo A. Relationship between esophageal motility and transit in patients with type I diabetes mellitus. *Am J Gastroenterol* 1999; **94**: 3150-3157
 - 42 **Jorgensen CS**, Ahrensberg JM, Gregersen H, Flyvberg A. Tension-strain relations and morphometry of rat small intestine in experimental diabetes. *Dig Dis Sci* 2001; **46**: 960-967
 - 43 **Zhao J**, Sha H, Zhou S, Tong X, Zhuang FY, Gregersen H. Remodelling of zero-stress state of small intestine in streptozotocin-induced diabetic rats. Effect of gliclazide. *Dig Liver Dis* 2002; **34**: 707-716
 - 44 **Karayalcin B**, Karayalcin U, Aburano T, Nakajima K, Hisada K, Morise T, Okada T, Takeda R. Esophageal clearance scintigraphy, in diabetic patients-a preliminary study. *Ann Nucl*

- Med* 1992; **6**: 89-93
- 45 **Sundkvist G**, Hillarp B, Lilja B, Ekberg O. Esophageal motor function evaluated by scintigraphy, video-radiography and manometry in diabetic patients. *Acta Radiol* 1989; **30**: 17-19
- 46 **Clouse RE**, Lustman PJ, Reidel WL. Correlation of esophageal motility abnormalities with neuropsychiatric status in diabetics. *Gastroenterology* 1986; **90**(5 Pt 1): 1146-1154
- 47 **Rathmann W**, Enck P, Frieling T, Gries FA. Visceral afferent neuropathy in diabetic gastroparesis. *Diabetes Care* 1991; **14**: 1086-1089
- 48 **Smith B**. Neuropathology of the oesophagus in diabetes mellitus. *J Neurol Neurosurg Psychiatry* 1974; **37**: 1151-1154
- 49 **Gregersen H**, Giversen IM, Rasmussen LM, Tottrup A. Biomechanical wall properties and collagen content in the partially obstructed opossum esophagus. *Gastroenterology* 1992; **103**: 1547-1551
- 50 **Mittal RK**, Ren J, McCallum RW, Shaffer HA Jr, Sluss J. Modulation of feline esophageal contractions by bolus volume and outflow obstruction. *Am J Physiol* 1990; **258**(2 Pt 1): G208-215
- 51 **Zhao J**, Lu X, Zhuang F, Gregersen H. Biomechanical and morphometric properties of the arterial wall referenced to the zero-stress state in experimental diabetes. *Biorheology* 2000; **37**: 385-400
- 52 **Mayhew TM**, Carson FL, Sharma AK. Small intestinal morphology in experimental diabetic rats: a stereological study on the effects of an aldose reductase inhibitor (ponalrestat) given with or without conventional insulin therapy. *Diabetologia* 1989; **32**: 649-654
- 53 **Zoubi SA**, Williams MD, Mayhew TM, Sparrow RA. Number and ultrastructure of epithelial cells in crypts and villi along the streptozotocin-diabetic small intestine: a quantitative study on the effects of insulin and aldose reductase inhibition. *Virchows Arch* 1995; **427**: 187-193
- 54 **Liu SQ**, Fung YC. Changes in the rheological properties of blood vessel tissue remodeling in the course of development of diabetes. *Biorheology* 1992; **29**: 443-457

Edited by Zhu LH Proofread by Chen WW and Xu FM

Angiogenic synergistic effect of basic fibroblast growth factor and vascular endothelial growth factor in an *in vitro* quantitative microcarrier-based three-dimensional fibrin angiogenesis system

Xi-Tai Sun, Yi-Tao Ding, Xiao-Gui Yan, Ling-Yun Wu, Qiang Li, Ni Cheng, Yu-Dong Qiu, Min-Yue Zhang

Xi-Tai Sun, Yi-Tao Ding, Xiao-Gui Yan, Qiang Li, Yu-Dong Qiu, Department of Hepatobiliary Surgery, Affiliated Gu Lou Hospital of Medical College, Hepatobiliary Research Institute, Nanjing University, Nanjing 210008, Jiangsu Province China

Ling-Yun Wu, Ni Cheng, State Key Laboratory of Pharmaceutical Biotechnology, Department of Biochemistry, Nanjing University, Nanjing 210093, Jiangsu Province China

Min-Yue Zhang, State Key Laboratory of Pharmaceutical Biotechnology, Model Animal Research Center, Department of Biochemistry, Nanjing University, Nanjing 210093, Jiangsu Province, China

Correspondence to: Dr. Min-Yue Zhang, State Key Laboratory of Pharmaceutical Biotechnology, Model Animal Research Center, Department of Biochemistry, Nanjing University, 10 Jinyin Street, Nanjing 210093, Jiangsu Province, China. zmy@nju.edu.cn

Telephone: +86-25-83595108 **Fax:** +86-25-83595108

Received: 2003-12-10 **Accepted:** 2004-01-12

Abstract

AIM: To develop an *in vitro* three-dimensional (3-D) angiogenesis system to analyse the capillary sprouts induced in response to the concentration ranges of basic fibroblast growth factor (bFGF) and vascular endothelial growth factor (VEGF) and to quantify their synergistic activity.

METHODS: Microcarriers (MCs) coated with human microvascular endothelial cells (HMVECs) were embedded in fibrin gel and cultured in 24-well plates with assay media. The growth factors bFGF, or VEGF, or both were added to the system. The wells ($n = 8$ /group) were digitally photographed and the average length of capillary-like sprouts (ALS) from each microcarrier was quantitated.

RESULTS: In aprotinin-stabilized fibrin matrix, human microvascular endothelial cells on the MCs invaded fibrin, forming sprouts and capillary networks with lumina. The angiogenic effects of bFGF or VEGF were dose-dependent in the range from 10 to 40 ng/mL. At d 1, 10 ng/mL of bFGF and VEGF induced angiogenesis with an ALS of $32.13 \pm 16.6 \mu\text{m}$ and $43.75 \pm 27.92 \mu\text{m}$, respectively, which were significantly higher than that of the control ($5.88 \pm 4.45 \mu\text{m}$, $P < 0.01$), and the differences became more significant as the time increased. In addition, the combination of 10 ng/mL of bFGF and VEGF each induced a more significant effect than the summed effects of bFGF (10 ng/mL) alone and VEGF (10 ng/mL) alone when analyzed using SPSS system for general linear model (GLM) ($P = 0.011$), and that also exceeded the effects by 20 ng/mL of either bFGF or VEGF.

CONCLUSION: A microcarrier-based *in vitro* three-dimensional angiogenesis model can be developed in fibrin. It offers a unique system for quantitative analysis of angiogenesis. Both bFGF and VEGF exert their angiogenic effects on HMVECs synergistically and in a dose-dependent manner.

Sun XT, Ding YT, Yan XG, Wu LY, Li Q, Cheng N, Qiu YD,

Zhang MY. Angiogenic synergistic effect of basic fibroblast growth factor and vascular endothelial growth factor in an *in vitro* quantitative microcarrier-based three-dimensional fibrin angiogenesis system. *World J Gastroenterol* 2004; 10 (17): 2524-2528

<http://www.wjgnet.com/1007-9327/10/2524.asp>

INTRODUCTION

Angiogenesis is a process by which new capillaries develop from an existing microvascular network. It is associated with a number of physiologic and pathologic conditions including malignancies, diabetic retinopathy, and rheumatoid arthritis. Angiogenesis in fibrin-based matrix is especially interesting because it is essential in tumor angiogenesis and wound healing.

Angiogenesis was first observed *in vitro* by Folkman and Haudenschild 20 years ago^[1]. After culture of endothelial cells, these cells organize spontaneously into capillary-like structures (CLS) with the presence of lumina. From a physiological point of view, an ideal *in vitro* system would take into account all the representative steps of *in vivo* angiogenesis, from detachment of endothelial cells from the vascular wall to final tubular morphogenesis and vascular network formation. It should be also rapid, easy to use, reproducible, and easily quantifiable. Depending on the way the cells reorganize, the *in vitro* models of angiogenesis described to date can be roughly classified into two categories: two-dimensional (2-D) and three-dimensional (3-D). While 2-D angiogenesis models lack the third dimension and obviously do not reflect all physiological steps, the 3-D models are closer to the *in vivo* environment, because they consider more steps of angiogenesis^[2].

A variety of 3-D *in vitro* models of angiogenesis have been developed in the past few years^[3-7] and have thus significantly increased our understanding of the roles of endothelial cells, extracellular matrix (ECM), growth factors and other bioactive molecules in angiogenesis.

In this study, we described an *in vitro* system of angiogenesis, which was based on microcarriers (MCs), human microvascular endothelial cells (HMVECs) and fibrin extracellular matrix. With this system, the angiogenic effect of basic fibroblast growth factor (bFGF) and vascular endothelial growth factor (VEGF) and their synergism were tested.

MATERIALS AND METHODS

Cell isolation and culture

HMVECs were isolated from juvenile foreskin as described previously^[8,9]. Briefly, the foreskin was cut into small pieces, washed with PBS and incubated with 15-20 mL of 2 g/L dispase in DMEM (Gibco BRL Cat# 11885-084) overnight (18-24 h) at 4 °C. The tissue pieces were transferred into DMEM and scratched with a scalpel. The remnants were discarded and the resulting cell suspension (containing HMVEC and other contaminating cell types) was centrifuged at 1 000 r/min for 5 min. The pellet was re-suspended in 10-15 mL of endothelial growth medium

(EGM) consisting of endothelial basal medium (EBM) (Clonetics, San Diego, CA), supplemented with 10 ng/mL epidermal growth factor (EGF) (Clonetics), 12 µg/mL bovine brain extract (BBE) (Clonetics), 1.0 µg/mL hydrocortisone (Clonetics), 100 U/mL penicillin (Clonetics), and 100 mg/mL streptomycin (Clonetics) in the presence of 150 mL/L normal human serum and seeded into a gelatin-coated 75-cm² tissue culture flask. Culture medium was changed every 2-3 d. Before the cultures were confluent (normally 5-7 d after seeding), the HMVECs were separated from the other cells in culture by immuno-magnetic isolation with CD31-Dynabeads following the manufacturer's instructions (DynaL A.S, Oslo, Norway). Endothelial cell cultures were characterized and determined to be >99% pure on the basis of the formation of typical cobblestone monolayer in culture and positive immuno-staining for factor VIII-related antigen (Beijing Zhongshan Biotechnology Co., Ltd). The purified HMVECs were cultured in EGM at 37 °C (50 mL/L CO₂) on gelatin-coated cell culture surfaces. All assays were conducted with cells in passages 6 to 8.

Microcarrier cell culture

Gelatin-coated cytodex-3 microcarriers (MCs) (Amersham Pharmacia Biotech, Piscataway, NJ) were prepared according to the recommendations of the supplier. Freshly autoclaved MCs were suspended in EGM and endothelial cells were added to a final density of 50-80 cells/MC. The cells were allowed to attach to the MCs in a 1.5 mL Eppendorf tube for 4 h at 37 °C. The MCs were then re-suspended in a larger volume of medium and cultivated for another 24-48 h at 37 °C (50 mL/L CO₂). MCs were gently agitated to prevent aggregation of individual MCs. MCs were used for angiogenesis assay when the endothelial cells on the MCs reached confluence^[10, 11].

Microcarrier-based fibrin gel angiogenesis assay

The microcarrier-based fibrin gel angiogenesis assay was performed as described^[10] with some modifications. Working solution of fibrinogen (Shanghai Raas Blood Product Co., Ltd) was prepared by dissolving the stock solution of fibrinogen (20 mg/mL in PBS) in EBM to a concentration of 1.0 mg/mL, supplemented with EGF and hydrocortisone at 10 ng/mL and 1.0 µg/mL, respectively. The 24-well plates were used for the assay. The bottom of each well was first covered with 250 µL fibrinogen solution, and the clotting was induced by addition of thrombin (0.5 U/mL). After 30 min of polymerization, another 250 µL of fibrinogen solution containing about 250 EC-coated MCs was added. The MCs were evenly distributed in the fibrinogen by gently shaking the culture plates, and polymerization was induced as described above. After complete polymerization, 1.0 mL of EBM supplemented with 10 ng/mL of EGF, 1.0 µg/mL of hydrocortisone and 50 mL/L adult human serum was added on the gel. To prevent excess fibrinolysis by fibrin-embedded cells, aprotinin was added to the growth media at 200 KIU/mL. For the experiments, which required bFGF (PeproTech EC Ltd) and/or VEGF (PeproTech EC Ltd), the components were added to both of the fibrinogen solution and the supernatant medium at the desired concentrations.

Quantification and statistics

At the time point of interest, six random fields of vision for every well were digitally photographed under inverted microscope, and the pictures were transferred to a computer. The quantification of capillary-like structure formation was performed as described by Xue and Greisler with some modifications^[12]. Briefly, a special grid was made by dividing a circle with radially oriented lines around 360 degrees with 10-degree intervals using Photoshop (version 6.0; Adobe Systems Inc). The digital photographs were transparently layered with

the grid. For each photographed microcarrier, the lengths of sprouts were measured on each of the grid lines and summed (Figure 1). The lengths of sprouts from each MC were averaged in each well. The average lengths of sprouts (ALS) from 8 replicate wells of each testing group were analyzed and expressed as mean±SD. SPSS system for one-way ANOVA was used to compare the differences during the time courses and the General Liner Model (GLM) was used to determine the synergism. $P < 0.05$ was considered statistically significant.

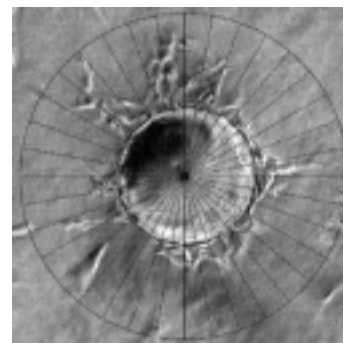


Figure 1 Quantification of angiogenesis. Each MC in random photographed fields was overlaid with a grid that was equally divided around 360° at 10-degree intervals (original magnification ×100). For each photographed microcarrier, the lengths of sprouts were measured on each of the grid lines and summed. The lengths of sprouts from each MC were averaged in each well. The average lengths of sprouts (ALS) from 8 replicate wells of each testing group were analyzed. Bar: 100 µm.

RESULTS

Sequential steps of capillary formation

In 1995, Nehls and Herrmann described a microcarrier-based *in vitro* model of angiogenesis^[9]. In their model, the endothelial cells coated on the microcarriers invaded the fibrin gel, forming elongated capillary-like structure in a response to angiogenic factors. However, this model was performed with large vascular endothelial cells of calf pulmonary artery origin. Although in later studies, they used human microvascular endothelial cells to investigate their response to the co-cultured tumor cells, but no positive result was found^[13]. In the present study, by modifying the system, we successfully established the microcarrier-based *in vitro* model of angiogenesis with human microvascular endothelial cells in fibrin.

In the early stages of capillary growth (about 16 h after polymerization of the fibrin gel), the HMVECs on microcarriers migrated into fibrin matrix to form sprouts without detectable lumina. At about 16-48 h, sprouts elongated, and small intracellular or intercellular lumina was formed. Usually, broad lumina developed at the base of the sprouts. The lumina frequently contained cellular debris, which could be seen to float by shaking the culture dishes, indicating that lumina contents had liquefied. The tips of capillary sprouts were generally solid or showed only primitive, slit-like lumina, which in later stages anastomosed to other sprouts, and finally formed capillary-like network (at about 5-7 d) (Figure 2). This result was not consistent with what was observed by Nehls and Herrmann, who assumed that due to the presence of serum, anastomosis of capillary sprouts occurred rarely^[14].

Capillary sprout formation induced by bFGF and VEGF

In the absence of growth factors, capillary sprout formation in our model was minimal. Both bFGF and VEGF induced obvious EC sprouting. The curves for both cytokines increase significantly with time. The angiogenic effects of both cytokines were dose-dependent over the range from 10 to 40 ng/mL. At d 1, 10 ng/mL

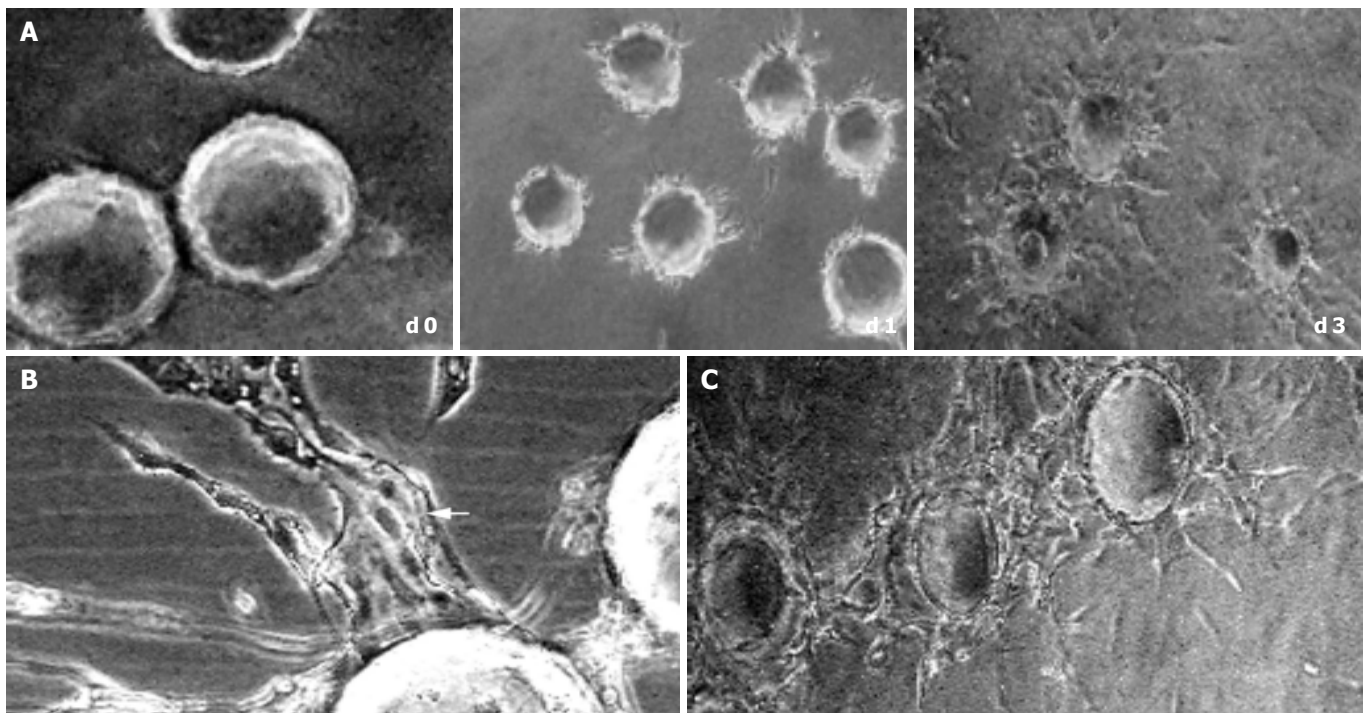


Figure 2 Sequential steps of capillary formation. During 3 d after polymerization of the fibrin gel, the HMVECs (bFGF 40 ng/mL) on microcarriers migrated into fibrin matrix to form sprouts, which elongated (A) with intracellular or intercellular lumina formed (bFGF 40 ng/mL). The lumina frequently contained cellular debris, which can be seen to float by shaking the culture dishes, indicating that lumina contents had liquefied (B, arrow). In the late stage (d 5), the capillary sprouts anastomosed to each other, and finally formed capillary-like network (C) (original magnification $\times 100$).

of bFGF and VEGF induced angiogenesis with an ALS of $32.13 \pm 16.6 \mu\text{m}$ and $43.75 \pm 27.92 \mu\text{m}$, respectively, which was significantly higher than that of the control ($5.88 \pm 4.45 \mu\text{m}$, $P < 0.01$). With the time going, on the difference became more significant (Figure 3). Within the dose range, angiogenesis increased correspondingly in both extent and rapidity as the concentration increased (Figure 4).

Exposure of ECs to both bFGF and VEGF in combination stimulated an angiogenic response that was greater than sum of their individual effects, and that occurred more rapidly than the response to either growth factor. The ALS induced by 10 ng/mL of bFGF plus 10 ng/mL of VEGF in combination was $590.75 \pm 289.15 \mu\text{m}$, which was greater than the total effects of 10 ng/mL of bFGF ($124.00 \pm 62.12 \mu\text{m}$) and 10 ng/mL of VEGF ($171.38 \pm 119.42 \mu\text{m}$) and also greater than that induced by 20 ng/mL of either bFGF ($187.25 \pm 98.14 \mu\text{m}$) or VEGF ($280.5 \pm 198.23 \mu\text{m}$) (Figure 5). The synergism of bFGF and VEGF was confirmed by the GLM test, which showed that the effect of the combination of bFGF plus VEGF was greater than the sum of the individual effects of bFGF and VEGF alone ($P = 0.011$) (Figure 5).

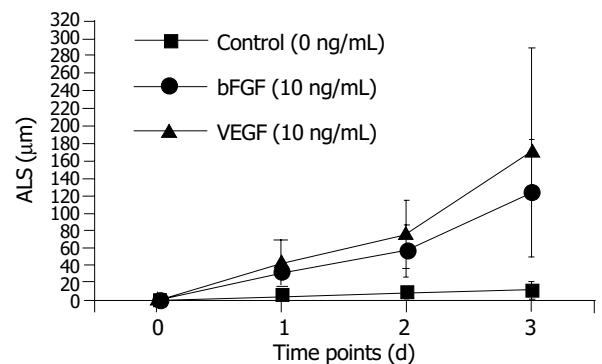


Figure 3 Time course of HMVEC angiogenesis in fibrin. Microcarriers coated with HMVECs were embedded in fibrin. The angiogenic effects of either bFGF or VEGF were dose-dependent over the range from 10 to 40 ng/mL. At day 1, 10 ng/mL of bFGF and VEGF induced angiogenesis with an ALS of $32.13 \pm 16.6 \mu\text{m}$ and $43.75 \pm 27.92 \mu\text{m}$, respectively, which were significantly higher than that of the control ($5.88 \pm 4.45 \mu\text{m}$, $P < 0.01$). The difference became more significant, as the time increased.

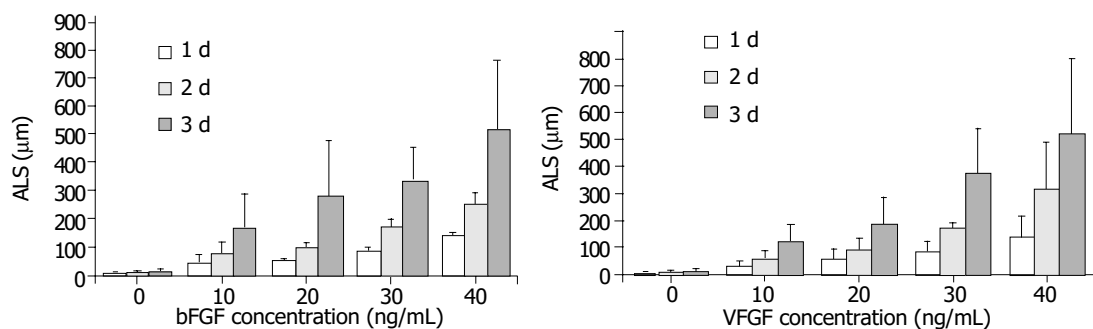


Figure 4 Dose responses of bFGF and VEGF on angiogenesis. Both bFGF and VEGF exhibited dose-dependent angiogenic effects in the range from 10 to 40 ng/mL. At d 1, 10 ng/mL of bFGF and VEGF induced angiogenesis with an ALS of $32.13 \pm 16.6 \mu\text{m}$ and $43.75 \pm 27.92 \mu\text{m}$, respectively, which were significantly higher than that of the control ($5.88 \pm 4.45 \mu\text{m}$, $P < 0.01$). With the concentration increasing, the difference became more significant.

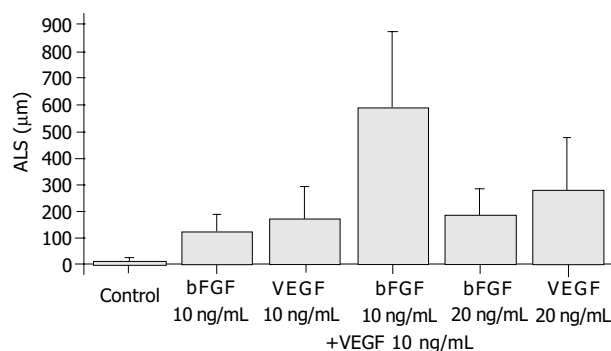


Figure 5 Synergism of bFGF and VEGF. The samples were quantitated at d 3. The combination of 10 ng/mL bFGF and 10 ng/mL VEGF induced an angiogenic response that was greater than the sum of the effects by each cytokine alone at the same dose ($P = 0.011$).

DISCUSSION

Three-dimensional angiogenesis assays are based on the capacity of activated endothelial cells to invade 3-D substrates. The matrix may consist of collagen gels, plasma clot, purified fibrin, matrigel, or a mixture of these proteins with others. The culture medium may be added to the gel before polymerization or on top of the gel. Depending on the culture medium composition (percentage of serum, addition of cytokines), cells can be induced to sprout, proliferate, migrate, differentiate, and tubular endothelial cell phenotypes in the 3-D configuration. Thus, one can *in vitro* observe the morphogenic responses of isolated ECs, which characterize the *in vivo* angiogenesis. In fact, a variety of 3-D angiogenesis models have provided great advances in the understanding of angiogenesis and the investigation of angiogenic/anti-angiogenic factors^[2].

In 3-D angiogenesis models, the ECs were usually reorganized in the following ways: directly overlaid by gels^[15,16], sandwiched between two gel layers^[17], seeded dispersedly^[18] or clustered as spheroids in gels^[3,4], or attached onto microcarrier beads. Microcarrier-based angiogenesis model was firstly developed by Nehls and Drenckhan^[10], who suggested, in their later studies, that in the presence of serum, the anastomosis of capillary sprouts occurred only rarely^[14].

In this study, we also established an *in vitro* angiogenesis system based on microcarrier, but it was with human dermal microvascular endothelial cells (HMVECs). With this system, we observed all of the angiogenic steps that characterize the *in vivo* angiogenesis, including sprouting (16-24 h), branching (24-48 h), and capillary network formation (after 72 h), as described above. However, not in agreement with the observation by Nehls and Drenckhan, we found that the anastomosis of capillary sprouts occurred commonly in the later stage (3-5 d), even in the presence of up to 100 mL/L serum in our system (data not shown). After 5 d, the capillary-like network could be seen around/between MCs.

Since one of our goals was to characterize the gene expression patterns at the different steps of angiogenesis including sprouting, branching and networking, our 3-D angiogenesis model thus gave a good supporting. However, because of the morphological complexity, the capillary-like network at the late stage of the model was difficult to be quantified. So, we confined our observation to the first 3 d of the culture for the angiogenic quantification of the growth factors.

Angiogenesis in physiological conditions is characterized by strict regulation and occurs mostly through a collagen-rich extracellular matrix and leads to the formation of an organized capillary network. In contrast, in different pathological conditions as they are associated with tumor growth or wound healing, capillary sprouting processes are known to primarily occur in a

fibrin-rich matrix and the stimulation of new vessels is exaggerated, leading to the formation of a disorganized^[4,19], capillary network. As one of the native ECM components involved in angiogenesis, fibrin is formed by the polymerization of fibrinogen after the proteolytic cleavage by thrombin. This scenario naturally takes place at sites of wound healing and tumor under the stimulation of VEGF and other factors, and leads to the deposition and stabilization of local fibrin clots. These fibrin clots serve as a temporary matrix that provides a solid support for invading cells, such as fibroblasts and endothelial cells.

In vitro angiogenesis in fibrin is affected by EC fibrinolysis involving both plasmin and metalloproteinase systems and the spatial structure of the gel^[20,21]. Cell surface fibrinolytic activity is crucial for EC invasion and migration in fibrin^[22,23]. The presence of aprotinin is necessary to maintain the integrity of fibrin. In the absence of aprotinin, fibrin was unable to support EC angiogenesis because it would be degraded before capillary-like structure formation. The configuration and mechanical properties of fibrin were determined by the conditions in which it polymerized. Various factors, including pH, ionic strength, fibrinogen and thrombin concentrations could affect the structural feature of fibrin^[24]. It is thus important to prepare fibrin at a well-controlled condition when performing fibrin matrix-based angiogenic experiments, and to avoid any modification between the groups when comparing the potency of different angiogenic factors.

Many growth factors have been found to have angiogenic effects. FGFs and VEGFs are the best characterized among them. FGFs and VEGFs bind with high specificity to their cognate receptor tyrosine kinases, inducing activation of the intrinsic enzymatic activity of these receptors. This activity leads to tyrosine phosphorylation of the receptors, as well as of substrates for the kinases. In some cases, growth factors may induce angiogenesis by regulating the expression of some other growth factors and their receptors^[19]. It is noteworthy that FGF and VEGF may act synergistically in induction of angiogenesis. Synergy of these growth factors in *in vivo* angiogenesis has been reported^[25], and combination of the two factors also yielded a synergistic response in collagen-based *in vitro* system^[26,27]. The mechanisms responsible for this synergism are that these two growth factors closely interact with each other in angiogenic process. bFGF could induce expression of endogenous VEGF and its receptors in ECs^[28-30], and VEGF-receptor antagonists inhibited bFGF-induced angiogenesis in spite of its lack of activities against bFGF receptors^[31]. The capacity of VEGF to induce u-PA-plasmin activity and angiogenesis depended on endogenous bFGF produced by ECs^[32]. In our fibrin and microcarrier-based angiogenesis model, we also found that both bFGF and VEGF demonstrated angiogenic effects on HMVECs in a dose-dependent manner, and when applied in combination these two factors also acted synergistically.

In conclusion, we have successfully established a microcarrier-based *in vitro* three-dimensional angiogenesis model that offers a unique system for quantitative analysis of angiogenesis. The model is especially applicable to *in vitro* evaluation and screening of novel angiogenic or angiostatic factors. It may also shed light on the study of molecular mechanism of angiogenesis.

REFERENCES

- 1 Folkman J, Haudenschild C. Angiogenesis *in vitro*. *Nature* 1980; **288**: 551-556
- 2 Vailhe B, Vittet D, Feige JJ. *In vitro* models of vasculogenesis and angiogenesis. *Lab Invest* 2001; **81**: 439-452
- 3 Korff T, Augustin HG. Integration of endothelial cells in multicellular spheroids prevents apoptosis and induces differentiation. *J Cell Biol* 1998; **143**: 1341-1352
- 4 Korff T, Augustin HG. Tensional forces in fibrillar extracellular matrices control directional capillary sprouting. *J Cell Sci*

- 1999; **112**(Pt 19): 3249-3258
- 5 **Vernon RB**, Sage EH. A novel, quantitative model for study of endothelial cell migration and sprout formation within three-dimensional collagen matrices. *Microvasc Res* 1999; **57**: 118-133
- 6 **Bell SE**, Mavila A, Salazar R, Bayless KJ, Kanagala S, Maxwell SA, Davis GE. Differential gene expression during capillary morphogenesis in 3D collagen matrices: regulated expression of genes involved in basement membrane matrix assembly, cell cycle progression, cellular differentiation and G-protein signaling. *J Cell Sci* 2001; **114**(Pt 15): 2755-2773
- 7 **Vailhe B**, Ronot X, Lecomte M, Wiernsperger N, Tranqui L. Description of an in vitro angiogenesis model designed to test antiangiogenic molecules. *Cell Biol Toxicol* 1996; **12**: 341-344
- 8 **Peters K**, Schmidt H, Unger RE, Otto M, Kamp G, Kirkpatrick CJ. Software-supported image quantification of angiogenesis in an *in vitro* culture system: application to studies of biocompatibility. *Biomaterials* 2002; **23**: 3413-3419
- 9 **Kubota Y**, Kleinman HK, Martin GR, Lawley TJ. Role of laminin and basement membrane in the morphological differentiation of human endothelial cells into capillary-like structures. *J Cell Biol* 1988; **107**: 1589-1598
- 10 **Nehls V**, Drenckhahn D. A novel, microcarrier-based *in vitro* assay for rapid and reliable quantification of three-dimensional cell migration and angiogenesis. *Microvasc Res* 1995; **50**: 311-322
- 11 **Nehls V**, Drenckhahn D. A microcarrier-based cocultivation system for the investigation of factors and cells involved in angiogenesis in three-dimensional fibrin matrices *in vitro*. *Histochem Cell Biol* 1995; **104**: 459-466
- 12 **Xue L**, Greisler HP. Angiogenic effect of fibroblast growth factor-1 and vascular endothelial growth factor and their synergism in a novel *in vitro* quantitative fibrin-based 3-dimensional angiogenesis system. *Surgery* 2002; **132**: 259-267
- 13 **von Bulow C**, Hayen W, Hartmann A, Mueller-Klieser W, Allolio B, Nehls V. Endothelial capillaries chemotactically attract tumour cells. *J Pathol* 2001; **193**: 367-376
- 14 **Nehls V**, Herrmann R, Huhnken M. Guided migration as a novel mechanism of capillary network remodeling is regulated by basic fibroblast growth factor. *Histochem Cell Biol* 1998; **109**: 319-329
- 15 **Schor AM**, Schor SL, Allen TD. Effects of culture conditions on the proliferation, morphology and migration of bovine aortic endothelial cells. *J Cell Sci* 1983; **62**: 267-285
- 16 **Montesano R**, Orci L, Vassalli P. *In vitro* rapid organization of endothelial cells into capillary-like networks is promoted by collagen matrices. *J Cell Biol* 1983; **97**(5 Pt 1): 1648-1652
- 17 **Chalupowicz DG**, Chowdhury ZA, Bach TL, Barsigian C, Martinez J. Fibrin II induces endothelial cell capillary tube formation. *J Cell Biol* 1995; **130**: 207-215
- 18 **Bayless KJ**, Salazar R, Davis GE. RGD-dependent vacuolation and lumen formation observed during endothelial cell morphogenesis in three-dimensional fibrin matrices involves the alpha(v) beta(3) and alpha(5) beta(1) integrins. *Am J Pathol* 2000; **156**: 1673-1683
- 19 **Gerwins P**, Skoldenberg E, Claesson-Welsh L. Function of fibroblast growth factors and vascular endothelial growth factors and their receptors in angiogenesis. *Crit Rev Oncol Hematol* 2000; **34**: 185-194
- 20 **Vailhe B**, Lecomte M, Wiernsperger N, Tranqui L. The formation of tubular structures by endothelial cells is under the control of fibrinolysis and mechanical factors. *Angiogenesis* 1998; **2**: 331-344
- 21 **van Hinsbergh VW**, Collen A, Koolwijk P. Role of fibrin matrix in angiogenesis. *Ann N Y Acad Sci* 2001; **936**: 426-437
- 22 **Koolwijk P**, van Erck MG, de Vree WJ, Vermeer MA, Weich HA, Hanemaaijer R, van Hinsbergh VW. Cooperative effect of TNF α , bFGF, and VEGF on the formation of tubular structures of human microvascular endothelial cells in a fibrin matrix. Role of urokinase activity. *J Cell Biol* 1996; **132**: 1177-1188
- 23 **Hiraoka N**, Allen E, Apel IJ, Gyetko MR, Weiss SJ. Matrix metalloproteinases regulate neovascularization by acting as pericellular fibrinolysins. *Cell* 1998; **95**: 365-377
- 24 **Nehls V**, Herrmann R. The configuration of fibrin clots determines capillary morphogenesis and endothelial cell migration. *Microvasc Res* 1996; **51**: 347-364
- 25 **Asahara T**, Bauters C, Zheng LP, Takeshita S, Bunting S, Ferrara N, Symes JF, Isner JM. Synergistic effect of vascular endothelial growth factor and basic fibroblast growth factor on angiogenesis *in vivo*. *Circulation* 1995; **92**(9 Suppl): II365-371
- 26 **Pepper MS**, Ferrara N, Orci L, Montesano R. Potent synergism between vascular endothelial growth factor and basic fibroblast growth factor in the induction of angiogenesis *in vitro*. *Biochem Biophys Res Commun* 1992; **189**: 824-831
- 27 **Goto F**, Goto K, Weindel K, Folkman J. Synergistic effects of vascular endothelial growth factor and basic fibroblast growth factor on the proliferation and cord formation of bovine capillary endothelial cells within collagen gels. *Lab Invest* 1993; **69**: 508-517
- 28 **Seghezzi G**, Patel S, Ren CJ, Gualandris A, Pintucci G, Robbins ES, Shapiro RL, Galloway AC, Rifkin DB, Mignatti P. Fibroblast growth factor-2 (FGF-2) induces vascular endothelial growth factor (VEGF) expression in the endothelial cells of forming capillaries: an autocrine mechanism contributing to angiogenesis. *J Cell Biol* 1998; **141**: 1659-1673
- 29 **Pepper MS**, Mandriota SJ, Jeltsch M, Kumar V, Alitalo K. Vascular endothelial growth factor (VEGF)-C synergizes with basic fibroblast growth factor and VEGF in the induction of angiogenesis *in vitro* and alters endothelial cell extracellular proteolytic activity. *J Cell Physiol* 1998; **177**: 439-452
- 30 **Pepper MS**, Mandriota SJ. Regulation of vascular endothelial growth factor receptor-2 (Flk-1) expression in vascular endothelial cells. *Exp Cell Res* 1998; **241**: 414-425
- 31 **Tille JC**, Wood J, Mandriota SJ, Schnell C, Ferrari S, Mestan J, Zhu Z, Witte L, Pepper MS. Vascular endothelial growth factor (VEGF) receptor-2 antagonists inhibit VEGF- and basic fibroblast growth factor-induced angiogenesis *in vivo* and *in vitro*. *J Pharmacol Exp Ther* 2001; **299**: 1073-1085
- 32 **Mandriota SJ**, Pepper MS. Vascular endothelial growth factor-induced *in vitro* angiogenesis and plasminogen activator expression are dependent on endogenous basic fibroblast growth factor. *J Cell Sci* 1997; **110**(Pt 18): 2293-2302

• CLINICAL RESEARCH •

Hematotesticular barrier is altered from early stages of liver cirrhosis: Effect of insulin-like growth factor 1

Inma Castilla-Cortázar, Nieves Diez, María García-Fernández, Juan Enrique Puche, Fernando Diez-Caballero, Jorge Quiroga, Matías Díaz-Sánchez, Alberto Castilla, Amelia Díaz Casares, Isabel Varela-Nieto, Jesús Prieto, Salvador González-Barón

Inma Castilla-Cortázar, Nieves Diez, María García-Fernández, Fernando Diez-Caballero, Matías Díaz-Sánchez, Department of Human Physiology, University of Navarra, Pamplona, Navarra, Spain
Jorge Quiroga, Jesús Prieto, Department of Internal Medicine, Liver Unit, University of Navarra, Pamplona, Navarra, Spain
Inma Castilla-Cortázar, María García-Fernández, Juan Enrique Puche, Amelia Díaz Casares, Salvador González-Barón, Department of Human Physiology, School of Medicine, University of Málaga, Malaga, Spain

Alberto Castilla, Department of Internal Medicine, Hospital Sierrallana, Tollevavega and School of Medicine, University of the Basque Country-Vitoria-Gasteiz, Spain

Isabel Varela-Nieto, Instituto de Investigaciones Biomédicas "Alberto Sols", Consejo Superior de Investigaciones Científicas-Universidad Autónoma de Madrid (CSIC-UAM), Madrid, Spain

Supported by the Spanish Program I+D, SAF 99/0072 and SAF 2001/1672

Correspondence to: Inma Castilla-Cortázar, MD, PhD, Department of Human Physiology, School of Medicine, University of Málaga, Campus Teatinos 29080, Málaga, Spain. iccortazar@uma.es

Telephone: +34-952131577 **Fax:** +34-952131650

Received: 2004-02-06 **Accepted:** 2004-03-04

Abstract

AIM: The pathogenesis of hypogonadism in liver cirrhosis is not well understood. Previous results from our laboratory showed that IGF-1 deficiency might play a pathogenetic role in hypogonadism of cirrhosis. The administration of IGF-1 for a short period of time reverted the testicular atrophy associated with advanced experimental cirrhosis. The aim of this study was to establish the historical progression of the described alterations in the testes, explore testicular morphology, histopathology, cellular proliferation, integrity of testicular barrier and hypophysogonadal axis in rats with no ascitic cirrhosis.

METHODS: Male Wistar rats with histologically-proven cirrhosis induced with carbon tetrachloride (CCl₄) for 11 wk, were allocated into two groups ($n = 12$, each) to receive recombinant IGF-1 (2 µg/100 g·d, sc) for two weeks or vehicle. Healthy rats receiving vehicle were used as control group ($n = 12$).

RESULTS: Compared to controls, rats with compensated cirrhosis showed a normal testicular size and weight and very few histopathological testicular abnormalities. However, these animals showed a significant diminution of cellular proliferation and a reduction of testicular transferrin expression. In addition, pituitary-gonadal axis was altered, with significant higher levels of FSH ($P < 0.001$ vs controls) and increased levels of LH in untreated cirrhotic animals. Interestingly, IGF-1 treatment normalized testicular transferrin expression and cellular proliferation and reduced serum levels of LH ($P = ns$ vs controls, and $P < 0.01$ vs untreated cirrhotic group).

CONCLUSION: The testicular barrier is altered from an

early stage of cirrhosis, shown by a reduction of transferrin expression in Sertoli cells, a diminished cellular proliferation and an altered gonadal axis. The treatment with IGF-1 could be also useful in this initial stage of testicular disorder associated with compensated cirrhosis.

Castilla-Cortázar I, Diez N, García-Fernández M, Puche JE, Diez-Caballero F, Quiroga J, Díaz-Sánchez M, Castilla A, Casares AD, Varela-Nieto I, Prieto J, González-Barón S. Hematotesticular barrier is altered from early stages of liver cirrhosis: Effect of insulin-like growth factor 1. *World J Gastroenterol* 2004; 10 (17): 2529-2534

<http://www.wjgnet.com/1007-9327/10/2529.asp>

INTRODUCTION

Hypogonadism (characterized by low testosterone levels and relative hyperestrogenism, loss of libido, sexual impotence and feminine body features in men) is a common complication of advanced liver cirrhosis^[1]. Previous data demonstrated that rats with advanced cirrhosis showed reduced testicular size and weight and severe histopathological testicular abnormalities, including reduced tubular diameters, loss of the germinal line, and diminutions in cellular proliferation and spermatogenesis and testicular transferrin expression, a good marker of the integrity of blood-testis barrier^[2]. In addition, low serum testosterone and high serum LH were present in cirrhotic animals, as well as decreased levels of serum IGF-1. Interestingly, the administration of IGF-1 at low doses for a short period of time reverted the testicular atrophy and improved the altered pituitary-testicular axis in these animals^[2]. In cirrhotic patients, hypogonadism has been attributed to a variety of mechanisms including gonadal toxicities of alcohol, malnutrition and increased production of estrogens from androgens in peripheral tissues due to the existence of portal systemic shunting^[3-9].

Insulin-like growth factor-1 (IGF-1) is an anabolic hormone produced in different tissues although the liver accounts for 90% of the circulating hormone, which is synthesized in response to growth hormone (GH) stimulation^[10,11]. In cirrhosis the reduction of receptors for GH in hepatocytes and the diminished synthesizing ability of the liver parenchyma caused a progressive fall of serum IGF-1 levels^[11-14]. Although in an early stage of cirrhosis serum levels of IGF-1 were normal, its bio-availability seemed to be diminished^[15]. The clinical impact of the reduced production or availability of IGF-1 in cirrhosis was largely unknown^[11-14]. Recent studies from our laboratory have demonstrated that short courses of treatment with low doses of IGF-1 were able to induce marked improvements in nutritional state^[15], nitrogen retention^[16], intestinal absorption^[17-19], osteopenia^[20,21], liver function reducing fibrogenesis^[22,23], and restore the reduced somatostatinergic tone^[24] in rats with experimental cirrhosis. These data suggest that IGF-1 deficiency plays a pathogenetic role in several systemic complications occurring in cirrhosis.

It is well known that IGF-1 stimulates testosterone synthesis and spermatogenesis^[25-32]. Its deficiency could contribute to the development of hypogonadism associated with cirrhosis as

the previous data supported^[2]. Since the pathogenesis of hypogonadism in cirrhosis is not yet well understood, the aim of the present study was to study the chronological progression of the described alterations in testes^[2] in advanced cirrhosis, explore testicular morphology, histopathology, cellular proliferation, integrity of testicular barrier and hypophyso-gonadal axis in rats with cirrhosis in an early stage, without ascites.

MATERIALS AND METHODS

Induction of liver cirrhosis

All experimental procedures were performed in conformity with The Guiding Principles for Research Involving Animals^[33]. Cirrhosis was induced as previously described^[15,16]. Briefly, male Wistar rats (3-week-old, 130-150 g) were subjected to CCl₄ inhalation (Merck, Darmstadt, Germany) twice a week for 11 wk with a progressively increasing exposure time from 1 to 5 min. During the whole period of cirrhosis induction animals received Phenobarbital (Luminal, Bayer, Leverkusen, Germany) in the drinking water (400 mg/L). Both food (standard semipurified diet for rodents; B.K. Universal, Sant Vicent del Horts, Spain) and water were given *ad libitum*. Healthy, age and sex-matched control rats were maintained under the same conditions but receiving neither CCl₄ nor Phenobarbital.

Study design

The treatment was administrated for 2 wk after stopping of CCl₄ exposure. In the morning of d 0, animals were weighed and blood samples were drawn from the retroocular venous plexus from all rats with capillary tubes (Marienfeld, Germany) and stored at -20 °C until used for analytical purposes. Cirrhotic rats were randomly assigned to receive either vehicle (saline) (group CI, *n* = 12) or recombinant human IGF-1 (Pharmacia-Uppsala, Sweden) (2 µg/100 g·d in two divided doses, subcutaneously) (group CI+IGF, *n* = 12) for two weeks. Control rats (group CO, *n* = 10) received saline during the same period.

In the morning of the 15th d, rats were weighed, blood was obtained from the retroocular plexus and animals were killed by decapitation. After the abdominal cavity was opened, the liver and testes were dissected and weighed. Samples from the left major liver lobe and testes were processed for histological examination (fixed in Bouin's solution). The testicular diameters (AP and LM) were measured using a precision calliper, Mituyoto® (±0.05 mm). Ascites was ruled out by direct exploration of abdominal cavity in all cirrhotic animals.

Liver histopathology

Bouin-fixed tissues were processed and sections (4-µm) were stained with Haematoxylin and Eosin and Masson's trichrome. Livers were scored (1 to 4) as previously reported^[15,22]. Preestablished criteria for inclusion of cirrhotic (CI) animals in the final analysis were the presence of: (1) altered baseline biochemical data of liver function; and (2) in retrospect, histologically proven liver cirrhosis (scores 3 or 4 of the classification) in CCl₄-treated-animals. All animals had compensated cirrhosis without ascites.

Testicular histopathology and PCNA and transferrin immunohistochemistry

For histopathological evaluation of testes, 30 seminiferous tubules from each rat of the three groups were blindly evaluated by two observers and the arithmetic mean of the scores was taken as the final result. Transverse sections of seminiferous tubuli were examined and evaluation of histological changes was made using a light projection microscope (Micro Promar Leitz GMBH, Wetzlar, Germany) at 150× magnification. The following parameters were studied: tubular diameter, quantitation of the presence of different types of cells in tubuli,

presence of peritubular fibrosis, and the number of proliferating cells. For general purposes haematoxylin & eosin stain and Masson's trichrome stain were used. Specific techniques for other purposes are specified in the corresponding paragraphs.

Changes in tubuli were classified into 5 categories (Category I: highest damage to Category V: full normality). Category I: presence of only Sertoli cells; category II: Sertoli cells plus spermatids; category III: Sertoli cells, plus spermatides, and spermatocytes; category IV: presence of all kinds of cells but showing some morphological alterations (i.e.: severe vacuolization, aberrant cells); category V: presence of all kinds of cells without morphological alterations. The presence of peritubular fibrosis was evaluated in Masson's trichrome preparations according to the thickness of the staining of collagen deposition surrounding tubuli. Proliferating cells were identified by immunostaining of proliferating cellular nuclear antigen (PCNA) using an avidin-biotin peroxidase method^[34] with retrieval of antigen by means of microwave irradiation. Specific anti-PCNA antibody (mouse anti-PCNA, clone PC 10, DAKO, Denmark) biotinylated rabbit anti-mouse IgG (DAKO, Denmark) were used and the avidin-biotin complex technique (ABC, DAKO kit) was performed. The bound antibodies were visualized by means of 3,3'-diaminobenzidine tetrahydrochloride (Sigma Chemical Company, St. Louis, MO) with nickel enhancement^[34]. Finally, samples were slightly counterstained (10 s) in hematoxylin, dehydrated, and mounted in DPX. Controls were performed by substitution of the primary antibody by TBS. The number of PCNA positive cells was recorded. The result was expressed as stained cells per tubuli (arithmetic mean of 30 screened tubuli).

In addition, the expression of transferrin^[35] in tubuli was evaluated by immunostaining using similar technique as for PCNA with specific anti-transferrin antibody (obtained from rabbit, RARa/TRf, Nordic Immunological Laboratories, Teknovas, The Netherlands). Transferrin expression was scored from 0 to 4 points. If 30 tubuli expressed transferrin normally all over the germinal epithelium, it was scored 0 points. The remaining scores were obtained according to the following formula: (30-tubuli showing expression of transferrin all over the germinal epithelium) × 0.075.

Analytical methods

Serum levels of albumin, total proteins, glucose, cholesterol, bilirubin, alkaline phosphatase, transferrin and aminotransferases (AST and ALT) were determined by routine laboratory methods using a Hitachi 747 autoanalyzer (Boehringer-Mannheim, Germany). Serum levels of the different hormones were assessed by RIA in a GammaChen 9612 Plus (Serono Diagnostics, Roma, Italy) using specific commercial assay systems: total and free testosterone and estradiol-6, Coat-a-Count, DPC (Diagnostic Products Corporation, Los Angeles, CA); rat luteinizing hormone (rLH) and rat follicle stimulating hormone (rFSH) from Amersham International Plc (Little Chalfont Buckinghamshire, England HP7 9NA); IGF-1 by extraction (Nichols Institute Diagnostics, San Juan Capistrano, CA, USA).

Lipid peroxidation assessment of testicular homogenates

Malondyaldehyde (MDA) was assessed after heating samples at 45 °C for 60 min in acid medium. It was quantitated by a colorimetric assay using LPO-586 (Bioxytech; OXIS International Inc., Portland, OR, USA), which after reacting with MDA, generated a stable chromophore that could be measured at 586 nm (Hitachi U2 000 Spectro; Roche).

Statistical analysis

Data are expressed as mean±SE. To assess the homogeneity between the three groups of rats a Kruskal-Wallis test was

used, followed by multiple post-hoc comparisons using Mann-Whitney *U* tests (two tailed) with Bonferroni adjustment. A regression model was fitted considering histopathological score, PCNA or transferrin expression scores and IGF-1 plasma concentration as the dependent and independent variables respectively. Within group differences between pre-and post-treatment values were assessed by means of Wilcoxon matched pairs signed rank sum test. Any *P* value less than 0.05 was considered to be statistically significant. Calculations were performed by SPSS Win v.6.0. program.

RESULTS

At baseline, CI groups showed abnormal values compared to controls (CO) in serum levels of alanine aminotransferase (CO = 26±2; CI = 273±49 IU/L, *P*<0.01), aspartate aminotransferase (CO = 55±5; CI = 297±49 IU/L, *P*<0.001), cholesterol (CO = 82±4; CI = 115±5 mg/dL, *P*<0.05), alkaline phosphatase (CO = 310±43; CI = 701±146 IU/L, *P*<0.05), bilirubin (CO = 0.4±0.0; CI = 1.2±0.3 mg/dL, *P*<0.05), total proteins (CO = 6.9±0.1; CI = 6.4±0.2 g/dL, *P*<0.05) and albumin (CO = 3.6±0.1; CI = 3.1±0.2 g/dL, *P*<0.05). No differences were found between cirrhotic groups.

At the end of the experimental period, all rats from groups CI and CI+IGF showed established cirrhosis (mixed micro-macronodular cirrhosis in liver histopathology) with some signs of portal hypertension (spleen weight, g, CO = 0.8±0.0; CI = 1.4±0.2; CI+IGF = 1.4±0.1, *P*<0.001 both cirrhotic groups vs controls). Ascites was absent in all of the cirrhotic animals.

Testicular morphology and morphometry

The testicular size and volume were normal in the cirrhotic groups as compared to controls. Morphometric study showed reduction in testicular weight (in absolute values but not if it was corrected by body mass) in untreated cirrhotic group as compared to controls and CI+IGF group. Findings regarding longitudinal and transverse testicular diameters were similar to those in testicular weight. Morphometric data in the three groups are summarized in Table 1.

Testicular histopathology

Figure 1 shows testicular morphology in the three experimental groups. Testicular histological section of normal rat (CO) demonstrated active spermatogenesis in normal-size seminiferous tubuli with thin basement membranes and minimal

peritubular fibrosis. Leydig cells were scarce, being widely separated by seminiferous tubuli. No evidence of peritubular fibrosis and other alterations was found in cirrhotic groups. Cellular analyses (see Methods) in 30 seminiferous tubuli were performed in each preparation and summarized in Table 2. No relevant findings were obtained in this morphologic study.

Testicular cellular proliferation, as evaluated by PCNA^[35], was significantly reduced in CI rats while CI+IGF rats showed values similar to controls (CO: 66±2, CI: 57±1, CI+IGF: 61±1, *P*<0.001 untreated cirrhotic group vs controls and *P*<0.05 CI+IGF vs controls and CI group). Figure 2 shows PCNA immunohistochemistry (PCNA+cells) in the three groups.

Testicular transferrin, a marker of the integrity of hemato-testicular barrier^[36-38], was evaluated from 0 to 4 points by immunohistochemistry in testicular slices (see Methods). Transferrin expression was decreased in CI rats (3.40±0.03 points, *P*<0.001 vs CO and CI+IGF groups) as compared to controls (3.98±0.04 points) and to cirrhotic rats receiving IGF-1 (3.76±0.05 points). Figure 3 shows transferrin expression in the three experimental groups.

Testicular levels of MDA in order to study the likely direct damage of CCl₄ to testes, MDA levels, an index of lipid peroxidation^[39], were assessed in testicular homogenates. No differences were found between the three experimental groups in testicular MDA content (nmol/mg protein, CO = 9.1±0.8, CI = 13.0±3.2, CI+IGF = 8.9±1.6).

Pituitary-gonadal axis

Serum levels of sexual hormones are summarized in Table 3. No significant differences were found between groups, either in total and free testosterone, or estradiol, or in the ratio of estradiol/testosterone. However, a significant increase of FSH (*P*<0.001 vs controls) and also high levels of LH (*P* = 0.06 vs controls) were observed in untreated rats with compensated cirrhosis, suggesting an altered negative feed-back since this early stage of the cirrhosis. On the other hand, LH concentrations were moved towards normal values in IGF-1 treated cirrhotic group (*P* = ns vs controls, and *P*<0.01 vs untreated cirrhotic rats).

Serum levels of IGF-1

At the time of animal sacrifice (d 15), no significant differences between the three groups were found in serum levels of IGF-1 (CO: 1030±67, CI: 1165±58, CI+IGF: 1030±38 ng/mL), similar to those described previously in early stage of cirrhosis^[16-18,24].

Table 1 Body mass and parameters of testicular size and weight in the three experimental groups (d 15)

	Healthy control rats (CO, n = 12)	Untreated cirrhotic rats (CI, n = 12)	Cirrhotic rats treated with IGF-1 (CI+IGF, n=12)
Body mass (g)	545.0±1.0	460.0±1.0 ^d	458.0±9.0 ^d
Right testis (g)	2.0±0.0	1.6±0.1 ^d	1.7±0.1 ^d
(×100 g/bm)	(0.4±0.0)	(0.3±0.0)	(0.4±0.0)
External testicular diameters (mm)			
• Longitudinal	20.4±0.26	18.56±0.22 ^d	18.37±0.34 ^d
• Transversal	10.3±0.24	9.41±0.23 ^b	9.64±0.14 ^a

^a*P*<0.05; ^b*P*<0.01; ^d*P*<0.001 vs CO group.

Table 2 Cellular analysis: Thirty seminiferous tubuli were examined in each preparation. The table summarizes the number of tubuli in each category: category I, only Sertoli's cells; category II, I+spermatids; category III, II+spermatocytes; category IV, all types of cells but with some alterations; category V, all types of cells with normal features

Category	I	II	III	IV	V
Controls (CO) (n = 10)×30 tubuli	0	0	0	2	298
Untreated cirrhotic rats (CI) (n = 10)×30 tubuli	0	0	5	20	275
IGF-treated cirrhotic rats (CI+IGF) (n = 10)×30 tubuli	0	0	0	8	292
Statistical analysis (<i>P</i>)	ns	ns	ns	^a <i>P</i> <0.05	ns

^a*P*<0.05, CI vs CO group.

Table 3 The pituitary-gonadal axis (on d 15) in the three experimental groups

	Healthy control rats (CO, n = 12)	Untreated cirrhotic rats (CI, n = 12)	IGF-1-treated cirrhotic rats (CI+IGF, n = 12)
Total testosterone (ng/dL)	62±13	77±17	64±7
Free testosterone (pg/mL)	0.36±0.09	0.36±0.10	0.41±0.05
Estradiol (pg/mL)	31±2	33±2	29±1
Estradiol/Total testosterone	0.5±0.1	0.5±0.1	0.6±0.1
LH (ng/mL)	4.8±0.6	6.0±0.5	3.8±0.7 ^d
FSH (ng/mL)	22±8	27±1 ^f	26±4 ^b

^bP<0.01 CI+IGF vs CO group; ^dP<0.01 CI+IGF vs CI group; ^fP<0.001 CI vs CO group.

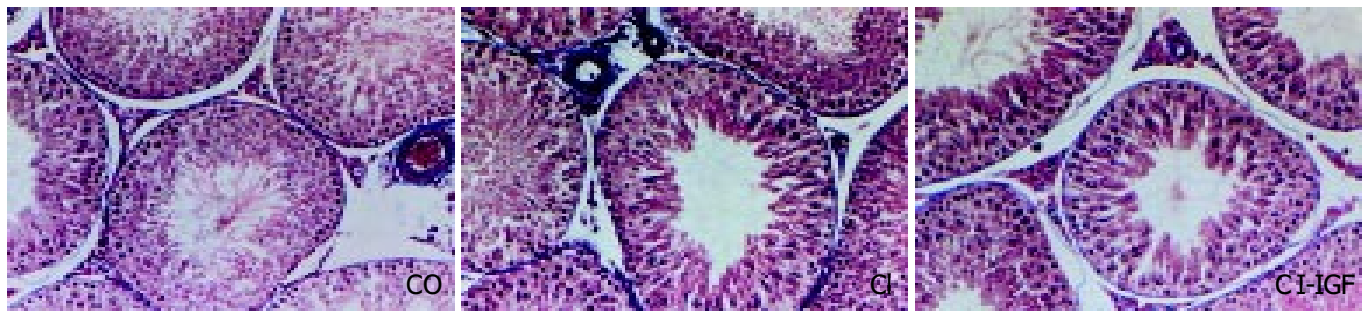


Figure 1 Microscopy of testes (×150 magnification, Masson's stain). Testicular histological sections of normal rat (CO) demonstrated active spermatogenesis in normal-size seminiferous tubuli with thin basement membranes and minimal peritubular fibrosis. Leydig cells were scarce, being widely separated by seminiferous tubuli. No evidence of peritubular fibrosis and other alterations were found in testes from cirrhotic animals.



Figure 2 Study of proliferative activity, assessed by PCNA immunostaining. A significant reduction of cellular proliferation were observed in rats with compensated cirrhosis. This reduction was normalized in IGF-1 treated cirrhotic group (CI+IGF). (×200 magnification, in the three pictures).



Figure 3 Immunohistochemistry for testicular transferrin in seminiferous tubuli. Transferrin immunostaining was observed at the level of Sertoli cells and in germ cells in normal rats (CO) and in cirrhotic rats treated with IGF-1 (CI+IGF) but a lower or absent transferrin immunostaining was observed in several tubuli of untreated cirrhotic rats (CI) (score, CI: 3.40±0.03, CO: 3.98±0.04, CI+IGF-1: 3.76±0.05).

DISCUSSION

This study demonstrates that rats with compensated CCl₄-induced cirrhosis show some testicular alterations and gonadal dysfunction, from early stages of liver cirrhosis. The main finding of this study is that there is an altered hemato-testicular barrier,

probably responsible for the reduction of cellular proliferation, as well as a paradoxical response of pituitary-testicular axis.

The occurrence of testicular atrophy and gonadal dysfunction in advanced cirrhosis is a well known clinical event^[1,3-9]. Both testicular histopathological abnormalities and low levels of serum testosterone have been described in patients with

alcoholic and nonalcoholic cirrhosis several years ago^[3-9]. Previous experimental data^[2] showed that severe testicular atrophy and gonadal insufficiency treated with low doses of IGF-1 recovered to normal in a very short time (21 d). Data regarding experimentally induced cirrhosis are, however, scarce. Our previous data showed a severe testicular damage^[2] as manifested by macroscopic testicular atrophy and a variety of histopathological abnormalities including a reduction in tubular diameters, presence of aberrant cells in tubular lumen, peritubular fibrosis, loss of the germinal line and a marked reduction in cellular proliferation. These alterations resembled those found in necropsic studies in alcoholic cirrhotics^[1] and those reported in experimental models of testicular damage such as chronic testicular ischemia^[35].

The mechanisms responsible for the described alterations are not fully understood, although the relationship between IGF-1 deficiency and testicular damage in cirrhosis was demonstrated in the mentioned work^[2]. In cirrhotic rats included in the current work, no IGF-1 deficiency was present but there was a reduced availability of this hormone as it has been suggested previously^[16-18,22]. Moreover, we have previously demonstrated that the changes induced by cirrhosis in the serum profile of IGF-1 binding proteins further reduce bio-availability of IGF-1 in cirrhotic rats^[16]. In fact, exogenous administration of IGF-1 was able to reverse several abnormalities (decreased food utility and intestinal absorption of nutrients, and somatostatinergic tone and osteopenia) associated with cirrhosis in animals with normal serum levels of this hormone^[16-20,22-24].

On the other hand, a direct effect of IGF-1 on testes seemed to be the most important factor to explain previous findings^[2]. This idea is supported by the existence of receptors for IGF-1 in Sertoli cells, germ cells and Leydig cells^[25-27] and by findings demonstrating a direct effect of IGF-1 on testes^[27-31]. Since IGF-1 is a well recognized trophic factor for testis, its deficiency could be a contributing factor to testicular damage in cirrhosis.

The present work was designed in order to gain more insights into the mechanisms involved in the pathogenesis of hypogonadism associated with liver cirrhosis. In fact, many factors that have been involved in this process, such as portal systemic shunting^[1,39,40] or undernutrition^[1,41] were minimized in this early stage of the liver disease. Specifically, this study was targeted to establish the historical progression of the described testicular alterations^[2].

The blood-testis barrier is considered nearly as specific as the blood-brain barrier^[42]. Although all cells require irons from serum transferrin produced by hepatocytes, cells that create a blood barrier such as Sertoli cells in the testis and choroid plexus epithelium in the brain also express the transferrin gene to provide irons to cells sequestered within the serum-free environment. Testicular transferrin expression was a good marker of the integrity of the hemato-testicular barrier^[36,37]. A major finding of this work was that transferrin expression by Sertoli cells was reduced in untreated cirrhotic rats. The medical bioavailability of IGF-1 could be due to the mechanism of testicular transferrin reduction. IGF-1 treatment increased the expression of this protein in Sertoli cells of cirrhotic rats (Figure 3). This possibility seemed to be plausible since several metabolic functions of Sertoli cells were also influenced by IGF-1^[32,43-45]. Interestingly, the recovery of transferrin expression in Sertoli cells observed in our study suggested a role for IGF-1 in maintaining the integrity of the hematotesticular barrier^[2,33-38].

The first step of the pathogenesis of testicular atrophy occurring in advanced cirrhosis seems to be the decreased expression of transferrin, showing a dysfunction of Sertoli cells and consequently the disruption in blood-testis barrier integrity. Therefore, the observed reduction of cellular proliferation finally affecting spermatogenesis^[2,46] would be its logical consequence.

A question arises as to whether direct toxicity of CCl₄ on testicular tissue could contribute to testicular injury. Alcohol was known to produce oxidative damage and to be able to pass across testicular barrier^[47,48]. This toxic possibility has been reasonably ruled out by the presence of similar levels of MDA, a marker of lipid peroxidation^[39], in testicular homogenates from the three experimental groups. Certainly, a slight increase of testicular MDA was found in untreated cirrhotic rats, but this did not reach statistical significance.

In the early stage of cirrhosis, testosterone levels were normal. However, both FSH and LH were increased in untreated cirrhotic animals. This abnormal response of the negative feedback could be an initial hormonal reaction of primary hypogonadism. In advanced stages of cirrhosis, we found increased levels of serum LH associated with a significant reduction of total and free serum testosterone defining a picture of primary hypogonadism, thus ruling out hypothalamic-pituitary dysfunction as the responsible mechanism^[2]. Interestingly, LH levels were reduced by IGF-1 treatment in this series with compensated cirrhosis and an incipient gonadal dysfunction. The significant increase of FSH could be related to the observed reduction of cellular proliferation in cirrhotic rats. Since a close relationship has been reported between IGF-1 and gonadotropins^[49-51], our findings require further investigation.

In summary, this study shows an altered hemato-testicular barrier from an early stage of cirrhosis and suggests that the reduction of IGF-1 bioavailability may play a critical role in the beginning stage of testicular damage and hypogonadism associated with liver cirrhosis. In addition, these results support the conclusion that the exogenous administration of IGF-1 may be useful for the treatment of testicular alterations in cirrhotic patients.

ACKNOWLEDGEMENTS

The authors wish to express their gratitude to Dr. Bruce Scharschmidt, Chiron, for generously granting the rhIGF-1 used in this study. We are as well deeply indebted to the "Real Academia de Medicina de Cataluña" (Barcelona) and Mrs.C. Alonso-Borrás and Mr. J. Celaya for financial collaboration.

REFERENCES

- 1 **Van Thiel DH.** Endocrine function. In *The liver: biology and pathobiology*. Raven Press 1982; 717-912
- 2 **Castilla-Cortázar I, García M, Quiroga J.** Insulin-like growth factor-I reverts testicular atrophy in rats with advanced cirrhosis. *Hepatology* 2000; **31**: 592-600
- 3 **Van Thiel GH, Gavaler JS, Slone FL.** Is feminization in alcoholic men due in part to portal hypertension?: a rat model. *Gastroenterology* 1980; **78**: 81-91
- 4 **Bennett HS, Baggenstoss AH, Butt H.** The testis, breast and prostate of men who die of cirrhosis of the liver. *Am J Clin Pathol* 1950; **20**: 814-828
- 5 **Van Steenberg W.** Alcohol, liver cirrhosis and disorders in sex hormone metabolism. *Acta Clin Belg* 1993; **48**: 269-283
- 6 **Galvao-Teles A, Monteiro E, Gavaler JS.** Gonadal consequences of alcohol abuse: lessons from the liver. *Hepatology* 1986; **6**: 123-128
- 7 **Guehot J, Vaubourdolle M, Ballet F.** Hepatic uptake of sex steroids in men with alcoholic cirrhosis. *Gastroenterology* 1987; **92**: 203-207
- 8 **Bannister P, Handley T, Chapman C, Losowsky MS.** Hypogonadism in chronic liver disease: impaired release of luteinising hormone. *Brit Med* 1986; **293**: 1191-1193
- 9 **Pajarinen JT, Karhunden PJ.** Spermatogenic arrest and "Sertoli cell-only" syndrome-common alcohol-induced disorders of the human testis. *Int J Androl* 1994; **17**: 292-299
- 10 **Sara VR, Hall K.** Insulin-like growth factors and their binding proteins. *Physiol Rev* 1990; **70**: 591-613
- 11 **Schimpf RM, Lebec D, Donadieu M.** Somatomedin production in normal adults and cirrhotic patients. *Acta Endocrinol* 1977; **86**: 355-362

- 12 **Hattori N**, Kurahachi H, Ikekubo K. Serum growth hormone-binding protein, insulin-like growth factor-I, and growth hormone in patients with liver cirrhosis. *Metab Clin Exp* 1992; **41**: 377-381
- 13 **Moller S**, Becker U, Juul A, Skakkebaek NE, Christensen E. Prognostic value of insulinlike growth factor I and its binding proteins in patients with alcohol-induced liver disease. *Hepatology* 1996; **23**: 1073-1078
- 14 **Moller S**, Gronbaek M, Main K, Becker U, Skakkebaek NE. Urinary growth hormone (U-GH) excretion and serum insulin-like growth factor 1 (IGF-1) in patients with alcoholic cirrhosis. *J Hepatol* 1993; **17**: 315-320
- 15 **Caufriez A**, Reding P, Urbain D, Goldstein J, Copinschi G. Insulin-like growth factor-I: a good indicator of functional hepatocellular capacity in alcoholic liver cirrhosis. *J Endocrinol Invest* 1991; **14**: 317-321
- 16 **Picardi A**, Costa de Oliveira A, Muguerza B, Tosar A, Quiroga J, Castilla-Cortázar I, Santidrián S, Prieto J. Low doses of insulin-like growth factor-I improve nitrogen retention and food efficiency in rats with early Cirrhosis. *J Hepatol* 1997; **24**: 267-279
- 17 **Castilla-Cortázar I**, Prieto J, Urdaneta E, Pascual M, Nuñez M, Zudaire E, García M, Quiroga J, Santidrián S. Impaired intestinal sugar transport in cirrhotic rats: correction by low doses of insulin-like growth factor I. *Gastroenterology* 1997; **113**: 1180-1187
- 18 **Castilla-Cortázar I**, Picardi A, Tosar A, Ainzua J, Urdaneta E, García M, Pascual M, Quiroga J, Prieto J. Effect of insulin-like growth factor I on *in vivo* intestinal absorption of D-galactose in cirrhotic rats. *Am J Physiol* 1999; **276**(1 Pt 1): G37-G42
- 19 **Pascual M**, Castilla-Cortázar I, Urdaneta E, Quiroga J, García M, Picardi A, Prieto J. Altered intestinal transport of amino acids in cirrhotic rats: the effect of insulin-like growth factor-I. *Am J Physiology* 2000; **279**: G319-G324
- 20 **Cemborain A**, Castilla-Cortázar I, García M, Quiroga J, Muguerza B, Picardi A, Santidrián S, Prieto J. Osteopenia in rats with liver cirrhosis: beneficial effects of IGF-1 treatment. *J Hepatol* 1998; **28**: 122-131
- 21 **Cemborain A**, Castilla-Cortázar I, García M, Muguerza B, Delgado G, Díaz-Sánchez M, Picardi A. Effects of IGF-1 treatment on osteopenia in rats with advanced liver cirrhosis. *J Physiol Biochem* 2000; **56**: 91-99
- 22 **Castilla-Cortázar I**, García M, Muguerza B, Pérez R, Quiroga J, Santidrián S, Prieto J. Hepatoprotective effects of insulin-like growth factor-I in rats with carbon-tetrachloride-induced cirrhosis. *Gastroenterology* 1997; **113**: 1682-1691
- 23 **Muguerza B**, Castilla-Cortázar I, García M, Quiroga J, Santidrián S, Prieto J. Antifibrogenic effect *in vivo* of low doses of Insulin-like growth factor-I (IGF-1) in cirrhotic rats. *BBA* 2001; **1536**: 185-195
- 24 **Castilla-Cortázar I**, Aliaga-Montilla MA, Salvador J, García M, Quiroga J, Delgado G, González-Barón S, Prieto J. Insulin-like growth factor-I restores the reduced somatostatinergic tone controlling GH secretion in cirrhotic rats. *Liver* 2001; **37**: 215-219
- 25 **Tajima Y**, Watanabe D, Koshimizu U, Matsuzawa T, Nishimune Y. Insulin-like growth factor-I and transforming growth factor-alpha stimulate differentiation of type A spermatogonia in organ culture of adult mouse cryptorchid testes. *Int J Androl* 1995; **18**: 8-12
- 26 **Spiteri-grech J**, Weinbauer GF, Bolze P, Chandolia RK, Bartlett JM, Nieschlag E. Effects of FSH and testosterone on intratesticular insulin-like growth factor-I and specific germ cell populations in rats treated with gonadotrophin-releasing hormone antagonist. *J Endocrinol* 1993; **137**: 81-89
- 27 **Zhou J**, Bondy C. Anatomy of the insulin-like growth factor system in the human testis. *Fertil Steril* 1993; **60**: 897-904
- 28 **Dubois W**, Gallard GV. Culture of intact Sertoli/germ cell units and isolated Sertoli cells from Squalus testis. II. Stimulatory effects of insulin and IGF-1 on DNA synthesis in premeiotic stages. *J Exp Zool* 1993; **267**: 233-244
- 29 **Moore A**, Morris JD. The involvement of insulin-like growth factor-I in local control of steroidogenesis and DNA synthesis of Leydig cells in the rat testicular interstitium. *J Endocrinol* 1993; **138**: 107-114
- 30 **Grizard G**. IGF(s) and testicular function. Secretion and action of IGF-1 on Leydig cells. *Contracept Fertil Sex* 1994; **22**: 551-555
- 31 **Lin T**, Wang D, Nagpal ML, Shimasaki S, Ling N. Expression and regulation of insulin-like growth factor-binding protein -1, -2, -3 and -4 messenger ribonucleic acids in purified rat Leydig cells and their biological effects. *Endocrinology* 1993; **132**: 1898-1904
- 32 **Rappaport MS**, Smith EP. Insulin-like growth factor (IGF) binding protein 3 in the rat testis: follicle-stimulating hormone dependence of mRNA expression and inhibition of IGF-1 action on cultured Sertoli cells. *Biol Reprod* 1995; **52**: 419-425
- 33 **The Guiding Principles for Research Involving Animals**. National Academy of Sciences and published by the *National Institute of Health -NIH-*, revised in 1991
- 34 **Shu SY**, Ju G, Fan LZ. The glucose oxidase-DAB-nickel method in peroxidase histochemistry of the nervous system. *Neurosci Lett* 1988; **85**: 169-171
- 35 **Santamaria L**, Martin R, Codesal J, Paniagua R. Myoid cell proliferation in rat seminiferous tubules after ischaemic testicular atrophy induced by epinephrine. Morphometric and immunohistochemical (bromo-deoxyuridine and PCNA) studies. *Int J Androl* 1995; **18**: 13-22
- 36 **Skinner MK**, Cosand WL, Griswold MD. Purification and characterization of testicular transferrin secreted by rat Sertoli cells. *Biochem J* 1984; **218**: 313-320
- 37 **Chaudhary J**, Skinner MK. Comparative sequence analysis of the mouse and human transferrin promoters: hormonal regulation of the transferrin promoter in sertoli cells. *Mol Reprod Dev* 1998; **50**: 273-283
- 38 **Gutteridge JMC**. Lipid peroxidation and antioxidants as biomarkers of tissue damage. *Clin Chem* 1995; **41**: 1819-1828
- 39 **Zaitoun AM**, Apelqvist G, Wikell C, Al-Mardini H, Bengtsson F, Record CO. Quantitative studies of testicular atrophy following portacaval shunt in rats. *Hepatology* 1998; **28**: 1461-1466
- 40 **Smanik EJ**, Mullen KD, Giroski WG, McCullough AJ. The influence of portacaval anastomosis on gonadal and anterior pituitary hormones in a rat model standardized for gender, food intake, and time after surgery. *Steroids* 1991; **56**: 237-241
- 41 **Mezey E**. Liver disease and nutrition. *Gastroenterology* 1978; **74**: 770-783
- 42 **Ghabriel MN**, Lu JJ, Hermanis G, Zhu C, Setchell BP. Expression of a blood-brain barrier-specific antigen in the reproductive tract of the male rat. *Reproduction* 2002; **123**: 389-397
- 43 **Itoh N**, Nanbu A, Tachiki H, Akagashi K, Nitta T, Mikuma N, Tsukamoto T, Kumamoto Y. Restoration of testicular transferrin, insulin-like growth factor I (IGF-1), and spermatogenesis by exogenously administered purified FSH and testosterone in medically hypophysectomized rats. *Arch Androl* 1994; **33**: 169-177
- 44 **Rappaport MS**, Smith EP. Insulin-like growth factor-I inhibits aromatization induced by follicle-stimulating hormone in rat Sertoli cell culture. *Biol Reprod* 1996; **54**: 446-452
- 45 **Prati M**, Palmero S, de Marco P, Trucchi P, Fugassa E. Effect of insulin-like growth factor-I on sertoli cell metabolism in the pubescent rats. *Boll Soc Ital Biol Sper* 1992; **68**: 121-128
- 46 **Waites GM**, Gladwell RT. Physiological significance of fluid secretion in the testis and blood-testis barrier. *Physiol Rev* 1982; **62**: 624-671
- 47 **Farghali H**, Williams DS, Gavalier J, Van Thiel DH. Effect of short-term ethanol feeding on rat testes as assessed by ³¹P NMR spectroscopy, ¹H NMR imaging, and biochemical methods. *Alcohol Clin Exp Res* 1991; **15**: 1018-1023
- 48 **Salonen J**, Eriksson CJ. Penetration of ethanol into the male reproductive tract. *Alcohol Clin Exp Res* 1989; **13**: 746-751
- 49 **Adam CL**, Gadd TS, Findlay PA, Wathes DC. IGF-1 stimulation of LH secretion, IGF-binding proteins (IGFBPs) and expression of mRNAs for IGFs, IGF receptors and IGFBPs in the ovine pituitary gland. *J Endocrinol* 2000; **166**: 247-254
- 50 **Carneiro G**, Lorenzo P, Pimentel C, Pegoraro L, Bertolini M, Ball B, Anderson G, Liu I. Influence of IGF-1 and its interaction with gonadotropins, estradiol, and fetal calf serum on *in vitro* maturation and parthenogenic development in equine oocytes. *Biol Reprod* 2001; **65**: 899-905
- 51 **Xia YX**, Weiss JM, Polack S, Diedrich K, Ortmann O. Interactions of IGF-1, insulin and estradiol with GnRH-stimulated luteinizing hormone release from female rat gonadotrophs. *Eur J Endocrinol* 2001; **144**: 73-79

• CLINICAL RESEARCH •

***Enterobius vermicularis* infection among population of General Mansilla, Argentina**

Betina C Pezzani, Marta C Minvielle, María M de Luca, María A Córdoba, María C Apezteguía, Juan A Basualdo

Betina C Pezzani, Marta C Minvielle, María M de Luca, María A Córdoba, Juan A Basualdo, Cátedra de Microbiología y Parasitología, Facultad de Ciencias Médicas, Universidad Nacional de La Plata 1900, Argentina

María C Apezteguía, Comisión de Investigaciones Científicas de la provincia de Buenos Aires

Supported by the Agencia Nacional de Promoción Científica y Técnica de la Argentina, the Alberto J. Roemmers Foundation, and the Universidad Nacional de La Plata, and it was declared of Municipal Interest by the town of Magdalena, Province of Buenos Aires, Argentina

Correspondence to: Juan A Basualdo, Cátedra de Microbiología y Parasitología, Facultad de Ciencias Médicas, Universidad Nacional de La Plata, Calle 60 y 120 s/n, La Plata 1900,

Argentina. jabasua@atlas.med.unlp.edu.ar

Telephone: +54-221-4258987 **Fax:** +54-221-4258987

Received: 2004-02-28 **Accepted:** 2004-04-29

Abstract

AIM: To evaluate the relationships between the personal, sociocultural, and environmental characteristics, and the presence or absence of symptoms with the detection of *Enterobius vermicularis* (*E. vermicularis*) in a population sample in our region (General Mansilla, Province of Buenos Aires, Argentina), by individual and familiar analyses.

METHODS: *E. vermicularis* was diagnosed in 309 people from 70 family units residing in the urban area and the rural area of the city of General Mansilla. Each of them was surveyed so as to register personal, environmental and sociocultural data. Questions about the presence or absence of anal itch, abdominal pain and sleeping disorder were also asked. Significant associations were determined by square chi tests. Logistic regression models were adjusted by using a backward conditional stepwise method to determine the presence of this parasite in the individuals and in the families.

RESULTS: The parasites were found in 29.12% (90/309) of the individuals, with a frequency of 14.28% (20/140) among the heads of the families and of 41.42% (70/169) among the children. The only variables showing a significant association were affiliation, where the risk category was "being the son/daughter of", and the symptoms were abdominal pain, sleeping disorder, and anal itch. Families with a member infected with parasite were considered Positive Families (PF) and they were 40/70 (57.14%), only 5% (2/40) of the PF had 100% of their members infected with the parasite. The logistic regression models applied showed that the risk categories were mainly affiliation (son/daughter) and housing (satisfactory) among others.

CONCLUSION: The presence of *E. vermicularis* was proved in one third of the studied population. The frequency of families with all their members infected with the parasite was very low. Most of the studied personal, sociocultural, and environmental variables did not turn out to be significantly associated with the presence of the parasite. An association

with the category of "son/daughter" and housing classified as "satisfactory" was determined. The latter may be due to the fact that the people living in that category of housing have hygienic practices at home that favour the distribution of the eggs in the environment. The presence of the analysed symptoms was associated with the presence of the parasite, thus strengthening the need of periodical control of the population showing at least one of these symptoms.

Pezzani BC, Minvielle MC, de Luca MM, Córdoba MA, Apezteguía MC, Basualdo JA. *Enterobius vermicularis* infection among population of General Mansilla, Argentina. *World J Gastroenterol* 2004; 10(17): 2535-2539

<http://www.wjgnet.com/1007-9327/10/2535.asp>

INTRODUCTION

Enterobius vermicularis (*E. vermicularis*) is a small whitish nematode whose evolution cycle differs from other intestinal helminths in the biological peculiarities^[1].

Enterobiosis is a cosmopolitan parasitosis. The peculiar biology of *E. vermicularis* contributes to the creation of contamination foci around the infected resident and the re-infections. The intra-family or cohabitating members' infection is very frequent. The most important infection routes are through oral and respiratory tract. The oral infection included the anus-hand-mouth route, onychophagia and/or ingestion of contaminated food. The respiratory tract infection would be from inhaling dust contaminated with the parasite eggs^[2].

The main source of contamination inside the house is found in the environmental dust and carried by children. This would be one of the infection routes for the family units.

It has been reported that no sex difference existed in the infection rates. The teen-age, however, infection rates remain unchanged in boys but decrease among girls, since girls start observing hygienic practices with higher precocity than boys^[3,4]. Among adults, the infection frequency is similar in both sexes, but it was commonly observed that many adults seemed not to get infected even when subjected to contaminated environments due to personal hygiene^[1-5].

Waste disposal little affects the distribution of the infection, since the oxyurus eggs are not found in excrement. Several groups in the population may be infected without depending on the socioeconomic conditions and environmental hygiene due to the biological characteristics of this parasite^[6,7].

Generally, this parasitosis is an asymptomatic illness, and in those cases where clinical manifestations are present, anal itch is the most frequent symptom. Indirectly, and mainly in children, it produces insomnia, fatigue and irritability, and sometimes abdominal pain^[2-8,9].

The objective of this study was to evaluate the relationship between the personal, socio-cultural and environmental characteristics, presence or absence of symptoms, and the detection of *E. vermicularis* in a sample population in our region (Province of Buenos Aires, Argentina), through individual and family analysis.

MATERIALS AND METHODS

Study area

The city of General Mansilla is located in the northeast of the Province of Buenos Aires, in the central-western area of the Argentine Republic (South America), 96 km from the city of Buenos Aires. Population is 2 300 in the urban area and 1 700 in the rural area. The urban area covers 250 hectares and the rural population is settled in a 15 km range around it (Figure 1).

Population

A total of 309 people constituting 70 family units, made up by mother, father and children (1 to 6 per family), were studied. Fifty families were analyzed from the urban area (221 people) and 20 from the rural area (88 people). Each member of the family was surveyed to record personal, environmental and socio-cultural data. The following variables were assessed: a) personal: sex, age, affiliation of each member, and number of children in each family; b) socio-cultural and environmental: habitat (urban area - rural area), water supply (water pump - running water), disposal of waste (sewer - no sewer), housing (satisfactory - unsatisfactory), home garbage (collected - not collected), bathroom (existent - non-existent), and overcrowding (yes - no). Housing was considered satisfactory when built of masonry with cement floors, and unsatisfactory when built of wood and/or metal with dirt floors. Overcrowding was considered when more than three individuals slept together in the same room. Besides, questions were asked about the presence or absence of the following symptoms: anal itch, abdominal pain and sleeping disorders, since they are considered to be typical of this parasitosis.

Parasitological analysis

A perianal swab method was performed to each surveyed individual for the detection of *E. vermicularis*. Each surveyed person was given five 10 cm×10 cm gauze pads and a bottle of 5% formaldehyde. At the same time, they were explained the procedure for sample taking. In the case of minors, instructions were given to their parents. Each of the testee collected the sample before getting up for 5 consecutive days, each day rubbing a gauze pad previously imbibed in water, on the perianal margins. Then, they put the sample in the container with formaldehyde and sent it to the lab.

Statistical analysis

The association between each of the variables studied and the presence of *E. vermicularis* was analyzed by means of the chi square test. In the case of finding statistically significant associations, the odds ratio (OR) was calculated.

Logistic regression models were adjusted by using backward conditional stepwise method to determine the presence of *E. vermicularis* in individuals and in families. In the case of individuals (total, rural and urban), socio-cultural and environmental characteristics, symptoms, age and sex were used as (independent) explanatory variables. In the case of families, only socio-cultural and environmental characteristics and affiliation were used. The logistic regression model predicts the probability of being infected with *E. vermicularis* according to the explanatory variables. From this prediction, individuals are classified according to their risk of infection as: high risk (when the probability is higher than 0.5), and low risk (when the probability is lower than 0.5). For this classification, sensitivity (S), specificity (E), positive predictive value and negative predictive value, and global adjustment (total percentage of correct predictions) in each of the models were estimated. The model can be used to obtain OR estimators for each variable. SPSS (Statistical Package for the Social Sciences) software version 11.5 was used.

RESULTS

The frequency of infected people in the total studied population (309) was 29.12% (90/309). Among the parents, it was 14.28% (20/140) and 41.42% (70/169) among the children.

Families with at least one infected member were called positive families (PF) and the rest, negative families (NF). The number of PF was 40/70 (57.14%). Of these, 8 families presented less than 25% of their members with the parasite, 20 had 26-50%, 6 between 51% and 75%, 4 between 76% and 99% and only two had 100% of their members infected.

The mean age of parents from PF and NF was 32.3 and 33.6, respectively. The mean age for children from PF and NF was 8.48 and 7.71, respectively. The mean age of positive children was 6.85. Thirty percent (12/40) of the mothers from PF were infected while only 20% (8/40) of the fathers were infected. Prevalence for adults from PF was 25% (20/80).

The number of children from PF was 103. Of these, 67.96% (70/103) were positive and 52.85% (37/70) were male. The number of children from NF was 66, 48.48% (32/66) of which were male.

The results obtained from socio-cultural and environmental aspects both from PF and NF and their statistical analysis are shown in Table 1.

Table 1 Sociocultural and environmental factors studied in 70 *E. vermicularis* infected and non-infected families in General Mansilla, Province of Buenos Aires, Argentina (n, %)

Variable		PF (n = 40)	FN (n = 30)	P
Habitat	Urban	29 (72.5)	21 (70)	0.8188
	Rural	11 (27.5)	9 (30)	
Water supply	Water pump	12 (30)	13 (43.33)	0.2493
	Running water	28 (70)	17 (56.66)	
Disposal of waste	Sewer	14 (35)	8 (26.66)	0.4573
	No sewer	26 (65)	22 (73.33)	
Housing	Satisfactory	30 (75)	20 (66.66)	0.4450
	Unsatisfactory	10 (25)	10 (33.33)	
Garbage	Collected	28 (70)	21 (70)	1.0000
	Not collected	12 (30)	9 (30)	
Bathroom	Existent	25 (62.5)	22 (73.33)	0.3396
	Non-existent	15 (37.5)	8 (26.66)	
Overcrowding	Yes	17 (42.5)	9 (30)	0.2841
	No	23 (57.5)	21 (60)	

PF: Families with some member infected with *E. vermicularis*; NF: Families with no member infected with *E. vermicularis*.
 1Satisfactory housing: With cement floors and masonry walls; unsatisfactory housing: Dirt floors and wood or metal walls.
 2Overcrowding: Yes: when more than three people sleep in a room; No: When less than three people sleep in a room.

When analyzing the association between the presence of *E. vermicularis* and each variable separately, the only one showing statistically significant association was affiliation, where the risk category was being the son/daughter ($P = 0.000$, $OR = 4.242$), and the symptoms of abdominal pain ($P = 0.001$, $OR = 2.680$), sleeping disorders ($P = 0.003$, $OR = 2.339$), and anal itch ($P = 0.001$, $OR = 2.662$).

Table 2 (a, b, c and d) shows the results from the logistic regression models built for the total of individuals, those residing in the urban area, those living in the rural area, and the families.

(1) In the whole population, the affiliation variable was the most significant, that is, children had greater probability of being infected than parents. In order of importance, the variables garbage collection and type of housing followed. Type of water supply and symptoms of abdominal pain and sleeping disorders

turned out to be of lesser importance. This model classified 22.2% of the infected individuals (S) and 92.2% of the non-infected individuals (E) correctly. Globally, it classified 71.8% of the individuals correctly.

(2) Among the rural population the affiliation variable had an even higher significance degree. It also turned out to be important age variable. This continuous variable had a positive coefficient, which implies that at an older age there is more risk to be infected. But being the affiliation variable present, older children are those with the higher risk of being infected. In order of importance, the symptom of sleeping disorders, type of housing and no bathroom available followed. This model classified 53.8% of the positive individuals (S), and 93.3% of the non-infected individuals (E) correctly. Globally, it classified 81.4% of the individuals correctly.

(3) Among the urban population, the affiliation variable was also the most significant. The symptom of abdominal pain, type of water supply and type of housing followed. This model classified 23.4% of the infected individuals (S) and 89.3% of the non-infected individuals (E) correctly. Globally, it classified 70.4% of the individuals correctly.

(4) Among the positive families, the variables of garbage collection, housing, water supply and bathroom had a similar degree of significance. This model classified 95% of the infected families (S) and 23% of the non-infected families (E) correctly. Globally, it classified 64.3% of the families correctly.

Table 2 Logistic regression models for the presence of *E. vermicularis* in 309 (88 rural and 221 urban) individuals, both individually and grouped into 70 families in General Mansilla, Argentina

Variable	Risk category	Coefficient	Odds Ratio
For the total of individuals, <i>n</i> = 309			
Affiliation	Son/daughter	1.267	3.550
Housing	Satisfactory	0.829	2.288
Garbage	Not collected	1.372	3.944
Water	Running	0.951	2.591
Abdominal pain	Present	0.555	1.742
Sleeping disorders	Present	0.561	1.752
Constant	-1.825		
For rural individuals, <i>n</i> = 88			
Affiliation	Son/daughter	10.246	28 167
Housing	Satisfactory	2.857	17.5
Age (yr)	Eldest son/daughter	0.316	1.372
Bathroom	Non-existent	2.160	8.670
Sleeping disorders	Present	1.967	7.151
Constant	-12.493		
For urban individuals, <i>n</i> = 221			
Affiliation	Son/daughter	1.176	3.241
Housing	Satisfactory	0.917	2.5
Water	Running	1.372	3.937
Abdominal pain	Present	0.690	1.993
Constant	-1.612		
For positive families, <i>n</i> = 40			
Housing	Satisfactory	2.749	15.625
Water	Running	2.614	13.699
Garbage	Not collected	2.75	15.636
Bathroom	Non-existent	2.403	11.056
Constant	0.338		

Regarding the three studied symptoms, the analysis showed anal itch in 19.41% (60/309) of the people. Of them, 27/60 (45%) were positive for *E. vermicularis* ($P = 0.0026$, OR = 2.42), 12/60 (20%) were negative but belonged to a PF, and 21/60 (35%)

were negative from NF. The presence of sleeping disorders was shown in 22.65% (79/309) of the studied population, 30/70 (42.85%) ($P = 0.0040$, OR = 2.24) of which were parasite infected, 17/70 (24.28%) showed no parasites but belonged to a PF, and 23/70 (32.85%) were negative from NF.

Abdominal pain was detected in 19.41% (60/309) of the testees, 28/60 (46.66%) ($P = 0.009$, OR = 2.64) of which were parasite infected individuals, 12/60 (20%) were negative for the parasite test but belonged to a PF, and 20/60 (33.33%) were negative from NF.



Figure 1 Geographical location of General Mansilla city in Argentina.

DISCUSSION

In the present study a high frequency of infection was found for *E. vermicularis*, going from 29.12% in the total population up to 41.42% if only the child population considered. These percentages are higher than those published in other countries. In Korea, a prevalence of this parasitosis was reported in 9.8% of school children^[10], 9.2% in pre-schoolers^[3], 14.8 in kindergarten children^[11], 12.6% in school children in the rural area^[4] and 9.8% in children of school age^[12]. In the town of Chennai, India, a prevalence of 0.50% was reported^[13] in school age children. In Thailand, in 5- to 10-year-old children, the prevalence was 21.91%^[7]. In Taiwan it was 11% in school age children^[14]. A prevalence of 10.5% was found for children between 7 and 13 years old in Turkey^[15]. A study carried out in 18- to 35-year-old adults in Malaysia, Kuala Lumpur, reported a frequency of 9.2%^[16,17]. In Poland, the frequency among 7-year-old children was 16.45%^[19]. And in Sweden, it was 21% in children from primary care centres^[18].

In America, a study carried out in New York (United States) on the prevalence of *E. vermicularis* in mentally and developmentally retarded children showed a prevalence of 4.5%^[19]. In Venezuela, the prevalence found in 5- to 14-year-old children was 19.1%^[20], and in Peru it was 1.1% in adults and children from different communities^[21]. In Argentina, a study carried out in two aboriginal communities from the province of Misiones, a prevalence of 0% and 5% for *E. vermicularis* was shown^[22]. In the Province of La Rioja, a percentage of 14.8% was reported in middle-class children^[23], and in the city of Buenos Aires, 20.50% was reported in hospital population^[24]. In Neuquen (Patagonia), 18.8% was reported in adults and children from deprived neighbourhoods^[25].

However, the high frequency shown in our study is similar to that reported by Norhayati *et al.*^[26] in 1994 in Malaysia (40.4%), Nithikathkul *et al.*^[6] in 2001 in Thailand (38.82%), Bahader *et al.*^[27] in 1995 in Egypt (43.8%), Gilman *et al.*^[28] in 1991 in Peru

(42.0%), and Mercado *et al.*^[29] in 1996 in Chile (35.2%) on studies done in diverse populations.

This study did not show significant sex and age differences regarding parasite infected parents, but there was a higher frequency among the mothers, probably due to the greater daily contact with their parasite infected children (regular behaviour among the inhabitants of this region).

The children had a higher probability of being infected than the parents. As to the infected children, no statistically verifiable differences could be found regarding sex or age but, unlike the parents, the highest level of infected people were male, probably in association with different hygienic practices for each sex. This difference agrees with Yoon *et al.*'s^[3] report about 10.1% of boys and 8.1% of girls with parasites, and Kim *et al.*'s^[10] about 10.8% in male and 8.7% in female schoolchildren. However, Kim^[10] reports 7.1% and 12.5% positive values for male and female kindergarten children, respectively. In our study, parasite infected kindergarten infantile population, sex distribution was 50% (13/26).

Among the PF there was a high percentage of non-infected parents and only 5% of these families had all of their members infected. With these results we could infer that when someone is detected to have parasites, the treatment of all the members of his/her family is not necessary, especially if we take into account that the cost of the treatment has to be afforded by each family in our region. This would make a regular control of the population so as to detect positive cases and treat them appropriately and thus reduce the prevalence of this parasitosis.

Socio-cultural and environmental factors studied in this study showed no statistically significant associations between PF and NF, which are in agreement with Nithikathkul *et al.*^[7] not with Kim *et al.*^[10].

Overcrowding was significantly associated for Acosta *et al.*^[1] ($P < 0.001$) with this parasitosis in children in Venezuela, but this association could not be shown in our study, in agreement with Norhayati *et al.*'s findings in children in Malaysia^[26].

In this study, a significant association was proved by the presence of anal itch, sleeping disorders and abdominal pain, and the detection of this parasite. But these symptoms were not exclusive for the parasite-infected population since 20% to 35% of the non-parasite infected people showed at least one of these symptoms. Venezuela^[1] reported that 53.9% of the parasite-infected population showed anal itch.

As a conclusion of this work we point out that enterobiosis was present in a percentage close to 30% of the general population and over 40% in children in our region (Province of Buenos Aires, Argentina).

Contrary to what was expected, the risk of getting this helminthosis was not related to age, sex, or most of the socio-cultural and environmental factors studied (habitat, consumption water, disposal of waste, garbage collection, bathroom characteristics and overcrowding). An association was determined between the variable affiliations, where the risk category was "being the son/daughter of".

The type of housing categorized as "satisfactory" was also related to this parasitosis. This contradictory situation could be due to the fact that people living in this type of housing show hygienic practices in the home favouring the distribution of eggs in the atmosphere (*e.g.*, shaking the sheets, using a feather dust for cleaning, *etc.*)

These results also strengthen the need of regular control of the population reporting at least one of these symptoms: anal itch, sleeping disorders, and/or abdominal pain.

ACKNOWLEDGEMENTS

The authors wish to thank Dr. Roberto Zungrí for his permanent "field work" contribution to this study.

REFERENCES

- 1 Acosta M, Cazorla D, Garvett M. Enterobiasis among school-children in a rural population from Estado Falcon, Venezuela, and its relation with socioeconomic level. *Invest Clin* 2002; **43**: 173-181
- 2 Atías A. Enterobiosis u Oxiuriasis. In: Atías A, ed. *Parasitología Médica. Editorial Mediterráneo, Santiago, Chile* 1999: 188-193
- 3 Yoon HJ, Choi YJ, Lee SU, Park HY, Huh S, Yang YS. Enterobius vermicularis egg positive rate of pre-school children in Chunchon, Korea (1999). *Korean J Parasitol* 2000; **38**: 279-281
- 4 Kim BJ, Yeon JW, Ock MS. Infection rates of Enterobius vermicularis and Clonorchis sinensis of primary school children in Hamyang-gun, Gyeongsangnam-do (province), Korea. *Korean J Parasitol* 2001; **39**: 323-325
- 5 Smolyakov R, Talalay B, Yanai-Inbar I, Pak I, Alkan M. Enterobius vermicularis infection of female genital tract: a report of three cases and review of literature. *Eur J Obstet Gynecol Reprod Biol* 2003; **107**: 220-222
- 6 Nithikathkul C, Changsap B, Wannapinyosheep S, Poister C, Boontan P. The prevalence of Enterobius vermicularis among primary school students in Samut Prakan Province, Thailand. *Southeast Asian J Trop Med Public Health* 2001; **32**(Suppl 2): 133-137
- 7 Nithikathkul C, Changsap B, Wannapinyosheep S, Poister C, Boontan P. The prevalence of enterobiasis in children attending mobile health clinic of Huachiew Chalermprakiet University. *Southeast Asian J Trop Med Public Health* 2001; **32** (Suppl 2): 138-142
- 8 Grecnis RK, Cooper ES. Enterobius, trichuris, capillaria, and hookworm including ancylostoma caninum. *Gastroenterol Clin North Am* 1996; **25**: 579-597
- 9 Nokes C, Bundiy DA. Compliance and absenteeism in school children: implications for helminth control. *Trans R Soc Trop Med Hyg* 1993; **87**: 148-152
- 10 Kim BJ, Lee BY, Chung HK, Lee YS, Lee KH, Chung HJ, Ock MS. Egg positive rate of Enterobius vermicularis of primary school children in Geoje island. *Korean J Parasitol* 2003; **41**: 75-77
- 11 Lee KJ, Lee IY, Im K. Enterobius vermicularis egg positive rate in a primary school in Chungchongnam-do (province) in Korea. *Korean J Parasitol* 2000; **38**: 177-178
- 12 Lee KJ, Ahn YK, Ryang YS. Enterobius vermicularis egg positive rates in primary school children in Gangwon-do (province), Korea. *Korean J Parasitol* 2001; **39**: 327-328
- 13 Fernandez MC, Verghese S, Bhuvaneshwari R, Elizabeth SJ, Mathew T, Anitha A, Chitra AK. A comparative study of the intestinal parasites prevalent among children living in rural and urban settings in and around Chennai. *J Commun Dis* 2002; **34**: 35-39
- 14 Fan PC. Review of enterobiasis in Taiwan and offshore islands. *J Microbiol Immunol Infect* 1998; **31**: 203-210
- 15 Gurses N, Ozkan Y, Peksen Y, Uysal S, Aydin M. Intestinal parasites in primary schools of different socioeconomic status and environmental conditions. *Mikrobiyol Bul* 1991; **25**: 57-62
- 16 Oothuman P, Noor Hayati MI, Mastura MH, Rampal L, Jeffery J, Rubiah M, Ismail G, Fatmah MS. Prevalence of Enterobius vermicularis amongst adults living in hostels by six successive day examination. *Southeast Asian J Trop Med Public Health* 1992; **23**: 82-86
- 17 Plonka W, Dzbeniski TH. The occurrence of intestinal parasites among children attending first classes of the elementary schools in Poland in the school year 1997/1998. *Przegl Epidemiol* 1999; **53**: 331-338
- 18 Herrstrom P, Fristrom A, Karlsson A, Hogstedt B. Enterobius vermicularis and finger sucking in young Swedish children. *Scand J Prim Health Care* 1997; **15**: 146-148
- 19 Schupf N, Ortiz M, Kapell D, Kiely M, Rudelli RD. Prevalence of intestinal parasite infections among individuals with mental retardation in New York State. *Ment Retard* 1995; **33**: 84-89
- 20 Devera R, Perez C, Ramos Y. Enterobiasis in students from Ciudad Bolívar, Venezuela. *Bol Chil Parasitol* 1998; **53**: 14-18
- 21 Maco Flores V, Marcos Raymundo LA, Terashima Iwashita A, Samalvides Cuba F, Gotuzzo Herencia E. Distribution of

- entero-parasitic infections in the Peruvian Highland: study carried out in six rural communities of the department of Puno, Peru. *Rev Gastroenterol Peru* 2002; **22**: 304-309
- 22 **Ilkow C**, Digiani MC, Navone GT. Prevalencias y cargas parasitarias intestinales en dos comunidades mbya guaraní (provincia de Misiones, Argentina). [Intestinal prevalences and burden in two mbya guaraní communities- province of Misiones, Argentina] 3º Congreso Argentino de Parasitología 2000. *Libro de Resúmenes. Tomo II*, p 393
- 23 **Flores J**, Páez S, Toro A, Bellegarde E, Córdoba P. Prevalencia de *Enterobius vermicularis* en la capital de la provincia de la rioja. [Prevalence of *Enterobius vermicularis* in the capital city of La Rioja's province] 3º Congreso Argentino de Parasitología 2002. *Libro de Resúmenes. Tomo II*, p 418
- 24 **Menghi C**, Clementel V, Zadcovich S, Gatta C, Fernández GG, Szmulewicz G, Mendez O. Enteroparasitosis halladas en una población asistida en un hospital de la ciudad de Buenos Aires. [Enteroparasitosis in hospital population of Buenos Aires city] 3º Congreso Argentino de Parasitología 2000. *Libro de Resúmenes. Tomo II*, p 425
- 25 **Soriano SV**, Barbieri LM, Pierangeli NB, Giayetto AL, Manacorda AM, Castronovo E, Pezzani BC, Minvielle M, Basualdo JA. Intestinal parasites and the environment: Frequency of intestinal parasites in children of Neuquen, Patagonia, Argentina. *Rev Latinoam Microbiol* 2001; **43**: 96-101
- 26 **Norhayati M**, Hayati MI, Oothuman P, Azizi O, Fatmah MS, Ismail G, Minudin YM. *Enterobius vermicularis* infection among children aged 1-8 years in a rural area in Malaysia. *Southeast Asian J Trop Med Public Health* 1994; **25**: 494-497
- 27 **Bahader SM**, Ali GS, Shaalan AH, Khalil HM, Khalil NM. Effects of *Enterobius vermicularis* infection on intelligence quotient (I.Q) and anthropometric measurements of Egyptian rural children. *J Egypt Soc Parasitol* 1995; **25**: 183-194
- 28 **Gilman RH**, Marquis GS, Miranda E. Prevalence and symptoms of *Enterobius vermicularis* infections in a Peruvian shanty town. *Trans R Soc Trop Med Hyg* 1991; **85**: 761-764
- 29 **Mercado R**, García M. Various epidemiological aspects of *enterobius vermicularis* infection inpatients served at public outpatient clinics and hospitals from the northern section of Santiago, Chile, 1995. *Bol Chil Parasitol* 1996; **51**: 91-94

Edited by Chen WW Proofread by Xu FM

• CLINICAL RESEARCH •

Possible causes of central pontine myelinolysis after liver transplantation

Jun Yu, Shu-Sen Zheng, Ting-Bo Liang, Yan Shen, Wei-Lin Wang, Qing-Hong Ke

Jun Yu, Shu-Sen Zheng, Ting-Bo Liang, Yan Shen, Wei-Lin Wang, Qing-Hong Ke, Department of Hepatobiliary Surgery, the First Affiliated Hospital, Medical School of Zhejiang University, Hangzhou 310003, Zhejiang Province, China

Correspondence to: Professor Shu-Sen Zheng, Department of Hepatobiliary Surgery, the First Affiliated Hospital, Medical School of Zhejiang University, Hangzhou 310003, Zhejiang Province, China. zhengss@mail.hz.zj.cn

Telephone: +86-571-87236616

Received: 2003-10-24 **Accepted:** 2003-12-22

Abstract

AIM: To sum up the clinical characteristics of patients with central pontine myelinolysis (CPM) after orthotopic liver transplantation (OLT) and to document the possible causes of CPM.

METHODS: Data of 142 patients undergoing OLT between January 1999 to May 2003 were analyzed retrospectively. Following risk factors during perioperation were analyzed in patients with and without CPM: primary liver disease, preoperative serum sodium level, magnesium level and plasma osmolality, fluctuation degree of serum sodium concentration, and immunosuppressive drug level, *etc.*

RESULTS: A total of 13 (9.2%) neurologic symptoms appeared in 142 patients post-operation including 5 cases (3.5%) with CPM and 8 cases (5.6%) with cerebral hemorrhage or infarct. Two patients developing CPM after OLT had a hyponatremia history before operation (serum sodium < 130 mmol/L), their mean serum sodium level was 130.6 ± 5.54 mmol/L. The serum sodium level was significantly lower in CPM patients than in patients without neurologic complications or with cerebral hemorrhage/infarct ($P < 0.05$). The increase in serum sodium during perioperative 48 h after OLT in patients with CPM was significantly greater than that in patients with cerebral hemorrhage/infarct but without neurologic complications (19.5 ± 6.54 mmol/L, 10.1 ± 6.43 mmol/L, 4.5 ± 4.34 mmol/L, respectively, $P < 0.05$). Plasma osmolality was greatly increased postoperation in patients with CPM. Hypomagnesemia was noted in all patients perioperation, but there were no significant differences between groups. The duration of operation on patients with CPM was longer than that on others (492 ± 190.05 min, $P < 0.05$). Cyclosporin A (CsA) levels were normal in all patients, but there were significant differences between patients with or without neurologic complications ($P < 0.05$).

CONCLUSION: CPM may be more prevalent following liver transplantation. Although the diagnosis of CPM after OLT can be made by overall neurologic evaluations including magnetic resonance imaging (MRI) of the head, the mortality is still very high. The occurrence of CPM may be associated with such factors as hyponatremia, rapid rise of serum sodium concentration, plasma osmolality increase postoperation, the duration of operation, and high CsA levels.

Yu J, Zheng SS, Liang TB, Shen Y, Wang WL, Ke QH. Possible causes of central pontine myelinolysis after liver transplantation. *World J Gastroenterol* 2004; 10(17): 2540-2543
<http://www.wjgnet.com/1007-9327/10/2540.asp>

INTRODUCTION

The morbidity and mortality of central nervous system (CNS) complications after orthotopic liver transplantation (OLT) was 19% and 47% respectively^[1]. Central pontine myelinolysis (CPM)^[2] is the most serious CNS complication that could be seen after OLT, and represents an important source of mortality early after OLT^[3]. CPM following liver transplantation was reported more and more in foreign literatures^[4,5], but it was rarely reported in our country^[6,7].

In this paper, we studied retrospectively 142 patients undergoing OLT in our center. Fifteen patients had CNS complications after OLT including 5 patients with CPM. The clinical features and possible causes of CPM after liver transplantation were analyzed.

MATERIALS AND METHODS

Clinical data

Between January 1999 to May 2003, consecutive OLT was performed on 142 patients at our center. Medical records and clinical data of the patients were retrospectively investigated. Of them 117 were males and 25 females, age from 19 to 65 years, their age was 45 ± 8.9 years. Indications for OLT included severe hepatitis 28 cases, hepatic cirrhosis (32 cases), liver carcinoma (53 cases), polycystic liver (3 cases), and others (24 cases). Operative procedures were performed with the standard technique and UW preservation solution. All patients had similar perioperative intensive care and received cyclosporin A (CsA) and methylprednisolone-based induction immunosuppression.

Observational indicators

Patients who developed posttransplant abnormal neurological symptoms underwent overall neurological evaluation. Magnetic resonance imaging (MRI) of head was performed in selected cases. CPM was diagnosed based on: (1) patients who had a variety of signs including mental status changes, quadriplegia, pseudobulbar palsy, and drowsiness, *etc.*; (2) MRI showed a hypointense signal in T1-weighted images and a hyperintense signal in T2-weighted images in the central pontine. The signal of T2 was slightly increased after contrast administration.

Following risk factors during perioperation were analyzed between patients with and without CPM: age, gender, primary liver disease, pretransplant serum sodium, magnesium levels, plasma osmolality, fluctuation degree of serum sodium and plasma osmolality 48 h after transplantation, duration of operation, and CsA level. Hyponatremia was defined as serum sodium < 130 mmol/L. Hypomagnesemia was defined as serum magnesium < 1.5 mg/L.

Statistical analysis

Data were expressed as mean ± SD. Comparisons of group

means were made with ANOVA for unpaired data, and Chi-Square test for enumeration data. $P < 0.05$ and $P < 0.01$ were considered statistically significant.

RESULTS

Clinical features of patients with CNS complications

Fifty-eight of 142 patients undergoing OLT developed abnormal neurological symptoms such as mania, tremor, confusion, drowsiness, and diminished state of responsiveness. Thirteen patients were diagnosed having CNS complications based on clinical features and MRI. The demographic characteristics of the patients are outlined in Table 1. There were 10 males and 3 females aged 40–55 years. Primary diseases included severe hepatitis in 6 cases; hepatic cirrhosis in 4 cases; liver carcinoma, drug liver failure, IgA nephropathy, and polycystic liver in 1 case, respectively. Patients developed neurological complications in the early postoperative period including cerebral hemorrhage/infarct in 8 cases, CPM in 5 cases. The incidence of cerebral hemorrhage/infarct and CPM was 5.6% (8/142) and 3.5% (5/142), respectively. The extent of CPM on MRI was variable, showing a hypointensity signal of T1-weighted images in the pontine without space occupying sign (Figure 1A), and increased signal intensity of T2-weighted images in central pontine (Figure 2A, 2B). None of the patients showed extrapontine myelinolysis. CNS complications occurred two weeks after liver transplantation, ranged from 2 to 18 d. The median time of survival of patients with CPM after OLT was 24 ± 16.1 d, ranged 7 to 48 d. The patients who were complicated with cerebral hemorrhage or infarct survived 2 to 96 d after transplantation, the mean time was 33 ± 30.7 d.

Comparison of clinical characteristics in patients with and without CPM (Table 2)

Pretransplant hyponatremia was present in all symptomatic patients with CPM. Two patients developing CPM after OLT had a severe hyponatremia history before operation (serum sodium level < 130 mmol/L). The average serum sodium level was 130.6 ± 5.54 mmol/L. The serum sodium level was significantly lower in patients with CPM than in patients without neurologic complications or with cerebral hemorrhage/infarct ($P < 0.05$). The average increase of perioperative serum sodium 48 h after OLT in patients with CPM, cerebral hemorrhage/infarct, and without CNS complications was 19.5 ± 6.54 mmol/L, 10.1 ± 6.43 mmol/L, 4.5 ± 4.34 mmol/L, respectively ($P < 0.01$). Plasma osmolality was greatly increased 48 h postoperation in patients with CPM. Despite this, the plasma osmolality was normal in patients without CPM, but no significant difference was noted between patient who had complication of cerebral hemorrhage/infarct and patients who had no CNS complication. Hypomagnesemia was noted in all patients perioperation, but there were no significant differences between groups. The operation time for patients with CPM was longer than that for others ($P < 0.05$). But no significant difference was found in operation time between patients who had complication of cerebral hemorrhage/infarct and those who had no CNS complication. Following transplantation, all patients received CsA-based induction immunosuppression. Though the mean CsA level in all patients was normal, the average CsA level was greatly higher in patients with CNS complications than in patients without CNS complications. Age, gender, primary liver disease were similar among three groups.

Table 1 Clinical characteristics of patients with CNS complications

Patient NO.	Hospital NO.	Age (yr)	Gender	Primary disease	CNS complication	Timing of onset (d)	Timing of survival (d)
1	287206	40	Male	Severe hepatitis	Cerebral hemorrhage	6	11
2	286967	48	Male	Severe hepatitis	CPM	10	15
3	291172	41	Female	Severe hepatitis	Cerebral hemorrhage	8	26
4	299921	54	Male	Severe hepatitis	CPM	6	23
5	306331	53	Female	polycystic liver	Cerebral infarct	4	28
6	312075	51	Male	Hepatic cirrhosis	Cerebral hemorrhage	2	9
7	314112	53	Male	Severe hepatitis	CPM	18	48
8	325113	49	Male	Liver carcinoma	Cerebral hemorrhage	2	2
9	315349	41	Male	Hepatic cirrhosis	CPM	3	20
10	328762	46	Male	Drug liver failure IgA nephropathy	CPM	5	7
11	351480	55	Female	Hepatic cirrhosis	Cerebral hemorrhage	14	56
12	362960	52	Male	Hepatic cirrhosis	Cerebral hemorrhage	3	36
13	363980	46	Male	Severe hepatitis	Cerebral hemorrhage	14	96

Table 2 Comparison of Clinical characteristics in patients with and without CPM

Index	CNS Complications		NO CNS Complication
	CPM	Cerebral hemorrhage /cerebral infarct	
Preoperative serum sodium (mmol/L)	130.6 ± 5.54^{bc}	135.9 ± 2.61	137.4 ± 3.83
Preoperative serum magnesium (mg/L)	0.8 ± 0.19	0.9 ± 0.20	1.0 ± 0.21
Preoperative sosm (mOsm/kg H ₂ O)	274.3 ± 33.09	290.2 ± 22.12	292.5 ± 26.05
Change in serum sodium After 48 h (mmol/L)	19.5 ± 6.54^{bd}	10.1 ± 6.43^b	4.5 ± 4.34
Postoperative sosm (mOsm/kg H ₂ O)	341.6 ± 14.99^{bc}	317.9 ± 29.76	308.8 ± 16.89
Surgery time (min)	492.0 ± 190.05^a	450.0 ± 93.50	399.9 ± 76.07
CsA level (ng/dL)	301.3 ± 9.23^b	273.8 ± 28.55^a	247.2 ± 35.44

Abbreviations: Sosm: Serum Osmolarity ^a $P < 0.05$ (0.016, 0.037), ^b $P < 0.01$ (0.000, 0.001) compared with no CNS complications; ^c $P < 0.05$ (0.017, 0.02), ^d $P < 0.01$ (0.000) compared with cerebral hemorrhage/infarct.

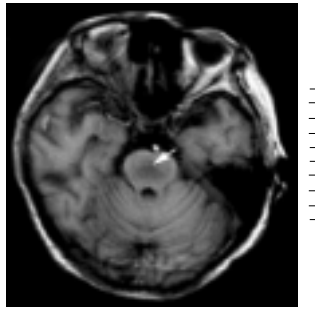


Figure 1 T1-Weighted axial magnetic resonance imaging scan shows symmetric area of hypointensity in the pons. (arrow).

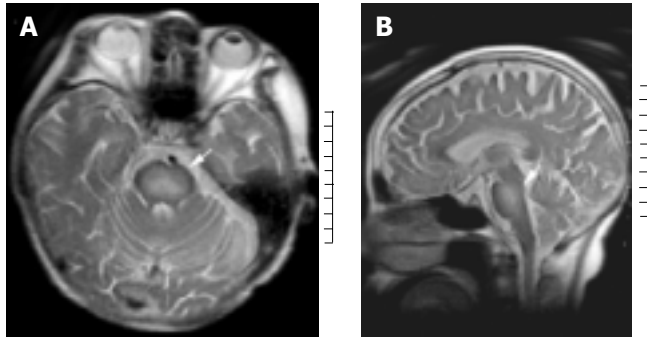


Figure 2 A: T2-Weighted axial magnetic resonance imaging shows bilaterally symmetric high-signal intensity is seen in the central pons. (arrow) B: T2-Weighted sagittal magnetic resonance imaging demonstrates hyperintensity area in central pons. (arrow).

DISCUSSION

CPM was first described in 1959 by Adams. CPM after OLT was first reported by Starzl^[8] in 1978. CPM^[9,10] was characterized by symmetrical loss of myelin in the pontine basalis, with relatively well-preserved axons and neuronal cell bodies. Acute CPM often occurred and had a variety of signs including quadriplegia, pseudobulbar palsy, and locked-in syndrome. As a severe neurological complication, the progress of CPM was usually dismal, with a high mortality rate^[11]. Most cases of CPM were diagnosed post-mortem. With the recognition of CPM and the development in MRI technology, more cases of CPM could be diagnosed while patients were alive. Liver transplant recipients constituted a high risk group for developing CPM. The incidence of CPM after OLT varied from 5-10%^[12-14], which was higher than that in other patients (0.16-5.8%)^[15]. The exact etiology of CPM is uncertain, the rapid correction of hyponatremia might be an important factor. However, controversy has been going on^[16-20].

Pathogenesis of CPM after OLT

End-stage hepatic insufficiency was a common feature of pretransplanted patients. Advanced liver failure was always associated with some degree of renal insufficiency. So almost all hyponatremic states associated with liver disease were chronic and difficult to be corrected^[21]. Input for patients after OLT was considerably increased as a consequence of bleeding during operation. The sodium content for fresh frozen plasma was around 165 mmol/L, 150 mmol/L for albumin solution, and 140 mmol/L for red blood cells, significantly higher than the serum sodium of patients with hyponatremia. Correction of blood loss would thus inevitably lead to a rapid rise in serum sodium concentration. A multicenter study showed^[22] that rapid correction of hyponatremia exceeding 18 mmol/L in the first 48 h was significantly associated with CPM. The present study

demonstrated that not all patients with hyponatremia developed CPM. But increase of serum sodium 48 h after OLT in patients with CPM was 19.5 ± 6.54 mmol/L, which was significantly higher than that in patients without CPM. Plasma osmolality was also greatly increased 48 h postoperation. The results of our study suggested that rapid correction of hyponatremia and abrupt change of plasma osmolality might account for the development of CPM. Liver failure might lead to disruption of astrocyte metabolism with resulting abnormalities of blood-brain barrier function and a decreased ability to generate new intracellular osmoles in response to osmotic changes. Thus, patients with liver transplantation were particularly susceptible to CPM^[23,24]. Lien *et al.*^[25] suggested that rapid correction of hyponatremia might produce acute dehydration of edematous brain, leading to high ion to organic osmolyte ratio, osmotic endothelial injury, and endothelial cell shrinkage with loosening of tight junctions. Subsequently, transvascular transport increased and myelinotoxic factors released. Because of an extensive gray-white matter admixture in the pontine, this anatomic arrangement could provide a suitable environment wherein myelinotoxic factors, chiefly derived from the richly vascular gray matter, could interact with surrounding bundles of myelin-containing white matter, then lead to demyelination viz development of CPM.

Dunn *et al.*^[26] demonstrated the neurotoxicity of CsA in transplanted patients. Three cases developing CsA associated akinetic mutism after liver transplantation were reported by Bird *et al.*^[27], two of three were identified by MRI. The CsA level in all patients was monitored and controlled in normal range. Although the mean in-hospital CsA level in CPM group was not different with that in cerebral hemorrhage/infarct group, the CsA levels in patients with CNS complications was higher than that in patients without CNS complications. In this study, pretransplant hypomagnesemia was noted in all patients after OLT. Previous study suggested^[28] that CsA neurotoxicity could lead to massive white matter lesions. Hypomagnesemia might contribute to CsA neurotoxicity and was associated with development of CPM after OLT, although the mechanism of CPM is unclear.

The results of our study also suggested that operation time in patients with CPM was significantly longer than that in patients without CNS complications. But there were no differences in operation time between patients with cerebral hemorrhage/infarct and without CNS complications, indicating that CNS lesions in liver transplant recipients may be related with intraoperative bleeding, prolonged low blood perfusion.

Prevention and therapy of CPM after OLT

To our knowledge, at present there is no definitive therapy for CPM. Therefore, prevention of this condition has become crucial^[29]. Slower correction of perioperative hyponatremia may be critical for patients undergoing OLT. The rate of correction should not exceed 15 mmol/L/24 h or 18 mmol/L/48 h. Major fluctuations in serum sodium during surgery should be avoided. Plasma osmolality level should be remained within normal reference, and aggressive magnesium replacement should be initiated for hypomagnesemia. To decrease the duration of operation and intraoperative bleeding, no venovenous bypass should be recommended. Immunosuppressive agent concentrations should be carefully monitored and controlled to avoid neurotoxicity^[30]. MRI of head should be performed when patients occurred neurologic and psychiatric symptoms after OLT^[31,32]. The best way of preventing CPM was to perform transplantation at an early stage of the disease. More recently, subclinical CPM after OLT was reported^[33], the patients were nearly asymptomatic, but MRI showed marked lesions in the pontine. According to these we suggest that the diagnosis of CPM should be considered in patients undergoing OLT with major electrolyte fluctuations, and high

immunosuppressive agent levels. MRI is currently the best modality available to identify CPM. Support treatment is very important for patients with CPM. It was reported that cortisol, vitamin, and serum replacement were used in CPM^[34]. Whether these therapies play a role in CPM remains to be determined.

Prognosis of CPM after OLT

A previous study showed^[35] that the occurrence of CPM after OLT varied from 2 to 11 d, average 7 d. The prognosis of CPM is usually dismal, with a high mortality rate. The results of the present study demonstrated that CPM occurred 3 to 18 d OLT. The median time of survival after OLT was 24.6±16.13 d, ranged 7 to 48 d, the mortality was 100%. These liver transplant recipients with CPM were associated with the following aspects. (1) Patients with CPM often had other complications^[36], such as infection, hemorrhage of digestive tract, and multi-organ failure. (2) Inadequate water intake and electrolyte derangements were not corrected due to CPM. (3) Venovenous bypass was used in part of transplantations^[37,38], which led to the increase in operation time, interoperative bleeding, time of low perfusion. The limited number of patients in this study may account for the high mortality of CPM after OLT.

REFERENCES

- Bonham CA, Dominguez EA, Fukui MB, Paterson DL, Pankey GA, Wagener MM, Fung JJ, Singh N. Central nervous system lesions in liver transplant recipients: prospective assessment of indications for biopsy and implications for management. *Transplantation* 1998; **66**: 1596-1604
- Kaiys-Wyllie M. Central pontine myelinolysis: a multidisciplinary approach to care. *J Neurosci Nurs* 1994; **26**: 36-41
- Lamp I, Yazdi K. Central pontine myelinolysis. *Eur Neurol* 2002; **47**: 3-7
- Singh N, Yu VL, Gayowski T. Central nervous system lesions in adult liver transplant recipients: Clinical review with implications for management. *Medicine* 1994; **73**: 110-118
- Fryer JP, Fortier MV, Metrakos P, Verran DJ, Asfar SK, Pelz DM, Wall WJ, Grant DR, Ghent CN. Central pontine myelinolysis and cyclosporine neurotoxicity following liver transplantation. *Transplantation* 1996; **61**: 658-661
- Xia SS. Current status of liver transplantation in China. *Shijie Huaren Xiaohua Zazhi* 1999; **7**: 645-646
- Qian YB, Cheng GH, Huang JF. Multivariate regression analysis on early mortality after orthotopic liver transplantation. *World J Gastroenterol* 2002; **8**: 128-130
- Starzl TE, Schneck SA, Mazzoni G, Aldrete JA, Porter KA, Schroter GPJ, Koep LJ, Putnam CW. Acute neurological complications after liver transplantation with particular reference to intraoperative cerebral air embolus. *Ann Surg* 1978; **187**: 236-240
- Ferreiro JA, Robert MA, Townsend J, Vinters HV. Neuropathologic findings after liver transplantation. *Acta Neuropathol* 1992; **84**: 1-14
- Wjodicks EF, Blue PR, Steers JL, Wiesner RH. Central pontine myelinolysis with stupor alone after orthotopic liver transplantation. *Liver Transplant Surg* 1996; **2**: 14-16
- Menger H, Jorg J. Outcome of central pontine and extrapontine myelindysis (n = 44). *J Neurol* 1999; **246**: 700-705
- Boon AP, Carey MP, Adams DH, Buckels J, McMaster P. Central pontine myelinolysis in liver transplantation. *J Clin Pathol* 1991; **44**: 909-914
- Estol CJ, Faris AA, Martinez AJ, Ahdab-Barmada M. Central pontine myelinolysis after liver transplantation. *Neurology* 1989; **39**: 493-498
- Bramhall SR, Minford E, Gunson B, Buckels JAC. Liver transplantation in the UK. *World J Gastroenterol* 2001; **7**: 602-611
- Kleinschmidt-DeMasters BK, Norenberg MD. Rapid correction of hyponatremia causes demyelination: relation to central pontine myelinolysis. *Science* 1981; **211**: 1068-1070
- Tien R, Arief AI, Kucharczyk W, Wasik A, Kucharczyk J. Hyponatremic encephalopathy: is central pontine myelinolysis a component? *Am J Med* 1992; **92**: 513-522
- Mast H, Gordon PH, Mohr JP, Tatemichi TK. Central pontine myelinolysis: clinical syndrome with normal serum sodium. *Eur J Med Res* 1995; **1**: 168-170
- Oh MS, Choi KC, Uribarri J, Sher J, Rao C, Carroll HJ. Prevention of myelinolysis in rats by dexamethasone or colchicine. *Am J Nephrol* 1990; **10**: 158-160
- Wszolek ZK, McComb RD, Pfeiffer RF, Steg RE, Wood RP, Shaw BW Jr, Markin RS. Pontine and extrapontine myelinolysis following liver transplantation. Relationship to serum sodium. *Transplantation* 1989; **48**: 1006-1012
- Soni BM, Vaidyanathan S, Watt JW, Krishnan KR. A retrospective study of hyponatremia in tetraplegic/paraplegic patients with a review of the literature. *Paraplegia* 1994; **32**: 597-607
- Palmer BF, Gates JR, Lader M. Causes and management of hyponatremia. *Pharmacother* 2003; **37**: 1694-1702
- Sterns RH, Cappuccio JD, Silver SM, Cohen EP. Neurologic sequelae after treatment of severe hyponatremia: a multicenter perspective. *J Am Soc Nephrol* 1994; **4**: 1522-1533
- Mueller AR, Platz KP, Bechstein WO, Schattenfroh N, Stoltenburg-Didinger G, Blumhardt G, Christe W, Neuhaus P. Neurotoxicity after orthotopic liver transplantation. A comparison between cyclosporine and FK506. *Transplantation* 1994; **58**: 155-170
- Kanwal F, Chen D, Ting L, Gornbein J, Saab S, Durazo F, Yersiz H, Farmer D, Ghobrial RM, Busuttill RW, Han SH. A model to predict the development of mental status changes of unclear cause after liver transplantation. *Liver Transpl* 2003; **9**: 1312-1319
- Lien YH. Role of organic osmolytes in myelinolysis. A topographic study in rats after rapid correction of hyponatremia. *J Clin Invest* 1995; **95**: 1579-1586
- Dunn CJ, Wagstaff AJ, Perry CM, Plosker GL, Goa KL. Cyclosporin: an updated review of the pharmacokinetic properties, clinical efficacy and tolerability of a microemulsion-based formulation (neoral) 1 in organ transplantation. *Drugs* 2001; **61**: 1957-2016
- Bird GL, Meadows J, Goka J, Polson R, Williams R. Cyclosporin-associated akinetic mutism and extrapyramidal syndrome after liver transplantation. *J Neurol Neurosurg Psychiatry* 1990; **53**: 1068-1071
- Abbasoglu O, Goldstein RM, Vodapally MS, Jennings LW, Levy MF, Husberg BS, Klintmalm GB. Liver transplantation in hyponatremic patients with emphasis on central pontine myelinolysis. *Clinical Transplantation* 1998; **12**: 263-269
- Harris CP, Townsend JJ, Baringer JR. Symptomatic hyponatremia: can myelinolysis be prevented by treatment? *J Neurol Neurosurg Psychiatry* 1993; **56**: 626-632
- Rodriguez J, Benito-Leon J, Molina JA, Ramos A, Bermejo F. Central pontine myelinolysis associated with cyclosporin in liver transplantation. *Neurologia* 1998; **13**: 437-440
- Bernsen HJ, Prick MJ. Improvement of central pontine myelinolysis as demonstrated by repeated magnetic resonance imaging in a patient without evidence of hyponatremia. *Acta Neurol Belg* 1999; **99**: 189-193
- Bekiesinska-Figatowska M, Bulski T, Rozyczka I, Furmanek M, Walecki J. MR imaging of seven presumed cases of central pontine and extrapontine myelinolysis. *Acta Neurobiol Exp* 2001; **61**: 141-144
- Kato T, Hattori H, Nagato M, Kiuchi T, Uemoto S, Nakahata T, Tanaka K. Subclinical central pontine myelinolysis following liver transplantation. *Brain Dev* 2002; **24**: 179-182
- Soupart A, Ngassa M, Decaux G. Therapeutic lowering of the serum sodium in a patient after excessive correction of hyponatremia. *Clin Nephrol* 1999; **51**: 383-386
- Bronster DJ, Emre S, Boccagni P, Sheiner PA, Schwartz ME, Miller CM. Central nervous system complications in liver transplant recipients-incidence, timing, and long-term follow-up. *Clin Transplant* 2000; **14**: 1-7
- Zheng SS, Liang TB, Xu X, Wang WL, Shen Y, Zhang M, Huang DS. Ten year's experience on liver transplantation in a single organ transplantation center. *Zhonghua Putong Waikexue Zazhi* 2003; **18**: 71-73
- Kokudo N, Sugawara Y, Imamura H, Sano K, Makuuchi M. Sling suspension of the liver in donor operation: a gradual tape-repositioning technique. *Transplantation* 2003; **76**: 803-807
- Yan LN, Wang W, Li B, Lu SC, Wen TF, Zeng Y, Cheng NS, Zhao JC, Lin QY, Chen XL, Wu XD, Jia QB, Zhou Y, Tu B, Wu YT. Venovenous bypass ahead of mobilization of the liver in orthotopic liver transplantation. *Hepatobiliary Pancreat Dis Int* 2003; **2**: 44-47

Ecologic study of serum selenium and upper gastrointestinal cancers in Iran

Mehdi Nouraei, Akram Pourshams, Farin Kamangar, Masood Sotoudeh, Mohammad Hossein Derakhshan, Mohammad Reza Akbari, Hafez Fakheri, Mohammad Javad Zahedi, Kathleen Caldwell, Christian C. Abnet, Philip R. Taylor, Reza Malekzadeh, Sanford M. Dawsey

Mehdi Nouraei, Akram Pourshams, Masood Sotoudeh, Mohammad Hossein Derakhshan, Mohammad Reza Akbari, Hafez Fakheri, Mohammad Javad Zahedi, Reza Malekzadeh, Digestive Disease Research Center, Tehran University of Medical Sciences, Tehran, Iran
Farin Kamangar, Christian C. Abnet, Philip R. Taylor, Sanford M. Dawsey, National Cancer Institute, NIH, Bethesda, MD20895-8314, USA

Kathleen Caldwell, Centers for Disease Control, Atlanta, Georgia, USA

Correspondence to: Dr. Sanford M. Dawsey, Senior Investigator, Cancer Prevention Studies Branch, CCR, NCI, 6116 Executive Blvd., Suite 705, Bethesda, MD 20895-8314, USA. dawseys@mail.nih.gov
Telephone: +1-301-594-2930 **Fax:** +1-301-435-8644

Received: 2004-03-06 **Accepted:** 2004-04-28

Abstract

AIM: Both observational and experimental studies have shown that higher selenium status reduces the risk of upper gastrointestinal cancers in selenium deficient populations. Recent cancer registry data have shown very different rates of esophageal cancer (EC) and gastric cancer (GC) in four Provinces of Iran, namely Ardabil, Mazandaran, Golestan, and Kerman. The aim of this study was to have a preliminary assessment of the hypothesis that high rates of EC in Golestan and high rates of GC in Ardabil may be partly attributable to selenium deficiency.

METHODS: We measured serum selenium in 300 healthy adults from Ardabil ($n = 100$), Mazandaran ($n = 50$), Golestan ($n = 100$), and Kerman ($n = 50$), using inductively coupled plasma, with dynamic reaction cell, mass spectrometry (ICP-DRC-MS) at the US Centers for Disease Control (Atlanta, Georgia).

RESULTS: The median serum selenium concentrations were very different in the four Provinces. The medians (IQR) for selenium in Ardabil, Mazandarn, Golestan, and Kerman were 82 (75-94), 123 (111-132), 155 (141-173), and 119 (110-128) $\mu\text{g/L}$, respectively ($P < 0.001$). The results of linear regression showed that the Province variable, by itself, explained 76% of the variance in log selenium ($r^2 = 0.76$). The proportion of the populations with a serum selenium more than 90 $\mu\text{g/L}$ (the concentration at which serum selenoproteins are saturated) was 100% in Golestan, Kerman, and Mazandaran but only 29% in Ardabil.

CONCLUSION: Our findings suggest that selenium deficiency is not a major contributor to the high incidence of EC seen in northeastern Iran, but it may play a role in the high incidence of GC in Ardabil Province.

Nouraei M, Pourshams A, Kamangar F, Sotoudeh M, Derakhshan MH, Akbari MR, Fakheri H, Zahedi MJ, Caldwell K, Abnet CC, Taylor PR, Malekzadeh R, Dawsey SM. Ecologic study of serum

selenium and upper gastrointestinal cancers in Iran. *World J Gastroenterol* 2004; 10(17): 2544-2546
<http://www.wjgnet.com/1007-9327/10/2544.asp>

INTRODUCTION

Esophageal cancer (EC) and gastric cancer (GC), collectively known as upper gastrointestinal (UGI) cancers, constitute 16% of all cancer deaths worldwide and are responsible for approximately one million deaths each year^[1].

Both observational and experimental studies have shown that higher selenium status reduces the risk of UGI cancers in selenium deficient populations^[2-5]. In a large-scale, prospective cohort study conducted in Finland, a low selenium region prior to a current supplementation program, Knekt and colleagues found a lower risk of stomach cancer in individuals with higher baseline serum selenium concentrations^[3]. In another large cohort study, Mark and colleagues also found a reduced risk of esophageal cancer and gastric cardia cancer among individuals with higher initial serum selenium concentrations in a selenium deficient population in Linxian, China^[4]. A double-blind, randomized clinical trial in this same Chinese population showed a reduced risk of both cardia and non-cardia gastric cancers in individuals supplemented with a combination of selenium, beta-carotene, and alpha-tocopherol^[2].

Iran also has high rates of both EC and GC^[6-8], and these cancers are the two most common causes of cancer death in Iran^[9]. However, recent cancer registry data showed highly varying rates of EC and GC in four Provinces of Iran, namely Ardabil^[7], Mazandaran, Golestan, and Kerman (unpublished data). The annual age-standardized incidence rates (ASRs) for EC were 15, 19, 40, and 3 per 10⁵, and ASRs for GC were 38, 22, 18, and 8 per 10⁵ in these four Provinces, respectively.

We hypothesized that differences in serum selenium may partly explain the highly varying rates of EC and GC in Iran. Here, we present the results of an ecologic study that compared serum selenium concentrations in randomly selected healthy subjects from Ardabil, Mazandaran, Golestan, and Kerman Provinces.

MATERIALS AND METHODS

Serum samples from 300 healthy adults were selected for this study. These subjects had all been recruited for previous studies. Ardabil serum samples (100 samples) were selected from participants in an endoscopic survey of gastric precancerous lesions conducted among rural and urban subjects ≥ 40 years old^[10]. These subjects were selected using simple random sampling, and all resided in Meshkinshahr, a major city in Ardabil, or its surrounding villages. Mazandaran and Kerman serum samples (50 samples each) were selected from participants in a survey of the prevalence of celiac disease among urban inhabitants ≥ 18 years old in these two Provinces. These subjects were selected randomly from the entire urban

population of Sari and Kerman, the two major cities of these Provinces. In Golestan, 100 serum samples were selected from urban and rural individuals ≥ 40 years of age who were recruited during the pilot phase of a cohort study of UGI cancers. In all of these studies, the only inclusion criteria were residence, age, and lack of life-threatening conditions. All samples were collected in the years 2002 and 2003. From these subjects, we selected our study samples such that they represented male and female participants equally (Table 1). Samples from Ardabil and Golestan included both urban and rural populations, but samples from Kerman and Mazandaran represented only urban subjects.

A single blood sample was collected from each person. Serum was separated and frozen in -20°C freezers in plastic vials, and the samples were transported to the U.S. Centers for Disease Control (Atlanta, Georgia) on dry ice, where serum selenium was measured using inductively coupled plasma, with dynamic reaction cell, mass spectrometry (ICP-DRC-MS). The analytical limit of detection for assessment was $5.2\ \mu\text{g/L}$ with a reference range of $80\text{--}300\ \mu\text{g/L}$ ^[11]. We pooled samples to make an internal quality control serum, and 20 quality control samples were randomly inserted among the other serum samples. The coefficient of variation in these samples was 0.04.

The distribution of serum selenium in the four Provinces was not normal. Therefore we used medians and interquartile ranges (IQRs) to present the descriptive results and the Kruskal-Wallis test to test the differences in serum selenium ranks among provinces, between males and females, and between urban and rural participants. The distribution of the natural logarithm of selenium (log selenium) in each province did not deviate from normal. Therefore we used linear regression to test the effect of age on log selenium values. We also used linear regression to find the proportion of variance of log selenium that was explained by the province. All statistical analyses were done using STATA[®] Software, version 8 (Stata Corporation, Tx).

RESULTS

The median age of all the study subjects was 45 years. Half of the subjects from each area (a total of 150) were males (Table 1). Half of the subjects from Ardabil and Golestan ($n = 100$) and all of the subjects from Mazandaran and Kerman ($n = 100$) were from urban areas.

The median serum selenium concentrations were very different in the four Provinces. The medians (IQR) for selenium in Ardabil, Mazandarn, Golestan, and Kerman were 82 (75-94), 123 (111-132), 155 (141-173), and 119 (110-128) $\mu\text{g/L}$, respectively ($P < 0.001$). The results of linear regression showed that the province variable, by itself, explained 76% of the variance in log selenium ($r^2 = 0.76$). The proportion of these populations with serum selenium concentrations more than $90\ \mu\text{g/L}$ (the concentration at which serum selenoproteins are saturated^[12]) was 100% in Golestan, Kerman, and Mazandaran, but only 29% in Ardabil.

The median (IQR) serum selenium concentrations in males

and females were 124 (95-145) and 116 (92-143) $\mu\text{g/L}$, respectively ($P = 0.49$).

Simple linear regression did not show a significant effect of age on log selenium in any of the four Provinces. The correlation coefficient between selenium and age in all samples combined was very low ($r = 0.006$).

Median (IQR) serum selenium concentrations in the urban and rural samples of Ardabil were 81 (76-86) and 83 (74-96) $\mu\text{g/L}$, respectively ($P = 0.57$). Median (IQR) serum selenium concentrations in urban and rural samples from Golestan were 150 (135-165) and 161 (144-183) $\mu\text{g/L}$ ($P = 0.003$).

DISCUSSION

Shamberger and Frost first suggested a role for selenium in the prevention of cancer in 1969, when they observed an inverse association between the geographic distribution of selenium in forage crops and cancer mortality rates in the United States^[13]. A growing body of evidence, from both laboratory and epidemiologic studies, has since shown that selenium may have anticarcinogenic effects, especially against cancers of the lung, prostate, skin, and gastrointestinal system^[14,15].

In this study, we measured serum selenium in 300 Iranian adults from four provinces with varying risks of EC and GC to have a preliminary assessment of the hypothesis that the high rates of EC in Golestan and GC in Ardabil may be partly attributable to selenium deficiency. The proportion of the populations with a serum selenium more than $90\ \mu\text{g/L}$ (the concentration at which the serum selenoproteins are saturated) was 100% in Golestan, Kerman, and Mazandaran, and these three provinces had medium to high concentrations of serum selenium compared with the other areas of the world. Therefore, it is unlikely that high incidence of EC in Golestan and Mazandaran is due to selenium deficiency. This is consistent with a case-control study in Mazandaran that did not find any difference in hair selenium between EC cases and controls^[16]. In Ardabil, however, only 29% of the population had a serum selenium concentration above $90\ \mu\text{g/L}$. This suggests that the high incidence of GC and pre-neoplastic gastric lesions in Ardabil^[10] could be partly due to selenium deficiency.

This is the first study that has examined serum selenium concentrations in different Iranian populations. Median serum selenium ranged widely, from $82\ \mu\text{g/L}$ in Ardabil to $155\ \mu\text{g/L}$ in Golestan. The median serum selenium concentration in these four provinces combined, weighted for the population of each province, was $123\ \mu\text{g/L}$. For comparison, median serum selenium in other areas of the world varies from very low concentrations ($< 50\ \mu\text{g/L}$) in some parts of China and Serbia to very high concentrations ($> 200\ \mu\text{g/L}$) in parts of the USA and some other regions of China. However, the majority of median serum selenium concentrations in the world range from $80\text{--}120\ \mu\text{g/L}$ ^[17].

The wide range of serum selenium concentrations among the four provinces and its small range within each province was an interesting finding. The major predictor of serum selenium is dietary intake^[14,17], and the observed differences

Table 1 Distribution of age, sex, location, and serum selenium in study sample

Province	Number of samples	Median age (yr)	Male (%)	Urban (%)	Annual incidence of EC/10 ⁵	Annual incidence of GC/10 ⁵	Median serum selenium (IQR) in $\mu\text{g/L}$
Ardabil	100	49	49 (49)	49 (49)	15	38	82 (75-94)
Mazandaran	50	35	24 (48)	50 (100)	19	22	123 (111-132)
Golestan	100	50	51 (51)	51 (51)	40	18	155 (141-173)
Kerman	50	33	26 (52)	50 (100)	3	8	119 (110-128)
Total	300	45	150 (50)	200 (67)	-	-	123 ¹

¹A weighted median based on the total population of each province.

among the provinces are most likely due to variation in the selenium content of their diets.

We plan to conduct further observational studies to confirm or refute the association of selenium intake and the risk of GC in Ardabil.

REFERENCES

- 1 **Parkin DM**, Bray F, Ferlay J, Pisani P. Estimating the world cancer burden: Globocan 2000. *Int J Cancer* 2001; **94**: 153-156
- 2 **Blot WJ**, Li JY, Taylor PR, Guo W, Dawsey S, Wang GQ, Yang CS, Zheng SF, Gail M, Li GY. Nutrition intervention trials in Linxian, China: supplementation with specific vitamin/mineral combinations, cancer incidence, and disease-specific mortality in the general population. *J Natl Cancer Inst* 1993; **85**: 1483-1492
- 3 **Knekt P**, Aromaa A, Maatela J, Alfthan G, Aaran RK, Hakama M, Hakulinen T, Peto R, Teppo L. Serum selenium and subsequent risk of cancer among finnish men and women. *J Natl Cancer Inst* 1990; **82**: 864-868
- 4 **Mark SD**, Qiao YL, Dawsey SM, Wu YP, Katki H, Gunter EW, Fraumeni JF Jr, Blot WJ, Dong ZW, Taylor PR. Prospective study of serum selenium levels and incident esophageal and gastric cancers. *J Natl Cancer Inst* 2000; **92**: 1753-1763
- 5 **Wei WQ**, Abnet CC, Qiao YL, Dawsey SM, Dong ZW, Sun XD, Fan JH, Gunter EW, Taylor PR, Mark SD. Prospective study of serum selenium concentrations and esophageal and gastric cardia cancer, heart disease, stroke, and total death. *Am J Clin Nutr* 2004; **79**: 80-85
- 6 **Mahboubi E**, Kmet J, Cook PJ, Day NE, Ghadirian P, Salmasizadeh S. Oesophageal cancer studies in the Caspian Littoral of Iran: the caspian cancer registry. *Br J Cancer* 1973; **28**: 197-214
- 7 **Sadjadi A**, Malekzadeh R, Derakhshan MH, Sepehr A, Nouraei M, Sotoudeh M, Yazdanbod A, Shokoohi B, Mashayekhi A, Arshi S, Majidpour A, Babaei M, Mosavi A, Mohagheghi MM, Alimohammadian M. Cancer occurrence in Ardabil: Results of a population-based cancer registry from Iran. *Int J Cancer* 2003; **107**: 113-118
- 8 **Saidi F**, Sepehr A, Fahimi S, Farahvash MJ, Salehian P, Esmailzadeh A, Keshoofy M, Pirmoazen N, Yazdanbod M, Roshan MK. Oesophageal cancer among the turkomans of northeast Iran. *Br J Cancer* 2000; **83**: 1249-1254
- 9 Iranian Disease Prevention and Control Department. Cancer Incidence in Iran. Tehran: *Ministry of Health and Medical Education* 2000: 6
- 10 **Malekzadeh R**, Sotoudeh M, Derakhshan MH, Mikaeli J, Yazdanbod A, Merat S, Yoonessi A, Tavangar M, Abedi BA, Sotoudehmanesh R, Pourshams A, Asgari AA, Doulatshahi S, Alizadeh BZ, Arshi S, Madjidpour A, Mir MS, Fleischer DE. Prevalence of gastric precancerous lesions in Ardabil, a high incidence province for gastric adenocarcinoma in the northwest of Iran. *J Clin Pathol* 2004; **57**: 37-42
- 11 Agency for Toxic Substance and Disease Registry. Toxicological Profile for Selenium. Atlanta, GA: *U.S. Department of Health and Human Services* 2001
- 12 Panel of dietary antioxidants and related compounds. Selenium. In: Panel of dietary antioxidants and related compounds, eds. Dietary reference intakes for vitamin C, vitamin E, selenium, and carotenoids. Washington DC: *National Academy Press* 2000: 284-324
- 13 **Shamberger RJ**, Frost DV. Possible protective effect of selenium against human cancer. *Can Med Assoc J* 1969; **100**: 682
- 14 **Combs GF Jr**, Gray WP. Chemopreventive agents: selenium. *Pharmacol Ther* 1998; **79**: 179-192
- 15 **Combs GF Jr**, Lü JX. Selenium as a cancer preventive agent. In: Hatfield DL, ed. Selenium: Its molecular biology and role in human health. Norwell, MA: *Kluwer Academic Publishers* 2001: 205-217
- 16 **Azin F**, Raie RM, Mahmoudi MM. Correlation between the levels of certain carcinogenic and anticarcinogenic trace elements and esophageal cancer in northern Iran. *Ecotoxicol Environ Saf* 1998; **39**: 179-184
- 17 **Alfthan G**, Neve J. Reference values for serum selenium in various areas-evaluated according to the TRACY protocol. *J Trace Elem Med Biol* 1996; **10**: 77-87

Edited by Chen WW Proofread by Xu FM

Changes of mRNA expression of enkephalin and prodynorphin in hippocampus of rats with chronic immobilization stress

Jia-Xu Chen, Wei Li, Xin Zhao, Jian-Xin Yang, Hong-Yan Xu, Zhu-Feng Wang, Guang-Xin Yue

Jia-Xu Chen, Wei Li, Xin Zhao, Jian-Xin Yang, Hong-Yan Xu, Zhu-Feng Wang, Guang-Xin Yue, School of Basic Medical Science, Beijing University of Traditional Chinese Medicine, Beijing 100029, China
Supported by the National Natural Science Foundation of China, No. 30000216, Teaching and Research Award Program for Outstanding Young Teachers in Higher Education Institutes of Ministry of Education, China, Foundation for the Authors of National Excellent Doctoral Dissertations of China, No. 200059, and Fok Ying Tong Education Foundation, No. 81037

Correspondence to: Dr. Jia-Xu Chen, Deputy of TCM Diagnosis Department, Beijing University of Traditional Chinese Medicine, Beijing 100029, China. chenjiayu@hotmail.com

Telephone: +86-10-64287074

Received: 2003-12-23 **Accepted:** 2004-01-16

Abstract

AIM: To observe the changes of enkephalin mRNA and prodynorphin mRNA in hippocampus of rats induced by chronic immobilization stress.

METHODS: Thirty rats were randomly divided into three groups of 10 each: the normal control group (group A), the group induced by chronic immobilization stress for 7 d (group B) and the group induced by chronic immobilization stress for 21 d (group C). The changes of the enkephalin mRNA and prodynorphin mRNA in the rat hippocampus were detected by reverse transcription-polymerase chain reaction (RT-PCR).

RESULTS: Expression levels of enkephalin mRNA and prodynorphin mRNA in rat hippocampus were significantly increased under chronic immobilization stress, and the expression of prodynorphin mRNA in the rat hippocampus in group C was remarkably higher than that in group B (0.624 ± 0.026 ; $n = 5$; $P < 0.01$).

CONCLUSION: The increased enkephalin mRNA and prodynorphin mRNA gene expressions in rat hippocampus were involved in chronic stress.

Chen JX, Li W, Zhao X, Yang JX, Xu HY, Wang ZF, Yue GX. Changes of mRNA expression of enkephalin and prodynorphin in hippocampus of rats with chronic immobilization stress. *World J Gastroenterol* 2004; 10(17): 2547-2549
<http://www.wjgnet.com/1007-9327/10/2547.asp>

INTRODUCTION

It is known that exposure to a variety of stressors can lead to the increase of plasma β -endorphin up to 10-15 times higher than normal. β -endorphin, enkephalin and dynorphin are termed as opioid peptides that are likely to exert influence on emotional and psychological state. Endogenous opioid peptides are extensively involved in the modulation of stress^[1] and regulation between central nervous system and immune system. We found that immune function was changed markedly (IL-1 β in serum was increased, while IL-2 and IL-6 in serum were decreased) in

rats under chronic immobilization stress^[2]. The average optical density of glucocorticoid receptor (GR) in hippocampus CA₁ and parietal lobe cortex was markedly increased after 7 d immobilization stress (180 min daily) exposure in comparison with normal control, but it was declined to the normal level after 21 d of stress exposure; the level of plasma adrenocorticotropin (ACTH) and serum cortisol had similar changes to that of GR^[3]. Are the opioid peptides in hippocampus implicated for the regulation of immune and internal secretion function under restrain stress? Here, we used animal models induced by chronic immobilization stress to observe the characteristic changes of expression of enkephalin mRNA and prodynorphin mRNA with reverse transcription-polymerase chain reaction (RT-PCR) in rat hippocampus.

MATERIALS AND METHODS

Subjects

Thirty male, Sprague-Dawley rats, weighing 180-220 g, were supplied by the Research Center of Experimental Animals "Weitong Lihua" in Beijing, with qualified certification No: SCXK-BJ2002-0003. They were randomly divided into three groups of 10 each: the normal control group (group A), the model group of 7 d (group B) and the model group of 21 d (group C). The rats were housed in groups of 5 rats in each cage and provided free access to food and water (20-24 °C, relative humidity of 30-40%).

All experiments conformed to the guidelines of NIH on the ethical use of animals. All efforts were made to minimize the animal suffering and maintain the number of animals necessary to produce reliable data.

Modeling methods

A T-form bound brace (self-made) was used: A frame with length of 20 cm and width of 10 cm and thickness of 2.8 cm was prepared. Its upper platform was of 22 cm in length and 6.6 cm in its widest part. A small frame for fixing the rat's head at the front end and grooves for rat's limbs were adapted. In the upper platform three adaptable soft bands, of which two are wide and one is thin, for fixing the rat in the head and neck, chest and loins, loins and back respectively were added. Means of chronic binding were applied in order to create stress models of rats. The rats were immobilized in the above-noted binding brace for 3 h daily and for either 7 or 21 consecutive days.

Extraction and measurement of total RNA

Extraction of total RNA of rat hippocampus: Rats were decapitated at the end of modeling and hippocampus tissues were rapidly taken bilaterally out and placed on the ice-plate. The tissues of 50-100 mg were mixed with 1 mL pre-cold TRIzol (Gibco) and were sufficiently ground in the appliance for grinding tissue. The homogenates produced were thereafter placed in ice for 5 min. Homogenates of hippocampus were added into 0.2 mL chloroform and drastically agitated for 15 s and placed in ice for 2-3 min. The resulting solution was then centrifuged at 12 000 g for 15 min. Supernatant was taken out and mixed with 0.5 mL isopropanol and placed for 5-10 min at room temperature. The resulting solution was then centrifuged at 12 000 g for 10 min at 4 °C and the supernatant produced was then removed. The

sediment was rinsed with 0.5 mL of 750 mL/L freshly made alcohol solution and centrifuged at 7 500 r/min for 5 min at 4 °C and the resulting supernatant was then removed. The sediment was dried at room temperature and then dissolved by 1 g/L diethyl pyrocarbonate (Sigma), in order to produce a concentration at which 1 µg RNA was resolved in 1 mL water.

Total RNA detection by electrophoresis

A 2-µL sample of the total RNA extracted was demonstrated by electrophoresis on 10 g/L agarose gel under constant voltage for 20 min. The strips of 28S, 18S and 5S were observed in the gel image system.

Quantification and purity identification of RNA

Certain amount of RNA sample was diluted (10- or 20- fold) and its concentration and purity were measured by ultraviolet spectrophotometer. Measurement of absorbance A_{260} was chosen to count the concentration of RNA (µg/µL) and ratios of A_{260}/A_{280} were chosen for its purity which was required as 1.8-2.0. Therefore, RNA with ratios less than 1.7 was deserted.

PCR primer design

Primers of β -actin, enkephalin and prodynorphin, of which β -actin was taken as inner-control of quasi-quantification PCR, were respectively designed by the software of Primer 5.0 according to the sequence of GenBank and synthesized by Sanboyuanzhi Company. Sequences of primers were as follows: β -actin: Primer of the upper stream: 5'-CATCTCTTGCTCGAAG TCCA-3', Primer of the down stream: 5'-ATCATGTTTGAGAC CTTCAACA-3'. Enkephalin: Primer of the upper stream: 5'-ATGGCGTTCCTGAGACTTTGA-3', Primer of the down stream: 5'-TAGAGTTTTGGCGTATTTTCGGAGGC-3'. Prodynorphin: Primer of the upper stream: 5'-ATGGCGTGGTCCAGGCTGATGC-3', Primer of the down stream: 5'-AGTTTGTTAGATTTA GAAGCCTTATCC-3'. Genes of enkephalin (810 bp) and prodynorphin (747 bp) were respectively amplified.

Reverse transcription reaction

A sample of RNA was kept at constant temperature of 70 °C for 10 min, centrifuged for several seconds and then placed in a water-bath. The following reaction (20 µL) happened in the centrifugal tube of PCR of 0.5 mL: 1 µL random primer 50 ng/µL; 1 µL dNTP (10 mmol/L) (Promega); 4 µL 5×RT buffer; 1 µL mixed solution of reverse transcriptase; 2 µL RNA sample; 1 µL DEPC-ddH₂O. The above-noted reaction system was placed at room temperature for 10 min and kept at constant temperature of 37 °C for 30 min, at 95 °C for 5 min, and then at 4 °C for 3 min prior to next procedures.

Amplification of target DNA by PCR

Enkephalin and prodynorphin were respectively amplified by PCR (PCT-100TM Programmable Thermal Controller, product of MJ RESEARCH, INC, America). The following materials were included in a 50 µL reaction system: 6 µL RT reaction product; 4.5 µL 10×PCR buffer; 1 µL dNTP (10 mmol/L); 1 µL (50 pmol) sense primer (enkephalin or prodynorphin); 1 µL (50 pmol) antisense primer (enkephalin or prodynorphin); 1 µL *Taq* DNA polymerase (Promega); 35.5 µL DEPC-ddH₂O. In the meantime, primer of enkephalin or prodynorphin was replaced by β -actin to perform PCR reaction with the rest reaction system noted above. The above systems were sufficiently mixed and centrifuged, then PCR reactions performed after adding 50 µL light mineral oil.

Temperatures of 46, 52 and 58 °C were respectively chosen as annealing temperature, so that three of them would be able to be used for amplification, while non-specific DNA segments would not occur. The last condition of optimized reaction was as follows: pre-degeneration at 94 °C for 3 min, tempering at

52 °C and extension at 72 °C, for 30 cycles, thereafter extension at 72 °C for another 15 min.

Amplified product was detected with 10 g/L agarose gel electrophoresis and analyzed with gel image analysis system FIT-5000 (Sweden). Ratio of optical density of the target genes and ratio of optical density of β -actin, which can be expressed as a stable value in the tissue (and it was therefore taken as interior control strip), were employed as data for quasi-quantified analysis.

Statistical analysis

Data were expressed as mean±SD and software of SPSS was applied for statistical analysis. ANOVA was performed for comparison among groups and followed by a post-hoc test. Significance was accepted at $P<0.05$.

RESULTS

General state of rats

Rats manifested symptoms such as lassitude, fewer activities, no gloss in hair, decreased food intake and loose stools.

Electrophoresis of total RNA

Three strips of 28S, 18S and 5S were observed after the extraction of the total RNA from the rat hippocampus with TRIzol RNA and electrophoresis.

Results of PCR amplification

Corresponding strips of target DNA were obtained via reverse transcription and PCR. The length of the strip of β -actin DNA was 300 bp, that of the enkephalin was 810 bp and that of the prodynorphin was 747 bp.

The expression of enkephalin mRNA was mildly increased in the rat hippocampus of group A, and significantly increased in the rat hippocampus of group C ($P<0.01$, $P<0.05$) when compared with rats in group A and B, respectively. The expression of prodynorphin mRNA was significantly increased in the rat hippocampus of group B and C when compared with rats in group A ($P<0.01$). The expression of prodynorphin mRNA in the rat hippocampus in group C was remarkably higher than that in group B ($P<0.01$). The results are shown in Table 1.

Table 1 Expression of enkephalin mRNA and prodynorphin mRNA in rat hippocampus ($n = 5$, mean ±SD)

Group	Enkephalin mRNA	Prodynorphin mRNA
A	0.284±0.013	0.360±0.017
B	0.308±0.018	0.492±0.036 ^b
C	0.352±0.028 ^{bc}	0.624±0.026 ^{bd}

Statistical analyses were performed by analysis of variance and post-hoc test. ^b $P<0.01$ vs group A; ^c $P<0.05$, ^d $P<0.01$ vs group B.

DISCUSSION

Endogenous opioid peptides, which mainly include enkephalin family (methionine enkephalin and leucine enkephalin), endorphin family (α -endorphin, β -endorphin and γ -endorphin) and dynorphin family (dynorphin A and dynorphin B), are one class of matters with opioid action, naturally generated in the brain of mammals. It has been reported that endogenous opioid peptides are extensively involved in the regulation of stress and exert important effect on mediating the central nervous system and immune system^[4-7].

The increased expression of opioid peptides including enkephalin mRNA and prodynorphin mRNA in our study, may influence hippocampal function and facilitate long-term depression (LTD) of the Schaffer collateral input to CA1 pyramidal neurons^[8]. Chronic stress increased the synthesis

of opioid peptides in the nervous system and increased plasma glucocorticoid^[9].

Enkephalin is extensively distributed inside the brain as a kind of endogenous opioid peptides. It plays several roles in analgesia, cardiovascular, respiratory and body temperature regulation via receptors of endogenous opioid peptides including widespread immunity modulation after it is generated and released. In addition, enkephalin can exert its effect on regulating the immune functions of body under both normal and stress conditions. Both methionine enkephalin and leucine enkephalin can influence the activity and the formation rate of rosettes of T lymphocyte, as well as the activity of natural killer cells in the body under physiological conditions^[6,10]. The mechanism of enkephalin involved in regulating immunity under physiological conditions has yet to be clarified. More researches have focused on the mechanism of enkephalin in regulating immunity in different stress situations. Researches suggested that methionine enkephalin and leucine enkephalin could markedly inhibit the cytotoxic action that can be stopped by naloxone, a substance that is produced by the natural killer cells, under the stress induced by electric shock in rats. Therefore, endogenous opioid peptides played an important role in immune regulation stimulated by stress^[11,12].

Hippocampus is a crucial structure in which enkephalin can regulate immune function via IL-1 α . A spleen lymphocyte proliferation reaction stimulated by Canavalia protein A could be markedly reinforced by microinjection of methionine enkephalin and leucine enkephalin into rat hippocampus (similar result obtained in the experiment of mice)^[13]. The inhibitive effect of enkephalin on IL-1 gene expression of the glia cell in hippocampus may shed lights on the mechanisms involved in the immunological amplification by microinjection of enkephalin, which inhibits gene expression of IL-1 α via opioid receptors in glia cells of hippocampus or in certain nerve cell membranes that possess the capacity of generating IL-1 α , and result in decreased activating effect of IL-1 α on the hypothalamus-pituitary-adrenal axis together with decreased synthesis of IL-1 α inside the brain, and simultaneous strengthening of the immune function of body by decreasing the blood plasma corticoid^[14-16].

It was demonstrated in the present study that expression of enkephalin mRNA was mildly increased after 7 d and significantly increased after 21 d under the conditions of chronic immobilization. In general, increase of enkephalin will result in poorer immune function. In line with our former research^[2], the substantial decrease of the transforming function of the spleen lymphocytes in rats most likely originated from the indirect inhibitive action of enkephalin. It means that the increase of enkephalin would inhibit gene expression of central IL-1 α and is likely to result in lower IL-1 α inside the brain.

Prodynorphin, containing the sequence of leucine enkephalin at N-terminal which was considered as its precursor at first, is another member of the endogenous opioid peptides with analogous distribution inside the brain in striatum, hippocampus and hypothalamus. It also exists in adrenal glands and genital organs. The splitting process of prodynorphin is complicated and its main products include dynorphin A₁₋₁₇, dynorphin B₁₋₂₉, dynorphin A₁₋₈ and neo-endorphin. In addition, generation of prodynorphin mRNA is affected by multiple factors in many regions of brain. For instance, gamma-aminobutyric acid (GABA) can decrease its generation in neo-striatum.

With dual action, dynorphin can not only protect, but also damage the nerve cells in some cases. It was indicated that the expression of prodynorphin in rat hippocampus was significantly increased and its change was likely to be earlier than that of

enkephalin under the condition of chronic immobilization stress. Taken together our previous and current experiments, increase of dynorphin is likely to result in certain nerve damage as fewer numbers of brain-derived neurotrophic factors (BDNF) and neurotrophin 3 (NT₃) might exert fewer protective effects on the nervous system under chronic immobilization stress. Whether and how dynorphin correlates with neurotrophins have yet to be established.

ACKNOWLEDGEMENTS

We greatly thank Qing-Hong Chen and Ioannis Solos for their kindly correcting grammar, spelling and punctuation of the manuscript.

REFERENCES

- 1 **Vaccarino AL**, Kastin AJ. Endogenous opiates: 1999. *Peptides* 2000; **21**: 1975-2034
- 2 **Li W**, Chen JX, Yang JX, Zhao X, Tang YT, Liu XL, Xu HY. The effect of compounds of soothing liver, invigorating spleen, tonifying kidney on the praxiology and immunological function of chronic immobilization stressed rats. *Acta Laboratorium Animalis Scientia Sinica* 2003; **11**: 33-37
- 3 **Tang YT**, Chen JX. Regulative effects of three TCM formulas on hypothalamus-pituitary-adrenal axis in the rats with chronic restrained stress. *J Beijing Univ Traditional Chine Med* 2002; **25**: 23-26
- 4 **Harbuz MS**, Lightman SL. Responses of hypothalamic and pituitary mRNA to physical and psychological stress in the rat. *J Endocrinol* 1989; **122**: 705-711
- 5 **Lightman SL**, Young WS 3rd. Influence of steroids on the hypothalamic corticotropin-releasing factor and preproenkephalin mRNA responses to stress. *Proc Natl Acad Sci U S A* 1989; **86**: 4306-4310
- 6 **Plotnikoff NP**, Murgu AJ, Miller GC, Corder CN, Faith RE. Enkephalins: immunomodulators. *Fed Proc* 1985; **44**: 118-122
- 7 **Kurumaji A**, Takashima M, Shibuya H. Cold and immobilization stress-induced changes in pain responsiveness and brain Met-enkephalin-like immunoreactivity in the rat. *Peptides* 1987; **8**: 355-359
- 8 **Wagner J**, Etemad LR, Thompson AM. Opioid-mediated facilitation of long-term depression in rat hippocampus. *J Pharmacol Exp Ther* 2001; **296**: 776-781
- 9 **Ahima RS**, Garcia MM, Harlan RE. Glucocorticoid regulation of preproenkephalin gene expression in the rat forebrain. *Brain Res Mol Brain Res* 1992; **16**: 119-127
- 10 **Miller GC**, Murgu AJ, Plotnikoff NP. Enkephalins-enhancement of active T-cell rosettes from normal volunteers. *Clin Immunol Immunopathol* 1984; **31**: 132-137
- 11 **Devi RS**, Namasivayam A, Prabhakaran K. Modulation of non-specific immunity by hippocampal stimulation. *J Neuroimmunol* 1993; **42**: 193-197
- 12 **Shavit Y**, Lewis JW, Terman GW, Gale RP, Liebeskind JC. Opioid peptides mediate the suppressive effect of stress on natural killer cell cytotoxicity. *Science* 1984; **223**: 188-190
- 13 **Ban E**, Milon G, Prudhomme N, Fillion G, Haour F. Receptors for interleukin-1 (alpha and beta) in mouse brain: mapping and neuronal localization in hippocampus. *Neuroscience* 1991; **43**: 21-30
- 14 **Blalock JE**. The syntax of immune-neuroendocrine communication. *Immunol Today* 1994; **11**: 504-511
- 15 **Payne LC**, Weigent DA, Blalock JE. Induction of pituitary sensitivity to interleukin-1: a new function for corticotropin-releasing hormone. *Biochem Biophys Res Commun* 1994; **198**: 480-484
- 16 **Wang AJ**, Yang YZ, Wu YM, Xie H, Hu MX, Gao N, Hong J, Sun CL. Effect of intrahippocampal microinjection of enkephalin on cellular immune function and brain IL-1 alpha gene expression in rat. *Acta Physiologica Sinica* 1996; **48**: 348-354

Differentiation of dermis-derived multipotent cells into insulin-producing pancreatic cells *in vitro*

Chun-Meng Shi, Tian-Min Cheng

Chun-Meng Shi, Tian-Min Cheng, Institute of Combined Injury, Third Military Medical University, 30 Gaotanyan street, 400038, Chongqing City, China

Supported by the National Key Basic Research Project, No. 1999054205

Correspondence to: Dr. Chun-Meng Shi, Institute of Combined Injury, Third Military Medical University, Gaotanyan 400038, Chongqing City, China. shicm@sina.com

Telephone: +86-23-68752355 **Fax:** +86-23-68752279

Received: 2003-12-28 **Accepted:** 2004-01-15

Abstract

AIM: To observe the plasticity of whether dermis-derived multipotent cells to differentiate into insulin-producing pancreatic cells *in vitro*.

METHODS: A clonal population of dermis-derived multipotent stem cells (DMCs) from newborn rat with the capacity to produce osteocytes, chondrocytes, adipocytes and neurons was used. The gene expression of cultured DMCs was assessed by DNA microarray using rat RGU34A gene expression probe arrays. DMCs were further cultured in the presence of insulin complex components (Insulin-transferrin-selenium, ITS) to observe whether DMCs could be induced into insulin-producing pancreatic cells *in vitro*.

RESULTS: DNA microarray analysis showed that cultured DMCs simultaneously expressed several genes associated with pancreatic cell, neural cell, epithelial cell and hepatocyte, widening its transcriptomic repertoire. When cultured in the specific induction medium containing ITS for pancreatic cells, DMCs differentiated into epithelioid cells that were positive for insulin detected by immunohistochemistry.

CONCLUSION: Our data indicate that dermal multipotent cells may serve as a source of stem/progenitor cells for insulin-producing pancreatic cells.

Shi CM, Cheng TM. Differentiation of dermis-derived multipotent cells into insulin-producing pancreatic cells *in vitro*. *World J Gastroenterol* 2004; 10(17): 2550-2552
<http://www.wjgnet.com/1007-9327/10/2550.asp>

INTRODUCTION

Organ-specific stem cells possess plasticity that can permit differentiation along new lineages and have significant implications for future therapies of diabetes. The production of endocrine pancreas and insulin-secreting beta cells from adult nonpancreatic stem cells and hepatic oval stem cell has been demonstrated^[1,2]. Zulewski *et al.* also showed that pancreatic islets contained a heretofore unrecognized distinct population of cells that expressed the neural stem cell-specific marker nestin. The nestin-positive islet-derived progenitor (NIP) cells are a distinct population of cells that reside within pancreatic islets and may participate in the neogenesis of islet endocrine

cells^[2]. According to this result, liver stem cells have been proved to differentiate into pancreatic islet-like cells^[3]. Dermis is a highly accessible tissue source for adult stem cells. Nestin-positive skin-derived stem cells have been isolated from dermis by Toma *et al.*^[4]. In our previous study, we isolated a clonal population of dermal multipotent cells by their adherence to tissue culture plastic (termed as plastic adherent DMCs) from newborn rat dermis. These cells showed the differentiation capacity to produce nestin-positive cells^[5]. In this study, we aimed to investigate whether plastic adherent DMCs had the differentiation capacity to produce insulin-producing pancreatic cells *in vitro*.

MATERIALS AND METHODS

Materials

A clonal population of dermis-derived multipotent stem cells (DMCs) was used in the experiments. The clonal population of DMCs were isolated and identified from primary dermal cells of male newborn Wistar rat as previously described^[5]. All tissue culture reagents, including Iscove's Modified Dulbecco's Medium (IMDM), ITS (insulin-transferrin selenium), epidermal growth factor, basic fibroblast growth factor, were purchased from Sigma (St. Louis, CA, USA). Fetal bovine serum (FBS) was purchased from Hyclone (Logan, UT, USA). The rat RGU34A gene expression probe arrays were purchased from Affymetrix (Santa Clara, CA). Mouse anti-insulin monoclonal antibody was purchased from Sigma (St. Louis, CA, USA). Horseradish peroxidase (HRP)-labeled goat anti-mouse IgG antibody was purchased from Boster (Wuhan, China).

Methods

Cell culture The DMCs were cultured in IMDM medium containing 10 mL/L fetal bovine serum and 100 U/mL penicillin and 100 µg/mL streptomycin. Cultures were maintained at 37 °C in a humidified atmosphere containing 50 mL/L CO₂. For differentiation induction, DMCs were transferred into specific inducing medium containing 10 µg/mL of keratocyte growth factor (KGF), 20 ng/mL of epidermal growth factor (EGF), 10 mmol/L of nicotinamide, and 1 mg/mL of ITS. The differentiated cells were examined for the insulin expression by immunohistochemistry.

DNA Microarray analysis Total RNA from cultured DMCs was isolated using QIAGEN's RNeasy total RNA isolation kit (Rneasy, Qiagen) following the manufacture's instructions, and quantified. Transcript profiling was conducted by means of rat RGU34A gene expression probe arrays, containing 8 799 probe sets, interrogating primarily annotated genes. The experiment was conducted according to the recommendations of the manufacturer (Affymetrix GeneChip expression analysis manual). The resulting "data-file" was processed further using the microarray analysis suite 5 software package (Affymetrix). According to the statistical expression analysis algorithm, the presence of a gene within a given sample was determined at a detection *P* value of <0.05 and was graded as absent (*A*), marginal (*M*), or present/positive (*P*).

Immunocytochemistry Immunocytochemistry study with peroxidase-labeled streptavidin biotin method was performed to detect the expression of insulin in differentiated cells. Before

detection, the cells were washed three times for 20 min with phosphate-buffered saline (PBS, PH = 7.2) to exclude the pollution of exogenous insulin in the culture medium. After washing, the cells were blocked for 30 min with 100 mL/L normal goat serum in PBS and were incubated with mouse anti-insulin antibody (1:100) at 4 °C for 24 h. Incubation at room temperature with anti-mouse secondary antibody and avidin-biotinylated peroxidase complexes was performed for 2 h. The specimens were washed for 15 min with 0.01 mol/L PBS between all steps. The reaction product was developed with 0.5 g/L 3,3'-diaminobenzine tetrahydrochloride (DAB). After staining, the result was observed microscopically. PBS was used as a substitute for primary antibody as negative control.

RESULTS

Biological properties of DMCs

Most adherent DMCs were of spindle-shaped cells (Figure 1). Phenotype analysis showed that DMCs were negative for some lineage-specific surface markers, including pan-cytokeratin, cytokeratin19, factor VIII, CD31, CD45, CD34, α -smooth muscle actin (α -SMA), desmin, collagen II and nestin, but were positive for CD59, CD90, CD44, vascular cell adhesion molecule-1 (VCAM-1) and intercellular adhesion molecule-1 (ICAM-1). The doubling time of cultured DMCs was about 40 h. Following induction, DMCs had the capacity to differentiate into cells with phenotypic characteristics of osteocytes (alkaline phosphatase activity and alizarin red staining), adipocytes (oil red staining), chondrocytes (collagen II and Alcian blue staining) and neurons (nestin and NF-200 staining) in specific induction media.



Figure 1 Morphology of cultured DMCs. (Inverted microscope, $\times 100$).

Gene expression profile of plastic-adherent DMCs

The gene expression of DMCs was assessed by DNA microarray analysis and the harbinger of a potential cell type was viewed by simultaneous expression of a panel of lineage-related genes. The result revealed that the cultured DMCs simultaneously expressed genes associated with pancreatic cells (Table 1). DMCs also simultaneously expressed transcripts for epithelial cell, neural cell, and hepatocyte as well (Table 1). These transcripts were developmentally related with pancreatic tissue and further widened the transcriptomic repertoire of DMCs. To confirm the data by DNA microarray, several genes were further tested by RT-PCR and the result was consistent with the result from microarray (data not shown).

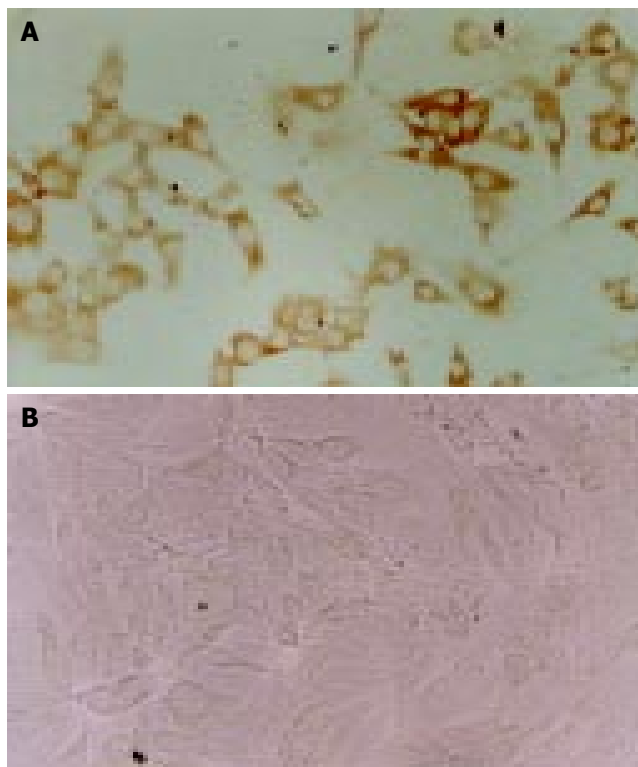


Figure 2 Differentiation of DMCs into insulin-producing cells. A: After induction in the medium containing ITS for 4 wk, cells were positive for insulin; B: Negative control (SP, $\times 200$).

Table 1 DMC gene lists (partial) associated with diverse cellular lineages

Cell lineage	Representative examples of associated genes
A: Pancreatic cell	Pancreatic eukaryotic initiation factor 2 alpha-subunit kinase (PEK), pancreatic secretory trypsin inhibitor-like protein (PSTI), pancreatic islet cDNA Rattus norvegicus cDNA similar to rapamycin-binding protein FKBP-13, insulin II gene, IRS-1 mRNA for insulin-receptor, mRNA for glucose-dependent insulinotropic polypeptide
B: Neural cell	Neural visinin-like Ca ²⁺ -binding protein type 3, neuron-specific enolase, neuronal nitric oxide synthase, GABA receptor-associated proteins, NCAM, brain-derived neurotrophic factor (BDNF), syntaxin 7, glial fibrillary acidic protein (GFAP), adrenomedullin, myelin protein SR13 (growth-arrest-specific Gas-3 homolog), neurotrimin; secretogranin II, synapse-associated protein 102, latexin, kexin-like protease PC7A, N-methyl-D-aspartate (NMDA) receptor
C: Epithelial cell	Epithelial membrane protein 1, epithelial cell transmembrane protein antigen precursor, epidermal growth factor precursor, heparin-binding EGF-like growth factor, mucin, parathyromosin and thy mosin 4 and 10
D: Hepatocyte	Liver glycogen phosphorylase enzyme, liver IL-6 receptor ligand binding chain, liver specific transcription factor LF-B, liver nuclear protein P47, liver α L-Fucosidase, hepatocyte nuclear factor 3 α (HNF-3beta)

Expression of a single gene can't define the phenotype of a particular cell type. Simultaneous expression of a panel of lineage-related genes in single isolated cell was viewed as the harbinger of a potential cell type. Representative examples of genes corresponding to each cell lineage are outlined in the above table.

Differentiation of DMCs into insulin-producing pancreatic cells

DMCs were further tested for their capacity to produce pancreatic cells in the inducing medium containing ITS. The morphology of DMCs were changed into epithelial cells-like cells when cultured in medium containing ITS for 2 wk and immunohistochemistry showed that a proportion of cells (less than 10 %) were positive for insulin when cultured in medium containing ITS for 4 wk (Figure 2). The negative control cells showed no positive staining for insulin. This result further indicated that DMCs could undergo differentiation to form insulin-producing cells.

DISCUSSION

Replacement of the insulin-producing pancreatic islet cells represents the ultimate treatment for type I diabetes. Recent advances in islet transplantation underscore the urgent need for developing alternatives to human tissue donors, which are scarce. The generation of insulin-producing cells from adult stem cells is one possible approach^[6-9]. Recent studies have suggested that there are closely developmental relationship between the nestin positive progenitors and the pancreatic cells^[10-13]. In addition to liver stem cells and neural stem cells, multipotent stem cells from dermis have been proved to have the capacity to produce nestin positive cells^[4,5]. In this study, we further reported that dermis-derived multipotent stem cells also showed a remarkable flexibility to differentiate into insulin-producing cells, when the appropriate stimuli were given. Since dermal cells are relatively easy to access and they also can be used for autologous use that may represent a safety advantage, dermis-derived multipotent cells may serve as a source of stem/progenitor cells for β cells.

Nevertheless, the efficiency of adult stem cells to differentiate into insulin-producing cells *in vitro* is low at present and expansion with large scale is needed for application. Genetic manipulation in tissue culture may be a choice and it is possible that new insights into endocrine pancreas development will lead to the manipulation of progenitor cell fate towards the β cell phenotype of insulin production, storage and regulated secretion^[14,15]. If successful, these approaches could lead to widespread cell replacement therapy for type I diabetes.

REFERENCES

- 1 Suzuki A, Zheng Yw YW, Kaneko S, Onodera M, Fukao K, Nakauchi H, Taniguchi H. Clonal identification and characterization of self-renewing pluripotent stem cells in the develop-

- ing liver. *J Cell Biol* 2002; **156**: 173-184
- 2 Zulewski H, Abraham EJ, Gerlach MJ, Daniel PB, Moritz W, Muller B, Vallejo M, Thomas MK, Habener JF. Multipotent nestin-positive stem cells isolated from adult pancreatic islets differentiate *ex vivo* into pancreatic endocrine, exocrine, and hepatic phenotypes. *Diabetes* 2001; **50**: 521-533
- 3 Meivar-Levy I, Ferber S. New organs from our own tissues: liver-to-pancreas transdifferentiation. *Trends Endocrinol Metab* 2003; **14**: 460-466
- 4 Toma JG, Akhavan M, Fernandes KJ, Barnabe-Heider F, Sadikot A, Kaplan DR, Miller FD. Isolation of multipotent adult stem cells from the dermis of mammalian skin. *Nat Cell Biol* 2001; **3**: 778-784
- 5 Shi C, Cheng T. Effects of acute wound environment on neonatal rat dermal multipotent cells. *Cells Tissues Organs* 2003; **175**: 177-185
- 6 Street CN, Rajotte RV, Korbitt GS. Stem cells: a promising source of pancreatic islets for transplantation in type 1 diabetes. *Curr Top Dev Biol* 2003; **58**: 111-136
- 7 Scharfmann R. Alternative sources of beta cells for cell therapy of diabetes. *Eur J Clin Invest* 2003; **33**: 595-600
- 8 Soria B, Skoudy A, Martin F. From stem cells to beta cells: new strategies in cell therapy of diabetes mellitus. *Diabetologia* 2001; **44**: 407-415
- 9 Pattou F, Kerr-Conte J, Gmyr V, Vandewalle B, Vantyghem MC, Lecomte-Houcke M, Proye C, Lefebvre J. Human pancreatic stem cell and diabetes cell therapy. *Bull Acad Natl Med* 2000; **184**: 1887-1899
- 10 Delacour A, Nepote V, Trumpp A, Herrera PL. Nestin expression in pancreatic exocrine cell lineages. *Mech Dev* 2004; **121**: 3-14
- 11 Esni F, Stoffers DA, Takeuchi T, Leach SD. Origin of exocrine pancreatic cells from nestin-positive precursors in developing mouse pancreas. *Mech Dev* 2004; **121**: 15-25
- 12 Humphrey RK, Bucay N, Beattie GM, Lopez A, Messam CA, Cirulli V, Hayek A. Characterization and isolation of promoter-defined nestin-positive cells from the human fetal pancreas. *Diabetes* 2003; **52**: 2519-2525
- 13 Lardon J, Rooman I, Bouwens L. Nestin expression in pancreatic stellate cells and angiogenic endothelial cells. *Histochem Cell Biol* 2002; **117**: 535-540
- 14 Suzuki T, Kadoya Y, Sato Y, Handa K, Takahashi T, Kakita A, Yamashina S. The expression of pancreatic endocrine markers in centroacinar cells of the normal and regenerating rat pancreas: their possible transformation to endocrine cells. *Arch Histol Cytol* 2003; **66**: 347-358
- 15 Ferber S, Halkin A, Cohen H, Ber I, Einav Y, Goldberg I, Barshack I, Seiffers R, Kopolovic J, Kaiser N, Karasik A. Pancreatic and duodenal homeobox gene 1 induces expression of insulin genes in liver and ameliorates streptozotocin-induced hyperglycemia. *Nat Med* 2000; **6**: 568-572

Edited by Kumar M Proofread by Xu FM

Heparin improves organ microcirculatory disturbances in caerulein-induced acute pancreatitis in rats

Marek Dobosz, Lucjanna Mionskowska, Stanislaw Haæ, Sebastian Dobrowolski, Dariusz Dymecki, Zdzislaw Wajda

Marek Dobosz, Lucjanna Mionskowska, Department of General and Gastroenterological Surgery, St. Vincent a'Paulo Hospital, Gdynia, Poland

Stanislaw Haæ, Sebastian Dobrowolski, Dariusz Dymecki, Zdzislaw Wajda, Department of General, Transplant and Endocrine Surgery, Medical University of Gdańsk, Poland

Supported by Medical University of Gdańsk, grant W-120, Poland
Correspondence to: Marek Dobosz, M.D., Ph.D., ul. Kossaka 2/7, 80-249 Gdańsk, Poland. marek-dobosz@wp.pl

Telephone: +48-58-6665540 **Fax:** +48-58-6665540

Received: 2004-02-06 **Accepted:** 2004-03-02

Abstract

AIM: Microcirculatory disturbances are important early pathophysiological events in various organs during acute pancreatitis. The aim of the study was to evaluate changes in microperfusion of the pancreas, liver, kidney, stomach, colon, skeletal muscle, and to investigate the influence of heparin on the organ microcirculation in caerulein-induced experimental acute pancreatitis.

METHODS: Acute pancreatitis was induced by 4 intraperitoneal injections of caerulein (Cn) (15 µg/kg). The organ microcirculation was measured by laser Doppler flowmetry. Serum interleukin 6 and hematocrit levels were analysed.

RESULTS: Acute pancreatitis resulted in a significant drop of microperfusion in all examined organs. Heparin administration (2×2.5 mg/kg) improved the microcirculation in pancreas (36.9±4% vs 75.9±10%), liver (56.6±6% vs 75.2±16%), kidney (45.1±6% vs 79.3±5%), stomach (65.2±8% vs 78.1±19%), colon (69.8±6% vs 102.5±19%), and skeletal muscle (59.2±6% vs 77.9±13%). Heparin treatment lowered IL-6 (359.0±66 U/mL vs 288.5±58 U/mL) and hematocrit level (53±4% vs 46±3%).

CONCLUSION: Heparin administration has a positive influence on organ microcirculatory disturbances accompanying experimental Cn-induced acute pancreatitis.

Dobosz M, Mionskowska L, Haæ S, Dobrowolski S, Dymecki D, Wajda Z. Heparin improves organ microcirculatory disturbances in caerulein-induced acute pancreatitis in rats. *World J Gastroenterol* 2004; 10(17): 2553-2556
<http://www.wjgnet.com/1007-9327/10/2553.asp>

INTRODUCTION

Pathophysiology of acute pancreatitis (AP) is heterogeneous and involves a complex cascade of events. Impaired tissue perfusion within the pancreatic gland is one of the early disorders accompanying the disease^[1,2]. Prolonged ischaemia and impaired tissue oxygenation, resulting from vasoconstriction, hemoconcentration, hypercoagulation, leukocyte adherence, increased vascular permeability, and interstitial oedema, play

an important role in the progression of the disease, leading to the development of pancreatic necrosis^[2-4]. Besides the pancreas, the microcirculatory disturbances, as a consequence of hypovolemia and systemic inflammatory response, are also observed in other organs^[1,5-8].

Although the hypovolemia and impairment of cardiac output can be normalized easily by vigorous fluid replacement, microcirculatory disturbances may be prevented merely by adequate fluid therapy, even though the cardiovascular parameters are stabilized at the baseline level^[9]. Various vasoactive mediators, as bradykinin, endothelin, thromboxan, platelet activating factor, and nitric oxide participate in the development of microcirculatory failure^[3,8]. In the last decade, the beneficial effect of therapeutic strategies in acute pancreatitis, affecting vasoactive mediators, is confirmed in several experimental studies.

One of the possible therapeutic agents, influencing microcirculatory disturbances by means of its anticoagulant and antiinflammatory properties, which could be applied in acute pancreatitis, is heparin. Some reports underlined beneficial impact of this well known polysaccharide on the course of the disease^[10-12]. In this study we examined whether heparin influenced splanchnic malperfusion in experimental caerulein-induced acute pancreatitis in rats.

MATERIALS AND METHODS

Animal models

The study was carried out on 34 male Wistar rats weighing 180-200 g. The rats were kept on a standard rat chow and fasted overnight before the experiment with water *ad libitum*. Acute pancreatitis was induced by four intraperitoneal injections of caerulein (Cn) (Sigma, St. Louis, USA) (15 µg/kg) in 1 mL of saline at 1h intervals: at the beginning, and consecutively after the first, second, and third hour of the experiment. Five hours after the first caerulein injection, rats were anaesthetized with pentobarbital sodium (40 mg/kg). Following the anaesthesia, a laparotomy was performed, and a fiberoptic probe of laser Doppler flowmeter (Periflux 4 001, Perimed Jarfalla, Sweden) was positioned against the surface of the pancreas, liver, kidney, stomach, colon, and skeletal muscle of thigh in order to estimate the organs' perfusion. Blood flow was measured in three different portions of each organ, the mean values were calculated, and presented as percent changes from basal values obtained in control rats (100%). After the measurements, blood was aspirated from the inferior caval vein for hematocrit and interleukin 6 tests, the pancreas was removed for microscopic evaluation, and the animals were exsanguinated.

The animals were randomly allocated into three groups: Group I ($n=10$), control; Group II ($n=12$), Cn-induced pancreatitis without treatment; and Group III ($n=12$), Cn-induced pancreatitis treated with heparin (Polfa, Warszawa, Poland) 2×2.5 mg/kg, given in the 3rd and 4th hafter the first Cn injection.

This study was approved by the Ethical Committee of the Medical University of Gdańsk.

Interleukin-6 functional assay

The IL-6 bioassay was performed using the IL-6 dependent

mouse hybridoma cell line B9 obtained from Dr. Lucien Aarden, Netherland Red Cross, Amsterdam. B9 cells were cultured in flat bottomed microtitre plates (10 000 cells/well) in the presence of serial dilutions of test sera. Starting serum dilutions were 1:10 for all specimens. After 48 h of incubation, proliferation of the B9 cells was measured using a rapid colorimetric MTT (tetrazolium) assay. The concentration of recombinant IL-6 producing half maximal proliferation was defined as one unit of activity, and the quantity of IL-6 in a serum sample was calculated by reference to a standard curve. Polyclonal anti-IL-6 antibody (Boehringer-Mannheim) was added into selected wells at concentrations: 1:10, 1:20, 1:50 in order to confirm the specificity of the assay. The antibody completely blocked IL-6 activity.

Statistical analysis

Data are presented as mean±SD. The differences between the groups were analysed by means of ANOVA test. Probability values less than 0.05 were considered significant.

RESULTS

Four intraperitoneal caerulein injections resulted in marked pancreatic oedema in all the rats. The microscopic examination revealed oedematous form of acute pancreatitis, with inter- and intralobular oedema, vacuolisation of parenchymal cells, and leukocyte infiltration within the pancreatic gland. No parenchymal necrosis was detected.

Microcirculatory values

Caerulein induced acute pancreatitis resulted in a significant drop of pancreatic microperfusion to 36.9±4% of basal values. Administration of heparin significantly improved the microcirculation of the pancreas up to 75.9±13%. Hepatic perfusion in rats with pancreatitis receiving no treatment was decreased to 56.6±6%, heparin injection raised this parameter to 75.2±16%. Renal blood flow in group II with pancreatitis was diminished to 45.1±6%, which was improved significantly with heparin treatment up to 79.3±15%. Microcirculatory values of stomach and colon wall in acute pancreatitis group were reduced to 65.2±8% and 69.8±6% respectively. Intraperitoneal injection of heparin caused improvement in the blood flow in stomach to 78.1±19%, and especially in colon to 102.55±19%. Similarly, skeletal muscle perfusion in rats with pancreatitis was significantly ameliorated after heparin administration from 59.2±3% to 77.9±13% (Figure 1).

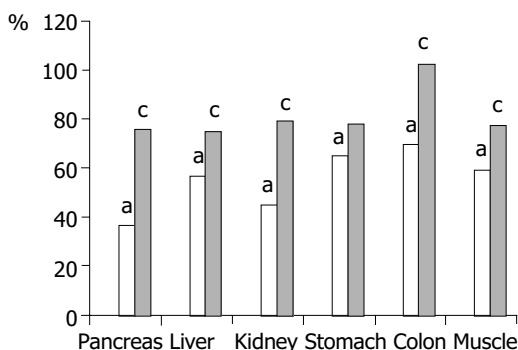


Figure 1 Microcirculatory parameters of pancreas, liver, kidney, stomach, colon and muscle (Mean values). Legend: grey bars: - control, white bars: - AP, black bars: - AP+heparin, ^a*P*<0.05 vs control, ^c*P*<0.05 vs AP group.

Serum interleukin 6 assay

Cn-induced acute pancreatitis caused a significant increase of serum IL-6 activity from 37.7±21 U/mL up to 359.0±66 U/mL in control rats. The heparin administration significantly diminished

IL-6 level to 288.5±58 U/mL (Table 1).

Hematocrit measurements

The mean hematocrit level of the control group without pancreatitis was 41±3%. In group II with Cn-induced pancreatitis the hematocrit was significantly increased to 53±4%. Heparin administration in animals with pancreatitis of group III significantly reduced the hematocrit to 46±3% (Table 1).

Table 1 Interleukin 6 and hematocrit levels in the three groups

Group	Interleukin 6 (U/mL)	Hematocrit (%)
Control	37.7±21	41±3
Acute pancreatitis	359.0±66 ^a	53±4 ^a
Acute pancreatitis + heparin	288.5±58 ^c	46±3 ^c

^a*P*<0.05 vs control, ^c*P*<0.05 vs acute pancreatitis group.

DISCUSSION

Caerulein-induced experimental pancreatitis was adopted by many authors to investigate microcirculatory changes of AP. The present study indicated that in Cn-induced acute pancreatitis the microperfusion of the pancreas decreased to 36.9% of basal values. These observations are in accordance with other investigations, which revealed the drop of local pancreatic blood flow in Cn induced pancreatitis^[2,13,14], although a majority of microcirculatory studies did not report such an obvious deterioration of the pancreatic perfusion as observed in the current study. Such a sharp decline of the pancreatic microperfusion might be influenced by the fact that the animals did not receive i.v. fluid administration, and could be elucidated also by an additional stress resulted from six i.p. injections of the drugs in conscious animals. In Liu's study^[14], the water immersion stress in rats with Cn-induced pancreatitis caused further pancreatic ischemia, diminishing the pancreatic blood flow to 37% of the normal value, and was considered as an aggravating factor in AP.

In contrast to these observations, the Heidelberg group described increased pancreatic capillary flow in experimental oedematous pancreatitis^[15,16]. The discrepancy of the results may be explained by various techniques of microcirculatory measurements and i.v. fluid administration. On the other hand, in the model of necrotizing pancreatitis, the authors observed a significant decrease of the pancreatic capillary flow^[16].

The disturbances of microcirculation in acute pancreatitis were not only confined to pancreatic capillary bed but were also observed in other organs^[5-8]. It was suggested that diffused microcirculatory disorders might play a crucial role in the development of the pancreatitis-associated multiorgan dysfunction syndrome^[7], some authors even defined severe AP as a systemic dysfunction syndrome^[7,17].

The present study confirmed these data. Besides the pancreas, reduced capillary perfusion was observed in liver, kidney, stomach, colon, and skeletal muscles, however the drop in perfusion of other organs was not so remarkable as in the pancreas. This suggests that in pancreatitis, pancreatic gland is especially susceptible to microcirculatory disorders. Kinnala *et al.* found that splanchnic malperfusion seemed to begin with pancreatic hypoperfusion before disturbances in gut microcirculation^[1]. On the other hand, Hotz *et al.* noted that in mild pancreatitis, pancreatic capillary perfusion remained unchanged, whereas mucosal and subserosal colonic capillary blood flow was significantly reduced. It was also shown in their experiment that severe pancreatitis was associated with a marked reduction in both pancreatic and colonic capillary perfusion^[18].

Microcirculatory disturbances in AP comprised many

components: decreased capillary blood flow and capillary density, increased capillary permeability, and enhanced leukocyte-endothelial interaction^[7]. It still remains unclear which of these factors is the initiating one or the most important. It seems to be logical that any effort to improve the microcirculation may be beneficial for all organs, irrespective of the underlying initiating factors.

Many studies documented positive impacts of various treatments on improving microcirculation in acute pancreatitis. In studies by Konturek *et al.* and Liu *et al.* pancreatic microperfusion was ameliorated with L-arginine (nitric oxide donor) treatment^[13,14]. Improvement of impaired pancreatic microcirculation by isovolemic hemodilution with dextran was observed by Klar *et al.*^[19]. Rheologic properties of pentoxifylline, its antiinflammatory effect, reduction of thrombus formation, and lowering of blood viscosity had a positive influence on Cn-induced pancreatitis in study of Gomez-Cambronero *et al.*^[20]. An advantageous effect of ICAM-1 antibodies on microcirculation in AP was shown by Foitzik *et al.*^[21], and Werner *et al.*^[22]. A single i.v. injection of bovine hemoglobin in an experiment by Strate *et al.* reduced microcirculatory dysfunction and pancreatic tissue damage in rodent pancreatitis^[4]. In a study by Zhao *et al.* Chinese natural medicines: Yuanhu (YHI) and Huoxuehuayu (HHI-I) had a positive impact on acute pancreatitis development, including pancreatic malperfusion and serum IL-6 level. Recently, it was shown that endothelin receptor blockade might be a promising therapeutic approach in AP, resulting in improvement of microcirculation, decreased capillary permeability and tissue injury^[7,23,24].

Intraperitoneal heparin administration in the current study significantly improved blood perfusion of examined organs. The beneficial effect of heparin on pancreatic microcirculation may in theory have an influence on severity of the disease, it could prevent or restrict the development of pancreatic necrosis. It was shown in our recent publication that heparin treatment in oedematous pancreatitis ameliorated the microscopic alterations of the pancreas: reduced leukocyte infiltration and diminished pancreatic oedema^[25].

By improving hepatic capillary blood flow, heparin could influence phagocytic Kupffer cell function in the liver which is important for eliminating antigens and toxic substances in acute pancreatitis. The study of Forgacs *et al.* showed a close relationship between liver phagocytic function and hepatic microperfusion in the early stage of experimental pancreatitis^[26]. On the other hand, Chen *et al.* revealed that a significant number of adherent leukocytes was observed in hepatic microcirculation 2 h after the induction of AP^[27]. This could impair hepatic perfusion, and might be a potential target for heparin treatment. In another study, Chen *et al.* observed beneficial effects of protease inhibitor gabexate mesilate on pancreatic and hepatic microcirculation^[8].

The pathophysiology of renal insufficiency, often observed as a complication of acute pancreatitis, is heterogeneous. The improvement of renal blood flow observed after heparin treatment in the rats with pancreatitis could also prevent this complication. Foitzik *et al.* using endothelin receptor blockers in severe acute pancreatitis, besides the enhancement of pancreatic perfusion, observed improved renal function^[7].

It was shown that decreased capillary blood flow in the colonic mucosa was associated with impaired gut barrier function and increased translocation of live bacteria through the morphologically intact colonic wall^[28]. The present study revealed that heparin treatment in the group with pancreatitis led the altered microperfusion of the colonic wall to the normal level. It suggests that heparin administration may play a role in prevention of secondary pancreatic infection.

Besides the organ microcirculatory improvement, heparin administration significantly decreased interleukin 6 activity,

and reduced hematocrit level. IL-6 was a reliable predictor of acute pancreatitis severity^[29]. Diminished IL-6 activity in the group with AP treated with heparin may indicate that this therapy could limit inflammatory response observed in AP. Beneficial influence of heparin on hematocrit level, observed in group III, may also suggest that heparin reduces capillary permeability, not just in the pancreatic gland, and prevent the fluid to the third space. Therefore heparin therapy may reduce the need for vigorous fluid resuscitation as applied in patients with AP.

The improvement of systemic microperfusion after heparin administration in rats with AP might be explained by its anticoagulatory effect which diminished blood viscosity and facilitated capillary blood flow. Besides its anticoagulant properties, heparin may play a positive role in AP treatment due to its antiinflammatory effects: TNF inhibition^[30], protection from oxygen free radicals^[31], the blockade of complement activity^[32] and histamine release^[33]. It was also shown that heparin prevented post-ischemic endothelial cell dysfunction^[34], neutrophil adhesion^[35], and had an inhibitory effect on the biosynthesis and release of endothelin-1, a very potent endogenous vasoconstrictor^[36,37].

In conclusion, heparin counteracts microcirculatory disorders, not only within the pancreas but also in other organs. The preservation of organ microperfusion with this treatment may be significant for diminishing and treating local and systemic complications in AP.

REFERENCES

- 1 **Kinnala PJ**, Kuttala KT, Gronroos JM, Havia TV, Nevalainen TJ, Niinikoski JH. Splanchnic and pancreatic tissue perfusion in experimental acute pancreatitis. *Scand J Gastroenterol* 2002; **37**: 845-849
- 2 **Zhou ZG**, Chen YD, Sun W, Chen Z. Pancreatic microcirculatory impairment in experimental acute pancreatitis in rats. *World J Gastroenterol* 2002; **8**: 933-936
- 3 **Zhou ZG**, Chen YD. Influencing factors of pancreatic microcirculatory impairment in acute pancreatitis. *World J Gastroenterol* 2002; **8**: 406-412
- 4 **Strate T**, Mann O, Kleinhans H, Schneider C, Knoefel WT, Yekebas E, Standl T, Bloechle C, Izibicki JR. Systemic intravenous infusion of bovine hemoglobin significantly reduces microcirculatory dysfunction in experimentally induced pancreatitis in the rat. *Ann Surg* 2003; **238**: 765-771
- 5 **Foitzik T**, Eibl G, Hotz B, Hotz H, Kahrau S, Kasten C, Schneider P, Buhr HJ. Persistent multiple organ microcirculatory disorders in severe acute pancreatitis: experimental findings and clinical implications. *Dig Dis Sci* 2002; **47**: 130-138
- 6 **Skoromnyi AN**, Starosek VN. Hemodynamic changes in the liver, kidney, small intestine and pancreas in experimental acute pancreatitis. *Klin Khir* 1998; **12**: 46-48
- 7 **Foitzik T**, Eibl G, Hotz HG, Faulhaber J, Kirchengast M, Buhr HJ. Endothelin receptor blockade in severe acute pancreatitis leads to systemic enhancement of microcirculation, stabilization of capillary permeability, and improved survival rates. *Surgery* 2000; **128**: 399-407
- 8 **Chen HM**, Hwang TL, Chen MF. The effect of gabexate mesilate on pancreatic and hepatic microcirculation in acute experimental pancreatitis in rats. *J Surg Res* 1996; **66**: 147-153
- 9 **Knol JA**, Inman MG, Strodel WE, Eckhauser FE. Pancreatic response to crystalloid resuscitation in experimental pancreatitis. *J Surg Res* 1987; **43**: 387-392
- 10 **Gabrylewicz A**, Kosidlo S, Prokopowicz J, Podkowicz K. Does heparin modify protease-antiprotease balance in acute experimental pancreatitis in rats. *Hepatogastroenterology* 1986; **33**: 79-82
- 11 **Goulbourne IA**, Watson H, Davies GC. 111In-platelet and 125I-fibrinogen deposition in the lungs in experimental acute pancreatitis. *J Surg Res* 1987; **43**: 521-526
- 12 **Rabenstein T**, Roggenbuck S, Framke B, Martus P, Fischer B, Nusko G, Muehldorfer S, Hochberger J, Ell C, Hahn EG, Schneider HT. Complications of endoscopic sphincterotomy:

- can heparin prevent acute pancreatitis after ERCP? *Gastrointest Endosc* 2002; **55**: 476-483
- 13 **Konturek SJ**, Szlachcic A, Dembinski A, Warzecha Z, Jaworek J, Stachura J. Nitric oxide in pancreatic secretion and hormone-induced pancreatitis in rats. *Int J Pancreatol* 1994; **15**: 19-28
- 14 **Liu X**, Nakano I, Yamaguchi H, Ito T, Goto M, Koyanagi S, Kirjoh M, Nawata H. Protective effect of nitric oxide on development of acute pancreatitis in rats. *Dig Dis Sci* 1995; **40**: 2162-2169
- 15 **Klar E**, Schratt W, Foitzik T, Buhr H, Herfarth C, Messmer K. Impact of microcirculatory flow pattern changes on the development of acute edematous and necrotizing pancreatitis in rabbit pancreas. *Dig Dis Sci* 1994; **39**: 2639-2644
- 16 **Schmidt J**, Ebeling D, Ryschich E, Werner J, Gebhard MM, Klar E. Pancreatic capillary blood flow in an improved model of necrotizing pancreatitis in the rat. *Surg Res* 2002; **106**: 335-341
- 17 **Gullo A**, Berlot G. Ingredients of organ dysfunction or failure. *World J Surg* 1996; **20**: 430-436
- 18 **Hotz HG**, Foitzik T, Rohweder J, Schulzke JD, Fromm M, Runkel NS, Buhr HJ. Intestinal microcirculation and gut permeability in acute pancreatitis: early changes and therapeutic implications. *J Gastrointest Surg* 1998; **2**: 518-525
- 19 **Klar E**, Mall G, Messmer K, Herfarth C, Rattner DW, Warshaw AL. Improvement of impaired pancreatic microcirculation by isovolemic hemodilution protects pancreatic morphology in acute biliary pancreatitis. *Surg Gynecol Obstet* 1993; **176**: 144-150
- 20 **Gomez-Cambronero L**, Camps B, de La Asuncion JG, Cerda M, Pellin A, Pallardo FV, Calvete J, Sweiry JH, Mann GE, Vina J, Sastre J. Pentoxifylline ameliorates cerulein-induced pancreatitis in rats: role of glutathione and nitric oxide. *J Pharmacol Exp Ther* 2000; **293**: 670-676
- 21 **Foitzik T**, Eibl G, Buhr HJ. Therapy for microcirculatory disorders in severe acute pancreatitis: comparison of delayed therapy with ICAM-1 antibodies and a specific endothelin A receptor antagonist. *J Gastrointest Surg* 2000; **4**: 240-246
- 22 **Werner J**, Hartwig W, Schmidt E, Gebhard MM, Herfarth C, Klar E. Reduction of local and systemic complications of acute pancreatitis by monoclonal antibody to ICAM-1. *Langenbecks Arch Chir Suppl Kongressbd.* 1998; **115** (Suppl I): 725-729
- 23 **Foitzik T**, Hotz HG, Eibl G, Faulhaber J, Kirchengast M, Buhr HJ. Endothelin receptor block in acute pancreatitis -improvement of microcirculation and decrease of capillary permeability also distant from the pancreas. *Langenbecks Arch Chir Suppl Kongressbd* 1998; **115**(Suppl I): 427-429
- 24 **Plusczyk T**, Witzel B, Menger MD, Schilling M. ETA and ETB receptor function in pancreatitis-associated microcirculatory failure, inflammation, and parenchymal injury. *Am J Physiol Gastrointest Liver Physiol* 2003; **285**: G145-153
- 25 **Dobosz M**, Wajda Z, Hac S, Myœliwska J, Bryl E, Mionskowska L, Roszkiewicz A, Mysliwski A. Nitric oxide, heparin and procaine treatment in experimental ceruleine-induced acute pancreatitis in rats. *Arch Immunol Ther Exp* 1999; **47**: 155-160
- 26 **Forgacs B**, Eibl G, Wudel E, Franke J, Faulhaber J, Kahrau S, Buhr HJ, Foitzik T. RES function and liver microcirculation in the early stage of acute experimental pancreatitis. *Hepatogastroenterology* 2003; **50**: 861-866
- 27 **Chen HM**, Sunamura M, Shibuya K, Yamauchi JI, Sakai Y, Fukuyama S, Mikami Y, Takeda K, Matsuno S. Early microcirculatory derangement in mild and severe pancreatitis models in mice. *Surg Today* 2001; **31**: 634-642
- 28 **Foitzik T**, Stufler M, Hotz HG, Klinnert J, Wagner J, Warshaw AL, Schulzke JD, Fromm M, Buhr HJ. Glutamine stabilizes intestinal permeability and reduces pancreatic infection in acute experimental pancreatitis. *J Gastrointest Surg* 1997; **1**: 40-47
- 29 **Bhatia M**, Brady M, Shokuhi S, Christmas S, Neoptolemos JP, Slavin J. Inflammatory mediators in acute pancreatitis. *J Pathol* 2000; **190**: 117-125
- 30 **Lantz M**, Thysell H, Nilsson E, Olsson I. On the binding of tumor necrosis factor (TNF) to heparin and the release *in vivo* of the TNF-binding protein I by heparin. *J Clin Invest* 1991; **88**: 2026-2031
- 31 **Hiebert LM**, Liu JM. Heparin protects cultured arterial endothelial cells from damage by toxic oxygen metabolites. *Atherosclerosis* 1990; **83**: 47-51
- 32 **Weiler JM**, Edens RE, Linhardt RJ, Kapelanski DP. Heparin and modified heparin inhibit complement activation *in vivo*. *J Immunol* 1992; **148**: 3210-3215
- 33 **Lucio J**, D'Brot J, Guo CB, Abraham WM, Lichtenstein LM, Kagey-Sobotka A, Ahmed T. Immunologic mast cell-mediated responses and histamine release are attenuated by heparin. *J Appl Physiol* 1992; **73**: 1093-1101
- 34 **Sternbergh WC 3rd**, Makhoul RG, Adelman B. Heparin prevents postischemic endothelial cell dysfunction by a mechanism independent of its anticoagulant activity. *J Vasc Surg* 1993; **17**: 318-327
- 35 **Leculier C**, Benzerara O, Couprie N, Francina A, Lasne Y, Archimbaud E, Fiere D. Specific binding between human neutrophils and heparin. *Br J Haematol* 1992; **81**: 81-85
- 36 **Imai T**, Hirata Y, Emori T, Marumo F. Heparin has an inhibitory effect on endothelin-1 synthesis and release by endothelial cells. *Hypertension* 1993; **21**: 353-358
- 37 **Inoue K**, Hirota M, Kimura Y, Kuwata K, Ohmuraya M, Ogawa M. Further evidence for endothelin as an important mediator of pancreatic and intestinal ischemia in severe acute pancreatitis. *Pancreas* 2003; **26**: 218-223

Helicobacter pylori in gastric corpus of patients 20 years after partial gastric resection

Christian Kirsch, Ahmed Madisch, Petja Piehler, Ekkehard Bayerdörffer, Manfred Stolte, Stephan Miehleke

Christian Kirsch, Ahmed Madisch, Stephan Miehleke, Medical Department I, Technical University Hospital, Dresden, Germany
Petja Piehler, Community Hospital, Kitzbühl, Germany
Ekkehard Bayerdörffer, Department of Internal Medicine, University Hospital, Marburg, Germany
Manfred Stolte, Institute of Pathology, Klinikum Bayreuth, Germany
Correspondence to: Dr. Stephan Miehleke, Medical Department I, Technical University Hospital Carl Gustav Carus, Fetscherstraße 74, D-01307 Dresden, Germany. miehleke@mk1.med.tu-dresden.de
Telephone: +49-351-4585645 **Fax:** +49-351-4584394
Received: 2004-03-23 **Accepted:** 2004-04-29

Abstract

AIM: To determine the long-term prevalence of *Helicobacter pylori* (*H. pylori*) gastritis in patients after partial gastric resection due to peptic ulcer, and to compare the severity of *H. pylori*-positive gastritis in the corpus mucosa between partial gastrectomy patients and matched controls.

METHODS: Endoscopic biopsies were obtained from 57 patients after partial gastric resection for histological examination using hematoxylin/eosin and Warthin-Starry staining. Gastritis was graded according to the updated Sydney system. Severity of corpus gastritis was compared between *H. pylori*-positive partial gastrectomy patients and *H. pylori*-positive duodenal ulcer patients matched for age and gender.

RESULTS: In partial gastrectomy patients, surgery was performed 20 years (median) prior to evaluation. In 25 patients (43.8%) *H. pylori* was detected histologically in the gastric remnant. Gastric atrophy was more common in *H. pylori*-positive compared to *H. pylori*-negative partial gastrectomy patients ($P < 0.05$). The severity of corpus gastritis was significantly lower in *H. pylori*-positive partial gastrectomy patients compared to duodenal ulcer patients ($P < 0.01$). There were no significant differences in the activity of gastritis, atrophy and intestinal metaplasia between the two groups.

CONCLUSION: The long-term prevalence of *H. pylori* gastritis in the gastric corpus of patients who underwent partial gastric resection due to peptic ulcer disease is comparable to the general population. The expression of *H. pylori* gastritis in the gastric remnant does not resemble the gastric cancer phenotype.

Kirsch C, Madisch A, Piehler P, Bayerdörffer E, Stolte M, Miehleke S. *Helicobacter pylori* in gastric corpus of patients 20 years after partial gastric resection. *World J Gastroenterol* 2004; 10(17): 2557-2559
<http://www.wjgnet.com/1007-9327/10/2557.asp>

INTRODUCTION

Helicobacter pylori (*H. pylori*) is the major etiological factor for peptic ulcer disease and gastric MALT lymphoma, and is strongly

linked to the development of gastric carcinoma^[1-3]. Recently, a gastric cancer phenotype of *H. pylori* gastritis has been proposed, which is characterized by an increased inflammation of the corpus mucosa^[4]. This phenotype of *H. pylori* gastritis is significantly more common in patients with early gastric cancer, and also in those with advanced stages of gastric cancer^[4,5]. An increased severity of corpus inflammation has also been described in particular risk groups for gastric cancer, such as first-degree relatives of gastric cancer patients^[6]. In contrast, patients with duodenal ulcer disease are characterized by a severe gastritis in the antrum, but a mild gastritis in the corpus^[7]. The risk for gastric cancer in duodenal ulcer patients is low compared to the general population^[8].

Patients underwent partial gastric resection for peptic ulcer are at high risk for developing cancer in the gastric remnant^[9]. Several mechanisms have been proposed for this phenomenon. It has been suggested that stump cancers uniformly develop upon a background of chronic mucosal changes in the gastric remnant^[10-12]. Factors that may contribute to cancer of the gastric remnant include enterogastric pancreaticobiliary reflux, hypochlorhydria, microflora, and N-nitroso compounds^[13,14].

The role of *H. pylori* gastritis with respect to cancer risk in patients underwent partial gastric resection for benign peptic ulcer disease is not clearly defined. Assuming that the majority of peptic ulcer patients were *H. pylori*-infected at the time of surgery, persisting *H. pylori* infection and long-term inflammation of the gastric corpus mucosa might contribute to carcinogenesis in these patients.

The aim of our study was therefore to determine the prevalence of *H. pylori* gastritis in the gastric remnant of patients who underwent partial gastric resection, and to test the hypothesis that *H. pylori*-positive patients with partial gastric resection may have a more severe corpus gastritis resembling the gastric cancer phenotype of *H. pylori* gastritis.

MATERIALS AND METHODS

The study included consecutive patients who were admitted to our institution for surveillance endoscopy after partial gastric resection due to peptic ulcer disease. Exclusion criteria included previous surgery for gastric cancer, previous treatment for *H. pylori* infection, and a present ulcer or tumor under endoscopy. Further exclusion criteria included pretreatment with antibiotics, proton-pump inhibitors, non-steroidal anti-inflammatory within the 4 wk before study entry.

Endoscopic biopsies were routinely obtained in 4 quadrants from the anastomosis, or from any suspicious macroscopic lesion. In addition, 2 biopsies were obtained from the middle of the remnant corpus and 2 from the cardia for assessing prevalence, severity of *H. pylori* gastritis, and gastric atrophy. All biopsy specimens were fixed in 40 g/L formaldehyde and embedded in paraffin. Sections were stained with hematoxylin and eosin and Warthin-Starry. The presence of *H. pylori* colonization as well as intestinal metaplasia and atrophy were judged as positive or negative. The grade of gastritis (infiltration of lymphocytes and plasma cells), the activity of gastritis (infiltration of neutrophil granulocytes), and the replacement of foveolar epithelium by regenerative epithelium were assessed by a semiquantitative

scale (grade 0 = negative, grade 1 = mild, grade 2 = moderate, grade 3 = severe) in accordance with the updated Sydney system^[15].

The control group consisted of *H pylori*-positive patients with duodenal ulcer disease who participated in previous clinical trials^[7] and who were age- and gender-matched. In these patients, endoscopic biopsies have been obtained from the antrum and the corpus, and were processed as described above. All histological slides were assessed by a single pathologist.

Data analysis was performed using the statistical software package SPSS 10.0 for Windows. The Chi-square test or Fisher exact test was used when appropriate. $P < 0.05$ was considered statistically significant.

RESULTS

A total of 57 patients with partial gastric resection were included into the study (19 males and 38 females, median age 64 years, range 26-92 years). The time period between surgery and histology assessment ranged from 8 to 47 years with a median of 20 years. None of the intraepithelial neoplasia was detected at the gastric anastomosis. In 25 patients (43.9%) *H pylori* was detected histologically in the gastric remnant.

Table 1 summarizes the histological features in the corpus and cardia of partial gastrectomy patients. For analysis purposes, patients with grade 0 and 1, and patients with grade 2 and 3 were combined, respectively. There was a higher proportion of patients with moderate or severe activity of gastritis in the corpus ($P < 0.0005$) and cardia ($P = 0.007$) among *H pylori*-positive patients compared to *H pylori*-negative partial gastrectomy patients. In addition, the proportion of patients with atrophy in the corpus mucosa was significantly higher among *H pylori*-positive compared to *H pylori*-negative patients ($P = 0.047$). No significant differences were found with regard to grade of gastritis, regenerative epithelium and the presence of intestinal metaplasia between *H pylori*-positive and *H pylori*-negative partial gastrectomy patients.

The comparison of corpus gastritis between *H pylori*-positive partial gastrectomy patients and *H pylori*-positive duodenal ulcer patients is summarized in Table 2. The proportion of patients with moderate or severe grade of gastritis in the corpus ($P = 0.001$) and with moderate or severe regenerative epithelium ($P = 0.004$) was significantly lower in *H pylori*-positive partial gastrectomy patients than that in *H pylori*-positive duodenal ulcer patients, respectively. A similar trend was observed for the activity of gastritis in the corpus, however

the differences were not statistically significant. The prevalence of intestinal metaplasia in the corpus mucosa was similar in both groups. The prevalence of atrophy in the corpus mucosa was higher in partial gastrectomy patients, however the difference did not reach statistical significance.

Table 2 Severity of corpus gastritis in *H pylori*-positive partial gastrectomy patients and *H pylori*-positive duodenal ulcer patients matched by age and gender

	Partial gastrectomy (n = 25)	Duodenal ulcer (n = 25)	P
Grade of gastritis			
Grade 0 or 1, n (%)	24 (96)	13 (52)	
Grade 2 or 3, n (%)	1 (4)	12 (48)	0.001
Activity of gastritis			
Grade 0 or 1, n (%)	16 (64)	11 (44)	
Grade 2 or 3, n (%)	9 (36)	14 (56)	0.256
Regenerative epithelium			
Grade 0 or 1, n (%)	25 (100)	17 (68)	
Grade 2 or 3, n (%)	0 (0)	8 (32)	0.004
Intestinal metaplasia			
Present, n (%)	5 (20)	5 (20)	1.00
Atrophy			
Present, n (%)	11 (44)	5 (20)	0.128

DISCUSSION

In the present study the prevalence of *H pylori* gastritis in patients underwent partial gastrectomy was 43.9% which is comparable to the average population in Germany and which is within the range of other studies on the *H pylori* prevalence in partial gastrectomy patients^[16-20].

An association between *H pylori* infection and an increased acute and chronic inflammatory response and a higher prevalence of chronic atrophic gastritis and intestinal metaplasia in the gastric remnant mucosa has been described^[16,18] while others were non-confirmatory^[20]. Our study suggests that *H pylori* leads to a higher proportion of atrophy in the corpus of the gastric remnant compared to *H pylori*-negative partial gastrectomy patients.

Several studies have shown that a severe although non-atrophic gastritis in the corpus mucosa is a particular risk factor for gastric cancer among those individuals infected with *H pylori*^[4-7]. These findings were recently confirmed by a prospective observational study from Japan where gastric cancer developed only in those patients infected with *H pylori*^[21] and where a

Table 1 Histology in the corpus and cardia of partial gastrectomy patients

	Corpus			Cardia		
	HP + n = 25	HP - n = 32	P	HP + n = 25	HP - n = 32	P
Grade of gastritis						
Grade 0 or 1, n (%)	24 (96)	32 (100)	-	24 (96)	32 (100)	-
Grade 2 or 3, n (%)	1 (4)	0	0.439	1 (4)	0	0.439
Activity of gastritis						
Grade 0 or 1, n (%)	16 (64)	32 (100)	-	16 (64)	32 (100)	-
Grade 2 or 3, n (%)	9 (36)	0	<0.0005	9 (36)	0	0.007
Regenerative epithelium						
Grade 0 or 1, n (%)	25 (100)	32 (100)	-	24 (96)	32 (100)	-
Grade 2 or 3, n (%)	0	0	-	1 (4)	0	0.439
Intestinal metaplasia						
Present, n (%)	5 (20)	7 (22)	1.00	4 (16)	4 (12.5)	0.720
Atrophy						
Present, n (%)	11 (44)	6 (19)	0.047	0	3 (9.5)	0.248

No partial gastrectomy patient had a grade 2 or 3 regenerative type of epithelium in the corpus. Based upon this result a statistical analysis with regard to regenerative type of epithelium in the corpus was not appropriate.

corpus-dominant gastritis or pangastritis was associated with an 34-fold increased risk for gastric cancer. Based upon the increased risk for gastric cancer in the presence of severe corpus gastritis we hypothesized that patients with partial gastrectomy due to ulcer disease may develop a corpus-dominant phenotype of *H pylori* gastritis, which may contribute as a risk factor for cancer in these patients. Surprisingly, we found a significant lower grade of gastritis in the corpus of *H pylori*-positive partial gastrectomy patients compared to the control group consisting of *H pylori*-positive duodenal ulcer patients. Possible explanation for this finding might include that in some patients the infection may have disappeared spontaneously due to an altered gastric milieu, or that some of the patients may have been operated due to *H pylori*-negative ulcer caused by nonsteroidal anti-inflammatory drugs. Other patients may have received antibiotic therapy for other indications that *H pylori* infection potentially leads to coincident eradication of the bacteria. Nevertheless, we conclude that partial gastrectomy patients should be tested for *H pylori* infection, and, if diagnosed positive, eradication therapy should be initiated to reduce the risk of ulcer relapse^[22].

Other factors than *H pylori* have been implicated in the pathogenesis of the mucosa alterations in partial gastrectomy patients, including enterogastric reflux, achlorhydria and increased mucosal proliferation, effects of vagotomy and dietary factors^[23-26]. Bile reflux may play a promotional role by increasing permeability to initiating carcinogens. This enterogastric reflux has been reported to be more pronounced after a gastrojejunostomy than after a gastroduodenostomy, which may explain the higher stomach cancer risk after a Billroth II operation^[27-29].

In conclusion, our study suggests that the *H pylori* prevalence in partial gastrectomy patients (former peptic ulcer patients) is comparable to the general population. *H pylori*-positive partial gastrectomy patients appear not to develop a corpus-dominant gastritis resembling the gastric cancer phenotype of *H pylori* gastritis.

REFERENCES

- Graham DY. *Helicobacter pylori* infection in the pathogenesis of duodenal ulcer and gastric cancer: a model. *Gastroenterology* 1997; **113**: 1983-1991
- Bayerdörffer E, Miehle S, Neubauer A, Stolte M. Gastric MALT-lymphoma and *Helicobacter pylori* infection. *Aliment Pharmacol Ther* 1997; **11**(Suppl 1): 89-94
- Schistosomes, liver flukes and *Helicobacter pylori*. IARC Working group on the evaluation of carcinogenic risks to humans. Lyon, 7-14 June 1994. *IARC Monogr Eval Carcinog Risks Hum* 1994; **61**: 1-241
- Meining A, Bayerdörffer E, Müller P, Miehle S, Lehn N, Hölzel D, Hatz R, Stolte M. Gastric carcinoma risk index in patients infected with *Helicobacter pylori*. *Virchows Arch* 1998; **432**: 311-314
- Miehle S, Hackelsberger A, Meining A, Hatz R, Lehn N, Malfertheiner P, Stolte M, Bayerdörffer E. Severe expression of corpus gastritis is characteristic in gastric cancer patients infected with *Helicobacter pylori*. *Br J Cancer* 1998; **78**: 263-266
- Meining AG, Bayerdörffer E, Stolte M. *Helicobacter pylori* gastritis of the gastric cancer phenotype in relatives of gastric carcinoma patients. *Eur J Gastroenterol Hepatol* 1999; **11**: 717-720
- Meining A, Stolte M, Hatz R, Lehn N, Miehle S, Morgner A, Bayerdörffer E. Differing degree and distribution of gastritis in *Helicobacter pylori*-associated diseases. *Virchows Arch* 1997; **431**: 11-15
- Hansson LE, Nyren O, Hsing AW, Bergström R, Josefsson S, Chow WH, Fraumeni JF Jr, Adami HO. The risk of stomach cancer in patients with gastric or duodenal ulcer disease. *N Engl J Med* 1996; **335**: 242-249
- Safatle-Ribeiro AV, Ribeiro U Jr, Reynolds JC. Gastric stump cancer: what is the risk? *Dig Dis* 1998; **16**: 159-168
- Safatle-Ribeiro AV, Ribeiro Junior U, Reynolds JC, Gama-Rodrigues JJ, Iriya K, Kim R, Bakker A, Swalsky PA, Pinotti HW, Finkelstein SD. Morphologic, histologic, and molecular similarities between adenocarcinomas arising in the gastric stump and the intact stomach. *Cancer* 1996; **78**: 2288-2299
- Kaminishi M, Shimizu N, Yamaguchi H, Hashimoto M, Sakai S, Oohara T. Different carcinogenesis in the gastric remnant after gastrectomy for gastric cancer. *Cancer* 1996; **77**(8 Suppl): 1646-1653
- Bajtai A, Hidvegi J. The role of gastric mucosal dysplasia in the development of gastric carcinoma. *Pathol Oncol Res* 1998; **4**: 297-300
- Langhans P, Bues M, Bunte H. Morphological changes in the operated stomach under the influence of duodenogastric reflux. Clinical follow-up over 20 years. *Scand J Gastroenterol Suppl* 1984; **92**: 145-148
- Sobala GM, Pignatelli B, Schorah CJ, Bartsch H, Sanderson M, Dixon MF, Shires S, King RF, Axon AT. Levels of nitrite, nitrate, N-nitroso compounds, ascorbic acid, and total bile acids in gastric juice of patients with and without precancerous conditions of the stomach. *Carcinogenesis* 1991; **12**: 193-198
- Dixon MF, Genta RM, Yardley JH, Correa P. Classification and grading of gastritis. The updated Sydney System. International Workshop on the Histopathology of Gastritis, Houston 1994. *Am J Surg Pathol* 1996; **20**: 1161-1181
- Leung WK, Lee YT, Choi CL, Chan FK, Ching J, Sung JJ. Diagnosis of *Helicobacter pylori* infection after gastric surgery for peptic ulcer: is the rapid urease test useful? *Scand J Gastroenterol* 1998; **33**: 586-589
- Ludtke FE, Maierhof S, Kohler H, Bauer FE, Tegeler R, Schauer A, Lepsien G. *Helicobacter pylori* colonization in surgical patients. *Chirurg* 1991; **62**: 732-738
- Leivonen MK, Haglund CH, Nordling SF. *Helicobacter pylori* infection after partial gastrectomy for peptic ulcer and its role in relapsing disease. *Eur J Gastroenterol Hepatol* 1997; **9**: 371-374
- Nagahata Y, Kawakita N, Azumi Y, Numata N, Yano M, Saitoh Y. Etiological involvement of *Helicobacter pylori* in "reflux" gastritis after gastrectomy. *Am J Gastroenterol* 1996; **91**: 2130-2134
- Rino Y, Imada T, Shiozawa M, Takahashi M, Fukuzawa K, Hasuo K, Nagano A, Tanaka J, Hatori S, Amano T, Kondo J. *Helicobacter pylori* of the remnant stomach and its eradication. *Hepatogastroenterology* 1999; **46**: 2069-2073
- Uemura N, Okamoto S, Yamamoto S, Matsumura N, Yamaguchi S, Yamakido M, Taniyama K, Sasaki N, Schlemper RJ. *Helicobacter pylori* infection and the development of gastric cancer. *N Engl J Med* 2001; **345**: 784-789
- Lee YT, Sung JJ, Choi CL, Chan FK, Ng EK, Ching JY, Leung WK, Chung SC. Ulcer recurrence after gastric surgery: is *Helicobacter pylori* the culprit? *Am J Gastroenterol* 1998; **93**: 928-931
- Offerhaus GJ, Rieu PN, Jansen JB, Joosten HJ, Lamers CB. Prospective comparative study of the influence of postoperative bile reflux on gastric mucosal histology and *Campylobacter pylori* infection. *Gut* 1989; **30**: 1552-1557
- Fukuzawa K, Noguchi Y, Matsumoto A. Alterations in DNA proliferation in gastric stump mucosa with special reference to topography. *Surgery* 1996; **119**: 191-197
- Ikeguchi M, Kondou A, Oka A, Tsujitani S, Maeta M, Kaibara N. Flow cytometric analysis of the DNA content of tumor cells in cases of gastric cancer in the upper third of the stomach and in the remnant stomach. *Oncology* 1995; **52**: 116-122
- Kaminishi M, Shimizu N, Shimoyama S, Yamaguchi H, Tsuji E, Aoki F, Nomura S, Yoshikawa A, Kuramoto S, Oohara T, Inada K, Tatematsu M. Denervation promotes the development of cancer-related lesions in the gastric remnant. *J Clin Gastroenterol* 1997; **25**(Suppl 1): S129-134
- Clarke MR, Safatle-Ribeiro AV, Ribeiro U, Sakai P, Reynolds JC. Bcl-2 protein expression in gastric remnant mucosa and gastric cancer 15 or more years after partial gastrectomy. *Mod Pathol* 1997; **10**: 1021-1027
- Kodera Y, Yamamura Y, Torii A, Uesaka K, Hirai T, Yasui K, Morimoto T, Kato T, Kito T. Gastric stump carcinoma after partial gastrectomy for benign gastric lesion: what is feasible as standard surgical treatment? *J Surg Oncol* 1996; **63**: 119-124
- Leivonen M, Nordling S, Haglund C. Does *Helicobacter pylori* in the gastric stump increase the cancer risk after certain reconstruction types? *Anticancer Res* 1997; **17**: 3893-3896

Cloning and expression and immunogenicity of *Helicobacter pylori* BabA₂ gene

Yang Bai, Ya-Li Zhang, Ye Chen, Jian-Feng Jin, Zhao-Shan Zhang, Dian-Yuan Zhou

Yang Bai, Ya-Li Zhang, Ye Chen, Dian-Yuan Zhou, PLA Institute for Digestive Medicine, Nanfang Hospital, the First Military Medical University, Guangzhou 510515, Guangdong Province, China
Jian-Feng Jin, Chemistry university of Beijing, Beijing 100071, China
Zhao-Shan Zhang, Institute of Biotechnology, Academy of Military Medical Sciences, Beijing 100071, China

Supported by the National Natural Science Foundation of China, No. 30270078

Correspondence to: Dr. Yang Bai, PLA Institute for Digestive Medicine, Nanfang Hospital, the First Military Medical University, Guangzhou 510515, Guangdong Province, China. Baiyang1030@hotmail.com
Telephone: +86-20-61641532

Received: 2003-08-06 **Accepted:** 2003-10-07

Abstract

AIM: To construct a recombinant strain which expresses BabA of *Helicobacter pylori* (*H pylori*) and to study the immunogenicity of BabA.

METHODS: BabA₂ DNA was amplified by PCR and inserted into the prokaryotic expression vector pET-22b (+) and expressed in the BL21 (DE3) *E. coli* strain. Furthermore, BabA immunogenicity was studied by animal test.

RESULTS: DNA sequence analysis showed the sequence of BabA₂ DNA was the same as the one published by GenBank. The BabA recombinant protein accounted for 34.8% of the total bacterial protein. The serum from *H pylori* infected patients and Balb/c mice immunized with BabA itself could recognize rBabA.

CONCLUSION: BabA recombinant protein may be a potential vaccine for control and treatment of *H pylori* infection.

Bai Y, Zhang YL, Chen Y, Jin JF, Zhang ZS, Zhou DY. Cloning and expression and immunogenicity of *Helicobacter pylori* BabA₂ gene. *World J Gastroenterol* 2004; 10(17): 2560-2562
<http://www.wjgnet.com/1007-9327/10/2560.asp>

INTRODUCTION

Helicobacter pylori (*H pylori*), a human-specific gastric pathogen, was first isolated in 1982 and has emerged as the causative agent of chronic active gastritis and peptic ulcer disease^[1-11]. Most infected individuals show no clinical symptoms, implicating additional factors, such as genetic predisposition and genotype of the infecting strain, are involved in disease pathogenesis. Chronic infection is associated with the development of gastric adenocarcinoma, one of the most common types of cancer in humans, and *H pylori* was recently defined as a class 1 carcinogen. In addition, seroprevalence studies indicate that *H pylori* infection is also associated with cardiovascular, respiratory, extra-gastrointestinal digestive, autoimmune disease. At present the main treatment to eradicate *H pylori* is combined antibiotics, but the cost of combination therapy and the emergency of antibiotic resistance provide further incentives for vaccine development.

In the development of *H pylori* vaccine, candidate vaccine antigens adopted currently such as urease, vacuolating cytotoxin, catalase, etc. basically focus on blocking toxicity factors of *H pylori* while considerably few candidate vaccine antigens focus on adhesins which are closely associated with *H pylori* colonizing human gastric mucosa by adhering to mucous epithelial cells and mucus layer lining the gastric epithelium. BabA is the only adhesin gene whose receptor has been confirmed. Studies indicate that BabA gene contains two alleles: BabA₁ and BabA₂. Gene BabA₁ is different from BabA₂ in the presence of a 10 bp repeat motif and in lack of Leb antigen-binding activity. No concerned study has been reported to date about BabA₂ in China. So in this study, recombinant plasmid of *H pylori* BabA₂ gene was constructed and expressed for development of *H pylori* vaccine.

MATERIALS AND METHODS

Materials

Bacterial strain BL21 (DE3) and plasmid pET-22 b (+) were provided by Institute of Biotechnology, Academy of Military Medical Sciences. *H pylori* SS1 was preserved in this research institute. Restriction enzyme *Not* I, *Nco* I and T4 DNA ligase, Vent DNA polymerase, isopropyl-β-D-thiogalactopyranoside (IPTG) were purchased from New England Biolabs Company. DNA molecular weight standard λ DNA/*Eco*RI+*Hind*III, goat anti-mouse and goat anti-human IgG-HRP were purchased from Huamei Bioengineering Company and His-Tag precolumn from Invitrogen Company. Specific-pathogen-free, female BALB/c mice were housed according to Health Research Council of China guidelines and allowed free access to food and water. Eight *H pylori* positive sera (which were detected positive by the urease test, pathological dying and germiculture) and three *H pylori* negative sera (which were detected negative by the above-mentioned three examinations) were from patients treated in the Endoscope Center of this institute. Other reagents were analytically pure reagents produced in China.

Recombinant DNA techniques

Unless otherwise stated, plasmid and chromosomal DNA extractions, restriction enzyme digests, DNA ligations, transformations into *E. coli* and other common DNA manipulations were performed by standard procedures. Genome of *H pylori* was prepared from the cells collected from the colonies on the agar plate. The gene of *H pylori* BabA₂ was amplified from the genome of *H pylori* by PCR using the primers BabA₂1 (5'-TG GCC ATG GAT AAA AAA CAC ATC CTT TCA-3') as upstream primer and BabA₂2 (5'-AG TGC GGCCGC ATA AGCGAA CAC ATA G-3') as downstream primer as described in the literature^[33]. BabA₂1 and BabA₂2 contained *Nco* I and *Not* I sites, respectively. PCR was performed with the hot start method. PCR condition was that after initial denaturing at 95 °C for 30 s, each cycle of amplification consisted of denaturing at 95 °C for 30 s, annealing at 55 °C for 30 s and polymerization at 72 °C for 60 s and further polymerization for 10 min after 35 PCR cycles. The PCR product was harvested from agarose gel, digested with *Nco* I and *Not* I, and inserted into the *Nco* I and *Not* I restriction fragment of the expression vector pET-22b(+) using T4 DNA ligase. The

resulting plasmid pET- BabA was transformed into competent *E. coli* BL21 (DE3) cells using ampicillin resistance for selection. The alkaline lysis method was chosen for large-scale preparations of recombinant plasmids which were identified by restriction enzymes. DNA sequence was performed with a DNA automatic sequencer.

Induced expression, purification and SDS-polyacrylamide gel electrophoresis

The recombinant strains were incubated overnight at 37 °C and shaken in 5 mL LB with 100 µg/mL ampicillin. A 50 mL LB was inoculated and the cells grew until the optical density at 600 nm reached 0.4-0.6. Isopropyl-β-D-thiogalactopyranoside (IPTG) was added to a final concentration of 0.1, 0.2, 0.4, 0.6, 0.8, 1.0 mmol/L, respectively. *E. coli* cells from a 50 mL growth 3 h or 5 h after induction were harvested by centrifugation at 12 000 g for 10 min and the pellet was resuspended in 1 mL 30 mmol/L Tris buffer (pH8.0) containing 1 mmol/L EDTA (pH8.0), 200 g/L sucrose. The suspension was put on ice for 10 min, and then centrifuged for 10 min at 12 000 g, and the resulting supernatant contained proteins from the periplasm. The resulting pellet was resuspended in 5 mL 50 mmol/L Tris buffer (pH8.0) containing 2 mmol/L EDTA, 0.1 mg/mL lysozyme and 10 g/L Triton X-100. The suspension was incubated at 30 °C for 20 min and then sonicated on ice until it became clarified. The lysate was centrifuged at 12 000 g for 15 min at 4 °C, then the resulting supernatant containing proteins from the cytoplasm was purified with Ni-NTA column. Whole-cell lysates, sonicated supernatant, osmotic shock liquid of recombinant strains expressing *H pylori* BabA2 genes and the purified rBabA were analyzed by electrophoresis analysis in a 100 g/L polyacrylamide gel.

Immunization of mice

Sixty-eight-week-old mice were immunized 4 times by hypodermic injection in the back of mice at weekly intervals. Each dose consisted of 20 µg of *H pylori* rBabA protein and 200 µg of adjuvant aluminum hydroxide gel. Age-matched control mice were not immunized. Four weeks after the last immunization, blood samples were taken from the retro-orbital sinus to measure the anti BabA systemic immune responses and stored at -20 °C until assay.

Serum antibody responses

Indirect ELISA as described previously evaluated serum samples from mice and patients for BabA-specific IgG. Purified *H pylori* rBabA was used as the coating antigen in ELISA immunoassays.

RESULTS

PCR amplification of *H pylori* BabA₂ gene

According to the literature, the gene encoding the BabA protein, was amplified by PCR with chromosomal DNA of *H pylori* Sydney strain (ss1) as the templates. The cloning products were electrophoresed and visualized on 8 g/L agarose gel (Figure 1). It revealed that BabA₂ DNA fragment amplified by PCR contained a gene of approximately 2 226 nucleotides, which was compatible with the previous reports.

Construction of recombinant plasmid and restriction enzyme confirmation

After the PCR products and pET-22 b (+) plasmid were cut by *Not* I and *Nco* I, directional cloning was performed, resulting in a recombinant plasmid named pET-22 b (+)/BabA. The recombinant plasmids pET-22 b (+)/BabA were all digested by *Not* I or *Nco* I, and by *Not* I and *Nco* I simultaneously, then digestive products were visualized on 8 g/L agarose gel electrophoresis (Figure 2). It demonstrated that recombinant plasmid contained the objective gene.

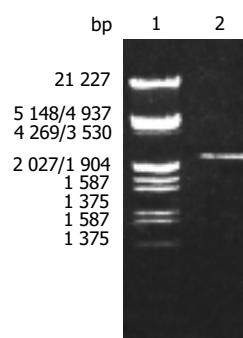


Figure 1 BabA₂ DNA fragment amplified by PCR from *Helicobacter pylori* electrophoresed on 8 g/L agarose gel. Lane 1: Nucleotide marker; Lane 2: PCR products.

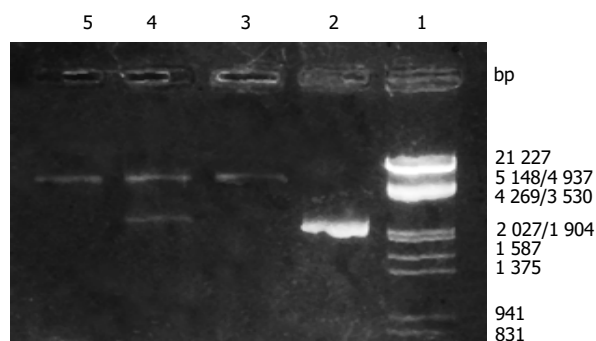


Figure 2 Identification of recombinant plasmid by restriction enzyme digestion. Lane 1: Nucleotide marker; Lane 2: PCR products; Lane 3: Recombinant plasmid/*Not* I; Lane 4: Recombinant plasmid/*Not* I and *Nco* I; Lane 5: pET22b(+)/*Not* I.

Sequence analysis of cloned BabA₂ nucleotide

The nucleotide sequence of cloned genes inserted in pET22 b(+) was analyzed by automatic sequencing across the cloning junction, using the universal primer T7. The results showed that cloned genes contained 2 226 nucleotides with a promoter and a start codon coding a putative protein of 741 amino acid residues with a calculated molecular mass of BabA. As compared with previously reports, the homogeneity was 100% between them.

Expression and purification of BabA₂ gene in *Escherichia coli*

Whole-cell lysate, sonicated supernatant, osmotic shock liquid of recombinant strains expressing *H pylori* BabA₂ genes and the purified rBabA were analyzed by electrophoresis analysis in a 100 g/L polyacrylamide gel for detection of fusion proteins (Figure 3). The result showed that the clearly identifiable band was 78 000 u highly expressed fusion proteins, which was similar to that predicted. Gel automatic scan analysis showed that it was 0.6 at D value and the final concentration of IPTG was 0.1 mmol/L and the expression of BabA rose remarkably after 5 h of induction, which accounted for 34.8% of total bacterial proteins. Among them, soluble substance accounted for 15.0% of supernatant. BabA was further analyzed with Ni-NTA column and finally BabA whose purity was 90%.

Antigenicity study of recombinant fusion protein

The positive results by the test of ELISA had colours, but the negative results had no colours, or weak colours. Serum from the eight mice serums immunized with rBabA showed positive results. In contrast, serum from the eight mice in the control group showed negative results. At the same time, serums from patients also showed the same results. *H pylori* positive serum from the eight patients showed positive results and *H pylori* negative serum from the three patients showed positive results.

It showed that anti-BabA antibody existed in the serum of infected patients and rBabA could enable the organism to generate specific humoral immunity.

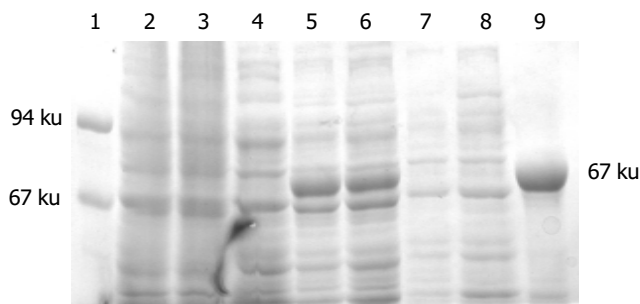


Figure 3 The 100 g/L SDS-PAGE analysis of fusion protein expressed in BL21 (DE3). Lane 1: Molecular mass marker (67, 94) $\times 10^3$; Lane 2: control strain BL21 (pET) before induction; Lane 3: control strain BL21 (pET) after 5-h induction with IPTG; Lane 4: BL21 (pET-BabA) cells before induction; Lane 5: BL21 (pET-BabA) cells after 3-h induction with IPTG; Lane 6: BL21 (pET-BabA) cells after 5-h induction with IPTG; Lane 7: BL21 (pET-BabA) cells periplasm protein after 3-h induction with IPTG; Lane 8: sonicated supernatant of BL21 (pET-BabA) cells after 3-h induction with IPTG; Lane 9: recombinant protein BabA purified.

DISCUSSION

At first Wadstr *et al.* suspected that the resting or slow growing cells of *H pylori* could interact with Lewis blood group substances in gastric mucin layer and on epithelium to facilitate initial colonization. Afterwards Liver *et al.* used receptor activity-directed affinity tagging to purify a kind of adhesin which mediated adherence of *H pylori* to human gastric epithelial cells by interacting with fucosylated Lewis b (Leb) histo-blood group antigen and named the adhesion BabA. Immunogold electron microscopy found BabA adhesin was located on the bacterial cell outer membrane by probing the Leb antigen. Receptor displacement analyses showed that receptor-adhesin complex was formed under conditions of equilibrium. Most of the cells (>90%) of the bacterial exhibited BAB activity, as determined by confocal microscopy and fluorescent Leb antigen. The K_a value for formation of the Leb antigen-BabA complex was -1×10^{10} mol/L. The number of Leb glycoconjugate molecules bound to BabA was calculated as -500 per bacterial cell. In addition, the prevalence of blood group antigen-binding activity was also assessed among 95 recent clinical isolates of *H pylori*, and 66% (63 isolates) were bound to the Leb antigen. Bosch *et al.* investigated the effects of acute stress on the salivary levels of the carbohydrate structure sulfo-Lewis (sulfo-Le). The results showed the stressor induced a strong increase in salivary sulfo-Le concentration (U/mL), sulfo-Le output (U/min), sulfo-Le/total protein ratio (U/mg protein), and saliva-mediated adherence (*ex vivo*) of *H pylori*. As expected, sulfo-Le concentration correlated with the adherence of *H pylori* ($r = 0.72$, $P < 0.05$). In a word, the adhesin BabA and its receptor Leb played an important role in the adherence mechanism of *H pylori*, especially when people were in the state of acute stress.

Isolates of *H pylori* differed in virulence and from individuals with peptic ulcers most often were type I strains that expressed vacuolating cytotoxin A (VacA) and cytotoxin-associated gene A (CagA) protein. By definition, type II strains could express neither marker. The bacterial Leb-binding phenotype was associated with the presence of the cag pathogenicity island among clinical isolates of *H pylori*. A vaccine strategy based on the BabA adhesin might serve as a means to target the

virulent type I strains of *H pylori*. So we selected *H pylori* ss1 chromosome DNA as a template, which has strong adhesin and is capable of colonizing firmly in the stomach of a mouse, designed specific primers and successfully screened the genes of BabA₂. To facilitate the expression and purification at the next stage, we cloned it into a fusion expression vector with 6 hercynine tails. The restriction enzyme digestion and the sequencing results showed that one open reading frame had the size of 2 226 bp. SDS-PAGE and scan analysis showed that the molecular mass of BabA was 78 ku and recombinant protein accounted for 34.8% of the total bacterial protein. Considering that the recombinant protein with bio-activity tended to preserve more integral and positive antigenicity, we selected supernatant of ultrasound disrupted live *E. coli* and performed repeated purification of rBabA with Ni-NTA resin, thus obtaining rBabA with activity whose purity was 90%. This has laid a foundation for further research on immune protection and molecular adhesin mechanism. In this study, serum from the mice immunized with purified recombinant protein BabA could be used to detect specific antibody against BabA, but serum from the mice in the control group could not. Serum from patients also showed the same results. These results suggest that BabA of *H pylori* maybe a good candidate as a vaccine component.

REFERENCES

- Bai Y, Zhang YL, Wang JD, Lin HJ, Zhang ZS, Zhou DY. Conservative region of the genes encoding four adhesins of *Helicobacter pylori*: cloning, sequence analysis and biological information analysis. *Diyi Junyi Daxue Xuebao* 2002; **22**: 869-871
- Vandenplas Y. *Helicobacter pylori* infection. *World J Gastroenterol* 2000; **6**: 20-31
- Bai Y, Chang SH, Wang JD, Chen Y, Zhang ZS, Zhang YL. Construction of the *E. coli* clone expressing adhesin BabA of *Helicobacter pylori* and evaluation of the adherence activity of BabA. *Diyi Junyi Daxue Xuebao* 2003; **23**: 293-295
- Morgner A, Miehle S, Stolte M, Neubauer A, Alpen B, Thiede C, Klann H, Hierlmeier FX, Ell C, Ehniger G, Bayerdörffer E. Development of early gastric cancer 4 and 5 years after complete remission of *Helicobacter pylori*-associated gastric low-grade marginal zone B-cell lymphoma of MALT type. *World J Gastroenterol* 2001; **7**: 248-253
- Bai Y, Zhang YL, Wang JD, Zhang ZS, Zhou DY. Construction of the non-resistant attenuated salmonella typhimurium strain expressing *Helicobacter pylori* catalase. *Diyi Junyi Daxue Xuebao* 2003; **23**: 101-105
- Solnick JV, Canfield DR, Hansen LM, Torabian SZ. Immunization with recombinant *Helicobacter pylori* urease in specific-pathogen-free rhesus monkeys (*Macaca mulatta*). *Infect Immun* 2000; **68**: 2560-2565
- Ilver D, Arnqvist A, Ogren J, Frick IM, Kersulyte D, Incecik ET, Berg DE, Covacci A, Engstrand L, Boren T. *Helicobacter pylori* adhesin binding fucosylated histo-blood group antigens revealed by retagging. *Science* 1998; **279**: 373-377
- Sambrook J, Fritsch EF, Maniatis T. Molecular cloning: a laboratory manual. 2nd ed. New York: Cold Spring Harbor Laboratory Press 1989: 35-400
- Wadstrom T, Hirno S, Boren T. Biochemical aspects of *Helicobacter pylori* colonization of the human gastric mucosa. *Aliment Pharmacol Ther* 1996; **10**(Suppl 1): 17-27
- Bosch JA, de Geus EJ, Ligtenberg TJ, Nazmi K, Veerman EC, Hoogstraten J, Amerongen AV. Salivary MUC5B-mediated adherence (*ex vivo*) of *Helicobacter pylori* during acute stress. *Psychosom Med* 2000; **62**: 40-49
- Covacci A, Censini S, Bugnoli M, Petracca R, Burrioni D, Macchia G, Massone A, Papini E, Xiang Z, Figura N. Molecular characterization of the 128-kDa immunodominant antigen of *Helicobacter pylori* associated with cytotoxicity and duodenal ulcer. *Proc Natl Acad Sci U S A* 1993; **90**: 5791-5795

Antisense imaging of colon cancer-bearing nude mice with liposome-entrapped ^{99m}Tc -labeled antisense oligonucleotides of *c-myc* mRNA

Jian-Guo Zheng, Tian-Zhi Tan

Jian-Guo Zheng, Department of Nuclear Medicine, Beijing Hospital, Beijing 100730, China

Tian-Zhi Tan, Department of Nuclear Medicine, West China Hospital, Sichuan University, Chengdu 610041, Sichuan Province, China

Supported by Natural Scientific Foundations of China, No: 39870200

Correspondence to: Tian-Zhi Tan, Department of Nuclear Medicine, West China Hospital, Sichuan University, Chengdu 610041, Sichuan Province, China. ttz@mcwccums.com

Telephone: +86-28-85422696 Fax: +86-28-85422696

Received: 2004-02-14 Accepted: 2004-02-24

Abstract

AIM: To investigate the feasibility for antisense imaging of the colon cancer with liposome-entrapped ^{99m}Tc -labeled antisense oligonucleotides as tracers.

METHODS: Fifteen mer single-stranded aminolinked phosphorothioate antisense oligonucleotides of *c-myc* mRNA were labeled with ^{99m}Tc -pertechnetate, then purified and finally entrapped with liposomes to form the labeling compounds, liposome-entrapped ^{99m}Tc -labeled antisense oligonucleotides. The LS-174-T cells (colon of adenocarcinoma cell line) were incubated with the labeling compounds to test the uptake rates of LS-174-T cells. Later on, a model of 30 tumor bearing nude mice was constructed by inoculating with 5×10^5 of LS-174-T cells at right flank of each nude mouse. About 10 d later, the model were administered by intravenous injection of the liposome-entrapped ^{99m}Tc -labeled antisense oligonucleotides. Then some of the tumour bearing nude mice were sacrificed at 0.5, 1, 2, and 4 h after intravenous injection, and proper quantity of liver, spleen, tumor, etc. was obtained. The tissues were counted in a gamma counter, and after correction for decay and background activity, expressed as a percentage of the injected dose. The others whose anterior and posterior whole-body scans were obtained at 1, 1.5, 2, 4, 6 and 24 h with a dual-head bodyscan camera equipped with parallel-hole low-energy collimators. The ratios of radioactive counts in tumor to that in contralateral equivalent region of abdomen were calculated.

RESULTS: The uptake rates of LS-174-T cells for liposome-entrapped ^{99m}Tc -labeled antisense oligonucleotides increased as time prolonged and reach the peak ($17.77 \pm 2.41\%$) at 7 h. The biodistributions showed that the radioactivity in the tumor ($13.46 \pm 0.20\%$) of injected dose was the highest at 2 h of intravenous injection of liposome-entrapped ^{99m}Tc -labeled antisense oligonucleotides, and then decreased sharply to $4.58 \pm 0.45\%$ at 4 h. The tumor was shown clearly in the whole-body scan at 2 h of intravenous injection. The ratios, radioactive counts in tumor to that in contralateral equivalent region of abdomen (1.7332 ± 0.2537), was the highest one at 2 h after intravenous injection of liposome-entrapped ^{99m}Tc -labeled antisense oligonucleotides.

CONCLUSION: The liposome-entrapped ^{99m}Tc -labeled antisense oligonucleotides deserve being developed into radiopharmaceuticals for the colon cancer imaging.

Zheng JG, Tan TZ. Antisense imaging of colon cancer-bearing nude mice with liposome-entrapped ^{99m}Tc -labeled antisense oligonucleotides of *c-myc* mRNA. *World J Gastroenterol* 2004; 10(17): 2563-2566

<http://www.wjgnet.com/1007-9327/10/2563.asp>

INTRODUCTION

Antisense imaging was referred to that antisense oligonucleotides of a gene were labeled with radionuclide, then administered to an organism to show its focus, especially the tumor^[1]. Colon cancer is a malignant tumor that seriously threatens human health. Its main oncogene, *c-myc*, whose overexpression can reach 30 times, is a target gene for antisense imaging^[2]. The oligonucleotides that are complementary to *c-myc* mRNA can prohibit many kinds of cancer cells from growing^[3]. Many nuclear medicine researchers are interested in this oncogene^[4,5]. At present, the antisense oligonucleotides of *c-myc* mRNA have been successfully labeled with ^{99m}Tc ^[6,7]. However, to the author's knowledge, their application in experimental researches on antisense imaging has not been reported as yet. Is the uptake rate of tumor tissue too small and the background too high to indicate the tumor? How can the uptake rates of tumor cells be increased? Do these limit the application of ^{99m}Tc -labeled antisense oligonucleotides? In order to explore the feasibility for antisense imaging of the colon carcinoma, develop a new radiolabeled-gene-pharmaceuticals, and promote the progress in the molecular nuclear medicine, the primary experimental studies, antisense imaging, on liposome-entrapped ^{99m}Tc -labeled antisense phosphorothioate oligonucleotides as a tracer were carried out.

MATERIALS AND METHODS

Materials

Fifteen mer, single-stranded phosphorothioate oligonucleotides, aminolinked, antisense oligonucleotides targeted at the translation initiation codon of *c-myc* mRNA were purchased from Gibco-BRL, US. Their base sequences were 5'-NH₂-FACGTTGAGGGGCAT-3' (F stood for phosphorothioate A). The molecular mass of the chain was about 300 u. These oligonucleotides were used directly without further purification, and generally handled under sterile conditions. All solutions were sterilized by terminal filtration through a 0.22 μm filter. All pipettes and tubes were autoclaved prior to use. The oligonucleotides were dissolved at a concentration of 4 mg/mL in sterile water and stored at -20 °C.

The hydrazino nicotinamide derivatives were synthesized elsewhere. ^{99m}Tc -pertechnetate was obtained from a ^{99}Mo - ^{99m}Tc radionuclide generator made by the Chinese Atomic Energy Institute. Tricine, SnCl₂·2H₂O and Dimethyl sulfoxide were

supplied by Sigma Company, US, lipofectamin reagent by Gibco-BRL, US, EDTA by Boehringer Mannheim Company, Germany, and Sep-Pak (C₁₈) reverse column by Waters Company, US.

The oligonucleotides were bound to hydrazino nicotinamide derivatives and then labeled with ^{99m}Tc following the methods described by Hnatowich *et al*^[8]. The ^{99m}Tc-labeled oligonucleotides were entrapped with liposome according to the manufacturer's protocols.

The cellular uptake rates of oligonucleotides

The LS-174-T cells were grown by adherent culture in media (RPMI-1 640, Gibco-BRL, US), supplemented with 100 mL/L fetal bovine serum at 37 °C, 50 mL/L CO₂. Thirty-six culture plates with diameter of 33 mm each was inoculated with about 1×10⁵ LS-174-T cells and cultured at 37 °C for 48 h. After the cells were grown to about 50% confluence in regular culture media, they were transfected using lipofectamin with 2 μg of freshly prepared liposome-entrapped ^{99m}Tc-labeled antisense oligonucleotides with radioactivity of about 29.60 MBq according to the manufacturer's protocols. The cellular uptake rates were determined at 1, 2, 5 and 7 h, and the testing steps were as follows: The cells were detached by 2.5 g/L trypsin to form suspension, then washed three times with the media by centrifugation (2 500 r/min, 10 min). The supernatant was collected into a 50 mL volumetric cylinder and the precipitation remained in the centrifugation tube. Then the radioactive counts in the precipitation and supernatant were counted in an automatic gamma well counter after correction for decay and background activity separately, and the cellular uptake rates were expressed as a percentage of the total counts. The uptake rate = radioactive counts in precipitation/the total counts in precipitation and supernatant ×100%.

The biodistribution of the antisense oligonucleotides in tumor-bearing nude mice

At first, the tumor model was constructed. Large-scale of LS-174-T cells collected by digestion, centrifugation and washing, were diluted with culture medium without serum and antibiotic to the concentration of 5×10⁶ cells per 0.2 mL. Thirty male nude mice, aged about 2 mo, were purchased from Experimental Animal Center of Sichuan University. The mice were maintained in a specific pathogen-free environment and cared in accordance with the institutional guidelines. Each of them was inoculated with 5×10⁶ cells at right flank. The tumor was allowed to grow for 10 d until diameter reached about 1 cm. Thus the tumor model was constructed successfully.

Biodistribution of liposome-entrapped ^{99m}Tc-labeled antisense oligonucleotides was determined in the 20 tumor-bearing nude mice. Each mouse received 0.3 mL of saline containing 3 to 5 μg (0.259 MBq) of liposome-entrapped ^{99m}Tc-labeled antisense oligonucleotides by tail vein administration. Meanwhile, the same injected dose of liposome-entrapped ^{99m}Tc-labeled antisense oligonucleotides was stored in a tube as standard, and double assays were carried out. Five mice were used at each time point of 0.5, 1, 2 and 4 h. After being bled from eye, they were sacrificed by cervical dislocation, and proper quantity of liver, spleen, kidney, lung, heart, bone, muscle, stomach, intestines, brain and tumor obtained. The tissues were washed cleanly with cool physiological saline and weighted by electronic balance (Denver, US). The tissues were counted against appropriate standards of known dilution in an automatic gamma well counter, and after correction for decay and background activity, expressed as a percentage of the injected dose.

Antisense imaging

The liposome-entrapped ^{99m}Tc-labeled antisense oligonucleotides containing oligonucleotides from 30 to 90 μg at the concentration

of 37 MBq/mL were freshly prepared. The 6 tumor-bearing nude mice were administered with 0.3 mL of the above products through tail vein. When these mice anesthetized with pentobarbital, anterior and posterior whole-body scans were obtained at 1, 1.5, 2, 4, 6 and 24 h with a dual-head bodyscan camera (Elcint Apex Helix, Israel) equipped with parallel-hole low-energy collimators. The ratios of radioactive counts in tumor to that in the contralateral equivalent region of abdomen were calculated.

RESULTS

The cellular uptake rates of oligonucleotides

The most important thing for antisense imaging is how much oligonucleotides are able to enter cells. High uptake rate is the key to success. The cellular uptake rates are as follows: 7.21±1.23% at 1 h, 15.19±2.81% at 2 h, 16.13±2.54% at 5 h, and 17.77±2.41% at 7 h. Within 7 h, the cellular uptake rate increased as the time prolonged, and reached the peak at 7 h. It was significantly higher than that at 1 and 2 h. However, the uptake rate at 7 h was not significantly higher than that at 5 h.

The biodistribution of liposome-entrapped ^{99m}Tc-labeled antisense oligonucleotides

The biodistribution of liposome-entrapped ^{99m}Tc-labeled antisense oligonucleotides are shown in Table 1. The endothelial system played a main role in biodistribution, and accumulated the greater part of the injected dose. The radioactive counts in the tumor tissue increased within 2 h and gradually reached the peak at 2 h, then dropped down sharply.

Table 1 Course of biodistribution of liposome-entrapped ^{99m}Tc-labeled antisense oligonucleotides in tumor-bearing nude mice (mean±SD, percent of injected dose, n = 5 mice for each time)

Tissue	0.5 h	1 h	2 h	4 h
Liver	8.78±0.63	9.16±1.14	7.92±0.38 ^c	8.97±0.12 ^c
Spleen	6.78±0.37 ^c	8.86±0.60	7.37±0.64 ^c	8.02±0.23 ^c
Kidney	4.89±0.67 ^a	2.90±1.19 ^a	3.07±0.18 ^{ac}	0.47±0.02 ^{ac}
Lung	10.23±1.02	13.37±0.84	12.21±0.42 ^a	10.20±0.50 ^c
Heart	7.18±0.13	8.78±1.01	7.25±0.18	5.28±0.45 ^{ac}
Blood	5.51±0.24 ^a	4.55±0.15	2.81±0.11 ^{ac}	2.61±0.06 ^{ac}
Bone	1.84±0.64 ^a	3.14±1.04 ^a	1.43±0.24 ^{ac}	1.02±0.32 ^{ac}
Muscle	2.27±0.37 ^a	1.36±0.60 ^{ac}	1.69±0.91 ^{ac}	2.85±0.26 ^a
Stomach	12.45±0.62 ^a	13.77±0.38	10.63±0.35	6.70±0.44 ^{ac}
Intestines	4.54±0.42 ^a	6.68±4.14	7.76±0.34 ^c	8.44±0.63 ^c
Brain	2.24±0.42 ^a	2.16±2.10 ^{ac}	0.68±0.06 ^{ac}	0.52±0.06 ^{ac}
Tumor	6.12±0.31 ^a	8.09±0.86	13.46±0.20 ^a	4.58±0.45 ^a

^aP<0.05 vs that of liver tissue ^cP<0.05 vs that of tumor tissue.

Antisense imaging

Anterior imaging at 1 h after intravenous injection of liposome-entrapped ^{99m}Tc-labeled antisense oligonucleotides showed that little accumulation of radioactivity might be seen in the right middle flank which was the place of tumor. Anterior imaging demonstrated a little accumulation of radioactivity in tumor site at 1.5 h (Figure 1), and a circular abnormal accumulation focus of radioactivity in the location of tumor at 2 h (Figure 2), but no accumulation of radioactivity in the location of tumor at 24 h.

The ratios of radioactive counts in tumor tissue to that in the contralateral equivalent region

The ratio was the highest one (1.7332±0.2537) at 2 h after intravenous injection of liposome-entrapped ^{99m}Tc-labeled antisense oligonucleotides. It was significantly higher than

that at 4 and 6 h ($P < 0.05$). Although it was higher than that at 1.0 and 1.5 h, there was no statistical difference. These ratios are shown in Table 2.

Table 2 Ratios of the radioactive counts in tumor to that in the contralateral equivalent region of abdomen (mean \pm SD, $n = 5$ for each time point)

Time point (h)	Ratios
1.0	1.2266 \pm 0.1259
1.5	1.5597 \pm 0.0190
2.0	1.7332 \pm 0.2537
4.0	1.0182 \pm 0.0495 ^a
6.0	1.0199 \pm 0.0131 ^a

^a $P < 0.05$ vs ratio of 2.0 h.

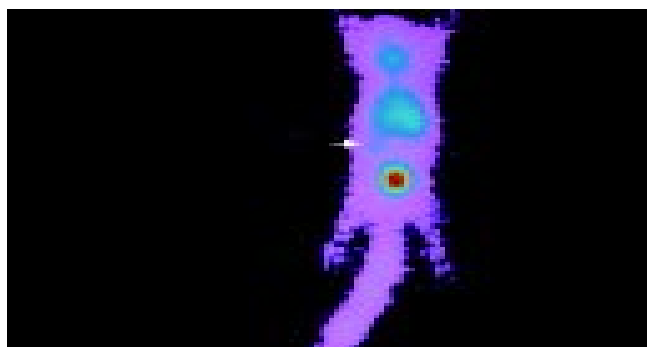


Figure 1 Anterior imaging at 1.5 h after intravenous injection of liposome-entrapped ^{99m}Tc-labeled antisense oligonucleotides. A little accumulation of radioactivity in tumor site, the right middle flank (arrow) could be observed.

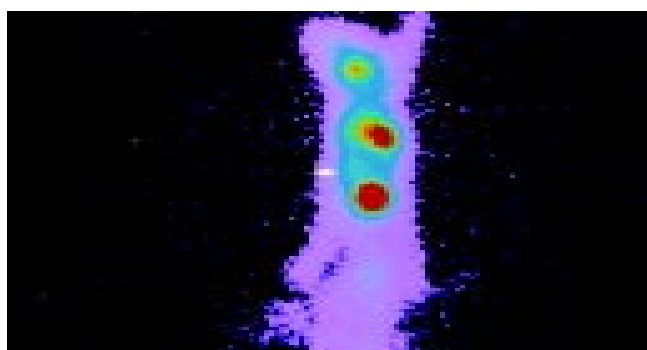


Figure 2 Anterior imaging at 2 h after intravenous injection of liposome-entrapped ^{99m}Tc-labeled antisense oligonucleotides. A circular abnormal accumulation focus was observed in the location of tumor (arrow).

DISCUSSION

The possible advantages of delivering oligonucleotides into cells by liposomes are not only to increase the uptake rates of dividing and mitostatic cells, but also protect the oligonucleotides against degeneration by nucleases. It has been confirmed that the amount of oligonucleotides used can be decreased greatly as liposomes are adopted as vectors *in vitro*^[9-13].

The cellular uptake rates of the liposome-entrapped ^{99m}Tc-labeled antisense oligonucleotides are the key parameter to antisense imaging. The maximum cellular uptake rate of the LS-174-T (17.77 \pm 2.41%) was plenty enough for the experimental or clinical use, and could be applied for the following experiments: biodistribution and antisense imaging.

The biodistribution assay showed that the radioactive counts

per gram of the tumor tissue was in the middle level at 0.5 h after injection, increased as time prolonged within 2 h, and reached the peak at 2 h. The proportion of radioactive counts per gram of the tumor tissue to the total was 13.46 \pm 0.20%, which was significantly higher than that of the liver, spleen, kidney, blood, bone, muscle, intestines and brain. The ratio of radioactive counts in the tumor to that in the blood was 4.79, and to that in the muscle was 7.96. It was thus evident that enough liposome-entrapped ^{99m}Tc-labeled antisense oligonucleotides were accumulated in the tumor tissue. The tumor could be observed clearly so long as radioactivity in the tissues around it was comparatively low.

Delong *et al.*^[14] studied the biodistribution of ^{99m}Tc-labeled phosphorothioate oligonucleotides without using liposomes as carriers. Their investigation demonstrated that radioactivity in the tumor tissue was only 2% to 3%. However, in our study, liposomes were used as vectors, and 4.58% to 13.46% of the total radioactivity could be accumulated in the tumor. Radioactivity was 2.29 to 4.49 times higher than that reported by Delong *et al.*^[14]. Thus, the uptake rates of the tumor tissue can be increased greatly by using liposomes as carriers. Accordingly, liposome is an effective vector in antisense imaging.

The whole body scan in the tumor bearing nude mice showed that the tumor was observed clearly at 2 h after intravenous injection of the liposome-entrapped ^{99m}Tc-labeled antisense oligonucleotides. It was evident that the imaging of the liver above the tumor and the bladder below the tumor was more clear than that of the tumor. They could influence the imaging of the tumor. However, the interference of the bladder can easily be decreased by diuretic or drinking a certain quantity of water, which is a routine clinical method of whole body bone scan. But the influence of the liver needs further investigation.

Although the imaging of the liver will influence the quality of the antisense imaging, our primary success on the tumor-bearing nude mice with ^{99m}Tc-labeled antisense oligonucleotides may contribute to the molecular nuclear medicine progress.

In conclusion, liposome-entrapped ^{99m}Tc-labeled antisense oligonucleotides with high cellular uptake rates can be accumulated by tumor in the tumor bearing-nude mice, and be able to show the colon carcinoma accurately, was worthy of being developed into a new radiopharmaceuticals for diagnosis^[15]. This will provide a new strategy for the early diagnosis of the colon carcinoma.

REFERENCES

- 1 Gauchez AS, Du Moulinet D'Hardemare A, Lunardi J, Vuillez JP, Fagret D. Potential use of radiolabeled antisense oligonucleotides in oncology. *Anticancer Res* 1999; **19**: 4989-4997
- 2 Zheng J, Tan T. The application of radionuclide antisense therapy for malignant tumours. *Nucl Med Commun* 2001; **22**: 469-472
- 3 Kang Y, Cortina R, Perry RR. Role of *c-myc* in tamoxifen-induced apoptosis estrogen-independent breast cancer cells. *J Natl Cancer Inst* 1996; **88**: 279-284
- 4 Dewanjee MK, Ghafouripour AK, Kapadvanjwala M, Dewanjee S, Serafini AN, Lopez DM, Sfakianakis GN. Noninvasive imaging of *c-myc* oncogene messenger RNA with indium-111-antisense probes in a mammary tumor-bearing mouse model. *J Nucl Med* 1994; **35**: 1054-1063
- 5 Hjelstuen OK, Tonnesen HH, Bremer PO, Verbruggen AM. 3'-^{99m}Tc-labeling and biodistribution of a CAPL antisense oligodeoxynucleotide. *Nucl Med Biol* 1998; **25**: 651-657
- 6 Zhang YM, Ruszkowski M, Liu N, Liu C, Hnatowich DJ. Cationic liposomes enhance cellular/nuclear localization of ^{99m}Tc-antisense oligonucleotides in target tumor cells. *Cancer Biother Radiopharm* 2001; **16**: 411-419
- 7 Liu G, Zhang S, He J, Liu N, Gupta S, Ruszkowski M, Hnatowich DJ. The influence of chain length and base sequence on the pharmacokinetic behavior of ^{99m}Tc-morpholinos in mice.

- Q J Nucl Med* 2002; **46**: 233-243
- 8 **Hnatowich DJ**, Mardirossian G, Fogarasi M, Sano T, Smith CL, Cantor CR, Rusckowski M, Winnard P Jr. Comparative properties of a technetium-99m-labeled single-stranded natural DNA and a phosphorothioate derivative *in vitro* and in mice. *J Pharmacol Exp Ther* 1996; **276**: 326-334
 - 9 **Ma DD**, Wei AQ. Enhanced delivery of synthetic oligonucleotides to human leukaemic cells by liposomes and immunoliposomes. *Leuk Res* 1996; **20**: 925-930
 - 10 **Roport C**, Lavignon M, Dubernet C, Couvreur P, Malvy C. Oligonucleotides encapsulated in pH sensitive liposomes are efficient toward Friend retrovirus. *Biochem Biophys Res Commun* 1992; **183**: 879-885
 - 11 **Zelphati O**, Zon G, Leserman L. Inhibition of HIV-1 replication in cultured cells with antisense oligonucleotides encapsulated in immunoliposomes. *Antisense Res Dev* 1993; **3**: 323-338
 - 12 **Kanamaru T**, Takagi T, Takakura Y, Hashida M. Biological effects and cellular uptake of *c-myc* antisense oligonucleotides and their cationic liposome complexes. *J Drug Target* 1998; **5**: 235-246
 - 13 **Moreira JN**, Hansen CB, Gaspar R, Allen TM. A growth factor antagonist as a targeting agent for sterically stabilized liposomes in human small cell lung cancer. *Biochim Biophys Acta* 2001; **1514**: 303-317
 - 14 **Delong RK**, Nolting A, Fisher M, Chen Q, Wickstrom E, Kligshsteyn M, Demirdji S, Caruthers M, Juliano RL. Comparative pharmacokinetics, tissue distribution, and tumor accumulation of phosphorothioate, phosphorodithioate, and methylphosphonate oligonucleotides in nude mice. *Antisense Nucleic Acid Drug Dev* 1997; **7**: 71-77
 - 15 **Zheng J**, Tan T, Zhang C, Li Y, Liang Z, Tu J. Preparation of liposome-mediated 99m-technetium-labeled antisense oligonucleotides of *c-myc* mRNA. *Shengwu Yixue Gongchengxue Zazhi* 2003; **20**: 704-707

Edited by Kumar M Proofread by Xu FM

Inhibition of mouse hepatocyte apoptosis via anti-Fas ribozyme

Min Zhang, Wei He, Fang Liu, Ping Zou, Juan Xiao, Zhao-Dong Zhong, Zhong-Bo Hu

Min Zhang, Wei He, Fang Liu, Ping Zou, Juan Xiao, Zhao-Dong Zhong, Zhong-Bo Hu, Institute of Hematology, Union Hospital, Tongji Medical College, Huazhong University of Science and Technology, Wuhan 430022, Hubei Province, China

Supported by the National Natural Science Foundation of China, No. 30240022

Correspondence to: Professor Ping Zou, Institute of Hematology, Union Hospital, Tongji Medical College, Huazhong University of Science and Technology, Wuhan 430022, Hubei Province, China. zhangmin35@yahoo.com.cn

Telephone: +86-27-85726880

Received: 2003-10-10 **Accepted:** 2003-12-16

Abstract

AIM: To investigate the effects of anti-Fas ribozyme on Fas expression and apoptosis in primary cultured mouse hepatocytes.

METHODS: Mouse hepatocytes were isolated by using collagenase irrigation. A hammerhead ribozyme targeting the Fas mRNA was constructed, and transfected into mouse hepatocytes via Effectene. Then Fas expression in mouse hepatocytes was detected by RT-PCR and western blotting. After being treated with anti-Fas antibody (JO₂), hepatocytes viability was measured with MTT assay. Caspase-3 proteolytic activity was detected, and cell apoptosis was measured according to Annexin V-FITC apoptosis detection kit.

RESULTS: Fas expressed in primary mouse hepatocytes. Fas expression in hepatocytes transfected with anti-Fas ribozyme was decreased remarkably and correlated with the resistance to Fas-mediated apoptosis as determined by flow cytometry and caspase-3 proteolytic activity.

CONCLUSION: Anti-Fas ribozyme can remarkably decrease the Fas expression in mouse hepatocytes, thus inhibit Fas-mediated apoptosis in hepatocytes. It is suggested that anti-Fas ribozyme could significantly increase the resistance of transplanted hepatocytes to apoptosis and improve the survival of transplanted hepatocytes.

Zhang M, He W, Liu F, Zou P, Xiao J, Zhong ZD, Hu ZB. Inhibition of mouse hepatocyte apoptosis via anti-Fas ribozyme. *World J Gastroenterol* 2004; 10(17): 2567-2570
<http://www.wjgnet.com/1007-9327/10/2567.asp>

INTRODUCTION

Liver transplantation is one of the efficient ways to treat liver function failure and liver necrosis induced by all kinds of diseases^[1,2]. But Fas expresses in hepatocytes and Fas-mediated apoptosis significantly impairs graft survival^[3-7]. Anti-Fas hammerhead ribozyme was designed and synthesized to target directly at position 596 of the Fas RNA, and cloned into a eukaryotic vector, which was transfected into primary cultured mouse hepatocytes via a vector named Effectene different from usual Lipofectamine reagents^[8]. Then the effects of anti-Fas ribozyme on Fas expression and apoptosis of mouse hepatocytes were investigated.

MATERIALS AND METHODS

Reagents and materials

E.coli DH-5 α was a kind gift from Department of Immunology, Tongji Medical College. Prokaryotic vector pBSKU6 and green fluorescent protein pEGFPC1 were given as presents by Dr. Kongxinjuan. All restriction endonucleases and T₄DNA ligase were products of Promega Company. Mini plasmid DNA extraction kit, gel DNA purification kit and DL-2000 DNA marker were purchased from TaKaRa Company. Transfection reagent Effectene was purchased from Qiagen Company. Reverse transcriptional kit, dNTP, Taq DNA polymerase were products of MBI Company. Fluorescein isothiocyanate (FITC)-conjugated Annexin V kit was product of Bender Company (purchased from Jingmei Company). FITC-conjugated anti-mouse Fas antibody (JO₂) was product of PharMingen Company. Caspase-3 activity detection kit was product of Clontech Company. MTT reagent was purchased from Sigma Company.

Synthesis and cloning of ribozyme

GUA triplets located at 596 of the mouse Fas RNA were selected as the cleavage site of ribozyme^[9], two small nucleotide sequences complementary to flanks of the cleavage site of target RNA were located before and after hammerhead structure—the conservative core catalytic sequence of ribozyme, which can form typical active cleavage structure through complementation^[10]. The cDNAs encoding the anti-Fas ribozyme were composed of two complementary strands each about 50 nt, which were terminated with *Bam*H I and *Xba* I: a 5' TCTAGAGATATATAAACTGATGAGTCCGTGAGGACGAAACAAGTGATCC 3', b 5' GGATC CACTTGT TTCGTCCTCACGGACTCATCAGTTTATATATCTCTAGA 3'. All cDNAs were synthesized by Shanghai Shenggong Company. The ribozyme was cloned into the *Bam*H I and *Xba* I sites of the pBSKU6, which was named as U6-RZ596, and digested and sequenced to be correct. Then this recombinant plasmid was used as template to get a fragment including U6 promoter and ribozyme by using PCR. The fragment was subcloned into the *Mlu* I site of the pEGFPC1, which was named as pU6-RZ596, and testified to be correct.

Isolation, cultivation and transfection of primary mouse hepatocytes

Healthy adult mice were spiled via portal vein after being anaesthetized and irrigated with a constant flux at about 9 mL/min. First Hanks solution was used without Ca²⁺ and Mg²⁺, then 0.2 g/L collagenase solution for 8 min^[11,12]. At last liver tissues were lacerated bluntly and digested vibrantly for 15 min in 37 °C bath water, and filtrated through nylon net and washed with PBS twice. Cells were resuspended in RPMI 1640 supplemented with 100 mL/L FBS and counted. Cell viability was 90-92%. Cell count was adjusted to 2×10⁶/mL and cells were cultured in a humidified 50 mL/L CO₂ atmosphere at 37 °C. Cells were collected and grouped as following: empty control; cells transfected with pEGFPC1; cells transfected with pU6-RZ596. Transfection was performed according to the instructions of Effectene reagent. Cells were cultured for 48 h, the stably transfected cells were selected by culturing in medium containing G418 (600 μg/mL).

Detection of Fas mRNA expressed in hepatocytes by using RT-PCR

Total RNA was extracted from all above-mentioned groups by using TriZol reagent. After cDNA was synthesized, PCR reaction was performed, β -actin was used as control. The employed primers were as follows: Fas sense primer 5'-GCTGCAGACATGCTGTGGATC-3' and anti-sense primer 5'-TCACAGCCAGGA GAATCGCAG-3', β -actin sense primer 5'-GACGATGATATTGCCGACT-3' and anti-sense primer 5'-GATACCACGCTTGC TCTGAG-3'. Reaction conditions for PCR were: pre-denaturation for 3 min at 95 °C, 30 cycles of denaturation for 30 s at 95 °C, annealing for 45 s at 58 °C, extension for 45 s at 72 °C, and extension for 3 min at 72 °C. PCR products were run on 15 g/L agarose gel.

Detection of Fas protein expressed in hepatocytes by western blot

Three groups of cells were collected regularly and lysed in soluble buffer, then the proteins were measured as 0.4 μ g/ μ L, and electrophoresed in 100 g/L SDS-polyacrylamide minigels. The first antibody was rabbit anti-mouse-Fas antibody (1:200). The second antibody was goat anti-rabbit-IgG (1:5 000). At last the color was developed by ECL system.

Detection of caspase-3 protease activity

Treated with JO₂ (5 μ g/mL) for 24 h under common growth condition, apoptosis of three-groups of cells were induced. Meanwhile the negative control without apoptosis and apoptosis cells treated with caspase-3 inhibitor (DEVD-fmk) were established. After being collected, cells were treated with cell lysis buffer sufficiently. The supernatant was retained (including protein needed), and then the procedure was performed according to the instructions of caspase-3 activity detection kit. The optical density (A) was measured at 405 nm.

Detection of cell viability via MTT assay

Grouped and treated as above, cells were inoculated into 96-well plates at a concentration about 10⁵/mL (100 μ L/well). After incubation with 10 μ L MTT(0.5 mg/mL) for 4 h at 37 °C, the formazan crystals were dissolved in 100 μ L DMSO, then the A was measured at 570 nm.

Detection of apoptosis through FACS

Three groups of cells treated with anti-Fas antibody JO₂ and the empty control were conjugated with Annexin V-FITC and PI respectively. Cell apoptosis was analyzed by flow cytometry.

RESULTS

Effects of ribozyme on Fas expression

Fas and β -actin PCR amplification generated amplicons of 419 bp and 186 bp respectively. Through scanning the luminescence, the ratio of Fas/ β -actin was analyzed by using gel image analysis system. The negative control was 1.1; mouse hepatocytes transfected with pEGFPC1 was 0.98; hepatocytes transfected with pU6-RZ596 was 0.43. It was clear that Fas mRNA expression in cells transfected with anti-Fas ribozyme was lower than that in control and cells transfected with empty vector (Figure 1).

Western blotting displayed Fas protein expressed in cells transfected with pU6-RZ596 was much lower than that expressed in control and cells transfected with pEGFPC1, which was consistent with the results of RT-PCR (Figure 2).

Effect of anti-Fas ribozyme on caspase-3 activity

After 24 h of stimulation with JO₂, caspase-3 activity of mouse hepatocytes was specifically inhibited by a caspase-3 inhibitor. Compared with negative control, caspase-3 activities of other groups transfected with pEGFPC1 and pU6-RZ596 were 95% and 45% respectively (Figure 3).

Effect of anti-Fas ribozyme on cell viability

After induction of apoptosis of mouse hepatocytes through stimulation with JO₂, cell viability was detected by MTT assay. Compared with negative control, cell viabilities of other groups transfected with pEGFPC1 and pU6-RZ596 were 98% and 208% respectively (Figure 4).

Inhibition of Fas-mediated apoptosis in mouse hepatocytes

Cell apoptosis was induced as the method mentioned above. Apoptosis rates of cells in control, mock-transfected and pU6-RZ596-transfected groups were 86%, 87% and 35%, respectively (Figure 5).

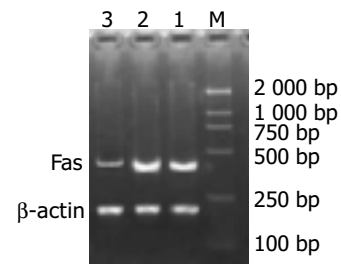


Figure 1 Fas gene transcription in all groups. M: DL-2000 DNA marker, Lanes 1-3: Empty control, mock-transfected group and pU6-RZ596-transfected group.

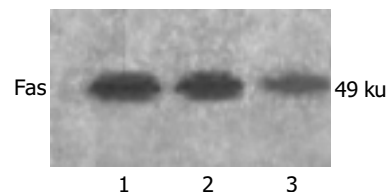


Figure 2 Fas protein expression in all groups. M: Marker; Lanes 1-3: Empty control, mock-transfected group and pU6-RZ596-transfected group.

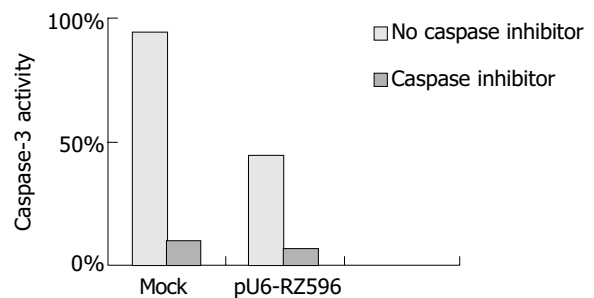


Figure 3 Detection of caspase-3 activity in all groups.

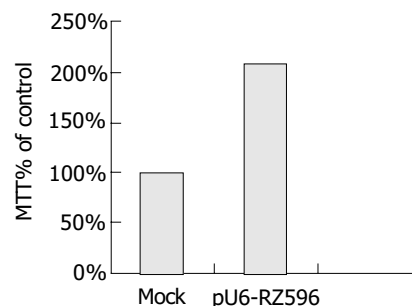


Figure 4 Stimulated with JO₂ for 24 h, cells viabilities of control, mock-transfected and pU6-RZ596-transfected groups were detected by MTT assay.

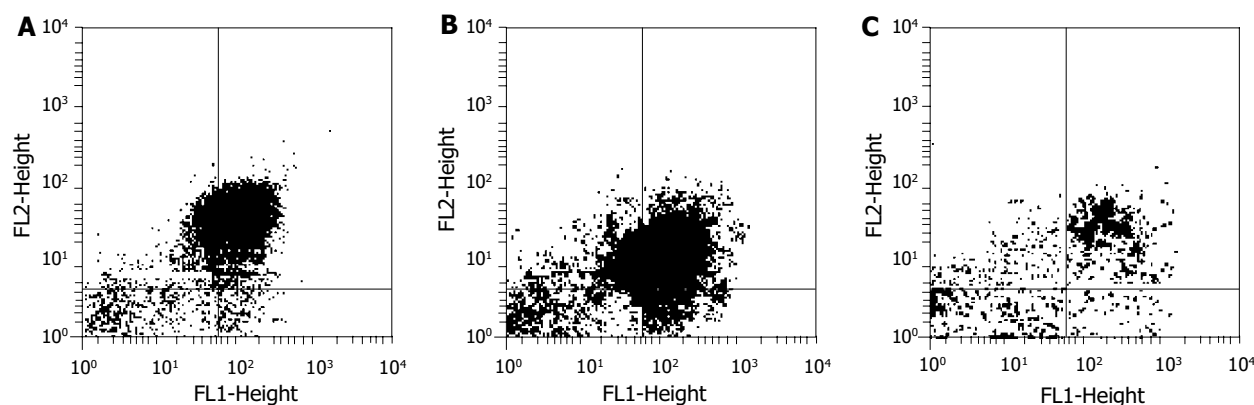


Figure 5 Detection of apoptosis of hepatocytes through cytometry. A: Apoptosis rate of control group was 86%; B: Apoptosis rate of mock-transfected cells was 87%; C: Apoptosis rate of pU6-RZ596-transfected cells was 35%.

DISCUSSION

Usually in clinic the hepatocytes of patients with acute or chronic liver failure show denaturation, necrosis and function failure. Existing pathogenic therapy and usual allopathy can not compensate functions of hepatocytes^[12,13]. Now, the most efficient way is liver transplantation, but grafts survival is one of the important factors to affect whether liver transplantation is successful.

Primary mouse hepatocytes were isolated through two-step irrigation method^[14], in which Fas expression was detected by RT-PCR and Western blotting. Treated with anti-Fas antibody JO₂, apoptosis of hepatocytes was induced with decreased viability. So hammerhead ribozyme targeting directly at 596 GUA triplets of Fas mRNA was constructed to efficiently block out Fas gene and decrease apoptosis of hepatocytes. As an RNA molecule with catalysis function^[15], ribozyme can bind and cleave target RNA to inhibit gene expression. Hammerhead ribozyme is widely used in gene therapy because of its many superiorities^[16], including small molecule weight, easy to design and synthesis, *etc.* Anti-Fas ribozyme was transfected into mouse hepatocytes by using Effectene reagent, then the stable clone was selected to investigate the inhibition action of ribozyme on Fas-mediated apoptosis. Results displayed that expression of Fas mRNA and protein in cells transfected with anti-Fas ribozyme was remarkably lower than that in control and mock-transfected cells. After stimulation with apoptosis inducer JO₂ (imitating the role of FasL *in vivo*) for 24 h, apoptosis rate of cells transfected with anti-Fas ribozyme was obviously lower than that of negative control and mock-transfected cells. Accordingly, caspase-3 activity of ribozyme-transfected cells was much lower than that of other groups, but cell viability was higher than the other two groups.

Apoptosis activates a series of proteases to induce programmed death of target cells through two ways including death receptor way and mitochondria way^[17,18]. The final effect of the two ways is activity of caspase-3, that is to say caspase-3 is the common channel of two apoptosis ways^[19]. Therefore, caspase-3 activity was increased in apoptosis and correlated with apoptosis rate positively. Anti-Fas ribozyme could not only decrease Fas expression but also weaken caspase-3 activity to reduce apoptosis induced by anti-Fas antibody. It is clear that hammerhead ribozyme targeting at 596 site of Fas RNA in this research can efficiently cleave Fas mRNA, which decreases not only the Fas expression but also its function. In existence of factors inducing apoptosis, ability of hepatocytes transfected with ribozyme against apoptosis was enhanced and cell viability was increased, which was coincident with study results of Dagmer about primary mouse islet β cells and insulinoma cells^[20,21].

In short, anti-Fas ribozyme not only prevents Fas expression in mouse hepatocytes but also inhibits Fas-mediated apoptosis to improve cell survival after being transfected into hepatocytes, which afford strong assurance for successful liver transplantation. Further research should be focused on clinical application of anti-Fas ribozyme and selection of more efficient, highly specific and low toxic vectors^[22-24].

REFERENCES

- 1 Sato Y, Yamamoto S, Takeishi T, Nakatsuka H, Kokai H, Hatakeyama K. New hepatic vein reconstruction by double expansion of outflow capacity of left-sided liver graft in living-donor liver transplantation. *Transplantation* 2003; **76**: 882-884
- 2 Akamatsu N, Sugawara Y, Kaneko J, Sano K, Imamura H, Kokudo N, Makuuchi M. Effects of middle hepatic vein reconstruction on right liver graft regeneration. *Transplantation* 2003; **76**: 832-837
- 3 Sorom AJ, Nyberg SL, Gores GJ. Keratin, fas, and cryptogenic liver failure. *Liver Transpl* 2002; **8**: 1195-1197
- 4 Rivero M, Crespo J, Mayorga M, Fabrega E, Casafont F, Pons-Romero F. Involvement of the Fas system in liver allograft rejection. *Am J Gastroenterol* 2002; **97**: 1501-1506
- 5 Uchiyama H, Kishihara K, Minagawa R, Hashimoto K, Sugimachi K, Nomoto K. Crucial Fas-Fas ligand interaction in spontaneous acceptance of hepatic allografts in mice. *Immunology* 2002; **105**: 450-457
- 6 Wang H, Chen XP, Qiu FZ. Overcoming multi-drug resistance by anti-MDR1 ribozyme. *World J Gastroenterol* 2003; **9**: 1444-1449
- 7 Dunham CM, Murray JB, Scott WG. A Helical twist-induced conformational switch activates cleavage in the hammerhead ribozyme. *J Mol Biol* 2003; **332**: 327-336
- 8 Nikcevic G, Kovacevic-Grujicic N, Stevanovic M. Improved transfection efficiency of cultured human cells. *Cell Biol Int* 2003; **27**: 735-737
- 9 Persson T, Hartmann RK, Eckstein F. Selection of hammerhead ribozyme variants with low Mg²⁺ requirement: importance of stem-loop II. *ChemBiochem* 2002; **3**: 1066-1071
- 10 Murray JB, Dunham CM, Scott WG. A pH-dependent conformational change, rather than the chemical step, appears to be rate-limiting in the hammerhead ribozyme cleavage reaction. *J Mol Biol* 2002; **315**: 121-130
- 11 Azuma H, Hirose T, Fujii H, Oe S, Yasuchika K, Fujikawa T, Yamaoka Y. Enrichment of hepatic progenitor cells from adult mouse liver. *Hepatology* 2003; **37**: 1385-1394
- 12 Tanimizu N, Nishikawa M, Saito H, Tsujimura T, Miyajima A. Isolation of hepatoblasts based on the expression of Dlk/Pref-1. *J Cell Sci* 2003; **116**(pt 9): 1775-1786
- 13 Wagner ME, Kaufmann P, Fickert P, Trauner M, Lackner C, Stauber RE. Successful conservative management of acute hepatic failure following exertional heatstroke. *Eur J Gastroenterol*

- Hepatology* 2003; **15**: 1135-1139
- 14 **Crossin JD**, Muradali D, Wilson SR. US of liver transplants: normal and abnormal. *Radiographics* 2003; **23**: 1093-1114
- 15 **Heneghan MA**, Zolfino T, Muiesan P, Portmann BC, Rela M, Heaton ND, O'grady JG. An evaluation of long-term outcomes after liver transplantation for cryptogenic cirrhosis. *Liver Transpl* 2003; **9**: 921-928
- 16 **Musallam L**, Ethier C, Haddad PS, Denizeau F, Bilodeau M. Resistance to Fas-induced apoptosis in hepatocytes: role of GSH depletion by cell isolation and culture. *Am J Physiol Gastrointest Liver Physiol* 2002; **283**: G709-718
- 17 **Steitz TA**, Moore PB. RNA, the first macromolecular catalyst: the ribosome is a ribozyme. *Trends Biochem Sci* 2003; **28**: 411-418
- 18 **Khan AU**, Lal SK. Ribozymes: a modern tool in medicine. *J Biomed Sci* 2003; **10**: 457-467
- 19 **Shi G**, Wu Y, Zhang J, Wu J. Death decoy receptor TR6/DcR3 inhibits T cell chemotaxis *in vitro* and *in vivo*. *J Immunol* 2003; **171**: 3407-3414
- 20 **Curtin JF**, Cotter TG. Live and let die: regulatory mechanisms in Fas-mediated apoptosis. *Cell Signal* 2003; **15**: 983-992
- 21 **Ientile R**, Campisi A, Raciti G, Caccamo D, Curro M, Cannavo G, Li Volti G, Macaione S, Vanella A. Cystamine inhibits transglutaminase and caspase-3 cleavage in glutamate-exposed astroglial cells. *J Neurosci Res* 2003; **74**: 52-59
- 22 **Klein D**, Denis M, Ricordi C, Pastori RL. Assessment of ribozyme cleavage efficiency using reverse transcriptase real-time PCR. *Mol Biotechnol* 2000; **14**: 189-195
- 23 **Klein D**, Ricordi C, Pugliese A, Pastori RL. Inhibition of Fas-mediated apoptosis in mouse insulinoma betaTC-3 cells via an anti-Fas ribozyme. *Hum Gene Ther* 2000; **11**: 1033-1045
- 24 **Mergia A**, Heinkelein M. Foamy virus vectors. *Curr Top Microbiol Immunol* 2003; **277**: 131-159

Edited by Zhu LH and Chen WW Proofread by Xu FM

A novel process for production of hepatitis A virus in Vero cells grown on microcarriers in bioreactor

Ming-Bo Sun, Yan-Jun Jiang, Wei-Dong Li, Ping-Zhong Li, Guo-Liang Li, Shu-De Jiang, Guo-Yang Liao

Ming-Bo Sun, Yan-Jun Jiang, Wei-Dong Li, Ping-Zhong Li, Guo-Liang Li, Shu-De Jiang, Guo-Yang Liao, Institute of Medical Biology, Chinese Academy of Medical Sciences, Peking Union Medical College, Kunming 650118, Yunnan Province, China
Supported by the Natural Science Foundation of Yunnan Province, No.1999C0023Q

Correspondence to: Guo-yang Liao, Institute of Medical Biology, Chinese Academy of Medical Sciences, 379 Jiaoling Road, Kunming 650118, Yunnan Province, China. liaogy@21cn.com

Telephone: +86-871-8334330

Received: 2003-12-28 **Accepted:** 2004-01-08

Abstract

AIM: To develop a novel process for production of HAV in Vero cells grown on microcarriers in a bioreactor.

METHODS: Vero cells infected with HAV strain W were seeded at an initial density of 1×10^5 cells/mL into a 7-L bioreactor containing Cytodex-I microcarriers. During the stage of cell proliferation, the following conditions were applied: pH 7.2 ± 0.2 , temperature 37 ± 0.2 °C, dissolved oxygen 40% of air saturation and agitation rate 40 r/min. After the stage of virus culture started, the culture conditions were altered to pH 7.2 ± 0.2 , temperature 35 ± 0.2 °C, dissolved oxygen 25% of air saturation, agitation rate 50 r/min and perfusion of fresh medium at a flux of 20 mL/h. During the course of fermentation, cell density, HAV antigen titre, glucose, lactate and ammonia levels were monitored. A control experiment using conventional static culture was conducted in the T150 flask.

RESULTS: After a 28-d cultivation, cell density increased to 14.0×10^5 cells/mL in the bioreactor, 5.6×10^9 viable cells and 4 000 mL virus suspension with a titre of 1:64 were harvested. The viral antigen output per cell unit in the bioreactor was 3-fold higher than that in the T150 flask. Meanwhile the metabolic mode of Vero cells did not change after the infection with HAV strain W.

CONCLUSION: The process for production of HAV in Vero cells grown on microcarriers in a bioreactor is a novel, efficient and practical way to obtain virus antigen for vaccine purpose. This approach produces more cells and HAV antigen than the conventional static culture. With further improvement, it is possible to be used for the production of hepatitis A vaccine.

Sun MB, Jiang YJ, Li WD, Li PZ, Li GL, Jiang SD, Liao GY. A novel process for production of hepatitis A virus in Vero cells grown on microcarriers in bioreactor. *World J Gastroenterol* 2004; 10(17): 2571-2573

<http://www.wjgnet.com/1007-9327/10/2571.asp>

INTRODUCTION

Hepatitis A continues to be one of the most frequently reported infectious diseases with a worldwide distribution, and the

continued occurrence of extensive community wide outbreaks indicates that hepatitis A remains a major public health problem. The availability of hepatitis A vaccine provides the opportunity to substantially lower disease incidence and potentially eliminate infection^[1,2]. Several inactivated and live-attenuated hepatitis A vaccines have been developed. Due to the high protective efficacy, immunogenicity and safety, the inactivated vaccines are more favored^[3-6]. At present several inactivated hepatitis A vaccines such as HAVRIX[®], VAQTA[®], AVAXIM[®] and EPAXAL[®] are commercially available^[7-9]. Inactivated hepatitis A vaccine is prepared by methods similar to those used for inactivated poliovirus vaccines. Cell-culture-adapted virus is propagated in human fibroblast cells, usually in MRC-5 cells, purified from cell lysates by ultrafiltration and exclusion gel chromatography or other methods, inactivated with formalin, and adsorbed to an aluminum hydroxide adjuvant. Compared with the production of live-attenuated vaccines, much larger quantities of HAV antigen are required for the production of inactivated vaccines. Thus the production of inactivated hepatitis A vaccines is usually hampered by the difficulty of preparation of large amounts of virus antigens in the conventional static flask or roller bottle cultures. The technique of microcarrier cell culture was first developed in the late 1960s and has been used successfully for the production of rabies and poliomyelitis vaccines. One definite advantage of microcarrier cell culture is the ability to offer a high product output, which may help to solve the shortage of virus antigens for production of inactivated hepatitis A vaccines^[10-13].

As mentioned above, most hepatitis A vaccines are commonly prepared by cultivation of HAV in human fibroblast cells including MRC-5 cells. No vaccine is produced by microcarrier technology due to the unsuitability of growth for MRC-5 cells on microcarriers. For HAV production in a microcarrier system it is necessary to establish suitable cells on microcarriers. Vero cells can grow well on microcarriers. But HAV is very difficult to adapt to grow in Vero cells. There are few reports about the isolation and adaptation of HAV in Vero cells. Until recently, no report about the production of hepatitis A vaccines in Vero cells grown on microcarriers in bioreactor is available. To verify the feasibility of this approach, HAV strain W was isolated and adapted in Vero cells in our previous work. This study described the production of HAV strain W in Vero cells grown on Cytodex-I microcarriers in a 7-L bioreactor.

MATERIALS AND METHODS

Bioreactor

A 7-L cell bioreactor (Applikon Co., Holland) was used. Its work volume is 4 L. The value of dissolved oxygen was regulated by importing air mixture with different ratios of O₂, N₂, CO₂ and air. The value of pH was controlled by addition of NaHCO₃.

Microcarrier

Cytodex-I microcarrier (Pharmacia Fine Chemicals, Uppsala, Sweden) was used.

Medium

Cells were grown in minimum essential medium (MEM; Gibco, Glasgow, UK) supplemented with 100 U/mL penicillin, 10 mmol/L

of glucose, 5 mmol/L of glutamine and 100 mL/L bovine calf serum. In both virus culture medium and the feeding medium, bovine calf serum was reduced to 2 %.

Cell line and virus

Vero cell line was obtained from ATCC and preserved at our laboratory. Vero cells were used between passages 142 and 146 in this study. HAV strain W was isolated and adapted in Vero cells at our laboratory. The antigen titre of HAV used for inoculation was 1:128.

Virus adsorption

Vero cells were seeded into the T150 flasks at the concentration allowing for the formation of a confluent monolayer in 4-5 d. The monolayer cells were trypsinized and collected to make cell suspension in a Bellco agitation bottle. The cell suspension was inoculated with HAV strain W and incubated at 35 °C with a stirring of 30 rpm for 6 h.

Bioreactor culture

Bioreactor culture was divided into two stages including cell proliferation and virus culture. Infected Vero cells were seeded into the 7-L bioreactor at an initial density of 1×10^5 cells/mL. During the stage of cell proliferation, the following conditions were applied: pH 7.2 ± 0.2 , temperature 37 ± 0.2 °C, dissolved oxygen 40% of air saturation and agitation rate 40 r/min. After the cell density reached to 1×10^6 cells/mL, stage of virus culture started and the used medium was replaced with maintenance medium. The culture conditions were altered to: pH 7.2 ± 0.2 , temperature 35 ± 0.2 °C, dissolved oxygen 25% of air saturation and agitation rate 50 r/min. Meanwhile, perfusion was started and the perfusion rate was modulated to 20 mL/h. After a 28-d culture, infected cells were trypsinized and collected for the harvest of HAV antigen.

In a further study, M199 medium was used instead of MEM during virus culture. A circulating equipment was used to increase the dissolved oxygen in the feeding medium.

Conventional static culture

Infected Vero cells were seeded at an initial density of 1×10^5 cells/mL into the T150 flask containing 150 mL MEM medium. The cultures were incubated at 35 °C and the medium was replaced each week. After a 28-d culture, infected cells were trypsinized and collected for the harvest of HAV antigen.

Metabolite analysis

Samples taken from the cultures in the bioreactor were centrifuged at 1 500 r/min for 10 min. The supernatants were stored at -20 °C until tested. Glucose, ammonia and lactate concentrations were monitored by enzymatic assays, using specific assay kits (16-UV, 171-UV and 826-UV for glucose, ammonia and lactate respectively; Sigma, St. Louis, USA).

HAV antigen titre assay

Harvested cells were applied to three cycles of freezing and thawing following ultrasonication. After centrifugation at 1 500 r/min for 10 min, HAV antigen titre in the supernatant was determined by ELISA.

RESULTS

Growth and metabolism of infected Vero cells in bioreactor

Seventy-eight hours after the seeding, infected Vero cell density increased from 1×10^5 cells/mL to 11.17×10^5 cells/mL. At this point, the mode of bioreactor culture was switched from cell proliferation to virus culture. During the stage of virus culture, the cell density was kept above 1×10^6 cells/mL, reaching a maximum

of 15.60×10^5 cells/mL at 402 h. It achieved 14.0×10^5 cells/mL at the end of virus culture, indicating a 14-fold increase over the initial cell density. The initial concentration of glucose was 7.8 mmol/L at the beginning of cell proliferation stage. As the cell density increased, the concentration declined. The rate of declination gradually became slow as a result of the feeding of fresh medium. The residual glucose concentration was 0.63 mmol/L at the end of virus culture. The initial concentrations of lactate and ammonia were 1.27 mmol/L and 0.18 mmol/L respectively at the beginning of cell proliferation and increased along with the increasing of cell density. The lactate level increased from 3.87 mmol/L to 12.68 mmol/L and ammonia level from 1.19 mmol/L to 2.68 mmol/L during the stage of virus culture. The rate of accumulation also became slow due to the feeding of fresh medium at the end of virus culture. Figure 1 shows the variations of cell density, glucose, lactate, and ammonia levels.

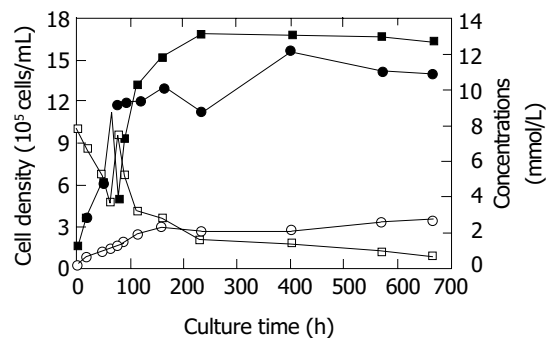


Figure 1 Growth and metabolism curves of Vero cells infected with HAV strain W. (●) Viable cell density (10^5 cells/mL), (□) Glucose (mmol/L), (■) Lactate (mmol/L), (○) Ammonia (mmol/L).

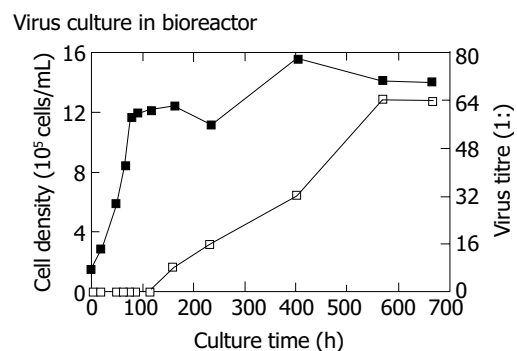


Figure 2 Production of HAV antigens by Vero cells grown on Cytodex-I microcarriers in a 7-litre bioreactor. (■) Viable cell density (10^5 cells/mL), (□) HAV antigen titre (1:).

Virus culture in bioreactor

No HAV antigen was detected during the stage of cell proliferation and at the early stage of virus culture. At 160 h, HAV antigen was first detected with a titre of 1:8 and achieved a maximum of 1:64 at 570 h (Figure 2). Four thousand millilitres of virus suspension with a titre of 1:64 was obtained at the end of virus culture.

Cell and antigen yields in flask

After a 28-d cultivation, 4×10^7 viable cells and 5 mL virus suspension with a titre of 1:128 were obtained from a T150 flask.

Improvement of virus culture in bioreactor

MEM medium was replaced by M199 medium, which contained richer nutrients and was more suitable for virus growth in cells. A circulating equipment was added to increase the dissolved oxygen in the feeding medium. With these

modifications, antigen titre achieved 1:128 in the harvested suspension.

DISCUSSION

In this study the growth kinetics and metabolic properties of Vero cells infected with HAV strain W were investigated. The results were similar to those of uninfected Vero cells in our previous work (Data not shown) and other studies^[14,15]. This indicated that the metabolic mode of Vero cells did not change after infection with HAV strain W.

The yield of viable cells was 5.6×10^9 in the bioreactor whereas 4×10^7 in the T150 flask. The former was 140-fold higher than the latter. The yield of HAV antigens was 4 000 mL with a titre of 1:64 in the bioreactor and equaled to the yield from 400 T150 flasks. Furthermore, per 10^5 cells produced 1 mL HAV antigens with a titre of 1:4.57 in a bioreactor compared with only a titre of 1:1.6 in the T150 flask, that is the antigen output per cell unit in the bioreactor was 3-fold higher than that in the T150 flask. The findings mentioned above demonstrated this process for the production of HAV in Vero cells grown on microcarriers in a bioreactor could provide much higher yields of viable cells and virus antigens than that in conventional static culture. The antigen output per cell unit was also apparently higher. The technique of microcarrier culture in a bioreactor could offer numerous advantages over traditional techniques, such as a high ratio of surface area to volume, an efficient monitoring and control of key process parameters including temperature, pH and dissolved oxygen. Moreover, the culture substrate conditions could be controlled exactly and regulated in batch or fed-batch operation. The optimal metabolism and physiological status of cells could be achieved through the feeding of fresh medium and removal of toxic metabolites. Thus a high cell density and product output rate could be easily achieved^[15-18].

In conclusion, the process for production of HAV in Vero cells grown on microcarriers in a bioreactor is a novel, efficient and practical way to obtain virus antigens for vaccine purpose. This approach produces more cells and HAV antigens than the conventional static culture. The optimal growth conditions for Vero cells and HAV strain W in a bioreactor are being further investigated to enhance the yield of virus antigens.

REFERENCES

- 1 **Zamir C**, Rishpon S, Zamir D, Leventhal A, Rimon N, Ben-Porath E. Control of a community-wide outbreak of hepatitis A by mass vaccination with inactivated hepatitis A vaccine. *Eur J Clin Microbiol Infect Dis* 2001; **20**: 185-187
- 2 **Van Damme P**, Banatvala J, Fay O, Iwarson S, McMahon B, Van Herck K, Shouval D, Bonanni P, Connor B, Cooksley G, Leroux-Roels G, von Sonnenburg F. Hepatitis A booster vaccination: is there a need? *Lancet* 2003; **362**: 1065-1071
- 3 **Demicheli V**, Tiberti D. The effectiveness and safety of hepatitis A vaccine: a systematic review. *Vaccine* 2003; **21**: 2242-2245
- 4 **Xu ZY**, Wang XY, Li RC, Meng ZD, Zhang Y, Gong J, Ma JC, Li YT, Zhao SJ, Li YP, Zhao YL, Huang QC, Lou D, Xia JL, Liu HB, Liu XL, Ouyang PY. Immunogenicity and efficacy of two live attenuated hepatitis A vaccines (H₂ strains and LA-1 strains). *Zhonghua Yixue Zazhi* 2002; **82**: 678-681
- 5 **Ren AG**, Ma JR, Feng FM, Xu YJ, Liu CB. Safety and immunogenicity of a new inactivated hepatitis A vaccine. *Zhonghua Shiyan He Linchuangbingduxue Zazhi* 2001; **15**: 357-359
- 6 **Ren YH**, Chen JT, Wu WT, Gong XJ, Zhang YC, Xue WH, Ren YF, Han LJ, Kang WX, Li SP, Liu CB. The study on the 0, 12 month vaccination schedule of Healive inactivated hepatitis A vaccine in children. *Zhonghua Liuxingbingxue Zazhi* 2003; **24**: 1013-1015
- 7 **Huang GB**, Wang ZG, Li RC. The investigation on the safety and immunogenicity of inactivated hepatitis A vaccine AVAXIM. *Zhonghua Liuxingbingxue Zazhi* 2000; **21**: 287-288
- 8 **Lingl6f T**, Van Hattum J, Kaplan KM, Corrigan J, Duval I, Jensen E, Kuter B. An open study of subcutaneous administration of inactivated hepatitis A vaccine (VAQTA®) in adults: safety, tolerability, and immunogenicity. *Vaccine* 2001; **19**: 3968-3971
- 9 **Usonis V**, Bakas6nas V, Valentelis R, Katiliene G, Vidzeniene D, Herzog C. Antibody titres after primary and booster vaccination of infants and young children with a virosomal hepatitis A vaccine (Epaxal®). *Vaccine* 2003; **21**: 4588-4592
- 10 **Williams JL**, Bruden DA, Cagle HH, McMahon BJ, Negus SE, Christensen CJ, Snowball MM, Bulkow LR, Fox-Leyva LK. Hepatitis A vaccine: immunogenicity following administration of a delayed immunization schedule in infants, children and adults. *Vaccine* 2003; **21**: 3208-3211
- 11 **Franco E**, Vitiello G. Vaccination strategies against hepatitis A in southern Europe. *Vaccine* 2003; **21**: 696-697
- 12 **Hennessey JP Jr**, Oswald CB, Dong ZY, Lewis JA, Sitrin RD. Evaluation of the purity of a purified, inactivated hepatitis A vaccine (VAQTA™). *Vaccine* 1999; **17**: 2830-2835
- 13 **Murdoch DL**, Goa K, Figgitt DP. Combined hepatitis A and B vaccines: a review of their immunogenicity and tolerability. *Drugs* 2003; **63**: 2625-2649
- 14 **Sun MB**, Zhang LJ, Liao GY, Li GL, Jiang SD. Physiology of Vero, CHO and Hybridoma cells cultured in bioreactor. *Zhongguo Shengwuzhipinxue Zazhi* 2001; **14**: 213-216
- 15 **Guan YH**, Kemp RB. Detection of the changing substrate requirements of cultured animal cells by stoichiometric growth equations validated by enthalpy balances. *J Biotechnol* 1999; **69**: 95-114
- 16 **Voigt A**, Zintl F. Hybridoma cell growth and anti-neuroblastoma monoclonal antibody production in spinner flasks using a protein-free medium with microcarriers. *J Biotechnol* 1999; **68**: 213-226
- 17 **Kallel H**, Rourou S, Majoul S, Loukil H. A novel process for the production of a veterinary rabies vaccine in BHK-21 cells grown on microcarriers in a 20-l bioreactor. *Appl Microbiol Biotechnol* 2003; **61**: 441-446
- 18 **Dürschmid M**, Landauer K, Simic G, Blüml G, Doblhoff-Dier O. Scalable inoculation strategies for microcarrier-based animal cell bioprocesses. *Biotechnol Bioeng* 2003; **83**: 681-686

Edited by Zhang JZ and Wang XL Proofread by Xu FM

Effect of interleukin-10 and platelet-derived growth factor on expressions of matrix metalloproteinases-2 and tissue inhibitor of metalloproteinases-1 in rat fibrotic liver and cultured hepatic stellate cells

Li-Juan Zhang, Yun-Xin Chen, Zhi-Xin Chen, Yue-Hong Huang, Jie-Ping Yu, Xiao-Zhong Wang

Li-Juan Zhang, Jie-Ping Yu, Department of Gastroenterology, People's Hospital, Medical School of Wuhan University, Wuhan 430060, Hubei Province, China

Yun-Xin Chen, Zhi-Xin Chen, Yue-Hong Huang, Xiao-Zhong Wang, Department of Gastroenterology, Union Hospital of Fujian Medical University, Fuzhou 350001, Fujian Province, China

Supported by the Science and Technology Fund of Fujian Province, No.2003D05

Correspondence to: Xiao-Zhong Wang, Department of Gastroenterology, Union Hospital of Fujian Medical University, Fuzhou 350001, Fujian Province, China. drwangxz@pub6.fz.fj.cn

Telephone: +86-591-3357896

Received: 2004-01-02 **Accepted:** 2004-01-12

Abstract

AIM: To examine the expressions of matrix metalloproteinases-2 (MMP-2) and tissue inhibitor of metalloproteinases-1 (TIMP-1) in rat fibrotic liver and in normal rat hepatic stellate cells, and to investigate the changes in their expressions in response to treatment with interleukin-10 (IL-10) and platelet-derived growth factor (PDGF).

METHODS: Rat models of CCl₄-induced hepatic fibrosis were established and the liver tissues were sampled from the rats with or without IL-10 treatment, and also from the control rats. The expressions of MMP-2 and TIMP-1 in liver tissues were detected by S-P immunohistochemistry, and their expression intensities were evaluated in different groups. Hepatic stellate cells (HSCs) were isolated from normal rat and cultured *in vitro* prior to exposure to PDGF treatment or co-treatment with IL-10 and PDGF. MMP-2 and TIMP-1 levels were measured by semi-quantitative reverse transcriptional polymerase chain reaction (RT-PCR).

RESULTS: CCl₄-induced rat hepatic fibrosis models were successfully established. The positive expressions of MMP-2 and TIMP-1 increased obviously with the development of hepatic fibrosis, especially in untreated model group (84.0% and 92.0%, $P < 0.01$). The positive signals decreased significantly following IL-10 treatment (39.3% and 71.4%, $P < 0.01$ and $P < 0.05$) in a time-dependent manner. TIMP-1 mRNA in PDGF-treated group was significantly increased time-dependently in comparison with that of the control group, but PDGF did not obviously affect MMP-2 expression. No difference was noted in TIMP-1 and MMP-2 expressions in HSCs after IL-10 and PDGF treatment ($P > 0.05$).

CONCLUSION: MMP-2 and TIMP-1 expressions increase in liver tissues with the development of fibrosis, which can be inhibited by exogenous IL-10 inhibitor. PDGF induces the up-regulation of TIMP-1 but not MMP-2 in the HSCs. IL-10 inhibits TIMP-1 and MMP-2 expressions in HSCs induced by PDGF.

Zhang LJ, Chen YX, Chen ZX, Huang YH, Yu JP, Wang XZ. Effect of interleukin-10 and platelet-derived growth factor on expressions of matrix metalloproteinases-2 and tissue inhibitor of metalloproteinases-1 in rat fibrotic liver and cultured hepatic stellate cells. *World J Gastroenterol* 2004; 10(17): 2574-2579

<http://www.wjgnet.com/1007-9327/10/2574.asp>

INTRODUCTION

Liver fibrosis and its end-stage sequelae cirrhosis represent a major worldwide health problem. By definition progressive fibrosis occurs when the rate of matrix synthesis exceeds matrix degradation^[1]. Considerable evidence suggests that the hepatic stellate cells (HSCs) are central to the fibrotic process. HSCs are normally located in the perisinusoidal space as quiescent vitamin A-storing cells secreting low levels of extracellular matrix (ECM). Following liver injury, increased synthesis of extracellular matrix constituents occurs in combination with other phenotypic changes (also called activation) of HSCs into myofibroblast-like cells. It has been demonstrated by the analysis of freshly isolated HSCs that a number of these phenotypic changes take place, including increased expression of extracellular matrix constituents and the expression of α -SMA^[2,3]. This activated phenotype of HSCs subsequently becomes the major source of the interstitial collagens^[4-6]. It has been suggested that HSCs are also a source of matrix-degrading metalloproteinases (MMPs), indicating their participation in matrix remodeling^[7-9]. As a family of neutral proteinases, MMPs act on a variety of substrates^[10]. Different expression profiles of MMPs influence the outcome of ECM components, resulting in preferential accumulation of interstitial collagens, type I in particular, in the fibrotic liver. MMPs are tightly regulated at the levels of transcription, secretion, and proteolytic activation, and their activities are governed by tissue-derived inhibitors^[11]. The expression of tissue inhibitors of MMPs (TIMP) has also been demonstrated in human fibrotic liver disease and animal models of liver fibrosis^[12]. At present, 4 TIMPs have been characterized^[13], all being low-molecular-weight proteins sharing structural similarities. Individual members of the TIMP family display selective affinities for different members of the MMP family^[14]. TIMP-1 controls mostly the activity of MMP, particularly MMP-1, whereas TIMP-2 is the major inhibitor of MMP-2^[15]. MMP/TIMP balance is thought to play a pivotal role in the development of liver fibrosis, but their direct interaction *in vivo* has not yet been clarified. In the present study, the expressions of MMP-2 and TIMP-1 in rat fibrotic liver and in HSCs were examined and their changes were investigated in the presence of interleukin (IL)-10 and PDGF.

MATERIALS AND METHODS

Materials

One hundred clean male Sprague-Dawley rats weighing 140-180 g

(provided by Shanghai Experimental Animal Center) were divided randomly into control group ($n = 24$), model group ($n = 40$) and IL-10 treatment group ($n = 36$). All the rats were bred under routine condition (room temperature of 22 ± 2 °C, humidity of $55 \pm 5\%$, with light/dark alternating every 12 h and free access to water and food. The feed was provided by BK Company in Shanghai, China).

Preparation of rats

Rats in control group were given intraperitoneal injection with saline at 2 mL/kg twice a week, and those in model and IL-10 treatment groups received intraperitoneal injection with 500 mL/L CCl_4 (dissolved in castor oil) at 2 mL/kg twice a week. From the third week, rats in treatment group were given intraperitoneal injection with IL-10 at 4 $\mu\text{g}/\text{kg}$ (dissolved in saline) 20 min prior to CCl_4 injection. All injections were performed on Mondays and Thursdays after measurement of the rats' body weight. In the 5th wk, 3 rats in model group and 2 in treatment group died; in the 7th wk, 8 and 4 rats in these two groups died, respectively, and in the 9th week, another 10 and 6 died. At this time point, 3 rats in control group also died. In the 5th, 7th and 9th wk, 7 to 10 rats in each group were sacrificed to collect their liver samples, which were fixed in 40 g/L formaldehyde and embedded with paraffin.

Immunohistochemistry

Rat liver tissues were sectioned at the thickness of 4 μm . After deparaffinization with xylene and dehydration with graded ethanol, the sections were incubated in PBS containing 30 mL/L H_2O_2 to remove endogenous peroxidases and then in PBS containing 0.1 mol/L citrate to saturate the nonspecific binding sites. After incubation with goat anti-rat MMP-2 and TIMP-1 monoclonal antibodies, the sections were treated with instant S-P immunohistochemical reagents (American Zymed Company) and then incubated in a buffer solution containing 3,3-diaminobenzidine tetrahydrochloride (DAB) and H_2O_2 for visualization, followed by dehydration and mounting procedures. Microscopic examination of the sections was then performed.

Result assessment

Reactions were graded and scored according to their intensities and percentage of the positive cells respectively as follows: Zero score for negative reaction, 1 score for pale yellowish staining, and 2 scores for dense yellow or brown staining; 0 score for a percentage of positive cells below 5%, 1 score for one between 6% and 25%, 2 scores for one between 26% and 50%, and 3 for one over 50%. The eventual score of the section was derived from the product of the 2 scores for staining intensity and positive cell percentage, and graded as negative (-) result for a score lower than 1, positive result (+) for one between 2 and 3, and strong positive result (++) for one over 4. Redit analysis was utilized to assess the difference between the groups.

Hepatic stellate cells isolation and culture

Male Sprague-Dawley rats weighing 450-500 g were used for isolation of HSCs. Rat liver nonparenchymal cells were isolated by means of sequential perfusion with collagenase and pronase E as described previously^[16]. Buoyant HSCs were separated from the resulted cell suspension by elutriation over a Nycodenz gradient centrifugation. Desmin immunocytochemistry demonstrated a purity of isolated HSCs over 95%. The HSCs were then seeded into plastic tissue culture flask at the density of $1 \times 10^6/\text{mL}$ in DMEM containing 100 mL/L fetal calf serum (FCS), and incubated at 37 °C with 50 mL/L CO_2 . The culture medium was replaced 24 h after plating and every 48-72 h thereafter. The subsequent passages of HSCs were diluted to

$5 \times 10^4/\text{mL}$ before seeded into 50 mL culture flask containing DMEM medium supplemented with FCS.

PDGF treatment of HSCs

The cultured HSCs were divided into 6 groups: the first and sixth groups serving as control were cultured in 3 mL DMEM medium for 2 and 24 h, respectively, with the second, third, fourth and fifth groups cultured in 3 mL DMEM medium in the presence of 20 ng/mL PDGF for 2, 4, 8 and 24 h, respectively. The cells were then harvested for reverse transcriptional-PCR (RT-PCR).

Co-treatment of HSCs with IL-10 and PDGF

Cultured HSCs were divided into 8 groups: the first and second groups (blank control) were cultured in 3 mL DMEM medium for 2 and 24 h, respectively, and the third, fifth and seventh groups (negative control) cultured in 3 mL DMEM medium containing 20 ng/mL PDGF for 2, 12 and 24 h, respectively, while the fourth, sixth and eighth groups were cultured in 3 mL DMEM medium containing both 20 ng/mL IL-10 and 20 ng/mL PDGF for 2, 12 h and 24 h, respectively. The cells were then harvested for RT-PCR.

RT-PCR for MMP-2 and TIMP-1

Total RNA was isolated from HSCs using Genra reagent (USA) according to the protocol provided by the manufacturer. The A_{260}/A_{280} of total RNA ranged between 1.8 and 2.0. After treatment with Dnase-I (1-2 μg), total RNA was reversely transcribed into complementary DNA (cDNA) with oligo (dT) using cDNA synthesis kit, and 2 μL cDNA product was then used as the template to amplify specific fragments in a 25 μL reaction system. PCRs using *Taq* polymerase reaction were carried out with an initial denaturation at 95 °C for 5 min, followed by 25 cycles at 94 °C for 45 s, annealing at 60 °C for 30 s, at 72 °C for 60 s, with a final extension at 72 °C for 7 min. The primer sequences used for MMP-2 were 5'-GTGCTGAAGGACACCCTCAAGAAGA-3' (sense) and 5'-TTGCCGTCCTTCTCAAAGTTGTACG-3' (antisense), and those for TIMP-1 were 5'-GCCATGGAGAGCCTCTGTGG-3' (sense) and 5'-GCAGGCAGCAAAGTGATCG-3' (antisense); the primers for β -actin as the internal control were 5'-GAGCTATGAGCTGCCTGACG-3' (sense) and 5'-AGCACTTGCGGTCCACGATG-3' (antisense).

Electrophoresis and semi-quantitative analysis

PCR products underwent 2% agarose gel electrophoresis and were visualized with ethidium bromide. The expected products' sizes were 604 bp for MMP-2, 310 bp for TIMP-1 and 410 bp for β -actin. Bio Imagine System was applied to detect the density of the bands of PCR products. The expression levels of MMP-2 and TIMP-1 were calculated by the ratio of their band densities of PCR products to that of β -actin. Semi-quantitative detection was repeated for 5 times. SPSS 10.0 software was used to analyze the difference between the groups.

RESULTS

MMP-2 and TIMP-1 expressions in liver tissues

The positive rate of MMP-2 in control group, model group and IL-10 treatment group was 9.5%, 84.0% and 39.3%, respectively, and that of TIMP-1 was 23.8%, 92.0% and 71.4%, respectively. The granular positive products were localized in the cytoplasm of hepatocytes and biliary epithelial cells. In control group, the positive expressions of MMP-2 and TIMP-1 were weak and found mainly in endothelial cells and hepatic cells. In model group, positive expressions increased obviously with the development of hepatic fibrosis, distributing in biliary epithelial cells, fibroblasts and muscular cells. In treatment group the

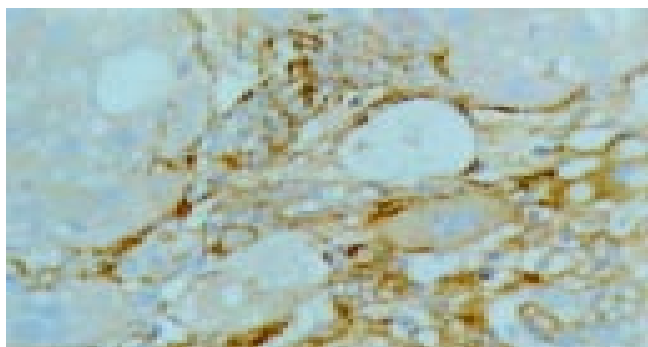


Figure 1 MMP-2-positive cells in the model group (S-P method, x200).

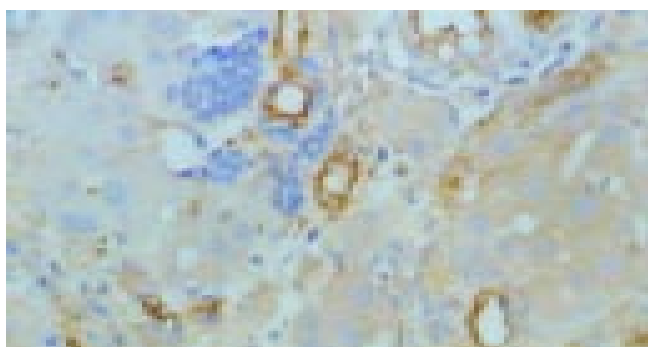


Figure 2 MMP-2-positive cells in IL-10 treatment group (S-P method, x200).

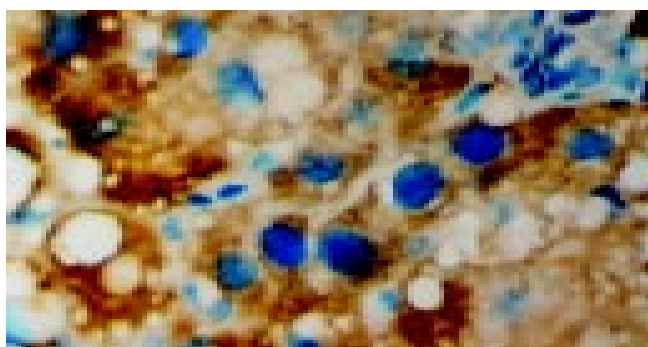


Figure 3 TIMP-1-positive cells in the model group (S-P method, x400).

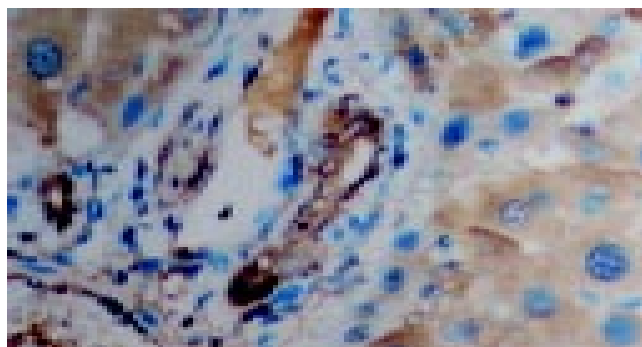


Figure 4 TIMP-1-positive cells in IL-10 treatment group (S-P method, x400).

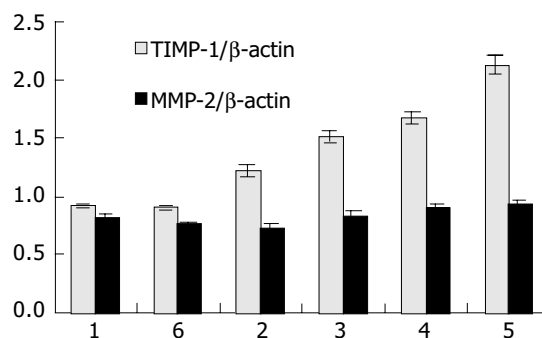


Figure 5 Effects of PDGF on TIMP-1 and MMP-2 expressions in HSCs. 1: Control group (2 h); 2: PDGF-treated group (2 h); 3: PDGF-treated group (4 h); 4: PDGF-treated group (8 h); 5: PDGF-treated group (24 h); 6: Control group (24 h).

Intensities of MMP-2 and TIMP-1 immunoreactivities

Comparison of MMP-2 and TIMP-1 positive expression levels between the 3 groups is shown in Table 1. Ridit analysis showed significant difference between the 3 groups ($P < 0.01$). Higher expression levels of MMP-2 and TIMP-1 in model group were detected than in control group ($P < 0.01$). In treatment group, IL-10 treatment resulted in decreased immunoreactivities for MMP-2 and TIMP-1 ($P < 0.01$ and $P < 0.05$ respectively). The expression levels of MMP-2 and TIMP-1 in different phases of hepatic fibrosis are listed in Table 2. With the development of hepatic fibrosis, the intensities of MMP-2 and TIMP-1 immunoreactivities increased gradually, and the difference was

Table 1 Comparison of MMP-2 and TIMP-1 immunoreactivities between control, model and treatment groups

Group	n	MMP-2			Ridit value	TIMP-1			Ridit value
		-	+	++		-	+	++	
Control	21	19	2	0	0.312	16	5	0	0.277 ^b
Model	25	4	13	8	0.712 ^d	2	14	9	0.684 ^d
Treatment	28	17	10	1	0.451 ^e	8	18	2	0.503 ^g

^b $P < 0.01$ vs treatment group; ^c $P < 0.05$; ^d $P < 0.01$ vs control group; ^e $P > 0.05$ vs control group; ^g $P < 0.05$ vs model group.

Table 2 Comparison of MMP-2 and TIMP-1 immunoreactivities measured at different time points in model group

Wk	n	MMP-2			Ridit value	TIMP-1			Ridit value
		-	+	++		-	+	++	
5	8	1	7	0	0.378	1	6	1	0.36 ^{ab}
7	8	2	5	1	0.388	1	5	2	0.418 ^c
9	9	1	1	7	0.709	0	2	7	0.698 ^c

^b $P < 0.01$ vs wk 7 and 9; ^a $P < 0.05$ vs wk 9; ^c $P < 0.05$ vs wk 7; ^e $P > 0.05$ vs wk 5.

significant ($P < 0.05$).

Relative quantities of MMP-2 and TIMP-1 mRNA in HSCs

Expression of TIMP-1 in PDGF-treated HSCs was significantly increased time-dependently as compared with that in control cells ($P < 0.01$). There was no difference in MMP-2 expression between PDGF-treated HSCs and control cells (Figure 5). After treatment with IL-10 and PDGF, expressions of TIMP-1 and MMP-2 in HSCs were similar to those in negative control groups ($P > 0.05$), without changes over time (Figure 6).

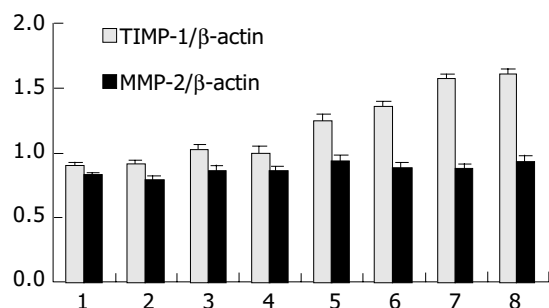


Figure 6 Effects of IL-10 and PDGF on TIMP-1 and MMP-2 expressions in HSCs. 1: Blank control group (2 h); 2: Blank control group (24 h); 3: Negative control group (2 h); 4: Treatment group (2 h); 5: Negative control group (12 h); 6: Treatment group (12 h); 7: Negative control group (24 h); 8: Treatment group (24 h).

DISCUSSION

Liver fibrosis is thought to be a progressive pathological process that leads ultimately to deposition of excess matrix proteins in extracellular space^[17], and destroys normal liver architecture to finally result in cirrhosis. In extracellular space, matrix degradation occurs predominantly consequent to the action of a family of enzymes known as matrix metalloproteinases^[18]. These enzymes are secreted by cells into extracellular space as proenzymes, which are then activated by a number of specific mechanisms. MMP-2 (gelatinase A) produced by activated HSCs, as demonstrated by immunohistochemistry and *in situ* hybridization^[19,20], plays an important role in remodeling the basement membranes as it degrades several of the collagen components including collagen IV, laminin and fibronectin^[21]. In other tissues, such as lung, kidney and heart, MMP-2 expression is also increased during fibrogenesis^[22-25]. Recent studies showed that inhibition of MMP-2 activity^[26] or blockade of MMP-2 synthesis^[21] might effectively prevent mesangial cell proliferation and collagen I synthesis *in vitro*, indicating the possible role of MMP-2 as a growth factor and activator for mesangial cells, performed probably through an autocrine pathway^[27]. In human liver fibrosis or in rat models of CCl₄-induced liver fibrosis, the expression of MMP-2 mRNA was increased by several fold, and HSCs expressed MMP-2 when activated by *in vitro* culture^[27,28], as is consistent with our findings in this study.

TIMPs are the most important family of molecules involved in regulation of extracellular MMP activity^[29-32]. TIMPs are produced by a wide variety of cells and often cosecreted with MMPs, providing local autoregulation of MMP activity. Recognized now as a multifunctional protein, TIMP-1 has been reported to stimulate steroidogenesis, inhibit angiogenesis, and induce changes in cell morphology^[11,33]. It has been shown that TIMP-1, but not TIMP-2, can enter the nuclei of several types of cells, which further suggests that TIMP-1 may also act as a transcription factor^[34,35]. We found that during the development of liver fibrosis, TIMP-1 expression in the liver was markedly up-regulated. Increased serum TIMP-1 levels

have been documented in patients with chronic active liver disease in correlation with histological degree of human liver fibrosis^[36]. Liver TIMP-1 protein levels are also closely correlated with the histological degree of liver fibrosis. The above findings suggest that TIMP-1 plays an important role in the development of liver fibrosis^[12,30,37]. Recent findings indicate that HOE077, a prolyl-4-hydroxylase inhibitor, may prevent fibrosis by inhibiting the expression of liver type I procollagen and TIMP-1 mRNAs as well as proline hydroxylation and stellate cell activation, resulting in reduced expression of procollagen and TIMP-1 mRNAs^[38]. Experiments with liver-targeted TIMP-1 transgenic (TIMP-Tg) mouse have shown significantly attenuated ability of reversing spontaneous liver fibrosis in TIMP-Tg mice as compared with the control mice^[39]. But the exact role of TIMP-1 in liver fibrogenesis has not yet been clarified. In another experiment with TIMP-Tg mice, the direct effect of TIMP-1 overexpression on CCl₄-induced liver fibrosis was examined, it was found that TIMP-1 did not induce liver fibrosis by itself, but strongly promoted liver fibrosis development, in other words, TIMP-1 behaved not as the initiation factor, but as a strong promoter of liver fibrosis^[40].

PDGF is a major mitogen for connective tissue cells and some other cell types. This dimeric molecule consists of disulfide-bonded, structurally similar A- and B-polypeptide chains that combine to form homo- and hetero-dimers, and is involved in autocrine and paracrine stimulation of cell growth in several different pathological conditions. Evidence showed that recombinant PDGF stimulated proliferation of nonconfluent myofibroblasts and collagen production in confluent cultures of myofibroblasts without increasing cell number, demonstrating the importance of PDGF in pathogenesis of liver fibrosis^[41-45]. It has been established that human and rat HSCs are able to migrate according to the concentration gradients of chemotactic factors^[46-48]. The best characterized chemotactic factor for HSCs identified so far is PDGF-BB^[46,47,49], known also as the most potent mitogen for HSCs and overexpression during active hepatic fibrogenesis^[50]. Our findings in this study showed that after PDGF treatment, the expression of TIMP-1 increased significantly in HSCs possibly because PDGF-promoted HSC proliferation and activation, indicating the importance of PDGF in pathogenesis of liver fibrosis. We also found that the expression of MMP-2 did not increase in HSCs after PDGF treatment, which is suggestive of the irrelevance of MMP-2 in fibrogenesis induced by PDGF.

IL-10, originally isolated from mouse helper T cells, is a cytokine that regulates a number of interleukins. It inhibits synthesis of several cytokines by T lymphocytes and activates monocytes, and was therefore originally named cytokine synthesis inhibitory factor^[51]. Recent studies showed that IL-10 also acted on connective tissue cells such as fibroblasts, inducing, for instance, transcriptional inhibition of the expression of type I collagen, which is the major component of extracellular matrix^[52]. IL-10 also possesses antifibrogenic properties by down-regulating profibrogenic cytokines like TGF- β_1 and TNF- α ^[53,54]. Our previous studies indicated that IL-10 could produce antifibrogenesis effect on CCl₄-induced rat hepatic fibrosis. In this study, we found that IL-10 down-regulated expression of MMP-2 and TIMP-1 in rat fibrotic liver, possibly another way that IL-10 exerts its effect of antifibrogenesis. In our previous study, PDGF was found to markedly promote the contraction and proliferation of HSCs and expressions of collagen type I and III as well as TGF- β_1 in HSCs, which was significantly inhibited by IL-10^[55]. But results of the present experiment showed that at the dose of 20 ng/mL, IL-10 did not inhibit TIMP-1 and MMP-2 expressions in PDGF-treated HSCs, indicating that the inhibitory effects of IL-10 on HSCs may not involve TIMP-1 and MMP-2.

In summary, the present study demonstrates that positive

expressions of MMP-2 and TIMP-1 in rat liver tissue increase with the development of hepatic fibrosis, and MMP-2 and TIMP-1 play an important role during the development of liver fibrosis. Exogenous IL-10 decreases the expression of MMP-2 and TIMP-1 in liver tissues. PDGF increases the expression of TIMP-1 in HSCs, possibly through promoting HSC proliferation and activation, and this effect is not inhibited by IL-10.

REFERENCES

- 1 **Bedossa P**, Paradis V. Liver extracellular matrix in health and disease. *J Pathol* 2003; **200**: 504-515
- 2 **Rockey DC**. The cell and molecular biology of hepatic fibrogenesis. Clinical and therapeutic implications. *Clin Liver Dis* 2000; **4**: 319-355
- 3 **Bataller R**, Brenner DA. Hepatic stellate cells as a target for the treatment of liver fibrosis. *Semin Liver Dis* 2001; **21**: 437-451
- 4 **Safadi R**, Friedman SL. Hepatic fibrosis-role of hepatic stellate cell activation. *Med Gen Med* 2002; **4**: 27
- 5 **Reeves HL**, Friedman SL. Activation of hepatic stellate cells-a key issue in liver fibrosis. *Front Biosci* 2002; **7**: d808-826
- 6 **Iredale JP**. Hepatic stellate cell behavior during resolution of liver injury. *Semin Liver Dis* 2001; **21**: 427-436
- 7 **Imai K**, Sato T, Senoo H. Adhesion between cells and extracellular matrix with special reference to hepatic stellate cell adhesion to three-dimensional collagen fibers. *Cell Struct Funct* 2000; **25**: 329-336
- 8 **Neubauer K**, Saile B, Ramadori G. Liver fibrosis and altered matrix synthesis. *Can J Gastroenterol* 2001; **15**: 187-193
- 9 **Benyon RC**, Arthur MJ. Extracellular matrix degradation and the role of hepatic stellate cells. *Semin Liver Dis* 2001; **21**: 373-384
- 10 **Okazaki I**, Watanabe T, Hozawa S, Arai M, Maruyama K. Molecular mechanism of the reversibility of hepatic fibrosis: with special reference to the role of matrix metalloproteinases. *J Gastroenterol Hepatol* 2000; **15**(Suppl): D26-32
- 11 **Will H**, Atkinson SJ, Butler GS, Smith B, Murphy G. The soluble catalytic domain of membrane type 1 matrix metalloproteinase cleaves the propeptide of progelatinase A and initiates autoproteolytic activation. Regulation by TIMP-2 and TIMP-3. *J Biol Chem* 1996; **271**: 17119-17123
- 12 **McCrudden R**, Iredale JP. Liver fibrosis, the hepatic stellate cell and tissue inhibitors of metalloproteinases. *Histol Histopathol* 2000; **15**: 1159-1168
- 13 **Gomez DE**, Alonso DF, Yoshiji H, Thorgeirsson UP. Tissue inhibitors of metalloproteinases: structure, regulation and biological functions. *Eur J Cell Biol* 1997; **74**: 111-122
- 14 **Arthur MJ**. Fibrogenesis II. Metalloproteinases and their inhibitors in liver fibrosis. *Am J Physiol Gastrointest Liver Physiol* 2000; **279**: G245-249
- 15 **Senoo H**, Imai K, Matano Y, Sato M. Molecular mechanisms in the reversible regulation of morphology, proliferation and collagen metabolism in hepatic stellate cells by the three-dimensional structure of the extracellular matrix. *J Gastroenterol Hepatol* 1998; **13**(Suppl): S19-32
- 16 **Ramm GA**. Isolation and culture of rat hepatic stellate cells. *J Gastroenterol Hepatol* 1998; **13**: 846-851
- 17 **Iredale JP**. Tissue inhibitors of metalloproteinases in liver fibrosis. *Int J Biochem Cell Biol* 1997; **29**: 43-54
- 18 **Benyon RC**, Arthur MJ. Extracellular matrix degradation and the role of hepatic stellate cells. *Semin Liver Dis* 2001; **21**: 373-384
- 19 **Takahara T**, Furui K, Yata Y, Jin B, Zhang LP, Nambu S, Sato H, Seiki M, Watanabe A. Dual expression of matrix metalloproteinase-2 and membrane-type 1-matrix metalloproteinase in fibrotic human livers. *Hepatology* 1997; **26**: 1521-1529
- 20 **Takahara T**, Furui K, Funaki J, Nakayama Y, Itoh H, Miyabayashi C, Sato H, Seiki M, Ooshima A, Watanabe A. Increased expression of matrix metalloproteinase-II in experimental liver fibrosis in rats. *Hepatology* 1995; **21**: 787-795
- 21 **Turck J**, Pollock AS, Lee LK, Marti HP, Lovett DH. Matrix metalloproteinase 2 (gelatinase A) regulates glomerular mesangial cell proliferation and differentiation. *J Biol Chem* 1996; **271**: 15074-15083
- 22 **Swiderski RE**, Dencoff JE, Floerchinger CS, Shapiro SD, Hunninghake GW. Differential expression of extracellular matrix remodeling genes in a murine model of bleomycin-induced pulmonary fibrosis. *Am J Pathol* 1998; **152**: 821-828
- 23 **Fukuda Y**, Ishizaki M, Kudoh S, Kitaichi M, Yamanaoka N. Localization of matrix metalloproteinases-1, -2, and -9 and tissue inhibitor of metalloproteinase-2 in interstitial lung diseases. *Lab Invest* 1998; **78**: 687-698
- 24 **Shimizu T**, Kuroda T, Hata S, Fukagawa M, Margolin SB, Kurokawa K. Pirfenidone improves renal function and fibrosis in the post-obstructed kidney. *Kidney Int* 1998; **54**: 99-109
- 25 **Bakowska J**, Adamson IY. Collagenase and gelatinase activities in bronchoalveolar lavage fluids during bleomycin-induced lung injury. *J Pathol* 1998; **185**: 319-323
- 26 **Steinmann-Niggli K**, Ziswiler R, Kung M, Marti HP. Inhibition of matrix metalloproteinases attenuates anti-Thy1.1 nephritis. *J Am Soc Nephrol* 1998; **9**: 397-407
- 27 **Benyon RC**, Hovell CJ, Da Gaca M, Jones EH, Iredale JP, Arthur MJ. Progelatinase A is produced and activated by rat hepatic stellate cells and promotes their proliferation. *Hepatology* 1999; **30**: 977-986
- 28 **Arthur MJ**, Stanley A, Iredale JP, Rafferty JA, Hembry RM, Friedman SL. Secretion of 72 kDa type IV collagenase/gelatinase by cultured human lipocytes. Analysis of gene expression, protein synthesis and proteinase activity. *Biochem J* 1992; **287**(Pt 3): 701-707
- 29 **Arthur MJ**, Iredale JP, Mann DA. Tissue inhibitors of metalloproteinases: role in liver fibrosis and alcoholic liver disease. *Alcohol Clin Exp Res* 1999; **23**: 940-943
- 30 **Arthur MJ**, Mann DA, Iredale JP. Tissue inhibitors of metalloproteinases, hepatic stellate cells and liver fibrosis. *J Gastroenterol Hepatol* 1998; **13**(Suppl): S33-38
- 31 **Murphy FR**, Issa R, Zhou X, Ratnarajah S, Nagase H, Arthur MJ, Benyon C, Iredale JP. Inhibition of apoptosis of activated hepatic stellate cells by tissue inhibitor of metalloproteinase-1 is mediated via effects on matrix metalloproteinase inhibition: implications for reversibility of liver fibrosis. *J Biol Chem* 2002; **277**: 11069-11076
- 32 **Bahr MJ**, Vincent KJ, Arthur MJ, Fowler AV, Smart DE, Wright MC, Clark IM, Benyon RC, Iredale JP, Mann DA. Control of the tissue inhibitor of metalloproteinases-1 promoter in culture-activated rat hepatic stellate cells: regulation by activator protein-1 DNA binding proteins. *Hepatology* 1999; **29**: 839-848
- 33 **Thorgeirsson UP**, Yoshiji H, Sinha CC, Gomez DE. Breast cancer; tumor neovasculature and the effect of tissue inhibitor of metalloproteinases-1 (TIMP-1) on angiogenesis. *In Vivo* 1996; **10**: 137-144
- 34 **Zhao WQ**, Li H, Yamashita K, Guo XK, Hoshino T, Yoshida S, Shinya T, Hayakawa T. Cell cycle-associated accumulation of tissue inhibitor of metalloproteinases-1 (TIMP-1) in the nuclei of human gingival fibroblasts. *J Cell Sci* 1998; **111**(Pt 9): 1147-1153
- 35 **Ritter LM**, Garfield SH, Thorgeirsson UP. Tissue inhibitor of metalloproteinases-1 (TIMP-1) binds to the cell surface and translocates to the nucleus of human MCF-7 breast carcinoma cells. *Biochem Biophys Res Commun* 1999; **257**: 494-499
- 36 **Iredale JP**, Benyon RC, Pickering J, McCullen M, Northrop M, Pawley S, Hovell C, Arthur MJ. Mechanisms of spontaneous resolution of rat liver fibrosis. Hepatic stellate cell apoptosis and reduced hepatic expression of metalloproteinase inhibitors. *J Clin Invest* 1998; **102**: 538-549
- 37 **Herbst H**, Wege T, Milani S, Pellegrini G, Orzechowski HD, Bechstein WO, Neuhaus P, Gressner AM, Schuppan D. Tissue inhibitor of metalloproteinase-1 and -2 RNA expression in rat and human liver fibrosis. *Am J Pathol* 1997; **150**: 1647-1659
- 38 **Sakaida I**, Uchida K, Hironaka K, Okita K. Prolyl 4-hydroxylase inhibitor (HOE 077) prevents TIMP-1 gene expression in rat liver fibrosis. *J Gastroenterol* 1999; **34**: 376-377
- 39 **Yoshiji H**, Kuriyama S, Yoshiji J, Ikenaka Y, Noguchi R, Nakatani T, Tsujinoue H, Yanase K, Namisaki T, Imazu H, Fukui H. Tissue inhibitor of metalloproteinases-1 attenuates spontaneous liver fibrosis resolution in the transgenic mouse. *Hepatology* 2002; **36**(4 Pt 1): 850-860

- 40 **Yoshiji H**, Kuriyama S, Miyamoto Y, Thorgeirsson UP, Gomez DE, Kawata M, Yoshii J, Ikenaka Y, Noguchi R, Tsujinoue H, Nakatani T, Thorgeirsson SS, Fukui H. Tissue inhibitor of metalloproteinases-1 promotes liver fibrosis development in a transgenic mouse model. *Hepatology* 2000; **32**: 1248-1254
- 41 **Zhang BB**, Cai WM, Weng HL, Hu ZR, Lu J, Zheng M, Liu RH. Diagnostic value of platelet derived growth factor-BB, transforming growth factor-beta₁, matrix metalloproteinase-1, and tissue inhibitor of matrix metalloproteinase-1 in serum and peripheral blood mononuclear cells for hepatic fibrosis. *World J Gastroenterol* 2003; **9**: 2490-2496
- 42 **Tangkijvanich P**, Melton AC, Chitapanarux T, Han J, Yee HF. Platelet-derived growth factor-BB and lysophosphatidic acid distinctly regulate hepatic myofibroblast migration through focal adhesion kinase. *Exp Cell Res* 2002; **281**: 140-147
- 43 **Di Sario A**, Bendia E, Svegliati-Baroni G, Marzioni M, Ridolfi F, Trozzi L, Ugili L, Saccomanno S, Jezequel AM, Benedetti A. Rearrangement of the cytoskeletal network induced by platelet-derived growth factor in rat hepatic stellate cells: role of different intracellular signalling pathways. *J Hepatol* 2002; **36**: 179-190
- 44 **Kinnman N**, Gorla O, Wendum D, Gendron MC, Rey C, Poupon R, Housset C. Hepatic stellate cell proliferation is an early platelet-derived growth factor-mediated cellular event in rat cholestatic liver injury. *Lab Invest* 2001; **81**: 1709-1716
- 45 **Kinnman N**, Hultcrantz R, Barbu V, Rey C, Wendum D, Poupon R, Housset C. PDGF-mediated chemoattraction of hepatic stellate cells by bile duct segments in cholestatic liver injury. *Lab Invest* 2000; **80**: 697-707
- 46 **Ikeda K**, Wakahara T, Wang YQ, Kadoya H, Kawada N, Kaneda K. *In vitro* migratory potential of rat quiescent hepatic stellate cells and its augmentation by cell activation. *Hepatology* 1999; **29**: 1760-1767
- 47 **Marra F**, Gentilini A, Pinzani M, Choudhury GG, Parola M, Herbst H, Dianzani MU, Laffi G, Abboud HE, Gentilini P. Phosphatidylinositol 3-kinase is required for platelet-derived growth factor's actions on hepatic stellate cells. *Gastroenterology* 1997; **112**: 1297-1306
- 48 **Marra F**, Romanelli RG, Giannini C, Failli P, Pastacaldi S, Arrighi MC, Pinzani M, Laffi G, Montalto P, Gentilini P. Monocyte chemotactic protein-1 as a chemoattractant for human hepatic stellate cells. *Hepatology* 1999; **29**: 140-148
- 49 **Carlioni V**, Romanelli RG, Pinzani M, Laffi G, Gentilini P. Focal adhesion kinase and phospholipase C gamma involvement in adhesion and migration of human hepatic stellate cells. *Gastroenterology* 1997; **112**: 522-531
- 50 **Pinzani M**. PDGF and signal transduction in hepatic stellate cells. *Front Biosci* 2002; **7**: d1720-1726
- 51 **Nelson DR**, Lauwers GY, Lau JY, Davis GL. Interleukin 10 treatment reduces fibrosis in patients with chronic hepatitis C: a pilot trial of interferon nonresponders. *Gastroenterology* 2000; **118**: 655-660
- 52 **Reitamo S**, Remitz A, Tamai K, Uitto J. Interleukin-10 modulates type I collagen and matrix metalloprotease gene expression in cultured human skin fibroblasts. *J Clin Invest* 1994; **94**: 2489-2492
- 53 **Kovalovich K**, DeAngelis RA, Li W, Furth EE, Ciliberto G, Taub R. Increased toxin-induced liver injury and fibrosis in interleukin-6-deficient mice. *Hepatology* 2000; **31**: 149-159
- 54 **Louis H**, Van Laethem JL, Wu W, Quertinmont E, Degraef C, Van den Berg K, Demols A, Goldman M, Le Moine O, Geerts A, Deviere J. Interleukin-10 controls neutrophilic infiltration, hepatocyte proliferation, and liver fibrosis induced by carbon tetrachloride in mice. *Hepatology* 1998; **28**: 1607-1615
- 55 **Chen YX**, Wang XZ, Weng SG, Chen ZX, Huang YH, Zhang LJ. Effects of IL-10 and PDGF on expression of TGF- β_1 at hepatic stellate cells. *Zhongxiyi Jiehe Ganbin Zazhi* 2002; **12**: 343-345

Edited by Chen WW Proofread by Zhu LH and Xu FM

Ischemic preconditioning protects liver from hepatectomy under hepatic inflow occlusion for hepatocellular carcinoma patients with cirrhosis

Shao-Qiang Li, Li-Jian Liang, Jie-Fu Huang, Zhi Li

Shao-Qiang Li, Li-Lian Liang, Jie-Fu Huang, Department of Hepatobiliary Surgery, the First Affiliated Hospital, Sun Yat-sen University, Guangzhou 510080, Guangdong Province, China

Zhi Li, Department of Pathology, Sun Yat-sen University, Guangzhou 510080, Guangdong Province, China

Correspondence to: Professor Li-Jian Liang, MD, PhD. Department of Hepatobiliary Surgery, the First Affiliated Hospital, Sun Yat-sen University, Guangzhou 510080, Guangdong Province, China. lianglijian@163.net

Telephone: +86-20-87755766 Ext. 8096

Fax: +86-20-87755766 Ext. 8663

Received: 2003-11-27 **Accepted:** 2003-12-22

Abstract

AIM: To investigate the protective effect of ischemic preconditioning (IPC) on hepatocellular carcinoma (HCC) patients with cirrhosis undergoing hepatic resection under hepatic inflow occlusion (HIO) and its possible mechanism.

METHODS: Twenty-nine consecutive patients with resectable HCC were randomized into two groups: IPC group: before HIO, IPC with 5 min of ischemia and 5 min of reperfusion was given; control group: no IPC was given. Liver functions, hepatic Caspase-3 activity, and apoptotic cells were compared between these two groups.

RESULTS: On postoperative days (POD) 1, 3 and 7, the aspartate transaminase (AST) and alanine transaminase (ALT) levels in the IPC group were significantly lower than those in the control group ($P < 0.05$). On POD 3 and 7, the total bilirubin level in the IPC group was significantly lower than that in the control group ($P < 0.05$). On POD 1, the albumin level in the IPC group was higher than that in the control group ($P = 0.053$). After 1 h of reperfusion, both hepatic Caspase-3 activity and apoptotic sinusoidal endothelial cells in the IPC group were significantly lower than those in the control group ($P < 0.05$).

CONCLUSION: IPC has a potential protective effect on HCC patients with cirrhosis. Its protective mechanism underlying the suppression of sinusoidal endothelial cell apoptosis is achieved by inhibiting Caspase-3 activity.

Li SQ, Liang LJ, Huang JF, Li Z. Ischemic preconditioning protects liver from hepatectomy under hepatic inflow occlusion for hepatocellular carcinoma patients with cirrhosis. *World J Gastroenterol* 2004; 10(17): 2580-2584

<http://www.wjgnet.com/1007-9327/10/2580.asp>

INTRODUCTION

Hepatic inflow occlusion (HIO), also called Pringle's maneuver^[1], is an effective and simple technique to control blood loss from the raw surface during hepatic parenchymal transaction, and

has been widely used during hepatectomy. However, HIO could also result in hepatic ischemic-reperfusion (I/R) injury, especially in case of cirrhosis. It is generally accepted that cirrhotic liver is particularly sensitive to ischemia. Although warm ischemia for cirrhotic liver should not exceed 30 min^[2], prolonged HIO might cause dysfunction of the remnant liver, which was a major risk factor associated with postoperative morbidity and mortality^[3]. Therefore, therapeutic modalities to ameliorate this injury are critically important in liver surgery.

Ischemic preconditioning (IPC), defined as giving a short period of ischemia and reperfusion and subsequently sustaining a prolonged ischemic insult, was first described by Murry *et al.*^[4] in 1986, and then this protective phenomenon was found in various visceral organs including the liver^[5-9].

However, up to now, the data of IPC available were most focused on animal models. Recently, Clavien *et al.*^[10] reported the first clinical trial, suggesting a beneficial effect of IPC during major hepatectomy on patients who were subjected to 30 min of ischemia. But there was no cirrhotic case in Clavien's series. In China and other Asia areas, more than 80% of hepatocellular carcinoma (HCC) patients had underlying cirrhosis or hepatitis due to hepatitis B virus infection^[11]. Whether IPC has the similar protective effect on I/R injury encountered in hepatectomy for cirrhotic liver is unclear. Hence, we conducted this prospective randomized clinical trial on cirrhotic HCC patients to test whether IPC could protect cirrhotic liver against I/R injury during tumor resection under HIO, and to explore its possible protective mechanism.

MATERIALS AND METHODS

Patients

Fifty-six consecutive patients with HCC were treated at the Department of Hepatobiliary Surgery, the First Affiliated Hospital of Sun Yat-Sen University between January 1, 2001 and April 30, 2001. Among them, 29 patients whose tumors were considered to be resectable after preoperative investigations, including liver function tests, liver function reserve (oral glucose tolerance test, OGTT)^[12], abdominal ultrasound, CT assessment and laparotomy, were recruited in this study. The resectable criteria we used were as follows. (1) The general condition of the patients was good and they could tolerate hepatectomy. (2) The tumor did not extend beyond half of the liver and had no distant metastasis. (3) Liver function belonged to Child A or B and liver function reserve was type P₁ or P₂ according to OGTT, which is a test widely used to evaluate liver function reserve^[12]. Briefly, patients were fasted overnight, and the fast blood glucose (FBS) was measured next morning, then 75 g of glucose diluted in pure water was given to the patients orally. One and 2 h after glucose solution was drunk, blood glucose concentration (BGC) was measured respectively. If BGC after 2 h was still higher than that after 1 h, it was the linear type (L type). If BGC after 2 h was between the FBS and that after 1 h, it was the parabolic type 2 (P₂ type). If BGC after 2 h was lower than 7.3 μmol/L, it was parabolic type 1 (P₁ type). P₁ type indicated the best liver function reserve, and patients could tolerate right

or left hepatectomy. P₂ type was moderate, and patients could tolerate segmentectomy or irregular hepatectomy. L type indicated the poor liver function reserve, and patients could only tolerate local tumor resection. The other 27 unresectable cases were excluded.

Then 29 resectable cases were randomized into IPC group ($n = 14$) and control group groups ($n = 15$) by permuted block without stratification. Our previous study indicated that IPC with 5 min of ischemia and 5 min of reperfusion produced the best protection on cirrhotic rat liver I/R model^[13]. Therefore, IPC with these time intervals was applied in these patients. Prior to liver parenchymal transection under HIO, IPC with 5 min of ischemia and 5 min of reperfusion was conducted in the IPC group. No IPC was given prior to liver parenchymal transection performed under HIO in the control group.

This protocol was performed under the consent of patients approved by the Ethical Committee of Sun Yat-sen University.

Procedures and biopsy

General anesthesia was performed. Bilateral subcoastal incision was made. A further abdominal exploration was conducted to exclude intra-abdominal metastasis. After mobilization of the liver prior to parenchymal transection, HIO was achieved by clamping the portal pedicles using a tourniquet. Blood inflow was initiated when hemostasis was achieved after removal of the tumor. The procedures available in these patients included irregular hepatectomy, segmentectomy and right/left hepatectomy according to the tumor's location and liver function tests. Liver parenchyma was transected by diathermy and crushing hepatic tissue with an artery forceps. Tubular structures on the raw surface were divided and ligated. All hepatectomies were finished within one time of HIO in our series, and the time of HIO not including the ischemic phase of IPC in the IPC group were recorded. Intraoperative blood loss was accurately calculated from the suction bottles and surgical pads. No cell saver was used in our series. Before HIO and 1 h after reperfusion, a small piece of liver tissue was harvested by wedge resection in remnant liver. The procedures were performed by the same surgical team.

Liver function test

Peripheral blood was sampled before operation and on postoperative days (POD) 1, 3, 7. Aspartate transaminase (AST), alanine transaminase (ALT), total bilirubin (TBIL), albumin (ALB) were measured using an auto biochemical analyzer (HITACHI 7170A, Japan).

Hepatic Caspase-3 activity assay

Caspase-3 activity was quantified by proteolytic cleavage of the fluorogenic substrate 7-amino-4-trifluoro-methylcoumarin-conjugated Asp-Glu-Val-Asp tetrapeptide (AMC-DEVD)^[14]. Briefly, fresh liver tissue (20 mg) was homogenized in a lysis buffer at 4 °C. After 4 times of freezing and thawing, lysates were centrifuged at 15 000 *g* for 10 min, supernatants were collected. Then Caspase-3 activity was measured using a fluorescence spectrophotometer (HITACHI F-3 010, Japan) and a Caspase-3 fluorescent kit (Sigma Co. USA) according to the manufacturer's instructions. Caspase-3 activity was expressed as nmol AMC release per hour per mg liver tissue.

TUNEL assay

Apoptosis was detected by terminal deoxynucleotidyl mediated nick end labeling (TUNEL) assay^[15]. Paraffin-embedded liver tissue was cut into 5- μ m thick sections. After deparaffinized in series of alcohol solutions, a TUNEL kit (Boehringer Mannheim Co. Germany) was used according to the manufacturer's protocols. Five high power fields ($\times 400$) were selected randomly in each specimen, for which apoptotic cells were calculated by a pathologist.

Statistical analysis

Data are expressed as mean \pm SD. Means were compared between these two groups by *t* test (continuous data) or chi-square test (categorical data). *P* value less than 0.05 was considered statistically significant.

RESULTS

Clinical characteristics of these two groups

The clinical characteristics (Table 1) including age, gender, Child's classification, tumor size, operation procedure, operation time, liver ischemic time and blood loss were compared between these two groups, and there was no statistical significance, indicating that the characteristics of the two groups were homogeneous and comparable.

Table 1 clinical characteristics of these two groups

Data	IPC group	control group	<i>P</i> value
Age (yr)	50.4 \pm 10.7	49.5 \pm 10.3	0.605
Gender			0.684
Male	12	12	
Female	2	3	
Child's classification			0.684
Grade A	12	12	
Grade B	2	3	
Grade C	0	0	
OGTT			0.867
P ₁ type	3	4	
P ₂ type	8	9	
L type	4	3	
Cirrhosis ¹			0.316
(+)	13	12	
(-)	1	3	
Tumor size (cm)	7.1 \pm 3.6	7.9 \pm 2.9	0.544
Procedures			0.971
Right/left hepatectomy	2	2	
Segmentectomy	4	4	
Irregular hepatectomy	8	9	
Operation times (min)	191.3 \pm 74.9	208.2 \pm 45.3	0.485
Ischemic times (min)	18.0 \pm 3.6	17.4 \pm 2.3	0.602
(Range)	(15-25)	13-22)	
Blood loss (mL)	469.2 \pm 292.6	602.0 \pm 310.6	0.257

¹Cirrhosis: (+) refers to macroscopic cirrhosis, which was diagnosed during surgery, (-) refers to that we could not diagnose cirrhosis during surgery by naked eyes, however, it was diagnosed mild cirrhosis and hepatitis by microscopic pathology. The etiology of cirrhosis was hepatitis B virus infection in our series.

IPC protected cirrhotic liver from I/R injury

Serum AST and ALT levels were sensitive parameters to assess the severity of liver injury. As shown in Table 2, on postoperative d 1, 3, 7, the AST and ALT levels in the IPC group were significantly lower than those in the control group ($P < 0.05$). On postoperative d 3, 7, the TBIL levels in the IPC group were also lower than those in the control group ($P < 0.05$). On postoperative d 1, the ALB level in the IPC group was higher than that in the control group, but it did not reach statistical significance. These data suggest that IPC could effectively protect cirrhotic liver from I/R injury. I/R injury could inhibit albumin synthesis, however IPC could ameliorate this albumin-synthesis inhibition.

Table 2 Comparison of liver functions between two groups before and after operation

Date	AST (U/L)		ALT (U/L)		TBIL ($\mu\text{mol/L}$)		ALB (g/L)	
	Control	IPC	Control	IPC	Control	IPC	Control	IPC
Preop	64.7 \pm 39.2	60.1 \pm 55.4	56.7 \pm 53.9	54.8 \pm 45.0	22.6 \pm 13.1	18.9 \pm 7.4	41.2 \pm 5.6	40.6 \pm 3.7
POD1	1856.4 \pm 310.9	433.8 \pm 143.8 ^b	802.9 \pm 280.1	430.9 \pm 179.4 ^b	33.1 \pm 23.9	26.7 \pm 10.3	32.9 \pm 4.6	36.2 \pm 3.9
POD 3	409.6 \pm 197.4	156.7 \pm 52.5 ^b	417.3 \pm 162.6	200.9 \pm 88.6 ^b	49.1 \pm 35.4	25.9 \pm 9.2 ^a		
POD 7	85.3 \pm 45.5	56.5 \pm 18.9 ^a	130.1 \pm 49.0	89.9 \pm 42.8 ^a	39.7 \pm 29.3	22.8 \pm 8.0 ^a		

Note: preop = preoperation. ^a $P < 0.05$, vs control (independent t test); ^b $P < 0.01$, vs control (independent t test).

Postoperative mortality, morbidity and hospitalized days

There was no operative and hospital mortality in both groups. The common postoperative morbidity was pleural effusion and liver failure. Pleural effusion was confirmed by chest X-ray. Postoperative liver failure was defined as the total bilirubin was higher than 2 times of its normal level, and massive ascites occurred. Pleural effusion occurred in 2 cases (14.3%) of the IPC group, and in 5 cases (33.3%) of the control group ($P = 0.390$), who needed repeated pleural tapping. No in the IPC group was complicated with liver failure after surgery. However, liver failure occurred in 3 cases of the control group after operation. These 3 patients recovered after conservative treatment. Other postoperative complications including subphrenic collection were found in 2 cases of the control group, who were treated by fine needle aspiration guided by ultrasound. Bile leakage from the transection surface was found in 1 case of the IPC group, who was cured by local drainage. No wound infection occurred in both groups. The mean hospitalized time of the IPC group was 12.8 d, which was significantly shorter than that of the control group (12.8 \pm 3.1 d vs 18.6 \pm 9.1 d, $P = 0.034$).

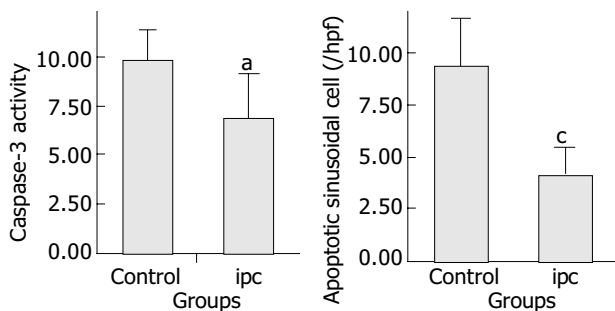


Figure 1 Comparison of Caspase-3 activity and SEC apoptosis between control group and IPC group ^a $P = 0.047$, vs control, ^c $P = 0.002$, vs control, (t test) (caspase-3 activity unit: nmol AMC · h⁻¹ · mg⁻¹ (tissue)) hpf: high power field.

Effect of IPC on Caspase-3 activity and apoptosis

To investigate the effect of IPC on Caspase-3 activity and apoptosis, 5 cases in each group were selected prospectively, whose hepatic Caspase-3 activity and apoptotic cells were detected respectively. One hour after reperfusion, the hepatic Caspase-3 activity in the IPC group was significantly lower than that in the control group ($P < 0.05$), and subsequently, the apoptotic sinusoidal endothelial cells (SECs) in the IPC group were also less than those in the control group ($P < 0.05$) (Figures 1, 2). Only few hepatocytes underwent apoptosis in the control group in this checking time point (Figure 2). These data indicated that IPC inhibited Caspase-3 activity and subsequently SEC apoptosis in the remnant liver.

DISCUSSION

Hemorrhage is the major lethal factor during hepatic resection. Hemostasis can be achieved by HIO or total vascular occlusion. The latter nevertheless was the safe choice for patients whose tumor involved major hepatic veins and inferior vena cava^[16]. But clinically, the vast majority of liver resections do not need this method for its detrimental effect of systemic circulation disturbance. HIO or Pringle's maneuver, which has the least hemodynamic effect, has been widely used in liver surgery^[17]. However, HIO could also result in liver I/R injury, which is one of the major factors leading to postoperative liver dysfunction. Cirrhotic liver is very vulnerable to ischemic injury. Though warm ischemia for cirrhotic liver should not exceed 30 min, and the majority of liver resections could be finished within this limit interval by using diathermy and crushing hepatic tissue with an artery forceps, the deleterious effect of ischemia could not be neglected. In order to minimize liver I/R injury, intermittent hepatic inflow occlusion (iHIO) has been used in HCC resection^[18,19]. However, massive bleeding might result from iHIO during reperfusion interval, which might increase blood transfusion and the possibility of postoperative morbidity and tumor recurrence^[20].

Our results demonstrated that HIO could cause massive

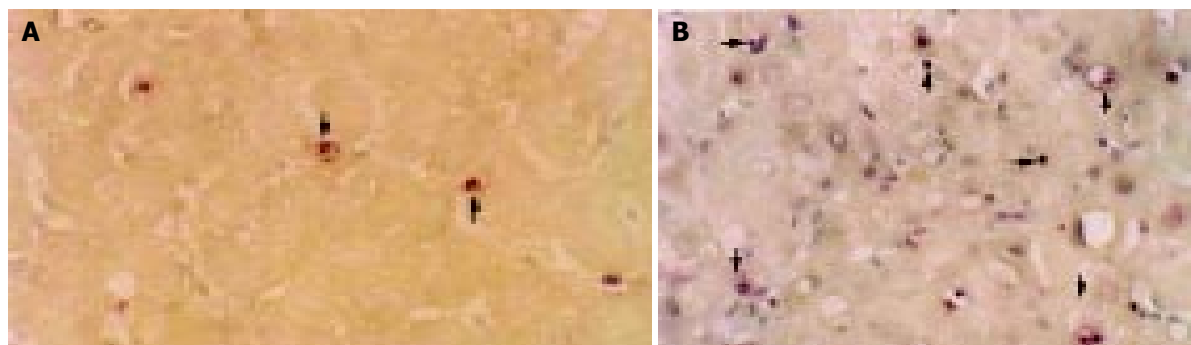


Figure 2 Typical features of apoptosis after 1 h of reperfusion (TUNEL assay, $\times 200$). Bold arrows show the SEC apoptosis and the black arrows indicate scanty of hepatocyte apoptosis. A: IPC group, B: control group.

liver injury and inhibit albumin synthesis in cirrhotic patients. However, IPC could significantly protect cirrhotic liver from I/R injury during hepatic resection under hepatic inflow occlusion in cirrhotic HCC patients. These were represented by a dramatically decrease in postoperative AST, ALT and TBIL levels; a relatively higher serum albumin level; an uneventful postoperative course and a relatively short hospital stay in the IPC group.

IPC is a simple procedure, which can produce dramatic protective effect on I/R injury. However, its clinical application is rare.

The protective mechanism of IPC has not been fully understood. Intrinsic nitric oxide (NO) synthesis, adenosine release^[18] and decreasing leukocyte/endothelial cell interactions^[21] have been reported to be the protective mechanisms underlying I/R injury.

Apoptosis, or programmed cell death, which is a distinct form of cell death from necrosis, has been documented to be a pivotal mechanism responsible for I/R injury encountered in liver surgery and liver graft preservation^[22-25]. However, this cell pathology was challenged by other authors, who documented that cell necrosis was the major cell death in rat liver I/R model subjected to 60 or 120 min of ischemia^[26]. Jaeschke *et al.*^[27], believed that both apoptosis and necrosis occurred in liver I/R. Actually, in our previous cirrhotic rat liver I/R model, we used H&E staining, TUNEL assay and electron microscope to investigate the cellular pathology, and found that there was no obvious necrosis but massive hepatocyte apoptosis mediated by Fas apoptotic pathway subjected to 30 min of liver ischemia and 6 h of reperfusion^[28]. This discrepancy might be due to the different time of ischemia and reperfusion used in each experiment.

In this clinical trial, we found that the major cell type undergoing apoptosis in the control group was SECs subjected to 1 h of reperfusion, only a few apoptotic hepatocytes were found at this checking time point. However, in our previous animal model^[28], after 6 h of reperfusion, massive apoptotic hepatocytes were seen, indicating that the cell type undergoing apoptosis might be time dependent. In the rat liver cell apoptosis model induced by intraperitoneal injection of Fas antibody^[29] and liver graft cold I/R model^[25], 1 h after antibody administration or reperfusion, SEC apoptosis was predominant. However, 2 to 6 h after antibody administration or reperfusion, hepatocytes were the major cell type undergoing apoptosis. Though we did not check apoptosis after 6 h of reperfusion in this clinical trial, we believed that during this period of time, hepatocytes might undergo apoptosis predominantly, thus subsequently resulting in liver injury and clinical manifestations.

As to the cellular mechanism of IPC related to apoptosis, Yadav *et al.*^[30], reported that the protective mechanism of IPC underlying hepatocyte and SEC apoptosis was achieved by inhibiting Caspase-3. It has been found that caspase-3 is a cysteine specific protease, an "executor" leading to DNA fragmentation in apoptotic signal cascades^[31]. We demonstrated that IPC could protect cirrhotic liver from I/R injury by inhibiting hepatocyte and SEC apoptosis through down-regulation of Fas expression and suppression of Caspase-3 activity in cirrhotic rat liver I/R model^[13]. In this study, we demonstrated again that the protective mechanism of IPC against liver I/R injury in cirrhotic patients was achieved by inhibiting Caspase-3 activity and subsequently apoptosis.

Why IPC down-regulates Caspase-3 activity is still under investigation. IPC could result in inhibition of intrinsic NO synthesis. *In vitro* and *in vivo* studies indicated that NO could inhibit Caspase-3 by S-nitrosation in Cys-163 residue of Caspase-3^[32].

In conclusion, IPC can protect potentially cirrhotic liver against I/R injury when hepatic resection is performed under hepatic inflow occlusion in HCC patients with cirrhosis. Its protective mechanism underlying SEC apoptosis is achieved

by inhibiting caspase-3 activity. IPC is a simple procedure with a potential protective effect, and it is recommended for clinical application.

REFERENCES

- 1 **Pringle JH.** Notes on the arrest of hepatic hemorrhage due to trauma. *Ann Surg* 1908; **48**: 541-549
- 2 **Nagasue N, Uchida M, Kubota H, Hayashi T, Kohno H, Nakamura T.** Cirrhotic livers can tolerate 30 minutes ischaemia at normal environmental temperature. *Eur J Surg* 1995; **161**: 181-186
- 3 **Belghiti J, Noun R, Zante E, Ballet T, Sauvanet A.** Portal triad clamping or hepatic vascular exclusion for major liver resection. A controlled study. *Ann Surg* 1996; **224**: 155-161
- 4 **Murry CE, Jennings RB, Reimer KA.** Preconditioning with ischemia: a delay of lethal cell injury in ischemic myocardium. *Circulation* 1986; **74**: 1124-1136
- 5 **Karck M, Tanaka S, Bolling SF, Simon A, Su TP, Oeltgen PR, Haverich A.** Myocardial protection by ischemic preconditioning and delta-opioid receptor activation in the isolated working rat heart. *J Thorac Cardiovasc Surg* 2001; **122**: 986-992
- 6 **Sola A, De Oca J, Gonzalez R, Prats N, Rosello-Catafau J, Gelpi E, Jaurrieta E, Hotter G.** Protective effect of ischemic preconditioning on cold preservation and reperfusion injury associated with rat intestinal transplantation. *Ann Surg* 2001; **234**: 98-106
- 7 **Ogawa T, Mimura Y, Hiki N, Kanauchi H, Kaminishi M.** Ischaemic preconditioning ameliorates functional disturbance and impaired renal perfusion in rat ischaemia-reperfused kidneys. *Clin Exp Pharmacol Physiol* 2000; **27**: 997-1001
- 8 **Peralta C, Prats N, Xaus C, Gelpi E, Rosello-Catafau J.** Protective effect of liver ischemic preconditioning on liver and lung injury induced by hepatic ischemia-reperfusion in the rat. *Hepatology* 1999; **30**: 1481-1489
- 9 **Yoshizumi T, Yanaga K, Soejima Y, Maeda T, Uchiyama H, Sugimachi K.** Amelioration of liver injury by ischaemic preconditioning. *Br J Surg* 1998; **85**: 1636-1640
- 10 **Clavien PA, Yadav S, Sindram D, Bentley RC.** Protective effects of ischemic preconditioning for liver resection performed under inflow occlusion in humans. *Ann Surg* 2000; **232**: 155-162
- 11 **Tang ZY, Yu YQ, Zhou XD, Ma ZC, Yang R, Lu JZ, Lin ZY, Yang BH.** Surgery of small hepatocellular carcinoma. Analysis of 144 cases. *Cancer* 1989; **64**: 536-541
- 12 **Lü MD, Huang JF, Liang LJ, Peng BG.** Oral glucose tolerance test and glucagons loading test as useful parameters for evaluating liver functional reserve. *Zhonghua Waike Zazhi* 1993; **31**: 532-534
- 13 **Li SQ, Liang LJ, Huang JF.** Effects of ischemic preconditioning on hepatocyte apoptosis induced by hepatic ischemia-reperfusion in cirrhotic rats. *Zhongguo Bingli Shengli Zazhi* 2002; **18**: 55-58
- 14 **Enari M, Talanian RV, Wong WW, Nagata S.** Sequential activation of ICE-like and CPP32-like proteases during Fas-mediated apoptosis. *Nature* 1996; **380**: 723-726
- 15 **Gavrieli Y, Sherman Y, Ben-Sasson SA.** Identification of programmed cell death in situ via specific labeling of nuclear DNA fragmentation. *J Cell Biol* 1992; **119**: 493-501
- 16 **Huguet C, Gavelli A, Chieco PA, Bona S, Harb J, Joseph JM, Jobard J, Gramaglia M, Lasserre M.** Liver ischemia for hepatic resection: where is the limit? *Surgery* 1992; **111**: 251-259
- 17 **Man K, Fan ST, Ng IO, Lo CM, Liu CL, Wong J.** Prospective evaluation of Pringle maneuver in hepatectomy for liver tumors by a randomized study. *Ann Surg* 1997; **226**: 704-713
- 18 **Selzner N, Rudiger H, Graf R, Clavien PA.** Protective strategies against ischemic injury of the liver. *Gastroenterology* 2003; **125**: 917-936
- 19 **Belghiti J, Noun R, Malafosse R, Jagot P, Sauvanet A, Pierangeli F, Marty J, Farges O.** Continuous versus intermittent portal triad clamping for liver resection: a controlled study. *Ann Surg* 1999; **229**: 369-375
- 20 **Asahara T, Katayama K, Itamoto T, Yano M, Hino H, Okamoto Y, Nakahara H, Dohi K, Moriwaki K, Yuge O.** Perioperative blood transfusion as a prognostic indicator in patients with

- hepatocellular carcinoma. *World J Surg* 1999; **23**: 676-680
- 21 **Cheng XD**, Jiang XC, Liu YB, Peng CH, Xu B, Peng SY. Effect of ischemic preconditioning on P-selectin expression in hepatocytes of rats with cirrhotic ischemia-reperfusion injury. *World J Gastroenterol* 2003; **9**: 2289-2292
- 22 **Kohli V**, Selzner M, Madden JF, Bentley RC, Clavien PA. Endothelial cell and hepatocyte deaths occur by apoptosis after ischemia-reperfusion injury in the rat liver. *Transplantation* 1999; **67**: 1099-1105
- 23 **Gao W**, Bentley RC, Madden JF, Clavien PA. Apoptosis of sinusoidal endothelial cells is a critical mechanism of preservation injury in rat liver transplantation. *Hepatology* 1998; **27**: 1652-1660
- 24 **Sasaki H**, Matsuno T, Tanaka N, Orita K. Activation of apoptosis during the reperfusion phase after rat liver ischemia. *Transplant Proc* 1996; **28**: 1908-1909
- 25 **Natori S**, Selzner M, Valentino KL, Fritz LC, Srinivasan A, Clavien PA, Gores GJ. Apoptosis of sinusoidal endothelial cells occurs during liver preservation injury by a caspase-dependent mechanism. *Transplantation* 1999; **68**: 89-96
- 26 **Gujral JS**, Bucci TJ, Farhood A, Jaeschke H. Mechanism of cell death during warm hepatic ischemia-reperfusion in rats: apoptosis or necrosis? *Hepatology* 2001; **33**: 397-405
- 27 **Jaeschke H**, Lemasters JJ. Apoptosis versus oncotic necrosis in hepatic ischemia/reperfusion injury. *Gastroenterology* 2003; **125**: 1246-1257
- 28 **Li SQ**, Liang LJ, Huang JF, Li Z. Hepatocyte apoptosis induced by hepatic ischemia-reperfusion injury in cirrhotic rats. *Hepatobiliary Pancreat Dis Int* 2003; **2**: 102-105
- 29 **Wanner GA**, Mica L, Wanner-Schmid E, Kolb SA, Hentze H, Trentz O, Ertel W. Inhibition of caspase activity prevents CD95-mediated hepatic microvascular perfusion failure and restores Kupffer cell clearance capacity. *FASEB J* 1999; **13**: 1239-1248
- 30 **Yadav SS**, Sindram D, Perry DK, Clavien PA. Ischemic preconditioning protects the mouse liver by inhibition of apoptosis through a caspase-dependent pathway. *Hepatology* 1999; **30**: 1223-1231
- 31 **Schulz JB**, Weller M, Moskowitz MA. Caspases as treatment targets in stroke and neurodegenerative diseases. *Ann Neurol* 1999; **45**: 421-429
- 32 **Rossig L**, Fichtlscherer B, Breitschopf K, Haendeler J, Zeiher AM, Mulsch A, Dimmeler S. Nitric oxide inhibits caspase-3 by S-nitrosation *in vivo*. *J Biol Chem* 1999; **274**: 6823-6826

Edited by Wang XL and Xu FM

Clinical analysis of primary small intestinal disease: A report of 309 cases

Jun Zhan, Zhong-Sheng Xia, Ying-Qiang Zhong, Shi-Neng Zhang, Lin-Yun Wang, Hong Shu, Zhao-Hua Zhu

Jun Zhan, Zhong-Sheng Xia, Ying-Qiang Zhong, Shi-Neng Zhang, Lin-Yun Wang, Hong Shu, Zhao-Hua Zhu, Gastrointestinal Division of Internal Medicine, Second Hospital, Sun Yat-Sen University, Guangzhou 510120, Guangdong Province, China

Correspondence to: Dr. Jun Zhan, Gastrointestinal Division of Internal Medicine, Second Hospital, Sun Yat-Sen University, Guangzhou 510120, Guangdong Province, China

Telephone: +86-20-81332598

Received: 2004-01-10 **Accepted:** 2004-03-06

Abstract

AIM: To evaluate the major clinical symptom, etiology, and diagnostic method in patients with primary small intestinal disease in order to improve the diagnosis.

METHODS: A total of 309 cases with primary small intestinal disease were reviewed, and the major clinical symptoms, etiology, and diagnostic methods were analyzed.

RESULTS: The major clinical symptoms included abdominal pain (71%), abdominal mass (14%), vomiting (10%), melaena (10%), and fever (9%). The most common disease were malignant tumor (40%), diverticulum (32%) and benign tumor (10%). Duodenal disease was involved in 36% of the patients with primary small intestinal diseases. The diagnostic rate for primary small intestinal diseases by double-contrast enteroclysis was 85.6%.

CONCLUSION: Abdominal pain is the most common clinical symptom in patients with primary small intestinal disease. Malignant tumors are the most common diseases. Duodenum was the most common part involved in small intestine. Double-contrast enteroclysis was still the simplest and the most available examination method in diagnosis of primary small intestinal disease. However, more practical diagnostic method should be explored to improve the diagnostic accuracy.

Zhan J, Xia ZS, Zhong YQ, Zhang SN, Wang LY, Shu H, Zhu ZH. Clinical analysis of primary small intestinal disease: A report of 309 cases. *World J Gastroenterol* 2004; 10(17): 2585-2587 <http://www.wjgnet.com/1007-9327/10/2585.asp>

INTRODUCTION

Clinically, primary small intestinal disease is relatively rare. Accounting for only 1-4% of digestive diseases^[1]. In spite of the development of techniques in endoscopy and the innovation of equipments, such as capsule endoscopy^[2,3] and double-balloon push enteroscopy^[4,5], diagnosis of primary small intestinal disease is still difficult. For example, uncontrollability in the movement of endoscopic capsule, the influence of fluid inside gastrointestinal tract, poor discrimination in images and unavailability of biopsy decrease the practicability of capsule endoscopy in clinical practice^[6]. Theoretically, there is no blind region in total small intestine for double-balloon push enteroscopy, as the new instrument has been put into practice recently. However, it is almost impossible for double-balloon

push enteroscopy to search all small intestines through either mouth or anus. Furthermore, double-balloon push enteroscopy has other limitations, such as long time of examination and patients' prolonged endurance^[7]. Therefore, the diagnosis of primary small intestinal disease is still difficult. In this study, by clinical analysis of 309 cases of patients with primary small intestinal disease, we aimed to investigate clinical symptoms, etiology, and diagnostic methods in primary small intestinal disease in order to increase the knowledge in primary small intestinal disease and improve the diagnosis.

MATERIALS AND METHODS

Criteria for selected patients

All selected patients had clinical symptoms or signs of the digestive system. The diagnosis of small intestinal disease was confirmed by means of laparotomy, pathology and other examinations. Primary small intestinal disease included duodenal disease, jejunal disease and ileal disease. However, duodenal bulb ulcer was not included. Secondary small intestinal diseases were also excluded.

Method of analysis

A total of 309 cases with primary small intestinal disease were reviewed, and the major clinical symptoms, etiology, and diagnostic methods were analyzed.

RESULTS

From January 1976 to July 2003, 309 cases with primary small intestinal disease were collected. Among them, there were 167 males, 142 females, with age ranging from 2 to 87 years old, and an average age of 51.2 years.

Among the 309 cases, 216 cases were confirmed by surgical operations, 53 by double-contrast enteroclysis, 24 by gastric endoscopy or enteroscopy and biopsy and 16 by a combination of clinical and other examinations. Among the 216 cases with surgical operations, diagnosis could not be definitely made in 142 cases until laparotomy was performed. Lesions were found in 89 of 104 cases examined by double-contrast enteroclysis, giving a positive rate of 85.6%. The major clinical symptoms were abdominal pain, abdominal mass, vomiting, melaena, fever, hematochezia and diarrhea. Some cases had two or more symptoms (Table 1). The most common diseases were malignant tumor (40%), diverticulum (32%) and benign tumor (10%). Duodenal disease was involved in 36% of the patients with primary small intestinal diseases. The distribution of the major diseases of 309 cases is listed in Table 2.

Table 1 Major clinical symptoms of 309 cases with primary small intestinal disease

Symptom	n (%)	Symptom	n (%)
Abdominal pain	218 (71)	Hematochezia	19 (6)
Abdominal mass	44 (14)	Diarrhea	14 (5)
Vomiting	32 (10)	Jaundice	13 (4)
Melaena	30 (10)	Haematemesis	3 (1)
Fever	27 (9)	Others	8 (3)

Table 2 Distribution of major diseases in 309 cases with primary small intestinal disease

Disease	n (%)
Small intestinal diverticulum	100 (32)
Small intestinal adenocarcinoma	35 (11)
Small intestinal leiomyosarcoma	34 (11)
Small intestinal lymphoma	29 (9)
Crohn's disease	15 (5)
Small intestinal leiomyomas	13 (4)
Hemorrhagic necrotizing enteritis	13 (4)
Ampullar carcinoma	11 (4)
Small intestinal malignant mesenchymoma	11 (4)
Small intestinal polyp	10 (3)
Small intestinal twist	8 (3)
Small intestine multiple perforation	4 (1)
Terminal ileal ulcer	3 (1)
Small intestinal cavernous hemangioma	2 (1)
Small intestinal malabsorption syndrome	2 (1)
Small intestinal internal hernia	2 (1)
Small intestinal fistula	2(1)
Others ¹	15(5)

¹Including jejunal malignant melanoma, jejunal malignant angioendothelioma, ileal liposarcoma, small intestinal malignant reticulosis, small intestinal fibrosarcoma, jejunal lipoma, jejunal fibroma, jejunal neurofibroma, ileal neurilemmoma, small intestinal benign mesenchymaloma, small intestinal teratoma, small intestinal inflammatory pseudotumor, terminal ilealitis, eosinophilic enteritis and idiopathic small intestinal obstruction which had 1 case respectively.

DISCUSSION

Distribution of major diseases in patients with primary small intestinal disease

In this study, 216 (70%) of 309 cases were diagnosed as having primary small intestinal disease by a combination of surgical operations and pathology. In addition, 24 of 309 cases were diagnosed by a combination of gastric endoscopy or enteroscopy and biopsy. Therefore, a total of 240 (78%) cases were diagnosed by pathology. Based on the analysis of the characteristics of the diseases, we found that malignant tumor was the most common disease in primary small intestinal disease. Overall, 125 patients had malignant tumors, 35 (11%) with adenocarcinoma, 34 (11%) with leiomyosarcoma, 29 (9%) with small intestinal lymphoma, and 11 (4) with ampullar carcinoma. These patients accounted for 40% of the cases with primary small intestinal disease. There were only 32 (10%) cases with small intestinal benign tumor, mainly including 13 (4%) cases of small intestinal leiomyomas, and 10 (3%) with small intestinal polyps. The ratio of small intestinal benign over malignant tumors was almost 1:4 (32:125), which indicates that most of small intestinal neoplasms are malignant, and thus small intestinal malignant tumors contribute significantly to small intestinal disease. This finding is consistent with previous domestic reports by Liu *et al.*^[8] and Shi *et al.*^[9], but different from the oversea reports that small intestinal benign tumor is more common than small intestinal malignant tumor^[10]. Our observations suggest that malignant tumors should be considered if small intestinal disease is under consideration, and further examinations should be taken as soon as possible to assure or exclude small intestinal malignant tumor. In this way, patients with small intestinal malignant tumor would receive optimum management through the early diagnosis and early treatment strategy, and thus prognosis would be significantly improved.

Among the 309 cases, 100 had small intestinal diverticulum, which contributed to 32% of cases and was the second common diagnosis in small intestinal disease. Among patients with small intestinal diverticulum, 72 (72%) had duodenal diverticulum, and 28 (28%) had jejunal or/and ileal diverticulum, which indicates that duodenal diverticulum is much more common than jejunal or/and ileal diverticulum. The data suggest that more attention should be paid to duodenal diverticulum, especially diverticulum of descending part of duodenum because diverticulum in this site is not only common but also detectable easily by gastric endoscopy or barium meal examination.

In addition, 84 cases had other small intestinal benign disease, which contributed to 27% of patients with small intestinal diseases, mainly including 32 (10%) with small intestinal benign tumor, 15 (5%) with Crohn's disease, 13 (4%) with hemorrhagic necrotizing enteritis and 8 (3%) with small intestinal twist. These data indicate that small intestinal benign tumor is the most common disease among small intestinal non-diverticular benign disease. It is also noticed that 111 cases with duodenal diseases contributed to 36% of the 309 patients with primary small intestinal disease. There were 72 cases with diverticulum accounting for 65% of patients with duodenal disease, 37 with malignant tumor accounting for 33% of patients with duodenal disease, and 2 with duodenal polyps. Since the human small intestine is 5 to 6 meters long, and duodenum is only 0.25 meter long, which is not longer than 1/20 of full length of small intestine. However, more than one third of small intestinal diseases were duodenal diseases. Therefore, duodenum is the most common part involved in small intestinal disease, and special attentions should be paid to duodenal disease, especially between descending part and ascending part of duodenum when small intestinal disease is under consideration, because duodenum is not only commonly involved but also shallow enough to be easily detected by gastric endoscopy or a barium meal examination without need for other complex examinations.

Major clinical symptoms in patients with primary small intestinal disease

Clinical symptoms of primary small intestinal disease in this study included abdominal pain, abdominal mass, vomiting, melaena, fever, hematochezia, diarrhea, jaundice, haematemesis, marasmus, abdominal distension, and constipation. Among these symptoms, abdominal pain was the most common clinical symptom as 218 cases had abdominal pain, which contributed to 71% of cases with primary small intestinal disease. The site of abdominal pain was mainly located around the navel. The second common symptom was abdominal mass. Altogether 44 cases had abdominal mass, which contributed to 14% of cases with primary small intestinal disease. The other common symptoms were vomiting, melaena and fever. Fever was caused mostly by small intestinal lymphoma and hemorrhagic necrotizing enteritis. However, hematochezia, diarrhea, jaundice, haematemesis were less common. Hematochezia was often characterized by dark-red stool and negative findings by enteroscopy. Haematemesis was a rare symptom, but if it occurred, then the volume of bleeding would be enormous. Therefore, the symptoms of patients with primary small intestinal disease are lacking of specificity as these symptoms may occur in patients with upper digestive disease and colon disease. So small intestinal disease could not be diagnosed only by symptoms, which is also one of the reasons for the difficulty in the diagnosis of primary small intestinal disease. However, when patients had above mentioned symptoms, especially melaena, hematochezia, haematemesis and enteremphraxis, but no positive findings were found by gastric endoscopy and enteroscopy at the same time, further examinations should be

given to patients to verify or exclude small intestinal disease. These examinations include double-contrast enteroclysis, selective arteriography, small intestinal endoscopy, capsule endoscopy, and double-balloon push enteroscopy.

Examinations methods for the diagnosis of primary small intestinal disease

In spite of so many examination methods, how to select appropriate examinations is a question to be often asked in clinical work. We found that some patients were finally definitely diagnosed as having primary small intestinal disease through almost all the examinations, which not only put heavy economical burden on patients, but also increased suffering of patients, and especially delayed the diagnosis of disease. However, if an examination was correctly selected, the diagnosis could be easily achieved. Capsule endoscopy is nontraumatic method for the examination of small intestinal disease, however, uncontrollability in movement of capsule endoscopy, poor discrimination in images and unavailability of biopsy, expensive price, and time-consuming decrease the practicability of this method in clinical practice. The traditional enteroscopy can only observe the digestive tract 1 meter above jejunum to Treitz ligament due to itself limitation, which means that most of small intestinal could not be diagnosed by the traditional enteroscopy. Radiography includes selective arteriography and double-contrast enteroclysis. Selective arteriography is a useful examination for patients with main clinical symptoms of melaena, hematochezia or haematemesis. The diagnosis rate of selective arteriography is increased especially when a patient is bleeding^[11]. Otherwise, double-contrast enteroclysis is a very valuable examination for patients with main clinical symptoms of abdominal pain, abdominal mass, vomiting, or diarrhea. In this study, among the 309 cases with primary small intestinal disease, 104 cases were examined by double-contrast enteroclysis, and 89 cases were found lesion in small intestine, with a positive rate of 85.6%, which was similar to report by Wang *et al*^[12]. This positive rate is significantly higher than that (70%) reported by Zhan *et al*, based on the hospitalized patients in our hospital before 1997^[13]. The improvement of diagnosis accuracy may be related to the better choice made by doctors for examinations, the improved experience of examiners and more attention paid to small intestinal disease over the past 6 years. Unfortunately, only one third of cases with primary small intestinal disease were examined by double-contrast enteroclysis in this study. The reasons for this included unawareness of double-contrast enteroclysis by physicians, emergency that did not allow patient for double-contrast enteroclysis but for laparotomy and situations that patients had a complete or incomplete intestinal obstruction. In fact, patients with incomplete intestinal obstruction can be examined by double-contrast enteroclysis with meglucamine diatrizoate instead of barium by placing a tube into duodenum during gastric endoscopy, which could not only increase the diagnosis rate, but also be more available and safer for patients^[14]. Because some endoscopic capsules can not move out of body in some patients until laparotomy was performed, it is suggested that double-contrast enteroclysis should be performed before capsule endoscopy. By this way, doctors not only obtain primary knowledge if there is a matter

with patient, but also obtain the information of the intestinal movement, which would help determine whether capsule endoscopy is suitable for the patient and thus avoid the situation which endoscopic capsule can not naturally move out of the body^[15]. Double-balloon push enteroscopy has been applied recently to provide a powerful tool for diagnosis of small intestinal disease. Therefore, we would draw a conclusion from what mentioned above that as a traditional nontraumatic or microtraumatic examination, double-contrast enteroclysis has advantages in simplicity and availability, little torment, high diagnosis accuracy and low price. Therefore, at present, double-contrast enteroclysis still plays an important role in diagnosis of small intestinal disease. We are hoping that double-balloon push enteroscopy and other newer and more practical examinations could aid in diagnosis of small intestinal disease with the development of technology in endoscopy and general use of endoscopic equipment.

REFERENCES

- 1 **Li YN.** Striving for improvement in diagnosis of small intestinal disease. *Zhonghua Xiaohua Zazhi* 1992; **12**: 249
- 2 **Yu M.** M2A capsule endoscopy. A breakthrough diagnostic tool for small intestine imaging. *Gastroenterol Nurs* 2002; **25**: 24-27
- 3 **Ell C, Remke S, May A, Helou L, Henrich R, Mayer G.** The first prospective controlled trial comparing wireless capsule endoscopy with push enteroscopy in chronic gastrointestinal bleeding. *Endoscopy* 2002; **34**: 685-689
- 4 **Yamamoto H, Sekine Y, Sato Y, Higashizawa T, Miyata T, Iino S, Ido K, Sugano K.** Total enteroscopy with a nonsurgical steerable double-balloon method. *Gastrointest Endosc* 2001; **53**: 216-220
- 5 **Yamamoto H, Sugano K.** A new method of enteroscopy- the double-balloon method. *Can J Gastroenterol* 2003; **17**: 273-274
- 6 **Lewis BS, Swain P.** Capsule endoscopy in the evaluation of patients with suspected small intestinal bleeding: Results of a pilot study. *Gastrointest Endosc* 2002; **56**: 349-353
- 7 **Zhong J, Zhang CL, Zhang J, Wu YL, Jiang SH.** Application of double-balloon push enteroscopy in diagnosis of small bowel diseases. *Zhonghua Xiaohua Zazhi* 2003; **23**: 591-594
- 8 **Liu DD, Wang JY, Sheng XZ.** Clinical analysis of small intestinal tumor in 93 cases. *Fudan Xuebao Yixue Kexueban* 2001; **28**: 145-147
- 9 **Shi HQ, Huang JY, Cheng J, Shao Z, Xu JW.** Clinical analysis of 142 cases of primary small intestinal tumor. *Zhejiang Linchuan Yixue* 2002; **4**: 642-643
- 10 **Lewis BS, Kornbluth A, Wayne JD.** Small bowel tumors: yield of enteroscopy. *Gut* 1991; **32**: 763-765
- 11 **Ding JZ, Li QY, Kuang J, Jin XT, Li HW.** The significance of auxiliary examinations in diagnosis of hemorrhagic small intestinal disease. *Shijie Huaren Xiaohua Zazhi* 2002; **10**: 603-604
- 12 **Wang AY, Lin SR, Liu X.** Clinical diagnostic value of double-contrast enteroclysis. *Zhonghua Xiaohua Zazhi* 1992; **12**: 27
- 13 **Zhan J, Gan XL, Wu XL, Li JG, Zeng ZY.** Clinical analysis of 224 cases of small intestinal disease. *Zhonghua Neike Zazhi* 2000; **39**: 592-593
- 14 **Chen MX.** Clinical diagnostic value of double-contrast enteroclysis by placing tube under endoscopy. *Zhonghua Xiaohua Zazhi* 2002; **22**: 444
- 15 **Costamagna G, Shah SK, Riccioni ME, Foschia F, Mutignani M, Perri V, Vecchioli A, Brizi MG, Piccicocchi A, Marano P.** A prospective trial comparing small bowel radiographs and video capsule endoscopy for suspected small bowel disease. *Gastroenterology* 2002; **123**: 999-1005

Edited by Xia HHX Proofread by Chen WW and Xu FM

Chylous ascites: Treated with total parenteral nutrition and somatostatin

Qi Huang, Zhi-Wei Jiang, Jun Jiang, Ning Li, Jie-Shou Li

Qi Huang, Zhi-Wei Jiang, Jun Jiang, Ning Li, Jie-Shou Li, Department of General Surgery, Jinling Hospital, School of Medicine, Nanjing University, Nanjing 210002, Jiangsu Province, China

Correspondence to: Dr. Zhi-Wei Jiang, Institute of General Surgery, Jinling Hospital, 305 Zhongshan East Road, Nanjing 210002, Jiangsu Province, China. doctorhq007@sina.com

Telephone: +86-25-4806187

Received: 2003-10-31 **Accepted:** 2003-12-16

Abstract

AIM: To determine the effects of total parenteral nutrition and somatostatin on patients with chylous ascites.

METHODS: Five patients were diagnosed with chylous ascites on the basis of laboratory findings of ascites sample from Nov 1999 to May 2003. Total parenteral nutrition and somatostatin or its analogue was administered to 4 patients, while the other one only received total parenteral nutrition. All the patients had persistent peritoneal drainage, with the quantity and quality of drainage fluid observed daily. Necessary supportive treatments were given to the patients individually during the therapy.

RESULTS: Two of 4 patients who received somatostatin therapy obtained complete recovery within 10 d without any recurrence while on a normal diet. In these 2 patients, the peritoneal drainage reduced to zero in one and the other's decreased from 2 000 mL to 80 mL with a clear appearance and negative qualitative analysis of chyle. Recurrent chylous ascites, though relieved effectively by the same method every time, developed in one patient with advanced pancreatic cancer. The other patient's lymphatic fistula was blocked with the fibrin glue after conservative treatment. The patient who only received total parenteral nutrition was cured 24 d after therapy.

CONCLUSION: Total parenteral nutrition along with somatostatin can relieve the symptoms and close the fistula in patients with chylous ascites rapidly. It appears to be an effective therapy available for the treatment of chylous ascites caused by various disorders.

Huang Q, Jiang ZW, Jiang J, Li N, Li JS. Chylous ascites: Treated with total parenteral nutrition and somatostatin. *World J Gastroenterol* 2004; 10(17): 2588-2591

<http://www.wjgnet.com/1007-9327/10/2588.asp>

INTRODUCTION

Chylous ascites, an uncommon disease usually caused by obstruction or rupture of the peritoneal or retroperitoneal lymphatic glands, is defined as the accumulation of chyle in the peritoneal cavity^[1]. It is a difficult disorder due to the serious mechanical, nutritional and immunological consequences of the constant loss of protein and lymphocytes^[2]. Morton's dramatic and detailed account in 1694 of a 2-year-old boy with tuberculosis who died of chylous ascites was the first clear report of chyloperitoneum.

Many pathological conditions can result in this disease, including congenital defects of the lymphatic system, nonspecific bacterial, parasitic and tuberculous peritoneal infection, liver cirrhosis, malignant neoplasm, blunt abdominal trauma and surgical injury^[1]. Over all, the most common cause in adults is believed to be abdominal malignancy, while congenital lymphatic abnormalities in pediatric population. Press *et al.* reported an incidence of 1 per 20 464 admissions at the Massachusetts General Hospital during a 20-year period^[3]. They found, however, a 1 per 11 589 incidence in the last years of their study. Most investigators believe that the incidence of chylous ascites is increasing because of more aggressive thoracic and retroperitoneal surgery and with the prolonged survival of patients with cancer^[4-8]. Some new techniques, such as laparoscopic surgery and transplantation, also lead to postoperative chylous ascites^[9-11]. Kaas *et al.* found that 12 (7.4%) of 163 patients with complex surgical procedures developed chylous ascites^[12].

Though the incidence of chylous ascites has increased in recent years, the treatment remains unsatisfactory in some cases because of prolonged duration of disease. Conservative treatment of chylous ascites, recommended in most patients, involves paracentesis, a medium chain triglyceride (MCT) based diet, total parenteral nutrition (TPN), recently used somatostatin and so on. Surgery is only recommended when conservative treatment fails^[2]. In a review of 156 patients with chylous ascites resolved after intervention, 51 patients were successfully treated surgically; 105 patients were treated conservatively^[13]. Usually the MCT based diet is the first choice, TPN is recommended after dietary manipulation has failed, and somatostatin therapy is attempted only if chylous ascites has been refractory to all conservative measures. It will take several weeks to 2 mo to close the lymphatic fistula adequately with routine conservative regimens^[13].

Here we report on our successful use of persistent peritoneal drainage, TPN as well as somatostatin in treatment of 5 cases of chylous ascites.

MATERIALS AND METHODS

Five adult patients with chylous ascites were admitted to our hospital from November 1999 to May 2003. On admission, computerized tomography (CT) examination was performed to reveal the etiology, and the diagnosis was confirmed by analyzing the cloudy ascites fluid obtained through paracentesis or peritoneal drainage. Table 1 shows the clinical features, CT findings and laboratory findings of ascites samples from 5 patients.

As soon as the diagnosis was confirmed, every patient was put in fasting state and received fluid replenishment until disturbance of water, electrolytes and acid-base was corrected. A single lumen central venous catheter was inserted into the peritoneal cavity for continuous drainage in 3 patients, while peritoneal cavity drainage tubes inserted during the operation were reserved in patient 4 and 5. The quality and quantity of drainage fluid were monitored daily. Then TPN (non-protein calorie 25 kcal/(kg·d), nitrogen 0.2-0.25 g/(kg·d), glucose: fat ratio 6:4) via central vein was administered to patients at gradually increasing dose. Somatostatin (Stilamin, Laboratoires Serono S. A.) was administered to patient 2 and 4 through continuous intravenous infusion at a dose of 3 mg per 12 h.

Patient 3 and 5 received subcutaneous administration of the somatostatin analogue, octreotide (Sandostatin, Novartis Pharma AG), at a dose from 100 µg to 200 µg 3 times daily. Necessary supportive treatments, such as albumin, diuretics and antibiotics, were given to the patients individually during the therapy. In addition, patient 5 received abdominal cavity and peripheral venous chemotherapy at the same time.

RESULTS

Figure 1 shows the change of drainage volume, the duration of TPN and somatostatin therapy of 5 patients. Once the peritoneal

drainage was zero (in patient 1 and 4) or was proved non-chylous ascites (in patient 2 and 3), TPN and somatostatin dose would diminish gradually along with the recovery of oral low fat diet. Patient 3 and 4, who received somatostatin therapy, obtained complete recovery within 10 d, while patient 1 who only received TPN was cured 24 d after therapy. The drainage of patient 3 decreased from 2 000 mL to 80 mL within 10 d with a clear appearance and negative qualitative analysis of chyle, and the volume remained unchanged when she received normal diet. Then patient 3 was referred to department of gastroenterology for further treatment of the established liver cirrhosis, which caused the remaining ascites. All these 3 patients' drainage

Table 1 Clinical features, CT and laboratory findings for 5 patients with chylous ascites

Patient	Age in yr/Sex	Medical/Surgical condition	CT findings	Laboratory findings of ascites			
				Qualitative analysis of chyle	Leukocyte count (/mm ³)/Lymphocyte (%)	Total protein/Albumin (g/L)	Cholesterol/Triglyceride (mmol/L)
1	48/M	Two wk after radical distal subtotal gastrectomy for gastric cancer	Large volume of ascites	+	1 600/95	49.4/30.9	1.92/7.14
2	50/M	Five mo after pancreaticoduodenectomy for pancreatic cancer	Large volume of ascites, multiple metastases involving liver and lymph nodes	+	120/95	15.0/10.1	1.59/2.41
3	65/F	Half a year after cure of the tuberculous peritoneal infection	Large volume of ascites, liver cirrhosis	+	560/50	23.2/14.2	2.11/5.68
4	50/F	One wk after finding of 400 mL milky fluid in pelvic cavity during laparoscopy cholecystectomy	Small volume of ascites in pelvic cavity	+	190/88	52.8/32.0	0.67/3.01
5	44/F	10 d after radical pelvic lymphadenectomy for ovarian cancer	Small volume of fluid in pelvic cavity	+	890/92	47.7/31.9	1.47/7.11

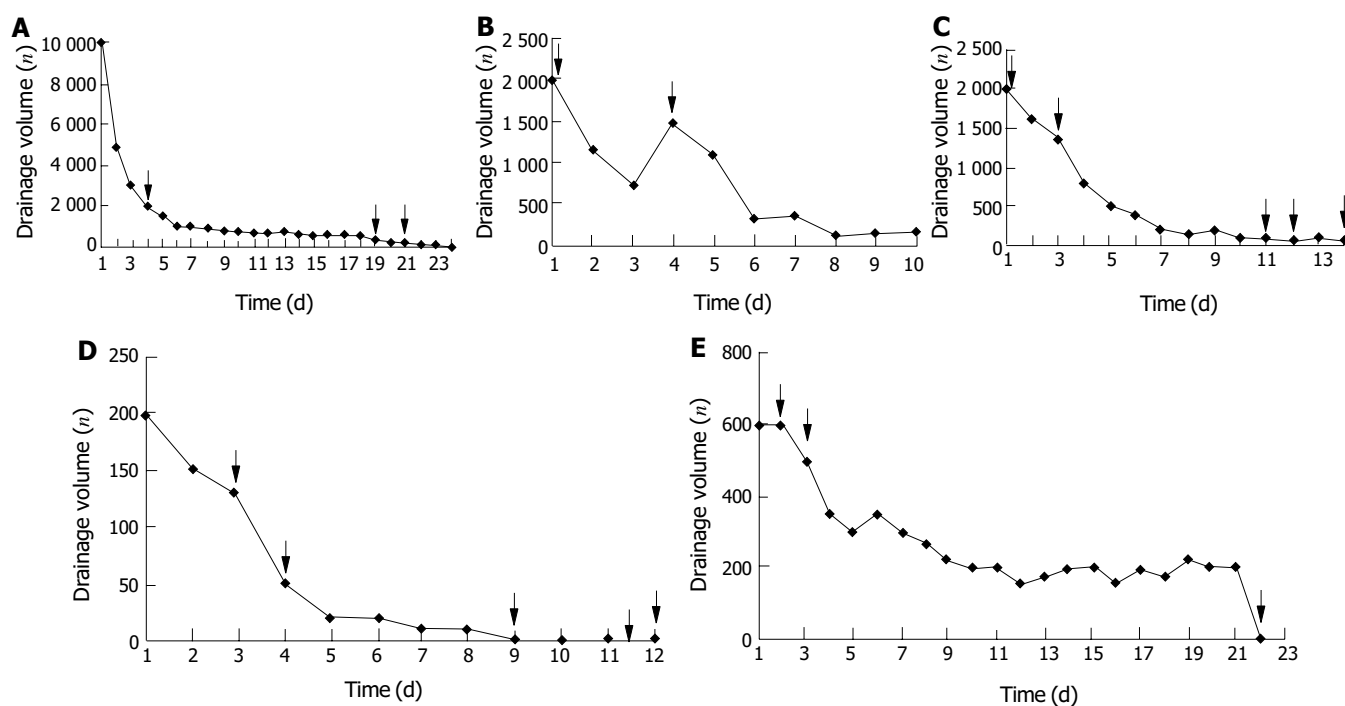


Figure 1 Change of drainage volume and the duration of TPN and somatostatin therapy in 5 patients. ↓The beginning and the end of TPN, ↓the beginning and the end of somatostatin therapy, ↓the beginning of food intake, ↓blockage of the fistula. A: Patient 1 who only received TPN recovered fully after 24 d of therapy; B: Patient 2 suffered from repeated recurrence though the drainage volume decreased from 2 000 mL to 100 mL within 11 d; C: Chylous ascites never recurred in patient 3 after the drainage volume decreased to 80 mL within 10 d with negative qualitative analysis of chyle; D: Patient 4 recovered fully within 9 d; E: Chylous fistula of patient 5 showed refractory to therapy and was sealed with fibrin glue.

catheters were removed after they had normal diet for 3 d. The drainage volume of patient 5, though dropped from 600 mL to 200 mL within 10 d, remained unchanged for 11 d with positive qualitative analysis of chyle. Then we successfully used fibrin glue to block up the lymphatic fistula that was proved mature with X-ray fistulography. CT follow-up examinations did not reveal the presence of ascitic fluid. The nutritional status of them was well maintained during therapy. Follow-up study found no recurrence in these 4 patients while on normal diet after 6 mo. Though the drainage decreased from 2 000 mL to 100 mL within 11 d and was proved non-chylous ascites, repeated recurrences developed in patient 2 who died of advanced pancreatic cancer 3 mo later.

DISCUSSION

Our results showed that TPN along with somatostatin appears to be an effective therapy available for the treatment of chylous ascites caused by various disorders.

There are multiple causes of chylous ascites. The most common ones in Western countries are abdominal malignancy and cirrhosis, which account for over two thirds of all cases. In contrast, infectious etiologies, such as tuberculosis and filariasis, account for the majority of cases of chylous ascites in Eastern and developing countries^[14]. Previous studies showed the effect of some regimen in the treatment of chylous ascites caused by one kind of pathological condition. In the present series, various etiological factors including surgical injury (patient 1 and 5), pancreatic cancer (patient 2), liver cirrhosis (patient 3) and idiopathic cause (patient 4) demonstrate the wide indications of our treatment. It also indicates the change of etiology spectrum in China, operation and cancer have become the common causes now.

Treatment of the underlying cause of chylous ascites is of pivotal importance in managing patients with chylous ascites, especially those having an infectious, inflammatory, or hemodynamic cause. But conservative treatment is usually vital for most patients to relieve the symptoms and restore nutritional deficits. Paracentesis is not only a diagnostic but also therapeutic method in the management of chylous ascites. Despite several definite drawbacks and complications, repeated paracentesis is commonly included in the nonoperative treatment regimens to relieve abdominal distention^[13]. In three patients of this series, repeated paracentesis was replaced by persistent peritoneal drainage with a single lumen central venous catheter, which permitted us to monitor the quality and quantity of drainage daily. In patient 4 and 5, peritoneal drainage tube inserted during the operation was reserved until recovery. No tube blockage, catheter-related sepsis or any other complications developed in all patients. So persistent peritoneal drainage may be a much better and accepted choice than repeated paracentesis.

Fasting, together with TPN, can decrease the lymph flow in thoracic duct dramatically from 220 mL/(kg·h) to 1 mL/(kg·h)^[13]. Furthermore, TPN restores nutritional deficits and balances metabolic impairments imposed by long-standing chylous ascites and repeat sessions of paracentesis. So fasting and TPN are essential in nonoperative management of chylous ascites. In the past, however, TPN was usually recommended as the second line treatment when enteral dietary manipulation failed^[13]. Routine conservative treatment, using TPN only or combined with an MCT diet, needed 2 to 6 wk to cure 60% to 100% of cases^[14,15]. In our study, patient 1 who only received fasting and TPN recovered completely after 24 d.

Initial experience with continuous intravenous high dose somatostatin for the closure of postoperative lymphorrhagia was reported in 1990 by Ulibarri *et al.* The exact mechanisms of somatostatin on drying lymphatic fistulas are not completely understood. It has been previously shown to decrease the

intestinal absorption of fats, lower triglyceride concentration in the thoracic duct and attenuate lymph flow in the major lymphatic channels^[16]. In addition, it also decreases gastric, pancreatic and intestinal secretions, inhibits motor activity of the intestine, slows the process of intestinal absorption and decreases splanchnic blood flow, which may further contribute to decreased lymph production. It has also been speculated that somatostatin improves chylous ascites by inhibition of lymph fluid excretion through specific receptors found in the normal lymphatic vessels of intestinal wall^[17,18]. Shapiro *et al.* reported rapid resolution of chylous ascites after liver transplantation within 2 d after administration of the octreotide combined with total parenteral nutrition^[17]. Satisfactory results were also achieved by others^[16,19-23]. To our knowledge, however, most of these articles included just one case. Somatostatin therapy also remains an indefinite or second-line method in treatment of chylous ascites. The recommended algorithm for the management of chylous ascites in a review in 2000, only regarded somatostatin in combination with TPN as an unproved alternative method^[13]. Another algorithm in 2002 recommended somatostatin therapy only after a period of combined dietary intervention and TPN had failed^[14]. Our results showed that 2 of 4 patients treated with somatostatin or its analogue recovered completely within 10 d with well maintained nutritional status and no significant side effect, while the symptoms of patient 2 relieved despite of relapse. As to patient 5, the conservative treatment decreased the fistula drainage greatly and paved the way for the subsequent management. In this case we are inclined to surmise that chemotherapy may affect the closure of lymphatic fistula. These results suggest that somatostatin along with TPN can close the lymphatic leakage or relieve the symptom effectively and rapidly, in comparison with conventional regimens.

The outcome of chylous ascites mostly depends on the underlying pathological condition causing lymphatic leakage. The mortality of chylous ascites, especially those caused by surgery, has decreased much than before^[15], but that caused by malignancy remains high. In our study, TPN and somatostatin could not control the chylous ascites completely in patient 2, so necessary adjustment of this regimen or more aggressive therapy should be applied to stop the lymphatic leakage in these patients. Peritoneovenous shunt has been proved to be a valuable method especially for those cancer patients who are refractory to conservative treatment^[24-26].

We conclude that TPN with somatostatin should be the first-line therapy for chylous ascites caused by various disorders, and started as soon as possible. Some other methods should also be attempted to close the fistula that is refractory to conservative treatment. Further studies of multicenter clinical trials involving more patients to compare the efficacy and cost between this regimen and the others are suggested.

REFERENCES

- 1 **Browse NL**, Wilson NM, Russo F, al-Hassan H, Allen DR. Aetiology and treatment of chylous ascites. *Br J Surg* 1992; **79**: 1145-1150
- 2 **Leibovitch I**. Postoperative chylous ascites-the urologist's view. *Drugs Today* 2002; **38**: 687-697
- 3 **Press OW**, Press NO, Kaufman SD. Evaluation and management of chylous ascites. *Ann Intern Med* 1982; **96**: 358-364
- 4 **Halkic N**, Abdelmoumene A, Suardet L, Mosimann F. Post-operative chylous ascites after radical gastrectomy. A case report. *Minerva Chir* 2000; **58**: 389-391
- 5 **Warner RR**, Croen EC, Zaveri K, Ratner L. A carcinoid tumor associated with chylous ascites and elevated tumor markers. *Int J Colorectal Dis* 2002; **17**: 156-160
- 6 **Amin R**. Chylous ascites from prostatic adenocarcinoma. *Urology* 2002; **59**: 773
- 7 **Tokiwa K**, Fumino S, Ono S, Iwai N. Results of retroperitoneal lymphadenectomy in the treatment of abdominal neuroblastoma.

- Arch Surg* 2003; **138**: 711-715
- 8 **Sexton WJ**, Wood CG, Kim R, Pisters LL. Repeat retroperitoneal lymph node dissection for metastatic testis cancer. *J Urol* 2003; **169**: 1353-1356
 - 9 **Senyuz OF**, Senturk H, Tasci H, Kaya G, Ozbay G, Sariyar M. Chylous ascites after liver transplantation with mesentero-portal jump graft. *J Hepatobiliary Pancreat Surg* 2001; **8**: 571-572
 - 10 **Shafizadeh SF**, Daily PP, Baliga P, Rogers J, Baillie GM, Rajagopalan PR, Chavin KD. Chylous ascites secondary to laparoscopic donor nephrectomy. *Urology* 2002; **60**: 345
 - 11 **Bacelar TS**, de Albuquerque AC, de Arruda PC, Ferraz AA, Ferraz EM. Postoperative chylous ascites: a rare complication of laparoscopic Nissen fundoplication. *JSLs* 2003; **7**: 269-271
 - 12 **Kaas R**, Rustman LD, Zoetmulder FA. Chylous ascites after oncological abdominal surgery: incidence and treatment. *Eur J Surg Oncol* 2001; **27**: 187-189
 - 13 **Aalami OO**, Allen DB, Organ CH Jr. Chylous ascites: A collective review. *Surgery* 2000; **128**: 761-778
 - 14 **Leibovitch I**, Mor Y, Golomb J, Ramon J. The diagnosis and management of postoperative chylous ascites. *J Urol* 2002; **167**(2pt 1): 449-457
 - 15 **Lee YY**, Soong WJ, Lee YS, Hwang B. Total parenteral nutrition as a primary therapeutic modality for congenital chylous ascites: report of one case. *Acta Paediatr Taiwan* 2002; **43**: 214-216
 - 16 **Collard JM**, Laterre PF, Boemer F, Reynaert M, Ponlot R. Conservative treatment of postsurgical lymphatic leaks with somatostatin-14. *Chest* 2000; **117**: 902-905
 - 17 **Shapiro AM**, Bain VG, Sigalet DL, Kneteman NM. Rapid resolution of chylous ascites after liver transplantation using somatostatin analog and total parenteral nutrition. *Transplantation* 1996; **61**: 1410-1411
 - 18 **Reubi JC**, Horisberger U, Waser B, Gebbers JO, Laissue J. Preferential location of somatostatin receptors in germinal centers of human gut lymphoid tissue. *Gastroenterology* 1992; **103**: 1207-1214
 - 19 **Rimensberger PC**, Muller-Schenker B, Kalangos A, Beghetti M. Treatment of a persistent postoperative chylothorax with somatostatin. *Ann Thorac Surg* 1998; **66**: 253-254
 - 20 **Laterre PF**, Dugernier T, Reynaert MS. Chylous ascites: diagnosis, causes and treatment. *Acta Gastroenterol Belg* 2000; **63**: 260-263
 - 21 **Al-Sebeih K**, Sadeghi N, Al-Dhahri S. Bilateral chylothorax following neck dissection: a new method of treatment. *Ann Otol Rhinol Laryngol* 2001; **110**: 381-384
 - 22 **Leibovitch I**, Mor Y, Golomb J, Ramon J. Chylous ascites after radical nephrectomy and inferior vena cava thrombectomy. Successful conservative management with somatostatin analogue. *Eur Urol* 2002; **41**: 220-222
 - 23 **Leong RW**, House AK, Jeffrey GP. Chylous ascites caused by portal vein thrombosis treated with octreotide. *J Gastroenterol Hepatol* 2003; **18**: 1211-1213
 - 24 **Wagayama H**, Tanaka T, Shimomura M, Ogura K, Shiraki K. Pancreatic cancer with chylous ascites demonstrated by lymphoscintigraphy: successful treatment with peritoneovenous shunting. *Dig Dis Sci* 2002; **47**: 1836-1838
 - 25 **Manolitsas TP**, Abdessalam S, Fowler JM. Chylous ascites following treatment for gynecologic malignancies. *Gynecol Oncol* 2002; **86**: 370-374
 - 26 **Camoglio FS**, Dipaola G, Cervellione RM, Chironi C, Giacomello L, Zanatta C, Ottolenghi A. Treatment of neonatal chylous ascites using a modified Denver peritoneovenous shunt: a case report. *Pediatr Med Chir* 2003; **25**: 145-147

Edited by Zhu LH Proofread by Chen WW and Xu FM

Glutamine supplemented parenteral nutrition prevents intestinal ischemia-reperfusion injury in rats

Guo-Hao Wu, Hao Wang, Yan-Wei Zhang, Zhao-Han Wu, Zhao-Guang Wu

Guo-Hao Wu, Hao Wang, Yan-Wei Zhang, Zhao-Han Wu, Zhao-Guang Wu, Department of General Surgery, Zhongshan Hospital, Fudan University, Shanghai 200032, China

Correspondence to: Guo-Hao Wu, Department of General Surgery, Zhongshan Hospital, Fudan University, Shanghai 200032, China. wugh@zshospital.net

Telephone: +86-21-64041990 Ext. 2365 **Fax:** +86-21-64038472

Received: 2004-02-02 **Accepted:** 2004-02-24

Abstract

AIM: To examine whether glutamine prevents the injury to the intestinal mucosa after intestinal ischemia-reperfusion (I/R) in rats.

METHODS: Thirty male Sprague-Dawley rats were randomly divided into 3 groups: a standard parenteral nutrition (PN) group ($n = 10$); an I/R-PN group ($n = 10$); an I/R-glutamine enriched PN (I/R-Gln) group ($n = 10$). The superior mesenteric artery (SMA) was clamped. After 60 min of ischemia, reperfusion was initiated and infusion was started. All rats received isocaloric and isonitrogenous nutritional support for 48 h. Spleen, liver, mesenteric lymph nodes (MLN), and intestinal segments were removed for morphological and biochemical analyses, and blood samples were collected for bacterial culture and measurement of endotoxin levels. The permeability of intestinal mucosa was assayed by measurement of D-(-)-lactate levels in plasma.

RESULTS: In I/R-PN group, extensive epithelial atrophy was observed, mucosal thickness, villous height, crypt depth and villous surface area were decreased significantly compared with PN group, whereas these findings did not occur in the I/R-Gln group. The incidence of intestinal bacterial translocation to spleen, liver, MLN, and blood was significantly higher in I/R-PN group than that in other groups. Plasma endotoxin levels significantly increased in the I/R-PN group compared with the I/R-Gln group. Remarkably higher values of D-(-)-lactate were also detected in PN group compared with that in I/R-Gln group.

CONCLUSION: Glutamine protects the morphology and function of intestinal mucosa from injury after I/R in rats.

Wu GH, Wang H, Zhang YW, Wu ZH, Wu ZG. Glutamine supplemented parenteral nutrition prevents intestinal ischemia-reperfusion injury in rats. *World J Gastroenterol* 2004; 10 (17): 2592-2594

<http://www.wjgnet.com/1007-9327/10/2592.asp>

INTRODUCTION

Ischemia-reperfusion (I/R) of the gut is a common event in a variety of clinical conditions, such as trauma, burn, septic shock, heart or aortic surgery, and liver or small bowel transplantation^[1,2]. Intestinal I/R results in many adverse events to the small intestine such as edema and disruption of the structural and

functional mucosa. This injury includes mucosal and vascular permeability, change bacterial translocation, and a high death rate^[3,4]. It has been proposed that most of the mucosal injury resulted from I/R are mediated by reactive oxygen derived free radicals produced and released when hypoxic tissues are reoxygenated during reperfusion. Clinical and experimental studies suggest that I/R-induced intestinal injury play a role in the pathogenesis of systemic inflammation, respiratory failure, and multiple-organ failure (MOF)^[5].

Glutamine (GLN) is the primary metabolic fuel of small intestinal enterocytes, and has been shown to be an essential metabolic component of the proliferative response of enterocytes. Studies have shown that glutamine reduced atrophy of intestinal mucosa in rats on total parenteral nutrition (TPN), prevented intestinal mucosal injury accompanying small bowel transplantation, chemotherapy, and radiation. It was also reported that glutamine supplemented TPN prevented intestinal I/R injury, and improved survival after intestinal I/R in animal models^[6,7]. Thus, GLN treatment seems to be a preventive and therapeutic method for gut I/R-induced organ injury. However, despite the positive result from previous studies, glutamine has not been used extensively to treat preexisting intestinal I/R injury. The purpose of this study was to examine whether glutamine prevented damage to the intestinal mucosa after intestinal I/R in rats.

MATERIALS AND METHODS

Experimental protocol/procedures

Thirty male Sprague-Dawley rats weighing 350 to 450 g were employed after a period of acclimatization. After an overnight fast, the rats were anesthetized with sodium pentobarbital 25 mg/kg intraperitoneally. Through a midline laparotomy, the superior mesenteric artery (SMA) was carefully isolated and clamped at its origin from the abdominal aorta. After 60 min of ischemia, the clamp was removed from the SMA and reperfusion was initiated. The abdominal incision was closed and infusion was started immediately. A silastic catheter was inserted through the right jugular vein, tunneled subcutaneously, and brought out through the skin of midscapular region. The rats were randomly divided into 3 groups: a standard parenteral nutrition (PN) group ($n = 10$); an I/R-PN group ($n = 10$); an I/R-glutamine enriched PN (I/R-Gln) ($n = 10$). The SMA of sham rats in PN group was isolated but not clamped. All rats were maintained in individual metabolic cages, and received parenteral nutritional support for 48 h. The composition of the TPN solution is shown in Table 1. Both solutions were isocaloric (174.3 kcal/kg-d) and isonitrogenous (1.0 g/kg-d). After 48 h' nutritional support, a 20-cm long intestinal segment was obtained from a point 10 cm distal to the ligament of Treitz for morphological and biochemical analysis. Spleen, liver, MLN, and blood samples were collected for bacterial culture and measurement of endotoxin levels.

Histologic evaluation and biochemical analysis

Intestinal samples corresponding to the first 5 cm of the resected intestinal segment were fixed in 40 g/L formaldehyde. All samples were embedded in paraffin and stained with hematoxylin and eosin. Three paraffin sections were prepared from each fixed tissue sample, and each slide was analyzed. A blinded

observer performed the histologic analyses using the histologic scoring system. Mucosal wall thickness, villous height, crypt depth and villous surface area were measured under light microscope. All measurements were made in triplicate, and mean values were obtained. The 15 cm of the intestinal segment left was sampled, and the mucosal sample was immediately scraped from the underlying muscular layer with a glass slide. The mucosa was weighed and stored at -70 °C until analysis. DNA and RNA content was measured by the fluorometric method. Protein content was determined by the bicichoninic acid method.

Intestinal permeability

The permeability of intestinal mucosa was assayed by measurement of D-lactate levels in plasma. The procedure used a glycine-hydrazine buffer at pH 9.5 and 25 °C. The assay was based on the enzymatic oxidation of D-lactate with a specific D-lactic dehydrogenase coupled to reduction of NAD⁺ with the spectrophotometric measurement of NADH at 340 nm. Plasma was separated from the blood sample by centrifugation and stored at -70 °C until analysis. Quantification of D-lactate was performed by fluorescence spectrometry as described by Shimojo *et al.*^[8]. The measurements were made with a Beckman DU fluorescence spectrophotometer at 340 nm. D-lactate standard stock solution was 0.47 mg/mL Li lactate (0.44 mg/mL D-lactic acid) and was diluted for standard curves. D-lactic dehydrogenase was from Sigma Biochemicals and was diluted with water to about 600 U/mL. Sigma assay kit 826-UV was used for D-lactate analysis.

Bacterial translocation measurements

Rats were killed, and their mesenteric lymph nodes, spleens and livers were removed. The tissues were transferred to grinding tubes containing sterile BHI to detect aerobic bacteria or sterile 10 A broth to detect lactobacilli. The tissues were homogenized, and BHI tubes were incubated aerobically, whereas the 10 A broth tubes were incubated in 100 mL/L carbon dioxide at 37 °C. After incubation, 0.2 mL of the tissues homogenates was spread on blood agar plates to detect aerobic bacteria, *E. coli* or lactobacilli. The tissues homogenates were Gram- stained to confirm that bacteria present in the homogenates grew on the agar plates.

Statistical analysis

Data were analyzed using standard statistical software (SPSS 10.0). For normally distributed data, a paired Student's *t* test was used for statistical analysis. A probability value less than or equal to 0.05 was considered statistically significant. All data were expressed as mean±SE.

RESULTS

The mortality rate was 0% (0/10), 28.6% (4/14), and 16.7% (2/12) in the PN, I/R-PN, and I/R-Gln groups, respectively. It was significantly higher in I/R-PN group compared with that in the PN group and I/R-Gln group ($P<0.05$).

In the I/R-PN group, extensive mucosal damage characterized by extensive edema, leukocytic infiltration, epithelial sloughing, mucosal ulceration of villous tips, and mucosal atrophy was observed. This did not occur in the PN group and I/R- Gln group, and no histologic difference was noted between the PN group and I/R- Gln group. Mucosal wall thickness, villous height, crypt depth and villous surface area decreased significantly in the I/R-PN group compared with those in the PN group and I/R-Gln group ($P<0.05$; Table 2). Mucosal wet weight, protein, DNA content and RNA content decreased significantly in the I/R-PN group compared with those in the PN group and I/R- Gln group ($P<0.05$; Table 3).

Plasma D-lactate levels significantly increased in the I/R-PN group (0.15±0.04 mmol/L) compared with those in the PN group (0.08±0.02 mmol/L; $P<0.05$) and I/R- Gln group (0.10±0.02 mmol/L;

$P<0.05$). No significant difference was observed between PN group and I/R- Gln group.

The incidence of intestinal bacterial translocation to MLN, spleen, liver, and blood was significantly higher in I/R-PN group compared with that in PN group and I/R- Gln group. There was no significant difference between PN group and I/R- Gln group ($P<0.05$; Table 4). The plasma endotoxin levels increased in I/R-PN group (14.5±0.12 pg/mL) compared with PN group (9.2±0.8 pg/mL; $P<0.05$) and I/R- Gln group (10.5±0.9 pg/mL; $P<0.05$).

Table 1 Composition of parenteral nutrition solutions (per 100 mL)

	PN	I/R- Gln
Glucose (g)	17.9	17.9
Fat emulsion (g)	5.6	5.6
Amino acid (g)	5.8	2.2
Ala- Glu (g)	0.0	3.6
Nitrogen (g)	0.93	0.93
NPC (kcal)	122.0	122.0
NPC/N	131.2	131.2

Table 2 Morphologic parameters

	PN (n = 10)	I/R-PN (n = 10)	I/R- Gln (n = 10)
Mucosal wall thickness (μm)	566.5±37.4 ^a	418.2±39.6	564.4±59.3 ^a
Villous height (μm)	404.2±39.1 ^a	290.8±48.8	396.4±60.5 ^a
Crypt depth (μm)	214.5±29.4 ^a	136.6±20.2	204.9±38.6 ^a
Villous surface area (mm ²)	0.118±0.010 ^a	0.065±0.006	0.112±0.012 ^a

^a $P<0.05$ vs I/R-PN; PN: parenteral nutrition; I/R: ischemia-reperfusion Gln: glutamine.

Table 3 Mucosal wet weight and biochemistry

	PN (n = 10)	I/R-PN (n = 10)	I/R- Gln (n = 10)
Mucosal wet weight (mg/cm)	74.6±16.3 ^a	55.2±12.0	82.8±18.2 ^a
Protein content (mg/cm)	3.25±0.92 ^a	1.73±0.60	3.16±0.47 ^a
DNA content (mg/cm)	1.42±0.20 ^a	0.64±0.12	1.33±0.17 ^a
RNA content (mg/cm)	4.53±0.58 ^a	3.26±0.78	4.45±0.84 ^a

^a $P<0.05$ vs I/R-PN; PN: parenteral nutrition; I/R: ischemia-reperfusion Gln: glutamine.

Table 4 Bacterial translocation measurements

	PN (n = 10)	I/R-PN (n = 10)	I/R- Gln (n = 10)
Rate of BT	10% (1/10)	100% (10/10)	20% (2/10)
MLN	1	9	2
Blood	1	7	1
Liver	0	5	0
Spleen	0	4	1

BT: bacterial translocation, MLN: mesenteric lymph mode.

DISCUSSION

Ischemia of the gut is a common event after trauma and a significant predisposing factor of MOF. Intestinal I/R injury results in

many adverse events to the small intestine such as interstitial edema and disruption of the structural and functional mucosa. These increase the permeability of the intestinal mucosa and promote bacterial translocation. Clinical and experimental studies suggest that I/R-induced intestinal injury plays a role in the pathogenesis of systemic inflammation, respiratory failure, and MOF^[9,10]. Glutamine is the primary metabolic fuel of small amino acid pool in the body, and has been shown to be an essential metabolic component of the proliferative response of enterocytes. Studies showed that glutamine supplementation of TPN improved survival after gut I/R injury^[6,11], reduced atrophy of intestinal mucosa in rats on total parenteral nutrition^[12], prevented intestinal mucosal injury accompanying short bowel, small bowel transplantation, chemotherapy, and radiation^[13-17]. In the present study, the mortality rate was 28.6% in the I/R-PN group and apparent mucosal damage, such as epithelial sloughing and mucosal ulceration was observed histologically. A 100% survival was achieved in the PN group, 16.7% in I/R-Gln group, and only minor histologic changes of the small intestine were observed in PN and I/R-Gln groups. The I/R-Gln rats had a greater villous height, more mucosal protein, DNA and RNA content, and a lower degree of intestinal permeability compared with the I/R-TPN rats. This suggests that Gln supplemented TPN plays an important role in the maintenance of intestinal structure and barrier function in I/R-injured rats.

The intestinal mucosa, especially in the region of villi, is especially susceptible to hypoxia because of the microvascular architecture and its high energy demand. Intestinal ischemia perpetuates the bacteremic condition by promoting translocation of bacteria into the circulation. Several experimental and clinical studies have shown that intestinal ischemia decreases barrier function of the gut and enhances translocation of bacteria and toxin^[18,19]. In our I/R model, the SMA of rats was clamped for 60 min, and the rats were killed 48 h after intestinal I/R. Mesenteric lymph nodes, spleens, livers and blood were then cultured quantitatively. Almost all MLN had positive cultures and grew significantly great numbers of enteric bacteria, spread to the blood, liver and spleen in I/R-PN group. The most common bacterium discovered from solid viscera was *E. coli*, other species included *enterococcus*, *pseudomonas*, *proteus*, and *staphylococcus*. While, only 20% MLN cultures were positive, less than 10% spread to blood and spleen in I/R-Gln group. Additionally, plasma D-lactate and endotoxin levels increased significantly in I/R-PN group compared with that in I/R-Gln group. These findings indicated that the increase of intestinal permeability and the incidence of bacterial translocation in the intestinal I/R rats were prevented by glutamine supplementation.

In conclusion, the present study demonstrates that glutamine supplemented TPN protects rat intestine from morphologic and functional mucosal injury after intestinal I/R. These results suggest that glutamine would be clinically useful in the treatment of intestinal I/R injury.

REFERENCES

- 1 Nowicki PT, Nankervis CA. The role of the circulation in the pathogenesis of necrotizing enterocolitis. *Clin Perinatol* 1994; **21**: 219-234
- 2 Grant D, Wall W, Mimeault R, Zhong R, Ghent C, Garcia B, Stiller C, Duff J. Successful small-bowel/liver transplantation. *Lancet* 1990; **335**: 181-184
- 3 Deitch EA, Morrison J, Berg R, Specian RD. Effect of hemorrhagic shock on bacterial translocation, intestinal morphology, and intestinal permeability in conventional and antibiotic-decontaminated rats. *Crit Care Med* 1990; **18**: 529-536
- 4 Deitch EA, Bridges W, Berg R, Specian RD, Granger DN. Hemorrhagic shock-induced bacterial translocation: the role of neutrophils and hydroxyl radicals. *J Trauma* 1990; **30**: 942-951
- 5 Deitch EA. Multiple organ failure. Pathophysiology and potential future therapy. *Ann Surg* 1992; **216**: 117-134
- 6 Ikeda S, Zarzaur BL, Johnson CD, Fukatsu K, Kudsk KA. Total parenteral nutrition supplementation with glutamine improves survival after gut ischemia/reperfusion. *J Parenter Enteral Nutr* 2002; **26**: 169-173
- 7 Tazuke Y, Wasa M, Shimizu Y, Wang HS, Okada A. Alanine-glutamine-supplemented parenteral nutrition prevents intestinal ischemia-reperfusion injury in rats. *J Parenter Enteral Nutr* 2003; **27**: 110-115
- 8 Shimojo N, Naka K, Nakajima C, Yoshikawa C, Okuda K, Okada K. Test-strip method for measuring lactate in whole blood. *Clin Chem* 1989; **35**: 1992-1994
- 9 Swank GM, Deitch EA. Role of the gut in multiple organ failure: bacterial translocation and permeability changes. *World J Surg* 1996; **20**: 411-417
- 10 Diebel LN, Dulchavsky SA, Brown WJ. Splanchnic ischemia and bacterial translocation in the abdominal compartment syndrome. *J Trauma* 1997; **43**: 852-855
- 11 Fukatsu K, Ueno C, Hashiguchi Y, Hara E, Kinoshita M, Mochizuki H, Hiraide H. Glutamine infusion during ischemia is detrimental in a murine gut ischemia/reperfusion model. *J Parenter Enteral Nutr* 2003; **27**: 187-192
- 12 Buchman AL. Glutamine: commercially essential or conditionally essential? A critical appraisal of the human data. *Am J Clin Nutr* 2001; **74**: 25-32
- 13 Gu Y, Wu ZH. The anabolic effects of recombinant human growth hormone and glutamine on parenterally fed, short bowel rats. *World J Gastroenterol* 2002; **8**: 752-757
- 14 Platell CFE, Coster J, McCauley RD, Hall JC. The management of patients with the short bowel syndrome. *World J Gastroenterol* 2002; **8**: 13-20
- 15 Frankel WL, Zhang W, Afonso J, Klurfeld DM, Don SH, Laitin E, Deaton D, Furth EE, Pietra GG, Naji A. Glutamine enhancement of structure and function in transplanted small intestine in the rat. *J Parenter Enteral Nutr* 1993; **17**: 47-55
- 16 Huang EY, Leung SW, Wang CJ, Chen HC, Sun LM, Fang FM, Yeh SA, Hsu HC, Hsiung CY. Oral glutamine to alleviate radiation-induced oral mucositis: a pilot randomized trial. *Int J Radiat Oncol Biol Phys* 2000; **46**: 535-539
- 17 Decker-Baumann C, Buhl K, Frohmuller S, von Herbay A, Dueck M, Schlag PM. Reduction of chemotherapy-induced side-effects by parenteral glutamine supplementation in patients with metastatic colorectal cancer. *Eur J Cancer* 1999; **35**: 202-207
- 18 Wischmeyer PE, Lynch J, Liedel J, Wolfson R, Riehm J, Gottlieb L, Kahana M. Glutamine administration reduces Gram-negative bacteremia in severely burned patients: a prospective, randomized, double-blind trial versus isonitrogenous control. *Crit Care Med* 2001; **29**: 2075-2080
- 19 Pscheidl E, Schywalsky M, Tschakowsky K, Boke-Prols T. Fish oil-supplemented parenteral diets normalize splanchnic blood flow and improve killing of translocated bacteria in a low-dose endotoxin rat model. *Crit Care Med* 2000; **28**: 1489-1496

Effects of dendritic cells transfected with full-length wild-type *p53* and stimulated by gastric cancer lysates on immune response

Hua-Wen Sun, Qi-Bing Tang, Yong-Jun Cheng, Sheng-Qian Zou

Hua-Wen Sun, Department of General Surgery, Renmin Hospital, Wuhan University, Wuhan 430060, Hubei Province, China

Qi-Bing Tang, Yong-Jun Cheng, Sheng-Qian Zou, Department of General Surgery, Tongji Hospital, Tongji Medical College, Huazhong University of Science and Technology, Wuhan 430030, Hubei Province, China

Correspondence to: Dr. Hua-Wen Sun, Department of General Surgery, Renmin Hospital, Wuhan University, Wuhan 430060, Hubei Province, China. sxshwyq@sina.com

Telephone: +86-27-88317091

Received: 2003-10-20 **Accepted:** 2003-12-16

Abstract

AIM: To investigate the effects of dendritic cells (DCs) transfected with full-length wild-type *p53* and stimulated by gastric cancer lysates on immune response.

METHODS: The wild-type *p53* was transduced to DCs with adenovirus, and the DCs were stimulated by gastric cancer lysates. The surface molecules (B7-1, B7-2, MHC-I, MHC-II) of all DCs were detected by FACS, and the ability of the DCs to induce efficient and specific immunological response in anti-⁵¹Cr-labeled target cells was studied. BALB/c mice injected with DCs and Mk28 were established, and CTL response in mice immunized with Lywt-p53DC was evaluated. Tumor-bearing mice were treated with Lywt-p53DC.

RESULTS: The surface molecules of Lywt-p53DC had a high expression of B7-1 (86.70±0.07%), B7-2 (18.77±0.08%), MHC-I (87.20±0.05%) and MHC-II (56.70±0.07%); T lymphocytes had a specific CTL lysis ability induced by Lywt-p53DC; the CTL lysis rate was as high as 81%. The immune protection of Lywtp-53DC was obvious, the tumor diameter in Lywtp-53DC group was 3.10±0.31 mm, 2.73±0.23 mm, 3.70±0.07 mm on d 13, 16 and 19, respectively, which were smaller than control, DC, wtp53DC and LyDC group ($P<0.05$). Tumor growth rate in Lywtp53DC group was slower than that in other groups ($P<0.05$).

CONCLUSION: DCs transfected with wild-type *p53* and stimulated by gastric cancer lysates have specific CTL killing activity.

Sun HW, Tang QB, Cheng YJ, Zou SQ. Effects of dendritic cells transfected with full-length wild-type *p53* and stimulated by gastric cancer lysates on immune response. *World J Gastroenterol* 2004; 10(17): 2595-2597

<http://www.wjgnet.com/1007-9327/10/2595.asp>

INTRODUCTION

Dendritic cells (DCs) are the most potent antigen-presenting cells and are actively used in cancer immunotherapy. The wild-type *p53* can be recognized as an antigen and can induce specific CTLs in the host body. It is an effective method to immunize body with *p53* in *p53*-overexpressing tumor cells. *p53*-based

immunization is an attractive approach to cancer immunotherapy due to the accumulation of *p53* protein in gastric cancer. We detected the effects of DCs transfected with full-length wild-type *p53* and modified by gastric cancer lysates on immune response and tried to make DC induce efficient and specific anti-tumor immunological response.

MATERIALS AND METHODS

Animals and cell lines

Eight-week-old female BALB/c mice were purchased from Hubei Animal Center and housed in pathogen-free units of Tongji Hospital experiment center.

Gastric cancer cells (Mk28) were obtained from Hubei cell culture center and cultured in complete culture medium (CCM) containing RPMI 1640 supplemented with 25 mL HEPES, 100 mL/LFCS, and antibiotics (100 U/mL penicillin, 100 µg/mL streptomycin, 0.25 µg/mL amphotericin B). It is a relatively immunogenic tumor that carries a mutant endogenous *p53* gene. P815 mastocytoma cells were obtained from ATC Company and cultured in CCM. The cell cultures were maintained at 37 in 50 mL/L CO₂ humidified atmosphere.

Reagents

Ad-mp53 was constructed by cloning the 1.5-kb murine *p53* cDNA (obtained from Sigma, Wuhan, China) into pAd1/CMV that contains CMV promoter and bovine growth hormone polyA signal sequence. This plasmid was co-transfected with pBHG10 into 293 cells. Recombinant adenovirus was selected based on PCR analysis of individual plaques. Control adenovirus (Ad-c) was prepared by deletion of E1 region from adenovirus serotype.

FITC-labeled mouse anti-mouse *p53* antibody and isotype mouse IgG2a were purchased from Serotec Company (New York, USA). FITC-labeled anti-mouse CD11c antibody and isotype mouse IgG2a, k, PE-labeled anti-mouse I-Ad, anti-mouse B7-1, B7-2, MHC-I, MHC-II antibody and isotype mouse IgG2a, k, as well as hamster anti-mouse CD40 (HM40-3) monoclonal antibody and anti-hamster IgM were purchased from Sigma Company.

Generation of DCs

DCs were generated from bone marrow of naive syngeneic mice in CCM supplemented with 20 ng/mL murine GM-CSF, 10 ng/mL IL-4, and 50 µmol/L 2-mercaptoethanol. The cells were maintained at 37 in a 50 mL/L CO₂ humidified atmosphere. Half of the medium was replaced on d 3. After 5-6 d in culture, cells were collected and enriched by centrifugation over a 135 g/L metrizamide gradient. The purity of DCs fraction was higher than 80% as determined by FACS analysis of surface molecules expression (B7-1, B7-2, MHC-I, MHC-II).

Infection of cells with adenovirus

DCs were infected with Ad-c or Ad-p53 (10 000 viral particles per cell) for 90 min in 0.5 mL serum-free RPMI 1 640 medium supplemented with 20 ng/mL GM-CSF and 10 ng/mL IL-4 in 24-well plates followed by culturing in CCM with the same cytokines for 48 h. This dose was selected after some preliminary

experiments, and did not affect cell viability (95% viable after trypan blue staining).

Preparation of lysates and DCs loaded with tumor cell lysates

DCs were washed twice in PBS and incubated with 14 $\mu\text{g}/\text{mL}$ hamster anti-mouse CD40 monoclonal antibody for 25 min on ice, then washed in RPMI 1640 twice and cultured in 1 mL CCM supplemented with 3.5 $\mu\text{g}/\text{mL}$ anti-hamster IgM, 20 ng/mL GM-CSF and 10 ng/mL IL-4 overnight. Four kinds of DCs such as DC, wtp53DC, LyDC, and Lywtp53 were collected and loaded with tumor cell lysates.

FACS analysis of four kinds of DCs surface molecules expression

DCs were estimated by intracellular staining followed by flow cytometry. Cells were washed in PBS twice, fixed by 2.5 g/L paraformaldehyde solution for 30 min on ice, washed in PBS, permeabilized by 2 g/L Tween 20 for 15 min at 37 $^{\circ}\text{C}$, washed in PBS, incubated with FITC-labeled mouse anti-mouse p53 antibody or isotype mouse IgG2a for 25 min on ice, washed twice in PBS and analyzed by FACScalibur low cytometer.

To study the expression of surface molecules, DCs were washed twice in PBS, incubated with 1 $\mu\text{g}/10^6$ cells FITC-labeled anti-mouse CD11c antibody and PE-labeled anti-mouse I-Ad or anti-mouse B7-1, B7-2, MHC-I, MHC-II antibody for 25 min on ice, washed twice in PBS and analyzed by flow cytometry. Non-specific binding was estimated using FITC-labeled isotype mouse IgG2a, k and PE-labeled isotype mouse IgG2b, k.

Immune protection effect of Lywtp53 and treatment in mice

DCs were generated from bone marrow of BALB/c mice and infected with adenovirus as described above. Forty-eight hours later cells were washed 3 times in PBS and injected to BALB/c mice (2×10^5 /mouse) 3 to 4 times with a 10-14 d interval. Seven days after the last immunization Mk28 tumor cells (3.5×10^5 /mouse) were inoculated s.c. and the size of the tumor was observed.

The same tumor model was used to evaluate the effectiveness of treatment. Five hundred thousand Mk28 cells were inoculated s.c. shaved backs of BALB/c mice. The treatment was started when tumors reached 4-6 mm in diameter (d 7). Mice were treated with DCs prepared as described above. The treatment was repeated 4 times with 5- to 6-d intervals. Tumor sizes were measured every 3-5 d for 4 wk.

CTL assay

Splenocytes (effector cells) freshly isolated or restimulated for 7 d with 4 kinds of DCs were mixed with different ^{51}Cr -labeled target cells: Mk28 cells pre-incubated for 48 h with 5 ng/mL murine IFN- γ or p815 cells infected with Ad-p53 or Ad-c. After 6-h incubation and harvesting of supernatants, the radioactivity was measured by gamma-counter. To estimate the maximum ^{51}Cr -release, 10 g/L triton X-100 was used. The percentage of cell lysis was calculated as follows: (experimental release-spontaneous release)/(maximum release-spontaneous release) $\times 100\%$.

RESULTS

DCs surface molecules expression

Surface molecules of lywt-p53DC highly expressed were detected by FACS: B7-1 ($86.70 \pm 0.07\%$), B7-2 ($18.77 \pm 0.08\%$), MCH-I ($87.20 \pm 0.05\%$), MCH-II ($56.70 \pm 0.07\%$).

Induction of CTL response in mice immunized with DCs

To induce an immune response against wild-type p53, we started with three immunizations of BALB/c mice with DCs generated from bone marrow progenitors of syngeneic mice and transduced with Ad-p53 loaded with lysates as described

in MATERIALS AND METHODS. We found statistically significant differences in tumor formation between mice immunized with Lywtp53 DCs and control groups (9 mice per group), and no differences between wtp53DC and LyDC.

The presence of Mk28-specific CTLs was evaluated in mice immunized with activated Ad-p53-transduced DCs. Six-hour standard CTL assay was performed 1 mo and 1 wk after the last immunization (1 mo after inoculation of Mk28 cells into immunized mice). Freshly isolated splenocytes were mixed with ^{51}Cr -labeled Mk28 cells at different ratios. Splenocytes from mice injected with Ad-c-infected DCs demonstrated no ability to lyse target cells, whereas splenocytes from mice immunized with Ad-p53-transduced DCs demonstrated low, but clearly significant cytotoxicity against Mk28 cells (Figure 1).

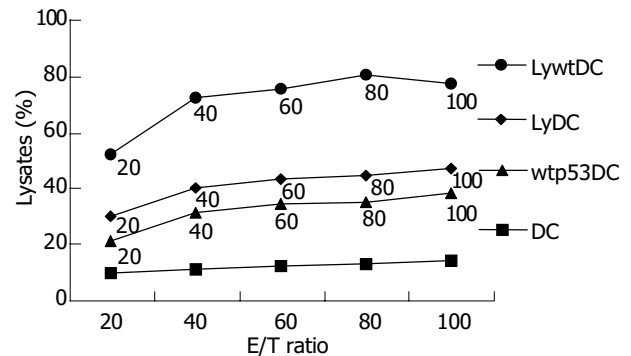


Figure 1 Lysis ability of DCs.

Table 1 Surface molecules expression of 4 kinds of DCs stimulated with lysates ($n = 10$, mean \pm SD, %)

Surface molecules	DC	Wtp53DC	LyDC	Lywtp53
B7-1	36.70 ± 0.07	61.77 ± 0.08	67.20 ± 0.05	86.70 ± 0.07^a
B7-2	5.27 ± 0.01	9.90 ± 0.04	9.13 ± 0.03	18.77 ± 0.08^a
MHC-I	44.03 ± 0.04	69.13 ± 0.05	68.10 ± 0.03	87.20 ± 0.05^a
MHC-II	17.13 ± 0.12	31.10 ± 0.31	32.73 ± 0.23	56.70 ± 0.07^a

^a $P < 0.05$ vs any group of DC, wtp53DC and LyDC.

Table 2 Immune protection of DCs (mean \pm SD, $n = 10$)

Group	Tumor diameter after inoculation (mm)			
	d 10	d 13	d 16	d 19
Control	3.72 ± 0.01	6.70 ± 0.02	7.10 ± 0.09	9.90 ± 0.02
DC	3.70 ± 0.01	5.70 ± 0.08	6.10 ± 0.04	9.70 ± 0.08
Wtp53DC	3.07 ± 0.01	6.90 ± 0.04	7.13 ± 0.03	8.22 ± 0.08
LyDC	4.03 ± 0.04	6.13 ± 0.05	7.10 ± 0.03	8.77 ± 0.05
Lywtp53	3.13 ± 0.02	3.10 ± 0.31^a	2.73 ± 0.23^a	3.70 ± 0.07^a

^a $P < 0.05$ vs control, DC, wtp53DC and LyDC group.

Table 3 Immune treatment of DCs (mean \pm SD, $n = 10$)

Group	Tumor diameter after inoculation (mm)			
	d 7	d 12	d 15	d 18
Control	5.72 ± 0.02	7.88 ± 0.09	9.20 ± 0.11	11.90 ± 0.09
DC	4.70 ± 0.03	7.71 ± 0.08	9.02 ± 0.04	10.70 ± 0.68
Wtp53DC	5.03 ± 0.09	6.90 ± 0.09	7.13 ± 0.11	8.29 ± 0.05
LyDC	5.06 ± 0.01	6.13 ± 0.08	7.10 ± 0.05	8.77 ± 0.03
Lywtp53	5.19 ± 0.09	5.10 ± 0.39	6.73 ± 0.66^a	6.79 ± 0.77^a

^a $P < 0.05$ vs control, DC, wtp53DC and LyDC group.

The immune protection of Lywtp53DC group was obvious, the tumor size of Lywtp53DC group was smaller than control, DC, wtp53DC and LyDC group on d 13, 16 and 19 (Table 2).

Treatment of tumor-bearing mice with Ad-p53-transduced DCs and CTL response are shown in Table 3. On d 15 and 18, the growth rate of tumor in Lywtp53DC group was slower than any of the other group (Table 3).

DISCUSSION

p53 protein is an attractive target for immunotherapy of cancer. Normal cells have very low levels of p53, whereas accumulation of this protein because of mutations or functional inactivation is observed in 50% of human malignancies. This provides, in theory, potential targets for CTLs that recognize class I MHC-bound epitopes^[1-3].

In this study we have demonstrated that activated DCs transfected with full-length wild-type p53 loaded with lysates are able to break tolerance to this self-protein and induce potent antitumor response with no detectable autoimmune abnormalities. Wild-type, p53-derived, self-MHC-self-peptide complexes expressed by bone marrow-derived cells in the thymus cause negative selection of immature thymic T cells with a high avidity for such complexes^[4,5]. These results in deletion of T cells with sufficient avidity to recognize natural wild-type p53 epitopes presented by MHC class I molecules on tumor cells and thus prevent immune response. Only low avidity CTLs survive during the induction of self-tolerance^[6-8].

We suggest here another method of immunotherapy based on the use of full-length wild-type p53. This approach may be devoid of many limitations of peptide-based immunization and would provide a valuable option for clinical trials. Overexpression of wild-type p53 in antigen-presenting cells would allow presentation of several different epitopes. The feasibility of such an approach was shown previously in model experiments in which each of the different minimal epitopes combined to a single fusion protein can be presented separately on the cell surface and be recognized by specific CTLs^[9,10].

The study demonstrated that the wild type p53 was transfected to DCs with adenovirus, and the DCs were stimulated by gastric cancer lysates. The T lymphocytes had specific CTL lysis ability induced by Lywtp53DC loaded with lysates, the CTL lysis rate was as high as 81%. The surface molecules of Lywtp53DC showed a high expression of B7-1 (86.70±0.07%), B7-2 (18.77±0.08%), MHC-I (87.20±0.05%), MHC-II (56.70±0.07%); There were significant differences in tumor sizes between Lywtp53DC group and any other group. In Lywtp53DC group, the growth rate of tumor was slower than any one of the other group ($P<0.05$). These studies showed that Lywtp53 DC had immune protection effect on mice, especially loaded with lysates^[11-14].

Because of a polyclonal nature of T cells generated after two rounds of stimulations with p53 DCs, it is possible that some level of cytotoxicity against tumor cells could be mediated by alloreactivity. When the DCs were loaded with lysates of tumor, the lysates will be presented to APC, and the process can increase immunogenicity in the body. DCs were recognized; the specificity of CTLs was enhanced^[15,16].

In conclusion, these data indicate that DCs transfected with full-length wild-type p53 loaded with lysates are able to generate a CTL response specifically for tumors with p53 overexpression. These findings demonstrate that this approach may overcome tolerance to self-protein and may serve as a valuable option in cancer immunotherapy.

REFERENCES

1 **Nikitina EY**, Clark JI, Van Beynen J, Chada S, Virmani AK, Carbone DP, Gabrilovich DI. Dendritic cells transfected with

- full-length wild-type p53 generate antitumor cytotoxic T lymphocytes from peripheral blood of cancer patients. *Clin Cancer Res* 2001; **7**: 127-135
- 2 **Nagayama H**, Sato K, Morishita M, Uchimaru K, Oyaizu N, Inazawa T, Yamasaki T, Enomoto M, Nakaoka T, Nakamura T, Maekawa T, Yamamoto A, Shimada S, Saida T, Kawakami Y, Asano S, Tani K, Takahashi TA, Yamashita N. Results of a phase I clinical study using autologous tumour lysate-pulsed monocyte-derived mature dendritic cell vaccinations for stage IV malignant melanoma patients combined with low dose interleukin-2. *Melanoma Res* 2003; **13**: 521-530
- 3 **Adams M**, Navabi H, Jasani B, Man S, Fiander A, Evans AS, Donniger C, Mason M. Dendritic cell (DC) based therapy for cervical cancer: use of DC pulsed with tumour lysate and matured with a novel synthetic clinically non-toxic double stranded RNA analogue poly [I]: poly [C (12) U] (Ampligen R). *Vaccine* 2003; **21**: 787-790
- 4 **Shimizu K**, Thomas EK, Giedlin M, Mule JJ. Enhancement of tumor lysate- and peptide-pulsed dendritic cell-based vaccines by the addition of foreign helper protein. *Cancer Res* 2001; **61**: 2618-2624
- 5 **Eura M**, Chikamatsu K, Katsura F, Obata A, Sobao Y, Takiguchi M, Song Y, Appella E, Whiteside TL, DeLeo AB. A wild-type sequence p53 peptide presented by HLA-A24 induces cytotoxic T lymphocytes that recognize squamous cell carcinomas of the head and neck. *Clin Cancer Res* 2000; **6**: 979-986
- 6 **Huang HL**, Wu BY, You WD, Shen MS, Wang WJ. Influence of dendritic cell infiltration on prognosis and biologic characteristics of progressing gastric cancer. *Zhonghua Zhongliu Zazhi* 2003; **25**: 468-471
- 7 **Ishigami S**, Natsugoe S, Tokuda K, Nakajo A, Xiangming C, Iwashige H, Aridome K, Hokita S, Aikou T. Clinical impact of intratumoral natural killer cell and dendritic cell infiltration in gastric cancer. *Cancer Lett* 2000; **159**: 103-108
- 8 **Weisbart RH**, Miller CW, Chan G, Wakelin R, Ferreri K, Koeffler HP. Nuclear delivery of p53 C-terminal peptides into cancer cells using scFv fragments of a monoclonal antibody that penetrates living cells. *Cancer Lett* 2003; **195**: 211-219
- 9 **Asai T**, Storkus WJ, Mueller-Berghaus J, Knapp W, DeLeo AB, Chikamatsu K, Whiteside TL. *In vitro* generated cytolytic T lymphocytes reactive against head and neck cancer recognize multiple epitopes presented by HLA-A2, including peptides derived from the p53 and MDM-2 proteins. *Cancer Immunol* 2002; **2**: 3
- 10 **Portefaix JM**, Rio MD, Granier C, Roquet F, Pau B, Navarro-Teulon I. Peptides derived from the two regulatory domains of p53 are recognized by two p53-activating antibodies. *Peptides* 2003; **24**: 339-345
- 11 **Takenobu T**, Tomizawa K, Matsushita M, Li ST, Moriwaki A, Lu YF, Matsui H. Development of p53 protein transduction therapy using membrane-permeable peptides and the application to oral cancer cells. *Mol Cancer Ther* 2002; **1**: 1043-1049
- 12 **Hoffmann TK**, Loftus DJ, Nakano K, Maeurer MJ, Chikamatsu K, Appella E, Whiteside TL, DeLeo AB. The ability of variant peptides to reverse the nonresponsiveness of T lymphocytes to the wild-type sequence p53 (264-272) epitope. *J Immunol* 2002; **168**: 1338-1347
- 13 **Portefaix JM**, Fanutti C, Granier C, Crapez E, Perham R, Grenier J, Pau B, Del Rio M. Detection of anti-p53 antibodies by ELISA using p53 synthetic or phage-displayed peptides. *J Immunol Methods* 2002; **259**: 65-75
- 14 **Kanovsky M**, Raffo A, Drew L, Rosal R, Do T, Friedman FK, Rubinstein P, Visser J, Robinson R, Brandt-Rauf PW, Michl J, Fine RL, Pincus MR. Peptides from the amino terminal mdm-2-binding domain of p53, designed from conformational analysis, are selectively cytotoxic to transformed cells. *Proc Natl Acad Sci U S A* 2001; **98**: 12438-12443
- 15 **Ferries E**, Connan F, Pages F, Gaston J, Hagnere AM, Vieillefond A, Thiounn N, Guillet J, Choppin J. Identification of p53 peptides recognized by CD8 (+) T lymphocytes from patients with bladder cancer. *Hum Immunol* 2001; **62**: 791-798
- 16 **Petersen TR**, Buus S, Brunak S, Nissen MH, Sherman LA, Claesson MH. Identification and design of p53-derived HLA-A2-binding peptides with increased CTL immunogenicity. *Scand J Immunol* 2001; **53**: 357-364

Combined hepatic resection with fenestration for highly symptomatic polycystic liver disease: A report on seven patients

Guang-Shun Yang, Qi-Gen Li, Jun-Hua Lu, Ning Yang, Hai-Bin Zhang, Xue-Ping Zhou

Guang-Shun Yang, Qi-Gen Li, Jun-Hua Lu, Ning Yang, Hai-Bin Zhang, Xue-Ping Zhou, Eastern Hepatobiliary Hospital, Second Military Medical University, Shanghai 200438, China

Correspondence to: Dr. Guang-Shun Yang, Eastern Hepatobiliary Hospital, Second Military Medical University, Shanghai 200438, China. guangshun@smmu.edu.cn

Telephone: +86-21-25070803

Received: 2003-03-02 **Accepted:** 2003-05-21

Abstract

AIM: To evaluate the immediate and long-term results in a series of patients with highly symptomatic polycystic liver disease (PLD) treated by combined hepatic resection with cystic fenestration.

METHODS: We reviewed our recent experience with a combined hepatic resection-fenestration procedure in seven highly symptomatic patients with PLD. Clinical data, liver manifestation of computed tomography (CT), and morbidity were recorded pre- and post-operation. Follow-up was made by clinical and CT examinations in all patients.

RESULTS: Symptomatic relief and reduction in abdominal girth were obtained in all patients during an average follow-up period of 20.4 mo. CT scans confirmed post-resection hypertrophy of the spared liver and lack of significant cyst progression. All patients had mild to severe ascites. Two patients were complicated with pleural effusion.

CONCLUSION: Some highly symptomatic patients with massive PLD may benefit from combined hepatic resection and fenestration at acceptable risk. To stitch the dissected hepatic ligaments could prevent the instable remnant liver from kinking and collapsing.

Yang GS, Li QG, Lu JH, Yang N, Zhang HB, Zhou XP. Combined hepatic resection with fenestration for highly symptomatic polycystic liver disease: A report on seven patients. *World J Gastroenterol* 2004; 10(17): 2598-2601

<http://www.wjgnet.com/1007-9327/10/2598.asp>

INTRODUCTION

Polycystic liver disease (PLD) is a rare, benign inherited condition, frequently associated with polycystic disease of the kidney^[1]. Unusually as liver failure appears, some patients may be highly symptomatic due to the compression of liver enlargement or liver complications, therefore requiring treatment.

Highly symptomatic patients with PLD almost exhaust all conservative therapeutic options, and surgery is considered as the best possible procedure^[2]. The purpose of this study was to evaluate the immediate surgical results and the short- and long-term outcome in patients treated with hepatic resection combined with cyst fenestration on the basis of our preliminary understanding and experience.

MATERIALS AND METHODS

From October 1995 to September 2002, we examined and operated on 6 women and 1 man with highly symptomatic PLD at our hospital. All operations were performed by a single surgeon (G.S. Yang). In this retrospective study, the medical records were reviewed. The mean interval from diagnosis of PLD to surgical treatment was 4.3 years, ranging from 2 to 11 years. Patient age ranged from 36-54 years, averaging 44.1 years. Specific symptoms included pain, massive abdominal distention, early satiety, regurgitation and supine dyspnea. Six patients were complicated with polycystic kidney disease but had no clinical evidence of abnormal renal function. Four patients had undergone percutaneous cyst aspiration with alcohol sclerotherapy before operation.

Preoperative workup included hematologic, hepatic and renal laboratory tests, and determinations of both respiratory and cardiovascular performance. CT scan was performed to delineate cyst distribution to assess portal vein patency and to serve as a baseline for follow-up comparison in each patient. No patient underwent angiography. The clinical features of these patients are summarized in Table 1.

Preoperative preparations of each patient were an overnight lavage bowel preparation and venous catheterization. The abdomen was explored through a bilateral subcostal incision. The hepatoduodenal ligament was exposed to provide access to a vascular clamping and identification of major vascular and biliary structures. The liver was mobilized by the division of hepatic peritoneal attachments, which was facilitated by sequential fenestration of accessible cysts according to the Lin technique^[3]. Liver segments spared of cystic involvement were identified to define limits to resection. Non-anatomic segmental or lobar resection was executed due to cystic distortion of normal anatomy. Significant islands of functional liver parenchyma were preserved as many as possible. After resection of major cystic segments, extensive fenestration of residual cysts was performed by excision of the cyst walls. Finally, cyst cavities exposed to the peritoneum were fulgurated by argon beam coagulation (Bard Electromedical Systems, USA) in an attempt to ablate secretory epithelium and reduce postoperative peritoneal fluid losses. Cholecystectomy in conjunction with hepatectomy was performed in three patients. The hepatic resection bed was drained by two large closed suction drains. After operation, patients were sent to the surgical intensive care unit for close monitoring.

All patients were followed up through telephone calls or at clinic. Special data included hepatic and renal function, symptomatic relief, the patients' working capacity and CT scans.

RESULTS

The surgical outcome of our patients is presented in Table 2. The histologic examination showed von Meyenburg's complexes in all cases. There was no hospital death. All patients had ascites, the majority of them were successfully managed with diuretics and drainage within one week. The average duration of drainage was 11 d, with a range of 5-26 d. Drainage

Table 1 Clinical findings of patients with PLD

Patient no.	Age (yr)	Gender	Family history	Symptoms	Other involved organs	Previous treatment
1	48	Female	No siblings	Abdominal distention, regurgitation	None	None
2	41	Female	Father, two sisters, brother	Abdominal pain and distention	Kidney	PCA+AS (5 times)
3	54	Female	Sister	Early satiety, regurgitation	Kidney	PCA+AS (2 times)
4	45	Male	Sister	Abdominal pain and distention	Kidney	PCA+AS (2 times)
5	43	Female	Sister, brother, grandmother	Abdominal pain and distention, early satiety, dyspnea	Kidney	PCA+AS (2 times)
6	36	Female	Mother, sister	Abdominal pain and distention, early satiety, supine dyspnea	Kidney	None
7	42	Female	Father	Abdominal distention, regurgitation	Kidney	None

PCA+AS, Percutaneous cyst aspiration with alcohol sclerotherapy.

Table 2 Operative data, surgical outcome, and follow-up of patients with PLD

Patient no.	Hepatic resection	Blood loss (mL)	Cystic fluid aspirated (mL)	Days of hospital stay (after operation)	Postoperative complications	Symptomatic relief	Reduction in size of liver
1	III, IVb, V	400	1 500	21 (12)	Acites	Marked	Marked
2	II, III, V	800	3 000	25 (14)	Acites	Marked	Marked
3	Right semi hepatectomy, cholecystectomy	200	1 200	16 (8)	Mild acites	Marked	Marked
4	Right smi hepatectomy, cholecystectomy	300	1 800	24 (16)	Moderate acites	Marked	Marked
5	II, III, IVb	1 500	6 500	83 (29)	Severe acites, left pleural effusion	Moderate	Moderate
6	II, III, VI, VII	3 400	4 000	42 (16)	Severe acites, right pleural effusion	Marked	Marked
7	II, III, VI	300	2 500	27 (11)	Acites	Marked	Marked

Table 3 Review of the literature: mortality, morbidity and outcome of patients with PLD treated by combined hepatic resection an cystic fenestration

Authors	No. of patients	Mortality (no.)	Morbidity (no.)	Follow-up (mos)	No. of symptom-free patients
Armitage <i>et al.</i> ^[12] (1984)	1	0	0	12	1
Iwatsuki <i>et al.</i> ^[13] (1988)	6	0	0	-	-
Newman <i>et al.</i> ^[2] (1990)	9	1	6	17	7
Sanchez <i>et al.</i> ^[8] (1991)	2	0	0	48	2
Vauthey <i>et al.</i> ^[11] (1992)	5	0	4	14	5
Henne-Bruns <i>et al.</i> ^[14] (1993)	8	0	3	15	6
Soravia <i>et al.</i> ^[15] (1995)	10	1	2	68	6
Que <i>et al.</i> ^[16] (1995)	31	1	18	29	28
Vons <i>et al.</i> ^[17] (1998)	12	1	10	34	10
Johnson <i>et al.</i> ^[18] (1999)	1	0	0	18	1
Our series	7	0	7	0	6
Total	92	4 (4.3%)	50 (54.3%)		72 (78.3%)

was continued by needle aspiration in Patients 5 and 6 immediately after a two-week closed suction drainage. The change was an attempt to prevent ascites from infection. Furthermore Patient 5 required thoracentesis due to left pleural effusion.

All patients experienced relief of abdominal symptoms and had normal hepatic and renal laboratory tests. Abdominal

girth was reduced markedly in six patients and moderately in one. Repeated abdominal CT scans in these patients failed to show significant development of cysts in the previously spared liver segments during a mean follow-up period of 20.4 mo, with a range from 2 to 86 mo. Indeed, as shown in Figure 1, CT scans confirmed post-resection hypertrophy of the spared liver and lack of clinically significant cyst progression.

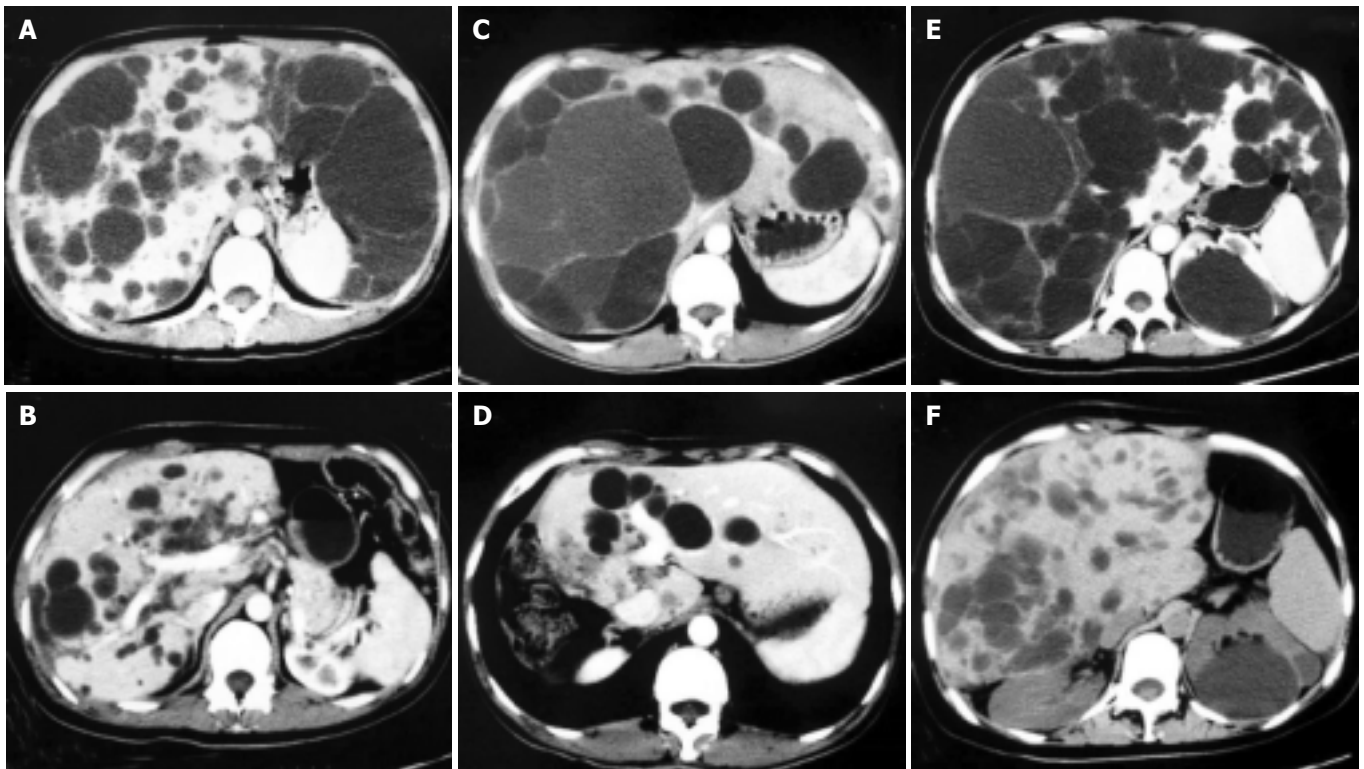


Figure 1 CT scans of livers in PLD patients before (left panels) and 3 mo (right panels) after operation, show that hypertrophy of spared liver and lack of clinically significant cyst progression, and that operative methods totally depend on cystic distribution in different patients, e.g., lateral segment removal from A to B, right semi-hepatectomy resection from C to D, whereas extensive fenestration of posterior and anterior cysts from E to F.

DISCUSSION

PLD is a rare disorder usually associated with autosomal dominant polycystic kidney disease, with an increasing prevalence associated with age and female sex^[4]. Symptoms arise from liver enlargement and compression of adjacent structures. Most symptomatic patients complained of increasing abdominal girth and a chronic dull abdominal pain. Liver enlargement may cause early satiety, weight loss, respiratory compromise, and physical disability. Complications such as ascites, esophageal varices, jaundice and hepatic failure, are rare^[5-7].

A variety of treatment have been advocated for the few patients with incapacitating symptoms. Percutaneous aspiration with alcohol sclerotherapy seems valuable for solitary cysts but does not provide relief for patients with PLD because cyst collapse may not be sufficient^[8]. Cyst fenestration with internal drainage into the peritoneal cavity, described by Lin in 1968, may fail to achieve long-term favorable outcome^[9]. In practice, the efficacy of the Lin decompression for PLD is limited by extent of cysts, access to central cysts, postoperative walling off of cysts, and the rigid architecture of the fenestrated liver, which does not completely collapse^[2]. Liver transplantation might be considered for patients with a "syndrome of lethal exhaustion" from PLD^[7,10,11].

Armitage and Blumgart^[12] described in 1984 a patient with PLD who underwent partial hepatic resection and cyst fenestration. This procedure allowed the excision of most prominent cysts with minimal resection of liver tissue; liver parenchyma was preserved despite the polycystic disease. Other reports have shown the feasibility of such an approach (Table 3)^[1,2,8,12-18]. We reported a similar favorable outcome. During a mean follow-up of 20.4 mo, six of seven patients were symptom free. Herein, we emphasize that the result might be achieved by a careful selection of patients and by an experienced surgeon. The head surgeon of our surgical team

has abundant experiences of more than 1400 hepatectomies for liver tumors during the same study period.

The postoperative morbidity rate in reviewed reports was 54.3%. The majority of immediately postoperative complications in our series were ascites and transient pleural effusion. Ascites was easily treated by diuretics and effective drainage or followed by needle aspiration. None of our patients had kidney failure requiring dialysis before or after operation. Ascites occurred in the patients with renal dysfunction may be refractory and even increased the chance to be infected or bring forth malnutrition^[17]. The elucidation for the mechanism of hepatic cystic epithelium secretion may be a key to solve this problem^[19].

The literature review showed an overall mortality rate of 4.3%. There is only one report that the cause of death was related to this procedure for patients with PLD^[15]. Acute Budd-Chiari syndrome developed shortly after fenestration of posterior cyst, which provoked a liver collapse. In practice, to stitch on the dissected triangular, falciform and round ligaments easily kept the stability of the remnant liver, which was weakened by extensive fenestration of posterior and anterior cysts. Patient 6 is a good example in our series. In patients 3 and 4, we found that the left lobes twisted towards right due to gravity after right semi-hepatectomy in operation. Connecting the falciform and round ligaments easily enabled the remnants fixed, avoiding occurrence of kinking. It may be unnecessary to avoid fenestration of posterior cysts and propose a frontal hepatectomy. Two patients in literature died from postoperative intracerebral bleeding, suggesting that evaluation of selected patients' cerebral vasculature to detect aneurismal disease is essential^[2,16].

Our follow-up duration is limited and our preliminary study includes just seven selected patients. Therefore, the long-term benefit of combined hepatic resection and fenestration should be further evaluated. On the basis of our experience and review of the available literature, however, this approach

could be feasible, with an acceptable risk as well as a favorable long-term outcome at follow-up. To stitch the dissected hepatic ligaments could prevent the instable remnant liver from kinking and collapsing.

REFERENCES

- 1 **Vauthey JN**, Maddern GJ, Blumgart LH. Adult polycystic disease of the liver. *Br J Surg* 1991; **78**: 524-527
- 2 **Newman KD**, Torres VE, Takela J, Nagorney DM. Treatment of highly symptomatic polycystic liver disease: preliminary experience with a combined hepatic resection-fenestration procedure. *Ann Surg* 1990; **212**: 30-37
- 3 **Lin TY**, Chen CC, Wang SM. Treatment of non-parasitic cystic disease of the liver: a new approach to therapy with polycystic liver. *Ann Surg* 1968; **168**: 921-927
- 4 **Grunfeld JP**, Albouze G, Jungers P, Landais P, Dana A, Droz D, Moynot A, Lafforgue B, Boursztyn E, Franco D. Liver changes and complications in adult polycystic kidney disease. *Adv Nephrol Necker Hosp* 1985; **14**: 1-20
- 5 **Ratcliffe PJ**, Teeders S, Theaker JM. Bleeding oesophageal varices and hepatic dysfunction in adult polycystic liver disease. *Br Med J* 1984; **288**: 1330-1331
- 6 **Wittig JH**, Burns R, Lonmire WP. Jaundice associated with polycystic liver disease. *Am J Surg* 1978; **138**: 383-386
- 7 **Washburn WK**, Johnson LB, Lewis WD, Jenkins RL. Liver transplantation for adult polycystic liver disease. *Liver Transpl Surg* 1996; **2**: 17-22
- 8 **Sanchez H**, Gagner M, Rossi RL, Lewis WD, Muson JL, Braasch JW. Surgical management of nonparasitic cystic liver disease. *Am J Surg* 1991; **161**: 113-119
- 9 **Tan YM**, Oli LL, Mack PO. Current status in the surgical management of adult polycystic liver disease. *Ann Acad Med Singapore* 2002; **31**: 216-222
- 10 **Swenson K**, Seu P, Kinkhabwala M, Marggard M, Martin P, Goss J, Brasuttil R. Liver transplantation for adult polycystic liver disease. *Hepatology* 1998; **28**: 412-415
- 11 **Starzl TE**, Reyes J, Tsakis A, Miele L, Todo S, Gordon R. Liver transplantation for polycystic liver disease. *Arch Surg* 1990; **125**: 575-577
- 12 **Armitage NC**, Blumgart LH. Partial resection and fenestration in the treatment of polycystic liver disease. *Br J Surg* 1984; **71**: 242-244
- 13 **Iwatsuki S**, Starzl TE. Personal experience with 411 hepatic resections. *Ann Surg* 1988; **208**: 421-434
- 14 **Henne-Bruns K**, Klomp HJ, Kremer B. Non-parasitic liver cysts and polycystic liver disease: results of surgical treatment. *Hepatogastroenterology* 1993; **40**: 1-5
- 15 **Soravia C**, Mentha G, Giostra E, Morel P, Rohner A. Surgery for adult polycystic liver disease. *Surgery* 1995; **117**: 272-275
- 16 **Que F**, Nagorney DM, Gross JB Jr, Torres VE. Liver resection and cyst fenestration in the treatment of severe polycystic liver disease. *Gastroenterology* 1995; **108**: 487-494
- 17 **Vons C**, Chauveau D, Martinod E, Smadja C, Capron F, Grunfeld JP, Franco D. Liver resection in patients with polycystic liver disease. *Gastroenterol Clin Biol* 1998; **22**: 50-54
- 18 **Johnson LB**, Kuo PC, Plotkin JS. Transverse hepatectomy for symptomatic polycystic liver disease. *Liver* 1999; **19**: 526-528
- 19 **Everson GT**, Emmett M, Brown WR, Redmond P, Thickman D. Functional similarities of hepatic cystic and biliary epithelium: studies of fluid constituents and *in vivo* secretion in response to secretin. *Hepatology* 1990; **11**: 557-565

Edited by Ma JY Proofread by Xu FM

Detection of *BCL2-IGH* rearrangement on paraffin-embedded tissue sections obtained from a small submucosal tumor of the rectum in a patient with recurrent follicular lymphoma

Naohisa Yoshida, Kenichi Nomura, Yosuke Matsumoto, Kazuhiro Nishida, Naoki Wakabayashi, Hideyuki Konishi, Shoji Mitsufuji, Keisho Kataoka, Takeshi Okanoue, Masafumi Taniwaki

Naohisa Yoshida, Naoki Wakabayashi, Hideyuki Konishi, Shoji Mitsufuji, Keisho Kataoka, Takeshi Okanoue, Molecular Gastroenterology and Hepatology, Kyoto Prefectural University of Medicine Graduate School of Medical Science, Kyoto 602-8566, Japan
Kenichi Nomura, Yosuke Matsumoto, Kazuhiro Nishida, Molecular Hematology and Oncology, Kyoto Prefectural University of Medicine Graduate School of Medical Science, Kyoto 602-8566, Japan
Masafumi Taniwaki, Clinical Molecular Genetics and Laboratory Medicine, Kyoto Prefectural University of Medicine Graduate School of Medical Science, Kyoto 602-8566, Japan

Correspondence to: Kenichi Nomura, M.D., Ph.D., Molecular Hematology and Oncology, Kyoto Prefectural University of Medicine Graduate School of Medical Science, Kawaramachi-Hirokoji, Kamigyoku, Kyoto 602-8566, Japan. nomuken@sun.kpu-m.ac.jp
Telephone: +81-75-251-5521 **Fax:** +81-75-251-0710
Received: 2004-01-15 **Accepted:** 2004-02-24

Abstract

A 59-year-old woman was admitted to our hospital because of recurrent follicular lymphoma (FL). Colonoscopic examination revealed a rectal submucosal tumor (SMT) without any erosions and ulcers. In this patient, it was difficult to distinguish non-Hodgkin's lymphoma (NHL) invasion from other disorders of the colon including carcinoid tumor merely based on endoscopic findings. Histopathologic and immunohistochemical studies on biopsy specimens showed an infiltration of atypical lymphocytes that were positive for CD20 and BCL2 but negative for UCHL-1. Fluorescence *in situ* hybridization on paraffin-embedded tissue sections (T-FISH) identified a translocation of *BCL2* with *IGH* gene. Based on these findings, the tumor was defined as an invasion of FL. T-FISH method is useful for the detection of a monoclonality of atypical lymphocytes in an SMT of the gastrointestinal tract, and particularly for the detection of chromosomal translocations specific to lymphoma subtypes.

Yoshida N, Nomura K, Matsumoto Y, Nishida K, Wakabayashi N, Konishi H, Mitsufuji S, Kataoka K, Okanoue T, Taniwaki M. Detection of *BCL2-IGH* rearrangement on paraffin-embedded tissue sections obtained from a small submucosal tumor of the rectum in a patient with recurrent follicular lymphoma. *World J Gastroenterol* 2004; 10 (17): 2602-2604
<http://www.wjgnet.com/1007-9327/10/2602.asp>

INTRODUCTION

Primary gastrointestinal (GI) lymphomas are uncommon tumors, constituting less than 2% of all GI malignancies^[1]. The stomach, however, is the most frequent site of extranodal NHL. Of all GI NHLs, the incidence of gastric lymphomas ranged from 51% to 86%^[2,3], while that of colonic lymphomas ranged from 1.6% to 16.2%^[4,5]. Diagnosis of GI lymphomas may be complicated due to difficulties in pathological diagnosis and in staging with

endoscopic biopsies. In fact, it is occasionally difficult not only to distinguish NHL from other tumors but also to define subtypes of NHL on the basis of endoscopic and histological findings of biopsy specimens^[6,7]. Although flowcytometric analysis is efficient for differential diagnosis of lymphomas, obtaining a diagnostic biopsy may sometimes be difficult because GI lymphomas spread submucosally and have normal surface qualities; therefore, a number of specimens are required for an accurate diagnosis.

On the other hand, chromosomal translocations are closely associated with distinctive subtypes of malignant lymphoma^[8]. Both chromosomal banding and fluorescence *in situ* hybridization (FISH) are used for the detection of specific translocation. In addition, we have developed a procedure using FISH directly on paraffin embedded tissue sections (T-FISH), enabling us to perform cytogenetic analyses on both archival and small biopsy specimens^[9,10].

In the current study, using T-FISH we detected rearrangement of the *BCL2* with immunoglobulin heavy chain (*IGH*) gene on biopsy specimens obtained from a small rectal submucosal tumor (SMT), thereby differentiating follicular lymphoma (FL) from other neoplastic tumors of colon as well as other types of lymphoma.

CASE REPORT

A 59-year-old woman was admitted to our hospital because of the swelling of multiple cervical lymph nodes. The patient had suffered from stage IV disease of FL since 1997. Although multiple chemotherapies including high dose regimen supported by autologous hematopoietic stem cell transplantation were administered, complete remission has not been achieved. At the current hospitalization, the patient showed elevated soluble interleukin-2 receptor (1 024 U/L), while no abnormal cells were detected in both the peripheral blood and bone marrow. Gallium-scintigraphy showed abnormal accumulation at cervical and supra-clavicular lesions. Gastroscopic examination revealed no remarkable abnormalities, whereas colonoscopic examination detected a small elevated lesion (7 mm×8 mm in size) on the rectum.

The surface of tumor was slightly reddish, but no erosions and ulcers were noted (Figure 1). No definitive deformity of colonic wall was detected with double-contrast barium enema (Figure 2). The tumor invasion was confined to the second layer of colonic wall based on the endoscopic ultrasonographic findings (Figure 3). Flowcytometric analyses were not able to be performed because of small specimens obtained from diagnostic biopsies. Histopathologic and immunohistochemical studies on biopsy specimens showed the aggregation of atypical medium-sized lymphocytes having irregularly enlarged nuclei that were positive for CD20, CD10 and BCL2, but negative for UCHL-1 and CD5 (Figures 4A-C).

Using DHAP regimen (cisplatin 70 mg/m², Ara-C 1.4 g/m²×2, dexamethasone 40 mg×4), the patient achieved a partial response, followed by the administration of rituximab. The rectal lesion disappeared on d 120.

In order to confirm a diagnosis of lymphoma and define specific chromosomal abnormalities, we performed T-FISH analyses on the sample obtained from a rectal SMT according to the protocol already described elsewhere^{9,10}. Briefly, sections from paraffin-embedded tissues were placed on slides, and then deparaffinized in xylene. Each slide was dehydrated in ethanol and treated with 0.2 mol/L HCl and 0.05 mg/mL proteinase K in TEN (0.05 mol/L tris-HCl, pH 7.8, 0.01 mol/L EDTA, and 0.01 mol/L NaCl buffer) for 10 min at 37 °C. FISH probes and samples were denatured simultaneously for 10 min at 90 °C, and were hybridized overnight at 42 °C. LSI IGH/BCL2, IGH/BCL1 and MALT1 probes (Vysis, CA, USA) were used for the detection of t (14; 18), t (11; 14), and 18q21 translocations, respectively. Images of signal were captured by a CCD camera. T-FISH detected fusion signals of *BCL2* and *IGH* genes on 75 of 100 nuclei (Figure 5), defining the invasion of FL with t (14; 18) (q32; q21). On the other hand, 95 of 100 nuclei showed negative results for both t (11; 14) and 18q21 translocations.



Figure 1 Endoscopic examination revealed a small submucosal tumor on rectum.

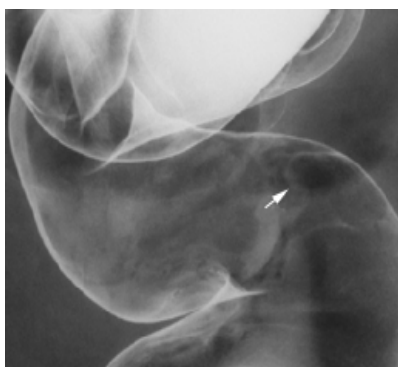


Figure 2 Double-contrast barium enema revealed no definite deformity of the GI wall at the lesion.

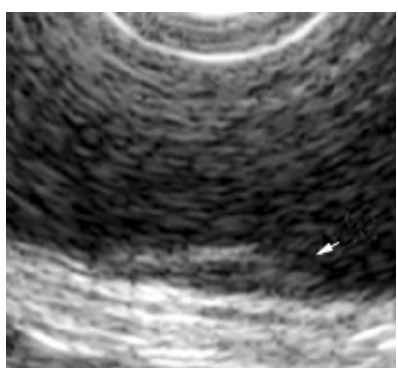


Figure 3 Endoscopic ultrasonography showed that the tumor was confined at the second layer of the colonic wall.

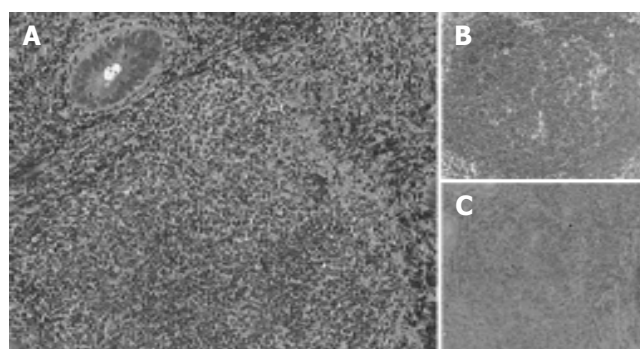


Figure 4 Histopathological studies showed aggregated atypical lymphocytes (A). Immunohistochemical analysis revealed that these lymphocytes were positive for CD20 and BCL2 (B and C).

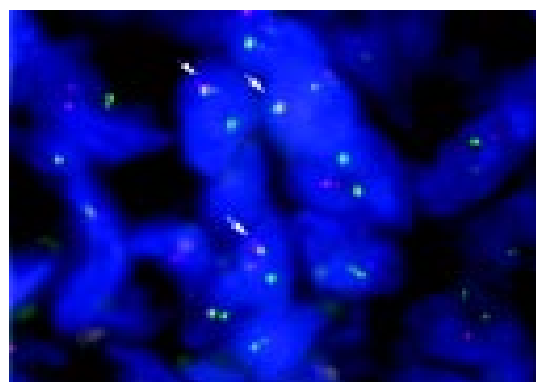


Figure 5 T-FISH detected fusion signals of IGH and BCL2 genes in nuclei as indicated by arrows.

DISCUSSION

We demonstrated rearrangement of *BCL2* with *IGH* gene on a small rectal SMT in a patient with recurrent lymphoma using T-FISH, thereby defining colonic involvement of FL. It is difficult to discriminate NHL from other disorders of the GI tract only based on endoscopic and histological findings¹¹. Although endoscopic procedures are important not only in the detection of other disorders involving GI tract, but also in providing a means for pathologic diagnosis through biopsy, it should be noted, however, that obtaining a diagnostic biopsy may be difficult because GI lymphomas spread submucosally and have normal surface qualities. Since most GI lymphomas and other malignancies including adenocarcinoma and carcinoid tumor frequently display a polypoid growth pattern involving the mucosa, submucosa and muscularis¹², it is sometimes difficult to make differential diagnosis based on the histological findings.

In the current patient, immunohistochemical studies defined a diagnosis of lymphoid lesion of a rectal SMT, although flowcytometric analysis was not successful because of small specimens obtained from diagnostic biopsy. There are many kinds of SMTs originating in the colon, for example, lipoma, malignant lymphoma, carcinoid tumor, *etc*¹³. Flowcytometric and immunocytochemical studies are useful for demonstration of a monoclonal population of lymphocytes of a lesion of interest, since most GI lymphomas are virtually always of the B-cell type. However, it should be noted that there are certain subtypes preferentially involving GI tract including mantle cell lymphoma, and mucosa-associated lymphoid tissue (MALT) lymphoma¹⁴. In this respect, cytogenetic study is necessary for the determination of these subtypes, since chromosomal translocations are closely associated with distinctive subtypes of NHL¹⁴. More than 90% of mantle cell lymphoma was related to the translocation of *IGH* with *BCL1* gene¹⁵. MALT lymphoma

was related to the translocation of *API2* with *MALT1* at frequencies of 18.8%^[9]. Approximately 60% of FL showed the translocation of *BCL2* with *IGH* (Matsumoto *et al.* in press). Hence, T-FISH is a useful method not only to make definitive diagnosis of NHL but also to define its subtypes. In addition, a few biopsy samples are enough for T-FISH analysis when compared with flowcytometric analysis and polymerase chain reaction (PCR). Furthermore, the tissues embedded for a period of 15 years were available for T-FISH analysis^[9,10].

At present there is considerable controversy concerning the treatment of primary and secondary GI lymphomas. Rituximab has recently included in treatment option^[16]. In our patient with recurrent FL, salvage therapy including high-dose Ara-C with rituximab was performed. Because *API2-MALT1*-positive lymphoma has demonstrated a more aggressive subgroup^[17], T-FISH will provide novel information for the selection of treatment for GI lymphomas.

In conclusion, our results indicate that T-FISH is a promising procedure for the routine detection of genetic alterations in GI lymphomas, it enables us to not only make definitive diagnosis of NHL but also to define its subtypes.

REFERENCES

- 1 Frazee RC, Roberts J. Gastric lymphoma treatment. Medical versus surgical. *Surg Clin North Am* 1992; **72**: 423-431
- 2 Radaszkiewicz T, Dragosics B, Bauer P. Gastrointestinal malignant lymphomas of the mucosa-associated lymphoid tissue: factors relevant to prognosis. *Gastroenterology* 1992; **102**: 1628-1638
- 3 Hansen PB, Vogt KC, Skov RL, Pedersen-Bjergaard U, Jacobsen M, Ralfkiaer E. Primary gastrointestinal non-Hodgkin's lymphoma in adults: a population-based clinical and histopathologic study. *J Intern Med* 1998; **244**: 71-78
- 4 Otter R, Bieger R, Klutin PM, Hermans J, Willemze R. Primary gastrointestinal non-Hodgkin's lymphoma in a population-based registry. *Br J Cancer* 1989; **60**: 745-750
- 5 Crump M, Gospodarowicz M, Shephers FA. Lymphoma of the gastrointestinal tract. *Semin Oncol* 1999; **26**: 324-337
- 6 Takenaga T, Yamamoto N, Yamanaka A, Yamada M, Takasimizu K, Sasabe M, Tamura Y, Kurosawa K, Fujimoto H, Ookusa T, Nakamura E, Hisayama Y. Gastrointestinal involvement of malignant lymphoma. *Gastroenterol Endosc* 1988; **30**: 2218-2224
- 7 Damaj G, Verkarre V, Delmer A, Solal-Celigny P, Yakoub-Agha I, Cellier C, Maurschhauser F, Bouabdallah R, Leblond V, Lefrere F, Bouscary D, Audouin J, Coiffier B, Varet B, Molina T, Brousse N, Hermine O. Primary follicular of the gastrointestinal tract: a study of 25 cases and a literature review. *Ann Oncol* 2003; **14**: 623-629
- 8 Ong ST, Le Beau MM. Chromosomal abnormalities and molecular genetics of non-Hodgkin's lymphoma. *Semin Oncol* 1998; **25**: 447
- 9 Nomura K, Yoshino T, Nakamura S, Akano Y, Tagawa H, Nishida K, Seto M, Nakamura S, Ueda R, Yamaguti H, Taniwaki M. Detection of t(11;18)(q21;q21) in marginal zone lymphoma of mucosa-associated lymphocytic tissue type on paraffin-embedded tissue sections by using fluorescence *in situ* hybridization. *Cancer Genet Cytogenet* 2003; **140**: 49-54
- 10 Nomura K, Sekoguchi S, Ueda K, Nakao M, Akano Y, Fujita Y, Yamashita Y, Horiike S, Nishida K, Nakamura S, Taniwaki M. Differentiation of follicular from mucosa-associated lymphoid tissue lymphoma by detection of t(14;18) on single-cell preparations and paraffin-embedded sections. *Genes Chromosomes Cancer* 2002; **33**: 213-216
- 11 Shepherd NA, Hall PA, Coates PJ, Levison DA. Primary malignant lymphoma of the colon and rectum. A histopathological and immunohistochemical analysis of 45 cases with clinicopathological correlations. *Histopathology* 1988; **12**: 235-252
- 12 Coulson WF. The Stomach. In: Coulson WF, ed. *Surgical Pathology*, Philadelphia:J.B. Lippincott Company 1988: 123-125
- 13 Kawamoto K, Yamada Y, Furukawa N, Utsunomiya T, Haraguchi Y, Mizuguchi M, Oiwa T, Takano H, Masuda K. Endoscopic submucosal tumorectomy for gastrointestinal submucosal tumors restricted to the submucosa. *Gastrointest Endosc* 1997; **46**: 311-317
- 14 Jaffe ES, Harris NL, Stein H, Vardiman JW, eds. *Tumours of Haematopoietic and Lymphoid Tissues*, 3rd ed. Lyon France: IARC 2001
- 15 Hui P, Howe JG, Crouch J, Nimmakayalu M, Qumsiyeh MB, Tallini G, Flynn SD, Smith BR. Real-time quantitative RT-PCR of cyclin D1 mRNA in mantle cell lymphoma: comparison with FISH and immunohistochemistry. *Leuk Lymphoma* 2003; **44**: 1385-1394
- 16 Press OW, Unger JM, Brazier RM, Maloney DG, Miller TP, LeBlanc M, Gaynor ER, Rivkin SE, Fisher RI. A phase 2 trial of CHOP chemotherapy followed by tositumomab/iodine I 131 tositumomab for previously untreated follicular non-Hodgkin lymphoma: Southwest Oncology Group Protocol S9911. *Blood* 2003; **102**: 1606-1612
- 17 Sakugawa ST, Yoshino T, Nakamura S, Inagaki H, Sadahira Y, Nakamine H, Okabe M, Ichimura K, Tanimoto M, Akagi T. *API2-MALT1* fusion gene in colorectal lymphoma. *Mod Pathol* 2003; **16**: 1232-1241

Edited by Zhu LH Proofread by Xu FM

• CASE REPORT •

Mesenteric Ischemia: An unusual presentation of fistula between superior mesenteric artery and common hepatic artery

Ertugrul Kayacetin, Serdar Karaköse, Aydin Karabacakoglu, Dilek Emlik

Ertugrul Kayacetin, Department of Gastroenterology, Meram Medical Faculty, Selcuk University, Konya-Turkey

Serdar Karaköse, Aydin Karabacakoglu, Dilek Emlik, Department of Radiology, Meram Medical Faculty, Selcuk University, Konya-Turkey

Correspondence to: Dr. Ertugrul Kayacetin, Selcuk Universitesi Meram Tip Fakultesi, Ic Hastalikleri AD, Gastroenterology BD, Konya-Turkey. ekayacetin@mynet.com

Telephone: +90-332-3218694

Received: 2004-03-05 **Accepted:** 2004-04-14

Abstract

Chronic mesenteric ischemia is an uncommon condition associated with a high morbidity and mortality. We reported a 36-year old women with postprandial abdominal pain due to chronic mesenteric ischemia caused by a fistula between superior mesenteric and common hepatic artery.

Kayacetin E, Karaköse S, Karabacakoglu A, Emlik D. Mesenteric Ischemia: An unusual presentation of fistula between superior mesenteric artery and common hepatic artery. *World J Gastroenterol* 2004; 10(17): 2605-2606

<http://www.wjgnet.com/1007-9327/10/2605.asp>

INTRODUCTION

Chronic mesenteric ischemia (CMI) is an uncommon condition associated with a high morbidity and mortality and the symptoms may be nonspecific until late in the course of disease^[1,2].

The most common cause of CMI is atherosclerosis. Involvement of the celiac, superior mesenteric, and inferior mesenteric arteries at their origins is typical^[3]. We reported an abnormal communication between the superior mesenteric artery (SMA) and common hepatic artery (CHA) which caused splanchnic hypoperfusion. To our knowledge, this entity has not been reported previously in the literature.

CASE REPORT

The patient was a 36-year old woman who had complained of severe postprandial abdominal pain and abdominal distention for 9 mo. The pain was described as a severe, poorly localized one radiating to the back. No fever, nausea or vomiting, hematochezia, or weight change was reported. She had no history of previous trauma, abdominal surgery, hepatic or pancreatic disease. Hematological and biochemical test results on admission were as follows: white blood cell count, 7 000/mm³ (normal, 4.0-10.0); hemoglobin, 13.4 g/dL (normal, 12.1-17.2); platelets, 177 10³/uL (normal, 150-400); total bilirubin, 0.36 mg/dL (normal, 0.1-1.3); albumin, 4.6 g/dL (normal, 3.5-5.2); aspartate aminotransferase, 29 u/L (normal, 10-31); alanine aminotransferase, 30 u/L (normal, 10-31); amylase, 74 u/L (normal, 0-90); lactate dehydrogenase, 335 u/L (normal, 220-450).

On physical examination, pulse rate was 84/min and arterial blood pressure was 110/70 mm Hg. Rectal examination revealed no mass and the stool was hemoccult negative. Computerized

tomography of the abdomen, plain abdominal radiography and upper endoscopy were normal. Abdominal ultrasonography showed a slightly enlarged liver with normal echo pattern and communication between the common hepatic artery and superior mesenteric artery (Figure 1). On Doppler ultrasound, arterial flow was observed within this fistula (Figure 2). We suspected CMI and consequently performed angiography. Celiac arteriogram revealed an abnormal fistula from the SMA to the CHA and not any other arterial communications (Figure 3).



Figure 1 Sonogram showing a fistula (thin arrow) between superior mesenteric artery (arrowhead) and common hepatic artery (thick arrow).

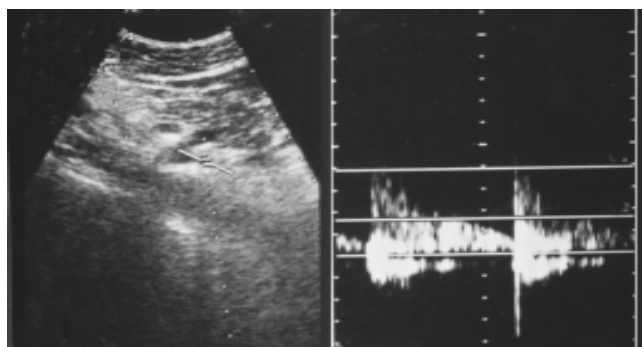


Figure 2 Color doppler sonogram of fistula revealing arterial flow.



Figure 3 Selective superior mesenteric artery angiography showing a fistula between superior mesenteric artery and common hepatic artery.

A small quantity diet with low fat content was advised to the patient who responded well to this measure and after one month she was free of abdominal pain, and also of abdominal distension, hence we did not plan to perform surgery or interventional radiology.

DISCUSSION

The major vascular supply of the bowel depends on the celiac, superior mesenteric and inferior mesenteric arteries. The superior mesenteric artery is the largest of all the aortic branches and carries over 10% of the cardiac output. Splanchnic circulation was about 30% of the circulating blood volume^[4,5].

CMI is a disputatious diagnostic problem. Most patients do not develop ischemic symptoms because of the abundant collateral circulation of these intestines. Usually at least two of the three mesenteric arteries must be significantly stenotic before symptoms developed^[6,7].

Classically, postprandial abdominal pain, known as "intestinal angina", was almost invariably the principal symptom. Other less consistent symptoms included bloating, flatulence, nausea, and variable changes in bowel habit^[2,8,9]. Superior mesenteric artery blood flow increased after ingestion of meals with a high fat content^[5]. Our patient reported significant crampy abdominal pain after heavy meal, meanwhile consuming small and low fat meal did not cause pain. The pathophysiological mechanism in this case was an arterial abnormality which was an abnormal communication between SMI and CHA. Under such a condition blood perfusion became impaired. A higher blood pressure in SMA could force flow towards CHA. Blood flow might be sufficient to sustain resting metabolic needs, but after a heavy meal, however, splanchnic blood flow did not increase because of this steal phenomenon.

A diagnosis of vasculogenic mesenteric ischemia was made on the basis of the clinical history and duplex ultrasonography findings. Other causes of abdominal pain were excluded. Large majority of cases of colonic ischemia were due to non-occlusive diseases^[10]. Other less common causes of CMI were vasculitis, SLE, sick cell disease, hypercoagulable states, medications (estrogen, danazol, vazopressin, gold, psychotropic drugs), and cocaine abuse^[1,11].

Clinical presentations of the patient might depend on the size and amount of blood flow through the fistula, ranging from asymptomatic cases to overt intestinal ischemia.

We suggested nutritional measures aiming at avoiding large meals and reduction of long-chain fat content.

In a patient with an unexplainable chronic abdominal pain, after exclusion of common reasons, vascular abnormalities must be suspected. Like in our case, there might be other abnormal vascular communications, thus even in a young patient vascular examinations might be necessary.

REFERENCES

- 1 **Rogers DM**, Thompson JE, Garrett WV, Talkington CM, Patman RD. Mesenteric vascular problems. A 26-year experience. *Ann Surg* 1982; **195**: 554-565
- 2 **Croft RJ**, Menon GP, Marston A. Does 'intestinal angina' exist? A critical study of obstructed visceral arteries. *Br J Surg* 1981; **68**: 316-318
- 3 **Kazmers A**. Operative management of chronic mesenteric ischemia. *Ann Vasc Surg* 1998; **12**: 299-308
- 4 **Muller AF**. Role of duplex Doppler ultrasound in the assessment of patients with postprandial abdominal pain. *Gut* 1992; **33**: 460-465
- 5 **Sidery MB**, Macdonald IA, Blackshaw PE. Superior mesenteric artery blood flow and gastric emptying in humans and the differential effects of high fat and high carbohydrate meals. *Gut* 1994; **35**: 186-190
- 6 **Thomas JH**, Blake K, Pierce GE, Hermreck AS, Seigel E. The clinical course of asymptomatic mesenteric arterial stenosis. *J Vasc Surg* 1998; **27**: 840-844
- 7 **Kolkman JJ**, Groeneveld AB. Occlusive and non-occlusive gastrointestinal ischaemia: a clinical review with special emphasis on the diagnostic value of tonometry. *Scand J Gastroenterol Suppl* 1998; **225**: 3-12
- 8 **Bower TC**. Ischemic colitis. *Surg Clin North Am* 1993; **73**: 1037-1053
- 9 **Zelenock GB**, Graham LM, Whitehouse WM Jr, Erlandson EE, Kraft RO, Lindenauer SM, Stanley JC. Splanchnic arteriosclerotic disease and intestinal angina. *Arch Surg* 1980; **115**: 497-501
- 10 **Marston A**, Clarke JM, Garcia Garcia J, Miller AL. Intestinal function and intestinal blood supply: a 20 year surgical study. *Gut* 1985; **26**: 656-666
- 11 **Patel A**, Kaleya RN, Sammartano RJ. Pathophysiology of mesenteric ischemia. *Surg Clin North Am* 1992; **72**: 31-41

Edited by Wang XL and Chen WW Proofread by Xu FM

• CASE REPORT •

Severe hypercholesterolemia associated with primary biliary cirrhosis in a 44-year-old Japanese woman

Tatsuo Kanda, Osamu Yokosuka, Hiroshige Kojima, Fumio Imazeki, Keiich Nagao, Ichiro Tatsuno, Yasushi Saito, Hiromitsu Saisho

Tatsuo Kanda, Osamu Yokosuka, Hiroshige Kojima, Fumio Imazeki, Hiromitsu Saisho, First Department of Medicine, Chiba University School of Medicine, Chiba 260-8670, Japan

Tatsuo Kanda, Keiich Nagao, Health Sciences Center, Chiba University, Chiba 260-8670, Japan

Ichiro Tatsuno, Yasushi Saito, Second Department of Medicine, Chiba University School of Medicine, Chiba 260-8670, Japan

Correspondence to: Osamu Yokosuka, M.D., First Department of Medicine, Chiba University School of Medicine, 1-8-1 Inohana, Chuo-ku, Chiba-City, Chiba 260-8670, Japan. kandat-cib@umin.ac.jp

Telephone: +81-43-226-2086 **Fax:** +81-43-226-2088

Received: 2004-02-02 **Accepted:** 2004-02-24

Abstract

A 44-year-old woman developed jaundice and was diagnosed as stage II of primary biliary cirrhosis (PBC). She showed a severely high total cholesterol level. This article focuses on atypical presentations of PBC and the need to test the total cholesterol level of PBC patients.

Kanda T, Yokosuka O, Kojima H, Imazeki F, Nagao K, Tatsuno I, Saito Y, Saisho H. Severe hypercholesterolemia associated with primary biliary cirrhosis in a 44-year-old Japanese woman. *World J Gastroenterol* 2004; 10(17): 2607-2608

<http://www.wjgnet.com/1007-9327/10/2607.asp>

CASE REPORT

A 44-year-old gentlewoman was admitted in August 1996 due to a feeling of itching and jaundice. She had no special past history, such as operation, blood transfusion, tattooing or illicit drug use. She did not drink or smoke. There were no particular familial histories such as liver disease or hyperlipidemia. The patient had been on medication for hyperlipidemia, with a daily intake of 10 mg of pravastatin sodium, 12 g of cholestyramine, and 600 mg of ursodeoxycholic acid since one month earlier.

On admission, her height, body mass and body mass index (BMI) were 154.5 cm, 46.0 kg and 19.3 kg/m², respectively. Her physical examination revealed mild anemia and jaundice. Xanthoma was noticed around her eyes, but thickened Achilles tendon was not seen on X-ray examination. Her liver and spleen were not enlarged. There was no pretibial edema in her feet.

Blood test results were compatible with the picture of primary biliary cirrhosis (PBC). The serum bilirubin level was 57 mg/L (normal 2-12 mg/L), direct bilirubin was 42 mg/L (normal <3 mg/L), alkaline phosphatase was 2 362 IU/L (normal 115-359 IU/L), and alanine aminotransferase was 105 IU/L (normal 8-42 IU/L). Prothrombin time was within normal limits at 11.8 seconds. Platelet count was 277×10⁹/L. Renal function was normal. Ultrasound scan showed normal liver size and biliary trees were normal. There were no gallstones or ascites. Intimal medial thickness (IMT) of the right common carotid artery did not show any increase on high-resolution B mode ultrasonography.

Serology tests for hepatitis B and C viruses were negative. Anti-mitochondrial antibody (AMA) and anti-mitochondrial M2 antibody were positive (×320) and 41.5 (normal <7). Anti-

nuclear antibody (ANA) and anti-smooth muscle antibody were both negative. IgG and IgM were 27.42 g/L (normal 8.7-17 g/L) and 11.89 g/L (normal 0.35-2.20 g/L), respectively. Thyroid gland functions were within normal limits at this time.

Her serum total cholesterol level was 13.90 g/L (normal 1.25-2.20 g/L), triglyceride 1.12 g/L (normal 0.35-1.50 g/L), high-density lipoprotein (HDL) cholesterol 1.03 g/L (normal >0.40 g/L), and blood glucose 1.03 g/L. She was positive for lipoprotein X. LCAT was not detectable, compatible with Frederickson type V hypercholesterolemia [apolipoprotein A-I 0.48 g/L (normal 1.26-1.65 g/L), A-II 0.24 g/L (normal 0.246-0.333 g/L), B 1.44 g/L (normal 0.66-1.01 g/L), C-II 333 mg/L (normal 15-38 mg/L), C-III 3.42 g/L (normal 26-46 mg/L) and E 450 mg/L (normal 29-53 mg/L)].

Liver biopsy showed no cirrhosis but revealed compatibility with PBC stage II (according to Ludwig). She was re-started on ursodeoxycholic acid at 900 mg/d and probucol at 500 mg/d. She was diagnosed as subclinical hypothyroidism [TSH 11.5 μIU/mL (normal 0.35-4.94 μIU/mL), free T3 1.45 pg/mL (normal 1.71-3.71 pg/mL) and free T4 8.2 ng/L (normal 7.0-14.8 ng/L)] in April 1999 and 0.05 mg/d of levothyroxine sodium was begun. However, her total cholesterol level remained quite similar to that before treatment as in October 2000 it was still high (10.11 g/L).

DISCUSSION

In PBC patients, a hyperlipidemic state is often observed; however, this case illustrated an unusual presentation of severe hypercholesterolemia. According to Talwalkar and Lindor^[1], up to 85% of patients presented with hypercholesterolemia at diagnosis. However, such a degree of hypercholesterolemia was not observed in many cases. In fact, our survey of more than 100 cases of PBC who visited our clinic revealed only this one case with a level of hypercholesterolemia higher than 10 g/L.

Earlier cross sectional studies reported higher levels of total cholesterol and lower levels of HDL cholesterol in patients with advanced disease compared with those in the earlier stages^[2,3]. On the other hand, Nikkila *et al.*^[4] reported that reduced hepatic synthesis and internal absorption in the terminal stage of PBC might lead to decreased total cholesterol levels. Although high levels of lipoprotein X, comprised of nonesterified cholesterol and phospholipids, were present in the serum of patients with PBC^[5], our patient was at stage II of early PBC, even if her serum bilirubin level was 57 mg/L. Hypothyroidism and subclinical hyperthyroidism often caused hyperlipidemia^[6,7]. In our patient, hypercholesterolemia did not improve after thyroid hormone therapy.

In PBC, marked hypercholesterolemia was not associated with an excess risk of cardiovascular disease, whereas less advanced patients with moderate hypercholesterolemia were exposed to an increased cardiovascular risk^[8]. There is no doubt that a reduction in serum cholesterol levels in PBC patients could be achieved with medical therapy^[9,10], so our patient continued to be observed with medical therapy.

In conclusion, we report a case of severe hypercholesterolemia, not familial, but associated with early-stage PBC. Further studies of severe hypercholesterolemia are warranted.

REFERENCES

- 1 Talwalkar JA, Lindor KD. Primary biliary cirrhosis. *Lancet* 2003;

- 362:** 53-61
- 2 **Jahn CE**, Schaefer EJ, Taam LA, Hoofnagle JH, Lindgren FT, Albers JJ, Jones EA, Brewer HB Jr. Lipoprotein abnormalities in primary biliary cirrhosis. Association with hepatic lipase inhibition as well as altered cholesterol esterification. *Gastroenterology* 1985; **89**: 1266-1278
 - 3 **Crippin JS**, Lindor KD, Jorgensen R, Kottke BA, Harrison JM, Murtaugh PA, Dickson ER. Hypercholesterolemia and atherosclerosis in primary biliary cirrhosis: what is the risk? *Hepatology* 1992; **15**: 858-862
 - 4 **Nikkila K**, Hockerstedt K, Miettinen TA. High cholestanol and low campesterol-to-sitosterol ratio in serum of patients with primary biliary cirrhosis before liver transplantation. *Hepatology* 1991; **13**: 663-669
 - 5 **Seidel D**, Alaupovic P, Furman RH, McConathy WJ. A lipoprotein characterizing obstructive jaundice. II. Isolation and partial characterization of the protein moieties of low density lipoproteins. *J Clin Invest* 1970; **49**: 2396-2407
 - 6 **Ganotakis ES**, Mandalaki K, Tampakaki M, Malliaraki N, Mandalakis E, Vrentzos G, Melissas J, Castanas E. Subclinical hypothyroidism and lipid abnormalities in older women attending a vascular disease prevention clinic: effect of thyroid replacement therapy. *Angiology* 2003; **54**: 569-576
 - 7 **Kong WM**, Sheikh MH, Lumb PJ, Naoumova RP, Freedman DB, Crook M, Dore CJ, Finer N, Naoumova P. A 6-month randomized trial of thyroxine treatment in women with mild subclinical hypothyroidism. *Am J Med* 2002; **112**: 348-354
 - 8 **Longo M**, Crosignani A, Battezzati PM, Squarcia Giussani C, Invernizzi P, Zuin M, Podda M. Hyperlipidaemic state and cardiovascular risk in primary biliary cirrhosis. *Gut* 2002; **51**: 265-269
 - 9 **Chauhan SS**, Zucker SD. Hypercholesterolemia in primary biliary cirrhosis: getting to the heart of the matter? *Gastroenterology* 2003; **124**: 854-856
 - 10 **Kanda T**, Yokosuka O, Imazeki F, Saisho H. Bezafibrate treatment: a new medical approach for PBC patients? *J Gastroenterol* 2003; **38**: 573-578

Edited by Zhu LH and Xu FM

EUS mini probes in diagnosis of cystic dystrophy of duodenal wall in heterotopic pancreas: A case report

Ivan Jovanovic, Srbislav Knezevic, Marjan Micev, Miodrag Krstic

Ivan Jovanovic, Miodrag Krstic, Clinic of Gastroenterology and Hepatology, Institute of Digestive Diseases, Belgrade, Serbia and Montenegro

Srbislav Knezevic, First Surgical Clinic, Belgrade, Serbia and Montenegro
Marjan Micev, Clinical Center of Serbia, Belgrade, Institute for Medical Research, Belgrade, Serbia and Montenegro

Correspondence to: Ivan Jovanovic, MD, PhD, Clinic of Gastroenterology and Hepatology, Clinical Center of Serbia, Belgrade, 6 Koste Todorovic, 11000 Belgrade, Serbia and Montenegro. ivangastro@beotel.yu

Telephone: +381-63-357080 **Fax:** +381-11-3614744

Received: 2004-01-16 **Accepted:** 2004-03-04

Abstract

Cystic dystrophy of the duodenal wall is a rare condition characterized by the development of cysts in heterotopic pancreatic tissue localized in the duodenal wall. A 38-year-old man was admitted to the hospital for abdominal pain and vomiting after food intake. The diagnosis of acute pancreatitis was initially suspected. Abdominal ultrasound examination revealed thickening of the second portion of duodenal wall within which, small cysts (diameter, less than 1 cm) were present in the vicinity of pancreatic head. The head of pancreas appeared enlarged (63 mm×42 mm) and hypoechoic. Upper endoscopy and barium X-ray series were performed revealing a severe circumferential deformation, as well as 4 cm long stenosis of the second portion of the duodenum. CT examination revealed multiple cysts located in an enlarged, thickened duodenal wall with moderate to strong post-contrast enhancement. We suspected that patient had cystic dystrophy of duodenal wall developed in the heterotopic pancreas and diagnosis was confirmed by endoscopic ultrasound (EUS). Endoscopic ultrasound (EUS) revealed circular stenosis from the duodenal bulb onwards. A twenty megaHertz mini-probe examination further showed diffuse (intramural) infiltration of duodenal wall limited to the submucosa and muscularis propria of the second portion of duodenum with multiple microcysts within the thickened mucosa and submucosa. Patient was successfully surgically treated and pancreatoduodenectomy was performed. The pathological examination confirmed a diagnosis of cystic dystrophy of a heterotopic pancreas. Endoscopic ultrasonography features allow preoperative diagnosis of cystic dystrophy of a heterotopic pancreas in duodenal wall, with intraluminal 20 MHz mini probe sonography being more efficient in cases of luminal stenosis.

Jovanovic I, Knezevic S, Micev M, Krstic M. EUS mini probes in diagnosis of cystic dystrophy of duodenal wall in heterotopic pancreas: A case report. *World J Gastroenterol* 2004; 10 (17): 2609-2612

<http://www.wjgnet.com/1007-9327/10/2609.asp>

INTRODUCTION

The most common type of heterotopic tissue in the gastrointestinal tract is pancreas. Pancreatic heterotopia is defined as the

presence of abnormally located (aberrant) pancreatic tissue with no contact (vascular, neural, and anatomical) with the normal pancreas, and possesses its own duct system and vascular supply^[1,2]. Heterotopic pancreatic tissue has been found in several abdominal and intrathoracic locations, most frequently in the stomach (25-60%) or duodenum (25-35%)^[3].

Cystic dystrophy of the duodenal wall in heterotopic pancreas is a relatively rare clinical disorder affecting young men in particular^[4]. Diagnosis is usually suspected during initial investigation of non-specific clinical symptoms such as abdominal pain, duodenal obstruction and weight loss and finally confirmed by imaging techniques, mainly endoscopic ultrasound which localizes precisely cysts in duodenal wall.

The purpose of this report was to present a case with this anomaly and provide up-to-date literature review on this topic.

CASE REPORT

A 38-year-old man who was admitted for clarification of several months of upper abdominal pain, vomiting after food intake accompanied by a weight loss. The patient had no history of alcohol abuse, and smoked 20 cigarettes per day. Physical examination revealed tachypnea and tachycardia, and a blood pressure 100/70 mmHg. There was abdominal tenderness in upper abdomen. Hematological and blood bio-chemical tests were performed (Tables 1, 2) showing a sevenfold increased level of serum amylase (625 U/L, range 20-90 U/L) accompanied by an elevated alkaline phosphatase, and markers of acute hepatocyte injury such as alanine (AST) and aspartate aminotransferase (ALT) and gamma GT. Bilirubin levels remained normal. The urine had a pH 6.5 and a specific gravity of 1.010. The sediment contained 3-5 red cells and 0-2 white cells per high-power field. A diagnosis of acute pancreatitis was initially suspected.

Ultrasonographic examination revealed an enlarged steatotic liver, no stones in gall bladder, and a common bile duct diameter of 8 mm with no signs of stone obstruction. Second portion duodenal wall appeared thicker within which, small cysts (diameter, less than 1 cm) were present in the vicinity of pancreatic head. The head of pancreas appeared enlarged (63 mm×42 mm) and hypoechoic.

An upper GI endoscopy also revealed a severe semispherical deformation of second portion of duodenum without mucosal lesions. Due to the stenosis the endoscope could not be passed distal to upper duodenal flexure. Biopsy of the duodenal mucosa detected moderate inflammatory changes (Figure 1).

A barium meal revealed a severe circumferential deformation, as well as 4 cm long stenosis of the second portion of the duodenum (Figure 2).

We suspected that the patient had cystic dystrophy of duodenal wall developed in the heterotopic pancreas which was highly indicated by computed tomography and endoscopic ultrasound (EUS).

CT examinations revealed multiple cysts located in an enlarged, thickened duodenal wall with moderate to strong post-contrast enhancement.

Endoscopic ultrasound (EUS) revealed circular stenosis from the duodenal bulb onwards. Twenty megaHertz mini-probe

examinations further showed diffuse (intramural) infiltration of duodenal wall limited to the submucosa and muscularis propria of the second portion of duodenum with multiple, very small anechoic spots, like microcysts (Figure 3A, B). EUS did not reveal any tumors of the pancreas.

MRI examinations showed a suspicious 6 cm×4 cm solid and partly cystic tumor of processus uncinatus of pancreas.

The patient was successfully surgically treated and pancreatoduodenectomy was performed (Figure 4). Pathological examinations confirmed a diagnosis of cystic dystrophy of a heterotopic pancreas (Figure 5).

Table 1 Hematologic tests

Variable	Value	Initial tests	Repeated tests
Hematocrit (%)	35-54	43	49.7
White cell count (×10 ⁹)	4.0-10.0	12.0	17.7
Differential count (×10 ⁹)			
Neutrophils	1.4-6.5	4.3	2.8
Lymphocytes	1.2-3.4	5.6	2.8
Monocytes	0.1-0.6	2.1	1.1
Prothrombin time (% quick)	75-120	114	115

Table 2 Blood bio-chemical tests

Variable	Initial test	Repeated test
Sodium (mmol/L)	132	148
Potassium (mmol/L)	2.5	4.6
Chloride (mmol/L)	75	107
Urea nitrogen (mmol/L)	9.4	2.8
Creatinine (μmol/L)	80	57
Glucose (mmol/L)	8.5	4.3
Bilirubin (μmol/L)	13	13
AST (U/L)	50	153
LT (U/L)	93	217
Alkaline phosphatase (U/L)	361	980
Alpha amylase (U/L)	627	354

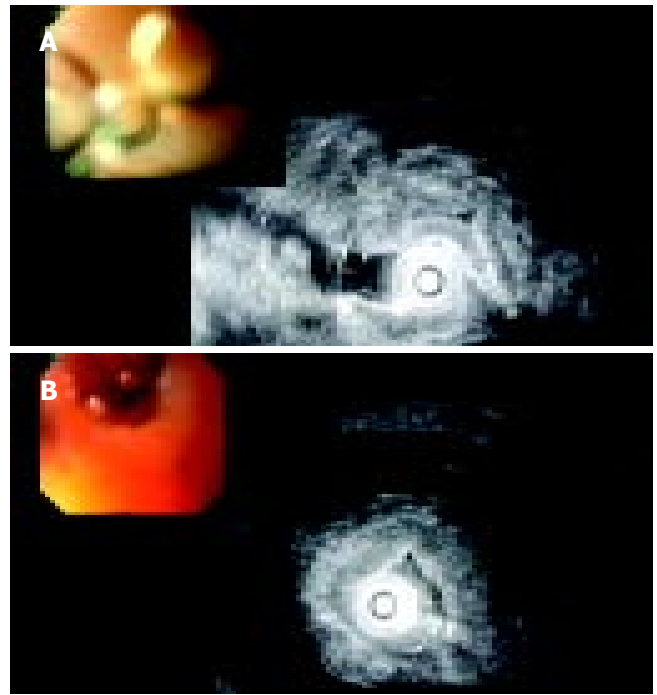


Figure 3 A: EUS image of diffusely thickened duodenal wall. B: EUS image of multiple microcysts in diffusely thickened duodenal wall.



Figure 1 Endoscopic image of the stenotic postbulbar duodenum.



Figure 2 Severe circumferential deformation, as well as 4 cm long stenosis of the second portion of the duodenum on X-ray series.



Figure 4 Surgical specimen of resected duodenal wall: Macrocysts in the thickened wall.



Figure 5 Irregular pseudocystic change in myofibroblastic stromal proliferation is considered as common histological findings in this lesion (HE, 112×).

DISCUSSION

The pancreas develops from two primitive diverticula, dorsal and ventral, that arise from the duodenum and the base of the liver, respectively, in the fifth week of gestation. During the seventh week, the two primordia fuse. The ventral portion gives rise to part of the head of the pancreas and the uncinat process,

and the dorsal portion becomes the body. In more than half the cases of pancreatic heterotopia, pancreatic tissue has been located in the duodenum or the pylorus but other sites have also been involved^[2].

Pancreatic heterotopia can develop due to either metaplasia of multipotent endodermal cells in situ or transplantation of embryonic pancreatic cells to adjacent structures^[2]. Heterotopic pancreatic tissues may be found in the mucosa or the muscularis or may be attached to the serosa of the gastrointestinal tract. Heterotopic pancreatic tissues that lack both acinar and endocrine cells have been called myoepithelial hamartoma, adenomyosis, or adenomyoma. Despite its congenital origin, pancreatic heterotopia was usually discovered in adults due to its complications^[5]. Most frequently it was found incidentally during autopsies, operations or during endoscopic examinations of the upper GI tract^[6]. The occurrence rate of heterotopic pancreas in autopsy series was estimated to be about 0.55% to 13.7%^[4,7].

Despite many advances of new diagnostic tools and methods, the diagnosis of heterotopic pancreas prior to surgery is still difficult. Heterotopic pancreas is usually asymptomatic and does not require treatment (i.e. surgical excision). However, sometimes, there were evident clinical symptoms^[8]. The most common symptoms attributed to heterotopic pancreas were: abdominal pain, nausea, vomiting, anemia, weight loss and melena^[9]. Rare manifestations and complications of heterotopic pancreas included acute and chronic pancreatitis^[10], biliary obstruction, intestinal obstruction, cystic dystrophy and malignant degeneration^[5,11,12].

The differential diagnosis of a cystic dystrophy of heterotopic pancreas includes disorders in three broad categories: inflammatory lesions, neoplasms, and congenital anomalies.

Complications of pancreatic heterotopia usually include inflammation with a formation of an inflammatory mass, ulceration, bleeding and obstruction with clinical manifestations of acute and chronic pancreatitis. Chronic pancreatitis with mucinous metaplasia of the ductal epithelium can further be complicated by prominent exudation of mucin into the stroma, mimicking mucinous carcinoma^[13].

The most challenging differential diagnosis of cystic dystrophy of heterotopic pancreas is cystic (mucinous) neoplasms. It has been demonstrated that pancreatic carcinomas or endocrine tumors can also develop in heterotopic pancreatic tissue^[14,15]. In this case, CT findings are non-specific. Endoscopic and upper GI barium X-ray series can reveal duodenal stenosis and submucosal masses if there are no mucosal lesions and biopsies from the lesions cannot always provide a representative tissue specimen. The introduction of endoscopic ultrasonography (EUS) makes the diagnosis of cystic dystrophy of the duodenal wall in heterotopic pancreas easier^[16]. Furthermore, endoscopic ultrasonography is a reliable method providing precise localization, extent and characteristics of the submucosal mass, making possible to differentiate it from all other causes of stenosis such as tumor and pancreas annulare^[17].

However, although there is good correlation between EUS^[16], computer tomography (CT) and nuclear magnetic resonance (NMR) findings with histological changes^[17,18], the definite diagnosis is often made only from surgical excision.

The treatment of this disease is controversial. There are reports of successful treatment with long-acting somatostatin synthetic stable analog^[19]. In some 40% of patients reduction in cyst size could be accomplished after three months of treatment^[16]. But, on the other hand, octreotide/analog treatment was of a limited value regarding already formed stenosis of the duodenum (in regards to persistent duodenal stenosis)^[20,21]. Furthermore, the necessary duration of treatment has not been established yet.

Ponchon *et al.* offered an alternative to surgical treatment for endoscopic fenestration of cysts, but that approach was feasible only for cases where cysts were fewer, not dispersed and relatively larger in size^[22].

Despite the encouraging attempts to treat cystic dystrophy of duodenal wall in heterotopic pancreas with conservative approaches, the treatment is still primarily surgical^[20,21,23,24].

Moreover, there is a difficult therapeutic dilemma: if such a lesion should be treated by duodenopancreatectomy or limited local excision?

Regarding the surgical procedures, there were data that conservative surgical procedures including segmental duodenal resection could be an alternative approach to the Whipple procedure^[25], but in other cases of pancreatic surgery, they were associated with a considerable morbidity and mortality^[26-28], and should be reserved for specialized centers^[29].

In conclusion, we demonstrated a rare case of cystic dystrophy of heterotopic pancreas in duodenal wall. Cystic dystrophy of aberrant pancreatic tissue can be either isolated or as in our case associated with acute pancreatitis and duodenal stenosis. Although the condition is benign, clinical symptoms vary and patients are usually referred for suspected pancreatic neoplasms or acute pancreatitis. Endoscopic ultrasonographic features allow preoperative diagnosis of cystic dystrophy of a heterotopic pancreas in duodenal wall, with intraluminal 20 MHz mini-probe sonography being more efficient in cases of luminal stenosis.

REFERENCES

- 1 **Dolan RV**, ReMine WH, Dockerthy MB. The fate of heterotopic pancreatic tissue. A study of 212 cases. *Arch Surg* 1974; **109**: 762-765
- 2 **Skandalakis JE**, Grey SW. Embryology for surgeons: the embryological basis for treatment of congenital anomalies. 2nd ed. Baltimore: *Williams Wilkins* 1994: 366-387
- 3 **Moen J**, Mack E. Small bowel obstruction caused by heterotopic pancreas in an adult. *Am Surg* 1989; **55**: 503-504
- 4 **Scarpelli DG**. The Pancreas In: Rubin E, Faber JL (Eds). *Pathology. Philadelphia: Lippincott* 1988: 811
- 5 **Burke GW**, Binder SC, Barron AM, Dratch PL, Umlas J. Heterotopic pancreas: gastric outlet obstruction secondary to pancreatitis and pancreatic pseudocyst. *Am J Gastroenterol* 1989; **84**: 52-55
- 6 **Jaffe R**. The pancreas. In: Wigglesworth JS, Singer DB, Eds. *Textbook of Fetal and Perinatal Pathology. Vol 2. Boston, Mass: Blackwell Scientific* 1991: 1021-1055
- 7 **Armstrong CP**, King PM, Dixon KM. The clinical significance of heterotopic pancreas in the gastrointestinal tract. *Br J Surg* 1981; **68**: 384-387
- 8 **Pang LC**. Pancreatic heterotopia: a reappraisal and clinicopathologic analysis of 32 cases. *South Med J* 1988; **81**: 1264-1275
- 9 **Hsia CY**, Wu CW, Lui WY. Heterotopic pancreas: a difficult diagnosis. *J Clin Gastroenterol* 1999; **28**: 144-147
- 10 **Chung JP**, Lee I, Kim KW. Duodenal ectopic pancreas complicated by chronic pancreatitis and pseudocyst formation: a case report. *J Korean Med Sci* 1994; **9**: 351-356
- 11 **Flejou JF**, Potet F, Molas G, Bernades P, Amouzal P, Fekete F. Cystic dystrophy of the gastric and duodenal wall developing in heterotopic pancreas: an unrecognized entity. *Gut* 1993; **34**: 343-347
- 12 **Jeng K**, Yang KC, Kuo H. Malignant degeneration of heterotopic pancreas. *Gastrointest Endosc* 1991; **37**: 196-198
- 13 **Nopajaroonsri C**. Mucus retention in heterotopic pancreas of the gastric antrum: a lesion mimicking mucinous carcinoma. *Am J Surg Pathol* 1994; **18**: 953-957
- 14 **Kaneda M**, Yano T, Yamamoto T, Suzuki T, Fujimori K, Itoh H, Mizumoto R. Ectopic pancreas in the stomach presenting as an inflammatory abdominal mass. *Am J Gastroenterol* 1989; **84**: 663-666
- 15 **Al-Jitawi SA**, Hiarat AM, Al-Majali SH. Diffuse myoepithe-

- lial hamartoma of the duodenum associated with adenocarcinoma. *Clin Oncol* 1984; **10**: 289-293
- 16 **Palazzo L**, Borotta E, Napoleon B. Is endoscopic ultrasonography accurate for the localization of pancreatic and duodenal tumors in patients with multiple endocrine neoplasia type I. *Gastroenterology* 1994; **106**: A313
- 17 **Vullierme MP**, Vilgrain V, Flejou JF, Zins M, O'Toole D, Ruszniewski P, Belghiti J, Menu Y. Cystic dystrophy of the duodenal wall in the heterotopic pancreas: radiopathological correlations. *J Comput Assist Tomogr* 2000; **24**: 635-643
- 18 **Procacci C**, Graziani R, Zamboni G, Cavallini G, Pederzoli P, Guarise A, Bogina G, Biasiutti C, carbognin G, Bergamo-Andreis IA, Pistolesi GF. Cystic dystrophy of the duodenal wall: radiologic findings. *Radiology* 1997; **205**: 741-747
- 19 **Basili E**, Allemand I, Ville E, Laugier R. Lanreotide acetate may cure cystic dystrophy in heterotopic pancreas of the duodenal wall. *Gastroenterol Clin Biol* 2001; **25**: 1108-1111
- 20 **Rubay R**, Bonnet D, Gohy P, Laka A, Deltour D. Cystic dystrophy in heterotopic pancreas of the duodenal wall: medical and surgical treatment. *Acta Chir Belg* 1999; **99**: 87-91
- 21 **Bittar I**, Cohen Solal JL, Cabanis P, Hagege H. Cystic dystrophy of an aberrant pancreas. Surgery after failure of medical therapy. *Presse Med* 2000; **29**: 1118-1120
- 22 **Ponchon T**, Napoleon B, Hedelius F, Bory R. Traitement endoscopique de la dystrophie kistique de la paroi duodenale. *Gastroenterol Clin Biol* 1997; **21**: A63
- 23 **Glaser M**, Roskar Z, Skalincky M, Krajnc I. Cystic dystrophy of the duodenal wall in a heterotopic pancreas. *Wien Klin Wochenschr* 2002; **114**: 1013-1016
- 24 **Wind P**, Pardies P, Rouillet MH, Rouzier R, Zinzindohoue F, Cugnenc PH. Cystic dystrophy of the duodenal wall in aberrant pancreas. *Ann Chir* 1999; **53**: 164-167
- 25 **Marmorale A**, Tercier S, Peroux JL, Monticelli I, Mc Namara M, Huguet C. Cystic dystrophy in heterotopic pancreas of the second part of the duodenum. One case of conservative surgical procedure. *Ann Chir* 2003; **128**: 180-184
- 26 **Lansing PB**, Blalock JB, Oschner JL. Pancreaticoduodenectomy: a retrospective review, 1949-1969. *Am Surg* 1972; **38**: 79-84
- 27 **Connolly MM**, Dawson PJ, Michelassi F, Moossa AR, Lowenstein F. Survival in 1001 patients with carcinoma of the pancreas. *Ann Surg* 1987; **206**: 366-372
- 28 **Herter FP**, Cooperman AM, Ahlborn TN, Antinori C. Surgical experience with pancreatic and periampullary cancer. *Ann Surg* 1982; **195**: 274-280
- 29 **Hanyu F**, Suzuki M, Imaizumi T. Whipple operation for pancreatic carcinoma: Japanese experiment. In: Berger HG, Buchler MW, Malfertheiner P, eds. Standards in Pancreatic Surgery Berlin Heidelberg: Springer Verlag 1993: 646

Edited by Zhu LH Proofread by Xu FM

Imaging findings of splenic hamartoma

Ri-Sheng Yu, Shi-Zheng Zhang, Jian-Ming Hua

Ri-Sheng Yu, Jian-Ming Hua, Department of Radiology, Second Affiliated Hospital, School of Medicine, Zhejiang University, Hangzhou 310009, Zhejiang Province, China

Shi-Zheng Zhang, Department of Radiology, Sir Run Run Shaw Hospital, School of Medicine, Zhejiang University, Hangzhou 310009, Zhejiang Province, China

Correspondence to: Dr. Ri-Sheng Yu, Department of Radiology, the Second Affiliated Hospital, School of Medicine, Zhejiang University, Hangzhou 310009, Zhejiang Province, China. yurisheng2003@yahoo.com.cn

Telephone: +86-571-87783860 **Fax:** +86-571-87783804

Received: 2003-10-08 **Accepted:** 2003-11-13

Abstract

AIM: To assess CT and MR manifestations and their diagnostic value in splenic hamartoma with review of literatures.

METHODS: We described a woman who was accidentally found to have a splenic tumor by ultrasound of the abdomen. CT and MR findings of this splenic hamartoma were proved by pathology retrospectively.

RESULTS: The CT and MR findings in this case included a ball-like mass with homogeneous mild-hypodensity lesions on non-enhanced CT scans or isointensity on T₁-weighted images and mild hypointensity on T₂-weighted images, progressive homogeneous enhancement on multiple-phase spiral CT and MR enhanced scans, and isodense enhancement on delayed post-contrast CT scans and obvious hyperintensity relative to the spleen on delayed MR images.

CONCLUSION: Splenic hamartoma has some specific radiological features. However, the diagnosis of this disease must be based on clinical features and confirmed by pathology.

Yu RS, Zhang SZ, Hua JM. Imaging findings of splenic hamartoma. *World J Gastroenterol* 2004; 10(17): 2613-2615
<http://www.wjgnet.com/1007-9327/10/2613.asp>

INTRODUCTION

Splenic hamartoma is a rare benign vascular tumor^[1]. Up to now,

less than 50 cases in Chinese literature or about 160 cases in the world have been reported after the first description by Rokitansky in 1861.

Imaging features of splenic hamartoma have been described by several researchers at computed tomography (CT), magnetic resonance imaging (MRI) and sonography^[2-8] and the imaging appearance of these lesions is considered as nonspecific and a histopathological confirmation is often required^[9-11].

This paper described the CT and MRI features of splenic hamartoma in a 40-year-old patient with review of the literature.

CASE REPORT

A 40-year-old woman was accidentally diagnosed having a splenic tumor by ultrasound of the abdomen. She did not complained about fever, fatigue, abdominal pain, or weight loss was complained. She denied any history of hepatitis or tuberculosis. Physical examination was entirely normal. There was no evidence of jaundice, peripheral lymphadenopathy or hepatosplenomegaly. Her hemoglobin was 125 g/L, the number of white blood cells was $7.3 \times 10^9/L$ and the number of platelets was $176 \times 10^9/L$. Both stool and urinate routine tests and hepatic and renal function tests were normal. Chest x-ray was also normal.

Spiral CT of the abdomen before contrast medium administration revealed a 3.8-cm diameter, homogeneous mild-hypodensity lesion within the spleen (Figure 1A). During hepatic artery phase following bolus injection of intravenous contrast, the lesion showed a slightly homogeneous enhancement (Figure 1B). During the portal venous phase and hepatic parenchymal phase, the lesion showed a progressively homogeneous enhancement. On delayed images up to 5 min after-contrast injection, the tumor was isodense with the spleen (Figure 1C). CT diagnosis was a splenic hemangioma.

MRI of the abdomen showed a 3.6 cm×3.8 cm×4.2 cm ball-like mass with isointensity on T₁-weighted images (Figure 2A) and mild hypointensity on T₂-weighted images (Figure 2B). The lesion demonstrated a diffuse heterogeneous enhancement on images obtained early after contrast medium administration (Figure 2C) and became more uniformly enhanced on the portal venous phase and hepatic parenchymal phase. It was hyperintense compared to the spleen on the delayed images (Figure 3). The MR examination yielded a diagnosis of splenic hemangioma. A 4.0-cm diameter tumor was found in the spleen during operation. The pathologic diagnosis was a splenic hamartoma (Figure 4).



Figure 1 CT scans of splenic hamartoma. A: Homogeneous mild hypodensity lesion within the spleen found by unenhanced CT scan, B: Mild-homogeneous enhancement of the mass found by enhanced CT scan on hepatic artery phase, C: Isodense tumor with normal spleen on delayed enhanced CT images.

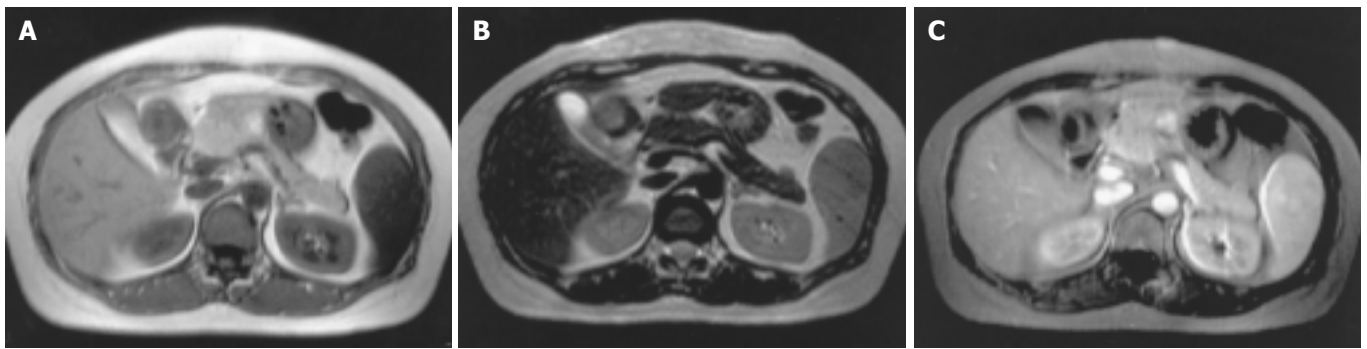


Figure 2 MR images of splenic hamartoma. A: Round-like mass with isointensity relative to the spleen on MR T₁-weighted images, B: Mild-hypointense mass on MR T₂-weighted images, C: Diffuse heterogeneous enhancement of mass by enhanced MR scan on early portal venous phase.



Figure 3 Obviously hyperintense tumor with normal spleen on delayed enhanced MR images.



Figure 4 Red marrow tissue and some blood sinusoid structures with lymphocytes and macrophages in hamartoma. Fibrosis was remarkable. (HE, original magnification×100).

DISCUSSION

Hamartoma of the spleen is a rare benign lesion and the diagnosis is difficult to make preoperatively. Histologically it is composed of an aberrant mixture of the normal tissue components of the spleen, so hamartoma of the spleen is often called splenoma, splenadenoma or nodular hyperplasia^[2,3].

Splenic hamartoma occurs most commonly in adults. About 14.3% of the reported cases of splenic hamartoma occurred in pediatric patients^[12]. Most patients were asymptomatic, they were incidentally found during imaging studies, laparotomy or autopsy^[2,3]. Our case was accidentally discovered by ultrasound examination of the abdomen. Symptomatic splenic hamartoma was rare but nearly half of splenic hamartoma pediatric patients had symptoms^[12]. A minority of these lesions had hematologic symptoms such as pancytopenia, anemia, and thrombocytopenia^[12-16]. Spontaneously ruptured splenic hamartoma has been reported^[17,18]. Symptomatic splenic hamartoma with renal, cutaneous abnormalities or portal hypertension and

heterotopic ovarian splenoma were described accidentally^[19-21].

A few radiological findings in splenic hamartoma have been described^[2-8]. Sonography was a more sensitive modality than CT in demonstrating the lesion, which showed hyperechoic masses with cystic components occasionally^[2]. But hypoechoic splenic mass was found and color Doppler sonography showed blood-flow signals inside the mass in a recent report^[4]. CT could reveal splenomegaly and homogeneous or heterogeneous low-density or isodense masses with calcification^[2,5,6] or fatty components, which are characteristic CT findings. Dense spreading enhancement on dynamic CT and prolonged enhancement on delayed post-contrast scans were noted in singular mass^[5]. But low-density masses relative to the spleen were seen in multiple splenic hamartomas after contrast medium administration^[2]. The CT findings in this case were similar to those in Ohtomo's report^[5], which included a homogeneous mild-hypodensity lesion on non-enhanced scans, a progressive homogeneous enhancement on multiple-phase spiral CT enhanced scans and an isodense enhancement on delayed post-contrast scans.

There were two types of MRI findings in splenic hamartomas, fibrous and non-fibrous splenic hamartomas. Histopathologically, fibrous splenic hamartomas had a dominant fibrous tissue and MRI showed isointensity or hyperintensity on T₁-weighted images, hypointensity on T₂-weighted images^[3,7]. We consider hypointensity on T₂-weighted images is one of the common MRI findings in splenic hamartomas. Non-fibrous splenic hamartomas are more common and MRI showed isointensity on T₁-weighted images, hyperintensity on T₂-weighted images^[6,8]. Both of the tumors demonstrated diffuse heterogeneous enhancement on the hepatic artery phase or early dynamic contrast-enhanced scans, which became more uniformly enhanced on delayed images^[3,5,8]. This case belonged to fibrous type and the MRI findings were similar to those in Fernandez-Canton's report besides obvious hyperintensity relative to the spleen on delayed images^[3]. We agree with that diffuse progressive enhancement and prolonged enhancement were the characteristic radiological findings^[5].

In short, the following clinical features and radiographic findings may suggest the diagnosis of splenic hamartomas: (1) asymptomatic and incidental findings in adults; (2) possible association with hematologic symptoms such as pancytopenia, anemia, and thrombocytopenia or spontaneous rupture of splenic mass; (3) splenic mass with calcification or fatty components on plain CT, and isointensity on T₁-weighted images, heterogeneous hyperintensity or hypointensity on T₂-weighted images; (4) dense spreading enhancement and obviously prolonged enhancement on postcontrast CT and MRI. Though splenic hamartomas have some clinical and CT features, the final and exact diagnosis depends on histopathologic examination.

Splenic haemangioma should be differentiated from splenic hamartomas^[8]. They have similar clinical and radiological findings. But the latter is manifested by splenic mass with calcification or fatty component on plain CT. The lesions appear isointense on T₁-weighted images, heterogeneous hyperintense or hypointense on T₂-weighted images. CT and MRI can demonstrate diffuse enhanced lesions on the hepatic artery phase or early dynamic contrast-enhanced scans. The typical CT and MRI features of the former include early peripheral nodular enhancement, hypointensity on T₁-weighted images and homogeneous hyperintensity on T₂-weighted images. Rare calcification and no fatty component of splenic haemangioma are seen on plain CT. In addition, splenic lymphoma and metastases were also considered to be different from splenic hamartomas^[5,8]. Most of splenic lymphomas are multiple, secondary lesions and often have extra-splenic lymphoma. Splenic metastases usually have a history of primary extra-splenic malignant neoplasms and hepatic metastases. Both splenic lymphoma and metastases seldom have dense spreading enhancement or prolonged enhancement on post-contrast CT and MRI.

REFERENCES

- 1 **Arber DA**, Strickler JG, Chen YY, Weiss LM. Splenic vascular tumors: a histologic, immunophenotypic, and virologic study. *Am J Surg Pathol* 1997; **21**: 827-835
- 2 **Zissin R**, Lishner M, Rathaus V. Case report: unusual presentation of splenic hamartoma; computed tomography and ultrasonic findings. *Clin Radiol* 1992; **45**: 410-411
- 3 **Fernandez-Canton G**, Capelastegui A, Merino A, Astigarraga E, Larena JA, Diaz-Otazu R. Atypical MRI presentation of a small splenic hamartoma. *Eur Radiol* 1999; **9**: 883-885
- 4 **Tang S**, Shimizu T, Kikuchi Y, Shinya S, Kishimoto R, Fujioka Y, Miyasaka K. Color Doppler sonographic findings in splenic hamartoma. *J Clin Ultrasound* 2000; **28**: 249-253
- 5 **Ohtomo K**, Fukuda H, Mori K, Minami M, Itai Y, Inoue Y. CT and MR appearances of splenic hamartoma. *J Comput Assist Tomogr* 1992; **16**: 425-428
- 6 **Thompson SE**, Walsh EA, Cramer BC, Pushpanathan CC, Hollett P, Ingram L, Price D. Radiological features of a symptomatic splenic hamartoma. *Pediatr Radiol* 1996; **26**: 657-660
- 7 **Chevallier P**, Guzman E, Fabiani P, Dib M, Oddo F, Padovani B. Fibrous splenic hamartoma: imaging features. *J Radiol* 1999; **80**: 1668-1671
- 8 **Ramani M**, Reinhold C, Semelka RC, Siegelman ES, Liang L, Ascher SM, Brown JJ, Eisen RN, Bret PM. Splenic hemangiomas and hamartomas: MR imaging characteristics of 28 lesions. *Radiology* 1997; **202**: 166-172
- 9 **Kumar PV**. Splenic hamartoma. A diagnostic problem on fine needle aspiration cytology. *Acta Cytol* 1995; **39**: 391-395
- 10 **Lee SH**. Fine-needle aspiration cytology of splenic hamartoma. *Diagn Cytopathol* 2003; **28**: 82-85
- 11 **Keogan MT**, Freed KS, Paulson EK, Nelson RC, Dodd LG. Imaging-guided percutaneous biopsy of focal splenic lesions: update on safety and effectiveness. *Am J Roentgenol* 1999; **172**: 933-937
- 12 **Hayes TC**, Britton HA, Mewborne EB, Troyer DA, Saldivar VA, Ratner IA. Symptomatic splenic hamartoma: case report and literature review. *Pediatrics* 1998; **101**: E10
- 13 **Fujii T**, Obara T, Shudo R, Tanno S, Maguchi H, Saitoh Y, Ura H, Kohgo Y. Splenic hamartoma associated with thrombocytopenia. *J Gastroenterol* 1997; **32**: 114-118
- 14 **Beham A**, Hermann W, Vennigerholz F, Schmid C. Hamartoma of the spleen with haematological symptoms. *Virchows Arch A Pathol Anat Histopathol* 1989; **414**: 535-539
- 15 **Wirbel RJ**, Uhlig U, Futterer KM. Case report: splenic hamartoma with hematologic disorders. *Am J Med Sci* 1996; **311**: 243-246
- 16 **Compton CN**, McHenry CR, Aijazi M, Chung-Park M. Thrombocytopenia caused by splenic hamartoma: resolution after splenectomy. *South Med J* 2001; **94**: 542-544
- 17 **Ferguson ER**, Sardi A, Beckman EN. Spontaneous rupture of splenic hamartoma. *J La State Med Soc* 1993; **145**: 48-52
- 18 **Yoshizawa J**, Mizuno R, Yoshida T, Kanai M, Kurobe M, Yamazaki Y. Spontaneous rupture of splenic hamartoma: a case report. *J Pediatr Surg* 1999; **34**: 498-499
- 19 **Kassarjian A**, Patenaude YG, Bernard C, Bell L. Symptomatic splenic hamartoma with renal, cutaneous, and hematological abnormalities. *Pediatr Radiol* 2001; **31**: 111-114
- 20 **Singh K**, Subbramaiah A, Choudhary SR, Bhasin DK, Wig JD, Radotra B, Nagi B. Splenic hamartoma with portal hypertension: a case report. *Trop Gastroenterol* 1992; **13**: 155-159
- 21 **Cualing H**, Wang G, Noffsinger A, Fenoglio-Preiser C. Heterotopic ovarian splenoma: report of a first case. *Arch Pathol Lab Med* 2001; **125**: 1483-1485

Edited by Zhang JZ and Wang XL Proofread by Xu FM

Brunner's gland adenoma of duodenum: A case report and literature review

Yu-Ping Gao, Jian-Shan Zhu, Wen-Jun Zheng

Yu-Ping Gao, Jian-Shan Zhu, Wen-Jun Zheng, Department of Pathology, Affiliated Renji Hospital, Shanghai Second Medical University, Shanghai 200001, China

Correspondence to: Dr Yu-Ping Gao, Department of Pathology, Affiliated Renji Hospital, Shanghai Second Medical University, 145 Shandong (c) Road, Shanghai 200001, China. jzmgyp@online.sh.cn

Telephone: +86-21-58752345 Ext. 3349

Fax: +86-21-58752345 Ext. 3349

Received: 2003-11-21 **Accepted:** 2004-01-15

Abstract

AIM: To analyze the clinicopathological features of Brunner's gland adenoma of the duodenum.

METHODS: A rare case of Brunner's gland adenoma of the duodenum was described and related literature was reviewed.

RESULTS: Brunner's gland adenoma of the duodenum appeared to be nodular hyperplasia of the normal Brunner's gland with an unusual admixture of normal tissues, including ducts, adipose tissue and lymphoid tissue. We suggested that it might be designated as a duodenal hamartoma rather than a true neoplasm.

CONCLUSION: The most common location of the lesion is the posterior wall of the duodenum near the junction of its first and second portions. It can result in gastrointestinal hemorrhage and duodenal obstruction. Endoscopic polypectomy is a worthy treatment for benign Brunner's gland adenomas, as malignant changes in these tumors have never been proven.

Gao YP, Zhu JS, Zheng WJ. Brunner's gland adenoma of duodenum: A case report and literature review. *World J Gastroenterol* 2004; 10(17): 2616-2617

<http://www.wjgnet.com/1007-9327/10/2616.asp>

INTRODUCTION

Brunner's gland adenoma, also known as Brunneroma or polypoid hamartoma, is a rare, benign, proliferative lesion arising from the Brunner's glands of the duodenum, accounting for 10.6% of benign tumors of the duodenum. The time patients are usually asymptomatic and lesions are discovered incidentally. These lesions manifest occasionally as a rare cause of duodenal obstruction or upper gastrointestinal hemorrhage, and require surgical excision^[1]. This article reports a case of Brunner's gland adenoma, and reviews briefly its clinical presentations, pathological features and therapy.

CASE REPORT

A 32-year-old Chinese man complained of two episodes of melenas and a two-month history of vague epigastric discomfort. The patient had in October 2001 his first tarry stool episode without nausea, vomiting and epigastralgia. Endoscopic examination revealed a mild ulcer in the duodenal bulb. The

symptoms were relieved by antacids and H₂ blockers. He reported however another tarry stool in September 2002 and complained about epigastric pain without nausea and vomiting during the preceding 2 mo. Antacids were taken and the pain was relieved. Vital signs were normal and no anemia was reported when he was admitted. The physical examination had no unremarkable finding. The abdomen was soft without palpating pain and jumping pain.

However, X-rays barium radiological examination of the upper gastrointestinal in October 2002 revealed a nodular, polypoid-filling defect mass measuring 3 cm×2.5 cm with a smooth surface and no ulceration in the duodenal bulb. A tumor was suspected. Follow-up endoscopy disclosed a lobulated, red-color tumor, occupying the anterior wall of the bulb. The surface of the tumor was smooth with mild depression at the top. The mucosa had no erosions and ulcers. Multiple biopsy specimens were taken and interpreted as "mucosal mild-medium atypia." CT scan was negative. A preoperative diagnosis of malignant tumor was made and the patient prepared for operation. On October 25, 2002, at the time of operation, a pedunculated polyp on a short broad-based stalk, 3.5 cm×3 cm×2 cm in size, was found in the anterior wall of the duodenal bulb. The common bile duct was normal. The lesion was amputated at the base of the stalk.

The resected specimen showed a lobulated, polypoid mass measuring 3.3 cm×2.5 cm×2.5 cm projecting into the duodenum. The stalk was measured 1.8 cm in diameter and 0.5 cm in length. The tumor was completely enveloped by the intact thin duodenal mucosa. The surface of the tumor was smooth without erosions and ulcers. The cut surface of tumor had a gray-red or gray-yellow color, revealing lobules. The consistency was moderate. On microscopic examination, the tumor was composed of hyperplasia of Brunner's glands. The hyperplasia formed lobules that were separated by intervening bands of fibrous tissue, adipose tissue, ducts and well developed aggregated lymphoid. No sign of malignancy was found in the hyperplasia, Brunner's glands as well as the surrounded duodenal mucosa. The frozen sections and the final pathologic diagnosis were assessed as Brunner's gland adenoma. The patient had an uneventful postoperative course and was discharged on the tenth postoperative day. He has remained symptom free ever since and no episode of recurrent melenas has been reported.

DISCUSSION

Besides the duodenal gland, the duodenum has Brunner's glands under the mucin. Its structure and function are similar to glands of the pylorus. Brunner's glands secrete an alkaline fluid composed of viscous mucin, whose function appears to protect the duodenal epithelium from acid chyme of the stomach. Brunner's glands consist of submucosal mucin-secreting glands located exclusively in the duodenum. They extend from the pylorus distally for a variable distance, usually stopping at the first and second portions of the duodenum, and less often stopping at the third and fourth portions.

In 1688 Brunner gave a precise anatomic description of the duodenal submucosal glands and coined the term "pancreas secundarium." In 1846 Middeldorpf correctly identified these glands as a separate entity, which he proposed be named Brunner's

glands. Salvioli reported the first adenoma of Brunner's gland in 1876. Since then, 150 cases or so have been reported in literature of English language^[2].

The etiology of Brunner's gland adenoma remains obscure. It tends to present predominantly in the fifth and sixth decades of man's life with no sex predominance. It has been found although the size of adenoma might extend from 1-12 cm, it is generally 1-2 cm in diameter^[3]. The most common location for the lesion is the posterior wall of the duodenum near the junction of its first and second portions. Brunner's gland adenoma was rarely found extending to the proximal jejunum^[4].

Brunner's gland adenoma has fallen into two categories: symptomatic tumors and asymptomatic ones that are only found incidentally. Symptomatic tumors can further be divided into hemorrhagic and obstructive tumors. The clinical manifestations of the former are gastrointestinal hemorrhage, due to ulceration or erosion of the tumor. Obstructive tumors occur when hyperplasia diffuses or a single adenoma grows too large, causing epigastric bloating, discomfort, vomiting or weight loss. Duodenal intussusception has been reported only in two patients^[2], probably because of the fixation of duodenum to the posterior abdominal wall. There are also reports about patients who complained of diarrhea owing to duodenal motor disturbances^[5].

Preoperative histological diagnosis at present is not always easy. In X-rays barium examination, the findings are often nonspecific because there is usually a sessile or pedunculated polypoid-filling defect in the duodenal bulb. Some doctors hold that hypotonic duodenography should play a vital role in establishing the diagnosis and should be treated as the best method to check the surface of the lesion. Endoscopy has an additional function in diagnosing and treating Brunner's gland adenoma, since it can verify the histological diagnosis and remove the tumor simultaneously. Endoscopic pinching biopsy however usually gave a negative result because the tumor was almost covered entirely with thick intact duodenal mucosa in the biopsy sites and the biopsy was often not deep enough to reach the submucosal tumor tissue^[6]. In our case, the endoscopic biopsy was negative, and the condition was diagnosed as chronic gastritis, although the final pathologic diagnosis indicated that the patient suffered from Brunner's gland adenoma. CT examination appeared to be unrevealing.

Pathomorphological features of Brunner's gland are characterized by the presence of nondysplastic, lobulated

Brunner's glands. Its hyperplasia is divided into diffuse hyperplasia, nodular hyperplasia and adenomatous hyperplasia with or without erosion or ulcer. In our opinion, the unusually admixture of normal tissues, including Brunner's glands, ducts, adipose tissue, and lymphoid tissue, supports the designation of these lesions as a hamartoma or nodular hyperplasia rather than a true neoplasm. It is a tumor without malignant predisposition. The malignant type is rare. Fujimaki *et al.* reported recently one patient with a focus atypical gland^[7].

It is still controversial whether asymptomatic Brunner's gland adenoma found incidentally needs surgical removal. Some people think that it needs no treatment, whereas others hold that it should undergo endoscopic excision in order to prevent complications. There have been several reports^[2,4] that Brunner's gland adenoma could give rise to acute profuse bleeding, which results in shock of patients. Symptomatic Brunner's gland adenoma, in our point of view, usually needs surgical treatment. When the tumor is small or pedunculated, endoscopic polypectomy is the first choice. Open surgical excision is reserved for cases where snaring has failed or when tumor is too large. The outcome of operation is usually excellent and there is no recurrent ever reported.

REFERENCES

- 1 **Matsumoto T**, Iida M, Matsui T, Yao T, Fujishima M. A large Brunner's gland adenoma removed by endoscopic polypectomy. *Endoscopy* 1990; **22**: 192-193
- 2 **Peetz ME**, Moseley HS. Brunner's gland hyperplasia. *Am Surg* 1989; **55**: 474-477
- 3 **Nakanishi T**, Takeuchi T, Hara K, Sugimoto A. A great Brunner's gland adenoma of the duodenal bulb. *Dig Dis Sci* 1984; **29**: 81-85
- 4 **Levine JA**, Burgart LJ, Batts KP, Wang KK. Brunner's gland hamartomas: clinical presentation and pathological features of 27 cases. *Am J Gastroenterol* 1995; **90**: 290-294
- 5 **Spellberg MA**, Vucelic B. A case of Brunner's glands hyperplasia with diarrhea responsive to cimetidine. *Am J Gastroenterol* 1980; **73**: 519-522
- 6 **Gourtsoyiannis NC**, Zarifi M, Gallis P, Mouchtouris A, Livaditou A. Radiologic appearances of Brunner's gland adenoma: a case report. *Eur J Radiol* 1990; **11**: 188-190
- 7 **Fujimaki E**, Nakamura S, Sugai T, Takeda Y. Brunner's gland adenoma with a focus of p53-positive atypical glands. *J Gastroenterol* 2000; **35**: 155-158

Edited by Qiu WS and Wang XL. Proofread by Xu FM

Production of a human single-chain variable fragment antibody against esophageal carcinoma

Ming-Yan Xu, Xiao-Hu Xu, Geng-Zhen Chen, Xiao-Ling Deng, Jonathan Li, Xiao-Jun Yu, Mei-Zhen Chen

Ming-Yan Xu, Xiao-Hu Xu, Xiao-Jun Yu, Mei-Zhen Chen, Department of Forensic Medicine, Medical College, Shantou University, Shantou 515041, Guangdong Province, China

Geng-Zhen Chen, Second Affiliated Hospital of Medical College, Shantou University, Shantou 515041, Guangdong Province, China

Xiao-Ling Deng, Department of Preventive Medicine, Medical College, Shantou University, Shantou 515041, Guangdong Province, China

Jonathan Li, University of California, San Francisco, USA

Supported by the National Natural Science Foundation of China, No. 30070291 and No. 30213914; Medical Scientific Foundation of Guangdong Province, No. A2000434

Correspondence to: Dr. Ming-Yan Xu, Department of Pathogenic biology, Medical College, Shantou University, 22 Xinling Road, Shantou 515041, Guangdong Province, China. xmycasey@sina.com.cn

Telephone: +86-754-8900431 **Fax:** +86-754-8900837

Received: 2003-08-05 **Accepted:** 2003-10-07

Abstract

AIM: To construct a phage display library of human single-chain variable fragment (scFv) antibodies associated with esophageal cancer and to preliminarily screen a scFv antibody against esophageal cancer.

METHODS: Total RNA extracted from metastatic lymph nodes of esophageal cancer patients was used to construct a scFv gene library. Rescued by M13K07 helper phage, the scFv phage display library was constructed. esophageal cancer cell line Eca 109 and normal human esophageal epithelial cell line (NHEEC) were used for panning and subtractive panning of the scFv phage display library to obtain positive phage clones. Soluble scFv was expressed in *E.coli* HB2151 which was transfected with the positive phage clone, then purified by affinity chromatography. Relative molecular mass of soluble scFv was estimated by Western blotting, its bioactivity was detected by cell ELISA assay. Sequence of scFv was determined using the method of dideoxynucleotide sequencing.

RESULTS: The size of scFv gene library was approximately 9×10^6 clones. After four rounds of panning with Eca109 and three rounds of subtractive panning with NHEEC cells, 25 positive phage clones were obtained. Soluble scFv was found to have a molecular mass of 31 ku and was able to bind to Eca109 cells, but not to HeLa and NHEEC cells. Variable heavy (V_H) gene from one of the positive clones was shown to be derived from the γ chain subgroup IV of immunoglobulin, and variable light (V_L) gene from the κ chain subgroup I of immunoglobulin.

CONCLUSION: A human scFv phage display library can be constructed from the metastatic lymph nodes of esophageal cancer patients. A whole human scFv against esophageal cancer shows some bioactivity.

Xu MY, Xu XH, Chen GZ, Deng XL, Li J, Yu XJ, Chen MZ. Production of a human single-chain variable fragment antibody

against esophageal carcinoma. *World J Gastroenterol* 2004; 10(18): 2619-2623

<http://www.wjgnet.com/1007-9327/10/2619.asp>

INTRODUCTION

Esophageal cancer is one of the most common malignancies in China with a relatively high mortality rate. In recent years, antibody-mediated tumor immunoscintigraphy and immunotherapy have been used in the diagnostic and therapeutic approaches of cancers^[1,2]. However, most antibodies are of murine origin, and repeated administration can induce human anti-mouse antibodies (HAMA). In addition, intact antibody is too large to penetrate into tumor masses, its application is limited. To overcome such deficiencies, many kinds of humanized antibodies including human-murine chimeric antibody and small molecular antibodies have been developed, but they are still of murine origin.

Recently, the emergence of genetically engineered antibodies and phage display libraries of human antibody fragments from immune or naïve donors has enabled the production of human antibody fragment targeting cancers^[3]. In the present study, phage antibody library techniques were used to construct a human phage single-chain Fv antibody library from metastatic lymph nodes of esophageal cancer patients. To obtain a single chain Fv AD09, panning and subtractive panning were performed with human esophageal cancer cell line (Eca109) and normal human esophageal epithelial cell line (NHEEC) respectively. Soluble AD09 was expressed in *E.coli* HB2151 and purified by affinity chromatography using anti-E tag antibody, its bioactivity was then detected by cell ELISA assay.

MATERIALS AND METHODS

Cell culture

Human esophageal carcinoma cell line Eca109 (Cytology Institute of Chinese Medical Academy, Beijing) and HeLa cell line (Shanghai Cytology Institute, China) were cultured at 37 in RPMI1640 medium supplemented with 100 mL/L fetal calf serum (Hyclone, USA) in a humidified atmosphere of 50 mL/LCO₂. Normal human esophageal epithelial cell (NHEEC) line was a primary cell line from a 20-wk conception fetus cultured in RPMI1640 with 200 mL/L fetal calf serum.

Primer design

Primer sequences were created as previously described^[4] with some modifications in PCR assembly part (Table 1B). We designed complementary coding sequences for a peptide linker at the 5'-end of J_H forward primers and the 3'-end of human V kappa (or lambda) back primers to optimize the diversity and efficiency of ligation. The primers were synthesized by Sunbiotech Company (Beijing, China) and the sequences are shown in Table 1. Sequences were given using the IUPAC nomenclature of mixed base (R = A or T, K = G or T, Y = C or T, S = G or C, H = A or C or T, N = A or C or G or T).

Library construction

Metastatic lymph nodes of 5 esophageal cancer patients were

Table 1 Oligonucleotide primers used for PCR of human immunoglobulin genes

A. Primary PCRs	
Human V _H back primers (sense)	
HuV _H 1aBACK	5'-CAG GTG CAG CTG GTG CAG TCT GG-3'
HuV _H 2aBACK	5'-CAG GTC AAC TTA AGG GAG TCT GG-3'
HuV _H 3aBACK	5'-GAG GTG CAG CTG GTG GAG TCT GG-3'
HuV _H 4aBACK	5'-CAG GTG CAG CTG CAG GAG TCG GG-3'
HuV _H 5aBACK	5'-GAG GTG CAG CTG TTG CAG TCT GC-3'
HuV _H 6aBACK	5'-CAG GTA CAG CTG CAG CAG TCA GG-3'
J _H forward primers (anti-sense)	
HuJ _H 1-2FOR	5'-TGA GGA GAC GGT GAC CAG GGT GCC-3'
HuJ _H 3FOR	5'-TGA AGA GAC GGT GAC CAT TGT CCC-3'
HuJ _H 4-5FOR	5'-TGA GGA GAC GGT GAC CAG GGT TCC-3'
HuJ _H 6FOR	5'-TGA GGA GAC GGT GAC CGT GGT CCC-3'
Human V kappa back primers (sense)	
HuV κ 1aBack	5'-GAC ATC CAG ATG ACC CAG TCT CC-3'
HuV κ 2aBack	5'-GAT GTT GTG ATG ACT CAG TCT CC-3'
HuV κ 3aBack	5'-GAA ATT GTG TTG ACG CAG TCT CC-3'
HuV κ 4aBack	5'-GAC ATC GTG ATG ACC CAG TCT CC-3'
HuV κ 5aBack	5'-GAA ACG ACA CTC ACG CAG TCT CC-3'
HuV κ 6aBack	5'-GAA ATT GTG CTG ACT CAG TCT CC-3'
Human J kappa forward primer (anti-sense)	
HuJ κ 1FOR	5'-ACG TTT GAT TTC CAC CTT GGT CCC-3'
HuJ κ 2FOR	5'-ACG TTT GAT CTC CAG CTT GGT CCC-3'
HuJ κ 3FOR	5'-ACG TTT GAT ATC CAC TTT GGT CCC-3'
HuJ κ 4FOR	5'-ACG TTT GAT CTC CAC CTT GGT CCC-3'
HuJ κ 5FOR	5'-ACG TTT AAT CTC CAG TCG TGT CCC-3'
Human V lambda back primers (sense)	
HuV λ 1BACK	5'-CAG TCT GTG TTG ACG CAG CCG CC-3'
HuV λ 2BACK	5'-CAG TCT GCC CTG ACT CAG CCT GC-3'
HuV λ 3aBACK	5'-TCC TAT GTG CTG ACT CAG CCA CC-3'
HuV λ 3bBACK	5'-TCT TCT GAG CTG ACT CAG GAC CC-3'
HuV λ 4BACK	5'-CAC GTT ATA CTG ACT CAA CCG CC-3'
HuV λ 5BACK	5'-CAG GCT GTG CTC ACT CAG CCG TC-3'
HuV λ 6BACK	5'-AAT TTT ATG CTG ACT CAG CCC CA-3'
Human J lambda forward primers (anti-sense)	
HuJ λ 1FOR	5'-ACC TAG GAC GGT GAC CTT GGT CCC-3'
HuJ λ 2-3FOR	5'-ACC TAG GAC GGT CAG CTT GGT CCC-3'
HuJ λ 4-5FOR	5'-ACC TAA AAC GGT GAG CTG GGT CCC-3'
B. PCR assembly	
Hu J _H -Linker primers	
HuJ _H 1-2Linker	5'-AGAGCCACCTCCGCCTGAACCGCCTCCACCTGAGGAGACGGT GACCAGGGTGCC-3'
HuJ _H 3Linker	5'-AGAGCCACCTCCGCCTGAACCGCCTCCACCTGAAGAGACGGT GACCATTGTCCC-3'
HuJ _H 4-5Linker	5'-AGAGCCACCTCCGCCTGAACCGCCTCCACCTGAGGAGACGGT GACCAGGGTTCC-3'
HuJ _H 6Linker	5'-AGAGCCACCTCCGCCTGAACCGCCTCCACCTGAGGAGACGGT GACCGTGGTCCC-3'
Linker-Hu V κ primers	
Linker-HuV κ 2-3-6 BACK	5'-GTTTCAGGCGGAGGTGGCTCTGGCGGTGGCGGATCGGAWRTTGTGHTGACKCAGTCTCC-3'
Linker-HuV κ 1-4 BACK	5'-gTTCAGGCGGAGGTGGCTCTGGCGGTGGCGGATCGGACATCSWGATGACCCAGTCTC C-3'
Linker- HuV κ 5 BACK	5'-GTTTCAGGCGGAGGTGGCTCTGGCGGTGGCGGATCGGAAACGACACTCAG CAGTCTCC-3'
Linker-Hu V λ primers	
Linker-HuV λ 1-2BACK	5'-GTTTCAGGCGGAGGTGGCTCTGGCGGTGGCGGATCGCAGTCTGYSYTGACKCAGCCCKS C-3'
Linker-HuV λ 3BACK	5'-GTTTCAGGCGGAGGTGGCTCTGGCGGTGGCGGATCGTCYMTGWGCTGACTCAGSMMCC-3'
Linker-HuV λ 4-5BACK	5'-GTTTCAGGCGGAGGTGGCTCTGGCGGTGGCGGATCGCASGYRTRCTSACTCARCCGYC-3'
Linker-HuV λ 6BACK	5'-GTTTCAGGCGGAGGTGGCTCTGGCGGTGGCGGATCGAATTTTATGCTGACTCAGCCC CA-3'
C. Reamplification with primers containing restriction sites	
Human V _H back (Sfi) primers (sense)	
HuV _H 1aBACKSfi	5'-GTCCTCGCAACTGCGGCCAGCCGGCCATGGCCCAGGTGCAGCTGGTGCAGTCTGG-3'
HuV _H 2aBACKSfi	5'-GTCCTCGCAACTGCGGCCAGCCGGCCATGGCCCAGGTCAACTTAAGGGAGTCTGG-3'
HuV _H 3aBACKSfi	5'-GTCCTCGCAACTGCGGCCAGCCGGCCATGGCCGAGGTGCAGCTGGTGGAGTCTGG-3'
HuV _H 4aBACKSfi	5'-GTCCTCGCAACTGCGGCCAGCCGGCCATGGCCCAGGTGCAGCTGCAGGAGTCCGG-3'
HuV _H 5aBACKSfi	5'-GTCCTCGCAACTGCGGCCAGCCGGCCATGGCCCAGGTGCAGCTGTTGCAGTCTGC-3'
HuV _H 6aBACKSfi	5'-GTCCTCGCAACTGCGGCCAGCCGGCCATGGCCCAGGTACAGCTGCAGCAGTCAAG-3'
Human J kappa forward (Not) primers (anti-sense)	
HuJ κ 1FORNot	5'-GAGTCATTCTCGACTTGCGGCCGCACGTTTGTATTTCCACCTTGGTCCC-3'
HuJ κ 2FORNot	5'-GAGTCATTCTCGACTTGCGGCCGCACGTTTGTATCTCCAGCTTGGTCCC-3'
HuJ κ 3FORNot	5'-GAGTCATTCTCGACTTGCGGCCGCACGTTTGTATATCCACTTTGGTCCC-3'
HuJ κ 4FORNot	5'-GAGTCATTCTCGACTTGCGGCCGCACGTTTGTATCTCCACCTTGGTCCC-3'
HuJ κ 5FORNot	5'-GAGTCATTCTCGACTTGCGGCCGCACGTTAATCTCCAGTCGTGTCCC-3'
Human J lambda forward (Not) primers (anti-sense)	
HuJ λ 1FORNot	5'-GAGTCATTCTCGACTTGCGGCCGCACCTAGGACGGTGACCTTGGTCCC-3'
HuJ λ 2-3FORNot	5'-GAGTCATTCTCGACTTGCGGCCGCACCTAGGACGGTCAGCTTGGTCCC-3'
HuJ λ 4-5FORNot	5'-GAGTCATTCTCGACTTGCGGCCGCACCTAAAACGGTGAGCTGGGTCCC-3'

collected for total RNA extraction (TRizol, Gibco BRL, UK). First-strand cDNA synthesis was performed in the presence of 40 U RNase inhibitor, 200 U Superscript II transcriptase (Gibco BRL, UK). The sample was finally treated with 2 U RNase H for 30 min at 37 °C and stored at -20 °C until use.

IgG-specific variable heavy (V_H) and light (V_L) chain gene fragments were amplified using Pyrobest PCR system (TarkaRa Biotechnology, Dalian, China) for 30 cycles (at 94 °C for 30 s, at 55 °C for 30 s and at 72 °C for 1 min), with each forward oligonucleotide primer and one of the back primers (Table 1A). The fragments were isolated from a 15 g/L agarose gel with the QIAex kit (QIAGEN, Germany). Then fragments were used as templates for PCR amplification to extend a linker, V_H fragments used human J_H -linker primers and human V_H back primers, V_L fragments used linker-human V_K primers (or linker-human V_L primers) and human J_K forward primers (or human J_L forward primers), respectively.

The amplified V_H -linker and V_L -linker PCR products were combined in a SOE-PCR reaction mixture. First, approximately 100 ng each of V_H -linker and V_L -linker was assembled by PCR without primers in which the short regions of complementarities built into the ends of primers drove hybridization of various fragments. An initial denaturation step (at 94 °C for 5 min) was followed by five cycles (at 94 °C for 1 min, at 60 °C for 1 min and at 72 °C for 1.5 min) in the absence of primers. After the outer primers containing restriction sites (Table 1C) were added, 30 cycles (at 94 °C for 30 s, at 60 °C for 1 min and at 72 °C for 1.5 min) were performed. These were gel-purified, digested with *SfiI* and *NotI* (TarkaRa Biotechnology, Dalian), cloned into the vector pCANTAB 5E (Amersham Pharmacia Biotech, Sweden) and transformed into electrocompetent *E.coli* TG1 (Amersham Pharmacia Biotech, Sweden). After electroporation, cells were plated on SOBAG medium (containing 20 g/L glucose and 100 mg/mL ampicillin) in 20 dishes and incubated overnight at 30 °C. The clones were scraped off the plates in 50 mL 2×YT medium with 100 mL/L glycerol and subsequently stored at -70 °C. Plasmid DNA was prepared from 10 randomly selected clones using Qiagen plasmid minikit (Qiagen, Germany). PCR and a *SfiI/NotI* double digestion reaction were performed to identify the positive insert clones.

Rescue of phagemid libraries

Ampicillin-resistant colonies were scraped into 2×YT medium and superinfected by M13K07 (Amersham Pharmacia Biotech, Sweden) helper phage. After an overnight induction in 2×YTAK medium without glucose, the phage preparation was precipitated in 40 g/L PEG/0.5 mol/L NaCl and resuspended in 10 g/L PBS.

Panning and subtractive panning of phage antibody library

To screen the positive phage clones, live Eca109 cell line as the antigen was used for panning. Live NHEEC was used for subtractive panning. The panning procedure was carried out essentially as described previously^[5]. After four rounds of panning and three rounds of subtractive panning, the unabsorbed phages were amplified.

Cell ELISA assay with phage

To detect the scFv-phage recombinant antibody, cell ELISA was performed. Eca109 cells (5×10^4) as antigens were grown in 96-well plates at 37 °C for 24 h, then fixed with 25 g/L glutaraldehyde and blocked with 10 g/L BSA. This was followed by incubation with scFv-phage at 37 °C for 2 h. After washed three times with PBS, HRP/anti-M13 monoclonal conjugate (1:5 000) (Amersham Pharmacia Biotech, Sweden) was added into wells with scFv-phage and they were incubated for 1 h at 37 °C. After washed again as above, 1×ABTS substrate solution was added, and incubated in darkness for 30 min and the reactions were read at 405 nm. PBS was used as negative control. The absorbance

reading for the positive was 0.2 or above at least three times higher than that for the negative control.

Expression and purification of soluble scFv

To produce soluble scFvs, strongly positive recombinant phage clones were used to infect log-phage *E.coli* HB2151 (Amersham Pharmacia Biotech, Sweden). Expression of soluble scFv was induced by adding isopropyl β -D-thiogalactopyranoside (IPTG) to a final concentration of 1 mmol/L and the cultures grown overnight at 30 °C. The induced culture was centrifuged at 1 500 r/min for 20 min. Cell pellets were resuspended in 2% of culture volume ice-cold 1×TES. Subsequently, 3% of culture volume ice-cold 0.2×TES was added, the mixture was incubated on ice for 30 min to induce a mild osmotic shock. The contents were centrifuged at 12 000 g for 10 min. The supernatant, containing the soluble antibodies from the periplasm, was transferred to the clean tubes and stored at -20 °C.

Soluble scFvs from periplasm were purified by affinity chromatography. Anti-E tag antibody (Amersham Pharmacia Biotech, Sweden) was covalently coupled to a protein G column (Amersham Pharmacia Biotech, Sweden) and soluble scFvs were selected by binding to anti-E tag antibody. After washed with 20 mmol/L phosphate buffer, pH 7.0, +0.5 g/L Na₃N, scFvs were eluted from the column with 0.1 mol/L glycine-HCl, pH 3.0, and neutralized immediately with 1 mol/L Tris/HCl, pH 8.2, +0.5 g/L Na₃N. Column fractions were assayed and positive fractions were pooled and stored at -70 °C. The expressed soluble scFv proteins were analyzed by 120 g/L sodium dodecyl sulfate (SDS)-polyacrylamide gel electrophoresis (PAGE), and confirmed by Western blotting. Purity and concentration of proteins were determined with Bradford assay.

Cell ELISA assay for activity of soluble scFv

To detect the activity of soluble scFv, HRP/anti-E tag antibody (Amersham Pharmacia Biotech, Sweden) was used. Eca109 cells, HeLa cells and NHEEC cells (5×10^4) were used as antigens. The cell ELISA assay procedure was performed as described above.

Sequencing

Plasmid DNA was prepared from recombinant clones using the Qiagen plasmid minikit (Qiagen, Germany). Nucleic acid sequencing was carried out on the ABI PRISM 377 DNA sequencer by the method of dideoxynucleotide sequencing. DNA and deduced amino acid sequence were compared with NCBI database.

RESULTS

Library construction and panning

The presence of V_H and V_L gene fragments obtained by RT-PCR was confirmed by electrophoresis, with their sizes being approximately 350 bp (Figure 1 A). The scFv genewas assembled successfully. Its size was about 750 bp (Figure 1B).

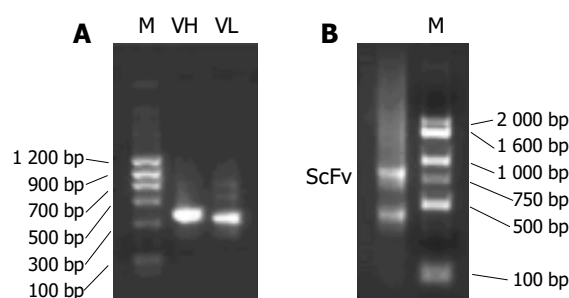


Figure 1 V_H and V_L and scFv fragments in 20 g/L agarose gel electrophoresis with staining of ethidium bromide (EB). (A) V_H and V_L fragments, (B) scFv fragment, M: DGL 2 000 marker.

After the scFv gene repertoires were transformed into *E. coli* TG1 cells, approximately 9×10^6 ampicillin-resistant clones grew. PCR and *SfiI/NotI* double digestion reactions showed the positive insert ratio was about 95% (19/20). Rescued by M13K07 helper phage, the recombinant phage antibody library (about 9×10^{11} cfu/mL) was constructed.

Four rounds of panning with Eca109 cells resulted in a 130-fold enrichment of tumor cell binding scFv-phage. After three rounds of subtractive panning with NHEEC cells, individual phage-displayed scFv fragments were tested for reactivity with Eca109 cells by cell ELISA. Of the 95 clones screened, 25 were positive. The highest A_{405} nm value was found in AD09 clone.

Expression and purification of soluble scFv

The soluble scFv was stably expressed in *E. coli* HB2151 transfected with AD09 positive phage clone. In pCANTAB 5E, the pel B signal peptide upstream from the scFv directed the expression to periplasmic compartment. The periplasmic extract of AD09 was run through anti-E tag antibody affinity chromatography column and soluble AD09 was eluted from the column as a single peak (data not shown). The expressed and purified AD09 was loaded on 120 g/L SDS-PAGE and analyzed by Western blot. This protein migrated with a molecular mass approximately 31 ku (Figure 2). The overall yield of soluble AD09 in *E. coli* flask culture was more than 0.55 mg/L. The purity was about 90%.

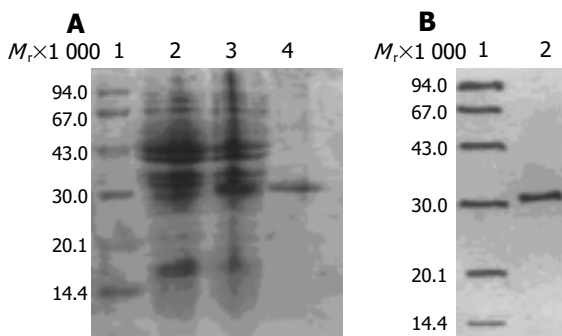


Figure 2 Expression and purification of AD09. A: SDS-PAGE. Lane 1: Markers (Amersham Pharmacia Biotech, Sweden). Lane 2: Product of *E. coli* HB2151 without scFv gene. Lane 3: Expression of AD09 in *E. coli* HB2151 with induction of IPTG. Lane 4: Purified AD09 protein. B: Western blot. Lane 1: Markers. Lane 2: Purified AD09 protein.

Determination of immunoreactivity of soluble scFv

The immunoreactivity of purified soluble AD09 was determined by ELISA. The result revealed that AD09 was highly specific and could bind to Eca109 cells, but not to HeLa and NHEEC cells (Table 2).

Table 2 Immunore activity of soluble scFv determined by ELISA

Sample	$A_{405\text{nm}}$ (mean \pm SD)		
	Eca109	HeLa	NHEEC
Soluble scFv	0.78 \pm 0.12	0.21 \pm 0.09 ^d	0.23 \pm 0.07 ^b
PBS	0.14 \pm 0.04	0.13 \pm 0.08	0.15 \pm 0.02

^d $P < 0.001$, ^b $P < 0.01$ vs Eca109 group.

Sequence analysis

Sequencing of six randomly selected antibodies from the positive clones was performed with an ABI PRISM 377 DNA sequencer using pCANTAB5 sequencing primer set (Amersham Pharmacia Biotech, Sweden). The sequence of AD09 clone is shown in

Figure 3. Compared using BLAST, both V_H and V_L had sequence similarities to the variable fragments of some known human antibodies. Alignment with the V_H and V_L sequences of Ig, blast analysis of immunoglobulin sequences showed that V_H was the γ chain subgroup IV of human immunoglobulin and V_L was the κ chain subgroup I of human immunoglobulin.

```

ATG CCA GCC GGC CAT GGC CGA GGT GCA GCT GGT GCA GTC TGC CCA GGA CTG
M P A G H G R G A A G A V C P G L
GTG AAG CCT TCG GAG ACC CTG TCC CTC ACC TGC ACT GTC TCT GGT GGC TCC
V K P S E T L S L T C T V S G G S
ATC AGT AGT TAC TAC TGG AGC TGG ATC CGG CAG CCC CCA GGG AAG GGA CTG
I S S Y Y W S W I R Q P P G K G L
                                CDR1
GAG TGG ATT GGG TAT ATC TAC AGT GGG AGC ACC AAC TAC AAC CCC TCC
E W I G Y I Y Y S G S T N Y N P S
                                CDR2
CTC AAG AGT CGA GTC ACC ATA TCA GTA GAC ACG TCC AAG AAC CAG TTC TCC
L K S R V T I S V D T S K N Q F S
CTG AAG CTG AGC TCT GTG ACC GCT GCG GAC ACG GCC GTG TAT TAC TGT GCG
L K L S S V T A A D T A V Y C A
AGA GAG CGT GCC GAG ATG GCT ACA ATC GGG GGT GCT TTT GAT ATC TGG GCG
R E R A E M A T I G G A F D I W G
                                CDR3
CAA GGG ACC ACG GTC ACC GTC TCC TCA GGT GGA GGC GGT TCA GGC GGA GGT
Q G T T V T V S S G G G G S G G G
                                Linker
GGC TCT GGC GGT GGC GGA TCG GAC ATC CTG ATG ACC CAG TCT CCA TCC TCC
G S G G G G S D I L M T Q S P S S
CTG TCT GCA TCT GTA GGA GAC AGA GTC ACC ATC ACT TGC CGG GCA AGT CAG
L S A S V G D R V T I T C R A S Q
AGC ATT AGC AGC TAT TTA AAT TGG TAT CAG CAG AAA CCA GGG AAA GCC CCT
S I S S Y L N W Y Q Q K P G K A P
                                CDR1
AAG CTC CTG ATC TAT GCT GCA TCC AGT TTG CAA AGT GGG GTC CCA TCA AGG
K L L I Y A A S S L Q S G V P S R
                                CDR2
TTC AGT GGC AGT GGA TCT GGG ACA GAT TTC ACT CTC ACC ATC AGC AGT CTG
F S G S G S G T D F T L T I S S L
CAA CCT GAA GAT TTT GCA ACT TAC TAC TGT CAA CAG AGT TAC AGT ACC CTG
Q P E D F A T Y Y C Q Q S Y S T L
                                CDR3
TAC ACT TTT GGC CAG GGG ACC A AG CTG GAT ATC AAA CGT GCG GCC GCA
Y T F G Q G T K L D I K R A A A

```

Figure 3 Sequence of AD09 gene.

DISCUSSION

The discovery of hybridoma technology by Kohler and Milstein in 1975^[6] has heralded a new era in antibody research and clinical development. However, until recently, there were few antibody-based products suitable for clinical trial. This delay can be largely explained by the fact that murine antibodies could trigger a human anti-mouse antibody response^[7-9]. Human monoclonal antibodies seldom triggered a harmful immune response and have been used in cancer immunotherapy^[10]. However, there are many difficulties in making human monoclonal antibodies by hybridoma technology. Phage display antibody library technique provides a powerful tool to produce human antibody. In this study, we selected a human single chain antibody against esophageal cancer from a phage displayed antibody library. It confirmed that this technique was feasible.

Since scFv could penetrate faster and deeper in solid tumors, scFv format of monoclonal antibody was selected. ScFv is a small antigen-binding antibody fragment consisting of V_H and V_L joined together by a flexible peptide linker. The main advantage of scFv over intact whole IgG or Fabs was its small size (one sixth of intact IgG), making it penetrate a solid tumor mass more rapidly and evenly^[11,12]. In addition, the lack of constant regions decreased retention by Fc receptors found in most tissues and organs, which further reduced the side effects^[13,14]. These characteristics rendered scFv an ideal vector for delivery of

agents such as radionuclide, enzyme, drugs or toxin *in vivo*^[14,15].

Normally, peripheral blood lymphocytes were the main source for the construction of antibody libraries^[16]. However, it was inconvenient to isolate at least 200 mL of peripheral blood to obtain 10^7 B-lymphocytes for constructing a large antibody library^[3]. There are thousands of B cells in metastatic peritumor lymph nodes which may be preimmunized by tumor-associated antigens in esophageal cancer patients. The preimmunized B cells are sufficient to construct a library, and can be directly used for screening recombinant antibodies, since the heavy and light chain genes have been rearranged and ligated to specific targets of tumor antigens. Therefore, it has become a better source of B cells for human antibody library construction^[17].

Recombinant antibodies in phage antibody library could be best captured with purified tumor antigens^[18]. Unfortunately, esophageal cancer associated specific antigens have not yet been identified. Human esophageal cancer cell line, Eca109 could express human esophageal cancer-associated specific antigens^[19]. In addition, live cells could facilitate the identification of antibodies better than fixed cells^[5,20] since the antibodies bound to native rather than denatured antigens. Moreover, using live cancer cells to screen phage antibody library was a feasible method^[20,21]. So we used live Eca109 as antigens to screen the phage antibody library, and live NHEEC cell line was used for subtractive panning to obviate the cross-reaction with normal human esophageal epithelial cells. This was done to facilitate subsequent expression cloning of corresponding antigens, as well as to enhance the therapeutic potential of the antibodies obtained.

Generation of large repertoires of scFv genes is a crucial step during phage antibody display. To construct a large scFv gene repertoire, a number of methods were used. (1) Multiple primers covering most of the immunoglobulin heavy and light chain variable genes were used. (2) To optimize the diversity and efficiency of ligation, linker sequences were designed in PCR assembly primers. These made the linker easily synthesized and increased the diversity of scFv genes. (3) Electroporation transformation was used to obtain an efficiency of 10^9 cfu/ug for pUC18 and 3×10^7 cfu/ug for ligation products. (4) The quality of mRNA appeared essential in the PCR amplification step and in subsequent construction of the library. To preserve intact mRNA, DEPC and RNase inhibitor were used during total RNA extraction and cDNA synthesis.

To further identify the bioactivity of scFv, soluble scFv protein was expressed in *E. coli* HB2151 induced by IPTG. SDS-PAGE and Western blot showed that the molecular mass was about 31 ku, which was consistent with the theoretically predicted product. The soluble expression level of scFv in *E. coli* HB2151 was still low, but it was sufficient for bioactivity detection. Cell ELISA assays showed that the soluble scFv had esophageal cancer associated antigen-binding activity. Whether this scFv shows affinity and specificity for tissue *in vivo* remains to be determined. Finally, DNA sequencing determined that scFv had common characteristics shared by other known scFvs^[3].

Our study demonstrated that specific human antibodies against tumor-associated antigens could be selected from a phage library constructed from the metastatic lymph nodes of esophageal cancer patients. The approach did not depend on immunization procedures. Since the antibody is entirely of human origin, it is expected to be much less immunogenic than murine antibodies and more efficient in targeting tumor cell surface. It may also be used as research reagents or a starting point for the development of therapeutic antibodies.

REFERENCES

- 1 **Souriau C**, Hudson PJ. Recombinant antibodies for cancer diagnosis and therapy. *Expert Opin Biol Ther* 2003; **3**: 305-318
- 2 **Trikha M**, Yan L, Nakada MT. Monoclonal antibodies as therapeutics in oncology. *Curr Opin Biotechnol* 2002; **13**: 609-614
- 3 **He J**, Zhou G, Liu KD, Qin XY. Construction and preliminary screening of a human phage single-chain antibody library associated with gastric cancer. *J Surg Res* 2002; **102**: 150-155
- 4 **Marks JD**, Hoogenboom HR, Bonnert TP, McCafferty J, Griffiths AD, Winter G. By-passing immunization human antibodies from V-gene libraries displayed on phage. *J Mol Biol* 1991; **222**: 581-597
- 5 **Cai XH**, Garen A. Anti-melanoma antibodies from melanoma patients immunized with genetically modified autologous tumor cells: Selection of specific antibodies from single-chain Fv fusion phage libraries. *Proc Natl Acad Sci U S A* 1995; **92**: 6537-6541
- 6 **Kohler G**, Milstein C. Continuous cultures of fused cells secreting antibody of predefined specificity. 1975. *Biotechnology* 1992; **24**: 524-526
- 7 **Isaacs JD**. The antiglobulin response to therapeutic antibodies. *Semin Immunol* 1990; **2**: 449-456
- 8 **Berkower I**. The promise and pitfalls of monoclonal antibody therapeutics. *Curr Opin Biotechnol* 1996; **7**: 622-628
- 9 **Frodin JE**, Lefvert AK, Mellstedt H. The clinical significance of HAMA in patients treated with mouse monoclonal antibodies. *Cell Biophys* 1992; **21**: 153-165
- 10 **Nilsson F**, Tarli L, Viti F, Neri D. The use of phage display for the development of tumour targeting agents. *Adv Drug Deliv Rev* 2000; **43**: 165-196
- 11 **Verhaar MJ**, Chester KA, Keep PA, Robson L, Pedley RB, Boden JA, Hawkins RE, Begent RH. A single chain Fv derived from a filamentous phage library has distinct tumor targeting advantages over derived from a hybridoma. *Int J Cancer* 1995; **61**: 497-501
- 12 **Mao SL**, Gao CS, Lo CHL, Wirsching P, Wong CH, Janda KD. Phage-display library selection of high-affinity human single-chain antibodies to tumor-associated carbohydrate antigens sialyl Lewis^x and Lewis^x. *Proc Natl Acad Sci U S A* 1999; **96**: 6953-6958
- 13 **Yamaguchi A**, Ding K, Maehara M, Goi T, Nakagawara G. Expression of nm23-H1, gene and Sialyl Lewis X antigen in breast cancer. *Oncology* 1998; **55**: 357-362
- 14 **Clark M**. Antibody humanization: a case of the 'Emperor's new clothes? *Immunol Today* 2000; **21**: 397-402
- 15 **Kim DJ**, Chung JH, Ryu YS, Rhim JH, Kim CW, Suh Y, Chung HK. Production and characterisation of a recombinant scFv reactive with human gastrointestinal carcinomas. *Br J Cancer* 2002; **87**: 405-413
- 16 **Hoogenboom HR**, Winter G. By-passing immunisation. Human antibodies from synthetic repertoires of germline VH gene segments rearranged *in vitro*. *J Mol Biol* 1992; **227**: 381-388
- 17 **Yip YL**, Hawkins NJ, Clark MA, Ward RL. Evaluation of different lymphoid tissue sources for the construction of human immunoglobulin gene libraries. *Immunotechnology* 1997; **3**: 195-203
- 18 **Poul MA**, Becerril B, Nielsen UB, Morisson P, Marks JD. Selection of tumor-specific internalizing human antibodies from phage libraries. *J Mol Biol* 2000; **301**: 1149-1161
- 19 **Hao MW**, Liang YR, Liu YF, Liu L, Wu MY, Yang HX. Transcription factor EGR-1 inhibits growth of hepatocellular carcinoma and esophageal carcinoma cells lines. *World J Gastroenterol* 2002; **8**: 203-207
- 20 **Ridgway JBB**, Ng E, Kern JA, Lee J, Brush J, Goddard A, Carter P. Identification of a human anti-CD55 single-chain Fv by subtractive panning of a phage library using tumor and nontumor cell lines. *Cancer Res* 1999; **59**: 2718-2723
- 21 **Kupsch JM**, Tidman NH, Kang NV, Truman H, Hamilton S, Patel N, Newton Bishop JA, Leigh IM, Crowe JS. Isolation of human tumor-specific antibodies by selection of an antibody phage library on melanoma cells. *Clin Cancer Res* 1999; **5**: 925-931

Pathobiological significance of vascular endothelial growth factor and Maspin expressions in human gastric carcinoma

Jian-Jun Li, Ying Chen, Su-Min Zhang, Dong-Ying Wu, Yan-Ping Wang, Yan Xin

Jian-Jun Li, Su-Min Zhang, Dong-Ying Wu, Yan-Ping Wang, Yan Xin, No.4 Laboratory, Cancer Institute, The First Affiliated Hospital, China Medical University, Shenyang 110001, Liaoning Province, China

Ying Chen, Shenyang Gynecology and Obstetrics Hospital, Shenyang 110014, Liaoning Province, China

Supported by the National Natural Science Foundation of China, No. 39370772, No.30070845

Correspondence to: Professor Xin Yan, No.4 Laboratory, Cancer Institute, The First Affiliated Hospital, China Medical University, Shenyang 110001, China. lijianjun@cmrt.com

Telephone: +86-24-23256666 Ext. 6351

Received: 2003-10-27 **Accepted:** 2003-12-16

Abstract

AIM: To investigate the correlation between expression of vascular endothelial growth factor (VEGF) and cell differentiation, invasion, metastasis and Maspin expression in gastric carcinoma.

METHODS: Formalin-fixed paraffin-embedded tissue specimens from 73 cases of gastric carcinoma were studied with SP immunohistochemistry, using anti-VEGF monoclonal antibody, and thirty-nine of them were studied using anti-Maspin monoclonal antibody. VEGF expression was compared with the clinical stage, lymph node metastasis, and Borrmann's and WHO's classification of gastric carcinoma.

RESULTS: The positive rate of VEGF expression was significantly higher in adjacent non-carcinoma epithelia (ANCE) than in non-metaplastic, non-carcinoma gastric epithelia (NMNCE), which were at least 4 cm distant from the primary tumor ($P = 0.000$, $\chi^2 = 73.03$). The positive rate of VEGF expression was significantly higher in advanced gastric carcinoma (AGC) than in early gastric carcinoma (EGC) ($P = 0.032$, $\chi^2 = 4.62$). The positive rate of VEGF expression in gastric carcinomas with lymph node metastases was significantly higher than that in those without metastasis ($P = 0.006$, $\chi^2 = 7.47$). Maspin was weakly expressed in 16 out of 39 cases of NMNCE, and the positive immunoreaction was limited to gland cells of the stomach body. There was no significant correlation between the expression of VEGF and histological or gross classifications, and correlation between the expressions of VEGF and Maspin in gastric carcinoma ($P = 0.648$, $\chi^2 = 0.21$).

CONCLUSION: Expression of VEGF is significantly correlated to the malignant biological behaviors of gastric carcinoma, but there is no significant correlation between the expression of VEGF and Maspin.

Li JJ, Chen Y, Zhang SM, Wu DY, Wang YP, Xin Y. Pathobiological significance of vascular endothelial growth factor and Maspin expressions in human gastric carcinoma. *World J Gastroenterol* 2004; 10(18): 2624-2627

<http://www.wjgnet.com/1007-9327/10/2624.asp>

INTRODUCTION

Tumor angiogenesis is one of the most important biological features. It has been shown that tumor angiogenesis plays an important role in its growth, invasion, metastasis and recurrence^[1-3]. Among the factors contributing to angiogenesis, VEGF is recognized as one of the most important molecules in the formation of new blood vessels. There is clinical and experimental evidence that VEGF plays a role in the progression of solid tumors, and its clinical significance in solid tumors has been demonstrated both immunohistochemically and quantitatively^[4]. Many studies demonstrated that over-expression of VEGF participated the growth and metastasis of malignant tumors depended on angiogenesis^[2,5]. VEGF increased the incidence rate of tumor metastasis by inducing tumor angiogenesis^[5]. Some studies demonstrated that the level of VEGF expression was of prognostic value in predicting metastasis of various malignant solid tumors and the level of VEGF expression correlated with tumor progression in human brain cancers and experimental tumor models^[6,7]. Hence, most studies in the field have focused on the regulation and inhibition of angiogenesis. The tumor suppressor gene Maspin, a unique member of the serpin super family, could inhibit cell motility, invasion, and metastasis in some cancers^[8-10]. Although at present the molecular and biological mechanisms of the function of Maspin remain unknown, there is evidence that Maspin interacts with the p53 tumor suppressor pathway and may function as an inhibitor of angiogenesis *in vitro* and *in vivo*^[11]. Pemberton *et al.*^[12] demonstrated the presence of Maspin in epithelia of several normal human organs (such as prostate, thymus, testis, small intestine, and colon). We are interested whether the tumor suppression function of Maspin in mammary or pancreatic carcinoma can be also detected in gastric carcinoma.

In this study, VEGF expression was immunohistochemically investigated in non-metaplastic, non-carcinoma gastric epithelia (NMNCE), which were at least 4 cm distant from the primary tumor, adjacent non-carcinoma epithelia (ANCE) and gastric carcinoma, and compared with the pathobiological behaviors of gastric carcinoma in order to clarify the clinical and pathobiological significance of the expression of VEGF. The relationship between the expressions of VEGF and Maspin was also explored.

MATERIALS AND METHODS

Tissue specimens

Seventy-three surgically removed specimens of gastric carcinoma were collected from Cancer Institute, China Medical University. The age of patients ranged from 32 to 80 years, mean age was 55.2 years; Forty-eight were males and 25 females. Carcinomas were staged according to pathological characteristics including depth of tumor invasion, tumor location, Borrmann's classification, and status of lymph node metastasis. According to clinical staging, 24 cases were in early stage (early gastric carcinoma, EGC), 49 cases in advanced stage (advanced gastric carcinoma, AGC). According to metastasis status, 40 cases had lymph node metastasis, of them 1 had ovary metastasis, 1 had liver metastasis (without lymph node metastasis), and 32 had not any metastasis. Seventy-three cases of gastric carcinoma were

studied with SP immunohistochemistry, using anti-VEGF monoclonal antibody, and thirty-nine of them were studied using anti-Maspin monoclonal antibody. Each specimen was classified according to the Borrmann's classification and WHO's histological classification criteria.

Immunohistochemistry

All specimens were fixed in 40 g/L formaldehyde solution and embedded in paraffin. Five μ m Sections were cut and mounted onto glass slides. Mouse anti-human monoclonal antibody against VEGF (ready to use) was from Maixin Biotech (Fuzhou, China) and mouse anti-human monoclonal antibody against Maspin was from Novo Castro (Newcastle, England). Immunohistochemical staining was performed using SP method. For control, sections were proceeded with PBS (0.01 mol/L, pH 7.4) instead of the primary antibodies. Counterstaining was performed with haematoxylin.

Evaluation of VEGF and Maspin expression

Clearly brown staining restricted to cytoplasm was considered as positive reaction for VEGF or Maspin. Two experienced pathologists assessed the positive rate according to the percent of positive cells in counted cells from 5 randomly selected representative fields. To evaluate the expression of VEGF and Maspin, immunostaining was classified into two groups, corresponding to the percentage of immunoreactive cells. The cut-off point to distinguish negative from positive VEGF or Maspin expression was 20% of positive cells.

Statistical analysis

Statistical evaluation was performed by χ^2 -test to differentiate the rates between two groups. $P < 0.05$ was considered statistically significant.

RESULTS

None of NMNCE expressed VEGF. VEGF expression was significantly higher in ANCE than in NMNCE ($P = 0.000$, $\chi^2 = 73.03$) (Table 1). Immunohistochemically, VEGF expression was significantly higher in AGC than in EGC ($P = 0.032$, $\chi^2 = 4.62$). There was no correlation between expression of VEGF and histology typing or gross typing (Table 2). VEGF expression in gastric carcinoma with lymph node metastases was significantly higher than that in those without metastasis ($P = 0.006$, $\chi^2 = 7.47$) (Table 3). Sixteen (41.0%) out of thirty-nine cases of NMNCE showed a weak Maspin expression that was limited to gland cells of the stomach body, while all gastric normal epithelia with intestinal metaplasia (GNEIM) strongly expressed Maspin (14/14) (Table 4). The positive rate of Maspin was 53.6% (15/28) in specimens of positive VEGF expression, whereas the positive rate of Maspin was 45.5% (5/11) in specimens of negative VEGF expression (Table 5). There was no significant correlation between the expressions of VEGF and Maspin in gastric carcinoma ($P = 0.648$, $\chi^2 = 0.21$) (Table 5).

Table 1 VEGF expression in NMNCE, ANCE and gastric carcinoma ($n = 73$)

Tissue origin	n	VEGF expression		Positive rate (%)
		-	+	
NMNCE	73	73	0	-
ANCE	73	23	50	68.5 ^b
Gastric carcinoma	73	14	59	80.8 ¹

^b $P = 0.000$ vs NMNCE (Yates corrected: $\chi^2 = 73.03$), ¹ $P = 0.086$ vs ANCE (Yates corrected: $\chi^2 = 2.93$).

Table 2 Relationship between VEGF expression and gross and histological types of gastric carcinoma ($n = 73$)

Type	n	VEGF expression		Positive rate (%)
		-	+	
Gross types				
EGC ^a	24	8	16	66.7
I	4	0	4	100.0
II	12	6	6	50.0
III	7	2	5	71.4
SS ¹	1	0	1	100.0
AGC	49	6	43	87.8
Bor. 0	3	0	3	100.0
Bor. I	1	0	1	100.0
Bor. II	6	0	6	100.0
Bor. III	36	5	31	86.1
Bor. IV	3	1	2	66.7
Histological type				
Papillary adenocarcinoma	8	1	7	87.5
Well-differentiated adenocarcinoma	3	2	1	33.3
Moderately-differentiated adenocarcinoma	11	3	8	72.7
Poorly-differentiated adenocarcinoma	30	5	25	83.3
Undifferentiated carcinoma	3	1	2	66.7
Signet-ring cell carcinoma	10	1	9	90.0
Mucinous adenocarcinoma	7	0	7	100.0
Carcinoid	1	1	0	-

^a $P = 0.032$ vs AGC ($\chi^2 = 4.62$), There was no correlation between the expression of VEGF and histology typing or gross typing ($P > 0.05$).

¹EGC SS (early gastric carcinomas of superficial spreading type).

Table 4 VEGF and Maspin expressions in NMNCE, GNEIM and gastric carcinoma

Histological type	n	VEGF			Maspin		
		+	-	+ %	+	-	+ %
NMNCE	39	0	39	0	16 ^a	23	41.0
GNEIM	14	-	-	-	14	0	100.0
Gastric carcinoma							
Papillary adenocarcinoma	3	3	0	100.0	2	1	66.7
Well-differentiated adenocarcinoma	3	2	1	66.7	2	1	66.7
Moderately-differentiated adenocarcinoma	6	5	1	83.3	2	4	33.3
Poorly-differentiated adenocarcinoma	21	14	7	66.7	11	10	52.4
Undifferentiated adenocarcinoma	3	2	1	66.7	1	2	33.3
Signet ring-cell carcinoma	3	2	1	66.7	2	1	66.7
Total of gastric carcinoma	39	28	11	71.8	20	19	51.3

Maspin was weakly expressed in gland cells of the stomach body, while it was not expressed in superficial epithelial cells and pyloric gland of the stomach.

Table 3 Relationship between VEGF expression and metastasis of gastric carcinoma (n = 73)

Metastasis status	n	VEGF expression		Positive rate (%)
		-	+	
No metastasis	32	12	20	62.5 ^b
Lymph node metastasis	39	4	35	89.7
Liver metastasis	1	1	0	0
Ovary metastasis	1	0	1	100.0

^bP = 0.006 vs lymph node metastasis ($\chi^2 = 7.47$).

Table 5 Relationship between VEGF and Maspin expressions in gastric carcinoma

Gastric carcinoma	Maspin +	Maspin -	Total
VEGF +	15	13	28
VEGF -	5	6	11
Total	20	19	39

There was no significant correlation between the expression of VEGF and Maspin in gastric carcinoma ($P = 0.648$, $\chi^2 = 0.21$).

DISCUSSION

Ferrara^[13] and his colleagues found that bovine pituitary follicular cells secreted a novel heparin-binding growth factor specific for vascular endothelial cells in 1989 and named it VEGF. VEGF is known to be a highly specific mitogen for endothelial cells which is almost specifically expressed in endothelial cells. VEGF might act as an autocrine and paracrine growth factor to induce the proliferation of tumor cells as well as tumor angiogenesis of tumor cells^[14].

Tumors require blood vessels for nutrient and oxygen supply to maintain their viability. In the first stage of growth, cloning proliferative phase does not need angiogenesis. To continue tumor expansion, additional blood supply was prerequisite, which was significantly correlated to tumor invasion, metastasis and recurrence^[15-18]. It has been widely accepted that tumor angiogenesis was one of the most crucial steps in tumor invasion and metastasis. There was a close relationship between VEGF expression and depth of invasion, lymph node metastasis and five-year survival rate of patients, which was an independent prognostic factor. Our study showed that there was no significant relationship between VEGF expression and histological or gross types of gastric carcinomas.

Yonemura further demonstrated the correlation between VEGF-C expression and lymphatic invasion or lymph node

metastasis^[19]. Tumors with high expression of VEGF-C had more remote lymph node involvement than those with low VEGF-C expression^[7,19,20]. These results strongly suggested that cancer cells producing VEGF-C might induce proliferation and dilation of lymphatic vessels, resulting in the development of invasion of cancer cells into lymphatic vessels and lymph nodes. These results were consistent with recent reports that showed a positive correlation of VEGF-C levels with lymph node metastasis in gastric carcinoma.

A number of observations and animal trials have spurred extensive investigations of VEGF inhibitors as possible therapies for cancer. In tumor cell lines VEGF was an autocrine growth factor, so that inhibitors of VEGF or VEGF receptors (VEGFR) compromised the viability of tumor cells. Lastly, inhibition of VEGF or VEGFR signaling would inhibit both tumor angiogenesis and tumor cell growth and viability when there was evidence that VEGFR was expression in tumor cells^[21,22].

Our study showed that VEGF was positively expressed in 76.7% of gastric carcinomas, which was significantly higher than that in NMNCE. The result indicated that VEGF was up-regulated and there might exist an autocrine mechanism of VEGF in gastric carcinoma. VEGF could promote tumor growth and metastasis by both direct and indirect pathways^[23].

Maspin, a member of the serpin family of protease inhibitors, is expressed in normal human mammary and prostate epithelial cells, and down-regulated during cancer progression. Biological studies demonstrated a tumor-suppressive role of Maspin, acting at the levels of tumor invasion and metastasis^[8,12]. Maass^[24] did not detect Maspin expression in any of 6 gastric cancer cells. Son^[25] studied Maspin expression in 30 cases of human gastric adenocarcinoma using immunohistochemistry and reverse transcripted-polymerase chain reaction. Twenty-seven cases (90%) of gastric adenocarcinoma, regardless of histological type, and all cases of GNEIM showed diffuse and strong immunoreactivity to Maspin. Eighteen of 26 cases (69.2%) of NMNCE showed weak and focal immunoreactivity. The level of Maspin expression was higher in GNEIM and lower in NMNCE than in adenocarcinoma cases. Akiyama^[26] examined Maspin expression and/or allele-specific methylation status in four gastric cancer cell lines, as well as normal, metaplastic, and carcinoma epithelia obtained from 50 gastric cancer patients. Three gastric cancer cell lines exhibiting Maspin overexpression showed hypomethylation on both alleles or a haploid allele. Dense and diffuse immunoreactivity to Maspin was observed in 40 (80%) of 50 gastric carcinomas and all GNEIM, but not in GNE without IM. Maspin gene promoter region of all GNE without IM was hypermethylated on both alleles whereas those with IM frequently represented the haploid type of hypomethylation

status. Maspin mRNA was amplified from GNEIM and cancerous crypts but not from GNE without IM. These results suggested that demethylation at the Maspin gene promoter disrupted the cell-type-specific gene repression in both GNE and gastric cancer. In our study, 41.0% (16/39) of NMNCE showed a weak Maspin expression that was limited to gland cells of the stomach body, and 51.3% (20/39) of gastric carcinomas expressed Maspin. The positive rate of Maspin expression in NMNCE and in gastric carcinoma in our study was significantly lower than that in Son and Akiyama's study. We considered that the cut-off point made the different results. The reason why all GNEIM showed immunoreactivity to Maspin in all studies should be studied further. In addition, the role of Maspin gene and its encoding protein in tumorigenesis and progression of gastric cancer need to be investigated further.

In our study, Maspin and VEGF showed no correlation in gastric carcinomas. The precise roles of VEGF and Maspin in cancer tumorigenesis, invasion, and metastasis should be studied further. The relationship between expression of VEGF and Maspin in gastric cancer needs to be proved by amplifying samples.

REFERENCES

- 1 **Tao H**, Lin Y, Yin H, Wang R. Prognostic value of tumor vascularity in gastric carcinoma. *Zhonghua Waikē Zazhi* 1998; **36**: 307-309
- 2 **Che X**, Hokita S, Natsugoe S, Tanabe G, Baba M, Takao S, Aikou T. Tumor angiogenesis related to growth pattern and lymph node metastasis in early gastric cancer. *Chin Med J* 1998; **111**: 1090-1093
- 3 **Yoshikawa T**, Yanoma S, Tsuburaya A, Kobayashi O, Sairenji M, Motohashi H, Noguchi Y. Angiogenesis inhibitor, TNP-470, suppresses growth of peritoneal disseminating foci. *Hepato-gastroenterology* 2000; **47**: 298-302
- 4 **Konno H**, Ohta M, Baba M, Suzuki S, Nakamura S. The role of circulating IL-8 and VEGF protein in the progression of gastric cancer. *Cancer Sci* 2003; **94**: 735-740
- 5 **Kabashima A**, Maehara Y, Kakeji Y, Sugimachi K. Overexpression of vascular endothelial growth factor C is related to lymphogenous metastasis in early gastric carcinoma. *Oncology* 2001; **60**: 146-150
- 6 **Xu L**, Fukumura D, Jain RK. Acidic extracellular pH induces vascular endothelial growth factor (VEGF) in human glioblastoma cells via ERK1/2 MAPK signaling pathway: mechanism of low pH-induced VEGF. *J Biol Chem* 2002; **277**: 11368-11374
- 7 **Giatromanolaki A**, Koukourakis MI, Stathopoulos GP, Kapsoritakis A, Paspatis G, Kakolyris S, Sivridis E, Georgoulivas V, Harris AL, Gatter KC. Angiogenic interactions of vascular endothelial growth factor, of thymidine phosphorylase, and of p53 protein expression in locally advanced gastric cancer. *Oncol Res* 2000; **12**: 33-41
- 8 **McGowen R**, Biliran H Jr, Sager R, Sheng S. The surface of prostate carcinoma DU145 cells mediates the inhibition of urokinase-type plasminogen activator by Maspin. *Cancer Res* 2000; **60**: 4771-4778
- 9 **Liu T**, Pemberton PA, Robertson AD. Three-state unfolding and self-association of Maspin, a tumor-suppressing serpin. *J Biol Chem* 1999; **274**: 29628-29632
- 10 **Sheng S**, Truong B, Fredrickson D, Wu R, Pardee AB, Sager R. Tissue-type plasminogen activator is a target of the tumor suppressor gene maspin. *Proc Natl Acad Sci U S A* 1998; **95**: 499-504
- 11 **Zou Z**, Gao C, Nagaich AK, Connell T, Saito S, Moul JW, Seth P, Appella E, Srivastava S. p53 regulates the expression of the tumor suppressor gene maspin. *J Biol Chem* 2000; **275**: 6051-6054
- 12 **Pemberton PA**, Tipton AR, Pavloff N, Smith J, Erickson JR, Mouchabeck ZM, Kiefer MC. Maspin is an intracellular serpin that partitions into secretory vesicles and is present at the cell surface. *J Histochem Cytochem* 1997; **45**: 1697-1706
- 13 **Ferrara N**, Henzel WJ. Pituitary follicular cells secrete a novel heparin-binding growth factor specific for vascular endothelial cells. *Biochem Biophys Res Commun* 1989; **161**: 851-858
- 14 **Tian X**, Song S, Wu J, Meng L, Dong Z, Shou C. Vascular endothelial growth factor: acting as an autocrine growth factor for human gastric adenocarcinoma cell MGC803. *Biochem Biophys Res Commun* 2001; **286**: 505-512
- 15 **Yonemura Y**, Fushida S, Bando E, Kinoshita K, Miwa K, Endo Y, Sugiyama K, Partanen T, Yamamoto H, Sasaki T. Lymphangiogenesis and the vascular endothelial growth factor receptor (VEGFR)-3 in gastric cancer. *Eur J Cancer* 2001; **37**: 918-923
- 16 **Maehara Y**, Kabashima A, Koga T, Tokunaga E, Takeuchi H, Kakeji Y, Sugimachi K. Vascular invasion and potential for tumor angiogenesis and metastasis in gastric carcinoma. *Surgery* 2000; **128**: 408-416
- 17 **Shimoyama S**, Kaminishi M. Increased angiogenin expression in gastric cancer correlated with cancer progression. *J Cancer Res Clin Oncol* 2000; **126**: 468-474
- 18 **Landuyt W**, Ahmed B, Nuyts S, Theys J, Op de Beeck M, Rijnders A, Anne J, van Oosterom A, van den Bogaert W, Lambin P. *In vivo* antitumor effect of vascular targeting combined with either ionizing radiation or anti-angiogenesis treatment. *Int J Radiat Oncol Biol Phys* 2001; **49**: 443-450
- 19 **Yonemura Y**, Endo Y, Fujita H, Fushida S, Ninomiya I, Bandou E, Taniguchi K, Miwa K, Ohoyama S, Sugiyama K, Sasaki T. Role of vascular endothelial growth factor C expression in the development of lymph node metastasis in gastric cancer. *Clin Cancer Res* 1999; **5**: 1823-1829
- 20 **Ishikawa M**, Kitayama J, Kazama S, Nagawa H. Expression of vascular endothelial growth factor C and D (VEGF-C and -D) is an important risk factor for lymphatic metastasis in undifferentiated early gastric carcinoma. *Jpn J Clin Oncol* 2003; **33**: 21-27
- 21 **Masood R**, Cai J, Zheng T, Smith DL, Hinton DR, Gill PS. Vascular endothelial growth factor (VEGF) is an autocrine growth factor for VEGF receptor-positive human tumors. *Blood* 2001; **98**: 1904-1913
- 22 **Vajkoczy P**, Farhadi M, Gaumann A, Heidenreich R, Erber R, Wunder A, Tonn JC, Menger MD, Breier G. Microtumor growth initiates angiogenic sprouting with simultaneous expression of VEGF, VEGF receptor-2, and angiopoietin-2. *J Clin Invest* 2002; **109**: 777-785
- 23 **Zhang H**, Wu J, Meng L, Shou CC. Expression of vascular endothelial growth factor and its receptors KDR and Flt-1 in gastric cancer cells. *World J Gastroenterol* 2002; **8**: 994-998
- 24 **Maass N**, Hojo T, Ueding M, Luttgies J, Kloppel G, Jonat W, Nagasaki K. Expression of the tumor suppressor gene Maspin in human pancreatic cancers. *Clin Cancer Res* 2001; **7**: 812-817
- 25 **Son HJ**, Sohn TS, Song SY, Lee JH, Rhee JC. Maspin expression in human gastric adenocarcinoma. *Pathol Int* 2002; **52**: 508-513
- 26 **Akiyama Y**, Maesawa C, Ogasawara S, Terashima M, Masuda T. Cell-type-specific repression of the Maspin gene is disrupted frequently by demethylation at the promoter region in gastric intestinal metaplasia and cancer cells. *Am J Pathol* 2003; **163**: 1911-1919

Effects of mifepristone on proliferation of human gastric adenocarcinoma cell line SGC-7901 *in vitro*

Da-Qiang Li, Zhi-Biao Wang, Jin Bai, Jie Zhao, Yuan Wang, Kai Hu, Yong-Hong Du

Da-Qiang Li, Zhi-Biao Wang, Jin Bai, Jie Zhao, Yuan Wang, Kai Hu, Yong-Hong Du, State Key Laboratory of Ultrasound Engineering in Medicine, Chongqing Medical University, Chongqing 400016, China
Supported by the National Key Research Project Foundation of China, No. 96-905-02-01, and the National Natural Science Foundation of China, No. 39630340

Correspondence to: Dr. Zhi-Biao Wang, State Key Laboratory of Ultrasound Engineering in Medicine, Chongqing Medical University PO Box 153, Chongqing 400016, China. wangzhibiao@netease.com
Telephone: +86-23-68485022 **Fax:** +86-23-68485023
Received: 2003-08-06 **Accepted:** 2003-12-06

Abstract

AIM: To explore the effects of mifepristone, a progesterone receptor (PR) antagonist, on the proliferation of human gastric adenocarcinoma cell line SGC-7 901 *in vitro* and the possible mechanisms involved.

METHODS: *In situ* hybridization was used to detect the expression of PR mRNA in SGC-7 901 cells. After treatment with various concentrations of mifepristone (2.5, 5, 10, 20 $\mu\text{mol/L}$) at various time intervals, the ultrastructural changes, cell proliferation, cell-cycle phase distribution, and the expression of caspase-3 and Bcl-X_L were analyzed using transmission electron microscopy (TEM), tetrazolium blue (MTT) assay, ³H-TdR incorporation, flow cytometry, and reverse transcription-polymerase chain reaction (RT-PCR).

RESULTS: Mifepristone markedly induced apoptosis and inhibited cell proliferation of PR- positive SGC-7 901 cells revealed by TEM, MTT assay and ³H-TdR incorporation, in a dose- and time-dependent manner. The inhibitory rate was increased from 8.98% to 51.29%. Flow cytometric analysis showed mifepristone dose-dependently decreased cells in S and G₂/M phases, increased cells in G₀/G₁ phase, reduced the proliferative index from 57.75% to 22.83%. In addition, mifepristone up-regulated the expression of caspase-3, and down- regulated the Bcl-X_L expression, dose-dependently.

CONCLUSION: Mifepristone effectively inhibited the proliferation of PR-positive human gastric adenocarcinoma cell line SGC-7 901 *in vitro* through multiple mechanisms, and may be a beneficial agent against human adenocarcinoma.

Li DQ, Wang ZB, Bai J, Zhao J, Wang Y, Hu K, Du YH. Effects of mifepristone on proliferation of human gastric adenocarcinoma cell line SGC-7901 *in vitro*. *World J Gastroenterol* 2004; 10 (18): 2628-2631
<http://www.wjgnet.com/1007-9327/10/2628.asp>

INTRODUCTION

Gastric adenocarcinoma is the second most common cancer with the second highest mortality rate^[1,2]. Presently, there is still no effective treatment means for patients with advanced

gastric adenocarcinoma^[3,4]. Chemotherapy or radiation therapy has generally shown some clinical response but little survival advantage and is not tolerated in many patients^[5,6]. Therefore, there is a need to identify other therapeutic agents against the tumor.

Mifepristone is a progesterone receptor (PR) antagonist that has been widely used as the first- line drug for the termination of early pregnancy^[7]. Interestingly, recent studies have proved that mifepristone could effectively inhibit the proliferation of PR-positive breast cancer^[8-10], ovarian cancer^[11,12], endometrial cancer^[13], and prostate cancer^[14] cells without serious side effects and drug resistance. However, the effects of mifepristone on gastric adenocarcinoma are still unknown. Therefore, the present study was undertaken to explore the effects of mifepristone on the proliferation of human gastric adenocarcinoma cell line SGC-7 901 *in vitro*. Results showed that mifepristone effectively inhibited the proliferation of cultured SGC-7 901 cells *in vitro* through multiple mechanisms.

MATERIALS AND METHODS

Cell culture and treatment

Human gastric adenocarcinoma cell line SGC-7 901, obtained from Wuhan University Type Culture Collection (Wuhan, China), was routinely maintained in phenol red-free RPMI1640 (Gibco BRL, Grand Island, NY) containing 100 mL/L fetal bovine serum (Hyclone, Logan, UT), 10⁵ U/L penicillin and 100 mg/L streptomycin at 37 °C in a humidified atmosphere with 50 mL/L CO₂ in air. When cells were grown to approximately 50% confluence, medium was replaced with serum-free RPMI1640. After 24 h, fresh media containing 2.5, 5, 10, 20 $\mu\text{mol/L}$ mifepristone (Sigma Chemical Co., St Louis, MO) were added, respectively. Control cells were treated with the same volumes of vehicle (ethanol). Unless otherwise indicated, the cells were harvested after 96 h of incubation.

In situ hybridization analysis of PR

The expression of PR mRNA in SGC-7 901 cells was detected by *in situ* hybridization (ISH) using an ISH detection kit for PR (Boster, Wuhan, China) according to the manufacturer's instructions. Unless otherwise stated, all steps were performed at room temperature. Briefly, after 24 h of culture on the RNase-free slides, cells were washed 3 times with phosphate buffered saline (PBS, pH7.4), fixed with 40 g/L paraformaldehyde in PBS containing 0.1 g/L diethylpyrocarbonate (DEPC-water) for 30 min, washed 3 times with 0.01 mol/L PBS, and then incubated with 5 mL/L hydrogen peroxide in methanol for 30 min to block endogenous peroxidase activity. After being rinsed with 0.01 mol/L PBS, cells were digested with proteinase K (10 g/mL in 0.01 mol/L PBS) at 37 °C for 15 min. Further washes with 0.5 mol/L PBS were performed before pre-hybridization for 3 h at 37 °C in the pre-hybridization solutions in a humidified environment. Hybridization was then performed with digoxigenin-labeled cRNA antisense probe (5 g/mL) overnight at 37 °C in a moist chamber. Subsequently cells were washed for 10 min with 2 SSC (1 SSC = 150 mmol/L NaCl, 15 mmol/L sodium citrate, pH7.0), followed by 0.5 SSC for 15 min, and finally 0.2 SSC for

15 min. After treatment with blocking reagent for 30 min, cells were incubated with biotin-labeled mouse anti-digoxigenin antibody at 37 °C for 1 h, washed 4 times, for 5 min each time, with 0.5 mol/L PBS, and then treated with SABC solutions at 37 °C for 20 min. Then cells were washed 3 times, for 5 min each time, with 0.5 mol/L PBS, incubated with biotin-labeled peroxidase (POD) at 37 °C for 20 min, washed three times with 0.5 mol/L PBS. Finally, cells were visualized with 3,3'-diaminobenzidine (DAB), counterstained with hematoxylin, dehydrated, cleared, mounted with neutral gum, and examined under a microscope. Brown-yellow deposits indicated the sites of hybridization. PR-positive breast cancer tissues were used as positive control, and probes were replaced by PBS as negative control.

Ultrastructural analysis

Harvested cells were washed 3 times with PBS, fixed for 2 h with 2.5 g/L glutaraldehyde in PBS, and then post-fixed for 2 h at 4 °C with 1 g/L OsO₄ in PBS. Cells were dehydrated using gradually increasing concentrations of ethanol from 50% to 100%, and then embedded in Epon 812. The ultra-thin sections (60 nm) were stained with uranyl acetate and lead citrate prior to examination at 50 kV with a Hitachi 600 transmission electron microscope (Hitachi Corp., Tokyo, Japan).

MTT assay

SGC-7901 cells were seeded into 96-well plates at a density of 1×10⁵/mL in RPMI1640. After 96 h of incubation with various concentrations of mifepristone, cell proliferation was measured by MTT (Sigma) reduction assay as described previously^[15]. Absorbance at 570 nm (*A*_{570nm}) was assayed. The inhibitory rate (IR) of SGC-7901 cells was calculated according to the equation as following: IR (%) = (*A*_{570nm} in control group - *A*_{570nm} in mifepristone-treated group) / *A*_{570nm} in control group × 100%.

³H-thymidine (³H-TdR) incorporation

Cells were incubated at various time intervals without or with various concentrations of mifepristone, followed by treatment with 10 μCi ³H-TdR (Amersham, Arlington Heights, IL) for an additional 6 h. Then, cells were washed twice with 100 mL/L trichloroacetic acid by centrifugation and resuspension, and were continuously incubated for 30 min at 60 °C with 0.5 mL of NaOH (0.3 mol/L). Finally, the cell lysates were collected, and the radioactivity was measured by a liquid scintillation counter (Beckman LS1 801, USA).

Cell cycle analysis by flow cytometry

The harvested cells were fixed with 700 mL/L ethanol at -20 °C for 30 min, and then stained with propidium iodide (Sigma) for 30 min in the dark. The stained cells were analyzed in a FACS Calibur flow cytometer (Becton Dickinson Labware, Lincoln Park, NJ) with excitation wavelength of 488 nm. The resulting histograms were analyzed by program MODFIT for cell distribution in cell cycle phase. Proliferative index (PI) was calculated according to the formula: PI (%) = (S + G₂/M) / (G₀/G₁ + S + G₂/M) × 100%.

Measurement of caspase-3 activity

Total proteins were extracted from harvested cells as described previously^[16], and protein concentrations were determined using the Bio-Rad protein assay (Bio-Rad Laboratories, Hercules, CA). An equal amount of cellular protein from extract of each group was added to a final volume of 100 μL of reaction mixture containing 0.2 mmol/L of a colorimetric caspase-3 substrate, acetyl-Asp-Glu-Val-Asp-p-nitroaniline (Ac-DEVD-pNA; Calbiochem, San Diego, CA), followed by incubation at 30 °C for 10 min. Free p-nitroaniline (pNA) released upon enzymatic cleavage was detected at 405 nm using a microplate reader (Bio-Rad). Caspase-3 activity correlated with the concentration of free

pNA generated in the reaction. Purified caspase-3 (Calbiochem) was used as positive control, whereas caspase-3 inhibitor I (Ac-DEVD-CHO, Calbiochem) was used as negative control.

RT-PCR analysis for Bcl-X_L

Total RNA was extracted from the cells using TRIzol reagent (Gibco BRL) according to the manufacturer's protocol. Two milligrams of total RNA were used for reverse transcription in a total volume of 20 μL with the SuperScript preamplification system (Promega, Madison, MI). Aliquots of 2 μL cDNA were subsequently amplified in a total volume of 50 μL using the GeneAmp PCR kit (Promega) following conditions recommended by the manufacturer. The sense and antisense primers for Bcl-X_L were 5'-AGGCAGGCGATGAGTTTGAAC-3' and 5'-GAACCACACCAGCCACA GTCA-3', respectively. The sense and antisense primers for -actin used as an internal control were 5'-ATCTGGCACCACACCTTCTACAATGAGCTGCG-3' and 5'-CGTCA TACTCCTGCTTGCTGATCCACATCTGC-3', respectively. The cycling conditions were 94 °C for 2 min, followed by 30 cycles of 92 °C for 30 s, at 62 °C for 30 s, and at 72 °C for 1 min and a final extension of 72 °C for 5 min. PCR products were separated on the 15 g/L agarose gel stained with ethidium bromide (EB) and viewed under ultraviolet light.

Statistical analysis

Data were expressed as mean ± SD. Statistical analysis was performed using the Student's *t* test and the chi-square test. *P* < 0.05 was considered statistically significant.

RESULTS

Expression of PR mRNA

In situ hybridization analysis showed that PR mRNA was highly expressed in the cultured SGC-7901 cells, which was mainly localized in the cytoplasm of the cells (Figure 1).

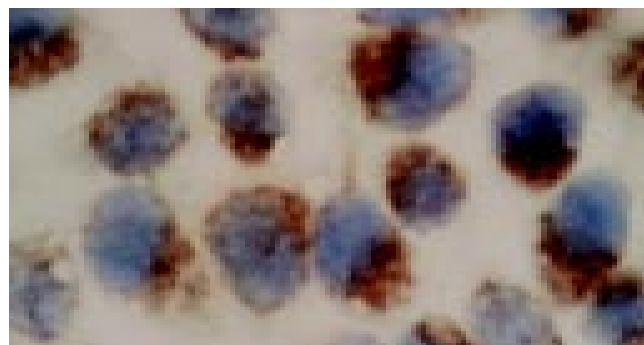


Figure 1 *In situ* hybridization (ISH) analysis of progesterone receptor (PR) expression in human gastric adenocarcinoma cell line SGC7901 (ISH, ×1000).

Morphological changes

To assess the effect of mifepristone on the ultrastructural changes of SGC-7901 cells, transmission electron microscopic analysis was performed. Results revealed that mifepristone dose-dependently induced apoptosis, which was especially remarkable at the 20 μmol/L concentration (Figure 2B). However, the irregular and enlarged nuclear, multiple nucleoli and increased nucleus-to-cytoplasm ratio were clearly seen in the cells of control group (Figure 2A).

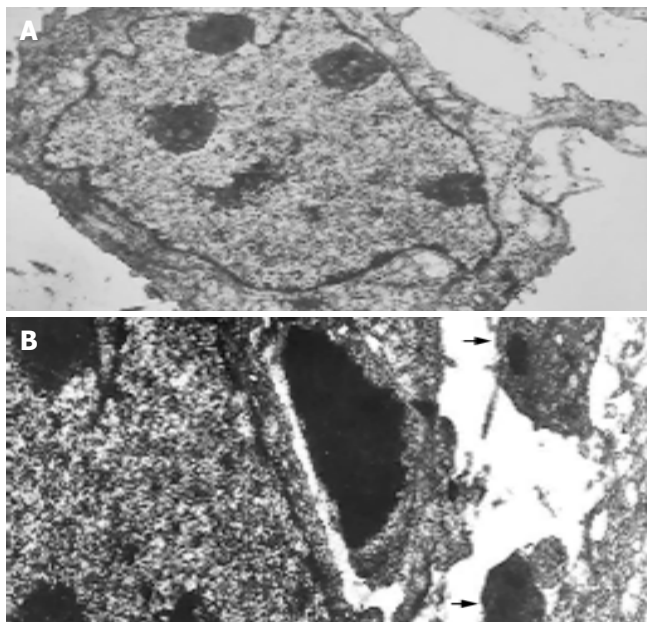
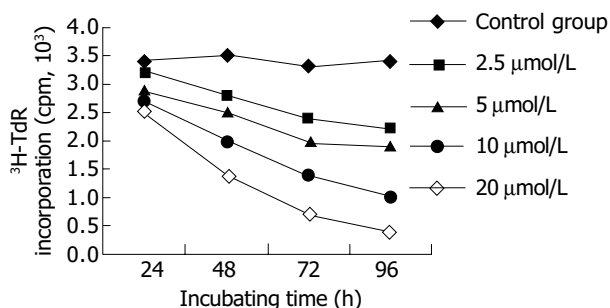
MTT assay and ³H-TdR incorporation

After 96 h of incubation with 2.5, 5, 10, 20 μmol/L mifepristone, MTT assay revealed *A*_{570nm} was markedly decreased in a dose-dependent manner, and the inhibitory rate (IR) of SGC-7901

Table 1 Effects of mifepristone on cell proliferation, cell-cycle phase distribution and caspase-3 activity of SGC7 901 cells *in vitro* (mean±SD)

Concentration (μmol/L)	A_{570nm} (MTT)	Cell cycle phase distribution (%)			Caspase-3 activity (U)
		G ₀ /G ₁	S	G ₂ /M	
0	1.125±0.048	42.25±4.20	35.68±3.98	22.07±3.01	1.28±0.28
2.5	1.024±0.030	49.47±5.68	30.82±4.36	19.71±2.41	2.79±0.36
5	0.896±0.035	52.23±6.22	28.68±3.64	19.01±1.36	5.04±0.29
10	0.678±0.026	65.80±5.63	25.93±3.01	8.27±1.10	9.46±0.20
20	0.548±0.031	77.16±8.25	15.54±2.54	7.29±0.82	15.23±0.41

cells by mifepristone was 8.98%, 20.36%, 39.73% and 51.29%, respectively (Table 1). Figure 3 shows that ³H-TdR incorporation into DNA of SGC-7 901 cells was significantly decreased in a dose- and time-dependent manner.

**Figure 2** Transmission electron microscopic photographs of the SGC7901 cells cultured for 96 h in the absence(A) or the presence of 20 μmol/L mifepristone (B) *in vitro* (TEM, ×2000). Arrows indicate apoptotic bodies which were formed in the cells of mifepristone-treated group.**Figure 3** Effect of various concentrations of mifepristone on the ³H-TdR incorporation of SGC7 901 cells at various time intervals *in vitro*.

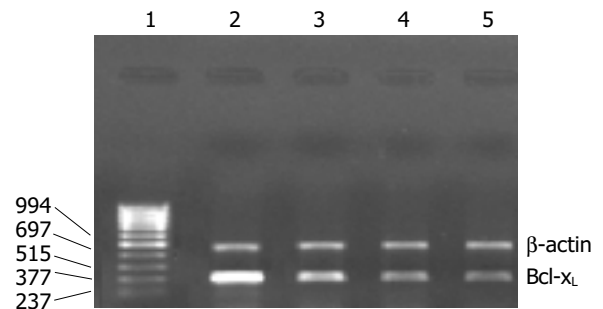
Cell-cycle phase distribution

The effect of mifepristone on the cell-cycle phase distribution of SGC-7 901 cells was determined by flow cytometry. After treatment with mifepristone, there was a strong dose-dependent decrease in the percentage of S- and G₂/M-phase cells, and with a concomitant increase in the percentage of cells in the

G₀/G₁ phases of the cell cycle (Table 1). Additionally, there is a significant decrease in the proliferative index (PI) of the mifepristone-treated cells (50.53%, 47.69%, 34.20% and 22.83%) as compared with control group (57.75%, $P<0.01$).

Expression of caspase-3 and Bcl-X_L

As shown in Table 1, mifepristone significantly up-regulated the activity of caspase-3 as compared with that in control group. Figure 4 shows the results of RT-PCR analysis for Bcl-x_L mRNA expression. Results indicated that mifepristone dose-dependently inhibited the expression of Bcl-X_L in the SGC-7 901 cells.

**Figure 4** RT-PCR analysis of Bcl-X_L mRNA expression in the SGC7 901 cells cultured for 96 h in the absence or the presence of various concentrations of mifepristone *in vitro*. Lanes 1-5: Marker (bp), contro l, 5, 10, 20 μmol/L mifepristone, respectively.

DISCUSSION

Accumulating evidence demonstrates that PR level is closely associated with proliferation, invasion and metastasis of human gastric adenocarcinoma, as well as prognosis of patients^[17-19]. Therefore, there has been increasing interest in the development of antiprogesterins for tumor treatment. Mifepristone has been proved to be a potent and effective PR antagonist by competing with progesterone for PR binding, followed by binding to progesterone response element (PRE)^[20]. In the present study, we proved that mifepristone effectively inhibited the proliferation of human gastric adenocarcinoma cell line SGC-7 901 *in vitro* through induction of apoptosis and arresting the cell cycle progression.

Previous studies^[21] found that the determination of PR levels was primarily used as a marker of a tumor's responsiveness to mifepristone. To determine the expression of PR mRNA in the SGC-7 901 cells, *in situ* hybridization was performed. We found that PR mRNA was highly expressed in cultured SGC-7 901 cells. Meanwhile, the result is in agreement with the work of Cui *et al.*^[22], who reported that the concentrations of PR protein in the cytoplasm and nuclei of cultured SGC-7901 cells were 20.3 fmoL/mg and 22.7 fmoL/mg, respectively, revealed by dextran-coated charcoal (DCC) assay. Thus, we speculate that the growth inhibitory effects of mifepristone in our study might be mediated, at least in part, by PR.

In our study, TEM, MTT assay and ³H-TdR incorporation were used to evaluate the effect of mifepristone on the proliferation of SGC-7901 cells *in vitro*. We found that mifepristone exerted significantly anti-proliferative effect on cultured SGC-7901 cells *in vitro* in a dose- and time-dependent manner. The results are in agreement with those of previous studies on other tumor cell lines *in vitro*^[9-11,23].

Although a number of studies have proved that mifepristone has the growth inhibitory effects on tumor cells, but the mechanisms remain unknown. These theoretically could be related with the changes of the dynamics of cell proliferation. The hypothesis was demonstrated by the work of Thomas *et al.*^[24], who proved that mifepristone inhibited the proliferation of the MCF-7 human breast cancer cells by arresting them in the G₀/G₁ phase of the cell cycle. Recently, Peters *et al.*^[25] reported that mifepristone up-regulated the expression of cell cycle protein p21^{WAF/cip1} in medroxyprogesterone acetate-induced ductal mammary adenocarcinoma. Thus, we further explored the effects of mifepristone on the cell cycle of SGC-7901 cell using flow cytometry. Results showed that mifepristone markedly increased the proportion of cells in G₀/G₁, and simultaneously decreased the percentage of cells in S- and G₂/M-phase. Taken together, it seems reasonable to conclude that the growth inhibitory effects of mifepristone on SGC-7901 cells is partially due to an accumulation of cells in G₀/G₁ phase.

To explore whether or not the apoptosis-related genes contributed to the inhibitory effect of mifepristone on the SGC-7901 cells, we assessed the activity of caspase-3, an executioner of apoptosis^[26,27], and mRNA level of Bcl-X_L, an anti-apoptotic gene. Our findings showed that mifepristone dose-dependently up-regulated caspase-3 activity and down-regulated Bcl-X_L mRNA expression. This result is supported by previous studies on prostate cells. El Etreby *et al.* reported that mifepristone significantly induced apoptosis in LNCaP prostate cancer cells in a time- and dose-dependent manner through down-regulation of Bcl-2 protein and induction of caspase-3 activity. Collectively, it is possible that the activation of caspase-3 and the degradation of Bcl-X_L are partially responsible for the antiproliferative effects of mifepristone on cultured SGC-7901 cells.

In conclusion, the study demonstrated that mifepristone exerted marked antiproliferative effect on the PR-positive SGC-7901 cells by inducing apoptosis, arresting cell cycle progression, up-regulating caspase-3 activity and down-regulating Bcl-X_L mRNA expression. These results indicate that mifepristone may be a useful agent against human gastric adenocarcinoma although further studies are clearly needed to prove the possibility.

REFERENCES

- 1 Albert C. Clinical aspects of gastric cancer. In: Rustgi AK, eds. *Gastrointestinal cancer: biology, diagnosis and therapy*. Philadelphia: Lippincott Raven 1995: 197-216
- 2 Lu JB, Sun XB, Dai DX, Zhu SK, Chang QL, Liu SZ, Duan WJ. Epidemiology of gastroenterologic cancer in Henan Province, China. *World J Gastroenterol* 2003; **9**: 2400-2403
- 3 Maehara Y, Kakeji Y, Masuda T, Sakoguchi T, Imamura M, Ohgaki K, Taniguchi K, Sakurai M, Futatsugi M, Kimura Y, Nakamura T, Tokunaga E, Oki E, Ushiro S, Watanabe M, Oda S, Tanaka S, Baba H. Treatment of gastric cancer: current state and future prospect. *Fukuoka Igaku Zasshi* 2003; **94**: 285-295
- 4 De Paoli A, Buonadonna A, Boz G, Lombardi D, Innocente R, Tumolo S, Tosolini G, Rossi C, Trovo MG, Frustaci S. Combined modality treatment for locally advanced gastric cancer. *Suppl Tumori* 2003; **2**: S58-S62
- 5 Macdonald JS. Chemotherapy in the management of gastric cancer. *J Clin Oncol* 2003; **21**: 276s-279s
- 6 Valentini V, Cellini F, D'Angelillo RM. Combined treatments in gastric cancer: radiotherapy. *Suppl Tumori* 2003; **2**: S39-S44
- 7 Mahajan DK, London SN. Mifepristone (RU486): a review. *Fertil Steril* 1997; **68**: 967-976
- 8 Liang Y, Hou M, Kallab AM, Barrett JT, El Etreby F, Schoenlein PV. Induction of antiproliferation and apoptosis in estrogen receptor negative MDA-231 human breast cancer cells by mifepristone and 4-hydroxytamoxifen combination therapy: a role for TGFbeta1. *Int J Oncol* 2003; **23**: 369-380
- 9 El Etreby MF, Liang Y, Wrenn RW, Schoenlein PV. Additive effect of mifepristone and tamoxifen on apoptotic pathways in MCF-7 human breast cancer cells. *Breast Cancer Res Treat* 1998; **51**: 149-168
- 10 El Etreby MF, Liang Y. Effect of antiprogestins and tamoxifen on growth inhibition of MCF-7 human breast cancer cells in nude mice. *Breast Cancer Res Treat* 1998; **49**: 109-117
- 11 Rose FV, Barnea ER. Response of human ovarian carcinoma cell lines to antiprogesterin mifepristone. *Oncogene* 1996; **12**: 999-1003
- 12 Roccereto TF, Saul HM, Aikins JA Jr, Paulson J. Phase II study of mifepristone (RU486) in refractory ovarian cancer. *Gynecol Oncol* 2000; **77**: 429-432
- 13 Schneider CC, Gibb RK, Taylor DD, Wan T, Gercel-Taylor C. Inhibition of endometrial cancer cell lines by mifepristone (RU 486). *J Soc Gynecol Investig* 1998; **5**: 334-338
- 14 El Etreby MF, Liang Y, Johnson MH, Lewis RW. Antitumor activity of mifepristone in the human LNCaP, LNCaP-C4, and LNCaP-C4-2 prostate cancer models in nude mice. *Prostate* 2000; **42**: 99-106
- 15 Saikawa Y, Kubota T, Furukawa T, Suto A, Watanabe M, Kumai K, Ishibiki K, Kitajima M. Single-cell suspension assay with an MTT end point is useful for evaluating the optimal adjuvant chemotherapy for advanced gastric cancer. *Jpn J Cancer Res* 1994; **85**: 762-765
- 16 Sridhar S, Ali AA, Liang YA, El Etreby MF, Lewis RW, Kumar MV. Differential expression of members of the tumor necrosis factor-related apoptosis-inducing ligand pathway in prostate cancer cells. *Cancer Res* 2001; **61**: 7179-7183
- 17 Matsui M, Kojima O, Kawakami S, Uehara Y, Takahashi T. The prognosis of patients with gastric cancer possessing sex hormone receptors. *Surg Today* 1992; **22**: 421-425
- 18 Oshima CT, Wonraht DR, Catarino RM, Mattos D, Forones NM. Estrogen and progesterone receptors in gastric and colorectal cancer. *Hepatogastroenterology* 1999; **46**: 3155-3158
- 19 Korenaga D, Orita H, Okuyama T, Kinoshita J, Maekawa S, Ikeda T, Sugimachi K. Sex hormone-receptor-negative tumors have a higher proliferative activity than sex hormone-receptor-positive tumors in human adenocarcinomas of the gastrointestinal tract. *Surg Today* 1998; **2**: 1007-1014
- 20 Meyer ME, Pormon A, Ji JW, Bocquel MT, Chambon P, Gronemeyer H. Agonistic and antagonistic activities of RU486 on the functions of the human progesterone receptor. *EMBO J* 1990; **9**: 3923-3932
- 21 Lin VC, Aw SE, Ng EH, Ng EH, Tan MG. Demonstration of mixed properties of RU486 in progesterone receptor (PR)-transfected MDA-MB-231 cells: a model for studying the functions of progesterone analogues. *Br J Cancer* 2001; **85**: 1978-1986
- 22 Cui H, Lu P, Yu QS, Chen ZH. Sex hormone receptor in the cytoplasm and nuclear of human gastric cancer cell line SGC-7901. *Zhongliu Fangzhi Yanjiu* 1998; **25**: 9-10
- 23 Yokoyama Y, Shinohara A, Takahashi Y, Wan X, Takahashi S, Niwa K, Tamaya T. Synergistic effects of danazol and mifepristone on the cytotoxicity of UCN-01 in hormone-responsive breast cancer cells. *Anticancer Res* 2000; **20**: 3131-3135
- 24 Thomas M, Monet JD. Combined effects of RU486 and tamoxifen on the growth and cell cycle phases of the MCF-7 cell line. *J Clin Endocrinol Metab* 1992; **75**: 865-870
- 25 Peters MG, Vanzulli S, Elizalde PV, Charreau EH, Goin MM. Effects of antiprogestins RU486 and ZK98 299 on the expression of cell cycle proteins of a medroxyprogesterone acetate (MPA)-induced murine mammary tumor. *Oncol Rep* 2001; **8**: 445-449
- 26 Cohen GM. Caspases: the executioners of apoptosis. *Biochem J* 1997; **326**: 1-16
- 27 Yang X, Stennicke HR, Wang B, Green DR, Janicke RU, Srinivasan A, Seth P, Salvesen GS, Froelich CJ. Granzyme B mimics apical caspases. Description of a unified pathway for trans-activation of executioner caspase-3 and -7. *J Biol Chem* 1998; **273**: 34278-34283

Mitotic cell death in BEL-7402 cells induced by enediyne antibiotic lidamycin is associated with centrosome overduplication

Yue-Xin Liang, Wei Zhang, Dian-Dong Li, Hui-Tu Liu, Ping Gao, Yi-Na Sun, Rong-Guang Shao

Yue-Xin Liang, Dian-Dong Li, Rong-Guang Shao, Institute of Medicinal Biotechnology, Chinese Academy of Medical Sciences and Peking Union Medical College, Beijing 100050, China

Wei Zhang, Hui-Tu Liu, Ping Gao, Yi-Na Sun, Key Laboratory of Cell Proliferation and Regulation Biology of Ministry of Education, College of Life Science, Beijing Normal University, Beijing 100875, China

Supported by Grants from the Major State Basic Research Development Program Foundation of China, No. G2000057010 and G1999053901 and Grants from the National Natural Science Foundation of China, No. 30271438 and 30300424 and Grant from the Key Laboratory of Cell Proliferation and Regulation Biology of the Ministry of Education, Beijing Normal University. No. CPR2001-004

Correspondence to: Professor Dian-Dong Li, Institute of Medicinal Biotechnology, Chinese Academy of Medical Science and Peking Union Medical College, Beijing 100050, China. ddli@public3.bta.net.cn

Telephone: +86-10-63165289 **Fax:** +86-10-63017302

Received: 2004-02-14 **Accepted:** 2004-02-21

Abstract

AIM: Mitotic cell death has been focused on in tumor therapy. However, the precise mechanisms underlying it remain unclear. We have reported previously that enediyne antibiotic lidamycin induces mitotic cell death at low concentrations in human epithelial tumor cells. The aim of this study was to investigate the possible link between centrosome dynamics and lidamycin-induced mitotic cell death in human hepatoma BEL-7402 cells.

METHODS: Growth curve was established by MTT assay. Cell multinucleation was detected by staining with Hoechst 33342. Flow cytometry was used to analyze cell cycle. Aberrant centrosomes were detected by indirect immunofluorescence. Western blot and senescence-associated β -galactosidase (SA- β -gal) staining were used to analyze protein expression and senescence-like phenotype, respectively.

RESULTS: Exposure of BEL-7402 cells to a low concentration of lidamycin resulted in an increase in cells containing multiple centrosomes in association with the appearance of mitotic cell death and activation of SA- β -gal in some cells, accompanied by the changes of protein expression for the regulation of proliferation and apoptosis. The mitochondrial signaling pathway, one of the major apoptotic pathways, was not activated during mitotic cell death. The aberrant centrosomes contributed to the multipolar mitotic spindles formation, which might lead to an unbalanced division of chromosomes and mitotic cell death characterized by the manifestation of multi- or micronucleated giant cells. Cell cycle analysis revealed that the lidamycin treatment provoked the retardation at G2/M phase, which might be involved in the centrosome overduplication.

CONCLUSION: Mitotic cell death and senescence can be induced by treatment of BEL-7402 cells with a low concentration of lidamycin. Centrosome dysregulation may play a critical role in mitotic failure and ultimate cell death following exposure to intermediate dose of lidamycin.

Liang YX, Zhang W, Li DD, Liu HT, Gao P, Sun YN, Shao RG. Mitotic cell death in BEL-7402 cells induced by enediyne antibiotic lidamycin is associated with centrosome overduplication. *World J Gastroenterol* 2004; 10(18): 2632-2636

<http://www.wjgnet.com/1007-9327/10/2632.asp>

INTRODUCTION

Liver cancer is one of the most malignant tumors in the world^[1,2]. Surgical resection is considered the most effective but not the most popular method for the treatment of hepatocellular carcinoma (HCC). Chemotherapy is indicated for a large member of HCC patients. Mitotic cell death is a cell death form different from apoptosis, on which has been focused in tumor therapy. It is also known as mitotic catastrophe or delayed reproductive death, and can be activated by radiation or antitumor agents at low doses or concentrations^[3-5]. Mitotic cell death is frequently characterized by enlargement of cell volume, appearance of multi- or micronucleation, and arrest in G2/M phase of cell cycle. Finally, these cells underwent death. Thus far, little is known about the mechanism responsible for mitotic cell death. Some researchers considered that defects in mitotic machinery, such as multiple rounds of DNA synthesis without an intervening cytokinesis, and chromosome missegregation, might play a key role in the process of lethal nuclear fragmentation^[6]. Previous reports have suggested that the absence or delay of the G1/S checkpoint and the subsequent absence of interphase apoptosis coupled to this checkpoint contribute to mitotic cell death^[7,8].

The centrosome, representing the major microtubule organizing centre in eukaryotic cells, contains a pair of centrioles surrounded by pericentriolar material. The centrosome duplicates once during each cell cycle. To complete the normal cell cycle, the centrosome duplication cycle and the centrosome quantity must be precisely regulated to couple the other events of cell cycle^[9]. If centrosome replication deviates from cycles of DNA synthesis and mitotic division, an unsuccessful mitosis will come out with the features associated with the formation of aberrant centrosomes and multiple mitotic spindles, and unbalanced chromosome segregation^[10].

Enediyne antibiotics have been focused on their potent antitumor activity due to their unique ability to damage the DNA of tumor cells by inducing single strand (SSB) and/or double strand (DSB) breaks through free radical attacks on the deoxyribose moieties in DNA^[11]. Lidamycin (also designated as C1027) is a member of the enediyne antibiotic family, which was isolated from a *Streptomyces globisporus* C1027 strain in China^[12,13]. Lidamycin consists of a chromophore and an apoprotein, and the former has the ability to attack DNA, whereas the latter plays the role as a protecting protein^[14]. The biological effects induced by lidamycin and ionizing radiation are similar^[11]. Previous reports have shown that lidamycin is highly cytotoxic toward tumor cells^[14-16]. As an attempt to investigate the mechanisms of lidamycin-induced mitotic cell death in human hepatoma BEL-7402 cells, we treated cells with lidamycin at low concentrations, and discovered centrosome overduplication, multipolar mitotic spindle formation, multinucleation, delayed reproductive death and changed patterns of protein expression associated with the regulation of proliferation and apoptosis.

These results indicate that mitotic cell death in BEL-7402 cells induced by lidamycin is associated with centrosome overduplication independently of mitochondria pathway.

MATERIALS AND METHODS

Chemical

Lidamycin was generously provided by Professor Lian-Fang Jin from our institute, and stored at -20°C as a 100 $\mu\text{mol/L}$ stock solution in 9 g/L NaCl solution.

Cell culture

Human hepatoma BEL-7402 cells (obtained from the Key Laboratory of Cell Proliferation and Regulation Biology of the Ministry of Education, Beijing Normal University) were cultured in DMEM (Gibco BRL) supplemented with 100 mL/L fetal bovine serum (HyClone), 100 U/mL penicillin and 100 $\mu\text{g/mL}$ streptomycin at 37°C in the presence of 50 mL/L CO_2 .

Growth curve assay

Growth curves establishments were performed at a 5-d interval as previously described^[17] with some modifications. Totally 2.0×10^3 cells were seeded into 96-well plates and then treated with lidamycin for 2 h. A 12 μL MTT (5 mg/mL) was added to each well before assay and incubated for an additional 4 h at 37°C , followed by treatment with 100 μL of 0.01 mol/L HCl-100 g/L SDS overnight. The value at each time point was read on a Microplate Reader (Model 550, Bio-Rad) at $\lambda_{570\text{nm}}$.

Cell multinucleation shown by staining with Hoechst 33342

Subconfluent cells were continuously incubated for 72 h after exposure to lidamycin for 2 h, and then were stained by the DNA-specific fluorescent dye Hoechst 33342 (2 $\mu\text{g/mL}$) (Sigma) for 15 min at 37°C . Next, cells were washed once, kept in PBS, and observed using a fluorescence microscope (BH2 system, Olympus) equipped with a $\lambda_{455\text{nm}}$ filter.

Flow cytometry

Cells were exposed to 0.5 nmol/L lidamycin for 2 h and then incubated in fresh, drug-free medium. Following a 3-d incubation, cells including the floating and the attached were harvested and washed with cold PBS twice. Cell suspensions were fixed in 700 mL/L ethanol at 4°C overnight. Next, the fixed cells were washed twice in PBS and incubated with 50 $\mu\text{g/mL}$ RNase (Sigma) for 30 min at 37°C . Samples were then stained with 50 $\mu\text{g/mL}$ propidium iodide (Sigma) in the dark at 4°C for 30 min, and analyzed on a fluorescence-activated cell sorter (EPICS XL, Coulter).

Indirect immunofluorescence

Cells were grown on coverslips. After 3 d following 2-h lidamycin treatment, the cells were washed in PHEM buffer (60 mmol/L PIPES, 25 mmol/L HEPES, 10 mmol/L EGTA and 2 mmol/L MgCl_2) twice briefly, and incubated with a permeabilization buffer (5 mL/L Triton X-100 in PHEM buffer) for 90 s. Then, the cells were fixed in 37 g/L paraform in PHEM buffer for 15 min at room temperature. After washed in PBS 3 times, the cells were incubated with a blocking solution (50 g/L defatted dry milk and 0.5 mL/L Tween-20 in PBS) for 30 min and used for indirect immunofluorescence. The primary antibodies included anti- α -tubulin monoclonal antibody (Zymed) and anti-centrin polyclonal antibody^[18] (kindly provided by Professor Da-Cheng He, the Key Laboratory of Cell Proliferation and Regulation Biology of the Ministry of Education, Beijing Normal University). Rhodamine-labeled goat anti-mouse antibody (Zymed) and Fluorescein isothiocyanate-labeled goat anti-rabbit antibody (Zymed) were used as second antibodies. The microscope slides were mounted with glycerol mounting medium (900 mL/L glycerol and 100 mL/L PBS) and observed under a laser-scanning

microscope (IX-70 system, Olympus). The cell with three or more centrosomes was considered aberrant.

Senescence-associated β -galactosidase (SA- β -gal) staining

Cells were treated with 0.1 nmol/L or 0.5 nmol/L lidamycin for 2 h and continuously maintained for 72 h. The attached cells were fixed in 5 mL/L glutaraldehyde and stained for SA- β -gal activity using X-gal at pH 6.0 as previously described^[19].

Western blot analysis

Cells incubated with lidamycin at 37°C for 2 h and then allowed to recover for 72 h at 37°C were harvested and washed in PBS. The cells were lysed on ice in lysis buffer (100 mmol/L Tris, pH 6.8, 25 g/L SDS, 100 mL/L β -mercaptoethanol, 1 mmol/L phenylmethylsulfonyl fluoride, and 100 mL/L glycerol) for 10 min, followed by ultrasonication. The cell lysates were cleared by centrifugation, and the protein concentration was estimated using the Bradford method with bovine serum albumin as a standard. Western blot analysis was performed as a protocol described previously^[20]. In brief, equal amounts of protein were electrophoresed on SDS-polyacrylamide gel (Fluka) and transferred onto a nitrocellulose membrane (Hybond-P, Amersham Pharmacia) for blotting with primary antibodies including anti-Bax (N-20, Santa Cruz), anti-Smac (a kind gift from Dr. Xiao-Dong Wang, University of Texas Southwestern Medical Center, Dallas, USA), anti-cyclin B1 (GNS-1, Santa Cruz), anti-p16 (16P04, NeoMarkers), anti-Rb (C-15, Santa Cruz), anti-p53 (DO-1, Santa Cruz), anti-p21 (F-5, Santa Cruz), and anti-actin (I-19, Santa Cruz) antibodies. Secondary antibodies conjugated with horseradish peroxidase (Amersham Pharmacia). Enhanced chemiluminescence (ECL Western Blot Kit, Amersham Pharmacia) was used according to the manufacturer's instructions.

RESULTS

Growth inhibition induced by lidamycin in BEL-7402 cells

Inhibition of cell growth and proliferation was measured by the MTT test. Exposing BEL-7402 cells to 0.1 and 0.5 nmol/L lidamycin resulted in a dose-dependent inhibition of cell growth (Figure 1).

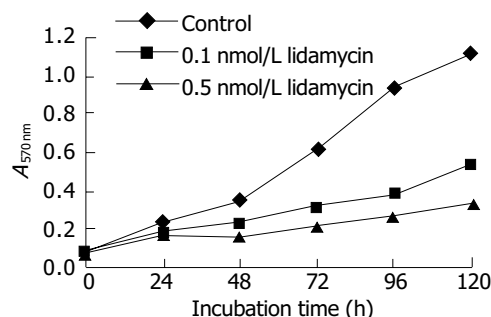


Figure 1 Effects of lidamycin treatment on BEL-7402 cells growth. Cells were seeded in 96-well plates and treated with 0.1 nmol/L or 0.5 nmol/L lidamycin for 2 h. Growth curves were established indirectly by detecting reactions with MTT. The value of each time point was derived from three samples.

Atypical chromatin condensation and multinucleation induced by lidamycin in BEL-7402 cells

With 0.1 nmol/L lidamycin for 2 h, followed by a 72-h incubation in drug-free medium, the treated BEL-7402 cells displayed a unique and atypical chromatin condensation characterized by appearance of small "dots" representing segregated condensed chromatin without apoptotic bodies (Figure 2B). Moreover, we did not observe detachment of these cells from the monolayer during the process of chromatin condensation. After 72-h incubation, multinucleation (three or more nuclei), one of the

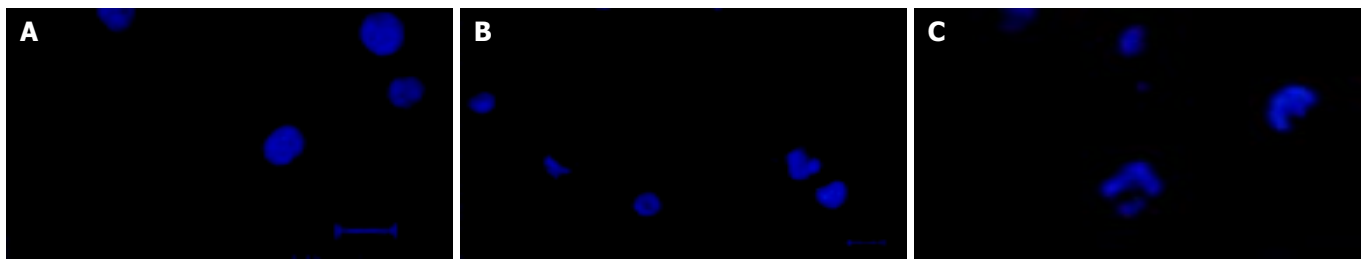


Figure 2 Induction by lidamycin of atypical chromatin condensation and multinucleation in BEL-7402 cells, determined by staining with the fluorescent dye Hoechst 33342 at 72 h after exposure to 0.1 nmol/L and 0.5 nmol/L lidamycin for 2 h. A: Untreated BEL-7402 cells; B: 0.1 nmol/L lidamycin treated BEL-7402 cells; C: 0.5 nmol/L lidamycin treated BEL-7402 cells.

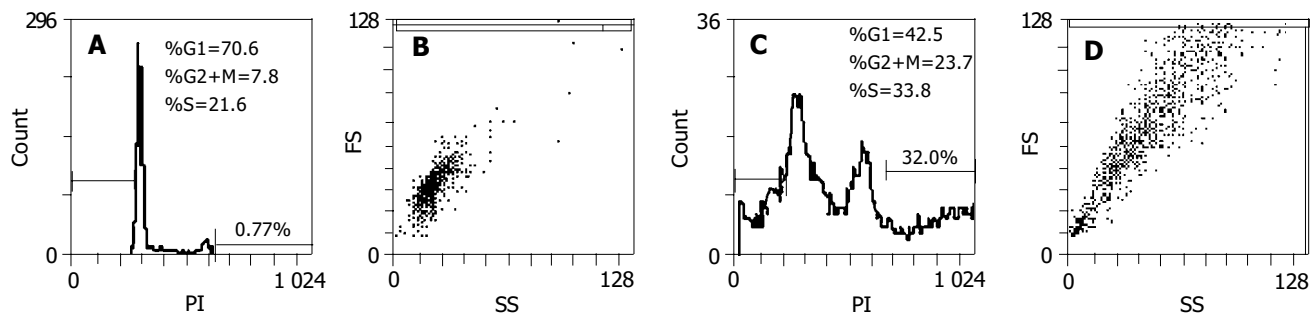


Figure 3 Effects of lidamycin on cell cycle. BEL-7402 cells were treated with 0.5 nmol/L lidamycin for 2 h, then washed and fed with fresh medium. After 72 h of incubation, the cells were stained with propidium iodide and sorted by flow cytometry. A,B: Untreated BEL-7402 cells; C, D: 0.5 nmol/L lidamycin treated BEL-7402 cells. The changes indicated in dot density maps were in accordance with those displayed in histograms.

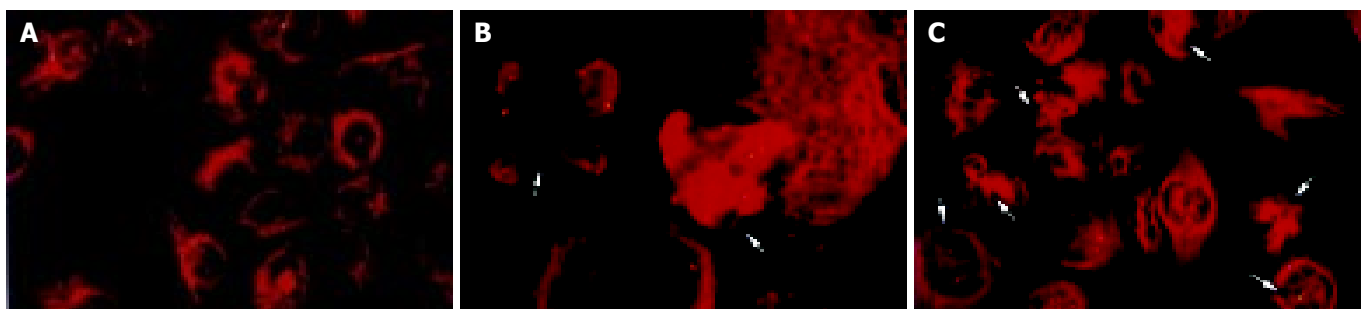


Figure 4 Immunofluorescence analysis of centrosomes and mitotic spindles in BEL-7402 cells at 72 h after treatments with 0.5 nmol/L lidamycin for 2 h. Cells grown on coverslips were fixed in paraform and doubly labeled with antibodies to α -tubulin (red) and centrin (green). Localization of centrosome on superimposed image showed yellow. A: Untreated BEL-7402 cells; B,C: 0.5 nmol/L lidamycin treated BEL-7402 cells. Arrows in B,C indicated the cells with multiple centrosomes, multipolar mitotic spindle or chromosome missegregation.



Figure 5 Phase contrast images of SA- β -gal stained BEL-7402 cells. At 72 h after incubation with lidamycin for 2 h, attached cells were fixed with 5 mL/L glutaraldehyde and stained for SA- β -gal activity for 16 h. A: Untreated BEL-7402 cells; B: 0.1 nmol/L lidamycin treated BEL-7402 cells; C: 0.5 nmol/L lidamycin treated BEL-7402 cells. The photographs were taken at 200-fold magnification (25 μ m scale bars).

main features of mitotic cell death, occurred at 0.5 nmol/L lidamycin-treated BEL-7402 cells (Figure 2C).

Changes of cell cycle progression and DNA polyploidy induced by lidamycin in BEL-7402 cells

The biochemical and cytological changes of multinucleated

giant cells remain poorly understood. To further characterize the etiology of mitotic cell death, we analyzed the cell cycle and DNA content of the lidamycin-treated BEL-7402 cells by flow cytometry. The cells were exposed to a low concentration of lidamycin for 2 h. At 72 h after treatment, ~23.7% of BEL-7402 cells arrested in G2/M phase, and the cells with >4N DNA

content were detected at 32.0% (Figure 3C).

Centrosome overduplication, multipolar spindle formation and unbalanced division induced by lidamycin in BEL-7402 cells

Immunofluorescence microscopy revealed that the abnormalities of multiple centrosomes and multipolar mitotic spindles markedly increased in BEL-7402 cells induced by lidamycin at a low concentration. Co-staining with antibodies to centrin and α -tubulin indicated that the increased centrosomes were localized at each pole of the multiple spindles, and the cells not deriving from equal division appeared (Figure 4B, C). However, to untreated cells, these defects rarely displayed (Figure 4A).

Induction by lidamycin of senescence-like phenotype in BEL-7402 cells

The induction of SA- β -gal activity and mitotic cell death were thought to be independent events^[21]. To investigate the effects of mitotic cell death on senescence-like phenotype of the lidamycin-treated cells, we observed SA- β -gal expression, a senescence marker, at 72 h after lidamycin treatment. The treated cells showed phenotypic changes that resembled features of normal senescence, including enlarged and flattened morphology, increased granularity, vacuolization, and enhanced SA- β -gal-positive cells (Figure 5). Moreover, the induction of senescence-like phenotype in BEL-7402 cells was increased dose-dependently.

Alterations of cell cycle related proteins in lidamycin-treated BEL-7402 cells

To understand some molecular changes that led to mitotic cell death, cell cycle proteins were analysed by Western blot analysis in lidamycin-treated cells. In BEL-7402 cells, lidamycin induced an increase in the levels of cyclin B1, p16 and pRb, meanwhile a decrease in expression of p53 and p21 (Figure 6).

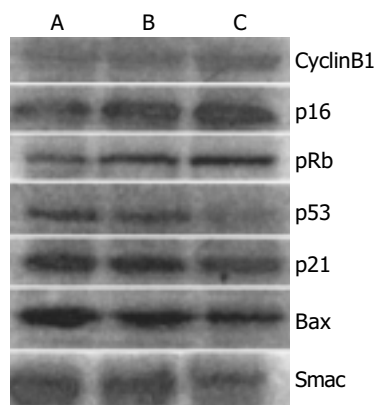


Figure 6 Western blot analysis of BEL-7402 cells. Cells were harvested at 72 h after 2-h lidamycin treatment, and total proteins (30 μ g/lane) were resolved by 8 to 15% SDS-PAGE and transferred onto nitrocellulose, and Western blot was performed using the indicated antibodies. Lane A, untreated BEL-7402 cells; lane B, 0.1 nmol/L lidamycin treated BEL-7402 cells; lane C, 0.5 nmol/L lidamycin treated BEL-7402 cells.

Alterations of apoptosis related proteins in lidamycin-treated BEL-7402 cells

To confirm that mitotic cell death induced by lidamycin was distinguished from typical apoptosis, and detect the correlation between them, proteins associated with apoptosis were examined. Bax is a regulator of apoptosis^[20]. Smac, an inhibitor of caspase suppressors, promotes cytochrome c-induced activation of caspases by sequestering the inhibitor of apoptosis protein family^[22]. As is shown in Figure 6, the protein levels of Bax and Smac declined in lidamycin-treated BEL-7402

cells. We were unable to detect the proteolytically activated caspase-3 and caspase-9, and found no significant alterations of the blots representing caspase-3 precursor and caspase-9 precursor after exposure to low concentrations of lidamycin in BEL-7402 cells (data not shown).

DISCUSSION

HCC is one of the most common malignant neoplasms in the world^[1]. The incidence of HCC in China exceeds 100 000 per year, and at least 110 000 HCC-related deaths occur every year. Lidamycin is a highly potent cytotoxic antitumor agent. We treated human hepatoma BEL-7402 cells with lidamycin at concentrations in the nanomolar range, and assessed the potential role of centrosome in lidamycin-induced mitotic cell death. The results indicated a series of abnormal events including centrosome overduplication, formation of multipolar mitotic spindles, multinucleation, and eventual mitotic catastrophe. In this study, we have described for the first time the association between centrosomes and enediyne antibiotics-induced cell death in human hepatoma cells.

Thus far, the modes of cell death induced by lidamycin can be divided into two classes, one is apoptosis, and the other is mitotic cell death^[5,23]. It has been reported that lidamycin can act directly as an endonuclease without dependence on caspase activities and is considered as an apoptosis-mimetic agent, at high concentrations^[24]. Cells exposed to low concentrations of lidamycin lost reproductive integrity due to inappropriate entry into mitosis, and apparently exhibited the morphological and biochemical changes associated with mitotic cell death: enlarged cell shape, multi- or micronucleation, accumulation of karyotypic abnormalities, and a G2/M arrest^[5]. Apoptosis, mitotic cell death and irreversible cell cycle arrest may all contribute to cell death after lidamycin treatment. The exact mechanism of mitotic cell death is unclear, and only a few studies have attempted to elucidate the effects of lidamycin on cells at moderate concentrations^[5,11]. In the present study, we used low-dose lidamycin to treat BEL-7402 cells, and mitotic cell death was observed predominantly after treatment. We demonstrate that lidamycin can induce multiple centrosomes which may be responsible for the assembly of multipolar mitotic spindles and the chromosomes missegregation. Most of the cells containing multiple nuclear fragments were temporarily viable but reproductively dead. However, in some cases, the cells undergoing mitotic death initiated endocycles, restituted mitosis and finally survival^[8]. We plan to continue this study to confirm the link between lidamycin-induced mitotic cell death and centrosome overduplication by using centrosome inhibitors and vectors containing antisense mRNAs to centrosome related proteins.

Because centrosome duplication was closely associated with DNA replication, cytokinesis and cell cycle regulation^[25,26], we analyzed the cell cycle progression of lidamycin-treated BEL-7402 cells to detect relationship between centrosome dysregulation and cell cycle distribution as well as to confirm the appearance of multinucleated cells, which is one of the main features of mitotic cell death. We found that lidamycin induced centrosome overduplication associated with induction of G2/M arrest. Previous reports showed that centrosome replication could dissociate from DNA synthesis cycle and mitotic division^[27], and cell cycle block in G2/M phase might be related to abnormal centrosome accumulation^[10], and endocycles starting from G2/M arrest could produce endopolyploid cells^[7]. We suppose that lidamycin-induced DNA replication cycle retardation in BEL-7402 cells could be helpful to trigger centrosome overduplication.

Analysis of gene expression may provide further insights into the molecular mechanisms mediating mitotic cell death. Cyclin B1, a component of the mitosis-promoting factor, plays an important role in G2/M regulation by forming a complex with

p34cdk1 to phosphorylate various substrates necessary for mitosis. The cells with the morphological features of mitotic catastrophe frequently undergo up-regulation of cyclin B1 level^[28,29], which is consistent with our results. Bax expression is a regulator of apoptosis. Ordinarily action of Bax facilitates apoptosis^[30]. However, our present study demonstrated that the levels of Bax and Smac both decreased along with no proteolytic activation of caspase-3 and caspase-9, and no DNA ladder was obtained (data not shown) after lidamycin treatments, which suggested that the mitochondrial apoptosis pathway might not be activated. The undetectable typical apoptosis is not caused by Bcl-2 involvement in BEL-7402 cells exposed to low concentrations of lidamycin (data not shown) and some other genes might play an essential role in this response. p21 is a p53-regulated protein. p53 inhibition was shown to increase mitotic death^[31]. We noticed decreased levels of p53 and p21 in BEL-7402 cells after lidamycin treatment. However, the expression of p16 and pRb proteins was upregulated in BEL-7402 cells, which might explain the increased intensity of staining for SA- β -gal in lidamycin-treated cells, since p16 is closely related to induction of senescence-like phenotype^[32]. Based on data presented here, we propose that the G2/M arrest of BEL-7402 cells may not be mediated by a classically driven cell cycle checkpoint mechanism correlated with p53. From a therapeutic standpoint, centrosome dysregulation might provide a valuable anticancer target. Further study to identify signaling pathways to mitotic cell death in tumor cells and normal somatocytes would help to improve the efficacy of HCC therapy with a low systemic toxicity.

ACKNOWLEDGMENTS

We thank Drs. Lian-Fang Jin, Da-Cheng He and Xiao-Dong Wang for providing lidamycin and antibodies to centrin and Smac. We thank Wei-Li Cai for technical assistance. Hong-Bin Deng, Jian-Ming Jiang and Guo Li are acknowledged for their helpful discussions.

REFERENCES

- Bosch FX, Ribes J, Borrás J. Epidemiology of primary liver cancer. *Semin Liver Dis* 1999; **19**: 271-285
- Shi YJ, Gong JP, Liu CA, Li XH, Mei Y, Mi C, Huo YY. Construction of a targeting adenoviral vector carrying AFP promoter for expressing EGFP gene in AFP-producing hepatocarcinoma cell. *World J Gastroenterol* 2004; **10**: 186-189
- Jonathan EC, Bernhard EJ, McKenna WG. How does radiation kill cells? *Curr Opin Chem Biol* 1999; **3**: 77-83
- Ianzini F, Mackey MA. Spontaneous premature chromosome condensation and mitotic catastrophe following irradiation of HeLa S3 cells. *Int J Radiat Biol* 1997; **72**: 409-421
- He QY, Liang YY, Wang DS, Li DD. Characteristics of mitotic cell death induced by enediyne antibiotic lidamycin in human epithelial tumor cells. *Int J Oncol* 2002; **20**: 261-266
- Allen CE, Wu LC. Downregulation of KRC induces proliferation, anchorage independence, and mitotic cell death in HeLa cells. *Exp Cell Res* 2000; **260**: 346-356
- Erenpreisa J, Cragg MS. Mitotic death: a mechanism of survival? A review. *Cancer Cell Int* 2001; **1**: 1
- Grafi G. Cell cycle regulation of DNA replication: the endoreduplication perspective. *Exp Cell Res* 1998; **244**: 372-378
- Winey M. Keeping the centrosome cycle on track. *Genome stability. Curr Biol* 1996; **6**: 962-964
- Shono M, Sato N, Mizumoto K, Minamishima YA, Nakamura M, Maehara N, Urashima T, Saimura M, Qian LW, Nishio S, Nagai E, Tanaka M. Effect of serum depletion on centrosome overduplication and death of human pancreatic cancer cells after exposure to radiation. *Cancer Lett* 2001; **170**: 81-89
- Dziegielewski J, Beerman TA. Cellular responses to the DNA strand-scission enediyne C-1027 can be independent of ATM, ATR, and DNA-PK kinases. *J Biol Chem* 2002; **277**: 20549-20554
- Hu JL, Xue YC, Xie MY, Zhang R, Otani T, Minami Y, Yamada Y, Marunaka T. A new macromolecular antitumor antibiotic, C-1 027. I. Discovery, taxonomy of producing organism, fermentation and biological activity. *J Antibiot* 1988; **41**: 1575-1579
- Otani T, Minami Y, Marunaka T, Zhang R, Xie MY. A new macromolecular antitumor antibiotic, C-1 027. II. Isolation and physico-chemical properties. *J Antibiot* 1988; **41**: 1580-1585
- Shao RG, Zhen YS. Relationship between the molecular composition of C1 027, a new macromolecular antibiotic with enediyne chromophore, and its antitumor activity. *Yaoxue Xuebao* 1995; **30**: 336-342
- Zhen YS, Ming XY, Yu B, Otani T, Saito H, Yamada Y. A new macromolecular antitumor antibiotic, C-1 027. III. Antitumor activity. *J Antibiot* 1989; **42**: 1294-1298
- Xu YJ, Zhen YS, Goldberg IH. C1 027 chromophore, a potent new enediyne antitumor antibiotic, induces sequence-specific double-strand DNA cleavage. *Biochemistry* 1994; **33**: 5947-5954
- Mosmann T. Rapid colorimetric assay for cellular growth and survival: application to proliferation and cytotoxicity assays. *J Immunol Meth* 1983; **65**: 55-63
- Chen XB, Wang YC, Li YZ, Cui JT. Identification of a novel resident protein in centrosome. *Kexue Tongbao* 2000; **45**: 1302-1307
- Dimri GP, Lee X, Basile G, Acosta M, Scott G, Roskelley C, Medranos EE, Linskens M, Rubelj I, Pereira-Smith O, Peacocke M, Campisi J. A biomarker that identifies senescent human cells in culture and in aging skin *in vivo*. *Proc Natl Acad Sci U S A* 1995; **92**: 9363-9367
- Liang Y, Yan CH, Schor NF. Apoptosis in the absence of caspase 3. *Oncogene* 2001; **20**: 6570-6578
- Chang BD, Broude EV, Dokmanovic M, Zhu HM, Ruth A, Xuan YZ. A senescence-like phenotype distinguishes tumor cells that undergo terminal proliferation arrest after exposure to anticancer agent. *Cancer Res* 1999; **59**: 3761-3767
- Lademann U, Cain K, Gyrd-Hansen M, Brown D, Peters D, Jaattela M. Diarylurea compounds inhibit caspase activation by preventing the formation of the active 700-kilodalton apoptosome complex. *Mol Cell Biol* 2003; **23**: 7829-7837
- Jiang B, Li DD, Zhen YS. Induction of apoptosis by enediyne antitumor antibiotic C1 027 in HL-60 human promyelocytic leukemia cells. *Biochem Biophys Res Commun* 1995; **208**: 238-244
- Wang Z, He QY, Liang YY, Wang DS, Li YY, Li DD. Non-caspase-mediated apoptosis contributes to the potent cytotoxicity of the enediyne antibiotic lidamycin toward human tumor cells. *Biochem Pharmacol* 2003; **65**: 1767-1775
- Hinchcliffe EH, Cassels GO, Rieder CL, Sluder G. The coordination of centrosome reproduction with nuclear events of the cell cycle in the sea urchin zygote. *J Cell Biol* 1998; **140**: 1417-1426
- Lacey KR, Jackson PK, Stearns T. Cyclin-dependent kinase control of centrosome duplication. *Proc Natl Acad Sci U S A* 1999; **96**: 217-2822
- Balczon R, Bao L, Zimmer WE, Brown K, Zinkowski RP, Brinkley BR. Dissociation of centrosome replication events from cycles of DNA synthesis and mitotic division in hydroxyurea-arrested Chinese hamster ovary cells. *J Cell Biol* 1995; **130**: 105-115
- Nabha SM, Mohammad RM, Dandashi MH, Coupaye-Gerard B, Aboukameel A, Pettit GR, Al-Katib AM. Combretastatin-A4 prodrug induces mitotic catastrophe in chronic lymphocytic leukemia cell line independent of caspase activation and poly (ADP-ribose) polymerase cleavage. *Clin Cancer Res* 2002; **8**: 2735-2741
- Hyun JW, Cheon GJ, Kim HS, Lee YS, Choi EY, Yoon BH, Kim JS, Chung MH. Radiation sensitivity depends on OGG1 activity status in human leukemia cell lines. *Free Radic Biol Med* 2002; **32**: 212-220
- Okuno S, Shimizu S, Ito T, Nomura M, Hamada E, Tsujimoto Y, Matsuda H. Bcl-2 prevents caspase-independent cell death. *J Biol Chem* 1998; **273**: 34272-34277
- Chang BD, Xuan YZ, Broude EV, Zhu HM, Schott B, Fang J, Roninson IB. Role of p53 and p21^{waf1/cip1} in senescence-like terminal proliferation arrest induced in human tumor cells by chemotherapeutic drugs. *Oncogene* 1999; **18**: 4808-4818
- Drayton S, Rowe J, Jones R, Vatcheva R, Cuthbert-Heavens D, Marshall J, Fried M, Peters G. Tumor suppressor p16(INK4a) determines sensitivity of human cells to transformation by co-operating cellular oncogenes. *Cancer Cell* 2003; **4**: 301-310

Safety of *Curcuma aromatica* oil gelatin microspheres administered via hepatic artery

Shi-Gui Deng, Zhi-Feng Wu, Wei-Ying Li, Zhi-Gang Yang, Gang Chang, Fan-Zhe Meng, Li-Li Mo

Shi-Gui Deng, Zhi-Feng Wu, Wei-Ying Li, Zhi-Gang Yang, Gang Chang, Fan-Zhe Meng, Li-Li Mo, Second Affiliated Hospital of Guangzhou University of Traditional Chinese Medicine, Guangzhou 510120, Guangdong Province, China

Supported by the National Medical Science and Technology Foundation during the 9th Five-Year Plan Period, No. 96-906-07-04

Correspondence to: Shi-Gui Deng, Second Affiliated Hospital of Guangzhou University of Traditional Chinese Medicine, Guangzhou 510120, 111 Dade Road, Guangdong Province, China. dengshigui@yahoo.com.cn

Telephone: +86-20-81887233-30904

Received: 2003-12-10 Accepted: 2004-02-01

Abstract

AIM: To evaluate the safety of *Curcuma aromatica* oil gelatin microspheres (CAO-GMS) infused via hepatic artery against primary liver cancer.

METHODS: The safety of CAO-GMS was evaluated in view of its acute toxicity in rats, long-term toxicity in Beagle dogs and general pharmacology in rats and mongrel dogs.

RESULTS: The 50% lethal dose (LD₅₀) of CAO-GMS infused via the hepatic artery was 17.19 mg/kg, and the serum biochemical indices of dying rats after the administration changed markedly while those of survived rats did not. Subsequent pathological examination of the tissues from the dead rats indicated improper embolism. Similar edema and small necrotic foci in the hepatic lobule were found in the hepatic tissue of rats receiving 10 and 5 mg/kg CAO-GMS and GMS 60 d after the last administration, while not in the rats of the blank control group, indicating that microspheres infused via the hepatic artery may induce irreversible liver damage dose-dependently. General pharmacological study showed that the activities (posture and gait), respiration frequency, blood pressure or heart rate of the dogs were not affected by CAO-GMS, nor were salivation, tremor or pupil changes of the rats observed or their balancing ability compromised, suggesting CAO-GMS infused via the hepatic artery did not significantly affect the nervous, respiratory and cardiovascular systems.

CONCLUSION: CAO-GMS embolization administered via the hepatic artery is safe but undesired embolization induced by vascular variation should be given due attention in its clinical application. Individualized embolization dosage and super-selective catheterization technique are recommended to avoid undesired embolism and reduce complications.

Deng SG, Wu ZF, Li WY, Yang ZG, Chang G, Meng FZ, Mo LL. Safety of *Curcuma aromatica* oil gelatin microspheres administered via hepatic artery. *World J Gastroenterol* 2004; 10(18): 2637-2642

<http://www.wjgnet.com/1007-9327/10/2637.asp>

INTRODUCTION

Curcuma aromatica oil (CAO) is the oil mixture extracted from

Curcuma aromatica consisting of multiple effective ingredients, such as β -elemene and curcumol^[1-7]. Researchers have demonstrated that CAO, with relatively low toxic effects, is the main anti-neoplasm ingredient of *Curcuma aromatica*^[8-12], which can be used for therapy against neoplastic diseases, especially liver neoplasm^[13-19]. Clinically, CAO has been applied in interventional therapy administered via the hepatic artery, and produced favorable effects in patients with primary liver cancer^[20-24] and experimentally, in rats with transplanted liver tumor as well^[25]. As an oil preparation, CAO is often difficult to achieve total embolization in interventional therapy with far too short retention time in the neoplastic lesions. CAO microsphere is suggested to be ideal for increasing the retention time, enhancing the inhibitory effects on cancer cells, and also for blocking the trophic vessels for the hepatoma, so to produce dual effects of chemotherapy and embolization. Therefore, we employed the microsphere degradation technique to entrap the CAO into the gelatin medium and prepared CAO-GMS^[26], which has shown potent therapeutic efficacy against transplanted liver cancer in rats^[27-29] and from which the released CAO exhibited marked dose-dependent inhibition of the growth of human hepatoma cell line SMMC-7721^[30].

CAO-GMS is a preparation of traditional Chinese herbal drugs possible for quality control^[26]. Considering its special pharmaceutical form and administration route, we adopted the interventional procedures described by Lindell *et al.*^[31] similar to clinical situations, so as to study CAO-GMS in view of its acute toxicity, long-term toxicity and general pharmacology in rats and dogs. The results may help evaluate the safety of the interventional therapy with CAO-GMS embolization administered via the hepatic artery in the treatment of primary liver cancer and provide experimental evidence for its potential clinical application.

MATERIALS AND METHODS

Drugs and reagents

CAO-GMS (50-100 μ m in diameter, Batch No.: 971006), 8% CAO and blank gelatin microspheres (50-100 μ m in diameter, Batch No.: 97050) were provided by the Department of Pharmaceutics, Shenyang Pharmaceutical University. Sodium carboxymethyl cellulose (CMC-Na) was purchased from Guangzhou Chemical Reagents and Glassware Co. (Batch No.: 950808). The microspheres were suspended in 3 g/L CMC-Na solution for use.

Animals

A total of 104 SD rats (clean animals, including 52 males and 52 females weighing 220-300 g, Certification No.: 152) used in this study were purchased from Shanghai Sino-British SIPPR/BK Lab Animal Co. Ltd. Twenty-one mongrel dogs (conventional animals, 11 males and 10 females, weighing 13.5-21.0 kg, Certification No.: 19980610) were purchased from Guangzhou Shima Experimental Animal Company and quarantined by the Experimental Animal Center of Guangzhou University of Traditional Chinese Medicine. Eighteen Beagle dogs (specific pathogen-free animals, 9 males and 9 females, weighing 12.5-13.1 kg, Certification No.: 97A025) were purchased from the Experimental Animal Center of Guangzhou Medicine Industry Institute.

Six-channel physiological recorder (Plugsys, Hugo Sachs Elektronik, Germany), blood pressure sensor (Isotec, Hugo Sachs Elektronik, Germany), thermosensitive recorder (WR500, Isotec, Hugo Sachs Elektronik, Germany), digital subtraction angiography-interventional therapy apparatus (DSA, Siemens, Germany), automated blood analyzer (Counter-5, Japan), automated blood coagulation analyzer (ACT-3000 plus, Germany), clinical biochemical analyzer (CL-7200, Japan) and electrocardiograph (ECG-6511, Japan) were used in this study.

Acute toxicity in rats

Seventy-four SD rats were randomly divided into 7 groups including CAO-GMS-1 group ($n = 10$) receiving CAO-GMS 5 mg/kg, CAO-GMS-2 group ($n = 12$) receiving CAO-GMS 10 mg/kg, CAO-GMS-3 group ($n = 14$) receiving CAO-GMS 20 mg/kg, CAO-GMS-4 group ($n = 12$) receiving CAO-GMS 40 mg/kg, GMS control group ($n=10$) receiving gelatin microspheres 40 mg/kg, blank control group ($n = 8$) receiving 3.5 mL/kg CMC-Na (3 g/L) in a volume equivalent to that of injected microspheres and ZT group ($n = 8$) receiving 3.2 mg/kg CAO. All rats were anesthetized with 45 mg/kg intraperitoneal pentobarbital injection prior to drug administration following the method described by Lidell *et al.*^[31] (Figure 1). In brief, a catheter was inserted through the gastroduodenal artery to the proper hepatic artery, the distal end of the gastroduodenal artery was ligated, and the common hepatic artery as well as the right branch of the proper hepatic artery was temporarily blocked to receive the agents through the left branch of the proper hepatic artery. The general activities, mortality and survival time of the rats were consecutively observed and recorded for 14 d after drug administration. Blood samples of the dying rats were collected and determined for ALT, AST, total bilirubin (T-BIL), direct bilirubin (D-BIL), blood creatinine (BCr) and blood urea nitrogen (BUN). Blood samples were also taken from the survived rats on d 14 for determination of the above indices. Autopsy was performed on the dead rats and the vital organs such as the liver, spleen, lung and kidney *etc.* were pathologically examined.

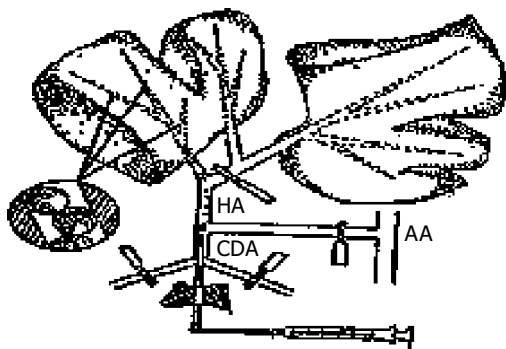


Figure 1 Administration method (from Lindell^[31]).

Long-term toxicity in Beagle dogs

Eighteen Beagle dogs were randomly divided into 4 groups including CAO-GMS high-dose group (CAO-GMS-H, 5 dogs) receiving 15 mg/kg CAO-GMS every 4 wk, CAO-GMS low-dose group (CAO-GMS-L, 5 dogs) receiving 7.5 mg/kg CAO-GMS every 4 wk, GMS control group (4 dogs) receiving 15 mg/kg gelatin microspheres every 4 wk, blank control group (4 dogs) receiving 10 mL/kg saline in the same volume as that of the microspheres every 4 wk. Each dog was anaesthetized with 30 mg/kg pentobarbital, and a catheter was super-selectively inserted into the hepatic artery through the femoral artery puncture under perspective monitor. The hepatic artery was examined by intra-arterial digital subtraction angiography with

the injection of 8 mL meglumine diatrizoate (760 g/L) at the rate of 2 mL/s, 150 Psi by a high-pressure syringe. The microspheres of specified doses were mixed with the contrast media and slowly injected. To prevent improper embolism due to reflux of the liquid, the injection rate was strictly controlled. The catheter was washed with saline after the injection, and angiography of the hepatic artery was performed for confirmation of the range and degree of embolization. The catheter was withdrawn after the surgery, and the puncture pressed for 15 min and bandaged with pressure. The procedures were repeated twice every 4 wk. Half of the dogs in each group were sacrificed on d 30 after the last treatment and the other half on d 60. The tissue samples were fixed in 40 g/L neutral formaldehyde, processed by the standard histological techniques, and stained with hematoxylin and eosin (HE) for light microscopic examination. The liver, kidney, lung, adrenal, pancreas, stomach, duodenum, ileum, colon, prostate, brain, spinal cord, heart, spleen, sternum (bone and marrow), bladder, uterus, ovary, thyroid, thymus and testis of the dogs were all examined pathologically to assess the long-term toxicity, reversible toxicity and delayed toxicity of CAO-GMS.

General effect on nervous system of rats

Thirty rats were randomly divided into 3 groups including high-dose CAO-GMS group (CAO-GMS-H, 12 rats) receiving 10 mg/kg CAO-GMS, low-dose CAO-GMS group (CAO-GMS-L, 10 rats) receiving 5 mg/kg CAO-GMS, and blank control group (8 rats) receiving 3.5 mL/kg CMC-Na (3 g/L, in equivalent volume). The administration of the agents followed the procedures described above. The general activities (posture and gait), salivation, tremor or pupil changes of rats were recorded. Balance test of rotarod model was performed on d 3, 5, 7 and 14, respectively, in which the rats were put on a 90-cm-long rod 2.5 cm in diameter to observe the dropping frequency. The rats dropping more than 3 times were defined to have incoordination with nervous system impairment.

General effect on respiratory and cardiovascular systems of dogs

Twenty-one mongrel dogs were randomly divided into 4 groups, namely high-dose CAO-GMS group (CAO-GMS-H, 6 dogs) receiving 0.10 g CAO-GMS, low-dose CAO-GMS group (CAO-GMS-L, 6 dogs) receiving 0.03 CAO-GMS, CAO group (4 dogs) receiving 6.4 μ L/kg CAO and blank control group (5 dogs) receiving 10 mL/kg CMC-Na (3 g/L, in equivalent volume). Under anesthesia with pentobarbital, the blood pressure of the dogs was measured with catheterization through the common carotid artery (connected by Isotec blood pressure sensor). Two-lead electrocardiogram and respiratory frequency were also recorded. Thirty minutes later, the dogs were given specified agents with the method described above. The respiratory frequency, blood pressure and electrocardiogram of the dogs before and 30, 60, 120, 180 min after administration were measured using six-channel physiology recorder.

Statistical analysis

Data were expressed as mean \pm SD. The 50% lethal dose (LD₅₀) was calculated with Bliss method. The biochemical indices were assessed by multiple ANOVA. Changes in blood pressure, respiratory frequency and heart rate before and after administration of the agents within the same group were assessed by paired *t* test using SPSS 10.0 statistical software. The difference was considered significant when *P* value was less than 0.05.

RESULTS

Acute toxicity in rats

All rats in CAO-GMS-4 group fell in a state of drowsiness with

hair erection and died within 24 h after administration of the agent. Death of the rats in CAO-GMS-3 group occurred 24-48 h after the administration, with the survived rats exhibiting signs of fatigue, hair erection, and emaciation accompanied by reduced activity and anorexia; 2 rats developed ascites and survived until d 14. The rats in CAO-GMS-2 group also showed fatigue within the first 2 d after administration of the agent but resumed normal condition on d 3. The rats in CAO-GMS-1, blank control and CAO group did not show signs of discomfort. The rats of GMS group exhibited changes similar to those of CAO-GMS-4 group. LD₅₀ of CAO-GMS embolization via the hepatic artery was 17.19 mg/kg, with the 95% confidential interval of 13.08-23.67 mg/kg (Table 1).

Compared with those of the blank control group, all the dying rats of the CAO-GMS groups showed marked increase in ALT, AST, T-BL, D-BL, BCr and BUN (Table 2), but none of the survived rats showed marked changes in these indices (Table 3).

The tissue samples of the rats in CAO-GMS and GMS groups showed damage of hepatic tissues, as were mostly manifested in CAO-GMS-3, 4 groups and GSM group. The rats in CAO-GMS-3 and -4 groups were found to have hemorrhagic damage in lung tissues and necrosis of renal tubules, indicating dose-dependent damage of the kidney and lung by CAO-GMS. We identified traces of the microspheres in a tissue sample of CAO-GMS-2 group, suggesting that the toxic effects on kidney tissues in CAO-GMS-1, -2, -3, -4 groups arose from improper

embolization of the renal artery. The tissue samples from the 4 groups showed dose-independent damage of the spleen tissues. Abnormal changes were not observed in vital organs in blank control and CAO groups.

We found that CAO-GMS induced untoward responses and death of the rats dose-dependently. Since the rats in blank control and CAO groups showed no untoward response as those in GMS group did, we presumed that GMS, instead of CAO, caused renal and hepatic injuries. The most probable cause of the renal damage might be undesired embolization of the renal artery by GMS.

Long-term toxicity in Beagle dogs

The dogs of CAO-GMS-H, CAO-GMS-L and GMS groups showed necrotic foci in the hepatic tissue with color attenuation 1-2 mm in diameter. The blank control group showed no marked change in the color and texture of the hepatic tissue.

Figure 2 displays the pathological changes in hepatic tissues of the dogs. Two dogs in CAO-GMS-H group exhibited whole lobule coagulation necrosis in the hepatic tissue with total destruction of the normal structures. The remaining hepatic tissue exhibited extensive moderate cellular edema with occasional cellular inflammatory edema in the necrotic region. In a dog died during the experiment, whole lobule coagulation necrosis was observed in the hepatic tissue, which was also seen in two dogs sacrificed on d 30 with mild cellular edema in the remaining hepatic tissue and destruction of normal structures.

Table 1 Deaths of the rats after administration of CAO-GMS

Group	Number of rats	Dosage (mg/kg)	Number of dead rats	Mortality (%)	Peak time of death occurrence (h)
CAO-GMS-1	10	5	0	0	-
CAO-GMS-2	12	10	4	33.33	24-48
CAO-GMS-3	14	20	8	57.14	24-48
CAO-GMS-4	12	40	12	100	<24
GMS	10	40	7	71.42	24-48
Blank control	8	3.5 ¹	0	0	-
CAO	8	3.2	0	0	-

¹Measured in mL/kg.

Table 2 Changes in biochemical indices of the dying rats receiving CAO-GMS (mean±SD)

Group	Number of rats	ALT (U/L)	AST (U/L)	T-BiL (mmol/L)	D-BiL (μmol/L)	BCr (μmol/L)	BUN (mmol/L)
CAO-GMS-1	0	-	-	-	-	-	-
CAO-GMS-2	4	200±54 ^b	805±533 ^b	12.0±5 ^b	46.0±90 ^b	50.0±34 ^b	20.0±12 ^a
CAO-GMS-3	8	186±89 ^b	700±522 ^b	12.4±8.6 ^b	59.0±88 ^b	49.0±43 ^b	20.0±14 ^a
CAO-GMS-4	12	241±289 ^b	715±614 ^b	15.0±19 ^b	78.0±162 ^b	58.0±43 ^b	22.0±13 ^a
GMS	7	232±168 ^b	685±503 ^b	13.8±9.6 ^b	54.0±126 ^b	52.0±36 ^b	20.0±13 ^a
Blank control	0	38±11	278±114	4.5±1.3	3.2±1.6	38.7±3.5	8.6±11.8
CAO	0	-	-	-	-	-	-

^aP<0.05; ^bP<0.01 vs blank control.

Table 3 Changes in biochemical indices of survived rats receiving CAO-GMS (mean±SD)

Group	Number of rats	ALT (U/L)	AST (U/L)	T-BiL (mmol/L)	D-BiL (μmmol/L)	BCr (μmmol/L)	BUN (mmol/L)
CAO-GMS-1	10	37.7±5.5	310±96	5.4±1.4	3.8±1.4	40.3±5.2	8.42±0.69
CAO-GMS-2	8	39.2±7.7	301±74	5.2±1.7	3.6±1.8	41.8±9.3	10.00±2.2
CAO-GMS-3	6	39.0±10	314±59	7.4±4.7	4.5±2.9	39.0±13	9.20±2.9
CAO-GMS-4	0	-	-	-	-	-	-
GMS	3	46.0±6.5	265±114	4.0±1.5	2.9±1.6	35.0±1.4	7.60±1.4
Blank control	8	38.0±11	278±114	4.5±1.3	3.2±1.6	38.7±3.5	8.60±1.8
CAO	8	36.0±7	307±84	4.8±1.9	3.2±1.7	39.4±2.4	8.00±1.6

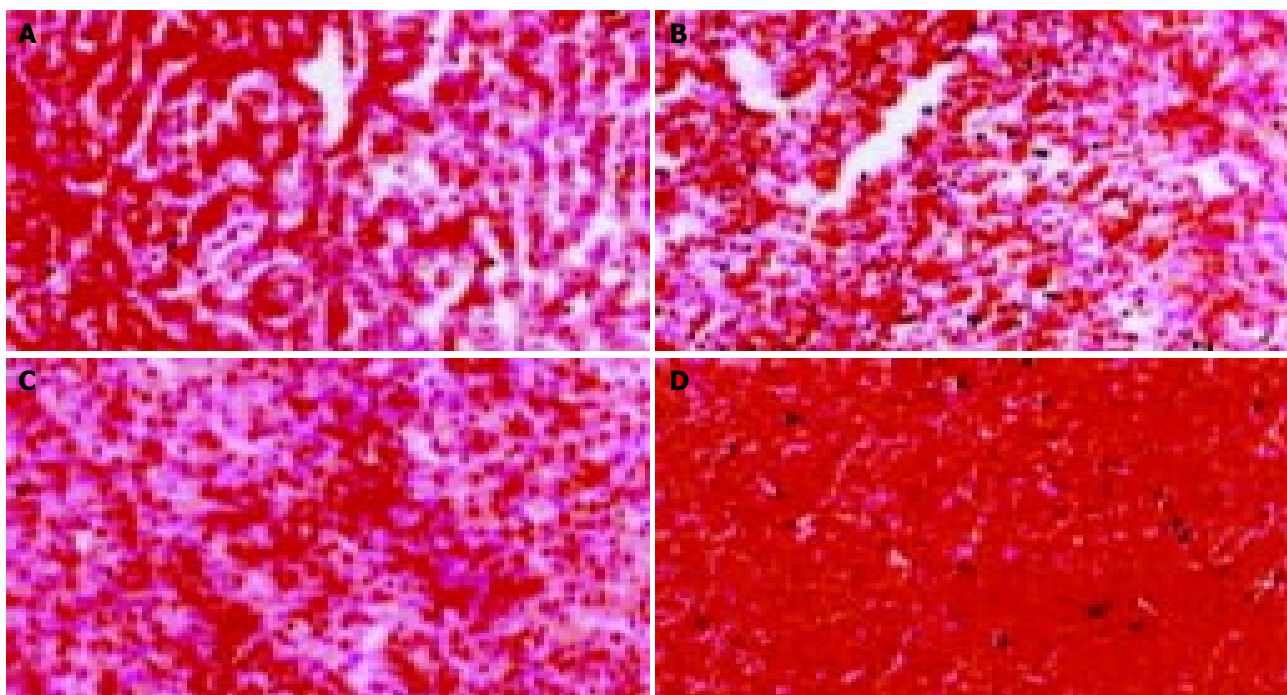


Figure 2 Long-term toxicity of CAO-GMS on the liver of dogs. A: CAO-GMS-H group receiving 15 mg/kg CAO-GMS every 4 wk; B: CAO-GMS-L group receiving 7.5 mg/kg CAO-GMS every 4 wk; C: GMS group receiving 15 mg/kg GMS every 4 wk; D: Blank control group receiving 10 mL/kg saline every 4 wk.

Two dogs of CAO-GMS-L group developed extensive moderate to severe hepatic cellular necrosis. The central region of the liver lobules showed moderate cellular edema with fatty degeneration and foci of coagulation necrosis, where neutrophilic leukocyte infiltration could be seen. Two dogs sacrificed on d 30 had extensive moderate cellular necrosis in the hepatic tissue and small necrotic foci, with ruptured normal structure.

In GMS group, two dogs were found to have whole lobular coagulation necrosis in the hepatic tissue where normal structure was disrupted. The other regions of the liver lobules showed moderate cellular edema with lymphocyte infiltration in the necrotic region. Two dogs sacrificed on d 30 exhibited extensive mild cellular necrosis in the hepatic tissue and spotty necrosis of the hepatic cells.

In the blank control group, mild cellular edema in the hepatic tissue was found in 2 dogs, with disrupted normal structure. Two dogs sacrificed on d 30 exhibited mild cellular necrosis in the hepatic tissue.

Pathological examination of the other vital organs showed no abnormal changes in the morphology of the kidney, lung, adrenal, pancreas, stomach, duodenum, ileum, colon, prostate, brain, spinal cord, heart, spleen, sternum (bone and marrow), bladder, uterus, ovary, thyroid, thymus and testis.

The above results demonstrated that CAO-GMS infused via the hepatic artery may cause irreversible ischemic necrosis

of the liver without visible damage on other organs. Delayed toxic response was not evident. The toxic effects on liver were identical with those observed in study of the acute toxicity. Partly due to the super-selective catheterization technique employed in this study, no improper embolization was found, indicating the importance of the technique in the clinical application for reducing complications.

Effects on nervous system of rats

The rats receiving 5 or 10 mg/kg CAO-GMS or 3 g/L CMC-Na showed emaciation, reduced activity and anorexia in the first 2 postoperative days, but resumed normal conditions on d 3, probably due to operative injury. No pupil abnormality or tremor was observed. All rats dropped less than 3 times in the balance test of rotarod model, indicating that CAO-GMS did not affect the balancing ability of the rats.

Effects on respiratory and cardiovascular systems of dogs

The effects of CAO-GMS on respiratory frequency, blood pressure and heart rate are shown in Table 4. CAO infused via the hepatic artery produced no marked effects on blood pressure and heart rate of the dogs ($P>0.05$). The respiratory frequency of the dogs within 3 h after administration of the agent was lowered, but not statistically ($P>0.05$ vs indices before embolization).

CAO-GMS or blank GMS produced no marked effects on blood pressure and heart rate of the dogs ($P>0.05$, Tables 5, 6).

Table 4 Changes in respiration, rates blood pressure and ECG in dogs at different time points after CAO (6.4 μ L/kg) interventional therapy (mean \pm SD)

Time point	Number of rats	Respiration frequency (breath/min)	Heart rate (beat/min)	Blood pressure (mmHg)	
				Systolic	Diastolic
Preoperation	4	17.0 \pm 10.2	198.5 \pm 38.4	147.8 \pm 8.2	116.0 \pm 11.5
30 min postoperative	4	15.0 \pm 7.0	193.5 \pm 36.1	141.5 \pm 8.2	114.8 \pm 9.7
60 min postoperative	4	16.0 \pm 8.5	189.3 \pm 27.1	140.5 \pm 8.9	115.8 \pm 9.3
120 min postoperative	4	17.8 \pm 9.5	190.5 \pm 23.6	141.5 \pm 3.3	117.0 \pm 5.0
180 min postoperative	4	13.8 \pm 6.0	189.0 \pm 28.4	143.5 \pm 5.8	119.0 \pm 6.3

Table 5 Changes in respiration, blood pressure and ECG in dogs at different time points after CAO-GMS interventional therapy (mean±SD)

Time point	Dosage	Number of rats	Respiration frequency (/min)	Heart rate (/min)	Blood pressure (mmHg)	
					Systolic	Diastolic
Preoperation	0.10	6	19.0±5.2	219.0±22.7	142.5±9.0	112.7±9.1
	0.03	6	13.5±4.9	196.0±28.5	144.7±12.2	116.2±9.8
30 min postoperative	0.10	6	20.5±6.7	214.7±19.1	142.7±7.3	113.0±8.6
	0.03	6	14.0±4.9	198.3±17.7	146.3±11.3	118.8±12.6
60 min postoperative	0.10	6	19.7±7.7	211.5±18.7	142.3±6.4	113.5±8.1
	0.03	6	12.3±3.4	194.0±16.6	144.0±10.7	119.2±13.6
120 min postoperative	0.10	6	19.5±7.8	211.7±25.0	142.3±10.0	114.0±10.7
	0.03	6	15.3±5.5	193.7±20.2	145.0±9.1	118.8±9.2
180 min postoperative	0.10	6	20.3±8.9	209.3±30.2	141.5±12.3	114.5±13.1
	0.03	6	16.8±6.8	193.7±21.6	143.8±9.5	119.2±9.5

Table 6 Changes in respiration, blood pressure and ECG in dogs at different time points after GMS (0.1 g) interventional therapy (mean±SD)

Time point	Number of rats	Respiration frequency (/min)	Heart rate (/min)	Blood pressure (mmHg)	
				Systolic	Diastolic
Preoperation	5	20.4±6.2	186.6±28.3	133.4±16.0	109.4±16.9
30 min postoperative	5	18.0±5.8	178.2±28.6	139.8±20.0	116.0±14.9
60 min postoperative	5	18.2±5.8	179.0±29.2	143.8±20.7	117.2±17.4
120 min postoperative	5	17.4±3.8	183.8±34.1	146.0±17.7	121.0±18.9
180 min postoperative	5	18.0±4.1	180.0±37.5	142.6±20.0	116.8±19.7

The respiratory frequency of the dogs within 3 h after the administration was lowered, but not significantly ($P>0.05$ vs indices before embolization).

Effects on respiratory blood pressure and heart rate graphs

The recorded graphical data also indicated the same results (Figure 3) as above.

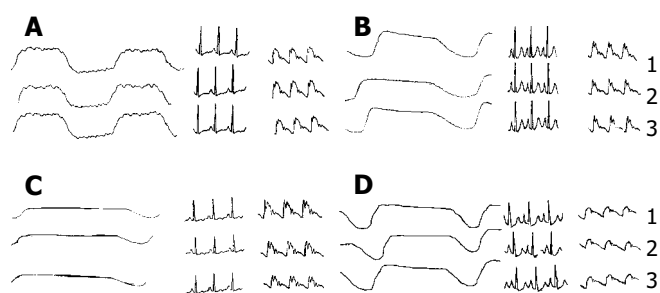


Figure 3 Effects of CAO-GMS infused via the hepatic artery on respiration, blood pressure and heart rate of dogs. A: Blank control group (with 3 g/L CMC-Na, 10 mL/kg); B: CAO-GMS group (with CAO-GMS, 0.1 g); C: CAO-GMS group (with CAO-GMS, 0.03 g); D: CAO group (with CAO, 6.4 µL/kg); 1: Before administration; 2: 60 min after administration; 3: 180 min after administration.

DISCUSSION

Transarterial chemoembolization (TACE) is most commonly adopted for palliative treatments in patients with hepatocellular carcinoma (HCC)^[32,33], but the shrinkage of neoplasm comes at the price of sacrificing the hepatic function and in the long-term effects, it does not significantly differ from conservative therapy^[34]. Improvement in the operative technique and in the agents used for interventional therapy is therefore much desired to produce better anti-tumor effect with low toxicity and liver

protection. By producing CAO-GMS, we take full advantage of CAO of its anti-tumor, immune-enhancing effects with low-toxicity^[12-26]. To enhance the effect of embolizing the trophic vessels for hepatoma, CAO was coupled with biodegradable microsphere (50-100 µm in diameter).

Previous studies demonstrated that CAO-GMS exhibited marked inhibitory effects on transplanted liver cancer in rats, which were attributed to the blocking of trophic vessels of the hepatoma by the microspheres and the therapeutic effects of CAO released slowly from the degraded microspheres^[27-30].

In this study, CAO-GMS was not found to affect respiration, blood pressure and heart rate, *etc.*, nor did it elicit acute or long-term toxic response, but at high doses, CAO-GMS embolization via the hepatic artery might induce significant increase in AST and ALT as well as irreversible ischemic necrosis of the liver. This was a sign of hyperreactive acute liver injury, as was similar to the clinical effect of other chemotherapeutic microspheres at high doses^[35,36], and predominantly responsible for its untoward, or even lethal effects.

CAO-GMS or blank GMS administered via the hepatic artery in normal animals caused embolization in the kidney and untargeted liver lobes, leading to the death of animals, which, however, did not happen with CAO or saline. This result indicates that CAO alone normally does not induce the adverse effects, which arise from undesired embolization of CAO-GMS as with other chemotherapeutic microspheres^[36,37]. Based on these facts, we concluded that the most probable reason for the acute hyperreactive response was the sudden accumulative embolization in the liver or undesired embolization as in the renal artery.

The dose adopted for embolization and the operation technique are crucial for clinical application of CAO-GMS. Most researchers preferred the use of computed tomography (CT) to determine individualized dosage rather than a conventionally fixed dosage, along with super-selective catheterization techniques to reduce reflux embolization of the microspheres. These techniques were believed to enhance the safety of the CAO-

GMS interventional therapy.

In general, the results of this study demonstrated that CAO-GMS is fairly safe for interventional therapy but individual difference should be fully considered in its clinical application. Clinicians are advised to determine the embolization dosage and interventional method individually to avoid the undesired embolization caused by the microspheres. We propose the use of superselective catheterization technique to precisely block the trophic artery of the hepatoma, and the exact dosage of CAO-GMS should be determined according to the size, location and trophic vessels of the tumors to prevent undesired embolization or complications after the interventional therapy.

REFERENCES

- 1 Wang Y, Wang MZ. Study on the quality of *Rhizoma Curcuma*. *Yaouxue Xuebao* 2001; **36**: 849-853
- 2 Li AQ, Hu XJ, Deng YH, Yao CS, Wang SJ, Chen JM. The chemical constituents of the volatile oil of *Curcuma Wenyujin* Y. H. Chen et C. Ling. *Zhongcaoyao* 2001; **33**: 782-783
- 3 Huang KX, Tao ZM, Zhang AJ, Peng SL, Ding LS. Studies on chemical constituents of *Curcuma aromatica* salisb. *Zhongguo Zhongyao Zazhi* 2000; **25**: 163-165
- 4 Guo YT, Chu XK, Chen YR, Wu XY, Chen G, Lu XR. Studies on constituents of wenezhu (*Curcuma aromatica Salise*). *Yaouxue Xuebao* 1980; **15**: 251-252
- 5 Yang SD, Chen YH. The determination of curcumol in the volatile oil of *Curcuma aromatica* by phloroglucinol spectrophotometry. *Yaouxue Xuebao* 1980; **15**: 228-233
- 6 Yang S, Chen J, Chen Y. Determination of curcumol in the volatile oil of *Curcuma aromatica*. *Yaouxue Xuebao* 1979; **14**: 356-361
- 7 Li CZ. Anti-inflammatory effect of the volatile oil from *Curcuma aromatica*. *Zhongyao Tongbao* 1985; **10**: 38-40
- 8 Fu NW. Antitumor effect and pharmacological actions of beta-elemene isolated from the rhizome of *Curcuma aromatica*. *Zhongyao Tongbao* 1984; **9**: 83-87
- 9 Zeng LL, Wang GY, Wang DX, Chen CH, Xu SY. Studies on the active ingredient of *Curcuma aromatica* Salisb and its effects. *Yaouxue Xuebao* 1982; **17**: 946-950
- 10 Dai LM, Chen MZ, Xu SY. The therapeutic effect of the Chinese drug Yu-Jin (*Curcuma aromatica salisb*) on experimental allergic encephalomyelitis of the guinea pig. *Yaouxue Xuebao* 1982; **17**: 692-695
- 11 Qian ZC, Liu JY, Zhao SR, Yu LH, Zhang DY, Wei WH. Prophylactic effect of active immunization with *Curcuma aromatica* treated tumor cells—exploration of mechanism of action of *Curcuma aromatica*. *Yaouxue Xuebao* 1981; **16**: 892-896
- 12 Li GD, Xu F, Shen AJ. Research progress of *Curcuma aromatica* oil. *Zhongguo Yaouxue Zazhi* 2002; **37**: 806-809
- 13 Tan M, Bin XN, Wu WY, Wang B, Zhang WB, Xiao CM. Effect of curcuma aromatica oil (CAO) on cellular apoptosis of hepatoma carried by mice. *Zhongxiyi Jiehe Ganbing Zazhi* 2002; **12**: 290-291
- 14 Wang J, Wang SQ, Ni H, Chen L, Song WQ. Experimental studies in the inhibitory effects of *Curcuma aromatica* oil on human hepatic cancer cell line SMMC-7721 growth. *Tianjin Zhongyiyao* 2003; **20**: 48-50
- 15 Shi LC, Wang B, Wu WY, Xiao CM, He QL. Study on molecule mechanism of inhibiting hepatoma of *Curcuma aromatica* oil in mice. *Zhongyao Yaoli Yu Linchuang* 2002; **18**: 6-7
- 16 Shi LC, Wu WY, Zhang WB, Ou YQ, Tan M, Xiao CM. Effect of curcuma aromatica oil on proliferating cell nuclear antigen of hepatoma in mice. *Shijie Huaren Xiaohua Zazhi* 1999; **7**: 156-157
- 17 Wu WY, Luo YJ, Cheng JH, Chang G, Xu Q, Liu WS, Li RX. Image cytometric DNA analysis of hepatic carcinomas carried by mice treated by *Curcuma aromatica* oil (CAO). *Zhongxiyi Jiehe Ganbing Zazhi* 1999; **9**: 18-20
- 18 Wu WY, Xu Q, Shi LC, Zhang WB. Inhibitory effects of *Curcuma aromatica* oil on proliferation of hepatoma in mice. *World J Gastroenterol* 2000; **6**: 216-219
- 19 Wu W, Liu K, Tang X. Preliminary study on the antitumor immuno-protective mechanism of beta-elemene. *Zhonghua Zhongliu Zazhi* 1999; **21**: 405-408
- 20 Li B, Liang N. Advances in the clinical application and experimental study of *Curcuma zedoaria* oil preparations. *Zhongyaocai* 2003; **26**: 68-71
- 21 Han MJ, Ren K, Zhao ZC, Zhang XT. Oleum curcuma compound used in hepatic arterial embolization to treat hepatocellular carcinoma: follow up report of 84 cases. *Linchuang Fangshexue Zazhi* 1998; **17**: 112-114
- 22 Cheng JH, Chang G, Wu WY. A controlled clinical study between hepatic arterial infusion with embolized curcuma aromatic oil and chemical drugs in treating primary liver cancer. *Zhongguo Zhongxiyi Jiehe Zazhi* 2001; **21**: 165-167
- 23 Chen CY, Xu K, Zhu DY, Wu WY, Deng H. Treatment of secondary hepatocarcinoma by hepatic artery perfusion embolism of oleum Curcumae: a clinical observation of 28 cases. *Xinzhongyi* 2003; **35**: 23-24
- 24 Cheng JH, Wu WY, Liu WS, Chang G, Liu YL, Yang ZG. Therapeutic effect of *Curcuma aromatica* oil infused via hepatic artery against primary liver neoplasms: 17 cases. *Shijie Huaren Xiaohua Zazhi* 1999; **7**: 92
- 25 Wu WY, Luo YJ, Cheng JH, Chang G, Liu WS, Li RX. Therapeutic effect of *Curcuma aromatica* oil infused via hepatic artery against transplanted hepatoma in rats. *Huaren Xiaohua Zazhi* 1998; **6**: 859-861
- 26 Deng R, Chen JM, Gao SC, Ding Y, Xu HD. Determination of Zedoary turmeric oil gelatin microspheres. *Zhongguo Yiyuan Yaouxue Zazhi* 2001; **21**: 79-81
- 27 Deng R, Chen JM, Wu WY. The anti-tumor activity of Zedoary turmeric oil gelatin microspheres for heparical arterial embolization. *Shenyang Yaoke Daxue Xuebao* 2000; **17**: 197-199
- 28 Wu WY, Deng R, Ou Y. Therapeutic efficacy of microsphere-entrapped curcuma aromatica oil infused via hepatic artery against transplanted hepatoma in rats. *Zhonghua Ganzangbing Zazhi* 2000; **8**: 24-26
- 29 Deng R, Chen JM, Yao CS, Wu WY. Zedoary turmeric oil gelatin microspheres for hepatic arterial embolization. *Yaouxue Xuebao* 2000; **35**: 539-543
- 30 Wu WY, Guo WJ, Chang G. Effect of CAO released from MS-CAO on human hepatoma cell line SMMC-7721. *Shijie Huaren Xiaohua Zazhi* 2003; **11**: 260-263
- 31 Lindell B, Aronsen KF, Rothman U. Repeated arterial embolization of rat livers by degradable microspheres. *Eur Surg Res* 1977; **9**: 347-356
- 32 Qian J, Feng GS, Vogl T. Combined interventional therapies of hepatocellular carcinoma. *World J Gastroenterol* 2003; **9**: 1885-1891
- 33 Cheng JH, Liu LH. Advances in research of primary liver cancer treatment with Chinese herbal medicine embolization. *Zhongguo Zhongxiyi Jiehe Zazhi* 1997; **17**: 187-190
- 34 Trinchet JC, Rached AA, Beaugrand M, Mathieu D, Chevret S, Chastang C. A comparison of lipiodol chemoembolization and conservative treatment for unresectable hepatocellular carcinoma. *N Engl J Med* 1995; **332**: 1256-1261
- 35 Li ZH, Li L, Yan LN, Lu WS, Xie XD, Luo YL. The side effect and its prevention of intra radioembolization using phosphorus-32 labelled glass microspheres for patients with nonresectable liver cancer. *Huaxi Yixue* 2002; **17**: 29-32
- 36 Luo YK, Liang P, Dong BW, Yu XL, Su L. Selective puncture to embolize the portal vein with NBCA injection in rats: study on its efficacy and safety. *Zhongguo Chaosheng Yixue Zazhi* 2002; **18**: 168-172
- 37 Li L, Yan LN, Chen XL, Wu YT, Sun WH, Li ML. The side effect and complication of intraarterial phosphorous -32 glass microspheres for patients with advanced hepatoma. *Shengwu Yixue Gongchengxue Zazhi* 1997; **14**: 376-379

Histone acetylation regulates $p21^{WAF1}$ expression in human colon cancer cell lines

Ying-Xuan Chen, Jing-Yuan Fang, Hong-Yin Zhu, Rong Lu, Zhong-Hua Cheng, De-Kai Qiu

Ying-Xuan Chen, Jing-Yuan Fang, Hong-Yin Zhu, Rong Lu, Zhong-Hua Cheng, De-Kai Qiu, Renji Hospital, Shanghai Second Medical University, Shanghai Institute of Digestive Disease, Shanghai 200001, China

Supported by the National Natural Science Foundation of China, No. 30170413 and Foundation for the Authors of National Excellent Doctoral Dissertation of China, No. 199946 and Foundation of Shanghai Education Committee, No. 02SG45

Correspondence to: Dr. Jing-Yuan Fang, Shanghai Institute of Digestive Disease, Renji Hospital, Shanghai Second Medical University, Shanghai 200001, China. jingyuanfang@yahoo.com

Telephone: +86-21-63200874 **Fax:** +86-21-63266027

Received: 2004-02-02 **Accepted:** 2004-02-24

Abstract

AIM: To investigate the effect of histone acetylation on regulation of $p21^{WAF1}$ gene expression in human colon cancer cell lines.

METHODS: Two cell lines, Colo-320 and SW1116 were treated with either trichostatin or sodium butyrate. Expressions of $p21^{WAF1}$ mRNA and protein were detected by real-time RT-PCR and Western blotting, respectively. Acetylation of two regions of $p21^{WAF1}$ gene-associated histones and total cellular histones were examined by chromatin immunoprecipitation assay and Western blotting.

RESULTS: Trichostatin or sodium butyrate re-activated $p21^{WAF1}$ transcription resulted in up-regulated $p21^{WAF1}$ protein level in colon cancer cell lines. Those effects were accompanied by an accumulation of acetylated histones in total cellular chromatin and $p21^{WAF1}$ gene-associated region of chromatin.

CONCLUSION: Histone acetylation regulates $p21^{WAF1}$ expression in human colon cancer cell lines, Colo-320 and SW1116.

Chen YX, Fang JY, Zhu HY, Lu R, Cheng ZH, Qiu DK. Histone acetylation regulates $p21^{WAF1}$ expression in human colon cancer cell lines. *World J Gastroenterol* 2004; 10(18): 2643-2646 <http://www.wjgnet.com/1007-9327/10/2643.asp>

INTRODUCTION

Cell cycle progression is controlled by various cyclin-dependent kinases (CDKs), whose activation is carefully regulated at multiple levels including the induction and degradation of cyclin protein, CDKs phosphorylation by cyclin-activating kinase, and the induction of CDK inhibitors (CDKIs)^[1]. CDKI $p21^{WAF1}$ was first cloned and characterized as an important effector that acts to inhibit CDK activity in p53 mediated cell cycle arrest in response to various agents^[2]. Increased expression of $p21^{WAF1}$ may play a crucial role in the G₁/S phase arrest induced in transformed cells, and may prevent the progression of neoplasia^[3].

Histone acetylation is emerging as a major regulatory mechanism thought to modulate gene expression by altering the accessibility of transcription factors to DNA and recent studies suggest that these alterations may also be important in the process of neoplasia formation^[4]. The level of histone acetylation depends on the activity of histone acetyltransferases (HATs) and histone deacetylases (HDACs). An important approach that has been used to study the function of chromatin acetylation is the use of specific inhibitors of HDAC. Trichostatin A^[5,6] (TSA, a hybrid polar compound of specific inhibitor) and sodium butyrate^[4] (a short chain fatty acid produced in human colon by bacterial fermentation of carbohydrate) were reported to inhibit HDAC activity.

Previously it was revealed that acetylation of gene-associated histone or total cellular histone alone regulated $p21^{WAF1}$ expression in colon cancer cell lines^[7,8]. We have shown^[9] that TSA or sodium butyrate induced G₁ phase cell cycle arrest was linked to increased expression of $p21^{WAF1}$. However, little is known about the regulation of acetylation of both gene-associated histone and total cellular histone on $p21^{WAF1}$ expression in human colon cancer. It is as yet not clear about the effect of histone acetylation on $p21^{WAF1}$ protein in Colo-320 and SW1116 cell lines. Therefore, in the present study, we further investigated whether TSA and sodium butyrate induced overexpression of $p21^{WAF1}$ resulted from hyperacetylation of gene-associated histones and histones in total cellular chromatin in two human colon cancer cell lines, Colo-320 and SW1116.

MATERIALS AND METHODS

Cell culture

Human colon cancer-derived cell lines Colo-320 and SW1116 were obtained from Shanghai Institute of Biochemistry and Cell Biology, SIBS, China and Shanghai Second Medical University Ruijin Hospital, respectively. Colo-320 and SW1116 cells were maintained in RPMI 1640 supplemented with 100 mL/L heat-inactivated fetal bovine serum, 2 mmol/L L-glutamine, 100 U/mL penicillin and 100 µg/mL streptomycin at 37 °C in a 50 mL/L CO₂ incubator.

Treatment of cells with TSA or sodium butyrate

Colon cancer cell lines were exposed to 1 µmol/L TSA or 5 mmol/L sodium butyrate (Sigma, St. Louis, MO) alone for 24 h, as described by Siavoshian *et al.*^[10]. The control cultures were treated simultaneously with phosphate-buffered saline (PBS) or alcohol (control for TSA treatment, because TSA can only be dissolved in alcohol).

Western blotting of acetylated histones and $p21^{WAF1}$

Colo-320 cells were cultured as described below with or without treatment. Cells were recovered by centrifugation, washed twice with ice-cold PBS, and resuspended for lysis in 1 mL buffer A (10 mmol/L HEPES, pH 7.4, 10 mmol/L KCl, 1.5 mmol/L MgCl₂, 0.5 mmol/L DTT, 0.2 mmol/L PMSF, 1 µg/mL protease inhibitors, 0.25 g/L NP40) for 15 min with rotation at 4 °C and the nuclear pellet was resuspended in 100 µL buffer B (20 mmol/L HEPES, pH 7.4, 420 mmol/L NaCl, 1.5 mmol/L MgCl₂, 0.2 mmol/L EDTA,

250 mL/L glycerol, 0.5 mmol/L DTT, 0.2 mmol/L PMSF, 1 µg/mL protease inhibitors) for 30 min, then the soluble nuclear protein was collected by centrifugation. Fifty µg (for acetylated histone H3 and H4) or 150 µg (for p21^{WAF1} protein) of nuclear extracts was boiled in loading buffer (125 mmol/L Tris-HCl, pH 6.8, 40 g/L SDS, 200 g/L glycerol, 0.05 g/L bromphenol blue) for 5 min and then loaded onto a 150 g/L SDS-polyacrylamide gel. After electrophoresis, proteins were transferred onto nitrocellulose membrane (0.45 µm). The following antibodies were used: rabbit polyclonal antibody against acetylated histone H3 or H4 (Upstate Biotechnology, Lake Placid, NY) and goat polyclonal antibody against p21^{WAF1} (C19, Santa Cruz, California). The bindings of antibodies were detected using ECL-system (Amersham Pharmacia Biotech, Piscataway, NJ, USA) and membranes were then exposed to Kodak BioMax film for 1 min. Antibody against β-actin (Sigma) in Western blot was used as a control for protein concentration.

Real-time RT-PCR for p21^{WAF1} mRNA

mRNA level of p21^{WAF1} was measured using a real-time quantitative PCR system. Total RNA samples from SW1116 and Colo-320 cells with or without treatment were prepared by TriZol Reagent. Gene-specific TaqMan probes and PCR primers were designed using Primer Express software (PE Biosystems, Foster City, CA). The sequence for forward and reverse primers and the probe are shown in Table 1. Triplicate PCR reactions were prepared for each cDNA sample. PCR consisted of 40 cycles of 95 °C denaturation (15 s) and 60 °C annealing/extension (60 s). Thermal cycling and fluorescent monitoring were performed using an ABI 7 700 sequence analyzer (PE Biosystems). The point at which the PCR product is first detected above a fixed threshold, termed cycle threshold (Ct), was determined for each sample, and the average Ct of triplicate samples was calculated. To determine the quantity of gene-specific transcripts present in treated cells cDNA relative to untreated cells, their respective Ct values were first normalized by subtracting the Ct value obtained from the β-actin control ($\Delta Ct = Ct_{FAM} - Ct_{VIC}$). The concentration of gene-specific mRNA in treated cells relative to untreated cells was calculated by subtracting the normalized Ct values obtained with untreated cells from those obtained with treated samples ($\Delta \Delta Ct = \Delta Ct_{treated} - \Delta Ct_{untreated}$), and the relative concentration was determined ($2^{-\Delta \Delta Ct}$). Altered mRNA expression was defined as 3-fold difference in the expression level in cells after the treatment relative to that before treatment^[11].

Chromatin immunoprecipitation (ChIP) assay

A ChIP assay kit from Upstate Biotechnology was used

according to the manufacturer's protocol and Richon's report^[12]. Colo-320 cells that were either treated with 1 µmol/L TSA or 5 mmol/L sodium butyrate for 24 h or untreated were plated at a density of 10×10^6 /T25 flask. Formaldehyde was then added to the cells to a final concentration of 10 g/L, and the cells were incubated at 37 °C for 10 min. The medium was removed, and the cells were suspended in 1 mL of ice-cold PBS containing protease inhibitors [1 mmol/L phenylmethylsulfonyl fluoride (PMSF), 1 µg/mL aprotinin and 1 µg/mL pepstatin A, Boehringer Mannheim]. Cells were pelleted, resuspended in 0.2 mL of SDS lysis buffer, and incubated on ice for 10 min. Lysates were sonicated. The majority of DNAs ranged from 200 bp to 1 000 bp. Debris was removed from samples by centrifugation for 10 min at 15 000 g at 4 °C in a microcentrifuge. An aliquot of the chromatin preparation (200 µL) was set aside and designated as the input. Supernatants were 10-fold diluted in ChIP dilution buffer containing the protease inhibitors as above, and 80 µL of a salmon sperm DNA/protein A-agarose beads was added and incubated for 30 min at 4 °C with rocking. Beads were pelleted by centrifugation, and supernatants were placed in tubes with 10 µg of antibody against acetylated histone H3 or H4, or normal rabbit IgG, and incubated overnight at 4 °C with rotation. Salmon sperm DNA/Protein A-agarose beads (60 µL) was added, and samples were rocked for 1 h at 4 °C. Protein A complexes were centrifuged and washed 5 times for 5 min each with low salt buffer, high salt buffer, LiCl buffer and TE buffer, respectively. Immune complexes were eluted twice with 250 µL of elution buffer (10 g/L SDS/0.1 mol/L NaHCO₃) for 15 min at room temperature. NaCl (5 mol/L, 20 µL) was added to the combined eluate, and the samples were incubated at 65 °C for 4 h. EDTA, Tris-HCl, pH 6.5, and proteinase K were then added to the samples at a final concentration of 10 mmol/L, 40 mmol/L, and 0.04 µg/µL, respectively, and the samples were incubated at 45 °C for 1 h. Immunoprecipitated DNA (both immunoprecipitation samples and input) was recovered by phenol/chloroform extraction and ethanol precipitation and analyzed by PCR. p21^{WAF1}-specific primers were used to carry out PCR. Sequences of two sets of primers for p21^{WAF1} PCR and PCR condition are shown in Table 2. The first set primer was used to amplify -576 to -293 and the second set primer was used to amplify -51 to +77 of p21^{WAF1} promoter and exon 1, which contained the transcription factor E2A binding sites.

RESULTS

HDAC inhibitors resulted in accumulation of acetylated core histones H3 and H4

Western blotting showed that before incubation with TSA or

Table 1 Sequence of primers and probes for real-time PCR

Gene	Primer (forward) (5'→3')	Primer (reverse) (5'→3')	Probe	GenBank accession number
p21 ^{WAF1}	CTG GAG ACT CTC AGG GTC GAA	GGA TTA GGG CTT CCT CTT GGA	ACG GCG GCA GAC CAG CAT GA	NM_078467
β-actin	CTG GCA CCC AGC ACA ATG	GGA CAG CGA GGC CAG GAT	ATC ATT GCT CCT CCT GAG	BC016045

Table 2 Sequence of primers and program of PCR for ChIPs

Primers	Sense (5'→3')	Antisense (5'→3')	Size of product and PCR condition	GenBank accession number
γ-actin	GGA CCT GGC TGG CCG GGA CC	GTG GCC ATC TCC TGC TCG AA	153 bp 95 °C 5 min 95 °C 1 min, 56 °C 1 min, 72 °C 1 min, 35 cycles	
p21 ^{WAF1} (P1)	CGT GGT GGT GGT GAG CTA GA	CTG TCT GCA CCT TCG CTC CT	296 bp 95 °C 5 min 95 °C 1 min, 58 °C 1 min, 72 °C 1 min, 35 cycles	U24170
p21 ^{WAF1} (P2)	GGT TGT ATA TCA GGG CCG	CTC TCA CCT CCT CTG AGT GC	128 bp 95 °C 5 min 95 °C 1 min, 58 °C 1 min, 72 °C 1 min, 35 cycles	U24170

sodium butyrate, the levels of acetylated H3 and H4 in colo-320 cells were low. Incubation with HDAC inhibitors resulted in the accumulation of acetylated histones H3 and H4 (Figure 1).

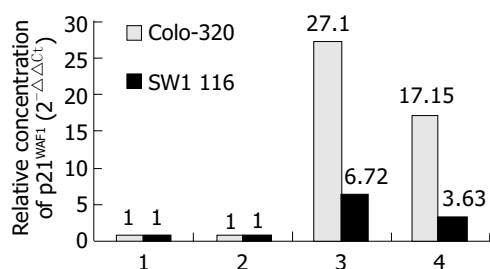


Figure 1 Western blotting of acetylated histones H3, H4 and $p21^{WAF1}$ protein in Colo-320 cells. Lane 1: Control (PBS); lane 2: Control (alcohol); lane 3: TSA 1 μmol/L, 24 h; lane 4: NaBu 5 mmol/L, 24 h.

Either TSA or sodium butyrate induced re-expression of $p21^{WAF1}$ mRNA and protein

To understand the change of $p21^{WAF1}$ expression level following HDAC inhibitors treatment, we examined accumulation of mRNA and protein by RT-PCR and Western blotting. As shown in Figures 1 and 2, $p21^{WAF1}$ mRNA and protein were activated after treatment of TSA and sodium butyrate. In addition, Colo-320 cells had an initial increase in $p21^{WAF1}$ expression to a higher level than that in SW1116 cells.

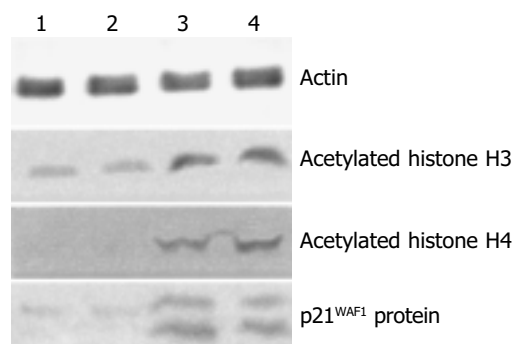


Figure 2 RT-PCR showed either TSA or sodium butyrate induced overexpression of $p21^{WAF1}$ mRNA in human colon cancer cell lines Colo-320 and SW1116. Lane 1: Control (PBS); lane 2: Control (alcohol); lane 3: TSA 1 μmol/L, 24 h; lane 4: NaBu 5 mmol/L, 24 h.

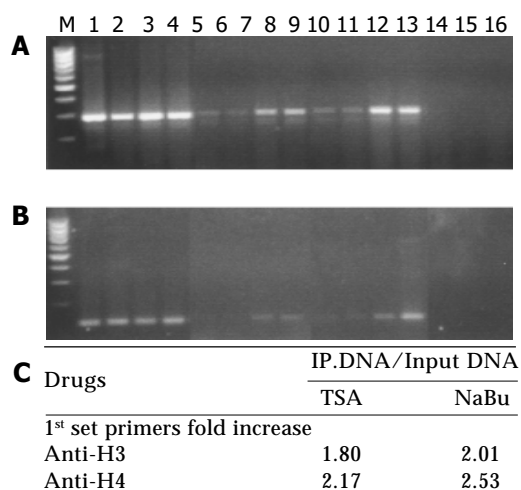


Figure 3 HDAC inhibitors induced accumulation of acetylated histones H3 and H4 in chromatin associated with $p21^{WAF1}$

gene. A: PCR products for the 1st set primer of $p21^{WAF1}$; B: PCR products for the 2nd set primer of $p21^{WAF1}$; C: The figure in A and B was scanned and quantified by using IMAGE analysis software. The ratio between input DNA and precipitated DNA was calculated for each treatment and primer set. The increase after treatment with either TSA or sodium butyrate was calculated from indicated ratios. PCR products of the 2nd primer were not visualized on agarose gel before treatment with HDAC inhibitor, so it could not be calculated. Input DNA, lanes 1-4: Soluble chromatin was immunoprecipitated with antiacetylated histone H3 antibody; lanes 5-8: Soluble chromatin was immunoprecipitated with antiacetylated histone H4 antibody; lanes 9-12: Normal rabbit serum as negative control; lanes 13-16, 1, 5, 9, 13: PBS control; lanes 2, 6, 10, 14: Alcohol control; lanes 3, 7, 11, 15: TSA 1 μmol/L, 24 h; lanes 4, 8, 12, 16: NaBu 5 mmol/L, 24 h.

$p21^{WAF1}$ gene-associated histone H3 was hyperacetylated in colon cancer cells treated with TSA or sodium butyrate

To determine whether histone acetylation reflected $p21^{WAF1}$ transcription and the functional interaction between $p21^{WAF1}$ and TSA or sodium butyrate treatment, ChIPs-PCR was performed. As shown in Figure 3, the densities of bands of $p21^{WAF1}$ gene-associated acetylated histones H4 and H3 were higher in chromatin extracted from Colo-320 cells treated with either TSA or sodium butyrate than that from cells mock treated, either the first or the second set PCR primer.

Taken together, TSA or sodium butyrate activated the transcription of $p21^{WAF1}$ through acetylation of histones H4- and H3-associated $p21^{WAF1}$ promoter.

DISCUSSION

Several lines of evidence suggest that histone acetylation plays a role in transcriptional regulation, probably by altering chromatin structure^[13]. Acetylation of core nucleosomal histones is regulated by the opposing activities of HATs and HDACs. The latter catalyze the removal of an acetyl group from the ε-amino group of lysine side chains of histones H2A, H2B, H3 and H4, thereby reconstituting the positive charge in lysine. Transcriptionally silent chromatin is composed of nucleosomes in which the histones have low levels of acetylation of lysine residues at their amino-terminal tails^[14,15]. Acetylation of histone neutralizes the positive charge in lysine residues and disrupts nucleosome structure, allowing unfolding of the associated DNA, access by transcription factors, and changes in gene expression. Chromatin fractions enriched in actively transcribed genes are also enriched in the more highly acetylated isoforms of the core histones^[16]. HDAC inhibitors appear to be selective with regard to the genes whose expression is altered^[17].

Total cellular histone acetylation is also involved in the regulation of gene expression. Several studies^[18] indicated that the effect of HDAC inhibitors on gene transcription was associated with an increased accumulation of acetylated histones H3 and H4 in total cellular chromatin. However, Lee's group^[19] showed an accumulation of acetylated histones H3 and H4 in total cellular chromatin after treatment with HDAC inhibitor (MS-275), but no change in the level of histone acetylation in chromatin-associated TGF-β I receptor gene. Therefore, we wanted to know whether HDAC inhibitor affected the acetylation level of histones in both gene-associated and total cellular chromatin. The data from ChIP and Western blotting suggested that $p21^{WAF1}$ transcription was dependent upon acetylation at the level of chromatin, since the level of $p21^{WAF1}$ promoter amplified from acetylated histone H3- or H4-associated chromatin was greater in chromatin isolated from HDAC inhibitor-treated cells than that from untreated cells. Accumulation of acetylated $p21^{WAF1}$ -associated histones induced by HDAC inhibitors was higher than that in total cellular chromatin, although there was accumulation of

acetylated histones H3 and H4 in total cellular chromatin.

It is noteworthy that, the level of acetylated histones H3 and H4 at the domain containing the transcriptional start site in *p21^{WAF1}* promoter and the binding sites of E2A was significantly higher than that at another domain or total cellular chromatin analyzed. The result of our observations suggested that *p21^{WAF1}* expression could be activated by histone acetylation of its transcription start domain in promoter. Therefore, a possible mechanism involved the binding of transcription factor E2A to *p21^{WAF1}* promoter at transcription start site of acetylated *p21^{WAF1}* gene-associated histones H3 and H4, and the enhancement of *p21^{WAF1}* gene transcription. It is known that histone acetylation can be targeted to specific promoters by gene-specific activator. E2A transcription factor belongs to the basic helix-loop-helix family of proteins^[20], which contains a conserved basic region responsible for DNA binding and a helix-loop-helix domain for dimerization^[21]. E2A binds *p21^{WAF1}* at the domain nearby TATA box in the promoter. TATA box-independent transcription of the *p21^{WAF1}* promoter has been previously reported^[22]. The proximal *p21^{WAF1}* promoter contains a TATA box^[23]. Some reports indicated that *p21^{WAF1}* was up-regulated by E2A binding to HTLV-1-infected T cells^[20]. Moreover, overexpression of E2A proteins, such as E47 has been shown to induce *p21^{WAF1}* promoter activity independent of p53 binding sites^[24,25].

Also, we showed that the levels of *p21^{WAF1}* mRNA and protein in colon cancer cells were very low, even difficult to detect before treatment. In Colo-320, *p21^{WAF1}* mRNA was increased by 27.1-fold and 17.15-fold after 1 μ mol/L TSA and 5 mmol/L sodium butyrate treatment, respectively. Accordingly, the protein level of *p21^{WAF1}* was elevated. Similar effects were shown in SW1116 cells (data not shown). Our data about TSA or sodium butyrate inducing *p21^{WAF1}* mRNA and protein expression are consistent with previous reports^[12].

In summary, this study demonstrated that HDAC inhibitor, TSA or sodium butyrate, activated the expressions of *p21^{WAF1}* mRNA and protein, and this increased expression was associated with an accumulation of acetylated histones in total cellular chromatin and the chromatin of *p21^{WAF1}* gene in these two colon cancer cell lines. It has been shown that *p21^{WAF1}* expression is reduced in adenomas and colorectal carcinomas. Our observations support the claim for the therapeutic potential of HDAC inhibitors in the treatment of colorectal carcinoma, because there is probably no mutation of the *p21^{WAF1}* gene in colorectal cancer.

ACKNOWLEDGEMENTS

Thanks are given to Mr. En-Lin Li, Ms. Wei-Qi Gu and Ms. Hong-Yin Zhu for performing cell culture and the real-time PCR assay and Western blotting.

REFERENCES

- 1 Sherr CJ. Mammalian G1 cyclins and cell cycle progression. *Proc Assoc Am Physicians* 1995; **107**: 181-186
- 2 Dulic V, Kaufmann WK, Wilson SJ, Tlsty TD, Lees E, Harper JW, Elledge SJ, Reed SI. p53-dependent inhibition of cyclin-dependent kinase activities in human fibroblasts during radiation-induced G1 arrest. *Cell* 1994; **76**: 1013-1023
- 3 Kim JS, Lee S, Lee T, Lee YW, Trepel JB. Transcriptional activation of p21(WAF1/CIP1) by apicidin, a novel histone deacetylase inhibitor. *Biochem Biophys Res Commun* 2001; **281**: 866-871
- 4 Archer SY, Hodin RA. Histone acetylation and cancer. *Curr Opin Genet Dev* 1999; **9**: 171-174
- 5 Magdinier F, Wolffe AP. Selective association of the methyl-CpG binding protein MBD2 with the silent p14/p16 locus in human neoplasia. *Proc Natl Acad Sci U S A* 2001; **98**: 4990-4995

- 6 Xiao H, Hasegawa T, Isobe K. p300 collaborates with Sp1 and Sp3 in p21 (waf1/cip1) promoter activation induced by histone deacetylase inhibitor. *J Biol Chem* 2000; **275**: 1371-1376
- 7 Hinnebusch BF, Meng S, Wu JT, Archer SY, Hodin RA. The effects of short-chain fatty acids on human colon cancer cell phenotype are associated with histone hyperacetylation. *J Nutr* 2002; **132**: 1012-1017
- 8 Hinnebusch BF, Henderson JW, Siddique A, Malo MS, Zhang W, Abedrapo MA, Hodin RA. Transcriptional activation of the enterocyte differentiation marker intestinal alkaline phosphatase is associated with changes in the acetylation state of histone H3 at a specific site within its promoter region *in vitro*. *J Gastrointest Surg* 2003; **7**: 237-244
- 9 Chen YX, Fang JY, Lu J. Epigenetics is involved in regulation of cell cycle and expression of tumor suppressor genes in human colon cancer cells. *Chin J Dig Dis* 2003; **4**: 105-110
- 10 Siavoshian S, Segain JP, Kornprobst M, Bonnet C, Cherbut C, Galmiche JP, Blottiere HM. Butyrate and trichostatin A effects on the proliferation/differentiation of human intestinal epithelial cells: induction of cyclin D3 and p21 expression. *Gut* 2000; **46**: 507-514
- 11 Scanlan MJ, Welt S, Gordon CM, Chen YT, Gure AO, Stockert E, Jungbluth AA, Ritter G, Jager D, Jager E, Knuth A, Old LJ. Cancer-related serological recognition of human colon cancer: identification of potential diagnostic and immunotherapeutic targets. *Cancer Res* 2002; **62**: 4041-4047
- 12 Richon VM, Sandhoff TW, Rifkind RA, Marks PA. Histone deacetylase inhibitor selectively induces *p21^{WAF1}* expression and gene-associated histone acetylation. *Proc Natl Acad Sci U S A* 2000; **97**: 10014-10019
- 13 Grunstein M. Histone acetylation in chromatin structure and transcription. *Nature* 1997; **389**: 349-352
- 14 Wolffe AP, Pruss D. Targeting chromatin disruption: transcription regulators that acetylated histones. *Cell* 1996; **84**: 817-819
- 15 Vettese-Dadey M, Grant PA, Hebbes TR, Crane-Robinson C, Allis CD, Workman JL. Acetylation of histone H4 plays a primary role in enhancing transcription factor binding to nucleosomal DNA *in vitro*. *EMBO J* 1996; **15**: 2508-2518
- 16 Struhl K. Histone acetylation and transcriptional regulatory mechanism. *Genes Dev* 1998; **12**: 599-606
- 17 Van Lint C, Emiliani S, Verdin E. The expression of a small fraction of cellular genes is changed in response to histone hyperacetylation. *Gene Expr* 1996; **5**: 245-253
- 18 Mishra N, Reilly CM, Brown DR, Ruiz P, Gilkeson G. Histone deacetylase inhibitors modulate renal disease in the MRL-lpr/lpr mouse. *J Clin Invest* 2003; **111**: 539-552
- 19 Lee BI, Park SH, Kim JW, Sausville EA, Kim HT, Nakanishi O, Trepel JB, Kim SJ. MS-275, a histone deacetylase inhibitor, selectively induces transforming growth factor beta type II receptor expression in human breast cancer cells. *Cancer Res* 2001; **61**: 931-934
- 20 de La Fuente C, Deng L, Santiago F, Arce L, Wang L, Kashanchi F. Gene expression array of HTLV type 1-infected T cells: Up-regulation of transcription factors and cell cycle genes. *AIDS Res Hum Retroviruses* 2000; **16**: 1695-1700
- 21 Murre C, McCaw PS, Baltimore D. A new DNA binding and dimerization motif in immunoglobulin enhancer binding, daughterless, MyoD and myc proteins. *Cell* 1989; **56**: 777-783
- 22 Datto MB, Yu Y, Wang XF. Functional analysis of the transforming growth factor beta responsive elements in the WAF1/Cip1/p21 promoter. *J Biol Chem* 1995; **270**: 28623-28628
- 23 Owen GI, Richer JK, Tung L, Takimoto G, Horwitz KB. Progesterone regulates transcription of the p21 (WAF1) cyclin-dependent kinase inhibitor gene through Sp1 and CBP/p300. *J Biol Chem* 1998; **273**: 10696-10701
- 24 Prabhu S, Ignatova A, Park ST, Sun XH. Regulation of the expression of cyclin-dependent kinase inhibitor p21 by E2A and Id proteins. *Mol Cell Biol* 1997; **17**: 5888-5896
- 25 Fang JY, Lu YY. Effects of histone acetylation and DNA methylation on p21^{WAF1} regulation. *World J Gastroenterol* 2002; **8**: 400-405

• COLORECTAL CANCER •

Clinical features and mismatch repair gene mutation screening in Chinese patients with hereditary nonpolyposis colorectal carcinoma

Shan-Run Liu, Bo Zhao, Zhen-Jun Wang, Yuan-Lian Wan, Yan-Ting Huang

Shan-Run Liu, Bo Zhao, Zhen-Jun Wang, Yuan-Lian Wan, Yan-Ting Huang, Department of Surgery, Peking University First Hospital, Beijing 100034, China

Supported by National Natural Science Foundation of China, No. 39970817, and Fund From Ministry of Education of China (the Former National Education Committee)

Correspondence to: Zhen-Jun Wang, Department of Surgery, Peking University First Hospital, 8 Xishiku Street, Xicheng District, Beijing 100034, China. wang3zj@sohu.com

Telephone: +86-10-66551122 Ext. 2270

Received: 2003-11-12 **Accepted:** 2003-12-29

Abstract

AIM: Hereditary nonpolyposis colorectal cancer (HNPCC) is an autosomal dominantly-inherited cancer-susceptibility syndrome that confers an increased risk for colorectal cancer and a variety of other tumors at a young age. It has been associated with germline mutations in five mismatch repair (MMR) genes (hMSH2, hMLH1, hPMS1, hPMS2, and hMSH6/GTBP). The great majority of germline mutations were found in hMSH2 and hMLH1. The purpose of this study was to analyze the clinical features of Chinese HNPCC patients and to screen hMSH2 and hMLH1 gene mutations.

METHODS: Twenty-eight independent Chinese families were collected, of which 15 met Amsterdam criteria I and 13 met the Japanese clinical diagnosis criteria. The data were recorded including sex, site of colorectal cancer (CRC), age of diagnosis, history of synchronous and/or metachronous CRC, instance of extracolonic cancers, and histopathology of tumors. Peripheral blood samples were collected from all pedigrees after formal written consents were signed. PCR and denaturing high-performance liquid chromatography (DHPLC) were used to screen the coding regions of hMSH2 and hMLH1 genes. The samples showing abnormal DHPLC profiles were sequenced by a 377 DNA sequencer.

RESULTS: One hundred and seventy malignant neoplasms were found in one hundred and twenty-six patients (multiple cancer in twenty-three), including one hundred and twenty-seven CRCs, fifteen gastric, seven endometrial, and five esophageal cancers. Seventy-seven point eight percent of the patients had CRCs, sharing the features of early occurrence (average age of onset, 45.9 years) and of the right-sided predominance reported in the literature. In Chinese HNPCC patients, gastric cancer occurred more frequently, accounting for 11.9% of all cancers patients and ranking second in the spectrum of HNPCC predisposing cancers. Synchronous CRCs occurred less frequently, only accounting for 3.1% of the total CRCs. Twenty percent of the colorectal patients had metachronous CRCs within 10 years after operation. Eight hMSH2 or hMLH1 gene sequence variations were found in twelve families, including the first Mongolian kindred with a hMSH2 gene mutation.

CONCLUSION: HNPCC is characterized by an early-age

onset, proximal predominance of CRC, multiple metachronous CRCs, and an excess of extra-colonic cancers. Frequent gastric cancer occurrence and less synchronous CRCs are the remarkable features in Chinese HNPCC patients. DHPLC is a powerful tool in hMSH2 and hMLH1 gene mutation screening. hMLH1 gene mutations, especially of the first nine exons, have been found more common than hMSH2 gene mutations in Chinese patients. Three of seven mutations have been found to be novel, and the germline G204X nonsense mutation in the third exon of hMSH2 has become the first MMR gene mutation found in Chinese Mongolian people.

Liu SR, Zhao B, Wang ZJ, Wan YL, Huang YT. Clinical features and mismatch repair gene mutation screening in Chinese patients with hereditary nonpolyposis colorectal carcinoma. *World J Gastroenterol* 2004; 10(18): 2647-2651
<http://www.wjgnet.com/1007-9327/10/2647.asp>

INTRODUCTION

Hereditary nonpolyposis colorectal cancer (HNPCC, or Lynch syndrome) is an autosomal dominantly-inherited cancer-susceptibility syndrome. It is estimated that HNPCC may account for 5-10% of the total colorectal cancers (CRC) worldwide^[1]. In Western countries, patients inheriting this predisposition are at a particularly high risk of developing CRC and endometrial cancer at a young age, and also at an increased risk of developing various other types of tumors, such as ovarian, uroepithelial, small intestine, biliary tract, stomach, brain, and skin cancers^[2]. Five mismatch repair (MMR) genes (hMSH2, hMLH1, hPMS1, hPMS2, and hMSH6/GTBP^[3-8]) have been known to be involved in this cancer susceptibility. Currently, more than 300 different mutations have been described in these genes, which account for approximately 500 HNPCC kindreds in the world^[9]. hMSH2 and hMLH1 germline mutations were found to be responsible for more than 90% of the HNPCC families^[10] (<http://www.nfdht.nl/>). Therefore, identification of the mutational incidence and spectrum of hMSH2 and hMLH1 genes is important. Identifying the clinical features of HNPCC in China, which might have some differences from those reported in Western countries, will facilitate its diagnosis and treatment. We described the clinical features and the results of mutation screening of both hMSH2 and hMLH1 genes in 28 HNPCC families registered in our hospital. We think that Chinese HNPCC patients have some unique clinic features and MMR gene defects.

MATERIALS AND METHODS

Clinical Data

Subjects were selected from 28 independent Chinese families from January 1992 to August 2003. Among these families, 15 met the Amsterdam criteria I^[11]. The criteria were as follows: (1) Three or more relatives had histologically-verified CRC, one of them was a first degree relative to the other two relatives; (2) At least two successive generations were affected; (3) One or

more CRC cases were diagnosed under 50 years of age; and (4) Familial polyposis of the colon was excluded. The Japanese clinical diagnosis criteria for HNPCC^[12] were used for the other 13 highly-suspected families that did not fully meet the Amsterdam criteria I. Families that met the following A or B were also clinically diagnosed as having HNPCC: A: a case with three or more CRCs within the first-degree relatives; B: a case with two or more CRCs within the first-degree relatives meeting one of the following criteria: age at onset of CRCs being under 50 years, right colon involvement, synchronous or metachronous multiple CRCs, or associated with synchronous or metachronous extracolorectal malignancies.

Detailed family and medical histories were obtained through interview with the proband, and a home visit to extended family members and an extensive review of medical records if available. Peripheral blood samples were collected from all participants after formal written consents were signed.

Eligible HNPCC families were registered and family members were followed up intensively. All patients were reviewed by telephone or outpatient visit at regular intervals. Data concerning sex, site of CRC, age of diagnosis, history of synchronous and/or metachronous CRC, instance of extracolonic cancers, and histopathology of tumors were documented and thoroughly verified.

DNA extraction and PCR amplification

Genomic DNA was isolated from peripheral blood lymphocytes according to the salting-out procedure^[13]. The entire hMLH1 and hMSH2 coding region and the splice junctions were amplified by PCR according to Weber methods^[14] with minor modifications.

DHPLC analysis

DHPLC analysis was performed on a Transgenomic WAVE system (Transgenomic Inc.) identical with that described previously^[15]. Briefly, PCR products (25 μ L) were denatured for 5 min at 95 °C and then gradually reannealed by decreasing sample temperature from 95 °C to 45 °C over a period of 30 min to form homo- and/or heteroduplexes. Crude PCR product (7-10 μ L) was loaded on the DHPLC column and eluted with a linear acetonitrile gradient at a flow rate of 0.9 mL/min. Gradient parameters were determined based on size and G-C content of the amplicon. Generally, an analysis took approximately 7 min, including column regeneration and re-equilibration to starting conditions. The column mobile phase consisted of a mixture of 0.1 mol/L triethylammonium acetate pH 7.0 (TEAA) with (buffer B) or without (buffer A) 250 mL/L acetonitrile. The temperature for heteroduplex analysis was primarily established by using the DHPLC melting algorithm WAVE MakerTM of the WAVETM instrument. The final temperature and denaturing condition for optimal resolution of homoduplexes and heteroduplexes of each fragment were experimentally determined.

DNA sequencing

PCR products displaying a double DHPLC peak indicating existence of heteroduplex were purified with micron microconcentrator filters (Amicon, Beverly, MA) to remove unwanted reagents from the PCR reaction and to concentrate the final products, which were then sequenced by a 377DNA sequencer. All mutations were sequenced in both directions and confirmed in other family members.

RESULTS

Statistics on patients and tumors

A total of 28 kindreds were studied, all of them met the Japanese clinical diagnosis criteria and 15 of them met the Amsterdam I criteria. There were 9 Lynch syndrome I families, in which only colorectal cancers were found, and 19 Lynch syndrome II families, which were characterized by concurrent extracolonic malignancies.

One hundred and seventy malignant neoplasms were found in 126 patients (multiple cancer in twenty-three), including 127 CRCs; 15 gastric, 7 endometrial, 5 esophageal, 2 skin, 2 pancreatic, 2 lung, 1 breast, 1 cervical, 1 ovarian, 1 hepatic, and 1 biliary cancers; 1 gastric leiomyosarcoma, 1 liposarcoma, 1 bone sarcoma, 1 leukemia, and 1 brain glioblastoma. In the present group, 77.8% of the patients had CRCs and 74.7% of the cancers were colorectal ones. There were 45 metachronous CRCs and 4 synchronous CRCs, accounting for 35.4% and 3.1% of the total CRCs, respectively. Right-sided colon cancers constituted 52.9% of the total tumors, and 70.9% of CRCs. Individuals suffering from gastric cancer amounted to 11.9% of total patients.

The average age of malignant neoplasm onset in all the patients was 47.0 years and the ratio of males to females was 1.2:1. Individuals developed CRCs at an average age of 45.9 years. Sixty-two point seven percent of colorectal tumors developed under 50 years of age, 33.3% under 40 years of age and less than 4% occurred above the age of 70 years. In the 28 pedigrees, the average age of tumor occurrence in the first, second, third, and fourth degree was 59.6, 50.0, 44.0, and 31.8 years, respectively.

Eighty-five percent of the patients received radical operations. The remaining patients received chemotherapy, irradiation, and traditional Chinese medicine treatment. Twenty percent of colorectal patients had metachronous CRCs within 10 years after the first operation and required re-operations.

hMSH2 and hMLH1 mutation results

Thirteen double peak profiles displayed in DHPLC were found among 28 probands of all the pedigrees. Finally, 12 probands were identified with a varying DNA sequence by sequencing, of which 7 developed different mutations and 5 had the same hMSH2 polymorphism (Table 1 and Figure 1). We also examined the relatives of affected probands for the same mutations, and found that cancers and mutations were co-segregated in all affected pedigrees.

Table 1 hMSH2/hMLH1 gene sequence variations identified by sequencing

Sample No.	Gene/Exon	Point of mutation	Mutation result	Reported previously by
23 ¹	hMSH2/3	g. ² 610G>T,GGA →TGA	G204X, Truncated protein (nonsense mutation)	None
10,12,15,16,28	hMSH2/10	g.1661+12A>G	In intron, polymorphism	Scott <i>et al.</i> ^[16]
26	hMSH2/14	g.2211-2 A>C	Truncated protein (splice point mutation)	None
11	hMLH1/3	g.265 G>T,GAG →TAG	E89X, Truncated protein (nonsense mutation)	Wang <i>et al.</i> ^[17]
14	hMLH1/6	g.545+3 A>G	Truncated protein (splice point mutation)	Pensotti <i>et al.</i> ^[18]
8	hMLH1/8	g.655 A>G,ATC →GTC	I219V (missense mutation)	Tomlinson <i>et al.</i> ^[19]
25	hMLH1/8	g.677 G>A,CGA →CAA	R226Q (missense mutation)	None
18	hMLH1/9	g.790+1 G>A	Truncated protein (splice point mutation)	Cunningham ^[20]

¹The first Mongolian family with hMSH2 gene mutation in China. ²G refers to genomic DNA.

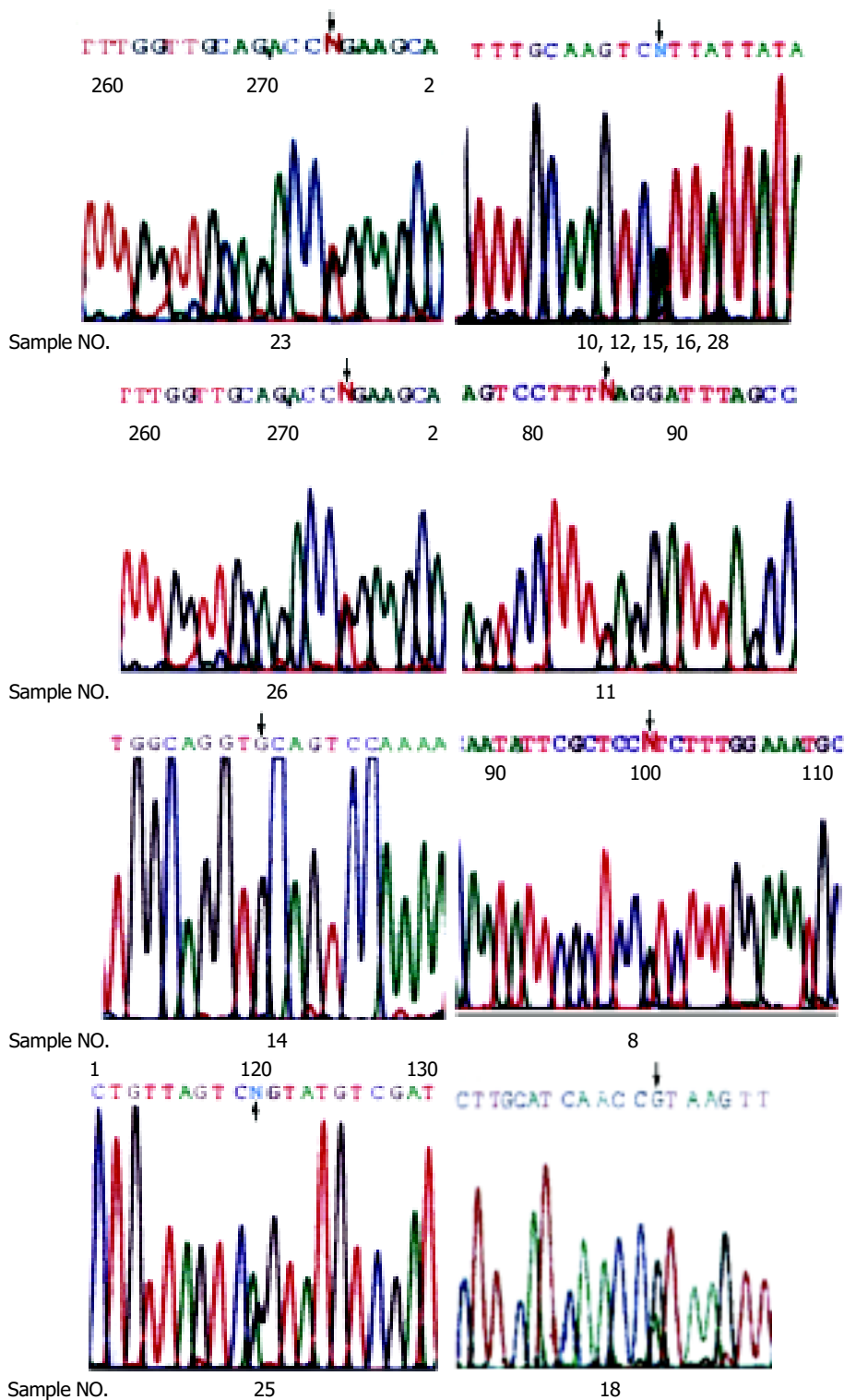


Figure 1 Sequencing graphs of mutations.

DISCUSSION

HNPCC was characterized by an early onset of colorectal cancers (proximal predominance, with 70% proximal to the splenic flexure), multiple synchronous and metachronous CRCs (about 18.1% and 24.2% respectively^[21]), and an excess of certain extracolonic cancers^[22]. In our study, patients with HNPCC developed CRC at an average age of 45.9 years, much earlier than the general population in China. According to our data, right-sided colon cancers amounted to 52.9% of the total cancers, and 70.9% of CRCs, similar to those reported in Western countries. Moreover, we also found the phenomenon of “generation anticipation”, that is, the later the generation was, the earlier the CRC developed. The fact that the family members

tended to be diagnosed early in the follow-up was an explanation for this phenomenon. Another reason for this phenomenon might be that there were carriers who harbored mutated MMR genes but did not become penetrant. Further studies should be carried out.

We found that the following two features were different from those reported in Western countries. Though Chinese patients had a high incidence of metachronous CRCs, synchronous cancer occurred quite rarely, only 3.1% in this study. Our previous studies also had a similar conclusion^[20], and the reason for the rare incidence of synchronous cancer in Chinese HNPCC patients remains unclear. The other striking feature was that gastric cancer was the second most common

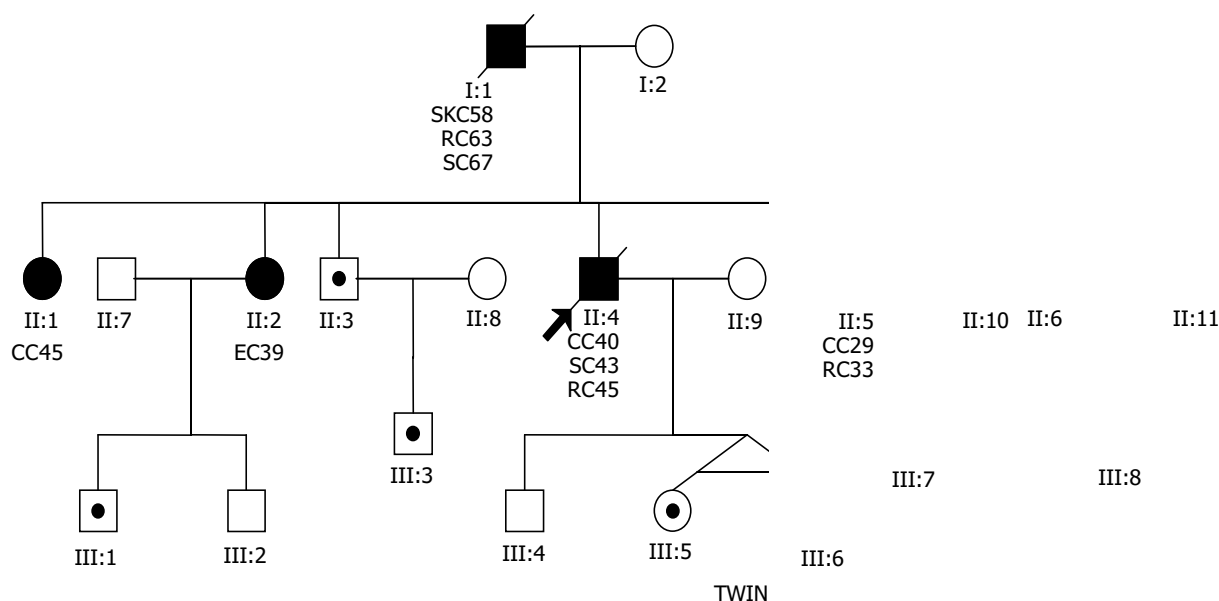


Figure 2 Pedigree of the first Mongolian family with hMSH2 gene mutation in China. ● Cancer patient, ○ Normal person, ⊙ Mutational gene carrier, SKC: skin cancer, RC: rectal cancer, CC: colonic cancer, EC: endometrial cancer, SC: stomach cancer.

cancer in Chinese HNPCC families, amounting to 11.9% of all cancers patients, much higher than the reported incidence in Western countries^[23,24]. Endometrial cancer ranked third, amounting to only 5.6%, and was followed by esophagus carcinoma. In Western countries, however, the second most commonly-seen tumor was endometrial cancer^[22,25]. In Japan and Korea, gastric cancer also occurred more frequently^[26]. We suppose that these features may represent the ethnic and geographical characteristics that may have some diagnostic significance in China and/or Asia.

The diagnosis of HNPCC depends on the detection of MMR genes. Single-strand conformation polymorphism (SSCP), denaturing gradient gel electrophoresis (DGGE), and direct sequencing have been used in MMR gene defect screening. Using DHPLC, we found a specificity of 92.3%, and recommended it as a hMSH2 and hMLH1 gene mutation screening method. In our study, 5 of 15 families (proband sample NO. 23, 11, 14, 8, 25), who met the Amsterdam I criteria, were found to have mutations and its mutation detection rate is 33.3%. But these criteria could only identify large families where the gene defect was highly penetrant and many small families were inappropriately excluded. In this study, 2 of 13 families (proband sample NO. 26, 18), which did not meet Amsterdam I criteria but fulfilled the Japan criteria, were also found to have mutations. Though the MMR gene defect rate of the latter is comparatively low (only 25%), it has been recommended as the clinical diagnosis criteria in HNPCC patients.

The mutations found in these families were compared with those described already in the human gene mutation database (HGMD) (<http://www.uwcm.ac.uk/uwcm/mg/hgmd0.html>). To our knowledge, apart from mutation of sample 11 (hMLH1, g. 265 G>T, GAG> TAG, E89X) reported before^[17], mutations of samples 14, 8, and 18 and the polymorphism of hMSH2 (g.1661+12A>G) were also reported previously^[18-20]. The other three mutations are novel. All the seven mutations resulted in an impaired capacity in MMR, which were consistent with their associations with penetrant tumors in the families. The probability of polymorphism of hMSH2 (g.1661+12A>G) being pathogenic was very small. Though there were no distinct "hot spot" mutations, we still noticed that hMLH1 gene mutations, especially of the first nine exons, were more common than hMSH2 gene mutations in China. Similarly, Baba^[12] and Yuan *et al.*^[27] described that hMLH1 gene mutations were more

frequently seen in Asia. So, it is worthwhile to initiate MMR gene mutation screening from the first nine exons of hMLH1 gene.

In this study, we identified the first Mongolian family with hMSH2 gene mutation in China. The pedigree is shown in Figure 2. In the large family, the nonsense alteration 610 (genomic DNA) G→T at codon 204 in exon3 of hMSH2 resulted in the substitution of stop codon TGA for glycine codon GGA. This mutation co-segregated with the disease in the family. In five phenotypic normal family members, the same mutated gene was found in the germline. These carriers remain to be followed up intensively.

REFERENCES

- Stephenson BM, Finan PJ, Gascoyne J, Garbett F, Murday VA, Bishop DT. Frequency of familial colorectal cancer. *Br J Surg* 1991; **78**: 1162-1166
- Wagner A, Tops C, Wijnen JT, Zwinderman K, Meer C, Kets M, Niermeijer MF, Klinjin JGM, Tibben A, Vasen HFA, Meijers-Heijboer H. Genetic testing in hereditary non-polyposis colorectal cancer families with a MSH2, MLH1, or MSH5 mutation. *J Med Genet* 2002; **39**: 833-837
- Fishel R, Lescoe MK, Rao MR, Copeland NG, Jenkins NA, Garber J, Kane M, Kolodner R. The human mutator gene homolog MSH2 and its association with hereditary nonpolyposis colon cancer. *Cell* 1994; **77**: 167
- Leach FS, Nicolaides NC, Papadopoulos N, Liu B, Jen J, Parsons R, Peltomaki P, Sistonen P, Aaltonen LA, Nystrom-Lahti M. Mutations of a mutS homolog in hereditary nonpolyposis colorectal cancer. *Cell* 1993; **75**: 1215-1225
- Bronner CE, Baker SM, Morrison PT, Warren G, Smith LG, Lescoe MK, Kane M, Earabino C, Lipford J, Lindblom A, Tannergård P, Bollag RJ, Godwin AR, Ward DC, Nordenskjöld M, Fishel R, Kolodner R, Liskay RM. Mutation in the DNA mismatch repair gene homologue hMLH1 is associated with hereditary non-polyposis colon cancer. *Nature* 1994; **368**: 258-261
- Papadopoulos N, Nicolaides NC, Wei YF, Ruben SM, Carter KC, Rosen CA, Haseltine WA, Fleischmann RD, Fraser CM, Adams MD, Venter JC, Hamilton SR, Petersen GM, Watson P, Lynch HT, Peltomäki P, Mecklin JP, Chapelle A, Kinzler KW, Vogelstein B. Mutation of a mutL homolog in hereditary colon cancer. *Science* 1994; **263**: 1625-1629
- Nicolaides NC, Papadopoulos N, Liu B, Wei YF, Carter KC, Ruben SM, Rosen CA, Haseltine WA, Fleischmann RD, Fraser CM, Adams MD, Venter JC, Dunlop MG, Hamilton SR, Petersen GM, Chapelle A, Vogelstein B, Kinzler KW. Mutations of two

- PMS homologues in hereditary nonpolyposis colon cancer. *Nature* 1994; **371**: 75-80
- 8 **Akiyama Y**, Sato H, Yamada T, Nagasaki H, Tsuchiya A, Abe R, Yuasa Y. Germ-line mutation of the hMSH6/GTBP gene in an atypical hereditary nonpolyposis colorectal cancer kindred. *Cancer Res* 1997; **57**: 3920-3923
 - 9 **Peltomaki P**, Gao X, Mecklin JP. Genotype and phenotype in hereditary nonpolyposis colon cancer: a study of families with different vs shared predisposing mutations. *Fam Cancer* 2001; **1**: 9-15
 - 10 **Peltomaki P**, Vasen HF. Mutations predisposing to hereditary nonpolyposis colorectal cancer: database and results of a collaborative study. The international collaborative group on hereditary nonpolyposis colorectal cancer. *Gastroenterology* 1997; **113**: 1146-1158
 - 11 **Vasen HF**, Mecklin JP, Khan PM, Lynch HT. The international collaborative group on hereditary non-polyposis colorectal cancer (ICG-HNPCC). *Dis Colon Rectum* 1991; **34**: 424-425
 - 12 **Baba S**. Hereditary nonpolyposis colorectal cancer: an update. *Dis Colon Rectum* 1997; **40**(10 Suppl): S86-S95
 - 13 **Miller SA**, Dykes DD, Polesky HF. A simple saltingout procedure for extracting DNA from human nucleated cells. *Nucleic Acids Res* 1988; **16**: 1215
 - 14 **Weber TK**, Conlon W, Petrelli NJ, Rodriguez-Bigas M, Keitz B, Pazik J, Farrell C, O'Malley L, Oshalim M, Abdo M, Anderson G, Stoler D, Yandell D. Genomic DNA-based hMSH2 and hMLH1 mutation screening in 32 Eastern United States hereditary nonpolyposis colorectal cancer pedigrees. *Cancer Res* 1997; **57**: 3798-3803
 - 15 **Gross E**, Arnold N, Goette J, Schwarz-Boeger U, Kiechle M. A comparison of BRCA1 mutation analysis by direct sequencing, SSCP and DHPLC. *Hum Genet* 1999; **105**: 72-78
 - 16 **Scott RJ**, McPhillips M, Meldrum CJ, Fitzgerald PE, Adams K, Spigelman AD, du Sart D, Tucker K, Kirk J. Hereditary nonpolyposis colorectal cancer in 95 families: differences and similarities between mutation-positive and mutation-negative kindreds. *Am J Hum Genet* 2001; **68**: 118-127
 - 17 **Zhao B**, Wang ZJ, Xu YF, Wan YL, Li P, Huang YT. Report of 16 kindreds and one kindred with hMLH1 germline mutation. *World J Gastroenterol* 2002; **8**: 263-266
 - 18 **Pensotti V**, Radice P, Presciuttini S, Calistri D, Gazzoli I, Grimalt Perez A, Mondini P, Buonsanti G, Sala P, Rossetti C, Ranzani GN, Bertario L, Pierotti MA. Mean age of tumor onset in hereditary nonpolyposis colorectal cancer (HNPCC) families correlates with the presence of mutations in DNA mismatch repair genes. *Genes Chromosomes Cancer* 1997; **19**: 135-142
 - 19 **Tomlinson IP**, Beck NE, Homfray T, Harocopos CJ, Bodmer WF. Germline HNPCC gene variants have little influence on the risk for sporadic colorectal cancer. *J Med Genet* 1997; **34**: 39-42
 - 20 **Cunningham JM**, Kim CY, Christensen ER, Tester DJ, Parc Y, Burgart LJ, Halling KC, McDonnell SK, Schaid DJ, Walsh Vockley C, Kubly V, Nelson H, Michels VV, Thibodeau SN. The frequency of hereditary defective mismatch repair in a prospective series of unselected colorectal carcinomas. *Am J Hum Genet* 2001; **69**: 780-790
 - 21 **Fitzgibbons RJ Jr**, Lynch HT, Stanislav GV, Watson PA, Lanspa SJ, Marcus JN, Smyrk T, Krieglner MD, Lynch JF. Recognition and treatment of patients with hereditary nonpolyposis colon cancer (Lynch syndromes I and II). *Ann Surg* 1987; **206**: 289-295
 - 22 **Lynch HT**, Smyrk T, Lynch J. An update of HNPCC (Lynch syndrome). *Cancer Genet Cytogenet* 1997; **93**: 84-99
 - 23 **Lynch HT**, Richardson JD, Amin M, Lynch JF, Cavalieri RJ, Bronson E, Fusaro RM. Variable gastrointestinal and urologic cancers in a Lynch syndrome II kindred. *Dis Colon Rectum* 1991; **34**: 891-895
 - 24 **Hakala T**, Mecklin JP, Forss M, Jarvinen H, Lehtovirta P. Endometrial carcinoma in the cancer family syndrome. *Cancer* 1991; **68**: 1656-1659
 - 25 **Froggatt NJ**, Green J, Brassett C, Evans DG, Bishop DT, Kolodner R, Maher ER. A common MSH2 mutation in English and North American HNPCC families: origin, phenotypic expression, and sex specific differences in colorectal cancer. *J Med Genet* 1999; **36**: 97-102
 - 26 **Park YJ**, Shin KH, Park JG. Risk of gastric cancer in hereditary nonpolyposis colorectal cancer in Korea. *Clin Cancer Res* 2000; **6**: 2994-2998
 - 27 **Yuan Y**, Han HJ, Zheng S, Park JG. Germline mutations of hMLH1 and hMSH2 genes in patients with suspected hereditary nonpolyposis colorectal cancer and sporadic early-onset colorectal cancer. *Dis Colon Rectum* 1998; **41**: 434-440

Edited by Wang XL and Chen ZR Proofread by Xu FM

Comparative study of proteome between primary cancer and hepatic metastatic tumor in colorectal cancer

Bo Yu, Shi-Yong Li, Ping An, Ying-Nan Zhang, Zhen-Jia Liang, Shu-Jun Yuan, Hui-Yun Cai

Bo Yu, Shi-Yong Li, Ping An, Ying-Nan Zhang, Zhen-Jia Liang, Shu-Jun Yuan, Hui-Yun Cai, Department of General Surgery, General Hospital of Beijing Military Command, Beijing 100700, China
Supported by the National Natural Science Foundation of China, No. 30070747 and No. 30271279

Correspondence to: Bo Yu, Department of General Surgery, General Hospital of Beijing Military Command, Beijing 100700, China. yubo66@126.com

Telephone: +86-10-66721189

Received: 2003-07-12 **Accepted:** 2003-08-16

Abstract

AIM: To identify the differential proteins associated with colorectal cancer genesis and hepatic metastasis.

METHODS: Hydrophobic protein samples were extracted from normal colorectal mucosa, primary cancer lesion and hepatic metastatic foci of colorectal cancer. With two-dimensional electrophoresis and image analysis, differentially expressed protein spots were detected, and the proteins were identified by matrix assisted laser desorption/ionization-time of flight-mass spectrometry and peptide mass fingerprint analysis.

RESULTS: Significant alterations of the proteins in number and expression levels were discovered in primary cancer and hepatic metastatic foci, the expression of a number of proteins was lost in 25-40 ku, but protein spots was increased in 14-21ku, compared with normal mucosa. Nine differentially expressed protein spots were identified. Three proteins expressed in normal mucosa, but lost in primary cancer and hepatic metastasis, were recognized as calmodulin, ribonuclease 6 precursor and mannosidase- α . Proapolipoprotein was expressed progressively from normal mucosa to primary cancer and hepatic metastasis. The differentially expressed protein of beta-globin was found in normal mucosa and hepatic metastatic tumor, but lost in primary cancer lesion. Cdc 42, a GTP-binding protein, was identified in hepatic metastasis. The protein spots of C4 from primary cancer, M7 and M9 from hepatic metastasis had less homology with the proteins in database.

CONCLUSION: Variations of hydrophobic protein expression in colorectal cancer initiation and hepatic metastasis are significant and can be observed with two-dimensional electrophoresis. The expression of calmodulin, ribonuclease 6 precursor and mannosidase- α is lost but the expression of proapolipoprotein is enhanced which is associated with colorectal cancer genesis and hepatic metastasis. Cdc 42 and beta-globin are expressed abnormally in hepatic metastasis. Protein C4, M7 and M9 may be associated with colorectal cancer genesis and hepatic metastasis.

Yu B, Li SY, An P, Zhang YN, Liang ZJ, Yuan SJ, Cai HY. Comparative study of proteome between primary cancer and hepatic metastatic tumor in colorectal cancer. *World J Gastroenterol* 2004; 10(18): 2652-2656
<http://www.wjgnet.com/1007-9327/10/2652.asp>

INTRODUCTION

Colorectal cancer genesis and metastasis are complex processes involving multiple changes in gene and protein expression^[1-5]. The liver is a common site of metastasis from colorectal cancer^[6-8]. Hepatic metastasis caused severe and fatal effects on patients who underwent radical excision for large intestine primary carcinoma^[9-12]. The success of metastatic hepatic cancer treatment is strongly dependent on early diagnosis and understanding of the molecular mechanisms and biological behaviors of colorectal cancer, especially its infiltration and metastasis. To unravel these alterations, genome and proteome approaches for the identification of qualitative and quantitative changes in gene and protein compositions provide theoretic and technical support^[13-16]. Our study was focused on the identification of differential expression proteins between primary colorectal cancer foci and hepatic metastasis with proteome approach. Hydrophobic proteins including membrane proteins play important roles in cellular signal transduction. Identification of the proteins is helpful to understand the molecular biological mechanisms of colorectal carcinogenesis and hepatic metastasis and to select tumor markers for colorectal cancer.

MATERIALS AND METHODS

Tissue sample collection

Samples of normal colorectal mucosa, primary cancer lesion and hepatic metastasis were collected from 12 colorectal cancer patients aged 36-68 years including 6 males and 6 females. The samples were stored in liquid nitrogen. Pathology examination was performed for all the specimens and the histological types consisted of moderately and poorly differentiated adenocarcinoma, signet-ring cell carcinoma and undifferentiated carcinoma, 4 cases in each type.

Protein sample preparation

A set of samples were taken from the same patient, 0.9 g of each, including normal colorectal mucosa, primary cancer and hepatic metastatic tumor. The samples were washed with PBS and then immediately ground by a liquid nitrogen cooled mortar, and homogenized in protease inhibitor buffer (cocktail formula: phenylmethylsulfonyl fluoride 40 μ g/mL, ethylenediamine tetraacetic acid 1 mmol/L, peptide inhibitin 0.7 μ g/mL, leupeptin 0.5 μ g/mL). Protein extraction was performed with Molloy procedure. Lysis buffer I (Tris 40 mmol/L, pH8.8) was added, stirred and mixed by an ultrasonic disintegrator. The mixture was centrifuged at 105 000 g for 1 h. Yellow lipids were discarded from the supernatant and the middle layer liquid was transferred and dried with a freezing dryer. The pellet was solubilized in lysis buffer II (Urea 8 mol/L, Tris 10 mmol/L, CHAPS 40 g/L, DTT 65 mmol/L) and centrifuged. The supernatant was dried and stored as *idem*. The pellet was solubilized in lysis buffer III (urea 5 mol/L, thiocarbamate 2 mol/L, SB3-10 20 g/L, 0.2 g, CHAPS 20 g/L, TBP 2 mmol/L), then the procedure was repeated once more. The proteins extracted with fractional procedure were stored at -20 °C.

Two-dimensional gel electrophoresis and image analysis

The first dimension of isoelectric focusing (IEF) was performed

in immobilized pH gradient (IPG) gel strips with nonlinear immobilized pH 3-10 gradient. Three hundred μg of protein sample from each tissue specimen of normal mucosa, primary cancer and hepatic metastatic tumor was loaded respectively. IPG strips were placed onto the rehydration buffer (urea 8 mol/L, CHAPS 40 g/L, TBP 2 mmol/L, IPG buffer 3 g/L) and added into the sample solution without trapping air bubbles. IEF with a low voltage (30 V, followed by 60 V and 200 V) was carried out according to the programmed settings. After IEF was terminated, the IPG strips were equilibrated for 20 min in equilibration buffer. The second dimension of SDS-PAGE was performed on vertical systems. IPG strips were loaded and run on a 125 g/L acrylamide SDS-PAGE gel in electrode buffer (Tris 0.025 mol/L, glycine 0.192 mol/L, SDS 1 g/L, pH8.3). Electrophoresis was performed with a current of 30 mA/gel for 15 min, then at maximum settings of 60 mA/gel for 4 h. The temperature of the cooling plate was set at 20 °C. After SDS-PAGE, the gels were stained with silver nitrate. Proteins were visualized by silver-staining and then scanned using Scan Prisa 640 UT. Two DE image computer analysis was carried out with Melanie 3.0 software (GeneBio, Geneva). Isoelectric points and molecular weights of individual proteins were evaluated with polypeptide SDS-PAGE-standards. Differential protein spots among normal colorectal mucosa, primary cancer lesion and hepatic metastasis were picked out by comparison of 2-DE images with Melanie 3.0 analysis.

Mass spectrometry and peptide mass fingerprint analysis

Selected differential protein spots were excised from 2-DE gels and transferred to a 96-well plate ready for trypsin digestion. The gel pieces were washed successively in water, Tris-HCl (20 mmol/L pH 8), Tris-HCl (20 mmol/L pH 8)/500 g/L acetonitrile and finally 1 000 g/L acetonitrile, and dried. The dried gel pieces were incubated in trypsin solution for 16 h at 37 °C. The resultant peptide mixture was extracted with 20 μL 5 g/L TFA/300 g/L

acetonitrile, followed by extraction with 20 μL 5 g/L TFA/600 g/L acetonitrile. α -cyano-4-hydroxycinnamic acid was used as matrix solution. Matrix assisted laser desorption/ionization-time of flight-mass spectrometry analysis were performed with MALDI-TOF mass spectrometer (Bruker, USA). The spectrum was obtained and recorded. Proteins were identified by searching NCBI and SwissProt databases using Profound peptide mass fingerprinting retrieval software (http://129.85.19.192/profound_bin/WebProFound.exe?FORM=1). Protein identities were assigned if at least four peptide masses were matched within a maximum of 100 ppm error spread across the data set and the candidate agreed with the estimated pI and molecular weight from the 2-DE gel.

Statistical analysis

Experimental data were analysed statistically with Crosstab chi-Square test and Student's *t*-test using SPSS 10.0. $P < 0.05$ was considered statistically significant.

RESULTS

2-DE image analysis of protein spots in matched sets of colorectal cancer

The hydrophobic protein profiles including partial membranous proteins from colorectal normal mucosa, primary cancer and metastatic foci in liver are displayed in Figures 1A-C. Comparing the 2-DE protein images of the three tissues, we found that the number of protein spots and protein expression level were significantly changed in primary cancer and hepatic metastatic lesion. Under the same experimental conditions, 390 ± 28 protein spots and 206 ± 22 , 236 ± 19 spots were found in normal colorectal mucosa and in primary cancer and hepatic metastasis, respectively. Compared with normal colorectal mucosa, the number of protein spots in primary cancer and metastatic tumor was significantly different $t = 53.116$, $t = 33.399$,

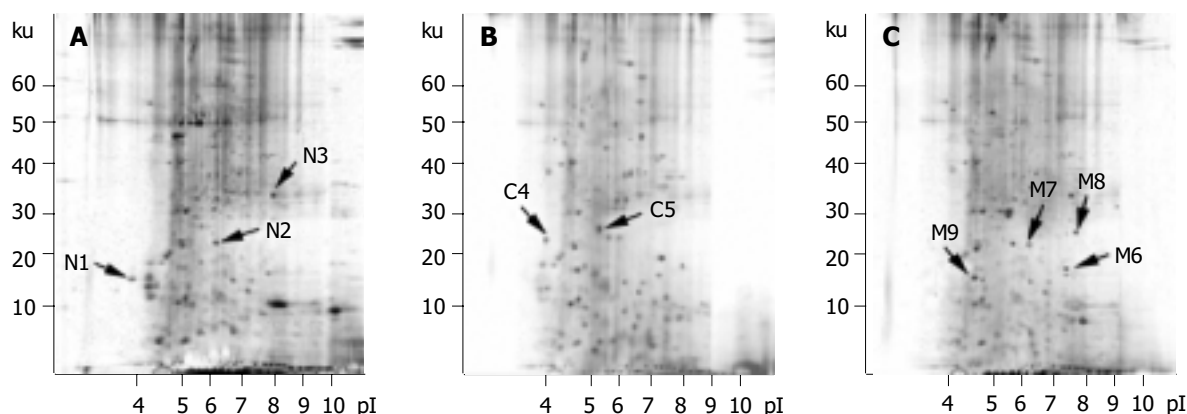


Figure 1 Silver-stained two-dimensional electrophoretic images of hydrophobic proteins from (A) Normal colon mucosa, (B) Primary colon cancer lesion, (C) Hepatic metastasis.

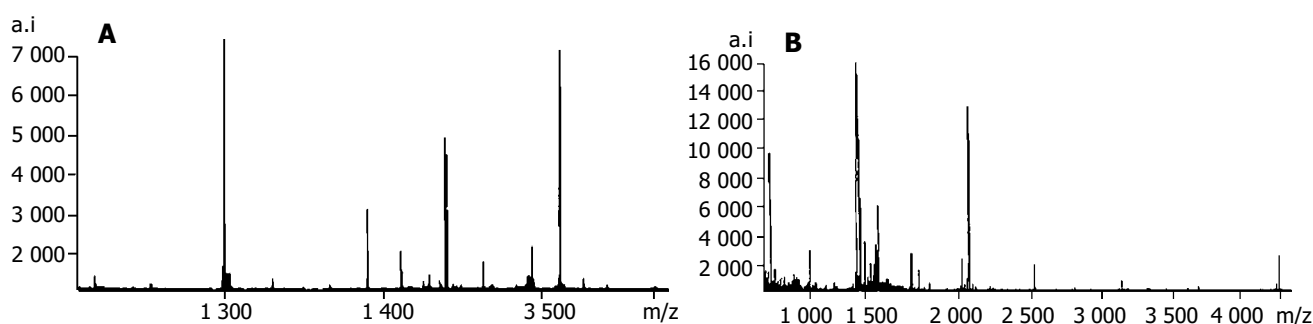


Figure 2 MALDI-TOF mass spectrometry and peptide mass fingerprint analysis of the differential protein spots (A) N2 protein spot from normal colon mucosa, (B) M6 protein spot from hepatic metastasis.

Table 1 Identification of nine differentially expressed proteins by peptide mass fingerprint and matching with proteins in databases

Spot No.	Accession (NCBI nr)	Theoretical pI	Theoretical M_r	Length (AA)	Protein name
N1	1CDL_B	4.0	16.56	147	Calmodulin complexed with calmodulin-binding peptide
N2	NP_003721	6.7	29.46	256	Ribonuclease 6 precursor
N3	XP_040720	8.4	32.76	287	Hypothetical protein XP_040720
C4		4.5	22.48	217	
C5	AAA51747	5.4	28.94	249	Proapolipoprotein
M6	AAA88054	6.8	15.96	147	Beta-globin
M7		5.5	22.57	203	
M8	XP_010554	6.8	21.25	191	Similar to cell division cycle 42
M9		4.5	14.72	127	

The difference of protein spot number between hepatic metastatic tumor and primary cancer was also significant ($t = 24.407, P < 0.01$).

Peptide mass fingerprinting of differential protein spots from 2-DE gels

Nine differential protein spots of the 2-DE gels were analysed using mass spectrometry. Three protein spots, N1, N2, N3, were taken from normal colorectal mucosa. C4 and C5 spots were from primary cancer lesions and four spots, M6, M7, M8, M9, from hepatic metastatic cancer. Molecular weight and isoelectric points of the nine protein spots were determined according to the standard molecular markers and peptide mass fingerprint analysis, and the data are shown in Table 1 and Figure 2.

Identification of differential expression proteins of colorectal cancer and hepatic metastasis

The peptide mass fingerprints obtained from the nine differential protein spots were compared to fingerprints obtained by theoretical cleavage of protein sequences in databases and the protein identities were assigned. Protein spots of N1, N2 and N3 from normal colorectal mucosa represented calmodulin, ribonuclease 6 precursor and hypothetical protein XP_040720, respectively. The expression of three proteins was lost in primary cancer and hepatic metastatic foci. Protein C5, matching to proapolipoprotein, expressed progressively from normal mucosa to primary cancer and hepatic metastatic tumor. Protein spot M6 was observed in normal mucosa and in hepatic metastatic cancer, but lost in primary carcinomas, being recognized as beta-globin. Expressed in hepatic metastasis, M8 was identified with cell division 42 (GTP-binding protein), but not found in normal mucosa and primary cancer lesion. Differential protein spots of C4 from primary carcinomas, M7 and M9 from hepatic metastasis were not identified by peptide mass fingerprint analysis because their peptide mass fingerprints had less homology with the known proteins in databases.

DISCUSSION

The initiation and hepatic metastasis of colorectal cancer involved multiple gene and protein alterations^[17-19]. Understanding the molecular basis of the disease is of great significance for its early detection and treatment. In this study, the proteome approach was applied to the identification of differential proteins between primary colorectal cancer lesion and its hepatic metastasis. We used 2-DE to isolate and analyze the set of hydrophobic proteins from normal colorectal mucosa, primary

cancer and hepatic metastatic tumor. It was of clinical importance to identify the differential expression proteins that had potentiality of being tumor markers and anticancer targets.

By comparison with 2-DE images, significant differences of protein expression were found in normal mucosa, primary cancer and hepatic metastasis, and the number and distribution of protein spots changed noticeably in the range of pH 4.0-9.0. Compared with normal mucosa, a number of protein spots with a molecular weight of 25-40 ku were lost in primary cancer and hepatic metastasis, but proteins with a molecular weight of 14-21 ku were observed in the same pH range. What the differential proteins were and what functions they performed in colorectal carcinogenesis and in hepatic metastasis attracted our attention. We identified nine protein spots and studied their roles in the course of initiation and hepatic metastasis of colorectal cancer.

Proteins of calmodulin (N1), ribonuclease 6 precursor (N2) and hypothetical protein XP_040720 (N3) were expressed in normal colorectal mucosa, but lost in primary cancer lesion and in hepatic metastasis. It indicated the loss of proteins was associated with colorectal carcinogenesis and hepatic metastasis. Calmodulin could regulate the concentration of calcium ions in cells and had important effects on normal cellular functions. Ca^{2+} regulation was necessary for cell differentiation and apoptosis. Combination of calcium ions and the receptors could influence cell signal transduction that controls cell differentiation and division. Low concentration of calcium ions made cell division easily, and the high concentration was advantageous to cell differentiation. Calcium ions promoted cancer cells into apoptosis. Thus, calcium was regarded as a chemoprophylaxis agent for colorectal cancer^[20,21]. We propose loss of calmodulin expression is connected with initiation and hepatic metastasis of colorectal cancer.

Ribonuclease 6 precursor protein belongs to the Rh/T2/S-glycoprotein class of extracellular ribonucleases and the gene is present in a single copy in the human genome and has been mapped to 6q27. This has been found to be a region of the human genome prone to rearrangements associated with several human malignancies^[22]. The family of the proteins possesses the function of ribozyme and self-splicing. They catalyze breaking of RNA, synthesis of polypeptide bonds and nucleotides. The protein can disintegrate DNA fragments, regulate cell biological behaviors and cell division. Loss of ribonuclease 6 precursor expression would facilitate carcinogenesis and infiltration. Ribozyme has been found useful in anticancer therapy^[23]. The loss of ribonuclease 6 precursor expression in primary colorectal cancer and hepatic metastasis could provide an experimental interpretation of ribozyme treatment.

XP_040720, a hypothetical protein is now defined as a

member of mannosidase- α class 1A. The protein is located in Golgi complex and participates in N-glycoprotein synthesis and oligosaccharide processing. It could play an important role in synthesis of membranous proteins and receptor proteins^[24]. But we do not know what functions the protein performs in colorectal carcinogenesis and metastasis. It could be regarded as a differentiation-related protein in normal mucosa cells, and loss of the protein expression is a dedifferentiation phenotype in the primary cancer lesion and hepatic metastasis, which is still lack of evidence.

Loss of the three protein expressions was considered to be connected with colorectal cancer initiation and hepatic metastasis. However proapolipoprotein expression was found stepwisely increased from normal mucosa to primary cancer and hepatic metastasis, and enhanced expression of the protein was in association with colorectal cancer. Proapolipoprotein was hydrolyzed by the signal peptidase and propeptidase, through which apolipoprotein was generated^[25]. Apolipoprotein is a carrier of lipids and regulates many cellular functions. It was found that apolipoprotein had an antiapoptosis effect and was related with carcinogenesis and progression. Enhanced expression of apolipoprotein has been reported in hepatoma^[26]. Our study provided an evidence of apolipoprotein in colorectal cancer.

A differentially expressed protein in our study was beta-globin. Its expression was found in normal mucosa and hepatic metastasis, but lost in primary cancer lesion. We suggested beta-globin was an associated protein with hepatic metastasis. The gene family of beta-globin consists of five functional genes and is located on chromosome 11. The family members expressed in order of the genes as they were arranged on the chromosome during various developmental stages. Beta-globin gene was activated and expressed continuously in late stage of pregnancy^[27,28]. Study on regulation of beta-globin showed that the variations of transcription frequency and cycle of phasic and specific expression of beta-globin family genes in developmental regulation were more important than changes of the gene transcription speed and expression quantity^[29]. Understanding the mechanisms of beta-globin regulation is helpful to researches on cell growth, carcinogenesis and progression. The cycle variation of beta-globin expression from the normal mucosa to primary cancer and hepatic metastasis implied genetic recombination and regulation changes in hepatic metastasis of colorectal cancer. It was reported that beta-globin expression was induced by treatment of chemotherapy agents in some cancer cells. This might indicate that the expression of beta-globin increased drug resistance of cancer cells and facilitated hepatic metastasis.

It has been found that Cdc 42, a differential protein expressed in hepatic metastasis, is a Rho-related member of the Ras superfamily, and acts as a GTP-binding protein^[30,31]. The protein performs the function of a molecular switch to control a diversity of cellular processes, and regulates cytoskeleton actin recombination, cell polarity and cell movement. Enhanced expression of Cdc 42 might facilitate cell division and accelerate cancer cell growth and proliferation, as well as interrupt signal transduction of apoptosis^[32]. Invasive behavior of cancer cells was reinforced by enhanced Cdc 42 expression through regulating cellular skeleton, cell adhesiveness and neovascularization. Therefore, Cdc 42 has been regarded as an associated protein in hepatic metastasis of colorectal cancer.

C4 expressed in primary cancer, M7 and M9 in hepatic metastasis, had low homology with the proteins known in database, and the three proteins were not identified. They manifested the possibility to be new proteins associated with colorectal cancer. Sequencing of the proteins and study of their functions are needed to help understand the mechanisms

of colorectal carcinogenesis and hepatic metastasis.

In summary, we identified 9 differentially expressed proteins that were associated with colorectal cancer genesis and hepatic metastasis. Relations of these proteins with colorectal cancer were not or seldom reported before. The differential proteins will help understand the mechanism of colorectal cancer genesis and hepatic metastasis. The results prove that proteome study represents a very useful and promising tool in discovering new tumor markers and anticancer targets of colorectal cancer.

REFERENCES

- 1 **Rooney PH**, Boonsong A, McKay JA, Marsh S, Stevenson DA, Murray GI, Curran S, Haites NE, Cassidy J, McLeod HL. Colorectal cancer genomics: evidence for multiple genotypes which influence survival. *Br J Cancer* 2001; **85**: 1492-1498
- 2 **Stulik J**, Hernychova L, Porkertova S, Knizek J, Macela A, Bures J, Jandik P, Langridge JJ, Jungblut PR. Proteome study of colorectal carcinogenesis. *Electrophoresis* 2001; **22**: 3019-3025
- 3 **Li XG**, Song JD, Wang YQ. Differential expression of a novel colorectal cancer differentiation-related gene in colorectal cancer. *World J Gastroenterol* 2001; **7**: 551-554
- 4 **Domon-Dell C**, Schneider A, Mouchadel V, Guerin E, Guenet D, Aguilon S, Duluc I, Martin E, Iovanna J, Launay JF, Duclos B, Chenard MP, Meyer C, Oudet P, Kedingner M, Gaub MP, Freund JN. Cdx1 homeobox gene during human colon cancer progression. *Oncogene* 2003; **22**: 5969-5977
- 5 **Jeong SY**, Shin KH, Shin JH, Ku JL, Shin YK, Park SY, Kim WH, Park JG. Microsatellite instability and mutations in DNA mismatch repair genes in sporadic colorectal cancers. *Dis Colon Rectum* 2003; **46**: 1069-1077
- 6 **Topal B**, Roskams T, Fevery J, Penninckx F. Aggregated colon cancer cells have a higher metastatic efficiency in the liver compared with nonaggregated cells: an experimental study. *J Surg Res* 2003; **112**: 31-37
- 7 **Schimanski CC**, Linnemann U, Galle PR, Arbogast R, Berger MR. Hepatic disseminated tumor cells in colorectal cancer UICC stage 4 patients: prognostic implications. *Int J Oncol* 2003; **23**: 791-796
- 8 **Nakamura S**, Suzuki S, Baba S. Resection of liver metastases of colorectal carcinoma. *World J Surg* 1997; **21**: 741-747
- 9 **Yamada H**, Kondo S, Okushiba S, Morikawa T, Katoh H. Analysis of predictive factors for recurrence after hepatectomy for colorectal liver metastases. *World J Surg* 2001; **25**: 1129-1133
- 10 **Cromheecke M**, de Jong KP, Hoekstra HJ. Current treatment for colorectal cancer metastatic to the liver. *Eur J Surg Oncol* 1999; **25**: 451-463
- 11 **Hugh TJ**, Kinsella AR, Poston GJ. Management strategies for colorectal liver metastases-Part I. *Surg Oncol* 1997; **6**: 19-30
- 12 **Hugh TJ**, Kinsella AR, Poston GJ. Management strategies for colorectal liver metastases-Part II. *Surg Oncol* 1997; **6**: 31-48
- 13 **Srivastava S**, Verma M, Henson DE. Biomarkers for early detection of colon cancer. *Clin Cancer Res* 2001; **7**: 1118-1126
- 14 **Srinivas PR**, Srivastava S, Hanash S, Wright GL Jr. Proteomics in early detection of cancer. *Clin Chem* 2001; **47**: 1901-1911
- 15 **Makin GB**, Breen DJ, Monson JRT. The impact of new technology on surgery for colorectal cancer. *World J Gastroenterol* 2001; **7**: 612-621
- 16 **Srinivas PR**, Verma M, Zhao Y, Srivastava S. Proteomics for cancer biomarker discovery. *Clin Chem* 2002; **48**: 1160-1169
- 17 **Aragane H**, Sakakura C, Nakanishi M, Yasuoka R, Fujita Y, Taniguchi H, Hagiwara A, Yamaguchi T, Abe T, Inazawa J, Yamagishi H. Chromosomal aberrations in colorectal cancers and liver metastases analyzed by comparative genomic hybridization. *Int J Cancer* 2001; **94**: 623-629
- 18 **Hishikawa Y**, Kohno H, Ueda S, Kimoto T, Dhar DK, Kubota H, Tachibana M, Koji T, Nagasue N. Expression of metallothionein in colorectal cancers and synchronous liver metastases. *Oncology* 2001; **61**: 162-167
- 19 **Seto S**, Onodera H, Kaido T, Yoshikawa A, Ishigami S, Arai S, Imamura M. Tissue factor expression in human colorectal carcinoma: correlation with hepatic metastasis and impact on

- prognosis. *Cancer* 2000; **88**: 295-301
- 20 **Chakrabarty S**, Radjendirane V, Appelman H, Varani J. Extracellular calcium and calcium sensing receptor function in human colon carcinomas: promotion of E-cadherin expression and suppression of beta-catenin/TCF activation. *Cancer Res* 2003; **63**: 67-71
- 21 **Lamprecht SA**, Lipkin M. Cellular mechanisms of calcium and vitamin D in the inhibition of colorectal carcinogenesis. *Ann N Y Acad Sci* 2001; **952**: 73-87
- 22 **Trubia M**, Sessa L, Taramelli R. Mammalian Rh/T2/S-glycoprotein ribonuclease family genes: cloning of a human member located in a region of chromosome 6 (6q27) frequently deleted in human malignancies. *Genomics* 1997; **42**: 342-344
- 23 **Pouckova P**, Soucek J, Jelinek J, Zadinova M, Hlouskova D, Polivkova J, Navratil L, Cinatl J, Matousek J. Antitumor action of bovine seminal ribonuclease. Cytostatic effect on human melanoma and mouse seminoma. *Neoplasma* 1998; **45**: 30-34
- 24 **Tremblay LO**, Herscovics A. Characterization of a cDNA encoding a novel human golgi α -1,2-mannosidase (IC) involved in N-Glycan biosynthesis. *J Biol Chem* 2000; **275**: 31655-31660
- 25 **Tricerri MA**, Behling Agree AK, Sanchez SA, Jonas A. Characterization of apolipoprotein A-I structure using a cysteine-specific fluorescence probe. *Biochemistry* 2000; **39**: 14682-14691
- 26 **Nassir F**, Bonen DK, Davidson NO. Apolipoprotein(a) synthesis and secretion from hepatoma cells is coupled to triglyceride synthesis and secretion. *J Biol Chem* 1998; **273**: 17793-17800
- 27 **Filipe A**, Li Q, Deveaux S, Godin I, Romeo PH, Stamatoyannopoulos G, Mignotte V. Regulation of embryonic/fetal globin genes by nuclear hormone receptors: a novel perspective on hemoglobin switching. *EMBO J* 1999; **18**: 687-697
- 28 **Guy LG**, Mei Q, Perkins AC, Orkin SH, Wall L. Erythroid Kruppel-like factor is essential for beta-globin gene expression even in absence of gene competition, but is not sufficient to induce the switch from gamma-globin to beta-globin gene expression. *Blood* 1998; **91**: 2259-2263
- 29 **Wijgerde M**, Gribnau J, Trimborn T, Nuez B, Philipsen S, Grosveld F, Fraser P. The role of EKLF in human beta-globin gene competition. *Genes Dev* 1996; **10**: 2894-2902
- 30 **Takai Y**, Sasaki T, Matozaki T. Small GTP-binding proteins. *Physiol Rev* 2001; **81**: 153-208
- 31 **Fritz G**, Just I, Kaina B. Rho GTPases are over-expressed in human tumors. *Int J Cancer* 1999; **81**: 682-687
- 32 **Tu S**, Cerione RA. Cdc42 is a substrate for caspases and influences Fas-induced apoptosis. *J Biol Chem* 2001; **276**: 19656-19663

Edited by Zhu LH and Wang XL Proofread by Xu FM

Polymerase synthesis and potential interference of a small-interfering RNA targeting hPim-2

Shu-Qun Zhang, Qing-You Du, Yang Ying, Zong-Zheng Ji, Sheng-Qi Wang

Shu-Qun Zhang, Zong-Zheng Ji, Second Hospital of Xi'an Jiaotong University, Xi'an 710004, Shaanxi Province, China

Qing-You Du, Yang Ying, Sheng-Qi Wang, Beijing Institute of Radiation Medicine, Beijing 100850, China

Correspondence to: Dr. Shu-Qun Zhang, Second Hospital of Xi'an Jiaotong University, 36 Western 5th Road, Xi'an 710004, Shaanxi Province, China. zhangshuqun1971@yahoo.com.cn

Telephone: +86-29-87679526

Received: 2003-12-12 **Accepted:** 2004-01-13

Abstract

AIM: To synthesize three small-interference RNAs (siRNAs) by T₇ RNA polymerase-catalyzed reaction, and to investigate their efficacy on modulating the expression of serine/threonine kinase Pim-2 in human colon cancer cell line.

METHODS: siRNA I, II and III were synthesized by T₇ RNA polymerase-directed *in vitro* transcription, then transfected into human colon cancer cells SW-480. After incubation for 6 h at 37 °C, 100 mL/L FBS in RPMI 1640 was substituted in each well. After the transfection was repeated twice to three times in each kind of siRNA, hPim-2 mRNA and protein expression were measured by RT-PCR and Western blotting, respectively.

RESULTS: Compared to the control group, after transfected for 48 h with hPim-2 siRNA I, II and III, the relative inhibition rates of hPim-2 mRNA expression in colon cancer cells were 65.4% ($P < 0.05$), 46.2% ($P < 0.05$) and 56.1% ($P < 0.05$), respectively. The protein level of hPim-2 was decreased at 72 h compared to the untransfected cells. The relative inhibition percentages of hPim-2 protein by siRNA I, II, III were 61.6% ($P < 0.05$), 45.8% ($P < 0.05$) and 55.6% ($P < 0.05$), respectively.

CONCLUSION: The *in vitro* transcribed siRNAs can be useful for silencing oncogene hPim-2 expression specifically and efficiently. This may open a new path toward the use of siRNAs as a gene-specific therapeutic tool.

Zhang SQ, Du QY, Ying Y, Ji ZZ, Wang SQ. Polymerase synthesis and potential interference of a small-interfering RNA targeting hPim-2. *World J Gastroenterol* 2004; 10 (18): 2657-2660

<http://www.wjgnet.com/1007-9327/10/2657.asp>

INTRODUCTION

RNAi is an evolutionarily conserved mechanism known to control insects, plants, and mammalian cells^[1-4]. In this process, introduced double-stranded RNAs (ds-RNAs) silence gene was expressed through specific degradation of their cognate mRNAs^[5,6]. Importantly, RNAi can be achieved in mammalian cells following transfection of synthetic 21- and 22-nucleotide (nt) small interfering (si) RNAs, indicating that RNAi may serve as a powerful tool to block the expression of target genes

specifically^[7-11].

Pim-2 is a member of a family of serine/threonine protein kinases that consists of two other members, Pim-1 and Pim-3, and it exists at high concentrations in many tumor cells^[12,13]. Though it was identified 20 years ago, its function that maintains the cell size and its role in the survival of cancer cells have been just determined recently^[14,15]. It is believed to be a cancer-causing gene, or oncogene. Here, we sought to use siRNA-targeting hPim-2 to determine whether this technique could be used to specifically inhibit hPim-2 expression.

MATERIALS AND METHODS

T₇ siRNA synthesis

siRNAs selection was based on the characterization of siRNA by Elbashir *et al.*^[16]. Three hPim-2 siRNA sequences are given in Figure 1. For *in vitro* transcription, 40-nt DNA template oligonucleotides were designed to produce 21-nt siRNAs. siRNA sequences of the form GN₁₇CN₂ were selected for each target. Uridines in the last two nt form the 3' overhang of the siRNA duplex. The template and a 19-nt T₇ promoter (GGT AAT ACG ACT CAC TATA) were synthesized by Applied Biosystems 393 DNA synthesizer and purified by OPC (Perkin-Elmer, Foster city, CA). The oligonucleotide-directed mutagenesis of small siRNA transcription with T₇ polymerase is as follows: for each transcription reaction, 1 nmol of each oligonucleotide was annealed in 50 µL of TE buffer (10 mmol/L Tris-HCl pH 8.0, and 1 mmol/L EDTA) by heating at 95 °C; after 5 min, the heating block was switched off and allowed to cool down slowly to obtain dsDNA. Transcription was performed in 50 µL of transcription mixture: 1×T₇ transcription buffer (40 mmol/L Tris-HCl pH 7.9, 6 mmol/L MgCl₂, 10 mmol/L DTT, 10 mmol/L NaCl and 2 mmol/L spermidine), 1 mmol/L rNTPs, 0.1 U yeast pyrophosphatase (Sigma), 40 U RNase (Life Technologies) and 100 U T₇ RNA polymerase (Fermentas) containing 200 pmol of the dsDNA as template. After incubation at 37 °C for 3 h, 1 U RNase free-DNase (Promega) was added at 37 °C for 30 min. Sense and antisense 21-nt RNAs (single strand RNA, ssRNA) generated in separate reactions were annealed by mixing both crude transcription reactions, incubating at 37 °C overnight to obtain "T₇ RNA polymerase synthesized small interfering double-strand RNA (T₇ siRNA, dsRNA)". The mixture (100 µL) was then extracted with TE-saturated (pH 4.5) phenol:chloroform:isoamyl alcohol (25:24:1), purified with chloroform:isoamyl alcohol(24:1), isopropanol and 0.2 mol/L sodium acetate (pH5.2). The pellet was washed once with 750 mL/L ethanol, dried, and resuspended in 50 µL of water.

Cell culture

Human colon cancer cell line SW-480 was obtained from Chinese National Cancer Institute. The cells were grown in RPMI 1640 medium (Invitrogen) supplemented with 100 mL/L fetal bovine serum (GIBCO BRL, Grand Island, NY), 100 U/mL penicillin and 100 µg/mL streptomycin at 37 °C with 50 mL/L CO₂.

Transfection with siRNA oligonucleotides

Cells were seeded the day before the experiment in 6-well plates at a density of 1.5×10⁵ per well to be 50% confluent on the day

hPim-2-I Target mRNA	5'	AAGUUUGCCCAGUUCUUCCUCC	3'	
siRNA	5'	GUUUGCCCAGUUCUUCCUCCU	3'	Sense strand
	3'	UUCAAACGGGUCAAGGGAAGG	5'	Antisense strand
hPim-2-II Target mRNA	5'	AAGACAUAACCAAGUUUGCC	3'	
siRNA	5'	GACAUAACCAAGUUUGCCU	3'	Sense strand
	3'	UUGUGUAUUUGGUUCAACGG	5'	Antisense strand
hPim-2-III Target mRNA	5'	AAGUUGUCCCAUUUUGAGCC	3'	
siRNA	5'	GUUGUCCCAUUUUGAGCCU	3'	Sense strand
	3'	UUACAACGGGUAACUCGG	5'	Antisense strand

Figure 1 Sequences of 21-nt siRNA duplex that were used to target at hPim-2.

of the experiment. Transfection of the RNA oligonucleotides was performed using Lipofectamine 2000 (Invitrogen) as directed by the manufacturer to result in a final RNA concentration of 50 nmol/L. After transfection (incubation for 6 h at 37 °C), cells were washed with PBS and incubated in fresh culture medium until additional analyses.

Analysis of hPim-2 mRNA by RT-PCR

After transfection, total RNA was isolated using TRIZOL (Invitrogen) by a single-step phenol-extraction. Subsequent RT-PCR was performed (RT-PCR kit, Promega, Madison, WI). Briefly, first strand cDNA was synthesized using an Oligo (dT)₁₅ primer at 42 °C for 30 min. PCR for hPim-2 and β-actin was performed in a single reaction of 20 μL volume. The latter served as a control following 28 cycles of denaturing at 95 °C for 45 s, annealing at 58 °C for 40 s, and extending at 72 °C for 40 s. Under this PCR condition, the amplification showed linearity as was determined experimentally (data not shown). PCR products were run on a 30 g/L agarose gel and visualized by ethidium bromide staining, and the intensities were then measured by scanning the gel with Gel Doc 1000 (Bio-Rad, Hercules, CA). Inhibition of hPim-2 mRNA was calculated according to the following formula:

$$\text{Inhibition percentage} = \frac{(1 - A_{\text{sample}} \times A_{0\text{control}})}{A_{\text{control}} \times A_{0\text{sample}}} \times 100\%.$$

A_{sample} : the intensity of hPim-2 PCR product in cells transfected with siRNA and Lipofectamine; $A_{0\text{sample}}$: the intensity of hPim-2 PCR product in cells transfected with Lipofectamine alone; A_{control} : the intensity of β-actin product in cells transfected with siRNA and Lipofectamine; $A_{0\text{control}}$: the intensity of β-actin product in cells transfected with Lipofectamine alone.

Analysis of hPim-2 protein

The expression levels of hPim-2 protein in cells transfected with siRNAs were measured by scanning the density of bands on Western blotting. The expression level of hPim-2 mRNA was analyzed by the method described above. After 72 h of transfection, cells were lysed in RIPA buffer [10 mmol/L Tris-HCl (pH 7.4), 10 g/L deoxycholate, 10 g/LNP40, 150 mmol/L NaCl, 1 g/L SDS, 0.2 mmol/L phenylmethyl sulfonyl fluoride, 1 μg/mL aprotinin and 1 μg/mL leupeptin] for 30 min on ice. The lysates were centrifuged at 15 000 r/min for 15 min to remove debris. Equal amounts (30 μg) of proteins were separated by 120 g/L SDS-PAGE and transferred onto PVDF membrane (Hybond-polyvinylidene difluoride membranes, Amersham Biosciences). The transferred membrane was incubated with anti-hPim-2 goat polyclonal or anti-β actin rabbit polyclonal antibodies (Santa Cruz Biotechnology, Santa Cruz, CA) and followed with peroxidase-linked secondary antibody. Finally, the

immunoreactive proteins were detected by an ECL-plus detection kit (Amersham Biosciences) and scanned by Gel Doc 1000 (Bio-Rad), and the inhibition percentage (%) was calculated according to the following formula: inhibition percentage = $(1 - A_{\text{sample}}/A_{\text{control}}) \times 100$.

Statistics

The data were expressed as mean ± standard deviation (mean ± SD). Statistical analysis was performed by Student's *t*-test (two tailed). All data represented at least two independent experiments.

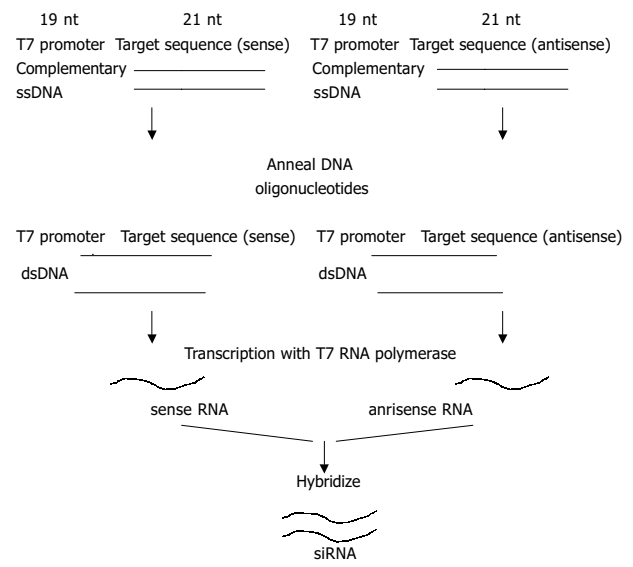


Figure 2 Strategy to generate T7 siRNA.

RESULTS

Synthesis of siRNA by *in vitro* transcription

To generate siRNAs by *in vitro* transcription, we designed the strategy presented in Figure 2. Target sequences for siRNA were identified by scanning the length of the hPim-2 gene with AA sequences. The AA and downstream 19 nucleotides were recorded and compared to an appropriate genome database to eliminate any sequences with significant homology to other genes. Those sequences that appear to be specific are the potential siRNA target sites. Besides, it is noteworthy that T₇ RNA polymerase can transcribe a template efficiently if only the first nucleotide of the RNA transcript is G. Thus, the design of T₇ siRNAs requires that the sequence starts with a G and has a C at position 19 (GN₁₇CN₂) to allow annealing with the complementary RNA, which also starts with a G^[17,18]. The T₇ promoter oligonucleotide is invariant and common to any target gene. A 40 mer DNA oligonucleotide template was synthesized

by a 21 mer oligonucleotide encompassing the T₇ promoter with complementary sequence preceded by two additional nucleotides (reading the sequence 5'---3'). Following transcription reactions, sense and antisense transcriptions were annealed, ethanol precipitated and yielded what we refer to as T₇siRNAs. The integrity of the transcriptions was checked on a 30 g/L agarose gel (Figure 3).

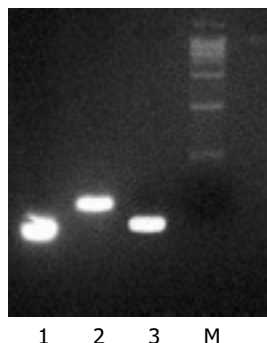


Figure 3 Lane 1: T7 *in vitro* transcribed single-strand RNA. Lane 2: annealed double-strand DNA template. Lane 3: hybridized double-strand small interference RNA.

Effect of siRNAs on hPim-2 expression

The mRNA level of hPim-2 was determined by semi-quantitative RT-PCR. A 237-bp DNA fragment of hPim-2 gene and a 317-bp DNA fragment of β -actin gene were amplified by RT-PCR with specific primers, respectively. As shown in Figure 4A, mRNA expression level of hPim-2 was decreased when compared to the uninduced cells, while the mRNA level of β -actin as the control was almost unchanged. As shown in Figure 4B, after transfection with hPim-2 siRNA I, II and III and compared with the

levels of β -actin, the relative inhibition rates of hPim-2 mRNA expression were 65.4% ($P < 0.05$), 46.2% ($P < 0.05$) and 56.1% ($P < 0.05$) in colon cancer cells, respectively.

In order to verify the decrease in mRNA expression, which corresponded to the decreases at protein levels, Western blotting was performed. Figure 5A shows that the protein level of hPim-2 was decreased at 72 h compared to the uninduced cells. The relative inhibition percentages of hPim-2 protein by siRNA I, II and III were 61.6% ($P < 0.05$), 45.8% ($P < 0.05$) and 55.6% ($P < 0.05$), respectively (Figure 5B).

DISCUSSION

Oncogene overexpression has been implicated in the development and progression of a variety of human cancers and, therefore, provides a potential target for cancer gene therapy^[19-22]. For years, research has been focused on effective tools to specifically down-regulate oncogene overexpression such as antisense oligonucleotide strategy. However, there has been only limited success because of the lack of specificity and potency for this method. For example, screening of more than 20 oligomers is usually required before identifying one antisense that functions effectively, and the dose required for inhibiting gene expression is often not much different from the doses that lead to nonselective toxicity^[23-25].

Recent progress of RNAi techniques has demonstrated the potential to overcome those limitations. The selection of targeting sequences of RNAi is less restricted, once the site is identified, sense and antisense oligonucleotides with 3'-UU overhangs can be designed, so the success rates of producing effective duplexes are higher. Just like in this experiment, siRNAs were designed complimentary to three different regions of the corresponding Pim-2 mRNA, and each of them has different level of inhibition efficacy, the suppression of hPim-2

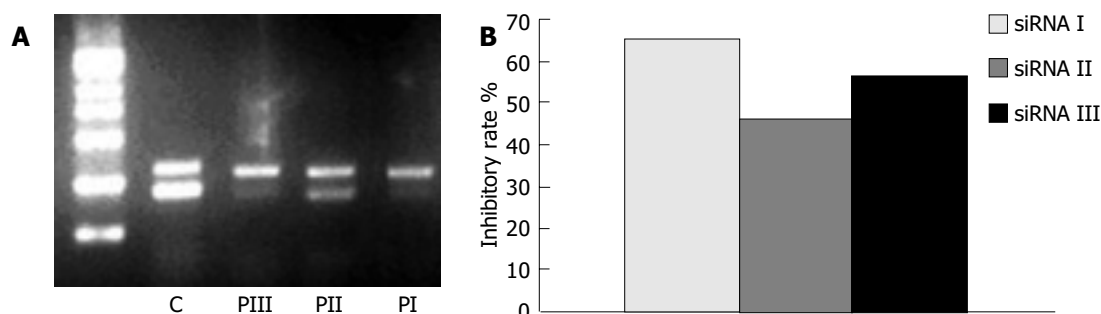


Figure 4 Inhibitory effects of siRNA on mRNA level of hPim-2. A: Electrophoresis of RT-PCR products of hPim-2 gene and β -actin gene in colon cancer cells transfected with siRNA I,II,III. B: Quantitation of inhibitory percentage of hPim-2 mRNA in transfected cells. Each level of PCR product of hPim-2 gene was quantitated and normalized to the level of β -actin. Inhibitory rate was calculated by comparing to the control cells. The results were expressed as mean \pm SD from independent experiments. $P < 0.05$ vs the cells transfected with lipofectamine alone.

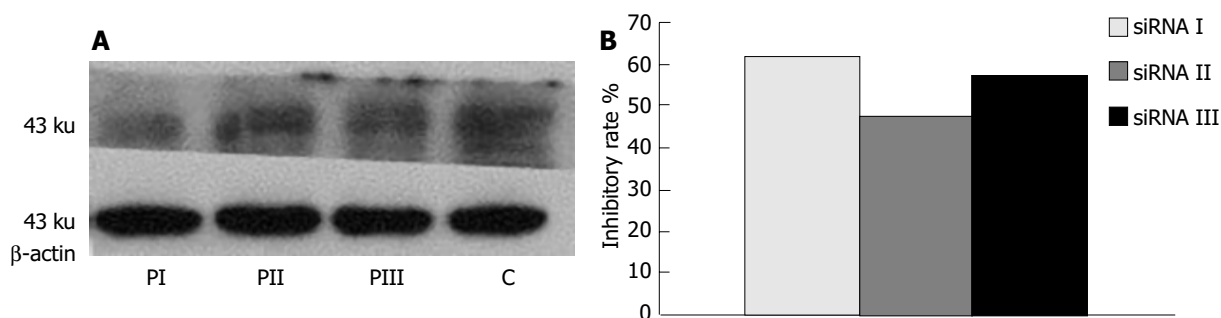


Figure 5 Inhibitory effects of siRNA on protein level of hPim-2. A: Western blot analysis of hPim-2 protein in colon cancer cells transfected with siRNA I, II, III. B: inhibitory percentage of hPim-2 protein in transfected cells compared to the control cells. Each level of hPim-2 protein was quantitated. Inhibitory rate was calculated by comparing to the control cells. The results were expressed as mean \pm SD from independent experiments. $P < 0.05$ vs the cells transfected with lipofectamine alone.

gene expression by these siRNAs directed at different sites varied from 45-65%. This indicates that screening potential target of RNAi is much more easy.

Besides, our results demonstrate that *in vitro* transcribed siRNA can effectively down-regulate oncogene expression with great efficiency. It has been suggested that siRNA may inhibit gene expression through diverse effects, inhibition of mRNA can occur through the formation of a nuclease complex called RISC (RNA-induced silencing complex) that targets and cleaves mRNA which is complementary to the siRNA. The damaged mRNA may deteriorate through the action of the RNA-dependent RNA polymerase (RdRP), producing new siRNAs to target other mRNA. This incessant waterfall-like amplification can produce RNA interference effect at a very small dose, and inhibit the protein translation quickly and efficiently^[26-30]. In our experiment, the dose required for inhibiting Pim-2 gene expression was 50 nmol/L, far below the dose required for the antisense oligonucleotide^[31], indicating that siRNA synthesized by the *in vitro* transcription strategy can suppress the hPim-2 gene expression sensitively.

Here, we used the *in vitro* transcription method for the synthesis of siRNAs by T₇ RNA polymerase and transferred them into cells. The main advantage of this technique is its simplicity. It provides a reproducible and highly efficient means to inhibit the target gene expression. Human Pim-2 gene, a regulated transcriptional apoptotic inhibitor, has a novel role in promoting cell autonomous survival. Over-expression of Pim-2 allows the tumour cells to ignore or become insensitive to boosters of the immune system^[14]. Application of Pim-2-directed siRNA can significantly reduce Pim-2 mRNA and protein levels efficiently. Our next step is to try to manipulate the action of Pim-2 with siRNA, so that we can interfere with the survival of cancer cells.

REFERENCES

- 1 **McCaffey AP**, Meuse L, Pham TT, Conklin DS, Hannon GJ, Kay MA. RNA interference in adult mice. *Nature* 2002; **418**: 38-39
- 2 **Tiscornia G**, Singer O, Ikawa M, Verma IM. A general method for gene knockdown in mice by using lentiviral vectors expressing small interfering RNA. *Proc Natl Acad Sci U S A* 2003; **100**: 1844-1848
- 3 **Brummelkamp TR**, Bernards R, Agami R. A system for state expressing short RNAs in mammalian cells. *Science* 2002; **296**: 550-553
- 4 **Elbashir SM**, Lendeckel W, Tuschl T. RNA interference is mediated by 21- and 22-nucleotide RNAs. *Genes Dev* 2001; **15**: 188-200
- 5 **Wang QC**, Nie QH, Feng ZH. RNA interference: Antiviral weapon and beyond. *World J Gastroenterol* 2003; **9**: 1657-1661
- 6 **Fire A**, Xu S, Montgomery MK, Kostas SA, Driver SE, Mello CC. Potent and specific genetic interference by double-stranded RNA in *Caenorhabditis elegans*. *Nature* 1998; **391**: 806-811
- 7 **Hammond SM**, Bernstein E, Beach D, Hannon GJ. An RNA-directed nuclease mediates post-transcriptional gene silencing in *Drosophila* cells. *Nature* 2000; **404**: 293-296
- 8 **McManus MT**, Petersen CP, Haines BB, Chen J, Sharp PA. Gene silencing using micro-RNA designed hairpins. *RNA* 2002; **8**: 842-850
- 9 **Novina CD**, Murray MF, Dykxhoorn DM, Beresford PJ, Riess J, Lee SK, Collman RG, Lieberman J, Shankar P, Sharp PA. siRNA-directed inhibition of HIV-1 infection. *Nat Med* 2002; **8**: 681-686
- 10 **Paddison PJ**, Caudy AA, Bernstein E, Hannon GJ, Conklin DS. Short hairpin RNAs induce sequence-specific silencing in mammalian cells. *Genes Dev* 2002; **16**: 948-958
- 11 **Yu JY**, DeRuiter SL, Turner DL. RNA interference by expression of short-interfering RNAs and hairpin RNAs in mammalian cells. *Proc Natl Acad Sci U S A* 2002; **99**: 6047-6052
- 12 **Datta SR**, Ranger AM, Lin MZ, Sturgill JF, Ma YC, Cowan CW, Dikkes P, Korsmeyer SJ, Greenberg ME. Survival factor-mediated BAD phosphorylation raises the mitochondrial threshold for apoptosis. *Dev Cell* 2002; **3**: 631-643
- 13 **Plas DR**, Thompson CB. Cell metabolism in the regulation of programmed cell death. *Trends Endo Met* 2002; **13**: 74-78
- 14 **Fox CJ**, Hammerman PS, Cinalli RM, Master SR, Chodosh LA, Thompson CB. The serine/threonine kinase Pim-2 is a transcriptionally regulated apoptotic inhibitor. *Genes Dev* 2003; **17**: 1841-1854
- 15 **Allen J**, Verhoeven E, Domen J, van der Valk M, Berns A. Pim-2 transgene induces lymphoid tumors, exhibiting potent synergy with *c-myc*. *Oncogene* 1997; **15**: 1133-1141
- 16 **Elbashir SM**, Harborth J, Lendeckel W, Yalcin A, Weber K, Tuschl T. Duplexes of 21-nucleotide RNAs mediate RNA interference in cultured mammalian cells. *Nature* 2002; **411**: 494-498
- 17 **Milligan JF**, Uhlenbeck OC. Synthesis of small RNAs using T7 RNA polymerase. *Methods Enzymol* 1989; **180**: 51-62
- 18 **Konarska MM**, Sharp PA. Structure of RNAs replicated by the DNA-dependent T7 RNA polymerase. *Cell* 1990; **63**: 609-618
- 19 **Gottlieb E**, Thompson CB. Targeting the mitochondria to enhance tumor suppression. *Methods Mol Biol* 2003; **223**: 543-554
- 20 **Watanabe RN**. Oncogene and tumor suppressor gene. *Rinsho Byori* 2002; **123**: 131-136
- 21 **Gerdes AM**. Cancer genetics. A review of oncological molecular biology seen in relation to the human genome. *Ugeskr Laeger* 2002; **164**: 2865-2871
- 22 **Willians JL**. Malignancy: an evolving definition of a cancer cell. *Clin Lab Sci* 2002; **15**: 37-43
- 23 **Miyagishi M**, Hayashi M, Taira K. Comparison of the suppressive effects of antisense oligonucleotides and siRNAs directed against the same targets in mammalian cells. *Antisense Nucleic Acid Drug Dev* 2003; **13**: 1-7
- 24 **Kretschmer-Kazemi Far R**, Sczakiel G. The activity of siRNA in mammalian cells is related to structural target: accessibility comparison with antisense oligonucleotides. *Nucleic Acid Res* 2002; **31**: 4417-4424
- 25 **Aoki Y**, Cioca DP, Oidaira H, Kamiya J, Kiyosawa K. RNA interference may be more potent than antisense RNA in human cancer cell lines. *Clin Exp Pharmacol Physiol* 2003; **30**: 96-102
- 26 **Chiu YL**, Rana TM. RNAi in human cells: basic structural and functional features of small interfering RNA. *Mol Cell* 2002; **10**: 549-561
- 27 **Scherr M**, Morgan MA, Eder M. Gene silencing mediated by small interfering RNAs in mammalian cells. *Curr Med Chem* 2003; **10**: 245-256
- 28 **Carthew RW**. Gene silencing by double-stranded RNA. *Curr Opin Cell Biol* 2001; **13**: 244-248
- 29 **Smith NA**, Singh SP, Wang MB, Stoutjesdijk PA, Green AG, Waterhouse PM. Total silencing by intron-spliced hairpin RNAs. *Nature* 2000; **407**: 319-320
- 30 **Doi N**, Zenno S, Ueda R, Ohki-Hamazaki H, Ui-Tei K, Saigo K. Short-interfering-RNA-mediated gene silencing in mammalian cells requires Dicer and eIF2C translation initiation factors. *Curr Biol* 2003; **13**: 41-46
- 31 **Bertrand JR**, Pottier M, Vekris A, Opolon P, Maksimenko A, Malvy C. Comparison of antisense oligonucleotide and siRNAs in cell culture and *in vivo*. *Biochem Biophys Res Commun* 2002; **296**: 1000-1004

• VIRAL HEPATITIS •

Effect of lamivudine treatment on plasma levels of transforming growth factor β_1 , tissue inhibitor of metalloproteinases-1 and metalloproteinase-1 in patients with chronic hepatitis B

Robert Flisiak, Haza Al-Kadasi, Jerzy Jaroszewicz, Danuta Prokopowicz, Iwona Flisiak

Robert Flisiak, Haza Al-Kadasi, Jerzy Jaroszewicz, Danuta Prokopowicz, Department of Infectious Diseases, Medical University, Bialystok, Poland

Iwona Flisiak, Department of Dermatology and Venereology, Medical University, Bialystok, Poland

Correspondence to: Robert Flisiak, M.D., Ph.D., Professor, Department of Infectious Diseases, Liver Unit, Medical University of Bialystok, 15-540 Bialystok, Zurawia str., 14, Poland. flisiakr@priv.onet.pl

Telephone: +48-85-7409481 **Fax:** +48-85-7434613

Received: 2004-01-15 **Accepted:** 2004-03-04

Abstract

AIM: Transforming growth factor (TGF)- β_1 , metalloproteinase (MMP)-1 and its tissue inhibitor (TIMP)-1 are considered predictive biomarkers of chronic hepatitis activity and fibrosis. The aim of this study was to evaluate the effect of lamivudine treatment on the plasma levels of these peptides in patients with chronic hepatitis B.

METHODS: TGF- β_1 , MMP-1 and TIMP-1 plasma concentrations were measured with an enzyme immunoassay in 40 patients treated with lamivudine for 48 wk. Elimination of HBV-DNA and HBV antigens was evaluated 24 wk after treatment completion.

RESULTS: Baseline TGF- β_1 (29.6 \pm 2.2 ng/mL) and TIMP-1 (1 578 \pm 93 ng/mL) significantly exceeded normal values (18.3 \pm 1.6 ng/mL and 1 102 \pm 67 ng/mL respectively). Lamivudine treatment resulted in a significant decrease of TGF- β_1 and TIMP-1 during treatment with an increase after 24 wk of treatment. Pretreatment MMP-1 levels (6.7 \pm 0.7 ng/mL) were significantly lower than normal values (11.9 \pm 0.9 ng/mL) and increased during treatment and follow-up. A significant correlation was noted between TGF- β_1 or TIMP-1 and aminotransferases as well as fibrosis scored in liver biopsy specimens. There were no statistically significant differences of TGF- β_1 , TIMP-1 and MMP-1 between four groups at baseline, 24 and 48 wk of treatment. TGF- β_1 and TIMP-1 levels increased significantly in non-responders and normalized in responders at wk 72. MMP-1 also normalized in responders and decreased to values significantly lower than normal in non-responders.

CONCLUSION: These findings support the role of TGF- β_1 , TIMP-1 and MMP-1 in the pathogenesis of chronic hepatitis B. Because of their association with hepatic injury and antiviral treatment efficacy, determination of these peptides may be useful in disease management.

Flisiak R, Al-Kadasi H, Jaroszewicz J, Prokopowicz D, Flisiak I. Effect of lamivudine treatment on plasma levels of transforming growth factor β_1 , tissue inhibitor of metalloproteinases-1 and metalloproteinase-1 in patients with chronic hepatitis B. *World J Gastroenterol* 2004; 10(18): 2661-2665

<http://www.wjgnet.com/1007-9327/10/2661.asp>

INTRODUCTION

Transforming growth factor- β_1 (TGF- β_1) is considered a pivotal inducer of liver fibrosis, acting mostly through activation of hepatic stellate cells (HSCs), which are the main source of extracellular matrix (ECM) proteins^[1-3]. The effect of TGF- β_1 on liver fibrosis is at least in part related to stimulation of the tissue inhibitor of metalloproteinases-1 (TIMP-1), which affects metalloproteinases (MMP) activity and is responsible for inhibition of ECM proteins breakdown^[4]. Apart from a profibrogenic role, TGF- β_1 inhibits DNA synthesis serving as a terminator of regenerative cell proliferation and induces apoptosis of hepatocytes in normal liver and during regression of liver hyperplasia^[5]. On the other hand, TGF- β may inhibit stellate cells apoptosis and promote their survival, which are at least in part a result of anti-apoptotic effect of TIMP-1^[6]. Additionally TGF- β_1 exerts regulatory, mostly immunosuppressive effects on the immune system. Since hepatitis B virus (HBV) infection is related to an immune response, cell proliferation and fibrosis, modulation of TGF- β_1 might affect the course of chronic viral hepatitis B^[7,8]. The possible role of TGF- β_1 , TIMP-1 and MMP-1 as predictive biomarkers of chronic hepatitis activity and progression was supported by recent clinical studies^[9-16], which demonstrated their association with hepatic function impairment or fibrosis, but did not evaluate their effect of antiviral treatment. We undertook this study to evaluate the effect of lamivudine, the most widespread antiviral medication for chronic HBV infection, on plasma TGF- β_1 , TIMP-1 and MMP-1 levels in patients with chronic hepatitis B.

MATERIALS AND METHODS

Patients

Ethical approval for the study was obtained from the Bioethical Committee of the Medical Academy of Bialystok. Informed consent was obtained from 40 patients (13 females and 27 males, mean age: 45 \pm 3 years) with chronic hepatitis B, who were included into the protocol of lamivudine (ZeffixTM, Glaxo-Smith-Kline) treatment. Normal values of TGF- β_1 , TIMP-1 and MMP-1 were collected from 13 healthy volunteers (5 females and 7 males, mean age: 47 \pm 2 years). The diagnosis of chronic hepatitis B was confirmed by the presence of HBs and HBe antigens with stable elevated alanine aminotransferase (ALT) activity for at least 6 mo. Additionally the disease activity was confirmed by the presence of viral replication and evaluation of liver biopsy specimens performed by means of the Hepafix System (Braun, Melsungen, Germany). Paraffin-embedded biopsy specimens were stained and evaluated using the Scheuer scoring system^[17]. Patients received 100 mg of lamivudine daily for 48 wk. Plasma levels of TGF- β_1 , TIMP-1 and MMP-1 were measured before treatment and at wk 24, 48 (end of the treatment) and 72. These results were compared to standard laboratory indices of liver injury. To evaluate treatment efficacy patients were divided into four groups with respect to elimination of HBV antigens and HBV-DNA at week 72 (24 wk after

completion of treatment). Criteria for inclusion into particular groups were as follows: group I (complete response): HBsAg (-), HBeAg (-), HBV-DNA (-); group II: HBsAg (+), HBeAg (-), HBV-DNA (-); group III: HBsAg (+), HBeAg (-), HBV-DNA (+); group IV (no response): HBsAg (+), HBeAg (+), HBV-DNA (+).

Methods

Venous blood for plasma TGF- β_1 , TIMP-1 and MMP-1 was collected on ice using tubes with EDTA. Samples for TGF- β_1 were immediately activated with acetic acid and urea and assayed with ELISA using recombinant human TGF- β soluble receptor type II (T β RII) as a solid phase precoated onto a microplate (Quantikine[®], R&D Systems Inc., Minneapolis, USA) as we described previously^[18]. TIMP-1 and MMP-1 were assayed by the two-site ELISA sandwich technique (Amersham Pharmacia Biotech, Little Chalfont, Buckinghamshire, England) using specific antibodies as a solid phase. MMP-1 assay recognises total human MMP-1, ie. free and complexed with TIMP-1. TIMP-1 assay recognises total human TIMP-1, including free and complexed with any metalloproteinases bound to the solid phase. TIMP-1 or MMP-1 bound to the solid phase, were detected by peroxidase labelled antibodies. There is no cross-reactivity between TIMP-1 and MMP-1 in these assays.

Liver function tests: ALT, aspartate aminotransferase (AST), alkaline phosphatase (ALP), gamma glutamyltranspeptidase (GGT) activity and bilirubin concentration were measured using a Cobas Mira instrument (Roche) and the prothrombin index (PI) was determined using Kselmed K-3002 (Poland).

Statistics

Values were expressed as the mean \pm SE. The significance of the difference was calculated by two-tailed Student's *t* test. For correlation analysis the Pearson product moment correlation was performed. Values of $P < 0.05$ were considered as statistically significant.

RESULTS

Plasma concentrations of TGF- β_1 and TIMP-1 were determined before lamivudine treatment (mean: 29.6 \pm 2.2 ng/mL and 1 578 \pm 93 ng/mL respectively) and significantly exceeded mean normal values (18.3 \pm 1.6 ng/mL and 1 102 \pm 67 ng/mL respectively). Treatment resulted in a significant decrease by wk 24 and a further decline at the end of the treatment. However 24 wk after treatment completion mean values of both TGF- β_1 and TIMP-1 increased (Table 1). In contrast, mean MMP-1 baseline level (6.7 \pm 0.7 ng/mL) was almost half the normal value (11.9 \pm 0.9 ng/mL) and increased during treatment. After completion of treatment the levels still remained lower than normal (Table 1). There was a significant positive correlation between TGF- β_1 , TIMP-1 and ALT or AST (Table 2). A significant correlation was also demonstrated between TIMP-1 and ALP or GGT, but there was no association between MMP-1 and the biochemical indices of liver injury (Table 2). As demonstrated in Figure 1 a significant positive correlation ($r = 0.435$; $P < 0.01$) was observed between TGF- β_1 and TIMP-1. There was no correlation between TGF- β_1 and MMP-1 ($r = 0.069$), or between TIMP-1 and MMP-1 ($r = -0.143$).

As demonstrated in Table 3 scored degree of hepatic inflammation and fibrosis was similar before and after the treatment. Histologic observations in biopsies performed before the treatment showed a significant correlation between the degree of fibrosis and plasma TGF- β_1 or TIMP-1 levels (Table 4). There was no association between scored inflammation or fibrosis and classical biochemical parameters of liver injury.

Table 1 Plasma concentrations of TGF- β_1 , TIMP-1 and MMP-1 during treatment with lamivudine (mean \pm SE)

	Normal values	Time since treatment beginning (wk)			
		0	24	48	72
TGF- β_1 (ng/mL)	18.3 \pm 1.6	29.6 \pm 2.2 ¹	22.6 \pm 1.2 ²	21.9 \pm 1.5 ²	24.1 \pm 2.4
TIMP-1 (ng/mL)	1 102.0 \pm 67	1 578.0 \pm 93 ¹	1 235.0 \pm 67 ²	927.0 \pm 50 ²	1 215.0 \pm 98 ²
MMP-1 (ng/mL)	11.9 \pm 0.9	6.7 \pm 0.7 ¹	8.3 \pm 0.5 ¹	9.6 \pm 0.5 ¹	9.7 \pm 0.7 ²

Statistical significance in comparison with normal ¹ and baseline ² values.

Table 2 Correlation expressed by *r*-value and its significance between analyzed biochemical indices and TGF- β_1 , TIMP-1 or MMP-1 in chronic hepatitis B patients treated with lamivudine

	mean \pm SE	TGF- β_1	TIMP-1	MMP-1
Bil (mg%)	1.02 \pm 0.06	0.049	0.119	-0.059
ALT (U/L)	74.50 \pm 5.9	0.201 ^a	0.247 ^a	0.005
AST (U/L)	60.10 \pm 5.2	0.244 ^a	0.269 ^a	-0.029
ALP (U/L)	96.10 \pm 3.8	0.114	0.295 ^a	-0.071
GGT (U/L)	47.70 \pm 4.9	0.062	0.247 ^a	-0.102
PI (%)	87.30 \pm 1.5	-0.109	0.006	-0.065

Bil: bilirubin; ALT: alanine aminotransferase; AST: aspartate aminotransferase; ALP: alkaline phosphatase; GGT: gamma glutamyltranspeptidase; PI: prothrombin index. ^a $P < 0.05$ vs other groups.

Table 3 Values of scored degree of hepatic inflammation and fibrosis in liver biopsy specimens obtained from patients before and after lamivudine treatment (mean \pm SE)

	Before the treatment	After the treatment
Portal inflammation	2.6 \pm 0.1	2.5 \pm 0.2
Lobular inflammation	1.9 \pm 0.1	1.8 \pm 0.1
Fibrosis	2.0 \pm 0.2	1.8 \pm 0.2

Table 4 Correlation expressed by *r*-value and significance between scored degree of hepatic inflammation or fibrosis and plasma levels of TGF- β_1 , TIMP-1 and MMP-1 in patients with chronic hepatitis B before lamivudine treatment

	Inflammation		Fibrosis
	Portal	Lobular	
TGF- β_1	0.207	0.179	0.391 ^a
TIMP-1	0.224	0.319	0.620 ^a
MMP-1	0.009	-0.094	-0.135

^a $P < 0.05$ vs others.

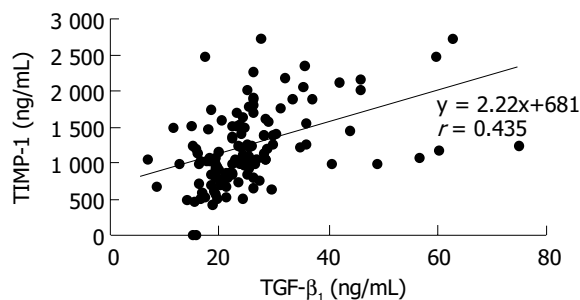
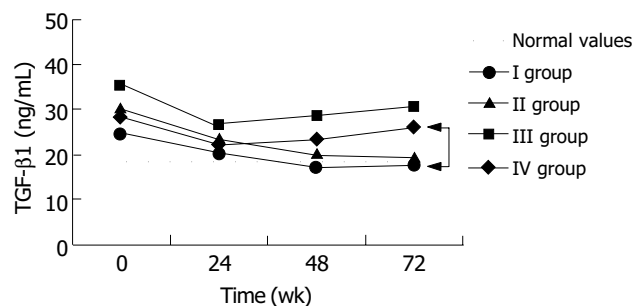
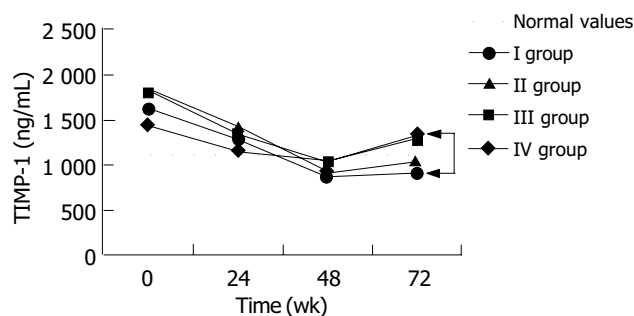
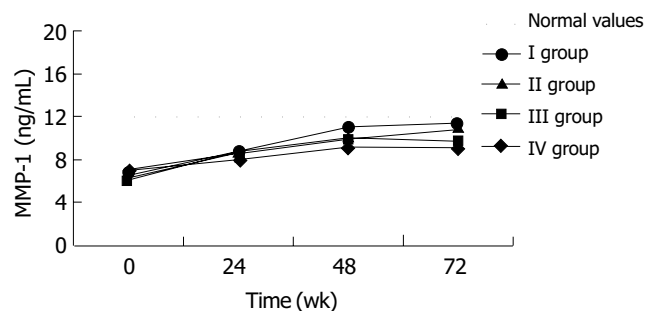
The majority of patients (23-57.5%) did not respond to treatment and were classified into group IV. A complete response (group I), with elimination of HBs and HBe antigens as well as HBV-DNA, was observed in 5 patients (12.5%). Six patients (15%) demonstrated a partial response (group II), and another six eliminated HBeAg with detectable viral replication (group III). Evaluation of baseline liver function tests and efficacy of treatment showed no statistically significant differences between the four groups. As demonstrated in Table 5, at the end of the treatment, patients in groups III and IV had significantly higher ALT activities than patients in group I. This difference was statistically significant in respect to both ALT and AST activities, 24 weeks after the treatment completion (Table 5). Histologic pictures did not demonstrate significant differences between groups in liver biopsies performed before

Table 5 Activities of alanine and aspartate aminotransferases during the treatment (0, 24 and 48 wk) and 24 wk after its completion (week 72) in four groups (mean \pm SE)

	ALT (U/L)				AST (U/L)			
	0	24	48	72	0	24	48	72
Group I	87.0 \pm 24.5	25.2 \pm 5.0	23.0 \pm 4.8	23.2 \pm 4.9	79.8 \pm 15.9	30.2 \pm 6.7	28.0 \pm 6.4	27.0 \pm 6.1
Group II	108.5 \pm 53	32.5 \pm 9.5	31.9 \pm 7.5	31.7 \pm 5.7	66.7 \pm 24.8	44.2 \pm 12.7	32.1 \pm 4.8	29.8 \pm 3.8
Group III	127.0 \pm 43.4	38.7 \pm 8.2	78.0 \pm 30.1 ^a	88.2 \pm 34 ^b	117 \pm 47.2	39.2 \pm 8.8	60.5 \pm 15.9	63.5 \pm 22 ^a
Group IV	101.0 \pm 11.8	78.6 \pm 8.3	69.2 \pm 6.3 ^b	68.5 \pm 4.2 ^b	65.9 \pm 6.4	65.2 \pm 21.2	59.7 \pm 8.4	58.7 \pm 3.9 ^a

Statistical significance in comparison with group I (complete response to treatment): ^a $P < 0.05$, ^b $P < 0.001$ vs other groups.

and after the treatment. During treatment TGF- β_1 , TIMP-1 and MMP-1 plasma levels were similar among all patients before divided into the response-related groups (Figures 2, 3, 4). And there were no statistically significant differences in their concentrations between groups at baseline, 24 and 48 weeks of treatment, either. Although at week 48 the mean TGF- β_1 in the non-responder groups (III and IV) tended to increase, whereas in groups I and II normalized, the difference was not significant (Figure 2). However 24 weeks after treatment completion (wk 72), the difference between TGF- β_1 levels in groups I and IV (17.5 \pm 0.6 and 26 \pm 1.8 ng/mL respectively) became significant ($P = 0.04$). Moreover the concentration in group IV was significantly ($P = 0.009$) higher than normal values. TIMP-1 mean concentrations were similar among all groups during the treatment period and normalized at week 48 (Figure 3). However 24 wk later, values in group IV (1 350 \pm 70 ng/mL) were significantly higher than normal, as well as that in group I (900 \pm 131 ng/mL). MMP-1 levels increased in all groups during the treatment. At wk 72, MMP-1 almost normalized in responders and slightly decreased in non-responders (Figure 4). The difference between MMP-1 concentrations in group IV after treatment completion (9.1 \pm 0.8 ng/mL) and normal values was statistically significant ($P = 0.037$).

**Figure 1** Correlation between plasma TGF- β_1 and TIMP-1 in patients with chronic hepatitis B treated with lamivudine.**Figure 2** Mean TGF- β_1 plasma concentrations before and during lamivudine therapy as well as 24 wk after its completion (wk 72) in respect to the final effect of the treatment. Statistical significance in comparison to normal values are indicated with asterisks and between groups with arrows.**Figure 3** Mean TIMP-1 plasma concentrations before and during lamivudine therapy as well as 24 wk after its completion (wk 72) in respect to the final effect of the treatment. Statistical significance in comparison to normal values are indicated with asterisks and between groups with arrows.**Figure 4** Mean MMP-1 plasma concentrations before and during lamivudine therapy as well as 24 wk after its completion (week 72) in respect to the final effect of the treatment. Statistical significance in comparison to normal values are indicated with asterisks and between groups with arrows.

DISCUSSION

The pivotal role of TGF- β_1 in fibrogenesis was finally proved in transgenic mice with an overexpression of TGF- β_1 , which caused an increase of TGF- β_1 plasma levels up to 700 ng/mL and a marked upregulation of TIMP-1 gene expression^[19-21]. Chronic liver injury leading to fibrosis displayed diminished ECM degradation mainly through TIMP induction and consequent MMP inhibition^[4]. As demonstrated recently by Nie *et al.* in the process of hepatic fibrosis, fibroblasts and myofibroblasts are the major cells that express TIMP-1 and TIMP-2, and their gene expressions correlate with degree of hepatic fibrosis.

The most important factor that affects the measurement of TGF- β_1 in human is the preparation of samples with minimal contamination from platelets which are an important source of this cytokine^[22]. The Quantikine ELISA System is recommended because of the relatively quick and simple activation with acid and urea, which disrupt the majority of TGF- β_1 complexes.

As we have demonstrated previously, TGF- β_1 correlates significantly with the degree of liver insufficiency in humans with liver cirrhosis^[18]. Moreover both TGF- β_1 and TIMP-1 measured in plasma of patients with chronic hepatitis B demonstrate a significant correlation with the degree of hepatocyte injury and fibrosis in liver biopsy specimens^[10]. We confirmed these observations in the present study. As demonstrated by Yoo *et al.*^[7] HBV antigens induce expression of TGF- β_1 in the early stages of infection. According to Lee *et al.*^[8] HBV encoded pX protein enhances transcriptional activity and response to TGF- β by amplification of Smad-mediated signaling, which can also contribute to HBV-associated liver fibrosis. Therefore the stimulatory effect of HBV antigens on TGF- β_1 seems to be an important mechanism of liver fibrosis in addition to TGF- β release caused by hepatocyte injury.

Association between circulating or tissue TGF- β_1 and liver fibrosis has also been confirmed in HCV infection^[10,11]. Recent studies of Neuman *et al.*^[23], Chen *et al.* and Lu *et al.*^[16] demonstrated a similar relationship between different chronic liver diseases including primary biliary cirrhosis and alcoholic liver disease and TGF- β_1 . Our previous study showed that the positive predictive value of TGF- β_1 plasma levels exceeding the upper normal range reached 96% for liver cirrhosis^[18]. As demonstrated recently by Zhang *et al.* serum level of TIMP-1 and TIMP-1/MMP-1 could be used as the indices for the diagnosis of hepatic fibrosis in chronic hepatitis B. According to Boeker *et al.*^[9], measurement of plasma TIMP-1 detected cirrhosis with a 100% sensitivity but lower specificity. These observations were also confirmed by the association between hepatic fibroproliferation and expression of hepatic TIMP and MMP mRNA^[12]. Walsh *et al.*^[15], who studied liver histology in patients with chronic hepatitis C, underlined the high sensitivity of TIMP-1 and TIMP-2 in detecting advanced liver disease. According to Nie *et al.*, there was a significant correlation between circulating and liver levels of TIMP-1 in cirrhotics, so its measurement in plasma might be useful in fibrosis management. These observations indicate the usefulness of both TGF- β_1 and TIMP-1 as possible early non-invasive biomarkers for liver fibrosis.

The rate of HBeAg seroconversion in our study (27.5%) was in range (18-32%) demonstrated by numerous authors in previous research with lamivudine treatment^[24-26]. In this study we confirmed the association between the degree of hepatocyte injury or liver fibrosis and plasma TGF- β_1 or TIMP-1 levels in patients with chronic hepatitis B. Aminotransferases, which are classical surrogate markers of hepatic injury, demonstrated similar association with the outcomes of the treatment. However, in contrast to TGF- β_1 and TIMP-1 their activities were not related to liver fibrosis. As the levels of TGF- β_1 , TIMP-1 and MMP-1 showed a similar change in all groups during therapy, it was unclear whether this was a direct effect of lamivudine on their expressions or an effect caused by HBV inhibition. However, their levels at 24 wk after therapy completion demonstrated their association with infection activity. This relationship was noted in respect to TGF- β_1 , which increased in group IV (non-responders) at the end of treatment. The effect on TIMP-1 was probably secondary to TGF- β_1 . The inhibitory activity of excessive TIMP-1 accumulation might be the reason for the decreased MMP-1 plasma concentration. These results are in accordance with our previous findings, demonstrating the strong association between TGF- β_1 or TIMP-1 plasma levels and scored hepatic fibrosis evaluated in biopsy specimens of patients with chronic hepatitis B and C^[10]. The findings of increased TGF- β_1 and TIMP-1 accompanied by an elevation in plasma carboxyterminal cross-linked telopeptide of type I procollagen (ICTP), indicative of type I collagen degradation. We suggested that collagenolytic mechanisms preceded TGF- β_1 /TIMP-1

dependent stimulation of liver fibrosis^[10]. Low MMP-1 plasma levels before treatment in the present study is consistent with this observation. It is also in accordance with the report by Murawaki *et al.*^[13], who demonstrated a decrease in MMP-1 concentration during histological progression of chronic hepatitis. Moreover, a significantly decreased baseline plasma MMP-1, followed by an increase during treatment, supports the role of TGF- β_1 /TIMP-1 dependent mechanism of liver fibrosis in patients with active chronic hepatitis B. Similar effects on MMP-1 and TIMP-1 were observed by Ninomiya *et al.*^[14] in patients with chronic hepatitis C who showed improvement of liver histology after treatment with interferon-alfa. Reduced progression of liver fibrosis during treatment of chronic hepatitis B with lamivudine has been demonstrated in numerous trials^[24-28]. Downregulation of TGF- β_1 /TIMP-1 causing an increase of MMP-1 activity should be considered as the probable mechanism underlying this effect of lamivudine. However, to confirm this hypothesis further research should be focused on the MMP-1 activity measurement.

These findings support the role of TIMP-1 and MMP-1 balance in the TGF- β_1 dependent mechanism of liver fibrosis related to HBV infection. The association of TIMP-1, MMP-1 and TGF- β_1 with hepatic injury and antiviral treatment efficacy suggest their possible usefulness in chronic hepatitis B management. Elevated TGF- β_1 plasma concentrations during antiviral therapy may indicate medication failure.

REFERENCES

- 1 Knittel T, Janneck T, Muller L, Fellmer P, Ramadori G. Transforming growth factor beta 1-regulated gene expression of Ito cells. *Hepatology* 1996; **24**: 352-360
- 2 Ramadori G, Saile B. The fibrogenic mediators, TGF- β and TNF- α , as surviving factors for activated hepatic stellate cells. In: Gressner AM, Heinrich PC, Matern S, eds. Cytokines in liver injury and repair. *Dordrecht/Boston/London: Kluwer Academic Publishers* 2002: 184-188
- 3 Williams EJ, Gaca MD, Brigstock DR, Arthur MJ, Benyon RC. Increased expression of connective tissue growth factor in fibrotic human liver and in activated hepatic stellate cells. *J Hepatol* 2000; **32**: 754-761
- 4 Knittel T, Mehde M, Kobold D, Saile B, Dinter C, Ramadori G. Expression patterns of matrix metalloproteinases and their inhibitors in parenchymal and non-parenchymal cells of rat liver: regulation by TNF- α and TGF- β_1 . *J Hepatol* 1999; **30**: 48-60
- 5 Fausto N. Liver regeneration. *J Hepatol* 2000; **32**(1 Suppl): 19-31
- 6 Saile B, Matthes N, Knittel T, Ramadori G. Transforming growth factor beta and tumor necrosis factor alpha inhibit both apoptosis and proliferation of activated rat hepatic stellate cells. *Hepatology* 1999; **30**: 196-202
- 7 Yoo YD, Ueda H, Park K, Flanders KC, Lee YI, Jay G, Kim SJ. Regulation of transforming growth factor-beta 1 expression by the hepatitis B virus (HBV) X transactivator. Role in HBV pathogenesis. *J Clin Invest* 1996; **97**: 388-395
- 8 Lee DK, Park SH, Yi Y, Choi SG, Lee C, Parks WT, Cho H, de Caestecker MP, Shaul Y, Roberts AB, Kim SJ. The hepatitis B virus encoded oncoprotein pX amplifies TGF-beta family signaling through direct interaction with Smad4: potential mechanism of hepatitis B virus-induced liver fibrosis. *Genes Dev* 2001; **15**: 455-466
- 9 Boeker KH, Haberkorn CI, Michels D, Flemming P, Manns MP, Lichtinghagen R. Diagnostic potential of circulating TIMP-1 and MMP-2 as markers of liver fibrosis in patients with chronic hepatitis C. *Clin Chim Acta* 2002; **316**: 71-81
- 10 Flisiak R, Maxwell P, Prokopowicz D, Timms PM, Panasiuk A. Plasma tissue inhibitor of metalloproteinases-1 and transforming growth factor β_1 -possible non-invasive biomarkers of hepatic fibrosis in patients with chronic B and C hepatitis. *Hepatogastroenterology* 2002; **49**: 1369-1372
- 11 Kanzler S, Baumann M, Schirmacher P, Dries V, Bayer E, Gerken G, Dienes HP, Lohse AW. Prediction of progressive liver fibrosis in hepatitis C infection by serum and tissue levels of transform-

- ing growth factor-beta. *J Viral Hepat* 2001; **8**: 430-437
- 12 **Lichtinghagen R**, Michels D, Haberkorn CI, Arndt B, Bahr M, Flemming P, Manns MP, Boeker KH. Matrix metalloproteinase (MMP)-2, MMP-7, and tissue inhibitor of metalloproteinase-1 are closely related to the fibroproliferative process in the liver during chronic hepatitis C. *J Hepatol* 2001; **34**: 239-247
- 13 **Murawaki Y**, Ikuta Y, Idobe Y, Kawasaki H. Serum matrix metalloproteinase-1 in patients with chronic viral hepatitis. *J Gastroenterol Hepatol* 1999; **14**: 138-145
- 14 **Ninomiya T**, Yoon S, Nagano H, Kumon Y, Seo Y, Kasuga M, Yano Y, Nakaji M, Hayashi Y. Significance of serum matrix metalloproteinases and their inhibitors on the antifibrogenetic effect of interferon-alfa in chronic hepatitis C patients. *Intervirology* 2001; **44**: 227-231
- 15 **Walsh KM**, Timms P, Campbell S, MacSween RN, Morris AJ. Plasma levels of matrix metalloproteinase-2 (MMP-2) and tissue inhibitors of metalloproteinases -1 and -2 (TIMP-1 and TIMP-2) as noninvasive markers of liver disease in chronic hepatitis C: comparison using ROC analysis. *Dig Dis Sci* 1999; **44**: 624-630
- 16 **Lu LG**, Zeng MD, Wan MB, Li CZ, Mao YM, Li JQ, Qiu DK, Cao AP, Ye J, Cai X, Chen CW, Wang JY, Wu SM, Zhu JS, Zhou XQ. Grading and staging of hepatic fibrosis, and its relationship with noninvasive diagnostic parameters. *World J Gastroenterol* 2003; **9**: 2574-2578
- 17 **Scheuer PJ**. Classification of chronic viral hepatitis: a need for reassessment. *J Hepatol* 1991; **13**: 372-374
- 18 **Flisiak R**, Pytel-Krolczuk B, Prokopowicz D. Circulating transforming growth factor β_1 as an indicator of hepatic function impairment in liver cirrhosis. *Cytokine* 2000; **12**: 677-681
- 19 **Kanzler S**, Lohse AW, Keil A, Henninger J, Dienes HP, Schirmacher P, Rose-John S, zum Buschenfelde KH, Blessing M. TGF-beta 1 in liver fibrosis: an inducible transgenic mouse model to study liver fibrogenesis. *Am J Physiol* 1999; **276**(4 Pt 1): G1059-1068
- 20 **Sanderson N**, Factor V, Nagy P, Kopp J, Kondaiah P, Wakefield L, Roberts AB, Sporn MB, Thorgeirsson SS. Hepatic expression of mature transforming growth factor beta 1 in transgenic mice results in multiple tissue lesions. *Proc Natl Acad Sci U S A* 1995; **92**: 2572-2576
- 21 **Clouthier DE**, Comerford SA, Hammer RE. Hepatic fibrosis, glomerulosclerosis, and a lipodystrophy-like syndrome in PEPCK-TGF-beta 1 transgenic mice. *J Clin Invest* 1997; **100**: 2697-2713
- 22 **Grainger DJ**, Mosedale DE, Metcalfe JC. TGF- β in blood: a complex problem. *Cytokine Growth Factor Rev* 2000; **11**: 133-145
- 23 **Neuman M**, Angulo P, Malkiewicz I, Jorgensen R, Shear N, Dickson ER, Haber J, Katz G, Lindor K. Tumor necrosis factor - alpha and transforming growth factor - beta reflect severity of liver damage in primary biliary cirrhosis. *J Gastroenterol Hepatol* 2002; **17**: 196-202
- 24 **Dienstag JL**, Schiff ER, Wright TL, Perrillo RP, Hann HW, Goodman Z, Crowther L, Condreay LD, Woessner M, Rubin M, Brown NA. Lamivudine as initial treatment for chronic hepatitis B in the United States. *N Engl J Med* 1999; **341**: 1256-1263
- 25 **Lai CL**, Chien RN, Leung NW, Chang TT, Guan R, Tai DI, Ng KY, Wu PC, Dent JC, Barber J, Stephenson SL, Gray DF. A one-year trial of lamivudine for chronic hepatitis B. Asia Hepatitis Lamivudine Study Group. *N Engl J Med* 1998; **339**: 61-68
- 26 **Schalm SW**, Heathcote J, Cianciara J, Farrell G, Sherman M, Willems B, Dhillon A, Moorat A, Barber J, Gray DF. Lamivudine and alpha interferon combination treatment of patients with chronic hepatitis B infection: a randomised trial. *Gut* 2000; **46**: 562-568
- 27 **Tassopoulos NC**, Volpes R, Pastore G, Heathcote J, Buti M, Goldin RD, Hawley S, Barber J, Condreay L, Gray DF. Efficacy of lamivudine in patients with hepatitis B e antigen - negative / hepatitis B virus DNA - positive (precore mutant) chronic hepatitis B. Lamivudine Precore Mutant Study Group. *Hepatology* 1999; **29**: 889-896
- 28 **Suzuki Y**, Kumada H, Ikeda K, Chayama K, Arase Y, Saitoh S, Tsubota A, Kobayashi M, Koike M, Ogawa N, Tanikawa K. Histological changes in liver biopsies after one year of lamivudine treatment in patients with chronic hepatitis B infection. *J Hepatol* 1999; **30**: 743-748

Edited by Zhu LH and Xu FM

Establishment and assessment of two methods for quantitative detection of serum duck hepatitis B virus DNA

Ya-Xi Chen, Ai-Long Huang, Zhen-Yuan Qi, Shu-Hua Guo

Ya-Xi Chen, Ai-Long Huang, Zhen-Yuan Qi, Shu-Hua Guo, Institute of Viral Hepatitis, Chongqing University of Medical Sciences, Chongqing, 400010, China

Supported by the Science Foundation of Education Commission of Chongqing, No. 000101

Correspondence to: Ya-Xi Chen, Institute of Viral Hepatitis, Chongqing University of Medical Sciences, Chongqing, 400010, China. zcyxi@sina.com

Telephone: +86-23-63849075-2227 Fax: +86-23-63822696

Received: 2003-12-10 Accepted: 2004-02-01

Abstract

AIM: To establish and assess the methods for quantitative detection of serum duck hepatitis B virus (DHBV) DNA by quantitative membrane hybridization using DHBV DNA probe labeled directly with alkaline phosphatase and fluorescence quantitative PCR (qPCR).

METHODS: Probes of DHBV DNA labeled directly with alkaline phosphatase and chemiluminescent substrate CDP-star were used in this assay. DHBV DNA was detected by autoradiography, and then scanned by DNA dot-blot. In addition, three primers derived from DHBV DNA S gene were designed. Semi-nested primer was labeled by AmpliSensor. Standard curve of the positive standards of DHBV DNA was established after asymmetric preamplification, semi-nested amplification and on-line detection. Results from 100 samples detected separately by alkaline phosphatase direct-labeled DHBV DNA probe with dot-blot hybridization and digoxigenin-labeled DHBV DNA probe hybridization. Seventy samples of duck serum were tested by fluorescent qPCR and digoxigenin-labeled DHBV DNA probe in dot-blot hybridization assay and the correlation of results was analysed.

RESULTS: Sensitivity of alkaline phosphatase direct-labeled DHBV DNA probe was 10 pg. The coincidence was 100% compared with digoxigenin-labeled DHBV DNA probe assay. After 30 cycles, amplification products showed two bands of about 180 bp and 70 bp by 20 g/L agarose gel electrophoresis. Concentration of amplification products was in direct proportion to the initial concentration of positive standards. The detection index was in direct proportion to the quantity of amplification products accumulated in the current cycle. The initial concentration of positive standards was in inverse proportion to the number of cycles needed for enough quantities of amplification products. Correlation coefficient of the results was (0.97, $P < 0.01$) between fluorescent qPCR and dot-blot hybridization.

CONCLUSION: Alkaline phosphatase direct-labeled DHBV DNA probe in dot-blot hybridization and fluorescent qPCR can be used as valuable means to quantify DHBV DNA in serum.

Chen YX, Huang AL, Qi ZY, Guo SH. Establishment and assessment of two methods for quantitative detection of serum duck hepatitis B virus DNA. *World J Gastroenterol* 2004; 10(18): 2666-2669

<http://www.wjgnet.com/1007-9327/10/2666.asp>

INTRODUCTION

Duck hepatitis B virus (DHBV) infection model is an important referenced animal model for studying HBV infection and viral replication and evaluating antiviral agents^[1-8]. HBV DNA level in serum is an important evidence for assessing antiviral effect. At present, it is difficult to accurately define the quantity of HBV DNA, though many methods^[9-15] such as competitive PCR, Chiron Quantiplex branched DNA (bDNA) assay, Abbott Genostics solution hybridization assay and Digene Hybrid Capture System have been reported which are not suitable for clinical application because of time- and cost-consuming process. HBV DNA quantitative PCR has been used in clinical detection^[16-18], but no reports were presented about DHBV DNA quantitative PCR. With the development of non-isotope-labeled nucleic acid probes, especially chemiluminescent-labeled probes^[19-21], the probe-sensitivity has been improved obviously. In order to establish a quick, sensitive and specific method for quantitative detection of DHBV DNA in serum, we detected DHBV DNA in serum sample with alkaline phosphatase direct-labeled DHBV DNA probe with dot-blot hybridization and fluorescent qPCR.

MATERIALS AND METHODS

Materials

DHBV serum was obtained from Institute of Viral Hepatitis, Chongqing University of Medical Sciences, Chongqing, China. pBR325 containing DHBV DNA sequence was extracted, digested with *EcoRI* and recovered according to the kit protocol. Then quantification was made with DU^R Series 600. DNA fragment diluted with water to a series concentrations of 2.76×10^6 to 2.76×10^1 copies/ μ L was used as positive standard. Reagents and instruments such as alkaline phosphatase direct-labeled kit (Amersham Pharmacia Biotech), Wizard Plus Midipreps DNA purification system (Promega), agarose gel DNA extraction kit (Roche), DU^R Series 600 (Beckman), scanning apparatus (Vuego Scan, Brisa-620ST), AmpliSensor kit (Biotronics), *Taq* DNA polymerase (Roche), AG-9 600 Analyzer and Amplicor monitor (Biotronics) were used in the study. Primers derived from DHBV DNA S gene were 5'-TGGCCTAATCGGATTACTGG-3' (Limited primer, 20 bp), 5'-CCTGGGCATCCCCACGGGCAGG-3' (Excess primer, 22 bp) and 5'-GGGACGCGCGCTTTCCAAGATACTG-3' (Semi-nested primer, 25 bp). The three primers were synthesized by Seagon, Shanghai.

Methods

Detection of serum DHBV DNA with a membrane hybridization assay using alkaline phosphatase direct-labeled DHBV DNA probe DHBV DNA fragment was diluted to a concentration of 10 ng/ μ L and labeled referring to alkaline phosphatase direct-labeling protocol. The probe can be stored in 50 mL/L glycerol at -20 °C for up to six months. DHBV DNA in the concentration series (100 ng, 10 ng, 1 ng, 100 pg, 10 pg) was dotted on nitric fibrous membrane in order to determine the probe sensitivity. The specificity was detected with human serum, duck serum and rat serum. The serum sample (40 μ L) was dotted on nitric fibrous membrane and 1 mol/L NaOH was used for DNA

degeneration. The membrane was baked at 80 °C for 2 h and prehybridized for at least 15 min, then 100 ng of the labeled probe was added to the buffer used for the prehybridization stage to hybridize at 55 °C overnight in a shaking water bath. The membrane was washed with the primary wash buffer for 20 min at 55 °C and with secondary wash buffer for 10 min at room temperature. The excess secondary wash buffer was drained from the blots and the membrane was placed on a clean, flat surface. Detection reagent was piped onto the blots (30–40 $\mu\text{L}/\text{cm}^2$) for 2–5 min. The DNA blots were placed side up in the film cassette and a sheet of autoradiography film was placed on top of the blots. The cassette was closed and exposed for 1 h at room temperature. The blots on the film were scanned with scanning apparatus and analysed with Discovery Series Quantity One [BioRad, volume (mm^3) = intensity \times Area].

Fluorescent qPCR for serum DHBV DNA ligation Five \times coupling reagent 10 μL , 5 \times AmpliSensor 10 μL , semi-nested primer 0.5 μg , water 30 μL were added to a microcentrifuge tube at room temperature. The tube was incubated for 90 min at 37 °C, then the reaction was terminated by adding 50 μL of deionized water and heating to 90 °C for 5 min to denature the enzymes. The ligated product was labeled as 5 \times AmpliSensor primer stock.

Ligation efficiency Two of the sample wells (5 \times AmpliSensor primer 1 μL , 1 \times PCR buffer 4 μL and PCR extension mixture 5 μL per well), two for negative control and two for standard (5 \times AmpliSensor primer 0.1 μL , 1 \times PCR buffer 4.9 μL and PCR extension mixture 5 μL per well), two for blank control (water 5 μL , PCR extension mixture 5 μL per well) were designated. The negative control served as a control of baseline signal, whereas the standard was a reference of maximum energy transfer. The reaction mixture was heated to 94 °C for 20 s, 55 °C for 20 s, 72 °C for 30 s, and then 20 °C for 30 s to equilibrate the signal. The fluorescence was read under the coupling mode using AG-9 600 Analyzer. Upon finishing, data were saved as baseline reading. One unit of *Taq* DNA polymerase was added to both the sample and standard wells and the reactions were subjected to three additional thermal cycles. Each cycle consists of 20 s at 94 °C, 20 s at 55 °C and 30 s at 72 °C. At the end of the cycling, reactions were cooled down to 20 °C for 30 s. The fluorescence reading was repeated under the same mode. When the data were saved, the coupling efficiency was displayed on the screen

Asymmetric preamplification Length of amplification fragment was 182 bp. Ten \times PCR buffer 110 μL , 40 mmol/L MgCl_2 110 μL , 10 \times dNTP 110 μL , 10 \times primer 110 μL , 10 \times terminal primer 110 μL , H_2O 330 μL were added. PCR master mix is intended for 100 reactions. The wells for negative (addition of 5 μL H_2O), Apex, standards (addition of 5 μL positive standards), sample (addition of 5 μL sample) were designated. PCR master mix 5 μL was added into each well except the well designated as Apex, to which 10 μL of 1 \times PCR buffer instead of 0.5 U *Taq* DNA polymerase was added. PCR cycle was repeated for 25 times: 20 s at 94 °C, 20 s at 55 °C and 30 s at 72 °C. At the end of the cycle, the reaction was at 72 °C for 30 s and cooled down to 4 °C for 2 min.

Semi-nested PCR and on-line detection A 700-bp fragment was amplified as follows: The 5 \times AmpliSensor primer stock 66 μL , 10 \times PCR buffer 33 μL , 40 mmol/L MgCl_2 33 μL and H_2O 198 μL were added into a 0.5 mL microcentrifuge tube to make the AmpliSensor mix. AmpliSensor mix 5 μL was aliquoted to each reaction. PCR cycles were: At 94 °C for 20 s, at 55 °C for 30 s and at 72 °C for 30 s. The reaction was cooled for 30 s at 20 °C to

establish a signal equilibrium, and then fluorescence reading was acquired under the standard mode using an AG-9 600 Analyzer. Data were saved as a baseline reading. Thermal cycling was resumed for a defined number of cycles. Fluorescence reading was repeated under the same mode, and data were saved as an assay reading. A detection index calculated by APAS software was derived from each reading. The magnitude of the detection index was directly proportional to the quantity of amplification product accumulated at the current cycle. The report window was activated to reveal the quantitative data of each sample.

Assessment of the two methods Alkaline phosphatase direct-labeled DHBV DNA probe with dot-blot hybridization was compared with digoxigenin-labeled DHBV DNA probe with dot-blot hybridization for 100 samples, and then the correlation of 70 samples between fluorescent qPCR and dot-blot hybridization with digoxigenin-labeled probe was analysed.

RESULTS

DHBV DNA fragment

The recovered DHBV DNA fragment after digestion of *EcoRI* was about 3.0 kb and the concentration was 28 $\mu\text{g}/\text{mL}$ ($A_{260}/A_{280} = 1.9$) (Figure 1).

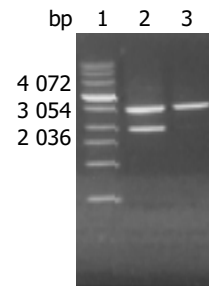


Figure 1 Detection of *EcoRI*-digested pBR325 and recovered long fragment by 10 g/L agarose gel electrophoresis. Lane 1: Molecular marker; lane 2: pBR325 digested with *EcoRI*; lane 3: Long fragment of pBR325 (DHBV DNA).

Sensitivity and specificity of alkaline phosphatase direct-labeled probe

Sensitivity of alkaline phosphatase direct-labeled probe was 10 pg without nonspecific signs (Figure 2, Table 1).

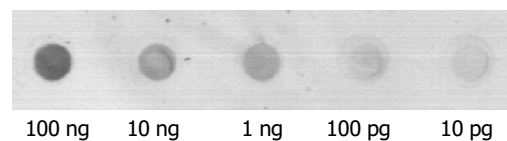


Figure 2 Sensitivity of alkaline phosphatase direct-labeled probe.

Comparison of alkaline phosphatase direct-labeled probe and digoxigenin-labeled DHBV DNA probe

Compared with digoxigenin-labeled DHBV DNA probe, the detection sensitivity of alkaline phosphatase direct-labeled probe was 100% (60/60), the specificity was 100% (40/40) and the coincidence was 100% (80/80) (Table 2).

Table 1 Results of serum samples from different genera detected by alkaline phosphatase direct-labeled probe

Genera	Samples (n)	DHBV DNA positive samples (n)	DHBV DNA negative samples (n)
Duck serum	20	10	10
Human serum	20	0	20
Rat serum	20	0	20

Ligation efficiency of semi-nested PCR and AmpliSensor assay

The detection indices of semi-nested PCR and AmpliSensor assay for sample wells were 424.79 and 551.28, respectively. A "+" status was assigned to samples with ligation efficiency greater than 70. The primer could be used in asymmetric preamplification.

Table 2 Comparison of the results of 100 serum samples detected with different probes

Probe	Positive samples (n)	Negative samples (n)
Digoxigenin-labeled probe	60	40
Alkaline phosphatase direct-labeled probe	60	40

Detection of DHBV DNA positive standard with qPCR

After 30 cycles, amplification products showed two bands of about 180 bp and 70 bp by 2% agarose gel electrophoresis. The concentration of amplification products was in direct proportion to the initial concentration of the positive standards (Figure 3).

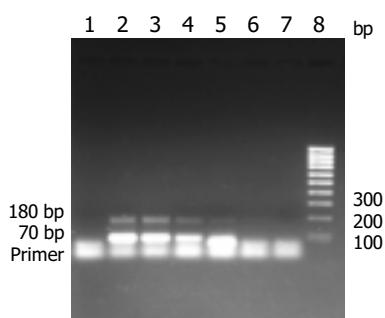


Figure 3 Detection of products of DHBV DNA positive standard with qPCR by 2% agarose gel electrophoresis. Lane 1: Negative control; lanes 2-7: DHBV DNA positive standard (2.76×10^6 - 2.76×10^1 copies/ μ L); lane 8: DNA marker.

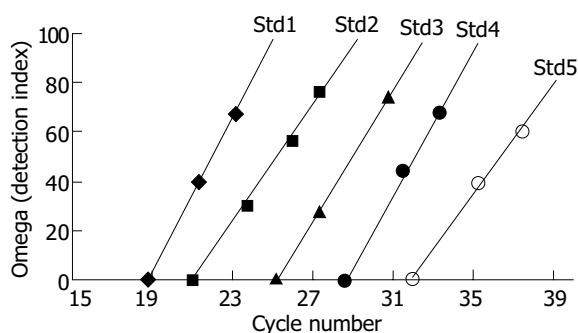


Figure 4 Amplification index standard curves of DHBV DNA positive standard.

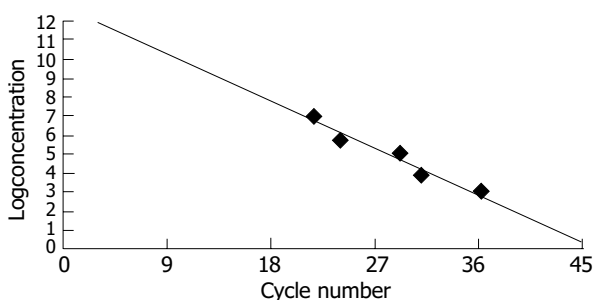


Figure 5 Concentration standard curve of DHBV DNA positive standard.

Standard curves of DHBV DNA positive standards with qPCR

The detection index curves Std1-Std5 showed that the detection index was in direct proportion to the quantities of amplification products at the current cycle (Figure 4). The concentration curve showed that the initial concentration of the positive standards was in inverse proportion to the number of cycles needed for enough quantities of amplification products and the correlation coefficient between initial concentration and number of cycles was 0.992 (Figure 5).

Detection of serum DHBV DNA

Seventy serum samples of ducks were tested by fluorescent qPCR and digoxigenin-labeled DHBV DNA probe with dot-blot hybridization, and the correlation of results was analysed. Correlation coefficient of the results was 0.97 ($P < 0.01$) between the two methods. DHBV DNA could not be found by dot-blot hybridization, but it could be detected by qPCR when DHBV DNA loads $< 10^2$ copies/mL (Table 3).

Table 3 Correlation analyses of DHBV DNA quantitative results of 70 serum samples detected by two methods

Serum samples (n)	qPCR (mean \pm SD) (copy/mL)	Dot-blot hybridization using digoxigenin-labeled probe (mean \pm SD) (volume, mm ³)
10	(2.37 ± 1.70) $\times 10^2$	-
10	(2.44 ± 1.71) $\times 10^3$	1 155 \pm 25
10	(4.47 ± 1.96) $\times 10^4$	1 241 \pm 32
10	(5.02 ± 2.14) $\times 10^5$	1 353 \pm 27
10	(1.83 ± 1.03) $\times 10^6$	1 428 \pm 25
10	(4.81 ± 2.61) $\times 10^7$	1 550 \pm 40
10	(5.16 ± 2.72) $\times 10^8$	1 748 \pm 118

DISCUSSION

Though probes labeled with radioisotope are still used to detect nucleic acids because of its high sensitivity and complete operation rule established many years ago, the safety and half-life of radioisotope must be taken into account. At present, labeling and detecting with non-radioisotope have made significant progress, and the sensitivity of the probe labeled with chemiluminescence has reached 50 fg. Two methods of labeling with non-radioisotope were available in the present study: non-direct-labeling such as random primed DNA-labeling with digoxigenin-dUTP^[22] and direct-labeling such as DNA-labeling with alkaline phosphatase^[23]. DNA-labeling with alkaline phosphatase is a new method with advantages of quickness, convenience and high sensitivity. Some procedures such as long time incubation with antibody and blocking reagent and elution can be omitted. The probe can be detached from hybridizing membrane and therefore the membrane can be used to hybridize with another probe sensitively and conveniently. Furthermore, alkaline phosphatase may be detected with chemiluminescence (dioxetane) and autoradiography or photoscanning apparatus. Chen *et al.*^[21] reported that the sensitivity of dot-blot hybridization with Epstein-Barr virus probe coupled with alkaline phosphatase was 4 pg, which is similar to our results that the sensitivity of dot-blot hybridization with DHBV probe labeled by alkaline phosphatase was 10 pg. It is necessary to optimize labeling method of alkaline phosphatase for improving the sensitivity of the probe. This study showed that the alkaline phosphatase direct-labeled probe could be used to evaluate antiviral activity in DHBV infection animal model.

AmpliSensor-PCR is a real-time, quantitative tool for PCR-based detection. The assay is based on the principle that fluorescence resonance energy transfer can be used to detect duplex formation between complementary nucleic acid strands. If the two complementary strands are labeled with donor and

acceptor fluorophores, respectively, fluorescence resonance energy transfer between the fluorophores is facilitated when the strands are base-paired, or eliminated when the base-pair is disrupted. In this way, the extent of energy transfer can be used to measure the amount of duplex formation between the fluorophore-labeled oligonucleotide duplexes, thereby the extent of duplex formation mediated DNA polymerase. The measured fluorescence intensity is in proportion to the quantity of AmpliSensor duplex left at the end of each amplification cycle. The decrease in the fluorescence intensity correlates proportionately to the initial target dosage and the extent of amplification. The signal-generating mechanism of AmpliSensor assay is tightly linked to the priming event. However, unlike typical PCR, where single-stranded primers are constantly subject to the possibility of nonspecific priming, the AmpliSensor primer is sequestered in a double-stranded form and stabilized against random priming. The AmpliSensor is a quasi-stable signal duplex of two oligonucleotides each labeled with an energy donor and acceptor fluorophore, respectively. Two strands of the AmpliSensor are unequal in length with the long strand 5' overhanging the short one by 7 nucleotides (5'-GCGTCCC-3'). For effective ligation, the semi-nested primer should encompass at its 5' end a "hook" sequence, that is, 5'-GGGACGC-3', complementing the overhang of the AmpliSensor. The fluorescence signal correlates to the overall energy transfer efficiency in a predictable, sequence-specific manner, and the amplified product can be monitored directly. As a simple, homogeneous assay for PCR quantification, AmpliSensor technology is target-specific, and it is amenable to the normalization of signal loading and sample loading. Thus it can reliably count the amplified product while it accounts for the efficiency difference among reactions.

At present, fluorescence quantitative PCR has been applied in the fields of clinical diagnosis for hepatitis B and C, evaluating and monitoring of antiviral effect, prediction of interferon effect, *etc.*^[24,25].

DHBV and HBV are two members of the hepadnavirus family of viruses. They both display similar molecular biological character and 40% nucleic acid sequence homology. We usually make use of DHBV model to learn human hepatitis B about its infection and replication strategies or antiviral effect and to screen new anti-HBV drugs. In previous studies, dot-blot hybridization, Southern blotting and *in situ* hybridization with digoxigenin-labeled probe were used to detect DHBV DNA in serum or liver, but the advanced AmpliSensor-PCR and a membrane hybridization assay with alkaline phosphatase direct-labeled DHBV DNA probe could provide more objective, more valuable experimental data for developing new anti-HBV drugs and elucidating pathogenesis of hepatitis B.

REFERENCES

- 1 Foster WK, Miller DS, Marion PL, Colonna RJ, Kotlarski I, Jilbert AR. Entecavir therapy combined with DNA vaccination for persistent duck hepatitis B virus infection. *Antimicrob Agents Chemother* 2003; **47**: 2624-2635
- 2 Cooper A, Paran N, Shaul Y. The earliest steps in hepatitis B virus infection. *Biochim Biophys Acta* 2003; **1614**: 89-96
- 3 Dong B, Shao XW, Tao PZ. Inhibition of duck hepatitis B virus DNA replication by antisense phosphorothioate oligodeoxynucleotides *in vitro* and *in vivo*. *Zhonghua Shiyan He Linchuangbingduxue Zazhi* 2003; **17**: 25-27
- 4 Seigneres B, Martin P, Werle B, Schorr O, Jamard C, Rimsky L, Trepo C, Zoulim F. Effects of pyrimidine and purine analog combinations in the duck hepatitis B virus infection model. *Antimicrob Agents Chemother* 2003; **47**: 1842-1852
- 5 Le Guerhier F, Thermet A, Guerret S, Chevallier M, Jamard C, Gibbs CS, Trepo C, Cova L, Zoulim F. Antiviral effect of adefovir in combination with a DNA vaccine in the duck hepatitis B virus infection model. *J Hepatol* 2003; **38**: 328-334
- 6 Zoulim F, Berthillon P, Guerhier FL, Seigneres B, Germon S, Pichoud C, Cheng YC, Trepo C. Animal models for the study of HBV infection and the evaluation of new anti-HBV strategies. *J Gastroenterol Hepatol* 2002; **17**(Suppl): S460-463
- 7 Thermet A, Rollier C, Zoulim F, Trepo C, Cova L. Progress in DNA vaccine for prophylaxis and therapy of hepatitis B. *Vaccine* 2003; **21**: 659-662
- 8 Lian Y, Tan J, Deng Z. Experimental study of shuangcao granule no. 1 on duck hepatitis B virus in ducklings. *Zhongguo Zhongxiyi Jiehe Zazhi* 2000; **20**: 530-532
- 9 Sidorkiewicz M, Bzorska A, Jozwiak B, Jablkowski M, Szemraj J, Lewandowska U. A competitor DNA template for the molecular quantification of the hepatitis B virus. *Cell Mol Biol Lett* 2003; **8**: 799-808
- 10 Drosten C, Weber M, Seifried E, Roth WK. Evaluation of a new PCR assay with competitive internal control sequence for blood donor screening. *Transfusion* 2000; **40**: 718-724
- 11 Pawlotsky JM, Bastie A, Hezode C, Lonjon I, Darthuy F, Remire J, Dhumeaux D. Routine detection and quantification of hepatitis B virus DNA in clinical laboratories: performance of three commercial assays. *J Virol Methods* 2000; **85**: 11-21
- 12 Gilbert N, Corden S, Ijaz S, Grant PR, Tedder RS, Boxall EH. Comparison of commercial assays for the quantification of HBV DNA load in health care workers: calibration differences. *J Virol Methods* 2002; **100**: 37-47
- 13 Jardi R, Rodriguez F, Buti M, Costa X, Cotrina M, Valdes A, Galimany R, Esteban R, Guardia J. Quantitative detection of hepatitis B virus DNA in serum by a new rapid real-time fluorescence PCR assay. *J Viral Hepat* 2001; **8**: 465-471
- 14 Hwang SJ, Lu RH, Wood ML, Wang YJ, Chang FY, Lee SD. Comparison of the nucleic acid-based crosslinking hybridization assay and the branched DNA signal amplification assay in the quantitative measurement of serum hepatitis B virus DNA. *J Clin Lab Anal* 1999; **13**: 296-300
- 15 Kao JH, Wood M, Chen PJ, Lai MY, Chen DS. Comparison of two methods for quantification of hepatitis B viral DNA. *J Gastroenterol Hepatol* 1999; **14**: 423-426
- 16 Nagata I, Colucci G, Gregorio GV, Cheeseman P, Williams R, Mieli-Vergani G, Vergani D. The role of HBV DNA quantitative PCR in monitoring the response to interferon treatment in chronic hepatitis B virus infection. *J Hepatol* 1999; **30**: 965-969
- 17 Kessler HH, Preininger S, Stelzl E, Daghofer E, Santner BI, Marth E, Lackner H, Stauber RE. Identification of different states of hepatitis B virus infection with a quantitative PCR assay. *Clin Diagn Lab Immunol* 2000; **7**: 298-300
- 18 Chen T, Luk JM, Cheung ST, Yu WC, Fan ST. Evaluation of quantitative PCR and branched-chain DNA assay for detection of hepatitis B virus DNA in sera from hepatocellular carcinoma and liver transplant patients. *J Clin Microbiol* 2000; **38**: 1977-1980
- 19 Kricka LJ. Stains, labels and detection strategies for nucleic acids assays. *Ann Clin Biochem* 2002; **39**(Pt 2): 114-129
- 20 Sander T, Olson S, Hall J, Siebert M, Grooms K, Heisler L, de Arruda M, Neri B. Comparison of detection platforms and post-polymerase chain reaction DNA purification methods for use in conjunction with Cleavase fragment length polymorphism analysis. *Electrophoresis* 1999; **20**: 1131-1140
- 21 Chen Y, Chen Y, Li H, Lu Z. Chemiluminescence detection of epstein-barr virus DNA with an oligonucleotide probe. *Clin Chim Acta* 2000; **298**: 45-53
- 22 Ying C, Van Pelt J, Yap SH, De Clercq E, Neyts J. Use of digoxigenin-labelled probes for the quantitation of HBV-DNA in antiviral drug evaluation. *J Virol Methods* 1999; **81**: 155-158
- 23 Chen Y, Huang A, Qi Z, Shan Y, Sun H. Establishment and evaluation of the method for detecting HBV DNA in serum using HBV DNA probe labeled directly by alkaline phosphatase. *Zhonghua Ganzangbing Zazhi* 2002; **10**: 429-431
- 24 Zhou X, Gao Z, Yao J. Relationship between HBV DNA serum level and acute exacerbation of the disease in chronic hepatitis B patients. *Zhonghua Shiyan He Linchuangbingduxue Zazhi* 1999; **13**: 335-339
- 25 Nie Q, Wang P, Zhou Y. Quantitation of hepatitis C virus RNA in amniotic fluid of gravida infected by hepatitis C virus. *Zhonghua Fuchanke Zazhi* 2002; **37**: 19-21

A vaccinia replication system for producing recombinant hepatitis C virus

Ying-Song Wu, Yu Feng, Wen-Qi Dong, Yan-Ming Zhang, Ming Li

Ying-Song Wu, Yu Feng, Wen-Qi Dong, Yan-Ming Zhang, Ming Li, Institute of Tropical Medicine, First Military Medical University, Guangzhou 510515, Guangdong Province, China

Supported by the "863" Program of China, No.2001AA215171

Correspondence to: Dr. Ming Li, Institute of Tropical Medicine, First Military Medical University, Guangzhou 510515, Guangdong Province, China. mingli@fimmu.com

Telephone: +86-20-61648303 **Fax:** +86-20-61648324

Received: 2003-10-20 **Accepted:** 2003-12-29

Abstract

AIM: To develop a cell culture system capable of producing high titer hepatitis C virus (HCV) stocks with recombinant vaccinia viruses as helpers.

METHODS: Two plasmids were used for the generation of recombinant HCV: one containing the full-length HCV cDNA cloned between T7 promoter and T7 terminator of pOCUS-T7 vector, and the other containing the HCV polyprotein open reading frame (ORF) directly linked to a vaccinia late promoter in PSC59. These two plasmids were co-transfected into BHK₂₁ cells, which were then infected with vTF7-3 recombinant vaccinia helper viruses.

RESULTS: After 5 d of incubation, approximately 3.6×10^7 copies of HCV RNA were present per milliliter of cell culture supernatant, as detected by fluorescence quantitative RT-PCR (FQ-PCR). The yield of recombinant HCV using this cell system increased 100- to 1 000- fold compared to *in vitro*-transcribed HCV genomic RNA or selective subgenomic HCV RNA molecule method.

CONCLUSION: This cell culture system is capable of producing high titer recombinant HCV.

Wu YS, Feng Y, Dong WQ, Zhang YM, Li M. A vaccinia replication system for producing recombinant hepatitis C virus. *World J Gastroenterol* 2004; 10(18): 2670-2674
<http://www.wjgnet.com/1007-9327/10/2670.asp>

INTRODUCTION

Hepatitis C virus (HCV) is a causative agent of acute and chronic liver diseases that infect millions of people worldwide^[1]. There is no vaccine for prevention of HCV infection, and interferon is the only known therapeutic drug, yet it is only 10-20% effective alone and less than 50% effective when used in combination with ribavirin^[2]. Overall, despite the epidemic significance of HCV infection, the development of anti-HCV drugs and vaccines has been impeded by the lack of functional cell culture systems capable of growing the virus on a large scale.

Several approaches have been taken for the propagation of HCV in cell cultures. One approach focuses on the identification of primary cells or cell lines that support replication of the virus. It has been reported that HCV isolated from infected patients is capable of infecting human primary hepatocytes^[3-5],

peripheral blood mononuclear cells^[6], and cell lines such as human T cell line HPBMa10-2, Daudi B cell line^[7-9] and various hepatocyte cell lines^[10-12]. However, HCV replication in these cell culture systems is generally transient and very inefficient. A second approach is to transfect *in vitro*-transcribed HCV genomic RNA into human hepatoma cell line, Huh7^[13]. Although it was reported that the transfected cells produced infectious viral particles, the replication efficiency of this method was very poor, and moreover, many research groups have reported failure to generate detectable HCV virions using this method. Recently, Lohmann *et al.* recovered high levels of selective subgenomic HCV RNA molecules from transfected Huh-7 cells. These replicons were derived from a cloned full-length HCV (genotype 1b) consensus sequence with the C-p7 or C-NS2 regions removed and a neomycin phosphotransferase gene (neo) inserted downstream of the HCV internal ribosome entry site IRES^[14-17]. However, HCV particles generated by this system may differ from the native virions, due to the alteration of full-length HCV genomic RNA. Thus, researchers continue to search for a HCV replication system that will produce large-scale quantities of native virions.

Compared to the infection of cell lines with HCV-containing patient serum, the introduction of cloned viral genomes was superior because the inoculum was well-defined and could be generated in high quantities^[18]. Here, we used recombinant vaccinia viruses as helper viruses to produce high-titer cloned HCV stocks in a cell culture system. This method has the advantages of being simple, highly efficient, and capable of producing large quantities of high-fidelity HCV particles.

MATERIALS AND METHODS

Plasmid construction

Plasmid pBRT703'X (NIHJ1) (generously provided by T. Suzuki), containing the full-length HCV cDNA, was cut with Hind III and inserted into vector pOCUS-T7 (plasmid pOCUS containing a T7 terminator) between *EcoR* I and Hind III sites, resulting in insertion of the HCV sequence between bacteriophage T7 promoter and terminator sequences to create plasmid pT7HCV. Next, plasmid O. pMKC1A (HCV) was cut with *EcoR* I and Hind III and inserted into PSC59 between *EcoR* I and *Stu* I sites to generate plasmid pVHCV, which contained the HCV polyprotein open reading frame (ORF) linked to a vaccinia late promoter. The correct sequences of pT7HCV and pVHCV were confirmed by restriction enzyme digestion and DNA sequencing.

HCV production

One day prior to use, BHK₂₁ cell cultures (5×10^5 cells per well) were seeded in 6-well plates and incubated in Dulbecco's modified Eagle's medium (DMEM) with high levels of glucose (4.5 g/L) supplemented with 100 mL/L fetal calf serum and antibiotics (100 U/mL penicillin and 100 U/mL streptomycin). Cultures were incubated overnight in a 37 °C CO₂ incubator. Cells were then transfected with either 5 µg pT7HCV, 5 µg pT7HCV plus 5 µg pVHCV, 5 µg pVHCV or control plasmid (pOCUS-T7) using the LIPOFECTAMINE™ 2000 reagent (Invitrogen) followed by infection with vTF7-3 vaccinia viruses^[19].

Two hours after inoculation, the inoculum was removed and the cells were cultured in a fresh medium in a 30 °C CO₂ incubator for 2-5 d.

Determination of HCV virions in cell culture supernatants

HCV virion RNA was used as an indicator for HCV virion production. Accordingly, cell culture supernatants were filtered through a 0.22 µm filter to remove residual cells and vaccinia viruses. Ten units of RNase A and 20 units of DNase I were added to 200 µL of each filtrate, and samples were incubated at 37 °C for 1 h for complete digestion of RNA and DNA. Protease K was then added to a final concentration of 100 µg/mL, and extraction of HCV genomic RNA was carried out using the high pure viral RNA kit (Roche). The resultant RNA was treated with DNase I and used as a template for RT-PCR (GIBCO BRL). For detection of positive strand HCV genomic RNA, a 416 bp fragment of the 5' region (nt 346 to 761) and a 488 bp fragment of the 3' region (nt 9378 to 8891) were amplified by RT-PCR. The primers used for reverse transcription and 5' and 3' region PCR reactions are shown in Table 1.

PCR amplification consisted of 30 cycles of denaturation at 94 °C for 30 s, annealing at 55 °C for 30 s, and extension at 72 °C for 30 s. Amplified fragments were confirmed by 10 g/L agarose gel electrophoresis, ethidium bromide staining and visualization under UV light.

Immunofluorescence and Western blot analysis of HCV proteins

For immunofluorescence, BHK₂₁ cells were grown on glass coverslips for 48 h and fixed after washed 3 times with PBS in an ice-cold mixture of 9:1 acetone and methanol. After 10 min of incubation at -20 °C, the cells were washed 3 times with PBS and incubated for 1 h in 1F buffer (PBS, 30 g/L bovine serum albumin and 1 g/L Triton X-100) at 4 °C. A mixture of NS3- and NS5a-specific mouse monoclonal antibodies (Bioscience) was added at a dilution of 1:100 in 1F buffer. After 1 h, the cells were washed 3 times with PBS followed by incubation with a mouse-specific antibody conjugated with fluorescein isothiocyanate (Sigma) in 1F buffer. Coverslips were washed 3 times with PBS and mounted on glass slides, and the cells were examined under a fluorescence microscope.

For Western blot analysis, cells were lysed with a buffer containing 10 g/L sodium deoxycholate, 1 g/L sodium dodecyl sulfate (SDS), 10 g/L Triton X-100, 10 mmol/L Tris, 140 mmol/L NaCl, 1 mmol/L phenylmethylsulfonyl fluoride (PMSF), 2 µg of aprotinin per mL, and 2 µg of leupeptin per mL (pH 8.0). The cell lysate was cleared of cell debris and nuclei by low-speed centrifugation (15 min at 15 000 g, 4 °C). A fraction of the supernatant was denatured by heating for 4 min at 100 °C in SDS sample buffer. The samples were electrophoresed on SDS-100/L polyacrylamide gels and transferred to nitrocellulose membranes. The membranes were then incubated overnight in blocking buffer (PBS containing 5 mL/L Tween 20 and 50 mL/L milk powder), and the mixture of NS3- and NS5a-specific mouse monoclonal antibodies was added at a dilution of 1:100 in blocking buffer for 1 h. After washed 3 times with 5 mL/L Tween 20 in PBS, the membranes were then incubated with a mouse-specific antibody conjugated with peroxidase (Sigma) in blocking buffer for 1 h, washed 3 times as described above, and bound antibodies were detected by DAB.

Immunoelectron microscopy

Transfected cells were grown in 6-well plates for 48 h. After washed 2 times with ice-cold PBS (pH 7.4), the cells were fixed in Petri dishes for 30 min in a mixture of 40 g/L formaldehyde, 2.5 g/L glutaraldehyde, and 2 mL/L picric acid in PIPES buffer. The fixed cells were washed 3 times with PBS, then cell pellets were embedded in 40 g/L melted agarose and cut into small blocks, which were stained in 10 g/L uranyl acetate dissolved in water for 30 min at 4 °C. The blocks were further dehydrated in ethanol and embedded in Epon-Araldite. Ultrathin sections were mounted on nickel grids without supporting films. All labeling was conducted on grids according to the method of Sparkman and White^[20]. Grids were etched with 10 g/L sodium periodate in water for 15 min, washed 3 times with PBS, and incubated with 30 g/L BSA in PBS for 30 min. The grids were then incubated for 1 h with a mixture of NS3- and NS5a-specific mouse monoclonal antibodies (diluted 1:100 in 10 g/L BSA-PBS) or in 10 g/L BSA-PBS only. After washed 5 times with PBS, the sections were treated for 1 h with goat anti-mouse antibody conjugated with colloidal gold (10-nm diameter, diluted 1:100 in PBS). Samples were rinsed five times with PBS. After counterstained with uranyl acetate and lead citrate, the sections were examined with an electron microscope.

Quantification virion RNA copy numbers

Fluorescence quantitative RT-PCR (FQ-PCR) was used to determine the amount of HCV virion RNA in cell culture supernatants treated with RNase A and DNase I as described above. Hepatitis C virus fluorescence polymerase chain reaction (PCR) diagnostic kit (Da Am Company, China) was used as directed to quantify virion RNA. Samples from ten transfections were detected by FQ-PCR.

RESULTS

Recombinant plasmids pT7HCV and pVHCV were confirmed by restriction endonuclease digestion. As expected, pT7HCV generated two fragments of 6.7 kb and 4.6 kb when digested with *Eco*R I, and pVHCV generated two fragments of 8 kb and 4.4 kb when digested with *Xho* I. DNA sequencing confirmed that the 3' and 5' sequences were as expected.

RT-PCR was used to detect HCV virion RNA in the cell culture supernatant as a measure of virion production. To ensure that the detected HCV RNA was the product of virions, we used RNase A treatment to remove HCV RNA that might release into the culture medium, as the virion envelope could protect the desired HCV RNA from digestion. To ensure that the fragments detected by RT-PCR did not come from the HCV DNA, the cell culture supernatants were also treated with DNase I. To ensure that the detected HCV RNA included the entire genome, the 5' and 3' ends of HCV genome were both amplified by RT-PCR. Positive samples amplified a 416 bp DNA fragment from the 5' UTR and a 488 bp DNA fragment from the 3' UTR. Transfection of BKH₂₁ cells with either pT7HCV or pT7HCV plus pVHCV resulted in samples that were positive for both the 3' and 5' fragments amplified by RT-PCR but not PCR alone. HCV RNA was not detected following transfection with pVHCV alone or with the control plasmid. These results confirmed that HCV virions existed in the culture supernatant of BKH₂₁ cells

Table 1 Primers for RT-PCR

Oligodeoxynucleotide	5' region	3' region
Reverse transcription primers	agccctggcagcggcccttagggggcgcc (nt 791 to 762)	gggggatggcctattggcctggagtgt (nt 9414 to 9388)
PCR primer 1	gcacaaatccaaaacccaagaaaa (nt 346-372)	cgctcatcggtggggagcaggtagatg (nt 9378 to 9351)
PCR primer 2	gacgagcgggaatgtaccatgaggtcggc (nt 761-732)	ccatcctctagcccaggagcaactga (nt 8891 to 8918)

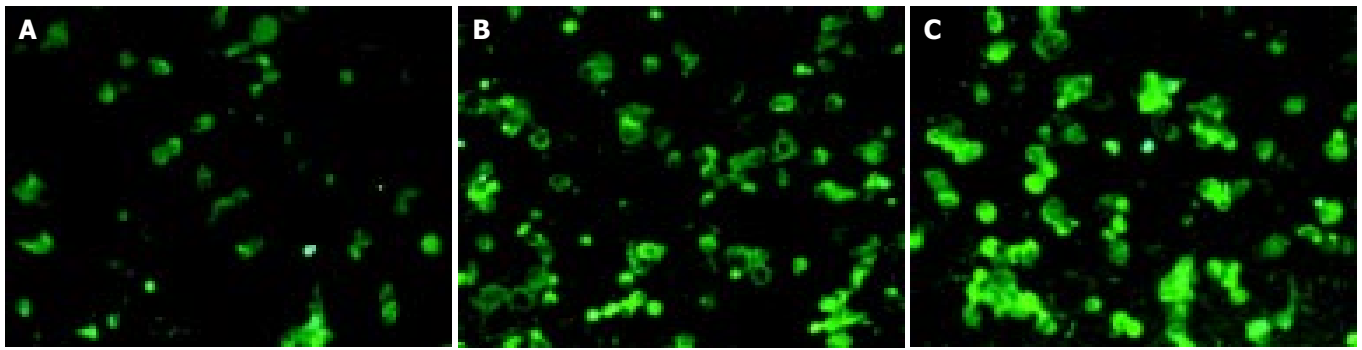


Figure 1 Immunofluorescent analysis of HCV nonstructural proteins expressed in BHK₂₁ cells using a mixture of NS3- and NS5a-specific mouse monoclonal antibodies. A: cells transfected with pT7HCV; B: cells cotransfected with pT7HCV and pVHCV; C: cells transfected with pVHCV.

transfected with pT7HCV or pT7HCV plus pVHCV.

Expression of HCV nonstructural proteins in the infected cells was detected by immunofluorescence and Western blot analysis using NS3- and NS5a-specific mouse monoclonal antibodies. BHK₂₁ cells transfected with pT7HCV, pT7HCV plus pVHCV or pVHCV were positive for immunofluorescence, though to varying degrees. Cells transfected with pVHCV showed the strongest signal, and cells transfected with pT7HCV showed the weakest (Figure 1). Expression of HCV nonstructural proteins in BHK₂₁ cells was further confirmed by Western blot analysis. Nonstructural proteins NS3 and NS5a were detected as bands of ~70 and 56 ku, respectively. Western blot analysis also showed that the expression of nonstructural proteins was highest in cells transfected with pVHCV and lowest in cells transfected with pT7HCV (Figure 2).

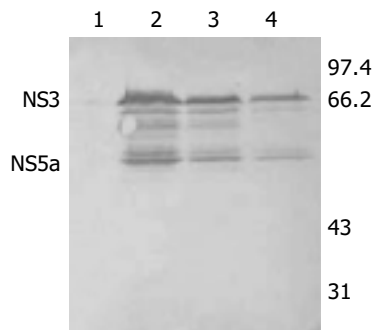


Figure 2 Western blotting of HCV gene products expressed in BHK₂₁ cells probed with a mixture of NS3- and NS5a-specific mouse monoclonal antibodies. 1: cells transfected with control plasmid (pOCUS-T7); 2: cells transfected with pVHCV; 3: cells cotransfected with pT7HCV and pVHCV; 4: cells transfected with pT7HCV.

NS3- and NS5a-specific mouse monoclonal antibodies were used to determine the subcellular localization of HCV proteins in cells transfected with pT7HCV plus pVHCV. Specific, though weak, signals were found in cytoplasm and vesicles (Figure 3), which were consistent with the results of Pietschmann *et al.*^[16], who reported that antisera monospecific for NS3, NS4b, NS5a or NS5b resulted in weak specific signals that were difficult to interpret. Our immunoelectron microscopy results identified positively stained small particles, about 40 to 60 nm in diameter, in cytoplasm and vesicles (Figure 3). The morphology and size of these particles were consistent with previous predictions regarding the HCV particles^[21-24]. No virion-like structures were identified in cells transfected with control plasmid and/or infected with vTF7-3 vaccinia alone.

Next, FQ-PCR was used to quantify the virion production in supernatants of cells transfected with pT7HCV, pT7HCV

plus pVHCV, pVHCV or the control plasmid. The copy number of HCV RNA per milliliter of culture supernatant 2, 3, 4 and 5 days after inoculation are shown in Table 2.

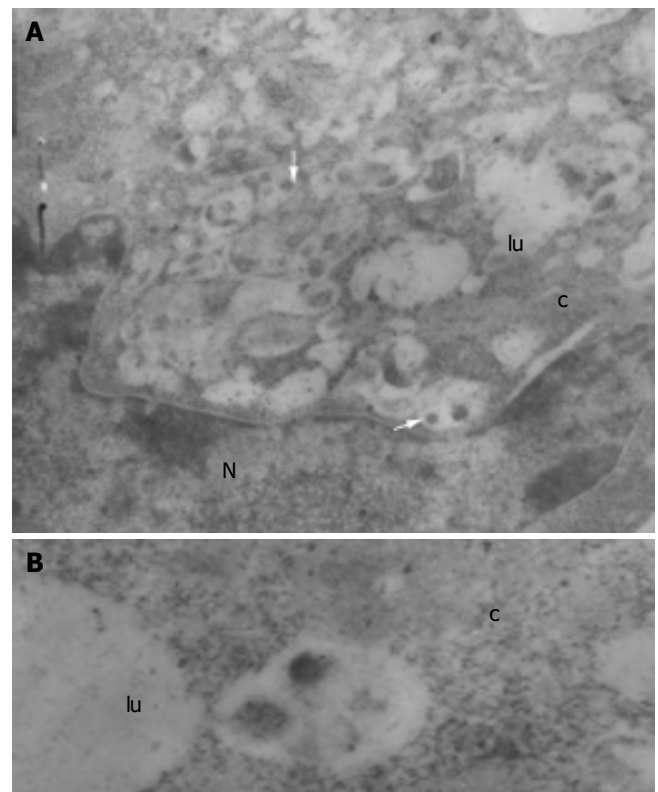


Figure 3 Immunoelectron microscopy of HCV-like virions in BHK₂₁ cells cotransfected with pT7HCV plus pVHCV and stained with mixed NS3- and NS5a-specific mouse monoclonal antibodies. Virions about 40 to 60 nm in diameter (arrows) were identified in cytoplasm and vesicles. Bar: 500 nm (A) and 200 nm (B). c: cytoplasm; lu: lumen; n: nucleus.

Table 2 Virion RNA quantitation in cell culture supernatants as measured by fluorescence quantitative RT-PCR (RNA copies per mL)

Culture time	RNA copies			
	PT7HCV	PT7HCV+ PvHCV	PvHCV	Control plasmid
48 h	1.12±0.18×10 ⁵	3.76±0.22×10 ⁵	0	0
72 h	4.08±0.20×10 ⁵	8.00±0.28×10 ⁵	0	0
96 h	1.28±0.27×10 ⁶	7.68±0.22×10 ⁶	0	0
120 h	3.24±0.25×10 ⁶	3.60±0.18×10 ⁷	0	0

DISCUSSION

Since HCV virions contain only genomic RNA and structural proteins, transfecting host cells with *in vitro* synthesized HCV viral genomic RNA could result in generation of HCV virions if the host cells were able to translate mRNA and properly processed the resulting polyprotein^[13]. However, because of low transfection efficiency, the short lifetime of viral RNA in the cytoplasm, and poor translation efficiency, viral production was generally very low by the RNA transfection method.

In this study, we used the vaccinia viral replication machinery to produce HCV virions in cell culture. The vaccinia expression system was previously tried for the production of HCV virions in cell culture. Selby *et al.* transfected Ost7-1 cells with a plasmid containing a cDNA of HCV genomic RNA downstream of a T7 promoter. The transfected cells were then infected with a recombinant vaccinia virus containing a T7 polymerase gene. Although HCV polyprotein was synthesized in Ost7-1 cells and correctly processed into individual viral proteins, no HCV virions were generated^[25], perhaps because the researchers did not place a T7 terminator downstream of HCV cDNA. Without terminator, transcripts synthesized by T7 RNA polymerase were heterogeneous concatemers that were too large to be packaged into a HCV virion. To correct this problem, Mizuno *et al.* cloned HCV cDNA between a T7 promoter and a T7 terminator^[21], resulting in the expression of both structural and nonstructural proteins in HeLa G cells, and the appearance of HCV core antigen-positive particle-like structures in cytosol and cisternae of the endoplasmic reticulum (ER). However, these particles were not tested for the presence of HCV RNA.

For identification of recombinant HCV virions, we detected the expression of HCV nonstructural proteins NS3 and NS5a in the supernatant of transfected cells. This has been reported by Mizuno *et al.* who detected the expression of structural proteins in HeLa G cells transfected with the full-length HCV genome sequence^[21]. Next, we used RT-PCR to detect the presence of positive strand HCV genomic RNA. Following digestion of HCV RNA from blocked cells, and residual plasmid DNA, RT-PCR of fragments from the 5' (nt 346 to 761) and 3' (nt 9378 to 8891) regions of HCV RNA showed that virions contained the entire sequence. This was in contrast to the report of Baumert *et al.*, who reported that HCV-like particles produced in insect cells using a recombinant baculovirus containing cDNA of HCV structural proteins contained various shortened HCV RNAs^[22]. Finally, we observed the expression of HCV proteins and virion-like structures using immunoelectron microscopy.

In this new culture system, cells were transfected with two plasmids. One contained the HCV genomic RNA-coding region between upstream T7 promoter and downstream T7 terminator, transcripts synthesized by bacteriophage T7 RNA polymerase would have a defined size. The other plasmid contained the open reading frame (ORF) of HCV polyprotein directly linked to a vaccinia late promoter. The doubly transfected cells were subsequently infected with vTF7-3 recombinant vaccinia viruses containing a T7 RNA polymerase gene under the control of a vaccinia promoter. Thus, T7 RNA polymerase was synthesized in the infected cells and in turn transcribed plasmid DNA encoding HCV genomic RNA. Meanwhile, vaccinia RNA polymerase transcribed DNA encoding HCV polyprotein. After polyprotein was processed, the resulting viral proteins packaged HCV genomic RNA and assembled it into virions, which were then released from cells via the secretory pathway. In the system, we took the advantage of the unique properties of vaccinia viruses. Vaccinia virus replicates entirely in cytoplasm and uses its own enzymes to replicate DNA and synthesize 5' capped and 3' polyadenylated mRNA. Vaccinia DNA polymerase is able to replicate plasmid DNA in cytoplasm, increase the number of DNA copies, and transcribe cytoplasmic DNA that is linked to a vaccinia promoter. Meanwhile, the viral capping enzyme

and poly(A) polymerase add a 5' cap and 3' poly(A) tail to the transcribes. The resulting mRNA can be translated by the host cell translation machinery. Because HCV genomic RNA is synthesized by T7 RNA polymerase of vaccinia while mRNA for the viral proteins is synthesized by vaccinia enzymes, RNA synthesis will not be restricted as RNA replication that is catalyzed by HCV enzymes.

For practical examination of this new system, we transfected BHK₂₁ cells with pT7HCV and pVHCV respectively, or cotransfected the cells with pT7HCV plus pVHCV for comparison. After 5 d of culture, we detected approximately $3.24 \pm 0.25 \times 10^6$ copies of HCV RNA per mL of supernatant from cells transfected with pT7HCV and $3.60 \pm 0.18 \times 10^7$ copies of HCV RNA per mL from cells cotransfected with pT7HCV plus pVHCV. HCV RNA was not detected in cells transfected with pVHCV alone. These results suggest that cotransfection with pT7HCV plus pVHCV could increase virion production. Evidence from a previous study with *in vitro*-transcribed HCV RNA showed that although transfection of cells with genomic HCV RNA could result in the production of HCV virions, cotransfection with both genomic RNA and 5' capped RNA in which 5' UTR is deleted could increase virion production^[13]. We hypothesize that it may be possible to further increase the production of viral particles by slight alterations of pT7HCV, including addition of mutations in the NS5a or NS3 regions (*e.g.*, serine to isoleucine at NS5 position 1179) to enhance replication^[26-29], or addition of a hairpin-ribozyme cassette right after the end of the 3' untranslated region^[30-32], which may also increase the titer of the resulting viral particles. However, the experimental benefits of these changes have yet to be determined.

Indeed, it also remains to be seen whether recombinant HCV virions identified in the present study are infectious. Evidence from a study with *in vitro*-transcribed full-length and subgenomic HCV RNA showed that recombinant viral particles were infectious and replication competent^[13]. To determine whether the virions produced by our new method are infectious, future work may include purification of the particles by sucrose and CsCl gradient centrifugation according to Baumert *et al.*^[22], to rule out interference by residual vaccinia viruses. Alternatively, we might generate a defective vaccinia virus that lacks D13L gene, which is essential for HCV production. Repression of D13L gene expression had no effect on viral replication and viral protein expression but could block formation of progeny virions^[33].

In conclusion, the yield of recombinant HCV using our cell system increased 100- to 1000-fold compared to *in vitro*-transcribed HCV genomic RNA method or selective subgenomic HCV RNA molecule method. This culture system may enable us to provide academic and medical researchers with high quality HCV preparations as well as to generate attenuated HCV for vaccine development. Furthermore, it may be useful as a system for future drug screening and vaccine selection.

REFERENCES

- 1 Alter MJ, Kruszon-Moran D, Nainan OV, McQuillan GM, Gao F, Moyer LA, Kaslow RA, Margolis HS. The prevalence of hepatitis C virus infection in the United States 1988-1994. *N Engl J Med* 1999; **341**: 556-562
- 2 Cohen J. The scientific challenge of hepatitis C. *Science* 1999; **285**: 26-30
- 3 Carloni G, Iacovacci S, Sargiacomo M, Ravagnan G, Ponzetto A, Peschle C, Battaglia M. Susceptibility of human liver cell cultures to hepatitis C virus infection. *Arch Virol Suppl* 1993; **8**: 31-39
- 4 Fournier C, Sureau C, Coste J, Ducos J, Pageaux G, Larrey D, Domergue J, Maurel P. *In vitro* infection of adult normal human hepatocytes in primary culture by hepatitis C virus. *J Gen Virol* 1998; **79**(Pt 10): 2367-2374
- 5 Iacovacci S, Sargiacomo M, Parolini I, Ponzetto A, Peschle C,

- Carloni G. Replication and multiplication of hepatitis C virus genome in human foetal liver cells. *Res Virol* 1993; **144**: 275-279
- 6 **Bouffard P**, Hayashi PH, Acevedo R, Levy N, Zeldis JB. Hepatitis C virus is detected in a monocyte/macrophage subpopulation of peripheral blood mononuclear cells of infected patients. *J Infect Dis* 1992; **166**: 1276-1280
- 7 **Bertolini L**, Iacovacci S, Ponzetto A, Gorini G, Battaglia M, Carloni G. The human bone-marrow-derived B-cell line CE, susceptible to hepatitis C virus infection. *Res Virol* 1993; **144**: 281-285
- 8 **Shimizu YK**, Iwamoto A, Hijikata M, Purcell RH, Yoshikura H. Evidence for *in vitro* replication of hepatitis C virus genome in a human T-cell line. *Proc Natl Acad Sci U S A* 1992; **89**: 5477-5481
- 9 **Sung VM**, Shimodaira S, Doughty AL, Picchio GR, Can H, Yen TS, Lindsay KL, Levine AM, Lai MM. Establishment of B-cell lymphoma cell lines persistently infected with hepatitis C virus *in vivo* and *in vitro*: the apoptotic effects of virus infection. *J Virol* 2003; **77**: 2134-2146
- 10 **Seipp S**, Mueller HM, Pfaff E, Stremmel W, Theilmann L, Goeser T. Establishment of persistent hepatitis C virus infection and replication *in vitro*. *J Gen Virol* 1997; **78**(Pt 10): 2467-2476
- 11 **Song ZQ**, Hao F, Min F, Ma QY, Liu GD. Hepatitis C virus infection of human hepatoma cell line 7721 *in vitro*. *World J Gastroenterol* 2001; **7**: 685-689
- 12 **Tagawa M**, Kato N, Yokosuka O, Ishikawa T, Ohto M, Omata M. Infection of human hepatocyte cell lines with hepatitis C virus *in vitro*. *J Gastroenterol Hepatol* 1995; **10**: 523-527
- 13 **Yoo BJ**, Selby MJ, Choe J, Suh BS, Choi SH, Joh JS, Nuovo GJ, Lee HS, Houghton M, Han JH. Transfection of a differentiated human hepatoma cell line (Huh7) with *in vitro*-transcribed hepatitis C virus (HCV) RNA and establishment of a long-term culture persistently infected with HCV. *J Virol* 1995; **69**: 32-38
- 14 **Lohmann V**, Korner F, Koch J, Herian U, Theilmann L, Bartenschlager R. Replication of subgenomic hepatitis C virus RNAs in a hepatoma cell line. *Science* 1999; **285**: 110-113
- 15 **Lohmann V**, Hoffmann S, Herian U, Penin F, Bartenschlager R. Viral and cellular determinants of hepatitis C virus RNA replication in cell culture. *J Virol* 2003; **77**: 3007-3019
- 16 **Pietschmann T**, Lohmann V, Kaul A, Krieger N, Rinck G, Rutter G, Strand D, Bartenschlager R. Persistent and transient replication of full-length hepatitis C virus genomes in cell culture. *J Virol* 2002; **76**: 4008-4021
- 17 **Pietschmann T**, Lohmann V, Rutter G, Kurpanek K, Bartenschlager R. Characterization of cell lines carrying self-replicating hepatitis C virus RNAs. *J Virol* 2001; **75**: 1252-1264
- 18 **Bartenschlager R**, Lohmann V. Replication of hepatitis C virus. *J Gen Virol* 2000; **81**(Pt 7): 1631-1648
- 19 **Fuerst TR**, Niles EG, Studier FW, Moss B. Eukaryotic transient-expression system based on recombinant vaccinia virus that synthesizes bacteriophage T7 RNA polymerase. *Proc Natl Acad Sci U S A* 1986; **83**: 8122-8126
- 20 **Sparkman DR**, White CL. A simple apparatus for processing large numbers of specimens for colloidal gold immunoelectron microscopy: application to paired helical filaments of Alzheimer's disease. *J Electron Microscop Tech* 1989; **13**: 152-153
- 21 **Mizuno M**, Yamada G, Tanaka T, Shimotohno K, Takatani M, Tsuji T. Virion-like structures in HeLa G cells transfected with the full-length sequence of the hepatitis C virus genome. *Gastroenterology* 1995; **109**: 1933-1940
- 22 **Baumert TF**, Ito S, Wong DT, Liang TJ. Hepatitis C virus structural proteins assemble into viruslike particles in insect cells. *J Virol* 1998; **72**: 3827-3836
- 23 **Wellnitz S**, Klumpp B, Barth H, Ito S, Depla E, Dubuisson J, Blum HE, Baumert TF. Binding of hepatitis C virus-like particles derived from infectious clone H77C to defined human cell lines. *J Virol* 2002; **76**: 1181-1193
- 24 **Blanchard E**, Brand D, Trassard S, Goudeau A, Roingard P. Hepatitis C virus-like particle morphogenesis. *J Virol* 2002; **76**: 4073-4079
- 25 **Selby MJ**, Choo QL, Berger K, Kuo G, Glazer E, Eckart M, Lee C, Chien D, Kuo C, Houghton M. Expression, identification and subcellular localization of the proteins encoded by the hepatitis C viral genome. *J Gen Virol* 1993; **74**(Pt 6): 1103-1113
- 26 **Blight KJ**, Kolykhalov AA, Rice CM. Efficient initiation of HCV RNA replication in cell culture. *Science* 2000; **290**: 1972-1974
- 27 **Blight KJ**, McKeating JA, Rice CM. Highly permissive cell lines for subgenomic and genomic hepatitis C virus RNA replication. *J Virol* 2002; **76**: 13001-13014
- 28 **Blight KJ**, McKeating JA, Marcotrigiano J, Rice CM. Efficient replication of hepatitis C virus genotype 1a RNAs in cell culture. *J Virol* 2003; **77**: 3181-3190
- 29 **Krieger N**, Lohmann V, Bartenschlager R. Enhancement of hepatitis C virus RNA replication by cell culture-adaptive mutations. *J Virol* 2001; **75**: 4614-4624
- 30 **Altschuler M**, Tritz R, Hampel A. A method for generating transcripts with defined 5' and 3' termini by autolytic processing. *Gene* 1992; **122**: 85-90
- 31 **Chung RT**, He W, Saquib A, Contreras AM, Xavier RJ, Chawla A, Wang TC, Schmidt EV. Hepatitis C virus replication is directly inhibited by IFN-alpha in a full-length binary expression system. *Proc Natl Acad Sci U S A* 2001; **98**: 9847-9852
- 32 **Yi M**, Lemon SM. Structure-function analysis of the 3' stem-loop of hepatitis C virus genomic RNA and its role in viral RNA replication. *RNA* 2003; **9**: 331-345
- 33 **Zhang Y**, Moss B. Immature viral envelope formation is interrupted at the same stage by lac operator-mediated repression of the vaccinia virus D13L gene and by the drug rifampicin. *Virology* 1992; **187**: 643-653

• *H pylori* •

Construction of prokaryotic expression system of *ItB-ureB* fusion gene and identification of the recombinant protein immunity and adjuvanticity

Jie Yan, Yuan Wang, Shi-He Shao, Ya-Fei Mao, Hua-Wen Li, Yi-Hui Luo

Jie Yan, Ya-Fei Mao, Hua-Wen Li, Yi-Hui Luo, Department of Medical Microbiology and Parasitology, Medical College, Zhejiang University, Hangzhou 310031, Zhejiang Province, China

Yuan Wang, Shi-He Shao, Faculty of Laboratory Medicine, Northern University, Jilin 132001, Jilin Province, China

Supported by the Foundation of Ministry of Education of China for Outstanding Young Teachers

Correspondence to: Jie Yan, Department of Medical Microbiology and Parasitology, Medical College, Zhejiang University, 353 Yan An Road, Hangzhou 310031, Zhejiang Province, China. yanchen@mail.hz.zj.cn

Telephone: +86-571-87217385 **Fax:** +86-571-87217044

Received: 2003-12-28 **Accepted:** 2004-01-12

Abstract

AIM: To construct *ItB-ureB* fusion gene and its prokaryotic expression system and identify immunity and adjuvanticity of the expressed recombinant protein.

METHODS: The *ureB* gene from a clinical *Helicobacter pylori* (*H pylori*) strain Y06 and the *ItB* gene from *Escherichia coli* (*E. coli*) strain 44851 were linked into *ItB-ureB* fusion gene by PCR. The fusion gene sequence was analyzed after T-A cloning. A prokaryotic recombinant expression vector *pET32a* inserted with *ItB-ureB* fusion gene (*pET32a-ItB-ureB*) was constructed. Expression of the recombinant LTb-UreB protein (rLTb-UreB) in *E. coli* BL21DE3 induced by isopropylthio- β -D-galactoside (IPTG) at different concentrations was detected by SDS-PAGE. Western blot assays were used to examine the immunoreaction of rLTb-UreB by a commercial antibody against whole cell of *H pylori* and a self-prepared rabbit anti-rUreB serum, respectively, and determine the antigenicity of the recombinant protein on inducing specific antibody in rabbits. GM₁-ELISA was used to demonstrate the adjuvanticity of rLTb-UreB. Immunoreaction of rLTb-UreB to the UreB antibody positive sera from 125 gastric patients was determined by using ELISA.

RESULTS: In comparison with the corresponding sequences of original genes, the nucleotide sequence homologies of the cloned *ItB-ureB* fusion gene were 100%. IPTG with different dosages of 0.1-1.0 mmol/L could efficiently induce *pET32a-ItB-ureB-E. coli* BL21DE3 to express the rLTb-UreB. The output of the target recombinant protein expressed by *pET32a-ureB-E. coli* BL21DE3 was approximately 35% of the total bacterial proteins. rLTb-UreB mainly presented in the form of inclusion body. Western blotting results demonstrated that rLTb-UreB could combine with the commercial antibody against whole cell of *H pylori* and anti-rUreB serum as well as induce rabbit to produce specific antibody. The strong ability of rLTb-UreB binding bovine GM₁ indicated the existence of adjuvanticity of the recombinant protein. All the UreB antibody positive sera from the patients (125/125) were positive for rLTb-UreB.

CONCLUSION: A recombinant prokaryotic expression

system with high expression efficiency of the target fusion gene *ItB-ureB* was successfully established. The expressed rLTb-UreB showed qualified immunogenicity, antigenicity and adjuvanticity. All the results mentioned above laid a firm foundation for further development of *H pylori* genetically engineered vaccine.

Yan J, Wang Y, Shao SH, Mao YF, Li HW, Luo YH. Construction of prokaryotic expression system of *ItB-ureB* fusion gene and identification of the recombinant protein immunity and adjuvanticity. *World J Gastroenterol* 2004; 10(18): 2675-2679

<http://www.wjgnet.com/1007-9327/10/2675.asp>

INTRODUCTION

In China, gastritis and peptic ulcer are the most prevalent gastric diseases and gastric cancer is one of the malignant tumors with high morbidities^[1]. *Helicobacter pylori* (*H pylori*), a microaerophilic, spiral and Gram-negative bacterium, is recognized as a human-specific gastric pathogen that colonizes the stomachs of at least half of the world's populations^[2]. Most infected individuals are asymptomatic. However, in some subjects, *H pylori* infection causes acute, chronic gastritis or peptic ulceration. Furthermore, the infection is also a high risk factor for the development of peptic ulcer and gastric adenocarcinoma, mucosa-associated lymphoid tissue (MALT) lymphoma and primary gastric non-Hodgkin's lymphoma^[3-8]. Recently, direct evidence of carcinogenesis of the microbe in an animal model has been presented^[9-11]. Immunization against the bacterium represents a cost-effective strategy to prevent *H pylori*-associated common peptic ulcer diseases and to reduce the incidence of global gastric cancers^[12]. However, no vaccines preventing *H pylori* infection have been commercially available so far.

Previous studies revealed many protective protein antigens of the microbe such as UreB, HpaA, FlaA, CagA, VacA *etc*^[13-18]. Among these protein antigens, UreB, one of the four subunits of an urease produced by almost all the isolated strains of *H pylori*, has been demonstrated to have the strongest antigenicity and protection in all known proteins of *H pylori*^[13,19,20]. *ureB* gene, responsible for encoding UreB with 569 amino acid residues, is a highly conserved nucleotide sequence with a similarity of approximately 95% in different *H pylori* isolates^[21-23]. These data strongly indicate that UreB can be used as an excellent antigen candidate for *H pylori* vaccine.

Since a genetically engineered vaccine composed of a single protein antigen usually showed a low immunization effect, it is necessary to increase immunogenicity of the antigen by co-administration with an appropriate adjuvant. *Escherichia coli* (*E. coli*) heat-labile toxin B subunit (LTB) and cholera toxin B subunit (CTB) were well-confirmed mucosal adjuvants^[24-28]. However, some of the previous studies demonstrated that the mucosal adjuvanticity of LTB was stronger than that of CTB^[26,29]. Furthermore, CTB activates Th2 pathway, and induces IL-4, a

cytokine closely related to IgE-mediated allergic reaction, but LTb mainly stimulates Th1 pathway^[26,30].

In order to simplify the procedure steps and further reduce cost in *H pylori* vaccine production, we constructed *ltB-ureB* fusion gene and its recombinant prokaryotic expression system. The immunogenicity, antigenicity and adjuvanticity of the expressed target recombinant protein (rLTB-UreB) were examined. The results of this study would benefit the mass production of *H pylori* UreB-associated genetically engineered vaccine at a lower cost.

MATERIALS AND METHODS

Materials

Both the *ureB* gene from a clinical *H pylori* strain Y06 and the *ltB* gene from *E. coli* strain 44851 (offered by National Institute for the Control of Pharmaceuticals and Biological Products of China) was cloned by our laboratory^[31]. A plasmid *pET32a* (Novagen, Madison, USA) and *E. coli* BL21DE3 (Novagen, Madison, USA) were used as the expression vector and host cell, respectively. Primers for PCR amplification were synthesized by BioAsia (Shanghai, China). *Taq*-plus high fidelity PCR kit and restriction endonucleases used were purchased from TaKaRa (Dalian, China). The T-A Cloning Kit, DNA Agarose Gel Purification Kit and sequencing service were provided by BBST (Shanghai, China). DAKO (Glostrup, Denmark) and Jackson ImmunoResearch (West Grove, USA) supplied rabbit antiserum against whole cell of *H pylori*, HRP-labeling sheep anti-rabbit IgG and anti-human IgG antibodies, respectively. The UreB antibody positive serum samples from 125 *H pylori* infected patients with gastritis or ulcer were stored at -70 °C in our laboratory^[31].

Methods

Extraction of DNA templates *E. coli* DH5 α strains respectively containing plasmid *pUCm-T-ureB*, *pUCm-T-ltB* were cultured in LB medium. The two plasmids were extracted by alkaline-denature method and then purified by DNase-free RNase treatment and routine phenol-chloroform method described by Sambrook *et al.*^[32]. The obtained DNA extracts were dissolved in TE buffer and their concentrations as well as purity were measured by ultraviolet spectrophotometry^[32]. The *pUCm-T-ureB* DNA was further digested with restriction endo-nucleases *EcoR* V and *Xho* I at 37 °C for 3 h. The target fragment of *ureB* gene was separated by agarose gel electrophoresis and then recovered by DNA Agarose Gel Purification Kit.

Amplification of *ureB* and *ltB* gene The sequence of *ltB* sense primer was: 5'-CCGGATATCATGAATAAAGTAA AATGTTA-3' (*EcoR* V). The sequence of antisense primer linking the 3'-end of *ltB* gene and the 5'-end of *ureB* gene was: 5'-AGAAACATATTCTTTTCTGCTAATGTTTCCATA CTGATTGCCGC-3'. Total volume per PCR was 100 μ L containing 2.5 mol/L each dNTP, 250 nmol/L each of the two primers, 15 mol/L MgCl₂, 2.5 U *Taq*-plus polymerase, 100 ng *pUCm-T-ltB* DNA template and 1 \times PCR buffer (pH8.3). Parameters for PCR of *ltB* gene were: at 94 °C for 5 min, \times 1; at 94 °C for 30 s, at 48 °C for 30 s, at 72 °C for 45 s, \times 10; at 94 °C for 30 s, at 48 °C for 30 s, at 72 °C for 50 s (an addition of 5 s for each of the following cycles), \times 20; finally at 72 °C for 7 min, \times 1. The results of PCR were observed under UV light after electrophoresis in 15 g/L agarose pre-stained with ethidium bromide. The expected size of target amplification fragment from *ltB* gene was 375 bp. The target fragment in the gel was recovered by using DNA Agarose Gel Purification Kit.

Construction of *ltB-ureB* fusion gene by PCR Total volume per tube was 90 μ L containing all the PCR reagents mentioned above but not the primers, 100 ng of the recovered *ltB* DNA fragment with a cohesive end and 400 ng of the recovered *ureB*

DNA fragment were added. Parameters for the following PCR were: at 94 °C for 5 min, \times 1; at 94 °C for 30 s, at 45 °C for 30 s, at 72 °C for 150 s, \times 10; at 72 °C for 10 min, \times 1. After this PCR, the two fragments of *ureB* and *ltB* produced a complex fragment of *ureB-ltB* dependent on the cohesive end in the *ltB* fragment, which would be used as a template for the next PCR. The sense primer for *ureB-ltB* amplification was as previously mentioned. The sequence of antisense primer was: 5'-CGACTCGAGGAA AAT GCTAAAGAGTTGTGC-3' (*Xho* I). The 250 nmol/L each of the two primers was added into each of the tubes. Parameters for *ltB-ureB* amplification were: at 94 °C for 3 min, \times 1; at 94 °C for 30 s, at 50 °C for 30 s, at 72 °C for 180 s, \times 10; at 94 °C for 30 s, at 50 °C for 30 s, at 72 °C for 195 s (an addition of 15 s for each of the following cycles), \times 15; at 72 °C for 12 min, \times 1. Examination of the results of this PCR and recovery of the target fragment were the same as described above. The expected size of target amplification fragment from *ureB-ltB* fusion gene was 2 070 bp.

T-A cloning, sequencing and subcloning of *ureB-ltB* fusion gene The *ltB-ureB* amplification DNA fragment was cloned into plasmid vector *pUCm-T* (*pUCm-T-ltB-ureB*) by using T-A Cloning Kit according to the manufacturer's instruction. The recombinant plasmid was amplified in *E. coli* DH5 α and then extracted by Sambrook's method^[32]. A professional company (BBST) was responsible for nucleotide sequence analysis of the inserted fragment. Two plasmids *pUCm-T-ltB-ureB* and *pET32a* in two different strains of *E. coli* DH5 α after amplified in LB medium were extracted and then digested with *EcoR* V and *Xho* I, respectively^[32]. The fragment *ltB-ureB* and *pET32a* were recovered and then ligated. The recombinant expression vector *pET32a-ltB-ureB* was transformed into *E. coli* BL21DE3, and the expression system was named as *pET32a-ltB-ureB-E. coli* BL21DE3. The *ltB-ureB* fragment inserted in *pET32a* was sequenced again.

Expression of the target recombinant protein *pET32a-ltB-ureB-E. coli* BL21DE3 was rotatively cultured in LB medium at 37 °C induced by isopropylthio- β -D-galactoside (IPTG) at different concentrations of 1.0, 0.5 and 0.1 mmol/L. The supernatant and precipitate were separated through centrifugation after the bacterial pellet was ultrasonically broken (300 V, 3 \times 5 s). The molecular mass and output of the target recombinant protein (rLTB-UreB) were measured by SDS-PAGE.

Identification of immunoreactivity and antigenicity of rLTB-UreB The expressed rLTB-UreB was collected by Ni-NTA affinity chromatography. The commercial rabbit antiserum against whole cell of *H pylori* or rabbit anti-rUreB serum prepared in our previous study and HRP-labeling sheep anti-rabbit IgG were used as the first and second antibodies, respectively, to determine the immunoreactivity of rLTB-UreB by Western blot. Rabbits were immunized with rUreB to prepare the antiserum and Western blot was applied again to determine the antigenicity of rLTB-UreB.

GM₁-ELISA GM₁-ELISA was used to demonstrate the adjuvanticity of rLTB-UreB. Briefly, 40-well plates were coated by bovine GM₁ (Sigma) and then added with rLTB-UreB. The rabbit anti-rLTB-UreB serum was used as the first antibody (1:100 dilution) and the commercial HRP-labeling sheep anti-human IgG (1:4 000 dilution) was applied as the second antibody. Each of the first antibody dilutions contained four wells. Negative controls without addition of rLTB-UreB with four repeated wells were set up and their mean A₄₉₀ value plus 3-fold SD values were used as the positive standard for each of the tested wells^[33].

ELISA By using rLTB-UreB as coated antigen at the concentration of 20 μ g/mL, each of the UreB antibody positive serum samples from the 125 patients (1:400 dilution) as the first antibody and HRP-labeling sheep anti-human IgG (1:4 000 dilution) as the second antibody, the immunoreaction of rLTB-UreB to the specific antibody in the sera were detected by

ELISA. In this assay, six UreB antibody negative serum samples were used as the control and the positive standard was similar to that in the GM₁-ELISA.

Statistical analysis

The nucleotide sequence of the cloned *ltB-ureB* fusion gene was compared for homologies with the original sequences^[31] by using a molecular biological analysis software.

RESULTS

PCR

The target fragments of *ureB*, *ltB* and *ltB-ureB* genes with the expected sizes are shown in Figure 1.

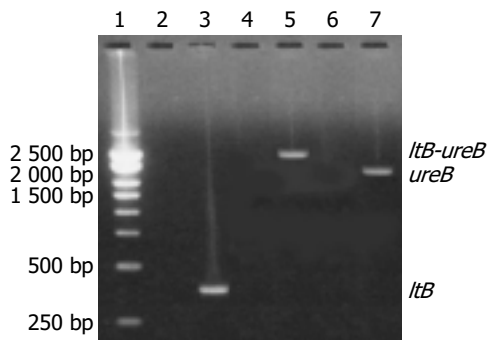


Figure 1 Target amplification fragments of *ltB* and *ureB* genes and *ltB-ureB* fusion gene. Lane 1: 250 bp DNA marker (BBST); Lanes 2, 4 and 6: Blank controls; Lanes 3 and 5: Target amplification fragments of *ltB* gene and *ltB-ureB* fusion gene, respectively; Lane 7: Target recovered fragment of *ureB* gene from *pUCM-T-ureB* after digestion with both *EcoR V* and *Xho I*.

Nucleotide sequence analysis

The homologies of the nucleotide sequences of the cloned *ltB-ureB* fusion gene compared with the original *ltB* and *ureB* gene sequences were 100%^[31]. The nucleotide and putative amino acid sequences of the *ltB-ureB* fusion gene are shown in Figure 2.

Expression of target fusion protein

IPTG at concentrations of 1.0, 0.5 and 0.1 mmol/L could efficiently induce the expression of rLTB-UreB in *pET32a-ltB-ureB-E.coli* BL21DE3 system. The product of rLTB-UreB was mainly presented in the ultrasonic precipitate and the output was approximately 35% of the total bacterial proteins (Figure 3).

Immunoreactivity and antigenicity of rLTB-UreB

Commercial rabbit antibody against the whole cell of *H pylori* could combine with rLTB-UreB and induce rabbit to produce specific antibody as confirmed by Western blotting (Figure 4), respectively.

GM₁-ELISA

Since the mean±SD of A₄₉₀ of the negative control in the four repeated wells was 0.28±0.09, the positive reference value was 0.55. The mean±SD of A₄₉₀ of the tested wells was 1.29±0.10, indicating that rLTB-UreB had the ability of binding to bovine GM₁.

ELISA

Since the mean±SD of A₄₉₀ values of the six UreB antibody negative serum samples was 0.17±0.03, the positive reference value for the specific antibody detection in patients' sera was 0.26. According to the reference value, 100% (125/125) of the tested patients' sera were positive for the antibodies against rLTB-UreB with an A₄₉₀ value ranging from 0.37-1.98.

```

1: ATGAATAAAGTAAATGTTATGTTTTATTACGGCGTACTATCCTCTCTATGTGCACAC
1: M N K V K C Y V L F T A L L S S L C A Y
61: GGAGCTCCCCAGTCTATTACAGAAGTATGTTCCGAAATATCGCAACACAAAATATATACG
21: G A P Q S I T E L C S E Y R N T Q I Y T
121: ATAAATGACAAGATACTATCATATACGGAATCGATGGCAGGCAAAAAGAGAAATGGTTATC
41: I N D K I L S Y T E S M A G K R E M V I
181: ATTACATTTAAGAGCGGCAACATTTTCAGGTCGAAGTCCCGGGCAGTCAACATATAGAC
61: I T F K S G A T F Q V E V P G S Q H I D
241: TCCCAAAAAGCCATTGAAAGGATGAAGGACACATTAAGAATCAATCATATCTGACCGGAG
81: S Q K K A I E R M K D T L R I T Y L T E
301: ACCAAAATGATAAATATGTGTATGGATAATAAAACCCCAATTCAAATGCGGCAATC
101: T K I D K L C V W N N K T P N S I A A T
    -ltB sequence | ureB sequence-
361: AGTATGGAAAACATTAGCAGAAAAGAATATGTTCTATGTATGGTCTACTACAGCGCAT
121: S M E N I S R K E Y V S M Y G P T T G D
421: AAAGTGAGATTGGGCGATACAGACTTGATCGCTGAAGTAGAACATGACTACACCTTTAT
141: K V R L G D T D L I A E V E H D Y T I Y
481: GCGGAAGAGCTTAAATTCGGTGCCGTAAGACTTTGAGGGAAGGCATGAGCCAATCCAAC
161: G E E L K F G R G K T L R E G M S Q S N
541: AACCTAGCAAGAAGAAGTGGATTAAATCATCACTAACGCTTTAATCGTGGATTACACC
181: N P S K E E L D L I I T N A L I V D Y T
601: GGTATTATAAGCGGATATTGGTATTAAAGATGGCAAAATCGCTGGCATTGGCAAAGGC
201: G I Y K A D I G I K D G K I A G I G K G
661: GGTAACAAGACATGCAAGATGGCGTTAAAAACAATCTTAGCGTGGTCTGCTACTGAA
221: G N K D M Q D G V K N N L S V G P A T E
721: GCCTTAGCTGGTGAAGTTGATCGTAACTGCTGGTGGTATTGACACACATCCACTTC
241: A L A G E G L I V T A G G I D T H I H F
781: ATCTCCCAACAACATCCCTACAGCTTTTGAAGCGGTGAACAACCATGATTGGTGGC
261: I S P Q Q I P T A F A S G V T T M I I G A
841: GGAACCTGCTGCTGATGGCACTAACGCAACCACTATCACTCCAGGCAAGAAGACTTA
281: G T G P A D G T N A T T I T P G R R N L
901: AAATGGAGTCTCAGAGCGGTAAGAATATTCATGAAGTCTAGGTTTCTAGCTAAAGGT
301: K W M L R A A E E Y S M N L G F L A K G
961: AACACTTCAACGATGCGAGCTTAGCCGATCAAAATGAAGCCGGTCCGATTGGTTTTAAA
321: N T S N D A S L A A G A I E A G A P L S I
1021: ATCCAGAAGACTGGGAACAACCTCTCTGCAATCAATACCGTITAGATGTTGGCGAC
341: I H E D W G T T P S A I N H A L D V A D
1081: AAATACGATGTGCAAGTCCGATATCCACACAGACACTTTGAATGAAGCCGGTGTGTAGAA
361: K Y D V Q V A I H T D T L N E A G C V E
1141: GACACTTGGCAGCCATTGCCGAGCCTATGCACACTTTCCACACTGAAGCGCGTGGT
381: D T M A A I A G R T M H T E F K D E G N
1201: GCGGACAGCTCTGATATTATAAAGTGGCCGCGCAACAACTTCTGCCCGCTCC
401: G G H A P D I I K V A G E H N I L P A S
1261: ACTAACCCCACTATCCCTTCTACTGTAATACAGAAGCAGAACACATGGACATGCTTATG
421: T N P T I P F T V N T E A E H M D M L M
1321: GTGTGCCACCCTTGGATAAAGCATTAAAGAAGATGTTCAAGTTCGCTGATTCAAGGATC
441: V H H L D K S I K E D V Q G F I A L S Q
1381: CGCCCTCAAATATTGCGGCTGAAGACACTTTCATGACATGGGGATTTCTCCATCACT
461: R P Q T I A A E D T L H D M G I F S I T
1441: AGTTCGACTCTCAAGCTATGGGTCTGTGGGTGAAGTTATCACTAGAAGTGGCAAAAC
481: S S D S Q A M G R V G E V I T R T W Q T
1501: GCTGACAAAAACAAAAAAGAAATTTGGCCGCTTGAAGAAGAAAAAGGCGATAACGCAAC
501: A D K N K K E F G R L K E F K G D E G N
1561: TTCAGGATCAAAAGCTACTTGTCTAAATACACCATTAAACCCAGCATCGCTCATGGGATT
521: F R I K R Y L S K Y T I N P A I A H G I
1621: AGCGAGTATGTAGGTTCTGTAGAAGTGGCAAGTGGCTGACTTGGTATTGTGGAGTCCA
541: S E Y V G S V E V G K V A D L V L W S P
1681: GCATTCCTTGGCGTGAACCAACATGATCATCAAGGCGGGTTCATTGCGTTAAGTCAA
561: A F F G V K P N M I I K G G F I A L S Q
1741: ATGGCGATGCGAACGCTTCTATCCCTACCCCAACACAGTTTATTACAGAGAAATGTTCC
581: M G D A N A S I P T P Q P V Y Y R E M F
1801: GCTCATCATGGTAAAGCCAAATACGATGCAAAACATCACTTTTGTCTCAAGCGCTTAT
601: A H H G K A K Y D A N I T F V S Q A G Y
1861: GACAAAGCATTAAAGAAGAAATTAGGCTTGAAGAAGCAAGTGTTCGCGTAAAAAATGCG
621: D K G I K E E L G L E R Q V L P V K N C
1921: AGAAACATCACTAAAAAGACATGCAATTAACGACACTACCGCTCACATTGAAGTCAAT
641: R N I T K K D M Q F N D T T A H I E V N
1981: CCTGAAACTTACCATGTGTTCTGGATGGCAAGAAGTAACTTCTAAACAGCACCATAAA
661: P E T Y H V F V D G K E V T S K P P A T K
2041: GTGAGCTTGGCACAACCTTTAGCATTTCCTCGAGCACCACCACCACCACCTGA
681: V S L A Q L F S I F L E H H H H H H *
    
```

Figure 2 Nucleotide and putative amino acid sequences of *ltB-ureB* fusion gene. Note: Underlined areas are sense, linking and antisense primers, respectively. The framed area is the sequence from plasmid *pET32a*. "*" means stop codon.

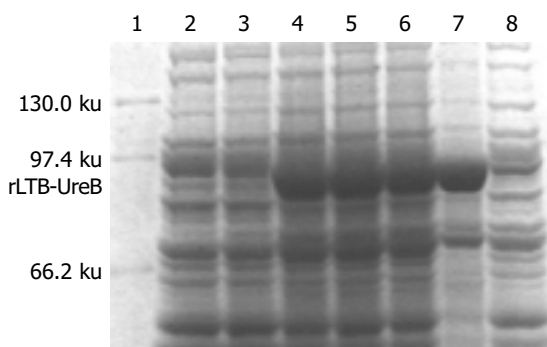


Figure 3 rLTB-UreB expression induced with different dosages of IPTG. Lane 1: Protein marker (Shanghai Shisheng); Lane 2: Blank control; Lane 3: Non-induced with IPTG; Lanes 4-6: Induced with 0.1, 0.5 and 1.0 mmol/L IPTG, respectively; Lanes 7 and 8: Bacterial precipitate and supernatant induced with 0.5 mmol/L IPTG, respectively.

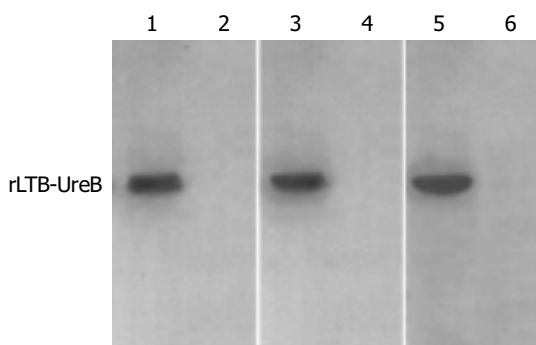


Figure 4 Western blotting of rLTB-UreB with rabbit antibody against whole cell of *H pylori* and rUreB- and rLTB-UreB-immunized rabbit antisera. Lanes 1, 3 and 5: rLTB-UreB with rabbit antibody against whole cell of *H pylori*, and rUreB- and rLTB-UreB-immunized rabbit antisera, respectively; Lanes 2, 4 and 6: Corresponding blank controls.

DISCUSSION

The selection of antigenic targets is critical in the design of *H pylori* vaccine. A large number of published data showed that UreB might be the most definitive antigen candidate for *H pylori* vaccine^[13,19-23]. On the other hand, LTB is found to be the most efficient mucosal adjuvant with few possibility of inducing allergic reaction^[24-30]. So UreB and LTB should be the optimal antigen and adjuvant for developing orally taken *H pylori* vaccine, respectively.

In the present study, *ltB-ureB* fusion gene was obtained by using three PCRs and the nucleotide sequence of the gene showed absolutely the same as the corresponding ones. This data indicated that the method used for constructing fusion gene was highly efficient and of high fidelity.

SDS-PAGE performed in this study confirmed that the constructed prokaryotic expression system *pET32a-ltB-ureB-E.coli* BL21DE3 could produce rLTB-UreB with high efficiency even when the concentration of IPTG was as low as 0.1 mmol/L. The inclusion body as a major form of rLTB-UreB and higher output (35% of the total bacterial proteins) of the recombinant protein was beneficial to industrial production.

The results of Western blotting in this study demonstrated that the rLTB-UreB could combine with both the commercial antibody against whole cell of *H pylori* and rabbit anti-rUreB serum. And this recombinant protein was able to efficiently induce rabbit to produce specific antibody. Furthermore, all the UreB antibody positive serum samples from 125 patients confirmed by our previous studies could recognize rLTB-UreB.

In the reports, the adjuvanticity of LTB was based on the binding ability to GM₁ receptor on the surface of cell^[27-33]. In this study, the strong binding to GM₁ receptor of rLTB-UreB was confirmed by GM₁-ELISA. Therefore, rLTB-UreB with qualified immunoreactivity, antigenicity and adjuvanticity could be used to develop *H pylori* genetically engineered vaccine at lower costs.

REFERENCES

- Zhang Z, Yuan Y, Gao H, Dong M, Wang L, Gong YH. Apoptosis, proliferation and p53 gene expression of *H pylori* associated gastric epithelial lesions. *World J Gastroenterol* 2001; 7: 779-782
- Michetti P, Kreiss C, Kotloff KL, Porta N, Blanco JL, Bachmann D, Herranz M, Saldinger PF, Cortesey-Theulaz I, Losonsky G, Nichols R, Simon J, Stolte M, Ackerman S, Monath TP, Blum AL. Oral immunization with urease and *Escherichia coli* heat-labile enterotoxin is safe and immunogenic in *Helicobacter pylori*-infected adults. *Gastroenterology* 1999; 116: 804-812
- Suganuma M, Kurusu M, Okabe S, Sueoka N, Yoshida M, Wakatsuki Y, Fujiki H. *Helicobacter pylori* membrane protein 1: a new carcinogenic factor of *Helicobacter pylori*. *Cancer Res* 2001; 61: 6356-6359
- Nakamura S, Matsumoto T, Suekane H, Takeshita M, Hizawa K, Kawasaki M, Yao T, Tsuneyoshi M, Iida M, Fujishima M. Predictive value of endoscopic ultrasonography for regression of gastric low grade and high grade MALT lymphomas after eradication of *Helicobacter pylori*. *Gut* 2001; 48: 454-460
- Uemura N, Okamoto S, Yamamoto S, Matsumura N, Yamaguchi S, Yamakido M, Taniyama K, Sasaki N, Schlemper RJ. *Helicobacter pylori* infection and the development of gastric cancer. *N Engl J Med* 2001; 345: 8298-8332
- Morgner A, Miehle S, Fischbach W, Schmitt W, Muller-Hermelink H, Greiner A, Thiede C, Schetelig J, Neubauer A, Stolte M, Ehninger G, Bayerdorffer E. Complete remission of primary high-grade B-cell gastric lymphoma after cure of *Helicobacter pylori* infection. *J Clin Oncol* 2001; 19: 2041-2048
- Kate V, Ananthakrishnan N, Badrinath S. Effect of *Helicobacter pylori* eradication on the ulcer recurrence rate after simple closure of perforated duodenal ulcer: retrospective and prospective randomized controlled studies. *Br J Surg* 2001; 88: 1054-1058
- Yao YL, Zhang WD. Relation between *Helicobacter pylori* and gastric cancer. *Shijie Huaren Xiaohua Zazhi* 2001; 9: 1045-1049
- Goto T, Nishizono A, Fujioka T, Ikewaki J, Mifune K, Nasu M. Local secretory immunoglobulin A and postimmunization gastritis correlate with protection against *Helicobacter pylori* infection after oral vaccination of mice. *Infect Immun* 1999; 67: 2531-2539
- Watanabe T, Tada M, Nagai H, Sasaki S, Nakao M. *Helicobacter pylori* infection induces gastric cancer in mongolian gerbils. *Gastroenterology* 1998; 115: 642-648
- Honda S, Fujioka T, Tokieda M, Satoh R, Nishizono A, Nasu M. Development of *Helicobacter pylori*-induced gastric carcinoma in mongolian gerbils. *Cancer Res* 1998; 58: 4255-4259
- Hatzifoti C, Wren BW, Morrow WJ. *Helicobacter pylori* vaccine strategies-triggering a gut reaction. *Immuno Today* 2000; 21: 615-619
- Cortesey-Theulaz I, Porta N, Glauser M, Saraga E, Vaney AC, Haas R, Kraehenbuhl JP, Blum AL, Michetti P. Oral immunization with *Helicobacter pylori* urease B subunit as a treatment against *Helicobacter* infection in mice. *Gastroenterology* 1995; 109: 115-121
- Opazo P, Muller I, Rollan A, Valenzuela P, Yudelevich A, Garcia-de la Guarda R, Urrea S, Venegas A. Serological response to *Helicobacter pylori* recombinant antigens in Chilean infected patients with duodenal ulcer, non-ulcer dyspepsia and gastric cancer. *APMIS* 1999; 107: 1069-1078
- Suerbaum S, Josenhans C, Labigne A. Cloning and genetic characterization of the *Helicobacter pylori* and *Helicobacter mustelae* *flaB* flagellin genes and construction of *H pylori* *flaA*- and *flaB*-negative mutants by electroporation-mediated allelic exchange. *J Bacteriol* 1993; 175: 3278-3288
- Ghiara P, Rossi M, Marchetti M, Di Tommaso A, Vindigni C, Ciampolini F, Covacci A, Telford JL, De Magistris MT, Pizza

- M, Rappuoli R, Del Giudice G. Therapeutic intragastric vaccination against *Helicobacter pylori* in mice eradicates an otherwise chronic infection and confers protection against reinfection. *Infect Immun* 1997; **65**: 4996-5002
- 17 **Nilsson I**, Utt M. Separation and surveys of proteins of *Helicobacter pylori*. *J Chromatogr B Analyt Technol Biomed Life Sci* 2002; **771**: 251-260
- 18 **Marchetti M**, Arico B, Burroni D, Figura N, Rappuoli R, Ghiara P. Development of a mouse model of *Helicobacter pylori* infection that mimics human disease. *Science* 1995; **267**: 1655-1658
- 19 **Rupnow MF**, Owens DK, Shachter R, Parsonnet J. *Helicobacter pylori* vaccine development and use: a cost-effectiveness analysis using the Institute of Medicine Methodology. *Helicobacter* 1999; **4**: 272-280
- 20 **Pappo J**, Thomas WD Jr, Kabok Z, Taylor NS, Murphy JC, Fox JG. Effect of oral immunization with recombinant urease on murine *Helicobacter felis* gastritis. *Infect Immun* 1995; **63**: 1246-1252
- 21 **Tomb JF**, White O, Kerlavage AR, Clayton RA, Sutton GG, Fleischmann RD, Ketchum KA, Klenk HP, Gill S, Dougherty BA, Nelson K, Quackenbush J, Zhou L, Kirkness EF, Peterson S, Loftus B, Richardson D, Dodson R, Khalak HG, Glodek A, McKenney K, Fitzgerald LM, Lee N, Adams MD, Venter JC. The complete genome sequence of the gastric pathogen *Helicobacter pylori*. *Nature* 1997; **388**: 539-547
- 22 **Akada JK**, Shirai M, Takeuchi H, Tsuda M, Nakazawa T. Identification of the urease operon in *Helicobacter pylori* and its control by mRNA decay in response to pH. *Mol Microbiol* 2000; **36**: 1071-1084
- 23 **Labigne A**, Cussac V, Courcoux P. Shuttle cloning and nucleotide sequences of *Helicobacter pylori* genes responsible for urease activity. *J Bacteriol* 1991; **173**: 1920-1931
- 24 **Verweij WR**, de Haan L, Holtrop M, Agsteribbe E, Brands R, van Scharrenburg GJ, Wilschut J. Mucosal immunoadjuvant activity of recombinant *Escherichia coli* heat-labile enterotoxin and its B subunit: induction of systemic IgG and secretory IgA responses in mice by intranasal immunization with influenza virus surface antigen. *Vaccine* 1998; **16**: 2069-2076
- 25 **Tochikubo K**, Isaka M, Yasuda Y, Kozuka S, Matano K, Miura Y, Taniguchi T. Recombinant cholera toxin B subunit acts as an adjuvant for the mucosal and systemic responses of mice to mucosally co-administered bovine serum albumin. *Vaccine* 1998; **16**: 150-155
- 26 **Yamamoto M**, McGhee JR, Hagiwara Y, Otake S, Kiyono H. Genetically manipulated bacterial toxin as a new generation mucosal adjuvant. *Scand J Immunol* 2001; **53**: 211-217
- 27 **de Haan L**, Feil IK, Verweij WR, Holtrop M, Hol WG, Agsteribbe E, Wilschut J. Mutational analysis of the role of ADP-ribosylation activity and GM1-binding activity in the adjuvant properties of the *Escherichia coli* heat-labile enterotoxin towards intranasally administered keyhole limpet hemocyanin. *Eur J Immunol* 1998; **28**: 1243-1250
- 28 **Saito K**, Shoji J, Inada N, Iwasaki Y, Sawa M. Immunosuppressive effect of cholera toxin B on allergic conjunctivitis model in guinea pig. *Jpn J Ophthalmol* 2001; **45**: 332-338
- 29 **Tamura S**, Hatori E, Tsuruhara T, Aizawa C, Kurata T. Suppression of delayed-type hypersensitivity and IgE antibody responses to ovalbumin by intranasal administration of *Escherichia coli* heat-labile enterotoxin B subunit-conjugated ovalbumin. *Vaccine* 1997; **15**: 225-229
- 30 **Douce G**, Fontana M, Pizza M, Rappuoli R, Dougan G. Intranasal immunogenicity and adjuvanticity of site-directed mutant derivatives of cholera toxin. *Infect Immune* 1997; **65**: 2821-2828
- 31 **Xia XP**, Yan J, Zhao SF. Cloning, expression and identification of *Escherichia coli* *LTB* gene and *Vibrio cholerae* *CTB* gene. *Zhejiang Daxue Xuebao Yixueban* 2003; **32**: 17-20
- 32 **Sambrook J**, Fritsch EF, Maniatis T. *Molecular Cloning, A Laboratory Manual* [M]. 2nd edition. New York: Cold Spring Harbor Laboratory Press 1989: pp1.21-1.52, 2.60-2.80, 7.3-7.35, 9.14-9.22
- 33 **de Haan L**, Holtrop M, Verweij WR, Agsteribbe E, Wilschut J. Mucosal immunogenicity of the *Escherichia coli* heat-labile enterotoxin: role of the A subunit. *Vaccine* 1996; **14**: 260-266

Edited by Zhu LH Proofread by Chen WW and Xu FM

Gene expression differences of regenerating rat liver in a short interval successive partial hepatectomy

Cun-Shuan Xu, An-Shi Zhang, Hong-Peng Han, Jin-Yun Yuan, Cui-Fang Chang, Wen-Qiang Li, Ke-Jin Yang, Li-Feng Zhao, Yu-Chang Li, Hui-Yong Zhang, Salman Rahman, Jing-Bo Zhang

Cun-Shuan Xu, Hong-Peng Han, Jin-Yun Yuan, Cui-Fang Chang, Ke-Jin Yang, Li-Feng Zhao, College of Life Sciences, Henan Normal University, Xinxiang 453007, Henan Province, China

Salman Rahman, Homophilia Research Center, London University, London SE17EH, United Kingdom

An-Shi Zhang, Wen-Qiang Li, Yu-Chang Li, Hui-Yong Zhang, Jing-Bo Zhang, State Key Laboratory of Cell Differentiation and Regulation of Province and Ministry, Xinxiang 453007, Henan Province, China

Supported by the National Natural Science Foundation of China, No. 30270673

Correspondence to: Professor Cun-Shuan Xu, College of Life Sciences, Henan Normal University, Xinxiang 453007, Henan Province, China. xucs@x263.net

Telephone: +86-373-3326001 **Fax:** +86-373-3326524

Received: 2003-10-29 **Accepted:** 2003-12-16

Abstract

AIM: To identify the genes expressed differentially in the regenerating rat liver in a short interval successive partial hepatectomy (SISPH), and to analyze their expression profiles.

METHODS: Five hundred and fifty-one elements selected from subtractive cDNA libraries were conformed to a cDNA microarray (cDNA chip). An extensive gene expression analysis following 0-36-72-96-144 h SISPH was performed by microarray.

RESULTS: Two hundred and sixteen elements were identified either up- or down-regulated more than 2-fold at one or more time points of SISPH. By cluster analysis and generalization analysis, 8 kinds of ramose gene expression clusters were generated in the SISPH. Of the 216 elements, 111 were up-regulated and 105 down-regulated. Except 99 unreported genes, 117 reported genes were categorized into 22 groups based on their biological functions. Comparison of the gene expression in SISPH with that after partial hepatectomy (PH) disclosed that 56 genes were specially altered in SISPH, and 160 genes were simultaneously up-regulated or down-regulated in SISPH and after PH, but in various amount and at different time points.

CONCLUSION: Genes expressed consistently are far less than that intermittently; the genes strikingly increased are much less than that increased only 2-5 fold; the expression trends of most genes in SISPH and in PH are similar, but the expression of 56 genes is specifically altered in SISPH. Microarray combined with suppressive subtractive hybridization can in a large scale effectively identify the genes related to liver regeneration.

Xu CS, Zhang AS, Han HP, Yuan JY, Chang CF, Li WQ, Yang KJ, Zhao LF, Li YC, Zhang HY, Rahman S, Zhang JB. Gene expression differences of regenerating rat liver in a short interval successive partial hepatectomy. *World J Gastroenterol* 2004; 10(18): 2680-2689

<http://www.wjgnet.com/1007-9327/10/2680.asp>

INTRODUCTION

In the liver regeneration (LR) after partial hepatectomy (PH), a great deal of genes is involved, and varied in the different phases of LR^[1-5]. Peak of DNA synthesis appears at 24 h and two small peaks occur at 36 h and 48 h after PH^[6]. Despite numerous related papers, the molecular mechanism of LR has not been thoroughly elucidated^[7-16]. To explore the hepatic regeneration mechanism, a 0-36-72-96-144 h short interval successive partial hepatectomy (SISPH) model was established in 2001, and has been proved an important tool for studying specific gene expression at various crucial points of LR^[17-19]. To uncover unknown differential display genes relevant to LR, the method of subtractive suppression hybridization (SSH) was used, and a bulk of up-regulated and down-regulated expressed sequence tags (ESTs) in the regenerating rat liver of 0-36-72-96-144 h SISPH were obtained. With development of cDNA microarray technology, genomewide expression of thousands of genes can be simultaneously analyzed facilitating differential expression monitoring of a large number of activated or suppressed genes under various biological conditions. To further display their expression variation in the LR, an in-house cDNA microarray was successfully performed to identify gene expression profiles in regenerating liver following the SISPH. Relevant information was achieved by data analysis of Microsoft Excel and GeneSpring.

MATERIALS AND METHODS

Short interval successive partial hepatectomy of rats

Male and female Sprague-Dawley (SD) rats, aged 10-12 wk and weighing 200-220 g, were raised in Experimental Animal Center of Henan Normal University. According to Xu *et al.*, lobule external sinister and lobus centralis sinister, lobus dexter, lobus centralis, and lobus caudatus were removed subsequently at four time points of 0, 36, 72, 96 h of 0-36-72-96-144 h SISPH^[20].

Sample preparation and RNA extraction

The removed liver lobes were rinsed in cold 1×PBS and immersed in -80 °C refrigerator for RNA and protein extraction. Total RNA was isolated from frozen liver lobes according to the manual of Trizol kit of Invitrogen. In brief, 50-100 mg liver tissue was homogenized in 1 mL Trizol reagent containing phenol and guanidinium isothiocyanate/cationic detergent, followed by phenol-chloroform extraction and isopropyl alcohol precipitation. The quantity and integrity of total RNA were examined by ultraviolet spectrometer and denaturing formaldehyde agarose electrophoresis stained by ethidium bromide (EB).

Subtracted cDNA library construction and screening

cDNA subtractive libraries were generated from total RNA by PCR-Select TM cDNA Subtraction kit (Clontech) following the manufacturer's instruction. Briefly, total RNA was reverse transcribed to double cDNA strands and digested with restriction enzymes, followed by subtractive hybridization with drivers and testers. Finally with suppression PCR, differential expression sequence tags were performed to construct

subtractive cDNA library, which was cloned into T-vector (Promega) and screened by PCR with nest primer 1 and 2.

Sequence analysis

The base sequence assay of ESTs was carried out according to the current protocols in molecular biology. All sequences were determined for both strands. Comparison analysis of the selected sequences was conducted with the DNAMAN and the National Center for Biotechnology Information (www.ncbi.nlm.nih.gov) GenBank database.

cDNA microarray construction

cDNA fragments amplified by polymerase chain reaction (PCR) with nested PCR primer 1 and primer 2, and purified by NaAc/isopropanol were spotted onto glass slides (Biostar) with the help of ProSys-5 510A spotting machine according to designed project. Then the gene chips were ready by hydrating, blocking and drying. Totally 1 152 elements (double spot chip) including 50 control systems (8 negative control, 12 blank control, 30 internal control) and 551 target genes to be studied comprised 8 submatrixes (12*12) occupying 9 mm*18 mm (Biostar).

Fluorescence-labeled cDNA preparation

RNA isolated from rat livers before SISPH served as a reference for all cDNA microarray analyses. Total denatured RNA was reverse transcribed with Cy3-conjugated dCTP (control group) and Cy5-conjugated dCTP (test group) (Amersham-Pharmacia Biotech) using MMLV reverse transcriptase (Promega) with olig (dT) primer. After bath incubation for 2 h, labeled buffer I and II were subsequently added to the reaction. The control group and test group were mingled together symmetrically and stored in the dark for use.

Hybridization and scanning

The glass slices were prehybridized at 42 °C for 5-6 h in hybridization buffer containing freshly cooked shared salmon sperm DNA. The labeled denatured probe was hybridized against cDNA microarrays with an overnight (16-18 h) incubation at 42 °C. The slides were then washed twice with 2×SSC containing 5 g/L SDS for 5 min at room temperature, once with 0.2×SSC containing 5 g/L SDS at 60 °C for 10 min, and finally with 0.2×SSC at 60 °C for 10 min. After that, the slices were photographed. Hybridized images were scanned by a fluorescence laser scanning device, Gene Pix 4 000 A (Axon Instruments, Inc., Foster City, CA). At least two hybridizations were performed at each time point. In addition, a semiquantitative inspection of the hybridization results was performed for (1) green signal (down regulation); (2) yellow signal (no obvious regulation); and (3) red signal (up regulation).

Data analysis

The cy3 and cy5 signal intensities were quantified by Gene Pix Pro 3.0 software (Axon Instruments, Inc., Foster City, CA). Subsequently, we normalized the obtained numerical data with classical linear regression techniques. In brief, quantified cy3 and cy5 signal intensities were obtained when foreground signal intensities were deducted by background signal intensities and cy5 signal intensities were replaced by 200 when it was <200. When R_i ($R_i = \text{cy5}/\text{cy3}$) was between 0.1 and 10, R_i was taken logarithms base natural to generate R_i' [$\log(R_i)$] and ND was taken by EXP (R) (averaged R_i'). The modified cy3^* was generated when ND was multiplied by cy3, and was replaced by 200 when it was <200. The ratio was expressed as $\text{cy5}/\text{cy3}^*$. Therefore, we selected genes whose ratio was more than 2 or less than 0.5 representing a 2-fold difference in expression level. To analyze the selected gene expression data, we applied κ -means cluster analysis, and performed

GeneMaths hierarchical clustering to appraise the number of groups. Whole analyses were executed with Microsoft Excel (Microsoft, Redmond, WA) and GeneSpring (Silicon Genetics, San Carlos, CA).

RESULTS

Category and expression changes of genes related to rat liver regeneration

Among the tested 551 genes, 216 were identified to be altered by more than 2-fold in intensity at least at one time point in the 0-36-72-96-144 h SISPH. Of the 216 identified genes, 111 were up-regulated and 105 were down-regulated. Ninety-nine of these 216 genes were unreported genes and the other 117 were reported, of which quite a few genes had not been reported to be involved in LR. Based on the functions and the time points at which they showed maximum up- or down-regulation, those reported genes were respectively involved in stress response, glycometabolism, fat and stearyl metabolism, oxidation and reduction response, regulation-proteins, glycoproteins, lipid-proteins, nucleolar proteins, receptors, factors, hemoglobins, immunological proteins, chaperonins, cytoskeletons, marker proteins, amino acid enzymes, proteolytic enzymes, proteinase inhibitors, phosphorylases, phosphatases, synthases and transferases (Table 1).

Gene expression differences at various time points of the 0-36-72-96-144 h SISPH

The gene expression profiles at different time points were generalized at 36, 36-72, 36-96, 36-144, 72, 72-96, 72-144, 96, 96-144, 144 h, and it was found that at 36 h of SISPH, 17 genes were up-regulated and 2 were down-regulated; at the time points of 36 h and 72 h of SISPH, 3 genes were up-regulated and 3 down-regulated; at the time points of 36 h and 96 h of SISPH, only 2 genes were up-regulated; at the time points of 36 h and 144 h of SISPH, 32 genes were up-regulated and 23 genes down-regulated, which is the largest group at all time points of SISPH; at 72 h of SISPH, 13 genes were down-regulated and 12 up-regulated. At the time points of 72 h and 96 h of SISPH, 5 genes were down-regulated and 4 up-regulated; at the time points of 72 h and 144 h of SISPH, 14 genes were up-regulated and 21 down-regulated; at 96 h of SISPH, one gene were up-regulated and 6 down-regulated; at the time points of 96 h and 144 h of SISPH, 10 genes were down-regulated and 7 up-regulated; at 144 h of SISPH, 11 genes were up-regulated and 31 down-regulated. Briefly, the LR of 0-36-72-96-144 h SISPH involved 216 elements, of which, 111 were up-regulated and 105 were down-regulated (Figure 1).

Gene expression level in the regenerating rat liver of 0-36-72-96-144 h SISPH

According to the up-regulated and down-regulated intensity of genes in the 0-36-72-96-144 h SISPH, we categorized the genes into 3 groups: (1) 105 genes were down-regulated by less than 50%; (2) 93 genes were up-regulated by 2-5 fold; (3) 18 genes were strongly up-regulated by more than 5-fold (Figure 2).

Hierarchical cluster analysis of genes expressed in the liver regeneration

The expression profile of the 216 genes altered by more than 2-fold in intensity at least at one time point in the 0-36-72-96-144 h SISPH was emanative to the last time point, indicating that at 144 h of SISPH, the liver regeneration has not been completed yet (Figure 3A). We undertook hierarchical clustering of 5 time points (0, 36, 72, 96 and 144 h) of SISPH using GeneSpring software and discovered that gene expression profiles had no similarity at the four time points (Figure 3B).

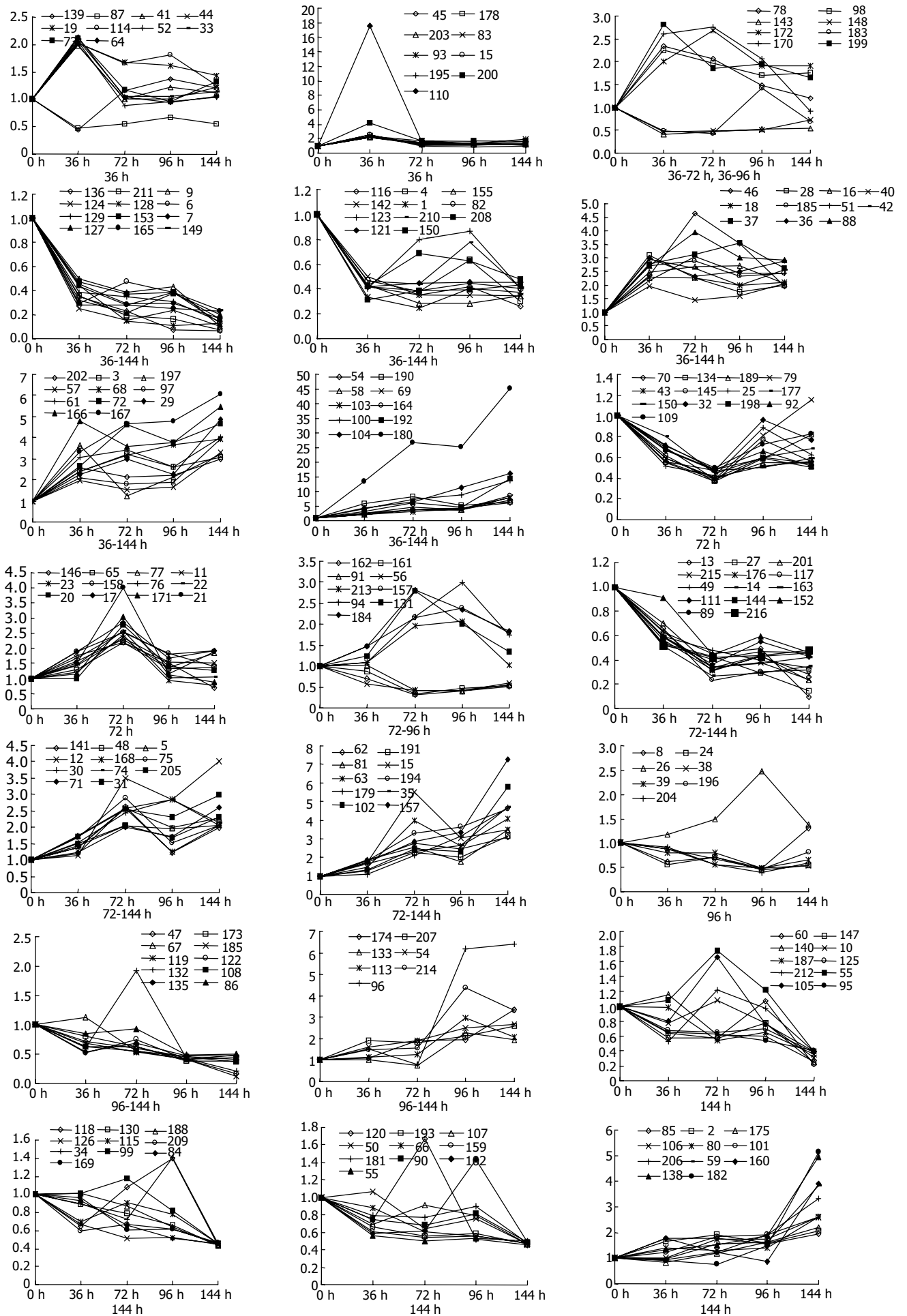


Figure 1 Gene expression differences in the regenerating rat liver of 0-36-72-96-144 h SISPH.

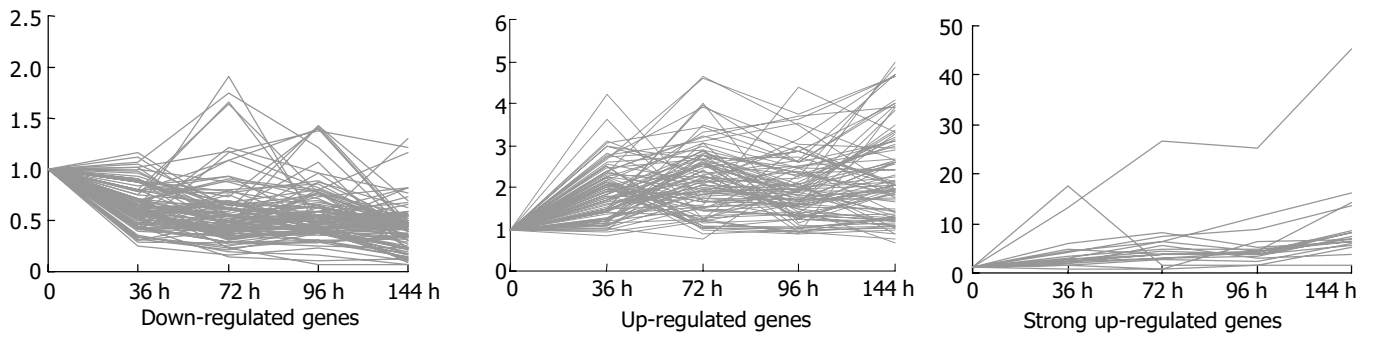


Figure 2 Expression level of genes in the regenerating rat liver of 0-36-72-96-144 h SISPH.

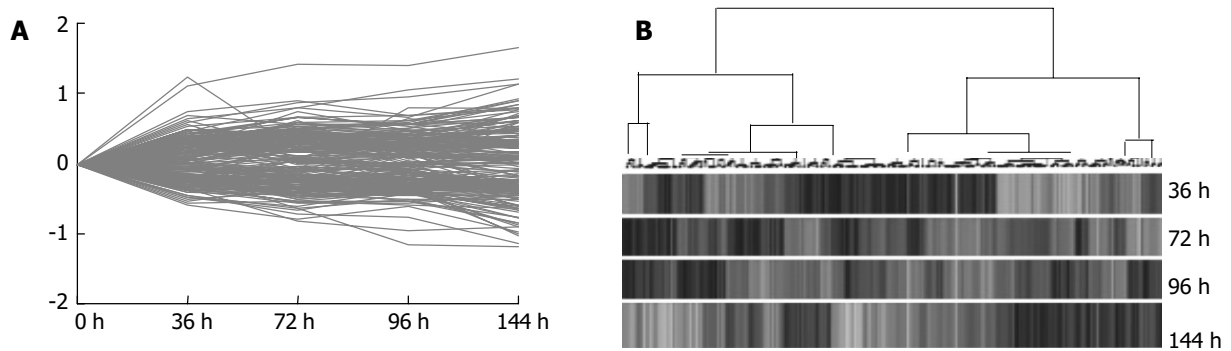


Figure 3 Cluster analysis of 216 elements. A: The difference of their intensity was identified more than two-fold at least at one time point. B: A hierarchical clustering of five time points indicated that the genes at these time points hardly had a common expression profile.

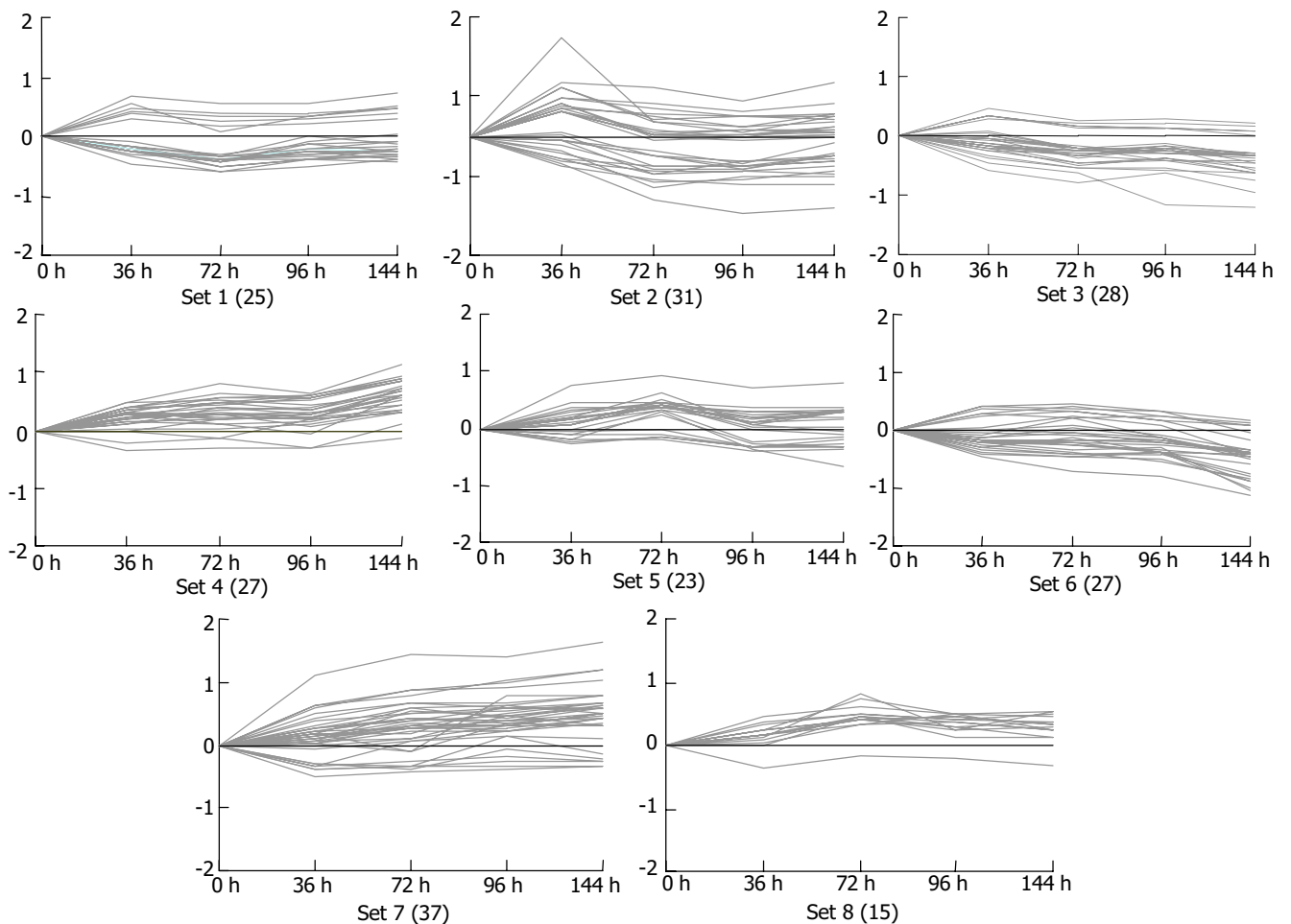


Figure 4 Cluster analysis of gene expression profiles identified by cDNA microarray. These genes were classified into 8 clusters by the κ -means method.

Table 1 The genes related to liver regeneration altered in 0-36-72-96-144h SISPH (*genes specially altered in SISPH)

No.	Gene description	Fold difference	No.	Gene description	Fold difference
Unreported genes					
1	AW558171	0.2	*93	RP24-176A1	2.4
2	CG31759-PA	2.0	94	RP24-347B22	3.0
*3	CH230-11N5	3.2	95	RP32-28p17	0.4
4	CH230-155H3	0.3	96	Adult male liver cDNA	6.4
5	CH230-155H3	2.6	97	DNA segment of Chr 1	3.9
6	CH230-186B23	0.1	98	12 d embryo liver cDNA	2.2
7	CH230-206C20	0.2	99	13 d embryo liver cDNA	0.5
8	CH230-329A5	0.5	Stress response		
9	CH230-372C24	0.1	100	Alpha-1 major acute phase protein prepeptide	13.6
10	CH230-403C20	0.3	101	Petaxin	2.6
*11	CH230-404C20	2.4	102	Angiotensinogen (Agt)	5.8
12	CH230-4L11	4.0	103	Kininogen	8.0
13	CH230-7A22	0.1	104	T-kininogen	16.1
14	Citb585c7	0.3	Glycometabolism		
*15	CTD-2328C19	2.5	105	Aldolase B	0.4
*16	FLJ20356	2.8	*106	C-reactive protein	2.6
17	KIAA1230	2.3	107	Glycerol 3-phosphate dehydrogenase (Gpd3)	0.5
18	LOC119392	2.0	108	Isoctrate dehydrogenase 1 (Idh1)	0.4
*19	LOC311304	2.8	*109	Maize aldolase	0.5
*20	LRRP Aa1-018	4.0	*110	3-phosphoglycerate dehydrogenase	17.6
21	LRRP Aa1027	2.6	Fatty and stearoyl metabolism		
*22	LRRP Aa1-076	2.4	111	Malonyl-CoA decarboxylase	0.4
*23	LRRP Aa1-114	0.5	112	NAD(P) dependent steroid hydrogenase	0.5
24	LRRP Aa2-020	0.4	113	P450 cholesterol 7- α -hydroxylase (P450 VII)	3.0
25	LRRP Aa2-066	2.5	114	Prostaglandin D2 synthase 2 (Ptgds2)	2.0
*26	LRRP Aa2-111	0.1	*115	Retinol dehydrogenase 11	0.5
27	LRRP Aa2-174	3.1	116	3- α -hydroxysteroid dehydrogenase	0.3
28	LRRP Aa2-296	4.9	Oxidation and reduction response		
29	LRRP Ab1-021	2.9	117	Acyl-coA oxidase	0.2
30	LRRP Ab1-046	3.0	118	Alcohol dehydrogenase (ADH)	0.4
31	LRRP Ab1-108	3.4	119	Cytochrom P450 15-beta (Cyp2c12)	0.1
32	LRRP Ab1-114	2.1	120	Cytochrome b	0.5
*33	LRRP Ab1-119	0.5	121	Cytochrome b5 (Cyb5)	0.4
34	LRRP Ab1-152	4.7	122	Cytochrome P450	0.2
35	LRRP Ab1-216	3.0	123	Cytochrome P450 (PNCN inducible, Cyp3A1)	0.4
36	LRRP Ab1-331	3.6	124	Cytochrome P450 2E1	0.1
37	LRRP Ab1-334	0.5	125	Cytochrome P450, 2c39 (Cyp2c39)	0.4
38	LRRP Ab2-001	0.5	*126	CytochromeP450, 2b19 (Cyp2b15)	0.4
39	LRRP Ab2-001	2.1	127	CytP450 arachidonic acid epoxygenase (cyp 2C23)	0.2
40	LRRP Ab2-008	2.0	128	Flavin-containing monooxygenase 1 (Fmo1)	0.1
*41	LRRP Ab2-018	3.0	129	Paraoxonase 1 (Pon1)	0.1
42	LRRP Ab2-034	0.4	*130	Peroxisome oxidin 1 (Prdx1)	0.4
*43	LRRP Ab2-057	2.0	*131	Plasma selenoprotein P1 (Sepp1)	2.8
*44	LRRP Ab2-079	2.1	132	Selenium-dependent glutathione peroxidase	0.2
*45	LRRP Ab2-093	4.6	Regulation-proteins		
46	LRRP Ab2-095	0.4	133	II-protein with tetratricopeptide repeats 3	2.3
47	LRRP Ab2-132	2.0	*134	Glu-Pro dipeptide repeat protein	0.4
48	LRRP Ab2-143	0.3	135	RAKB	0.5
49	LRRP Ab2-225	0.5	Glycoproteins		
*50	LRRP Ab2-255	3.1	136	Alpha-1-B glycoprotein (A1bg)	0.1
51	LRRP Ab2-379	2.1	137	Fibrinogen, gamma polypeptide (Fgg)	7.2
*52	LRRP Ab2-390	0.4	138	Fibronectin 1 (Fn1)	5.0
53	LRRP Ab2-402	2.7	139	Histidine-rich glycoprotein (Hrg)	0.4
54	LRRP Ac1-060	0.5	140	Myelin-associated glycoprotein (L-MAG)	0.3
55	LRRP Ac1-163	0.4	141	TRAM1	2.6
56	LRRP Ac1177	3.3	142	UDP-glucuronosyltransferase 2B3 (Udpgt)	0.3
57	LRRP Ac1-233	7.1	Lipid-proteins		
58	LRRP Ac1873	3.8	143	Apolipoprotein C-I (ApoC1)	0.4
59	LRRP Ac2-061	0.2	144	Apolipoprotein C-II	0.3
60	LRRP Ac2-125	4.0	145	Apolipoprotein C-III	0.4
61	LRRP Ac2-143	3.1	146	C57BL/6j	2.2
62	LRRP Ac2-193	4.1	147	Fatty acid binding protein 1 (Fabp1)	0.2
63	LRRP Ac2-202	2.1	148	Plasma retinol-binding protein (PRBP)	0.5
64	LRRP Ac2-223	2.2	149	Transferrin-related protein (TTN)	0.2
*65	LRRP Ac2-256	0.5	Nucleolar proteins		
*66	LRRP Ac2-282	0.4	150	RNase A family 4	0.4
*67	LRRP Ac2-300	0.4	Receptors		
68	LRRP Ba1-647	3.9	151	Cocoa protein	5.5
69	LRRP Bm403207	7.9	*152	Golgi SNAP receptor member 1 (Gosr1)	0.4
70	LRRP Cc1-27	0.4	153	Nuclear receptor subfamily 0, mem 2 (Nr0b2)	0.2
71	LRRP Cc1-8	2.6	154	Type I interleukin 1 receptor (Il1r1)	6.2
72	LRRP Cc1-9	4.7	Factors		
*73	LRRP Da1-10	2.1	155	Angiogenin	0.3
74	LRRP Da1-24	2.8	156	Angiopoietin-like 3	0.5
75	LRRP Da1-6	2.9	157	Early growth response factor 1 (Egr1)	2.4
*76	LRRP Da2-19	2.6	158	Eukaryotic translation initiation factor 4A1	2.5
*77	LRRP Da2-35	2.3	159	Insulin-like growth factor I	0.5
*78	LRRP Da2-4	0.4	160	Neuropeptide Y (Npy)	3.9
79	LRRP zbs559	2.6	Hemoglobins		
*80	MGC38937	3.5	161	Hemoglobin, alpha 1 (Hba1)	0.3
81	RIKEN 1110061A24	0.4	162	Hemoglobin beta chain (Hbb)	0.3
82	RIKEN 1300002A08	2.2	Immunological proteases		
*83	RIKEN 1500012D08	0.5	163	Achaete-scute complex homolog-like 1 (Ascl1)	0.3
*84	RIKEN 2310045J23	2.0	164	Complement component 5 (C5)	8.6
85	RIKEN 2810051A14	0.5	165	Immunoglobulin C kappa	0.2
*86	RIKEN 4930408O21	0.5	*166	Fc-gamma receptor class III	5.5
87	RP11-281N10	0.5	167	JE/MCP-1	6.1
88	RP23-195K1	3.9	191	Alpha-1-macroglobulin	3.1
89	RP23-235O1	0.4	192	Contrapsin-like protease inhibitor (CPI-26)	14.1
90	RP23-35D4	0.5	193	Leuserpin-2 (Serpind1)	0.5
91	RP23-417P22	0.4	194	Serine protease inhibitor 1	4.6
92	RP23-480P21	0.5	Phosphorylases		
Chaperonins					
*168	DnaI (Hsp40), subfamily B, mem 11 (DnaIb11)	2.6	*195	CDK103	2.5
*169	TCP-1 containing cytosolic chaperonin (CCT)	0.5	196	CDK110	0.5
Cytoskelets					
170	Actin gamma	2.7	197	Mss4 protein	3.6
*171	Actin beta (Actb)	3.0	*198	Rho-associated kinase beta (Rock1)	0.5
172	Clathrin, heavy polypeptide (Hc) (Cltc)	2.7	199	Thymidylate kinase (dTMP kinase)	2.8
173	Karyopherin (importin) alpha 2	0.4	Phosphatases		
*174	Mutant beta-actin (beta-actin)	3.4	200	Pyrophosphatase/phosphodiesterase 1(Enpp1)	4.2
*175	Ribosomal protein S12 (Rps12)	2.2	201	Phosphatase 1 (GL-subunit)	0.2
Marker proteins					
176	ATP-binding cassette, sub-family C	0.3	202	Phosphatidylserine-specific phospholipase A1	3.0
*177	CD164 antigen (Cd164)	0.4	*203	Secreted phosphoprotein 1 (Spp1)	2.2
*178	CD44 antigen (Cd44)	2.2	*204	UTP-glucose-1-phosphate	0.4
179	Pregnancy-zone protein (Pzp)	4.7	Synthases		
180	Serum amyloid a-5 protein	45.1	*205	ATPase synthase subunit 6	2.3
181	Subchromosomal transferable fragment 4	0.5	206	Carbamyl phosphate synthetase I	3.3
Amino acid enzymes					
182	Cytosolic aspartate aminotransferase	5.1	*207	Glutamyl-prolyl-tRNA synthetase (Eprs)	2.6
*183	Phenylalanine hydroxylase (Pah)	0.4	Transferases		
*184	Tissue-type transglutaminase (Tgm2)	2.8	208	Carnitine O-octanoyltransferase (Crot)	0.3
185	2-hydroxyphytanoyl-CoA lyase (Hpcl2)	0.4	209	Glutathione S-transferase 1 (Mgst1)	0.5
Proteolytic enzymes					
*186	Alpha/beta hydrolase domain containing protein 1	2.9	*210	Glutathione S-transferase Y(b) subunit	0.4
187	Cathepsin C (Ctsc)	0.4	211	Glutathione S-transferase, alpha 1 (Gsta1)	0.1
*188	Proteasome (macropain subunit, beta type 6 Psmb6)	0.4	212	Glutathione S-transferase, type 3 (Yb3) (Gstm3)	0.4
Proteinase inhibitors					
189	Alpha-1 microglobulin/bikunin (Ambp)	0.4	213	Serine hydroxymethyl transferase 1	2.1
190	Alpha-2-macroglobulin (A2m)	8.1	214	Sialyltransferase 1 (Siat1)	4.4
			215	Sulfotransferase K2	0.2
			216	UDP-glucuronosyltransferase 2, mem 5 (Ugt2b5)	0.4

Table 2 The comparison of difference of gene expression in SISPH with that after in PH

Gene description	Fold difference		Gene description	Fold difference	
	SISPH	PH		SISPH	PH
Unreported genes					
AW558171	0.2	0.3	Cytochrome P450 (PNCN inducible, Cyp3A1)	0.4	0.2
CG31759-PA	2.0	2.9	Cytochrome P450 2E1	0.1	0.1
CH230-155H3	0.3	0.3	Cytochrome P450, 2c39 (Cyp2c39)	0.4	0.1
CH230-155H3	2.6	2.2	CytP450 arachidonic acid epoxygenase (cyp 2C23)	0.2	0.2
CH230-186B23	0.1	0.2	Flavin-containing monooxygenase 1 (Fmo1)	0.1	0.1
CH230-206C20	0.2	0.3	Paraoxonase 1 (Pon1)	0.1	0.2
CH230-329A5	0.5	0.3	Selenium-dependent glutathione peroxidase	0.2	0.4
CH230-372C24	0.1	0.1	Regulation-proteins		
CH230-403C20	0.3	0.2	II-protein with tetratricopeptide repeats 3	2.3	0.2
CH230-4L11	4.0	4.5	RAKb	0.5	0.2
CH230-7A22	0.1	0.1	Glycoproteins		
Citb585c7	0.3	0.2	Alpha-1-B glycoprotein (A1bg)	0.1	0.1
KIAA1230	2.8	2.6	Fibrinogen, gamma polypeptide (Fgg)	7.2	7.2
LOC119392	2.3	2.1	Fibronectin 1 (Fn1)	5.0	7.2
LRRP Aa1027	4.0	2.1	Histidine-rich glycoprotein (Hrg)	0.4	0.1
LRRP Aa2-020	0.5	0.4	Myelin-associated glycoprotein (L-MAG)	0.3	7
LRRP Aa2-066	0.4	0.4	TRAM1	2.6	5.1
LRRP Aa2-174	0.1	0.1	UDP-glucuronosyltransferase 2B3 (Udpgt)	0.3	0.3
LRRP Aa2-296	3.1	2.1	Lipid-proteins		
LRRP Ab1-021	4.9	8.1	Apolipoprotein C-I (ApoC1)	0.4	3.3
LRRP Ab1-046	2.9	0.5	Apolipoprotein C-II	0.3	0.3
LRRP Ab1-108	3.0	2.9	Apolipoprotein C-III	0.4	0.5
LRRP Ab1-114	3.4	4.2	C57BL/6J	2.2	7.3
LRRP Ab1-152	0.5	0.4	Fatty acid binding protein 1 (Fabp1)	0.2	0.3
LRRP Ab1-216	4.7	6.8	Plasma retinol-binding protein (PRBP)	0.5	0.4
LRRP Ab1-331	3.0	2.2	Transthyretin-related protein (TTN)	0.2	0.3
LRRP Ab1-334	3.6	2.7	Nucleolar proteins		
LRRP Ab2-001	0.5	0.2	RNase A family 4	0.4	0.2
LRRP Ab2-001	0.5	0.2	Receptors		
LRRP Ab2-008	2.1	2.1	Cocoa protein	5.5	4.6
LRRP Ab2-034	3.0	2.3	Nuclear receptor subfamily 0, mem 2 (Nr0b2)	0.2	0.2
LRRP Ab2-095	4.6	3.1	Type I interleukin 1 receptor (Il1r1)	6.2	7.8
LRRP Ab2-132	0.4	0.1	Factors		
LRRP Ab2-143	2.0	3.3	Angiogenin	0.3	0.2
LRRP Ab2-225	0.3	0.3	Angiotensin-like 3	0.5	0.2
LRRP Ab2-379	3.1	2.2	Early growth response factor 1 (Egr1)	2.4	3.6
LRRP Ab2-402	0.4	0.1	Eukaryotic translation initiation factor 4A1	2.5	3.8
LRRP Ac1-060	2.7	0.4, 2.3	Insulin-like growth factor I	0.5	0.5
LRRP Ac1-163	0.5	0.4	Neuropeptide Y (Npy)	3.9	18.2
LRRP Ac1177	0.4	0.4, 3.3	Hemoglobins		
LRRP Ac1-233	3.3	4.2	Hemoglobin, alpha 1 (Hba1)	0.3	0.3
LRRP Ac1873	7.1	6	Hemoglobin beta chain (Hbb)	0.3	0.3
LRRP Ac2-061	3.8	7.6	Immunological proteases		
LRRP Ac2-125	0.2	0.3	Achaete-scute complex homolog-like 1 (Ascl1)	0.3	0.4
LRRP Ac2-143	4.0	3.3	Complement component 5 (C5)	8.6	8.8
LRRP Ac2-193	3.1	2.3	Immunoglobulin C kappa	0.2	0.2
LRRP Ac2-202	4.1	2.5	JE/MCP-1	6.1	4
LRRP Ac2-223	2.1	2.4	Cytoskeletons		
LRRP Ba1-647	3.9	3.2	Actin gamma	2.7	4.7
LRRP Bm403207	7.9	5.7	Clathrin, heavy polypeptide (Hc) (Cltc)	2.7	3.3
LRRP Ccl-27	0.4	2.2	Karyopherin (importin) alpha 2	0.4	0.4
LRRP Ccl-8	2.6	2.3	Marker proteins		
LRRP Ccl-9	4.7	2.5	ATP-binding cassette, sub-family C	0.3	0.4
LRRP Da1-24	2.8	3.5	Pregnancy-zone protein (Pzp)	4.7	2.4
LRRP Da1-6	2.9	2.0	Serum amyloid a-5 protein	45.1	90.5
LRRP zbs559	0.4	3.1	Subchromosomal transferable fragment 4	0.5	0.3
RIKEN 1110061A24	3.5	3	Amino acid enzymes		
RIKEN 1300002A08	0.4	0.3, 2.4	Cytosolic aspartate aminotransferase	5.1	5.3
RIKEN 2810051A14	2.0	2.7	2-hydroxyphytanoyl-CoA lyase (Hplc2)	0.4	0.4
RP11-281N10	0.5	0.3	Proteolytic enzyme		
RP23-195K1	3.9	2.4	Cathepsin C (Ctsc)	0.4	0.4
RP23-235O1	0.4	0.2	Proteinase inhibitor		
RP23-35D4	0.5	0.4, 2.8	Alpha-1 microglobulin/bikunin (Ambp)	0.4	2.1
RP23-417P22	0.4	0.1	Alpha-2-macroglobulin (A2m)	8.1	21.3
RP23-480P21	0.5	0.4	Alpha-1-macroglobulin	3.1	2
RP24-347B22	3.0	2.2	Contrapsin-like protease inhibitor (CPI-26)	14.1	6.6
RP32-28p17	0.4	0.3	Leuserpin-2 (Serpind1)	0.5	0.2
Adult male liver cDNA	6.4	0.1	Serine protease inhibitor 1	4.6	5
DNA segment of Chr 1	3.9	6.1	Phosphorylases		
13 d embryo liver cDNA	0.5	5.9	CDK110	0.5	0.5
Stress response					
Alpha-1 major acute phase protein prepeptide	13.6	6.2	Mss4 protein	3.6	2.1
Petaxin	2.6	2.2	Thymidylate kinase (dTMP kinase)	2.8	3
Angiotensinogen (Agt)	5.8	8.4	Phosphatases		
Kininogen	8.0	3.4	Pyrophosphatase/phosphodiesterase 1(Enpp1)	4.2	6.6
T-kininogen	16.1	5.9	Phosphatase 1 (GL-subunit)	0.2	0.2
Glycometabolism					
Aldolase B	0.4	0.3	Phosphatidylserine-specific phospholipase A1	3.0	2.8
Glycerol 3-phosphate dehydrogenase (Gpd3)	0.5	0.4	Synthase		
Isoctrate dehydrogenase 1 (Idh1)	0.4	0.3	Carbamyl phosphate synthetase I	3.3	2.9
Fatty and stearoyl metabolism					
Malonyl-CoA decarboxylase	0.4	0.3	Transferases		
NAD(P) dependent steroid hydrogenase	0.5	0.4	Carnitine O-octanoyltransferase (Crot)	0.3	0.3
P450 cholesterol 7- α -hydroxylase (P450 VII)	3.0	0.5, 2.3	Glutathione S-transferase 1 (Mgst1)	0.5	0.4
Prostaglandin D2 synthase 2 (Ptgds2)	2.0	3	Glutathione S-transferase Y(b) subunit	0.4	0.3
3-alpha-hydroxysteroid dehydrogenase	0.3	0.2	Glutathione S-transferase, alpha 1 (Gsta1)	0.1	0.1
Oxidation and reduction response					
Acyl-coA oxidase	0.2	0.4, 2.7	Glutathione S-transferase, type 3 (Yb3) (Gstm3)	0.4	0.3
Alcohol dehydrogenase (ADH)	0.4	0.1, 2.4	Sialyltransferase 1 (Siat1)	4.4	2.6
Cytochrom P450 15-beta (Cyp2c12)	0.1	0.2	Sulfotransferase K2	0.2	0.3
Cytochrome b	0.5	0.5	UDP-glucuronosyltransferase 2, mem 5 (Ugt2b5)	0.4	0.3
Cytochrome b5 (Cyb5)	0.4	0.2			
Cytochrome P450	0.2	0.2			

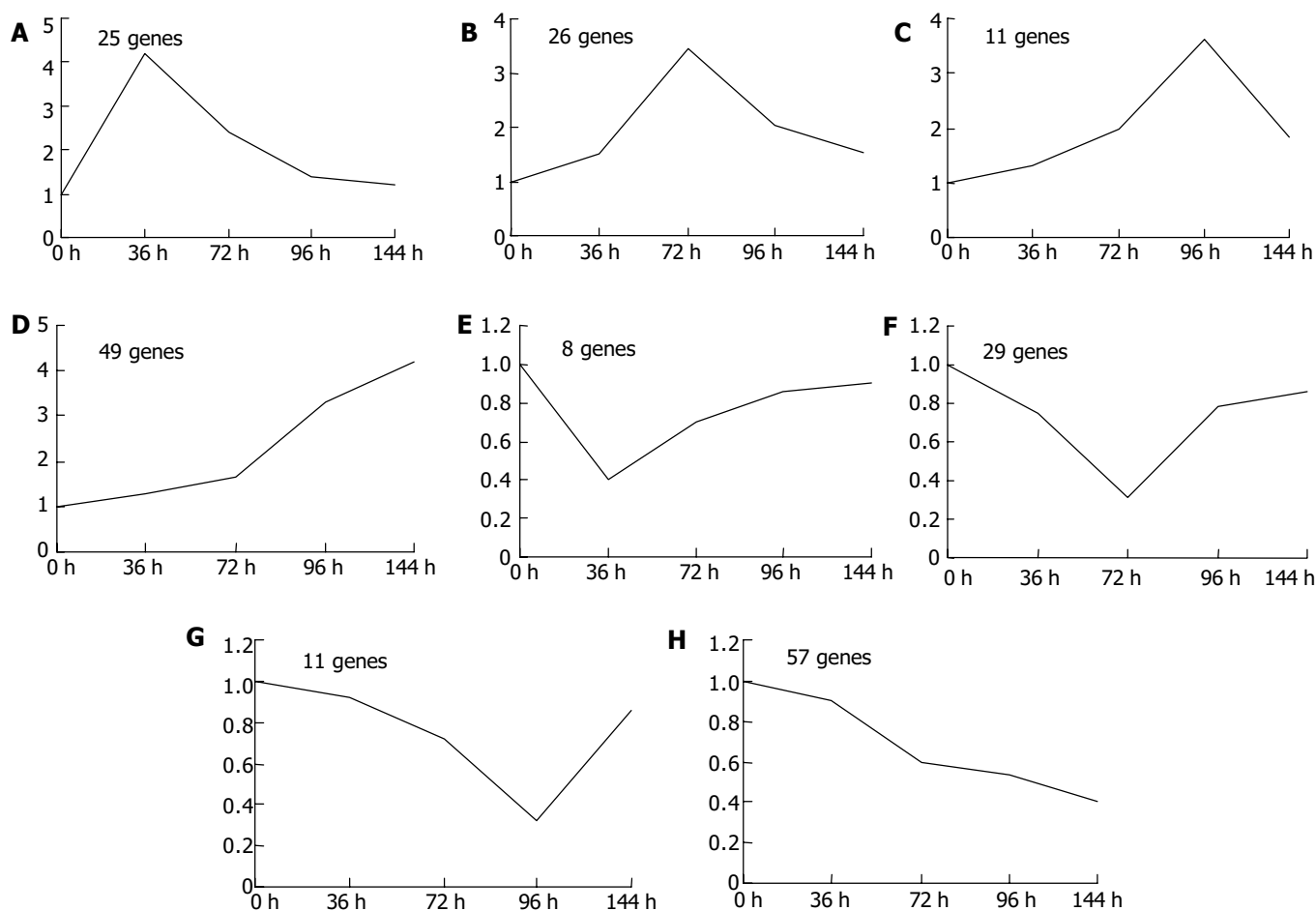


Figure 5 Category of the 216 elements. Based on the results of the cluster analysis, eight distinct temporal patterns were designated. A: Immediate induction, B: Middle induction, C: Late induction, D: Consistent induction, E: Immediate suppression, F: Middle suppression, G: Late suppression, H: Consistent suppression.

To facilitate the visualization and interpretation of the gene expression program presented in this very large body of data, we used the method of κ -means to order genes on the basis of similarities in their expression patterns and displayed the results in a compact graphical format, generating 8 kinds of ramose gene expression clusters (Figure 4). We then categorized the selected elements into 8 distinct temporal induction or suppression patterns: immediate induction, middle induction, late induction, consistent induction, immediate suppression, middle suppression, late suppression, consistent suppression (Figure 5).

Comparison of gene expression in SISPH with that after PH

Comparison of gene expression profile in SISPH with that after PH revealed that 56 genes were specially induced by SISPH, and the expression of 160 genes was altered simultaneously with the same trend in both SISPH and PH, but the time points of their expression and degree of up-regulation and down-regulation were different (Table 2).

DISCUSSION

This study found that 111 genes were up-regulated in the 0-36-72-96-144 h SISPH, suggesting that they could promote the liver growth, development and regeneration. It was also found that a large number of genes were related to positive and negative acute phase reaction to the successive hepatectomy, which suggests that these genes might regulate the balance of cell proliferation and death in the acute-phase response.

In the 25 genes up-regulated to reach the highest level at 36 h

of 0-36-72-96-144 h SISPH, 20 genes were decreased immediately to control level after the peak of 36 h, but 5 kept a high level until 144 h of SISPH. Among them, 3-phosphoglycerate dehydrogenase (PGDH) was reported to catalyze the first step in serine biosynthesis and was increased in regenerating liver^[21-23]. Prostaglandin D2 synthase 2 was confirmed to play an important role in reproduction as a PGD2-producing enzyme and a retinoid transporter^[24,25]. Phosphoprotein 1 was involved in regulation of hepatocyte proliferation in LR^[26]. The maximum expression of these genes at 36 h of SISPH showed that they could regulate hepatocyte multiplication after the peak of DNA replication in LR.

In the 27 genes up-regulated to reach the highest level at 72 h of 0-36-72-96-144 h SISPH, 12 of them declined gradually to control level at 96-144 h, and 6 did not decline until 144 h of SISPH, of which *eIF4A1* was reported to control melanoma cell proliferation by over expression^[27], whose up-regulation was assumed to accelerate protein synthesis at 72 h of SISPH. Actin γ played specific roles in the growth of liver parenchymal cells in the LR of SISPH^[28]. Cocoa extract could protect against early alcohol-induced liver injury in the rat^[29], whose conduction at 72 h was presumed to be involved in relieving hepatocytes from alcohol damage in LR of SISPH. Alpha-2-macroglobulin (A2M) was confirmed to reduce paracrine- and autocrine-stimulated extracellular matrix synthesis by scavenging TGF- β ^[30]. The successive induction of alpha 2-macroglobulin, a multifunctional binding protein with protease and cytokine scavenging properties^[31], may restrain protein degradation and termination of TGF- β in LR. The increase of HSP40 at 72 h means that lots of newly synthesized proteins need to correctly

fold with help of HSP40 in LR of SISPH.

In the 11 genes up-regulated to reach the highest level at 96 h of 0-36-72-96-144 h SISPH, cytochrome P450 cholesterol 7- α -hydroxylase (CYP7) is confirmed to regulate the protein modeling and the mRNA level in response to multiple physiological activities, including liver cholesterol synthesis, bile acid feedback inhibition, and diurnal rhythm^[32,33]. The conduction of CYP7 at 96 h is supposed to relate with cholesterol synthesis and hormone regulation in LR of SISPH.

In the 48 genes up-regulated to reach the highest level at 144 h of 0-36-72-96-144 h SISPH, plasma fibronectin was decreased in favor of LR impairment^[34-36], its expression at 144 h indicated that fibronectin-mediated function between the cells and the extracellular matrix was active in LR of SISPH. α -1-macroglobulin, serine protease inhibitor 1, angiotensinogen (Agt), fibrinogen γ , pregnancy-zone protein (Pzp) were always up-regulated from 36 h to 144 h of 0-36-72-96-144 h SISPH, suggesting that they are necessary for inhibiting proteolysis and facilitating cell growth and connection at these time points of SISPH. α -1 major acute phase protein (alpha 1-MAP) is one of the cysteine protease inhibitors^[37]. Complement component 5 can increase hepatic glycogenolysis by a prostanoid-mediated intercellular communication between Kupffer cells and hepatocytes^[38]. Fc- γ receptor III is responsible for IgG-dependent cell cytotoxicity and production of several cytokines and chemokines and involved in macrophage inflammatory protein 1 α (MIP-1 α) and neutrophil influx^[39-41]. JE/MCP-1 is known as a CC chemokine attracting monocytes, basophils and T-lymphocytes^[42,43]. Serum amyloid A-5 (SAA-5) is a major acute-phase protein synthesized and secreted mainly by the liver^[44], and is increased in response to acute inflammation in LR of SISPH. T-kininogen and kininogen are promoters to IL-6 as LR signal. These genes were always up regulated from 36 h to 144 h of 0-36-72-96-144 h SISPH, suggesting that they are necessary for relinquishing inflammation and promoting growth in whole SISPH.

This study found that 105 genes were suppressed in 0-36-72-96-144 h SISPH and a large number of them were related to energy metabolism, suggesting that they restrain LR by various paths, and that the need for energy in LR of SISPH is not as important as for other demand, which is different after PH.

Eight genes were suddenly down-regulated at 36 h after SISPH, including histidine-rich glycoprotein (HRG), apolipoprotein C-I (Apo C-I), retinol-binding protein (PRB), cytochrome P450 3A1 (Cyp3A1), RNase A family 4, carnitine O-octanoyltransferase (Crot), cytochrome b5 (Cyb5), *etc.* Histidine-rich glycoprotein (HRG) is confirmed an abundant serum exhibit protein in diverse biological systems, whose combination with zinc could be used as an antidote for heparin^[45,46]. Therefore, the down-regulation of HRG at 36 h indicated that the increased activity of heparin is essential for LR of SISPH. Apo C-I is known associated with the lipid surface of the plasma chylomicron, VLDL, and HDL subfractions, and reverse transfer from VLDL to HDL and to SBV^[47], acting as a major plasma inhibitor of cholesteryl ester transfer protein and phospholipase inhibitor^[48,49]. From the above evidence, a low level of Apo C-I at 36 h is supposed to facilitate lipoprotein linkage to LDL receptor, LDL receptor-related protein, and VLDL receptor, as well as fatty acid uptake of hepatocytes in LR of SISPH. Cyp3A1 enzymes belong to the most abundant subfamily of the cytochrome P-450 system that is predominantly found in the liver where they metabolize numerous drugs and endogenous substances such as oestrogens^[50]. The down-regulation of cyp 3A1 suggested that the harm induced by hepatectomy was presumably distinct from that by drugs and endogenous substances in rat liver.

Twenty-nine genes were suppressed and had a minimum expression at 72 h in after SISPH. Among them, angiopoietin-like protein 3 (Angptl3) is reported to activate lipolysis in adipocytes

as a vascular endothelial growth factor by response to the liver X receptor (LXR)^[51]. The extensive suppression of angiopoietin-like protein 3 mRNA at 72 h suggested that the activity of lipolysis of hepatocytes was very low in LR of SISPH. Acyl-CoA can play many important roles in numerous biochemical reactions, such as tricarboxylic acid cycle, glycoylate bypass, fatty acid synthesis. The mRNA level of acyl-coA oxidase was first dropped to meet the condition and later increased to eliminate over expressed acyl-CoA in LR of SISPH.

Hpcl 2 was expressed at 96 h in SISPH, and involved in the carbon-carbon bond cleavage as peroxisomal pyrophosphate-dependent enzyme during α -oxidation of 3-methyl-branched fatty acids^[52,53]. Down-regulation of Hpcl 2 can protect phytanic acid against being broken down, which may store energy during LR of SISPH. Fmo1 can lead to the decrease of cytochrome P-450^[54], which was repressed at 96 h to accommodate electronic environment for hepatocyte multiplication in LR of SISPH.

Retinoic acid is known necessary for the maintenance of many lining epithelia of the body, whereas retinol dehydrogenase can catalyze the first step in retinoic acid biosynthesis^[55]. Its suppression at 144 h after SISPH demonstrates that retinoic acid is not necessary in late phase of LR. In normal liver the activity of ADH is in excess, while in regenerating rat liver, the rate of ethanol elimination may be limited by the activity of alcohol dehydrogenase in SISPH^[56]. Cathepsin C (Ctsc) and dipeptidyl aminopeptidase I are regarded to play an important role in protein degradation and the activation of proenzyme in rat liver^[57]. The down-regulation of cathepsin C may be due to the indispensability of peptide for protein construction in LR of SISPH. Hepatectomy is reported to decrease liver cytochrome P450 levels by inducing heme oxygenase and inhibiting ALA synthase activities^[58], which was inhibited at 144 h to regulate the oxidation reaction of hepatocytes in LR of SISPH. Glutathione S-transferase (GST) is a family of conjugative enzymes that catalyze nucleophilic addition of tripeptide glutathione to xenobiotics carcinogens and endogenous lipophilic compounds^[59]. It was manifested that xenobiotics carcinogens and endogenous lipophilic might produce some uncertain toxic effect on LR of SISPH. Glutathione S-transferase type 3 (Yb3) mRNA was always hampered, implying that over accumulation of Yb3 could lead to contrary reaction. Fatty binding protein is well known to transfer fat from cytoplasm to nuclear or membrane, and fatty acid elongase 1 (rELO1) catalyzes short chain fat transition to long chain fat. The repression of its mRNA in SISPH indicates that long chain fatty acid was not in badly need until 144 h in LR of SISPH. Leuserpin-2 (Sperpind1) was confirmed to participate in complement activation in fibrinolysis and inflammatory response^[60], which was continuously repressed in SISPH, suggesting that it can regulate inflammatory response to improve severely injured hepatocytes in LR of SISPH. Myelin-associated glycoprotein (MAG)-binding activity of novel sulfated GM1b, high-affinity ligands for neural singlets is important to nervous system regeneration^[61]. The repression of MAG at 144 h of SISPH may result in mild damage of hepatocytes and nerve system in late phase of LR.

In conclusion, further experiments will be done by using sham surgical rats as control, so as to confirm which genes reported in this paper are related to surgical operation, and which are really related to liver regeneration.

ACKNOWLEDGEMENTS

The authors gratefully acknowledge BioStar for microarray.

REFERENCES

- 1 Michalopoulos GK, DeFrances MC. Liver regeneration. *Science* 1997; 276: 60-66

- 2 **Taub R.** Liver regeneration 4: transcriptional control of liver regeneration. *FASEB J* 1996; **10**: 413-427
- 3 **Fausto N.** Liver regeneration. *J Hepatol* 2000; **32**(1 Suppl): 19-31
- 4 **Zimmermann A.** Liver regeneration: the emergence of new pathways. *Med Sci Moimt* 2002; **8**: RA53-63
- 5 **Nagy P, Bisgaard HC, Schnur J, Thorgeirsson SS.** Studies on hepatic gene expression in different liver regenerative models. *Biochem Biophys Res Commun* 2000; **272**: 591-595
- 6 **Gressner AM.** Cytokines and cellular crosstalk involved in the activation of fat-storing cells. *J Hepato* 1995; **22**(2 Suppl): 28-36
- 7 **Cressman DE, Diamond RH, Taub R.** Rapid activation of the Stat3 transcription complex in liver regeneration. *Hepatology* 1995; **21**: 1443-1449
- 8 **FitzGerald MJ, Webber EM, Donovan JR, Fausto N.** Rapid DNA binding by nuclear factor κ B in hepatocytes at the start of liver regeneration. *Cell Growth Differ* 1995; **6**: 417-427
- 9 **Fukuhara Y, Hirasawa A, Li XK, Kawasaki M, Fujino M, Funeshima N, Katsuma S, Shiojima S, Yamada M, Okuyama T, Suzuki S, Tsujimoto G.** Gene expression profile in the regenerating rat liver after partial hepatectomy. *J Hepatol* 2003; **38**: 784-792
- 10 **Sato Y, Igarashi Y, Hakamata Y, Murakami T, Kaneko T, Takahashi M, Seo N, Kobayashi E.** Establishment of Alb-DsRed2 transgenic rat for liver regeneration research. *Biochem Biophys Res Commun* 2003; **311**: 478-481
- 11 **Qin JM, Fu XY, Li SJ, Liu SQ, Zeng JZ, Qiu XH, Wu MC, Wang HY.** Gene and protein expressions of p28^{GANK} in rat with liver regeneration. *World J Gastroenterol* 2003; **9**: 2523-2527
- 12 **Mars WM, Kim TH, Stolz DB, Liu ML, Michalopoulos GK.** Presence of urokinase in serum-free primary rat hepatocyte cultures and its role in activating hepatocyte growth factor. *Cancer Res* 1996; **56**: 2837-2843
- 13 **Jensen SA.** Liver gene regulation in rats following both 70 or 90% hepatectomy and endotoxin treatment. *J Gastroenterol Hepatol* 2001; **16**: 525-530
- 14 **Enami Y, Kato H, Murakami M, Fujioka T, Aoki T, Niiya T, Murai N, Ohtsuka K, Kusano M.** Anti-transforming growth factor-beta1 antibody transiently enhances DNA synthesis during liver regeneration after partial hepatectomy in rats. *J Hepatobiliary Pancreat Surg* 2001; **8**: 250-258
- 15 **Xia M, Xue SB, Xu CS.** Shedding of TNFR1 in regenerative liver can be induced with TNF alpha and PMA. *World J Gastroenterol* 2002; **8**: 1129-1133
- 16 **Tang W, Liang K, Wang J, Du L, Zhang W.** Effects of pHGF on hepatocyte DNA synthesis after partial hepatectomy in rats. *J Tongji Med Univ* 1998; **18**: 25-27
- 17 **Xu CS, Lu AL, Xia M, Li XY, Li YH, Zhao XY.** The effect of heat shock before rat partial hepatectomy on HSC70/HSP68, expression and phosphatase activities. *Shiyan Shengwu Xuebao* 2000; **33**: 1-11
- 18 **Li YC, Lin JT, Li WQ, Zhang HY, Wei MX, Xu CS.** Cloning and functional analysis of up-regulated expressed genes in rat liver regeneration following short interval successive partial hepatectomy. *Dev Rep Biol* 2002; **11**: 151-160
- 19 **Li YC, Ma ZQ, Xu CS.** Change of TNF- α , c-myc, p53, p21, PCNA, Bcl-2, TGF- β related with the cell proliferation in rat liver regeneration following short interval successive partial hepatectomy. *Dev Rep Biol* 2002; **11**: 253-260
- 20 **Xu CS, Li YH, Duan RF, Lu AL, Xia M, Gu AL.** Effects of the short interval successive partial hepatectomy on rat survival and liver tissue structure. *Dongwu Xuebao* 2001; **47**: 659-665
- 21 **Bell JK, Pease PJ, Bell JE, Grant GA, Banaszak LJ.** De-regulation of D-3-phosphoglycerate dehydrogenase by domain removal. *Eur J Biochem* 2002; **269**: 4176-4184
- 22 **Yamasaki M, Yamada K, Furuya S, Mitoma J, Hirabayashi Y, Watanabe M.** 3-Phosphoglycerate dehydrogenase, a key enzyme for l-serine biosynthesis, is preferentially expressed in the radial glia/astrocyte lineage and olfactory ensheathing glia in the mouse brain. *J Neurosci* 2001; **21**: 7691-7704
- 23 **Snell K, Weber G.** Enzymic imbalance in serine metabolism in rat hepatomas. *Biochem J* 1986; **233**: 617-620
- 24 **Samy ET, Li JC, Grima J, Lee WM, Silvestrini B, Cheng CY.** Sertoli cell prostaglandin D2 synthetase is a multifunctional molecule: its expression and regulation. *Endocrinology* 2000; **141**: 710-721
- 25 **Saito S, Tsuda H, Michimata T.** Prostaglandin D2 and reproduction. *Am J Reprod Immunol* 2002; **47**: 295-302
- 26 **Kikuchi K, Kitamura K, Kakinoki Y, Nakamura K, Matsuzawa S, Saadat M, Mizuno Y.** Gene expressions and activities of protein phosphatases 1 alpha, 2A and 2C in hepatocarcinogenesis and regeneration after partial hepatectomy. *Cancer Detect Prev* 1997; **21**: 36-43
- 27 **Eberle J, Fecker LF, Bittner JU, Orfanos CE, Geilen CC.** Decreased proliferation of human melanoma cell lines caused by antisense RNA against translation factor eIF-4A1. *Br J Cancer* 2002; **86**: 1957-1962
- 28 **Tanahashi T, Suzuki M, Itoh N, Mitsui Y.** Enhancement of gamma-actin protein during liver regeneration: its accumulation in a region adjacent to the hepatocyte plasma membrane. *J Biochem* 1995; **118**: 355-363
- 29 **McKim SE, Konno A, Gabele E, Uesugi T, Froh M, Sies H, Thurman RG, Arteel GE.** Cocoa extract protects against early alcohol-induced liver injury in the rat. *Arch Biochem Biophys* 2002; **406**: 40-46
- 30 **Smorenburg SM, Griffini P, Tiggelman AB, Moorman AF, Boers W, Van Noorden JF.** Alpha2-Macroglobulin is mainly produced by cancer cells and not by hepatocytes in rats with colon carcinoma metastases in liver. *Hepatology* 1996; **23**: 560-570
- 31 **Schuftan GG, Bachem MG.** Alpha2-macroglobulin reduces paracrine-and autocrine-stimulated matrix synthesis of cultured rat hepatic stellate cells. *Eur J Clin Invest* 1999; **29**: 519-528
- 32 **Lee YH, Alberta JA, Gonzalez FJ, Waxman DJ.** Multiple, functional DBP sites on the promoter of the cholesterol 7 alpha-hydroxylase P450 gene, CYP7. Proposed role in diurnal regulation of liver gene expression. *J Biol Chem* 1994; **269**: 14681-14689
- 33 **Massimi M, Lear SR, Huling SL, Jones AL, Erickson SK.** Cholesterol 7alpha-hydroxylase (CYP7A): patterns of messenger RNA expression during rat liver development. *Hepatology* 1998; **28**: 1064-1072
- 34 **Kwon AH, Inada Y, Uetsuji S, Yamamura M, Hioki K, Yamamoto M.** Response of fibronectin to liver regeneration after hepatectomy. *Hepatology* 1990; **11**: 593-598
- 35 **Chijiwa K, Nakano K, Kameoka N, Nagai E, Tanaka M.** Proliferating cell nuclear antigen, plasma fibronectin, and liver regeneration rate after seventy percent hepatectomy in normal and cirrhotic rats. *Surgery* 1994; **116**: 544-549
- 36 **Milliano MT, Luxon BA.** Initial signaling of the fibronectin receptor (alpha5beta1 integrin) in hepatic stellate cells is independent of tyrosine phosphorylation. *J Hepatol* 2003; **39**: 32-37
- 37 **Anderson KP, Heath EC.** The relationship between rat major acute phase protein and the kininogens. *J Biol Chem* 1985; **260**: 12065-12071
- 38 **Hespeling U, Puschel GP, Jungermann K, Gotze O, Zwirner J.** Stimulation of glycogen phosphorylase in rat hepatocytes via prostanoid release from Kupffer cells by recombinant rat anaphylatoxin C5a but not by native human C5a in hepatocyte/Kupffer cell co-cultures. *FEBS Lett* 1995; **372**: 108-112
- 39 **Arase N, Arase H, Hirano S, Yokosuka T, Sakurai D, Saito T.** IgE-mediated activation of NK cells through Fc gamma RIII. *J Immunol* 2003; **170**: 3054-3058
- 40 **Taube C, Dakhama A, Rha YH, Takeda K, Joetham A, Park JW, Balhorn A, Takai T, Poch KR, Nick JA, Gelfand EW.** Transient neutrophil infiltration after allergen challenge is dependent on specific antibodies and Fc gamma III receptors. *J Immunol* 2003; **170**: 4301-4309
- 41 **Song X, Shapiro S, Goldman DL, Casadevall A, Scharff M, Lee SC.** Fc gamma receptor I- and III-mediated macrophage inflammatory protein 1alpha induction in primary human and murine microglia. *Infect Immun* 2002; **70**: 5177-5184
- 42 **Kawahara RS, Deng ZW, Denking DJ, Deuel TF.** Role of serine/threonine protein kinases in the induction of JE, a platelet-derived growth factor inducible gene. *Biochem Biophys Res Commun* 1994; **203**: 1815-1820
- 43 **DiPietro LA, Polverini PJ, Rahbe SM, Kovacs EJ.** Modulation of JE/MCP-1 expression in dermal wound repair. *Am J Pathol* 1995; **146**: 868-875
- 44 **Bing Z, Reddy SA, Ren Y, Qin J, Liao WS.** Purification and

- characterization of the serum amyloid A3 enhancer factor. *J Biol Chem* 1999; **274**: 24649-24656
- 45 **Gorgani NN**, Smith BA, Kono DH, Theofilopoulos AN. Histidine-rich glycoprotein binds to DNA and Fc gamma RI and potentiates the ingestion of apoptotic cells by macrophages. *J Immunol* 2002; **169**: 4745-4751
- 46 **Fu CL**, Horn MK 3rd. Histidine-rich glycoprotein plus zinc to neutralize heparin. *J Lab Clin Med* 2002; **139**: 211-217
- 47 **McKeone BJ**, Massey JB, Knapp RD, Pownall HJ. Apolipoproteins C-I, C-II, and C-III: kinetics of association with model membranes and intermembrane transfer. *Biochemistry* 1988; **27**: 4500-4505
- 48 **Shachter NS**. Apolipoproteins C-I and C-III as important modulators of lipoprotein metabolism. *Curr Opin Lipidol* 2001; **12**: 297-304
- 49 **Poensgen J**. Apolipoprotein C-1 inhibits the hydrolysis by phospholipase A2 of phospholipids in liposomes and cell membranes. *Biochim Biophys Acta* 1990; **1042**: 188-192
- 50 **Galant C**, Gala JL, Van Den Berge V, Berliere M, Haumont E, Horsmans Y. Immunolocalisation of cytochrome P-450 3A enzymes in human breast carcinoma: relationship with tumour differentiation and steroid receptors. *Pharmacol Toxicol* 2001; **88**: 142-146
- 51 **Shimamura M**, Matsuda M, Kobayashi S, Ando Y, Ono M, Koishi R, Furukawa H, Makishima M, Shimomura I. Angiotensin-like protein 3, a hepatic secretory factor, activates lipolysis in adipocytes. *Biochem Biophys Res Commun* 2003; **301**: 604-609
- 52 **Foulon V**, Antonenkov VD, Croes K, Waelkens E, Mannaerts GP, Van Veldhoven PP, Casteels M. Purification, molecular cloning, and expression of 2-hydroxyphytanoyl-CoA lyase, a peroxisomal thiamine pyrophosphate-dependent enzyme that catalyzes the carbon-carbon bond cleavage during alpha-oxidation of 3-methyl-branched fatty acids. *Proc Natl Acad U S A* 1999; **96**: 10039-10044
- 53 **Jansen GA**, Verhoeven NM, Denis S, Romeijn G, Jakobs C, ten Brink HJ, Wanders RJ. Phytanic acid alpha-oxidation: identification of 2-hydroxyphytanoyl-CoA lyase in rat liver and its localisation in peroxisomes. *Biochim Biophys Acta* 1999; **1440**: 176-182
- 54 **Kedderis GL**, Rickert DE. Loss of rat liver microsomal cytochrome P-450 during methimazole metabolism. Role of flavin-containing monooxygenase. *Drug Metab Dispos* 1985; **13**: 58-61
- 55 **Rexer BN**, Ong DE. A novel short-chain alcohol dehydrogenase from rats with retinol dehydrogenase activity, cyclically expressed in uterine epithelium. *Biol Reprod* 2002; **67**: 1555-1564
- 56 **Poso AR**, Poso H. Ethanol elimination in regenerating rat liver: the roles of alcohol dehydrogenase and acetaldehyde. *Acta Chem Scand B* 1979; **33**: 249-255
- 57 **Cigic B**, Pain RH. Location of the binding site for chloride ion activation of cathepsin. *Eur J Biochem* 1999; **264**: 944-951
- 58 **Solangi K**, Sacerdoti D, Goodman AI, Schwartzman ML, Abraham NG, Levere RD. Differential effects of partial hepatectomy on hepatic and renal heme and cytochrome P450 metabolism. *Am J Med Sci* 1988; **296**: 387-391
- 59 **Atkins WM**, Wang RW, Bird AW, Newton DJ, Lu AY. The catalytic mechanism of glutathione S-transferase (GST). Spectroscopic determination of the pKa of Tyr-9 in rat alpha 1-1 GST. *J Biol Chem* 1993; **268**: 19188-19191
- 60 **Ragg H**, Ulshofer T, Gerewitz J. On the activation of human leuserpin-2, a thrombin inhibitor, by glycosaminoglycans. *J Biol Chem* 1990; **265**: 5211-5218
- 61 **Ito H**, Ishida H, Collins BE, Fromholt SE, Schnaar RL, Kiso M. Systematic synthesis and MAG-binding activity of novel sulfated GM1b analogues as mimics of Chol-1 (alpha-series) gangliosides: highly active ligands for neural siglecs. *Carbohydr Res* 2003; **338**: 1621-1639

Edited by Zhu LH Proofread by Chen WW and Xu FM

Protective effect of melatonin against liver injury in mice induced by *Bacillus Calmette-Guerin* plus lipopolysaccharide

Hua Wang, Wei Wei, Yu-Xian Shen, Chen Dong, Ling-Ling Zhang, Ni-Ping Wang, Li Yue, Shu-Yun Xu

Hua Wang, Wei Wei, Yu-Xian Shen, Chen Dong, Ling-Ling Zhang, Ni-Ping Wang, Li Yue, Shu-Yun Xu, Institute of Clinical Pharmacology, Anhui Medical University, Hefei 230032, Anhui Province, China
Supported by Funds From State Key Programs of Science and Technology of China, No. 969010652

Correspondence to: Professor Wei Wei, Institute of Clinical Pharmacology, Anhui Medical University, Hefei 230032, Anhui Province, China. wwei@ahmu.edu.cn

Telephone: +86-551-5161208 Fax: +86-551-5161208

Received: 2003-11-13 Accepted: 2003-12-22

Abstract

AIM: To investigate the effects and mechanisms of melatonin on immunological liver injury in mice.

METHODS: A model of liver injury was induced by tail vein injection of *Bacillus Calmette Guerin* (BCG) and lipopolysaccharide (LPS) in mice. Kupffer cells and hepatocytes were isolated and cultured according to a modified two-step collagenase perfusion technique. Levels of alanine aminotransferase (ALT), aspartate aminotransferase (AST) and nitric oxide (NO), content of malondialdehyde (MDA), activity of superoxide dismutase (SOD), were measured by biochemical methods. Tumor necrosis factor- α (TNF- α) activity was determined by RIA. Interleukin (IL)-1 activity was measured by thymocyte proliferation bioassay. Hepatic tissue sections were stained with hematoxylin and eosin and examined under a light microscope.

RESULTS: Immunological liver injury induced by BCG+LPS was successfully duplicated. Serum transaminase (ALT, AST) activities were significantly decreased by melatonin (0.25, 1.0, 4.0 mg/kg bm). Meanwhile, MDA content was decreased and SOD in liver homogenates was upregulated. Furthermore, pro-inflammatory mediators (TNF- α , IL-1, NO) in serum and liver homogenates were significantly reduced by melatonin. Histological examination demonstrated that melatonin could attenuate the area and extent of necrosis, reduce the immigration of inflammatory cells. In *in vitro* experiment, TNF- α was inhibited at the concentrations of 10^{-8} - 10^{-6} mol/L of melatonin, while IL-1 production of Kupffer cells induced by LPS (5 μ g/mL) was decreased only at the concentration of 10^{-6} mol/L of melatonin, but no effect on NO production was observed. Immunological liver injury model *in vitro* was established by incubating hepatocytes with BCG- and LPS-induced Kupffer cells. Activities of ALT, TNF- α , IL-1, and MDA in supernatant were significantly increased. Melatonin had little effect on the level of ALT, but reduced the content of TNF- α and MDA at concentrations of 10^{-7} - 10^{-5} mol/L and decreased the content of IL-1 at concentrations of 10^{-6} - 10^{-5} mol/L.

CONCLUSION: Melatonin could significantly protect liver injury in mice, which was related to free radical scavenging, increased SOD activity and pro-inflammatory mediators.

Wang H, Wei W, Shen YX, Dong C, Zhang LL, Wang NP, Yue L,

Xu SY. Protective effect of melatonin against liver injury in mice induced by *Bacillus Calmette-Guerin* plus lipopolysaccharide. *World J Gastroenterol* 2004; 10(18): 2690-2696
<http://www.wjgnet.com/1007-9327/10/2690.asp>

INTRODUCTION

Viral infection, alcoholic or drug toxicity, or any other factors that cause damage to hepatocytes elicit an inflammatory reaction in the liver. The damaged hepatocytes, their membrane components, metabolites of toxic agents, and infiltrating inflammatory cells are the activators of Kupffer cells. Kupffer cells, the resident macrophages in the sinusoids of the liver, play significant roles in immunomodulation, phagocytosis, and biochemical attack^[1,2]. It has been reported that Kupffer cells to be activated are considered the key evidence in the pathophysiology of many animal models of hepatic injury^[3-8]. Activated Kupffer cells contribute to the onset of liver injury by producing and releasing cytotoxic agents such as pro-inflammatory cytokines including tumor necrosis factor alpha (TNF- α)^[9,10], interleukin-1 (IL-1)^[9], interleukin-6 (IL-6) and active oxygen^[11], nitric oxide (NO)^[8] which damage sinusoidal endothelial cells and hepatocytes. Previous studies have shown that elimination of Kupffer cells by gadolinium chloride^[5] and TNF- α antibodies are effective on reducing hepatic damage *in vivo*.

Ferluga *et al.* first reported the *P. acnes*-primed LPS-induced hepatic shock model in mice in 1978^[12], and three years later Ferluga also reported that LPS injection subsequent to the priming of *Bacillus Calmette-Guerin* (BCG) provoked the same hepatic injury in mice^[13]. Since then, many investigators have tried to explain the mechanism of the above two similar models^[14,15]. It is known that *P. acnes* or BCG priming and LPS challenge in mice cause massive liver injury, which consists of priming and eliciting phases. *P. acnes* or BCG priming induces mononuclear cell infiltration into the liver lobules and granuloma formation^[16]. The subsequent LPS injection elicits acute and massive hepatic injury, with a concomitant release of various cytokines and active free radicals^[17-21]. Thus, in immunological liver injury model induced by BCG and LPS, hepatocyte damage is presumably caused by immunological mechanisms. Pro-inflammatory cytokines and active free radicals produced by activated Kupffer cells play an important role in the progress of the resulted liver injury. This experimental immunological liver injury has frequently been used as a model for testing and developing new drugs^[12,13,22-24].

The hormone melatonin (N-acetyl-5-methoxytryptamine) is synthesized by pineal gland. Melatonin participates in many important physiological functions, including anti-inflammation^[25] and immunoregulation^[26,27], as well as acting as a broad spectrum antioxidant^[28-30]. In addition, melatonin protects against liver injury induced by endotoxin shock^[31,32] and ischemia/reperfusion^[33,34] in rats through its antioxidant action. The purpose of this study was to investigate whether exogenous melatonin would protect against BCG- and LPS-induced immunological liver injury in mice via antioxidative and immunoregulatory mechanisms. Meanwhile, the direct effect of melatonin on isolated Kupffer cells or co-cultured Kupffer cells and hepatocytes *in vitro* was studied.

MATERIALS AND METHODS

Materials

Melatonin, purchased from Sigma Chemical Co. (St Louis, Mo, USA), was dissolved in 9 g/L saline with absolute ethanol ($<=0.1$ mL/L) and stored at -20°C . 3-[4,5-dimethylthiazol-2-yl]-2,5-diphenyltetra-zolium bromide (MTT), RPMI 1640, Hepes buffer, collagenase IV, Pronase E, DNase, Nycodenz and LPS from *Escherichia coli* were obtained from Sigma Chemical Co (St Louis, Mo, USA). Commercial kits used for determining lipid peroxidation and superoxide dismutase (SOD) activity were obtained from the Jiancheng Institute of Biotechnology (Nanjing, China). Other chemicals used in these experiments were of analytical grade from commercial sources.

Animals

Male Sprague-Dawley (SD) rats (300 ± 20 g), C57BL/6J mice (18 ± 2 g) and male Kunming mice (20 ± 2 g), obtained from the Animal Department of Anhui Medical University, were maintained on a 12 h light/ dark cycle from 6AM to 6PM in a controlled environment ($20\pm 1^{\circ}\text{C}$). Animals were housed in plastic cages with free access to food and water. All experimental protocols described in this study were approved by the Ethics Review Committee for Animal Experimentation of Institute of Clinical Pharmacology, Anhui Medical University.

Establishment of immunological liver injury model^{8,13}

A 2.5 mg dose of BCG (viable bacilli) suspended in 0.2 mL saline was injected via the tail vein into each animal, and 10 d later, 7.5 μg LPS dissolved in 0.2 mL saline was injected. Mice were anesthetized with ether, then sacrificed by cervical dislocation 16 h after LPS injection and trunk blood was collected into heparinized tubes (50 U/mL) and centrifuged (1 500 r/min, 10 min, 4°C). Serum was aspirated and stored at -70°C until assayed as described below. The liver was also removed and stored at -70°C until required.

Drug treatment

In vivo experiment, the animals were equally divided into 5 groups randomly, including normal, model control and melatonin groups (3 different doses). Mice in melatonin groups were received daily doses of 0.25, 1.0 or 4.0 mg/kg bm of melatonin using an 18-gauge stainless steel animal feeding needle for 10 d prior to LPS injection. Mice in normal and model control group were only fed the same volume of vehicle.

In vitro experiment, after Kupffer cells were isolated from normal rat, the cells were divided into 7 groups randomly, including control cells, cells added with LPS (5 $\mu\text{g}/\text{mL}$) alone, cells added with LPS (5 $\mu\text{g}/\text{mL}$) simultaneously with melatonin (5 different concentrations including 10^{-9} , 10^{-8} , 10^{-7} , 10^{-6} , 10^{-5} mol/L). Every group had triplicate wells and the experiment above was repeated twice.

In another *in vitro* experiment, after Kupffer cells were isolated from BCG priming rat and hepatocytes isolated from normal rat, the two types of cells were divided into 7 groups randomly, including control cells, cells added with LPS (5 $\mu\text{g}/\text{mL}$) alone, cells added with LPS (5 $\mu\text{g}/\text{mL}$) simultaneously with melatonin (5 different concentrations including 10^{-9} , 10^{-8} , 10^{-7} , 10^{-6} , 10^{-5} mol/L). Every group had triplicate wells and the experiment above was repeated twice.

Isolation and culture of Kupffer cells and hepatocytes

In vitro experiment, the direct effect of melatonin on Kupffer cells was studied by isolating Kupffer cells from the livers of normal rat. Rat liver perfusion was performed using a modification of the two-step collagenase perfusion technique introduced by previous studies^{35,36}.

In brief, the rat liver was perfused through the portal vein with D-Hank's until blood free, and then with Hank's containing 0.5 g/L collagenase IV. The latter was administered by recirculation until the vessels were digested (up to 20 min). The liver was then scraped using a cell scraper, filtered through a 100- μm filter, and stirred in Hank's containing 2.5 g/L pronase and 0.05 g/L DNase for 20 min at 37°C . After three times of centrifugation and washing at $300\times g$ for 10 min at 4°C in Gey's balanced salt solution (GBSS), cells were centrifuged in an 180 g/L Nycodenz gradient at $2\,500\times g$ for 20 min. Kupffer cells were carefully sucked by cusp-straws at the pearl layer interphase. At last, purified Kupffer cell fractions were obtained by centrifugal elutriation. The viability of Kupffer cells prepared was more than 95% as determined by trypan blue exclusion. The purity of Kupffer cells was greater than 90% based on a peroxidase activity assay³⁷.

Kupffer cells, obtained as described above, were washed with Hanks' and resuspended in RPMI 1640 medium containing antibiotics (penicillin, 100 U/mL; streptomycin, 100 mg/mL), 2 mmol/L glutamine, and 100 mL/L fetal calf serum. One-milliliter aliquots containing 1×10^6 cells were added to 24-well culture plates. The cells were incubated for 60 min in a humidified atmosphere containing 50 mL/L CO_2 at 37°C . Nonadherent cells were removed, and adherent cells were washed twice with PBS. The cells at a density of $1\times 10^6/\text{mL}$ were incubated with different concentrations of melatonin (10^{-9} , 10^{-8} , 10^{-7} , 10^{-6} , 10^{-5} mol/L). They ($1\times 10^6/\text{well}$) were cultured for 48 h with 5 $\mu\text{g}/\text{mL}$ LPS and the supernatants were collected and TNF- α and NO concentration measured with the methods described below.

In *in vitro* liver injury model, BCG induced Kupffer cells were isolated from the livers of the rats which were injected via the tail vein with 3 mg of BCG 10 d before, at the same time hepatocytes isolated from normal rat. The hepatocytes at a density of $1\times 10^9/\text{mL}$ were incubated with different concentrations of melatonin (10^{-9} , 10^{-8} , 10^{-7} , 10^{-6} , 10^{-5} mol/L) and BCG-induced Kupffer cells ($1\times 10^6/\text{well}$). They were co-cultured for 48 h with 5 $\mu\text{g}/\text{mL}$ LPS and the supernatants were collected.

Measurement of serum ALT and AST

Serum ALT and AST were determined using commercial kits produced by Jiancheng Institute of Biotechnology (Nanjing, China). Their activities were expressed as an international unit (U/L).

Measurement of NO in serum and cell culture supernatants

Nitric oxide (NO) in Kupffer cells was measured by a microplate assay using Griess reagent, which produces a chromophore with the nitrite³⁸. Briefly, 100 μL of cell culture supernatants was removed and incubated with 100 μL of Griess reagent (10 g/L sulfanilamide and 1 g/L N-1-naphthylethylenediamine dihydrochloride in 25 mL/L phosphoric acid) in a 96-well plate. The plate was incubated for 10 min at room temperature. Nitrite production was quantified spectrophotometrically using an automated colorimetric procedure. Absorbance at 540 nm was measured using a microplate reader (Bio-Tek, USA). The nitrite concentration was calculated by comparing samples with standard solutions of sodium nitrite produced in the culture medium. All samples were assayed in triplicate. Results were expressed as $\mu\text{mol}/\text{L}$.

Measurement of MDA and SOD in liver homogenates

Livers were thawed, weighed and homogenized with Tris-HCl (5 mmol/L containing 2 mmol/L EDTA, pH 7.4). Homogenates were centrifuged (1 000 r/min, 10 min, 4°C) and the supernatant was used immediately for the assays of MDA and SOD. MDA and SOD were determined following the instructions of the kit. In brief, MDA in liver tissue was determined by the thiobarbituric

acid method^[39]. All samples were assayed in triplicate. The content of MDA was expressed as nmol per gram liver tissue. The assay for total SOD was based on its ability to inhibit the oxidation of oxyamine by the xanthine-xanthine oxidase system. The red product (nitrite) produced by the oxidation of oxyamine has an absorbance at 550 nm. One unit (U) of SOD activity was defined as the quantity that reduced the absorbance at 550 nm by 50%. All samples were assayed in triplicate. Results were expressed as U per gram liver tissue.

Measurement of TNF- α in serum and cell culture supernatants

Serum was assayed according to procedures described by the instruction of the commercial kits. The standard curve of TNF- α measured was between 2 and 160 pg/mL.

Bioassay of IL-1 activity in serum and cell culture supernatants

IL-1 activity was measured by mouse thymocyte activation assayed by MTT (Sigma) reduction^[40]. MTT was dissolved in sterile PBS to a concentration of 5 mg/mL and stored in the dark at 4 °C for up to 1 wk. Immediately before use, stock MTT was filtered (0.22 μ m) to remove any formazan precipitate. Thymocytes (2×10^6 /well) from mice were cultured for 48 h in 96-well plates containing RPMI 1640 medium supplemented with 5 μ g/mL concanavalin A and 0.1 mL collected supernatants in triplicate. Three hours before the termination of culture, cells were pulsed with MTT stock (20 μ L/well), returned to 37 °C and incubated for another 3 h. The plates were centrifuged for 10 min at 1 000 g to cell pellets and MTT formazan products. The supernatant was carefully aspirated without disturbing the pellets, and formazan was solubilized by addition of isopropanol (100 μ L/200 μ L supernatant). Insoluble material was then removed by centrifugation for 10 min at 1 000 g. The solubilized formazan in isopropanol was collected and distributed into 12-well flat-bottom ELISA plates at a final volume of 100 μ L/well. Plates were read at 570 nm in EL 301 Strip Reader (Bio-Tek, USA) within 1 h of addition of isopropanol. Values were expressed as mean absorbance (A) of triplicate wells.

Histological analysis

Formalin-fixed specimens were embedded in paraffin and stained with hematoxylin and eosin for conventional morphological evaluation. After decapitation of rats, small liver specimens were placed in 100 mL/L formalin solution and processed routinely by embedding in paraffin. Tissue sections (4-5 μ m) were stained with hematoxylin and eosin and examined under light microscope (Olympus). An experienced histologist who was unaware of the treatment conditions made histological assessments.

Statistical analyses

All values were presented as mean \pm SE. Statistical analysis of the data for multiple comparisons was performed by one-way analysis of variance (ANOVA) followed by Duncan's test. For a single comparison, the significance of differences between means was determined by the *t*-test, A level of $P < 0.05$ was accepted as statistical significant.

RESULTS

Effect of melatonin on serum ALT and AST

Activities of both serum AST and ALT, indices of hepatic cell damage, were significantly higher in BCG- and LPS-induced group than in the control group. Melatonin (0.25, 1.0, 4.0 mg/kg bm) significantly reduced the activities of serum AST and ALT (Table 1).

Effect of melatonin on liver homogenate MDA and total SOD

Liver homogenate malondialdehyde (MDA) content in BCG-

and LPS-induced group was significantly higher than that in the control group while liver total SOD activity was lower. Melatonin (0.25, 1.0, 4.0 mg/kg bm) significantly attenuated MDA generation and increased liver total SOD activity (Table 2).

Table 1 Effects of melatonin on serum ALT and AST activities in immunological liver injury in mice ($n = 10$, mean \pm SE)

Group	Dose (mg/kg bm)	ALT (U/L)	AST (U/L)
Normal	---	28.2 \pm 8.8	26.8 \pm 8.5
Model	---	224 \pm 40 ^d	205 \pm 40 ^d
Melatonin	0.25	187 \pm 21 ^a	129 \pm 13 ^b
	1.0	119 \pm 41 ^b	124 \pm 36 ^b
	4.0	163 \pm 44 ^b	162 \pm 33 ^a

^a $P < 0.05$, ^b $P < 0.01$ vs model group; ^d $P < 0.01$ vs normal control group.

Table 2 Effects of melatonin on MDA level and SOD activity of liver homogenates of immunological injury mice ($n = 10$, mean \pm SE)

Group	Dose (mg/kg bm)	MDA (nmol/g tissue)	SOD (U/g tissue)
Normal	---	92 \pm 26	297 \pm 22
Model	---	439 \pm 25 ^d	202.46 \pm 26 ^d
Melatonin	0.25	335 \pm 37 ^b	266 \pm 71 ^b
	1.0	332 \pm 28 ^b	273 \pm 31 ^b
	4.0	346 \pm 17 ^b	244 \pm 27 ^b

^a $P < 0.05$, ^b $P < 0.01$ vs model group; ^d $P < 0.01$ vs normal control group.

Effect of melatonin on serum and liver homogenate TNF- α , IL-1 and NO concentration

As shown in Table 3, when mice were first injected with BCG and then challenged with LPS, the levels of TNF- α , IL-1 and NO were elevated significantly. Melatonin (0.25, 1.0 and 4.0 mg/kg bm) obviously reversed these effects. Similarly, in liver homogenates of immunological injury mice the levels of above three indices increased and melatonin (0.25, 1.0 and 4.0 mg/kg bm) significantly inhibited the production of TNF- α and NO while melatonin (4 mg/kg bm) inhibited IL-1 (Table 4).

Table 3 Effects of melatonin on serum TNF- α , IL-1 and NO levels in immunological liver injury mice ($n = 10$, mean \pm SE)

Group	Dose (mg/kg bm)	TNF- α (ng/L)	IL-1 ($A_{570\text{nm}}$)	NO (μ mol/L)
Normal	---	1.61 \pm 0.76	0.107 \pm 0.001	9.82 \pm 1.92
Model	---	4.80 \pm 1.61 ^d	0.242 \pm 0.03 ^d	73 \pm 19 ^d
Melatonin	0.25	3.42 \pm 1.08 ^a	0.183 \pm 0.07 ^a	55 \pm 18 ^a
	1.0	3.26 \pm 0.73 ^a	0.131 \pm 0.04 ^b	28 \pm 14 ^b
	4.0	2.64 \pm 1.19 ^b	0.158 \pm 0.04 ^b	56 \pm 19 ^a

^a $P < 0.05$, ^b $P < 0.01$ vs model group; ^d $P < 0.01$ vs normal control group.

Effect of melatonin on NO, TNF- α and IL-1 production of isolated Kupffer cells

In vitro, melatonin at the concentrations of 10^{-8} - 10^{-6} mol/L was able to inhibit directly the production of TNF- α while only at the concentrations of 10^{-6} mol/L decreased IL-1 production of Kupffer cells co-cultured with LPS (5 μ g/mL). However, melatonin had no effect on NO production (Table 5).

Table 4 Effects of melatonin on TNF- α , IL-1 and NO levels of liver homogenates in immunological injury mice ($n = 10$, mean \pm SE)

Group	Dose (mg/kg bm)	TNF- α (ng/L)	IL-1 ($A_{570\text{ nm}}$)	NO ($\mu\text{mol/L}$)
Normal	---	3.1 \pm 8.3	0.15 \pm 0.03	9.5 \pm 2.7
Model	---	26.6 \pm 2.3 ^d	0.41 \pm 0.03 ^d	45.0 \pm 9.8 ^d
Melatonin	0.25	13.9 \pm 2.9 ^b	0.38 \pm 0.13	25.6 \pm 9.5 ^b
	1.0	12.4 \pm 2.9 ^b	0.22 \pm 0.05 ^b	17 \pm 11 ^b
	4.0	17.9 \pm 4.8 ^b	0.35 \pm 0.04 ^b	24 \pm 10 ^b

^a $P < 0.05$, ^b $P < 0.01$ vs model group; ^d $P < 0.01$ vs normal control group.

Table 5 Effect of melatonin on TNF- α , IL-1 and NO released from cultured normal Kupffer cells of rats ($n = 10$, mean \pm SE)

Group	Concentration of melatonin (mol/L)	TNF- α (ng/L)	IL-1 ($A_{570\text{ nm}}$)	NO ($\mu\text{mol/L}$)
KC	---	4.25 \pm 0.79	0.137 \pm 0.03	13.65 \pm 0.21
KC+LPS	---	11.21 \pm 1.63 ^d	0.233 \pm 0.03 ^d	18.85 \pm 0.88 ^d
KC+LPS +melatonin	10 ⁻⁹	9.96 \pm 0.24	0.238 \pm 0.02	19.08 \pm 0.40
	10 ⁻⁸	9.31 \pm 0.53 ^a	0.223 \pm 0.02	19.13 \pm 0.46
	10 ⁻⁷	8.35 \pm 0.82 ^b	0.201 \pm 0.01	18.90 \pm 0.77
	10 ⁻⁶	8.01 \pm 0.38 ^b	0.177 \pm 0.01 ^b	18.65 \pm 0.61
	10 ⁻⁵	9.74 \pm 0.39	0.216 \pm 0.02	18.70 \pm 0.57

KC: Kupffer cells; ^a $P < 0.05$, ^b $P < 0.01$ vs model group; ^d $P < 0.01$ vs normal control group.

Effect of melatonin on liver injury in mice *in vitro*

Immunological liver injury model *in vitro* was established by hepatocytes incubated with BCG- and LPS-induced Kupffer cells. Activities of ALT, TNF- α , IL-1 and MDA in supernatant

were significantly increased. Melatonin had little effect on the level of ALT, but at concentrations of 10⁻⁷-10⁻⁵ mol/L it reduced the content of TNF- α and MDA while at concentrations of 10⁻⁶-10⁻⁵ mol/L it decreased the content of IL-1 (Table 6).

Histological results

In normal group, there was no pathological abnormality. Liver parenchyma was in good morphology and hepatocytes were arranged around the central vein. No congestion and inflammation were observed in the sinusoids (Figure 1A).

In model group, there was a severe pathological abnormality. Hepatocytes were with marked vacuolization, moreover, hepatocytes dot necrosis, striped necrosis, bridging necrosis appeared and inflammatory cells arranged around the necrotic tissue. Congestion in liver sinusoids was significant with scattered infiltration of inflammatory cells (Figure 1B).

In melatonin-treated group, the area and extent of necrosis attenuated and the immigration of inflammatory cells reduced. Liver parenchyma was well preserved with radially arranged hepatocytes around the central vein. Regular sinusoidal structures were seen without congestion (Figure 1C).

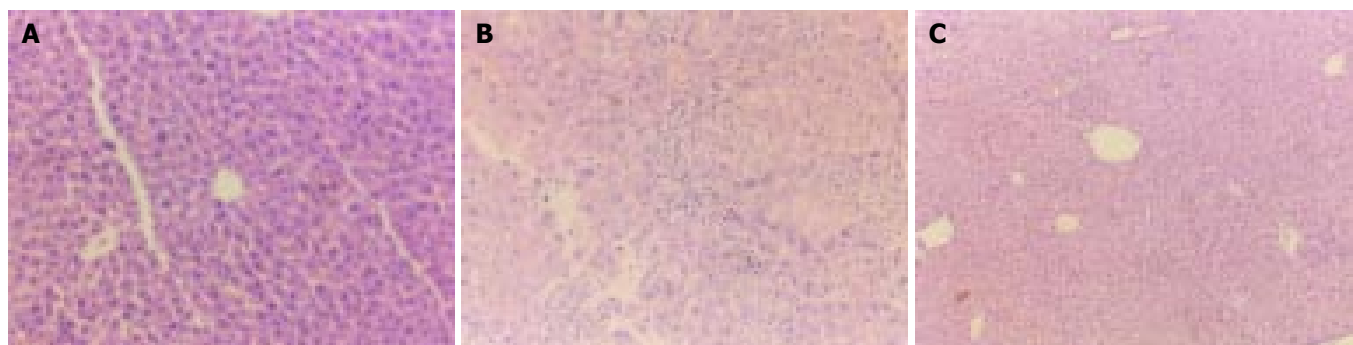
DISCUSSION

Injection of BCG followed by LPS is useful for the creation of experimental models of acute hepatic damage^[13,16,22,41]. In the present study, immunological liver injury in mice was successfully induced by BCG and LPS and the model *in vitro* also duplicated. On this basis, administration of melatonin *in vivo* resulted in marked reduction of acute liver injury, as demonstrated by significant reduction of serum transaminase concentration and amelioration of severe hepatic pathological abnormalities. Meanwhile, melatonin decreased MDA content and increased total SOD activity in liver homogenates. Furthermore, melatonin significantly reduced TNF- α , IL-1 and NO production in serum and liver homogenates. The *in vitro* experiment also supported

Table 6 Effects of melatonin on MDA, TNF- α and IL-1 released from co-cultured normal rat hepatocytes and Kupffer cells activated by BCG ($n = 5$, mean \pm SE)

Group	Concentration of melatonin (mol/L)	ALT (U/L)	MDA (nmol/L)	TNF- α (ng/L)	IL-1 ($A_{570\text{ nm}}$)
KC+HC	---	37.1 \pm 3.7	0.506 \pm 0.029	4.50 \pm 0.78	0.16 \pm 0.03
KC+HC+LPS	---	81.4 \pm 6.4 ^d	0.849 \pm 0.062 ^d	11.36 \pm 1.6 ^d	0.25 \pm 0.03 ^d
KC+HC+LPS+Melatonin	10 ⁻⁹	82.4 \pm 4.3	0.809 \pm 0.015	10.13 \pm 0.23	0.26 \pm 0.02
	10 ⁻⁸	79.6 \pm 5.4	0.789 \pm 0.036	9.49 \pm 0.52	0.24 \pm 0.02
	10 ⁻⁷	74.9 \pm 4.2	0.706 \pm 0.014 ^b	8.54 \pm 0.81 ^b	0.22 \pm 0.01
	10 ⁻⁶	72.9 \pm 6.6	0.676 \pm 0.043 ^b	8.21 \pm 0.37 ^b	0.19 \pm 0.01 ^a
	10 ⁻⁵	83.8 \pm 3.3	0.69 \pm 0.04 ^b	8.39 \pm 1.22 ^b	0.20 \pm 0.01 ^b

KC: Kupffer cell; ^a $P < 0.05$, ^b $P < 0.01$ vs model group; ^d $P < 0.01$ vs normal control group.

**Figure 1** Histological results of tissues stained with hematoxylin and eosin under light microscope. A: Normal control group; B: Model group; C: Melatonin-treated group.

the direct protective role of melatonin in suppression of Kupffer cell function. Although melatonin had no direct protection on hepatocytes injury *in vitro* induced by BCG and LPS, it could inhibit the production of MDA and pro-inflammatory cytokines such as TNF- α and IL-1. Based on the current results, we propose that the mode of melatonin's hepatic protective action is, at least in part, related to its antioxidative and immunoregulatory properties.

As it is well known, melatonin, the chief secretory product of the pineal gland, was found to be a multi-faceted free radical scavenger and antioxidant. It detoxifies a variety of free radicals and reactive oxygen intermediates, including the hydroxyl radical, singlet oxygen, peroxynitrite anion and nitric oxide^[29,30]. In both *in vitro* and *in vivo* experiments, melatonin has been found to protect cells, tissues, and organs against oxidative damage induced by a variety of free-radical-generating agents and processes, *e.g.*, the carcinogen safrole, LPS, carbon tetrachloride, ischemia-reperfusion, amyloid-protein, and ionizing radiation^[42,43]. Melatonin also has been reported to stimulate the activities of enzymes and increase gene expression that improves the total antioxidative defense capacity of the organism, *i.e.*, SOD, glutathione peroxidase, glutathione reductase^[44,45]. Moreover, recent studies indicate that melatonin is effective on inhibiting oxidative liver damage. Calvo *et al.* found that melatonin protected against ANIT-induced liver injury with cholestasis in rats, and suggested that this protective effect was likely due to its antioxidative properties and above all to its capacity to inhibit liver neutrophil infiltration, a critical factor in the pathogenesis of ANIT-induced liver injury^[46]. Melatonin also could dose-dependently reduce liver lipid peroxide content in CCl₄ treated rats. This indicated that melatonin exerted a therapeutic effect on CCl₄-induced acute liver injury in rats, possibly through its antioxidant action. Melatonin plays a cytoprotective role in the liver insulted by ischemia and reperfusion by virtue of its ability to prevent hepatic malfunction and inhibit the generation of free radicals and accumulation of neutrophils in the damaged hepatic tissue^[35]. In the present study, the effects of melatonin on immunological liver injury model were firstly investigated. The results showed that melatonin decreased MDA content in liver homogenates, meanwhile, SOD activity rose significantly. Those results are in accordance with the findings of melatonin's antioxidative properties.

A growing body of evidence suggests that nitric oxide (NO) may also modulate different experimental liver injuries. The role, that NO plays in the process of liver injury has been the subject of active debate. *In vitro* and *in vivo* data suggest that NO may act to protect tissue by virtue of its ability to react with and decompose superoxide radical^[47-49]. It has also been suggested that NO may act to modulate the activity of certain transcription factors such as NF- κ B^[50]. Although some studies demonstrate that NO may act to limit or down-regulate liver injury, there are other reports suggesting that NO may actually promote hepatocellular damage possibly due to the formation of strongly oxidizing species peroxynitrite^[51]. Much of the controversy may be related to the use of non-specific inhibitors of different NOS isoforms and the concentration of NO^[52]. Melatonin is reported to inhibit peroxynitrite induced oxidative reactions. Additionally, melatonin under or near physiological concentration inhibits the prooxidative enzyme nitric oxide synthase (NOS) activity^[14,49] and thereby influences NO production. It was also reported that melatonin had protective effect in an endotoxic and non-septic shock partly related to prevention of NO overproduction. The present study showed that melatonin significantly inhibited serum NO and did not directly inhibit Kupffer cells and generate NO *in vitro*. The results demonstrated that melatonin might modulate the generation of NO at a whole body level but had no direct effect on Kupffer cells. It seems

likely that melatonin regulated NO production to a certain extent, but more studies should be carried out to clarify it.

As it is well known, TNF- α is a multifunctional cytokine mostly secreted by inflammatory cells and is involved in numerous pathological states. TNF- α is considered to be a common early effector molecule for liver injury, in addition to its direct cytotoxic effects, this cytokine is able to induce chemokines, macrophage chemoattractant protein-1 and adhesive molecules, vascular-cell adhesion molecule-1, which are key to inflammation and consequent liver damage^[9-11]. Prevention of liver injury has been observed upon neutralization of TNF- α with anti-TNF- α antibody, prevention of translation of primary RNA transcript of TNF- α by antisense oligonucleotide and interaction of TNF- α with soluble TNF- α receptors^[53]. Although IL-1 itself does not exert damage on liver, its elevation could stimulate inflammatory cells to excrete many other cytokines including TNF- α , IL-6 and IL-8. Our results suggest that the elevation of inflammatory cytokines including TNF- α and IL-1 in serum, liver homogenates and Kupffer cell culture supernatants contributes to the mechanisms of immunological liver injury.

It is now well recognized that melatonin plays an important immunoregulatory role. Shin *et al.* found that low levels of *Bacillus anthracis* were known to induce release of cytokines such as TNF- α , and thereby exposure of melatonin (10^{-7} - 10^{-6} mol/L) to anthrax lethal toxin-treated macrophages also decreased the release of TNF- α to extracellular medium as compared to the control^[54]. Sacco found that administration of melatonin to mice (5 mg/kg bm, s.c. 30 min before or simultaneously with LPS) inhibited serum TNF- α levels by 50-80% and improved survival of mice treated with a lethal dose of LPS. Melatonin did not increase serum corticosterone and did not modify the elevation of serum corticosterone levels by LPS or by IL-1. Furthermore, it exerted its inhibitory effect in adrenalectomized or hypophysectomized mice also, indicating that its effect is independent of the hypothalamus-pituitary-adrenal axis^[55]. It was previously reported melatonin had a protective role in LPS-induced septic shock by suppressing pro-inflammatory cytokines, prostaglandins and NO production^[31,32]. However, other studies indicated melatonin did not alter cytokines including TNF- α and IL-1 secretion by LPS-stimulated macrophages^[56]. The inconsistencies in the literature suggested that the effect of melatonin on macrophages was complex. In our experimental condition, we found that in *in vitro* experiments melatonin at the concentrations of 10^{-8} - 10^{-6} mol/L directly inhibited production of TNF- α while only at the concentrations of 10^{-6} mol/L decreased IL-1 production of Kupffer cell co-cultured with LPS (5 μ g/mL). In *in vitro* liver injury model, we also found that melatonin at the concentrations of 10^{-7} - 10^{-5} mol/L reduced the content of TNF- α while at concentrations of 10^{-6} - 10^{-5} mol/L decreased the content of IL-1. Even more, *in vivo* experiment showed that melatonin at the dose between 0.25 mg/kg bm and 4.0 mg/kg bm significantly inhibited serum TNF- α and IL-1 level. Thus suppression of TNF- α and IL-1 could be one of the means by which melatonin attenuated immunological liver injury in mice.

Therefore, the protective effects of melatonin on immunological liver injury might relate to free radical scavenging, increased content of SOD, decreased expression of procytokines.

REFERENCES

- 1 Decker K. Biologically active products of stimulated liver macrophages (Kupffer cells). *Eur J Biochem* 1990; **192**: 245-261
- 2 Edwards MJ, Keller BJ, Kauffman FC, Thurman RG. The involvement of Kupffer cells in carbon tetrachloride toxicity. *Toxicol Appl Pharmacol* 1993; **119**: 275-279
- 3 el Sisi AE, Earnest DL, Sipes IG. Vitamin A potentiation of carbon tetrachloride hepatotoxicity: role of liver macrophages and active oxygen species. *Toxicol Appl Pharmacol* 1993; **119**: 295-301

- 4 **Shiratori Y**, Kawase T, Shiina S, Okano K, Sugimoto T, Teraoka H, Matano S, Matsumoto K, Kamii K. Modulation of hepatotoxicity by macrophages in the liver. *Hepatology* 1988; **8**: 815-821
- 5 **Kukam M**, Vajdova K, Horecky J, Nagyova A, Mehendale HM, Trnovec T. Effects of blockade of Kupffer cells by gadolinium chloride on hepatobiliary function in cold ischemia-reperfusion injury of rat liver. *Hepatology* 1997; **26**: 1250-1257
- 6 **Kayano K**, Sakaida I, Kubota M, Yasunaga M, Okita K. Functional differences between activated and normal rat liver macrophages: LPS uptake capacity by flow cytometric analysis in contrast with TNF-alpha release. *Liver* 1995; **15**: 253-259
- 7 **Arthur MJ**, Kowalski-Saunders P, Wright R. *Corynebacterium parvum* -elicited hepatic macrophages demonstrate enhanced respiratory burst activity compared with resident Kupffer cells in the rat. *Gastroenterology* 1986; **91**: 174-181
- 8 **Zhang GL**, Wang YH, Ni W, Teng HL, Lin ZB. Hepatoprotective role of ganoderma lucidum polysaccharide against BCG-induced immune liver injury in mice. *World J Gastroenterol* 2002; **8**: 728-733
- 9 **Muto Y**, Nouri-Aria KT, Meager A, Alexander GJ, Eddleston AL, Williams R. Enhanced tumour necrosis factor and interleukin-1 in fulminant hepatic failure. *Lancet* 1988; **2**: 72-74
- 10 **Nagakawa J**, Hishinuma I, Hirota K, Miyamoto K, Yamanaka T, Tsukidate K, Katayama K, Yamatsu I. Involvement of tumor necrosis factor- α in the pathogenesis of activated macrophage-mediated hepatitis in mice. *Gastroenterology* 1990; **99**: 758-765
- 11 **Arthur MJ**, Bentley IS, Tanner AR, Saunders PK, Millward-Sadler GH, Wright R. Oxygen-derived free radicals promote hepatic injury in the rat. *Gastroenterology* 1985; **89**: 1114-1122
- 12 **Ferluga J**, Allison AC. Role of mononuclear infiltrating cells in pathogenesis of hepatitis. *Lancet* 1978; **2**: 610-611
- 13 **Ferluga J**. Tuberculin hypersensitivity hepatitis in mice infected with *Mycobacterium bovis* (BCG). *Am J Pathol* 1981; **105**: 82-90
- 14 **Tsutsui H**, Nakanishi K, Matsui K, Higashino K, Okamura H, Miyazawa Y, Kaneda K. IFN- γ -inducing factor up-regulates Fas ligand-mediated cytotoxic activity of murine natural killer cell clones. *J Immunol* 1996; **157**: 3967-3973
- 15 **Smith SR**, Calzetta A, Bankowski J, Kenworthy-Bott L, Terminelli C. Lipopolysaccharide-induced cytokine production and mortality in mice treated with *Corynebacterium parvum*. *J Leuka Biol* 1993; **54**: 23-29
- 16 **Tsuji H**, Harada A, Mukaida N, Nakanuma Y, Bluethmann H, Kaneko S, Yamakawa K, Nakamura SI, Kobayashi KI, Matsushima K. Tumor necrosis factor receptor p55 is essential for intrahepatic granuloma formation and hepatocellular apoptosis in a murine model of bacterium-induced fulminant hepatitis. *Infect Immun* 1997; **65**: 1892-1898
- 17 **Fujioka N**, Mukaida N, Harada A, Akiyama M, Kasahara T, Kuno K, Ooi A, Mai M, Matsushima K. Preparation of specific antibodies against murine IL-1ra and the establishment of IL-1ra as an endogenous regulator of bacteria-induced fulminant hepatitis in mice. *J Leukoc Biol* 1995; **58**: 90-98
- 18 **Ikeda N**, Mukaida N, Kaneko S, Fujioka N, Su S, Nariuchi H, Unoura M, Harada K, Nakanuma Y, Kobayashi K, Matsushima K. Prevention of endotoxin-induced acute lethality in Propionibacterium acnes-primed rabbits by an antibody to leukocyte integrin β_2 with concomitant reduction of cytokine production. *Infect Immun* 1995; **63**: 4812-4817
- 19 **Liu P**, Ohnishi H, Moriwaki H, Muto Y. Enhanced tumor necrosis factor and interleukin-1 in an experimental model of massive liver cell necrosis/fatal hepatitis in mice. *Gastroenterol Jpn* 1990; **25**: 339-342
- 20 **Tsuji H**, Mukaida N, Harada A, Kaneko S, Matsushita E, Nakanuma Y, Tsutsui H, Okamura H, Nakanishi K, Tagawa Y, Iwakura Y, Kobayashi K, Matsushima K. Alleviation of lipopolysaccharide-induced acute liver injury in Propionibacterium acnes-primed IFN- γ -deficient mice by a concomitant reduction of TNF- α , IL-12, and IL-18 production. *J Immunol* 1999; **162**: 1049-1055
- 21 **Tsutsui H**, Matsui K, Kawada N, Hyodo Y, Hayashi N, Okamura H, Higashino K, Nakanishi K. IL-18 accounts for both TNF- α - and Fas ligand-mediated hepatotoxic pathways in endotoxin-induced liver injury in mice. *J Immunol* 1997; **159**: 3961-3967
- 22 **Yao HW**, Li J, Jin Y, Zhang YF, Li CY, Xu SY. Effect of leflunomide on immunological liver injury in mice. *World J Gastroenterol* 2003; **9**: 320-323
- 23 **Shands JW Jr**, Senterfitt VC. Endotoxin-induced hepatic damage in BCG-infected mice. *Am J Pathol* 1972; **67**: 23-40
- 24 **Nagai H**, Yakuo I, Yamada H, Shimazawa T, Koda A, Niu K, Asano K, Shimizu T, Kasahara M. Liver injury model in mice for immunopharmacological study. *Jpn J Pharmacol* 1988; **46**: 247-254
- 25 **Cuzzocrea S**, Reiter RJ. Pharmacological actions of melatonin in acute and chronic inflammation. *Curr Top Med Chem* 2002; **2**: 153-165
- 26 **Guerrero JM**, Reiter RJ. Melatonin-immune system relationships. *Curr Top Med Chem* 2002; **2**: 167-179
- 27 **Skwarlo-Sonta K**. Melatonin in immunity: comparative aspects. *Neuroendocrinol Lett* 2002; **23**(Suppl 1): 61-66
- 28 **Reiter RJ**, Tan DX, Manchester LC, Qi W. Biochemical reactivity of melatonin with reactive oxygen and nitrogen species: a review of the evidence. *Cell Biochem Biophys* 2001; **34**: 237-256
- 29 **Reiter RJ**, Tan DX, Osuna C, Gitto E. Actions of melatonin in the reduction of oxidative stress. A review. *J Biomed Sci* 2000; **7**: 444-458
- 30 **Tan DX**, Reiter RJ, Manchester LC, Yan MT, El-Sawi M, Sainz RM, Mayo JC, Kohen R, Allegra M, Hardeland R. Chemical and physical properties and potential mechanisms: melatonin as a broad spectrum antioxidant and free radical scavenger. *Curr Top Med Chem* 2002; **2**: 181-197
- 31 **Sewerynek E**, Melchiorri D, Reiter RJ, Ortiz GG, Lewinski A. Lipopolysaccharide-induced hepatotoxicity is inhibited by the antioxidant melatonin. *Eur J Pharmacol* 1995; **293**: 327-334
- 32 **Maestroni GJ**. Melatonin as a therapeutic agent in experimental endotoxic shock. *J Pineal Res* 1996; **20**: 84-89
- 33 **Sewerynek E**, Reiter RJ, Melchiorri D, Ortiz GG, Lewinski A. Oxidative damage in the liver induced by ischemia-reperfusion: protection by melatonin. *Hepatogastroenterology* 1996; **43**: 898-905
- 34 **Sener G**, Tosun O, Sehirli AO, Kacmaz A, Arbak S, Ersoy Y, Ayanoglu-Dulger G. Melatonin and N-acetylcysteine have beneficial effects during hepatic ischemia and reperfusion. *Life Sci* 2003; **72**: 2707-2718
- 35 **Lepay DA**, Nathan CF, Steinman RM, Murray HW, Cohn ZA. Murine Kupffer cells. Mononuclear phagocytes deficient in the generation of reactive oxygen intermediates. *J Exp Med* 1985; **161**: 1079-1096
- 36 **Hasegawa T**, Sakurai K, Kambayashi Y, Saniabadi AR, Nagamoto H, Tsukada K, Takahashi A, Kuwano H, Nakano M. Effects of OPC-6535 on lipopolysaccharide-induced acute liver injury in the rat: involvement of superoxide and tumor necrosis factor-alpha from hepatic macrophages. *Surgery* 2003; **134**: 818-826
- 37 **Mustafa SB**, Gandhi CR, Harvey SA, Olson MS. Endothelin stimulates platelet-activating factor synthesis by cultured rat Kupffer cells. *Hepatology* 1995; **21**: 545-553
- 38 **Kiechle FL**, Malinski T. Nitric oxide. Biochemistry, pathophysiology, and detection. *Am J Clin Pathol* 1993; **100**: 567-575
- 39 **Gavino VC**, Miller JS, Ikharebha SO, Milo GE, Cornwell DG. Effect of polyunsaturated fatty acids and antioxidants on lipid peroxidation in tissue cultures. *J Lipid Res* 1981; **22**: 763-769
- 40 **Mosmann T**. Rapid colorimetric assay for cellular growth and survival: application to proliferation and cytotoxicity assays. *J Immunol Methods* 1983; **65**: 55-63
- 41 **Wang GS**, Liu GT. Influences of Kupffer cell stimulation and suppression on immunological liver injury in mice. *Zhongguo Yaoli Xuebao* 1997; **18**: 173-176
- 42 **Reiter RJ**, Melchiorri D, Sewerynek E, Poeggeler B, Barlow-Walden L, Chuang J, Ortiz GG, Acuna-Castroviejo D. A review of the evidence supporting melatonin's role as an antioxidant. *J Pineal Res* 1995; **18**: 1-11
- 43 **Marchiafava PL**, Longoni B. Melatonin as an antioxidant in retinal photoreceptors. *J Pineal Res* 1999; **26**: 184-189
- 44 **Kotler M**, Rodriguez C, Sainz RM, Antolin I, Menendez-Pelaez A. Melatonin increases gene expression for antioxidant enzymes

- in rat brain cortex. *J Pineal Res* 1998; **24**: 83-89
- 45 **Antolin I**, Rodriguez C, Sainz RM, Mayo JC, Uria H, Kotler ML, Rodriguez-Colunga MJ, Tolivia D, Menendez-Pelaez A. Neurohormone melatonin prevents cell damage: Effect on gene expression for antioxidant enzymes. *FASEB J* 1996; **10**: 882-890
- 46 **Calvo JR**, Reiter RJ, Garcia JJ, Ortiz GG, Tan DX, Karbownik M. Characterization of the protective effects of melatonin and related indoles against alpha-naphthylisothiocyanate-induced liver injury in rats. *J Cell Biochem* 2001; **80**: 461-470
- 47 **Harbrecht BG**, Wu B, Watkins SC, Billiar TR, Peitzman AB. Inhibition of nitric oxide synthesis during severe shock but not after resuscitation increases hepatic injury and neutrophil accumulation in hemorrhaged rats. *Shock* 1997; **8**: 415-421
- 48 **Symington PA**, Ma XL, Lefer AM. Protective actions of S-nitroso-N-acetylpenicillamine (SNAP) in a rat model of hemorrhagic shock. *Methods Find Exp Clin Pharmacol* 1992; **14**: 789-797
- 49 **Mojena M**, Hortelano S, Castrillo A, Diaz-Guerra MJ, Garcia-Barchino MJ, Saez GT, Bosca L. Protection by nitric oxide against liver inflammatory injury in animals carrying a nitric oxide synthase-2 transgene. *FASEB J* 2001; **15**: 583-585
- 50 **Marshall HE**, Merchant K, Stamler JS. Nitrosation and oxidation in the regulation of gene expression. *FASEB J* 2000; **14**: 1889-1900
- 51 **Isoke M**, Katsuramaki T, Hirata K, Kimura H, Nagayama M, Matsuno T. Beneficial effects of inducible nitric oxide synthase inhibitor on reperfusion injury in the pig liver. *Transplantation* 1999; **68**: 803-813
- 52 **Wang Y**, Lawson JA, Jaeschke H. Differential effect of 2-aminoethyl-isothiourea, an inhibitor of the inducible nitric oxide synthase, on microvascular blood flow and organ injury in models of hepatic ischemia-reperfusion and endotoxemia. *Shock* 1998; **10**: 20-25
- 53 **Van Zee KJ**, Kohno T, Fischer E, Rock CS, Moldawer LL, Lowry SF. Tumor necrosis factor soluble receptors circulate during experimental and clinical inflammation and can protect against excessive tumor necrosis factor α *in vitro* and *in vivo*. *Proc Natl Acad Sci U S A* 1992; **89**: 4845-4849
- 54 **Shin S**, Hur GH, Kim YB, Yeon GB, Park KJ, Park YM, Lee WS. Dehydroepiandrosterone and melatonin prevent Bacillus anthracis lethal toxin-induced TNF production in macrophages. *Cell Biol Toxicol* 2000; **16**: 165-174
- 55 **Sacco S**, Aquilini L, Ghezzi P, Pinza M, Guglielmotti A. Mechanism of the inhibitory effect of melatonin on tumor necrosis factor production *in vivo* and *in vitro*. *Eur J Pharmacol* 1998; **343**: 249-255
- 56 **Williams JG**, Bernstein S, Prager M. Effect of melatonin on activated macrophage TNF, IL-6, and reactive oxygen intermediates. *Shock* 1998; **9**: 406-411

Edited by Chen WW and Zhu LH Proofread by Xu FM

Effects of endothelin-1 on hepatic stellate cell proliferation, collagen synthesis and secretion, intracellular free calcium concentration

Chuan-Yong Guo, Jian-Ye Wu, Yun-Bin Wu, Min-Zhang Zhong, Han-Ming Lu

Chuan-Yong Guo, Jian-Ye Wu, Yun-Bin Wu, Min-Zhang Zhong,
Department of Gastroenterology, Shanghai Tenth People Hospital of
Tongji University, Shanghai 200072, China

Han-Ming Lu, Department of Gastroenterology, Xinhua Hospital
of Shanghai Second Medical University, Shanghai 200092, China
Supported by the Grant for Nature and Science from Shanghai, No.
03ZR14097

Correspondence to: Dr. Chuan-Yong Guo, Department of
Gastroenterology, Shanghai Tenth People Hospital of Tongji
University, Shanghai 200072, China. guochuanrong@hotmail.com

Telephone: +86-21-56779971 **Fax:** +86-21-66303983

Received: 2003-09-06 **Accepted:** 2003-10-29

Abstract

AIM: To explore the effects of endothelin-1(ET-1) on hepatic stellate cells (HSCs) DNA uptake, DNA synthesis, collagen synthesis and secretion, inward whole-cell calcium concentration ($[Ca^{2+}]_i$) as well as the blocking effect of verapamil on ET-1-stimulated release of inward calcium (Ca^{2+}) of HSC *in vitro*.

METHODS: Rat hepatic stellate cells (HSCs) were isolated and cultivated. 3H -TdR and 3H -proline incorporation used for testing DNA uptake and synthesis, collagen synthesis and secretion of HSCs cultured *in vitro*; Fluorescent calcium indicator Fura-2/AM was used to measure $[Ca^{2+}]_i$ inward HSCs.

RESULTS: ET-1 at the concentration of 5×10^{-8} mol/L, caused significant increase both in HSC DNA synthesis ($2\ 247 \pm 344$ cpm, $P < 0.05$) and DNA uptake ($P < 0.05$) when compared with the control group. ET-1 could also increase collagen synthesis ($P < 0.05$ vs control group) and collagen secretion ($P < 0.05$ vs control group). Besides, inward HSC $[Ca^{2+}]_i$ reached a peak concentration (422 ± 98 mol/L, $P < 0.001$) at 2 min and then went down slowly to 165 ± 51 mol/L ($P < 0.01$) at 25 min from resting state (39 ± 4 mol/L) after treated with ET-1. Verapamil (5 mol/L) blocked ET-1-activated $[Ca^{2+}]_i$ inward HSCs compared with control group ($P < 0.05$). Fura-2/AM loaded HSC was suspended in no Ca^{2+} buffer containing 1 mol/L EGTA, 5 min later, 10^{-8} mol/L of ET-1 was added, $[Ca^{2+}]_i$ inward HSCs rose from resting state to peak 399 ± 123 mol/L, then began to come down by the time of 20 min. It could also raise $[Ca^{2+}]_i$ inward HSCs even without Ca^{2+} in extracellular fluid, and had a remarkable dose-effect relationship ($P < 0.05$). Meanwhile, verapamil could restrain the action of ET-1 ($P < 0.05$).

CONCLUSION: Actions of ET-1 on collagen metabolism of HSCs may depend on the transportation of inward whole-cell calcium.

Guo CY, Wu JY, Wu YB, Zhong MZ, Lu HM. Effects of endothelin-1 on hepatic stellate cell proliferation, collagen synthesis and secretion, intracellular free calcium concentration. *World J Gastroenterol* 2004; 10(18): 2697-2700
<http://www.wjgnet.com/1007-9327/10/2697.asp>

INTRODUCTION

Hepatic fibrosis associated with the activation of hepatic stellate cells (HSCs), the major source of extracellular matrix (ECM) proteins^[1]. It is generally believed that HSCs are the main cells producing ECM, from resting state to active myofibroblasts, which is the key point of formation and development of hepatic fibrosis^[2-6]. Endothelin-1(ET-1) is currently known as a polypeptide with a stronger activity to contract blood vessel. So, based on prophase researches^[7-9], we chose ET-1 to observed its direct effect on DNA ingestion and synthesis as well as collagen synthesis and secretion of HSCs in cultivating. Meanwhile, as we know that Ca^{2+} is an important intracellular messenger, relate to HSC proliferation and ECM synthesis^[10-13]. The effects of ET-1 on regulation and intracellular $[Ca^{2+}]_i$ of HSCs isolated and cultivated *in vitro* were studied.

MATERIALS AND METHODS

MATERIALS

Animals Wistar male rats, weighting (450 ± 50) g, were provided by Shanghai Experimental Animals Center of Chinese Academy of Sciences.

Reagents ET-1, calcium fluorescence probes Fura-2/AM, Triton X-100, pronase, trypsin, DMEM, DAB- H_2O_2 were from Sigma; verapamil from Knoll; collagenase from Medical Industry Academy of Shanghai; RPMI 1640 from Gibco; HEPES from EMK; 3H -L-proline from Academy of Atomic Energy in China (66.6 GBq/mmol, radioactivity purity $> 90\%$). 3H -TdR was from Institute of Atomic Energy in Shanghai (814 GBq/mmol, radioactivity purity $> 95\%$).

Methods

Isolation and cultivation of rat HSCs Rat HSCs were isolated referring to Knook^[14-17]. Rats were anaesthetized with pentobarbitone (200 mg/kg) by abdominal injection, then heparin sodium (10 mg/kg) was injected into the caudal vein. The abdominal cavity was opened and portal vein and dorsal vein were exposed. Blood was released through vein and D-Hank's solution was perfused (20-25 mL/min) until pale yellow appeared. Liver was taken out and undergone extracorporeal circulation when perfusion fluid was changed to GBSS containing 0.5 g/L pronase E, 0.5 g/L collagenase and 10 mmol/L HEPES. Circle perfusion was performed for 30 min (15 mL/min). Liver was taken out and cut to pieces, then put into GBSS containing 0.25 g/L pronase E, 0.25 g/L collagenase and 10 mmol/L HEPES, shocked at 37 °C for 30 min, little suspended deposit was put in culture media on the top of three-layer density gradient centrifugation fluid containing 80 g/L and 130 g/L metrizamide, 2 800 r/min centrifugation for 20 min, Cells were sucked between top layer and 80 mL/L density layer. DMEM containing 200 mL/L calf serum was used to regulate the number of cells to 1×10^5 /mL.

DNA and collagen synthesis of HSCs HSCs in 2 to 4 th generation were digested by pancreatin and cultured with DMEM supplemented with 100 g/L calf serum and 100 mL/L horse serum. Cells were adjusted to 1×10^8 /mL and inoculated on a 48-well plate, cultured for 24 h, then different concentration of ET-1 and the same dosage of drug was added, respectively

and triplicated for each concentration. ^3H -TdR and ^3H -proline were used to assay the incorporation.

HSC ingestion of DNA ^3H -TdR 18.5 GBq/mmol was added at 10, 20, 30 and 60 min respectively, washed 3 times with PBS of 1×10^5 mmol/L, centrifuged 1000 r/min 10 min, the top layer fluid was removed, 2 mL of 100 g/L TCA was added and centrifuged 1000 r/min 10 min again. Top layer fluid was collected and deposited, washed 3 times with 800 mL/L ethanol at 4 °C. The top layer fluid was removed and dried in vacuum. 1 mol/L NaOH was added to lyse the deposit and 1N HCl was used to adjust pH to 7.0 Radioactivity of specimens was measured on Beckman scintillation counter.

Collagen secretion of HSC In experiment of ^3H -TdR, before transferred to F_{49} filter paper, 1 mL culture media was taken out and put into a tube. A 5 mmol/L acetic acid was used to adjust pH to 2 to 3, then 25 μL of 2.5 g/L pepsin was added to digest. A 50 μL of proline was added at 4 °C for 3 h, 1, 1.2 mol/L trichloroacetic acid was fixed for 2 h, transferred to F_{4a} filter paper, closed with saline, 0.6 mol/L trichloroacetic acid was used again, then bleached with anhydrous alcohol, baked at 80 °C. Radioactivity of specimens was measured on YSJ-75 liquid scintillation counter.

$[\text{Ca}^{2+}]_i$ in Fura-2/AM loaded HSC HSCs were cultured on a rectangle glass when HSCs grew and covered the glass. Then cells were taken out of the glass and RPMI 1640 containing Fura-2/AM (10 nmol/L) was added to incubate at 37 °C for 50 min, D-Hank's solution was used to wash extracellular free Fura-2/AM and incubated for another 30 min, 1 g/L trypsin was used to digest the cells and the number of cells was adjusted to $10^6/\text{mL}$ by buffer.

Fluorescence spectrum About 2 mL of Fura-2/AM loaded HSCs was suspended for the test with a fluorescence spectrophotometer. Raster (EX) 5 nm, radiate raster (EM) 10 nm were excited at a middle scan speed (32 mm/min), excitation light scan ranged 300-400 nm, emission light scan ranged 440-540 nm.

Intracellular fluorescence intensity Fluorescence intensity F was detected first (laser wave-length 340 nm, EX 5 nm, emission wave-length 510 nm, EM 10 nm), then different concentrations of ET-1 and verapamil and EGTA (last concentration 8 mmol/L) were added for the detection of minimum fluorescence intensity (F min).

Calculation of $[\text{Ca}^{2+}]_i$ Intracellular $[\text{Ca}^{2+}]_i$ (nmol/L) = kd (F-F min)/(F max-F). Kd is a dissociation constant for Fura-2/ Ca^{2+} compound which equals to 224 nmol/L.

Statistical analysis Variance homogeneity tests were used to make comparisons.

RESULTS

HSC activity

Trypan blue staining revealed an activity above 90% for HSCs. The purity of HSCs was more than 80% assessed by fluorescence microscope. The nuclei of HSC were stained blue among the desmin-positive satellite cells.

Effect of ET-1 on HSC DNA synthesis

As shown in Table 1, ET-1 could accelerate ^3H -TdR incorporation into HSCs and HSC DNA synthesis and proliferation ($P < 0.05$), in a concentration-dependent manner.

Effect of ET-1 on HSC ingested ^3H -TdR

ET-1 could accelerate the rate of HSC ingested DNA, the rate increased with the time prolonged ($P < 0.05$ or $P < 0.01$, Figure 1).

Effect of ET-1 on HSC collagen synthesis

ET-1 could accelerate ^3H -Proline incorporation into HSCs and

collagen synthesis at the concentration of 5×10^{-8} mol/L ($P < 0.05$), in a concentration-dependent manner.

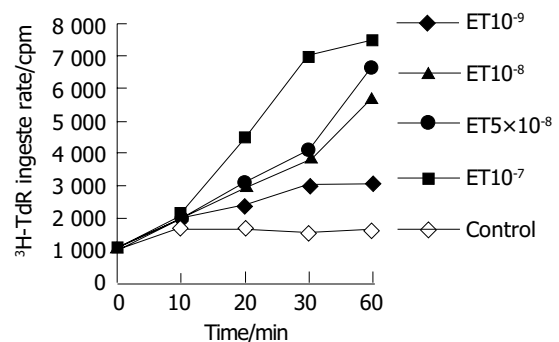


Figure 1 Effect of ET-1 on HSC ingested ^3H -TdR.

Table 1 Effects of ET-1 on HSC DNA synthesis, collagen synthesis and secretion (cpm, mean±SD)

Group	DNA synthesis	Collagen Synthesis	Collagen secretion
Control	1 370±113	2 167±454	1 431±389
ET 10 ⁻⁹ mol/L	1 489±305	2 206±725	1 528±242
ET 5×10 ⁻⁸ mol/L	1 986±457 ^a	2 698±304 ^a	1 903±552 ^a
ET 10 ⁻⁸ mol/L	2 247±344 ^a	2 876±396 ^a	2 087±128 ^a
ET 10 ⁻⁷ mol/L	4 015±102 ^a	3 056±401 ^a	2 794±397 ^b

^a $P < 0.05$, ^b $P < 0.01$ vs control group.

Effect of ET-1 on HSC collagen secretion

As shown in Table 1, ET-1 could remarkably accelerate HSC collagen secretion compared with the control group ($P < 0.05$).

Effect of ET-1 (10⁻⁸ mol/L) on intracellular $[\text{Ca}^{2+}]_i$

As shown in Figure 2, when ET-1 was added to the suspension of Fura-2/AM loaded HSCs and kept for 25 min ($n = 3$), $[\text{Ca}^{2+}]_i$ in HSCs rose from (39±4) mol/L (resting state) to (165±51) mol/L ($P < 0.01$) and rose to peak (422±98) mol/L ($P < 0.001$) after another 2 min, then it began to go down slowly and remained a higher concentration even after another 18 min compared with the resting $[\text{Ca}^{2+}]_i$ ($P < 0.01$). It suggested that the effect of ET-1 on $[\text{Ca}^{2+}]_i$ in HSCs could be divided into 2 phases, a fast phase (I P) and a slow phase (II P).

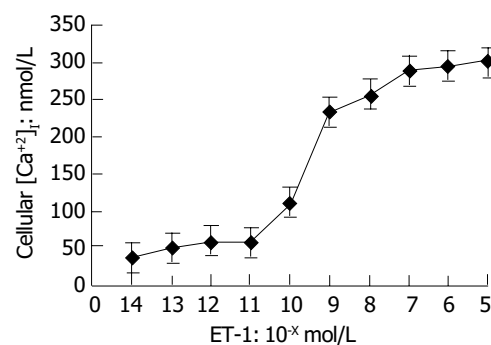


Figure 2 Effect of ET-1 on $[\text{Ca}^{2+}]_i$ peak value in HSCs.

Effect of ET-1 on peak concentration of $[\text{Ca}^{2+}]_i$ in HSCs

As shown in Figure 3, $[\text{Ca}^{2+}]_i$ in HSCs was in a ET-1 concentration-dependent manner. No change of $[\text{Ca}^{2+}]_i$ occurred in HSCs when ET-1 was less than 10^{-11} mol/L. $[\text{Ca}^{2+}]_i$ reached its peak in a ET-1-dose-dependent manner when ET-1 was greater than 10^{-9} mol/L.

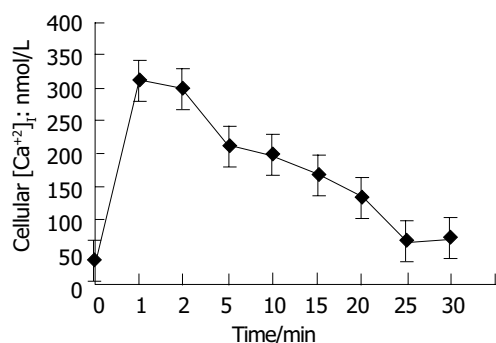


Figure 3 Effect of ET-1 on $[Ca^{2+}]_i$ in HSCs (10^{-10} mol/L).

Blocking effect of verapamil

As shown in Figure 4, calcium channel blocking agent verapamil (5 μ mol/L) could significantly restrain I P and II P effects on $[Ca^{2+}]_i$ in HSCs excited by ET-1 compared with control group ($P < 0.05$). Fura-2/AM loaded HSCs suspended in Ca^{2+} -free buffer containing 1 mol/L EGTA made $[Ca^{2+}]_i$ in HSCs raise from resting state to peak (399 ± 123) mol/L, then go down to (49 ± 17) mol/L at the time of 20 min when first treated with 10^{-8} mol/L of ET-1, suggesting that Ca^{2+} -free buffer had no remarkable effect on I P of $[Ca^{2+}]_i$ in HSCs excited by ET-1 but completely blocked II P.

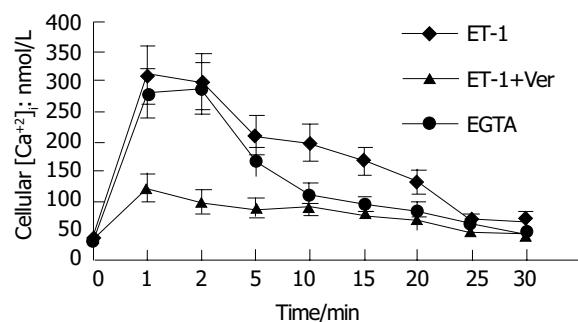


Figure 4 Effect of ET-1 increase $[Ca^{2+}]_i$ in HSCs.

DISCUSSION

HSCs were first detected by Ito and Nemoto in 1952, which provided a new way to study episode mechanism of hepatic fibrosis and deepened the cognition of hepatic fibrosis from an angle of source cells of collagen production^[2-6,15,16]. HSCs is also named Ito cell, VitA storing cell, liver antrum around cell, fat-storing cell, and is one of the liver interstitial cells. The main function of HSC is to store and metabolize VitA. It has been found to be able to synthesize and secrete ECM and synthesize collagenase^[2-6]. When hepatic fibrosis occurred, HSC turned into fibroblasts or myofibroblasts that were the cause of liver synthesis of ECM. This change of HSC was called activation or conversion^[2,3]. It has been certificated that interstitial cells especially HSCs are the main cells which producte collagen when hepatic fibrosis occurs. So it has become a central link in hepatic fibrosis occurrence mechanism.

ET distributes widely in liver and portal vein system, and has important biological effects on liver^[18-24]. This experiment showed that ET could remarkably accelerate HSC proliferation, DNA synthesis, collagen synthesis and secretion. It is thus clear that ET-1 had double roles during hepatic fibrosis, accelerating not only HSC synthesis of collagen but also selective excretion of collagen. Besides^[25,26], endothelial cells in hepatic sinusoid secrete endothelins that can activate HSCs. It has been reported that ET could raise $[Ca^{2+}]_i$ in smooth muscle cells^[27-29]. This study showed that ET-1 could raise $[Ca^{2+}]_i$ in

HSCs and appeared double phase reaction, fast phase and slow phase. Both phases had a dose-dependent manner. It turns out that when the cells are at resting state, if there is extracellular Ca^{2+} , the $[Ca^{2+}]_i$ in HSCs will be higher than that without extracellular Ca^{2+} . ET-1 can remarkably raise $[Ca^{2+}]_i$ in HSC with or without extracellular Ca^{2+} . It implies that ET-1 can accelerate HSC release of intracellular Ca^{2+} .

Three different ways have been found to elevate $[Ca^{2+}]_i$ ^[30-33]. Plenty of calcium flows into cell through Ca^{2+} channel, Ca^{2+} -ATP enzyme or Na^+ - Ca^{2+} changing system is restrained which can transfer Ca^{2+} out of cells; Ca^{2+} -storing systems such as mitochondrion and endoplasm increase Ca^{2+} . We used Ca^{2+} -free buffer and found it had no effect on $[Ca^{2+}]_i$ in I P in HSC excited by ET-1 but could block $[Ca^{2+}]_i$ in II P. It implies that elevated $[Ca^{2+}]_i$ in I P is caused by increased Ca^{2+} stored in cells, while elevated $[Ca^{2+}]_i$ in II P is caused by Ca^{2+} flowing out of cells. It has been currently accepted by some of scholars that the raise of Ca^{2+} in HSC is through the way of phospholipase C (PLC)-inositol triphosphate (IP_3)-diacylglycerol (DAG)^[34-51]. ET-1 excites PLC on cell membrane through G protein that makes 4,5-biphosphate inositol divide into IP_3 and DAG- IP_3 . Mitochondrion, endoplasm and sarcoplasm that make Ca^{2+} in cell release to cytoplasm and increase free $[Ca^{2+}]_i$ in cells. IP_3 works only a very short time, and is quickly converted to IP_4 by special enzymes. So peak I P lasts for a very short time, but IP_4 can accelerate the opening of Ca^{2+} channel on cell membrane, which makes an increase of calcium flowing out of cells and at last results in a fast raise of $[Ca^{2+}]_i$ in cells.

Physiological and pathological significance of elevated free Ca^{2+} in HSCs excited by ET is still not clear. Maybe it could participate the series of signals in cells and physiological effect of ET^[25,27]. In conclusion, ET-1 can remarkably accelerate HSC proliferation, collagen synthesis and secretion, increase of $[Ca^{2+}]_i$ in HSC and of release of Ca^{2+} in cells, thus accelerating proliferation of fibrous tissues and repair of injury tissues.

REFERENCES

- Huang ZG, Zhai WR, Zhang YE, Zhang XR. Study of heteroserum-induced rat liver fibrosis model and its mechanism. *World J Gastroenterol* 1998; **4**: 206-209
- Kawada N. The hepatic perisinusoidal stellate cell. *Histol Histopathol* 1997; **12**: 1069-1080
- Schuppan D, Porov Y. Hepatic fibrosis: From bench to bedside. *J Gastroenterol Hepatol* 2002; **17**(Suppl 3): S300-S305
- Marra F, Pinzani M. Role of hepatic stellate cells in the pathogenesis of portal hypertension. *Nefrologia* 2002; **22**(Suppl 5): 34-40
- Mann DA, Smart DE. Transcriptional regulation of hepatic stellate cell activation. *Gut* 2002; **50**: 891-896
- Ramadori G, Saile B. Mesenchymal cells in the liver—one cell type or two? *Liver* 2002; **22**: 283-294
- Hasegawa T, Kimura T, Sasaki T, Okada A. Plasma endothelin-1 level as a marker reflecting the severity of portal hypertension in biliary atresia. *J Pediatr Surg* 2001; **36**: 1609-1612
- Tsuchiya Y, Suzuki S, Inaba K, Sakaguchi T, Baba S, Miwa M, Konno H, Nakamura S. Impact of endothelin-1 on microcirculatory disturbance after partial hepatectomy under ischemia/reperfusion in thioacetamide-induced cirrhotic rats. *J Surg Res* 2003; **111**: 100-108
- Hasselblatt M, Bunte M, Dringen R, Tabernero A, Medina JM, Giaume C, Siren AL, Ehrenreich H. Effect of endothelin-1 on astrocytic protein content. *Glia* 2003; **42**: 390-397
- Raue F. Epidemiology of medullary thyroid carcinoma. *Recent Results Cancer Res* 1992; **125**: 47-54
- Raue F, Zink A. Measurement of free cytosolic calcium in single cells: method and application. *Methods Find Exp Clin Pharmacol* 1992; **14**: 327-332
- Lyall V, Alam RI, Phan TH, Phan DQ, Heck GL, DeSimone JA. Excitation and adaptation in the detection of hydrogen ions by taste receptor cells: a role for cAMP and Ca^{2+} . *J Neurophysiol*

- 2002; **87**: 399-408
- 13 **Satin LS**, Kinard TA. Neurotransmitters and their receptors in the islets of Langerhans of the pancreas: what messages do acetylcholine, glutamate, and GABA transmit? *Endocrine* 1998; **8**: 213-223
- 14 **Brouwer A**, Barelds RJ, de Leeuw AM, Blauw E, Plas A, Yap SH, van den Broek AM, Knook DL. Isolation and culture of Kupffer cells from human liver. Ultrastructure, endocytosis and prostaglandin synthesis. *J Hepatol* 1988; **6**: 36-49
- 15 **Hendriks HF**, Brouwer A, Knook DL. The role of hepatic fat-storing (stellate) cells in retinoid metabolism. *Hepatology* 1987; **7**: 1368-1371
- 16 **de Leeuw AM**, McCarthy SP, Geerts A, Knook DL. Purified rat liver fat-storing cells in culture divide and contain collagen. *Hepatology* 1984; **4**: 392-403
- 17 **Knook DL**, Seffelaar AM, de Leeuw AM. Fat-storing cells of the rat liver. Their isolation and purification. *Exp Cell Res* 1982; **139**: 468-471
- 18 **Housset C**, Rockey DC, Bissell DM. Endothelin receptors in rat liver: lipocytes as a contractile target for endothelin 1. *Proc Natl Acad Sci U S A* 1993; **90**: 9266-9270
- 19 **Yokomori H**, Oda M, Yasogawa Y, Nishi Y, Ogi M, Takahashi M, Ishii H. Enhanced expression of endothelin receptor subtypes in cirrhotic rat liver. *Liver* 2001; **21**: 114-122
- 20 **Moore K**, Wendon J, Frazer M, Karani J, Williams R, Badr K. Plasma endothelin immunoreactivity in liver disease and the hepatorenal syndrome. *N Engl J Med* 1992; **327**: 1774-1778
- 21 **Serradeil-Le Gal C**, Jouneaux C, Sanchez-Bueno A, Raufaste D, Roche B, Preaux AM, Maffrand JP, Cobbold PH, Hanoune J, Lotersztajn S. Endothelin action in rat liver. Receptors, free Ca²⁺ oscillations, and activation of glycogenolysis. *J Clin Invest* 1991; **87**: 133-138
- 22 **Moller S**, Emmeluth C, Henriksen JH. Elevated circulating plasma endothelin-1 concentrations in cirrhosis. *J Hepatol* 1993; **19**: 285-290
- 23 **Salo J**, Francitorra A, Follo A, Navasa M, Gines A, Jimenez W, Gines P, Arroyo V, Rivera F, Rodes J. Increased plasma endothelin in cirrhosis. Relationship with systemic endotoxemia and response to changes in effective blood volume. *J Hepatol* 1995; **22**: 389-398
- 24 **Yokomori H**, Oda M, Yasogawa Y, Nishi Y, Ishii H. Signal detection of endothelin receptor subtypes in human cirrhotic liver by a new in situ hybridization method. *Med Electron Microsc* 2000; **33**: 207-216
- 25 **Yokomori H**, Oda M, Ogi M, Yoshimura K, Nomura M, Fujimaki K, Kamegaya Y, Tsukada N, Ishii H. Endothelin-1 suppresses plasma membrane Ca⁺⁺-ATPase, concomitant with contraction of hepatic sinusoidal endothelial fenestrae. *Am J Pathol* 2003; **162**: 557-566
- 26 **Oda M**, Han JY, Yokomori H. Local regulators of hepatic sinusoidal microcirculation: recent advances. *Clin Hemorheol Microcirc* 2000; **23**: 85-94
- 27 **Gasull X**, Bataller R, Gines P, Sancho-Bru P, Nicolas JM, Gorbign MN, Ferrer E, Badia E, Gual A, Arroyo V, Rodes J. Human myofibroblastic hepatic stellate cells express Ca(2+)-activated K(+) channels that modulate the effects of endothelin-1 and nitric oxide. *J Hepatol* 2001; **35**: 739-748
- 28 **Reinehr RM**, Kubitz R, Peters-Regehr T, Bode JG, Haussinger D. Activation of rat hepatic stellate cells in culture is associated with increased sensitivity to endothelin 1. *Hepatology* 1998; **28**: 1566-1577
- 29 **Shao R**, Rockey DC. Effects of endothelins on hepatic stellate cell synthesis of endothelin-1 during hepatic wound healing. *J Cell Physiol* 2002; **191**: 342-350
- 30 **Kriebel ME**, Keller B. The unitary evoked potential at the frog nerve-muscle junction results from synchronous gating of fusion pores at docked vesicles. *Cell Biol Int* 1999; **23**: 527-532
- 31 **Smogorzewski MJ**. Central nervous dysfunction in uremia. *Am J Kidney Dis* 2001; **38**(4 Suppl 1): S122-128
- 32 **Satin LS**. Localized calcium influx in pancreatic beta-cells: its significance for Ca²⁺-dependent insulin secretion from the islets of Langerhans. *Endocrine* 2000; **13**: 251-262
- 33 **Murthy KS**, Zhou H. Selective phosphorylation of the IP3R-1 *in vivo* by cGMP-dependent protein kinase in smooth muscle. *Am J Physiol Gastrointest Liver Physiol* 2003; **284**: G221-230
- 34 **Inoue A**, Yanagisawa M, Kimura S, Kasuya Y, Miyauchi T, Goto K, Masaki T. The human endothelin family: three structurally and pharmacologically distinct isopeptides predicted by three separate genes. *Proc Natl Acad Sci U S A* 1989; **86**: 2863-2867
- 35 **Xu D**, Emoto N, Giaid A, Slaughter C, Kaw S, deWit D, Yanagisawa M. ECE-1: a membrane-bound metalloprotease that catalyzes the proteolytic activation of big endothelin-1. *Cell* 1994; **78**: 473-485
- 36 **Clozel M**, Gray GA, Breu V, Loffler BM, Osterwalder R. The endothelin ETB receptor mediates both vasodilation and vasoconstriction *in vivo*. *Biochem Biophys Res Commun* 1992; **186**: 867-873
- 37 **Sakurai T**, Yanagisawa M, Masaki T. Molecular characterization of endothelin receptors. *Trends Pharmacol Sci* 1992; **13**: 103-108
- 38 **Higuchi H**, Satoh T. Endothelin-1 induces vasoconstriction and nitric oxide release via endothelin ET(B) receptors in isolated perfused rat liver. *Eur J Pharmacol* 1997; **328**: 175-182
- 39 **Jouneaux C**, Mallat A, Serradeil-Le Gal C, Goldsmith P, Hanoune J, Lotersztajn S. Coupling of endothelin B receptors to the calcium pump and phospholipase C via Gs and Gq in rat liver. *J Biol Chem* 1994; **269**: 1845-1851
- 40 **Kuddus RH**, Nalesnik MA, Subbotin VM, Rao AS, Gandhi CR. Enhanced synthesis and reduced metabolism of endothelin-1 (ET-1) by hepatocytes-an important mechanism of increased endogenous levels of ET-1 in liver cirrhosis. *J Hepatol* 2000; **33**: 725-732
- 41 **Leivas A**, Jimenez W, Bruix J, Boix L, Bosch J, Arroyo V, Rivera F, Rodes J. Gene expression of endothelin-1 and ET(A) and ET(B) receptors in human cirrhosis: relationship with hepatic hemodynamics. *J Vasc Res* 1998; **35**: 186-193
- 42 **Gerbes AL**, Moller S, Gulberg V, Henriksen JH. Endothelin-1 and -3 plasma concentrations in patients with cirrhosis: role of splanchnic and renal passage and liver function. *Hepatology* 1995; **21**: 735-739
- 43 **Uchihara M**, Izumi N, Sato C, Marumo F. Clinical significance of elevated plasma endothelin concentration in patients with cirrhosis. *Hepatology* 1992; **16**: 95-99
- 44 **Asbert M**, Gines A, Gines P, Jimenez W, Claria J, Salo J, Arroyo V, Rivera F, Rodes J. Circulating levels of endothelin in cirrhosis. *Gastroenterology* 1993; **104**: 1485-1491
- 45 **Matsumoto H**, Uemasu J, Kitano M, Kawasaki H. Clinical significance of plasma endothelin-1 in patients with chronic liver disease. *Dig Dis Sci* 1994; **39**: 2665-2670
- 46 **Moller S**, Gulberg V, Henriksen JH, Gerbes AL. Endothelin-1 and endothelin-3 in cirrhosis: relations to systemic and splanchnic haemodynamics. *J Hepatol* 1995; **23**: 135-144
- 47 **Tsai YT**, Lin HC, Yang MC, Lee FY, Hou MC, Chen LS, Lee SD. Plasma endothelin levels in patients with cirrhosis and their relationships to the severity of cirrhosis and renal function. *J Hepatol* 1995; **23**: 681-688
- 48 **Martinet JP**, Legault L, Cernacek P, Roy L, Dufresne MP, Spahr L, Fenyves D, Pomier-Layrargues G. Changes in plasma endothelin-1 and Big endothelin-1 induced by transjugular intrahepatic portosystemic shunts in patients with cirrhosis and refractory ascites. *J Hepatol* 1996; **25**: 700-706
- 49 **Bernardi M**, Gulberg V, Colantoni A, Trevisani F, Gasbarrini A, Gerbes AL. Plasma endothelin-1 and -3 in cirrhosis: relationship with systemic hemodynamics, renal function and neurohumoral systems. *J Hepatol* 1996; **24**: 161-168
- 50 **Nagasue N**, Dhar DK, Yamanoi A, Emi Y, Udagawa J, Yamamoto A, Tachibana M, Kubota H, Kohno H, Harada T. Production and release of endothelin-1 from the gut and spleen in portal hypertension due to cirrhosis. *Hepatology* 2000; **31**: 1107-1114
- 51 **Rieder H**, Ramadori G, Meyer zum Buschenfelde KH. Sinusoidal endothelial liver cells *in vitro* release endothelin: augmentation by transforming growth factor [beta] and Kupffer cell-conditioned media. *Klin Wochenschr* 1991; **69**: 387-391

Proteomics to display tissue repair opposing injury response to LPS-induced liver injury

Xiao-Wei Liu, Fang-Gen Lu, Guang-Sen Zhang, Xiao-Ping Wu, Yu You, Chun-Hui Ouyang, Dong-Ye Yang

Xiao-Wei Liu, Fang-Gen Lu, Xiao-Ping Wu, Yu You, Chun-Hui Ouyang, Dong-Ye Yang, Department of Gastroenterology, the Second Xiangya Hospital, Central South University, Changsha 410011, Hunan Province, China

Guang-Sen Zhang, Department of Hematology, the Second Xiangya Hospital, Central South University, Changsha 410011, Hunan Province, China

Supported by the Science and Development Foundation of Hunan Province No.99SSY2002-22

Correspondence to: Professor Fang-Gen Lu, Department of Gastroenterology, the Second Xiangya Hospital, Central South University, Changsha 410011, Hunan Province, China. xw_liu@msn.com

Telephone: +86-731-5550366 **Fax:** +86-731-5533525

Received: 2003-10-08 **Accepted:** 2003-12-16

Abstract

AIM: To examine the protein expression alterations in liver injury/repair network regulation as a response to gut-derived lipopolysaccharide (LPS) treatment, in order to anticipate the possible signal molecules or biomarkers in signaling LPS-related liver injury.

METHODS: Male BALB/c mice were treated with intra-peritoneal (i.p.) LPS (4 mg/kg) and sacrificed at 0, 6, 24 and 30 h to obtain livers. The livers were stained with hematoxylin and eosin for histopathologic analyses. Total liver protein was separated by two-dimensional gel electrophoresis (2-DE). The peptide mass of liver injury or repair related proteins were drawn up and the protein database was searched to identify the proteins.

RESULTS: Observations were as follows: (1) TRAIL-R2 was down regulated in livers of LPS-treated mice. TNFAIP1 was significantly up regulated at 6 h, then down-regulated at 24, 30 h with silent expression during senescent stage. (2) The amount of metaxin 2 and mitochondria import inner membrane translocase subunit TIM8a (TIMM8A) was increased upon treatment with LPS. (3) P34 cdc2 kinase was significantly up-regulated 30 h after LPS administration with silent expression during senescent, 6, 24 h treated stage. (4) The amount of proteasome activator 28 alpha subunit (PA28), magnesium dependent protein phosphatase (MDPP) and lysophospholipase 2 was decreased 6 h after LPS treatment but recovered or up-regulated 24 and 30 h after LPS treatment.

CONCLUSION: LPS-treated mouse liver displaying a time-dependent liver injury can result in expression change of some liver injury or repair related proteins.

Liu XW, Lu FG, Zhang GS, Wu XP, You Y, Ouyang CH, Yang DY. Proteomics to display tissue repair opposing injury response to LPS-induced liver injury. *World J Gastroenterol* 2004; 10 (18): 2701-2705

<http://www.wjgnet.com/1007-9327/10/2701.asp>

INTRODUCTION

Human intestinal tract accumulates Gram-negative bacteria that supply lipopolysaccharide (LPS). Gut-derived LPS reaches the first target organ liver through portal venous flow and results in hepatic clearance or tissue damage. Recent studies have shown that peritoneal macrophages in cirrhotic patients may secrete angiogenic products when stimulated by LPS and accumulate in liver injury^[1-3]. *In vivo* experiments also indicate LPS may cause liver injury in normal subjects and exaggerate liver injury in alcoholic liver disease^[4-7]. That is, chronic liver diseases suffering from subsequent LPS attack would result in much severer clinical findings. The precise mechanisms underlying LPS-treated liver injury remain unclear. Several studies of liver protein expression exposed to some hepatotoxic agents have revealed certain changes which illustrated the pathogenesis of liver injury in some extent^[2,4,8,9]. However, most reported researches focused only on some partial signaling or effector molecules on a limited view^[4,5,7]. Protein expression changes of liver exposed to LPS remains to be established.

The goal of the present study was to dynamically examine protein expression alterations in liver tissues from mice exposed to LPS administration, in order to anticipate of the possible signal molecules or biomarkers in signaling LPS-related liver injury.

MATERIALS AND METHODS

Reagents

Ultra pure reagents for polyacrylamide gel preparation were obtained from Bio-Rad. Eighteen cm immobilized pH gradient (IPG) strips (pH3-10 L), IPG buffer and dry strip cover fluid were purchased from Amersham Pharmacia Biotech (Uppsala, Sweden). 3-[(3-cholamidopropyl) dimethylammonio]-propanesulfonate (CHAPS), glycine, ammonium persulphate (APS), TEMED, trifluoroacetic acid were obtained from Amresco (Solon, OH, USA). Dithiothreitol (DTT), PMSF, Iodoacetamide, urea, thiourea, α -cyano-4-hydroxycinnamic acid (CCA), TPCK-Trypsin, *E. Coli* LPS 0111:B4 were purchased from Sigma Chemical (St Louis, MO, USA). Acetonitrile was HPLC grade. Ten μ L ZipTipTMC18 tip were purchased from Millipore Company (USA).

Animal treatment protocol

Male BALB/c mice (supplied by Laboratory Research Animal Center, 2nd Xiangya Hospital, Central South University), 6 wk of age and weighing 19-21 g, were used. The animals were housed individually in mouse gang cages in cleaning-grade controlled room. The Hunan Association accredited the house facility for Accreditation of Laboratory Animal Care, and all animal handling procedures were in conform to the Guide for the Care and Use of Laboratory Animals. Four groups of five mice each received intra-peritoneal (i.p) RPMI-1640 medium treatment (control) and LPS (diluted in RPMI-1640 medium) 4 mg/kg for 6, 24, 30 h, respectively. Mice were killed by decapitation, liver samples were removed and flash-frozen in liquid nitrogen and kept at -70 °C until proteomics analysis. For histopathologic research, liver slices from the right lateral lobes were immersion-fixed in 40 g/L neutral buffered formaldehyde,

routinely processed to 5- μ m thick paraffin sections, stained with hematoxylin and eosin (HE) and examined by light microscopy.

Sample preparation^[10]

Liver samples were homogenized in eight volumes of 8 mol/L urea, 2 mol/L thiourea, 40 g/L CHAPS, 20 g/L Triton X-100, 5 g/L DTT, 1 mmol/L PMSF, 1 mmol/L EDTA, 40 mmol/L Tris. Homogenates were centrifuged at 42 000 g at 20 °C for 1 h (LE-80 K ultracentrifuge, Type 90 rotor, Beckman). Supernatant was removed, divided into several aliquots and stored at -70 °C until to be used. Protein concentration of each sample was measured by Bradford method^[11].

Two-dimensional gel electrophoresis^[11,12]

The first-dimensional isoelectrical focus (IEF) was performed on precast 18 cm IPG strips at 20 °C with a maximum current setting of 50 μ A/strip using an Amersham Pharmacia IPGphor IEF unit. The strips were rehydrated at 30 V for 16 h in 350 μ L samples containing 8 mol/L urea, 20 g/L CHAPS, 20 mmol/L DTT, 5 g/L IPG buffer. Eight hundred μ g proteins was applied to each IPG strip. After rehydration, IEF run was carried out using the following conditions: 500 V, 500 Vh; 1 000 V, 1 000 Vh; 8 000 V, 40 000 Vh. Then, the strips were subjected to a two-step equilibration. The first was with an equilibration buffer consisting of 6 mol/L urea, 300 g/L glycerol, 20 g/L SDS, 50 mmol/L Tris (pH8.8) and 10 g/L DTT. The second equilibration buffer was the same, only with DTT substituted by 25 g/L iodoacetamide. After the strips were transferred onto the second-dimensional 0.75 mm thick 125 g/L sodium dodecyl sulfate-polyacrylamide gel electrophoresis (SDS-PAGE) gel, the strips were sealed in place with 7.5 g/L agarose. Electrophoresis was carried out at a constant current of 25 μ A/gel at 12 °C until bromophenol blue reached the edge of gels.

Silver staining

Gels were fixed in 400 mL/L ethanol, 100 mL/L acetic acid in water for 30 min, and then sensitized with 2 g/L sodium thiosulfate for 30 min. After the gels were rinsed twice with water for 5 min each, they were incubated in 2.5 g/L silver nitrate for 20 min. After the silver nitrate was discarded and rinsed with three changes of distilled water for 5 min each, the gels were visualized in 25 g/L sodium carbonate in 0.004% formalin until the desired intensity was attained. Then the gels were incubated with 14.6 g/L EDTA disodium dihydrate for 10 min to stop the development. The staining procedure was performed by three rinses with water for 5 min each.

Quantitative gel pattern analysis

Stained 2-D gels were scanned on a UMAX powerLook III scanner (Amersham Biosciences). Image analysis and Group Wise statistical comparisons were performed using the Image Master 2D v3.01 software (Amersham Pharmacia). The protein spot intensity was arbitrarily calculated by integrating the optical density over the spot area to search for treatment-related protein change. The amount of protein was marked by volumes ($A \times \text{area}$) and expressed as mean \pm SD. Statistical difference was analyzed by analysis of Variance (ANOVA). The cutoff of quantitative protein changes between control and treated groups was made at $P < 0.05$.

Protein digestion and protein identification by MALDI-TOF-MS^[10,12]

Destaining Protein spots of interest were excised from the 2-D gels and washed 3 times in distilled water, destained with 15 mmol/L potassium ferricyanide in 50 mmol/L sodium thiosulfate, dehydrated in acetonitrile and finally dried in a centrifugal vaporizer.

Reduction and alkylation Gel pieces were incubated in 100 mmol/L

NH_4HCO_3 by adding 10 mmol/L DTT at 57 °C for 1 h. After they were cooled, 100 mmol/L NH_4HCO_3 with 55 mmol/L iodoacetamide was added and incubated at room temperature in dark for 30 min. Supernatant was removed and samples were washed twice in 100 mmol/L NH_4HCO_3 and dehydrated in 1 000 g/L acetonitrile, finally dried in a centrifugal vaporizer.

In-gel digestion Gel pieces were rehydrated in a digestion buffer containing 0.1 mg/mL TPK-trypsin for 30 min. After excess buffer was discarded, the gel pieces were covered with digestion buffer and proteins were in-gel digested for 24 h at 37 °C.

Deionization Digested peptides were pipetted out and into to make them attached in a 10 μ L ZipTipTMC18 tip, washed twice with 1 mL/L trifluoroacetic acid.

MALDI-TOF-MS for protein identification The matrix solution was saturated in 500 g/L acetonitrile, 1 g/L TFA in water. Peptides were eluted with 5 μ L MALDI matrix, 2.0 μ L mixed solution was loaded to the sample plate target and allowed to air-evaporate. MALDI experiments were performed on a Perspective Biosystem Voyager-DE STR time-of-flight mass spectrometer (Applied Biosystems Voyager system 4307, USA) equipped with delayed ion extraction. Data were acquired in the delayed ion extraction mode using a 20 KV accelerating voltage and a 100 ns extraction delay time. Dual microchannel plate detection was utilized in the reflector mode with the ion signal recorded using a transient digitizer. The performance of the mass spectrometer produced sufficient mass resolution to produce isotopic multiplet for each ion species below a mass-to-charge (m/z) of 3 000. All MALDI mass spectra were internally calibrated using masses from two trypsin autolysis products (monoisotopic masses 2163.05 and 2273.15). The software package Protein Prospector (*prospector.ucsf.edu*) was used to identify protein spots. The mouse nonredundant (NR) database Genpept.5.1.2002 was used in searches. The search parameters used were as follows: Cysteines modification mode as carbamidomethylation, maximum allowed peptide mass error 50 ppm, more than four peptide mass hits required for protein match, up to one enzymatic missed cleavage. A restriction was placed on species of origin, pI (experimental pI \pm 1.00 pH unit) and protein mass (experimental molecular mass \pm 50%).

RESULTS

General health and histopathology

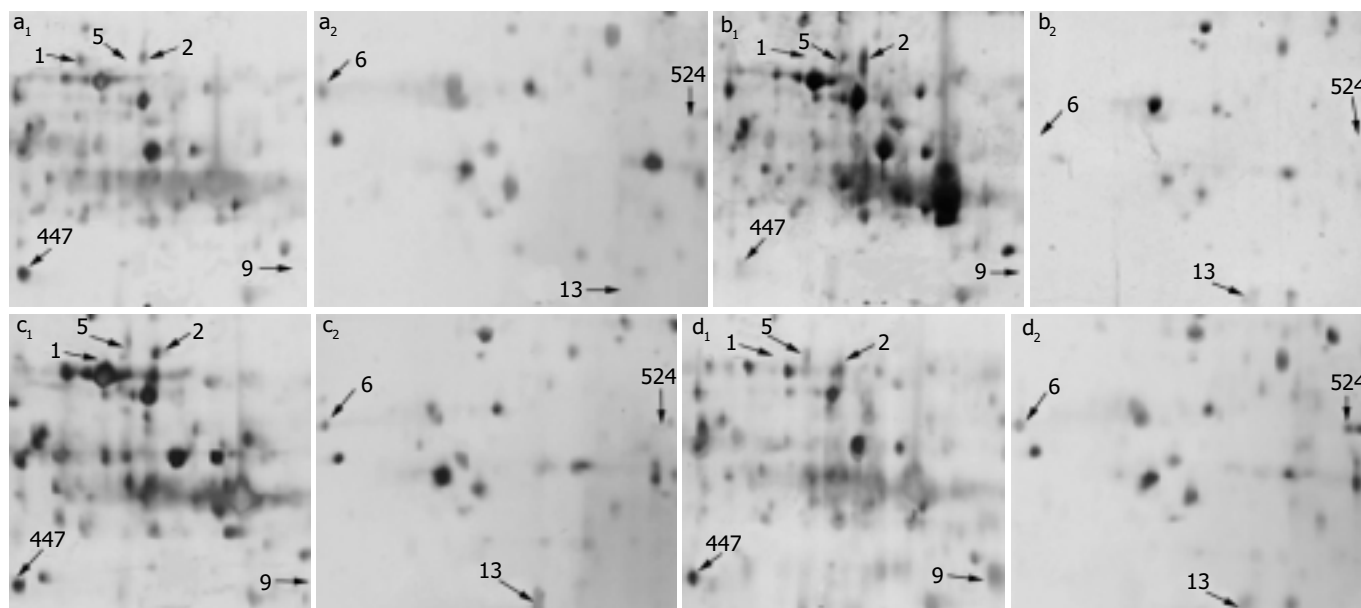
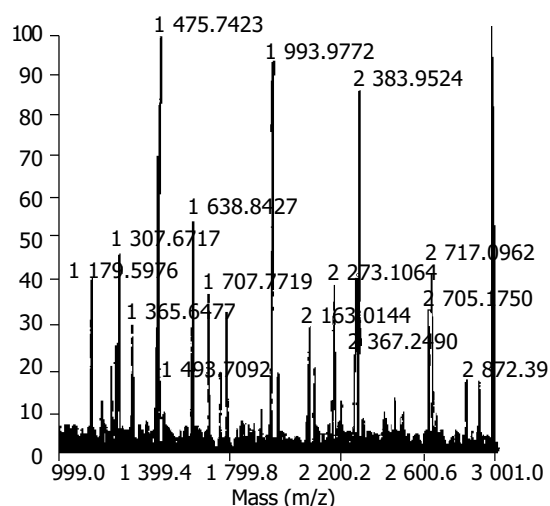
All subjects were inspected for general health before, during and after LPS exposure. Throughout the study, no animal experienced mortality that was determined to be related to the exposure. Nine of 10 animal that were treated by exposure to LPS for 24, 30 h experienced visible signs of laziness and retardation. Light microscopic examination of HE sections from LPS-treated mice revealed that a large number of inflammatory cells infiltrated portal areas with additional focal hepatocellular necrosis 24, 30 h after i.p. LPS (4 mg/kg)^[13].

Table 1 Relative amount of 8 injury/repair related liver proteins in response to LPS treatment (mean \pm SD)

Liver protein	Control	LPS		
		6 h	24 h	30 h
1	9 800 \pm 32	1 130 \pm 41	absent	absent
2	9 952 \pm 21	11 020 \pm 26	34 060 \pm 19	29 800 \pm 24
5	absent	38 040 \pm 18	19 500 \pm 42	20 540 \pm 34
6	12 420 \pm 24	absent	15 500 \pm 32	17 200 \pm 30
9	absent	absent	1 200 \pm 35	41 500 \pm 29
13	absent	4 500 \pm 42	8 900 \pm 44	10 500 \pm 32
447	43 200 \pm 21	3 200 \pm 35	absent	54 400 \pm 32
524	absent	absent	absent	9 500 \pm 23

Table 2 Results from search of Genpept.5.1.2002 database for *Musculus* protein sequences with tryptic peptide masses

Protein NO.	MOWSE score	Masses matched	Coverage (%)	Protein M_r	Protein PI	Accession NO.	Protein name
1	36.2	4	27	42 677	6.5	Q9QZM4	TRAIL receptor 2
2	56.3	5	45	35 646	6.0	P47802	Metaxin 2
5	29.5	4	32	36 134	8.0	O70479	TNF- α induced protein 1
6	47.9	4	26	28 673	5.7	P97371	Proteasome activator 28-alpha subunit (PA28)
9	76.1	4	20	34 191	7.8	P11440	P34 cdc2 kinase
13	25.3	4	26	11 043	5.1	Q9WVA2	Mitochondria import inner membrane translocase subunit TIM8 A (TIMM8A)
447	23.2	4	22	42 795	5.0	452526	Magnesium dependent protein phosphatase (MDPP)
524	37.3	4	25	24 794	6.7	P47713	Lysophospholipase 2

**Figure 1** Partial 2-D images of mouse liver proteins from (a₁, a₂) a control animal and animals treated with 4 mg/kg i.p LPS (b₁, b₂) 6 h, (c₁, c₂) 24 h, (d₁, d₂) 30 h. The spots representing proteins whose levels changed following LPS treatment are shown. a₁, b₁, c₁, d₁ represent the relative same partial map after different LPS-treated onset. a₂, b₂, c₂, d₂ represent another relative same partial map.**Figure 2** Peptide mass fingerprint of MDPP (spot 447). The spot was in-gel digested with trypsin. After desalted, the peptide mixture was analyzed by MALDI-TOF-MS. All MALDI mass spectra were internally calibrated using masses from two trypsin autolysis products (monoisotopic masses 2 163.05 and 2 273.15).

2-DE and relative abundance change

The resolution in 2-DE silver-stained gels resulted in approximately 1000 spots. The volumes ($A \times \text{area}$) and coordinates of each spot (pI and MW) were determined to select the fine right proteins

among candidates. There were significant alterations in 40 protein spots following LPS treatment when compared with each other, $P < 0.01$. These 40 proteins were identified by MALDI-TOF-MS (data not shown). Figure 1 (A-D) shows the location of 8 injury/repair related proteins in illustrated partial 2-DE maps of control and LPS-treated mice, respectively. Table 1 summarizes the relative amount of these considered proteins. The amount of protein 1 was 9 800 in the control and down-regulated to 1 130 in 6-h group, absent in 24-, 30-h group. Protein 5 was significantly up-regulated 6 h after LPS treatment, then down-regulated 24 h and 30 h after LPS treatment with silent expression in the control. Proteins 2 and 13 were increased upon treatment with LPS. Protein 9 was significantly up-regulated 30 h after LPS treatment with silent expression in control, 6, 24 h treated stage. Proteins 6, 447 and 524 were decreased in amount 6 h after LPS treatment, recovered and up-regulated 24 and 30 h after LPS treatment.

Identity of injury/repair related proteins

The proteins were cut from 2-DE gels and subjected to tryptic digestion. The 8 proteins analyzed by peptide mass fingerprinting yielded searchable masses and resulted in the identification (Table 2). Figure 2 indicates the peptide mass fingerprint of MDPP (spot 447) as a representative.

DISCUSSION

It has been proved that gut-derived LPS provokes liver inflammation

with focal hepatocyte injury and increases the sensitivity of hepatotoxicity to carbon tetrachloride, concanavalin A, D-galactosamine and ethanol induced liver damage^[4-6,14]. The role of LPS signaling pathway in the initiation and early propagation of immune response has been deeply demonstrated^[8,9,15]. In this study, liver injury occurred apparently 24 h after LPS administration. It indicated that LPS could promote hepatotoxicity by indirect mechanisms. Some immediate signaling or effector molecules may play a pivotal role in this delayed injurious response.

In our research, TNF-related apoptosis-inducing ligand receptor 2 (TRAIL-R2), TNF- α inducible endothelial protein 1 (TNFAIP1) and mitochondria apoptosis signaling related proteins metaxin 2, mitochondria import inner membrane translocase subunit TIM8a (TIMM8A) were demonstrated to be involved in the initiation of liver injury of LPS-treated mice and consistent with the histological change of liver tissue.

A recent research showed that LPS administration could result in elevated circulating TNF- α and up-regulation of gene transcription for TNF- α as early as 2 h after administration^[16]. Then, TNF- α related apoptosis pathway played a control role in mediating the tissue injury. TRAIL was recently reported to promote apoptosis of carcinogenic cells by binding to the transmembrane receptors. The resulting death-inducing signaling complex consisting of TRAIL, TRAIL-R2 and caspase-8, initiated the subsequent cascade of Caspases mediating apoptosis^[17,18]. The down-regulation of TRAIL-R2 in livers of LPS-treated mice could result in rather a protective mode of normal hepatocytes. The induction of TNFAIP1 has been shown to be apoptosis-specific, suggesting that TNF- α related apoptosis is triggered in liver cells of LPS-treated mice at earlier stage^[19].

Metaxin 2 is bound to the cytosolic face of mitochondria outer membrane by its interaction with membrane-bound metaxin 1, and this complex may play a role in protein import into mammalian mitochondria. The requirement of metaxin in TNF-induced cell death has been confirmed by *in vitro*^[20,21]. It has been found that TIMM8A exists in the mitochondria intermembrane space which mediates the import and insertion of inner membrane proteins^[22-24]. These two mitochondria proteins are required for normal physiological balance. Treatment-mediated changes of these proteins were likely to associated with mitochondria apoptosis. How mitochondria related pro- or anti-apoptotic proteins are involved in liver injury needs to be further demonstrated.

Tissue repair associated proteins, p34 cdc2 kinase and proteasome related proteins, showed some controversial expression in response to LPS-treated liver injury. p34 cdc2 kinase belongs to the Ser/Thr family of protein kinases. The sequential activation and inactivation of p34 cdc2 kinase of eukaryotic cells are required for it to entry into mitosis and to exit from it. In addition, a sustained activation of it during mitotic arrest has been associated with anti-microtubule agents-induced apoptosis^[25,26]. In this study, we found significant histopathological changes in mice livers 24 h after LPS treatment. p34 cdc2 kinase of mice livers was significantly up-regulated 30 h after LPS administration with silent expression during senescent, 6-, 24-h treated stage. It indicated that the enhanced expression of p34 cdc2 kinase was subsequently present to severe hepatic damage. It is likely that up-regulation of p34 cdc2 kinase in LPS-treated mice was more reflective of mitogenic response rather than antimitogenic activities. That is, cell division and tissue repair occurred as events opposing to tissue injury and could limit the extent of liver injury. It seemed possible that p34 cdc2 kinase could act by promoting mitosis and tissue repair, thus contributing to tissue repair response to LPS-treated liver injury.

The biological implications of amount in abundance of proteasome related proteins in mice liver response, including

proteasome activator 28 alpha subunit (PA28), magnesium dependent protein phosphatase (MDPP) and lysophospholipase 2, which decreased in amount 6 h after LPS treatment but recovered or up-regulated 24 and 30 h after LPS treatment, were even less clear. Previous study demonstrated that PA28 could bind to and activate the proteasome by the alpha subunit^[27]. MDPP is a new member of the halo acid dehalogenase family which has been found to be competent to catalyzing dephosphorylation of tyrosine-phosphorylated proteins^[28]. Lysophospholipase 2 was implicated in the initiation of inflammatory response by mediating cell division and differentiation^[1,29].

It is concluded that proteasome related proteins play a major role in the initiation of tissue repair program opposing to tissue damage. While the function, pathway interactions and ultimate biological outcomes of these changes in protein expression remains to be explained by further research.

In summary, the current investigation used 2-DE to characterize the proteome of LPS-treated mice liver that displayed a time-dependent liver injury in some liver injury or repair related proteins. In this study, 8 liver injury or repair related proteins were identified whose expression levels were altered at different time points after LPS treatment. TNF related apoptosis induced by LPS treatment could provoke an initiation response in tissue repair.

REFERENCES

- 1 **Perez-Ruiz M**, Ros J, Morales-Ruiz M, Navasa M, Colmenero J, Ruiz-del-Arbol L, Cejudo P, Claria J, Rivera F, Arroyo V, Rodes J, Jimenez W. Vascular endothelial growth factor production in peritoneal macrophages of cirrhotic patients: regulation by cytokines and bacterial lipopolysaccharide. *Hepatology* 1999; **29**: 1057-1063
- 2 **Hanck C**, Manigold T, Bocker U, Kurimoto M, Kolbel CB, Singer MV, Rossol S. Gene expression of interleukin 18 in unstimulated peripheral blood mononuclear cells of patients with alcoholic cirrhosis. *Gut* 2001; **49**: 106-111
- 3 **Mathurin P**, Deng QG, Keshavarzian A, Choudhary S, Holmes EW, Tsukamoto H. Exacerbation of alcoholic liver injury by enteral endotoxin in rats. *Hepatology* 2000; **32**: 1008-1017
- 4 **Uesugi T**, Froh M, Arteel GE, Bradford BU, Thurman RG. Toll-like receptor 4 is involved in the mechanism of early alcohol-induced liver injury in mice. *Hepatology* 2001; **34**: 101-108
- 5 **Josephs MD**, Bahjat FR, Fukuzuka K, Ksontini R, Solorzano CC, Edwards CK 3rd, Tannahill CL, MacKay SL, Copeland EM 3rd, Moldawer LL. Lipopolysaccharide and D-galactosamine-induced hepatic injury is mediated by TNF- α and not by Fas ligand. *Am J Physiol Regul Integr Comp Physiol* 2000; **278**: R1196-R1201
- 6 **Han DW**. Intestinal endotoxemia as a pathogenetic mechanism in liver failure. *World J Gastroenterol* 2002; **8**: 961-965
- 7 **Seki E**, Tsutsui H, Nakano H, Tsuji N, Hoshino K, Adachi O, Adachi K, Futatsugi S, Kuida K, Takeuchi O, Okamura H, Fujimoto J, Akira S, Nakanishi K. Lipopolysaccharide-induced IL-18 secretion from murine Kupffer cells independently of Myeloid differentiation factor 88 that is critically involved in induction of production of IL-12 and IL-1 β . *J Immunol* 2001; **166**: 2651-2657
- 8 **Kinser S**, Copple BL, Roth RA, Ganey PE. Enhancement of allyl alcohol hepatotoxicity by endotoxin requires extrahepatic factors. *Toxicol Sci* 2002; **69**: 470-481
- 9 **Wang B**, Cai SR, Gao C, Sladek FM, Ponder KP. Lipopolysaccharide results in a marked decrease in hepatocyte nuclear factor 4 alpha in rat liver. *Hepatology* 2001; **34**: 979-989
- 10 **Steiner S**, Gatlin CL, Lennon JJ, McGrath AM, Aponte AM, Makusky AJ, Rohrs MC, Anderson NL. Proteomics to display lovastatin-induced protein and pathway regulation in rat liver. *Electrophoresis* 2000; **21**: 2129-2137
- 11 **Kristensen DB**, Kawada N, Imamura K, Miyamoto Y, Tateno C, Seki S, Kuroki T, Yoshizato K. Proteome analysis of rat hepatic stellate cells. *Hepatology* 2000; **32**: 268-277
- 12 **Fountoulakis M**, Berndt P, Boelsterli UA, Cramer F, Winter

- M, Albertini S, Suter L. Two-dimensional database of mouse liver proteins: changes in hepatic protein levels following treatment with acetaminophen or its nontoxic regioisomer 3-acetamidophenol. *Electrophoresis* 2000; **21**: 2148-2161
- 13 Liu XW, You Y, Lu FG. TLR4 mRNA expression and liver injury in LPS-induced mouse. *Hunan Yike Daxue Xuebao* 2003; **28**: 217-220
- 14 Enomoto N, Takei Y, Hirose M, Ikejima K, Miwa H, Kitamura T, Sato N. Thalidomide prevents alcoholic liver injury in rats through suppression of Kupffer cell sensitization and TNF- α production. *Gastroenterology* 2002; **123**: 291-300
- 15 Muta T, Takeshige K. Essential roles of CD14 and lipopolysaccharide-binding protein for activation of toll-like receptor (TLR) 2 as well as TLR4 Reconstitution of TLR2- and TLR4-activation by distinguishable ligands in LPS preparations. *Eur J Biochem* 2001; **268**: 4580-4589
- 16 Barton CC, Barton EX, Ganey PE, Kunkel SL, Roth RA. Bacterial lipopolysaccharide enhances aflatoxin B1 hepatotoxicity in rats by a mechanism that depends on tumor necrosis factor α . *Hepatology* 2001; **33**: 66-73
- 17 Wu GS, Burns TF, Zhan Y, Alnemri ES, El-Deiry WS. Molecular cloning and functional analysis of the mouse homologue of the KILLER/DR5 tumor necrosis factor-related apoptosis-inducing ligand (TRAIL) death receptor. *Cancer Res* 1999; **59**: 2770-2775
- 18 Srivastava RK. TRAIL/Apo-2L: mechanisms and clinical applications in cancer. *Neoplasia* 2001; **3**: 535-546
- 19 Swift S, Blackburn C, Morahan G, Ashworth A. Structure and chromosomal mapping of the TNF-alpha inducible endothelial protein 1 (Edp1) gene in the mouse. *Biochim Biophys Acta* 1998; **1442**: 394-398
- 20 Abdul KM, Terada K, Yano M, Pyan MT, Streimann I, Hoogenraad NJ, Mori M. Functional analysis of human metaxin in mitochondria protein import in cultured cells and its relationship with the Tom complex. *Biochem Biophys Res Commun* 2000; **276**: 1028-1034
- 21 Wang X, Ono K, Kim SO, Kravchenko V, Lin SC, Han J. Metaxin is required for tumor necrosis factor-induced cell death. *EMBO Rep* 2001; **2**: 628-633
- 22 Roesch K, Curran SP, Tranebjaerg L, Koehler CM. Human deafness dystonia syndrome is caused by a defect in assembly of the DDP1/TIMM8a-TIMM13 complex. *Hum Mol Genet* 2002; **11**: 477-486
- 23 Ye K, Zhou J, Landen JW, Bradbury EM, Joshi HC. Sustained activation of p34 (cdc2) is required for nescapine-induced apoptosis. *J Biol Chem* 2001; **276**: 46697-46700
- 24 Hofmann S, Rothbauer U, Muhlenbein N, Neupert W, Gerbitz KD, Brunner M, Bauer MF. The C66W mutation in the deafness dystonia peptide 1 (DDP1) affects the formation of functional DDP1. TIM13 complexes in the mitochondrial intermembrane space. *J Biol Chem* 2002; **277**: 23287-23293
- 25 Selengut JD. MDP-1 is a new and distinct member of the halo acid dehalogenase family of aspartate-dependent phosphohydrolases. *Biochemistry* 2001; **40**: 12704-12711
- 26 Schoemaker MH, Ros JE, Homan M, Trautwein C, Liston P, Poelstra K, van Goor H, Jansen PL, Moshage H. Cytokine regulation of pro- and anti-apoptotic genes in rat hepatocytes: NF-kappaB-regulated inhibitor of apoptosis protein 2 (cIAP2) prevents apoptosis. *J Hepatol* 2002; **36**: 742-750
- 27 Song X, von Kampen J, Slaughter CA, DeMartino GN. Relative functions of the alpha and beta subunits of the proteasome activator, PA28. *J Biol Chem* 1997; **272**: 27994-28000
- 28 Wang A, Johnson CA, Jones Y, Ellisman MH, Dennis EA. Subcellular localization and PKC-dependent regulation of the human lysophospholipase A/acyl-protein thioesterase in WISH cells. *Biochim Biophys Acta* 2000; **1484**: 207-214
- 29 Khan S, van den Broek M, Schwarz K, de Giuli R, Diener RA, Groettrup M. Immunoproteasomes largely replace constitutive proteasomes during an antiviral and antibacterial immune response in the liver. *J Immunol* 2001; **167**: 6859-6868

Edited by Wang XL and Xu FM

Effects of platelet-derived growth factor and interleukin-10 on Fas/Fas-ligand and Bcl-2/Bax mRNA expression in rat hepatic stellate cells *in vitro*

Xiao-Zhong Wang, Sheng-Jun Zhang, Yun-Xin Chen, Zhi-Xin Chen, Yue-Hong Huang, Li-Juan Zhang

Xiao-Zhong Wang, Sheng-Jun Zhang, Yun-Xin Chen, Zhi-Xin Chen, Yue-Hong Huang, Li-Juan Zhang, Department of Gastroenterology, Union Hospital of Fujian Medical University, Fuzhou 350001, Fujian Province, China

Supported by the Science and Technology Foundation of Fujian Province, No. 2003D05

Correspondence to: Xiao-Zhong Wang, Department of Gastroenterology, Union Hospital of Fujian Medical University, Fuzhou 350001, Fujian Province, China. drwangxz@pub6.fz.fj.cn

Telephone: +86-591-3357896 Ext. 8482

Received: 2004-03-05 Accepted: 2004-03-12

Abstract

AIM: To investigate the effects of platelet-derived growth factor (PDGF) and interleukin-10 (IL-10) on Fas/Fas-ligand and Bcl-2/Bax mRNA expressions in rat hepatic stellate cells.

METHODS: Rat hepatic stellate cells (HSCs) were isolated and purified from rat liver by *in situ* digestion of collagenase and pronase and single-step density Nycodenz gradient. After activated by culture *in vitro*, HSCs were divided into 4 groups and treated with nothing (group N), PDGF (group P), IL-10 (group I) and PDGF in combination with IL-10 (group C), respectively. Semi-quantitative reverse-transcriptase polymerase chain reaction (RT-PCR) analysis was employed to compare the mRNA expression levels of Fas/FasL and Bcl-2/Bax in HSCs of each group.

RESULTS: The expression levels of Fas between the 4 groups had no significant differences ($P > 0.05$). FasL mRNA level in normal culture-activated HSCs (group N) was very low. It increased obviously after HSCs were treated with IL-10 (group I) (0.091 ± 0.007 vs 0.385 ± 0.051 , $P < 0.01$), but remained the low level after treated with PDGF alone (group P) or PDGF in combination with IL-10 (group C). Contrast to the control group, after treated with PDGF and IL-10, either alone or in combination, Bcl-2 mRNA expression was down-regulated and Bax mRNA expression was up-regulated, both following the turn from group P, group I to group C. Expression of Bcl-2 mRNA in group C was significantly lower than that in group P (0.126 ± 0.008 vs 0.210 ± 0.024 , $P < 0.01$). But no significant difference was found between group C and group I, as well as between group I and group P ($P > 0.05$). Similarly, the expression of Bax in group C was higher than that in group P (0.513 ± 0.016 vs 0.400 ± 0.022 , $P < 0.01$). No significant difference was found between group I and group P ($P > 0.05$). But compared with group C, Bax expressions in group I tended to decrease (0.449 ± 0.028 vs 0.513 ± 0.016 , $P < 0.05$).

CONCLUSION: PDGF may promote proliferation of HSCs but is neutral with respect to HSC apoptosis. IL-10 may promote the apoptosis of HSCs by up-regulating the expressions of FasL and Bax and down-regulating the expression of Bcl-2, which may be involved in its antifibrosis mechanism.

Wang XZ, Zhang SJ, Chen YX, Chen ZX, Huang YH, Zhang LJ. Effects of platelet-derived growth factor and interleukin-10 on Fas/Fas-ligand and Bcl-2/Bax mRNA expression in rat hepatic stellate cells *in vitro*. *World J Gastroenterol* 2004; 10(18): 2706-2710

<http://www.wjgnet.com/1007-9327/10/2706.asp>

INTRODUCTION

Liver fibrosis is a progressive pathological process involving multi-cellular and molecular events that ultimately lead to deposition of excess matrix proteins in the extracellular space. It is generally accepted that hepatic stellate cells (HSCs) are central to the process of fibrosis as the major source of extracellular matrix (ECM) components^[1-10]. Following acute or chronic liver tissue injury, HSCs undergo a process of activation towards a phenotype characterized by increasing proliferation, motility, contractility and synthesis of ECM components. Cytokines play an important role in the formation, development and reversibility of fibrosis^[9-14]. Activated HSCs secrete many important cytokines through autocrine and paracrine, of which platelet-derived growth factor (PDGF) can activate secretory cells and those quiescent HSCs around^[15,16] and promote the proliferation of HSCs^[17]. IL-10 is a potent anti-inflammatory cytokine that inhibits the synthesis of pro-inflammatory cytokines by T helper type 1 T cells and mono/macrophages. Previous studies have shown that endogenous IL-10 has the ability to inhibit the inflammation in injured liver and block the advance of fibrosis^[18-21]. Previous works by our group have demonstrated that exogenous IL-10 has an anti-fibrogenic function^[22]. But the underlying mechanism remains obscure. In this study, in order to investigate the effects of IL-10 and PDGF on the proliferation and apoptosis of rat HSCs, culture-activated HSCs were treated with IL-10 and PDGF. Fas/FasL and Bcl-2/Bax mRNA expressions in each group were assayed by semiquantitative reverse-transcriptase polymerase chain reaction (RT-PCR) analysis.

MATERIALS AND METHODS

Materials

Male Wistar rats, weighing 450-500 g, were provided by Shanghai Center for Laboratory Animals. Total RNA isolation kit was obtained from Jingmei Biotechnology Company of Shenzhen. Moloney murine leukemia virus (M-MLV) reverse transcriptase was purchased from Promega. PCR reagent and Dulbecco's modified Eagle's medium (DMEM) were respectively provided by Shanghai Biotechnology Company and GibcoB. PCR primers were synthesized by Shanghai Biotechnology Company.

Isolation, culture and evaluation of HSCs

HSCs were isolated from normal male Wistar rats by *in situ* digestion of collagenase and pronase and single-step density Nycodenz gradient as Ramm GA^[23] and Friedman SL^[24] previously described, and cultured in DMEM supplemented with 100 mL/L FBS. Desmin immunocytochemistry was employed to determine the

isolated HSCs' purity. HSCs were subcultured 4 d after primary culture. Alpha smooth muscle actin (α -SMA) immunocytochemistry and electron microscope were employed to confirm that HSCs were activated by culture *in vitro* and transformed into myofibroblasts.

Intervention and division of HSCs

The subcultured HSCs were diluted to a concentration of 5×10^4 /mL with DMEM containing 100 mL/L FBS and seeded onto the 24-well plastic tissue culture plates. When HSCs spread the plate fully, the culture medium was replaced with DMEM containing 10 mL/L FBS. After incubated for 24 h, HSCs were divided randomly into 4 groups: one as control group cultured in 1 mL DMEM containing 10 mL/L FBS, the other three were cultured in the same medium and treated with 20 ng PDGF or 20 ng IL-10, either alone or in combination, respectively. We named them group N, group P, group I and group C, respectively. Each group included 5 wells.

RNA extraction

Total RNA was extracted from the above treated HSCs after incubated for 24 h according to the RNA isolation kit instructions. The content and purity of total RNA were determined by spectrophotography. A_{260}/A_{280} of total RNA was between 1.8-2.0.

RT-PCR for Fas/FasL and Bcl-2/Bax

For RT-PCR, total RNA was reverse-transcribed using M-MLV reverse transcriptase and oligo (dT) at 37 °C for 60 min, followed by at 70 °C for 10 min. Approximately 2 μ g total RNA was used in each reverse transcription reaction and the final volume was 25 μ L. β -actin was used as internal control. The PCR reaction volume was 50 μ L, including 5 μ L 10 \times PCR buffer, 2 mmol/L $MgCl_2$, 1 μ L 10 mmol/L dNTP, 1 μ L 20 pmol/ μ L target gene sense and anti-sense primers, 1 μ L 20 pmol/ μ L β -actin primer pair, 2 μ L RT product, 1.5 U Tag DNA polymerase. The specific sets of primers and the target gene amplification conditions are shown in Table 1.

Result determination

PCR products were run on 20 g/L agarose gel electrophoresis and visualized with ethidium bromide staining. Bio imagine system was used to detect the densities of bands of the PCR products. The ratio of target gene density to β -actin density was used to represent the relative levels of Fas/FasL and Bcl-2/Bax mRNA expressions. The semi-quantitative detection was analyzed 5 times repeatedly.

Statistical analysis

All data were expressed as mean \pm SE. The significance for the

difference between the groups was assessed with SPSS 10.0 by one-way ANOVA. $P < 0.05$ was considered statistically significant.

RESULTS

Evaluation of HSCs

Freshly isolated HSCs were round-shaped with many yellow droplets in cytoplasm. After cultured for 5-6 d, the spread cells showed a typical 'star'-like configuration. Desmin immunocytochemistry showed that the positive percentage was about 95% (Figure 1A), indicating that 95% of the isolated cells were HSCs. α -SMA immunocytochemistry showed that 98% of the cells were α -SMA positive (Figure 1B), indicating that most of the cells were activated. The myofilament could be seen in cytoplasm under the electron microscope, confirming that HSCs were activated and transformed into myofibroblasts after cultured *in vitro* (Figure 2).

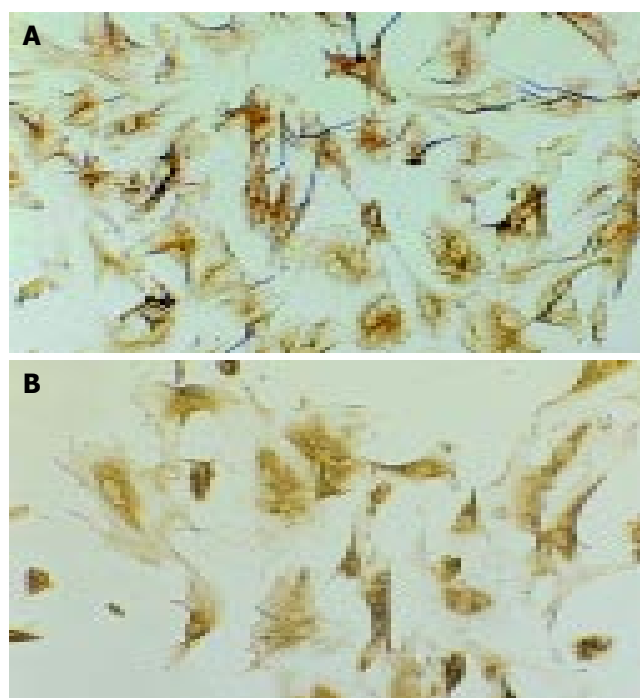


Figure 1 Desmin and α -SMA immunocytochemistry (SP, original magnification: $\times 100$). A: Desmin immunocytochemistry of HSCs 7 d after isolation; B: α -SMA immunocytochemistry of HSCs 7 after isolation.

Table 1 Primer sequences for PCR and amplification conditions for each target gene

Primer (base)	Sequence	Amplification conditions
Fas 414	5'-GAATGCAAGGGACTGATAGC-3' 5'-TGGTTCGTGTGCAAGGCTC-3'	Denaturation at 94 °C for 45 s, Annealing at 55 °C for 30 s and synthesizing at 72 °C for 1 min for 25 cycles
FasL 239	5'-GGAATGGGAAGACACATATGGAAGTGC -3' 5'-CATATCTGGCCAGTAGTGCAGTAATTC-3'	Denaturation at 94 °C for 45 s, Annealing at 55 °C for 30 s and synthesizing at 72 °C for 1 min for 33 cycles
Bcl-2 525	5'-TATGATAACCGGGAGATCGTGATC-3' 5'-GTGCAGATGCCGGTTCAGGTACTC-3'	Denaturation at 94 °C for 45 s, Annealing at 60 °C for 30 s and synthesizing at 72 °C for 1 min for 33 cycles
Bax 310	5'-GACACCTGAGCTGACCTTGG-3' 5'-GAGGAAGTCCAGTGTCAGC-3'	Denaturation at 94 °C for 45 s, Annealing at 60 °C for 30 s and synthesizing at 72 °C for 1 min for 30 cycles
β -actin 660	5'-CCAACCGTGAAAAGATGACC-3' 5'-CAGGAGGAGCAATGATCTTG-3'	Changed according to different target genes

All initial denaturations were at 94 °C for 5 min. Finally an additional extension step at 72 °C for 7 min was done.

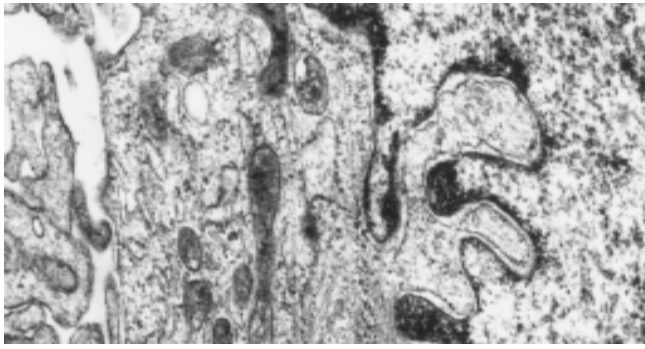


Figure 2 Activated HSCs under the electron microscope. The myofilament can be seen in the cytoplasm as the arrow point shows.

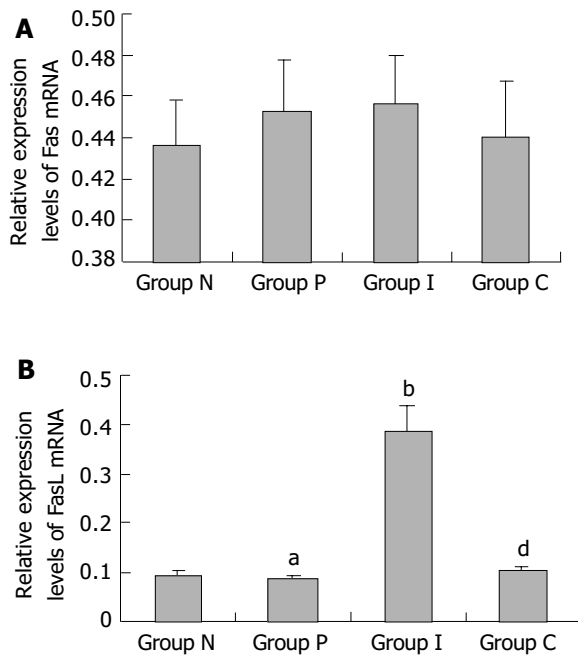


Figure 3 Relative Fas/ FasL mRNA expression levels in HSCs of different groups assessed by RT-PCR. A: Relative Fas mRNA expression levels ($P>0.05$ between random two groups.); B: Relative FasL mRNA expression levels (^a $P>0.05$ vs group N, ^b $P<0.01$ vs group N, ^d $P<0.01$ vs group I); group N: Normal group as control; group P: PDGF treated group; group I: IL-10 treated group; group C: Combined PDGF and IL-10 treatment group.

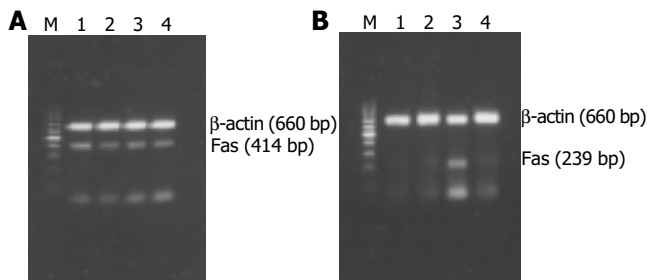


Figure 4 RT-PCR results of Fas/FasL mRNA expression in HSCs of different groups. A: RT-PCR results of Fas mRNA expression; B: RT-PCR results of FasL mRNA expression; M: 100 bp DNA ladder (upper to lower: 1 000, 900, 800, 700, 600, 500, 400, 300, 200, and 100 bp); Lane 1: Normal group as control; Lane 2: PDGF treatment group; Lane 3: IL-10 treatment group; Lane 4: Combined PDGF and IL-10 treatment group.

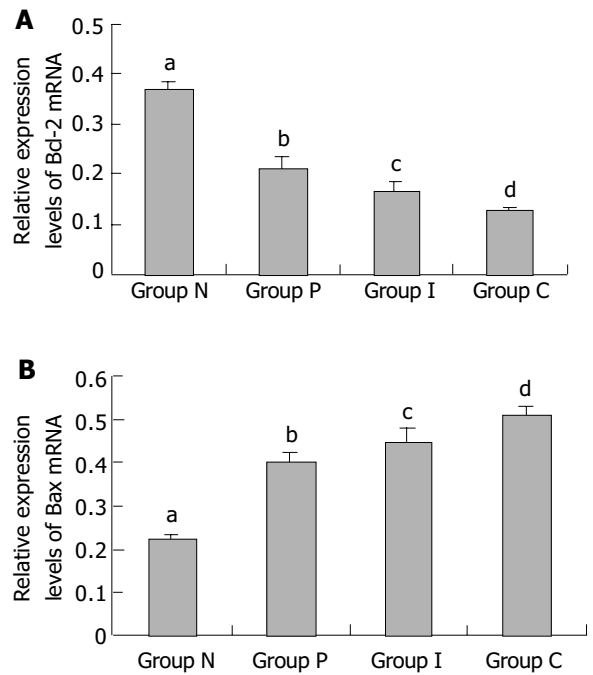


Figure 5 Relative Bcl-2/Bax mRNA expression levels in HSCs of different groups assessed by RT-PCR. A: Relative Bcl-2 mRNA expression levels (^b $P<0.01$ vs group P, group I and group C, respectively; ^a $P>0.05$ vs group I, ^c $P>0.05$ vs group C, ^d $P<0.01$ vs group P.). B: Relative Bax mRNA expression levels (^b $P<0.01$ vs group P, group I and group C, respectively; ^a $P>0.05$ vs group I, ^c $P = 0.045<0.05$ vs group C, ^d $P<0.01$ vs group P.). Group N: Normal group as control; group P: PDGF treated group; group I: IL-10 treated group; group C: Combined PDGF and IL-10 treatment group.

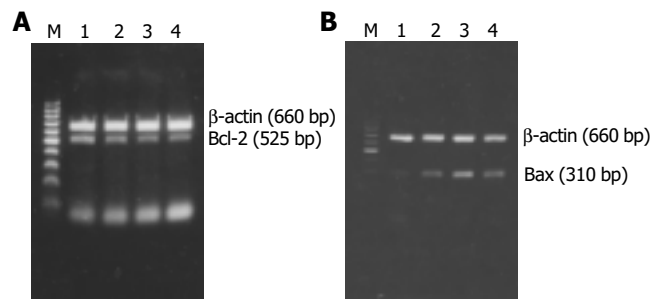


Figure 6 RT-PCR results of Bcl-2/Bax mRNA expression in HSCs of different groups. A: Bcl-2 mRNA expression. B: Bax mRNA expression. M: 100 bp DNA ladder (upper to lower: 1 000, 900, 800, 700, 600, 500, 400, 300, 200, and 100 bp); Lane 1: Normal group as control; Lane 2: PDGF treatment group; Lane 3: IL-10 treatment group; Lane 4: Combined PDGF and IL-10 treatment group.

Effects of PDGF and IL-10 on Fas and FasL expressions in HSCs

Fas mRNA was expressed in HSCs of each group and the expression levels had no significant difference among the 4 groups, as shown in Figures 3A, 4A, indicating that neither PDGF nor IL-10 had effect on Fas mRNA expression in HSCs. As it could be informed from Figures 3B, 4B, FasL mRNA level in normal culture-activated HSCs (group N) was very low. It increased obviously after HSCs were treated with IL-10 (group I) (0.091 ± 0.007 vs 0.385 ± 0.051 , $P<0.01$), but remained the low level after treated with PDGF alone (group P) or PDGF in combination with IL-10 (group C) (0.085 ± 0.006 , 0.101 ± 0.008 , respectively). The data suggested that IL-10 could improve FasL mRNA expression in culture-activated HSCs and PDGF could not. Furthermore, PDGF tended to abolish this effect of IL-10.

Effects of PDGF and IL-10 on Bcl-2 and Bax expressions in HSCs

Bcl-2 and Bax mRNA were expressed in normal culture-activated HSCs. Both of their expression levels were significantly changed after treated with PDGF and IL-10, either alone or in combination. Bcl-2 mRNA expression was down-regulated and Bax mRNA expression was up-regulated, following the turn from group P, group I to group C. The expression of Bcl-2 in group C was significantly lower than that in group P (0.126 ± 0.008 vs 0.210 ± 0.024 , $P<0.01$). But no significant difference was found between group C and group I, as well as between group I and group P (0.210 ± 0.024 vs 0.166 ± 0.017 , 0.166 ± 0.017 vs 0.126 ± 0.008 , $P>0.05$) (Figures 5A, 6A). Similarly, the expression of Bax in group C was higher than that in group P (0.513 ± 0.016 vs 0.400 ± 0.022 , $P<0.01$). No significant difference was found between group I and group P (0.400 ± 0.022 vs 0.449 ± 0.028 , $P>0.05$). But compared with combined treatment group, Bax expressions in group I tended to decrease (0.449 ± 0.028 vs 0.513 ± 0.016 , $P=0.045<0.05$) (Figures 5B, 6B). These results showed that both PDGF and IL-10 promoted the Bax mRNA expression in HSCs and inhibited the Bcl-2 expression, but the differences of their effects were not significant. Intervention with PDGF and IL-10 seemed to be able to manifest effects on Bax expression than intervention alone. IL-10 showed similar influences on culture-activated HSCs and reactivated HSCs by PDGF.

DISCUSSION

It is generally accepted that hepatic stellate cells (HSCs) are central to the process of hepatic fibrosis. They are the major source of extracellular matrix and during fibrogenesis undergo an activation process characterized by increased proliferation and collagen synthesis^[1-10,24]. So the activation, proliferation and apoptosis of HSCs have close relationship with the formation and development of liver fibrosis. To inhibit the activation and proliferation of the HSCs and promote their apoptosis has become the most important therapeutic approach for liver fibrosis^[7-10,14,25-28].

There is evidence that HSCs can be successfully isolated by *in situ* digestion of collagenase and pronase and single-step density Nycodenz gradient^[23,24,29]. Desmin is a marker for muscle cells and expressed by all muscle lineages including HSCs (either quiescent or activated) in the liver. Alpha smooth muscle actin (α -SMA) is an intermediate filament protein that is expressed by activated HSCs and is widely accepted to be a marker of activation. Both of them were used to identify and quantify HSCs and their activation. The desmin immunocytochemistry result showed that the purity of the isolated HSCs by this method was satisfying (Figure 1A). The results of α -SMA immunocytochemistry (Figure 1B) and electron microscope (Figure 2) confirmed that HSCs were activated and transformed into myofibroblasts after cultured *in vitro*.

PDGF, which is produced by HSCs, Kuffer cells and platelets, is a major mitogen for connective tissues and certain other cells. It was viewed as one of the most important growth factors serving as the matrix-bound cytokines^[11] and plays an important role in the pathogenesis of liver fibrosis via promoting the activation and proliferation of HSCs^[12,15,25,30-32]. The best characterized chemotactic factor for HSCs identified so far is the PDGF-BB^[33-35] which is also known as the most potent mitogen for HSCs over-expressed during active hepatic fibrosis^[36]. But there is also evidence that PDGF is proapoptotic for fibroblasts in conditions of low serum^[37]. Saile B^[38] reported that resting HSCs displayed no sign of apoptosis and spontaneous apoptosis became detectable in parallel with HSCs activation, suggesting that apoptosis might represent an important mechanism terminating proliferation of activated HSCs. He also found that Fas and Fas-ligand in HSCs became increasingly expressed during the course of activation. But our data demonstrated that PDGF

alone had no effect on the expression of Fas and FasL during further activating the culture-activated HSCs, which was supported by Issa R^[39]. Bax and Bcl-2 are known as the representatives of proapoptotic factor and contra-apoptotic factor of Bcl-2 family, respectively^[40,41]. In our study, evidences showed that PDGF could promote Bax mRNA expression in HSCs and inhibited Bcl-2 mRNA expression as well, resulting in the apoptosis of HSCs^[41]. All the above data demonstrated that PDGF can accelerate the apoptosis of HSCs through Bcl-2/Bax pathway in parallel with their proliferation^[42]. In other words, PDGF may promote proliferation but is neutral with respect to HSCs apoptosis. But the proportion of apoptosis-inducing forces and apoptosis-inhibiting forces would determine that PDGF-activated HSCs tend to proliferate and increase^[22].

Cytokine interleukin-10 (IL-10), produced by lymphocytes and macrophages as well as cells within liver such as Kuffer cells, hepatocytes and HSCs, has profound inhibitory actions on macrophages and inflammation. The present studies showed that IL-10 had additional effects on connective tissue cells, such as HSCs and fibroblast. IL-10 could inhibit the activation of HSCs by inflammatory cells^[43], relieve the inflammation of liver^[18,19,44], suppress the function of NF- κ B^[45] and affect the expression of collagen I and collagenase^[20], thus exerting an antifibrogenesis effect^[46]. Failure for HSCs to sustain IL-10 expression might underlie pathologic progression to liver cirrhosis^[18,20]. Our previous studies also implied that IL-10 had an antagonism on CCL₄-induced rat hepatic fibrosis^[22]. But the underlying mechanism remains obscure. In this study, our results showed that IL-10 could promote the expression of FasL and Bax mRNA in culture-activated HSCs and meanwhile could inhibit Bcl-2 mRNA expression, implying that IL-10 may induce the apoptosis of HSCs through binding FasL to Fas on the cell membranes of HSCs and increasing the proportion of Bax and Bcl-2. Saile B^[38] found that apoptosis could be fully blocked by Fas-blocking antibodies in normal cells and HSCs already entering the apoptotic cycle, implying that Fas/FasL system is the key pathway for the apoptosis of HSCs. Our data, however, showed that Bax/Bcl-2 system was another important pathway involving in HSCs' apoptosis^[40,41]. In short, IL-10 could promote the apoptosis of HSCs, which may be related to its mechanism of antifibrosis.

There is evidence that activated-HSCs could express IL-10 as well as its receptor^[20,47]. In this study, PDGF had a similar effect to IL-10 on Bax/Bcl-2 mRNA expression in HSCs. This promotes us to hypothesize that PDGF may regulate the expression of Bax and Bcl-2 mRNA by affecting the expression of IL-10 in HSCs. But PDGF in combination with IL-10 did not show a satisfying synergistic action, thus we can not exclude the possibility that PDGF and IL-10 affect in different ways, and further works are demanded.

REFERENCES

- 1 Gressner AM. Transdifferentiation of hepatic stellate cells (Ito cells) to myofibroblasts: a key event in hepatic fibrogenesis. *Kidney Int Suppl* 1996; **54**: S39-45
- 2 Brenner DA, Waterboer T, Choi SK, Lindquist JN, Stefanovic B, Burchardt E, Yamauchi M, Gillan A, Rippe RA. New aspects of hepatic fibrosis. *J Hepatol* 2000; **32**(1 Suppl): 32-38
- 3 Benyon RC, Iredale JP. Is liver fibrosis reversible? *Gut* 2000; **46**: 443-446
- 4 Murphy FR, Issa R, Zhou X, Ratnarajah S, Nagase H, Arthur MJ, Benyon C, Iredale JP. Inhibition of apoptosis of activated hepatic stellate cells by tissue inhibitor of metalloproteinase-1 is mediated via effects on matrix metalloproteinase inhibition: implications for reversibility of liver fibrosis. *J Biol Chem* 2002; **277**: 11069-11076
- 5 Rockey DC. The cell and molecular biology of hepatic fibrogenesis. Clinical and therapeutic implications. *Clin Liver Dis* 2000; **4**: 319-355
- 6 Du WD, Zhang YE, Zhai WR, Zhou XM. Dynamic changes of

- type I, III and IV collagen synthesis and distribution of collagen-producing cells in carbon tetrachloride-induced rat liver fibrosis. *World J Gastroenterol* 1999; **5**: 397-403
- 7 **Bataller R**, Brenner DA. Hepatic stellate cells as a target for the treatment of liver fibrosis. *Semin Liver Dis* 2001; **21**: 437-451
- 8 **Reeves HL**, Friedman SL. Activation of hepatic stellate cells—a key issue in liver fibrosis. *Front Biosci* 2002; **7**: d808-826
- 9 **Albanis E**, Friedman SL. Hepatic fibrosis. Pathogenesis and principles of therapy. *Clin Liver Dis* 2001; **5**: 315-334
- 10 **Li D**, Friedman SL. Liver fibrogenesis and the role of hepatic stellate cells: new insights and prospects for therapy. *J Gastroenterol Hepatol* 1999; **14**: 618-633
- 11 **Friedman SL**. Cytokines and fibrogenesis. *Semin Liver Dis* 1999; **19**: 129-140
- 12 **Pinzani M**, Marra F. Cytokine receptors and signaling in hepatic stellate cells. *Semin Liver Dis* 2001; **21**: 397-416
- 13 **Gressner AM**. The up-and-down of hepatic stellate cells in tissue injury: apoptosis restores cellular homeostasis. *Gastroenterology* 2001; **120**: 1285-1288
- 14 **Gressner AM**. The cell biology of liver fibrogenesis - an imbalance of proliferation, growth arrest and apoptosis of myofibroblasts. *Cell Tissue Res* 1998; **292**: 447-452
- 15 **Kinnman N**, Francoz C, Barbu V, Wendum D, Rey C, Hultcrantz R, Poupon R, Housset C. The myofibroblastic conversion of peribiliary fibrogenic cells distinct from hepatic stellate cells is stimulated by platelet-derived growth factor during liver fibrogenesis. *Lab Invest* 2003; **83**: 163-173
- 16 **Oh SJ**, Kurz H, Christ B, Wilting J. Platelet-derived growth factor-B induces transformation of fibrocytes into spindle-shaped myofibroblasts *in vivo*. *Histochem Cell Biol* 1998; **109**: 349-357
- 17 **Chen A**, Zhang L. The antioxidant (-)-epigallocatechin-3-gallate inhibits rat hepatic stellate cell proliferation *in vitro* by blocking the tyrosine phosphorylation and reducing the gene expression of platelet-derived growth factor- β receptor. *J Biol Chem* 2003; **278**: 23381-23389
- 18 **Thompson K**, Maltby J, Fallowfield J, McAulay M, Millward-Sadler H, Sheron N. Interleukin-10 expression and function in experimental murine liver inflammation and fibrosis. *Hepatology* 1998; **28**: 1597-1606
- 19 **Louis H**, Van Laethem JL, Wu W, Quertinmont E, Degraef C, Van den Berg K, Demols A, Goldman M, Le Moine O, Geerts A, Deviere J. Interleukin-10 controls neutrophilic infiltration, hepatocyte proliferation, and liver fibrosis induced by carbon tetrachloride in mice. *Hepatology* 1998; **28**: 1607-1615
- 20 **Wang SC**, Ohata M, Schrum L, Rippe RA, Tsukamoto H. Expression of interleukin-10 by *in vitro* and *in vivo* activated hepatic stellate cells. *J Biol Chem* 1998; **273**: 302-308
- 21 **Demols A**, Van Laethem JL, Quertinmont E, Degraef C, Delhaye M, Geerts A, Deviere J. Endogenous interleukin-10 modulates fibrosis and regeneration in experimental chronic pancreatitis. *Am J Physiol Gastrointest Liver Physiol* 2002; **282**: G1105-1112
- 22 **Chen YX**, Wang XZ, Weng SG, Chen ZX, Huang YH, Zhang LJ. Effects of Interleukin-10 on the proliferation and Fas/Fas ligand expression of hepatic stellate cells. *Zhonghua Ganzhangbing Zazhi* 2003; **11**: 637
- 23 **Ramm GA**. Isolation and culture of rat hepatic stellate cells. *J Gastroenterol Hepatol* 1998; **13**: 846-851
- 24 **Friedman SL**, Rockey DC, McGuire RF, Maher JJ, Boyles JK, Yamasaki G. Isolated hepatic lipocytes and Kupffer cells from normal human liver: morphological and functional characteristics in primary culture. *Hepatology* 1992; **15**: 234-243
- 25 **Friedman SL**. Molecular regulation of hepatic fibrosis, an integrated cellular response to tissue injury. *J Biol Chem* 2000; **275**: 2247-2250
- 26 **Safadi R**, Friedman SL. Hepatic fibrosis-role of hepatic stellate cell activation. *MedGenMed* 2002; **4**: 27
- 27 **Arthur MJ**, Mann DA, Iredale JP. Tissue inhibitors of metalloproteinases, hepatic stellate cells and liver fibrosis. *J Gastroenterol Hepatol* 1998; **13**(Suppl): S33-38
- 28 **Iredale JP**, Benyon RC, Pickering J, McCullen M, Northrop M, Pawley S, Hovell C, Arthur MJ. Mechanisms of spontaneous resolution of rat liver fibrosis. Hepatic stellate cell apoptosis and reduced hepatic expression of metalloproteinase inhibitors. *J Clin Invest* 1998; **102**: 538-549
- 29 **Riccalton-Banks L**, Bhandari R, Fry J, Shakesheff KM. A simple method for the simultaneous isolation of stellate cells and hepatocytes from rat liver tissue. *Mol Cell Biochem* 2003; **248**: 97-102
- 30 **Marra F**, Choudhury GG, Pinzani M, Abboud HE. Regulation of platelet-derived growth factor secretion and gene expression in human liver fat-storing cells. *Gastroenterology* 1994; **107**: 1110-1117
- 31 **Kinnman N**, Gorla O, Wendum D, Gendron MC, Rey C, Poupon R, Housset C. Hepatic stellate cell proliferation is an early platelet-derived growth factor-mediated cellular event in rat cholestatic liver injury. *Lab Invest* 2001; **81**: 1709-1716
- 32 **Liu X**, Zhang J, Zhang Y. Effects of platelet-derived growth factor on the proliferation of hepatic stellate cells and their expressions of genes of collagens and platelet-derived growth factor. *Zhonghua Binglixue Zazhi* 2000; **29**: 27-29
- 33 **Ikeda K**, Wakahara T, Wang YQ, Kadoya H, Kawada N, Kaneda K. *In vitro* migratory potential of rat quiescent hepatic stellate cells and its augmentation by cell activation. *Hepatology* 1999; **29**: 1760-1767
- 34 **Marra F**, Gentilini A, Pinzani M, Choudhury GG, Parola M, Herbst H, Dianzani MU, Laffi G, Abboud HE, Gentilini P. Phosphatidylinositol 3-kinase is required for platelet-derived growth factor's actions on hepatic stellate cells. *Gastroenterology* 1997; **112**: 1297-1306
- 35 **Carloni V**, Romanelli RG, Pinzani M, Laffi G, Gentilini P. Focal adhesion kinase and phospholipase C gamma involvement in adhesion and migration of human hepatic stellate cells. *Gastroenterology* 1997; **112**: 522-531
- 36 **Pinzani M**. PDGF and signal transduction in hepatic stellate cells. *Front Biosci* 2002; **7**: d1720-1726
- 37 **Kim HR**, Upadhyay S, Li G, Palmer KC, Deuel TF. Platelet-derived growth factor induces apoptosis in growth-arrested murine fibroblasts. *Proc Natl Acad Sci U S A* 1995; **92**: 9500-9504
- 38 **Saile B**, Knittel T, Matthes N, Schott P, Ramadori G. CD95/CD95L-mediated apoptosis of the hepatic stellate cell. A mechanism terminating uncontrolled hepatic stellate cell proliferation during hepatic tissue repair. *Am J Pathol* 1997; **151**: 1265-1272
- 39 **Issa R**, Williams E, Trim N, Kendall T, Arthur MJ, Reichen J, Benyon RC, Iredale JP. Apoptosis of hepatic stellate cells: involvement in resolution of biliary fibrosis and regulation by soluble growth factors. *Gut* 2001; **48**: 548-557
- 40 **Saile B**, Matthes N, El Armouche H, Neubauer K, Ramadori G. The bcl, NFkappaB and p53/p21WAF1 systems are involved in spontaneous apoptosis and in the anti-apoptotic effect of TGF-beta or TNF-alpha on activated hepatic stellate cells. *Eur J Cell Biol* 2001; **80**: 554-561
- 41 **Gong W**, Pecci A, Roth S, Lahme B, Beato M, Gressner AM. Transformation-dependent susceptibility of rat hepatic stellate cells to apoptosis induced by soluble Fas ligand. *Hepatology* 1998; **28**: 492-502
- 42 **Eng FJ**, Friedman SL. Fibrogenesis I. New insights into hepatic stellate cell activation: the simple becomes complex. *Am J Physiol Gastrointest Liver Physiol* 2000; **279**: G7-G11
- 43 **Weng S**, Leng X, Wei Y. Interleukin-10 inhibits the activation of cultured rat hepatic stellate cells induced by Kupffer cells. *Zhonghua Yixue Zazhi* 2002; **82**: 104-107
- 44 **Leifeld L**, Cheng S, Ramakers J, Dumoulin FL, Trautwein C, Sauerbruch T, Spengler U. Imbalanced intrahepatic expression of interleukin 12, interferon gamma, and interleukin 10 in fulminant hepatitis B. *Hepatology* 2002; **36**(4 Pt 1): 1001-1008
- 45 **Yoshidome H**, Kato A, Edwards MJ, Lentsch AB. Interleukin-10 inhibits pulmonary NF-kappaB activation and lung injury induced by hepatic ischemia-reperfusion. *Am J Physiol* 1999; **277**(5 Pt 1): L919-923
- 46 **Nelson DR**, Lauwers GY, Lau JY, Davis GL. Interleukin 10 treatment reduces fibrosis in patients with chronic hepatitis C: a pilot trial of interferon nonresponders. *Gastroenterology* 2000; **118**: 655-660
- 47 **Thompson KC**, Trowern A, Fowell A, Marathe M, Haycock C, Arthur MJ, Sheron N. Primary rat and mouse hepatic stellate cells express the macrophage inhibitor cytokine interleukin-10 during the course of activation *in vitro*. *Hepatology* 1998; **28**: 1518-1524

• CLINICAL RESEARCH •

Effects of 24 h ultra-marathon on biochemical and hematological parameters

Huey-June Wu, Kung-Tung Chen, Bing-Wu Shee, Huan-Cheng Chang, Yi-Jen Huang, Rong-Sen Yang

Huey-June Wu, Department of Physical Education, Chinese Culture University, Taipei 111, Taiwan, China

Kung-Tung Chen, Department of General Education, Ming Hsin University of Science and Technology Hsin-chu 304, Taiwan, China

Bing-Wu Shee, Huan-Cheng Chang, Li-shin hospital Pingjen City, Taoyuan County, Taiwan, China

Yi-Jen Huang, Department of Physical Education, Soochow University, Taipei 112, Taiwan, China

Rong-Sen Yang, Department of Orthopaedics, College of Medicine, National Taiwan University & Hospital, Taipei 10043, Taiwan, China

Supported by the National Science Council of Taiwan, NSC91-2413-H-159-001

Correspondence to: Dr. Bing-Wu Shee M.D., Department of Orthopaedics, Li-shin Hospital No.77, Kuang-Tai Rd. Pingjen City, Taoyuan County 324, Taiwan, China. sbeebw@ush.com.tw

Telephone: +886-3-4941234 Ext. 2910 **Fax:** +886-3-4021057

Received: 2003-10-24 **Accepted:** 2003-11-20

Abstract

AIM: To analyze detailed changes in hematology and biochemistry tests parameters before and after a long-distance race in ultramarathon runners.

METHODS: Blood samples of 11 participants were obtained for standard analysis before, immediately after, two days after and nine days after the 2002 International Ultramarathon 24 h Race and the International Association of Ultrarunners (IAU) Asia 24 h Championship.

RESULTS: Total bilirubin (BIL-T), direct bilirubin (BIL-D), alkaline phosphatase (ALP), aspartate aminotransferase (AST), alanine aminotransferase (ALT) and lactate dehydrogenase (LDH) increased statistically significantly ($P < 0.05$) the race. Significant declines ($P < 0.05$) in red blood cell (RBC), hemoglobin (Hb) and hematocrit (Hct) were detected two days and nine days after the race. 2 d after the race, total protein (TP), concentration of albumin and globulin decreased significantly. While BIL, BIL-D and ALP recovered to their original levels. High-density lipoprotein cholesterol (HDL-C) remained unchanged immediately after the race, but it was significantly decreased on the second and ninth days after the race.

CONCLUSION: Ultra-marathon running is associated with a wide range of significant changes in hematological parameters, several of which are injury related. To provide appropriate health care and intervention, the man who receives athletes on high frequent training program high intensity training programs must monitor their liver and gallbladder function.

Wu HJ, Chen KT, Shee BW, Chang HC, Huang YJ, Yang RS. Effects of 24 h ultra-marathon on biochemical and hematological parameters. *World J Gastroenterol* 2004; 10(18): 2711-2714

<http://www.wjgnet.com/1007-9327/10/2711.asp>

INTRODUCTION

Numerous reports have been published on the effects on the body of endurance sports such as the 5 000 m, the 10 000 m, the marathon, cross-country running, rowing and cycling^[1-14]. In recent years, more athletes have become involved in ultra-endurance races, such as the iron-man triathlon, the 100 km race and the 24 h marathon, and a few investigations have addressed the related hematological and biochemical changes. Strenuous physical activities are becoming increasingly popular around the world, and this work may benefit participants in future competitions.

Some of these previous studies have involved staged races with long rest periods; while others made comparisons before and after competition. This study examines, athletes who have completed a long-distance run lasting 24 h, and detailing the related hematological and biochemical changes before, immediately after, two days after and nine days after the race.

MATERIALS AND METHODS

Anthropometric data

A 24 h ultra-marathon was held at Soo-Chow University on March 2, 2002. The runners ran around a 400 m oval track for 24 h, covering a distance of at least 100 km. The runners changed direction every 4 h. The temperature during the 24 h race ranged from 19.0 to 26.8 °C and the relative humidity ranged from 63 to 91%. The runners were permitted to rest and to ingest water and food freely. Ten males (10/36) and one female (1/1) participated in this study, having previously given their informed consent. Table 1 lists the anthropometric data.

Table 1 Anthropometric data of the study population ($n = 11$)

	Range	Mean	Standard Deviation
Age (yr)	26.00-55.00	45.10	±2.64
Height (cm)	155.00-177.00	166.80	±6.23
Body weight (kg)	47.00-69.30	60.60	±9.69
Distance completed (km)	106.70-194.40	158.60	±26.78
BMI(body mass index)	19.56-22.12	21.79	±0.24

Parameter of blood tests

20 mL blood samples were obtained from the antecubital vein 24 h before the race, immediately after the race, two days after the race and nine days after the race. The blood was analyzed in 1 h using an ABBOTT CELL DYN 3 000 autoanalyser (Abbott Diagnostics, Mountain View, CA., USA) and HITACHI 7150 autoanalyser (Hitachi High Technologies, Tokyo, Japan).

Statistical significance of paired differences in means and standard deviations of the related hematological and biochemical changes among pre-race, immediately post-race, two days post-race, and nine days post-race values were calculated using by one-way ANOVA analysis. The level of significance was set at $P < 0.05$.

RESULTS

Hb. Hct. platelet data

The pre-race red cell count, Hb and Hct levels were not significantly

immediately after the race, but were significantly reduced two and nine days after the race, being lowest at two days after the race. The mean cell volume was not significantly changed immediately after the race or on day two post-race, but was significantly increased by day nine post-race. Mean cell Hb concentration was significantly lower on day two than before the race, but had recovered on day nine.

Mean cell Hb and red cell distribution width remained unchanged at all times. The platelet concentration immediately after the race and on day nine following the race was increased significantly compared to pre-race values, but had decreased significantly on day two. (Table 2).

Total WBC and differential count

The white blood cell count was significantly increased at the end of the race and remained high until day nine. Moreover, the number of neutrophils was increased at the end of race but recovered two days later. Furthermore, the lymphocytes, eosinophils and basophils were decreased immediately after the race but recovered two days later. Finally, the number of monocytes was increased immediately after the race and on day two post-race, but returned to the pre-race level by day nine post-race. (Table 3).

Ferritin, TIBC

The ferritin level, total iron binding capacity (TIBC) and transferrin saturation rose significantly immediately post-race along with ferritin level, and remained at the end higher on day two and nine. All of the parameters remained normal

mean values. (Table 4).

Liver function tests

The BIL-T and BIL-D concentrations were significantly raised immediately after the race and normalized two days later. TP, albumin and globulin concentrations were unchanged immediately after the race but were significantly reduced on day two, recovering gradually after day nine, though TP and albumin remained below pre-race levels.

ALP, AST and ALT had increased significantly by the end of the race. ALP returned to its pre-race level after day two. Moreover, AST declined by day two and resumed its pre-race level by day nine. Furthermore, ALT continued to rise until day two and had recovered by day nine. Gamma glutamyl transferase (γ -GT) remained unchanged until the end of race and beyond the end of the event. Finally, LDH was significantly raised by the end of the race and was decreased on day two post-race, but remained above their pre-race level on day nine. (Table 5).

Lipid metabolism

Triglyceride (TG), cholesterol/low-density lipoprotein cholesterol (CHO/LDL-C) ratio and LDL-C were lower immediately after the race had finished. TG level and CHO/LDL-C ratio recovered by day two post-race, while LDL-C recovered by day nine. Cholesterol was not significantly changed at the end of the race, but was significantly lower on day two.

HDL-C was highest immediately after the race but had reduced by day two and nine post-race. (Table 6).

Table 2 Changes in Hb, Hct, red cell parameters and platelet count before and after the race

	Pre-race	0 h post-race	2 d post-race	9 d post-race
Red cell count ($\times 10^{12}/L$)	4.71 \pm 0.25 ^{ce}	4.71 \pm 0.45	4.07 \pm 0.27	4.42 \pm 0.21
Hb (g/dL)	14.63 \pm 0.91 ^{ce}	14.58 \pm 1.17	12.52 \pm 0.86	13.81 \pm 0.69
Hct (%)	42.34 \pm 2.73 ^{ce}	42.37 \pm 3.82	37.33 \pm 3.15	40.27 \pm 1.84
Mean cell volume (fl)	89.91 \pm 3.11 ^e	90.05 \pm 3.37	90.29 \pm 3.50	91.15 \pm 3.19
Mean cell Hb (pg)	31.09 \pm 1.23	31.02 \pm 1.44	30.90 \pm 1.29	31.22 \pm 1.34
Mean cell Hb Concentration (g/dL)	34.59 \pm 0.45 ^e	34.44 \pm 0.60	34.24 \pm 0.47	34.25 \pm 0.64
Red cell distribution width (%)	12.84 \pm 0.60	12.94 \pm 0.88	12.69 \pm 0.57	12.80 \pm 0.65
Platelet ($\times 10^9/L$)	235.45 \pm 47.27 ^{ace}	248.91 \pm 46.95	209.82 \pm 58.28	280.27 \pm 67.23

^a P <0.05 vs statistically significant when pre-race compared with 0 h post-race. ^c P <0.05 vs statistically significant when pre-race compared with 2 d post-race. ^e P <0.05 vs statistically significant when pre-race compared with 9 d post-race.

Table 3 Total and differential white cell counts before and after the race

	Pre-race	0 h post-race	2 d post-race	9 d post-race
White cell count ($\times 10^9/L$)	4.95 \pm 1.05 ^{ace}	11.87 \pm 1.46	5.83 \pm 1.09	5.95 \pm 1.45
Neutrophils (%)	56.02 \pm 6.69 ^a	76.43 \pm 6.28	57.66 \pm 7.28	57.93 \pm 9.16
Lymphocytes (%)	33.10 \pm 6.94 ^a	14.47 \pm 4.82	30.89 \pm 6.42	32.15 \pm 8.07
Monocytes (%)	7.83 \pm 3.58	8.21 \pm 2.84	9.34 \pm 2.77	7.15 \pm 1.91
Eosinophils ($\times 10^9/L$)	2.07 \pm 1.01 ^a	0.20 \pm 0.19	1.75 \pm 0.76	1.80 \pm 1.20
Basophils ($\times 10^9/L$)	0.96 \pm 0.19 ^a	0.68 \pm 0.24	0.82 \pm 0.26	0.99 \pm 0.28

^a P <0.05 vs statistically significant when pre-race compared with 0 h post-race. ^c P <0.05 vs statistically significant when pre-race compared with 2 d post-race. ^e P <0.05 vs statistically significant when pre-race compared with 9 d post-race.

Table 4 Comparisons of parameters related to iron metabolism before and after the race

	Pre-race	0 h post-race	2 d post-race	9 d post-race
Ferritin (μ g/L)	64.45 \pm 27.95 ^{ae}	117.00 \pm 52.66	70.18 \pm 44.88	103.36 \pm 42.15
TIBC (μ mol/L)	361.00 \pm 31.38 ^{ae}	372.18 \pm 30.93	357.64 \pm 35.43	356.36 \pm 30.75
Transferrin saturation (%)	17.73 \pm 8.05 ^{ae}	31.09 \pm 13.32	19.27 \pm 11.62	29.18 \pm 11.70

^a P <0.05 vs statistically significant when pre-race compared with 0 h post-race. ^c P <0.05 vs statistically significant when pre-race compared with 2 d post-race. ^e P <0.05 vs statistically significant when pre-race compared with 9 d post-race.

Table 5 Serum enzyme activity before and after the ultra marathon race

	Pre-race	0 h post-race	2 d post-race	9 d post-race
BIL-T ($\mu\text{mol/L}$)	11.63 \pm 2.91 ^a	25.65 \pm 9.75	13.68 \pm 7.70	12.14 \pm 4.10
BIL-D ($\mu\text{mol/L}$)	2.57 \pm 0.68 ^a	7.01 \pm 2.91	3.25 \pm 1.54	2.74 \pm 1.20
TP (g/L)	72.51 \pm 4.70 ^{ce}	72.50 \pm 6.21	66.14 \pm 3.90	67.00 \pm 4.91
Albumin (g/L)	44.82 \pm 2.83 ^{ce}	45.42 \pm 2.92	38.55 \pm 5.83	42.43 \pm 2.84
Globulin (g/L)	27.53 \pm 2.51 ^c	27.25 \pm 3.74	25.56 \pm 2.01	27.53 \pm 2.42
ALP (U/L)	132.85 \pm 56.50 ^a	160.55 \pm 33.00	131.36 \pm 34.00	134.27 \pm 34.40
AST (U/L)	37.10 \pm 19.10 ^{ac}	536.70 \pm 311.10	271.30 \pm 227.80	34.30 \pm 8.70
ALT (U/L)	35.10 \pm 13.10 ^{ace}	118.40 \pm 75.10	126.00 \pm 68.30	50.50 \pm 18.90
γ -GT (U/L)	20.18 \pm 6.23	24.18 \pm 14.30	19.18 \pm 9.00	20.91 \pm 8.00
LDH (U/L)	367.50 \pm 105.60 ^{ace}	1 420.50 \pm 598.50	1 120.30 \pm 605.10	582.70 \pm 207.90

^a P <0.05 vs statistically significant when pre-race compared with 0 h post-race. ^c P <0.05 vs statistically significant when pre-race compared with 2 d post-race. ^e P <0.05 vs statistically significant when pre-race compared with 9 d post-race.

Table 6 Changes in parameters related to lipid metabolism before and after the ultra marathon race

	Pre-race	0 h post-race	2 d post-race	9 d post-race
TG (mmol/L)	0.95 \pm 0.27 ^a	0.67 \pm 0.28	0.84 \pm 0.32	1.09 \pm 0.55
CHO (mmol/L)	4.87 \pm 1.06 ^c	4.63 \pm 1.09	4.13 \pm 0.57	4.51 \pm 0.50
HDL-C (mmol/L)	1.92 \pm 0.47	2.02 \pm 0.50	1.68 \pm 0.24	1.77 \pm 0.32
LDL-C (mmol/L)	2.51 \pm 0.78 ^{ac}	2.30 \pm 0.72	2.02 \pm 0.49	2.24 \pm 0.39
CHO/ HDL-C	2.50 \pm 0.48 ^a	2.30 \pm 0.37	2.40 \pm 0.38	2.60 \pm 0.43

^a P <0.05 vs statistically significant when pre-race compared with 0 h post-race. ^c P <0.05 vs statistically significant when pre-race compared with 2 d post-race. ^e P <0.05 vs statistically significant when pre-race compared with 9 d post-race.

DISCUSSION

Few studies have extensively addressed the hematological and biochemical changes in endurance runners. This investigation elucidates the effects of intensive exercise on athlete health and the findings can be used to help participants in future competitions.

Red cell count, Hb and Hct, three indicators of anemia, were normal before the race. Significant decreases was found by day two, consistent with the accelerated destruction of RBC in endurance athletes. The three indicators remained reduced between days two and nine; so-called sports anemia^[15], is not only caused by hemolysis owing to mechanical trauma but also by oxidative injuries of the red cells^[16]. Under normal conditions, red cells with a mean life of 120 d are renewed at approximately 1% daily. However, this turnover rate increases following endurance training, as reflected in the participants in this study. The increased turnover rate is good for the athletes as the young red cells can carry oxygen more efficiently than the older cells.^[17,18] The mean cell volume, mean cell hemoglobin and mean cell hemoglobin concentration remained normal throughout. The transient sports anemia was caused by reduced red cell numbers rather than red cell size or amount of Hb^[19,20]. The change in platelets number was inconsistent with previous studies. The platelet count was higher at the end of the race and on day nine, but remained within the normal range, and no coagulopathy was detected. Further study can clarify the significance of the increase. The white cell count increased markedly race and subsequently declined. The initial increase followed from to a rise in peripheral reserves and was mostly associated with neutrophils. Neutrophilia and numbers of lymphocytes were related to catecholamine, cortisol and some chemotactic factors: transient immunological dysfunction may occur under such conditions^[21,22]. This study found on decrease in absolute lymphocyte count and no signs of infection in a follow-up questionnaire administered 2 wk after the race.

The concentration of serum ferritin was significantly increased immediately after the race and on day nine post-race, owing to the acute phase response of the destruction of red cells, consistent with previous reports. Total iron binding capacity and transferrin saturation were markedly increased by

the end of race, reflecting the acute release of iron.

BIL and BIL-D increased at the end of the race and normalized after day two, associated with hemolysis that follows from ultra-long running. The hemolysis was related to a decline in haptoglobin concentration and structural changes in the red cell membranes^[23,24]. AST, ALT, γ -GT, LDH and ALP all increased by the end of the race, implying damage to the skeletal muscle cells and hepatic cells. Serum BIL normalized by day two as red cell turnover reduced, but AST, ALT and LDH continued to exceed pre-race levels, representing a continued release of enzymes from the muscles and liver^[25-27].

Albumin is involved in protein synthesis by the liver. Albumin reduced significantly by day two, reflecting damage to the anabolic functioning of hepatic cells. TP fell after day two, mainly owing to the decrease in albumin and had not recovered by day nine. Despite the reduced protein level, no clinical pitting edema was found. The pre-race mean AST, ALT and LDH exceeded the normal range, possibly indicating chronic damage to the liver following long-term strenuous exercise.

Most hepatic function parameters displayed no correlation with age, except for negatively correlated globulin, reflecting the lower immunological functioning of older runners following endurance exercise^[28,29]. AST, ALT and LDH were positively correlated with runner performance and unrelated to BIL and ALP, implying that changes in hepatobiliary parameters resulted mainly from damage to hepatic cells. Long-term regular exercise has been recognized to contribute to reducing cholesterol^[30-32], triglyceride and LDL-C and increasing HDL-C. In this study the lipid parameters of all of the participants were in the normal ranges, supporting the beneficial effect of rhythmic aerobic exercise. However, the effects of long-term ultra-endurance activities deserve further investigation.

Most fat is stored as triglyceride in fat and muscle cells. Plasma and muscular triglyceride were consumed equally during the first stage of endurance exercise, and subsequently the free fatty acid became the major source of energy explaining the reduction in triglyceride at the end of the race^[33,34]. The TG and LDL-C were significantly lower at the end of the race and on day agreeing with previous reports. Cholesterol is a major

risk factor for coronary artery disease and deserves extensive investigation. Cholesterol levels were not significantly changed at the end of the race, and were decreased by day two, but the cholesterol/HDL-C ratio, which is not affected by plasma volume, was significantly reduced by the end of the race. This phenomenon may result from the increase in HDL-C and the decrease in LDL-C.

Ultramarathon running is associated with numerous changes in hematological parameters, many of which are injury related. These changes should not be confused with indicators of disease. Increasing liver enzyme levels in runners indicated damage to liver cells, but increased BIL resulted from higher clearance rates of RBC. The liver damage was directly proportional to workload. Acute reduction of TG might result from the use of body fat as the major energy source. An ultra-long endurance run effectively reduced LDL-C for two days post-race, but did not significantly change HDL-C.

Safety guidelines, protective equipment and prevention education are crucial to reducing sports injuries. Then, preventing liver and gall bladder injuries and ensuring safe health management program are necessary for ultramarathon athletes. In summary, efforts to minimize these injuries are warranted both to ensure the long-term health of runners and to reduce medical costs. The key to management of ultramarathon runner osteoporosis involves identifying the potential risk for osteoporosis and osteoporotic fracture, followed by measures that focus on reducing modifiable risk factors through health management program^[33-34].

REFERENCES

- 1 **Pestell RG**, Hurley DM, Vandongen R. Biochemical and hormonal changes during a 1000 km ultramarathon. *Clin Exp Pharmacol Physiol* 1989; **16**: 353-361
- 2 **Noakes TD**, Carter JW. Biochemical parameters in athletes before and after having run 160 kilometres. *S Afr Med J* 1976; **50**: 1562-1566
- 3 **Nagel D**, Seiler D, Franz H. Biochemical, hematological and endocrinological parameters during repeated intense short-term running in comparison to ultra-long-distance running. *Int J Sports Med* 1992; **13**: 337-343
- 4 **Seiler D**, Nagel D, Franz H, Hellstern P, Leitzmann C, Jung K. Effects of long-distance running on iron metabolism and hematological parameters. *Int J Sports Med* 1989; **10**: 357-362
- 5 **Dickson DN**, Wilkinson RL, Noakes TD. Effects of ultra-marathon training and racing on hematologic parameters and serum ferritin levels in well-trained athletes. *Int J Sports Med* 1982; **3**: 111-117
- 6 **Taylor C**, Rogers G, Goodman C, Baynes RD, Bothwell TH, Bezwoda WR, Kramer F, Hattingh J. Hematologic, iron-related, and acute-phase protein responses to sustained strenuous exercise. *J Appl Physiol* 1987; **62**: 464-469
- 7 **Davidson RJ**, Robertson JD, Galea G, Maughan RJ. Hematological changes associated with marathon running. *Int J Sports Med* 1987; **8**: 19-25
- 8 **Rama R**, Ibanez J, Riera M, Prats MT, Pages T, Palacios L. Hematological, electrolyte, and biochemical alterations after a 100-km run. *Can J Appl Physiol* 1994; **19**: 411-420
- 9 **Fellmann N**, Bedu M, Giry J, Pharmakis-Amadieu M, Bezou MJ, Barlet JP, Coudert J. Hormonal, fluid, and electrolyte changes during a 72-h recovery from a 24-h endurance run. *Int J Sports Med* 1989; **10**: 406-412
- 10 **Zuliani U**, Mandras A, Beltrami GF, Bonetti A, Montani G, Novarini A. Metabolic modifications caused by sport activity: effect in leisure-time cross-country skiers. *J Sports Med Phys Fitness* 1983; **23**: 385-392
- 11 **Fallon KE**, Broad E, Thompson MW, Reull PA. Nutritional and fluid intake in a 100-km ultramarathon. *Int J Sport Nutr* 1998; **8**: 24-35
- 12 **van Rensburg JP**, Kielblock AJ, van der Linde A. Physiologic and biochemical changes during a triathlon competition. *Int J Sports Med* 1986; **7**: 30-35
- 13 **Thompson PD**, Crouse SF, Goodpaster B, Kelley D, Moyna N, Pescatello L. The acute versus the chronic response to exercise. *Med Sci Sports Exerc* 2001; **33**: S438-S445
- 14 **Fallon KE**, Sivyver G, Sivyver K, Dare A. The biochemistry of runners in a 1600 km ultramarathon. *Br J Sports Med* 1999; **33**: 264-269
- 15 **Weight LM**. 'Sports anaemia'. Does it exist? *Sports Med* 1993; **16**: 1-4
- 16 **Szygula Z**. Erythrocytic system under the influence of physical exercise and training. *Sports Med* 1990; **10**: 181-197
- 17 **Jordan J**, Kiernan W, Merker HJ, Wenzel M, Beneke R. Red cell membrane skeletal changes in marathon runners. *Int J Sports Med* 1998; **19**: 16-19
- 18 **Smith JA**. Exercise, training and red blood cell turnover. *Sports Med* 1995; **19**: 9-31
- 19 **Newmark SR**, Toppo FR, Adams G. Fluid and electrolyte replacement in the ultramarathon runner. *Am J Sports Med* 1991; **19**: 389-391
- 20 **Staubli M**, Roessler B. The mean red cell volume in long distance runners. *Eur J App Physiol Occup Physiol* 1986; **55**: 49-53
- 21 **Natale VM**, Brenner IK, Moldoveanu AI, Vasiliou P, Shek P, Shephard RJ. Effects of three different types of exercise on blood leukocyte count during and following exercise. *Sao Paulo Med J* 2003; **121**: 9-14
- 22 **Pyne DB**. Regulation of neutrophil function during exercise. *Sports Med* 1994; **17**: 245-258
- 23 **Spitler DL**, Alexander WC, Hoffler GW, Doerr DF, Buchanan P. Haptoglobin and serum enzymatic response to maximal exercise in relation to physical fitness. *Med Sci Sports Exerc* 1984; **16**: 366-370
- 24 **Nagel D**, Seiler D, Franz H, Jung K. Ultra-long-distance running and the liver. *Int J Sports Med* 1990; **11**: 441-445
- 25 **Priest JB**, Oei TO, Moorehead WR. Exercise-induced changes in common laboratory tests. *Am J Clin Pathol* 1982; **77**: 285-289
- 26 **Elosua R**, Molina L, Fito M, Arquer A, Sanchez-Quesada JL, Covas MI, Ordóñez-Llanos J, Marrugat J. Response of oxidative stress biomarkers to a 16-week aerobic physical activity program, and to acute physical activity, in healthy young men and women. *Atherosclerosis*. 2003 ;**167**: 327-334
- 27 **Yao HW**, Li J, Jin Y, Zhang YF, Li CY, Xu SY. Effect of leflunomide on immunological liver injury in mice. *World J Gastroenterol* 2003; **9**: 320-323
- 28 **Nieman DC**, Pedersen BK. Exercise and immune function. Recent developments. *Sports Med* 1999; **27**: 73-80
- 29 **Nieman DC**, Nehlsen-Cannarella SL, Fagoaga OR, Henson DA, Shannon M, Hjertman JM, Schmitt RL, Bolton MR, Austin MD, Schilling BK, Thorpe R. Immune function in female elite rowers and non-athletes. *Br J Sports Med* 2000; **34**: 181-187
- 30 **Lamon-Fava S**, McNamara JR, Farber HW, Hill NS, Schaefer EJ. Acute changes in lipid, lipoprotein, apolipoprotein, and low-density lipoprotein particle size after an endurance triathlon. *Metabolism* 1989; **38**: 921-925
- 31 **Crouse SF**, O'Brien BC, Grandjean PW, Lowe RC, Rohack JJ, Green JS. Effects of training and a single session of exercise on lipids and apolipoproteins in hypercholesterolemic men. *J Appl Physiol* 1997; **83**: 2019-2028
- 32 **Nicklas BJ**, Katzell LI, Busby-Whitehead J, Goldberg AP. Increases in high-density lipoprotein cholesterol with endurance exercise training are blunted in obese compared with lean men. *Metabolism* 1997; **46**: 556-561
- 33 **Ginsburg GS**, Agil A, O'Toole M, Rimm E, Douglas PS, Rifai N. Effects of a single bout of ultraendurance exercise on lipid levels and susceptibility of lipids to peroxidation in triathletes. *JAMA* 1996; **276**: 221-225
- 34 **Kratz A**, Lewandrowski KB, Siegel AJ, Chun KY, Flood JG, Van Cott EM, Lee-Lewandrowski E. Effect of marathon running on hematologic and biochemical laboratory parameters, including cardiac markers. *Am J Clin Pathol* 2002; **118**: 856-863

Assessment of autonomic function in untreated adult coeliac disease

Gian Marco Giorgetti, Antonio Tursi, Cesare Iani, Flavio Arciprete, Giovanni Brandimarte, Ambrogio Capria, Luigi Fontana

Gian Marco Giorgetti, Department of Internal Medicine, Clinical Nutrition Unit, "S. Eugenio" Hospital, Rome, Italy

Antonio Tursi, Digestive Endoscopy Unit, "Lorenzo Bonomo" Hospital, Andria (BA), Italy

Cesare Iani, Flavio Arciprete, Division of Neurology, "S. Eugenio" Hospital, Rome, Italy

Giovanni Brandimarte, Department of Internal Medicine, Division of Gastroenterology, "Cristo Re" Hospital, Rome, Italy

Ambrogio Capria, Luigi Fontana, Department of Internal Medicine and Immunology, "Tor Vergata" University, Rome, Italy

Correspondence to: Dr. Antonio Tursi, Galleria Pisani, 4, 70031 Andria (BA), Italy. antotursi@tiscali.it

Fax: +39-883-290225

Received: 2004-01-10 **Accepted:** 2004-03-02

Abstract

AIM: Some recent studies showed that alteration of upper-gut motility in coeliac disease may be related to dysfunction of autonomic nervous system. The aim of our study was to investigate whether autonomic nervous system was altered in untreated and unselected coeliac disease patients.

METHODS: We studied 8 untreated and consecutive coeliac disease patients (2 males and 6 females, age range 37 ± 14.5 years). Histological evaluation of duodenal mucosa, anti-gliadin antibodies (AGA), antiendomysial antibodies (EMA) and anti-tTG antibodies and sorbitol H2 breath test were performed in all patients. Extrinsic autonomic neuropathy was assessed by the standardized measurement of cardiovascular reflexes (lying-to-standing, Valsalva manoeuvre, deep breathing, sustained handgrip). The results obtained were compared with a healthy, asymptomatic control group (6 males and 7 females, age range 42.3 ± 13.5 years).

RESULTS: Coeliac patients exhibited a lower increase of PAS as a response to isometric effort, a reduction of spectral power LF as a response to clinostatic position, but without statistical significance. Also they showed a lower tolerance to orthostatic position, associated with a latent disequilibrium of sympathetic-vagal balance, a relative prevalence of parasympathetic component of the autonomic function. However, these results were not statistically significant when compared with control group ($P = n.s.$). And they were unchanged after 6 and 12 mo of gluten-free diet.

CONCLUSION: This study failed to confirm a significant correlation between autonomic dysfunction and coeliac disease, yet we could not exclude a role of autonomic dysfunction in the genesis of systemic symptoms in some coeliacs.

Giorgetti GM, Tursi A, Iani C, Arciprete F, Brandimarte G, Capria A, Fontana L. Assessment of autonomic function in untreated adult coeliac disease. *World J Gastroenterol* 2004; 10(18): 2715-2718

<http://www.wjgnet.com/1007-9327/10/2715.asp>

INTRODUCTION

Coeliac disease (CD) is the most common severe food intolerance in the Western world^[1]. It is a clinical syndrome of intestinal malabsorption, a characteristic though not specific histological lesion involving total, subtotal or partial small bowel villous atrophy (predominating in its proximal segments). It is the result of sensitiveness to ingested gluten in genetically susceptible people with the subsequent immune reaction leading to small bowel inflammation^[2]. The classical malabsorptive symptoms of diarrhoea and weight loss are only one aspect of the spectrum of manifestations of this relatively common disease^[3,4], since symptoms may be subtle and many patients have subclinical or silent disease^[5,6]. A proper gluten-free diet (GFD) would lead to a clinical and histological improvement^[7-9]. In particular, GFD played a key role in preventing nutritional deficiency, especially of micronutrients, and in reducing the risk of the development of intestinal malignancies^[10].

It is quite frequently seen in clinical practice that coeliac patients present gastrointestinal motor abnormalities^[11]. It has been recently shown that alteration of upper-gut motility may be related to dysfunction of autonomic nervous system^[12]. The aim of our study was to investigate whether autonomic nervous system (ANS) was altered even in untreated and unselected coeliac patients and to assess the effect of GFD on ANS dysfunctions.

MATERIALS AND METHODS

Patients

We studied 8 untreated, consecutive and unselected coeliac disease patients (2 males and 6 females, age range 37 ± 14.5 years). Both the original^[13] and revised^[14] criteria for the diagnosis of CD were used in this study. CD was defined as a permanent gluten-sensitive enteropathy, primarily manifested by the presence of characteristic small intestinal lesions^[15]. Small-bowel biopsy was performed in all patients, as well as esophagogastroduodenoscopy (Fujinon EG300 videogastroscope; Fujinon, Omiya, Japan). At least six small-bowel biopsies were obtained from the second part of the duodenum using a disposable biopsy forceps with spike (U.S. Endoscopy Inc., Mentor, Ohio, U.S.A.) and evaluated by haematoxylin/eosin staining. Histopathology was expressed according to the Marsh classification of 1992^[16]: "infiltrative" lesions with >30 lymphocytes/100 epithelial cells were defined as Marsh type I, "infiltrative/hyperplastic" lesions as Marsh II and "partial (sub)total villous atrophy (VA) as type III. We subdivided the Marsh III type into partial VA (Marsh IIIa), subtotal VA (Marsh IIIb) and total VA (Marsh IIIc), according to Oberhuber's modified classification^[17].

Other possible causes of villous atrophy or duodenal damage, such as *Giardia Lamblia* infection, tropical sprue, collagenous sprue, food protein hypersensitiveness (cow's milks, eggs, fish, rice, chicken) were excluded, as well as other causes of inflammatory infiltration of duodenum, such as peptic duodenitis^[17].

Methods

IgA and IgG anti-gliadin antibodies (AGA) were measured in all patients by enzyme-linked immunosorbent assay (kit Alfa-gliatest, Eurospital, Trieste - Italy); the lower limit of positivity

of IgA-class was 0.2 EU/mL and of IgG-class 10.0 EU/mL. IgA antiendomysial antibodies (EMA) were screened by the indirect immunofluorescent method on monkey oesophagus (kit Antiendomysium, Eurospital, Trieste - Italy). IgA anti-tissue transglutaminase antibodies were also screened by enzyme-linked immunosorbent assay using human recombinant tTG (kit Eu-tTG, Eurospital, Trieste - Italy); the lower limit of positivity of these antibodies was 7 UA/mL.

Also sorbitol H₂ breath test (H₂-BT) was performed. All patients were studied after an overnight fasting having been instructed to consume a meal of rice and meat; they were also requested not to smoke on the morning of the test day. End expiratory samples were collected before the patients drank the test solution (5 g of sorbitol in 150 mL of tap water) and every 30 min for 4 h. Hydrogen concentrations in each collected sample were measured with a breath-hydrogen analyzer (EC60 Gastrolyzer Breath Hydrogen Monitor, Bedford Scientific Ltd, Upchurch - Kent, England [U.K.]). An increase in H₂ concentration of at least 20 ppm over fasting baseline was considered positive for sorbitol malabsorption. The cut-off for calculating the validity of the test was shifted every 30 min, and a response operating characteristics (ROC) curve was plotted on the basis of the obtained results.

The clinical, endoscopic, histological and serological pattern of the studied coeliacs are described in Tables 1, 2.

Table 2 Non- invasive tests in the studied coeliac population

Patient No.	AGA IgA	AGA IgG	EMA	Anti-tTG	Sorbitol H ₂ -BT
1	+	+	+	+	+
2	+	+	+	+	+
3	+	+	+	+	+
4	+	+	-	-	+
5	+	+	+	+	+
6	+	+	-	+	+
7	-	-	+	-	+
8	+	-	-	+	+

Abbreviations: AGA: Anti-gliadin antibodies; EMA: anti-endomysium antibodies; anti-tTG: anti-tissue transglutaminase; H₂-BT: Hydrogen₂-breath test.

Table 1 Demographic, clinical, endoscopic and histological data of the coeliac patients

Patient No.	Sex	Age (yr)	Clinical finding	Endoscopic finding	Histology
1	F	71	Weakness, diarrhoea	Absence of Kerckring's folds	Marsh IIIc
2	M	58	Diarrhoea, weight loss	Absence of Kerckring's folds	Marsh IIIb
3	F	31	Aphtous stomatitis, IDA	Reduction of Kerckring's folds	Marsh IIIb
4	F	31	IDA	"Scalloping" of duodenal folds	Marsh IIIa
5	F	38	Diarrhoea, abdominal pain, weight loss	Reduction of Kerckring's folds, micronodular mucosa	Marsh IIIc
6	M	33	IDA	Reduction of Kerckring's folds	Marsh IIIa
7	F	24	IDA, Grave's disease	Reduction of Kerckring's folds	Marsh IIIa
8	F	32	IDA, weakness	Reduction of Kerckring's folds	Marsh IIIa

Abbreviations: IDA: iron-deficiency anaemia.

Table 3 Evaluation of autonomic function in coeliac patients and control group

Group	LS	VR	DB	△PAS Handgrip	△PAD Handgrip
Coeliac disease	1.22±0.1	1.73±0.38	35.5±16.4	35.7±16.4	24.6±13.2
Control group	1.24±0.19	1.62±0.25	32.5±7.67	55.5±24.2	27.1±11.1
P	NS	NS	NS	NS	NS

LS: Lying-to-standing; VR: Valsalva reaction; DB: Deep breathing.

No patient had other associated organic (such as hereditary, toxic, infectious, inflammatory) or metabolic diseases.

Extrinsic autonomic neuropathy was assessed by the standardized measurement of cardiovascular reflexes. Tests were performed in the morning and at constant temperatures. Autonomic function was evaluated by means of electrocardiograph Personal 120 (Esaote Biomedica, Firenze, Italy) and a Finapres set (Ohmeda, Louisville, Colorado, USA). We evaluated the heart rate variation (R-R interval) and systolic (SBP) and diastolic (DBP) blood pressures in response to a variety of stimuli: lying-to-standing (evaluation of R-R variation with a 30.15 ratio); Valsalva manoeuvre (forced expiration for 15 s with a 40 mm Hg pressure); deep breathing (6 expiratory cycles throughout one minute, evaluating the average of differences between the maximal and minimal duration of R-R interval during three subsequent deep breath [DB3]); sustained handgrip (performing isometric sub-maximal work for 3 min and evaluating blood pressure and heart rate variations); and tilt tests. The results of each test were scored according to Ewing's modified criteria^[18,19].

The results obtained were compared with a healthy, asymptomatic control group (13 people, 6 males and 7 females, age range 42.3±13.5 years). All coeliac patients were re-evaluated about the autonomic function 6 and 12 mo after GFD has started.

Statistical analysis

The Student's *t*-test for unpaired data was used, and data are presented as mean±SD. *P*<0.05 was considered as statistically significant.

RESULTS

We noted that coeliac patients showed a lower increase of PAS in response to isometric effort. Moreover, they showed a reduction of spectral power LF in response to clinostatic position, but without statistical significance (Tables 3, 4).

Only one female patient (Table 5, patient number 8) showed symptomatic orthostatic hypotension (defined as SBP decrease ≥/≤ 20 mm Hg and DBP ≥/≤ 10 mmHg within 3 min in orthostatic position) as responsiveness to orthostatic position.

The overall results of ANS in coeliacs showed a tendency

Table 4 Evaluation of Heart rate variance in coeliac patients and control group

Group	LF Clino	LF Ortho	HF Clino	HF Ortho	LF/HF Clino	LF/HF Ortho
Coeliac disease	35.9±18.1	73.5±15.3	35.7±18.9	13.21±9.3	1.56±1.85	8.63±6.34
Control group	52.8±21.0	67.1±25.9	31.1±15.6	17.90±12.9	2.35±1.65	6.94±5.5
P	NS	NS	NS	NS	NS	NS

Table 5 Overall results of autonomic tests in coeliac patients

Patient No.	Basal SBP	Basal DBP	Ortho SBP	Ortho DBP	Clino. LF	Ortho. LF	Clino. HF	Ortho. HF	Clino. LF/HF	Ortho. LF/HF	LS	VR	DB	Syst. SH	Diast. SH	Syst. Tilt Test	Diast. Tilt Test
1	127	82	120	82	40.99	61.65	48.00	32.82	0.85	1.88	1.03	1.46	19.2	54	27	-9	7.00
2	130	87	135	87	21.41	60.74	30.09	10.73	0.71	5.66	1.37	1.90	35.9	36	14	-9	5.00
3	130	80	125	80	77.04	92.52	12.89	5.96	5.98	15.52	1.20	1.40	33.3	35	25	19	14.00
4	105	70	105	85	38.26	63.87	20.19	17.85	1.9	3.58	1.20	2.30	40.1	39	36	3	7.00
5	115	80	120	82	31.15	58.43	62.16	16.49	0.5	3.54	1.20	1.40	39.3	48	28	7	14.00
6	120	80	108	75	27.16	87.79	27.33	11.00	0.99	7.98	1.18	1.50	40.2	50	47	2	12.00
7	105	70	115	75	20.30	94.00	61.00	4.79	0.3	19.6	1.30	2.30	44.3	7	6	-7	15.00
8	115	70	80	60	30.93	68.81	23.81	6.06	1.3	11.35	1.30	1.60	31.8	17	14	-10	2.00
Mean	118.38	77.38	113.50	78.25	35.91	73.48	35.68	13.21	1.57	8.64	1.22	1.73	35.51	35.75	24.63	-0.50	9.50
SD	10.20	6.52	16.50	8.51	18.13	15.27	18.88	9.28	1.85	6.34	0.10	0.39	7.74	16.37	13.20	10.23	4.87

to lower systolic-diastolic values of blood pressure both in clinostatic position and in active and passive orthostatic positions. However, these results had no statistical difference compared with those of control group (Table 4).

The spectral analysis of heart rate variance (HRV), performed with autoregressive method, confirmed these findings. The autoregressive analysis of HRV showed an important, but not significant, reduction of the power LF according to a considerable reductive activity of sympathetic tone at rest with a relative prevalence of parasympathetic tone. Passive orthostatic, evaluated by tilt tests, induced a marked sympathetic response (with increase of spectral power LF) (Table 5).

All patients were re-evaluated about the autonomic function 6 and 12 mo after GFD has started. In none of them we noted change of the results, and the symptomatic orthostatic hypotension persisted in patient number 8 despite strict adherence to GFD.

DISCUSSION

In recent years a discrete frequency of autonomic neuropathy has been disclosed in coeliac patients^[12,20], similar to that reported in other functional gastrointestinal disorders, but lower than that described in diabetic subjects^[21]. Pathogenetic factors involved in autonomic dysfunction in coeliac disease were unknown, and autoimmune damage or metabolic derangement have been hypothesized^[22-24].

We investigated our coeliac patients, exploring their autonomic function using the cardiovascular tests because they were easily available reproducible, and not very expensive^[25,26]. Our study showed quite different results from those recent studies about autonomic function in coeliacs. In particular, they differed from Usai's study, which reported ANS abnormalities in 45% of coeliacs affected by upper gastrointestinal symptoms^[12]. Thus, we can hypothesize that ANS abnormalities may play a role in upper gastrointestinal symptoms rather than in systemic symptoms. In fact we recorded ANS abnormalities only in 1/5 patient without gastrointestinal symptoms. On the other hand, it is noteworthy that we did not find ANS abnormalities in any of the 3 patients complaining about gastrointestinal symptoms (Table 5). However, a role of ANS dysfunction in some coeliac patients cannot be excluded, since the patient No. 8 of our studied population (a 32-year-old

female), the only one with ANS dysfunction, did not show dyspeptic symptoms but only systemic symptoms.

What a role could then the autonomic neuropathy play? Can it really play a role in the systemic symptoms in coeliac disease? We knew that several coeliac patients experienced weakness or chronic fatigue in clinical practice. In most cases it was related to malabsorption (such as iron-deficiency anaemia or folic acid deficiency), but in some cases autonomic neuropathy might be suspected. Our study unfortunately failed to demonstrate a significant autonomic dysfunction in CD; however, we cannot exclude that in some patients ANS dysfunction might play a role in the genesis of some systemic symptoms, such as weakness or chronic fatigue. In fact we noted that coeliac patients showed a lower tolerance to orthostatism, associated with a latent disequilibrium of sympathetic-vagal balance, ie, a relative prevalence of the parasympathetic component of the autonomic function. These alterations, and in particular the reduced tolerance to orthostatism, may explain the above mentioned symptoms in some cases, as we noted in patient No. 8 (Table 5).

But another very finding was that ANS dysfunction did not improve in this patient after GFD. It is difficult to explain why ANS did not improve after gluten withdrawal. We speculate that ANS dysfunction may be a two step process. In the first phase it may be gluten-related, and may improve after GFD. This phase may have a variable length, probably related to age, gender and time to gluten exposure. In the second phase it may be gluten - independent, probably related to autoimmune axonal aggression to autonomic nervous system, in which autoimmunity may perpetuate the neurological damage. Recent studies of Luostarinen *et al.*^[27] may in part confirm this hypothesis. They showed that axonal neuropathy in CD might be also subclinical without any sign of malabsorption and it often persisted despite good compliance to GFD^[27]. This hypothesis may justify the persistence of the orthostatic hypotension in patient 8 after six and twelve months of GFD, and it may also explain why some coeliacs experienced persistence or recurrence of chronic fatigue despite GFD. We consider that the recurrence of systemic symptoms is related to incidental gluten ingestion from unknown sources: the autonomic neuropathy, with consequent disequilibrium of sympathetic-vagal balance may be the cause of these systemic symptoms.

REFERENCES

- 1 **Catassi C**, Ratsch IM, Fabiani E, Rossigni M, Mordicchia F, Candela F, Coppa GV, Giorgi PL. Coeliac disease in the year 2000: exploring the iceberg. *Lancet* 1994; **343**: 200-203
- 2 **Lundin KE**. Coeliac disease – all questions answered? *Digest Liver Dis* 2002; **34**: 238-242
- 3 **Johnston SD**, Watson RG, Mcmillan SA, Sloan J, Love AH. Prevalence of coeliac disease in Northern Ireland. *Lancet* 1997; **350**: 1370
- 4 **Volta U**, Bellentani S, Bianchi FB. High prevalence of celiac disease in Italian General population. *Dig Dis Sci* 2001; **46**: 1500-1505
- 5 **Tursi A**, Giorgetti G, Brandimarte G, Rubino E, Lombardi D, Gasbarrini G. Prevalence and clinical presentation of subclinical/silent coeliac disease in adults: an analysis on a 12-year observation. *Hepatogastroenterology* 2001; **48**: 462-464
- 6 **Brandimarte G**, Tursi A, Giorgetti GM. Changing trends in clinical form of coeliac disease: which is now the main form of coeliac disease in clinical practice? *Minerva Gastroenterol Dietol* 2002; **48**: 121-130
- 7 **Walker-Smith JA**, Guandalini S, Schmitz J, Schmerling DH, Visakorpi JK. On behalf of Working Group of European Society of Paediatric Gastroenterology and Nutrition. Revised criteria for diagnosis of coeliac disease. *Arch Dis Child* 1990; **65**: 909-911
- 8 **Green PH**, Jabri B. Coeliac disease. *Lancet* 2003; **362**: 383-391
- 9 **O'Mahoney S**, Howdle PD, Losowsky MS. Review article: management of patients with non-responsive coeliac disease. *Aliment Pharmacol Ther* 1996; **10**: 671-678
- 10 **Holmes GKT**, Prior P, Lane MR, Pope D, Allan RN. Malignancy in coeliac disease – effect of a gluten free diet. *Gut* 1989; **30**: 333-338
- 11 **Tursi A**. Gastrointestinal motility disturbances in celiac disease. *J Clin Gastroenterol* 2004; **38**: (in press)
- 12 **Usai P**, Usai Satta P, Lai M, Corda MG, Piras E, Calcara C, Boy MF, Morelli A, Balestrieri A, Bassotti G. Autonomic dysfunction and upper digestive functional disorders in untreated adult coeliac disease. *Eur J Clin Invest* 1997; **27**: 1009-1015
- 13 **Meuwisse GH**. Diagnostic criteria in coeliac disease. *Acta Paediatr* 1970; **59**: 461-463
- 14 **Walker-Smith JA**, Guandalini S, Schmitz J, Schmerling DH, Visakorpi JK. Revised criteria for diagnosis of celiac disease. *Arch Dis Child* 1990; **65**: 909-911
- 15 **Feighery C**, Weir DG, Whelan A, Willoughby R, Youngprapakorn S, Lynch S, O'Morain C, McEneaney P, O'Farrelly C. Diagnosis of gluten-sensitive enteropathy: is exclusive reliance on histology appropriate? *Eur J Gastroenterol Hepatol* 1998; **10**: 919-925
- 16 **Marsh MN**. Gluten, major histocompatibility complex, and the small intestine. A molecular and immunologic approach to the spectrum of gluten sensitivity (celiac sprue). *Gastroenterology* 1992; **102**: 330-354
- 17 **Oberhuber G**, Grandisch G, Vogelsang H. The histopathology of coeliac disease: time for a standardized report scheme for pathologists. *Eur J Gastroenterol Hepatol* 1999; **11**: 1185-1194
- 18 **Ewing DJ**, Clarke BF. Diagnosis and management of diabetic autonomic neuropathy. *BMJ* 1982; **285**: 916-918
- 19 **Cardone C**, Paiusco P, Marchetti GP, Burelli F, Feruglio M, Fedele D. Cough test to assess cardiovascular autonomic reflexes in diabetes. *Diabetes Care* 1990; **13**: 719-724
- 20 **Usai P**, Usai Satta P, Savarino V, Boy MF. Autonomic neuropathy in adult's celiac disease. *Am J Gastroenterol* 1996; **91**: 1676-1677
- 21 **Bhaurucha AE**, Camilleri M, Low PA, Zinsmeister AM. Autonomic dysfunction in gastrointestinal motility disorders. *Gut* 1993; **34**: 397-401
- 22 **Pengiran Tengah DS**, Wills AJ, Holmes GK. Neurological complications of coeliac disease. *Postgrad Med J* 2002; **78**: 393-398
- 23 **Kaplan JG**, Pack D, Horoupian D, DeSouza T, Brin M, Schaumburg H. Distal axonopathy associated with chronic gluten enteropathy: a treatable disorder. *Neurology* 1988; **38**: 642-645
- 24 **Willis A**, Howell CJ. Neurological complications of enteric disease. *Gut* 1996; **39**: 501-504
- 25 **Piha SJ**, Puukka P, Seppanen A. Short and long-term reproducibility of cardiovascular tests of autonomic function in normal subjects. *Clin Auton Res* 1991; **1**: 115-118
- 26 **Nyarco-Adomfeh C**. The long-term reproducibility of clinical tests of autonomic cardiovascular function in normal subjects. *Clin Auton Res* 1992; **2**: 257-265
- 27 **Luostarinen L**, Himanen SL, Luostarinen M, Collin P, Pirttila T. Neuromuscular and sensory disturbances in patients with well treated coeliac disease. *J Neurol Neurosurg Psychiatry* 2003; **74**: 490-494

Edited by Zhu LH and Xu FM

Detection of frameshift mutations of *RIZ* in gastric cancers with microsatellite instability

Kai-Feng Pan, You-Yong Lu, Wan-Guo Liu, Lian Zhang, Wei-Cheng You

Kai-Feng Pan, Lian Zhang, Wei-Cheng You, Department of Cancer Epidemiology, Peking University School of Oncology, Beijing Institute for Cancer Research, Beijing Cancer Hospital, Beijing 100034, China
You-Yong Lu, Beijing Laboratory of Molecular Oncology, Peking University School of Oncology, Beijing Institute for Cancer Research, Beijing Cancer Hospital, Beijing 100034, China

Wan-Guo Liu, Division of Experimental Pathology, Department of Laboratory Medicine and Pathology, Mayo Clinic/Mayo Medical School, Rochester, MN 55905, USA

Supported by the Major State Basic Research Development Program of the Ministry of Science and Technology of China, No. G1998051203, and Beijing Municipal Commission Foundation for Science and Technology, No. H020920030130

Correspondence to: Dr. Wei-Cheng You, Department of Cancer Epidemiology, Peking University School of Oncology, Beijing Institute for Cancer Research, Beijing Cancer Hospital, Beijing 100034, China. weichengyou@yahoo.com

Telephone: +86-10-88141035 **Fax:** +86-10-66175832

Received: 2003-12-28 **Accepted:** 2004-02-18

Abstract

AIM: To study the frameshift mutations of the retinoblastoma protein-interacting zinc finger gene *RIZ* in gastric cancer with microsatellite instability, and to identify two coding polyadenosine tracts of *RIZ*.

METHODS: Frameshift mutations at (A)₈ and (A)₉ tracts of *RIZ* were detected in 70 human gastric cancer (HGC) specimens by DHPLC and DNA sequencing. Microsatellite instability (MSI) status was assessed by two mononucleotide markers, BAT26 and BAT25, by means of denaturing high-performance liquid chromatography (DHPLC).

RESULTS: In 70 HGC samples, 8 (11.4%) were found positive for instabilities at BAT26 and BAT25. In 7 of the 8 cases with instabilities at both BAT26 and BAT25 (MSI-H), 1 was unstable at BAT26 but stable at BAT25. Frameshift mutations were identified in 4 (57.1%) of the 7 samples with MSI-H in the (A)₉ tract of *RIZ* without mutations in the (A)₈ tract. In contrast, frameshift mutations were found in neither of the polyadenosine tracts in 63 samples of MSI-L or MSI stable tumors. Pro704 LOH detection in 4 cases with frameshift mutations did not find LOH in these cases.

CONCLUSION: Frameshift mutations of *RIZ* may play an important role in gastric cancers with MSI.

Pan KF, Lu YY, Liu WG, Zhang L, You WC. Detection of frameshift mutations of *RIZ* in gastric cancers with microsatellite instability. *World J Gastroenterol* 2004; 10(18): 2719-2722
<http://www.wjgnet.com/1007-9327/10/2719.asp>

INTRODUCTION

Two major pathways of genomic instabilities have been recently recognized, namely the chromosomal instability pathway (CIN) and the microsatellite instability (MSI) pathway (MIN), the

former is characterized by the loss of heterozygosity (LOH) whereas the latter by MSI^[1]. Some genes contain repetitive regions in their coding sequences that are often targets of MSI. Gastrointestinal tumors with DNA mismatch repair (MMR) defects often present MSI and harbor frameshift mutations in coding mononucleotide repeats of cancer-related genes. MSI (+) tumors arise from the defects in the MMR system through the mechanism presumably involving frameshift mutations of the microsatellite repeats within the coding regions of the affected target genes, whose function loss is believed to contribute to tumorigenesis^[2-5].

The retinoblastoma protein-interacting zinc finger gene *RIZ* is a candidate tumor suppressor gene locus on 1p36, a region that commonly harbors alterations in many types of human cancers^[6]. The interaction of *RIZ* with the retinoblastoma protein (Rb) suggests its involvement in the control of proliferation by an alternative mechanism. *RIZ* gene encodes two protein products, RIZ1 and RIZ2, which differ for a motif present in the N-terminal domain, defined as the PR domain that was previously identified as a common motif in several transcription factors. RIZ1 contains a PR domain indicative of tumor suppressor function, whereas RIZ2 does not contain this motif^[7,8]. RIZ1 has the capacity to induce cell cycle arrest at G₂/M phase and cell apoptosis, and suppresses tumorigenicity in nude mice^[9-11]. A role for *RIZ* has been recently proposed in cell cycle arrest and cell apoptosis through a transcriptional repression mechanism^[7,12].

In MSI(+) tumors, *RIZ* was found to be affected by frequent frameshift mutations of one or two coding poly(A) tract, an (A)₈ tract at the coding nucleotide sequence 4273-4280 and an (A)₉ tract at 4462-4471 in exon 8. These mutations generate truncated RIZ1 proteins lacking the COOH-terminal PR-binding motif and are expected to have serious deleterious effects on the PR domain-specific function of RIZ1. *RIZ* plays an important role in hereditary tumors of the MIN pathway as suggested by the frequent frameshift mutations in HNPCC tumors^[11]. The role of *RIZ* in gastric MSI(+) tumors remains to be investigated. In this study, we used denaturing high-performance liquid chromatography (DHPLC), a highly productive method, to rapidly detect frameshift mutations of (A)₈ and (A)₉ tracts and LOH of pro704 in gastric cancer specimens and to explore the role of *RIZ* gene in gastric carcinogenesis.

MATERIALS AND METHODS

Tissue specimen and DNA extraction

Gastric cancer samples and matched adjacent normal gastric tissues were obtained from 41 male and 29 female patients during surgical resection of the tumors with informed consent from the patients at Beijing Institute for Cancer Research, Beijing Cancer Hospital. The fresh samples were collected at the time of surgery and frozen at -80 °C. The sections from each specimen were examined by a pathologist. There were 39 intestinal-type tumors and 31 diffuse-type tumors. High-molecular weight genomic DNA was extracted by standard proteinase K digestion and phenol/ chloroform extraction^[13].

Primers and PCR

Primers used for (A)₈ tract and (A)₉ tract in the *RIZ* gene amplification

were as follows: *RIZA8-F5'*-GAGCTCAGCAAAATGTCGTC-3', *RIZA8-R5'*-CAAGTCGGCCTTCTGCTTTG-3'; *RIZA9-F5'*-TCTCACATCTGCCCTTACTG-3', *RIZA9-R5'*-GTGATGAGTGTCCACCTTTG-3'. The *RIZ* Pro704 deletion polymorphism was assayed by PCR followed by DHPLC. The PCR primers were: RP145 5'-CCCAAGATAAACTAATCTCT-3', RP105 5'-ACTCCATGCTGGTGAGTC-3'.

The samples used for mutation screening and sequencing were amplified in 25 μ L reaction solution containing 50 ng genomic DNA, 0.4 μ mol/L sense and antisense primers for each tract, 200 μ mol/L dNTPs (Perkin-Elmer, Foster City, CA, USA), 0.2 μ L Taq polymerase (Ampli Taq Gold: Perkin-Elmer), and 2.0 mmol/L MgCl₂. After an initial activation of the enzyme by denaturation at 95 °C for 9 min, PCR amplification was performed for 35 cycles in the following sequence: at 94 °C for 30 s, at optimized annealing temperature for 45 s, and at 72 °C for 45 s, with a final extension at 72 °C for 10 min. The annealing temperature for various primer sets was: 58 °C for *RIZ* A₈ tract, 60 °C for *RIZ* A₉ tract, and 55 °C for pro704.

Mutation analysis

For examining the heteroduplex content, 50-100 ng of the PCR products were subjected to DHPLC (WAVE™ system, Transgenomic, USA) under partial denaturation condition. The mobile phase consisted of a mixture of 0.1 mol/L triethylamine acetate (TEAA, pH 7.0) with or without 25% acetonitrile. The flow rate used in this study was 0.9 mL/min. The column temperatures for the PCR products were 57 °C for *RIZ* (A)₈ tract and 56 °C for *RIZ* (A)₉ tract. The PCR products were heated to 95 °C for 3 min followed by cooling to 25 °C over 45 min. Homozygous mutant DNA must be combined with the wild

type at the ratio of approximately 1:1 prior to hybridization.

LOH analysis

The pro704 PCR products were directly used without a denaturation and reannealing process under non-denaturing conditions on the WAVE™ system. The gradient of buffer B from 1 to 7 min was 49-55%. The column temperature was 50 °C and flow rate was 0.75 mL/min.

DNA sequencing

The PCR product was treated with exonuclease and shrimp alkaline phosphatase based on the protocol provided by the United States Biochemical and sequenced by the Mayo Clinic DNA sequencing facility. Sequencing reactions were performed in the GeneAmp PCR System 9600 with fluorescent terminations, and the products were analyzed on an ABI 377 sequencer (Perkin-Elmer, Foster City, CA, USA). All sequence alterations were confirmed by bidirectional sequencing of the PCR products generated by at least two independent reactions.

MSI analysis by DHPLC

MSI analysis by DHPLC was performed as described previously^[14]. Briefly, the PCR products were examined by DHPLC under fully denaturing conditions. The flow rate used in this study was 0.9 mL/min, with the column temperature of 80 °C. The gradient of buffer B from 0.1 to 7.1 min was 30-51%.

RESULTS

A total of 70 HGC samples and their matched normal tissues were analyzed for MSI status by two mononucleotide markers,

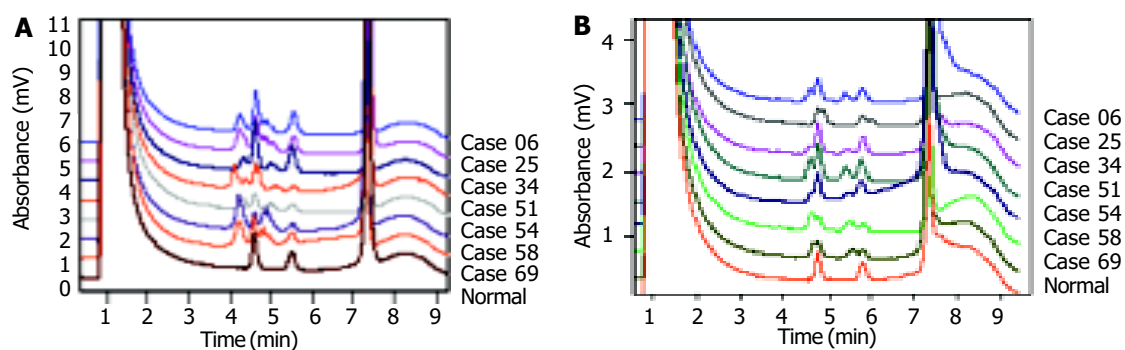


Figure 1 MSI analysis of 70 paired HGCs by DHPLC. Curves at the bottom in both Panels A and B represent normal DNA as indicated by the specification on the bottom right, and the rest curves represent tumor DNA in specified cases. Column: DNASep™; mobile phase: 0.1 mol/L TEAA (pH 7.0); linear gradient: 30-51% B in 7 min; flow rate: 0.9 mL/min; temperature: 80 °C; detection: UV at 260 nm. Panel A: DHPLC chromatograms of HGCs at BAT26; Panel B: DHPLC chromatograms of HGCs at BAT25.

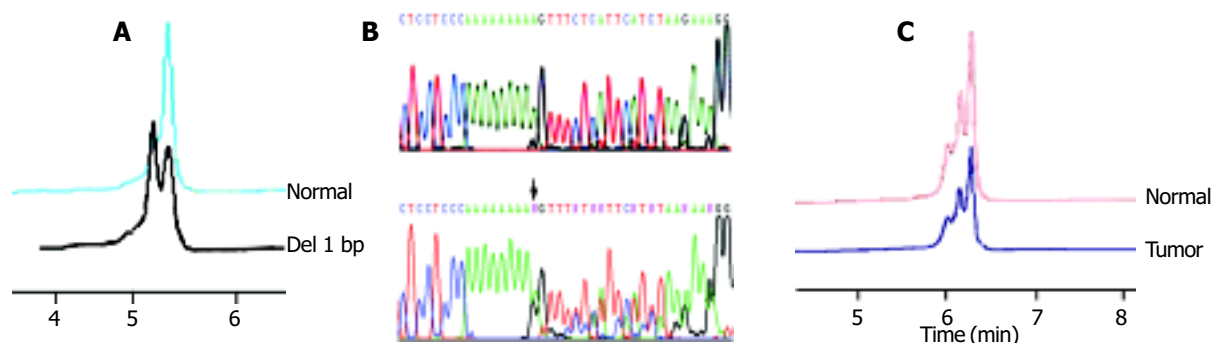


Figure 2 Typical elution profiles of DHPLC analysis and sequencing. Panel A: DHPLC elution profiles for *RIZ*(A)₉ tract, column temperature: 56 °C, flow rate: 0.9 mL/min, mobile phase: 0.1 mol/L TEAA (pH 7.0), linear gradient: 51-60% B in 4.5 min, detected with UV at 260 nm; Panel B: Sequence tracings for the same samples. The upper panel is a normal control, and the lower is a frameshift mutation (1-bp deletion). The arrow indicates the mutant nucleotide; Panel C: DHPLC elution profiles for pro704 LOH, column temperature: 50 °C, flow rate: 0.75 mL/min, mobile phase: 0.1 mol/L TEAA (pH 7.0), linear gradient: 49-55% B in 7 min, detected with UV at 260 nm.

BAT26 and BAT25, by means of DHPLC. In 70 HGC samples, 8 (11.4%) were found to contain sequence variation at BAT26 and BAT25 and 7 of them were shown to be unstable at both BAT26 and BAT25 (Figure 1), classified as MSI-H. One was unstable at BAT26 but stable at BAT25.

Frameshift mutations of *RIZ* (A)₉ and (A)₈ tract were identified. HCT-116 cell line had been studied previously and frameshift mutations were identified in the polyadenosine tracts^[11], which served as the positive control in this study. In 7 samples with MSI-H, 4 (57.1%) were found to have mutations in the (A)₉ tract of *RIZ* by DHPLC and DNA sequencing, including 3 intestinal-type tumors and 1 diffuse-type tumor. All of them had a 1-bp deletion (Figure 2A, B). No mutations were detected in the (A)₈ tract. No mutations in the (A)₉ or (A)₈ tract were found in the 63 MSI-L or MSI stable samples.

To determine whether *RIZ* was also affected by chromosomal deletion in MSI(+) tumors, pro704 LOH studies were performed on 4 samples with frameshift mutations for which the matched normal DNAs were available. We observed that both the PCR products of the tumor DNA and matched normal DNA resulted in the same peak chromatogram on DHPLC under the condition used for DNA sizing at 50 °C. LOH was not found at the *RIZ* locus in these tumors (Figure 2C).

DISCUSSION

Approximately 10-15% of gastrointestinal tumors are caused by defective MMR^[15], characterized by the presence of tumor MSI (MSI-H) and the absence of protein expression for any of the various genes involved in DNA MMR including hMLH1, hMSH2, hMSH6 or hPMS2^[16]. Gastric cancer with an MSI-H phenotype often harbors somatic frameshift mutations in the coding mononucleotide repeats of cancer-related genes. Frameshift mutations in *TGFβRII*, *BAX*, *IGFIR* and *E2F4* genes are often observed in cancers exhibiting a high frequency of MSI^[17]. Recently, the new candidate tumor suppressor gene, *RIZ*, which may be targeted for deletion, was identified. *RIZ* is a protein with two alternative forms of *RIZ1* and *RIZ2*, which differ for a PR domain present in the N-terminal domain. The PR domain is necessary for the negative regulatory function of *RIZ*. Frameshift mutations in either (A)₈ or (A)₉ tract are thought to lead to C-terminal domain loss of the *RIZ* protein involved in PR binding. In this study, we detected frameshift mutations in *RIZ* (A)₉ tract, whereas no mutation was found in (A)₈ tract. All of the frameshift mutations here found in *RIZ* are assumed to lead to the production of the COOH-terminal domain-truncated protein, which is likely to seriously affect *RIZ1* functions.

Frameshift in short mononucleotide tracts is common in gastrointestinal tumors of the microsatellite mutator phenotype (MMP). MSI is considered a hallmark of the mutator phenotype, and determination of MSI is critical for understanding tumor biology. Separation of HGCs based on their mutator phenotypes is an effective first step to allow the distinction of these two different pathways of carcinogenesis. In the present study, we analyzed MSI status by two mononucleotide markers, and detected *RIZ* mutations in 4 (57.1%) of the 7 MSI-H tumors but in none of the 63 MSI-L or MSI stable gastric cancers, indicating that these mutations are specific for MSI-H tumors that exhibit a tendency to accumulate frameshift mutations in reiterated sequence of the coding regions of cancer-related genes known to facilitate cancer development and progression. These mutations may contribute to cancer progression either by inactivating their tumor suppressor functions or acting as secondary mutator mutations in MMP(+) gastric tumors^[18]. Our study has shown that MSI-H gastric cancers accumulate frameshift mutations in the *RIZ* gene. On the basis of our findings, we suppose that *RIZ* is a candidate target gene in MSI tumorigenesis.

Two kinds of genetic instability, MIN and CIN, have been

documented in colorectal cancers. To determine whether *RIZ* is also affected by chromosomal deletion in MSI-H cancers, we detected the pro704 LOH in the 4 cases with frameshift mutations but failed to find LOH at the *RIZ* locus in these tumors, suggesting that *RIZ* frameshift mutations are common in MSI(+) gastric cancers, whereas LOH is not. More extensive studies on gastric cancers are needed to clarify whether *RIZ* is affected by two different ways. In MSI(+) tumors (MIN pathway), frameshift mutations in the COOH-terminal interfere with the interactions between the C terminus of the protein and its PR domain. In MSI(-) tumors (CIN pathway), mutations or deletions of the PR domain of *RIZ1* may have similar effects.

In this study, we detected MSI status and LOH by DHPLC analysis. DHPLC has been described as a novel technology for the detection of gene mutations in inherited diseases or cancers and for the identification of single nucleotide polymorphisms (SNPs)^[19]. The present study demonstrates the efficacy of DHPLC in analysis of the MSI status and LOH, which allows automated examination of MSI and LOH with considerable precision at relatively low cost, without any special labeling procedure.

REFERENCES

- 1 **Lengauer C**, Kinzler KW, Vogelstein B. Genetic instabilities in human cancers. *Nature* 1998; **17**: 643-649
- 2 **Parsons R**, Myeroff LL, Liu B, Willson JK, Markowitz SD, Kinzler KW, Vogelstein B. Microsatellite instability and mutations of the transforming growth factor beta type II receptor gene in colorectal cancer. *Cancer Res* 1995; **55**: 5548-5550
- 3 **Shin KH**, Park JG. Microsatellite instability is associated with genetic alteration but not with low levels of expression of the human mismatch repair proteins hMSH2 and hMLH1. *Eur J Cancer* 2000; **36**: 925-931
- 4 **Markowitz S**, Wang J, Myeroff L, Parsons R, Sun L, Lutterbaugh J, Fan RS, Zborowska E, Kinzler KW, Vogelstein B. Inactivation of the type II TGF-beta receptor in colon cancer cells with microsatellite instability. *Science* 1995; **268**: 1336-1338
- 5 **Rampino N**, Yamamoto H, Ionov Y, Li Y, Sawai H, Reed JC, Perucho M. Somatic frameshift mutations in the BAX gene in colon cancers of the microsatellite mutator phenotype. *Science* 1997; **275**: 967-969
- 6 **Huang S**. The retinoblastoma protein-interacting zinc finger gene *RIZ* in 1p36-linked cancers. *Front Biosci* 1999; **4**: D528-532
- 7 **Huang S**, Shao G, Liu L. The PR domain of the Rb-binding zinc finger protein *RIZ1* is a protein binding interface and is related to the SET domain functioning in chromatin-mediated gene expression. *J Biol Chem* 1998; **273**: 15933-15939
- 8 **Abbondanza C**, Medici N, Nigro V, Rossi V, Gallo L, Piluso G, Belsito A, Roscigno A, Bontempo P, Puca AA, Molinari AM, Moncharmont B, Puca GA. The retinoblastoma-interacting zinc-finger protein *RIZ* is a downstream effector of estrogen action. *Proc Natl Acad Sci U S A* 2000; **97**: 3130-3135
- 9 **He L**, Yu JX, Liu L, Buyse IM, Wang MS, Yang QC, Nakagawara A, Brodeur GM, Shi YE, Huang S. *RIZ1*, but not the alternative *RIZ2* product of the same gene, is underexpressed in breast cancer, and forced *RIZ1* expression causes G2-M cell cycle arrest and/or apoptosis. *Cancer Res* 1998; **58**: 4238-4244
- 10 **Jiang G**, Liu L, Buyse IM, Simon D, Huang S. Decreased *RIZ1* expression but not *RIZ2* in hepatoma and suppression of hepatoma tumorigenicity by *RIZ1*. *Int J Cancer* 1999; **83**: 541-546
- 11 **Chadwick RB**, Jiang GL, Bennington GA, Yuan B, Johnson CK, Stevens MW, Niemann TH, Peltomaki P, Huang S, de la Chapelle A. Candidate tumor suppressor *RIZ* is frequently involved in colorectal carcinogenesis. *Proc Natl Acad Sci U S A* 2000; **97**: 2662-2667
- 12 **Xie M**, Shao G, Buyse IM, Huang S. Transcriptional repression mediated by the PR domain zinc finger gene *RIZ*. *J Biol Chem*

- 1997; **272**: 26360-26366
- 13 **Albrecht S**, von Deimling A, Pietsch T, Giangaspero F, Brandner S, Kleihues P, Wiestler OD. Microsatellite analysis of loss of heterozygosity on chromosomes 9q, 11p and 17p in medulloblastomas. *Neuropathol Appl Neurobiol* 1994; **20**: 74-81
- 14 **Pan KF**, Liu W, Lu YY, Zhang L, Li ZP, Lu WL, Thibodeau SN, You WC. High throughput detection of microsatellite instability by denaturing high-performance liquid chromatography. *Hum Mutat* 2003; **22**: 388-394
- 15 **Peltomaki P**. Deficient DNA mismatch repair: a common etiologic factor for colon cancer. *Hum Mol Genet* 2001; **10**: 735-740
- 16 **Aaltonen LA**, Salovaara R, Kristo P, Canzian F, Hemminki A, Peltomaki P, Chadwick RB, Kaariainen H, Eskelinen M, Jarvinen H, Mecklin JP, de la Chapelle A. Incidence of hereditary nonpolyposis colorectal cancer and the feasibility of molecular screening for the disease. *N Engl J Med* 1998; **338**: 1481-1487
- 17 **Wu MS**, Lee CW, Shun CT, Wang HP, Lee WJ, Chang MC, Sheu JC, Lin JT. Distinct clinicopathologic and genetic profiles in sporadic gastric cancer with different mutator phenotypes. *Genes Chromosomes Cancer* 2000; **27**: 403-411
- 18 **Piao Z**, Fang W, Malkhosyan S, Kim H, Horii A, Perucho M, Huang S. Frequent frameshift mutations of RIZ in sporadic gastrointestinal and endometrial carcinomas with microsatellite instability. *Cancer Res* 2000; **60**: 4701-4704
- 19 **Liu W**, Smith DI, Rechtzigel KJ, Thibodeau SN, James CD. Denaturing high performance liquid chromatography (DHPLC) used in the detection of germline and somatic mutations. *Nucleic Acids Res* 1998; **26**: 1396-1400

Edited by Chen WW Proofread by Zhu LH and Xu FM

Ovarian hormone modulates 5-hydroxytryptamine 3 receptors mRNA expression in rat colon with restraint stress-induced bowel dysfunction

Tian-Jin Li, Bao-Ping Yu, Wei-Guo Dong, He-Sheng Luo, Long Xu, Mu-Qi Li

Tian-Jin Li, Bao-Ping Yu, Wei-Guo Dong, He-Sheng Luo, Long Xu, Mu-Qi Li, Department of Gastroenterology, Renmin Hospital, Wuhan University, Wuhan 430060, Hubei Province, China

Supported by the Key Technologies Programme of Hubei, No. 2003AA304B12

Correspondence to: Dr. Bao-Ping Yu, Department of Gastroenterology, Renmin Hospital, Wuhan University, Wuhan 430060, Hubei Province, China. yubaoping62@yahoo.com.cn

Telephone: +86-27-88075814

Received: 2003-11-18 Accepted: 2004-01-15

Abstract

AIM: To examine the effects of ovarian hormone on the expression of 5-hydroxytryptamine 3 receptors (5-HT₃R) in rat colon of restraint stress-induced bowel dysfunction.

METHODS: Twenty-four female Sprague-Dawley rats were randomly divided into three groups of 8 each: sham operation, ovariectomy (OVX) and ovariectomy with estrogen (E₂) and progesterone (P) replacement therapy (OVX+E₂+P). The rats were subjected to 1-h restraint stress 4 wk after operation. The changes of defecation were monitored by collection of fecal pellets. The gonadal steroids were measured in duplicate by radioimmunoassay (RIA). The expression of 5-HT₃R mRNA in the colon was studied by RT-PCR.

RESULTS: Compared with sham group and OVX+E₂+P group, OVX group showed increase in fecal pellets and decrease in the time of vitreous pellets excretion ($P < 0.01$). Serum levels of E₂ and P were suppressed in OVX group and restored following treatment with ovarian steroids ($P < 0.01$), and the levels of 5-HT₃R mRNA in the colon of ovariectomized rats were significantly increased, the expression of 5-HT₃R mRNA was significantly decreased in hormone replacement therapy group ($P < 0.01$).

CONCLUSION: Ovarian hormone plays a role in the regulation of 5-HT₃R expressions in restraint stress-induced bowel dysfunction of rats. The interactions between ovarian steroids and gastrointestinal tract may have major pathophysiological implications in 5-HT-related disorders, such as irritable bowel syndrome (IBS).

Li TJ, Yu BP, Dong WG, Luo HS, Xu L, Li MQ. Ovarian hormone modulates 5-hydroxytryptamine 3 receptors mRNA expression in rat colon with restraint stress-induced bowel dysfunction. *World J Gastroenterol* 2004; 10(18): 2723-2726
<http://www.wjgnet.com/1007-9327/10/2723.asp>

INTRODUCTION

IBS is characterized by intermittent or continuous abdominal pain and alterations in bowel patterns^[1,2]. The syndrome is one of the most common gastrointestinal (GI) disorders seen in primary care and specialist practices^[3,4]. There is a female-to-male ratio of 2/1 in North American population studies of IBS^[5],

and epidemiologic surveys indicate that women seek health care services for IBS more frequently than men^[4,6]. In menstruating women, symptoms are influenced by menstrual cycle. Peri- and postmenopausal women have a high prevalence of altered bowel function and IBS-like gastrointestinal complaints^[7]. For many women, symptoms become amplified around the time of menses^[8]. However, the exact mechanism (e.g. ovarian hormones, stress response) accounting for these cyclic changes is still unknown.

Studies suggested that the female sex steroid hormones, including estrogen and progesterone, could affect the myoelectric and mechanical activity of colonic smooth muscle *in vitro*. By geometric center method, estrogen and progesterone pretreatment of ovariectomized rats resulted in a significant decrease in colonic transit compared with untreated ovariectomized rats^[9].

5-HT₃R is a ligand-gated ion channel and probably involved in the modulation of colonic motility and visceral pain in the gut^[10]. Clinically, 5-HT₃R antagonists are important in the treatment of symptoms in IBS and more effective on diminishing bowel pattern symptom in women as compared to men^[11]. Rat with wrap restraint stress is an appropriate animal model to study stress-related colonic dysfunction like IBS^[12]. Previous studies have suggested that restraint stress results in an increase of fecal pellet output in rats via peripheral 5-HT₃ receptors^[13].

Earlier research has shown that E₂ can suppress gastric motility response to thyrotropin-releasing hormone (TRH) and restraint stress in conscious rats^[14], low dose of P (1 mg/kg) increased intestinal transit while higher dose (10-20 mg/kg) had no effect. Recently, it has been demonstrated that both forskolin and 17-beta-estradiol inhibit the function of 5-HT₃R in a noncompetitive manner and that this inhibition is independent of cAMP levels^[15]. Based on the research mentioned above, we suggested that this change, in part, be due to the increased activity of 5-HT₃R innervating these organs. Therefore, we decided to assess whether both of these sex steroids could modulate mRNA expression of 5-HT₃R in rat colon with restraint stress-induced colonic dysfunction and the potential mechanisms involved. Ovariectomized rats were treated with or without E₂ and P in combination, after that changes in fecal pellets and the time of vitreous pellets output were assessed. Furthermore, we used RT-PCR to determine whether there was a decrease in 5-HT₃R mRNA expression after treatment with sex steroids.

MATERIALS AND METHODS

Animals

Twenty-four adult female Sprague-Dawley rats (weighing 220-250 g), purchased from the Animal Department of Tongji Medical College, Huazhong University of Science and Technology were housed individually in a light and temperature controlled room with light-dark cycles of 12:12 h, where the temperature (24±2 °C) and relative humidity (65-70%) were kept constant. The animals were fed on a standard pellet diet, and food was withdrawn overnight before surgery and emptying experiments, but free access to water was allowed *ad libitum*. Experimental protocols followed standards and policies of the Animal Care and Use Committee, School of Medicine, Wuhan University.

Surgical procedures

Rats were housed for 7 d before experiments. At 6 wk of age, rats were randomly divided into three groups of eight each: sham-operated group, OVX group and OVX+E₂+P group. Under aseptic conditions, bilateral ovariectomy or sham operation was performed under general anesthesia with ketamine (100 mg/kg, ip). For OVX, two dorsolateral incisions, in the skin and the peritoneum, were made and the ovaries and uterine horn removed. Sham operations consisted of skin and peritoneum incisions. After operation, animals were housed four per cage under previous conditions. On the same day, rats in OVX+E₂+P group were subcutaneously injected a mixture of estradiol benzoate (E₂, 5 µg/d) and progesterone (P, 0.2 mg/d). Four weeks after E₂ and P combination treatment, wrap restraint stress experiments were performed in the three groups.

Restraint stress-induced bowel dysfunction

The method described by Williams *et al.*^[16] was used with slight modifications. Rats were acclimated to metal mesh cage placed on a tray for 5 h (9:00-14:00). After the acclimation, they were lightly anesthetized with ether. Then, their forelimbs were restrained with adhesive tapes (12.5 mm in width). The restrained limbs and thoracic trunk were wrapped with other adhesive tapes (50 mm in width). Immediately after those rats were returned to the cages, the number of feces dropped on the tray was counted 1 h after the wrapping. Test compounds were administered 1 h or 30 min before the restraint.

Hormone assays

The blood was collected from the heart of anesthetized animals and serum was separated by centrifugation at 1 500 r/min for 20 min and kept at -70 °C until assayed for E₂ and P. The gonadal steroids were measured in duplicate by radioimmunoassay using kits (Tianjin Depu Biotech). Aliquots of serum were added to tubes that had been coated with antibodies to steroid hormone followed by addition of ¹²⁵I-hormone. Mixtures were vortexed gently and incubated for 2-3 h at room temperature. Incubation was terminated by aspirating excess of ¹²⁵I-hormone and tubes were counted.

RNA extraction and RT-PCR

Distal colon tissues were harvested from animals in various treatment groups and frozen in liquid nitrogen. Total RNA from the frozen tissues was extracted using TRIzol as described by the manufacturer's protocol (Invitrogen). RNA was dissolved in RNase-free water and the concentration was determined by measuring the optical density (A) at 260 nm. The purity of the RNA was assessed by the ratio of A₂₆₀/A₂₈₀. Two micrograms of total RNA from each sample was transcribed into cDNA using M-MLV reverse transcriptase (Promega). Briefly, total RNA was mixed with M-MLV reverse transcriptase (200 U/µL), oligo (dT)₁₈ (50 µmol/L, Sangon, Shanghai), RNase inhibitor (40 U/µL), and dNTPs (1.25 mmol/L each, TaKaRa, Dalian) in a buffer containing 37.5 mmol/L KCl, 25 mmol/L Tris-HCl, and 1.5 mmol/L MgCl₂ (pH 8.3) in a total volume of 25 µL. The mixture was incubated at 42 °C for 90 min, heated to 95 °C for 5 min and cooled to 58 °C for 5 min. The resulted cDNA samples were amplified by PCR using Biometra PCR machine (Standard Power Pack P25, Germany) and the following specific primer pairs were used (SBS Genetech, Beijing): rats 5-HT_{2R} sense, 5'-GAG ACC ATC TTC ATT GTG CAG CTG GTG CA-3'; antisense, 5'-ACA GCA GCG TGT CCA GCA CAT ATC CCA CC-3', for the 397-bp product^[17]. Amplification of the rat β-actin gene transcript was used to control the efficiency of RT-PCR among the samples, β-actin sense, 5'-GTC ACC CAC ACT GTG CCC ATC T-3'; antisense, 5'-ACA GAG TAC TTG CGC TCA GGA G-3' for the 542-bp product^[18]. PCR mixes contained 25 pmol each of sense

and antisense primers, 2.0 U Taq DNA polymerase (Biostar), the buffer supplemented with 1.5 mmol/L MgCl₂, 0.2 mmol/L dNTPs and 1 µL cDNA in 25 µL. The amplification cycles were carried out under the following conditions: first denaturing at 94 °C for 3 min, then denaturing at 92 °C for 45 s, annealing at 55 °C for 45 s, and extension at 72 °C for 45 s for a total of 35 cycles, finally a 7 min extension at 72 °C was conducted. The resulted PCR products were analyzed on 20 g/L agarose gels in TBE buffer (40 mmol/L Tris-acetate, 1 mmol/L EDTA, pH 8.3) containing 0.05 µg/mL ethidium bromide. Appropriate molecular weight markers (100 bp ladder, MBI) were used to verify the required size of the final PCR product. The gels were scanned and the mean density of the products were visualized and photographed under the BIO-PROFIL (VILBER LOURMAT, France).

Statistical analysis

Results are expressed as mean±SD. The statistical significance of difference was evaluated with one-way analysis of variance (ANOVA), and analyzed by SPSS 10.0. A confidence level of P<0.05 was considered significant.

RESULTS

Fecal pellets output

Table 1 shows the effects of E₂+P combination and blank control on restraint stress-induced fecal pellet output in rats. The number of fecal pellets counted during observation period was negligible in unrestrained normal rats. In the restraint stress rats, fecal pellet output was measured with pellet counts of 5.6±0.5 for ovarian hormone-induced sham group. The number of fecal pellets was significantly increased in OVX vehicle-treated group compared with sham and E₂+P-treated group (vehicle-treated, 8.6±0.6; sham group, 5.6±0.5; E₂+P-treated, 4.1±0.5; P<0.01). Meanwhile, the time of vitreous pellets output was significantly decreased (P<0.01). The number of fecal pellets was significantly decreased (E₂+P-treated, 4.1±0.5; sham group, 5.6±0.5; P<0.01) and the time of vitreous pellets output was significantly increased in E₂+P-treated group (P<0.01).

Table 1 Effects of ovarian hormone on fecal pellets output in the ovariectomized restraint stress rats (mean±SD, n = 8)

Group	Fecal pellets (number)	Time of vitreous pellet output (min)
Sham-operated	5.6±0.5	4.8±0.26
OVX	8.6±0.6 ^d	1.3±0.22 ^f
OVX+E ₂ +P	4.1±0.5 ^{db}	5.8±0.29 ^f

^bP=0.000 vs OVX group; ^dP=0.000 vs sham-operated group; ^fP=0.000 vs sham-operated group.

Table 2 Serum concentration of estrogen and progesterone (mean±SD, n = 8)

Group	E ₂ (pmol/L)	P (nmol/L)
Sham-operated	104±6	26±1
OVX	15.7±0.8 ^d	3.2±0.6 ^b
OVX+E ₂ +P	168±8 ^d	44±2 ^b

^bP=0.000 vs sham-operated group; ^dP=0.000 vs sham-operated group.

Serum concentration of estrogen and progesterone

As expected, serum levels of E₂ were suppressed in OVX rats and restored after treatment with ovarian steroids (sham-operated, 104±6; OVX: vehicle-treated 15.7±0.8; E₂+P-treated 168±8; P<0.01, Table 2). Serum levels of P were also decreased

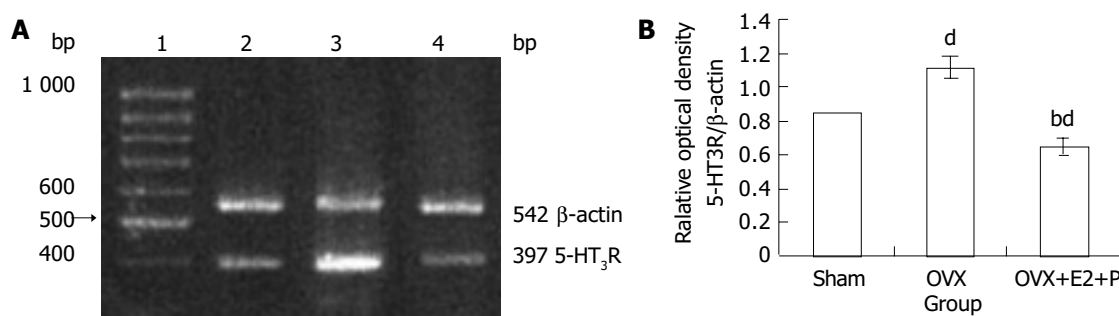


Figure 1 A: 5-HT₃R mRNA expression in the colon of restraint stress rats. Lane 1: Markers, 100-bp ladder; lane 2: sham-operated group; lane 3: OVX group; lane 4: OVX+E₂+P group. B: 5-HT₃R mRNA expression in the colon of restraint stress rats. The bar shows the relative optical density of 5-HT₃R band obtained from different groups. Values were reported as the ratio of 5-HT₃R to β-actin signals and normalized by the corresponding RT-PCR products for β-actin, used as the internal control. PCR was carried out for 35 cycles. Amplified cDNA products were separated by 20 g/L agarose gel electrophoresis. ^b*P* = 0.000 vs OVX group; ^d*P* = 0.000 vs sham-operated group.

in OVX rats and increased following treatment with E₂+P (sham-operated, 26±1; OVX: vehicle-treated, 3.2±0.6; E₂+P-treated, 44±2; *P* < 0.01).

Expression of 5-HT₃R in the colon of restraint stressed rats

Effects of ovarian hormone on the expressions of 5-HT₃R mRNA in colon tissues of restraint stress-induced rats were examined by RT-PCR as shown in Figure 1, which revealed a marked increase in OVX vehicle-treated group (relative optical density: 1.12±0.07). The expression of 5-HT₃R mRNA in colon was increased to a maximum in OVX vehicle-treated group (sham: 0.85±0.06, *P* < 0.01) and significantly decreased after E₂+P-treatment (0.65±0.05, *P* < 0.01, Figure 1B). Furthermore, 5-HT₃R mRNA expression was decreased by 1.3-fold in E₂+P-treated group (*P* < 0.01 compared with sham group, Figure 1B). However, there was a trend of lower expression of 5-HT₃R mRNA in colon with the increasing serum levels of E₂ and P.

DISCUSSION

IBS is a complex GI disorder with a poorly understood pathophysiology in which three major mechanisms interact: altered gastrointestinal motility, increased sensory function of the intestine and psychosocial factors^[19]. Various observations suggested that fluctuations in sex hormones in women might have an influential role in IBS: for many women, symptoms became amplified around the time of menses^[8]. In menstruating women, symptoms are influenced by menstrual cycle and bloating, abdominal pain, and diarrhea tend to be amplified during the late luteal and early menses phases^[20,21]. GI symptoms increase and intestinal transit decreases during pregnancy (a time of high E₂ and P levels)^[22], and rectal sensitivity is greater during menses compared with other menstrual-cycles in women with IBS^[8]. The precise mechanism responsible for the changes in gastrointestinal motility is still unknown. Earlier research has shown that E₂ can delay gastric emptying and GI transit in rats^[23], low dose of P (1 mg/kg, i.p.) enhanced the gastric emptying and high dose of P (5 mg/kg, i.p.) inhibited it. P (1 mg/kg) increased the intestinal transit while higher dose (10–20 mg/kg) had no effect. E₂ suppresses gastric motility response to thyrotropin-releasing hormone (TRH) and restraint stress in conscious rats^[14]. The precise sex steroid that is responsible for these changes is controversial. It appears that sex steroids play an important role in modulating these effects as postmenopausal women being treated with sex hormone-replacement therapy (HRT) had a decreased rate of gastric emptying of solids compared with men. In contrast, postmenopausal women without hormone replacement had rates of solid emptying similar to those of men^[24]. Results in pre- and postmenopausal women taking sex HRT showed they had slower gastric emptying than men^[25]. Whereas

recent studies have also confirmed that HRT is associated with an increased risk of IBS^[26].

Stress is known to be an important factor in causing IBS, since it significantly alters bowel functions. Several rodent models of bowel dysfunction caused by restraint stress have been investigated for pharmacological analysis of a stress-related bowel disorder like IBS^[12,13,27]. There were similarities between the intestinal effects of wrap restraint stress in rats and IBS in human. Therefore, wrap restraint stress rat is an appropriate animal model to study stress-related intestinal dysfunction. The role of sex hormones in the development of IBS is the subject of ongoing study. Our results indicate that in the restraint stress rats, serum levels of E₂ and P were suppressed in OVX rats and restored following chronic treatment with ovarian steroids. Meanwhile, OVX vehicle-treatment significantly increased the number of fecal pellets, moreover, the time of vitreous pellets output was significantly decreased. E₂+P treatment significantly decreased the number of fecal pellets and increased the time of vitreous pellets output. Our study indicated that E₂ and P could relieve the rat colon contractile response to restraint stress, thus decrease the number of fecal pellets and increase the number of fecal pellets output.

5-HT₃R is expressed by most myenteric neurons, including those that excite gastrointestinal muscle^[28–30]. In contrast to other serotonin receptor subtypes, these receptors are ligand-gated ion channels involved in rapid excitatory responses in peripheral and central nervous system^[31]. 5-HT₃R mediates a fast inward current in myenteric neurons^[29,30], and their activation is thought to enhance cholinergic transmission via the release of acetylcholine from parasympathetic nerve terminals^[13], thus resulting in an increase in gastrointestinal motility, fluid secretion and pain. Clinically, 5-HT₃R antagonists are important in the treatment of symptoms in IBS^[32].

Previous studies demonstrated that restraint stress resulted in an increase in fecal pellet output in rats fed the diet, as well as diarrhea in food-deprived rats, which are equally mediated through the endogenous activation of the 5-HT₃R^[13,14]. Clinically, 5-HT₃R antagonist drugs appeared to more effectively diminish bowel pattern disruption in women with IBS as compared to men^[11]. Recently, it has been demonstrated that both forskolin and 17-beta-estradiol inhibit the function of 5-HT₃R in a noncompetitive manner and that this inhibition is independent of cAMP levels^[15]. Because 5-HT₃R plays a role in the pathogenesis of IBS, it is possible that the attenuated development of IBS in female rats might be related to the modulation of gonadal hormones on 5-HT₃R and GI system. This study focused on the effects of gonadal steroid hormones on 5-HT₃R mRNA expression in colon of wrap restraint stress rats. We observed an increase in 5-HT₃R gene expression in OVX rats. The increase in 5-HT₃R gene

expression was prevented by treating the OVX rats with a combination of E₂ and P. These results suggest that 5-HT₃R mRNA expression is sensitive to the absence of E₂ and P. Their roles in regulation of 5-HT₃R mRNA expression deserve further study. If the increase in the density of 5-HT₃R gene expression induced by E₂ and P deficiency reflects overactivity of 5-HT₃R, then such changes may be relevant to hormone- and age-related GI dysfunction.

In conclusion, we suggest that female gonadal hormones may play an important role in regulation of colon 5-HT₃R. Exploration of 5-HT₃R expression by gonadal steroid hormones could contribute to a better understanding of the interactions between ovarian steroids and GI and may have major pathophysiological implications for 5-HT-related bowel disorders, such as IBS.

REFERENCES

- 1 Heitkemper M, Jarrett M. Irritable bowel syndrome: causes and treatment. *Gastroenterol Nurs* 2000; **23**: 256-263
- 2 Leahy A, Epstein O. Non-pharmacological treatments in the irritable bowel syndrome. *World J Gastroenterol* 2001; **7**: 313-316
- 3 Olden KW. Diagnosis of irritable bowel syndrome. *Gastroenterology* 2002; **122**: 1701-1714
- 4 Foxx-Orenstein AE, Clarida JC. Irritable bowel syndrome in women: the physician-patient relationship evolving. *J Am Osteopath Assoc* 2001; **101**(12 Suppl Pt 2): S12-16
- 5 Camilleri M. Management of the irritable bowel syndrome. *Gastroenterology* 2001; **120**: 652-668
- 6 Saito YA, Schoenfeld P, Locke GR 3rd. The epidemiology of irritable bowel syndrome in North America: a systematic review. *Am J Gastroenterol* 2002; **97**: 1910-1915
- 7 Triadafilopoulos G, Finlayson M, Grellet C. Bowel dysfunction in postmenopausal women. *Women Health* 1998; **27**: 55-66
- 8 Houghton LA, Lea R, Jackson N, Whorwell PJ. The menstrual cycle affects rectal sensitivity in patients with irritable bowel syndrome but not healthy volunteers. *Gut* 2002; **50**: 471-474
- 9 Ryan JP, Bhojwani A. Colonic transit in rats: effect of ovariectomy, sex steroid hormones, and pregnancy. *Am J Physiol* 1986; **251**(1 Pt 1): G46-50
- 10 Hunt RH, Tougas G. Evolving concepts in functional gastrointestinal disorders: promising directions for novel pharmaceutical treatments. *Best Pract Res Clin Gastroenterol* 2002; **16**: 869-883
- 11 Viramontes BE, Camilleri M, McKinzie S, Pardi DS, Burton D, Thomforde GM. Gender-related differences in slowing colonic transit by a 5-HT₃ antagonist in subjects with diarrhea-predominant irritable bowel syndrome. *Am J Gastroenterol* 2001; **96**: 2671-2676
- 12 Li J, Liu X, Xie P, Gu Q, Li J, Zhang Y, Tang Z. The regulation of calcium in the movement of colonic smooth muscle in wrap restraint stress rats. *Zhonghua Neike Zazhi* 2000; **39**: 588-591
- 13 Miyata K, Kamato T, Nishida A, Ito H, Yuki H, Yamano M, Tsutsumi R, Katsuyama Y, Honda K. Role of the serotonin₃ receptor in stress-induced defecation. *J Pharmacol Exp Ther* 1992; **261**: 297-303
- 14 Bond EF, Heitkemper MM, Bailey SL. Estrogen suppresses gastric motility response to thyrotropin-releasing hormone and stress in awake rats. *Res Nurs Health* 1998; **21**: 221-228
- 15 Oz M, Zhang L, Spivak CE. Direct noncompetitive inhibition of 5-HT₃ receptor-mediated responses by forskolin and steroids. *Arch Biochem Biophys* 2002; **404**: 293-301
- 16 Williams CL, Villar RG, Peterson JM, Burks TF. Stress-induced changes in intestinal transit in the rat: a model for irritable bowel syndrome. *Gastroenterology* 1988; **94**: 611-621
- 17 Isenberg KE, Ukhun IA, Holstad SG, Jafri S, Uchida U, Zorumski CF, Yang J. Partial cDNA cloning and NGF regulation of a rat 5-HT₃ receptor subunit. *Neuroreport* 1993; **5**: 121-124
- 18 Dou DB, Huang YW, Wang SP, Cai G, Lin J. Influence of Zhishi Xiaopi pill on gene expression of CCK and CCK-A receptor in upper-alimentary tract of rats. *Shijie Huaren Xiaohua Zazhi* 2002; **10**: 927-930
- 19 Camilleri M. Pathophysiology in irritable bowel syndrome. *Drug News Perspect* 2001; **14**: 268-278
- 20 Heitkemper MM, Jarrett M. Pattern of gastrointestinal and somatic symptoms across the menstrual cycle. *Gastroenterology* 1992; **102**: 505-513
- 21 Heitkemper MM, Jarrett M, Cain KC, Shaver J, Walker E, Lewis L. Daily gastrointestinal symptoms in women with and without a diagnosis of IBS. *Dig Dis Sci* 1995; **40**: 1511-1519
- 22 Wald A, Van Thiel DH, Hoechstetter L, Gavalier JS, Egler KM, Verm R, Scott L, Lester R. Gastrointestinal transit: the effect of the menstrual cycle. *Gastroenterology* 1981; **80**: 1497-1500
- 23 Bond EF, Heitkemper MM, Perigo R. Gastric emptying and gastric-intestinal transit in rats with varying ovarian hormone status. *Nurs Res* 1996; **45**: 218-224
- 24 Perez Gutthann S, Garcia Rodriguez LA, Castellsague J, Duque Oliart A. Hormone replacement therapy and risk of venous thromboembolism: population based case-control study. *BMJ* 1997; **314**: 796-800
- 25 Hutson WR, Roehrkasse RL, Wald A. Influence of gender and menopause on gastric emptying and motility. *Gastroenterology* 1989; **96**: 11-17
- 26 Ruigomez A, Garcia Rodriguez LA, Johansson S, Wallander MA. Is hormone replacement therapy associated with an increased risk of irritable bowel syndrome? *Maturitas* 2003; **44**: 133-140
- 27 Muraoka M, Mine K, Kubo C. A study of intestinal dysfunction induced by restraint stress in rats. *Scand J Gastroenterol* 1998; **33**: 806-810
- 28 Glatzle J, Sternini C, Robin C, Zittel TT, Wong H, Reeve JR Jr, Raybould HE. Expression of 5-HT₃ receptors in the rat gastrointestinal tract. *Gastroenterology* 2002; **123**: 217-226
- 29 Zhai J, Gershon MD, Walsh JH, Wong HC, Kirchgessner AL. Inward currents in neurons from newborn guinea pig intestine: mediation by 5-hydroxytryptamine type 3 receptors. *J Pharmacol Exp Ther* 1999; **291**: 374-382
- 30 Zhou X, Galligan JJ. Synaptic activation and properties of 5-hydroxytryptamine (3) receptors in myenteric neurons of guinea pig intestine. *J Pharmacol Exp Ther* 1999; **290**: 803-810
- 31 Gutierrez B, Arranz MJ, Huez-Diaz P, Dempster D, Matthiasson P, Travis M, Munro J, Osborne S, Kerwin RW. Novel mutations in 5-HT_{3A} and 5-HT_{3B} receptor genes not associated with clozapine response. *Schizophr Res* 2002; **58**: 93-97
- 32 Camilleri M, Mayer EA, Drossman DA, Heath A, Dukes GE, McSorley D, Kong S, Mangel AW, Northcutt AR. Improvement in pain and bowel function in female irritable bowel patients with alosetron, a 5-HT₃ receptor antagonist. *Aliment Pharmacol Ther* 1999; **13**: 1149-1159

Edited by Chen WW and Zhu LH Proofread by Xu FM

Meta-analysis of intraperitoneal chemotherapy for gastric cancer

Da-Zhi Xu, You-Qing Zhan, Xiao-Wei Sun, Su-Mei Cao, Qi-Rong Geng

Da-Zhi Xu, You-Qing Zhan, Xiao-Wei Sun, Department of Abdominal Surgery, Cancer Center, Sun Yat-sen University, Guangzhou 510060, Guangdong Province, China

Su-Mei Cao, Department of Nasopharyngeal Cancer, Department of Clinical Epidemiology, Cancer Center, Sun Yat-sen University, Guangzhou 510060, Guangdong Province, China

Qi-Rong Geng, Department of Medical Oncology, Cancer Center, Sun Yat-sen University, Guangzhou 510060, Guangdong Province, China

Supported by the Natural Science Foundation of Guangdong Province, No.20030245

Correspondence to: You-Qing Zhan, Department of Abdominal Surgery, Cancer Center, Sun Yat-sen University, Guangzhou 510060, Guangdong Province, China. yq_zhan@21cn.com

Telephone: +86-20-87343123

Received: 2004-01-02 **Accepted:** 2004-01-12

Abstract

AIM: To assess the efficacy and safety of intraperitoneal chemotherapy in patients undergoing curative resection for gastric cancer through literature review.

METHODS: Medline (PubMed) (1980-2003/1), Embase (1980-2003/1), Cancerlit Database (1983-2003/1) and Chinese Biomedicine Database (1990-2003/1) were searched. Language was restricted to Chinese and English. The statistical analysis was performed by RevMan4.2 software provided by the Cochrane Collaboration. The results were expressed with odds ratio for the categorical variables.

RESULTS: Eleven trials involving 1 161 cases were included. The pooled odds ratio was 0.51, with a 95% confidence interval (0.40-0.65). Intraperitoneal chemotherapy may benefit the patients after curative resection for locally advanced gastric cancer, and the combination of intraperitoneal chemotherapy with hyperthermia or activated carbon particles may provide more benefits to patients due to the enhanced antitumor activity of drugs. Sensitivity analysis and fail-safe number suggested that the result was comparatively reliable. However, of 11 trials, only 3 studies were of high quality.

CONCLUSION: Intraperitoneal chemotherapy after curative resection for locally advanced gastric cancer may be beneficial to patients. Continuous multicenter, randomized, double blind, rigorously designed trials should be conducted to draw definitive conclusions.

Xu DZ, Zhan YQ, Sun XW, Cao SM, Geng QR. Meta-analysis of intraperitoneal chemotherapy for gastric cancer. *World J Gastroenterol* 2004; 10(18): 2727-2730

<http://www.wjgnet.com/1007-9327/10/2727.asp>

INTRODUCTION

Gastric cancer is the second most common cause of cancer death worldwide. Surgery is the main choice of radical treatment, however, even for patients with apparently completely resection, the five-year survival rate is about 30-60%, which has been disappointing. Peritoneal metastasis is the most common type of recurrence after surgery and has the worst prognosis in

patients with advanced stomach cancer. To improve the survival of the patients with gastric cancer, intraperitoneal chemotherapy (IPT) as a possible effective treatment for peritoneal dissemination in locally advanced gastric cancer has been investigated clinically, but the results among these studies are still different and disputed. To evaluate whether IPT benefited the patients undergoing radical resection for locally advanced gastric cancer, we summarized all the available randomized trials and combined the results for meta-analysis.

MATERIALS AND METHODS

Materials

Medline (PubMed) (1980-2003/1), Embase (1980-2003/1), Cancerlit Database (1983-2003/1) and Chinese Biomedicine Database (1990-2003/1) were searched. Languages were restricted to Chinese and English.

Inclusion and exclusion criteria

To be included, trials had to be randomised and controlled. Trials could be single-blind, double-blind or not blind. Chemotherapy groups were treated intraperitoneally, including intraperitoneal chemotherapy with or without activated carbon particles (CH), intraperitoneal hyperthermic perfusion. No oral or intravenous chemotherapy, chemoimmunotherapy, or radiotherapy were used. Those receiving gastrectomy alone were included in control group. All patients must have had a potential curative surgery for locally advanced gastric cancer.

Data extracted included the baseline data of intraperitoneal chemotherapy group and control group, assessments of eligibility and trial quality, number of survival and death and the statistical consideration.

Methods

Data collection The content terms of stomach neoplasms, intraperitoneal chemotherapy and surgery, and the methodological terms of clinical trial, phase III, randomized trial, double blind method were used. These searches were supplemented by hand searching of the reference lists of identified trials and review articles. Two reviewers assessed independently the outcome data using a pre-designed strategy. They also evaluated study quality using Jadad-scale⁽¹⁾ plus allocation concealment. Intention-to-treat analyses were also performed. Agreement was achieved through discussion when they have different evaluations.

Statistical analysis

The results of eligible trials were pooled using RevMan4.2 software provided by the Cochrane Collaboration. The result was expressed with odds ratio (OR) for the categorical variables. *Q* statistic test was used for gross statistical heterogeneity. Sensitivity analysis was performed by excluding the trials in which Jadad-scale was low. Publication bias was assessed by calculating the Rosenthal's fail-safe number. Subgroup analysis was performed by collecting summaries for subsets of studies with different characteristics.

RESULTS

Study selection

There was good agreement between the two reviewers on the eligibility, quality scores and data extraction of analysis. Eighteen

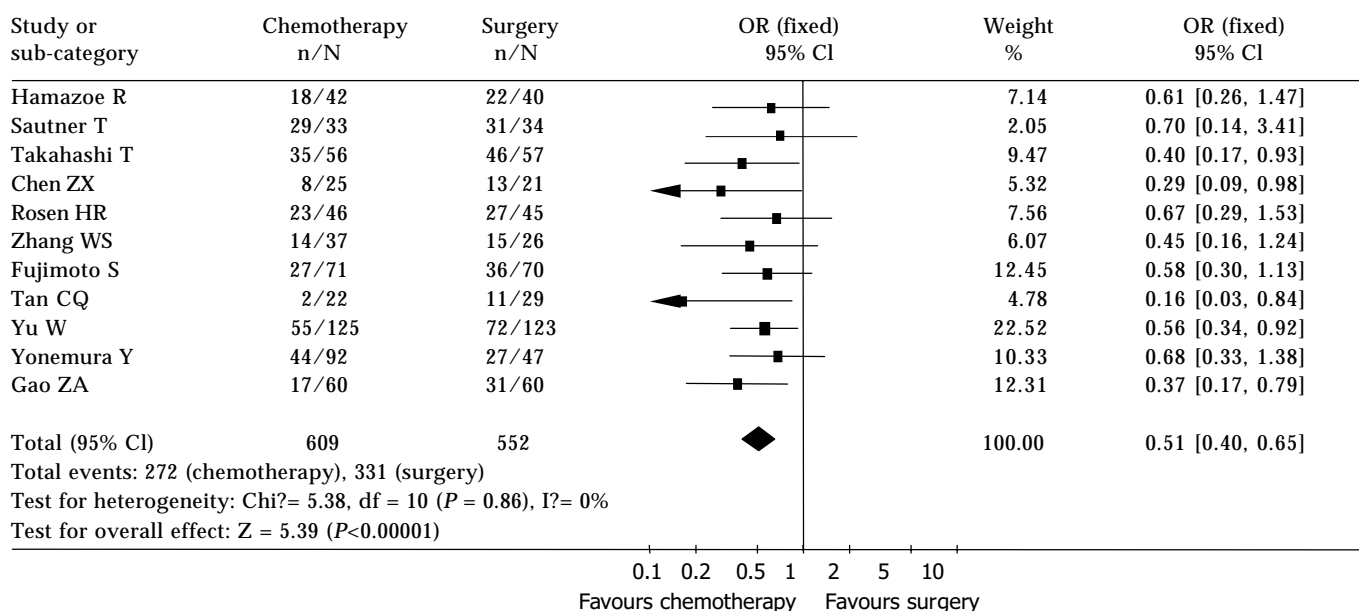
Table 1 Data from 11 randomized controlled trials

Author	Country	Publication time	Chemotherapy regimens	IPT (number of death/total)	Surgery (number of death/total)	Follow-up (mo)	Quality score
Rosen HR	Austria	1998	MMC+Carbon	23/46	27/45	36	4
Sautner T	Austria	1994	Cisplatin	29/33	31/34	60	3
Takahashi T	Japan	1995	MMC+Carbon	35/56	46/57	36	3
Yu W	Korea	2001	MMC+5-Fu	55/125	72/123	60	2
Yonemura Y	Japan	2001	MMC+CDDP	44/92	27/47	60	1
Hamazoe R	Japan	1993	MMC	18/42	22/40	60	1
Chen ZX	China	1996	DDP	8/25	13/21	18	1
Zhang WS	China	1998	5-Fu	14/37	15/26	36	1
Fujimoto S	Japan	1998	MMC	27/71	36/70	96	1
Tan CQ	China	2000	MMC	2/22	11/29	36	1
Gao ZA	China	2002	MMC+DDP+HCPT	17/60	31/60	36	2

Review: Intraperitoneal chemotherapy after curative resection for gastric cancer: meta- analysis of randomized trials

Compariso: 01 chemotherapy vs surgery

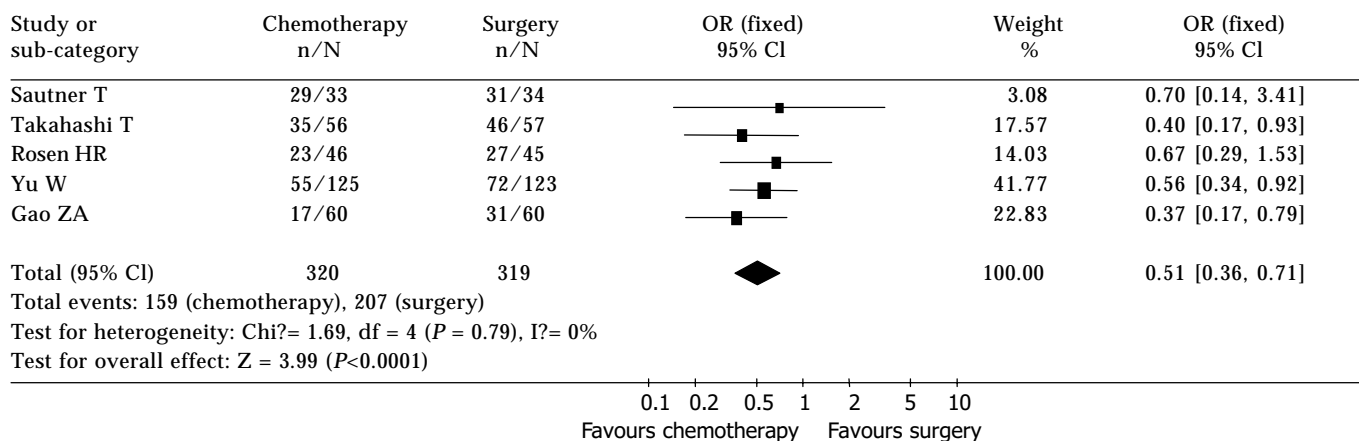
Outcome: 01 OR

**Figure 1** Odds ratio for 11 randomized controlled trial.

Review: Intraperitoneal chemotherapy after curative resection for gastric cancer: meta- analysis of randomized trials

Compariso: 01 chemotherapy vs surgery

Outcome: 01 OR

**Figure 2** Sensitivity analysis 1 (by excluding trials according to Jadad-scale with 1 score).

Review: Intraperitoneal chemotherapy after curative resection for gastric cancer: meta- analysis of randomized trials
 Compariso: 01 chemotherapy vs surgery
 Outcome: 01 OR

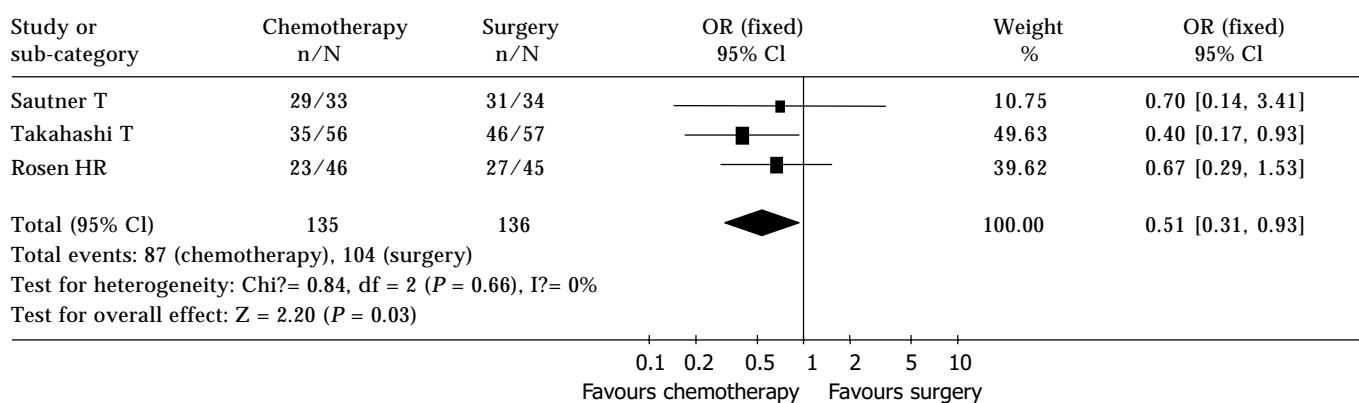


Figure 3 Sensitivity analysis 2 (by excluding the low quality trials).

random trials including surgery plus intraperitoneal chemotherapy, preliminary surgery alone were analysed, from which 7 reports were excluded for repetitive studies. Table 1 shows the details of the 11 trials^[2-12] included in the analysis with a total enrollment of 1 161 patients, in which 609 patients were assigned to the treatment group and 552 to the control group. The average sample size was 106 patients. Of 11 trials, three studies were of high quality according to the Jadad-scale (with three scores), one trial mentioned double-blind design and sample-size calculation, and two studies described intention-to-treat analysis. The fail-safe number of 104 suggested that no important publication bias existed in this meta-analysis.

Meta-analysis

Figure 1 shows the result of the meta-analysis. There was no statistically significant heterogeneity in our analysis, so a fixed effect model was used and the odds ratio was 0.51 (95% CI 0.40 to 0.65). The sensitivity analysis was performed by excluding trials with Jadad-scale scores between 1 and 3 and revealed the same difference between intraperitoneal chemotherapy and surgery alone (odds ratio 0.51, 95% CI 0.36 to 0.71: odds ratio 0.54, 95% CI 0.31 to 0.93) (Figures 2, 3).

Subgroup analysis

As shown in Table 2, intraperitoneal hyperthermic chemoperfusion (IHCP) or chemotherapy with activated carbon particles (CH) produced more benefits to patients than those without hyperthermia or CH; the group of trials from Asian countries exhibited a trend towards a more significant effect than those from non-Asian countries, which showed no effect with IPT; for trials with more than 5 years of follow-up, the effects were less obvious than those of shorter follow-up, if indicated that IPT might afford long-term survival by delaying relapse and recurrence.

Table 2 Subgroup analysis

Characteristic	No. of trials	OR	95% CI
IPT (without CH and IHCP)	2	0.57	(0.35-0.92)
IPT (only with CH)	2	0.52	(0.29-0.94)
IHCP	7	0.48	(0.35-0.67)
Follow-up time (mo) <60	6	0.40	(0.27-0.59)
Follow-up time (mo) ≥60	5	0.60	(0.44-0.82)
Asia	9	0.49	(0.38-0.64)
Non-Asia (Austria)	2	0.67	(0.32-1.41)

IPT: intraperitoneal chemotherapy; CH: carbon particles; IHCP: intraperitoneal hyperthermic chemoperfusion.

Side effect analysis

All studies described the side effects of medicine, including anastomotic leakage, leukocytopenia, fever, intestinal obstruction, fistula, intraabdominal bleeding, and prolonged abdominal pain, *etc.* Of 11 trials, 5 had mild complications; 3 had no significant differences in adverse effects between the surgery group and the chemotherapy group; 2 trials produced complications in the chemotherapy group: one was bowel fistula, the other was intraabdominal abscess which turned better after effective treatment. One trial from Austria reported serious side effects by IPT, the complications of the treatment group and control group were respectively 35% and 16%, the death rates, 11% and 2%, which terminated the trial ahead of schedule.

DISCUSSION

IPT is applied to kill residual tumor cells left behind during surgery, which can not be achieved by the intravenous approach, especially for stage 3 and 4 gastric carcinomas. It is of much importance to extirpate the free tumor cells in the abdominal cavity and micrometastases on the peritoneal surface to attain longer survival. Animal trials and phase II clinical trials have revealed that IPT could be effective to prevent peritoneal dissemination and liver metastasis^[13].

The aim of meta-analysis is to provide a comprehensive, up-to-date summary of average effect of all the relevant randomized controlled trials, to provide reliable guidance for clinical practice and future research^[14]. Based on our results, IPT may benefit the patient after curative resection for locally advanced gastric cancer, and the combination of IPT with hyperthermia or activated carbon particles may provide more benefit to patients due to the enhanced antitumor activity of drugs^[15]. Sensitivity analysis and fail-safe number suggested that the results were comparatively reliable.

Two trials from Austria showed that intraperitoneal chemotherapy was not beneficial to patients, one of them terminated ahead of time because of serious adverse effects. Nine Asian studies (from China, Japan, Korea) confirmed a significant survival benefit for patients with tolerable side effects of antitumor drugs. Considering the difference between western studies and Asian studies^[16,17], we speculate that they may have different aetiology or biology methods^[18].

The adverse effect was an important factor to influence the result of intraperitoneal chemotherapy. However, only 4 trials described the side effects of medicine on the basis of World Health Organization classification, and the different forms of illustration made it difficult to analyze the effect according to evidence based medicine. There fore, we should observe and

describe the toxicity of medicine by WHO standard in future clinical research.

Of included 11 trials, only 3 trials were of high quality (Jadad-scale with 3 scores) and the other 8 trials were of low quality, which weakened our evidence. On the other hand, reliance on published trials alone might distort the outcome of meta-analysis, because positive studies were more likely to be published than negative ones.

At present, the treatment effect of gastric cancer is still disappointing. Many surgeons hold that the stomach cancer patients cannot benefit from IPT, which is different from our meta-analysis results. To draw definitive conclusions, more effective multicenter, randomized, double blind, rigorously designed trials are needed.

REFERENCES

- 1 **Moher D**, Jadad AR, Nichol G, Penman M, Tugwell P, Walsh S. Assessing the quality of randomized controlled trials: an annotated bibliography of scales and checklists. *Control Clin Trials* 1995; **16**: 62-73
- 2 **Yu W**, Whang I, Chung HY, Averbach A, Sugarbaker PH. Indications for early postoperative intraperitoneal chemotherapy of advanced gastric cancer: results of a prospective randomized trial. *World J Surg* 2001; **25**: 985-990
- 3 **Rosen HR**, Jatzko G, Repse S, Potrc S, Neudorfer H, Sandbichler P, Zacherl J, Rabl H, Holzberger P, Lisborg P, Czejka M. Adjuvant intraperitoneal chemotherapy with carbon-adsorbed mitomycin in patients with gastric cancer: results of a randomized multicenter trial of the Austrian Working Group for Surgical Oncology. *J Clin Oncol* 1998; **16**: 2733-2738
- 4 **Takahashi T**, Hagiwara A, Shimotsuma M, Sawai K, Yamaguchi T. Prophylaxis and treatment of peritoneal carcinomatosis: intraperitoneal chemotherapy with mitomycin C bound to activated carbon particles. *World J Surg* 1995; **19**: 565-569
- 5 **Sautner T**, Hofbauer F, Depisch D, Schiessel R, Jakesz R. Adjuvant intraperitoneal cisplatin chemotherapy does not improve long-term survival after surgery for advanced gastric cancer. *J Clin Oncol* 1994; **12**: 970-974
- 6 **Hamazoe R**, Maeta M, Kaibara N. Intraperitoneal thermochemotherapy for prevention of peritoneal recurrence of gastric cancer. Final results of a randomized controlled study. *Cancer* 1994; **73**: 2048-2052
- 7 **Fujimoto S**, Takahashi M, Mutou T, Kobayashi K, Toyosawa T. Successful intraperitoneal hyperthermic chemoperfusion for the prevention of postoperative peritoneal recurrence in patients with advanced gastric carcinoma. *Cancer* 1999; **85**: 529-534
- 8 **Yonemura Y**, de Aretxabala X, Fujimura T, Fushida S, Katayama K, Bandou E, Sugiyama K, Kawamura T, Kinoshita K, Endou Y, Sasaki T. Intraoperative chemohyperthermic peritoneal perfusion as an adjuvant to gastric cancer: final results of a randomized controlled study. *Hepatogastroenterology* 2001; **48**: 1776-1782
- 9 **Chen ZX**, Hu JK, Chen Z, Cheng JP, Peng DX, Tao QP. Positive results of therapy of gastric cancer patients after operation by intraperitoneal hyperthermic chemotherapy. *Zhonghua Shiyong Yixue* 2001; **3**: 39-40
- 10 **Gao ZA**, Jiang ZX, Zhou F. Clinical survey of early intraperitoneal hyperthermic chemoperfusion for gastric cancer patients after operation. *Zhongguo Zhongliu Linchuang* 2002; **29**: 294-295
- 11 **Tang CQ**, Wang XJ, Xu YK, Jiang BN, Zeng FH. Study for prevention of peritoneal dissemination of advanced gastric cancer by intraperitoneal thermochemotherapy. *Shiyong Zhongliu Zazhi* 2000; **15**: 165-167
- 12 **Zhang WS**, Su DM, Wang K, Yi PT, Zhou HT, Guo JJ. Clinical study in prophylactic use of intraperitoneal hyperthermic chemoperfusion for the prevention of peritoneal metastasis in patients with advanced gastric carcinoma. *Shanxi Yiyao Zazhi* 1998; **27**: 67-69
- 13 **Devita VT**, Hellman S, Rosenberg SA. Cancer principles practice of oncology (6th edition). (USA) Philadelphia: *Lippincott Williams wilkins Press* 2001: 1109-1110
- 14 **Li Jing**, Wang JL. Method and principle of systematic reviews. *Zhonghua Yixue Zazhi* 2001; **81**: 53-55
- 15 **Teicher BA**, Kowal CD, Kennedy KA, Sartorelli AC. Enhancement by hyperthermia of the *in vitro* cytotoxicity of mitomycin C toward hypoxic tumor cells. *Cancer Res* 1981; **41**: 1096-1099
- 16 **Bonenkamp JJ**, Hermans J, Sasako M, van de Velde CJ. Extended lymph-node dissection for gastric cancer. Dutch Gastric Cancer Group. *N Engl J Med* 1999; **340**: 908-914
- 17 **Shimada K**, Ajani JA. Adjuvant therapy for gastric carcinoma patients in the past 15 years: a review of western and oriental trials. *Cancer* 1999; **86**: 1657-1668
- 18 **Gulmann C**, Hegarty H, Grace A, Leader M, Patchett S, Kay E. Differences in proximal (cardia) versus distal (antral) gastric carcinogenesis via retinoblastoma pathway. *World J Gastroenterol* 2004; **10**: 17-21

Edited by Chen WW and Zhu LH Proofread by Xu FM

Diallyl disulfide-induced G2/M arrest of human gastric cancer MGC803 cells involves activation of p38 MAP kinase pathways

Jing-Ping Yuan, Gui-Hua Wang, Hui Ling, Qi Su, Yue-Hong Yang, Ying Song, Rong-Jun Tang, Yao Liu, Chen Huang

Jing-Ping Yuan, Gui-Hua Wang, Yue-Hong Yang, Department of Pathology, Central Hospital of Wuhan, Wuhan 430014, Hubei Province, China

Hui Ling, Qi Su, Ying Song, Rong-Jun Tang, Yao Liu, Chen Huang, Institute of Oncology, Medical College, Nanhua University, Hengyang 421001, Hunan Province, China

Supported by the Natural Science Foundation of Hunan Province, No. 02JJY2026, 01JJY2146 and the Foundation of Hunan Province Education Department, No. 01A016

Correspondence to: Professor Qi Su, Institute of Oncology, Nanhua University, Hengyang 421001, Hunan Province, China. suqi1@hotmail.com

Telephone: +86-734-8281547 **Fax:** +86-734-8281547

Received: 2003-04-02 **Accepted:** 2003-05-21

Abstract

AIM: To determine the role of p38 MAP kinase signal transduction pathways in diallyl disulfide (DADS)-induced G2/M arrest in human gastric cancer MGC803 cells.

METHODS: MGC803 cell growth inhibition was measured by MTT assay. Phase distribution of cell cycle was analyzed by flow cytometry. Expression of Cdc25C, p38, phosphorylation of p38 (pp38) were determined by Western blotting.

RESULTS: MTT assay showed that SB203580, a specific p38 MAPK inhibitor blocked DADS-induced growth inhibition. Flow cytometry analysis revealed that treatment of MGC803 cells with 30 mg/L DADS increased the percentage of cells in the G2/M phase from 9.3% to 39.4% ($P < 0.05$), whereas inhibition of p38 activity by SB203580 abolished induction of G2/M arrest by DADS. Western blotting showed that phosphorylation of p38 was increased 3.52-fold following treatment of MGC803 cells with 30 mg/L DADS for 20 min ($P < 0.05$), whereas Cdc25C was decreased 68% following treatment of MGC803 cells with 30 mg/L DADS for 24 h ($P < 0.05$). Decreased Cdc25C protein expression by DADS was attenuated by SB203580 ($P < 0.05$).

CONCLUSION: DADS-induced G2/M arrest of MGC803 cells involves activation of p38 MAP kinase pathways. Decreased Cdc25C protein expression by p38 MAPK played a crucial role in G2/M arrest after treatment with DADS.

Yuan JP, Wang GH, Ling H, Su Q, Yang YH, Song Y, Tang RJ, Liu Y, Huang C. Diallyl disulfide-induced G2/M arrest of human gastric cancer MGC803 cells involves activation of p38 MAP kinase pathways. *World J Gastroenterol* 2004; 10 (18): 2731-2734

<http://www.wjgnet.com/1007-9327/10/2731.asp>

INTRODUCTION

Unlimited and uncontrolled cell proliferation is obviously characteristics of tumor cells^[1,2]. Given that disruption of cell cycle plays a crucial role in cancer progression^[3], its modulation

by phytochemicals seems to be a logical approach in controlling carcinogenesis. Thus cell cycle regulation and its modulation by various natural (plant-derived) and synthetic agents are gaining widespread attention in recent years^[4-18]. Most of the plant products with anticancer activity are strong antioxidants and some of them are effective modulators of protein kinase/phosphatases that are associated with cell cycle regulation. DADS is a major component of cooked garlic and oil-soluble organosulfur compound in processed garlic, which inhibits the proliferation of human breast, hepatoma, lung, bladder, colon cancer cells and human leukemia HL-60 cells^[19-25]. Previous studies showed that the ability of DADS to suppress HCT-15, HT-29 cell proliferation was related to its propensity to induce a G2/M arrest^[23,24]. However, the molecular mechanisms by which DADS exerts its effects on tumor cells leading to inhibition of cell growth and induction of G2/M arrest are largely unknown. p38 MAP kinase (p38) is a member of the mitogen-activated protein (MAP) kinase signaling cascade which has been shown to regulate a variety of cellular events such as cell proliferation, differentiation, and apoptosis^[26-28], and may therefore be a potential target of DADS action. Gastric cancer is one of the most common malignant tumors in China^[29-30]. Our previous studies showed that DADS could inhibit human gastric cancer MGC803 cell growth^[31]. In this study, signaling pathways of p38 MAPK-induced G2/M arrest in DADS treated MGC803 cells were investigated for their involvement in the mechanisms of DADS-induced growth inhibition.

MATERIALS AND METHODS

Materials

Human gastric cancer cell line MGC803 was purchased from Cancer Research Institute of Hunan Medical University. DADS was purchased from Fluka Chemika (Ronkonkoma, NY). Monoclonal anti-p38, anti-pp38 antibodies and SB203580 were purchased from Cell Signaling (Beverly, MA). Polyclonal anti-Cdc25C antibody was purchased from Santa Cruz Biotechnology (Santa Cruz, CA).

Methods

Cell culture and MTT assay MGC803 cells were cultured in RPMI 1640 medium (Gibco) supplemented with 100 mL/L fetal bovine serum (Sijiqing Co.1 Hangzhou) with addition of 100 U/mL penicillin, 100 U/mL streptomycin. Cells in suspension (50 μ L) were added to each well of a 96-well culture plate and incubated for 24 h at 37 °C in a humidified atmosphere of 50 mL/L CO₂ in air. The 96-well culture plate was divided into 4 sections, with one section being treated by culture media, the others were treated by one of the followings at 50 μ L: culture media containing 2 \times reagents (10 μ mol/L SB203580, 30 mg/L DADS, 30 mg/L DADS+10 μ mol/L SB203580). In the latter group, SB203580 was added 1 h prior to DADS. The cultures were again incubated as above. After 72 h, 20 μ L 5 g/L MTT solution was added to each well, and the cultures were further incubated in 100 μ L DMSO solution. A microplate reader was used to measure absorbance at 570 nm for each well. Growth inhibition rate was calculated as follows: growth inhibition rate = $(1 - A_{570nm} \text{ of treated cells} / A_{570nm} \text{ of control cells}) \times 100\%$.

Cell cycle analysis Cells were incubated in culture media alone or culture media containing reagents (10 $\mu\text{mol/L}$ SB203580, 30 mg/L DADS, 30 mg/L DADS+10 $\mu\text{mol/L}$ SB203580), at 37 °C for 24 h. In the latter group, SB203580 was added 1 h prior to DADS. Cells were harvested in cold PBS, fixed in 700 mL/L ethanol, and stored at 4 °C for subsequent cell cycle analysis. Fixed cells were washed with PBS once and suspended in 1 mL of PI staining reagents (20 mg/L ribonuclease and 50 mg/L propidium iodide). Samples were incubated in the dark for 30 min before cell cycle analysis. The distribution of cells in the cell cycle was measured by a flow cytometer.

Western blotting MGC803 cells treated with different reagents were harvested, rinsed twice with cold PBS, and incubated in the lysis buffer containing 50 mmol/L Tris (pH7.5), 150 mmol/L NaCl, 10 mL/L NP-40, 1 g/L SDS, 10 g/L sodium deoxycholate, 1 mmol/L DTT, 1 mmol/L PMSF, 2.5 mg/L leupeptin, 25 mg/L aprotinin on ice for 20 min. Following the centrifugation at 12 000 g for 30 min at 4 °C. The amount of protein in the supernatant was determined using BCA protein assay reagent. Equal amount of protein sample was completely vortexed with 2 \times SDS-gel buffer, and boiled for 5 min at 100 °C to dissolve the bound proteins. The samples were segregated on 100 g/L SDS-acrylamide gel, transferred onto a nitrocellulose membrane and blocked with 50 g/L defatted milk, then probed with different primary antibodies. Anti-mouse or anti-rabbit IgG conjugated peroxidase was as a secondary antibody. The filters were then incubated in SuperSignal ECL-HRP detection reagent for 1 min followed by exposure to X-ray film.

Statistical analysis

Results were analyzed by SPSS10.0 statistical software. Data were expressed as mean \pm SD. Comparisons between different groups were made by one-way ANOVA (with LSD for post hoc analysis) or χ^2 test. $P < 0.05$ was taken as statistically significant.

RESULTS

Effect of reagents on growth inhibition of MGC803 cells

As shown in Table 1, 30 mg/L DADS suppressed MGC803 growth by 58.6% ($P < 0.05$). SB203580 10 $\mu\text{mol/L}$ alone slightly reduced cell growth, In contrast, SB203580 blocked DADS-induced growth inhibition ($P < 0.05$). Thus, addition of SB203580 to the cells decreased the inhibitory ability of DADS to MGC803 cells growth.

Table 1 $A_{570\text{nm}}$ of MGC803 cells exposed to reagents

$n = 12$	Control	SB203580 (10 $\mu\text{mol/L}$)	DADS (30 mg/L)	DADS (30 mg/L) +SB203580 (10 $\mu\text{mol/L}$)
χ	0.78	0.076	0.32	0.53
S	0.038	0.035	0.028	0.024
IR (%)		3.4	58.6 ^a	31.7 ^a

^a $P < 0.05$ vs control; IR: inhibition rate.

Table 2 Distribution of MGC803 cells in cell cycle (%)

	Control	SB203580 (10 $\mu\text{mol/L}$)	DADS (30 mg/L)	DADS (30 mg/L) +SB203580 (10 $\mu\text{mol/L}$)
G1	62.5 \pm 0.9	62.8 \pm 1.3	33.7 \pm 1.2	54.0 \pm 1.5
S	28.2 \pm 1.2	27.3 \pm 0.8	27.9 \pm 0.8	24.8 \pm 1.1
G2	9.3 \pm 0.8	9.9 \pm 1.1	39.4 \pm 1.3 ^a	21.2 \pm 0.9 ^a

^a $P < 0.05$ vs control.

Effect of reagents on cell cycle distribution of MGC803 cells

Flow cytometry revealed that the proportion of cells in the G2/M phase after treatment with 30 mg/L DADS for 24 h was 39.4%, three times more than that in untreated cells (9.3%). SB203580 10 $\mu\text{mol/L}$ alone had no effect on cell growth ($P > 0.05$). But inhibition of p38 activity by SB203580 abrogated induction of G2/M arrest by DADS. MGC803 cells treated with DADS in the presence of SB203580 decreased the G2/M phase to 21.2%, compared to 39.4% by DADS alone ($P < 0.05$).

Expression of p38, pp38, and Cdc25C after reagents treatment of MGC803 cells

Western blotting revealed that phosphorylation of p38 was increased 3.52-fold following treatment of cells with 30 mg/L DADS for 20 min. At the same time, the total p38 amount did not change. Furthermore, DADS-induced-phosphorylation of p38 was completely inhibited by SB203580 (10 $\mu\text{mol/L}$) (Figure 1).

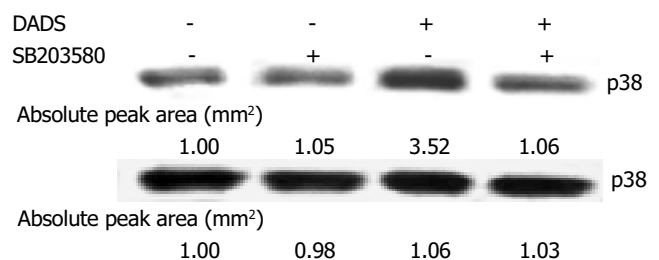


Figure 1 Expression of p38, phosphorylation of p38 proteins in MGC803 cells following treatment of reagents for 20 min.

DADS treatment for 24 h decreased the level of Cdc25C by 68%, and pretreatment of MGC803 cells with SB203580 partially reversed the down-regulation of Cdc25C level by DADS. In contrast, SB203580 alone had no significant effect on Cdc25C expression (Figure 2).

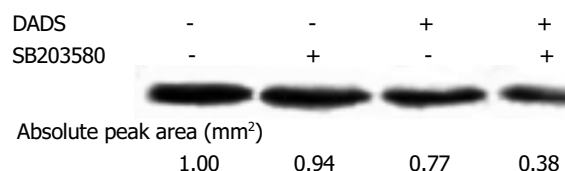


Figure 2 Expression of Cdc25C protein in MGC803 cells following treatment of reagents for 24 h.

DISCUSSION

Mitogen-activated protein kinase (MAPK) pathway has a central role in transducing extracellular signals into cellular responses. p38 kinase is a member of the mitogen-activated protein kinase family that is activated by a variety of environmental stress. Rapid initiation of G2 arrest after UV radiation is mediated by p38 kinase^[32]. Inhibition of p38 blocks the rapid initiation of G2 delay in both human and murine cells after ultraviolet radiation. p38 kinase is responsible for rapid initiation of the G2 delay in IME cells after the hypertonic stress created by addition of NaCl^[33]. Inhibition of p38 kinase blocks the rapid initiation of this checkpoint both in an immortalized cell line (mIMCDs) and in second-passage IME cells from mouse inner medulla. Genistein-induced G2/M arrest is associated with the activated p38 mitogen-activated protein kinase^[34]. Thus p38 is a critical event for initiating the G2/M checkpoint and inducing G2/M arrest. Our research showed that DADS-induced MGC803 cells

G2/M arrest and growth inhibition correlated with increased p38 phosphorylation. We used SB203580, a specific inhibitor of p38 to address the potential role of p38 kinase in the regulation of cell-cycle progression. Inhibition of p38 activity by SB203580 abolished induction of G2/M arrest by DADS. Therefore, our research data demonstrated that DADS-induced G2/M arrest of MGC803 cells involved activation of p38 MAP kinase pathways.

p34^{cdc2} is the key regulator of cell-cycle progression through G2-M^[35]. In particular, activation of p34^{cdc2} kinase activity is required for progression from G2 to M. phosphorylation of the inhibitory residues Thr14/Tyr15 of p34^{cdc2} leads to decreased kinase activity and subsequent arrest at the G2/M phase^[36]. The Cdc25C protein phosphatase is a key regulator of p34^{cdc2} phosphorylation status and kinase activity by dephosphorylating Thr14/Tyr15 residues^[37]. *In vitro*, p38 binds and phosphorylates Cdc25C at serine 216^[32]. Phosphorylation of Cdc25C triggers cell-cycle arrest by the sequestration of Cdc25C by 14-3-3^[38]. Frey *et al.* found that p38 was involved in genistein-induced G2/M arrest and down-regulation of Cdc25C expression in immortalized human mammary epithelial cell line MCF-10F^[35]. Hepatitis B virus X protein (pX) is implicated in hepatocarcinogenesis by an unknown mechanism. Research data^[39] showed that pX-dependent activation of p38 MAPK inactivated Cdc25C by phosphorylation of Ser216, thus initiating activation of the G2/M checkpoint, resulting in 4pX-1 cell growth retardation. These data suggest that p38 participation in down-regulation of the Cdc25C level may be an important way to impair its actions and an important event in G2/M checkpoint regulation. In the present studies, decreased Cdc25C protein phosphatase by DADS was attenuated by SB203580. Thus it indicates that regulation of Cdc25C protein expression by p38 is a critical event for G2/M arrest after treatment with DADS.

In summary, DADS-induced G2/M arrest and growth inhibition of MGC803 cells involves activation of p38 MAP kinase pathways. Decreased Cdc25C protein expression by p38 is a critical event for G2/M arrest by DADS. However, it should be noted that although p38 inhibitor SB203580 abrogated DADS-induced G2/M arrest, the reversal was not total. SB203580 could not completely abolish induction of G2/M arrest by DADS. This implies that p38 activation is not the sole prerequisite for DADS induced G2/M arrest, other mechanisms may be involved in G2/M arrest. Additional studies are needed to clarify these mechanisms. A deeper understanding of the molecular mechanisms involved in the regulation of cell cycle control is very important for the development of novel anticancer strategies.

REFERENCES

- 1 **Lopez-Saez JF**, de la Torre C, Pincheire J, Gimenez-Martin G. Cell proliferation and cancer. *Histol Histopathol* 1998; **13**: 1197-1214
- 2 **Rew DA**, Wilson GD. Cell production rates in human tissues and tumours and their significance. *Part II: clinical data. Eur J Surg Oncol* 2000; **26**: 405-417
- 3 **Hartell LH**, Kastan MB. Cell cycle control and cancer. *Science* 1994; **266**: 1821-1828
- 4 **Agarwal R**. Cell signaling and regulators of cell cycle as molecular targets for prostate cancer prevention by dietary agents. *Biochem Pharmacol* 2000; **60**: 1051-1059
- 5 **Weinstein IB**. Disorders in cell circuitry during multistage carcinogenesis: the role of homeostasis. *Carcinogenesis* 2000; **21**: 857-864
- 6 **Agarwal C**, Sharma Y, Agarwal R. Anticarcinogenic effect of a polyphenolic fraction isolated from grape seeds in human prostates carcinoma DU145 cells: modulation of mitogenic signaling and cell cycle regulators and induction of G1 arrest and apoptosis. *Mol Carcinogenesis* 2000; **28**: 129-138
- 7 **Mo H**, Elson CE. Apoptosis and cell-cycle arrest in human and murine tumor cells are initiated by isoprenoids. *J Nutr* 1999; **129**: 804-813
- 8 **Singh RP**, Dhanalakshmi S, Agarwal R. Phytochemicals as cell cycle modulators—a less toxic approach in halting human cancers. *Cell Cycle* 2002; **1**: 156-161
- 9 **Lin JK**. Cancer chemoprevention by tea polyphenols through modulating signal transduction pathways. *Arch Pharm Res* 2002; **25**: 561-571
- 10 **Sun J**, Chu YF, Wu X, Liu RH. Antioxidant and antiproliferative activities of common fruits. *J Agric Food Chem* 2002; **50**: 7449-7454
- 11 **Katdare M**, Osborne M, Telang NT. Soy isoflavone genistein modulates cell cycle progression and induces apoptosis in HER-2/neu oncogene expressing human breast epithelial cells. *Int J Oncol* 2002; **21**: 809-815
- 12 **Katdare M**, Osborne MP, Telang NT. Inhibition of aberrant proliferation and induction of apoptosis in pre-neoplastic human mammary epithelial cells by natural phytochemicals. *Oncol Rep* 1998; **5**: 311-315
- 13 **Chinni SR**, Li Y, Upadhyay S, Koppolu PK, Sarkar FH. Indole-3-carbinol (I3C) induced cell growth inhibition, G1 cell cycle arrest and apoptosis in prostate cancer cells. *Oncogene* 2001; **20**: 2927-2936
- 14 **Zi X**, Grasso AW, Kung HJ, Agarwal R. A flavonoid antioxidant, silymarin, inhibits activation of erbB1 signaling and induces cyclin-dependent kinase inhibitors, G1 arrest, and anticarcinogenic effects in human prostate carcinoma DU145 cells. *Cancer Res* 1998; **58**: 1920-1929
- 15 **Park MJ**, Kim EH, Park IC, Lee HC, Woo SH, Lee JY, Hong YJ, Rhee CH, Choi SH, Shim BS, Lee SH, Hong SI. Curcumin inhibits cell cycle progression of immortalized human umbilical vein endothelial (ECV304) cells by up-regulating cyclin-dependent kinase inhibitor, p21WAF1/CIP1, p27KIP1 and p53. *Int J Oncol* 2002; **21**: 379-383
- 16 **Moragoda L**, Jaszewski R, Majumdar AP. Curcumin induced modulation of cell cycle and apoptosis in gastric and colon cancer cells. *Anticancer Res* 2001; **21**: 873-878
- 17 **Tyagi AK**, Singh RP, Agarwal C, Chan DC, Agarwal R. Silibinin strongly synergizes human prostate carcinoma DU145 cells to doxorubicin-induced growth inhibition, G2-M arrest, and apoptosis. *Clin Cancer Res* 2002; **8**: 3512-3519
- 18 **Lin L**, Lin G, Chen W, Guo W, Lin X. Paclitaxel-induced apoptosis in ACC-2 cells is associated with the arrest of G2(M). *Zhonghua Kouqiang Yixue Zazhi* 2002; **37**: 94-96
- 19 **Nakagawa H**, Tsuta K, Kiuchi K, Senzaki H, Tanaka K, Hioki K, Tsubura A. Growth inhibition effects of diallyl disulfide on human breast cancer cell lines. *Carcinogenesis* 2001; **22**: 891-897
- 20 **Iciek MB**, Rokita HB, Wlodek LB. Effects of diallyl disulfide and other donors of sulfane sulfur on the proliferation of human hepatoma cell line (HepG2). *Neoplasma* 2001; **48**: 307-312
- 21 **Hong YS**, Ham YA, Choi JH, Kim J. Effects of allyl sulfur compounds and garlic extract on the expression of Bcl-2, Bax, and p53 in non small cell lung cancer cell lines. *Exp Mol Med* 2000; **32**: 127-134
- 22 **Chung JG**. Effects of garlic components diallyl sulfide and diallyl disulfide on arylamine N-acetyltransferase activity in human bladder tumor cells. *Drug Chem Toxicol* 1999; **22**: 343-358
- 23 **Knowels LM**, Milner JA. Depressed p34cdc2 kinase activity and G2/M phase arrest induced by diallyl disulfide in HCT-15 cells. *Nutrition Cancer* 1998; **30**: 169-174
- 24 **Robert V**, Mouille B, Mayeur C, Michaud M, Blachier F. Effect of the garlic compound diallyl disulfide on the metabolism, adherent and cell cycle of HT-29 Colon carcinoma cells: evidence of sensitive and resistant sub-populations. *Carcinogenesis* 2001; **22**: 1155-1161
- 25 **Kwon KB**, Yoo SJ, Ryu DG, Yang JY, Rho HW, Kim JS, Park JW, Kim HR, Park BH. Induction of apoptosis by diallyl disulfide through activation of caspase-3 in human leukemia HL-60 cells. *Biochem Pharmacol* 2002; **63**: 41-47
- 26 **Olson JM**, Hallahan AR. p38 MAP kinase: a convergence point

- in cancer therapy. *Trends Mol Med* 2004; **10**: 125-129
- 27 **Sutter AP**, Maaser K, Barthel B, Scherubl H. Ligands of the peripheral benzodiazepine receptor induce apoptosis and cell cycle arrest in oesophageal cancer cells: involvement of the p38MAPK signaling pathway. *Br J Cancer* 2003; **89**: 564-572
- 28 **Kondoh M**, Tasaki E, Araragi S, Takiguchi M, Higashimoto M, Watanabe Y, Sato M. Requirement of caspase and p38MAPK activation in zinc-induced apoptosis in human leukemia HL-60 cells. *Eur J Biochem* 2002; **269**: 6204-6211
- 29 **Liu T**, Wang XY, Song WJ, Zhu CZ, Li Y. Incidence of gastric malignant tumors during the past 20 years in Tianjin. *Shijie Huaren Xiaohua Zazhi* 2004; **12**: 20-22
- 30 **Chen XM**, Chen GY, Wang ZR, Zhu FS, Wang XL, Zhang X. Detection of micrometastasis of gastric carcinoma in peripheral blood circulation. *World J Gastroenterol* 2004; **10**: 804-808
- 31 **Zhang LY**, Ling H, Su Q, Song Y, Liang XQ. Inhibitory effect of diallyl disulfide on human gastric cancer cell line MGC803 *in vitro*. *Shijie Huaren Xiaohua Zazhi* 2003; **11**: 1290-1293
- 32 **Bulavin DV**, Higashimoto Y, Popoff I, Gaarde W, Basrur V, Potapova O, Appella E, Fornace A. Initiation of a G2/M checkpoint after ultraviolet radiation require p38 kinase. *Nature* 2001; **411**: 102-106
- 33 **Dmitrieva N**, Bulavin D, Fornace A, Brug M. Rapid activation of G2/M checkpoint after hypertonic stress in renal inner medullary epithelial (IME) cells is protective and requires p38 kinase. *Proc Natl Acad Sci U S A* 2002; **99**: 184-189
- 34 **Frey RS**, Singletary KW. Genistein activates p38 mitogen-activated protein kinase, inactivates ERK1/ERK2 and decreases Cdc25C expression in immortalized human mammary epithelial cells. *J Nutr* 2003; **133**: 266-231
- 35 **King RW**, Jackson PK, Kirschner MW. Mitosis in transition. *Cell* 1994; **79**: 563-571
- 36 **Coleman TR**, Dunphy WG. Cdc2 regulatory factors. *Curr Opin Cell Biol* 1994; **6**: 877-882
- 37 **Obaya AJ**, Sedivy JM. Regulation of cyclin-Cdk activity in mammalian cells. *Cell Mol Life Sci* 2002; **59**: 126-142
- 38 **Peng CY**, Graves PR, Thoma RS, Wu Z, Shaw AS, Piwnicka-Worms H. Mitotic and G2 checkpoint control: regulation of 14-3-3-protein binding by phosphorylation of cdc25C on serine-216. *Science* 1997; **277**: 1501-1505
- 39 **Tarn C**, Zou L, Hullinger RL, Andrisani OM. Hepatitis B virus X protein activates the p38 mitogen-activated protein kinase pathway in dedifferentiated hepatocytes. *J Virus* 2002; **76**: 9763-9772

Edited by Zhu LH Proofread by Chen WW and Xu FM

ADAM17 mRNA expression and pathological features of hepatocellular carcinoma

Xiang Ding, Lian-Yue Yang, Gen-Wen Huang, Wei Wang, Wei-Qun Lu

Xiang Ding, Lian-Yue Yang, Gen-Wen Huang, Wei Wang, Wei-Qun Lu, Liver Cancer Laboratory, Department of General Surgery, Xiangya Hospital, Central South University, Changsha 410008, Hunan Province, China

Supported by the National Key Research and Development Program, No. 2001BA703B05 and the National Natural Science Foundation of China, No. 30371595

Correspondence to: Lian-Yue Yang, Department of General Surgery, Xiangya Hospital, Central South University, Changsha 410008, Hunan Province, China. lianyueyang@hotmail.com

Telephone: +86-731-4327326 **Fax:** +86-731-4327332

Received: 2003-12-12 **Accepted:** 2004-01-15

Abstract

AIM: To study the expression of a disintegrin and metalloproteinase 17 (ADAM17) mRNA in hepatocellular carcinoma (HCC) and to evaluate the relationship between ADAM17 mRNA expression and clinicopathological features of HCC.

METHODS: Hepatocellular carcinomas (HCC) from 31 cases were divided into small HCC (SHCC), nodular HCC (NHCC) and solitary large HCC (SLHCC) according to tumor diameter and the number of nodes. ADAM17 mRNA expressions were compared among those groups by means of semi-quantitative reverse transcription polymerase chain reaction (RT-PCR). The relationship between ADAM17 mRNA expression level and clinicopathological features of HCC was evaluated.

RESULTS: NHCC had lower differentiation and was more frequently of microvascular invasion (10/12) than SHCC (3/11) and SLHCC (3/8) ($P < 0.05$), but no statistical difference was observed between SHCC and SLHCC comparing their clinicopathological features. ADAM17 mRNA expression was detected in 77.4% (24/31) of HCC tissues and was significantly higher than that in paired non-cancerous liver tissues in which only 35.5% (11/31) of the samples were detected of the expression ($P < 0.05$). The expression of ADAM17 mRNA was much higher in NHCC than in SHCC and SLHCC ($P < 0.05$), while no significant difference was discovered between SHCC and SLHCC. The quantities of ADAM17 mRNA were significantly higher in poorly differentiated HCC than in well or moderately differentiated HCC, but no statistical difference was found concerning liver cirrhosis, tumor capsule formation or microvascular invasion of the cancer.

CONCLUSION: The increased expression of ADAM17 may play a key role in the development of HCC. The expression levels of ADAM17 mRNA varied among different pathological types of HCC. Lower mRNA expression of ADAM17 mRNA in SLHCC may be associated with the better molecular pathological features of SLHCC.

Ding X, Yang LY, Huang GW, Wang W, Lu WQ. ADAM17 mRNA expression and pathological features of hepatocellular carcinoma. *World J Gastroenterol* 2004; 10(18): 2735-2739 <http://www.wjgnet.com/1007-9327/10/2735.asp>

INTRODUCTION

Hepatocellular carcinoma (HCC) is one of the most common malignant diseases in the world. Approximately 560 000 new cases of HCC are diagnosed each year, constituting 6% of all new human cancers^[1]. The HCC mortality rate in China is approximately 20.4/100 000 and is the second leading cause of cancer death among Chinese males^[2]. The prognosis of large hepatocellular carcinoma (LHCC) is generally considered to be worse than small hepatocellular carcinoma (SHCC), but long-term survival of some LHCC, especially solitary large hepatocellular carcinoma (SLHCC), could be frequently observed after curative resection^[3-5]. From the clinical observation and our research, we hypothesized that SLHCC was of relatively better biological behavior^[2]. Furthermore, we have preliminarily proved our hypothesis in a series of researches by showing that SLHCC was of relatively better pathological features and surgical prognosis^[2,3,6]. Although many systemic studies have been performed, the unique clinical and molecular pathological features of SLHCC are still far from a clear deep understanding and need further investigation.

A disintegrin and metalloproteinase 17 (ADAM17) is a kind of transmembrane metalloproteinase^[7], which can cleave the ectodomain of many transmembrane proteins. The substrates of ADAM17 mediated cleavage include tumor necrosis factor- α (TNF- α), tumor necrosis factor receptor type I, (TNFR I) and tumor necrosis factor receptor type II (TNFR II), interleukin1 receptor type II (IL1R II), Notch receptor, L-selectin, mucin1 (MUC1), CD30, tumor necrosis factor-related activation-induced cytokine (TRANCE) and many ligands of epidermal growth factor receptor (EGFR), such as transforming growth factor- α (TGF- α), heparin-binding epidermal growth factor-like growth factor (HB-EGF), amphiregulin and so on^[8-19]. Hassan reported that the oxygen radicals generated by smoke stimulated ADAM17 to cleave transmembrane amphiregulin. The binding of amphiregulin to EGFR then promoted proliferation of lung cancer cells^[20]. The cleavage function of ADAM17 was required for the activation of EGFR by TGF- α in Hela cells, and the high expression level of ADAM17 in mammary tumors was correlated with high activation rate of EGFR^[21]. Another experiment showed that single metastatic lung cancer cell in bone marrow presented overexpression of ADAM17^[22]. All these suggested that ADAM17 played a key role in the development of some cancers. It is well known that the EGFR mediated pathway played an important role in HCC development^[23,24]. The overexpression of EGFR and its ligands were observed in HCC tissue and were related to the prognosis of HCC patients^[25,26]. However, much less is known about the mechanisms involved in signal transduction, which activate the EGFR in HCC. It is even not sure whether there is an increased activation rate of EGFR in HCC besides the overexpression of EGFR and its ligands. As ADAM17 played an important role in the activation of EGFR^[27] and up to now, there is no report about the expression and function of ADAM17 in HCC, so to have a better understanding of the molecular mechanisms involved in HCC development and the unique molecular pathological features of SLHCC, we studied the expression of ADAM17 in HCC and paired non-cancerous liver tissues.

MATERIALS AND METHODS

Materials

Thirty-one fresh HCC specimens (26 from males and 5 from females) were obtained by surgical resection in Xiangya Hospital, Central South University between May 2002 and February 2003. Tissues 1 cm away from the edge of the cancer were used as the paired non-cancerous control. The tissues used for RNA extraction were immediately snap-frozen in liquid nitrogen and stored at -70°C . The specimens used for pathological study were fixed with 10% formalin, dehydrated by conventional methods, embedded in paraffin, cut into slices of 5 μm thick and stained by haematoxylin and eosin.

The specimens were divided into SHCC group (largest diameter less than 5 cm for single tumor nodule or the sum of diameters less than 5 cm for two tumor nodules, $n = 11$), SLHCC group (single tumor nodule with largest diameter more than 5 cm, $n = 8$) and NHCC group (two or more tumor nodules in the liver, only two tumor nodules and the sum of diameters less than 5 cm were excluded, $n = 12$).

Clinicopathological study

All specimens were examined under a microscope after haematoxylin-eosin staining by two pathologists. Four aspects of clinicopathological features including liver cirrhosis, Edmondson classification, capsule formation and microvascular invasion were studied.

RT-PCR

The total RNA was extracted from HCC tissue and paired non-cancerous liver tissue by using the TRIzol (Invitrogen, USA). The quality of RNA was checked through the ribosomal RNA bands on the gel. Two μg of each intact total RNA sample was reverse-transcribed to complementary DNA (cDNA) by using RT-PCR kit (MBI, USA). The PCR primer sequences used were as follows: sense: 5'-GCACAGGTAATAGCAGTGAGTGC-3' and antisense: 5'-CACACAATGGACAAGAATGCTG-3' for ADAM17; sense: 5'-TTCCAGCCTTCCTTCCTGG-3' and antisense: 5'-TTGCGCTCAGGAGGAGC AAT -3' for β -actin. The sizes of PCR products were 440 bp for ADAM17 and 218 bp for β -actin. The procedure was as follows: denaturation at 94°C for 5 min, then 40 cycles of denaturation at 94°C for 50 s; annealing at 52°C for 1 min and extension at 72°C for 1 min. The PCR products were electrophoresed in 20 g/L agarose gels, and visualized under ultraviolet light. The expression ratio of ADAM17 mRNA to β -actin was determined by Eagle Eye II photo-analysis system.

Statistical analysis

The χ^2 test was used for quantitative enumeration data. The student's t test and one-way analysis of variance were used for qualitative data. The statistic analysis was performed by statistical software SPSS11.0. P value less than 0.05 was considered significant.

RESULTS

Clinicopathological features of HCC in three groups

According to the results of pathological study (shown in Table 1), the NHCC group had higher incidences of microvascular invasion (10/12) compared with SLHCC (3/8) and SHCC (3/11) ($P < 0.05$). Only 8.3% NHCC (1/12) was classified as Edmondson I-II, while 62.5% SLHCC (5/8) and 63.6% SHCC (7/11) were classified as Edmondson I-II. The differentiation of NHCC was significantly poorer than SLHCC and SHCC ($P < 0.05$). The other two pathological features of SLHCC and SHCC were also better than NHCC but the difference did not reach statistical significance. No statistical difference of the four pathological features was observed between SLHCC and SHCC.

Table 1 Pathological features of HCC in three groups

Pathological features	SHCC ($n = 11$)	SLHCC ($n = 8$)	NHCC ($n = 12$)
Liver cirrhosis			
Present	7	6	9
Absent	4	2	3
Microvascular invasion			
Present	3	3 ^a	10
Absent	8	5 ^a	2
Capsule formation			
Present	8	6	4
Absent	3	2	8
Edmondson classification			
I-II	7	5	1
III-IV	4	3	11

^a $P < 0.05$ vs NHCC.

Expression of ADAM17 mRNA in HCC and paired non-cancerous liver tissue

As shown in Figure 1, RT-PCR products of ADAM17 and β -actin presented at the same site as previously designed. The expression of ADAM17 mRNA was detected in 77.4% (24/31) of HCC tissues, much higher than that in paired non-cancerous liver tissues in which only 35.5% (11/31) tissues were detected of the expression ($P < 0.05$).

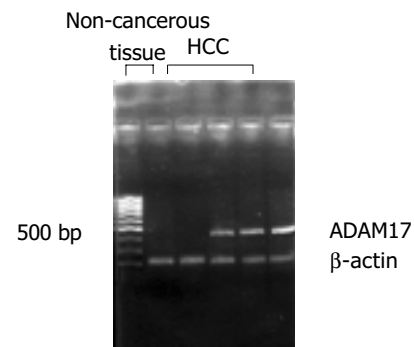


Figure 1 ADAM17 transcription was detected in HCC but no obvious transcription was observed in paired non-cancerous tissues.

Transcription level of ADAM17 in SLHCC, SHCC and NHCC

As shown in Figures 2, 3, the transcription level of ADAM17 was 0.8 ± 0.7 (mean \pm SD) in SLHCC and 0.9 ± 0.6 in SHCC. Both were significantly lower than that in NHCC (1.6 ± 0.5) ($P < 0.05$). No statistical difference in transcription level of ADAM17 was observed between SLHCC and SHCC.

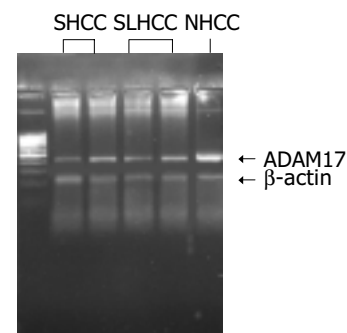


Figure 2 The expression of ADAM17 mRNA was higher in NHCC compared with SHCC and SLHCC.

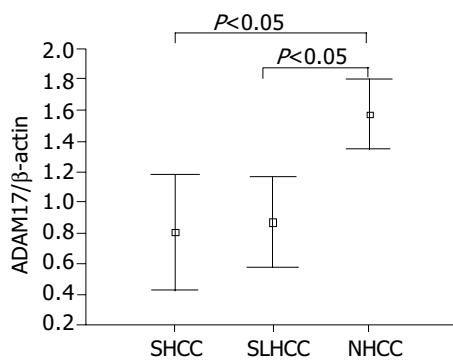


Figure 3 Transcription level of ADAM17 in three groups of HCC.

Relationship between transcription level of ADAM17 and clinicopathological features of HCC

The transcription level of ADAM17 was compared between different pathological types of HCC. The ADAM17 transcription level was much higher in HCC samples classified as Edmondson I-II compared with those classified as Edmondson III-IV ($P < 0.05$). While no statistical difference in transcription level of ADAM17 was observed when capsule formation, liver cirrhosis, and microvascular invasion were concerned (Table 2).

Table 2 Relationship between ADAM17 transcription and pathological features of HCC

	Sample (n)	Transcription level of ADAM17 (mean±SD)	P
Liver cirrhosis			
Present	22	1.141±0.743	>0.05
Absent	9	0.996±0.662	
Microvascular invasion			
Present	16	1.279±0.648	>0.05
Absent	15	0.893±0.750	
Capsule formation			
Present	18	1.058±0.157	>0.05
Absent	13	1.187±0.800	
Edmondson classification			
I-II	13	0.768±0.204	<0.05
III-IV	18	1.349±0.157	

DISCUSSION

HCC ranks fifth in frequency worldwide among all malignancies^[1]. Surgery is the only potential curative treatment of HCC^[28]. The post-operative survival of SHCC was generally considered to be better than LHCC, but long-term disease-free survival of some LHCC was also frequently observed after curative resection. Furthermore, some clinical investigation showed that the 5-year survival rate of LHCC after curative resection was not statistically different from SHCC^[4,5]. This kind of LHCC was named SLHCC because it was of some unique characters such as: isolated lesion, expanding growth and relatively integrated fibrous capsule formation *et al.*^[2]. Previous studies showed that SLHCC had relative better prognosis after curative resection^[2,3,6]. Consistent with this, the relatively better pathological features of SHCC were found in this study. The differentiation of SLHCC was much better than that of NHCC, and NHCC was more frequently of microvascular invasion compared with SLHCC. No statistic difference in pathological features was observed between SHCC and SLHCC.

ADAM17 is a sheddase of many transmembrane proteins. The substrates of ADAM17 mediated shedding include many

ligands of EGFR such as TGF- α , HB-EGF, amphiregulin *et al.*^[14]. It has been well known that the activation of EGFR is essential for the carcinogenesis and metastasis of many cancers, while ADAM17 mediated shedding is a key mechanism of sending signals to activate EGFR^[19-21]. Overexpression of ADAM17 has been observed in gastric tumor, mammary cancer, leukemia cell lines and prostate cancer cell lines^[20,21,29-32]. In this study the transcription of ADAM17 was detected in 77.4% (24/31) HCC samples and was statistically higher than that in paired non-cancerous samples in which only 35.5% (11/31) were detected ($P < 0.05$). This suggests that ADAM17 may play a key role in HCC development.

Previous studies showed that SLHCC had relative better prognosis after curative resection. To understand the underlying molecular mechanism, the transcription levels of ADAM17 in SLHCC, SHCC and NHCC were also studied. As expected, the transcription level of ADAM17 was much higher in NHCC than in SLHCC and SHCC, while no statistical difference was observed between SLHCC and SHCC. The transcription level of ADAM17 mRNA was also detected to be statistically higher in samples classified as Edmondson III-IV compared with those classified as I-II. The higher expression of ADAM17 mRNA in NHCC as well as in poorly differentiated HCC suggested that it might facilitate tumor invasiveness. The lower transcription level of ADAM17 in SLHCC was probably associated with the relatively better molecular pathological features of SLHCC.

The relationship between ADAM17 mRNA expression and the other two tumor features: microvascular invasion and tumor capsule formation was also studied in this study. Although much higher ADAM17 mRNA level was detected in tumors with microvascular invasion and those without integrated capsule formation, the difference did not reach statistical significance. This maybe due to the relatively small sample size in this study. As only 31 samples were used in the study, especially after the samples were divided into three groups, the significance of the research results may be impaired. The role of ADAM17 in HCC invasiveness needs further investigation with a larger sample size.

The increased transcription of ADAM17 may facilitate the growth and invasiveness of HCC in several ways. (1) Overexpressions of EGFR and its ligands were observed in HCC and were related to the prognosis. However, ADAM17 mediated shedding is a key mechanism of sending signals to activate EGFR. ADAM17 is required for the activation of EGFR by TGF-alpha or amphireglin in several cancer cells and the high expression of ADAM17 in mammary tumors was correlated with a high activation rate of EGFR^[20,21]. As ADAM17 regulates the ligands production and activity of EGFR, the overexpression of ADAM17 is probably as important as the increased expression of EGFR and its ligands for HCC development; (2) ADAM17 can function as an effector of G protein-coupled receptor (GPCR) -mediated signaling. Activation of GPCR specifically results in ADAM17 cleavage and release of amphiregulin, which could activate EGFR and regulate the proliferation and motility of squamous cell carcinoma^[32]. Overexpression of GPCR was also observed in HCC and was strongly correlated with carcinogenesis of HCC^[33]. ADAM17 may be a key element of communication between GPCR and EGFR in HCC and facilitates HCC development; (3) TRANCE could activate osteoclast and help cancer cells metastasize to bones. Overexpression of TRANCE was found in bone metastatic lesion of several cancers^[34]. ADAM17 may play a role in the bone metastasis of HCC by cleaving TRANCE; (4) The shedding of TNFR by ADAM17 may cause disorder of host immune system as the soluble form of TNFR could bind to the TNF and block its attack to cancer cells^[35].

Other transmembrane proteins associated with HCC

metastasis such as Fas ligand, CXCL12, E-cadherin, interleukin-6 α ^[36-39] were also the suspected substrates of ADAM17 mediated shedding, so it is of particular significance to study the sheddase role of ADAM17 in HCC development. The ADAM metalloproteinase family includes more than 30 members by now^[40]. Many of them not only function as metalloproteinases to shed transmembrane proteins^[41-43] in cancer but also can work as adhesion molecules^[44,45]. In contrast to the matrix metalloproteinases, relatively few data on expression of ADAMs in cancer tissue are available. The expression of ADAM12 and ADAM9 were recently studied in HCC tissue and were of particular importance^[46]. To study the role of other ADAM family members may help us better understand HCC development.

REFERENCES

- Parkin DM. Global cancer statistics in the year 2000. *Lancet Oncol* 2001; **2**: 533-543
- Yang LY, Huang GW. Surgical strategy of large hepatocellular carcinoma. *Linchuang Waiké Zazhi* 2001; **9**: 4-5
- Yang LY, Huang GW, Huang JH, Yang JQ, Lü XS, Han M. Surgical excision of 114 cases of large hepatocellular carcinomas. *Zhongguo Shiyong Waiké Zazhi* 2002; **22**: 353-355
- Poon RT, Fan ST, Wong J. Selection criteria for hepatic resection in patients with large hepatocellular carcinoma larger than 10 cm in diameter. *J Am Coll Surg* 2002; **194**: 592-602
- Regimbeau JM, Farges O, Shen BY, Sauvanet A, Belghiti J. Is surgery for large hepatocellular carcinoma justified? *J Hepatol* 1999; **31**: 1062-1068
- Yang LY, Huang GW, Huang JH, Yang JQ. Resection of large hepatocellular carcinoma without employment of pringle maneuver. *Zhonghua Gandan Waiké Zazhi* 2003; **9**: 331-333
- Black RA. Tumor necrosis factor-alpha converting enzyme. *Int J Biochem Cell Biol* 2002; **34**: 1-5
- Black RA, Rauch CT, Kozlosky CJ, Peschon JJ, Slack JL, Wolfson MF, Castner BJ, Stocking KL, Reddy P, Srinivasan S, Nelson N, Boiani N, Schooley KA, Gerhart M, Davis R, Fitzner JN, Johnson RS, Paxton RJ, March CJ, Cerretti DP. A metalloproteinase disintegrin that releases tumour-necrosis factor-alpha from cells. *Nature* 1997; **385**: 729-733
- Reddy P, Slack JL, Davis R, Cerretti DP, Kozlosky CJ, Blanton RA, Shows D, Peschon JJ, Black RA. Functional analysis of the domain structure of tumor necrosis factor-alpha converting enzyme. *J Biol Chem* 2000; **275**: 14608-14614
- Condon TP, Flournoy S, Sawyer GJ, Baker BF, Kishimoto TK, Bennett CF. ADAM17 but not ADAM10 mediates tumor necrosis factor-alpha and L-selectin shedding from leukocyte membranes. *Antisense Nucleic Acid Drug Dev* 2001; **11**: 107-116
- Slack BE, Ma LK, Seah CC. Constitutive shedding of the amyloid precursor protein ectodomain is up-regulated by tumour necrosis factor-alpha converting enzyme. *Biochem J* 2001; **357**(Pt 3): 787-794
- Wang X, He K, Gerhart M, Huang Y, Jiang J, Paxton RJ, Yang S, Lu C, Menon RK, Black RA, Baumann G, Frank SJ. Metalloprotease-mediated GH receptor proteolysis and GHBP shedding. Determination of extracellular domain stem region cleavage site. *J Biol Chem* 2002; **277**: 50510-50519
- Thathiah A, Blobel CP, Carson DD. Tumor necrosis factor-alpha converting enzyme/ADAM 17 mediates MUC1 shedding. *J Biol Chem* 2003; **278**: 3386-3394
- Sunnarborg SW, Hinkle CL, Stevenson M, Russell WE, Raska CS, Peschon JJ, Castner BJ, Gerhart MJ, Paxton RJ, Black RA, Lee DC. Tumor necrosis factor-alpha converting enzyme (TACE) regulates epidermal growth factor receptor ligand availability. *J Biol Chem* 2002; **277**: 12838-12845
- Garton KJ, Gough PJ, Blobel CP, Murphy G, Greaves DR, Dempsey PJ, Raines EW. Tumor necrosis factor-alpha-converting enzyme (ADAM17) mediates the cleavage and shedding of fractalkine (CX3CL1). *J Biol Chem* 2001; **276**: 37993-38001
- Brou C, Logeat F, Gupta N, Bessia C, LeBail O, Doedens JR, Cumano A, Roux P, Black RA, Israel A. A novel proteolytic cleavage involved in Notch signaling: the role of the disintegrin-metalloprotease TACE. *Mol Cell* 2000; **5**: 207-216
- Rio C, Buxbaum JD, Peschon JJ, Corfas G. Tumor necrosis factor-alpha-converting enzyme is required for cleavage of erbB4/HER4. *J Biol Chem* 2000; **275**: 10379-10387
- Lum L, Wong BR, Josien R, Becherer JD, Erdjument-Bromage H, Schlondorff J, Tempst P, Choi Y, Blobel CP. Evidence for a role of a tumor necrosis factor-alpha (TNF-alpha)-converting enzyme-like protease in shedding of TRANCE, a TNF family member involved in osteoclastogenesis and dendritic cell survival. *J Biol Chem* 1999; **274**: 13613-13618
- Peschon JJ, Slack JL, Reddy P, Stocking KL, Sunnarborg SW, Lee DC, Russell WE, Castner BJ, Johnson RS, Fitzner JN, Boyce RW, Nelson N, Kozlosky CJ, Wolfson MF, Rauch CT, Cerretti DP, Paxton RJ, March CJ, Black RA. An essential role for ectodomain shedding in mammalian development. *Science* 1998; **282**: 1281-1284
- Lemjabbar H, Li D, Gallup M, Sidhu S, Drori E, Basbaum C. Tobacco smoke-induced lung cell proliferation mediated by tumor necrosis factor alpha-converting enzyme and amphiregulin. *J Biol Chem* 2003; **278**: 26202-26207
- Borrell-Pages M, Rojo F, Albanell J, Baselga J, Arribas J. TACE is required for the activation of the EGFR by TGF-alpha in tumors. *EMBO J* 2003; **22**: 1114-1124
- Klein CA, Seidl S, Petat-Dutter K, Offner S, Geigl JB, Schmidt-Kittler O, Wendler N, Passlick B, Huber RM, Schlimok G, Baeuerle PA, Riethmuller G. Combined transcriptome and genome analysis of single micrometastatic cells. *Nat Biotechnol* 2002; **20**: 387-392
- Hisaka T, Yano H, Haramaki M, Utsunomiya I, Kojiro M. Expressions of epidermal growth factor family and its receptor in hepatocellular carcinoma cell lines: relationship to cell proliferation. *Int J Oncol* 1999; **14**: 453-460
- Miyaki M, Sato C, Sakai K, Konishi M, Tanaka K, Muraoka M, Kikuchi-Yanoshita R, Nadaoka Y, Kanda H, Kitagawa T. Malignant transformation and EGFR activation of immortalized mouse liver epithelial cells caused by HBV enhancer-X from a human hepatocellular carcinoma. *Int J Cancer* 2000; **85**: 518-522
- Daveau M, Scotte M, Francois A, Coulouarn C, Ros G, Tallet Y, Hiron M, Hellot MF, Salier JP. Hepatocyte growth factor, transforming growth factor alpha, and their receptors as combined markers of prognosis in hepatocellular carcinoma. *Mol Carcinog* 2003; **36**: 130-141
- Ito Y, Takeda T, Sakon M, Tsujimoto M, Higashiyama S, Noda K, Miyoshi E, Monden M, Matsuura N. Expression and clinical significance of erb-B receptor family in hepatocellular carcinoma. *Br J Cancer* 2001; **84**: 1377-1383
- Lee DC, Sunnarborg SW, Hinkle CL, Myers TJ, Stevenson MY, Russell WE, Castner BJ, Gerhart MJ, Paxton RJ, Black RA, Chang A, Jackson LF. TACE/ADAM17 processing of EGFR ligands indicates a role as a physiological convertase. *Ann N Y Acad Sci* 2003; **995**: 22-38
- Yu AS, Keefe EB. Management of hepatocellular carcinoma. *Rev Gastroenterol Disord* 2003; **3**: 8-24
- Yoshimura T, Tomita T, Dixon MF, Axon AT, Robinson PA, Crabtree JE. ADAMs (a disintegrin and metalloproteinase) messenger RNA expression in Helicobacter pylori-infected, normal, and neoplastic gastric mucosa. *J Infect Dis* 2002; **185**: 332-340
- McCulloch DR, Harvey M, Herington AC. The expression of the ADAMs proteases in prostate cancer cell lines and their regulation by dihydrotestosterone. *Mol Cell Endocrinol* 2000; **167**: 11-21
- Wu E, Croucher PI, McKie N. Expression of members of the novel membrane linked metalloproteinase family ADAM in cells derived from a range of haematological malignancies. *Biochem Biophys Res Commun* 1997; **235**: 437-442
- Gschwind A, Hart S, Fischer OM, Ullrich A. TACE cleavage of proamphiregulin regulates GPCR-induced proliferation and motility of cancer cells. *EMBO J* 2003; **22**: 2411-2421
- Yamamoto Y, Sakamoto M, Fujii G, Tsuiji H, Kenetaka K, Asaka M, Hirohashi S. Overexpression of orphan G-protein-coupled receptor, Gpr49, in human hepatocellular carcinomas with beta-catenin mutations. *Hepatology* 2003; **37**: 528-533

- 34 **Huang L**, Cheng YY, Chow LT, Zheng MH, Kumta SM. Tumour cells produce receptor activator of NF-kappaB ligand (RANKL) in skeletal metastases. *J Clin Pathol* 2002; **55**: 877-878
- 35 **Wallach D**, Engelmann H, Nophar Y, Aderka D, Kemper O, Hornik V, Holtmann H, Brakebusch C. Soluble and cell surface receptors for tumor necrosis factor. *Agents Actions Suppl* 1991; **35**: 51-57
- 36 **Ethell DW**, Kinloch R, Green DR. Metalloproteinase shedding of Fas ligand regulates beta-amyloid neurotoxicity. *Curr Biol* 2002; **12**: 1595-1600
- 37 **Marin V**, Montero-Julian F, Gres S, Bongrand P, Farnarier C, Kaplanski G. Chemotactic agents induce IL-6Ralpha shedding from polymorphonuclear cells: involvement of a metalloproteinase of the TNF-alpha-converting enzyme (TACE) type. *Eur J Immunol* 2002; **32**: 2965-2970
- 38 **Steinhausen U**, Weiske J, Badock V, Tauber R, Bommert K, Huber O. Cleavage and shedding of E-cadherin after induction of apoptosis. *J Biol Chem* 2001; **276**: 4972-4980
- 39 **Scotton CJ**, Wilson JL, Scott K, Stamp G, Wilbanks GD, Fricker S, Bridger G, Balkwill FR. Multiple actions of the chemokine CXCL12 on epithelial tumor cells in human ovarian cancer. *Cancer Res* 2002; **62**: 5930-5938
- 40 **Brachvogel B**, Reichenberg D, Beyer S, Jehn B, von der Mark K, Bielke W. Molecular cloning and expression analysis of a novel member of the Disintegrin and Metalloprotease-Domain (ADAM) family. *Gene* 2002; **288**: 203-210
- 41 **Moss ML**, Lambert MH. Shedding of membrane proteins by ADAM family proteases. *Essays Biochem* 2002; **38**: 141-153
- 42 **Gutwein P**, Oleszewski M, Mechtersheimer S, Agmon-Levin N, Krauss K, Altevogt P. Role of Src kinases in the ADAM-mediated release of L1 adhesion molecule from human tumor cells. *J Biol Chem* 2000; **275**: 15490-15497
- 43 **Blobel CP**. Functional and biochemical characterization of ADAMS and their predicted role in protein ectodomain shedding. *Inflamm Res* 2002; **51**: 83-84
- 44 **Thodeti CK**, Albrechtsen R, Grauslund M, Asmar M, Larsson C, Takada Y, Mercurio AM, Couchman JR, Wewer UM. ADAM12/syndecan-4 signaling promotes beta 1 integrin-dependent cell spreading through protein kinase Calpha and RhoA. *J Biol Chem* 2003; **278**: 9576-9584
- 45 **Zhu P**, Sun Y, Xu R, Sang Y, Zhao J, Liu G, Cai L, Li C, Zhao S. The interaction between ADAM 22 and 14-3-3zeta: regulation of cell adhesion and spreading. *Biochem Biophys Res Commun* 2003; **301**: 991-999
- 46 **Le Pabic H**, Bonnier D, Wewer UM, Coutand A, Musso O, Baffet G, Clement B, Theret N. ADAM12 in human liver cancers: TGF-beta-regulated expression in stellate cells is associated with matrix remodeling. *Hepatology* 2003; **37**: 1056-1066

Edited by Chen WW Proofread by Zhu LH and Xu FM

Clinical significance of serum IGF-I, IGF-II and IGFBP-3 in liver cirrhosis

Yun-Lin Wu, Jing Ye, Shu Zhang, Jie Zhong, Rong-Ping Xi

Yun-Lin Wu, Jing Ye, Shu Zhang, Jie Zhong, Rong-Ping Xi, Department of Gastroenterology, Ruijin Hospital, Shanghai Second Medical University, Shanghai 200025, China

Supported by the Medical Development Project of Asahi Fund of Japan

Correspondence to: Dr. Yun-Lin Wu, Department of Gastroenterology, Ruijin Hospital, Shanghai Second Medical University, Shanghai 200025, China. carlionje8@hotmail.com

Telephone: +86-21-64370045 Ext. 665246

Received: 2003-07-17 **Accepted:** 2004-01-07

Abstract

AIM: To investigate the relationship between insulin-like growth factor-I, -II (IGF-I and IGF-II), IGF-binding protein 3 (IGFBP-3) and Child-Pugh score in patients with liver cirrhosis, and to search for potential clinical markers of liver function.

METHODS: Forty-four patients with advanced liver cirrhosis of viral origin were divided into 3 groups according to severity of cirrhosis (Child-Pugh score) and 38 healthy subjects served as controls. Serum levels of IGF-I, IGF-II and IGFBP-3 were measured by immunoradiometric assay.

RESULTS: Serum IGF-I, IGF-II and IGFBP-3 levels were significantly lower in patients with cirrhosis than in controls, and serum concentrations of IGF-I, IGF-II and IGFBP-3 were associated with the severity of liver dysfunction, and dropped sharply during the progression of liver failure. Among these 3 parameters, serum IGF-II was the most sensitive and effective indicator for liver dysfunction. Concentrations of IGF-I <30 ng/mL, IGF-II <200 ng/mL and IGFBP-3 <6 ng/mL implied a negative prognosis for patients with liver cirrhosis.

CONCLUSION: Serum IGF-I, IGF-II and IGFBP-3 may provide a new dimension in the assessment of liver dysfunction. Combined detection of serum IGF-I, IGF-II and IGFBP-3 with Child-Pugh score is more effective in predicting prognosis than Child-Pugh score alone.

Wu YL, Ye J, Zhang S, Zhong J, Xi RP. Clinical significance of serum IGF-I, IGF-II and IGFBP-3 in liver cirrhosis. *World J Gastroenterol* 2004; 10(18): 2740-2743

<http://www.wjgnet.com/1007-9327/10/2740.asp>

INTRODUCTION

Insulin-like growth factor-I and II (IGF-I, IGF-II), two major forms of insulin-like growth factors (IGFs) family, are single-chain molecules with three intrachain disulfide bridges consisting of 70 (*M_r* 7 646) and 67 (*M_r* 7 471) amino acid residues respectively^[1,2]. Both of them may be considered as important anabolic hormones which are active throughout one's life, inducing anabolic metabolism and stimulating DNA synthesis, cell proliferation and meiotic division^[3,4]. Compared with IGF-I, IGF-II is more well-known as a tumor genesis marker^[5]. As serum IGF-II may be produced and secreted by hepatoma cells, the hormone

could accelerate or magnify its function of continuously stimulating cell growth by directly or indirectly combining with its receptor in neighboring cells or hepatoma cells themselves to form intracellular shortcuts^[6,7].

Insulin-like growth factor binding protein-3 (IGFBP-3) consisting of 264 amino acid residues binds nearly 95% circulating IGFs in the human body, forming a stable ternary complex (*M_r* 150 000) with the acid-labile subunit (ALS). The complex is believed to serve as a reservoir in circulation to prolong half-lives of both IGF-I and IGF-II^[8,9]. Since most circulating IGF-I, IGF-II and IGFBP-3 are synthesized by hepatocytes, lower levels of the above three parameters should be found in patients with liver diseases^[10]. This study was designed to clarify the influences of associated liver cirrhosis as assessed by Child-Pugh score (CP score) on these parameters, to determine whether measurement of these three parameters could reflect the severities of cirrhosis and liver dysfunction, to reveal whether the combination of these three parameters with CP score could be a more reasonable clinical option for evaluating liver function.

MATERIALS AND METHODS

Patients

From February to September 2001, 44 patients with hepatitis B-induced liver cirrhosis (30 males and 14 females with a mean age of 57.41 years, ranging from 38 to 83) were studied. Patients with liver cirrhosis were diagnosed by liver biopsy and/or by computerized tomography, ultrasonography and clinical biochemical examinations, according to Chinese diagnostic criteria of liver cirrhosis set up in 1995. Patients were divided into 3 groups by CP score: Fifteen people in the group of CP A (scored 5-6), 19 in the group of CP B (scored 7-10) and 10 in the group of CP C (scored 11-15). A total of 38 healthy subjects were served as controls (23 males and 15 females, mean age of 49.97 years, ranging from 35 to 82). After detection of serum IGF-I, IGF-II and IGFBP-3 levels, patients were followed-up in the liver clinic for a period of 6 mo.

Study protocols

Serum IGF-I was quantified by immunoradiometric assay kit (Immunotech A BECKMAN Company). Serum levels of IGF-II and IGFBP-3 were detected by DSL-2 600 ACTIVETM immunoradiometric assay kits (Diagnostic System Laboratories Inc, USA).

Sample collection, procession and storage were referred to the following: A 6 mL venipuncture blood was collected into a dry, heparinized tube in the morning from every subject. Then serum or plasma was separated from cells by centrifugation. Samples should be kept at below -30 °C after aliquoting so as to avoid repeated freezing and thawing.

Assay procedures were firmly accorded to instructions of the kits. Briefly, taking protocol of IGF-II for example, first, 100 µL of the reconstituted standards, controls and pretreated samples were added to appropriate tubes. Then all the tubes were mixed and incubated at room temperature for 3 h, centrifuged at 180 r/m, and decanted except for total count tubes by simultaneous inversion. The tubes were shaken violently to facilitate complete drainage and allowed to drain on absorbent for 1-2 min. Two

milliliters of deionized water was added to all tubes, except total count tubes, and the tubes were decanted. After 100 μ L of anti-IGF-II [125 I] reagents was added, all tubes were mixed by shaking and were incubated at room temperature for 1 h on a shaker at 180 r/min, then were decanted except for total count tubes by simultaneous inversion. The tubes were struck sharply on absorbent material for 1-2 min and analyzed, after 2 mL of wash solution being added to each tube except for total count tubes. All tubes were counted in a gamma counter for 1 min after decantation.

Statistical analysis

Data were listed as mean \pm SD. Comparison between means was tested by Student's *t* test, Friedman's ANOVA and Duncan test in SAS. *P* value less than 0.05 was considered significant.

RESULTS

Serum IGF-I, IGF-II and IGFBP-3 in cirrhotic liver tissues and matched controls

The mean values for IGF-I, IGF-II and IGFBP-3 in 44 cirrhotic patients (66 \pm 58, 367 \pm 193 and 12.0 \pm 7.6 ng/mL, respectively) were significantly lower than those in 38 healthy subjects (260 \pm 74, 1 094 \pm 119 and 39 \pm 7 ng/mL, respectively, *P*<0.001, Table 1). Since mean values of the three parameters were negatively correlated to age according to our statistical show (*r* = -0.646, -0.612, -0.609), data were revised with covariance analysis to obviate age-related effect on three parameters, and similar result was obtained (*P*<0.001).

Serum IGF-I, IGF-II and IGFBP-3 levels in patients with different CP scores

The mean values for IGF-I, IGF-II and IGFBP-3 were 119 \pm 67, 507 \pm 185 and 19 \pm 8 ng/mL, respectively, in CP A; 45 \pm 29, 343 \pm 154 and 10 \pm 5 ng/mL, respectively, in CP B. The mean values for IGF-I, IGF-II and IGFBP-3 in patients classed as Child-Pugh C stage, the worst stage of liver dysfunction with incurable ascites and elongation of APTT (activated partial thromboplastin time), were 27 \pm 11, 201 \pm 115 and 6 \pm 3 ng/mL, respectively. Significant difference of the three parameters was found between control group and any stage of cirrhosis (*P*<0.001). These three parameters gradually diminished, along with disease progression. Statistic analysis also showed that the mean levels for IGF-I and IGFBP-3 in CP A were significantly higher than those in CP B/C (*P*<0.001), and these values were a little higher in CP B than in CP C, however no significant difference of the two parameters was observed between these 2 categories (*P*>0.05). Only mean levels of IGF-

II showed clear statistical difference in patients between CP B and CP C (*P*<0.05), suggesting that IGF-II reduced significantly due to the severity of liver dysfunction (Table 2, Figure 1). Thus serum IGF-II was a more sensitive and effective indicator than IGF-I and IGFBP-3. Furthermore, the depressed IGF-II level was significantly correlated with the IGF-I variation, as well as with CP score (*P*<0.001).

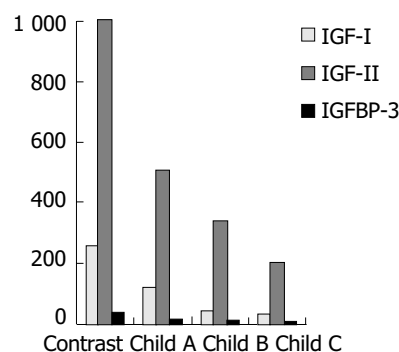


Figure 1 Serum IGF-I, IGF-II and IGFBP-3 levels in patients with different Child-Pugh scores.

DISCUSSION

Low levels of circulating IGF-I in cirrhosis have been described^[11]. In recent studies, Assy *et al.*^[12] confirmed that basal IGF-I and IGFBP-3 levels were significantly lower in patients with liver cirrhosis in their pilot study of IGF-I generation test, in which the two parameters were observed before and after stimulation with recombinant human growth hormone (rhGH). It was also approved by Donaghy *et al.*^[13] that basal IGF-I and IGFBP-3 levels dropped markedly in cirrhosis due to severe GH resistance in these patients, caused by the feedback maladjustment of GH-IGF-I-IGFBP-3 axis. He considered that the fact of impaired IGF-I and IGFBP-3 production and the severity of GH resistance seen in cirrhosis likely reflected the effect of injury to the liver, the central organ of the endocrine GH-IGF-I-IGFBP-3 axis. GH resistance, an increasingly recognized feature related to the reduction of IGF-I, IGF-II and IGFBP-3 in liver dysfunction, may have been further pathogenically effected by the severity of liver dysfunction, disorder of portosystemic shunting and malnutrition of hepatic storage. In addition, the production/secretion of GH receptor was also markedly reduced due to severely damaged hepatocytes, thus leading to the disturbance of feedback maladjustment and GH resistance^[14,15].

Table 1 Serum concentrations of IGF-I, IGF-II and IGFBP-3 in patients with liver cirrhosis and healthy subjects

Category	<i>n</i>	IGF-I (ng/mL)	IGF-II (ng/mL)	IGFBP-3 (ng/mL)
Cirrhosis	44	66 \pm 58 ^b	367 \pm 193 ^b	12 \pm 8 ^b
Control	38	260 \pm 74	1 094 \pm 119	39 \pm 7

^b*P*<0.001 vs control.

Table 2 Serum concentrations of IGF-I, IGF-II and IGFBP-3 in healthy subjects and patients with different CP scores

Category	<i>n</i>	IGF-I (ng/mL)	<i>P</i> ¹	IGF-II (ng/mL)	<i>P</i> ¹	IGFBP-3 (ng/mL)	<i>P</i> ¹
Control	38	260 \pm 75	0.001	109 \pm 119	0.001	39 \pm 7	0.001
CP A	15	119 \pm 67	0.001	507 \pm 185	0.001	19 \pm 8	0.001
CP B	19	45 \pm 29	0.001	343 \pm 154	0.001	10 \pm 5	0.001
CP C	10	27 \pm 11	0.001	201 \pm 115	0.001	6 \pm 3	0.001

¹*P* represents the statistical comparison in columns between healthy subjects and patients with different Child Pugh scores (A: scored 5-6; B: scored 7-10; C: scored 11-15). *P*<0.001 vs between different groups of the same parameter.

Our data confirmed that serum IGF-I, IGF-II and IGFBP-3 levels were significantly lower in patients with liver cirrhosis than those in control group. Circulating concentrations of IGF-I, IGF-II and IGFBP-3 were decreased in patients with liver cirrhosis and apparently correlated with the degree of liver dysfunction. These lines of evidence indicate that impaired hepatic IGF-I, IGF-II and IGFBP-3 levels may be the real potential indicators for evaluation of liver dysfunction and clinical outcome.

Though no significant difference of serum IGF-I and IGFBP-3 was observed between CP B and CP C in our study, serum IGF-II responded comparably lower in patients with CP C than with CP B, confirming that fluctuation of serum IGF-II level remained statistically significant even in patients with severe liver dysfunction assessed by CP score, and the range of serum IGF-II concentrations was much more clearly delineated from normal to excessively low in patients with severe dysfunction than the case for serum IGF-I and IGFBP-3. With regards to the facts above, serum IGF-II concentration could be an important indicator for hepatic dysfunction and clinical prognosis, and was more sensitive and effective than serum IGF-I and IGFBP-3. The assumption was also supported by Nicolici^[16], who recently reported that serum IGF-II was lower in patients of cirrhosis than in healthy subjects, and that serum IGF-II was markedly lower in patients with Child-Pugh B/C score ($P < 0.05$). Moreover, he found that serum IGF-II was significantly correlated with IGF-I and CP score ($P = 0.007$). So Nicolici suggested that single IGF-II determination, a safe, reliable and convenient measurement, may be applicable for the assessment of patients with liver cirrhosis instead of GH stimulated IGF-I generation test and combined measurement of serum IGF-I, IGF-II and IGFBP-3. Other studies showed that both IGF-II and IGF-I were synthesized by hepatocytes, however, specific IGF-II mRNA has been found in hepatocytes, which indicated the impaired serum IGF-II production was the direct effect of decreased liver function, while baseline IGF-I and IGFBP-3 levels were decreased under other circumstances, besides liver dysfunction, such as low serum albumin, malnutrition and glucose metabolic abnormality, most of which are the complications of cirrhosis^[17-19].

Our research confirmed that serum concentrations of IGF-I, IGF-II and IGFBP-3 were correlated with CP scores ($P < 0.001$), which is consistent with previous studies^[20,21]. Thus, we investigated serum levels of IGF-I, IGF-II and IGFBP-3 that had similar effects on evaluation of hepatic dysfunction and proposed that the combined detection of serum IGF-I, IGF-II and IGFBP-3 effectively predicted functional liver reserve, prognostic and clinical states of the patients. More relation has been found between IGF-I and the degree of portal hypertension and portosystemic shunting compared with the degree of liver function impairment^[22,23]. In agreement with our results, IGFBP-3 has been reported suitable to predict liver synthetic capacity, because IGFBP-3 uniquely reflects GH activity, so it is down-regulated during depletion of either GH or its receptor, and diminished even in the presence of rebounded GH concentration^[24,25]. Biological functions of IGF-I and IGF-II are modulated by specific high-affinity IGFBP-3. IGFBP-3 level might be less age-dependent than IGF-I level^[26-28]. The significance of IGF-II detection has been described above.

Assy *et al*^[29] measured serum levels of IGF-I and IGFBP-3 before and 24 h after a single subcutaneous injection of rhGH (0.14 U/kg bw). IGF-I level below 10 nmol/L was considered indicative of a poor prognosis with 15% survival at one year, whereas above 10 nmol/L indicated a 100% survival rate in 1-2 years. He then concluded that stimulated IGF-I of less than 10 nmol/L might be a true predictor of a negative prognosis in patients with liver cirrhosis. Castilla-Cortazar *et al*^[30-32] obtained similar results in their study.

In our research, all patients were followed up in the liver clinic for a period of 6 months after the measurement, among

which 6 patients' levels were below the specific levels (IGF-I < 30 ng/mL, IGF-II < 200 ng/mL and IGFBP-3 < 6 ng/mL), and 5 (83%, 4 in CP C, 1 in CP B) of them died of liver failure or bleeding in less than half a year. It is suggested that hepatic cirrhosis patients with low baseline IGF-I, IGF-II and IGFBP-3 levels have a lower survival rate than those with high levels. In agreement with our result, Assy^[12] also speculated that CP score alone could not be regarded as an ideal predictive method for patients with liver cirrhosis.

So, combined evaluation of baseline IGF-I, IGF-II and IGFBP-3 with CP score gives better prediction than CP score alone of patients' liver function. It appears to be a good predictor of survival and an early indicator of liver dysfunction. However, long-term follow-up with multi-center and large sampled studies are expected.

REFERENCES

- 1 **Mirpuri E**, Garcia-Trevijano ER, Castilla-Cortazar I, Berasain C, Quiroga J, Rodriguez-Ortigosa C, Mato JM, Prieto J, Avila MA. Altered liver gene expression in CCl4-cirrhotic rats is partially normalized by insulin-like growth factor-I. *Int J Biochem Cell Biol* 2002; **34**: 242-252
- 2 **Mazziotti G**, Sorvillo F, Morisco F, Carbone A, Rotondi M, Stornaiuolo G, Precone DF, Cioffi M, Gaeta GB, Caporaso N, Carella C. Serum insulin-like growth factor I evaluation as a useful tool for predicting the risk of developing hepatocellular carcinoma in patients with hepatitis C virus-related cirrhosis: a prospective study. *Cancer* 2002; **95**: 2539-2545
- 3 **Garcia-Fernandez M**, Castilla-Cortazar I, Diaz-Sanchez M, Diez Caballero F, Castilla A, Diaz Casares A, Varela-Nieto I, Gonzalez-Baron S. Effect of IGF-I on total serum antioxidant status in cirrhotic rats. *J Physiol Biochem* 2003; **59**: 145-146
- 4 **Muguerza B**, Castilla-Cortazar I, Garcia M, Quiroga J, Santidrian S, Prieto J. Antifibrogenic effect *in vivo* of low doses of insulin-like growth factor-I in cirrhotic rats. *Biochim Biophys Acta* 2001; **1536**: 185-195
- 5 **Scharf JG**, Braulke T. The role of the IGF axis in hepatocarcinogenesis. *Horm Metab Res* 2003; **35**: 685-693
- 6 **Tannapfel A**, Wittekind C. Genes involved in hepatocellular carcinoma: deregulation in cell cycling and apoptosis. *Virchows Arch* 2002; **440**: 345-352
- 7 **Fan ZR**, Yang DH, Cui J, Qin HR, Huang CC. Expression of insulin like growth factor II and its receptor in hepatocellular carcinoma. *World J Gastroenterol* 2001; **7**: 285-288
- 8 **Wang XZ**, Chen ZX, Zhang LJ, Chen YX, Li D, Chen FL, Huang YH. Expression of insulin-like growth factor 1 and insulin-like growth factor 1 receptor and its intervention by interleukin-10 in experimental hepatic fibrosis. *World J Gastroenterol* 2003; **9**: 1287-1291
- 9 **Moller S**, Juul A, Becker U, Henriksen JH. The acid-labile subunit of the ternary insulin-like growth factor complex in cirrhosis: relation to liver dysfunction. *J Hepatol* 2000; **32**: 441-446
- 10 **Nedic O**, Nikolic JA, Prusic S, Acimovic J, hajdukovic-Dragojlovic L. Reactivity of IGF binding protein-3 isoforms towards concanavalin A in healthy adults and subjects with cirrhosis. *Addict Biol* 2003; **8**: 81-88
- 11 **Vyzantiadis T**, Theodoridou S, Giouleme O, Harsoulis P, Evgenidis N, Vyzantiadis A. Serum concentrations of insulin-like growth factor-I (IGF-I) in patients with liver cirrhosis. *Hepatogastroenterology* 2003; **50**: 814-816
- 12 **Assy N**, Hochberg Z, Amit T, Shen-Orr Z, Enat R, Baruch Y. Growth hormone-stimulated insulin-like growth factor (IGF) I and IGF-binding protein-3 in liver cirrhosis. *J Hepatol* 1997; **27**: 796-802
- 13 **Donaghy AJ**, Delhanty PJ, Ho KK, Williams R, Baxter RC. Regulation of the growth hormone receptor/binding protein, insulin-like growth factor ternary complex system in human cirrhosis. *J Hepatol* 2002; **36**: 751-758
- 14 **Ottesen LH**, Bendtsen F, Flyvbjerg A. The insulin-like growth factor binding protein 3 ternary complex is reduced in cirrhosis. *Liver* 2001; **21**: 350-356
- 15 **Fernandez-Rodriguez CM**, Prada I, Andrade A, Moreiras M,

- Guitian R, Aller R, Lledo JL, Cacho G, Quiroga J, Prieto J. Disturbed synthesis of insulinlike growth factor I and its binding proteins may influence renal function changes in liver cirrhosis. *Dig Dis Sci* 2001; **46**: 1313-1320
- 16 **Nikolic JA**, Todorovic V, Bozic M, Tosic L, Bulajic M, Alempijevic J, Nedic O, Masnikosa R. Serum insulin-like growth factor (IGF)-II is more closely associated with liver dysfunction than is IGF-I in patients with cirrhosis. *Clin Chim Acta* 2000; **294**: 169-177
- 17 **Caregato L**, Alberino F, Amodio P, Merkel C, Angeli P, Plebani M, Bolognesi M, Gatta A. Nutritional and prognostic significance of insulin-like growth factor I in patients with liver cirrhosis. *Nutrition* 1997; **13**: 185-190
- 18 **Petersen KF**, Jacob R, West AB, Sherwin RS, Shulman GI. Effects of insulin-like growth factor I on glucose metabolism in rats with liver cirrhosis. *Am J Physiol* 1997; **273**(6 Pt 1): E1189-1193
- 19 **Nunez M**, Urdaneta E, Santidrian S. Effect of insulin-like growth factor-I on nitrogen balance and intestinal galactose transport in rats with moderate liver cirrhosis. *Br J Nutr* 2003; **90**: 929-937
- 20 **Sedlaczek N**, Hasilik A, Neuhaus P, Schuppan D, Herbst H. Focal overexpression of insulin-like growth factor 2 by hepatocytes and cholangiocytes in viral liver cirrhosis. *Br J Cancer* 2003; **88**: 733-739
- 21 **Inaba T**, Saito H, Inoue T, Han I, Furukawa S, Matsuda T, Ikeda S, Muto T. Growth hormone/insulin-like growth factor 1 axis alterations contribute to disturbed protein metabolism in cirrhosis patients after hepatectomy. *J Hepatol* 1999; **31**: 271-276
- 22 **Mirpuri E**, Garcia-Trevijano ER, Castilla-Cortazar I, Berasain C, Quiroga J, Rodriguez-Ortigosa C, Mato JM, Prieto J, Avila MA. Altered liver gene expression in CCl4-cirrhotic rats is partially normalized by insulin-like growth factor-I. *Int J Biochem Cell Biol* 2002; **34**: 242-252
- 23 **Zietz B**, Lock G, Plach B, Drobnik W, Grossmann J, Scholmerich J, Straub RH. Dysfunction of the hypothalamic-pituitary-glandular axes and relation to Child-Pugh classification in male patients with alcoholic and virus-related cirrhosis. *Eur J Gastroenterol Hepatol* 2003; **15**: 495-501
- 24 **Scharf JG**, Schmitz F, Frystyk J, Skjaerbaek C, Moesus H, Blum WF, Ramadori G, Hartmann H. Insulin-like growth factor-I serum concentrations and patterns of insulin-like growth factor binding proteins in patients with chronic liver disease. *J Hepatol* 1996; **25**: 689-699
- 25 **Moller S**, Juul A, Becker U, Flyvbjerg A, Skakkebaek NE, Henriksen JH. Concentrations, release, and disposal of insulin-like growth factor (IGF)-binding proteins (IGFBP), IGF-I, and growth hormone in different vascular beds in patients with cirrhosis. *J Clin Endocrin Metabol* 1995; **80**: 1146-1157
- 26 **Cuneo RC**, Hickman PE, Wallace JD, Teh BT, Ward G, Veldhuis JD, Waters MJ. Altered endogenous growth hormone secretory kinetics and diurnal GH-binding protein profiles in adults with chronic liver disease. *Clin Endocrinol* 1995; **43**: 265-275
- 27 **Canturk NZ**, Canturk Z, Ozden M, Dalcik H, Yardimoglu M, Tulubas F. Protective effect of IGF-1 on experimental liver cirrhosis-induced common bile duct ligation. *Hepatogastroenterology* 2003; **50**: 2061-2066
- 28 **Guo X**, Chen Y, Jin R. Experimental and clinical studies of recombinant human growth hormone treatment of hypoproteinemia of liver cirrhosis patients. *Zhonghua Shiyan He Linchuangbingduxue Zazhi* 2001; **15**: 339-341
- 29 **Assy N**, Hochberg Z, Enat R, Baruch Y. Prognostic value of generation of growth hormone-stimulated insulin-like growth factor-I (IGF-I) and its binding protein-3 in patients with compensated and decompensated liver cirrhosis. *Dig Dis Sci* 1998; **43**: 1317-1321
- 30 **Castilla-Cortazar I**, Aliaga-Montilla MA, Salvador J, Garcia M, Delgado G, Gonzalez-Baron S, Quiroga J, Prieto J. Insulin-like growth factor-I restores the reduced somatostatinergic tone controlling growth hormone secretion in cirrhotic rats. *Liver* 2001; **21**: 405-409
- 31 **Seehofer D**, Steinmueller T, Graef KJ, Rayes N, Wiegand W, Tullius SG, Settmacher U, Neuhaus P. Pituitary function test and endocrine status in patient with cirrhosis of the liver before and after hepatic transplantation. *Ann Transplant* 2002; **7**: 32-37
- 32 **De Palo EF**, Bassanello M, Lancerin F, Spinella P, Gatti R, D'Amico D, Cillo U. GH/IGF system, cirrhosis and liver transplantation. *Clin Chim Acta* 2001; **310**: 31-37

Edited by Chen WW and Zhu LH Proofread by Xu FM

Expression of TREM-1 mRNA in acute pancreatitis

Da-Yu Wang, Ren-Yi Qin, Zheng-Ren Liu, Manoj Kumar Gupta, Qing Chang

Da-Yu Wang, Ren-Yi Qin, Zheng-Ren Liu, Manoj Kumar Gupta, Qing Chang, Department of Surgery, Tongji Hospital, Tongji Medical College, Huazhong University of Science and Technology, Wuhan, 430030, Hubei Province, China

Correspondence to: Professor Ren-Yi Qin, Department of Surgery, Tongji Hospital, Tongji Medical College, Huazhong University of Science and Technology, Wuhan, 430030, Hubei Province, China. ryqin@tjh.tjmu.edu.cn

Telephone: +86-27-83662389

Received: 2003-09-06 **Accepted:** 2003-10-07

Abstract

AIM: To explore the expression of triggering receptor expressed on myeloid cells (TREM-1) mRNA in acute pancreatitis (AP).

METHODS: Using the reverse transcription polymerase chain reaction (RT-PCR), we examined the expression of TREM-1 mRNA in 10 cases of mild acute pancreatitis (MAP), 8 cases of severe acute pancreatitis (SAP), and 10 cases of healthy control subjects. And we also examined the expression of TREM-1 mRNA in 14 cases of AP (including 10 MAP and 4 SAP) before treatment, after successful therapy and clinically cured.

RESULTS: The expression of TREM-1 mRNA in the groups of MAP, SAP patients and healthy control subjects was 0.771 ± 0.274 , 1.092 ± 0.331 and 0.459 ± 0.175 , respectively; there was a significant difference among the three groups ($P < 0.05$). And there was also a significant difference between the AP patients (0.914 ± 0.341) and healthy control subjects (0.459 ± 0.175) ($P < 0.05$). Moreover, in the 14 cases of AP, before treatment, after successful therapy and clinically cured, the expression of TREM-1 mRNA was 0.905 ± 0.226 , 0.739 ± 0.169 and 0.633 ± 0.140 , respectively, and there was a significant difference among the three stages ($P < 0.05$).

CONCLUSION: The expression of TREM-1 mRNA in the patients with AP increases obviously, and correlates with the degree of AP. Furthermore, the expression of TREM-1 mRNA is distinctly different at the different stages of AP. It indicates TREM-1 may play an important role in the occurrence and development of AP.

Wang DY, Qin RY, Liu ZR, Gupta MK, Chang Q. Expression of TREM-1 mRNA in acute pancreatitis. *World J Gastroenterol* 2004; 10(18): 2744-2746

<http://www.wjgnet.com/1007-9327/10/2744.asp>

INTRODUCTION

TREM-1 is a new activating receptor of the Ig superfamily expressed on human myeloid cells. And it is selectively expressed on blood neutrophils and a subset of monocytes and up-regulated by bacterial lipopolysaccharide (LPS)^[1]. Researchers have demonstrated that TREM-1 mediates activation of neutrophil and monocytes, and may have a predominant role in inflammatory responses such as septic shock and systemic inflammatory response syndrome (SIRS)^[1,2]. In this study, we aimed to explore the expression of TREM-1 mRNA in AP and

tried to reveal etiology of AP and underlying mechanism.

MATERIALS AND METHODS

Patients and specimens

Data obtained from 18 AP patients without any treatment during 48 h of the onset of the disease and 10 healthy control subjects were explored. According to the standards of diagnosis and classification of AP proposed at the Sixth National Conference on Pancreatic Surgery of China in 1996^[3], we divided the AP patients into two groups: 10 cases of MAP, and 8 of SAP. Among the AP patients, we examined the expression of TREM-1 in 14 patients at different stages of the disease (before treatment, after successful therapy and clinically cured). We collected 2 mL of blood from the patients and controls before breakfast in the morning and stored them in the EDTA tube. The total leucocytes in the blood were separated by centrifugation at 1 200 r/min for 15 min.

Reagents and primers

Trizol reagents, Oligo (dt) 15, M-MLV reverse transcriptase and DEPC were the products of Promega Co. (USA). Taq DNA polymerase were purchased from Sangon Co. (Shanghai). The RNase inhibitor was from Takara Co. (Japan). According to the human TREM-1 and β -actin cDNA sequence reported in GeneBank, we designed two sets of primers: TREM-1 sense 5'-GTG TGT GAT CTA CCA GCC T-3', antisense 5'-TTC AGA GTC AGG AGT GGA G-3' (amplified fragment length: 232 bp); β -actin sense 5'-GTG CGT GAC ATT AAG GAG-3', antisense 5'-CTA AGT CAT AGT CCG CCT-3' (amplified fragment length: 520 bp).

Total RNA extraction

The total RNA was extracted from the leucocytes by Trizol reagent. The extracted RNA concentrations and purity were determined at A_{260} and A_{280} spectrophotometrically (Beckman DU650, USA). Then 750 mL/L ethanol was used to preserve total RNA at -20 °C.

Reverse transcription polymerase chain reaction

The total RNA was denatured by incubation for 5 min at 70 °C and rapidly cooled on ice for about 2-3 min. Single-stranded cDNA was synthesized by mixing 1-2 μ g denatured RNA with 0.5 μ L (40 u/ μ L) RNase inhibitor, 1 μ L (200 u/ μ L) M-MLV reverse transcriptase, 4 μ L reaction buffer, 1 μ L Oligodt (15), 1 μ L (10 mmol/L) dNTP, and adding DEPC-treated water up to 20 μ L. The RT reaction mixture was incubated at 37 °C for 60 min, followed by 95 °C for 5 min to inactivate M-MLV reverse transcriptase, and stored at 4 °C for use. A 5 μ L of the cDNA was used as template in PCR amplification for TREM-1. The mixture (50 μ L) consisting of 1 μ L of primers (p1/p2 of TREM-1 and β -actin) each, Taq DNA polymerase (0.5 μ L (5 U/ μ L)), 10 \times PCR buffer 5 μ L, MgCl₂ 3 μ L (25 mmol/L), by addition of deionised water up to 50 μ L, was reacted on a programmable thermocycler (Perkinelmer 9600). The DNA was predenatured at 95 °C for 5 min, followed by 35 cycles of denaturation (45 s at 95 °C), annealing (45 s at 56 °C), and extension (45 s at 72 °C). Then the mixture was finally extended for 10 min at 72 °C, and stored at -20 °C. β -actin was served as internal control in each experiment under the same conditions.

Electrophoresis identification and quantitative scanning

PCR products (7-9 μ L) with DL 2 000 marker were electrophoresed through 10 g/L agarose gel in 1 \times TBE at 70 V for 30 min. The samples were stained with ethidium bromide (0.5 mg/L) and observed by ultraviolet illumination and photographed. Each lane was scanned longitudinally. The A values of TREM-1 and β -actin bands were measured by a gel imaging analysis system (GELWORKS 1D advanced v4.01). The A ratios of TREM-1/ β -actin representing the relative levels of the expression of TREM-1 mRNA were calculated for semi-quantitative analysis.

Statistical analysis

Results were presented as mean \pm SD. Statistical comparisons were analyzed through the SAS 8.1 software. Analysis of variance was used. $P < 0.05$ was considered statistically significant.

RESULTS

Expression of TREM-1 mRNA and semi-quantitative analysis

The expression of TREM-1 mRNA in the groups of MAP, SAP patients and healthy control subjects were 0.771 ± 0.274 , 1.092 ± 0.331 and 0.459 ± 0.175 , respectively. There was a significant difference among the three groups ($P < 0.05$). The difference was also significant ($P < 0.05$) (Figures 1, 3) between the AP patients (0.914 ± 0.341) and healthy control subjects (0.459 ± 0.175). In AP patients of before treatment, after successful therapy and clinically cured, the expression of TREM-1 mRNA was 0.905 ± 0.226 , 0.739 ± 0.169 and 0.633 ± 0.140 , respectively. There was a significant difference among the three stages ($P < 0.01$ or $P < 0.05$). And the expression of TREM-1 mRNA was higher in clinically cured group than in healthy control subjects ($P < 0.05$) (Figures 2, 4).

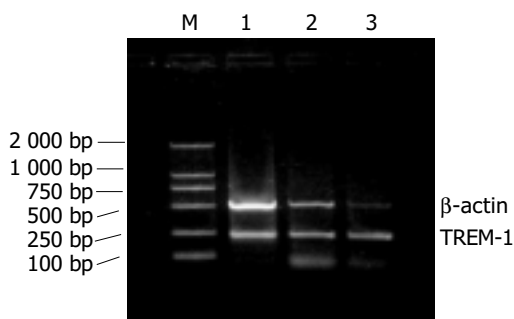


Figure 1 Electrophoresis of the PCR products. M: DL2000 marker; 1: the PCR product of normal subject; 2: the PCR product of MAP; 3: the PCR product of SAP. The amplified fragment lengths of β -actin and TREM-1 are 520 bp and 232 bp respectively.

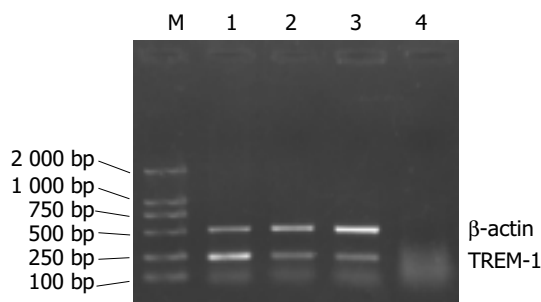


Figure 2 Electrophoresis of the PCR products. M: DL2 000 marker; 1: the AP patient before treatment; 2: the same patient after successful therapy; 3: the same AP patient after clinically cured; 4: negative control. The amplified fragment length of β -actin is 520 bp, of TREM-1 is 232 bp. 10 g/L agarose gel.

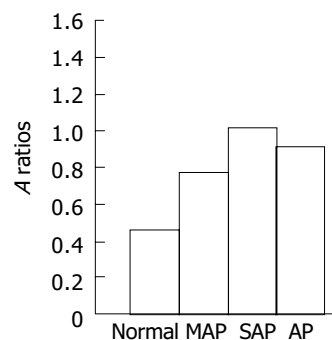


Figure 3 The A ratios of TREM-1/ β -actin in different degree of AP: There was a significant difference among the three groups in the expressions of TREM-1 mRNA ($P < 0.05$). And between the AP patients and healthy control subjects, the difference was significant ($P < 0.05$).

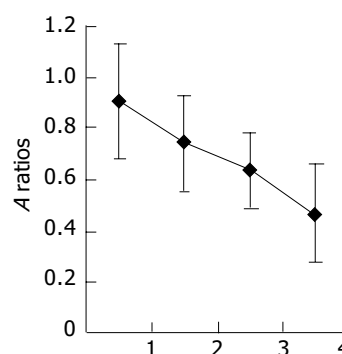


Figure 4 The A ratios of TREM-1/ β -actin in different stage of AP: 1, the group in the stage of before treatment. 2, the group in the stage after successful therapy. 3, the group in the stage of clinically cured. 4, the group of normal subject. There was a significant difference among the three stages in the expression of TREM-1 mRNA (groups 1, 2 and 3. $P < 0.05$). And in the group of clinically cured the ratio was higher than in healthy control subjects ($P < 0.05$).

DISCUSSION

AP is a disease of self-digestive chemical inflammation with unclear etiology. In most cases, they present a self-limited course. Twenty percent of patients with AP have a severe form of the disease. SAP is such a severe disease that it may be associated with both systemic and local complications, such as respiratory insufficiency with adult respiratory distress syndrome (ARDS), renal failure, the development of pancreatic and peripancreatic infection. The mortality of SAP is higher than 40%^[4,5]. Even now, there are no efficient and sensitive methods to treat AP successfully because the pathogenesis of AP still remains obscure^[6]. Recent studies^[7] show that factors like the pancreatic enzymes activated abnormally lead the body to secrete and amplify large quantities of cytokines. Finally, the cytokines increase vascular permeability, activate complement components, resulting in microcirculatory impairment and imbalance of thrombo-fibrinolytic system. Many of these events occur not only in the pancreas itself, but also in the other vital organs and tissues, leading to SAP and complications^[8,9]. Generally, there are three phases of AP progression: local acinar injury, systemic response, and general sepsis^[7]. Moreover, some data suggest that the changes in concentration of proinflammatory cytokines can be an early diagnostic criterion for AP^[10,11]. Most authors have realized that the pathogenesis of SAP is very complicated. It is a multifactorial as well as multifaceted disease. First of all, the etiologic agents initiate the pancreatic acinar injury by release of pancreatic enzymes and over-stimulation of

macrophages and neutrophils, and then the cytokines and inflammatory mediators are delivered^[12,13].

In 2000, Bouchon *et al.* had identified a new activating receptor of the Ig superfamily expressed on human myeloid cells, called triggering receptor expressed on myeloid cells (TREM). TREM-1 is selectively expressed on blood neutrophils and a subset of monocytes and up-regulated by bacterial LPS. Engagement of TREM-1 triggers secretion of IL-8, monocyte chemoattractant protein-1, and TNF- α and induces neutrophil degranulation. Intracellularly, TREM-1 induces Ca²⁺ mobilization and tyrosine phosphorylation of extracellular signal-related kinase 1 (ERK1), ERK2 and phospholipase C- γ . To mediate activation, TREM-1 associates with the transmembrane adapter molecule DAP12^[14]. Furthermore Bleharski *et al.*^[15] suggested that activation of TREM-1 on monocytes participated in the early induced and adaptive immune responses involved in host defense against microbial challenges. Thus, TREM-1 was considered mediating the activation of neutrophil and monocytes, and might have a predominant role in inflammatory responses.

Wilson *et al.*^[16] discovered that SAP had many similarities to sepsis syndrome and septic shock. The haemodynamic features of cardiovascular instability, reduced ejection fraction and decreased systemic vascular resistance were indistinguishable in each of these conditions. In addition, there are many striking similarities in the cytokine and inflammatory mediator profiles, suggesting that the haemodynamic abnormalities may result from the same pathogenic mechanisms, albeit as a result of different inflammatory stimuli.

In 2001 through their experiments, Bouchon *et al.*^[2] believed that inflammatory responses to microbial products were amplified by a pathway mediated by TREM-1. TREM-1 was an activating receptor expressed at high levels in neutrophils and monocytes that infiltrate human tissues infected with bacteria. Furthermore, it was up-regulated in peritoneal neutrophils of patients with microbial sepsis and mice with experimental LPS-induced shock. Notably, blockade of TREM-1 protected mice against LPS-induced shock, as well as microbial sepsis caused by live *Escherichia coli* or caecal ligation and puncture. Their results demonstrate a critical function of TREM-1 in acute inflammatory responses to bacteria and implicate TREM-1 as a potential therapeutic target for septic shock. A recent study shows that TREM-1 amplifies Toll-like receptor-initiated responses against microbial challenges and potentiates the secretion of proinflammatory chemokines and cytokines in response to bacterial and fungal infections. Blockade of TREM-1 reduced inflammation and increased survival in animal models of bacterial infections that caused systemic hyper-inflammatory syndromes^[17]. But nobody knows how TREM-1 expressed in AP as yet. According to the theory mentioned above, we carried out a study of the expression of TREM-1 in AP.

We demonstrated that the expression of TREM-1 in leucocytes of patients with AP was much higher than that in healthy control subjects and correlated with the degree of AP. Furthermore, significant differences in the expression of TREM-1 mRNA were found at the different stages of AP. The expression of TREM-1 decreased gradually with the improvement of severity of the AP patients. This experiment indicates that the expression of TREM-1 is relevant to progression of AP. Because of lack of

relevant data about the patients after they were discharged from the hospital, we only compared the expression of TREM-1 between the cured group and healthy control subjects and found that there was still a significant difference between them. Therefore, we suggest that the pathological changes of the pancreas continued even after the patients were cured clinically.

This study may help reveal the etiology of AP and the mechanism of its progression. It may provide a new standard for the diagnosis and classification of AP as well as an efficient method to cure AP by blocking the expression of TREM-1.

REFERENCES

- 1 Bouchon A, Dietrich J, Colonna M. Cutting edge: inflammatory responses can be triggered by TREM-1, a novel receptor expressed on neutrophils and monocytes. *J Immunol* 2000; **164**: 4991-4995
- 2 Bouchon A, Facchetti F, Welgand MA, Colonna M. TREM-1 amplifies inflammation and is a crucial mediator of septic shock. *Nature* 2001; **410**: 1103-1107
- 3 The Pancrea Study Group. Chinese medical association of surgery. The standards on diagnosis and classification of acute pancreatitis (1996). *Zhonghua Waikexue* 1997; **35**: 773-775
- 4 Abu-Zidan FM, Bonham MJ, Windsor JA. The severity of acute pancreatitis: a multivariate analysis of oxidative stress markers and modified. Glasgow criteria. *Br J Surg* 2000; **87**: 1019-1023
- 5 Bradley EL. A clinically based classification system for acute pancreatitis: summary of the Atlanta Symposium. *Arch Surg* 1993; **128**: 586-590
- 6 Nam JH, Murthy S. Acute pancreatitis-the current status in management. *Expert Opin Pharmacother* 2003; **4**: 235-241
- 7 Makhija R, Kingsnorth AN. Cytokine storm in acute pancreatitis. *J Hepatobiliary Pancreat Surg* 2002; **9**: 401-410
- 8 Bentrem DJ, Joehl RJ. Pancreas: healing response in critical illness. *Crit Care Med* 2003; **31**: S582-589
- 9 Zhang Q, Ni Q, Cai D, Zhang Y, Zhang N, Hou L. Mechanisms of multiple organ damages in acute necrotizing pancreatitis. *Chin Med J* 2001; **114**: 738-742
- 10 Riche FC, Cholley BP, Laisne MJ, Vicaut E, Panis YH, Lajeunie EJ, Boudiaf M, Valleur PD. Inflammatory cytokines, C reactive protein, and procalcitonin as early predictors of necrosis infection in acute necrotizing pancreatitis. *Surgery* 2003; **133**: 257-262
- 11 Demydov VM, Zaporozhchenko BS, Demidov SM. Changes of cytokine levels in the serum in patients with acute pancreatitis as an early symptom for diagnosis. *Klin Khir* 2003; **3**: 29-32
- 12 Norman J. The role of cytokines in the pathogenesis of acute pancreatitis. *Am J Surg* 1998; **175**: 76-83
- 13 Bhatia M, Brady M, Shokui S, Christmas S, Neoptolemos JP, Slavin J. Inflammatory mediators in acute pancreatitis. *J Pathol* 2000; **190**: 117-125
- 14 Nochi H, Aoki N, Oikawa K, Yanai M, Takiyama Y, Atsuta Y, Kobayashi H, Sato K, Tateno M, Matsuno T, Katagiri M, Xing Z, Kimura S. Modulation of hepatic granulomatous responses by transgene expression of DAP12 or TREM-1-Ig molecules. *Am J Pathol* 2003; **162**: 1191-1201
- 15 Bleharski JR, Kiessler V, Buonsanti C, Sieling PA, Stenger S, Colonna M, Modlin RL. A role for triggering receptor expressed on myeloid cells-1 in host defense during the early-induced and adaptive phases of the immune response. *J Immunol* 2003; **170**: 3812-3818
- 16 Wilson PG, Manji M, Neoptolemos JP. Acute pancreatitis as a model of sepsis. *J Antimicrob Chemother* 1998; **41**: 51-63
- 17 Colonna M, Facchetti F. TREM-1 (triggering receptor expressed on myeloid cells): a new player in acute inflammatory responses. *J Infect Dis* 2003; **187**: S397-401

Development of an ELISA kit using monoclonal antibody to *Clostridium difficile* toxin A

Si-Wu Fu, Ya-Li Zhang, Dian-Yuan Zhou

Si-Wu Fu, Ya-Li Zhang, Dian-Yuan Zhou, PLA Institute for Digestive Medicine, Nanfang Hospital, First Military Medical University, Guangzhou 510515, Guangdong province, China

Correspondence to: Dr. Si-Wu Fu, M.D. PLA Institute for Digestive Medicine, Nanfang Hospital, First Military Medical University, Guangzhou 510515, Guangdong Province, China. fusiwu2001@sina.com

Telephone: +86-20-61641544

Received: 2003-12-28 **Accepted:** 2004-01-12

Abstract

AIM: To establish an ELISA kit using monoclonal antibodies against *Clostridium difficile* (*C. difficile*) toxin A.

METHODS: An indirect sandwich ELISA was described using the purified rabbit monospecific antiserum as capturing antibody. After the polystyrene microtitre plates with 96 flat-bottomed wells were coated with rabbit antiserum, the wells were blocked with 100 g/L BSA in PBS-T. *C. difficile* toxin A or culture filtrates were added to each well and then monoclonal antibodies IgG-horseradish peroxidase conjugate was added as detecting antibody, tetramethylbenzidine was used as substrate and A_{450} of the stopped reacting product was recorded in an automated plate reader.

RESULTS: The tested specimens included culture filtrates of 2 strains of toxigenic *C. difficile*, 2 strains of non-toxigenic *C. difficile*, 26 strains of *E. coli*, 2 strains of *S. dysenteriae*, 1 strain of *Bif. infantis*, 5 strains of *V. cholera*, 2 strains of *S. typhi*, 7 strains of *C. botulinum*, 1 strain of toxigenic *C. sordellii*, and 1 strain of *C. butyricum*. A total of 47 strains of culture filtrates were all negative except for 2 strains of toxigenic *C. difficile*. The detective limitation of toxin A was 0.1 ng/mL.

CONCLUSION: An ELISA kit with high specificity and excellent sensitivity for the rapid detection of *C. difficile* toxin A was established. It will be a useful tool for diagnostic test of *C. difficile* toxin A.

Fu SW, Zhang YL, Zhou DY. Development of an ELISA kit using monoclonal antibody to *Clostridium difficile* toxin A. *World J Gastroenterol* 2004; 10(18): 2747-2749

<http://www.wjgnet.com/1007-9327/10/2747.asp>

INTRODUCTION

Clostridium difficile (*C. difficile*), which has been reported as the major cause of antibiotic-associated colitis (AAC) and pseudomembranous colitis (PMC) in humans and experimental animals, produces at least two toxins, named toxin A and B. Toxin A, a tissue-damaging enterotoxin, can lead to hemorrhagic fluid accumulation in rabbit ileal loops and is cytotoxic for cultured fibroblasts. Toxin B is an extremely potent cytotoxin for many cultured cells^[1,2].

Polyclonal antibodies are used in immunoassays and detection for *C. difficile* toxin in many clinical researches. They

are against toxin A and toxin B, and may be against other antigens at the same time, causing false positive results^[3-5]. The problem may be solved when monoclonal antibodies were used. They can not only improve the specificity of the method, but also decrease the false positive results as well. The present report describes an enzyme-linked immunosorbent assay (ELISA) which used monospecific antibody as a capture antibody, and monoclonal antibody as a detection antibody, for detection of *C. difficile* toxin A in clinical specimens.

MATERIALS AND METHODS

Bacterial strains and culture filtrates

The 49 strains of bacteria included 2 strains of toxigenic *C. difficile*, 2 strains of non-toxigenic *C. difficile*; 26 strains of *E. coli*, 2 strains of *S. dysenteriae*; 1 strain of *Bif. infantis*; 5 strains of *V. cholera*; 2 strains of *S. typhi*; 7 strains of *C. botulinum*; 1 strain of *C. sordellii*; and 1 strain of *C. butyricum*. All strains were cultured with proper medium separately and the culture filtrates were used for the assay.

Purification of *C. difficile* toxin A

Toxigenic *C. difficile* VPI 10463 was grown anaerobically at 37 °C for 72 h in brain heart infusion (Difco) by the dialysis bag methods. Toxin A was purified by precipitation with 500 g/L $(\text{NH}_4)_2\text{SO}_4$ and acid precipitation at pH5.5, then by ion-exchange chromatography on DEAE-Toyopearl 650 mol/L.

Preparation of monospecific toxin A antiserum

Purified toxin A was inactivated with 4 g/L formaldehyde at 37 °C for 72 h, mixed with SEPPIC adjuvant (5.41:4.6 v/v, Montanide ISA206, France), and then injected in to a New Zealand white male rabbit of 2 kg weight every 2 wk over a period of 4 wk. Booster injections of 0.2 mg of toxoid A were prepared with adjuvant and injected subcutaneously at 4 wk intervals over a period of 32 wk, and antiserum was collected 1 wk after the final booster dose.

Production of monoclonal antibody

Purified toxin A of *C. difficile* (100 µg) was inactivated with 4 g/L formaldehyde at 37 °C for 72 h, and mixed with SEPPIC adjuvant, BALB/c mice were injected intraperitoneally with 0.5 mL of toxoid A at 2 wk intervals over a period of 8 wk. Three days before fusion, one mouse was boosted with the same quantity of toxoid A without the adjuvant. The splenocytes from immunized mice were fused with myeloma cells Sp2/0. The hybridoma cells were screened by indirect ELISA and cloned by limiting dilution method.

Purification of antibodies

Antibodies were purified by precipitation with 400 g/L $(\text{NH}_4)_2\text{SO}_4$ followed by precipitation with 330 mL/L $(\text{NH}_4)_2\text{SO}_4$ for 3 times, centrifuged at 6 000 r/min for 30 min, and then loaded on Sephacryl-300 chromatography column.

Conjugate of monoclonal antibody to horseradish peroxidase^[6]

Sodium periodate solution (0.3 mL, 0.1 mol/L) and 5 mg horseradish peroxidase dissolved in 1 mL of water, the mixture was stirred

for 30 min at 4 °C and dialyzed at 4 °C against 0.01 mol/L sodium acetate buffer (pH4.4) overnight, followed by addition of 0.5 mL of 0.16 mol/L ethylene glycol, stirred for 1 h at 4 °C. Monoclonal IgG of 5 mg in 1 mL of 0.05 mol/L sodium carbonate buffer (pH9.6) was added immediately, stirred and dialyzed at 4 °C with same buffer overnight before any unconjugated enzyme was removed by addition of 0.2 mL sodium borohydride solution (5 mg/mL, 4 °C, 3 h), then precipitated by addition of equal volumes of 100% ammonium sulfate (4 °C, 2.5 h), centrifuged (6 000 r/min, 15 min), dialyzed against 0.01 mol/L PBS (pH7.4) at 4 °C overnight, and stored at 4 °C after diluted with 500 mL/L glycerol (1:1).

Indirect sandwich ELISA

Ninety-six-well polystyrene flat-bottomed microtitre plates were coated with 100 µL of purified rabbit monospecific antitoxin (8 µg/mL, capture antibody) in 0.05 mol/L carbonate buffer (pH9.6) and incubated overnight at 4 °C, the plates were washed once in PBS-T (0.01 mol/L PBS containing 0.5 g/L Tween-20, pH7.4). After 200 µL of 100 g/L BSA in PBS-T was added to the wells and incubated at 37 °C for 2 h, washed 5 times in PBS-T with 3 min incubation at room temperature between each wash, 100 µL of *C. difficile* toxin A or test samples in PBS-T were added to each well and incubated for 1 h at 37 °C, washed for 5 times. Then 100 µL of 1:1 000 diluted monoclonal antibodies IgG-horseradish peroxidase conjugate (detecting antibody) was added for 1 h at 37 °C, wells were washed 5 times with PBS-T, and 0.1 mL of TMB(3,3',5,5'-tetramethylbenzidine) substrate was added to each well. After 15 min at 37 °C in the dark, the reaction was stopped by the addition of 1 drop of 2 mol/L sulfuric acid and A_{450} was measured. ELISA titers of positivity were expressed as $A_{450} \geq 0.10$. Non. toxigenic *C. difficile* culture filtrate was used as negative control.

Protein determination

Protein concentration was determined by the method of Coomassie brilliant blue G-250, and bovine serum albumin was purchased from Sigma Company of USA.

RESULTS

Properties of the antibodies

Six hybridoma cell lines (2H7, 3E9, 4B5, 5C10, 6G8 and 8A1) secreting mAbs against *C. difficile* toxin A were produced. The Ig subclasses of mAbs 2H7, 3E9 and 6G8 were IgM, mAbs 4B5 and 8A1 were IgG1, mAb 5C10 was IgG2a. All 6 mAbs had no neutralization activity. Epitope recognized by 5 mAbs (2H7, 4B5, 5C10, 6G8 and 8A1) differed from mAb 3E9. Relative affinities of mAbs 8A1 and 4B5 were all above 10^5 , and those of the other 4 mAbs were 10^4 . mAbs 8A1 were conjugated to horseradish peroxidase for ELISA, A_{403}/A_{280} was 0.40 and the optimal dilution was 1:1000. The monospecific antiserum could neutralize all activities of *C. difficile* toxin A. The ELISA titer was 10^6 /mL.

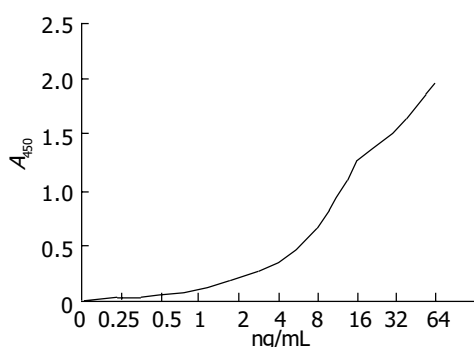


Figure 1 Detection of *C. difficile* toxin A with ELISA.

Sensitivity of ELISA

Purified *C. difficile* toxin A was detected with ELISA and a high sensitivity of 0.1 ng/mL was found.

Specificity of ELISA

The tested specimens were from culture filtrates of 49 strains. Forty-seven strains were all negative except that 2 strains were positive. Table 1 illustrates the ELISA results with a high specificity.

Table 1 Detection of *C. difficile* toxin A in culture filtrates by ELISA

Strain	Number	Culture supernatant	
		Positive (n)	Negative (n)
<i>C. difficile</i> toxigenic	2	2	0
<i>C. difficile</i> non-toxigenic	2	0	2
<i>E. coli</i>	26	0	26
<i>S. dysenteriae</i>	2	0	2
<i>Bif. infantis</i>	1	0	1
<i>V. cholera</i>	5	0	5
<i>S. typhi</i>	2	0	2
<i>C. botulinum</i>	7	0	7
<i>C. sordellii</i>	1	0	1
<i>C. butyricum</i>	1	0	1

Stability of the ELISA kit

Ninety-six-well polystyrene flat-bottomed microtitre plates were coated with 100 µL of purified rabbit monospecific antitoxin (8 µg/mL) in carbonate buffer (pH9.6) and incubated overnight at 4 °C, the plates were washed once in PBS containing 0.5 g/L Tween-20, pH 7.4 (PBS-T). After 200 µL of 100 g/L BSA in PBS-T was added to the wells and incubated at 37 °C for 3 h, and then vacuumed and kept in plastic bag at 37 °C for 6 d, the titer was detected, indicating that the kit can be kept at 4 °C for at least 1 year.

DISCUSSION

A number of rapid (enzyme immunoassay and latex agglutination) and conventional (direct plating and tissue culture) tests have been developed as aids in the diagnosis of *C. difficile* infection: (1) Tissue culture cytotoxicity assay is the best available laboratory test for determination of the role of *C. difficile* in the pathology of a given patient diarrhea, it has an excellent sensitivity and specificity, but its utility is limited because of its inherent technical complexity, time requirement, specimen-handling requirements, and high costs; (2) Latex agglutination test was found to be nearly as sensitive as the cytotoxicity assay and it did not detect toxin A but a *C. difficile* cell-associated protein; (3) Organism culture: first, the asymptomatic carriage rate of this organism may be as high as 20% in patients receiving antibiotics making interpretation of positive culture data difficult. Second, organisms that do not produce toxin are thought to be avirulent. Isolates must be proved to produce toxin to be considered pathogenic; (4) ELISA. ELISA has the potential of greatly simplifying and improving the efficiency of the laboratory diagnosis of *C. difficile* associated diseases. It has the high sensitivity and excellent specificity comparable with tissue culture cytotoxicity assay. Using the commercial enzyme immunoassays for the detection of toxin A or toxin B, the results could be available in 2-4 h. ELISA was a perfect method to detect toxin A in feces^[7,8].

The advantage of ELISA for detection is that: first, as a clinical expression of *C. difficile* infection, toxin A was more stable than toxin B. Second, toxin A was easy to be purified and its antibodies were easy to produce. Third, the monoclonal antibodies can be prepared in unlimited quantities and are more reproducible reagents than other antibodies. After comparing

the antibody preparations by indirect ELISA, Lyerly *et al.* reported that ELISA with monoclonal antibodies could detect 4 ng of toxin A, but the polyclonal antibodies purified by affinity chromatography and monospecific antiserum could detect 1 ng of toxin A^[8]. Laughon *et al.* reported that they could detect 0.1 ng (1.0 ng/mL) of toxin A with a monospecific antiserum^[9]. In this study we present ELISA kits which used the purified rabbit monospecific antitoxin as capturing antibody and monoclonal antibodies IgG-horseradish peroxidase conjugate as detecting antibody, the detective limitation of toxin A was 0.1 ng/mL.

Antibiotic-associated diarrhea and PMC are the major problems in a variety of health care settings. Requests for the laboratory diagnosis of *C. difficile*-associated diseases are frequently made, but there have been no diagnostic reagents in China until now. Thus, rapid diagnosis of *C. difficile* in patients with PMC and antibiotic-associated diarrhea is very important and guides both the treatment and control of nosocomial spread of infection. The ELISA kits with a high specificity, sensitivity and stability for the rapid detection of *C. difficile* toxin A are presented here. The usefulness of the ELISA kits awaits further studies in clinic.

REFERENCES

- 1 **John GB.** Antibiotic-associated diarrhea. *Clin Infect Dis* 1992; **15**: 573-581
- 2 **John GB.** *Clostridium difficile*: History of its role as an enteric pathogen and the current state of knowledge about the organism. *Clin Infect Dis* 1994; **18**: S265-272
- 3 **Schue V, Green GA, Monteil H.** Comparison of the ToxA test with cytotoxicity assay and culture for the detection of *Clostridium difficile*-associated diarrhoeal disease. *J Med Microbiol* 1994; **41**: 316-318
- 4 **Krishnan C.** Detection of *Clostridium difficile* toxins by enzyme immunoassay. *J Hyg* 1986; **96**: 5-12
- 5 **Merz CS, Kramer C, Forman M, Gluck L, Mills K, Senft K, Steiman I, Wallace N, Charache P.** Comparison of four commercially available rapid enzyme immunoassays with cytotoxin assay for detection of *Clostridium difficile* toxins from stool specimens. *J Clin Microb* 1994; **32**: 1142-1147
- 6 **Jie Y, Luo HB, Lu DY.** Modern microbiological technology and its application 1st edition, people health press. *Beijing* 1997: 173-183
- 7 **David ML, Carol JP, Tracy DW.** Monoclonal and Specific Polyclonal Antibodies for Immunoassay of *Clostridium difficile* Toxin A. *J Clin Microb* 1985; **21**: 12-14
- 8 **David ML, Howard CK, Tracy DW.** *Clostridium difficile*: its disease and toxins. *Clin Microb Rev* 1988; **1**: 3-18
- 9 **Laughon BE, Viscidi RP, gdovinSL, Yolken RH, Bartlett JG.** Enzyme immunoassays for detection of *Clostridium difficile* toxin A and B in fecal specimens. *J Infect Dis* 1984; **149**: 781-788

Edited by Chen WW and Zhu LH Proofread by Xu FM

Relationship between urokinase-type plasminogen activator receptor and vascular endothelial growth factor expression and metastasis of gallbladder cancer

Shu-Qiang Yue, Yan-Ling Yang, Jing-Shi Zhou, Kai-Zong Li, Ke-Feng Dou

Shu-Qiang Yue, Yan-Ling Yang, Jing-Shi Zhou, Kai-Zong Li, Ke-Feng Dou, Department of Hepatobiliary Surgery, Xijing Hospital, Fourth Military Medical University, Xi'an 710032, Shaanxi Province, China
Correspondence to: Ke-Feng Dou, Department of Hepatobiliary Surgery, Xijing Hospital, Fourth Military Medical University, Xi'an 710032, Shaanxi Province, China. gdwk@fmmu.edu.cn
Telephone: +86-29-3375259 **Fax:** +86-29-3375561
Received: 2003-12-10 **Accepted:** 2004-01-15

Abstract

AIM: To investigate the relationship of urokinase type plasminogen activator receptor (uPAR) and vascular endothelial growth factor (VEGF) expression with clinical and pathological characteristics of human gallbladder cancer.

METHODS: uPAR and VEGF expressions in 68 gallbladder cancer tissues were detected with anti-receptor immunohistochemical stain.

RESULTS: Expression rate of uPAR was 57.4% (39/68), and VEGF 51.5% (35/68) in gallbladder cancer tissues. Expression of both uPAR and VEGF was significantly related to metastasis, but not significantly correlated with differentiation stage and size of gallbladder cancer.

CONCLUSION: Expression of uPAR and VEGF may be an invasive phenotype of gallbladder cancer and indicator for predicting prognoses, and uPAR expression is significantly correlated with the expression of VEGF.

Yue SQ, Yang YL, Zhou JS, Li KZ, Dou KF. Relationship between urokinase-type plasminogen activator receptor and vascular endothelial growth factor expression and metastasis of gallbladder cancer. *World J Gastroenterol* 2004; 10(18): 2750-2752
<http://www.wjgnet.com/1007-9327/10/2750.asp>

INTRODUCTION

The main lethal cause of patients with malignant tumor is the invasion and metastasis of tumor cells. Tumor blood vessels can not only get rich nutrient from hosts, but also spread many malignant cells to hosts. And all these result in unceasing tumor growth and metastasis^[1-4]. Urokinase-type plasminogen activator (uPA) is a kind of serine protease, which can activate plasminogen to fibrinolysin, the latter can degrade most kinds of extracellular matrix, which then form extracellular local lysis region, thus constructing the path for metastasis. The role of uPA *in vivo* is dependent on the expression of corresponding receptor (uPAR) in cell membrane. The conjugation of uPA and uPAR can reinforce tumor cells' infiltration ability^[5,6]. Formation of tumor blood vessels is a very complicated process. Vascular endothelial growth factor (VEGF) has an important role in the formation of tumor blood vessels, as well as in growth and metastasis of tumor, because it can adjust angiogenesis and is specific^[7-9]. Prognosis

of operation of gallbladder cancer is poor, and its relapse rate is very high. So investigation of metastasis and recurrence of gallbladder cancer has great clinical significance. We made use of immunohistochemistry to detect the expression of uPAR and VEGF in gallbladder cancer, and investigated the relationship between the expression of uPAR and VEGF and pathologic characteristics, invasion and metastasis of gallbladder cancer. Image analyses were also used to quantitatively analyze the relationship between them.

MATERIALS AND METHODS

Materials

Sixty-eight specimens of gallbladder cancer resected or biopsied from 1990 to 2001 were pathologically diagnosed. Retrospective analyses were performed on these routine paraffin embedded sections of 4 μ m thick. According to WHO classification standard of gallbladder cancer differentiation, 21 cases were in grade I, 27 cases grade II, 20 cases grade III. Twenty-six cases had a diameter of tumor \leq 2 cm, 23 cases 2-4 cm, 19 cases $>$ 4 cm. Metastasis was found in 31 cases by clinic examination and in surgical operation. Murine anti-uPA, -VEGF and -SABC monoclonal antibodies were purchased from Wuhan Bosted Co, and uPA from Guangdong Tipus Co.

Methods

Anti-ligand antibodies were used to determine uPAR^[10-13]: routine de-waxing, trypsin digestion, non-specific antigen blocking. A 1 mg/L of urokinase was used to saturate receptors; anti-uPA monoclonal antibody was added; the rest procedures were according to routine SABC. The procedures of VEGF mAb staining was according to instruction of SABC test kit. There were blank, substitute and normal controls. Positive cells were defined as cytoplasm and/or cell membrane stained clearly buffy or brown. Samples were analyzed by image analyzer. Firstly, strong positive expression regions were selected under low power visual field, then, 10 high power visual fields (400 times) were randomly selected, their grey scales were detected, the average value was used as average expression intensity of the sample.

Statistics

Analyses were performed by χ^2 -test, *t*-test and correlation-test. $P < 0.05$ was considered significant.

RESULTS

Results of immunohistochemistry

Positivity rates of uPAR and VEGF expressions in tissue of gallbladder cancer were 57.4% (39/68) and 51.5% (35/68), respectively. uPAR and VEGF were negatively stained in corresponding noncancerous tissues, including relatively normal liver tissue and normal mucosa tissue of gallbladder.

Expression of uPAR and VEGF and clinical pathological stages

Analysis of the relationship between expression rate and

intensity of uPAR and VEGF and clinical features revealed that expression of uPAR and VEGF was closely correlated to metastasis of gallbladder cancer, but not significantly correlated to the differentiation stage and size of gallbladder cancer (Tables 1, 2).

Table 1 Relationship between uPAR expression and clinical pathological stages of gallbladder cancer

Tumor	Patients (n)	uPAR-positive patients (n)	Positive rate (%)
Diameter of tumor			
</=2 cm	26	15	57.7
2-4 cm	23	11	47.8
>/=4 cm	19	13	68.4
Pathological stage			
I	21	12	57.1
II	27	16	59.3
III	20	11	55.0
Metastasis			
Positive	31	27 ^b	87.1 ^b
Negative	37	12	32.4

^bP<0.01 vs others.

Table 2 Relationship between VEGF expression and clinical pathological stage of gallbladder cancer

Tumor	Patients (n)	uPAR-positive patients (n)	Positive rate (%)
Diameter of tumor			
</=2 cm	26	14	53.8
2-4 cm	23	12	52.2
>/=4 cm	19	9	47.4
Pathological stage			
I	21	12	57.1
II	27	15	55.6
III	20	8	40.0
Metastasis			
Positive	31	24 ^b	77.4 ^b
Negative	37	11	29.7

^bP<0.01 vs others.

Image analysis of expression of uPAR and VEGF

Grey scales for positively expressed uPAR and VEGF were 238.4±6.2 and 231.2±4.1, respectively, that for negative expression were 32.1±4.3 and 36.2±3.7, respectively. Correlation analysis showed that the expression intensity of uPAR was significantly positively correlated to that of VEGF ($\gamma = 0.671$).

DISCUSSION

Human uPAR is composed of 313 amino acid residues. The binding site for uPAR and its ligand-uPA is domain I which is close to N-terminal. Amino acid residues involved in the interaction with ligand are mediated by hydrophobic interaction^[14-17]. uPAR and its ligand-uPA's binding is highly specific. Moreover, this kind of highly effective binding ($K_d = 0.1-1.0$ nmol/L) makes uPA strongly gather on cell surface, thus activating plasminogen to fibrinolysin locally, leading to extracellular matrix hydrolyzing^[18-21]. On the other hand, uPAR also has high avidity to pro-uPA. After pro-uPA binding to its membrane receptor, pro-uPA is easily activated into uPA by fibrinolysin around, then pre-fibrinolysin is activated into fibrinolysin by uPA, forming positive feedback enlargement effect. In addition,

fibrinolysin on cell membrane is not easily hydrolyzed to inactive form by its inhibitor- α_2 anti-fibrinolysin^[22-25]. Furthermore, uPAR also activates pre-fibrinolysin by taking part in complex formation of pro-uPA and pre-fibrinolysin on cell surface. Therefore, expression of uPAR in tumor cells has an important localizing role in process of local extracellular matrix hydrolysis, and closely correlates to metastasis^[26-30].

VEGF is a kind of specific vascular endothelial cell stimulating factor. It high-effectively and specifically acts on vascular endothelial cells, and intensively promotes splitting and chemotaxis by: (1) increasing microvessel permeability, leading to plasm fibrous protein exosmose, thus providing a fiber network for cell migration during the process of vascularization^[31-34]; (1) directly stimulating endothelial cell proliferation by acting on two special receptors flt and flk (kdk) of endothelial cell, and producing plasminogen activator (tissue-type and urokinase-type) and collagenase^[35-37]. It not only promotes endothelial cell movement, which is in favor of vascularization, but also benefits cancer cells shedding and entrance to blood vessel or infiltrating to neighboring fibrous protein and connective tissue matrix. This specificity provides conditions for tumor invasion and metastasis.

Our results display that expression of uPAR and VEGF is closely correlated to invasion and metastasis of gallbladder cancer, but not significantly correlated to the differentiation stage and size of gallbladder cancer. uPAR and VEGF can be regarded as an invasive phenotype of gallbladder cancer and used for predicting the prognoses, and as evaluation marker for therapeutic efficacy as well. The results also revealed the correlation between the incidence of gallbladder cancer and expression of uPAR and VEGF. On the one hand, extracellular matrix hydrolysis by uPAR provides advantages over vascularization; on the other hand, plasminogen activator induced by VEGF stimulates endothelial cell growth and increases microvascular permeability by interacting with uPAR, herein, extracellular matrix hydrolysis is reinforced by uPAR^[38-40]. The regulatory mechanism between uPAR and VEGF, and effective gene therapy methods need further investigation.

REFERENCES

- 1 **Braun S**, Harbeck N. Molecular markers of metastasis in breast cancer: current understanding and prospects for novel diagnosis and prevention. *Expert Rev Mol Med* 2001; **6**: 1-14
- 2 **Liu LX**, Zhang WH, Jiang HC. Current treatment for liver metastases from colorectal cancer. *World J Gastroenterol* 2003; **9**: 193-200
- 3 **Quaranta V**, Giannelli G. Cancer invasion: watch your neighbourhood. *Tumori* 2003; **89**: 343-348
- 4 **Townson JL**, Naumov GN, Chambers AF. The role of apoptosis in tumor progression and metastasis. *Curr Mol Med* 2003; **3**: 631-642
- 5 **Reuning U**, Sperl S, Kopitz C, Kessler H, Kruger A, Schmitt M, Magdolen V. Urokinase-type plasminogen activator (uPA) and its receptor (uPAR): development of antagonists of uPA/uPAR interaction and their effects *in vitro* and *in vivo*. *Curr Pharm Des* 2003; **9**: 1529-1543
- 6 **Cunningham O**, Andolfo A, Santovito ML, Iuzzolino L, Blasi F, Sidenius N. Dimerization controls the lipid raft partitioning of uPAR/CD87 and regulates its biological functions. *EMBO J* 2003; **22**: 5994-6003
- 7 **Nakamura Y**, Yasuoka H, Tsujimoto M, Yang Q, Imabun S, Nakahara M, Nakao K, Nakamura M, Mori I, Kakudo K. Flt-4-positive vessel density correlates with vascular endothelial growth factor-d expression, nodal status, and prognosis in breast cancer. *Clin Cancer Res* 2003; **9**: 5313-5317
- 8 **Jiang CQ**, Liu ZS, Qian Q, He YM, Yuan YF, Ai ZL. Relationship of Hypoxia-Inducible Factor 1 Alpha (HIF-1alpha) Gene Expression with Vascular Endothelial Growth Factor (VEGF) and Microvessel Density (MVD) in Human Colorectal Adenoma and Adenocarcinoma. *Aizheng* 2003; **22**: 1170-1174

- 9 **Zhu Z**, Bohlen P, Witte L. Clinical development of angiogenesis inhibitors to vascular endothelial growth factor and its receptors as cancer therapeutics. *Curr Cancer Drug Targets* 2002; **2**: 135-156
- 10 **Viereck V**, Grundker C, Blaschke S, Niederkleine B, Siggelkow H, Frosch KH, Raddatz D, Emons G, Hofbauer LC. Raloxifene concurrently stimulates osteoprotegerin and inhibits interleukin-6 production by human trabecular osteoblasts. *J Clin Endocrinol Metab* 2003; **88**: 4206-4213
- 11 **Hudelist G**, Kostler WJ, Attems J, Czerwenka K, Muller R, Manavi M, Steger GG, Kubista E, Zielinski CC, Singer CF. Her-2/neu-triggered intracellular tyrosine kinase activation: *in vivo* relevance of ligand-independent activation mechanisms and impact upon the efficacy of trastuzumab-based treatment. *Br J Cancer* 2003; **89**: 983-991
- 12 **Michael-Robinson JM**, Pandeya N, Cummings MC, Walsh MD, Young JP, Leggett BA, Purdie DM, Jass JR, Radford-Smith GL. Fas ligand and tumour counter-attack in colorectal cancer stratified according to microsatellite instability status. *J Pathol* 2003; **201**: 46-54
- 13 **Machner A**, Baier A, Wille A, Drynda S, Pap G, Drynda A, Mawrin C, Buhling F, Gay S, Neumann W, Pap T. Higher susceptibility to Fas ligand induced apoptosis and altered modulation of cell death by tumor necrosis factor-alpha in periarthritic tenocytes from patients with knee joint osteoarthritis. *Arthritis Res Ther* 2003; **5**: 253-261
- 14 **Andreasen PA**, Egelund R, Petersen HH. The plasminogen activation system in tumor growth, invasion, and metastasis. *Cell Mol Life Sci* 2000; **57**: 25-40
- 15 **Hemsen A**, Riethdorf L, Brunner N, Berger J, Ebel S, Thomssen C, Janicke F, Pantel K. Comparative evaluation of urokinase-type plasminogen activator receptor expression in primary breast carcinomas and on metastatic tumor cells. *Int J Cancer* 2003; **107**: 903-909
- 16 **Korte W**. Changes of the coagulation and fibrinolysis system in malignancy: their possible impact on future diagnostic and therapeutic procedures. *Clin Chem Lab Med* 2000; **38**: 679-692
- 17 **Van Hensbergen Y**, Broxterman HJ, Peters E, Rana S, Elderkamp YW, Van Hinsbergh VW, Koolwijk P. Aminopeptidase inhibitor bestatin stimulates microvascular endothelial cell invasion in a fibrin matrix. *Thromb Haemost* 2003; **90**: 921-929
- 18 **Wang Y**. The role and regulation of urokinase-type plasminogen activator receptor gene expression in cancer invasion and metastasis. *Med Res Rev* 2001; **21**: 146-170
- 19 **Ramont L**, Pasco S, Hornebeck W, Maquart FX, Monboisse JC. Transforming growth factor-beta1 inhibits tumor growth in a mouse melanoma model by down-regulating the plasminogen activation system. *Exp Cell Res* 2003; **291**: 1-10
- 20 **De Bock CE**, Wang Y. Clinical significance of urokinase-type plasminogen activator receptor (uPAR) expression in cancer. *Med Res Rev* 2004; **24**: 13-39
- 21 **Le Gat L**, Gogat K, Bouquet C, Saint-Geniez M, Darland D, Van Den Berghe L, Marchant D, Provost A, Perricaudet M, Menasche M, Abitbol M. *In vivo* adenovirus-mediated delivery of a uPA/uPAR antagonist reduces retinal neovascularization in a mouse model of retinopathy. *Gene Ther* 2003; **10**: 2098-2103
- 22 **Harvey SR**, Hurd TC, Markus G, Martinick MI, Penetrante RM, Tan D, Venkataraman P, DeSouza N, Sait SN, Driscoll DL, Gibbs JF. Evaluation of urinary plasminogen activator, its receptor, matrix metalloproteinase-9, and von Willebrand factor in pancreatic cancer. *Clin Cancer Res* 2003; **9**: 4935-4943
- 23 **Rabbani SA**, Mazar AP. The role of the plasminogen activation system in angiogenesis and metastasis. *Surg Oncol Clin N Am* 2001; **10**: 393-415
- 24 **Mabrouk RA**, Ali-Labib R. Detection of urokinase plasminogen activator receptor and c-erbB-2 in sera of patients with breast and ovarian carcinoma. *Clin Biochem* 2003; **36**: 537-543
- 25 **Hamdi HK**, Castellon R. ACE inhibition actively promotes cell survival by altering gene expression. *Biochem Biophys Res Commun* 2003; **310**: 1227-1235
- 26 **Shin YC**, Folk WR. Formation of polyomavirus-like particles with different VP1 molecules that bind the urokinase plasminogen activator receptor. *J Virol* 2003; **77**: 11491-11498
- 27 **Zhang F**, Tom CC, Kugler MC, Ching TT, Kreidberg JA, Wei Y, Chapman HA. Distinct ligand binding sites in integrin alpha3beta1 regulate matrix adhesion and cell-cell contact. *J Cell Biol* 2003; **163**: 177-188
- 28 **Leung YK**, Ng TB, Ho JW. Transcriptional regulation of fosl-1 by licorice in rat Clone 9 cells. *Life Sci* 2003; **73**: 3109-3121
- 29 **Lloyd FP Jr**, Slivova V, Valachovicova T, Sliva D. Aspirin inhibits highly invasive prostate cancer cells. *Int J Oncol* 2003; **23**: 1277-1283
- 30 **Roelofs JJ**, Rowshani AT, van den Berg JG, Claessen N, Aten J, ten Berge IJ, Weening JJ, Florquin S. Expression of urokinase plasminogen activator and its receptor during acute renal allograft rejection. *Kidney Int* 2003; **64**: 1845-1853
- 31 **Baker EA**, Bergin FG, Leaper DJ. Plasminogen activator system, vascular endothelial growth factor, and colorectal cancer progression. *Mol Pathol* 2000; **53**: 307-312
- 32 **Konno H**, Abe J, Kaneko T, Baba M, Shoji A, Sunayama K, Kamiya K, Tanaka T, Suzuki S, Nakamura S, Urano T. Urokinase receptor and vascular endothelial growth factor are synergistically associated with the liver metastasis of colorectal cancer. *Jpn J Cancer Res* 2001; **92**: 516-523
- 33 **Poulaki V**, Mitsiades CS, McMullan C, Sykourti D, Fanourakis G, Kotoula V, Tseleni-Balafouta S, Koutras DA, Mitsiades N. Regulation of vascular endothelial growth factor expression by insulin-like growth factor I in thyroid carcinomas. *J Clin Endocrinol Metab* 2003; **88**: 5392-5398
- 34 **Koide N**, Nishio A, Kono T, Hiraguri M, Watanabe H, Igarashi J, Hanazaki K, Adachi W, Amano J. Histochemical study of angiogenesis in basaloid squamous carcinoma of the esophagus. *Dis Esophagus* 2000; **13**: 142-147
- 35 **Koshida K**, Konaka H, Kato H, Miyagi T, Egawa M, Uchibayashi T, Namiki M. Correlation between expression of metastasis-related genes and lymph node metastasis in testicular cancer. *Hinyokika Kyo* 2000; **46**: 775-781
- 36 **Oh CW**, Hoover-Plow J, Plow E. The role of plasminogen in angiogenesis *in vivo*. *J Thromb Haemost* 2003; **1**: 1683-1687
- 37 **Dazzi C**, Cariello A, Maioli P, Magi S, Rosti G, Giovanis P, Giovannini G, Lanzanova G, Marangolo M. A high cytosol value of urokinase-type plasminogen activator (uPA) may be predictive of early relapse in primary breast cancer. *Cancer Invest* 2003; **21**: 208-216
- 38 **Kaneko T**, Konno H, Baba M, Tanaka T, Nakamura S. Urokinase-type plasminogen activator expression correlates with tumor angiogenesis and poor outcome in gastric cancer. *Cancer Sci* 2003; **94**: 43-49
- 39 **Gruss CJ**, Satyamoorthy K, Berking C, Lininger J, Nesbit M, Schaidt H, Liu ZJ, Oka M, Hsu MY, Shirakawa T, Li G, Bogenrieder T, Carmeliet P, El-Deiry WS, Eck SL, Rao JS, Baker AH, Bennet JT, Crombleholme TM, Velazquez O, Karmacharya J, Margolis DJ, Wilson JM, Detmar M, Skobe M, Robbins PD, Buck C, Herlyn M. Stroma formation and angiogenesis by overexpression of growth factors, cytokines, and proteolytic enzymes in human skin grafted to SCID mice. *J Invest Dermatol* 2003; **120**: 683-692
- 40 **Behzadian MA**, Windsor LJ, Ghaly N, Liou G, Tsai NT, Caldwell RB. VEGF-induced paracellular permeability in cultured endothelial cells involves urokinase and its receptor. *FASEB J* 2003; **17**: 752-754

Adjustment of lipiodol dose according to tumor blood supply during transcatheter arterial chemoembolization for large hepatocellular carcinoma by multidetector helical CT

Hong-Yan Cheng, Yi Shou, Xiang Wang, Ai-Min Xu, Dong Chen, Yu-Chen Jia

Hong-Yan Cheng, Yi Shou, Xiang Wang, Ai-Min Xu, Dong Chen, Yu-Chen Jia, Department of Radiology, Eastern Hepatobiliary Surgery Hospital, Second Military Medical University, Shanghai 200438, China
Correspondence to: Dr. Hong-Yan Cheng, Department of Radiology, Eastern Hepatobiliary Surgery Hospital, Shanghai 200438, China
Telephone: +86-21-25070861 **Fax:** +86-21-25070861
Received: 2003-12-28 **Accepted:** 2004-01-12

Abstract

AIM: To work out an individualized lipiodol dose in transcatheter arterial chemoembolization (TACE) for large hepatocellular carcinoma (HCC) according to its blood supply evaluated by CT.

METHODS: One hundred patients with large HCC (more than 8 cm in diameter) were studied by multidetector helical CT. Patterns of blood supply of HCC were divided into sufficient blood supply, poor blood supply, mixed blood supply and arteriovenous (A-V) shunt. The dose of ultra-fluid lipiodol was determined by diameter and blood supply type of HCC. Patients were divided into two groups (50 cases each): lipiodol perfusion group and iodized oil perfusion group according to tumor diameter and the blood supply type of tumor.

RESULTS: The confirmation and effective rates were 82%, 84% in the first group and 36%, 46% in the second group ($P < 0.01$).

CONCLUSION: A relatively individualized lipiodol dose may be determined according to the blood supply pattern and the tumor diameter by CT imaging.

Cheng HY, Shou Y, Wang X, Xu AM, Chen D, Jia YC. Adjustment of lipiodol dose according to tumor blood supply during transcatheter arterial chemoembolization for large hepatocellular carcinoma by multidetector helical CT. *World J Gastroenterol* 2004; 10(18): 2753-2755

<http://www.wjgnet.com/1007-9327/10/2753.asp>

INTRODUCTION

A critical issue in treating large hepatocellular carcinoma (HCC) is determining the optimum lipiodol and antitumor drug dose before transcatheter arterial chemoembolization (TACE). Over-dose will damage hepatic function and inadequate dose will lead to poor treatment effect. Tumor blood supply is the crucial factor for determining lipiodol dose. Lipiodol dose was worked out according to the HCC blood supply check by CT scan, then the actual perfusion dose and curative effect were compared in order to assess the therapeutic efficacy.

MATERIALS AND METHODS

Patients

One hundred patients (91 male and 9 female, age range 20-72 years,

mean age 48 years) with large HCC (diameter larger than 8 cm) were prepared for TACE. All HCC cases were confirmed by clinic, laboratory and image examinations.

Methods

CT scan CT scan patterns were as follows: multi-slice helical CT (Lightspeed QX/I, GE Corporation); 5 mm-thick-section; Pitch 3:1; non-enhanced scanning performed along with arterial phase, portal-venous phase and delayed-phase at 20-25 s, 45-50 s and 2-3 min, respectively; at 120 kV; 270-300 mA; high pressure injector as well as nonionic-contrast media injected at a rate of 3 mL/s (standard 1.2-1.5 mL/kg). The images were obtained by picture archiving and communication system (PACS) and relevant diagnostic reports writing workstation (DELL 21 in monitor, resolving power 1 920 × 1 920). Radiologists analyzed the CT images by using analysis software on Radworks 5.1 to determine the tumor contrast features and confirm the blood supply patterns and further work out the lipiodol dose.

DSA examination DSA (Advantx TC, GE Corporation) was selected and the hepatic artery, coeliac artery and mesenteric artery were detected; the contrast media was injected to reveal the tumor blood supply; the correlation between CT and DSA images was analyzed. Catheter was put into nourishing artery with super-selection skill and anti-carcinoma drug and iodine oil were perfused.

Perfusion dose All cases were randomly divided into two groups. In testing group, dose was determined based on maximum tumor diameter along with the pattern of blood supply. When the sufficient blood supply was concerned, lipiodol dose would be 2-3 times tumor's diameter (If tumor diameter of sufficient blood supply was about 10 cm, the lipiodol dose would be about 20-30 mL). As for the poor blood supply, the dose would be equal to its diameter; lipiodol was perfused till tumor volume was filled completely. To mixed blood supply, the dose was adjusted according to its sufficient blood supply area. When A-V shunt existed, lipiodol amount was determined according to actual condition during TACE. In control group dose was determined based on tumor size (If tumor was about 10 cm, lipiodol dose would be 10 mL accordingly).

Reference standard of lipiodol congreation In CT film, we took the area which lipiodol actually occupied within tumor as a criterion after first TACE: over 75% area as complete filling, area between 50-74% as relatively complete filling, below 49% area as partial filling. Through CT scanning, complete filling and relatively complete filling accorded with pre-operation criterion and partial filling did not.

Evaluation criterion for curative effect With short term follow-up of 6 mo, according to evaluation criterion established by WHO, curative effect could be divided into: complete response (CR), partial response (PR), no change (NC), and progressive deterioration (PD). The three former items were regarded as effective and PD ineffective.

Statistics Confirmation rate and effective rate were assessed by χ^2 test.

RESULTS

Four types of blood supply patterns of large HCC

Type I, abundant blood supply, which could be further divided into Ia and Ib subtype. Ia subtype: Tumor displayed obviously homogeneous or non-homogeneous hyper-dense contrast in arterial phase after enhancement in which broadened nourishing vessels were like radiated, piebald, petal or tuberous shape, and were still in enhancement at portal-venous phase and tailed off at delayed-phase. In DSA, tumor's nourishing arteries broadened and small vessel was hyperplasia in radiated and clasp shape. Ib subtype: Compared with surroundings of hepatic parenchyma in CT, tumor presented slight enhancement and were still in relative hypodense in arterial and portal-venous phases where slightly broadened or nodular arteries at arterial phase could be seen. And palisade shape enhancement could be found at portal-venous phase. Many small vessels showed in DSA film.

Type II, poor blood supply, tumor showed no or mild enhancement during arterial phase, portal-venous phase or delayed phase. In DSA, the nourishing arteries presented no or slight widening and small vessels were in absence; during parenchyma phase, the tumor showed slightly staining.

Type III, mixed blood supply, tumor consisted of sufficient blood supply areas and poor blood supply areas, some areas took on apparent contrast while others did slightly. In DSA, sufficient blood supply areas and poor supply areas co-existed in a tumor.

Type IV, A-V shunt portal vein showed at arterial phase in advance while tumor rarely contrasted at arterial or portal venous phase. In DSA, the normal hepatic artery evidently enlarged rather than tumor arteries. A great amount of contrast media could flow into fistula existed in tumor through portal vein or hepatic vein so that involved veins visualized.

From Tables 1, 2, types I-III in CT scan accorded to that in DSA, and the type of A-V shunt in CT scan is very different from that in DSA. The confirmation rate of lipiodol perfusion was 82% in testing group and 36% in control group. In terms of the effective rate, the difference was significant between testing group (84%) and control group (46%).

Table 1 Blood supply of 100 cases large HCC classified in CT and DSA

Item	Case	Sufficient blood supply		Poor blood supply		Mixed blood supply		A-V shunt	
		Case	%	Case	%	Case	%	Case	%
CT	100	75	75	14	14	7	7	4	4
DSA	100	72	72	12	12	6	6	10	10

Table 2 Curative effects in two groups

Group	Case	PR	NC	PD	Effective rate (%)
Testing group	50	24	18	8	84.0
Control group	50	7	16	27	46.0

CP: Complete response; PR: Partial response; NC: No change; PD: Progressive deterioration.

DISCUSSION

Lipiodol dose is determined by tumor blood supply, patients' general conditions, tolerance to operation, catheter position, etc., of which tumor blood supply plays a crucial role. CT and DSA can display the tumor blood supply well. With sufficient blood supply, tumors in CT scan show apparent enhancement and in DSA display a large amount of inordinately dilated vessels, even "blood lake". With poor blood supply, tumors

reveal little enhancement as well as a small number of vessels. The display rate and staining extent of the vessels were different when the catheter ends reached coeliac trunk, common hepatic artery or proper hepatic artery. Tumor staining extent was significantly higher in latter two because most of blood stream could flow back to splenic artery when catheter was in coeliac trunk. In addition, display rate and staining extent of small vessels were in direct proportion to contrast media amount and injection rate. Two cases revealing no classical trabecula and roundish contrast features in CT were misdiagnosed as poor blood supply type, but the nourishing arteries were presented in arterial phase and a large amount of small vessels appeared in portal venous phase and in DSA lipiodol filled in the tumor completely.

It is of great significance to work out a set of individualized therapy before TACE. Previously, lipiodol dose was determined by tumor's size^[1]. In another word, lipiodol dose should correspond to tumor size and if lipiodol dose is equal to tumor diameter or 1.5 times the diameter, it will produce good curative effect, and if dose is beyond twice the diameter, it will have fewer effects and even damage the hepatic function, leading to cirrhosis. Matsuo^[2] believed that in conventional TACE, lipiodol should be over 5 mL if tumor diameter is less than 5 cm, and the maximum dose will be 10 mL when the tumor develops to more than 5 cm in diameter. With the improvement of the catheter quality and the development of the superselective skills, the catheter can be superselected directly into tumor supply arteries with ease, and lipiodol dose can rise up to 20 mL to fill the tumor less than 10 cm in diameter and 30 mL or more to the tumor more than 10 cm. But in poor blood supply cases, the lipiodol dose should not be over its necessity because lipiodol can flow back and disperse into the normal liver parenchyma. As for mixed blood supply, the dose will rely on the sufficient blood supply area in tumor. Tumor has its shape and volume, supposing to make the lipiodol fill in the tumor as much as possible, it is not enough to inject lipiodol dose into tumor just as its maximum diameter, especially in sufficient blood supply tumor. The tumor will survive if lipiodol dose is not sufficient. Theoretically, tumor cell can be killed only when lipiodol has obstructed all supply vessels and drug flows completely into the tumor. Over dose of drug and lipiodol will make hepatic function get worse in the case of the liver cirrhosis. For these reasons above, to make the drug and lipiodol fill as completely in the tumor as possible, lipiodol dose ought to be based not only on tumor diameter but also on individual blood supply.

CT film can reflect tumor's position, shape, size, quantity as well as blood supply, thus providing guidance for therapy. Patterns of tumor blood supply can be divided into 3 types at arterial phase in CT scan: sufficient blood supply, poor blood supply and mixed blood supply. The survival rate of sufficient blood supply is obviously higher than that of poor blood supply^[3,4]. Vogl^[5] held that lipiodol filling over 75% area of tumor was complete filling and 50-70% area was comparatively complete filling, and the survival rate was encouraging in these two circumstances.

Chung suggested that over-dose lipiodol injection could lead to pulmonary artery embolism when obvious artery-vein shunt exists, especially in hepatic arterial-venous fistula of large HCC. CT can illustrate obvious A-V shunt and provide guidance for therapy. In such cases, lipiodol dose should be decreased and fistula embolized by gelfoam, then correct dose of lipiodol injected to perfuse tumors.

In the first time of therapy, lipiodol dose should be relatively excessive to completely fill in the tumor, because tumor cells can produce the drug resistance with the increase of TACE operation, the artery will be impaired more or less by lipiodol even produce stenosis or obstruction, and finally, the sufficient blood supply of tumor may turn into poor blood supply, meanwhile, the normal hepatic parenchyma may gradually

become cirrhosis, or deteriorated from intrinsic cirrhosis, which would bring side effects and even interrupt the treatment.

REFERENCES

- 1 **Nakao N**, Uchida H, Kamino K, Nishimura Y, Ohishi H, Takayasu Y, Miura K. Determination of the optimum dose level of lipiodol in transcatheter arterial embolization of primary hepatocellular carcinoma based on retrospective multivariate analysis. *Cardiovasc Intervent Radiol* 1994; **17**: 76-80
- 2 **Matsuo N**, Uchida H, Sakaguchi H, Nishimine K, Nishimura Y, Hirohashi S, Ohishi H. Optimal lipiodol volume in transcatheter arterial chemoembolotherapy for hepatocellular carcinoma: study based on lipiodol accumulation patterns and histopathologic findings. *Semin Oncol* 1997; **24**(2 Suppl 6): 61-70
- 3 **Katyal S**, Oliver JH, Peterson MS, Chang PJ, Baron RL, Carr BI. Prognostic significance of arterial phase CT for prediction of response to transcatheter arterial chemoembolization in unresectable hepatocellular carcinoma: a retrospective analysis. *Am J Roentgenol* 2000; **175**: 1665-1672
- 4 **Vogl TJ**, Trapp M, Schroeder H, Mack M, Schuster A, Schmitt J, Neuhaus P, Felix R. Transarterial chemoembolization for hepatocellular carcinoma: volumetric and morphologic CT criteria for assessment of prognosis and therapeutic success-results from a liver transplantation center. *Radiology* 2000; **214**: 349-357
- 5 **Chung JW**, Park JH, Im JG, Han JK, Han MC. Pulmonary oil embolism after transcatheter oily chemoembolization of hepatocellular carcinoma. *Radiology* 1993; **187**: 689-693

Edited by Zhu LH and Chen WW Proofread by Xu FM

Simplified purification method for *Clostridium difficile* toxin A

Si-Wu Fu, Jing Xue, Ya-Li Zhang, Dian-Yuan Zhou

Si-Wu Fu, Jing Xue, Ya-Li Zhang, Dian-Yuan Zhou, PLA Institute for Digestive Medicine, Nanfang Hospital, First Military Medical University, Guangzhou 510515, Guangdong Province, China
Correspondence to: Dr. Si-Wu Fu, PLA Institute for Digestive Medicine, Nanfang Hospital, First Military Medical University, Guangzhou 510515, Guangdong Province, China. fusiwu2001@sina.com
Telephone: +86-20-61641544
Received: 2003-12-17 **Accepted:** 2004-01-12

Abstract

AIM: To establish the purification method for *Clostridium difficile* (*C. difficile*) toxin A.

METHODS: *C. difficile* VPI 10463 filtrate was cultured anaerobically by the dialysis bag methods. And then the toxin A was purified by precipitation with 500 g/L (NH₄)₂SO₄ and acid precipitation at pH 5.5, followed by ion-exchange chromatography on DEAE-Toyopearl.

RESULTS: Purified toxin A exhibited only one band on native polyacrylamide gel electrophoresis (native-PAGE) and Ouchterlony double immunodiffusion. The molecular weight of toxin A was estimated to be 550 000. The purified toxin A had a protein concentration of 0.881 mg/mL. The minimum lethal dose was 1×10⁶ MLD/mL (i.p.mice). The cytotoxic titer was 10⁷ CU/mg. The haemagglutinate activity was at a concentration of 1.72 µg/mL. The ratio of fluid volume (mL) accumulated to the length (cm) of the loop was 2.46.

CONCLUSION: The modified method for purification of toxin A of *C. difficile* was simple and convenient. It may be even more suitable for purification of toxin A on large scales.

Fu SW, Xue J, Zhang YL, Zhou DY. Simplified purification method for *Clostridium difficile* toxin A. *World J Gastroenterol* 2004; 10(18): 2756-2758
<http://www.wjgnet.com/1007-9327/10/2756.asp>

INTRODUCTION

Clostridium difficile (*C. difficile*) is one major causative agent of pseudomembranous colitis (PMC) and a large number of antibiotic-associated diarrhea in humans and animals. It has been reported that this organism produces at least two toxins, designated A (enterotoxin) and B (cytotoxin). Toxin A, a tissue-damaging enterotoxin, causes hemorrhagic fluid accumulation in rabbit ileal loops and is cytotoxic to cultured fibroblasts. Toxin B is an extremely potent cytotoxin for many cultured cells^[1]. The importance of toxin A in the pathogenesis of *C. difficile* enteritis has been documented and several investigators have established the purification method of enterotoxin^[2]. In this report, we presented a simple method for purification of toxin A. The highly purified toxin A was obtained and analyzed for its biological and immunological properties.

MATERIALS AND METHODS

Bacterial strains and culture filtrates

C. difficile VPI 10463 was grown anaerobically at 37 °C for 72 h

in Brain Heart Infusion (Difco) by the dialysis bag methods.

Purification of toxin A

C. difficile VPI 10463 culture filtrates were centrifuged at 8 000 r/min for 20 min and filtrated through a 0.45 µm membrane filter. The culture supernatant of 200 mL was precipitated by 500 g/L saturated (NH₄)₂SO₄ overnight at 4 °C, centrifuged at 8 000 r/min for 15 min. The precipitation was dissolved in 50 mmol/L Tris-HCl buffer (pH7.5) and dialyzed in 10 mmol/L acetic buffer(pH5.5) at 4 °C for 24 h, centrifuged twice, The precipitate was dissolved in 50 mmol/L Tris-HCl (pH7.5) and dialysed against the same buffer, concentrated by PEG 10000 at 4 °C. The sample was then loaded onto anion-exchange DEAE-Toyopearl 650 mol/L chromatography column, the sample was equilibrated by 300 mL of 50 mmol/L Tris-HCl buffer (pH7.5, containing 50 mmol/L NaCl), and then eluted first with 200 mL of a linear NaCl gradient (50-250 mmol/L NaCl), followed by 200 mL of 50 mmol/L Tris-HCl buffer (pH7.5) containing 300 mmol/L NaCl. A second elution using 200 mL of a linear gradient (300-600 mmol/L NaCl) in the same buffer was performed. The toxins that eluted in the first NaCl gradient were designated toxins A. The toxin was pooled and concentrated, and analyzed for its biological and immunological properties.

Tissue culture assay

Cytotoxic activity was determined by using African green monkey kidney (Vero) cells as previously described by Kamiya *et al.*^[3]. For the analysis, tenfold dilutions of test samples were prepared and assayed for activity. The cytotoxic titer, which was expressed as the reciprocal of the highest dilution that caused 100% rounding of the cells by 24 h, was determined by serially diluted 100 µL samples transferring to microtiter wells containing Vero cells (10⁵/mL) in 100 µL of MEM medium. The specific activity, which was determined from the cytotoxic titer, was defined as the number of cytotoxic units per microgram.

Haemagglutinate activity

In reference to the methods described by Meng *et al.*^[3], rabbit blood cells were washed 3 times with PBS (0.15 mol/L, pH7.2) and then diluted to 25 mL/L suspension. 2×serial dilution of specimens (50 µL) was performed with PBS buffer in microplate wells and 50 µL of blood cells were added to each well. The HA titer was expressed as the highest dilution that agglutinated rabbit blood cells at 4 °C for 3 h.

Rabbit ileal loop assay

Enterotoxic activity was determined by the rabbit ileal loop assay as previously described^[3]. Results were obtained approximately 18 h after injection of 1 mL of test samples and expressed as the ratio of the accumulated fluid (volume) to the length (centimeters) of the loop. Heat-inactivated toxin preparations were used as negative controls.

Determination of lethal activity

The minimum lethal dose was determined by intraperitoneally injecting mice (14-16 g) with 0.5 mL aliquots of tenfold serial dilutions of test samples and observing the mice over 72 h for toxicity. Two mice were used for each dose of toxin.

Polyacrylamide gel electrophoresis (PAGE)

Native polyacrylamide gel electrophoresis was performed in 75 g/L and 40-300 g/L gel. Samples were electrophoresed at 120 V for 15 h after initial electrophoreses at 70 V for 30 min. After electrophoresis, gels were stained with Coomassie brilliant blue R-250 and destained. Molecular weights were estimated by comparison with high molecular weight standards (Pharmacia).

Immunological methods

Ouchterlony double immunodiffusion was done in 10 g/L agarose. Crossed immunoelectrophoresis (CIP) was performed as previously described^[3]. Goat antiserum against toxin A used in the analyses was prepared in our laboratory.

Protein assay

Protein concentration was determined by the method of Coomassie brilliant blue G-250. Bovine serum albumin was purchased from Sigma Company of USA.

RESULTS

High purified toxin A was obtained by precipitation with 500 g/L $(\text{NH}_4)_2\text{SO}_4$ and acid precipitation at pH5.5, followed by DEAE-Toyopearl 650 mol/L column chromatography. The elution profile of toxin A by DEAE-Toyopearl 650 mol/L column chromatography is shown in Figure 1. The purified toxin A exhibited only one band on 40-300 g/L native polyacrylamide gel electrophoresis, the molecular mass of toxin A was estimated to be 550 000 (Figure 2). The toxin preparation also gave a single component when analyzed by Ouchterlony double immunodiffusion (Figure 3) and cross immunoelectrophoresis.

The purified toxin A had a protein concentration of 0.881 mg/mL, the cytotoxic titer was 10^7 CU units per mg. The HA activity was at a concentration of 1.72 $\mu\text{g}/\text{mL}$, the ratio of fluid accumulated volume (mL) to the length (cm) of the loop was 2.46. The minimum lethal dose was 1×10^6 MLD/mL (Table 1). All biological properties of purified toxin A were neutralized by the antiserum of *C. difficile* toxin A.

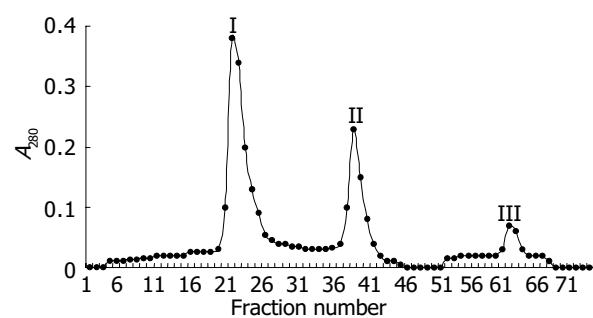


Figure 1 Purification of *Clostridium difficile* toxin A by DEAE-Toyopearl 650 mol/L chromatography. Fractions 1-34 were eluted with 50 mmol/L Tris-HCl buffer (pH7.5) containing a linear NaCl gradient (50 mmol/L-250 mmol/L), then fractions 35-50 were eluted with 300 mmol/L NaCl and fractions 51-75 were eluted with linear gradient (300 mmol/L-600 mmol/L NaCl) in the same buffer.

Table 1 Purification of *C. difficile* toxin A

Purification step	Vol (mL)	Protein(mg/mL)	Lethal dose(Mice, MLD/mL)	Cytotoxicity (CU/mg)
Crude culture supernatant	200	1.86	6×10^4	10^{10}
50% $(\text{NH}_4)_2\text{SO}_4$ precipitation	10	ND	ND	ND
Acid precipitation	10	6.15	2×10^6	10^{10}
DEAE-Toyopearl 650 mol/L	6	0.881	1×10^6	10^7

ND: not detected.

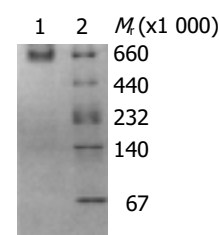


Figure 2 Analysis of toxin A preparations by native-PAGE (4-30%). Line 1: Purified *C. difficile* toxin A; Line 2: High molecular mass markers, thyroglobulin (M_r 669 000), ferritin (M_r 440 000), catalase (M_r 232 000), lactate dehydrogenase (M_r 140 000), bovine serum albumin (M_r 67 000).

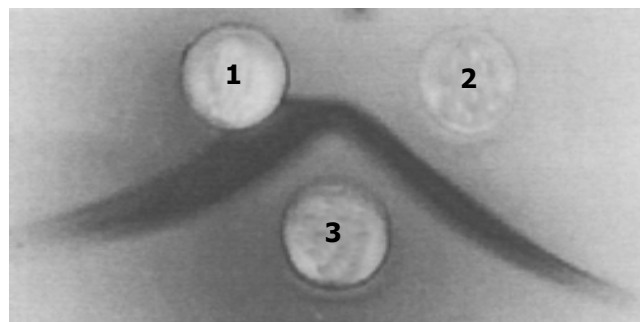


Figure 3 Analysis of toxin A by Ouchterlony double immunodiffusion. Well 3 contained 20 μL of antiserum against strain 10463 culture filtrate, well 1 and well 2 contained 20 μL of purified toxin A by acid precipitation and DEAE-Toyopearl 650 mol/L chromatography respectively.

DISCUSSION

Affinity chromatography used to purify toxin A in the present study was first described by Krivan *et al.* The methods using bovine thyroglobulin for purification of *C. difficile* toxin A which depends on the temperature was dependent on binding between toxin A and thyroglobulin. A change of the temperature from 4 to 37 $^{\circ}\text{C}$ toxin A was released from the glycoprotein molecule^[2]. In addition to toxin A, there were trace amounts of toxin B and a few other proteins at low level. As thyroglobulin is an expensive biological reagent, this method might not be suitable for purification of toxin A in some laboratories.

Sullivan *et al.* (1982) described a procedure for preparing milligram amounts of homogeneous toxin A from culture filtrate^[4]. The method consisted of ultrafiltration through an Amicon XM100 membrane filter, anion-exchange chromatography on DEAE-Sepharose CL-6B, and precipitation at pH5.5. We purified toxin A from culture filtrate with the method and found that except for a major protein band, there was a faint band as well on native PAGE. High purified toxin A was obtained by precipitation with 500 g/L $(\text{NH}_4)_2\text{SO}_4$ and acid precipitation at pH5.5, followed by DEAE-Toyopearl 650 mol/L column chromatography.

In the studies on the toxins of *C. difficile*, researchers have reported the cytotoxicity of *C. difficile* toxin A for human colonic and pancreatic carcinoma cell lines^[5]. Although there are a lot

of problems to be solved before the toxin being used in clinic, the modified method for purification of toxin A of *C. difficile* was simple and convenient, it may be even more suitable for purification of toxin A on large scale.

REFERENCES

- 1 **Bartlett JG**. *Clostridium difficile*: history of its role as an enteric pathogen and the current state of knowledge about the organism. *Clin Infect Dis* 1994; **18**(Suppl 4): S265-272
- 2 **Kamiya S**, Reed PJ, Borriello SP. Purification and characterisation of *Clostridium difficile* toxin A by bovine thyroglobulin affinity chromatography and dissociation in denaturing conditions with or without reduction. *J Med Microbiol* 1989; **30**: 69-77
- 3 **Meng XQ**, Kamiya S, Yamakawa K, Ogura H, Nakamura S. Purification and characterisation of intracellular toxin A of *Clostridium difficile*. *J Med Microbiol* 1993; **38**: 69-73
- 4 **Sullivan NM**, Pellett S, Wilkins TD. Purification and Characterization of toxins A and B of *Clostridium difficile*. *Infect Immun* 1982; **35**: 1032-1040
- 5 **Kushnaryov VM**, Redlich PN, Sedmak JJ, Lysterly DM, Wilkins TD, Grossberg SE. Cytotoxicity of *Clostridium difficile* toxin A for human colonic and pancreatic carcinoma cell lines. *Cancer Res* 1992; **52**: 5096-5099

Edited by Zhu LH Proofread by Chen WW and Xu FM

Expression of Survivin in pancreatic cancer and its correlation to expression of Bcl-2

Jian-Guo Qiao, Yu-Qing Zhang, Yu-Chun Yin, Zui Tan

Jian-Guo Qiao, Yu-Chun Yin, Zui Tan, Department of General Surgery, Zhongnan Hospital Affiliated to Wuhan University, Wuhan 430071, Hubei Province, China

Yu-Qing Zhang, Medical Department of Wuhan University, Wuhan 430071, Hubei Province, China

Correspondence to: Zui Tan, Department of General Surgery, Zhongnan Hospital Affiliated to Wuhan University, Wuhan 430071, Hubei Province, China. txh728@public.wh.hb.cn

Telephone: +86-27-87325822

Received: 2003-10-24 **Accepted:** 2003-12-22

Abstract

AIM: To investigate the expression of Survivin in pancreatic cancer and its correlation to the expression of Bcl-2.

METHODS: Survivin and Bcl-2 expressions were examined by immunohistochemistry in 42 tissue samples from pancreatic cancer and 10 from normal pancreas.

RESULTS: No survivin expression was detected in the tissue samples from normal pancreas, while it was detected in 34 of 42 tissue samples from pancreatic cancer (81.95%). There was a correlation between survivin expression and differentiation and stages of pancreatic cancer. Survivin positive cases were strongly correlated to Bcl-2 expression (28/30 vs 6/12, $P < 0.05$).

CONCLUSION: Overexpression of survivin plays an important role in the development and progression of pancreatic cancer, and correlates to the expression of Bcl-2. Survivin expression can be used as a prognostic factor.

Qiao JG, Zhang YQ, Yin YC, Tan Z. Expression of Survivin in pancreatic cancer and its correlation to expression of Bcl-2. *World J Gastroenterol* 2004; 10(18): 2759-2761
<http://www.wjgnet.com/1007-9327/10/2759.asp>

INTRODUCTION

The inhibitor of apoptosis protein (IAP) is a member of the widely-expressed gene family of apoptosis inhibitors. It can inhibit apoptosis induced by a variety of stimuli and plays a critical role in the physiologic activities of cells. Survivin is a recently-characterized gene, a member of the IAP family, and has a close relation between anti-apoptosis and tumors. Overexpression of survivin has been reported to play an important role in the development and progression of pancreatic cancer^[1-5]. In this study, we investigated the relationship between the expression of survivin in patients with pancreatic cancer and the expression of Bcl-2 in order to provide a theoretical basis for the prevention, diagnosis, and treatment of pancreatic cancer.

MATERIALS AND METHODS

Materials

Ten samples from normal pancreatic tissue and 42 samples from

pancreatic cancer were collected. Normal pancreatic tissues were obtained from autopsy specimens in Department of Anatomy, Medical College, Wuhan University, and their mean age was 49.3 years (range, 33-78). Pancreatic cancer samples were obtained from surgically-resected specimens in Zhongnan Hospital, Wuhan University. All these cancers were diagnosed pathologically.

Reagents

Primary antibody for survivin was purchased from Novus Co., Ltd (USA) and Bcl-2 was purchased from Boster Biological Technology Ltd (Wuhan). SP kit was purchased from Zhongshan Biotechnology Co., Ltd (Beijing).

Methods

Fixed in routinely-processed formalin and then embedded in paraffin, 4- μ m thick sections were prepared from the cut surface of blocks at the maximum cross-section. For morphological analysis, the sections were routinely stained with hematoxylin and eosin. Immunohistochemical staining for survivin and Bcl-2 antigen was made by the standard streptavidin/peroxidase (SP) technique. The positive section was used as a positive control. As a negative control, PBS was used instead of the primary antibody for survivin and Bcl-2.

Scoring criteria

Cytoplasm staining with light yellow or brown was defined as a marker of positive cells. All sections were analyzed by an image analysis system. The mean percentage of positive cells for the expression of survivin and Bcl-2 was determined in at least 10 areas at 400-fold magnification, and the cases with less than 5% positively-stained cells were defined as being negative. The cases with 5% to 10% positively-stained cells were defined as having a positivity rate of "+", 11% to 60% as "++", and more than 60% as "+++".

Statistical analysis

All statistical analyses were performed with SPSS 11.0 software. Difference and correlation were analyzed by χ^2 test. $P < 0.05$ was considered statistically significant.

RESULTS

Immunohistochemistry

With immunohistochemical staining, we examined the expression of survivin in pancreatic cancer. The results are shown in Figure 1. The expression of survivin was localized in cytoplasm of tumor cells, which are shown as brown granules in Figure 1 (SP), and in Figure 2 (HE). Survivin was expressed in 34 of 42 pancreatic cancer samples, but not expressed in the 10 samples from normal pancreatic tissue. The expression rate was 81.95%.

To study the relationship between the expressions of survivin and Bcl-2, 42 cases were analyzed. The results are shown in Table 2.

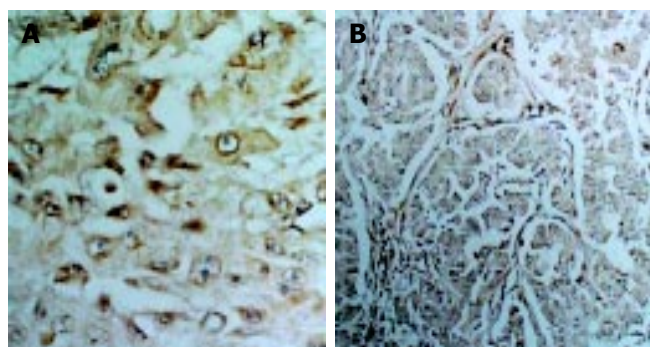


Figure 1 Expression of survivin in poorly and well differentiated pancreatic cancer. A: Expression of survivin in poorly differentiated pancreatic cancer (SPx400). B: Expression of survivin in well differentiated pancreatic cancer (SPx200).

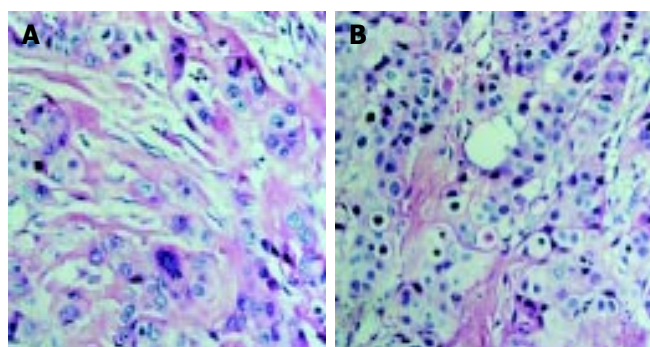


Figure 2 Poorly and well differentiated pancreatic cancer. A: poorly differentiated pancreatic cancer (HEx400). B: well differentiated pancreatic cancer (HEx400).

Table 1 Relationship between survivin expression in pancreatic cancer and clinicopathologic parameters

		Survivin expression		P	r
		(-,+)	(++,+++)		
Sex	Male	11	7	>0.05	
	Female	13	11		
Location	Head	16	14	>0.05	
	Body,Tail	8	4		
Differentiation	High	14	4	<0.05	0.361
	Low	10	14		
Distant metastasis	Present	8	8	>0.05	
	Absent	16	10		
Stage	I-II	18	8	<0.05	0.311
	III-IV	6	10		

Table 2 Correlation between expressions of survivin and Bcl-2

	Survivin expression		P	r
	(+)	(-)		
Bcl-2 (+)	28	2	<0.01	0.499
Bcl-2 (-)	6	6		

DISCUSSION

Survivin, a recently-characterized member of IAP family, was isolated from the human gene bank by Altieri *et al.* in 1997 using effector cell protease receptor-1(EPR-1) cDNA^[6]. Recently, great progress has been made in the structure and function of survivin and its correlation to malignant tumors.

Many findings have suggested that survivin may express selectively in different tissues. Survivin was max expressed or poorly expressed in normal terminally-differentiated tissues, whereas it was extensively expressed in many kinds of human tumor tissues^[7-14].

Studies have shown that Caspase is responsible for apoptosis, which can activate in cascade and lyze protein, thus determining the pattern of apoptosis. Survivin could directly inhibit the activities of Caspase-3 and 7 and block the process of apoptosis and indirectly inhibit Caspase through P21. Therefore survivin would bind to cell cycle apoptosis factor CDK4 to form survivin-CDK4 complex, and then release of P21 from CDK4 complex. When P21 was bound to mitochondrial Caspase-3, it could inhibit its activity, thus preventing apoptosis^[15-17].

The results of our study showed that survivin was highly expressed in pancreatic tumor tissues, but not in normal pancreatic tissues, suggesting that it might play a critical role in the development and progression of pancreatic cancer. Furthermore, there was a positive correlation between survivin expression and tumor TNM staging and differentiation grade. It can be concluded that survivin expression is indicative of higher invasiveness or poor prognosis in pancreatic cancer.

Bcl-2 was the first characterized anti-apoptotic gene with an inhibiting apoptotic pathway different from that of survivin. Bcl-2 could regulate apoptosis by preventing cytochrome C release from mitochondrion to cytoplasm. Whereas, survivin acted by direct inhibition of the terminal effector proteases of apoptosis, i.e., Caspase-3 and Caspase-7.

Our study demonstrated that the expression of survivin was positively correlated with that of Bcl-2. It might be caused by the same transcription and activation mechanism of survivin and Bcl-2, or both might be regulated by GC-rich promoters, and were then transcribed and activated to enhance cell proliferation, acting synergistically to inhibit apoptosis^[18-29].

Asanuma *et al.*^[2,5] investigated whether survivin expression could directly regulate cancer sensitivity to radiotherapy using gene-transduced pancreatic cancer cell strain (MIAPaCa-2). Their results showed that survivin expression could directly down-regulate pancreatic cancer sensitivity to radiotherapy.

In addition, Rohayem *et al.*^[12,30,31] observed that specific anti-survivin antibody could be detected in serum of patients with cancers of the lung and colon, suggesting that this antibody could be used as a new diagnostic marker for cancers of the lung and colon. Furthermore, Smith *et al.*^[32], Moore *et al.*^[33], and Swana *et al.*^[34] found that survivin levels in urine could be used to diagnose primary and recurrent bladder carcinomas, thus providing a new idea for the diagnosis of pancreatic cancer^[35-39].

In conclusion, Survivin can be used as a cancer therapeutic target because of its selective expression in the tissue concerned. Moreover, natural antisense nucleic acid for Survivin-endogenous EPR-1 has become a new hot issue for the tumor gene therapy.

REFERENCES

- Satoh K, Kaneko K, Hirota M, Masamune A, Satoh A, Shimosegawa T. Expression of survivin is correlated with cancer cell apoptosis and is involved in the development of human pancreatic duct cell tumors. *Cancer* 2001; **92**: 271-278
- Asanuma K, Kobayashi D, Furuya D, Tsuji N, Yagihashi A, Watanabe N. A role for survivin in radio resistance of pancreatic cancer cells. *Jpn J Cancer Res* 2002; **93**: 1057-1062
- Sarella AI, Verbeke CS, Ramsdale J, Davies CL, Markham AF, Guillou PJ. Expression of Survivin, a novel inhibitor of apoptosis and cell cycle regulatory protein, in pancreatic adenocarcinoma. *Br J Cancer* 2002; **86**: 886-892
- Jinfeng M, Kimura W, Sakurai F, Moriya T, Takeshita A, Hirai I. Histopathological study of intraductal papillary mucinous tumor of the pancreas: special reference to the roles of Survivin and p53 in tumorigenesis of IPMT. *Int J Gastrointest Cancer*

- 2002; **32**: 73-81
- 5 **Asanuma K**, Moriai R, Yajima T, Yagihashi A, Yamada M, Kobayashi D, Watanabe N. Survivin as a radio resistance factor in pancreatic cancer. *Jpn J Cancer Res* 2000; **91**: 1204-1209
 - 6 **Ambrosini G**, Adida C, Altieri DC. A novel anti-apoptosis gene, Survivin, expressed in cancer and lymphoma. *Nat Med* 1997; **3**: 917-921
 - 7 **Hausladen DA**, Wheeler MA, Altieri DC, Colberg JW, Weiss RM. Effect of intravesical treatment of transitional cell carcinoma with bacillus Calmette-Guerin and mitomycin C on urinary Survivin levels and outcome. *J Urol* 2003; **170**: 230-234
 - 8 **Altieri DC**. Validating survivin as a cancer therapeutic target. *Nat Rev Cancer* 2003; **3**: 46-54
 - 9 **Altieri DC**. Survivin and apoptosis control. *Adv Cancer Res* 2003; **88**: 31-52
 - 10 **Altieri DC**. The molecular basis and potential role of survivin in cancer diagnosis and therapy. *Trends Mol Med* 2001; **7**: 542-547
 - 11 **Carter BZ**, Milella M, Altieri DC, Andreeff M. Cytokine-regulated expression of survivin in myeloid leukemia. *Blood* 2001; **97**: 2784-2790
 - 12 **Kawasaki H**, Altieri DC, Lu CD, Toyoda M, Tenjo T, Tanigawa N. Inhibition of apoptosis by Survivin predicts shorter survival rates in colorectal cancer. *Cancer Res* 1998; **58**: 5071-5074
 - 13 **Lu CD**, Altieri DC, Tanigawa N. Expression of a novel anti-apoptosis gene, survivin, correlated with tumor cell apoptosis and p53 accumulation in gastric carcinomas. *Cancer Res* 1998; **58**: 1808-1812
 - 14 **Li F**, Ackermann EJ, Bennett CF, Rothermel AL, Plescia J, Tognin S, Villa A, Marchisio PC, Altieri DC. Pleiotropic cell-division defects and apoptosis induced by interference with Survivin function. *Nat Cell Biol* 1999; **1**: 461-466
 - 15 **Suzuki A**, Ito T, Kawano H, Hayashida M, Hayasaki Y, Tsutomi Y, Akahane K, Nakano T, Miure M, Shiraki K. Survivin initiates procaspase 3/p21 complex formation as a result of interaction with Cdk4 to resist Fas-mediated cell death. *Oncogene* 2000; **19**: 1346-1353
 - 16 **Ito T**, Shiraki K, Sugimoto K, Yamanaka T, Fujikawa K, Ito M, Takase K, Moriyama M, Kawano H, Hayashida M, Nakano T, Suzuki A. Survivin promotes cell proliferation in human hepatocellular carcinoma. *Hepatology* 2000; **31**: 1080-1085
 - 17 **Garcia JF**, Camacho FI, Morente M, Fraga M, Montalban C, Alvaro T, Bellas C, Castano A, Diez A, Flores T, Martin C, Martinez MA, Mazorra F, Menárguez J, Mestre MJ, Mollejo M, Sáez AI, Sánchez L, Piris MA. Hodgkin and Reed-Sternberg cells harbor alterations in the major tumor suppressor pathways and cell-cycle checkpoints: analyses using tissue microarrays. *Blood* 2003; **101**: 681-689
 - 18 **Rohayem J**, Diestelkoetter P, Weigle B, Oehmichen A, Schmitz M, Mehlhorn J, Conrad K, Rieber EP. Antibody response to the tumor-associated inhibitor of apoptosis protein Survivin in cancer patients. *Cancer Res* 2000; **60**: 1815-1817
 - 19 **Sharief MK**, Semra YK. Down-regulation of Survivin expression in T lymphocytes after interferon beta-1a treatment in patients with multiple sclerosis. *Arch Neurol* 2002; **59**: 1115-1121
 - 20 **Agui T**, McConkey DJ, Tanigawa N. Comparative study of various biological parameters, including expression of Survivin, between primary and metastatic human colonic adenocarcinomas. *Anticancer Res* 2002; **22**: 1769-1776
 - 21 **Gradilone A**, Gazzaniga P, Ribuffo D, Scarpa S, Cigna E, Vasaturo F, Bottoni U, Innocenzi D, Calvieri S, Scuderi N, Frati L, Aglianò AM. Survivin, bcl-2, bax, and bcl-X gene expression in sentinel lymph nodes from melanoma patients. *J Clin Oncol* 2003; **21**: 306-312
 - 22 **Yoshida H**, Ishiko O, Sumi T, Matsumoto Y, Ogita S. Survivin, bcl-2 and matrix metalloproteinase-2 enhance progression of clear cell-and serous-type ovarian carcinomas. *Int J Oncol* 2001; **19**: 537-542
 - 23 **Konno R**, Yamakawa H, Utsunomiya H, Ito K, Sato S, Yajima A. Expression of survivin and Bcl-2 in the normal human endometrium. *Mol Hum Reprod* 2000; **6**: 529-534
 - 24 **Rodel F**, Hoffmann J, Grabenbauer GG, Papadopoulos T, Weiss C, Günther K, Schick C, Sauer R, Rodel C. High Survivin expression is associated with reduced apoptosis in rectal cancer and may predict disease-free survival after preoperative radiochemotherapy and surgical resection. *Strahlenther Onkol* 2002; **178**: 426-435
 - 25 **Guan J**, Chen J, Luo Y, Gao J, Qiu H. Effects of antisense bcl-2 or survivin on the growth of human neuroblastoma cell line SK-N-MC. *Zhonghua Yixue Zazhi* 2002; **82**: 1536-1540
 - 26 **Sarella AI**, Scott N, Ramsdale J, Markham AF, Guillou PJ. Immunohistochemical detection of the anti-apoptosis protein, survivin, predicts survival after curative resection of stage II colorectal carcinomas. *Ann Surg Oncol* 2001; **8**: 305-310
 - 27 **Hiroshima K**, Iyoda A, Toyozaki T, Supriatna Y, Shibuya K, Shimamura F, Haga Y, Yoshida S, Fujisawa T, Ohwada H. Proliferative activity and apoptosis in thymic epithelial neoplasms. *Mod Pathol* 2002; **15**: 1326-1332
 - 28 **Mikami T**, Yoshida T, Akino F, Motoori T, Yajima M, Okayasu I. Apoptosis regulation differs between ulcerative colitis-associated and sporadic colonic tumors. Association with Survivin and Bcl-2. *Am J Clin Pathol* 2003; **119**: 723-730
 - 29 **Park JW**, Choi YJ, Suh SI, Baek WK, Suh MH, Jin IN, Min DS, Woo JH, Chang JS, Passaniti A, Lee YH, Kwon TK. Bcl-2 overexpression attenuates resveratrol-induced apoptosis in U937 cells by inhibition of caspase-3 activity. *Carcinogenesis* 2001; **22**: 1633-1639
 - 30 **Rohayem J**, Diestelkoetter P, Weigle B, Oehmichen A, Schmitz M, Mehlhorn J, Conrad K, Rieber EP. Antibody response to the tumor-associated inhibitor of apoptosis protein Survivin in cancer patients. *Cancer Res* 2000; **60**: 1815-1817
 - 31 **Monzó M**, Rosell R, Felip E, Astudillo J, Sánchez JJ, Maestre J, Martin C, Font A, Barnadas A, Abad A. A novel anti-apoptosis gene: Re-expression of survivin messenger RNA as a prognosis marker in non-small-cell lung cancers. *J Clin Oncol* 1999; **17**: 2100-2104
 - 32 **Smith SD**, Wheeler MA, Plescia J, Colberg JW, Weiss RM, Altieri DC. Urine detection of Survivin and diagnosis of bladder cancer. *JAMA* 2001; **285**: 324-328
 - 33 **Moore M**. Urine detection of Survivin and diagnosis of bladder cancer. *J Insur Med* 2001; **33**: 202-203
 - 34 **Swana HS**, Grossman D, Anthony JN, Weiss RM, Altieri DC. Tumor content of the anti apoptosis molecule Survivin and recurrence of bladder cancer. *N Engl J Med* 1999; **341**: 452-453
 - 35 **Yamamoto T**, Tanigawa N. The role of Survivin as a new target of diagnosis and treatment in human cancer. *Med Electron Microsc* 2001; **34**: 207-212
 - 36 **Sela B**. Survivin: anti-apoptosis protein and a prognostic marker for tumor progression and recurrence. *Harefuah* 2002; **141**: 103-107
 - 37 **Xia C**, Xu Z, Yuan X, Uematsu K, You L, Li K, Li L, McCormick F, Jablons DM. Induction of apoptosis in mesothelioma cells by anti Survivin oligonucleotides. *Mol Cancer Ther* 2002; **1**: 687-694
 - 38 **Carter BZ**, Wang RY, Schober WD, Milella M, Chism D, Andreeff M. Targeting Survivin expression induces cell proliferation defect and subsequent cell death involving mitochondrial pathway in myeloid leukemic cells. *Cell Cycle* 2003; **2**: 488-493
 - 39 **Li F**. Survivin study: what is the next wave? *J Cell Physiol* 2003; **197**: 8-29

Effects of Antiadhesion preparation on free fibrinogen and fibrin degrading products in abdominal exudates of rabbits postoperatively

You-Li Wang, Cheng-En Pan, Ping-Lin Yang, Yuan Tian, Shu-Wen Pei, Ming Dong

You-Li Wang, Cheng-En Pan, Department of Hepatobiliary Surgery, Xi'an Jiaotong University First Hospital, Xi'an 710061, Shaanxi Province, China

Ping-Lin Yang, Department of Orthopedics Surgery, Xi'an Jiaotong University Second hospital, Xi'an 710061, Shaanxi Province, China

Yuan Tian, Shu-Wen Pei, Ming Dong, Department of Gastroenterology, Shaanxi College of TCM Hospital, Xianyang 712000, Shaanxi Province, China

Correspondence to: Dr You-Li Wang, Xi'an Jiaotong University Medical College, Xi'an 710061, Shaanxi Province, China. stage 9909 @ sina.com

Telephone: +86-29-85274659 **Fax:** +86-29-85323201

Received: 2003-12-19 **Accepted:** 2004-01-15

Abstract

AIM: To observe effects of ACOL on fibrinogen (FIB), fibrin degrading products (FDP) and changes of FIB and FDP concentration in rabbits with intra-abdominal exudates during 7 d after major abdominal surgery.

METHODS: Sixty New Zealand rabbits were randomly divided into 4 groups: ACOL group, the control group, DCT group and the normal group. After being modeled, except the normal group, the other 3 groups were treated with different ways for a week; the intra-abdominal exudates of rabbits in the 4 groups were drawn for FIB and FDP measurement once daily during 7 d after major abdominal surgery.

RESULTS: FIB and FDP in the intra-abdominal exudates altered in a regular way and ACOL could change the concentration of FIB and FDP in the intra-abdominal exudates after major abdominal surgery.

CONCLUSION: ACOL can prevent intestinal adhesion by reducing the concentration of FIB and raising that of FDP in the intra-abdominal exudates after major abdominal surgery.

Wang YL, Pan CE, Yang PL, Tian Y, Pei SW, Dong M. Effects of Antiadhesion preparation on free fibrinogen and fibrin degrading products in abdominal exudates of rabbits postoperatively. *World J Gastroenterol* 2004; 10(18): 2762-2766

<http://www.wjgnet.com/1007-9327/10/2762.asp>

INTRODUCTION

With a high incidence of 90%^[1-2], intra-abdominal adhesions are the most common complications after major abdominal surgery, and overall 70% patients of intra-abdominal adhesion have the history of previous laparotomies^[3]. The exact mechanisms about this complication have widely been explored. The damage of peritoneum and its base during laparotomies leads to intra-abdominal traumatic inflammation, and thus the normal intra-abdominal physical condition is destroyed, inflammatory cells and medias are released. Coagulation, kinin

peptide, fibrinolysis, arachidonic acid (AA) participate in this process. The activity of plasminogen activator (t-PA), matrix metalloproteinase (MMP) and their inhibitor changes accordingly^[4-8]. The related factors of adhesion, such as TNF- α , TGF- β , and VEG-F, are involved in regulations of the whole process^[9-11], which results in the abnormally higher concentration of free FIB and FDP in the intra-abdominal exudates. The disturbance of the intra-abdominal homeostasis among secreting, dissolving and absorbing together with over-deposition of fibrin in the abdominal cavity finally leads to fibrous adhesion^[12]. In this research, occurrence and development of intra-abdominal adhesions will be discussed by observing the dynamical changes of FIB and FDP in rabbits' intra-abdominal exudates continuously during 7 d postoperatively. Antiadhesion concentrated oral liquid (ACOL) was used as soon as possible to improve the intra-abdominal physical condition and help to regain the homeostasis of internal environments to prevent the formation of the fibrous jelly in the abdominal cavity. This experiment provided evidence for the punctual and strategic prevention and treatment of the postoperative intra-abdominal adhesion.

MATERIALS AND METHODS

Experimental animal

Sixty healthy New Zealand rabbits of both sexes, weighing from 2.5-3.5 kg, were purchased from Laboratory Animal Center, Medical College of Xi'an Jiaotong University.

Drugs, reagents and instruments

ACOL consisted of Rubarb, Cotex Magnoliae Officinalis, Fructus Auvantii Immature, Caucklandiu Lappal, Folium Raphani Radish Seed, Radix Aucklandiae, Radix Astragali, Cortex Cinnamomi, Fructu Amomi, Radix Angelicae Cinensis, Rhizoma Zingiberis and Radix Salvia Miltiorrhiza. Da-Cheng-Qi Tang (DCT) consisted of Rubarb, Ctex Magnoliae Officinalis, Fructus Aurantii Immature and Natrli Sulfas. Both were provided by Shaanxi College of TCM, and decocted with water and concentrated through reflux with distillatory and water bath to extract the decoction containing 1.0 g crude /mL. FIB test kit was purchased from Changzheng Medical Scientific Limited Company, Shanghai, (batch number f4900704). FDP test kit was purchased from Institute of Microbiology and Epidemiology, Academy of Military Medical Sciences, (batch number 900325). Automatic Biochemical Analyzer 7170 type was from Hitachi, Tokyo, Japan.

Animal models

The experiment was carried out in the clean but not sterile condition under 30 g/L procaine anesthesia (0.5 mL/kg, iv). After shaving and skin-disinfecting, the laparoscopy was performed through a 4 cm vertical midline incision to enable the following performances: (1) appendectomy, (2) perforation of an incision (1 cm in diameters) at 5 cm off pylorus on the lesser curvature with punching device, then repair of the perforation, (3) 2×2 cm² area of the cecal parietal peritoneum being carefully stripped, (4) injection of the solution of Talc powder 1mL/kg and 5 mL distilled water into the abdominal cavity prior to skin closure, (5) splenectomy, and (6) leaving a tube for drainage in the

spleen pit because all the animals were fasted for 8 h after operation. The study protocol was in accordance with the guideline for animal research and was approved by the Research Committee of the hospital.

Grouping and medication

The 60 New Zealand rabbits were randomly divided into 4 groups: normal group, ACOL group, control group and DCT group, with 15 rabbits in each group. From the second day postoperation, rabbits in ACOL group were administered ACOL (5 mL/kg) gastrogavage twice daily, the DCT group was administered DCT, the control group was given normal saline (NS) instead, while the normal group had none treatment. The medication was carried out from the second day of modeling and lasted for 1 wk. 15 mL NS was injected through the drainage cube into the abdominal cavity of each model animal once daily, and 5 min later the abdominal exudates was drawn for FDP and FIB detection.

Statistical analysis

All data were expressed as mean±SD, and statistical analysis were performed by Student-Newman-Keuls test, ANOVA analysis, Difference between groups were compared by SNK-*q* test, with *P*<0.05 considered to have statistical significance.

RESULTS

Concentration curves of FIB and FDP in rabbits abdominal exudates during the 7 d postoperatively

The concentration curve of FIB in the rabbits' intra-abdominal exudates showed an increasing trend in the initial 5 d, and reached its peak on the 5th d. After that, it showed a decreasing trend, while on the 7th d still above the preoperative value (0.1±0.017) g/L. (Figure 1). At the same time, the concentration curve of FDP in the exudates showed increase in the first 4 d, arriving at its peak on the 3rd or the 4th d. After that, it showed decrease, while the value of the 7th d was also still above the preoperative value (0.3±0.012) µg/mL. (Figure 2). In comparison with the concentration curve of FIB and FDP in the exudates during the 7 d postoperatively, the DCT group was similar to the ACOL group while the normal group similar to the control group. (Figure 1, 2). In comparison with the average concentration

of FIB and FDP in intra-abdominal exudates during 7 d postoperatively, there was remarkable difference among the DCT group, normal group, and control group (*P*<0.05). The ACOL group showed a remarkable difference (*P*<0.05), compared with the other three groups. (Tables 1, 2).

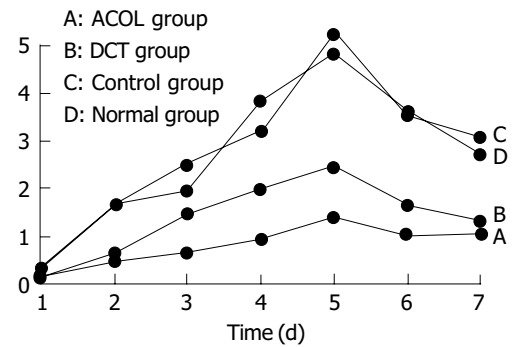


Figure 1 Concentration variety of FIB in healthy rabbits' abdominal cavity during 7 d after operation.

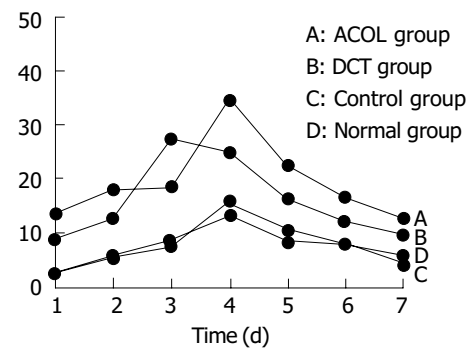


Figure 2 Concentration variety of FDP in healthy rabbits' abdominal cavity during 7 d after operation.

Analyses of the average concentration of FIB and FDP in rabbits abdominal exudates

Compared with the control group and the normal group, FIB and FDP in the DCT group showed a significant difference

Table 1 Concentration of FIB and FDP in healthy rabbits' abdominal cavity during 7 d after operation

Group	d 1	d 2	d 3	d 4	d 5	d 6	d 7
FIB (g/L)							
Normal group	0.236±0.052	1.621±0.083	1.927±0.121	3.813±0.154	4.823±0.183	3.612±0.076	2.721±0.055
Control group	0.27±0.071	1.587±0.012	2.471±0.134	3.224±0.126	5.256±0.113	3.533±0.054	3.081±0.046
DCT group	0.145±0.021 ^a	0.652±0.046 ^a	1.432±0.061 ^a	1.961±0.051 ^a	2.431±0.112 ^a	1.621±0.107 ^a	1.321±0.062 ^a
ACOL group	0.121±0.032 ^a	0.457±0.054 ^a	0.628±0.052 ^a	0.927±0.072 ^a	1.367±0.077 ^a	1.024±0.068 ^a	1.026±0.059
FDP (µg/mL)							
Normal group	2.328±0.072	5.821±0.176	8.368±0.372	13.472±0.961	8.462±0.371	7.721±0.262	5.642±0.078
Control group	2.452±0.077	5.262±0.132	7.526±0.327	15.641±0.625	10.431±0.362	7.651±0.241	4.326±0.062
DCT group	8.675±0.323 ^a	12.638±0.672 ^a	27.236±2.331 ^a	24.638±2.725 ^a	16.369±1.026 ^a	12.445±0.328 ^a	9.652±0.375 ^a
ACOL group	13.372±0.541 ^a	19.338±1.321 ^a	17.328±1.124 ^a	34.325±4.68 ^a	22.438±1.372 ^a	16.367±0.554 ^a	12.771±0.366

^a*P*<0.05 vs other groups.

Table 2 Average concentration of FIB and FDP in healthy rabbits' abdominal cavity during 7 d after operation

	Normal group	Control group	DCT group	ACOL group
Concentration of FIB (g/L)	2.679±0.096	2.760±0.079	1.36±0.066 ^a	0.793±0.059 ^a
Concentration of FDB (µg/mL)	7.442±0.268	7.613±0.261	15.947±0.121 ^a	19.424±1.417 ^a

^a*P*<0.05 vs the normal group and the control group.

($P < 0.05$); while in comparison with the other 3 groups, those of the ACOL group showed a significant difference ($P < 0.05$).

DISCUSSION

So far, there is no safe and effective prophylaxis available for intra-abdominal adhesions. Scientists try to find the answer from studying the exact mechanism of intra-abdominal adhesions, thus various experiments have been conducted to elaborate the exact mechanism of intra-abdominal adhesions and its prevention. The theory of traumatic inflammation is prevalent in elucidating the mechanism of intra-abdominal adhesions^[14]. Actually, multiple factors are involved in the development of postoperative intra-abdominal adhesions, such as operative injury, tissue ischemia and foreign materials left during operation^[14-15]. Any damage to the peritoneum and its base can lead to the release of inflammatory exudates, which contained FIB that causes fibrous adhesion and eventually results in the following two consequences: First, the fibrin is eliminated through the phagocytosis and endogenous fibrinolysis system, and the regeneration of mesothelial cell will cover the wound surface thus to get it repaired physiologically. Second, the wound is not covered by the regenerated mesothelial cells and no physiological repair occurs. Instead, fibrous adheres to other serosa in 12-24 h after operation, and then fibroblasts forms in place of the fibrous matrix, which causes the production of the fibrous collagen and eventually leads to fibrous adhesion. The adhesion can be absorbed completely if mesothelial cells are intact, but when the mesothelial cells are seriously destroyed, its plasminogen activator activity (PAA) is depressed, and with the depression value to that low as 60% or less, the fibrous adhesion will form as a consequence^[16-19].

In this experiment, the postoperative concentration levels of FIB and FDP in the rabbits' intra-abdominal exudates were constantly observed during the postoperative period of 7 d. The values of both FIB and FDP in intra-abdominal exudates increased considerably after 24 h postoperatively, arrived at its peak on the 4th or 5th d after operation, and then started to decrease till the 7th d, but still not being able to recover to the its normal preoperative level. The whole process is rather similar to the traumatic inflammation process. Giving the experimental animals some drugs which had been proved effective in promoting the ability of intestinal movement, the incidence of intestinal adhesion decreased remarkably, which indicates that the intestinal adhesion is related to traumatic inflammation, intestinal movement, and intra-abdominal physical conditions.

Under normal condition, there is a little serous fluid in the peritoneal cavity, which, on one hand, is necessary to keep the surface of the viscera moist and reduce the friction among the viscera, and on the other hand, functions to help recover the viscera and defend it against damage. Normally, the omentum, parietal and visceral peritoneum keeps a balance between releasing and absorbing serous fluid in the peritoneal cavity. Maintenance of this balance depends upon the normal sequential movement of intestines and the unobstructed movement of intestinal contents. After abdominal surgery, ileuses paralysis and the retention of the intestinal contents can effect the normal sequential movement of intestines and the smooth movement of intestinal contents. With intestines paralyzed postoperation, the contents are retained in the intestinal cavity. Endotoxin and bacteria in the stool are absorbed from intestines, which results in the abnormally high level endotoxin in the blood, which, in turn, stimulates intestines and worsens their paralysis, thus weakening the intestines' sequential movement and obstructing the smooth movement of their contents. Inflammatory reaction is indispensable to the healing of gastrointestinal and peritoneal damage in operation.

Tissue injury, local hemorrhage, cell inactivity and coagulation will call for the inflammation response, which originates from the following vascular reaction: the inflammatory mediums such as histamine, 5-HT, bradykinin, and prostaglandin. cause small blood vessels to first contract transiently, then dilate with congestion, and thus increase the permeability of blood vessels, which enables water, electrolyte, serum proteins, neutrophils and monocytes to enter tissue inter-space, so traumatic inflammatory reaction happens to help heal the damage. The FIB that has permeated into the wound gaps can turn into fibrin and fill the gaps to function as the network for cells to proliferate. However these inflammatory exudes can also enter peritoneal cavity from the wound, and the homeostasis of intra-abdominal serous postoperation is destroyed. During the damage, the serous secretion is far beyond the absorbing capability of peritoneal cavity. At the same time, high concentration of FIB in the wound exudes increases the concentration of FIB in peritoneal cavity. With the weakened movement of intestines in the early stage of postoperation and the temporarily destroyed normal physical condition, the exudes among viscera containing higher concentration of FIB easily constitute early fibrous adhesion, which is although still fragile at its early stage. Such traumatic inflammatory response arrives at the climax around 48 to 72 h postoperation, then disappears gradually. The early fragile adhesion can turn into tight one through endometrial stage and mould stage. We can see that the early recovery of the intestinal movement and abdominal physical condition postoperation is vital for prevention of the intestinal adhesion^[20-23].

The present study also indicates the traumatic inflammation caused by major abdominal surgery can cause the release of cytokines, the subsequent effects on endothelial cells, inflammatory cells and mesothelini cells, which produce and release plasminogen activator activity inhibitor I or II (PAI1, PAI2). Previous research showed TNF- α , IL-1, TGF β , alone or combined, can stimulate the cultured mesothelini cells to produce plasminogen activator activity inhibitor I or II (PAI1 and PAI2), which ultimately causes the disturbance of homeostasis between FIB and FDP intra-abdominal exudes. Consequently fibrin depositing on the surface of intra-abdominal viscera constitutes adhesion^[24-27].

In essence, intestinal adhesion is that the normal physical condition of peritoneum and the homeostasis between secreting and absorbing sera is destroyed, with higher FIB concentration in the peritoneal cavity, the weakened sequential movement of intestines and the dysfunctional movement of the intestinal contents, so that the wound healing appears among intestine, peritoneal and other viscera. The incidence of intestinal adhesion is related to the degree of the completeness of the peritoneal mesothelial cells in that when mesothelial cells are destroyed seriously, the fibrous adhesion forms. The damage of peritoneal mesothelium cannot be avoided in laparoscopy no matter how gentle the operation is. Since intestinal adhesions postoperation are almost inevitable to some extent^[28], recovery of the physical condition in abdominal cavity after operation as soon as possible can reduce the incidence and the adventure of intestinal adhesion^[29].

Now we can see, how to shorten the time of traumatic inflammation caused by major abdominal surgery, how to recover the normal physical condition of intra-peritoneum, and how to recover the homeostasis between FIB and FDP, is the vital to prevent the intra-abdominal adhesion postoperatively. The pharmaceuticals of laxative remedies represented by Rhubarb start with purgation of intestinal contents, improve the early recovery of intestinal movement as soon as possible. The pharmacologic research of Rhubarb develops quickly, clinic application is wider and wider. The main components of Rhubarb include: Anthraquinones (emodin, rhein, aloe-emodin),

Polysacchavide from *Rheum palmatum* (DHP₁, DHP₂) Tannins (hydrolysates type, condensed type), Modern pharmacology finds the effective component in *Rhubarb* of purgation is Anthraquinone, which effects on colon and increases the tension of the middle and far parts of colon to make them move faster, while no affection on the function of small bowels to absorb the nutritions. experiments reported: if vasectomy the part between colon and small bowels, then inject Anthraquinone into small bowels, but the medicine affects on the colon. Emodin combines with the muscle albumen of affected organ, then behavior cholinergic reaction, which can excite the M receptors of intestinal smooth muscle, increasing intestinal movement, inhibiting Na⁺ K⁺ ATP enzyme in intestinal cell membrane. It also can hinder the absorption and transportation of Na⁺, increase osmotic pressure of intra-intestines, keep lots of water, promote intestinal movement to defecate.^[30] On one hand through relieving the temporary enterogenic bacterial translocation caused by intestine paralyzed. *Rhubarb* prevent intestines from ischemia-reperfusion injury, protect gut barrier function, lower the level of endotoxin in blood to demodulate the release of cytokine and inflammatory mediums intra-peritoneum. on the other hand, it can lower the ability of endotoxin in blood which stimulates the target cells such as mesothelial cell, platelet *et al.*, Lower the sensitivity of these target cells to the stimulus of endotoxin in blood, make the injuries caused by cytokine, inflammatory mediums easy to be controled. It also can reduce the level of PGE and CAMP in cerebrolate. Lots of experiments prove: *Rhubarb* remarkably inhibits the functions of cytokine secreted by Macrophage cells which are stimulated by endotoxin. emodin strongly inhibits proliferations of T lymphocyte. Perhaps it is realized through reducing the expression of inflammatory mediums IL-2mRNA and concentration of Ca²⁺ in cell membrane^[31], emodin has excellent Antagonism to early inflammatory exudes, increasing penetration of microvascular, and leucocytes migration^[32]. In the condition of injures, such as tissue ischemia, endometrial injury, leucocytes Infiltration, and platelet aggregation, lots of free radicals are brought out, which cause pathologic lipidoxidation and induce production of cytotoxic lipid free radical and lipid peroxides malondiadehyde (MDA). *Rhubarb* can inhibit the production of MDA, relieve the injure of tissue and organ. *Rhubarb* is a kind of strongly free radical scavengers, and an inhibitor of lipidoxidation, it has function to remove most of free radicals^[33]. *Rhubarb* can remove O₂, H₂O₂ and other peroxides, inhibit lipid oxidation, *Rhubarb* themselves on pharmacology have the function of immune regulate two-wayly. emodin improve Indraft of Ca²⁺ outside of leucocytes, this function have some relations with improving immune of leucocytes; while Polysacchavide from *Rheum palmatum* inhibits Indraft of Ca²⁺ outside of leucocytes and release of Ca²⁺ inside of leucocytes, and the degree of inhibition have some relations with its dosage, so for leucocytes it has inhibit function^[34], *Rhubarb* can inhibits the production of red blood corpuscles antibody, and inhibit the function of T cell, improve phagocytosis of macrophage, it is benefit to regulate immunation. It also can inhibits synthetic of germ's protein and nucleic acid, ACOL adds some medicine such as Radix Astragali, Radix Salvia Miltiorrhiza, Rhizoman Zingiberis to DCT. Those functions lie in invigorating qi and strengthening asthenia, activating blood to resolve stagnation, and improving the whole condition of patients postoperatively. They also can enhance the resistance of human being, improve the microcirculation. It is benefits to the recovery of the normal physical condition of intra-peritoneum postoperatively. Altogether, ACOL can suppress bacterial and anti-inflammation, protect organs, improve microcirculation through exclude from accumulating. It relieves the accumulation of excrement and bacterial through improving intestinal movement, so it can lower temporary high level toxin in blood, reduce the release and

production of histamine, bradykinin, 5-HT, prostaglandin, *et al.*, improve the perfusion of blood, relieve the traumatic inflammation intra-peritoneum postoperatively, recover the homeostasis between FIB and FDP as soon as possible, reduce the incidence of adhesion intra-peritoneum.

REFERENCES

- 1 **Scott-Coombes DM**, Whawell SA, Thompson JN. The operative peritoneal fibrinolytic response to abdominal operation. *Eur J Surg* 1995; **161**: 395-399
- 2 **Liakakos T**, Thomakos N, Fine PM, Dervenis C, Young RL. Peritoneal adhesions: etiology, pathophysiology, and clinical significance. Recent advances in prevention and management. *Dig Surg* 2001; **18**: 260-273
- 3 **Parker MC**, Ellis H, Moran BJ, Thompson JN, Wilson MS, Menzies D, McGuire A, Lower AM, Hawthorn RJ, O'Brien F, Buchan S, Crowe AM. Postoperative adhesions: ten-year follow-up of 12,584 patients undergoing lower abdominal surgery. *Dis Colon Rectum* 2001; **44**: 822-829
- 4 **Edelstam G**, Lecander I, Larsson b, Astedt B. Fibrinolysis in the peritoneal healing and adhesion, endometriosis and ongoing pelvic inflammatory disease. *Inflammation* 1998; **22**: 341-351
- 5 **Saed GM**, Diamond MP. Modulation of the expression of tissue plasminogen activator and its inhibitor by hypoxia in human peritoneal and adhesion fibroblasts. *Fertil Steril* 2003; **79**: 164-168
- 6 **Hellebrekers BW**, Trimbo-Kemper GC, Bakkum EA, Trimbo JB, Declerck PJ, Kooistra T, Emeis JJ. Short-term effect of surgical trauma on rat peritoneal fibrinolytic activity and its role in adhesion formation. *Thromb Haemost* 2000; **84**: 876-881
- 7 **Saed GM**, Zhang W, Diamond MP. Molecular characterization of fibroblasts isolated from human peritoneum and adhesions. *Fertil Steril* 2001; **75**: 763-768
- 8 **Chegini N**, Zhao Y, Kotseos K, Ma C, Bennett B, Diamond MP, Holmdahl L, Skinner K. Differential expression of matrix metalloproteinase and tissue inhibitor of MMP in serosal tissue of intraperitoneal organs and adhesions. *BJOG* 2002; **109**: 1041-1049
- 9 **Chegini N**, Kotseos K, Zhao Y, Bennett B, McLean FW, Diamond MP, Holmdahl L, Burns J. Differential expression of TGF-beta1 and TGF-beta3 in serosal tissues of human intraperitoneal organs and peritoneal adhesions. *Hum Reprod* 2001; **16**: 1291-1300
- 10 **Zeng J**, Li XF. Molecular mechanism and medicinal prevention and treatment of peritoneal adhesions. *World J Digestol* 2003; **11**: 1429-1432
- 11 **Diamond MP**, El-Hammady E, Wang R, Saed G. Transforming growth factor-beta, type III Regulation of transforming growth factor-beta, type III collagen, and fibronectin by dichloroacetic acid in human fibroblasts from normal peritoneum and adhesions. *Fertil Steril* 2003; **79**: 1168-1175
- 12 **Liu JY**, Zeng GX, Zheng YB. Observe the peritoneal constitution morphology during the development of wounded intestine adhesion. *Chine J Sterol Image Anal* 2003; **8**: 97-101
- 13 **Treutner KH**, Schumpelick V. Prevention of adhesions. Wish and reality. *Chirurg* 2000; **71**: 510-517
- 14 **Chegini N**. Peritoneal molecular environment, adhesion formation and clinical implication. *Front Biosci* 2002; **7**: e91-115
- 15 **Duron JJ**, Olivier L, Khosrovani C, Gineste D, Jost JL, Keilani K. Natural history of postoperative intraperitoneal adhesions. Surely, a question of the day. *J Chir* 1993; **130**: 385-390
- 16 **Molinas CR**, Mynbaer O, Pauwels A, Novak P, Koninckx PR. Peritoneal mesothelial hypoxia during pneumoperitoneum is a cofactor in adhesion formation in laparoscopic mouse model. *Fertil Steril* 2001; **76**: 560-567
- 17 **Lai HS**, Chen Y, Chang KJ, Chen WJ. Effects of octreotide on epidermal growth factor receptor, tissue plasminogen activator, and plasminogen activator inhibitor during intraperitoneal adhesion formation. *J Gastroenterol* 2003; **38**: 555-560
- 18 **Molinas CR**, Elkemani O, Campo R, Luttun A, Carmeliet P, Koninckx PR. Role of the plasminogen system in basal adhesion formation and carbon dioxide pneumoperitoneum-enhanced adhesion formation after laparoscopic surgery in

- transgenic mice. *Fertil Steril* 2003; **80**: 184-192
- 19 **Witz CA**, Thomas MR, Montoya-Rodriguez IA, Nair AS, Centonze VE, Schenken RS. Short-term culture of peritoneum explants confirms attachment of endometrium to intact peritoneal mesothelium. *Fertil Steril* 2001; **75**: 385-390
- 20 **Alatas E**, Gunal O, Alatas O, Colak O. Octreotide prevents postoperative adhesion formation by suppressing peritoneal myeloperoxidase activity. *Hepatogastroenterology* 2000; **47**: 1034-1036
- 21 **Haney AF**. Identification of macrophages at the site of peritoneal injury: evidence supporting a direct role for peritoneal macrophages in healing injured peritoneum. *Fertil Steril* 2000; **73**: 988-995
- 22 **Toh H**, Torisu M, Shimura H, Kitsuki H, Uchiyama A, Itoh H, Ohsato K. *In vitro* analysis of peritoneal adhesions in peritonitis. *J Surg Res* 1996; **61**: 250-255
- 23 **Vural B**, Canturk NZ, Esen N, Solakoglu S, Canturk Z, Kirkali G, Sokmensuer C. The role of neutrophils in the formation of peritoneal adhesions. *Hum Reprod* 1999; **14**: 49-54
- 24 **Cheong YC**, Shelton JB, Laird SM, Richmond M, Kudesia G, Li TC, Ledger WL. IL-1, IL-6 and TNF-alpha concentrations in the peritoneal fluid of women with pelvic adhesions. *Hum Reprod* 2002; **17**: 69-75
- 25 **Lindholt JS**, Jorgensen B, Shi GP, Henneberg EW. Relationships between activators and inhibitors of plasminogen, and the progression of small abdominal aortic aneurysms. *Eur J Vasc Endovasc Surg* 2003; **25**: 546-551
- 26 **Falk K**, Bjorquist P, Stromqvist M, Holmdahl L. Reduction of experimental adhesion formation by inhibition of plasminogen activator inhibitor type 1. *Br J Surg* 2001; **88**: 286-289
- 27 **Xiao Y**, Li H, Bunn C, Bartold PM. The expression of plasminogen activator system in a rat model of periodontal wound healing. *J Periodontol* 2001; **72**: 849-857
- 28 **Wang XC**, Gui CQ, Zheng QS. Combined therapy of allantoin, metronidazole, dexamethasone on the prevention of intra-abdominal adhesion in dogs and its quantitative analysis. *World J Gastroenterol* 2003; **9**: 568-571
- 29 **Ricketts SA**, Sibbons PD, Green CJ. Quantitative analysis of the development of experimentally induced post surgical adhesions: a microstereological study. *Int J Exp Pathol* 1999; **80**: 325-334
- 30 **Guo WX**. The pharmacologic research of Rhubarb. *J Jiangnan University* 2002; **30**: 60-61
- 31 **Kuo YC**, Meng HC, Tsai WJ. Regulation of cell proliferation, inflammatory cytokine production and calcium mobilization in primary human T lymphocytes by emodin from *Polygonum hypoleucum* Ohwi. *Inflamm Res* 2001; **50**: 73-82
- 32 **Qi H**. Anti-inflammation of emodine. *Zhongcaoyao* 1999; **30**: 550-552
- 33 **Matsuda H**, Morikawa T, Toguchida I, Park JY, Harima S, Yoshikawa M. Antioxidant constituents from rhubarb: structural requirements of stilbenes for the activity and structures of two new anthraquinone glucosides. *Bioorg Med Chem* 2001; **9**: 41-50
- 34 **Chen D**, Qiao L, Jing B. Effect of rhubarb on oxygen radicals leakage from mitochondria of intestinal mucosa in burned rats. *Zhongxiyi Jiehe Zazhi* 2000; **20**: 849-852

Edited by Zhang JZ and Xu FM

Endoscopic identification of Peyer's patches of the terminal ileum in a patient with Crohn's disease

Hiroshi Ishimoto, Hajime Isomoto, Saburo Shikuwa, Chun Yang Wen, Takashi Suematu, Masahiro Ito, Ikuo Murata, Hiromi Ishibashi, Shigeru Kohno

Hiroshi Ishimoto, Saburo Shikuwa, Hiromi Ishibashi, Department of Internal Medicine, National Nagasaki Medical Center, 2-1001 Kubara, Omura, Nagasaki 856-8562, Japan

Hiroshi Ishimoto, Gastrointestinal Unit, Massachusetts General Hospital, Department of Medicine, Harvard Medical School, Jackson 706, 55 Fruit Street, Boston, MA 02114, USA

Hajime Isomoto, Ikuo Murata, Shigeru Kohno, Second Department of Internal Medicine, Nagasaki University School of Medicine, Nagasaki, 852-8501, Japan

Chun Yang Wen, Department of Molecular Pathology, Atomic Bomb Disease Institute, Nagasaki University School of Medicine, 1-7-1 Sakamoto, Nagasaki, 852-8501, Japan

Takashi Suematu, Central Electroscopy Laboratory, Nagasaki University School of Medicine, Nagasaki, 852-8501, Japan

Masahiro Ito, Department of Pathology, National Nagasaki Medical Center, j2-1001 Kubara, Omura, Nagasaki 856-8562, Japan

Correspondence to: Hajime Isomoto, MD, Gastrointestinal Unit, Massachusetts General Hospital, Jackson 706, 55 Fruit Street, Boston, MA 02114, USA. hajime2002@yahoo.co.jp

Telephone: +1-617-724-8977 **Fax:** +1-617-726-3673

Received: 2004-01-16 **Accepted:** 2004-03-18

Abstract

We presented a 20-year-old patient with Crohn's disease (CD). Colonoscopy revealed longitudinal ulceration in the terminal ileum and rectal aphthoid ulcers. After treatment with mesalamine and total parenteral nutrition, repeat colonoscopy revealed a granular elevated area in the terminal ileum, which appeared as an irregular dome-like elevation with irregularly arranged villi on magnifying endoscopy. Biopsy specimens taken from the region showed microgranulomas and lymphoid hyperplasia. Scanning electron microscopy revealed the presence of M cells, confirming that the area corresponded to Peyer's patches. Peyer's patches by magnifying endoscopy and electron microscopy may provide insights into the pathogenesis of CD.

Ishimoto H, Isomoto H, Shikuwa S, Wen CY, Suematu T, Ito M, Murata I, Ishibashi H, Kohno S. Endoscopic identification of Peyer's patches of the terminal ileum in a patient with Crohn's disease. *World J Gastroenterol* 2004; 10(18): 2767-2768
<http://www.wjgnet.com/1007-9327/10/2767.asp>

INTRODUCTION

The gut-associated lymphoid tissue (GALT) is composed of Peyer's patches, peripheral lymphoid tissues and appendix and plays an important role in the immune system of the gastrointestinal tract^[1]. The importance of Peyer's patches in the development of Crohn's disease (CD) is generally accepted^[1-8], but there have been only a few reports focusing on the endoscopic appearance of Peyer's patches of the terminal ileum in CD^[3-5].

We presented a patient with CD in whom specific CD lesions were found in the Peyer's patches of the terminal ileum by magnifying endoscopy, histopathology and scanning electron microscopy. We also discussed the importance of endoscopic observation of the Peyer's patches of the terminal ileum in the diagnosis and assessment of the pathogenesis of CD.

CASE REPORT

A 20-year-old man was admitted to our hospital with right lower abdominal pain, diarrhea and anal fistula for 4 wk. Physical examination revealed localized guarding with tenderness in the right lower quadrant of the abdomen as well as anal discharge. Laboratory analysis showed leukocytosis (10 700/ μ L), elevated C-reactive protein (27 mg/L) and slight hypoproteinemia, while other biochemical and serological data were within normal limits. Repeated stool cultures yielded no enteric pathogens including *Yersinia* and *tubercle* bacilli. Colonoscopy showed longitudinal ulcers in the terminal ileum (Figure 1A), ileocecal valve, hepatic flexure, and anal canal. A subsequent radiological examination of the small bowel disclosed three discrete longitudinal ulcers with cobblestone appearance in the ileum. After treatment with a total of 2 250 mg of mesalamine for 2 wk under total parenteral nutrition, repeat colonoscopy revealed improvement of the above lesions, leaving deformity of the ileocecal valve and anal stenosis. In addition to multiple aphthoid ulcers in the rectum, a granular elevated area was noted in the terminal ileum, which corresponded to the lymph follicle type of the Peyer's patches according to a classification proposed by Fujikura (Figure 1B)^[9]. On magnifying endoscopy, the surface of the Peyer's patches appeared as an irregular dome-like elevation with irregularly arranged villi (Figure 1C). Histopathological examination of the biopsy specimens taken from the region and rectal aphthoid ulcers disclosed the presence



Figure 1 Endoscopic findings. A: Endoscopic view showing an ulceration of the terminal ileum. B: Endoscopic view showing granularly elevated mucosa consistent with the lymphoid follicle type of the Peyer's patches. C: Magnifying endoscopy showing the irregular villi and the dome.

of microgranulomas and lymphoid hyperplasia (Figure 2). Scanning electron microscopy of the specimen taken from the Peyer's patch revealed the presence of M cells (Figure 3).

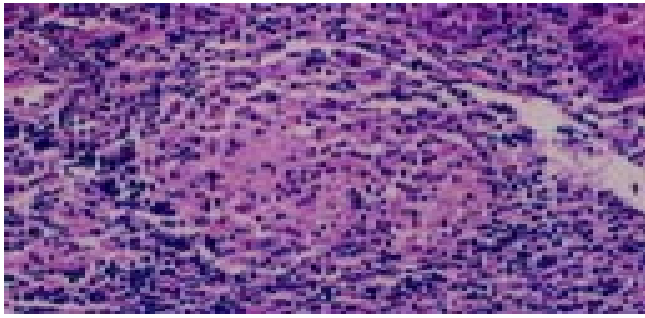


Figure 2 Histological finding of a biopsy specimen obtained from the Peyer's patches in the terminal ileum disclosing the presence of a microgranuloma and lymphoid hyperplasia.

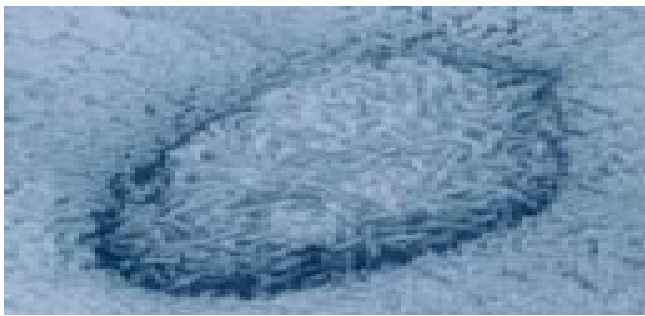


Figure 3 Scanning electron microscopy of the Peyer's patches demonstrating M cells with microfolds.

DISCUSSION

Major advances have been made in every aspect of CD and ulcerative colitis (UC), but several problems in the etiology and pathogenesis of inflammatory bowel diseases (IBD) remain unresolved^[1-8]. It has been recognized that the disorder of GALT plays a crucial role in the development of IBD^[1-8]. Peyer's patches and related lymphoid follicles have specialized follicle-associated epithelia (FAE) which serve as sites for the induction of mucosal immune responses^[4,5]. In particular, it has been found that M cells serve as an important first step in this process^[1,4,5], and Peyer's patches are abundantly distributed in the terminal ileum^[7,9], an area predisposed to CD. However, little attention has been paid to endoscopic observation of Peyer's patches, and therefore, only a few studies^[3-5] have described endoscopic appearance of Peyer's patches in the terminal ileum. In this regard, Fujikura^[9] examined the terminal ileum by colonoscopy in 110 normal cases and grossly in 48 autopsy cases, and classified Peyer's patches into three categories as follows; lymph follicle, lymph border and lymphocyte aggregation types^[9]. Macroscopically, the lymph follicle type appeared as granular or convolute elevation and was associated with lymphoid hyperplasia. The lymphocyte aggregation type appeared as a flat area associated with mild lymphocytic infiltration and few lymphoid follicles^[9]. Recently, Van Kruiningen *et al.*^[7] examined 55 adults without intestinal disease and reported that Peyer's patches were concentrated in the distal 25 cm of ileum but extended proximally to 200 cm from the ileac end.

In the present case, magnifying endoscopy identified the irregular surface of Peyer's patches, which harbored microgranulomas and lymphoid hyperplasia when examined histopathologically. Scanning electron microscopy identified the presence of M cells, confirming that the specimens were taken from the Peyer's patches.

Our findings pose an important question: does the CD lesion

selectively originate from the Peyer's patch? In this regard, Lockhart-Mummery and Morson^[2] reported in 1960 that the earliest microscopic change in CD was ulceration of the lymphoid follicles and Peyer's patches in the terminal ileum. Since then, several investigators have reported that CD initially occurs as tiny aphthoid lesions at the sites of mucosal lymphoid follicles in the gastrointestinal tract^[3-5]. Recently, Fujishima *et al.*^[3-5] investigated ultrastructurally the epithelium covering solitary lymphoid nodules using biopsy samples obtained from the colonoscopy during colonoscopy, and indicated that the red halo appearance of such epithelia seemed to precede visible aphthoid ulcers. They suggested that ulcerations in CD might originate from the follicle-associated epithelium (FAE), possibly related to its role as a portal entry for potentially pathogenic agents. These studies have led to the concept that CD could originate from GALT including Peyer's patches and lymphoid follicles in the terminal ileum^[3-8]. With this concept^[3-7], one can explain the reason for the occurrence of the skip lesions and the frequent involvement of the terminal ileum in CD.

Fujikura^[9] showed that M cells of the Peyer's patches were more frequently seen in the dome area of the lymph follicle and lymph border types than in that of the lymphocyte aggregation type, emphasizing its pathogenetic functions. Further studies of the ultrastructure of M cells should enhance our understanding of their role in the development of IBD. However, it is difficult to obtain M cells by conventional endoscopic biopsy because they are located in the dome area (FAE), but not in the villi of Peyer's patches^[9]. Our experience indicates that biopsy using magnifying endoscopy is beneficial for accurate biopsy sampling to obtain tissue segments containing M cells, because this tool allows us to clearly recognize the dome area.

In conclusion, we identified CD-specific lesions in the Peyer's patch of the terminal ileum by endoscopy and histopathological examination. Although the pathogenic role of M cells in the development of IBD is still unknown, examination of the Peyer's patches by magnifying endoscopy and electron microscopy may provide insights into the pathogenesis of CD.

REFERENCES

- 1 **Elson CO**. The Immunology of inflammatory bowel disease. In: Kirsner JB, ed. *Inflammatory bowel disease*. Philadelphia: Saunders 2000: 208-239
- 2 **Lockhart-mummery HE**, Morson BC. Crohn's disease (regional enteritis) of the large intestine and its distinction from ulcerative colitis. *Gut* 1960; **1**: 87-105
- 3 **Hizawa K**, Iida M, Aoyagi K, Fujishima M. The significance of colonic mucosal lymphoid hyperplasia and aphthoid ulcers in Crohn's disease. *Clin Radiol* 1996; **51**: 706-708
- 4 **Fujimura Y**, Kamoi K, Iida M. Pathogenesis of aphthoid ulcers in Crohn's disease: correlative findings by magnifying colonoscopy, electron microscopy, and immunohistochemistry. *Gut* 1996; **38**: 724-732
- 5 **Fujimura Y**, Owen R. The intestinal Epithelial M cell: Properties and function. In: Kirsner JB, ed. *Inflammatory bowel disease*. 5th ed. Philadelphia: Saunders 2000: 33-44
- 6 **Van Kruiningen HJ**, Ganley LM, Freda BJ. The role of Peyer's patches in the age-related incidence of Crohn's disease. *J Clin Gastroenterol* 1997; **25**: 470-475
- 7 **Van Kruiningen HJ**, West AB, Freda BJ, Holmes KA. Distribution of Peyer's patches in the distal ileum. *Inflamm Bowel Dis* 2002; **8**: 180-185
- 8 **Chiba M**, Komatsu M, Iizuka M, Masamune O, Hoshina S, Kono M. Microbiology of the intestinal lymph follicle: a clue to elucidate causative microbial agent(s) in Crohn's disease. *Med Hypotheses* 1998; **51**: 421-427
- 9 **Fujikura S**. A study of Peyer's patch of the terminal ileum (part 1): A study of the mucosal surface appearance and histological finding in endoscopic cases and autopsy cases (in Japanese). *Gastroenterol Endosc* 1984; **26**: 1246-1261

• CASE REPORT •

Intestinal perforation after combined liver-kidney transplantation for a case of congenital polycystic disease

Tao Peng, Min-Hao Peng, Le-Qun Li, Yao-Liang Deng, Ding-Hua Yang, Bang-Yu Lu, Xi-Gang Chen, Ya Guo, Kai-Yin Xiao, Bin Chen, Qin Zhong, Min-Yi Wei

Tao Peng, Min-Hao Peng, Le-Qun Li, Ding-Hua Yang, Bang-Yu Lu, Xi-Gang Chen, Ya Guo, Kai-Yin Xiao, Bin Chen, Qin Zhong, Department of Hepatobiliary Surgery, First Affiliated Hospital, Guangxi Medical University, Nanning 530021, Guangxi Zhuang Autonomous Region, China

Yao-Liang Deng, Department of Urology Surgery, First Affiliated Hospital, Guangxi Medical University, Nanning 530021, Guangxi Zhuang Autonomous Region, China

Min-Yi Wei, Department of Pathology, First Affiliated Hospital, Guangxi Medical University, Nanning 530021, Guangxi Zhuang Autonomous Region, China

Correspondence to: Dr. Peng Tao, Department of Hepatobiliary Surgery, First Affiliated Hospital, Guangxi Medical University, Nanning 530021, Guangxi Zhuang Autonomous Region, China. pengpang@hotmail.com

Telephone: +86-771-5352400

Received: 2004-01-10 **Accepted:** 2004-02-21

Abstract

AIM: To highlight the intestinal perforation (IP), an uncommon and catastrophic complication after combined liver-kidney transplantation.

METHODS: Combined liver-kidney transplantation (LKTx) with left kidney excision and a cyst fenestration procedure on the right kidney were performed on a case of 46-year-old female with congenital polycystic disease (CPCD).

RESULTS: Two sites of IP were noted 40-50 cm proximal to ileocecal area during emergent laparotomy 10 d postoperatively. Despite aggressive surgical and medical management, disease progressed toward a fatal outcome due to sepsis and multiple organ failure 11 d later.

CONCLUSION: Long duration of operation without venovenous bypass, overdose of steroid together with postoperative volume excess may all contribute to the risk of idiopathic multiple IPs. Microbiology and pathology inspections suggested that the infected cyst of the fenestrated kidney might be one reason for the fatal intra-peritoneal infection. Thus for the CPCD patients who seem to be very susceptible to infectious complications, any sign of suspected renal-infection found before or during LKTx is indication for the excision of original kidney. And the intensity of immunosuppression therapy should be controlled cautiously.

Peng T, Peng MH, Li LQ, Deng YL, Yang DH, Lu BY, Chen XG, Guo Y, Xiao KY, Chen B, Zhong Q, Wei MY. Intestinal perforation after combined liver-kidney transplantation for a case of congenital polycystic disease. *World J Gastroenterol* 2004; 10(18): 2769-2771

<http://www.wjgnet.com/1007-9327/10/2769.asp>

INTRODUCTION

Intestinal perforation (IP) is a catastrophic complication after

liver or kidney transplantation and well documented in literatures separately^[1,2]. Herein we report a case of IP after combined liver-kidney transplantation (LKTx).

CASE REPORT

The recipient was a 46-year-old female who had a history of 6-year aggravating abdominal girth and pain, with symptoms of gross hematuria, intermittent fever and anorexia in the recent one and a half year. The above symptoms severely affected her daily life as well as her profession. She had obvious abdominal protuberance with a liver palpable 5 cm below the right costal margin, the lower edge of left kidney aligned with the navel level and the right kidney 3 cm lower. Percussion tenderness was found in bilateral areas of kidney. Her liver function was Child B. Her serum creatinine was 132 $\mu\text{mol/L}$ and the glomerular filtration rate was 19.3 mL/min. In urine sediment Gram-negative bacillus was found (1/hpf). ABO typing was "O". HLA typing results were: A3, 26 (10); B39 (16), 54 (22); Bw6; DR4, 8; DRw53; DQw7 (3), 8 (3). Preoperative diagnosis was congenital polycystic disease (CPCD) with chronic renal failure and urinary tract infection.

Allografts came from an "O" type, 23-year-old male cadaver. HLA typing results were: A203 (2), 1102 (11); B27, 38 (16); Bw4; DR15 (2), 16 (2); DRw51; DQw5 (1), 6 (1); DTT-PRA negative; lymphocytotoxic crossmatch negative. Liver and kidney were harvested and preserved routinely.

Bacillus in urine sediment and culture turned negative after therapy whereas WBC counting was $4.1 \times 10^9/\text{L}$ (neutrophils 80.5%) before operation. Left kidney excision + right kidney fenestration + combined liver-kidney transplantation were performed on June 23, 2000. About 1 000 mL ascites was found in laparotomy. The fluid in the cysts of right kidney and liver was clear, in contrast to those muddy yellow-white liquids in the cysts of left kidney. Culture of the fluid from left cysts showed Gram-negative bacilli. The recipient hepatectomy and graft liver implant (Piggyback) were done routinely with modification (the hepatic artery and portal vein anastomosis was performed subsequently and revascularized simultaneously). No venovenous bypass was done. The left kidney resection, right kidney depression and graft kidney implantation (in right iliac fossa) were performed in the usual manner. Totally 650 mL urine was collected from recipient's kidneys but no urine drainage was found from the implanted kidney. The whole operation lasted 18 h and 47 min (anhepatic period 2 h 7 min; warm ischemic 0 min, cold ischemic 794 min for liver and 1 143 min for kidney). Bleeding during operation (about 7 000 mL) mainly came from the right kidney. The haemodynamic was stable.

Immunosuppression regimen was initially based on cyclosporine. Oral cyclosporine 500 mg was given the night before operation and 1 000 mg methylprednisolone was given intravenously before revascularization. However, due to the delayed recovery of function of the implanted kidney, postoperative immunosuppression protocol shifted to methylprednisolone + mycophenolate mofetil (MMF, Roche Corp.). The dosage of methylprednisolone during the 8-d post transplantation were 200, 160, 260, 220, 160, 100, 40, 20 mg separately and, maintained

at a dosage of prednisolone 20 mg/d. MMF 2 g/d was given orally until the 16th d, when bone marrow suppression was manifested. Sandostatin (somatostatin, Sandoz Corp.) and Losec (Astra) were given daily after operation. Beta-lactam antibiotics, ganciclovir (Cymevene, Roche Corp.) and injection fluconazole (Diflucan, Pfizer Corp.) were used for prophylaxis of bacterial, cytomegalovirus (CMV) and fungus infections separately.

The patient woke up 2 h after returning to ICU. Due to transfusion overload (6 000 mL positive balance in the first 24 h) and retention of sodium and water, acute left heart failure, pulmonary edema and ARDS presented in turn. All were reversed 6 d later. The liver function recovered well. Drainage from left side subdiaphragmatic location increased continuously. Its creatinine concentration was 2-fold higher than that of blood (1 114 $\mu\text{mol/L}$ vs 586 $\mu\text{mol/L}$), which indicated urine leakage from the right kidney. Since d 5 postoperatively (POD), daily urine decreased from 900 mL to 40 mL, and serum creatinine peaked to 626 mmol/L (glomerular rate 22.6 mL/min). Haemodialysis was performed daily since d 8 postoperatively. Passage of flatus and green stools began from d 6 postoperatively, and changed to water like, with frequent discharge and urgency to defecate. Temperature mounted since d 7 postoperatively. Obvious abdominal pain and distention with lower abdominal tenderness presented on d 10 postoperatively. White blood cell count rose to $17.35 \times 10^9/\text{L}$. No vascular problem of implanted liver and kidney was found in real-time ultrasound examination. In emergent exploration on d 10, two sites of bowel perforation at a diameter of 1.2 cm and 0.6 cm were noted 40-50 cm proximal to ileocecal area; and multiple ulcerative lesions with purulence were scattered on the serosa of terminal ileum. Postoperative pathology found no sign of rejection in the implanted liver and kidney except that, acute tubular necrosis in the graft kidney; acute purulence with multiple acute perforations on the ileum wall; and especially, the inflammation on the serosa side was more severe than that of the mucosa side (Figure 1). Ileum of 60 cm (30 cm proximal to the ileocecal) long was resected and an end-to-end anastomosis was done. Distention and abdominal pain were not relieved after laparotomy. And multiple ulcers appeared on the buccal mucosa, with skin rash on the forehead and chest. The temperature rose to 39.5 °C on d 15 postoperatively, accompanied with decreased counting of WBC and PLT ($1.3 \times 10^9/\text{L}$, $1.8 \times 10^9/\text{L}$ separately). A bone marrow aspiration showed severe marrow suppression that was not ultimately reversed by granulocyte macrophage colony stimulating factors. Culture findings included: *Pseudomonas cepacia* (blood, urine, secretion from trachea, and abdominal drainage), *Staphylococcus haemolyticus* (abdominal drainage and wound secretion), *Klebsiella pneumoniae*, *Acinetobacter junii* (secretion from trachea), *Candida parapsilosis*, *Candida sake* (urine). Serology supervision of CMV, herpes simplex virus and EB virus were always negative. No reperforation was found except multiple superficial ulcers scattered on the

whole bowel wall and mesentery in reexploration on d 20 postoperatively. Biopsy of graft liver/kidney and chest rash indicated no evidence of rejection and GVHD. The case progressed to death on d 21 for multiple organ failure (Data shown in Figure 2).

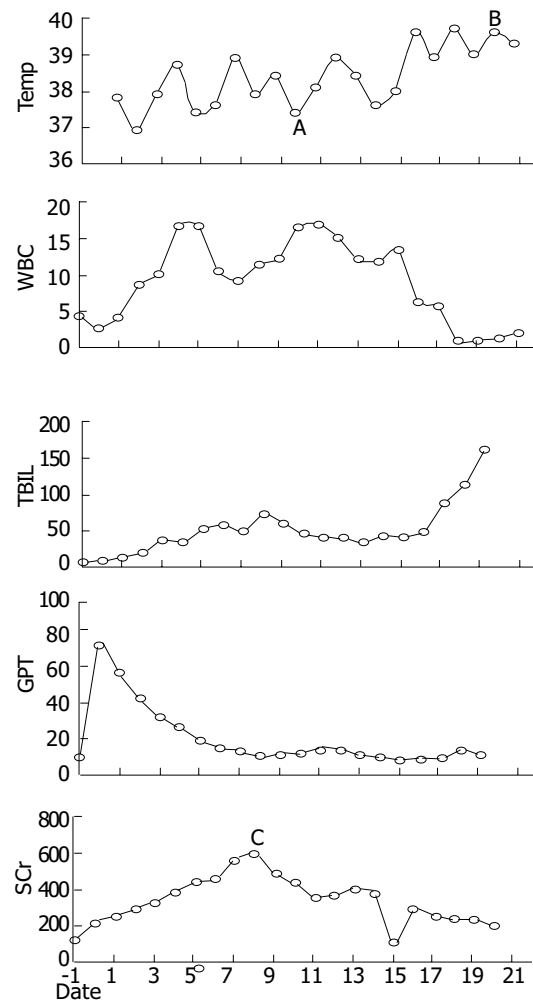


Figure 2 Alterations of body temperature, white blood cell count, liver and renal function after combined liver-kidney transplantation. Temperature (°C) = daily maximum of body temperature; WBC = white blood cell count ($\times 10^9/\text{L}$); TBIL = total bilirubin ($\mu\text{mol/L}$); GPT = glutamic pyruvic transaminase (IU/L); SCr = serum creatinine ($\mu\text{mol/L}$); DATE = date posttransplant; Point A: the first emergent laparotomy on the 10th d posttransplantation; Point B: the second laparotomy on the 20th d; Point C: inception of haemodialysis on the 8th d.

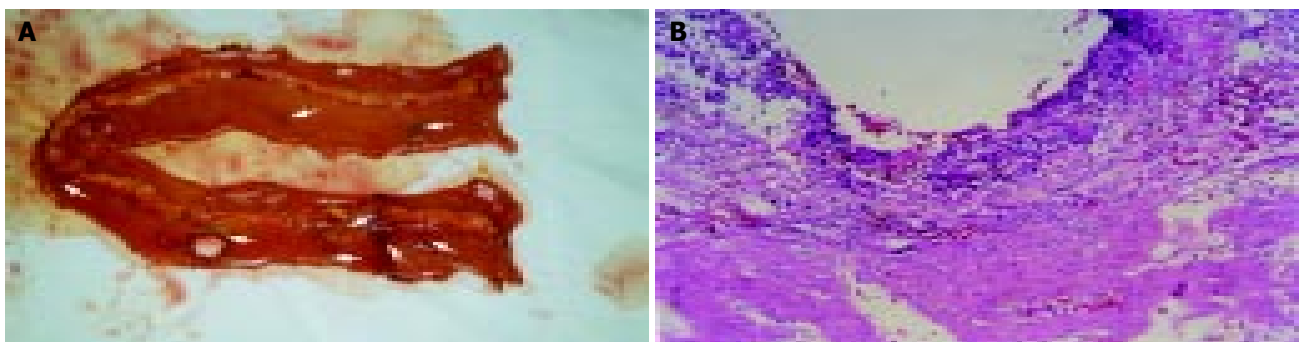


Figure 1 A: Lesions of bowel perforation and multiple ulcerative lesions 40-50 cm proximal to ileocecal area; attached with purulent secretion scattered on the serosa of terminal ileum. B: Photomicrograph of mucosal ulceration in ileum wall (HE staining, original magnification: $\times 100$).

DISCUSSION

For liver transplantation, postoperative IP mostly happens among pediatric recipients (6.4-20%)^[1,3], especially in those who have had previous abdominal surgery but rarely seen in adults. The median delay between transplantation and perforation was 13 d, according to Soubrane O.^[3] The sites tended to locate in small intestine^[4,5] and, according to Marujo, the typical intraoperative findings in whom developed the syndrome of multiple bowel perforations were pinpoint perforations in areas of normal bowel^[6]. The cause remains obscure and is probably of multifactorial origin. Risk factors have been implicated as following: a previous history of abdominal operation (especially those who received Kasai operation for congenital biliary atresia), steroid therapy, CMV infection, long time duration of operation, relaparotomy for postoperative bleeding, early portal vein embolism and venovenous bypass^[3,6,7]. Incidence of reperforation was as high as 31-53%^[7,8]. Even though there was report of 100% success rescue^[6] and 70% 3-year survival^[3], we noticed Shaked's report of 50% (12/24) mortality in primary perforation and 78% (7/9) in reperforation group^[4].

The incidence of IP in renal transplant recipients ranged from 0.62% to 3.4%^[9,10] or, in reports of larger sample, differed from 1.1% to 2.1%^[11,12]. Most perforations occurred within a few weeks or months after engraftment, the period of most intense immunosuppression^[9,12]. The pathogenesis was related to a high incidence of diverticular disease in patients with polycystic kidneys and/or chronic renal failure^[11]. Other risk factors included overimmunosuppression^[9,12], CMV infection^[13], and the transplant procedure^[11]. The average mortality rate was 56.5%^[14]. This high mortality appeared to be related to the effects of immunosuppression and associated response to sepsis^[9]. Clinical findings in these patients, such as fever or leucocytosis, might be masked by the immunosuppressive agents^[12]. And pneumoperitoneum on abdominal roentgenograms was not necessarily positive^[1,4]. Therefore, prompt diagnosis, aggressive surgical care consisting of resectional therapy, broad-spectrum antibiotics, and a reduced immunosuppressive protocol are crucial to outcome^[2].

In our case, without a previous history of abdominal surgery and consequent adhesion, resections of the original liver and left kidney as well as implantation of graft liver and kidney were smooth, although the whole duration of operation lasted 18 h due to the limitation of personnel in the renal transplantation group. Diverticulosis and CMV infection were also cautiously excluded by inspection during operation and postoperative supervision separately. Furthermore, no pathologic evidence of GVHD was found in the examinations of either the perforated ileum or biopsy skin rash in this case. In our case, it is hard to blame just the absence of venovenous bypass during the anhepatic phase as the only risk factor in inducing gastrointestinal congestion thus responsible for the perforation^[6]. But the postoperative sodium and water retention aggravated the bowel edema and stasis authentically. In addition, an obvious risk factor herein, is the relatively high dose of steroid that has not tapered down routinely because of the withdrawal of cyclosporine. Overimmunosuppression may increase risk of IP through inducing damage to the barrier of intestinal mucosa^[9,12]. Thus we propose that, the long duration of operation without venovenous bypass, overdose of steroid together with postoperative volume excess may all contribute to the risk of idiopathic multiple IPs in the present case.

Also, we suggest that intraperitoneal infection in this case might originate first from the infected cyst of the fenestrated kidney and might be prior to the occurrence of IP, based on the following evidences: (1) Neutrophils counting was above normal before operation. (2) *G. bacillus* was found in the fluid

from left cysts during operation. (3) Evidence of urine leakage from the right kidney was present. (4) The inflammation on the serosa side was more severe than that of the mucosa side under pathologic inspection. This supports Jeyarajah's observation in 6 cases of CPCD who received liver and kidney transplantation and that, possibly due to overimmunosuppression or the presence of infectious foci in residual cysts, these patients seemed to be very susceptible to infectious complications after transplantation^[15]. Unfortunately, the intraperitoneal infection of this case was masked and deteriorated by the post-transplant leukopenia. The cause of marrow suppression in this case might be multifactorial but most likely to be drug-induced. Leukopenia and/or thrombocytopenia, the frequent side effects of MMF, ganciclovir and beta-lactam antibiotics that had been applied in this case, might be accentuated by her renal dysfunction.

In summary, the lesson we learn from this particular case is, for the CPCD, any sign of suspect renal infection found before or during LKTx is indication for the excision of original kidney and, the intensity of immunosuppression therapy should be controlled with caution.

REFERENCES

- 1 **Beierle EA**, Nicolette LA, Billmire DF, Vinocur CD, Weintraub WH, Dunn SP. Gastrointestinal perforation after pediatric orthotopic liver transplantation. *J Pediatr Surg* 1998; **33**: 240-242
- 2 **Pirenne J**, Lledo-Garcia E, Benedetti E, West M, Hakim NS, Sutherland DE, Gruessner RW, Najarian JS, Matas AJ. Colon perforation after renal transplantation: a single-institution review. *Clin Transplant* 1997; **11**: 88-93
- 3 **Soubrane O**, el Meteini M, Devicor D, Bernard O, Houssin D. Risk and prognostic factors of gut perforation after orthotopic liver transplantation for biliary atresia. *Liver Transpl Surg* 1995; **1**: 2-9
- 4 **Shaked A**, Vargas J, Csete ME, Kiai K, Jurim O, Colquhoun S, McDiarmid SV, Ament ME, Busuttil RW. Diagnosis and treatment of bowel perforation following pediatric orthotopic liver transplantation. *Arch Surg* 1993; **128**: 994-998
- 5 **Bilik R**, Yellen M, Superina RA. Surgical complications in children after liver transplantation. *J Pediatr Surg* 1992; **27**: 1371-1375
- 6 **Marujo WC**, Stratta RJ, Langnas AN, Wood RP, Markin RS, Shaw BW Jr. Syndrome of multiple bowel perforations in liver transplant recipients. *Am J Surg* 1991; **162**: 594-598
- 7 **Vilca Melendez H**, Vougas V, Muiesan P, Andreani P, Mieli-Vergani G, Rela M, Heaton ND. Bowel perforation after paediatric orthotopic liver transplantation. *Transpl Int* 1998; **11**: 301-304
- 8 **Yamanaka J**, Lynch SV, Ong TH, Balderson GA, Strong RW. Posttransplant gastrointestinal perforation in pediatric liver transplantation. *J Pediatr Surg* 1994; **29**: 635-638
- 9 **Bardaxoglou E**, Maddern G, Ruso L, Siriser F, Champion JP, Le Pogamp P, Catheline JM, Launois B. Gastrointestinal surgical emergencies following kidney transplantation. *Transpl Int* 1993; **6**: 148-152
- 10 **Morcillo Rodenas MA**, Garcia Espinosa R, Moliner Quiles C, Pallardo Mateu L, Planells Roig M, Rodero Rodero D. Colonic perforation in patients with kidney transplant. *Rev Esp Enferm Dig* 1990; **77**: 49-51
- 11 **Church JM**, Fazio VW, Braun WE, Novick AC, Steinmuller DR. Perforation of the colon in renal homograft recipients. A report of 11 cases and a review of the literature. *Ann Surg* 1986; **203**: 69-76
- 12 **Stelzner M**, Vlahakos DV, Milford EL, Tilney NL. Colonic perforations after renal transplantation. *J Am Coll Surg* 1997; **184**: 63-69
- 13 **Toogood GJ**, Gillespie PH, Gujral S, Warren BF, Roake JA, Gray DW, Morris PJ. Cytomegalovirus infection and colonic perforation in renal transplant patients. *Transpl Int* 1996; **9**: 248-251
- 14 **Lin HS**, Yang CR, Chang CH, Chang CL, Wu HC, Ho HC. Bowel perforation-a fatal complication following renal transplantation: a report of two cases. *Zhonghua Yixue Zazhi* 1994; **54**: 442-446
- 15 **Jeyarajah DR**, Gonwa TA, Testa G, Abbasoglu O, Goldstein R, Husberg BS, Levy MF, Klintmalm GB. Liver and kidney transplantation for polycystic disease. *Transplantation* 1998; **66**: 529-532

Why a *World Journal of Gastroenterology*?

Pelayo Correa

Pelayo Correa, Boyd Professor, Department of Pathology, Louisiana State University, LSU Health Sciences Center, 1901 Perdido Street, Box P5-1, New Orleans, LA 70112, USA

Correspondence to: Pelayo Correa, Boyd Professor, Department of Pathology, Louisiana State University, LSU Health Sciences Center, 1901 Perdido Street, Box P5-1, New Orleans, LA 70112, USA. correa@lsuhsc.edu

Telephone: +1-504-568-6035 **Fax:** +1-504-599-1278

Received: 2004-06-11 **Accepted:** 2004-06-22

Correa P. Why a *World Journal of Gastroenterology*? *World J Gastroenterol* 2004; 10(19): 2773-2774

<http://www.wjgnet.com/1007-9327/10/2773.asp>

When a new medical journal is launched, the reaction is frequent: Why? Do we have already so much to read that we feel overwhelmed? But, the litmus test of a good new journal is: Does it find its way into the reading time of physicians and medical scientists? The new *World Journal of Gastroenterology* has the opportunity to pass that litmus test.

We already have excellent journals of gastroenterology. All have originated as local publications. Some have reached an international status because of the quality of the published materials. Clear examples in the Western world are journals originated in Great Britain, Scandinavia and the United States of America. But they all keep their original flavor which permeates their published materials and reflects mostly the experience and the interest of physicians in the countries they represent.

Gastroenterologists, as most clinicians, tend to draw conclusions from their own experience, which they tend to generalize to "the world". That experience represents the pattern of diseases in their community. But gastrointestinal diseases display radically different patterns in different populations. In the case of cancer, for instance, the incidence of cancers of the colon, liver, biliary system, and stomach displayed rates in some populations that were several times higher than in other populations, as regularly published and illustrated by the International Agency for Research on Cancer^[1].

The phenomenon is well illustrated by gastric cancer and its precursor lesions. Their morphologic characteristics were first masterfully described and illustrated by European pioneers such as Faber, Fenwick, Magnus and Kupfer approximately a century ago^[2-5]. In those days pernicious anemia was a major medical problem in Europe and was, with good reasons, linked to gastric carcinogenesis. At the present time pernicious anemia has drastically decreased in frequency perhaps due to improved nutrition and sanitation. However, the genes for the predisposition to the syndrome remain in the population. The type of gastric adenocarcinoma originally described in association with pernicious anemia (the papillary type, located in the corpus) has become very rare^[6]. But it is entirely possible that the genes that predispose to pernicious anemia in one set of environmental conditions may manifest themselves as a different disease in another set of conditions. It has been suggested in populations susceptible to pernicious anemia, the initial trigger for chronic gastritis may be *Helicobacter pylori* infection. In such populations gastritis may be severe in the corpus leading to atrophy of the oxyntic mucosa^[7].

Most clinicians attending only populations of non-European

extraction have never seen a case of pernicious anemia. The genes linked to that disease are either rare or not present in their population and gastritis associated with *Helicobacter pylori* in their patients is multifocal but antral predominant, with minimal or absent corpus involvement. Some medical writers concentrated on corpus atrophy as a cancer precursor and ignore the gastric antrum^[8]. They might not appreciate that outside Europe, most gastric cancer precursors were predominantly in the antrum, not in the corpus.

Some publications insist that the high cancer risk gastritis phenotype depends on the grade and activity of gastritis in the corpus. The general experience presently showed that the antrum and the antrum-corpus transition zones (mostly the area of the incisura) were the sites of the most advanced lesions, including intestinal metaplasia, dysplasia and carcinoma^[9].

The Jarvi-Lauren classification of tumors as "intestinal" or "diffuse" has been challenged. Some reports have concluded that gastric carcinomas may arise as "gastric type" and later convert to a mixed type, expressing gastric and intestinal mucins. It has been suggested that stem cells, from which carcinomas are supposed to arise, are "primarily gastric type" (meaning they encode for gastric mucins only)^[10]. Normal stem cells have a minimal amount of acid (intestinal) mucins, indicating repressed genes and explaining their multi-potential characteristics^[11]. Obviously the ultimate mechanism of carcinogenesis is not well understood. An attractive hypothesis has been recently discussed by Kirchner *et al.*^[12]. They presented scientific evidence in support of a mechanism of carcinogenesis based on atrophy (loss of differentiated cells) followed by re-differentiation of stem cells, which may be abnormal. This would explain the carcinogenic process of the gastric and cardiac mucosae. After atrophy, the so-called complete intestinal metaplasia expresses preferentially small intestinal (sialic) mucins. Later the so called "incomplete" metaplasia appears and expresses several types of mucins, including gastric MUC-5AC and MUC-6, small intestinal MUC-2 and large intestinal DAS-1^[13]. These findings do not support gastric carcinoma classification based on mucin expressions as "gastric", "intestinal" or "mixed". Mucins expressed by pre-neoplastic and neoplastic cells represent abnormal re-differentiation which is not a permanent but rather a represent dynamic expression of mucin genes present in stem cells.

We hope that the *World Journal of Gastroenterology* will minimize the "provincial" bias and inspire the authors to be less dogmatic and more eclectic. We also hope that future authors adopt some of the basic teachings of epidemiology. For example, (1) Disease patterns are strongly influenced by the geographic and demographic characteristics of the populations under study. The local experience may not be applicable to all populations. Frequently, more than one demographic group share the same geography, comparison of such groups offers opportunities for etiologic research. (2) Disease frequency determines population risk and there are clear rules to assign causality. As an example, cancer frequency is often measured in the number of cases per 100 000 populations. Invasive gastric carcinoma is the final stage of a prolonged precancerous process involving chronic gastritis, atrophy, metaplasia and dysplasia. As in precancerous processes in other organs, the earlier stages are very frequent but less predictive of eventual neoplastic outcomes. Later stages have a lower prevalence in the population but are better indicators of cancer risk. Let us

remember that the skin of all people is exposed to the effects of sun rays which may lead to several degrees of actinic damage. But very few develop skin cancer. Large cohorts observed for many years may provide more valid data than small cohorts followed-up for a few years. Large cohorts have been reported in Finland, Yugoslavia and Japan^[14-16]. (3) As in all medical sciences, epidemiologic observations may be biased. But epidemiologists have figured out how to deal with bias. Causal vs non-causal associations are distinguished by epidemiologic criteria such as strength, consistency, temporality, and plausibility of the associations.

Recent advances in medicine and biology have made it possible to depend less on experimental animals to test causality. Molecular changes can be traced in human cells, tissues and fluids, but molecular techniques are not an end in themselves. Clinicians and medical scientists should remember that these new techniques are merely tools to explore causality in human beings. The new science of molecular epidemiology in some way should make molecular biologists use the epidemiologic techniques to analyze their findings. Similarly, classical epidemiologists need to become acquainted with the new powerful tools provided by molecular biologists. More than ever, multidisciplinary teams are needed to make real progresses in our understanding of the complex processes of carcinogenesis.

REFERENCES

- 1 **Parkin DM**, Whelan S, Ferlay S. Cancer incidence in five continents. Vol. VII. International Agency for Research on Cancer Publication. Lyon, France 1993: 143
- 2 **Faber K**, Block CE. Uber die pathologischen Verenderungen am digestion tractus bei die perniciosen anemia und ulcer die Sogennante. *Dermat Z Klin Med* 1900; **40**: 98
- 3 **Fenwick S**. On atrophy of the stomach. *Lancet* 1870; **2**: 78-80
- 4 **Kupfer C**. Festschrift. *Arz Verein Munch* 1883: 7
- 5 **Magnus HA**. A re-assessment of the gastric lesion in pernicious anaemia. *J Clin Path* 1958; **11**: 289-295
- 6 **Elsborg L**, Mosbech J. Pernicious anemia as a risk factor in gastric cancer. *Acta Medica Scandinavica* 1979; **206**: 315-318
- 7 **Carmel R**, Perez-Perez G, Blaser MJ. *Helicobacter pylori* infection and food cobalamine malabsorption. *Dig Dis Sci* 1994; **39**: 309-314
- 8 **Meining A**, Morgner A, Miehle S, Bayerdorffer E, Stolte M. Atrophy-metaplasia-dysplasia-carcinoma sequence in the stomach: a reality or merely a hypotheses? *Best Pract Res Clin Gastroenterol* 2001; **15**: 983-998
- 9 **Rugge M**, Cassaro M, Pennelli G. Atrophic gastritis: pathology and endoscopy in the reversibility assessment. *Gut* 2003; **52**: 1387-1388
- 10 **Endoh Y**, Sakata K, Tamura G, Ohmura K, Ajioka Y, Watanabe H, Motoyama T. Cellular phenotypes of differentiated type adenocarcinoma and precancerous lesions of the stomach are dependent on the genetic path ways. *J Path* 2000; **191**: 257-263
- 11 **Jass JR**, Filipe MI. The mucin profiles of normal gastric mucosa, intestinal metaplasia and its variants and gastric carcinoma. *Histochem J* 1981; **13**: 931-939
- 12 **Kirchner T**, Muller S, Hattori T, Mukaisyo K, Papadopoulos T, Brabletz T, Jung A. Metaplasia, intraepithelial neoplasia and early cancer of the stomach are related to dedifferentiated epithelial cells defined by cytokeration - 7 expressions in gastritis. *Virchow's Arch* 2001; **439**: 512-522
- 13 **Piazuelo MB**, Haque S, Delgado A. Phenotypic differences between esophageal and gastric intestinal metaplasia. *Mod Pathol* 2004; **19**: 62-74
- 14 **Siurala M**, Isokoski M, Varis K. Prevalence of gastritis in a rural population. *Scand J Gastroenterol* 1968; **3**: 211-223
- 15 **Filipe MI**, Munoz N, Matko I, Kato I, Pompe-Kirn V, Jutersek A, Teuchmann S, Benz M, Prijon T. Intestinal metaplasia types and the risk of gastric cancer: a cohort study in Slovenia. *In J Cancer* 1994; **57**: 324-329
- 16 **Ohata H**, Kitauchi S, Yoshimura N, Mugitani K, Iwane M, Nakamura H, Yoshikawa A, Yanaoka K, Arii K, Tamai H, Shimizu Y, Takeshita T, Mohara O, Ichinose M. Progression of chronic atrophic gastritis associated with *Helicobacter pylori* infection increases risk of gastric cancer. *Int J Cancer* 2004; **109**: 138-143

Edited by Xu XQ, Wang XL and Zhang JZ Proofread by Xu FM

p53 polymorphism in human papillomavirus-associated Kazakh's esophageal cancer in Xinjiang, China

Xiao-Mei Lu, Yue-Ming Zhang, Ren-Yong Lin, Xiao-Hui Liang, Ya-Lou Zhang, Xing Wang, Yan Zhang, Yan Wang, Hao Wen

Xiao-Mei Lu, Ren-Yong Lin, Xiao-Hui Liang, Ya-Lou Zhang, Xing Wang, Yan Zhang, Yan Wang, Hao Wen, Medical Research Center, 1st Teaching Hospital, Xinjiang Medical University, Urumqi 830054, Xinjiang Uygur Autonomous Region, China

Yue-Ming Zhang, Public and Health College, Xinjiang Medical University, Urumqi 830054, Xinjiang Uygur Autonomous Region, China
Supported by Xinjiang Key Laboratory Foundation, No. XJDX0202-2003-05

Correspondence to: Hao Wen, Ph.D., Professor, Medical Research Center, 1st Teaching Hospital, Xinjiang Medical University, No.1 Liyushan Road, Urumqi 830054, Xinjiang Uygur Autonomous Region, China. wenhao2002@hotmail.com

Telephone: +86-991-4362844 **Fax:** +86-991-4324139

Received: 2004-03-26 **Accepted:** 2004-04-05

Abstract

AIM: To investigate the relationship between *p53* codon 72 polymorphism and human papillomavirus (HPV) type 16 infection in Kazakh's esophageal cancer (EC) in Xinjiang, China.

METHODS: Encoding regions of *p53* codon 72 and HPV-16 *E6* were amplified by polymerase chain reaction-restriction fragment length polymorphism (PCR-RFLP) and polymerase chain reaction (PCR) methods using pairs of primary esophageal squamous cell carcinoma (SCC) tissue and corresponding normal mucosa, which were collected from 104 patients of Kazakh in Xinjiang, China.

RESULTS: Only arginine allele was detected in 70.1% (39/55) of HPV-16-*E6*-positive cases but only in 40.8% (20/49) of HPV-16-*E6*-negative cases ($P < 0.05$; *OR*, 3.53; 95% *CI*, 1.57-7.98). In contrast, such a significant correlation between *p53* polymorphism and HPV infection was not evident in corresponding normal mucosae. The allele frequency of *Arg* allele in cancer cases (0.68) was higher than that in normal mucosa samples (0.54) ($P < 0.05$; *OR*, 1.80; 95% *CI*, 1.21-2.69).

CONCLUSION: *p53* codon 72 *Arg* homozygous genotype is one of the high-risk genetic factors for HPV-associated SCC of Kazakh. Individuals carrying *Arg* allele compared to those with *Pro* allele have an increased risk for esophageal SCC.

Lu XM, Zhang YM, Lin RY, Liang XH, Zhang YL, Wang X, Zhang Y, Wang Y, Wen H. *p53* polymorphism in human papillomavirus-associated Kazakh's esophageal cancer in Xinjiang, China. *World J Gastroenterol* 2004; 10(19): 2775-2778

<http://www.wjgnet.com/1007-9327/10/2775.asp>

INTRODUCTION

Esophageal cancer is common in several areas of central Asia, including Xinjiang Uygur Autonomous Region, China. The incidence of Kazakh's EC is the highest among population in Xinjiang and its age-adjusted mortality rate up to 91/100 000

has been reported in Kazakh's population^[1]. The population size of Kazakh was estimated to be 13 million around the world and 10 million Kazakh distributed in Kazakhstan and 2 million in Xinjiang, China. The population in the present study was a Kazakh isolated community located at the Northeast of Xinjiang. The genetic homogeneity and geography stability of the population, along with shared exposure to common environmental variables, provide an excellent opportunity for the study of genetic influence on EC. These cancers are mostly SCC, and show a high frequency of mutation in the *p53* tumor suppressor^[2]. Epidemiological studies have suggested that a number of risk factors are involved in the carcinogenesis of Kazakh's SCC, including deficiencies in vitamins and minerals, consumption of pickled foods and environmental exposure to specific nitrosamines, etc^[3,4]. Viral infections, in particular HPV infection, have been reported in esophageal cancers from China, and HPV DNA has been detected in 0-60.0% of cancer tissues by polymerase chain reaction analysis^[5,6]. HPV is implicated in the pathogenesis of squamous cell carcinoma of the cervix and esophagus. HPV-16 encodes *E6* protein, which binds to cellular tumor-suppressor protein *p53* and directs degradation through the ubiquitin pathway^[7]. This event is mediated by another cellular protein termed *E6-AP*, a component of the ubiquitin pathway^[8,9]. The arginine allele at codon 72 of *p53* was found to be more susceptible to degradation by HPV *E6* protein than the proline allele *in vivo*, thus resulting in a high frequency of esophageal SCC in individuals homozygous for arginine at the codon^[8]. On the basis of these experiments, it has been widely assumed that *p53* is functionally inactivated by the viral *E6* protein in HPV-associated cancer cells and that infection with high-risk HPV types leads to the same phenotype as a loss of *p53* function because of *p53* gene mutations or direct degradation^[9]. The association of *p53* codon 72 polymorphism with HPV-16-associated esophagus SCC risk has been studied by several groups but with inconsistent results. Kawaguchi *et al.*^[10] reported that the form of *p53* protein carrying an *Arg* residue at this position in HPV-16/18 positive samples was found to be significantly more susceptible to degradation by *E6* protein than that in HPV-16/18 negative samples. There are controversial results from several clinical studies of esophagus SCC^[11,12]. A part of Kazakh's esophageal SCC correlated with the presence of HPV-16/18^[13]. To our knowledge, *p53* polymorphism in Kazakh's esophageal SCC has apparently not been documented. In this study, we investigated the genotypic frequency of *p53* codon 72 polymorphism and HPV-16 *E6* in Kazakh's esophageal SCC patients in Xinjiang, China. The data we obtained seemed to be the first regarding the association of this polymorphism with HPV-associated risk for cancer of the esophagus.

MATERIALS AND METHODS

Tissue specimens

Pairs of primary Kazakh's esophageal SCC tissue and corresponding normal mucosa were obtained from 63 patients who underwent surgery in the Department of Surgery, 1st Teaching Hospital of Xinjiang Medical University, from 1999 to 2003, and from 41 patients who underwent surgery in

Department of Surgery, the People's Hospital of Xinjiang Uygur Autonomous Region, China, between 1998 and 2000. No patient had been given treatment prior to the study. In all cases the histopathological type of tumors was squamous cell carcinoma. Cancer tissues and well-separated normal esophageal mucosae obtained from surgically resected esophageal SCC patients were fixed in 40 g/L formaldehyde and embedded in paraffin. Genomic DNA was prepared by proteinase K digestion and phenol/chloroform extraction, followed by ethanol precipitation, as described by Greer *et al.*^[14].

HPV detection and identification

First, as a control, purified genomic DNA was successfully amplified by PCR using primers specific for the β -globin gene, indicating a suitable quality and quantity of DNA. PCR analysis was then performed using HPV-16 E6 oligodeoxynucleotide primers as follows: HPV-16E6 forward, 5'-GCAAGCAACAGTTACTGCGA-3' and reverse, 5'-CAACAAGACATACATCGACC-3'. Amplified PCR products were then determined by electrophoresis on 15 g/L agarose gels stained with ethidium bromide. Finally, the gels were analyzed by DC-2000 image system (Bio-Rad, USA).

Analysis of codon 72 polymorphism

p53 exon 4 (codons 33-125) containing codon 72 was amplified by PCR using oligodeoxynucleotide primers 5'-TGAGGACC TGGTCTCTGAC-3' (forward) and 5'-AGAGGAATCCCAA GTTCCA-3' (reverse), under the following conditions: denaturation at 94 °C for 30 s, primary annealing at 54 °C for 30 s, and extension at 72 °C for 30 s for 35 cycles. PCR products (412 bp) were digested overnight at 37 °C with *Acc* II, which was cut within the sequence corresponding to the *Arg* codon (CGC) at position 72 to generate two fragments of 252 bp and 160 bp^[15]. The DNA fragments were then resolved by electrophoresis on 30 g/L agarose gels stained with ethidium bromide. Presence of uncut (412 bp) DNA was indicative of the *Pro* allele and heterozygous for *Arg/Pro* genotypes showed three fragments of 412, 252 and 160 bp.

Statistical analysis

Chi-square test was used to examine the correlation between the *p53* codon 72 polymorphism of the esophageal SCC patients and the presence of HPV-16E6 by SPSS software(12.0).

RESULTS

Frequency of HPV-16E6 among Kazakh's esophageal SCC patients

Pairs of 104 DNA sample from primary Kazakh's esophageal SCC tissues and corresponding normal mucosae were analyzed for the presence of oncogenic HPV-16-E6 using PCR methods (Figure 1). The frequency of HPV-16-E6 gene in cancer cases (52.9%) was higher than that in corresponding normal mucosae (39.4%) (Tables 1, 2). These results were similar to previous reports^[16].

Table 1 *Arg* and *Pro* alleles of *p53* in SCCs of Kazakh's esophagus (n, %)

	<i>Pro</i>	<i>Pro/Arg</i>	<i>Arg</i>
Esophageal SCC (n = 104)	21 (20.2)	25 (24.0)	58 (55.8)
HPV16E6 positive (n=55)	8 (14.5)	8 (14.5)	39 (71.0) ^a
HPV16E6 negative (n=49)	13 (26.5)	16(32.7)	20 (40.8)

^a*P*<0.05 vs negative.

Arg allele at the codon 72 in HPV-associated esophageal SCC
PCR-RFLP was carried out on 104 DNA samples from primary

Kazakh's esophageal SCC tissues and corresponding normal mucosae to analyze the association between the *p53* codon 72 polymorphism and HPV-associated esophageal SCC by DC-2000 image system (Figure 2). It showed a typical pattern of codon 72 evaluated by restriction analysis. Presence of the *Pro* allele resulted in resistance of the PCR amplified DNA fragment to digestion by *Acc* II. The comparison between the distribution of *p53* alleles at codon 72 in HPV-positive esophageal SCC with the HPV-negative group is shown in Table 1. The frequency of presence of *Arg* allele alone from the Kazakh's esophageal cancer specimens was similar (55.8%, 58 of 104) to other population cases of esophageal cancer^[10]. Moreover, there was a marked difference in the frequency of *Pro/Arg* alleles between HPV-positive and HPV-negative groups. *p53 Arg* allele alone was detected in 71.0% (39/55) in the HPV-positive group, whereas in 40.8% (20/49) in the HPV-negative group (*P*<0.05; *OR*, 3.53; 95% *CI*, 1.57-7.98) (Table 1). The allele frequency of *Arg* alleles in cancer cases (0.68) was higher than that in normal mucosa samples (0.54) (*P*<0.05; *OR*, 1.80; 95% *CI*, 1.21-2.69).

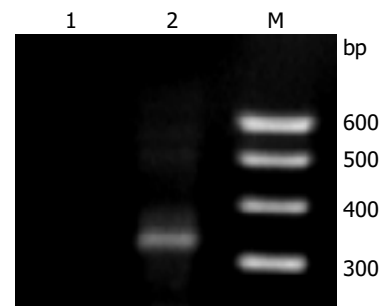


Figure 1 Agarose gel electrophoresis of HPV-16 E6 PCR-amplified fragments. Lane M: 100 bp DNA ladder marker; Lane 1: negative sample; and Lane 2: positive sample.

Table 2 *Arg* and *Pro* alleles of *p53* in normal mucosae of Kazakh's esophagus (n, %)

	<i>Pro</i>	<i>Pro/Arg</i>	<i>Arg</i>
Normal mucosa (n = 104)	28 (26.9)	40 (38.5)	36 (34.6)
HPV16E6 positive (n = 41)	10 (24.4)	18 (43.9)	13 (31.7)
HPV16E6 negative (n = 63)	10 (15.9)	30 (47.6)	23 (36.5)

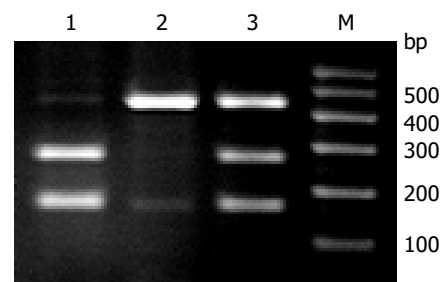


Figure 2 Restriction analysis of *p53* codon 72 polymorphism. The PCR product from the proline alleles had a single band with a fragment of 412 bp in length. The arginine was cleaved by *Acc* II, yielding two small fragments (252 and 160 bp). Lane M: 100 bp DNA ladder marker; Lane 1: homozygous for arginine; Lane 2: homozygous for proline; and Lane 3: digested sample, heterozygous for the polymorphism.

Arg allele at the codon 72 in surrounding normal mucosae in HPV-associated esophageal cancer

Differences in *p53* polymorphism in the corresponding normal mucosae were not significant between HPV-positive and -negative tissues (*P*>0.05; *OR*, 0.81; 95% *CI*, 0.35-1.86) (Table 2).

DISCUSSION

Infection with human papilloma virus is an important etiological factor in the development of SCC and it has been proposed that individuals homozygous for *Arg/Arg* at codon 72 of *p53* are several times more susceptible to HPV-mediated cancer^[10,17]. In agreement with the result, studies in India and Mexico also found a strong increase in SCC risk associated with *p53* polymorphism and the presence of HPV infection^[18,19]. In China similar research has been carried out on esophageal SCC, ovarian carcinoma, and breast carcinoma^[20]. However, several studies conducted in different countries failed to reproduce this observation^[21-25]. This polymorphism has been shown to vary with ethnic and geographical distribution. However, its influence has not been elucidated in the Kazakh population.

In the present study, the frequency of HPV-16-*E6* gene in Kazakh's esophageal SCC cases was higher than that in corresponding normal mucosae, suggesting that there is a trend towards an association between the carcinogenesis of Kazakh's esophageal SCC and the presence of HPV-16 infection. These results were similar to previous report^[16], which suggested that infection with HPV-16 might be involved in carcinogenesis of Kazakh's esophageal SCC. In addition, the distribution of *p53* codon 72 *Arg* homozygous genotype in Kazakh's esophageal SCC was significantly higher than that in corresponding normal mucosae, indicating that an individual homozygous for *p53 Arg* would be more likely to develop esophageal SCC than a *Pro/Arg* heterozygote or a *Pro* homozygote. Furthermore, it is noteworthy that the distribution of *p53* codon 72 *Arg* homozygous genotype in HPV positive samples of Kazakh's esophageal SCC was at a 3.53-folds higher risk for the development of esophageal SCC compared with HPV negative samples. In contrast, such a significant correlation between *p53* polymorphism and HPV infection was not evident in corresponding normal mucosae. From the above analyses, when stratified with HPV infection, the frequency of *p53* codon 72 *Arg* homozygous genotype was at a 1.48-folds increased risks for developing Kazakh's esophageal SCC compared with *p53 Arg* homozygosity (*Arg/Arg*) solely. Therefore, this implied *p53* codon 72 *Arg* polymorphism in combination with HPV infection could increase the risk of development of SCC in Kazakhs.

p53 tumor-suppressor protein accumulates rapidly through post-transcriptional mechanisms and is also activated as a transcriptional factor, thus leading to growth arrest or apoptosis when DNA damage has occurred^[26]. The ubiquitin-dependent proteolytic pathway plays a major role in selective protein deregulation. *E6* oncoprotein of oncogenic HPV-16/18 might use this cellular proteolytic system to target *p53* protein^[7] and bind to a cellular protein of *E6-AP*, and the *E6-AP* complex might interact with *p53*, resulting in the rapid ubiquitin-dependent degradation of *p53*^[27]. The level and half-life of *p53* in *E6* immortalized cell lines or in HPV-positive cervical carcinoma cells have been reported to be generally decreased^[28,29]. Certain HPV types such as HPV-16/18 found in SCC of esophagus suggested a model by which *E6* degraded cell growth control by elimination of the *p53* tumor suppresser protein and led to HPV-associated esophageal SCC^[10,30].

In conclusion, the current study reveals the potential role of the polymorphism of *p53* at codon 72 in HPV-associated carcinogenesis of esophageal SCC in Kazakh population. Individuals carrying *Arg* alleles compared to those with *Pro* alleles have an increased risk for esophageal SCC.

ACKNOWLEDGMENTS

We thank Professor Zhen-Zhu Sun (Department of Pathology, the People's Hospital of Xinjiang Uygur Autonomous Region, China) for providing the samples of Kazakh's esophageal SCC.

REFERENCES

- 1 Zhang YM. The distribution of esophageal cancer in Xinjiang. *Xinjiang Yixueyuan Xuebao* 1988; **11**: 139-144
- 2 Liang YY, Esteve A, Martel-Planche G, Takahashi S, Lu SH, Montesano R, Hollstein M. *p53* mutations in esophageal tumors from high-incidence areas of China. *Int J Cancer* 1995; **61**: 611-614
- 3 Munoz N, Wahrendorf J, Bang LJ, Crespi M, Thurnham DI, Day NE, Ji ZH, Grassi A, Yan LW, Lin LG. No effect of riboflavin, retinol, and zinc on prevalence of precancerous lesions of oesophagus. Randomised double-blind intervention study in high-risk population of China. *Lancet* 1985; **2**: 111-114
- 4 Lin K, Shen W, Shen Z, Cai S, Wu Y. Estimation of the potential for nitrosation and its inhibition in subjects from high- and low-risk areas for esophageal cancer in southern China. *Int J Cancer* 2003; **10**: 891-895
- 5 He D, Zhang DK, Lam KY, Ma L, Ngan HY, Liu SS, Tsao SW. Prevalence of HPV infection in esophageal squamous cell carcinoma in Chinese patients and its relationship to the *p53* gene mutation. *Int J Cancer* 1997; **72**: 959-964
- 6 Chen B, Yin H, Dhurandhar N. Detection of human papilloma-virus DNA in esophageal squamous cell carcinomas by the polymerase chain reaction using general consensus primers. *Hum Pathol* 1994; **25**: 920-923
- 7 Scheffner M, Werness BA, Huibregtse JM, Levine AJ, Howley PM. The *E6* oncoprotein encoded by human papillomavirus types 16 and 18 promotes the degradation of *p53*. *Cell* 1990; **63**: 1129-1136
- 8 Huibregtse JM, Scheffner M, Howley PM. A cellular protein mediates association of *p53* with the *E6* oncoprotein of human papillomavirus types 16 or 18. *EMBO J* 1991; **10**: 4129-4135
- 9 Huibregtse JM, Scheffner M, Howley PM. Localization of the *E6-AP* regions that direct human papillomavirus *E6* binding, association with *p53*, and ubiquitination of associated proteins. *Mol Cell Biol* 1993; **13**: 4918-4927
- 10 Kawaguchi H, Ohno S, Araki K, Miyazaki M, Saeki H, Watanabe M, Tanaka S, Sugimachi K. *p53* polymorphism in human papillomavirus-associated esophageal cancer. *Cancer Research* 2000; **60**: 2753-2755
- 11 Peixoto Guimaraes D, Hsin Lu S, Snijders P, Wilmette R, Herrero R, Lenoir G, Montesano R, Meijer CJ, Walboomers J, Hainaut P. Absence of association between HPV DNA, TP53 codon 72 polymorphism, and risk of oesophageal cancer in a high-risk area of China. *Cancer Lett* 2001; **162**: 231-235
- 12 Lu ZM, Chen KN, Guo M. Detection of HPV in human esophageal cancer in high-incidence area and its correlation with *p53* expression. *Zhonghua Zhongliu Zazhi* 2001; **23**: 220-223
- 13 Zou SY, Si JY, Liu XM, Tang XP. PCR in detection of human papillomavirus DNA in esophageal carcinoma in Xingjiang. *Aizheng* 1998; **17**: 32-34
- 14 Greer CE, Whee Le CM, Manos MM. PCR Primer A Laboratory Manual. *Cold Spring Harbor Laboratory Press* 1995: 64-69
- 15 de la Calle-Martin O, Fabregat V, Romero M, Soler J, Vives J, Yague J. AccII Polymorphism of the *p53* gene. *Nucleic Acids Res* 1990; **18**: 4963
- 16 Chang F, Syrjanen S, Shen Q, Cintorino M, Santopietro R, Tosi P, Syrjanen K. Human papillomavirus involvement in esophageal carcinogenesis in the high-incidence area of China. A study of 700 cases by screening and type-specific in situ hybridization. *Scand J Gastroenterol* 2000; **35**: 123-130
- 17 Ojeda JM, Ampuero S, Rojas P, Prado R, Allende JE, Barton SA, Chakraborty R, Rothhammer F. *p53* codon 72 polymorphism and risk of cervical cancer. *Biol Res* 2003; **36**: 279-283
- 18 Saranath D, Khan Z, Tandle AT, Dedhia P, Sharma B, Contractor R, Shrivastava S, Dinshaw K. HPV16/18 prevalence in cervical lesions/cancers and *p53* genotypes in cervical cancer patients from India. *Gynecol Oncol* 2002; **86**: 157-162
- 19 Sifuentes Alvarez A, Reyes Romero M. Risk factors for cervico-uterine cancer associated to HPV: *p53* codon 72 polymorphism in women attending hospital care. *Ginecol Obstet Mex* 2003; **71**: 12-15
- 20 Li T, Lu ZM, Guo M, Wu QJ, Chen KN, Xing HP, Mei Q, Ke Y. *p53* codon 72 polymorphism (C/G) and the risk of human papillomavirus-associated carcinomas in China. *Cancer* 2002; **95**: 2571-2576

- 21 **Humbey O**, Cairey-Remonnay S, Guerrini JS, Algros MP, Mouglin C, Bittard H, Aubin F. Detection of the human papillomavirus and analysis of the TP53 polymorphism of exon 4 at codon 72 in penile squamous cell carcinomas. *Eur J Cancer* 2003; **39**: 684-690
- 22 **Inserra P**, Abrahamsen M, Papenfuss M, Giuliano AR. Ethnic variation of the P53 codon 72 polymorphism, HPV persistence, and cervical cancer risk. *Int J STD AIDS* 2003; **14**: 800-804
- 23 **Comar M**, Molin GD, Guaschino S, Campello C. p53 at codon 72 polymorphism, human papillomavirus infection and cervical lesions: a cross-sectional study from northeastern Italy. *Eur J Obstet Gynecol Reprod Biol* 2004; **114**: 210-214
- 24 **Tanara G**, Falugi C, Cesario A, Margaritora S, Russo P, Cosimi A. TP53 codon 72 polymorphism does not affect risk of cervical cancer in patients from The Gambia. *Int J Biol Markers* 2003; **18**: 280-283
- 25 **Ngan HY**, Liu VW, Liu SS, Cheng DK, Ng TY, Wong LC. Homozygous arginine at codon 72 of p53 has no prognostic significance in cervical cancer. *Tumour Biol* 2000; **21**: 135-138
- 26 **Levine AJ**. p53, the cellular gatekeeper for growth and division. *Cell* 1997; **88**: 323-331
- 27 **Scheffner M**, Huibregtse JM, Vierstra RD, Howley PM. The HPV-16 E6 and E6-AP complex functions as a ubiquitin-Protein ligase in the ubiquitination of p53. *Cell* 1993; **75**: 495-505
- 28 **Scheffner M**, Munger K, Byrne JC, Howley PM. The state of the p53 and retinoblastoma genes in human cervical carcinoma cell lines. *Proc Natl Acad Sci U S A* 1991; **88**: 5523-5527
- 29 **Hengstermann A**, Linares LK, Ciechanover A, Whitaker NJ, Scheffner M. Complete switch from Mdm2 to human papillomavirus E6-mediated degradation of p53 in cervical cancer cells. *Proc Natl Acad Sci U S A* 2001; **98**: 1218-1223
- 30 **Vos M**, Adams CH, Victor TC, van Helden PD. Polymorphisms and mutations found in the regions flanking exons 5 to 8 of the TP53 gene in a population at high risk for esophageal cancer in South Africa. *Cancer Genet Cytogenet* 2003; **140**: 23-30

Edited by Kumar M and Wang XL Proofread by Xu FM

Inhibitory effect of ubiquitin-proteasome pathway on proliferation of esophageal carcinoma cells

Wei-Guo Zhang, Jie-Ping Yu, Qing-Ming Wu, Qiang Tong, Sheng-Bao Li, Xiao-Hu Wang, Guo-Jian Xie

Wei-Guo Zhang, Qing-Ming Wu, Qiang Tong, Sheng-Bao Li, Xiao-Hu Wang, Guo-Jian Xie, Digestive Department, Taihe Hospital, Yunyang Medical College, Shiyan 442000, Hubei Province, China

Jie-Ping Yu, Digestive Department, Renmin Hospital of Wuhan University, Wuhan 430060, Hubei Province, China

Correspondence to: Wei-Guo Zhang, Digestive Department, Taihe Hospital, Yunyang Medical College, Shiyan 442000, Hubei Province, China. zwg789@sina.com

Telephone: +86-719-8801431

Received: 2004-02-02 **Accepted:** 2004-02-18

Abstract

AIM: To investigate the inhibitory effect of ubiquitin-proteasome pathway (UPP) on proliferation of esophageal carcinoma cells.

METHODS: Esophageal carcinoma cell strain EC9706 was treated with MG-132 to inhibit its UPP specificity. Cell growth suppression was evaluated with 3-(4,5-dimethylthiazole-2-yl)-2,5-diphenyl tetrazolium bromide (MTT) assay. DNA synthesis was evaluated by ³H-thymidine (³H-TdR) incorporation. Morphologic changes of cells were observed under microscope. Activity of telomerase was examined by telomeric repeat amplification protocol (TRAP) of PCR-ELISA. Cell cycle and apoptosis were detected by flow cytometry (FCM). DNA fragment analysis was used to confirm the presence of apoptosis. Expression of p27^{kip1} was detected by immunocytochemical technique.

RESULTS: After exposed to MG-132, the growth and value of ³H-TdR incorporation of EC9706 cells were obviously inhibited. Cells became round, small and exfoliative under microscope. TRAP PCR-ELISA showed that light absorption of cells gradually decreased after exposed to 5 μmol/L of MG-132 for 24, 48, 72 and 96 h ($P < 0.01$). The percentage of cells at G₀/G₁ phase was increased and that at S and G₂/M was decreased ($P < 0.01$). The rate of apoptotic cells treated with 5 μmol/L of MG-132 for 48 and 96 h was 31.7% and 66.4%, respectively. Agarose electrophoresis showed marked ladders. In addition, the positive signals of p27^{kip1} were located in cytoplasm and nuclei in MG-132 group in contrast to cytoplasm staining in control group.

CONCLUSION: MG-132 can obviously inhibit proliferation of EC9706 cells and induce apoptosis. The mechanisms include upregulation of p27^{kip1} expression, G₁ arrest and depression of telomerase activity. The results indicate that inhibiting UPP is a novel strategy for esophageal carcinoma therapy.

Zhang WG, Yu JP, Wu QM, Tong Q, Li SB, Wang XH, Xie GJ. Inhibitory effect of ubiquitin-proteasome pathway on proliferation of esophageal carcinoma cells. *World J Gastroenterol* 2004; 10 (19): 2779-2784

<http://www.wjgnet.com/1007-9327/10/2779.asp>

INTRODUCTION

Esophageal carcinoma is common in China. Previous studies have shown that its occurrence and progression are complicated, and are associated with the changes of multi-genes and molecules^[1-3]. The ubiquitin-proteasome pathway (UPP) is the major system employed by eukaryotes for the selective degradation of cellular proteins that play key roles in cellular processes such as cell cycle regulation, differentiation, signal transduction, gene transcription, antigen presenting and transmembrane localization of proteins^[4,5]. In this study, we investigated the inhibitory effect of UPP on proliferation of esophageal carcinoma cells by using specific ubiquitin proteasome to find a new strategy for esophageal carcinoma therapy.

MATERIALS AND METHODS

Materials

Esophageal carcinoma cell strain EC9706 was presented by professor Ming-Rong Wang, China Academy of Medical Sciences. MG-132 was purchased from Calbiochem Co. Ltd (USA), and dissolved in dimethylsulfoxide (DMSO) as a 40 mmol/L stock solution and stored at -20 °C. 3-(4,5-dimethylthiazole-2-yl)-2,5-diphenyl tetrazolium bromide (MTT) and DMSO were bought from Sigma Co. Ltd (USA). ³H-thymidine (³H-TdR) was provided by Beijing Atomic Power Research Institute. Telomeric repeat amplification protocol (TRAP) ELISA telomerase detection kit was obtained from Intergen Company (USA). Monoclonal mouse antibody of p27^{kip1}, ultra sensitive S-P kit, and 3,3-diaminobenzidine (DAB) kit were purchased from Fuzhou Maixin Biotechnology Co. Ltd. RPMI 1640 medium was obtained from GIBCOBRL Company (USA). Low melting-temperature agarose was obtained from Promega Company (USA). DNA-PREP™ LPR and DNA-PREP™ stain were obtained from America Beckman Coulter Company.

Cell culture

Human esophageal carcinoma cell strain EC9706 was maintained in RPMI 1640 medium supplemented with 100 mL/L fetal calf serum (FCS), 100 kU/L penicillin, 100 mg/L streptomycin and 2 mmol/L *l*-glutamine in a humidified incubator containing 50 mL/L CO₂ at 37 °C, the medium was changed every 2-3 d.

MTT assay

EC9706 cells growing exponentially were chosen. Cell density in the suspension was adjusted to 2×10⁵ cells/mL. After addition of 200 mL/well of the final cell suspension, 96-well plates were incubated for 24 h. Then the cells were treated with 0.5, 1.0, 2.5, 5.0, 10, 15, 20 μmol/L (DMSO ≤ 0.5 g/L) of MG-132, respectively, as the different observation groups. The cells treated with an equal amount of DMSO instead of MG-132 served as the control. The background was conducted using only cell-free culture medium. After cultivated for 24, 48, 72 and 96 h, 10 μL of stock MTT solution (5 g/L) was added to the cells in each well, followed by a further incubation at 37 °C for 4 h. The culture medium was carefully removed, 100 μL of DMSO was added to each well and culture was vibrated for 20 min. The absorbance

of samples was measured three times for each group with three wells at a wavelength of 550 nm with the enzyme linked immunosorbent assay meter (PR 2100, SANOFI company, France). The inhibitory rate (IR) was calculated according to the formula: $IR = [1 - (\text{absorbance of MG-132 group} - \text{absorbance of background group}) / (\text{absorbance of control group} - \text{absorbance of background group})] \times 100\%$.

Incorporation test of $^3\text{H-TdR}$

As described above, experimental group and control group were cultured for 3 h with 100 mL/L FCS RPMI 1640, and then for 12 h with FCS-free RPMI 1640. MG-132 and $1 \mu\text{Ci } ^3\text{H-TdR}$ were added to each group, which was rinsed with PBS after 24, 48, 72 and 96 h and fixed with methyl alcohol and absolute ethyl alcohol for 10 min each. Finally, 200 μL of 0.1 mol/L NaOH was added, then 200 μL of each was taken after blowing, and mixed in 5 mL scintillation liquid for overnight. On the following day, the count per minute (CPM) of ^3H was tested three times for each group with three wells.

Morphologic changes of cells

Morphologic changes of EC9706 cells were observed under microscope 24, 48, 72 and 96 h after treated with MG-132 (5 $\mu\text{mol/L}$).

Telomerase assay

The cells (10^5 - 10^6) treated with MG-132 (5 $\mu\text{mol/L}$) for 24, 48, 72 and 96 h were collected, respectively. After addition of 300 μL telomerase assay lysis buffer (1 \times CHAPS), the cells were lysed on ice. The lysate was incubated on ice for 30 min and then centrifuged at 13 000 g for 25 min at 4 $^\circ\text{C}$. The supernatant (2 μL) was added to reaction solution containing 10 μL of TRAP buffer, 2 units of Taq polymerase and 48 μL of DH_2Oqs . PCR was carried out through 33 amplification cycles, each cycle consisting of denaturation at 94 $^\circ\text{C}$ for 30 s, primer annealing at 55 $^\circ\text{C}$ for 30 s, and extension at 72 $^\circ\text{C}$ for 30 s. The amplified product was added to block/dilution buffer (250 μL), and incubated at 37 $^\circ\text{C}$ for 30 min, and 5 μL of TRAP reactant was then added and mixed. After incubated at 37 $^\circ\text{C}$ for 60 min, 100 μL working solution of anti-DNP Ab was added and incubated for 30 min, then 100 μL of 3,3',5,5'-tetramethylbenzidine (TMB) substrate solution and 100 μL of stop reagent were added. The absorbance value in each well was read at the wave lengths of 450 nm and 690 nm on an enzyme linked immunosorbent assay meter. Telomerase activity was considered positive when the absorbance value of a sample was at least 0.8 units. When those were lower than 0.2 units, they were regarded as negative.

Flow cytometry detection

After cell cycle was synchronic, the cells of experiment group were treated with MG-132 (5 $\mu\text{mol/L}$) for 48 h and 96 h. The collected cells were added with DNA-PREPTM LPR and DNA-PREPTM stain, respectively, after they were washed with PBS and centrifuged. Cell cycle and apoptosis were detected by

flow cytometry (Epics XL, Beckman Coulter Company, USA) and SYSTEM IITM software was used to dispose the data.

DNA ladder demonstration

As described above, the cells (7×10^6 /sample, both attached and detached cells) were lysed with hypotonic lysis buffer (10 mmol/L edetic acid, 5 g/L Triton X-100, Tris-HCl, pH 7.4) for 15 min on ice and precipitated with 25 g/L polyethylene glycol and 1 mol/L NaCl for 15 min at 4 $^\circ\text{C}$. After centrifugation at 16 000 g for 10 min at room temperature, the supernatant was treated with proteinase K (0.3 g/L) at 37 $^\circ\text{C}$ for 1 h and precipitated with isopropanol. After centrifugation, each pellet was dissolved in 10 μL of Tris-EDTA (pH 7.6) and electrophoresed on a 17 g/L agarose gel containing ethidium bromide. DNA ladder pattern was identified under ultraviolet light.

Immunocytochemical staining

EC9706 cells cultured with MG-132 (5 $\mu\text{mol/L}$) for 48 h were fixed with dimethyl ketone at 4 $^\circ\text{C}$. The cells carrying the detected antigen were stained following SP immunocytochemical staining method using anti-p27kip1 as primary antibody^[6]. PBS was substituted for primary antibody as negative control.

Statistics

The data were expressed as mean \pm SD. The difference between each group was analyzed by *t*-test. $P < 0.05$ was considered statistically significant.

RESULTS

Inhibitory effect of MG-132 on EC9706 cell growth

The growth of EC9706 cells treated with 0.5-20 $\mu\text{mol/L}$ of MG-132 was significantly inhibited compared with that of control group. While the cells exposed to MG-132 for 24 h produced a certain inhibitory effect, but only exceeding 48 h did MG-132 show significant effect. When the dose of MG-132 exceeded 5 $\mu\text{mol/L}$, only slight increases in IR of the cells were observed (Figure 1).

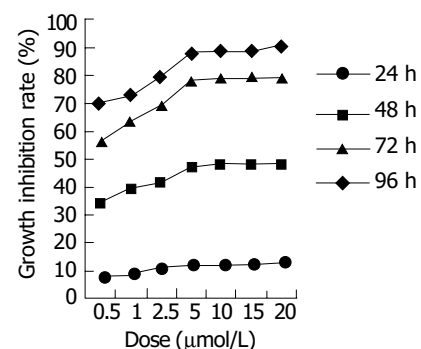


Figure 1 MTT assay of EC9706 cells after exposed to MG-132.

Table 1 Evaluation of DNA synthesis by $^3\text{H-TdR}$ incorporation (mean \pm SD)

Group	24 h	48 h	72 h	96 h
Control MG-132 ($\mu\text{mol/L}$)	4 295.52 \pm 136.32	5 236.17 \pm 221.36	5 642.92 \pm 105.41	5 863.43 \pm 206.58
0.5	3 764.68 \pm 97.37 ^a	2 879.83 \pm 86.25 ^b	1 918.73 \pm 76.49 ^b	1 759.29 \pm 89.23 ^b
1.0	3 526.14 \pm 101.42 ^a	2 643.29 \pm 79.38 ^b	1 547.25 \pm 68.94 ^b	1 366.18 \pm 52.49 ^b
2.5	3 402.34 \pm 93.44 ^a	2 567.76 \pm 68.21 ^b	1 260.37 \pm 51.27 ^b	910.25 \pm 45.37 ^b
5.0	3 324.78 \pm 65.43 ^a	2 411.56 \pm 69.34 ^b	840.79 \pm 41.17 ^b	517.83 \pm 41.26 ^b
10.0	3 301.29 \pm 59.28 ^a	2 360.40 \pm 49.28 ^b	820.56 \pm 39.76 ^b	498.71 \pm 40.14 ^b
15.0	3 294.12 \pm 67.33 ^a	2 324.25 \pm 47.30 ^b	810.17 \pm 45.61 ^b	485.26 \pm 37.56 ^b
20.0	3 280.54 \pm 62.46 ^a	2 320.60 \pm 46.83 ^b	804.63 \pm 51.34 ^b	476.90 \pm 38.41 ^b

^a $P < 0.05$, ^b $P < 0.01$ vs control.

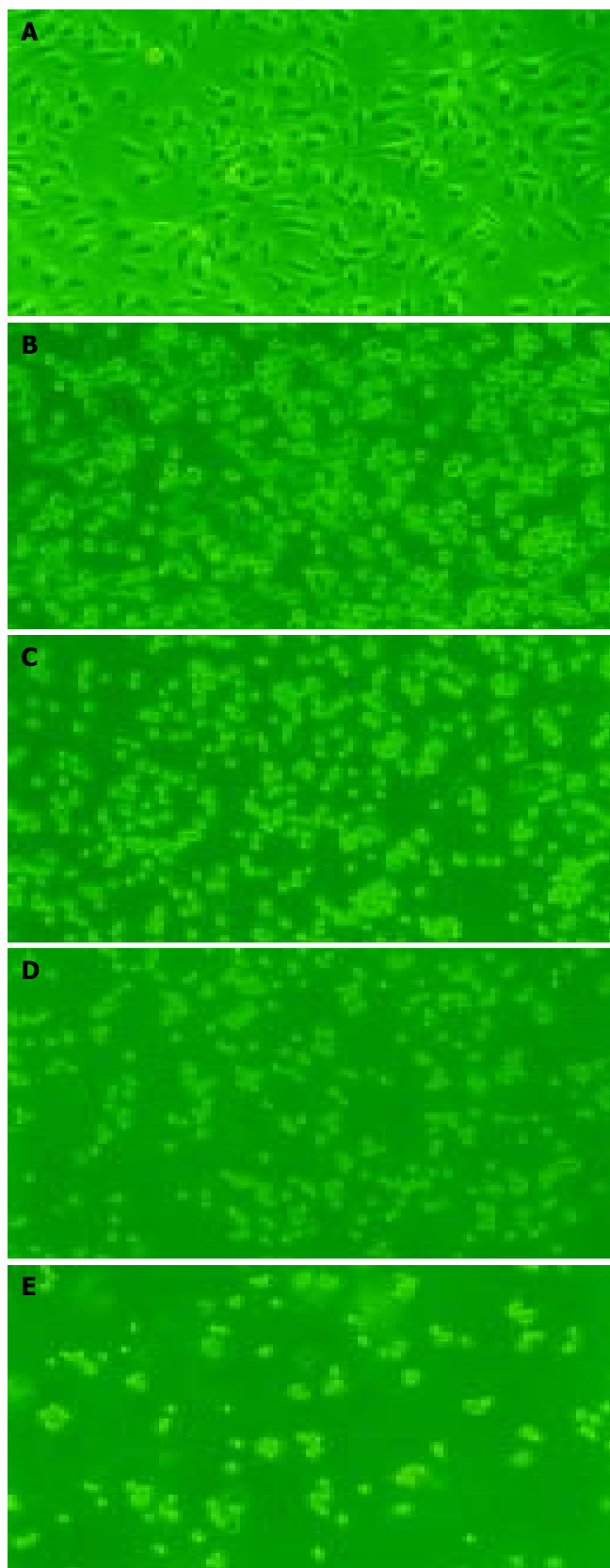


Figure 2 Morphologic changes of EC9706 cells observed under microscope after treated with 5 $\mu\text{mol/L}$ of MG-132. A: control group; B: EC9706 cells treated with MG-132 for 24 h; C: EC9706 cells treated with MG-132 for 48 h; D: EC9706 cells treated with MG-132 for 72 h; E: EC9706 cells treated with MG-132 for 96 h ($\times 200$).

Inhibition of DNA synthesis

The values of $^3\text{H-TdR}$ incorporation of MG-132 group were decreased compared with the control group (Table 1).

Morphologic changes of cells

EC9706 cells became round, small and exfoliative after exposed to MG-132 under microscope (Figure 2).

Inhibition of telomerase activity

After treated with MG-132 (5 $\mu\text{mol/L}$) for 24, 48, 72 and 96 h, respectively, EC9706 cells showed a gradual decrease in values of A compared with the control group ($P < 0.01$). Furthermore, telomerase activity was negative (Table 2).

Table 2 Effect of MG-132 on telomerase activity of EC9706 cells (mean \pm SD)

Groups	Light absorption (A)			
	24 h	48 h	72 h	96 h
Control	1.871 \pm 0.061	2.234 \pm 0.092	2.907 \pm 0.113	3.025 \pm 0.120
MG-132	0.154 \pm 0.008 ^b	0.085 \pm 0.006 ^b	0.072 \pm 0.004 ^b	0.067 \pm 0.003 ^b

^b $P < 0.01$ vs control group.

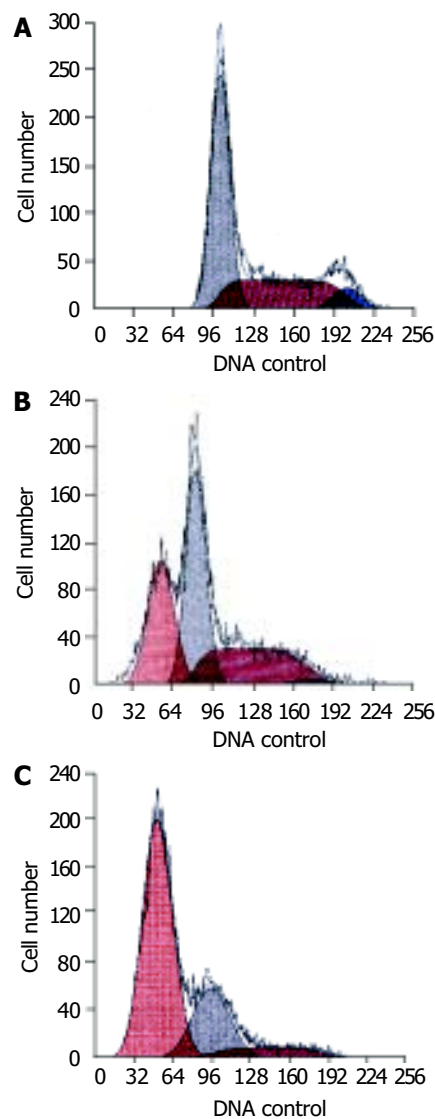


Figure 3 Cell cycle and apoptosis of EC9706 cells exposed to 5 $\mu\text{mol/L}$ of MG-132. A: control group. Apoptotic sub- G_1 peak was not found; B: EC9706 cells exposed to MG-132 for 48 h. The ratio of apoptotic cells was 31.7%; C: EC9706 cells exposed to MG-132 for 96 h. The ratio of apoptotic cells was 66.4%.

Changes of cell cycle and apoptosis

The percentage of cells at G_0/G_1 phase was increased and that

at G₂/M and S was decreased ($P < 0.01$). The rate of apoptotic cells treated with 5 $\mu\text{mol/L}$ of MG-132 for 48 and 96 h was 31.7% and 66.4%, respectively (Table 3, Figure 3).

Table 3 Effect of MG-132 on cell cycle of EC9706 cells (mean \pm SD, %)

Groups	48 h			96 h		
	G ₀ /G ₁	S	G ₂ /M	G ₀ /G ₁	S	G ₂ /M
Control	40.4 \pm 3.9	46.5 \pm 4.3	13.1 \pm 1.0	44.6 \pm 4.1	40.9 \pm 2.3	14.5 \pm 1.4
MG-132	67.5 \pm 5.1 ^b	29.3 \pm 2.8 ^b	3.2 \pm 0.2 ^b	73.1 \pm 5.2 ^b	24.6 \pm 2.1 ^b	2.3 \pm 0.1 ^b

^b $P < 0.01$ vs control group.

DNA ladder

Agarose electrophoresis showed marked ladders in MG-132 group, while the ladder was not detected in control group. Furthermore, DNA fragmentation was more apparent at 96 h (Figure 4).

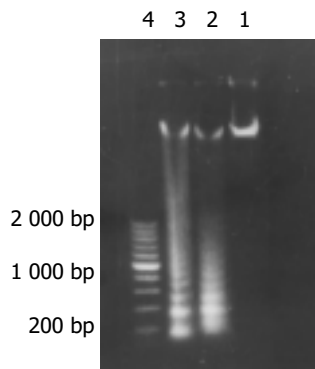


Figure 4 Results of DNA agarose electrophoresis. Lane 1: control group; Lane 2: EC9706 cells exposed to 5 $\mu\text{mol/L}$ of MG-132 for 48 h; Lane 3: EC9706 cells exposed to 5 $\mu\text{mol/L}$ of MG-132 for 96 h; Lane 4: 200, 400, 600, 800, 1 000, 1 200, 1 400, 1 600, 1 800, 2 000 bp ladder markers.

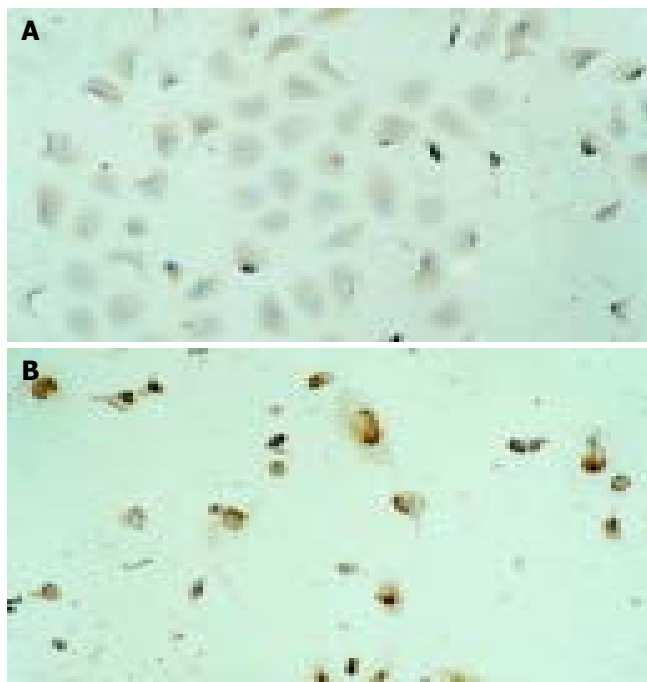


Figure 5 Results of immunohistochemical staining of EC9706 cells. A: control group. Immunohistochemical staining of p27^{kip1} protein located in cytoplasm of EC9706 cells; B: MG-132 group.

Immunohistochemical staining of p27^{kip1} protein located in cytoplasm and nuclei ($\times 200$).

Expression of p27^{kip1}

In the control group, the cytoplasm was stained in brownish yellow and the nuclei were stained in blue. In the experiment group, both the cytoplasm and nuclei were stained in brownish yellow, indicating that the expression of p27^{kip1} in EC9706 cells was increased after treated with MG-132 (Figure 5).

DISCUSSION

Proteolytic degradation by ubiquitin-proteasome system involves ATP-dependent covalent attachment of a macromolecular chain of ubiquitin (Ub) molecules to the target protein, followed by degradation through the multicatalytic 26S proteasome. The conjugation of Ub, a highly conserved 8.6 kDa protein, to its target protein is mediated by the serial actions of three enzymes. E1, the Ub-activating enzyme, activates Ub in an ATP-dependent manner. E2, the Ub-conjugating enzyme, catalyzes the attachment of Ub to the substrate protein. E3, the Ub-ligase, serves as a scaffold between E2 and the substrate and provides recognition specificity of the substrate^[7-10]. A protein tagged with a polyubiquitin chain is recognized and degraded by the 26S proteasome complex. This complex is composed of a 19S regulatory subcomplex and two 20S catalytic subcomplexes. UPP is extensively involved in physiological and biochemical processes. Some experiments showed that the low expression of some anti-oncogene including p53, p27^{kip1} in tumor cells was associated with the increasing activity of ubiquitin proteasome which leads to degradation of expression products of anti-oncogene, and have proved that deubiquitination of p53 is an important pathway for p53 stabilization^[11,12]. Moreover, the degradation accommodation of some transcription factors was regulated by UPP, such as *NF- κ B*, *c-fos*, *c-jun*, *c-mos*, *c-myc* and *MATa*^[13-17]. So UPP is closely associated with the occurrence and development of malignant tumor.

Ubiquitin proteasome inhibitors include peptide aldehyde, borofax peptide and 3, 4-dichloro isocoumarin. MG-132, also known as carbobenzoxy-L-leucyl-L-leucyl-L-leucinal, a reversible, effective and specific peptide aldehyde inhibitor of ubiquitin-proteasome, could block UPP through inhibiting ubiquitin-mediated proteolysis by binding to and inactivating 20S and 26S proteasomes^[18-22].

In our study, esophageal cancer cell line EC9706 was exposed to MG-132 to observe whether UPP could be inhibited. We found that the proliferation of cells was obviously inhibited in a dose- and time-dependent manner. The results also revealed some anti-tumor mechanisms of MG-132. First, MG-132 could up-regulate the expression of p27^{kip1}. p27^{kip1} was recently found^[23] as an anti-oncogene with function of negative regulation of cell cycle, getting involved in the inhibitive reaction of cytokines, inducing cell differentiation and apoptosis, enhancing cell's adherence and regulating the resistance to medicines for nonmenal tumors. p27^{kip1} protein is a cyclin dependent kinase inhibitor (CDKI) that could block G₁/S transition of cell cycle by inhibiting the action of cyclin E-CDK2 complex and cyclin D-CDK4 complex^[24-26]. p27^{kip1} expression decreases in esophageal cancer and it may correlate with the histologic differentiation. Reduction of p27^{kip1} has been considered to be an independent prognostic indicator of esophageal cancer^[27-30]. The nuclear localization signal of p27^{kip1} contains a protein kinase B (PKB/Akt) consensus site at threonine 157, and phosphorylation of p27^{kip1} by PKB/Akt has been found to impair its nuclear import^[31,32], which is a key procedure to play its functional role^[33]. We found that p27^{kip1} protein localized in cytoplasm of EC9706 cells showed low expression, but that localized both in cytoplasm

and nuclei of EC9706 cells showed high expression after treated with MG-132. Our previous studies^[6,34] demonstrated that the growth of EC9706 cells and tumors implanted in nude mice was obviously inhibited, apoptosis was induced and cell cycle was arrested in G₁ phase by up-regulating p27^{kip1}. Second, MG-132 could depress telomerase activity. The activation of telomerase was closely associated with cyclin. It has been reported that inhibition of UPP could not only increase the expression of p27^{kip1}, but also increase the expression of p53^[35]. Moreover p27^{kip1} and p21 regulated by p53 could inhibit cyclin and result in decreased telomerase activity^[36,37]. Third, MG-132 could cause G₁ arrest, which may be involved in changes of cell cycle regulatory factors such as p27^{kip1}. Fan *et al.*^[38] obtained the same results as ours. But Ling *et al.*^[39] tended to consider ubiquitin proteasome inhibitors to cause G₂ arrest. The difference may be involved in the different types of cells. The last, MG-132 could induce apoptosis, which may be closely associated with the functions mentioned above.

In conclusion, MG-132 can obviously inhibit proliferation of EC9706 cells and induce apoptosis. The mechanisms include upregulation of p27^{kip1} expression, G₁ arrest and depression of telomerase activity. The results indicate that inhibiting UPP is a novel strategy for esophageal carcinoma therapy.

REFERENCES

- Zhang WG, Wu QM, Wang XH, Xie GJ, Yu JP. Relationship between expression of survivin gene and biological characteristics in human esophageal carcinoma. *J Chinese Physician* 2003; **5**: 1378-1380
- Wu QM, Li SB, Wang Q, Wang DH, Li XB, Liu CZ. The expression of COX-2 in esophageal carcinoma and its relation to clinicopathologic characteristics. *Shijie Huaren Xiaohua Zazhi* 2001; **9**: 11-14
- Li SB, Wu QM, Wang Q, Wang XH, Xie GJ. Effects of adenovirus-mediated human COX-2 antisense RNA on synthesis of DNA and proteins in esophageal carcinoma cell line. *Shijie Huaren Xiaohua Zazhi* 2003; **11**: 517-521
- King RW, Deshaies RJ, Peters JM, Kirschner MW. How proteolysis drives the cell cycle. *Science* 1996; **274**: 1652-1659
- Fuchs SY. The role of ubiquitin-proteasome pathway in oncogenic signaling. *Cancer Biol Ther* 2002; **1**: 337-341
- Wu QM, Yu JP, Tong Q, Wang XH, Xie GJ. Inhibition of adenovirus-mediated p27^{kip1} gene on growth of esophageal carcinoma cell strain. *World J Gastroenterol* 2003; **9**: 2404-2408
- Hellmann H, Estelle M. Plant development: regulation by protein degradation. *Science* 2002; **297**: 793-797
- Whitehouse AS, Tisdale MJ. Increased expression of the ubiquitin-proteasome pathway in murine myotubes by proteolysis-inducing factor (PIF) is associated with activation of the transcription factor NF-kappaB. *Br J Cancer* 2003; **89**: 1116-1122
- von der Lehr N, Johansson S, Larsson LG. Implication of the ubiquitin/proteasome system in Myc-regulated transcription. *Cell Cycle* 2003; **2**: 403-407
- Yun J, Lee WH. Degradation of transcription repressor ZBRK1 through the ubiquitin-proteasome pathway relieves repression of Gadd45a upon DNA damage. *Mol Cell Biol* 2003; **23**: 7305-7314
- Lim MS, Adamson A, Lin Z, Perez-Ordóñez B, Jordan RC, Tripp S, Perkins SL, Elenitoba-Johnson KS. Expression of Skp2, a p27^{kip1} ubiquitin ligase, in malignant lymphoma: correlation with p27^{kip1} and proliferation index. *Blood* 2002; **100**: 2950-2956
- Li M, Chen D, Shiloh A, Luo J, Nikolaev AY, Qin J, Gu W. Deubiquitination of p53 by HAUSP is an important pathway for p53 stabilization. *Nature* 2002; **416**: 648-653
- McDade TP, Perugini RA, Vittimberga FJ Jr, Callery MP. Ubiquitin-proteasome inhibition enhances apoptosis of human pancreatic cancer cells. *Surgery* 1999; **126**: 371-377
- Salvat C, Aquaviva C, Jariel-Encontre I, Ferrara P, Pariat M, Steff AM, Carillo S, Piechaczyk M. Are there multiple proteolytic pathways contributing to c-Fos, c-Jun and p53 protein degradation *in vivo*? *Mol Biol Rep* 1999; **26**: 45-51
- Lafarga M, Berciano MT, Pena E, Mayo I, Castano JG, Bohmann D, Rodrigues JP, Tavanez JP, Carmo-Fonseca M. Clastosome: a subtype of nuclear body enriched in 19S and 20S proteasomes, ubiquitin, and protein substrates of proteasome. *Mol Biol Cell* 2002; **13**: 2771-2782
- Gregory MA, Hann SR. c-Myc proteolysis by the ubiquitin-proteasome pathway: stabilization of c-Myc in Burkitt's lymphoma cells. *Mol Cell Biol* 2000; **20**: 2423-2435
- von der Lehr N, Johansson S, Wu S, Bahram F, Castell A, Cetinkaya C, Hydbring P, Weidung I, Nakayama K, Nakayama KI, Soderberg O, Kerppola TK, Larsson LG. The F-box protein Skp2 participates in c-Myc proteosomal degradation and acts as a cofactor for c-Myc-regulated transcription. *Mol Cell* 2003; **11**: 1189-1200
- Mailhes JB, Hilliard C, Lowery M, London SN. MG-132, an inhibitor of proteasomes and calpains, induced inhibition of oocyte maturation and aneuploidy in mouse oocytes. *Cell Chromosome* 2002; **1**: 2
- Steinhilb ML, Turner RS, Gaut JR. The protease inhibitor, MG132, blocks maturation of the amyloid precursor protein Swedish mutant preventing cleavage by beta-Secretase. *J Biol Chem* 2001; **276**: 4476-4484
- Bonuccelli G, Sotgia F, Schubert W, Park DS, Frank PG, Woodman SE, Insabato L, Cammer M, Minetti C, Lisanti MP. Proteasome inhibitor (MG-132) treatment of mdx mice rescues the expression and membrane localization of dystrophin and dystrophin-associated proteins. *Am J Pathol* 2003; **163**: 1663-1675
- Shibata T, Imaizumi T, Tamo W, Matsumiya T, Kumagai M, Cui XF, Yoshida H, Takaya S, Fukuda I, Satoh K. Proteasome inhibitor MG-132 enhances the expression of interleukin-6 in human umbilical vein endothelial cells: Involvement of MAP/ERK kinase. *Immunol Cell Biol* 2002; **80**: 226-230
- Banerjee D, Liefshitz A. Potential of the proteasomal inhibitor MG-132 as an anticancer agent, alone and in combination. *Anticancer Res* 2001; **21**: 3941-3947
- Polyak K, Kato JY, Solomon MJ, Sherr CJ, Massague J, Roberts JM, Koff A. p27^{kip1}, a cyclin-Cdk inhibitor, links transforming growth factor-beta and contact inhibition to cell cycle arrest. *Genes Dev* 1994; **8**: 9-22
- Manne U, Jhala NC, Jones J, Weiss HL, Chatla C, Meleth S, Suarez-Cuervo C, Grizzle WE. Prognostic significance of p27^{kip1} expression in colorectal adenocarcinomas is associated with tumor stage. *Clin Cancer Res* 2004; **10**: 1743-1752
- Center DM, Cruikshank WW, Zhang Y. Nuclear pro-IL-16 regulation of T cell proliferation: p27^(kip1)-dependent G0/G1 arrest mediated by inhibition of Skp2 transcription. *J Immunol* 2004; **172**: 1654-1660
- Wang G, Reisdorph R, Clark RE Jr, Miskimins R, Lindahl R, Miskimins WK. Cyclin dependent kinase inhibitor p27^(kip1) is upregulated by hypoxia via an ARNT dependent pathway. *J Cell Biochem* 2003; **90**: 548-560
- Yasunaga M, Tabira Y, Nakano K, Iida S, Ichimaru N, Nagamoto N, Sakaguchi T. Accelerated growth signals and low tumor-infiltrating lymphocyte levels predict poor outcome in T4 esophageal squamous cell carcinoma. *Ann Thorac Surg* 2000; **70**: 1634-1640
- Shamma A, Doki Y, Tsujinaka T, Shiozaki H, Inoue M, Yano M, Kawanishi K, Monden M. Loss of p27^(kip1) expression predicts poor prognosis in patients with esophageal squamous cell carcinoma. *Oncology* 2000; **58**: 152-158
- Shibata H, Matsubara O, Wakiyama H, Tanaka S. The role of cyclin-dependent kinase inhibitor p27 in squamous cell carcinoma of the esophagus. *Pathol Res Pract* 2001; **197**: 157-164
- Taniere P, Martel-Planche G, Saurin JC, Lombard-Bohas C, Berger F, Scoazec JY, Hainaut P. TP53 mutations, amplification of P63 and expression of cell cycle proteins in squamous cell carcinoma of the oesophagus from a low incidence area in Western Europe. *Br J Cancer* 2001; **85**: 721-726

- 31 **Liang J**, Zubovitz J, Petrocelli T, Kotchetkov R, Connor MK, Han K, Lee JH, Ciarallo S, Catzavelos C, Beniston R, Franssen E, Slingerland JM. PKB/Akt phosphorylates p27, impairs nuclear import of p27 and opposes p27-mediated G1 arrest. *Nat Med* 2002; **8**: 1153-1160
- 32 **Viglietto G**, Motti ML, Bruni P, Melillo RM, D'Alessio A, Califano D, Vinci F, Chiappetta G, Tsichlis P, Bellacosa A, Fusco A, Santoro M. Cytoplasmic relocalization and inhibition of the cyclin-dependent kinase inhibitor p27kip1 by PKB/Akt-mediated phosphorylation in breast cancer. *Nat Med* 2002; **8**: 1136-1144
- 33 **Singh SP**, Lipman J, Goldman H, Ellis FH Jr, Aizenman L, Cangi MG, Signoretti S, Chiaur DS, Pagano M, Loda M. Loss or altered subcellular localization of p27 in Barrett's associated adenocarcinoma. *Cancer Res* 1998; **58**: 1730-1735
- 34 **Zhang WG**, Wu QM, Tong Q, Yu JP. Inhibitory effect of p27kip1 mediated by adenovirus on model of esophageal carcinoma in nude mice. *Shijie Huaren Xiaohua Zazhi* 2003; **11**: 512-516
- 35 **Fan XM**, Wong BC, Wang WP, Zhou XM, Cho CH, Yuen ST, Leung SY, Lin MC, Kung HF, Lam SK. Inhibition of proteasome function induced apoptosis in gastric cancer. *Int J Cancer* 2001; **93**: 481-488
- 36 **Liu XJ**, Wu QM, Tong Q, Zhang WG, Liu CZ, Yu JP. The effect of p27kip1 cDNA on the telomerase activity and cell cycle of SGC7901 cells. *Shiyong Aizheng Zazhi* 2003; **18**: 253-256
- 37 **Harada K**, Kurisu K, Sadatomo T, Tahara H, Tahara E, Ide T, Tahara E. Growth inhibition of human glioma cells by transfection-induced P21 and its effects on telomerase activity. *J Neurooncol* 2000; **47**: 39-46
- 38 **Fan XM**, Wong BC, Wang WP, Zhou XM, Cho CH, Yuen ST, Leung SY, Lin MC, Kung HF, Lam SK. Inhibition of proteasome function induced apoptosis in gastric cancer. *Int J Cancer* 2001; **93**: 481-488
- 39 **Ling YH**, Liebes L, Ng B, Buckley M, Elliott PJ, Adams J, Jiang JD, Muggia FM, Perez-Soler R. PS-341, a novel proteasome inhibitor, induces Bcl-2 phosphorylation and cleavage in association with G2-M phase arrest and apoptosis. *Mol Cancer Ther* 2002; **1**: 841-849

Edited by Kumar M and Wang XL Proofread by Xu FM

Are gap junction gene connexins 26, 32 and 43 of prognostic values in hepatocellular carcinoma? A prospective study

I-Shyan Sheen, Kuo-Shyang Jeng, Po-Chuan Wang, Shou-Chuan Shih, Wen-Hsing Chang, Horng-Yuan Wang, Chung-Chu Chen, Li-Rung Shyung

I-Shyan Sheen, Division of Hepatogastroenterology, Chang Gung Memorial Hospital, Taipei, Taiwan, China

Kuo-Shyang Jeng, Departments of Surgery, Mackay Memorial Hospital, Taipei, Taiwan, China

Po-Chuan Wang, Shou-Chuan Shih, Wen-Hsing Chang, Horng-Yuan Wang, Chung-Chu Chen, Li-Rung Shyung, Department of Internal Medicine, Mackay Memorial Hospital, Taipei, Taiwan, China

Kuo-Shyang Jeng, Mackay Junior School of Nursing, Taipei, Taiwan, China

Supported by grants from Department of Health, National Science Council, Executive Yuan, Taiwan, China NSC-89-2314-B-195-027

Correspondence to: Kuo-Shyang Jeng, M.D., F.A.C.S., Department of Surgery, Mackay Memorial Hospital, No.92, Sec 2, Chung-San North Road, Taipei, Taiwan, China. issheen.jks@msa.hinet.net

Telephone: +886-2-25433535 **Fax:** +886-2-27065704

Received: 2004-02-02 **Accepted:** 2004-02-23

Abstract

AIM: To investigate the prognostic value of the expression of connexin (Cx) 26, 32 and 43 messenger RNA (mRNA) in hepatocellular carcinoma (HCC) tissues.

METHODS: Using a reverse-transcriptase polymerase chain reaction (RT-PCR), Cx 26, Cx 32 and Cx 43 mRNAs were determined in the liver tissues of 15 controls and in HCC tissues of 25 patients undergoing curative hepatic resection. The patients were followed up clinically.

RESULTS: Cx 26 and Cx 32 mRNAs were significantly lower in HCC tissues compared with controls (both $P < 0.01$). By multivariate analysis, a lower level of Cx 26 and Cx 32 mRNA correlated significantly with a risk of HCC recurrence ($P = 0.033$) and recurrence-related mortality ($P = 0.031$, $P = 0.031$). Cx 43 mRNA was higher in HCC tissues compared with controls but did not correlate with postoperative recurrence or recurrence-related mortality. Other significant predictors of HCC recurrence included cellular dedifferentiation ($P = 0.033$), less encapsulation ($P = 0.050$), vascular permeation ($P = 0.046$), and daughter nodules ($P = 0.046$). Significant variables related to recurrence-related mortality consisted of cell dedifferentiation ($P = 0.031$), vascular permeation ($P = 0.048$), and daughter nodules ($P = 0.048$). The levels of Cx 26 and Cx 32 mRNAs correlated significantly with cell differentiation ($P = 0.031$).

CONCLUSION: A low expression of Cx 26 and Cx 32 mRNAs in HCC tissues is predictive of postoperative recurrence of HCCs.

Sheen IS, Jeng KS, Wang PC, Shih SC, Chang WH, Wang HY, Chen CC, Shyung LR. Are gap junction gene connexins 26, 32 and 43 of prognostic values in hepatocellular carcinoma? A prospective study. *World J Gastroenterol* 2004; 10(19): 2785-2790

<http://www.wjgnet.com/1007-9327/10/2785.asp>

INTRODUCTION

Hepatocellular carcinoma (HCC) is a leading cause of death in Taiwan and many Asian countries, where hepatitis B and C have a high prevalence. During the last 10 years, efforts have been made worldwide toward early detection and curative surgical resection of HCC. However, despite diagnostic and therapeutic advances, postoperative recurrence is still common^[1-7]. Predicting which patients are likely to have a recurrence is a challenge.

Gap junctional intercellular communication (GJIC) occurs via intercellular hemichannels, which are formed by six basic protein subunits expressed in neighboring cells. These subunits are called connexins (Cx)^[8]. Six connexins locate around a central pore, through which adjacent cells directly exchange low weight molecules providing information or energy. GJIC plays important roles in embryonic development, metabolic cooperation, growth control, cell proliferation, and differentiation^[9-12]. Many authors believed that disorders of GJIC were involved in carcinogenesis^[12-21].

Connexin 32 (Cx 32) and connexin 26 (Cx 26) are the major gap junction proteins in hepatocytes. Some authors have reported that Cx 32 and Cx 43 mRNAs and their proteins were significantly decreased in HCC tissues and cell lines. In contrast, Cx 43 protein was increased in the hepatoma cell line SMMC-7721^[22-25].

To the best of our knowledge, little is known about the prognostic significance of connexin mRNA expression in the prediction of postresection recurrence of HCCs. We conducted this prospective study to investigate the correlation between connexin mRNA expression in HCC tissues and postoperative recurrence of the tumor.

MATERIALS AND METHODS

Study population

From July 1999 to August 2000, 25 (18 men and 7 women, with a mean age of 56.4 ± 12.6 years) of 34 consecutive patients with HCC undergoing curative hepatectomy were enrolled in this prospective study. The 9 patients who were excluded had a previous hepatectomy, preoperative neoadjuvant ethanol injection, hepatic arterial chemoembolization (TACE), or surgical morbidity. The surgical procedures performed included 23 major resections (6 extended right lobectomies, 10 right lobectomies, 3 left lobectomies and 4 double segmentectomies) and 2 minor resections (single segmentectomy). Clinical details were available from medical records on all patients (Table 1). Connexins were assayed in both cancerous and noncancerous liver tissues obtained at the time of resection. A control group including 5 healthy volunteers, 5 individuals with chronic active hepatitis without HCCs, and 5 individuals with liver cirrhosis but no HCC also underwent liver biopsies during exploratory laparotomies for other reasons. The surgically removed liver samples were immediately transferred to the pathology laboratory, dissected, frozen in liquid nitrogen, and stored at -80°C until RNA extraction. Frozen and formalin-fixed samples of the dissected tumor and surrounding tissues were also studied by routine pathology. No obvious ischemic change

was observed in the surrounding tissues, suggesting that the time between removal and freezing of samples did not result in problematic artifacts.

After discharge, the patients were assessed regularly to detect tumor recurrence with abdominal ultrasonography (every 2-3 mo during the first 5 years, then every 4-6 mo thereafter), serum alpha fetoprotein (AFP) and liver biochemistry (every 2 mo during the first 2 years, then every 4 mo during the following 3 years, and every 6 mo thereafter), abdominal computed tomography (CT) (every 6 mo during the first 5 years, then annually), and chest X-ray and bone scans (every 6 mo). Hepatic arteriography was obtained if the other studies suggested possible recurrences. A recurrence was defined as detection of a tumor on any imaging study.

Clinicopathologic parameters analyzed included sex (male vs female), age, presence of liver cirrhosis, hepatitis B virus (HBV) infection (hepatitis B surface antigen-positive), hepatitis C virus (HCV) infection (anti-hepatitis C virus antibody-positive), serum AFP level (<20 ng/mL vs 20 to 1 000 ng/mL vs >1 000 ng/mL), cirrhosis, Child-Pugh class of liver functional reserve (A vs B), tumor size (<3 cm vs 3 to 10 cm vs >10 cm in diameter), tumor encapsulation (complete vs incomplete or absent), presence of daughter nodules, vascular permeation (including vascular invasion and/or tumor thrombi in either the portal or hepatic vein), and cell differentiation grade (Edmondson and Steiner grades I to IV) (Table 1).

Table 1 Demographic, clinical and pathological variables in patients with HCC undergoing curative resections (n = 25)

Variables	Patients (n, %)
Age (mean, yr)	56.4±12.6
Male	18 (72)
Child- Pugh class A	
Serum AFP <20 ng/mL	3 (12)
20-10 ³ ng/mL	10 (40)
>10 ³ ng/mL	12 (48)
HBsAg (+)	12 (48)
Anti-HCV (+)	10 (40)
Diameter of HCC <3 cm	2 (8)
3-10 cm	10 (40)
>10 cm	13 (52)
Cirrhosis	20 (80)
Edmondson-Steiner's grade I	11 (44)
grade II	
grade III	14 (56)
grade IV	
Complete capsule	9 (36)
Vascular permeation	14 (56)
Daughter nodules	13 (52)
Multinodular HCC	5 (20)
Tumor necrosis	5 (20)
Tumor hemorrhage	1 (4)

AFP: serum alpha fetoprotein; HBsAg (+): positive hepatitis B surface antigen; Anti-HCV(+): positive hepatitis C virus antibody; Edmondson Steiner grade: differentiation grade.

Detection of connexin mRNA in liver tissues

We chose measuring connexin mRNA instead of measuring protein because RT-PCR was thought to provide better quantification method than immunohistochemistry.

Extraction of RNA Resected tissues were completely homogenized in 1 mL of RNA-bee™ (Tel-Test, Protech Technology Enterprises

Co., Ltd, Friendswood, TX, USA), 0.2 mL chloroform was added, and the mixture was shaken vigorously for 15 to 30 s. The samples were stored on ice for 5 min and then centrifuged at 12 000 g for 15 min. The supernatant was transferred to a new 1.5 mL Eppendorf tube, precipitated with 0.5 mL of isopropanol for 5 min at 4 °C, and centrifuged at 12 000 g for 5 min at 4 °C. The supernatant was removed and the RNA pellet was washed with 1 mL of isopropanol and shaken to dislodge the pellet from the side of the tube. The pellet was centrifuged again at 12 000 g for 5 min at 4 °C, the supernatant was removed, and the RNA pellet was washed once again with 750 mL/L ethanol. The pellet was resuspended in at least 1 mL of 750 mL/L ethanol and centrifuged at 7 500 r/min for 5 min at 4 °C, after which the ethanol was carefully removed. The RNA was allowed to dry in air and then dissolved in DEPC-H₂O (50 to 100 µL) and stored at -80 °C.

Reverse transcription The RNA sample was heated at 55 °C for 10 min and chilled on ice. The following reagents were then added: (1) 4 µL 5×RT buffer containing Tris-HCl (pH 8.3), 75 mmol/L KCl, 3 mmol/L MgCl₂, and 10 mmol/L DTT (dithiothreitol), (2) 3 µL 10 mmol/L dNTP (deoxyribonucleoside triphosphate), (3) 1.6 µL Oligo-d(T)₁₈ and 0.4 µL random hexamers (N) 6 (1 µg/µL), (4) 0.5 µL RNase inhibitor (40 U/µL), (5) 3 µL 25 mmol/L MnCl₂, (6) 6 µL RNA in DEPC-H₂O, and (7) 0.5 µL DEPC-H₂O. The mixture was incubated at 70 °C for 2 min and then chilled to 23 °C to anneal the primer to the RNA. We then added 1 µL of M-MLV RTase (moloney murine leukemia virus reverse transcriptase, 200 U/µL, Promega) and the mixture was incubated for 10 min at 23 °C followed by 60 min at 40 °C. It was heated at 94 °C for 5 min, then chilled on ice. The cDNA was stored -20 °C.

Amplification of connexins 26, 32, 43, and GAPDH cDNA by PCR First-strand cDNA synthesis was carried out using 2 µg of total RNA purified from 50 mg tissue. Reverse transcription was performed in a final volume of 20 µL containing 2 µg of random hexamer (Gene Tek Bioscience Inc., Taipei), and 1.5 mmol/L each of dATP, dCTP, dGTP, and dTTP. Each reaction mixture was incubated for 8 min at 23 °C with 20 U of rRNasin (RNase inhibitor; Promega, Madison, WI) followed by incubation with 200 U of moloney murine leukemia virus reverse transcriptase (Gibco-BRL, Paisley, UK) for 60 min at 40 °C, followed by 5 min at 94 °C. PCR was performed in a final volume of 50 µL, by using 2 µL of cDNA solution in a mixture containing 0.4 mmol/L deoxynucleotide triphosphates, 40 pmol/L of both sense and antisense oligonucleotide primers for Cx 26, Cx 32 or Cx 43, 2.5 mmol/L MgCl₂, 2.5U of Taq DNA polymerase (Promega) and 5 µL of 10x Taq DNA polymerase reaction buffer (500 mmol/L KCl, 100 mmol/L Tris-HCl (pH9.0), 10 g/L Triton-X-100). PCR primer sequences of the sense and antisense oligonucleotides for Cx 26, Cx 32 and Cx 43 as well as the direction, size and reaction conditions are shown in Table 2. For example, Cx 26 anti-sense oligonucleotide (5'-CCGAAGTTCATGAAGGGAGA GAT-3') and its related scrambled sequence (5'-GGTCTTTTGG ACTTCCCTGAGCA -3') were synthesized (by Sigma-Genosys Ltd, Woodlands, TX, USA). GAPDH was used as a control, with the quantities of the other mRNA products reported as their intensity as a fraction of that of GAPDH mRNA. To eliminate any possibility of genomic DNA contamination, PCR amplification reaction was carried out on each sample from the RNA extraction. As another internal contamination control, PCR amplification was also carried out on a sample of reaction mixture in the absence of cDNA.

The intensity of bands was measured using Fujifilm Science Lab 98 (Image Gauge V3.12). The sensitivity of our assay was assessed using human hepatocytes. A HepG2 (hepatoblastoma) cell line served as a positive control for connexin mRNA expression. For negative controls, we used EDTA-treated water (filtered and vaporized).

Statistical analysis

A statistical software package (SPSS for windows, version 8.0, Chicago, Illinois) was used. Student's *t*-test was used to analyze continuous variables and chi-square or Fisher's exact test was used for categorical variables. A Cox proportional hazards model was used for multivariate stepwise analysis to identify the significant factors predicting recurrence and mortality. Significance was taken as a *P* value <0.05.

Table 2 Nucleotide sequences of the primer sets and specific oligonucleotide probes to each type of connexin 5'-noncoding mRNA

Type of connexin mRNA	Primer probes	Nucleotide sequences
Cx 26	Sense	5' CCGAAGTTCATGAAGGGAGAGAT
	Antisense	5' GGTCTTTTGGACTTCCCTGAGCA
Cx 32	Sense	5' CTGCTCTACCCGGGCTATGC
	Antisense	5' CAGGCTGAGCATCGGTGCTCTT
Cx 43	Sense	5' TACCATGCGACCAGTGGTGCGCT
	Antisense	5'GAATTCTGTTATCATCGTGGGGAA

RESULTS

RT-PCR analysis of connexin transcripts in liver and HCC tissues

The mean values of Cx 26 mRNA and Cx 32 mRNA in HCC tissues were significantly lower than those in the control samples ($P < 0.01$, $P < 0.01$ respectively). There was no significant difference in Cx 43 mRNA between cancerous and control tissues (Table 3).

Table 3 Correlation of Cx 26, Cx 32, and Cx 43 mRNAs in cancerous and noncancerous liver tissues of 25 patients with HCC and liver tissues of 15 control patients

Tissues	mRNA (mean value)		
	Connexin 26	Connexin 32	Connexin 43
HCC patients			
Cancerous liver ¹	0.745	0.775	0.241
Controls ²	1.205	1.225	0.100

$P < 0.01$ for connexin 26 mRNA; $P < 0.01$ for connexin 32 mRNA; $P > 0.05$ for connexin 43 mRNA.

Correlation of connexin mRNA expression and tumor recurrence

Patients were followed up for a median of 45 mo (range 38 to 51 mo). Fourteen (56%) had clinically detectable recurrences, of whom 6 died. A low Cx 26 mRNA correlated significantly with tumor recurrences by both univariate ($P < 0.001$, $P < 0.001$) and multivariate analyses ($P = 0.033$, $P = 0.033$). No such correlation was found with Cx 43 mRNA. By multivariate analyses, other significant predictors of recurrences included poor cell differentiation ($P = 0.033$), less encapsulation ($P = 0.050$), vascular permeation ($P = 0.046$) and the presence of daughter nodules ($P = 0.046$) (Table 4).

Correlation of connexin mRNA expression and recurrence-related death

A low level of Cx 26 mRNA and Cx 32 mRNA in HCC tissues was significantly correlated with death from recurrent tumors by both univariate ($P < 0.001$, $P < 0.001$) and multivariate analyses ($P = 0.031$, $P = 0.031$) (Table 5). By multivariate analyses, poor cell differentiation, vascular permeation, and daughter nodules correlated significantly with mortality ($P = 0.031$, 0.048, and 0.048

respectively), and less encapsulation correlated with mortality with a marginal significance ($P = 0.053$).

Table 4 Predictors of HCC recurrence

Variable	<i>P</i> values	
	UV	MV
Sex	1.000	-
Age (yr)	0.030	0.071
Tumor diameter (<3 cm, >10 cm)	0.250	-
Liver cirrhosis	0.009	0.067
Child-Pugh class	0.528	-
Serum AFP	0.744	-
HBsAg (+)	1.000	-
Anti-HCV (+)	1.000	-
Edmondson Steiner grade	<0.001	0.033
Capsule	<0.001	0.050
Vascular permeation	<0.001	0.046
Daughter nodules	<0.001	0.046
Tumor necrosis	0.046	-
Tumor hemorrhage	0.046	-
Connexin 26 mRNA	<0.001	0.033
Connexin 32 mRNA	<0.001	0.033
Connexin 43 mRNA	0.280	0.071

UV: univariate analysis; MV: multivariate analysis; AFP: serum alpha fetoprotein; HBsAg(+): positive hepatitis B surface antigen; Anti-HCV(+): positive hepatitis C virus antibody; Edmondson Steiner grade: differentiation grades I, II vs III, IV.

Table 5 Correlation between clinical and pathological variables and recurrence-related mortality

Parameters	<i>P</i> values	
	UV	MV
Sex	0.888	-
Age (yr)	0.005	0.356
Tumor diameter (<3 cm, >10 cm)	0.324	-
Liver cirrhosis	0.030	0.324
Child-Pugh class	0.548	-
HBsAg (+)	0.956	-
Anti-HCV (+)	0.785	-
Edmondson Steiner grade	0.000	0.031
Capsule	0.000	0.053
Vascular permeation	0.000	0.048
Daughter nodules	0.039	0.048
Multinodular HCC	0.007	0.324
Tumor necrosis	0.373	-
Tumor hemorrhage	0.356	-
Connexin 26 mRNA	<0.001	0.031
Connexin 32 mRNA	<0.001	0.031
Connexin 43 mRNA	0.461	-

UV: univariate analysis; MV: multivariate analysis; AFP: serum alpha fetoprotein; HBsAg (+): positive hepatitis B surface antigen; Anti-HCV(+): positive hepatitis C virus antibody; Edmondson Steiner grade: differentiation grades I, II vs III, IV; n.s.: not significant.

Correlation between connexin mRNA expression and clinical and histopathologic features

Cx 26 and Cx 32 mRNAs were significantly correlated with cell differentiation but not with gender, age, serum AFP level, chronic HBV or HCV carriage, tumor size, coexisting cirrhosis, encapsulation, vascular permeation, daughter nodules, tumor necrosis, or tumor hemorrhage (all $P > 0.05$).

DISCUSSION

Our study showed that a low value of Cx 26 and Cx 32 mRNAs in resected HCC tissues was significantly associated with an increased risk of postoperative recurrences and death. While increased Cx 43 mRNA was not significantly predictive of outcomes.

Most tumors studied had a reduction in either homologous or heterologous GJIC. This presumably contributed to neoplastic progression by allowing tumor cells to escape intercellular signals involved in regulation of cell proliferation, differentiation, and apoptosis^[8,10,12,13]. Cx 32 and Cx 26, the components of hepatocyte gap junctions, were also found in a variety of other cell types. Cx 43 (or $\alpha 1$) was prominent in the liver capsule and between other types of liver cells, including Ito (fat-storing) cells, cholangiocytes, and endothelial cells lining the venules. We speculated that, because the Cx 32 and Cx 26 genes were expressed in normal liver tissues, they might serve as tumor suppressor genes. Other authors have suggested Cx 32 and Cx 43 for this role^[16]. Eghbali *et al.*^[18] found that transfection of tumor cells with Cx 32 cDNA retarded tumor growth *in vivo*. They demonstrated that the growth rate of tumor cells correlated negatively with the strength of intercellular communication.

Since Lowenstein *et al.*^[12] used electrophysiologic techniques to demonstrate a lack of communication between rat liver cancer cells, an interest has been attracted to changes in cell-to-cell communications in carcinoma tissues. In studies of rat hepatocarcinogenesis, several laboratories have found that a significant decrease in the major liver gap junction protein Cx 32 at the mRNA or protein level occurred in preneoplastic nodules and HCCs induced by chemicals^[14,17,19,21]. Loss of GJIC due to down-regulated expression of Cx genes appears to be an important event in cell transformation and is associated with uncontrolled tumor cell growth. Transformed cells *in vitro* and *in vivo* had a decreased GJIC capacity between themselves or with surrounding normal cells^[18,20]. Disruption of GJIC activity could contribute to the multi-step process of carcinogenesis.

Oyamada *et al.*^[25] reported that GJIC was altered in human HCCs by molecular mechanisms different from those in rat hepatocarcinogenesis. It is possible that defects in post-translational processing of Cx 32 and Cx 43 proteins may be an obstacle in their transportation to cell membranes. Some studies suggested that multiple mechanisms could likely contribute to block of GJIC, including decreased expressions of gap junction proteins and abnormal pathways of signal transduction resulted from decreased levels of intracellular Ca^{2+} , phosphorylation of the tyrosine of Cx proteins^[19]. Other potential mechanisms included control of cell recognition and gating of established gap junctions^[19,20,24].

Different authors have proposed various mechanisms by which changes in connexin mRNA might contribute to the biological behaviors of HCC. These include rapid proliferation of tumor cells, changes in the interaction between host and tumors, aberrant localization of connexins, and change in connexin expression during tumor differentiation. Whether the rapid growth of preneoplastic tissues is the cause or the effect of a decrease in connexin mRNA remains unknown.

Some authors have found a great decrease in the number of gap junctions after partial hepatectomy. A reciprocal correlation between the expression of Cx32 and the mitotic activities of hepatocytes during liver regeneration was noted. Based on their findings of a significant reduction of Cx 32 expression in S-phase cells, it seems that quantitative changes in gap junction expression may play an important role in the control of proliferation of liver cells. Since neoplastic liver tissues had a higher proliferation rate than the surrounding tissues, it might have fewer gap junctions. It was found that the partial loss of gap junctions provided a selective advantage for those preneoplastic liver cells which developed into rapidly proliferating tumor cells. It is possible that preneoplastic cells with a reduced number of gap junctions might have an increased capability of proliferating and are therefore more likely to develop into HCC^[14].

With regard to changes in the interaction between host and tumors, Krutovskikh *et al.*^[24] highlighted the role such an interaction might play in natural host resistance against neoplastic growth, with an emphasis on the underlying mechanisms of both connexin function and impairment.

Some other authors attributed the possible contribution of connexins to aberrant localization of the gap junction proteins. Some studies showed that the levels of Cx 32 and Cx 43 mRNAs were not decreased in HCCs compared with normal liver tissues, but the proteins were aberrantly located in HCCs^[25]. Krutovskikh *et al.*^[26] thought abnormal location of Cx 32 was more important than its translational dysregulation. Omori *et al.*^[17] drew a similar conclusion regarding Cx 32.

Another mechanism leading to a loss of heterologous host-cancer cell coupling is a change in the expression of connexin species in tumors during differentiation. According to Markert *et al.*^[27] three important characteristics of cell differentiation were the rate of cell division, the adhesive properties of the cell membrane that determine the capacity of the cell of migrating or metastasizing, and specific patterns of cell metabolism. Connexins are likely related to adhesive properties. An altered pattern of adhesion molecules on the surface of tumorigenic hepatocytes may influence the distribution of gap junctions in neoplastic tissues.

A characteristic feature of a cancerous phenotype is dedifferentiation. In some tissues, cells at different stages of differentiation express different sets of connexin proteins. HCC cells may express the same connexins as surrounding normal hepatocytes and therefore adhere well to each other. However, because of the inability of Cx 32 hemichannels expressed by normal hepatocytes to assemble functional gap junctional channels with Cx 43 hemichannels in neoplastic cells, they failed to communicate with each other^[28,29].

The high recurrence rate after resection is the main cause of the poor outcomes of HCC. Variables correlated with tumor recurrence included high serum AFP, hepatitis, vascular permeation, grade of cell differentiation, infiltration or absence of capsule, tumor size, coexisting cirrhosis, presence of daughter nodules, and multiple lesions^[1-7, 30-33]. According to our study, connexin was significantly correlated with the grade of cell differentiation. In our series, tumors with higher levels of Cx26 and Cx32 mRNAs, that were closer to normal, were more likely to be well-differentiated (Edmondson and Steiner grade I) and less likely to recur than those tumors of grade II to IV. The association between the grade of anaplasia and connexin positivity also varied in other reports. We attribute these differences to the possibility that different histologic grades may coexist within a particular HCC. Additionally, the regulation of connexin may be complex, particularly at different grades of dedifferentiation.

There is also discrepancy in the expression of Cx 43 in human HCCs. Ma *et al.*^[34] suggested that decreased expression of Cx 32 and Cx 43 might be closely related to liver carcinogenesis.

We found a similar decrease in Cx32 mRNA, but Cx 43 mRNA was increased. The discrepancy might be due to a difference in study samples and examination methods, as well as the background liver diseases. Furthermore, it should be noted that the benign liver tissue surrounding HCC was not normal. Oyamada *et al.*^[25] studied 6 patients with HCC and found various abnormalities in the surrounding tissues, including cholestasis in 2, fatty liver in 1, chronic persistent hepatitis in 1, cirrhosis in 1, and possible hemochromatosis in 1. In our 25 patients, we found a different distribution of background liver diseases, including cirrhosis in 20 (80%), hepatitis B virus hepatitis in 12 (48%) and hepatitis C virus hepatitis in 10 (40%); 3 patients had both hepatitis B and C hepatitis. We used RT-PCR and Northern and Southern blot analyses. Oyamada *et al.*^[25] found no decrease in Cx 32 mRNA, while the level of Cx 43 mRNA was higher than that in the surrounding nontumorous tissues but without any amplification of Cx 43 gene. They attributed the increased expression of Cx 43 to a large amount of connective tissues in HCC.

However, another possible explanation for elevated expression of Cx 43 is the stem cell concept of tumor cell origins. This theory proposes that the target cells in carcinogenesis are stem cells present in normal tissues. Assuming that a stem cell that expresses Cx 43 is the target cell in human hepatocarcinogenesis, the resulting neoplasm would be expected to express connexin 43. The mechanism of switching on the Cx 43 gene in human HCC remains to be investigated, which may include DNA methylation, a stabilization of RNA, or positive or negative trans-acting factors^[25].

Carcinogenesis is believed to result from block, arrest, or derangement in differentiation. Based on this concept, we could explain the increased expression of Cx 43 by the appearance of isozymes, for example, aldolase and γ -glutamyl transpeptidase, in human HCC.

We proposed that not all HCCs contained connexin mutations, in another word, there might be both connexin-dependent and connexin-independent pathways leading to liver cancer. The selective advantage conferred on liver cells by a mutant connexin gene seems to be significant in later steps of tumorigenesis, after the accumulation of additional genetic changes. The identification of genetic alterations related to connexin changes remains a considerable challenge in the field of liver cancer research.

Surgery remains the best possible therapy for patients with HCC. Examination of connexin mRNA in HCC tissues may provide information about the risk of postoperative recurrences, and our results support this hypothesis. Addition of neoadjuvant therapy after surgery, might be considered for the risk patients. Furthermore, serial measurement of circulating connexin mRNAs after surgery to monitor the effects of therapy or screen for recurrences needs further investigation.

REFERENCES

- 1 **Poon RT**, Fan ST, Lo CM, Liu CL, Wong J. Intrahepatic recurrence after curative resection of hepatocellular carcinoma. Long-term results of treatment and prognostic factors. *Ann Surg* 1999; **229**: 216-222
- 2 **Yamamoto J**, Kosuge T, Takayama T, Shimada K, Yamasaki S, Ozaki H, Yamaguchi N, Makuuchi M. Recurrence of hepatocellular carcinoma after surgery. *Br J Surg* 1996; **83**: 1219-1222
- 3 **Lee PH**, Lin WJ, Tsang YM. Clinical management of recurrent hepatocellular carcinoma. *Ann Surg* 1995; **222**: 670-676
- 4 **Jeng KS**, Sheen IS, Chen BF, Wu JY. Is the p53 gene mutation of prognostic value in hepatocellular carcinoma after resection? *Arch Surg* 2000; **135**: 1329-1333
- 5 **Jeng JS**, Sheen IS, Tsai YC. Gamma glutamyl transpeptidase messenger RNA may serve as a diagnostic aid in hepatocellular carcinoma. *Br J Surg* 2001; **88**: 986-987
- 6 **Jeng KS**, Chen BF, Lin HJ. En bloc resection for extensive hepatocellular carcinoma. Is it advisable? *World J Surg* 1994; **18**: 834-849
- 7 **Jeng K**, Yang FS, Chiang HJ, Ohta I. Is it advisable to perform a second operation for nodular recurrent hepatocellular carcinoma within the cirrhotic liver remnant? A comparison with TACE. *World J Surg* 1992; **16**: 1188-1191
- 8 **Bennett MV**, Barrio LC, Bargiello TA, Spray DC, Hertzberg E, Saez JC. Gap junctions: new tools, new answers, new questions. *Neuron* 1991; **6**: 305-320
- 9 **Robenek H**, Rassat J, Themann H. A quantitative freeze-fracture analysis of gap and tight junctions in the normal and cholestatic human liver. *Virchows Arch B Cell Pathol Incl Mol Pathol* 1981; **38**: 39-56
- 10 **Wilson MR**, Close TW, Trosko JE. Cell population dynamics (apoptosis, mitosis, and cell-cell communication) during disruption of homeostasis. *Exp Cell Res* 2000; **254**: 257-268
- 11 **Yamaoka K**, Nouchi T, Kohashi T, Marumo F, Sato C. Expression of gap junction protein connexin 32 in chronic liver diseases. *Liver* 2000; **20**: 104-107
- 12 **Loewenstein WR**, Kanno Y. Intercellular communication and the control of tissue growth: lack of communication between cancer cells. *Nature* 1966; **209**: 1248-1249
- 13 **Niessen H**, Willecke K. Strongly decreased gap junctional permeability to inositol 1,4,5-triphosphate in connexin32 deficient hepatocytes. *FEBS Lett* 2000; **466**: 112-114
- 14 **Janssen-Timmen U**, Traub O, Dermietzel R, Rabes HM, Willecke K. Reduced number of gap junctions in rat hepatocarcinomas detected by monoclonal antibody. *Carcinogenesis* 1986; **7**: 1475-1482
- 15 **Lee SW**, Tomasetto C, Paul D, Keyomarsi K, Sager R. Transcriptional downregulation of gap-junction proteins blocks junctional communication in human mammary tumor cell lines. *J Cell Biol* 1992; **118**: 1213-1221
- 16 **Hirschi KK**, Xu CE, Tsukamoto T, Sager R. Gap junction genes Cx26 and Cx43 individually suppress the cancer phenotype of human mammary carcinoma cells and restore differentiation potential. *Cell Growth Differ* 1996; **7**: 861-870
- 17 **Omori Y**, Krutovskikh V, Mironov N, Tsuda H, Yamasaki H. Cx32 gene mutation in a chemically induced rat liver tumour. *Carcinogenesis* 1996; **17**: 2077-2080
- 18 **Eghbali B**, Kessler JA, Reid LM, Roy C, Spray DC. Involvement of gap junctions in tumorigenesis: transfection of tumor cells with connexin 32 cDNA retards growth *in vivo*. *Proc Natl Acad Sci U S A* 1991; **88**: 10701-10705
- 19 **Krutovskikh VA**, Mesnil M, Mazzoleni G, Yamasaki H. Inhibition of rat liver gap junction intercellular communication by tumor-promoting agents *in vivo*. Association with aberrant localization of connexin proteins. *Lab Invest* 1995; **72**: 571-577
- 20 **Rose B**, Mehta PP, Loewenstein WR. Gap-junction protein gene suppresses tumorigenicity. *Carcinogenesis* 1993; **14**: 1073-1075
- 21 **Iwai M**, Harada Y, Muramatsu A, Tanaka S, Mori T, Okanoue T, Katoh F, Ohkusa T, Kashima K. Development of gap junctional channels and intercellular communication in rat liver during ontogenesis. *J Hepatol* 2000; **32**: 11-18
- 22 **Rahman S**, Carlile G, Evans WH. Assembly of hepatic gap junctions. Topography and distribution of connexin 32 in intracellular and plasma membranes determined using sequence-specific antibodies. *J Biol Chem* 1993; **268**: 1260-1265
- 23 **Zhang JT**, Nicholson BJ. Sequence and tissue distribution of a second protein of hepatic gap junctions, Cx26, as deduced from its cDNA. *J Cell Biol* 1989; **109**: 3391-3401
- 24 **Krutovskikh V**, Mazzoleni G, Mironov N, Omori Y, Aguelon AM, Mesnil M, Berger F, Partensky C, Yamasaki H. Altered homologous and heterologous gap-junctional intercellular communication in primary human liver tumors associated with aberrant protein localization but not gene mutation of connexin 32. *Int J Cancer* 1994; **56**: 87-94
- 25 **Oyamada M**, Krutovskikh VA, Mesnil M, Partensky C, Berger F, Yamasaki H. Aberrant expression of gap junction gene in primary human hepatocellular carcinomas: increased expres-

- sion of cardiac-type gap junction gene connexin 43. *Mol Carcinog* 1990; **3**: 273-278
- 26 **Krutovskikh VA**, Mesnil M, Mazzoleni G, Yamasaki H. Inhibition of rat liver gap junction intercellular communication by tumor-promoting agents *in vivo*. Association with aberrant localization of connexin proteins. *Lab Invest* 1995; **72**: 571-577
- 27 **Markert CL**. Neoplasia: a disease of cell differentiation. *Cancer Res* 1968; **28**: 1908-1914
- 28 **Shimoyama Y**, Hirohashi S. Cadherin intercellular adhesion molecule in hepatocellular carcinomas: loss of E-cadherin expression in an undifferentiated carcinoma. *Cancer Lett* 1991; **57**: 131-135
- 29 **Yamaoka K**, Nouchi T, Tazawa J, Hiranuma S, Marumo F, Sato C. Expression of gap junction protein connexin 32 and E-cadherin in human hepatocellular carcinoma. *J Hepatol* 1995; **22**: 536-539
- 30 **Ng IO**, Lai EC, Fan ST, Ng MM, So MK. Prognostic significance of pathologic features of hepatocellular carcinoma. A multivariate analysis of 278 patients. *Cancer* 1995; **76**: 2443-2448
- 31 **Sakamoto M**, Ino Y, Fujii T, Hirohashi S. Phenotype changes in tumor vessels associated with the progression of hepatocellular carcinoma. *Jpn J Clin Oncol* 1993; **23**: 98-104
- 32 **Terada T**, Nakanuma Y. Arterial elements and perisinusoidal cells in borderline hepatocellular nodules and small hepatocellular carcinomas. *Histopathology* 1995; **27**: 333-339
- 33 **Nakashima O**. Pathological diagnosis of hepatocellular carcinoma. *Nippon Rinsho* 2001; **59**(Suppl 6): 333-341
- 34 **Ma XD**, Ma X, Sui YF, Wang WL, Wang CM. Signal transduction of gap junctional genes, connexin32, connexin43 in human hepatocarcinogenesis. *World J Gastroenterol* 2003; **9**: 946-950

Edited by Zhu LH and Wang XL Proofread by Xu FM

Postoperative adjuvant arterial chemoembolization improves survival of hepatocellular carcinoma patients with risk factors for residual tumor: A retrospective control study

Zheng-Gang Ren, Zhi-Ying Lin, Jing-Lin Xia, Sheng-Long Ye, Zeng-Chen Ma, Qing-Hai Ye, Lun-Xiu Qin, Zhi-Quan Wu, Jia Fan, Zhao-You Tang

Zheng-Gang Ren, Zhi-Ying Lin, Jing-Lin Xia, Sheng-Long Ye, Zeng-Chen Ma, Qing-Hai Ye, Lun-Xiu Qin, Zhi-Quan Wu, Jia Fan, Zhao-You Tang, Liver Cancer Institute and Zhongshan Hospital, Fudan University, Shanghai 200032, China

Correspondence to: Dr. Zhao-You Tang, Liver Cancer Institute and Zhongshan Hospital, Fudan University, Shanghai 200032, China. zytang@srcap.stc.sh.cn

Telephone: +86-21-64037181 Fax: +86-21-64037181

Received: 2003-10-09 Accepted: 2003-12-06

Abstract

AIM: To evaluate the effect of postoperative adjuvant transcatheter arterial chemoembolization (TACE) on the prognosis of hepatocellular carcinoma (HCC) patients with or without risk factors for the residual tumor.

METHODS: From January 1995 to December 1998, 549 consecutive HCC patients undergoing surgical resection were included in this research. There were 185 patients who underwent surgical resection with adjuvant TACE and 364 patients who underwent surgical resection only. Tumors with a diameter more than 5 cm, multiple nodules, and vascular invasion were defined as risk factors for residual tumor and used for patient stratification. Kaplan-Meier method was used to analyze survival curve and Cox proportional hazard model was used to evaluate the prognostic significance of adjuvant TACE.

RESULTS: In the patients without any risk factors for the residual tumor, the 1-, 3-, 5-year survival rates were 93.48%, 75.85%, 62.39% in the control group and 97.39%, 70.37%, 50.85% in the adjuvant TACE group, respectively. There was no significant difference in the survival between two groups ($P = 0.3956$). However, in the patients with risk factors for residual tumor, postoperative adjuvant TACE significantly prolonged the patients' survival. There was a statistically significant difference in survival between two groups ($P = 0.0216$). The 1-, 3-, 5-year survival rates were 69.95%, 49.86%, 37.40% in the control group and 89.67%, 61.28%, 44.36% in the adjuvant TACE group, respectively. Cox proportional hazard model showed that tumor diameter and cirrhosis, but not the adjuvant TACE, were the significantly independent prognostic factors in the patients without risk factors for residual tumor. However, in the patients with risk factors for residual tumor adjuvant TACE, and also tumor diameter, AFP level, vascular invasion, were the significantly independent factors associated with the decreasing risk for patients' death from HCC.

CONCLUSION: Postoperative adjuvant TACE can prolong the survival of patients with risk factors for residual tumor, but can not prolong the survival of patients without risk factors for residual tumor.

Ren ZG, Lin ZY, Xia JL, Ye SL, Ma ZC, Ye QH, Qin LX, Wu ZQ, Fan J, Tang ZY. Postoperative adjuvant arterial chemoembolization improves survival of hepatocellular carcinoma patients with risk factors for residual tumor: A retrospective control study. *World J Gastroenterol* 2004; 10(19): 2791-2794

<http://www.wjgnet.com/1007-9327/10/2791.asp>

INTRODUCTION

Hepatocellular carcinoma is the fifth most common malignant death in the world and is estimated to cause half a million deaths annually^[1]. In China, primary liver cancer mortality ranked second after stomach cancer. The age-standardized mortality rate (adjusted by the world population) was 33.7 per 100 000 in male Chinese and 12.3 per 100 000 in female Chinese^[2]. Surgical resection is a major treatment for hepatocellular carcinoma (HCC)^[3]. However, postoperative recurrence is still high and the main death cause after resection of HCC^[4]. The overall recurrence was 30.1%, 62.3% and 79.0% in 1, 3, 5 years after resection of HCC, respectively^[5]. Adjuvant therapies were used to prolong the survival and decrease the recurrence of HCC in different centers, such as transcatheter arterial chemoembolization (TACE)^[6-13], polyphenolic acid^[14], adoptive immunotherapy^[15], interferon^[16], and iodine-131-labeled lipiodol^[17-19]. TACE was one of the most commonly used adjuvant managements for preventing recurrence and prolonging the survival of patients postoperatively. However, the benefits of adjuvant TACE were controversial. From January 1995 to December 1998, a consecutive series of 549 HCC patients with partially hepatectomy were included in this study. Of them, 185 patients received adjuvant TACE and 364 patients received surgical resection only. The aim of this research was to evaluate the benefits of adjuvant TACE in our series and to determine whether the characteristics of HCC such as diameter of tumor size, tumor nodules and vascular invasion could affect the benefits of adjuvant TACE to the patients' survival.

MATERIALS AND METHODS

Patients

This study included 549 patients with HCC who underwent partial hepatectomy. The entry criteria included: 1) All the tumor lesions were removed, which were judged by surgeon's gross inspection; 2) no lymphnode involvement; and 3) no distant metastasis. For all the 549 patients, hepatectomy was performed in Liver Cancer Institute, Zhongshan Hospital, Fudan University from January 1995 to December 1998. There were 465 males and 84 females with a median age of 50 years. According to the UICC TNM classification, 48 patients were in stage I, 382 in stage II, 86 in stage IIIA, and 33 in stage IVA. For their liver function defined by Child-Pugh classification, 539 patients were in class A, 10 in class B, and no patients in class C.

Adjuvant TACE

In the entire series, 185 patients underwent adjuvant TACE and 364 patients who did not undergo adjuvant TACE were assigned as control. Adjuvant TACE was performed 2 mo after hepatectomy. Hepatic arterial angiography was performed and then preventive or therapeutic chemoembolization was done depending on the patients with or without tumor stain in the remnant liver, respectively. The regimen for preventive adjuvant TACE consisted of 5-fluorouracil (5-FU) 0.75 g, cisplatin (DDP) 60 mg, and the emulsion mixed with mitomycin C (MMC) 16 mg and lipiodol 5 mL. Two months later a repeated preventive adjuvant TACE was performed and the regimen was finished. For therapeutic adjuvant TACE, the regimen consisted of 5-FU 1.0 g, DDP 80 mg, and the emulsion of MMC 20 mg and lipiodol 5-10 mL (the volume of lipiodol used for a patient depending on the tumor volume in the patient). TACE was repeated every one and a half month. The interval and times of repeated TACE depended on the response of the patients.

Patient stratification and grouping

The patients were retrospectively stratified into patients without risk factors for the residual tumor and patients with any risk factors for the residual tumor. These risk factors were evaluated according to preoperative ultrasonography, CT scan and postoperative pathological examination. Risk factors were defined as tumor diameter >5 cm, multiple nodules or vascular invasion. These factors were reported to have a close relation with residual tumor or recurrence in the remnant liver of HCC patients^[4,20-23]. After stratification, there were 251 patients without risk factors for the residual tumor and 298 patients with risk factors for the residual tumor. After stratification, the patients were further grouped as the adjuvant TACE group and the control group.

Follow-up and statistics

The patients were followed up every 2 to 3 mo with ultrasonography and alpha-fetoprotein (AFP) during the first 2 years after HCC resection and every 3-6 mo afterwards. If the patients were unable to undergo this procedure, they were followed up with telephone or letter every year. The follow-up termination time for all patients was December 31, 2002. The significance of differences in clinical and pathological characteristics between groups was examined with Chi-square test and Student *t* test. Cumulative survival rates were obtained by the Kaplan-Meier method. Cumulative survival comparison between groups was performed with log-rank test. Multivariate analysis for the independent prognostic factors was determined by Cox proportional hazards model. *P* values <0.05 were considered statistically significant.

RESULTS

Clinical and pathological characteristics of adjuvant TACE and control groups

Clinical and pathological characteristics of the patients with or without risk factors for residual tumor in adjuvant TACE and control groups were summarized in Tables 1 and 2, respectively. There were no significant differences in their age, HBsAg positive rate, Child-Pugh class, AFP level, TNM class between two groups, except that the ratio of female vs male patients was lower in the adjuvant TACE group than that in control group (*P* = 0.005) without risk factor for residual tumor.

Survival of patients in adjuvant TACE group and control group

Figure 1A presents the Kaplan-Meier survival analysis comparing the patients in control group and adjuvant TACE group without risk factors for the residual tumor. There were

no differences in their survival curves between two groups (*P* = 0.3956). The 1-, 3-, 5-year survival rates were 93.48%, 75.85%, 62.39% in the control group and 97.39%, 70.37%, 50.85% in the adjuvant TACE group, respectively. However, for the patients with risk factors for the residual tumor improved survival rates were observed in the adjuvant TACE group, as showed by Figure 2B. There were significant differences between two groups (*P* = 0.0216). The 1-, 3-, 5-year survival rates were 69.95%, 49.86%, 37.40% in the control group and 86.67%, 61.28%, 44.36% in the adjuvant TACE group.

Table 1 Clinical and pathological characteristics in control and adjuvant TACE groups patients without risk factors for residual tumor

Characteristics	Control (n = 174)	Adjuvant TACE group (n = 77)	<i>P</i> value
Gender			
Female	34	5	0.009
Male	140	72	
Age (mean±SD)	50.86±11.61	49.35±10.04	0.323
HBsAg			
Positive	43	11	0.135
Negative	131	66	
Cirrhosis			
Absent	22	6	0.130
Mild	53	33	
Severe	99	38	
Child-pugh Class			
A	165	77	0.134
B	5	0	
AFP (mean±SD, ug/L)	333.91±529.92	406.04±735.16	0.381
TNM classification			
I	28	19	0.108
II	146	58	

Table 2 Clinical and pathological characteristics in control and adjuvant TACE groups patients with risk factors for residual tumor

Characteristics	Control (n = 190)	Adjuvant TACE group (n = 108)	<i>P</i> value
Gender			
Female	33	12	0.147
Male	157	96	
Age (mean±SD)	51.50±11.72	49.63±10.07	0.105
HBsAg			
Positive	47	27	0.588
Negative	143	81	
Cirrhosis			
Absent	41	24	0.563
Mild	69	45	
Severe	80	39	
Child-pugh Class			
A	187	106	0.860
B	3	2	
AFP (mean±SD, ug/l)	501.39±807.14	518.25±707.99	0.856
TNM classification			
II	113	66	0.926
IIIA	55	31	
IVA	22	11	

Multivariate analysis

Cox proportional hazards models were constructed to predict the survival of the patients with adjuvant TACE and other variables including sex, age, HBsAg, cirrhosis, Child-Pugh class, AFP levels, tumor diameter, tumor nodules, and vascular invasion. In the patients without risk factors for residual tumor, the tumor diameter and cirrhosis were statistically significant independent factors associated with an increased risk of death from HCC, but adjuvant TACE had no effect on the survival of patients (Table 3). However, in the patients with risk factors for residual tumor, adjuvant TACE was statistically significant independent factor associated with a decreased risk of the death of patients with HCC. Tumor diameter, AFP level and vascular invasion were significantly independent factors associated with death of patients with HCC (Table 4). These results indicated that adjuvant TACE could improve the survival of patients with risk factors for residual tumor, but did not affect the survival of patients without risk factors for residual tumor.

Table 3 Multivariate Cox proportional hazard analysis to evaluate independent variables in patients without risk factors for residual tumor

Variables	B	Wald	Significance	HR	95% CI	
					lower	upper
Cirrhosis	0.689	14.443	0.000	1.991	1.396	2.841
Absent = 1						
Mild = 2						
Severe = 3						
Tumor diameter (cm)	0.235	6.019	0.014	1.264	1.048	1.525

Table 4 Multivariate Cox proportional hazard analysis to evaluate independent variables in patients with risk factors for residual tumor

Variables	B	Wald	Significance	HR	95% CI	
					lower	upper
AFP ($\mu\text{g/L}$)	0.212	5.333	0.021	1.236	1.033	1.480
<20 = 1						
21-400 = 2						
>400 = 3						
Adjuvant TACE	-0.406	6.041	0.014	0.666	0.482	0.921
Without = 1						
With = 2						
Tumor diameter (cm)	0.076	16.327	0.000	1.079	1.040	1.119
Vascular invasion	0.245	7.691	0.006	1.278	1.075	1.520
Absent = 1						
Present = 2						

DISCUSSION

The frequent postoperative recurrence was a main obstacle for long survival after resection of HCC and intrahepatic metastasis was thought to have a close relation with the postoperative recurrence^[24]. However, it is difficult to detect the minimal intrahepatic metastasis before or during operation and the existence of this minimal intrahepatic metastasis contributes to intrahepatic recurrence. Theoretically, treatment of this minimal intrahepatic metastasis should play an important role in preventing of postoperative recurrence of HCC. However, though TACE has been widely used in unresectable HCC patients^[25-27], the clinical trial showed there was no confirmed evidence supporting the benefits of adjuvant TACE to patients with resectable HCC^[6]. Tanaka and Izumi showed that postoperative adjuvant TACE improved the survival of HCC patients^[28,29]. The patients selected in their clinical trials had advanced stages (TNM III or TNM IV) or characteristics of uncompleted encapsulated, intrahepatic metastasis, or vascular invasion which was thought to have a close relation with residual tumor and earlier massive recurrence^[22,30]. For these patients postoperative adjuvant TACE played a role in earlier therapy of the residual tumor and could decrease the earlier recurrence and prolong survival. However, TACE has been known to damage remnant liver and deteriorate liver function. This adverse impact is possible to affect long survival of patients with resectable HCC if the resection is truly curative. One of the clinical trials showed that adjuvant chemembolization using the regimen of intravenous epirubicin in combination with transarterial infusion of an emulsion of iodized oil and cisplatin, was even associated with more frequent extrahepatic recurrences and a worse outcome in their group of patients^[31]. In that clinical trial, all the patients had no demonstrable evidence of residual disease on ultrasonography and hepatic angiography 1 mo after surgery. These evidences suggested that the benefits of adjuvant TACE depended on the selection of patients. In patients who had high risks of residual tumor or intrahepatic metastasis in remnant liver, adjuvant TACE could improve their survival due to therapeutic actions on the residual tumor. However, in patients with lower risks of residual tumor or intrahepatic metastasis, adjuvant TACE might have less usefulness or even worse actions due to deterioration of remnant liver function.

Our results showed that postoperative adjuvant TACE could improve the survival of patients with risk factors for the residual tumor but not the survival of patients without risk factors for the residual tumor. For further evaluation of the effect of adjuvant TACE on patients with resectable HCC, Cox proportional hazards models were constructed to study if adjuvant TACE was the significantly independent factor associated with the survival. The results showed that in patients without risk factors for residual tumor, the significantly independent prognostic factors

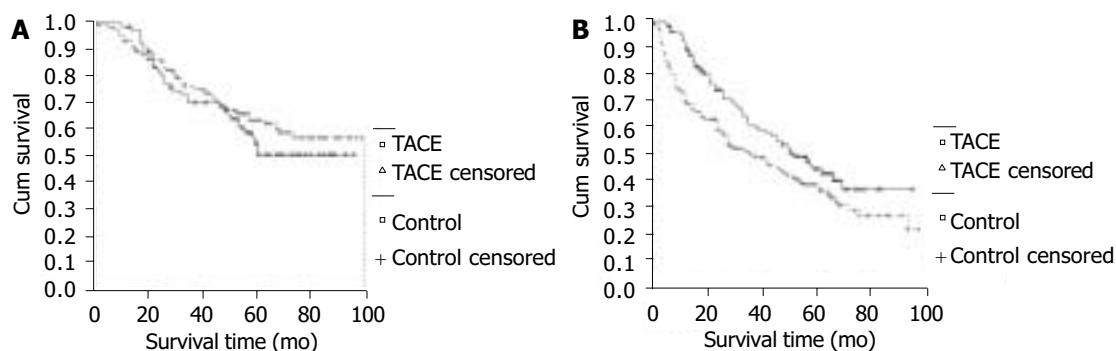


Figure 1 Survival curves of patients in control group and adjuvant TACE group without or with risk factors for residual tumor. A: Survival curve of patients in control group and adjuvant TACE group without risk factor for residual tumor. B: Survival curve of patients in control group and adjuvant TACE group with risk factors for residual tumor.

were tumor diameter and cirrhosis but not the adjuvant TACE. However, in patients with risk factors for residual tumor, adjuvant TACE was the significant prognostic factor. This result suggested that the benefits of adjuvant TACE to patients with resectable HCC depended on the selected patients with or without risk factors for the residual tumor. Therefore adjuvant TACE should be used in patients with higher risks of residual tumor but not in patients with lower risks of residual tumor.

REFERENCES

- 1 **El-Serag HB.** Hepatocellular carcinoma: an epidemiologic view. *J Clin Gastroenterol* 2002; **35**(5 Suppl 2): S72-78
- 2 **Zhang S, Li L, Lu F.** Mortality of primary liver cancer in China from 1990 through 1992. *Zhonghua Zhongliu Zazhi* 1999; **21**: 245-249
- 3 **Tang ZY.** Hepatocellular carcinoma. *J Gastroenterol Hepatol* 2000; **15**(Suppl): G1-7
- 4 **Cha C, Fong Y, Jarnagin WR, Blumgart LH, DeMatteo RP.** Predictors and patterns of recurrence after resection of hepatocellular carcinoma. *J Am Coll Surg* 2003; **197**: 753-758
- 5 **Imamura H, Matsuyama Y, Tanaka E, Ohkubo T, Hasegawa K, Miyagawa S, Sugawara Y, Minagawa M, Takayama T, Kawasaki S, Makuuchi M.** Risk factors contributing to early and late phase intrahepatic recurrence of hepatocellular carcinoma after hepatectomy. *J Hepatol* 2003; **38**: 200-207
- 6 **Schwartz JD, Schwartz M, Mandeli J, Sung M.** Neoadjuvant and adjuvant therapy for resectable hepatocellular carcinoma: review of the randomised clinical trials. *Lancet Oncol* 2002; **3**: 593-603
- 7 **Fukuda S, Okuda K, Imamura M, Imamura I, Eriguchi N, Aoyagi S.** Surgical resection combined with chemotherapy for advanced hepatocellular carcinoma with tumor thrombus: report of 19 cases. *Surgery* 2002; **131**: 300-310
- 8 **Ono T, Yamanoi A, Nazmy El Assal O, Kohno H, Nagasue N.** Adjuvant chemotherapy after resection of hepatocellular carcinoma causes deterioration of long-term prognosis in cirrhotic patients: metaanalysis of three randomized controlled trials. *Cancer* 2001; **91**: 2378-2385
- 9 **Shimoda M, Bando T, Nagata T, Shirosaki I, Sakamoto T, Tsukada K.** Prophylactic chemolipiodolization for postoperative hepatoma patients. *Hepatogastroenterology* 2001; **48**: 493-497
- 10 **Huang YH, Wu JC, Lui WY, Chau GY, Tsay SH, Chiang JH, King KL, Huo TI, Chang FY, Lee SD.** Prospective case-controlled trial of adjuvant chemotherapy after resection of hepatocellular carcinoma. *World J Surg* 2000; **24**: 551-555
- 11 **Kohno H, Nagasue N, Hayashi T, Yamanoi A, Uchida M, Ono T, Yukaya H, Kimura N, Nakamura T.** Postoperative adjuvant chemotherapy after radical hepatic resection for hepatocellular carcinoma (HCC). *Hepatogastroenterology* 1996; **43**: 1405-1409
- 12 **Yamamoto M, Arie S, Sugahara K, Tobe T.** Adjuvant oral chemotherapy to prevent recurrence after curative resection for hepatocellular carcinoma. *Br J Surg* 1996; **83**: 336-340
- 13 **Takenaka K, Yoshida K, Nishizaki T, Korenaga D, Hiroshige K, Ikeda T, Sugimachi K.** Postoperative prophylactic lipiodolization reduces the intrahepatic recurrence of hepatocellular carcinoma. *Am J Surg* 1995; **169**: 400-404
- 14 **Muto Y, Moriwaki H, Ninomiya M, Adachi S, Saito A, Takasaki KT, Tanaka T, Tsurumi K, Okuno M, Tomita E, Nakamura T, Kojima T.** Prevention of second primary tumors by an acyclic retinoid, polypropenoic acid, in patients with hepatocellular carcinoma. Hepatoma Prevention Study Group. *N Engl J Med* 1996; **334**: 1561-1567
- 15 **Takayama T, Sekine T, Makuuchi M, Yamasaki S, Kosuge T, Yamamoto J, Shimada K, Sakamoto M, Hirohashi S, Ohashi Y, Kakizoe T.** Adoptive immunotherapy to lower postsurgical recurrence rates of hepatocellular carcinoma: a randomised trial. *Lancet* 2000; **356**: 802-807
- 16 **Kubo S, Nishiguchi S, Hirohashi K, Tanaka H, Shuto T, Kinoshita H.** Randomized clinical trial of long-term outcome after resection of hepatitis C virus-related hepatocellular carcinoma by postoperative interferon therapy. *Br J Surg* 2002; **89**: 418-422
- 17 **Lau WY, Leung TW, Ho SK, Chan M, Machin D, Lau J, Chan AT, Yeo W, Mok TS, Yu SC, Leung NW, Johnson PJ.** Adjuvant intra-arterial iodine-131-labelled lipiodol for resectable hepatocellular carcinoma: a prospective randomised trial. *Lancet* 1999; **353**: 797-801
- 18 **Partensky C, Sassolas G, Henry L, Paliard P, Maddern GJ.** Intra-arterial iodine 131-labeled lipiodol as adjuvant therapy after curative liver resection for hepatocellular carcinoma: a phase 2 clinical study. *Arch Surg* 2000; **135**: 1298-1300
- 19 **Boucher E, Corbinais S, Rolland Y, Bourguet P, Guyader D, Boudjema K, Meunier B, Raoul JL.** Adjuvant intra-arterial injection of iodine-131-labeled lipiodol after resection of hepatocellular carcinoma. *Hepatology* 2003; **38**: 1237-1241
- 20 **Lee WC, Jeng LB, Chen MF.** Estimation of prognosis after hepatectomy for hepatocellular carcinoma. *Br J Surg* 2002; **89**: 311-316
- 21 **Sun HC, Tang ZY.** Preventive treatments for recurrence after curative resection of hepatocellular carcinoma-A literature review of randomized control trials. *World J Gastroenterol* 2003; **9**: 635-640
- 22 **Lin Z, Ren Z, Xia J.** Appraisal of postoperative transcatheter arterial chemoembolization (TACE) for prevention and treatment of hepatocellular carcinoma recurrence. *Zhonghua Zhongliu Zazhi* 2000; **22**: 315-317
- 23 **Poon RT, Ng IO, Fan ST, Lai EC, Lo CM, Liu CL, Wong J.** Clinicopathologic features of long-term survivors and disease-free survivors after resection of hepatocellular carcinoma: a study of a prospective cohort. *J Clin Oncol* 2001; **19**: 3037-3044
- 24 **Ouchi K, Sugawara T, Fujiya T, Kamiyama Y, Kakugawa Y, Mikuni J, Yamanami H, Nakagawa K.** Prediction of recurrence and extratumor spread of hepatocellular carcinoma following resection. *J Surg Oncol* 2000; **75**: 241-245
- 25 **Tzoracoleftherakis EE, Spiliotis JD, Kyriakopoulou T, Kakkos SK.** Intra-arterial versus systemic chemotherapy for non-operable hepatocellular carcinoma. *Hepatogastroenterology* 1999; **46**: 1122-1125
- 26 **Rose DM, Chapman WC, Brockenbrough AT, Wright JK, Rose AT, Meranze S, Mazer M, Blair T, Blanke CD, Debelak JP, Pinson CW.** Transcatheter arterial chemoembolization as primary treatment for hepatocellular carcinoma. *Am J Surg* 1999; **177**: 405-410
- 27 **Wallace S, Kan Z, Li C.** Hepatic chemoembolization: clinical and experimental correlation. *Acta Gastroenterol Belg* 2000; **63**: 169-173
- 28 **Tanaka K, Shimada H, Togo S, Takahashi T, Endo I, Sekido H, Yoshida T.** Use of transcatheter arterial infusion of anticancer agents with lipiodol to prevent recurrence of hepatocellular carcinoma after hepatic resection. *Hepatogastroenterology* 1999; **46**: 1083-1088
- 29 **Izumi R, Shimizu K, Miyazaki I.** Postoperative adjuvant locoregional chemotherapy in patients with hepatocellular carcinoma. *Hepatogastroenterology* 1996; **43**: 1415-1420
- 30 **Yamanaka J, Yamanaka N, Nakasho K, Tanaka T, Ando T, Yasui C, Kuroda N, Takata M, Maeda S, Matsushita K, Uematsu K, Okamoto E.** Clinicopathologic analysis of stage II-III hepatocellular carcinoma showing early massive recurrence after liver resection. *J Gastroenterol Hepatol* 2000; **15**: 1192-1198
- 31 **Lai EC, Lo CM, Fan ST, Liu CL, Wong J.** Postoperative adjuvant chemotherapy after curative resection of hepatocellular carcinoma: a randomized controlled trial. *Arch Surg* 1998; **133**: 183-188

Heparanase mRNA expression and point mutation in hepatocellular carcinoma

Xiao-Peng Chen, Yin-Bib Liu, Jing Rui, Shu-You Peng, Cheng-Hong Peng, Zi-Yan Zhou, Liang-Hui Shi, Hong-Wei Shen, Bin Xu

Xiao-Peng Chen, Jing Rui, Zi-Yan Zhou, Liang-Hui Shi, Department of Surgery, Affiliated Yijishan Hospital, Wannan Medical College, Wuhu 241001, Anhui Province, China

Yin-Bib Liu, Shu-You Peng, Cheng-Hong Peng, Hong-Wei Shen, Bin Xu, Department of Surgery, Second Affiliated Hospital, Medical School of Zhejiang University, Hangzhou 310009, Zhejiang Province, China

Correspondence to: Dr. Xiao-Peng Chen, Department of Surgery, Affiliated Yijishan Hospital, Wannan Medical College, Wuhu 241001, Anhui Province, China. drcxp@sohu.com

Telephone: +86-553-5866103 **Fax:** +86-10-85381893

Received: 2003-06-05 **Accepted:** 2003-08-16

Abstract

AIM: To explore the expression of heparanase mRNA and point mutation in hepatocellular carcinoma (HCC).

METHODS: Reverse transcription polymerase chain reaction was used to measure the expression of heparanase mRNA in the primary tumor tissues and surrounding liver tissues of 33 HCC patients. T-A cloning and sequencing were used to detect whether there was any mutation in the amplified PCR products.

RESULTS: The expression of heparanase mRNA was positive in 16 primary tumor tissues of HCC, and the positive rate was 48.5%, which was significantly higher than that in the surrounding liver parenchyma ($P < 0.01$). The positive rate for heparanase gene in high-tendency to metastatic recurrence group (71.4%, 10/14) was obviously higher than that in low-tendency to metastatic recurrence group (31.6%, 6/19) ($P = 0.023$). The positive rate for heparanase gene in patients with metastatic recurrence during postoperative follow-up (78.6%, 11/14) was also significantly higher than that in those without metastatic recurrence (21.4%, 3/14) ($P = 0.003$). Sequence analysis of the HPA PCR products was made in 7 patients, and 2-point mutations were found in 4 patients, one of which was sense mutation, neither base insertion nor deletion was detected. The mutation rate was 57.1% (4/7).

CONCLUSION: The expression rate of heparanase mRNA increases in HCC, and HPA mRNA may be one of the reliable markers for the metastatic activity gained by the liver tumor cells and could be used clinically in predicting metastatic recurrence of HCC. Point mutation may be one of the causes for enhanced heparanase mRNA expression.

Chen XP, Liu YB, Rui J, Peng SY, Peng CH, Zhou ZY, Shi LH, Shen HW, Xu B. Heparanase mRNA expression and point mutation in hepatocellular carcinoma. *World J Gastroenterol* 2004; 10(19): 2795-2799

<http://www.wjgnet.com/1007-9327/10/2795.asp>

INTRODUCTION

Primary hepatocellular carcinoma (HCC) is a common malignant

tumor, especially in China and southeast Asia. Although the resection rate of HCC has improved in recent 20 years, the general therapeutic efficacy is still not satisfactory yet. The death rate of HCC ranks second in all malignant tumors in China, due to postoperative metastatic recurrence as the main cause. Tumor invasion and metastasis can break through the tissue barriers, which are formed of extracellular matrix (ECM) and basement membranes (BMs) and are composed of structural proteins, including collagen, laminin and vitronectin, etc. and glycosaminoglycans (GSGs). The chief components of GSG are heparan sulfate proteoglycans (HSPGs) that are principally composed of a core protein covalently linked to several heparan sulfate side chains^[1]. Over the past ten years, most studies about neoplasm metastasis including HCC, focused on some proteases, such as matrix metalloproteinases (MMPs)^[2-4], u-PA^[5,6], serine and cysteine protease^[7,8] whose substrates were structural proteins, but heparanase (HPA), whose substrate was GSGs, was ignored. In recent years, mammalian HPA gene has successfully been cloned and sequenced in Israel and U.S.A^[9-13], and HPA was found to play an important role in tumor invasion and metastasis. El-Assal *et al.*^[14] found that HPA mRNA expression in HCC patients was related to the tumor sizes, staging, classification, infection of hepatitis C virus (HCV), vascularization, postoperative metastasis and prognosis. However, in their studies, over half of HCC patients (52.7%, 29/55) were accompanied with HCV infection, and few were associated with hepatitis B virus (HBV). Ikeguchi *et al.*^[15] found that relative heparanase mRNA expression level in HCC was significantly lower than that in noncancerous liver tissues ($P < 0.001$), and that tumor heparanase expression did not correlate to tumor differentiation, tumor stage, or patient prognosis. They concluded that enhanced heparanase mRNA expression might not be a good biological marker for HCC. In addition, the possible mechanism of HPA expression has not been explored in both studies. It is well known that most HCCs in China are HBV-associated, which is different from the HCCs reported in Japan, but whether there is some difference of HPA expression in HCCs between in China and Japan or other regions is still unknown. In the present study, we tried to find out whether HPA mRNA expression was related to the clinicopathological indexes, including infection of HBV and postoperative metastatic recurrence of Chinese HCC patients, whether there was mutation in HPA gene, and whether the mutation of HPA gene was associated with HPA mRNA expression.

MATERIALS AND METHODS

Patients

Thirty-three patients (28 men and 5 women) undergoing curative hepatic resection for HCC between October 2000 and April 2001, were included in the present study. None of the patients received preoperative chemo- or embolic therapy. The patients' ages ranged from 27 to 73 years (49 ± 7 years, mean \pm SD). Among the 33 patients, the biggest diameter of tumors was >5 cm in 25 cases and ≤ 5 cm in 8. Tumor capsules were integrated in 14 and disintegrated in 19 cases. Serum AFP was positive in 21 and negative in 12; HBsAg was positive in 24 and negative in 9. Liver cirrhosis was detected in 18 cases. Thirteen patients

belonged to Edmondson grade I or II, and the remaining 20 patients to Edmondson grade III or IV. Eighteen patients belonged to TNM staging I or II, and 15 to TNM staging III or IV. According to the operative records and postoperative pathologic data, 14 HCC patients with cancer emboli, intrahepatic dissemination (satellite foci or multiple nodules) and/or lymph node metastasis were demarcated to high-tendency to metastatic recurrence group, and the other 19 patients without emboli, dissemination and/or metastasis belonged to low-tendency to metastatic recurrence group. A total of 28 patients were followed up 6-16 mo after operation, during which neoplasm metastasis or recurrence was found in 14 patients.

Tissue selection

After the neoplasm was resected, HCC tissues from all the patients were selected from the most viable areas of the tumors immediately. This aimed at excluding areas of tissue necrosis and hemorrhages, which might influence the quality and the quantity of the extracted RNA. For selection of surrounding non-tumor liver tissues, specimens were obtained from tissues at a clear distance from the edge of tumors (>1cm), if there was no evidence of nearby tumor invasion. Tissues were at once preserved in liquid nitrogen after the resection and kept at -80 °C until the experiment began.

RNA extraction and cDNA synthesis

About 100 mg tumor or liver tissue was used for total RNA isolation using TRIzol reagent (Gibco-BRL), according to the instructions of the manufacturer. First-strand cDNA was synthesized using 5 L total RNA with oligo (dT)₁₆ primer in a 50-L reverse transcription mixture containing 10 L of 5× first-strand buffer, 2.5 L dNTP mixture containing 25 mmol/L each deoxynucleotide triphosphate base (Pharmacia Biotech, Tokyo, Japan), 2.5 L ribonuclease inhibitor (TaKaRa Biochemicals, Ohotsu, Japan), 25 L ddH₂O (managed with DEPC in advance), and 2.5 L avian myeloblastosis virus reverse transcriptase (TaKaRa Biochemicals, Ohotsu, Japan).

PCR amplification of HPA and β-actin genes

The resulting cDNA was used for PCR amplification using Taq polymerase (TaKaRa Biochemicals, Ohotsu, Japan). The primers for HPA PCR amplification were designed according to the literature^[9]. The sequences of the oligonucleotides were: forward, 5'-TTCGATCCCAAGAAGGAATCAAC-3'; and reverse, 5'-GATTCACTTACATGGCATCACTAC-3'. The first and final bases of the amplified HPA segment were at the 409th and 993rd positions of the HPA cDNA, respectively, and the amplified segment should be 585 bp in length. The primers used for β-actin had the following sequences: forward, 5'-TTCCAGCCTTCCTTCCTGG-3', and reverse, 5'-ATTGCTCCTCTGAGCGCAA-3', as generated by Oligo 4.0 S computer software. The amplified β-actin segment was 224 bp in length. The PCR conditions included initial denaturation at 94 °C for 4 min, followed by 35 cycles of amplification with subsequent denaturation at 94 °C for 30 s, annealing at 57 °C for 45 s, and extension for 1 min at 72 °C. Ten μL PCR products underwent electrophoresis using 12 g/L agarose and was visualized by UV absorption and ethidium bromide.

T-A cloning and sequencing

By using *Escherichia coli*, competent cell DH5α was routinely prepared and stored at -80 °C. One hundred μL liquid HPA PCR products was used for purification. Five liters of purified preparation, 1 L pGEM-Teasy vector (3 015 bp in length) and 1 L T4-DNA ligase (Promega, New York, U.S.A) were mixed and incubated overnight at 4 °C for ligation reaction. After 200 L competent cell suspension was thawed at room temperature, 5 L

ligated products was added for transformation test. The recombinant plasmid was screened, and the plasmid DNA was extracted by the alkaline lysis method. Five liters plasmid DNA was digested with 0.5 L restriction endonuclease *EcoR* I for 2-3 h at 37 °C, then the enzyme digestion products were identified by electrophoresis. Results of enzyme digestion analysis were essentially identical with expected ones. Using the recombinant plasmid DNA as a template, DNA sequencing for both strands was performed on an ALF express DNA automatic sequencer (Pharmacia Co.) by the dideoxy terminal termination method. The sequenced HPA segment was 585 bp in length. The sequence of amplified HPA segment was compared with the gene bank database and analyzed for homogeneity using BLAST program at NCBI.

Statistical analysis

The significance of difference between two groups was tested with Chi-square analysis or exact probabilities in fourfold table. A *P* value less than 0.05 was considered statistically significant.

RESULTS

Expression of HPA mRNA in HCC

HPA mRNA was amplified in the tumor tissues from 16 patients. Electrophoretic analysis showed a bright band about 550-600 bp in length in these patients. No amplification strand was found in the other 17 patients (Figure 1). The HPA mRNA expression rate in the tumor tissues of HCC was 48.5% (16/33) and significantly higher than that in the surrounding non-tumor liver tissues (*P*<0.01) in which HPA mRNA was positive in only one patient.

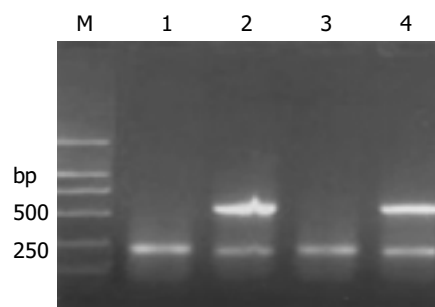


Figure 1 Expression of HPA mRNA in HCC. M: molecular mass markers (DL2 000); lanes 1 and 3: the noncancerous liver tissue; lanes 2 and 4: the HPA positive samples of cancer tissues both with a bright band at 585 bp.

Relationship between HPA expression and clinicopathological indexes

By statistical analysis, no significant difference in HPA mRNA expression was found among the tumor size, capsule, AFP, HBsAg and liver cirrhosis groups (*P*>0.05) (Table 1). HPA expression rate in Edmondson grade I or II group was significantly lower than that in Edmondson grade III or IV group (*P* = 0.019), and the rate in TNM staging I or II group was also obviously lower than that in TNM staging III or IV group (*P* = 0.047) (Table 1).

Relationship between HPA expression and metastatic recurrence of HCC

HPA mRNA expression rate in high-tendency to metastatic recurrence group was obviously higher than that in low-tendency to metastatic recurrence group (*P* = 0.023), and the rate in metastatic recurrence group was also significantly higher than that in non-metastatic recurrence group (*P*=0.003) (Table 2).

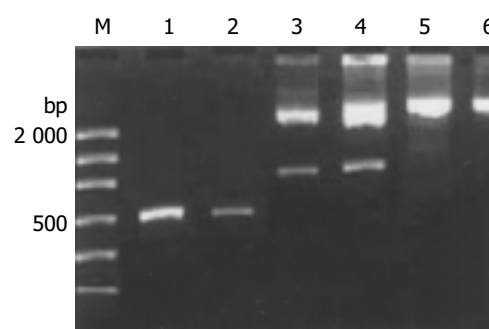
Table 1 Relationship between the HPA expression and the clinicopathological parameters of HCC

Items	Number	HPA positive	HPA negative	P value
Size of tumor				
>5 cm	25	13	12	0.250
≤5 cm	8	3	5	
Tumor capsule				
Integrated	14	5	9	0.130
Disintegrated	19	11	8	
AFP				
Positive	21	12	9	0.125
Negative	12	4	8	
HBsAg				
Positive	24	12	12	0.292
Negative	9	4	5	
Liver cirrhosis				
Yes	18	8	10	0.241
No	15	8	7	
Edmondson grade				
I, II	13	3	10	0.019
III, IV	20	13	7	
TNM staging				
I, II	18	6	12	0.047
III, IV	15	10	5	

Point mutation

After the recombinant plasmid DNA was digested by *Eco*R I and run in 10 g/L agarose gel electrophoresis, 2 bright bands could be seen, which were about 750 and 2 900 bp in length, respectively, according to the markers. The recombinant plasmid that was not digested by the enzyme showed only one band about 3 600 bp in length, and the pure HPA RT-PCR products only produced one strip about 550-600 bp in length

in the same agarose gel. These results proved that it was successful to purify HPA RT-PCR products, ligate them with plasmid DNA to be digested by restriction endonuclease (Figure 2). Seven samples of HPA mRNA positive PCR products were cDNA sequenced, and the results confirmed that the target gene segment in all the 7 samples of PCR products was human HPA cDNA. Two point mutations (at the 513th and 878th base of the HPA cDNA, respectively) were observed in 4 samples, and no insertion or deletion was found. The mutation rate was 57.1% (4/7). One of the point mutations of G to A transversion was at the third base position of codon 138. Because the varied codon was still translated to glutamic acid resulting in no alternation of amino acid residues, the mutation belonged to nonsense mutation. The other point mutation of A to G transversion at nucleotide 878 corresponded to the second base position of codon 260. After transversion, the codon became AGU from AAU, resulting in alternation of amino acid residues (asparagine to serine), it was therefore sense mutation (Table 3, Figure 3).

**Figure 2** Electrophoretogram of the recombinant plasmid DNA digested by *Eco*R I. M: molecular mass markers (DL2 000); lanes 1 and 2: the pure HPA RT-PCR products; lanes 3 and 4: the products of digestion; lanes 5 and 6: the products without digestion.**Table 2** Relationship between HPA expression and metastatic recurrence of HCC

Items	Number	HPA positive	HPA negative	P value
Tendency to metastatic recurrence				
High	14	10	4	0.023
Low	19	6	13	
Metastatic recurrence				
Yes	14	11	3	0.003
No	14	3	11	

Table 3 Sequencing and corresponding series number

Number	Nucleotide sequence						Remarks
409-468	TTGG	GCCCACGTC	GCATGCTCCC	GGCCGCCATG	GCGGCCGCGG	GAATTCGATT	Plasmid DNA
469-528	<i>TTCCGATCCCA</i>	<i>AGAAGGAATC</i>	<i>AA'CCTTTGAA</i>	GAGAGAAGTT	ACTGGCAATC	TCAAGTCAAC	HPAcDNA
529-588	CAGGATATTT	GCAAATATGG	ATCCATCCCT	CCTGATGTGG	<i>AGGAA^{3,5}AAGTT</i>	ACGGTTGGAA	HPAcDNA
589-648	TGGCCCTACC	AGGAGCAATT	GCTACTCCGA	GAACACTACC	AGAAAAAGTT	CAAGAACAGC	HPAcDNA
649-708	ACCTACTCAA	GAAGCTCTGT	AGATGTGCTA	TACACTTTTG	CAAACCTGTC	AGGACTGGAC	HPAcDNA
709-768	TTGATCTTTG	GCCTAAATGC	GTTATTAAGA	ACAGCAGATT	TGCAGTGGAA	CAGTTCTAAT	HPAcDNA
769-828	GCTCAGTTGC	TCCTGGACTA	CTGCTCTTCC	AAGGGGTATA	ACATTTCCTG	GGAAGTGGC	HPAcDNA
829-888	AATGAACCTA	ACAGTTTCTT	TAAGAAGGCT	GATATTTTCA	TCAATGGGTC	GCAGTTAGGA	HPAcDNA
889-948	GAAGATTTTA	TTC AATTGCA	TAAACTTCTA	AGAAAGTCCA	<i>CCTTCAAAG⁴</i>	<i>T⁶GCAAAACTC</i>	HPAcDNA
949-993	TATGGTCTCTG	ATGTTGGTCA	GCCTCGAAGA	AAGACGGCTA	AGATGCTGAA	GAGCTTCTCTG	HPAcDNA
	AAGGCTGGTG	GAGAAGTGAT	<i>TGATTCAGTT</i>	<i>ACATGGCATC</i>	<i>ACTAC²</i>		HPAcDNA
	AATCACTAGT	GAATTCGCGG	CCGCCTGCAG	GTCCACCATA	TGGGAGAGCT	CCCAACGCGT	Plasmid DNA
	TGAATCACTA	GTGAATTCGC	GGCCGCCTGC	AGGTCGACCA	TATGGGAGAG	CTCCAACGC	Plasmid DNA
	GTTG						Plasmid DNA

^{1,2}The segments with italics and boldface corresponded to the primers used in RT-PCR. ^{3,4}The letters represented the mutated bases. ^{5,6}The parts with underline represented the codons.

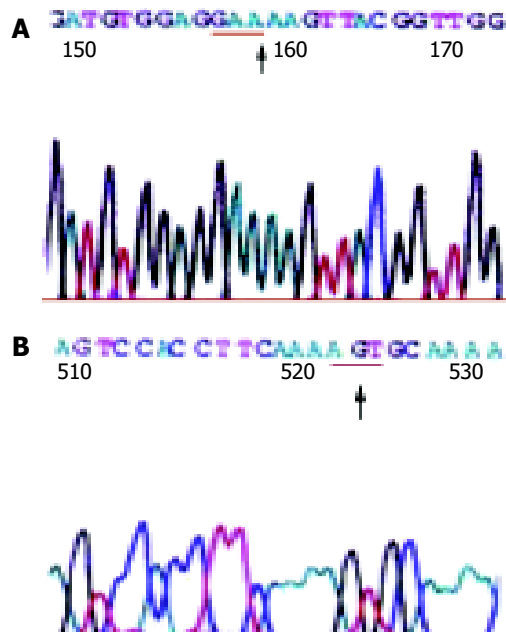


Figure 3 The sequencing map 1(A) and map 2(B) ↑, the mutated base; the parts with underline, the codons.

DISCUSSION

Mammalian genes including human HPA gene have been cloned and identified in recent years^[9-13]. It is known that the gene is on chromosome 4q22^[16] and includes 14 exons separated by 13 introns. The complete cDNA of HPA is 1 758^[9] or 1 629 bp in length^[10], and contains an open reading frame encoding a polypeptide of 543 amino acids, with a calculated molecular weight of 61 192 daltons. The HPA enzymes of about 50 ku isolated from human placenta and hepatoma cell line (SK-hep-1) may represent a processed or mature form of the native protein. In normal state, HPA is mainly identified in placenta, fetus liver, thymus gland, spleen, platelets, neutrophils, and activated T- and B-lymphocytes. HPA plays important physiological roles in embryonic morphogenesis, wound healing, inflammatory and autoimmune conditions by degrading GAGs. Many tumors and their stroma cells also produce or secrete HPA and use the same molecular machinery to induce neoplasm metastasis. RT-PCR analysis showed that most highly metastatic tumor cells expressed higher levels of HPA mRNA or HPA activity, but nonmetastatic carcinoma cells and low metastatic cells expressed no or only very weak HPA activity. HPA expression correlates with the metastatic potential of breast cancers^[17], and antisense-mediated suppression of human heparanase gene expression may inhibit pleural dissemination of human cancer cells^[18]. It has been found that high levels of HPA can be detected in a variety of malignant tissues or cells with high malignance or powerfully metastatic potential, among which are lymphoma, fibrosarcoma^[9,19], oral cancer cell lines and oral cancer^[20], esophageal carcinomas^[21], lung cancer^[18,22], malignant melanoma^[19,23,24], breast cancer^[9,25], gastric carcinoma and carcinoma of colon^[26,27], pancreatic carcinoma^[28,29], prostate cancer^[30], bladder carcinoma^[31], pheochromocytoma and ovarian cancer, and that no or only very weak HPA could be observed in some tumor cells with low or no metastatic potential. We detected the HPA mRNA expression of cancerous tissues in 33 HCC patients, and found that it was positive in 16 HCC samples (48.5%, 16/33). The expression rate of HPA mRNA in our study was similar to that of El-Assal *et al.* (47%)^[14]. In addition, we detected the HPA mRNA expression in the surrounding non-tumor liver tissues, and found that it was positive in only one sample. These results showed that about half of HCC tissues could

synthesize or secrete HPA, and the surrounding non-tumor liver tissues could hardly produce the enzyme on the whole.

HPA could degrade HSPG by cleaving the glycosidic linkages^[24] with a hydrolase mechanism, destroy and degrade the ECM and BM barricade in coordination with other proteases to promote the invasion and metastasis of tumor cells^[9,24]. Moreover, HPA could not only activate plasminogen and MMPs by means of promoting the release of urokinase-type plasminogen activator (u-PA) and tissue-type plasminogen activator (t-PA) but also facilitate the release of HS-binding active basic fibroblast growth factor (bFGF) and vascular endothelial growth factor (VEGF) to deliver its effect of enhancing cell metastasis and angiogenesis. It has been proved that HPA in cancerous tissues is closely related to tumor invasion, metastasis and angiogenesis^[9,10]. Both metastatic recurrence and tumor microvessel density (MVD) in tumors might significantly increase with high levels of HPA. By analyzing statistically the relationship between HPA mRNA and clinicopathological parameters in HCC patients, El-Assal *et al.*^[14] found that HPA mRNA expression was related to the tumor size, staging, classification, infection of HCV, vascularization, postoperative metastasis and prognosis, but was not related to other clinicopathological parameters. In this study, the expression rate in HCC was 48.5%, and HPA expression was associated with the pathological classification and TNM staging, which were similar to the conclusions drawn by El-Assal *et al.*^[14] The obvious difference in HPA expression between low- and high-tendency to metastatic recurrence groups in our study preliminarily indicated that HPA was associated with the invasion and metastasis of HCC. The significant difference between metastatic recurrence group and nonmetastatic recurrence group in our study was also similar to that of El-Assal^[14], and further proved that HPA expression was associated with metastatic recurrence, and that there were stronger invasiveness and tendency of postoperative recurrence in patients with positive HPA compared with HPA negative patients, and that HPA might provide a potential and valuable index to predict clinically postoperative metastatic recurrence.

No relationship was found between HPA expression and the integrity of tumor size or capsule in this study, which was different from the study of El-Assal *et al.*^[14] We speculate that the probable cause is that there were relatively fewer patients with tumors ≤ 5 cm in diameter (only 8 cases). In addition, HPA expression was not found to be associated with AFP, HBsAg and liver cirrhosis in this study perhaps because the types of causative viruses were different. Patients in the study of El-Assal *et al.*^[14] were mainly infected with HCV, but most HCCs in China were related to HBV infection and posthepatitic cirrhosis, few were infected with HCV. In addition, our conclusions are different from those of Ikeguchi *et al.*^[15], in which relative heparanase mRNA expression level in HCC was significantly lower than that in noncancerous liver tissues, and tumor heparanase expression did not correlate with tumor differentiation, tumor stage, or patient prognosis. Both the discrepancy of hepatitis virus and experimental methods could contribute to the different results. The surrounding non-tumor liver tissues in our study were at a clear distance from the edge of tumors (>1 cm), but they could be close to the tumor tissues in the study of Ikeguchi *et al.*

Both the positive rates of HPA mRNA in the study of El-Assal *et al.*^[14] and ours were close to 50% (47% and 48.5%, respectively), but very few HPAs were expressed in the surrounding non-tumor liver tissues. To our knowledge, no concrete mechanism of enhanced HPA mRNA expression in tumor tissues has been evaluated so far. To explore the probable mechanism of enhanced HPA expression in cancerous tissues, the positive PCR products of 7 patients were randomly selected and sequenced by T-A cloning. Two-point mutations including

a G to A transversion at nucleotide 513 and a A to G at nucleotide 878 of the HPA cDNA were found in 4 cases. By sequence analysis, we did not find base insertion and deletion, and the mutation rate was 57.1%. The point mutation of G to A transversion at nucleotide 513 resulting in GAG to GAA at codon 138 was a nonsense mutation because the amino acid residue was still glutamic acid after translation. The other point mutation of A to G transversion at nucleotide 878 leading to AAU to AGU at codon 260 belonged to sense mutation because it resulted in the alteration of amino acid residue (asparamide to serine), which may cause HPA structure to change and HPA activity to increase, resulting in the acceleration of ECM and BM barrier degrading and the final metastasis of tumor cells. Therefore, we guess that the point mutation at HPA gene might be one of the important mechanisms of increased HPA expression and enhanced metastasis of carcinoma cells, and it deserves further study.

REFERENCES

- 1 **Eccles SA.** Heparanase: breaking down barriers in tumors. *Nat Med* 1999; **5**: 735-736
- 2 **Airola K,** Karonen T, Vaalamo M, Lehti K, Lohi J, Kariniemi AL, Keski-Oja J, Saarialho-Kere UK. Expression of collagenases-1 and -3 and their inhibitors TIMP-1 and -3 correlates with the level of invasion in malignant melanomas. *Br J Cancer* 1999; **80**: 733-743
- 3 **Fan YZ,** Zhang JT, Yang HC, Yang YQ. Expression of MMP-2, TIMP-2 protein and the ratio of MMP-2/TIMP-2 in gallbladder carcinoma and their significance. *World J Gastroenterol* 2002; **8**: 1138-1143
- 4 **Tang Z,** Zhou X, Lin Z, Yang B, Ma Z, Ye S, Wu Z, Fan J, Liu Y, Liu K, Qin L, Tian J, Sun H, He B, Xia J, Qiu S, Zhou J. Surgical treatment of hepatocellular carcinoma and related basic research with special reference to recurrence and metastasis. *Chin Med J* 1999; **112**: 887-891
- 5 **Zheng Q,** Tang ZY, Xue Q, Shi DR, Song HY, Tang HB. Invasion and metastasis of hepatocellular carcinoma in relation to urokinase-type plasminogen activator, its receptor and inhibitor. *J Cancer Res Clin Oncol* 2000; **126**: 641-646
- 6 **Morita Y,** Hayashi Y, Wang Y, Kanamaru T, Suzuki S, Kawasaki K, Ohta K, Yamamoto M, Saitoh Y, Itoh H, Doe WF. Expression of urokinase-type plasminogen activator receptor in hepatocellular carcinoma. *Hepatology* 1997; **25**: 856-861
- 7 **Herszenyi L,** Plebani M, Carraro P, De Paoli M, Roveroni G, Cardin R, Tulassay Z, Naccarato R, Farinati F. The role of cysteine and serine proteases in colorectal carcinoma. *Cancer* 1999; **86**: 1135-1142
- 8 **Liu Y,** Xiao S, Shi Y, Wang L, Ren W, Sloane BF. Cathepsin B on invasion and metastasis of gastric carcinoma. *Chin Med J* 1998; **111**: 784-788
- 9 **Vlodavsky I,** Friedmann Y, Elkin M, Aingorn H, Atzmon R, Ishai-Michaeli R, Bitan M, Pappo O, Peretz T, Michal I, Spector L, Pecker I. Mammalian heparanase: gene cloning, expression and function in tumor progression and metastasis. *Nat Med* 1999; **5**: 793-802
- 10 **Hulett MD,** Freeman C, Hamdorf BJ, Baker RT, Harris MJ, Parish CR. Cloning of mammalian heparanase, an important enzyme in tumor invasion and metastasis. *Nat Med* 1999; **5**: 803-809
- 11 **Toyoshima M,** Nakajima M. Human heparanase. Purification, characterization, cloning, and expression. *J Biol Chem* 1999; **274**: 24153-24160
- 12 **Kussie PH,** Hulmes JD, Ludwig DL, Patel S, Navarro EC, Seddon AP, Giorgio NA, Bohlen P. Cloning and functional expression of a human heparanase gene. *Biochem Biophys Res Commun* 1999; **261**: 183-187
- 13 **Miao HQ,** Navarro E, Patel S, Sargent D, Koo H, Wan H, Plata A, Zhou Q, Ludwig D, Bohlen P, Kussie P. Cloning, expression, and purification of mouse heparanase. *Protein Expr Purif* 2002; **26**: 425-431
- 14 **El-Assal ON,** Yamanoi A, Ono T, Kohno H, Nagasue N. The clinicopathological significance of heparanase and basic fibroblast growth factor expressions in hepatocellular carcinoma. *Clin Cancer Res* 2001; **7**: 1299-1305
- 15 **Ikeguchi M,** Ueta T, Yamane Y, Hirooka Y, Kaibara N. Quantitative analysis of heparanase messenger RNA expression in hepatocellular carcinoma. *J Surg Oncol* 2002; **81**: 148-154
- 16 **Dong J,** Kukula AK, Toyoshima M, Nakajima M. Genomic organization and chromosome localization of the newly identified human heparanase gene. *Gene* 2000; **253**: 171-178
- 17 **Maxhimer JB,** Quiros RM, Stewart R, Dowlathshahi K, Gattuso P, Fan M, Prinz RA, Xu X. Heparanase-1 expression is associated with the metastatic potential of breast cancer. *Surgery* 2002; **132**: 326-333
- 18 **Uno F,** Fujiwara T, Takata Y, Ohtani S, Katsuda K, Takaoka M, Ohkawa T, Naomoto Y, Nakajima M, Tanaka N. Antisense-mediated suppression of human heparanase gene expression inhibits pleural dissemination of human cancer cells. *Cancer Res* 2001; **61**: 7855-7860
- 19 **Nakajima M,** Irimura T, Di Ferrante D, Di Ferrante N, Nicolson GL. Heparan sulfate degradation: relation to tumor invasive and metastatic properties of mouse B16 melanoma sublines. *Science* 1983; **220**: 611-613
- 20 **Ikuta M,** Podyma KA, Maruyama K, Enomoto S, Yanagishita M. Expression of heparanase in oral cancer cell lines and oral cancer tissues. *Oral Oncol* 2001; **37**: 177-184
- 21 **Mikami S,** Ohashi K, Usui Y, Nemoto T, Katsube K, Yanagishita M, Nakajima M, Nakamura K, Koike M. Loss of syndecan-1 and increased expression of heparanase in invasive esophageal carcinomas. *Jpn J Cancer Res* 2001; **92**: 1062-1073
- 22 **Sasaki M,** Ito T, Kashima M, Fukui S, Izumiyama N, Watanabe A, Sano M, Fujiwara Y, Miura M. Erythromycin and clarithromycin modulation of growth factor-induced expression of heparanase mRNA on human lung cancer cells *in vitro*. *Mediators Inflamm* 2001; **10**: 259-267
- 23 **Staquicini FI,** Moreira CR, Nascimento FD, Tersariol IL, Nader HB, Dietrich CP, Lopes JD. Enzyme and integrin expression by high and low metastatic melanoma cell lines. *Melanoma Res* 2003; **13**: 11-18
- 24 **Marchetti D,** Li J, Shen R. Astrocytes contribute to the brain-metastatic specificity of melanoma cells by producing heparanase. *Cancer Res* 2000; **60**: 4767-4770
- 25 **Zcharia E,** Metzger S, Chajek-Shaul T, Friedmann Y, Pappo O, Aviv A, Elkin M, Pecker I, Peretz T, Vlodavsky I. Molecular properties and involvement of heparanase in cancer progression and mammary gland morphogenesis. *J Mammary Gland Biol Neoplasia* 2001; **6**: 311-322
- 26 **Endo K,** Maejara U, Baba H, Tokunaga E, Koga T, Ikeda Y, Toh Y, Kohnoe S, Okamura T, Nakajima M, Sugimachi K. Heparanase gene expression and metastatic potential in human gastric cancer. *Anticancer Res* 2001; **21**: 3365-3369
- 27 **Friedmann Y,** Vlodavsky I, Aingorn H, Aviv A, Peretz T, Pecker I, Pappo O. Expression of heparanase in normal dysplastic, and neoplastic human colonic mucosa and stroma. Evidence for its role in colonic tumorigenesis. *Am J Pathol* 2000; **157**: 1167-1175
- 28 **Koliopanos A,** Friess H, Kleeff J, Shi X, Liao Q, Pecker I, Vlodavsky I, Zimmermann A, Buchler MW. Heparanase expression in primary and metastatic pancreatic cancer. *Cancer Res* 2001; **61**: 4655-4659
- 29 **Rohloff J,** Zinke J, Schoppmeyer K, Tannapfel A, Witzigmann H, Mossner J, Wittekind C, Caca K. Heparanase expression is a prognostic indicator for postoperative survival in pancreatic adenocarcinoma. *Br J Cancer* 2002; **86**: 1270-1275
- 30 **Kosir MA,** Wang W, Zukowski KL, Tromp G, Barber J. Degradation of basement membrane by prostate tumor heparanase. *J Surg Res* 1999; **81**: 42-47
- 31 **Gohji K,** Okamoto M, Kitazawa S, Toyoshima M, Dong J, Katsuoka Y, Nakajima M. Heparanase protein and gene expression in bladder cancer. *J Urol* 2001; **166**: 1286-1290

Lymphatic metastasis and nm23H₁ genetic instability in Chinese colon cancer patients

Zhi-Hong Su, Ji-Cheng Li

Zhi-Hong Su, Ji-Cheng Li, Department of Histology and Embryology, Zhejiang University Medical College, Hangzhou 310031, Zhejiang Province, China

Correspondence to: Dr. Ji-Cheng Li, Department of Histology and Embryology, Zhejiang University Medical College, Hangzhou 310031, Zhejiang Province, China. lijc@mail.hz.zj.cn

Telephone: +86-571-87217451 **Fax:** +86-571-87217139

Received: 2004-02-02 **Accepted:** 2004-02-21

enhanced expression of nm23H₁ protein can effectively inhibit colon cancer metastasis and improve prognosis of sporadic colon cancer patients.

Su ZH, Li JC. Lymphatic metastasis and nm23H₁ genetic instability in Chinese colon cancer patients. *World J Gastroenterol* 2004; 10(19): 2800-2804

<http://www.wjgnet.com/1007-9327/10/2800.asp>

Abstract

AIM: To investigate the pathogenic mechanism of colon cancer at the molecular level and to elucidate the relationship between intercellular adhesion molecule-1 (ICAM-1) and nm23H₁ genes and Chinese patients with colon cancer.

METHODS: DNA was extracted from paraffin-embedded materials. Polymerase chain reaction-single strand conformation polymorphism (PCR-SSCP) was used to analyze MSI and LOH. Expression of ICAM-1 was detected by Envision immunohistochemistry. Experimental results were analyzed with Leica-Qwin computer imaging techniques and SPSS software of statistics.

RESULTS: ICAM-1 expression of lymphatic endothelium was negative in normal colon and positive in colon cancer respectively. The number of lymphatics positive for ICAM-1 was gradually increased with degree of cancer invasion ($P < 0.01$). In the group with metastasis of colon cancer, the number of lymphatics positive for ICAM-1 in lymph nodes was more than that in the group with no metastasis ($P < 0.01$). The frequency of MSI, LOH and nm23H₁ protein was 26.67%, 20.00% and 53.33% in colon cancer, respectively. In TNM staging, MSI (43.75%) and nm23H₁ protein (81.25%) in stages I+II were detected more easily than the corresponding indexes (MSI: 7.14%, $P < 0.05$ and nm23H₁: 21.43%, $P < 0.01$) in stages III+IV. By comparison, the frequency of LOH (35.71%) in stages III+IV was more than that of LOH (6.25%, $P < 0.05$) in stages I+II. LOH exhibited a rising trend along with the Duke's staging. nm23H₁ protein in the group of tubular adenocarcinoma (60.00%) was higher expressed than that in the group of mucoid adenocarcinoma (20.00%) ($P < 0.01$), and exhibited a rising trend with the differentiation degrees of tubular adenocarcinoma. nm23H₁ protein in MSI positive group was higher expressed (75%) than that in MSI negative group (45.45%, $P < 0.05$).

CONCLUSION: The expression of ICAM-1 in lymphatic vessels is beneficial to the judgement of the invasion and metastasis ability of colon cancer and the anti-tumor immunity function, and shows an important clinical significance in predicting lymphatic metastasis of colon cancer. MSI and LOH may separately control the development of sporadic colon cancer with different pathways. LOH mostly arises in the late period of sporadic colon cancer and endows a high aggressive and poor prognostic phenotype. By comparison, MSI may be an early period molecule marker for sporadic colon cancer,

INTRODUCTION

Colon cancer is one of the common malignant tumors. A series of investigations have revealed that the main reason why it gives rise to death of patients lies in its invasiveness and metastasis^[1]. Therefore, preventing colon deterioration and decreasing the death rate of colon cancer is of great significance. So far, it has been known that many factors may have an influence on colon cancer, such as anti-oncogenes, adhesion molecular E-selectin and E-cadherin, vascular endothelial growth factor and matrix metal protein (MMP-2)^[2-5]. Among these factors, anti-oncogene and adhesion molecules have become the "hot spots" in research of colon cancer^[6-8].

Intercellular adhesion molecule-1 (ICAM-1), an important transmembrane glycoprotein, is negatively expressed on endothelial cells of lymphatic vessels in normal conditions^[9,10]. ICAM-1 could induce attachment of cells such as lymphocytes to endothelial cells of blood vessels, and traverse blood vessels, aggregate antigens and take part in immune and inflammatory reactions. When tumors appeared in the body, lymphatic vessels became the main pathway for tumor cells to be transferred as a result of their own permeability^[11]. In the process, recognition, adhesion, morphologic change and penetration between cells were involved. Vasse *et al.*^[12], reported that breast cancer cells could over-express the specific ligands of ICAM-1 (lymphocyte function associated antigen 1, LFA-1). With the development of cancer, the expression of LFA-1 went to an ascending trend on cancer cells. All the results indicated that ICAM-1 might take part in the metastasis. How endothelial cells of lymphatic vessels express ICAM-1? Few reports are available about whether endothelial cells of lymphatics express ICAM-1 or not in cancer tissue and whether ICAM-1/LFA-1 take part in the process of cancer cells attached to endothelial cells of lymphatics and metastasis.

nm23H₁ is one of the main anti-oncogenes. A great number of experiments indicated that inactivation of these genes, that is, genetic instability, resulted in metastasis^[13,14]. However, there were few researches of these genes on colon cancers^[15]. In order to further investigate the pathogenic mechanism of colon, we examined the instability of D17S396 of nm23H₁ in unrelated patients with the single strand conformation polymorphism analysis of polymerase chain reaction products (PCR-SSCP).

MATERIALS AND METHODS

Case selection and extraction of DNA

Thirty-two specimens were obtained during 2000 to 2002. There were 21 males and 11 females, aged 27-77 years. Twenty-seven cases were patients with tubular adenocarcinoma, 5 cases were

patients with mucoid adenocarcinoma in histological types. A senior pathologist made the final diagnosis on the basis of histological examination. No patient received radioactive therapy, chemotherapy before operation. Fresh surgical tissue samples were fixed immediately in formaldehyde solution for 12-24 h and paraffin-embedded for PCR-SSCP and immunohistochemical assay.

DNA extraction

DNA was extracted according to the standard protocols.

PCR amplification

Designed primers were synthesized by Shanghai Shengyou Biology Company. The primer sequences were (sense) 5'-TTGACCGGGGTAGAGAACTC-3', (antisense) 5'-TCTCAGTACTTCCCCTGACC-3'. PCR mixture contained 200 ng of template-DNA and PCR reaction buffer containing 50 mmol/L KCl, 10 mmol/L Tris-HCl (pH 8.4), 1.5 mmol/L MgCl₂, 0.5 μmol/L each of two fragment-specific primers, 100 μmol/L each of dATP, dGTP, dTTP and dCTP, and 2 units of Taq DNA polymerase (Shanghai Shengyou Biology Company) for a reaction volume of 50 μL. The conditions for all PCR amplifications were at 94 °C for 5 min for pre-denaturation, at 94 °C for 45 s, at 62 °C for 45 s and at 72 °C for 45 s. Amplification was carried out for 35 cycles with a final extension for 10 min at 72 °C. The amplified fragments were run in 1% agarose gel.

SSCP analysis

SSCP analysis of fragments was performed on a mini electrophoresis Unit (Bio-Rad Company, USA). Ten microlitre of the PCR product was diluted with 10 μL of sample buffer containing 90% formamide, 0.05% bromphenol blue dye and 0.05% xylene cyanol. The samples were heated at 100 °C for 8 min, transferred into an ice-cold water bath for 3 min, and analysed by 8% PAGE in 45 mmol/L-Tris-borate (pH8.0)/1 mmol/L-EDTA (TBE) buffer under 13 v/cm at 10 °C.

DNA silver staining

Gels were stained with silver as follows. Gels were firstly fixed in 100 mL/L alcohol for 10 min and then oxidized in 100 mL/L nitric acid for 3 min. After washed for 1 min with double distilled water, they were stained in 2 g/L silver nitric acid for 5 min and washed for 1 min with double distilled water. Gels showed appropriate color in 15 g/L anhydrous sodium carbonate and 4 mL/L formalin and then the reaction was terminated by 7.5 mL/L glacial acetic acid. Finally they were washed with double distilled water.

Immunohistochemical assay

Immunohistochemical study was performed using Envision method. Briefly, 5 μm thick sections of the tissue were deparaffinized and rehydrated. Endogenous peroxidase activity was blocked with 3% hydrogen peroxide for 20 min. After three times of rinsing with 0.01 mol/L phosphate-buffered saline (PBS) (pH = 7.4), the slides were incubated with 10% normal goat serum

at room temperature for 10 min to block the nonspecific reaction, and incubated for two hours with anti-ICAM-1 antibody. After rinsed in PBS for five min, they were incubated with Envision complex for two hours at room temperature, and stained with DAB after washed in PBS.

Statistical analyses

The experimental results were expressed as mean±SD. The correlation was analyzed with SPSS 8.0 software. *P* value less than 0.05 was regarded as statistically significant.

RESULTS

Expression of ICAM-1 in lymphatic endothelial cells

In the submucosa of normal colon, there existed a few lymphatic vessels with large, irregular cavities and thin walls. Simple squamous epithelia lined on them had no expression of ICAM-1 (Figure 1A). But in the submucosa and peripheral area of colon cancer, the number of lymphatic vessels was increased. Significant differences existed between them (*P*<0.01) (Table 1). The expression of lymphatic endothelial cell was positive for ICAM-1 in colon cancer (Figure 1B). With the degree of cancer invasion, lymphatic vessels positive for ICAM-1 showed an increasing trend (*P*<0.01) (Table 2). When cancer metastasis appeared in the peripheral lymph node, ICAM-1 was strongly expressed in endothelial cells of their peripheral lymphatic vessels, and the number of lymphatic vessels positive for ICAM-1 was to the highest (Table 2).

Table 1 Comparison of ICAM-1 expression between colon cancer and normal colon (mean±SD)

Group	Cases	ICAM-1/15HPF
Normal colon	5	11.001±1.58
Colon cancer	32	26.131±9.19 ^b

^a*P*<0.05, ^b*P*<0.01, vs normal colon group.

Genetic instability at D17S396 of nm23H1

Microsatellite fragments of D17S396 were amplified. The positive rate of D17S396 MSI (Figures 2A, B), LOH (Figure 2C) and nm23H₁ protein (Figure 2D) was 26.67%, 20.00% and 53.33% respectively in 30 cases of colon cancer (Table 3).

MSI and LOH were independent of the histological type of colon cancer, the degree of differentiation and Duke's stage were related to the clinical TNM stage. In TNM staging, the frequency of MSI (43.75%) in stages I+II was more than that in stages III+IV (7.14%, *P*<0.05). In contrast, LOH (35.71%) in stages III+IV was detected more easily than that (6.25%, *P*<0.05) in stages I+II. In addition, LOH exhibited an ascending trend with the Duke's stage (*P*<0.01).

Expression of nm23H₁ protein

The positive rate of nm23H₁ protein was related with the histological type of colon cancer, differentiation degree and

Table 2 ICAM-1 expression in colon cancer (mean±SD)

Dukes stage	Cases	ICAM-1		ICAM-1/15HPF	<i>P</i> Value
		Low-expression	High-expression		
A	5	3	2	19.671±5.59	
B	15	6	9	23.571±9.65	
C	10	3	7	25.591±8.07	<0.01
D	2	0	2	35.681±2.51	
Metastasis	12	3	9	28.091±8.33	
No metastasis	20	11	9	22.621±8.99	

Table 3 Relationship between clinical pathological parameter and nm23H₁ genetic instability in colon cancer (mean±SD)

	Cases	MSI(%)	LOH(%)	nm23(%)	nm23 expression
Histological types	30	8 (26.67)	6 (20.00)	16 (53.33)	40.21±3.29
Tubular adenocarcinoma	25	7 (28.00)	5 (20.00)	15 (60.00)	40.76±2.74
High differentiation	8	2 (25.00)	1 (12.50)	8 (100.00)	41.49±2.01
Intermediate differentiation	13	5 (38.46)	2 (15.38)	6 (46.15)	40.41±1.98
Poor differentiation	4	0 (0.00)	2 (50.00)	1 (25.00) ^d	40.18±2.17
Mucoid adenocarcinoma	5	1 (20.00)	1 (20.00)	1 (20.00) ^b	39.53±2.61
TNM stage					
Stage I+II	16	7 (43.75)	1 (6.25)	13 (81.25)	42.42±1.08
Stage III+IV	14	1 (7.14) ^e	5 (35.71) ^e	3 (21.43) ^f	39.49±2.57
Dukes stage					
A	5	2 (40.00)	0 (0.00)	4 (80.00)	41.32±2.18
B	15	5 (33.33)	3 (20.00)	8 (53.33)	40.69±2.11
C	8	1 (12.50)	1 (12.50)	4 (50.00)	42.32±1.66
D	2	0 (0.00)	2 (100.0) ^h	0 (0.00)	39.24±2.32

^a $P<0.05$, ^b $P<0.01$, vs tubular adenocarcinoma group; ^c $P<0.05$, ^d $P<0.01$ vs high differentiation group; ^e $P<0.05$, ^f $P<0.01$, vs stage I+II group; ^g $P<0.05$, ^h $P<0.01$ vs A, B, C groups respectively.

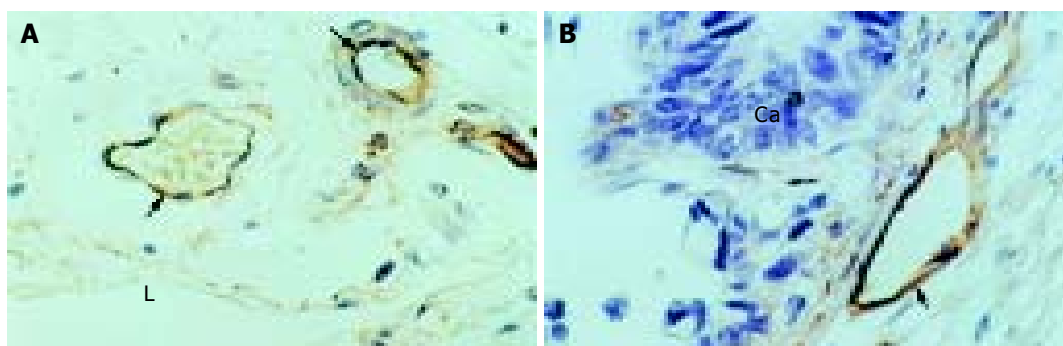


Figure 1 Expression of ICAM-1 in lymphatic endothelial cells. A: Negative expression of ICAM-1 in the lymphatic endothelium (L) of normal colon and positive expression of ICAM-1 in blood vessel endothelium (arrow) (Envision, original magnification ×400); B: Positive expression of ICAM-1 in the lymphatic endothelium (arrow) of colon cancer (Ca) (Envision, original magnification ×400).

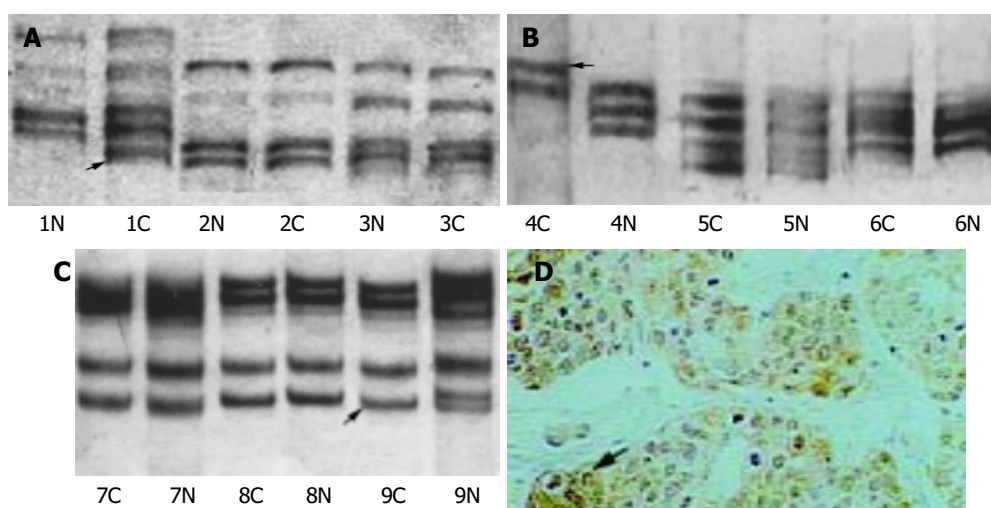


Figure 2 Positive D17S396 MSI, LOH and nm23H₁ in 30 cases of colon cancer. A: Positive MSI (arrow-headed) with an additional allele band (1C) compared with normal tissue (1N); B: Positive MSI (arrow-headed) with a removed allele band (4C) compared with normal tissue (4N); C: Positive LOH (arrow-headed) with a lacked allele band (9C) compared with normal tissue (9N); D: Positive nm23H₁ protein (arrow-headed) in cytoplasm, and nucleoli and membranes (Envision, original magnification ×200).

clinical stage. The expression of nm23H₁ protein in the group of tubular adenocarcinoma (60.00%) was apparently higher than that in the group of mucoid adenocarcinoma (20.00%, $P<0.01$), and exhibited a rising trend with the differentiation degrees of tubular adenocarcinoma ($P<0.01$). The positive rate of nm23H₁ in stages I+II (81.25%) was greater than that in stages III+IV

(21.43%) ($P<0.01$). The same phenomenon occurred between the group positive for MSI (75%) and the group negative for MSI (45.45%) ($P<0.05$) (Table 4). However, LOH had no effect on the expression of nm23H₁ protein (Table 4). Computer imaging analysis showed that there was a difference among the groups in nm23H₁ protein expression level.

Table 4 Relationship between LOH, MSI and nm23 protein expression (mean±SD)

Groups	Cases	Expression of nm23 protein(%)	Intensity of nm23 protein
Positive to MSI	8	6/8 (75.00)	39.06±2.14
Negative to MSI	22	10/22(45.45)	41.14±2.36
Positive to LOH	6	2/6 (33.33)	41.23±2.27
Negative to LOH	24	14/24 (58.33)	39.44±2.52

DISCUSSION

Metastasis, the spread of cells from primary neoplasms to distant sites and their growth at that location, is the most harmful aspect of cancer. Despite great improvements in early diagnosis, surgical techniques, general patient care, local and systemic adjuvant therapies, most deaths from cancer are attributable to metastases that are resistant to conventional therapies. During metastatic cascade, tumor cells interact with various host cells as well as extracellular matrices and basement membrane components including laminin, fibronectin, and type I collagen through certain adhesion molecules such as integrins. Such adhesive interactions may lead to the enhancement of survival, arrest, or invasiveness of tumor cells and is one of the most important events in the metastatic process^[14-17].

Intercellular adhesion molecule-1 (ICAM-1) is a single transmembrane glycoprotein and has two patterns in the body. One is located on the endothelial cells of blood vessels and is consisted of outmembrane region, transmembrane region and cytoplasmic region. The other (sICAM-1) is soluble in serum and is consisted of extracellular domains and originates from leucocytes, endothelial cells and hepatocytes^[18-20]. The specific ligand of ICAM-1, LFA-1, can be expressed on the surfaces of leucocytes and lymphocytes. In normal conditions, ICAM-1/LFA-1 plays an important role in various immune responses.

How ICAM-1 expresses when tumors appear in the body? In the present case, ICAM-1 was expressed on endothelial cells of lymphatic vessels in colon cancer. With the degree of cancer invasion, lymphatic vessels positive for ICAM-1 showed an increasing trend. When cancer metastasis appeared in peripheral lymph nodes, ICAM-1 was strongly expressed on endothelial cells of peripheral lymphatic vessels, and the number of lymphatic vessels positive for ICAM-1 was the highest. The results might give a hint that cancer cells can be transferred into lymphatic vessels in combination with LFA-1. Furthermore, sICAM-1 transformed from ICAM-1 could inhibit natural killer cells, which could activate lymphocytes and restrict major histocompatibility complex (MHC) to react with T cells and tumor cells, thus promoting tumor cells to escape^[21-23]. Therefore, sICAM-1 could strengthen and promote cancer cells to survive and transfer in lymphatic vessels when tumor metastasis occurred.

Genetic instability is the main reason why tumors appear and transfer^[24-31]. MSI and LOH could induce canceration in the body. MSI was firstly found in hereditary non-polyposis colorectal cancer (HNPCC), and then in some kinds of sporadic tumors such as colon cancer, gastric cancer, uterus cancer, breast cancer, prostate cancer and pancreatic cancer. Our results showed that DNA from thirty Chinese patients at the site of D17S396 appeared microsatellite instability, the incidence was 26.67%. Subsequent experiments indicated that the incidence of MSI at the site of D17S396 in the stage of TNM I+II was greater than that in the stage of TNM III+IV, suggesting that MSI might be one of the markers for early colon cancer.

In contrast to MSI, the incidence of LOH at the site of D17S396 increased with the degree of Duke stage. Therefore, our results made it clear that LOH of nm23H₁ appeared at the later stage of colon cancer, which endowed colon cancer with

a high invasiveness and a poor prognosis.

The expression of nm23H₁ has a negative relationship with tumor metastasis. Leone *et al.*^[32] found that nm23H₁ had a function on the prevention of tumor metastasis by inhibiting the ability of cancer cells to clone. With the degree of tumor stage, the expression of nm23H₁ decreased. Our results indicate that with the development of colon cancer, the expression of nm23H₁ decreases.

REFERENCES

- 1 **Bodey B**, Bodey B Jr, Siegel SE, Kaiser HE. Failure of cancer vaccines: the significant limitations of this approach to immunotherapy. *Anticancer Res* 2000; **20**: 2665-2676
- 2 **Dudda JC**, Simon JC, Martin S. Dendritic cell immunization route determines CD8⁺ T cell trafficking to inflamed skin: role for tissue microenvironment and dendritic cells in establishment of T cell-homing subsets. *J Immunol* 2004; **172**: 857-863
- 3 **Launay D**, Peyrat JP, Verdier A, Hornez L, Hatron PY, Hachulla E, Devulder B, Hebbar M. Multiplex reverse transcription polymerase chain reaction assessment of sialyltransferase expression in peripheral blood mononuclear cells in systemic sclerosis. *J Rheumatol* 2004; **31**: 88-95
- 4 **Perdikogianni CH**, Dimitriou H, Stiakaki E, Markaki EA, Kalmanti M. Adhesion molecules, endogenous granulocyte colony-stimulating factor levels and replating capacity of progenitors in autoimmune neutropenia of childhood. *Acta Paediatr* 2003; **92**: 1277-1283
- 5 **Kwei S**, Stavrakis G, Takahas M, Taylor G, Folkman MJ, Gimbrone MA Jr, Garcia-Cardena G. Early adaptive responses of the vascular wall during venous arterialization in mice. *Am J Pathol* 2004; **164**: 81-89
- 6 **Benkoel L**, Doderer F, Hardwigsen J, Benoliel AM, Bongrand P, Botta-Fridlund D, Le Treut YP, Chamlian A, Lombardo D. Expression of intercellular adhesion molecule-1 (ICAM-1) during ischemia-reperfusion in human liver tissue allograft: image analysis by confocal laser scanning microscopy. *Dig Dis Sci* 2003; **48**: 2167-2172
- 7 **Nyska A**, Moomaw CR, Ezov N, Shabat S, Levin-Harrus T, Nyska M, Redlich M, Mittelman M, Yedgar S, Foley JF. Ocular expression of vascular cell adhesion molecule (VCAM-1) in 2-butoxyethanol-induced hemolysis and thrombosis in female rats. *Exp Toxicol Pathol* 2003; **55**: 231-236
- 8 **Somersalo K**, Anikeeva N, Sims TN, Thomas VK, Strong RK, Spies T, Lebedeva T, Sykulev Y, Dustin ML. Cytotoxic T lymphocytes form an antigen-independent ring junction. *J Clin Invest* 2004; **113**: 49-57
- 9 **Chattopadhyay R**, Taneja T, Chakrabarti K, Pillai CR, Chitnis CE. Molecular analysis of the cytoadherence phenotype of a Plasmodium falciparum field isolate that binds intercellular adhesion molecule-1. *Mol Biochem Parasitol* 2004; **133**: 255-265
- 10 **Einstein O**, Karussis D, Grigoriadis N, Mizrachi-Kol R, Reinhartz E, Abramsky O, Ben-Hur T. Intraventricular transplantation of neural precursor cell spheres attenuates acute experimental allergic encephalomyelitis. *Mol Cell Neurosci* 2003; **24**: 1074-1082
- 11 **Toyama H**, Takada M, Suzuki Y, Kuroda Y. Brain death-induced expression of ICAM-1 and VCAM-1 on rat hepatocytes. *Hepatogastroenterology* 2003; **50**: 1854-1856
- 12 **Vasse M**, Thibout D, Paysant J, Legrand E, Soria C, Crepin M. Decrease of breast cancer cell invasiveness by sodium phenylacetate (NaPa) is associated with an increased expression of adhesive molecules. *Br J Cancer* 2001; **84**: 802-807
- 13 **Soufir N**, Daya-Grosjean L, de La Salmoniere P, Moles JP, Dubertret L, Sarasin A, Basset-Seguin N. Association between INK4a-ARF and p53 mutations in skin carcinomas of xeroderma pigmentosum patients. *J Natl Cancer Inst* 2000; **92**: 1841-1847
- 14 **Berney CR**, Fisher RJ, Yang J, Russell PJ, Crowe PJ. Genomic alterations (LOH, MI) on chromosome 17q21-23 and prognosis of sporadic colorectal cancer. *Int J Cancer* 2000; **89**: 1-7
- 15 **Chow NH**, Liu HS, Chan SH. The role of nm23H1 in the progression of transitional cell bladder cancer. *Clin Cancer Res* 2000; **6**: 3595-3599

- 16 **Kawamura A**, Miura S, Murayama T, Iwata A, Zhang B, Nishikawa H, Tsuchiya Y, Matsuo K, Tsuji E, Saku K. Increased Expression of Monocyte CD11a and intracellular adhesion molecule-1 in patients with initial atherosclerotic coronary stenosis. *Circ J* 2004; **68**: 6-10
- 17 **Burns S**, Hardy SJ, Buddle J, Yong KL, Jones GE, Thrasher AJ. Maturation of DC is associated with changes in motile characteristics and adherence. *Cell Motil Cytoskeleton* 2004; **57**: 118-132
- 18 **DesJardin LE**, Kaufman TM, Potts B, Kutzbach B, Yi H, Schlesinger LS. Mycobacterium tuberculosis-infected human macrophages exhibit enhanced cellular adhesion with increased expression of LFA-1 and ICAM-1 and reduced expression and/or function of complement receptors, FcγRII and the mannose receptor. *Microbiology* 2002; **148**(Pt 10): 3161-3171
- 19 **Masamune A**, Sakai Y, Kikuta K, Satoh M, Satoh A, Shimosegawa T. Activated rat pancreatic stellate cells express intercellular adhesion molecule-1 (ICAM-1) *in vitro*. *Pancreas* 2002; **25**: 78-85
- 20 **Becker A**, van Hinsbergh VW, Jager A, Kostense PJ, Dekker JM, Nijpels G, Heine RJ, Bouter LM, Stehouwer CD. Why is soluble intercellular adhesion molecule-1 related to cardiovascular mortality? *Eur J Clin Invest* 2002; **32**: 1-8
- 21 **Rescigno M**, Valzasina B, Bonasio R, Urbano M, Ricciardi-Castagnoli P. Dendritic cells, loaded with recombinant bacteria expressing tumor antigens, induce a protective tumor-specific response. *Clin Cancer Res* 2001; **7**(3 Suppl): 865S-870S
- 22 **Zhou Y**, Bosch ML, Salgaller ML. Current methods for loading dendritic cells with tumor antigen for the induction of antitumor immunity. *J Immunother* 2002; **25**: 289-303
- 23 **Ishigami S**, Natsugoe S, Tokuda K, Nakajo A, Xiangming C, Iwashige H, Aridome K, Hokita S, Aikou T. Clinical impact of intratumoral natural killer cell and dendritic cell infiltration in gastric cancer. *Cancer Lett* 2000; **159**: 103-108
- 24 **Storchova Z**, Pellman D. From polyploidy to aneuploidy, genome instability and cancer. *Nat Rev Mol Cell Biol* 2004; **5**: 45-54
- 25 **Ko EC**, Wang X, Ferrone S. Immunotherapy of malignant diseases. Challenges and strategies. *Int Arch Allergy Immunol* 2003; **132**: 294-309
- 26 **Kleist B**, Junghans D, Lorenz G, Bankau A, Poetsch M. The supplementary diagnostic power of selected immunohistochemical, molecular genetic and infective parameters in epithelial hyperplastic laryngeal lesions. *Oncology* 2003; **65**: 347-354
- 27 **Kovesi G**, Szende B. Changes in apoptosis and mitotic index, p53 and ki67 expression in various types of oral leukoplakia. *Oncology* 2003; **65**: 331-336
- 28 **Hayashi H**, Furihata M, Kuwahara M, Kagawa S, Shuin T, Ohtsuki Y. Infrequent alteration in the P53R2 gene in human transitional cell carcinoma of the urinary tract. *Pathobiology* 2004; **71**: 103-106
- 29 **Bai Y**, Murnane JP. Telomere instability in a human tumor cell line expressing NBS1 with mutations at sites phosphorylated by ATM. *Mol Cancer Res* 2003; **1**: 1058-1069
- 30 **Alexander J**, Watanabe T, Wu TT, Rashid A, Li S, Hamilton SR. Histopathological identification of colon cancer with microsatellite instability. *Am J Pathol* 2001; **158**: 527-535
- 31 **Rouba A**, Kaisi N, Al-Chaty E, Badin R, Pals G, Young C, Worsham MJ. Patterns of allelic loss at the BRCA1 locus in Arabic women with breast cancer. *Int J Mol Med* 2000; **6**: 565-569
- 32 **Leone A**, Flatow U, van Houtte K, Steeg PS. Transfection of human nm23-H1 into the human MDA-MB-435 breast carcinoma cell line: effects on tumor metastatic potential, colonization and enzymatic activity. *Oncogene* 1993; **8**: 2325-2333

Edited by Wang XL and Zhang JZ Proofread by Xu FM

Cytochrome C oxidase III interacts with hepatitis B virus X protein *in vivo* by yeast two-hybrid system

Dan Li, Xiao-Zhong Wang, Jie-Ping Yu, Zhi-Xin Chen, Yue-Hong Huang, Qi-Min Tao

Dan Li, Jie-Ping Yu, Department of Gastroenterology, Renmin Hospital of Wuhan University, Wuhan 430060, Hubei Province, China

Xiao-Zhong Wang, Zhi-Xin Chen, Yue-Hong Huang, Department of Gastroenterology, Union Hospital of Fujian Medical University, Fuzhou 350001, Fujian Province, China

Qi-Min Tao, Research Institute of Hepatology, Beijing University, Beijing 100044, China

Supported by Science and Technology Program of Fujian Province, No. 2001Z157

Correspondence to: Dr. Dan Li, Department of Gastroenterology, Renmin Hospital of Wuhan University, Wuhan 430060, Hubei Province, China. lidan2006@hotmail.com

Telephone: +86-27-88043424-8508

Received: 2003-12-10 **Accepted:** 2004-02-01

Abstract

AIM: To screen and identify the proteins which interact with hepatitis B virus (HBV) X protein in hepatocytes by yeast two-hybrid system and to explore the effects of X protein in the development of hepatocellular carcinoma (HCC).

METHODS: With HBV X gene amplified by polymerase chain reaction (PCR), HBV X bait plasmid, named pAS2-1-X, was constructed by yeast-two hybridization system³ and verified by auto-sequencing assay. pAS2-1-X was transformed into the yeast AH109, and X-BD fusion protein expressed in the yeast cells was detected by Western blotting. The yeast cells cotransformed with pAS2-1-X and normal human liver cDNA library were grown in selective SC/-trp-leu-his-ade medium. The second screen was performed with β -gal activity detection, and false positive clones were eliminated by segregation analysis, true positive clones were amplified, sequenced and analyzed with bioinformatics. Mating experiment was performed to confirm the binding of putative proteins to X protein in the yeast cells.

RESULTS: Bait plasmid pAS2-1-X was successfully constructed and pAS2-1-X correctly expressed BD-X fusion protein in yeast AH109. One hundred and three clones grew in the selective SC/-trp-leu-his-ade medium, and only one clone passed through β -gal activity detection and segregation analysis. The inserted cDNA fragment showed high homology with Homo sapiens cytochrome C oxidase III (COXIII). Furthermore, mating experiment identified that the binding of COXIII to X protein was specific.

CONCLUSION: COXIII protein is a novel protein that can interact with X protein *in vivo* by yeast two-hybrid system, and may contribute to the development of HCC through the interaction with X protein.

Li D, Wang XZ, Yu JP, Chen ZX, Huang YH, Tao QM. Cytochrome C oxidase III interacts with hepatitis B virus X protein *in vivo* by yeast two-hybrid system. *World J Gastroenterol* 2004; 10(19): 2805-2808

<http://www.wjgnet.com/1007-9327/10/2805.asp>

INTRODUCTION

Hepatitis B virus (HBV) belongs to the family hepadnaviridae which replicate their genome by reverse transcription, and causes acute and chronic hepatitis and is strongly associated with the development of primary hepatocellular carcinoma (HCC)^[1,2]. HBV has a unique open reading frame, with the sequence being highly conserved among different mammalian hepadnaviruses, coding for a 16.5 kDa protein known as hepatitis B virus X protein (HBx). X gene is a multifunctional regulatory factor which has been identified as a potential oncogene. Transcriptional activation of diverse cellular genes by the HBx has been suggested as one of the mechanisms for HBV-associated HCC^[2]. HBx has been shown to activate a wide variety of cellular and viral genes in trans activation including the HBV enhancers, tumor suppressor *p53*^[3,4], and proto-oncogenes *c-jun*, *c-fos* and *c-myc*^[5,6]. HBx-responsive elements also include nuclear factor kappa B (NF- κ B), activator protein-1 (AP-1), activator protein-2 (AP-2) and cAMP-response element (CRE)^[7,8]. Since HBx has no ability to bind to dsDNA, protein-protein interaction seems to be crucial for HBx transactivation. The interaction of HBx with cellular proteins may trigger a cascade of phosphorylation and dephosphorylation events which might lead to a general up-regulation of gene expression^[9]. Identification of cellular X-interactive proteins would provide insights into the mechanism of HBV cellular effects. Several techniques have been used to study possible protein-protein interaction with HBx. Using these approaches, HBx has been discovered to interact with many proteins^[9]. Nonetheless, to the author's knowledge, the functional significance of these interactions has not yet been elucidated. In the present study, we screened a clone encoding a novel X-interactive protein which was homologous to Homo sapiens cytochrome C oxidase III (COXIII) from normal human liver cDNA library by the *Saccharomyces cerevisiae* two-hybrid system.

MATERIALS AND METHODS

Plasmids and cells

Plasmids pAS2-1, PCL1, PLAM5'-1, normal human liver pACT2-cDNA library and *Saccharomyces cerevisiae* AH109 were purchased from Clontech, USA. *Saccharomyces cerevisiae* AH109 was grown in YPD medium (10 g/L yeast extract, 20 g/L peptone, 20 g/L dextrose). This yeast strain carried LacZ, HIS3 and ADE2 reporter genes under the control of Gal4-binding site and was used to screen the liver cDNA library. *Escherichia coli* JM105 was provided as a gift from Research Institute of Hepatology, Beijing University, China.

Reagents

Restriction enzymes (*Eco*RI and *Pst* I), TaqDNA polymerase and T4 DNA ligase were purchased from Promega, USA. DNA gel extraction kit was provided by Jingmei Company, China. Gal4 DNA-BD monoclonal antibody, matchmaker AD LD-insert screening amplifiers and yeast culture medium were purchased from Clontech, USA. Glass beads (acid-washed) were purchased from Sigma, USA. Alkaline phosphatase-conjugated goat anti-mouse IgG was purchased from Wuhan Boster Biological Technology Company, China.

pAS2-1-X construction

The X region of the HBV genome was amplified by PCR with XF and XR as forward and reverse primers which contained an *EcoRI* site and a *PstI* site, respectively, for convenience of cloning. The sequences of the primers with the restriction enzyme sites underlined were: XF, 5'-ACGGAATTCATGGCTGCTAGGCTGTG-3'; XR, 5'-ATCCTGCAGAGGTGAAAAAGTTGCAT-3'. The fragment amplified was from nucleotides 1 374 to 1 838 on HBV genome. The template for this reaction was extracted from sera of HBV DNA-positive patients. The reaction mixture was subjected to 30 cycles of PCR amplification. Each cycle included denaturation at 94 °C for 30 s, annealing at 58 °C for 1 min, and extension at 72 °C for 30 s, and a final extension for 7 min at 72 °C. The approximate 464 bp fragment was digested by *EcoRI* and *PstI*, and recombined into the plasmid pAS2-1 by T4 DNA ligase. The reconstructed plasmid was subsequently named pAS2-1-X and identified by PCR and auto-sequencing assay. Auto-sequencing assay was performed in Bioasia Biologic Technology Company and the resulting sequence was analyzed in the database of EMBL\GeneBank by the BLAST program.

Transformation of pAS2-1-X into AH109

Yeast AH109 was transformed with pAS2-1-X by lithium acetate-mediated method demonstrated by Gietz *et al.*^[10] and plated in selective SC/-trp medium. Plasmids were isolated from transformants and X gene was amplified. Filter assay was used to exclude the auto-activation function of pAS2-1-X in AH109. Expressed X-BD fusion protein in yeasts transformed with pAS2-1-X was detected by Western blotting. The cells were collected by centrifugation and yeast protein extract was prepared according to urea/SDS method. SDS-polyacrylamide gel electrophoresis was performed and protein extracts were electroblotted onto nitrocellulose membrane. After being blocked with nonfat milk, the membrane was added to 1:3 000 diluted Gal4 DNA-BD monoclonal antibodies and incubated for 1 h, after washed with TBST. Then, the secondary alkaline phosphatase-conjugated goat anti-mouse IgG was added and incubated for 2 h. The proteins were visualized with 5-bromo-4-chloro-3-indolyl phosphate and nitro blue tetrazolium. Protein extracts of untransformed yeast cells were used as negative control.

Screening of human liver cDNA library by the yeast two-hybrid system

The screening procedure used here was a modification of the method described by Gietz *et al.*^[10]. Yeast cells were transformed with pAS2-1-X and pACT2-cDNA library by lithium acetate-mediated method, plated in selective SC/-trp-leu-his-ade medium, incubated at 30 °C for 7 d and selected for histidine, leucine and tryptophan prototrophy. The freshly growing clones were assayed for β -gal activity by replicating the yeast transformants onto Whatman filter paper. The filters were then snap frozen twice in liquid nitrogen for 10 s and incubated in a buffer containing 5-bromo-4-chloro-3-indolyl- β -D-galactopyranoside solution at 30 °C for 1-8 h. Positive interactions were detected by appearance of blue clones. Plasmids PCL1 and PLAM5'-1 were transformed into AH109 as positive and negative controls, respectively. Segregation analysis was performed to eliminate false positive clones and thus true positive clones were obtained.

Analysis of positive clones

pACT2-cDNA plasmid genome was isolated following the method described by Gietz *et al.*^[10]. Briefly, the true positive clones were incubated with SC/-leu liquid medium at 30 °C overnight, followed by spinning down the cells by centrifuging at 14 000 g for 5 min, and resuspension of pellets in lysis buffer

(20 g/L Triton 100, 10 g/L SDS, 10 mmol/L NaCl, 10 mmol/L Tris-HCl, pH8.0, 1 mmol/L Na₂EDTA) was added with phenol, chloroform and isoamyl alcohol (volume fraction 25:24:1). Then the suspension was vortexed vigorously with acid-washed glass beads, lysate was centrifuged and plasmid DNA was harvested. The pACT2-cDNA plasmid was purified by CsCl gradient centrifugation to permit PCR using the matchmaker AD LD-insert screening amplimers which annealed to GAL4-AD. The PCR reaction consisted 30 amplification cycles, each cycle included denaturation at 94 °C for 30 s, annealing at 68 °C for 3 min, and a final extension for 7 min at 72 °C. Auto-sequencing assay was performed in Shanghai Sangon Biological Engineering Technology and Service Corporation, the resulting sequences were compared against the databases of EMBL\GenBank by the BLAST program.

Mating experiment

pAS2-1-X, pAS2-1, pLAM5'-1 transformed yeasts in SC/-trp medium and positive clones were incubated in SC/-leu medium at 30 °C for 2 d, respectively, then removed. Two types of transformants were incubated into YPD medium at 30 °C for 4 h. Finally, transformants were subcultured in SC/-leu-trp medium, incubated at 30 °C for 2 d and assayed for β -gal activity.

RESULTS

Identification of the pAS2-1-X

The fragment of approximately 460 bp was amplified from the reconstructed plasmid pAS2-1-X, and auto-sequencing assay confirmed the fragment inserted into plasmid pAS2-1 had a high identity (99.9%) with X gene.

Detection of the transformed yeast AH109

X gene was amplified from the plasmid isolated from the transformed yeast cells (Figure 1). Filter assay excluded the auto-activation function of pAS2-1-X in the cells. Staining for X-BD was obtained in yeast cells transformed with pAS2-1-X (Figure 2). pAS2-1-X could be used as a bait plasmid in yeast two-hybrid system.

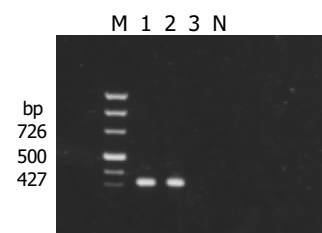


Figure 1 Result of detection of X gene in yeasts transformed with pAS2-1-X. M: PCR marker; lanes 1 and 2: transformed yeasts; lanes 3: untransformed yeasts; N: negative control.

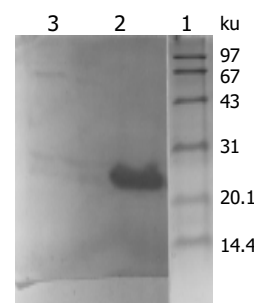


Figure 2 Western blot analysis of expressed fusion protein in yeasts transformed with pAS2-1-X. Lane 1: protein molecular weight standard; lane 2: protein extracted from transformed yeasts; lane 3: protein extracted from untransformed yeasts.

Screening of the liver cell cDNA library

Of the 5×10^6 transformants screened, 103 were grown in the selective SC/-trp-leu-his-ade medium, 19 were positive for β -gal activity, and only 1 clone passed through the segregation analysis.

Analysis of positive clones

The fragment of approximately 900 bp was amplified from the true positive clones (Figure 3). DNA sequence analysis of the fragment revealed that the yeast plasmid insert had a high identity (98%) with the Homo sapiens COXIII gene (GeneBank ID:BC013930).

Mating experiment

The transformants containing pAS2-1-X and positive pACT2-cDNA gave a blue colour by filter assay, whereas the transformants containing pAS2-1 or pLAM5'-1 and positive pACT2-cDNA gave a white colour. Mating experiment confirmed the specific interaction between positive clones and HBx (Figure 4).

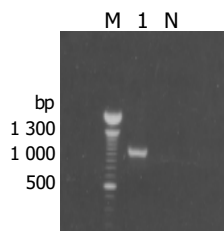


Figure 3 Results of amplification for cDNA fragment by PCR from the positive clones. M: 100 bp DNA ladder; lane 1: positive clone; N: negative control.



Figure 4 Mating experiment for the interaction between COXIII and X protein in yeast cells.

DISCUSSION

Chronic HBV infection is strongly associated with the development of HCC, but the mechanisms by which HBV induces events leading to the genesis of HCC remains unclear. Several studies have suggested a possible role of HBx in the process of HCC, a few studies have reported transformation of certain cell types *in vitro* by HBx^[11] and initiation of HCC in HBx transgenic mice^[12,13], but its direct oncogenicity seems to depend on the strength, and duration of protein expression and the genetic background of mice and cells. It is more likely that HBx causes transactivation of cell regulatory genes or interacts with one or more cellular proteins to initiate the development of human HCC through upregulation of cell growth and mutagenesis. The transactivation function of HBx has been shown to involve both direct interaction with transcriptional factors, such as RPB5 of RNA polymerases^[14], TATA-binding protein^[15] or activating transcription factor (ATF)/CRE-binding protein (CREB)^[16] and activation of signal transduction pathways, such as ras/raf/MAP-kinase^[17], protein kinase C (PKC)^[18] and SAPK/JNK^[19,20]. HBx is predominantly localized in the cytoplasm with a low level of nuclear distribution, whereas recent findings from two independent laboratories

indicated that HBx could localize at the mitochondria. Confocal laser microscopy of hepatoma cells transfected with respective expression vectors showed colocalization of the third member of the family of human genes that encode the voltage-dependent anion channel (HVDAC3) and HBx in mitochondria. Moreover, stable cationic fluorophore dye showed that HBx expression in hepatoma cells led to alteration of mitochondrial transmembrane potential, an abnormal aggregation of mitochondrial structures, release of cytochrome C from mitochondria, decrease of mitochondrial membrane potential and membrane blebbing of cells, which are characteristics of cell death. These functional roles of HBx in affecting mitochondrial physiology are associated with HBV-induced liver injury and development of HCC^[21,22].

Since HBx seems to accomplish its functions via protein-protein interaction, identification of the HBx-interactive cellular proteins represents a major goal in order to define the function of HBx in HBV replication and liver carcinogenesis. The yeast two-hybrid system using a genetic approach, offers a way to clone and identify genes that interact with a protein of interest through *in vivo* complementation in yeast cells^[23,24]. In the present study, we screened and cloned a novel HBx-interactive protein from a normal human liver cDNA library. Sequence analysis revealed it was the homolog of Homo sapiens COXIII. The interaction of HBx with COXIII was confirmed by yeast-two hybridization system 3. The growth of yeast cells harboring both pAS-1-X and pACT2-COXIII recombinant plasmids in His-independent medium, formation of blue-colonies detected by the β -gal assay, and the behaviors of the cells in false-positive elimination tests suggested that the binding of COXIII was HBx specific. Mating experiment further identified the interaction between COXIII and HBx in yeast cells.

Cytochrome C oxidase (COX), the terminal enzyme of the mitochondrial respiratory chain, catalyzes the transfer of electrons from reduced cytochrome C to molecular oxygen. COXIII, which is encoded by the mitochondrial DNA and synthesized within the mitochondria, represents one of the large subunits of COX and acts as the catalytic core of the enzyme^[25]. Defective COX activity resulting in deficient adenosine triphosphate generation may contribute to the development of Alzheimer's disease^[26], cardiomyopathy^[27], neonatal giant cell hepatitis^[28] and other clinically heterogeneous diseases^[29,30]. Incorrect assembly of the critical subunits including COXI, COXII and COXIII, is a major mechanism leading to COX deficiencies. COX also plays a key role in inducing apoptosis in multiple cell types through transcriptional activation of the respective genes^[31]. Mitochondrial dysfunction and transcriptional function changes have been identified to be associated with chronic liver disease and oncogenic processes^[32]. Kuo *et al.*^[33] reported the integration of HBV with human hepatoma cells might cause mitochondrial defects in the ATP synthase 6 and COXIII genes. Studies on the effects of HBx on apoptotic pathways indicated that HBx blocked the activation of caspases 8, 9 and 3 and the release of cytochrome c, it also upregulated PKC, extracellular signal-regulated kinase (ERK), phosphatidylinositol-3-kinase (PI-3-K) and NF- κ B activity^[34]. The study of NF- κ B and HBx expression in human HCC tissues detected by immunohistochemistry SP method strongly suggested that NF- κ B was abnormally activated in HCC, which was probably related to HBx. The ability of HBx to induce the activation of NF- κ B has been demonstrated by mobility shift and reporter gene expression assays with lysates from HBx-transfected HepG2 cells^[35]. Furthermore, HBx was shown to bind to a voltage-dependent anion channel and alter the mitochondrial transmembrane potential and consequently induce activation of transcription factors, which include STAT-3 and NF- κ B^[21]. Cogswell *et al.*^[36] reported that the NF- κ B regulatory pathway existed in mitochondria and NF- κ B could negatively regulate the expression of both COXIII and cytochrome B mRNAs. Whether and how the interaction of HBx with COXIII

regulates the activity of transcription factor NF- κ B has remained obscure. However, based on our data, we hypothesize that HBx might impair mitochondrial respiration chain and energy metabolism by combining COXIII.

Future investigations will focus on the identification of COXIII properties and physiological significance of interaction of HBx with COXIII and probably with other mitochondrial proteins. Further inquiries in this area may pave the way for investigation of possible mechanisms leading to chronic infection and subsequent progression to HCC in the context of mitochondrial association of HBx.

REFERENCES

- 1 **Su Q**, Schroder CH, Hofmann WJ, Otto G, Pichlmayr R, Bannasch P. Expression of hepatitis B virus protein in HBV-infected human livers and hepatocellular carcinomas. *Hepatology* 1998; **27**: 1109-1120
- 2 **Koike K**, Tsutsumi T, Fujie H, Shintani Y, Kyoji M. Molecular mechanism of viral hepatocarcinogenesis. *Oncology* 2002; **62** (Suppl 1): 29-37
- 3 **Huo TI**, Wang XW, Forgues M, Wu CG, Spillare EA, Giannini C, Brechot C, Harris CC. Hepatitis B virus X mutants derived from human hepatocellular carcinoma retain the ability to abrogate p53-induced apoptosis. *Oncogene* 2001; **20**: 3620-3628
- 4 **Shiota G**, Oyama K, Udagawa A, Tanaka K, Nomi T, Kitamura A, Tsutsumi A, Noguchi N, Takano Y, Yashima K, Kishimoto Y, Suou T, Kawasaki H. Occult hepatitis B virus infection in HBs antigen-negative hepatocellular carcinoma in a Japanese population: involvement of HBx and p53. *J Med Virol* 2000; **62**: 151-158
- 5 **Sirma H**, Giannini C, Poussin K, Paterlini P, Kremsdorf D, Brechot C. Hepatitis B virus X mutants, present in hepatocellular carcinoma tissue abrogate both the antiproliferative and transactivation effects of HBx. *Oncogene* 1999; **18**: 4848-4859
- 6 **Natoli G**, Avantaggiati ML, Chirillo P, Puri PL, Ianni A, Balsano C, Levrero M. Ras- and Raf-dependent activation of c-jun transcriptional activity by the hepatitis B virus transactivator pX. *Oncogene* 1994; **9**: 2837-2843
- 7 **Cao XY**, Liu J, Lian ZR, Clayton M, Hu JL, Zhu MH, Fan DM, Feitelson M. Cloning of differentially expressed genes in human hepatocellular carcinoma and nontumor liver. *World J Gastroenterol* 2001; **7**: 579-582
- 8 **Shamay M**, Barak O, Doitsh G, Ben-Dor I, Shaul Y. Hepatitis B virus pX interacts with HBXAP, a PHD finger protein to coactivate transcription. *J Biol Chem* 2002; **277**: 9982-9988
- 9 **Yeh CT**. Hepatitis B virus X protein: searching for a role in hepatocarcinogenesis. *J Gastroenterol Hepatol* 2000; **15**: 339-341
- 10 **Gietz RD**, Triggs-Raine B, Robbins A, Graham KC, Woods RA. Identification of proteins that interact with a protein of interest: applications of the yeast two-hybrid system. *Mol Cell Biochem* 1997; **172**: 67-69
- 11 **Tarn C**, Bilodeau ML, Hullinger RL, Andrisani OM. Differential immediate early gene expression in conditional hepatitis B virus pX-transforming versus nontransforming hepatocyte cell lines. *J Biol Chem* 1999; **274**: 2327-2336
- 12 **Murakami S**. Hepatitis B virus X protein: a multifunctional viral regulator. *J Gastroenterol* 2001; **36**: 651-660
- 13 **Kim CM**, Koike K, Saito I, Miyamura T, Jay G. HBx gene of hepatitis B virus induces liver cancer in transgenic mice. *Nature* 1991; **351**: 317-320
- 14 **Cheong JH**, Yi M, Lin Y, Murakami S. Human RPB5, a subunit shared by eukaryotic nuclear RNA polymerases, binds human hepatitis B virus X protein and may play a role in X transactivation. *EMBO J* 1995; **14**: 143-150
- 15 **Haviv I**, Matza Y, Shaul Y. pX, the HBV-encoded coactivator, suppresses the phenotypes of TBP and TAFII250 mutants. *Genes Dev* 1998; **12**: 1217-1226
- 16 **Maguire HF**, Hoefler JP, Siddiqui A. HBV X protein alters the DNA binding specificity of CREB and ATF-2 by protein-protein interactions. *Science* 1991; **252**: 842-844
- 17 **Chirillo P**, Falco M, Puri PL, Artini M, Balsano C, Levrero M, Natoli G. Hepatitis B virus pX activates NF-kappa B-dependent transcription through a Raf-independent pathway. *J Virol* 1996; **70**: 641-646
- 18 **Cong YS**, Yao YL, Yang WM, Kuzhandaivelu N, Seto E. The hepatitis B virus X-associated protein, XAP3, is a protein kinase C-binding protein. *J Biol Chem* 1997; **272**: 16482-16489
- 19 **Diao J**, Khine AA, Sarangi F, Hsu E, Iorio C, Tibbles LA, Woodgett JR, Penninger J, Richardson CD. X protein of hepatitis B virus inhibits Fas-mediated apoptosis and is associated with up-regulation of the SAPK/JNK pathway. *J Biol Chem* 2001; **276**: 8328-8340
- 20 **Arbuthnot P**, Capovilla A, Kew M. Putative role of hepatitis B virus X protein in hepatocarcinogenesis: effects on apoptosis, DNA repair, mitogen-activated protein kinase and JAK/STAT pathways. *J Gastroenterol Hepatol* 2000; **15**: 357-368
- 21 **Rahmani Z**, Huh KW, Lasher R, Siddiqui A. Hepatitis B virus X protein colocalizes to mitochondria with a human voltage-dependent anion channel, HVDAC3, and alters its transmembrane potential. *J Virol* 2000; **74**: 2840-2846
- 22 **Takada S**, Shirakata Y, Kaneniwa N, Koike K. Association of hepatitis B virus X protein with mitochondria causes mitochondrial aggregation at the nuclear periphery, leading to cell death. *Oncogene* 1999; **18**: 6965-6973
- 23 **Fields S**, Song O. A novel genetic system to detect protein-protein interactions. *Nature* 1989; **340**: 245-246
- 24 **Bartel PL**, Fields S. Analyzing protein-protein interactions using two-hybrid system. *Methods Enzymol* 1995; **254**: 241-263
- 25 **Lenka N**, Vijayarathay C, Mullick J, Avadhani NG. Structural organization and transcription regulation of nuclear genes encoding the mammalian cytochrome c oxidase complex. *Prog Nucleic Acid Res Mol Biol* 1998; **61**: 309-344
- 26 **Maurer I**, Zierz S, Moller HJ. A selective defect of cytochrome c oxidase is present in brain of Alzheimer disease patients. *Neurobiol Aging* 2000; **21**: 455-462
- 27 **Quigley AF**, Kapsa RM, Esmore D, Hale G, Byrne E. Mitochondrial respiratory chain activity in idiopathic dilated cardiomyopathy. *J Card Fail* 2000; **6**: 47-55
- 28 **Muller-Hocker J**, Muntau A, Schafer S, Jaksch M, Staudt F, Pongratz D, Taanman JM. Depletion of mitochondrial DNA in the liver of an infant with neonatal giant cell hepatitis. *Hum Pathol* 2002; **33**: 247-253
- 29 **von Kleist-Retzow JC**, Vial E, Chantrel-Groussard K, Rotig A, Munnich A, Rustin P, Taanman JW. Biochemical, genetic and immunoblot analyses of 17 patients with an isolated cytochrome c oxidase deficiency. *Biochim Biophys Acta* 1999; **1455**: 35-44
- 30 **Aguilera I**, Garcia-Lozano JR, Munoz A, Arenas J, Campos Y, Chinchon I, Roldan AN, Bautista J. Mitochondrial DNA point mutation in the COI gene in a patient with McArdle's disease. *J Neurol Sci* 2001; **192**: 81-84
- 31 **Chandra D**, Liu JW, Tang DG. Early mitochondrial activation and cytochrome c up-regulation during apoptosis. *J Biol Chem* 2002; **277**: 50842-50854
- 32 **Valgimigli M**, Valgimigli L, Trere D, Gaiani S, Pedulli GF, Gramantieri L, Bolondi L. Oxidative stress EPR measurement in human liver by radical-probe technique. Correlation with etiology, histology and cell proliferation. *Free Radic Res* 2002; **36**: 939-948
- 33 **Kuo KW**, Yang PY, Huang YS, Shieh DZ. Variations in gene expression and genomic stability of human hepatoma cells integrated with hepatitis B virus DNA. *Biochem Mol Biol Int* 1998; **44**: 1133-1140
- 34 **Li J**, Xu Z, Zheng Y, Johnson DL, Ou JH. Regulation of hepatocyte nuclear factor 1 activity by wild-type and mutant hepatitis B virus X proteins. *J Virol* 2002; **76**: 5875-5881
- 35 **Waris G**, Huh KW, Siddiqui A. Mitochondrially associated hepatitis B virus X protein constitutively activates transcription factors STAT-3 and NF-kappa B via oxidative stress. *Mol Cell Biol* 2001; **21**: 7721-7730
- 36 **Cogswell PC**, Kashatus DF, Keifer JA, Guttridge DC, Reuther JY, Bristow C, Roy S, Nicholson DW, Baldwin AS Jr. NF-kappaB and I kappa B alpha are found in the mitochondria. Evidence for regulation of mitochondrial gene expression by NF-kappaB. *J Biol Chem* 2003; **278**: 2963-2968

Roles of *Helicobacter pylori* infection and cyclooxygenase-2 expression in gastric carcinogenesis

Wei-Hao Sun, Qian Yu, Hong Shen, Xi-Long Ou, Da-Zhong Cao, Ting Yu, Cheng Qian, Feng Zhu, Yun-Liang Sun, Xi-Ling Fu, Han Su

Wei-Hao Sun, Department of Geriatrics, The First Affiliated Hospital of Nanjing Medical University, Nanjing 210029, Jiangsu Province, China
Qian Yu, Xi-Long Ou, Da-Zhong Cao, Ting Yu, Cheng Qian, Feng Zhu, Yun-Liang Sun, Xi-Ling Fu, Han Su, Department of Gastroenterology, Zhongda Hospital of Southeast University, Nanjing 210009, Jiangsu Province, China

Hong Shen, Department of Gastroenterology, Jiangsu Provincial Hospital of Traditional Chinese Medicine, Nanjing 210029, Jiangsu Province, China

Supported by the Scientific Research Foundation for the Returned Overseas Chinese Scholars, State Education Ministry, No. 9247342057

Correspondence to: Dr. Wei-Hao Sun, Department of Geriatrics, The First Affiliated Hospital of Nanjing Medical University, 300 Guangzhou Road, Nanjing 210029, China. weihaosun@hotmail.com

Telephone: +86-25-83718836-6044 **Fax:** +86-25-83783506

Received: 2003-10-20 **Accepted:** 2003-12-08

Abstract

AIM: Cyclooxygenase (COX)-2 is over expressed in gastrointestinal neoplasm. *Helicobacter pylori* (*H pylori*) infection is causally linked to gastric cancer. However, the expression of COX-2 in various stages of *H pylori*-associated gastric carcinogenesis pathway has not been elucidated. Therefore, the aim of this study was to clarify the role of *H pylori* induced COX-2 expression during carcinogenesis in the stomach.

METHODS: Gastric biopsies from 138 subjects [30 cases of chronic superficial gastritis (CSG), 28 cases of gastric glandular atrophy (GA), 45 cases of gastric mucosal intestinal metaplasia (IM), 12 cases of moderate gastric epithelial dysplasia and 23 cases of gastric cancer] were enrolled. *H pylori* infection was assessed by a rapid urease test and histological examination (modified Giemsa staining). The expression of COX-1 and COX-2 in human gastric mucosa was detected by immunohistochemical staining.

RESULTS: *H pylori* infection rate was 64.3% in GA and 69.5% in gastric cancer, which was significantly higher than that (36.7%) in CSG ($P < 0.05$). The positive expression rates of COX-2 were 10.0%, 35.7%, 37.8%, 41.7% and 69.5% in CSG, GA, IM, dysplasia and gastric cancer, respectively. From CSG to GA, IM, dysplasia and finally to gastric cancer, expression of COX-2 showed an ascending tendency, whereas COX-1 expression did not change significantly in the gastric mucosa. The level of COX-2 expression in IM and dysplasia was significantly higher in *H pylori*-positive than in *H pylori*-negative subjects ($P < 0.01$).

CONCLUSION: COX-2 expression induced by *H pylori* infection is a relatively early event during carcinogenesis in the stomach.

Sun WH, Yu Q, Shen H, Ou XL, Cao DZ, Yu T, Qian C, Zhu F, Sun YL, Fu XL, Su H. Roles of *Helicobacter pylori* infection and cyclooxygenase-2 expression in gastric carcinogenesis. *World J Gastroenterol* 2004; 10(19): 2809-2813
<http://www.wjgnet.com/1007-9327/10/2809.asp>

INTRODUCTION

Gastric cancer remains the world's second, and the Chinese first, commonest cause of cancer related deaths^[1]. There is epidemiological evidence that *Helicobacter pylori* (*H pylori*) infection is causally linked to gastric cancer^[2,3]. It has been classified as a class I biological carcinogen by the World Health Organization^[4]. However, the exact mechanism responsible for the development of gastric cancer in *H pylori*-infected patients still remains obscure. According to Correa's^[5] model, gastric cancer develops in a multistep process from chronic active gastritis, gastric glandular atrophy (GA), intestinal metaplasia (IM), dysplasia, and finally to gastric cancer. Recent studies have shown that *H pylori* infection induces cyclooxygenase-2 (COX-2) expression in human gastric mucosa^[6-8]. COX-2, an inducible isoform of cyclooxygenase enzyme, which converts arachidonic acid to prostanoids, is strongly expressed in colorectal cancer^[9,10], pancreatic cancer^[11], hepatocellular carcinoma^[12,13], esophageal cancer^[14,15], and gastric cancer^[16,17]. Several studies have also shown that COX-2 expression is increased in premalignant lesions including colonic adenoma^[9], Barrett's esophagus^[18,19], and gastric adenomas^[20], indicating that this enzyme may be involved in the early process of carcinogenesis.

It is well known that *H pylori* infection causes inflammation, and COX-2 is involved in inflammatory responses and also related to carcinogenesis. However, COX-2 expression in various stages of *H pylori*-associated gastric carcinogenesis pathway has not been elucidated. To clarify the role of *H pylori* induced COX-2 expression during carcinogenesis in the stomach, COX-1 and COX-2 expression at different stages of gastric carcinogenesis from inflammation, premalignant lesions, to gastric cancer was investigated by using immunohistochemical analysis in the present study.

MATERIALS AND METHODS

Patients

A total of 138 patients were studied. Of these, 78 were males and 60 were females. The mean age was 52 years (range, 19-74). Endoscopies with biopsy were performed in all patients. Patients who took non-steroidal anti-inflammatory drugs (NSAIDs), H₂ receptor antagonists, proton pump inhibitors, antimicrobials, bismuth compounds, over last 4 wk prior to the examination, were excluded. The Medical Ethics Committee of Nanjing Medical University approved this study and written informed consent was obtained from all patients.

Endoscopic and histological assessment

All endoscopic examinations were performed under local anesthesia with lidocaine. Four biopsy specimens, 2 from the antrum within 2 cm of the pyloric channel and 2 from the corpus, were taken during the procedure. When lesions suspected to be cancerous were noted, additional biopsies were taken from the site of lesions. Of these specimens, 2 (each from antrum and corpus) were submitted to a rapid urease test (RUT), and the others were processed for hematoxylin and eosin (H&E) stain and modified Giemsa stain. The pathologic assessment

was performed by one pathologist according to the updated Sydney system^[21]. GA was defined as loss of glandular tissue and fibrous replacement of lamina propria. IM or exchange of crypts by intestinal epithelium was recognized by the presence of goblet cells and absorptive cells.

Detection of *H pylori* infection

H pylori infection was identified by histological examination using modified Giemsa stain and RUT (CLO test, Delta West, Bentley, Australia). Patients were classified as *H pylori* positive if any of the two examinations yielded a positive result. Subjects were considered to be *H pylori* negative only when both assays were negative for the organism.

Immunohistochemistry

Immunohistochemical staining for COX-1 and COX-2 was performed by the avidin-biotin-peroxidase complex (ABC) method using a Vectastain kit (Vector Laboratories, Burlingame, CA). In brief, paraffin-embedded blocks were sectioned at about 4- μ m thickness, deparaffinized, and rehydrated. After microwave pretreatment in citrate buffer (pH 6.0) for antigen retrieval, slides were immersed in 3 mL/L H₂O₂ in methanol for 30 min to block the endogenous peroxidase activity. Nonspecific binding was blocked with 50 mL/L rabbit serum (DAKO, Glostrup, Denmark) in phosphate-buffered saline (PBS), and the tissues were then incubated with goat polyclonal antibody against COX-1 or COX-2 (1:200, Santa Cruz Biotechnology, Inc. Santa Cruz, CA) in PBS containing 20 mL/L rabbit serum and 1 mL/L Triton 100 overnight at 4 °C in a humidity chamber. After being rinsed with PBS, the sections were subsequently incubated with biotinylated secondary rabbit anti-goat immunoglobulins (1:400) for 45 min and then with avidin-biotin-peroxidase complex for another 45 min. The color was developed in 3,3'-diaminobenzidine tetrahydrochloride (Sigma Chemical Co., St. Louis, MO) solution containing 0.3 mL/L H₂O₂. Nuclei were counterstained with Mayer's hematoxylin (Merck, Darmstadt, Germany). Tissues of part sections were incubated with PBS containing 20 mL/L rabbit serum and 1 mL/L Triton 100 without the primary antibody as a negative control.

Evaluation of COX-1 and COX-2 immunostaining

In each section, 5 high-power fields were selected, and a total of at least 1 000 cells were calculated. The percentage of positive staining cells was graded semiquantitatively, and each sample was assigned to one of the following categories: - (negative, 0% to 4%); + (weak, 5% to 29%); ++ (moderate, 30% to 59%); or +++ (strong, more than 60%). All immunostained sections were evaluated independently by two investigators who were blind to the pathological and clinical data. Evaluations were similar among assessors, with less than 10% disagreement. A final consensus was achieved between the 2 assessors using a multihead microscope.

Statistical analysis

Expressions of COX-1 and COX-2 between the 5 study groups (CSG, GA, IM, dysplasia and gastric cancer) were compared by Kruskal-Wallis nonparametric analysis of variance test, using Dunn's multiple comparison tests for *post hoc* comparison. The association between COX-2 expression and *H pylori* infection was analyzed using Fisher's exact test. Statistical significance was taken at $P < 0.05$.

RESULTS

Histopathologic characteristics and the prevalence of *H pylori* infection

Of the 138 patients, 63 were *H pylori*-positive and 75 were *H pylori*-

negative. Table 1 shows the histopathologic characteristics and *H pylori* status. Histopathologic diagnosis in this population included CSG ($n = 30$), GA ($n = 28$), IM ($n = 45$), moderate dysplasia ($n = 12$) and gastric cancer ($n = 23$). The rates of *H pylori* infection in GA and gastric cancer were significantly higher than that in CSG.

Table 1 Rates of *H pylori* infection in various gastric mucosal lesions

Pathological diagnosis	<i>n</i>	<i>H pylori</i> rate (%)
CSG	30	36.7
GA	28	64.3 ^a
IM	45	31.1
Dysplasia	12	33.3
Gastric cancer	23	69.5 ^a

^a $P < 0.05$ vs CSG.

Expression of COX-1 and COX-2 in human gastric mucosa with various lesions

COX-1 was clearly detected in the gastric foveolar and glandular epithelium including parietal cells. Patchy cytoplasmic staining for COX-1 was also seen in the inflammatory mononuclear cells and macrophages, myofibroblasts, as well as endothelial cells in the lamina propria. Spotty cytoplasmic staining for COX-1 was seen in gastric cancer cells (Figure 1). Perinuclear and cytoplasmic staining for COX-2 was mainly seen in the foveolar and glandular epithelium, and mild staining in mononuclear inflammatory cells and macrophages in the lamina propria. Strong expression of COX-2 was also found on glandular epithelium of IM and dysplasia. Immunoreactivity of COX-2 protein showed diffuse staining in the cytoplasm of gastric cancer cells (Figure 2). Furthermore, scattered expression for COX-2 was detected in interstitial cells such as vascular endothelial cells and myofibroblasts. Table 2 shows the positive rates of COX-1 and COX-2 expression in the gastric mucosa with various lesions. From CSG to GA, IM, dysplasia and finally to gastric cancer, the expression of COX-2 showed an ascending tendency, whereas COX-1 expression did not change significantly in the gastric mucosa with various lesions.

Table 2 Expression of COX-1 and COX-2 in gastric mucosa with various lesions

Pathological diagnosis	<i>n</i>	COX-1 expression (%)	COX-2 expression (%)
CSG	30	56.6	10.0
GA	28	53.8	35.7 ^a
IM	45	53.3	37.8 ^b
Dysplasia	12	41.7	41.7 ^a
Gastric cancer	23	43.4	69.5 ^{bc}

^a $P < 0.05$; ^b $P < 0.01$ vs CSG; ^c $P < 0.05$ vs GA.

Relationship between *H pylori* infection and COX-2 expression in the gastric mucosa

COX-2 expression was found in 57% (36/63) *H pylori*-infected patients, including one case of CSG, eight cases of GA, twelve cases of IM, four cases of dysplasia, and eleven cases of gastric cancer, with intensity scoring ranged from + to +++ (Table 3). *H pylori*-associated gastritis exhibited strong expression of COX-2 in foveolar and glandular epithelium but with a lower intensity in mononuclear inflammatory cells. On the contrary, only 20% (15/75) of non-infected patients expressed COX-2 protein in the gastric biopsy. The intensity of COX-2 expression in IM and dysplasia was significantly higher in *H pylori*-

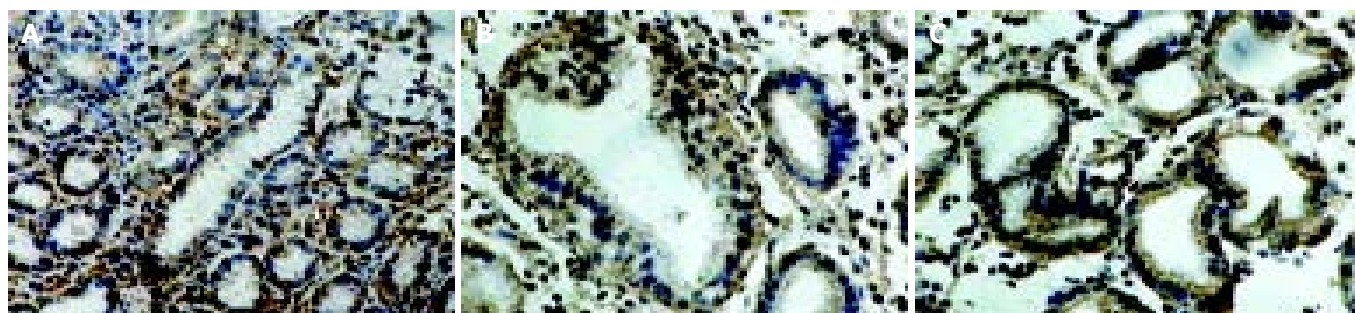


Figure 1 Immunostaining of cyclooxygenase-1 in the gastric mucosa with CSG (A), dysplasia (B) and gastric cancer (C) as shown by immunostaining. In the gastric biopsies of cases of CSG, GA, IM and dysplasia, COX-1 immunostaining was detected in the foveolar and glandular epithelium including parietal cells, and in the subepithelial mononuclear inflammatory cells. Spotty cytoplasmic staining for COX-1 was seen in the gastric cancer cells.

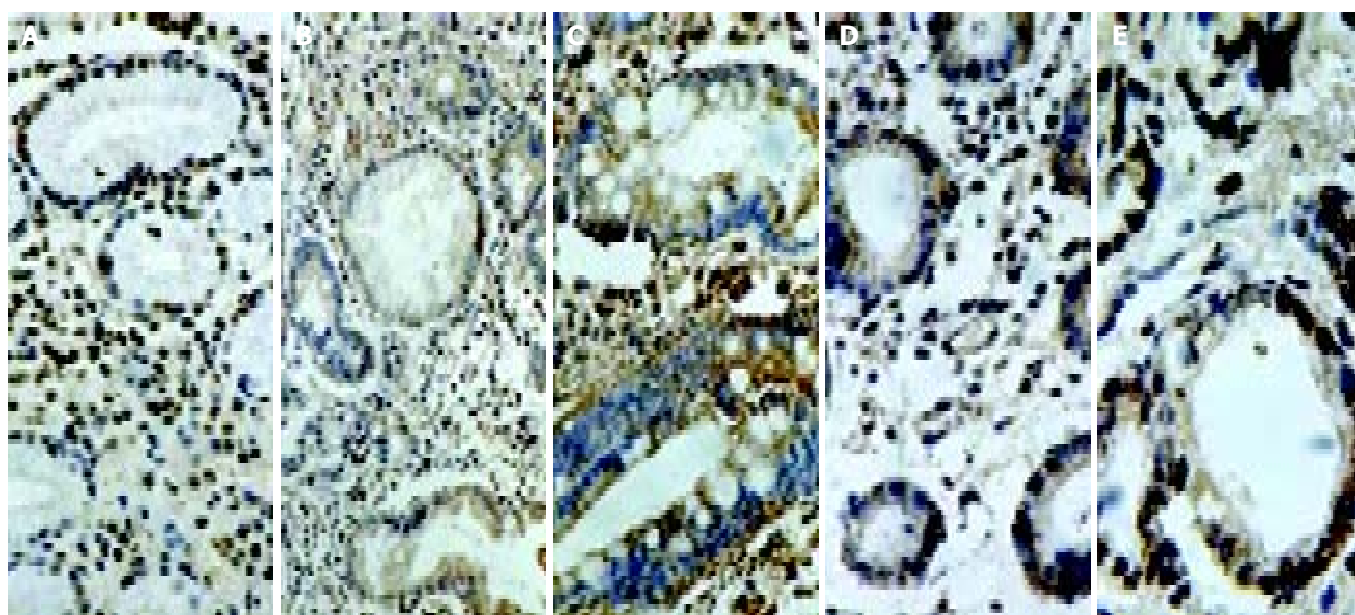


Figure 2 Immunostaining of cyclooxygenase-2 in the gastric mucosa with CSG (A), GA (B), IM (C), dysplasia (D) and gastric cancer (E). CSG showing strong expression in foveolar and glandular epithelium and weak expression in mononuclear inflammatory cells, myofibroblasts, and endothelial cells in the lamina propria; GA showing strong expression in the atrophic glands of the gastric mucosa; IM showing strong expression in intestinal epithelium and goblet cells; and gastric cancer showing strong expression in cancer cells.

Table 3 Relationship between *H pylori* infection and COX-1/COX-2 expression in the gastric mucosa with various lesions

Pathological diagnosis	<i>n</i>	COX-1				COX-2				
		-	+	++	+++	-	+	++	+++	
CSG	<i>H pylori</i> (+)	11	5	1	3	2	10	0	0	1
	<i>H pylori</i> (-)	19	8	3	4	4	17	1	1	0
GA	<i>H pylori</i> (+)	18	9	2	4	3	10	1	3	4
	<i>H pylori</i> (-)	10	4	2	2	2	8	1	1	0
IM	<i>H pylori</i> (+)	14	6	3	2	3	2	2	4	6 ^b
	<i>H pylori</i> (-)	31	15	5	5	6	26	3	2	0
Dysplasia	<i>H pylori</i> (+)	4	2	0	1	1	0	0	2	2 ^b
	<i>H pylori</i> (-)	8	5	0	1	2	7	0	1	0
Gastric cancer	<i>H pylori</i> (+)	16	9	2	2	3	5	1	3	7
	<i>H pylori</i> (-)	7	4	2	0	1	2	1	2	2

^b $P < 0.01$ vs *H pylori* (-).

positive than in *H pylori*-negative subjects ($P < 0.01$). However, there was no significant difference in COX-2 expression in CSG, GA and gastric cancer patients with or without *H pylori* infection (Table 3).

DISCUSSION

Epidemiological studies have shown that long-term use of NSAIDs reduces the risk of colon cancer development by 40%^[22,23] and the risk of esophageal cancer development by up to 90%^[24,25].

In addition, NSAIDs could induce regression of adenomatous polyps in patients with familial adenomatous polyposis^[26,27], as well as in an Apc Min mouse model^[28]. Although the exact mechanisms of NSAIDs on cancer prevention have not been clarified, one possible role of NSAIDs is via the inhibition of COX enzymes, leading to chemopreventive effect. COX exists in two isoforms, of which COX-1 is constitutively expressed in many tissues, including the stomach, and COX-2 showing 61% homology with COX-1 is expressed at low concentrations or is even undetectable in unstimulated cells or tissues, but is readily induced by various stimuli including mitogens, cytokines, growth factors, and tumor promoters in inflammatory and certain cell types, such as fibroblasts, macrophages and endothelial cells^[29,30]. It is well known that COX-2 is strongly expressed in gastric cancer^[17,20]. More than 90% of gastric cancers are adenocarcinomas, which are divided into intestinal and diffuse histological types. Pathogenesis of the intestinal-type gastric cancer has been connected to precursor changes such as GA, IM, and dysplasia. The present study clearly showed that COX-2 protein was expressed not only in gastric cancer cells but also in the glandular epithelium of IM and dysplasia as detected by immunohistochemistry. From CSG, GA to IM and dysplasia and finally to gastric cancer, the expression of COX-2 showed an ascending tendency, whereas COX-1 expression did not change significantly in premalignant and malignant gastric lesions. These results provided evidence that COX-2 might contribute to an early event in gastric carcinogenesis^[31], and suggesting the possibility that the use of selective COX-2 inhibitors may provide a chemopreventive strategy against gastric carcinogenesis.

H. pylori infection is an important risk factor for adenocarcinoma of the distal stomach in humans^[2-5], but the mechanism whereby *H. pylori* infection contributes to gastric carcinogenesis is still hypothetical. Recent studies have shown that *H. pylori* infection induces COX-2 expression in human gastric mucosa^[6-8]. Furthermore, McCarthy *et al.*^[32] showed that COX-2 expression in antral mucosa was reduced but not eliminated in the epithelium after successful eradication of *H. pylori*. Kimura *et al.*^[33] reported that immunoreactivity of COX-2 was observed in all cases of IM even after the cure of *H. pylori* infection. Thus, cure of *H. pylori* infection may decrease the risk of gastric carcinogenesis due to COX-2-related compounds in gastric mucosa but not in those patients with IM. In this study, we demonstrated that COX-2 was expressed in epithelial lining of the stomach in the *H. pylori*-associated gastric carcinogenesis pathway from CSG, to GA and IM and dysplasia, and finally to gastric cancer. The level of COX-2 expression in patients with IM and dysplasia was significantly higher in *H. pylori*-positive than in *H. pylori*-negative subjects. In contrast, COX-1 protein was constitutively expressed in different gastric mucosal lesions with or without *H. pylori* infection. Thus, COX-1 is considered as a housekeeping gene, and prostanoids synthesized via the COX-1 pathway are thought to be responsible for cytoprotection of the stomach, for vasodilatation in the kidney, and for production of a proaggregative prostanoid, thromboxane, by the platelets. In contrast, COX-2 is an inducible immediate-early gene, and its role has been connected to inflammation, reproduction, and carcinogenesis. Although the exact mechanism of COX-2 expression in carcinogenesis is still unclear, some studies have suggested that overexpression of COX-2 is associated with cellular resistance to apoptosis whereas treatment with specific COX-2 inhibitors could suppress cell proliferation and induces apoptosis^[14,34-36]. It has been hypothesized that the alteration of the balance between apoptosis and proliferation of gastric epithelial cells, induced by *H. pylori* infection, contributes to either gastric injury or carcinogenesis of the stomach^[37-39]. Although *H. pylori* could decrease epithelial cell proliferation and induce apoptosis *in vitro*^[40-43], *H. pylori* infection *in vivo* was associated with both increased apoptosis and proliferation^[44-46].

These differences between the *in vivo* and *in vitro* results suggest that *in vivo* factors including inflammatory cells, extracellular matrix proteins, cytokines, and adhesion molecules may also contribute to epithelial cell turnover. On the other hand, COX-2 expression has been reported to correlate with invasion of the lymphatic vessels, lymph node metastasis, and advanced tumor stage in gastric cancer^[47,48].

In conclusion, COX-2 overexpression plays an important role in the initiation of gastric carcinogenesis. The use of selective COX-2 inhibitors may provide a chemopreventive strategy against gastric carcinogenesis.

REFERENCES

- 1 Stadlander CT, Waterbor JW. Molecular epidemiology, pathogenesis and prevention of gastric cancer. *Carcinogenesis* 1999; **20**: 2195-2208
- 2 Wang RT, Wang T, Chen K, Wang JY, Zhang JP, Lin SR, Zhu YM, Zhang WM, Cao YX, Zhu CW, Yu H, Cong YJ, Zheng S, Wu BQ. *Helicobacter pylori* infection and gastric cancer: evidence from a retrospective cohort study and nested case-control study in China. *World J Gastroenterol* 2002; **8**: 1103-1107
- 3 Welin M, Holmgren NM, Nilsson P, Enroth H. Statistical model of the interactions between *Helicobacter pylori* infection and gastric cancer development. *Helicobacter* 2003; **8**: 72-78
- 4 Infection with *Helicobacter pylori*. *IARC Monogr Eval Carcinog Risks Hum* 1994; **61**: 177-240
- 5 Correa P. *Helicobacter pylori* and gastric carcinogenesis. *Am J Surg Pathol* 1995; **19**(Suppl 1): S37-S43
- 6 Fu S, Ramanujam KS, Wong A, Fantry GT, Drachenberg CB, James SP, Meltzer SJ, Wilson KT. Increased expression and cellular localization of inducible nitric oxide synthase and cyclooxygenase 2 in *Helicobacter pylori* gastritis. *Gastroenterology* 1999; **116**: 1319-1329
- 7 Tatsuguchi A, Sakamoto C, Wada K, Akamatsu T, Tsukui T, Miyake K, Futagami S, Kishida T, Fukuda Y, Yamanaka N, Kobayashi M. Localisation of cyclooxygenase 1 and cyclooxygenase 2 in *Helicobacter pylori* related gastritis and gastric ulcer tissues in humans. *Gut* 2000; **46**: 782-789
- 8 Chan FK, To KF, Ng YP, Lee TL, Cheng AS, Leung WK, Sung JJ. Expression and cellular localization of COX-1 and -2 in *Helicobacter pylori* gastritis. *Aliment Pharmacol Ther* 2001; **15**: 187-193
- 9 Eberhart CE, Coffey RJ, Radhika A, Giardiello FM, Ferrenbach S, DuBois RN. Up-regulation of cyclooxygenase 2 gene expression in human colorectal adenomas and adenocarcinomas. *Gastroenterology* 1994; **107**: 1183-1188
- 10 Sano H, Kawahito Y, Wilder RL, Hashimoto A, Mukai S, Asai K, Kimura S, Kato H, Kondo M, Hla T. Expression of cyclooxygenase-1 and -2 in human colorectal cancer. *Cancer Res* 1995; **55**: 3785-3789
- 11 Tucker ON, Dannenberg AJ, Yang EK, Zhang F, Teng L, Daly JM, Soslow RA, Masferrer JL, Woerner BM, Koki AT, Fahey TJ 3rd. Cyclooxygenase-2 expression is up-regulated in human pancreatic cancer. *Cancer Res* 1999; **59**: 987-990
- 12 Koga H, Sakisaka S, Ohishi M, Kawaguchi T, Taniguchi E, Sasatomi K, Harada M, Kusaba T, Tanaka M, Kimura R, Nakashima Y, Nakashima O, Kojiro M, Kurohiji T, Sata M. Expression of cyclooxygenase-2 in human hepatocellular carcinoma: relevance to tumor dedifferentiation. *Hepatology* 1999; **29**: 688-696
- 13 Shiota G, Okubo M, Noumi T, Noguchi N, Oyama K, Takano Y, Yashima K, Kishimoto Y, Kawasaki H. Cyclooxygenase-2 expression in hepatocellular carcinoma. *Hepatogastroenterology* 1999; **46**: 407-412
- 14 Zimmermann KC, Sarbia M, Weber AA, Borchard F, Gabbert HE, Schror K. Cyclooxygenase-2 expression in human esophageal carcinoma. *Cancer Res* 1999; **59**: 198-204
- 15 Ratnasinghe D, Tangrea J, Roth MJ, Dawsey S, Hu N, Anver M, Wang QH, Taylor PR. Expression of cyclooxygenase-2 in human squamous cell carcinoma of the esophagus; an immunohistochemical survey. *Anticancer Res* 1999; **19**: 171-174
- 16 Sung JJ, Leung WK, Go MY, To KF, Cheng AS, Ng EK, Chan FK. Cyclooxygenase-2 expression in *Helicobacter pylori*-associ-

- ated premalignant and malignant gastric lesions. *Am J Pathol* 2000; **157**: 729-735
- 17 **Uefuji K**, Ichikura T, Mochizuki H, Shinomiya N. Expression of cyclooxygenase-2 protein in gastric adenocarcinoma. *J Surg Oncol* 1998; **69**: 168-172
 - 18 **Wilson KT**, Fu S, Ramanujam KS, Meltzer SJ. Increased expression of inducible nitric oxide synthase and cyclooxygenase-2 in Barrett's esophagus and associated adenocarcinomas. *Cancer Res* 1998; **58**: 2929-2934
 - 19 **Shirvani VN**, Ouatu-Lascar R, Kaur BS, Omary MB, Triadafilopoulos G. Cyclooxygenase 2 expression in Barrett's esophagus and adenocarcinoma: Ex vivo induction by bile salts and acid exposure. *Gastroenterology* 2000; **118**: 487-496
 - 20 **Uefuji K**, Ichikura T, Mochizuki H. Expression of cyclooxygenase-2 in human gastric adenomas and adenocarcinomas. *J Surg Oncol* 2001; **76**: 26-30
 - 21 **Dixon MF**, Genta RM, Yardley JH, Correa P. Classification and grading of gastritis. The updated Sydney System. International Workshop on the Histopathology of Gastritis, Houston 1994. *Am J Surg Pathol* 1996; **20**: 1161-1181
 - 22 **Thun MJ**, Namboodiri MM, Heath CW Jr. Aspirin use and reduced risk of fatal colon cancer. *N Engl J Med* 1991; **325**: 1593-1596
 - 23 **Rosenberg L**, Palmer JR, Zauber AG, Warshauer ME, Stolley PD, Shapiro S. A hypothesis: nonsteroidal anti-inflammatory drugs reduce the incidence of large-bowel cancer. *J Natl Cancer Inst* 1991; **83**: 355-358
 - 24 **Thun MJ**, Namboodiri MM, Calle EE, Flanders WD, Heath CW Jr. Aspirin use and risk of fatal cancer. *Cancer Res* 1993; **53**: 1322-1327
 - 25 **Funkhouser EM**, Sharp GB. Aspirin and reduced risk of esophageal carcinoma. *Cancer* 1995; **76**: 1116-1119
 - 26 **Giardiello FM**, Hamilton SR, Krush AJ, Piantadosi S, Hylind LM, Celano P, Booker SV, Robinson CR, Offerhaus GJ. Treatment of colonic and rectal adenomas with sulindac in familial adenomatous polyposis. *N Engl J Med* 1993; **328**: 1313-1316
 - 27 **Waddell WR**, Loughry RW. Sulindac for polyposis of the colon. *J Surg Oncol* 1983; **24**: 83-87
 - 28 **Jacoby RF**, Marshall DJ, Newton MA, Novakovic K, Tutsch K, Cole CE, Lubet RA, Kelloff GJ, Verma A, Moser AR, Dove WF. Chemoprevention of spontaneous intestinal adenomas in the Apc Min mouse model by the nonsteroidal anti-inflammatory drug piroxicam. *Cancer Res* 1996; **56**: 710-714
 - 29 **Lee SH**, Soyoola E, Channugam P, Hart S, Sun W, Zhong H, Liou S, Simmons D, Hwang D. Selective expression of mitogen-inducible cyclooxygenase in macrophages stimulated with lipopolysaccharide. *J Biol Chem* 1992; **267**: 25934-25938
 - 30 **Mitchell JA**, Larkin S, Williams TJ. Cyclooxygenase-2: regulation and relevance in inflammation. *Biochem Pharmacol* 1995; **50**: 1535-1542
 - 31 **Lim HY**, Joo HJ, Choi JH, Yi JW, Yang MS, Cho DY, Kim HS, Nam DK, Lee KB, Kim HC. Increased expression of cyclooxygenase-2 protein in human gastric carcinoma. *Clin Cancer Res* 2000; **6**: 519-525
 - 32 **McCarthy CJ**, Crofford LJ, Greenson J, Scheiman JM. Cyclooxygenase-2 expression in gastric antral mucosa before and after eradication of *Helicobacter pylori* infection. *Am J Gastroenterol* 1999; **94**: 1218-1223
 - 33 **Kimura A**, Tsuji S, Tsujii M, Sawaoka H, Iijima H, Kawai N, Yasumaru M, Kakiuchi Y, Okuda Y, Ali Z, Nishimura Y, Sasaki Y, Kawano S, Hori M. Expression of cyclooxygenase-2 and nitrotyrosine in human gastric mucosa before and after *Helicobacter pylori* eradication. *Prostaglandins Leukot Essent Fatty Acids* 2000; **63**: 315-322
 - 34 **Sheng H**, Shao J, Morrow JD, Beauchamp RD, DuBois RN. Modulation of apoptosis and Bcl-2 expression by prostaglandin E2 in human colon cancer cells. *Cancer Res* 1998; **58**: 362-366
 - 35 **Sawaoka H**, Kawano S, Tsuji S, Tsujii M, Gunawan ES, Takei Y, Nagano K, Hori M. Cyclooxygenase-2 inhibitors suppress the growth of gastric cancer xenografts via induction of apoptosis in nude mice. *Am J Physiol* 1998; **274**(6 Pt 1): G1061-G1067
 - 36 **Erickson BA**, Longo WE, Panesar N, Mazuski JE, Kaminski DL. The effect of selective cyclooxygenase inhibitors on intestinal epithelial cell mitogenesis. *J Surg Res* 1999; **81**: 101-107
 - 37 **Anti M**, Armuzzi A, Gasbarrini A, Gasbarrini G. Importance of changes in epithelial cell turnover during *Helicobacter pylori* infection in gastric carcinogenesis. *Gut* 1998; **43**(Suppl 1): S27-S32
 - 38 **Correa P**, Miller MJ. Carcinogenesis, apoptosis and cell proliferation. *Br Med Bull* 1998; **54**: 151-162
 - 39 **Mannick EE**, Bravo LE, Zarama G, Realpe JL, Zhang XJ, Ruiz B, Fontham ET, Mera R, Miller MJ, Correa P. Inducible nitric oxide synthase, nitrotyrosine, and apoptosis in *Helicobacter pylori* gastritis: effect of antibiotics and antioxidants. *Cancer Res* 1996; **56**: 3238-3243
 - 40 **Chen G**, Sordillo EM, Ramey WG, Reidy J, Holt PR, Krajewski S, Reed JC, Blaser MJ, Moss SF. Apoptosis in gastric epithelial cells is induced by *Helicobacter pylori* and accompanied by increased expression of BAK. *Biochem Biophys Res Commun* 1997; **239**: 626-632
 - 41 **Ricci V**, Ciacci C, Zarrilli R, Sommi P, Tummuru MK, Del Vecchio Blanco C, Bruni CB, Cover TL, Blaser MJ, Romano M. Effect of *Helicobacter pylori* on gastric epithelial cell migration and proliferation *in vitro*: role of VacA and CagA. *Infect Immun* 1996; **64**: 2829-2833
 - 42 **Rudi J**, Kuck D, Strand S, von Herbay A, Mariani SM, Krammer PH, Galle PR, Stremmel W. Involvement of the CD95 (APO-1/Fas) receptor and ligand system in *Helicobacter pylori*-induced gastric epithelial apoptosis. *J Clin Invest* 1998; **102**: 1506-1514
 - 43 **Wagner S**, Beil W, Westermann J, Logan RP, Bock CT, Trautwein C, Bleck JS, Manns MP. Regulation of gastric epithelial cell growth by *Helicobacter pylori*: offence for a major role of apoptosis. *Gastroenterology* 1997; **113**: 1836-1847
 - 44 **Fraser AG**, Sim R, Sankey EA, Dhillon AP, Pounder RE. Effect of eradication of *Helicobacter pylori* on gastric epithelial cell proliferation. *Aliment Pharmacol Ther* 1994; **8**: 167-173
 - 45 **Peek RM Jr**, Wirth HP, Moss SF, Yang M, Abdalla AM, Tham KT, Zhang T, Tang LH, Modlin IM, Blaser MJ. *Helicobacter pylori* alters gastric epithelial cell cycle events and gastrin secretion in Mongolian gerbils. *Gastroenterology* 2000; **118**: 48-59
 - 46 **Peek RM Jr**, Moss SF, Tham KT, Perez-Perez GI, Wang S, Miller GG, Atherton JC, Holt PR, Blaser MJ. *Helicobacter pylori* cagA+ strains and dissociation of gastric epithelial cell proliferation from apoptosis. *J Natl Cancer Inst* 1997; **89**: 863-868
 - 47 **Murata H**, Kawano S, Tsuji S, Tsujii M, Sawaoka H, Kimura Y, Shiozaki H, Hori M. Cyclooxygenase-2 overexpression enhances lymphatic invasion and metastasis in human gastric carcinoma. *Am J Gastroenterol* 1999; **94**: 451-455
 - 48 **Yamamoto H**, Itoh F, Fukushima H, Hinoda Y, Imai K. Overexpression of cyclooxygenase-2 protein is less frequent in gastric cancers with microsatellite instability. *Int J Cancer* 1999; **84**: 400-403

Lansoprazole ameliorates intestinal mucosal damage induced by ischemia-reperfusion in rats

Hiroshi Ichikawa, Norimasa Yoshida, Tomohisa Takagi, Naoya Tomatsuri, Kazuhiro Katada, Yutaka Isozaki, Kazuhiko Uchiyama, Yuji Naito, Takeshi Okanoue, Toshikazu Yoshikawa

Hiroshi Ichikawa, Department of Food Sciences and Nutritional Health, Faculty of Human Environment, Kyoto Prefectural University, 606-8522, Japan

Norimasa Yoshida, Yuji Naito, Takeshi Okanoue, Department of Molecular Gastroenterology and Hepatology, Graduate School of Medical Sciences, Kyoto Prefectural University of Medicine, 606-8522, Japan

Tomohisa Takagi, Naoya Tomatsuri, Kazuhiro Katada, Yutaka Isozaki, Kazuhiko Uchiyama, Toshikazu Yoshikawa, Department of Inflammation and Immunology, Graduate School of Medical Sciences, Kyoto Prefectural University of Medicine, 606-8522, Japan

Correspondence to: Dr. Norimasa Yoshida, Department of Molecular Gastroenterology and Hepatology, Graduate School of Medical Sciences, Kyoto Prefectural University of Medicine, 465 Kajii-cho, Kawaramachi-Hirokoji, Kamigyo-ku, Kyoto 602-8566, Japan. nyoshida@koto.kpu-m.ac.jp

Telephone: +81-75-251-5508 **Fax:** +81-75-252-3721

Received: 2004-03-18 **Accepted:** 2004-04-29

Abstract

AIM: To investigate the protective effect of lansoprazole on ischemia and reperfusion (I/R)-induced rat intestinal mucosal injury *in vivo*.

METHODS: Intestinal damage was induced by clamping both the superior mesenteric artery and the celiac trunk for 30 min followed by reperfusion in male Sprague-Dawley rats. Lansoprazole was given to rats intraperitoneally 1 h before vascular clamping.

RESULTS: Both the intraluminal hemoglobin and protein levels, as indices of mucosal damage, significantly increased in I/R-groups comparison with those of sham-operation groups. These increases in intraluminal hemoglobin and protein levels were significantly inhibited by the treatment with lansoprazole at a dose of 1 mg/kg. Small intestine exposed to I/R resulted in mucosal inflammation that was characterized by significant increases in thiobarbituric acid-reactive substances (TBARS), tissue-associated myeloperoxidase activity (MPO), and mucosal content of rat cytokine-induced neutrophil chemoattractant-1 (CINC-1). These increases in TBARS, MPO activities and CINC-1 content in the intestinal mucosa after I/R were all inhibited by pretreatment with lansoprazole at a dose of 1 mg/kg. Furthermore, the CINC-1 mRNA expression was increased during intestinal I/R, and this increase in mRNA expression was inhibited by treatment with lansoprazole.

CONCLUSION: Lansoprazole inhibits lipid peroxidation and reduces development of intestinal mucosal inflammation induced by I/R in rats, suggesting that lansoprazole may have a therapeutic potential for I/R injury.

Ichikawa H, Yoshida N, Takagi T, Tomatsuri N, Katada K, Isozaki Y, Uchiyama K, Naito Y, Okanoue T, Yoshikawa T. Lansoprazole ameliorates intestinal mucosal damage induced by ischemia-

reperfusion in rats. *World J Gastroenterol* 2004; 10(19): 2814-2817

<http://www.wjgnet.com/1007-9327/10/2814.asp>

INTRODUCTION

Reactive oxygen species such as superoxide radicals, hydrogen peroxide, and hydroxyl radicals, have been implicated in the pathogenesis of ischemia-reperfusion (I/R) injury in a variety of organs, including the brain^[1], large intestine^[2], and heart^[3]. Intestinal I/R is an especially grave condition resulted from acute mesenteric ischemia, small bowel transplantation, abdominal aortic aneurysm, hemorrhagic, traumatic, or septic shock, and severe burns^[4,5]. I/R injury of the small intestine is characterized by a number of microvascular and mucosal alterations, including endothelial cell swelling, capillary plugging, prolonged reduction in intestinal blood flow, and mucosal barrier dysfunction^[6-8]. Previous studies have demonstrated that neutrophils are critically involved in I/R injury. This hypothesis based on experiments shows that neutrophil depletion^[9,10] and inhibition of neutrophil-endothelial cell interactions^[11] could protect against injury after I/R.

Proton-pump inhibitors (PPIs)^[12] such as omeprazole and lansoprazole are extensively used for therapeutic control of acid-related disorders, including gastroesophageal reflux disease and peptic-ulcer diseases caused by stress, nonsteroidal anti-inflammatory drugs and *Helicobacter pylori* infection^[13-16]. PPIs are strong antisecretory agents that act on gastric (H⁺/K⁺) ATPase of parietal cells^[17]. Recently, it has been suggested that PPIs inhibit neutrophil functions such as chemotaxis, superoxide production and degradation^[18]. We have already reported that PPIs can attenuate neutrophil adherence to endothelial cells via inhibition of the expression of adhesion molecules^[19]. These results have indicated that PPIs have anti-inflammatory effects and can inhibit acid secretion.

The present study was to evaluate anti-inflammatory effects of lansoprazole, which has dramatically influenced the management of acid-peptic disorders in recent years, using I/R-induced rat intestinal mucosal injury model unrelated to acid secretion.

MATERIALS AND METHODS

Experimental animals

Male Sprague-Dawley (SD) rats weighing 190-210 g were obtained from Kearsy Co. Ltd. (Osaka, Japan). The rats were housed in stainless steel cages with wire bottoms and maintained on a 12-h light and dark cycle, with the temperature and relative humidity of the animal room controlled at 21-23 °C and 55-65%, respectively. The rats were not fed for 18 h prior to the experiments, but allowed free access to water. All experimental procedures described below were approved by the Animal Care Committee of the Kyoto Prefectural University of Medicine (Kyoto, Japan).

Preparation of rats for intestinal ischemia-reperfusion

Intestinal ischemia was induced for 30 min by applying a small clamp to the superior mesenteric artery after ligating the celiac artery in rats given intraperitoneal urethane anesthesia (1 000 mg/kg). Reoxygenation was produced by removal of the clamp. Sixty minutes after reperfusion, the rats were killed by exsanguinations via the abdominal aorta under urethane anesthesia (1 000 mg/kg). 2-[[[3-methyl-4-(2,2,2-trifluoroethoxy)-2-pyridyl] methyl] sulfinyl] benzimidazole (Lansoprazole), a gift from Takeda Chemical Industries Ltd. Japan, was diluted with physiological saline at a dose of 0.3-1 mg/kg after dissolved in dimethylsulfoxide, and was given to rats intraperitoneally 1 h before the vascular clamping. In the control groups, rats received an equivalent volume of the vehicle.

Assessment of intestinal mucosal injury induced by ischemia-reperfusion

To estimate the severity of the intestinal mucosal damage by I/R, leakage of intraluminal protein and intraluminal hemoglobin levels were measured as mg/cm intestine.

The concentrations of thiobarbituric acid-reactive substances (TBARS) in the intestinal mucosa, an index of lipid peroxidation, were measured by the method of Ohkawa *et al.*^[20]. In brief, the small intestine was opened by a longitudinal incision, and the intestinal mucosa was scraped off using two glass slides. Mucosal tissue was then homogenized with 10 mmol/L potassium phosphate buffer (pH 7.8) containing 30 mmol/L KCl in a Teflon Potter-Elvehjem homogenizer. The levels of TBARS in the mucosal homogenates were expressed as nmol of malondialdehyde per gram of wet weight using 1,1,3,3-tetramethoxypropane as the standard.

Myeloperoxidase (MPO) activity in the intestinal mucosa, an index of polymorphonuclear leukocyte accumulation, were determined by a modification of the method of Grisham *et al.*^[21]. Two milliliters of mucosal homogenate was centrifuged at 20 000 g for 15 min at 4 °C to pellet the insoluble cellular debris. The pellet was then rehomogenized in an equivalent volume of 0.05 mol/L potassium phosphate buffer (pH 5.4) containing 5 g/L hexadecyltrimethylammonium bromide. Samples were centrifuged at 20 000 g for 15 min at 4 °C, and the supernatants were saved. MPO activity was assessed by measuring the H₂O₂-dependent oxidation of 3,3',5,5'-tetramethylbenzidine. One unit of enzyme activity was defined as the amount of MPO that caused a change in the absorbance of 1.0/min at 655 nm and 25 °C.

The content of cytokine-induced neutrophil chemoattractant-1 (CINC-1) in the intestinal mucosal homogenates was determined by enzyme-linked immunosorbent assay (ELISA) using a kit (Immuno Biological Laboratories, Gunma, Japan) according to the manufacturer's instructions. The absorbance of each well was read at 490 nm by a microplate reader (MPR-A4i; Tosoh, Tokyo, Japan).

The expression of intestinal CINC-1 was determined using the RT-PCR method. Samples of intestinal tissue for mRNA isolation were prepared from the whole intestine. Total RNA was isolated using the acid-guanidium-phenol-chloroform (AGPC) method with ISOGEN (NIPPON GENE). The concentration of RNA was determined by the absorbance at

260 nm in relation to that at 280 nm. The RNA was stored at -70 °C until used for RT-PCR. One microliter of RT-PCR products was added to 3 mmol/L of each primer, CINC-1 and β -actin (for internal standard purpose), and a solution of 0.5 U of *Taq* DNA polymerase (Takara Biochemicals) in a final volume of 50 L. The primers had the following sequences: for CINC-1, sense 5'-ACAGTGGCAGGGATTCACCTT-3', and antisense 5'-CTAGCA CAGTGGTTGACACT-3'; for β -actin, sense 5'-TCCTGTGG CATCCATGAAACT-3', and antisense 5'-GAAGCATTGCGG TGCACGAT-3'. The mixture was subjected to 30 cycles (1 min at 94 °C, 1 min at 54 °C, 1 min at 72 °C) of amplification. Then the reaction products were separated by electrophoresis on 25 g/L agarose gel and stained with ethidium bromide.

Statistical analysis

All values were expressed as mean \pm SE. The data were compared by one-way analysis of variance (ANOVA) followed by Dunnett's multiple comparison test. All analyses were performed using the Stat View 5.0-J program (Abacus Concepts Inc. Berkeley, CA). $P < 0.05$ was considered statistically significant.

RESULTS

Intraluminal protein and hemoglobin levels of the small intestine

Intraluminal hemoglobin and protein levels, the reflections of intestinal mucosal injury, were significantly increased above basal levels after 60 min of reperfusion. These increases in intraluminal protein and hemoglobin levels induced by I/R were significantly decreased by lansoprazole treatment at a dose of 1 mg/kg (Table 1).

TBARS in the intestinal mucosa

TBARS in the intestinal mucosa, an index of lipid peroxidation, significantly increased 60 min after reperfusion (13.0 \pm 2.5 nmol/100 g wet wt). These levels were significantly decreased to 7.98 \pm 1.98 nmol/100 g wet wt after lansoprazole treatment at a dose of 1 mg/kg (Figure 1A).

MPO activity in the intestinal mucosa

The I/R group showed a significant increase in mucosal MPO activity (0.167 \pm 0.046 mU/mg wet wt) compared with the sham-operation group (0.014 \pm 0.001 mU/mg wet wt). However, this increase in MPO activity significantly decreased to 0.028 \pm 0.008 mU/mg wet wt after lansoprazole treatment at a dose of 1 mg/kg (Figure 1B).

Inflammatory cytokine in the intestinal mucosa

The content of mucosal CINC-1 in the I/R groups was significantly increased compared with the levels in sham-operated groups. This increase in the levels of inflammatory cytokines was significantly inhibited by lansoprazole at a dose of 1 mg/kg (Figure 1C).

Intestinal expression of CINC-1 mRNA during ischemia-reperfusion

The expression of CINC-1 mRNA in the intestinal mucosa was up-regulated by I/R injury. This increase in the expression of CINC-1 mRNA was also inhibited by lansoprazole at a dose of 1 mg/kg (Figure 2).

Table 1 Effect of lansoprazole on intraluminal hemoglobin and protein levels in small intestine of I/R-induced rats (mean \pm SE)

	Sham-operation (Normal)	Ischemia-reperfusion (Control)	Lansoprazole (mg/kg)	
			0.3	1
Intraluminal hemoglobin (mg/cm)	0.000043 \pm 0.000002	0.0043 \pm 0.0006 ^a	0.0035 \pm 0.0007	0.0010 \pm 0.0004 ^c
Intraluminal protein (mg/cm)	0.065 \pm 0.012	0.172 \pm 0.016 ^a	0.156 \pm 0.022	0.087 \pm 0.010 ^c

^a $P < 0.05$ vs normal; ^c $P < 0.05$ vs control.

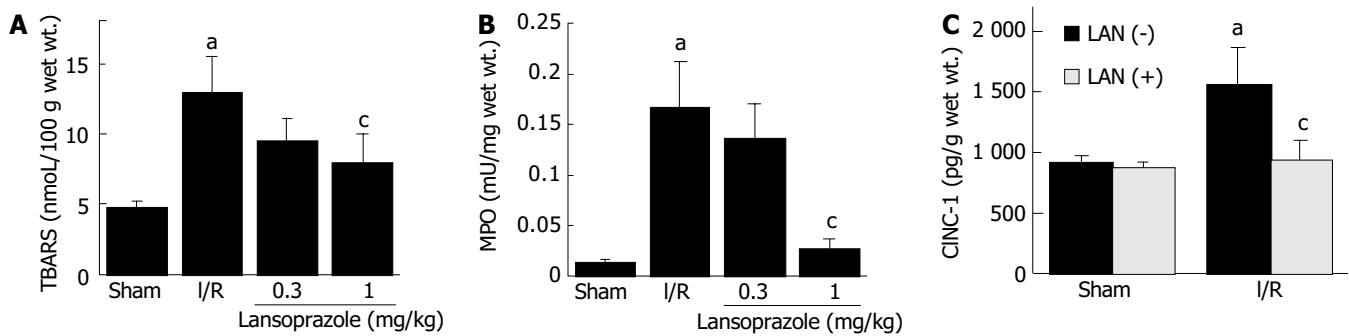


Figure 1 Effect of lansoprazole on the level of thiobarbituric-acid reactive substances (TBARS), mucosal myeloperoxidase (MPO) activity, and cytoline induced neutrophil chemo-attractant-1 (CINC-1) in intestinal mucosa of I/R-induced rats. A: Effect of lansoprazole on the level of TBARS in intestinal mucosa of I/R-induced rats. ^a*P*<0.05 vs normal; ^c*P*<0.05 vs control. Sham group and I/R group received an equivalent volume of vehicle instead of lansoprazole. B: Effect of lansoprazole on the level of mucosal myeloperoxidase (MPO) activities in intestinal mucosa of I/R-induced rats. ^a*P*<0.05 vs normal; ^c*P*<0.05 vs control. Sham group and I/R group received an equivalent volume of vehicle instead of lansoprazole. C: Effect of lansoprazole on cytokine induced neutrophil chemoattractant-1 (CINC-1) of intestinal mucosa of I/R-induced rats. ^a*P*<0.05 vs normal; ^c*P*<0.05 vs control. LAN(+): with lansoprazole; LAN(-): without lansoprazole.

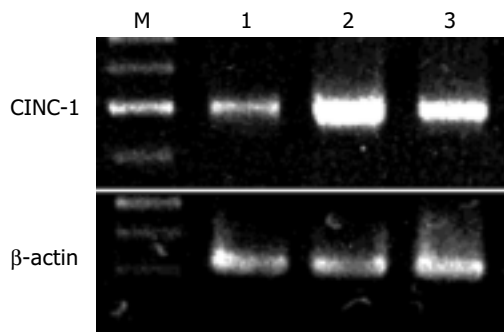


Figure 2 Intestinal CINC-1 mRNA expression during I/R in rats. M: Marker; Lane 1: Before ischemia; Lane 2: After I/R; Lane 3: I/R + lansoprazole.

DISCUSSION

Our results clearly showed that lansoprazole had a protective effect against reperfusion-induced intestinal mucosal injury in rats. In addition, increases in TBARS contents, MPO activity and CINC-1 contents were inhibited by the treatment of lansoprazole. In I/R-induced tissue injury, oxygen radicals have been suggested to be generated via several mechanisms, including the xanthine/xanthine oxidase reaction^[22], NADPH oxidase and myeloperoxidase of activated leukocytes migrating into the previously ischemic area^[23], and mitochondrial respiratory system^[24]. We have already reported that oxygen-derived free radicals and lipid peroxidation played a role in the formation of gastrointestinal mucosal damage induced by I/R^[25,26]. Furthermore, it is well known that neutrophils that adhere to post-capillary venules and subsequently emigrate into the interstitium are implicated in the I/R-related tissue injury^[27,28]. Activated neutrophils release a variety of cytotoxic substances, including proteases, collagenases, cytokines, leukotrienes, and cationic proteins, thereby causing tissue damage. In addition, adhered and aggregated neutrophils can physically disturb capillary flow and induce a non-reflow phenomenon.

Little is known about the protective mechanism of lansoprazole against I/R injury. However, there have been some reports about the anti-inflammatory action of PPIs. We have shown that the expression of adhesion molecules on neutrophils and endothelial cells elicited by *H. pylori* extract and IL-1 was inhibited by lansoprazole and omeprazole at clinical relevant doses^[19]. Other reports have also revealed that PPIs could prevent the neutrophil-endothelial cell adhesion reaction^[29,30]. Recently, some reports regarding the anti-oxidative effects of PPIs have also appeared. Suzuki *et al.*^[31] reported that PPIs inhibited the production of oxygen-derived free radicals from neutrophils activated by

chemotactic peptides or opsonized zymosan. Other studies have concluded that PPIs block stress-induced increased reactive oxygen intermediates and associated lipid peroxidation and protein oxidation, indicating that its antioxidant properties play a major role in preventing oxidative damage^[32-34].

Lansoprazole has been widely used in the treatment of acid-related diseases including reflux esophagitis. This drug is thought to be transformed into two active species which inhibit acid secretion by (H⁺, K⁺)-ATPase within the parietal cell canaliculi. However, acid secretion was not directly involved in the pathogenesis of I/R-induced intestinal injury model we used. In the present study, lansoprazole was found to prevent lipid peroxidation and to reduce the development of intestinal mucosal inflammation via inhibition of the production of inflammatory cytokines such as CINC-1. These results suggest that lansoprazole may protect against I/R injury via an anti-inflammatory effect but not inhibition of acid secretion.

It was previously reported that CINC levels were increased during small intestinal I/R injury, and that CINC-1 was related with the extent of mucosal damage^[35]. It was reported that CINC could be produced by many types of cells, including macrophages, monocytes, and endothelial cells^[36]. In the present study, lansoprazole inhibited both CINC-1 protein and mRNA in the small intestine after I/R injury. These results suggest that lansoprazole may prevent CINC-1 production by scavenging active oxygen species that are related to signal transduction for the promotion of CINC-1 synthesis. Further study needs to be done to determine the molecular mechanisms involved in the inhibition of CINC-1 production by lansoprazole.

In conclusion, lansoprazole protects against acid-unrelated intestinal injury induced by I/R via inhibition of neutrophil-dependent inflammation. We suggest that lansoprazole has potential as a new therapeutic agent for reperfusion injury.

REFERENCES

- 1 Walder CE, Green SP, Darbonne WC, Mathias J, Rae J, Dinauer MC, Curnutte JT, Thomas GR. Ischemic stroke injury is reduced in mice lacking a functional NADPH oxidase. *Stroke* 1997; **28**: 2252-2258
- 2 Panes J, Granger DN. Leukocyte-endothelial cell interactions: molecular mechanisms and implications in gastrointestinal disease. *Gastroenterology* 1998; **114**: 1066-1090
- 3 Jolly SR, Kane WJ, Baile MB, Abrams GD, Lucchesi BR. Canine myocardial reperfusion injury. Its reduction by the combined administration of superoxide dismutase and catalase. *Circ Res* 1984; **54**: 277-285
- 4 Cappell MS. Intestinal (mesenteric) vasculopathy. I. Acute

- superior mesenteric arteriopathy and venopathy. *Gastroenterol Clin North Am* 1998; **27**: 783-825
- 5 **Homer-Vanniasinkam S**, Crinnion JN, Gough MJ. Post-ischaemic organ dysfunction: a review. *Eur J Vasc Endovasc Surg* 1997; **14**: 195-203
 - 6 **Schoenberg M**, Muhl E, Sellin D, Younes M, Schildberg F, Haglund U. Posthypotensive generation of superoxide free radicals: possible role in the pathogenesis of the intestinal mucosal damage. *Acta Chir Scand* 1984; **150**: 301-309
 - 7 **Granger DN**, Hollwarth ME, Parks DA. Ischemia-reperfusion injury; role of oxygen-derived free radicals. *Acta Physiol Scand suppl* 1986; **548**: 47-53
 - 8 **Haglund U**, Bulkley GB, Granger DN. On the pathophysiology of intestinal ischemic injury. Clinical review. *Acta Chir Scand* 1987; **153**: 321-324
 - 9 **Hernandez LA**, Grisham MB, Twohig B, Arfors KE, Harlan JM, Granger DN. Role of neutrophils in ischemic-reperfusion-induced microvascular injury. *Am J Physiol* 1987; **253**: H699-H703
 - 10 **Sisley AC**, Desai T, Harig JM, Gewertz BL. Neutrophil depletion attenuates human intestinal reperfusion injury. *J Surg Res* 1994; **57**: 192-196
 - 11 **Kurose I**, Anderson DC, Miyasaka M, Tamatani T, Paulson JC, Todd RF, Rusche JR, Granger DN. Molecular determinants of reperfusion-induced leukocyte adhesion and vascular protein leakage. *Circ Res* 1994; **74**: 336-343
 - 12 **Horn J**. The proton-pump inhibitors: similarities and differences. *Clin Ther* 2000; **22**: 266-280
 - 13 **Langtry HD**, Wilde MI. Omeprazole. A review of its use in *Helicobacter pylori* infection, gastro-oesophageal reflux disease and peptic ulcers induced by nonsteroidal anti-inflammatory drugs. *Drugs* 1998; **56**: 447-486
 - 14 **Garnett WR**. Lansoprazole: a proton pump inhibitor. *Ann Pharmacother* 1996; **30**: 1425-1436
 - 15 **Zimmermann AE**, Katona BG. Lansoprazole: a comprehensive review. *Pharmacotherapy* 1997; **17**: 308-326
 - 16 **Wolfe MM**, Sachs G. Acid suppression: optimizing therapy for gastroduodenal ulcer healing, gastroesophageal reflux disease, and stress-related erosive syndrome. *Gastroenterology* 2000; **118**: S9-31
 - 17 **Fellenius E**, Berglindh T, Sachs G, Olbe L, Elander B, Sjostrand SE, Wallmark B. Substituted benzimidazoles inhibit gastric acid secretion by blocking (H⁺ + K⁺)ATPase. *Nature* 1981; **290**: 159-161
 - 18 **Wandall JH**. Effects of omeprazole on neutrophil chemotaxis, super oxide production, degranulation, and translocation of cytochrome b-245. *Gut* 1992; **33**: 617-621
 - 19 **Yoshida N**, Yoshikawa T, Tanaka Y, Fujita N, Kassai K, Naito Y, Kondo M. A new mechanism for anti-inflammatory actions of proton pump inhibitors-inhibitory effects on neutrophil-endothelial cell interactions. *Aliment Pharmacol Ther* 2000; **14**: 74-81
 - 20 **Ohkawa H**, Ohnishi N, Yagi K. Assay for lipid peroxides for animal tissues by thiobarbituric acid reaction. *Anal Biochem* 1979; **95**: 351-358
 - 21 **Grisham MB**, Hernandez LA, Granger DN. Xanthine oxidase and neutrophil infiltration in intestinal ischemia. *Am J Physiol* 1986; **251**: G567-G574
 - 22 **McCord JM**. Oxygen-derived free radicals in post ischemic tissue injury. *N Engl J Med* 1985; **312**: 159-163
 - 23 **Fantone JC**, Ward PA. Role of oxygen derived free radicals and metabolites in leukocyte dependent inflammatory reactions. *Am J Pathol* 1982; **107**: 395-418
 - 24 **Chance B**, Sies H, Boveris A. Hydroperoxide metabolism in mammalian tissues. *Physiol Rev* 1979; **59**: 527-605
 - 25 **Yoshikawa T**, Naito Y, Ueda S, Ichikawa H, Takahashi S, Yasuda M, Kondo M. Ischemia-reperfusion injury and free radical involvement in gastric mucosal disorders. *Adv Exp Med Biol* 1992; **316**: 231-238
 - 26 **Yoshikawa T**, Ueda S, Naito Y, Takahashi S, Oyamada H, Morita Y, Yoneta T, Kondo M. Role of oxygen-derived free radicals in gastric mucosal injury induced by ischemia or ischemia-reperfusion in rats. *Free Rad Res Comms* 1989; **7**: 285-291
 - 27 **Granger DN**. Role of xanthine oxidase and granulocytes in ischemia-reperfusion injury. *Am J Physiol* 1988; **255**: H1269-H1275
 - 28 **Yoshida N**, Granger DN, Anderson DC, Rothlein R, Lane C, Kvietys PR. Anoxia/reoxygenation-induced neutrophil adherence to cultured endothelial cells. *Am J Physiol* 1992; **262**: H1891-H1898
 - 29 **Suzuki M**, Mori M, Fukumura D, Suzuki H, Miura S, Ishii H. Omeprazole attenuates neutrophil-endothelial cell adhesive interaction induced by extracts of *Helicobacter pylori*. *J Gastroenterol Hepatol* 1999; **14**: 27-31
 - 30 **Ohara T**, Arakawa T. Lansoprazole decreases peripheral blood monocytes and intercellular adhesion molecule-1-positive mononuclear cells. *Dig Dis Sci* 1999; **44**: 1710-1715
 - 31 **Suzuki M**, Mori M, Miura S, Suematsu M, Fukumura D, Kimura H, Ishii H. Omeprazole attenuates oxygen-derived free radical production from human neutrophils. *Free Radic Biol Med* 1996; **21**: 727-731
 - 32 **Biswas K**, Bandyopadhyay U, Chattopadhyay I, Varadaraj A, Ali E, Banerjee RK. A novel antioxidant and antiapoptotic role of omeprazole to block gastric ulcer through scavenging of hydroxyl radical. *J Biol Chem* 2003; **278**: 10993-11001
 - 33 **Zedtwitz-Liebenstein K**, Wenisch C, Patruta S, Parschalk B, Daxböck F, Graninger W. Omeprazole treatment diminishes intra- and extracellular neutrophil reactive oxygen production and bactericidal activity. *Crit Care Med* 2002; **30**: 1118-1122
 - 34 **Noble DW**. Proton pump inhibitors and stress ulcer prophylaxis: pause for thought? *Crit Care Med* 2002; **30**: 1175-1176
 - 35 **Tsuruma T**, Yagihashi A, Tarumi K, Hirata K. Anti-rat IL-8 (CINC) monoclonal antibody administration reduces ischemia-reperfusion injury in small intestine. *Transplant Proc* 1998; **30**: 2644-2645
 - 36 **Yagihashi A**, Tsuruma T, Tarumi K, Kameshima T, Yajima T, Yanai Y, Watanabe N, Hirata K. Prevention of small intestinal ischemia-reperfusion injury in rat by anti-cytokine-induced neutrophil chemoattractant monoclonal antibody. *J Surg Res* 1998; **78**: 92-96

Hepatic differentiation capability of rat bone marrow-derived mesenchymal stem cells and hematopoietic stem cells

Sai-Nan Shu, Lai Wei, Jiang-Hua Wang, Yu-Tao Zhan, Hong-Song Chen, Yu Wang

Sai-Nan Shu, Lai Wei, Jiang-Hua Wang, Hong-Song Chen, Yu Wang, Institute of Hepatology, People's Hospital, Peking University, Beijing 100044, China

Yu-Tao Zhan, Gastroenterology Department, Tong-Ren Hospital, Capital Medical University, Beijing 100730, China

Supported by the National High Technology Research and Development Program of China (863 Program), No. 2001AA216031

Correspondence to: Dr. Lai Wei, Institute of Hepatology, People's Hospital, Peking University, 11 Xizhimen South Street, Beijing 100044, China. w1114@hotmail.com

Telephone: +86-10-68314422 Ext.5730 **Fax:** +86-10-68318386

Received: 2003-12-23 **Accepted:** 2004-01-12

Abstract

AIM: To investigate the different effects of mesenchymal stem cells (MSCs) and hematopoietic stem cells (HSCs) on hepatic differentiation.

METHODS: MSCs from rat bone marrow were isolated and cultured by standard methods. HSCs from rat bone marrow were isolated and purified by magnetic activated cell sorting. Both cell subsets were induced. Morphology, RT-PCR and immunocytochemistry were used to identify the hepatic differentiation grade.

RESULTS: MSCs exhibited round in shape after differentiation, instead of fibroblast-like morphology before differentiation. Albumin mRNA and protein were expressed positively in MSCs, without detection of alpha-fetoprotein (AFP). HSCs were polygonal in shape after differentiation. The expression of albumin signal decreased and AFP signal increased. The expression of CK18 was continuous in MSCs and HSCs both before and after induction.

CONCLUSION: Both MSCs and HSCs have hepatic differentiation capabilities. However, their capabilities are not the same. MSCs can differentiate into mature hepatocyte-like cells, never expressing early hepatic specific genes, while Thy-1.1⁺ cells are inclined to differentiate into hepatic stem cell-like cells, with an increasing AFP expression and a decreasing albumin signal. CK18 mRNA is positive in Thy-1.1⁺ cells and MSCs, negative in Thy-1.1⁻ cells. It seems that CK18 has some relationship with Thy-1.1 antigen, and CK18 may be a predictive marker of hepatic differentiation capability.

Shu SN, Wei L, Wang JH, Zhan YT, Chen HS, Wang Y. Hepatic differentiation capability of rat bone marrow-derived mesenchymal stem cells and hematopoietic stem cells. *World J Gastroenterol* 2004; 10(19): 2818-2822

<http://www.wjgnet.com/1007-9327/10/2818.asp>

INTRODUCTION

In recent years, liver related stem cells have become a hot spot of research. One of the important findings is that liver stem cells might be derived from bone marrow. Petersen *et al.*^[1] first identified this phenomenon in rat model of liver injury. Later

many researchers have reported similar *in vivo* and *in vitro* findings^[2-8]. Bone marrow cells have been hypothesized as the third recruitment source in liver regeneration besides hepatocytes and endogenous liver stem cells^[9].

Among bone marrow cells, there are two subsets, hematopoietic stem cells (HSCs) and mesenchymal stem cells (MSCs). Hepatic oval cells^[10], well known endogenous liver stem cells, can express CD34^[11], c-kit^[12, 13], Thy-1^[14] and flt-3 receptor mRNA^[15], all of which are markers of HSCs. So HSCs are regarded as the exact source of hepatocytes. However, some studies have found that non-hematopoietic subsets (CD45⁻ subsets) also play such a role^[7]. In this paper, we isolated two subsets of stem cells from rat bone marrow. One was MSCs, isolated and cultured by standard methods, the other was Thy-1.1⁺ cells, isolated and purified by magnetic activated cell sorting (MACS), which were recognized as HSCs of rats. We imitated the circumstances of liver development to define the different capacities of hepatic differentiation of the two subsets *in vitro*.

MATERIALS AND METHODS

Animals

Male Sprague-Dawley (SD) rats at 6-7 wk of age were obtained from Charles River China. All animal experiments were performed in accordance with the animal guidelines of Peking University Health Science Center.

Isolation and culture of MSCs from rat bone marrow

Rat bone marrow was harvested from rat femurs and tibias, and collected into Dulbecco's modified Eagle's medium (DMEM), filtered (40 μm), and centrifuged at 300 r/min to pellet cells. After rinsed in PBS, bone marrow cells were loaded onto 5 mL 57% Percoll (1.073 g/mL in 0.01 mol/L PBS) and centrifuged at 400 r/min for 30 min. Mononuclear cells were collected at the Percoll interface, rinsed twice in PBS, and seeded at 2×10⁵/cm² in 600 g/L low glucose DMEM (DMEM-LG, Sigma-Aldrich), 400 g/L MCDB-201 (Sigma-Aldrich), with 100 mL/L fetal bovine serum (FBS; Hyclone, USA) and 1 000 U/mL rat leukemia inhibitory factor (rLIF; Chemicon, USA). Non-adherent cells were removed after 24 h and culture media were replaced every 3 d. After about 7 d, isolated colonies of MSCs were apparent. Then the cells were trypsinized and replated at 8 000/cm², and the cells from passage 3 were used for differentiation protocol.

Differentiation protocols

MSCs from passage 3 were seeded at 2×10⁴/cm² on 10 ng/mL fibronectin (FN, Sigma-Aldrich, USA) in culture medium as above. After 12 h, media were removed and cells were cultured in 600 g/L DMEM-LG, 400 g/L MCDB-201 supplemented with 50 mL/L FBS, 10⁻⁶ mol/L dexamethasone (Dex, Sigma-Aldrich, USA), 10 ng/mL epithelial growth factor (EGF, R&D, USA), 1×insulin/transferrin/selenium (ITS, Sigma-Aldrich, USA). In some experiments, inducing growth factors were added into culture medium (20 ng/mL acid fibroblast growth factors, aFGF; 10 ng/mL basic fibroblast growth factors, bFGF; and 20 ng/mL hepatocyte growth factor, HGF). aFGF, bFGF, and HGF were all from R&D System Inc, USA.

Isolation, culture and differentiation of Thy-1.1⁺ stem cells from rat marrow

After Percoll gradient centrifugation, bone marrow mononuclear cells were collected, then incubated with mouse anti-rat Thy-1.1 monoclonal antibody (Serotech, UK) at 4 °C for 30 min. Unbound antibodies were removed by washing twice. Secondary marking was done by incubation with rat-anti-mouse IgG bound magnetic microbeads (MiltenyiBiotec, Germany). The positive cells were absorbed in magnetic field by Mini-MACS columns (MiltenyiBiotec, Germany). The column was removed from the magnetic field and the Thy-1.1⁺ cells were washed out.

Thy-1.1⁺ cells were cultured in differentiation media, 600 g/L DMEM-LG, 400 g/L MCDB-201 supplemented with 150 mL/L FBS, 10⁻⁶ mol/L Dex, 10 ng/mL EGF, 1×ITS, 20 ng/mL aFGF, 10 ng/mL bFGF, and 20 ng/mL HGF. After about 7-10 d, apparent colonies of Thy-1.1⁺ cells appeared.

Flow cytometry determination of cell-surface antigen

The cells were resuspended in washing buffer (10 mL/L bovine serum, 2 g/L sodium azide in PBS), and stained on ice according to the manufacturer's recommendations with the monoclonal antibodies as follows: R-PE conjugated mouse anti-rat-Thy1.1 (Pharmingen, USA), FITC conjugated mouse anti-rat-CD45 (HarlanSera-Lab, UK), PE conjugated mouse anti-rat-CD34 (Santa Cruz, USA). After washed three times with washing buffer, the stained cells were resuspended in 300 µL fixation buffer (20 g/L formaldehyde in PBS) and run on a flow cytometer (FACS Calibur, BectonDi-ckinson, USA). The results were analyzed by CellQuest software (BD, USA).

Reverse transcription-polymerase chain reaction (RT-PCR)

Total RNA was extracted by using TRIzol (Invitrogen, USA) according to the manufacturer's instructions and quantified by UV spectroscopy. To prepare RNA for PCR analysis, 2 µg total RNA was converted to the cDNA using SuperScript II reverse transcriptase (Invitrogen, USA) with oligo (dT) (Promega, USA) and random hexamer primers (Promega, USA). PCR was performed by using *Taq* DNA polymerase (Gibco BRL, USA). For each gene, the DNA primers were originated from different exons to ensure that the PCR products represented the specific mRNA species and not genomic DNA. All PCR experiments were performed using

a GeneAmp PCR system 2 400 (Perkin-Elmer, USA).

The following specific oligonucleotide primers were used: albumin (5'-AAGGCACCCCGATTACTCCG-3' (sense), 5'-TGCGAAGTCACCCATCACCG-3' (antisense)), AFP (5'-AGGCTGTACTCATCATTAAGT-3' (sense), 5'-ATATTGTCC TGGCATTTCG-3' (antisense)), CK18 (5'-GGACCTCAGCAAG ATCATGGC-3' (sense), 5'-CCACGATCTTACGGGTAGTTG-3' (antisense)), β-actin (5'-AGAGGGAAATCGTGGCGTGAC-3' (sense), 5'-AGGAGCCAGGCAGTAATC-3' (anti-sense)).

Amplification reactions were carried out for 35 cycles (25 cycles for β-actin) at 94 °C for 1 min, 58 °C for 1 min, and at 72 °C for 1 min for albumin; at 94 °C for 45 s, at 51 °C for 45 s and at 72 °C for 45 s for AFP; at 94 °C for 1 min, at 60 °C for 1 min and at 72 °C for 1 min for CK18 and at 94 °C for 30 s, at 55 °C for 45 s, and at 72 °C for 45 s for β-actin. The reaction products were subjected to 12 g/L agarose gel electrophoresis and visualized by ethidium bromide staining. The reaction products were 649 bp (albumin), 484 bp (AFP), 515 bp (CK18), and 353 bp (β-actin), respectively. Housekeeping gene β-actin was used as an internal control. Adult liver tissue or newborn rat liver tissue was used as a positive control.

Immunocytochemistry

Cell cultures were washed with PBS twice and fixed with 95% alcohol/acetic acid (99:1) for 10 min at room temperature, then permeabilized with 2 g/L Triton X-100 for 10 min. After washed, cells were incubated overnight at 4 °C with primary antibodies, including mouse anti-human CK18 (Sigma, USA), mouse anti-human albumin (Dako, Denmark) and goat anti-human AFP (SantaCruz, USA). Subsequently, the cells were washed with PBS three times and incubated with fluorescence labeled second antibody, FITC labeled goat anti-mouse IgG1 and rhodamine labeled donkey anti-goat IgG at 37 °C for 1 h. After washed with PBS, cells were mounted with glycerol-PBS (9:1). The cells were visualized and photomicrographed by a fluorescence microscope (Olympus Provis AX80, Japan).

RESULTS

Cell yield and shape of MSC and Thy-1.1⁺ cells before and after differentiation

The number of mononuclear cells by 57% Percoll gradient centrifugation was about 6.44×10⁷ per rat. After MACS

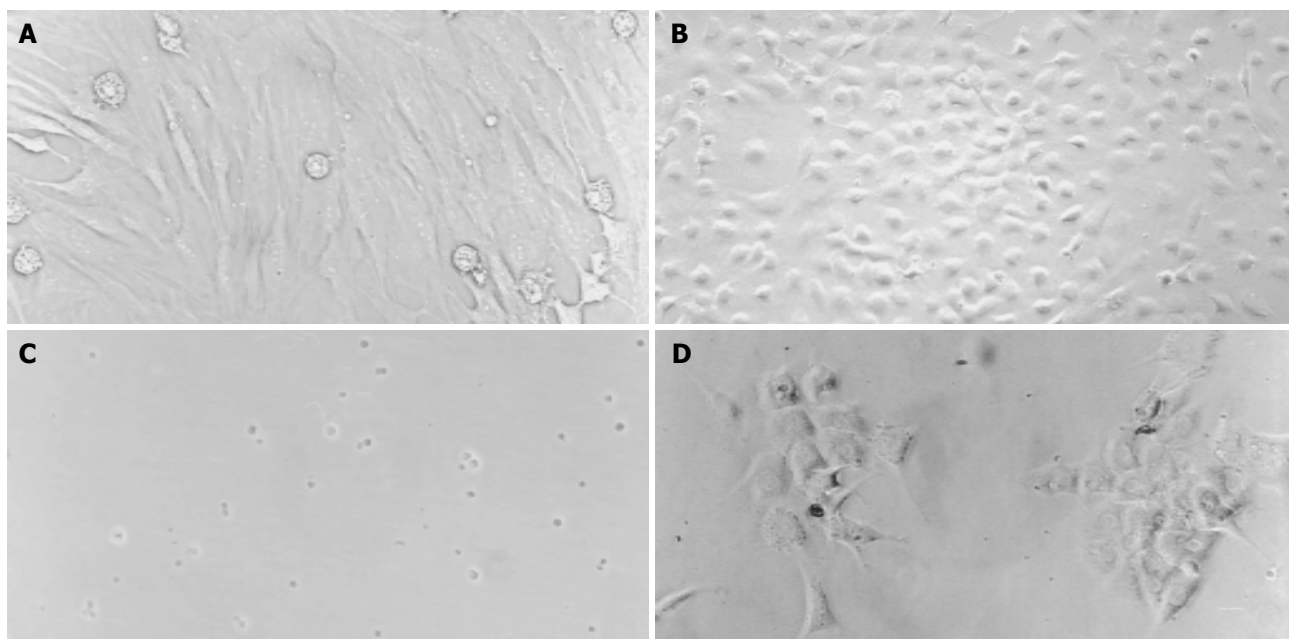


Figure 1 A-D Cell morphology before and after differentiation (Original magnification, 200×). A: Fibroblast-like MSC before differentiation, B: Round MSC after differentiation, C: Freshly isolated Thy1.1⁺ cells, D: Thy1.1⁺ cells 10 d after differentiation.

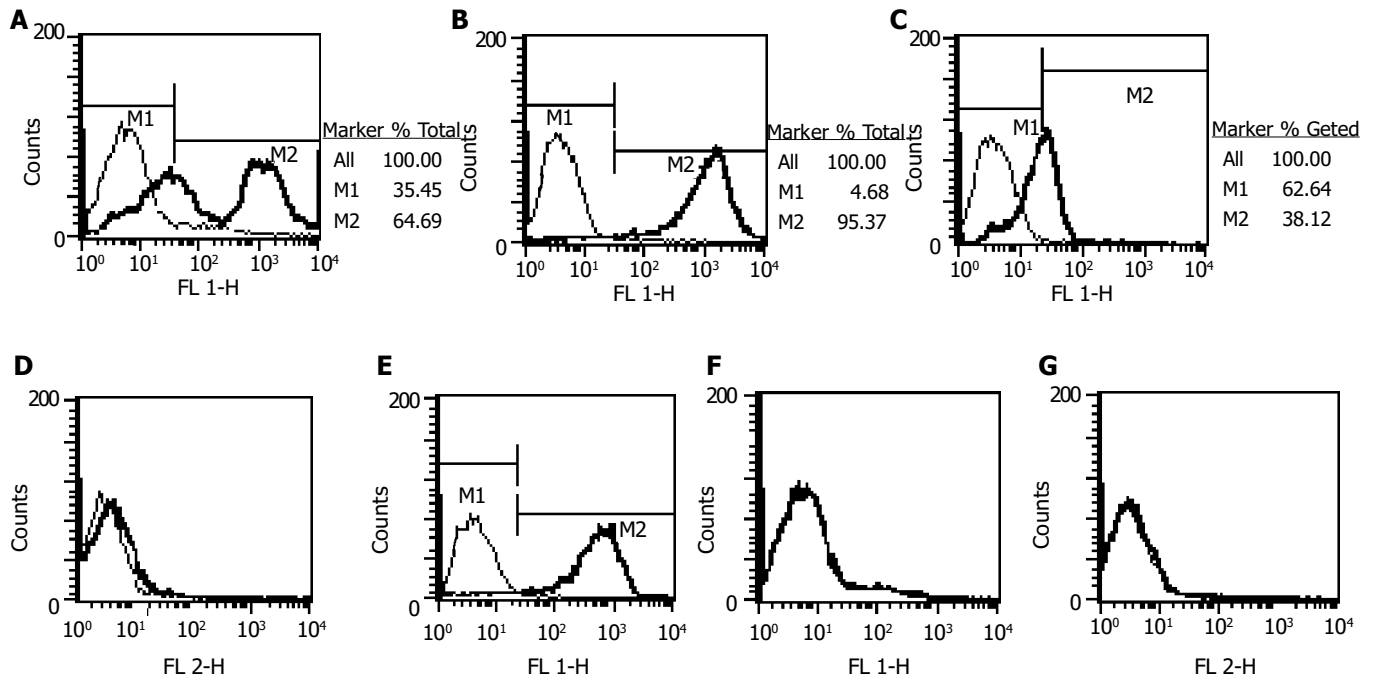


Figure 2 Phenotype analysis of MSCs and Thy-1.1⁺ cells. A: Thy-1.1 of mononuclear bone marrow cells before MACS; B, C, D: Thy-1.1, CD45, CD34 after MACS purification; E, F, G: Thy-1.1, CD45, CD34 of MSCs.

purification, the number of Thy1.1⁺ cells was about 2.36×10⁷. The recovery rate of Thy1.1⁺ cells from mononuclear bone marrow cells was 64.65%. Before differentiation, MSCs exhibited a fibroblastic morphology with spindle cell bodies (Figure 1A), while after differentiation, the cells contracted obviously and were inclined to be round in shape (Figure 1B). This change occurred early on d 4 after MSC differentiation protocol. Thy1.1⁺ cells were small and round in shape when freshly isolated (Figure 1C), and became typical polygonal, much bigger in size after cultured in differentiation media (Figure 1D).

Quantitative analysis of cell-surface antigen expression

The percentage of Thy-1.1⁺ of rat bone marrow mononuclear cells was 56.65%. After MACS, this percentage was 93.45% in positive subset (Figure 2A, B). Thy-1.1⁺ subset was CD34⁺, and partial CD45⁺ (Figure 2C, D). The percentage of CD45 positivity in Thy-1.1⁺ subset was 36.68%. As displayed in Figure 2E-2G, MSC was Thy-1.1⁺, CD45⁺, CD34⁺.

RT-PCR analysis of hepatic gene expression of CK18, albumin, and AFP

We analyzed hepatic gene expression of the cells before and after differentiation protocol. Adult rat liver or newborn rat liver tissue

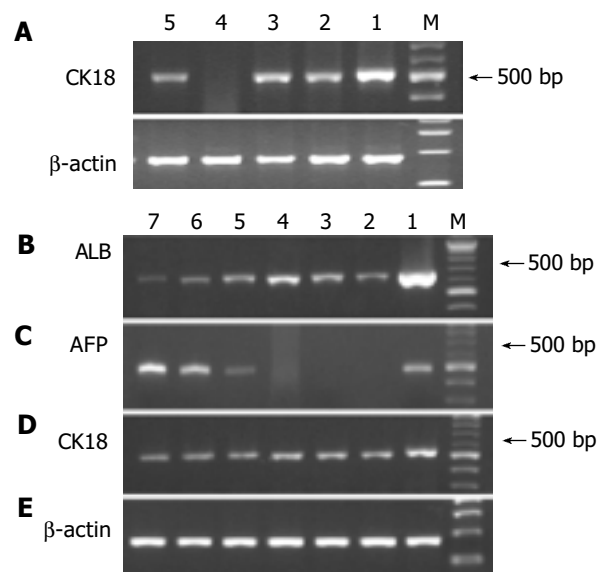


Figure 3 RT-PCR analysis of hepatic gene expression before and after differentiation. A: Analysis of CK18 mRNA before differentiation, lane 1: Adult liver, lane 2: Mononuclear BM cells.

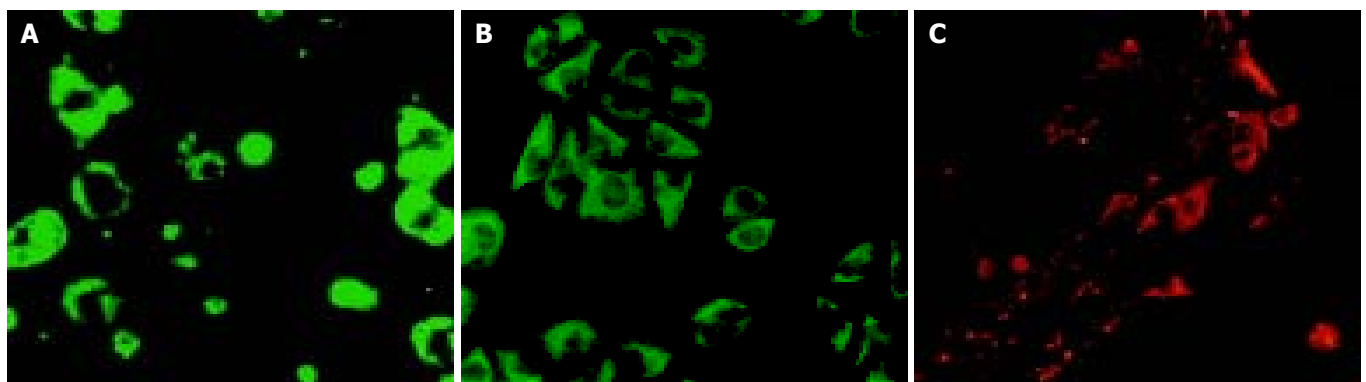


Figure 4 Immunocytofluorescence. A: MSCs-albumin, B: Thy1.1⁺ cells-CK18, C: Thy1.1⁺ cells-AFP.

was used as positive control. Before differentiation, Thy-1.1⁺ cells showed a CK18 signal, so did MSCs. However, Thy-1.1⁻ cells did not express CK18 (Figure 3A). After differentiation, Thy-1.1⁺ cells were AFP mRNA positive and had decreased signals of albumin, while MSCs expressed albumin only and the signals of albumin increased with the extension of differentiation time (Figure 3B, C). Both cells had a continuous CK18 expression during the process of induction (Figure 3D).

Immunocytochemical analysis

MSCs showed positive staining for albumin (Figure 4A), and Thy1.1⁺ cells showed CK18 and AFP positive staining (Figure 4B, C).

DISCUSSION

As stromal cells of bone marrow, MSCs could differentiate into cells of all mesodermal origin, including adipocytes, osteocytes, chondrocytes and myocytes^[16-19], *etc.* Besides these, MSCs are also capable of "transdifferentiation" into ectodermal cells, such as neural cells^[20,21]. So MSCs are multipotential adult stem cells. Regarding hepatic differentiation of MSCs, there has been no specific report yet. Schwartz *et al.*^[7] isolated a non-hematopoietic stem cell subset (CD45⁻GlyA⁺ in humans or CD45⁻Ter119⁻ in mice) from bone marrow, termed multipotent adult progenitor cells (MAPCs). MAPCs should be ascribed to MSCs, since they were copurified with MSCs at the same time^[22]. Under serial conditions, Schwartz *et al.*^[7] induced MAPCs into cells with morphological, phenotypic, and functional characteristics of hepatocytes *in vitro*. In our study, we tried to induce standard MSCs into hepatocytes, and found hepatic specific gene CK18 was already expressed by MSCs without differentiation protocol. After induction, MSCs also expressed albumin besides CK18. Albumin mRNA appeared early on d 4 after differentiation (data not shown), coinciding with the change of morphology. Albumin signals had a gradual increase with the extension of differentiation time. Immunocytochemical staining confirmed the results of the PCR analysis at protein-level. There were no early markers of hepatocytes before or during differentiation protocol. Morphologic change of MSCs was apparent. Cell shape changed from spindle and fibroblast-like to round and epithelia-like.

HSCs are another subset of stem cells from bone marrow. A large number of papers demonstrated that HSCs could differentiate into hepatocytes or hepatocyte-like cells. Among the papers, CD34, the most general marker of HSCs in humans and mice, was used. Theise *et al.*^[2] reported 200 CD34⁺ marrow cells produced the same degree of hepatic engraftment as 20 000 unfractionated bone marrow cells in gender mismatch bone marrow transplantation model of mice. Human investigations with G-CSF mobilized CD34⁺ stem cells have shown that these cells were also able to transdifferentiate into hepatocytes^[23]. Thy1.1 antigen has been a well-accepted marker of rat HSCs since 1978^[24]. Recently, Avital *et al.*^[25] identified a population of bone marrow-derived hepatocyte stem cells in rats, which were beta 2 microglobulin-negative and Thy-1-positive ($\beta_2m^-/Thy-1^+$). Moreover, according to Petersen *et al.*^[26], Thy-1 is a new marker for identification of hepatic oval cells. Using Thy-1 would facilitate both *in vivo* and *in vitro* studies of hepatic oval cells. There was no colony-formation in Thy-1.1⁻ bone marrow cells in our studies (data not shown). Thy-1.1⁻ cells did not express CK18 mRNA when freshly isolated, while Thy-1.1⁺ cells had a strong CK18 expression. During hepatic differentiation, Thy-1.1⁺ cells expressed AFP mRNA and had a weak albumin signal. Expression of CK18 of Thy-1.1⁺ cells continued. The cells were polygonal in shape, exhibiting epithelial morphology.

HSCs and MSCs are two separate stem cell subsets of bone marrow. They have different functions in hematopoiesis. Previous studies have explored the ability of hepatic differentiation of different subsets from bone marrow. However, what

relationship they have or what similarity or difference exists among the two subsets is unknown. Our study combined two subsets for the first time, and investigated their different abilities of hepatic differentiation simultaneously. Our results indicated that both of them had hepatic differentiation ability, however, they were different. MSCs could differentiate into mature hepatocyte-like cells, not expressing early hepatic specific genes. Under a similar induction condition, Thy-1.1⁺ cells were inclined to become hepatic stem cell-like cells, with a continuous AFP expression and weak albumin signal. To our interest, CK18 mRNA was positive in Thy-1.1⁺ cells and MSCs, negative in Thy-1.1⁻ cells. It seemed that CK18 had some relationship with Thy-1.1 antigen, and it would be an indicative marker of hepatic differentiation ability.

Hepatic stem cells, especially bone marrow-derived hepatic stem cells may be therapeutically useful for treating a variety of diseases that affect the liver. This has been proved in some animal models^[3,27]. Compared with other liver-related stem cells, such as embryonic stem cells^[28], pancreatic stem cells^[29], and neural stem cells^[30], bone marrow-derived stem cells provide several advantages: (1) Bone marrow can be obtained from living donors or recipients themselves using a moderately invasive procedure. There is no problem of limited donors, which restrict liver transplantation and hepatocyte transplantation greatly. (2) Based on its ability of high self-renewal, the amplification of bone marrow stem cells could be obtained. (3) Utilizing patients' own bone marrow or repopulation of both bone marrow and hepatic system from the same donor could avoid or reduce immunological rejection, which usually affects recipients for a life-long time.

REFERENCES

- Petersen BE, Bowen WC, Patrene KD, Mars WM, Sullivan AK, Murase N, Boggs SS, Greenberger JS, Goff JP. Bone marrow as a potential source of hepatic oval cells. *Science* 1999; **284**: 1168-1170
- Theise ND, Badve S, Saxena R, Henegariu O, Sell S, Crawford JM, Krause DS. Derivation of hepatocytes from bone marrow cells in mice after radiation-induced myeloablation. *Hepatology* 2000; **31**: 235-240
- Lagasse E, Connors H, Al-Dhalimy M, Reitsma M, Dohse M, Osborne L, Wang X, Finegold M, Weissman IL, Grompe M. Purified hematopoietic stem cells can differentiate into hepatocytes *in vivo*. *Nat Med* 2000; **6**: 1229-1234
- Alison MR, Poulosom R, Jeffery R, Dhillion AP, Quaglia A, Jacob J, Novelli M, Prentice G, Williamson J, Wright NA. Hepatocytes from non-hepatic adult stem cells. *Nature* 2000; **406**: 257
- Theise ND, Nimmakayalu M, Gardner R, Illei PB, Morgan G, Teperman L, Henegariu O, Krause DS. Liver from bone marrow in humans. *Hepatology* 2000; **32**: 11-16
- Oh SH, Miyazaki M, Kouchi H, Inoue Y, Sakaguchi M, Tsuji T, Shima N, Higashio K, Namba M. Hepatocyte growth factor induces differentiation of adult rat bone marrow cells into a hepatocyte lineage *in vitro*. *Biochem Biophys Res Commun* 2000; **279**: 500-504
- Schwartz RE, Reyes M, Koodie L, Jiang Y, Blackstad M, Lund T, Lenvik T, Johnson S, Hu WS, Verfaillie CM. Multipotent adult progenitor cells from bone marrow differentiate into functional hepatocyte-like cells. *J Clin Invest* 2002; **109**: 1291-1302
- Fiegel HC, Lioznov MV, Cortes-Dericks L, Lange C, Kluth D, Fehse B, Zander AR. Liver-specific gene expression in cultured human hematopoietic stem cells. *Stem Cells* 2003; **21**: 98-104
- Zhang Y, Bai XF, Huang CX. Hepatic stem cells: existence and origin. *World J Gastroenterol* 2003; **9**: 201-204
- Theise ND, Saxena R, Portmann BC, Thung SN, Yee H, Chiriboga L, Kumar A, Crawford JM. The canals of Hering and hepatic stem cells in humans. *Hepatology* 1999; **30**: 1425-1433
- Petersen BE, Goff JP, Greenberger JS, Michalopoulos GK. Hepatic oval cells express the hematopoietic stem cell marker Thy-1 in the rat. *Hepatology* 1998; **27**: 433-435

- 12 **Baumann U**, Crosby HA, Ramani P, Kelly DA, Strain AJ. Expression of the stem cell factor receptor c-kit in normal and diseased pediatric liver: identification of a human hepatic progenitor cell? *Hepatology* 1999; **30**: 112-117
- 13 **Ma X**, Qiu DK, Peng YS. Immunohistochemical study of hepatic oval cells in human chronic viral hepatitis. *World J Gastroenterol* 2001; **7**: 238-242
- 14 **Omori N**, Omori M, Evarts RP, Teramoto T, Miller MJ, Hoang TN, Thorgeirsson SS. Partial cloning of rat CD34 cDNA and expression during stem cell-dependent liver regeneration in the adult rat. *Hepatology* 1997; **26**: 720-727
- 15 **Omori M**, Omori N, Evarts RP, Teramoto T, Thorgeirsson SS. Coexpression of flt-3 ligand/flt-3 and SCF/c-kit signal transduction system in bile-duct-ligated SI and W mice. *Am J Pathol* 1997; **150**: 1179-1187
- 16 **Pittenger MF**, Mackay AM, Beck SC, Jaiswal RK, Douglas R, Mosca JD, Moorman MA, Simonetti DW, Craig S, Marshak DR. Multilineage potential of adult human mesenchymal stem cells. *Science* 1999; **284**: 143-147
- 17 **Gerson SL**. Mesenchymal stem cells: no longer second class marrow citizens. *Nat Med* 1999; **5**: 262-264
- 18 **Jaiswal N**, Haynesworth SE, Caplan AI, Bruder SP. Osteogenic differentiation of purified, culture-expanded human mesenchymal stem cells *in vitro*. *J Cell Biochem* 1997; **64**: 295-312
- 19 **Wakitani S**, Saito T, Caplan AI. Myogenic cells derived from rat bone marrow mesenchymal stem cells exposed to 5-azacytidine. *Muscle Nerve* 1995; **18**: 1417-1426
- 20 **Woodbury D**, Schwarz EJ, Prockop DJ, Black IB. Adult rat and human bone marrow stromal cells differentiate into neurons. *J Neurosci Res* 2000; **61**: 364-370
- 21 **Sanchez-Ramos J**, Song S, Cardozo-Pelaez F, Hazzi C, Stedeford T, Willing A, Freeman TB, Saporta S, Janssen W, Patel N, Cooper DR, Sanberg PR. Adult bone marrow stromal cells differentiate into neural cells *in vitro*. *Exp Neurol* 2000; **164**: 247-256
- 22 **Reyes M**, Lund T, Lenvik T, Aguiar D, Koodie L, Verfaillie CM. Purification and ex vivo expansion of postnatal human marrow mesodermal progenitor cells. *Blood* 2001; **98**: 2615-2625
- 23 **Korbling M**, Katz RL, Khanna A, Ruitrok AC, Rondon G, Albitar M, Champlin RE, Estrov Z. Hepatocytes and epithelial cells of donor origin in recipients of peripheral-blood stem cells. *N Engl J Med* 2002; **346**: 738-746
- 24 **Goldschneider I**, Gordon LK, Morris RJ. Demonstration of Thy-1 antigen on pluripotent hemopoietic stem cells in the rat. *J Exp Med* 1978; **148**: 1351-1366
- 25 **Avital I**, Inderbitzin D, Aoki T, Tyan DB, Cohen AH, Ferrareso C, Rozga J, Arnaout WS, Demetriou AA. Isolation, characterization, and transplantation of bone marrow-derived hepatocyte stem cells. *Biochem Biophys Res Commun* 2001; **288**: 156-164
- 26 **Petersen BE**, Goff JP, Greenberger JS, Michalopoulos GK. Hepatic oval cells express the hematopoietic stem cell marker Thy-1 in the rat. *Hepatology* 1998; **27**: 433-445
- 27 **Zhan YT**, Wei L, Chen HS, Cong X, Fei R, Wang Y. Differentiation of bone marrow stem cells in rat hepatic fibrogenesis environment. *Zhonghua Ganzangbing Zazhi* 2003; **11**: 673-675
- 28 **Hamazaki T**, Iiboshi Y, Oka M, Papst PJ, Meacham AM, Zon LI, Terada N. Hepatic maturation in differentiating embryonic stem cells *in vitro*. *FEBS Lett* 2001; **497**: 15-19
- 29 **Wang X**, Al-Dhalimy M, Lagasse E, Finegold M, Grompe M. Liver repopulation and correction of metabolic liver disease by transplanted adult mouse pancreatic cells. *Am J Pathol* 2001; **158**: 571-579
- 30 **Clarke DL**, Johansson CB, Wilbertz J, Veress B, Nilsson E, Karlstrom H, Lendahl U, Frisen J. Generalized potential of adult neural stem cells. *Science* 2000; **288**: 1660-1663

Edited by Chen WW and Wang XL. Proofread by Zhu LH and Xu FM

Effects of Zuogui Wan on neurocyte apoptosis and down-regulation of TGF- β_1 expression in nuclei of arcuate hypothalamus of monosodium glutamate -liver regeneration rats

Han-Min Li, Xiang Gao, Mu-Lan Yang, Jia-Jun Mei, Liu-Tong Zhang, Xing-Fan Qiu

Han-Min Li, Xiang Gao, Hepatopathy Institute, Affiliated Hospital of Hubei Traditional Chinese Medicine College, Wuhan 430061, Hubei Province, China

Mu-Lan Yang, Ultramicropathology Laboratory, Tongji Medicine College, Huazhong Scientific University, Wuhan 430030, Hubei Province, China

Jia-Jun Mei, Liu-Tong Zhang, Xing-Fan Qiu, Hubei Traditional Chinese Medicine College, Wuhan 430061, Hubei Province, China

Supported by National Natural Science Foundation of China, No. 30271562 and Natural Science Foundation of Hubei Province, China, No. 2001ABB171

Correspondence to: Han-Min Li, Hepatopathy Institute, Affiliated Hospital of Hubei Traditional Chinese Medicine College, Wuhan 430061, Hubei Province, China

Telephone: +86-27-88929180 **Fax:** +86-27-88929180

Received: 2003-08-08 **Accepted:** 2003-10-22

Abstract

AIM: To inquire into the effects and mechanism of Zuogui Wan (Pills for Kidney Yin) on neurocyte apoptosis in nuclei of arcuate hypothalamus (ARN) of monosodium glutamate (MSG)-liver regeneration rats, and the mechanism of liver regeneration by using optic microscope, electron microscope and *in situ* end labeling technology to adjust nerve-endocrine-immunity network.

METHODS: Neurocyte apoptosis in ARN of the experiment rats was observed by using optic microscope, electron microscope and *in situ* end labeling technology. Expression of TGF- β_1 in ARN was observed by using immunohistochemistry method.

RESULTS: The expression of TGF- β_1 in rats of model group was increased with the increase of ARN neurocyte apoptosis index (AI) ($t = 8.3097, 12.9884, P < 0.01$). As compared with the rats of model group, the expression of TGF- β_1 in rats of Zuogui Wan treatment group was decreased with the significant decrease of ARN neurocyte apoptosis ($t = 4.5624, 11.1420, P < 0.01$).

CONCLUSION: Brain neurocyte calcium ion overexertion and TGF- β_1 protein participate in the adjustment and control of ARN neurocyte apoptosis in MSG-liver regeneration-rats. Zuogui Wan can prevent ARN neurocyte apoptosis of MSG-liver regeneration in rats by down-regulating the expression of TGF- β_1 , and influence liver regeneration through adjusting nerve-endocrine-immune network.

Li HM, Gao X, Yang ML, Mei JJ, Zhang LT, Qiu XF. Effects of Zuogui Wan on neurocyte apoptosis and down-regulation of TGF- β_1 expression in nuclei of arcuate hypothalamus of monosodium glutamate -liver regeneration rats. *World J Gastroenterol* 2004; 10(19): 2823-2826

<http://www.wjgnet.com/1007-9327/10/2823.asp>

INTRODUCTION

MSG-liver regeneration rat model is very useful in study about the correlative mechanism of liver regeneration with high-grade nerve center, hypothalami-hypophysis-liver axial and nerve-endocrine-immune network (NEIN). Experiment results showed that the process of liver regeneration in MSG-liver regeneration rats was disproportional, liver regeneration was faster in the initial stage (the postoperative 1st d), significantly restrained in the intermediate and advanced periods, finally the degree of liver regeneration, meiosis index of liver cells (MI) and the ratio of liver mass to body mass all could not recover the normal level^[1-2], but the above mentioned indexes could be significantly improved after MSG-liver regeneration rats were treated with Zuogui Wan^[2-5]. Functional disorder of NEIN is probably one of the important mechanisms of serious imbalance of liver regenerative process. In order to research the effects of Zuogui Wan on neurocyte apoptosis of MSG-liver regeneration in rat hypothalamus and the mechanism to interfere with liver regeneration by adjusting nerve-endocrine-immunity network, we studied the apoptosis of neurocytes on experimental rats' nuclei of arcuate hypothalami (ARN) and the expression of apoptosis related gene TGF- β_1 with *in situ* end-labeling technique (ISEL), optic microscope, electronic microscope and immunohistochemical method.

MATERIALS AND METHODS

Materials

Wistar rats were offered by the Animal Laboratory, Academy of Medical Sciences of Hubei Province, YDZ19-008. Monosodium glutamate (MSG) was provided by Sigma Co. ISEL apoptosis test kit was from Boehringer Mannheim Co. Strept avidin-biotin complex (SABC) was used to detect the expression of TGF- β_1 by immunohistochemical method (Wuhan Boshide Limited Company).

Establishment of MSG-liver regeneration-rat model

Wistar rats were divided into two groups: Treatment group which was given monosodium glutamate dissolved in saline solution, the other group which served as control was given the vehicle only. MSG 4 mg/g.b.mb was injected on d 2, 4, 6, 8, and 10 after birth. On the 28th d, pups were weaned and caged in 8 groups (4 groups were male rats, 4 groups were female rats). The rats were maintained in an air-conditioned (temperature 24±1 °C) animal room with controlled lighting (12 h light, 12 h dark). They were provided with commercial diet and water. From the 6th week to the experiment end, treatment group rats were treated by gastrogavage of Zuogui Wan (Radix Rehmanniae Praeparata, Rhizoma Dioscoreae, Fructus Lycii, Fructus Corni, Semen Cuscutae, Radix Cyathulae, Colla Cornus Cervi, and Colla Plastris Testudinis) 5 g/kg^[1]. In the 8 wk, partial hepatectomy was performed by excision of the median and left hepatic lobes (occupying about 68% of whole liver) according to the method of Higgins and Anderson under pentobarbital anesthesia^[1]. Shamly-operated rats (MSG-rats) were anesthetized, and their

livers were exposed but not removed. All operations above were clean operations. Rats were operated and killed between 8 and 12 h a.m. to avoid the effects of diurnal variation. Rats subjected to partial hepatectomy were killed on the 1st, 3rd, 5th, 11th d after operation, and 6 were taken randomly in each group per batch (3 males and 3 females).

Neurocyte apoptosis observation

Using *in situ* end labeling (ISEL) method, the nuclei of positively apoptotic neurocytes were stained into blue purple, the starches of cells were intact. Each slice was randomly taken under five fields of vision, the positively stained area was surveyed, and the positive cell number was calculated on the unit area. Then five fields of vision were averaged to calculate the proportion of positive cells in the slice. The percentage of positive cells (apoptosis index, AI) was used to show the apoptosis degree in the tissue.

Pathology-histology observation

Hypothalamus tissue specimens were fixed in 10% formalin, embedded in paraffin, cut into 4 μm thick sections, dewaxed and evaporated with routine procedures, stained with HE, observed with optic microscope. Hypothalamus specimens were embedded and sliced for observation under electron microscope (using ultramicrotome of AO type) and transmission electron microscope (EM10C, Germany OPTON).

Immunohistochemistry

We used SABC method. The cerebral nerve cells showing brown, homogeneous or fine grains were positive. These fine grains distributed all over the cell membranes and cytoplasm,

mainly in cell membranes. Five visual fields were taken randomly in each microsection, then the number of stained areas was surveyed and the number of positive cells was calculated according to the total count of cells in unit area. Finally, the number of positive cells in five visual fields was averaged, and the proportion of positive cells in the microsection was obtained. The percentage of positive cells was used to show the content of fine grains in the tissue.

Statistical analysis

The experimental data were statistically analyzed with HPIAS-1000 high acuity colored pathology image measurement system and Microsoft's Excel.

RESULTS

Effect of Zuogui Wan on MSG-liver regeneration rat hypothalamus pathology-histology alteration

Under light microscope, the neurocytes in arcuatus hypothalami (ARN) of MSG-liver regeneration rats reduced significantly and astrocytes increased significantly. Under electron microscope, neurocyte nucleus chromatin collected at the edge was stained deeply, and nuclear membrane was not regular, cytoplasm was concentrated. Neurocyte nucleus shape factor (approach 1 was regular, and >1 was not regular), circularity (approach 1 was round, and <1 was not round) and heteromorphic index (approach 3 was low for the heterotype degree, >3 was high for the heterotype degree) had significant differences ($P < 0.05$). Pathological changes in Zuogui Wan treatment group were distinguished (Table 1, Figure 1).

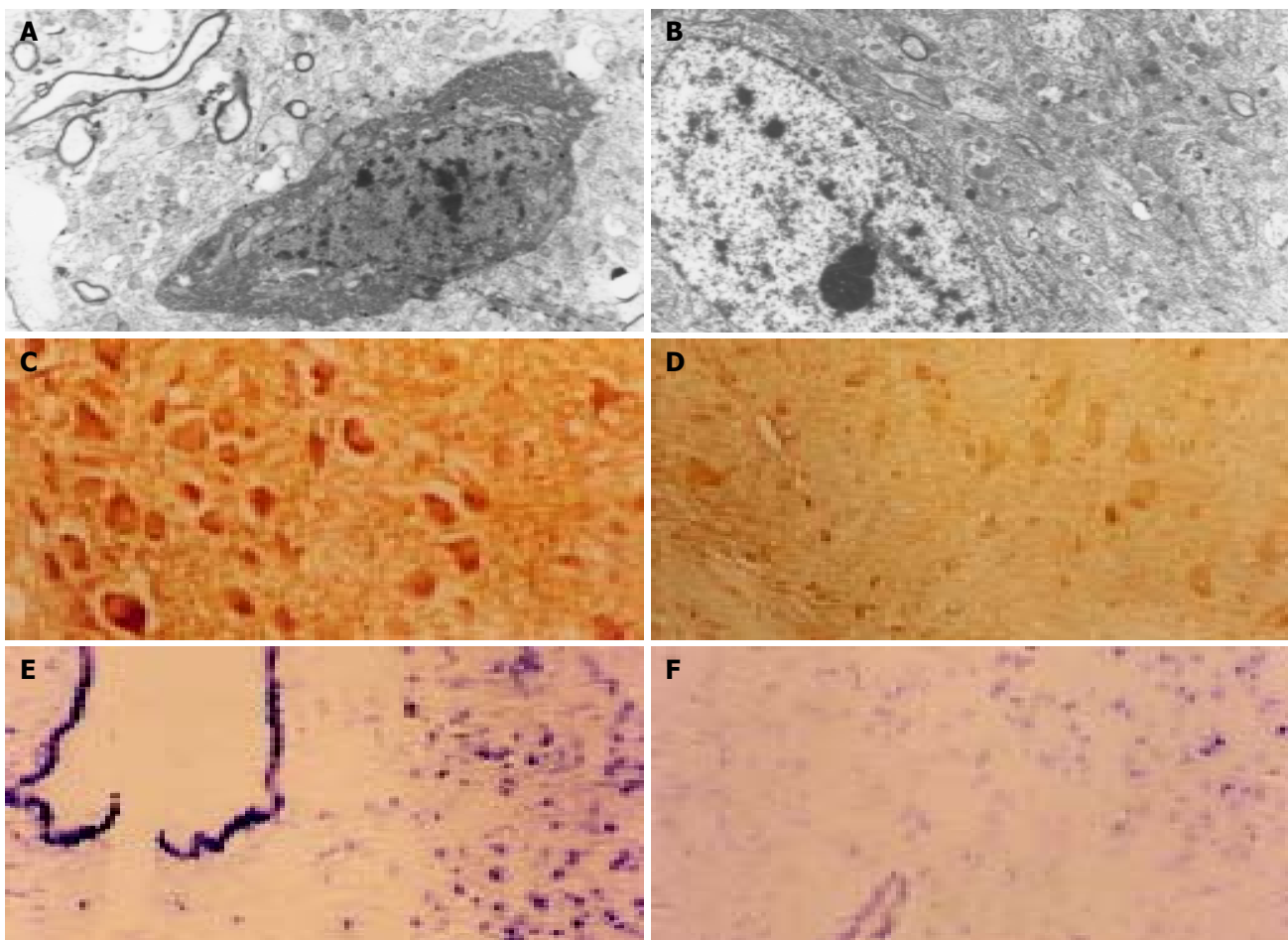


Figure 1 Effect of Zuogui Wan on alteration, apoptosis and TGF- β_1 expression in ARN of MSG-liver regeneration rats. A, B: Effect of Zuogui Wan on alteration in ARN of MSG-liver regeneration rats. C, D: Effect of Zuogui Wan on apoptosis in ARN of MSG-liver regeneration rats. E, F: Effect of Zuogui Wan on TGF- β_1 expression in ARN of MSG-liver regeneration rats.

Table 1 Effect of Zuogui Wan on alterations of ARN nuclei in MSG-liver regeneration rat on the postoperative 11th d ($n = 10$, mean \pm SD)

Group	Shape factor	Circular degree	Heteromorphic index
Normal saline	1.14 \pm 0.45	0.88 \pm 0.16	3.80 \pm 0.8
Model	3.10 \pm 1.14 ^b	0.32 \pm 0.17 ^b	6.24 \pm 1.83 ^b
Zuogui Wan	1.68 \pm 0.33 ^d	0.60 \pm 0.32 ^a	4.60 \pm 0.74 ^a

¹ $t = 5.0572, 7.5856, 3.8633$, ^b $P < 0.01$ vs control (Normal saline); ² $t = 2.4436, 2.6273$, ^a $P < 0.05$, ³ $t = 3.7836$, ^d $P < 0.01$ vs model.

Effect of Zuogui Wan on apoptosis index of MSG-liver regeneration rats in ARN

Apoptosis index (AI) of MSG-liver regeneration rats in ARN was higher than that of saline treated and shamly-operated MSG-rats, and the difference was significant ($P < 0.01$ or $P < 0.05$). AI of Zuogui Wan treated group reduced significantly on the postoperative 5th and 11th days compared to model group ($P < 0.01$) (Table 2).

Table 2 Effect of Zuogui Wan on ARN neurocyte apoptosis in MSG-liver regeneration rats (positive cells %, $n = 6$, mean \pm SD)

Group	Postoperative 1 st d	Postoperative 5 th d	Postoperative 11 th d
Normal saline	0.07 \pm 0.08	0.08 \pm 0.04	0.09 \pm 0.03
MSG-rats	2.45 \pm 0.32 ^d	2.32 \pm 0.45 ^d	2.56 \pm 0.59 ^d
Model	2.62 \pm 0.72 ^d	3.32 \pm 0.81 ^{ad}	4.23 \pm 1.22 ^{ad}
Zuogui Wan	1.62 \pm 0.65	1.43 \pm 0.75 ^f	1.12 \pm 1.14 ^f

¹ $t = 2.6435, 3.0185$, ^a $P < 0.05$ vs MSG-rats; ² $t = 17.6741, 12.1451, 10.2414, 8.6222, 9.7860, 8.3097$, ^d $P < 0.01$ vs control (Normal saline); ³ $t = 4.1938, 4.5624$, ^f $P < 0.01$ vs Model.

Effect of Zuogui Wan on expression of TGF- β_1 in ARN of MSG-liver regeneration rats

Results indicated that, the expression of TGF- β_1 in ARN of MSG-liver regeneration rats was significantly higher than that in saline control group and shamly-operated group (MSG-rats) ($P < 0.01$). Along with increased apoptotic index (AI) in ARN neurocytes, the expression of TGF- β_1 improved correspondingly, namely, the more the TGF- β_1 expressed, the larger the AI was. Besides, along with the weakened expression of TGF- β_1 , AI of ARN in Zuogui Wan treatment group decreased significantly ($P < 0.01$, Table 3).

DISCUSSION

Some studies found that neonate rats who were given high dose MSG on the 2nd, 4th, 6th, 8th, 10th days could destroy nucleus arcuatus hypothalami (ARN) selectively, and swelling and necrosis in ARN neurocytes were the main pathological lesions, and its mechanism in nervous poison might be concerned with the overexertion of calcium ions in cerebral neurocytes^[6-11]. Our experiment results showed that MSG could induce neurocyte apoptosis in the intermediate and advanced stage

after rats were injected with MSG, leading to acute swelling and necrosis in ARN neurocytes. We also could find apoptosis in cerebral neurocytes under electron microscopy and the number of apoptotic cells in model group is larger than that in control group, 8-10 wk after hypodermic injection of MSG. Furthermore, the shape factor, circularity and heteromorphic index that reflected the changes of neurocyte nuclei in ARN were different compared with saline control group. Quantitating apoptotic neurocytes in cerebra by *in situ* end-labeling technique also showed that cerebral IA was larger than that of control group. In ordinary physiological state, most neurons can survive all the life and do not renew, therefore, apoptosis can seldom be found. As a common secondary messenger of apoptosis, MSG could lead to overexertion of calcium ions in neuron cytoplasm, which may be one of the mechanisms underlying apoptosis in MSG-rats' and MSG-liver regeneration-rats' cerebral neurocytes. But the phenomenon that cerebral neurocyte apoptosis of MSG-liver regeneration rats was more conspicuous than that of MSG-rat group can not be explained completely with the mechanism, i.e. MSG leading to overexertion of calcium ions in neuron cytoplasm could induce neurocyte apoptosis. These studies showed that it probably involved other factors leading to cerebral neurocyte apoptosis, besides overexertion of calcium ions in neuron cytoplasm induced by MSG^[4].

TGF- β_1 can enhance apoptosis, so the considerable expression of TGF- β_1 is an important signal that apoptosis takes place. TGF- β_1 expressed excessively in cerebral neurocytes of MSG-liver regeneration rats, and the quantity was larger than that in MSG-rat group and saline control group, and the differences were significant^[12-22]. That overexertion of calcium ions in cerebral neurocytes induced by MSG and the considerable expression of TGF- β_1 induced by partial hepatectomy in ARN of MSG-liver regeneration rats hint that both of them have synergistic effects on inducing MSG-liver regeneration-rat cerebral neurocyte apoptosis. AI of MSG-liver regeneration rat cerebellar neurocytes is closely correlated with considerable expression of TGF- β_1 . Neurocyte apoptosis in ARN of MSG-liver regeneration rats is one of the important mechanisms of functional disorder in nerve-endocrine-immune network. TGF- β_1 protein could participate in the regulation of neurocyte apoptosis in ARN of MSG-liver regeneration rats^[2-5].

One of the major research achievements of the kidney's essence is deficiency of kidney-yang in hypothalamus, and deficiency of kidney-yang is closely correlated with functional disorder in nerve-endocrine-immune network^[23-30]. Our results showed that deficiency of kidney-yin was located in hypothalamus also^[2-5,27], and neurocyte apoptosis in ARN of MSG-liver regeneration rats significantly lessened and indexes such as shape factor, circularity, heteromorphism which reflect the changes of ARN neurocyte nuclei improved significantly by replenishing kidney-yin with Zuogui Wan. Meanwhile, its expression of TGF- β_1 was also less than that in model group.

In summary, Zuogui Wan could prevent cerebral neurocyte apoptosis MSG-liver regeneration rats and down-regulate the overexpression of TGF- β_1 and its acceptors. Thus Zuogui Wan

Table 3 Effect of Zuogui Wan on TGF- β_1 expression of ARN in MSG-liver regeneration-rats (positive cells %, $n = 6$, mean \pm SD)

Group	Postoperative 1 st d	Postoperative 3 rd d	Postoperative 5 th d	Postoperative 11 th d
Normal saline	10.9 \pm 2.7	13.7 \pm 2.5	16.8 \pm 2.9	12.6 \pm 1.6
MSG-rats	12.8 \pm 3.1	13.5 \pm 2.8	12.3 \pm 3.2	14.5 \pm 2.9
Model	19.4 \pm 2.4 ^{bd}	21.3 \pm 2.6 ^{bd}	25.1 \pm 2.9 ^{bd}	29.7 \pm 2.8 ^{bd}
Zuogui Wan	11.3 \pm 2.1 ^f	12.9 \pm 3.2 ^f	18.8 \pm 2.2 ^f	14.8 \pm 1.7 ^f

¹ $t = 5.7635, 5.1612, 4.9573, 12.9884$, ^b $P < 0.01$ vs control (Normal saline); ² $t = 4.1237, 5.0003, 7.2602, 9.2362$, ^d $P < 0.01$ vs MSG-rats; ³ $t = 6.2216, 4.9903, 4.2394, 11.1420$, ^f $P < 0.01$ vs Model.

can influence liver regeneration by adjusting nerve-endocrine-immune network.

REFERENCES

- Li HM, Zhang LT, Mei JJ, Qiu XF, Wang P. The establishment of L-monosodium glutamate-liver regeneration-rat model. *Shijie Huaren Xiaohua Zazhi* 2000; **8**: 824-826
- Li HM, Zhang LT, Qiu XF. Research of "liver and kidney are all origin from the same origin of brain" and the essence of liver and kidney. *Zhongyi Zazhi* 2000; **41**: 69-71
- Li HM, Zhang LT, Qiu XF, Mei JJ, Wang P. Study about the effect and the mechanism of Zuogui Pill on the kidney-essence and liver-blood deficiency syndrome of model of MSG-regeneration-rats. *Hubei Zhongyixueyuan Xuebao* 2001; **3**: 30-33
- Li HM, Yang ML, Mei JJ, Zhang LT, Qiu XF. Neurocyte apoptosis and expression of TGF- β_1 in ARN of MSG-Regeneration-Rats. *China J Appl Physiol* 2003; **19**: 46-47
- Yang ML, Li HM, Mei JJ, Zhang LT, Qiu XF. Dig marked probe *in situ* hybridization detected TGF- β_1 mRNA in MSG-liver regeneration-rats' nucleus arcuatus hypothalami. *Zhongguo Zuzhihuaxue Yu Xibaohuaxue Zazhi* 2002; **11**: 202-204
- Liu YF, Cai DF. The effect of L-monosodium glutamate on nerve-endocrine-immune network. External medicine-endocrine fascicle. *Guowai Yixue Neifenmixie Fence* 1997; **17**: 143-145
- Olney JW. Brain lesions, obesity, and other disturbances in mice treated with monosodium glutamate. *Science* 1969; **164**: 719-721
- Belluardo N, Mudo G, Biondi M. Effects of early destruction of the mouse arcuate nucleus by monosodium glutamate on age-dependent natural killer activity. *Brain Res* 1990; **534**: 225-233
- Kure S, Tominaga T, Yoshimoto T, Tada K, Narisawa K. Glutamate triggers internucleosomal DNA cleavage in neuronal cells. *Biochem Biophys Res Commun* 1991; **179**: 39-45
- Terry LC, Epelbaum J, Martin JB. Monosodium glutamate: acute and chronic effects on rhythmic growth hormone and prolactin secretion, and somatostatin in the undisturbed male rat. *Brain Res* 1981; **217**: 129-142
- Hu L, Fernstrom JD, Goldsmith PC. Exogenous glutamate enhances glutamate receptor subunit expression during selective neuronal injury in the ventral arcuate nucleus of postnatal mice. *Neuroendocrinology* 1998; **68**: 77-88
- Yamamoto M, Fukuda K, Miura N, Suzuki R, Kido T, Komatsu Y. Inhibition by dexamethasone of transforming growth factor beta1-induced apoptosis in rat hepatoma cells: a possible association with Bcl-xL induction. *Hepatology* 1998; **27**: 959-966
- Roberts RA, James NH, Cosulich SC. The role of protein kinase B and mitogen-activated protein kinase in epidermal growth factor and tumor necrosis factor alpha-mediated rat hepatocyte survival and apoptosis. *Hepatology* 2000; **31**: 420-427
- Choi KS, Lim IK, Brady JN, Kim SJ. ICE-like protease (caspase) is involved in transforming growth factor beta1-mediated apoptosis in FaO rat hepatoma cell line. *Hepatology* 1998; **27**: 415-421
- Tsukada T, Eguchi K, Migita K, Kawabe Y, Kawakami A, Matsuoka N, Takashima H, Mizokami A, Nagataki S. Transforming growth factor beta 1 induces apoptotic cell death in cultured human umbilical vein endothelial cells with down-regulated expression of bcl-2. *Biochem Biophys Res Commun* 1995; **210**: 1076-1082
- Derynck R, Zhang Y, Feng XH. Smads: transcriptional activators of TGF-beta responses. *Cell* 1998; **95**: 737-740
- Ribeiro A, Bronk SF, Roberts PJ, Urrutia R, Gores GJ. The transforming growth factor beta 1-inducible transcription factor, TIEG1, mediates apoptosis through oxidative stress. *Hepatology* 1999; **30**: 1490-1497
- Bissell DM, Wang SS, Jarnagin WR, Roll FJ. Cell-specific expression of transforming growth factor-beta in rat liver. Evidence for autocrine regulation of hepatocyte proliferation. *J Clin Invest* 1995; **96**: 447-455
- Oberhammer F, Bursch W, Tiefenbacher R, Fröschl G, Pavelka M, Purchio T, Schulte-Hermann R. Apoptosis is induced by transforming growth factor-beta 1 within 5 hours in regressing liver without significant fragmentation of the DNA. *Hepatology* 1993; **18**: 1238-1246
- Khosla S, Oursler MJ, Schroeder MJ, Eberhardt NL. Transforming growth factor-beta 1 induces growth inhibition of a human medullary thyroid carcinoma cell line despite an increase in steady state *c-myc* messenger ribonucleic acid levels. *Endocrinology* 1994; **135**: 1887-1893
- Gruppiso PA, Mead JE, Fausto N. Transforming growth factor receptors in liver regeneration following partial hepatectomy in the rat. *Cancer Res* 1990; **50**: 1464-1469
- Massague J. TGFbeta signaling: receptors, transducers, and mad proteins. *Cell* 1996; **85**: 947-950
- Cai DF, Shen ZY, Zhang LJ, Wang WJ. The effect of Yougui-ying on the hypothalamus-pituitary-adrenal thymus axis of rats inhibited by corticosterone. *Zhongguo Mianyixue Zazhi* 1994; **10**: 236-239
- Song CF, Yin GS, Zhao JH, Sun SJ, Li En, Lü PY. The effect of tonifying kidney herbs on CaMPKII of hypothalamus-pituitary-adrenal axis in kidney-yang deficiency rats. *Zhongguo Zhongyi Jichuyixue Zazhi* 2001; **7**: 605-607
- Song CF, Yin GS, Li E, Li XY. The effect of Yougui-ying on median eminence ependymocytes of hypothalamus in kidney-yang deficiency rats. *Zhongguo Zhongyi Jichu Yixue Zazhi* 2001; **7**: 19-22
- Gao B, Yao YX, Zhang XY, Yin GS. Expression of NosmRNA in hypothalamus neuron on rats of kidney-yang deficiency and regulation of notifying kidney medicines. *Zhongguo Zhongyi Jichu Yixue Zazhi* 2001; **8**: 583-584
- Cai DF, Liu YF, Cheng XH, Li WW, Bo J, Shen SY, Lin QW, Chen XQ, Ruan QM. The effect of Zuogui Pill on hypothalamus-pituitary-adrenal axis of MSG-rats. *Zhongguo Zhongyi Jichu Yixue Zazhi* 1999; **5**: 24-27
- Wu ZK, Jiang BH, Li CJ, Chen SH, Liu FY, Cui JH, Chen YY, Zheng J, Huang XZ, Lü XX. Modern study on the theory of "kidney manufactures the marrow". *Zhongyi Zazhi* 1999; **10**: 626-628
- Shen ZY. Contrasting research between kidney deficiency and senile in microcosmic. *Zhongyi Zazhi* 2002; **43**: 565-567
- Shen ZY. Study on the localization of kidney-yang deficiency. *Zhongguo Zhongxiyi Jiehe Zazhi* 1997; **17**: 50-52

Edited by Wang XL Proofread by Xu FM

Autocrine expression of hepatocyte growth factor and its cytoprotective effect on hepatocyte poisoning

Yong He, Jun Zhou, Ke-Feng Dou, Yong Chen, Qing-Guo Yan, Hai-Min Li

Yong He, Ke-Feng Dou, Yong Chen, Hai-Min Li, Department of Hepatobiliary Surgery, Xijing Hospital, the Fourth Military Medical University, Xi'an 710032, Shaanxi Province, China

Jun Zhou, Department of Pathology, Qindu Hospital, the Fourth Military Medical University, Xi'an 710032, Shaanxi Province, China

Qing-Guo Yan, Department of Pathology, the Fourth Military Medical University, Xi'an 710032, Shaanxi Province, China

Supported by National Natural Science Foundation of China, No. 30170927 and No. 3007021

Correspondence to: Dr. Yong He, Department of Hepatobiliary Surgery, Xijing Hospital, the Fourth Military Medical University, 127 ChangLe West Road, Xi'an 710032, Shaanxi Province, China. heyong007@yahoo.com

Telephone: +86-29-83375259 **Fax:** +86-29-83375261

Received: 2004-02-21 **Accepted:** 2004-04-13

Abstract

AIM: To construct pEGFP-hepatocyte growth factor (HGF) expression vector, to detect its expression in transfected human hepatocytes, and to investigate the influence of autocrine HGF expression on the proliferative potential and cytoprotective effects in human hepatocytes.

METHODS: Human HGF cDNA was ligated to the pEGFP vector. Recombinant plasmid was transfected into human hepatocyte line QZG with liposome. Expression of HGF protein was observed by fluorescence microscopy and immunohistochemistry. Hepatic cells were collected 24, 48, and 72 h after transfection to detect the number of [³H]-TdR uptake in DNA. DNA synthesis was observed by using PCNA stain immunohistochemistry. Acute liver cell damage was induced by carbon tetrachloride. Cytoprotective effect was observed by examining the survival rate of hepatocytes and leakage of intracellular alanine transaminase (ALT) and potassium ions.

RESULTS: HGF identification of pEGFP-HGF by enzyme digestion showed that HGF fragment was cloned into *Bam*H I and *Sal*I sites of pEGFP-N3. Expression of GFP in transfected hepatocytes was observed with fluorescence microscopy. The [³H]-TdR uptake became 7 times as many as in the control group 96 h after transfection. After HGF transfection, the survival rate of hepatocytes poisoned by CCl₄ significantly increased (83% vs 61%, *P*<0.05), and the leakage of intracellular alanine transaminase and potassium ions decreased (586 nkat/L vs 1089 nkat/L, *P*<0.01; and 5.59 mmol/L vs 6.02 mmol/L, *P*<0.01 respectively). Culture of transfected hepatic cells promoted the proliferation of other non-transfected cells.

CONCLUSION: Transfected HGF is expressed in hepatic cells and has the activity of promoting cell division and protecting hepatic cells against poisoning.

He Y, Zhou J, Dou KF, Chen Y, Yan QG, Li HM. Autocrine expression of hepatocyte growth factor and its cytoprotective effect on hepatocyte poisoning. *World J Gastroenterol* 2004; 10(19): 2827-2830

<http://www.wjgnet.com/1007-9327/10/2827.asp>

INTRODUCTION

Hepatocyte growth factor (HGF) was originally isolated as the most potent mitogen for primary hepatocytes. HGF has subsequently been revealed to be a multifunctional cytokine in a wide variety of epithelial cells, endothelial cells, and some mesenchymal cells during the past two decades^[1-7]. In addition to mitogenic activity, HGF has some unique morphogenic activities such as an induction of epithelial tubulogenesis including in cells derived from the kidney, liver and mammary gland^[8,9]. Characterization of scatter factor, which enhances epithelial cell motility, revealed that it had the same molecule as HGF. HGF is a heterodimeric glycoprotein composed of a 69 ku α -chain and a 34 ku β -chain, and has four homologous kringle domains in the α -chain^[10]. The receptor capable of signal transduction of HGF is a c-met protooncogene product of heterodimeric tyrosine kinase^[11,12]. Extensive studies on the physiological function of HGF have established that the growth factor functions as a potent hepatotrophic factor for liver injuries, but elevated plasma HGF levels have not been noted in patients with hepatic diseases^[13-19].

HGF and its receptor MET, ordinarily constitute a paracrine signaling system in which cells of mesenchymal origin produce the ligand (HGF) which binds to its receptor (MET) that is predominantly expressed in cells of epithelial origin^[10]. While the effects of exogenous HGF on promoting normal hepatocyte growth have been well characterized, there appears to have a controversy on effect of autocrine HGF on hepatocytes. In this study, the effects of forced autocrine expression of HGF in hepatocytes were examined. huHGF was expressed by transducing hepatocytes with a vector containing huHGF cDNA. It was demonstrated that the forced expression of HGF in hepatocytes led to an increase in the population of transduced hepatocytes compared to non-transduced hepatocytes in the same cultures. The results suggest that autocrine expression presents an advantage for the proliferation and survival of hepatocytes poisoning.

MATERIALS AND METHODS

Materials

PBS-7 vector containing human HGF cDNA was donated by Professor Toshikazu Nakamura (Division of Biochemistry, Osaka University Medical School, JaPan). The transfer vector pEGFPN₃ containing a humanized green fluorescence protein (GFP) cDNA was purchased from Clontech Biology Company (USA).

Culture of hepatocytes

Human hepatocyte QZG (donated by the Department of Pathology, Fourth Military Medical University) was cultured in RPMI 1640 medium (Gibco) supplemented with 150 mL/L fetal bovine serum (100 kU/L penicillin, 100 kU/L streptomycin) and incubated at 37 °C in humidified atmosphere of 50 mL/L CO₂ incubator.

Construction of pEGFP-HGF vectors

Construction of pEGFP-HGF vector was previously described^[20]. The human HGF cDNA was isolated from pBluescript SK⁺ as a 2.3 kb *Bam*H I-*Sal*I fragment. The resulting cDNA fragment

was then inserted into the *Sal* I and *Bam*HI-sites of the pEGFP-N₃ vector.

Transduction of rat hepatocytes

Exponentially growing QZG cells were seeded into 35 mm tissue culture dishes and grown to 60-70% confluency in culture medium. Each culture dish was then transfected with 5 µg pEGFP-HGF constructs by using lipofectamine according to the instructions of the manufacturer (Gibco BRL, Eggenstein, Germany). Encapsulated pEGFP-HGF was incubated for 5 h on cells in serum free medium, then in medium containing 15 mL/L bovine serum. After a further incubation of the cells for 24 h, the culture medium was discarded and replaced by normal culture medium. Seventy-two hours after transfection, the QZG cells and their media were harvested for further analysis.

Analysis for HGF expression in hepatocyte

After transfected with pEGFP-HGF, the cells were examined for the presence of green fluorescence by using an inverted fluorescent light microscope. Immunocytochemical staining was performed by using HGF antibody on logarithmically growing cell lines. Firstly, the cells were plated onto coverslips, adhered overnight. Then, after rinsed three times with PBS, the cells were fixed in cold acetone for 8-10 min. Endogenous peroxidase was blocked with 10 mL/L hydrogen peroxide in absolute methanol for 30 min. The primary antibodies were applied for 2 h at 37 °C at 1:50 dilution in a humidified chamber. Then the typical SABC strategy followed.

Assay of DNA synthesis by ³H-TdR incorporation

The cells were cultured in an appropriate medium for 24 h prior to beginning the experiment, and incubated with [³H] thymidine (18.5 MBq/L, 37 kBq/well). After 6 h the cells were harvested with trypsin/EDTA, and collected from the acetic fiber filter with a cellular collector and washed three times with PBS. The filter was dried overnight at 37 °C, and transferred into a liquid scintillation counter (containing 10 g/L PO and 20 g/L POP in xylene) and cpm value was determined by the liquid scintillation counter (LS6500, Beckmen Co.)

Cell proliferation

The level of expression of proliferating cell nuclear antigen (PCNA) was used as a marker of cell proliferation. In the present study PCNA was measured by ABC immunohistochemical method.

Cytoprotective effects on CCl₄-intoxicated human hepatocytes

For assaying cytoprotective effect of autocrine HGF, hepatocyte QZG was poisoned by carbon tetrachloride (CCl₄). After treated with 15 mmol/L CCl₄ for 40 min, survival rate of cells was measured by trypan blue method. Aspartate aminotransferase (AST) and alanine aminotransferase (ALT) in supernatant were measured by using a biochemical analyzer. Leakage of intracellular potassium ions was measured by using an ion analyzer.

In situ hybridisation

This was performed as previously described. Hepatocytes were transfected with pEGFP-HGF, trypsinized after 48 h and centrifuged onto slides (roughly 40 000 cells/cm²). These slides were used for *in situ* hybridization. Results were evaluated by counting at least 3 viewing fields per slide at a magnification ×200.

Statistical analysis

The results are expressed as mean±SE. Statistical analysis was performed by the Student's *t*-test. *P*<0.05 was considered statistically significant.

RESULTS

Identification of recombinant pEGFP-HGF expression vector

The recombinant pEGFP-HGF vector was digested by *Bam*HI and *Sal* I. pEGFP-HGF contained a 2300-bp and a 4700-kb gene fragments separated by electrophoresis in 12 g/L agarose gel (Figure 1). It proved that the HGF gene was correctly inserted in pEGFP-HGF.

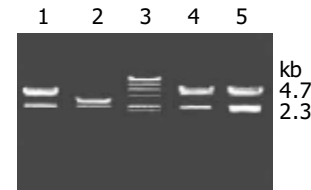


Figure 1 Identification of recombinant plasmids digested with restriction enzymes *Bam*HI and *Sal* I. 1, 4, 5: pEGFP-HGF plasmid digested with *Bam*HI and *Sal* I; 2: pBS-7 plasmid digested with *Bam*HI+*Sal* I; 3: λDNA/*Hind*III marker.

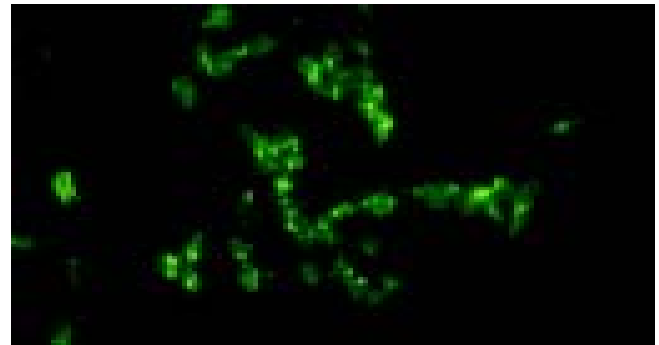


Figure 2 Green fluorescence in QZG cells transfected with pEGFP-HGF fusion constructs, Inverted fluorescent light microscope ×200.



Figure 3 Expression of HGF protein in QZG cells transfected with pEGFP-HGF. SABC ×400.

Expression of pEGFP-HGF fusion proteins in QZG cell line

Green fluorescence was visible after transfection with pEGFP-HGF fusion constructs (Figure 2). The pEGFP-HGF fusion proteins were localized primarily in cytoplasm. The expression of HGF in the transfected QZG cells was also detected by immunohistochemical staining. A lot of brown granules were seen in HGF transfected QZG cell cytoplasm (Figure 3) proving that HGF gene could be expressed in QZG cells.

Effect on DNA synthesis

DNA synthesis as mirrored by [³H]thymidine uptake of QZG cells was determined after transfection with pEGFP-HGF. DNA synthesis in QZG cells transfected by pEGFP-HGF was accelerated

in a time-dependent fashion increased by 7-fold compared to control group after 96 h transfection with pEGFP-HGF (Figure 4).

Cell proliferation

As shown in Figure 5, the expression rate of PCNA on QZG cells increased after transfection with pEGFP-HGF.

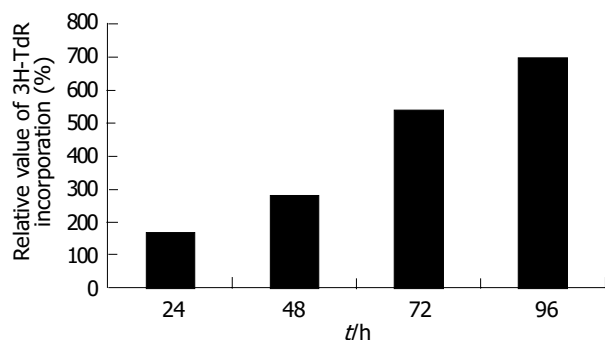


Figure 4 Relative values of ³H-TdR incorporation in QZG cells transfected with pEGFP-HGF (relative to QZG cells transfected with pEGFP).

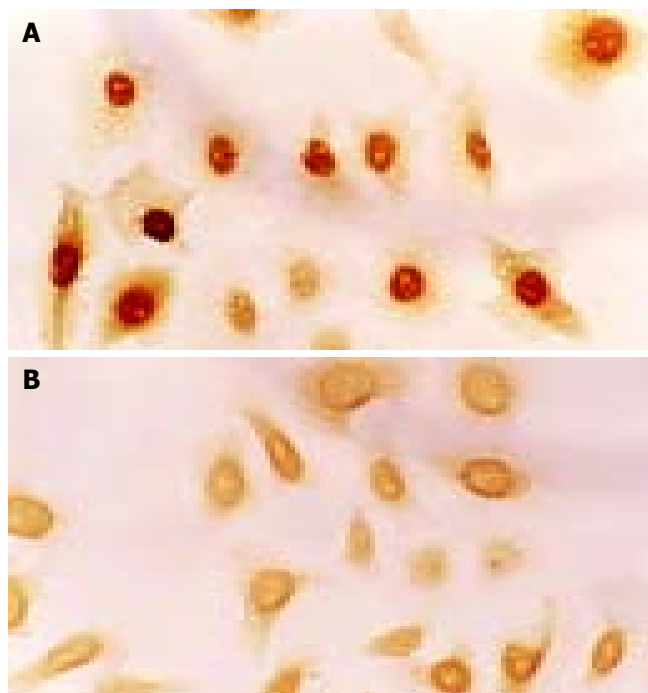


Figure 5 Expression of PCNA protein in QZG cells transfected with pEGFP-HGF (A) and transfected with pEGFP (B). $\times 200$.

Table 1 Survival rate of hepatocytes and leakage of intracellular ALT and K⁺

Group	Survival rate (%)	ALT (nkat/L)	K ⁺ (mmol/L)
QZG	96 \pm 2	403 \pm 70	5.21 \pm 0.04
pEGFP-HGF	98 \pm 1	429 \pm 80	5.18 \pm 0.02
QZG intoxicated by CCL ₄	61 \pm 7 ^a	1 089 \pm 223 ^b	6.02 \pm 0.17 ^b
pEGFP-HGF intoxicated by CCL ₄	83 \pm 6 ^c	586 \pm 124 ^d	5.59 \pm 0.07 ^d

^a $P < 0.05$, ^b $P < 0.01$, vs QZG group; ^c $P < 0.05$, ^d $P < 0.01$, vs QZG intoxicated by CCL₄ group.

Cytoprotective effect on hepatocytes injured by CCl₄

After pEGFP-HGF was transfected, the survival rate of QZG cells intoxicated by CCl₄ was significantly increased (83% vs 61%, $t = 3.89$, $P < 0.05$). The leakage of intracellular alanine transaminase (ALT) (586 nkat/L vs 1 089 nkat/L, $t = 13.07$, $P < 0.01$) and potassium ions (5.59 mmol/L vs 6.02 mmol/L, $t = 12.91$, $P < 0.01$) was decreased (Table 1).

DISCUSSION

Hepatocyte growth factor (HGF) is well known as a pleiotropic substance with mitogenic, motogenic, morphogenic, and tumor suppressor activities. HGF was found in the serum of partially hepatectomized rat and in rat platelets as the most potent stimulator of hepatocyte growth and DNA synthesis *in vitro*^[21]. The mitogenic function of HGF was confirmed *in vivo*. In normal rats as well as partially hepatectomized rats, infusion of HGF stimulated a 6-fold increase in the mitotic labeling index of hepatocytes. It also stimulated protein synthesis, seen as increased hepatic messenger RNA content and serum albumin levels. HGF has been intensively investigated in terms of its beneficial effects on hepatic injury^[22-24]. It has been documented that HGF reduced the hepatotoxicity of alpha-naphthylisothiocyanate, D-galactosamine, and carbon tetrachloride in rats^[25,26]. Moreover, HGF increased survival of cirrhotic rats subjected to a major hepatic resection and treatment with dimethylnitrosamine^[27-29]. These results suggest that HGF may play important roles in protection from and regeneration of hepatic injury and serve as a therapeutic agent.

HGF and its receptor MET, ordinarily constitute a paracrine signaling system in which cells of mesenchymal origin produce the ligand (HGF) which binds to its receptor (MET) that is predominantly expressed in cells of epithelial origin. In the present study, we demonstrated that HGF gene transfer into hepatocytes caused increased proliferation of hepatocytes by method of PCNA stain and increased DNA synthesis by method of [³H]thymidine uptake. Forced HGF expression by cultured human hepatocytes had a mitogenic effect. The detection of HGF protein assessed by immunocytochemical staining confirmed the successful transfection of HGF gene.

Accumulated evidence has revealed that HGF has a cytoprotective effect on various types of liver cells. In hepatocytes, HGF attenuated the liver injury induced by lipopolysaccharide and D-galactosamine^[30]. Moreover, HGF abrogated Fas-induced massive liver apoptosis and lethal hepatic failure by inducing Bcl-xL expression, with subsequent blockage of a Fas-mediated signaling pathway upstream of CPP32 in the liver, suggesting that HGF has an inhibitory effect on Fas-mediated apoptosis. HGF could also ameliorate hepatocellular dysfunction and posthepatectomy hyperbilirubinemia in an α -naphthylisothiocyanate-induced cholestasis model, in which the epithelia of bile ducts, as well as hepatocytes, became necrotic. This finding indicates that HGF could promote tissue repair of both epithelial cells and hepatocytes^[31,32]. In the present study we demonstrated the cytoprotective effect of HGF transgene on hepatocyte injury by CCl₄. HGF transgene markedly increased the survival rate of hepatocytes against CCl₄ injury, decreased the leakage of intracellular alanine transaminase and potassium ions.

Since its introduction into cell biological research, the green fluorescent protein (GFP) of jellyfish *Aequorea victoria* has become a versatile tool for the analysis of protein function and dynamics at the cellular level. GFP, consisting of 238 amino acids, has been used as a tag for localization of a broad range of proteins in a wide variety of eukaryotic cells. A mutant of GFP, S65T with an excitation peak of 489 nm and an emission peak of 511 nm, could emit 4 to 6 times more fluorescence energy compared with wild-type GFP. GFP may be fused generically to

a target protein, and the fluorophore of GFP forms spontaneously in the presence of oxygen, thus rendering it an ideal probe for *in vivo* applications. The *in vivo* expression of GFP could obviate the fixation and permeabilization of cells for immunofluorescence or the microinjection of labeled proteins. GFP fusion proteins constitute a major advance in the study of the dynamics of intracellular processes in living cells^[33-37]. A major concern in the application of GFP as a fluorescent tag relates to whether the distribution of GFP fluorescence is identical to that of the protein to which it is fused. We have constructed GFP-HGF fusion gene and transfected into hepatocytes. The results indicate that the fusion protein can still be expressed in the nuclei of hepatocytes. Because liver disease, especially viral liver diseases are common in China, our study is of much more significance.

REFERENCES

- 1 Yu SL, Yang FH. Molecular biological progress of hepatocyte growth factor (HGF). *Shengwu Gongcheng Xuebao* 2002; **18**: 1-4
- 2 Morishita R, Aoki M, Yo Y, Ogihara T. Hepatocyte growth factor as cardiovascular hormone: role of HGF in the pathogenesis of cardiovascular disease. *Endocr J* 2002; **49**: 273-284
- 3 Ricci G, Catizone A, Galdieri M. Pleiotropic activity of hepatocyte growth factor during embryonic mouse testis development. *Mech Dev* 2002; **118**: 19-28
- 4 Skibinski G. The role of hepatocyte growth factor/c-met interactions in the immune system. *Arch Immunol Ther Exp* 2003; **51**: 277-282
- 5 Liu Y. Hepatocyte growth factor promotes renal epithelial cell survival by dual mechanisms. *Am J Physiol* 1999; **277**: F624-633
- 6 Natsume M, Tsuji H, Harada A, Akiyama M, Yano T, Ishikura H, Nakanishi I, Matsushima K, Kaneko S, Mukaida N. Attenuated liver fibrosis and depressed serum albumin levels in carbon tetrachloride-treated IL-6-deficient mice. *J Leukoc Biol* 1999; **66**: 601-608
- 7 He Y, Zhou J, Dou K. Autocrine expression of hepatocyte growth factor and its cytoprotective effect on hepatocyte poisoning. *Zhonghua Yixue Zazhi* 2002; **82**: 275-278
- 8 Ohnishi T, Daikuhara Y. Hepatocyte growth factor/scatter factor in development, inflammation and carcinogenesis: its expression and role in oral tissues. *Arch Oral Biol* 2003; **48**: 797-804
- 9 Kokuzawa J, Yoshimura S, Kitajima H, Shinoda J, Kaku Y, Iwama T, Morishita R, Shimazaki T, Okano H, Kunisada T, Sakai N. Hepatocyte growth factor promotes proliferation and neuronal differentiation of neural stem cells from mouse embryos. *Mol Cell Neurosci* 2003; **24**: 190-197
- 10 Funakoshi H, Nakamura T. Hepatocyte growth factor: from diagnosis to clinical applications. *Clin Chim Acta* 2003; **327**: 1-23
- 11 Zhang YW, Vande Woude GF. HGF/SF-met signaling in the control of branching morphogenesis and invasion. *J Cell Biochem* 2003; **88**: 408-417
- 12 Sun W, Funakoshi H, Nakamura T. Localization and functional role of hepatocyte growth factor (HGF) and its receptor c-met in the rat developing cerebral cortex. *Brain Res Mol Brain Res* 2002; **103**: 36-48
- 13 Nozato E, Shiraishi M, Nishimaki T. Up-regulation of hepatocyte growth factor caused by an over-expression of transforming growth factor beta, in the rat model of fulminant hepatic failure. *J Surg Res* 2003; **115**: 226-234
- 14 Hata J, Ikeda E, Uno H, Asano S. Expression of hepatocyte growth factor mRNA in rat liver cirrhosis induced by N-nitrosodimethylamine as evidenced by *in situ* RT-PCR. *J Histochem Cytochem* 2002; **50**: 1461-1468
- 15 Chijiwa K, Saiki S, Tanaka M. Serum interleukin-6 and hepatocyte growth factor levels in patients after hepatectomy. *Hepatogastroenterology* 2002; **49**: 467-471
- 16 Borawski J, Mysliwiec M. Serum hepatocyte growth factor is associated with viral hepatitis, cardiovascular disease, erythropoietin treatment, and type of heparin in haemodialysis patients. *Nephrol Dial Transplant* 2002; **17**: 637-644
- 17 Chen P, Li K, Dong JH, Han BL. Changes of TGF- α , HGF, PCNA and IGFBP-1s mRNA after partial hepatectomy in rat liver. *Shijie Huaren Xiaohua Zazhi* 2003; **11**: 434-437
- 18 Xu W, Wu SG. The possible relationship between hepatomegaly and release of HGF into plasma induced by clofibrate in rats. *World J Gastroenterol* 1999; **5**: 440-442
- 19 Yamagami H, Moriyama M, Tanaka N, Arakawa Y. Detection of serum and intrahepatic human hepatocyte growth factor in patients with type C liver diseases. *Intervirol* 2001; **44**: 36-42
- 20 He Y, Zhou J, Dou KF. Construction of hepatocyte growth factor expression vector and detection of expression in human hepatocytes. *Shijie Huaren Xiaohua Zazhi* 2001; **9**: 1143-1146
- 21 Luo YQ, Wu MC. Hepatocyte growth factor. *Xin Xiaohuabingxue Zazhi* 1997; **5**: 198-199
- 22 Okamoto K, Suzuki S, Kurachi K, Sunayama K, Yokoi Y, Konno H, Baba S, Nakamura S. Beneficial effect of deletion variant of hepatocyte growth factor for impaired hepatic regeneration in the ischemically damaged liver. *World J Surg* 2002; **26**: 1260-1266
- 23 Takeda Y, Arii S, Kaido T, Imamura M. The impairment of hepatocytes and sinusoidal endothelial cells during cold preservation in rat fatty liver induced by alcohol and the beneficial effect of hepatocyte growth factor. *Transpl Int* 2003; **16**: 241-249
- 24 Yamashita Y, Fujise N, Imai E, Masunaga H. Reduction of monocrotaline-induced hepatic injury by deleted variant of hepatocyte growth factor (dHGF) in rats. *Liver* 2002; **22**: 302-307
- 25 Otsuka T, Takagi H, Horiguchi N, Toyoda M, Sato K, Takayama H, Mori M. CCl₄-induced acute liver injury in mice is inhibited by hepatocyte growth factor overexpression but stimulated by NK2 overexpression. *FEBS Lett* 2002; **532**: 391-395
- 26 Xue F, Takahara T, Yata Y, Minemura M, Morioka CY, Takahara S, Yamato E, Dono K, Watanabe A. Attenuated acute liver injury in mice by naked hepatocyte growth factor gene transfer into skeletal muscle with electroporation. *Gut* 2002; **50**: 558-562
- 27 Matsuno Y, Iwata H, Umeda Y, Takagi H, Mori Y, Kosugi A, Matsumoto K, Nakamura T, Hirose H. Hepatocyte growth factor gene transfer into the liver via the portal vein using electroporation attenuates rat liver cirrhosis. *Gene Ther* 2003; **10**: 1559-1566
- 28 Ueki T, Kaneda Y, Tsutsui H, Nakanishi K, Sawa Y, Morishita R, Matsumoto K, Nakamura T, Takahashi H, Fujimoto J. Hepatocyte growth factor gene therapy of liver cirrhosis in rats. *Nature Med* 1999; **5**: 226-230
- 29 Oe S, Fukunaka Y, Hirose T, Yamaoka Y, Tabata Y. A trial on regeneration therapy of rat liver cirrhosis by controlled release of hepatocyte growth factor. *J Control Release* 2003; **88**: 193-200
- 30 Kosai K, Matsumoto K, Funakoshi H, Nakamura T. Hepatocyte growth factor prevents endotoxin-induced lethal hepatic failure in mice. *Hepatology* 1999; **30**: 151-159
- 31 Kondo H, Tani T, Kodama M. Effects of deletion-type human hepatocyte growth factor on murine septic model. *J Surg Res* 1999; **85**: 88-95
- 32 Zeng C, Pesall JE, Gilkerson KK, McFarland DC. The effect of hepatocyte growth factor on turkey satellite cell proliferation and differentiation. *Poult Sci* 2002; **81**: 1191-1198
- 33 Cheng H, Liu YF, Zhang HZ, Shen WA, Zhang SZ. Construction and expression of anti-HCC immunotoxin of sFv-TNF- α and GFP fusion proteins. *Shijie Huaren Xiaohua Zazhi* 2001; **9**: 640-644
- 34 Lin T, Ding J, Meng FP, Han QL, Yu ZC, Guo CC, Liu ZG, Fan DM. Construction and identification of recombinant adenovirus vaccines of gastric cancer MG7-Ag mimotope. *Shijie Huaren Xiaohua Zazhi* 2003; **11**: 14-17
- 35 Fujikawa T, Hirose T, Fujii H, Oe S, Yasuchika K, Azuma H, Yamaoka Y. Purification of adult hepatic progenitor cells using green fluorescent protein(GFP)-transgenic mice and fluorescence-activated cell sorting. *J Hepatol* 2003; **39**: 162-170
- 36 Scarff KL, Ung KS, Sun J, Bird PL. A retained selection cassette increases reporter gene expression without affecting tissue distribution in SPI3 knockout/GFP knock-in mice. *Genesis* 2003; **36**: 149-157
- 37 Waldo GS. Improving protein folding efficiency by directed evolution using the GFP folding reporter. *Methods Mol Biol* 2003; **230**: 343-359

Effects of herbal compound 861 on human hepatic stellate cell proliferation and activation

Lin Wang, Jian Wang, Bao-En Wang, Pei-Gen Xiao, Yan-Jiang Qiao, Xue-Hai Tan

Lin Wang, Yan-Jiang Qiao, School of Chinese Materia Medica, Beijing University of Chinese Medicine, Beijing 100102, China
Xue-Hai Tan, Jian Wang, Beijing Genomic Institute, Beijing 101300, China

Bao-En Wang, Liver Research Center, Beijing Friendship Hospital, Capital University of Medical Sciences, Beijing 100050, China

Pei-Gen Xiao, Institute of Medicinal Plant Development, Chinese Academy of Medical Sciences, Beijing 100094, China

Supported by the Fund of One Hundred Scientist Plan of Chinese Academy of Sciences and the Knowledge Innovation Program Foundation of Chinese Academy of Sciences, No. KSCX2-SW-207

Co-correspondents: Jian Wang

Correspondence to: Dr. Xue-Hai Tan, Beijing Genomic Institute, Beijing 101300, China. tanxh@genomics.org.cn

Telephone: +86-10-80481755 **Fax:** +86-10-80498676

Received: 2004-03-23 **Accepted:** 2004-04-16

Abstract

AIM: To investigate the effects of herbal compound 861 (Cpd 861) on cell proliferation in human hepatic stellate cells (LX-2) and human hepatocellular liver carcinoma cells (HepG2), and expression of α -smooth muscle actin (α -SMA) in LX-2 cells.

METHODS: LX-2 and HepG2 cells were incubated with various concentrations of Cpd 861 (0.1-0.003 mg/mL) for 1, 2, 3, 5 and 7 d. Cell proliferation was analyzed by 3-(4, 5-dimethylthiazol-2-yl)-5-(3-carboxymethoxyphenyl)-2-(4-sulfophenyl)-2H-tetrazolium (MTS) assay. Effects of Cpd861 on the expression of α -SMA mRNA in LX-2 cells were measured by real-time quantitative PCR method using SYBR Green I technology.

RESULTS: Cpd 861, at 0.1 mg/mL, significantly inhibited LX-2 cell proliferation (15% decrease relative to control, $P < 0.05$) after 3 d of incubation. The inhibitory effects seemed to increase with the treatment time (25% decrease after 5 d of incubation and 35% decrease after 7 d of incubation, $P < 0.01$). However, Cpd 861 did not affect HepG2 cell proliferation at the same concentration used for LX-2 cells. The expression levels of α -SMA mRNA decreased significantly when LX-2 cells were exposed to Cpd 861 for 48 h (59% decrease relative to control, $P < 0.05$) or 72 h (60% decrease relative to control, $P < 0.01$).

CONCLUSION: Cpd 861 can significantly inhibit LX-2 cell proliferation in a dose-dependant manner, and reduce the expression levels of α -SMA mRNA in LX-2 cells. Since hepatic cell proliferation and high level of α -SMA are associated with liver fibrosis, the results suggest that Cpd 861 may be useful in the treatment of this disease.

Wang L, Wang J, Wang BE, Xiao PG, Qiao YJ, Tan XH. Effects of herbal compound 861 on human hepatic stellate cell proliferation and activation. *World J Gastroenterol* 2004; 10 (19): 2831-2835

<http://www.wjgnet.com/1007-9327/10/2831.asp>

INTRODUCTION

Hepatic fibrosis is a reversible wound healing response to chronic liver injury due to a variety of insults, including viral hepatitis (especially hepatitis B and C), alcohol abuse, drugs, metabolic diseases, autoimmune attack of hepatocytes or congenital abnormalities^[1,2]. As shown in many recent studies, hepatic stellate cells (previously called Ito cells, lipocytes, perisinusoidal cells, or fat-storing cells) are primary cell types to mediate fibrogenesis^[1,2]. In normal liver, hepatic stellate cells (HSCs) are nonparenchymal quiescent cells with functions to store vitamin A. Following liver injury of any etiology, HSCs undergo a process of activation, transform from quiescent vitamin A-rich cells to proliferative, fibrogenic, contractile myofibroblasts. Activated HSCs lose lipid droplets, feature high level expression of α -smooth muscle actin (α -SMA), and also are responsible for the deposition of the majority of excess extracellular matrix (ECM, predominantly types I and III collagen), which leads to form action of scar tissue in the fibrotic liver^[1-4].

Herbal compound 861 (Cpd 861) is an extract of 10 herbs with *Salvia miltiorrhiza*, *Astragalus membranaceus* and *Spatholobus suberectus* as its chief components. The recipe of this mixed compound was based on the therapeutically indications of Chinese medicine. Clinical studies showed Cpd 861 could significantly improve clinical symptoms in hepatic fibrosis patients as well as the biochemical parameters associated with diseases in clinical tests for patients^[5,6]. Experimental researches also showed that Cpd 861 could inhibit cell proliferation, reduce the level of α -SMA and reverse the process of liver fibrosis on rat model^[5-7]. In this study, we aimed to investigate the effects of Cpd 861 on LX-2 and HepG2 cell proliferation and expression of α -SMA in LX-2 cells.

MATERIALS AND METHODS

Materials

Human activated hepatic stellate cell line LX-2 was a gift from Dr. Friedman of Mount Sinai School of Medicine. LX-2 cells were a low-passaged human cell line from normal human stellate cells that were spontaneously immortalized^[8,9]. The cells exhibited typical features of stellate cells and expressed α -SMA under all culture conditions and were regarded as at least partially activated even after immediate replating. LX-2 cells underwent further activation during growth and expansion on plastic surfaces^[8].

Human hepatocellular carcinoma cell line HepG2 was purchased from the Chinese Academy of Medical Sciences (Beijing, China). Dulbecco's modified Eagle's medium (DMEM), L-glutamine and streptomycin were purchased from Gibco, Invitrogen, Carlsbad, CA. Fetal bovine serum (FBS) was from Hyclone, USA. Penicillin and phenazine methosulfate (PMS) were from Sigma, USA. MTS and oligo (dT)₁₅ primers were acquired from Promega, USA. TRIzol reagent and Moloney murine leukemia virus reverse transcriptase (M-MLV RT) were the products of Invitrogen, CA. SYBR Green I was purchased from OPE Technology Development Company, Shanghai, China. Hotstar Taq DNA polymerase was purchased from TW-Biotech, China.

Cell culture and cell proliferation assay

LX-2 cells were cultured in DMEM supplemented with 50 mL/L heat-inactivated FBS, 200 mmol/L *L*-glutamine, 100 U/mL penicillin and 100 µg/mL streptomycin. HepG2 cells were cultured in DMEM containing 100 mL/L FBS, 200 mmol/L *L*-glutamine, 100 U/mL penicillin and 100 µg/mL streptomycin.

MTS assay was used to determine the effect of Cpd 861 on the proliferation of LX-2 and HepG2 cells. In metabolically active cells, MTS was reduced by dehydrogenase enzymes into an aqueous, soluble formazan product. The absorbance was measured directly at 490 nm from 96-well assay plates without additional processing. The quantity of formazan was considered to be directly proportional to the number of viable cells in the culture^[10,11].

LX-2 and HepG2 cells were seeded into 96-well tissue culture plates containing 100 µL DMEM containing 50 mL/L FBS (5000 LX-2 cells/well and 8000 HepG2 cells/well). After 24 h of incubation (37 °C, 50 mL/L CO₂), the medium was carefully removed and 100 µL fresh medium containing various concentrations of Cpd 861 was added into the wells. The cells were treated continuously with Cpd 861 for 1, 2, 3, 5 and 7 d and the medium containing Cpd 861 was changed every other day. At the end of experiments, 20 µL/well of combined MTS/PMS solution was added. After 3 h of incubation at 37 °C in a humidified incubator, the absorbance was analyzed on a VERSAmax microplate reader at 490 nm. Absorbance values were the mean±SE of 3 replicates for each treatment. The cells in only controls and compound controls were included.

RNA isolation and reverse transcription

LX-2 cells were seeded into 60 mm dishes in DMEM containing 50 mL/L FBS. After 3 d of seeding, the medium was carefully removed and fresh medium containing Cpd 861 (0.01 mg/mL) was added. After 24, 48 and 72 h of Cpd 861 treatment, total RNA was extracted from LX-2 cells using TRIzol reagent as the lysis buffer. Complementary DNA (cDNA) was synthesized using oligo (dT)₁₅ primers and M-MLV RT.

Real-time quantitative PCR using SYBR Green I

After the reverse-transcription reaction, cDNA templates were amplified by quantitative real-time PCR. The reaction was performed using the iCycler iQ real-time PCR detection system (Bio-Rad, USA) with SYBR Green I. Human α-SMA and G3PDH (glyceraldehyde-3-phosphate dehydrogenase) primers were designed using Primer 3 software (Table 1).

Each experiment was performed in 25 µL of reaction volume [1.25 µL of 20× SYBR Green, 1 µL of first strand cDNA (50 ng RNA), 2 µL of each 5 nmolar primer, 0.75 U Hotstar Taq DNA polymerase, 2.5 µL of 10× amplification buffer (Mg⁺⁺ free), 2.5 µL of 25 mmol/L MgCl₂, 0.5 µL of 10 mmol/L

solution of four dNTP and 15.1 µL of dH₂O]. In the last tube, 1 µL of ddH₂O was added as a non-template control. The conditions of amplification cycles were as follows: 40 cycles consisting of denaturation at 95 °C for 40 s, annealing at 59 °C (for α-SMA) or at 60 °C (for G3PDH) for 40 s, and extension at 72 °C for 30 s.

The iCycler apparatus was used to measure the fluorescence of each sample in every cycle at the end of the extension^[12]. A series of consecutive 10 fold dilution of α-SMA and G3PDH plasmid DNA ranging from 10⁹ copies/µL to 10³ copies/µL were used as the templates for the standard curves. The iCycler software was used to construct the calibration curve by plotting the Ct (threshold cycle) vs the logarithm of the number of copies for each calibrator. The number of copies in unknown samples was calculated by comparing their Cts with the standard calibration curve. The quality and quantities of samples were normalized based on that of G3PDH.

After PCR, a melting curve was obtained by increasing the temperature from 55 °C to 95 °C with a temperature transition rate of 0.1 °C/s. The melting curves of all final PCR products were analyzed. The differences in melting temperature of PCR products allowed us to distinguish genuine products from nonspecific products, and primer dimers. To ensure that the correct product was amplified in the reaction, all samples were also separated on 20 g/L agarose gel electrophoresis. All PCR conditions and primers were optimized to produce a single product of the correct basepair size.

Table 1 Oligonucleotide PCR primers for human α-SMA and G3PDH

Oligonucleotide	Oligonucleotide primer sequence	Fragment size
α-SMA		
sense	ACT GGG ACG ACA TGG AAA AG	265 bp
antisense	TAG ATG GGG ACA TTG TGG GT	
G3PDH		
sense	ACC CAG AAG ACT GTG GAT GG	125 bp
antisense	TTC AGC TCA GGG ATG ACC TT	

Statistical analysis

Data were expressed as mean±SE. Statistical analysis was performed using GraphPad Prism (version 3.0) software. The *t* test was used for comparison between the groups. *P*<0.05 was considered statistically significant.

RESULTS

Cell proliferation assay

We examined the effects of Cpd 861 on the proliferation of LX-2 and HepG2 cells (Figures 1, 2). Cells were incubated

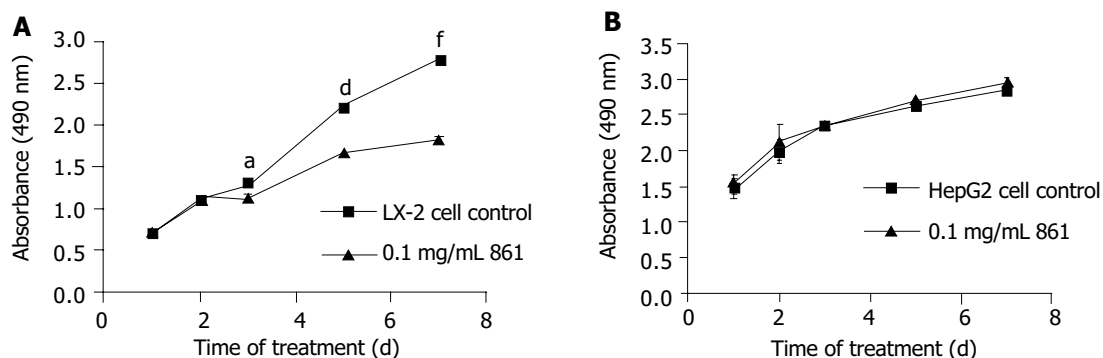


Figure 1 Regulation of proliferation in LX-2 and HepG2 cells by Cpd 861. A: Effect of 0.1 mg/mL Cpd 861 on LX-2 cell proliferation. B: Effect of 0.1 mg/mL Cpd 861 on HepG2 cell proliferation. Data are expressed as the mean±SE of 3 replicates. ^a*P*<0.05 vs LX-2 cell controls after 3 d of incubation. ^d*P*<0.01 vs LX-2 cell controls after 5 d of incubation. ^f*P*<0.01 vs LX-2 cell controls after 7 d of incubation.

with 0.1 mg/mL, 0.03 mg/mL, 0.01 mg/mL and 0.003 mg/mL of Cpd 861 for different days (Figure 1). Cell proliferation was performed by MTS assay. As shown in Figure 2, the effects of Cpd 861 on LX-2 cell proliferation seemed to be correlated with the dose. A significant proliferation inhibition was observed when Cpd 861 concentration was over 0.03 mg/mL (Figure 2). As shown in Figure 1A, 0.1 mg/mL Cpd 861 significantly inhibited LX-2 cell proliferation (15% decrease relative to control, $P < 0.05$) after 3 d of incubation. The inhibition effects seemed to increase with the treatment time (25% decrease after 5 d of incubation and 35% decrease after 7 d of incubation, $P < 0.01$). The inhibition of cell proliferation Cpd 861 at 0.03 mg/mL concentration was also observed on d 3 (15% decrease relative to control) and on d 5 (21% decrease relative to control) (data not shown), and still could be observed on d 7 (18% decrease relative to control) (Figure 2). However, Cpd 861, at 0.01 mg/mL and 0.003 mg/mL concentrations, did not inhibit LX-2 proliferation evidently. The effects of Cpd 861 on LX-2 cell proliferation seemed low at early time points (on day 1 and day 2). We also examined the effects of Cpd 861 on the proliferation of HepG2 cells. As shown in Figures 1B and 2, Cpd 861 did not affect HepG2 cell proliferation.

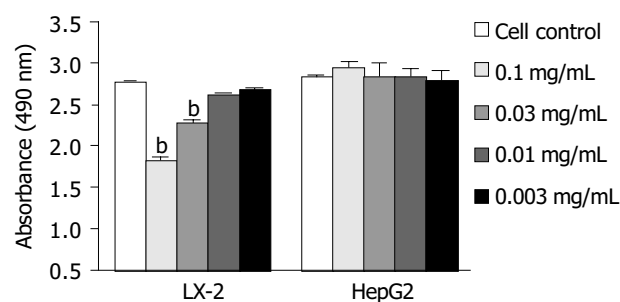


Figure 2 Dose dependent effects of Cpd 861 on cell proliferation in LX-2 and HepG2 7 d after incubation. Data are expressed as the mean \pm SE of 3 replicates. ^b $P < 0.01$ vs LX-2 cell controls.

Quantification of expression of α -SMA mRNA in Cpd 861-treated LX-2 cells

We examined the effect of Cpd 861 on the expression of α -SMA, a phenotypic marker of activated HSCs. The PCR amp/cycle graph and standard curve graph of α -SMA are shown in Figure 3. The standard curve showed a correlation coefficient

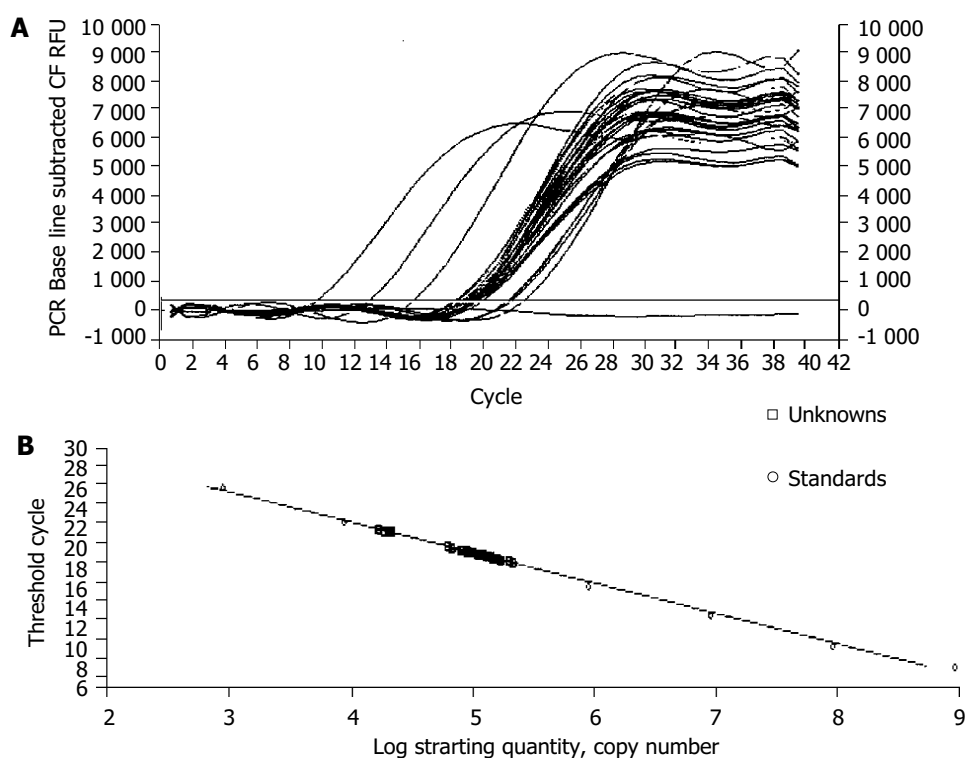


Figure 3 Fluorescence data (A) and standard curve (B) for α -SMA generated on iCycler iQ real-time PCR detection system. Plasmids containing the fragments for α -SMA were diluted from 10^9 to 10^3 copies.

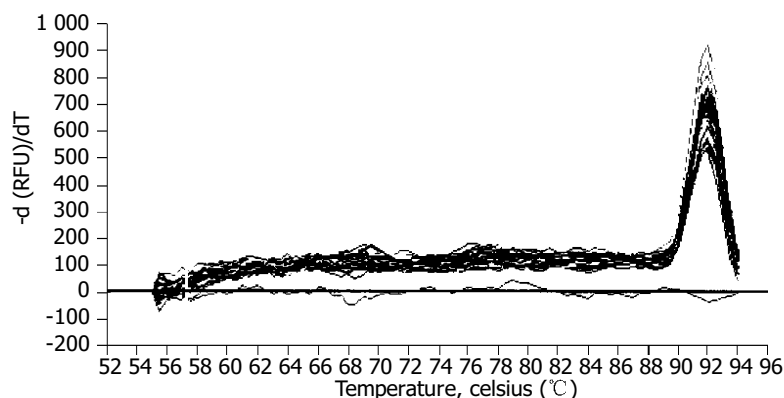


Figure 4 Melting curve for all PCR products after amplification.

>0.99, indicating a precise log-linear relationship. As shown in melt curve graph (Figure 4), single and sharply defined melting curves with narrow peaks were obtained for PCR products of α -SMA gene. Bands visible after electrophoresis on 2% agarose gel and ethidium bromide staining correlated well with the quantitative PCR results. As shown in Figure 5, Cpd 861 could reduce the expression levels of α -SMA in LX-2 cells after treatment. When LX-2 cells were exposed to Cpd 861 for 48 or 72 h, the expression levels of α -SMA decreased significantly (59% decrease relative to control at 48 h, $P < 0.05$, and 60% decrease relative to control at 72 h, $P < 0.01$) (Figure 5).

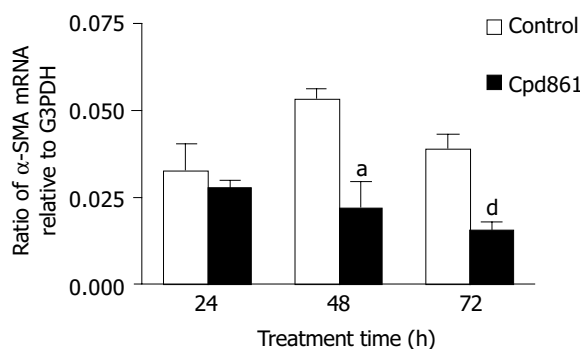


Figure 5 Effects of Cpd 861 on expression of α -SMA mRNA in LX-2 cells. LX-2 cells were incubated with 0.01 mg/mL Cpd 861 for different time. The relative number of molecules of α -SMA mRNA after normalization to G3PDH was calculated. The data represent mean \pm SE of 4 replicates for each treatment. ^a $P < 0.05$ vs LX-2 cell controls after 48 h of incubation. ^d $P < 0.01$ vs LX-2 cell controls after 72 h of incubation.

DISCUSSION

In the liver, activated stellate cells are the key mediators of fibrosis^[4]. During hepatic fibrogenesis, HSCs undergo an activation process, becoming highly proliferative and α -SMA positive myofibroblast-like cells.

Cpd 861 is an effective herbal compound for treatment of patients with hepatic fibrosis^[5]. Its function to effectively reverse hepatic fibrosis has been confirmed by liver biopsies^[5-7]. In other studies, data showed that Cpd 861 also could suppress inflammation and fibrogenesis of the liver tissue^[7, 13, 14] and reduce expression of collagens and fibrosis related cytokines^[14-19]. It could also inhibit rat hepatic stellate cell proliferation in a dose-dependent manner and decrease activation of rat HSCs *in vivo* and *in vitro*^[20,21].

Our results suggested that Cpd 861 could significantly inhibit human hepatic stellate cell LX-2 proliferation in a dose-dependant manner when its concentration was over 0.03 mg/mL. The inhibition function increased obviously with the incubation time. However, the results showed that Cpd 861 did not inhibit HepG2 cell proliferation at the same concentration, indicating that Cpd 861 probably could specifically inhibit hepatic stellate cell proliferation, although further study is needed.

RT-PCR is a technique that has been widely used to quantify physiological changes in gene expression^[22]. However, there is lack of accurate quantification in most of the cases^[22,23]. Real-time PCR techniques developed during the last decade could offer much more accurate and precise quantitation of DNA and RNA^[23,24]. In our study a reliable and accurate real-time PCR method using SYBR Green I technology^[25,26] was taken to measure the effects of Cpd 861 on expression of α -SMA mRNA in LX-2 cells. To quantify the number of molecules of α -SMA mRNA, standard curves were constructed with plasmids containing the fragments for α -SMA and

G3PDH as the templates. A high linearity was observed over a dynamic range of at least 5 orders of magnitude (from 10^9 to 10^3 copies). All PCR conditions and primers were optimized to produce the target products of the correct basepair size just as shown in melt curves. Quantities of α -SMA were expressed as relative ratio to the copy number of G3PDH. The results indicated that the expression levels of α -SMA mRNA decreased significantly when LX-2 cells were exposed to Cpd 861 at 0.01 mg/mL concentration for 48 or 72 h. Although at the same concentration, Cpd 861 did not inhibit LX-2 cell proliferation.

In conclusion, Cpd 861 can significantly inhibit LX-2 proliferation in a dose-dependant manner when its concentration is over 0.03 mg/mL. Additionally, Cpd 861 can reduce the expression levels of α -SMA mRNA in LX-2 cells and this function seems independent of its effects on inhibition of cell proliferation.

ACKNOWLEDGEMENT

We thank Dr. Friedman and Mount Sinai, School of Medicine, for their help in providing the LX-2 cell line.

REFERENCES

- Friedman SL. Molecular regulation of hepatic fibrosis, an integrated cellular response to tissue injury. *J Biol Chem* 2000; **275**: 2247-2250
- Iredale JP. Hepatic stellate cell behavior during resolution of liver injury. *Semin Liver Dis* 2001; **21**: 427-436
- Battaller R, Brenner DA. Hepatic stellate cells as a target for the treatment of liver fibrosis. *Semin Liver Dis* 2001; **21**: 437-451
- Reeves HL, Friedman SL. Activation of hepatic stellate cells - a key issue in liver fibrosis. *Front Biosci* 2002; **7**: d808-826
- Wang BE, Wang TL, Jia JD, Ma H, Duan ZP, Li XM, Li J, Wang AM, Qian LX. Experiment and clinical study on inhibition and reversion of liver fibrosis with integrated Chinese and Western Medicine. *CJIM* 1999; **5**: 6-11
- Yin SS, Wang BE, Wang TL. The effect of Cpd 861 on chronic hepatitis B related fibrosis and early cirrhosis: A randomized, double blind, placebo controlled clinical trial. *Zhonghua Ganzangbing Zazhi* 2004; **12**: 467-470
- Wang TL, Wang BE, Zhang HH, Liu X, Duan ZP, Zhang J, Ma H, Li XM, Li NZ. Pathological study of the therapeutic effect on HBV -related liver fibrosis with herbal compound 861. *Weichangbingxue He Ganbingxue Zazhi* 1998; **7**: 148-153
- Taimr P, Higuchi H, Kocova E, Rippe RA, Friedman SL, Gores GJ. Activated stellate cells express the TRAIL Receptor-2/Death receptor-5 and undergo TRAIL-mediated apoptosis. *Hepatology* 2003; **37**: 87-95
- Cao Q, Mak KM, Ren C, Lieber CS. Leptin stimulates tissue inhibitor of metalloproteinase-1 in human hepatic stellate cells: respective roles of the JAK/STAT and JAK-mediated H2O2-dependant MAPK pathways. *J Biol Chem* 2004; **279**: 4292-4304
- Sutherland MW, Learmonth BA. The tetrazolium dyes MTS and XTT provide new quantitative assays for superoxide and superoxide dismutase. *Free Radic Res* 1997; **27**: 283-289
- Dunigan DD, Waters SB, Owen TC. Aqueous soluble tetrazolium/formazan MTS as an indicator of NADH- and NADPH-dependent dehydrogenase activity. *Biotechniques* 1995; **19**: 640-649
- Stagliano KE, Carchman E, Deb S. Real-time polymerase chain reaction quantitation of relative expression of genes modulated by p53 using SYBR Green I. *Methods Mol Biol* 2003; **234**: 73-91
- Zhang FK, Wang BE, Wang TL, Jia JD, Dong Z, Zhang J. Effect of different pharmaceuticals of herbal compound 861 on experimental liver fibrosis. *Zhonghua Zhongxiyi Jiehe Zazhi* 2000; **10**: 15-16
- Jia JD, Wang BE, Dong Z, Cui L, Zhu JX, Che JT. The effect of herbal compound 861 on mRNA levels for type I, III, and IV collagens and TGF- β in immune complex rat liver fibrosis. *Zhonghua Ganzangbing Zazhi* 1996; **4**: 214-216
- Ma H, Wang BE, Ma XM, Jia JD. Effect of herbal compound

- 861 on rat hepatic stellate cell collagen synthesis and degradation *in vitro*. *Zhonghua Ganzangbing Zazhi* 1999; 7(Suppl): 30-32
- 16 **Ding HG**, Tang SZ, Wang BE, Jia JD, Zhao CH. Effects of herbal compound 861 in hepatic stellate cell expressing endothelin-1 protein and mRNA. *Zhonghua Ganzangbing Zazhi* 2003; 11: 308
- 17 **Yin CH**, Ma H, Wang AM, Ma XM, Jia JD, Wang BE. Effect of compound 861 on tissue inhibitor of metalloprotease 1 gene expression of HSC-T6 cells. *Zhonghua Ganzangbing Zazhi* 2002; 10: 197-199
- 18 **Ding HG**, Wang BE, Shang HW. Effect of herbal compound 861 on expression and activity of nitric oxide synthase in hepatic stellate cells. *Zhonghua Zhongxiyi Jiehe Zazhi* 2002; 22: 362-364
- 19 **Yin CH**, Ma H, Wang AM, Ma XM, Jia JD, Wang BE. Effect of compound 861 on stromelysin gene expression of HSC-T6 cell. *Linchuang Ganzangbing Zazhi* 2002; 18: 168-170
- 20 **You H**, Wang EN, Wang TL, Ma XM, Zhang J. Proliferation and apoptosis of hepatic stellate cells and effects of compound 861 on liver fibrosis. *Zhonghua Ganzangbing Zazhi* 2000; 8: 78-80
- 21 **Ma H**, Wang BE, Ma XM, Jia JD. Effect of compound 861 on hepatic stellate cell proliferation and collagen synthesis. *Zhongguo Linchuang Yaolixue Yu Zhilixue Zazhi* 1998; 3: 172-175
- 22 **Wall SJ**, Edwards DR. Quantitative reverse transcription-polymerase chain reaction (RT-PCR): a comparison of primer-dropping, competitive, and real-time RT-PCRs. *Anal Biochem* 2002; 300: 269-273
- 23 **Pérez C**, Vandesompele J, Vandenbroucke I, Holtappels G, Speleman F, Gevaert P, Cauwenberge PV, Bachert C. Quantitative real time polymerase chain reaction for measurement of human Interleukin - 5 receptor alpha spliced isoforms mRNA. *BMC Biotechnol* 2003; 3: 17-23
- 24 **Ginzinger DG**. Gene quantification using real-time quantitative PCR: an emerging technology hits the mainstream. *Exp Hematol* 2002; 30: 503-512
- 25 **Ponchel F**, Toomes C, Bransfield K, Leong FT, Douglas SH, Field SL, Bell SM, Combaret V, Puisieux A, Mighell A, Robinson PA, Inglehearn CF, Isaacs JD, Markham AF. Real-time PCR based on SYBR-Green I fluorescence: An alternative to the TaqMan assay for a relative quantification of gene rearrangements, gene amplifications and micro gene deletions. *BMC Biotechnol* 2003; 3: 18-31
- 26 **Ramos-Payan R**, Aguilar-Medina M, Estrada-Parra S, Gonzalez-Y-Merchand JA, Favila-Castillo L, Monroy-Ostria A, Estrada-Garcia IC. Quantification of cytokine gene expression using an economical real-time polymerase chain reaction method based on SYBR Green I. *Scand J Immunol* 2003; 57: 439-445

Edited by Kumar M and Wang XL. Proofread by Xu FM

Tegaserod inhibits noxious rectal distention induced responses and limbic system c-Fos expression in rats with visceral hypersensitivity

Hong-Mei Jiao, Peng-Yan Xie

Hong-Mei Jiao, Peng-Yan Xie, Department of Gastroenterology, First Hospital of Peking University, Beijing 100034, China

Correspondence to: Peng-Yan Xie, Department of Gastroenterology, First Hospital of Peking University, Beijing 100034, China. pengyanx2002@yahoo.com

Telephone: +86-10-66551122 Ext. 2581

Received: 2004-03-15 **Accepted:** 2004-04-17

Abstract

AIM: To examine the effects of tegaserod, a serotonin (5-HT) 4 receptor partial agonist, on abdominal withdrawal reflex (AWR) to rectal distention (RD) and c-Fos expression in limbic system.

METHODS: Neonatal Sprague-Dawley rats randomly received colonic irritation by acetic acid from postnatal day 8 to d 21 as a visceral hypersensitive model (group H) or by intrarectal saline as a control group (group C). When they became adults, rectal distention (RD) was performed by a balloon (6F; Fogarty arterial embolectomy catheter; length, 20 mm; diameter, 2 mm) which was rapidly inflated with increasing volumes of saline (0.4, 0.8 and 1.2 mL) for 20 s at five-minute intervals. Five subgroups of group H (H-saline, H-vehicle, H-Teg0.1, H-Teg0.3 and H-Teg1.0) were injected randomly with saline, vehicle (1-methyl-2-thpyrrolidone) or tegaserod at doses of 0.1, 0.3 and 1.0 mg/kg ip, respectively. Two subgroups of group C (C-Saline and C-Teg1.0) were injected with saline or tegaserod (1.0 mg/kg) ip. RD was performed 10 min after injection, AWR was recorded and c-Fos expression in limbic system was analyzed quantitatively by immunohistochemistry.

RESULTS: Compared to saline, tegaserod significantly inhibited AWR in group H (0.4 mL: from 2.0 to 0.5; 0.8 mL: from 3.5 to 1.5; 1.2 mL: from 4.0 to 3.0, $P < 0.01$), but had no significant effect on group C. Tegaserod dose-dependently attenuated the number of c-Fos positive neurons in limbic structures, anterior cingulate cortex (ACC) showed the greatest attenuation. In group H, tegaserod (1.0 mg/kg) resulted in a significant overall decrease to 57% of H-saline (283 ± 41 vs 162 ± 16 , $P < 0.01$), in ACC to 42% of H-saline (72 ± 10 vs 31 ± 8 , $P < 0.01$). In group C, tegaserod (1.0 mg/kg) resulted in an overall decrease to 77% of C-saline (214 ± 13 vs 164 ± 22 , $P < 0.01$), in ACC to 65% of C-saline (48 ± 8 vs 31 ± 7 , $P < 0.01$).

CONCLUSION: Tegaserod inhibits the response to rectal distention in rats with visceral hypersensitivity and dose-dependently attenuates c-Fos expression in limbic system, especially in anterior cingulate cortex.

Jiao HM, Xie PY. Tegaserod inhibits noxious rectal distention induced responses and limbic system c-Fos expression in rats with visceral hypersensitivity. *World J Gastroenterol* 2004; 10(19): 2836-2841

<http://www.wjgnet.com/1007-9327/10/2836.asp>

INTRODUCTION

Irritable bowel syndrome (IBS) is a common disorder characterized by abdominal pain and altered bowel habits, consisting of constipation, diarrhea, or both. Several pathophysiological mechanisms have been suggested to play a role in the genesis of symptoms in patients with IBS, among others visceral hypersensitivity, autonomic nervous system dysregulation^[1], alterations of gastrointestinal (GI) motility^[2], and abnormalities in neurotransmitter systems^[3]. It has been shown that at least a subgroup of IBS patients shows a hyperalgesic response to visceral stimuli, and discomfort in response to colorectal balloon distension under experimental conditions^[3,4]. Abnormalities which upregulate afferent (sensory) signal intensity anywhere in the "brain-gut axis" could induce visceral hypersensitivity^[5].

It has been shown in experimental rats that rectal distention is a non-invasive, reproducible visceral stimulus, which can induce a range of pseudoaffective responses, including vasomotor, visceromotor, and respiratory responses^[3]. Abdominal withdrawal reflex (AWR) is an involuntary motor reflex similar to the visceromotor reflex^[6]. Intestinal distention can be considered to as an appropriate stimulus for studies of visceral nociception^[7].

In previous studies, it has been shown that noxious distention of hollow viscera induces a specific pattern of c-Fos expression in rat limbic brain structures^[3,8], which involved in higher cognitive functions (*i.e.* emotion, memory, motivation) and led to the perception of visceral pain^[9]. Induction of c-Fos expression is a well established marker of neuronal activation, and immunohistological detection of c-Fos-like immunoreactivity allows a mapping of activated brain nuclei on a single cell level^[3].

Serotonin (5-HT) is thought to play a role in visceral nociceptive mechanisms. There is considerable evidence that serotonin is involved in the regulation of motility and sensation in the gut^[3]. In animal studies, tegaserod was reported to inhibit abdominal contraction response to noxious intestinal distention^[10]. Tegaserod, a 5-HT₄ receptor partial agonist, could relieve symptoms in irritable bowel syndrome patients with abdominal pain, bloating and constipation^[11]. However, little is known about the effect of tegaserod on neuronal activity in limbic structures at noxious rectal distention. Therefore, in the present study, we established a rat model to investigate the role of 5-HT₄ receptors in mediating activation of limbic structures at rectal distention, as assessed by c-Fos expression. We aimed to establish a mechanism of the action of 5-HT₄ receptors specific to visceral nociceptive neurotransmission.

MATERIALS AND METHODS

Animals

Experiments were performed using Sprague-Dawley rats obtained as preweaning neonates (younger than 8 d) from the Animal Center in the First Hospital of Peking University. Rats were housed in plastic cages containing corn chip bedding and maintained on a 12:12-h light-dark cycle (lights on at 7 AM) at 22 to 23 °C and in 60-65% humidity. The irritation procedure and the experimental testing were conducted during the light component of the cycle. The neonates were housed

12 in a cage with their mothers until they were 25 d old. Mothers had access to food and water *ad libitum*. After separation, the rats were housed 4 in a cage with access to food and water *ad libitum*. The animals were deprived of food but water 18 h before rectal distention (RD). Animal care and experimental procedures were followed institutional ethics guidelines and conformed to the requirements of the State Authority for Animal Research Conduct.

Weight

Each rat was weighed every 3 d from days 9 to 40.

Colon irritation

Neonatal Sprague-Dawley rats (8 d old) were divided into 2 groups (group C: control and group H: hypersensitivity) undergoing different treatments. Forty-eight rats in group H received intracolonic injections of 5 mL/L acetic acid (0.5 mL) daily between the ages of 8 and 21 d. Acetic acid was injected into the colon via the PE90 tube inserted to 2 cm from the anus. Twenty-four rats in group C received intracolonic injections of 9 g/L saline (0.5 mL) daily between the ages of 8 and 21 d^[12].

Drug administration protocol

Because tegaserod (HTF 919; Novartis Pharma AG, Basel, Switzerland) is poorly soluble in water, the fractions were made up using 0.1 mL of 1-methyl-2-pyrrolidinone (vehicle)^[10]. After dissolved in the vehicle, distilled water was added to make the solution up to 0.5 mL. According to the drugs injected intraperitoneally 10 min before RD, 48 rats in group H were divided into 6 subgroups (H0, H-saline, H-vehicle, H-Teg0.1, H-Teg0.3, and H-Teg1.0), and 24 rats in group C were divided into 3 subgroups (C0, C-saline, and C-Teg1.0), eight rats in each subgroup. Rats in group C-saline and H-saline were injected with saline (0.5 mL), in group C-Teg1.0 with tegaserod (1.0 mg/kg), in group H-vehicle with vehicle (0.1 mL and distilled water 0.4 mL) and in group H-Teg0.1, H-Teg0.3, and H-Teg1.0 with tegaserod at a dose of 0.1, 0.3 or 1.0 mg/kg, respectively. Groups H0 and C0 were not distended and only histological examination and myeloperoxidase (MPO) activity assay were done.

Histological examination and myeloperoxidase (MPO) activity assay

Three weeks after cessation of the irritation protocol, in groups H0 and C0, the distal 4–5 cm of the descending colon and rectum was removed and histological analysis and MPO activity assay were performed. MPO activity assay was performed as described previously^[13,14]. MPO activity was expressed as U/g protein.

Behavioral testing^[6,12]

Behavioral responses to RD were assessed in all groups 3 wk after cessation of the irritation protocol by measuring the abdominal withdrawal reflex (AWR) using a semiquantitative score. AWR is an involuntary motor reflex similar to the visceromotor reflex. However, the advantage of AWR over the visceromotor reflex is that the latter requires additional surgery to implant recording electrodes and wires in the abdominal muscles, which may cause additional sensitization in an already sensitized system. Distention balloons (described below) were placed in the rectum of lightly sedated adult rats (ether) and secured by taping the attached tube to the rat's tail. The rats were then housed in small Lucite cubicles (20 cm×8 cm×8 cm) on an elevated Plexiglas platform and allowed to wake up and adapt (20 min). Measurement of the AWR consisted of visual observation of animal response to graded RD (0.4, 0.8 and 1.2 mL) by blinded observers and assignment of AWR scores: 0, no behavioral response to RD; 1, brief head movement followed by immobility; 2, contraction of abdominal muscles; 3, lifting of

abdomen; 4, body arching and lifting of pelvic structures. The rats were given RD for 20 s every 5 min. To achieve an accurate measure, distensions were repeated 5 times for each volume. The data for each animal were averaged for analysis. The results obtained were compared among groups. A change in the magnitude of an evoked response indicated a change in visceral pain processing.

Colon stimuli^[12]

Colon stimulation consisted of graded RD produced by inflating a balloon inside the rectum. The balloon, 2 cm in length and 2 mm in diameter (6F, Fogarty arterial embolectomy catheter, Baxter, USA), was carefully inserted intrarectally and fixed at a distance of 1 cm with an adhesive tape at the tail of the rat. Distension was produced by rapidly inflating the balloon to the desired volumes with saline (0.4, 0.8 or 1.2 mL) for 20 s at 5-min intervals. Before they were used, the balloons were blown up and left overnight so the latex stretched and the balloons became compliant. Tegaserod (0.1, 0.3 or 1.0 mg/kg) or saline or vehicle was administered 10 min prior to RD. Only a single dose was tested in each animal.

c-Fos immunohistochemistry^[15]

Within 30 min following the end of the distention procedure, the animals were deeply anesthetized with an overdose of sodium pentobarbitone (60 mg/kg intraperitoneally) and then perfused through the ascending aorta with saline (9 g/L), followed by 500 mL of cold 0.1 mol/L phosphate buffer (PB, 4 °C) containing 40 g/L paraformaldehyde (pH 7.4). The brain was immediately removed and postfixed in the same fixative at 4 °C overnight, and then placed in 300 g/L sucrose with 0.1 mol/L PB for 72 h at 4 °C. Coronal sections (40 µm thick) were cut from frozen blocks at the levels of brain regions of interest (1.5 mm to 5 mm posterior to bregma, according to the atlas of Paxinos and Watson). Every fifth section was stained for c-Fos-like immunoreactivity (c-Fos-ir) using the method of free floating for immunohistochemistry. Briefly, sections were first washed 3 times in phosphate buffered saline plus 3 g/L Triton X-100 (PBS-T) (5 min each time) at room temperature, and incubated for 10 min with PBS-T containing 50 mL/L normal goat serum to block nonspecific binding sites and facilitate tissue penetration. Then sections were washed with PBS-T and incubated for 24 h at room temperature with PBS-T containing rabbit polyclonal anti-Fos protein antiserum (Zhongshan, China) (diluted 1:200). After washed with PBS-T, sections were incubated with biotinylated anti-rabbit IgG (1:300, Zhongshan, China) for 120 min. The sections were then incubated with strepta-vidin-peroxidase conjugate (1:300) for 120 min and subsequently visualized using diaminobenzidine (DAB) as chromogen. Sections were mounted on gelatin-coated glass slides, air dried, dehydrated in ethanol, and xylene, then coverslipped with DePeX. Brain sections were examined using bright-field microscopy. The same lot of antibody was used for each study outlined below. The primary c-Fos antibody was omitted in one well of each immunohistological reaction as a negative control. In each study, every staining process included free-floating sections of all groups using the same buffers and solutions.

Fos-like immunoreactive nuclei

The number of c-Fos-like immunoreactive (c-Fos-ir) nuclei was counted in 5 sections of each rat as identified by morphology using an image analysis package (Leica Q550CW running QWIN software; Leica UK Ltd, Milton Keynes, UK). In the anterior cingulate cortex (ACC), thalamus (TH), hippocampus (HP), hypothalamus (HypoTH) and amygdala (Amy), c-Fos-ir nuclei were counted individually and expressed as the number per 600×500 pixel. All brain regions were counted bilaterally in

each section. The total number of c-Fos-ir nuclei in five sections was used for subsequent data analysis. The counts comprising all those nuclear immunoreactive signals could be clearly distinguished from the background.

Data and statistical analysis

Statistical analysis was done using SPSS for windows 11.0. The results of weight, MPO activity and the number of c-Fos-ir were expressed as mean±SD, and statistical significances were determined using Student's paired *t* test or one way analysis of variance (ANOVA), followed by Dunnett's post hoc test. The median values of the AWR scores among all groups at each volume of RD were compared using the Mann-Whitney *U*-test. *P*<0.05 was considered statistically significant.

RESULTS

Comparison of body masses of rats in each group

Masses on d 9 and 40 were not statistically different between groups H and C (18.9±3.2 g vs 19.6±3.2 g, 154.4±12.7 g vs 149.3±16.5 g, respectively). The model did not alter the growth rate of the rats.

Histological analysis and MPO activity assay

The identifiable histopathology was absent in the adult colons. The tissues showed no significant structural damage or loss of crypts. Mucin depletion or increase in intraepithelial lymphocytes was not seen in any of the tissues examined. MPO activity was not statistically different between groups H and C (20.49±1.64 U/g protein and 17.49±6.35 U/g protein, respectively).

Table 1 AWR scores in group H (median, min-max) (*n* = 8)

	0.4 mL	0.8 mL	1.2 mL
H-saline	2.0 (1-3)	3.5 (3-4)	4.0 (4-4)
H-vehicle	2.0 (0-3)	3.0 (2-4)	4.0 (3-4)
H-Teg0.1	1.0 (0-2) ^b	2.0 (1-3) ^{a, b}	3.0 (3-4) ^{a, b}
H-Teg0.3	1.0 (0-1) ^b	1.5 (0-3) ^b	3.0 (3-4) ^{a, b}
H-Teg1.0	0.5 (0-1) ^b	1.5 (1-2) ^b	3.0 (1-3) ^b

^b*P*<0.01 vs H-saline; Difference between H-Teg0.1 and H-Teg0.3 was not significant at all volumes; ^a*P*<0.05 H-Teg0.1, H-Teg0.3 vs H-Teg1.0.

Table 2 AWR scores in group C (median, min-max, *n* = 8)

	0.4 mL	0.8 mL	1.2 mL
C-saline	1.0 (0-2)	2.5 (2-3)	3.0 (3-4)
C-Teg1.0	0.0 (0-2)	2.0 (2-2)	3.0 (3-4)
Z value	1.465	2.236	0
P value	0.195	0.105	1.000

The differences between C-saline and C-Teg1.0 were not significant at all volumes.

Comparison of tegaserod effects on AWR (Tables 1, 2)

H-saline vs C-saline Median AWR scores at volumes of 0.4, 0.8, and 1.2 mL were significantly higher in H-saline than in C-saline (2.0, 3.5, and 4.0, vs 1.0, 2.5, and 4.0, respectively) (*P*<0.05). These results suggested that the model of visceral hypersensitivity in this study was reliable (Figure 1A).

AWR in subgroups of group H Median AWR scores were similar in H-saline and in H-vehicle, so the effect of vehicle could be negligible. AWR scores were significantly higher in H-saline than in H-Teg0.1, H-Teg0.3, and H-Teg1.0. The 5-HT₄ receptor agonist tegaserod (0.1, 0.3, and 1.0 mg/kg) significantly inhibited

the response to rectal distention in rats with hypersensitivity (*P*<0.01). The difference between H-Teg0.1 and H-Teg0.3 was not significant at all volumes. The difference between H-Teg0.1 and H-Teg1.0 was significant at the volumes of 0.8 mL and 1.2 mL (*P*<0.05). The difference between H-Teg0.3 and H-Teg1.0 was significant only at 1.2 mL (*P*<0.05). At the volume of 0.4 mL, differences of AWR scores in H-Teg0.1, H-Teg0.3, and H-Teg1.0 were not significant (Figure 1B, Table 1).

C-saline vs C-Teg1.0 Median AWR scores were similar in C-saline and in C-Teg1.0 at all volumes. These results suggested that tegaserod (1.0 mg/kg) had little effect on the AWR response to RD in control rats (Figure 1C, Table 2).

C-Teg1.0 vs H-Teg1.0 At 1.2 mL, AWR scores were higher in C-Teg1.0 than in H-Teg1.0 (*P*<0.05). While at 0.4 mL and 0.8 mL, the differences between H-Teg1.0 and C-Teg1.0 were not significant. It seemed that the inhibitory effect on AWR at largest volume (1.2 mL) was stronger in hypersensitive condition than in normal condition (Figure 1D).

Table 3 Number of c-Fos positive neurons in limbic structures in group H (mean±SD, *n* = 8)

	ACC	Hippocampus	HypoTH	Amygdala	Thalamus	Overall
H-saline	72±10	54±13	51±17	44±16	62±19	283±41
H-vehicle	72±10	54±13	49±15	43±15	62±19	281±37
H-Teg0.1	53±14 ^b	48±10	47±13	42±11	50±13	239±31 ^a
H-Teg0.3	40±11 ^b	45±7	41±11 ^a	37±11	45±11 ^a	208±25 ^b
H-Teg1.0	31±8 ^b	36±9 ^b	31±10 ^b	30±8 ^b	34±10 ^b	162±16 ^b
F value	60.583	11.605	8.199	5.362	14.574	61.989
P value	0.000	0.000	0.000	0.000	0.000	0.000

^a*P*<0.05, ^b*P*<0.01 vs H-saline.

Table 4 Number of c-Fos positive neurons in limbic structures in group C (mean±SD, *n* = 8)

	ACC	Hippocampus	HypoTH	Amygdala	Thalamus	Overall
C-saline	48±8	46±7	36±8	39±7	45±11	214±13
C-Teg1.0	31±7 ^b	36±8 ^b	30±9	33±10	34±7 ^a	164±22 ^b

^a*P*<0.05, ^b*P*<0.01 vs C-saline.

Comparison of tegaserod effects on c-Fos expression in limbic structures (Tables 3, 4)

Repetitive RD significantly induced changes in neuronal activity in all animals, as determined by increased density of c-Fos-ir cells (Figure 2). c-Fos expression was located bilaterally in discrete areas of limbic structures. The overall number of c-Fos-ir cells in H-saline was significantly more than that in C-saline (283±41 vs 214±13, *P*<0.001), but the difference was not significant in hippocampus (54±13 vs 46±7, *P* = 0.374). Tegaserod given ip 10 min prior to RD produced a significant, dose-dependent attenuation in the total number of c-Fos-ir nuclei in limbic brain compared with saline. These effects were especially clear in anterior cingulate cortex (ACC). In the hippocampus and amygdala, the effect of tegaserod was significant only at the high-dose (1.0 mg/kg). Tegaserod (0.1 mg/kg) decreased the overall c-Fos-ir to 85% of saline (*P*<0.05). The greatest attenuation was in ACC (74% of H-saline), while amygdala was least affected (95% of H-saline). Tegaserod (0.3 mg/kg) significantly attenuated c-Fos expression in ACC, hypothalamus, and thalamus (to 56%, 80% and 73% of saline, respectively). A high dose of tegaserod (1.0 mg/kg) resulted in a significant (*P*<0.01) overall decrease of c-Fos in five areas, the overall number was decreased to 57% of saline. Similar to the low dose, ACC showed the greatest attenuation (42% of H-saline), while other regions were decreased to approximately 60% of H-saline (Figure 3A).

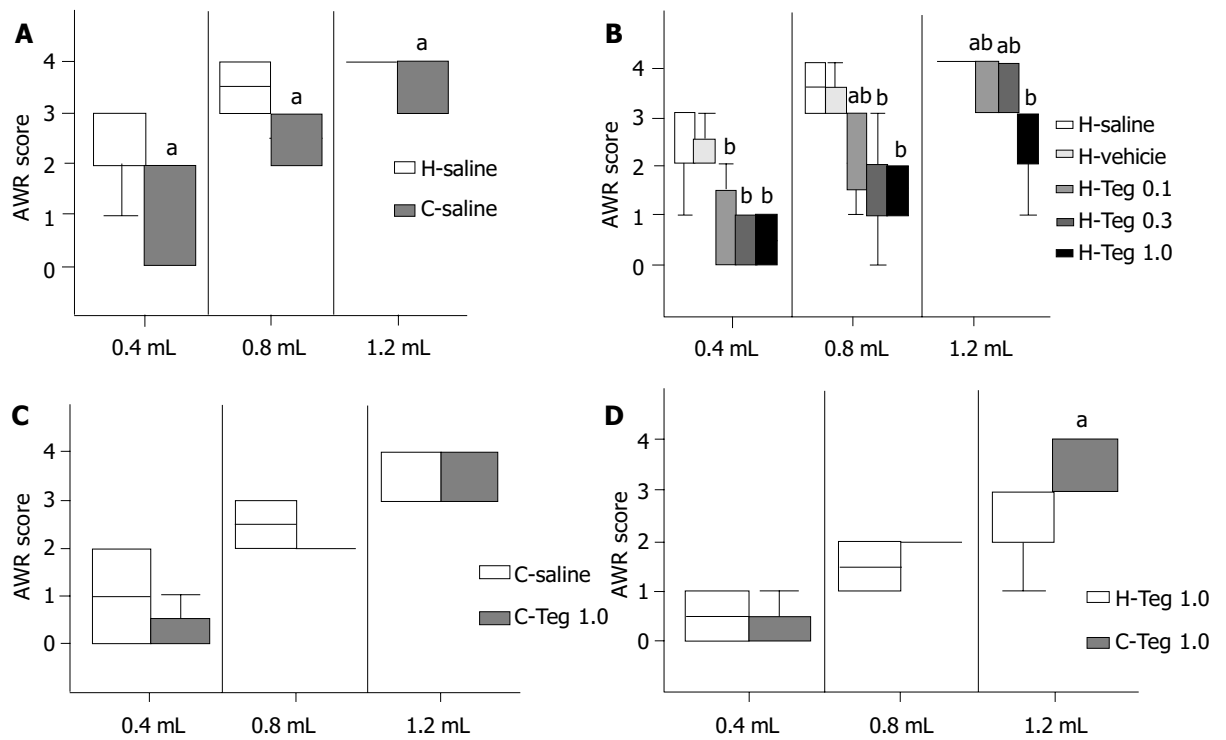


Figure 1 AWR scores of H-saline and C-saline, group H, group C, H-Teg1.0 and C-Teg1.0, ^a $P < 0.05$; ^b $P < 0.01$. A: AWR scores of H-saline and C-saline. B: AWR scores of group H. C: AWR scores of group C. D: AWR scores of H-Teg1.0 and C-Teg1.0.

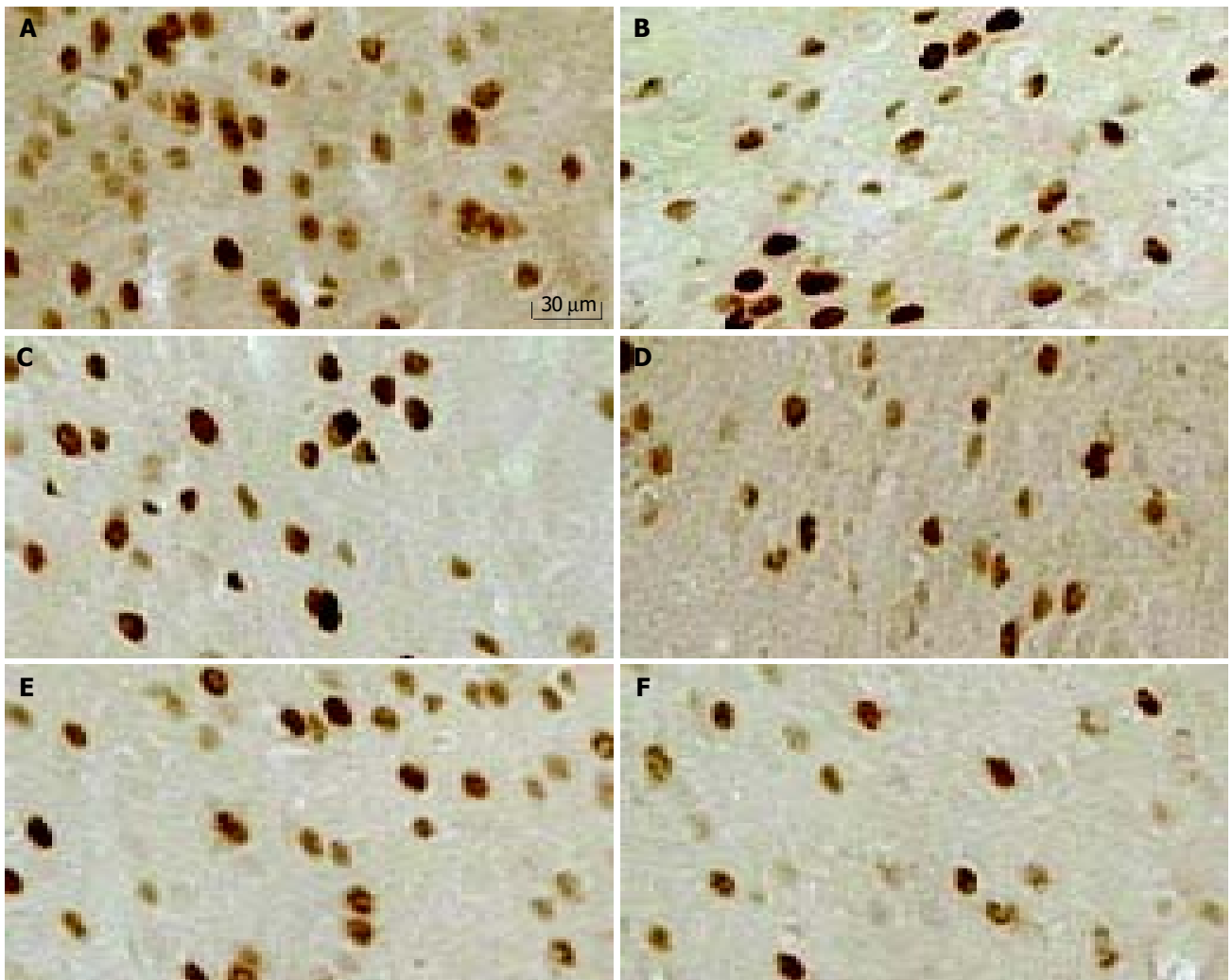


Figure 2 c-Fos-ir nuclei in anterior cingulate cortex (ACC) (200 \times). A: H-saline; B: H-Teg0.1; C: H-Teg0.3; D: H-Teg1.0; E: C-saline; F: C-Teg1.0.

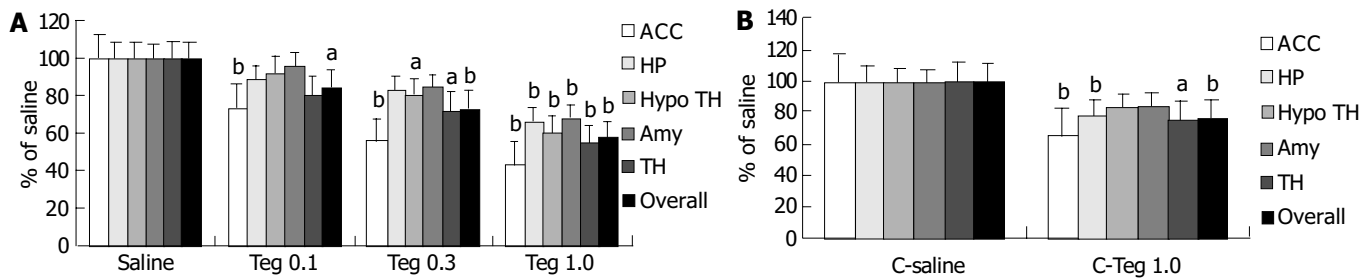


Figure 3 Number of overall c-Fos-ir nuclei and in each of the 5 areas as a percent of H-saline and C-saline. A: Number of overall c-Fos-ir nuclei and in each of the 5 areas as a percent of H-saline. B: Number of overall c-Fos-ir nuclei and in each of the 5 areas as a percent of C-saline.

In group C, although the inhibitory effect of tegaserod on AWR was not significant, the attenuation effect on c-Fos expression was also observed. Tegaserod (1.0 mg/kg) resulted in a significant overall decrease in c-Fos to 77% of C-saline. Similarly, ACC also was the greatest attenuation (65% of C-saline). In addition, tegaserod could decrease c-Fos in thalamus and hippocampus (76% and 78% of C-saline, respectively) (Figure 3B).

DISCUSSION

Experimental data suggested that patients with IBS had visceral sensory dysfunction so that physiological stimuli could induce their symptoms. Visceral afferent input is modulated by a variety of mechanisms operating between the gastrointestinal tract and the brain, and dysfunction of these regulatory mechanisms could distort gastrointestinal perception^[16]. Intestinal discomfort reaches awareness via neural connections termed the “brain-gut axis”. Abnormalities which upregulate afferent (sensory) signal intensity anywhere in this system could induce hypersensitivity, pain, and discomfort. Several features of IBS suggest involvement of the brain’s emotional limbic system, such as higher prevalence of anxiety and psychosocial stressors, augmented intestinal and stress responses and response to centrally acting medication. Recent brain imaging data suggested that pathways involved in visceral pain perception overlapped with limbic pathway^[17,18]. In the brain, increased thalamic activation has been seen in IBS, which could indicate increased afferent output from lower levels. Activation of the anterior cingulate cortex, the limbic center that encodes pain suffering, appeared to be enhanced in IBS, especially under the influence of anxiety^[5].

Colonic irritation with acetic acid in neonatal rats could lead to a state of chronic visceral hypersensitivity in adults^[19-21]. This model did not alter the growth rate of the rats. This hypersensitivity occurs in the absence of identifiable histopathology in the adult colon and does not change MPO activity of colonic tissue. Myeloperoxidase (MPO), a hydrogen peroxide (H₂O₂) oxidoreductase, is specifically found in mammalian granulocytic leukocytes, including polymorphonuclear leukocytes (PMNs), monocytes, basophils and eosinophils. MPO activity has been widely accepted as an enzyme marker to measure and quantitate the PMN content in a variety of tissues. It has been suggested that measurement of MPO provides a simple and specific method to quantitate PMN accumulation or infiltration in a variety of pathological processes accompanied with inflammation^[22].

5-HT₄ receptors have been found to be involved in regulating the sensitivity of rectal mechanoreceptive afferents^[23]. Tegaserod is a 5-HT₄ receptor partial agonist with a relatively long half-life (approximately 11 h in dogs and humans)^[24]. It could dose-dependently inhibit the abdominal contraction response to noxious intestinal distention not linked to alterations in compliance^[10]. In our study, in rats with hypersensitivity but

not in control rats, tegaserod potently inhibited AWR at all volumes of distention. It seemed that the inhibitory effect on AWR at the highest volume (1.2 mL) was more powerful in hypersensitive condition than in normal condition. The results are inconsistent with the study of Coelho *et al.*^[10]. Two reasons may have been responsible for these phenomena. One reason might be that the patterns of intestinal distention were different. In the study of Coelho *et al.*, the balloon was an inflated 5 min step of 15 mmHg, from 0 to 60 mmHg. The other reason might be that 5-HT₄ receptors played a relatively modest role in modulating visceral sensation under basal physiological condition^[25]. Thus, we tentatively suggest that the number of 5-HT₄ receptors may be upregulated and/or the effect followed by the activity of 5-HT₄ receptor may be increased under hypersensitive status. The exact mechanisms of its action need to be further researched.

c-fos, an immediate-early gene, could be expressed within the neurons following voltage-gated calcium entry into the cells^[26]. *c-fos* was induced by noxious stimulus, generally as the result of an injury^[27]. *c-Fos* protein encoded by *c-fos*, has been regarded as a third messenger molecule which couples the short term extracellular signals with the long term alteration in cell function when neurons are excited^[28]. *c-Fos* could be interpreted as an increase in activity of those neurons expressing the protein^[27], so it is usually used as a marker to indicate the activation of neurons^[29]. Following injury there was a correlation between the expression of *c-Fos* and magnitude of hyperalgesia, and *c-Fos* expression following noxious intensities of intestinal distention could reflect the intensity of stimuli and the degree of discomfort^[27]. Previous study has demonstrated that *c-Fos* is expressed in limbic brain structures in response to noxious rectal distention^[9]. Limbic structures play an important role in visceral pain processing. The present report provided quantitative data on expression of *c-Fos* protein induced by rectal distention and the effect of tegaserod at different doses on *c-Fos* expression in brain nuclei, such as hypothalamus, thalamus, amygdala, hippocampus, and anterior cingulate cortex following noxious rectal distention. Functional brain imaging researches have demonstrated that colorectal distention could cause abnormal activation in ACC^[17] and thalamus in IBS patients compared with control^[17,18]. From our results, we conclude that tegaserod dose-dependently attenuates *c-Fos* expression in limbic structures. Especially in ACC and thalamus, the effect of tegaserod is more evident. This may do good for IBS patients.

5-HT₄ receptors are widely distributed in peripheral and central sites. In gut, 5-HT₄ receptors are located primarily on the enterochromaffin cells and less on smooth muscle cells, enterocytes, and neurons^[24]. 5-HT₄ receptors are highly expressed in several brain regions, such as limbic areas, periaqueductal grey matter and sensory terminals^[30] and in spinal cord and dorsal root ganglion neurons^[25]. The site of action of tegaserod was not established in the present study, but could be at the level of enteric or primary sensory neurons,

or via spinal or supraspinal neuronal circuits concerned with the modulation of nociceptive transmission. A study by Schikowski *et al.*^[23] demonstrated that tegaserod might have a direct effect on the mechanoreceptive afferents. We supposed that 5-HT₄ receptors might directly decrease the signals ascending to the central nervous system (CNS) or might decrease the activity of CNS (as demonstrated by c-Fos-ir nuclei), which would benefit for IBS patients. Little is known about the effect of tegaserod on response following intracerebroventricular injection. Further studies are needed to determine the central action of 5-HT₄ receptors.

In conclusion, tegaserod inhibits response to noxious distention, and the effect is more evident in hypersensitive condition than in control. Tegaserod dose-dependently attenuates c-Fos expression in limbic structures, especially in anterior cingulate cortex. Therefore, tegaserod decreases central sensitization. Tegaserod may be of potential use in the treatment of visceral pains.

ACKNOWLEDGMENTS

The authors are grateful to Professor Xin-Guang Liu and Hua-Hong Wang for advice, and to Novartis Pharmaceuticals Corp for providing the drugs for this study.

REFERENCES

- 1 **Tougas G.** Irritable bowel syndrome: new approaches to its pharmacological management. *Can J Gastroenterol* 2001; **15** (Suppl B): 12B-13B
- 2 **Monnikes H, Tebbe JJ, Hildebrandt M, Arck P, Osmanoglou E, Rose M, Klapp BF, Wiedenmann B, Heymann-Monnikes I.** Role of stress in functional gastrointestinal disorders. Evidence for stress-induced alterations in gastrointestinal motility and sensitivity. *Dig Dis* 2001; **19**: 201-211
- 3 **Monnikes H, Ruter J, König M, Grote C, Kobelt P, Klapp BF, Arnold R, Wiedenmann B, Tebbe JJ.** Differential induction of c-fos expression in brain nuclei by noxious and non-noxious colonic distension: role of afferent C-fibers and 5-HT₃ receptors. *Brain Res* 2003; **966**: 253-264
- 4 **Miura M, Lawson DC, Clary EM, Mangel AW, Pappas TN.** Central modulation of rectal distension-induced blood pressure changes by alosetron, a 5-HT₃ receptor antagonist. *Dig Dis Sci* 1999; **44**: 20-24
- 5 **Mertz H.** Role of the brain and sensory pathways in gastrointestinal sensory disorders in humans. *Gut* 2002; **51**(Suppl 1): i29-i33
- 6 **Al-Chaer ED, Kawasaki M, Pasricha PJ.** A new model of chronic visceral hypersensitivity in adult rats induced by colon irritation during postnatal development. *Gastroenterology* 2000; **119**: 1276-1285
- 7 **Ness TJ.** Intravenous lidocaine inhibits visceral nociceptive reflexes and spinal neurons in the rat. *Anesthesiology* 2000; **92**: 1685-1691
- 8 **Monnikes H, Lauer G, Arnold R.** Peripheral administration of cholecystokinin activates c-fos expression in the locus coeruleus/subcoeruleus nucleus, dorsal vagal complex and paraventricular nucleus via capsaicin-sensitive vagal afferents and CCK-A receptors in the rat. *Brain Res* 1997; **770**: 277-288
- 9 **Traub RJ, Silva E, Gebhart GF, Solodkin A.** Noxious colorectal distention induced-c-Fos protein in limbic brain structures in the rat. *Neurosci Lett* 1996; **215**: 165-168
- 10 **Coelho AM, Rovira P, Fioramonti J, Bueno L.** Antinociceptive properties of HTF 919 (Tegaserod), a 5-HT₄ receptor partial agonist, on colorectal distension in rats. *Gastroenterology* 2000; **118**(4 Suppl 2): A835
- 11 **Muller-Lissner SA, Fumagalli I, Bardhan KD, Pace F, Pecher E, Nault B, Ruegg P.** Tegaserod, a 5-HT₄ receptor partial agonist, relieves symptoms in irritable bowel syndrome patients with abdominal pain, bloating and constipation. *Aliment Pharmacol Ther* 2001; **15**: 1655-1666
- 12 **Liu YB, Yuan YZ, Tao RJ, Zhai ZK, Chen HZ.** Establishment of a rat model of gut hypersensitivity and for evaluation of visceral sensitivity. *Chin J Dig* 2003; **23**: 34-37
- 13 **Al-Awadi FM, Khan I.** Studies on purine enzymes in experimental colitis. *Mol Cell Biochem* 1999; **194**: 17-22
- 14 **Bradford MM.** A rapid and sensitive method for the quantitation of microgram quantities of protein utilizing the principle of protein-dye binding. *Anal Biochem* 1976; **72**: 248-254
- 15 **Chowdhury GM, Fujioka T, Nakamura S.** Induction and adaptation of Fos expression in the rat brain by two types of acute restraint stress. *Brain Res Bull* 2000; **52**: 171-182
- 16 **Azpiroz F.** Hypersensitivity in functional gastrointestinal disorders. *Gut* 2002; **51**(Suppl 1): i25-i28
- 17 **Mertz H, Margan V, Tanner G, Pickens D, Price R, Shyr Y, Kessler R.** Regional cerebral activation in irritable bowel syndrome and control subjects with painful and nonpainful rectal distention. *Gastroenterology* 2000; **118**: 842-848
- 18 **Yuan YZ, Tao RJ, Xu B, Sun J, Chen KM, Miao F, Zhang ZW, Xu JY.** Functional brain imaging in irritable bowel syndrome with rectal balloon-distention by using fMRI. *World J Gastroenterol* 2003; **9**: 1356-1360
- 19 **Lin C, Al-Chaer ED.** Long-term sensitization of primary afferents in adult rats exposed to neonatal colon pain. *Brain Res* 2003; **971**: 73-82
- 20 **Lidow MS, Song ZM, Ren K.** Long-term effects of short-lasting early local inflammatory insult. *Neuroreport* 2001; **12**: 399-403
- 21 **Ruda MA, Ling QD, Hohmann AG, Peng YB, Tachibana T.** Altered nociceptive neuronal circuits after neonatal peripheral inflammation. *Science* 2000; **289**: 628-631
- 22 **Xia Y, Zweier JL.** Measurement of myeloperoxidase in leukocyte-containing tissues. *Anal Biochem* 1997; **245**: 93-96
- 23 **Schikowski A, Thewissen M, Mathis C, Ross HG, Enck P.** Serotonin type-4 receptors modulate the sensitivity of intramural mechanoreceptive afferents of the cat rectum. *Neurogastroenterol Motil* 2002; **14**: 221-227
- 24 **Lacy BE, Yu S.** Tegaserod: a new 5-HT₄ agonist. *J Clin Gastroenterol* 2002; **34**: 27-33
- 25 **Bharucha AE, Camilleri M, Haydock S, Ferber I, Burton D, Cooper S, Tompson D, Fitzpatrick K, Higgins R, Zinsmeister AR.** Effects of a serotonin 5-HT₄ receptor antagonist SB-207266 on gastrointestinal motor and sensory function in humans. *Gut* 2000; **47**: 667-674
- 26 **Premkumar DR, Adhikary G, Overholt JL, Simonson MS, Cherniack NS, Prabhakar NR.** Intracellular pathways linking hypoxia to activation of c-fos and AP-1. *Adv Exp Med Biol* 2000; **475**: 101-109
- 27 **Traub RJ, Stitt S, Gebhart GF.** Attenuation of c-Fos expression in the rat lumbosacral spinal cord by morphine or tramadol following noxious colorectal distention. *Brain Res* 1995; **701**: 175-182
- 28 **Saria A, Fischer HS, Humpel C, Pfattner A, Schatz DS, Schuligoi R.** Margatoxin and iberiotoxin, two selective potassium channel inhibitors, induce c-fos like protein and mRNA in rat organotypic dorsal striatal slices. *Amino Acids* 2000; **19**: 23-31
- 29 **Harris JA.** Using c-fos as a neural marker of pain. *Brain Res Bull* 1998; **45**: 1-8
- 30 **Espejo EF, Gil E.** Antagonism of peripheral 5-HT₄ receptors reduces visceral and cutaneous pain in mice, and induces visceral analgesia after simultaneous inactivation of 5-HT₃ receptors. *Brain Res* 1998; **788**: 20-24

Inhibitory effects of berberine on ion channels of rat hepatocytes

Fang Wang, Hong-Yi Zhou, Gang Zhao, Li-Ying Fu, Lan Cheng, Jian-Guo Chen, Wei-Xing Yao

Fang Wang, Hong-Yi Zhou, Li-Ying Fu, Lan Cheng, Jian-Guo Chen, Wei-Xing Yao, Department of Pharmacology, Tongji Medical College of Huazhong University of Science and Technology, Wuhan 430030, Hubei Province, China

Gang Zhao, Pancreatic Surgery Center, Union Hospital, Tongji Medical College of Huazhong University of Science and Technology, Wuhan 430022, Hubei Province, China

Correspondence to: Dr. Fang Wang, Department of Pharmacology, Tongji Medical College of Huazhong University of Science and Technology, Wuhan 430030, Hubei Province, China. wangfang0322@yahoo.com.cn

Telephone: +86-27-83691760

Received: 2004-02-03 **Accepted:** 2004-02-18

Abstract

AIM: To examine the effects of berberine, an isoquinoline alkaloid with a long history used as a tonic remedy for liver and heart, on ion channels of isolated rat hepatocytes.

METHODS: Tight-seal whole-cell patch-clamp techniques were performed to investigate the effects of berberine on the delayed outward potassium currents (I_k), inward rectifier potassium currents (I_{K1}) and Ca^{2+} release-activated Ca^{2+} currents (I_{CRAC}) in enzymatically isolated rat hepatocytes.

RESULTS: Berberine 1-300 $\mu\text{mol/L}$ reduced I_k in a concentration-dependent manner with EC_{50} of $38.86 \pm 5.37 \mu\text{mol/L}$ and n_H of 0.82 ± 0.05 ($n = 8$). When the bath solution was changed to tetraethylammonium (TEA) 8 mmol/L, I_k was inhibited. Berberine 30 $\mu\text{mol/L}$ reduced I_k at all examined membrane potentials, especially at potentials positive to +60 mV ($n = 8$, $P < 0.05$ or $P < 0.01$ vs control). Berberine had mild inhibitory effects on I_{K1} in rat hepatocytes. Berberine 1-300 $\mu\text{mol/L}$ also inhibited I_{CRAC} in a concentration-dependent fashion. The fitting parameters were $EC_{50} = 47.20 \pm 10.86 \mu\text{mol/L}$, $n_H = 0.71 \pm 0.09$ ($n = 8$). The peak value of I_{CRAC} in the I-V relationship was decreased by berberine 30 $\mu\text{mol/L}$ at potential negative to -80 mV ($n = 8$, $P < 0.05$ vs control). But the reverse potential of I_{CRAC} occurred at voltage 0 mV in all cells.

CONCLUSION: Berberine has inhibitory effects on potassium and calcium currents in isolated rat hepatocytes, which may be involved in hepatoprotection.

Wang F, Zhou HY, Zhao G, Fu LY, Cheng L, Chen JG, Yao WX. Inhibitory effects of berberine on ion channels of rat hepatocytes. *World J Gastroenterol* 2004; 10(19): 2842-2845
<http://www.wjgnet.com/1007-9327/10/2842.asp>

INTRODUCTION

Many natural drugs for liver diseases are currently used in popular medicine. For example, quaternary protoberberine alkaloids from *Flissitigma* and *Goniothalamus* have been used in popular medicine for hepatomegaly and hepatosplenomegaly^[1,2]. The use of alkaloids from *Berberis aristata* for liver injury induced by chemical carcinogenesis and alkaloids from *Enantica* for disorders of bilirubin has also been reported^[3,4].

Berberine is an isoquinoline alkaloid with a long history in

both Ayurvedic and Chinese medicine. It exists in *Hydrastis canadensis* (golden seal), *Coptis chinensis* (Coptis or golden thread), *Berberis aquifolium* (Oregon grape), *Berberis vulgaris* (barberry), and *Berberis aristata* (tree turmeric). Berberine alkaloid can be found in roots, rhizomes, and stem bark of plants^[5]. Berberine has been extensively studied and is known to exhibit multiple pharmacological activities such as antiprotozoal, antihypertensive^[6], antibacterial^[7], anti-inflammatory, anticholinergic^[8] and antiarrhythmic activities^[9]. Hwang *et al.* reported that berberine inhibited hepatotoxicity induced by *tert*-butyl hydroperoxide (*t*-BHP) via its antioxidant potential and could function as a chemopreventive agent in living systems^[10]. Previous studies have shown that berberine could block delayed rectifier potassium currents, inward rectifier potassium currents (I_{K1}) and L-type calcium currents ($I_{Ca,L}$) in guinea pig ventricular myocytes^[11,12]. So far, however, its hepatoprotective mechanism still remains unknown. No data are available on the relationship between ion currents in hepatocytes and the hepatoprotective effect of berberine.

Therefore, this study used patch-clamp techniques to record the whole-cell currents in isolated rat hepatocytes in order to investigate the hepatoprotective mechanism of berberine.

MATERIALS AND METHODS

Cell preparation

Rat hepatocytes were enzymatically isolated from Sprague-Dawley (SD) rats of either sex (150-200 g) by using slightly modified procedures described previously^[13]. Briefly, adult animals were anesthetized with an intraperitoneal injection of pentobarbital sodium (30 mg/kg) in strict accordance to the guidelines established by the Institutional Animal Care and Use Committee, which follow all applicable state and federal laws. Portal vein and inferior vena cava were cannulated. The liver was initially perfused at a flow rate of 25 mL/min via a constant-flow system with modified oxygenated Ca^{2+} , Mg^{2+} -free Hanks' solution for several minutes, followed by perfusion with a Ca^{2+} , Mg^{2+} -free Hanks' solution containing collagenase (0.3 g/L, type I) for 10 min. The solutions were gassed with 950 mL/L O_2 +50 mL/L CO_2 and heated to 37 °C. After these perfusions, the liver was excised and then minced in Ca^{2+} , Mg^{2+} -free Hanks' solution at 0 °C. The cells were filtered through a 200 μm nylon mesh, and washed 3 times by centrifugation at 50 g for 2 min. The cell pellets were resuspended in KB medium that yielded approximately 85% to 95% viable hepatocytes. A small aliquot of the medium containing single cells was transferred into a 1-mL chamber mounted on the stage of an inverted microscope (IX-70, Olympus, Japan). Spherical and smooth cells were used for the whole-cell patch-clamp studies. All experiments were performed at room temperature (20 °C to 22 °C).

Voltage-clamp recording

A programmable vertical puller (pp-83, Narishige, Japan) was used to pull the electrodes. The resistance of capillary glass electrodes (GC150TF-10, Clark Electromedical Instruments, UK) used was 2 to 4 M Ω when filled with internal solution. A patch-clamp amplifier (EPC-9, Germany) was used to record the whole-cell currents with four-pole Bessel filter set at 1 kHz, digitized at 5 kHz. The protocols for voltage-clamp and data analysis were established with routines using pClamp 6.0 software (Axon Instrument, USA), and data

were stored in computer for subsequent analysis. Drug actions were measured only after steady-state conditions reached, which were judged by the amplitudes and time courses of currents remaining constant with further perfusion of drugs.

Drugs and solutions

Berberine hydrochloride was obtained from Yichang Pharmaceutical Company of China as base powders, dissolved in distilled water and made into a stock solution at 0.1 mol/L. Berberine was added to bath solutions for extracellular application. All drugs were purchased from Sigma (USA) unless otherwise indicated.

Ca²⁺, Mg²⁺-free Hanks' solution for cell-isolation (mmol/L) contained NaCl 137, KCl 5.4, NaH₂PO₄ 0.5, Na₂HPO₄ 0.58, NaHCO₃ 4.16 and glucose 5.5 (pH 7.3). Kraft-bruhe (KB) medium for cell-preservation (mmol/L) contained L-glutamic acid 70, KCl 130, taurine 15, KH₂PO₄ 10, MgCl₂ 0.5, glucose 11, N-(hydroxyethyl) piperazine-N'-2-ethanesulphonic acid (HEPES) 10 and ethylene glycol-O-O'-bis (2-aminoethyl) -N,N,N',N'-tetraacetic acid (EGTA) 0.5 (pH 7.4).

In studies of I_K, the bath solution was a modified Tyrode's solution (mmol/L) containing NaCl 144, KCl 4.0, CaCl₂ 1.8, MgCl₂ 0.53, Na₂HPO₄ 0.33, HEPES 5 and glucose 5.5 (pH 7.3). The patch pipette solution contained (mmol/L) KCl 130, K₂ATP 5.0, creatine phosphate 5.0 and HEPES 5.0 (pH 7.4).

For experiments on I_{K1}, both the bath solution and the pipette solution contained (mmol/L) KCl 7, MgCl₂ 2, EGTA 1, K-glutamate 130 and HEPES 10 (pH 7.4).

For I_{CRAC} recording, the bath solution (mmol/L) contained NaCl 140, KCl 2.8, CaCl₂ 10, MgCl₂ 0.5, glucose 11 and HEPES 10 (pH 7.4). The pipette solution used (mmol/L) contained K-glutamate 145, NaCl 8, MgCl₂ 1, MgATP 0.5, EGTA 10 and HEPES 10 (pH 7.2).

Data analysis

All the data were expressed as mean±SD and error bars were plotted as SD. Statistical significance was evaluated by a *t* test. Statistical differences were considered to be significant when *P* value was less than 0.05.

RESULTS

Effects of berberine on I_K

Under conventional whole-cell patch-clamp mode, the membrane potential was clamped at -50 mV, and I_K was elicited in isolated rat hepatocytes by depolarizing pulse to +140 mV for 900 ms. The current at the end point of the test pulse was measured as the amplitude of I_K.

The percentage block of I_K was defined as (I_{Control}-I_{berberine})/I_{Control} and plotted as a function of logarithm [berberine] in

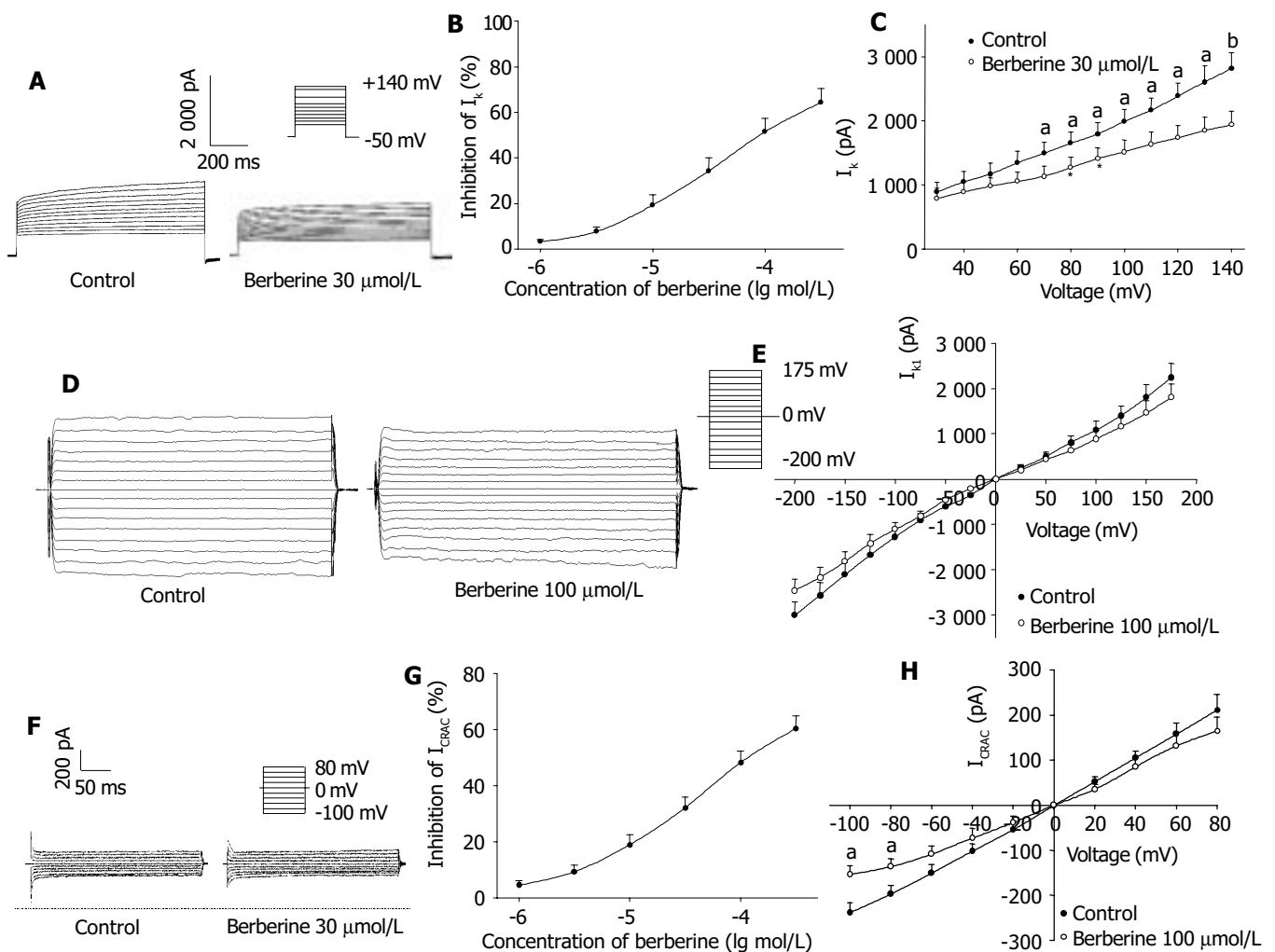


Figure 1 Effects of berberine on I_K. **A**: Families of I_K recorded with changes in the absence or presence of berberine 30 μmol/L and 100 μmol/L. Dotted line indicates zero current level; **B**: Dose-response curve for effects of berberine on I_K; **C**: I-V relationship of I_K under control (●) and berberine 30 μmol/L (○). **D**: Families of I_{K1} recorded with changes in the absence or presence of berberine 100 μmol/L. Dotted line indicates zero current level; **E**: I-V relationship of I_{K1} under control (●) and berberine 100 μmol/L (○). **F**: Families of I_{CRAC} recorded with changes in the absence or presence of berberine 30 μmol/L. Dotted line indicates zero current level; **G**: Dose-response curve for effects of berberine on I_{CRAC}. **H**: I-V relationship of I_{CRAC} under control (●) and berberine 30 μmol/L (○). The voltage steps used to elicit I_K are shown in the inset. *n* = 8, mean±SD, ^a*P*<0.05, ^b*P*<0.01 vs control.

Figure 1B. At +140 mV, berberine 1-300 $\mu\text{mol/L}$ decreased the I_K amplitude concentration-dependently in all cells tested, which was poorly reversible after washout. The data points were fitted according to the Hill equation: Inhibition of current (%) = $100/[1 + (\text{EC}_{50}/C)^{n_H}]$, and an EC_{50} value of $38.86 \pm 5.37 \mu\text{mol/L}$ and n_H of 0.82 ± 0.05 were obtained ($n = 8$). When the bath solution was changed to tetraethylammonium (TEA) 8 mmol/L, I_K was inhibited.

Figure 1A shows the effects of berberine 30 $\mu\text{mol/L}$ on the steady-state I-V relationship for I_K generated by applying 12 steps voltage command pulse from +30 mV to +140 mV for 900 ms with a 10 mV increment from a holding potential of -50 mV. By comparing these two I-V curves shown in Figure 1C, I_K was reduced by berberine 30 $\mu\text{mol/L}$ at all membrane potentials examined, especially at potentials positive to +60 mV ($n = 8$, $P < 0.05$ or $P < 0.01$ vs control). The results clearly indicated that berberine had a depressant action on I_K in rat hepatocytes.

Effects of berberine on I_{K1}

Hyperpolarizing and depolarizing potentials over a range from -200 mV to +175 mV with a 25 mV increment for 40 ms were applied from a holding level of 0 mV. The absolute value at the end of test pulse was measured as the amplitude of I_{K1} . After administration of berberine 100, 300 $\mu\text{mol/L}$, the I_{K1} amplitude at -200 mV was decreased from -3044.75 ± 262.06 pA to -2451.33 ± 226.45 pA and -2310.66 ± 182.65 pA, respectively. The inhibition rates were $17.49 \pm 2.51\%$ and $24.11 \pm 3.60\%$, respectively. Figures 1D and 1E shows the I-V relations of berberine 100 $\mu\text{mol/L}$ on I_{K1} . As shown in Figures 1D and 1E, berberine only had mild inhibitory effects on I_{K1} in isolated rat hepatocytes.

Effects of berberine on I_{CRAC}

When the holding potential was 0 mV, and the cells were depolarized to -100 mV for 200 ms at a frequency of 0.2 Hz, I_{CRAC} was evoked. As shown in Figure 1G, I_{CRAC} also was blocked by berberine in a concentration-dependent fashion, with an EC_{50} value of $47.20 \pm 10.86 \mu\text{mol/L}$ and n_H of 0.71 ± 0.09 ($n = 8$). Figure 1H shows the effect of berberine 30 $\mu\text{mol/L}$ on the steady-stated I-V relationships generated by applying a series depolarizing pulses from a holding potential of 0 mV to different membrane potentials (-100 mV to +80 mV) with a 20 mV increment. The peak value of I_{CRAC} was reduced on either inward or outward components, especially from -100 mV through -80 mV ($n = 8$, $P < 0.05$ vs control). But the reverse potential of I_{CRAC} occurred at voltage 0 mV in all cells.

DISCUSSION

In this study, for the first time, we characterized the effects of berberine on I_K , I_{K1} and I_{CRAC} by patch-clamp techniques and demonstrated that berberine mainly inhibited I_K , I_{CRAC} and I_{K1} in isolated rat hepatocytes.

Potassium channels are ubiquitous in eukaryotic cells and could play roles in resting membrane potential, frequency of action potential, membrane potential repolarization rates and cell functions. It has been found that membrane potential is important in regulating metabolic processes in the liver, including gluconeogenesis, amino acid transport, and the rate of uptake of bile salts^[14,15]. Changes in K^+ permeability could affect the transmembrane potential. Bile formation was involved in anion accumulation within the apical lumen of hepatocytes. Potassium flux through hepatocellular basolateral membrane channels might provide the counterion for apical anion efflux^[16]. Transcellular bile acid transport could be integrated in the regulation of intracellular pH, K^+ homeostasis and membrane potential. Hepatocellular K^+ -depletion could result in the inhibition of bile acid secretion despite increasing the intracellular concentration^[17-19].

During ischemia and hypoxia, hepatocellular volume and K^+ conductance were increased and would lead to cell death^[20,21].

Nietsch *et al.* demonstrated TNF (25 ng/mL) elicited a 2- and 5-fold increase in K^+ current in hepatoma tissue culture cells. K^+ channel activation might participate in pathways that leading to TNF-mediated cell death, thus representing potential therapeutic targets to attenuate liver injury from TNF^[22]. The inhibition of K^+ channels could delay hepatocyte apoptosis and death. Churchill *et al.* reported that potassium channel antagonists had protective effects on rat liver via regulating the energy metabolism^[23].

Previous studies showed that berberine (0.5, 5 mg/kg, i.p.) protected rat liver from hepatotoxicity induced by *t*-BHP^[10]. As shown previously, *t*-BHP could shrink hepatocytes by release of cellular K^+ . Single-channel patch-clamp studies demonstrated *t*-BHP activated a 35-pS K^+ channel and contributed to the K^+ release of hepatocytes following exposure to *t*-BHP^[24]. In this study, we observed that the concentration of berberine on I_K was consistent with the dose reported by Hwang^[10]. The hepatoprotective effect of berberine on *t*-BHP may have some relations with the inhibitory effect on potassium channel.

However, as we reported previously, AP-Q had a protective effect on CCl_4 -induced liver injury, probably by selectively increasing I_K . In this experiment, we observed that berberine had a protective effect on *t*-BHP induced liver injury by decreasing I_K . The contradiction may be due to the different mechanism of CCl_4 -induced and *t*-BHP induced liver injury. CCl_4 -induced hepatocyte injury paralleled with membrane depolarization by blocking the potassium channel in damaged hepatocytes^[25-27]. However, *t*-BHP-induced liver injury is concerned with the release of cellular K^+ by activating potassium channel. A previous study showed that berberine had not any protective effects on CCl_4 -induced liver injury^[28].

Calcium has been demonstrated to play an important role in hepatocyte damage. An increase in calcium ion concentration in cytoplasm due to the influence of various toxic agents caused disturbances in the structure and function of hepatocytes, leading to their damage and even death^[29]. Previous studies showed that hepatocellular Ca^{2+} overload and impaired Ca^{2+} signaling were related to hemorrhage/resuscitation liver injury. Increased Ca^{2+} uptake could result from a receptor-gated Ca^{2+} influx and/or oxygen-free radical induced membrane Ca^{2+} leaks. A protective effect of calcium channel blockers on hepatotoxins has been reported^[30].

Calcium ions could enter the cells mostly through calcium channels. However, hepatocytes as the nonexcitable cells were short of the voltage-dependent Ca^{2+} channels but possessed plasma membrane Ca^{2+} channels that had a high selectivity for Ca^{2+} , and were activated by a decrease in the concentration of Ca^{2+} in intracellular stores, which was named I_{CRAC} ^[31,32]. Berberine inhibited I_{CRAC} with EC_{50} of 47.20 $\mu\text{mol/L}$, which was different from the EC_{50} of I_{CaL} in cardiac myocytes^[33]. The differential drug sensitivity of the two currents also provided further support for the idea that I_{CRAC} is different from voltage-gated Ca^{2+} channel.

Berberine inhibited I_K , I_{K1} and I_{CRAC} concentration-dependently in isolated rat hepatocytes and the inhibitory extent was $I_K > I_{CRAC} > I_{K1}$. Therefore, berberine could block K^+ channel and decrease the extracellular K^+ to regulate the metabolic processes in the liver. Berberine could also inhibit I_{CRAC} effectively and protect hepatocytes from calcium overload via the inhibition of I_{CRAC} . The inhibitory effects on potassium and calcium current may partly contribute to the hepatoprotective action of berberine. As berberine has already been used for liver damage in human beings^[34], it may be a good candidate for further study and used in treatment of liver damage.

REFERENCES

- 1 Virtanen P, Lassila V, Njimi T, Mengata DE. Natural protoberberine alkaloids from *Enantia chlorantha*, palmatine,

- columbamine and jatrorrhizine for thioacetamide-traumatized rat liver. *Acta anat* 1988; **131**: 166-170
- 2 **Virtanen D**, Lassila V, Njimi T, Ekotto Mengata D. Regeneration of D-galactosamine-traumatized rat liver with natural protoberberine alkaloids from *Enantia chlorantha*. *Acta Anat* 1988; **132**: 159-163
 - 3 **Virtanen D**, Lassila V, Njimi T, Mengata DE. Effect of splenectomy on hepasor treatment in allyl-alcohol-traumatized rat liver. *Acta Anat* 1989; **134**: 301-304
 - 4 **Anis KV**, Rajeshkumar NV, Kuttan R. Inhibition of chemical carcinogenesis by berberine in rats and mice. *J Pharm Pharmacol* 2001; **53**: 763-768
 - 5 **Lau CW**, Yao XQ, Chen ZY, Ko WH, Huang Y. Cardiovascular actions of berberine. *Cardiovasc Drug Rev* 2001; **19**: 234-244
 - 6 **Bova S**, Padrini R, Goldman WF, Berman DM, Cargnelli G. On the mechanism of vasodilating action of berberine: possible role of inositol lipid signaling system. *J Pharmacol Exp Ther* 1992; **261**: 318-323
 - 7 **Amin AH**, Subbaiah TV, Abbasi KM. Berberine sulfate: antimicrobial activity, bioassay, and mode of action. *Can J Microbiol* 1969; **15**: 1067-1076
 - 8 **Tsai CS**, Ochillo RF. Pharmacological effects of berberine on the longitudinal muscle of the guinea-pig isolated ileum. *Arch Int Pharmacodyn Ther* 1991; **310**: 116-131
 - 9 **Wang YX**, Zheng YM. Ionic mechanism responsible for prolongation of cardiac action-potential duration by berberine. *J Cardiovasc Pharmacol* 1997; **30**: 214-222
 - 10 **Hwang JM**, Wang CJ, Chou FP, Tseng TH, Hsieh YS, Lin WL, Chu CY. Inhibitory effect of berberine on *tert*-butyl hydroperoxide-induced oxidative damage in rat liver. *Arch Toxicol* 2002; **76**: 664-670
 - 11 **Li BX**, Yang BF, Zhou J, Xu CQ, Li YR. Inhibitory effects of berberine on I_{K1} , I_K , and HERG channels of cardiac myocytes. *Acta Pharmacol Sin* 2001; **22**: 125-131
 - 12 **Li Y**, Fu LY, Yao WX, Xia GJ, Jiang MX. Effects of benzyltetrahydro-palmatine on potassium currents in guinea pig and rat ventricular myocytes. *Acta Pharmacol Sin* 2002; **23**: 612-616
 - 13 **Seglen PO**. Preparation of isolated rat liver cells. *Methods Cell Biol* 1976; **13**: 29-83
 - 14 **Bernardi P**, Azzone GF. Regulation of Ca^{2+} efflux in rat liver mitochondria. Role of membrane potential. *Eur J Biochem* 1983; **134**: 377-383
 - 15 **Einarsson C**, Ellis E, Abrahamsson A, Ericzon BG, Björkhem I, Axelsson M. Bile acid formation in primary human hepatocytes. *World J Gastroenterol* 2000; **6**: 522-525
 - 16 **Roman R**, Feranchak AP, Troetsch M, Dunkelberg JC, Kilic G, Schlenker T, Schaack J, Fitz JG. Molecular characterization of volume-sensitive SK (Ca) channels in human liver cell lines. *Am J Physiol Gastrointest Liver Physiol* 2002; **282**: G116-G122
 - 17 **vom Dahl S**, Hallbrucker C, Lang F, Haussinger D. Regulation of cell volume in the perfused rat liver by hormones. *Biochem J* 1991; **280**(Pt 1): 105-109
 - 18 **Devin A**, Espie P, Guerin B, Rigoulet M. Energetics of swelling in isolated hepatocytes: a comprehensive study. *Mol Cell Biochem* 1998; **184**: 107-121
 - 19 **Kiss L**, Immke D, LoTurco J, Korn SJ. The interaction of Na^+ and K^+ in voltage-gated potassium channels. Evidence for cation binding sites of different affinity. *J Gen Physiol* 1998; **111**: 195-206
 - 20 **Hill CE**, Jacques JE. Cholestatic effects of the K^+ channel blockers Ba^{2+} and TEA occur through different pathways in the rat liver. *Am J Physiol* 1999; **276**(1 Pt 1): G43-G48
 - 21 **Hill CE**, Briggs MM, Liu J, Magtanong L. Cloning, expression, and localization of a rat hepatocyte inwardly rectifying potassium channel. *Am J Physiol Gastrointest Liver Physiol* 2002; **282**: G233-G240
 - 22 **Nietsch HH**, Roe MW, Fiekers JF, Moore AL, Lidofsky SD. Activation of potassium and chloride channels by tumor necrosis factor α . Role in liver cell death. *J Biol Chem* 2000; **275**: 20556-20561
 - 23 **Churchill TA**, Fuller BJ. Effects of sodium and potassium channel antagonists on the energy metabolism of rat liver during cold storage. *Transplantation* 1995; **59**: 904-907
 - 24 **Breit S**, Kolb HA, Haussinger D, Lang F. Effects of tetrabutylhydroperoxide on hepatocyte ion channels. *Cell Physiol Biochem* 1999; **9**: 133-138
 - 25 **Wands JR**, Smuckler EA, Woodbury WJ. Transmembrane potential changes in liver cells following CCl_4 intoxication. *Am J Pathol* 1970; **58**: 499-508
 - 26 **Olson JR**, Hosko MJ, Fujimoto JM. Alterations in the liver cell transmembrane potential following CCl_4 and bile salt treatment of rats. *Life Sci* 1979; **25**: 2043-2050
 - 27 **Burczynski FJ**, Wang GQ, Minuk GY, Rosser B. Altered transmembrane ionic flux in hepatocytes isolated from cirrhotic rats. *J Hepatol* 1999; **30**: 492-497
 - 28 **Janbaz KH**, Gilani AH. Studies on preventive and curative effects of berberine on chemical-induced hepatotoxicity in rodents. *Fitoterapia* 2000; **71**: 25-33
 - 29 **Isozaki H**, Fujii K, Nomura E, Hara H. Calcium concentration in hepatocytes during liver ischaemia-reperfusion injury and the effects of diltiazem and citrate on perfused rat liver. *Eur J Gastroenterol Hepatol* 2000; **12**: 291-297
 - 30 **Farghali H**, Kmonickova E, Lotkova H, Martinek J. Evaluation of calcium channel blockers as potential hepatoprotective agents in oxidative stress injury of perfused hepatocytes. *Physiol Res* 2000; **49**: 261-268
 - 31 **Takanashi H**, Sawanobori T, Kamisaka K, Maezawa H, Hiraoka M. Ca^{2+} -activated K^+ channel is present in guinea-pig but lacking in rat hepatocytes. *Jpn J Physiol* 1992; **42**: 415-430
 - 32 **Rychkov G**, Brereton HM, Harland ML, Barritt GJ. Plasma membrane Ca^{2+} release-activated Ca^{2+} channels with a high selectivity for Ca^{2+} identified by patch-clamp recording in rat liver cells. *Hepatology* 2001; **33**: 938-947
 - 33 **Xu SZ**, Zhang Y, Ren JY, Zhou ZN. Effects of berberine on L- and T-type calcium channels in guinea pig ventricular myocytes. *Zhongguo Yaoli Xuebao* 1997; **18**: 515-518
 - 34 **Brunton CC**. In pharmacological basis of therapeutics edited by Hardman JG, Limbird LE, Molinoff PB, Ruddon RW, Gilman AG. *New York: McGraw Hill* 1996: 917-936

Edited by Wang XL Proofread by Xu FM and Chen WW

Surgical management of esophageal strictures after caustic burns: A 30 years of experience

Yong Han, Qing-Shu Cheng, Xiao-Fei Li, Xiao-Ping Wang

Yong Han, Qing-Shu Cheng, Xiao-Fei Li, Xiao-Ping Wang,
Department of Thoracic Surgery, Tangdu Hospital, the Fourth Military
Medical University, Xi'an 710038, Shaanxi Province, China

Correspondence to: Dr. Yong Han, Department of Thoracic Surgery,
Tangdu Hospital, the Fourth Military Medical University, Xi'an
710038, Shaanxi Province, China. han2003002@vip.sina.com

Telephone: +86-29-83377736 **Fax:** +86-29-83246270

Received: 2004-02-14 **Accepted:** 2004-03-02

Abstract

AIM: To analyze a 30-year historical series of patients treated in our hospital, who ingested corrosive substances, and to assess the effectiveness of surgical therapy administered in patients with strictures after caustic injury in esophagus during this period.

METHODS: A total of 79 cases of caustic burns in esophagus were treated in Tangdu Hospital from 1971 to 2001. Their clinical and pathological data were reviewed, and collected from the medical records of patients and interviews with them.

RESULTS: More men ($n = 61$) than women ($n = 18$) ingested caustic substances with a sex ratio of 3.4:1 during the 30-year period. The caustic materials were liquid lye and acids (54 cases and 25 cases, respectively). Sixty-eight patients were given esophageal replacement in more than three months after caustic injury with no postoperative death, of which 17 cases developed postoperative complications making a complication rate of 25%. The most common one was cervical anastomotic leakage. All patients had improvement in swallowing afterwards.

CONCLUSION: The presence and severity of injuries are correlated with the amount of caustic substances ingested. Surgical treatment is a good option in patients with severe strictures, and colonic interposition might be the best surgical process. The most important factors to guarantee a successful outcome for surgery are good vascular supply and absence of tension in the anastomosis.

Han Y, Cheng QS, Li XF, Wang XP. Surgical management of esophageal strictures after caustic burns: A 30 years of experience. *World J Gastroenterol* 2004; 10(19): 2846-2849
<http://www.wjgnet.com/1007-9327/10/2846.asp>

INTRODUCTION

Potentially catastrophic presentation and life long complications resulting from caustic ingestion make it one of the most challenging clinical situations in gastroenterology. Caustic material ingestion is most frequently encountered in children who accidentally swallowed caustic materials or in adults who ingested caustic materials for suicidal purposes^[1,2]. Alkaline caustics and acids are the commonest chemicals implicated in caustic burns. Burns from ingestion of such agents may include

the oral, pharynx, larynx, esophagus and stomach. Destruction of tissues or of these organs may lead to complications, of which respiratory compromise, esophageal and gastric perforation, septicemia, or even death might occur. Stricture formation with inability to swallow food after the injury is inevitable in some cases. Many different therapies have been recommended. The literature regarding the treatment of these patients is quite controversial and inconclusive. Repeated dilations to maintain an adequate lumen diameter were given in patients with chronic strictures. As for the complications and ineffectiveness of the dilation in more severe strictures, surgical replacement of esophagus may be required. The objective of this study was to analyze a 30-year historical series of patients treated in our hospital who ingested caustic substances, and to assess the effectiveness of surgical therapy administered in patients with strictures after caustic injury in esophagus as well as the best time for operation.

MATERIALS AND METHODS

Subjects

From 1971 to 2001, 79 cases of caustic burns in esophagus were treated in Tangdu Hospital. Their clinical and pathological data were reviewed, and collected from the medical records of patients and interviews with them. Sixty-one men and 18 women ingested caustic substances (sex ratio 3.4:1), respectively. Patients aged from 2 to 72 years (mean, 20.8 ± 2.5 years). The caustic materials for injuries were liquid lye and acids (54 cases and 25 cases, respectively). Ingestion was associated with suicidal intent in 70% of cases and accidental in 29% of cases. The amount of substances ingested ranged from 5-15 mL to as much as 40 mL, with the amount tending to be larger in the suicide attempts. To determine the amount of caustic substances ingested, patients or witnesses were asked to compare the amount ingested to the amount of water in a cup. The time intervals the patient came to our hospital after ingestion varied from several hours to several days. A total of 73 cases presented lesions of the esophagus. Two patients, who ingested a large amount of more than 60 mL caustic substances, died of stomach and esophageal perforation during the acute phase as a result of generalized infection and bleeding. Four patients, who ingested less than 15 mL, did not present severe complications. Esophageal strictures were found in 72 cases, the presence of stenosis was determined 2 wk after ingestion (chronic phase) by endoscopy and radiological signs.

Treatment

All the patients were given early emergency managements including early administration of an appropriate neutralizing agent such as ingesting water or milk after the ingestion, although it did not seem to prevent stenosis^[3], and antibiotics, as well as the correction of any apparent hydration deficiency or acid-base imbalance, and corticosteroid treatment to the patients with signs of esophagitis. Forty-eight patients of 77 cases underwent emergent endoscopy to assess the degree of damage after patients were stabilized, which was very important for the diagnosis and evaluation of the degree of injuries. Patients with ulceration, blisters, even areas of extensive

necrosis always tended to develop esophageal strictures^[4,5]. Among the 79 patients, 72 might undergo a long period of dysphagia, and gastrostomy or jejunostomy was performed for feed routinely soon after the injury except 4 patients who were lucky enough to escape severe injury and suffered from only oral burn, and 1 patient refused for further treatment because of economical reasons. No emergency thoracotomy was performed for the esophagectomy or gastrectomy in this group. Sixteen patients were performed repeated dilations 1-2 mo after ingestion (Table 1).

Table 1 Previous management before esophagus replacement ($n = 79$)

Procedures	<i>n</i>	%
Gastrostomy	25	31.6
Jejunostomy and pyloroplasty	12	15.2
Jejunostomy	19	24.1
Repeated dilation after gastrostomy or jejunostomy	15	19.0
Dilation and stent placement after gastrostomy or jejunostomy	1	1.2
No surgery	7	8.8

Esophageal replacement

Sixty-eight patients, among whom 12 had been given repeated dilation with failure therapy, were performed esophagus replacement for diffuse or multiple caustic esophageal strictures and 3 patients were cured after corticosteroid treatment and repeated dilations, 1 patient was performed stent placement. Among the 68 patients, 65 underwent the operation 6 mo and 3 three months after the injury. Stomach, jejunum and colon were used for esophageal replacement (Table 2). The colon (63/68) was commonly used as an esophageal substitute in reconstruction, and all went through the substernal route.

Table 2 Operation procedure of esophageal replacement ($n = 68$)

Procedure	<i>n</i>	%
Colonic interposition	63	92.6
Esophagogastronomy	3	4.4
Jejunal interposition	2	3.0

Surgical procedure of colonic interposition

As colonic interposition was mostly used in our study, the surgical procedure was prescribed. The operation was carried out through an upper abdominal incision and a cervical oblique incision along the inner border of the sternocleidomastoid muscle in 62 patients and in 1 patient with a right thoracotomy respectively. The cervical esophagus was explored. It was transected in the level that esophagus was normal. In case the cervical esophagus was thickened and stiff in consistency, indicating that the organ was too extensively injured, a hypopharyngocolostomy had to be performed. This was occurred in 7 cases in this series.

A sufficient colon segment for graft was mobilized from colonic mesentery. The middle and left colonic arteries were identified and freed respectively. The root of the vessels elected was clamped with bulldog clamps for about 15 min. In the same time, the estimated ends of graft were clamped with intestinal clamps and watched. If the colon acted as replacement expressed normal in color, peristalsis and marginal arterioles would be pulsating (especially those in both ends of the segment), it would be transected. The colonic segment used in this group consisted of left colon in 30 cases, right colon and transverse colon in 33 cases. The peristaltic orientation of graft consisted

of isoperistalsis in 40 cases and antiperistalsis in 23 cases.

The substernal tunnel in 61 cases and the subcutaneous tunnel in 2 were prepared. The proximal end of graft was elevated gently from abdomen up to the neck through the tunnel. A proximal esophagocolic or hypopharyngocolic anastomosis was performed in an end-to-end or end-to-side fashion with hand-suturing single-layer technique in 56 and 7 cases, respectively.

Cologastric anastomosis was performed over the midportion of the anterior wall of the stomach without extensively injuring the stomach, and the anastomosis between the distal portion of graft and a Rouxeny loop of jejunum was performed.

Additional procedure included resection of upper portion of sternum in 5 patients in order to avoid or decrease compression on the proximal colonic graft at the level of the thoracic inlet.

RESULTS

After early emergency management in these patients, 2 patients who ingested more than 60 mL of caustic substances died of stomach and esophageal perforation during the acute phase as a result of generalized infection and bleeding. Four patients, who ingested less than 10 mL, did not present complications in the present study. On this basis, we believed that the presence and severity of injuries were correlated with the amount of caustic substances ingested, which was similar with the result of Chien *et al.*^[6]. Sixteen patients were performed repeated dilation 1-2 mo after ingestion in fear of perforation in earlier dilations and 12 patients needed further surgical treatment.

Sixty-eight cases were performed esophageal replacement because of the later stricture, which caused persistent dysphagia and weight loss in these patients. Results of operation were satisfactory with no postoperative death and improved swallowing ability, among which 17 cases developed postoperative complications making a complication rate of 25% (Table 3). The most common one was cervical anastomotic leakage, which occurred in 9 cases in this series. Postoperatively, swallow ability was considered good in 65 patients (95.7%) after an average of 22-mo follow-up (six months to eight years). The swallow ability was determined through the questionnaire about the sorts and amounts of food that could be swallowed compared with the condition before injury and operation in a general analysis.

Table 3 Postoperative complications ($n = 17$)

Complication	<i>n</i>	%
Cervical anastomotic leakage	9	52.9
Cervical wound infection	2	11.7
Anastomotic stenosis	3	17.6
Intestinal obstruction	1	5.8
Pneumothorax	1	5.8
Aspiration pneumonitis	1	5.8

DISCUSSION

A successful management of corrosive injury involves prompt recognition and early treatment. Unfortunately, it is sometimes not possible to maintain an esophageal lumen despite all the measures. Clinically apparent esophageal strictures occurred in 10-30% of patients with a caustic injury^[7], even higher in some other reports^[8,9]. In our study, 68 patients (85%) presented strictures that needed replacement, which might be due to the ingestion of relatively large amount of caustic substances for suicidal intent. Treatment of the strictures after esophageal injury was very difficult, and dilation has been used in many hospitals^[10]. Even after many times of dilation, strictures were

found in about 48% cases^[11], and although the danger of severe complications, such as perforation of the esophagus per procedure, was low (0.9-1.5%)^[12,13], a significant number of people, especially children were at risk with a relatively high mortality^[14,15]. Dilatation therapy, furthermore, required frequent admissions to hospital and multiple anesthetics with inherent risks. Surgical intervention, which is a good way to solve the problem of strictures, in the form of esophageal replacement, was carried out in more than half patients with established esophageal strictures^[16].

Most beneficial time for surgery

The time for operation of esophageal replacement after corrosive injury is still under controversy. Certainly, emergency surgical exploration is indicated if perforation or penetration is demonstrated.

Bassiouny *et al.*^[17] found in rats that collagen deposition peaked during the second week but continued for a long time after corrosive injury of esophagus. Scar retraction began as early as the end of the second week, and lasted for about six months. It took about 6-12 mo before full fibrosis stopped to develop after the injury^[18], which showed that the edge of the stricture in the esophagus might not be confirmed until then. A too earlier operation, when the scar has not completely formed, may promote the risk of anastomotic stenosis. So, it is believed that the chance of successful surgical management is greater if the operation is carried out at least six months after the injury. In our study, 3 patients with strictures in the lower segment of esophagus, who developed severe dysphagia and refused gastrostomy, were performed partial esophagectomy and esophagogastrostomy about 90 d after caustic injury. However, anastomotic stenosis occurred in 2 patients (67%) 2 mo after operation, a higher incidence of stenosis. The other 65 patients were performed operation 6 mo after injury with only one esophageal stenosis occurred.

Although it was reported that esophageal replacement could be performed even 2-3 mo after injury^[19], but many conditions must be met and the mucosa in the pharynx must be normal. So we think that the most beneficial time for surgery is no less than six months after the injury.

Choice of replacement organs

The organs used for esophageal replacement in patients after caustic injuries included stomach, jejunum and colon in previous studies^[20,21]. Stomach has the disadvantages of long-term gastroesophageal reflux, possible ulceration, anastomotic stenosis and progressive dysfunctional propulsion^[22]. The stomach is always not long enough to reestablish a continuity of esophagus when anastomosis had to be performed in the neck because the diffused injuries of esophagus, when patients had to be given partial gastrectomy after caustic injuries. In our study partial esophagectomy and esophagogastrostomy were performed only in 3 patients on the condition that strictures were located in the lower segment of esophagus. Jejunal interposition is seldom used because of the difficulty for operation since blood vessels of jejunum are too thin and easier to be affected after anastomosis. Furthermore, the jejunum is fragile to the erosion of acid in a long run, so the jejunum should not be the first choice. In our study, only 2 cases of jejunal interposition were performed, because the patients had undergone abdominal operation before and the stomach and colon were unable to be mobilized. With good blood supply and improved somatic growth, colon is long enough for esophageal replacement, and it causes fewer late complications of esophagitis and stricture because of the resistance to acid. So colon could offer potential advantages over other organs^[20,23], and is believed to be an ideal organ for the replacement. We used colon for replacement in 63 cases, and the result was

satisfactory. Our experiences support the idea that colon interposition is the best process for reconstruction of esophagus in caustic injury strictures.

Choice of colon segment as a graft is also a key point for reconstruction of esophagus. The left colon has been considered by many surgeons to be a preferable conduit for several reasons. But left colon interposition could always be used in an antiperistaltic fashion, which may cause inflammation of the anastomosis, and affect the healing process. In our study, leakage of cervical anastomosis appeared in 7 cases of the antiperistaltic anastomosis group, which was much higher than the isoperistaltic groups. So, it is suggested that the reversed peristalsis might cause more complications of anastomosis than isoperistalsis. The choice of a colon segment for substitution in our study was also affected by the supply of blood vessels during operation, and the color of intestine, and pulsation of marginal arteries after the supplying artery of colon was clamped. The mortality and morbidity in the literature after colonic interposition was very high^[24]. The most severe complication was complete necrosis of the transplanted colon. When it happened, a more complex reconstruction procedure should be considered. We had no experience in facing such a catastrophe. In 1 case, local necrosis in the proximal end of transplanted colon was observed when anastomotic leakage was diagnosed 3 d after the procedure. The anastomotic leakage was the most common complication in 9 of 63 cases, making an incidence as high as 13.3%. Considering the fact that most patients in whom esophageal disease was caused by caustic injury accompanied with bad nutritional status, this rate of postoperative complication after colon interposition is acceptable. Anastomotic leakage of the patients was managed by opening the cervical wound, and it seemed to have no effect on the late swallow ability of patients after anastomotic leakage compared with the patients without leakage in the follow up interviews. There was no death in the group. The outcome was favorable when compared with published literature^[24].

Residual esophagus

It is still a subject of a controversy whether the residual esophagus should be resected after colonic interposition. Many studies have focused on the relation between esophageal injury and carcinoma. Although the scarred and damaged esophagus might have an increased incidence of carcinoma^[25,26], there is no evidence that has been reported. In our study, esophagectomy was only performed in the esophagogastrostomy and jejunal interposition groups, and no residual esophagus was resected in the colonic interposition group. In our follow-up study, no carcinoma of residual esophagus occurred even 8 years after operation. In our experience, an additional thoracotomy or esophagectomy to resect the injured esophagus is a big burden for patients, when an abdominal incision is enough in colonic interposition procedure. Adhesion and inflammation of the residual esophagus after long time caustic injuries may be a great strike for patients to receive esophagectomy, with a higher risk of complications, even death than expected. It is therefore suggested that a long term follow-up and observation for the residual esophagus may be a preferable option for the treatment of caustic injuries of esophagus. Resection of the residual esophagus should be seriously considered anyhow.

Keys for success of surgical procedure

Certainly good nutrition and careful peri-operation treatment are important for the healing process of anastomosis. Gastrostomy or jejunostomy must be performed for the nutrition of patients. In addition to an effective nutritional support, the pivotal keys for a successful surgical procedure are the adequate and good vascular supply for the esophageal replacement, as well as the absence of tension at the anastomosis. Thus, an

enough length of substitutes must be prepared. Resection of parts of the sternum should be considered for colonic interposition to allow a spacious room for the graft colon, if the sternum exerts pressure upon the graft colon .

REFERENCES

- 1 **Havanond C.** Clinical features of corrosive ingestion. *J Med Assoc Thai* 2003; **86**: 918-924
- 2 **Rodriguez MA, Meza Flores JL.** Clinical-epidemiological characteristics in caustics ingestion patients in the Hipolito Unanue National Hospital. *Rev Gastroenterol Peru* 2003; **23**: 115-125
- 3 **Ramasamy K, Gumaste VV.** Corrosive ingestion in adults. *J Clin Gastroenterol* 2003; **37**: 119-124
- 4 **Tseng YL, Wu MH, Lin MY, Lai WW.** Massive upper gastrointestinal bleeding after acid-corrosive injury. *World J Surg* 2004; **28**: 50-54
- 5 **Havanond C.** Is there a difference between the management of grade 2b and 3 corrosive gastric injuries? *J Med Assoc Thai* 2002; **85**: 340-344
- 6 **Chien WC, Pai L, Lin CC, Chen HC.** Epidemiology of hospitalized burns patients in Taiwan. *Burns* 2003; **29**: 582-588
- 7 **Schaffer SB, Hebert AF.** Caustic ingestion. *J La State Med Soc* 2000; **152**: 590-596
- 8 **de Jong AL, Macdonald R, Ein S, Forte V, Turner A.** Corrosive esophagitis in children: a 30-year review. *Int J Pediatr Otorhinolaryngol* 2001; **57**: 203-211
- 9 **Lopez Vallejos P, Garcia Sanchez MV, Naranjo Rodriguez A, Galvez Calderon C, Hervas Molina A, Chicano Gallardo M, Mino Fugarolas G.** Endoscopic dilatation of caustic esophageal strictures. *Gastroenterol Hepatol* 2003; **26**: 147-151
- 10 **Shao YX, Chen ZH, Ning JW.** Treatment of esophageal stricture and leakage with dilation stents. *Shijie Huaren Xiaohua Zazhi* 2002; **10**: 249-251
- 11 **Ogunleye AO, Nwaorgu GB, Grandawa H.** Corrosive oesophagitis in Nigeria: clinical spectrums and implications. *Trop Doct* 2002; **32**: 78-80
- 12 **Lan LC, Wong KK, Lin SC, Sprigg A, Clarke S, Johnson PR, Tam PK.** Endoscopic balloon dilatation of esophageal strictures in infants and children: 17 years' experience and a literature review. *J Pediatr Surg* 2003; **38**: 1712-1715
- 13 **Poddar U, Thapa BR.** Benign esophageal strictures in infants and children: results of Savary-Gilliard bougie dilation in 107 Indian children. *Gastrointest Endosc* 2001; **54**: 480-484
- 14 **Erdogan E, Eroglu E, Tekant G, Yeker Y, Emir H, Sarimurat N, Yeker.** Management of esophagogastric corrosive injuries in children. *Eur J Pediatr Surg* 2003; **13**: 289-293
- 15 **Lew RJ, Kochman ML.** A review of endoscopic methods of esophageal dilation. *J Clin Gastroenterol* 2002; **35**: 117-126
- 16 **Adegboye VO, Brimmo A, Adebo OA.** Transhiatal esophagectomy in children with corrosive esophageal stricture. *Afr J Med Med Sci* 2000; **29**: 223-226
- 17 **Bassiouny IE, Al-Ramadan SA, Al-Nady A.** Long-term functional results of transhiatal oesophagectomy and colonic interposition for caustic oesophageal stricture. *Eur J Pediatr Surg* 2002; **12**: 243-247
- 18 **Demirbilek S, Aydin G, Yucesan S, Vural H, Bitiren M.** Polyunsaturated phosphatidylcholine lowers collagen deposition in a rat model of corrosive esophageal burn. *Eur J Pediatr Surg* 2002; **12**: 8-12
- 19 **Munoz-Bongrand N, Gornet JM, Sarfati E.** Diagnostic and therapeutic management of digestive caustic burns. *J Chir* 2002; **139**: 72-76
- 20 **Erdogan E, Emir H, Eroglu E, Danismend N, Yeker D.** Esophageal replacement using the colon: a 15-year review. *Pediatr Surg Int* 2000; **16**: 546-549
- 21 **Hirschl RB, Yardeni D, Oldham K, Sherman N, Siplovich L, Gross E, Udassin R, Cohen Z, Nagar H, Geiger JD, Coran AG.** Gastric transposition for esophageal replacement in children: experience with 41 consecutive cases with special emphasis on esophageal atresia. *Ann Surg* 2002; **236**: 531-539
- 22 **Helardot P.** Caustic burns of the esophagus, esophagectomy and replacement with gastric tube: comparative study with other procedures. *Saudi Med J* 2003; **24**: S39
- 23 **Deschamps C.** History of esophageal surgery for benign disease. *Chest Surg Clin N Am* 2000; **10**: 135-144
- 24 **Ma QF, Liu K, Wang YJ, Cheng QS, Wang XP, Zhou YA.** Colonic interposition for 40 patients with benign esophageal disease. *Disi Junyi Daxue Xuebao* 2001; **22**: 708-713
- 25 **Kim YT, Sung SW, Kim JH.** Is it necessary to resect the diseased esophagus in performing reconstruction for corrosive esophageal stricture? *Eur J Cardiothorac Surg* 2001; **20**: 1-6
- 26 **Dauids PH, Bartelsman JF, Tilanus HW, van Lanschot JJ.** Consequences of caustic damage of the esophagus. *Ned Tijdschr Geneesk* 2001; **145**: 2105-2108

Edited by Kumar M and Wang XL Proofread by Xu FM

• CLINICAL RESEARCH •

Laparoscopic resection of submucosal tumor on posterior wall of gastric fundus

Zhong-Wei Ke, Cheng-Zhu Zheng, Ming-Gen Hu, Dan-Lei Chen

Zhong-Wei Ke, Cheng-Zhu Zheng, Ming-Gen Hu, Dan-Lei Chen,
Department of Minimally Invasive Surgery, Changhai Hospital, Second
Military Medical University, Shanghai 200433, China

Correspondence to: Dr. Zhong-Wei Ke, Department of Minimally
Invasive Surgery, Changhai Hospital, Second Military Medical University,
174 Changhai Road, Shanghai 200433, China. weiz@miscenter.cn

Telephone: +86-21-25072014 **Fax:** +86-21-25074527

Received: 2004-02-14 **Accepted:** 2004-03-04

Abstract

AIM: Laparoscopic resection of tumors on the posterior wall of gastric fundus, especially when they are next to the esophagocardiac junction (ECJ), is both difficult and time-consuming. Furthermore, it can lead to inadvertent esophagus stenosis and injury to the spleen. In order to overcome these difficulties, laparoscopically extraluminal resection of gastric fundus was designed to manage submucosal tumors located on the posterior wall of gastric fundus and next to ECJ.

METHODS: From January 2001 to September 2003, laparoscopically extraluminal resection of gastric fundus was successfully carried out on 15 patients. There were 11 males and 4 females with an average age of 58 years (range, 38 to 78 years). The mean diameter of the tumors was 4.8 cm. The distance of the tumor border from ECJ was about 1.5-2.5 cm. The four-portal operation procedures were as follows: localization of the tumor, dissection of the omentum, mobilization of the gastric fundus and the upper polar of spleen, exposure of ECJ, and resection of the gastric fundus with Endo GIA.

RESULTS: The laparoscopic operation time averaged (66.2±10.4) min, the average amount of bleeding was (89.4±21.7) mL. The mean post-operative hospital stay was (5.3±1.1) d. Within 36 h post-operation, 73.3% of all the patients recovered their gastrointestinal function and began to eat something and to walk. In all the operations, no apparent tumor focus was left and no complication or conversion to open surgery occurred.

CONCLUSION: Our newly designed procedure, laparoscopically extraluminal resection of the gastric fundus, can avoid contamination of the abdominal cavity, injury to the spleen and esophageal stenosis. The procedure seems to be both safe and effective.

Ke ZW, Zheng CZ, Hu MG, Chen DL. Laparoscopic resection of submucosal tumor on posterior wall of gastric fundus. *World J Gastroenterol* 2004; 10(19): 2850-2853
<http://www.wjgnet.com/1007-9327/10/2850.asp>

INTRODUCTION

Malignant gastric tumors are still considered a contraindication for laparoscopic surgery by many surgeons. However, the

removal of benign tumors laparoscopically has been widely accepted as a feasible alternative to laparotomy^[1-6]. The most frequent benign gastric tumor is leiomyoma, and extensive resection is indicated because it is difficult to differentiate it from leiomyosarcoma only by biopsy. When a gastric submucosal tumor is laparoscopically removed, it is recommended to resect a sufficient margin of the surrounding normal tissues in the event that the tumor is malignant^[5,7-14].

Laparoscopic resection of a gastric fundus tumor on the anterior wall is relatively easy, in which a wedge of stomach can be resected under laparoscopic vision using an Endo GIA after the lesion is marked endoscopically. However, laparoscopic resection of tumors on the posterior wall of gastric fundus, especially when they are next to the esophagocardiac junction (ECJ), is both difficult and time-consuming. Furthermore, it can lead to inadvertent esophagus stenosis and injury to the spleen^[14-18]. In order to overcome these difficulties, we proposed a new technique for the management of submucosal tumors located on the posterior wall of gastric fundus and next to ECJ, which was *laparoscopically extraluminal resection of the gastric fundus*.

MATERIALS AND METHODS

Materials

From January 2001 to September 2003, 15 procedures of laparoscopically extraluminal resection of the gastric fundus were carried out for the submucosal tumors located on the posterior wall of gastric fundus and next to ECJ. There were 11 male and 4 female patients with an average age of 58 years (range, 38 to 78 years). The complaints at admission included upper gastrointestinal bleeding (10 cases, 66.7%) and abdominal pain (4 cases, 26.7%). The remaining one (6.7%) was diagnosed when having a physical checkup. Preoperative examinations included gastroscopy, ultrasonic gastroscopy, and barium swallow examination of the upper gastrointestinal tract, all of which revealed a submucosal lesion on the posterior wall of gastric fundus near the ECJ with a regular margin. Since these tumors could not be lifted by intrasubmucosal injection of normal saline, gastroscopic local tumor resections were not indicated. Besides, gastroscopy suggested the presence of ulcers at the center of tumor surfaces in 11 patients. The neoplasm diameter ranged 3.0-6.5 cm with a mean value of 4.8 cm. The distance of the neoplasm margin from ECJ was about 1.5-2.5 cm (Figure 1).

Surgical Methods

Anesthesia and position After general anesthesia under bronchial intubation, the patient was placed in a supine position with both legs abducted 30°. The surgeon stood between the patient's legs while the laparoscopic holder and the operative assistant on the right and left sides of the patient, respectively. **Portal positions** Trocars with 5 mm or 10-12 mm in diameter were placed in the umbilicus, the left or right midclavicular line, and under the xiphoid (Figure 2).

Localization of tumors Under laparoscopy, three methods could be used for neoplasm localization: naked eye inspection, instrument exploration, and intra-operative gastroscopy^[19]. In

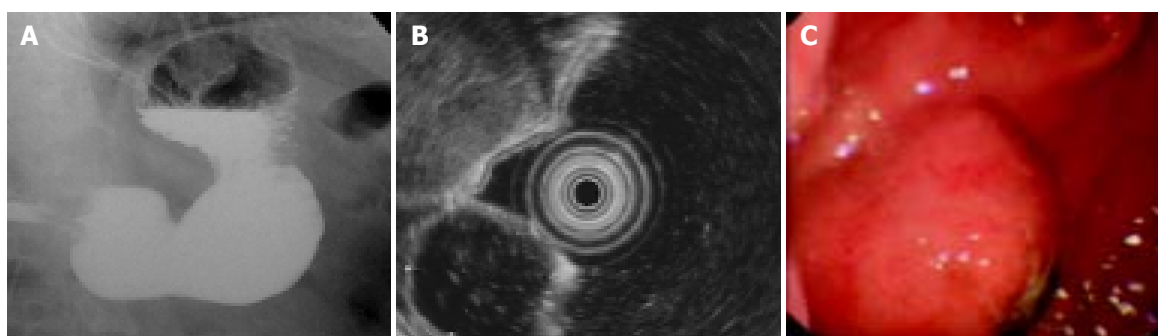


Figure 1 Submucosal tumors on gastric fundus diagnosed in preoperative examinations. A: A lesion near to ECJ with a clear-cut margin shown in barium swallow examination of upper gastrointestinal; B: A lesion with a clear-cut margin protruded into gastric lumen shown in ultrasonic gastroscopy; C: A hemisphere-like projection in the posterior wall of gastric fundus and an ulcer in its center shown in gastroscopy.

this series, the neoplasms had a relative large diameter. So the localization was realized via naked eye inspection and instrument exploration except in four cases under the help of gastroscopy. To perform this operation, it was also important to confirm the distances between tumors and ECJ after the tumors were localized. **Dividing omentum, entering omental bursa, and dividing splenogastric ligament** Omentum dissection was begun from the middle-inferior pole of spleen and proceeded along outside of gastroepiploic vascular arch. After entering the omental bursa, the gastric posterior wall was turned to right by three-finger forceps. Next, the short gastric vessels were coagulated and cut with the ultrasonically activated scalpel to completely divide the gastric fundus from the superior pole of spleen.

Dissection of the left side of cardiac orifice to expose ECJ

Resection of gastric fundus using Endo GIA Figure 3A shows the cutting line of Endo GIA. The firing times of Endo GIA depended on the size of tumors. Complete resection of tumors with a sufficient margin usually required 2-3 sequential firings. When Endo GIA was placed near the left side of cardia, special care was taken to ensure that ECJ was not involved (Figure 3B).

Taking out of specimens Specimens were taken out through portal B after they were put in the specimen bag. Pathological examination was routinely carried out during the procedure.

The surgical field was irrigated and drainage tube was placed under the left diaphragm.

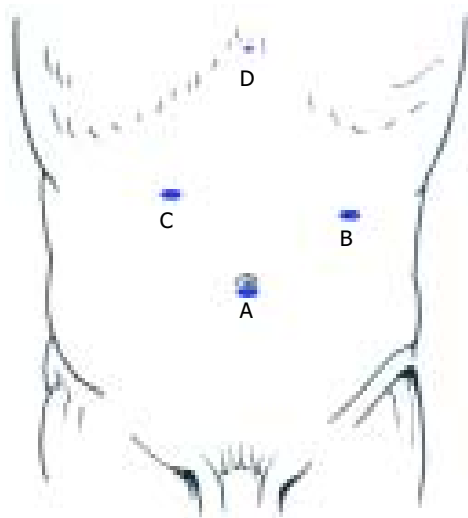


Figure 2 Trocar positions for laparoscopically extraluminal resection of gastric fundus. A: Endoscope portal (10 mm); B, C: Main working portals (10-12 mm); D: Assisting working portal (5 mm).

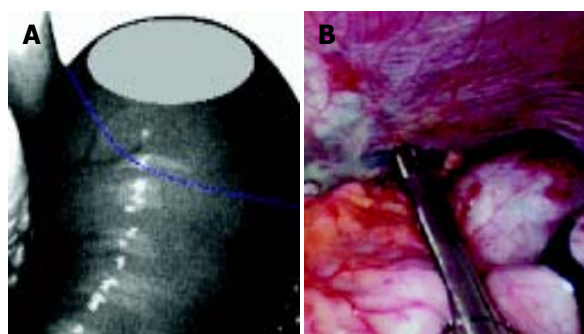


Figure 3 Resection of gastric fundus with Endo GIA. A: The blue line represents the Endo GIA resection line; B: When Endo GIA was placed near the cardia, special care was taken to ensure that ECJ was not involved.

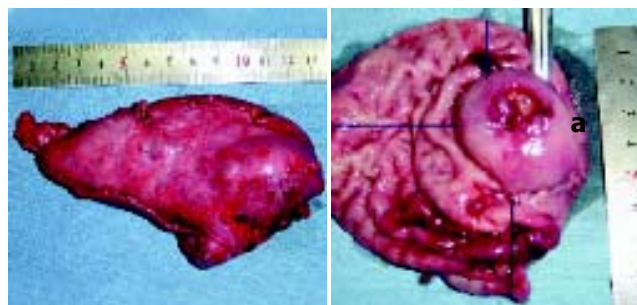


Figure 4 Resected specimens. Line a: the distance of the tumor to ECJ.

RESULTS

In this series, the mean operative time, blood loss, and postoperative hospital stay were 66.2 ± 10.4 min (range, 55 to 90 min), 89.4 ± 21.7 mL (range, 50-200 mL), and 5.3 ± 1.1 d (range, 4-7 d), respectively. On the first postoperative day, the abdominal drainage was 40-180 mL (average, 60.7 ± 14.3 mL). Of all the patients, 73.3% recovered their gastrointestinal function within 36 h after operation and began to eat and to walk. The slowest recovery of gastrointestinal function occurred 60 h post-operation.

Figure 4 shows the resected specimens. The distance of the tumor to the section edge was: (1) 1-1.5 cm to ECJ, with an average of 1.1 ± 0.3 cm; (2) 2.5-6 cm to the other three edges, with an average of 3.9 ± 1.2 cm. The intra-operative frozen sections suggested that all the tumors were benign. But the postoperative paraffin-embedded sections revealed two cases of mesenchymoma with a low malignancy. In these two cases, the distance of the tumor to ECJ was 1.3 cm and 1.5 cm respectively, and the distance to the other three edges was greater than 3 cm. The

extensive salvage operation was not carried out, and a follow-up period of 18 mo and 22 mo, respectively, did not find any recurrence and metastasis. In the other 13 cases, leiomyoma was diagnosed in 8 cases, mesenchymoma in 4 cases, and neurofibroma in 1 case.

All the 15 laparoscopic surgeries were carried out successfully with no apparent lesion left, and no complication and conversion to open surgery occurred. Follow-up was continued for 3.5-33 mo and revealed no abnormality.

DISCUSSION

Clinically, gastric benign tumors are difficult to differentiate into malignancy. Even in benign tumors, canceration and severe complications of obstruction and bleeding may take place latter. So, active measures should be taken to surgically resect the tumors. As to the resection depth, the tendency was to remove the total layer of gastric wall^[20-22]. Under gastroscopy, some gastric tumors could be excised via the intrasubmucosal injection of normal saline. However, this technique is applied mainly to the resection of mucosal tumors and not effective on submucosal neoplasms. Furthermore, the whole thickness of gastric wall could not be removed using this method. In the past, laparotomy was primarily performed to resect gastric submucosal tumors. With the advent of minimally invasive surgery, laparoscopic resection has become the first choice of many surgeons^[23-26].

Submucosal tumors in the fundus or cardia of stomachs can be managed via laparoscopic proximal gastrectomy. However, postoperative reflux esophagitis is common. For most benign gastric submucosal tumors, the range of excision is too large and the procedure is too invasive^[27-31]. Laparoscopic wedge resection of stomachs is the most commonly seen procedure for submucosal tumors of gastric fundus^[31-34]. The tumor on the anterior wall of fundus is easy to excise with Endo GIA^[20]. But for submucosal tumors on the posterior wall of gastric fundus, especially when next to ECJ, the wedge resection of stomachs is quite difficult, and caution should be taken to protect ECJ from postoperative esophageal stenosis and the spleen from injury, especially its superior polar.

In our early experience, we managed to resect submucosal tumors on the posterior wall of gastric fundus through the window of gastrotomy on the anterior gastric wall. The procedure was performed as follows: to cut open the anterior wall of the gastric body or fundus firstly (gastrotomy on the anterior gastric wall), to extract the posterior wall of gastric fundus through this cut, and to excise the tumor on the posterior gastric wall with Endo GIA or the method of stripping plus endoscopic suturing^[35]. This method, though relatively easy to carry out and with quite a good outcome, has the disadvantage of seriously intra-operative abdominal contamination of gastric juice. Furthermore, this method cannot achieve good exposure of ECJ and has not been used in the excision of tumors on the posterior wall near ECJ. Sekimoto *et al.*^[20] reported that intraluminal resection of the full thickness of posterior gastric wall lesion was performed to manage submucosal tumors on the posterior wall of gastric fundus near ECJ. In this study, balloon-tip trocars were inserted directly into the gastric lumen and gas was charged into the stomach through the trocars, then wedge resection of the posterior wall tumor was completed under direct vision with Endo GIA. The authors believe that the procedure has fewer traumas to patients and less opportunity of intraperitoneal contamination by gastric juice than gastrotomy on the anterior gastric wall. ECJ was always in the surgeon's sight, so the distance between the resection line and ECJ could be continuously monitored, which means less morbidity of postoperative esophageal stenosis. However, we think that the above two methods have the same disadvantage

of a limited range of resection and a higher incidence of spleen injury in that the short gastric vessels were not cut and especially that the superior pole of the spleen was not completely divided from gastric fundus. Moreover, care must be taken that the lateral tension to the gastric wall from gas inflation cannot be excessive, otherwise, injury of splenic capsule or gastric wall laceration might occur^[15-18,20].

In order to solve these problems, we proposed a new laparoscopic approach to surgical resection of submucosal tumors on the posterior wall of gastric fundus. In this technique, the omentum is dissected to get access to the omental bursa. So, the splenogastric ligament could be severed to completely dissect the gastric fundus away from the superior pole of spleen. Then the left side of cardiac orifice is dissected to expose ECJ, and the gastric fundus is resected with the Endo GIA. Through these measures, the newly designed approach, *laparoscopically extraluminal resection of gastric fundus*, could avoid intraperitoneal contamination, the spleen injury and the postoperative esophagus stenosis. Meanwhile, it could also provide a sufficient range of gastric resection. The main disadvantage is the increased steps required. However, with necessary training and skills in the laparoscopic surgery, the procedure can be accomplished not quite both difficult and time consuming. The average operation time in our series was only 66.2±10.4 min. The procedure, we think, is both safe and effective in that the ECJ and the superior pole of spleen are under the continuous supervision of the operator when resecting the gastric fundus, and that the procedure can provide a more sufficient range of resection.

When the laparoscopically extraluminal resection of gastric fundus is performed, two key points must be stressed. One is that the interspace between gastric fundus and superior pole of spleen must be adequately dissected. The other is that when Endo GIA is placed near the cardia, special care must be taken to ensure that ECJ is not involved. So long as the above key points are fulfilled, our method is safe, easy and beneficial to the laparoscopic resection of submucosal tumors on the posterior wall of gastric fundus.

REFERENCES

- 1 Shimizu S, Noshiro H, Nagai E, Uchiyama A, Tanaka M. Laparoscopic gastric surgery in a Japanese institution: analysis of the initial 100 procedures. *J Am Coll Surg* 2003; **197**: 372-378
- 2 Cuschieri A. Laparoscopic gastric resection. *Surg Clin North Am* 2000; **80**: 1269-1284
- 3 Giger U, Schafer M, Krahenbuhl L. Technique and value of staging laparoscopy. *Dig Surg* 2002; **19**: 473-478
- 4 Croce E, Olmi S, Magnone S, Russo R. Laparoscopic surgery of the stomach: state of the art. *Chir Ital* 2003; **55**: 811-820
- 5 Ludwig K, Weiner R, Bernhardt J. Minimally invasive resections of gastric tumors. *Chirurg* 2003; **74**: 632-637
- 6 Saikawa Y, Kumai K, Otani Y, Yoshida M, Furukawa T, Kitagawa Y, Kubota T, Kitajuma M. Present status of laparoscopic surgery for gastrointestinal neoplasms. *Nippon Naika Gakkai Zasshi* 2003; **92**: 53-57
- 7 Yang W, Wu YL, Chu Y, Sheng H, He JH, Xiong FB, Wang Y, Cheng SD. Difference of tumor size between endoscopic estimation and postoperative pathological measurement in early gastric carcinoma. *Shijie Huaren Xiaohua Zazhi* 2003; **11**: 51-53
- 8 Avital S, Brasesco O, Szomstein S, Liberman M, Rosenthal R. Technical considerations in laparoscopic resection of gastric neoplasms. *Surg Endosc* 2003; **17**: 763-765
- 9 Yuan Y, Lin HZ, Zhang YC, Wang XJ, Wu YQ, Gao H, Wang L, Liu YH, Lu F, Lou SQ. Study on the pathogenetic effect of salted pork from a high risk area of stomach cancer in China. *China Nati J New Gastroenterol* 1997; **3**: 93-94
- 10 Qin DX, Wang GQ, Yuan FL, Tang MZ, Li MS, Zhang ZL. Screening for upper digestive tract cancer with an occult blood bead detector. Investigation of a normal north China population.

- Cancer* 1988; **62**: 1030-1034
- 11 **Cheng YS**, Li MH, Chen WX, Zhuang QX, Chen NW, Shang KZ. Follow-up evaluation for benign stricture of upper gastrointestinal tract with stent insertion. *World J Gastroenterol* 2003; **9**: 2609-2611
 - 12 **Hsieh CC**, Shih CS, Wu YC, Huang BS, Hsu WH, Huang MH, Wang LS. Leiomyosarcoma of the gastric cardia and fundus. *Zhonghua Yixue Zazhi* 1999; **62**: 418-424
 - 13 **Alecu L**, Costan I, Vitalariu A, Obrocea F, Pacuraru E, Gulinescu L. Gastric stromal tumor treated by laparoscopic surgery. *Chirurgia* 2002; **97**: 297-304
 - 14 **Pross M**, Wolff S, Nestler G, Schubert D, Kahl S, Lippert H. A technique for endo-organ resection of gastric wall tumors using one intragastric trocar. *Endoscopy* 2003; **35**: 613-615
 - 15 **Motson RW**, Fisher PW. A new technique for laparoscopic resection of a submucosal tumor on the posterior wall of the gastric fundus. *Surg Endosc* 2000; **14**: 205-206
 - 16 **Pross M**, Wolff S, Schubert D, Meyer L, Lippert H. Combined minimal-invasive procedures for resection of benign gastric wall tumors. *Zentralbl Chir* 2003; **128**: 191-194
 - 17 **Bouillot JL**, Bresler L, Fagniez PL, Samama G, Champault G, Parent Y. Laparoscopic resection of benign submucosal stomach tumors. A report of 65 cases. *Gastroenterol Clin Biol* 2003; **27**(3 Pt 1): 272-276
 - 18 **Moesta KT**, Hunerbein M, Schlag PM. Treatment procedures for adenocarcinoma of the esophagogastric junction. *Chirurg* 2003; **74**: 381-392
 - 19 **Ke ZW**, Zheng CZ, Qiu M, Li JH, Yin K, Hua JD. Laparoscopic small bowel resection. *Zhonghua Weichang Waiké Zazhi* 2002; **5**: 92-94
 - 20 **Sekimoto M**, Tamura S, Hasuike Y, Yano M, Murata A, Inoue M, Shiozaki H, Monden M. A new technique for laparoscopic resection of a submucosal tumor on the posterior wall of the gastric fundus. *Surg Endosc* 1999; **13**: 71-74
 - 21 **Xu GW**. The gastric tumor. In: Wu JP, Qiu FZ, eds. Huang Jia-Si Waiké Xue. 6th Edition. Beijing: Renmin WeiSheng Press 1999: 1031-1052
 - 22 **Tangoku A**, Yamamoto K, Hirazawa K, Takao T, Mori N, Tada K, Oka M. Laparoscopic resection of large leiomyomas of the gastric fundus. *Surg Endosc* 1999; **13**: 1050-1052
 - 23 **Rohatgi A**, Singh KK. Laparoendoscopic management of gastrointestinal stromal tumors. *J Laparoendosc Adv Surg Tech A* 2003; **13**: 37-40
 - 24 **Tonouchi H**, Mohri Y, Tanaka K, Konishi N, Ohmori Y, Kobayashi M, Watanabe Y, Matsumura K, Takeda K, Kusunoki M. Lymphatic mapping and sentinel node biopsy during laparoscopic gastrectomy for early cancer. *Dig Surg* 2003; **20**: 421-427
 - 25 **Kobayashi T**, Kazui T, Kimura T. Surgical local resection for early gastric cancer. *Surg Laparosc Endosc Percutan Tech* 2003; **13**: 299-303
 - 26 **Nguyen NT**, Jim J, Nguyen A, Lee J, Chang K. Laparoscopic resection of gastric stromal tumor: a tailored approach. *Am Surg* 2003; **69**: 946-950
 - 27 **Uyama I**, Ogiwara H, Takahara T, Kikuchi K, Iida S. Laparoscopic and minilaparotomy proximal gastrectomy and esophagogastrostomy: technique and case report. *Surg Laparosc Endosc* 1995; **5**: 487-491
 - 28 **Zhang G**, Miao L, Zhang H, Lu J. Clinical study on reservation of part of stomach for patients with cardiac cancer of the gastric stump. *Chin Med J* 1998; **111**: 630-633
 - 29 **Usui S**, Inoue H, Yoshida T, Fukami N, Kudo SE, Iwai T. Hand-assisted laparoscopic total gastrectomy for early gastric cancer. *Surg Laparosc Endosc Percutan Tech* 2003; **13**: 304-307
 - 30 **Dostalík J**, Martinek L, Satinsky I, Richter V, Stigler J. Laparoscopic total gastrectomy-initial experience. *Rozhl Chir* 2003; **82**: 353-356
 - 31 **Walsh RM**, Ponsky J, Brody F, Matthews BD, Heniford BT. Combined endoscopic/laparoscopic intragastric resection of gastric stromal tumors. *J Gastrointest Surg* 2003; **7**: 386-392
 - 32 **Jess P**, Jensen KH. Laparoscopic wedge resection of stromal gastric tumor guided by laparoscopic ultrasonographic scanning. *Ugeskr Laeger* 2003; **165**: 1038-1039
 - 33 **Ozmen MM**, Zulfikaroglu B, Ozalp N, Ziraman I, Hengirmen S, Sahin B. Staging laparoscopy for gastric cancer. *Surg Laparosc Endosc Percutan Tech* 2003; **13**: 241-244
 - 34 **Onate-Ocana LF**, Ochoa-Carrillo FJ. The role of minimal invasion surgery in the management of patients with gastric carcinoma. *Cir Cir* 2003; **71**: 324-328
 - 35 **Ke Z**, Zheng C, Qiu M, Shen Y, Hua J. Laparoscopic gastric resection. *Zhonghua Waiké Zazhi* 2000; **38**: 680-682

Edited by Kumar M and Wang XL Proofread by Xu FM

• CLINICAL RESEARCH •

First two cases of living related liver transplantation with complicated anatomy of blood vessels in Beijing

Wen-Han Wu, Yuan-Lian Wan, Long Lee, Yin-Mo Yang, Yan-Ting Huang, Chao-Long Chen, Sheung-Tat Fan

Wen-Han Wu, Yuan-Lian Wan, Long Lee, Yin-Mo Yang, Yan-Ting Huang, Department of Surgery, The First Hospital, Peking University, Beijing 100034, China

Chao-Long Chen, Department of Surgery, Chang Gung Memorial Hospital, 123 Ta-Pei Road, Niao-Sung, Kaohsiung, Taiwan, China

Sheung-Tat Fan, Department of Surgery, Queen Mary Hospital, University of Hong Kong Medical Centre, 102 Pokfulam Road, Hong Kong, China

Correspondence to: Dr. Wen-Han Wu, Department of Surgery, The First Hospital, Peking University, Beijing 100034, China

Received: 2003-07-17 **Accepted:** 2003-10-12

Abstract

AIM: Living related liver transplantation (LRLT) has been developed in response to the paediatric organ donor shortage. Though it has been succeeded in many centers worldwide, the safety of the donor is still a major concern, especially in donors with anatomy variation. We succeeded in performing the first two cases of living related liver transplantation with complicated anatomy of blood vessels as a way to overcome cadaveric organ shortage in Beijing.

METHODS: Two patients, with congenital liver fibrosis and congenital biliary atresia were performed with living donor liver transplantation in our hospital and then followed up from November 12 to December 13, 2001. The two living donors, mother and father, were healthy aged 34 and 35 years. One right lobe (segment V, VI, VII, VIII) and one left lateral lobe (segment II and III) were used. The grafts weighed 394 g and 300 g. The ratio of graft weight to the standard liver volume (SLV) of donors was 68% and 27%. The graft weight to recipient body weight ratio was 3.2% and 4.4%. The graft weight to recipient estimated standard liver mass (ESLM) ratio was 63% and 85%. The two donors had complicated blood vessel variation.

RESULTS: Two patients undergone living donor liver transplantation had good results. Abnormal liver function with high bilirubin level appeared in a few days after operation, but liver function returned to normal one month after operation with bilirubin level almost decreased to near normal. No bleeding, thrombosis, infection and bile leakage occurred. One had an acute rejection and recovered. The two donors recovered in two weeks. One had slight fever because of a little collection in abdomen and recovered after paracentesis and drainage.

CONCLUSION: Living donor liver transplantation has been proved to be a good way that offers a unique opportunity of getting a timely liver graft as a response to shortage of pediatric donors, though it could be a technically difficult operation if there is anatomical variation.

Wu WH, Wan YL, Lee L, Yang YM, Huang YT, Chen CL, Fan ST. First two cases of living related liver transplantation with complicated anatomy of blood vessels in Beijing. *World J Gastroenterol* 2004; 10(19): 2854-2858
<http://www.wjgnet.com/1007-9327/10/2854.asp>

INTRODUCTION

Orthotopic liver transplantation is an effective therapy for end-stage liver disease and has been proved to be a major advance in the treatment of children with liver disease. But the development of liver transplantation in infants and young children has been hampered by the shortage of donors, especially the scarcity of size-matched donors. Though reduced-size liver transplantation (RLT) was used in some centers, it does not expand the pool of potential donors and the mortality rate of recipients on the waiting list has remained high.

From November 12 to December 13 of 2001, the first two cases of living related liver transplantation in Beijing were successfully performed in our hospital. The donors were mother and father. The recipients were their 12-year-old and 31-month-old daughters. The donors and recipients all recovered about two months after operation. These two cases indicate the potential benefit of living related liver transplantation in Beijing.

MATERIALS AND METHODS

Patients

Between November 12 and December 13 of 2001, living related liver transplantation was successfully performed on two cases in the First Hospital, Peking University. They were two girls. Underlying diseases were congenital liver fibrosis and congenital biliary atresia.

Donor selection and evaluation

The living donors were mother and father with ABO identical blood group to the patients. There was no biochemical or serologic evidence of liver disease. Computerized tomography (CT) with volumetric measurement was performed to assess the volume of the right lobe and the left lateral lobe in order to determine the graft to be harvested. Angiographies to assess the vascular anatomy were performed in both donors. We found that both donors had blood vessel variations. In donor 1, the right hepatic artery (RHA) was from the superior mesenteric artery (SMA) (Figure 1A). The two branches of right portal veins (anterior and posterior right portal vein, ARPV and PRPV) of the mother were combined to the left portal veins (LPV) separately inside the liver parenchyma, no common trunk of right portal vein was found (Figure 1B). In donor 2, the left hepatic artery was derived from the right anterior hepatic artery, which was nearly inside the liver parenchyma (Figure 1C).

Donor operation

Laparotomy was performed via bilateral subcostal incision with an upward midline extension to the xiphoid process. Cholecystectomy was performed and the cystic duct was cannulated for cholangiography using undiluted radiographic contrast in order to delineate the ductal anatomy.

In donor 1, the cholangiography showed that it had the similar variation to the portal vein, the two branches of right bile ducts (anterior and posterior right bile ducts, ARBD and PRBD) of the mother were combined to the left bile duct separately which were inside the liver parenchyma (Figure 2).

Intraoperative ultrasonography was then performed to

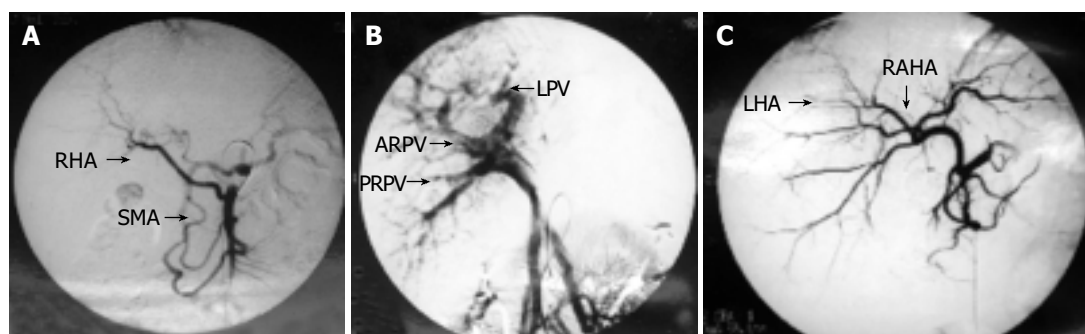


Figure 1 Angiography of the donors. A: Right hepatic artery (RHA) from superior mesenteric artery (SMA). B: Two branches of right portal veins (anterior and posterior right portal veins, ARPV and PRPV) of the mother. C: Left hepatic artery (LHA) derived from right anterior hepatic artery (RAHA).

determine the configuration of the right hepatic vein, the junction of the middle hepatic vein with the left hepatic vein and to mark on the liver surface the position of the middle hepatic vein, which would be the liver transection plane. No right inferior hepatic veins were found in these two donors. The transection line was determined by the optimal graft volume and the anatomy of its drainage veins. The entire drainage area of the right and left hepatic veins were also identified by intraoperative ultrasonography. All of the right and left hepatic venous branches were traced to the periphery in the medial segment and marked with electrocautery on the liver surface. Hilar dissection was performed to free the right hepatic artery and portal vein. Branches of the right and left portal veins supplying the caudate process were divided and ligated.

In donor 1, dissection of the right portal veins (ARPV and PRPV) and the right hepatic ducts (ARBD and PRBD) was not made until the liver was transected, because they were inside the liver parenchyma due to anatomical variation. Parenchymal transection was performed by intraoperative ultrasonography with an ultrasonic dissector without vascular occlusion. The right hepatic ducts (the anterior and posterior ducts) were divided near the confluence of the bile ducts. The defect on the left hepatic duct was closed with 5-0 PDS monofilament absorbable sutures. After mobilization of the right liver, the right portal veins (the anterior and posterior veins), the right hepatic artery (from superior mesenteric artery) and vein were clamped at the junction with the main trunks and divided. At the back table, the graft was immersed in ice sludge and flushed with University of Wisconsin (UW) solution through the right portal venous cannula. The stumps of the right hepatic artery, the right hepatic vein and portal vein on the donor liver remnant were sutured.

In donor 2, The left hepatic artery, portal vein and hepatic vein were freed and hepatic parenchymal transection was accomplished using an ultrasonic dissector without vascular occlusion. Because the left hepatic artery was from the anterior right hepatic artery, the dissection of the left hepatic artery was partly inside the liver parenchyma when the liver transection was finished. The left duct was divided close to the cut surface of the liver, with an intact Glissonian sheath. The left hepatic duct was divided near the confluence of the bile ducts. The isolated graft was perfused in situ with the left portal vein clamped and cannulated by a catheter connected with cold lactated Ringer's solution followed by a cold UW solution, when the left hepatic vein was opened.

Recipient operation

The abdomen was entered through a bilateral subcostal incision with midline extension. Hilar dissection was performed to isolate and divide branches of the hepatic artery and portal vein. Then, total hepatectomy was performed with the inferior

vena cava preserved.

In recipient 1, the graft right hepatic vein (RHV-D) was anastomosed end-to-end to the recipient right hepatic vein (RHV-R). The graft anterior right portal vein (ARPV-D) was anastomosed end-to-end to the recipient left portal vein (LPV-R) and the graft posterior right portal vein (PRPV-D) was anastomosed end-to-end to the recipient right portal vein (RPV-R). The similar method was used to reconstruct the bile duct without stenting after the hepatic artery anastomosis (Figure 3).



Figure 2 Cholangiography of the donor 1 Two branches of right bile duct (anterior and posterior right bile ducts, ARBD and PRBD) of the mother.

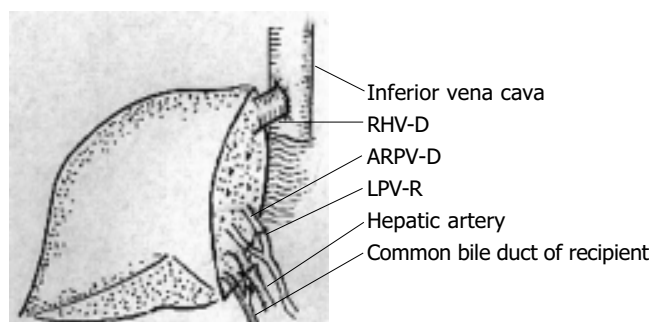


Figure 3 End-to-end anastomosis of the graft right hepatic vein (RHV-D) to the recipient right hepatic vein (RHV-R).

In recipient 2, the graft left hepatic vein was anastomosed end-to-end to the confluence of the recipient left and middle hepatic veins. The graft left portal vein was anastomosed end-to-end to the truncated bifurcation of the recipient portal vein. The left hepatic duct was anastomosed to the Roux-en-Y limb of jejunum with an internal stent after the hepatic artery anastomosis.

The hepatic artery of the graft was anastomosed to the recipient hepatic artery using microvascular techniques.

Postoperative immunosuppression

Induction and maintenance immunosuppressive therapy consisted of a triple-drug regimen of steroid, cyclosporine A, and azathioprine. Acute rejection episode suspected on clinical and biochemical features and confirmed by percutaneous liver biopsy, was treated by intravenous bolus of methyl-predimetholone.

RESULTS

There was no operative mortality in the two living donors. One donor had postoperative complication of abdominal collection about two weeks after operation and recovered by percutaneous drainage about three weeks after operation. Blood losses during the donor operations were 150 mL and 70 mL respectively, and no blood transfusion was required in these two donor operations. Blood losses during the recipient operations were 50 mL and 100 mL respectively, and recipient 2 received 200 mL blood transfusion in the operation. The first warm ischaemia time of the grafts was 30 s and almost 0 s. The cold ischaemia time of the grafts was 120 min and 180 min. The second warm ischaemia time of the graft was 40 min and 50 min. The portal and arterial reperfusion interval time was 70 min and 90 min.

Table 1 Laboratory findings of donor 1

Content	Pre-operation	1 d post-operation	3 d post-operation	7 d post-operation	14 d post-operation
ALT (IU/L)	12	372	110	48	45
AST (IU/L)	9	404	105	43	40
TBIL (ug/L)	10.5	80.2	32.5	7.4	8.2
DBIL (ug/L)	3.8	37.5	4	3.94	2.1
PTA (%)	78.0	32.0	29.0	56.0	72.0

Table 2 Laboratory findings of donor 2

Content	Pre-operation	1 d post-operation	3 d post-operation	7 d post-operation	14 d post-operation
ALT (IU/L)	37	816	305	42	
AST (IU/L)	30	817	58	37	
TBIL (ug/L)	7.7	21.8	9.7	5.0	
DBIL (ug/L)	3.5	3.24	2.3	0.78	
PTA (%)	82	127	151	127	

The weight of grafts was 394 g and 300 g, respectively. The ratio of graft weight to the standard liver volume (SLV) of donor

was 68% and 27%, respectively. The graft weight to recipient body weight ratio was 3.2% and 4.4% respectively, and the graft weight to recipient estimated standard liver mass (ESLM) was 63% and 85%.

The duration of postoperative hospital stay of the donors was 7 d and 21 d. Most laboratory profiles returned to normal about two weeks after operation. The two donors had normal liver function and were able to return to their preoperative activities 3 mo after the operation.

Both patient and graft survived well 3 mo after operation. No postoperative complication occurred in recipient 1. Recipient 2 had an attack of acute rejection one week after the operation, and recovered after bolus treatment of methylprednisolone (1 g methylprednisolone per day for three days, iv).

Data on the postoperative serum total bilirubin (TBIL), direct bilirubin (DBIL), alanine aminotransferase (ALT), aspartate aminotransferase (AST) and prothrombin activities (PTA) are shown in Tables 1-4.

DISCUSSION

The well-known inverse relationship between the availability of cadaveric pediatric organs and the epidemiology of pediatric liver disease has resulted in a substantial mortality rate among children on the waiting list^[1,2]. Although RLT could alleviate the shortage of small donor organs, it did not expand the pool of potential donors, but induced a shift of grafts from a limited pool of adult cadaveric donors to pediatric recipients^[3]. The use of liver donors has provided a means for increasing the overall supply of livers^[4,5].

Though liver consists of paired structures anatomically, safe separation of liver into its right and left halves requires considerable experience^[6,7]. Fan *et al.*^[14] identified the reasons for unsatisfactory outcomes such as the presence of necrotic tissue on the liver transection surface, inadequate hepatic venous drainage, missed right posterior hepatic duct, and more than one right hepatic duct orifice on the graft. All these made its reconstruction difficult^[8]. We followed the procedure "living donor liver transplantation using right lobe graft" by preferring the division of liver parenchyma along the Cantlie line^[9]. To define the Cantlie line, we used the middle hepatic vein as a reference by using the intraoperative ultrasonogram^[10,11]. To reduce the bleeding in the operation, we also decreased the central venous pressure to about 5 cm H₂O^[12].

The blood supply to the hepatic duct is dependent on a peribiliary plexus^[13]. In the harvesting of the right or the left

Table 3 Laboratory findings of recipient 1

Content	Pre-operation	1 d post-operation	3 d post-operation	7 d post-operation	14 d post-operation	21 d post-operation	28 d post-operation
ALT (IU/L)	40	372	189	103	80	24	28
AST (IU/L)	44	418	78	53	19	17	22
TBIL (ug/L)	17.4	73.4	63.3	80.6	58.6	53.6	23.8
DBIL (ug/L)	5.0	45.28	30.6	46.6	30.2	26.6	6.6
PTA (%)	89	18	31	43	41	73	81

Table 4 Laboratory findings of recipient 2

Content	Pre-operation	1 d post-operation	3 d post-operation	7 d post-operation	14 d post-operation	21 d post-operation	28 d post-operation
ALT (IU/L)	105	1 054	1 397	496	185	47	42
AST (IU/L)	250	3 028	414	107	70	35	31
TBIL (ug/L)	480.4	87.7	209.3	216.2	205.4	96.7	44.2
DBIL (ug/L)	373.8	44.79	124.4	178.1	161.1	82.1	30.7
PTA (%)	92	7	16	58	72	76	78

lobe graft, the blood supply is mainly from tiny arterial arcades from the right or the left portion of the caudate lobe^[13]. So, the liver tissue cranial to the hepatic duct was cleared by ultrasonic dissector down to the caudate process and care was taken to avoid thinning the wall of the hepatic duct with ultrasonic dissector. We also noticed to maintain the blood pressure stable in the operation because hypotensive episodes would render the hepatic duct stump vulnerable to ischemia and necrosis^[14].

In our group, the two donors had complicated anatomy variation. In donor 1, ARPV and PRPV were parallelly combined to the left portal vein, which were inside the liver parenchyma, no common trunk of right portal vein was found in extraparenchyma of the liver. The right hepatic duct had the similar anatomical variation with two parallel branches. This was rare in our past experiences and made the operation quite complicated. A series of 990-arteriportographic studies and 3 000-endoscopic retrograde cholangio-pancreatic-graphic studies of the liver showed that the incidence of this kind of portal vein variation and hepatic bile duct variation was 0.15% and 5.08%, respectively^[15-17]. When we tried to expose the ARPV and PRPV, we did not follow the main trunk of portal vein from the hilum, but dissected the hepatic parenchyma with intraoperative ultrasonography by an ultrasonic dissector without vascular occlusion in combination with hilar dissection to free the ARPV and PRPV^[11]. Dissection of right hepatic ducts was not carried out until the liver was transected. Chen *et al.*^[4] reported that 83.33% intrahepatic ducts had the similar anatomy variation as the portal veins^[18]. We paid more attention to intraoperative cholangiography and certified the similar anatomical variation in our group. We performed the same procedure to finish the dissection of anterior right hepatic duct and posterior right hepatic vein^[19,20].

In donor 2, angiographic study showed that the left hepatic artery was from the anterior right hepatic artery. To avoid ischemia due to excessive hepatic artery dissection, which might cause biliary stricture or leakage^[21], we dissected the left hepatic artery just on the left side of the common hepatic duct and carefully preserved the posterior right hepatic artery from the left side of the left hepatic artery. We also performed a little dissection in liver parenchyma with an ultrasonic dissector to get enough length of left hepatic artery for anastomosis^[4]. It is important not to isolate the left hepatic artery too far into the left side of the liver parenchyma to avoid devascularization of the left hepatic duct^[22].

Since these are the first two cases of living related liver transplantation in Beijing, ethical issues need to be considered when one contemplates liver transplantation from parent to child. These issues are similar to those associated with the transplantation of renal grafts from living related donors^[23]. With the experience in liver resection, we conclude that the surgical risk is low enough to be acceptable for a parent or other close relatives if they volunteer to be an organ donor. Sure, it is an ethical dilemma of subjecting a healthy person to major hepatic resection to obtain a graft for a patient with end-stage liver disease^[24-26]. We all agree with the consensus that living-donor liver transplantation is not justified when there are sufficient cadaveric donors. However, the procedure could be justified for a patient with fulminant hepatic failure when no cadaver donor was available and when the recipient had a reasonable chance of a successful outcome^[27].

The success of these first two cases has led to the acceptance of living related liver transplantation (LRLT) for clinical application in our center. With the excellent results in many centers and our present study^[28,29], we consider that LRLT should be a good way for the care of patients with end-stage liver diseases or fulminant liver failure, particular in countries where cadaveric organ donation is limited or not available^[30,31]. Though it might be very difficult technically, we should not give it up when we consider safety of the donor as our absolute

priority first.

REFERENCES

- 1 Kelly D, Sibal A. Current status of liver transplantation. *Indian J Pediatr* 2003; **70**: 731-736
- 2 Ogura Y, Kaihara S, Haga H, Kozaki K, Ueda M, Oike F, Fujimoto Y, Ogawa K, Tanaka K. Outcomes for pediatric liver retransplantation from living donors. *Transplantation* 2003; **76**: 943-948
- 3 Abouljoud M, Yoshida A, Dagher F, Moonka D, Brown K. Living donor and split-liver transplantation: an overview. *Transplant Proc* 2003; **35**: 2772-2774
- 4 Chen CL, Chen YS, Liu PP, Chiang YC, Cheng YF, Huang TL, Eng HL. Living related donor liver transplantation. *J Gastroenterol Hepatol* 1997; **12**: S342-345
- 5 Malago M, Testa G, Frilling A, Nadalin S, Valentin-Gamazo C, Paul A, Lang H, Treichel U, Cicinnati V, Gerken G, Broelsch CE. Right living donor liver transplantation: an option for adult patients: single institution experience with 74 patients. *Ann Surg* 2003; **238**: 853-863
- 6 Kamel IR, Lawler LP, Fishman EK. Variations in anatomy of the middle hepatic vein and their impact on formal right hepatectomy. *Abdom Imaging* 2003; **28**: 668-674
- 7 Yersiz H, Renz JF, Farmer DG, Hisatake GM, McDiarmid SV, Busuttil RW. One hundred in situ split-liver transplantations: a single-center experience. *Ann Surg* 2003; **238**: 496-505
- 8 Fan ST, Lo CM, Liu CL. Technical refinement in adult-to-adult living donor liver transplantation using right lobe graft. *Ann Surg* 2000; **231**: 126-131
- 9 Akamatsu N, Sugawara Y, Kaneko J, Sano K, Imamura H, Kokudo N, Makuuchi M. Effects of middle hepatic vein reconstruction on right liver graft regeneration. *Transplantation* 2003; **76**: 832-837
- 10 Cheng YF, Huang TL, Chen CL, Chen TY, Huang CC, Ko SF, Lee TY. Variations of the left and middle hepatic veins: application in living related hepatic transplantation. *J Clin Ultrasound* 1996; **24**: 11-16
- 11 Ko EY, Kim TK, Kim PN, Kim AY, Ha HK, Lee MG. Hepatic vein stenosis after living donor liver transplantation: evaluation with doppler US. *Radiology* 2003; **229**: 806-810
- 12 Johnson M, Mannar R, Wu AV. Correlation between blood loss and inferior vena caval pressure during liver resection. *Br J Surg* 1998; **85**: 188-190
- 13 Stapleton GN, Hickman R, Terblanche J. Blood supply of the right and left hepatic ducts. *Br J Surg* 1998; **85**: 202-207
- 14 Fan ST, Lai EC, Lo CM, Chu KM, Liu CL, Wong J. Hepatectomy with an ultrasonic dissector for hepatocellular carcinoma. *Br J Surg* 1996; **83**: 117-120
- 15 Cheng YF, Huang TL, Lee TY, Chen TY, Chen CL. Variation of the intrahepatic portal vein; angiographic demonstration and application in living-related hepatic transplantation. *Transplant Proc* 1996; **28**: 1667-1668
- 16 Huang TL, Cheng YF, Chen CL, Chen TY, Lee TY. Variants of the bile ducts: clinical application in the potential donor of living-related hepatic transplantation. *Transplant Proc* 1996; **28**: 1669-1670
- 17 Kornasiewicz O, Krawczyk M, Paluszkiwicz R, Zieniewicz K, Hevelke P, Grzelak I, Pacho R, Rowinski O, Kalicinski P, Kaminski A, Pawlowska J. Anatomical alteration of the vascular tree observed during living related liver transplantation. *Transplant Proc* 2003; **35**: 2245-2247
- 18 Cheng YF, Huang TL, Shen CL, Sheen-Chen SM, Liu CC, Chen TY, Lee TY. Anatomic dissociation between the intrahepatic bile duct and portal vein: risk factors for left hepatectomy. *World J Surg* 1997; **21**: 297-300
- 19 Kornberg A, Heyne J, Schotte U, Hommann M, Scheele J. Hepatic venous outflow reconstruction in right lobe living-donor liver graft using recipient's superficial femoral vein. *Am J Transplant* 2003; **3**: 1444-1447
- 20 Hisatsune H, Yazumi S, Egawa H, Asada M, Hasegawa K, Kodama Y, Okazaki K, Itoh K, Takakuwa H, Tanaka K, Chiba T. Endoscopic management of biliary strictures after duct-to-duct biliary reconstruction in right-lobe living-donor liver

- transplantation. *Transplantation* 2003; **76**: 810-815
- 21 **Sanchez-Urdazpal L**, Gores GJ, Ward EM, Maus TP, Buckel EG, Steers JL, Wiesner RH, Krom RAF. Diagnostic features and clinical outcome of ischemic-type biliary complications after liver transplantation. *Hepatology* 1993; **17**: 605-609
- 22 **Kanazawa A**, Kubo S, Tanaka H, Takemura S, Yamazaki K, Hirohashi K, Shiomi S. Bile leakage after living donor liver transplantation demonstrated with hepatobiliary scan using ^{99m}Tc-PMT. *Ann Nucl Med* 2003; **17**: 507-509
- 23 **D'Alessandro AM**, Sollinger HW, Knechtle SJ, Kalayoglu M, Kishen WA, Uehling DT, Moon TD, Messing EM, Bruskewitz RC, Pirsch JD. Living related and unrelated donors for kidney transplantation. A 28-year experience. *Ann Surg* 1995; **222**: 353-362
- 24 **Broelsch CE**, Whittington PF, Emond JC, Heffron TG, Thistlethwaite JR, Stevens L, Piper J, Whittington SH, Lichtor JL. Liver transplantation in Children from living related donors. Surgical techniques and results. *Ann Surg* 1991; **214**: 428-437
- 25 **Basaran O**, Karakayali H, Emiroglu R, Tezel E, Moray G, Haberal M. Donor safety and quality of life after left hepatic lobe donation in living-donor liver transplantation. *Transplant Proc* 2003; **35**: 2768-2769
- 26 **Lan AK**, Luk HN, Goto S, Chen SM, Eng HL, Chen YS, de Villa VH, Wang CC, Cheng YF, Chen CL, Lee JH, Jawan B. Stress response to hepatectomy in patients with a healthy or a diseased liver. *World J Surg* 2003; **27**: 761-764
- 27 **Majno P**, Mentha G, Berney T, Buhler LH, Giostra E, Gelez P, Morard I, Bednarkiewicz M, Huber O, Morel P. Adult-to-adult living-donor liver transplantation. A summary of current status and an outline of the program in Geneva. *Swiss Surg* 2003; **9**: 227-236
- 28 **Imamura H**, Seyama Y, Kokudo N, Maema A, Sugawara Y, Sano K, Takayama T, Makuuchi M. One thousand fifty-six hepatectomies without mortality in 8 years. *Arch Surg* 2003; **138**: 1198-1206
- 29 **Ghobrial RM**, Busuttill RW. Future of adult living donor liver transplantation. *Liver Transpl* 2003; **9**(10 Suppl 2): S73-79
- 30 **Zimmerman MA**, Trotter JF. Living donor liver transplantation in patients with hepatitis C. *Liver Transpl* 2003; **9**: S52-57
- 31 **Sugawara Y**, Makuuchi M, Kaneko J, Akamatsu N, Imamura H, Kokudo N. Living donor liver transplantation for hepatitis B cirrhosis. *Liver Transpl* 2003; **9**: 1181-1184

Edited by Xu JY and Wang XL Proofread by Xu FM

Transcutaneous perianal sonography: A sensitive method for the detection of perianal inflammatory lesions in Crohn's disease

Jochen Wedemeyer, Timm Kirchhoff, Gernot Sellge, Oliver Bachmann, Joachim Lotz, Michael Galanski, Michael P. Manns, Michael J. Gebel, Jörg S. Bleck

Jochen Wedemeyer, Gernot Sellge, Oliver Bachmann, Michael P. Manns, Michael J. Gebel, Jörg S. Bleck, Department of Gastroenterology, Hepatology and Endocrinology, Medical School of Hannover, Carl Neuberg Str. 1, 30623 Hannover, Germany

Timm Kirchhoff, Joachim Lotz, Michael Galanski, Department of Diagnostic Radiology, Medical School of Hannover, Carl Neuberg Str. 1, 30623 Hannover, Germany

Correspondence to: Jochen Wedemeyer M.D., Department of Gastroenterology, Hepatology and Endocrinology, Medical School of Hannover, Carl Neuberg Str. 1, 30625 Hannover, Germany. wedemeyer.jochen@mh-hannover.de

Telephone: +49-511-5323157 **Fax:** +49-511-5328157

Received: 2004-03-18 **Accepted:** 2004-04-29

Abstract

AIM: Pelvic magnetic resonance imaging (MRI) and endoanal ultrasound which are established imaging methods for perianal inflammatory lesions in patients with Crohn's disease require expensive specialized equipments and expertise. We investigated the feasibility and sensitivity of transcutaneous perianal ultrasound (PAUS) using regular ultrasound probes in the imaging of perianal inflammatory lesions. The sonographic findings were correlated to pelvic MRI-scans.

METHODS: We performed PAUS in 25 patients with Crohn's disease and clinical signs of perianal inflammatory disease. Within a median of 10 d (range 0-75) these patients underwent MRI of the pelvis. Regular convex and linear high resolution probes were used for PAUS. The sonographic findings were correlated to the MRI findings by blinded investigators.

RESULTS: The sonographic investigations were well tolerated by all patients. Fistulae typically presented as hypoechoic tracks. Twenty-nine fistulae were detected in 22 patients. Abscesses were detected in 7 patients and presented as hypo- or anechoic formations. Twenty-six of 29 fistulae and 6 of 7 abscesses could be confirmed by MRI. Kappa statistics showed an excellent agreement ($\kappa > 0.83$) between the two imaging methods.

CONCLUSION: PAUS is a simple, painless, feasible, real-time method that can be performed without specific patient preparation which is comparable in its sensitivity to pelvic MRI in the detection of perianal fistulae and/or abscesses. PAUS can especially be recommended as a screening tool in acute perianal disorders such as perianal abscess and for follow-up studies of perianal inflammatory disease.

Wedemeyer J, Kirchhoff T, Sellge G, Bachmann O, Lotz J, Galanski M, Manns MP, Gebel MJ, Bleck JS. Transcutaneous perianal sonography: A sensitive method for the detection of perianal inflammatory lesions in Crohn's disease. *World J Gastroenterol* 2004; 10(19): 2859-2863
<http://www.wjgnet.com/1007-9327/10/2859.asp>

INTRODUCTION

Perianal disease is a common complication in Crohn's disease. Approximately 20% of patients with Crohn's disease would suffer from perianal fistulae and/or sinus tracks^[1,2]. The diagnosis and treatment of perianal fistulae can be difficult and represent a challenge for physicians. Treatment modalities include conservative as well as surgical approaches. Therefore comprehensive imaging is necessary in order to develop adequate treatment strategies and to evaluate treatment outcomes^[3]. Endoanal ultrasound (EAUS) as well as MRI of the pelvis are frequently used for imaging of perianal fistulae, sinus tracks or abscesses. The combination of MRI and EAUS is capable of detecting perianal fistulae with a sensitivity of 100%^[4,5]. Recent studies for the medical treatment of perianal disease used either MRI of the pelvis or transanal ultrasound as a follow-up tool to evaluate the therapy outcomes after infliximab treatment^[6-8].

However, both imaging methods require specialized and fairly expensive equipments as well as an experienced investigator. The use of a rigid EAUS probe can be painful or even impossible in patients with inflammatory perianal disease due to anal stenosis. Furthermore, EAUS does not allow the assessment of pathological changes extending to the gluteal region. MRI allows the evaluation of the whole pelvic region, however, it lacks the real time capacity of ultrasound and the high resolution of high frequency linear ultrasound probes.

Transcutaneous perineal/perianal ultrasound (PAUS) represents another method to detect perianal inflammatory disease which can be performed using regular ultrasound probes without special patient preparation. Furthermore, it can be used in patients with anal stenosis. However, despite its methodical simplicity, PAUS is not yet widely used in the detection of perianal fistulae and/or abscesses. Several investigators have applied perineal ultrasound in female patients for diagnosis of incontinence including postpartum anal sphincter tears^[9-15]. These investigations were regularly performed in the lithotomy position and supplemented or compared with transvaginal or transrectal ultrasound. Rubens *et al.*^[16] described PAUS as a valuable tool to image perianal inflammatory disease in their pictorial essay, while Stewart *et al.*^[17] recently described PAUS using a combination of transvaginal and transperineal ultrasound in female and transperineal ultrasound in male patients to detect perianal fistulas and abscesses. Beside a linear probe, Parks *et al.*^[18] used a transvaginal probe for the PAUS to take advantage of its small footprints and they were able to classify fistulae according to the Parks classification. In their recent published study Mallouhi *et al.*^[19] showed a high correlation of perineal ultrasound findings and surgical examination. However, as Mallouhi *et al.*^[19] pointed out correctly surgical exploration in some cases, might not allow the detection of every perianal fistula. Despite the obvious advantages of perianal/perineal ultrasound no studies exist so far that compared the effectiveness of PAUS with the established imaging methods such as MRI and/or EAUS. Therefore, we investigated patients with clinical signs of perianal fistulae or abscesses using PAUS and compared the detected pathology with results of MRI scans of the pelvis as the gold standard. Also, we performed follow-up

studies in certain patients to monitor the treatment effectiveness.

MATERIALS AND METHODS

Patients were recruited either from the inflammatory bowel disease outpatient clinic or from the gastroenterology wards of our institution. Ultrasound examinations were performed in 25 patients (17 females, 8 males) with a mean age of 36.2 ± 2.5 years. All patients had prediagnosed Crohn's disease confirmed by biopsy and presented with complaints suspicious of perianal disease. No specific preparations of the patients such as enemas were performed. Either a Toshiba Aplio (3.3 Mhz [Tissue Harmonic Imaging, THI] and 12 Mhz transducer), a Toshiba Powervision (6 Mhz and 12 Mhz transducer, Toshiba, Neuss, Germany) or a Siemens Elegra (3.75 [THI] and 9 Mhz transducer, Siemens, Erlangen, Germany) was used depending on availability for the ultrasound examination. Colour Doppler ultrasound was applicable with all probes. The ultrasound probe was covered with contact gel, and introduced into a regular latex examination glove with the fingers of the glove tied up in knots for hygienic reasons (Figure 1A). For sufficient contact, contact gel was spread on the outside of the glove before the examination was performed. PAUS was performed with the patient in the left lateral position by placing the probe directly above the anus in the sagittal plane (Figure 1B). For better orientation, the examination was started with a convex transducer identifying bladder, rectum and prostate/vagina (Figure 2). Details and pathological findings were imaged and further investigated using the linear high resolution probes. The maximal penetration for good visualisation using linear transducers was 6 cm. Depending on the specific findings the probe was turned or shifted in the perianal area. The probe was placed above any pathological opening. Colour Doppler was used to distinguish blood vessels from other anechoic/hypoechoic lesions such as fistulae. All ultrasound examinations were checked by either J.S.B. or M.J.G. who both held the highest DEGUM (German society for ultrasound in medicine) ultrasound certificates (DEGUM III, Seminarleiter). Colour Doppler ultrasound was applicable with all probes. Fistulae were categorized as superficial, intersphincteric, transsphincteric, suprasphincteric, extrasphincteric, recto-vaginal fistulae and/or abscesses.

Within a median of 10 d (range 0-75) the patients were also examined by pelvic MRI. MRI was performed to identify inflammatory changes, abscess formations and fistulae. A 1.5 Tesla MR scanner (GE Signa Horizon Echospeed, Milwaukee, Wisconsin) was used. A phased array surface coil was placed on the pelvis. Transverse and sagittal T1-spin echo (T1SE), fat-saturated T2-fast spin echo (fsT2FSE) sequences were applied. Also, transverse and oblique coronal (angulated adjacent to the anal canal) T2FSE sequences without fat saturation were applied in order to detect fistulous tracks. Either respiratory compensation or respiratory trigger was used to avoid artefacts from respiratory motion. After intravenous gadolinium administration (0.1 mmol/kg Gd-DTPA, Magnevist, Schering, Berlin, Germany) transverse and oblique coronal fat-saturated T1-spin echo (fsT1SEpostGd) sequences were performed. Raised signal intensity in the T2-weighted images and an increased uptake of Gd-DTPA served as markers for active inflammatory changes, whereas low signal intensity bands distorting normal fibrofatty tissue in both T1 and T2 weighted images were considered to be fibrous scarring. The results were reviewed by two radiologists in consensus reading. The investigators of either method were not aware of the results generated by the other.

Results were compared by calculating the kappa coefficient according to Cohen.

RESULTS

General Images

PAUS was well tolerated in all patients. In cases of subcutaneous perianal abscesses or significant inflammatory changes, slight local pain was reported during the examination when pressure was applied with the ultrasound probe. Two patients who had a history of significant anal stenosis and repeated surgical anal dilations were included in the study and evaluated with PAUS, because endoanal ultrasound could not be performed in these cases.

A general view was achieved using a regular convex probe (as listed in the Materials and Methods section) that showed rectum, bladder, prostate gland and urethra or vagina and uterus (Figure 2). Small intestinal bowel loops could be shown as well as pathological pelvic intraabdominal fluid collections. However, for comprehensive imaging of perianal inflammatory disease, a high frequency linear probe provided a much more detailed imaging. The penetration that could be achieved using a linear transducer (as listed in Materials and Methods) was sufficient to detect most of the perianal inflammatory changes. The anal canal presented as an anechoic area (Figure 3A,B). The external anal sphincter presented with hyperechoic striped bands while the internal sphincter had a homogenic hypoechoic texture (Figure 3B).

Pathological findings were detected in 96% (24/25) of the patients examined with PAUS. Pathological findings included entero-cutaneous perianal fistulae, sinus tracts without cutaneous openings, bifurcated complex perianal fistulae, perianal or subcutaneous abscesses, rectovaginal fistulae and inflammatory remnants post perianal abscess.

Fistulas

In 88% (22/25) of patients investigated, fistulae and/or sinus tracts could be visualized by PAUS. A total of 29 fistulae were detected. Fistulae and sinus tracks presented as hypo/anechoic tracks. Figure 3 shows typical PAUS images of entero-cutaneous perianal fistulae. Regularly small hyperechoic dots could be detected representing air bubbles within the fistulous tracks. In 45% (10/22) of the fistulae, it was possible to trace small hyperechoic dots which would move within the fistulae and therefore enabling the investigator to detect even minor fistulous tracks indicating active fistulae.

MRI confirmed 90% (26/29) fistulae in 91% (20/22) of these patients. All fistulae detected by MRI were also detected by PAUS. The kappa coefficient for fistulae was calculated as 0.83 resembling an excellent agreement. In two patients both methods described incomplete fistulae (sinus tracks with no visible cutaneous opening). Figure 4 shows a perianal enterocutaneous fistula imaged by PAUS and MRI.

As PAUS included inspection of the anoderm, cutaneous openings of fistulae could easily be detected. In two cases MRI was not able to confirm perianal fistulae that were detected by PAUS. However, discharge from a cutaneous opening proved the presence of a perianal fistula in both of these cases, which could be visualized with PAUS. Both of these fistulae were short intersphincteric fistulae of type 1 according to the Parks classification^[18]. In one of these cases the fistula described in PAUS could be detected in a repeat MRI performed using a vaginal tampon for better anatomical differentiation. However, the investigators were aware of the findings made in the PAUS in this second examination.

Follow-up PAUS investigations were performed in 8 of the 25 patients. Improvement under therapy was noted in 4 cases, no change in 2 cases and progressive disease in 2 patients. The sonographical improvement was consistent with clinical findings. In one case follow-up MRI was performed confirming the PAUS findings as both imaging methods described an abscess within the fistulous track.

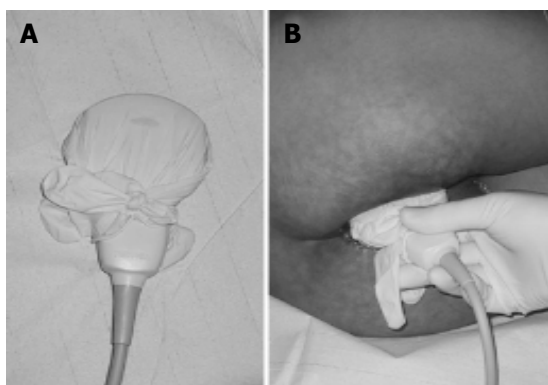


Figure 1 A regular latex examination glove filled with ultrasound contact gel was used to cover the probes for hygienic reasons (A). The examinations were performed in the left lateral position with the probe placed above the anus (B).

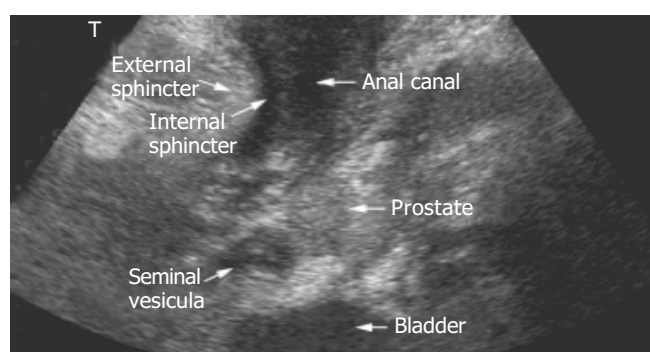


Figure 2 A general overview over perianal anatomy and pathology can be obtained using a regular convex 3.5 Mhz probe.

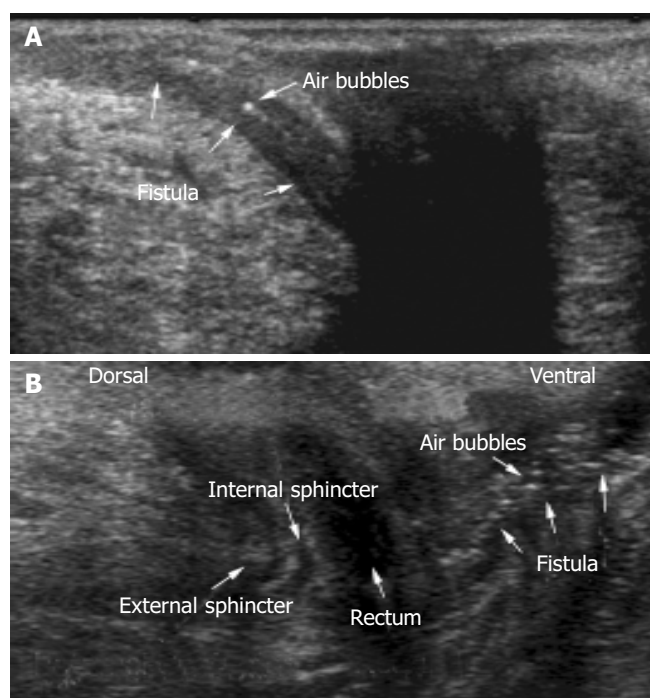


Figure 3 Perianal imaging of entero-cutaneous fistulae using a 10 MHz ultrasound probe. Hyperechoic dots resemble air bubbles within the fistulous track. The rectum represents as hypo- anechoic structure. External and internal anal sphincter can be distinguished.

Recto-vaginal fistulae

PAUS was able to visualize rectovaginal fistulae in 3 cases.

MRI confirmed recto-vaginal fistulae in two of the three cases. In the remaining case MRI showed a fistula from the sigmoid colon to the vagina, in contrast, PAUS described a recto-vaginal fistula. While gynaecological examination did not confirm the presence of any fistula, drainage of blue stain into the vagina after the introduction of a methylene blue soaked swab into the rectum finally proved the presence of a recto-vaginal fistula as was described by PAUS. The sigmoid-vaginal fistula was not detected in the PAUS examination.

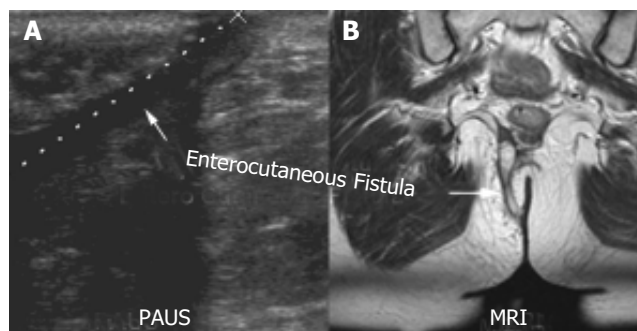


Figure 4 Enterocutaneous fistula detected with PAUS (A) was confirmed using MRI (oblique coronary T2-FSE sequence without fat saturation) (B).

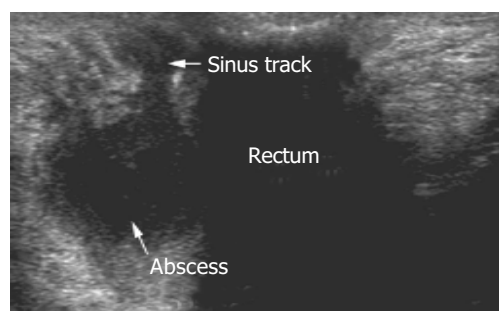


Figure 5 Typical appearance of a pararectal abscess, dorsal of the rectum. Furthermore a sinus track could be detected that perforated the external sphincter and ceased in multiple small sinus tracks that did not have a cutaneous opening.

Abscesses

Perianal fluid collections/abscesses were detected by PAUS in 28% (7/25) of the patients. Abscesses presented as oval shaped hypo- to anechoic masses which were demarcated off the regular tissue by a hypoechoic seam (Figure 5). In 5 cases a direct association of a fistulous and/or sinus track to the abscess formation could be demonstrated. Figure 5 shows a perianal sonographic scan of a male patient that presented to our outpatient clinic with severe perianal discomfort. While inspection and digital examination of the anus were inconspicuous, the transcuteaneous perianal ultrasound examination revealed hypoechoic fluid collections dorsal of the rectum in this patient. The abscess shown in Figure 5 had a fistulous track connecting the rectum and a complex intrasphincteric fistulous system. In 6 cases fluid collections could be confirmed using MRI, and no fluid collection detected in MRI was missed by PAUS. In one case MRI could not confirm a fluid collection. However the two examinations were performed at an interval of 23 d. The smallest abscess detected in PAUS measured 14 mm×12 mm× 8 mm. In three of the cases with significant, drainable abscesses examination under anaesthesia (EUA) could confirm PAUS/MRI findings.

Figure 6 shows an example of a perianal abscess as imaged by PAUS and MRI. Clinical inspection of the anal region did not show any abnormalities in this patient. However anal

discharge upon digital examination was observed and further imaging was initiated. Both PAUS and MRI showed a significant fluid collection with a diameter of approximately 4.5 cm. In contrast to MRI, PAUS detected a fistulous connection to the rectum. In addition to the abscess, a sinus track was detected that emanated from the abscess, and ended within the gluteal fat. The sinus tract could clearly be visualized by both methods (Figure 6). Interestingly, EUA failed to reproduce the pathological findings in the first place and had to be repeated to confirm the PAUS/MRI findings and to achieve appropriate drainage of the abscess. In Figure 7 a small subcutaneous abscess was imaged by PAUS and MRI. Both methods were able to show an active fistulous track reaching from the rectum to the subcutaneous fluid collection.

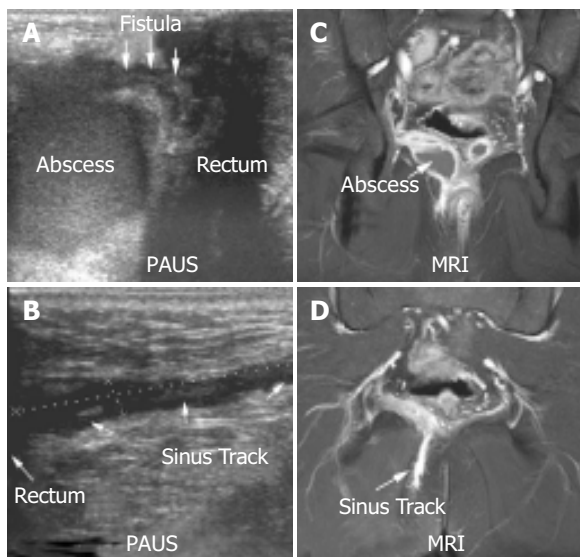


Figure 6 PAUS (A+B) and MRI (C+D) imaging (coronary fat-saturated T1-SE sequence after gadolinium administration) of a perianal abscess. In contrast to MRI, PAUS was able to clearly identify a connection between the rectum and the abscess (A+C). Both methods could identify a sinus track that began within the abscess and ended in the gluteal fat (B+D). A scale (cm) is shown on the left side of the PAUS images for orientation.

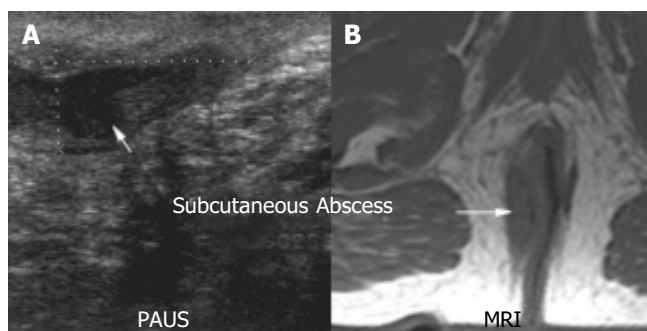


Figure 7 Comparison of PAUS (A) and MRI (B) imaging (transverse T1-SE sequence) of a subcutaneous abscess. A small fistula from the rectum to the abscess could be detected with PAUS and MRI.

DISCUSSION

In this study we investigated the feasibility of transcutaneous PAUS for the evaluation of perianal inflammatory disorders in patients with Crohn's disease.

We showed that perianal fistulae, complex fistulous systems as well as perianal abscesses could be detected with high sensitivity using PAUS. The results were comparable to pelvic MRI that

currently represents in combination with EAUS, the gold standard for the imaging of perianal inflammatory disease. However, PAUS still has certain limitations when performed in the left lateral position compared to EAUS and MRI. The localization of fistulae within the sphincter apparatus is important when surgical interventions are indicated. While imaging of the internal anal sphincter is difficult using PAUS, the external sphincter can be clearly distinguished due to its hyperechoic striped appearance. In terms of impact on treatment, the definite description of the anatomical relationship of pathological changes to the external anal sphincter according to the Parks classification is most important^[18]. Still, accurate localization of pathological changes to the internal/external sphincter requires an experienced investigator.

Despite the limitations stated above, we believe that PAUS has several advantages compared to EAUS and MRI. PAUS is as effective as MRI in the detection of perianal fistulae, but the detection of air bubbles within a fistulous track can clearly indicate active fistulae. Real time imaging in sonography is an advantage that can be helpful in detecting possible connection to the rectal lumen. In two cases investigated by MRI and PAUS, MRI was not able to detect a short perianal fistulae, while the cutaneous openings of the fistulae were obvious on clinical inspection. While EAUS is limited to pathological changes associated to the rectal lumen, perianal ultrasound can be used to identify fistulous tracks in the gluteal region. PAUS therefore combines the high resolution and real time capabilities of EAUS and the panoramic view generated by MRI.

The presence of perianal abscesses is an important condition for surgical interventions in patients with perianal Crohn's disease. Abscesses were detected by PAUS with the same sensitivity as by MRI. PAUS therefore is a valuable tool in the screening for perianal disease. Especially when immediate action is necessary and sophisticated diagnostic imaging could delay diagnosis due to limited availability, PAUS might be a feasible alternative to EAUS and MRI. For example, we were able to detect perianal abscesses in two patients that presented with severe perianal discomfort using PAUS. These patients did not have a history of perianal inflammatory disease and neither inspection of the anus nor digital rectal examination revealed pathological findings. These two patients underwent immediate surgical drainage of their abscesses without further imaging and therefore had to be excluded from this study. Vice versa a perianal abscess was suspected in a patient that presented with a painful perianal swelling with typical redness and induration. An abscess was ruled out using PAUS and the patient was spared a surgical intervention and had complete remission of symptoms. Again no further imaging was performed in this patient. In the future, a mobile application of PAUS in the operating room to guide drainage operations is conceivable. This, however, has not been tested in this study yet.

With more advanced imaging techniques in medicine, the costs of diagnosis and treatment have become a serious and important issue. Especially in chronic diseases, such as Crohn's disease which require regular examination for follow-up and treatment-evaluation alternative, easily available methods to EAUS and MRI as rather expensive diagnostic tools are more than welcome. We believe that PAUS represents such an alternative for it can be performed with regular ultrasound probes and is therefore widely available. It is fast and does not require special patient preparations such as enemas or injection of contrast agents. Basically it can be performed in any outpatient radiology or internal medicine practice. Depending on on-site experience additional imaging of perianal disease with EAUS or MRI might be necessary. However, after initial comparison with the established methods, follow-up can easily be performed with PAUS alone. In follow-up studies the application of more sophisticated imaging methods such as

EAUS or MRI would then be limited to investigate significant clinical changes not detectable by the transcutaneous approach.

In general PAUS was well tolerated by our patients. As a matter of fact one of the reasons to perform this study was that several patients refused diagnosis with EAUS. As perianal inflammatory disease can result in fibrosis and consecutive anal stenosis, EAUS might not be applicable at all in some patients.

The use of contrast agents such as hydrogen peroxide or Levovist might improve the imaging quality of perianal ultrasound^[20-23]. However, the main goal of this study was to determine whether a simple alternative approach was helpful in the imaging of perianal disorders.

We would like to encourage the readers of this article who perform EAUS to employ PAUS using regular ultrasound probes. Since PAUS has been established in our department, the use of EAUS for inflammatory disease has been drastically reduced and is now limited to very few cases that can not be clarified with PAUS and/or MRI.

In conclusion, PAUS represents a sensitive, non-invasive tool that can be used for initial screening and follow-up in the detection of perianal inflammatory disease.

REFERENCES

- 1 **Hellers G**, Bergstrand O, Ewerth S, Holmstrom B. Occurrence and outcome after primary treatment of anal fistulae in Crohn's disease. *Gut* 1980; **21**: 525-527
- 2 **Schwartz DA**, Loftus EV Jr, Tremaine WJ, Panaccione R, Harmsen WS, Zinsmeister AR, Sandborn WJ. The natural history of fistulizing Crohn's disease in Olmsted County, Minnesota. *Gastroenterology* 2002; **122**: 875-880
- 3 **Sandborn WJ**, Fazio VW, Feagan BG, Hanauer SB. AGA technical review on perianal Crohn's disease. *Gastroenterology* 2003; **125**: 1508-1530
- 4 **Orsoni P**, Barthet M, Portier F, Panuel M, Desjeux A, Grimaud JC. Prospective comparison of endosonography, magnetic resonance imaging and surgical findings in anorectal fistula and abscess complicating Crohn's disease. *Br J Surg* 1999; **86**: 360-364
- 5 **Schwartz DA**, Wiersema MJ, Dudiak KM, Fletcher JG, Clain JE, Tremaine WJ, Zinsmeister AR, Norton ID, Boardman LA, Devine RM, Wolff BG, Young-Fadok TM, Diehl NN, Pemberton JH, Sandborn WJ. A comparison of endoscopic ultrasound, magnetic resonance imaging, and exam under anesthesia for evaluation of Crohn's perianal fistulas. *Gastroenterology* 2001; **121**: 1064-1072
- 6 **van Bodegraven AA**, Sloots CE, Felt-Bersma RJ, Meuwissen SG. Endosonographic evidence of persistence of Crohn's disease-associated fistulas after infliximab treatment, irrespective of clinical response. *Dis Colon Rectum* 2002; **45**: 39-45
- 7 **Bell SJ**, Halligan S, Windsor AC, Williams AB, Wiesel P, Kamm MA. Response of fistulating Crohn's disease to infliximab treatment assessed by magnetic resonance imaging. *Aliment Pharmacol Ther* 2003; **17**: 387-393
- 8 **Van Assche G**, Vanbeckevoort D, Bielen D, Coremans G, Aerden I, Noman M, D'Hoore A, Penninckx F, Marchal G, Cornillie F, Rutgeerts P. Magnetic resonance imaging of the effects of infliximab on perianal fistulizing Crohn's disease. *Am J Gastroenterol* 2003; **98**: 332-339
- 9 **Roche B**, Deleaval J, Fransioli A, Marti MC. Comparison of transanal and external perineal ultrasonography. *Eur Radiol* 2001; **11**: 1165-1170
- 10 **Bernstein I**, Juul N, Gronvall S, Bonde B, Klarskov P. Pelvic floor muscle thickness measured by perineal ultrasonography. *Scand J Urol Nephrol Suppl* 1991; **137**: 131-133
- 11 **Cornelia L**, Stephan B, Michel B, Antoine W, Felix K. Transperineal versus endo-anal ultrasound in the detection of anal sphincter tears. *Eur J Obstet Gynecol Reprod Biol* 2002; **103**: 79-82
- 12 **Kiilholma PJ**, Makinen JI, Pitkanen YA, Varpula MJ. Perineal ultrasound: an alternative for radiography for evaluating stress urinary incontinence in females. *Ann Chir Gynaecol Suppl* 1994; **208**: 43-45
- 13 **Piloni V**. Dynamic imaging of pelvic floor with transperineal sonography. *Tech Coloproctol* 2001; **5**: 103-105
- 14 **Pregazzi R**, Sartore A, Bortoli P, Grimaldi E, Troiano L, Guaschino S. Perineal ultrasound evaluation of urethral angle and bladder neck mobility in women with stress urinary incontinence. *BJOG* 2002; **109**: 821-827
- 15 **Schaer GN**, Koechli OR, Schuessler B, Haller U. Perineal ultrasound for evaluating the bladder neck in urinary stress incontinence. *Obstet Gynecol* 1995; **85**: 220-224
- 16 **Rubens DJ**, Strang JG, Bogineni-Misra S, Wexler IE. Transperineal sonography of the rectum: anatomy and pathology revealed by sonography compared with CT and MR imaging. *Am J Roentgenol* 1998; **170**: 637-642
- 17 **Stewart LK**, Mc Gee J, Wilson SR. Transperineal and transvaginal sonography of perianal inflammatory disease. *Am J Roentgenol* 2001; **177**: 627-632
- 18 **Parks AG**, Gordon PH, Hardcastle JD. A classification of fistula-in-ano. *Br J Surg* 1976; **63**: 1-12
- 19 **Mallouhi A**, Bonatti H, Peer S, Lugger P, Conrad F, Bodner G. Detection and characterization of perianal inflammatory disease: accuracy of transperineal combined gray scale and color Doppler sonography. *J Ultrasound Med* 2004; **23**: 19-27
- 20 **Chew SS**, Yang JL, Newstead GL, Douglas PR. Anal fistula: Levovist-enhanced endoanal ultrasound: a pilot study. *Dis Colon Rectum* 2003; **46**: 377-384
- 21 **Kruskal JB**, Kane RA, Morrin MM. Peroxide-enhanced anal endosonography: technique, image interpretation, and clinical applications. *Radiographics* 2001; **21**: S173-S189
- 22 **Poen AC**, Felt-Bersma RJ, Eijsbouts QA, Cuesta MA, Meuwissen SG. Hydrogen peroxide-enhanced transanal ultrasound in the assessment of fistula-in-ano. *Dis Colon Rectum* 1998; **41**: 1147-1152
- 23 **Sloots CE**, Felt-Bersma RJ, Poen AC, Cuesta MA, Meuwissen SG. Assessment and classification of fistula-in-ano in patients with Crohn's disease by hydrogen peroxide enhanced transanal ultrasound. *Int J Colorectal Dis* 2001; **16**: 292-297

Edited by Zhang JZ and Wang XL. Proofread by Xu FM

Low plasma apolipoprotein A-I level is not a reliable marker of fibrosis in children with chronic hepatitis B

Mukadder Ayse Selimoglu, Rasit Vural Yagci, Gül Yüce

Mukadder Ayse Selimoglu, Department of Pediatric Gastroenterology, Hepatology and Nutrition, Faculty of Medicine, Atatürk University, Erzurum, Turkey

Rasit Vural Yagci, Department of Pediatric Gastroenterology, Hepatology and Nutrition, Faculty of Medicine, Ege University, Izmir, Turkey

Gül Yüce, Department of Pathology, Faculty of Medicine, Ege University, Izmir, Turkey

Correspondence to: Dr. Mukadder-Ayşe Selimoglu, Atatürk Üniversitesi, Tıp Fakültesi, Çocuk Sağlığı ve Hastalıkları AD, Erzurum 25240, Turkey. ayseselimoglu@hotmail.com

Telephone: +90-442-2361212 Ext. 1635 **Fax:** +90-442-2361301

Received: 2004-02-14 **Accepted:** 2004-04-29

Abstract

AIM: To evaluate the clinical value of plasma apolipoprotein A-I (Apo A-I) as a marker of fibrosis in children with chronic hepatitis B (CHB).

METHODS: Liver biopsy specimens from 49 children with CHB were evaluated by using Knodell index. Plasma Apo A-I level was measured after 12-h fasting. Student's *t* test, Spearman's correlation test and receptor-operating characteristic (ROC) curve were used for statistical evaluation.

RESULTS: Mean Apo A-I level of the patients was not different from that of controls ($P > 0.05$). Six (8.7%) children had fibrosis score of more than 2 (severe fibrosis). No difference in the level of mean plasma Apo A-I was found among children with and without severe fibrosis ($P > 0.05$). No correlation between Apo A-I level and fibrosis scores was found ($P > 0.05$). The area under the ROC curve was 0.407 ± 0.146 ($P > 0.05$).

CONCLUSION: Severe fibrosis is not common in children with CHB and plasma Apo A-I level is not a reliable indicator of fibrosis.

Selimoglu MA, Yagci RV, Yüce G. Low plasma apolipoprotein A-I level is not a reliable marker of fibrosis in children with chronic hepatitis B. *World J Gastroenterol* 2004; 10(19): 2864-2866 <http://www.wjgnet.com/1007-9327/10/2864.asp>

INTRODUCTION

Apolipoprotein A-I (Apo A-I) is produced mainly by hepatocytes and its level varies according to the degree of liver fibrosis^[1-4]. In our previous study, we demonstrated the inverse correlation of Apo A-I with the Child-Pugh score^[3] in children with cirrhosis. Data of Apo A-I levels in chronic hepatitis were mainly from studies performed in adults with hepatitis C^[5,6]. A recent study showed that serum Apo A-I level was inversely correlated with liver fibrosis in adult patients with chronic hepatitis B (CHB)^[7].

Liver biopsy is an invasive procedure especially for children. It is well known that serum alanine transaminase (ALT) is a good indicator of portal inflammation in chronic hepatitis^[8],

but a reliable biochemical fibrosis index is not available for children. The aim of this study was to determine if low plasma Apo A-I level was a reliable indicator of fibrosis in childhood CHB.

MATERIALS AND METHODS

Forty-nine hepatitis Be antigen (HBeAg) positive children (13 females and 36 males) with pathology verified chronic HBV infection were included in this study. Their mean age was 9.1 ± 4.1 years (3 to 18 years). Patients were excluded if they had hepatitis D or C or HIV infection. No patient had evidence of decompensated liver diseases or autoimmune hepatitis. Parents of the patients were required to give written informed consent before entering the study.

Pretreatment liver biopsy specimens were obtained from all patients and scored with the use of the Knodell index^[9], which grades the histological activity of hepatitis on a scale from 0 to 22, with higher scores indicating more severe abnormalities. The overall Knodell score is the sum of the scores for periportal/bridging necrosis (0 to 10), intralobular degeneration and focal necrosis (0 to 4), portal inflammation (0 to 4), and fibrosis (0 to 4). Before the patients entered the study, blood samples were taken for the test of blood cell counts, serum alanine aminotransferase (ALT), Apo A-I, hepatitis B surface antigen (HBsAg), HBeAg, antibody to HBeAg, antibody to HBsAg and HBV DNA.

Plasma Apo A-I levels of 20 gender- and age-matched healthy children were used as controls. Student's *t* test, Spearman's correlation test and ROC curve were used for statistical analysis.

RESULTS

Pre treatment ALT, Apo A-I, hepatic activity index (HAI), portal fibrosis, inflammation and necrosis scores, and HBV DNA levels of the children are shown in Table 1. Mean plasma Apo A-I level of 49 children with CHB was not different from that of controls ($39.3 \pm 5.8 \mu\text{mol/L}$ vs $40.71 \pm 4.8 \mu\text{mol/L}$, $P > 0.05$).

Table 1 Some pretreatment biochemical, pathological and serological findings in children with chronic hepatitis B

Parameter	mean \pm SD	Range
ALT (IU/l)	80 \pm 80	21-396
Apo A-I ($\mu\text{mol/L}$)	39.3 \pm 5.8	29.2-57.5
Hepatic activity index	7.0 \pm 3.0	3-17
Portal fibrosis	1.4 \pm 0.9	0-4
Portal inflammation	2.0 \pm 1.2	0-4
Focal necrosis	1.6 \pm 0.9	0-4
Bridging necrosis	2.0 \pm 1.6	0-6
HBV DNA (ng/L)	1 537 \pm 712	118-3 111

Children with CHB were divided into 2 groups according to their fibrosis stage: group 1, whose portal fibrosis scores were 0, 1 or 2; group 2, whose portal fibrosis scores were 3 or 4. In groups 1 and 2, the mean Apo A-I levels were $39.6 \pm 5.6 \mu\text{mol/L}$

and $36.9 \pm 6.8 \mu\text{mol/L}$, respectively ($P > 0.05$). Only 6 (8.7%) children had a fibrosis score of more than 2.

No correlation among Apo A-I and HAI, portal inflammation, portal fibrosis, focal necrosis, bridging necrosis scores was found ($P > 0.05$). A positive correlation between ALT and portal inflammation scores and between ALT and HAI was found ($P < 0.05$ and $P < 0.01$, respectively).

The area under the ROC curve of Apo A-I was 0.407 ± 0.146 ($P > 0.05$, Figure 1).

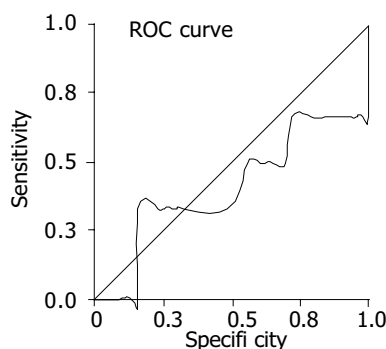


Figure 1 ROC curve of Apo A-I.

DISCUSSION

Fibronectin, a major liver extracellular matrix component, can interact with Apo A-I both by downregulating its mRNA level in liver cells and by binding to this molecule after its secretion in the extracellular space^[1,2]. Since fibronectin is the first matrix component to be produced in excess and deposited in liver fibrosis, it has been thought to be involved in the decrease in Apo A-I in alcoholic patients with liver fibrosis and cirrhosis^[1,2].

Because liver biopsy is an invasive method with a 1/10 000 mortality rate, noninvasive serum markers of liver fibrosis are under investigation^[10]. Furthermore, although histological analysis is considered to be the gold standard for the diagnosis of extensive fibrosis and cirrhosis, the rate of false-negative results was approximately 15-20%^[10]. Clinical investigations on fibrosis markers were generally focused on hepatitis C rather than hepatitis B^[5,6]. One of the few studies performed of patients with CHB was the study Huang *et al.*^[7]. They investigated the value of serum biochemical markers in the diagnosis of liver fibrosis of patients with hepatitis B and observed that levels of ALT, total bilirubin, alpha 2-macroglobulin, GGT and Apo A-I were significantly correlated with the clinical staging of liver fibrosis, and concluded that a combined assessment of these indices might help obtain an accurate diagnosis of liver cirrhosis with less need of pathological biopsy in this population^[7].

Besides noninvasive biochemical markers, some studies strongly recommended using some historical features such as sex, age at biopsy and alcohol consumption as independent predictors of fibrosis in chronic hepatitis C adults^[5]. They demonstrated that a simple index including age, sex, and five biochemical markers could accurately predict significant hepatitis C-related fibrosis^[5].

Teare *et al.*^[11] compared aminoterminal type III procollagen propeptide (PIIP) with the PGA index, which combines the prothrombin time, gamma-glutamyl transpeptidase activity, and serum Apo A-I concentration, in predicting liver fibrosis in patients with alcoholic liver disease, primary biliary cirrhosis, and CHB. They stated that PGA and PIIP values were increased in all patients with CHB in comparison with controls. For the detection of cirrhosis they found that PGA was 91% sensitive and 81% specific^[11]. Similarly Ding *et al.*^[12] evaluated the diagnostic value of serum liver fibrosis markers by analyzing the correlation between liver fibrosis stage in patients with

CHB and serum liver fibrosis markers, such as hyaluronate, type III procollagen, laminin, and type IV collagen in 278 patients. They found that liver fibrosis stage was correlated to inflammation degree and that serum hyaluronate, type III procollagen, laminin, and type IV collagen could reflect the state of liver fibrosis^[12].

The difference between mean Apo A-I level of children with CHB and controls was not significant ($39.3 \pm 5.8 \mu\text{mol/L}$ vs $40.71 \pm 4.8 \mu\text{mol/L}$). In 2002, we reported similar figures for children with chronic hepatitis, most of them had CHB^[4]. However, Norton *et al.*^[13] reported that Apo A-I and apo C-III steady-state mRNA levels were suppressed by HBV replication and/or gene expression. Other studies revealed that the levels of Apo A-I and Apo A-II were reduced during acute hepatitis, when virus levels were high, and normalized after viral clearance^[14,15]. Similar results were reported for chronic HBV infection. Reduced levels of circulating lipoproteins and apolipoproteins have been correlated with increased viral replication^[16-18]. In our study no correlation between HBV DNA and Apo A-I levels was detected.

Of the 49 children, only 8.7% had significant fibrosis according to Knodell index (>2), suggesting that fibrosis is not prevalent in this age group. Although the mean plasma Apo A-I level was lower in this small population compared to children with mild/no fibrosis ($36.9 \pm 6.8 \mu\text{mol/L}$ vs $39.6 \pm 5.6 \mu\text{mol/L}$), statistical significance was not detected.

Recently it has been recommended to use ROC curves in determination of the indices of hepatic fibrosis in clinical practice^[19,20]. In this study, plasma Apo A-I level as a fibrosis marker was measured in children with CHB and compared with Knodell scores to determine if it had any clinical value as a marker of fibrosis. In conclusion, severe fibrosis and Knodell score higher than 2, are not common in CHB children and plasma Apo A-I level is not a reliable indicator of fibrosis.

REFERENCES

- 1 Paradis V, Laurent A, Mathurin P, Poynard T, Vidaud D, Vidaud M, Bedossa P. Role of liver extracellular matrix in transcriptional and post-transcriptional regulation of apolipoprotein A-I by hepatocytes. *Cell Mol Biol* 1996; **42**: 525-534
- 2 Paradis V, Mathurin P, Ratziu V, Poynard T, Bedossa P. Binding of apolipoprotein A-I and acetaldehyde-modified apolipoprotein A-I to liver extracellular matrix. *Hepatology* 1996; **23**: 1232-1238
- 3 Selimoglu MA, Aydogdu S, Yagci RV. Low plasma apolipoprotein A-I level: new prognostic criterion in childhood cirrhosis? *Turk J Pediatr* 2001; **43**: 307-311
- 4 Selimoglu MA, Aydogdu S, Yagci RV. Lipid parameters in childhood cirrhosis and chronic liver disease. *Pediatr Int* 2002; **44**: 400-443
- 5 Myers RP, Ratziu V, Imbert-Bismut F, Charlotte F, Poynard T. Biochemical markers of liver fibrosis: a comparison with historical features in patients with chronic hepatitis C. *Am J Gastroenterol* 2002; **97**: 2419-2425
- 6 Poynard T, Imbert-Bismut F, Ratziu V, Chevret S, Jardel C, Moussalli J, Messous D, Degos F. Biochemical markers of liver fibrosis in patients infected by hepatitis C virus: longitudinal validation in a randomized trial. *J Viral Hepat* 2002; **9**: 128-133
- 7 Huang W, Gong FY. Diagnostic value of serum biochemical markers for liver fibrosis in patients with hepatitis B virus. *Diyi Junyi Daxue Xuebao* 2002; **22**: 1034-1036
- 8 Tang TJ, Kwekkeboom J, Laman JD, Niesters HG, Zondervan PE, de Man RA, Schalm SW, Janssen HL. The role of intrahepatic immune effector cells in inflammatory liver injury and viral control during chronic hepatitis B infection. *J Viral Hepat* 2003; **10**: 159-167
- 9 Knodell RG, Ishak KG, Black WC, Chen TS, Craig R, Kaplowitz N, Kiernan TW, Wollman J. Formulation and application of a numerical scoring system for assessing histological activity in asymptomatic chronic active hepatitis. *Hepatology* 1981; **1**: 431-435
- 10 Cadranet JF, Mathurin P. Prothrombin index decrease: a use-

- ful and reliable marker of extensive fibrosis? *Eur J Gastroenterol Hepatol* 2002; **14**: 1057-1059
- 11 **Teare JP**, Sherman D, Greenfield SM, Simpson J, Bray G, Catterall AP, Murray-Lyon IM, Peters TJ, Williams R, Thompson RP. Comparison of serum procollagen III peptide concentrations and PGA index for assessment of hepatic fibrosis. *Lancet* 1993; **342**: 895-898
- 12 **Ding H**, Chen Y, Feng X, Liu D, Wu A, Zhang L. Correlation between liver fibrosis stage and serum liver fibrosis markers in patients with chronic hepatitis B. *Zhonghua Ganzangbing Zazhi* 2001; **9**: 78-80
- 13 **Norton PA**, Gong Q, Mehta AS, Lu X, Block TM. Hepatitis B virus-mediated changes of apolipoprotein mRNA abundance in cultured hepatoma cells. *J Virol* 2003; **77**: 5503-5506
- 14 **Vergani C**, Trovato G, Delu A, Pietrogrande M, Dioguardi N. Serum total lipids, lipoprotein cholesterol, and apolipoprotein A in acute viral hepatitis and chronic liver disease. *J Clin Pathol* 1978; **31**: 772-778
- 15 **Vergani C**, Trovato G, Pietrogrande M, Crocchiolo P, Dioguardi N. Behavior of total lipids, cholesterol, lipoproteins and apolipoprotein A in the blood of subjects with acute hepatitis and chronic hepatopathy. *Minerva Med* 1978; **69**: 2081-2094
- 16 **Chen Z**, Keech A, Collins R, Slavin B, Chen J, Campbell TC, Peto R. Prolonged infection with hepatitis B virus and association between blood cholesterol and liver cancer. *BMJ* 1993; **306**: 890-894
- 17 **Cordova C**, Musca A, Violi F, Alessandri C, Iuliano L. Apolipoproteins A-I, A-II and B in chronic active hepatitis and in liver cirrhotic patients. *Clin Chim Acta* 1984; **137**: 61-66
- 18 **Fehér J**, Romics L, Jakab L, Fehér E, Szilvási I, Papp G. Serum lipids and lipoproteins in chronic liver disease. *Acta Med Acad Sci Hung* 1976; **33**: 217-223
- 19 **Zheng M**, Cai WM, Weng HL, Liu RH. ROC curves in evaluation of serum fibrosis indices for hepatic fibrosis. *World J Gastroenterol* 2002; **8**: 1073-1076
- 20 **Walsh KM**, Timms P, Campbell S, Macsween RNM, Morris AJ. Plasma levels of matrix metalloproteinases-2 (MMP-2) and tissue inhibitors of metalloproteinases-1 and -2 (TIMP-1,2) as noninvasive markers of liver disease in chronic hepatitis C disease in chronic hepatitis C comparison using ROC analysis. *Dig Dis Sci* 1999; **44**: 624-630

Edited by Chen WW and Wang XL. Proofread by Xu FM

Prospective study in 142 cases of hepatitis C virus infection

Wen-Mei Fan, Wan-Fu Zhu, Li-Min Yin, Lai Wei, Xiao-Yuan Xu, Hui Zhuang

Wen-Mei Fan, Wan-Fu Zhu, Li-Min Yin, Hui Zhuang, Department of Microbiology, School of Basic Medicine, Peking University Health Science Center, Beijing 100083, China

Lai Wei, Hepatology Institute, People's Hospital, Peking University, Beijing 100044, China

Xiao-Yuan Xu, Department of Infectious Diseases, First Hospital, Peking University, Beijing 100034, China

Supported by the National Key Technologies Research and Development Program of China during the 10th Five-Year period, No. 2001BA705B06

Correspondence to: Professor Wan-Fu Zhu, Department of Microbiology, School of Basic Medicine, Health Science Center, Peking University, Beijing 100083, China. zhuwanfu@sun.bjmu.edu.cn

Telephone: +86-10-82801599 **Fax:** +86-10-82801599

Received: 2004-03-05 **Accepted:** 2004-04-05

Abstract

AIM: There is limited information on the natural history of HCV infection in China. We investigated the outcome of HCV infection after nine-year follow-up and the risk factors in blood donors in China in order to provide the foundation for prevention and therapy.

METHODS: A total of 172 cases of HCV infection with anti-HCV positive and ALT abnormality were enrolled in the archives when was screened blood in Hebei Province in 1993. In them 142 blood donors were followed up till July 2002. No antiviral treatment was applied to them during the period of infection. In the present study, anti-HCV, HCV-RNA and aminotransferase were detected and genotyping was conducted by the method of restriction fragment length polymorphism(RFLP). B-type ultrasound detection was performed in all the patients. Age, sex, alcohol consumption and clinical symptoms were questioned.

RESULTS: After nine years' follow-up, 10.56% (15/142) of the cases were negative for anti-HCV and 16.42% (12/134) of them were negative for HCV-RNA. The genotypes 1b, 2a and 1b/2a were 91.07%, 6.25% and 2.68% respectively. Twelve cases (8.45%) were negative for both HCV RNA and anti-HCV. The rate of chronicity in this group was 83.58% (112/134), and the rate of viral spontaneous resolution was 16.42% (22/134). The mean level of ALT, AST, γ -GT in HCV RNA positive cases was significantly higher than that in HCV RNA negative cases ($P < 0.001$). The abnormal rate of ALT and/or AST in male donors was significantly higher than that in female donors ($P = 0.005$). The rate of progression to liver cirrhosis from chronic hepatitis C was significantly higher in the cases of super-infection with HBV than that in the cases of single HCV infection. Overdose alcohol consumption promoted the progression to chronicity.

CONCLUSION: This area (Hebei Province) has a higher rate of chronicity in HCV infection, and measures should be taken to prevent its progression to serious liver diseases, especially for patients super-infected with HCV and HBV.

Fan WM, Zhu WF, Yin LM, Wei L, Xu XY, Zhuang H. Prospective

study in 142 cases of hepatitis C virus infection. *World J Gastroenterol* 2004; 10(19): 2867-2869

<http://www.wjgnet.com/1007-9327/10/2867.asp>

INTRODUCTION

Hepatitis C virus is the major cause of post-transfusion hepatitis. It has been estimated that nearly 170 million people are infected with HCV in the world. High chronicity is an obvious characteristic of HCV infection. Eighty-five percent of infected patients developed chronic infection and 8-45% of them could resolve. Liver cirrhosis developed in 10-50%, hepatocellular carcinoma in 1-23%, liver disease related mortality in 4-15%^[1-3] in twenty years of natural infection. There is limited information about the long-term follow-up study in China. Many donors were infected with HCV by means of plasmapheresis in the 1990 s^[4]. In the present study, 172 cases of blood donors infected with HCV were diagnosed in August of 1993, and 142 of them were followed up till July 2002. The outcome in natural history of HCV infection and related factors affecting the outcome were investigated.

MATERIALS AND METHODS

Patients

A total of 172 cases of blood donors from a rural area of Zhao County in Hebei Province were diagnosed as HCV infection by etiology and biochemistry detection (including anti-HCV and hepatitis B surface antigen) in August of 1993. Thirteen cases of them were co-infected with hepatitis C virus and hepatitis B virus. Nine years later, only 142 persons (66 men and 76 women with a mean age of 36.67±9.10 years at time of infection and 45.70±9.11 years at time of investigation) were followed up. Additionally, three children with aged of 2 to 8 years at the time of infection were checked-up in our series. It was noted that all of the donors received no antiviral treatment during the nine years of infection.

Methods

Anti-HCV antibodies Five-milliliter peripheral vein blood was collected for biochemical and etiology detection. All patients were tested for the presence of anti-HCV antibodies with Abbott diagnostic test kit (Abbott, USA) according to the manufacturer's instructions in 1993 and 2002. The rest of the blood samples were stored at -80 °C.

HCV RNA detection and genotyping Primers were designed from the conserved 5'-noncoding (5'-NC) region of the HCV genome. P1: 5'-GTGTGAGGAAGTACTGTGTT-3', P1': 5'-AACACTACTCGGCTAGCAGT-3', and P2: 5'-TTCACGCAGAAAGCGTCTAG-3', P2': 5'-GTTTATCAAGAAAGGACCCG-3'. RT-PCR procedure was performed as previously described^[5]. PCR products positive for HCV RNA were genotyped with restriction fragment length polymorphism (RFLP) method^[5].

Risk factors for HCV chronicity All data of risk factors for HCV chronicity were collected by using special questionnaires, including sex, age, symptoms, alcohol consumption, alanine aminotransferase (ALT), aspartate aminotransferase (AST), γ -glutamyltransferase (γ -GT), alkaline phosphatase (ALP), total bilirubin (Tbil), direct bilirubin (Dbil), total protein (TP) and

albumin (ALB) in 12 by using fully automatic biochemical analysis compliance 7071A (Hitachi, Japan). HBV markers were also detected by Abbott diagnostic kit.

Diagnostic criterion Chronic hepatitis C and liver cirrhosis were diagnosed based on the criteria modified at the Sixth (Xi'an) National Convention of Infectious, Parasitic and Liver Diseases^[6].

Statistical analysis

Quantitative values were expressed as mean±SE. Unpaired Student's *t* test, χ^2 and Fisher's exact test were used for statistical comparison of the data. $P < 0.05$ was considered statistically significant.

RESULTS

Outcome of HCV infection

In the 172 cases enrolled in this study in 1993, seven cases were already died at the time of investigation. Two (1.16%) out of seven cases died of suspected hepatocellular carcinoma. Twenty-three cases were out of follow-up. In the present study, only 142 cases were followed-up under the investigation. Out of the 142 cases, HCV RNA was detected in 134 cases. The result showed that 112 cases (83.58%) of the donors were positive for HCV RNA and 16.42% were negative for HCV RNA; 89.44% were positive for anti-HCV and 10.56% were negative for anti-HCV; 8.45% of them were negative for both anti-HCV and HCV RNA. Out of the 142 infected persons, most but one (who was with chronic moderate hepatitis C) with mild chronic hepatitis C had no obvious clinical symptoms according to the viral hepatitis prevention project. In the cases with persistent infection, B-type ultrasound detection showed 2.68% with liver cirrhosis, 86.61% with chronic hepatitis and 10.71% with fatty liver.

Anti-HCV, HCV RNA and abnormality of liver function

Ninety-one point sixty percent of the cases were positive for HCV RNA in the positive group of anti-HCV. Eight cases of severe hepatitis and three cases of liver cirrhosis were positive for both anti-HCV and HCV RNA. Another two patients with liver cirrhosis and severe hepatitis were co-infected with both HCV and HBV in 1993 and turned positive for anti-HCV, negative for HCV RNA and positive for hepatitis B surface antigen in the present study. The rate of ALT and/or AST abnormalities in the positive group of anti-HCV was 28.57% (34/119), while that in the negative group of anti-HCV was zero (Table 1). The average level of ALT, AST and γ -GT in the positive group of HCV RNA was significantly higher than that in the negative group ($P < 0.001$) (Table 2). On the other hand, the abnormal rate of ALT and / or AST in the positive group was also significantly higher than that in negative group (29.46% vs 4.55%, $P = 0.014$).

Clinical symptoms

Fifty out of 112 cases (44.64%) of chronic HCV infection had mild symptoms, including abdominal pain (18.75%), fatigue (17.86%), and arthralgia (16.96%). The rates of cases with symptoms in the group of liver cirrhosis was 50.0%. Surprisingly, six cases with negative viral markers had fatigue.

Table 1 Abnormal of serum alanine aminotransferase in patients infected with HCV after 9 years' follow-up in different groups

Group	Liver function	
	Normal cases (%)	Abnormal cases (%)
Anti-HCV(+)/HCV RNA(+)	76 (69.72)	33 (30.28)
Anti-HCV(+)/HCV RNA(-)	9 (90.00)	1 (10.00)
Anti-HCV(-)/HCV RNA(+)	3 (100.0)	0
Anti-HCV(-)/HCV RNA(-)	12 (100.0)	0
Anti-HCV(+)/HCV RNA(undetected)	4 (50.00)	4 (50.00)
Total	104 (73.24)	38 (26.76)

Note: The number in the bracket is the percentage of normal and abnormal cases in each group.

Co-infection with HBV and alcohol consumption

Thirteen of 142 cases had co-infection with HBV in 1993. Twelve cases of them were positive for hepatitis B surface antigen (HBsAg) and the rest were negative for HBsAg and positive for anti-hepatitis B core (anti-HBc). Nine years later, three of them turned negative for HbsAg, suggesting that spontaneous resolution of HBsAg per year was 2.77% similar to the of standard rate of resolution (2.01%) in our country^[7]. The rate of spontaneous resolution of anti-HCV was 7.69% in the group of co-infection with HBV while 8.53% in the group of single HCV infection. There was no significant difference between the two groups. Thirty point seventy-seven percent lost their HCV RNA in the group super-infected with HCV and HBV and 14.88% lost their HCV RNA in the group with single HCV infection. However, there was no significant difference between them. Two (15.38%) out of thirteen cases with co-infection developed liver cirrhosis while two (1.55%) out of 129 cases with single HCV infection also developed liver cirrhosis. The progression to liver cirrhosis due to co-infection was significant faster than that due to single infection ($P < 0.05$). Thirteen of 142 cases had alcohol consumption of more than 100 g every day and all developed persistent infection. We also found that all cases with viral resolution had no history of excessive alcohol consumption, suggesting that alcohol consumption might promote the progression of HCV infection to chronicity.

Age at the time of primary infection

We divided the donors into three groups according to the age of infection: 18-30 years, 31-40 years and ≥ 41 years. The rate of spontaneous viral resolution in the three groups was 17.95%, 15.09% and 16.67% respectively. There was no significant difference. There was no linear correlation between the age of infection and the viral load ($r = -0.144$). Liver function was normal in the three investigated children. One of them was negative for viral markers and the other two developed persistent infection.

Influence of sex on the viral resolution

Sixty-two male cases and seventy-two female cases were detected for HCV RNA. The rate of viral resolution was 12.90% in the male group and 19.44% in the female group. No significant

Table 2 Comparison of ALT, AST, ALP, γ -GT, TBIL and DBIL between positive (+) and negative (-) HCV RNA patients (mean±SE)

HCV RNA	Case	ALT (IU/L)	AST (IU/L)	ALP (IU/L)	γ -GT (IU/L)	Tbil (μ mol/L)	DBil (μ mol/L)
+	112	31.2±32.6 ^b	34.8±27.0 ^b	82.0±36.6	20.0±17.6 ^b	13.2±5.6	6.0±2.3
-	22	16.1±8.6	22.9±6.5	78.9±40.1	12.4±5.8	12.1±7.4	5.4±2.2

^b $P < 0.001$ vs the negative group of HCV RNA.

difference was found between them. Four cases of liver cirrhosis were all male cases. The rate of ALT and/or AST abnormalities was significantly higher in male donors than in female donors ($P=0.005$).

Related factors affecting the outcome of HCV might include co-infection with HBV and long-term excessive alcohol consumption, which could promote the progression of HCV infection to chronicity and liver cirrhosis. In the present study, we could not find the significant correlation between the outcome of HCV and age of infection and sex.

DISCUSSION

The harm of hepatitis C is only next to hepatitis B in our country. The epidemic rate is 3.2% in Chinese population and it is estimated that 41 million people were infected^[8]. Economic burden for HCV is 11.7-21.6 billion RMB per year in China. New cases have been decreased through the detection of blood donors since 1990 s, but part of patients would progress to chronic hepatitis, liver cirrhosis and hepatocellular carcinoma. Although there are many reports on this aspect in Western countries^[9-13], few similar researches have been carried out in China. So it is very necessary to summarize the natural outcome of HCV in China.

Chronicity rate

The rate of spontaneous resolution in the present study was 16.42%, lower than 29.01%^[14] reported before in China after 12-25 years of infection. It may be because the qualitative method used in the study was more sensitive than quantitative method used in another area. Additionally, during our investigation, the infection was spontaneously resolved in some cases, which might be one of the causes of high chronicity in HCV infection in this study. Two patients died of suspected liver disease, and the case fatality rate was 1.16% in the group studied, which was lower than the previously reported^[10]. B-type ultrasound detection reflected liver inflammation in some degree under the condition that liver biopsy was not taken. After nine years of infection, 2.68% of the patients developed liver cirrhosis, which was lower than 7-16% after 8-16 years of infection^[1]. Our results showed that the clinical symptoms were latent in the donors studied. Compared with the patients with HBV infection, higher chronicity and faster progression to liver cirrhosis were observed in the patients with HCV infection.

Factors affecting the outcome

Age As described previously^[15-17], age appear to be an important determinant of progression. The data suggest that the younger the age at infection, the lower the rate of progression. In the present study, no difference was found in the rate of viral resolution in the different age groups, which is consistent with a previous report^[14]. The rate of chronicity was higher in the group than in children and young women of other countries.

Sex Regarding sex, there is evidence that the rate of progression of liver disease was lower in women than in men. The cases who progressed to liver cirrhosis in our study were all males. The rate of ALT and/or AST abnormalities in males was significantly higher than that in females, indicating that males might relate with the more serious liver disease.

Super-infection with HBV The rate of viral resolution in the donors super-infected with HBV was a little higher than in the donors without HBV infection, but there was no significant difference. The rate of progression to liver cirrhosis in the cases super-infected with HCV and HBV was significantly higher than that in the cases only infected with HCV, which is consistent with previous reports.

Alcohol consumption Several reports showed that overdose alcohol consumption might contribute to the progression to liver cirrhosis and hepatocellular carcinoma. In the present study, alcohol consumption was shown the progression to chronicity. Whether alcohol consumption affects the progression of liver diseases, needs to be further studied.

In summary, this area (Hebei province) has a higher rate of chronicity in HCV infection, and measures should be taken to prevent the progression to serious liver diseases, especially for the patients super-infected by HCV and HBV.

REFERENCES

- 1 **Alberti A**, Chemello L, Benvegno L. Natural history of hepatitis C. *J Hepatol* 1999; **31**(Suppl 1): 17-24
- 2 **Seeff LB**. Natural history of chronic hepatitis C. *Hepatology* 2002; **36**(5 Suppl 1): S35-46
- 3 **Hoofnagle JH**. Course and outcome of hepatitis C. *Hepatology* 2002; **36**(5 Suppl 1): S21-S29
- 4 **Wang SP**, Ding H, Zhang HQ, Lu YZ, Yang JC, Zhao XK, Geng HH, Zhu WF. Hepatitis C virus infection in the plasmapheresis donors. *Zhonghua Liuxingbing Zazhi* 1994; **15**: 71-73
- 5 **Du SC**, Tao QM, Zhu L. Typing on 5'-terminal noncoding region of hepatitis C virus genome with restrict endonuclease. *Zhonghua Yixue Zazhi* 1993; **73**: 7-9
- 6 Modified at the Sixth (Xi'an) National Convention of Infectious, Parasitic and Liver Disease. Viral hepatitis prevention project. *Zhonghua Chuanranbing Zazhi* 2001; **19**: 56-62
- 7 **Luo KX**. Hepatitis B basic biology and clinical science. 1sted. Beijing: People's Medical Publishing House 1997: 159
- 8 **Cheng JM**. Modern epidemiology. 1sted. Beijing: People's Military Medical Publishing House 1999: 269
- 9 **Bellentani S**, Pozzato G, Saccoccio G, Crovatto M, Croce LS, Mazzoran L, Masutti F, Cristianini G, Tiribelli C. Clinical course and risk factors of hepatitis C virus related liver disease in the general population: report from the Dionysos study. *Gut* 1999; **44**: 874-880
- 10 **Seeff LB**, Miller RN, Rabkin CS, Buskell-Bales Z, Straley Eason KD, Smoak BL, Johnson LD, Lee SR, Kaplan EL. 45-year follow-up of hepatitis C virus infection in healthy young adults. *Ann Intern Med* 2000; **132**: 105-111
- 11 **Datz C**, Cramp M, Haas T, Dietze O, Nitschko H, Froesner G, Muss N, Sandhofer F, Vogel W. The natural course of hepatitis C virus infection 18 years after an epidemic outbreak of non-A, non-B hepatitis in a plasmapheresis centre. *Gut* 1999; **44**: 563-567
- 12 **Yokosuka O**, Kojima H, Imazeki F, Tagawa M, Saisho H, Tamatsukuri S, Omata M. Spontaneous negatiation of serum hepatitis C virus RNA is a rare event in type C chronic liver diseases: analysis of HCV RNA in 320 patients who were followed for more than 3 years. *J Hepatol* 1999; **31**: 394-399
- 13 **Mazzeo C**, Azzaroli F, Giovanelli S, Dormi A, Festi D, Colecchia A, Miracolo A, Natale P, Nigro G, Alberti A, Roda E, Mazzella G. Ten year incidence of HCV infection in northern Italy and frequency of spontaneous viral clearance. *Gut* 2003; **52**: 1030-1034
- 14 **Wei L**, Wang QX, Xu XY, Wan H, Gao Y, Tian XL, Yu M, Sun DG, Fan CL, Jin J, Fan WM, Yi LM, Zhu WF, Chen HS, Zhuang H, Wang Y. 12-25-year follow-up of hepatitis C virus infection in a rural area of Hebei province, China. *Beijing Daxue Xuebao* 2002; **34**: 574-578
- 15 **Minola E**, Prati D, Suter F, Maggiolo F, Caprioli F, Sonzogni A, Fraquelli M, Paggi S, Conte D. Age at infection affects the long-term outcome of transfusion-associated chronic hepatitis C. *Blood* 2002; **99**: 4588-4591
- 16 **Bellentani S**, Tiribelli C. The spectrum of liver disease in the general population: lesson from the Dionysos study. *J Hepatol* 2001; **35**: 531-537
- 17 **Alter MJ**, Kruszon-Moran D, Nainan OV, McQuillan GM, Gao F, Moyer LA, Kaslow RA, Margolis HS. The prevalence of hepatitis C virus infection in the United States, 1988 through 1994. *N Engl J Med* 1999; **341**: 556-562

Ability of luteinizing hormone releasing hormone-*Pseudomonas aeruginosa* exotoxin 40 binding to LHRH receptor on human liver cancer cells

Shou-Liang Gong, Gang Zhao, Hong-Guang Zhao, Wen-Tian Lü, Guang-Wei Liu, Ping Zhu

Shou-Liang Gong, Gang Zhao, Hong-Guang Zhao, Wen-Tian Lü, Guang-Wei Liu, Radiobiology Research Unit of Ministry of Public Health, School of Public Health, Jilin University, Changchun 130021, Jilin Province, China

Ping Zhu, Institute of Military Veterinary Medicine, Quartermaster University of Chinese PLA, Changchun 130062, Jilin Province, China
Supported by the Key Programs of National Science and Technology, No. 96-901-05-101

Correspondence to: Shou-Liang Gong, Radiobiology Research Unit of Ministry of Public Health, School of Public Health, Jilin University, Changchun 130021, Jilin Province, China. gongsl@163.com

Telephone: +86-431-5622028 **Fax:** +86-431-5645486

Received: 2003-11-18 **Accepted:** 2003-12-16

Abstract

AIM: To explore the ability of recombinant toxin luteinizing hormone releasing hormone-*Pseudomonas aeruginosa* exotoxin 40 (LHRH-PE40) and LHRH binding to LHRH receptor (LHRHR) on the membrane surface of human liver cancer HEPG cells.

METHODS: LHRH was labeled by using ^{125}I with enzymatic reaction. The affinity and receptor volume of LHRH-PE40 and LHRH binding to LHRHR on the membrane surface of human liver cancer cells were measured with radioligand receptor assay.

RESULTS: The specific activity of LHRH labeled with ^{125}I was 2.7×10^4 kBq/ μL , and its radiochemical purity reached to 99.2-99.7%. The binding of ^{125}I to LHRH was maximal for 240 min in the warm cultivation, and this binding was stabilized. The inhibiting rates of ^{125}I -LHRH and LHRH on the proliferation of human liver cancer HEPG cells were not significantly different. On the basis of the saturation curve of ^{125}I -LHRH binding to the membrane LHRHR of HEPG cells, ^{125}I -LHRH of 1×10^5 cpm was selected for radioligand receptor assay. The affinity constants (Kd) of LHRH-PE40 and LHRH binding to the membrane LHRHR of HEPG cells were 0.43 ± 0.12 nmol/L and 4.86 ± 1.47 nmol/L, respectively, and their receptor volumes were 0.37 ± 0.15 $\mu\text{mol/g}$ and 0.42 ± 0.13 $\mu\text{mol/g}$, respectively. The binding of LHRH-PE40 to the membrane protein of normal liver cells was not observed.

CONCLUSION: The recombinant toxin LHRH-PE40 binding to the membrane surface of LHRHR of human liver cancer HEPG cells was very strong, while the specific binding of it to normal liver cells was not observed. The results provide an important experimental basis for the clinical application of LHRH-PE.

Gong SL, Zhao G, Zhao HG, Lü WT, Liu GW, Zhu P. Ability of luteinizing hormone releasing hormone-*Pseudomonas aeruginosa* exotoxin 40 binding to LHRH receptor on human liver cancer cells. *World J Gastroenterol* 2004; 10(19): 2870-2873

<http://www.wjgnet.com/1007-9327/10/2870.asp>

INTRODUCTION

Guide medicine is currently one of the focuses in the field of medicine and biology. We can couple some tumor specific antibodies, cytokines or hormones, etc. with toxins (such as animal and plant toxin, radiotherapy and chemotherapy medicines or bacterial toxins, etc.) through chemical method or connection by gene fusing technology, and then express fusing protein to make a guide medicine with specific target characteristics and killing cell toxicity, that is biological missile, which can selectively kill homologous antigen-associated cells or antibody-associated cells, while exerts little effect on irrespective cells^[1]. So far, a series of recombinant immune toxins have shown perfect effects through *in vitro* and animal experiment^[2-4], moreover the results in some clinic investigations are also satisfactory^[5,6]. DAB389IL-2 which IL-2 receptor used as a guide medicine of target has passed FAD's warrant and come into use^[7].

Luteinizing hormone-releasing hormone (LHRH) is also termed gonadotropin-releasing hormone (GnRH). It is a peptide hormone synthesized and secreted mostly from hypothalamus. *Pseudomonas aeruginosa* exotoxin 40 (PE40) was obtained by removing I a region of PE. A fusing protein LHRH-PE40 was recombined by the fusion of both LHRH gene and PE40 gene with genetic engineering *in vitro*. LHRH-PE40 is a guide medicine to treat cancer. PE40 has effect on antitumor and immune regulation. The key of LHRH-PE40 biological effect is selectively to kill carcinoma cells. This effect is gained by the distributing difference of membrane surface LHRH receptor (LHRHR) in live cancer cells and normal liver cells. Many experimental results showed that LHRHR expressed greatly in the membrane surface of some carcinoma cells, but not in that of normal liver cells^[8-13]. The results provide an important basis for studying and preparing guide medicine to treat cancer^[14]. Therefore, LHRHR is acted as a sign to distinguish carcinoma cells from normal cells. The abilities of LHRH-PE40 binding to the membrane surface LHRHR of liver cancer cells and normal liver cells were observed with radioligand receptor assay for providing an important experimental basis for LHRH-PE40 clinical application.

MATERIALS AND METHODS

Liver cancer cell line and normal liver tissues

Human liver cancer HEPG cell line was bought from the Cell Center, Institute of Cell Biology, Chinese Academy of Medical Sciences (Beijing, China). Human liver tissues (3 cases) were provided by the Center of Medicolegal Examination, Criminal and Police Team, Liaoyuan City, Jilin, China.

Human liver cancer HEPG cell line was maintained in 75 cm² culture flasks at 37 °C in a humidified 50 mL/L CO₂-in-air mixture. The cells were passed weekly. After cells were harvested in exponential growth phase, they were dissociated with a non-enzymatic cell dissociation solution (Sigma, USA), and then counted by a hemacytometer. The cells were washed twice with phosphate-buffered saline (PBS) before cell membrane protein was prepared.

Reagents and hormones

^{125}I was from Amersham, UK. LHRH and thyrotropin releasing hormone (TRH) were bought from Institute of Biochemistry, Shanghai. LHRH-PE40 was synthesized by the Institute of Military Veterinary Medicine, Quartermaster University of PLA. Lactoperoxidase, glucoseoxidase and Sephadex G-25 gel were made in Sigma, USA.

LHRH labeled with ^{125}I of enzymatic reaction

The lactoperoxidase-glucoseoxidase method by Piyachaturawata *et al.*^[15] was slightly modified to label LHRH using ^{125}I with enzymatic reaction. Half mol/L PBS of 20 μL (pH 7.6), LHRH of 5 μg (dissolved in 0.1 mol/L NaAc of 5 μL), 2.3 mU lactoperoxidase (dissolved in 0.1 mol/L NaAc of 10 μL , pH 5.6), 2.8 mU glucoseoxidase (dissolved in 0.1 mol/L NaAc of 10 μL , pH 5.6) and 5 g/L $\beta\text{-D}$ (+) glucose of 5 μL in proper order were added into the test tube with 3.7×10^4 kBq fresh ^{125}I of non-reducer, oscillated and mixed, to make ^{125}I quickly labeling to LHRH. After the reaction for 5 min at 22-25 $^{\circ}\text{C}$, 0.1 mol/L boric acid buffer of 50 μL was added into the test tube to stop the reaction. The reactant of LHRH labeled with ^{125}I in test tube was separated and purified by column chromatography (the column of 1 cm \times 25 cm) with Sephadex G-25 gel to removing free ^{125}I , eluted with 0.1 mol/L boric acid buffer (containing 1 g/L gelatin and 0.2 g/L sodium azide, pH 9.2, flow rate: 3 mL/3 min, 3 mL/tube). Thirty-six tubes were collected. The radioactivity (counts per minute, cpm) of ^{125}I -LHRH of 10 μL in each tube was determined. The specific activity of ^{125}I -LHRH determined with self-displacement curve was $2.69\text{-}3.7 \times 10^4$ GBq/g LHRH.

Inhibiting rate of liver cancer cell proliferation measured with MTT

Inhibiting rates of both ^{125}I -LHRH and LHRH on the proliferation of human liver cancer HEPG cells were measured using enzyme-linked immunosorbent assay meter (Bio-Rad, USA) with MTT (thiazolyl blue) method^[16].

Preparation of cell membrane protein

The preparation of the membrane protein in human liver cancer HEPG cells: The cells were centrifuged in culture fluid, counted, washed once with PBS and centrifuged (500 r/min, 4 $^{\circ}\text{C}$, 5 min). The centrifuged sediment was suspended in ice-cold sucrose buffer for 20 min. The suspension was again centrifuged (300 r/min, 4 $^{\circ}\text{C}$, 5 min) after the cells in the suspension were ground with ultrasonic meter at ice bath. The centrifuged supernatant was further centrifuged (18 000 g, 4 $^{\circ}\text{C}$, 30 min). The centrifuged sediment was a membrane protein. Then the purer membrane protein of liver cancer cells was gained after the membrane protein was washed once with PBS.

Preparation of membrane protein in normal human liver cells: The liver tissue was sheared into fragments with ophthalmic scissors after the frozen tissue was thawed in sucrose buffer. The fragments were homogenized at ice bath for 1 min and centrifuged (1 500 r/min, 4 $^{\circ}\text{C}$, 10 min). The centrifuged supernatant was again centrifuged (31 000 g, 4 $^{\circ}\text{C}$, 15 min). Then the purer membrane protein of normal liver cells was gained after the membrane protein was washed once with PBS.

Competitive binding of LHRH-PE40 and LHRH to LHRHR of HEPG cell membrane

Polypropylene test tubes dried after soak with 10 g/L bovine serum albumin (BSA) were used as the reactive tubes. The tri-tube was used as a determined value. LHRH-PE40 or LHRH of different concentrations and ^{125}I -LHRH (1×10^5 cpm) of 100 μL in proper order were added into the reactive tube in ice bath, respectively, and mixed. Then, 100 μL suspension of the cell membrane (containing 180-220 μg protein) was added into the reactive tube. The reactive tubes were cultivated at 4 $^{\circ}\text{C}$ for 4 h

after oscillation. Excessive LHRH-PE40 or LHRH (200 μg) was added into the non-specific binding tube. The total volume in the reactive tube was 0.3 mL. The reactant was filtrated by using a microfilter with 32# glass fiber filter paper at 93.3 kPa negative pressure vacuum. The reactive tube and filter pore were washed 3 times with 0.5 mL of precolded 0.5 mol/L PBS (pH 7.4): physiological saline at 1:50. The radioactivity of the sediment on the filter paper filtered at vacuum and dried for 5 min was measured with ^{125}I automatic radio-immunity analyzer. The protein was measured with Lowry modification, and its standard curve was done with human serum albumin.

RESULTS

Characteristics of LHRH labeled with ^{125}I

The specific activity of LHRH labeled with ^{125}I of enzymatic reaction was 2.7×10^4 kBq/ μg . Its radiochemical purity measured using paper chromatography with the developer of 5% KI and 1 mol/L HCl (1:1) reached 99.2-99.7%. ^{125}I -LHRH did not produce free ^{125}I 3 and 7 d after preservation at -80 $^{\circ}\text{C}$, and produced 5% free ^{125}I after 10 d. The inhibiting rate of ^{125}I -LHRH on the proliferation of cancer cells was not significantly different as compared with that of LHRH (Figure 1).

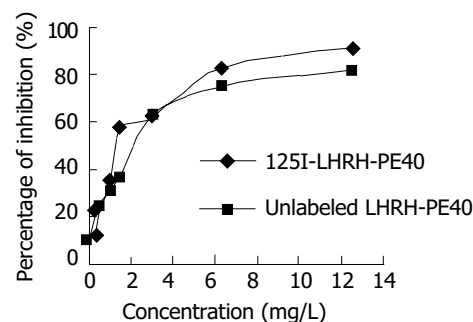


Figure 1 Inhibitory rates of unlabeled LHRH and ^{125}I -LHRH on human liver cancer HEPG cell proliferation.

Warm cultivation time of ^{125}I -LHRH binding to HEPG cell membrane protein

The ^{125}I -LHRH binding to HEPG cell membrane protein was observed for 60, 90, 120, 150, 180, 240 and 300 min in warm cultivation. The binding increased with the prolongation of warm cultivation time, and reached the peak value at 240 min. If the time in the warm cultivation was prolonged further, the binding decreased.

Radioligand receptor assay of competitive binding of LHRH-PE40 and LHRH to HEPG cell membrane protein with ^{125}I -LHRH

The specific binding of HEPG cell membrane protein to ^{125}I -LHRH increased with the protein concentration. The increase of the binding was not obvious as protein concentration exceeded 250 μg per 0.3 mL, while the non-specific binding increased obviously. According to the experimental results, the protein concentration of 180-220 μg per 0.3 mL was used as radioligand receptor assay.

The saturation curve of ^{125}I -LHRH binding to LHRHR of HEPG cells was firstly done. ^{125}I -LHRH of 1×10^5 cpm in 50% linear range of the saturation curve was selected as radioligand receptor assay (Figure 2). Figure 3 shows the inhibiting curve of competitive binding of non-labeled LHRH-PE40 and LHRH to HEPG cell membrane protein LHRHR with ^{125}I -LHRH. ^{125}I -LHRH binding to LHRHR reduced with increase of the non-labeled ligands to demonstrate a specific inhibiting curve of competitive binding. LHRH-PE40 could bind to HEPG cell surface LHRHR, while TRH could not. Figure 4 was drawn with Scatchard method

to gain two straight lines. The affinity constants (Kd) of binding of LHRH-PE40 and LHRH to LHRHR of HEPG cells were $0.43 \pm 0.12 \mu\text{mol/g}$ and $4.86 \pm 1.47 \mu\text{mol/g}$, respectively, and their receptor volumes were $0.37 \pm 0.15 \mu\text{mol/g}$ and $0.42 \pm 0.13 \mu\text{mol/g}$, respectively.

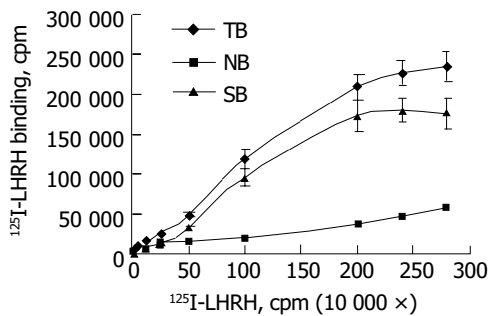


Figure 2 Saturation curve of ^{125}I -LHRH binding to LHRHR of human liver cancer HEPG cells. TB: total binding, NB: non-specific binding, SB: specific binding.

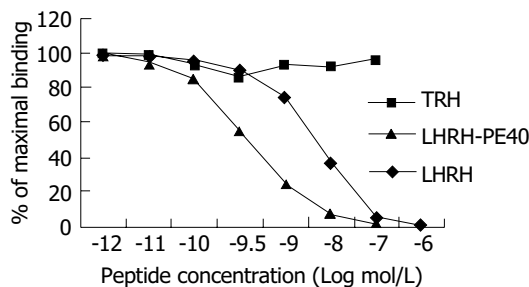


Figure 3 Inhibiting curve of competitive binding of non-labeled LHRH-PE40, LHRH and TRH to human liver cancer HEPG cell LHRHR with ^{125}I -LHRH.

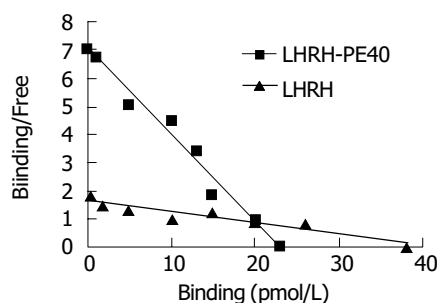


Figure 4 Scatchard analysis of LHRH-PE40 and LHRH binding to LHRHR of human liver cancer HEPG cells.

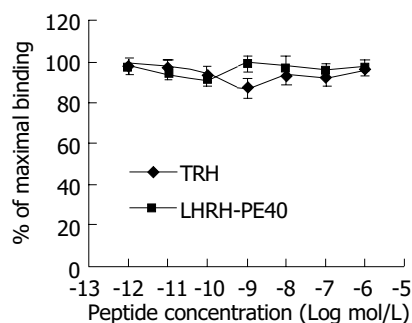


Figure 5 Inhibiting curve of competitive binding of non-labeled LHRH-PE40 and TRH to normal human liver cell LHRHR with ^{125}I -LHRH.

The binding curve of LHRH-PE40 to the membrane protein of normal liver cells was not significantly different from that of negative control TRH (Figure 5). The labeled ligand ^{125}I -LHRH binding to the membrane protein of normal liver cells did not change with increase of the non-labeled ligand LHRH-PE40. The result suggested that LHRH-PE40 binding to trace LHRHR in the membrane of normal human liver cells could not be examined.

DISCUSSION

The specific activity of LHRH labeled with ^{125}I of enzymatic reaction was $2.7 \times 10^4 \text{ kBq}/\mu\text{L}$, and its radiochemical purity reached 99.2-99.7%. The ^{125}I binding to LHRH was maximal at 240 min in the warm cultivation. This binding was stabilized, i.e. ^{125}I -LHRH did not produce free ^{125}I 3 and 7 d after preservation at -80°C , and produced 5% free ^{125}I after 10 d. The inhibiting rates of ^{125}I -LHRH and LHRH on the proliferation of human liver cancer HEPG cells measured with MTT (thiazolyl blue) method were not significantly different. The results suggest that LHRH satisfactorily labeled with ^{125}I of enzymatic reaction may be used as radioligand receptor assay.

LHRH-PE40 is a guide medicine to treat cancer. It is composed of the guide fraction of LHRH peptides and the toxicity fraction of PE40 protein. The active principle of LHRH-PE40 is that its toxicity fraction PE40 enters in cells through transmembrane transport to kill cancer cells after its guide fraction LHRH binds to LHRHR of cancer cell membrane surface. The expression of LHRH and its receptor as a part of a negative autocrine regulatory system of cell proliferation has been demonstrated in a number of human malignant tumors. Moreover, the dose-dependent antiproliferative effects of LHRH agonists on cell lines derived from these cancers have been observed by various investigators^[17-19]. The effect exerts through the signal transduction in cancer cells^[20, 21]. So, the specific binding of guide fraction LHRH to LHRHR of cancer cell membrane surface becomes the key in the treatment of carcinoma. It has been currently demonstrated that there also are LHRH and its receptor LHRHR in some tissues besides hypothalamus and pituitary. Some literatures indicated that there was LHRHR in the membrane surface of normal liver cells, but its content was very low^[18, 9]. The fact brings forward a challenge against the LHRHR specificity of killing cancer cells. However, our experimental results showed that specific binding of LHRH-PE40 to the membrane surface LHRHR of human liver cancer HEPG cells occurred, while did not to normal human liver cell membrane surface where there may be trace LHRHR. Of course, the negative result of this non-specific binding may be affected by the precision limitation in the experimental method itself. For example, some methods could be used only when the Kd of sample was less than 10^{-8} nmol/L ^[22]. Both epidermal growth factor (EGF) and interleukin-2 (IL-2) used as the guide medicines are also faced with the same problem that their trace receptors exist on the surface of normal liver and kidney cells, but they have been used in clinic. Although this kind of medicines may also have a weak liver toxicity, their side effects are less as compared with chemotherapy. So, LHRH-PE40 has some value in curing liver cancer with numeric proliferation of LHRHR.

The binding of hormone to its receptor was limited by many factors^[23]. Among these factors the space of hormone protein can directly affect the binding to its receptor. LHRH is a decapeptide without free amino and carboxyl. The amino acids at its 4-6 sites can form β -sheet like a barrette, which makes it binding to receptor. Furthermore, the amino acids at this hormone's first and 4-10 sites can bind to its receptor too. LHRH of LHRH-PE40 replaces I a section of PE. A linking bridge of both His and Met amino acids added between two molecules maintains the primary structure of LHRH. But whether LHRH's space configuration of this fusing protein changes should be

further explored. The results from this experiment were that the affinity constants (Kd) of LHRH-PE40 and LHRH binding to LHRHR of HEPG cells were 0.43 ± 0.12 nmol/g and 4.86 ± 1.47 nmol/L, respectively, and their receptor volumes were 0.37 ± 0.15 μ mol/g and 0.42 ± 0.13 μ mol/g, respectively. The affinity constant of LHRH-PE40 is nearly one-tenth of LHRH. Therefore, we can infer that LHRH-PE40 maintains the characteristics of LHRH binding to its receptor, and its binding capacity is stronger than LHRH itself. The result is identical with the report published elsewhere^[6]. This enhancing binding capacity may be caused by its molecular mass being larger than LHRH, which makes itself more stable and decomposed difficultly *in vitro*. These results proved that LHRH-PE40 can bind to LHRHR on the surface of liver cancer cells, and then exerts its guide action.

Up till now, some problems still need to be resolved on the guide medicine for the treatment of cancer. Somebody testified that positive rate of LHRHR in adjacent tissues of cancers was even higher than that in cancer tissues^[24], which should be attached importance. The articles demonstrated that the signal transduction pathways mediated by LHRHR were different^[25], LHRHR of cancer cell surface could mediate cell apoptosis^[26,27].

ACKNOWLEDGEMENTS

We are grateful to Dr. Zhang PY and Dr. Li JZ for their excellent technical assistance, and Dr. Wu GM and Dr. Zhang GL for their providing experimental materials.

REFERENCES

- 1 **Panchal RG**. Novel therapeutic strategies to selectively kill cancer cells. *Biochem Pharmacol* 1998; **55**: 247-252
- 2 **Reiter Y**, Pastan I. Recombinant Fv immunotoxins and Fv fragments as novel agents for cancer therapy and diagnosis. *Trends Biotechnol* 1998; **16**: 513-520
- 3 **Perentesis JP**, Gunther R, Waurzyniak B, Yanishevsky Y, Myers DE, Ek O, Messinger Y, Shao Y, Chelstrom LM, Schneider E, Evans WE, Uckun FM. *In vivo* biotherapy of HL-60 myeloid leukemia with a genetically engineered recombinant fusion toxin directed against the human granulocyte macrophage colony-stimulating factor receptor. *Clin Cancer Res* 1997; **3**(12 Pt 1): 2217-2227
- 4 **Saleh MN**, LeMaistre CF, Kuzel TM, Foss F, Platanius LC, Schwartz G, Ratain M, Rook A, Freytes CO, Craig F, Reuben J, Sams MW, Nichols JC. Antitumor activity of DAB389IL-2 fusion toxin in mycosis fungoides. *J Am Acad Dermatol* 1998; **39**: 63-73
- 5 **Kreitman RJ**, Wilson WH, Robbins D, Margulies I, Stetler-Stevenson M, Waldmann TA, Pastan I. Responses in refractory hairy cell leukemia to a recombinant immunotoxin. *Blood* 1999; **94**: 3340-3348
- 6 **Haggerty HG**, Warner WA, Comereski CR, Peden WM, Mezza LE, Damle BD, Siegall CB, Davidson TJ. BR96 sFv-PE40 immunotoxin: nonclinical safety assessment. *Toxicol Pathol* 1999; **27**: 87-94
- 7 **Duvic M**, Kuzel TM, Olsen EA, Martin AG, Foss FM, Kim YH, Heald PW, Bacha P, Nichols J, Liepa A. Quality-of-life improvements in cutaneous T-cell lymphoma patients treated with denileukin diftitox (ONTAK(R)). *Clin Lymphoma* 2002; **2**: 222-228
- 8 **Zhao G**, Gong SL, Yue Y, Zhu P. Distribution of human LHRH receptors in normal and carcinomatous tissues outside pituitary. *Jilin Daxue Xuebao* 2002; **28**: 445-447
- 9 **Zhao G**, Gong SL, Zhu P. Binding ability of LHRH-PE40 to LHRH receptors on the surface of cancer cell line. *Jilin Daxue Xuebao* 2003; **29**: 5-8
- 10 **Dharap SS**, Qiu B, Williams GC, Sinko P, Stein S, Minko T. Molecular targeting of drug delivery systems to ovarian cancer by BH3 and LHRH peptides. *J Control Release* 2003; **91**: 61-73
- 11 **Grundker C**, Gunthert AR, Millar RP, Emons G. Expression of gonadotropin-releasing hormone II (GnRH-II) receptor in human endometrial and ovarian cancer cells and effects of GnRH-II on tumor cell proliferation. *J Clin Endocrinol Metab* 2002; **87**: 1427-1430
- 12 **Volker P**, Grundker C, Schmidt O, Schulz KD, Emons G. Expression of receptors for luteinizing hormone-releasing hormone in human ovarian and endometrial cancers: frequency, autoregulation, and correlation with direct antiproliferative activity of luteinizing hormone-releasing hormone analogues. *Am J Obstet Gynecol* 2002; **186**: 171-179
- 13 **Halmos G**, Arencibia JM, Schally AV, Davis R, Bostwick DG. High incidence of receptors for luteinizing hormone-releasing hormone (LHRH) and LHRH receptor gene expression in human prostate cancers. *J Urol* 2000; **163**: 623-629
- 14 **Plonowski A**, Schally AV, Nagy A, Groot K, Krupa M, Navone NM, Logothetis C. Inhibition of *in vivo* proliferation of MDA-MDA-PCa-2b human prostate cancer by a targeted cytotoxic analog of luteinizing hormone-releasing hormone AN-207. *Cancer Lett* 2002; **176**: 57-63
- 15 **Piyachaturawata P**, Pedroza E, Huang WY, Arimura A, Schally AV. Studies on the iodination of LH-RH and the biological and immunological activities of the products. *Life Sci* 1980; **26**: 1309-1318
- 16 **Xu N**, Shi AP, Wang YD, Wang CX, Guo WH. Effect of telomerase oligonucleotides on the inhibition of telomerase activity and cell growth in bladder. *Jilin Daxue Xuebao* 2003; **29**: 630-633
- 17 **Gunthert AR**, Grundker C, Hollmann K, Emons G. Luteinizing hormone-releasing hormone induces JunD-DNA binding and extends cell cycle in human ovarian cancer cells. *Biochem Biophys Res Commun* 2002; **294**: 11-15
- 18 **Grundker C**, Gunthert AR, Westphalen S, Emons G. Biology of the gonadotropin-releasing hormone system in gynecological cancers. *Eur J Endocrinol* 2002; **146**: 1-14
- 19 **Shacham S**, Cheifetz MN, Lewy H, Ashkenazi IE, Becker OM, Seger R, Naor Z. Mechanism of GnRH receptor signaling: from the membrane to the nucleus. *Ann Endocrinol* 1999; **60**: 79-88
- 20 **Grundker C**, Schlotawa L, Viereck V, Emons G. Protein kinase C-independent stimulation of activator protein-1 and c-Jun N-terminal kinase activity in human endometrial cancer cells by the LHRH agonist triptorelin. *Eur J Endocrinol* 2001; **145**: 651-658
- 21 **Grundker C**, Volker P, Schulz KD, Emons G. Luteinizing hormone-releasing hormone agonist triptorelin and antagonist cetrotorelix inhibit EGF-induced c-fos expression in human gynecological cancers. *Gynecol Oncol* 2000; **78**: 194-202
- 22 **Lü BZ**, Tian Y. Receptorology outline. 1st Ed. *Beijing Sciences Press* 1991: 27-32
- 23 **Luo HB**, Zhu P, Li LJ. Bacterial toxin and clinic. 1st Ed. *Beijing People Health Press* 1999: 91-99
- 24 **Zhang JS**, Huang GS, Huang WQ, Zhang YQ. Immunohistochemical localization of gonadotropin releasing hormone and its receptor in hepatocellular carcinoma tissues. *Disi Junyi Daxue Xuebao* 1998; **19**: 235-236
- 25 **Limonta P**, Moretti RM, Marelli MM, Dondi D, Parenti M, Motta M. The luteinizing hormone-releasing hormone receptor in human prostate cancer cells: messenger ribonucleic acid expression, molecular size, and signal transduction pathway. *Endocrinology* 1999; **140**: 5250-5256
- 26 **Imai A**, Tamaya T. GnRH receptor and apoptotic signaling. *Vitam Horm* 2000; **59**: 1-33
- 27 **Grundker C**, Schulz K, Gunthert AR, Emons G. Luteinizing hormone-releasing hormone induces nuclear factor κ B-activation and inhibits apoptosis in ovarian cancer cells. *J Clin Endocrinol Metab* 2000; **85**: 3815-3820

Human endostatin gene transfer, either naked or with liposome, has the same inhibitory effect on growth of mouse liver tumor cells *in vivo*

Chun-Hong Ma, Yan Zhang, Xiao-Yan Wang, Li-Fen Gao, Hua Liu, Chun Guo, Su-Xia Liu, Ying-Lin Cao, Li-Ning Zhang, Wen-Sheng Sun

Chun-Hong Ma, Yan Zhang, Xiao-Yan Wang, Li-Fen Gao, Hua Liu, Chun Guo, Su-Xia Liu, Ying-Lin Cao, Li-Ning Zhang, Wen-Sheng Sun, Institute of Immunology, Medical College of Shandong University, Jinan 250012, Shandong Province, China

Supported by the National Natural Science Foundation of China, No. 30100078 and Huo Yingdong Educational Fund, No.81035

Correspondence to: Dr. Chun-Hong Ma, Institute of Immunology, Medical College of Shandong University, Jinan 250012, Shandong Province, China. machunhong@sdu.edu.cn

Telephone: +86-531-8382038

Received: 2003-11-21 **Accepted:** 2003-12-22

Abstract

AIM: To explore a safe and efficient strategy of tumor therapy using anti-angiogenetic agents.

METHODS: Endostatin gene with a signal sequence of human IgG γ chain was amplified by PCR and cloned into pVAX1 plasmid which was the only vector authorized by FDA in clinical trial to construct a recombinant plasmid named as pVAX-sEN. The recombinant plasmid was detected with *EcoRI/KpnI* and DNA sequencing. BALB/c mice bearing hepatocarcinoma cell line H22 were treated with naked pVAX-sEN or liposome-DNA complex in which the dose of DNA and the ratio of DNA and liposome were different from each other. To compare the efficiency of gene transfection, expression of endostatin at the treated tumor site was assayed with ELISA. To investigate the effect of pVAX1-sEN on hepatocellular carcinoma, pVAX-sEN either naked or in liposome-DNA complex was injected into BALB/c mice bearing H22, then the diameter of tumors was measured, microvessel density was detected by immunohistochemistry, endostatin expression *in vivo* was assayed at different time points.

RESULTS: DNA sequencing showed the endostatin gene with the signal peptide was correctly cloned. *In situ* gene expression assay indicated that both the ratio of DNA and liposome and the dose of DNA could affect the gene transfection efficiency. Interestingly, naked pVAX-sEN had a similar *in situ* endostatin expression to pVAX-sEN with liposome. Animal experiments showed that pVAX-sEN together with pVAX-sEN-liposome complex could efficiently suppress the growth of mouse hepatoma cells.

CONCLUSION: Naked endostatin plasmid intratumoral injection can get a similar gene transfection efficiency to liposome-DNA complex when used *in situ*.

Ma CH, Zhang Y, Wang XY, Gao LF, Liu H, Guo C, Liu SX, Cao YL, Zhang LN, Sun WS. Human endostatin gene transfer, either naked or with liposome, has the same inhibitory effect on growth of mouse liver tumor cells *in vivo*. *World J Gastroenterol* 2004; 10(19): 2874-2877

<http://www.wjgnet.com/1007-9327/10/2874.asp>

INTRODUCTION

Tumor neovascularization is necessary to the growth and metastasis of tumors^[1]. Anti-angiogenesis is an effective method to treat cancer^[2,3]. Endostatin, an endogenous angiogenesis inhibitor, was found in 1997^[4]. It can specifically suppress endothelial cell proliferation. Animal experiments have demonstrated that endostatin can strikingly inhibit the growth of many kinds of tumor cells without drug resistance and toxicity. Endostatin is a promising agent to treat cancer^[5,6]. However, to produce a large quantity of biologically active proteins has been proven difficult, the treatment requires repeated administration and high doses of recombinant protein, which limits endostatin's clinical application. Gene therapy can overcome the above disadvantages and become a potential method for cancer therapy. In this article, we constructed the recombinant eukaryotic plasmid using pVAX1 which is the only vector authorized by FDA in clinical trial. It can express secretive endostatin *in vivo*. Efficient gene transfer and expression are the key to gene therapy. In order to explore an efficient and easy gene transfer method, we also compared the inhibitory effect of liposome and naked DNA transfection on mouse hepatoma cells *in vivo*.

MATERIALS AND METHODS

Plasmids

Eukaryotic expression vector pVAX1 authorized by FDA in clinical trial was purchased from Invitrogen(USA). Cloning vector pGEM-T-EN containing human endostatin genes was constructed and preserved in our laboratory^[7].

Cells and cultures

Mouse hepatoma cell line H22 was purchased from Shandong Medical Science Institute and grown in BALB/c abdominal cavity.

Animals

BALB/c female mice, 5-6 wk of age, were provided by Experimental Animal Center of Shandong University. A total of 1×10^6 H22 cells were transplanted subcutaneously into mice. Treatment began 1 wk later, when tumor volume ranged between 0.4 to 0.5 cm³.

Primer design

According to the sequences in GeneBank, primers were designed to amplify endostatin genes. In order to get a secretory protein, signal sequence of human IgG γ chain was added to the 5' end of forward primer, and sequences recognized by *KpnI* and *EcoRI* were respectively added to the forward primer and reverse primer: forward(P1): 5' TTAGGTACCATGGAAGCCCCAGCTCAGCTTCTCTTCTCCTGCTACTCTGGCTCCCAGATACCACCGGACACAGCCACCGC 3'; reverse(P2): 5' CGGCGAATTCC TTGGAGG CAGTC 3'. All of these oligonucleotide primers were synthesized by Shanghai BioAsia Bio-technology Co.Ltd.

PCR

The endostatin gene containing signal sequence of human

IgG γ chain was amplified by PCR taking pGEM-T-EN as template and P1 and P2 as primers. PCR reaction was performed in 25 μ L volume containing: 1 μ L of plasmid DNA, 2.5 μ L of 10 \times buffer, 0.5 mmol/L Mg⁺⁺, 5 nmol/L dNTP, 3 units of Taq polymerase, 10 nmol/L primers (forward and reverse). Reaction conditions were at 95 $^{\circ}$ C for 5 min, then 30 cycles each at 95 $^{\circ}$ C for 1 min, at 62 $^{\circ}$ C for 1 min, at 72 $^{\circ}$ C for 3 min, followed by a final extension at 72 $^{\circ}$ C for 5 min. PCR products were purified by UNIQUE-10 Kit (Shanghai Shenggong Biological Co.Ltd) after 20 g/L agarose gel electrophoresis.

Construction of recombinant eukaryotic plasmid expressing secretive endostatin

PCR products and pVAX1 were digested by *Eco*RI and *Kpn*I (TaKaRa Biotechnology, Dalian) respectively, then purified and ligated with T4DNA ligase (TaKaRa Biotechnology, Dalian) at room temperature overnight. *E. coli*, DH5 α , competent cells were transfected using CaCl₂. Recombinant clones were detected by *Eco*RI and *Kpn*I and then sequenced by Shanghai BioAsia Biotechnology Co.Ltd.

In situ expression of secretary endostatin

Five-to-six week old female BALB/c mice were injected subcutaneously with 1 \times 10⁶ logarithmically growing H22 cells to axillary. One week later, when tumor volume was about 0.4 to 0.5 cm³, naked plasmid or liposome-DNA complex (LipofectamineTM2000 from Invitrogen) was administered intratumorally. The ratio of liposome and recombinant plasmid in liposome-DNA complex was 1:1, 1:3, 1:8 respectively. Animals were sacrificed 3 d after injection and about 0.5 cm³ of tumor was separated and cut into pieces, then cultured in 0.5 mL MEM medium with 100 mL/L of FCS at 37 $^{\circ}$ C, 50 mL/L CO₂ atmosphere for 24 h. Supernatants were collected and centrifuged at 1 000 r/min for 5 min, then stored at -20 $^{\circ}$ C for gene expression assay.

In vivo inhibition assay

One week after BALB/c mice were injected subcutaneously with 1 \times 10⁶ logarithmically growing H22 cells to axillary, naked recombinant plasmid (20 μ g) or the liposome-DNA complex containing 20 μ g recombinant plasmid was administered intratumorally once a week for two weeks. The ratio of liposome and recombinant plasmid in liposome-DNA complex was 1:1. pVAX1 and NS were respectively injected into animals as control. The length (a) and width (b) of tumor were measured twice a week. The tumor volumes were then calculated using the formula: Volume=a \times b² \times 0.52.

The experiment was done in triplicate with 5 animals in each group.

In vivo expression assay of endostatin

In order to determine the association of anti-tumor effects and the expression level of endostatin, peripheral blood was prepared from tail at different time point and serum was used to detect the expression of endostatin with ELISA.

ELISA

Expression of endostatin was detected with human endostatinTM protein accucyte^REIA kit (Oncogene) following the manufacturer's instructions.

Immunohistochemistry

Mice were killed 3 d after the fourth administration. Tumors were excised, fixed in formalin and prepared for paraffin-embedded sections. Factor VIII-related antigen was detected with S-P immunohistochemistry kit (Beijing Zhongshan Biocompany) according to the manufacturer's instructions.

Tumor microvessel density (MVD) was evaluated as described by Weidner^[8].

Statistical analysis

All data were expressed as mean \pm SD. Student's *t*-test was used for statistical analysis. A *P* value <0.05 was considered statistically significant.

RESULTS

Plasmid construction

Endostatin gene with signal sequence of human IgG γ chain was amplified by PCR and cloned into eukaryotic vector pVAX1 named as pVAX-sEN. Two percent agarose gel electrophoresis demonstrated two bands about 3 kb and 610 bp in size as expected after the recombinant plasmid was digested by *Kpn*I and *Eco*RI (Figure 1). DNA sequencing analysis indicated both the sequence of endostatin and signal peptide were in accordance with those in the GenBank.

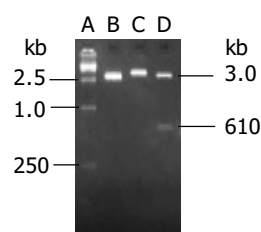


Figure 1 Detection of the recombinant plasmid pVAX-sEN using *Eco*RI and *Kpn*I digestion. A: Marker 15 000; B: pVAX1 digested by *Eco*RI; C: Recombinant plasmid pVAX-sEN digested by *Eco*RI; D: Recombinant plasmid pVAX-sEN digested by *Eco*RI and *Kpn*I.

In situ gene expression assay of naked DNA and liposome-DNA complex

To compare the efficiency of gene transfection, expression of endostatin transgenic protein at the tumor site of the treated group was assayed with ELISA. Endostatins were detected in all samples treated with naked or liposome-DNA complex but not in the control groups (Figure 2). Endostatin expression was about 30 ng/mL when the ratio of liposome and DNA was 1:1. With the addition of the liposome into complex the expression of endostatin was increased gradually. When the ratio reached 1:8, the endostatin was 92 ng/mL. Interestingly, naked DNA administration could get a pretty high gene expression which was about 86 ng/mL.

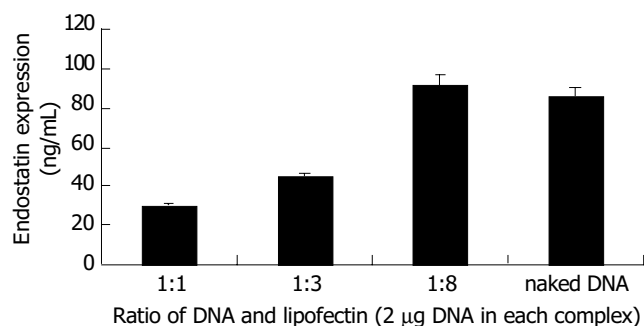


Figure 2 Comparison of *in vivo* transfection using different ratios of liposome and DNA in liposome-DNA complex and naked DNA.

To compare gene transfection using liposome-DNA complex containing different doses of DNA *in vivo*, liposome-DNA

complex was prepared with the ratio of liposome and DNA 1:1 which contained different doses of DNA. Twenty-four hours after transfection endostatins were detected by ELISA (Figure 3). The result indicated that when DNA was less than 20 μg , with the elevation of DNA doses, the expression of endostatin increased. When the DNA dose reached 20 μg , endostatin reached 152 ng/mL, the peak expression. On the contrary, when the DNA reached 50 μg , the expression of endostatin dropped to 80 ng/mL.

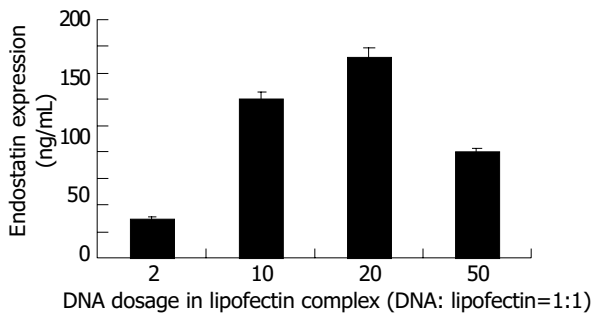


Figure 3 Comparison of *in vivo* transfection using liposome complex (the ratio of liposome and DNA is 1:1) containing different doses of DNA.

In vivo inhibitory effect of pVAX-sEN on mouse hepatoma cells

Changes of tumor volumes indicated pVAX-sEN-liposome complex could obviously inhibit the growth of mouse hepatoma cells when administered intratumorally (Figure 4). The tumor volume was only $0.451 \pm 0.26 \text{ cm}^3$, obviously less than that in NS treated group ($1.86 \pm 0.62 \text{ cm}^3$) and pVAX1 treated group ($1.56 \pm 0.37 \text{ cm}^3$) ($P < 0.05$). The inhibition rate was about 73%. Interestingly, pVAX-sEN alone could produce an inhibitory effect. The tumor size in pVAX-sEN treated group was $0.4 \pm 0.25 \text{ cm}^3$, and the inhibitory rate was about 80%, which was not significant from pVAX-sEN-liposome complex treated group ($P > 0.05$).

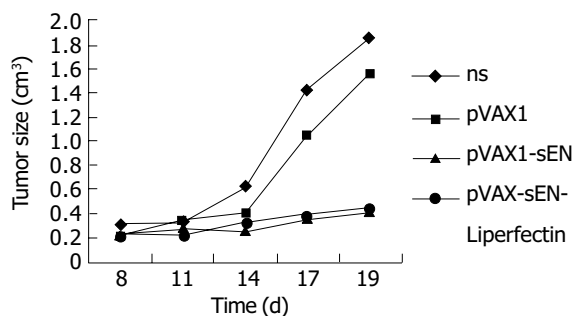


Figure 4 Inhibitory effect of recombinant secretive endostatin on mouse hepatoma cells.

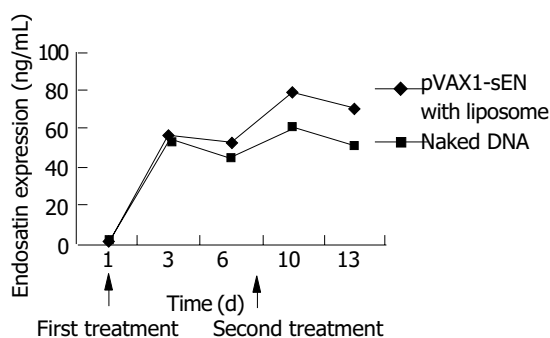


Figure 5 *In vivo* endostatin expression in peripheral blood of treated mice.

In vivo expression of endostatin

ELISA showed that the expression of endostatin in peripheral blood varied with the administration of recombinant plasmid. Three days after the first treatment of recombinant plasmid, both naked and in combination with liposome, the expression of endostatin could be detected ($56.8 \pm 3.8 \text{ ng/mL}$ and $54 \pm 5.8 \text{ ng/mL}$, respectively. $P > 0.05$) and then the expression decreased 2 d later. After the second administration the expression raised to $79.8 \pm 6.1 \text{ ng/mL}$ and $60.43 \pm 8.3 \text{ ng/mL}$ and it could be lasted for another 3 d. The expression level in naked plasmid treated mice was lower than that in DNA-liposome complex treated mice ($50.1 \pm 6.3 \text{ ng/mL}$ vs $70.4 \pm 6.4 \text{ ng/mL}$, $P < 0.05$) (Figure 5).

Inhibition of tumor angiogenesis by pVAX-sEN

Immunohistochemical analysis showed a potent inhibition of angiogenesis in tumors treated by pVAX-sEN. The MVD was counted and results are shown in Figure 6. Expression of endostatin mediated by naked pVAX-sEN or liposome-DNA complex injection caused a significant reduction in MVD compared with the NS control group or the pVAX1 treated group ($P < 0.05$). However, the difference in MVD between naked DNA and liposome-DNA complex injection groups was not statistically significant.

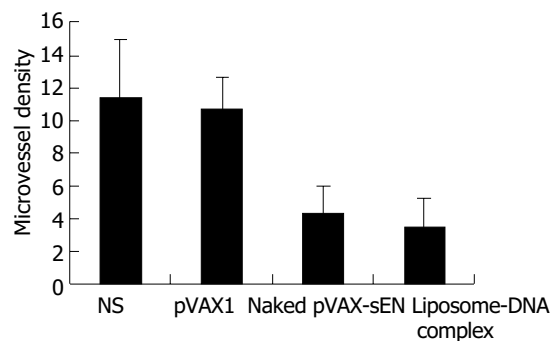


Figure 6 Inhibition of tumor neovascularization by injecting recombinant plasmid.

DISCUSSION

Growth and metastasis of tumor depend on the neovascularization. Anti-angiogenesis can effectively suppress tumor growth. Endostatin was found to specifically inhibit endothelial cell proliferation but not actively proliferating cells such as carcinoma cells, intestinal cells, epithelial cells, bone marrow cells^[4]. So the application of endostatin did not cause bone marrow ablation, stomach and intestinal reaction, and other side effects^[5]. Moreover, endostatin could be used for a long time without drug resistance since its target cells, endothelial cells have a relatively stable gene structure and low mutation rate^[5,6]. Consequently endostatin is an attractive new strategy in cancer therapy.

Recombinant endostatin protein has been used in clinical trials at present^[9]. However poor solubility of recombinant endostatin protein and its high effective dose have limited its wide spread application^[4]. Gene therapy by which endostatin can express *in vivo* is an efficient method for anti-angiogenesis cancer therapy^[10-12].

The key point of gene therapy is to establish an effective gene delivering system. Vectors used to deliver genes nowadays mainly include viral and non-viral vectors. Because of limitations of viral vectors such as potent danger, immune response and limitations of the gene length^[13-15], more and more researchers have paid their attention to non-viral vectors. In this paper, a highly safe vector pVAX1 authorized by FDA in clinical trial was selected to construct a recombinant vector expressing

secretive endostatin which was named as pVAX-sEN. DNA sequencing indicated endostatin gene together with a signal peptide was correctly cloned. Animal experiments showed pVAX-sEN could efficiently suppress the growth of mouse hepatoma cells. This study provides an experimental basis for further study on safe and efficient gene therapy with endostatin.

Non-viral gene can be transferred by physical and chemical methods. The cationic liposome-mediated gene transfer system is popular because of its low immunity, high safety, easy preparation, no limitation to gene sequence and potential to be used repeatedly^[16,17]. Gene transfer efficiency of liposome can be affected by many factors. Studies indicated that a suitable quantity ratio of DNA and liposome was one of the essential factors^[18]. Naked DNA injection is another simple safe gene transfer method. Many researchers have verified that naked DNA administration could induce a high gene expression level^[19,20]. In 2003 VEGF administered into cardiac muscle using naked DNA was applied to clinical trial^[21]. In our study, cationic liposome was used to transfer endostatin DNA into mouse hepatoma cells *in vivo*. It showed that when the quantity ratio of liposome and DNA was 1:1, the expression of endostatin was pretty high. When the quantity ratio was 1:8, endostatin reached the highest expression (92 ng/mL). With the elevation of DNA dose, the expression of endostatin increased. When the DNA dose reached 20 µg, the expression of endostatin amounted to 152 ng/mL. However, if DNA dose reached 50 µg, the expression of endostatin dropped to 80 ng/mL. The possible reason was that the high dose of liposome in the complex might be deposited^[18]. So the transfection efficiency was lower. Results also indicated that naked DNA could also get a pretty high gene expression (86 ng/mL). Our *in vivo* inhibition assay even showed that naked DNA could get an inhibition as efficient as DNA-liposome complex. In 2002, Shi *et al.*^[22] compared the transfection rate of naked DNA with liposome-DNA complex and found the expression of IL-12 was equal. Their result is in accordance with ours. However, *in vivo* gene expression assay indicated that the peripheral expression of endostatin in naked DNA treated mice decreased more quickly than that in DNA-liposome complex treated mice.

In conclusion, we successfully constructed the recombinant vector secretively expressing endostatin using highly safe vector pVAX1 named pVAX-sEN. Animal experiments showed it could efficiently suppress the growth of hepatoma cells. It is a promising method in cancer therapy. At the same time we compared the transfection efficiency of naked pVAX-sEN DNA with liposome-DNA complex. Results indicated naked DNA could produce both a high endostatin gene expression and a good tumor inhibition effect when used *in situ*, strongly suggesting that naked DNA administration is a simple, safe and efficient gene transfer method.

REFERENCES

- 1 Folkman J. What is the Evidence that tumors are angiogenesis dependent. *J Natl Cancer Inst* 1990; **82**: 4-6
- 2 Marx J. Angiogenesis. A boost for tumor starvation. *Science* 2003; **301**: 452-454
- 3 Brem S, Brem H, Folkman J, Finkelstein D, Patz A. Prolonged tumor dormancy by prevention of neovascularization in the vitreous. *Cancer Res* 1976; **36**: 2807-2812
- 4 O'Reilly MS, Boehm T, Shing Y, Fukai N, Vasios G, Lane WS,

- Flynn E, Birkhead JR, Folkman J, Fukai N, Vasios G, Lane WS, Elynn E, Birkhead JR, Folkman J. Endostatin: an endogenous inhibitor of angiogenesis and tumor growth. *Cell* 1997; **88**: 277-285
- 5 Boehm T, Folkman J, Browder T, O'Reilly MS. Antiangiogenic therapy of experimental cancer does not induce acquired drug resistance. *Nature* 1997; **390**: 404-407
- 6 Kerbel RS. A cancer therapy resistant to resistance. *Nature* 1997; **390**: 335-336
- 7 Ma CH, Sun WS, Zhang LN, Wang XY, Li X. Expression of human endostatin in picha yeast and its inhibition effect on tumor. *J Shandong Med University* 2001; **39**: 334-336
- 8 Weidner N. Current pathologic methods for measuring intratumoral microvessel density within breast carcinoma and other solid tumors. *Breast Cancer Res Treat* 1995; **36**: 169-180
- 9 Eder JP Jr, Supko JG, Clark JW, Puchalski TA, Garcia-Carbonero R, Ryan DP, Shulman LN, Proper J, Kirvan M, Rattner B, Connors S, Keogan MT, Janicek MJ, Fogler WE, Schnipper L, Kinchla N, Sidor C, Phillips E, Folkman J, Kufe DW. Phase I clinical trial of recombinant human endostatin administered as a short intravenous infusion repeated daily. *J Clin Oncol* 2002; **20**: 3772-3784
- 10 Wang X, Liu F, Li X, Li J, Xu G. Anti-tumor effect of human endostatin mediated by retroviral gene transfer in nude mice. *Chin Med J* 2002; **115**: 1664-1669
- 11 Nakashima Y, Yano M, Kobayashi Y, Moriyama S, Sasaki H, Toyama T, Yamashita H, Fukai I, Iwase H, Yamakawa Y, Fujii Y. Endostatin gene therapy on murine lung metastases model utilizing cationic vector-mediated intravenous gene delivery. *Gene Ther* 2003; **10**: 123-130
- 12 Li X, Fu GF, Fan YR, Shi CF, Liu XJ, Xu GX, Wang JJ. Potent inhibition of angiogenesis and liver tumor growth by administration of an aerosol containing a transferrin-liposome-endostatin complex. *World J Gastroenterol* 2003; **9**: 262-266
- 13 Bramson JL, Hitt M, Gaudie J, Graham FL. Pre-existing immunity to adenovirus does not prevent tumor regression following intratumoral administration of a vector expressing IL-12 but inhibits virus dissemination. *Gene Ther* 1997; **4**: 1069-1076
- 14 Lehrman S. Virus treatment questioned after gene therapy death. *Nature* 1999; **401**: 517-518
- 15 Rochlitz CF. Gene therapy of cancer. *Drugs Today* 2000; **36**: 619-629
- 16 Ota T, Maeda M, Tatsuka M. Cationic liposomes with plasmid DNA influence cancer metastatic capability. *Anticancer Res* 2002; **22**: 4049-4052
- 17 Kaiser S, Toborek M. Liposome-mediated high-efficiency transfection of human endothelial cells. *J Vasc Res* 2001; **38**: 133-143
- 18 Clark PR, Stopeck AT, Ferrari M, Parker SE, Hersh EM. Studies of direct intratumoral gene transfer using cationic lipid-complexed plasmid DNA. *Cancer Gene Ther* 2000; **7**: 853-860
- 19 Kim JM, Jeong JG, Ho SH, Hahn W, Park EJ, Kim S, Yu SS, Lee YW, Kim S. Protection against collagen-induced arthritis by intramuscular gene therapy with an expression plasmid for the interleukin-1 receptor antagonist. *Gene Ther* 2003; **10**: 1543-1550
- 20 Imboden M, Shi F, Pugh TD, Freud AG, Thom NJ, Hank JA, Hao Z, Staelin ST, Sondel PM, Mahvi DM. Safety of interleukin-12 gene therapy against cancer: a murine biodistribution and toxicity study. *Hum Gene Ther* 2003; **14**: 1037-1048
- 21 Fortuin FD, Vale P, Losordo DW, Symes J, DeLaria GA, Tyner JJ, Schaer GL, March R, Snell RJ, Henry TD, Van Camp J, Lopez JJ, Richenbacher W, Isner JM, Schatz RA. One-year follow-up of direct myocardial gene transfer of vascular endothelial growth factor-2 using naked plasmid deoxyribonucleic acid by way of thoracotomy in no-option patients. *Am J Cardiol* 2003; **92**: 436-439
- 22 Shi F, Rakhmilevich AL, Heise CP, Oshikawa K, Sondel PM, Yang NS, Mahvi DM. Intratumoral injection of interleukin-12 plasmid DNA, either naked or in complex with cationic lipid, results in similar tumor regression in a murine model. *Mol Cancer Ther* 2002; **1**: 949-957

Expression of plasma vascular endothelial growth factor in patients with hepatocellular carcinoma and effect of transcatheter arterial chemoembolization therapy on plasma vascular endothelial growth factor level

Xin Li, Gan-Sheng Feng, Chuan-Sheng Zheng, Chen-Kai Zhuo, Xi Liu

Xin Li, Gan-Sheng Feng, Chuan-Sheng Zheng, Chen-Kai Zhuo, Xi Liu, Department of Interventional Radiology, Union Hospital, Tongji Medical College, Huazhong University of Science and Technology, Wuhan 430022, Hubei Province, China
Supported by the National Natural Science Foundation of China, No. 39770839

Correspondence to: Xin Li, M.D., Department of Radiology, the Affiliated Union Hospital, Tongji Medical College, Huazhong University of Science and Technology, Wuhan 430022, Hubei Province, China. wxyao2001@yahoo.com.cn

Telephone: +86-27-85726373

Received: 2004-03-27 **Accepted:** 2004-04-05

invasion. TACE increases the level of P-VEGF only temporarily which may be associated with tumor ischemia. P-VEGF may be useful in predicting treatment response, monitoring disease course after TACE and judging the effect of different TACE regimens.

Li X, Feng GS, Zheng CS, Zhuo CK, Liu X. Expression of plasma vascular endothelial growth factor in patients with hepatocellular carcinoma and effect of transcatheter arterial chemoembolization therapy on plasma vascular endothelial growth factor level. *World J Gastroenterol* 2004; 10(19): 2878-2882

<http://www.wjgnet.com/1007-9327/10/2878.asp>

Abstract

AIM: To investigate the expression level of plasma vascular endothelial growth factor (P-VEGF) in patients with hepatocellular carcinoma (HCC) and its relationship with the clinicopathologic characteristics, and to examine the changes of P-VEGF in the course of transcatheter arterial chemoembolization (TACE).

METHODS: Peripheral blood samples were taken from 45 HCC patients before and 1, 3, 7 d, and 1 mo after TACE. Plasma VEGF level was measured with the quantitative sandwich enzyme-linked immunosorbent assay (ELISA). Twenty patients with benign liver lesions and 17 healthy control subjects were also included in this study.

RESULTS: Plasma VEGF levels in HCC patients were significantly elevated as compared to those in patients with benign liver lesions ($P = 0.006$) and in the normal controls ($P = 0.003$). Significant differences were observed when P-VEGF was categorized by tumor size ($P = 0.006$), portal vein thrombosis ($P = 0.011$), distant metastasis ($P = 0.017$), arterial-portal vein shunting ($P = 0.026$), and International Union Against Cancer (UICC) TNM stage ($P = 0.044$). There was no correlation between plasma level of VEGF and the level of alpha fetoprotein (α -FP) ($r = 0.068$, $P = 0.658$) and weakly correlated with the number of platelets ($r = 0.312$, $P = 0.038$). P-VEGF levels increased significantly and reached the peak value on the first day after TACE, and then decreased gradually. The change rate of P-VEGF concentration (one month post-TACE/pre-TACE \times 100%) was correlated with the retention rate of lipiodol oil ($r_s = 0.494$, $P = 0.001$) and the tumor volume change ($r_s = 0.340$, $P = 0.034$). The patients who achieved a partial or complete response to TACE therapy showed significantly less pre-treatment P-VEGF than those nonresponders ($P = 0.025$). A high pre-therapeutic P-VEGF level was associated with poor response to treatment ($P = 0.018$).

CONCLUSION: A high pre-treatment P-VEGF level is a useful marker for tumor progression, especially for vascular

INTRODUCTION

Transcatheter arterial chemoembolization (TACE) is the most frequently applied palliative treatment in HCC patients who are considered to be unsuitable candidates for surgery. But the indications and outcome of TACE are not clearly defined in the literature^[1,2]. TACE therapy is invasive and associated with high financial costs^[3]. To predict which patients are likely to benefit from TACE would be useful to both oncologists and patients.

Tumor angiogenesis is essential for solid tumorigenesis, growth, invasion and metastasis^[4-6]. Tumor angiogenesis is mediated by angiogenic factors and vascular endothelial growth factor (VEGF) is one of the most potent factors. Strong VEGF expression has been demonstrated in various solid tumor types. In HCC, VEGF expression in tumor tissue has been reported to be correlated with aggressive behavior, early metastasis spread, and poor prognosis^[7,8]. Recently, the expression of VEGF in patients with various malignancies has been made possible by measuring circulating VEGF concentrations with the enzyme-linked immunosorbent assay (ELISA)^[9]. The elevation of VEGF in blood implies a promotion of tumor angiogenesis, and several studies have revealed the predictive value of circulating VEGF level in disease progression and prognosis in various types of cancer^[10,11]. Raised pre-treatment circulation VEGF levels in small-cell lung carcinoma, esophageal carcinoma, gastrointestinal cancer and non-Hodgkin's lymphoma have been associated with a poor outcome^[12-15].

Although elevated circulation VEGF levels have been measured in patients with various tumors. To our knowledge few data are available with regard to plasma VEGF (P-VEGF) levels in patients with HCC^[16]. Data concerning the change of P-VEGF in the course of TACE therapy and its significance in prediction of patient's response to chemoembolization have not been reported to date.

Therefore, in this prospective study, we analyzed the P-VEGF level in patients with HCC prior to treatment to determine the clinicopathologic significance of P-VEGF, and to assess the clinical usefulness of pre-treatment P-VEGF as a predictor of outcome in patients undergoing TACE therapy for HCC.

MATERIALS AND METHODS

Patients and treatment design

The study consisted of 45 patients (37 males, 8 females, mean age 50 years, range 29-77 years) with unresectable HCC who underwent TACE at the Department of Interventional Radiology, Wuhan Union Hospital between October 2000 and February 2002. HCC was diagnosed by distinctive radiographic findings, serum alpha fetoprotein, and with ($n = 8$) or without histological proof. All patients were treated with TACE therapy alone without any other therapies such as surgery, percutaneous ethanol injection, or systemic chemotherapy. The chemoembolization agents consisted of 100 mg/m² of carboplatin, 50 mg/m² of doxorubicin hydrochloride, 1 g of 5-fluorouracil and 5-25 mL of iodized oil (Lipiodol; Guerbet, Aulnay-sous-Bois, France). For those with hepatic arterial-portal vein fistula, gelfoam piece was used to block the fistula before iodized oil was used.

Twenty patients underwent TACE therapy for benign diseases (ten patients underwent partial hepatic artery embolization for hepatic cavernous angioma, ten patients underwent partial spleen artery embolization for hypersplenism) and seventeen healthy volunteers were also involved in this study, served as control to evaluate the P-VEGF cut-off level.

Clinicopathologic data

Physical examination, chest X-ray, routine liver function test were performed. Complete blood count, hepatitis B surface antigen status and serum alpha fetoprotein (α -FP) were prospectively collected from each patient. Tumor characteristics such as size, location, capsular, portal vein involvement, lymph node or extrahepatic metastasis, were assessed on the basis of radiographic findings. Tumor vascularity and arteio-portal vein shunting (A-V shunting) were studied by superselective digital subtraction angiography (DSA). Tumor staging was performed using the International Union Against Cancer (UICC) TNM classification^[17].

Blood sampling and enzyme immunoassay of P-VEGF concentration

Peripheral venous blood was taken before ($n = 45$) and 1 ($n = 30$), 3 ($n = 44$), 7 ($n = 18$) and 1 mo ($n = 45$) after TACE therapy. Blood samples were collected in sterile glass tubes containing 0.057 mL of 15% EDTA. Plasma was separated by centrifugation at 2000 r/min for 15 min to eliminate platelets and stored at -70 °C till use.

Plasma VEGF was measured in duplicate by commercially available ELISA kits (Quantikine human VEGF, R&D System, Minneapolis, MN, USA). According to the manufacturer the minimal detectable dose of VEGF was <5.0 ng/L, the intra-assay and the inter-assay variabilities were 6.7-5.1% and 8.8-6.2%, respectively. Absorbance was determined using a biokinetics reader EL312e (Bio-Tek Instruments, Winooski, VT, USA) at 450nm.

Definition of response to TACE treatment

Response to treatment was assessed by image examinations one month after TACE Therapy. Treatment was evaluated according to the tumor volume change and retention rate of the iodized oil. The tumor volume was calculated using the summed products of the longest dimensions of the lesion, and patients were categorized as responding group (tumor size decrease or stable, no new-born nest) and non-responding group (enlargement of the tumor or the presents of new-born nest). According to the retention rate of the oil, patients were categorized as groups >75%, 50-75%, 25-50% and <25%.

Statistical analysis

Statistical analysis was carried out by the SPSS 10.0 packed program. To investigate the relationships between P-VEGF

levels and other variables, *t* test, ANOVA test, Chi-square test, Fisher exact probability test, correlation coefficient (*r*) and spearman's rank correlation (*rs*) were used when appropriate. $P < 0.05$ based on a two-tailed test was considered statistically significant.

RESULTS

Pre-TACE P-VEGF in patients with HCC

The pre-operative P-VEGF levels were significantly higher in HCC patients (63.83 ± 51.09 ng/L) than those in benign liver diseases (28.99 ± 6.67 ng/L) ($P = 0.006$) and in healthy controls (25.60 ± 5.47 ng/L) ($P = 0.003$). There was no significant difference in P-VEGF levels between the patients with benign liver diseases and healthy control. The sensitivity of P-VEGF in detecting HCC, using the mean P-VEGF of the patients with benign liver diseases (28.99 ng/L) as cut-off level, was found to be 73.3% with 62.2% specificity.

Correlation between pre-TACE P-VEGF and clinicopathologic features

There was no significant association between pre-TACE P-VEGF levels and various clinical and laboratory variables, except the gender ($t = 4.111$, $P = 0.003$). There was a weak correlation between P-VEGF levels and the platelet number (PLT) ($r = 0.312$, $P = 0.038$) and no correlation with the levels of α -FP ($r = 0.068$).

There was no significant association between the P-VEGF level and the presence of cirrhosis, tumor location, tumor capsule, ascites, lymph node metastasis, or the tumor vascularity. Significant differences were observed when P-VEGF was categorized by tumor size ($P = 0.006$), distant metastasis ($P = 0.017$), portal vein thrombosis ($P = 0.011$), arterio-portal vein shunting ($P = 0.026$), and advanced TNM stage ($P = 0.044$) (Table 1, Figure 1).

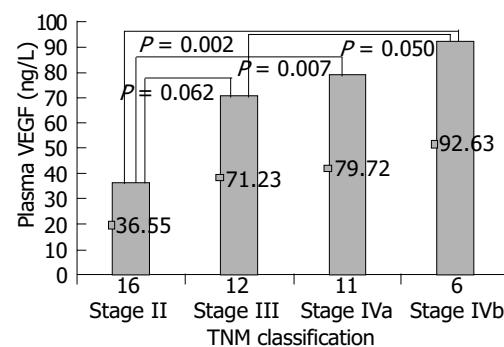


Figure 1 Mean plasma vascular endothelial growth factor levels at each disease stage in patients with hepatocellular carcinoma.

Using mean concentration of TII tumors as cut-off level, P-VEGF was able to predict TIII/TIV tumors with 75.9% sensitivity and 62.5% specificity. Using mean concentration of portal vein thrombosis of negative tumors as cut-off level, P-VEGF was found to have a sensitivity of 62.5% and a specificity of 64.9% in detecting portal vein thrombosis of positive tumors. Using mean concentration of the distant metastasis-free group as cut-off level, P-VEGF was able to exclude distant metastasis with a negative predictive value of 89.3%, a sensitivity of 50% and a specificity of 64.1%. P-VEGF could predict the presence of A-V shunting with 75% sensitivity and 67.6% specificity by using mean concentration of the non-A-V shunting patients as cut-off level (Table 2).

Change of P-VEGF levels during TACE course

P-VEGF levels were significantly elevated in patients with HCC

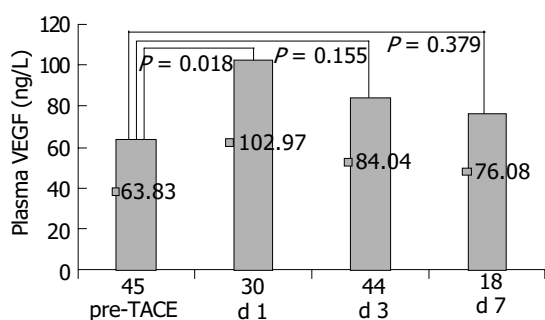
Table 1 Pre-TACE plasma VEGF levels in patients categorized by radiological parameters

	Group	No. of patients	Median plasma VEGF (ng/L)	Statistic value	P value
Cirrhotic liver	No	13	80.15	$t = 1.380$	0.175
	Yes	32	57.19		
Tumor location	Left lobe	4	77.82	$F = 0.275$	0.843
	Right lobe	26	66.62		
	Spiegel's lobe	5	50.38		
	Multiple lobe	10	57.68		
Tumor capsule	No	32	68.15	$t = 0.888$	0.379
	Yes	13	53.18		
Ascites	No	37	62.81	$t = 1.151$	0.280
	Yes	8	82.60		
Lymph node involvement	No	39	61.68	$t = 1.677$	0.101
	Yes	6	101.31		
Tumor vascularity	Hypervascularity	31	75.59	$F = 0.922$	0.406
	Median	9	55.31		
	Hypovascularity	3	39.1		
Tumor size	<5 cm	7	27.57	$F = 5.804$	0.006
	5-10 cm	22	55.59		
	>10 cm	11	101.54		
Portal vein thrombosis	No	37	57.97	$t = 2.669$	0.011
	Yes	8	104.79		
Extra hepatic metastasis	No	39	59.39	$t = 2.483$	0.017
	Yes	6	116.18		
TNM classification	Stage II	16	36.55	$F = 2.937$	0.044
	Stage III	12	71.23		
	Stage Iva	11	79.72		
	Stage Ivb	6	92.63		
Arterio-portal vein shunting	No	37	56.03	$t = 2.283$	0.026
	Yes	8	99.9		

TNM: tumor-node-metastasis. Tumor vascularity and arterial-portal vein shunting were studied by superselective digital subtraction angiographic (DSA).

Table 2 Effect of different VEGF levels on specificity and sensitivity in predicting tumor load in patients with HCC

	Cut-off VEGF value (ng/L)	Sensitivity (%)	Specificity (%)	Positive predictive value (%)	Negative predictive value (%)
TII and TIII/IV	36.55	75.9	62.5	78.6	58.8
Portal vein thrombosis	57.97	62.5	64.9	27.8	88.8
Extra hepatic metastasis	59.39	50	64.1	17.6	89.3
Arterio-portal vein shunting	56.03	75	67.6	33.3	92.6

**Figure 2** Effect of TACE on mean plasma vascular endothelial growth factor levels.

on the first post-TACE day (102.97 ± 89.26 ng/L) compared to pre-TACE (63.83 ± 51.09) ($P = 0.018$). Then VEGF level decreased gradually to 84.04 ± 79.16 ng/L on the third day and 76.08 ± 45.38 ng/L on the seventh day post-TACE, showing no statistical difference with pre-TACE P-VEGF levels (Figure 2).

A similar change of P-VEGF was found in patients who underwent TACE for treatment of benign liver diseases (data not shown).

One month after TACE, the P-VEGF level was 71.47 ± 50.87 ng/L, no statistical difference was found between them and pre-TACE P-VEGF levels.

Correlation between P-VEGF and response to TACE therapy

Treatment response was evaluated according to the change in tumor volume and retention of the oil. Forty five patients were categorized as responding group (18 cases) and non-responding group (27 cases). The change rate of P-VEGF levels was associated with the change in tumor volume ($r_s = 0.340$, $P = 0.034$). No statistic difference was found between changes in α -FP levels and tumor volume ($r_s = 0.230$, $P = 0.138$).

The pre-TACE P-VEGF level in non-responding group (73.33 ± 70.32 ng/L) was significantly higher than that in the responding group (49.52 ± 25.33 ng/L, $P = 0.025$). The response rate of the low VEGF group (P-VEGF < 49.5 ng/L) was significantly higher than that of the high VEGF group (P-VEGF > 49.5 ng/L) (51.6% vs 14.29%; $P = 0.018$, Fisher exact probability test) (Table 3).

Table 3 Correlation between plasma VEGF concentration and response to treatment

Clinical response	Plasma VEGF (ng/L)		No. of patients		
			Low VEGF	High VEGF	
Responder	49.52±25.33	$t = 2.285$	16	2	$\chi^2 = 5.599$
Non-responder	73.33±70.32	$P = 0.025$	15	12	$P = 0.018$

According to the retention rate of the iodized oil, 45 patients were classified as follows: 11 cases >75%, 16 cases 50 - 75%, 9 cases 25 - 50% and 9 cases <25%. The change rate of P-VEGF levels was strongly associated with oil retention ($r_s = 0.494$, $P = 0.001$). No statistical difference was found between the change rate of α -FP and oil retention ($r_s = 0.209$, $P = 0.179$).

DISCUSSION

By alternate splicing of the VEGF gene, VEGF could exist at least in one of the four forms, namely, VEGF206 (tissue bound), VEGF189 (tissue bound), VEGF165 (the most abundant form, soluble, and partly tissue bound) and VEGF121 (soluble)^[18]. Compared with bioassays, detection of soluble VEGF isoforms with immunoassay was characterized by low detection limits and greater specificity, reproducibility, and practicability^[19,20].

Recently, serum VEGF was measured by an enzyme-linked immunosorbent assay (ELISA) in patients with various types of cancer^[20]. Increased levels of VEGF were demonstrated in most patients with cancer and closely related to tumor progression and metastasis^[21,22]. However, some studies have shown that VEGF is not only secreted from tumor cells but also from a variety of CD34⁺ hematological cells (including platelets, megakaryocytes, monocytes, T-lymphocytes and leukocytes) during clotting^[23]. Serum VEGF concentrations could reflect blood platelet counts rather than VEGF synthesis by tumor tissues, and plasma rather than serum should be considered suitable for the measurement of circulating VEGF^[24]. So in our study, plasma VEGF concentrations were analyzed and ethylenediamine tetraacetic acid (EDTA) was used as anticoagulant.

Hepatocellular carcinoma (HCC) is a highly vascular tumor characterized by neovascularization and a high propensity for venous invasion. A strong VEGF expression was observed in the tissue of HCC and closely associated with tumor progression and metastasis^[6]. Recently, Poon *et al.*^[25] reported that serum VEGF level was significantly elevated in patients with HCC, and significantly high serum VEGF levels were associated with the absence of tumor capsule, the presence of venous invasion and microsatellite modules, and advanced TNM stage. Li *et al.*^[26] also considered that serum VEGF was a predictor of invasion and metastasis of HCC. To our knowledge, only one previous study measured P-VEGF changes in HCC patients. Jinno *et al.*^[16] reported that P-VEGF was a promising tumor marker for remote metastasis of HCC and its specificity, sensitivity and overall accuracy were high enough to be clinically useful.

In the current study, pre-TACE P-VEGF was found to be markedly elevated in the majority of patients with HCC and the increase was closely related to a more advanced stage of diseases. This finding suggested that HCC cells were an important source of P-VEGF. But the lower P-VEGF levels in HCC patients overlapped considerably with those in normal controls, thus limiting the application of VEGF as a tumor marker in early detection of HCC.

We found that high P-VEGF levels were associated with the presence of extrahepatic metastasis and portal vein involvement. Because vascular invasion by tumor cells is indispensable for remote metastasis, metastasis, portal vein involvement and A-V shunting can reflect the ability of tumor cells to invade blood vessels. These results indicated that P-VEGF could be used as a tumor marker in detecting vascular invasive phenotypes of

HCC. It is clinically important to search for the metastasis radiologically in patients with high P-VEGF levels.

In the present study, there was a weak correlation of PLT number with P-VEGF level. It has been suggested that platelets aggregate at metastatic sites, due to factors released from metastatic cells and vascular invasion, resulting in microthrombosis, tumor adhesion, and may release VEGF to the circulation^[27,28]. Therefore, we considered that in metastatic HCC patient platelet activation was a part of the sources of plasma VEGF.

The finding that there was no significant association between the P-VEGF level and tumor vascularity shown by DSA is of great interest. This might suggest that circulation VEGF levels could reflect the formation of new vessels rather than the degree of existing tumor vascularity.

No correlation was found between P-VEGF and serum α -FP, suggesting that they had different mechanisms of production, and P-VEGF might be an independent predictive factor.

Suzuki *et al.*^[29] found serum VEGF increased significantly and reached the peak value 7 d after TACE, suggesting that VEGF might play a role as a sensitive marker for tumor ischemia. We observed that P-VEGF increased and reached the peak value on the first day after TACE and then decreased gradually. We thought that the changes of serum VEGF during TACE might be associated with chemotherapy-induced thrombocytopenia and a subsequent rebound increase in platelet number^[30]. Although the exact mechanism is currently unknown, hypoxia caused by TACE, clotting and platelets aggregation after TACE, tumor cell lysis (and release of VEGF)^[31], elevation of VEGF in acute hepatitis^[32], and tissue trauma^[33] might contribute to the increase of P-VEGF in the early post-TACE period.

It has been reported that high pre-treatment levels of circulating VEGF are correlated with a poor response to the conventional chemotherapy^[12-15]. Similar results were found that the mean P-VEGF of the responding group was significantly higher than that of the non-responding group. Two treatment response indicators (tumor volume change and retention of the iodized oil) were associated with the change rate of P-VEGF levels rather than the change rate of α -FP. These results indicated that P-VEGF might act as a follow-up marker for post-TACE monitoring of the disease course and evaluation of curative effect, especially in α -FP negative patients. It may be useful in predicting treatment response and judging the effect of different TACE regimens.

In summary, P-VEGF level is an independent predictive factor of tumor progression, especially vascular invasion. TACE increases the level of P-VEGF only temporarily which may be associated with tumor ischemia. P-VEGF may be useful in predicting treatment response, monitoring disease course after TACE and judging the effect of different TACE regimens.

REFERENCES

- 1 Okada S. Transcatheter arterial embolization for advanced hepatocellular carcinoma: the controversy continues. *Hepatology* 1998; 27: 1743-1744
- 2 Llad Inverted Question Marko L, Virgili J, Figueras J, Valls C, Dominguez J, Rafecas A, Torras J, Fabregat J, Guardiola J, Jaurrieta E. A prognostic index of the survival of patients with unresectable hepatocellular carcinoma after transcatheter arterial chemoembolization. *Cancer* 2000; 88: 50-57

- 3 **Katyal S**, Oliver JH, Peterson MS, Chang PJ, Baron RL, Carr BI. Prognostic significance of arterial phase CT for prediction of response to transcatheter arterial chemoembolization in unresectable hepatocellular carcinoma: a retrospective analysis. *Am J Roentgenol* 2000; **175**: 1665-1672
- 4 **Hanahan D**, Folkman J. Patterns and emerging mechanisms of the angiogenic switch during tumorigenesis. *Cell* 1996; **86**: 353-364
- 5 **Kirsch M**, Schackert G, Black PM. Metastasis and angiogenesis. *Cancer Treat Res* 2004; **117**: 285-304
- 6 **Gupta MK**, Qin RY. Mechanism and its regulation of tumor-induced angiogenesis. *World J Gastroenterol* 2003; **9**: 1144-1155
- 7 **Yamaguchi R**, Yano H, Iemura A, Ogasawara S, Haramaki M, Kojiro M. Expression of vascular endothelial growth factor in human hepatocellular carcinoma. *Hepatology* 1998; **28**: 68-77
- 8 **Poon RT**, Lau CP, Ho JW, Yu WC, Fan ST, Wong J. Tissue factor expression correlates with tumor angiogenesis and invasiveness in human hepatocellular carcinoma. *Clin Cancer Res* 2003; **9**: 5339-5345
- 9 **Kondo S**, Asano M, Matsuo K, Ohmori I, Suzuki H. Vascular endothelial growth factor/vascular permeability factor is detectable in the sera of tumor-bearing mice and cancer patients. *Biochim Biophys Acta* 1994; **1221**: 211-214
- 10 **Kraft A**, Weindel K, Ochs A, Marth C, Zmija J, Schumacher P, Unger C, Marme D, Gastl G. Vascular endothelial growth factor in the sera and effusions of patients with malignant and nonmalignant disease. *Cancer* 1999; **85**: 178-187
- 11 **Fuhrmann-Benzakein E**, Ma MN, Rubbia-Brandt L, Mentha G, Ruefenacht D, Sappino AP, Pepper MS. Elevated levels of angiogenic cytokines in the plasma of cancer patients. *Int J Cancer* 2000; **85**: 40-45
- 12 **Salven P**, Teerenhovi L, Joensuu H. A High pretreatment serum VEGF concentration is associated with poor outcome in non-Hodgkin's lymphoma. *Blood* 1997; **90**: 3167-3172
- 13 **Salven P**, Ruotsalainen T, Mattson K, Joensuu H. High pretreatment serum level of vascular endothelial growth factor (VEGF) is associated with poor outcome in small-cell lung cancer. *Int J Cancer* 1998; **79**: 144-146
- 14 **Shimada H**, Takeda A, Nabeya Y, Okazumi SI, Matsubara H, Funami Y, Hayashi H, Gunji Y, Kobayashi S, Suzuki T, Ochiai T. Clinical significance of serum vascular endothelial growth factor in esophageal squamous cell carcinoma. *Cancer* 2001; **92**: 663-669
- 15 **Hyodo I**, Doi T, Endo H, Hosokawa Y, Nishikawa Y, Tanimizu M, Jinno K, Kotani Y. Clinical significance of plasma vascular endothelial growth factor in gastrointestinal cancer. *Eur J Cancer* 1998; **13**: 2041-2045
- 16 **Jinno K**, Tanimizu M, Hyodo I, Nishikawa Y, Hosokawa Y, Doi T, Endo H, Yamashita M, Okada Y. Circulating vascular endothelial growth factor (VEGF) is a possible tumor marker for metastasis in human hepatocellular carcinoma. *J Gastroenterol* 1998; **33**: 376-382
- 17 **Zhang ZJ**, Wu MC, Shen F, He J, Chen H, Yang GS, Cong WM, Zong M. Significance of TNM classification in prognostic evaluation of hepatocellular carcinoma following surgical resection. *Zhonghua Zhongliu Zazhi* 1999; **21**: 293-295
- 18 **Houck KA**, Ferrara N, Winer J, Cachianes G, Li B, Leung DW. The vascular endothelial growth factor family: Identification of a fourth molecular species and characterization of alternative splicing of RNA. *Mol Endocrinol* 1991; **5**: 1806-1814
- 19 **Bienvenu JA**, Monneret G, Gutowski MC, Fabien N. Cytokine assays in human sera and tissues. *Toxicology* 1998; **129**: 55-61
- 20 **Yamamoto Y**, Toi M, Kondo S, Matsumoto T, Suzuki H, Kitamura M, Tsuruta K, Taniguchi T, Okamoto A, Mori T, Yoshida M, Ikeda T, Tominaga T. Concentrations of vascular endothelial growth factor in the sera of normal controls and cancer patients. *Clin Cancer Res* 1996; **2**: 821-826
- 21 **Zhao J**, Hu J, Cai J, Yang X, Yang Z. Vascular endothelial growth factor expression in serum of patients with hepatocellular carcinoma. *Chin Med J* 2003; **116**: 772-776
- 22 **Dirix LY**, Vermeulen PB, Pawinski A, Prove A, Benoy I, De Pooter C, Martin M, Van Oosterom AT. Elevated levels of the angiogenic cytokines basic fibroblast growth factor and vascular endothelial growth factor in sera of cancer patients. *Br J Cancer* 1997; **76**: 238-243
- 23 **Lee JK**, Hong YJ, Han CJ, Hwang DY, Hong SI. Clinical usefulness of serum and plasma vascular endothelial growth factor in cancer patients: which is the optimal specimen? *Int J Oncol* 2000; **17**: 149-152
- 24 **Jelkmann W**. Pitfalls in the measurement of circulating vascular endothelial growth factor. *Clin Chem* 2001; **47**: 617-623
- 25 **Poon RT**, Ng IO, Lau C, Zhu LX, Yu WC, Lo CM, Fan ST, Wong J. Serum vascular endothelial growth factor predicts venous invasion in hepatocellular carcinoma: a prospective study. *Ann Surg* 2001; **233**: 227-235
- 26 **Li XM**, Tang ZY, Qin LX, Zhou J, Sun HC. Serum vascular endothelial growth factor is a predictor of invasion and metastasis in hepatocellular carcinoma. *J Exp Clin Cancer Res* 1999; **18**: 511-517
- 27 **Pinedo HM**, Verheul HM, D'Amato RJ, Folkman J. Involvement of platelets in tumor angiogenesis? *Lancet* 1998; **352**: 1775-1777
- 28 **Mohle R**, Green D, Moore MA, Nachman RL, Raffi S. Constitutive production and thrombin-induced release of vascular endothelial growth factor by human megakaryocytes and platelets. *Proc Natl Acad Sci U S A* 1997; **94**: 663-668
- 29 **Suzuki H**, Mori M, Kawaguchi C, Adachi M, Miura S, Ishii H. Serum vascular endothelial growth factor in the course of transcatheter arterial embolization of hepatocellular carcinoma. *Int J Oncol* 1999; **14**: 1087-1090
- 30 **Verheul HM**, Hoekman K, Luyckx-de Bakker S, Eekman CA, Folman CC, Broxterman HJ, Pinedo HM. Platelet: transporter of vascular endothelial growth factor. *Clin Cancer Res* 1997; **3**: 2187-2190
- 31 **Nasu R**, Kimura H, Akagi K, Murata T, Tanaka Y. Blood flow influences vascular growth during tumor angiogenesis. *Br J Cancer* 1999; **79**: 780-786
- 32 **Akiyoshi F**, Sata M, Suzuki H, Uchimura Y, Mitsuyama K, Matsuo K, Tanikawa K. Serum vascular endothelial growth factor levels in various liver diseases. *Dig Dis Sci* 1998; **43**: 41-45
- 33 **Bondestam J**, Salven P, Jaaskela-Saari H, Ikonen T, Lepantalo M, Mattila S, Joensuu H. Major surgery increases serum levels of vascular endothelial growth factor only temporarily. *Am J Surg* 2000; **179**: 57-59

Quantifying anti-HBV effect of targeted ribonuclease by real-time fluorescent PCR

Jun Liu, Ying-Hui Li, Jin Ding, Wei-Dong Gong, Cai-Fang Xue, Ya Zhao, Yu-Xiao Huang

Jun Liu, Ying-Hui Li, Jin Ding, Wei-Dong Gong, Cai-Fang Xue, Ya Zhao, Yu-Xiao Huang, Department of Etiology, Fourth Military Medical University, Xi'an 710032, Shaanxi Province, China
Supported by the National Natural Science Foundation of China, No. 30100157; Medical Research Fund of Chinese PLA, No. 01MA184; Innovation Project of FMMU, No. CX99005

Co-correspondents: Cai-Fang Xue

Correspondence to: Dr. Jun Liu, Department of Etiology, Fourth Military Medical University, Xi'an 710033, Shaanxi Province, China. etiology@fmmu.edu.cn

Telephone: +86-29-83374536 **Fax:** +86-29-83374594

Received: 2004-03-11 **Accepted:** 2004-04-13

Abstract

AIM: To quantify the inhibition of HBV replication by targeted ribonuclease by using real-time fluorescent PCR.

METHODS: Targeted ribonuclease was introduced into 2.2.15 cells by liposome-mediated transfection or HIV-TAT mediated protein transduction. Forty-eight hours after the transfection and 24 h after the transduction, supernatants of 2.2.15 cells were collected and HBV DNA in the supernatants was quantified by real-time fluorescent PCR with a commercial kit.

RESULTS: HBV DNA concentrations in the supernatants of 2.2.15 cells transfected or transduced with targeted ribonuclease were $4.9 \pm 2.4 \times 10^8$ copies/L and $8.3 \pm 4.0 \times 10^8$ copies/L, respectively. Compared with controls, transfection or transduction of targeted ribonuclease reduced HBV DNA concentration in the supernatants of 2.2.15 cells by 90.4% and 90.1%, respectively ($P < 0.05$).

CONCLUSION: Targeted ribonuclease can inhibit HBV replication in 2.2.15 cells.

Liu J, Li YH, Ding J, Gong WD, Xue CF, Zhao Y, Huang YX. Quantifying anti-HBV effect of targeted ribonuclease by real-time fluorescent PCR. *World J Gastroenterol* 2004; 10 (19): 2883-2885

<http://www.wjgnet.com/1007-9327/10/2883.asp>

INTRODUCTION

Chronic hepatitis B virus (HBV) infection is a major health problem worldwide. Globally, more than 350 million people are infected with HBV, and some of them will evolve into liver cirrhosis and hepatocellular carcinoma (HCC). Current treatment regimens for chronic HBV infection, including interferon- γ , lamivudine, adefovir, or different combinations of these drugs, have only a limited long-term efficacy, but many adverse effects and drug resistance^[1,2]. Therefore, the exploration of novel treatment strategies for HBV infection is both necessary and urgent. In fact, many ingenious treatment strategies have been tested for inhibition of HBV replication, such as antisense nucleotides, ribozymes, intracellular antibodies, targeted nucleases, RNA interference^[3-13]. All of them can inhibit HBV replication to various degrees.

To explore alternative treatment methods against HBV

infection, targeted ribonuclease (TN), a fusion protein of HBVc and human eosinophil-derived neurotoxin (hEDN), was constructed and its effect on HBV replication was tested. After the targeted ribonuclease was introduced by transfection or transduction into 2.2.15 cells, a cell model of HBV infection, we found that it significantly reduced the serological markers of HBV replication, namely HBsAg and HBeAg, in the supernatants of 2.2.15 cells, suggesting that the targeted ribonuclease could inhibit HBV replication.

To further characterize the anti-HBV effect of the targeted ribonuclease, the HBV DNA was quantified in the supernatants of 2.2.15 cells treated by the targeted ribonuclease. Our results showed that the targeted ribonuclease markedly reduced HBV DNA concentration in the supernatants, which together with our previous findings, demonstrate that HBV replication can be inhibited by targeted ribonuclease.

MATERIALS AND METHODS

Cell culture

2.2.15 cells, a human hepatoblastoma Hep G2 cell line stably transfected by HBV genome, were cultured in Dulbecco's modified Eagle's medium (DMEM, purchased from Gibco Life Technologies, Grand Island, NY) supplemented with 100 mL/L fetal calf serum (Sijiqing Biotech Company, Hangzhou, China).

Transfection

The transfection methods were previously described^[14]. Briefly, twenty-four hours before transfection, 2.2.15 cells were seeded into a culture plate at the density of 2×10^8 /L. LipofectamineTM 2000 reagent (Gibco Life Technologies) was used for the transfection of 2.2.15 cells by p/TN, p/TNm, p/hEDN, p/HBVc, pcDNA3.1 (-), or mock solution (DMEM plus LipofectamineTM 2000 reagent containing no plasmid) according to the manufacturer's protocol. p/TN, p/TNm, p/hEDN and p/HBVc are the eukaryotic expression plasmids for targeted ribonuclease, point-mutated targeted ribonuclease without ribonuclease activity, human eosinophil-derived neurotoxin, and HBV core protein, respectively.

Transduction

2.2.15 cells were seeded into a culture plate at the density of 2×10^8 /L. Twenty-four hours later, purified recombinant proteins with protein transduction domain, TAT-TN, TAT-TNm, TAT-hEDN, and TAT-HBVc were added into the culture medium. For mock transduction, an equal volume of DMEM instead of protein was added into the culture medium.

Real-time fluorescent PCR

Forty-eight hours after transfection and 24 h after transduction, the supernatants of 2.2.15 cells were collected and HBV DNA in the supernatants was quantified by using fluorescent PCR kit for quantification of HBV DNA (Daan Gene Company, Guangzhou, China) according to the manufacturer's protocol. PCR primers were: P1: 5' ATCCTGCTGCTATGCCTCATCTT3', P2: 5' ACAGTGGGGAAAGCCCTACGAA3'. The probe was 5' TGGCTAGTTTACTAGTGCCATTTTG3'. PCR reaction was analyzed by PE 5700 (Perkin Elmer, USA).

Statistical analysis

All data were analyzed by SPSS 10.0 software. Differences were considered statistically significant when $P < 0.05$.

RESULTS

HBV DNA in the supernatants of 2.2.15 cells transfected or transduced with the targeted ribonuclease and controls was quantified by real-time fluorescent PCR. The results are shown in Figure 1. Compared with the controls, HBV DNA concentration in the supernatant of 2.2.15 cells was markedly reduced by the targeted ribonuclease, which was introduced into the cells by both pathways, *i.e.* transfection and transduction. The transfected targeted ribonuclease reduced HBV DNA concentration by 90.4% and the transduced targeted ribonuclease by 90.1% ($P < 0.05$). Either hEDN or HBVc alone had no such an effect, indicating that it was the fusion protein itself, *i.e.* the targeted ribonuclease, but not its constituent molecules that exerted the anti-HBV effect. Interestingly, TNm which was mutated at just one amino acid residue (Lys113→Arg) but had no ribonuclease activity as compared with TN, did not decrease HBV DNA concentration either, suggesting that the ribonuclease activity was needed in the anti-HBV effect of the targeted ribonuclease. To exclude the possibility that the anti-HBV effect of the targeted ribonuclease was due to nonspecific killing of 2.2.15 cells, we also detected cell viability of the transfected and transduced cells by MTT assay. The results showed that the targeted ribonuclease had no adverse effects on cell viability and proliferation as compared with controls ($P > 0.05$, data not shown).

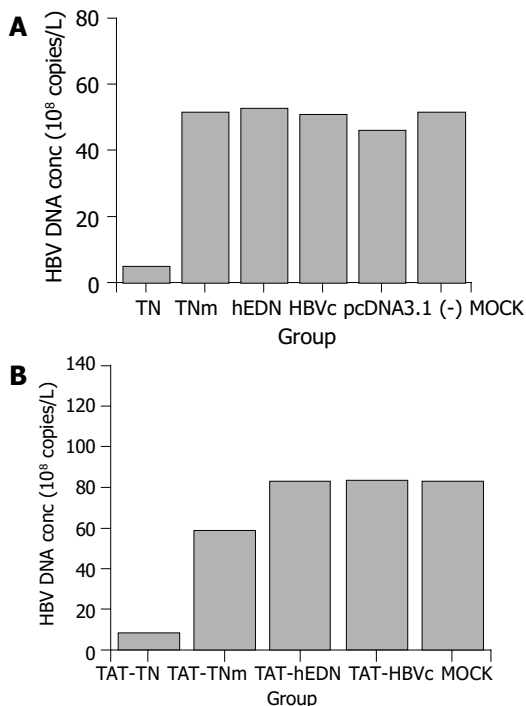


Figure 1 HBV DNA concentration in the supernatants of transfected and transduced 2.2.15 cells. A: HBV DNA concentration in the supernatants of transfected 2.2.15 cells. TN, TNm, hEDN, HBVc, pcDNA3.1 (-), and MOCK represent the supernatants collected from 2.2.15 cells transfected by p/TN, p/TNm, p/hEDN, p/HBVc, pcDNA3.1 (-), or mock solution (DMEM plus Lipofectamine™ 2000 reagent containing no plasmid), respectively. B: HBV DNA concentrations in the supernatants of transduced 2.2.15 cells. TAT-TN, TAT-TNm, TAT-hEDN, TAT-HBVc, and MOCK represent the supernatants collected from 2.2.15 cells transduced by purified proteins of TAT-TN, TAT-TNm, TAT-hEDN, TAT-HBVc, or mock solution (DMEM), respectively.

DISCUSSION

Real-time fluorescent PCR is a simple, sensitive, specific and precise method to quantitate nucleic acids over a vast dynamic range^[15]. Due to these advantages, real-time fluorescent PCR has been widely used in both basic research and clinical diagnosis to measure the quantity of nucleic acids. As for HBV, real-time fluorescent PCR has been used in monitoring viral load during the course of antiviral treatment to evaluate the efficacy of the treatment and predict the possibility of emergence of drug-resistant variants, in the analysis of anti-HBV effect of small interfering RNA transfected into HBV-producing cell lines, and in the study of HBV pathogenesis^[10,16-19]. In the current research, we also used real-time fluorescent PCR to precisely quantify HBV DNA in the supernatants of 2.2.15 cells to detect the effect of the targeted ribonuclease on HBV replication. The targeted ribonuclease reported here is a fusion protein against HBV infection constructed by us, based on the principle of capsid-targeted viral inactivation (CTVI)^[5,20]. Our previous studies showed that it significantly reduced HBsAg and HBeAg in the supernatants of 2.2.15 cells, suggesting that the targeted ribonuclease could inhibit HBV replication. In consistent with our previous findings, in this study we observed the targeted ribonuclease notably reduced HBV DNA in the supernatants of 2.2.15 cells. Taken together, these results demonstrate that the targeted ribonuclease strongly inhibits HBV replication. The targeted ribonuclease may therefore be one of the promising alternative anti-HBV agents which are being studied in the pursuing of a satisfactory treatment for chronic HBV infection.

Although the precise mechanism of anti-HBV effect of targeted ribonuclease still remains unknown and awaits further study, the principle of capsid-targeted viral inactivation (CTVI) implies that it may specifically recognize pregenomic RNA (pgRNA) of HBV, the template for HBV replication, intracellularly by the HBVc domain of fusion protein, and then degrades pgRNA by the hEDN domain. This will in turn lead to a decrease in the replication of HBV DNA and synthesis of viral proteins, which finally results in a reduction of extracellular HBV DNA and viral proteins (HBsAg and HBeAg). In fact, we have found that purified targeted ribonuclease can degrade RNA *in vitro* (unpublished data) which supports this mechanism. Experiments are ongoing in this laboratory to clarify the mechanism and to apply the targeted ribonuclease to small animal models.

REFERENCES

- 1 **Conjeevaram HS**, Lok AS. Management of chronic hepatitis B. *J Hepatol* 2003; **38**(Suppl 1): S90-S103
- 2 **Jaboli MF**, Fabbri C, Liva S, Azzaroli F, Nigro G, Giovanelli S, Ferrara F, Miracolo A, Marchetto S, Montagnani M, Colecchia A, Festi D, Reggiani LB, Roda E, Mazzella G. Long-term alpha interferon and lamivudine combination therapy in non-responder patients with anti-HBe-positive chronic hepatitis B: Results of an open, controlled trial. *World J Gastroenterol* 2003; **9**: 1491-1495
- 3 **Li JG**, Lian JQ, Jia ZS, Feng ZH, Nie QH, Wang JP, Huang CX, Bai XF. Effect of ribozymes on inhibiting expression of HBV mRNA in HepG2 cells. *Shijie Huaren Xiaohua Zazhi* 2003; **11**: 161-164
- 4 **Lu YY**, Wang L, Liu Y, Yu M, Li K, Wang YD, Zhang LX, Cheng J. Inhibitory effect of HBeAg ScFv on hepatitis B virus. *Shijie Huaren Xiaohua Zazhi* 2002; **10**: 765-769
- 5 **Beterams G**, Nassal M. Significant interference with hepatitis B virus replication by a core-nuclease fusion protein. *J Biol Chem* 2001; **276**: 8875-8883
- 6 **Giladi H**, Ketzinel-Gilad M, Rivkin L, Felig Y, Nussbaum O, Galun E. Small interfering RNA inhibits hepatitis B virus replication in mice. *Mol Ther* 2003; **8**: 769-776
- 7 **McCaffrey AP**, Nakai H, Pandey K, Huang Z, Salazar FH,

- Xu H, Wieland SF, Marion PL, Kay MA. Inhibition of hepatitis B virus in mice by RNA interference. *Nat Biotechnol* 2003; **21**: 639-644
- 8 **Shlomai A**, Shaul Y. Inhibition of hepatitis B virus expression and replication by RNA interference. *Hepatology* 2003; **37**: 764-770
- 9 **Hamasaki K**, Nakao K, Matsumoto K, Ichikawa T, Ishikawa H, Eguchi K. Short interfering RNA-directed inhibition of hepatitis B virus replication. *FEBS Lett* 2003; **543**: 51-54
- 10 **Ying C**, De Clercq E, Neyts J. Selective inhibition of hepatitis B virus replication by RNA interference. *Biochem Biophys Res Commun* 2003; **309**: 482-484
- 11 **Chen Y**, Du D, Wu J, Chan CP, Tan Y, Kung HF, He ML. Inhibition of hepatitis B virus replication by stably expressed shRNA. *Biochem Biophys Res Commun* 2003; **311**: 398-404
- 12 **Konishi M**, Wu CH, Wu GY. Inhibition of HBV replication by siRNA in a stable HBV-producing cell line. *Hepatology* 2003; **38**: 842-850
- 13 **Klein C**, Bock CT, Wedemeyer H, Wustefeld T, Locarnini S, Dienes HP, Kubicka S, Manns MP, Trautwein C. Inhibition of hepatitis B virus replication *in vivo* by nucleoside analogues and siRNA. *Gastroenterology* 2003; **125**: 9-18
- 14 **Liu J**, Li YH, Xue CF, Ding J, Gong WD, Zhao Y, Huang YX. Targeted ribonuclease can inhibit replication of hepatitis B virus. *World J Gastroenterol* 2003; **9**: 295-299
- 15 **Klein D**. Quantification using real-time PCR technology: applications and limitations. *Trends Mol Med* 2002; **8**: 257-260
- 16 **Werle B**, Cinquin K, Marcellin P, Pol S, Maynard M, Trepo C, Zoulim F. Evolution of hepatitis B viral load and viral genome sequence during adefovir dipivoxil therapy. *J Viral Hepat* 2004; **11**: 74-83
- 17 **Kohmoto M**, Enomoto M, Yano Y, Otani S, Minamitani S, Tamori A, Habu D, Takeda T, Shiomi S, Seki S, Arakawa T, Nishiguchi S. Detection of serum hepatitis B virus DNA by real-time quantitative polymerase chain reaction (TaqMan PCR) during lamivudine treatment: comparison with three other assays. *Hepatol Res* 2003; **26**: 125-133
- 18 **Ide T**, Kumashiro R, Koga Y, Tanaka E, Hino T, Hisamochi A, Murashima S, Ogata K, Tanaka K, Kuwahara R, Sata M. A real-time quantitative polymerase chain reaction method for hepatitis B virus in patients with chronic hepatitis B treated with lamivudine. *Am J Gastroenterol* 2003; **98**: 2048-2051
- 19 **Wieland SF**, Spangenberg HC, Thimme R, Purcell RH, Chisari FV. Expansion and contraction of the hepatitis B virus transcriptional template in infected chimpanzees. *Proc Natl Acad Sci U S A* 2004; **101**: 2129-2134
- 20 **Natsoulis G**, Boeke JD. New antiviral strategy using capsid-nuclease fusion proteins. *Nature* 1991; **352**: 632-635

Edited by Zhang JZ and Wang XL Proofread by Xu FM

Expression of survivin and its significance in colorectal cancer

Wei-Chang Chen, Qiang Liu, Jian-Xin Fu, Su-Ya Kang

Wei-Chang Chen, Qiang Liu, Department of Gastroenterology, The First Affiliated Hospital of Suzhou University, Suzhou 215006, Jiangsu Province, China

Jian-Xin Fu, Jiangsu Institute of Hematology, The First Affiliated Hospital of Suzhou University, Suzhou 215006, Jiangsu Province, China

Su-Ya Kang, Department of Pathology, The First Affiliated Hospital of Suzhou University, Suzhou 215006, Jiangsu Province, China

Supported by 135 Medical Important Talent Foundation of Jiangsu Province, No. 37RC 2002037

Correspondence to: Dr. Wei-Chang Chen, Department of Gastroenterology, The First Affiliated Hospital of Suzhou University, Suzhou 215006, Jiangsu Province, China. cwc-sz@hotmail.com

Telephone: +86-512-65223637 Ext. 8374

Received: 2003-11-21 **Accepted:** 2003-12-22

Abstract

AIM: To study the expression of survivin, a novel member of inhibitors of apoptosis protein (IAP) and its significance in colorectal carcinoma.

METHODS: Survivin mRNA expression was evaluated by semi-quantitative reverse transcriptase polymerase chain reaction (RT-PCR) in 52 colorectal carcinoma samples and 48 adjacent normal colorectal tissue samples. PCR product was sequenced to verify the desired result. Expressions of survivin protein, proliferating cell nuclear antigen labelling index (PI) and apoptotic index (AI) were detected immunohistochemically in 52 human colorectal carcinomas.

RESULTS: The expression of survivin mRNA was detected in a significantly greater proportion of colorectal carcinoma samples than in adjacent normal colorectal tissues (67.3% vs 25%; $P < 0.01$). There was no relationship between survivin mRNA expression in colorectal carcinomas and sex, tumor size, histological types, lymphnode metastasis, distant metastasis and Dukes' stage. The PCR product shared 99% of homology with human counterparts. Survivin expression was observed immunohistochemically in 27 of 52 cases of colorectal carcinoma (51.9%). The AI was significantly lower in survivin positive group than in survivin negative group ($0.67 \pm 0.18\%$ vs $1.14 \pm 0.42\%$; $P < 0.001$), while the PI was greater in survivin positive group than in survivin negative group ($51 \pm 22\%$ vs $27 \pm 18\%$, $P < 0.001$).

CONCLUSION: Survivin is a special tumor marker independent of histopathological characteristics. It may play an important role during human colorectal tumorigenesis by inhibiting apoptosis and accelerating proliferative activity of colorectal tumor cells.

Chen WC, Liu Q, Fu JX, Kang SY. Expression of survivin and its significance in colorectal cancer. *World J Gastroenterol* 2004; 10(19): 2886-2889

<http://www.wjgnet.com/1007-9327/10/2886.asp>

INTRODUCTION

Apoptosis is an evolutionally conserved genetic program of

cellular suicide and also central to the homeostasis of adult tissues by maintaining the balance between cell production and cell elimination. There is compelling evidence that defects in apoptosis contribute to human diseases such as malignancies. In the evolution of colorectal cancer (CRC) the imbalance between cell proliferation and cell apoptosis may be an important potential factor. A large number of evidences show that many molecules such as p53 and bcl-2 are involved in the regulation of apoptosis during colorectal tumorigenesis. The inhibitor of apoptosis proteins (IAPs), which are widely expressed in all kinds of malignancies, is encoded by the highly-conservative anti-apoptosis gene family and plays an important role in the regulation of apoptosis. IAP molecules contain 1-3 copies of a -70 amino acid zinc-finger fold, and designate the baculovirus IAP repeat (BIR) and their mechanism of action has been directly attributed to the binding of Caspases, thus preventing enzyme activity of the Caspases^[1,2]. Among molecules of the IAP family, survivin, a novel anti-apoptosis gene is prominently expressed in CRC and several other malignancies^[3,13-18]. The role of survivin in blocking apoptosis is unclear and its ability to inhibit Caspase-3 activity has been widely debated^[3-5]. Survivin may play an important role in the development of CRC. The present study was to examine the expression of survivin in CRC and to evaluate the association between expression of survivin and clinicopathological characteristics of patients with CRC. We also investigated the significance of survivin expression in CRC.

MATERIALS AND METHODS

Patients

Specimens used for this study were obtained from 52 carcinomas and 48 adjacent normal tissues from the resection margins at the First Affiliated Hospital of Suzhou University. The suspected de novo cancers and patients with a known familial colon cancer syndrome history were excluded. All patients had received neither chemotherapy nor radiation therapy before tumor resection. The diagnosis and histopathologic classification were determined according to the General Rules for Pathologic Studies of National CRC Cooperation Group. In CRC patients, there were 31 males and 21 females, and the mean age of the patients was 61.1 years. According to histological differentiation grade, 52 cases of CRC were classified as well, moderately and poorly differentiated subgroups which included 6, 39 and 7 cases respectively. Seven, 19, 17 and 9 cases were staged as Dukes' A, B, C and D respectively. After washed with physiological saline, all cancer tissue samples were cut into two pieces by sterile blade. One piece was fixed with formalin for H&E, the other was frozen in liquid nitrogen immediately after the lesion was resected and stored at -80 °C for subsequent assay.

Semi-quantitative RT-PCR

Briefly, total RNAs were extracted from colorectal cancer and normal mucosae, using TRIzol reagent (Life Technologies, Rockville, MD). Prepared RNA (2 µg) was mixed with the random hexamer (100 ng), incubated for 5 min at 70 °C, and then quickly chilled at 4 °C for 5 min. RNA samples were reverse-transcribed at 37 °C for 60 min into first-strand cDNA in reverse transcription solution [50 mmol/L Tris-HCl (pH8.3), 40 mmol/L KCl, 8 mmol/L

MgCl₂, 0.5 mmol/L each dNTP, 225 mg/mL BSA, 5 mmol/L DTT, 25 units of RNasin (Promega, Madison, WI), and 200 units of Mo-MLV reverse transcriptase (Life Sciences, Rockville, MD)] with a total volume of 40 µL. The cDNA samples were incubated at 95 °C for 5 min to inactivate the reverse transcriptase and then chilled. The samples were amplified by adding of 50 µL of PCR mixture [50 mmol/L Tris-HCl (pH 8.3), 40 mmol/L KCl, 2 mmol/L MgCl₂, 0.2 mmol/L each dNTP, 10 pmol of each sense and antisense primer, and 1.5 units of Taq polymerase (MBI)]. Amplification of β₂-microglobulin (β₂-MG) gene was performed 28 cycles, each for 30 s at 94 °C, for 30 s at 58 °C, and 60 s at 72 °C, followed by an extension at 72 °C for 7 min. Amplification of survivin gene was performed 32 cycles, each for 45 s at 94 °C, 45 s at 61 °C, and for 60 s at 72 °C, followed by an extension at 72 °C for 7 min. The products were electrophoresed on 15 g/L agarose gels and then scanned. Specific primers for survivin gene, targeting a 528-bp fragment, were: 5'-TTGAA TCGCG GGACC CGTTG G-3' (sense) and 5'-CAGAG GCCTC AATCC ATGGC A-3' (antisense). As internal standards, β₂-microglobulin (β₂-MG) gene was used. Primer pairs specific to β₂-MG gene, targeting a 330-bp fragment, were used sense: 5'-CTCGC GCTAC TCTCT CTTTC-3' and antisense: 5'-CATGT CTCGA TCCCACTTAA-3'.

Sequencing of survivin

The PCR products of survivin were isolated and purified using UNIQ-10 purification kit (MBI) and then ligated with pGEM easy T vector by T4 DNA ligase and transformed *E. coli* JM109. Recombinant vectors were identified through *Eco*RI digestion and agarose gel electrophoresis. Positive plasmids were sequenced by an ABI PRISM 377 DNA sequencer (Perkin-Elmer Company).

Immunohistochemistry

Immunohistochemical staining of survivin was performed by SP method. For PCNA, SABC method was performed. TUNEL assay was used to detect apoptosis. In brief, paraffin sections (4 µm thick) were dewaxed, dehydrated, and then immersed in a 10⁻³ mol/L sodium citrate buffer (pH 6.0). For detection of survivin, antigen retrieval was performed by boiling the sections for 20 min in a pressure cooker. For detection of PCNA, the sections were heated in a microwave oven for 10 min to retrieve the antigens. Endogenous peroxidase was inactivated by incubating the sections with 30 mL/L hydrogen peroxide. Nonspecific reactions were blocked by bovine serum. The sections were incubated with a primary antibody overnight at 4 °C. The antibody used was an 8E2 monoclonal antibody (Chemcon, USA) at 1:5 dilution. Rinsed with PBS, the sections were incubated for 30 min at 37 °C with biotinylated secondary antibody and streptavidin conjugated to horseradish peroxidase, respectively. After three rinse with PBS, the sections were incubated with diaminobenzidine substrate, then rinsed with distilled water and counterstained with hematoxylin. As a negative control, PBS was used instead of the primary antibody. PCNA (Maxim, USA) and TUNEL (Roche, USA) assay were performed according to the manufacturer's instructions.

Scoring criteria

The mean percentage of positive tumor cells for the expression of survivin was determined in at least five areas at 400-fold magnification, and cases with less than 10% positively stained cells were defined as negative. Cases with 10-29% positively stained cells were defined as "+", 30-59% as "++", and 60% or more as "+++". These scorings were performed in a blind fashion.

PI and AI were expressed as the ratio of positively stained tumor cells to all tumor cells. If possible, five areas were randomly selected for counting under 400-fold magnification. Otherwise, the whole section underwent assessment.

Statistical analysis

All results were analyzed by software of SPSS 10.00. *P*<0.05 was considered statistically significant.

RESULTS

Expressions of survivin mRNA in colorectal carcinoma samples and adjacent normal mucosa samples

Fifty two CRC samples and forty eight normal mucosa samples were available for analyses. The expressions of survivin mRNA were detected in a significantly greater proportion of CRC than in normal mucosa samples (67.3% vs 25% *P*<0.01). Survivin mRNA was not detected in normal tissue when the associated cancer was survivin negative (Figure 1).

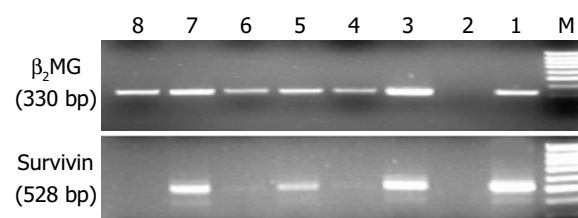


Figure 1 RT-PCR products of paired samples from normal colonic mucosae (lanes 4, 6, 8) and CRC (lanes 3, 5, 7) from three different resection specimens. Lane 1: positive control (U937 cell line), lane 2: negative control, lane M: DNA mark. Expression of β₂MG confirmed the fidelity of reverse transcription.

Relationship between expressions of survivin mRNA and clinicopathological characteristics of patients with CRC

No relationship was found between survivin mRNA expression in CRC and sex, tumor size, histological types, lymphnode metastasis, distant metastasis and Dukes' stage (Table 1).

Table 1 Correlation between expression of survivin mRNA and clinicopathological characteristics of patients with CRC

Variable	Total No β ₂ MG	Survivin	<i>P</i> Value
Sex			
Male	31	0.74±0.63	>0.05
Female	21	0.77±0.56	
Tumor size			
≥5 cm	20	0.71±0.59	>0.05
<5 cm	32	0.78±0.61	
Histological type			
High	7	0.62±0.51	>0.05
Middle	39	0.75±0.59	
Low	6	0.92±0.74	
Lymphnode metastasis			
Positive	22	0.80±0.65	>0.05
Negative	30	0.72±0.57	
Distant metastasis			
Positive	9	0.93±0.18	>0.05
Negative	43	0.72±0.65	
Duke stage			
A	7	0.55±0.57	>0.05
B	19	0.73±0.62	
C	17	0.77±0.73	
D	9	0.93±0.18	

Correlations between expression of survivin, AI and PI

The expression of survivin protein was observed in cytoplasm of malignant tumor cells. Survivin expression was observed immunohistochemically in 27 of 52 cases of colorectal carcinoma (51.9%). To examine whether the expression of survivin correlated with AI and PI, tissue samples obtained from

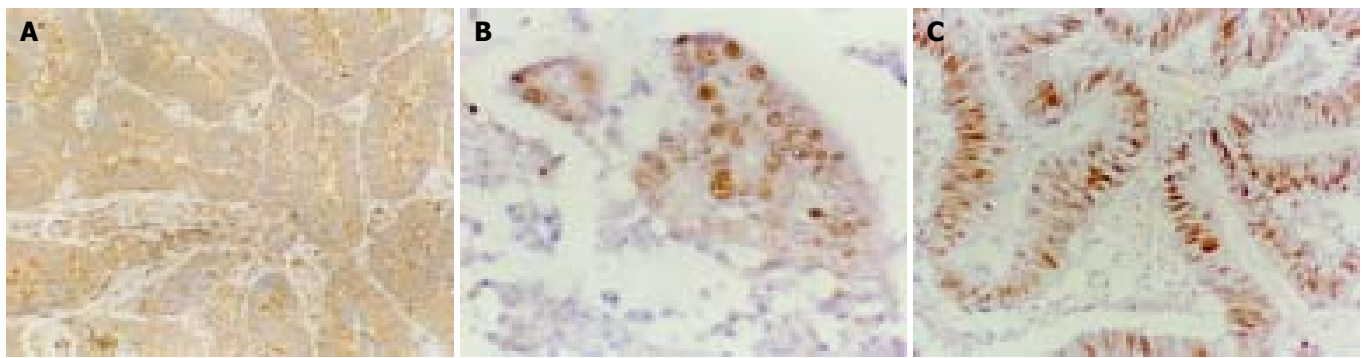


Figure 3 Immunohistochemical analysis of apoptosis, proliferation, and survivin in CRC. Survivin expression was restricted to the cytoplasm of cancer cells (brown staining, $\times 400$ fold). Apoptotic cells and proliferative cells were detected in the nuclei of cancer cells (brown staining, $\times 400$ fold).

carcinoma were divided into two groups according to the expression of survivin and compared to AI and PI (Figure 2). Survivin positive tumors had significantly lower values for AI than survivin negative tumors ($P < 0.001$), and PI in survivin positive tumors was higher than in survivin negative tumors ($P \leq 0.001$, Figure 3).

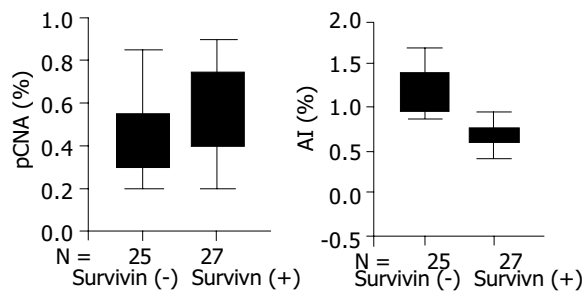


Figure 2 Correlations between survivin expression and AI and PI. $P < 0.001$ as PI in survivin positive tumors ($51 \pm 22\%$) compared with survivin negative tumors ($27 \pm 18\%$), $P < 0.001$ as AI in survivin positive tumors ($0.67 \pm 0.18\%$) compared with survivin negative tumors ($1.14 \pm 0.42\%$).

DISCUSSION

Hybridization screening of a human PI genomic library with the cDNA of effector cell protease receptor-1 (EPR-1) yielded a new gene spanning -15 kb containing four exons and three introns, and located to band 17q25 by Ambrosini *et al.* in 1997^[6]. Survivin is the smallest member of the IAP gene family, structurally characterized by a single BIR module and a -COOH-terminus α -helix coiled domain, substituting a canonical ring finger^[6]. Prominently expressed in a variety of apoptosis-regulated organs during embryonic and fetal development^[7], survivin is undetectable in most normal adult tissues, and becomes abundantly reexpressed in a variety of human cancers. The PCR based approach used in our study is exquisitely sensitive and may detect gene transcripts even in a single cell or cell cluster with a comparable specificity. The present study showed that expression of survivin mRNA was detected in a significantly greater proportion of CRC samples than in adjacent normal colorectal tissues (67.3% vs 25% , $P < 0.01$). The data were consistent with a study by Adida *et al.*^[8]. Furthermore, the prevalence of survivin mRNA expression in the present study correlated well with the expression of survivin protein (unpublished data). Recent studies demonstrated that the novel splice variants survivin- Δ Ex3 and survivin-2B were expressed in malignancies^[9,10]. Survivin- Δ Ex3, which lacks exon 3, exhibited a pronounced anti-apoptotic activity, whereas survivin-2B containing a part of intron 2 as an additional cryptic

exon, largely lost its anti-apoptotic activity. These alternative splice variants have not been explored so far. In gastric carcinomas, Mahotka *et al.*^[10] showed that survivin-2B might act as a naturally occurring antagonist of survivin and might play a role in tumor progression. We found that CRC also expressed survivin- Δ Ex3, survivin-2B and survivin. The latter was a dominant transcript (Figure 1), and shared 99% of homology with human counterparts by sequencing.

The expression of survivin mRNA was independent of clinical pathological characteristics. The result was consistent with previous studies^[8,11]. However, in endometrial carcinoma, survivin expression correlated with clinical stage, histological grade, invasive behavior and survival rate^[12]. The expression of survivin has been proved as a prognostic mark in non-small cell lung cancer^[13], breast carcinoma^[14], oesophageal carcinoma^[15] and hepatocellular carcinoma^[16]. In CRC, Adida *et al.*^[8] reported that the predictive value of survivin expression was limited to patients with stage II CRC, those with survivin negative tumors had a five year survival rate of 94.4% compared with 44.8% for patients with survivin positive tumors. Recent studies showed the phenomena of chemo-radioresistance were prevalent in survivin positive tumors and molecular manipulation of survivin expression might enhance chemotherapy and radiation therapy^[17-22]. These findings indicate that survivin may play an important role in chemoresistance of cancer cells. However, the clinical importance of survivin expression remains unclear in patients with cancer.

We found that survivin positive tumors had significantly lower values for AI than survivin negative tumors, and PI was higher in survivin positive tumors than in survivin negative tumors ($P < 0.001$ for both). These findings indicate that the overexpression of survivin not only inhibits cell death but also reflects the presence of a greater number of proliferating cells. By inhibiting apoptosis and promoting proliferation, survivin plays an important role in colorectal tumorigenesis.

There has been a considerable interest in survivin biomedical researches. The exploitation of survivin might provide important predictive and prognostic clues in diagnosis, and offer new therapeutic alternatives for cancer. Further studies are required to identify the potential role and mechanism of survivin in the development of CRC.

REFERENCES

- 1 Miller LK. An exegesis of IAPs: salvation and surprises from BIR motifs. *Trends Cell Biol* 1999; 9: 323-328
- 2 Altieri DC. The molecular basis and potential role of survivin in cancer diagnosis and therapy. *Trends Mol Med* 2001; 7: 542-547
- 3 Zhu XD, Lin GJ, Qian LP, Chen ZQ. Expression of survivin in human gastric carcinoma and gastric carcinoma model of rats.

- World J Gastroenterol* 2003; **9**: 1435-1438
- 4 **Kasof GM**, Gomes BC. Livin, a novel inhibitor of apoptosis protein family member. *J Biol Chem* 2001; **276**: 3238-3246
 - 5 **Shin S**, Sung BJ, Cho YS, Kim HJ, Ha NC, Hwang JI, Chung CW, Jung YK, Oh BH. An anti-apoptotic protein human survivin is a direct inhibitor of caspase-3 and -7. *Biochemistry* 2001; **40**: 1117-1123
 - 6 **Shankar SL**, Mani S, O'Guin KN, Kandimalla ER, Agrawal S, Shafit-Zagardo B. Survivin inhibition induces human neural tumor cell death through caspase-independent and -dependent pathways. *J Neurochem* 2001; **79**: 426-436
 - 7 **Ambrosini G**, Adida C, Altieri DC. A novel anti-apoptosis gene, survivin, expressed in cancer and lymphoma. *Nat Med* 1997; **3**: 917-921
 - 8 **Adida C**, Crotty PL, McGrath J, Berrebi D, Diebold J, Altieri DC. Developmentally regulated expression of the novel cancer anti-apoptosis gene survivin in human and mouse differentiation. *Am J Pathol* 1998; **152**: 43-49
 - 9 **Sarela AI**, Macadam RC, Farmery SM, Markham AF, Guillou PJ. Expression of the antiapoptosis gene, survivin, predicts death from recurrent colorectal carcinoma. *Gut* 2000; **46**: 645-650
 - 10 **Mahotka C**, Wenzel M, Springer E, Gabbert HE, Gerharz CD. Survivin- Δ Ex3 and survivin-2B: two novel splice variants of the apoptosis inhibitor survivin with different antiapoptotic properties. *Cancer Res* 1999; **59**: 6097-6102
 - 11 **Krieg A**, Mahotka C, Krieg T, Grabsch H, Muller W, Takeno S, Suschek CV, Heydthausen M, Gabbert HE, Gerharz CD. Expression of different survivin variants in gastric carcinomas: first clues to a role of survivin-2B in tumour progression. *Br J Cancer* 2002; **86**: 737-743
 - 12 **Lin LJ**, Zheng CQ, Jin Y, Ma Y, Jiang WG, Ma T. Expression of survivin protein in human colorectal carcinogenesis. *World J Gastroenterol* 2003; **9**: 974-977
 - 13 **Takai N**, Miyazaki T, Nishida M, Nasu K, Miyakawa I. Survivin expression correlates with clinical stage, histological grade, invasive behavior and survival rate in endometrial carcinoma. *Cancer Lett* 2002; **184**: 105-116
 - 14 **Monzo M**, Rosell R, Felip E, Astudillo J, Sanchez JJ, Maestre J, Martin C, Font A, Barnadas A, Abad A. A novel anti-apoptosis gene: Re-expression of survivin messenger RNA as a prognosis marker in non-small-cell lung cancers. *J Clin Oncol* 1999; **17**: 2100-2104
 - 15 **Tanaka K**, Iwamoto S, Gon G, Nohara T, Iwamoto M, Tanigawa N. Expression of survivin and its relationship to loss of apoptosis in breast carcinomas. *Clin Cancer Res* 2000; **6**: 127-134
 - 16 **Ikeguchi M**, Kaibara N. survivin messenger RNA expression is a good prognostic biomarker for oesophageal carcinoma. *Br J Cancer* 2002; **87**: 883-887
 - 17 **Ikeguchi M**, Hirooka Y, Kaibara N. Quantitative analysis of apoptosis-related gene expression in hepatocellular carcinoma. *Cancer* 2002; **95**: 1938-1945
 - 18 **Asanuma K**, Moriai R, Yajima T, Yagihashi A, Yamada M, Kobayashi D, Watanabe N. Survivin as a radioresistance factor in pancreatic cancer. *Jpn J Cancer Res* 2000; **91**: 1204-1209
 - 19 **Ikeguchi M**, Liu J, Kaibara N. Expression of survivin mRNA and protein in gastric cancer cell line (MKN-45) during cisplatin treatment. *Apoptosis* 2002; **7**: 23-29
 - 20 **Kato J**, Kuwabara Y, Mitani M, Shinoda N, Sato A, Toyama T, Mitsui A, Nishiwaki T, Moriyama S, Kudo J, Fujii Y. Expression of survivin in esophageal cancer: correlation with the prognosis and response to chemotherapy. *Int J Cancer* 2001; **95**: 92-95
 - 21 **Ambrosini G**, Adida C, Sirugo G, Altieri DC. Induction of apoptosis and inhibition of cell proliferation by survivin gene targeting. *J Biol Chem* 1998; **273**: 11177-11182
 - 22 **O'Connor DS**, Grossman D, Plescia J, Li F, Zhang H, Villa A, Tognin S, Marchisio PC, Altieri DC. Regulation of apoptosis at cell division by p34cdc 2 phosphorylation of survivin. *Proc Natl Acad Sci U S A* 2000; **97**: 13103-13107

Edited by Wang XL and Xu FM

Expression of toll-like receptor 4 and MD-2 gene and protein in Kupffer cells after ischemia-reperfusion in rat liver graft

Yong Peng, Jian-Ping Gong, Chang-An Liu, Xu-Hong Li, Ling Gan, Shou-Bai Li

Yong Peng, Jian-Ping Gong, Chang-An Liu, Xu-Hong Li, Ling Gan, Shou-Bai Li, Department of Hepatobiliary Surgery, the Second Affiliated Hospital of Chongqing Medical University, Chongqing 400010, China

Supported by the National Natural Science Foundation of China, No. 30300337, 30200278, 30170919

Correspondence to: Dr. Jian-Ping Gong, Department of Hepatobiliary Surgery, the Second Affiliated Hospital of Chongqing Medical University, 74 Linjiang Road, Chongqing 400010, China. gongjianping11@hotmail.com

Telephone: +86-23-63766701 **Fax:** +86-23-63829191

Received: 2004-03-11 **Accepted:** 2004-04-13

Abstract

AIM: To investigate the expression of toll-like receptor 4 (TLR4) and MD-2 gene and protein in Kupffer cells (KCs) and their role in ischemia-reperfusion (IR) injury of rat liver graft.

METHODS: KCs were isolated at 0 (control group), 2, 12, 24 h (IR group) following IR in rat liver graft. mRNA expression of TLR4 and MD-2 was detected by RT-PCR analysis, protein expression of TLR4/MD-2 was detected by flow cytometric (FCM) analysis, and tumor necrosis factor- α (TNF- α) level in supernatant was measured by ELISA. Then isolated KCs were incubated with anti-TLR4 polyclonal antibody (anti-TLR4 group), and TNF- α level was measured again.

RESULTS: The mRNA and protein expression of TLR4/MD-2 and the level of TNF- α in IR group increased significantly at 2 h following IR, and reached the maximum at 12 h, and slightly decreased at 24 h, but were still significantly higher than those in the control group ($P < 0.01$). The expression of these factors was markedly decreased after anti-TLR4 antibody treatment as compared with the IR group ($P < 0.01$).

CONCLUSION: Lipopolysaccharide (LPS) following IR can up-regulate TLR4/MD-2 gene and protein expression in KCs, and synthesize cytokine TNF- α . Anti TLR4 antibody can inhibit the production of TNF- α induced by LPS. TLR4 and its partner molecule MD-2 may play an important role in Kupffer cell activation and IR injury.

Peng Y, Gong JP, Liu CA, Li XH, Gan L, Li SB. Expression of toll-like receptor 4 and MD-2 gene and protein in Kupffer cells after ischemia-reperfusion in rat liver graft. *World J Gastroenterol* 2004; 10(19): 2890-2893

<http://www.wjgnet.com/1007-9327/10/2890.asp>

INTRODUCTION

Toll-like receptor 4 (TLR4) is a transmembrane protein, mainly existed in monocytes/macrophages^[1-3]. It plays an important role in recognizing endotoxin (lipopolysaccharide, LPS) or LPS-CD14 complex, and mediating monocyte/macrophage activation and pro-inflammatory cytokine release^[2,4,5]. MD-2 molecule is

a secreting protein, linking with the exocytic area of TLR4, and facilitating the binding of TLR4 and LPS to enhance cell activation induced by LPS^[6-10]. Kupffer cells (KCs) are not only the biggest residing macrophages in the body, but also are the main participant of ischemia-reperfusion injury (IRI) in liver transplantation^[11-14]. Therefore, studying the expression of TLR4 and MD-2 gene and protein in KCs following IR is very important to clarify the source of cytokines involved in IRI. The aim of the current study was to investigate the expression of TLR4 and MD-2 gene and protein, and the production of cytokines in liver graft by isolating and culturing KCs following IRI, and to probe the role of TLR4 and MD-2 in IRI injury.

MATERIALS AND METHODS

Establishment of animal model of IRI following liver transplant in rat

Male Wistar rats weighing 210-250 g, supplied by Chongqing Medical University, were used as donors and recipients. Orthotopic liver transplantation was performed with improved two-cuff technique introduced by Peng *et al.*^[15] as following: (1) Graft procurement: portal vein (PV), hepatic artery (HA), infrahepatic vena cava (IHVC), and bile duct were divided. Then the graft was infused and harvested for preparation. PV and IHVC were prepared by cuff technique, and a drainage Teflon catheter was inserted into the bile duct. (2) Implantation of graft: the graft was placed orthotopically in the recipient's abdominal cavity after the original liver was removed. The suprahepatic vena cava was sutured end to end, and the portal vein was anastomosed by cuff method, then the liver was perfused. After the anastomosis of IHVA and HA was completed, the bile duct was reestablished end to end by Teflon catheter.

KC isolation and culture

KCs were isolated at 0, 2, 12, 24 h following IR with *in situ* collagenase perfusion technique described by Gong *et al.*^[16]. In brief, the liver was removed with portal vein perfusion with Hank's balance salt solution (HBSS) and digested in a solution of 0.5 g/L collagenase (type IV, Sigma, USA). The digest was washed thoroughly and plated on plastic dishes in RPMI medium containing 100 mL/L fetal calf serum (FCS). After 6 h incubation at 37 °C in humidified atmosphere containing 50 mL/L CO₂ in air, the nonadherent cells were removed by pipet. The adherent cells were collected with a rubber policeman. KC purity exceeded 90% as assessed by light microscopy, and viability was greater than 95% as determined by trypan blue exclusion assay. The KCs at 0 h were regarded as control group, and those at 2, 12 and 24 h were as IR group.

RNA isolation and complementary DNA synthesis

Total RNA was isolated from rat KCs using the TRIZOL reagent (Life Technologies, USA). The quality of RNA was controlled by the intactness of ribosomal RNA bands. A total of 5 μ g of each intact total RNA sample was reverse-transcribed to complementary DNA (cDNA) using AMV reverse transcriptase (Roche, USA).

Determination of TLR4 and MD-2 mRNA by RT-PCR

The PCR primers used are shown in Table 1. The conditions for

amplification were as follows: denaturation at 94 °C for 1 min, annealing at 58 °C for 1 min, and extension at 72 °C for 1 min for 30 cycles, and extension at 72 °C for 7 min again. The PCR products were electrophoresed on 20 g/L agarose gels containing ethidium bromide, and video photographed on an ultraviolet transilluminator, and the results were shown as the ratio of relative absorbance of TLR4 or MD-2/ β -actin analyzed with Quantity one 4.1.0 software.

Table 1 Primer used for PCR amplification of TLR4 and MD-2 gene

	Primer sequence	Size (bp)
TLR4	5' TGGATACGTTTCCTTATAAG 3'	311
	5' GAAATGGAGGCACCCCTTC3'	
MD-2	5'ATGGTCTTCTGGCGAGTTT3'	332
	5'CCATGGCACAGAACTTCCTT3'	
β -actin	5'ATCATGTTTGAGACCTTCAACA 3'	300
	5'CATCTCTTGCTCGAAGTCCA 3'	

Flow cytometric analysis

Expression of TLR4 and MD-2 membrane protein in KCs was determined by flow cytometric analysis. In brief, KCs were incubated with rabbit anti-rat TLR4 polyclonal antibody (1 μ g/mL) labeled with FITC and goat anti-rat MD-2 polyclonal antibody (1 μ g/mL) labeled with PE (Sigma, USA). After washed three times, 10 000 cells were analyzed by flow cytometry (Coulter, USA), and the percentage and mean fluorescence intensity (MFI) of TLR4 and MD-2-positive cells were taken as the indexes.

TNF- α level in supernatant

Supernatants were collected to measure the levels of TNF- α with ELISA kit (Jingmei Biotechnology Company, China) following the manufacturer's instructions.

Blocking test of anti-TLR4 antibody

To determinate the role of TLR4 and MD-2 in LPS-induced KC activation, KCs were harvested and adjusted to the concentration of 1×10^6 (mL/well). Then, 0.2 mL of anti-TLR4 antibody (1: 100) was added to the medium, and incubated for 30 min at 37 °C. The supernatants were collected again for measuring the levels of TNF- α by ELISA analysis following the manufacturer's instructions.

Statistical analysis

All results were expressed as mean \pm SD. Statistical difference between means was determined by Student's *t* test using SigmaPlot 2000 software (SPSS Inc., USA). A *P* value <0.01 was considered statistically significant.

RESULTS

Expression of TLR4 and MD-2 mRNA in KCs

RT-PCR analysis showed that KCs from control group had low but detectable levels of TLR4 and MD-2 mRNA. The mRNA level was significantly increased with time, reaching its maximum of nine-fold at 12 h following IR, and slightly declined 24 h after IR, but was still significantly higher than that in the control group (*P*<0.01) (Figure 1).

Binding of FITC, PE to KCs

To confirm the expression of TLR4 and MD-2 membrane protein on KCs, we examined the binding of FITC/PE to the cells. TLR4 and MD-2 positive cells were 7.94% and 6.51% in control group. But in the rats with IR, the mean fluorescence intensity (MFI) was significantly increased, and TLR4 positive cells were 45.71%,

78.46%, and 61.72% and PE positive cells were 38.64%, 74.15%, and 58.47%, respectively, at 2 h, 12 h and 24 h following IR, which were significantly higher compared with the control group (*P*<0.01) (Figure 2).

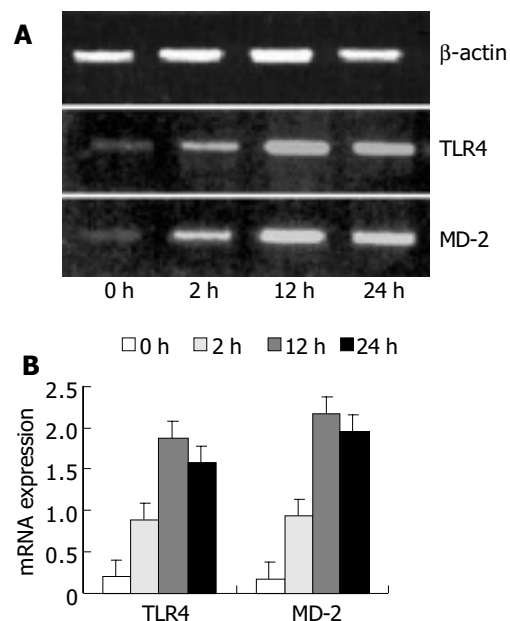


Figure 1 Expression of TLR4 and MD-2 mRNA by RT-PCR analysis. A: PCR products were electrophoresed on agarose gels and photographed. B: Quantitative data of mRNA levels were shown as the ratio of relative absorbance and expressed as mean \pm SD. Expression of TLR4 and MD-2 mRNA were significantly increased in the IR group compared with the control group (*P*<0.01).

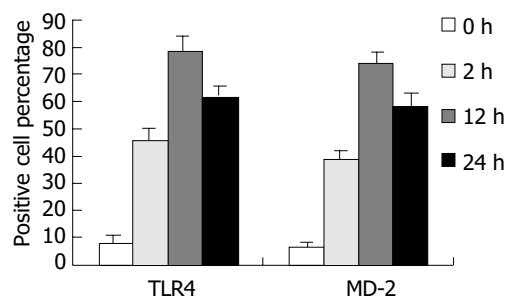


Figure 2 Percentage of TLR4 and MD-2 positive cells. The percentage of TLR4 and MD-2 positive cells was significantly increased after IR compared with the control group.

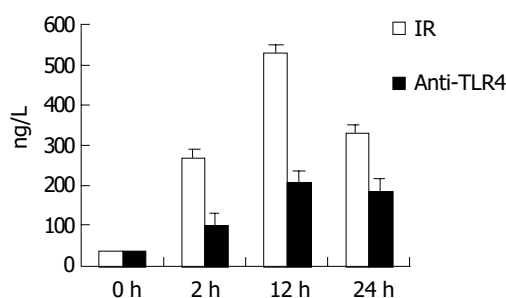


Figure 3 Comparison of TNF- α production in supernatant of KCs. In IR group, the TNF- α level in supernatant was increased with time, and reached the maximum (529.1 \pm 30.9 ng/mL) at 12 h. But in anti-TLR4 group, the production of TNF- α was obviously inhibited by Ab against TLR4 compared with the IR group (*P*<0.01).

Decrease of TNF- α levels after anti-TLR4 treatment

In IR group, the level of TNF- α in supernatant of KCs was 267.4 \pm 24.1, 529.1 \pm 30.9, and 329.7 \pm 24.6 ng/mL at 2, 12 and 24 h after IR, respectively. In group of anti-TLR4 antibody blockade, the production of TNF- α in supernatant was obviously inhibited by Ab against TLR4 when compared with that in IR group ($P < 0.01$), and it was 102.5 \pm 10.4, 207.6 \pm 18.4, and 185.3 \pm 12.7 ng/mL at 2, 12 and 24 h after IR, respectively (Figure 3).

DISCUSSION

Toll protein is a transmembrane protein which mainly acts as a necessary tool for immune defence to microorganism^[6,17-20]. The first toll-like protein in human cells was reported by Janeway, and named toll-like receptor (TLR)^[3,21]. About ten members of TLR superfamily in mammals have been reported in recent years. Among them, TLR4 plays a key role in LPS signal transduction^[4,22,23].

When LPS enters blood, it first binds to LBP (LPS binding protein), forming a LPS-LBP compound, and then binds to TLR4 on cell membranes leading to activation of cells^[18,24,25]. Recent studies have confirmed that the activation of cells induced by LPS needs another important molecule, namely MD-2. MD-2 is a key regulator protein, which could promote LPS signal transduction through connecting with TLR4 on cell membranes and forming the TLR4/MD-2 compound^[26-28].

Kupffer cells are special macrophages residing in hepatic sinusoids, which constitute 80% to 90% of total fixed macrophages in the body^[13,29]. Because of their special location, KCs act as an important defensive barrier for gut-derived endotoxemia. A large amount of endotoxins contact with KCs through portal circulation following ischemia-reperfusion after liver transplantation, and activate the KCs^[30,31]. Thus, it is very important to study the expression of TLR4 and MD-2 in KCs to clarify the origin of cytokines and the mechanism of IRI.

In our study, we found there were weak expressions of TLR4 and MD-2 gene and protein in resting KCs, which might play a critical role in maintaining the normal function of KCs, and might be essential for keeping KCs to be ready for activation after stress. But after IR, a large amount of LPS entered liver sinusoids, activated KCs, resulting in increased release of harmful cytokines such as TNF- α , which reached the maximum at 12 h after IR. To correctly illuminate the relation between TLR4 and MD-2 and downstream cytokines, we used anti-TLR4 antibody to inhibit the binding function of TLR4, and found that the production of TNF- α was greatly decreased, suggesting that the expression of TLR4 and MD-2 protein is indispensable to the secretion of downstream cytokines.

In summary, the present data suggest that there are weak expressions of TLR4 and MD-2 mRNA and protein in Kupffer cells. Expressions of TLR4 and MD-2 can significantly increase following ischemia-reperfusion in rat liver transplantation. LPS can induce activation of KCs by combining with TLR4 and MD-2, and subsequently release harmful cytokines, which ultimately attack the graft. Further studies are needed for elucidating TLR4/MD-2-mediated signal transduction pathways which lead to the secretion of cytokines during IRI on liver graft.

ACKNOWLEDGEMENT

This work was supported by the Key Laboratory of Hepatobiliary Surgery Department of Chongqing Medical University.

REFERENCES

1 Latz E, Visintin A, Lien E, Fitzgerald KA, Espevik T, Golenbock DT. The LPS receptor generates inflammatory signals from the

cell surface. *J Endotoxin Res* 2003; **9**: 375-380

- 2 Espevik T, Latz E, Lien E, Monks B, Golenbock DT. Cell distributions and functions of Toll-like receptor 4 studied by fluorescent gene constructs. *Scand J Infect Dis* 2003; **35**: 660-664
- 3 Kimoto M, Nagasawa K, Miyake K. Role of TLR4/MD-2 and RP105/MD-1 in innate recognition of lipopolysaccharide. *Scand J Infect Dis* 2003; **35**: 568-572
- 4 Harada K, Ohira S, Isse K, Ozaki S, Zen Y, Sato Y, Nakanuma Y. Lipopolysaccharide activates nuclear factor-kappaB through toll-like receptors and related molecules in cultured biliary epithelial cells. *Lab Invest* 2003; **83**: 1657-1667
- 5 Fujihara M, Muroi M, Tanamoto K, Suzuki T, Azuma H, Ikeda H. Molecular mechanisms of macrophage activation and deactivation by lipopolysaccharide: roles of the receptor complex. *Pharmacol Ther* 2003; **100**: 171-194
- 6 Re F, Strominger JL. Separate functional domains of human MD-2 mediate Toll-like receptor 4-binding and lipopolysaccharide responsiveness. *J Immunol* 2003; **171**: 5272-5276
- 7 Guillot L, Medjane S, Le-Barillec K, Balloy V, Danel C, Chignard M, Si-Tahar M. Response of human pulmonary epithelial cells to lipopolysaccharide involves Toll-like receptor 4 (TLR4)-dependent signaling pathways: evidence for an intracellular compartmentalization of TLR4. *J Biol Chem* 2004; **279**: 2712-2718
- 8 Asai Y, Hashimoto M, Ogawa T. Treponemal glycoconjugate inhibits Toll-like receptor ligand-induced cell activation by blocking LPS-binding protein and CD14 functions. *Eur J Immunol* 2003; **33**: 3196-3204
- 9 Totemeyer S, Foster N, Kaiser P, Maskell DJ, Bryant CE. Toll-like receptor expression in C3H/HeN and C3H/HeJ mice during *Salmonella enterica* serovar Typhimurium infection. *Infect Immun* 2003; **71**: 6653-6657
- 10 Akashi S, Saitoh S, Wakabayashi Y, Kikuchi T, Takamura N, Nagai Y, Kusumoto Y, Fukase K, Kusumoto S, Adachi Y, Kosugi A, Miyake K. Lipopolysaccharide interaction with cell surface Toll-like receptor 4-MD-2: higher affinity than that with MD-2 or CD14. *J Exp Med* 2003; **198**: 1035-1042
- 11 Schauer RJ, Gerbes AL, Vonier D, Meissner H, Michl P, Leuderer R, Schildberg FW, Messmer K, Bilzer M. Glutathione protects the rat liver against reperfusion injury after prolonged warm ischemia. *Ann Surg* 2004; **239**: 220-231
- 12 Cavaliere B, Perrelli MG, Aragno M, Ramadori P, Poli G, Cutrin JC. Ischaemic preconditioning modulates the activity of Kupffer cells during *in vivo* reperfusion injury of rat liver. *Cell Biochem Funct* 2003; **21**: 299-305
- 13 Carini R, Albano E. Recent insights on the mechanisms of liver preconditioning. *Gastroenterology* 2003; **125**: 1480-1491
- 14 Giakoustidis DE, Iliadis S, Tsantilas D, Papageorgiou G, Kontos N, Kostopoulou E, Botsoglou NA, Gerasimidis T, Dimitriadou A. Blockade of Kupffer cells by gadolinium chloride reduces lipid peroxidation and protects liver from ischemia/reperfusion injury. *Hepatogastroenterology* 2003; **50**: 1587-1592
- 15 Peng Y, Gong JP, Yan LN, Li SB, Li XH. Improved two-cuff technique for orthotopic liver transplantation in rat. *Hepatobiliary Pancreat Dis Int* 2004; **3**: 33-37
- 16 Gong JP, Wu CX, Liu CA, Li SW, Shi YJ, Yang K, Li Y, Li XH. Intestinal damage mediated by Kupffer cells in rats with endotoxemia. *World J Gastroenterol* 2002; **8**: 923-927
- 17 Visintin A, Latz E, Monks BG, Espevik T, Golenbock DT. Lysines 128 and 132 enable lipopolysaccharide binding to MD-2, leading to Toll-like receptor-4 aggregation and signal transduction. *J Biol Chem* 2003; **278**: 48313-48320
- 18 Tamai R, Asai Y, Hashimoto M, Fukase K, Kusumoto S, Ishida H, Kiso M, Ogawa T. Cell activation by monosaccharide lipid A analogues utilizing Toll-like receptor 4. *Immunology* 2003; **110**: 66-72
- 19 Uehori J, Matsumoto M, Tsuji S, Akazawa T, Takeuchi O, Akira S, Kawata T, Azuma I, Toyoshima K, Seya T. Simultaneous blocking of human Toll-like receptors 2 and 4 suppresses myeloid dendritic cell activation induced by *Mycobacterium bovis* bacillus Calmette-Guerin peptidoglycan. *Infect Immun* 2003; **71**: 4238-4249
- 20 Vives-Pi M, Somoza N, Fernandez-Alvarez J, Vargas F, Caro P, Alba A, Gomis R, Labeta MO, Pujol-Borrell R. Evidence of expression of endotoxin receptors CD14, toll-like receptors TLR4 and TLR2 and associated molecule MD-2 and of sensitivity to

- endotoxin (LPS) in islet beta cells. *Clin Exp Immunol* 2003; **133**: 208-218
- 21 **Tamai R**, Sugawara S, Takeuchi O, Akira S, Takada H. Synergistic effects of lipopolysaccharide and interferon-gamma in inducing interleukin-8 production in human monocytic THP-1 cells is accompanied by up-regulation of CD14, Toll-like receptor 4, MD-2 and MyD88 expression. *J Endotoxin Res* 2003; **9**: 145-153
- 22 **Suzuki M**, Hisamatsu T, Podolsky DK. Gamma interferon augments the intracellular pathway for lipopolysaccharide (LPS) recognition in human intestinal epithelial cells through coordinated up-regulation of LPS uptake and expression of the intracellular Toll-like receptor 4-MD-2 complex. *Infect Immun* 2003; **71**: 3503-3511
- 23 **Thompson PA**, Tobias PS, Viriyakosol S, Kirkland TN, Kitchens RL. Lipopolysaccharide (LPS)-binding protein inhibits responses to cell-bound LPS. *J Biol Chem* 2003; **278**: 28367-28371
- 24 **Ohnishi T**, Muroi M, Tanamoto K. MD-2 is necessary for the toll-like receptor 4 protein to undergo glycosylation essential for its translocation to the cell surface. *Clin Diagn Lab Immunol* 2003; **10**: 405-410
- 25 **Miyake K**, Nagai Y, Akashi S, Nagafuku M, Ogata M, Kosugi A. Essential role of MD-2 in B-cell responses to lipopolysaccharide and Toll-like receptor 4 distribution. *J Endotoxin Res* 2002; **8**: 449-452
- 26 **Medvedev AE**, Vogel SN. Overexpression of CD14, TLR4, and MD-2 in HEK 293T cells does not prevent induction of *in vitro* endotoxin tolerance. *J Endotoxin Res* 2003; **9**: 60-64
- 27 **Okamoto M**, Sato M. Toll-like receptor signaling in anti-cancer immunity. *J Med Invest* 2003; **50**: 9-24
- 28 **Schroder NW**, Morath S, Alexander C, Hamann L, Hartung T, Zahringer U, Gobel UB, Weber JR, Schumann RR. Lipoteichoic acid (LTA) of *Streptococcus pneumoniae* and *Staphylococcus aureus* activates immune cells via Toll-like receptor (TLR)-2, lipopolysaccharide-binding protein (LBP), and CD14, whereas TLR-4 and MD-2 are not involved. *J Biol Chem* 2003; **278**: 15587-15594
- 29 **Zhu X**, Qiu Y, Shi M, Ding Y. Matrine protects sinusoidal endothelial cells from cold ischemia and reperfusion injury in rat orthotopic liver transplantation. *Ann Clin Lab Sci* 2003; **33**: 216-225
- 30 **Kojima Y**, Suzuki S, Tsuchiya Y, Konno H, Baba S, Nakamura S. Regulation of pro-inflammatory and anti-inflammatory cytokine responses by Kupffer cells in endotoxin-enhanced reperfusion injury after total hepatic ischemia. *Transpl Int* 2003; **16**: 231-240
- 31 **Kiemer AK**, Gerwig T, Gerbes AL, Meissner H, Bilzer M, Vollmar AM. Kupffer-cell specific induction of heme oxygenase 1 (hsp32) by the atrial natriuretic peptide-role of cGMP. *J Hepatol* 2003; **38**: 490-498

Edited by Kumar M and Wang XL Proofread by Xu FM

Protective effects of recombinant human growth hormone on cirrhotic rats

Shuang Chen, Hong-Tao Wang, Bin Yang, Yu-Ru Fu, Qing-Jia Ou

Shuang Chen, Hong-Tao Wang, Bin Yang, Qing-Jia Ou,
Department of General Surgery, Sun Yat-Sen Memorial Hospital, the
Second Affiliated Hospital, Sun Yat-Sen University, Guangzhou
510120, Guangdong Province, China

Yu-Ru Fu, Medical Research Center, Sun Yat-Sen Memorial Hospital,
the Second Affiliated Hospital, Sun Yat-Sen University, Guangzhou
510120, Guangdong Province, China

Supported by the Natural Science Foundation of Guangdong Province,
No. 984213 and Academic Foundation of Sun Yat-Sen University and
Ministry of Public Health for Project 211, No. F000099075

Correspondence to: Dr. Shuang Chen, M.D., Ph.D., Department of
General Surgery, Sun Yat-Sen Memorial Hospital, the Second Affiliated
Hospital, Sun Yat-Sen University, Guangzhou 510120, Guangdong
Province, China. mdchens@yahoo.com

Telephone: +86-20-81332539 **Fax:** +86-20-81332853

Received: 2004-03-11 **Accepted:** 2004-04-05

Abstract

AIM: To investigate the effects and molecular mechanisms of recombinant human growth hormone (rhGH) on protecting liver function and alleviating portal hypertension of liver cirrhotic rats.

METHODS: Liver cirrhosis of male Sprague-Dawley rats was induced by administration of thioacetamide. The rats with or without liver cirrhosis were randomly divided into four groups. Group A consisted of the normal rats was treated with normal saline (NS), group B consisted of the normal rats was treated with rhGH, group C consisted of cirrhotic rats was treated with NS, and group D consisted of cirrhotic rats was treated with rhGH. The rats of different groups were subcutaneously injected with 0.5 mL of NS or 333 ng/kg of rhGH daily for 7 d. After treatments, the following parameters were examined, including GH-binding capacity (R_T) by ^{125}I -hGH binding, growth hormone receptor mRNA (GHR mRNA) expression by RT-PCR, relative content of collagen (RCC) by histomorphometry, and level of malon-dialdehyde (MDA) and superoxide dismutase (SOD) in liver tissue by thiobarbituric acid reaction and pyrogallol acid self-oxidation, respectively. Serum albumin (ALB), alanine transaminase (ALT) and portal vein pressure (PVP) were also examined.

RESULTS: rhGH up-regulated both the GH-binding capacity (R_T) and the expression of GHR mRNA *in vivo*. R_T in group A (72 ± 12 fmol/mg protein) was significantly higher than that in group C (31 ± 4 fmol/mg protein) ($P < 0.05$). R_T in group B (80 ± 9 fmol/mg protein) increased markedly compared to group A ($P < 0.05$). R_T in group D (40 ± 7 fmol/mg protein) raised remarkably compared with group C ($P < 0.05$), but less than that in group A, and there was no significant GH binding affinity contrast (Kd) change. The GHR mRNA level (IOD, pixel) in group A (29 ± 3) was significantly higher than that in group C (23 ± 3) ($P < 0.05$). GHR mRNA levels were significantly raised in group B (56 ± 4) and group D (42 ± 8) compared with groups A and C (29 ± 3 and 23 ± 3 , respectively) ($P < 0.05$). Compared with the normal liver,

MDA level was higher and SOD level was lower in cirrhotic livers. After rhGH treatment, MDA level was significantly declined to 12.0 ± 2.2 nmol/mg protein and SOD was raised to 1029 ± 76 U/mg protein in group D ($P < 0.05$). ALB levels in groups B and D (42 ± 7 g/L and 37 ± 7 g/L, respectively) were significantly raised compared with those in groups A and C (35 ± 5 g/L and 29 ± 4 g/L, respectively) ($P < 0.05$). ALT level was markedly lower in group D (69 ± 7 U/L) compared to group C (89 ± 15 U/L) ($P < 0.05$), and close to group A (61 ± 10 U/L). RCC in group C ($22.30 \pm 3.86\%$) was significantly higher than that in group A ($1.14 \pm 0.21\%$) and group D ($14.70 \pm 2.07\%$) ($P < 0.05$). In addition, rhGH markedly alleviated portal hypertension in liver cirrhotic rats (group D *vs* C, 9.3 ± 1.5 cmH₂O *vs* 14.4 ± 2.0 cmH₂O) ($P < 0.05$).

CONCLUSION: Pharmacological doses of rhGH can increase R_T and GHR mRNA expression, ameliorate liver functions, repress fibrosis and decline portal hypertension, suggesting it has potentially clinical usage as a hepatotropic factor.

Chen S, Wang HT, Yang B, Fu YR, Ou QJ. Protective effects of recombinant human growth hormone on cirrhotic rats. *World J Gastroenterol* 2004; 10(19): 2894-2897
<http://www.wjgnet.com/1007-9327/10/2894.asp>

INTRODUCTION

Liver cirrhosis is a common pathway of a variety of chronic liver diseases^[1], and is associated with high protein catabolism, low anabolism and negative nitrogen balance^[2], resulting in hypoproteinemia which contributes to ascites, dysfunction of coagulation and suppression of immune response^[3]. Early reports showed that cirrhotic patients undergone emergency abdominal surgery exhibited a higher mortality^[4]. In retrospective studies of liver transplant recipients, protein-calorie malnutrition has been associated with adverse outcomes in patients with end-stage liver diseases^[5,6]. A prospective study showed that cirrhotic patients with hypermetabolism and emaciation had a much higher mortality rate after liver transplantation than those with normal metabolism^[7]. It is critical for patients with hepatic cirrhosis to correct malnutrition. To date, studies have shown that nutritional support is always not effective enough to prevent protein loss and optimize the care of these patients in severe catabolic illnesses, including cirrhosis^[8,9].

Growth hormone (GH) is essential for body growth in children. In adults, GH continues to stimulate many anabolic processes. GH secreted by the pituitary gland is pulsatile, and its action depends on its binding to growth hormone receptor on cell membrane^[10-13]. New insights have initiated new applications and a growing potential for GH replacement therapy in adults. Recombinant human growth hormone (rhGH) has been clinically used in many states, such as after abdominal operation^[14], organ transplantation^[15], major trauma^[16] and severe burns^[17], to enable the patients to survive an aggressive surgery^[18]. After treatment with rhGH, donor site healing rate

in children with severe burns was enhanced and hospitalization time was decreased^[19-21]. It significantly enhanced cell-mediated immunity and decreased wound infection rates and length of hospitalization in a large group of postoperative patients^[22]. Some clinical trials reported that growth hormone enhanced nitrogen retention of patients with chronic obstructive lung diseases^[23], severe sepsis^[24,25] and emaciated AIDS^[26,27], in addition to fasted adult volunteers. Although there are many controversies^[28-32], it has been confirmed that rhGH is an effective drug to accelerate protein anabolism^[33] and plays a central role in metabolic intervention with a significant cost-effect benefit^[34].

In this study, we investigated the effects and molecular mechanism of pharmacological doses of recombinant human growth hormone (rhGH) on expression of growth hormone receptor (GHR) in liver tissue, liver function and portal vein pressure in a rat cirrhotic model with portal hypertension.

MATERIALS AND METHODS

Induction of liver cirrhosis

Male SD rats were purchased from Medical Animal Center of Sun Yat-Sen University. Rat liver cirrhosis was induced by daily intraperitoneal injection of 30 g/L thioacetamide (TAA, 50 mg/kg for 9 to 12 wk). Twenty normal rats (body mass 200-300 g) were randomly divided into two groups: group A ($n = 10$) was treated with normal saline (NS), and group B ($n = 10$) was treated with rhGH. Twenty cirrhotic rats (body mass, 200-300 g) were randomly divided into two groups: group C ($n = 10$) was treated with NS and group D ($n = 10$) was treated with rhGH. The rats were injected subcutaneously with 0.5 mL of NS or 333 ng/kg of rhGH daily for 7 d.

Experimental methods and observation indexes

Rats were anesthetized with pentobarbital (30 mg/kg, subcutaneous injection), weighed, antiseptised. Then peritoneum was incised to explore the liver.

Measurement of portal vein pressure (PVP) After the portal vein was punctured, PVP was measured directly.

Estimation of liver function Blood samples from inferior vena cava were collected to measure serum albumin (ALB) and alanine transaminase (ALT) levels by biochemical autoanalyzers.

Tissue sampling Partial liver tissue samples were frozen in liquid nitrogen immediately, then stored at -80°C for use. The rest part was fixed in 100 g/L formaldehyde solution and stained with Masson trichrome stain for regular pathological examination.

GH binding capacity (R_T) analysis One hundred μL (approximately 20 000 cpm) of ^{125}I -hGH (NEN inc, USA) with a specific activity of about 108 $\mu\text{Ci}/\mu\text{g}$, 100 μL of unlabelled hGH with various concentrations (0-3 nmol/L was divided into 7-9 concentration gradients, standard samples were bought from Northern Biological Technical Company), and 100 μL of liver membrane microsomes (preparation with gradient centrifugation technique) were mixed and incubated at 4°C overnight. Dissociated ligands were eliminated by filtration.

The precipitates were subjected to a radioactive counter, and then ^{125}I -GH binding capacity (R_T , fmol/mg protein) and binding affinity contrast (kd, nmol/L) were calculated by Scatchard analysis.

Expression of GHR mRNA in liver tissue Self-designed primers were as follows: forward, 5'-ATGTGAGATCCAGACAACG-3', and reverse, 5'-ATGTCAGGGTCATAACAGC-3'. The amplification segment containing introns was supposed to be 499 bp in length. Total RNA of the rats' liver tissues was extracted with Trizol following the manufacturer's instructions. RT-PCR was performed with RT-PCR kits (Epicentre inc. USA) as previously described^[35]. After thirty amplification cycles were performed, the PCR products were detected by gel electrophoresis. The level of GHR mRNA was expressed as iOD (pixel, the integral optical density of amplification segment).

Level of malon-dialdehyde (MDA) and superoxide dismutase (SOD) Thiobarbituric acid reaction and pyrogallol acid self oxidation method were adopted to measure the amount of MDA (the degradation products of peroxide lipid in liver) and the activity of SOD, respectively.

Measurement of relative content of collagen (RCC) in liver Liver fibrosis levels was expressed as RCC. After stained with Masson's trichrome stain, liver collagen content was calculated by histomorphometric measurement. Three random areas were chosen and analyzed by computers with Kontron IBAS2.5 system (Germany) for digital image analysis. The total area and the fibrotic area with positive staining were automatically selected, outlined and evaluated by planimetry. RCC was calculated as a percentage of positive staining area in the total area.

Statistical analysis

The data were processed with duplex factor χ^2 analysis by software statistica 5.0. Least significant difference (LSD) was adopted to compare the inter-group variance. Values were expressed as mean \pm SD. $P < 0.05$ was considered statistically significant.

RESULTS

GH-binding capacity (R_T) analysis

As shown in Table 1, R_T in group A was significantly higher than that in group C ($P < 0.05$). R_T in group B increased markedly compared with group A ($P < 0.05$). It significantly increased in group D compared with group C ($P < 0.05$), but was lower than that in group A. There was no significant difference in Kd.

GHR mRNA expression in liver tissue

As shown in Table 1 and Figure 1, the expression of GHR mRNA (iOD, pixel) in group A was significantly higher than that in group C ($P < 0.05$). It was significantly raised in groups B and D after rhGH treatment, which was 1.9 and 1.8 times higher than that in groups A and C, respectively ($P < 0.05$). It was higher in group D than in group A.

Serum ALB and ALT level

Without rhGH treatment, ALB level in cirrhotic rats (group C)

Table 1 Effects of rhGH treatment on various parameters (mean \pm SD)

Group	R_T (fmol/mg protein)	GHR mRNA (iOD)	ALB (g/L)	ALT (U/L)	MDA (nmol/mg protein)	SOD (U/mg)	RCC (%)	PVP (cmH ₂ O)
A	72 \pm 12	29 \pm 3	35 \pm 5	61 \pm 10	10.2 \pm 1.4	1078 \pm 185	1.14 \pm 0.21	5.6 \pm 0.7
B	80 \pm 9 ^c	56 \pm 4 ^c	42 \pm 7 ^c	55 \pm 11	9.4 \pm 1.2	1057 \pm 159	1.13 \pm 0.18	5.8 \pm 0.7
C	31 \pm 4 ^a	23 \pm 3 ^a	29 \pm 4 ^a	89 \pm 15 ^a	18.7 \pm 3.2 ^a	824 \pm 108 ^a	22.30 \pm 3.86 ^a	14.4 \pm 2.0 ^a
D	40 \pm 7 ^{ac}	42 \pm 8 ^{ac}	37 \pm 7 ^c	69 \pm 7 ^{ac}	12.0 \pm 2.2 ^{ac}	1029 \pm 76 ^c	14.70 \pm 2.07 ^{ac}	9.3 \pm 1.5 ^{ac}

^a $P < 0.05$ vs control groups A and B, ^c $P < 0.05$ vs before rhGH treatment (group A or C).

was significantly lower than that in normal rats (group A), and ALT in cirrhotic rats was markedly higher than that in normal rats ($P < 0.05$) (Table 1). After rhGH administration, ALB in groups B and D increased significantly ($P < 0.05$), ALT in group D decreased remarkably ($P < 0.05$), which was close to normal rats (Table 1).

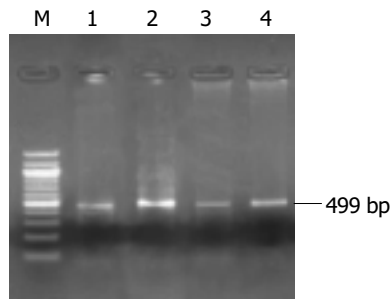


Figure 1 Expression of GHR mRNA in normal and cirrhotic liver tissues after NS or rhGH administration. Lane 1: control group +NS (group A); Lane 2: control group +rhGH (group B); Lane 3: cirrhotic group +NS (group C); Lane 4: cirrhotic group +rhGH (group D); and Lane M: DNA standard marker of 100, 200, 300, 400, 500, 600, 700, 800, 900, 1 000, 1 100 and 1 200 bp, respectively.

Changes of MDA and SOD in liver tissue

Before the treatment with rhGH, the amount of MDA in cirrhotic rats (group C) was significantly higher than that in normal rats (group A) ($P < 0.05$), and SOD in cirrhotic rats was significantly lower than that in normal rats ($P < 0.05$). After rhGH administration, MDA and SOD in group B were not obviously changed, but in group D, MDA was significantly lower than that in group C ($P < 0.05$), while SOD was significantly higher than that in group C ($P < 0.05$). The curve correlation analysis manifested a significant correlation between SOD and MDA ($P < 0.01$). (Table 1, Figure 2).

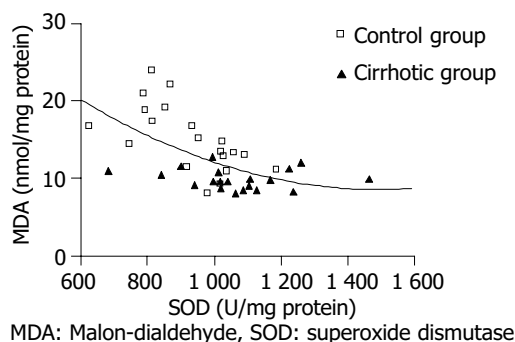


Figure 2 Correlation analysis of SOD and MDA.

RCC in liver tissue

As shown in Table 1, RCC in group C was significantly higher than that in group A ($P < 0.05$). Compared with group C, it was significantly lower in group D ($P < 0.05$).

Changes of PVP

As shown in Table 1, PVP in cirrhotic rats (group C) was significantly higher than that in normal rats (group A) ($P < 0.05$). After rhGH administration, no significant change was found in normal rats, however PVP in cirrhotic rats (group D) was significantly lower than that in group C ($P < 0.05$).

DISCUSSION

In cirrhotic patients, nutritional status was an important predictor

of morbidity, mortality, and survival after transplantation^[36]. The poor status of these patients was associated with the state of acquired GH resistance^[37,38], which is common in conditions associated with malnutrition and protein catabolism, trauma or surgery, organ failure and critical illness. Much has been done regarding the expression of GHR and signal transduction^[10-13], but the expression of GHR and GHR mRNA in some pathological states such as cirrhotic hepatocytes, malignant cells, remains to be established. Chang *et al.*^[39] reported that ¹²⁵I-rhGH binding activity in 6 cases of hepatocellular carcinoma and adjacent cirrhotic liver tissues could not be detected and they believed that GHR in cirrhotic hepatic tissues disappeared although the study only examined one aspect of the GHR and GH binding. Another study^[40] showed that specific binding of ¹²⁵I-hGH in liver tissues from liver transplant of 17 patients with end-stage liver diseases was lower than that in normal controls, but only in 3 cirrhotic livers Scatchard analysis was performed for calculation of GH binding capacity and affinity. In this setting of tissue-based GH binding assay, there was still a controversy about the expression of GHR on cirrhotic liver cells.

Our study showed that rhGH could significantly increase serum ALB and SOD levels, decrease ALT and MAD to nearly the normal level in liver cirrhotic rats. In addition, after rhGH treatment, both the liver fibrosis level and PVP were remarkably decreased.

In our study, the expression of GHR mRNA in cirrhotic liver tissue was lower than that in normal liver tissue, suggesting that liver cirrhosis could down-regulate GHR gene transcription and result in decrease of GHR, which might be an important reason of malnutrition in liver cirrhosis.

Simultaneously, we found that rhGH up-regulated GHR and its mRNA in both cirrhotic and normal liver tissues. In normal liver, the changes before and after rhGH treatment were not obvious. We hypothesized that the up-regulation of GHR and its mRNA in cirrhotic rats could improve liver function, and decrease liver fibrosis levels and PVP. This implied that the effects of rhGH on the expression of GHR and GHR mRNA in cirrhotic liver tissues might play an important role in ameliorating the sensibility of cirrhotic liver tissues to rhGH, thereby exerting a therapeutic effect on liver cirrhosis.

In conclusion, rhGH can up-regulate the expression of GHR and its mRNA in livers, particularly in cirrhotic livers, which can increase the sensibility of cirrhotic liver tissue to growth hormones. Thus, rhGH can protect liver function, repress fibrosis, alleviate portal hypertension of cirrhotic livers.

REFERENCES

- 1 Strong RW. Liver transplantation: current status and future prospects. *J R Coll Surg Edinb* 2001; **46**: 1-8
- 2 Dichi JB, Dichi I, Maio R, Correa CR, Angeleli AY, Bicudo MH, Rezende TA, Burini RC. Whole-body protein turnover in malnourished patients with child class B and C cirrhosis on diets low to high in protein energy. *Nutrition* 2001; **17**: 239-242
- 3 Sobhonslidsuk A, Roongpisuthipong C, Nantiruj K, Kulapongse S, Songchitsomboon S, Sumalnop K, Bussagorn N. Impact of liver cirrhosis on nutritional and immunological status. *J Med Assoc Thai* 2001; **84**: 982-988
- 4 Maul KI, Turnage B. Trauma in the cirrhotic patient. *South Med J* 2001; **94**: 205-207
- 5 Moukarzel AA, Najm I, Vargas J, McDiarmid SV, Busuttill RW, Ament ME. Effect of nutritional status on outcome of orthotopic liver transplantation in pediatric patients. *Transplant Proc* 1990; **22**: 1560-1563
- 6 Harrison J, McKiernan J, Neuberger JM. A prospective study on the effect of recipient nutritional status on outcome in liver transplantation. *Transpl Int* 1997; **10**: 369-374
- 7 Muller MJ, Lantz HU, Plogmann B, Burger M, Korber J, Schmidt FW. Energy expenditure and substrate oxidation in patients with cirrhosis: the impact of cause, clinical staging

- and nutritional state. *Hepatology* 1992; **15**: 782-794
- 8 **Streat SJ**, Beddoe AH, Hill GL. Aggressive nutritional support does not prevent protein loss despite fat gain in septic intensive care patients. *J Trauma* 1987; **27**: 262-266
 - 9 **Le Cornu KA**, McKiernan FJ, Kapadia SA, Neuberger JM. A prospective randomized study of preoperative nutritional supplementation in patients awaiting elective orthotopic liver transplantation. *Transplantation* 2000; **69**: 1364-1369
 - 10 **Carter-Su C**, Schwartz J, Smit LS. Molecular mechanism of growth hormone action. *Annu Rev Physiol* 1996; **58**: 187-207
 - 11 **Hocquette JF**, Postel-Vinay MC, Kayser C, de Hemptinne B, Amar-Costesec A. The human liver growth hormone receptor. *Endocrinology* 1989; **125**: 2167-2174
 - 12 **Husman B**, Andersson G, Norstedt G, Gustafsson JA. Characterization and subcellular distribution of somatogenic receptor in rat liver. *Endocrinology* 1985; **116**: 2605-2611
 - 13 **van Neste L**, Husman B, Moller C, Andersson G, Norstedt G. Cellular distribution of somatogenic receptors and insulin-like growth factor-I mRNA in the rat liver. *J Endocrinol* 1988; **119**: 69-74
 - 14 **Wong WK**, Soo KC, Nambiar R, Tan YS, Yo SL, Tan IK. The effect of recombinant growth hormone on nitrogen balance in malnourished patients after major abdominal surgery. *Aust N Z J Surg* 1995; **65**: 109-113
 - 15 **Rodeck B**, Kardorff R, Melter M, Ehrich JH. Improvement of growth after growth hormone treatment in children who undergo liver transplantation. *J Pediatr Gastroenterol Nutr* 2000; **31**: 286-290
 - 16 **Petersen SR**, Holaday NJ, Jeevanandam M. Enhancement of protein synthesis efficiency in parenterally fed trauma victims by adjuvant recombinant human growth hormone. *J Trauma* 1994; **36**: 726-733
 - 17 **Singh KP**, Prasad R, Chari PS, Dash RJ. Effect of growth hormone therapy in burn patients on conservative treatment. *Burns* 1998; **24**: 733-738
 - 18 **Iglesias P**, Diez JJ. Clinical applications of recombinant human growth hormone in adults. *Expert Opin Pharmacother* 1999; **1**: 97-107
 - 19 **Herndon DN**, Hawkins HK, Nguyen TT, Pierre E, Cox R, Barrow RE. Characterization of growth hormone enhanced donor site healing in patients with large cutaneous burns. *Ann Surg* 1995; **221**: 649-656
 - 20 **Aili Low JF**, Barrow RE, Mittendorfer B, Jeschke MG, Chinkes DL, Herndon DN. The effect of short-term growth hormone treatment on growth and energy expenditure in burned children. *Burns* 2001; **27**: 447-452
 - 21 **Hart DW**, Herndon DN, Klein G, Lee SB, Celis M, Mohan S, Chinkes DL, Wolf SE. Attenuation of posttraumatic muscle catabolism and osteopenia by long-term growth hormone therapy. *Ann Surg* 2001; **233**: 827-834
 - 22 **Vara-Thorbeck R**, Guerrero JA, Rosell J, Ruiz-Requena E, Capitan JM. Exogenous growth hormone: effects on the catabolic response to surgically produced acute stress and on postoperative immune function. *World J Surg* 1993; **17**: 530-537
 - 23 **Pape GS**, Friedman M, Underwood LE, Clemmons DR. The effect of growth hormone on weight gain and pulmonary function in patients with chronic obstructive lung disease. *Chest* 1991; **99**: 1495-1500
 - 24 **Koea JB**, Breier BH, Douglas RG, Gluckman PD, Shaw JH. Anabolic and cardiovascular effects of recombinant human growth hormone in surgical patients with sepsis. *Br J Surg* 1996; **83**: 196-202
 - 25 **Li W**, Li J, Xu B, Yin L, Wang L, Gu J, Ren J, Quan Z. Effect of recombinant human growth hormone with total parenteral nutrition on albumin synthesis in patients with peritoneal sepsis. *Zhonghua Waike Zazhi* 1998; **36**: 643-645
 - 26 **Schambelan M**, Mulligan K, Grunfeld C, Daar ES, LaMarca A, Kotler DP, Wang J, Bozzette SA, Breitmeyer JB. Recombinant human growth hormone in patients with HIV-associated wasting. A randomized, placebo-controlled trial. Serostim Study Group. *Ann Intern Med* 1996; **125**: 873-882
 - 27 **Waters D**, Danska J, Hardy K, Koster F, Qualls C, Nickell D, Nightingale S, Gesundheit N, Watson D, Schade D. Recombinant human growth hormone, insulin-like growth factor 1, and combination therapy in AIDS-associated wasting. A randomized, double-blind, placebo-controlled trial. *Ann Intern Med* 1996; **125**: 865-872
 - 28 **O'Leary MJ**, Ferguson CN, Rennie M, Hinds CJ, Coakley JH, Preedy VR. Effect of growth hormone on muscle and liver protein synthesis in septic rats receiving glutamine-enriched parenteral nutrition. *Crit Care Med* 2002; **30**: 1099-1105
 - 29 **Losada F**, Garcia-Luna PP, Gomez-Cia T, Garrido M, Pereira JL, Marin F, Astorga R. Effects of human recombinant growth hormone on donor-site healing in burned adults. *World J Surg* 2002; **26**: 2-8
 - 30 **Carroll PV**, Van den Berghe G. Safety aspects of pharmacological GH therapy in adults. *Growth Horm IGF Res* 2001; **11**: 166-172
 - 31 **Takala J**, Ruokonen E, Webster NR, Nielsen MS, Zandstra DF, Vundelinckx G, Hinds CJ. Increased mortality associated with growth hormone treatment in critically ill adults. *N Engl J Med* 1999; **341**: 785-792
 - 32 **Jeschke MG**, Barrow RE, Herndon DN. Recombinant human growth hormone treatment in pediatric burn patients and its role during the hepatic acute phase response. *Crit Care Med* 2000; **28**: 1578-1584
 - 33 **Raguso CA**, Genton L, Kyle U, Pichard C. Management of catabolism in metabolically stressed patients: a literature survey about growth hormone application. *Curr Opin Clin Nutr Metab Care* 2001; **4**: 313-320
 - 34 **Wilmore DW**. Postoperative protein sparing. *World J Surg* 1999; **23**: 545-552
 - 35 **Zhao J**, van Tol HT, Taverne MA, van der Weijden GC, Bevers MM, van den Hurk R. The effect of growth hormone on rat pre-antral follicles *in vitro*. *Zygote* 2000; **8**: 275-283
 - 36 **Mendenhall CL**, Tosch T, Weesner RE, Garcia-Pont P, Goldberg SJ, Kiernan T, Seeff LB, Sorell M, Tamburro C, Zetterman R. VA cooperative study on alcoholic hepatitis. II: Prognostic significance of protein-calorie malnutrition. *Am J Clin Nutr* 1986; **43**: 213-218
 - 37 **Moller S**, Becker U, Gronbaek M, Juul A, Winkler K, Skakkebaek NE. Short-term effect of recombinant human growth hormone in patients with alcoholic cirrhosis. *J Hepatol* 1994; **21**: 710-717
 - 38 **Donaghy A**, Ross R, Gimson A, Hughes SC, Holly J, Williams R. Growth hormone, insulin like growth factor-1, and insulin like growth factor binding proteins 1 and 3 in chronic liver disease. *Hepatology* 1995; **21**: 680-688
 - 39 **Chang TC**, Lin JJ, Yu SC, Chang TJ. Absence of growth-hormone receptor in hepatocellular carcinoma and cirrhotic liver. *Hepatology* 1990; **11**: 123-126
 - 40 **Shen XY**, Holt RI, Miell JP, Justice S, Portmann B, Postel-Vinay MC, Ross RJ. Cirrhotic liver expresses low levels of the full-length and truncated growth hormone receptors. *J Clin Endocrinol Metab* 1998; **83**: 2532-2538

Tumor necrosis factor α antibody prevents brain damage of rats with acute necrotizing pancreatitis

Yan-Ling Yang, Ji-Peng Li, Kai-Zong Li, Ke-Feng Dou

Yan-Ling Yang, Ji-Peng Li, Kai-Zong Li, Ke-Feng Dou, Department of Hepatobiliary Surgery, Xijing Hospital, Fourth Military Medical University, Xi'an 710032, Shaanxi Province, China

Correspondence to: Ke-Feng Dou, Department of Hepatobiliary Surgery, Xijing Hospital, Fourth Military Medical University, Xi'an 710032, Shaanxi Province, China. gdwk@fmmu.edu.cn

Telephone: +86-29-3375259 **Fax:** +86-29-3375561

Received: 2003-12-12 **Accepted:** 2004-02-20

Abstract

AIM: To study the protective effects of tumor necrosis factor α (TNF α) antibody on pancreatic encephalopathy in rats.

METHODS: One hundred and twenty SD rats were randomly divided into normal control group, acute necrotizing pancreatitis group and TNF α antibody treated group. Acute hemorrhage necrotizing pancreatitis model in rats was induced by retrograde injection of 50 g/L sodium taurocholate into the pancreatobiliary duct. Serum TNF α was detected and animals were killed 12 h after drug administration. Changes in content of brain water, MDA and SOD as well as leucocyte adhesion of brain microvessels were measured.

RESULTS: In TNF α antibody treated group, serum TNF α level was decreased. Content of brain water, MDA and SOD as well as leucocyte adhesion were decreased significantly in comparison with those of acute necrotizing pancreatitis group ($P < 0.05$).

CONCLUSION: TNF α antibody can alleviate the brain damage of rats with acute hemorrhage necrotizing pancreatitis.

Yang YL, Li JP, Li KZ, Dou KF. Tumor necrosis factor α antibody prevents brain damage of rats with acute necrotizing pancreatitis. *World J Gastroenterol* 2004; 10(19): 2898-2900 <http://www.wjgnet.com/1007-9327/10/2898.asp>

INTRODUCTION

Pancreatic encephalopathy, a syndrome of mental retardation induced by severe acute pancreatitis, has been greatly concerned by clinicians. Unfortunately, the pathogenesis and mechanism of pancreatic encephalopathy are still unclear although many factors are thought to be related to it, such as pancreatin, epiphyte infection, electrolyte disturbance, lack of vitamin, alcoholism, hypoxemia^[1-3]. Recent reports have shown that overactivation of leucocytes and overexpression of cytokines play important roles in the pathogenesis of pancreatic encephalopathy. Moreover, the high level of TNF α in patients has a remarkable correlation with pancreatic encephalopathy^[4-9]. In the present study, we attempted to block or relieve pancreatic encephalopathy by using TNF α antibody.

MATERIALS AND METHODS

Animals

One hundred and twenty male Spargue-Dawley (SD) rats

weighing 230 ± 20 g, were obtained from Animal Research Center of Shaanxi Academy of Traditional Medicine, and fed with standard rat chow.

Drugs

Sodium taurocholate (Sigma) was diluted to 50 g/L with saline prior to use. TNF α monoclonal antibody (Jingmei Co.Ltd., Guangdong, China) was diluted at 1:100 with saline prior to use.

Experimental grouping

One hundred and twenty SD rats were randomly divided into three groups: Group I: normal control group ($n = 40$), sham operation was performed and saline was retrograde injected into the pancreatobiliary duct of the rats; Group II: acute necrotizing pancreatitis group ($n = 40$), in which an acute hemorrhage necrotizing pancreatitis model was induced by retrograde injection of 50 g/L sodium taurocholate into the pancreatobiliary duct; Group III: TNF α antibody treated group ($n = 40$), in which 1 mL TNF α antibody (2.0 mg/kg) was injected into the rats through dorsum veins of penis 5 min prior to operation. Blood samples (2 mL) were taken from inferior vena cava of all animals in each group 12 h after operation. Then the rats were killed and samples were obtained for analysis.

Operation

The animals were fasted but free to drink water 12 h before operation. Then the rats were intraabdominally anesthetized by 100 g/L pentobarbital sodium (30 mg/kg), and incised through median incision of the abdomen. After the common bile duct was clamped in hepatoduodenal ligament by small artery clamps, a cannula was inserted into pancreatobiliary duct through mammary papilla from anterior wall of duodenum. Then sodium taurocholate (50 g/L) was injected by the cannula with even speed of 0.1 mL/min, the scatheless vascular clamp was removed 10 min later. Finally, the abdomen incisions were closed and the animals were given gentamicin to prevent infection^[10,11].

Evaluation of TNF α in serum

Evaluation of serum TNF α was performed by sandwich ELISA method with double antibodies. The kit was purchased from Endogen Company (USA) and the procedures were made according to the manufacturer's instructions.

Evaluation of water content in brain

Evaluations of water content in brain of 20 rats in each group were completed by the methods of dry and wet weight estimation. Water content in brain = (wet weight - dry weight) \div wet weight $\times 100\%$.

Evaluation of brain MDA and SOD content

Skulls of 20 rats in each group were opened to get frontal lobe of the brain. Then brain tissues were homogenized and centrifuged. MDA and SOD contents were gained by chemical colorimetry (kit purchased from Bioengineer Institute of Nanjing Jiancheng, China).

Congregation of leucocytes and mural counting in blood capillary

After stained by HE, the whole number of leucocytes in 20 sections

Table 1 Serum TNF α level, content of brain water, MDA and SOD as well as leucocyte mural counting in brain blood capillary in three groups

Group	Serum TNF α level (pg/mL)	Brain water content (%)	Brain MDA content (nmol/mL)	Brain SOD content (nmol/mL)	Mural leucocytes (per 20 capillary)
I ^a	25.17 \pm 2.26	77.09 \pm 0.51	5.32 \pm 1.40	13.40 \pm 2.77	6.12 \pm 1.60
II	264.58 \pm 4.39	83.17 \pm 1.42	17.26 \pm 3.18	35.52 \pm 3.10	62.15 \pm 5.18
III ^c	74.33 \pm 1.78	81.41 \pm 1.52	11.71 \pm 3.26	23.65 \pm 1.93	38.37 \pm 3.43

^a P <0.05 vs II, ^c P <0.05 vs II.

of brain tissues was counted under light microscope to obtain the mean number.

Statistical analysis

The data were expressed as mean \pm SD and analyzed by software of SPSS10.0. P <0.05 was considered statistically significant.

RESULTS

Serum TNF α level

The level of TNF α in blood serum in acute necrotizing pancreatitis group (264.58 \pm 4.39 pg/mL) was increased markedly (P <0.05) compared with that in the normal control group (25.17 \pm 2.26 pg/mL). But the level of TNF α in blood serum in the TNF α antibody treated group (74.33 \pm 1.78 pg/mL) was decreased markedly (P <0.05) compared with that in acute necrotizing pancreatitis group.

Brain water content

Brain water content in the acute necrotizing pancreatitis group (83.17 \pm 1.42%) was significantly higher than that in the normal control group (77.09 \pm 0.51%). But it was significantly lower in the TNF α antibody treated group (81.41 \pm 1.52%) than in the acute necrotizing pancreatitis group (P <0.05).

Brain MDA content

Brain MDA content of in the acute necrotizing pancreatitis group (17.26 \pm 3.18 nmol/mL) was increased remarkably (P <0.05) compared with that in the normal control group (5.32 \pm 1.40 nmol/mL). It was decreased remarkably in the TNF α antibody treated group (11.71 \pm 3.26 nmol/mL) in comparison with acute necrotizing pancreatitis group (P <0.05).

Brain SOD content

Brain SOD content in the acute necrotizing pancreatitis group (35.52 \pm 3.10 nmol/mL) was increased remarkably compared with that in the normal control group (13.40 \pm 2.77 nmol/mL). It was decreased remarkably in the TNF α antibody treated group (23.65 \pm 1.93 nmol/mL) in comparison with acute necrotizing pancreatitis group (P <0.05).

Leucocyte mural counting of brain blood capillary

The number of leucocyte mural counts in blood capillary in every 20 blood capillaries in the TNF α antibody treated group (38.37 \pm 3.43) was significantly lower (P <0.05) than that in the acute necrotizing pancreatitis group (62.15 \pm 5.18).

DISCUSSION

Cytokines, mainly excreted by immunocytes in human body, are soluble peptides, which play important roles in immune activation and inflammatory reactions. In normal conditions, the content of cytokines is very low. However, the expression of cytokines is increased remarkably following multiple stimulations, such as infection and trauma. It is well known that the overactivation of cytokines could induce or even aggravate

tissue damage^[12-16]. Acute severe pancreatitis could always lead to systemic inflammatory response syndrome (SIRS) and multiple organ dysfunction syndrome (MODS)^[17-24]. The present studies have focused on the pathogenesis and therapy of respiratory failure, kidney failure, hepatic failure and cardiovascular function failure complicated by acute severe pancreatitis. However, investigations on mechanism of brain damage and related preventive measures after acute severe pancreatitis remain ineffective.

TNF α is excreted by activated macrophages, endothelial cells and B lymphocytes with multiple functions. It can play important roles in inflammatory reactions. Animal experiments suggested that serum TNF α in patients with acute severe pancreatitis could induce pancreatic and other organs' damages. In the early period of acute severe pancreatitis, TNF α was involved in occurrence and progress of acute severe pancreatitis. On the other hand, TNF α was closely related with the severity and mortality of this disease^[25-31].

In acute severe pancreatitis, the mechanisms of TNF α - induced brain damage included^[32-40]: (1) TNF α could stimulate differentiation of phospholipase A2 or directly activate phospholipase, aggregate and activate leucocytes to release cellular media, thus reinforcing permeability of blood capillary including platelet active factor (PAF), leukotriene B4 (LTB4), nitrogen monoxide (NO), thromboxane A2 (TXA2), prostaglandin (PG) and oxygen-derived free radicals. The media in positive feedback could accelerate the yield of TNF α , and thereby form "waterfall" cascade reaction. (2) TNF α could directly increase the permeability of blood endothelial cells, and also act through leucocytes, up-regulate adhesive factors of endothelial cells, such as ELAM-1 and ICAM-1, thus facilitating adhesiveness and contraction of leucocytes to cause leakage of blood capillary and tissue damage. (3) TNF α could induce inflammatory injuries of myelin sheath by direct toxicity or activating immune cells.

In the present study, we attempted to relieve pancreatic encephalopathy by using TNF α antibody. The results showed that the level of serum TNF α , content of brain water, MDA and SOD as well as mural leucocyte count of the rats in TNF α antibody treated group, reduced significantly compared with those in acute necrotizing pancreatitis group. The present data suggest that TNF α antibody plays an important protective role in pancreatic encephalopathy in rats. But the optimal concentration of TNF α antibody and its influence on body immune system still need further investigation.

REFERENCES

- 1 Chan C, Fryer J, Herkes G, Prelog K, Harrington T. Fatal brain stem event complicating acute pancreatitis. *J Clin Neurosci* 2003; **10**: 351-358
- 2 Ruggieri RM, Lupo I, Piccoli F. Pancreatic encephalopathy: a 7-year follow-up case report and review of the literature. *Neurol Sci* 2002; **23**: 203-205
- 3 Chen L, Zhang X. Pancreatic encephalopathy and Wernicke encephalopathy. *Zhonghua Neike Zazhi* 2002; **41**: 94-97
- 4 Ammori BJ. Role of the gut in the course of severe acute pancreatitis. *Pancreas* 2003; **26**: 122-129
- 5 Nam JH, Murthy S. Acute pancreatitis-the current status in management. *Expert Opin Pharmacother* 2003; **4**: 235-241

- 6 **Demols A**, Deviere J. New frontiers in the pharmacological prevention of post-ERCP pancreatitis: the cytokines. *JOP* 2003; **4**: 49-57
- 7 **Algul H**, Tando Y, Schneider G, Weidenbach H, Adler G, Schmid RM. Acute experimental pancreatitis and NF-kappaB/Rel activation. *Pancreatology* 2002; **2**: 503-509
- 8 **Noji T**, Karasawa A, Kusaka H. Pharmacological study on the effects of the adenosine uptake inhibitor KF24345 on inflammatory diseases. *Nippon Yakurigaku Zasshi* 2003; **122**: 121-134
- 9 **Park BK**, Chung JB, Lee JH, Suh JH, Park SW, Song SY, Kim H, Kim KH, Kang JK. Role of oxygen free radicals in patients with acute pancreatitis. *World J Gastroenterol* 2003; **9**: 2266-2269
- 10 **Dib M**, Zhao X, Wang X, Andersson E, Drewsen G, Andersson R. Acute phase response in acute pancreatitis: a comparison with abdominal sepsis. *Scand J Gastroenterol* 2003; **38**: 1072-1077
- 11 **Strate T**, Mann O, Kleinhans H, Schneider C, Knoefel WT, Yekebas E, Standl T, Bloechle C, Izbicki JR. Systemic intravenous infusion of bovine hemoglobin significantly reduces microcirculatory dysfunction in experimentally induced pancreatitis in the rat. *Ann Surg* 2003; **238**: 765-771
- 12 **Nakane A**, Sasaki S. Effect of cytokines on the expression of Shiga toxin toxicity. *Nippon Rinsho* 2002; **60**: 1089-1094
- 13 **Klar E**, Werner J. New pathophysiologic knowledge about acute pancreatitis. *Chirurg* 2000; **71**: 253-264
- 14 **Ogawa M**. Acute pancreatitis and cytokines: "second attack" by septic complication leads to organ failure. *Pancreas* 1998; **16**: 312-315
- 15 **Miller AP**, Chen YF, Xing D, Feng W, Oparil S. Hormone replacement therapy and inflammation: interactions in cardiovascular disease. *Hypertension* 2003; **42**: 657-663
- 16 **Herrera MT**, Toledo C, Valladares F, Muros M, Diaz-Flores L, Flores C, Villar J. Positive end-expiratory pressure modulates local and systemic inflammatory responses in a sepsis-induced lung injury model. *Intensive Care Med* 2003; **29**: 1345-1353
- 17 **Bhatia M**. Novel therapeutic targets for acute pancreatitis and associated multiple organ dysfunction syndrome. *Curr Drug Targets Inflamm Allergy* 2002; **1**: 343-351
- 18 **Fang BW**, Qiu Q, Wu XZ, Kong L, Qin MF, Zhou ZL, Cui NQ. Changes in pro-inflammatory cytokines and media and peptide hormones during multiple organ dysfunction syndrome following acute abdominal diseases. *Zhongguo Weizhongbing Jijiu Yixue* 2003; **15**: 19-22
- 19 **Austrums E**, Pupelis G, Snippe K. Postoperative enteral stimulation by gut feeding improves outcomes in severe acute pancreatitis. *Nutrition* 2003; **19**: 487-491
- 20 **Isenmann R**, Rau B, Zoellner U, Beger HG. Management of patients with extended pancreatic necrosis. *Pancreatology* 2001; **1**: 63-68
- 21 **Buter A**, Imrie CW, Carter CR, Evans S, McKay CJ. Dynamic nature of early organ dysfunction determines outcome in acute pancreatitis. *Br J Surg* 2002; **89**: 298-302
- 22 **Zhang Q**, Ni Q, Cai D, Zhang Y, Zhang N, Hou L. Mechanisms of multiple organ damages in acute necrotizing pancreatitis. *Chin Med J* 2001; **114**: 738-742
- 23 **Gloor B**, Uhl W, Tcholakov O, Roggo A, Muller CA, Worni M, Buchler MW. Hydrocortisone treatment of early SIRS in acute experimental pancreatitis. *Dig Dis Sci* 2001; **46**: 2154-2161
- 24 **Desiateryk VI**, Kryvyts'kyi IuM, Shapovaliuk VV. Inflammation response syndrome, sepsis and multi-organ insufficiency in patients operated for destructive pancreatitis. *Klin Khir* 2001; **4**: 24-26
- 25 **Makhija R**, Kingsnorth AN. Cytokine storm in acute pancreatitis. *J Hepatobiliary Pancreat Surg* 2002; **9**: 401-410
- 26 **Bhatia M**, Brady M, Shokuhi S, Christmas S, Neoptolemos JP, Slavin J. Inflammatory mediators in acute pancreatitis. *J Pathol* 2000; **190**: 117-125
- 27 **Holtmann MH**, Schutz M, Galle PR, Neurath MF. Functional relevance of soluble TNF-alpha, transmembrane TNF-alpha and TNF-signal transduction in gastrointestinal diseases with special reference to inflammatory bowel diseases. *Z Gastroenterol* 2002; **40**: 587-600
- 28 **Farrow B**, Evers BM. Inflammation and the development of pancreatic cancer. *Surg Oncol* 2002; **10**: 153-169
- 29 **Bhatia M**, Neoptolemos JP, Slavin J. Inflammatory mediators as therapeutic targets in acute pancreatitis. *Curr Opin Investig Drugs* 2001; **2**: 496-501
- 30 **Reinheckel T**, Deussing J, Roth W, Peters C. Towards specific functions of lysosomal cysteine peptidases: phenotypes of mice deficient for cathepsin B or cathepsin L. *Biol Chem* 2001; **382**: 735-741
- 31 **Yamauchi J**, Shibuya K, Sunamura M, Arai K, Shimamura H, Motoi F, Takeda K, Matsuno S. Cytokine modulation in acute pancreatitis. *J Hepatobiliary Pancreat Surg* 2001; **8**: 195-203
- 32 **Brady M**, Christmas S, Sutton R, Neoptolemos J, Slavin J. Cytokines and acute pancreatitis. *Baillieres Best Pract Res Clin Gastroenterol* 1999; **13**: 265-289
- 33 **Markert R**, Modzelewski B. Inflammatory mediators in the acute pancreatitis. *Pol Merkuriusz Lek* 1999; **6**: 100-103
- 34 **Zang GQ**, Zhou XQ, Yu H, Xie Q, Zhao GM, Wang B, Guo Q, Xiang YQ, Liao D. Effect of hepatocyte apoptosis induced by TNF-alpha on acute severe hepatitis in mouse models. *World J Gastroenterol* 2000; **6**: 688-692
- 35 **Silveira RC**, Procianoy RS. Interleukin-6 and tumor necrosis factor-alpha levels in plasma and cerebrospinal fluid of term newborn infants with hypoxic-ischemic encephalopathy. *J Pediatr* 2003; **143**: 625-629
- 36 **Gimenez F**, Barraud de Lagerie S, Fernandez C, Pino P, Mazier D. Tumor necrosis factor alpha in the pathogenesis of cerebral malaria. *Cell Mol Life Sci* 2003; **60**: 1623-1635
- 37 **Kawada J**, Kimura H, Ito Y, Hara S, Iriyama M, Yoshikawa T, Morishima T. Systemic cytokine responses in patients with influenza-associated encephalopathy. *J Infect Dis* 2003; **188**: 690-698
- 38 **Miura Y**, Koyanagi Y, Mizusawa H. TNF-related apoptosis-inducing ligand (TRAIL) induces neuronal apoptosis in HIV-encephalopathy. *J Med Dent Sci* 2003; **50**: 17-25
- 39 **Ichiyama T**, Isumi H, Ozawa H, Matsubara T, Morishima T, Furukawa S. Cerebrospinal fluid and serum levels of cytokines and soluble tumor necrosis factor receptor in influenza virus-associated encephalopathy. *Scand J Infect Dis* 2003; **35**: 59-61
- 40 **Okamoto M**, Ono M, Baba M. Suppression of cytokine production and neural cell death by the anti-inflammatory alkaloid cepharanthine: a potential agent against HIV-1 encephalopathy. *Biochem Pharmacol* 2001; **62**: 747-753

Effects of narcotic analgesic drugs on human Oddi's sphincter motility

Shuo-Dong Wu, Zhen-Hai Zhang, Jun-Zhe Jin, Jing Kong, Wei Wang, Qiang Zhang, Dong-Yan Li, Min-Fei Wang

Shuo-Dong Wu, Zhen-Hai Zhang, Jun-Zhe Jin, Jing Kong, Wei Wang, Qiang Zhang, Dong-Yan Li, Min-Fei Wang, Department of Hepatobiliary Surgery, the Second Affiliated Hospital, China Medical University, Shenyang 110004, Liaoning Province, China

Correspondence to: Dr. Shuo-Dong Wu, Department of Hepatobiliary Surgery, the Second Affiliated Hospital, China Medical University, Shenyang 110004, Liaoning Province, China

Telephone: +86-24-83955062

Received: 2004-02-11 **Accepted:** 2004-02-26

Abstract

AIM: To assess the effects of intramuscular analgesics (morphine, Ap-237, pethidine and tramadol) on human Oddi's sphincter motility with choledochoscope manometry.

METHODS: A total of 70 patients having T tubes after cholecystectomy and choledochotomy were assessed by choledochoscope manometry. They were randomly divided into morphine group, Ap-237 group, pethidine group and tramadol group. Basal pressure of Oddi's sphincter (BPOS), amplitude of phasic contractions (SOCA), frequency of phasic contractions (SOF), duration of phasic contractions (SOD), duodenal pressure (DP) and common bile duct pressure (CBDP) were scored and analyzed. All narcotic analgesic drugs were administered intramuscularly.

RESULTS: Levels of BPOS, SOCA and SOF were increased after injection of morphine and Ap-237 ($P < 0.05$), level of CBDP was increased from 4.97 ± 3.87 mmHg to 8.62 ± 7.43 mmHg (10 min later) and 7.32 ± 5.95 mmHg (20 min later) after injection of morphine ($P < 0.01$). No apparent change occurred after intramuscular injection of pethidine. Level of BPOS was increased from 7.01 ± 5.50 mmHg to 2.87 ± 2.78 mmHg 10 min after injection of tramadol and SOCA was decreased from 63.34 ± 35.29 mmHg to 45.90 ± 27.86 mmHg (10 min later, $P < 0.05$) and 35.97 ± 24.30 (20 min later, $P < 0.01$) after administration of tramadol.

CONCLUSION: All these findings indicate that Oddi's sphincter manometry via choledochoscope is a practical and new way to study the dynamics of Oddi's sphincter. The regular dose of morphine and Ap-237 could increase BPOS, SOF and SOCA. Morphine could increase the level of CBDP, demonstrating an excitatory effect on the sphincter of Oddi. Pethidine had no effect on Oddi's sphincter motility. Tramadol shows an inhibitory effect on the motility of the sphincter of Oddi and decreases levels of BPOS and SOCA.

Wu SD, Zhang ZH, Jin JZ, Kong J, Wang W, Zhang Q, Li DY, Wang MF. Effects of narcotic analgesic drugs on human Oddi's sphincter motility. *World J Gastroenterol* 2004; 10(19): 2901-2904

<http://www.wjgnet.com/1007-9327/10/2901.asp>

INTRODUCTION

Morphine can cause excitatory effect on Oddi's sphincter motility and therefore induces upper abdominal pain with

characteristics of biliary colic in some patients. Morphine could increase intrabiliary duct pressure^[1-3], and delay bile flow to the duodenum^[4], for this reason, other opioid analgesics rather than morphine are recommended clinically to relieve the pain, especially biliary pain. It is believed that pethidine has less effect on the sphincter than morphine and therefore is usually the drug of choice for pain relief in acute pancreatitis. Pethidine is also commonly used during endoscopic retrograde cholangiopancreatography (ERCP). Because of potential interference, all narcotic analgesic drugs, including pethidine, are proscribed during Oddi's sphincter manometry (OSM). However, the performance of OSM with only diazepam sedation was difficult as pethidine markedly improves ERCP tolerance.

The aim of this study was to evaluate the effects of four analgesic drugs on human Oddi's sphincter motility by choledochoscope manometry, and to understand the different clinical responses to analgesics.

MATERIALS AND METHODS

Patients

OSM was performed for 70 patients (25 men, 45 women, and mean age 55.5 years, range 35-77 years) with PENTAX choledochoscope at the Second Affiliated Hospital of China Medical University between November 2001 and December 2003. All patients underwent cholecystectomy and choledochotomy, at least 1.5 mo (mean 2.5 mo) after T tube drainage. The patients were fasted overnight before manometry.

Methods

A triple lumen polyethylene manometry catheter 200 cm in length with an outer diameter of 1.7 mm was used for manometry. The three side holes in the distal end were located 2 mm apart. Sterile water was infused through the catheter at a flow rate of 0.5 mL/min by a hydraulic capillary infusion system. PC polygraph HR (Swedish CTD-Synetics medical company) and relevant program were used to record and analyze the tracings. Manometry was performed after all the stones were removed from the common bile duct. The catheter was introduced via the side-pore of choledochoscope into duodenum directly, when the pressure was stable, duodenal pressure-curve was recorded. It was then withdrawn in a stepwise fashion, the position of catheter in the sphincter could be confirmed by direct observation through choledochoscope or by the characteristic pressure changes on the screen. The Oddi's sphincter and common bile duct motility tracings were recorded respectively. Drugs were administered intramuscularly at 10 min intervals.

Patients were randomly administered one of the four different drugs. Morphine was administered in a dose of 0.1 mg/kg after the first measurement, the second and third manometries were performed respectively 10 min and 20 min later. Each of the other three analgesics was administered in a dose of 1 mg/kg. The procedures were same as in morphine group.

Basal pressure of Oddi's sphincter (BPOS), amplitude of phasic contractions (SOCA), frequency of phasic contractions (SOF), duration of phasic contractions (SOD), duodenal pressure (DP) and common bile duct pressure (CBDP) were recorded and analyzed with a special computer program. Statistical analysis was carried out using the Student's *t*-test.

Data were expressed as mean±SD. A single-tailed *P* value <0.05 was considered statistically significant.

RESULTS

Seventy patients with T-tubes had no evidence of ampullary abnormality underwent OSM. Clear tracings of pressure and phasic contractions were acquired. Data were compared.

Effect of morphine on Oddi's sphincter motility

Morphine at the dose of 0.1 mg/kg produced an immediate and marked stimulatory effect on the sphincter of Oddi and bile duct, which was obvious 10 min after injection. Levels of BPOS, SOCA, SOF and CBDP were all significantly increased (*P*<0.01) and the effect persisted for 20 min (Table 1). Ten patients (25%) had an increased BPOS between 30-40 mmHg, four patients had an increased BPOS over 40 mmHg after drug administration.

Effect of pethidine on Oddi's sphincter motility

No statistical difference before and after administration of pethidine (1 mg/kg). Pethidine showed no apparent effect on

Oddi's sphincter motility (Table 2).

Effect of Ap-237 on Oddi's sphincter motility

Marked increased levels of BPOS, SOCA and SOF were observed 10 min after injection of Ap-237, and high levels of BPOS and SOF persisted for 20 min, which showed an excitatory effect on Oddi's sphincter motility (Table 3).

Effect of tramadol on Oddi's sphincter motility

Levels of BPOS and SOCA were obviously reduced 10 min after administration of tramadol, which maintained at low levels for 20 min and showed an inhibitory effect of tramadol on Oddi's sphincter motility. (Table 4)

DISCUSSION

The most important development in our understanding of Oddi's sphincter motility came with the advent of Oddi's sphincter manometry (OSM) in the mid-1970s. Then, it was considered as the gold standard method for evaluating the function of Oddi's sphincter. OSM could be directly performed during surgery, or

Table 1 Manometric data before and after administration of morphine in 40 patients (mean±SD)

	Before morphine administration (n = 40)	10 min after morphine administration (n = 40)	20 min after morphine administration (n = 10)
Oddi's sphincter basal pressure (mmHg)	8.90±9.11	22.23±16.04 ^b	20.51±13.46 ^b
Amplitude of phasic contractions (mmHg)	50.85±36.66	104.97±49.15 ^d	89.04±62.37 ^d
Frequency of phasic contractions (n/min)	7.22±2.89	9.29±1.93 ^f	8.85±2.42 ^f
Common bile duct pressure (mmHg)	4.97±3.87	8.62±7.43 ^h	7.32±5.95 ^h

^b*P*, ^d*P*, ^f*P*, ^h*P*<0.01 vs themselves, n represents the number of patients involved in the research.

Table 2 Manometric data before and after administration of pethidine in 10 patients (mean±SD)

	Before pethidine administration (n = 10)	10 min after pethidine administration (n = 10)	19 min after pethidine administration 20 (n = 10)
Oddi's sphincter basal pressure (mmHg)	7.06±5.07	11.24±6.11	6.68±4.32
Amplitude of phasic contractions (mmHg)	78.52±40.23	95.65±45.49	70.35±31.67
Frequency of phasic contractions (n/min)	7.31±1.95	6.49±2.81	7.92±2.07
Common bile duct pressure (mmHg)	4.23±2.83	4.70±3.87	3.91±3.36

n represents the number of patients involved in the research.

Table 3 Manometric data before and after administration of Ap-237 in 10 patients (mean±SD)

	Before Ap-237 administration (n = 10)	10 min after Ap-237 administration (n = 10)	20 min after Ap-237 administration (n = 10)
Sphincter of Oddi basal pressure (mmHg)	6.42±5.10	11.33±9.39 ^a	11.34±8.40 ^a
Amplitude of phasic contractions (mmHg)	52.56±30.99	87.03±51.72 ^c	50.06±29.11
Frequency of phasic contractions (n/min)	5.62±1.34	7.72±2.16 ^e	9.28±3.98 ^f
Common bile duct pressure (mmHg)	4.20±3.97	4.82±2.30	3.25±2.30

^a*P*, ^c*P*, ^e*P*<0.05, ^f*P*<0.01 vs themselves, n represents the number of patients involved in the research.

Table 4 Manometric data before and after administration of tramadol in 10 patients (mean±SD)

	Before tramadol administration (n = 10)	10 min after tramadol administration (n = 10)	20 min after tramadol administration (n = 10)
Sphincter of Oddi basal pressure (mmHg)	7.01±5.50	2.87±2.78 ^a	6.39±5.37
Amplitude of phasic contractions (mmHg)	63.34±35.29	45.90±27.86 ^c	35.97±24.30 ^d
Frequency of phasic contractions (n/min)	7.24±2.52	8.14±2.54	7.07±3.70
Common bile duct pressure (mmHg)	4.41±2.65	3.97±4.69	4.96±2.82

^a*P*, ^c*P*<0.05, ^d*P*<0.01 vs themselves, n represents the number of patients involved in the research.

indirectly during ERCP, via a T-tube or percutaneously. A basal pressure and phasic contractions of Oddi's sphincter could be obtained with OSM.

OSM during ERCP is a useful tool in the evaluation of patients with unexplained pancreaticobiliary pain or recurrent idiopathic pancreatitis^[5-7]. However, it might provoke serious pancreatitis^[8,9]. It is a technical procedure, because it requires selective deep bile duct and/or pancreatic duct cannulation during active duodenal peristalsis and in suboptimally anesthetized patients. These features account for the relatively high failure rate (up to 20%) even in expert hands^[10].

OSM *via* choledochoscopic approach allows easy and accurate recording of Oddi's sphincter pressure and makes a long time maneuver of manometry possible. The position of manometric catheter in the sphincter can be monitored on the screen with the characteristic phasic contractions. It also could be confirmed by direct observation through choledochofiberoscopy. And it is easy to get enough patients for manometry. However, it is difficult to get a relative normal value of the sphincter of Oddi *via* choledochoscope manometry, for patients with a T-tube tract often suffer from hepatobiliary or pancreatic diseases. Furthermore, whether irrigation of natural cold saline and the semi-closed state of bile duct during choledochoscopic procedure affect the motility of the sphincter of Oddi is unknown.

Morphine and pethidine are the two most commonly used analgesic drugs. Their effects on the sphincter of Oddi have well been researched. Helm *et al.*^[11] studied the effect of morphine on SO using OSM during ERCP. In a small cumulative dose of 2.5-5 µg/kg, morphine increased the frequency of phasic contractions to a maximum of 10-12/min, but it did not affect the mean amplitude of phasic contractions and the mean SO basal pressure. As the cumulative dose was increased from 10 to 20 µg/kg, no further increase in the frequency of phasic pressure waves was seen. Instead, the phasic wave amplitude and the mean SO basal pressure increased. Blaut *et al.*^[12] found that morphine increased the intraductal biliary pressure (IDP) with OSM *via* a T-tube, but the high intraductal biliary pressure caused by morphine could be counteracted by transcutaneous electrical nerve stimulation (TENS). Elta *et al.*^[13] performed ERCP manometry to evaluate the effect of pethidine at therapeutic doses on SO manometry, and found that after administration of pethidine the frequency of phasic contractions increased, but the mean SO basal pressure did not change. Using the same method, Sherman *et al.*^[14] found that biliary sphincter basal pressure and phasic wave amplitude were not significantly altered by pethidine, but phasic frequency increased and phasic duration decreased slightly after administration of pethidine, sphincter basal pressure of the pancreatic and the common channel's sphincters was not significantly altered, but their phasic wave amplitude decreased, phasic frequency increased, and phasic duration decreased.

The only study directly comparing morphine to pethidine with OSM was done in 1990 by Thune *et al.*^[15] They compared the effect of morphine and pethidine on patients intraoperatively after surgical placement of a catheter across the SO. Morphine was associated with an increase in phasic wave frequency, but no change was found in basal sphincter pressure, amplitude, or wave propagation direction. Pethidine showed a dose-dependent decrease in phasic wave frequency but without significant changes in the basal sphincter pressure, contraction amplitude or wave propagation direction.

We found that morphine could increase the basal pressure of Oddi's sphincter, common bile duct pressure, frequency and amplitude of phasic contractions. Morphine showed an excitatory effect on the sphincter of Oddi, and might be a cause of Oddi's sphincter dysfunction(SOD). SO may function as a peristaltic pump to actively expel fluid from the sphincter segment into the duodenum. The SO segment fills with fluid from the

common bile duct (CBD) only during the diastolic interval between phasic contractions. Outflow of fluid from the CBD is reduced or arrested when (1) the frequency of phasic contractions increases sufficiently to compromise diastolic filling of the sphincter segment, (2) phasic contractions propagate retrograde or occur simultaneously along the sphincter segment, or (3) passive filling of the sphincter segment is prevented by a BPOS that exceeds the CBDP. Morphine could cause functional obstruction of the SO by all three of these mechanisms^[11]. OSM shows a diagnostic value for Oddi's sphincter dysfunction. Elevated basal pressure (>40 mmHg) was the most important manometric finding in Oddi's sphincter dysfunction and its borderline was about 30-40 mmHg. Our study found that 10 patients (25%) had an increased BPOS between 30-40 mmHg, four patients had an increased BPOS over 40 mmHg. So morphine can cause spasm of SO and should not be used during ERCP manometry or choledochoscope examination. After administration of pethidine, no patients had an elevated BPOS up to 30 mmHg. Pethidine could be used for an additional analgesia during OSM. This may improve both patient's tolerance and the success rate of the procedure. But we should be cautious in patients with renal failure, hepatic failure or central nervous system diseases. For the pethidine metabolite, normeperidine, might invoke seizures at high doses or in patients with renal failure. Hubbard^[16] reports that pethidine invoked seizures in a patient with Oddi's sphincter dysfunction.

Tramadol has the same analgesic effect as morphine. But it has little effect on the respiratory system and circulation system, and can be used in old patients with respiratory system diseases. There were only a few researches about its effect on the sphincter of Oddi. Staritz *et al.*^[17] and Brandstatter *et al.*^[18] performed ERCP manometry to evaluate the effect of tramadol on SO manometry, and found that it had no apparent effect on Oddi's sphincter motility. Our study indicated that tramadol could decrease BPOS and the amplitude of phasic contractions, showing an inhibitory effect on the sphincter of Oddi, and tramadol could be used during ERCP manometry and choledochoscope examination.

As a fast acting analgesic, Ap-237 has little effect on visceral pain. A MEDLINE search found no report about its effect on the sphincter of Oddi. We found that Ap-237 could increase BPOS, amplitude and frequency of phasic contractions, showing an excitatory effect on the sphincter of Oddi, and Ap-237 should not be used in patients with hepatobiliary and pancreatic diseases.

REFERENCES

- 1 Sarles JC, Midejean A, Devaux MA. Electromyography of the sphincter of Oddi. Technic and experimental results in the rabbit: Effect of certain drugs. *Am J Gastroenterol* 1975; **63**: 221-231
- 2 Dedrick DF, Tanner WW, Bushkin FL. Common bile duct pressure during enflurane anesthesia. Effects of morphine and subsequent naloxone. *Arch Surg* 1980; **115**: 820-822
- 3 Radnay PA, Duncalf D, Novakovic M, Lesser ML. Common bile duct pressure changes after fentanyl, morphine, meperidine, butorphanol, and naloxone. *Anesth Analg* 1984; **63**: 441-444
- 4 Joehl RJ, Koch KL, Nahrwold DL. Opioid drugs cause bile duct obstruction during hepatobiliary scans. *Am J Surg* 1984; **147**: 134-138
- 5 Coyle WJ, Pineau BC, Tarnasky PR, Knapple WL, Aabakken L, Hoffman BJ, Cunningham JT, Hawes RH, Cotton PB. Evaluation of unexplained acute and acute recurrent pancreatitis using endoscopic retrograde cholangiopancreatography, sphincter of Oddi manometry and endoscopic ultrasound. *Endoscopy* 2002; **34**: 617-623
- 6 Lehman GA. Acute recurrent pancreatitis. *Can J Gastroenterol* 2003; **17**: 381-383
- 7 Mariani A, Curioni S, Zanello A, Passaretti S, Masci E, Rossi M, Del Maschio A, Testoni PA. Secretin MRCP and endoscopic

- pancreatic manometry in the evaluation of sphincter of Oddi function: a comparative pilot study in patients with idiopathic recurrent pancreatitis. *Gastrointest Endosc* 2003; **58**: 847-852
- 8 **Rolny P**, Anderberg B, Ihse I, Lindstrom E, Olaison G, Arvill A. Pancreatitis after sphincter of Oddi manometry. *Gut* 1990; **31**: 821-824
- 9 **Maldonado ME**, Brady PG, Mamel JJ, Robinson B. Incidence of pancreatitis in patients undergoing sphincter of Oddi manometry (SOM). *Am J Gastroenterol* 1999; **94**: 387-390
- 10 **Kowalski T**, Kanchana T, Pungpapong S. Perceptions of gastroenterology fellows regarding ERCP competency and training. *Gastrointest Endosc* 2003; **58**: 412-414
- 11 **Helm JF**, Venu RP, Geenen JE, Hogan WJ, Dodds WJ, Toouli J, Arndorfer RC. Effects of morphine on the human sphincter of Oddi. *Gut* 1988; **29**: 1402-1407
- 12 **Blaut U**, Marecik J, Hartwich A, Herman RM, Laskiewicz J, Thor PJ. The effect of transcutaneous nerve stimulation on intraductal biliary pressure in post-cholecystectomy patients with T-drainage. *Eur J Gastroenterol Hepatol* 2003; **15**: 21-26
- 13 **Elta GH**, Barnett JL. Meperidine need not be proscribed during sphincter of Oddi manometry. *Gastrointest Endosc* 1994; **40**: 7-9
- 14 **Sherman S**, Gottlieb K, Uzer MF, Smith MT, Khusro QE, Earle DT, Brunelle RL, Hawes RH, Lehman GA. Effects of meperidine on the pancreatic and biliary sphincter. *Gastrointest Endosc* 1996; **44**: 239-242
- 15 **Thune A**, Baker RA, Saccone GT, Owen H, Toouli J. Differing effects of pethidine and morphine on human sphincter of Oddi motility. *Br J Surg* 1990; **77**: 992-995
- 16 **Hubbard GP**, Wolfe KR. Meperidine misuse in a patient with sphincter of Oddi dysfunction. *Ann Pharmacother* 2003; **37**: 534-537
- 17 **Staritz M**, Poralla T, Manns M, Meyer Zum Buschenfelde KH. Effect of modern analgesic drugs (tramadol, pentazocine and buprenorphine) on the bile duct sphincter in man. *Gut* 1986; **27**: 567-569
- 18 **Brandstatter G**, Schinzel S, Wurzer H. Influence of spasmolytic analgesics on motility of sphincter of Oddi. *Dig Dis Sci* 1996; **41**: 1814-1818

Edited by Wang XL and Ren SY Proofread by Xu FM

Angiographic findings of gastrointestinal stromal tumor

Song-Hua Fang, Dan-Jun Dong, Shi-Zheng Zhang, Mei Jin

Song-Hua Fang, Dan-Jun Dong, Shi-Zheng Zhang, Department of Radiology, Sir Run Run Shaw Hospital, Zhejiang University, Hangzhou 310016, Zhejiang Province, China

Mei Jin, Department of Pathology, Sir Run Run Shaw Hospital, Zhejiang University, Hangzhou 310016, Zhejiang Province, China

Correspondence to: Song-Hua Fang, Department of Radiology, Sir Run Run Shaw Hospital, Zhejiang University, Hangzhou 310016, Zhejiang Province, China. fangsonghua@163.com

Telephone: +86-571-86090073 Ext. 4609

Received: 2004-02-06 **Accepted:** 2004-03-04

Abstract

AIM: To discuss the angiographic features of gastrointestinal stromal tumor (GIST) and to evaluate their diagnostic role.

METHODS: Twelve patients with pathologically proved GIST underwent angiography (DSA) 1 wk before operation, using Puck and digital subtraction DSA. The origin, size, morphology and angiographic appearance of the lesions were reviewed.

RESULTS: Two tumors arose from stomach, 8 from jejunum, and 2 from ileum. Seven cases were benign and 5 were malignant. Obviously thickened supplying arteries were detected in 8 tumors, and early-developed veins were found in 3. Two types of angiographic changes of GIST were observed. Four cases had twisted irregular neoplastic vessels with partially coarse and indistinct margins, which were all malignant. Eight cases had ball-like neoplastic vessels with uniform tumor staining, of which 7 were benign and 1 was malignant.

CONCLUSION: Angiography facilitates localization and diagnosis of GIST, helps define their size, range and location, and is especially valuable to patients suffering from melena with unknown reasons.

Fang SH, Dong DJ, Zhang SZ, Jin M. Angiographic findings of gastrointestinal stromal tumor. *World J Gastroenterol* 2004; 10(19): 2905-2907

<http://www.wjgnet.com/1007-9327/10/2905.asp>

INTRODUCTION

Gastrointestinal stromal tumor and its imaging features have been reported^[1-3]. However, to our knowledge, the appearance of GIST at angiography has been seldom discussed. We analyzed retrospectively the angiographic appearance of 12 cases of GIST, which was proved by surgical pathology (immunohistochemistry), and the diagnostic value of angiography was discussed.

MATERIALS AND METHODS

Subjects

Twelve patients (4 women and 8 men, aged 40-70 years with a mean age of 53.3 years) with pathologically proved GIST (immunohistochemistry) who underwent angiography 1 wk before surgery were included. All the patients suffered from

recurrent melena for 3 mo to 3 years, with syncope in 2 cases, a palpable abdominal mass in 1 case, and concomitant abdominal pain in another case.

After routine preparations, Seldinger's puncture of femoral artery and super selective catheterization, angiographies of superior mesenteric artery, inferior mesenteric artery and coeliac trunk were performed sequentially using 6-7 F catheters. Omnipaque (iodine content: 350 mg/mL) as contrast medium was administered with a dose of 30 mL and at a rate of 8 mL/s for superior mesenteric artery, 20 mL/s and 6 mL/s for inferior mesenteric artery, and 40 mL/s and 8 mL/s for coeliac trunk. Puck changer was used in all angiographies (with the sequence 2 films/s×3 s, 1 film/s×4 s, 1 film/2 s×4 s), and DSA was selected necessarily (with acquisition sequence 3.1 films/s×5 s, 1.6 films/s×5 s, 1 film/s×2 s). The dose and rate of contrast medium were same in two methods. The apparatus was GE medical systems, Hiline.

RESULTS

Size origin and morphology of the tumors

Two tumors arose from stomach, 8 from jejunum (Figures 1,2), and 2 from ileum. Most of them were originated from the jejunum with a percentage of 66.7% (8/12). The lesions had different sizes, ranged from 3 cm×3 cm×2 cm to 5 cm×6 cm×4 cm (mean 4 cm×4.5 cm×3 cm) in 7 benign lesions, of which 5 lesions were malignant (Figure 3). The smallest was 5.5 cm×4.5 cm×3 cm and the largest was 6.5 cm×10 cm×7 cm. All tumors were round or oval in shape, except an irregular malignant tumor and another dumbbell-shaped benign tumor growing endophytically and exophytically from the intestinal lumen at the same time.

Angiographic appearance

Thickened supplying arteries were observed in 8 tumors (Figure 1), of which 6 were benign and 2 were malignant. Early-developed veins were found in 3 cases (Figure 1), all of which were benign. Four cases having irregular twisted neoplastic vessels with different vessel size and partially coarse and obscure vessel margin were all malignant (Figure 3). Eight cases have ball-like neoplastic vessels with clear margins, included 7 benign and 1 malignant cases. However, the 7 benign cases all had predominantly homogeneous tumor staining with distinct margins (Figures 1, 2).

Boundary of tumors and relationship to surrounding structures

Four malignant tumors had an indistinct border, and the others had a clear margin. The surrounding organs were pushed by the tumors. Intestinal intussusception was found in 1 patient with recurrent abdominal pain.

Pathology

The neoplastic cells were fusiform or polygon in shape, and arranged in interlacing or swirl or fence-like. LSAB label was used in immunohistochemistry. Leiomyomas or leiomyosarcomas of other organs (uterus and soft tissue) and schwannomas of soft tissue were chosen for comparisons. High positive presentation of Vim, CD₁₁₇ and CD₃₄ was found in 12 cases of GIST. Negative presentation of CD₃₄ was found in leiomyomas or leiomyosarcomas, and positive S-100 and negative CD₃₄ were found in schwannomas.



Figure 1 Benign stromal tumor in a 54-year-old male.

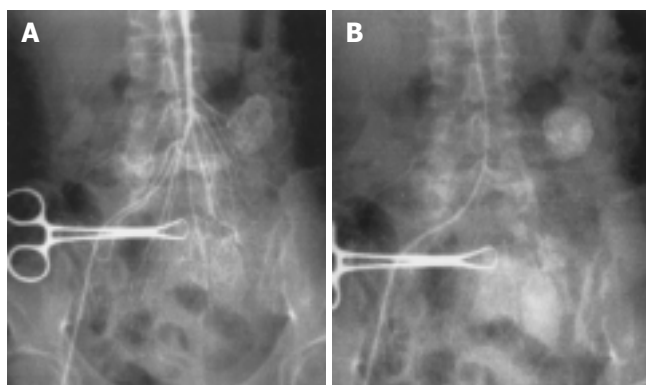


Figure 2 Benign stromal tumor and marked homogeneous tumor-staining in a 41-year-old male. A: Benign stromal tumor; B: Marked homogeneous tumor staining.

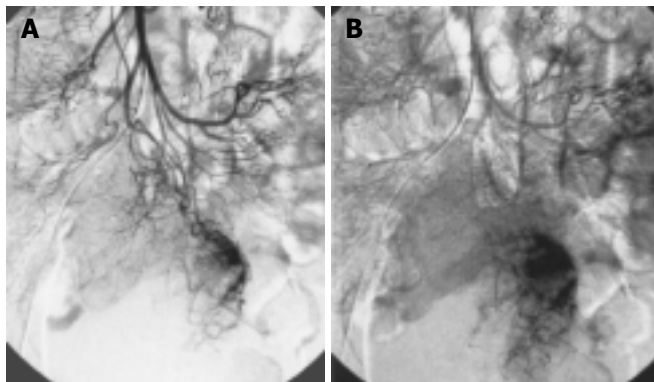


Figure 3 Malignant stromal tumor and heterogeneous tumor staining in a 35-year-old female. A: Malignant stromal tumor; B: Heterogeneous tumor staining with irregular morphology.

Others

Five malignant tumors contained necrotic or cystic changes with different degrees and two possessed central hemorrhage. Six patients in this study underwent CT at the same time. Masses were revealed by CT in 4 cases, only intestinal intussusception was seen in 1 patient, and diagnosis could not be established with confidence in the other case because of the relatively small size. Of the 3 patients who underwent barium examinations, one was normal, one had an intestinal filling defect and another had his intestines pushed away. No metastasis was found before surgery and no lymphadenopathy was demonstrated during operation.

DISCUSSION

GIST included the majority of primary non-epithelial tumors of gastrointestinal (GI) tract. These tumors were originated from

cells located in the wall of the organ and showed a remarkable variability in their differentiation pathways. They can be divided into 4 major categories on the basis of their phenotypical features: tumors showing differentiation toward smooth muscle, tumors showing apparent differentiation toward neural elements, tumors showing dual differentiation toward smooth muscle and neural elements, tumors lacking differentiation toward either cell type even after exhaustive immunohistochemical and ultrastructural probing^[4,5]. However, with the development in immunohistochemistry and ultrastructural probing, it has been agreed generally that GIST is an independent kind of tumors originated from primitive mesenchymal cells of GI tract with non-directive differentiation, some of which have incomplete differentiation parts of smooth muscles and/or nerve sheath cells^[1,6-8]. Micro superstructures of these tumors are similar to those of primitive mesenchymal cells without any characteristics of differentiated cellularity. Vim, CD₁₁₇ and CD₃₄ are highly presented in immunohistochemistry. The standards were all compliant in this study.

GIST could be localized in any portion of the GI tract, but was most often found in the gastric part^[9,10]. The jejunum as the most frequent place (66.7%) in this group did not reflect the fact, because it is not necessary for gastric lesion to do angiography when endoscopy, endoluminal ultrasonography or barium study was available and effective.

CT and MR imaging features have been reported previously^[1-3,10]. To our knowledge, however, few articles included a description of the appearance of GIST on angiography. According to our study, two types of angiographic changes could be concluded. First, abnormally distributed twisted neoplastic vessels with different thickness and obscure margin were one of the malignant features, and heterogeneous tumor blush with ill-defined border in capillary phase was another. Second ball like vessels with a clear margin, well defined homogeneous tumor staining in round or oval shape, and early-developed veins, suggested a benign GIST. The differentiation points have been described in many previous documents already, including that the malignant tumor was characterized by a larger size more than 5 cm, necrosis, hemorrhage, an indistinct border, and adherence to or direct invasion of the structures nearby^[5,11]. The tumors in our group with first type of manifestations were all malignant, but they were found in a relatively small number of patients.

There are many diagnostic approaches for GIST, including barium meal, double-contrast barium study, ultrasonography, fibro-endoscopy, endoluminal ultrasonography, CT, MR imaging and angiography. The sensitivity of these procedures varied according to the different sites of lesions. CT has been considered as the most effective method^[1,9]. Therefore, angiography is used less and less in diagnosing tumors of GI, as a result, angiography is only recommended for patients with melena when no abdominal mass is palpable and the examination of upper GI is negative. It helps indicate the supplying arteries, differentiate benign from malignant tumors, and define their size, range and origin, despite the tumors grow exophytically or endophytically. On the other hand, we do not suggest routine use of this procedure because of its traumatic property, high risk and relative complicated technique.

REFERENCES

- 1 **Belloni M**, De Fiori E, Mazzarol G, Curti A, Crosta C. Endoscopic ultrasound and computed tomography in gastric stromal tumours. *Radiol Med* 2002; **103**: 65-73
- 2 **Pisanu A**, Ambu R, Uccheddu A. Uncommitted gastrointestinal stromal tumour. Case report. *G Chir* 2001; **22**: 217-221
- 3 **Kitabayashi K**, Seki T, Kishimoto K, Saitoh H, Ueno K, Kita I, Takashimas, Kurose N, Nojima T. A spontaneously ruptured

- gastric stromal tumor presenting as generalized peritonitis: report of a case. *Surg Today* 2001; **31**: 350-354
- 4 **LaRock RG**, Ginn PE. Immunohistochemical staining characteristics of canine gastrointestinal stromal tumors. *Vet Pathol* 1997; **34**: 303-311
 - 5 **Rosai J**. Gastrointestinal tract. In: Rosai J, ed. Ackerman's surgical pathology. 8th ed. *Mosby-year Book Inc U S A* 1996: 645-648
 - 6 **Tworek JA**, Appelman HD, Singleton TP, Greenson JK. Stromal tumors of the jejunum and ileum. *Mod Pathol* 1997; **10**: 200-209
 - 7 **Spivach A**, Zanconati F, Bonifacio Gori D, Pellegrino M, Sinconi A. Stromal tumors of the small intestine (GIST). Prognostic differences based on clinical, morphological and immunophenotypic features. *Minerva Chir* 1999; **54**: 717-724
 - 8 **Mignon F**, Julie C, Izzillo R, Luciani A, Guichoux F, Mesurolle B, El Hajam M, Qanadli SD, Chagnon S, Lacombe P. Imaging features of gastric stromal tumors: radiologic-pathologic correlation. Report of 4 cases. *J Radiol* 2000; **81**: 874-881
 - 9 **Wiener Y**, Gold R, Zehavy S, Sandbank J, Halevy A. Primary gastrointestinal stromal tumors. *Harefuah* 2001; **14**: 377-380
 - 10 **Hasegawa S**, Semelka RC, Noone TC, Woosley JT, Marcos HB, Kenney PJ, Siegelman ES. Gastric stromal sarcomas: correlation of MR imaging and histopathologic findings in nine patients. *Radiology* 1998; **208**: 591-595
 - 11 **Lin SC**, Huang MJ, Zeng CY, Wang TI, Liu ZL, Shiay RK. Clinical manifestations and prognostic factors in patients with gastrointestinal stromal tumors. *World J Gastroenterol* 2003; **9**: 2809-2812

Edited by Wang XL and Chen WW Proofread by Xu FM

Expression of growth hormone and its receptor in chronic atrophic gastritis and its clinical significance

Jian-Min Si, Qian Cao, Min Gao

Jian-Min Si, Qian Cao, Min Gao. Gastroenterology Laboratory, Institute of Clinical Medicine, Sir Run Run Shaw hospital, School of Medicine, Zhejiang University, Hangzhou 310016, Zhejiang Province, China

Correspondence to: Dr. Qian Cao, Department of Gastroenterology of Sir Run Run Shaw Hospital, Zhejiang University, School of Medicine, Hangzhou 310016, Zhejiang Province, China. wjgd@public.bta.net.cn

Telephone: +86-571-86090073-4503 **Fax:** +86-571-86044718

Received: 2002-11-30 **Accepted:** 2003-03-16

Abstract

AIM: To investigate the growth hormone (GH) and growth hormone receptor (GHR) expression of and its clinical significance in patients with chronic atrophic gastritis (CAG).

METHODS: A total of 90 cases were enrolled in the study. Thirty were healthy controls, the other 60 patients were divided into two groups according to the endoscopic and histological diagnosis. Blood samples were drawn in the morning (menarche did not occur during the blood extraction in female patients), gastric mucosa was obtained by endoscopy. Serum GH and gastric mucosal GHR levels were measured using radioimmunoassay (RIA) and En Vision technique.

RESULTS: The average GH level was 1.021 ± 0.132 $\mu\text{g/L}$ in CAG patients, in controls it was 2.869 ± 0.512 $\mu\text{g/L}$. There was a significant difference between these two groups ($P < 0.01$). The positive rate of GHR in CAG patients was 10%, in controls the rate was 100%. There was a significant difference ($P < 0.01$). There was no significant change of GH level (3.176 ± 0.421 $\mu\text{g/L}$) in patients with gastric carcinoma compared with controls ($P > 0.05$).

CONCLUSION: The study shows that levels of GH and GHR expression are low in CAG patients. CAG pathogenesis has a correlation with mucosal nutrient deficiency, decreased levels of GH and GHR have an adverse effect on the repair and regeneration of CAG. There is no significant change of GH in gastric carcinoma patients, GH does not play a role in the pathogenesis of gastric cancer.

Si JM, Cao Q, Gao M. Expression of growth hormone and its receptor in chronic atrophic gastritis and its clinical significance. *World J Gastroenterol* 2004; 10(19): 2908-2910
<http://www.wjgnet.com/1007-9327/10/2908.asp>

INTRODUCTION

Growth factor family is a group of protein hormones discovered during the 20th century. This family includes growth hormone (GH), insulin-like growth factor (IGF), epidermal growth factor (EGF), transfer growth factor (TGF), and vascular endothelial growth factor (VEGF), etc. These factors can stimulate cell DNA, RNA and protein synthesis, control cell growth and differentiation,

and promote regeneration of injured epithelia^[1-7]. Studies in recent years have shown that there is an intimate relationship between growth factor and gastric mucosal disease^[6]. Growth hormone (GH) is a type of mono-peptide strain hormone released from anterior pituitary eosinophilic cells. In the gastrointestinal (GI) tract, GH is known to promote water and electrolyte transport and calcium absorption. The proliferative functions of GH have been reported as well. Administration of GH restores the intestinal and gastric mucosal weight after hypophysectomy in rats, it is regarded as an important nutrient factor^[8].

Chronic atrophic gastritis (CAG) is a gastric precancerous lesion and has a high morbidity in China^[9]. Gastric mucosal malnutrition is considered as an important factor in the pathogenesis of CAG^[10-13].

Since CAG was recognized as a precancerous condition of the stomach by the World Health Organization in the early 1980 s, a number of methods have been tested for their ability to reverse and prevent the development of cancer. Most gastric mucosa protectors promote the growth and repair of gastric mucosa by promoting the aggregation and secretion of growth factors such as EGF, TGF. In a previous animal study, GH/GHR expression was measured on atrophic gastritis rats. The levels of GH and GHR expression in rats with CAG were low^[14]. However, the effect and safety of GH in clinical use are uncertain in CAG. The purpose of the present study was to investigate the expression of GH/GHR in patients with CAG and gastric cancers.

MATERIALS AND METHODS

Research subjects

Ethical approval for this study was given by the Sir Run Run Shaw Hospital in May 1999. Clinical data were obtained by review of case records for all patients. Patients were selected at random from adult out-patients attending the gastroenterology clinics. Diagnosis was made on the basis of clinical, endoscopic and histological data according to standard criteria. We excluded the patients who had abnormal findings in other vital organs (such as the heart, liver, lung, pancreas and pituitary). Patients were divided in two groups. Thirty patients in group B were diagnosed as moderate-severe gastritis and 30 patients in group C were diagnosed as gastric cancer, 30 unrelated individuals served as controls. Characteristics of the research subjects are shown in Table 1.

Sample collection and processing

After an overnight fast, 3 mL of blood was taken from cubital vein. Blood samples were set for two hours, then centrifuged at 3 500 rpm for 15 min. Supernatant was saved and stored at -20 °C. Two samples were taken from gastric antrum tissue and two from gastric body tissue, or four from the primary focus, and immediately immersed in 10% buffered formalin and embedded in paraffin wax using standard techniques. Five μm thick sections were cut and stained with hematoxylin and eosin for histopathological analysis. Each slide was assessed.

Analytical methods

The level of serum GH was measured by radioimmunoassay

(RIA) (Reagents were from DPC Company in Tianjing). The detection of gastric mucosal GHR expression was carried out by immunohistochemistry and En Vision assay (reagents from Biogenesis Company).

Table 1 Base-line characteristics of the patients

Characteristic	Group A (n = 30)	Group B (n = 30)	Group C (n = 30)
Age (yr)	48±7	50±6	52±9
Male	19	17	20
Female	11	13	10
Endoscopical finding	normal gastric mucosa	chronic atrophic gastritis(CAG)	gastric cancer
Pathologic finding	mild superficial gastritis(non-active)	moderate-severe CAG with or without intestinal malplasia	gastric cancer

Statistical analysis

Concentrations of serum GH were expressed as mean±SD. Differences between the two groups were evaluated by *t*-test. Significance was shown as $P < 0.05$. The expression of GHR was expressed as positive rate. Differences between groups were evaluated by χ^2 test. Significance was shown as $P < 0.05$. All experimental data were analyzed with Spss-pc+ software.

RESULTS

The average level of serum GH was lower in group B than in groups A and C. There were significant differences between them, but there was no significant difference between groups A and C.

Table 2 Serum GH Level (ng/mL) in the studied groups (mean±SD)

Group	A group (n = 30)	B group (n = 30)	C group (n = 30)
GH level	2.869±0.512 ^{1,2}	1.021±0.132 ¹	3.176±0.421 ²

¹t_{AB} = 3.135 $P < 0.01$ ¹t_{BC} = 3.537 $P < 0.01$ ²t_{AC} = 1.893 $P > 0.05$.

Table 3 Positive rate of gastric mucosal GHR expression in the studied groups (%)

Group	A group (n = 30)	B group (n = 30)	C group (n = 30)
GHR expression	100 (30/30) ¹	10 (3/30) ²	13 (4/30) ^{1,2}

¹ $\chi^2_{AB} = 49$ $P < 0.01$ ¹ $\chi^2_{AC} = 45$ $P < 0.01$ ² $\chi^2_{BC} = 0.16$ $P > 0.05$.

The positive rate of gastric mucosal GHR expression in groups B and C was lower than that in group A. There were significant differences between them, but there was no difference between groups B and C.

DISCUSSION

Growth hormone (GH) is a type of mono-peptide strain hormones released from anterior pituitary eosinophilic cells. Growth hormone receptor (GHR) is widely distributed in the gastrointestinal tracts. GH takes its effect on target tissues by combining with GHR. In the stomach, GHR is mainly distributed among parietal and chief cells. In 1995, Nagano *et al.* by using reverse transcription PCR technology and Southern blot analysis, found the wide distribution of GHR in the gastrointestinal tract especially in epidermal cells, suggesting that GH and GHR could play an

important role in the regulation of metabolism, growth, and differentiation of gastric mucosal cells. GH and GHR could improve protein synthesis, promote wound healing, stimulate gastrointestinal tract proliferation and repair, regulate immunological responses, and improve absorption of nutrients^[8]. Presently, clinical applications of recombinant human growth hormone (rhGH) in various gastrointestinal ailments such as malabsorption and short bowel syndrome were reported^[15-19].

Chronic atrophic gastritis (CAG) is a gastric precancerous lesion and listed as the first of cancer prevention by WHO. CAG pathogenesis has a correlation with mucosal nutrient deficiency. CAG patients had a decreased serum level of trace elements and beta-carotene with malnutrition^[20-21].

During the last several years, we have focused on exploring the correlation between CAG and GH. In a previous animal study, we measured the GH/GHR expression in atrophic gastritis rats, and found the levels of GH and GHR expression in rats with CAG were rather low. After removing the pituitary glands from rats, Crean GP discovered that there were gastric mucosal atrophy, shrinkage and decreased expression of parietal and chief cells. Increased secretion of gastric acid and pepsin, and exogenous GH have been shown to promote protein synthesis and increase gastrointestinal absorption of nutrients. We have considered using GH to treat CAG^[14].

Our present study showed the same results as before^[14]. The levels of GH/GHR expression in patients with CAG were significantly lower than normal. GH and GHR could regulate the metabolism, growth and differentiation of gastrointestinal epidermal cells, therefore, a decreased GH/GHR level would hinder the repair and recovery of CAG. Decreased levels of GH and GHR had an adverse effect on the progression of CAG. This study suggests that when CAG is treated, GH or GH-like drugs may be considered in the treatment regimen to promote mucosal repair and stop the progression of CAG.

Exogenous GH has been shown to significantly increase the expression of c-myc oncogene^[22]. Watanabe *et al.*^[23] showed that by using N-methyl-N-nitrosourea solution to induce gastric cancer in F344 rats, GH levels were elevated, suggesting that high concentrations of GH play a role in the pathogenesis of gastric cancer. Studies have shown that acromegalic patients, had an increased risk of developing gastrointestinal tumor and carcinoma^[24-28]. Therefore, cautions should be taken to monitor the possibilities of gastrointestinal cancers. Whether clinical usage of growth hormone and medicine which stimulates the release of growth hormone causes the carcinogenesis of atrophic gastritis is concerned. Our study showed that the serum GH level in gastric cancer patients and normal individuals was similar, the positivity rate of GHR expression was not high, suggesting that GH dose not play a role in the development of gastric cancer. Lobie *et al.*^[29] investigated the effect of GH on gastric structure and function in GH-deficient Lewis (dwarf) rats, Bovine GH (65 micrograms/100 g body wt), was administered twice daily to adult male dwarf rats for 6 d (DW+) while control animals received vehicle only (DW-). Administration of GH produced a significant increase in body ,stomach wt and stomach to body wt ratio. GH administration also resulted in an increase of total gastric DNA, RNA, and protein. The density of differentiated (parietal and chief) cell types was not significantly different in DW- and DW+ animals. They demonstrated that GH could stimulate proliferation and enlargement of the gastric mucosae without significant alterations in cellular composition. So we recommend using GH as a treatment agent for CAG, but a definite conclusion needs further clinical observations.

REFERENCES

- 1 Arzt E, Pereda MP, Castro CP, Pagotto U, Renner U, Stalla GK. Pathophysiological role of the cytokine network in the an-

- terior pituitary gland. *Front Neuroendocrinol* 1999; **20**: 71-95
- 2 **Li HW**, Wang JB. Study on TGF β ₁, TGF β ₂, TGF β ₃ expression in the chick basilar papilla following gentamicin toxicity. *Lingchuang Erbiyanhouke Zazhi* 1998; **12**: 463-465
- 3 **Shirakata Y**, Komurasaki T, Toyoda H, Hanakawa Y, Yamasaki K, Tokumaru S, Sayama K, Hashimoto K. Epiregulin, a novel member of the epidermal growth factor family, is an autocrine growth factor in normal human keratinocytes. *J Biol Chem* 2000; **275**: 5748-5753
- 4 **Kobayashi T**, Hashimoto K, Okumura H, Asada H, Yoshikawa K. Endogenous EGF-family growth factors are necessary for the progression from the G1 to S phase in human keratinocytes. *J Invest Dermatol* 1998; **111**: 616-620
- 5 **Zushi S**, Shinomura Y, Kiyohara T, Miyazaki Y, Tsutsui S, Sugimachi M, Higashimoto Y, Kanayama S, Matsuzawa Y. Role of heparin-binding EGF-related peptides in proliferation and apoptosis of activated ras-stimulated intestinal epithelial cells. *Int J Cancer* 1997; **73**: 917-923
- 6 **Abe S**, Sasano H, Katoh K, Ohara S, Arikawa T, Noguchi T, Asaki S, Yasui W, Tahara E, Nagura H, Toyota T. Immunohistochemical studies on EGF family growth factors in normal and ulcerated human gastric mucosa. *Dig Dis Sci* 1997; **42**: 1199-1209
- 7 **Ono I**, Gunji H, Zhang JZ, Maruyama K, Kaneko F. Studies on cytokines related to wound healing in donor site wound fluid. *J Dermatol Sci* 1995; **10**: 241-245
- 8 **Nagano M**, Chastre E, Choquet A, Bara J, Gespach C, Kelly PA. Expression of prolactin and growth hormone receptor genes and their isoforms in the gastrointestinal tract. *Am J Physiol* 1995; **268**(3 Pt 1): G431-G442
- 9 **Pan GZ**, Chao SZ, Liu TH, Lu XH, Chen YF, Chen SP. Contemporary Gastroenterology. 1st ed. Beijing: *Science Pub* 1998: 991
- 10 **You WC**, Blot WJ, Li JY, Chang YS, Jin ML, Kneller R, Zhang L, Han ZX, Zeng XR, Liu WD. Precancerous gastric lesions in a population at high risk of stomach cancer. *Cancer Res* 1993; **53**: 1317-1321
- 11 **Fukao A**, Hisamichi S, Ohsato N, Fujino N, Endo N, Iha M. Correlation between the prevalence of gastritis and gastric cancer in Japan. *Cancer Causes Control* 1993; **4**: 17-20
- 12 **Jin GQ**, Yao JS, Jiang YN, Zhu HW, Ye YG, He MJ, Xiao SD. Observation on gastric mucosa of the healthy elderly. *Zhonghua Xiaohua Zazhi* 1984; **4**: 18-19
- 13 **Krasinski SD**, Russell RM, Samloff IM, Jacob RA, Dallal GE, McGandy RB, Hartz SC. Fundic atrophic gastritis in an elderly population. Effect on hemoglobin and several serum nutritional indicators. *J Am Geriatr Soc* 1986; **34**: 800-806
- 14 **Cao Q**, Si JM, Li XL. GH/GHR expression on atrophic gastritis in rats. *Zhonghua Xiaohua Zazhi* 2001; **21**: 627-628
- 15 **Jeppesen PB**, Mortensen PB. Enhancing bowel adaptation in short bowel syndrome. *Curr Gastroenterol Rep* 2002; **4**: 338-347
- 16 **Zhu WM**, Li N, Ren JA, Gu J, Jiang J, Li JS. Rehabilitation therapy for short bowel syndrome. *Chin Med J* 2002; **115**: 776-778
- 17 **Scolapio JS**. Treatment of short-bowel syndrome. *Curr Opin Clin Nutr Metab Care* 2001; **4**: 557-560
- 18 **Gu Y**, Wu ZH, Xie JX, Jin DY, Zhou HC. Effects of growth hormone (rhGH) and glutamine supplemented parenteral nutrition on intestinal adaptation in short bowel rats. *Clin Nutr* 2001; **20**: 159-166
- 19 **Ukleja A**, Tammela LJ, Lankisch MR, Scolapio JS. Nutritional support for the patient with short-bowel syndrome. *Curr Gastroenterol Rep* 1999; **1**: 331-334
- 20 **Bukin YV**, Zaridze DG, Draudin-Krylenko VA, Orlov EN, Sigacheva NA, Dawei F, Kurtzman MYA, Schlenskaya IN, Gorbacheva ON, Nechipai AM. Effect of beta-carotene supplementation on the activity of ornithine decarboxylase (ODC) in stomach mucosa of patients with chronic atrophic gastritis. *Eur J Cancer Prev* 1993; **2**: 61-68
- 21 **Palli D**, Decarli A, Cipriani F, Forman D, Amadori D, Avellini C, Giacosa A, Manca P, Russo A, Salkeld RM. Plasma pepsinogens, nutrients, and diet in areas of Italy at varying gastric cancer risk. *Cancer Epidemiol Biomarkers Prev* 1991; **1**: 45-50
- 22 **Murphy J**, Bell GI, Friesen HG. Growth hormone stimulates sequential induction of c-myc and insulin-like growth factor I expression *in vivo*. *Endocrinology* 1987; **120**: 1806-1812
- 23 **Watanabe H**, Fujimoto N, Kawamoto K, Ando Y, Yamada K, Okamoto T, Kanin GN, Ito A. Elevated serum growth hormone accelerates gastric tumorigenesis in F344 rats after treatment with N-methyl-N-nitrosourea in their drinking water. *Jpn J Cancer Res* 1995; **86**: 631-637
- 24 **Ezzat S**, Strom C, Melmed S. Colon polyps in acromegaly. *Ann Intern Med* 1991; **114**: 754-755
- 25 **Pines A**, Rozen P, Ron E, Gilat T. Gastrointestinal tumors in acromegalic patients. *Am J Gastroenterol* 1985; **80**: 266-269
- 26 **Asai K**, Shimoyama S, Sanno N, Kaminishi M, Oohara T. A rare case of gastric cancer in an acromegalic patient. *J Gastroenterol* 1997; **32**: 528-532
- 27 **Kojima K**, Miyake M, Nakagawa H, Yunoki Y, Ogurusu K, Saino S, Wani T, Kawaguchi Y. Multiple gastric carcinoids and pituitary adenoma in type A gastritis. *Intern Med* 1997; **36**: 787-789
- 28 **Papotti M**, Cassoni P, Volante M, Deghenghi R, Muccioli G, Ghigo E. Ghrelin-producing endocrine tumors of the stomach and intestine. *J Clin Endocrinol Metab* 2001; **86**: 5052-5059
- 29 **Lobie PE**, Garcia-Aragon J, Waters MJ. Growth hormone (GH) regulation of gastric structure and function in the GH-deficient rat: up-regulation of intrinsic factor. *Endocrinology* 1992; **130**: 3015-3024

Clinical and experimental study of oxaliplatin in treating human gastric carcinoma

Wan-Long Lin, Ding-Guo Li, Qiang Chen, Han-Ming Lu

Wan-Long Lin, Ding-Guo Li, Qiang Chen, Han-Ming Lu, Department of Gastroenterology, Affiliated Xinhua Hospital, Shanghai Second Medical University, Shanghai 200092, China

Correspondence to: Dr. Wan-Long Lin, Department of Gastroenterology, Affiliated Xinhua Hospital, Shanghai Second Medical University, Shanghai 200092, China. linwanlong155@sohu.com

Telephone: +86-21-56748087

Received: 2003-09-18 **Accepted:** 2003-10-27

Abstract

AIM: To evaluate the therapeutic effectiveness of oxaliplatin on human gastric carcinoma and to explore its mechanisms.

METHODS: Twenty-two cases of stage IV gastric carcinoma received 4-6 (mean 4.6) cycles of first line combined chemotherapy with oxaliplatin (oxaliplatin 85 mg/m², iv, gtt, 1 h, d 1; leukovorin 200 mg/m², iv, gtt, 1 h, d 1 and d 2; 5-FU 300 mg/m², iv, d 1 and d 2, 5-FU, continuous iv, gtt, 48 h; 1 cycle/2 wk). Response rate, progression-free survival (PFS), total survival time, toxic side effects were evaluated. The inhibitory effect of oxaliplatin on human gastric cell line SGC-7901 was detected and IC₅₀ was calculated by MTT. Transmission electron microscopy, flow cytometry and TUNEL were performed to evaluate the apoptosis of cell line induced by the drug. The expression of Caspase-3 m-RNA was detected by RT-PCR. AC-DEVD-CHO, a Caspase-3 specific inhibitor, was used to elucidate the role of activated Caspase-3 in the process of apoptosis induced by oxaliplatin.

RESULTS: Total response (complete and partial) occurred in 9 (40.9%) patients. Mean PFS was 4.2 mo and mean total survival time was 7.2 mo. Cumulative neurotoxicity (all grade I-II), vomiting and diarrhea, myelosuppression appeared in 93.5%, 20%, 32.9% patients, respectively. IC₅₀ was calculated to be 0.71 mg/L by MTT assay. A maximal inhibitory rate reached 85.3%. Apoptosis index was elevated after incubated with 1 mmol/L oxaliplatin for 30 min, but without statistic significance ($P > 0.05$). However it could be detected at a much higher degree both by flowcytometry and by TUNEL with a statistical significance ($68.47 \pm 7.92\%$ and $8.23 \pm 2.67\%$, respectively, $P < 0.05$) after incubated with 1 mmol/L oxaliplatin for 2 d. By means of RT-PCR, we detected an enhancement of Caspase-3 m-RNA expression induced by oxaliplatin which was also in positive correlation with the apoptotic level. AC-DEVD-CHO, a Caspase-3 specific inhibitor, could significantly inhibit and delay apoptosis induced by oxaliplatin.

CONCLUSION: Oxaliplatin is effective and well-tolerated in patients with advanced gastric carcinoma. Oxaliplatin could significantly inhibit the growth of human gastric cell line SGC-7901. The induction of Caspase-3 m-RNA expression, activation of Caspase-3 and promotion of apoptosis may be some of the therapeutic mechanisms of oxaliplatin on gastric carcinoma. Annexin-V-fluorescein labeling flow cytometry is much more sensitive than TUNEL in detecting

early stage apoptosis.

Lin WL, Li DG, Chen Q, Lu HM. Clinical and experimental study of oxaliplatin in treating human gastric carcinoma. *World J Gastroenterol* 2004; 10(19): 2911-2915

<http://www.wjgnet.com/1007-9327/10/2911.asp>

INTRODUCTION

Gastric cancer is one of the common carcinomas in human being. Drug treatment draws more and more attention as an essential part of comprehensive treatment of gastric malignancy. Gastric carcinoma is relatively sensitive to chemotherapy. It is generally considered that chemotherapy may prolong patient's life and decrease relapse. Oxaliplatin (L-OHP) is an innovative third generation platinum compound with powerful anti-neoplasm competence, lack of cross drug resistance with CDDP, with a synergistic effect with 5-FU and satisfactory safety profile. This new anticancer drug provides us more choices in fighting against malignancy, especially colon cancer. At present, treating gastric cancer with oxaliplatin and the relationship between chemotherapy and cancer cell apoptosis draw more and more attention. The discovery of Caspase family (cysteine proteases) that is implicated in the execution of programmed cell death in organisms ranging from nematodes to humans, brings the fresh air to the research of malignant cell apoptosis. The Caspase family is big and family members interact with each other to promote or inhibit the process of apoptosis. Caspase-3 locates in the downstream of the Caspase cascade. The proteolytic activation of Caspase-3 plays a key role in apoptotic process. This article summarizes the effect and side effects of chemotherapy with oxaliplatin on 22 cases of stage IV human gastric cancer, and tries to elucidate the mechanisms of chemotherapy by detecting apoptosis of cancer cells and evaluating the role Caspase-3 plays in apoptotic process.

MATERIALS AND METHODS

Patients

A total of 22 cases of stage IV human gastric cancer patients who underwent chemotherapy in the Affiliated Xinhua Hospital of Shanghai Second Medical University from January 1999 to September 2002 were enrolled in this study. There were 17 men and 5 women, and their age ranged from 25 to 70 years (mean, 60±10 years). Among the 22 patients, 16 had poorly differentiated adenocarcinoma and 6 had signet ring cell carcinoma.

Methods

Each case received a combination chemotherapy containing L-OHP (L-OHP 85 mg/m² by continuous intravenous infusion for 2 h on d 1, leukovorin 200 mg/m² by continuous intravenous infusion for 1 h on d 1 and d 2, 5-FU 300 mg/m² by bolus intravenous injection on d 1 and d 2, 5-FU 1200 mg/m² by continuous intravenous infusion for 48 h, one course lasting 2 wk for 4-6 courses).

Cell culture

Human gastric adenocarcinoma cell line SGC-7901, purchased

from the Shanghai Institute of Cell Biology, Chinese Academy of Sciences, was routinely maintained in RPMI 1640 containing 100 mL/L fetal bovine serum (FBS), 100 U/mL penicillin, 100 U/mL streptomycin at 37 °C in a humidified atmosphere containing 50 mL/L CO₂.

MTT assay

Cells were seeded at the density of 5×10³ per well in 96-well plates in RPMI-1640 containing 100 mL/L FBS. After 24 h, fresh medium was added, containing oxaliplatin at concentrations of 0 to 10 mg/L. After 48 h incubation, MTT assay was performed, 150 μL of stock MTT (0.5 mg/mL) was added to each well, and the cells were further incubated at 37 °C for 4 h. The supernatant was removed and 150 μL DMSO was added to each well. An ELISA reader was used to measure the absorbance at a wavelength of 525 nm.

Transmission electron microscopy

The cells treated with 0.1 mg/L oxaliplatin were trypsinized and harvested after 24 h. Subsequently the cells were fixed in 40 g/L glutaral and immersed with Epon 821, embedded in capsules and converged for 72 h at 60 °C, then prepared into ultrathin sections (60 nm) and stained with uranyl acetate and lead citrate. Cell morphology was examined by transmission electron microscopy.

Flow cytometry

SGC-7901 cells were treated with oxaliplatin or oxaliplatin plus AC-DEVD-CHO at oxaliplatin concentrations of 0 to 10 mg/L for 30 min. Cells were digested by 2.5 g/L trypsin, washed in 0.01 mol/L PBS, fixed by cold alcohol at 4 °C and dyed with annexin-V (according to the description of annexin-V kit), and then analyzed by flow cytometry.

TUNEL

SGC-7901 cells were added to 6-well plates with cover glass-slides at 6×10⁴ cells/well, after incubated with oxaliplatin or oxaliplatin plus AC-DEVD-CHO at different oxaliplatin concentrations of 0 to 10 mg/L and fixed in 40 g/L formaldehydum polymerisatum for 1 h. After washed in 0.01 mol/L PBS twice, the cells were treated with reaction buffer, labeled with fluorescein dUTP in a humid box for 1 hour at 37 °C, then combined with anti-fluorescein antibody, colorized with NBT/BCIP. Cells were visualized with light microscopy. The apoptotic index (AI) was calculated as follows: AI = (number of apoptotic cells/total number) × 100%.

RT-PCR

Total RNA was extracted from cells using an RNA extraction reagent, TRIZOL (Life Technologies, USA), according to standard acid-guanidium-phenol-chloroform method^[17]. About 4 μg of total RNA as reversely transcribed at 42 °C for 60 min in a total of 30 μL reaction volume using a first-strand cDNA synthesis kit (Boehringer Mannheim, Germany). cDNA was incubated at 95 °C for 5 min to inactivate the reverse transcriptase, and served as template DNA for 28 rounds of amplification using the GeneAmp PCR system 2400 (Perkin-Elmer Applied

Biosystems, CA, USA). PCR was performed in a standard 25 μL reaction mixture consisting of 1.5 mmol/L magnesium chloride (pH 8.3), 2.5 mmol/L dNTPs, 12.5 pmol each of sense and antisense primers and 2.5 U of Taq DNA polymerase (M BI, Canada). Amplification was performed for 1 min at 94 °C, for 1 min at 62 °C and for 1 min at 72 °C after heat-start for 5 min. Finally, an additional extension step was carried out for 10 min at 72 °C. As control, the DNA template of Caspase-3 was replaced by that of β-actin in the reaction. The amplification products were separated on 12 g/L agarose gels and visualized by ethidium bromide staining. PCR primers for Caspase-3 were as follows: forward primer, 5'- ATG GAG AAC ACT GAA AAC TCA -3'; reverse primer, 5'- TTA GTG ATA AAA ATA GAG TTC -3': according to the Caspase-3 gene structure in GeneBank. An 834 bp PCR product of Caspase-3 and a 315 bp product of β-actin were obtained.

Statistical analysis

The difference between each two groups was analyzed by ANOVA. *P*<0.05 was considered statistically significant.

RESULTS

Clinical results

Nine cases achieved objective responses (including 1 complete response and 8 partial responses), the response rate was 40.9% progression-free survival (PFS) 4.2 mo, and total survival time 7.2 mo. The rate of accumulative neurotoxicity, vomiting and diarrhea, bone marrow depression was 93.5%, 20% and 32.9%, respectively (Table 1).

Inhibitory effect of oxaliplatin on SGC-7901

Taking the means of data from MTT assay, we got a smooth inhibition curve, which was a typical inverse 'S', and the IC₅₀ was calculated to be 0.71 mg/L by GraphPaol Prism software (Figure 1). The inhibition of L-OHP on SGC-7901 cell line was typically dose dependent. A maximal inhibitory rate reached 85.3%.

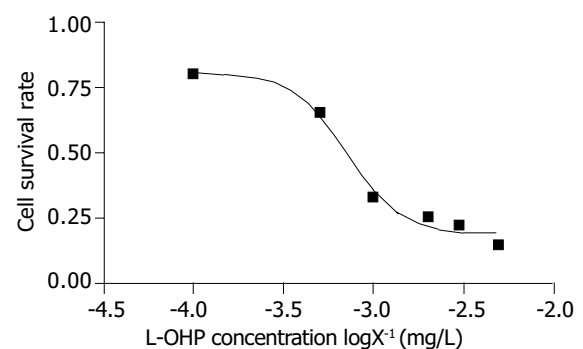


Figure 1 Relationship between SGC-7901 cell survival rate and L-OHP concentration.

Apoptosis induced by L-OHP

We used transmission electron microscopy, TUNEL and

Table 1 Side effects of combined chemotherapy with oxaliplatin in treating stage IV gastric carcinoma (cycles, *n* = 102)

Side effects	Anemia	Neutropenia	Thrombo-cytopenia	Nausea& vomiting	Diarrhea	Mucositis	Dysaesthesia
I	27	17	7	14	16	9	89
II	7	6	3	6	3	1	6
III	0	0	0	0	1	0	0
IV	0	0	0	0	0	0	-
Incidence (%)	32.9	22.9	10	20	20	10	93.5

Annexin-V labeling flowcytometry to quest for the mechanism of its anti-neoplastic effect. After treatment of SGC-7901 cells with oxaliplatin (0.1 mg/L) for 24 h, some cells showed apoptotic characteristics including chromatin condensation, chromatin crescent formation, nucleus fragmentation and apoptotic body formation by transmission electron microscopy (Figure 2). Apoptotic index was 0.38% in the control group. In the experimental group, the apoptotic index determined by the TUNEL method was 7.35% while receiving L-OHP 1mg/L (slightly higher than IC_{50}) for 4 h and 14.35% while increasing the L-OHP concentration to 5 mg/L. As time went on, the apoptotic index remained stable in the control group, and was significantly increased in two experimental groups (0.5 mg/L and 1 mg/L) which reached a peak of 7.93% and 10.15%, respectively on the 4th d and decreased slightly on the 7th d. The two experimental groups had a similar trend. We could conclude that the increase in apoptotic index correlated with the L-OHP concentration and time. The apoptotic level was positively correlated with L-OHP at a concentration within 0-2.0 mg/L, as detected by Annexin-V labeling flowcytometry. The apoptotic index reached a peak of 76.47% when the concentration of L-OHP was 2 mg/L. On the contrary, the apoptotic index dropped when the concentration reached 5 mg/L.

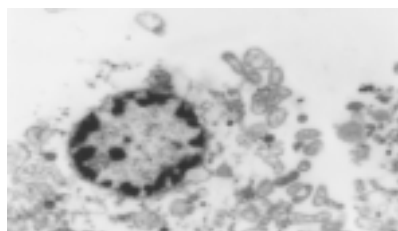


Figure 2 Oxaliplatin-induced apoptosis in SGC-7901 cells with transmission electron microscopy. It shows apoptotic cells with chromatin condensation, chromatin crescent formation, nucleus fragmentation ($\times 4000$).

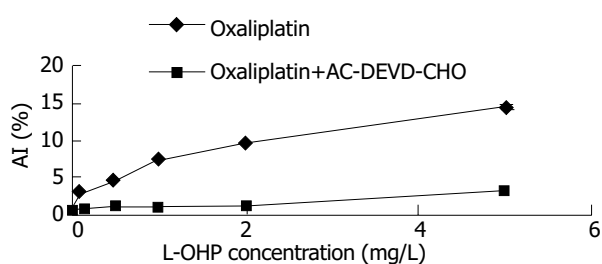


Figure 3 Inhibitory effect of AC-DEVD-CHO on apoptosis detected by TUNEL.

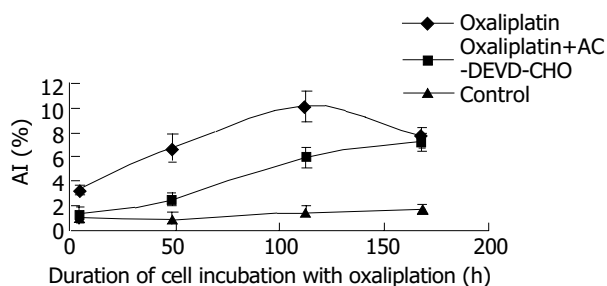


Figure 4 Effect of AC-DEVD-CHO on apoptosis at different times detected by TUNEL.

Expression of Caspase-3 m-RNA

By means of RT-PCR, we detected an enhancement of Caspase-3

m-RNA expression (0.48 ± 0.47 vs 0.18 ± 0.20 , $P < 0.05$) induced by L-OHP which was also in positive correlation with the apoptotic level.

Role of activated Caspase-3 in apoptotic process induced by oxaliplatin

AC-DEVD-CHO, a Caspase-3 specific inhibitor, could significantly inhibit and delay apoptosis induced by L-OHP (Figures 3, 4).

DISCUSSION

Gastric carcinoma is one of the major causes of cancer morbidity and mortality in China. The natural history shows a high metastatic potential since many patients with gastric carcinoma at advanced stage will relapse or initially present with metastasis. One of the first issues solved by clinical research over the last decade is the value of chemotherapy in the metastatic setting. Indeed, chemotherapy has been shown to have a favorable impact on survival and quality of life compared with supportive care alone. However, in this disease some traditional chemotherapy regimens were considered as poorly tolerated or less effective^[1-4]. Oxaliplatin is an innovative platinum compound indicated as a first-line therapy in combination with 5-FU and folinic acid for metastatic colorectal cancer^[5-8]. Oxaliplatin has a powerful anti-neoplasm competence, little cross drug resistance with CDDP, a synergistic effect with 5-FU and a satisfactory safety profile^[9-11]. We replaced CDDP with oxaliplatin in a traditional FLP protocol, trying to explore its anti-neoplasm activity and side effects in treating advanced gastric carcinoma. In 22 patients, 9 cases achieved objective responses (including 1 complete response and 8 partial responses), the overall response rate reached 40.9%, PFS 4.2 mo, and overall survival time 7.2 mo. The toxicity was tolerable, the rate of vomiting and diarrhea (1 case with grade III diarrhea), bone marrow depression was 20% and 32.9%, respectively. No alopecia and skin toxicity were encountered. Although the incidence of accumulative neurotoxicity was as high as 93.5%, all of them were grade I-II. Acute symptoms manifesting as transient dysaesthesia and/or paraesthesia of the extremities were commonly observed, their occurrence was triggered or enhanced by exposure to cold. No patient experienced pharyngolaryngeal dysaesthesia characterized by a transient sensation of difficulty in breathing or swallowing without any objective evidence of respiratory distress, which was encountered during the multi-center research in treating colorectal cancer after 9 cycles^[12-14]. In all the cases in this study, symptoms improved after treatment discontinuation. It is suggested that oxaliplatin is effective and well-tolerated in patients with stage IV gastric carcinoma.

We chose human gastric cancer cell line SGC-7901 for experimental study. First, we used MTT to prove if L-OHP could inhibit SGC-7901 growth. using the means of our data from the experiments, we obtained a smooth inhibition curve, which was a typical inverted 'S'. IC_{50} was 0.71 mg/L and the maximal inhibitory rate reached 85.3%. The inhibition of L-OHP on SGC-7901 cell line was typically dose dependent.

Naturally occurring or programmed cell death can regulate cell number, facilitate morphogenesis, remove harmful or otherwise abnormal cells, and eliminate cells that have already performed their functions during the life development as well as in tissue homeostasis and aging. The role of apoptosis in the process of carcinogenesis, development of cancer and malignancy treatment has drawn more and more attention in recent years^[15-17]. In this study, we tried to evaluate the level of apoptosis induced by oxaliplatin. Transmission electron microscopy could reveal the changes of cell ultrastructure during the apoptotic process. TUNEL assay is a traditional method for detecting apoptosis, but its selectivity is poor. It could hardly differentiate the apoptotic cells from the necrotic ones.

Phosphatidylserine (PS) only exists in the cytoplasm side of cell plasma membrane, and externalization of PS occurs in the early stage of apoptosis. Annexin-V could specifically conjugate to the PS to detect the apoptotic cells^[18]. So we combined traditional transmission electron microscopy and TUNEL assay with relatively highly selective annexin-V labeling flowcytometry to detect SGC-7901 cell line apoptosis induced by oxaliplatin. After treatment of SGC-7901 cells with oxaliplatin, some cells showed typical morphologic changes of apoptosis including chromatin condensation, chromatin crescent formation, nucleus fragmentation and apoptotic body formation under transmission electron microscope. TUNEL assay showed the AI positively correlated with drug concentration and treatment time. Annexin-V-fluorescein labeling flowcytometry was much more sensitive than TUNEL in detecting the early stage apoptosis. The apoptotic level positively correlated with L-OHP at a concentration within 0-2.0 mg/L, as detected by annexin-V labeling flowcytometry. The apoptotic index reached a peak, when the concentration of L-OHP was 2 mg/L. On the contrary, the apoptotic index dropped while the concentration reached 5 mg/L. To put these results together, we believed that the induction of apoptosis played a key role in inhibiting malignant cells at a low drug concentration of L-OHP, and that cytotoxicity and apoptosis coexisted while the drug concentration was high. This discovery may provide a theoretical basis for this type of treatment.

The discovery of cytosolic aspartate-specific proteases, called Caspases, which are responsible for the deliberate disassembly of a cell into apoptotic bodies, brings the fresh air to the research of malignant cell apoptosis. The Caspase family is big and dozens of family members interact with each other to promote or inhibit the process of apoptosis. Caspases are present as inactive pro-enzymes, most of which are activated by proteolytic cleavage. There are two pathways of Caspase activation, namely the cell surface death receptor pathway and the mitochondria-initiated pathway. In the cell surface death receptor pathway, activation of Caspase-8 following its recruitment to the death-inducing signaling complex (DISC) is the critical event that transmits the death signal. This event is regulated at several different levels by various viral and mammalian proteins. Activated Caspase-8 can activate downstream Caspases, such as Caspase-3 by direct cleavage or by indirectly cleaving bid and inducing cytochrome C release from the mitochondria. In the mitochondrial-initiated pathway, Caspase activation is triggered by the formation of an Apaf-1/cytochrome C complex that is fully functional in recruiting and activating proCaspase-9. Activated Caspase-9 will then cleave and activate downstream Caspases such as Caspase-3, -6, and -7^[19-23]. So we can find out that Caspase-3 locates in the downstream of the Caspase cascade. The proteolytic activation of Caspase-3 has been found to play a key role in apoptotic process^[24-26]. Caspase-3 may then cleave vital cellular proteins or activate additional Caspases by proteolytic cleavage. In this study, we detected an enhancement of Caspase-3 m-RNA expression induced by oxaliplatin by means of RT-PCR. Caspase-3 m-RNA expression was also positively correlated with the apoptotic level. AC-DEVD-CHO, a Caspase-3 specific inhibitor, could significantly inhibit and delay apoptosis induced by oxaliplatin. Taken together, we believe that Caspase-3 synthesis and activation play a key role in the apoptotic process of SGC-7901 cell line induced by oxaliplatin.

Our research demonstrates that oxaliplatin is effective and well tolerable in treating gastric cancer. Inducing cancer cell apoptosis may be one of the anti-neoplasm mechanisms. This apoptosis may be mediated by up-regulation of Caspase-3 synthesis and activation. The efficacy and safety profile of oxaliplatin as a chemotherapeutic drug in combined anti-gastric carcinoma chemotherapy regimen should be further confirmed by double blind multi-center clinical studies.

REFERENCES

- 1 **Cascinu S**, Scartozzi M, Labianca R, Catalano V, Silva RR, Barni S, Zaniboni A, D'Angelo A, Salvagni S, Martignoni G, Beretta GD, Graziano F, Berardi R, Franciosi V. High curative resection rate with weekly cisplatin, 5-fluorouracil, epidoxorubicin, 6S-leucovorin, glutathione, and filgastrim in patients with locally advanced, unresectable gastric cancer: a report from the Italian Group for the Study of Digestive Tract Cancer (GISCAD). *Br J Cancer* 2004; **90**: 1521-1525
- 2 **Park YH**, Ryoo BY, Choi SJ, Kim HT. A phase II study of capecitabine and docetaxel combination chemotherapy in patients with advanced gastric cancer. *Br J Cancer* 2004; **90**: 1329-1333
- 3 **Yamamura Y**, Kodera Y, Tanemura H, Oshita H, Miyashita K, Fujimura T. A phase I study of combination chemotherapy using TS-1 and pirarubicin (THP) for advanced gastric cancer. *Gan To Kagaku Ryoho* 2004; **31**: 361-365
- 4 **Ramos-De La Medina A**, Salgado-Nesme N, Torres-Villalobos G, Medina-Franco H. Clinicopathologic characteristics of gastric cancer in a young patient population. *J Gastrointest Surg* 2004; **8**: 240-244
- 5 **Braun AH**, Achterrath W, Wilke H, Vanhoefer U, Harstrick A, Preusser P. New systemic frontline treatment for metastatic colorectal carcinoma. *Cancer* 2004; **100**: 1558-1577
- 6 **Santini D**, Massacesi C, D'Angelillo RM, Marcucci F, Campisi C, Vincenzi B, Pilone A, Bianco V, Bonsignori M, Tonini G. Raltitrexed plus weekly oxaliplatin as first-line chemotherapy in metastatic colorectal cancer: a multicenter non-randomized phase ii study. *Med Oncol* 2004; **21**: 59-66
- 7 **Di Leo A**, Buyse M, Bleiberg H. Is overall survival a realistic primary end point in advanced colorectal cancer studies? A critical assessment based on four clinical trials comparing fluorouracil plus leucovorin with the same treatment combined either with oxaliplatin or with CPT-11. *Ann Oncol* 2004; **15**: 545-549
- 8 **Link K**, Happich K, Schirner I, Jungert B, Bruckl V, Mannlein G, Bruckl WM, Merkel S, Gohl J, Hohenberger W, Hahn EG, Wein A. Palliative second-line treatment with weekly high-dose 5-fluorouracil as 24-hour infusion and folinic acid (AIO) plus oxaliplatin after pre-treatment with the AIO-regimen in colorectal cancer (CRC). *Anticancer Res* 2004; **24**: 385-391
- 9 **Arnould S**, Hennebelle I, Canal P, Bugat R, Guichard S. Cellular determinants of oxaliplatin sensitivity in colon cancer cell lines. *Eur J Cancer* 2003; **39**: 112-119
- 10 **Marchetti P**, Galla DA, Russo FP, Ricevuto E, Flati V, Porzio G, Ficorella C, Cifone MG. Apoptosis induced by oxaliplatin in human colon cancer HCT15 cell line. *Anticancer Res* 2004; **24**: 219-226
- 11 **Ravaioli A**, Marangolo M, Pasquini E, Rossi A, Amadori D, Cruciani G, Tassinari D, Oliverio G, Giovanis P, Turci D, Zumaglini F, Nicolini M, Panzini I. Bolus fluorouracil and leucovorin with oxaliplatin as first-line treatment in metastatic colorectal cancer. *J Clin Oncol* 2002; **20**: 2545-2550
- 12 **Chiara S**, Nobile MT, Gozza A, Taveggia P, Heouaine A, Pastrone I, Percivale PL, Lionetto R, Sanguineti O, Rosso R. Phase II study of weekly oxaliplatin and high-dose infusional 5-fluorouracil plus leucovorin in pretreated patients with metastatic colorectal cancer. *Anticancer Res* 2004; **24**: 355-360
- 13 **Lehky TJ**, Leonard GD, Wilson RH, Grem JL, Floeter MK. Oxaliplatin-induced neurotoxicity: acute hyperexcitability and chronic neuropathy. *Muscle Nerve* 2004; **29**: 387-392
- 14 **Cavaletti G**, Petruccioli MG, Marmioli P, Rigolio R, Galbiati S, Zoia C, Ferrarese C, Tagliabue E, Dolci C, Bayssas M, Griffon Etienne G, Tredici G. Circulating nerve growth factor level changes during oxaliplatin treatment-induced neurotoxicity in the rat. *Anticancer Res* 2002; **22**: 4199-4204
- 15 **Onizuka S**, Kawakami S, Taniguchi K, Fujioka H, Miyashita K. Pancreatic carcinogenesis: apoptosis and angiogenesis. *Pancreas* 2004; **28**: 317-319
- 16 **Correa P**. The biological model of gastric carcinogenesis. *IARC Sci Publ* 2004; **157**: 301-310
- 17 **Schrenk D**, Schmitz HJ, Bohnenberger S, Wagner B, Worner W. Tumor promoters as inhibitors of apoptosis in rat hepatocytes. *Toxicol Lett* 2004; **149**: 43-50

- 18 **Kim SJ**, Kim JE, Moon IS. Paraquat induces apoptosis of cultured rat cortical cells. *Mol Cells* 2004; **17**: 102-107
- 19 **Del Bello B**, Valentini MA, Comporti M, Maellaro E. Cisplatin-induced apoptosis in melanoma cells: role of caspase-3 and caspase-7 in Apaf-1 proteolytic cleavage and in execution of the degradative phases. *Ann N Y Acad Sci* 2003; **1010**: 200-204
- 20 **Twiddy D**, Brown DG, Adrain C, Jukes R, Martin SJ, Cohen GM, MacFarlane MM, Cain K. Pro-apoptotic proteins released from the mitochondria regulate the protein composition and caspase-processing activity of the native Apaf-1/caspase-9 apoptosome complex. *J Biol Chem* 2004; **279**: 19665-19682
- 21 **Cain K**. Chemical-induced apoptosis: formation of the Apaf-1 apoptosome. *Drug Metab Rev* 2003; **35**: 337-363
- 22 **Del Bello B**, Valentini MA, Mangiavacchi P, Comporti M, Maellaro E. Role of caspases-3 and -7 in Apaf-1 proteolytic cleavage and degradation events during cisplatin-induced apoptosis in melanoma cells. *Exp Cell Res* 2004; **293**: 302-310
- 23 **Jazirehi AR**, Gan XH, De Vos S, Emmanouilides C, Bonavida B. Rituximab (anti-CD20) selectively modifies Bcl-xL and apoptosis protease activating factor-1 (Apaf-1) expression and sensitizes human non-Hodgkin's lymphoma B cell lines to paclitaxel-induced apoptosis. *Mol Cancer Ther* 2003; **2**: 1183-1193
- 24 **Dong ML**, Zhu YC, Hopkins JV. Oil A induces apoptosis of pancreatic cancer cells via caspase activation, redistribution of cell cycle and GADD expression. *World J Gastroenterol* 2003; **9**: 2745-2750
- 25 **Fu YG**, Qu YJ, Wu KC, Zhai HH, Liu ZG, Fan DM. Apoptosis-inducing effect of recombinant Caspase-3 expressed by constructed eukaryotic vector on gastric cancer cell line SGC7901. *World J Gastroenterol* 2003; **9**: 1935-1939
- 26 **Boulares AH**, Ren T. Mechanism of acetaminophen-induced apoptosis in cultured cells: roles of caspase-3, DNA fragmentation factor, and the Ca²⁺ and Mg²⁺ endonuclease DNAS1L3. *Pharmacol Toxicol* 2004; **94**: 19-29

Edited by Wang XL. Proofread by Zhu LH and Xu FM

A new method of preventing bile duct injury in laparoscopic cholecystectomy

Fang Xu, Cheng-Gang Xu, De-Zheng Xu

Fang Xu, Cheng-Gang Xu, De-Zheng Xu, Department of General Surgery, Hangzhou Second Hospital, Hangzhou 310015, Zhejiang Province, China

Correspondence to: Fang Xu, Department of General Surgery, Hangzhou Second Hospital, Hangzhou 310015, Zhejiang Province, China. xufangsurg@zj165.com

Telephone: +86-571-88303636 **Fax:** +86-571-88021730

Received: 2003-12-12 **Accepted:** 2004-02-01

Abstract

AIM: Of all the complications of laparoscopic cholecystectomy, bile duct injury (BDI) is the most serious complication. The prevention of injury to the common bile duct (CBD) remains a significant concern in laparoscopic cholecystectomy (LC). Different kinds of methods have been advanced to avoid this injury but no single method has gained wide acceptance. Because of various limitations of current methodologies we began a study using cold light illumination of the extrahepatic biliary system (light cholangiography LCP) to better visualize this area and thereby reduce the risk of bile duct injury.

METHODS: Thirty-six patients with cholelithiasis were divided into two groups. Group I (16 cases) received LCP and group II (20 cases) received methelenum coeruleum cholangiography (MCCP). In group I cold light was used to illuminate the common bile duct by leading an optical fiber into the common duct with a duodenoscope at the time of LC. The light coming from the fiber in the CBD could clearly illuminate the location of CBD and hepatic duct establishing its location relative to the cystic duct. This method was compared with the dye injection technique using methelenum coeruleum.

RESULTS: In group I thirteen cases were successfully illuminated and three failed. The cause of three failed cases was due to the difficulty in inserting the fiber into the ampulla of Vater. No complications occurred in the thirteen successful cases. In each of these successful cases the location of the common and hepatic ducts was clearly seen differentiating the ductal system from surrounding anatomy. In ten cases both the left and right hepatic ducts could be seen and in three only the right hepatic ducts were seen. In four of the thirteen cases, cystic ducts were also seen. In group II, eighteen of the twenty cases were successful. The location of extrahepatic ducts became blue differentiating the ductal system from surrounding anatomy. Two cases failed due to a stone obstructing the cystic duct, and extravasation of the dye turned the entire area blue. LCP showed the common and hepatic ducts more clearly than MCCP.

CONCLUSION: LCP is the only technique that can clearly and directly show the location of the extrahepatic biliary system and may be useful in selecting cases of uncertain anatomy in the prevention of bile duct injury.

Xu F, Xu CG, Xu DZ. A new method of preventing bile duct

injury in laparoscopic cholecystectomy. *World J Gastroenterol* 2004; 10(19): 2916-2918

<http://www.wjgnet.com/1007-9327/10/2916.asp>

INTRODUCTION

Bile duct injury continues to be one of the most serious complications of LC. The principal cause is the difficulty in recognition of the junction of the cystic duct to the hepatic duct. A number of methods have been advanced to avoid this error but no single method has gained wide acceptance. From March 2001 to October 2003 we used LCP for illumination of the biliary system in 36 cases and believe it is quite useful.

MATERIALS AND METHODS

Patients

Thirty-six patients with cholelithiasis, including 16 males and 20 females aged 41 to 66 years (mean age: 56 years) were selected for the procedure and divided into two groups. Group I (16 cases) received LCP and group II (20 cases) received MCCP.

Materials

Laparoscopic equipments were produced by Stryker and duodenoscopes with a channel diameter of 3.5 cm and 4.2 cm respectively were from Olympus. Optical fibers were specially produced according to our own design.

Methods

All patients drank 500 mL 100 g/L mannitol 15 h before operation and were fasted during this period. All cases received general anesthesia. In group I, Calot's triangle was dissected carefully and the relationship of the cystic duct to the hepatic and common bile ducts was noted. Duodenoscope was then introduced and the optic fiber was advanced into the common duct. When the light was turned on, the extra hepatic ducts were clearly seen. In group II, instead of placing the duodenoscope, a needle guided with the laparoscope was percutaneously punctured into the gall bladder. Five mL of bile was aspirated from the gall bladder. After that 5 mL of MCCP dye was injected. The bile ducts became blue.

RESULTS

In group I, thirteen cases were successfully illuminated and three failed. The cause of three failed cases was due to the difficulty in inserting the fiber into the ampulla of Vater. The time required for this examination ranged from 15 to 100 min with a median time of 35 min. No complications occurred in the thirteen successful cases. In each of these cases, the location of the common and hepatic ducts was seen clearly differentiating the ductal system from surrounding anatomy. In ten cases both the left and right hepatic ducts could be seen and in three only the right hepatic ducts were seen. In four of the thirteen cases, the cystic ducts were also seen. In two cases the ducts were clearly seen in spite of considerable fat over Calot's triangle.

In group II, eighteen of the twenty cases were successful.

The extrahepatic duct became blue differentiating the ductal system from surrounding anatomy. Two cases failed due to a stone obstructing the cystic duct, and extravasation of the dye turned the entire area blue.

DISCUSSION

Prevention of injury to the ductal system continues to be a matter of considerable concern of surgeons performing laparoscopic cholecystectomy. The accurate incidence of bile duct injury (BDI) during laparoscopic cholecystectomy (LC) is not known^[1]. The principal causes of CBD in LC are the uncertain anatomy and the laparoscopic view that is quite different from open cholecystectomy. A few methods have been practiced, *e.g.* using 30° laparoscope, applying three dimensional laparoscope and inserting laparoscope through the right side of umbilicus were used. Greater efforts have been concentrated on dealing with the uncertain anatomy. The key point continues to be how to best identify the anatomy and thereby avoid injury. Currently the primary means of preventing injury resulted from uncertain anatomy include careful dissection, the judgment of an experienced surgeon, conversion to open cholecystectomy and intraoperative cholangiography (IOC).

The major causes of uncertain anatomy are anatomic variation and unclear anatomy. Kurumi *et al.*^[2] classified confluent forms of the cystic duct and the bile duct into five different types, including four abnormal types. Sixteen instances (3.13%) of anatomic variation of the biliary tract were found among 511 patients, and four cases (4.35%) were found in 92 cadavers. Anatomic variation of the biliary tract is both common and complicated and can create a pitfall during laparoscopic cholecystectomy. Unclear anatomy resulted from inflammation and adhesion at Calot's triangle is an important factor associated with injury^[3-5]. The judgment of an experienced surgeon^[1,4,6] and conversion from laparoscopic to open cholecystectomy^[5,7] are now considered the primary means of preventing bile duct injury resulted from uncertain anatomy. Unfortunately these means do not always work effectively. Injuries are likely to occur despite better procedures and increased experience^[4]. Calvete *et al.* believed that no relation could be found between the experience of surgeons and the number of BDI over different periods of time^[8]. Therefore, BDI during LC can not be attributed solely to the learning curve. One approach is to convert to open cholecystectomy when the anatomy is uncertain. But even open cholecystectomy can not avoid CBD injury due to the uncertain anatomy. Yang *et al.*^[9] reported iatrogenic extrahepatic bile duct injury in 182 patients. Bile duct injury occurred in 152 patients during open cholecystectomy and in 30 patients during laparoscopic cholecystectomy. The incidence of BDI after LC was similar to that in the open procedure^[1].

Cautious dissection is necessary and essential to prevent BDI in LC^[4,6,10-12]. Illegible anatomy often poses dissection difficultly to operators and renders them quite helpless. Surgeons are seeking assisting measures to help them identify the anatomy during LC. Some surgeons recommended that IOC be attempted on all patients undergoing LC. They deemed that the routine use of IOC during laparoscopic cholecystectomy could not prevent bile duct injuries, but minimized the extent of the injuries so that they could be repaired easily, thus decreasing the rate of BDI^[13-16]. But its routine use during LC remains controversial. Routine IOC yields very little useful clinical information compared to selective policies. A large number of unnecessary IOC were performed under routine IOC policy, and therefore a selective policy has been advocated^[17]. IOC depends on the radiopaque dye introduced into the ductal system via the cystic duct and displayed by either a static film or fluoroscopy which does not always identify the relationship of the ductal system to adjacent anatomy. The primary purpose

of IOC is to identify anatomy and any aberration as well as to identify stones. The image of IOC obtained from static film or fluoroscopy is completely different from that obtained from the monitor and can not really tell where the cystic duct or common bile duct is. The information afforded by IOC can only help operators realize if there are continuity, stones, tumor and injury of the ducts but can not help them dissect easily and safely. Thus it is of limited value during dissection of the area. Nevertheless it has become the most common method of visualizing the area.

The use of MCCP has been advocated by Xu *et al.*^[18]. This technique does give a direct image but it is blurry. A mixture is got by injecting methylenum coeruleum into gall bladder. The color of the mixture is close to that of the tissue surrounding the extrahepatic duct, so that the bile ducts can not be identified clearly. The image is even more indistinct when there is much fatty tissue over the ducts. If there is extravasation, the entire area turns blue making dissection more difficult since the dye is not easily washed away. CBD does not keep the dye long enough. The dye diluted by the bile flows into duodenum soon, so that the operator can not observe Calot's triangle repeatedly. Finally, the procedure can not be used if the duct is blocked by a stone.

Because of these limitations of current methodologies, we advocated the new method of direct illumination of the extrahepatic ductal system (LCP). By adjusting the optic fiber, it can go into right or left hepatic duct and cystic duct. The movement of the fiber must be slow and soft. It is not very easy sometimes to insert the fiber into cystic duct for the duct may pass behind the common hepatic duct to enter on its posterior wall or on its left lateral aspect. If the inserting was difficult, we gave the attempt up in case that the duct wall was injured by the fiber. We do not think the illumination of cystic duct is absolutely necessary. The important thing is to know the locations of CBD and common hepatic duct, though the illumination of cystic duct may make the image of Calot's triangle appear completely.

Table 1 Comparison between group I and group II

	Group I (n=16)	Group II (n=20)
Examine method	LCP	MCCP
Examine time (min)		
Range	15-100	5-10
Median	35	7
Examination cost	\$ 200	\$ 5
Image	direct	direct
Legibility	clear	blurry
Observed time	unlimited	limited

Additional observations we made during this study revealed the importance of releasing any adhesions in the area of the ductal system to straighten the ductal system out facilitating the introduction of the optical fiber. The initial dissection of the ductal system along with our observations as to the probable location of the various elements was also helpful. In our opinion it is best to keep the optical fiber in the right hepatic duct until the dissection of the gall bladder and cystic duct is completed. This is particularly true in the occasional case when the cystic duct comes off the right hepatic duct. We do not feel routine LCP examination of the ductal system is indicated but in selected cases. The examination with LCP is extremely rewarding and not terrifically difficult in any hospital where the intraoperative endoscopic retrograde cholangiopancreatography (ERCP) is practiced. As far as the cost is concerned, the increase is quite acceptable (Table 1). Of course, if there is any reason

for intraoperative ERCP to be done, it can be easily accomplished during LCP, though it needs not to be done as a routine. LCP can not help operators realize if there are continuity, stones, tumor and injury of the ducts. When the forgoing conditions are suspected, cholangiography should be done with intraoperative ERCP.

LCP is currently the most effective way to directly observe the extrahepatic ductal system during laparoscopic cholecystectomy and may play a useful role in clarifying uncertain anatomy in selected cases. As a useful assisting measure, it plays an important role in preventing extrahepatic duct injury in LC.

REFERENCES

- 1 **Savassi-Rocha PR**, Almeida SR, Sanches MD, Andrade MA, Frerreira JT, Diniz MT, Rocha AL. Iatrogenic bile duct injuries. *Surg Endosc* 2003; **17**: 1356-1361
- 2 **Kurumi Y**, Tani T, Hanasawa K, Kodama M. The prevention of bile duct injury during laparoscopic cholecystectomy from the point of view of anatomic variation. *Surg Laparosc Endosc Percutan Tech* 2000; **10**: 192-199
- 3 **Mahatharadol V**. Bile duct injuries during laparoscopic cholecystectomy: an audit of 1522 cases. *Hepatogastroenterology* 2004; **51**: 12-14
- 4 **Francoeur JR**, Wiseman K, Buczkowski AK, Chung SW, Scudamore CH. Surgeons' anonymous response after bile duct injury during cholecystectomy. *Am J Surg* 2003; **185**: 468-475
- 5 **Bingener-Casey J**, Richards ML, Strodel WE, Schwesinger WH, Sirinek KR. Reasons for conversion from laparoscopic to open cholecystectomy: a 10-year review. *J Gastrointest Surg* 2002; **6**: 800-805
- 6 **Panpimanmas S**, Kanyaprasit K. Complications of laparoscopic cholecystectomy and their management. *Hepatogastroenterology* 2004; **51**: 9-11
- 7 **Fathy O**, Zeid MA, Abdallah T, Fouad A, Eleinien AA, el-Hak NG, Eleibiedy G, el-Wahab MA, Sultan A, Anwar N, Ezzat F. Laparoscopic cholecystectomy: a report on 2000 cases. *Hepatogastroenterology* 2003; **50**: 967-971
- 8 **Calvete J**, Sabater L, Camps B, Verdu A, Gomez-Portilla A, Martin J, Torrico MA, Flor B, Cassinello N, Lledo S. Bile duct injury during laparoscopic cholecystectomy: myth or reality of the learning curve? *Surg Endosc* 2000; **14**: 608-611
- 9 **Yang FQ**, Dai XW, Wang L, Yu Y. Iatrogenic extrahepatic bile duct injury in 182 patients: causes and management. *Hepatobiliary Pancreat Dis Int* 2002; **1**: 265-269
- 10 **Panzer F**, Ghisio S, Grosso A, Vigezzi P, Vitale M, Cariaggi RM, Mistrangelo M. Laparoscopic cholecystectomy. Our experience. *Minerva Chir* 2000; **55**: 489-492
- 11 **Luo D**, Chen XR, Mao JX, Li SH, Zhou ZD, Yu SM. Three-dimensional identification of the cystic infundibulum-cystic duct junction: a technique for identification of the cystic duct in laparoscopic cholecystectomy. *Hepatobiliary Pancreat Dis Int* 2003; **2**: 441-444
- 12 **Bassi M**. Bile duct injuries due to unwarranted duct catheterization during cholangiography (prevention and treatment). *Chir Ital* 2003; **55**: 41-44
- 13 **Polat FR**, Abci I, Coskun I, Uranues S. The importance of intraoperative cholangiography during laparoscopic cholecystectomy. *JSLs* 2000; **4**: 103-107
- 14 **Ludwig K**, Bernhardt J, Steffen H, Lorenz D. Contribution of intraoperative cholangiography to incidence and outcome of common bile duct injuries during laparoscopic cholecystectomy. *Surg Endosc* 2002; **16**: 1098-1104
- 15 **Flum DR**, Dellinger EP, Cheadle A, Chan L, Koepsell T. Intraoperative cholangiography and risk of common bile duct injury during cholecystectomy. *JAMA* 2003; **289**: 1639-1644
- 16 **Vezakis A**, Davides D, Ammori BJ, Martin IG, Larvin M, McMahon MJ. Intraoperative cholangiography during laparoscopic cholecystectomy. *Surg Endosc* 2000; **14**: 1118-1122
- 17 **Metcalfe MS**, Ong T, Bruening MH, Iswariah H, Wemyss-Holden SA, Maddern GJ. Is laparoscopic intraoperative cholangiogram a matter of routine? *Am J Surg* 2004; **187**: 475-481
- 18 **Xu JJ**, Xiong XH, Yu HL, Xi JS, Bu YB, Jin SS. The effect of methylenum coeruleum in laparoscope cholecystectomy. *Zhonghua Waike Zazhi* 2000; **38**: 756-757

Edited by Wang XL and Zhang JZ Proofread by Xu FM

• CASE REPORT •

An unusual presentation of "silent" disseminated pancreatic neuroendocrine tumor

Dragomir Marisavljevic, Natasa Petrovic, Nikola Milinic, Vesna Cemerikic, Miodrag Krstic, Olivera Markovic, Dragoljub Bilanovic

Dragomir Marisavljevic, Natasa Petrovic, Nikola Milinic, Olivera Markovic, Dragoljub Bilanovic, Medical Center "Bezanijska kosa", Belgrade, Yugoslavia

Vesna Cemerikic, Miodrag Krstic, Clinical Center Serbia, Belgrade, Yugoslavia

Correspondence to: Petrovic Natasa, Medical Center "Bezanijska kosa", Bezanijska kosa bb, 11080 Belgrade, Yugoslavia. naca@infosky.net

Telephone: +381-11-3010748 **Fax:** +381-11-606520

Received: 2003-06-30 **Accepted:** 2003-11-06

Abstract

To present a patient diagnosed with pancreatic carcinoid that was extremely rare and produced an atypical carcinoid syndrome. We reported a 58-year old male patient who presented with long standing, prominent cervical lymphadenopathy and occasional watery diarrhea. Pathohistological and immunohistochemical examination of lymph node biopsy showed a metastatic neuroendocrine tumor, which was histological type A of carcinoid (EMA+, cytokeratin+, CEA-, NSE+, chromogranin A+, synaptophysin+, insulin-). Bone marrow biopsy showed identical findings. Primary site of the tumor was pancreas and diagnosis was made according to cytological and immunocytochemical analysis of the tumor cells obtained with aspiration biopsy of pancreatic mass (12 mm in diameter) under endoscopic ultrasound guidance. However, serotonin levels in blood and urine samples were normal. It is difficult to establish the precise diagnosis of a "functionally inactive" pancreatic carcinoid and aspiration biopsy of pancreatic tumor under endoscopic ultrasound guidance can be used as a new potent diagnostic tool.

Marisavljevic D, Petrovic N, Milinic N, Cemerikic V, Krstic M, Markovic O, Bilanovic D. An unusual presentation of "silent" disseminated pancreatic neuroendocrine tumor. *World J Gastroenterol* 2004; 10(19): 2919-2921

<http://www.wjgnet.com/1007-9327/10/2919.asp>

INTRODUCTION

In 1907, Obendorfer applied the term "karzinoide" to describe a set of ileal tumors that behaved in a more benign manner than carcinomas. Since then, carcinoid tumors have been found to be relatively uncommon neuroendocrine tumors arising from neural crest cells known as "amine precursor uptake and decarboxylation cells" (APUD), which are derived from gut endoderm. Recent consensus meetings suggested that a more appropriate term "neuroendocrine tumor" should be used for all endocrine tumors of the digestive system, because these tumors derive from the diffuse neuroendocrine system^[1]. Pancreas, mucosa of the gastrointestinal tract^[2] and endocrine cells scattered in other endodermal sites (such as thyroid, lung, biliary tree and the urogenital tract) belong to APUD system. Neuroendocrine tumors can be subclassified into those with or without clinical syndromes and are termed "functionally active" and "functionally inactive" pancreatic carcinoid, respectively^[3].

Carcinoid of the pancreas is extremely rare and the diagnosis may puzzle physicians and pathologists^[4]. Pancreatic carcinoids produce an atypical carcinoid syndrome, skin flushing was reported in only 34%, the main symptom is pain, followed by diarrhea and weight loss.

We hereby described a patient with disseminated "functionally inactive" neuroendocrine tumor who presented with lymph node metastases, but without characteristic symptoms of carcinoid syndrome. The primary site of the tumor was pancreas.

CASE REPORT

A 58-years old male was admitted to Hematology Department in June 2001 with complaint of a left anterior neck mass and occasional massive, watery diarrhea. The patient noticed slow enlargement of neck mass for two years prior to admission, and also stated that in the last 12 mo he had episodes of diarrhea 1-2 times/wk. Diarrhea was massive and watery (up to 1 L/d) without visible blood or mucous and usually self-limited. Diarrhea was not associated with abdominal pain, tenesmus or with food intake. He lost 5 kg in 3-4 mo, inspite of good appetite. His previous medical history was unremarkable. Physical examination showed a left anterior neck mass (7 cm×6 cm in diameter), painless and movable in all directions. Chest X-ray showed paratracheal infiltrate. On bronchoscopy, external compression on posterior and lateral tracheal walls was seen. CT of chest showed enlarged mediastinal lymph nodes (up to 40 mm). CT of abdomen showed an enlarged pancreatic head (46 mm) with a mild hypodense area (12 mm in diameter). Pathohistological findings of tissue samples from the neck tumor (cuneiform biopsy) and bone marrow (trephine biopsy) were identical, namely a metastatic neuroendocrine tumor, which was histological type A of carcinoid. Immunophenotyping of cells from the neck tissue sample showed well-differentiated neuroendocrine tumor (APUDOMA) that was immunostained as follows: EMA+, cytokeratin 8+, CEA-, NSE+, *chromogranin A+*, *synaptophysin+*, insulin-. In an effort to find the primary site of APUDOMA, esophagogastroduodenoscopy, endoscopic enteroscopy, colonoscopy, small bowel barium enema, radial endoscopic ultrasound (radial EUS - Olympus device) were done (Figure 1). Ultrasound (linear EUS) guided aspiration biopsy of the pancreatic mass was performed (Figure 2). Cytological examination showed solid nodular nests of small uniform, epitheloid cells of dense heterochromatin. Immunocytochemical analysis revealed groups of epithelial cells with positive cytoplasmatic staining on NSE and chromogranin A that implied on tumor with neuroendocrine differentiation (Figure 3). Pathohistological examination of aspiration liver biopsy was normal, excluding possible liver micro-metastasis. To exclude MEN syndrome, X-ray and MRI of sellar region as well as thyroid US were done and all tests were normal. On 2D ultrasound the right heart was anatomically and functionally within normal limits. Blood count and biochemistry were normal except for occasional hypokalemia and mild hypoproteinaemia (with proportional decrease in all electrophoresis fractions). CEA was significantly increased (535.5 ng/mL), but pancreatic tumor marker (CA 19-9) and alpha-feto protein were within normal

limits. Serotonin level in blood and urine was normal (0.25 mmol/L and 359 mmol/24 h, respectively). 5-HIAA in the urine sample was increased (84 μ mol/L, reference range: 10.4-41.6 μ mol/L). Periodical diarrhea was controlled with loperamid and oral potassium supplementation. During hospitalization, patient developed urinary retention. Rectal examination and US revealed a prostatic adenoma (size 44 mm \times 54 mm \times 54 mm, 60 g weight) with normal values of prostate serum antigen. Transvesical adenectomy was performed, and pathohistologic findings confirmed it to be an adenoma. Postoperative period was complicated with prolonged wound healing and vesicodermal fistula. The patient also had changes of mental status, but CT of the head did not show any abnormalities. The patient was regularly followed up. In December 2001 he was doing well, still complaining of frequent diarrhea and minimal enlargement of the neck mass. Blood tests continued to show hypoproteinemia and hypokalemia, easily controlled with potassium supplementation. However, the patient died in January 2002 at home. His family recorded no particular circumstances related to his death.



Figure 1 Pancreatic mass (radial endoscopic ultrasound, Olympus device).



Figure 2 Ultrasound (linear EUS) guided aspiration biopsy of the pancreatic mass.

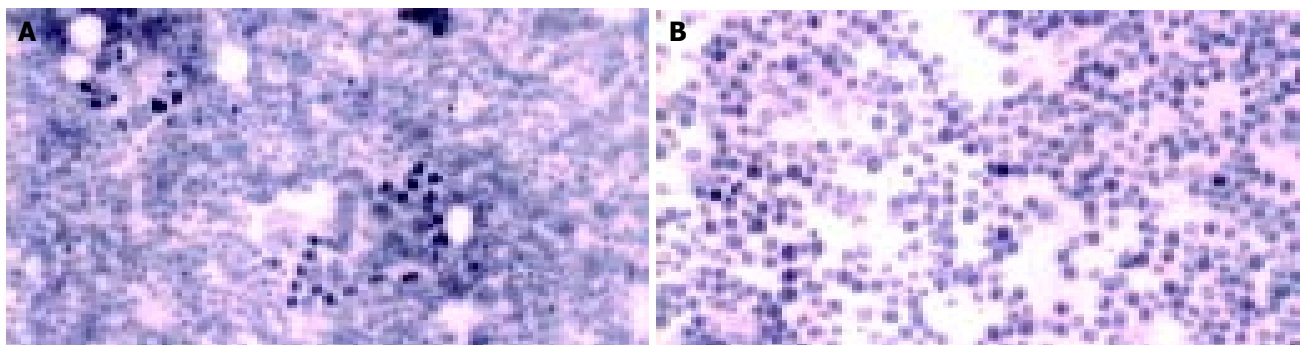


Figure 3 Groups of epithelial cells with positive cytoplasmic staining on chromogranin (A) and NSE (B) (immunocytochemical analysis).

DISCUSSION

Functionally active neuroendocrine tumors are presented with clinical symptoms because of excessive hormone release from the tumor cells as in insulinoma, gastrinoma, VIPoma, glucagonoma and carcinoid syndrome^[5]. Carcinoid tumors, except those originating from rectum, produced a variety of endocrine substances, the most frequent one was serotonin and kallikrein^[6-8]. Carcinoid syndrome that includes diarrhea, flushing, wheezing, and right-sided heart disease^[9] is caused by systemic serotonin release. Less than 10% of carcinoids had some of these symptoms^[10]. Explanation is efficient hepatic metabolism of vasoactive amines, and that is also the reason why carcinoid syndrome rarely occurred in the absence of liver metastasis. Exceptions are circumstances in which venous blood from a large tumor was drained directly into systemic circulation^[11].

Functionally inactive neuroendocrine tumors can be diagnosed in several ways: a) accidentally during routine ultrasonography performed for unexplained abdominal complaints, b) when a large tumor of the pancreatic head is causing obstruction and consequently extrahepatic jaundice, c) when a patient presents with abdominal pain secondary to bowel pseudo-obstruction, and d) as complications of the tumor such as bleeding. Our patient had occasional diarrhea that was not significant (less than 1L per day). Besides he had no other symptoms, and his blood tests failed to show any endocrine abnormalities. Histopathological and immunohistochemical analyses of the tissue sample from the neck mass showed a well-differentiated neuroendocrine tumor, which was histological type A of carcinoid (APUDOMA). At the time of diagnosis, metastatic disease of cervical and mediastinal lymph nodes, and bone marrow already existed which was confirmed by histopathological finding. Aspiration liver biopsy was done to exclude micro-metastases, that otherwise could not be visualized by imaging methods, and the result was negative. Primary site of the tumor was unknown. Because the most frequent localization of carcinoid was in the gastrointestinal tract, it was explored in whole, but primary tumor was not found. Aspiration biopsy of the pancreatic mass under endoscopic ultrasound guidance was done for the first time in Yugoslavia. Immunocytochemical report confirmed that the pancreatic mass was the primary site that only occurred in 2-3% of all cases^[4,12,13]. Also, carcinoid tumors up to 1 cm rarely metastasize, but that was not the case with our patient.

The slow growth rate and late invasion of adjacent organs rendered local resection of pancreatic carcinoid tumor possible, but the high incidence of distant metastases (69%) prevented long-term survival in the majority of patients^[4]. Diarrhea with hypokalemia and hypoproteinemia, as a manifestation of carcinoid syndrome in this case could be explained by increased release of vasoactive substances most probably from the

extensive metastasis in the bone marrow, and lymph nodes. However, these metabolic abnormalities were well controlled and could not be the main cause of his death.

In summary, atypical presentation in this and other reported cases of pancreatic carcinoids suggests that metastatic potential of functionally inactive neuroendocrine cells is originated from the pancreas.

REFERENCES

- 1 **Polak JM.** Diagnostic histopathology of neuroendocrine tumors. *Edinburgh: Churchill-Livingstone* 1993
- 2 **Solcia E, Capella C, Riocca R.** Disorders of the endocrine system. In: Ming SC, Goldman H, eds. *Pathology of the gastrointestinal tract. Philadelphia: Williams and Wilkins* 1998: 295-322
- 3 **Arnold R.** Diagnosis and Management of Neuroendocrine Tumors. 8th United European Gastroenterology Week, Brussels, *Belgium* 2001
- 4 **Maurer CA, Baer HU, Dyong TH, Mueller-Garamvoelgyi E, Friess H, Ruchti C, Reubi JC, Buchler MW.** Carcinoid of the pancreas: clinical characteristics and morphological features. *Eur J Cancer* 1996; **32A**: 1109-1116
- 5 **Eriksson B, Oberg K, Stridsberg M.** Tumor markers in neuroendocrine tumors. *Digestion* 2000; **62**: 33-38
- 6 **Sweeney JF, Rosemurgy AS.** Carcinoid tumors of the gut. *Cancer Control* 1997; **4**: 18-24
- 7 **Shebani KO, Souba WW, Finkelstein DM, Stark PC, Elgadi KM, Tanabe KK, Ott MJ.** Prognosis and survival in patients with gastrointestinal tract carcinoid tumors. *Ann Surg* 1999; **229**: 815-821
- 8 **Kulke MH, Mayer RJ.** Carcinoid tumors. *N Engl J Med* 1999; **340**: 858-868
- 9 **Anderson AS, Krauss D, Lang R.** Cardiovascular complications of malignant carcinoid disease. *Am Heart J* 1997; **134**: 693-702
- 10 **Vinik AI, Thompson N, Eckhauser F, Moattari AR.** Clinical features of carcinoid syndrome and the use of somatostatin analogue in its management. *Acta Oncol* 1989; **28**: 389-402
- 11 **Onaitis MW, Kirshbom PM, Hayward TZ, Quayale FJ, Feldman JM, Seigler HF, Tyler DS.** Gastrointestinal Carcinoids: Characterization by site of origin and hormone production. *Ann Surg* 2000; **232**: 549-556
- 12 **Varshney S, Johnson CD.** Neuroendocrine tumors of the pancreas. *Indian J Gastroenterol* 2000; **19**: 181-183
- 13 **Jensen RT.** Pancreatic endocrine tumors: recent advances. *Ann Oncol* 1999; **10**: 170-176

Edited by Wang XL and Xu JY Proofread by Xu FM

• LETTERS@WJGNET.COM •

Regulation of plasma erythropoietin in chronic liver disease

Frank Tacke, Tom Luedde, Michael P. Manns, Christian Trautwein

Frank Tacke, Tom Luedde, Michael P. Manns, Christian Trautwein, Department of Gastroenterology, Hepatology and Endocrinology, Hannover Medical School 30625 Hannover, Germany

Correspondence to: Christian Trautwein, M.D., Professor of Medicine, Hannover Medical School, Department of Gastroenterology, Hepatology and Endocrinology, Carl-Neuberg-Strasse 1, D-30625, Hannover, Germany. trautwein.christian@mh-hannover.de

Telephone: +49-511-5326620 **Fax:** +49-511-5324896

Received: 2004-05-25 **Accepted:** 2004-06-22

Tacke F, Luedde T, Manns MP, Trautwein C. Regulation of plasma erythropoietin in chronic liver disease. *World J Gastroenterol* 2004; 10(19): 2922

<http://www.wjgnet.com/1007-9327/10/2922.asp>

To the Editor:

In a May-issue of the *World Journal of Gastroenterology*, there is a very interesting study by Bruno *et al.* on erythropoietin (EPO) levels in patients with chronic liver disease^[1]. We have very recently reported a similar, but much larger study by Tacke *et al.*^[2] on the role of EPO in chronic liver disease. By comparing Bruno's results with our patient cohort and applying their criteria in a re-evaluation of our study population, we uncovered interesting differences between the two studies and could answer some of the key questions in the article raised by Bruno *et al.*, e.g. on the correlation of EPO with liver dysfunction and potential regulating factors in the clinical setting of liver cirrhosis.

Therefore, we would like to briefly present our data and compare the results with Bruno's recent study. We think the role of EPO is important in the pathophysiology of chronic liver disease, and the recent studies provided new insights into its regulation in liver cirrhosis.

Chronic anemia is a common clinical complication in patients with liver cirrhosis and is regarded as an important prognostic factor^[3]. The great progress in the understanding of cytokine alterations in chronic liver diseases as well as the discovery and clinical application of different hematopoietic growth factors have raised attention to the potential pathophysiological role of erythropoietin (EPO) in liver diseases^[4,5]. In a recent issue of the *World Journal of Gastroenterology*, Bruno *et al.* reported that increased EPO plasma levels were only detected in cirrhotic patients with hemoglobin concentrations below 12 g/dL and that this EPO response was inadequate compared to patients with iron-deficiency anemia^[1]. Furthermore, the authors did not observe an association between EPO levels and the stage of liver cirrhosis or liver synthesis function. The regulating factors in the pathophysiological setting of advanced liver diseases as well as possible clinical consequences remained an open question.

We analyzed 111 patients with chronic liver diseases who were evaluated for potential liver transplantation and 220 healthy (non-anemic) controls with the same EPO ELISA (R&D Systems, Wiesbaden, Germany) kit. In contrast to Bruno *et al.* who studied mainly patients with viral hepatitis and advanced stages of cirrhosis, our much larger cohort comprised all Child's stages of cirrhosis in a fairly equal number of patients as well as different etiology subgroups. As we reported recently, EPO plasma levels

clearly increased with Child's stage of liver cirrhosis, independent of the disease etiology (Figure 1)^[2]. EPO also correlated directly with the markers of liver synthesis function, e.g. cholinesterase activity ($r = -0.448, P < 0.001$), albumin concentration ($r = -0.358, P < 0.001$), or prothrombin time ($r = 0.300, P = 0.001$). Interestingly, the absolute values of measured EPO levels in Bruno *et al.* and our studies were relatively similar (e.g. mean EPO 11.6 U/L for chronic hepatitis by Bruno *et al.*, median EPO 11.3 U/L for our "non cirrhosis" group), thereby raising the question whether the clear association between EPO and stage of liver cirrhosis could have been observed if the number of patients included in Bruno *et al.* study was high enough. Furthermore, it is hard to believe that EPO was normally distributed in anemic or non-anemic cirrhotic patients as the mean±SD values suggested by Bruno *et al.*, thus a different statistical analysis using median and U-test could possibly uncover these important correlations.

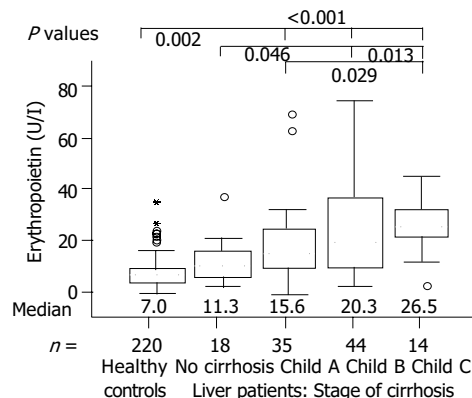


Figure 1 Erythropoietin plasma levels and stage of cirrhosis. EPO was significantly higher in patients with liver cirrhosis than in healthy controls and increased with Child's stages of cirrhosis.

We also found a significant inverse correlation between EPO levels and hemoglobin in patients with chronic liver diseases ($r = -0.498, P < 0.001$, Spearman rank correlation analysis). As this was described by Bruno *et al.* only for patients with iron-deficiency anemia, this correlation could not be observed when we divided our liver disease patient group by the criteria of Bruno *et al.* into so-called anemic or non-anemic patients ($hb \leq 12, n = 48$, vs $hb > 120$ g/L, $n = 63$). However, in accordance with Bruno *et al.*, we also found significantly elevated EPO levels in anemic vs non-anemic liver disease patients (median EPO 29.3 vs 11.4 U/L, $P < 0.001$, U-test). In contrast, the non-anemic liver disease patients also had elevated EPO levels as compared with controls ($P < 0.05$), which could be possibly explained by the much larger control group in our study.

In further investigating the potential regulating factors, one should consider the complex clinical picture of advanced liver cirrhosis. As we could show, the degrees of anemia and liver dysfunction not only were independent parameters associated with elevated EPO in chronic liver disease, but also impaired pulmonary function^[2]. Changes in pulmonary function test and blood gas analysis were commonly found in our study population, and EPO was inversely correlated with carbon dioxide tension (pCO_2) and elevated in patients with reduced (carbon monoxide) diffusion capacity. In addition, we noticed a positive correlation between interleukin-6 and EPO, thereby possibly linking the EPO response to a common protective cytokine response usually seen in liver cirrhosis^[6].

In conclusion, the recent studies by Bruno *et al.* and our group provide some new important insights in the regulation of plasma EPO in chronic liver diseases. EPO plasma levels are apparently upregulated in patients with liver cirrhosis, and one might speculate whether this increase is sufficient in the setting of chronic anemia when compared with other forms of anemia,

e.g. iron-deficiency. However, the regulation of plasma EPO is complex and multifactorial, and the degrees of anemia, liver dysfunction, impaired pulmonary function and cytokine alterations are the major factors in regulating plasma erythropoietin in patients with chronic liver diseases.

REFERENCES

- 1 **Bruno CM**, Neri S, Sciacca C, Bertino G, Di Prima P, Cilio D, Pellicano R, Caruso L, Cristaldi R. Plasma erythropoietin levels in anaemic and non-anaemic patients with chronic liver diseases. *World J Gastroenterol* 2004; **10**: 1353-1356
- 2 **Tacke F**, Schoffski P, Luedde T, Meier PN, Ganser A, Manns MP, Trautwein C. Analysis of factors contributing to higher erythropoietin levels in patients with chronic liver disease. *Scand J Gastroenterol* 2004; **39**: 259-266
- 3 **Orrego H**, Israel Y, Blake JE, Medline A. Assessment of prognostic factors in alcoholic liver disease: toward a global quantitative expression of severity. *Hepatology* 1983; **3**: 896-905
- 4 **Pirisi M**, Fabris C, Falletti E, Soardo G, Toniutto P, Gonano F, Bartoli E. Evidence for a multifactorial control of serum erythropoietin concentration in liver disease. *Clin Chim Acta* 1993; **219**: 47-55
- 5 **Yang YY**, Lin HC, Lee WC, Huang YT, Hou MC, Lee FY, Chang FY, Lee SD. Plasma erythropoietin level in patients with cirrhosis and its relationship to the severity of cirrhosis and renal function. *J Gastroenterol Hepatol* 2003; **18**: 1156-1161
- 6 **Streetz KL**, Tacke F, Leifeld L, Wustefeld T, Graw A, Klein C, Kamino K, Spengler U, Kreipe H, Kubicka S, Muller W, Manns MP, Trautwein C. Interleukin 6/gp130-dependent pathways are protective during chronic liver diseases. *Hepatology* 2003; **38**: 218-229

Edited by Xu XQ, Wang XL and Zhang JZ

• LETTERS@WJGNET.COM •

Comment on "Eosinophilic gastroenteritis: Clinical experience with 15 patients"

Peter J Kerr

Peter J Kerr, BEng (Hons) CEng, MIEE, MIMechE
Correspondence to: Mr Peter J Kerr, 6 Middledyke Lane, Cottingham, East Yorkshire, HU16 4NH, United Kingdom. pkerr@pkerr.karoo.co.uk
Telephone: +44-1482-847201 **Fax:** +44-1482-847201
Received: 2004-06-15 **Accepted:** 2004-06-22

Kerr PJ. Comment on "Eosinophilic gastroenteritis: Clinical experience with 15 patients". *World J Gastroenterol* 2004; **10**(19): 2923

<http://www.wjgnet.com/1007-9327/10/2923.asp>

To the Editor:

I recently read the paper by Chen *et al.*^[1] published in your Journal. The paper shows that there have been a few cases where medications have caused eosinophilia. Clozapine is an antipsychotic medication that can cause eosinophilia. It is pointed out in your paper "The diagnostic criteria included . . . 5), exclusion of intestinal lymphoma, Crohn's disease or other tumors." Table 2 shows symptoms associated with eosinophilic gastroenteritis, which are very like those in Crohn's disease.

Miss Z, a 29 years old female received a diagnosis of Crohn's disease five years ago. It seemed to be the more aggressive fistulizing form of Crohn's disease. The inflammation seemed

to be located in her colon. She had several perianal abscesses. Miss Z took the antipsychotic, clozapine. Clozapine can cause constipation, diarrhea^[2-7], nausea^[6,8], vomiting^[3,6,8], allergic reactions, *etc.* Clozapine has also been linked with colitis^[5,14], gastrointestinal symptoms^[7], hepatotoxicity^[12], eosinophilia^[5,7,9], neutropenia^[5,6], colon perforation^[13], necrotizing colitis^[13], perianal abscesses^[9], and increased levels of TNF-alpha^[10], *etc.*

When Miss Z was growing up, she had no prodromal symptoms that, even with the benefit of hindsight one might be able to say, this was the beginning of Crohn's disease. The sickness and diarrhea started 32 d after the clozapine was titrated to its full dose of 300 mg/d in November 1998.

Tumor necrosis factor α (TNF α) is a proinflammatory cytokine that has an important role in the pathogenesis of Crohn's disease. Infliximab-a chimeric anti-TNF α monoclonal antibody binds to TNF α with high affinity, thereby neutralising its biological activity. Pollmacher *et al.*^[10], found that clozapine significantly increased the plasma levels of TNF-alpha.

Miss Z responded very well to infliximab. Steroids (prednisolone) had little effect on the symptoms. Stopping clozapine was not an option unless we were to be reasonably sure that it was responsible for causing or exacerbating the inflammation in Miss Z's colon.

I am particularly interested in the effect of clozapine. If it were to cause eosinophilia it might have effects on the colon. I wondered if the symptoms of nausea, vomiting, *etc.*, might persist all the time when clozapine was taken.

REFERENCES

- 1 **Chen MJ**, Chu CH, Lin SC, Shih SC, Wang TE. Eosinophilic gastroenteritis: Clinical experience with 15 patients. *World J Gastroenterol* 2003; **9**: 2813-2816
- 2 **Harvey RJ**, Bullock T, Montgomery SA. Diarrhoea during treatment with clozapine: association with lymphocyte count. *BMJ* 1992; **305**: 810
- 3 **Patterson BD**, Jennings JL. Spiking fever and profuse diarrhea with clozapine treatment. *American J Psychiatry* 1993; **150**: 1126
- 4 **Druss BG**, Mazure CM. Transient fever and hematologic abnormalities during clozapine use. *J Clin Psychopharmacol* 1993; **13**: 155-156
- 5 **Lucht MJ**, Rietschel M. Clozapine-induced eosinophilia: subsequent neutropenia and corresponding allergic mechanisms. *J Clin Psychiatry* 1998; **59**: 195-197
- 6 **Beck DA**, Miller DD. Clozapine-associated neutropenic enterocolitis. *Ann Clin Psychiatry* 1994; **6**: 185-188
- 7 **Galletly C**, Wilson D, McEwen S. Eosinophilia associated with decreasing neutrophil count in a clozapine treated patient. *J Clin Psychiatry* 1996; **57**: 40-41
- 8 **Maria DD**. Clozapine-induced gastrointestinal symptoms. Llorente, Annual Meeting - American Psychiatric Association. *New Research Abstracts* 1997; **150**: 132
- 9 **Amital D**, Gross R, Amital H, Zohar I. Coexistence of eosinophilia and agranulocytosis in a clozapine treated patient. *British J Psychiatry* 1997; **170**: 194
- 10 **Pollmacher T**, Hinze-Selch D, Mullington J. Effects of clozapine on plasma cytokine and soluble cytokine receptor levels. *J Clin Psychopharmacol* 1996; **16**: 403-409
- 11 **John JP**, Chengappa KN, Baker RW, Gupta B, Mortimer MT. Assessment of changes in both weight and frequency of use of medications for the treatment of gastrointestinal symptoms among clozapine-treated patients. *Ann Clin Psychiatry* 1995; **7**: 119-125
- 12 **Macfarlane B**, Davies S, Mannan K, Sarsam R, Pariente D, Dooley J. Fatal acute fulminant liver failure due to clozapine: a case report and review of clozapine-induced hepatotoxicity. *Gastroenterology* 1997; **112**: 1707-1709
- 13 **Freudenreich O**, Goff DC. Colon perforation and peritonitis associated with clozapine. *J Clin Psychiatry* 2000; **61**: 950-951
- 14 **Friedberg JW**, Frankenburg FR, Burk J, Johnson W. Clozapine-caused eosinophilic colitis. *Ann Clin Psychiatry* 1995; **7**: 97-98

Edited by Xu XQ, Wang XL and Zhang JZ

e.g. iron-deficiency. However, the regulation of plasma EPO is complex and multifactorial, and the degrees of anemia, liver dysfunction, impaired pulmonary function and cytokine alterations are the major factors in regulating plasma erythropoietin in patients with chronic liver diseases.

REFERENCES

- 1 **Bruno CM**, Neri S, Sciacca C, Bertino G, Di Prima P, Cilio D, Pellicano R, Caruso L, Cristaldi R. Plasma erythropoietin levels in anaemic and non-anaemic patients with chronic liver diseases. *World J Gastroenterol* 2004; **10**: 1353-1356
- 2 **Tacke F**, Schoffski P, Luedde T, Meier PN, Ganser A, Manns MP, Trautwein C. Analysis of factors contributing to higher erythropoietin levels in patients with chronic liver disease. *Scand J Gastroenterol* 2004; **39**: 259-266
- 3 **Orrego H**, Israel Y, Blake JE, Medline A. Assessment of prognostic factors in alcoholic liver disease: toward a global quantitative expression of severity. *Hepatology* 1983; **3**: 896-905
- 4 **Pirisi M**, Fabris C, Falletti E, Soardo G, Toniutto P, Gonano F, Bartoli E. Evidence for a multifactorial control of serum erythropoietin concentration in liver disease. *Clin Chim Acta* 1993; **219**: 47-55
- 5 **Yang YY**, Lin HC, Lee WC, Huang YT, Hou MC, Lee FY, Chang FY, Lee SD. Plasma erythropoietin level in patients with cirrhosis and its relationship to the severity of cirrhosis and renal function. *J Gastroenterol Hepatol* 2003; **18**: 1156-1161
- 6 **Streetz KL**, Tacke F, Leifeld L, Wustefeld T, Graw A, Klein C, Kamino K, Spengler U, Kreipe H, Kubicka S, Muller W, Manns MP, Trautwein C. Interleukin 6/gp130-dependent pathways are protective during chronic liver diseases. *Hepatology* 2003; **38**: 218-229

Edited by Xu XQ, Wang XL and Zhang JZ

• LETTERS@WJGNET.COM •

Comment on "Eosinophilic gastroenteritis: Clinical experience with 15 patients"

Peter J Kerr

Peter J Kerr, BEng (Hons) CEng, MIEE, MIMechE
Correspondence to: Mr Peter J Kerr, 6 Middledyke Lane, Cottingham, East Yorkshire, HU16 4NH, United Kingdom. pkerr@pkerr.karoo.co.uk
Telephone: +44-1482-847201 **Fax:** +44-1482-847201
Received: 2004-06-15 **Accepted:** 2004-06-22

Kerr PJ. Comment on "Eosinophilic gastroenteritis: Clinical experience with 15 patients". *World J Gastroenterol* 2004; **10**(19): 2923

<http://www.wjgnet.com/1007-9327/10/2923.asp>

To the Editor:

I recently read the paper by Chen *et al.*^[1] published in your Journal. The paper shows that there have been a few cases where medications have caused eosinophilia. Clozapine is an antipsychotic medication that can cause eosinophilia. It is pointed out in your paper "The diagnostic criteria included . . . 5), exclusion of intestinal lymphoma, Crohn's disease or other tumors." Table 2 shows symptoms associated with eosinophilic gastroenteritis, which are very like those in Crohn's disease.

Miss Z, a 29 years old female received a diagnosis of Crohn's disease five years ago. It seemed to be the more aggressive fistulizing form of Crohn's disease. The inflammation seemed

to be located in her colon. She had several perianal abscesses. Miss Z took the antipsychotic, clozapine. Clozapine can cause constipation, diarrhea^[2-7], nausea^[6,8], vomiting^[3,6,8], allergic reactions, *etc.* Clozapine has also been linked with colitis^[5,14], gastrointestinal symptoms^[7], hepatotoxicity^[12], eosinophilia^[5,7,9], neutropenia^[5,6], colon perforation^[13], necrotizing colitis^[13], perianal abscesses^[9], and increased levels of TNF-alpha^[10], *etc.*

When Miss Z was growing up, she had no prodromal symptoms that, even with the benefit of hindsight one might be able to say, this was the beginning of Crohn's disease. The sickness and diarrhea started 32 d after the clozapine was titrated to its full dose of 300 mg/d in November 1998.

Tumor necrosis factor α (TNF α) is a proinflammatory cytokine that has an important role in the pathogenesis of Crohn's disease. Infliximab-a chimeric anti-TNF α monoclonal antibody binds to TNF α with high affinity, thereby neutralising its biological activity. Pollmacher *et al.*^[10], found that clozapine significantly increased the plasma levels of TNF-alpha.

Miss Z responded very well to infliximab. Steroids (prednisolone) had little effect on the symptoms. Stopping clozapine was not an option unless we were to be reasonably sure that it was responsible for causing or exacerbating the inflammation in Miss Z's colon.

I am particularly interested in the effect of clozapine. If it were to cause eosinophilia it might have effects on the colon. I wondered if the symptoms of nausea, vomiting, *etc.*, might persist all the time when clozapine was taken.

REFERENCES

- 1 **Chen MJ**, Chu CH, Lin SC, Shih SC, Wang TE. Eosinophilic gastroenteritis: Clinical experience with 15 patients. *World J Gastroenterol* 2003; **9**: 2813-2816
- 2 **Harvey RJ**, Bullock T, Montgomery SA. Diarrhoea during treatment with clozapine: association with lymphocyte count. *BMJ* 1992; **305**: 810
- 3 **Patterson BD**, Jennings JL. Spiking fever and profuse diarrhea with clozapine treatment. *American J Psychiatry* 1993; **150**: 1126
- 4 **Druss BG**, Mazure CM. Transient fever and hematologic abnormalities during clozapine use. *J Clin Psychopharmacol* 1993; **13**: 155-156
- 5 **Lucht MJ**, Rietschel M. Clozapine-induced eosinophilia: subsequent neutropenia and corresponding allergic mechanisms. *J Clin Psychiatry* 1998; **59**: 195-197
- 6 **Beck DA**, Miller DD. Clozapine-associated neutropenic enterocolitis. *Ann Clin Psychiatry* 1994; **6**: 185-188
- 7 **Galletly C**, Wilson D, McEwen S. Eosinophilia associated with decreasing neutrophil count in a clozapine treated patient. *J Clin Psychiatry* 1996; **57**: 40-41
- 8 **Maria DD**. Clozapine-induced gastrointestinal symptoms. Llorente, Annual Meeting - American Psychiatric Association. *New Research Abstracts* 1997; **150**: 132
- 9 **Amital D**, Gross R, Amital H, Zohar I. Coexistence of eosinophilia and agranulocytosis in a clozapine treated patient. *British J Psychiatry* 1997; **170**: 194
- 10 **Pollmacher T**, Hinze-Selch D, Mullington J. Effects of clozapine on plasma cytokine and soluble cytokine receptor levels. *J Clin Psychopharmacol* 1996; **16**: 403-409
- 11 **John JP**, Chengappa KN, Baker RW, Gupta B, Mortimer MT. Assessment of changes in both weight and frequency of use of medications for the treatment of gastrointestinal symptoms among clozapine-treated patients. *Ann Clin Psychiatry* 1995; **7**: 119-125
- 12 **Macfarlane B**, Davies S, Mannan K, Sarsam R, Pariente D, Dooley J. Fatal acute fulminant liver failure due to clozapine: a case report and review of clozapine-induced hepatotoxicity. *Gastroenterology* 1997; **112**: 1707-1709
- 13 **Freudenreich O**, Goff DC. Colon perforation and peritonitis associated with clozapine. *J Clin Psychiatry* 2000; **61**: 950-951
- 14 **Friedberg JW**, Frankenburg FR, Burk J, Johnson W. Clozapine-caused eosinophilic colitis. *Ann Clin Psychiatry* 1995; **7**: 97-98

Edited by Xu XQ, Wang XL and Zhang JZ

- tinal dysfunction. *World J Gastroenterol* 2004; **10**: 875-880
- 2 **Reeve JR Jr**, Green GM, Chew P, Eysselein VE, Keire DA. CCK-58 is the only detectable endocrine form of cholecystokinin in rat. *Am J Physiol Gastrointest Liver Physiol* 2003; **285**: G255-G265
 - 3 **Paloheimo PI**, Clemmesen O, Dalhoff O, Dalhoff K, Rehfeld JF. Plasma cholecystokinin and its precursors in hepatic cirrhosis. *J Hepatol* 1997; **27**: 299-305
 - 4 **Xiao R**, Cui ZJ. Mutual dependence of VIP/PACAP and CCK receptor signaling for a physiological role in duck exocrine pancreatic secretion. *Am J Physiol Regul Integr Comp Physiol* 2004; **286**: R189-R198

Edited by Xu XQ, Wang XL and Zhang JZ

• LETTERS@WJGNET.COM •

Plagiarized and inaccurate papers in the *World Journal of Gastroenterology*

Thomas E. Adrian

Thomas E. Adrian, Northwestern University Feinberg School of Medicine, 303 E. Chicago Avenue, Tarry 4-711, Chicago, IL 60611, USA
Correspondence to: Professor Thomas E. Adrian, Edward Elcock Professor of Surgical Research, Northwestern University Feinberg School of Medicine, 303 E. Chicago Avenue, Tarry 4-711, Chicago, IL 60611, USA. tadrian@northwestern.edu
Telephone: +1-312-503 3493 **Fax:** +1-312-503 3491
Received: 2004-04-24 **Accepted:** 2004-06-22

Adrian TE. Plagiarized and inaccurate papers in the *World Journal of Gastroenterology*. *World J Gastroenterol* 2004; **10**(19): 2925
<http://www.wjgnet.com/1007-9327/10/2925.asp>

To the Editor:

I was astonished to find this paper [Dong ML, Ding XZ, Collin P, Adrian TE. Red oil A5 inhibits proliferation and induces apoptosis in pancreatic cancer cells. *World J Gastroenterol* 2004; **10**(1): 105-111] published in your journal. This has been done without my knowledge or the other coauthor, Dr. Ding. There are numerous errors. These include (1) the exclusion of an important collaborating contributor; (2) the appearance that the work was carried out in China, when it was actually carried out at Northwestern University in Chicago; (3) an incorrect name for the compound being used; (4) an incorrect company name where the compound originated from. The following are the correct information. The authors list should be: Dong ML^[1], Ding XZ^[1], Collin P^[2], Adrian TE^[1]. The title should have been: CR-A5 inhibits proliferation and induces apoptosis in pancreatic cancer cells (the term oil A5 is meaningless; the product is called CR-A5). The address where the work was carried out was: ¹"Department of Surgery and Robert H. Lurie Comprehensive Cancer Center, Northwestern Feinberg School of Medicine, Chicago, IL" and ²"Coastside Research, Stonington, Maine". The funding sources that should have been acknowledged were: The American Institute of Cancer Research, the RAPID Program of the RAPID Program of the Chemoprevention Branch of the National Cancer Institute, the Michael Rolfe Foundation and the Maine Technology Institute. Dr. Dong did carry out this work in my laboratory with the help of others, however, we never discussed where the work would be published and I certainly did not sanction its publication in your journal. I consider what Dr. Dong has done to be dishonest. Most journals require the signature of all authors before a paper can be

accepted for publication, this would be a good policy for the World Journal of Gastroenterology to adopt. More seriously, regarding Dr. Dong, I have now found another paper that he has published in your journal [Dong ML, Zhu YC, Hopkins JV. Oil A induces apoptosis of pancreatic cancer cells via caspase activation, redistribution of cell cycle and GADD expression. *World J Gastroenterol* 2003; **(9)**: 2745-2750]. Again this paper was published without my knowledge. The other authors are unknown to me and the name John V. Hopkins appears to have been fabricated. The contents of this paper have been almost entirely plagiarized from a previous publication from a Medical Oncologist, Dr. Xin-Quan Li who worked in my laboratory and Xian-Zhong Ding in the laboratory (Li X, Ding XZ, Adrian TE. Arsenic trioxide induces apoptosis in pancreatic cancer cells via changes in cell cycle, caspase activation, and GADD expression. *Pancreas* 27: 174-179, 2003). More disturbingly, at least some of the data have clearly been fabricated. The data in Figure 5 of the *World Journal of Gastroenterology* paper have been entirely lifted from the arsenic trioxide data in Figures 6 and 7 in the Pancreas paper. Please find the enclosed MS Powerpoint file where I have indicated the stolen data in red. Furthermore, careful perusal of the data in Figures 3 and 7 has been assembled in the computer by cutting and pasting sections from different gels. Since some of the data have clearly been fabricated this sheds doubt on all of the other findings in the manuscript. I never saw the raw data for most of these experiments and doubt that they were ever performed. I request that this paper is immediately retracted from the journal with an explanation published. I am sure you will want to do this for the integrity of the journal. An internal committee will be set up at Northwestern University to investigate this matter. I will attempt to contact the Dean of Wenzhou Medical College to inform him of this situation with one of his faculty. Since my NIH grant number was also copied onto the WJG paper, I am informing the NIH of this matter. Please let me know if I should inform your editorial board of what has happened. Finally, as you have requested, I state that the contents of this letter represent my viewpoints rather than those of the journal.

Apology to Dr. Thomas E. Adrian

After we received the letter of Dr Thomas E. Adrian, Dr Mi-Lian Dong wrote a letter for Dr Thomas E. Adrian and the following is the statement from Dr Mi-Lian Dong (the letter was provided by Dr. Thomas E. Adrian). Statement from Dr Mi-Lian Dong for Dr Thomas E. Adrian. From: Mi-Lian Dong (mdong2@hotmail.com). Sent: Monday, June 28, 2004 8:54 AM. To: tadrian@northwestern.edu. Subject: Dear Dr. Thomas Adrian, I don't know how to start this letter, but I have to face it. I can imagine your anger and your disappointment for my unacceptable behavior. I feel very sorry and apologize for what stupid things I did. When I was in Chicago, my former supervisor-Dr. White from Lutheran General Hospital, a very nice gentleman, took care of me and introduced me to your lab. In your Lab, you and Dr. Ding trained me and I learned a lots new stuff, some I never heard before as a clinician in China. I believe I worked very hard and did my best in your lab to repay your generous help. I never forget those wonderful days. But now, I destroyed all those wonderful memories. Dr. Thomas Adrian, I already sent a letter to the journal to ask them to remove that article. Such stupid things never happened in my 40 years life. I cannot sleep well and cannot focus my daily work as a busy doctor. I took a few days off. I believe I got punishment from this, but I accept it. It is unforgettable lesson for my future life. But now, besides sorry and regret, I really don't know what else I can do. Again, I apologize for what I did. Sincerely, Mi-Lian Dong.

Edited by Xu XQ, Zhang JZ and Wang XL

Construction of pETNF-P16 plasmid and its expression properties in EC9706 cell line induced by X-ray irradiation

Cong-Mei Wu, Tian-Hua Huang, Qing-Dong Xie, De-Sheng Wu, Xiao-Hu Xu

Cong-Mei Wu, Tian-Hua Huang, Qing-Dong Xie, Research Center of Reproductive Medicine, Shantou University Medical College, Shantou 515041, Guangdong Province, China

Xiao-Hu Xu, Department of Forensic Medicine, Shantou University Medical College, Shantou 515041, Guangdong Province, China

De-Sheng Wu, Lanzhou Medical College, Lanzhou 730000, Gansu Province, China

Supported by the National Natural Science Foundation of China, No. 30210103904 and the Science and Technology Program of Guangdong Province, No.2003C30304

Correspondence to: Dr. Tian-Hua Huang, Research Center of Reproductive Medicine, Shantou University Medical College, Shantou 515041, Guangdong Province, China. thhuang@stu.edu.cn

Telephone: +86-754-8900442 **Fax:** +86-754-8557562

Received: 2003-11-17 **Accepted:** 2003-12-08

Abstract

AIM: Recombined plasmid pETNF-P16 was constructed to investigate its expression properties in esophageal squamous carcinoma cell line EC9706 induced by X-ray irradiation and the feasibility of gene-radiotherapy for esophageal carcinoma.

METHODS: Recombined plasmid pETNF-P16 was constructed and transfected into EC9706 cells with lipofectamine. ELISA, Western blot, and immunocytochemistry were performed to determine the expression properties of pETNF-P16 in EC9706 after transfection induced by X-ray irradiation.

RESULTS: Eukaryotic expression vector pETNF-P16 was successfully constructed and transfected into EC9706 cells. TNF α expressions were significantly increased in the transfected cells after different doses of X-ray irradiation than in those after 0Gy irradiation (1 192.330-2 026.518 pg/mL, $P < 0.05-0.01$), and the TNF α expressions and P16 were significantly higher 6-48 h after 2 Gy X-ray irradiation (358.963-585.571 pg/mL, $P < 0.05-0.001$). No P16 expression was detected in normal EC9706 cells. However, there was strong expression in the transfected and irradiation groups.

CONCLUSION: X-ray irradiation induction could significantly enhance TNF α and P16 expression in EC9706 cells transfected with pETNF-P16 plasmid. These results may provide important experimental data and therapeutic potential for gene-radiotherapy of esophageal carcinoma.

Wu CM, Huang TH, Xie QD, Wu DS, Xu XH. Construction of pETNF-P16 plasmid and its expression properties in EC9706 cell line induced by X-ray irradiation. *World J Gastroenterol* 2004; 10(20): 2927-2930
<http://www.wjgnet.com/1007-9327/10/2927.asp>

INTRODUCTION

Esophageal carcinoma is one of the most frequent malignant tumors. Its treatment choices include surgical resection,

radiation, chemotherapy and biological therapy. However, their limitations and adverse effects influence the therapeutic results. In 1992, Wechselbaum proposed the theory of gene-radiation combination treatment, that is, to ligate the promoter with irradiation-induced function and treatment gene so as to take advantages of the combined therapeutic functions of both modalities^[1].

In this study, pETNF-P16 plasmid was constructed and transfected into human esophageal cancer cell line EC9706. The expressions of TNF α and P16 in the transfected cells exposed to different doses of X-ray irradiation and the time course of the expressions after 2Gy X-ray irradiation were detected to explore the feasibility of gene-radiotherapy for esophageal carcinoma.

MATERIALS AND METHODS

Cell line and vectors

The EC9706 was maintained in Dulbecco's modified Eagle's medium (DMEM), high glucose media (Life Technologies) and generously supplemented with 100 mL/L fetal bovine serum (Hyclone Laboratories), penicillin, streptomycin and nonessential amino acids (Life Technologies). PIRES1 vector was bought from Promega-Biotech (Shanghai, Promega Corporation).

Construction of pETNF-P16 plasmid

The expression vector for TNF α and P16 was constructed as Figure 1.

Transfection

Transfection of EC9706 cells was carried out in a 6-well plate. The transfection procedure began when the cells reached 70% confluence on the surface of plate wells. Solution A was prepared by separate addition of 10 μ g of pETNF-P16 or PIRES1 to 100 μ L serum-free medium (SFM), and solution B by addition of 10 μ L liposome to 100 μ L SFM. Solutions A and B were combined at room temperature for 30 min then 0.8 mL SFM was added to the tube containing the above solutions, and then the mixture was added to rinsed cells. The medium was replaced with a fresh and complete medium after 6 h in transfection. The cells were exposed to irradiation after 36 h in transfection.

Protein determination

TNF α protein was detected using ELISA kit (Genzyme). P16 protein was studied using Western blot analysis and immunocytochemistry (P16 antibody, Boster).

Ionizing irradiation

X-rays of 180 kV and 12 mA with 0.25 mmCu and 1.08 mm Al as filter were given at a dose-rate of 0.8639 Gy/min for doses of 2-20Gy.

Statistical analysis

Student's *t* test was used to determine the difference between groups. *P* values of less than 0.05 were considered statistically significant.

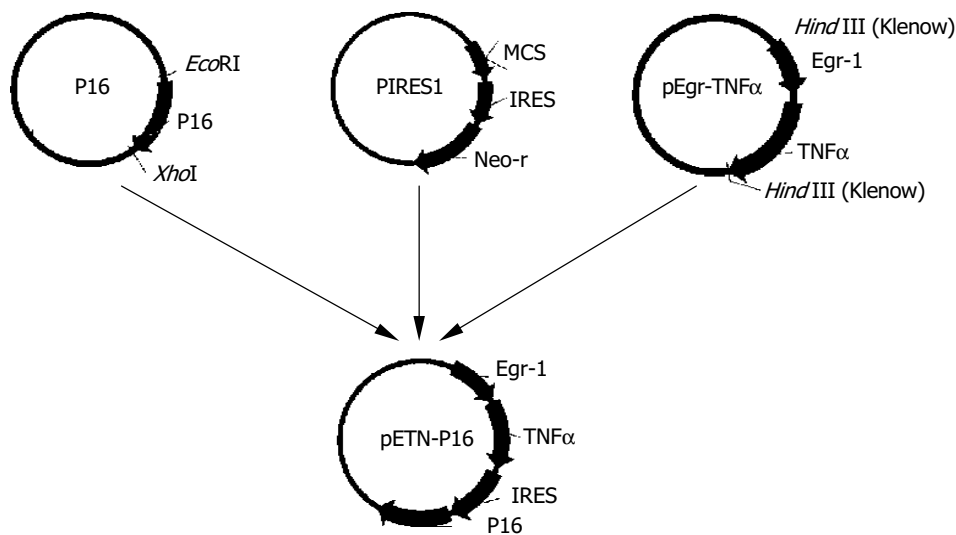


Figure 1 Construction of plasmid pETNF-P16.

RESULTS

TNFα expressions in EC9706 cells transfected with pETNF-P16 after different doses of X-irradiation

EC9706 cells transfected with pETNF-P16 received different doses of X-ray irradiation. The cells of control group were transfected with PIRES1. Eight hours after irradiation, the protein was extracted and TNFα expression was detected by ELISA.

The results showed that TNFα expression in the 2, 4, 10 Gy groups was significantly higher than that in 0 Gy group ($P < 0.05-0.01$) (Figure 2).

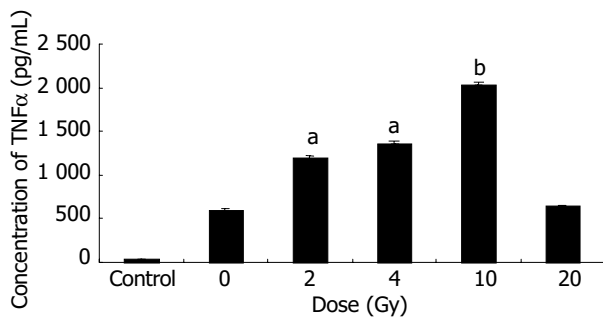


Figure 2 TNFα expression in EC9706 cells after irradiation with different doses of X-ray (mean±SD, $n = 3$). ^a $P < 0.05$, ^b $P < 0.01$ vs 0 Gy group.

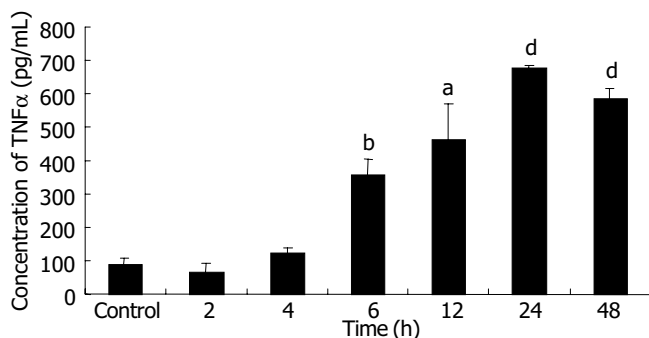


Figure 3 Expression time course of TNFα in EC9706 cells after 2 Gy of X-ray irradiation (mean±SD, $n = 3$). ^a $P < 0.05$, ^b $P < 0.01$, ^d $P < 0.001$ vs control group.

TNFα and P16 expressions in EC9706 cells transfected with pETNF-P16 at different time points after 2 Gy irradiation

EC9706 cells transfected with pETNF-P16 received 2 Gy of

X-ray irradiation while the control group did not receive. Proteins of TNFα and P16 were isolated at different time points after irradiation and detected by ELISA and Western blot.

ELISA results showed that TNFα expression increased from 2 to 24h, and reached the peak level at the 24th h, about 7.5 times of control group ($P < 0.01$). TNFα expression in 48 h group was significantly higher than that in control group ($P < 0.001$), but lower than that in 24 h group ($P > 0.05$) (Figure 3).

The results of Western blot analysis showed no P16 expression in cells transfected with PIRES1 plasmid. After 2Gy X-ray irradiation, P16 expression in the cells transfected with pETNF-P16 plasmid increased between 2 h and 48 h. The expression in the control group was lower than that in 4 h to 48 h groups (Figure 4).

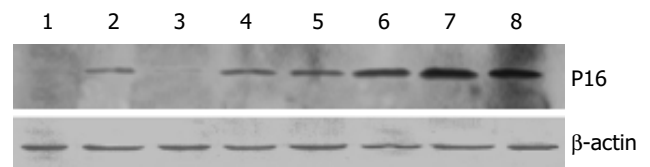


Figure 4 Expression time course of P16 in EC9706 cells after 2 Gy x-ray irradiation Lane 1: transfected with PIRES1 plasmid Lane 2: control group Lane 3: 2 h after irradiation Lane 4: 4 h after irradiation Lane 5: 6 h after irradiation Lane 6: 12 h after irradiation Lane 7: 24 h after irradiation Lane 8: 48 h after irradiation.

Immunocytochemistry

Thirty-six hours after transfected with pETNF-P16 plasmids, EC9706 cells received 2 Gy X-ray irradiation while the control group did not receive. After 24 h, anti-P16 IgG and Biotin-labeled secondary antibody were used to detect the P16 expression in treated cells. P16 protein was positive in the nucleus, cytoplasm and cellular membrane as judged by the brown color.

Immunocytochemical analysis demonstrated that all the normal EC9706 cells had no P16 expression. After transfected with pETNF-P16 plasmid, positive P16 expression in EC9706 cells was detected. Then, the transfected cells received 2 Gy X-ray irradiation and P16 expression remained positive, but morphological changes of EC9706 cells occurred.

DISCUSSION

It was reported that Egr-1 was transcriptionally induced

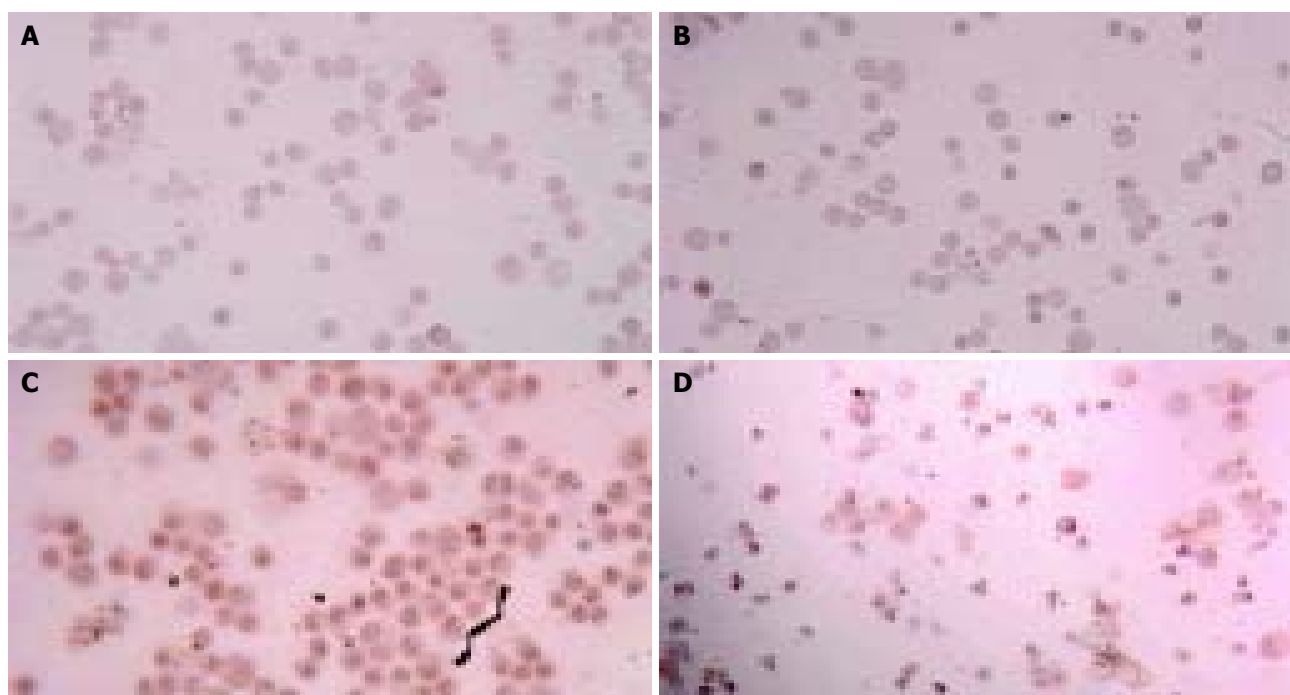


Figure 5 P16 expression in EC9706 cells transfected with pETNF-P16 plasmid after 2Gy X-ray irradiation. A: Negative control group; B: Untransfected group; C: Transfected group; D: Transfected and irradiated group.

following exposure to irradiation^[2]. Sequences responsive to ionizing radiation-induced signals were determined by deletion analysis of the Egr-1 promoter. The results demonstrated that induction of Egr-1 by X-rays was conferred by serum response or CC (A/T) rGG elements. Further analysis confirmed that the region encompassing the three distal or upstream CC(A/T)rGG elements was functional in X-ray response^[3-5].

Weichselbaum *et al.*^[6] were forerunners in tumor gene-radiotherapy. In 1992 they put forward that ionizing radiation could be used to activate the transcription of exogenous genes encoding cytotoxic proteins, and established the techniques that might be used to target gene therapy during the treatment of human neoplasms.

Combination of gene therapy with radiation therapy could overcome some problems and side effects of either radiation or gene therapy alone, including radioresistance of some tumors and toxicities to normal tissues. Weichselbaum *et al.*^[7] linked DNA sequences from the promoter region of Egr-1 to a cDNA sequence that encoded human tumor necrosis factor (TNF) alpha. Egr-TNF construction was transfected into a human cell line of hematopoietic origin, HL525 (clone 2). The latter was injected into human xenografts of the radioresistant human squamous cell carcinoma cell line SQ-20B. Animals treated with radiation and clone 2 demonstrated an improvement compared with those treated with radiation or injections of clone 2 alone. Thereafter, a variety of downstream genes were introduced to Egr-1 promoter to treat different tumors and similar results were obtained^[8-10].

TNF has complex *in-vivo* anti-tumor actions and involves a series of biochemical reactions, and varies according to host metabolism. It could not only kill tumor cells directly, but also act indirectly by occluding the feeding vessels of tumors, promoting inflammation reaction of the host, stimulating cytotoxic activities of megalocytes and producing tumor-specific cytotoxic antibody. Up to now, TNF has been found to have the strongest direct tumor-killing action. However, severe side effects made the effects of systemic treatment unsatisfactory. By contrast, regional administration into the tumor had better therapeutic effects. It has been widely reported that intra-tumor TNF injection had no severe side effects on patients with malignant tumors^[11-12]. We constructed pEgr-TNF α plasmid

and injected it into mouse melanoma locally to induce its expression by X-ray irradiation. The results showed that pEgr-TNF α gene in combination with radiotherapy could significantly inhibit tumor and had no side effects^[13].

P16 is a tumor suppressor gene product. Serrano *et al.*^[14] demonstrated that P16 bound to CDK4 and inhibited the catalytic activity of CDK4/cyclin D enzymes. P16 seemed to act in a regulatory feedback circuit with CDK4, D-type cyclins and retinoblastoma protein. Overexpression of P16 gene could block cell cycle progression through the G₁-to-S phase boundary in a pRB-dependent manner^[15,16]. Many P16 mutants identified from human tumors have been shown to have defects in this activity^[17-19]. These suggested that the CDK4-inhibitory activity of p16 was involved in regulating cell cycle progression through the G₁/S boundary.

On the basis of anti-tumor function of TNF α and P16, we constructed pETNF-P16 plasmid and transfected EC9706 cells to investigate the expression properties of plasmid induced by X-ray irradiation. The results showed that TNF α expression in pETNF-P16-transfected cells induced by irradiation was higher than that in control group ($P < 0.05-0.01$). Time-course studies between 6 h and 48 h after 2Gy irradiation revealed that TNF α expression in X-ray induced groups was higher than that in the control group ($P < 0.05-0.001$). It gradually increased and peaked at the 24th h with the expression level of 7.5 times of control group ($P < 0.01$). Immunocytochemistry showed no P16 expression in the control group, but strong expressions in the transfected and irradiated group. However, the cellular morphology was altered in the latter group and the mechanism is to be clarified.

Esophageal carcinoma still has high morbidity and mortality in China^[20-22], and its treatment is still difficult^[23-30]. Our work might have laid some theoretical basis for further study on esophageal cancer gene-radiotherapy, which should have promising therapeutic potential.

ACKNOWLEDGEMENTS

We are very grateful to Professor Ming-Rong Wang, Institute of Cancer, Chinese Academy of Medical Sciences for his kindness in providing us with the EC9706 cell line.

REFERENCES

- 1 Weichselbaum RR, Hallahan DE, Beckett MA, Mauceri HJ, Lee H, Sukhatme VP, Kufe DW. Gene therapy targeted by radiation preferentially radiosensitizes tumor cells. *Cancer Res* 1994; **54**: 4266-4269
- 2 Christy B, Nathans D. DNA binding site of the growth factor-inducible protein Zif268. *Proc Natl Acad Sci U S A* 1989; **86**: 8737-8741
- 3 Sukhatme VP. Early transcriptional events in cell growth: The Egr family. *J Am Soc Nephrol* 1990; **1**: 859-866
- 4 Cao XM, Koski RA, Gashler A, McKiernan M, Morris CF, Gaffney R, Hay RV, Sukhatme VP. Identification and characterization of the Egr-1 gene product, a DNA-binding zinc finger protein induced by differentiation and growth signals. *Mol Cell Biol* 1990; **10**: 1931-1939
- 5 Tsai-Morris CH, Cao XM, Sukhatme VP. 5' flanking sequence and genomic structure of Egr-1, a murine mitogen inducible zinc finger encoding gene. *Nucleic Acids Res* 1988; **16**: 8835-8846
- 6 Weichselbaum RR, Kufe DW, Advani SJ, Roizman B. Molecular targeting of gene therapy and radiotherapy. *Acta Oncol* 2001; **40**: 735-738
- 7 Datta R, Taneja N, Sukhatme VP, Qureshi SA, Weichselbaum R, Kufe DW. Reactive oxygen intermediates target CC(A/T) 6GG sequences to mediate activation of the early growth response 1 transcription factor gene by ionizing radiation. *Proc Natl Acad Sci U S A* 1993; **90**: 2419-2422
- 8 Hanna NN, Seetharam S, Mauceri HJ, Beckett MA, Jaskowiak NT, Salloum RM, Hari D, Dhanabal M, Ramchandran R, Kalluri R, Sukhatme VP, Kufe DW, Weichselbaum RR. Antitumor interaction of short- course endostatin and ionizing radiation. *Cancer J* 2000; **6**: 287-293
- 9 Takahashi T, Namiki Y, Ohno T. Induction of the suicide HSV-TK gene by activation of the Egr-1 promoter with radioisotopes. *Hum Gene Ther* 1997; **8**: 827-833
- 10 Griscelli F, Li H, Cheong C, Opolon P, Bennaceur Griscelli A, Vassal G, Soria J, Soria C, Lu H, Perricaudet M, Yeh P. Combined effects of radiotherapy and angiostatin gene therapy in glioma tumor model. *Proc Natl Acad Sci U S A* 2000; **97**: 6698-6703
- 11 Vilcek J, Lee TH. Tumor necrosis factor. New insights into the molecular mechanisms of its multiple actions. *J Biol Chem* 1991; **266**: 7313-7316
- 12 Rothe J, Gehr G, Loetscher H, Lesslauer W. Tumor necrosis factor receptors-structure and function. *Immunol Res* 1992; **11**: 81-90
- 13 Wu CM, Li XY, Liu SZ. Construction of pEgr.p-TNF α and its expression in NIH3T3 cells induced by ionizing irradiation. *Chin J Radiol Med Prot* 2001; **21**: 332-334
- 14 Serrano M, Hannon GJ, Beach D. A new regulatory motif in cell-cycle control causing specific inhibition of cyclin D/CDK4. *Nature* 1993; **366**: 704-707
- 15 Koh J, Enders GH, Dynlacht BD, Harlow E. Tumour-derived p16 alleles encoding proteins defective in cell-cycle inhibition. *Nature* 1995; **375**: 506-510
- 16 Lukas J, Parry D, Aagaard L, Mann DJ, Bartkova J, Strauss M, Peters G, Bartek J. Retinoblastoma-protein-dependent cell-cycle inhibition by the tumour suppressor p16. *Nature* 1995; **375**: 503-506
- 17 Monzon J, Liu L, Brill H, Goldstein AM, Tucker MA, From L, McLaughlin J, Hogg D, Lassam NJ. CDKN2A mutations in multiple primary melanomas. *N Engl J Med* 1998; **338**: 879-887
- 18 Nobori T, Miura K, Wu DJ, Lois A, Takabayashi K, Carson DA. Deletions of the cyclin-dependent kinase-4 inhibitor gene in multiple human cancers. *Nature* 1994; **368**: 753-756
- 19 Soufir N, Avril MF, Chompret A, Demenais F, Bombléd J, Spatz A, Stoppa-Lyonnet D, Benard J, Bressac-de-Paillerets B. Prevalence of p16 and CDK4 germline mutations in 48 melanoma-prone families in France. The French Familial Melanoma Study Group. *Hum Mol Genet* 1998; **7**: 209-216
- 20 Zhao XJ, Li H, Chen H, Liu YX, Zhang LH, Liu SX, Feng QL. Expression of e-cadherin and beta-catenin in human esophageal squamous cell carcinoma: relationships with prognosis. *World J Gastroenterol* 2003; **9**: 225-232
- 21 Heidecke CD, Weighardt H, Feith M, Fink U, Zimmermann F, Stein HJ, Siewert JR, Holzmann B. Neoadjuvant treatment of esophageal cancer: Immunosuppression following combined radiochemotherapy. *Surgery* 2002; **132**: 495-501
- 22 Tsunoo H, Komura S, Ohishi N, Yajima H, Akiyama S, Kasai Y, Ito K, Nakao A, Yagi K. Effect of transfection with human interferon-beta gene entrapped in cationic multilamellar liposomes in combination with 5-fluorouracil on the growth of human esophageal cancer cells *in vitro*. *Anticancer Res* 2002; **22**: 1537-1543
- 23 Nemoto K, Zhao HJ, Goto T, Ogawa Y, Takai Y, Matsushita H, Takeda K, Takahashi C, Saito H, Yamada S. Radiation therapy for limited-stage small-cell esophageal cancer. *Am J Clin Oncol* 2002; **25**: 404-407
- 24 Tachibana M, Dhar DK, Kinugasa S, Yoshimura H, Fujii T, Shibakita M, Ohno S, Ueda S, Kohno H, Nagasue N. Esophageal cancer patients surviving 6 years after esophagectomy. *Langenbecks Arch Surg* 2002; **337**: 77-83
- 25 Wilson KS, Wilson AG, Dewar GJ. Curative treatment for esophageal cancer: Vancouver Island Cancer Centre experience from 1993 to 1998. *Can J Gastroenterol* 2002; **16**: 361-368
- 26 Liu HH, Yoshida M, Momma K, Oohashi K, Funada N. Detection and treatment of an asymptomatic case of early esophageal cancer using chromoendoscopy and endoscopic mucosal resection. *J Formos Med Assoc* 2002; **101**: 219-222
- 27 Wang AH, Sun CS, Li LS, Huang JY, Chen QS. Relationship of tobacco smoking, CYP1A1, GSTM1 gene polymorphism and esophageal cancer in Xi'an. *World J Gastroenterol* 2002; **8**: 49-53
- 28 Muto M, Ohtsu A, Miyata Y, Shioyama Y, Boku N, Yoshida S. Self-expandable metallic stents for patients with recurrent esophageal carcinoma after failure of primary chemoradiotherapy. *Jpn J Clin Oncol* 2001; **31**: 270-274
- 29 Yeh AM, Mendenhall WM, Morris CG, Zlotecki RA, Desnoyers RJ, Vogel SB. Factors predictive of survival for esophageal carcinoma treated with preoperative radiotherapy with or without chemotherapy followed by surgery. *J Surg Oncol* 2003; **83**: 14-23
- 30 Lew JI, Gooding WE, Ribeiro U Jr, Safatle-Ribeiro AV, Posner MC. Long-term survival following induction chemoradiotherapy and esophagectomy for esophageal carcinoma. *Arch Surg* 2001; **136**: 737-742

Endoscopic survey of esophageal cancer in a high-risk area of China

Xu-Jing Lu, Zhi-Feng Chen, Cui-Lan Guo, Shao-Sen Li, Wen-Long Bai, Guo-Liang Jin, Yu-Xia Wang, Fan-Shu Meng, Feng Gao, Jun Hou

Xu-Jing Lu, Zhi-Feng Chen, Jun Hou, Hebei Cancer Institute and Fourth Affiliated Hospital of Hebei Medical University, Shijiazhuang 050011, Hebei Province, China

Cui-Lan Guo, Shao-Sen Li, Wen-Long Bai, Guo-Liang Jin, Yu-Xia Wang, Fan-Shu Meng, Feng Gao, Cixian Cancer Institute, Cixian 056500, Hebei Province, China

Supported by the National Tenth Five-Year Scientific Championship Project, No. 2001BA703B10

Correspondence to: Dr. Jun Hou, Hebei Cancer Institute, Jiankanglu 12, Hebei Medical University, Shijiazhuang 050011, Hebei Province, China. luxujing@csc.org.cn

Telephone: +86-311-6033511 **Fax:** +86-311-6077634

Received: 2003-10-09 **Accepted:** 2003-12-16

Abstract

AIM: To characterize the histological types of esophageal and cardiac mucosa by endoscopic survey of a population in a high-risk area of esophageal cancer of China.

METHODS: A selected cohort of residents in Cixian County during December 2001 and May 2002 was surveyed by using Lugol's staining, followed by computer-based statistical analysis of the data with SPSS 10.0 software.

RESULTS: Histologically, the detection rates of squamous epithelial acanthosis, squamous epithelial atrophy, and basal cell hyperplasia in the esophagus were 1.9% (38/2 013), 0.1% (3/2 013) and 0.9% (18/2 013) respectively, and those of mild, moderate, and severe esophagitis were 34.9% (703/2 013), 1.6% (33/2 013) and 0.2% (2/2 013) respectively. Mild, moderate, and severe esophageal dysplasia were detected in 8.6% (172/2 013), 7.8% (157/2 013) and 2.6% (53/2 013) respectively in the selected population, whereas *in situ* carcinoma, intramucosal carcinoma, invasive squamous carcinoma of the esophagus in 2.5% (50/2 013), 0.2% (4/2 013) and 0.7% (14/2 013) respectively. The detection rates of non-atrophic gastritis and atrophic gastritis of the cardia were 36.3% (730/2 013) and 11.5% (232/2 013) respectively, with mild and severe dysplasia of the cardia detected in 2.5% (51/2 013) and 0.8% (17/2 013), respectively, in this population; the rates of intramucosal adenocarcinoma and invasive adenocarcinoma of the cardia were 0.1% (3/2 013) and 0.8% (17/2 013) respectively. The detection rate of esophageal cancer at early stage was 79.4% (54/68). The survey rate (ratio of examined population to expected population) was 73.8% (2 013/2 725).

CONCLUSION: Histologic types of the esophageal and cardiac mucosa were characterized by endoscopic survey in a high-risk population of esophageal cancer, which may help the early detection and treatment of esophageal and cardiac cancers and dysplasia, and reduce the mortality of such malignancies.

Lu XJ, Chen ZF, Guo CL, Li SS, Bai WL, Jin GL, Wang YX, Meng FS, Gao F, Hou J. Endoscopic survey of esophageal cancer in a high-risk area of China. *World J Gastroenterol* 2004; 10(20): 2931-2935

<http://www.wjgnet.com/1007-9327/10/2931.asp>

INTRODUCTION

Esophageal cancer (EC) is one of the most common malignant tumors with a high incidence in such regions as China, Iran, South Africa, Uruguay, France and Italy^[1], of which China has almost half of the total cases with also the highest mortality rate, the fourth leading cause of cancer-related deaths in China. According to the data derived from 1/10 sample death investigation in the whole population of China in 1990-1992, the mortality rate of esophageal cancer was 27.73/100 000 for men and 13.63/100 000 for women, which were 3.1 and 3.6 times, that reported by the World Health Organization (WHO) in 1998 respectively^[2]. Some southern regions of the Taihang Mountains on the borders of Henan, Shanxi and Hebei provinces have significantly higher mortality rates of esophageal cancer. Cixian County in Hebei Province is also one of the areas with the highest mortality rate in China, where an endoscopic survey was conducted by Hebei Cancer Institute during the period between December 2001 and May 2002, and in this paper the results are reported.

MATERIALS AND METHODS

Cixian County is located at 36.30° northern latitude, 114.40° eastern longitude, on the east side of the Taihang Mountains along the Zhanghe River. It occupies an area about 1 014 square kilometers with a population of 634 470. This region contains greatly diverse geographic conditions, ranging from mountainous, hilly regions to long-stretched plains, each constituting about one-third of its total area. The climate is mainly under the influence of the warm seasonal wind from the mainland, with an annual average temperature of 18-25 °C and a rainfall between 600-700 mm. The dominant brown and light-colored soil yields mainly such farm products as wheat, corn, millet, rice, sweet potato and beans. Iron and coal are the main mineral resources, and the residents use coal mainly for daily cooking and heating^[3].

As a key science research project sponsored by the National Tenth Five-Year Plan of China, the survey was conducted among the residents of 9 villages aged between 40 and 69 years in the hilly region of Cixian County, which is known for a higher incidence of esophageal cancer than the plain regions. The total population of the 9 villages was 12 048, and the annual incidence and mortality rate of esophageal cancer in this region during 1996-2000 were 176.0/100 000 and 126.2/100 000 respectively.

Before the survey, a county-wide conference was convened by the local government participated by the local county, countryside and village leaders and cancer prevention professionals. At the conference, special committees were set up at each of the 3 administrative levels to be responsible for the execution of the survey in the areas where they perform daily duties. After the conference, the residents in the target areas were acknowledged of the benefits of such a massive survey through a propaganda campaign. On the basis of the government record of the residents, 2 000 potential target subjects from the 9 villages were selected by the cancer prevention professionals, and two days prior to the survey, personal contacts with the subjects were made by local physicians to arrange for the details of the survey. At the

beginning of the survey, the subjects were asked to fill an epidemiological questionnaire, followed by physical examination performed by the physicians to exclude persons with serious contraindications to endoscopy. Endoscopic examinations were then performed by specialists following the procedures described by Wang *et al.*^[4]. The detailed results were recorded and the biopsy specimens obtained were fixed in 80% alcohol and stained by hematoxylin-eosin (HE) for subsequent pathological diagnosis by pathologists.

Finally, the data were input into a computer to set up a survey information database and statistical analysis was performed using SPSS 10.0 software with chi-square test.

RESULTS

Survey rate

Of the totally 12 048 residents of the 9 villages, 2 992 were within the age range between 40 and 69 years, and after exclusion of 267 residents with contraindications (including 32 patients with cancer, 22 with heart diseases, 29 with cerebrovascular diseases, 55 with hypertension, 56 with other diseases, 59 already died, and 14 emigrants), the total number of subjects enrolled in this survey was 2 013 (including 973 male and 1 040 female subjects, with the male to female ratio of 0.94:1), and the survey rate was therefore 73.8% (Table 1).

Endoscopic findings of the esophagus

As shown in Table 2, the histologic detection rates of *in situ* carcinoma, intramucosal carcinoma, and invasive squamous carcinoma were 2.5% (50/2013), 0.2% (4/2013), and 0.7% (14/2013), respectively; early cancerous changes were detected in 2.7% (54/2013) of the subjects, which occupied 79.4% (54/68) of total esophageal cancer cases. Male subjects had comparable incidence of esophagitis [35.9% (349/973)] with that in female subjects [37.6% (391/1 040), $\chi^2 = 0.645$, $P = 0.422$], but had significantly higher incidence of dysplasia [23.1% (225/973) vs 15.1% (157/1 040) in female, $\chi^2 = 21.072$, $P = 0.000$]. The incidence of esophageal cancer did not vary significantly between the male and female subjects [3.3% (32/973) vs 3.5% (36/1 040), $\chi^2 = 0.001$, $P = 0.98$].

Table 3 shows that with a 5-year increase in age, the histologic incidence of esophageal cancer and dysplasia all tended to be increased from the relatively low level in the 40-year-old group to the highest in the 65-year-old group (trend $\chi^2 = 135.943$, $^aP = 0.000$; trend $\chi^2 = 182.782$, $^bP = 0.000$). The rates of esophagitis in different age groups varied significantly ($\chi^2 = 12.475$, $P = 0.029$), as well as the rates of dysplasia ($\chi^2 = 141.184$, $P = 0.000$), and esophageal cancer ($\chi^2 = 74.855$, $P = 0.000$).

Table 2 Detection rates of the histologic changes in the esophagus (%)

Type	Male (%)	Female (%)	Total (%)
Normal squamous epithelium	308 (31.7)	392 (37.7)	700 (34.8)
Squamous epithelial acanthosis	19 (2.0)	19 (1.8)	38 (1.9)
Squamous epithelial atrophy	1 (0.1)	2 (0.2)	3 (0.1)
Esophagitis			
Mild	337 (34.6)	366 (35.2)	703 (34.9)
Moderate	11 (1.1)	22 (2.1)	33 (1.6)
Severe	1 (0.1)	3 (0.3)	4 (0.2)
Dysplasia			
Mild	114 (11.7)	58 (5.6)	172 (8.6)
Moderate	82 (8.4)	75 (7.2)	157 (7.8)
Severe	29 (3.0)	24 (2.3)	53 (2.6)
<i>In situ</i> carcinoma	25 (2.6)	25 (2.4)	50 (2.5)
Intramucosal carcinoma	2 (0.2)	2 (0.2)	4 (0.2)
Invasive carcinoma	5 (0.5)	9 (0.9)	14 (0.7)
Others	31 (3.2)	33 (3.2)	64 (3.2)
Total	973 (100.0)	1040 (100.0)	2013 (100.0)

Endoscopic findings of the gastric cardia

The incidence of cardiac cancer was much lower than that of esophageal cancer ($\chi^2 = 26.767$, $P = 0.000$), and early cardiac cancer only occupied 15% (3/20) of cardiac cancer cases. The rates of gastritis involving the cardia were 44.5% (433/973) in male and 50.8% (529/1 040) in female subjects, showing significant difference between them ($\chi^2 = 8.159$, $P = 0.004$). The rates of dysplasia also varied significantly between them [4.9% (48/973) in male vs 1.9% (20/1 040) in female, $\chi^2 = 13.955$, $P = 0.000$], but not that of cardiac cancer, [1.3% (13/973) in male vs 0.7% (7/1 040) in female, $\chi^2 = 2.246$, $P = 0.134$], as shown in Table 4.

At a 5-year interval, the incidence of cardiac cancer and dysplasia both increased from the level in the 40-year-old group to the highest in the 65-year-old group (trend $\chi^2 = 84.875$, $^aP = 0.000$; trend $\chi^2 = 36.209$, $^bP = 0.000$, Table 5). The rates of gastritis involving the cardia and dysplasia of the cardia also varied significantly ($\chi^2 = 11.223$, $P = 0.047$; $\chi^2 = 18.901$, $P = 0.002$), as well as that of cardiac cancer ($\chi^2 = 43.351$, $P = 0.000$).

Table 1 Statistics of the residents of the 9 target villages enrolled in this survey

Village	Total population	Aged between 40-69 (yr %)	Contraindication	Expected population	Examined population	Survey rate (%)
Hebei Village	1 184	304 (25.7)	29	275	220	80.0
Taichen Village	1 648	412 (25.0)	39	373	287	76.9
Xichengji Village	1 682	381 (22.7)	53	328	283	86.3
Zhonghao Village	699	183 (26.2)	23	160	130	81.3
Donghao Village	1 860	494 (26.6)	26	468	208	44.4
Chejiao Village	1 618	383 (23.7)	38	345	276	80.0
Bai Village	1 679	415 (24.7)	27	388	284	73.2
Donghelan Village	1 076	271 (25.2)	17	254	208	81.9
Xihelan Village	602	149 (24.8)	15	134	117	87.3
Total	12 048	2 992 (24.8)	305	2 725	2 013	73.8

The percentages in bracket indicate the rates of the population aged 40-69 years.

Table 4 Incidence of pathological changes detected histologically in the cardia (%)

Type	Male (%)	Female (%)	Total (%)
Normal	301 (31.0)	329 (31.7)	630 (31.4)
adenoepithelium			
Non-atrophic	323 (33.2)	407 (39.1)	730 (36.3)
gastritis			
Atrophic gastritis	110 (11.3)	122 (11.7)	232 (11.5)
Dysplasia			
Mild	36 (3.7)	15 (1.4)	51 (2.5)
Severe	12 (1.2)	5 (0.5)	17 (0.8)
Intramucosal	1 (0.1)	2 (0.2)	3 (0.1)
adenocarcinoma			
Invasive	12 (1.2)	5 (0.5)	17 (0.8)
adenocarcinoma			
Others	178 (18.3)	155 (14.9)	333 (16.5)
Total	973 (100.0)	1 040 (100.0)	2 013 (100.0)

DISCUSSION

The prognosis of esophageal and cardiac cancer is the poorest among the patients with digestive carcinomas as more than 90% of them are not clinically identified until at an advanced stage, when surgery is defied due to either local tumor invading the surrounding tissues or distant metastasis, and therefore the 5-year survival rate of esophageal cancer is below 10%^[5-7]. Early-stage asymptomatic esophageal cancer is basically curable with, for instance, conventional surgery and endoscopic resection, resulting in a 5-year survival rate of the patients reaching 90% or above^[8-10].

For esophageal cancer prevention and treatment, a series of systematic researches including clinical, laboratory and field investigation were carried out in high-risk areas such as Linxian and Cixian counties since 1959^[11-16], but at present the etiological factors have not yet been identified, and the incidence and mortality rates of esophageal cancer still remain high in those areas. A variety of detecting methods have been attempted by Chinese scientists to identify early esophageal cancer and precancerous lesions, such as exfoliative balloon cytology (EBC), occult blood bead (OBB), conventional endoscopy with

Table 3 Age-related distribution of the incidence of pathological changes in esophagus

Type	Age [yr (%)]					
	40-	45-	50-	55-	60-	65-69
Normal squamous epithelium	355 (44.8)	176 (38.4)	92 (28.6)	56 (24.9)	14 (9.4)	7 (10.4)
Squamous epithelial acanthosis	11 (1.4)	4 (0.9)	10 (3.1)	7 (3.1)	5 (3.4)	1 (1.5)
Squamous epithelial atrophy	1 (0.1)	1 (0.2)	1 (0.3)	-	-	-
Basal cell hyperplasia	6 (0.8)	6 (1.3)	3 (0.9)	1 (0.4)	2 (1.3)	-
Esophagitis						
Mild	304 (38.4)	167 (36.5)	90 (28.0)	71 (31.6)	53 (35.6)	18 (26.9)
Moderate	17 (2.1)	2 (0.4)	9 (2.8)	4 (1.8)	1 (0.7)	-
Severe	-	1 (0.2)	2 (0.6)	1 (0.4)	-	-
Dysplasia						
Mild	37 (4.7)	36 (7.9)	41 (12.7)	26 (11.6)	21 (14.1)	11 (16.4)
Moderate	19 (2.4)	30 (6.6)	43 (13.4)	26 (11.6)	26 (17.4)	13 (19.4)
Severe	12 (1.5)	12 (2.6)	12 (3.7)	6 (2.7)	9 (6.0)	2 (3.0)
<i>In situ</i> carcinoma	3 (0.4)	8 (1.7)	10 (3.1)	14 (6.2)	8 (5.4)	7 (10.4)
Intramucosal carcinoma	-	2 (0.4)	-	-	2 (1.3)	-
Invasive carcinoma	-	2 (0.4)	3 (0.9)	4 (1.8)	3 (2.0)	2 (3.0)
Others	27 (3.4)	11 (2.4)	6 (1.8)	9 (4.0)	5 (3.4)	6 (9.0)
Total	792 (100.0)	458 (100.0)	322 (100.0)	225 (100.0)	149 (100.0)	67 (100.0)

Table 5 Age-related distribution of detection rates of pathological changes in gastric cardia

Type	Age [yr (%)]					
	40-	45-	50-	55-	60-	65-
Normal adenoepithelium	295 (37.2)	156 (34.1)	81 (25.2)	61 (27.1)	27 (18.1)	10 (14.9)
Non-atrophic gastritis	319 (40.3)	169 (36.9)	116 (36.0)	60 (26.7)	47 (31.5)	19 (28.4)
Atrophic gastritis	90 (11.4)	45 (9.8)	38 (11.8)	34 (15.1)	14 (9.4)	11 (16.4)
Dysplasia						
Mild	13 (1.6)	8 (1.7)	10 (3.1)	8 (3.6)	8 (5.4)	4 (6.0)
Severe	-	8 (1.7)	2 (0.6)	3 (1.3)	4 (2.7)	-
Intramucosal adenocarcinoma	-	-	1 (0.3)	-	1 (0.7)	1 (1.5)
Invasive adenocarcinoma	-	1(0.2)	1 (0.3)	3 (1.3)	5 (3.4)	7 (10.4)
Others	75 (9.5)	71 (15.5)	73 (22.6)	56 (24.9)	43 (28.9)	15 (22.4)
Total	792 (100.0)	458 (100.0)	322 (100.0)	225 (100.0)	149 (100.0)	67 (100.0)

smear or biopsy, sparse hydrochloric acid preliminary screening, serum total salicylic acid detection (TSA), otolaryngologic examination and so forth, but all these methods are marred by certain disadvantages besides their respective advantages in the early detection of esophageal cancer and precancerous lesions^[17-19].

A massive screening in the population of 126 187 in Cixian was carried out by Hebei Cancer Institute and 16 748 high risk participants aged 40 years and older were screened with exfoliative balloon cytology, the survey rate was 71.4%, resulting in the identification of 179 cases of esophageal cancer, 172 esophageal precancerous lesions, 866 stage II severe esophageal epithelial dysplasia (SEED II), 3 179 stage I severe esophageal epithelial dysplasia (SEED I) and 5 346 mild esophageal epithelium dysplasia (MEED), with the detection rates of MEED, SEED I, SEED II, esophageal precancerous lesions and esophageal cancer being 31.92%, 18.98%, 5.17%, 1.03% and 1.07%, respectively^[20]. Most of the researches indicate that exfoliative balloon cytology is an effective, economic and practicable method, having higher detection rate for esophageal cancer than conventional endoscopy, but only cytological diagnosis is obtained and a further endoscopic biopsy and histopathologic confirmation are necessary. This method is now insufficient for esophageal cancer screening because of the severe discomfort and low acceptance by the target subjects.

Esophageal chromoendoscopy with multi-point biopsy and histopathologic examination has developed rapidly since 1974, which greatly increased the detection rate of esophageal cancer and precancerous lesions, and at the same time it is capable of characterizing and defining the scope of the lesions to provide guidance for treatment and follow-up, also suitable for the secondary prevention of esophageal cancer^[4,21-33]. Currently the secondary prevention with early detection, early diagnosis and early treatment through chromoendoscopy survey has become the major research concern in the prevention and control of esophageal cancer.

The occurrence and development of esophageal cancer is a slow process involving multiple factors and genes and undergoing multiple stages. Prior to cancerization of the squamous esophageal epithelium, the basal cell hyperplasia or simple hyperplasia takes place and evolves into mild, moderate, severe dysplasia cells that develop, in sequence, into *in situ* carcinoma, early invasive cancer and advanced cancer^[34-36]. As a part of the entire research project, a massive esophageal chromoendoscopic survey was initially conducted in the high-risk area without preliminary screening, and the high survey rate reaching 73.8% indicates that the population's compliance to the survey was high after adequate health education. The distribution of histologic types of the esophageal and cardiac mucosa in high-risk area can be accurately obtained by esophageal chromoendoscopic survey, which possesses the advantage of accurate pathologic diagnosis and differentiation of the histologic types, well defined scope of the lesions and their invasive depth.

This study will, after defining the incidences of the pathological changes of the esophageal and cardiac mucosa in the population, contribute to the early treatment of esophageal and cardiac cancer and dysplasia, increase their cure rates, and reduce the mortality of such malignancies.

REFERENCES

- 1 Lu S, Lin P, Wang G, Luo X, Wu M. Comprehensive prevention and treatment for esophageal cancer. *Chin Med J* 1999; **112**: 918-923
- 2 Qiao YL, Hou J, Yang L, He YT, Liu YY, Li LD, Li SS, Lian SY, Dong ZW. The trends and preventive strategies of esophageal cancer in high-risk areas of Taihang Mountains, China. *Zhongguo Yixue Kexueyuan Xuebao* 2001; **23**: 10-14
- 3 Hou J, Lin PZ, Chen ZF, Ding ZW, Li SS, Men FS, Guo LP, He YT, Qiao CY, Duan JP, Wen DG. Field population-based blocking treatment of esophageal epithelia dysplasia. *World J Gastroenterol* 2002; **8**: 418-422
- 4 Wang GQ, Zhou MH, Cong QW, Cui HH. Lugol's solution in endoscopic diagnosis of early esophageal cancer. *Zhonghua Yixue Zazhi* 1995; **75**: 417-418
- 5 Wang GQ, Wei WQ, Hao CQ, Zhang XH, Lai SQ, Yu GX, Ju FH, Ma YH, Qiao YL, Dong ZW, Wang GQ. Minimal invasive treatment of early esophageal cancer and its precancerous lesion: endoscopic mucosal resection using transparent cap-fitted endoscope. *Zhonghua Yixue Zazhi* 2003; **83**: 306-308
- 6 Liu HF, Liu WW, Fang DC. Study of the relationship between apoptosis and proliferation in gastric carcinoma and its precancerous lesion. *Shijie Huaren Xiaohua Zazhi* 1999; **7**: 649-651
- 7 Chen KN, Xu GW. Diagnosis and treatment of esophageal cancer. *Shijie Huaren Xiaohua Zazhi* 2000; **8**: 196-202
- 8 Wang GQ, Wei WQ, Lu N, Hao CQ, Lin DM, Zhang HT, Sun YT, Qiao YL, Wang GQ, Dong ZW. Significance of screening by iodine staining of endoscopic examination in the area of high incidence of esophageal carcinoma. *Aizheng* 2003; **22**: 175-177
- 9 Urba SG, Orringer MB, Perez-Tamayo C, Bromberg J, Forastiere A. Concurrent preoperative chemotherapy and radiation therapy in localized esophageal adenocarcinoma. *Cancer* 1992; **69**: 285-291
- 10 Wolfe WG, Vaughn AL, Seigler HF, Hathorn JW, Leopold KA, Duhaylongsod FG. Survival of patients with carcinoma of the esophagus treated with combined-modality therapy. *J Thorac Cardiovasc Surg* 1993; **105**: 749-755
- 11 Hu SP, Yang HS, Shen ZY. Study on etiology of esophageal carcinoma: retrospect and prospect. *Zhongguo Aizheng Zazhi* 2001; **11**: 171-174
- 12 Hou J, Qiao CY, Meng FS, Zhang GS, He YT, Chen ZF, Liu JB, Song GH, Li SS, Hao SM, Ji HX. A case-control study on risk factor of esophageal cancer in cixian county of Hebei Province. *Zhongguo Zhongliu* 1999; **8**: 252-255
- 13 Ding Z, Gao F, Lin P. Long-term effect of treating patients with precancerous lesions of the esophagus. *Zhonghua Zhongliu Zazhi* 1999; **21**: 275-277
- 14 Dawsey SM, Fleischer DE, Wang GQ, Zhou B, Kidwell JA, Lu N, Lewin KJ, Roth MJ, Tio TL, Taylor PR. Mucosal iodine staining improves endoscopic visualization of squamous dysplasia and squamous cell carcinoma of the esophagus in Linxian, China. *Cancer* 1998; **83**: 220-231
- 15 Hou J, Yan FR. Treatment of esophageal precancerous lesion with cang dlou pill. *Zhongguo Zhongxiyi Jiehe Zazhi* 1992; **12**: 604-606
- 16 Qiu SL, Yang GR. Precursor lesions of esophageal cancer in high-risk populations in Henan Province, China. *Cancer* 1988; **62**: 551-557
- 17 Lin PZ, Chen ZF, Hou J, Liu TG, Wang JX, Ding ZW, Guo LP, Li SS, Men FS, Du CL. Chemical prevention of esophageal cancer. *Zhongguo Yixue Kexueyuan Xuebao* 1998; **20**: 413-417
- 18 Cai L, Yu SZ. A molecular epidemiologic study on gastric cancer in Changle, Fujian Province. *Shijie Huaren Xiaohua Zazhi* 1999; **7**: 652-655
- 19 Hou J, Chen ZF, He YT. Screening of esophageal cancer. *Hebei Zhigong Yixueyuan Xuebao* 2001; **18**: 32-34
- 20 Hou J, Lin PZ, Chen ZF, Wang GQ, Liu TG, Li SS, Meng FS, Du CL. A study survey of esophageal cancer in chixian of Hebei. *Zhongliu Fangzhi Yanjiu* 1998; **25**: 73-75
- 21 Roth MJ, Liu SF, Dawsey SM, Zhou B, Copeland C, Wang GQ, Solomon D, Baker SG, Giffen CA, Taylor PR. Cytologic detection of esophageal squamous cell carcinoma and precursor lesions using balloon and sponge samplers in asymptomatic adults in Linxian, China. *Cancer* 1997; **80**: 2047-2059
- 22 Qin DX, Wang GQ, Wang ZY. Double blind randomized trial on occult blood bead (OBB) and gastroscopy-pathology screening for gastro-oesophageal cancer. *Eur J Cancer Prev* 1997; **6**: 158-161
- 23 Wang GQ. 30-year experiences on early detection and treatment of esophageal cancer in high risk areas. *Zhongguo Yixue Kexueyuan Xuebao* 2001; **23**: 69-72
- 24 Mitsunaga N, Tsubouchi H. Detection of early esophageal and gastric cancers by mass screening. *Nippon Rinsho* 1996; **54**:

- 1415-1420
- 25 **Meyer V**, Burtin P, Bour B, Blanchi A, Cales P, Oberti F, Person B, Croue A, Dohn S, Benoit R, Fabiani B, Boyer J. Endoscopic detection of early esophageal cancer in a high-risk population: does Lugol staining improve videoendoscopy? *Gastrointest Endosc* 1997; **45**: 480-484
- 26 **Hou J**, Chen ZF, Li SS, Li ZY, Yan FR. Clinical study on treatment of esophageal precancerous lesion with Cangdouwan PILL. *Zhongguo Zhongliu Linchuang* 1996; **23**: 117-119
- 27 **Shimizu Y**, Tukagoshi H, Fujita M, Hosokawa M, Kato M, Asaka M. Endoscopic screening for early esophageal cancer by iodine staining in patients with other current or primary cancers. *Gastrointest Endosc* 2001; **53**: 1-5
- 28 **Freitag CP**, Barros SG, Krueh CD, Putten AC, Dietz J, Gruber J, Diehl AS, Meurer L, Breyer HP, Wolff F, Vidal R, Arruda CA, Luz LP, Fagundes RB, Prolla JC. Esophageal dysplasias are detected by endoscopy with Lugol in patients at risk for squamous cell carcinoma in southern Brazil. *Dis Esophagus* 1999; **12**: 191-195
- 29 **Misao Y**, Kumiko M, Tomoko H, Yosuke I, Nobuhiro S. Endoscopic evaluation of depth of cancer invasion in cases with superficial esophageal cancer. *Stomach And Intestine* 2001; **36**: 295-306
- 30 **Hiroyasu M**, Hideo S, Osamu C, Yoshifumi K. Long term prognosis of m₃,sm₁ cancer of the esophagus-comparison between EMR and radical surgery cases. *Stomach And Intestine* 2002; **37**: 53-63
- 31 **Junji Y**. Comparison of histological picture and ultrasonographic picture of the alimentary tract wall. *Stomach And Intestine* 2001; **36**: 276-282
- 32 **Tsuneo O**. Lymph nodal metastasis of m₃,sm₁ esophageal cancer. *Stomach And Intestine* 2002; **37**: 71-74
- 33 **Dawsey SM**, Shen Q, Nieberg RK, Liu SF, English SA, Cao J, Zhou B, Wang GQ, Lewin KJ, Liu FS, Roth MJ, Taylor PR. Studies of esophageal balloon cytology in Linxian, China. *Cancer Epidemiol Biomarkers Prev* 1997; **6**: 121-130
- 34 **Wang GQ**. Clinical preventive strategies to decrease incidence and death rates of esophageal cancer in high-risk areas. *Zhonghua Zhongliu Zazhi* 1999; **21**: 223
- 35 **Wang LD**, Zhou Q, Feng CW, Liu B, Qi YJ, Zhang YR, Gao SS, Fan ZM, Zhou Y, Yang CS, Wei JP, Zheng S. Intervention and follow-up on human esophageal precancerous lesions in Henan, northern China, a high-incidence area for esophageal cancer. *Gan To Kagaku Ryoho* 2002; **29**(Suppl 1): 159-172
- 36 **Wang GQ**. The trends and strategies of esophageal cancer and precancerous lesions. *Zhonghua Zhongliu Zazhi* 2002; **24**: 206

Edited by Chen WW Proofread by Zhu LH and Xu FM

Alteration of cyclin D1 in gastric carcinoma and its clinicopathologic significance

Peng Gao, Geng-Yin Zhou, Yuan Liu, Jin-Song Li, Jun-Hui Zhen, Yin-Ping Yuan

Peng Gao, Geng-Yin Zhou, Jin-Song Li, Jun-Hui Zhen, Yin-Ping Yuan, Department of Pathology, School of Medicine, Shandong University, Jinan 250012, Shandong Province, China

Yuan Liu, Qilu Hospital, Shandong University, Jinan 250012, Shandong Province, China

Supported by the National Natural Science Foundation of China, No. 30300124

Correspondence to: Peng Gao, Department of Pathology, School of Medicine, Shandong University, Jinan 250012, Shandong Province, China. gaopeng@sdu.edu.cn

Telephone: +86-531-8382045 **Fax:** +86-531-8382045

Received: 2003-11-17 **Accepted:** 2004-03-18

Abstract

AIM: To detect the genetic alteration and abnormal expression of cyclin D1 in gastric carcinoma and investigate its clinicopathologic significance in advanced gastric carcinoma.

METHODS: Proteins of cyclin D1 were detected by immunohistochemistry in 42 cases of advanced gastric carcinoma with their follow-up data available, 27 cases of early stage carcinoma, 21 cases of gastric adenoma, 22 cases of hyperplastic polyp and 20 cases of normal mucosa adjacent to adenocarcinomas. Genetic alteration of cyclin D1 was detected by Southern blot and expression of cyclin D1 mRNA was detected by PT-PCR in 42 cases of advanced gastric carcinoma.

RESULTS: Cyclin D1 protein was not expressed in normal mucosa, hyperplastic polyp and gastric adenoma, while it was only positively expressed in gastric carcinoma. The expression rate of cyclin D1 protein in early stage gastric carcinoma, advanced gastric carcinoma and lymph node metastasis was 48.1%, 47.4% and 50.0%, respectively. The amplification of cyclin D1 gene was detected in 16.6% of advanced gastric carcinomas. The overexpression of cyclin D1 mRNA was detected in 40.5% of the samples. There was no significant correlation between cyclin D1 protein expression and age, lymph-node metastasis and histological grading in patients with advanced gastric carcinoma ($\chi^2 = 0.038, 0.059, 0.241, P > 0.05$). Significant correlation was observed between the expression of cyclin D1 protein and the 5-year survival rate ($\chi^2 = 3.92, P < 0.05$).

CONCLUSION: Detection of cyclin D1 protein by immunohistochemistry may be useful in the diagnosis of early gastric carcinomas. Patients with positive expression of cyclin D1 protein tend to have a worse prognosis.

Gao P, Zhou GY, Liu Y, Li JS, Zhen JH, Yuan YP. Alteration of cyclin D1 in gastric carcinoma and its clinicopathologic significance. *World J Gastroenterol* 2004; 10(20): 2936-2939 <http://www.wjgnet.com/1007-9327/10/2936.asp>

INTRODUCTION

Hyperplasia is an essential characteristic of malignant tumors.

Close attention has been paid to the role of cell-cycle regulators associated with cell proliferation in oncogenesis. Under the stimulation of proliferation signals, cells could produce early stage transcription factors such as *c-fos*, *c-jun*. These factors could bind to DNA specifically in nuclei and initiate cell cycles^[1]. During the cell cycle, the progression from G1 phase to S phase (DNA synthesis phase) is essential for initiation of the cell cycle^[2]. Cyclin D1, a protooncogene identified in recent years, plays a positive-regulation role in the progression^[3]. The expression of cyclin D1 is an early event that is stimulated by growth factors or other mitogens. The major targets of cyclin D1-Cdk complexes are the retinoblastoma family of protein Rb^[4]. Phosphorylation of Rb in mid-G₁ leads to the release of active forms of the E2F family of transcription factors. Free E2F mediates transcription of E2f-dependent genes, including DNA polymerase, thymidine kinase^[5]. The role of cyclin D1 in the oncogenesis of gastric carcinoma is worth investigating^[6]. So far, there are few reports about the alteration of cyclin D1 in gastric carcinoma in China. In order to understand the alteration of cyclin D1 in gastric carcinoma, the protein expression of cyclin D1 in normal mucosa, hyperplastic polyp, adenoma, early stage carcinoma and advanced carcinoma of stomach was detected by immunohistochemistry. Genetic amplification and mRNA expression of cyclin D1 in advanced gastric carcinoma were detected by Southern blot and PT-PCR. The expression of cyclin D1 was also investigated in combination with other prognostic markers in advanced gastric cancer, such as patient's age, LN metastasis, histological grade and 5-year survival rate.

MATERIALS AND METHODS

Tissue specimens

Tissues from 132 cases were collected in Qilu Hospital of Shandong University. They included 42 cases of advanced gastric carcinoma with their follow-up data available (among them 16 cases had lymph node metastasis), 27 cases of early stage carcinoma (among them 7 cases had carcinomas *in situ*, the other 20 cases had early infiltrating carcinomas), 21 cases of gastric adenoma, 22 cases of hyperplastic polyp, 20 cases of normal mucosa adjacent to adenocarcinomas. All samples were fixed in 40 g/L formaldehyde and embedded in paraffin for histological diagnosis and immunohistochemistry study. Fresh tissues from advanced gastric carcinoma were obtained and stored in liquid nitrogen for DNA and RNA analyses.

Immunohistochemical staining

Immunohistochemistry was performed by the labeled streptavidin biotin (LSAB) method by using vectastain Elite kit (vector, Burlingame, CA). Monoclonal antibody to cyclin D1 was used at 1:100 dilution. The technique was performed as described^[6] except for an antigen retrieval step. Sections were placed in plastic coplin jars containing 10 mmol/L citrate buffer and heated in microwave oven for 10 min at 675 W for antigen retrieval. A positive section produced in preparative experiments was used as positive control.

Detection of cyclin D1 mRNA by reverse transcription polymerase chain reaction (RT-PCR)

Total RNA from cells was extracted by using acid guanidium-phenol-chloroform as described^[7] and converted to single-strand cDNA by using random 9 mers. PCR was performed by using a thermal cycler as described^[8]. The sequence of primer for cyclinD1 was : 5'-CTGGAGCCCCGTGAAAAAGAGC-3', 5'-CTGGAGAGGAAGCGTGTGAGG-3'. A 10 μ L of each mixture was analysed by electrophoresis on 20 g/L agarose gel. Each band was quantitated by gel figure analysis system (Alpha, No.IS-1220). β -actin was used as control. The sequence of primer for β -actin was: 5'-CTACAATGAGCTGCGTGTGGC-3', 5'-CAGGTCCAGACGCAGGATGGC-3'. CyclinD1 index = cyclin D1 data / β -actin data.

Detection of genetic alteration of cyclin D1 by Southern blot

Nucleic acids were prepared by the guanidinium thiocyanate method as described^[9]. Sample DNA (5 μ g) was digested with restriction endonuclease *EcoR* I and fractionated by electrophoresis on 20 g/L agarose gel. The gel was denatured and DNA was transferred to nitrocellulose filters. The probe used for detection of cyclin D1 was 18-mer of oligodeoxynucleotide complementary to the initial stretch of bases in cyclin D1 mRNA from -1 to +17. The probe was labeled by 32p-dCTP. The filters were prehybridized and hybridized in conditions as described^[10], dried and exposed at -70 $^{\circ}$ C with intensifying screen for various periods of time to XAR5 Kodak films. β -actin was used as control for DNA loading amount, and normal tissue near carcinoma was used as normal control.

Statistical analysis

χ^2 test was used to evaluate the differences between two groups.

RESULTS

Expression of cyclin D1 protein in gastric carcinomas and its correlation with other prognostic factors

The cyclin D1 immunohistochemical signal was located exclusively in nuclei (Figure 1A) and variable in terms of staining intensity and the proportion of positive nuclei among the cells of an individual case. One thousand tumor cells in 10 visual fields chosen randomly were counted for each case. The case was defined as positive if the proportion of stained cells was more than 10% of the tumor cells. In 20 cases of normal mucosa, 22 cases of hyperplastic polyp and 21 cases of gastric adenoma (Figure 1A), only weak to undetectable staining was seen and no one was defined as positive. On the other hand, 13/27 (48.1%) cases of early stage gastric carcinoma (Figure 1B), 20/42 (47.6%) cases of advanced gastric carcinoma (Figure 1C), 8/16 (50.0%) cases of lymph node metastasis were defined as positive. There was no significant difference among the positive rates of them (Table 1, $P > 0.05$). In the 20 cases of carcinoma with early stage infiltration, there was a good consistency of cyclin D1 expression between the *in situ* components and infiltration components. Seventeen cases showed the same immunostaining pattern in two components (85.0%). In the 16 cases of carcinoma with lymph node metastasis, 12 cases showed the same cyclin D1 immunostaining pattern in metastasis as in its primary lesion (75.0%).

Positive expression of cyclin D1 was observed in 9/24 (37.5%) patients who survived 5 years after operation. While in patients who died within 5 years, 11/18 (61.5%) cases had positive expression. There was a significant difference between the two groups (Table 1, $\chi^2 = 3.92$, $P < 0.05$). No significant correlation was observed between cyclin D1 protein expression and age, lymph-node metastasis, histological grading in patients with advanced gastric carcinoma (Table 2, $\chi^2 = 0.038$, 0.059,

0.241, $P > 0.05$).

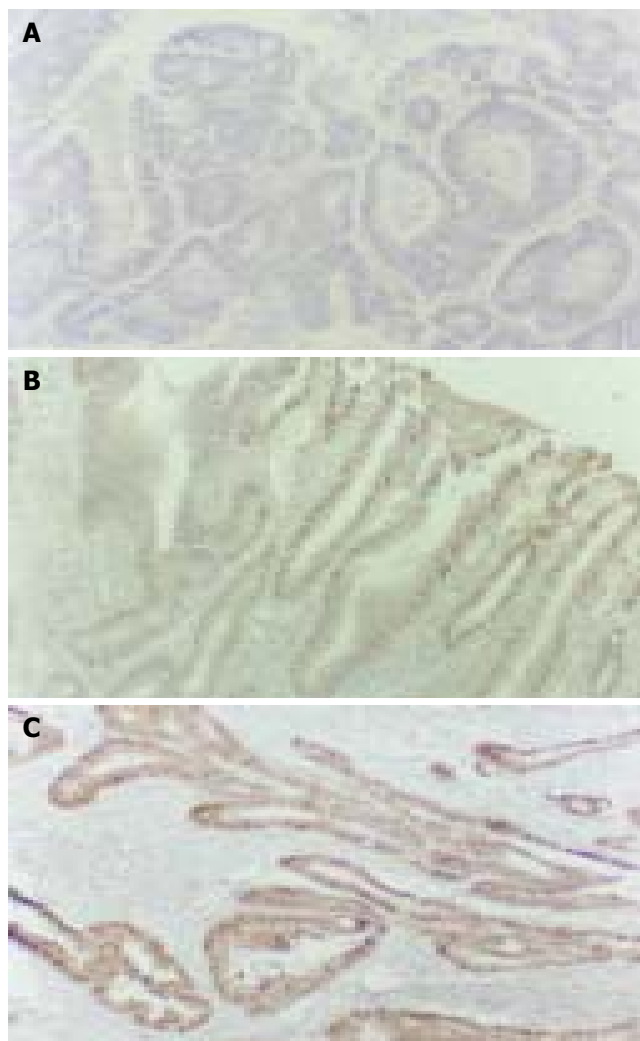


Figure 1 Expression of cyclin D1 protein. LSAB $\times 200$. A: Gastric adenoma; B: Early stage gastric carcinoma; C: Advanced gastric carcinoma.

Table 1 Cyclin D1 expression in early stage gastric carcinoma (EC), advanced gastric carcinoma (AC) and lymph node metastasis (LNM) and five-year survival

Cyclin D1	EC	AC	LNM	5-year survival rate	
				Alive	Dead
Positive	13	20	8	9	11
Negative	14	22	8	15	7
Total	27	42	16	24	18

Table 2 Relationship between cyclin D1 expression with age, lymph node metastasis (LDM) and histological grades (HG) in patients with advanced gastric carcinoma

Cyclin D1	Age (yr)		LDM		HD		
	>60	<60	Positive	Negative	I	II	III
Positive	14	6	8	12	5	11	5
Negative	16	6	8	14	4	12	4

Abnormal expression of cyclin D1 mRNA and genetic alteration of cyclin D1 gene in advanced gastric carcinoma

The amplification products of cyclin D1 and β -actin by RT-PCR were 434 bp and 206 bp respectively. Overexpression of cyclin

D1 mRNA (Figure 2) was observed in 17/42 cases (40.5%) and all these cases showed positive expression of cyclin D1 protein.

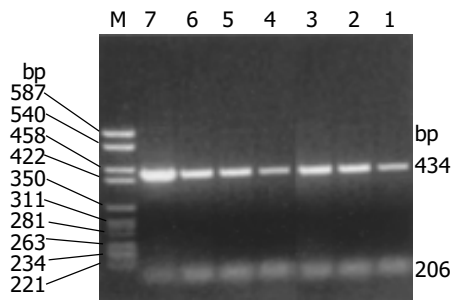


Figure 2 Overexpression of cyclin D1 mRNA detected by RT-PCR. M: marker; 1: Normal control; 3, 6, 7: Overexpression of cyclin D1 mRNA.

The level of amplification was estimated by densitometric tracing of the 4.0 kb cyclin D1 fragments of carcinomas and normal tissue. In this study, 7/42 (16.6%) cases had cyclin D1 gene amplification (2 to 4 fold), which also showed positive expression of cyclin D1 protein and overexpression of cyclin D1 mRNA. No gene rearrangement of cyclin D1 was observed in our study (Figure 3).

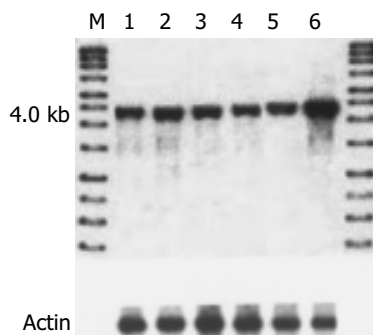


Figure 3 Genetic alteration of cyclin D1 in advanced gastric carcinoma detected by Southern blot. M: DNA marker; 1: Normal control; 6: Cyclin D1 gene amplification.

DISCUSSION

Cyclin D1 gene is located in the 11q13 region. Cyclin D1 protein consists of 295 amino acids, its function in normal cells is to regulate the progression through G1 phase of the cell cycle in combination with CDKs by phosphorylation of pRb. In normal human tissues, the expression of cyclin D1 protein was rather low and negative by immunohistochemistry^[11]. In our study, no one was positive in normal mucosa adjacent to adenocarcinomas. Negative staining was also observed in hyperplastic polyp and gastric adenoma. However, in 33/69 (47.8%) cases of gastric carcinoma, including 42 cases of advanced gastric carcinoma and 27 cases of early stage carcinoma, the expression of cyclin D1 was positive. The detection of cyclin D1 protein by immunohistochemistry is helpful in the diagnosis of early stage gastric carcinoma and could distinguish these cases from hyperplastic polyp. The expression of cell cycle regulators could be used as prognostic markers in some malignant tumors. Some studies showed that the positive expression of cyclin D1 was statistically associated with well-differentiated tumors^[12]. In our study, the expression of cyclin D1 protein had no correlation with age, lymph node metastasis and histological grading of the patients. But a significant correlation was observed between cyclin D1 expression and 5-year survival rate. The patients

with positive expression of cyclin D1 tended to have a worse prognosis.

Bartkora revealed a very good correlation in the expression of cyclin D1 between the *in situ* components and the invasive components of carcinoma^[13]. Our results were in accordance with it. In our study, the positive rates of cyclin D1 protein in early stage carcinoma, advanced gastric carcinoma and lymph node metastases were similar, with no significant difference among them. A very high degree of consistence was found in the same section of early stage carcinoma between carcinoma *in situ* and its infiltration component (89.5%). The consistence between primary tumors and lymph node metastases in the same patient with advanced gastric carcinoma was also high (75.0%). These results suggested that positive expression of cyclin D1 protein might be an early event in gastric carcinoma pathogenesis, and it tended to maintain stable throughout the progression of infiltration and metastasis.

Genetic alteration of cyclin D1 was observed in several kinds of human tumors such as breast carcinoma^[14], squamous cell carcinoma of the lung^[15], endometrial carcinoma^[16] and malignant gliomas^[17]. Yang *et al.*^[18] reported that a characteristic translocation, t(11:14)(q13;q32) involving rearrangement of cyclin D1 gene, was detected in centrocytic lymphoma and could be used in its diagnosis. In this study, cyclin D1 gene amplification accompanying positive expression of cyclin D1 protein and overexpression of cyclin D1 mRNA in advanced gastric carcinoma was observed in 7/42 (16.6%) cases. The expression rate of cyclin D1 protein (47.4%) was significantly higher than that of cyclin D1 gene amplification (16.6%). It was similar to the overexpression rate of cyclin D1 mRNA (42.1%). We considered that the expression of cyclin D1 protein was affected more directly by mRNA level rather than gene level. Besides gene amplification, other factors including alteration in cyclin D1 promoter or abnormal regulation by transcription factors could both up-regulate the expression of mRNA and induce more cyclin D1 protein production. The discrepancy between the expression rates of cyclin D1 mRNA and protein might be caused by stroma cells in tumor tissues, which make the overexpression rate of cyclin D1 mRNA lower.

REFERENCES

- 1 Shaulian E, Karin M. AP-1 as a regulator of cell life and death. *Nat Cell Biol* 2002; 4: E131-E136
- 2 Blagosklonny MV, Pardee AB. The restriction point of the cell cycle. *Cell Cycle* 2002; 1: 103-110
- 3 Ortega S, Malumbres M, Barbacid M. Cyclin D-dependent kinases, INK4 inhibitors and cancer. *Biochim Biophys Acta* 2002; 1602: 73-87
- 4 Rafferty MA, Fenton JE, Jones AS. An overview of the role and inter-relationship of epidermal growth factor receptor, cyclin D and retinoblastoma protein in the carcinogenesis of squamous cell carcinoma of the larynx. *Clin Otolaryngol* 2001; 26: 317-320
- 5 Coqueret O. Linking cyclins to transcriptional control. *Gene* 2002; 299: 35-55
- 6 Chen B, Zhang XY, Zhang YI, Zhou P, Gu Y, Fan DM. Antisense to cyclin D1 reverses the transformed phenotype of human gastric cancer cells. *World J Gastroenterol* 1999; 5: 18-21
- 7 Shoker BS, Jarvis C, Davies MP, Iqbal M, Sibson DR, Sloane JP. Immunodetectable cyclin D(1) is associated with oestrogen receptor but not Ki67 in normal, cancerous and precancerous breast lesions. *Br J Cancer* 2001; 84: 1064-1069
- 8 Chomczynski P, Sacchi N. Single-step method of RNA isolation by acid guanidinium thiocyanate-phenol-chloroform extraction. *Anal Biochem* 1987; 162: 156-159
- 9 Wan QH, Qian KX, Fang SG. A simple DNA extraction and rapid specific identification technique for single cells and early embryos of two breeds of *Bos taurus*. *Anim Reprod Sci* 2003; 77: 1-9

- 10 **Renado M**, Martinez-Delgado B, Arranz E, Garcia M, Urioste M, Martinez-Ramirez A, Rivas C, Cigudosa JC, Benitez I. Chromosomal changes pattern and gene amplification in T cell non-Hodgkin's lymphomas. *Leukemia* 2001; **15**: 1627-1632
- 11 **Turner HE**, Nagy Z, Sullivan N, Esiri MM, Wass JA. Expression analysis of cyclins in pituitary adenomas and the normal pituitary gland. *Clin Endocrinol* 2000; **53**: 337-344
- 12 **Naidu R**, Wahab NA, Yadav MM, Kutty MK. Expression and amplification of cyclin D1 in primary breast carcinomas: relationship with histopathological types and clinico-pathological parameters. *Oncol Rep* 2002; **9**: 409-416
- 13 **Bartkova J**, Lukas J, Muller H, Lutzhoft D, Strauss M, Bartek J. Cyclin D1 protein expression and function in human breast cancer. *Int J Cancer* 1994; **57**: 353-361
- 14 **Steeg PS**, Zhou Q. Cyclins and breast cancer. *Breast Cancer Res Treat* 1998; **52**: 17-28
- 15 **Qiuling S**, Yuxin Z, Suhua Z, Cheng X, Shuguang L, Fengsheng H. Cyclin D1 gene polymorphism and susceptibility to lung cancer in a Chinese population. *Carcinogenesis* 2003; **24**: 1499-1503
- 16 **Moreno-Bueno G**, Rodriguez-Perales S, Sanchez-Estevez C, Hardisson D, Sarrio D, Prat J, Cigudosa JC, Matias-Guiu X, Palacios J. Cyclin D1 gene (CCND1) mutations in endometrial cancer. *Oncogene* 2003; **22**: 6115-6118
- 17 **Buschges R**, Weber RG, Actor B, Lichter P, Collins VP, Reifenberger G. Amplification and expression of cyclin D genes (CCND1, CCND2 and CCND3) in human malignant gliomas. *Brain Pathol* 1999; **9**: 435-442
- 18 **Yang WI**, Zukerberg LR, Motokura T, Arnold A, Harris NL. Cyclin D1 (Bcl-1, PRAD1) protein expression in low-grade B-cell lymphomas and reactive hyperplasia. *Am J Pathol* 1994; **145**: 86-96

Edited by Wang XL and Xu CT Proofread by Pan BR and Xu FM

Comparison of quality of life between urban and rural gastric cancer patients and analysis of influencing factors

Jun Tian, Zhen-Chun Chen, Bin Wu, Xin Meng

Jun Tian, Bin Wu, Xin Meng, Department of Epidemiology and Health Statistics, Fujian Medical University, Fuzhou 350004, Fujian Province, China

Zhen-Chun Chen, Fujian Cancer Hospital, Fuzhou 350014, Fujian Province, China

Correspondence to: Jun Tian, Department of Epidemiology and Health Statistics, Fujian Medical University, Fuzhou 350004, Fujian Province, China. tianjun@mail.fjmu.edu.cn

Telephone: +86-591-3569264

Received: 2003-11-18 **Accepted:** 2003-12-08

Abstract

AIM: The conception of quality of life has been widely accepted by clinic doctors. Evaluations of the treatment effect of chronic diseases have been changed to depend not only on the survival time, but also on the quality of life of the patients. Fuzhou City and Changle County are high-incidence areas of the gastric cancer in Fujian Province. The aims of this research were to compare the quality of life of urban patients with that of rural patients and analyze the factors influencing quality of life of gastric cancer patients in Fujian Province.

METHODS: The samples were drawn with cluster sampling. The urban sample consisted of 162 patients aged 25 to 75 with 143 males and 19 females. The rural sample consisted of 200 patients aged 32 to 78 with 166 males and 34 females. The patients in both the urban and rural areas were investigated, and their scores on 21 items reflecting the quality of life were measured. The methods of *t* test and stepwise regression were used to analyze the data.

RESULTS: The average total scores of quality of life of the urban patients and rural patients were 64.11 and 68.69 respectively. There was a significant difference between the means of two samples ($P = 0.0004$). Seven variables in the regression model estimated by the urban sample and 4 variables in the model by the rural sample were at the level of significance $\alpha = 0.05$. Family income, nutrition and rehabilitative exercise were selected into both the urban and rural regression models.

CONCLUSION: Most of the gastric cancer patients have poor quality of life in Fujian Province and the rural patients have lower quality of life than that of urban patients. The patients having more family income have better quality of life, and enhanced nutrition and doing rehabilitative exercise are helpful in improving the quality of life of the gastric cancer patients.

Tian J, Chen ZC, Wu B, Meng X. Comparison of quality of life between urban and rural gastric cancer patients and analysis of influencing factors. *World J Gastroenterol* 2004; 10(20): 2940-2943

<http://www.wjgnet.com/1007-9327/10/2940.asp>

INTRODUCTION

Along with the changes of medical pattern and health care practice, evaluations of the treatment effect of chronic diseases have been changed to depend not only on the survival time, but also on the quality of life of the patients. The quality of life of a person is his personal feeling in sections of physiology, psychology and society^[1,2]. The quality of life of the cancer patients can reflect not only treatment effect but also rehabilitation effect, so it has attracted much attention since 1980. Many studies have been done regarding the quality of life of the cancer patients in western countries and Japan^[3-8], and there also have been several relevant studies in China^[9-11]. Another important aspect of research on the quality of life is analyzing factors influencing the quality of life. Since many factors can impact on the quality of life of the cancer patients, it is important to analyze which factors may be related to the quality of life in order to improve the quality of life of the patients. Fuzhou City and Changle County are high-incidence areas of gastric cancer in Fujian Province. Every year, there are many new cases reported in the two areas^[12]. A lot of efforts have been made in prevention and treatment of gastric cancer. However, little attention has been paid to the quality of life of the gastric cancer patients and few studies have been done on how to improve the quality of life of the patients. In order to understand the levels of quality of life of the gastric cancer patients in Fujian Province, we made an epidemiological survey from May 1999 to July 1999. In this paper, we describe the levels of the quality of life of the urban patients and rural patients, compare the quality of life of the urban patients with that of the rural patients, and analyze the factors influencing the quality of life. The results of this research may be useful to doctors and nurses in the community health center to help improve the quality of life of the gastric cancer patients.

MATERIALS AND METHODS

Materials

The populations of the gastric cancer patients diagnosed between 1997 and 1998 were provided by the Tumor Registration Office of Fujian Province. The samples were drawn from the populations with cluster sampling. All of the gastric cancer patients in the urban sample were residents in Fuzhou City and diagnosed by the provincial-level hospitals. The patients in the rural sample were residents in Changle County and diagnosed by the county-level above hospitals. All of the patients in the two samples had survived for no less than one year.

Methods

The questionnaire was composed of two sections, one with 16 items related to the disease, treatment and rehabilitation of the gastric cancer patients (Table 1), and the other with 21 items related to the quality of life of the patients (Table 2). Each of the 21 items of survival quality was scored from 1 to 5 indicating the function from the worst to the best. The internal consistency and stability index, Cronbach $\alpha = 0.9866$, confirmed the reliability of the 21 items describing the quality of life. The investigators

Table 1 List of factors that may affect the quality of life of gastric cancer patients

Factor	Definition
Gender	Male 1 Female 2
Age (yr)	
Marital status	Single 1 Married 2 Divorced 3 Widowed 4
Education	Primary school 1 Middle school 2 High school 3 University 4
Family income (per capita, Yuan)	
Medical insurance	Yes 1 No 0
Clinical stage of tumor	1-4
Survival time (mo)	
Surgery	2/3 gastrectomy 1, 4/5 gastrectomy 2, total gastrectomy 3
Number of chemotherapy programs	
Time from the latest chemotherapy to the enrollment (mo)	
Treatment of traditional Chinese medicine	Yes 1 No 0
Home nursing staff	Spouse 1 Other relatives 2 Housekeepers 3 None 4
Chemotherapy	Yes 1 No 0
Enhanced nutrition	Yes 1 No 0
Rehabilitating exercise	Yes 1 No 0

visited the patient’s family and asked the patient to complete the questionnaire except the contents of the disease stage and treatments which were collected from the medical records at the hospitals. The scores for the individual items shown in Table 2 were summed to produce a ‘total score’, representing the quality of life of each patient.

Numerical descriptive statistics were used in summarizing the total score of quality of life in urban patients and rural patients respectively, *t* test was used for testing the difference between the means of two samples and stepwise regression^[13] was used for analyzing the factors influencing quality of life. SAS software package was used for all analyses^[14].

Table 2 The 21 parameters of the quality of life

Items	Items
1 Sleep	12 Knowledge of cancer
2 Range of activities	13 Mental status
3 Eating	14 Fear of disease
4 Ability of using traffic vehicles independently	15 Psychological pain
5 Ability of body movement	16 Connection with relatives and friends
6 Ability to live independently	17 Social contact
7 Housework	18 Disappointment
8 Pain	19 Confidence of fighting the disease
9 Recreational activities	20 Intellectual activities
10 Watching TV or listening to radio	21 Attitude towards treatment
11 Interest or hobby	

RESULTS

Description of samples

The urban sample consisted of 162 patients aged 25 to 75. There were 143 male and 19 female patients in the urban sample, about 88.3% and 11.7% of the urban sample size respectively. The rural sample consisted of 200 patients aged 32 to 78. There were 166 male and 34 female patients in the rural sample, about 83.0% and 17.0% of the rural sample size respectively. In the urban sample, the workers represented 42.6% and government functionaries took up 23.5%. All of the patients in the rural sample were peasants.

The quality of life

The distributions of total scores of urban patients and rural patients are shown in Table 3. Among the urban patients, the highest score was 96 and the lowest score 22, and 36.42% of the patients, the largest group, had total scores between 70 and 80 and 1.23%, the smallest group, had total scores between 90-105. Among the rural patients, the highest score was 81 and the lowest score 19, and 34.5% had total scores between 60 and 70 and none had a total score between 90-105. Table 4 shows the means and standard deviations of the total scores of the urban and rural patients. The difference of total scores between the urban and rural patients was significant (*P* = 0.0004). These results suggest that most of the gastric cancer patients had poor quality of life in Fujian Province and the qualities of life of rural patients were worse than those of urban patients.

Table 3 Distributions of total scores in urban patients and rural patients

Total score	Urban		Rural	
	<i>n</i>	Percentage (%)	<i>n</i>	Percentage (%)
<30	3	1.85	4	2.00
30-	3	1.85	6	3.00
40-	8	4.94	16	8.00
50-	17	10.49	54	27.00
60-	43	26.54	69	34.50
70-	59	36.42	41	20.50
80-	27	16.67	10	5.00
90-105	2	1.23	0	0.00

Table 4 Means and standard deviations of total scores in the two samples

	Number of the patients	mean	SD	95% confidence interval
Urban	162	68.69	12.98	66.69-70.69
Rural	200	64.11	11.29	62.54-65.67
		<i>t</i> = 3.5885	<i>P</i> = 0.0004	

Factors influencing the quality of life

The relationship between the total scores, also called dependent variables, and the factors shown in Table 1, also called independent variables, was analyzed by using method of stepwise regression.

Setting the level of significance $\alpha = 0.05$, we had the result

of regression analysis with urban patients (Table 5). Table 5 shows the factors influencing quality of life of gastric cancer patients and the regression coefficients. This result suggests that the factors related to the total score of urban patients were age ($P = 0.0001$), family income ($P = 0.0032$), clinical stage of the tumor ($P = 0.0375$), the time from the latest chemotherapy to the enrollment ($P = 0.0095$), home nursing staff ($P < 0.0001$), enhanced nutrition ($P = 0.0431$) and rehabilitative exercise ($P = 0.0115$). As indicated by the regression coefficients, the quality of life of elder patients was worse than that of the younger ones, the patient in the early stage of gastric cancer had a better quality of life than that in the late stage and patients with a longer time period from the latest chemotherapy to the enrollment had a better quality of life than one with a shorter time period.

Table 5 Results of stepwise regression with urban patients

Variable	Regression coefficient	SEM	<i>t</i>	<i>P</i>
Age (yr)	-0.10620	0.02654	-4.00	0.0001
Family income	1.11909	0.36949	3.03	0.0032
Clinical stage of the tumor	-1.10772	0.52498	-2.11	0.0375
Time from the latest chemotherapy to the enrollment	0.09199	0.03876	2.37	0.0095
Home nursing staff	-2.98233	0.57659	-5.17	<0.0001
Enhanced nutrition	1.80669	0.88221	2.05	0.0431
Rehabilitating exercise	1.01185	0.39245	2.58	0.0115

At $\alpha = 0.05$, the results of regression analysis of the rural patients are shown in Table 6. The results suggested that the factors related to the total score of rural patients were family income ($P = 0.0193$), surgical operation ($P < 0.0001$), enhanced nutrition ($P = 0.0488$) and rehabilitative exercise ($P = 0.0125$). Based on regression coefficients, patients with total gastrectomy had a worse quality of life than those with a partial gastrectomy.

Table 6 Results of stepwise regression with rural patients

Variable	Parameter estimated	SEM	<i>t</i>	<i>P</i>
Family income	1.0860	0.45974	2.36	0.0193
Surgery	-14.24462	2.77803	5.12	<0.0001
Enhanced nutrition	-2.73243	1.37834	1.98	0.0488
Rehabilitating exercise	-2.20909	0.87618	2.52	0.0125

Three factors: family income, nutrition and rehabilitative exercise, in both regression models, might be important for improving the quality of life of the gastric cancer patients. The patients having more economic incomes had a better quality of life, and increased nutrition and doing rehabilitative exercise are helpful in improving the quality of life of the gastric cancer patients.

DISCUSSION

Traditionally, the effects of treatments were evaluated by such quantitative indexes as survival rate, survival time and the volumes of tumors. The conception of quality of life is proposed, along with the changes of medical and health care practice patterns and progress of medical science. It is used to evaluate the effects of treatments for chronic diseases and cancers. The purpose of this study was to obtain the information about quality of life of gastric cancer patients in Fujian Province and explore which factors impacted on the quality of life of gastric cancer patients.

For most of gastric cancer patients, the prognosis and their qualities of life were poor since the cancers had been in advanced stages when they were diagnosed^[15,16]. Our results show that most of the gastric cancer patients have low quality of life in Fujian Province, and the quality of life of rural gastric cancer patients are worse than that of urban patients. It may be that the rural patients suffered more physical and psychological pain because of their lower levels of education and economic income compared with the urban patients.

Some researchers held that patient's nutritional status played a critical role in maintaining a positive quality of life from both physical and emotional points of view^[17-20]. Nutrient depletion adversely affects immune function, the patient's enjoyableness and social interactions with family and friends, which can further depress appetite^[17]. Low hemoglobin levels were associated with fatigue, poor overall quality of life, and decreased ability to work. Interventions that reverse fatigue and other anemia-related symptoms should have a positive effect on quality of life^[19]. Our results also showed that improved nutrition was one of the factors influencing quality of life both in rural and urban areas. This may suggest that appropriate nutritional care can help maintain the patient's body weight and protein status, reduce fatigue and improve quality of life.

Rehabilitating exercise has been thought to be a factor influencing quality of life of breast cancer patients. A review on 24 studies dealing with physical exercise and quality of life of cancer patients published between 1980 and 1997 demonstrated that physical exercise had a positive effect on quality of life including physical, functional, psychological, and emotional well-being^[21-27]. In our research, rehabilitative exercise was related to quality of life of gastric cancer patients, which is consistent with previous researches. Not only can taking rehabilitative exercise improve the patient's body function, but it can also please his mood, strengthen his confidence of defeating the disease and improve his ability of contacting society.

Our results also showed that the quality of life of urban patients could be affected by the home nursing staff and rural patients affected by the surgery. The psychological status of the nursing staff may have more influence on the physiological and psychological functions of the patient. Good nutritional care for the patient requires full support from the home nursing staff^[28-32]. Patients who have been given a partial gastrectomy achieved a better quality of life than those having a total gastrectomy. When the entire gastric is removed, the patients should adjust to a different eating schedule involving eating small quantities of food more frequently and high-protein foods, so the home nursing staff should be educated on providing cancer care and nutritional support. The family members should have adequate knowledge as to how to support the patient.

In summary, our data obtained by epidemiological survey show that most of the gastric cancer patients have poor quality of life in Fujian Province, and the quality of life of the rural patients are worse than that of the urban patients. The patients having more family income have better quality of life, and enhanced nutrition and doing rehabilitative exercise are helpful in improving the quality of life of the gastric cancer patients.

REFERENCES

- 1 Mellette SJ. Cancer rehabilitation. *J Natl Cancer Inst* 1993; **85**: 781-784
- 2 Wang JP, Cui JN, Chen ZG, Lin WJ, Luo J, Sun Y. Quality of life and factors that influence it among cancer patients in China. *Zhongguo Linchuang Xinlixue Zazhi* 2000; **8**: 23-26
- 3 Bottomley A. The cancer patient and quality of life. *Oncologist* 2002; **7**: 120-125
- 4 Repetto L, Ausili-Cefaro G, Gallo C, Rossi A, Manzione L. Quality of life in elderly cancer patients. *Ann Oncol* 2001; **3**

- (Suppl): S49-52
- 5 **Efficace F**, Bottomley A, van Andel G. Health related quality of life in prostate carcinoma patients: a systematic review of randomized controlled trials. *Cancer* 2003; **97**: 377-388
 - 6 **Rustoen T**, Wiklund I, Hanestad BR, Burckhardt CS. Validity and reliability of the Norwegian version of the Ferrans and Powers Quality of Life Index. *Scand J Caring Sci* 1999; **13**: 96-101
 - 7 **Andersen BL**. Quality of life for women with gynecologic cancer. *Curr Opin Obstet Gynecol* 1995; **7**: 69-76
 - 8 **Arora NK**, Gustafson DH, Hawkins RP, McTavish F, Cella DF, Pingree S, Mendenhall JH, Mahvi DM. Impact of surgery and chemotherapy on the quality of life of younger women with breast carcinoma: a prospective study. *Cancer* 2001; **92**: 1288-1298
 - 9 **Deng XL**, Wang W, Wang LS. Relationship between the Quality of life and therapeutic modalities in patients with gastric cancer. *Zhongguo Zhongliu* 2001; **10**: 78-80
 - 10 **Tian J**, Zhang JY, Wu B, Chen JL, Chen ZC. A multifactor study on the quality of survival of aged cancer patients. *Zhonghua Laonian Yixue Zazhi* 1996; **15**: 339-342
 - 11 **Tian J**, Wu B, Chen JL, Chen ZC, Chen JS. An influencing factors study on the quality of life of gastric carcinoma patients. *Shuli Tongji Yu Guanli* 2000; **19**: 35-38
 - 12 Quanguo Zhongliu Fangzhi Yanjiu Bangongshi. The cancer incidences and death rates in China (1988-1992). Bejin: *Zhongguo Yiyao Keji Chubanshe* 2001: 22-200
 - 13 **Katz MH**. Multivariable Analysis: A Practical Guide for Clinicians. H.K.: *Science Culture Publishing House LTD* 2000: 26-45
 - 14 **Hong N**, Hou J. SAS for Windows. Beijing: *Dianzi Gongye Chubanshe* 2001: 107-138
 - 15 **Luo J**, Sun Y. The research on quality of life in cancer patients. *Zhongguo Zhongliu* 2001; **10**: 76-78
 - 16 **LENA-MARIE Petersson**. Group rehabilitation for cancer patients: effects, patient satisfaction, utilisation and prediction of rehabilitation need. Sweden: *Tryck Medier* 2003: 14-73
 - 17 **Small W**, Carrara R, Danford L, Logemann JA, Cella D. Quality of life and nutrition in the patient with cancer. *Oncology* 2002(Suppl): 13-14
 - 18 **Brown J**, Byers T, Thompson K, Eldridge B, Doyle C, Williams AM. Nutrition during and after cancer treatment: A guide for informed choices by cancer survivors. *CA Cancer J Clin* 2001; **51**: 153-187
 - 19 **Cella D**. Factors influencing quality of life in cancer patients: anemia and fatigue. *Semin Oncol* 1998; **25**(3 Suppl 7): 43-46
 - 20 **Peltz G**. Nutrition support in cancer patients: a brief review and suggestion for standard indications criteria. *Nutr J* 2002; **1**: 1
 - 21 **Salmon PG**, Swank AM. Exercise-based disease management guidelines for individuals with cancer: Potential applications in a high-risk mid-southern state. *J Exercise Physiol* 2002; **5**: 1-10
 - 22 **Watson PG**. Cancer rehabilitation. The evolution of a concept. *Cancer Nurs* 1990; **13**: 2-12
 - 23 **Courneya KS**, Friedenreich CM. Physical exercise and quality of life following cancer diagnosis: a literature review. *Ann Behav Med* 1999; **21**: 171-179
 - 24 **Andersen BL**. Psychological interventions for cancer patients to enhance the quality of life. *J Consult Clin Psychol* 1992; **60**: 552-568
 - 25 **Courneya KS**, Friedenreich CM. Framework PEACE: an organizational model for examining physical exercise across the cancer experience. *Ann Behav Med* 2001; **23**: 263-272
 - 26 **Blanchard CM**, Courneya KS, Laing D. Effects of acute exercise on state anxiety in breast cancer survivors. *Oncol Nurs Forum* 2001; **28**: 1617-1621
 - 27 **Courneya KS**. Exercise interventions during cancer treatment: biopsychosocial outcomes. *Exerc Sport Sci Rev* 2001; **29**: 60-64
 - 28 **Rustoen T**, Wiklund I, Hanestad BR, Moum T. Nursing intervention to increase hope and quality of life in newly diagnosed cancer patients. *Cancer Nurs* 1998; **21**: 235-245
 - 29 **Rustoen T**, Wiklund I. Hope in newly diagnosed patients with cancer. *Cancer Nurs* 2000; **23**: 214-219
 - 30 **Andersen BL**. Biobehavioral outcomes following psychological interventions for cancer patients. *J Consult Clin Psychol* 2002; **70**: 590-610
 - 31 **Velikova G**, Booth L, Smith AB, Brown PM, Lynch P, Brown JM, Selby PJ. Measuring quality of life in routine oncology practice improves communication and patient well-being: a randomized controlled trial. *J Clin Oncol* 2004; **22**: 714-724
 - 32 **Wan GJ**, Counte MA, Cella DF. The influence of personal expectations on cancer patients' reports of health-related quality of life. *Psychooncology* 1997; **6**: 1-11

Edited by Hu DK and Zhu LH Proofread by Chen WW and Xu FM

Down-modulation of heat shock protein 70 and up-modulation of Caspase-3 during schisandrin B-induced apoptosis in human hepatoma SMMC-7721 cells

Yi-Feng Wu, Ming-Fu Cao, Yan-Ping Gao, Fei Chen, Tao Wang, Edward P. Zumbika, Kai-Xian Qian

Yi-Feng Wu, Yan-Ping Gao, Kai-Xian Qian, College of Life Sciences, Zhejiang University, Hangzhou 310027, Zhejiang Province, China

Ming-Fu Cao, College of Life Sciences, Hangzhou Teachers college, Hangzhou 310012, Zhejiang Province, China

Fei Chen, Tao Wang, Edward P. Zumbika, School of Medicine, Zhejiang University, Hangzhou 310027, Zhejiang Province, China

Supported by the National Key Technologies Research and Development Program of China during the 10th Five-Year Plan Period, No. 2002BA760C

Correspondence to: Kai-Xian Qian, College of Life Sciences, Zhejiang University, Hangzhou 310027, Zhejiang Province, China. biozell@zju.edu.cn

Telephone: +86-571-87952761

Received: 2004-02-02 **Accepted:** 2004-02-21

Abstract

AIM: To investigate the effect of schisandrin B (Sch B) on proliferation and apoptosis of human hepatoma SMMC-7721 cells *in vitro* and regulation of Hsp70 and Caspases-3, 7, 9 expression by Sch B.

METHODS: Human hepatoma cell line SMMC-7721 was cultured and treated with Sch B at various concentrations. Growth suppression was detected with MTT colorimetric assay. Cell apoptosis was confirmed by DNA ladder detection and flow cytometric analysis. The expression of Hsp70, Caspases-3, 7, 9 were analyzed by Western blot analysis.

RESULTS: Sch B inhibited the growth of hepatoma SMMC-7721 cells in a dose-dependent manner, leading to a 50% decrease in cell number (LC50) value of 23.50 mg/L. Treatment with Sch B resulted in degradation of chromosomal DNA into small internucleosomal fragments, evidenced by the formation of a 180-200 bp DNA ladder on agarose gels. FCM analysis showed the peak areas of subdiploid at the increased concentration of Sch B. The results of Western blot analysis showed that Hsp70 was down-regulated and Caspase-3 was up-regulated, while the activity of Caspases-7, -9 had no significant change.

CONCLUSION: Sch B is able to inhibit the proliferation of human hepatoma SMMC-7721 cells and induce apoptosis, which goes through Caspase-3-dependent and Caspase-9-independent pathway accompanied with the down-regulation of Hsp70 protein expression at an early event.

Wu YF, Cao MF, Gao YP, Chen F, Wang T, Zumbika EP, Qian KX. Down-modulation of heat shock protein 70 and up-modulation of Caspase-3 during schisandrin B-induced apoptosis in human hepatoma SMMC-7721 cells. *World J Gastroenterol* 2004; 10(20): 2944-2948

<http://www.wjgnet.com/1007-9327/10/2944.asp>

INTRODUCTION

Schisandrin B (Sch B, Figure 1) is a dibenzocyclooctadiene

compound isolated from *Fructus Schisandrae* (FS, the fruit of *Schisandra chinensis*), an herb commonly prescribed in tonic and sedative formulae in Chinese medicine^[1,2]. In clinical situations, FS was also found to produce beneficial effects on patients suffering from viral hepatitis^[3]. Recently, the pharmacological profile of FS, which includes the enhancement of liver functions and inhibitory/sedative effects on the central nervous system, has been established by laboratory investigations^[4-9]. We presented evidence that Sch B was able to inhibit the proliferation of human hepatoma SMMC-7721 cells and induce apoptosis *in vitro*.

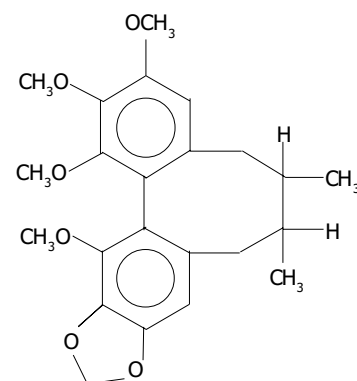


Figure 1 Chemical structure of Schisandrin B.

Apoptosis is an essential physiological process required for normal development and maintenance of tissue homeostasis^[10,11]. Insufficient or excessive cell death can contribute to human diseases, including cancer, acquired immunodeficiency syndrome and some neurodegenerative disorders^[12]. Although many factors are involved in apoptotic program^[13-16], Caspases, a family of cysteine proteases have been shown to play a major role in the transduction of apoptotic signals and the execution of apoptosis in mammalian^[17-21], which has become recognized as key components of the apoptotic machinery^[22]. Most of the biochemical and morphological events of apoptosis are a direct result of Caspase-mediated cleavage of specific substrates^[23,24].

Inhibition of Caspases following treatment with apoptotic stimuli has been shown to prevent some features of apoptosis. The heat shock protein 70 (Hsp70) family of proteins has been demonstrated to be a potent inhibitor of apoptosis induced by a wide range of stimuli^[25,26]. It can protect against apoptosis at an early event in the apoptotic pathway. A role for Hsp70 in tumorigenesis has been suggested, based on the observations that many transformed cells have elevated levels of Hsp70 and overexpression of Hsp70 in transgenic mice results in T-cell lymphoma^[27-30].

In this study, Sch B induced human hepatoma SMMC-7721 cell apoptosis was confirmed by DNA ladder detection and flow cytometric analysis. At the same time, the down-modulation of Hsp70 and Caspases was observed to study the mechanism of Sch B induced apoptosis in human hepatoma SMMC-7721 cells.

MATERIALS AND METHODS

Reagents

Sch B was purchased from National Institute for the Control of Pharmaceutical and Biological Products, China (NICBPB). The drug was dissolved in dimethyl sulfoxide (DMSO) at a concentration of 10 g/L. For cell treatments, the samples were further diluted in culture medium with the final DMSO concentration <5 g/L. Antibodies to Hsp70, Caspases-3, 7, 9 were purchased from Boster Biotech, China. RPMI-1640 culture medium was obtained from Gibco Co. USA. Fetal calf serum was supplied by Si-Ji-Qing Biotechnology Co. (Hangzhou, China). 96-well plates and culture bottles were purchased from Costar Co. USA. All other chemicals were purchased from Sigma Chemical (St. Louis, MO, USA).

Cell lines and culture

Human hepatoma cell line SMMC-7721 and human hepatic cell line HL-7702 were purchased from American Type Culture Collection (ATCC). Human endothelial cell line ECV-304 was obtained from Tumor Institute, Zhejiang University. Primary human fibroblast cell line was derived from fresh muscle tissues by enzymatic dissociation. Human lymphocytes were derived from umbilical blood by Ficoll-Hyaque separation method, and seeded in 96-well microplates with the concentration of phytoagglutinin (PHA). All the cell lines were grown as monolayers in RPMI1640 medium supplemented with 100 mL/L fetal calf serum and antibiotics (100 unit/mL penicillin and 100 µg/mL streptomycin), incubated at 37 °C in a humidified incubator containing 50 mL/L CO₂ in air.

Assay of cell proliferation

SMMC-7721 cells (100 µL of cell suspension per well) were seeded at a density of 1.5×10^5 /mL in 96-well plates. Each group had three wells with a non-treated group as control. When the cells anchored to the plates, various concentrations of Sch B were added and the slides were incubated at 37 °C in humidified atmosphere containing 50 mL/L CO₂. When the cells described above were cultured for 48 h, 50 µL of MTT (2 mg/mL in PBS) was added to each well and cultured for another 4 h. After the supernatant was discarded, MTT formazan precipitates were dissolved in 100 µL of DMSO, shaken mechanically for 10 min and then read immediately at 570 nm in a plate reader. Cell proliferation inhibition rate (CPIR) was calculated using the following equation: CPIR = (1 - average absorbance (A) value of experimental group / average A value of control group) × 100%.

Cell toxicity on primary cells or normal cell lines

HL-7702 cells, ECV-304 cells, primary human fibroblast cells, human lymphocytes (100 µL cell suspension per well) were seeded at a density of 1.0×10^5 /mL in 96-well plates. Following treatment at the concentration of 10, 20, 40, 80, 160 mg/L Sch B for 24 h, cell viability was estimated by trypan blue exclusion. Six wells were measured for each concentration of test compound. All toxicity experiments were repeated at least three independent occasions.

DNA ladder demonstration

After exposed to Sch B for 12 h, SMMC-7721 cells (5×10^6 /sample, both attached and detached cells) were collected and lysed with lysis buffer containing 50 mmol/L Tris-HCl buffer (pH 7.5), 20 mmol/L EDTA, and 10 g/L NP-40. Then 10 g/L SDS and RNase (5 µg/mL) were added to the supernatant, and incubated at 56 °C for 2 h, followed by incubation with proteinase K (2.5 µg/mL) at 37 °C for 2 h. After the DNA was precipitated by addition of both ammonium acetate (3.3 mol/L) and ethanol (995 mL/L), it was dissolved in a gel loading buffer. DNA fragmentation was detected by electrophoresis on 15 g/L agarose gels and visualized with ethidium bromide staining.

Flow cytometric analysis

SMMC-7721 cells were seeded in culture flasks. When the cells were anchored to the plates, various concentrations (0, 10 µmol/L, 20 µmol/L, 40 µmol/L) of Sch B were added and the cells were incubated at 37 °C in humidified atmosphere containing 50 mL/L CO₂ for 2 d. Then each group of cells were washed with PBS, trypsinized and fixed with 700 mL/L ethanol at -20 °C for 30 min, and they were stained with 1.0 µg/mL propidium iodide (PI, Boehringer Mannheim, Germany). The red fluorescence of DNA-bound PI in individual cells was measured at 488 nm with an Altra flow cytometer. The results were analyzed using the ExpoII software (Beckman Coulter, USA). Ten thousand events were analyzed for each sample.

Western blotting analysis

The cells were lysed in a lysis buffer (25 mmol/L hepes, 15 g/L Triton X-100, 10 g/L sodium deoxycholate, 1 g/L SDS, 0.5 mol/L NaCl, 5 mmol/L edetic acid, 50 mmol/L NaF, 0.1 mmol/L sodium vanadate, 1 mmol/L phenylmethylsulfonyl fluoride (PMSF) and 0.1 g/L leupeptin, pH7.8) at 4 °C with sonication. The lysates were centrifuged at 15 000 g for 15 min and the concentration of the protein in each lysate was determined with Coomassie brilliant blue G-250. Loading buffer (42 mmol/L Tris-HCl, containing 100 mL/L glycerol, 23 g/L SDS, 50 g/L 2-mercaptoethanol and 0.02 g/L bromophenol blue) was then added to each lysate, which was subsequently boiled for 3 min and then electrophoresed on a SDS-polyacrylamide gel. Proteins were transferred onto a nitrocellulose filter and incubated separately with antibodies against Hsp70, Caspases-3,7,9, then labeled with peroxidase-conjugated secondary antibodies. The reactions were visualized using the enhanced chemiluminescence reagent (Sigma). The results were approved by repeating the reactions twice.

Statistical analysis

All data were expressed as mean ± SD. Statistical analysis was performed by *t* test using software SPSS 11.0 for Windows. *P* < 0.05 was considered statistically significant.

RESULTS

Effect of Sch B on cell proliferation

Treatment of human hepatoma SMMC-7721 cells with Sch B resulted in a dose-dependent cytotoxicity. As shown in Figure 2, Sch B-mediated cytotoxicity occurred at a concentration greater than 20 mg/L for 48 h. A significant decrease in cell number was seen in the cells treated with Sch B at 20 mg/L. The concentration of Sch B leading to a 50% decrease in cell number (LC50) was about 23.5 mg/L.

Effect of Sch B on primary cells or normal cell line toxicity

As indicated in Figure 3, Sch B had little cytotoxic effect on primary human fibroblast cells and human lymphocyte cells even if at the concentration of 160 mg/L. Treatment of human HL-7702, ECV-304 with Sch B resulted in a dose-dependent cytotoxicity. But human hepatic HL-7702 cells were more resistant to the Sch B-mediated cytotoxicity than human endothelial cells, ECV-304 cells and human hepatoma SMMC-7721.

Detection of DNA fragmentation in SMMC-7721 cells treated with Sch B

As shown in Figure 4, treatment with Sch B resulted in degradation of chromosomal DNA into small internucleosomal fragments, evidenced by the formation of a 180-200 bp DNA ladder on agarose gels, hallmark of cells undergoing apoptosis. No DNA ladders were detected in the samples isolated from control cultures. These results indicated that Sch B induced an apoptotic cell death in SMMC-7721 cells.

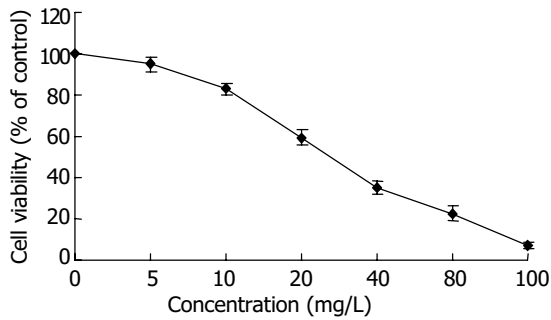


Figure 2 Inhibition rate of Sch B on proliferation of SMMC-7721 cells. Cells were incubated at concentrations of Sch B for 48 h.

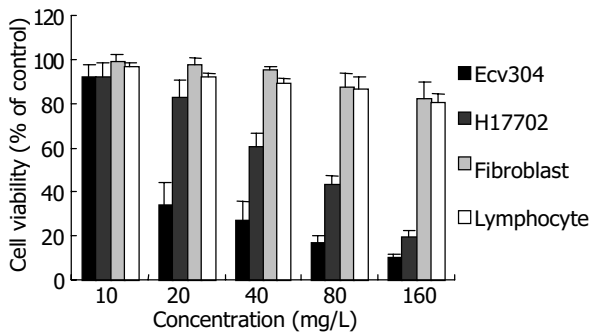


Figure 3 Cytocidal effect of Sch B on growth of human endothelial ECV-304 cells, human hepatic HL-7702 cells, primary human fibroblast cells and human lymphocyte cells. Cells were incubated at concentrations (10, 20, 40, 80, 160 mg/L) of Sch B for 48 h.

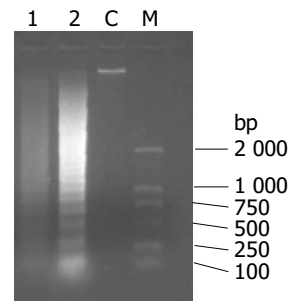


Figure 4 DNA fragmentation in SMMC-7721 cells treated with Sch B for 12 h. M: size marker; C: control culture; lane 1: 20 mg/L Sch B treatment; lane 2: 40 mg/L Sch B treatment.

Flow cytometric analysis of cell apoptosis

SMMC-7721 cells were exposed to increased concentrations of Sch B (10 mg/L, 20 mg/L, 40 mg/L) for 48 h, and the growth of the cells was analyzed using flow cytometry (Figure 5). The peak value appearing before the G1 peak is called apoptotic peak. As shown in Figure 5 and Table 1, the apoptotic peak areas and rate increased with increased concentrations of Sch B.

Table 1 Apoptosis rate of SMMC-7721 cells induced by Sch B

Sch B concentration (mg/L)	Apoptosis rate (%)
0	0.95±0.17
10	3.44±0.21 ^a
20	10.73±1.17 ^b
40	30.25±1.76 ^b

^aP<0.05, ^bP<0.01 vs control group.

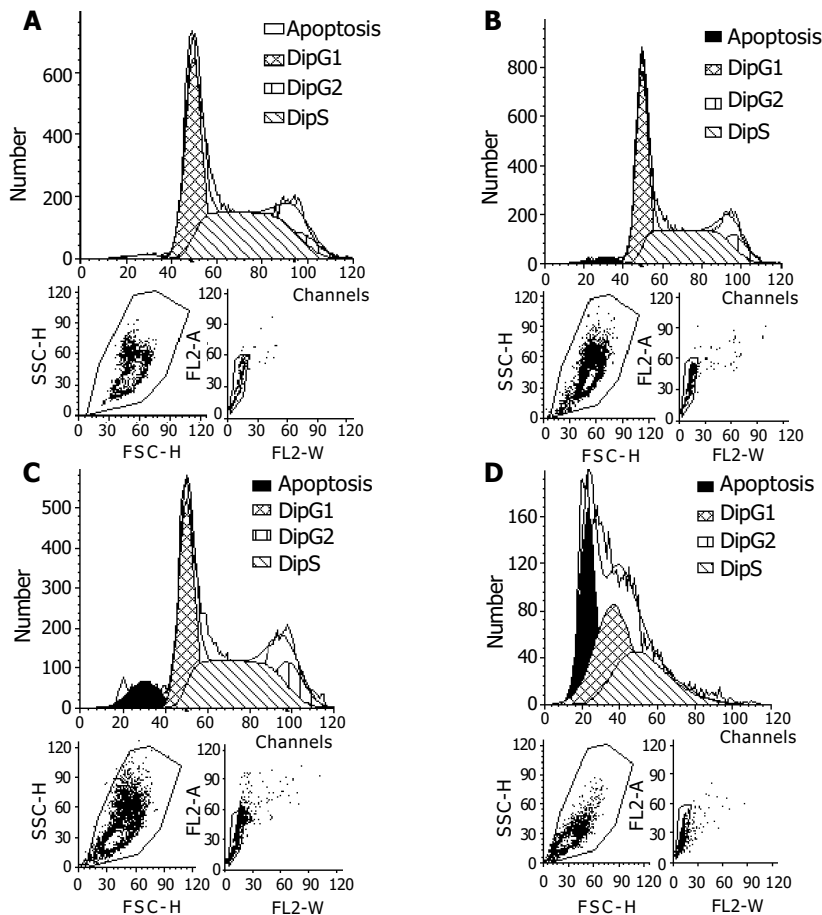


Figure 5 Cell apoptosis determined by flow cytometry. SMMC-7721 cells were treated with Sch B at various concentrations (0, 10, 20, 40 mg/L, respectively A to D) for 48 h.

Effects of Sch B on expression of Hsp70 and Caspases-3,-7,-9

Recent reports suggested that Hsp70 might help to protect cells from apoptosis at an early event in the apoptotic pathway. To elucidate whether Hsp70 was modulated during Sch B induced apoptosis, we examined the expression of Hsp70 by Western blot. Moreover, it was shown that Caspases were the main factor in the apoptotic pathway. We investigated whether Caspases were involved in inducing SMMC-7721 cell apoptosis treated with Sch B. SMMC-7721 cells treated with Sch B for 48 h were analyzed for the enzymatic activity by Western blot. The results showed that Hsp70 was down-regulated and Caspase-3 was activated, while the activity of Caspases-7,-9 had no significant change (Figure 6).

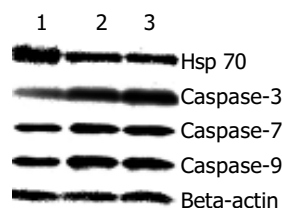


Figure 6 Effect of Sch B on expression of Hsp70, Caspases-3, -7, -9 proteins. SMMC-7721 cells were treated with Sch B for 48 h. After treatment, cell lysates were extracted, and the level of Hsp70, Caspases-3, -7, -9 proteins were analyzed by Western bolt analysis. Beta-actin was used as an internal loading control. Lane 1: control; Lane 2: 20 mg/L Sch B treatment; lane 3: 40 mg/L Sch B treatment.

DISCUSSION

After human hepatoma SMMC-7721 cells were treated at various concentrations of Sch B for 48 h, MTT colorimetric analysis showed that Sch B could significantly inhibit the proliferation of SMMC-7721 cells, with LC50 value of 23.50 mg/L. While human hepatic HL-7702 cells were more resistant to the Sch B mediated cytotoxic activity than human endothelial ECV-304 cells and human hepatoma SMMC-7721 cells. It is interesting that Sch B had an un conspicuous cytotoxic effect on primary human fibroblast cells and human lymphocyte cells.

Current antineoplastic therapies, including chemotherapy and radiation-therapy, are likely to be affected by the apoptotic tendency of cells. During apoptosis, certain characteristic morphologic events, such as nuclear condensation, nuclear fragmentation, and cell shrinkage, and biochemical events, such as DNA fragmentation, would occur^[31-35]. In this study, we showed that Sch B induced human hepatoma SMMC-7721 cell apoptosis was confirmed by DNA ladder and cell cycle analyses.

The commitment of cell apoptosis requires the integration of numerous inputs involving multiple signal transduction pathways. Some cellular pathways and molecular regulators/ effectors of apoptosis have been identified. Many lines of evidence demonstrated that activation of Caspases is a central mechanism of apoptosis. So far, more than 15 members of Caspases have been reported in the literature, and most of them played a major role in apoptosis, participating in the initiation and execution of programmed cell death^[36,37]. Based on their structure and function, Caspases are classified into two groups: initiator Caspases (such as Caspases-2,-8 and-9) and executor Caspases (such as Caspases-3, -6 and -7)^[38,39]. In this study, Sch B-induced apoptosis of SMMC-7721 cells was accompanied with up-regulation of Caspase-3, but did not involve the regulation of Caspase-7 and Caspase-9 protein expression. These results suggested that Caspase-3 but not Caspase-7 was the "executors" of Sch B induced SMMC-7721 cell apoptosis that did not go through Caspase-9-dependent

pathway.

Recent results indicated that Hsp70 might help to protect cells from apoptosis. Jaattela *et al.*^[40] reported that Hsp70 exerted its anti-apoptotic function on downstream of Caspase-3. Creagh *et al.*^[41] revealed that Hsp70 acted on upstream of the Caspases. In the presence of Hsp70, Caspase-3 was not processed or activated and the release of cytochrome C from the mitochondrial intermembrane space, a major Caspase activating mechanism, was inhibited. In this study, the down-modulation of Hsp70 was observed, indicating that Sch B could help Caspase-3 to release from the blockade of Hsp70 so as to promote human hepatoma SMMC-7721 cells to apoptosis.

In conclusion, Sch B is able to inhibit the proliferation of human hepatoma SMMC-7721 cells and induce apoptosis, which goes through Caspase-3-dependent and Caspase-9-independent pathways accompanied with the down-regulation of Hsp70 protein expression at an early event. Further investigation will focus on the identification of other signal modulations in this apoptosis pathway.

ACKNOWLEDGMENTS

The authors are grateful to Professor Shu Zheng for her help in this study.

REFERENCES

- 1 Liu JH, Ho SC, Lai TH, Liu TH, Chi PY, Wu RY. Protective effects of Chinese herbs on D-galactose-induced oxidative damage. *Methods Find Exp Clin Pharmacol* 2003; **25**: 447-452
- 2 Hsieh MT, Tsai ML, Peng WH, Wu CR. Effects of Fructus schizandrae on cycloheximide-induced amnesia in rats. *Phytother Res* 1999; **13**: 256-257
- 3 Li XY. Bioactivity of neolignans from fructus Schizandrae. *Mem Inst Oswaldo Cruz* 1991; **86**(Suppl 2): 31-37
- 4 Chiu PY, Tang MH, Mak DH, Poon MK, Ko KM. Hepatoprotective mechanism of schisandrin B: role of mitochondrial glutathione antioxidant status and heat shock proteins. *Free Radic Biol Med* 2003; **35**: 368-380
- 5 Chiu PY, Mak DH, Poon MK, Ko KM. *In vivo* antioxidant action of a lignan-enriched extract of Polygonum root and an anthraquinone-containing extract of Polygonum root in comparison with schisandrin B and emodin. *Planta Med* 2002; **68**: 951-956
- 6 Ko KM, Lam BY. Schisandrin B protects against tert-butylhydroperoxide induced cerebral toxicity by enhancing glutathione antioxidant status in mouse brain. *Mol Cell Biochem* 2002; **238**: 181-186
- 7 Pan SY, Han YF, Carlier PR, Pang YP, Mak DH, Lam BY, Ko KM. Schisandrin B protects against tacrine- and bis(7)-tacrine-induced hepatotoxicity and enhances cognitive function in mice. *Planta Med* 2002; **68**: 217-220
- 8 Ip SP, Yiu HY, Ko KM. Schisandrin B protects against menadione-induced hepatotoxicity by enhancing DT-diaphorase activity. *Mol Cell Biochem* 2000; **208**: 151-155
- 9 Yim TK, Ko KM. Schisandrin B protects against myocardial ischemia-reperfusion injury by enhancing myocardial glutathione antioxidant status. *Mol Cell Biochem* 1999; **196**: 151-156
- 10 Souto PC, Brito VN, Gameiro J, da Cruz-Hofling MA, Verinaud L. Programmed cell death in thymus during experimental paracoccidioidomycosis. *Med Microbiol Immunol* 2003; **192**: 225-229
- 11 Hu W, Kavanagh JJ. Anticancer therapy targeting the apoptotic pathway. *Lancet Oncol* 2003; **4**: 721-729
- 12 Thompson CB. Apoptosis in the pathogenesis and treatment of disease. *Science* 1995; **267**: 1456-1462
- 13 Wajant H, Pfizenmaier K, Scheurich P. TNF-related apoptosis inducing ligand (TRAIL) and its receptors in tumor surveillance and cancer therapy. *Apoptosis* 2002; **7**: 449-459
- 14 Inoue H, Shiraki K, Yamanaka T, Ohmori S, Sakai T, Deguchi M, Okano H, Murata K, Sugimoto K, Nakano T. Functional expression of tumor necrosis factor-related apoptosis-induc-

- ing ligand in human colonic adenocarcinoma cells. *Lab Invest* 2002; **82**: 1111-1119
- 15 **Wei XC**, Wang XJ, Chen K, Zhang L, Liang Y, Lin XL. Killing effect of TNF-related apoptosis inducing ligand regulated by tetracycline on gastric cancer cell line NCI-N87. *World J Gastroenterol* 2001; **7**: 559-562
- 16 **MacFarlane M**, Harper N, Snowden RT, Dyer MJ, Barnett GA, Pringle JH, Cohen GM. Mechanisms of resistance to TRAIL-induced apoptosis in primary B cell chronic lymphocytic leukaemia. *Oncogene* 2002; **21**: 6809-6818
- 17 **Held J**, Schulze-Osthoff K. Potential and caveats of TRAIL in cancer therapy. *Drug Resist Updat* 2001; **4**: 243-252
- 18 **de Almodovar CR**, Ruiz-Ruiz C, Munoz-Pinedo C, Robledo G, Lopez-Rivas A. The differential sensitivity of Bcl-2-overexpressing human breast tumor cells to TRAIL or doxorubicin-induced apoptosis is dependent on Bcl-2 protein levels. *Oncogene* 2001; **20**: 7128-7133
- 19 **Ibrahim SM**, Ringel J, Schmidt C, Ringel B, Muller P, Koczan D, Thiesen HJ, Lohr M. Pancreatic adenocarcinoma cell lines show variable susceptibility to TRAIL-mediated cell death. *Pancreas* 2001; **23**: 72-79
- 20 **Ohshima K**, Sugihara M, Haraoka S, Suzumiya J, Kanda M, Kawasaki C, Shimazaki K, Kikuchi M. Possible immortalization of Hodgkin and Reed-Sternberg cells: telomerase expression, lengthening of telomere, and inhibition of apoptosis by NF-kappaB expression. *Leuk Lymphoma* 2001; **41**: 367-376
- 21 **Wall NR**, O'Connor DS, Plescia J, Pommier Y, Altieri DC. Suppression of survivin phosphorylation on Thr34 by flavopiridol enhances tumor cell apoptosis. *Cancer Res* 2003; **63**: 230-235
- 22 **Thornberry NA**, Lazebnik Y. Caspases: enemies within. *Science* 1998; **281**: 1312-1316
- 23 **Rheume E**, Cohen LY, Uhlmann F, Lazure C, Alam A, Hurwitz J, Sekaly RP, Denis F. The large subunit of replication factor C is a substrate for Caspase-3 *in vitro* and is cleaved by a Caspase-3-like protease during Fas-mediated apoptosis. *EMBO J* 1997; **16**: 6346-6354
- 24 **Song Q**, Burrows SR, Smith G, Lees-Miller SP, Kumar S, Chan DW, Trapani JA, Alnemri E, Litwack G, Lu H, Moss DJ, Jackson S, Lavin MF. Interleukin-1 beta-converting enzyme-like protease cleaves DNA-dependent protein kinase in cytotoxic T cell killing. *J Exp Med* 1996; **184**: 619-626
- 25 **Samali A**, Cotter TG. Heat shock proteins increase resistance to apoptosis. *Exp Cell Res* 1996; **223**: 163-170
- 26 **Lasunskaja EB**, Fridlianskaia II, Darieva ZA, da Silva MS, Kanashiro MM, Margulis BA. Transfection of NS0 myeloma fusion partner cells with HSP70 gene results in higher hybridoma yield by improving cellular resistance to apoptosis. *Biotechnol Bioeng* 2003; **81**: 496-504
- 27 **Liu TS**, Musch MW, Sugi K, Walsh-Reitz MM, Ropeleski MJ, Hendrickson BA, Pothoulakis C, Lamont JT, Chang EB. Protective role of HSP72 against Clostridium difficile toxin A-induced intestinal epithelial cell dysfunction. *Am J Physiol Cell Physiol* 2003; **284**: C1073-1082
- 28 **Diez-Fernandez C**, Andres D, Cascales M. Attenuating effects of heat shock against TGF-beta1-induced apoptosis in cultured rat hepatocytes. *Free Radic Biol Med* 2002; **33**: 835-846
- 29 **Neuhof W**, Lugmayr K, Fraek ML, Beck FX. Regulated overexpression of heat shock protein 72 protects Madin-Darby canine kidney cells from the detrimental effects of high urea concentrations. *J Am Soc Nephrol* 2001; **12**: 2565-2571
- 30 **Gibbons NB**, Watson RW, Coffey RN, Brady HP, Fitzpatrick JM. Heat-shock proteins inhibit induction of prostate cancer cell apoptosis. *Prostate* 2000; **45**: 58-65
- 31 **Mariggio MA**, Cafaggi S, Ottone M, Parodi B, Vannozzi MO, Mandys V, Viale M. Inhibition of cell growth, induction of apoptosis and mechanism of action of the novel platinum compound cis-diaminechloro-[2-(diethylamino) ethyl 4-amino-benzoate, N(4)]-chloride platinum (II) monohydrochloride monohydrate. *Invest New Drugs* 2004; **1**: 3-16
- 32 **Dong YG**, Chen DD, He JG, Guan YY. Effects of 15-deoxy-delta12, 14-prostaglandin J2 on cell proliferation and apoptosis in ECV304 endothelial cells. *Acta Pharmacol Sin* 2004; **1**: 47-53
- 33 **Liu JB**, Gao XG, Lian T, Zhao AZ, Li KZ. Apoptosis of human hepatoma HepG2 cells induced by emodin *in vitro*. *Aizheng* 2003; **22**: 1280-1283
- 34 **Yoo HG**, Jung SN, Hwang YS, Park JS, Kim MH, Jeong M, Ahn SJ, Ahn BW, Shin BA, Park RK, Jung YD. Involvement of NF-kappaB and Caspases in silibinin-induced apoptosis of endothelial cells. *Int J Mol Med* 2004; **13**: 81-86
- 35 **Eriguchi M**, Nonaka Y, Yanagie H, Yoshizaki I, Takeda Y, Sekiguchi M. A molecular biological study of anti-tumor mechanisms of an anti-cancer agent Oxaliplatin against established human gastric cancer cell lines. *Biomed Pharmacother* 2003; **57**: 412-415
- 36 **Dalen H**, Neuzil J. alpha-Tocopheryl succinate sensitises a T lymphoma cell line to TRAIL-induced apoptosis by suppressing NF-kappaB activation. *Br J Cancer* 2003; **88**: 153-158
- 37 **Biswas DK**, Martin KJ, McAlister C, Cruz AP, Graner E, Dai SC, Pardee AB. Apoptosis caused by chemotherapeutic inhibition of nuclear factor-kappaB activation. *Cancer Res* 2003; **63**: 290-295
- 38 **Fernandes-Alnemri T**, Litwack G, Alnemri ES. CPP32, a novel human apoptotic protein with homology to Caenorhabditis elegans cell death protein Ced-3 and mammalian interleukin-1 beta-converting enzyme. *J Biol Chem* 1994; **269**: 30761-30764
- 39 **Tormanen-Napankangas U**, Soini Y, Kahlos K, Kinnula V, Paakko P. Expression of Caspases-3, -6 and -8 and their relation to apoptosis in non-small cell lung carcinoma. *Int J Cancer* 2001; **93**: 192-198
- 40 **Jaattela M**, Wissing D, Kokholm K, Kallunki T, Egeblad M. Hsp70 exerts its anti-apoptotic function downstream of Caspase-3-like proteases. *EMBO J* 1998; **17**: 6124-6134
- 41 **Creagh EM**, Carmody RJ, Cotter TG. Heat shock protein 70 inhibits Caspase-dependent and -independent apoptosis in Jurkat T cells. *Exp Cell Res* 2000; **257**: 58-66

Edited by Kumar M and Wang XL. Proofread by Xu FM

• COLORECTAL CANCER •

Microscopic spread of low rectal cancer in regions of mesorectum: Pathologic assessment with whole-mount sections

Zhao Wang, Zong-Guang Zhou, Cun Wang, Gao-Ping Zhao, You-Dai Chen, Hong-Kai Gao, Xue-Lian Zheng, Rong Wang, Dai-Yun Chen, Wei-Ping Liu

Zhao Wang, Zong-Guang Zhou, Cun Wang, Gao-Ping Zhao, You-Dai Chen, Hong-Kai Gao, Xue-Lian Zheng, Rong Wang, Department of Gastroenterology Surgery and Institution of Digestive Surgery, West China Hospital, Sichuan University, Chengdu 610041, Sichuan Province, China

Dai-Yun Chen, Wei-Ping Liu, Department of Pathology, West China Hospital, Sichuan University, Chengdu 610041, Sichuan Province, China
Supported by the Key Project of National Outstanding Youth Foundation of China, No. 39925032 and National Natural Science Foundation of China, No. 30271283

Correspondence to: Dr. Zong-Guang Zhou, Department of Gastroenterology Surgery and Institute of Digestive Surgery, West China Hospital, Sichuan University, Chengdu 610041, Sichuan Province, China. zhou767@21cn.com

Telephone: +86-28-85422525 **Fax:** +86-28-85422484

Received: 2004-02-02 **Accepted:** 2004-02-18

Abstract

AIM: To assess the microscopic spread of low rectal cancer in mesorectum regions to provide pathological evidence for the necessity of total mesorectal excision (TME).

METHODS: A total of 62 patients with low rectal cancer underwent low anterior resection and TME, surgical specimens were sliced transversely on the serial embedded blocks at 2.5 mm interval, and stained with hematoxylin and eosin (HE). The mesorectum on whole-mount sections was divided into three regions: outer region of mesorectum (ORM), middle region of mesorectum (MRM) and inner region of mesorectum (IRM). Microscopic metastatic foci were investigated microscopically on the sections for the metastatic mesorectal regions, frequency, types, involvement of lymphatic vessels and correlation with the original rectal cancer.

RESULTS: Microscopic spread of the tumor in mesorectum and ORM was observed in 38.7% (24/62) and 25.8% (16/62) of the patients, respectively. Circumferential resection margin (CRM) with involvement of microscopic metastatic foci occurred in 6.5% (4/62) of the patients, and distal mesorectum (DMR) involved was 6.5% (4/62) with the spread extent within 3 cm of low board of the main lesions. Most (20/24) of the patients with microscopic metastasis in mesorectum were in Dukes C stage.

CONCLUSION: Results of the present study support that complete excision of the mesorectum without destruction of the ORM is essential for surgical management of low rectal cancer, an optimal DMR clearance resection margin should be no less than 4 cm, further pathologic assessment of the regions in extramesorectum in the pelvis is needed.

Wang Z, Zhou ZG, Wang C, Zhao GP, Chen YD, Gao HK, Zheng XL, Wang R, Chen DY, Liu WP. Microscopic spread of low rectal cancer in regions of mesorectum: Pathologic assessment with whole-mount sections. *World J Gastroenterol* 2004; 10(20): 2949-2953

<http://www.wjgnet.com/1007-9327/10/2949.asp>

INTRODUCTION

Local tumor recurrence after surgical resection of rectal cancer remains a major problem. Since Heald *et al.*^[1] first reported evidence of isolated tumor deposits in the mesorectum, more authors have demonstrated that residual foci of the tumor within pelvis resulting from inadequate excision of the mesorectum were the cause of such recurrence^[2,3]. Further studies revealed that remnant of microscopic tumor nodules in the mesorectum, which cannot easily be detected by imaging preoperatively or by palpation intraoperatively, other than large nodules, contributes to most of local failures^[4,5].

Comparison of clinical outcomes between conventional surgery^[6,7] and total mesorectal excision (TME)^[1,8] showed that a proportion of microscopic tumor nodules of rectal cancer causing local pelvic collapse might settle in the outer region of mesorectum (ORM). Unfortunately, investigations on discrete tumor nodules spread in this region are rare. A comprehensive assessment of ORM in patients with low rectal cancer may provide further pathological evidence for supporting the TME procedure.

Although TME has been extensively employed as a standard procedure for surgical treatment of patients with low rectal cancer in western countries, conventional resection has been dominated in China due to little pathological information standing for TME. The present study investigated the regional spread of microscopic tumor nodules in mesorectum using whole-mount sections.

MATERIALS AND METHODS

Patients

Sixty-two consecutive patients with biopsy-proven adenocarcinoma of the rectum underwent TME at the Division of Gastroenterology Surgery of Affiliated West China Hospital of Sichuan University between November 2001 and June 2002, and specimens were examined prospectively by the same pathologist (Chen DY). Patients (30 males) had a mean age of 58 years (range, 21-78). Lesions were classified as upper or low rectal cancers based on the location of peritoneal reflection, and all diseases from our series were categorized as low rectal cancers with sigmoidoscopy preoperatively. Thirty-two patients had the lower board of primary tumors within 5 cm of anal verge, and another 30 patients had the lower board located not farther than 10 cm from anal verge and above the level of 5 cm from anal verge. None of the patients received any preoperative adjuvant therapy.

Surgical techniques

All patients were operated on by the same chief surgeon (Professor. Zhou ZG) and two assistants according to TME principles^[1]. The rectum and mesorectum were mobilized as a package enveloped within the fascia propria with the preservation of autonomic nerves. Under direct vision, electrocautery was used to divide the rectosacral ligament posterior, the peritoneum posterior to the seminal vesicle in the males and the peritoneal reflection in Douglas' pouch in the females anteriorly, lateral ligaments medial to the pelvic plexus laterally. Sharp dissection

was continued down to the pelvic floor in front of Denonvilliers' fascia anteriorly and along the fascia propria posteriorly. Eventually, over 2 cm of distal clearance margin of rectal wall and over 4 cm of mesorectum were attained by transecting the rectum without stretching the bowel wall^[9].

Whole-mount sections

Each specimen was straightened without stretching and pinned to a cork board, different from Quirke's method^[2]. The specimens were not opened longitudinally along the antimesenteric border, and fixed in 40 g/L buffered formaldehyde for 48 h. Serial longitudinal tissue blocks were cut at 5 mm intervals from the distal portion. Each block, consisting of the full thickness of the rectal wall with the mesorectum, was fixed in 40 g/L buffered formaldehyde for another 48 h, and then embedded in paraffin. Whole-mount sections of the bowel wall and mesorectum were sliced transversely on the embedded tissue blocks in 4 μm at 2.5 mm intervals, stained with hematoxylin and eosin (HE), and examined for discrete tumor nodules microscopically (Figure 1). Circumferential resection margin (CRM) involvement was assessed in the conventional manner^[10].

Parameters

The following pathological parameters were used for analysis, namely Dukes stage, differentiation grade, presence of microscopic tumor nodules, local metastasis of lymph nodes, outer region of mesorectum (ORM), distal mesorectum (DMR), CRM (involved ≤1 mm, or clear >1 mm), and distant metastases. Microscopic metastatic nodules of rectal cancer were defined as tumor nodules ≤1 mm in diameter, which could not be detected either preoperatively or intraoperatively. Large metastatic nodules of rectal cancer were defined as tumor nodules >5 mm in diameter, most of which could be easily detected by palpation during operation. The mesorectum on the transverse whole-mount section was divided into three regions (Figure 2).

Discrete tumor nodule spread in the mesorectum 1 mm or less away from the outermost board of CRM was recorded as involvement of CRM, and discrete tumor nodule spread in the mesorectum below the lowest board of primary tumor was defined as involvement of DMR.

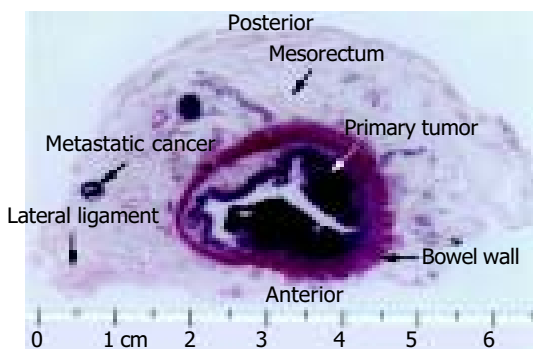


Figure 1 Illustration for regions of mesorectum.

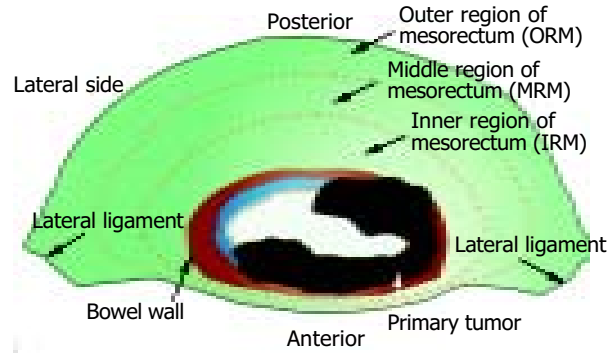


Figure 2 Transverse whole-mount sections of the specimen, HE staining, macroscopic view.

RESULTS

The clinicopathologic characteristics of the patients are summarized in Table 1. All the 62 patients underwent low anterior resection. In 52 patients (83.9%) the operation was potentially curative, while residual tumors in 2 patients (3.3%) were noticed to remain in pelvis on operation and distant metastases were observed in 8 patients (12.9%).

Table 1 Clinicopathologic characteristics of the 62 patients

Parameters	Results
Age (yr, range, mean)	20-78, 58
Sex (No. of patients)	
Male	30
Female	32
Dukes stage (No. of patients)	
A	2
B	10
C	42
D	8
Differentiation grade (No. of patients)	
High	4
Medium	34
Low	24
Distance of the primary tumor from anal verge (No. of patients)	
≤5 cm	32
>5 cm	30
Diameter of the primary tumor (No. of patients)	
<5 cm	24
≥5 cm	38

Microscopic spread types and involvement of mesorectum

Four types of microscopic spread of the tumor were observed in mesorectum: discrete microscopic tumor nodules, blood vessel invasion, lymphatic vessel invasion and perineural invasion (Figure 3). Microscopic spread in mesorectum was observed in 38.7% (24 of 62) of the patients (Table 2).

Table 2 Mesorectal regions with involvement of discrete tumor nodules (%)

	Involved mesorectal regions					
	MR	ORM	MRM	IRM	DMR	CRM
Tumor nodules	58.1 (36/62)	45.2 (28/62)	35.5 (22/62)	41.9 (26/62)	6.5 (4/62)	6.5 (4/62)
Microscopic tumor nodules	38.7 (24/62)	25.8 (16/62)	25.8 (16/62)	29.0 (18/62)	6.5 (4/62)	6.5 (4/62)

MR: mesorectum; ORM: outer region of mesorectum; MRM: middle region of mesorectum; IRM: inner region of mesorectum; DMR: distal mesorectum; CRM: circumferential resection margin.

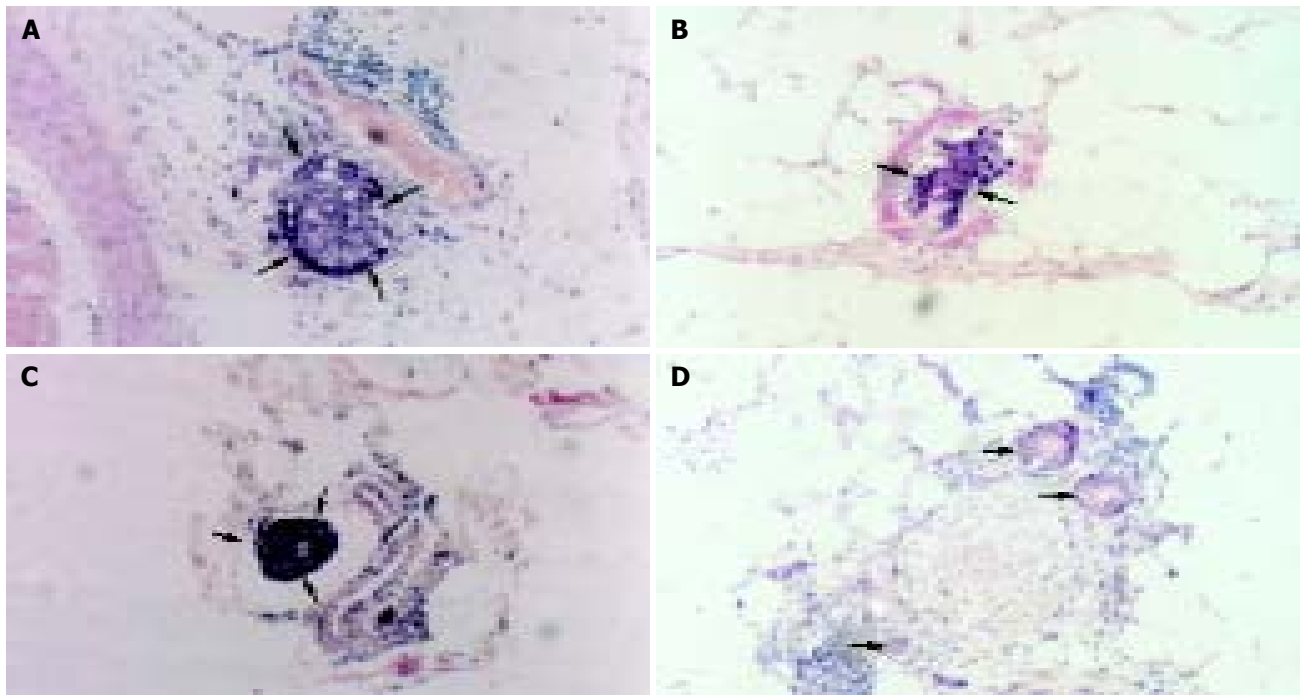


Figure 3 Spread types of microscopic tumor nodules (→) in the mesorectum, HE, ×100. A: Discrete microscopic tumor nodules; B: Blood vessel invasion; C: Lymphatic vessel invasion; D: Perineural invasion.



Figure 4 Microscopic tumor nodule spread (→) in outer region of the mesorectum (ORM) (4a), CRM (4b) and DMR(4c) , HE, ×100.

Microscopic spread of the tumor in outer region of mesorectum

Microscopic spread in ORM (Figure 4) occurred in 25.8% (16 of 62) of the patients (Table 2).

Microscopic spread of the tumor in circumferential resection margin

Four of 36 patients with tumor involvement of mesorectum and 2 of the 52 patients having potentially curative resections had microscopic spread in CRM.

Table 3 Mesorectal regional discrete microscopic tumor nodules involving lymph nodes or lymphatic vessels

	Involvement of MR	Involvement of ORM
L type (No. of patients)	16	14
NL type (No. of patients)	18	13

MR: mesorectum; ORM: outer region of mesorectum; L type: involving lymph nodes or lymphatic vessel; NL type: without involving lymph nodes or lymphatic vessels.

Microscopic spread of the tumor in distal mesorectum

DMR with involvement of microscopic tumor nodules was observed in 4 patients. The utmost spread was 3.0 cm or less from the low edge of primary carcinoma. The most extensive distal infiltration was seen in two cases of Dukes stage C.

Table 4 Correlation between mesorectal microscopic spread and primary tumors

Primary tumor	Spread in MR (No. of patients)	Spread in ORM (No. of patients)
Diameter:	10/14	8/8
<5 cm/ ≥5 cm		
Differentiation grade:	0/10/14	0/8/8
high/medium/low		
Dukes stage:	0/2/20/2	0/2/12/2
A/B/C/D		
From anal verge:	12/12	8/8
≤5 cm/>5 cm		

MR: mesorectum; ORM: outer region of mesorectum.

Microscopic spread of the tumor in mesorectal lymph nodes or lymphatic vessels

Microscopic spread nodules without involvement of lymph nodes or lymphatic vessels in mesorectum were observed in 18 patients, and such a spread in ORM was found in 13 patients (Table 3).

Correlation between regional mesorectal microscopic spread and primary tumors

Most patients (20 of 24) with mesorectal microscopic spread in

MR and 12 of 16 microscopic spreads in ORM were Dukes C stage (Table 4).

Correlation between microscopic tumor nodules and large tumor nodules

Microscopic tumor nodules coexisting with large tumor nodules were observed in 14 of 24 (58.3%) patients with microscopic spread in mesorectum.

DISCUSSION

Whole-mount sections were used to facilitate the precise and effective assessment of rectal cancer, especially in mesorectal regional spread of discontinuous microscopic tumor nodules. All whole-mount sections showed that whole morphological features of the surgical specimen enclosing the primary tumor, bowel wall and the mesorectum, could be directly observed with naked eyes and by microscopy, which enabled the investigators to obtain valuable pathological outcomes on rectal cancer^[2,11].

The present study showed the incidence of discrete microscopic tumor nodules was 38.7% (24 of 62) of patients in mesorectum and 25.8% (16 of 62) of patients in ORM. The high frequency of microscopic tumor nodules in mesorectum (especial ORM) highlighted the importance of complete excision of mesorectum with fascia propria circumferentially intact for low rectal cancer. Disturbance of ORM during operation would predispose local recurrence because the undetected microscopic foci in the mesorectum, especially in ORM were easily left behind in pelvis^[4,12,13]. Frequency of CRM involvement after conventional resection was reported up to 27%^[2,11,14,15], compared with 6.5% after TME^[16,17], which is consistent with our findings. The decrease of CRM involvement rates after TME justified the theory: the frequency of microscopic spread in ORM could be very high, and destruction of ORM which often occurred in conventional resection, could easily lead to positive CRM.

Distal mesorectal spread can be evaluated pathologically after TME, after standard resection of the rectal cancer, the DMR remained inside pelvis^[18]. Frequency of discrete tumor cancer spread 3 cm or more from the primary lesions in DMR varied from 0 to 10% of the cases^[4,17,19-22], and discontinuous spread in DMR could be found even up to 5 cm beyond the lower margin of the primary tumor^[1,6], some patients with DMR spread had poor prognosis^[21-23]. The present study showed that four cases with tumor involvement of DMR had the spread within 3 cm of primary mural tumors, with a maximum of 3.0 cm. Therefore, we support a safe DMR resection margin of no less than 4 cm for lower rectal cancer, and consider that failure to adequate excision of the involved DRM would risk in leaving behind residual microscopic cancer foci in a significant percentage of patients. The most common pattern of pelvic recurrence is extramural diseases emanating from the sacral hollow or pelvic floor, which is entirely compatible with this hypothesis^[24]. But others argued that pathological evidence of DMR spread in itself did not necessarily justify total removal of DMR in all cases because the local recurrence rate and survival rate were not improved significantly even after TME^[4,17].

Cawthorn^[25] reported that mesorectal involvement of large tumor nodules (greater than 4 mm) was associated with significant poorer prognosis than that of small ones (less than 4 mm). However, the author cautioned that the poor prognosis might result from residual microscopic tumor nodules, which coexist with large nodules and can easily be overlooked and left behind during operation. Ueno *et al.*^[13] demonstrated that large tumor nodules and microscopic tumor nodules correlated closely, and that large tumor nodules had a predicting value for existence of microscopic tumor nodules. The present study showed that 58.3% (14/24) patients with microscopic tumor

foci involvement of the mesorectum had large tumor nodules (greater than 5 mm) in the mesorectum, which was lower than that reported by Ueno *et al.*

Kapiteijn *et al.* recently reported that standardized TME in combination with preoperative radiotherapy could significantly decrease the local recurrence rate in patients with rectal cancer, though its benefits in survival were not demonstrated because of a relatively short time of follow-up^[26]. Other authors also concluded that preoperative radiotherapy could improve the prognosis of patients with rectal cancer^[27]. In our series, no patients were treated with adjuvant therapy due to the high frequency of postoperative complications and its controversial impact on prognosis.

Extended lateral dissection beyond the extent of TME has been widely accepted in Japan as the improvement in survival rates was reported^[28,29], but some argued that it had a limited advantage in prognosis and the functional problems were considerable^[30,31]. Microscopic tumor nodule involvement of CRM after TME in our series suggested that a proportion of the patients had microscopic tumor spread in the extramesorectal regions in the pelvis. Further comprehensive pathological assessment of the extramesorectum is required to evaluate the curative value of TME in rectal cancer.

REFERENCES

- 1 Heald RJ, Husband EM, Ryall RD. The mesorectum in rectal cancer surgery—the clue to pelvic recurrence? *Br J Surg* 1982; **69**: 613-616
- 2 Quirke P, Durdey P, Dixon MF, Williams NS. Local recurrence of rectal adenocarcinoma due to inadequate surgical resection. Histopathological study of lateral tumour spread and surgical excision. *Lancet* 1986; **2**: 996-999
- 3 Ratto C, Ricci R, Rossi C, Morelli U, Vecchio FM, Doglietto GB. Mesorectal microfoci adversely affect the prognosis of patients with rectal cancer. *Dis Colon Rectum* 2002; **45**: 733-742
- 4 Ono C, Yoshinaga K, Enomoto M, Sugihara K. Discontinuous rectal cancer spread in the mesorectum and the optimal distal clearance margin *in situ*. *Dis Colon Rectum* 2002; **45**: 744-749
- 5 Andreola S, Leo E, Belli F, Gallino G, Sirizzotti G, Sampietro G. Adenocarcinoma of the lower third of the rectum: metastases in lymph nodes smaller than 5 mm and occult micrometastases; preliminary results on early tumor recurrence. *Ann Surg Oncol* 2001; **8**: 413-417
- 6 Reynolds JV, Joyce WP, Dolan J, Sheahan K, Hyland JM. Pathological evidence in support of total mesorectal excision in the management of rectal cancer. *Br J Surg* 1996; **83**: 1112-1115
- 7 McCall JL, Cox MR, Wattoo DA. Analysis of local recurrence rates after surgery alone for rectal cancer. *Int J Colorectal Dis* 1995; **10**: 126-132
- 8 Enker WE. Total mesorectal excision—the new golden standard of surgery for rectal cancer. *Ann Med* 1997; **29**: 127-133
- 9 Zhou ZG, Wang Z, Yu YY, Shu Y, Cheng Z, Li L, Lei WZ, Wang TC. Laparoscopic total mesorectal excision of low rectal cancer with preservation of anal sphincter: A report of 82 cases. *World J Gastroenterol* 2003; **9**: 1477-1481
- 10 Quirke P, Dixon MF. The prediction of local recurrence in rectal adenocarcinoma by histopathological examination. *Int J Colorectal Dis* 1988; **3**: 127-131
- 11 Ng IO, Luk IS, Yuen ST, Lau PW, Pritchett CJ, Ng M, Poon GP, Ho J. Surgical lateral clearance in resected rectal carcinomas. A multivariate analysis of clinicopathologic features. *Cancer* 1993; **71**: 1972-1976
- 12 Paty PB, Enker WE, Cohen AM, Lauwers GY. Treatment of rectal cancer by low anterior resection with coloanal anastomosis. *Ann Surg* 1994; **219**: 365-373
- 13 Ueno H, Mochizuki H, Tamakuma S. Prognostic significance of extranodal microscopic foci discontinuous with primary lesion in rectal cancer. *Dis Colon Rectum* 1998; **41**: 55-61
- 14 Adam JJ, Mohamdee MO, Martin IG, Scott N, Finan PJ, Johnston D, Dixon MF, Quirke P. Role of circumferential margin involvement in the local recurrence of rectal cancer. *Lancet* 1994; **344**: 707-711

- 15 **de Haas-Kock DF**, Baeten CG, Jager JJ, Langendijk JA, Schouten LJ, Volovics A, Arends JW. Prognostic significance of radial margins of clearance in rectal cancer. *Br J Surg* 1996; **83**: 781-785
- 16 **Cawthorn SJ**, Gibbs NM, Marks CG. Clearance technique for the detection of lymph nodes in colorectal cancer. *Br J Surg* 1986; **73**: 58-60
- 17 **Scott N**, Jackson P, al-Jaberi T, Dixon MF, Quirke P, Finan PJ. Total mesorectal excision and local recurrence: a study of tumour spread in the mesorectum distal to rectal cancer. *Br J Surg* 1995; **82**: 1031-1033
- 18 **McCall JL**. Total mesorectal excision: evaluating the evidence. *Aust N Z J Surg* 1997; **67**: 599-602
- 19 **Madsen PM**, Christiansen J. Distal intramural spread of rectal carcinomas. *Dis Colon Rectum* 1986; **29**: 279-282
- 20 **Williams NS**. The rationale for preservation of the anal sphincter in patients with low rectal cancer. *Br J Surg* 1984; **71**: 575-581
- 21 **Shirouzu K**, Isomoto H, Kakegawa T. Distal spread of rectal cancer and optimal distal margin of resection for sphincter-preserving surgery. *Cancer* 1995; **76**: 388-392
- 22 **Williams NS**, Dixon MF, Johnston D. Reappraisal of the 5 centimetre rule of distal excision for carcinoma of the rectum: a study of distal intramural spread and of patients' survival. *Br J Surg* 1983; **70**: 150-154
- 23 **Penfold JC**. A comparison of restorative resection of carcinoma of the middle third of the rectum with abdominoperineal excision. *Aust N Z J Surg* 1974; **44**: 354-356
- 24 **Pilipshen SJ**, Heilweil M, Quan SH, Sternberg SS, Enker WE. Patterns of pelvic recurrence following definitive resections of rectal cancer. *Cancer* 1984; **53**: 1354-1362
- 25 **Cawthorn SJ**, Parums DV, Gibbs NM, A'Hern RP, Caffarey SM, Broughton CI, Marks CG. Extent of mesorectal spread and involvement of lateral resection margin as prognostic factors after surgery for rectal cancer. *Lancet* 1990; **335**: 1055-1059
- 26 **Kapiteijn E**, Marijnen CA, Nagtegaal ID, Putter H, Steup WH, Wiggers T, Rutten HJ, Pahlman L, Glimelius B, van Krieken JH, Leer JW, van de Velde CJ. Preoperative radiotherapy combined with total mesorectal excision for resectable rectal cancer. *N Engl J Med* 2001; **345**: 638-646
- 27 **Camma C**, Giunta M, Fiorica F, Pagliaro L, Craxi A, Cottone M. Preoperative radiotherapy for resectable rectal cancer: A meta-analysis. *JAMA* 2000; **284**: 1008-1015
- 28 **Koyama Y**, Moriya Y, Hojo K. Effects of extended systematic lymphadenectomy for adenocarcinoma of the rectum-significant improvement of survival rate and decrease of local recurrence. *Jpn J Clin Oncol* 1984; **14**: 623-632
- 29 **Moriya Y**, Hojo K, Sawada T, Koyama Y. Significance of lateral node dissection for advanced rectal carcinoma at or below the peritoneal reflection. *Dis Colon Rectum* 1989; **32**: 307-315
- 30 **Glass RE**, Ritchie JK, Thompson HR, Mann CV. The results of surgical treatment of cancer of the rectum by radical resection and extended abdomino-iliac lymphadenectomy. *Br J Surg* 1985; **72**: 599-601
- 31 **Scholefield JH**, Steup WH. Surgery for rectal cancer in Japan. *Lancet* 1992; **340**: 1101

Edited by Ren SY and Wang XL Proofread by Xu FM

Targeting cyclooxygenase-2 with sodium butyrate and NSAIDs on colorectal adenoma/carcinoma cells

Zhi-Hong Zhang, Qin Ouyang, Hua-Tian Gan

Zhi-Hong Zhang, Qin Ouyang, Hua-Tian Gan, Department of Gastroenterology, First Hospital, Western China University of Medical Sciences, Chengdu 610041, Sichuan Province, China

Supported by the Scientific Foundation of Sichuan Province, No. 174

Correspondence to: Zhi-Hong Zhang, Department of Gastroenterology, First Hospital, Western China University of Medical Sciences, Chengdu 610041, Sichuan Province, China. zhang-821@21cn.com

Telephone: +86-28-85081923

Received: 2002-07-17 **Accepted:** 2002-11-04

Abstract

AIM: The protective effects of sodium butyrate and NSAIDs (especially the highly selective COX-2 inhibitors) have attracted considerable interest recently. In this study, primary adenoma cells and HT-29 were used to investigate whether the above drugs would be effective for reducing proliferation and inducing apoptosis. Additionally, it was investigated whether NSAIDs would strengthen the effects of sodium butyrate and its possible mechanisms.

METHODS: *In vitro* primary cell culture of colorectal adenomas and HT-29 were used for this investigation. PGE₂ isolated from HT-29 cell culture supernatants was investigated by ELISA. MTT was employed to detect the anti-proliferative effects on both adenoma and HT-29 culture cells. FCM was used for apoptosis rate and cell cycle analysis. The morphology of apoptotic cells was investigated by means of electromicroscopy.

RESULTS: Sodium butyrate could stimulate the secretion of PGE₂, while NSAIDs inhibited it to below 30 pg/10⁶ cells. Both butyrate and NSAIDs could inhibit cell proliferation and induce apoptosis. The effects were time- and dose-dependent ($P < 0.05$). Aspirin and NS-398 could enhance the effects of sodium butyrate. The effects were stronger while sodium butyrate was used in combination with NS-398 than it was used in combination with Aspirin.

CONCLUSION: Butyrate and NSAIDs could inhibit cell proliferation and induce apoptosis respectively. NSAIDs could enhance the effects of sodium butyrate by down-regulating COX-2 expression. Selective COX-2 inhibitor is better than traditional NSAIDs.

Zhang ZH, Ouyang Q, Gan HT. Targeting cyclooxygenase-2 with sodium butyrate and NSAIDs on colorectal adenoma/carcinoma cells. *World J Gastroenterol* 2004; 10(20): 2954-2957
<http://www.wjgnet.com/1007-9327/10/2954.asp>

INTRODUCTION

Colorectal cancer remains the major cause of cancer-related mortality in the developed countries. With improvement in economic status, the incidence of colorectal cancer is increasing in China. Prevention of the disease is a more attractive approach to dealing with the problem than treatment of existing disease

for both medical and fiscal reasons. Clinical evidences showed that removal of colorectal adenoma could attenuate 76-90% risk of colorectal cancer, but the yearly relapse rate has reached 10-15%. Therefore, the urgent task is to develop new strategies to prevent the disease. With regard to chemoprevention, butyrate sodium (sodium butyrate) and non-steroidal anti-inflammatory drugs (NSAIDs), especially selective COX-2 inhibitors have attracted more attention.

Evidences have shown that low fat and high dietary fiber diet could protect against colorectal cancer. Dietary fiber could be fermented by symbiotic bacteria in the large bowel and then a short chain fatty acid-butyrate, could be released. Clinical and laboratory studies showed that butyrate might be beneficial to the development of colorectal cancer and even in the early stage of its premalignant status^[1].

NSAIDs have shown its promising role in colorectal cancer chemoprevention in recent years. Epidemic studies demonstrated that it might reduce 40-50% risk of colorectal cancer in persons who took aspirin or other NSAIDs on a regular basis^[2]. The most recognized target for NSAIDs was cyclooxygenase (COX), because COX-2 showed 86% and 43% expression in colorectal adenoma and carcinoma tissues respectively^[17]. Furthermore, COX-2 selective inhibitors have attracted more attention because of their minimal risk of gastrointestinal side effects.

Although the precise mechanisms are unclear, sodium butyrate and NSAIDs are involved in chemoprevention of colorectal cancer. In this study, colorectal adenoma cells and HT-29 cells were used to investigate whether the above agents were effective in reducing proliferation and inducing apoptosis, and whether NSAIDs could strengthen the effects of sodium butyrate and its possible mechanisms.

MATERIALS AND METHODS

Materials

NS-398 was a gift from Dr. W Sternson (Washington University). EGF was from Dr. Ouyang Xueshong (Hong Kong University). Sodium butyrate, aspirin, collagenase type IV, hyaluronidase type IV were purchased from Sigma Chemical Co. Prostaglandin E₂ EIA kit was from Cayman Chemical. Arachidonic acid, insulin, FBS was from GIBCO Co.

Colorectal adenoma specimens were from resection through colonoscopy in the Endoscopic Center, First Hospital of Western China University of Medical Sciences. HT-29 was a gift from Immuno-Transplantation Laboratory, First Hospital of Western China University of Medical Sciences.

Methods

Cell cultures Adenoma specimens were washed at least 10 times in PBS containing penicillin (1 000 U/mL), streptomycin (1 000 U/mL), amphotericin B (3 µg/mL). The minced tissues were digested by DMEM containing collagenase type IV (1.5 mg/mL), hyaluronidase type IV (0.25 mg/mL) for 2 h until the tissues were dispersed into individual crypts, then they were incubated at 37 °C, 50 mL/L CO₂ in growth medium consisting of DMEM, 50 mL/L FBS, 0.5 µg/mL insulin, 1 µg/mL hydrocortisone, 5 µg/mL transferrin, 20 ng/mL EGF, 5 × 10⁻⁹ Na₂SeO₃, 0.1 µg/mL pentagastrin, 2 mmol/L glutamine, 200 U/mL penicillin, 200 U/mL

streptomycin. The culture cells were identified as epithelial origin by immunohistochemical staining and electro microscopy (data not shown). HT-29 was cultured in standard growth condition containing DMEM, 100 g/L LBS, 200 U/mL penicillin and streptomycin.

Preparation of drugs

Sodium butyrate was dissolved in culture medium. Aspirin and NS-398 were in DMSO, and the final concentration was less than 3.3 mL/L. The drugs below were used to measure PGE₂, MTT and FCM. Sodium butyrate: 2 mmol/L, 4 mmol/L, 6 mmol/L; Aspirin: 1 mmol/L, 5 mmol/L, 10 mmol/L, 20 mmol/L; NS-398: 0.1 μmol/L, 1 μmol/L, 10 μmol/L, 50 μmol/L; 2 mmol/L Sodium butyrate+10 mmol/L Aspirin; 2 mmol/L Sodium butyrate+10 μmol/L NS-398. For electro microscopy, 2 mmol/L Sodium butyrate, 10 mmol/L aspirin or 10 μmol/L NS-398 was used.

Prostaglandin E₂ (PGE₂) immunoassay

HT-29 cells were seeded at a density of 1×10⁶ cells/T25 flask for 48 h, and then treated with medicine for 24 h or 72 h separately. Aliquots of culture medium (1 mL) were stored at -70 °C until assayed (In NSAIDs treatments and control groups, an exogenous supply of 10 μmol/L AA was added to pre-treat for 30 min individually). Immunoassay was carried out according to the manufacturer's protocol. The sensitivity of the assay was 10 pg/mL.

Proliferation assays

Cell proliferation of both primary adenoma cells and HT-29 was assessed by MTT. After seeded at a density of 2×10⁴ cells/well for 96 well plates with 100 μL media for 48 h, the cells were treated with medicine for 24 h or 72 h separately. At the end of incubation, the medium was removed and 20 μL MTT solution was added to each well. Then DMSO was added to each well, the optical density of each well was read on the plate reader at 570 nm.

The inhibition rate = (1 - tested group optical density/the control optical density)×100%.

Flow cytometric analysis

After HT-29 cells were harvested, they were fixed in 700 mL/L ethanol overnight at 4 °C, mixed with PI staining fluid for 20 min at 4 °C and then filtered. At last, the samples were examined by FCM.

Electro microscopy

The collected HT-29 cells were fixed in 30 g/L glutaraldehyde, then rinsed in 10 g/L osmium tetroxide for 30 min at 4 °C, dehydrated through a series of acetone, embedded in EPON polymerized at 60 °C, stained with uranyl acetate and Reynold lead citrate. Finally, the sections were examined under an electron microscope.

Statistical analysis

PGE₂ expression and growth inhibition were statistically analyzed by two-way ANOVA. Comparison among the groups was analyzed by L-S-D. The apoptotic rate was analyzed by χ^2 . All data were analyzed by SPSS.

RESULTS

PGE₂ production in HT-29 cells

With the increase of optical density, PGE₂ production was decreased in standard culture condition. Sodium butyrate 2 mmol/L was enough for stimulating the secretion of PGE₂ 1 306 pg/10⁶ cells compared with control values of 69 pg/10⁶ cells in 24 h ($P<0.05$), but it was not time- and dose-dependent. 2 mmol/L\4 mmol/L\6 mmol/L sodium butyrate separately stimulated the secretion of PGE₂ 1306\1230\1385 (pg/10⁶ cells). And the same concentration of sodium butyrate had no statistical differential effects in 24 h and 72 h. In contrast, NSAIDs (aspirin and NS-398) could completely inhibit PGE₂ secretion in a time- and dose-independent manner ($P<0.001$). After incubated for 30 min with 10 μmol/L AA, PGE₂ production reached 1 470 pg/10⁶ cells in control, while 1-20 mmol/L aspirin reduced the PGE₂ levels to below 30 pg/10⁶ cells and 0.1-50 μmol/L NS-398 reached 477 pg/10⁶ cells-25 pg/10⁶ cells. NS-398 was different in time- and concentration-dependence from aspirin. Sodium butyrate in combination with NSAIDs showed PGE₂ production inhibition (<30 pg/10⁶ cells) (Table 1).

Sodium butyrate and NSAIDs had dose- or time-dependent anti-proliferative effects on HT-29 and adenoma cells

The anti-proliferative effects on HT-29 and adenoma cells were obvious concentration- and time- dependent ($P<0.05$). 2-6 mmol/L sodium butyrate after 24 h showed 4.3-12.6% on HT-29 and 5.7-11.9% on adenoma cells. They reached 23.7-62.9% and 19-30.5% after 72 h. In agreement with NS-398 and aspirin, the effect was stronger on NS-398 than on aspirin with the same concentration. 1-20 mmol/L aspirin could inhibit the cell proliferation 18.5-57.1% after 24 h and 48.5-76.6% after 72 h, while 0.1-50 μmol/L NS-398 reached 4.5-24% after 24 h and 52.2-68.5% after 72 h. The effects were more obvious on the adenoma cells. Treatment with both Sodium butyrate and NSAIDs resulted in an increase in anti-proliferative effects compared with Sodium butyrate treatment alone for HT-29, and the effects were time-dependent (Table 2).

But for adenoma cells, the results were different in repeated experiments. Only treatment with Sodium butyrate and NS-398 for 72 h showed the synergistic effects on 28.6% adenoma specimens ($P<0.05$).

Moreover, HT-29 cell cycle distribution was analyzed by FCM. Both Sodium butyrate and NSAIDs could arrest the cell cycle in S phase compared with the control ($P<0.05$), but the response to G₁/G₁ or G₂ phase was different.

Induction of apoptosis effects was dose-dependent in HT-29

Normal primary culture cells and HT-29 showed irregular polygon-appearances. The cells treated with the drugs shrank and became round, then shad from the wall and floated in the fluid. The floating cells showed blue coloration by trypan blue staining, while the attached cells were achromatical.

As expected, the dose-dependent apoptotic effects on HT-29 cells treated with Sodium butyrate or NSAIDs could be seen

Table 1 PGE₂ (pg/10⁶ cells) production in HT-29 treated with Sodium butyrate and/or NSAIDs

Production of PGE ₂	2 mmol/L sodium butyrate	10 mmol/L aspirin	10 μmol/L NS-398	Sodium butyrate+aspirin	Sodium butyrate+NS-398
24 h	1 306±5.6	13.2±4.1	35.2±3.5	14.9±1.9	45.9±2.9
72 h	1 427±7.1	5.61±2.7	5.95±2.2	6.5±1.0	8.49±1.3

Table 2 Comparison of growth inhibition effects on HT-29 with Sodium butyrate alone or in combination with NSAIDs (%)

Time	2 mmol/L sodium butyrate	10 mmol/L aspirin	10 μmol/L NS-398	Sodium butyrate+aspirin	Sodium butyrate+NS-398
24 h	4.28	55	10.2	58.3	26
72 h	23.7	72.2	63.9	81.9	70.5

Table 3 Percentage of HT-29 apoptotic cell rate (%)

Concentration	Control				Aspirin (mmol/L)				NS-398 ($\mu\text{mol/L}$)				Sodium butyrate (mmol/L)		
	1	5	10	20	0.1	1	10	50	2	4	6				
Apoptotic rate	4.2 \pm 1.3	8.3 \pm 1.6	10.9 \pm 2.0	11.9 \pm 2.7	29.7 \pm 3.1	6 \pm 1.4	7.8 \pm 1.7	12.5 \pm 3.1	19.5 \pm 3.4	10.7 \pm 2.5	15.9 \pm 0.9	23.2 \pm 4.1			

($P < 0.05$) (Table 3). Sodium butyrate with NS-398 had more preferential apoptotic effects (14.7%) compared with Sodium butyrate alone (10.7%) or Sodium butyrate in combination with aspirin (13.3%).

To confirm the induction of apoptosis, the morphological appearances of HT-29 cells were examined by electron microscopy. Typical apoptotic appearances are shown in Figure 1, which included cell shrinkage, nuclear condensation, and formation of apoptotic bodies, etc.

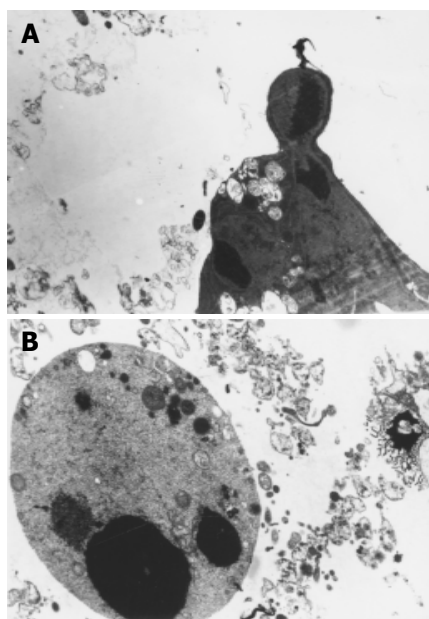


Figure 1 Morphological appearances of HT-29 cells. A: Typical appearances of apoptotic cells; B: Illustration of apoptotic bodies.

DISCUSSION

In recent years, the incidence of colorectal cancer is increasing in China. Prevention of the disease is a more attractive approach in the early stage of adenoma-cancer progression. Butyrate and NSAIDs (especially highly selective COX-2 inhibitors) have attracted considerable attention recently.

As a byproduct of carbohydrates fermented by symbiotic bacteria, butyrate has been demonstrated its important role in inhibiting cell growth and in inducing apoptosis of colorectal cancer cells *in vitro*^[3]. Clinical case-control and cohort studies have shown a 40-50% reduction in colorectal cancer-related mortality in individuals taking aspirin and other NSAIDs on a regular basis compared with those not taking these agents^[2]. Aspirin serves as a typical representative of classical NSAID agents. As a highly selective COX-2 inhibitor, NS-398 showed higher selective effects than others. Its IC_{50} (COX-2/COX-1) was 0.0005, while L-745, 337 was 0.003, flosulide was 0.001^[4], rofecoxib was 0.0012^[5]. Although the precise mechanism underlying the protective effects of NSAIDs is unclear, COX-2 could play a key role in intestinal tumorigenesis^[6] and has been a widely recognized target because of its high expression in colorectal adenoma and cancer tissues^[7-10]. The COX-2-dependent mechanism involving in increased angiogenesis^[11-13], could reduce apoptotic susceptibility by inhibiting the cytochrome c-dependent apoptotic pathway^[14]. Down-regulation of bcl₂ and

CD44v6 expression and up-regulation of nm23 expression^[15] could inhibit death receptor 5 expression and confer resistance to tumor necrosis factor-related apoptosis-inducing ligand (TRAIL)-induced apoptosis^[16]. However, some COX-independent ways, such as lipoxigenase (LOX) another AA metabolic enzyme, could modulate sodium butyrate-induced apoptosis and cell differentiation^[17]. Leukotriene (LT) D₄/CysLT₁ R signaling could facilitate survival of colon cancer cells and LTs were accessible targets for pharmacologic treatment like COX-2^[18]. NF-KB/I-KB system^[19]. Activated Ras and TGF- β could collaborate to increase the invasive response^[20], etc, which have been shown to be involved in the protective mechanism. In this study, adenoma cells and HT-29 were investigated whether Sodium butyrate and aspirin/NS-398 were the effective adjuvants for the protective effects.

The relationship between PGE₂ (an AA metabolize product) and colorectal carcinogenesis is still disputed. Generally, PGE₂ could combine with the transcription factor PPAR α , which activates the target gene transcription and promotes carcinogenesis^[21]. PGE₂ could also increase bcl-2 expression and inhibit cell apoptosis^[22] and was involved in the angiogenesis of cancers. So it has been implicated that PGE₂ inhibition is the main mechanism of anticarcinogenesis of NSAIDs. But a positive result showed that exogenous PGE₂ could not reverse the antineoplastic effects of sulindac sulfone^[23]. In this study, PGE₂ production was investigated to reflect the COX-2 enzyme activity indirectly. For HT-29, Sodium butyrate could stimulate its PGE₂ secretion in a time- and dose-independent manner, suggesting that it could increase its COX-2 enzyme activity. In contrast, NSAIDs inhibited PGE₂ production. Although previous evidence displayed that the expression of COX-2 was increased by some NSAIDs and TGF- β ^[24], we proposed that the inhibited enzyme activity would still down-regulate the effects of NSAIDs.

Sodium butyrate could reduce cell proliferation and induce cell apoptosis in a time- and dose-dependent manner. The possible mechanism has been known to involve in a large number of parameters, including inhibition of histone deacetylase and induction of caspase-3 protease activity with a mitochondrial/cytochrome c-dependent pathway^[25], enhancement of Fas-mediated apoptosis^[26], inhibition of P53 expression^[25]. Down-regulation of GATA-6 and up-regulation of 15-LO-1 were observed after treatment with sodium butyrate (sodium butyrate), which was also involved in stimulating cell apoptosis and cell differentiation^[27]. NSAIDs had the same effects on both cell lines. This was not in a time- and dose-dependent manner. Therefore, it implied that anti-neoplastic mechanisms of NSAIDs were COX-2-dependent and COX-2-independent.

Compared with the effects on adenoma and carcinoma cells, NSAIDs had stronger inhibitory effects on carcinoma cells than on adenoma cells with MTT. Maybe the cause laid in the primarily cultured adenoma cells from different specimens, which resulted in the individual characterization of COX-2 expression and cell proliferation. Other studies gave the same conclusion that NSAIDs had stronger effects on HT-29 carcinoma cells (high COX-2 expression) than on S/KS cells (lack of COX-2 expression).

Previous studies revealed that COX-2 expression up-regulation would induce resistance to apoptosis induced by sodium butyrate. Because NSAIDs could down-regulate COX-2

expression, whether NSAIDs could sensitize the cells to the action of sodium butyrate and reduce the potential side-effects and increase the efficacy by using both drugs was investigated in this study. The data showed that NSAIDs inhibited the growth of HT-29 by sodium butyrate by down-regulating COX-2 expression. It was in agreement with the previous studies. In contrast, other studies reported that cooperation with the two agents was greatly dependent on the category of cell lines and NSAIDs, especially highly selective COX-2 inhibitors showed more preferential effects. Only HT-29 cell line was investigated in this study, so it was necessary to investigate other cell lines for more precise results. Cooperation with the two drugs could affect the two cell lines differently. The effects on HT-29 were completely shown, but only 28.6% was positive for primary adenoma specimens. The main cause depended on the adenoma samples. Additionally, treatment with NS-398 and sodium butyrate had more preferential effects than that with aspirin and sodium butyrate, suggesting that specific selective COX-2 inhibitor NS-398 had a more promising future in clinical application.

In summary, sodium butyrate and NSAIDs could inhibit the cell proliferation and induce cell apoptosis through a number of mechanisms. Combination of two kinds of agents would enhance the above effects by down-regulating COX-2 expression, which could serve as a promising chemoprevention for colorectal neoplasm.

REFERENCES

- 1 Young GP, McIntyre A, Albert V, Folino M, Muir JG, Gibson PR. Wheat bran suppresses potato starch-potentiated colorectal tumorigenesis at the aberrant crypt stage in a rat model. *Gastroenterology* 1996; **110**: 508-514
- 2 Smalley WE, DuBois RN. Colorectal cancer and nonsteroidal anti-inflammatory drugs. *Adv Pharmacol* 1997; **39**: 1-20
- 3 Hernandez A, Thomas R, Smith F, Sandberg J, Kim S, Chung DH, Evers BM. Butyrate sensitizes human colon cancer cells to TRAIL-mediated apoptosis. *Surgery* 2001; **130**: 265-272
- 4 Cromlish WA, Kennedy BP. Selective inhibition of cyclooxygenase-1 and -2 using intact insect cell assays. *Biochem Pharmacol* 1996; **52**: 1777-1785
- 5 Ehrich EW, Dallob A, De Lepeleire I, Van Hecken A, Riendeau D, Yuan W, Porras A, Wittreich J, Seibold JR, De Schepper P, Mehlisch DR, Gertz BJ. Characterization of rofecoxib as a cyclooxygenase-2 isoform inhibitor and demonstration of analgesia in the dental pain model. *Clin Pharmacol Ther* 1999; **65**: 336-347
- 6 Sonoshita M, Takaku K, Oshima M, Sugihara K, Taketo MM. Cyclooxygenase-2 expression in fibroblasts and endothelial cells of intestinal polyps. *Cancer Res* 2002; **62**: 6846-6849
- 7 Eberhart CE, Coffey RJ, Radhika A, Giardiello FM, Ferrenbach S, DuBois RN. Up-regulation of cyclooxygenase 2 gene expression in human colorectal adenomas and adenocarcinomas. *Gastroenterology* 1994; **107**: 1183-1188
- 8 Takeuchi M, Kobayashi M, Ajioka Y, Honma T, Suzuki Y, Azumaya M, Narisawa R, Hayashi S, Asakura H. Comparison of cyclo-oxygenase 2 expression in colorectal serrated adenomas to expression in tubular adenomas and hyperplastic polyps. *Int J Colorectal Dis* 2002; **17**: 144-149
- 9 McEntee MF, Cates JM, Neilsen N. Cyclooxygenase-2 expression in spontaneous intestinal neoplasia of domestic dogs. *Vet Pathol* 2002; **39**: 428-436
- 10 Zhang H, Sun XF. Overexpression of cyclooxygenase-2 correlates with advanced stages of colorectal cancer. *Am J Gastroenterol* 2002; **97**: 1037-1041
- 11 Chapple KS, Scott N, Guillou PJ, Coletta PL, Hull MA. Interstitial cell cyclooxygenase-2 expression is associated with increased angiogenesis in human sporadic colorectal adenomas. *J Pathol* 2002; **198**: 435-441
- 12 Deng WG, Saunders MA, Gilroy DW, He XZ, Yeh H, Zhu Y, Shtivelband MI, Ruan KH, Wu KK. Purification and characterization of a cyclooxygenase-2 and angiogenesis suppressing factor produced by human fibroblasts. *FASEB J* 2002; **16**: 1286-1288
- 13 Cianchi F, Cortesini C, Bechi P, Fantappie O, Messerini L, Vannacci A, Sardi I, Baroni G, Boddi V, Mazzanti R, Masini E. Up-regulation of cyclooxygenase 2 gene expression correlates with tumor angiogenesis in human colorectal cancer. *Gastroenterology* 2001; **121**: 1339-1347
- 14 Sun Y, Tang XM, Half E, Kuo MT, Sinicrope FA. Cyclooxygenase-2 overexpression reduces apoptotic susceptibility by inhibiting the cytochrome c-dependent apoptotic pathway in human colon cancer cells. *Cancer Res* 2002; **62**: 6323-6328
- 15 Yu HG, Huang JA, Yang YN, Huang H, Luo HS, Yu JP, Meier JJ, Schrader H, Bastian A, Schmidt WE, Schmitz F. The effects of acetylsalicylic acid on proliferation, apoptosis, and invasion of cyclooxygenase-2 negative colon cancer cells. *Eur J Clin Invest* 2002; **32**: 838-846
- 16 Tang X, Sun YJ, Half E, Kuo MT, Sinicrope F. Cyclooxygenase-2 overexpression inhibits death receptor 5 expression and confers resistance to tumor necrosis factor-related apoptosis-inducing ligand-induced apoptosis in human colon cancer cells. *Cancer Res* 2002; **62**: 4903-4908
- 17 Ikawa H, Kamitani H, Calvo BF, Foley JF, Eling TE. Expression of 15-lipoxygenase-1 in human colorectal cancer. *Cancer Res* 1999; **59**: 360-366
- 18 Ohd JF, Nielsen CK, Campbell J, Landberg G, Lofberg H, Sjolander A. Expression of the leukotriene D4 receptor CysLT1, COX-2, and other cell survival factors in colorectal adenocarcinomas. *Gastroenterology* 2003; **124**: 57-70
- 19 Yin MJ, Yamamoto Y, Gaynor RB. The anti-inflammatory agents aspirin and salicylate inhibit the activity of I(kappa)B kinase- β . *Nature* 1998; **396**: 77-80
- 20 Roman CD, Morrow J, Whitehead R, Beauchamp RD. Induction of cyclooxygenase-2 and invasiveness by transforming growth factor-beta (1) in immortalized mouse colonocytes expressing oncogenic Ras. *J Gastrointest Surg* 2002; **6**: 304-309
- 21 Lefebvre AM, Chen I, Desreumaux P, Najib J, Fruchart JC, Geboes K, Briggs M, Heyman R, Auwerx J. Activation of the peroxisome proliferator-activated receptor γ promotes the development of colon tumors in C57BL/6J-APCMin/+ mice. *Nat Med* 1998; **4**: 1053-1057
- 22 Sheng H, Shao J, Morrow JD, Beauchamp RD, DuBois RN. Modulation of apoptosis and Bcl-2 expression by prostaglandin E2 in human colon cancer cells. *Cancer Res* 1998; **58**: 362-366
- 23 Piazza GA, Rahm AL, Krutzsch M, Sperl G, Paranka NS, Gross PH, Brendel K, Burt RW, Alberts DS, Pamukcu R. Anti-neoplastic drugs sulindac sulfide and sulfone inhibit cell growth by inducing apoptosis. *Cancer Res* 1995; **55**: 3110-3116
- 24 Sheng H, Shao J, O'Mahony CA, Lamps L, Albo D, Isakson PC, Berger DH, DuBois RN, Beauchamp RD. Transformation of intestinal epithelial cells by chronic TGF- β 1 treatment results in downregulation of the type II TGF- β receptor and induction of cyclooxygenase-2. *Oncogene* 1999; **18**: 855-867
- 25 Medina V, Edmonds B, Young GP, James R, Appleton S, Zalewski PD. Induction of caspase-3 protease activity and apoptosis by butyrate and trichostatin A (inhibitors of histone deacetylase): dependence on protein synthesis and synergy with a mitochondrial/cytochrome c-dependent pathway. *Cancer Res* 1997; **57**: 3697-3707
- 26 Bonnotte B, Favre N, Reveneau S, Micheau O, Droin N, Garrido C, Fontana A, Chauffert B, Solary E, Martin F. Cancer cell sensitization to fas-mediated apoptosis by sodium butyrate. *Cell Death Differ* 1998; **5**: 480-487
- 27 Kamitani H, Kameda H, Kelavkar UP, Eling TE. A GATA binding site is involved in the regulation of 15-lipoxygenase-1 expression in human colorectal carcinoma cell line, caco-2. *FEBS Lett* 2000; **467**: 341-347

• COLORECTAL CANCER •

A novel mouse model for colitis-associated colon carcinogenesis induced by 1,2-dimethylhydrazine and dextran sulfate sodium

Jian-Guo Wang, Dong-Fei Wang, Bing-Jian Lv, Jian-Min Si

Jian-Guo Wang, Dong-Fei Wang, Jian-Min Si, Department of Gastroenterology, Sir Run Run Shaw Hospital, Zhejiang University Medical School, Hangzhou 310016, Zhejiang Province, China
Bing-Jian Lv, Department of Pathology, Sir Run Run Shaw Hospital, Zhejiang University Medical School, Hangzhou 310016, Zhejiang Province, China

Correspondence to: Jian-Guo Wang, Department of Gastroenterology, Sir Run Run Shaw Hospital, Hangzhou 310016, Zhejiang Province, China. roshy@163.com

Telephone: +86-571-86090073 Ext. 4535

Received: 2003-12-23 **Accepted:** 2004-01-08

Abstract

AIM: To develop an efficient animal colitis-associated carcinogenesis model and to detect the expression of β -catenin and p53 in this new model.

METHODS: Dysplasia and cancer were investigated in mice pretreated with a single intraperitoneal injection of 20 mg/kg body mass of 1,2-dimethylhydrazine prior to three repetitive oral administrations of 30 g/L dextran sulfate sodium to give conditions similar to the clinically observed active and remission phases. Immunohistochemical staining of β -catenin and p53 was performed on paraffin-embedded specimens of animals with cancer and/or dysplasia, those without dysplasia and the normal control animals.

RESULTS: At wk 11, four early-invasive adenocarcinomas and 36 dysplasia were found in 10 (90.9%) of the 11 mice that underwent 1,2-dimethylhydrazine-pretreatment with 3 cycles of 30 g/L dextran sulfate sodium-exposure. Dysplasia and/or cancer occurred as flat lesions or as dysplasia-associated lesion or mass (DALM) as observed in humans. Colorectal carcinogenesis occurred primarily on the distal portion of the large intestine. No dysplasia and/or cancer lesion was observed in the control groups with 1,2-dimethylhydrazine pretreatment or 3 cycles of 30 g/L dextran sulfate sodium exposure alone. Immunohistochemical investigation revealed that β -catenin was translocated from cell membrane to cytoplasm and/or nucleus in 100% of cases with dysplasia and neoplasm, while normal membrane staining was observed in cases without dysplasia and the normal control animals. Nuclear expression of p53 was not detected in specimens.

CONCLUSION: A single dose of procarcinogen followed by induction of chronic ulcerative colitis results in a high incidence of colorectal dysplasia and cancer. Abnormal expression of β -catenin occurs frequently in dysplasia and cancer. This novel mouse model may provide an excellent vehicle for studying colitis-related colon carcinogenesis.

Wang JG, Wang DF, Lv BJ, Si JM. A novel mouse model for colitis-associated colon carcinogenesis induced by 1,2-dimethylhydrazine and dextran sulfate sodium. *World J Gastroenterol* 2004; 10(20): 2958-2962
<http://www.wjgnet.com/1007-9327/10/2958.asp>

INTRODUCTION

The incidence of colorectal cancer (CRC) has been increasing in patients with ulcerative colitis (UC) and the risk of CRC increases with increased extent and duration^[1-4]. The mechanisms underlying the frequent development of CRC in patients with UC are still unknown.

Through the study of animal models which do not allow experiments in humans, we could better understand the cause and mechanisms of various diseases. There are many animal ulcerative colitis models, but only a few of them are applicable to the study of dysplasia-cancer sequence. Among them, the most widely used is a mouse model with dextran sulfate sodium (DSS). DSS could be used to induce UC in mice. Acute colitis was observed by administration of 50-100 g/L DSS to mice for 4-9 d^[5-8]. A chronic colitis could be induced by feeding 30-50 g/L DSS in drinking water for 7 d followed by 7-14 d of water^[6,8-10]. In recent years, some researchers have described the occurrence of dysplasia and/or cancers in mice when they are subjected to repeated administration of DSS in a long term^[11-13]. Before the occurrence of cancer, the features of colitis in this model were very similar to those in patients in terms of both clinical and histopathological characteristics, i.e. diarrhea, occult blood, melena, mucosal inflammatory cell infiltration, crypt abscess formation, and mucosal erosion. But this kind of models needs a long period to be established and the incidence of induced tumors is relatively low.

1,2-dimethylhydrazine (DMH) is a toxic environmental pollutant which was reported as a specific colon procarcinogen. Animal studies showed that experimental colonic tumors induced by DMH were of epithelial origin with a similar histology, morphology and anatomy to human colonic neoplasms^[14]. This procarcinogen could thus provide an adequate model for studying colorectal cancer. However, multiple treatments with DMH (20-40 mg/kg body mass) and a long-term experimental period are needed to induce large bowel neoplasms^[15-17].

We present here a newly developed colitis-associated CRC mouse model in which dysplasia and cancer developed within 10 wk when mice were given a single, low dose of DMH followed by three repeated administrations of 30 g/L DSS in drinking water. We used DSS to induce recurrence-remission cycle of chronic colitis which was similar to humans and added a low dose of DMH, in order to shorten CRC development period since chronic exposure to a small amount of environmental carcinogens is also a main cause of human CRC. In addition, we found dysplasias and cancers in this model showed positive reactivity for β -catenin, but not for p53.

MATERIALS AND METHODS

Animals

Forty-five specific pathogen-free BALB/c male mice weighing 25-30 g (Slaccas Experimental Animal Co. Ltd. Shanghai, China), 7 wk of age, were used. They were housed in plastic cages (5 or 6 mice/cage) with wood shavings under standard laboratory conditions (24±0.5 °C temperature, 50±10% humidity, and 12 h of light from 06.00 to 18.00). All mice were permitted free access

to a commercial diet and DSS-supplemented or normal drinking tap water in bottles at the Animal Laboratory Center of our hospital.

Study design

The design for inducing colitis-associated dysplasia and/or cancer is shown in Figure 1. At the age of 8 wk, the animals were divided into one experimental group (group A) and 3 control groups (groups B-D), 10-12 mice each group. The animals in group A were subjected to three cycles of alternating administration of distilled water containing 30 g/L synthetic dextran sulfate sodium (DSS; mol mass 5000; Wako Pure Chemical Industries, Ltd. Japan) for 7 d followed by distilled water for the subsequent 14 d after intraperitoneal pretreatment with 20 mg/kg 1,2-dimethylhydrazine (DMH; Sigma-Aldrich Corp. St. Louis, MO, USA). For comparison, control groups B to D received each of the treatment alone or maintained as untreated control. Three mice from group A, B, and D were sacrificed during the experiment. Forty-two mice were anesthetized with ether and sacrificed at the age of 18 wk.

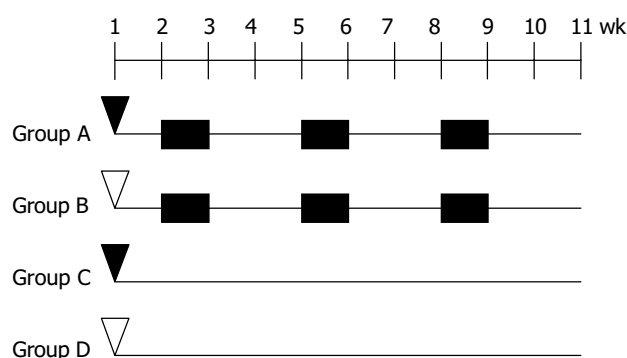


Figure 1 Experimental protocol for inducing colitis-related colon cancer in mice. ▼DMH, 20 mg/kg body mass, intraperitoneal injection; ▽ Saline 0.5 mL/mice intraperitoneal injection; 30 g/L ■ DSS in drinking water.

Observation of colitis

Changes in body weight were recorded every week throughout the experiment. Occult blood was examined on d 3 or 4 of DSS feeding, when DSS feeding was stopped, and once a week thereafter. Presence of gross blood and stool consistency were observed daily. The individuals who examined the mice were blinded as to the experimental group to which the animals belonged.

Histopathological evaluation

After death, the entire colorectum from the colocolic junction to the anal verge was examined. Their length was measured, and then the specimen was opened longitudinally and washed with saline. After colorectum was macroscopically inspected, it was immediately fixed in a 40 g/L formaldehyde buffer solution (pH 7.2).

Part of the colon was divided into three equal portions (proximal, middle and distal). Five-six pieces/portion and 14-17 pieces/colorectum were stained with hematoxylin and eosin (H&E) for histological processing.

The severity of UC of each colon was histologically graded on a scale from 0-4 and expressed using the pathological index corresponding to the following modified standard scoring system^[18]: 0, normal; 1, focal inflammatory cell infiltration including polymorphonuclear leucocytes; 2, gland loss with inflammatory cell infiltration or crypt abscess formation; 3, mucosal ulceration, or five or more foci of gland loss with inflammatory cell infiltration; 4, two or more areas of mucosal

ulceration.

Dysplasia (low and high grades) was scored according to the criteria described by Riddell *et al.*^[19]. Cancer was divided into early invasive and advanced cancer. Early invasive cancer was defined as cancer cells invading into muscularis mucosa and/or into submucosa. Advanced cancer was defined as cancer cells invading into muscularis propria or beyond.

A single experienced pathologist reviewed all cases blindly.

The evaluation of β -catenin and p53

To detect the expression of β -catenin and p53, we utilized the two step immunostaining technique. Four μ m thick tissue sections were dewaxed and rehydrated through changes of xylene and graded alcohol, then to water. Endogenous peroxidase activity was blocked by incubating the sections with 30 g/L hydrogen peroxidase for 15 min. Heat-mediated antigen retrieval was performed by heating the sections (immersed in 0.01 mol/L citrate buffer, pH 6.0) in a microwave oven (750 W) for 15 min. The slides were then washed with phosphate-buffered saline (PBS) before incubated with primary antibody overnight at 4 °C. The antibody to β -catenin (Santa Cruz Biotechnology, Inc. USA) was a mouse monoclonal IgG1 antibody corresponding to amino acids 680-781 and was used at a dilution of 1:800. p53 antibody (Santa Cruz Biotechnology, Inc. USA) was a rabbit polyclonal antibody that reacts with both wild-type and mutant p53 and was used at a dilution of 1:200. After washed with PBS, the slides were incubated for 30 min with the EnVision+peroxidase reagent (Zhongshan Biological Technology Co., LTD, Beijing, China). After further washed in PBS, the slides were developed with 3,3'-diaminobenzidine (DAB; Sigma-Aldrich Corp. St. Louis, MO, USA) for 5 min, and the reaction was terminated in water. The slides were then counterstained with hematoxylin, dehydrated in alcohol, and evaluated under a light microscope. Positive controls for β -catenin expression were normal human colonic epithelia. Human colonic adenocarcinoma were used as positive controls for p53 antibody. Omission of the primary antibody of β -catenin and p53 was used as a negative control.

Lesions were classified as positive for β -catenin if cytoplasmic/nuclear staining was detected (1+: \leq 50% cells positive, 2+: \geq 50% cell positive). Staining for p53 was considered positive if nuclear expression was detected in more than 10% of cells. Two experienced pathologists who were blinded to the specimen independently examined slides, and a high level of concordance (90%) was achieved. In case of disagreement, the slides were reviewed and a consensus view was achieved.

Statistical analysis

Statistical analysis was carried out by SPSS 11.5 for windows statistic software. Variance tests and One-way ANOVA test were used to compare the means of weight, length of large bowel in different groups, the number of neoplasms, and pathological index in different sites. $P < 0.05$ was considered statistically significant.

RESULTS

Body growth, fecal examination and colorectal length

At the end of the first DSS treatment period, 75.0% (18/24) mice in groups A and B had diarrhea and occult blood or gross blood in the feces, and these signs disappeared after the mice drank distilled water for 14 d. However, during the second and third administrations of DSS, only 45.5% (10/22) and 36.4% (8/22) mice had diarrhea or occult blood, respectively.

Body growth rate was slightly lower in the mice that received 3 cycles of DSS treatment. The mean body weight of group A and B at the end of study was significantly smaller than that of

group D ($P < 0.05$, Table 1).

Although the colorectal length was not affected by DMH-treatment alone, it was shortened by DSS treatment. The mean length of colorectum of mice in groups A and B was significantly shorter than that of mice in group D ($P < 0.01$, Table 1).

Table 1 Body mass and colorectal length (mean \pm SD)

Groups	A	B	C	D
Body mass (g)	24.09 \pm 2.02 ^a	25.9 \pm 2.020 ^a	31.00 \pm 2.10	30.01 \pm 1.02
Colon length (cm)	8.80 \pm 0.98 ^b	9.37 \pm 0.90 ^b	12.21 \pm 0.94	12.66 \pm 0.73

Significantly different from group D (^a $P < 0.05$, ^b $P < 0.01$).

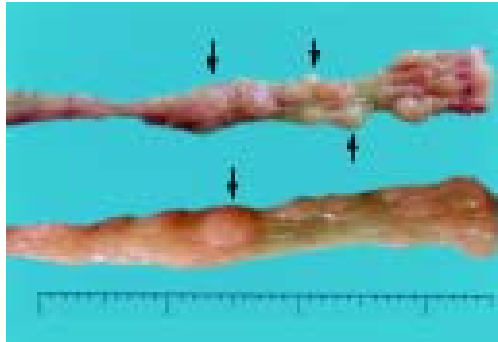


Figure 2 Induced colorectal tumors. Gross polypoid lesions are evident on the distal and middle portions of the large intestine (arrows).

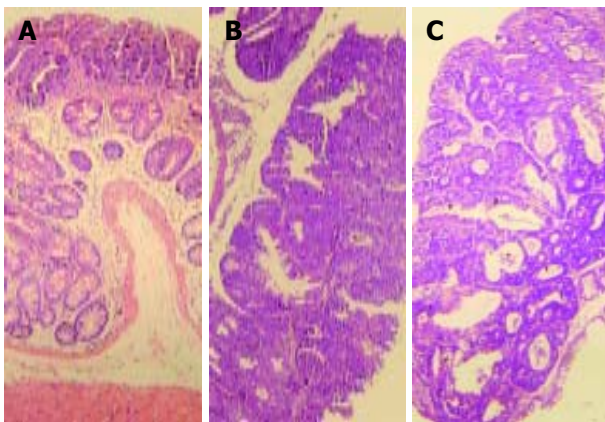


Figure 3 Histopathology showing dysplastic and cancer lesions developed in the colon of mice from group A. A: Whole-mount view of DALM with low-grade dysplasia, B: A slightly or non-elevated lesion diagnosed as high-grade dysplasia, C: whole-mount view of an early invasive cancer arising out of DALM. Hematoxylin and eosin stain. Original magnification, $\times 10$.

Incidence and distribution of dysplasia and cancer

Group A mice that received DMH pretreatment and repeated administrations of 30 g/L DSS developed multiple tumours in the colorectal region. Ten of 11 (90.9%) animals were detected to have at least one dysplasia and/or cancer lesion. Gross lesions were noted in 5 animals (all in group A). These lesions were dome shaped and ranged 2 to 4 mm in size, which appeared in the distal portion of the large intestine mainly, then in the middle portion, and none in the proximal part. (Table 2, Figure 2).

Most tumor tissues were tubular lesions with atypical severe cellular and structural high-grade dysplasia. A small number of lesions revealed relatively moderate dysplasia. Ten dysplasias were categorized as low-grade dysplasia (Figure 3A), and 26 dysplasias as high-grade dysplasia (Figure 3B), 22 out of 36 (61.1%)

dysplasia lesions were DALMs. Four out of 26 tumours on the distal portion of the large intestine were confirmed to be early invasive adenocarcinomas (Figure 3C), and 3 of them arose within a DALM. No signs of tumor development were detected in control groups B to D.

Among the animals with dysplasia and/or cancer, the incidence of dysplasia and/or cancer was 15.0% (6/40), 20.0% (8/40) and 65.0% (26/40) in the proximal, middle and distal colon segments, respectively, 4 of 10 (40.0%) animals with dysplasia and/or cancer had lesions limited to only one colon segment, 3 animals (30.0%) had lesions in two different segments, and 3 animals (30.0%) had lesions in all three segments. Of the 3 animals with cancers, one had two synchronous cancers.

Pathology score/cancer relationship

The mice that received repeated administrations of 30 g/L DSS showed mild colitis regardless of DMH pretreatment. Mice in group A and B demonstrated multiple foci of gland loss with inflammatory cell infiltration, but not many crypt abscess formations and mucosal ulcerations. Pathological scores in these two groups were statically significantly higher than those in group D (Table 2). However, there was no significant relationship between pathology scores among three portions of group A and B. This did not correlate well with the locations of CRC that developed mainly on the distal segment of colorectum.

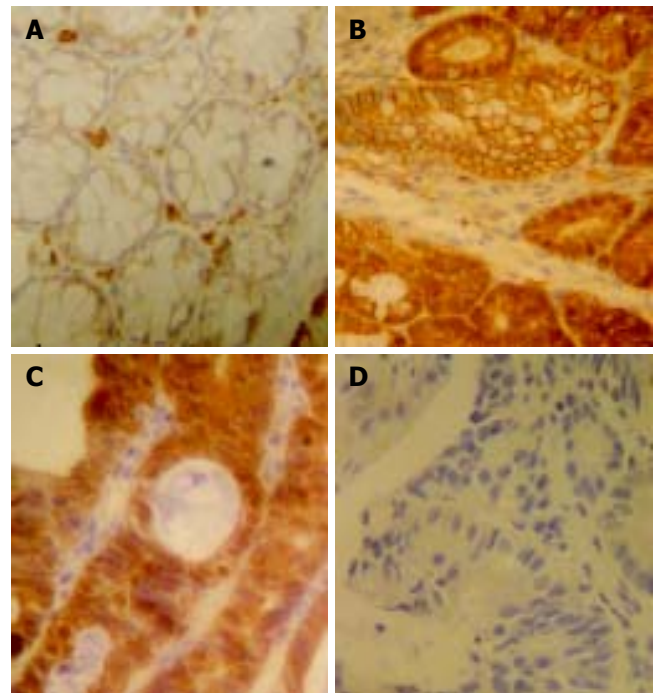


Figure 4 Immunohistochemistry of β -catenin and p53 in dysplastic lesions found in the colon of mice from group A. A: Control colon. β -catenin was expressed exclusively on the cell membrane. No cytoplasmic or nuclear staining was observed, B: Dysplasia cells expressed strong cytoplasmic and partly nuclear staining of β -catenin while other adjacent dysplastic cells showed membrane pattern of β -catenin, C: Lesions of early invasive cancer showing strong nuclear and cytoplasmic staining of β -catenin, D: No nuclear expression of p53 in lesions with high-grade dysplasia was observed. Original magnification, $\times 40$.

β -catenin and p53 expression

Four cancers, 25 dysplasias (10 of low-grade, 15 of high-grade), 10 negative dysplasias and 10 control animals were studied for β -catenin and p53 expression, respectively.

In normal colon epithelial cells, β -catenin was mainly localized at the membranes of cell-cell borders (Figure 4A).

Table 2 Incidence of dysplasia/cancer and pathology score of UC (mean±SD)

Group number	Mice	Number of dysplasias/cancers			Pathology score of UC		
		Proximal	Middle	Distal	Proximal	Middle	Distal
A	11	0.55±0.82	0.73±0.79	2.36±1.12 ^a	1.82±0.40	1.72±0.46	1.82±0.40 ^c
B	11	0.0±0.0	0.0±0.0	0.0±0.0	2.00±0.63	1.82±0.40	2.09±0.54 ^c
C	10	0.0±0.0	0.0±0.0	0.0±0.0	0.0±0.0	0.0±0.0	0.0±0.0
D	10	0.0±0.0	0.0±0.0	0.0±0.0	0.0±0.0	0.0±0.0	0.0±0.0

^a $P < 0.05$, significantly different from proximal and middle portion of group A; ^c $P < 0.05$ significantly different from group D.

Strong (2+) β -catenin expression was seen in nuclei and cytoplasm of cancer cells of 4 specimens (Figure 4C). Although the intensity was relatively weaker than that in carcinoma cells, dysplastic cells showed positivity for β -catenin in their nuclei, cytoplasm, and cell membranes (Figure 4B). The intensity was greater in high-grade dysplasias (73.3% were 2+) than in low-grade dysplasias (30.0% were 2+). In addition, positive reaction against β -catenin antibody was found in vascular endothelia and infiltrated inflammatory cells. However, nuclear p53 staining was not seen in tumor cells and dysplastic cells (Figure 4D).

DISCUSSION

The results of our experiment indicate that neither DMH pretreatment nor repeated administration of 3% DSS induced any tumorous lesions in the colorectum. However, their combination induced 4 invasive adenocarcinomas and 36 lesions with dysplasia in 11 mice within the relatively short term of 10 wk. Therefore, a clear synergism between the two agents was established. The histopathology of dysplasia and cancer in this model was very similar to that seen in humans. First, the animals developed dysplasia in both flat mucosa and DALM identical to that seen in humans. Second, early invasive cancer was revealed in 4 out of 40 lesions, and the data provided evidence of a dysplasia-adenocarcinoma sequence in this experimental system. Finally, the distribution of dysplasia/cancer was also similar. Colon cancers in patients with UC developed mainly on the left side of the large intestine and transverse colon. In our experiment, DMH and DSS induced colitis-related tumors dominant in the distal part of colon followed by in the middle part. In human UC, dysplasia was found in two or more segments in 42-75% of the cases and the incidence of multiple synchronous cancers was reported to vary from 22-50%^[20-22]. In the current study, the result also showed that dysplasia was present in two or more segment in 60% of the animals and the incidence of synchronous cancers was 33.3%. However, we finished the experiment in 10 wk and only induced four early invasive cancers.

β -catenin played a role in both cell adhesion and intracellular signaling^[23,24]. Cytoplasmic/nuclear translocation of β -catenin was reported in human colitis-associated neoplasms^[25-27] and DSS-induced CRC mice models^[28,29]. In our study, we also found aberrant β -catenin expression immunohistochemical in dysplasia and cancer in mice treated with DMH and DSS. Furthermore, we noticed that carcinoma, high- and low-grade dysplasias had different intensities and distributions of β -catenin. However, we don't know whether the translocation of β -catenin was due to loss of APC function or a direct mutation of β -catenin itself. This change might be associated with the progression from dysplasia to cancer. Our model are dissimilar regarding the role of p53. Nuclear expression of p53 was a relatively early event in UC-related CRC compared with sporadic colon neoplasia^[30-32]. However, in the current study, p53 immunohistochemical expression was not detected in colonic dysplasia and cancer. This findings might be due to the absence or low frequency of p53 mutations in colitis-related cancer mouse model. It is also

possible that p53 mutations occurred at a later stage of cancer.

In conclusion, this study provides a novel colitis-associated mouse colon neoplasm model which features a single dose of procarcinogen followed by induction of chronic UC in a relatively short term. Further studies on molecular mechanism or chemopreventive agents of this model may help us better understand CRC in patients with UC.

ACKNOWLEDGEMENTS

The authors wish to thank Dr. Mei Jin, Department of Pathology, Sir Run Run Shaw Hospital, Zhejiang University, Hangzhou, China, for her technical assistance in immunohistochemical analysis. We are also very grateful to Ming-Juan Jin, Department of Epidemiology and Public Health Statistics, Medical College of Zhejiang University, Hangzhou, China, for her statistical analysis.

REFERENCES

- 1 **Ekbom A**, Helmick C, Zack M, Adami HO. Ulcerative colitis and colorectal cancer. A population-based study. *N Engl J Med* 1990; **323**: 1228-1233
- 2 **Delco F**, Sonnenberg A. A decision analysis of surveillance for colorectal cancer in ulcerative colitis. *Gut* 2000; **46**: 500-506
- 3 **Eaden JA**, Abrams KR, Mayberry JF. The risk of colorectal cancer in ulcerative colitis: a meta-analysis. *Gut* 2001; **48**: 526-535
- 4 **van Hogezaand RA**, Eichhorn RF, Choudry A, Veenendaal RA, Lamers CB. Malignancies in inflammatory bowel disease: fact or fiction? *Scand J Gastroenterol Suppl* 2002; **236**: 48-53
- 5 **Okayasu I**, Hatakeyama S, Yamada M, Ohkusa T, Inagaki Y, Nakaya R. A novel method in the induction of reliable experimental acute and chronic ulcerative colitis in mice. *Gastroenterology* 1990; **98**: 694-702
- 6 **Kullmann F**, Messmann H, Alt M, Gross V, Bocker T, Scholmerich J, Ruschoff J. Clinical and histopathological features of dextran sulfate sodium induced acute and chronic colitis associated with dysplasia in rats. *Int J Colorectal Dis* 2001; **16**: 238-246
- 7 **Aghdassi E**, Carrier J, Cullen J, Tischler M, Allard JP. Effect of iron supplementation on oxidative stress and intestinal inflammation in rats with acute colitis. *Dig Dis Sci* 2001; **46**: 1088-1094
- 8 **Hans W**, Scholmerich J, Gross V, Falk W. The role of the resident intestinal flora in acute and chronic dextran sulfate sodium-induced colitis in mice. *Eur J Gastroenterol Hepatol* 2000; **12**: 267-273
- 9 **Cooper HS**, Murthy SN, Shah RS, Sedergran DJ. Clinicopathologic study of dextran sulfate sodium experimental murine colitis. *Lab Invest* 1993; **69**: 238-249
- 10 **Clapper ML**, Adrian RH, Pfeiffer GR, Kido K, Everley L, Cooper HS, Murthy S. Depletion of colonic detoxication enzyme activity in mice with dextran sulphate sodium-induced colitis. *Aliment Pharmacol Ther* 1999; **13**: 389-396
- 11 **Okayasu I**, Yamada M, Mikami T, Yoshida T, Kanno J, Ohkusa T. Dysplasia and carcinoma development in a repeated dextran sulfate sodium-induced colitis model. *J Gastroenterol Hepatol* 2002; **17**: 1078-1083
- 12 **Mitamura T**, Sakamoto S, Sassa S, Suzuiki S, Kudo H, Okayasu I. The more an ulcerative colitis is repeated, the more the risk of

- colorectal carcinogenesis is increased in mice. *Anticancer Res* 2002; **22**: 3955-3961
- 13 **Seril DN**, Liao J, Ho KL, Yang CS, Yang GY. Inhibition of chronic ulcerative colitis-associated colorectal adenocarcinoma development in a murine model by N-acetylcysteine. *Carcinogenesis* 2002; **23**: 993-1001
- 14 **Ma Q**, Hoper M, Anderson N, Rowlands BJ. Effect of supplemental L-arginine in a chemical-induced model of colorectal cancer. *World J Surg* 1996; **20**: 1087-1091
- 15 **Tsunoda A**, Shibusawa M, Tsunoda Y, Yokoyama N, Nakao K, Kusano M, Nomura N, Nagayama S, Takechi T. Antitumor effect of S-1 on DMH induced colon cancer in rats. *Anticancer Res* 1998; **18**(2A): 1137-1141
- 16 **Balansky R**, Gyosheva B, Ganchev G, Mircheva Z, Minkova S, Georgiev G. Inhibitory effects of freeze-dried milk fermented by selected *Lactobacillus bulgaricus* strains on carcinogenesis induced by 1, 2-dimethylhydrazine in rats and by diethylnitrosamine in hamsters. *Cancer Lett* 1999; **147**: 125-137
- 17 **Schmelz EM**, Sullards MC, Dillehay DL, Merrill AH Jr. Colonic cell proliferation and aberrant crypt foci formation are inhibited by dairy glycosphingolipids in 1, 2-dimethylhydrazine-treated CF1 mice. *J Nutr* 2000; **130**: 522-527
- 18 **Onderdonk AB**, Bartlett JG. Bacteriological studies of experimental ulcerative colitis. *Am J Clin Nutr* 1979; **32**: 258-265
- 19 **Riddell RH**, Goldman H, Ransohoff DF, Appelman HD, Fenoglio CM, Haggitt RC, Ahren C, Correa P, Hamilton SR, Morson BC, Sommers SC, Yardley JH. Dysplasia in inflammatory bowel disease: standardized classification with provisional clinical applications. *Hum Pathol* 1983; **14**: 931-968
- 20 **Connell WR**, Lennard-Jones JE, Williams CB, Talbot IC, Price AB, Wilkinson KH. Factors affecting the outcome of endoscopic surveillance for cancer in ulcerative colitis. *Gastroenterology* 1994; **107**: 934-944
- 21 **Taylor BA**, Pemberton JH, Carpenter HA, Levin KE, Schroeder KW, Welling DR, Spencer MP, Zinsmeister AR. Dysplasia in chronic ulcerative colitis: implications for colonoscopic surveillance. *Dis Colon Rectum* 1992; **35**: 950-956
- 22 **Vatn MH**, Elgjo K, Bergan A. Distribution of dysplasia in ulcerative colitis. *Scand J Gastroenterol* 1984; **19**: 893-895
- 23 **Ilyas M**, Tomlinson IP. The interactions of APC, E-cadherin and β -catenin in tumour development and progression. *J Pathol* 1997; **182**: 128-137
- 24 **Morin PJ**, Sparks AB, Korinek V, Barker N, Clevers H, Vogelstein B, Kinzler KW. Activation of β -catenin-Tcf signaling in colon cancer by mutations in β -catenin or APC. *Science* 1997; **275**: 1787-1790
- 25 **Tomlinson I**, Ilyas M, Johnson V, Davies A, Clark G, Talbot I, Bodmer W. A comparison of the genetic pathways involved in the pathogenesis of three types of colorectal cancer. *J Pathol* 1998; **184**: 148-152
- 26 **Brabletz T**, Jung A, Kirchner T. Beta-catenin and the morphogenesis of colorectal cancer. *Virchows Arch* 2002; **441**: 1-11
- 27 **Mikami T**, Mitomi H, Hara A, Yanagisawa N, Yoshida T, Tsuruta O, Okayasu I. Decreased expression of CD44, α -catenin, and deleted colon carcinoma and altered expression of β -catenin in ulcerative colitis-associated dysplasia and carcinoma, as compared with sporadic colon neoplasms. *Cancer* 2000; **89**: 733-740
- 28 **Cooper HS**, Murthy S, Kido K, Yoshitake H, Flanagan A. Dysplasia and cancer in the dextran sulfate sodium mouse colitis model. Relevance to colitis-associated neoplasia in the human: a study of histopathology, β -catenin and p53 expression and the role of inflammation. *Carcinogenesis* 2000; **21**: 757-768
- 29 **Tanaka T**, Kohno H, Suzuki R, Yamada Y, Sugie S, Mori H. A novel inflammation-related mouse colon carcinogenesis model induced by azoxymethane and dextran sodium sulfate. *Cancer Sci* 2003; **94**: 965-973
- 30 **Kern SE**, Redston M, Seymour AB, Caldas C, Powell SM, Kornacki S, Kinzler KW. Molecular genetic profiles of colitis associated neoplasms. *Gastroenterology* 1994; **107**: 420-428
- 31 **Brentnall TA**, Crispin DA, Rabinovitch PS, Haggitt RC, Rubin CE, Stevens AC, Burmer GC. Mutations in the p53 gene: an early marker of neoplastic progression in ulcerative colitis. *Gastroenterology* 1994; **107**: 369-378
- 32 **Ilyas M**, Talbot IC. p53 expression in ulcerative colitis: a longitudinal study. *Gut* 1995; **37**: 802-804

Edited by Ren SR and Wang XL Proofread by Xu FM

Impact of cigarette smoking on response to interferon therapy in chronic hepatitis C Egyptian patients

A. El-Zayadi, Osaima Selim, H. Hamdy, A. El-Tawil, Hanaa M. Badran, M. Attia, A. Saeed

A. El-Zayadi, H. Hamdy, Departments of Tropical Medicine, Ain Shams University, Cairo, Egypt

Osaima Selim, Department of Clinical Pathology, Ain Shams University, Cairo, Egypt

A. El-Tawil, Department of Pathology, Ain Shams University, Cairo, Egypt

Hanaa M. Badran, Department of Hepatology, National Liver Institute, Menoufeya, Egypt

M. Attia, Department of Hepatology and Gastroenterology, Theodor Bilharz Research Institute, Cairo, Egypt

A. Saeed, Cairo Liver Center, Giza, Egypt

Correspondence to: Professor A. El-Zayadi, Cairo Liver Center, 5 El-Gergawy St., Dokki, Giza, Egypt. clcz@tedata.net.eg

Telephone: +202-7603002 **Fax:** +202-7481900

Received: 2004-02-03 **Accepted:** 2004-03-13

Abstract

AIM: Smoking may affect adversely the response rate to interferon- α . Our objective was to verify this issue among chronic hepatitis C patients.

METHODS: Over the year 1998, 138 chronic hepatitis C male Egyptian patients presenting to Cairo Liver Center, were divided on the basis of smoking habit into: group I which comprised 38 smoker patients (>30 cigarettes/d) and group II which included 84 non-smoker patients. Irregular and mild smokers (16 patients) were excluded. Non eligible patients for interferon- α therapy were excluded from the study and comprised 3/38 (normal ALT) in group I and 22/84 in group II (normal ALT, advanced cirrhosis and thrombocytopenia). Group I was randomly allocated into 2 sub-groups: group Ia comprised 18 patients who were subjected to therapeutic phlebotomy while sub-group Ib consisted of 17 patients who had no phlebotomy. In sub-group Ia, 3 patients with normal ALT after repeated phlebotomies were excluded from the study. Interferon- α 2b 3 MU/TIW was given for 6 mo to 15 patients in group Ia, 17 patients in group Ib and 62 patients in group II. Biochemical, virological end-of- treatment and sustained responses were evaluated.

RESULTS: At the end of interferon- α treatment, ALT was normalized in 3/15 patients (20%) in group Ia and 2/17 patients (11.8%) in group Ib compared to 17/62 patients (27.4%) in group II ($P=0.1$). Whereas 2/15 patients (13.3%) in group Ia. and 2/17 patients (11.8%) in group Ib lost viraemia compared to 13/62 patients (26%) in group II ($P=0.3$). Six months later, ALT was persistently normal in 2/15 patients (13.3%) in group Ia and 1/17 patients (5.9%) in group Ib compared to 9/62 patients (14.5%) in group II ($P=0.47$). Viraemia was eliminated in 1/15 patients (6.7%) in group Ia and 1/17 patients (5.9%) in group Ib compared to 7/62 patients (11.3%) in group II, but the results did not mount to statistical significance ($P=0.4$).

CONCLUSION: Smokers suffering from chronic hepatitis C tend to have a lower response rate to interferon- α compared

to non-smokers. Therapeutic phlebotomy improves the response rate to interferon- α therapy among this group.

El-Zayadi A, Selim O, Hamdy H, El-Tawil A, Badran HM, Attia M, Saeed A. Impact of cigarette smoking on response to interferon therapy in chronic hepatitis C Egyptian patients. *World J Gastroenterol* 2004; 10(20): 2963-2966

<http://www.wjgnet.com/1007-9327/10/2963.asp>

INTRODUCTION

It has been reported that cigarette smoking causes a variety of life threatening disorders such as pulmonary, cardiovascular, neoplastic, secondary polycythemia and others^[1]. In addition, cigarette smoking has hepatotoxicity independent from alcoholic cirrhosis^[2,3] and chronic hepatitis B virus carriers^[4]. It increases the 5-year mortality rates of patients with alcoholic cirrhosis^[5]. Furthermore, tobacco consumption has been associated with an increased risk of hepatocellular carcinoma (HCC) in patients with viral hepatitis^[6-8]. A recent report has found that cigarette smoking was associated with increased fibrosis and histological activity in chronic hepatitis C (CHC) patients. It suggested that cigarette smoking could influence liver disease either by direct hepatotoxicity through its various constituents or secondary to erythrocytosis, immunological impact or synergistic effect with other factors such as alcohol^[9].

The spectrum of liver injury in patients with CHC is broad and many factors influence the severity and progression of the lesion such as age^[10], route of infection^[11], genotype^[12], concomitant chronic hepatitis B virus (HBV) infection^[13] and others. Furthermore, many factors influence the natural history of CHC, clinical picture, and response to therapy, yet not all identified factors^[12]. The adverse effects of heavy smoking particularly the response to therapy among CHC patients have been overlooked. Accordingly, we were motivated to study the impact of heavy smoking on clinical presentation, laboratory parameters and response to interferon- α (IFN- α) therapy in these patients.

MATERIALS AND METHODS

Over the year 1998, 138 CHC Egyptian male patients presenting to Cairo Liver Center for assessment of eligibility to interferon therapy were recruited. All patients met the following inclusion criteria: hepatitis C virus (HCV) antibody positive for ELISA, detectable HCV-RNA (Innolipa PCR) in serum, negative for HBsAg (Abbot ELISA), absent clinical and ultrasonographic evidence of cirrhosis, no ascites or hepatocellular carcinoma. No patient had received previous course of IFN- α therapy.

A standardized questionnaire to assess the smoking history was used^[14] and accordingly all patients were divided into: smokers (group I) which consisted of 38 patients who smoked >30 cigarettes/d and non-smokers (group II) which included 84 patients who never smoked. Sixteen patients who were irregular, mild and passive smokers as well as pipe water and cigar smokers were excluded owing to difficulty in calculating smoking index. All patients in both groups were residents away from known

districts of high carbon monoxide pollution. None of the patients received drugs causing haemolysis over the preceding 6 mo period. All patients in both groups were assessed for haemoglobin, haematocrit, serum iron, and liver profile before liver biopsy. Patients who had persistently normal transaminases or had thrombocytopenia (platelet count less than 80 000/mm³, 1 patient from group 1 and 16 patients from group 2) were considered non-eligible to interferon therapy and therefore excluded from the study.

Liver biopsy was performed using a true-cut needle to 37 patients from group I and 68 patients from group II scheduled for IFN- α therapy. All liver biopsy specimens were fixed in formalin, embedded in paraffin and routinely processed. The histological grade of disease activity and fibrosis was assessed using a reproducible scoring system^[15] as follows: A 1 to A 3 for the degree of necroinflammatory activity (A 1 = mild, A3 = marked) and stage F0 to F4 for the degree of fibrosis (F0 = no fibrosis, F4 = cirrhosis). Two patients from group 1 and 6 patients from group 2 who had F4 (established cirrhosis) were also eliminated from IFN- α therapy. Iron staining using Perl's stain was done to non-cirrhotic specimen in both groups and scored according to percentage of iron stained hepatocyte.

Phlebotomy at a 2-wk interval till achieving low normal serum iron level was performed to 18 randomly allocated cases in group I patients (Ia), whereas 17 smoker patients had no phlebotomy and formed group Ib. Before undergoing phlebotomy all patients were instructed about its possible complications and all gave informed consent. None of the patients developed serious complications and all continued their schedule of phlebotomy. On serial ALT follow up, persistent normalization of ALT was observed in 3 patients in group Ia and therefore they were excluded from interferon therapy.

Thirty two smoker patients (15 from group Ia and 17 from group Ib) and 62 non smoker patients from group II with persistent elevation of ALT received IFN- α therapy -3 MU TIW for 6 mo with serial evaluation of transaminases and test for HCV-RNA at the end of treatment and 6 mo later.

Statistical data was presented as mean \pm SD for the numeric variables. *t*-test was performed to compare both groups to each other. Response to therapy was categorized into responders and non-responders then presented into cross tables. χ^2 analysis was performed to assist the difference between the two groups. A *P* value of less than 0.05 was accepted as a level of significance.

RESULTS

Patients in group 1 had a significantly higher haemoglobin level ranging 16.1-19.1 g/dL with a mean of 16.9 \pm 0.54 g/dL compared to the patients in group 2 whose haemoglobin level ranged 13.5-16.3 g/dL with a mean of 15.3 \pm 0.59 g/dL. All patients in group 1 (100%) had a haemoglobin level exceeding 16 g/dL compared to 12/84 (14.3%) in patients of group 2.

The haematocrit level among group 1 patients ranged 56.1-61.4% with a mean of 56.3 \pm 0.86%, while group 2 patients had a haematocrit level ranging 45-55.9% with a mean of 54.8 \pm 1.16%, the difference was statistically significant (*P*<0.005). All patients in group 1 had a haematocrit value exceeding 55% compared to 14.3% of group 2 patients.

The mean serum iron level was significantly higher in group 1 (160.4 \pm 38.36 μ g/dL) with a range of 100.3-283 μ g/dL compared to group 2 (148.8 \pm 28.11 μ g/dL) with a range of 90-194.3 μ g/dL (*P*<0.05). Serum iron in 12 (31.5%) patients of group 1 was above normal level.

The mean serum uric acid level was 5.4 \pm 1.0 mg/dL in group 1 (range of 4-9 mg/dL) compared to 5.0 \pm 0.7 mg/dL (range of 3.8-6.9 mg/dL) in group 2, and the results were statistically significant (*P*<0.01).

Liver biopsy was performed to 37 patients from group 1 and 68 patients from group 2. Mild hepatitis was recorded in 10 (27%) patients of group 1 and 39 (57.4%) of group 2, whereas 17 patients (45.9%) of group 1 and 20 patients (29.4%) of group 2 had moderate hepatitis. Severe hepatitis was recorded in 8 patients (21.6%) of group 1 and 3 patients (4.4%) of group 2. Cirrhosis was recorded in 2 patients (5.4%) of group 1 and 6 patients (8.8%) of group 2. Iron staining using semiquantitative Perl's stain was positive with predominant periportal localization and associated steatosis in 3 (8.6%) patients of group 1 and 1 patient (1.5%) of group 2.

The end treatment biochemical response (ETBR) was reported in 5 patients (15.6%) of group 1 and 17 patients (27.4%) of group 2. Six months later only 3 patients (9.4%) of group 1 showed sustained normal ALT compared to 9 patients (14.5%) of group 2. The end treatment virological response (ETVR) was reported in 4 patients (12.5%) of group 1 and 3 patients (26%) of group 2. Six-months later, the sustained virological response (SVR) was reported in 2 patients (6.3%) of group 1 and 7 patients (11.3%) of group 2, but the differences did not reach statistical significance (*P*>0.05).

Among group I patients, ETBR in patients who had phlebotomy (group Ia) was recorded in 3 patients (20%) compared to 2 patients (11.8%) in those underwent no phlebotomy (group Ib). Two patients (13.3%) in group Ia had sustained biochemical response (SBR) compared to 1 patient (5.9%) in group 2b.

ETVR was found in 2 patients (13.3%) of group Ia compared to 2 patients (11.8%) of group Ib. SVR after 6 mo obtained in 1 patient of both groups (6.7% and 5.9%) respectively. Therefore, repeated phlebotomy increased both ETBR and SBR, but had no effect on virological responses (ETVR or SVR).

In group Ia repeated phlebotomy led to a significant decrease in mean ALT level from 167 \pm 50.3 to 112 \pm 37.7 IU/L (*P*<0.01).

DISCUSSION

Many studies have shown that smoking is an independent factor contributing to progression of HBV induced cirrhosis^[4], alcoholic cirrhosis^[11] and HCC development^[6-8]. A recent French study has shown similarly that smoking favors progression to cirrhosis in chronic HCV infection independent of other co-morbid conditions^[9].

The impact of smoking on various liver disorders has been extrapolated from experimental studies. It has been suggested that tobacco induced liver injury is ascribed to oxidative stress associated with lipid peroxidation^[16,17]. In patients with CHC, the reduction in the concentration of hepatic, plasmatic and lymphocytic glutathione could favor the hepatotoxic effect of smoking^[18]. Data from experimental studies suggest that nicotine, a major component of tobacco smoke, was rapidly absorbed through the lungs and released into circulation. Thereafter, it is mainly metabolized through the liver inducing lesions characterized by steatosis and focal or confluent necrosis^[19].

A recent study demonstrated that smoking was mainly related to increased inflammatory activity but not to the stage of fibrosis^[20], whereas Pessione *et al.*^[9] provided evidence that smoking could worsen the degree of fibrosis in CHC independent of other co-morbid conditions. Advanced fibrosis adversely affected the response to interferon therapy^[21,22], but this could not explain why smokers had lower response to interferon therapy compared to non-smokers as patients in both groups had comparable histopathological affection at entry of study. Cigarette smoking could increase generation of oxygen radicals. Chronic viral hepatitis patients who were cigarette smokers tended to have lower levels of natural anti-oxidants compared to non-smokers^[23].

Smoking could induce a secondary form of polycythemia.

Smoker's polycythemia was attributable to increased carbon monoxide. The latter interfered with oxygen transport and utilization^[24]. Secondary polycythemia may be associated with increased red cell turnover and subsequent rise of serum iron and tissue iron. In support of this hypothesis in our study, all smoker groups had higher hemoglobin and haematocrit compared to non-smoker group. In our study all HCV smoker patients had higher serum iron compared to HCV non-smoker patients as well.

It has long been recognized that hepatic iron overload could promote hepatic fibrosis in hereditary haemochromatosis^[25]. Serum iron stores were frequently increased in patients with CHC^[26]. Enhanced liver fibrosis has been reported in HCV infected patients with stainable iron in liver biopsy compared with controls with no detectable liver iron^[27]. The mechanism by which iron accumulates in CHC patients has not been established but might in part be the result of iron release from damaged hepatocytes^[28].

Another possible mechanism is that smoker polycythemia contributes to increased serum iron by increased cell turnover.

In support of this point of view, it was found that phlebotomy ameliorated not only symptoms related to smoker's polycythemia, but also transaminase level and resulted in persistent normalization of ALT level in 3/38 smoker patients. In our study, non-smoker patients had a better-sustained virological response rate compared to smoker patients. Although, phlebotomy resulted in a slight amelioration response rate, but results did not reach statistical significance. Many reports^[29,30] showed significant improvement in serum ALT levels in interferon non-responders when they underwent iron reduction by therapeutic venesection. Three prospective, randomized controlled trials showed that iron reduction could increase the response rate to interferon therapy. While another multi-center trials showed no significant improvement in response of CHC to iron reduction treatment, although, histological improvement was documented even in patients with iron therapy alone^[31].

This could be explained by other possible mechanisms such as immune alterations. Cigarette smoking may induce immune impairment by increasing apoptosis of lymphocytes, and counteracting interferon effect^[32]. It was shown that tobacco smoking had a suppressive effect on human immunity as a result of decreased serum concentration of immunoglobulins and lysosome decreased absolute number of (CD16+) NK-cells and elevated population of (CD8+) T-cytotoxic lymphocytes entailing a decrease in CD4+/CD8+ ratio^[33]. Cigarette smokers exhibited impaired NK cytotoxic activity and unbalanced production of pro- and anti-inflammatory cytokines^[34]. Smoking could alter immune response either directly through impairment of antigen receptor mediated signal transduction pathways leading to T cell anergy^[35] or indirectly through brain immune interactions^[36].

In conclusion, smokers suffering from CHC tend to have lower response to IFN- α compared to non-smokers. Therapeutic phlebotomy improves the response rate to IFN- α therapy among this group. This deserves further evaluation in prospective study. Chronic hepatitis C patients should be advised to avert smoking before embarking on interferon therapy.

REFERENCES

- 1 Klatsky AL, Armstrong MA. Alcohol smoking coffee and cirrhosis. *Am J Epidemiol* 1992; **136**: 1248-1257
- 2 Corrao G, Lepore AR, Torchio P, Valenti M, Galatola G, D'Amicis A, Arico S, di Orio F. The effect of drinking coffee and smoking cigarettes on the risk of cirrhosis associated with alcohol consumption: a case-control study. *Eur J Epidemiol* 1994; **10**: 657-664
- 3 Pessione F, Ramond MJ, Peters L, Pham BN, Batel P, Rueff B, Valla DC. Five-year survival predictive factors in patients with excessive alcohol intake and cirrhosis. Effect of alcoholic hepatitis, smoking and abstinence. *Liver Int* 2003; **23**: 45-53
- 4 Yu MW, Hsu FC, Sheen IS, Chu CM, Lin DY, Chen CJ, Liaw YF. Prospective study of hepatocellular carcinoma and liver cirrhosis in asymptomatic chronic hepatitis B virus carrier. *Am J Epidemiol* 1997; **145**: 1039-1047
- 5 Mori M, Hara M, Wada I, Hara T, Yamamoto K, Honda M, Naramoto J. Prospective study of hepatitis B and C viral infection, cigarette smoking, alcohol consumption and other factors associated with hepatocellular carcinoma risk in Japan. *Am J Epidemiol* 2000; **151**: 131-139
- 6 Mukaiya M, Nishi M, Miyake H, Hirata K. Chronic liver disease for the risk of hepatocellular carcinoma: a case control study in Japan. Etiologic association of alcohol consumption, cigarette smoking and the development of chronic liver diseases. *Hepatology* 1998; **45**: 2328-2332
- 7 Yu MW, Chiu YH, Yang SY, Santella RM, Chern HD, Liaw YF, Chen CJ. Cytochrome P450 1A1 genetic polymorphisms and risk of hepatocellular carcinoma among chronic hepatitis B carriers. *Br J Cancer* 1999; **80**: 598-603
- 8 Alberti A, Chemello L, Benvegno L. Natural history of hepatitis C. *J Hepatol* 1999; **31**(Suppl 1): 17-24
- 9 Pessione F, Ramond MJ, Njapoum C, Duchatelle V, Degott C, Erlinger S, Rueff B, Valla DC, Degos F. Cigarette smoking and hepatic lesions in patients with chronic hepatitis C. *Hepatology* 2001; **34**: 121-125
- 10 Poynard T, Bedossa P, Opolon P. Natural history of liver fibrosis progression in patients with chronic hepatitis C. The OBSVIRC, METAVIR, CLINIVIR, and DOSVIRC groups. *Lancet* 1997; **349**: 825-832
- 11 Lopez-Morante A, Saez-Royuela F, Echevarria C, Llanos C, Martin-Lorente JL, Yuguero L, Ojeda C. Influence of the transmission route and disease duration in the histopathology of chronic hepatitis C: a study of 101 patients. *Eur J Gastroenterol Hepatol* 1998; **10**: 15-19
- 12 Tran TT, Martin P. Chronic Hepatitis C. *Curr Treat Options Gastroenterol* 2001; **4**: 503-510
- 13 Pontisso P, Ruvoletto MG, Fattovich G, Chemello L, Gallorini A, Ruol A, Alberti A. Clinical and virological profiles in patients with multiple hepatitis virus infection. *Gastroenterology* 1993; **105**: 1529-1533
- 14 Baum GIL, Wolinsky E. Textbook of pulmonary disease. 5th Edn, vol 11. Boston: Little Brown 1994: 257
- 15 Intraobserver and interobserver variations in liver biopsy interpretation in patients with chronic hepatitis C. The French METAVIR Cooperative Study Group. *Hepatology* 1994; **20**(1Pt 1): 15-20
- 16 Husain K, Scott BR, Reddy SK, Somani SM. Chronic ethanol and nicotine interaction on rat tissue antioxidant defense system. *Alcohol* 2001; **25**: 89-97
- 17 Watanabe K, Eto K, Furuno K, Mori T, Kawasaki H, Gomita Y. Effect of cigarette smoke on lipid peroxidation and liver function tests in rats. *Acta Med Okayama* 1995; **49**: 271-274
- 18 Barbaro G, Di Lorenzo G, Ribersani M, Soldini M, Giancaspro G, Bellomo G, Belloni G, Grisorio B, Barbarini G. Serum ferritin and hepatic glutathione concentrations in chronic hepatitis C patients related to the hepatitis C virus genotype. *J Hepatol* 1999; **30**: 774-782
- 19 Yuen ST, Gogo AR, Luk IS, Cho CH, Ho JC, Loh TT. The effect of nicotine and its interaction with carbon tetrachloride in the rat liver. *Pharmacol Toxicol* 1995; **77**: 225-230
- 20 Hezode C, Lonjon I, Roudot-Thoraval F, Mavrier JP, Pawlotsky JM, Zafrani ES, Dhumeaux D. Impact of smoking on histological liver lesions in chronic hepatitis C. *Gut* 2003; **52**: 126-129
- 21 McHutchison J. Hepatitis C therapy in treatment-naive patients. *Am J Med* 1999; **107**: 56S-61S
- 22 Poynard T, Marcellin P, Lee SS, Niederau C, Minuk GS, Ideo G, Bain V, Heathcote J, Zeuzem S, Trepo C, Albrecht J. Randomized trial of interferon alpha 2b plus ribavirin for 48 weeks or for 24 weeks versus interferon-a 2b plus placebo for 48 weeks for treatment of chronic interferon with hepatitis C virus. *Lancet* 1998; **352**: 1426-1432
- 23 Yu MW, Horng IS, Hsu KH, Chiang YC, Liaw YF, Chen CJ. Plasma selenium levels and risk of hepatocellular carcinoma among men with chronic hepatitis virus infection. *Am J Epidemiol*

- 1999; **150**: 367-374
- 24 **Panda K**, Chattopadhyay R, Chattopadhyay DJ, Chatterjee IB. Vitamin C prevents cigarette smoke-induced oxidative damage *in vivo*. *Free Radic Biol Med* 2000; **29**: 115-124
- 25 **Bacon BR**, Tavill AS. Haemochromatosis and the iron overload syndromes. In: Zakim B, Boyer TD, eds. *Hepatology: a text book of liver disease*, 3rd ed. Philadelphia: *Saunders* 1996: 1439-1489
- 26 **Riggio O**, Montagnese F, Fiore P, Folino S, Giambartolomei S, Gandin C, Merli M, Quinti I, Violante N, Caroli S, Senofonte O, Capocaccia L. Iron overload in patients with chronic viral hepatitis: how common is it? *Am J Gastroenterol* 1997; **92**: 1298-1301
- 27 **Beinker NK**, Voigt MD, Arendse M, Smit J, Stander IA, Kirsch RE. Threshold effect of liver iron content on hepatic inflammation and fibrosis in hepatitis B and C. *J Hepatol* 1996; **25**: 633-638
- 28 **Bonkovsky HL**, Banner BF, Rothman AL. Iron and chronic viral hepatitis. *Hepatology* 1997; **25**: 759-768
- 29 **Hayashi H**, Takikawa T, Nishimura N, Yano M, Isomura T, Sakamoto N. Improvement of serum aminotransferase levels after phlebotomy in patients with chronic active hepatitis C and excess hepatic iron. *Am J Gastroenterol* 1994; **89**: 986-988
- 30 **Piperno A**, Sampietro M, D'Alba R, Roffi L, Fargion S, Parma S, Nicoli C, Corbetta N, Pozzi M, Arosio V, Boari G, Fiorelli G. Iron stores, response to alpha- interferon therapy, and effects of iron depletion in chronic hepatitis C. *Liver* 1996; **16**: 248-254
- 31 **Di Bisceglie AM**, Bonkovsky HL, Chopra S, Flamm S, Reddy RK, Grace N, Killenberg P, Hunt C, Tamburro C, Tavill AS, Ferguson R, Krawitt E, Banner B, Bacon BR. Iron reduction as an adjuvant to interferon therapy in patients with chronic hepatitis C who have previously not responded to interferon: A multi-center, prospective, randomized, controlled trial. *Hepatology* 2000; **32**: 135-138
- 32 **Suzuki N**, Wakisaka S, Takeba Y, Mihara S, Sakane T. Effects of cigarette smoking on Fas/Fas ligand expression of human lymphocytes. *Cell Immunol* 1999; **192**: 48-53
- 33 **Moszczynski P**, Zabinski Z, Moszczynski P, Rutowski J, Slowinski S, Tabarowski Z. Immunological findings in cigarette smokers. *Toxic Lett* 2001; **118**: 121-127
- 34 **Zeidel A**, Beilin B, Yardeni I, Mayburd E, Smirnov G, Bessler H. Immune response in asymptomatic smokers. *Acta Anaesthesiol Scand* 2002; **46**: 959-964
- 35 **Kalra R**, Singh SP, Savage SM, Finch GL, Sopori ML. Effects of cigarette smoke on immune response: chronic exposure to cigarette smoke impairs antigen-mediated signaling in T cells and depletes IP3-sensitive Ca(2+) stores. *J Pharmacol Exp Ther* 2000; **293**: 166-171
- 36 **Sopori ML**, Kozak W, Savage SM, Geng Y, Soszynski D, Kluger MJ, Perryman EK, Snow GE. Effect of nicotine on the immune system: possible regulation of immune responses by central and peripheral mechanisms. *Psychoneuroendocrinology* 1998; **23**: 189-204

Edited by Wang XL and Chen WW Proofread by Xu FM

siRNA-mediated inhibition of HBV replication and expression

Xiao-Nan Zhang, Wei Xiong, Jia-Dong Wang, Yun-Wen Hu, Li Xiang, Zheng-Hong Yuan

Xiao-Nan Zhang, Wei Xiong, Jia-Dong Wang, Yun-Wen Hu, Li Xiang, Zheng-Hong Yuan, Key Laboratory of Medical Molecular Virology, Ministry of Education and Health, Shanghai Medical College, Fudan University, Shanghai 200032, China

Supported by the State Basic Research Foundation of China, No. G19999054105 and Med-X Foundation of Fudan University

Correspondence to: Zheng-Hong Yuan, Key Laboratory of Medical Molecular Virology, Ministry of Education and Health, Shanghai Medical College, Fudan University, 138 Yi Xue Yuan Road Shanghai 200032, China. zhyuan@shmu.edu.cn

Telephone: +86-21-64161928 **Fax:** +86-21-64227201

Received: 2004-03-05 **Accepted:** 2004-04-13

Abstract

AIM: RNA interference (RNAi) is a newly discovered phenomenon provoked by dsRNA. The dsRNA is initially cleaved by Dicer into 21-23 nt small interfering RNA (siRNA) and can then specifically target homologous mRNA for degradation by cellular ribonucleases. RNAi has been successfully utilized to down-regulate the endogenous gene expression or suppress the replication of various pathogens in mammalian cells. In this study, we investigated whether vector-based siRNA promoted by U6 (pSilencer1.0-U6) could efficiently inhibit HBV replication in cell culture.

METHODS: pSilencer vectors with inserts targeting on different regions of HBV genome were constructed. These plasmids were co-transfected with pHBV3.8 into Huh-7 cells via lipofection and viral antigens were measured by ELISA. Viral RNA was analyzed by Northern blot. The mRNA of Mx_A and 2'-5'OAS was reverse transcribed and quantified by real-time PCR.

RESULTS: Vector-based siRNA could potently reduce hepatitis B virus antigen expression in transient replicative cell culture. Furthermore, Northern blot analysis showed that viral RNA was effectively degraded, thus eliminating the messengers for protein expression as well as template for reverse transcription. Real-time PCR analysis of cellular Mx_A and 2'-5'OAS gene expression revealed that vector-based siRNA did not provoke the interferon pathway which reassured the specificity of the vector-based RNA interference technique.

CONCLUSION: Our results indicate that RNA interference may be a potential tool to control HBV infection.

Zhang XN, Xiong W, Wang JD, Hu YW, Xiang L, Yuan ZH. siRNA-mediated inhibition of HBV replication and expression. *World J Gastroenterol* 2004; 10(20): 2967-2971
<http://www.wjgnet.com/1007-9327/10/2967.asp>

INTRODUCTION

Hepatitis B virus is a severe infectious pathogen causing chronic liver diseases and increasing risk of hepatocellular carcinoma^[1]. Although recombinant vaccines are widely available^[2], HBV infection is still a big challenge to the societies

all over the world. Until now, interferon- α and nucleoside analogs, such as lamivudine, are of the few drugs capable of inhibiting HBV replication. However, interferon treatment usually results in a limited percentage of complete response and relapses generally occur without further treatment. Lamivudine, a strong inhibitor of HBV's reverse-transcriptase, has been proved to be highly effective in blocking its genome replication. Nevertheless, a significant portion of patients relapsed after cessation of treatment. With prolonged treatment, escape mutants would develop^[3].

RNA interference is a newly discovered phenomenon present in almost all eukaryotes^[4,5]. It is activated by dsRNA, which is subsequently cleaved by Dicer into 21-23 nt small interfering RNAs (siRNA). The siRNAs are then unwound by RISC (siRNA induced silencing complex) in the presence of ATP. The activated RISC binds to and degrades target mRNA guided by the single strand siRNA. In mammals, long dsRNA can activate protein kinase R (PKR) and RNaseL, which are key components of the interferon signaling pathway, thus causing unspecific effects, whereas 21-23 nt siRNAs are short enough to bypass them^[6]. Many studies have been carried out to silence a number of RNA viruses by RNA interference, such as human immunodeficiency virus (HIV), hepatitis C virus (HCV) and poliovirus, *etc*^[7-11]. As hepatitis B virus (HBV) utilizes pregenomic RNA for synthesis of viral DNA via reverse transcription, it is also an ideal candidate for RNAi. Recently, vector-based RNAi technique, which uses endogenous U6 or H1 promoter to generate small interfering RNA (siRNA) *in vivo*, has become a new and economical system to achieve gene silencing^[12,13]. In this study, we investigated whether vector-based siRNA promoted by U6 (pSilencer1.0-U6) could efficiently inhibit HBV replication in cell culture.

MATERIALS AND METHODS

Materials

TRIzol reagent, Dulbecco's modified Eagle's medium (DMEM), fetal calf serum and antibiotics were from GIBCO BRL. Restriction endonucleases were supplied by MBI Fermentas. SuperScript II reverse transcriptase was from Invitrogen, Carlsbad. DNA sequence primers were synthesized by CASarray, Shanghai. pSilencer 1.0-U6 was from Ambion, Austin. HBsAg and HBeAg ELISA kit were purchased from Shanghai SIIC Kehua Biotech. pHBV3.8 plasmid encoding the whole transcript of HBV DNA (adr subtype) from the core promoter to the polyA signal region (nucleotides 1403-3215 plus 1 to 1987), was constructed as a 1.2 copy insert of the full-length HBV genome into vector pBS+ (Stratagene) via restriction enzyme *EcoRI* and *PstI* sites (kindly provided by Professor. Yuan Wang, Institute of Biochemistry, Academia Sinica, Shanghai). After transfected into Huh-7 cells, the pHBV3.8 could express both HBV surface antigen (HBsAg) and E antigen (HBeAg), and the replication of HBV could be initiated. Plasmid pcDNA-CAT containing the chloramphenicol acetyltransferase (CAT) gene under control of the CMV promoter was co-transfected as internal control. The expression of CAT could be measured by CAT ELISA kit (Roche, Mannheim, Germany).

Cell culture and transfection

Huh-7 cell line was maintained in Dulbecco's modified Eagle's

medium supplemented with 100 mL/L fetal calf serum, 2 mmol/mL L-glutamine, 100 µg/mL penicillin and 100 units/mL streptomycin (GIBCO BRL). The cells were incubated in a humidified incubator at 37 °C containing 50 mL/L CO₂. Cell viability was estimated by the trypan blue dye exclusion method. Huh-7 cells were transfected using FuGENE6 cationic liposome (Roche, Mannheim, Germany), and cells were harvested 48 h and 72 h after transfection, respectively. Experiments were performed in triplicate.

Target sequence selection and insertion sequence synthesis

By aligning different subtypes of HBV genome and using the Ambion web-based software, we selected 3 regions of high conservation designated as si-HBV1, 2 and 3 to be the target sequence. The target sequence of si-HBV1 was located in S region as well as P region of the HBV genome (nt 310 to 328), si-HBV2 and 3 were both in the C region (nt 1868 to 1886 for HBV2, nt 2373 to 2391 for HBV3). si-HBV1, 2 and 3 had the siRNA sequences completely identical to the target sequence of pHBV3.8. To create pSilencer plasmids, we used the primers: 5'-TTCGCAGTCCCCAACCTCCTTCAAGAGAGGAGGTTGGGACTGCGAATTTTT-3' (sense) and 5'-AGCTAAAAAATTCGAGTCCCCAACCTCCTTGAAGGAGGTTGGGGACTGCGAAGGCC-3' (antisense) for pSi-HBV1; 5'-GCCTCCAAGCTGTGCCTTGTTCAAGAGACAAGGCACAGCTTGGAGGCTTTT-3' (sense) and 5'-AGCTAAAAAAGCCTCCAAGCTGTGCC TTGTCTCTTGAACAAGGCACAGCTTGGAGGCGGCC-3' (antisense) for pSi-HBV2; 5'-GAAGAACTCCCTCGCCTCGTTCAAGAGACGAGGCGAGGGAGTTCTTCTTTTTT-3' (sense) and 5'-AGCTAAAAAAGAAGAACTCCCTCGCCTCGTCTCTTGAACGAGGCGAGGGAGTTCTTCGGCC-3' (antisense) for pSi-HBV3.

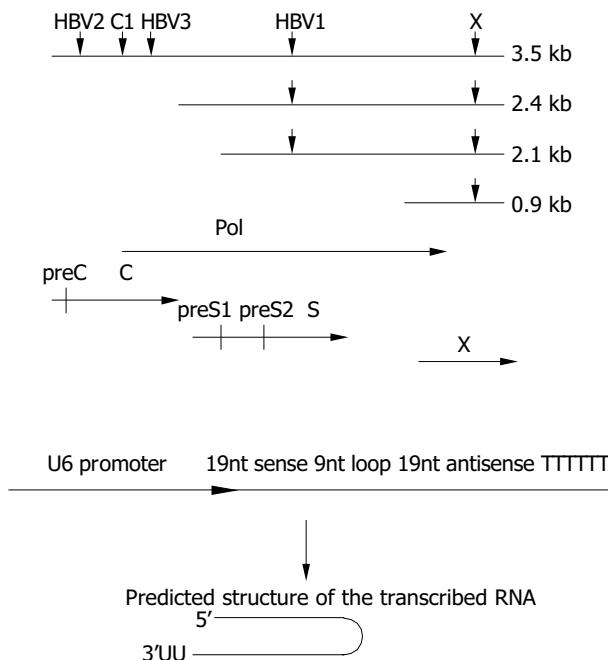


Figure 1 Design of siRNAs specific for HBV genome. A: Downward arrows show the target sites within the RNA transcripts. The HBV ORFs are shown below aligned with HBV mRNA. B: Schematic presentation of U6 promoter constructs. The inverted 19 nt sequences are separated by a 9 nt loop, transcription ends with 5Ts. The resulting shRNA (short hairpin RNA) are predicted to fold back to form a hairpin RNA.

In this study, the target sequences used by Shlomai *et al.*^[14] for pSuper core1 (nt 2191 to 2209) and pSuper X (nt 1649 to 1667)

were also included for comparison (Figure 1) with slight modifications to suit the DNA sequence of pHBV3.8. The oligo sequences were: 5'-AATCAGACAACACTACTGTGGTTCAAGA GACCACAGTAGTTGTCTGATTTTTTTTT-3' (sense) and 5'-AGCTAAAAAAATCAGACAACACTACTGTGGTCTCTTGAACC ACAGTAGTTGTCTGATTGGCC-3' (antisense) for pSi-core1; 5'-GGTCTTACATAAGAGCACTTTCAAGAGAAGTGCTCTT ATGTAAGACCTTTTTT-3' (sense) and 5'-AGCTAAAAAAG GTCTTACATAAGAGCACTTCTCTTGAAGAGTGCTCTTATGTA AGACCGGCC-3' (antisense) for pSi-X.

pSi-EGFP-h was a control vector with insertion sequence targeting on EGFP gene. The synthesized oligos were: 5'-GACGTAAACGGCCACAAGTTTCAAGAGAAGTTGTGG CCGTTTACGTCTTTTTT-3' (sense) and 5'-AGCTAAAAAAG ACGTAAACGGCCACAAGTTCTCTTGAAGACTTGTGGCCGTT TACGTCCGCC-3' (antisense).

Plasmid constructs

The oligos were annealed and cloned into *ApaI-HindIII* sites of pSilencer as described in the pSilencer 1.0 U6 manual (Ambion). All the plasmids constructed were confirmed by DNA sequencing.

Quantitation of HBsAg and HBeAg

The HBsAg and HBeAg secreted into the culture media were measured by diagnostic ELISA kit (Shanghai SIIC Kehua Biotech).

Northern blot analysis of viral RNA

Total RNA was extracted directly from transfected cells using TRIzol reagent (Gibco BRL). After 30 min of DNaseI digestion of remaining DNA, total RNA was re-extracted by TRIzol, precipitated and dissolved in DEPC-H₂O. Ten micrograms of total RNA was electrophoresed on 10 g/L formaldehyde-agarose gel and then transferred to nylon membranes (Roche, Mannheim, Germany). After fixation at 120 °C for 30 min, the membrane was prehybridized for 6 h at 42 °C in 5×SSC, 5×Denhardt's solution, 10 g/L SDS, 50 g/L formaldehyde, 0.1 mg/mL salmon sperm DNA, followed by hybridization with full-length HBV DNA probes labeled with [α -³²P] dCTP by hexamer random labeling kit (Roche, Mannheim, Germany) under the same condition of prehybridization at 42 °C for 16 h. After a stringent washing process at 68 °C, the signals were detected by autoradiography, then the blots were quantified by densitometry. The 28 s and 18 s rRNA were visualized under ultraviolet light for equal loading control. The values of HBV blots were normalized by monitoring the expression of an internal control CAT by CAT ELISA (Roche, Mannheim, Germany).

Quantitative real-time PCR

Huh-7 cells in 6-well plates were transfected with 2 µg of various plasmids. After 48 h of transfection, total RNA was extracted as described above. RNA was denatured for 5 min at 65 °C in the presence of random hexamer, immediately cooled in ice water, then reverse transcribed using SuperScript II reverse-transcriptase according to the manufacturer's instructions. Real-time PCR (iCycler, Bio-Rad) was performed as instructed by iCycler resource guide. Reactions with no reverse transcriptase enzyme added were performed in parallel. Briefly, reactions were carried out in 25 µL volume containing 2 µL of template (cDNA or RNA), 400 nmol/L of each forward and reverse primer and 1X SybrGreenI PCR Master Mix (Roche). To quantitate cellular transcripts, dilutions of plasmids containing the human GAPDH gene were run in parallel. The experiment was performed twice. The primer sequences used included: 5'-GGTATCGTGAAGG ACTCATGAC3' (sense) and 5'-ATGCCAGTGAGCTTCCCGT TCAGC3' (antisense) for GAPDH; 5'-GCTACACACCGTGACG GATATGG3' (sense) and 5'-CGAGCTGGATTGGAAAGCCC3'

(antisense) for MxA; 5'-TCAGAAGAGAAGCCAACGTGA-3' (sense) and 5'-CGGAGACAGCGAGGGTAAAT-3' (antisense) for 2'-5'OAS.

RESULTS

Inhibition of HBV gene expression in transiently transfected Huh-7 cells by RNAi

pSilencer, pSi-EGFP-h and other derivatives targeting on different regions of HBV genome were co-transfected with pHBV3.8 in the ratio of 10:1 into Huh-7 cells. pcDNA-CAT was also transfected as internal control. The secreted viral antigens, HBsAg and HBeAg in the culture media were quantified 48 h and 72 h after transfection. Transfection efficiencies were standardized by measurement of CAT using CAT ELISA Kit. Compared with control vector, HBsAg and HBeAg expressions were reduced by about 60% in average when measured 48 h after transfection (Figure 2). When the antiviral effect of siRNA was assessed 72 h post-transfection, the silencing effect was still apparent, indicating the stability of the transcribed RNAi. Among all the siRNAs used, pSi-HBV1 targeting on S gene as well as P gene of HBV genome was most potent, as HBsAg and HBeAg were reduced 86% and 83% 72 h after transfection, respectively.

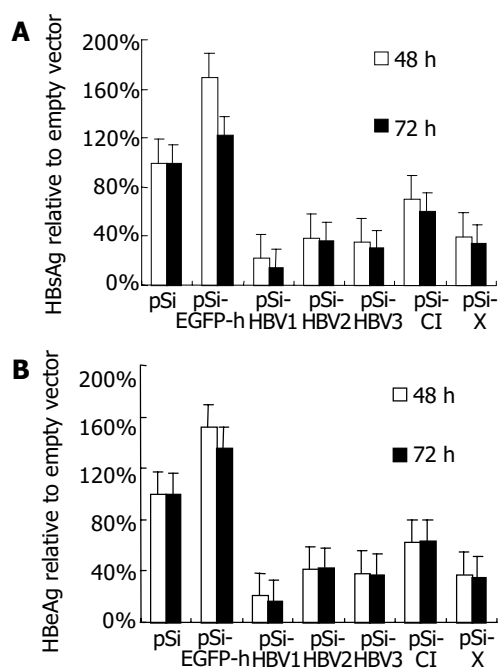


Figure 2 Effect of RNAi on HBV protein expression in transiently transfected Huh-7 cells.

Reduction of HBV viral transcripts by RNAi

To determine whether viral pregenomic RNA and other transcripts were efficiently degraded by siRNA, Northern blot assay was carried out using ³²P-labeled full length HBV fragment as the probe generated with a random-primed labeling kit. Compared with control vector pSi-EGFP-h, significant reduction of all the viral transcripts was observed when pSilencer vectors targeting on specific HBV RNA were used (Figure 3). Among them, pSi-HBV1 and pSi-HBV2 were much more efficient with over 90% reduction in viral RNAs.

Vector-based siRNA could not activate interferon response

To rule out the possibility that inhibition of HBV gene expression and replication by vector-based siRNA was due to the dsRNA-induced activation of IFN pathway, we compared the mRNA

levels of IFN-induced genes 2'-5'OAS and MxA by quantitative real-time PCR 48 h after transfection of siRNA generating plasmids. Compared with mock-transfected Huh-7 cells, IFN induced about 10 000 and 100-fold increase in 2'-5'OAS and MxA mRNA levels, respectively. While the transfection of pSi-HBV plasmids only led to 1.67-fold and 0.71-fold (in average) induction of MxA and 2'-5'OAS, respectively, thus eliminating the non-specific effect of siRNAs (Figure 4).

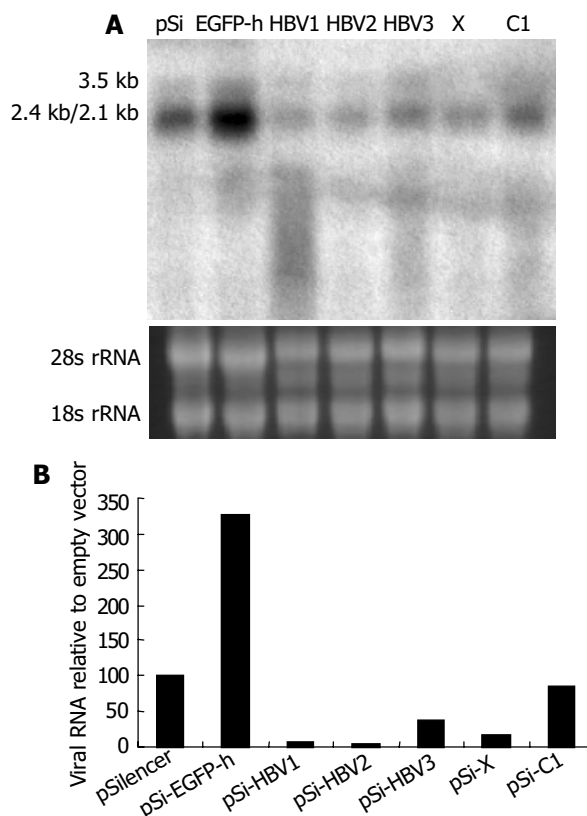


Figure 3 Effect of RNAi on HBV gene transcription detected by Northern blot. A: Northern blot experiment of HBV transcripts. The 28 s and 18s rRNAs were visualized under ultraviolet light for equal loading control. B: The hybridization signal was quantitatively evaluated by Smartview™ image analysis software (Shanghai Fu-ri Inc).

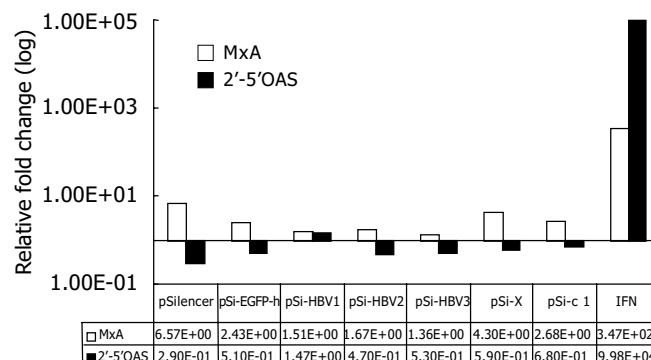


Figure 4 Effect of RNAi on IFN-induced genes. Real-time PCR quantification of MxA and 2'-5'OAS. The copy number of MxA and 2'-5'OAS were normalized with GAPDH. The relative fold induction of each gene compared with mock transfection is shown.

DISCUSSION

Numerous reports have demonstrated that RNAi can block replication of various types of mammalian viruses, including

two retroviruses, human immunodeficiency virus (HIV)^[7,15-17] and Rous sarcoma virus^[18]; a negative-strand RNA virus, respiratory syncytial virus (RSV)^[19], two positive-stranded RNA virus, hepatitis C virus (HCV)^[9,20,21] and poliovirus^[10]; and a DNA virus, human papillomavirus^[22]. Although HBV is a DNA virus, its replication requires a key step of reverse transcription for synthesis of viral DNA from pregenomic RNA, which is quite different from other DNA viruses. Therefore, HBV is assumed to be susceptible to siRNA not only at the level of post-transcription, but also at the level of replication.

In this study, we demonstrated that vector-based siRNA could significantly inhibit HBV antigen expression (both HBsAg and HBeAg) in hepatocytes. Furthermore, Northern blot analysis revealed that HBV pregenomic RNA and other shorter transcripts were diminished in the presence of specific siRNAs. Our results were different from a previous report^[14], which demonstrated that pSuper-core1 and pSuper-core2 did not inhibit HBsAg and resulted in only a minor reduction of about 13% in the 3.5-kb transcript whereas pSuper-X reduced both HBsAg and HBeAg, and resulted in a significant reduction of about 68% at the level of all the viral transcripts. However, they were consistent with McCaffrey *et al.*^[23] that siRNA targeting on the pregenomic RNA in the overlap region of the C and P open reading frames (ORF) reduced the levels of 2.4- and 2.1-kb RNAs and serum HBsAg even though it did not directly target on these RNAs. It can be assumed that HBV-specific siRNA first recognizes and degrades the corresponding sequence of viral pregenomic RNA, consequently depleting template for reverse transcription. Decreased synthesis of viral DNA then further influences the life cycle of HBV genome, especially in transcription and translation, thereby resulting in the overall inhibition of viral RNA and proteins.

Among the selected siRNAs, si-HBV1 is the most potent in inhibiting HBV replication. As si-HBV1 targeted on S region of the virus, multiple viral RNAs would be inhibited. Besides, it could also down-regulate the expression of P gene (the S ORF is within the P ORF), thus inhibiting viral replication *in trans*. These factors might explain, at least in part, why si-HBV1 has the highest efficacy.

Compared with the general nonspecific shutdown of cellular protein synthesis by double-stranded RNA (dsRNA) mediated primarily by IFN- α/β through the induction of protein kinase R (PKR) and RNaseL, the main known advantage of RNAi strategies is its high specificity on gene silencing. Attention has been paid to the potential non-specific effects of RNAi recently. Bridge *et al.*^[24] found that a substantial number of siRNA vectors could trigger an interferon response. Sledz *et al.*^[25] reported that transfection of siRNA resulted in interferon mediated activation of the Jak-Stat pathway and global up-regulation of IFN-stimulated genes. Although Kapadia *et al.*^[20] and we did not detect the activation of known IFN-inducible pathways after transfection of siRNA or siRNA generating plasmids, the overall inhibition of viral RNAs by RNAi in our study and others still raise the possibility that RNAi may have some sequence-independent antiviral effects at certain doses. Overdose of siRNA or accumulation of unprocessed or aberrantly processed Pol III transcripts may trigger interferon response. Hence, further studies are required to optimize the dose and structure of short-hairpin RNA as well as the delivery strategy to minimize the non-specific effects.

Taken together, our data show that RNAi is an attractive new strategy to inhibit the replication of hepatitis B virus. But to really apply this phenomenon to medical therapy, many problems are yet to be solved. One major problem is the selection of target sequence. Although there have been some online tools to help select the target sequence, the result is not always satisfactory. Recently, a theory has been proposed that siRNAs with relative stability at the 5' end of the sense strand, relative

instability at the 5' end of the antisense strand and the cleavage site will most probably be the most effective ones^[26-28]. These findings have significantly enlarged our knowledge of target selection, but the best siRNA should still be selected empirically. Therefore, a simple method of finding out the best target is urgently needed. Another major problem is how to efficiently and specifically deliver the siRNA-expressing vectors to the target cell types^[29]. At present, retroviral or lentiviral vectors containing RNAi cassettes seem to be a good delivery system in carrying out gene silencing *in vivo*^[30,31]. Chemically modified synthetic siRNA, which could be delivered into cells without cationic lipid carrier also holds promise for a future therapeutic agent^[8]. With the advance in newly established techniques, RNAi may provide an effective therapeutic solution for HBV infection in the near future.

ACKNOWLEDGEMENTS

Wei Xiong is supported by the PhD studentship from the Ministry of Education P.R.C.

REFERENCES

- 1 **Tang ZY.** Hepatocellular carcinoma-Cause, treatment and metastasis. *World J Gastroenterol* 2001; **7**: 445-454
- 2 **Kao JH, Chen DS.** Global control of hepatitis B virus infection. *Lancet Infect Dis* 2002; **2**: 395-403
- 3 **Lee WM.** Hepatitis B virus infection. *N Engl J Med* 1997; **337**: 1733-1745
- 4 **Hannon GJ.** RNA interference. *Nature* 2002; **418**: 244-251
- 5 **Dykxhoorn DM, Novina CD, Sharp PA.** Killing the messenger: short RNAs that silence gene expression. *Nat Rev Mol Cell Biol* 2003; **4**: 457-467
- 6 **Elbashir SM, Harborth J, Lendeckel W, Yalcin A, Weber K, Tuschl T.** Duplexes of 21-nucleotide RNAs mediate RNA interference in cultured mammalian cells. *Nature* 2001; **411**: 494-498
- 7 **Novina CD, Murray MF, Dykxhoorn DM, Beresford PJ, Riess J, Lee SK, Collman RG, Lieberman J, Shankar P, Sharp PA.** siRNA-directed inhibition of HIV-1 infection. *Nat Med* 2002; **8**: 681-686
- 8 **Capodici J, Kariko K, Weissman D.** Inhibition of HIV-1 infection by small interfering RNA-mediated RNA interference. *J Immunol* 2002; **169**: 5196-5201
- 9 **Wilson JA, Jayasena S, Khvorova A, Sabatino S, Rodrigue-Gervais IG, Arya S, Sarangi F, Harris-Brandts M, Beaulieu S, Richardson CD.** RNA interference blocks gene expression and RNA synthesis from hepatitis C replicons propagated in human liver cells. *Proc Natl Acad Sci U S A* 2003; **100**: 2783-2788
- 10 **Gitlin L, Karelsky S, Andino R.** Short interfering RNA confers intracellular antiviral immunity in human cells. *Nature* 2002; **418**: 430-434
- 11 **Wang QC, Nie QH, Feng ZH.** RNA interference: Antiviral weapon and beyond. *World J Gastroenterol* 2003; **9**: 1657-1661
- 12 **Sui G, Soohoo C, Affar el B, Gay F, Shi Y, Forrester WC, Shi Y.** A DNA vector-based RNAi technology to suppress gene expression in mammalian cells. *Proc Natl Acad Sci U S A* 2002; **99**: 5515-5520
- 13 **Brummelkamp TR, Bernards R, Agami R.** A system for stable expression of short interfering RNAs in mammalian cells. *Science* 2002; **296**: 550-553
- 14 **Shlomai A, Shaul Y.** Inhibition of hepatitis B virus expression and replication by RNA interference. *Hepatology* 2003; **37**: 764-770
- 15 **Jacque JM, Triques K, Stevenson M.** Modulation of HIV-1 replication by RNA interference. *Nature* 2002; **418**: 435-438
- 16 **Stevenson M.** Dissecting HIV-1 through RNA interference. *Nat Rev Immunol* 2003; **3**: 851-858
- 17 **Martinez MA, Clotet B, Este JA.** RNA interference of HIV replication. *Trends Immunol* 2002; **23**: 559-561
- 18 **Hu WY, Myers CP, Kilzer JM, Pfaff SL, Bushman FD.** Inhibition of retroviral pathogenesis by RNA interference. *Curr Biol* 2002; **12**: 1301-1311
- 19 **Bitko V, Barik S.** Phenotypic silencing of cytoplasmic genes using sequence-specific double-stranded short interfering RNA

- and its application in the reverse genetics of wild type negative-strand RNA viruses. *BMC Microbiol* 2001; **1**: 34
- 20 **Kapadia SB**, Brideau-Andersen A, Chisari FV. Interference of hepatitis C virus RNA replication by short interfering RNAs. *Proc Natl Acad Sci U S A* 2003; **100**: 2014-2018
- 21 **Yokota T**, Sakamoto N, Enomoto N, Tanabe Y, Miyagishi M, Maekawa S, Yi L, Kurosaki M, Taira K, Watanabe M, Mizusawa H. Inhibition of intracellular hepatitis C virus replication by synthetic and vector-derived small interfering RNAs. *EMBO Rep* 2003; **4**: 602-608
- 22 **Jiang M**, Milner J. Selective silencing of viral gene expression in HPV-positive human cervical carcinoma cells treated with siRNA, a primer of RNA interference. *Oncogene* 2002; **21**: 6041-6048
- 23 **McCaffrey AP**, Nakai H, Pandey K, Huang Z, Salazar FH, Xu H, Wieland SF, Marion PL, Kay MA. Inhibition of hepatitis B virus in mice by RNA interference. *Nat Biotechnol* 2003; **21**: 639-644
- 24 **Bridge AJ**, Pebernard S, Ducraux A, Nicoulaz AL, Iggo R. Induction of an interferon response by RNAi vectors in mammalian cells. *Nat Genet* 2003; **34**: 263-264
- 25 **Sledz CA**, Holko M, de Veer MJ, Silverman RH, Williams BR. Activation of the interferon system by short-interfering RNAs. *Nat Cell Biol* 2003; **5**: 834-839
- 26 **Khvorova A**, Reynolds A, Jayasena SD. Functional siRNAs and miRNAs exhibit strand bias. *Cell* 2003; **115**: 209-216
- 27 **Schwarz DS**, Hutvagner G, Du T, Xu Z, Aronin N, Zamore PD. Asymmetry in the assembly of the RNAi enzyme complex. *Cell* 2003; **115**: 199-208
- 28 **Silva JM**, Sachidanandam R, Hannon GJ. Free energy lights the path toward more effective RNAi. *Nat Genet* 2003; **35**: 303-305
- 29 **Robinson R**. RNAi Therapeutics: How Likely, How Soon? *PLoS Biol* 2004; **2**: E28
- 30 **Brummelkamp TR**, Bernards R, Agami R. Stable suppression of tumorigenicity by virus-mediated RNA interference. *Cancer Cell* 2002; **2**: 243-247
- 31 **Rubinson DA**, Dillon CP, Kwiatkowski AV, Sievers C, Yang L, Kopinja J, Rooney DL, Ihrig MM, McManus MT, Gertler FB, Scott ML, Van Parijs L. A lentivirus-based system to functionally silence genes in primary mammalian cells, stem cells and transgenic mice by RNA interference. *Nat Genet* 2003; **33**: 401-406

Edited by Kumar M and Wang XL Proofread by Xu FM

• VIRAL HEPATITIS •

Expression of hepatitis C virus envelope protein 2 induces apoptosis in cultured mammalian cells

Li-Xin Zhu, Jing Liu, You-Hua Xie, Yu-Ying Kong, Ye Ye, Chun-Lin Wang, Guang-Di Li, Yuan Wang

Li-Xin Zhu, Jing Liu, You-Hua Xie, Yu-Ying Kong, Ye Ye, Chun-Lin Wang, Guang-Di Li, Yuan Wang, State Key Laboratory of Molecular Biology, Institute of Biochemistry and Cell Biology, Shanghai Institutes for Biological Sciences, Chinese Academy of Sciences, Shanghai 200031, China

Supported by the National High Technology Research and Development Program of China, No. 2001AA215171

Correspondence to: Professor Yuan Wang, Institute of Biochemistry and Cell Biology, Chinese Academy of Sciences, Yueyang Road 320, Shanghai 200031, China. wangyuan@server.shnc.ac.cn

Telephone: +86-21-54921103

Received: 2003-12-24 **Accepted:** 2004-02-13

Abstract

AIM: To explore the role of hepatitis C virus (HCV) envelope protein 2 (E2) in the induction of apoptosis.

METHODS: A carboxyterminal truncated E2 (E2-661) was transiently expressed in several cultured mammalian cell lines or stably expressed in Chinese hamster ovary (CHO) cell line. Cell proliferation was assessed by ³H thymidine uptake. Apoptosis was examined by Hoechst 33258 staining, flow cytometry and DNA fragmentation analysis.

RESULTS: Reduced proliferation was readily observed in the E2-661 expressing cells. These cells manifested the typical features of apoptosis, including cell shrinkage, chromatin condensation and hypodiploid genomic DNA content. Similar apoptotic cell death was observed in an E2-661 stably expressing cell line.

CONCLUSION: HCV E2 can induce apoptosis in cultured mammalian cells.

Zhu LX, Liu J, Xie YH, Kong YY, Ye Y, Wang CL, Li GD, Wang Y. Expression of hepatitis C virus envelope protein 2 induces apoptosis in cultured mammalian cells. *World J Gastroenterol* 2004; 10(20): 2972-2978

<http://www.wjgnet.com/1007-9327/10/2972.asp>

INTRODUCTION

Hepatitis C virus (HCV) is the major causative agent of post-transfusion and community-acquired hepatitis. HCV has been classified in the Hepacivirus genus within the *Flaviviridae* family that includes flaviviruses, such as yellow fever and dengue viruses, and animal pestiviruses, such as bovine viral diarrhea virus (BVDV). Infection with HCV usually leads to chronic hepatitis. Although the mechanism for virus persistence is poorly understood, the high mutation rate of viral envelope proteins^[1,2] and the suppression of the host immune system^[3-5] are believed to contribute to the chronic infection. Analysis of peripheral blood mononuclear cells and liver biopsies from chronic patients suggested that HCV infection could induce apoptosis, which may help the virus escape the immune surveillance and causes liver injuries^[6-11]. *In vitro* studies with

either HCV full length RNA^[12] or cDNA^[13] have demonstrated that apoptosis could be induced by viral proteins. Several independent studies suggested that the viral core protein could induce apoptosis in cultured mammalian cell lines^[14,15], while others using similar systems obtained different results^[16-18]. Therefore, the viral molecule (s) responsible for the induction of apoptosis has not been clearly identified.

Some members in the *Flaviviridae* family, e.g. dengue and Langkat viruses, could induce apoptosis during infection^[19-22]. Duarte dos Santos *et al.* showed that determinants in the envelope protein of dengue type 1 virus could influence the induction of apoptosis^[21]. Prikhod'ko *et al.* demonstrated that apoptosis could be induced by Langkat flavivirus infection. Moreover, expression of the viral envelope protein alone was sufficient to induce apoptosis in cultured mammalian cells^[22].

Since HCV envelope protein 2 (E2) displays a similar genetic organization as the envelope proteins of these viruses^[23], it is possible that E2 may also induce apoptosis. It has been reported that a carboxyterminal truncated E2 (E2-661) without the transmembrane domain is properly folded in cultured mammalian cells^[24,25] and has since been used in HCV studies, such as E2-CD81 binding analysis^[26] and post-translational processing of E2^[27]. In this study, we observed reduced cell proliferations of several cultured mammalian cell lines transiently expressing E2-661. These cells showed the typical features of apoptosis, including cell shrinkage, chromatin condensation and hypodiploid genomic DNA content. Similar apoptotic cell death was observed in an E2-661 stably expressing cell line. This is the first report that HCV E2 can induce apoptosis in cultured mammalian cells.

MATERIALS AND METHODS

Plasmid

pSecTagB/sE2 and pSecTagB/sS1E2 containing the insert of E2-661 (aa384-661 of the HCV polyprotein) coding sequence downstream to a signal sequence of Igk and under the control of the CMV promoter (Figure 1A) were used in the study. To construct pSecTagB/sE2, E2-661 was PCR-amplified from pUC18/E (a gift from Dr. Wang *et al.*^[28], Beijing University, GenBank accession# D10934) with primers 5'-GGCGTTAAGCTTAA CACCTACG TG-3' (*Hind*III site underlined) and 5'-CAG GAATTCTCACTCTGATCTATC-3' (*Eco*RI site underlined). The PCR product was digested with *Hind*III/*Eco*RI and cloned in the pSecTagB (Invitrogen). pSecTagB/sS1E2 was constructed by the insertion of a short tag derived from hepatitis B virus (HBV) preS1 polypeptide (aa21-47) upstream to the E2-661 coding sequence in pSecTagB/sE2. These constructs were verified by sequencing.

Cell culture

Human liver carcinoma Huh7 and hepatoma HepG2, human cervical carcinoma HeLa and baby hamster kidney BHK-21 cell lines were grown in DMEM supplemented with 100 mL/L fetal calf serum (FCS). Chinese hamster ovary (CHO) cells were grown in DMEM/F12 (1:1) supplemented with 100 mL/L FCS. The stable E2-661 expressing cell line, CHO/sS1E2 was constructed by transfection

of CHO cells with pSecTagB/sS1E2 and selection in DMEM/F12 (1:1) medium containing 400 µg/mL Zeocin (Invitrogen)^[24].

Transient expression

Expression plasmids or empty vectors were introduced into cells grown to 60% confluence with LipofectAMINE (Gibco). Transfection efficiency was monitored by co-transfection of pEGFP-C2 (Clontech) which encodes an enhanced green fluorescent protein. Two days after transfection, cells were subjected to Western blot, cell proliferation and apoptosis analysis.

Western blot analysis

Proteins were resolved on 100 g/L SDS-polyacrylamide gels and electroblotted onto nitrocellulose membranes. Membranes were blocked with 50 mL/L skimmed milk in PBS, followed by incubation with rabbit polyclonal anti-E2 antibody RE2116^[29]. The blots were then incubated with horseradish peroxidase conjugated anti-rabbit IgG (Dako) and developed with SuperSignal West Pico stable peroxide solution (Pierce).

Immunofluorescence analysis

CHO and CHO/sS1E2 cells were fixed in ice-cold CMA solution (chloroform: methanol: acetone=1:2:1), incubated with anti-preS1 monoclonal antibody 125E11^[30] 1 000-fold diluted in 10 g/L BSA (prepared in PBS) and followed by incubation with FITC conjugated anti-mouse IgG (Santa Cruz). Fluorescence was viewed under a fluorescence microscope.

Deglycosylation analysis

CHO and CHO/sS1E2 cells were washed twice with PBS and then harvested. Cells were lysed by boiling in the denaturing buffer provided by the manufacturer. Cell lysates were then digested with PNGase F or Endo H (NEB) for 2 h at 37 °C. To analyze the secreted expression products, CHO and CHO/sS1E2 cells were grown in serum free OptiMEM/F12 (1:1) for 12 h. Medium was clarified by centrifugation at 20 000 g for 30 min at 4 °C. Expression products were precipitated by an equal volume of ice-cold ethanol, resuspended in a small volume of PBS and subjected to Western blot analysis.

Cell proliferation analysis

Cell proliferation was measured by ³H thymidine uptake according to a standard protocol^[31]. Cells were incubated with 0.05 µCi ³H thymidine (Amersham Pharmacia) for 4 h in complete medium with 100 mL/L FCS. Cells were then washed once with PBS and 100 mL/L trichloroacetic acid (TCA) followed by incubation in 100 mL/L TCA for 10 min at 37 °C. After TCA was removed from the culture dishes, cells were lysed in the lysis buffer containing 0.33 mol/L NaOH and 10 g/L SDS. ³H thymidine incorporation in the cell lysates was measured by liquid scintillation counting.

Apoptosis analysis

Apoptosis in stable and transient E2 expressing cells was analyzed by three methods: (1) Hoechst 33258 staining: Cells were seeded on sterile cover glasses placed in the 6-well plates the day before transfection. Two days after transfection, cells were fixed, washed twice with PBS and stained with Hoechst 33258 staining solution according to the manufacturer's instructions (Beyotime). Stained nuclei were observed under a fluorescence microscope. For the stable cell lines, similar staining procedures were performed without DNA transfection. (2) Flow cytometry: Cells were washed twice with PBS, trypsinized, and resuspended in complete medium with 100 mL/L FCS. Cells were then washed twice again with PBS and fixed with ice-cold 700 mL/L ethanol at 4 °C for 1 h. After the removal of ethanol, cells were incubated in PBS containing 250 µg/mL RNase A

and 50 µg/mL propidium iodide (Sigma) at room temperature for 15 min, and stored in the dark at 4 °C until further analysis. Ten thousand cells per sample were analyzed with a FACSCalibur flow cytometer (Beckton-Dickinson). (3) DNA fragmentation: CHO and CHO/sS1E2 cells were washed twice with PBS and harvested. Cells were incubated in lysis buffer [10 mmol/L Tris, 1 mmol/L EDTA, 100 mmol/L NaCl, 5 g/L SDS, 1 µg/µL RNase A, pH8.0] at 37 °C for 30 min. At the end of incubation, proteinase K was added to a final concentration of 0.1 mg/mL and the incubation was continued at 55 °C for 4 h. DNA was extracted with phenol/chloroform and precipitated with ethanol. DNA pellets were dissolved in TE buffer and analyzed on a 20 g/L agarose gel.

Statistical analysis

Statistical analysis was performed with unpaired 2-sided Student *t* test. *P*<0.05 was regarded as statistically significant.

RESULTS

Transient expression of E2-661 in mammalian cells

DNA fragments encoding aa384-661 of the HCV polyprotein (E2-661) were cloned in the expression vector pSecTagB to generate pSecTagB/sE2 and pSecTagB/sS1E2 (Figure 1A). Compared to pSecTagB/sE2, E2-661 expressed by pSecTagB/sS1E2 had a small 27-aa preS1 tag located at the N-terminus to facilitate the characterization of the expression products. The above plasmids were used to transfect Huh7, HepG2, HeLa and BHK-21 cells. Cell lysates were analyzed by Western blot with anti-E2 antibody. E2-661 was detected in E2-661 transient expressing cells (Figure 1B). The expressed protein exhibited a heterogeneous pattern typical of a glycoprotein. The expression of E2-661 could also be detected in the cells (transiently) transfected with pSecTagB/sS1E2 (see below).

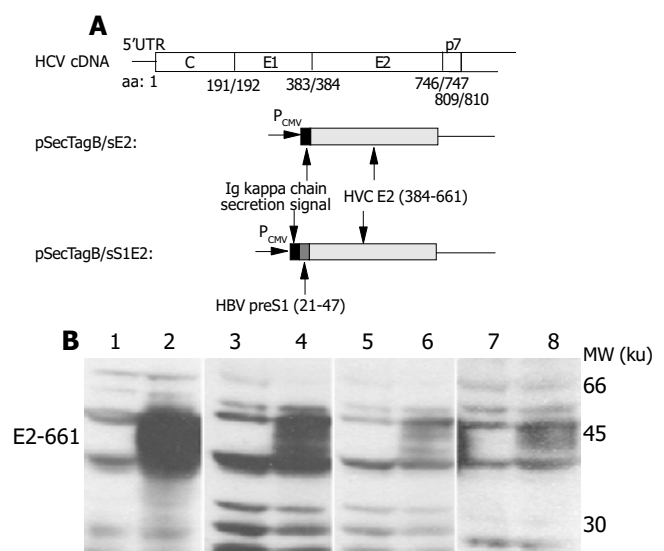


Figure 1 Transient expression of E2-661 in mammalian cells. A: Schematic representation of plasmids encoding E2-661. HBV preS1 (21-47) tag and HCV E2-661 (384-661) signal peptide are indicated. Numbers refer to amino acids of the HCV polyprotein. B: Western blot analysis of E2-661 expressed in mammalian cells with a rabbit polyclonal anti-E2 antibody RE2116. Lanes on the left of all blots were transfected with the empty vector while those on the right were transfected with pSecTagB/sE2. 1-2, BHK-21; 3-4, HeLa; 5-6, Huh7 and 7-8, HepG2. E2-661 was indicated by arrowhead.

E2 expressing cells showed reduced cell proliferation

Cells transfected with pSecTagB/sE2 showed significant cell death upon microscope observation (Figure 2A). Reduced cell

density, cell rounding and cell shrinkage were the common features of all the cell lines transfected with pSecTagB/sE2. The effect of E2 expression on the cell proliferation was further analyzed by ^3H thymidine uptake assay (Figure 2B). Reductions in ^3H incorporation were observed with all the cell lines assayed ($P < 0.05$ for HepG2, $P < 0.001$ for Huh7, HeLa and BHK-21). Transfection efficiencies were monitored by cotransfection with pEGFP-C2. Since a similar amount of EGFP expressing cells were observed between pSecTagB and pSecTagB/sE2 transfected cells (data not shown), the reduced cell proliferation

of E2 expressing cells was not due to the transfection procedure (e.g. transfection reagent and EGFP expression). Similar results were observed with the E2 expressing plasmid pSecTagB/sS1E2 (data not shown). These results suggested that the expression of E2 was responsible for the reduction in cell proliferation.

Apoptosis induced by transient expression of E2

The reduced proliferation might be due to various reasons. To determine if apoptosis contributed to the reduced cell proliferation of E2 expressing cells, cells transfected with pSecTagB/sE2 or

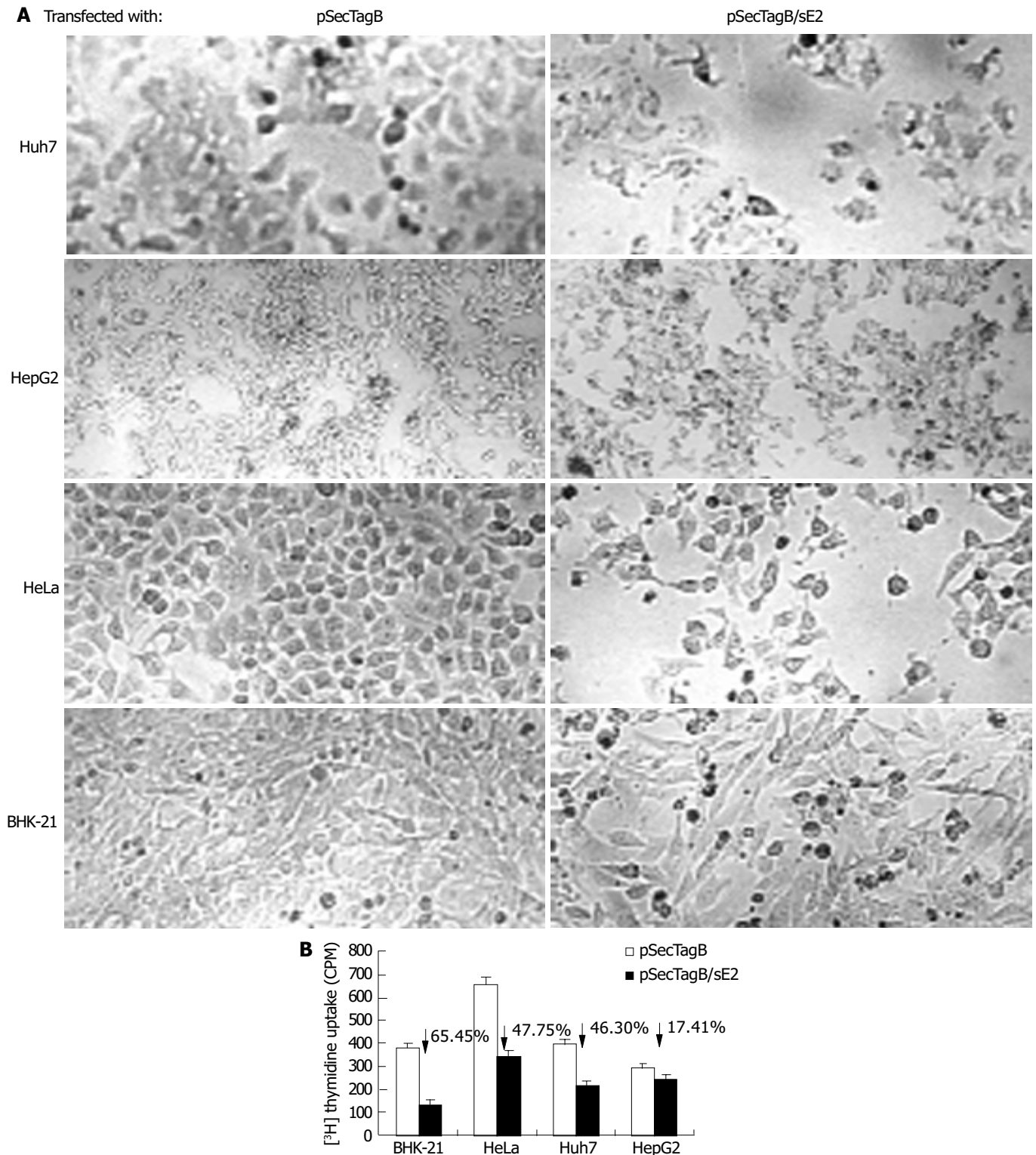


Figure 2 Reduced cell proliferation in E2 expressing cells. A: Morphology of Huh7, HepG2, HeLa, BHK-21 cells 48 h after transfection with pSecTagB or pSecTagB/sE2 (original magnification 40 \times). B: Reduced ^3H thymidine uptake by E2 expressing cells. $P < 0.05$ between all the cells tested.

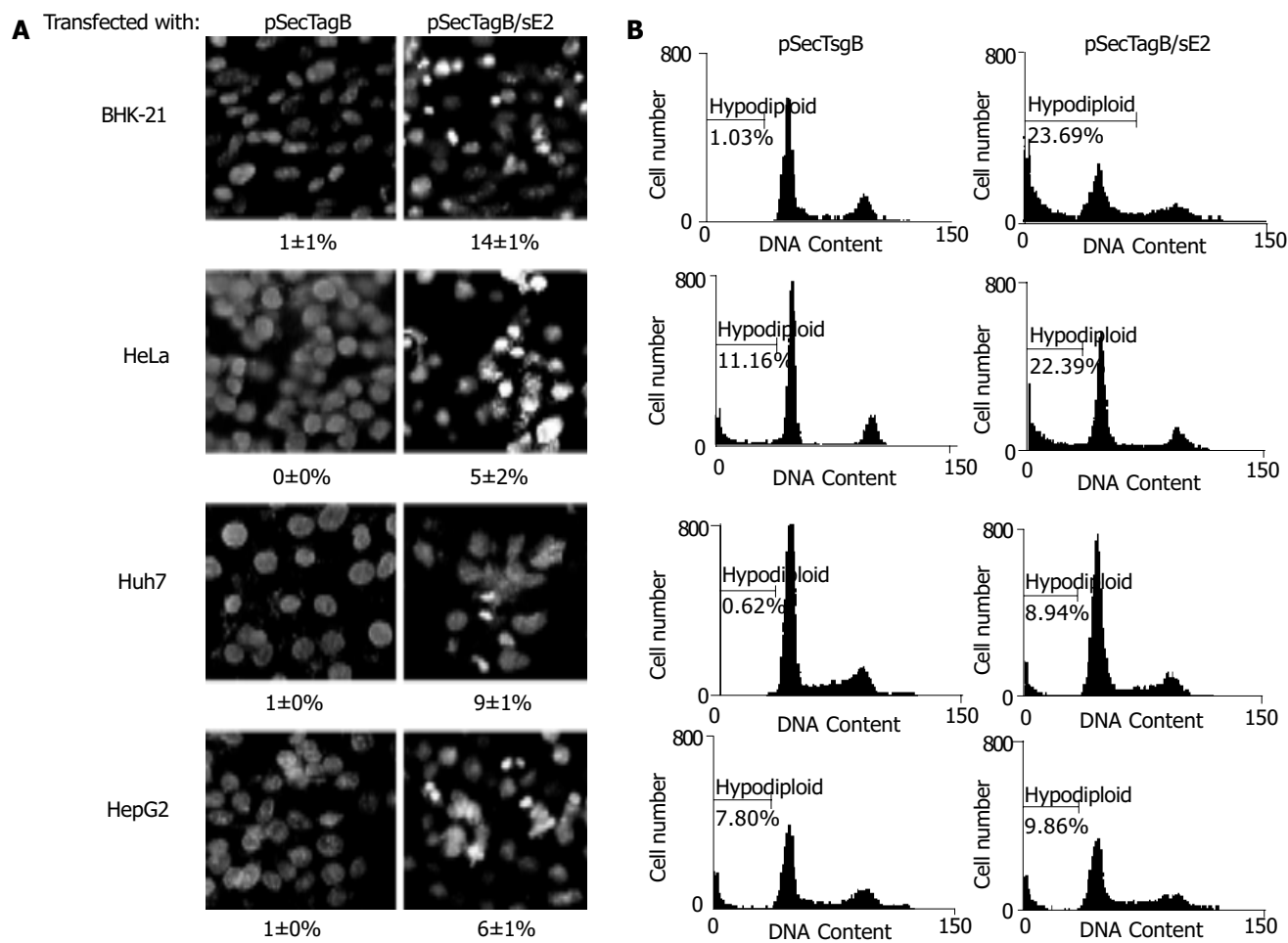


Figure 3 Apoptosis induced by transient expression of E2. A: Hoechst staining of BHK-21, HeLa, Huh7 and HepG2 cells 48 h after transfection with pSecTagB or pSecTagB/sE2. Note the bright nuclei among cells transfected with pSecTagB/sE2. Photograph is a representative experiment repeated three times (original magnification 400×). B: Flow cytometry analysis of PI stained cells 48 h after transfection with pSecTagB or pSecTagB/sE2. The percentage of cells with hypodiploid genomic DNA are indicated on each of the histogram. Results were a representative experiment repeated twice.

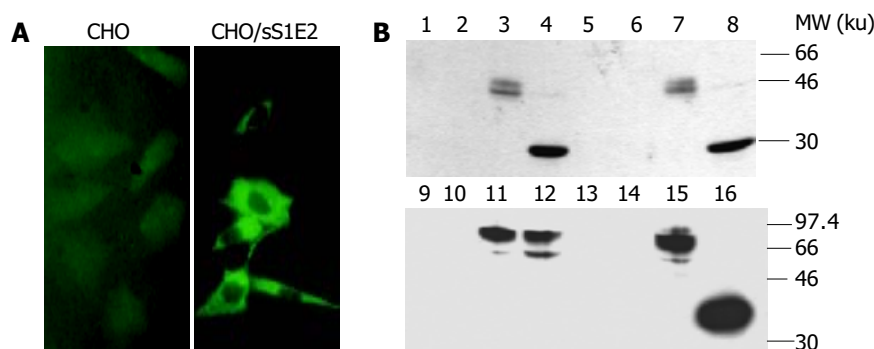


Figure 4 Expression of E2-661 in CHO/sS1E2 cells. A: Immunofluorescence of E2 in CHO/sS1E2 cells analyzed with a monoclonal anti-preS1 antibody 125E11 (original magnification 400×). B: Western blot analysis of the E2 products from CHO/sS1E2 cells. Cell lysates and proteins precipitated from culture medium were analyzed with anti-E2 polyclonal antibody RE2116 after N-glycosidase treatment. Lanes 1, 2, 5, 6: cell lysates from CHO cells; lanes 3, 4, 7, 8: cell lysates from CHO/sS1E2 cells; lanes 9, 10, 13, 14: culture medium from CHO cells; lanes 11, 12, 15, 16: culture medium from CHO/sS1E2 cells; lanes 1, 3, 9, 11: samples incubated with Endo H digestion buffer; lanes 2, 4, 10, 12: samples digested with Endo H; lanes 5, 7, 13, 15: samples incubated with PNGase F digestion buffer; lanes 6, 8, 14, 16, samples digested with PNGase F.

pSecTagB were stained with Hoechst 33258, respectively (Figure 3A). Condensed bright apoptotic nuclei were readily observed amidst the pSecTagB/sE2 transfected cells. The presence of apoptotic cells in E2 expressing cells was further confirmed by flow cytometry. Huh7, HepG2, BHK-21, HeLa cells transfected with pSecTagB/sE2 or control pSecTagB were stained with PI and analyzed by flow cytometry (Figure 3B). Hypodiploid DNA appeared in the sub-G0/G1 region, which

represented dead cells. A higher percentage of dead cells was observed in all the four cell lines transfected with pSecTagB/sE2.

Apoptosis in a CHO cell line stably expressing E2

E2 induced apoptosis was also investigated in a CHO cell line CHO/sS1E2 stably expressing E2-661. This cell line showed the expression of E2-661 as detected by indirect fluorescence assay with the monoclonal antibody against the preS1 tag (Figure 4A).

The fluorescence in CHO/sS1E2 cells suggested the localization of expressed proteins in the cytoplasm. In further characterization by Western blot analysis, cell-associated and secreted E2 proteins (from 10^5 and 10^7 cells) were detected with the E2 polyclonal antibody (Figure 4B). The cell-associated E2 protein was sensitive to Endo H (lane 4), suggesting that the glycans carried on it were ER-restricted. On the other hand, secreted E2 was resistant to Endo H (lane 12), suggesting that the glycans on this species of E2 underwent the modification by Golgi enzymes.

Similar to cells transiently transfected with pSecTagB/sE2, the morphology of CHO/sS1E2 was different from that of the original CHO cell line (Figure 5A). There were obvious differences in cell size and shape between these two cell lines. A significant number of dead cells were readily observed for CHO/sS1E2 and cells could hardly grow to 100% confluency. Similar morphology and growth curve were also observed in other CHO/sS1E2 clones (data not shown), suggesting that they are not the result of clonal selection. ^3H incorporation analysis showed that there was a significant reduction (72.0%, $P < 0.001$) of cell proliferation for CHO/sS1E2 in comparison with CHO

cells (Figure 5B).

Hoechst 33258 staining of CHO/sS1E2 showed condensed bright nuclei typical of apoptotic dead cells which reached about 14% of the total cells, while almost no apoptotic nuclei were observed in control CHO cells (Figure 6A). Flow cytometry analysis confirmed that there were a significant number of dead cells for CHO/sS1E2 (Figure 6B).

Since the cleavage of chromosomal DNA into fragments of oligonucleosomal size is a biochemical hallmark of apoptosis^[32], DNA fragmentation in CHO/sS1E2 was examined by DNA laddering assay. With the freshly seeded CHO/sS1E2 cells, no obvious DNA fragmentation was observed, while clear DNA laddering in -180 bp interval was detected 48 h after cell seeding. No apoptotic DNA fragmentation was observed in CHO cells at either time points (Figure 6C).

DISCUSSION

In this study, HCV E2 was transiently expressed in several mammalian cells. All tested cells showed shrinkage in morphology and reduced cell proliferation due to the expression

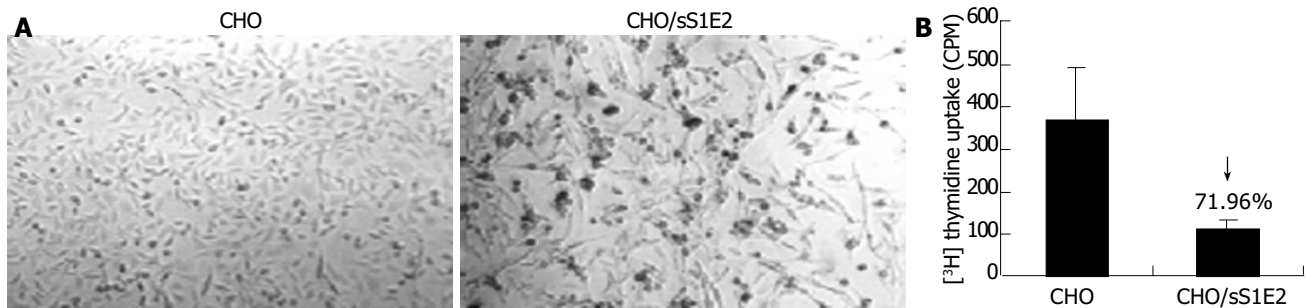


Figure 5 Reduced cell proliferation in CHO/sS1E2 cells. A: Morphology of CHO and CHO/sS1E2 cells (original magnification 40 \times). B: Reduced ^3H thymidine uptake by CHO/sS1E2 cells. CHO and CHO/sS1E2 cells were subjected to ^3H thymidine uptake assay 24 h after seeding. Each sample was done in quadruplicates. The differences in ^3H incorporation between CHO and CHO/sS1E2 cells were significant ($P < 0.001$).

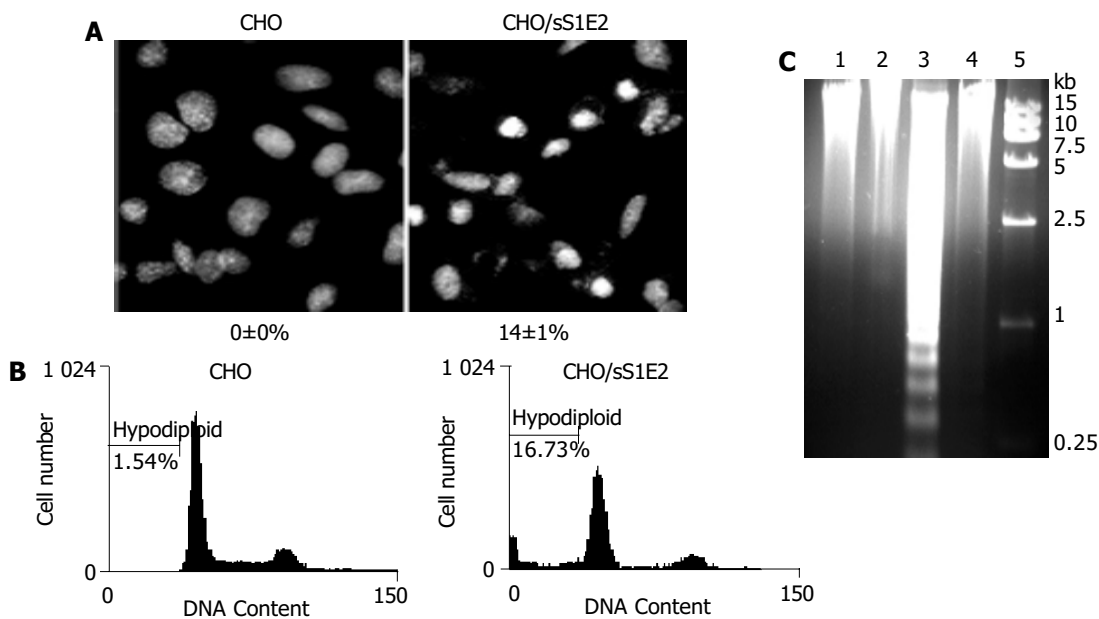


Figure 6 Apoptosis of CHO/sS1E2 cells. A: Hoechst staining of CHO and CHO/sS1E2 cells 24 h after seeding. Photograph is a representative experiment repeated three times (original magnification 400 \times). The percentage of condensed and fragmented nuclei is indicated at the bottom of each photo. Numbers are presented as mean \pm SD. B: Flow cytometry analysis of PI stained cells 24 h after seeding. The percentage of cells with hypodiploid genomic DNA is indicated on each of the histogram. Results were a representative experiment repeated twice. C: Fragmentation of CHO/sS1E2 cell DNA. Lane 1: CHO cells 48 h post-seeding; lane 2: CHO cells freshly seeded; lane 3: CHO/sS1E2 cells 48 h post-seeding; lane 4: CHO/sS1E2 cells freshly seeded; lane 5: DNA size marker.

of E2. Further evidences, such as condensed chromatin, demonstrated that apoptosis contributed, at least in part, to the cell death induced by E2. E2 induced apoptosis was also observed in a stable E2 expressing cell line CHO/sS1E2. Again there was a significant reduction in cell proliferation of CHO/sS1E2 in comparison to CHO cells. Hoechst 33258 staining, flow cytometry analysis and DNA laddering assay demonstrated that apoptosis contributed to the reduced cell proliferation. Apoptosis in CHO/sS1E2 was not due to the expression of the small preS1 tag because toxicity was not observed when preS1 was transiently expressed in cultured mammalian cells^[33]. In conclusion, our results demonstrate that the expression of HCV E2 could induce apoptosis in cultured mammalian cells.

It has been reported that apoptosis is involved in the pathogenesis of hepatitis C. Immunohistochemical study suggested that the Fas system played an important role in liver injuries of viral hepatitis^[34]. There is evidence that immune response (cytotoxic T lymphocyte) might be involved in the apoptosis of hepatocytes in HCV infected patients^[35]. Recent studies suggested that apoptosis of hepatocytes might also be due to the cytopathic effect of viral proteins^[13,14]. Our result that E2 expression induced apoptosis in cultured mammalian cells including human hepatic cells supports this hypothesis. On the other hand, E2-induced apoptosis may also partly contribute to the escape of HCV from the host immune surveillance. It awaits further investigation whether the expression of E2 can induce apoptosis in lymphocytes.

Studies of Langkat flavivirus^[22] demonstrated that expression of envelope (E) protein could induce apoptosis via the Caspase 3 pathway. Since HCV E2 and the E protein of Langkat flavivirus share similar genetic organization and hydropathy profile^[23], it is possible that E2 could induce apoptosis through a similar mechanism. Increased Fas expression observed in HCV patients^[7] also suggested the involvement of the caspase-3 pathway. However, comparing the expression levels of secreted and cell-associated E2, we found that in our system, E2 was mainly cell-associated and localized in the cytoplasm. By glycosidase digestion analysis, we found that most of the cell-associated E2 were high-mannose type glycoproteins, which suggested the localization of E2 to the endoplasmic reticulum (ER). Many other mammalian expression systems also showed the ER localization of the expressed HCV E2, and a large portion of them formed disulfide-linked aggregates^[36-38]. The accumulation of large amount of proteins in the ER might induce ER stress and apoptosis could be triggered via the Caspase 12-mediated apoptosis pathway^[39]. Further study is required for understanding the possible pathway of HCV E2 induced apoptosis.

ACKNOWLEDGEMENTS

The authors thank Professor Jia-Rui Wu for providing CHO cell line and Professor Yu Wang for the HCV cDNA for this study.

REFERENCES

- Bassett SE, Thomas DL, Brasky KM, Lanford RE. Viral persistence, antibody to E1 and E2, and hypervariable region 1 sequence stability in hepatitis C virus-inoculated chimpanzees. *J Virol* 1999; **73**: 1118-1126
- Farci P, Purcell RH. Clinical significance of hepatitis C virus genotypes and quasispecies. *Semin Liver Dis* 2000; **20**: 103-126
- Crotta S, Stilla A, Wack A, D'Andrea A, Nuti S, D'Oro U, Mosca M, Filliponi F, Brunetto RM, Bonino F, Abrignani S, Valiante NM. Inhibition of natural killer cells through engagement of CD81 by the major hepatitis C virus envelope protein. *J Exp Med* 2002; **195**: 35-41
- Large MK, Kittleson DJ, Hahn YS. Suppression of host immune response by the core protein of hepatitis C virus: possible implications for hepatitis C virus persistence. *J Immunol* 1999; **162**: 931-938
- Bain C, Fatmi A, Zoulim F, Zarski JP, Trepo C, Inchauspe G. Impaired allostimulatory function of dendritic cells in chronic hepatitis C infection. *Gastroenterology* 2001; **120**: 512-524
- Hiramatsu N, Hayashi N, Katayama K, Mochizuki K, Kawanishi Y, Kasahara A, Fusamoto H, Kamada T. Immunohistochemical detection of Fas antigen in liver tissue of patients with chronic hepatitis C. *Hepatology* 1994; **19**: 1354-1359
- Calabrese F, Pontisso P, Pettenazzo E, Benvegno L, Vario A, Chemello L, Alberti A, Valente M. Liver cell apoptosis in chronic hepatitis C correlates with histological but not biochemical activity or serum HCV-RNA levels. *Hepatology* 2000; **31**: 1153-1159
- Emi K, Nakamura K, Yuh K, Sugyo S, Shijo H, Kuroki M, Tamura K. Magnitude of activity in chronic hepatitis C is influenced by apoptosis of T cells responsible for hepatitis C virus. *J Gastroenterol Hepatol* 1999; **14**: 1018-1024
- Toubi E, Kessel A, Goldstein L, Slobodin G, Sabo E, Shmuel Z, Zuckerman E. Enhanced peripheral T-cell apoptosis in chronic hepatitis C virus infection: association with liver disease severity. *J Hepatol* 2001; **35**: 774-780
- Taya N, Torimoto Y, Shindo M, Hirai K, Hasebe C, Kohgo Y. Fas-mediated apoptosis of peripheral blood mononuclear cells in patients with hepatitis C. *Br J Haematol* 2000; **110**: 89-97
- Pianko S, Patella S, Ostapowicz G, Desmond P, Sievert W. Fas-mediated hepatocyte apoptosis is increased by hepatitis C virus infection and alcohol consumption, and may be associated with hepatic fibrosis: mechanisms of liver cell injury in chronic hepatitis C virus infection. *J Viral Hepat* 2001; **8**: 406-413
- Kalkeri G, Khalap N, Garry RF, Fermin CD, Dash S. Hepatitis C virus protein expression induce apoptosis in HepG2 cells. *Virology* 2001; **282**: 26-37
- Kalkeri G, Khalap N, Akhter S, Garry RF, Fermin CD, Dash S. Hepatitis C viral proteins affect cell viability and membrane permeability. *Exp Mol Pathol* 2001; **71**: 194-208
- Zhu N, Khoshnan A, Schneider R, Matsumoto M, Dennert G, Ware C, Lai MM. Hepatitis C virus core protein binds to the cytoplasmic domain of tumor necrosis factor (TNF) receptor 1 and enhances TNF-induced apoptosis. *J Virol* 1998; **72**: 3691-3697
- Honda M, Kaneko S, Shimazaki T, Matsushita E, Kobayashi K, Ping LH, Zhang HC, Lemon SM. Hepatitis C virus core protein induces apoptosis and impairs cell-cycle regulation in stably transformed Chinese hamster ovary cells. *Hepatology* 2000; **31**: 1351-1359
- Marusawa H, Hijikata M, Chiba T, Shimotohno K. Hepatitis C virus core protein inhibits Fas- and tumor necrosis factor alpha-mediated apoptosis via NF-kappaB activation. *J Virol* 1999; **73**: 4713-4720
- Ray RB, Meyer K, Ray R. Suppression of apoptotic cell death by hepatitis C virus core protein. *Virology* 1996; **226**: 176-182
- Ray RB, Meyer K, Steele R, Shrivastava A, Aggarwal BB, Ray R. Inhibition of tumor necrosis factor (TNF-alpha)-mediated apoptosis by hepatitis C virus core protein. *J Biol Chem* 1998; **273**: 2256-2259
- Despres P, Flamand M, Ceccaldi PE, Deubel V. Human isolates of dengue type 1 virus induce apoptosis in mouse neuroblastoma cells. *J Virol* 1996; **70**: 4090-4096
- Avirutnan P, Malasit P, Seliger B, Bhakdi S, Husmann M. Dengue virus infection of human endothelial cells leads to chemokine production, complement activation, and apoptosis. *J Immunol* 1998; **161**: 6338-6346
- Duarte dos Santos CN, Frenkiel MP, Courageot MP, Rocha CF, Vazeille-Falcoz MC, Wien MW, Rey FA, Deubel V, Despres P. Determinants in the envelope E protein and viral RNA helicase NS3 that influence the induction of apoptosis in response to infection with dengue type 1 virus. *Virology* 2000; **274**: 292-308
- Prikhod'ko GG, Prikhod'ko EA, Cohen JI, Pletnev AG. Infection with Langkat Flavivirus or expression of the envelope protein induces apoptotic cell death. *Virology* 2001; **286**: 328-335
- Hijikata M, Kato N, Ootsuyama Y, Nakagawa M, Shimotohno K. Gene mapping of the putative structural region of the hepatitis C virus genome by *in vitro* processing analysis. *Proc Natl Acad Sci U S A* 1991; **88**: 5547-5551
- Wang CL, Zhu LX, Liu J, Zhang ZC, Wang Y, Li GD. Expression and characterization of hepatitis C Virus E2 glycoprotein

- fused to hepatitis B virus preS1 (21-47) fragment in CHO cells. *Shengwuhuaxue Yu Shengwuwuli Xuebao* 2002; **34**: 400-404
- 25 **Michalak JP**, Wychowski C, Choukhi A, Meunier JC, Ung S, Rice CM, Dubuisson J. Characterization of truncated forms of hepatitis C virus glycoproteins. *J Gen Virol* 1997; **78**(Pt 9): 2299-2306
- 26 **Pileri P**, Uematsu Y, Campagnoli S, Galli G, Falugi F, Petracca R, Weiner AJ, Houghton M, Rosa D, Grandi G, Abrignani S. Binding of hepatitis C virus to CD81. *Science* 1998; **282**: 938-941
- 27 **Zhu LX**, Liu J, Li YC, Kong YY, Staib C, Sutter G, Wang Y, Li GD. Full-length core sequence dependent complex-type glycosylation of hepatitis C virus E2 glycoprotein. *World J Gastroenterol* 2002; **8**: 499-504
- 28 **Wang Y**, Okamoto H, Tsuda F, Nagayama R, Tao QM, Mishiro S. Prevalence, genotypes, and an isolate (HC-C2) of hepatitis C virus in Chinese patients with liver disease. *J Med Virol* 1993; **40**: 254-260
- 29 **Liu J**, Zhu L, Zhang X, Lu M, Kong Y, Wang Y, Li G. Expression, purification, immunological characterization and application of Escherichia coli-derived hepatitis C virus E2 proteins. *Biotechnol Appl Biochem* 2001; **34**(Pt 2): 109-119
- 30 **Yang HL**, Jin Y, Cao HT, Xu X, Li GD, Wang Y, Zhang ZC. Affinity purification of hepatitis B virus surface antigen containing preS1 region. *Shengwuhuaxue Yu Shengwuwuli Xuebao* 1996; **28**: 412-417
- 31 **Tolleson WH**, Melchior WB Jr, Morris SM, McGarrity LJ, Domon OE, Muskhelishvili L, James SJ, Howard PC. Apoptotic and anti-proliferative effects of fumonisins B1 in human keratinocytes, fibroblasts, esophageal epithelial cells and hepatoma cells. *Carcinogenesis* 1996; **17**: 239-249
- 32 **Wyllie AH**. Glucocorticoid -induced thymocyte apoptosis is associated with endogenous endonuclease activation. *Nature* 1980; **284**: 555-556
- 33 **Hui J**, Mancini M, Li G, Wang Y, Tiollais P, Michel ML. Immunization with a plasmid encoding a modified hepatitis B surface antigen carrying the receptor binding site for hepatocytes. *Vaccine* 1999; **17**: 1711-1718
- 34 **Hayashi N**, Mita E. Fas system and apoptosis in viral hepatitis. *J Gastroenterol Hepatol* 1997; **12**: S223-S226
- 35 **Onji M**, Kikuchi T, Kumon I, Masumoto T, Nadano S, Kajino K, Horiike N, Ohta Y. Intrahepatic lymphocyte subpopulations and HLA class I antigen expression by hepatocytes in chronic hepatitis C. *Hepatogastroenterology* 1992; **39**: 340-343
- 36 **Selby MJ**, Choo QL, Berger K, Kuo G, Glazer E, Eckart M, Lee C, Chien D, Kuo C, Houghton M. Expression, identification and subcellular localization of the proteins encoded by the hepatitis C viral genome. *J Gen Virol* 1993; **74**(Pt 6): 1103-1113
- 37 **Dubuisson J**, Hsu HH, Cheung RC, Greenberg HB, Russell DG, Rice CM. Formation and intracellular localization of hepatitis C virus envelope glycoprotein complexes expressed by recombinant vaccinia and Sindbis viruses. *J Virol* 1994; **68**: 6147-6160
- 38 **Dubuisson J**, Rice CM. Hepatitis C virus glycoprotein folding: disulfide bond formation and association with calnexin. *J Virol* 1996; **70**: 778-786
- 39 **Yoneda T**, Imaizumi K, Oono K, Yui D, Gomi F, Katayama T, Tohyama M. Activation of caspase-12, an endoplasmic reticulum (ER) resident caspase, through tumor necrosis factor receptor-associated factor 2-dependent mechanism in response to the ER stress. *J Biol Chem* 2001; **276**: 13935-13940

Edited by Wang XL and Xu XQ Proofread by Xu FM

• VIRAL HEPATITIS •

Construction of exogenous multiple epitopes of helper T lymphocytes and DNA immunization of its chimeric plasmid with HBV pre-S2/S gene

Wen-Jun Gao, Xiao-Mou Peng, Dong-Ying Xie, Qi-Feng Xie, Zhi-Liang Gao, Ji-Lu Yao

Wen-Jun Gao, Department of Infectious Diseases, Zhongshan People's Hospital, Zhongshan 528400, Guangdong Province, China
Xiao-Mou Peng, Dong-Ying Xie, Qi-Feng Xie, Zhi-Liang Gao, Ji-Lu Yao, Department of Infectious Diseases, Third Hospital, Sun Yat-Sen University, Guangzhou 510630, Guangdong Province, China
Supported by the National Natural Science Foundation of China, NO. 39970677 and the Science Foundation of Guangdong Province, NO. 99M04801G

Correspondence to: Xiao-Mou Peng, Department of Infectious Diseases, Third Hospital, Sun Yat-Sen University, Guangzhou 510630, Guangdong Province, China. xiaomoupeng@hotmail.com
Telephone: +86-20-85516867 Ext. 2019 **Fax:** +86-20-85515940
Received: 2004-01-01 **Accepted:** 2004-02-26

Abstract

AIM: To design and construct an exogenous multiple epitope of helper T lymphocytes (HTL), and to evaluate its effect on anti-HBs response through DNA immunization.

METHODS: Artificial HTL epitope, PADRE and four other HTL epitopes from different proteins were linked together using splicing by overlap extension to generate exogenous multiple epitopes of HTL, MTE5. pcMTE5 and pcHB were generated by cloning MTE5 and fragments of HBV pre-S2/S gene into mammalian expression plasmid pcDNA3. Four chimeric plasmids were constructed by cloning MTE5 into the region of pre-S2 gene (*Bam* HI), 5' terminal of S gene (*Hinc*II, *Xba* I) and 3' terminal of S gene (*Acc* I) of pcHB respectively. BALB/c mice were used in DNA immunization of the recombinant plasmids. Anti-HBs was detected using Abbott IMx AUSAB test kits.

RESULTS: The sequences of MTE5 and the 6 constructs of recombinant plasmids were confirmed to be correct by DNA sequencing. The anti-HBs response of the co-inoculation of pcHB and pcMTE5 was much higher than that of the inoculation of pcHB only (136.7 ± 69.1 mIU/mL vs 27.6 ± 17.3 mIU/mL, $P < 0.01$, $t = -6.56$). Among the 4 chimeric plasmids, only the plasmid in which MTE5 was inserted into the pre-S2 region had good anti-HBs response (57.54 ± 7.68 mIU/mL), and had no significant difference compared with those of pcHB and the co-inoculation of pcHB and pcMTE5.

CONCLUSION: Exogenous multiple epitopes of HTL had immune enhancement when they were co-inoculated with pre-S2/S gene or inoculated in the chimeric form at a proper site of pre-S2/S gene of HBV. It might suggest that it was possible to improve hepatitis B vaccine using exogenous multiple epitopes of HTL. The antibody responses were very low using DNA immunization in the study. Thus, the immune enhancement effect of exogenous multiple epitopes of HTL has to be confirmed and the effect on overcoming the drawback of the polymorphism of HLA II antigens should also be evaluated after these chimeric plasmids are expressed in mammalian cell lines.

Gao WJ, Peng XM, Xie DY, Xie QF, Gao ZL, Yao JL.

Construction of exogenous multiple epitopes of helper T lymphocytes and DNA immunization of its chimeric plasmid with HBV pre-S2/S gene. *World J Gastroenterol* 2004; 10 (20): 2979-2983

<http://www.wjgnet.com/1007-9327/10/2979.asp>

INTRODUCTION

There are more than 300 millions of HBsAg carriers all over the world. Most of them have active infection of hepatitis B virus. Chronic hepatitis B virus infection may cause significant incidence of chronic hepatitis, cirrhosis, and hepatocellular carcinoma^[1,2]. Hepatitis B vaccine inoculation is an important measure for prevention of HBV infection. Considerable variability exists, however, in response to hepatitis B vaccines, and 5-10% of healthy young adults demonstrate no or inadequate responses following a standard vaccination schedule^[3-8]. The frequency of non- and low-responders is up to 40-50% in vaccinated subjects with depressed immune responses, such as patients on maintenance hemodialysis. Only some of the non- or low-responders to hepatitis B vaccine are responsive to the novel recombinant triple antigen hepatitis B vaccine (pre-S1/S2 and HBsAg)^[9]. These non- or low-responders usually carry specific type of class II human leukocyte antigens (HLA II antigens), such as DRB1*3, DRB1*7, DQB1*20 or DPB1*1101^[10-13]. The antigen presentation is blocked because these HLA II antigen molecules on the surface of helper T lymphocytes (HTL) cannot combine efficiently with the epitope of HTL on the vaccine protein, hepatitis B surface antigen (HBsAg)^[14,15]. Adding exogenous multiple epitopes of HTL, which can combine with much more types of HLA II antigens to hepatitis B vaccine may be a good way to solve this problem. Conducting HTL epitopes from tetanus toxoids (aa73-99, aa830-845) and artificial epitopes of PADRE into HBsAg can enhance the immunogenicity of HbsAg^[16,17]. Adding exogenous HTL epitopes to HBsAg can let natural non-responder mice respond to HbsAg^[18]. These data suggest that it is possible to use exogenous HTL epitopes to improve hepatitis B vaccine. For these reasons, an exogenous multiple epitope of HTL, MTE5, consisting of five HTL epitopes from different origins was designed and constructed. Its effect on anti-HBs response was evaluated through DNA immunization after it was inserted in different loci of HBV pre-S2/S gene.

MATERIALS AND METHODS

Reagents

pTZ19U-HBV containing double copies of HBV DNA (adw) was a gift from professor Zhi-Min Huang, Sun Yat-Sen University. T4 DNA ligase and pfu DNA polymerase were purchased from Promega Company (USA). DNA gel extraction kits and plasmid isolation kits were purchased from Qiagen Company (German). Polyclonal antibodies of anti-HBs and LSAB test kit for immunohistochemistry were purchased from DAKO Company (USA). Primers and oligonucleotide fragments shown in Table 1 were synthesized in Bioasia Biological Engineering Company (Shanghai, China).

Table 1 Primers and oligonucleotide fragments used in *mte5* splicing and construction of eukaryotic expression plasmids

	Sequences (5'→3')
F1	ATGGCTAAAA CCATCGCCTA TGATGAAGAA GCTCGTCGTG GTCTGGAACG TGGTCTGAAT GCCTCCGAT
F2	GTCCAGGCAG CAACGAATT AGCTCCCTGC AGCCAGTGTC CAGGCAGAAC ATCGGAGGCA TTCAGACCA
F3	AATTCGTTGC TGCCTGGACC CTGAAAGCTG CCGCTGGAAG ACACGTTGTT ATCGATAAGA GCTTCGGAA
F4	TTCGGTGATT CCGATAAACT TGAATTAGC TTTGATGTAC TGCTGAGGGC TTCCAAGGCT CTTATCGAT M' TE-
MTE-P1	TGGGATCCCA TGGCTAAAAC CATCGCC
MTE-P2	GCTCTAGACT TTCGGTGATT CCGATAA
HBV-P1	CCTAAGCTTA TGCAGTGGAA CTCCACT
HBV-P2	TGGAATTCCT TAAATGTATA CCCAGAG
Bam-1	TGGGATCCCA TGGCTAAAAC CATCGCC
Bam-2	GCGGATCCCT TTCGGTGATT CCGATAA
Hinc-1	TCGTTGACAA TGGCTAAAAC CATCGCC
Hinc-2	GCGTTGACAA TTCGGTGATT CCGATAA
Xba-1	TCTCTAGACA TGGCTAAAAC CATCGCC
Xba-2	GCTCTAGACT TTCGGTGATT CCGATAA
Acc-1	TCGTATACAT GGCTAAAACC ATCGCCT
Acc-2	GCGGTATACT TCGGTGATTC CGATAAA

Animal

Eight to 12 week-old female inbred BALB/c mice were obtained from Guangzhou Traditional Chinese Medicine University.

MTE5 splicing and cloning MTE5 was designed to consist of HTL epitopes from heat shock protein 65 of *mycobacterium tuberculosis* (aa1-20), E2 polyprotein of *rubella* virus (aa54-65), artificial epitope (PADRE), heat shock protein 60 of *chlamydia trachomatis* (aa35-48) and tetanus toxoid (aa830-843). These epitopes were translated into a 219-bp fragment of DNA sequence. Then, it was synthesized in four oligonucleotide fragments, which were linked together at last using splicing by overlap extension^[19,20]. The oligonucleotide fragments F1 and F2, F3 and F4 were spliced by PCR respectively at first. Their purified products were spliced together again to generate MTE5. The construct of pUMTE5 was generated by cloning MTE5 into plasmid pUC18 at the site between restriction endonucleases *Bam* HI and *Xba* I. pcMTE5 then was obtained by sub-cloning MTE5 from pUMTE5 into mammalian expression plasmid, pcDNA3. The sequence of MTE5 in pcMTE5 was confirmed using automatic DNA sequencing in Bioasia Biological Engineering Company.

HBV pre-S2/S gene cloning Pre-S2/S fragment of HBV was obtained using pTZ19U-HBV as template, and HBV-P1 and HBV-P2 as primers. The purified product was then cloned into pUC18 at the site between the restriction endonucleases *Hind* III and *Eco* RI to generate recombinant plasmid pUHB. pCHB was constructed by sub-cloning the fragment of HBV pre-S2/S gene into pcDNA3. pCHB was denominated after its sequence was confirmed by automatic DNA sequencing.

Construction of chimeric plasmids of MTE5 and HBV pre-S2/S gene MTE5 was designed to insert into the region of pre-S2 gene (*Bam* HI), 5' terminal of S gene (*Hinc* II, *Xba* I) and 3' terminal of S gene (*Acc* I) respectively. All the inserting sites were far from the α determinant to avoid decreasing the antigenicity of HBsAg. In order to obtain these chimeric plasmids, four fragments of MTE5 with different types of restriction endonuclease site in its two terminals were generated through PCR with different primers at first. Then four chimeric plasmids, pCHB-MTEB, pCHB-MTEH, pCHB-MTEX and pCHB-MTEA were constructed by cloning MTE5 into pUHB at first since pcDNA3 had some similar restriction endonuclease sites of its own, and then by sub-cloning the chimeric fragment of MTE5 and pre-S2/S into pcDNA3. The sequences of these recombinant plasmids were confirmed by automatic DNA sequencing.

Large-scale DNA preparation, DNA immunization Large-scale plasmid DNA of recombinant plasmids was prepared using

Qiagen's Max-Prep kits. Plasmid DNA of pcDNA3 was used as control. Plasmid DNA was adjusted to 1 μ g/mL in normal saline. Seventy BLBA/c mice were randomly divided into 8 groups. Every mouse was injected a total 100 μ L of plasmid DNA which was distributed over five different sites into the anterior tibialis muscle 5 d after the injection of an equal volume of 2 g/L Bupivacaine. Boost injection was carried out every 3 wk for 3 times with an equal amount of plasmid DNA. Four weeks after the last boost injection, all mice were put to death for serum.

Detecting anti-HBs in serum Anti-HBs in serum was detected using AUSAB kits (Abbott Laboratory, USA). The tests were carried out following the manufacturer's instructions.

Pathological examination and HBsAg detection in muscle cell Pathological examination and HBsAg detection using immunohistochemistry in the mouse muscle of inoculation site from all groups were carried out after the samples were routinely embedded by paraffin in our laboratory. The muscles from the opposite leg were used as negative controls.

Statistical analysis For anti-HBs level, geometric mean titer (GMT) for each group was calculated at first. Then Student-Newman-Keuls-q was used for statistical analysis. For positive rate, Fisher's exact probability analysis was used. SPSS 10.0 for Windows was used for all statistical analyses.

RESULTS

MTE5 splicing and cloning

The theoretical products of the first and second round splicing were 120 bp and 219 bp, respectively. The actual products shown in Figure 1 were same as the design. Restriction fragment length polymorphism (RFLP) analysis was used to identify the positive clones after the 219-bp fragment was inserted into pUC18 to generate recombinant plasmid pUMTE5, which is shown in Figure 2. Two correct clones were selected by DNA sequencing among 13 positive clones of pUMTE5. The rest clones usually carried deletions or mismatches in the region longer than 50 bp of the synthesized oligonucleotide fragments, which implied that the synthesized DNA oligonucleotide fragment longer than 50 bp would not be reliable. The DNA sequence and amino acid sequence of MTE5 are shown in Figure 3. MTE5 was successfully cloned into pcDNA3 to generate pcMTE5 at last.

HBV pre-S2/S gene cloning

The theoretical base pair number of PCR products of HBV pre-S2/S fragment was about 847 bp. It was cloned into pUC18 to

generate recombinant plasmid pUHB. Then, the fragment of pre-S2/S was sub-cloned into pcDNA3 to generate recombinant plasmid pcHB. RFLP analysis was used to identify the positive clones of pcHB, which is shown in Figure 4A. After its sequence was confirmed by DNA sequencing, the recombinant plasmid was denominated as pcHB.

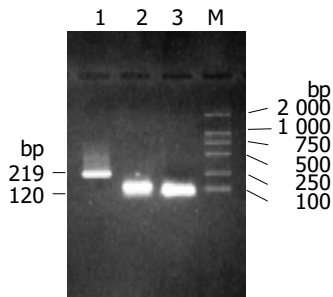


Figure 1 Electrophoresis of ultimate product of MTE5 and its middle oligonucleotide fragments. Lane 1: Ultimate product of MTE5; Lanes 2 and 3: The middle oligonucleotide fragments of MTE5; Lane M: DNA marker.

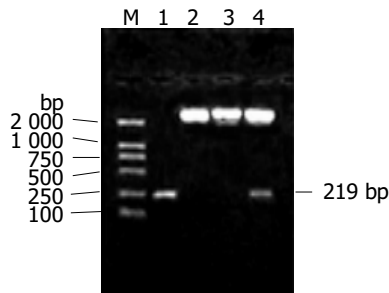


Figure 2 RFLP analysis of recombinant plasmid pUMTE5. Lane M: DNA marker; Lane 1: Splicing product of MTE5; Lanes 2 and 3: Plasmid pUC18 and recombinant plasmid pUMTE5 digested with restriction endonuclease *Xba* I; Lane 4: Recombinant plasmid pUMTE5 digested with restriction endonucleases *Xba* I and *Bam* HI.

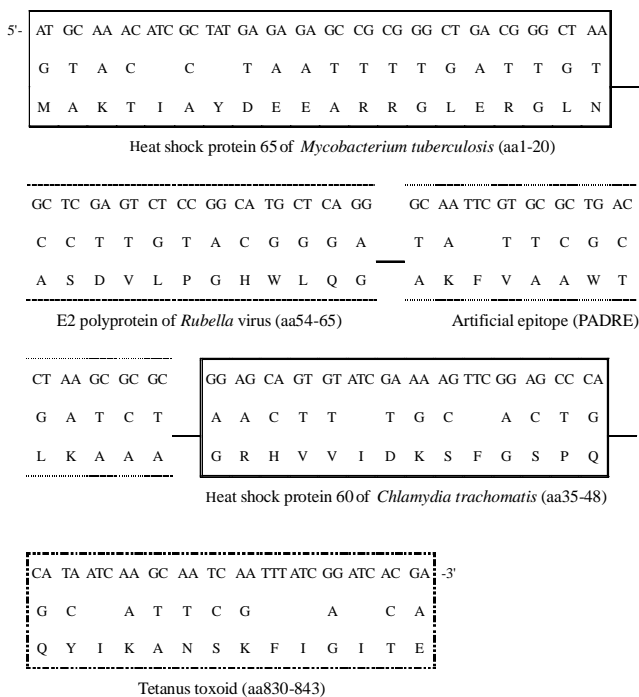


Figure 3 DNA and amino acid sequences of MTE5.

Construction of chimeric plasmids of MTE5 and HBV pre-S2/S gene

Four fragments of MTE5 with different types of restriction endonuclease site in its two terminals were successfully obtained by PCR. They were cloned into pUHB to generate their recombinant plasmids at first. The chimeric fragments of MTE5 and pre-S2/S were sub-cloned into pcDNA3 to generate their mammalian expression plasmids at last. RFLP analysis was used to identify positive clones. The results of RFLP analysis of the recombinant plasmid pcHB-MTEX with MTE5 inserted in site of *Xba* I is shown in Figure 4B as an example. The sequence of all chimeric plasmids was confirmed to be correct by DNA sequencing.

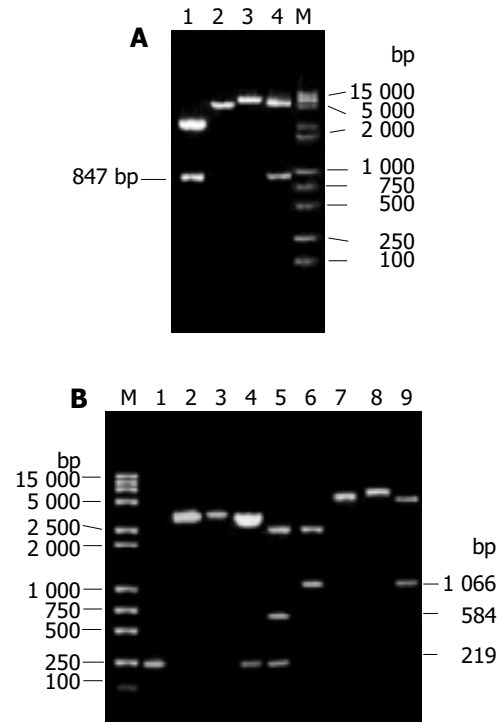


Figure 4 A: RFLP analysis of recombinant plasmid pcHB and chimeric plasmid pcHB-MTEX. Lane 1: Recombinant plasmid pUHB digested with restriction endonucleases *Hind* III and *Eco* RI; Lanes 2 and 3: Plasmid pcDNA3 and recombinant plasmid pcHB digested with restriction endonuclease *Hind* III; Lane 4: Recombinant plasmid pcHB digested with restriction endonucleases *Hind* III and *Eco* RI; Lane M: DNA marker. B: RFLP analysis of the chimeric plasmid pcHB-MTEX. Lane M: DNA marker; Lane 1: MTE5; Lanes 2 and 3: Recombinant plasmid pUHB and pUHB-MTEX digested with restriction endonuclease *Eco* RI; Lane 4: Recombinant plasmid pUHB-MTEX digested with restriction endonuclease *Xba* I; Lane 5: recombinant plasmid pUHB-MTEX digested with restriction endonucleases *Xba* I and *Eco* RI; Lane 6: Recombinant plasmid pUHB-MTEX digested with restriction endonucleases *Hind* III and *Eco* RI; Lanes 7 and 8: Recombinant plasmid pcHB and pcHB-MTEX digested with restriction endonuclease *Eco* RI; Lane 9: Recombinant plasmid pcHB-MTEX digested with restriction endonucleases *Hind* III and *Eco* RI.

Anti-HBs responses

All mice were alive after the inoculation schedule was finished. The anti-HBs levels are shown in Table 2. The anti-HBs level was negative in groups of normal saline and plasmid pcDNA3. The anti-HBs response to co-inoculation of pcHB and pcMTE5 was much higher than that of inoculation of pcHB only (136.7±69.1 mIU/mL vs 27.6±17.3 mIU/mL, the positive rate was 8/10 vs 6/10, $P < 0.01$, $t = -6.56$). Among the 4 chimeric plasmids, only pcHB-MTE-B with MTE5 inserted into pre-S2 region had a good anti-HBs response, which was 57.54±7.68 mIU/mL, and

slightly higher than that of pcHB, and lower than that of the co-inoculation of pcHB and pcMTE5. However, the difference was not statistically significant ($P>0.05$).

Table 2 Effect of MTE5 on anti-HBs response of HBV pre-S2/S gene

Group	Anti-HBs		Enhancement
	Positive ratio	MIU/L (GMT±SE)	
Empty control	0/5	-	-
PcDNA3	0/5	-	-
PcHB	6/10	27.60±17.3	-
PcHB/pcMTE5	8/10	136.70±69.1 ^b	4.95
PcHB-MTEB	7/10	57.540±7.68	2.09
PcHB-MTEX	0/10	-	-
PcHB-MTEH	1/10	1.50	-
PcHB-MTEA	0/10	-	-

GMT: Geometric mean titer; Enhancement: GMT ratio of given group to pcHB, immune enhancement was considered when the ratio was larger than 1. "-" means anti-HBs negative or the enhancement could not be detected. ^b $P<0.01$, $t = -6.56$ vs pcHB group.

Histological findings and HBsAg in mouse muscle cells

Compared with the control groups and the sample from the opposite leg, all experimental groups had obvious inflammation cell filtration in the inoculation sites and HBsAg expression in muscle cells with disassembling and rupture. HBsAg was prominently expressed in cytoplasm of cells. Some cells had membrane expressions simultaneously. The positive signal of HBsAg was usually expressed in cytoplasm, and inflammation was more obvious in non- or low-anti-HBs response groups of chimeric plasmids.

DISCUSSION

The simple way for a given protein to obtain exogenous multiple epitopes was to link them to a higher molecular weight protein. The immune responses were not always good enough because of the interfering effects of immune responses of the carrying protein^[21]. The spliced exogenous multiple epitopes of HTL used in this study, however, might not have immune responses of its own, and were thus preferable. The exogenous multiple epitopes of HTL, MTE5, constructed in this study consisted of 2 universal HTL epitopes and 3 unique HTL epitopes. Two universal epitopes of tetanus toxoid (aa830-843) and artificial epitope PADRE were both effective for 95% individuals of the population^[22-26]. They might cover more individuals when used together. Three unique epitopes from *Mycobacterium tuberculosis* (aa1-20), E2 polyprotein of *rubella* virus (aa54-65) and heat shock protein 60 of *Chlamydia trachomatis* (aa35-48) were selected for HLA-DRB1*3, HLA-DRB1*7 and HLA-DR4 respectively^[27-29]. They could improve the anti-HBs responses of hepatitis B vaccine in individuals who carried these types of HLA II antigens. Thus, the overall response rate of HB vaccine in population could rise dramatically. During the course of splicing, many deletions or mismatches were found in the spliced sequences, especially in the region of synthesized oligonucleotide fragments longer than 50 bp. It implied that synthesized DNA oligonucleotide fragments shorter than 50 bp would be preferable.

A satisfactory anti-HBs response was obtained when MTE5 and pre-S2/S were co-inoculated through DNA immunization, suggesting that MTE5 had immune enhancement. Among the 4 chimeric plasmids, only the recombinant plasmid with MTE5 inserted into the region of pre-S2 had a detectable anti-HBs

response, suggesting that the insertion location of MTE5 was critical for anti-HBs response. The insertion was far from the antigen determinant of HBsAg. Thus, the non-response cause of the rest chimeric plasmids was not clear. HBsAg could be detected in muscle cells at the inoculation site, suggesting that the construction of recombinant plasmids was successful. HBsAg positive signals were mainly located in cytoplasm, suggesting that the poor anti-HBs response might result in failure to secrete the large particles like HBsAg^[30-32].

The chimeric plasmid of pcHB-MTEB had an equal or better anti-HBs response as comparing with that of pcHB, and might be a good candidate for new hepatitis B vaccine in further research. DNA immunization is a simple and quick way to evaluate recombinant plasmids. The response rate of recombinant plasmids, however, was very low in this study. A considerable portion of mice did not develop anti-HBs at all. Its reason is not clear. It might be the nature of DNA immunization because this phenomenon also occurred in other researches^[31]. The exact value should be evaluated after purified recombinant protein is obtained through mammalian expression. The effect on overcoming the drawback of the polymorphism of HLA II antigens should also be evaluated in the future.

REFERENCES

- Liaw YF. Management of patients with chronic hepatitis B. *J Gastroenterol Hepatol* 2002; **17**: 406-408
- Block TM, Mehta AS, Fimmel CJ, Jordan R. Molecular viral oncology of hepatocellular carcinoma. *Oncogene* 2003; **22**: 5093-5107
- Das K, Gupta RK, Kumar V, Kar P. Immunogenicity and reactogenicity of a recombinant hepatitis B vaccine in subjects over age of forty years and response of a booster dose among nonresponders. *World J Gastroenterol* 2003; **9**: 1132-1134
- Kubba AK, Taylor P, Graneek B, Strobel S. Non-responders to hepatitis B vaccination: a review. *Commun Dis Public Health* 2003; **6**: 106-112
- van Zonneveld M, van Nunen AB, Niesters HG, de Man RA, Schalm SW, Janssen HL. Lamivudine treatment during pregnancy to prevent perinatal transmission of hepatitis B virus infection. *J Viral Hepat* 2003; **10**: 294-297
- Wang J, Zhu Q, Zhang X. Effect of delivery mode on maternal-infant transmission of hepatitis B virus by immunoprophylaxis. *Chin Med J* 2002; **115**: 1510-1512
- Kao JH, Chen DS. Global control of hepatitis B virus infection. *Lancet Infect Dis* 2002; **2**: 395-403
- Tsebe KV, Burnett RJ, Hlungwani NP, Sibara MM, Venter PA, Mphahlele MJ. The first five years of universal hepatitis B vaccination in South Africa: evidence for elimination of HBsAg carriage in under 5-year-olds. *Vaccine* 2001; **19**: 3919-3926
- Page M, Jones CD, Bailey C. A novel, recombinant triple antigen hepatitis B vaccine (Hepacare). *Intervirology* 2001; **44**: 88-97
- Thio CL, Thomas DL, Karacki P, Gao X, Marti D, Kaslow RA, Goedert JJ, Hilgartner M, Strathdee SA, Duggal P, O'Brien SJ, Astemborski J, Carrington M. Comprehensive analysis of class I and class II HLA antigens and chronic hepatitis B virus infection. *J Virol* 2003; **77**: 12083-12087
- Hohler T, Reuss E, Evers N, Dietrich E, Rittner C, Freitag CM, Vollmar J, Schneider PM, Fimmers R. Differential genetic determination of immune responsiveness to hepatitis B surface antigen and to hepatitis A virus: a vaccination study in twins. *Lancet* 2002; **360**: 991-995
- Desombere I, Willems A, Leroux-Roels G. Response to hepatitis B vaccine: multiple HLA genes are involved. *Tissue Antigens* 1998; **51**: 593-604
- Watanabe H, Matsushita S, Kamikawaji N, Hirayama K, Okumura M, Sasazuki T. Immune suppression gene on HLA-B*54-DR4-Drw53 haplotype controls nonresponsiveness in human to hepatitis B surface antigen via CD8+ suppressor T cells. *Hum Immunol* 1988; **22**: 9-17
- Hohler T, Meyer CU, Notghi A, Stradmann-Bellinghausen B, Schneider PM, Starke R, Zepp F, Sanger R, Clemens R, Meyer zum Buschenfelde KH, Rittner C. The influence of major histo-

- compatibility complex class II genes and T-cell Vbeta repertoire on response to immunization with HBsAg. *Hum Immunol* 1998; **59**: 212-218
- 15 **Mineta M**, Tanimura M, Tana T, Yssel H, Kashiwagi S, Sasazuki T. Contribution of HLA class I and class II alleles to the regulation of antibody production to hepatitis B surface antigen in humans. *Int Immunol* 1996; **8**: 525-531
- 16 **Chengalvala MV**, Bhat RA, Bhat BM, Vernon SK, Lubeck MD. Enhanced immunogenicity of hepatitis B surface antigen by insertion of a helper T cell epitope from tetanus toxoid. *Vaccine* 1999; **17**: 1035-1041
- 17 **Peng XM**, Xie DY, Gu L, Huang YS, Gao ZL, Yao JL. Effect of exogenous epitopes of helper T lymphocyte on humoral immunity of HBV S gene DNA immunity. *Zhonghua Yixue Zazhi* 2003; **83**: 232-236
- 18 **Hervas-Stubbs S**, Berasain C, Golvano JJ, Lasarte JJ, Prieto I, Sarobe P, Prieto J, Borrás-Cuesta F. Overcoming class II-linked non-responsiveness to hepatitis B vaccine. *Vaccine* 1994; **12**: 867-871
- 19 **Horton RM**, Hunt HD, Ho SN, Pullen JK, Pease LR. Engineering hybrid genes without the use of restriction enzymes: gene splicing by overlap extension. *Gene* 1989; **77**: 61-68
- 20 **An LL**, Whitton JL. A multivalent minigene vaccine, containing B-cell, cytotoxic T-lymphocyte, and Th epitopes from several microbes, induces appropriate responses *in vivo* and confers protection against more than one pathogen. *J Virol* 1997; **71**: 2292-2302
- 21 **Barzu S**, Arondel J, Guillot S, Sansonetti PJ, Phalipon A. Immunogenicity of IpaC-hybrid proteins expressed in the *Shigella flexneri* 2a vaccine candidate SC602. *Infect Immun* 1998; **66**: 77-82
- 22 **Panina-Bordignon P**, Tan A, Termijtelen A, Demotz S, Corradin G, Lanzavecchia A. Universally immunogenic T cell epitopes: promiscuous binding to human MHC class II and promiscuous recognition by T cells. *Eur J Immunol* 1989; **19**: 2237-2242
- 23 **Boitel B**, Blank U, Mege D, Corradin G, Sidney J, Sette A, Acuto O. Strong similarities in antigen fine specificity among DRB1*1302-restricted tetanus toxin tt830-843-specific TCRs in spite of highly heterogeneous CDR3. *J Immunol* 1995; **154**: 3245-3255
- 24 **Valmori D**, Sabbatini A, Lanzavecchia A, Corradin G, Matricardi PM. Functional analysis of two tetanus toxin universal T cell epitopes in their interaction with DR1101 and DR1104 alleles. *J Immunol* 1994; **152**: 2921-2929
- 25 **Franke ED**, Hoffman SL, Sacci JB Jr, Wang R, Charoenvit Y, Appella E, Chesnut R, Alexander J, Del Guercio MF, Sette A. Pan DR binding sequence provides T-cell help for induction of protective antibodies against *Plasmodium yoelii* sporozoites. *Vaccine* 1999; **17**: 1201-1205
- 26 **Alexander J**, Sidney J, Southwood S, Ruppert J, Oseroff C, Maewal A, Snoke K, Serra HM, Kubo RT, Sette A, Grey HW. Development of high potency universal DR-restricted helper epitopes by modification of high affinity DR-blocking peptides. *Immunity* 1994; **1**: 751-761
- 27 **Young SP**, Epstein E, Potter V. Determinant capture by MHC class II DR3 during processing of mycobacteria leprae 65kD heat shock protein by human B cells. *Hum Immunol* 1998; **59**: 259-264
- 28 **Ou D**, Chong P, Choi Y, McVeigh P, Jefferies WA, Koloitis G, Tingle AJ, Gillam S. Identification of T-cell epitopes on E2 protein of rubella virus, as recognized by human T-cell lines and clones. *J Virol* 1992; **66**: 6788-6793
- 29 **Deane KH**, Jecock RM, Pearce JH, Gaston JS. Identification and characterization of a DR4-restricted T cell epitope within chlamydia heat shock protein 60. *Clin Exp Immunol* 1997; **109**: 439-445
- 30 **Davis HL**, Michel ML, Whalen RG. DNA-based immunization induces continuous secretion of hepatitis B surface antigen and high levels of circulating antibody. *Hum Mol Genet* 1993; **2**: 1847-1851
- 31 **Geissler M**, Tokushige K, Chante CC, Zurawski VR Jr, Wands JR. Cellular and humoral immune response to hepatitis B virus structural proteins in mice after DNA-based immunization. *Gastroenterology* 1997; **112**: 1307-1320
- 32 **Geissler M**, Schirmbeck R, Reimann J, Blum HE, Wands JR. Cytokine and hepatitis B virus DNA co-immunizations enhance cellular and humoral immune responses to the middle but not to the large hepatitis B virus surface antigen in mice. *Hepatology* 1998; **28**: 202-210

Edited by Wang XL and Chen WW Proofread by Xu FM

Effect of artificial liver support system on patients with severe viral hepatitis: A study of four hundred cases

Lan-Juan Li, Qian Yang, Jian-Rong Huang, Xiao-Wei Xu, Yue-Mei Chen, Su-Zhen Fu

Lan-Juan Li, Qian Yang, Jian-Rong Huang, Xiao-Wei Xu, Yue-Mei Chen, Su-Zhen Fu, Department of Infectious Diseases, First Hospital, College of Medicine, Zhejiang University, Hangzhou 310003, Zhejiang Province, China

Supported by the National High Technology Research and Development Program of China (863 Program), No. 2003AA205015 and the Major Science Foundation of Zhejiang Province, No. 021107689 and No. 021103126 and the Health Foundation of Zhejiang Province, No. 2003A031

Correspondence to: Dr. Lan-Juan Li, Department of Infectious Disease, First Hospital, College of Medicine, Zhejiang University, 79 Qingchun Road, Hangzhou 310003, Zhejiang Province, China. ljli@zjwst.gov.cn

Telephone: +86-571-87236759 **Fax:** +86-571-87236755

Received: 2004-01-10 **Accepted:** 2004-03-02

Abstract

AIM: To assess the effect of artificial liver support system (ALSS) on patients with severe viral hepatitis, who were divided into treatment group and control group.

METHODS: Four hundred in-hospital patients enrolled during 1995-2003 who received ALSS therapy were studied as the treatment group. Four hundred in-hospital patients enrolled during 1986-1994 who received other medical therapies served as the control group. The methods of ALSS used included plasma exchange, hemoperfusion, hemofiltration, continuous hemodiafiltration (CHDF). The effect of ALSS treatment was studied in patients at different stages of the disease.

RESULTS: The cure rate of acute and subacute severe hepatitis in the treatment group was 78.9% (30/38), and was 11.9% (5/42) in the control group. The improved rate of chronic severe hepatitis in the treatment group was 43.4% (157/362), and was 15.4% (55/358) in the control group. We found that patients treated with ALSS in the early or middle stage of the disease had much higher survival rates than patients in the end stage of the disease.

CONCLUSION: ALSS is an effective and safe therapy for severe viral hepatitis.

Li LJ, Yang Q, Huang JR, Xu XW, Chen YM, Fu SZ. Effect of artificial liver support system on patients with severe viral hepatitis: A study of four hundred cases. *World J Gastroenterol* 2004; 10(20): 2984-2988

<http://www.wjgnet.com/1007-9327/10/2984.asp>

INTRODUCTION

Severe viral hepatitis is the main cause of hepatic failure in China because of the great population of hepatitis B patients, which is different from the Western countries where drugs or alcohol usually is the major cause. Despite a combination of all available treatments, the mortality of hepatic failure is more than 70%^[1,2].

It is believed that damaged liver has the ability to regenerate

and restore normal function of metabolism, synthesis and biotransformation. Liver transplantation remains the only effective therapeutic modality for chronic patients in end-stage^[3-5]. There is also a need to develop a liver support system that can serve as a bridge to transplantation^[6,7], so that patients can be supported until a liver becomes available or the condition of patients is improved. ALSS has been used to treat hepatic failure and has significantly decreased the mortality^[8-11].

We designed an artificial liver support system for severe hepatitis patients. In this report, we described 400 patients with hepatic failure treated with ALSS in our hospital. Data such as concentrations of endotoxin and blood HBV, and serum amino acid spectrum were recorded. The effect of ALSS treatment was also compared in patients at different stages of the disease.

MATERIALS AND METHODS

The treatment group consisting of 400 viral severe hepatitis patients was treated with ALSS at the First Hospital of College of Medicine, Zhejiang University during 1995 to 2003. Two hundred and ninety-five were males and 105 were females. The age ranged from 20 to 64 years, with an average of 34.3±16.5 years. The control group consisting of 400 viral severe hepatitis patients was treated in Department of Internal Medicine at the same hospital during 1986 to 1994, of them 273 were males and 127 were females. The age ranged from 19 to 68 years, with an average of 32.5±18.8 years.

The patients were diagnosed according to the criteria established in the 1995 National Infectious Disease Meeting in Beijing^[12]. Type A hepatitis was diagnosed by the identification of HAV-RNA and/or IgM anti-HAV. The diagnosis of hepatitis B was based on positive HBsAg. Acute type B hepatitis was diagnosed by the presence of HBsAg and/or IgM anti-HBc antibody. Three patients among them were negative for HBsAg but had positive IgM anti-HBc and they were diagnosed as type B hepatitis. All were positive for HBV DNA by PCR. An acute exacerbation of HB in a HBV carrier was diagnosed by a history of known HBsAg positivity for more than 6 mo, the presence of HBV-DNA and a markedly elevated IgG anti-HBc level. Type C hepatitis was diagnosed by the presence of either HCV RNA or anti-HCV antibody. Type B+D hepatitis was diagnosed by the presence of HBsAg and HDV-RNA. Type E hepatitis was diagnosed by the identification of IgM anti-HEV antibody.

Three types of severe viral hepatitis have been found in our country: acute, subacute and chronic severe hepatitis. Violent symptoms of acute severe hepatitis occurred within 10 d after the appearance of clinical manifestations, including malignant jaundice, hepatic encephalopathy (above phase II) and prolonged prothrombin time (PTA<40%). These patients were usually accompanied with shrinking live dullness, rapidly rising blood bilirubin (TB>171 μmol/L) and obvious abnormal liver functions. Subacute severe hepatitis patients were those who had prolonged prothrombin time (PTA<40%) after the occurrence of manifestations for more than 10 d, and meanwhile, they had any one of the following symptoms, namely hepatic encephalopathy (above phase II⁰), rapid rising of blood bilirubin (blood TB more than 171 μmol/L within several days), severe damage of liver functions, extremely fatigue, loss of appetite,

nausea, abdominal distention or hydroperitoneum, sometimes with a tendency to bleed. Chronic severe hepatitis was clinically similar to acute or subacute severe hepatitis, but was distinguished by a known history of HBV carriage, chronic hepatitis or cirrhosis, or by the results of imaging, endoscopy or biopsy showing the existence of chronic hepatitis. Subacute and chronic severe hepatitis was classified into early, middle and end stages. Symptoms of the early stage included fulminant liver failure but without hepatic encephalopathy or ascites. The serum level of bilirubin (TB) was above 171 $\mu\text{mol/L}$, while the prothrombin time rate (PTA) was less than 40%. Liver biopsy was also taken into account when available. In addition, patients in the middle stage had hepatic encephalopathy (II^o above), ascites, or a tendency to bleed with a PTA $\leq 30\%$. End stage patients had severe complications such as hepatorenal syndrome, infection, hepatoencephalopathy (II^o above), electrolytic disturbance, with a PTA $\leq 20\%$.

In the treatment group there were 38 cases of acute or subacute severe hepatitis (6 type A, 8 type A+B, 5 type B+E, 17 type B, 2 type E), while the other 362 were cases of chronic severe hepatitis (310 type B, 18 type A+B, 14 type C, 12 type B+D, 7 type B+E, 1 type B+C+D). The average prothrombin time of the patients on admission was 31.8 ± 7.2 s (the normal was 12 s). Sixty-eight cases were treated with ALSS in the early stage, 186 in the middle stage and 146 in the end stage. In the control group there were 42 cases of acute or subacute severe hepatitis (8 type A, 9 type A+B, 3 type B+E, 20 type B, 1 type E, 1 type B+C+D), while the other 358 were cases of chronic severe hepatitis (313 type B, 16 type A+B, 10 type C, 13 type B+D, 5 type B+E, 1 type B+C+D) (Table 1). The average prothrombin time of the patients in control group on admission was 30.9 ± 8.4 s. Seventy-four patients were diagnosed as early stage, 168 cases as middle stage and 158 as end stage acute or subacute severe hepatitis, respectively. There were no significant differences in sex, ages, etiology and conditions between two groups.

Table 1 Types of severe hepatitis in two groups

Types	Treatment group		Control group	
	Acute and subacute	Chronic	Acute and subacute	Chronic
A	6	0	8	0
B	17	310	20	313
C	0	14	0	10
E	2	0	1	0
B+D	0	12	0	13
A+B	8	18	9	16
B+E	5	7	3	5
B+C+D	0	1	1	1
Total	38	362	42	358

The methods of ALSS included plasma exchange, hemoperfusion, hemofiltration, continuous hemodiafiltration (CHDF). We chose therapy based on the condition of patients. The ALSS treatment room was thoroughly sterilized by UV light before each treatment. The external circulation system and the separator were connected under sterile condition, washed with 0.9% saline solution at 38 °C to remove the micro bubbles in the line, and then filled with 2 mg/500 mL heparin saline solution. The main parts of ALSS were 160-200 g activated carbon absorber, membrane plasma separator, bilirubin absorbent, dialyser, *etc.* Plasma exchange was performed by using a membrane separation method marketed as Plasmacure PS-06 (Kuraray Co., Japan) (Figure 1). Fresh frozen plasma (FFP) was supplied by the Hangzhou Blood Center, Chinese Red Cross. Filtration was performed at a flow rate of 4-6 liters/h using a

bicarbonate buffer, pH 7.4, having a potassium concentration of 4.0 mmol/L. The volume of substitution fluid was adjusted over a range of 6-30 L, depending on the patient's response (Figure 3). Dialysis was performed concurrently at a flow rate of 500 mL/min using a conventional acetate buffer.

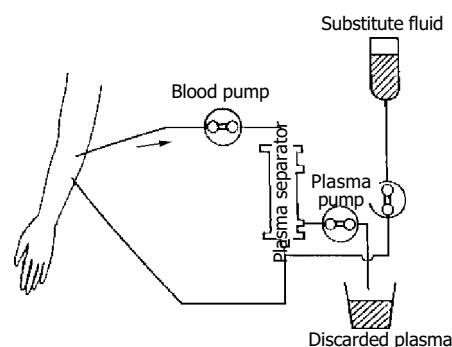


Figure 1 Circuit diagram of plasma exchange.

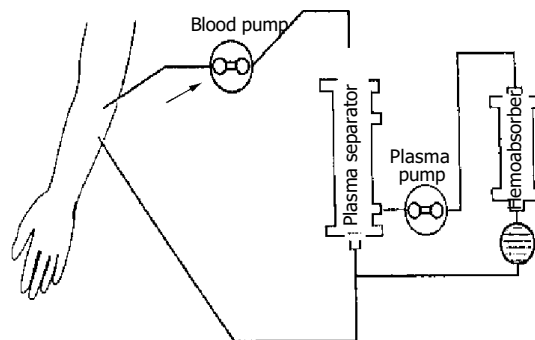


Figure 2 Circuit diagram of plasmapheresis plus plasma absorption. Special absorbers could be used to treat patients with hyperbilirubinemia or hepatic encephalopathy such as bilirubin and carbon absorbers.

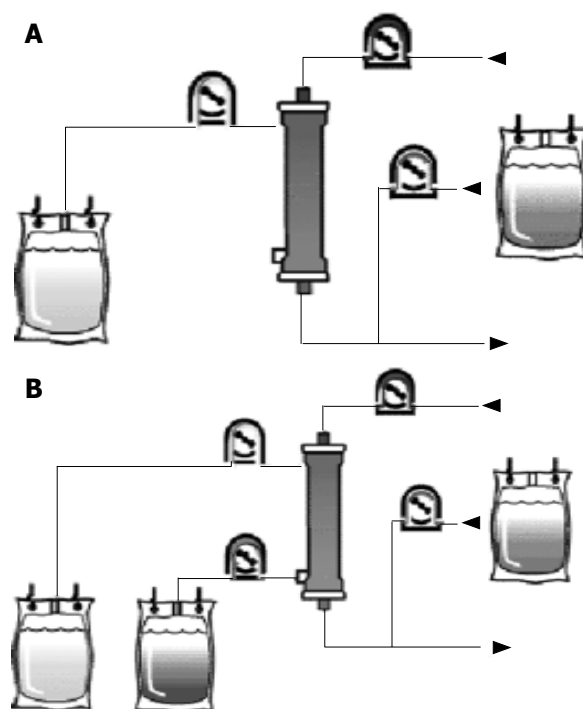


Figure 3 Continuous hemofiltration and hemodiafiltration with aid of a blood pump. A: Continuous hemofiltration with aid of a blood pump; B: Continuous hemodiafiltration with aid of a blood pump.

Before ALSS therapy, blood access was established with a double-lumen catheter inserted into the patient's jugular or femoral vein, and heparin was then used to block the catheter after each session. The circuit diagrams for plasma exchange and perfusion are shown in Figures 1, 2. During each session of ALSS therapy which was lasted for 4-6 h, the total volume of exchanged plasma was about 3 500 mL, and the exchange rate of plasma was 25-30 mL/min. A total of 3 000-4 500 mL of fresh frozen plasma and its substitute fluid, and 20-40 g albumin were supplied. The flow rate of blood was adjusted to 60-130 mL/min, and blood pressure and pulse were recorded continuously during treatment. Prophylactic antibiotics were used before and after therapy. Five mg dexamethasone and 10-20 mg heparin were injected routinely before therapy. During the session, the prothrombin time was tested constantly to allow the dose of heparin to be adjusted. A total of 10-108 mg heparin was used for each session. At the end of each ALSS treatment heparin was neutralized by injection of 10-50 mg of protamine sulphate. ALSS therapy was carried out two or three times in the first or second week, then one time each week till the patient's condition was stable.

Liver function and endotoxin levels were monitored during the therapy. Amino acid spectra were determined for 25 subjects by auto amino acid analyzing system, performed at the Analyzing Center of the Second Medical University in Shanghai. Endotoxin level was measured by quantitative Azo color test. HBV-DNA concentration in 10 cases was measured by chiron branched chain DNA assay, performed at the Virus Center of Luebrek Medical University, Germany.

Statistical analysis

All data were presented as mean±SE. The data were analyzed by SPSS 10.0. The Student's *t* test or Fischer's exact test was used to determine the level of significance between groups. A *P*-value <0.05 was considered statistically significant.

RESULTS

Nearly 90% patients experienced an improvement in symptoms such as fatigue or abdominal distention after each treatment. Results of liver function tests improved significantly in all subjects. The serum ALT, AST and TBA levels declined significantly (*P*<0.001), the level of serum bilirubin decreased from 511.36±192.81 μmol/L to 257.38±123.48 μmol/L (*P*<0.001), while the prothrombin time decreased from 31.8±7.2 s to 23.6±6.8 s (Table 2). The serum endotoxin levels before therapy in all hepatic failure patients were above the upper limit of normal which was 40 ng/L. After ALSS therapy, serum endotoxin levels declined from 58.2±12.3 ng/L to 32.4±7.8 ng/L (*P*<0.001). In the 10 patients tested, the HBV-DNA concentration declined from an average of 2 588±1 534 copies/mL to 1 815±620 copies/mL (*P*<0.05) as a result of ALSS therapy. The serum level of aromatic amino acids (AAA), such as methionine, tyrosine, phenylalanine, cysteine, arginine, especially methionine declined significantly (*P*<0.05) in 25 subjects. Meanwhile, the ratio of branched-chain amino acid/aromatic amino acid (BCAA/AAA) increased significantly (*P*<0.05) (Table 3). No significant difference in TNF, rIL-2R and IL-2 levels before and after the ALSS treatment was observed (Table 4). There was no disturbance of electrolytes after ALSS therapy.

Seventeen candidates for orthotopic liver transplantation (OLT) received 2-3 runs of ALSS and were "bridged" successfully to OLT. After OLT, ALSS was used to replace liver function in non-function period. Twelve of 17 patients were completely recovered and 3 died of infection, acute rejection and abdominal bleeding.

Among the 38 patients with acute or subacute severe hepatitis treated with ALSS 3-5 times, 30 of them (78.9%)

survived for at least half a year but 8 died in 1 mo. One hundred and fifty-seven of 362 patients with chronic severe hepatitis were cured or greatly improved, 107 patients were discharged as their own will, and 98 patients died in the next 3 months, so the cure rate was 43.4%. In the control group, the cure rate of acute and subacute severe hepatitis was 11.9% (5/42), while cure and improved rate of chronic severe hepatitis was only 15.4% (55/358) (Table 5). There were significant differences in the cure rate between two groups (*P*<0.001). More importantly, in the treatment group, the cure rate of patients in early or middle stage (76.5% and 61.8%, respectively) was much higher than that those in end-stage (13.7%, Table 6).

Table 2 Result of liver function test before and after ALSS therapy (mean±SE)

Liver function	Pre-treatment	Post-treatment	<i>P</i>
ALT (U/L)	123.35±281.32	53.15±94.21	<0.001
AST (U/L)	126.84±115.25	63.71±58.45	<0.001
ALP (U/L)	127.97±66.74	81.45±39.62	<0.001
TBil (μmol/L)	511.36±192.81	257.38±123.48	<0.001
ChE (U/L)	2 572.58±2 236.95	3 119.24±1 812.62	0.001
γ-GT (U/L)	42.38±53.85	20.91±25.58	<0.001
TBA (μmol/L)	256.36±48.69	119.42±49.37	<0.001
PT (s)	31.8±7.2	23.6±6.8	<0.001

Table 3 Serum amino acid levels in 25 cases before and after the first ALSS therapy (mean±SE)

	Pre-therapy (μmol/L)	After therapy (μmol/L)
Cys	65.63±41.40	53.74±26.86 ^a
Phe	94.78±62.00	80.92±40.75 ^a
Ala	256.51±123.73	267.84±138.32
Gly	194.89±83.43	212.50±106.07
Glu	118.50±89.65	116.85±91.26
Gln	494.16±218.91	515.84±208.81
Met	185.85±142.33	149.91±134.16 ^b
Arg	170.44±231.69	143.18±175.92 ^a
Lys	220.72±168.05	190.29±136.28
Tyr	121.98±82.82	104.44±59.94 ^a
Leu	73.73±58.81	78.17±43.74
Orn	113.99±94.58	92.84±52.93
Tau	46.41±27.34	43.51±32.90
Ser	123.78±64.83	122.22±61.29
Thr	165.60±83.34	152.94±83.42
Asp	16.22±10.72	13.38±7.87
Asn	59.40±46.09	64.52±49.46
Val	121.69±75.01	126.35±68.72
Ile	44.86±36.61	46.29±25.88
His	96.18±73.85	87.86±51.56
BCAA/AAA	1.18±0.39	1.52±0.77 ^a

^a*P*<0.05; ^b*P*<0.001 vs pre-therapy group.

Table 4 Endotoxin, TNF, rIL-2R, IL-2 in patients with hepatic failure before and after ALSS therapy (mean±SE)

	Pre-treatment	Post-treatment	<i>P</i>
Endotoxin (ng/L)	58.2±12.3	32.4±7.8	<0.005
TNF (ng/L)	3.4±1.2	3.2±1.2	>0.05
rIL-2R (U/mL)	1 040.1±309.2	951.0±285.6	>0.05
IL-2 (ng/mL)	20.1±1.9	9.7±1.8	>0.05

Complications occurred during ALSS therapy included skin rash, hypotension, blood coagulation in perfusion apparatus,

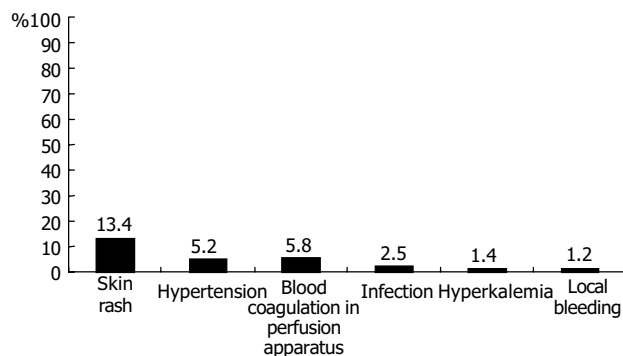
Table 5 Prognosis of ALSS treatment group and control group

	ALSS treatment group				Control group			
	Acute and subacute severe hepatitis		Chronic severe hepatitis		Acute and subacute severe hepatitis		Chronic severe hepatitis	
	Cases	Ratio (%)	Cases	Ratio (%)	Cases	Ratio (%)	Cases	Ratio (%)
Cured	30	78.9	157	43.4	5	11.9	55	15.4
Discharged as their own will	2	5.3	107	29.6	16	38.1	122	34.0
Died	6	15.8	98	27.0	21	50.0	181	50.6
Total	38	100	362	100	42	100	358	100

infection, hyperkalemia, and local bleeding (Figure 4). All patients recovered after management of these complications, except one patient who died of intracranial bleeding.

Table 6 Outcome of patients in different stages after ALSS treatment

Stages	Cured		Discharged		Died		Total
	Cases	%	Cases	%	Cases	%	
Early stage	52	76.5	9	13.2	7	10.3	68
Middle stage	115	61.8	34	18.3	37	19.9	186
End stage	20	13.7	68	46.6	58	39.7	146
Total	187	46.8	111	27.8	102	25.5	400

**Figure 4** Incidence rate of complications of ALSS therapy.

DISCUSSION

In acute liver failure, the liver parenchyma injured by viral, toxic, or some other insults failed to function sufficiently. Temporary support of normal liver function would promote the damaged liver to restore its normal function. Artificial liver support system could serve this purpose. Moreover, when the liver lost its ability to function normally, then an artificial liver support system might be used as a “bridge” to liver transplantation^[6,7]. Although various liver assistant devices have been introduced during the past 40 years, a complete artificial liver system that can support patients with severe hepatic failure till the damaged liver restores its normal function has not yet been developed^[8].

We modified the artificial liver support system for treatment of patients with severe hepatic failure. We substituted the usual 50 g activated carbon absorber with 160-200 g one to remove toxic substances of intermediate molecular weight from blood. The 160-200 g carbon absorber proved to be appropriate, as a larger carbon absorber might destroy blood cells and cause side effects. The bilirubin absorbent could absorb excess bilirubin from the plasma, so that the cleaned plasma could be retransmitted to patients directly. The membrane plasma separator could separate and discard plasma containing toxic substances, and supply normal fresh plasma containing albumin and coagulation factors for patients. The volume exchanged

utilizing this method was about 3 500 mL each time, much more than that utilizing traditional centrifugation methods, which exchanged only 800-1 000 mL each time. Continuous hemodiafiltration (CHDF) could eliminate middle and small molecular toxic substances, and keep the balance of internal environment^[13]. These methods were used in different combinations based on the symptoms of patients (Figures 1-3). For example, when patients had hepatic encephalopathy, we performed plasma exchange in combination with plasma perfusion. For patients with hepatorenal syndrome, we chose plasma exchange and hemodialysis or hemofiltration or CHDF. For those with hyperbilirubinemia, plasma bilirubin absorption in combination with hemoperfusion was used. When the balance of water or electrolytes was disturbed, we used plasma exchange and hemofiltration or CHDF. Sometimes, more than three methods were used together for one patient. In addition, we carefully adjusted the dose of heparin and protamine according to PT, and maintained fluid balance to decrease complications such as bleeding, hemolysis, hypotension. This was crucial to decrease the mortality of hepatic failure.

Changes in the spectrum of amino acids might be another benefit of ALSS therapy. It has been shown that the concentration of aromatic amino acids (AAA) was increased in patients with fulminant hepatitis failure^[14,15]. Moreover, the concentration of methionine was a sensitive indicator of liver injury because methionine was released while liver necrosis^[16]. Methionine was toxic to the central nervous system, and one of the main causes of hepatic encephalopathy^[17]. After ALSS therapy, the serum level of aromatic amino acids, especially methionine declined and the ratio of BCAA/AAA was significantly increased.

In this study, we found that the cure rate of treatment group was significantly higher than that of the control group, indicating that ALSS is an effective therapy in treating patients with severe hepatitis. We also compared the efficiency of ALSS therapy in different stages of severe liver disease and concluded that the cure rate of early or middle stage severe hepatitis was much higher than that of end stage severe hepatitis (76.5%, 61.8% vs 13.7%, respectively). It is possible that ALSS may provide a favorable internal environment for hepatocytes to regenerate and restore normal function in patients at early or middle stage. However, there was massive necrosis of hepatocytes in hepatitis patients at end stage, and liver regeneration was not sufficient to recover liver function. Our data suggested that ALSS therapy might be an effective method to treat hepatitis patients at early stages.

Liver transplantation could provide good results in the treatment of hepatic failure, with a 5-year survival rate of 60%^[6,18]. However, its use has been greatly limited because of the lack of sufficient liver donors. Therefore, a system that can serve as a “bridge” to eventual OLT would greatly extend the survival rate^[19,20]. Based on our data, the artificial liver support system could serve as an effective “bridge” to OLT. Plasmapheresis was also beneficial, as the levels of coagulation factors and albumin could be increased by several plasma exchanges^[19]. Hemoperfusion was effective in improving the neurologic status

of patients with hepatic failure^[8,21]. Hemodialysis, hemofiltration or CHDF could correct the disturbance of water or electrolytes of patients^[13,22]. So ALSS could improve the condition of patients until a donor liver was available. Complications of the transplantation included acid-base imbalance, hyperbilirubinemia, disturbance of electrolytes, dysfunction of blood coagulation, acute rejection, etc.^[23]. ALSS treatment could improve the internal environment to support patients in pre- and post-transplantation periods. In addition ALSS could therefore improve the result of OLT in patients with severe liver disease. Further appropriately controlled trials are being initiated to confirm this observation.

REFERENCES

- 1 **Shakil AO**, Kramer D, Mazariegos GV, Fung JJ, Rakela J. Acute liver failure: clinical features, outcome analysis, and applicability of prognostic criteria. *Liver Transpl* 2000; **6**: 163-169
- 2 **Mas A**, Rodes J. Fulminant hepatic failure. *Lancet* 1997; **349**: 1081-1085
- 3 **Ostapowicz G**, Lee WM. Acute hepatic failure: a western perspective. *J Gastroenterol Hepatol* 2000; **15**: 480-488
- 4 **van Hoek B**, de Boer J, Boudjema K, Williams R, Corsmit O, Terpstra OT. Auxiliary versus orthotopic liver transplantation for acute liver failure. EURALT Study Group. European Auxiliary Liver Transplant Registry. *J Hepatol* 1999; **30**: 699-705
- 5 **Miwa S**, Hashikura Y, Mita A, Kubota T, Chisuwa H, Nakazawa Y, Ikegami T, Terada M, Miyagawa S, Kawasaki S. Living-related liver transplantation for patients with fulminant and subfulminant hepatic failure. *Hepatology* 1999; **30**: 1521-1526
- 6 **Amy L**, Friedman. Why bioartificial liver support remains the holy grail. *ASAIO J* 1998; **44**: 241-243
- 7 **Abouna GM**, Ganguly PK, Hamdy HM, Jabur SS, Tweed WA, Costa G. Extracorporeal liver perfusion system for successful hepatic support pending liver regeneration or liver transplantation: a pre-clinical controlled trial. *Transplantation* 1999; **67**: 1576-1583
- 8 **Uchino J**, Matsushita M. Strategies for the rescue of patients with liver failure. *ASAIO J* 1994; **40**: 74-77
- 9 **Lanjuan L**, Qian Y, Jianrong H, Xiaowei X, Yuemei C, Yagang C, Weihang M, Zhi C, Suzhen F. Severe hepatitis treated with an artificial liver support system. *Int J Artif Organs* 2001; **24**: 297-303
- 10 **Sussman NL**, Gislason GT, Conlin CA, Kelly JH. The hepatic extracorporeal liver assist device: initial clinical experience. *Artif Organs* 1994; **18**: 390-396
- 11 **Li L**, Yang Q, Huang J, Xu X, Chen Y, Chen Y, Ma W, Chen Z, Fu S. Treatment of hepatic failure with artificial liver support system. *Chin Med J* 2001; **114**: 941-945
- 12 **Si CW**, Zhang H, Wang BE. Prevention and cure project of viral hepatitis. Revised Statement 5th National Infectious Disease Meeting, Beijing, 1995. *Zhonghua Chuanranbing Zazhi* 1995; **13**: 241-247
- 13 **Sadahiro T**, Hirasawa H, Oda S, Shiga H, Nakanishi K, Kitamura N, Hirano T. Usefulness of plasma exchange plus continuous hemodiafiltration to reduce adverse effects associated with plasma exchange in patients with acute liver failure. *Crit Care Med* 2001; **29**: 1386-1392
- 14 **Kato A**, Suzuki K, Sato S. Imbalance of amino acid metabolism in fulminant hepatitis and its management. *Nippon Rinsho* 1992; **50**: 1599-1603
- 15 **Takahashi Y**. Evaluation of the special therapies in fulminant viral hepatitis - a multi-institution study. *Nippon Shokakibyo Gakkai Zasshi* 1995; **92**: 7-18
- 16 **Higashi T**. Impaired metabolism of methionine in severe liver diseases: I. Clinical and pathophysiological significance of elevated serum methionine levels. *Gastroenterol Jpn* 1982; **17**: 117-124
- 17 **Toborek M**, Kopiczna-Grzebieniak E, Drozd M, Wieczorek M. Increased lipid peroxidation and antioxidant activity in methionine induced hepatitis in rabbits. *Nutrition* 1996; **12**: 534-537
- 18 **Goss JA**, Shackleton CR, Maggard M, Swenson K, Seu P, McDiarmid SV, Busuttill RW. Liver transplantation for fulminant hepatic failure in the pediatric patient. *Arch Surg* 1998; **133**: 839-846
- 19 **Agishi T**, Nakagawa Y, Teraoka S, Kubo K, Nakazato S, Ota K. Plasma exchange as a rescue strategy for hepatic failure. *ASAIO J* 1994; **40**: 77-79
- 20 **Larsen FS**, Hansen BA, Jorgensen LG, Secher NH, Bondesen S, Linkis P, Hjortrup A, Kirkegaard P, Agerlin N, Kondrup J. Cerebral blood flow velocity during high volume plasmapheresis in fulminant hepatic failure. *Int J Artif Organs* 1994; **17**: 353-361
- 21 **Ash SR**. Hemodiabsorption in the treatment of acute hepatic failure. *ASAIO J* 1994; **40**: 80-82
- 22 **Kaplan AA**, Epstein M. Extracorporeal blood purification in the management of patients with hepatic failure. *Semin Nephrol* 1997; **17**: 576
- 23 **Zhu XF**, Chen GH, He XS, Lu MQ, Wang GD, Cai CJ, Yang Y, Huang JF. Liver transplantation and artificial liver support in fulminant hepatic failure. *World J Gastroenterol* 2001; **7**: 566-568

Edited by Wang XL Proofread by Chen WW and Xu FM

• VIRAL HEPATITIS •

Yeast expression and DNA immunization of hepatitis B virus S gene with second-loop deletion of α determinant region

Hui Hu, Xiao-Mou Peng, Yang-Su Huang, Lin Gu, Qi-Feng Xie, Zhi-Liang Gao

Hui Hu, Xiao-Mou Peng, Yang-Su Huang, Lin Gu, Qi-Feng Xie, Zhi-Liang Gao, Department of Infectious Diseases, the Third Affiliated Hospital, Sun Yat-Sen University, Guangzhou 510630, Guangdong Province, China

Supported by the National Natural Science Foundation of China, No. 39970677 and the Science Foundation of Guangdong Province, No. 99M04801G

Correspondence to: Xiao-Mou Peng, Department of Infectious Diseases, the Third Affiliated Hospital, Sun Yat-Sen University, Guangzhou 510630, Guangdong Province, China. xiaomoupeng@hotmail.com

Telephone: +86-20-85516867 Ext. 2019 Fax: +86-20-85515940

Received: 2004-03-23 Accepted: 2004-04-13

Abstract

AIM: Immune escape mutations of HBV often occur in the dominant epitope, the second-loop of the α determinant of hepatitis B surface antigen (HBsAg). To let the hosts respond to the subdominant epitopes in HBsAg may be an effective way to decrease the prevalence of immune escape mutants. For this reason, a man-made clone of HBV S gene with the second-loop deletion was constructed. Its antigenicity was evaluated by yeast expression analysis and DNA immunization in mice.

METHODS: HBV S gene with deleted second-loop, amino acids from 139 to 145, was generated using splicing by overlap extension. HBV deleted S gene was then cloned into the yeast expression vector pPIC9 and the mammalian expression vector pcDNA3 to generate pHB-SDY and pHB-SD, respectively. The complete S gene was cloned into the same vectors as controls. The deleted recombinant HBsAg expressed in yeasts was detected using Abbott IMx HBsAg test kits, enzyme-linked immunoadsorbent assay (ELISA) and immune dot blotting to evaluate its antigenicity *in vitro*. The anti-HBs responses to DNA immunization in BALB/c mice were detected using Abbott IMx AUSAB test kits to evaluate the antigenicity of that recombinant protein *in vivo*.

RESULTS: Both deleted and complete HBsAg were successfully expressed in yeasts. They were intracellular expressions. The deleted HBsAg could not be detected by ELISA, in which the monoclonal anti-HBs against the α determinant was used, but could be detected by Abbott IMx and immune dot blotting, in which multiple monoclonal anti-HBs and polyclonal anti-HBs were used, respectively. The activity of the deleted HBsAg detected by Abbott IMx was much lower than that of complete HBsAg (the ratio of sample value/cut off value, 106 ± 26.7 vs $1\ 814.4 \pm 776.3$, $P < 0.01$, $t = 5.02$). The anti-HBs response of pHB-SD to DNA immunization was lower than that of complete HBV S gene vector pHB (the positive rate $2/10$ vs $6/10$, 4.56 ± 3.52 mIU/mL vs 27.60 ± 17.3 mIU/mL, $P = 0.02$, $t = 2.7$).

CONCLUSIONS: HBsAg with deleted second-loop of the α determinant still has antigenicity, and can also raise weak anti-HBs response in mice to DNA immunization, suggesting

that it is possible to develop a subdominant vaccine for preventing infections of immune escape mutants of HBV.

Hu H, Peng XM, Huang YS, Gu L, Xie QF, Gao ZL. Yeast expression and DNA immunization of hepatitis B virus S gene with second-loop deletion of α determinant region. *World J Gastroenterol* 2004; 10(20): 2989-2993

<http://www.wjgnet.com/1007-9327/10/2989.asp>

INTRODUCTION

The prevalence of hepatitis B virus (HBV) is still high in some areas of the world^[1,2]. Universal inoculation of hepatitis B vaccine helps to sharply decrease the prevalence of HBsAg carriers from about 10% to 2% among the urban children in China^[3]. However, there are about 5-10% of healthy individuals demonstrating no or inadequate responses following a standard vaccination schedule^[4,5]. A portion of these non-responders may be with a breakthrough infection of immune escape mutants^[6,7]. The escape mutant infections were also frequently occurred in liver transplant recipients under hepatitis B immunoglobulin prophylaxis^[8,9]. The prevalence of the mutants, usually as occult HBV infections, will progressively increase in the future since certain mutants are stable enough to be horizontally transmittable^[10,11] and have a potential to be transmitted through blood transfusion because of escaping the routine screening assays. The second-loop from aa139 to aa147 of the α determinant of HBsAg is the dominant epitope. The escape mutants usually have mutations in this region, including K141E, P142S, D144E and G145R^[8,9,12-16], though there are mutations in the rest part of HBsAg^[17,18], and induce an altered immunity against the second-loop so that the mutants can escape vaccine-raised antibodies or rabbit polyclonal antibodies to some extent^[19,20]. Fortunately, recent researches suggested that weak epitopes, such as subdominant epitopes, might not be escaped^[21,22]. To let hosts respond to subdominant epitopes or to both dominant and subdominant epitopes may be an effective way for the prevention of escape mutant infections. For these reasons, a man-made clone of HBV S gene with the second-loop deletion of the α determinant region was constructed in order to destroy the dominant epitope and let the subdominant epitopes be responded by the hosts. The antigenicity of that deleted S gene was evaluated by means of yeast expression analysis and DNA immunization in mice.

MATERIALS AND METHODS

Reagents

pTZ19U-HBV containing double copies of HBV DNA (adw) was presented from professor Zhi-Min Huang, Zhongshan University, Guangzhou, China. pcDNA3 and pPIC9 were purchased from Invitrogen Company (the United States of America). T4 DNA ligase and pfu DNA polymerase were purchased from Promega Company (the United States of America). DNA gel extraction kits and plasmid isolation kits were purchased from Qiagen Company (Germany). Primers shown in Table 1 were synthesized by Bioasia Biological

Table 1 Primers used in construction of eukaryotic expression vectors

Name	Sequences (5'→3')
HBS-SD1	TCC AAG CTT ATG GGA TCC GAG AAC ATC ACA TCA GGA TTC
HBS-SD2	GCA ACA TGA GGG AAA CAT AG
HBS-SD3	TCT ATG TTT CCC TCA TGT TGC AAT TGC ACC TGT ATT CCC ATC
HBS-SD4	TCC GAA TTC TTT TGT TAG GGT TTA AAT GTA TAC C
HBPIC9-1	CCG GAA TTC GAC GAT GAC GAT AAG GAG AAC ATC ACA TCA GGA TTC
HBPIC9-2	CAA CGC GGC CGC TTA AAT GTA TAC CCA GAG AC

Engineering Company (Shanghai, China). ELISA HBsAg kit was purchased from Zhongshan Biological Engineering Company (Guangdong, China). Abbott IMx HBsAg and AUSAB test kits were purchased from Abbott Laboratory (the United States of America). Sheep polyclonal anti-HBs and labeled streptavidin biotin detecting kit were purchased from DAKO Company (the United States).

Animal

Eight to twelve week-old inbred BALB/c female mice were obtained from Guangzhou Traditional Chinese Medicine University.

Construction of HB-SD and HB-SDY fragments

HB-SD was the fragment of HBV S gene with deletion of seven amino acid residues from 139 to 145 of the second-loop of the α determinant. In order to construct HB-SD, Two fragments of HBV S gene from codon 1 to codon 138 and from codon 146 to codon 226 were obtained by polymerase chain reaction (PCR) using HBS-SD1/HBS-SD2 and HBS-SD3/HBS-SD4 as primers, respectively, and pTZ19U-HBV as template. The fragments were then connected using splicing by overlap extension after the PCR products were run on 20 g/L agarose gel and a given band was extracted using DNA gel extraction kit^[23]. HB-SD was obtained at last by purifying the spliced products. HB-SDY was obtained by PCR using HB-SD as template and HBSPIC9-1/HBSPIC9-2 as primers. The control fragments of complete HBV S gene were obtained using pTZ19U-HBV as template, and HBS-SD1/HBS-SD4 or HBSPIC9-1/HBSPIC9-2 as primers.

Construction of recombinant vector pHB-SDY and pHB-SD

For construction of pHB-SDY, the fragments of HB-SD and pPIC9 were digested by restriction endonucleases *Eco*RI and *Not* I, respectively. For construction of pHB-SD, the fragment of HB-SD was digested by restriction endonucleases *Hind* III and *Eco* RI, respectively as well as pcDNA3. Digested DNA fragment and vector DNA were ligated using T4 DNA ligase after purification. Plasmid DNA was obtained after *Escherichia coli* was transformed by ligated products. Candidate recombinant plasmids were selected by restriction fragment length polymorphism (RFLP) analysis and automatic DNA sequencing by Bioasia Biological Engineering Company. Control vectors pHB and pHBV were generated using the control fragments of complete HBV S gene in the same way.

Expression of pHB-SDY in yeast

The recombinant vector DNA of pHB-SDY and pHBV was prepared from transformed bacteria using Qiagen's Max-Prep kits. Yeast cells from a single colony of *Pichia pastoris* GS115 strain were cultivated using YPD culture. Vector DNA was transformed into yeast cells by lithium chloride transformation method. Transformants were grown on minimal dextrose and minimal methanol plates to screen Mut⁺ and Mut^S phenotypes. PCR using AOX1 primers was utilized to screen integrants. Mut^S strain was cultivated in BMGY culture and induced using 5 mL/L methanol. Protein expression of the supernatants and cell pellets

was analyzed by Coomassie-stained SDS-PAGE, ELISA, Abbott IMx and immune dot blotting assay. ELISA and IMx tests were carried out as the manufacturer's protocol. Immune dot blotting was carried out using sheep polyclonal anti-HBs as first antibody and LSAB kit to demonstrate the results.

DNA immunization analysis of pHB-SD

Large scale plasmid DNA of recombinant plasmids pHB-SD and pHB was prepared using Qiagen's Max-Prep kits. Plasmid DNA of pcDNA3 was also prepared to be used as control. Plasmid DNA was adjusted to 1 μ g/ μ L in normal saline. Thirty BLBA/c mice were randomly divided into 4 groups. Each mouse was injected 100 μ L of plasmid DNA which was distributed over five different sites into the anterior tibialis muscle 5 d after the injection of an equal volume of 2 g/L bupivacaine. Boost injection was carried out 3 times every 3 wk with equal amount of plasmid DNA. Four weeks after the last boost injection, all mice were put to death for serum. Anti-HBs in serum was detected using Abbott AUSAB kits.

Statistical analysis

For anti-HBs level, geometric mean titer (GMT) for each group was calculated at first. Then Student-Newman-Keuls-q was used for statistical analysis. For positive rate, Fisher exact probability analysis was used. SPSS 10.0 for Windows was used for all statistical analysis. $P < 0.05$ was considered statistically significant.

RESULTS

Construction of HB-SD and HB-SDY

Two fragments for constructing HB-SD fragment (Figure 1) were successfully obtained with base pair number as expected. The base pair number of spliced HB-SD fragment (Figure 1) was just a little smaller than that of HB fragment (Figure 1), which was the PCR fragment of complete HBV S gene with 711 bp in length. That was conformed to the fact that HB-SD fragment was only 21 bp smaller than HB fragment. HBV and HB-SDY fragments are shown in Figure 1. Their base pair numbers were the same as designed.

Construction of pHB-SD and pHB-SDY

HB-SD fragment was inserted into the vector of pcDNA3 between restriction endonucleases *Hind* III and *Eco*RI. When recombinant plasmids were digested with the two restriction endonucleases, the molecular weight of the small restriction fragment was the same as that of HB-SD (Figure 2). After its sequence was confirmed by DNA sequencing, the recombinant plasmid was denominated as pHB-SD. The HB fragment was cloned into the same vector to obtain a recombinant plasmid of pHB as control. HB-SDY fragment was inserted into the vector of pPIC9 between restriction endonucleases *Eco* RI and *Not* I. The digested fragment shown in Figure 2 was the same as designed in base pair numbers. The recombinant vector was denominated as pHB-SDY after its sequence was confirmed by DNA sequencing. HBV fragment was cloned into the pPIC9 to obtain recombinant vector of pHBV as control.

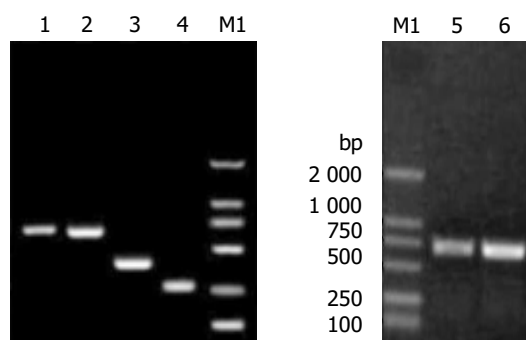


Figure 1 Electrophoresis of the fragments of HBV S gene. Lane 1: HB fragment of complete HBV S gene; Lane 2: HB-SD fragment with the second-loop deletion of the α determinant; Lane 3: DNA fragment of HBV S gene from codon 1 to codon 138; Lane 4: DNA fragment of HBV S gene from codon 146 to codon 226; Lane 5: HBV fragments; Lane 6: HB-SDY fragments; Lane M1: DNA marker.

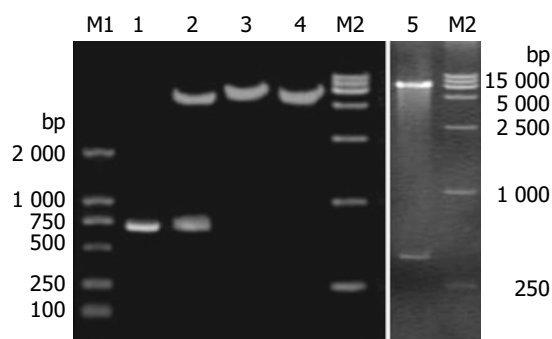


Figure 2 RFLP analysis of recombinant vectors of pHB-SD and pHB-SDY. Lane M1: DNA marker; Lane 1: HB-SD fragment; Lane 2: pHB-SD candidate digested by restriction endonuclease *Hind* III and *Eco* RI; Lane 3: pHB-SD candidate digested by restriction endonuclease *Bam* HI; Lane 4: pcDNA3 digested by restriction endonuclease *Bam* HI; Lane 5: pHB-SDY candidate digested by restriction endonuclease *Not* I and *Eco* RI; Lane M2: DNA marker.

Expression of recombinant plasmid pHB-SDY in yeast

Mut^s transformants for pHB-SDY and its control pHB-Y were successfully selected though growing on plates of minimal dextrose and minimal methanol. The integrant screening results of transformants are shown in Figure 3. The PCR product of Mut^r transformants without gene of interest was 2.2 kb (Figure 3A). The PCR product of pPIC9 alone was 492 bp (Figure 3A). The PCR products of integrants of pHB-Y and pHB-SDY were 1 200 bp and 1 179 bp respectively. These transformants shown in Figure 3A were recombinants with the genes of interest, and belonged to Mut^s transformants since they had no bands of wild-type *AOX1* gene. The results of Coomassie-stained SDS-PAGE analysis of the protein expression of Mut^s transformants with pHB-Y and pHB-SDY are shown in Figure 3B. No recombinant protein was visible. The results of HBsAg antigenicity detection using ELISA and immune dot blotting are shown in Figure 4. The expression of transformants with pHB-Y was intracellular. The recombinant protein of pHB-SDY could not be detected by ELISA, and only weakly demonstrated by immune dot blotting assay. The IMx results are shown in Table 2. The ratio of sample value/cut off value of pHB-SDY was much lower than that of pHB-Y ($P < 0.01$, $t = 5.02$).

DNA immunization

All mice were alive after the inoculation schedule was finished. The anti-HBs levels are shown in Table 2. The anti-HBs was

negative in groups of normal saline and plasmid pcDNA3. The positive rate of anti-HBs was 2/10 in pHB-SD group and 6/10 in pHB group. The amount of anti-HBs induced in groups of HBV S gene with deleted second-loop of the α determinant was less than that in the complete HBV S gene groups ($P = 0.02$, $t = 2.7$).

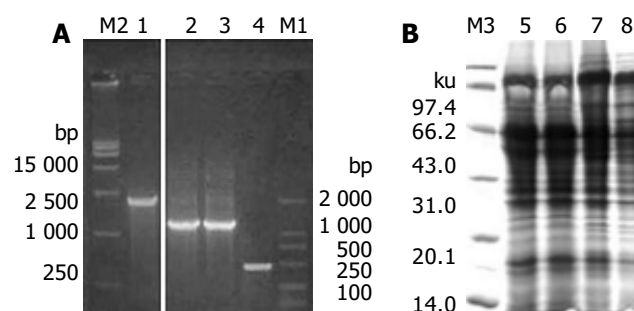


Figure 3 Screening integrants and SDS-PAGE analysis. A: Screening integrants using PCR with *AOX1* primers. Lane M2: DNA marker; Lane 1: PCR products of Mut^r transformant without gene of interest; Lane 2: PCR products of Mut^s transformants with pHB-Y; Lane 3: PCR products of Mut^s transformants with pHB-SDY; Lane 4: PCR products of pPIC9 alone. Lane M1 were DNA markers. B: Coomassie-stained SDS-PAGE analysis of the recombinant proteins of pHB-SDY and pHB-Y. Lane M3: protein marker; Lane 5: cell lysate supernatants of yeast alone; Lane 6: yeast transformed with pPIC9; Lane 7: yeast transformed with pHB-Y; Lane 8: yeast transformed with pHB-SDY.

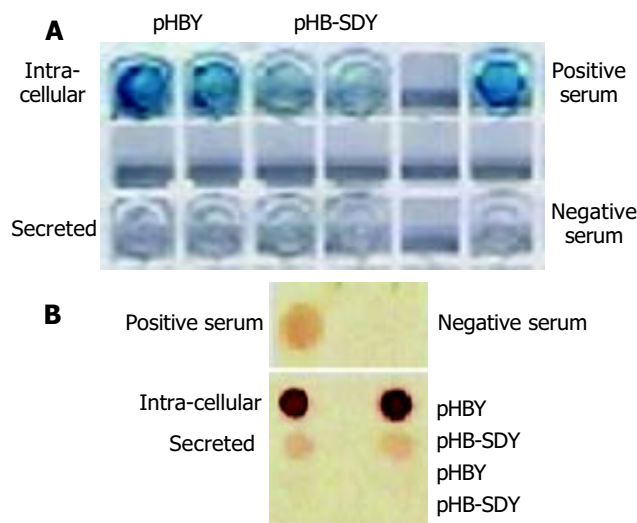


Figure 4 Antigenicity analysis of recombinant proteins using ELISA and immune dot blotting assay. (A) ELISA, (B) immune dot blotting assay.

Table 2 Antigenicity of HBsAg with second-loop deletion of α determinant

Groups	HBsAg titer by IMx S/CO value	Anti-HBs responses in DNA immunization	
		Positive rate	mIU/L (GMT \pm SE)
Empty control	-	0/5	-
pcDNA3	-	0/5	-
pHB	1 589 \pm 234.5 ^b	6/10	27.60 \pm 17.3 ^c
pHB-SD	106 \pm 26.8	2/10	4.56 \pm 3.52

S/CO: the ratio of sample against cut off value. GMT: geometric mean titer. ^b $P < 0.01$, $t = 5.02$ vs groups of pHB-SD; ^c $P = 0.02$, $t = 2.7$ vs groups of pHB-SD.

DISCUSSION

The hosts usually do not respond to the subdominant epitopes in both vaccinated individuals and patients because of the dominant negative mechanism. Since they usually have no escape mutations and are not tolerant in patients, the subdominant epitopes have been widely used to overcome immunological tolerance in the fields of tumor and chronic infections^[24-27]. Many subdominant epitopes were successfully responded by the hosts with chronic infections or tumor carrying patients^[24-29]. However, the most data were limited in CD8+ cells or cytotoxic T lymphocytes. There are few such literatures about the epitopes of B lymphocytes. As a protective antigen, HBsAg is of great significance for prevention of HBV infection. It has been confirmed that there are more than three B-lymphocyte epitopes in HBsAg. The second-loop of α determinant is the strongest one among them^[30]. It is the dominant epitope, and the rest ones are the subdominant epitopes.

To completely destroy the dominant epitope may be able to eliminate the dominant negative mechanism, and let the subdominant epitopes be responded by the hosts. In our study even after deletion of the second-loop of HBsAg α determinant, the recombinant protein expressed in yeasts still had a weak antigenicity. Though it escaped the monoclonal anti-HBs derived from the α determinant, the recombinant protein might react with polyclonal anti-HBs or monoclonal anti-HBs derived from other parts of HBsAg because it could be detected by immune dot blotting and Abbott IMx kits, in which the demonstrating antibodies consisted of monoclonal anti-HBs derived from α determinant and the rest part of HBsAg^[31]. These results are similar to that of the α determinant variants that could be detected by monoclonal antibody from the rest part of HBsAg too^[22]. Mammalian expression vector with deleted HBV S gene could raise a weak anti-HBs response to DNA immunization. It was not sure that this anti-HBs was protective. However, it might be able to react with HBV particles since the anti-HBs derived from the first-loop of the α determinant of HBsAg could be accessible on native HBsAg^[21]. These suggested that it was possible to develop a subdominant vaccine for the prevention of immune escape mutant infections of HBV.

The response rate of recombinant plasmids was very low in our study. It might be the nature of DNA immunization because this phenomenon also occurred in researches of other scientists^[32]. The deleted HBV S gene was successfully expressed in yeasts. However, the expression conditions need to be improved. The exact value of deleted HBsAg should be evaluated after purified recombinant proteins are obtained in the future. The effect of anti-HBs raised by subdominant epitopes of HBsAg on the infectivity of HBV should also be evaluated in the future.

HBsAg with deleted second-loop of the α determinant still has antigenicity, and can also raise weak anti-HBs response in mice to DNA immunization, suggesting that it is possible to develop a subdominant vaccine for preventing infections of immune escape mutants of HBV.

REFERENCES

- Kao JH**, Chen DS. Global control of hepatitis B virus infection. *Lancet Infect Dis* 2002; **2**: 395-403
- Huang P**, Ye G, Zhong J, Sha Q. Assessment of current epidemiological status of viral hepatitis in Guangdong Province, China. *Southeast Asian J Trop Med Public Health* 2002; **33**: 832-836
- Kane MA**. Global control of primary hepatocellular carcinoma with hepatitis B vaccine: the contributions of research in Taiwan. *Cancer Epidemiol Biomarkers Prev* 2003; **12**: 2-3
- Tao Q**, Feng B. Prevention and therapy of hepatitis B. *Chin Med J* 1999; **112**: 942-946
- Andre FE**, Zuckerman AJ. Review: protective efficacy of hepatitis B vaccines in neonates. *J Med Virol* 1994; **44**: 144-151
- He C**, Nomura F, Itoga S, Isobe K, Nakai T. Prevalence of vaccine-induced escape mutants of hepatitis B virus in the adult population in China: a prospective study in 176 restaurant employees. *J Gastroenterol Hepatol* 2001; **16**: 1373-1377
- Jeaentet D**, Chemin I, Mandrand B, Zoulim F, Trepo C, Kay A. Characterization of two hepatitis B virus populations isolated from a hepatitis B surface antigen-negative patient. *Hepatology* 2002; **35**: 1215-1224
- Kim KH**, Lee KH, Chang HY, Ahn SH, Tong S, Yoon YJ, Seong BL, Kim SI, Han KH. Evolution of hepatitis B virus sequence from a liver transplant recipient with rapid breakthrough despite hepatitis B immune globulin prophylaxis and lamivudine therapy. *J Med Virol* 2003; **71**: 367-375
- Poovorawan Y**, Theamboonlers A, Chongsrisawat V, Sanpavatt S. Molecular analysis of the a determinant of HBsAg in children of HBeAg-positive mothers upon failure of postexposure prophylaxis. *Int J Infect Dis* 1998; **2**: 216-220
- Levicnik-Stežinar S**. Hepatitis B surface antigen escape mutant in a first time blood donor potentially missed by a routine screening assay. *Clin Lab* 2004; **50**: 49-51
- Chakravarty R**, Neogi M, Roychowdhury S, Panda CK. Presence of hepatitis B surface antigen mutant G145R DNA in the peripheral blood leukocytes of the family members of an asymptomatic carrier and evidence of its horizontal transmission. *Virus Res* 2002; **90**: 133-141
- Thakur V**, Kazim SN, Guptan RC, Malhotra V, Sarin SK. Molecular epidemiology and transmission of hepatitis B virus in close family contacts of HBV-related chronic liver disease patients. *J Med Virol* 2003; **70**: 520-528
- Cooreman MP**, Leroux-Roels G, Paulij WP. Vaccine- and hepatitis B immune globulin-induced escape mutations of hepatitis B virus surface antigen. *J Biomed Sci* 2001; **8**: 237-247
- Koyanagi T**, Nakamuta M, Sakai H, Sugimoto R, Enjoji M, Koto K, Iwamoto H, Kumazawa T, Mukaide M, Nawata H. Analysis of HBs antigen negative variant of hepatitis B virus: unique substitutions, Glu129 to Asp and Gly145 to Ala in the surface antigen gene. *Med Sci Monit* 2000; **6**: 1165-1169
- Hou J**, Wang Z, Cheng J, Lin Y, Lau GK, Sun J, Zhou F, Waters J, Karayiannis P, Luo K. Prevalence of naturally occurring surface gene variants of hepatitis B virus in nonimmunized surface antigen-negative Chinese carriers. *Hepatology* 2001; **34**: 1027-1034
- Karthigesu VD**, Allison LM, Fortuin M, Mendy M, Whittle HC, Howard CR. A novel hepatitis B virus variant in the sera of immunized children. *J Gen Virol* 1994; **75**(Pt 2): 443-448
- Chen HB**, Fang DX, Li FQ, Jing HY, Tan WG, Li SQ. A novel hepatitis B virus mutant with A-to-G at nt551 in the surface antigen gene. *World J Gastroenterol* 2003; **9**: 304-308
- Komatsu H**, Fujisawa T, Sogo T, Isozaki A, Inui A, Sekine I, Kobata M, Ogawa Y. Acute self-limiting hepatitis B after immunoprophylaxis failure in an infant. *J Med Virol* 2002; **66**: 28-33
- Shizuma T**, Hasegawa K, Ishikawa K, Naritomi T, Iizuka A, Kanai N, Ogawa M, Torii N, Joh R, Hayashi N. Molecular analysis of antigenicity and immunogenicity of a vaccine-induced escape mutant of hepatitis B virus. *J Gastroenterol* 2003; **38**: 244-253
- Oon CJ**, Chen WN, Goh KT, Mesenas S, Ng HS, Chiang G, Tan C, Koh S, Teng SW, Toh I, Moh MC, Goo KS, Tan K, Leong AL, Tan GS. Molecular characterization of hepatitis B virus surface antigen mutants in Singapore patients with hepatocellular carcinoma and hepatitis B virus carriers negative for HBsAg but positive for anti-HBs and anti-HBc. *J Gastroenterol Hepatol* 2002; **17**(Suppl): S491-S496
- Ijaz S**, Ferns RB, Tedder RS. A 'first loop' linear epitope accessible on native hepatitis B surface antigen that persists in the face of 'second loop' immune escape. *J Gen Virol* 2003; **84**(Pt 2): 269-275
- Jolivet-Reynaud C**, Lesenechal M, O'Donnell B, Becquart L, Foussadier A, Forge F, Battail-Poirot N, Lacoux X, Carman W, Jolivet M. Localization of hepatitis B surface antigen epitopes present on variants and specifically recognised by anti-hepatitis B surface antigen monoclonal antibodies. *J Med Virol* 2001; **65**: 241-249

- 23 **Horton RM**, Hunt HD, Ho SN, Pullen JK, Pease LR. Engineering hybrid genes without the use of restriction enzymes: gene splicing by overlap extension. *Gene* 1989; **77**: 61-68
- 24 **Marastoni M**, Bazzaro M, Micheletti F, Gavioli R, Tomatis R. Peptide analogues of a subdominant epitope expressed in ebv-associated tumors: synthesis and immunological activity. *J Med Chem* 2001; **44**: 2370-2373
- 25 **Hudrisier D**, Riond J, Gairin JE. Molecular and functional dissection of the H-2Db-restricted subdominant cytotoxic T-cell response to lymphocytic choriomeningitis virus. *J Virol* 2001; **75**: 2468-2471
- 26 **Barouch DH**, Craiu A, Santra S, Egan MA, Schmitz JE, Kuroda MJ, Fu TM, Nam JH, Wyatt LS, Lifton MA, Krivulka GR, Nickerson CE, Lord CI, Moss B, Lewis MG, Hirsch VM, Shiver JW, Letvin NL. Elicitation of high-frequency cytotoxic T-lymphocyte responses against both dominant and subdominant simian-human immunodeficiency virus epitopes by DNA vaccination of rhesus monkeys. *J Virol* 2001; **75**: 2462-2467
- 27 **Nelson D**, Bundell C, Robinson B. *In vivo* cross-presentation of a soluble protein antigen: kinetics, distribution, and generation of effector CTL recognizing dominant and subdominant epitopes. *J Immunol* 2000; **165**: 6123-6132
- 28 **Tourdout S**, Oukka M, Manuguerra JC, Magafa V, Vergnon I, Riche N, Bruley-Rosset M, Cordopatis P, Kosmatopoulos K. Chimeric peptides: a new approach to enhancing the immunogenicity of peptides with low MHC class I affinity: application in antiviral vaccination. *J Immunol* 1997; **159**: 2391-2398
- 29 **Chengalvala MV**, Bhat RA, Bhat BM, Vernon SK, Lubeck MD. Enhanced immunogenicity of hepatitis B surface antigen by insertion of a helper T cell epitope from tetanus toxoid. *Vaccine* 1999; **17**: 1035-1041
- 30 **Maillard P**, Pillot J. At least three epitopes are recognized by the human repertoire in the hepatitis B virus group a antigen inducing protection; possible consequences for seroprevention and serodiagnosis. *Res Virol* 1998; **149**: 153-161
- 31 **Shah DO**, Coleman P, Chen J, Peterson B, Dimarco A, Stewart J. The detection of recombinant hepatitis B surface antigen from "vaccine escape mutants" in two HBsAg immunoassays. *Clin Lab* 2000; **46**: 161-163
- 32 **Geissler M**, Tokushige K, Chante CC, Zurawski VR Jr, Wands JR. Cellular and humoral immune response to hepatitis B virus structural proteins in mice after DNA-based immunization. *Gastroenterology* 1997; **12**: 1307-1320

Edited by Kumar M and Wang XL Proofread by Xu FM

Prominent role of γ -glutamyl-transpeptidase on the growth of *Helicobacter pylori*

Min Gong, Bow Ho

Min Gong, Bow Ho, Department of Microbiology, Faculty of Medicine, National University of Singapore, Singapore 117597, Republic of Singapore

Supported by NMRC Grant No. 0415/2000. Gong Min is a National University of Singapore research scholar

Correspondence to: Bow Ho, Department of Microbiology, Faculty of Medicine, National University of Singapore, Science Drive 2, Singapore 117597, Republic of Singapore. michob@nus.edu.sg

Telephone: +65-68743672 **Fax:** +65-67766872

Received: 2003-10-10 **Accepted:** 2003-12-03

Abstract

AIM: γ -glutamyl transpeptidase (GGT) has been reported as a virulence and colonizing factor of *Helicobacter pylori* (*H pylori*). This study examined the effect of GGT on the growth of *H pylori*.

METHODS: Standard *H pylori* strain NCTC 11637 and 4 clinical isolates with different levels of GGT activity as measured by an enzymatic assay were used in this study. Growth inhibition and stimulation studies were carried out by culturing *H pylori* in brain heart infusion broth supplemented with specific GGT inhibitor (L-serine sodium borate complex, SBC) or enhancer (glutathione together with glycyl-glycine), respectively. The growth profiles of *H pylori* were determined based on viable bacterial count at time interval.

RESULTS: Growth was more profuse for *H pylori* isolates with higher GGT activity than those present with lower GGT activity. However, in the presence of SBC, growth of *H pylori* was retarded in a dose dependent manner ($P = 0.034$). In contrast, higher growth rate was observed when GGT activity was enhanced in the presence of glutathione and glycyl-glycine.

CONCLUSION: Higher GGT activity provides an advantage to the growth of *H pylori in vitro*. Inhibition of GGT activity by SBC resulted in growth retardation. The study shows that GGT plays an important role on the growth of *H pylori*.

Gong M, Ho B. Prominent role of γ -glutamyl-transpeptidase on the growth of *Helicobacter pylori*. *World J Gastroenterol* 2004; 10(20): 2994-2996

<http://www.wjgnet.com/1007-9327/10/2994.asp>

INTRODUCTION

Helicobacter pylori (*H pylori*) is a gram-negative spiral bacterium that causes chronic infection of the human stomach in adults^[1-5] as well as children^[6]. The chronic *H pylori* infection may lead to peptic ulceration^[7-9] and may be a potential risk factor for gastric carcinoma^[10-12].

The exact mechanism on how *H pylori* promotes gastric neoplasia is not known but is hypothesized to have occurred through the production of reactive oxygen species leading to oxidative stress and DNA damage in gastric epithelial cells^[13-15].

The level of reduced form of the tripeptide thiol, glutathione (GSH), one of the major endogenous defense mechanisms against oxidative stress, was shown to be decreased in gastric mucosal after *H pylori* infection^[16,17]. Furthermore, it has been well established that GGT plays a major role in glutathione metabolism. This enzyme catalyses transpeptidation reaction in which a γ -glutamyl moiety is transferred from γ -glutamyl compounds, such as glutathione, a non-protein sulphhydryl molecule, to amino acids. In addition, GGT can use γ -glutamyl peptides as substrates in the reciprocal hydrolysis reaction, thus playing a role in the synthesis of glutathione^[18,19].

It has been reported that GGT activity could be inhibited by the presence of inhibitors like L-serine sodium borate complex (SBC)^[20] and acivicin^[21]. Although acivicin is a more effective GGT inhibitor, it is nonspecific and inhibits a number of glutamine amino-transferase^[21]. In contrast, SBC is a highly specific GGT inhibitor but substantially higher concentration of SBC as compared to acivicin is needed for an effective inhibition of GGT activity^[20].

GGT being a constitutive enzyme of *H pylori* was shown to participate in the colonization of *H pylori* in Swiss specific pathogen-free mice^[22]. However, a later study using a different animal model demonstrated that GGT was not essential for colonization but acted as a virulence factor^[23]. The present study examined the effect of GGT on *H pylori* growth *in vitro* in the presence of GGT inhibitor as well as enhancer.

MATERIALS AND METHODS

Bacterial strains and culture conditions

A standard *H pylori* strain NCTC 11 637 and 4 clinical isolates with different levels of GGT activity were used in this study. Strains 712 and 1 018 showed high GGT activity (>1 U/mg protein) while strains 1 082 and 888 had low GGT activity (<0.4 U/mg protein).

H pylori was grown for 3 d at 37 °C on chocolate blood agar containing 40 g/L blood agar base No.2 (Oxoid) and 50 mL/L horse blood (Gibco) in a humidified incubator (Forma Scientific) supplied with 50 mL/L CO₂^[24]. The bacterial cells were harvested and washed with PBS buffer (pH 7.4) to give a suspension of ca. 5×10⁷ CFU/mL ($A_{600} = 0.2$) in either PBS or brain heart infusion (BHI, Gibco) broth.

Inhibitory effect of SBC on *H pylori* GGT activity

A bacterial population of 3 d old 10⁷ CFU/mL *H pylori* NCTC 11 637 was incubated in BHI broth containing various concentrations (2-10 mmol/L) of SBC (Sigma) at 37 °C for 30 min. GGT activity of *H pylori* cells was then measured by an enzymatic assay as described by Meister *et al.*^[25].

Growth inhibition and stimulation studies

H pylori NCTC 11 637 was suspended in fresh BHI broth at a final cell concentration of approximately 5×10⁵ CFU per ml. For growth inhibition study, appropriate volumes of filter-sterilized (pore size, 0.2 μ m; Nalgene sterile syringe filter) SBC stock solution (100 mmol/L) were added to sterile BHI broth to provide final concentrations of SBC in BHI in the range of 2-10 mmol/L. For growth stimulation study, filter-sterilized glycyl-glycine

(Sigma) and GSH (Sigma) were added to BHI broth at a final concentration of 1 mmol/L and 0.1 mmol/L, respectively.

Growth inhibition and stimulation curves were constructed based on viable bacterial count at different time interval.

Growth of various *H pylori* strains that expressed different levels of GGT activity

Two strains each with high GGT activity (strains 1 018 and 712) and low GGT activity (strains 1 082 and 888) were grown in BHI broth at 37 °C over a period of 3 wk. The bacterial populations of the various strains were enumerated at time interval.

Statistical analysis

Data was analyzed using one-way ANOVA test (SPSS). A value of $P \leq 0.05$ was considered statistically significant.

RESULTS

SBC inhibits GGT activity of *H pylori*

Figure 1 shows that *H pylori* strain NCTC 11 637 GGT activity was inhibited in a dose dependent manner upon exposure to a range of SBC concentrations (2-10 mmol/L) for 30 min at 37 °C, where >90% GGT activity was inhibited by ≥ 4 mmol/L SBC. The maximum inhibitory effect of 96% of GGT activity was achieved at the concentration of 10 mmol/L SBC.

Effect of GGT on *H pylori* growth

Since SBC has inhibitory effect on *H pylori* GGT activity, *H pylori* NCTC 11 637 was cultured in BHI broth supplemented with different concentrations of SBC (2-10 mmol/L). Figure 2 shows that the *H pylori* cultured in the presence of various concentrations of SBC (2-10 mmol/L) over 3 wk displayed marked inhibition on the growth of *H pylori* in a dose dependent manner (ANOVA, $P = 0.034$). A >99% decrease in viability of the bacterial population was observed within 72 h after culturing *H pylori* in the presence of 10 mmol/L SBC. In contrast, *H pylori* proliferated at twice the normal growth rate in the presence of GSH and glycyl-glycine with increased GGT activity as compared to the control. And this acceleration in growth lasted over a period of more than two weeks. Similar growth profile was observed with another *H pylori* strain SS1 (data not shown).

Growth of different *H pylori* strains

Growth of the four *H pylori* strains with disparate GGT activities was followed over a period of 3 wk. Figure 3 shows that *H pylori* isolates with higher GGT activity (strains 1 018 and 712) grew better and more abundant than those with lower GGT activity (strains 1 082 and 888) by 10-100 folds depending on the age of culture. However, all 4 cultures showed similar growth rate at 3 wk-old.

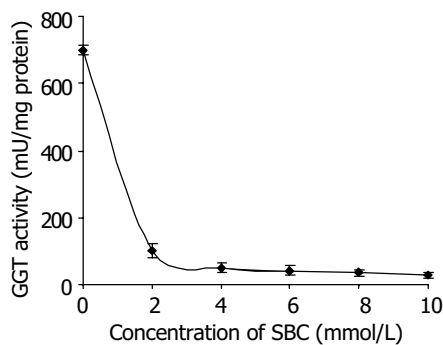


Figure 1 Inhibitory effect of SBC on *H pylori* GGT activity. Inhibition of 85%, 92%, 94%, 95% and 96% were obtained by incubating *H pylori* in 2, 4, 6, 8 and 10 mmol/L SBC, respectively at 37 °C for 30 min.

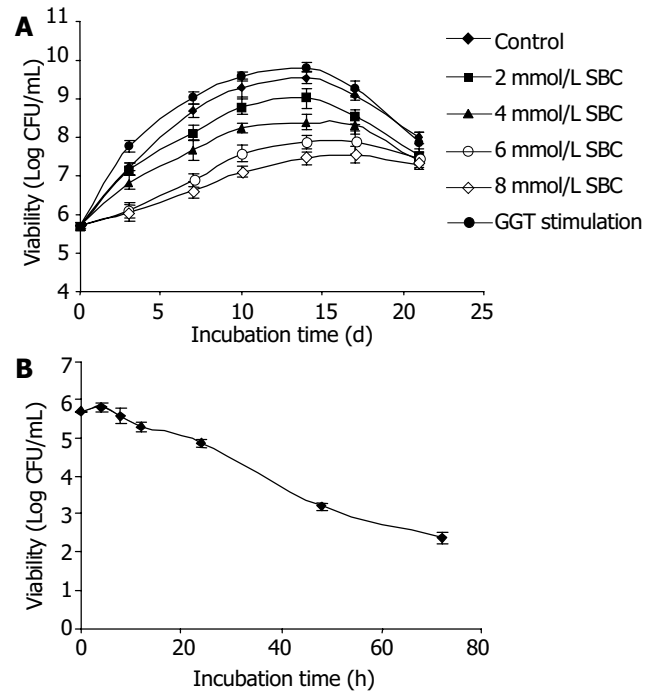


Figure 2 Effect of GGT on the growth of *H pylori*. *H pylori* strain NCTC 11 637 was cultured microaerobically in BHI broth medium supplemented with 10% fetal bovine serum at 37 °C and in the presence of either different concentration of GGT inhibitor or stimulator. A: Effect of 2 mmol/L (■ square), 4 mmol/L (▲ triangle), 6 mmol/L (× cross), 8 mmol/L (* star) SBC and GGT stimulation (0.1 mol/L GSH+1 mol/L glycyl-glycine, ● circle) on NCTC 11 637 over 21 d. Control (◆ diamond). B: Effect of 10 mmol/L SBC on NCTC 11 637 over 72 h. Viability was determined continuously at time intervals. (CFU: colony-forming units).

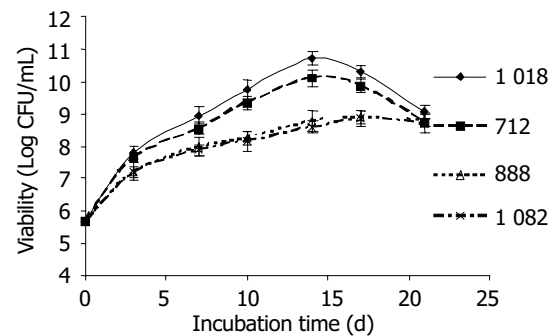


Figure 3 Growth of 4 *H pylori* strains with different levels of GGT activity. *H pylori* strains 1 018 and 712 expressed high GGT activity (>1 U/mg protein) while strains 888 and 1 082 produced low GGT activity (<0.4 U/mg protein). *H pylori* strains 1 018 (◆ diamond), 712 (■ square), 888 (△ triangle), and 1 082 (× cross) were cultured in BHI medium microaerobically over 3 wk. Viability was determined continuously at time intervals.

DISCUSSION

Inhibition of GGT activity by SBC was caused by competition with respect to γ -glutamyl substrate, and it was suggested that a serine-borate complex is formed which may bind to the active site of the enzyme by interacting with a carbohydrate residue of the enzyme^[20]. Although acivicin is 20 times more effective in inhibiting GGT activity as compared to SBC (data not shown), it was not used for the growth inhibition study because it is a non-specific GGT inhibitor^[21]. In this study, more than 90% of GGT activity was suppressed by 4 mmol/L SBC. Inhibition of

GGT activity by SBC resulted in retarding the growth of *H pylori* in a dose dependent manner indicating that GGT is an essential enzyme in the growth of *H pylori*. In contrast, when physiological concentration of GSH and glycyl-glycine^[26,27] were supplemented into the culture medium, growth of *H pylori* was accelerated by more than two folds. The results show that the growth of *H pylori* was enhanced under GGT stimulation condition demonstrating the possibility of such event in *in vivo* situation.

In this study, it is interesting to note that *H pylori* with higher GGT activity (>1 U/mg protein) grows better than those with lower GGT activity (<0.4 U/mg protein). However, in the presence of SBC, a specific GGT inhibitor, the growth of *H pylori* was shown to be retarded. This finding that GGT is vital for the growth of *H pylori* could possibly explain why there was a reduction in the recovery of GGT isogenic mutant in the postinfected mice in the *in vivo* study carried out by McGovern *et al.*^[23], while no *ggt* mutant *H pylori* were recovered in the animal model of Chevalier *et al.*^[22]. The explanation supports the role of GGT activity in the ability of *H pylori* to proliferate in *in vivo* condition. However, the variation could also be due to the difference in animal model as suggested by McGovern *et al.*^[23], or owing to strain difference in terms of the level of GGT activity expressed as demonstrated in this study.

It has been reported that GGT plays a significant role in *H pylori*-mediated apoptosis^[28]. It was therefore suggested that *H pylori* induces apoptosis by GGT and that the bacteria gain essential nutrients from the apoptotic cells, thus establishing a permanent colony *in vivo*^[28,29]. The results of earlier studies^[22,23,28] indicated that GGT is an important enzyme for the growth and survival of *H pylori in vivo* while our findings that growth of *H pylori* is relative to the level of bacterial GGT activity and that higher GGT activity favors its growth *in vitro*. It is therefore proposed that GGT has a vital and prominent role to play on the growth of *H pylori*.

REFERENCES

- 1 Israel DA, Peek RM. Pathogenesis of *Helicobacter pylori*-induced gastric inflammation. *Aliment Pharmacol Ther* 2001; **15**: 1271-1290
- 2 Sanders MK, Peura DA. *Helicobacter pylori*-Associated Diseases. *Curr Gastroenterol Rep* 2002; **4**: 448-454
- 3 Min K, Hong SM, Kim KR, Ro JY, Park MJ, Kim JS, Kim JM, Jung HC, Yu E. Intramucosal *Helicobacter pylori* in the human and murine stomach: its relationship to the inflammatory reaction in human *Helicobacter pylori* gastritis. *Pathol Res Pract* 2003; **199**: 1-8
- 4 Shibata K, Moriyama M, Fukushima T, Une H, Miyazaki M, Yamaguchi N. Relation of *Helicobacter pylori* infection and lifestyle to the risk of chronic atrophic gastritis: a cross-sectional study in Japan. *J Epidemiol* 2002; **12**: 105-111
- 5 Cave DR. Chronic gastritis and *Helicobacter pylori*. *Semin Gastrointest Dis* 200; **12**: 196-202
- 6 Ng BL, Quak SH, Aw M, Goh KT, Ho B. Immune responses to differentiated forms of *Helicobacter pylori* in children with Epigastric pain. *Clin Diagn Lab Immunol* 2003; **10**: 866-869
- 7 Lai YC, Wang TH, Huang SH, Yang SS, Wu CH, Chen TK, Lee CL. Density of *Helicobacter pylori* may affect the efficacy of eradication therapy and ulcer healing in patients with active duodenal ulcers. *World J Gastroenterol* 2003; **9**: 1537-1540
- 8 Nomura AM, Perez-Perez GI, Lee J, Stemmermann G, Blaser MJ. Relation between *Helicobacter pylori cagA* status and risk of peptic ulcer disease. *Am J Epidemiol* 2002; **155**: 1054-1059
- 9 Stack WA, Atherton JC, Hawkey GM, Logan RF, Hawkey CJ. Interactions between *Helicobacter pylori* and other risk factors for peptic ulcer bleeding. *Aliment Pharmacol Ther* 2002; **16**: 497-506
- 10 Dawsey SM, Mark SD, Taylor PR, Limburg PJ. Gastric cancer and *H pylori*. *Gut* 2002; **51**: 457-458
- 11 Blaser MJ. Linking *Helicobacter pylori* to gastric cancer. *Nat Med* 2000; **6**: 376-377
- 12 Takahashi S. Long-term *Helicobacter pylori* infection and the development of atrophic gastritis and gastric cancer in Japan. *J Gastroenterol* 2002; **37**(Suppl 13): 24-27
- 13 Davies GR, Simmonds NJ, Stevens TR, Sheaff MT, Banatvala N, Laurenson IF, Blake DR, Rampton DS. *Helicobacter pylori* stimulates antral mucosal reactive oxygen metabolite production *in vivo*. *Gut* 1994; **35**: 179-185
- 14 Obst B, Wagner S, Sewing KF, Beil W. *Helicobacter pylori* causes DNA damage in gastric epithelial cells. *Carcinogenesis* 2000; **21**: 1111-1115
- 15 Farinati F, Cardin R, Degan P, Rugge M, Mario FD, Bonvicini P, Naccarato R. Oxidative DNA damage accumulation in gastric carcinogenesis. *Gut* 1998; **42**: 351-356
- 16 Beil W, Obst B, Sewing KF, Wagner S. *Helicobacter pylori* reduces intracellular glutathione in gastric epithelial cells. *Dig Dis Sci* 2000; **45**: 1769-1773
- 17 Shirin H, Pinto JT, Liu LU, Merzianu M, Sordillo EM, Moss SF. *Helicobacter pylori* decreases gastric mucosal glutathione. *Cancer Letters* 2001; **164**: 127-133
- 18 Meister A, Anderson ME. Glutathione. *Annu Rev Biochem* 1983; **52**: 711-760
- 19 Tate SS, Meister A. γ -glutamyl transpeptidase catalytic, structural and functional aspects. *Mol Cell Biochem* 1981; **39**: 357-368
- 20 Tate SS, Meister A. Serine-borate complex as a transition-state inhibitor of γ -glutamyl transpeptidase. *Proc Natl Acad Sci U S A* 1978; **75**: 4806-4809
- 21 Anderson ME, Meister A. Inhibition of γ -glutamyl transpeptidase and glutathionuria produced by γ -glutamyl amino acids. *Proc Natl Acad Sci U S A* 1986; **83**: 5029-5032
- 22 Chevalier C, Thiberge JM, Ferrero RL, Labigne A. Essential role of *Helicobacter pylori* γ -glutamyl transpeptidase for the colonization of the gastric mucosa of mice. *Mol Microbiol* 1999; **31**: 1359-1372
- 23 McGovern KJ, Blanchard TG, Gutierrez JA, Czinn SJ, Krakowka S, Youngman P. γ -glutamyltransferase is a *Helicobacter pylori* virulence factor but is not essential for colonization. *Infect Immun* 2001; **69**: 4168-4173
- 24 Zheng PY, Hua J, Yeoh KG, Ho B. Association of peptic ulcer with increased expression of Lewis antigens but not *cagA*, *iceA*, and *vacA* in *Helicobacter pylori* isolates in an Asian population. *Gut* 2000; **47**: 18-22
- 25 Meister A, Tate SS, Griffith OW. γ -Glutamyl transpeptidase. *Methods Enzymol* 1981; **77**: 237-253
- 26 Tate SS, Meister A. γ -Glutamyl transpeptidase from kidney. *Meth Enzymol* 1985; **113**: 400-419
- 27 Paroni R, Vecchi ED, Cighetti G, Arcelloni C, Fermo I, Grossi A, Bonini P. HPLC with o-phthalaldehyde precolumn derivatization to measure total, oxidized, and protein-bound glutathione in blood, plasma, and tissue. *Clin Chem* 1995; **41**: 448-454
- 28 Shibayama K, Kamachi K, Nagata N, Yagi T, Nada T, Doi Y, Shibata N, Yokoyama K, Yamane K, Kato H, Iinuma Y, Arakawa Y. A novel apoptosis-inducing protein from *Helicobacter pylori*. *Mol Microbiol* 2003; **47**: 443-451
- 29 Shibayama K, Doi Y, Shibata N, Yagi T, Nada T, Iinuma Y, Arakawa Y. Apoptotic signaling pathway activated by *Helicobacter pylori* infection and increase of apoptosis-inducing activity under serumstarved conditions. *Infect Immun* 2001; **69**: 3181-3189

• *H pylori* •

Detection of anti-*Helicobacter pylori* antibodies in serum and duodenal fluid in peptic gastroduodenal disease

Angelo Locatelli, Wilson Roberto Catapani, Claudio Rufino Gomes Junior, Claudilene Battistin Paula Silva, Jaques Waisberg

Angelo Locatelli, Wilson Roberto Catapani, Claudio Rufino Gomes Junior, Claudilene Battistin Paula Silva, Jaques Waisberg, Department of Surgery, ABC Faculty of Medicine, Avenida Principe de Gales 821, Santo Andre, Sao Paulo, 09060-650, Brazil
Correspondence to: Dr. Jaques Waisberg, Rua das Figueiras 550, apto.134, Santo Andre - Sao Paulo 09080-300, Brazil. jaqueswaisberg@uol.com.br
Telephone: +55-11-44362461 Fax: +55-11-44362160
Received: 2004-02-20 Accepted: 2004-03-13

Gastroenterol 2004; 10(20): 2997-3000
<http://www.wjgnet.com/1007-9327/10/2997.asp>

Abstract

AIM: To study the diagnosis of *Helicobacter pylori* (*H pylori*) infection through the determination of serum levels of anti-*H pylori* IgG and IgA antibodies, and the levels of anti-*H pylori* IgA antibodies in duodenal fluid.

METHODS: Data were collected from 93 patients submitted to upper digestive endoscopy due to dyspeptic symptoms. The patients were either negative (group A) or positive (group B) to *H pylori* by means of both histological detection and urease tests. Before endoscopy, peripheral blood was collected for the investigation of anti-*H pylori* IgG and IgA antibodies. To perform the urease test, biopsies were obtained from the gastric antrum. For the histological evaluation, biopsies were collected from the gastric antrum (greater and lesser curvatures) and the gastric body. Following this, duodenal fluid was collected from the first and second portions of the duodenum. For the serological assaying of anti-*H pylori* IgG and IgA, and anti-*H pylori* IgA in duodenal fluids, the ELISA method was utilized.

RESULTS: The concentration of serum IgG showed sensitivity of 64.0%, specificity of 83.7%, positive predictive value of 82.0%, negative predictive value of 66.6% and accuracy of 73.1% for the diagnosis of *H pylori* infection. For the same purpose, serum IgA showed sensitivity of 72.0%, specificity of 65.9%, positive predictive value of 72.0%, negative predictive value of 67.4% and accuracy of 69.8%. If the serological tests were considered together, i.e. when both were positive or negative, the accuracy was 80.0%, sensitivity was 86.6%, specificity was 74.2%, positive predictive value was 74.2% and negative predictive value was 86.6%. When values obtained in the test for detecting IgA in the duodenal fluid were analyzed, no significant difference ($P = 0.43$) was observed between the values obtained from patients with or without *H pylori* infection.

CONCLUSION: The results of serum IgG and IgA tests for *H pylori* detection when used simultaneously, are more efficient in accuracy, sensitivity and negative predictive value, than those when used alone. The concentration of IgA antibodies in duodenal fluid is not useful in identifying patients with or without *H pylori*.

Locatelli A, Catapani WR, Junior GCR, Silva CBP, Waisberg J. Detection of anti-*Helicobacter pylori* antibodies in serum and duodenal fluid in peptic gastroduodenal disease. *World J*

INTRODUCTION

Knowledge about peptic ulcers has changed profoundly since Warren and Marshall^[1] managed to cultivate *Helicobacter pylori* (*H pylori*) from gastric biopsies. This raised great interest in the study of how it colonized the upper gastrointestinal tract and more specifically, in its direct relationship with peptic disease^[1-3].

In epidemiological studies, serum tests could offer high sensitivity and specificity^[4]. Serum assaying of anti-*H pylori* IgG and IgA antibodies could be used for the determination of prevalence of acute and chronic infections^[5-7]. In general, the serum levels of anti-*H pylori* IgG antibodies were increased in the presence of infection and could be used as a marker. On the other hand, anti-*H pylori* IgA antibodies were less appropriate for this purpose^[8,9], nevertheless serological findings of anti-*H pylori* IgA antibodies in symptomatic patients might have significant clinical values for the diagnosis of infection, especially if the patient was seronegative for IgG^[10].

In treatment of peptic diseases among *H pylori*-infected patients, local immune responses of the host, as well as the inherent factors of the microorganism, such as the presence of cytotoxin-associated gene A (*cagA*) were important^[11,12]. Few studies have analyzed the effect of local immune response on diseases induced by *H pylori*^[13,14].

H pylori infection could result in a major increase in cells secreting IgA in human gastroduodenal mucosa^[15,16] and usually induce high serum levels of anti-*H pylori* antibodies. Moreover, significant concentrations of antibodies were demonstrated in saliva, gastric fluid and feces^[17]. Despite the antibody response, this microorganism has been rarely eliminated from the stomach and when it was not treated adequately the infection generally persisted in the rest of an individual's life^[18].

However, the use of serological tests based on the determination of serum levels of anti-*H pylori* IgG and IgA antibodies to clinically diagnose *H pylori* infection has not yet been fully clarified^[5,7,10,16].

The objective of the present study was to analyze the use of serum levels of anti-*H pylori* IgG and IgA antibodies, and the levels of anti-*H pylori* IgA antibodies in duodenal fluid for the diagnosis of *H pylori* infection.

MATERIALS AND METHODS

Patients

Examinations were done on 93 patients with peptic symptoms from November 2000 to September 2001.

The inclusion criteria were: adult patients with a normal endoscopic examination or showing a peptic disease^[19,20]. The followings were considered to be exclusion criteria: presence of malignant disease of the upper digestive tract, previous gastrectomy, use of hormonal or non-hormonal anti-inflammatory medications, proton pump inhibitors, histamine H₂ receptor

blockers or antibiotics or antacids over the past twelve months, previous treatment for the elimination of *H pylori* over the past twelve months, presence of intestinal inflammatory disease or immunodeficiency of any nature, and pediatric age.

The patients ($n = 93$) were divided into two groups. Group A ($n = 43$) that had urease test and was histology negative for *H pylori*, and group B ($n = 50$) that had urease test and was histology positive for *H pylori*. These criteria (patients simultaneously positive or negative in histological and urease tests) were used for diagnosis of *H pylori*. In group A, 22 (51.2%) patients were males and 21 (48.8%) were females, the mean age was 34.77 ± 12.89 years (range: 17 to 71 years). In group B, 25 (50.0%) patients were males and 25 (50.0%) were females, the mean age was 41.6 ± 14.6 years (range: 21 to 71 years).

Methods

Endoscopic examination, biopsies of gastric mucosa and sampling of duodenal fluid To perform urease test, two biopsies were obtained from the gastric antrum (greater and lesser curvatures) at least 2 cm from the pylorus. For the histological analysis, four biopsies were collected, two of which from the gastric antrum (greater and lesser curvatures), and two of which from the gastric body on the anterior and posterior walls. Following this, a minimum of 2 mL of secreted duodenal fluid was collected from the first and second portions of the duodenum.

Processing of biopsy material The material collected from the gastric biopsies was placed in flasks containing 40 g/L buffered formaldehyde for fixation and then sent for histological examination. Slides were stained with hematoxylin and eosin and the modified Giemsa method (1% Lugol's solution and 25 g/L gentian violet solution). The four biopsy fragments removed from the gastric antrum were placed in flasks containing urease medium (Probac, Sao Paulo, Brazil), with 2 mL of solution in each. The flasks were maintained at 37 °C and read by the main author 6 and 12 h later.

Determination of serum levels of anti-*H pylori* IgG and IgA and anti-*H pylori* IgA in duodenal fluid Before endoscopy, peripheral blood was collected to determine the serum levels of anti-*H pylori* IgG and IgA. Two-milliliter aliquots from duodenal fluid were diluted with distilled water until a final volume of 10 mL was reached. This solution was centrifuged at 1 500 r/min for 10 min and the supernatant was stored at -20 °C.

ELISA method (Accubind®, Monobind, Inc., Costa Mesa, California, USA) was used to determine the levels of serum anti-*H pylori* IgG and IgA and anti-*H pylori* IgA in the duodenal fluid. The serum samples were diluted to 1/100 while the samples of duodenal fluids were diluted to 1/1 000. Other steps were performed according to the instructions of manufacturer.

For both the anti-*H pylori* IgG and IgA serum antibodies, optical density values greater than 20 U/mL were considered as positive results. For the anti-*H pylori* IgA antibodies in the duodenal fluid, no reference optical density value for a positive or negative test was available. Thus, a receiver operating characteristic (ROC) curve was constructed, taking the results obtained in ELISA test *versus* the gold standard.

Statistical analysis

Statistical analysis was performed by the Mann-Whitney, Fisher's exact and Kruskal-Wallis tests. The ROC curve was constructed in order to assess the sensitivity and specificity of anti-*H pylori* IgA assays in the duodenal fluid at different cutoff levels. An alpha value less than or equal to 5% was adopted for rejection of the null hypothesis. The results were expressed as mean \pm SD to illustrate the distribution of variables.

RESULTS

Findings of endoscopic and histological examination

The findings of endoscopic and histological examination were

gastritis alone in 32 (34.4%) patients, gastritis in association with duodenal peptic ulcer and/or moderate to severe enanthematic or erosive bulboduodenitis in 18 (19.4%), gastritis in association with hiatal hernia and/or esophagitis in 16 (17.2%), gastritis and slight bulboduodenitis in 11 (11.8%), gastritis in association with gastric ulcer and duodenal ulcer simultaneously in 4 (4.3%) and gastritis and gastric polyps in one (1.0%). Eleven (11.8%) patients presented normal endoscopic and histological examination of the gastric mucosa.

Value of serum tests for diagnosis of *H pylori* infection

The sensitivity, specificity, positive and negative predictive values and accuracy of the serum tests for anti-*H pylori* IgG and IgA were analyzed in relation to the gold standard. The accuracy of serum IgG levels was 73.1%, the sensitivity was 64.0%, specificity was 83.7%, positive predictive value was 82.0% and negative predictive value was 66.6%. With regard to serum IgA levels, the accuracy was 69.8%, sensitivity was 72.0%, specificity was 65.9%, positive predictive value was 72.0% and negative predictive value was 67.4%. If the serological tests were considered together, i.e. when both were positive or negative in comparison with the gold standard (Table 1), the accuracy was 80.0%, sensitivity was 86.6%, specificity was 74.2%, positive predictive value was 74.2% and negative predictive value was 86.6%.

Table 1 Frequency of patients positive or negative for serum anti-*H pylori* IgG, positive or negative for serum anti-*H pylori* IgA and negative or positive simultaneously for serum anti-*H pylori* IgG and IgA in comparison to the gold standard

	IgG (+) <i>n</i>	IgG (-) <i>n</i>	IgA (+) <i>n</i>	IgA (-) <i>n</i>	IgG and IgA (+) ^f <i>n</i>	IgG and IgA (-) ^f <i>n</i>
Histology and urease (+)	32 ^b	18 ^b	36 ^d	14 ^d	26 ^f	4 ^f
Histology and urease (-)	7	36	14	29	9	26

n: Number of patients; ^b $P < 0.0001$, ^d $P = 0.0002$, ^f $P < 0.0001$ vs histology and urease (-) group.

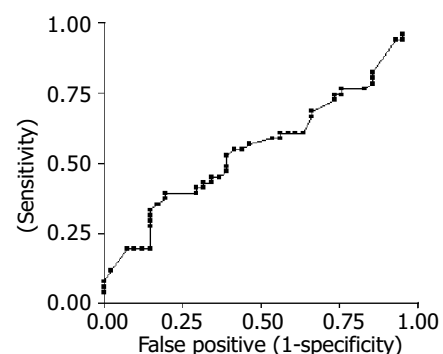


Figure 1 Sensitivity and specificity of anti-*H pylori* IgA in duodenal fluid for diagnosis of infection determined by ROC curve.

Compared with the frequencies of individuals with positive or negative results in the serological test for identifying anti-*H pylori* IgG and IgA antibodies, the serological tests were efficient in the diagnosis of the presence or absence of *H pylori* infection. The difference in the frequencies of positive and negative test results between the groups was highly significant (Table 1). With regard to the ELISA serological tests for anti-*H pylori* IgG and IgA considered together (Table 1), the difference between the frequencies of patients in each group was highly

significant ($P < 0.0001$).

In comparison between the values obtained in the ELISA tests in patients positive or negative for *H pylori*, the difference was significant in relation to anti-*H pylori* serological IgA and IgG.

Value of anti-*H pylori* IgA antibodies in duodenal fluid for diagnosis of *H pylori* infection

Sensitivity, specificity and false positive ratio for IgA in the duodenal fluid were defined by the ROC curve at different cutoff levels, as compared to the gold standard (Figure 1).

When values obtained in the ELISA test for determination of anti-*H pylori* IgA antibodies in the duodenal fluids were analyzed, no significant difference ($P = 0.43$) was observed between the patients with or without *H pylori* infection.

DISCUSSION

Martin-de-Argila *et al.*^[21] concluded that ELISA serum test for the detection of anti-*H pylori* IgA and IgG antibodies was sensitive and specific and should preferentially be utilized in population-based studies. Peura^[22] found that the sensitivity and specificity of ELISA test ranged from 75% to 95%. Perez-Perez *et al.*^[23], examined the detection of anti-*H pylori* IgA and IgG in serological samples from patients with positive cultures for *H pylori* and a histological diagnosis of gastritis, and verified that tests using both antibodies simultaneously had a sensitivity of 93.1% and a specificity of 94.4%. In our study, if the serological tests were considered together, the sensitivity was 86.6% and specificity was 74.2%. A possible explanation for this difference could be the different methods utilized as the gold standard. Indeed, the *H pylori* culture method performed by those authors could possibly have revealed smaller quantities of bacteria in the gastric mucosa. With few bacteria in the mucosa, the urease test and histology could give a false negative result.

Our results also pointed to an increased sensitivity when both anti-*H pylori* IgG and IgA were considered together, in relation to IgG or IgA alone, but the improvement in specificity occurred only in relation to IgA, and it was reduced in comparison with IgG alone. The association between IgG and IgA resulted in a marked improvement of the negative predictive value in comparison with the two assays alone, but did not offer advantages in relation to the positive predictive value.

Certainly, other variables than these might be responsible for the differences observed between the various studies, such as the severity and staging of peptic disease and the different strains of microorganism might also play a role. Strains with cytotoxin-associated gene A (cagA) exhibited more intense immunological responses^[11,16,23,24].

Watanabe *et al.*^[14], found that patients who presented high titers of anti-*H pylori* IgA in the gastric secretion presented a lower degree of neutrophilic infiltration on histological examination. These results suggest that anti-*H pylori* IgA antibodies have a protective function, even though this is insufficient to completely eliminate the organism.

In the present study, when the titers of anti-*H pylori* IgA in the duodenal fluid in patients with and without *H pylori* were analyzed, no significant difference was found in these values. The ROC curve, constructed using the values obtained from the determination of duodenal anti-*H pylori* IgA, compared to the gold standard, showed that the levels of this immunoglobulin in the duodenal fluid presented high sensitivity and low specificity, or even the opposite, depending on the cutoff level considered. Thus, if a cutoff level of 1.0 is adopted, it can be predicted that an individual will be negative for *H pylori* if the anti-*H pylori* IgA values in the duodenal fluid are below this reference level (sensitivity 82.4%). However, at this cutoff level,

individuals with anti-*H pylori* IgA above this value will be at increased risk of being considered as false positive, i.e. with a specificity of 14.5%, the number of false positives will reach 85.4%.

Crabtree *et al.*^[24], using ELISA method, evaluated the local immunological response of anti-*H pylori* IgA and IgG antibodies in patients with duodenitis. These authors observed that the local immunological response of anti-*H pylori* IgA antibodies was greater than that of anti-*H pylori* IgG antibodies. They also noted that there was a direct relationship between the titers of anti-*H pylori* antibodies and the severity of the inflammatory process found, or in other words, the more severe the duodenitis, the higher the levels of local antibodies and especially those of IgA. However, their investigation into these antibodies was done by evaluating the supernatant material from *in vitro* culture of biopsies taken from the first and second portions of the duodenum. In our study, duodenal fluid was collected from these same locations for investigating the anti-*H pylori* IgA antibodies. Often, studies performed *in vitro* could not be directly correlated with *in vivo* results because of the absence of other conditions frequently encountered *in vivo*, such as the presence of proteolytic enzymes in the intestine that could change the concentration of secreted IgA, although this immunoglobulin is very resistant to the action of these enzymes^[14]. Our results expressed the concentration of IgA in the duodenal fluid, but the total amount of IgA in this fluid was unknown, because the quantity of fluid in the first and second portions of the duodenum varied between patients. Crabtree *et al.*, studied anti-*H pylori* antibodies in the duodenal mucosa, and observed notable differences in antibody concentrations between the first and second portions of the duodenum. These authors observed that, in the second portion of the duodenum, the concentrations of anti-*H pylori* IgA and IgG antibodies were lower than those in the first portion. This could have had a decisive influence on our results, since the duodenal fluid presented a greater volume in the second portion of the duodenum and it was often difficult to obtain samples of duodenal fluid from the first portion.

In conclusion, the results from the present investigation demonstrate that anti-*H pylori* IgA and IgG serum immunoglobulins are useful in distinguishing between patients with and without *H pylori* infection, whereas the concentration of anti-*H pylori* IgA in the duodenal fluid is not useful in identification of infected or uninfected patients.

REFERENCES

- 1 Warren JR, Marshall BJ. Unidentified curved bacilli on gastric epithelium in active chronic gastritis. *Lancet* 1983; **1**: 1273-1275
- 2 Olbe L, Fandriks L, Hamlet A, Svennerholm AM, Thoreson AC. Mechanisms involved in *Helicobacter pylori* induced duodenal ulcer disease: an overview. *World J Gastroenterol* 2000; **6**: 619-623
- 3 Svennerholm AM, Quiding-Järbrink M. Priming and expression of immune responses in the gastric mucosa. *Microbes Infect* 2003; **5**: 731-739
- 4 Jensen AK, Andersen LP, Wachmann CH. Evaluation of eight commercial kits for *Helicobacter pylori* IgG antibody detection. *APMIS* 1993; **101**: 795-801
- 5 Andersen LP, Rosenstock SJ, Bonnevie O, Jorgensen T. Seroprevalence of immunoglobulin G, M and A antibodies to *Helicobacter pylori* in an unselected Danish population. *Am J Epidemiol* 1996; **143**: 1157-1164
- 6 Morris A, Nicholson G. Ingestion of *Campylobacter pyloridis* causes gastritis and raised fasting gastric pH. *Am J Gastroenterol* 1987; **82**: 192-199
- 7 Sobala GM, Crabtree JE, Dixon MF, Schorah CJ, Taylor JD, Rathbone BJ, Heatley RV, Axon AT. Acute *Helicobacter pylori* infection: clinical features, local and systemic immune response, gastric mucosal histology, and gastric juice ascorbic acid concentrations. *Gut* 1991; **32**: 1415-1418

- 8 **Andersen LP**, Kiilerick S, Pedersen G, Thoreson AC, Jorgensen F, Rath J, Larsen NE, Borup O, Kroghfelt K, Scheibel J, Rune S. An analysis of seven different methods to diagnose *Helicobacter pylori* infections. *Scand J Gastroenterol* 1998; **33**: 24-30
- 9 **Kosunen TU**, Höök J, Rautelin HI, Myllylä G. Age-dependent increase of *Campylobacter pylori* antibodies in blood donors. *Scand J Gastroenterol* 1989; **24**: 110-114
- 10 **Jaskowski TD**, Martins TB, Hill HR, Litwin CM. Immunoglobulin A antibodies to *Helicobacter pylori*. *J Clin Microbiol* 1997; **35**: 2999-3000
- 11 **Rathbone BJ**, Wyatt JI, Worsley BW, Shires SE, Trejdosiewicz LK, Heatley RV, Losowsky MS. Systemic and local antibody responses to gastric *Campylobacter pyloridis* in non-ulcer dyspepsia. *Gut* 1986; **27**: 642-647
- 12 **Atalay C**, Atalay G, Altinok M. Serum *Helicobacter pylori* IgG and IgA levels in patients with gastric cancer. *Neoplasma* 2003; **50**: 185-190
- 13 **Doweck J**, Quintana C, Barrios A, Monastra L, Lopetegui G, Zerbo O, Schenone L, Giordano A, Valero J, Kogan Z, Bartellini MA, Corti R. Evaluation of sensitivity, specificity and predictive value of six qualitative serological methods for the detection of *Helicobacter pylori* antibodies. *Acta Gastroenterol Latinoam* 1997; **27**: 259-261
- 14 **Watanabe T**, Goto H, Arisawa T, Hase S, Niwa Y, Hayakawa T, Asai J. Relationship between local immune response to *Helicobacter pylori* and the diversity of disease: investigation of *H pylori*-specific IgA in gastric juice. *J Gastroenterol Hepatol* 1997; **12**: 660-665
- 15 **Mattsson A**, Quiding-Järbrink M, Lönroth H, Hamlet A, Ahlstedt I, Svennerholm A. Antibody-secreting cells in the stomachs of symptomatic and asymptomatic *Helicobacter pylori*-infected subjects. *Infect Immun* 1998; **66**: 2705-2712
- 16 **Xia HHX**, Talley NJ, Blum AL, O'Morain CA, Stolte M, Bolling-Sternevald E, Mitchell HM. Clinical and pathological implications of IgG antibody responses to *Helicobacter pylori* and its virulence factors in non-ulcer dyspepsia. *Aliment Pharmacol Ther* 2003; **17**: 935-943
- 17 **Wyatt JI**, Rathbone BJ. Immune response of the gastric mucosa to *Campylobacter pylori*. *Scand J Gastroenterol Suppl* 1988; **142**: 44-49
- 18 **Luzza F**, Imeneo M, Maletta M, Monteleone G, Doldo P, Biancone L, Pallone F. Isotypic analysis of specific antibody response in serum, saliva, gastric and rectal homogenates of *Helicobacter pylori*-infected patients. *FEMS Immunol Med Microbiol* 1995; **10**: 285-288
- 19 **Dixon MF**, Genta RM, Yardley JH, Correa P. Classification and grading of gastritis. The updated Sydney System. International Workshop on the Histopathology of Gastritis, Houston 1994. *Am J Surg Pathol* 1996; **20**: 1161-1181
- 20 **Garza-González E**, Bosques-Padilla FJ, Tijerina-Menchaca R, Flores-Gutiérrez JP, Maldonado-Garza HJ, Pérez-Pérez GI. Comparison of endoscopy-based and serum-based methods for the diagnosis of *Helicobacter pylori*. *Can J Gastroenterol* 2003; **17**: 101-106
- 21 **Martín-de-Argila C**, Boixeda D, Cantón R, Valdezate S, Mir N, De Rafael L, Gisbert JP, Baquero F. Usefulness of the combined IgG and IgA antibody determinations for serodiagnosis of *Helicobacter pylori* infection. *Eur J Gastroenterol Hepatol* 1997; **9**: 1191-1196
- 22 **Peura DA**. *Helicobacter pylori*: a diagnostic dilemma and a dilemma of diagnosis. *Gastroenterology* 1995; **109**: 313-315
- 23 **Perez-Perez GI**, Dworkin BM, Chodos JE, Blaser MJ. *Campylobacter pylori* antibodies in humans. *Ann Intern Med* 1988; **109**: 11-17
- 24 **Crabtree JE**, Shallcross TM, Wyatt JI, Taylor JD, Heatley RV, Rathbone BJ, Losowsky MS. Mucosal humoral immune response to *Helicobacter pylori* in patients with duodenitis. *Dig Dis Sci* 1991; **36**: 1266-1273

Edited by Wang XL Proofread by Chen WW and Xu FM

Relationship between focal adhesion kinase and hepatic stellate cell proliferation during rat hepatic fibrogenesis

Hui-Qing Jiang, Xiao-Lan Zhang, Li Liu, Chang-Chun Yang

Hui-Qing Jiang, Xiao-Lan Zhang, Li Liu, Department of Gastroenterology, The Second Hospital of Hebei Medical University, Shijiazhuang 050000, Hebei Province, China

Chang-Chun Yang, Department of Medicine, the Armed Police Hospital of Hebei Province, Shijiazhuang 050081, Hebei Province, China

Supported by the Natural Science Foundation of Hebei Province, No. 301361

Correspondence to: Professor Hui-Qing Jiang, Department of Gastroenterology, The Second Hospital of Hebei Medical University, Shijiazhuang 050000, Hebei Province, China. huiqingj@heinfo.net

Telephone: +86-311-7222951

Received: 2003-08-23 **Accepted:** 2003-09-05

Abstract

AIM: To investigate the dynamic expression of focal adhesion kinase (FAK) protein and FAK mRNA in fibrotic rat liver tissue, and the relationship between FAK and hepatic stellate cell (HSC) proliferation.

METHODS: Rat hepatic fibrosis was induced by bile duct ligation (BDL). Histopathological changes were evaluated by hematoxylin and eosin staining, and by Masson's trichrome method. FAK mRNA in the rat livers was determined by reverse transcription-polymerase chain reaction (RT-PCR), and the distributions of FAK were assessed immunohistochemically. The number of activated HSCs was quantified after alpha smooth muscle actin (α -SMA) staining.

RESULTS: With the development of hepatic fibrosis, the positively stained cells of α -SMA increased obviously, which were mainly resided in the portal ducts, fiber septa and perisinuses accompanied with proliferating bile ducts. The positively stained areas of the rat livers in model groups 1 to 4 wk after ligation of common bile duct ($12.88 \pm 2.63\%$, $22.65 \pm 2.16\%$, $27.45 \pm 1.86\%$, $35.25 \pm 2.34\%$, respectively) were significantly larger than those in the control group ($5.88 \pm 1.46\%$) ($P < 0.01$). The positive staining for FAK significantly increased, which was mainly situated in portal ducts, fiber septa and around the bile ducts, vascular endothelial cells and perisinusoidal cells. The expression of FAK was positively correlated with α -SMA expression ($r = 0.963$, $P < 0.05$). FAK mRNA expression was obviously up-regulated in the model groups compared to the control group.

CONCLUSION: These data suggest that expressions of FAK protein and mRNA are greatly increased in fibrotic rat livers, which may play an important role in HSC proliferation and hepatic fibrogenesis.

Jiang HQ, Zhang XL, Liu L, Yang CC. Relationship between focal adhesion kinase and hepatic stellate cell proliferation during rat hepatic fibrogenesis. *World J Gastroenterol* 2004; 10(20): 3001-3005

<http://www.wjgnet.com/1007-9327/10/3001.asp>

INTRODUCTION

Focal adhesion kinase (FAK) is a cytoplasmic protein tyrosine kinase that has been implicated to play an important role in integrin-mediated signal transduction pathways. Furthermore, some lines of evidence indicate FAK as a point of convergence of other signaling pathways. The *in vitro* expression of FAK and its level of phosphorylation appear to be related to several physiological phenomena, including cell adhesion, spreading, migration, cytoskeleton organization, proliferation and apoptosis^[1-3]. It has been accepted that hepatic stellate cells (HSCs) represent the pivot of fibrotic process^[4-9]. In healthy livers, HSCs are perisinusoidal mesenchymal elements with characteristic intracytoplasmic lipid droplets rich in retinyl esters. In contrast, in chronic liver injury, HSCs undergo a process of activation from the resting fat-storing phenotype towards a myofibroblast-like phenotype^[10].

Current evidence indicates that activated HSCs are responsible for the majority of extracellular matrix protein depositions in liver fibrosis^[11]. Although a recent study has focused on the roles of FAK in cultured cells^[12], little is known about its regulation *in vivo* or its relevance to HSC proliferation. In addition, it is not known whether FAK is up-regulated in response to liver injury by bile duct ligation (BDL). To assess whether FAK was associated with fibrogenesis or the survival of HSCs in biliary fibrosis, we investigated the expression of FAK in liver tissues from rats with BDL-induced biliary fibrosis using immunohistochemistry and reverse transcription-polymerase chain reaction (RT-PCR), we also used immunohistochemistry method to examine the expression of α -smooth muscle actin (α -SMA) as a marker of activated HSCs.

MATERIALS AND METHODS

Reagents

Monoclonal antibodies against FAK and α -SMA were products of Santa Cruz Biotech Inc. Streptavidin peroxidase (SP) immunohistochemical kit was purchased from Zhongshan Biological Technology Co. (Beijing). Trizol reagent was obtained from Life Technologies, Inc (USA). One tube RT-PCR kit was from Promega Co (USA). Primers for rat FAK and β -actin were designed by ourselves in accordance with gene sequence in GeneBank, synthesized and purified by Bao Biological Engineering Co. (Dalian). All other reagents were analytically pure.

Animal model and experimental protocol

A total of 80 adult male Sprague-Dawley rats weighing 350-400 g were purchased from the Experimental Animal Center of Hebei Medical University (Clearing Grade, Certificate No. 04057). All rats were housed in plastic cages and allowed free access to food and water. For the purpose of this study, rats were randomly divided into eight groups (ten rats in each group) as follows: Control group (sham-operated group), with BDL for 2 h, 6 h, 2 d, 1 wk, 2 wk, 3 wk and 4 wk, respectively. The rats were subjected to laparotomy with their common bile ducts completely ligated while they were intraperitoneally injected with ketamine hydrochloride at a dose of 100 mg/kg^[13]. Under deep anaesthesia, the peritoneal cavity was opened and the common bile duct

was double-ligated with 3-0 silk and cut between the ligatures. Control animals underwent a sham operation that consisted of exposure but not ligation of the common bile duct. At various intervals postoperation, animals were anaesthetised and the livers were harvested. Liver tissue specimens were routinely fixed in 40 g/L phosphate-buffered formaldehyde and embedded in paraffin. Some liver tissue specimens were used for light microscopy and immunohistochemistry using anti α -SMA and FAK, while others were snap-frozen in liquid nitrogen and stored at -80 °C for RNA analysis. In addition, control livers were harvested 4 wk after sham operation.

Histopathology

For light microscopic examination, liver specimens were routinely fixed overnight in 40 g/L phosphate-buffered formaldehyde, embedded in paraffin. Tissue sections (5- μ m thick) were stained with haematoxylin and eosin (HE) for morphological evaluation and Masson's trichrome for assessment of fibrosis.

Immunohistochemical detection of α -SMA and FAK

All immunohistochemical studies using the streptavidin-peroxidase technique were performed on 5- μ m thick sections of paraformaldehyde-fixed and paraffin-embedded liver block tissue mounted on APES-coated slides. Slides were deparaffinised in xylene, and rehydrated in graded ethanol. Endogenous peroxidase activity was quenched with a 30 mL/L hydrogen peroxide solution in methanol at room temperature for 30 min, followed by rinsing in pH 6.0 phosphate-buffered saline (PBS). After antigen retrieval in a water bath set in a 10 mmol/L citrate buffer (pH 6.0) at 94 °C for 8 min, 10 min, respectively, the slides were immediately cooled for 20 min at room temperature. Non-specific binding sites were blocked by incubation with washing buffer containing 100 mL/L normal goat serum at 37 °C for 30 min. Sections might at 4 °C with a mouse monoclonal antibody directed against α -SMA or FAK at a dilution of 1:100. The secondary antibody bindings were localized using a biotin conjugated rabbit anti-mouse IgG (1:100 dilution), followed by incubation with streptavidin-peroxidase complex (1:200 dilution). Peroxidase conjugates were subsequently visualised using diaminobenzidine (DAB) solution in hydrogen peroxide as a chromogen yielding a brown reaction product. Sections were then counterstained in Mayer's hematoxylin and mounted over cover slips. All incubations were performed in a moist chamber. Furthermore, between each incubation step, the slides were washed three times with PBS for 5 min. To ensure antibody specificity, negative control samples were processed in parallel under the same conditions but with omission of the first antibody, which was replaced by an equal volume of PBS. The α -SMA-positive parenchyma and the FAK-positive parenchyma were measured by a video-image analysis system and expressed as a percentage of area occupied by the signal.

RNA extraction and RT-PCR assay

Expression of FAK mRNA was evaluated with RT-PCR. Total RNA from liver specimens (100 mg) was isolated using a monophasic solution of phenol and guanidine thiocyanate (Trizol), precipitated in ethanol and resuspended in sterile RNAase-free water for storage at -80 °C until use, as recommended by the suppliers. Total RNA was quantified spectrometrically at 260 nm, and the quality of isolated RNA was analysed on agarose gels under standard conditions. One-step RT-PCR was performed according to the manufacturer's instructions. Two micrograms of RNA was added to each reaction and RT-PCR was routinely performed using 5 units of AMV reverse transcriptase, 5 units of *T7* DNA polymerase, 10 pmol of each oligonucleotide primer, 10 pmol of dNTP mix and 25 mmol/L MgSO₄ in a final reaction volume of 50 μ L. Primer sequences were as follows:

FAK, forward 5'-ACT TGG ACG CTG TAT TGG AG-3' and reverse 5'-CTG TTG CCT GCT TTC TGG AT-3', fragment length 833 bp; β -actin, forward 5'-AGC TGA GAG GGA AAT CGT GCG-3' and reverse 5'-GTGCCACCA GAC AGC ACT GTG-3', fragment length 300 bp. RT-PCR was performed in the following steps: reverse transcription was performed at 41 °C for 45 min, pre-denaturation at 94 °C for 2 min; then amplification was performed in a thermal controller for 35 cycles (denaturation at 94 °C for 40 s, annealing at 52 °C for 1 min and extension at 72 °C for 1.5 min), and a final extension at 72 °C for 10 min after the last cycle. A 10 μ L of the PCR products was analyzed on 15 g/L agarose gel containing ethidium bromide with TAE buffer at 80 V for 40 min and photographed under UV illumination. The band intensities were quantified by densitometry. FAK/ β -actin quotient indicated the relative expression of FAK. Experiments were performed at least three times with similar results.

Statistical analysis

The data were expressed as mean \pm SD. The mean values were compared by using analysis of variance, followed by the Student-Newman-Keuls test if the former was significant. The correlation between the expressions of FAK and α -SMA was analyzed for statistical significance by the simple linear regression analysis. *P* values less than 0.05 were considered statistically significant.

RESULTS

Histology of progressive fibrotic liver injury

In accordance with previous reports^[13], a marked liver fibrosis was apparently observed in the SD rats after BDL. In the present study, the results of HE and Masson's trichrome staining confirmed spotted (or scattered) perivenular degeneration of hepatocytes, an increase in the inflammatory infiltrates in the necrotic areas and bile ductular proliferation in the portal triads after 1 wk of BDL. After 2 wk of BDL, all rats showed expanded portal tracts with fibrous tissues, portal-to-portal fibrous bridging, nodular transformation and widespread proliferating bile ductules that extended into the parenchyma in places without clear-cut cirrhosis. After BDL for 3-4 wk, the animals developed severe fibrosis associated with proliferating bile ducts that formed a continuous meshwork of connective tissues with complete distortion of lobular architecture, whereas there was no notable histological abnormality or evidence of stainable collagen in any of the shamly operated control livers (Figure 1A-D).

Identification of proliferating and activated HSC

Since α -SMA was expressed in activated HSCs, immunostaining for this protein was used to detect and quantify the numbers of activated HSCs. A weak staining for α -SMA positive cells in the shamly operated control livers was observed in vascular smooth muscle cells and sinusoids. With the development of hepatic fibrosis, the positive stainings for α -SMA were greatly increased in the cells of portal ducts, fibrotic septa, perisinuses and around the proliferated bile ducts. The positively stained areas of the rat livers in model groups 1 to 4 wk after ligation of common bile duct (12.88 \pm 2.63%, 22.65 \pm 2.16%, 27.45 \pm 1.86%, 35.25 \pm 2.34%, respectively) were significantly larger than that in control group (5.88 \pm 1.46%) (*P*<0.01, Figure 2 A-C).

Distribution of FAK protein in common bile duct ligated rat liver

To explore the distribution of FAK, the sections of rat livers in sham operation and BDL groups were immunostained using specific monoclonal anti-FAK antibody. In the sections from sham operation group, expression of FAK was found in vascular smooth muscle cells and perisinusoidal cells. In contrast, the positive staining of BDL rat liver was obviously visible in and

around α -SMA-positive areas, which were prevailingly detected in portal ducts, fibrotic septa, perisinusoidal cells and cells around the bile ducts as well as vascular endothelial cells. The positive areas of the rat livers in model groups 1 to 4 wk after

ligation of common bile duct ($13.05 \pm 1.32\%$, $18.43 \pm 2.18\%$, $23.45 \pm 2.73\%$, $31.00 \pm 2.77\%$, respectively) were significantly larger than that in control group ($3.98 \pm 1.27\%$) ($P < 0.01$, Figure 3A-C).

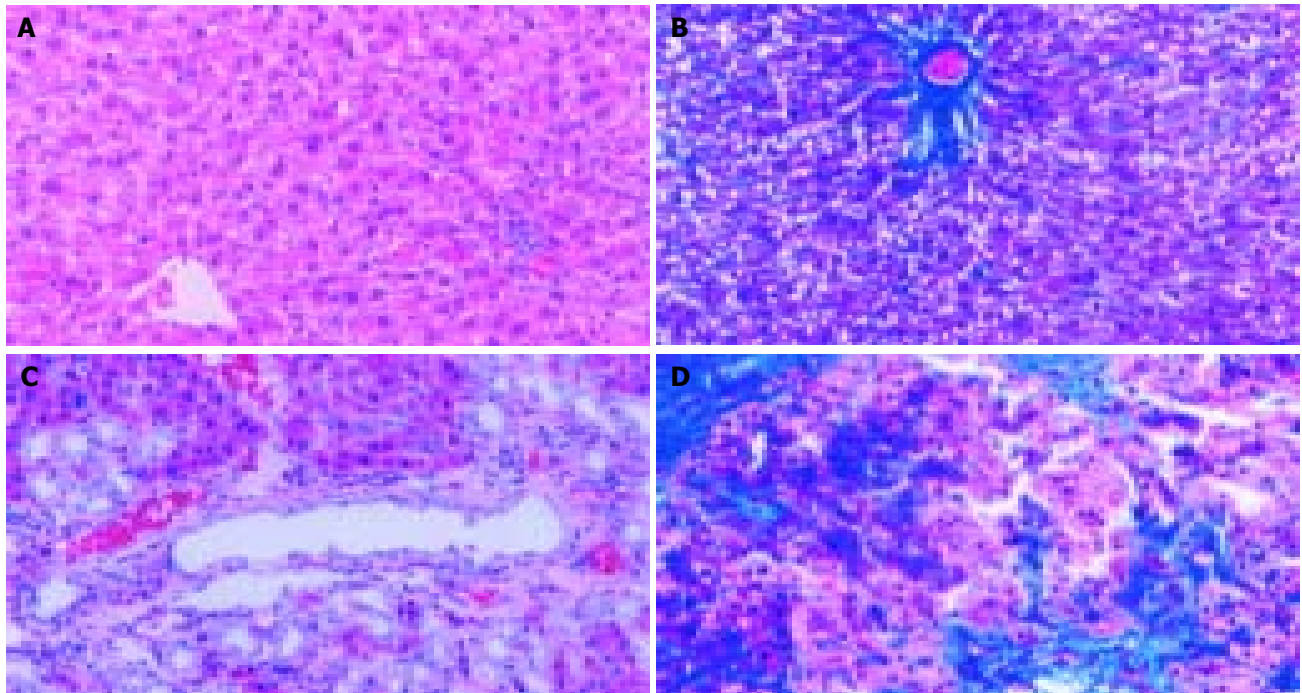


Figure 1 Histopathological changes in liver tissue (100 \times) A: Normal hepatic lobular architecture in sham operation group (HE); B: Few ECM deposition in sham operation group (Masson trichrome); C: Extensive ductular proliferation and ECM deposition 4 wk after BDL (HE); D: Extensive connective tissue deposition 4 wk after BDL (Masson trichrome).

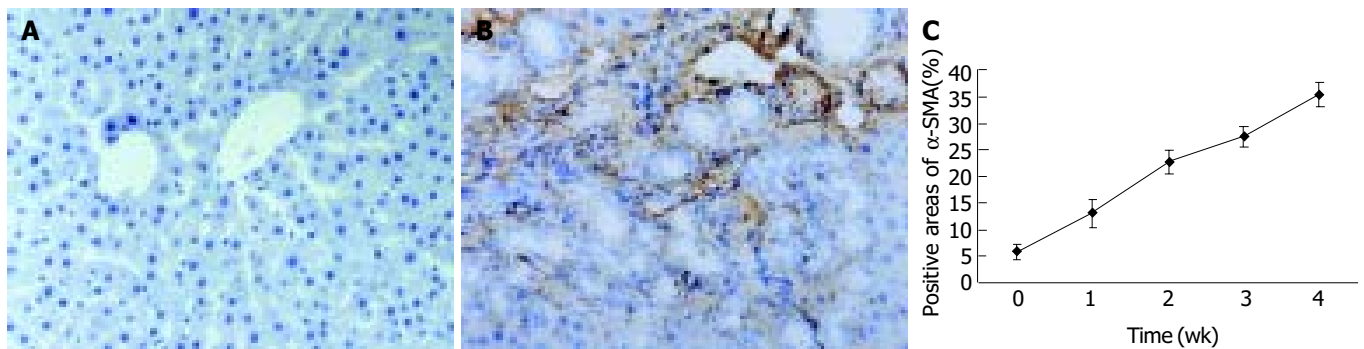


Figure 2 α -SMA protein expression in liver tissue stained by immunohistochemistry (SP 200 \times) A: Few α -SMA expressions in sham operation group; B: Positive cells of α -SMA resided in portal ducts, fiber septa, perisinuses and around proliferated bile ducts after 2 wk BDL; C: Positively stained areas of α -SMA expression in model groups 1 to 4 wk after common bile duct ligation.

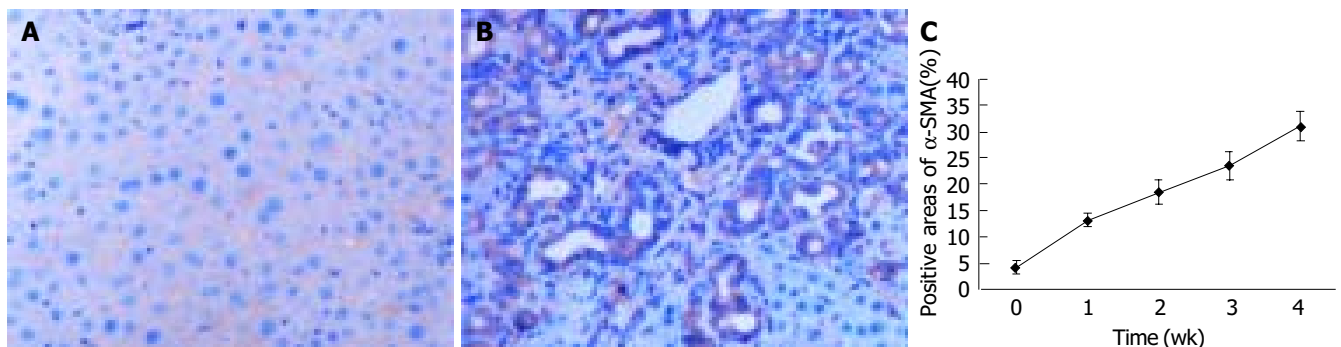


Figure 3 FAK protein expression in liver tissue stained by immunohistochemistry (SP 200 \times) A: FAK protein expression in sham operation group; B: FAK protein expression 2 wk after BDL; C: Time course of FAK expression in hepatic fibrogenesis stained by immunohistochemistry.

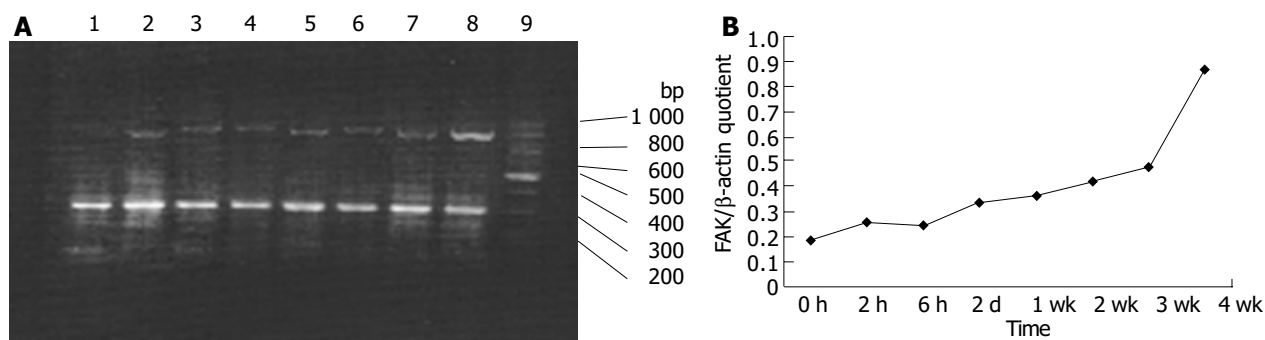


Figure 4 RT-PCR analysis of mRNA encoding FAK in hepatic fibrogenesis. A: RT-PCR analysis of mRNA encoding FAK in hepatic fibrogenesis at different time points. Lane 1: sham operation group; lane 2: BDL 2 h; lane 3: BDL 6 h; lane 4: BDL 2 d; lane 5: BDL 1 wk; lane 6: BDL 2 wk; lane 7: BDL 3 wk; lane 8: BDL 4 wk; lane 9: Marker. B: Band intensities were quantified by densitometry. FAK/ β -actin quotient indicated the relative expression of FAK.

FAK mRNA expression in common bile duct ligated rat livers

Although it was shown that FAK protein was produced by liver tissues *in vivo*, it was not clear whether the FAK mRNA level under fibrogenic response was increased *in vivo*. Therefore, we investigated the production of FAK mRNA in the liver. RT-PCR results revealed faint bands for FAK mRNA in the sham operation group, whereas obvious and specific bands for FAK mRNA in fibrotic liver of BDL groups. Moreover, FAK mRNA expression was initially up-regulated and reached the peak level 4 wk after BDL. The levels housekeeping gene, β -actin, did not show any significant differences between normal and BDL rat liver tissues (Figure 4A, B).

Correlation between FAK and α -SMA

Immunohistochemistry experiments were performed to analyze whether FAK protein distribution was correlated with α -SMA between sham operation group and BDL group. The results indicated that FAK was positively correlated with α -SMA ($r=0.963$, $P<0.05$).

DISCUSSION

HSCs, a principal cellular source of extracellular matrix during chronic liver injury, undergo a transition into α -SMA-expressing myofibroblast-like cells in response to injury. Furthermore, HSC activation is associated with stellate cell proliferation, increased contractility, enhanced matrix production, and expression of a number of fibrogenic and proliferative cytokines and their cognate receptors. Therefore, HSCs could play a pivotal role in cellular and molecular events that lead to fibrosis^[14-17]. As above, expressing α -SMA is one of the characteristics of activated HSCs. Cassiman *et al.*^[18] and α -SMA-positive cells mainly reside in the portal triads and fibrotic septa accompanied with proliferating bile ducts. Namely, α -SMA-positive cells was coincident with collagen deposition. The results of the present study verified that the positive cells of α -SMA, which mainly reside in portal ducts, fibrotic septa, perisinuses and around the proliferated bile ducts, were greatly increased with the development of hepatic fibrosis compared with sham operation group. Thus, our results are consistent with the others mentioned above.

Various factors and signal transduction pathways have been shown to regulate the activation and proliferation of HSCs^[8,9,19-21]. However, the mechanism by which *in vivo* factors impact HSC activation is not clear as yet. To better understand the mechanism by which FAK is generated in liver tissues might influence HSC activation, proliferation, and hepatic fibrogenesis, we performed the current research.

FAK, a 125 kD molecule, is a cytoplasmic nonreceptor tyrosine kinase that has been shown to play a key role in the

regulation of cell adhesion, spreading, migration, cytoskeleton organization, proliferation and apoptosis. Furthermore, some lines of evidence has indicated FAK is a point of convergence of many signaling pathways^[22]. The co-localization of FAK with integrins in focal adhesion plaque (FAP) is a trigger for cell adhesion-dependent activation of FAK signals^[22]. Subsequently, its autophosphorylation at Tyr397 in the N-terminal domain is prerequisite, which may initiate a number of signaling pathways. Among them, RAS-dependent mitogen-activated protein kinase (MAPK) pathway is the clearest. It has been found that the RAS-RAF-MEK (ERK kinase)-ERK (extracellular signal-regulated kinase) pathway is involved in many cellular behaviors^[22,23], such as proliferation, apoptosis. FAK knockout mice showed extensive mesodermal defects and embryonic death^[24]. Moreover, the monoclonal antibody specific for FAK microinjected into fibroblasts could inhibit FAK activity and give rise to apoptosis of fibroblasts^[25]. The results presented herein demonstrated that FAK protein was obviously expressed in portal ducts, fibrotic septa, perisinusoidal cells in BDL rat livers, which was in accordance with the distribution α -SMA-positive loci. In addition, FAK mRNA expression was also elevated with the progression of hepatic fibrosis. Importantly, FAK protein distribution was positively correlated with α -SMA. So, we suggested that activation of FAK in BDL rat liver tissues might activate downstream signal molecules, which could modulate gene expression of HSCs and give rise to hepatic fibrosis.

To date, the mechanism of FAK elevation during hepatic fibrogenesis remains unknown. But increasing *in vitro* evidence supports that HSCs are a major cell source of FAK. First, extracellular matrix components, including collagen and fibronectin could activate FAK in HSCs via integrin signal pathway^[26-28]. Second, cytokines such as platelet derived growth factor (PDGF), endothelin (ET), insulin-like growth factor-1 (IGF-1) and tumor necrosis factor (TNF), could increase the production of FAK^[29]. Third, reactive oxygen species (ROS) like H_2O_2 could also elevate the expression of FAK^[30,31]. In contrast, antioxidants such as *Salvia Miltiorrhiza*, might have opposite effects on FAK expression in HSCs^[32,33].

In conclusion, FAK-mediated activation of HSCs can result in hepatic fibrogenesis. Inhibition of FAK activity by various methods would be expected to attenuate liver fibrosis and, therefore, deserve further study.

REFERENCES

- 1 Taylor JM, Mack CP, Nolan K, Regan CP, Owens GK, Parsons JT. Selective expression of an endogenous inhibitor of FAK regulates proliferation and migration of vascular smooth muscle cells. *Mol Cell Biol* 2001; 21: 1565-1572
- 2 Sonoda Y, Matsumoto Y, Funakoshi M, Yamamoto D, Hanks

- SK, Kasahara T. Anti-apoptotic role of focal adhesion kinase (FAK). Induction of inhibitor-of-apoptosis proteins and apoptosis suppression by the overexpression of FAK in a human leukemic cell line, HL-60. *J Biol Chem* 2000; **275**: 16309-16315
- 3 Almeida EA, Ilic D, Han Q, Hauck CR, Jin F, Kawakatsu H, Schlaepfer DD, Damsky CH. Matrix survival signaling: from fibronectin via focal adhesion kinase to c-Jun NH(2)-terminal kinase. *J Cell Biol* 2000; **149**: 741-754
- 4 Jiang HQ, Zhang XL. Progress in the study of pathogenesis in hepatic fibrosis. *Shijie Huaren Xiaohua Zazhi* 2000; **8**: 687-689
- 5 Gressner AM. The cell biology of liver fibrogenesis - an imbalance of proliferation, growth arrest and apoptosis of myofibroblasts. *Cell Tissue Res* 1998; **292**: 447-452
- 6 Friedman SL. Molecular mechanisms of hepatic fibrosis and principles of therapy. *J Gastroenterol* 1997; **32**: 424-430
- 7 Friedman SL. Cytokines and fibrogenesis. *Semin Liver Dis* 1999; **19**: 129-140
- 8 Pinzani M, Marra F, Carloni V. Signal transduction in hepatic stellate cells. *Liver* 1998; **18**: 2-13
- 9 Huang GC, Zhang JS. Signal transduction in activated hepatic stellate cells. *Shijie Huaren Xiaohua Zazhi* 2001; **9**: 1056-1060
- 10 Iredale JR. Hepatic stellate cell behavior during resolution of liver injury. *Semin Liver Dis* 2001; **21**: 427-436
- 11 Benyon RC, Arthur MJ. Extracellular matrix degradation and the role of hepatic stellate cells. *Semin Liver Dis* 2001; **21**: 373-384
- 12 Su JM, Gui L, Zhou YP, Zha XL. Expression of focal adhesion kinase and alpha5 and beta1 integrins in carcinomas and its clinical significance. *World J Gastroenterol* 2002; **8**: 613-618
- 13 Liu H, Song D, Lee SS. Role of heme oxygenase-carbon monoxide pathway in pathogenesis of cirrhotic cardiomyopathy in the rat. *Am J Physiol Gastrointest Liver Physiol* 2001; **280**: G68-G74
- 14 Iredale JP, Benyon RC, Pickering J, McCullen M, Northrop M, Pawley S, Hovell C, Arthur MJ. Mechanisms of spontaneous resolution of rat liver fibrosis. Hepatic stellate cell apoptosis and reduced hepatic expression of metalloproteinase inhibitors. *J Clin Invest* 1998; **102**: 538-549
- 15 Issa R, Williams E, Trim N, Kendall T, Arthur MJ, Reichen J, Benyon RC, Iredale JP. Apoptosis of hepatic stellate cells: involvement in resolution of biliary fibrosis and regulation by soluble growth factors. *Gut* 2001; **48**: 548-557
- 16 Cales P. Apoptosis and liver fibrosis: antifibrotic strategies. *Biomed Pharmacother* 1998; **52**: 259-263
- 17 Greenwel P, Dominguez-Rosales JA, Mavi G, Rivas-Estilla AM, Rojkind M. Hydrogen peroxide: a link between acetaldehyde-elicited $\alpha 1$ (I) collagen gene up-regulation and oxidative stress in mouse hepatic stellate cells. *Hepatology* 2000; **31**: 109-116
- 18 Cassiman D, Libbrecht L, Desmet V, Deneef C, Roskams T. Hepatic stellate cell/myofibroblast subpopulations in fibrotic human and rat livers. *J Hepatol* 2002; **36**: 200-209
- 19 Ramm GA, Carr SC, Bridle KR, Li L, Britton RS, Crawford DH, Vogler CA, Bacon BR, Tracy TF. Morphology of liver repair following cholestatic liver injury: resolution of ductal hyperplasia, matrix deposition and regression of myofibroblasts. *Liver* 2000; **20**: 387-396
- 20 Zhang XL, Jiang HQ. Intracellular signal transduction pathway of integrin and hepatic stellate cell behavior. *Zhongguo Bingli Shengli Zazhi* 2003; **18**: 987-991
- 21 Svegliati-Baroni G, Ridolfi F, Di Sario A, Saccomanno S, Bendia E, Benedetti A, Greenwel P. Intracellular signaling pathways involved in acetaldehyde-induced collagen and fibronectin gene expression in human hepatic stellate cells. *Hepatology* 2001; **33**: 1130-1140
- 22 Guan JL. Role of focal adhesion kinase in integrin signaling. *Int J Biochem Cell Biol* 1997; **29**: 1085-1096
- 23 Zhao JH, Guan JL. Role of focal adhesion kinase in signaling by the extracellular matrix. *Prog Mol Subcell Biol* 2000; **25**: 37-55
- 24 Schaller MD. Biochemical signals and biological responses elicited by the focal adhesion kinase. *Biochim Biophys Acta* 2001; **1540**: 1-21
- 25 Hungerford JE, Compton MT, Matter ML, Hoffstrom BG, Otey CA. Inhibition of pp125FAK in cultured fibroblasts results in apoptosis. *J Cell Biol* 1996; **135**: 1383-1390
- 26 Boudreau NJ, Jones PL. Extracellular matrix and integrin signalling: the shape of things to come. *Biochem J* 1999; **339**(Pt 3): 481-488
- 27 Zhang XL, Jiang HQ, Liu L, Bai Y, Song M. Effects of Arg-Gly-Asp-Ser tetrapeptide on integrin signaling and apoptosis in hepatic stellate cells. *Zhonghua Ganzangbing Zazhi* 2003; **11**: 479-482
- 28 Iwamoto H, Sakai H, Tada S, Nakamuta M, Nawata H. Induction of apoptosis in rat hepatic stellate cells by disruption of integrin-mediated cell adhesion. *J Lab Clin Med* 1999; **134**: 83-89
- 29 Carloni V, Pinzani M, Giusti S, Romanelli RG, Parola M, Bellomo G, Failli P, Hamilton AD, Sebti SM, Laffi G, Gentilini P. Tyrosine phosphorylation of focal adhesion kinase by PDGF is dependent on ras in human hepatic stellate cells. *Hepatology* 2000; **31**: 131-140
- 30 Jiang HQ, Zhang XL, Liu L. Induction of apoptosis with Salvia miltiorrhiza monomer IH764-3 via downregulating focal adhesion kinase in H₂O₂-stimulated hepatic stellate cells. *Zhongguo Bingli Shengli Zazhi* 2003; **19**: 18-21
- 31 Liu L, Jiang HQ, Zhang XL. The effect and mechanism of Salvia miltiorrhiza monomer IH764-3 on proliferation and collagen of hepatic stellate cells stimulated by H₂O₂. *Zhongguo Yingyong Shengli Zazhi* 2003; **19**: 78-81
- 32 Zhang XL, Jiang HQ, Liu L, Zhao DQ. The apoptosis-inducing role of Salvia miltiorrhiza monomer IH764-3 in hepatic stellate cells. *Zhonghua Neike Zazhi* 2002; **41**: 166-167
- 33 Zhao DQ, Jiang HQ, Xiu HM, Zhang XL, Yao XX. Effects of IH764-3 on proliferation and apoptosis of HSCs. *Zhonghua Ganzangbing Zazhi* 2002; **10**: 265-274

Gene expression profile in liver of hB1F transgenic mice

Shui-Liang Wang, Hua Yang, You-Hua Xie, Yuan Wang, Jian-Zhong Li, Long Wang, Zhu-Gang Wang, Ji-Liang Fu

Shui-Liang Wang, Hua Yang, Jian-Zhong Li, Ji-Liang Fu, Department of Medical Genetics, Second Military Medical University, Shanghai 200433, China

Shui-Liang Wang, PLA Center for Laboratory Medicine, Fuzhou General Hospital, Fuzhou 350025, Fujian Province, China

You-Hua Xie, Yuan Wang, State Key Laboratory for Molecular Biology, Institute of Biochemistry and Cell Biology, Shanghai Institutes for Biological Sciences, Chinese Academy of Sciences, Shanghai 200031, China

Long Wang, Zhu-Gang Wang, Ji-Liang Fu, Shanghai Nanfang Research Center for Model Organisms, Shanghai 201203, China

Supported by the National Natural Science Foundation of China, No.39830360; the National "863" High Technology Research and Development Program of China, No.2001AA221261; the Qi Ming Xing Program from Shanghai Science and Technology Committee, No. 01QA14046

Correspondence to: Professor Ji-Liang Fu, Department of Medical Genetics, Second Military Medical University, 800 Xiangyin Road, Shanghai 200433, China. jlfu@guomai.sh.cn

Telephone: +86-21-25070027 **Fax:** +86-21-25070027

Received: 2003-10-15 **Accepted:** 2003-12-08

Abstract

AIM: To analyze the tissue morphologic phenotype and liver gene expression profile of hB1F transgenic mice.

METHODS: Transgene expression was analyzed with RT-PCR and Western blotting. For one of the transgenic mouse lines, tissue expression pattern of the transgene was also examined with immunochemical methods. Pathological analysis was used to examine the tissue morphologic phenotype of established transgenic mice. The liver gene expression profile of transgenic mice was analyzed with microchip, and some of the differentially expressed genes were verified with RT-PCR.

RESULTS: The expressions of hB1F were shown in livers from 6 of 7 transgenic mouse lines. The overexpression of hB1F transgene did not cause pathological changes. Expressions of three genes were up-regulated, while down-regulation was observed for 25 genes.

CONCLUSION: The overexpression of hB1F transgene may cause changes of gene expression profiles in the liver of transgenic mice.

Wang SL, Yang H, Xie YH, Wang Y, Li JZ, Wang L, Wang ZG, Fu JL. Gene expression profile in liver of hB1F transgenic mice. *World J Gastroenterol* 2004; 10(20): 3006-3010
<http://www.wjgnet.com/1007-9327/10/3006.asp>

INTRODUCTION

Human hepatitis B virus enhancer II B1 binding factor (hB1F, also known as LRH-1, hFTF, CPF) belongs to the *fushi tarazu* factor 1 (FTZ-F1) nuclear receptor subfamily, which was formally designated as NR5A2^[1-3]. Like other FtsTZ-F1 receptors, hB1F contains a particular FTZ-F1 box which is located at the C-terminus of the DNA-binding domain (DBD) and binds to the response element as monomer^[1]. The biological function of

hB1F is just being unveiled. It has been reported that hB1F and/or its rodent homologs play an important role in regulating the liver-specific expression of several genes^[4,5]. Recent findings pinpoint hB1F as a critical transcription regulator in bile acid biosynthesis^[2,6,7], cholesterol homeostasis^[8-10], sex hormone biosynthesis^[11-13], and lipid metabolism^[14].

To facilitate the study on the function of hB1F, we have established 7 transgenic mouse lineages carrying hB1F transgene^[15]. In this study, we analyzed the expression of the transgene in livers of these transgenic mouse lines with RT-PCR and Western blotting. Tissue expression pattern of the transgene in one of the transgenic mouse lines was also examined with immunochemical methods. The results of pathological analysis demonstrated that the overexpression of hB1F transgene did not cause pathological changes. We then analyzed the gene expression profile in the liver of transgenic mice with microchip and found that the expression of 3 genes was up-regulated while the expression of 25 genes was down-regulated. Some of the differentially expressed genes were verified with RT-PCR. The expression of farnesyl pyrophosphate synthase, a key enzyme in cholesterol biosynthesis, was inhibited in hB1F transgenic mice.

MATERIALS AND METHODS

Animals

C57 mice were maintained by Shanghai Nanfang Research Center for Model Organisms (SNRCMO). hB1F transgenic mice were produced in SNRCMO, maintained and bred in the Laboratory Animal Center of the Second Military Medical University.

Expression of the transgene

Total RNA was isolated from tissues with the TRIzol reagent (Invitrogen) according to the manufacturer's instructions. Semiquantitative RT-PCR reactions were performed with primer pair sets 5'-CCGACAAGTGGTACATGGAA-3' and 5'-CTGCTGCGGG TAGTTACA CA-3' for hB1F cDNA, and 5'-AACTTTGGCATTGTGGAAGG-3' and 5'-TGTGAGGGAG ATGCTCAGTG-3' for mouse glyceraldehyde-3-phosphate dehydrogenase (GAPDH) cDNA, which resulted in the generation of 300 bp and 600 bp products, respectively. PCR reactions were performed 30 cycles at 94 °C for 1 min, at 57 °C for 1 min, and at 72 °C for 1 min. PCR products were electrophoresed on 15 g/L agarose gels.

For Western blotting, protein samples from tissues were prepared according to the protocol from Santa Cruz Biotechnology, Inc. Each protein sample (50 µg) was electrophoresed on 100 g/L SDS-polyacrylamide gel and transferred to PVDF membrane. Membranes were blocked with 50 g/L non-fat milk in Tween-TBS (TBST) overnight at 4 °C and incubated with the anti-Flag antibody (Sigma) at a dilution of 1:500 in TBST for 2 h at room temperature. Membranes were washed three times with TBST and incubated with a horseradish peroxidase-conjugated anti-mouse IgG at a dilution of 1:2 000 at room temperature for 1 h. Immunodetection was carried out with an enhanced chemiluminescence kit (Amersham Pharmacia Biotech) according to the manufacturer's instructions.

Immunohistochemistry and pathological analysis

Tissue samples were fixed in 10% (vol/vol) neutral formalin,

embedded in paraffin, and sectioned for staining. Immunohistochemistry was performed on deparaffinized sections. Tissue sections were permeabilized with 3 g/L Triton X-100 in PBS for 30 min. After washed with PBS, sections were saturated for 30 min at room temperature with PBS containing 50 mL/L milk and then incubated for 1 h at room temperature with the anti-Flag antibody (1/250 dilution). This incubation was followed by five washes for 5 min in PBS-10 mL/L milk and then incubated with a sheep anti-mouse IgG (1/100 dilution) in PBS-milk for 1 h at room temperature. Sections were then washed five times for 5 min in PBS and coverslipped with 500 mL/L glycerol in PBS and examined under a microscope and photographed. Immunohistochemistry and pathological analyses were carried out at the Department of Pathology, Changhai Hospital of the Second Military Medical University.

Microchip analysis of gene expression profile change

RNAs were isolated from livers of two male transgenic mice (TGM-4) and a male C57 mouse. Expressions of 8,315 genes of the mice were analyzed by using BiostarM-80s cDNA arrays (Biostar genechip Inc., Shanghai, China). Control C57 mouse liver cDNA was labeled with fluorescence Cy3 and TGM-4 liver cDNA was labeled with fluorescence Cy5. Cy3 intensity values were adjusted to Cy3* by multiplying a normalization coefficient. The ratios of Cy5/Cy3* were calculated and genes were identified as either up-regulated when the ratio >2, or down-regulated when the ratio <0.5.

Semi-quantitative RT-PCR analysis

Primers used in PCR for CBG gene were 5'-TGTCGTCGCTGCACTTAATC-3' and 5'-AGCACATTCCCTTCATCCAG-3', and

for FPPS gene 5'-GGCCATGTGGATCT TGGTAG-3' and 5'-GAGGAGAGGCTCGTAGCAGA-3', which resulted in generations of 255 bp and 301 bp products, respectively. The cycling parameters were at 94 °C for 5 min, followed by 30 cycles at 94 °C for 1 min, at 57 °C for 1 min, and at 72 °C for 1 min. The PCR products were separated on 1.5% agarose gels. Signals were quantified by density analysis of the digital images using Alpha image software (Alpha Co., Ltd).

Statistical analysis

Differences in CBG and FPPS mRNA expressions (comparing CBG/GAPDH or FPPS/GAPDH ratios) were analyzed using one-way ANOVA and by the Student-Newman-Keuls multiple range test.

RESULTS

Transgene expression in livers of transgenic mice

Since the liver is the main organ that expresses hB1F which is involved in the regulation of the liver-specific expression of several important genes, the overexpression of hB1F transgene in mouse liver may serve as an *in vivo* model to study the function of hB1F in liver. We examined the expression of hB1F transgene in livers of seven transgenic mouse lines. RT-PCR results showed that except TGM-2, six out of seven transgenic mouse lines examined had expression of the transgene (Figure 1). Western blot results demonstrated the expression of the transgene was found in livers of all lines with a relatively higher expression in lines TGM-3, TGM-6, and TGM-7 (Figure 2).

Morphology of TGM tissues

Pathological analysis was performed to examine whether the

Table 1 Genes up- or down-regulated in liver of TGM-4

Gene	Ratio 1	Ratio 2	Average Ratio	GenBank ID
Down-regulated: Trypsin 4	0.279	0.355	0.317	NM_011646
PAS Ser/Thr kinase	0.223	0.412	0.318	NM_080850
Elongation of very long chain fatty acids-like 3	0.274	0.402	0.338	NM_007703
4933406J07Rik RIKEN cDNA	0.363	0.352	0.358	AK016694
Similar to hypothetical protein MGC3169 clone MGC:25675	0.367	0.372	0.369	BC014728
Farnesyl pyrophosphate synthase	0.328	0.419	0.374	AF309508
Similar to hypothetical protein DKFZp434G2226 clone MGC:27627	0.422	0.328	0.375	BC016095
T cell immunoglobulin mucin-3	0.333	0.434	0.384	AF450241
Malate dehydrogenase mitochondrial	0.419	0.350	0.385	NM_008617
1810009A17Rik RIKEN cDNA	0.362	0.430	0.396	AK007392
Tetratricopeptide repeat domain	0.386	0.412	0.399	NM_009441
1810007A24Rik RIKEN cDNA	0.342	0.461	0.402	NM_026925
1810015P03Rik RIKEN cDNA	0.371	0.432	0.402	NM_025458
4930563E19Rik RIKEN cDNA	0.424	0.394	0.406	AK016201
1700030E05Rik RIKEN cDNA	0.400	0.422	0.411	BC017608
2700007P21Rik RIKEN cDNA	0.364	0.458	0.411	AK012215
Capping protein alpha 3	0.455	0.383	0.419	NM_007605
Trefoil factor 1	0.378	0.464	0.421	NM_009362
Ketohexokinase	0.447	0.444	0.446	NM_008439
Mus musculus cDNA	0.429	0.467	0.448	AV079172
Amylase 1 salivary	0.430	0.470	0.450	NM_007446
Elastase 2	0.495	0.448	0.472	NM_007919
Transient receptor protein 2	0.446	0.499	0.472	NM_011644
Clone IMAGE:3587716	0.491	0.458	0.474	BC012849
Heavy polypeptide 8 skeletal muscle	0.486	0.489	0.488	M12289
Up-regulated:				
602390464F1 Mus musculus cDNA	2.097	2.512	2.305	BG293529
Corticosteroid binding globulin	2.154	2.577	2.366	NM_007618
602843872F1 Mus musculus cDNA	3.259	2.292	2.775	BG974154

expression of hB1F transgene might cause any pathological changes in tissues of the transgenic mice. As shown in Figure 3, no obvious pathological change was observed in all tissues from the transgenic mouse line TGM-4. Therefore, as far as the tissues were examined, the expression of hB1F transgene did not result in pathological consequences in TGM-4. Similar results were obtained with other lines (data not shown).

Gene expression profile in livers of TGM-4

Microchip analysis was performed to investigate whether the gene expression profile of the host mice might be altered in the transgenic lines due to the expression of hB1F transgene. The gene expression profiles of cells from the livers of two independent TGM-4 mice were compared with that of the non-transgenic control mouse. Figure 4 represents a visual demonstration of the comparison of gene expression profiles between TGM-4 and C57. The expressions of 28 genes in the livers of TGM-4 mice were found to have changed compared with the C57 control mouse. Among them, 25 genes were down-regulated and 3 genes were up-regulated (Table 1).

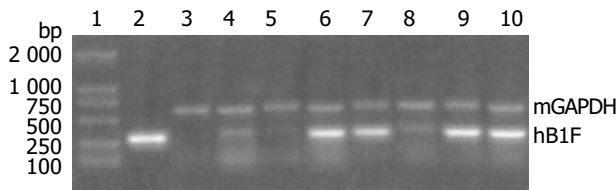


Figure 1 Semi-quantitative RT-PCR results of transgene expression in livers of TGMs lane 1: DNA molecular weight marker DL2 000 (Takara Inc.); lane 2: Positive control, pcDNA3-hB1F; lane 3: Negative control, liver of C57 mouse; lanes 4-10: livers of different lines of transgenic mice, TGM-1 to 7.

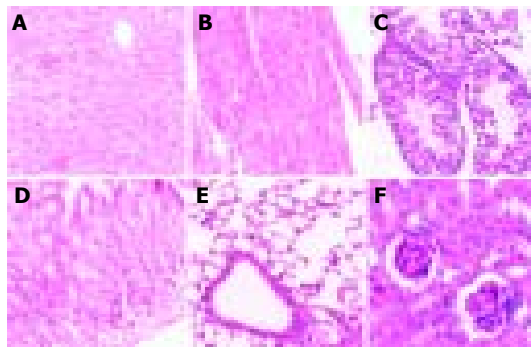


Figure 3 Morphology of TGM-4 tissues A: liver; B: heart; C: testicle; D: stomach; E: lung; F: kidney.

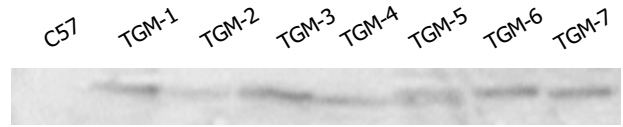


Figure 2 Western blot analysis of hB1F transgene expression in livers of TGMs.

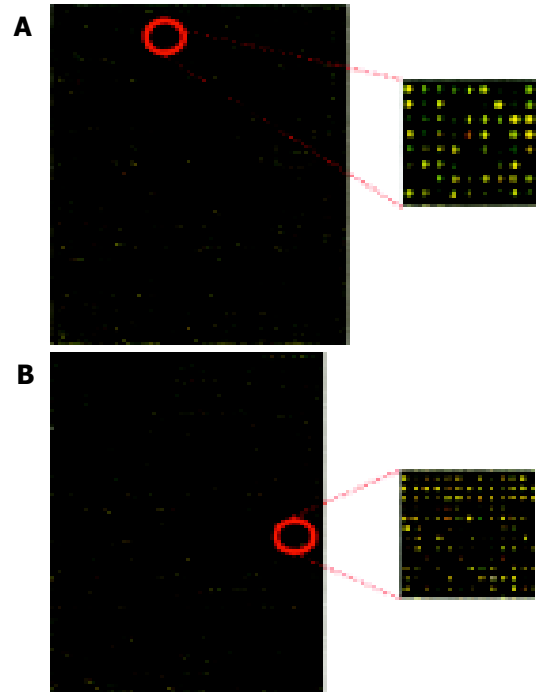


Figure 4 Visual demonstration of gene expression profiles between C57 control mouse and hB1F TGM4 A. chip 1; B. chip 2. Red signals stand for the up-regulated genes and green ones for the down-regulated genes. Yellow signals stand for non-differentially expressed genes.

RT-PCR analysis of differentially expressed genes

Based on the results of the microchip analysis, some of the differentially expressed genes including corticosteroid-binding globulin (CBG) and farnesyl pyrophosphate synthase (FPPS) were subjected to further analysis. Semi-quantitative RT-PCR was performed with samples used in the microchip analysis and also with additional samples from other transgenic lines, TGM-1, TGM-3, TGM-6, and TGM-7. The corticosteroid binding globulin (serine/cysteine proteinase inhibitor) gene was up-regulated in the liver of TGM-4 (Figure 5) and the farnesyl

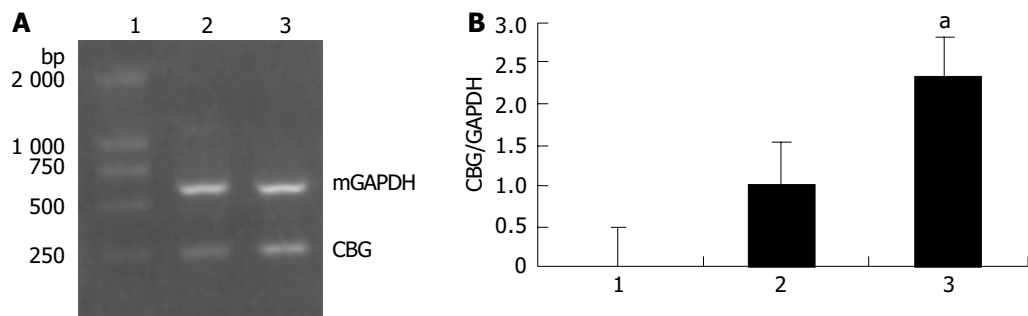


Figure 5 Semi-quantitative RT-PCR results of CBG expression in livers of TGM-4 and C57 control mouse. A: lane 1: DNA molecular weight marker DL2 000; lane 2: C57 control mouse; lane 3: TGM-4. B: The ratio of CBG/GAPDH was calculated for each sample and used as an indication for the relative expression of CBG. The average value for the control was taken as 1. RT-PCR was repeated three times and the results were presented as mean±SE. Statistical significance was subjected to one-way ANOVA and Student-Newman-Keuls multiple range test. ^aP<0.05 vs control.

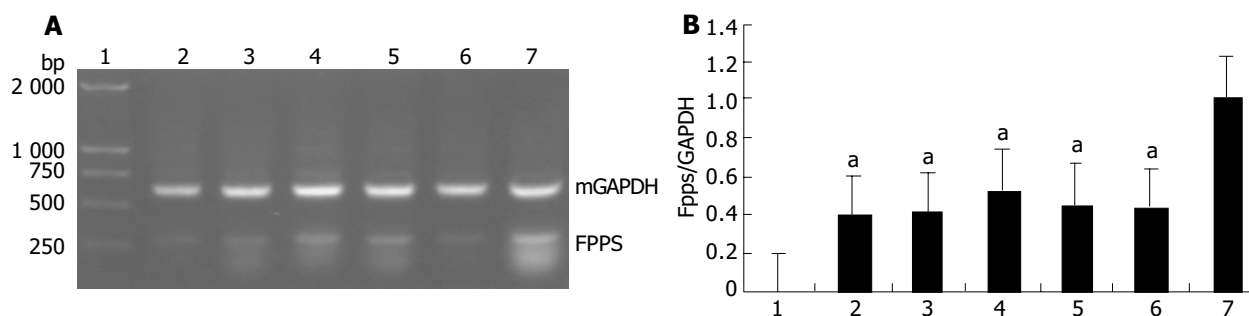


Figure 6 Semi-quantitative RT-PCR results of FPPS expression in livers of TGMs and C57 control mouse. A: lane 1: DNA molecular weight marker DL2000; lane 2: TGM-1; lane 3: TGM-3; lane 4: TGM-4; lane 5: TGM-6; lane 6: TGM-7; lane 7: C57 control mouse. B: The ratio of FPPS/GAPDH was calculated for each sample and used as an indication for the relative expression of FPPS. The average value for the control was taken as 1. RT-PCR was repeated three times and results were presented as mean \pm SE. Statistical significance was subjected to one-way ANOVA and Student-Newman-Keuls multiple range test. * P <0.05 vs control.

pyrophosphate synthase gene was down-regulated in all transgenic mouse lines (Figure 6). These results were well consistent with the microchip analysis data.

DISCUSSION

In this report, we verified the expression of hB1F transgene in several transgenic lines we have constructed previously. Results from RT-PCR and Western blotting analysis indicated that hB1F transgene was expressed in livers of all transgenic lines but with different expression levels. Besides liver, the transgene was also expressed in other organs such as stomach and testis (data not shown). The tissue expression pattern of hB1F transgene was expected since the transcription of the transgene was under the control of the CMV early promoter which has a relative broad tissue expression range. Although hB1F was thought previously to be present mainly in liver and pancreas, recent data revealed that it could be expressed in many types of tissues, such as intestine^[10,16], ovary^[17], adrenal gland^[12], and preadipocytes^[11,18]. Therefore, the transgenic lines established and verified in this study would provide a valuable animal model for studying the function of hB1F in multiple tissues.

Given that hB1F plays an important role in cholesterol homeostasis and bile acid biosynthesis, it is somewhat unexpected that no discernable pathological changes resulting from the overexpression of hB1F transgene have occurred in these transgenic lines. It is possible that the overexpression of hB1F might negatively feedback on the expression of the endogenous mouse counterpart of hB1F, mLRH-1. It remains to determine whether the expression of the endogenous mLRH-1 changes in cells overexpressing hB1F. On the other hand, it is apparent from the microchip analysis that the expression of some genes were altered in livers of these transgenic lines. Since disturbance to metabolic pathways such as the cholesterol homeostasis might require a long incubation time before any pathological phenotypes could be observed, it is necessary to perform a long term follow-up investigation on the possible pathological changes.

Among the genes identified to exhibit altered expressions in hB1F transgenic mice, the gene that encodes the farnesyl pyrophosphate synthase (FPPS) is the most interesting one. FPPS could catalyse the formation of farnesyl pyrophosphate (FPP) through the condensation of dimethylallyl pyrophosphate with two molecules of isopentenyl pyrophosphate. FPP is a key cellular intermediate for the biosynthesis of isoprenoids and a precursor of cholesterol, steroid hormones, dolichols, haem A and ubiquinone. Furthermore, it has been found that FPP and its derivative geranylgeranyl pyrophosphate are involved in prenylation, a post-translational modification of a variety of cellular proteins that influence their proper cellular

localizations and biological functions^[19]. The semi-quantitative RT-PCR results confirmed the down-regulated expression of FPPS in all transgenic lines, suggesting that inhibition of the expression of FPPS has a general effect on hB1F transgenic mice, unrelated to other reasons such as the position effect due to the integration of the transgene. Given the complexity of the regulatory network for the cholesterol homeostasis, it is still early to speculate on the molecular mechanism underlying the inhibition of expression of FPPS in hB1F transgenic mice. Whether hB1F directly or indirectly inhibits the expression of FPPS awaits future study.

REFERENCES

- Li M, Xie YH, Kong YY, Wu X, Zhu L, Wang Y. Cloning and characterization of a novel human hepatocyte transcription factor, hB1F, which binds and activates enhancer II of hepatitis B virus. *J Biol Chem* 1998; **273**: 29022-29031
- Nitta M, Ku S, Brown C, Okamoto AY, Shan B. CPF: an orphan nuclear receptor that regulates liver-specific expression of the human cholesterol 7 α -hydroxylase gene. *Proc Natl Acad Sci U S A* 1999; **96**: 6660-6665
- Nuclear Receptors Nomenclature Committee. A unified nomenclature system for the nuclear receptor superfamily. *Cell* 1999; **97**: 161-163
- Galarneau L, Pare JF, Allard D, Hamel D, Levesque L, Tugwood JD, Green S, Belanger L. The alpha1-fetoprotein locus is activated by a nuclear receptor of the Drosophila FTZ-F1 family. *Mol Cell Biol* 1996; **16**: 3853-3865
- Pare JF, Roy S, Galarneau L, Belanger L. The mouse fetoprotein transcription factor (FTF) gene promoter is regulated by three GATA elements with tandem E box and Nkx motifs, and FTF in turn activates the Hnf3beta, Hnf4alpha, and Hnf1alpha gene promoters. *J Biol Chem* 2001; **276**: 13136-13144
- Goodwin B, Jones SA, Price RR, Watson MA, McKee DD, Moore LB, Galardi C, Wilson JG, Lewis MC, Roth ME, Maloney PR, Willson TM, Kliewer SA. A regulatory cascade of the nuclear receptors FXR, SHP-1, and LRH-1 represses bile acid biosynthesis. *Mol Cell* 2000; **6**: 517-526
- Lu TT, Makishima M, Repa JJ, Schoonjans K, Kerr TA, Auwerx J, Mangelsdorf DJ. Molecular basis for feedback regulation of bile acid synthesis by nuclear receptors. *Mol Cell* 2000; **6**: 507-515
- Luo Y, Liang CP, Tall AR. The orphan nuclear receptor LRH-1 potentiates the sterol-mediated induction of the human CETP gene by liver X receptor. *J Biol Chem* 2001; **276**: 24767-24773
- Schoonjans K, Annicotte JS, Huby T, Botrugno OA, Fayard E, Ueda Y, Chapman J, Auwerx J. Liver receptor homolog 1 controls the expression of the scavenger receptor class B type I. *EMBO Rep* 2002; **3**: 1181-1187
- Inokuchi A, Hinoshita E, Iwamoto Y, Kohno K, Kuwano M, Uchiumi T. Enhanced expression of the human multidrug resistance protein 3 by bile salt in human enterocytes: A transcriptional control of a plausible bile acid transporter. *J Biol Chem* 2001; **276**: 46822-46829

- 11 **Clyne CD**, Speed CJ, Zhou J, Simpson ER. Liver receptor homologue-1 (LRH-1) regulates expression of aromatase in preadipocytes. *J Biol Chem* 2002; **277**: 20591-20597
- 12 **Wang ZN**, Bassett M, Rainey WE. Liver receptor homologue-1 is expressed in the adrenal and can regulate transcription of 11 beta-hydroxylase. *J Mol Endocrinol* 2001; **27**: 255-258
- 13 **Sirianni R**, Seely JB, Attia G, Stocco DM, Carr BR, Pezzi V, Rainey WE. Liver receptor homologue-1 is expressed in human steroidogenic tissues and activates transcription of genes encoding steroidogenic enzymes. *J Endocrinol* 2002; **174**: R13-17
- 14 **Fayard E**, Schoonjans K, Annicotte JS, Auwerx J. Liver receptor homolog 1 controls the expression of carboxyl ester lipase. *J Biol Chem* 2003; **278**: 35725-35731
- 15 **Wang SL**, Yang H, Xie YH, Wang Y, Li JZ, Wang L, Wang ZG, Fu JL. Establishment of transgenic mice carrying the gene of human nuclear receptor NR5A2 (hB1F). *World J Gastroenterol* 2003; **6**: 1333-1336
- 16 **Rausa FM**, Galarneau L, Belanger L, Costa RH. The nuclear receptor fetoprotein transcription factor is coexpressed with its target gene HNF-3beta in the developing murine liver, intestine and pancreas. *Mech Dev* 1999; **89**: 185-188
- 17 **Falender AE**, Lanz R, Malenfant D, Belanger L, Richards JS. Differential expression of steroidogenic factor-1 and FTF/LRH-1 in the rodent ovary. *Endocrinology* 2003; **144**: 3598-3610
- 18 **Iwaki M**, Matsuda M, Maeda N, Funahashi T, Matsuzawa Y, Makishima M, Shimomura I. Induction of adiponectin, a fat-derived antidiabetic and antiatherogenic factor, by nuclear receptors. *Diabetes* 2003; **52**: 1655-1663
- 19 **Zhang FL**, Casey PJ. Protein prenylation: molecular mechanisms and functional consequences. *Annu Rev Biochem* 1996; **65**: 241-269

Edited by Wang XL Proofread by Xu FM

Anti-tumor effect of *pEgr-IFN γ* gene-radiotherapy in B16 melanoma-bearing mice

Cong-Mei Wu, Xiu-Yi Li, Tian-Hua Huang

Cong-Mei Wu, Tian-Hua Huang, Research Center of Reproductive Medicine, Shantou University Medical College (SUMC), Shantou 515041, Guangdong Province, China

Xiu-Yi Li, The Ministry of Public Health Radiobiology Research Unit of Jilin University, Changchun 130021, Jilin Province, China
Supported by the National Natural Science Foundation of China, No. 39970229

Correspondence to: Dr. Cong-Mei Wu, Research Center of Reproductive Medicine, Shantou University Medical College, Shantou 515041, Guangdong Province, China. cmwu@stu.edu.cn

Telephone: +86-754-8900442 **Fax:** +86-754-8557562

Received: 2003-12-10 **Accepted:** 2004-03-02

Abstract

AIM: To construct a *pEgr-IFN γ* plasmid and to investigate its expression properties of interferon- γ (INF- γ) induced by irradiation and the effect of gene-radiotherapy on the growth of melanoma.

METHODS: A recombinant plasmid, *pEgr-IFN γ* , was constructed and transfected into B16 cell line with lipofectamine. The expression properties of *pEgr-IFN γ* were investigated by ELISA. Then, a B16 melanoma-bearing model was established in mice, and the plasmid was injected into the tumor tissue. The tumor received 20 Gy X-ray irradiation 36 h after injection, and IFN- γ expression was detected from the tumor tissue. A tumor growth curve at different time points was determined.

RESULTS: The eukaryotic expression vector, *pEgr-IFN γ* , was successfully constructed and transfected into B16 cells. IFN- γ expression was significantly increased in transfected cells after X-ray irradiation in comparison with 0 Gy group (77.73-94.60 pg/mL, $P < 0.05-0.001$), and was significantly higher at 4 h and 6 h than that of control group after 2 Gy X-ray irradiation (78.90-90.00 pg/mL, $P < 0.01-0.001$). When the transfected cells were given 2 Gy irradiation 5 times at an interval of 24 h, IFN- γ expression decreased in a time-dependent manner. From d 3 to d 15 after IFN γ gene-radiotherapy, the tumor growth was significantly slower than that after irradiation or gene therapy alone.

CONCLUSION: The anti-tumor effect of *pEgr-IFN γ* gene-radiotherapy is better than that of gene therapy or radiotherapy alone for melanoma. These results may establish an important experimental basis for gene-radiotherapy of cancer.

Wu CM, Li XY, Huang TH. Anti-tumor effect of *pEgr-IFN γ* gene-radiotherapy in B16 melanoma-bearing mice. *World J Gastroenterol* 2004; 10(20): 3011-3015
<http://www.wjgnet.com/1007-9327/10/3011.asp>

INTRODUCTION

Radiotherapy is one of the treatments for cancer. However, its therapeutic effect is still unsatisfactory, and thus new therapeutic

strategy must be adopted. Gene therapy in combination with radiotherapy is one of the most important advances^[1-4]. The introduction of Egr-1 promoter induced by irradiation has provided a possible approach to this combination therapy^[5-6].

IFN γ is the first cytokine produced by gene engineering and used for treatment of carcinoma, and has anti-tumor effects. Its antitumor mechanism includes direct inhibition of tumor cell proliferation, and indirect action by activating cytotoxic activities^[7-18]. In the present study we constructed the *pEgr-IFN γ* plasmid by connecting IFN γ cDNA to Egr-1 promoter to investigate its expression properties in B16 cells and its antitumor effect in mice.

MATERIALS AND METHODS

Construction of *pEgr-IFN γ* Plasmid

The expression vector for *pEgr-IFN γ* is shown in Figure 1.

Cell line and transfection

B16 cell line was cultured in MH Radiobiology Research Unit of Jilin University and maintained in RPMI 1640 (Life Technologies) with 100 mL/L fetal bovine serum (Hyclone Laboratories), L-glutamine, 100 μ g/mL of streptomycin, and 100 U/mL of penicillin. The cell line was incubated at 37 °C in 50 mL/L CO₂.

B16 cells were transfected in a 6-well plate when the cells reached 70% confluence. Solution A was prepared by addition of 10 μ g of *pEgr-IFN γ* or pcDNA3.1+ to 100 μ L serum-free medium (SFM), and solution B by addition of 10 μ L liposome to 100 μ L SFM. Solutions A and B were mixed at room temperature for 30 min, then mixed with 0.8 mL SFM, the mixture was added to the rinsed cells. The medium was replaced with fresh and complete medium 6 h after transfection.

Protein determination

Supernatants from different groups were collected for detection of the IFN γ expression with ELISA kit (Genzyme).

Establishment of B16 melanoma-bearing model

Adult female Kunming mice were provided by the Experimental Animal Center of Jilin University, with an average weight of 18 \pm 2 g.

A melanoma-bearing model was established by subcutaneous injection at right hind limb with 0.1 mL B16 cells (5 \times 10⁶/mL), 10 d later, tumor tissue received multi-focus injection of plasmids packaged with liposome (20 μ g plasmid and 0.1 mL liposome per mouse) for the experimental groups.

Tumor size was measured. Then, tumor volume (V) was calculated according to the formula: V (mm³) = $L \times W^2 / 2$, where, L: the longest diameter of tumor; W: the diameter at right angles on the largest horizontal section. Tumor growth rate (f) was the ratio of the volume at different time points over the initial volume (V₀).

Ionizing irradiation

X-rays of 200 kV and 10 mA with 0.5 mm copper and 1.0 mm aluminum filter were given at a dose-rate of 0.8639 Gy/min for a total dose of 2--20 Gy.

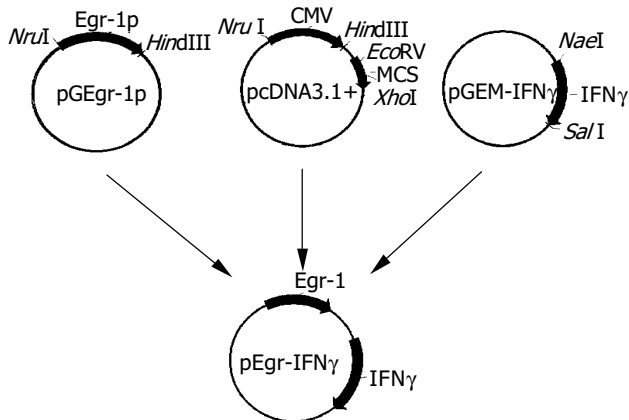


Figure 1 Construction of plasmid pEgr-IFN γ .

B16 cells were seeded in a 6-well plate and randomly divided into different groups. The experiment groups received X-ray irradiation of various doses or at different time points, control groups received sham irradiation simultaneously.

Mice bearing B16 xenografts ($n = 40$) were randomly divided into five groups: control group, 20 Gy group, pcDNA3.1+20 Gy group, pEgr-IFN γ group and pEgr-IFN γ +20 Gy group. Thirty-six hours before irradiation, melanoma tissue was injected with plasmids or buffer at 5 separate sites. Tumor beds were given 20 Gy X-ray irradiation. Animals of 20 Gy group, pcDNA3.1+20 Gy group and pEgr-IFN γ +20 Gy group were shielded with lead except for the tumor-bearing hind limb, animals in the other 2 groups were given sham-irradiation at the same time. Tumors were measured and recorded as previously described.

RT-PCR

Total RNA were extracted from EC9706 cells and tumor tissue for RT-PCR. GAPDH was used as an internal reference. Primers were as follows: GAPDH, forward primer 5'-TGCACCACCAAC TGCTTAGC -3' and reverse one 5'-GGCATGGACTGTGG TCATGAG-3', mouse IFN γ cDNA, forward primer 5'-GATCCT TTGGACCCTCTG ACTT-3' and reverse one 5'-AGACAGTGA TAAACTATAAATGAGCG-3'.

RT-PCR was performed as following: denaturation at 95 °C for 3 min, 30 cycles at 95 °C for 45 s, at 56 °C for 45 s, at 72 °C for 40 s and extension at 72 °C for 10 min.

Statistical analysis

Student's *t* test was used to determine comparability between groups. *P* values less than 0.05 were considered statistically significant.

RESULTS

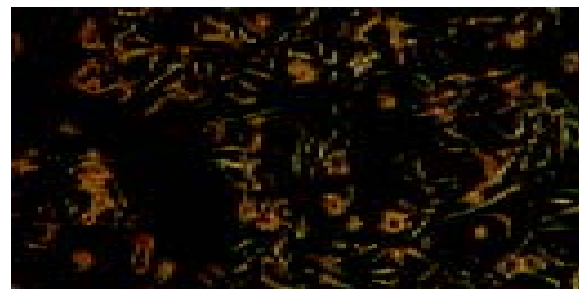
B16 cell line transfected with pEgr-IFN γ plasmid

Pre- and post-transfection of B16 cells are shown in Figure 2.

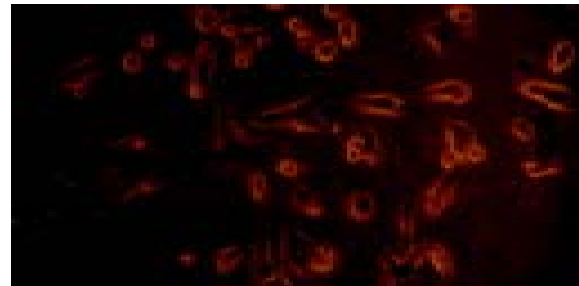
IFN γ expressions in B16 cells transfected with pEgr-IFN γ after different doses of X-irradiation

After transfection B16 cells received different doses of X-ray irradiation. The cells of control group were transfected with pcDNA3.1+ plasmid. Six hours after irradiation IFN γ expression and mRNA level were detected.

The results showed that IFN γ expression in 2-20 Gy groups was significantly higher than that in 0 Gy group ($P < 0.05-0.01$) (Figure 3).



B16 cells before transfection



B16 cells after transfection

Figure 2 Pre- and post-transfection of B16 cells.

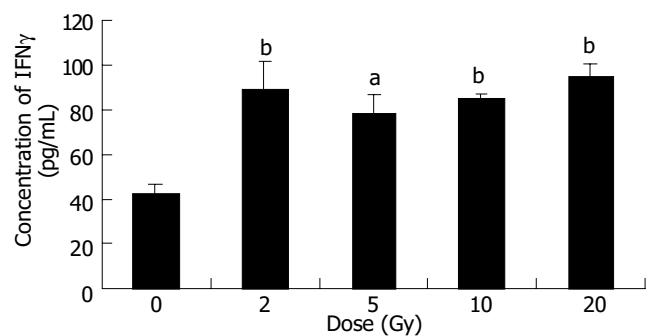


Figure 3 Expression of IFN γ in B16 cells after different doses X-ray irradiation. (mean \pm SD, $n = 3$) ^a $P < 0.05$ and ^b $P < 0.01$ vs 0 Gy group.

After irradiation IFN γ mRNA could be detected in B16 cells (Figure 4). The level of IFN γ mRNA was compared with that of GAPDH, and their ratios are shown in Table 1. The IFN γ mRNA levels in 2-20 Gy groups were higher than that of 0 Gy group.

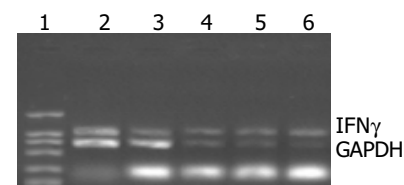


Figure 4 IFN γ mRNA level in B16 cells after different doses of X-ray irradiation. Lane 1: DL2000 Marker; Lane 2: 0 Gy group; Lane 3: 2 Gy group; Lane 4: 5 Gy group; Lane 5: 10 Gy group; Lane 6: 20 Gy group.

IFN γ expressions in B16 cells transfected with pEgr-IFN γ at different time points after 2Gy irradiation

After transfection B16 cells received 2 Gy of X-ray irradiation while the control group received sham irradiation. IFN γ protein was detected at different time points after irradiation. ELISA results showed that the IFN γ expression increased with time from 2 h to 6 h in a time-dependent manner, and peaked at 6 h, about 1.8 times of that in control group ($P < 0.001$). However,

from 8 h to 48 h post-radiation IFN γ expressions were not significantly different from that in control group (Figure 5).

Table 1 IFN γ mRNA level in B16 cells after irradiation with different doses

Dose (Gy)	Ratio of IFN γ mRNA level
0	0.819
2	0.972
5	1.347
10	1.950
20	2.144

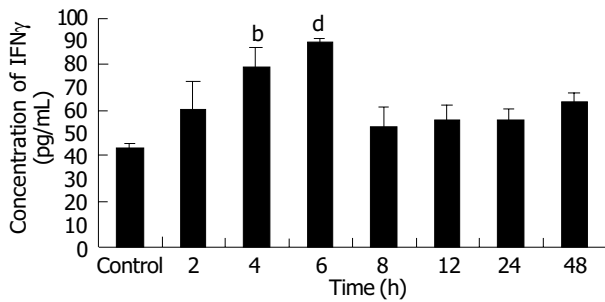


Figure 5 Expression time course of IFN γ in B16 cells after 2 Gy X-ray irradiation (mean \pm SD, *n* = 3) ^b*P*<0.01 and ^d*P*<0.001 vs control group.

Expression of IFN γ in B16 cells at different time points after X-ray irradiation

After transfection B16 cells received 2 Gy irradiation while the

Table 2 Tumor growth rate after gene-radiotherapy (mean \pm SD, *n* = 8)

Group	f (V/V ₀) on days after irradiation				
	3 d	6 d	9 d	2 d	15 d
Control	1.23 \pm 0.37	3.11 \pm 1.5	12.29 \pm 4.83	20.21 \pm 7.62	22.80 \pm 8.50
20 Gy	1.57 \pm 0.19	2.34 \pm 0.40	3.28 \pm 0.68 ^b	4.18 \pm 0.66 ^b	6.18 \pm 1.40 ^b
PcDNA3.1+20 Gy	1.86 \pm 0.54	1.67 \pm 0.40 ^{ad}	2.26 \pm 0.50 ^{bd}	2.86 \pm 0.58 ^{bd}	5.19 \pm 0.66 ^b
PEgr-IFN γ	1.38 \pm 0.23	1.76 \pm 0.56 ^b	2.61 \pm 0.75 ^b	5.23 \pm 0.98 ^b	8.03 \pm 2.14 ^b
PEgr-IFN γ +20 Gy	0.48 \pm 0.10 ^{bf}	0.34 \pm 0.11 ^{bf}	0.38 \pm 0.14 ^{bf}	0.43 \pm 0.11 ^{bf}	0.35 \pm 0.10 ^{bf}

^a*P*<0.05, ^b*P*<0.001 vs control group; ^d*P*<0.01, ^f*P*<0.001 vs 20 Gy group.

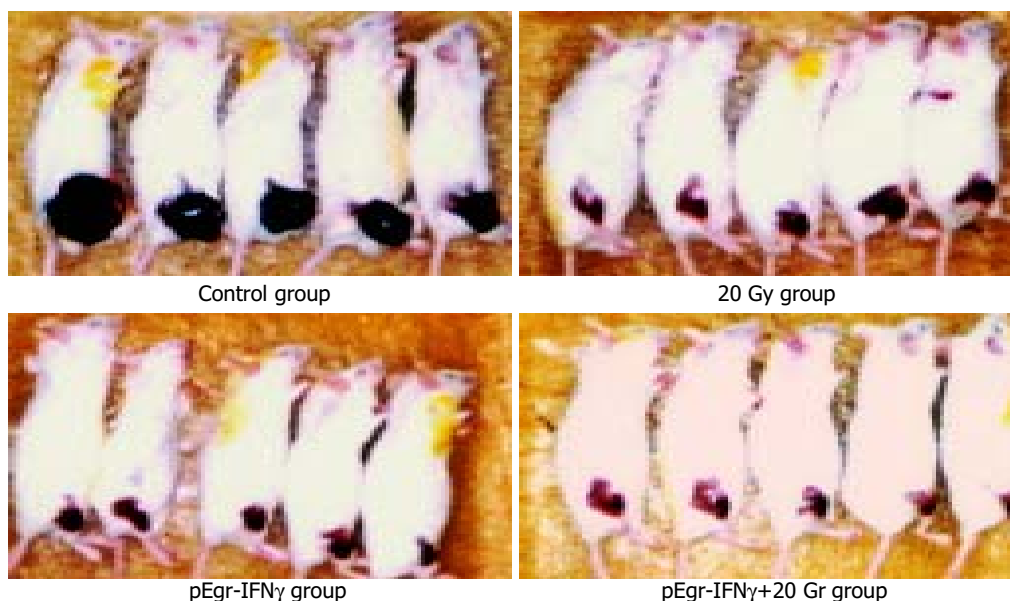


Figure 7 Melanoma-bearing mice 15 d after treatment.

control group received sham irradiation. IFN γ expression was detected 6 h later. Irradiation and detection were repeated 5 times at an interval of 24 h.

The result showed that the IFN γ expression after the first irradiation was the highest, then decreased in a time-dependent manner. The expressions after the first 2 times of irradiation were higher than that in control group (*P*<0.01-0.001) (Figure 6).

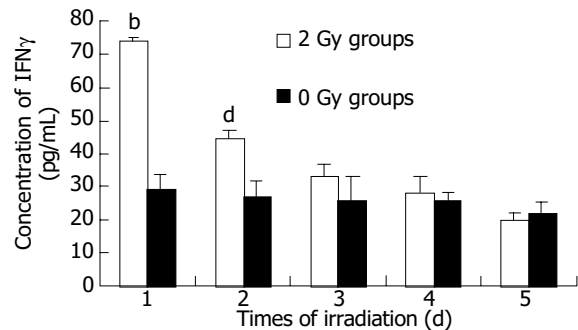


Figure 6 Expression of IFN γ in B16 cells at different time points after X-ray irradiation (mean \pm SD, *n* = 3) ^b*P*<0.01 and ^d*P*<0.001 vs 0 Gy groups.

Effect of gene-radiotherapy on tumor growth

Melanoma-bearing mice of different groups were shown in Figure 7.

Tumor growth rate of pEgr-IFN γ group was significantly slower than that of control group (*P*<0.001) between 6 d and 15 d after irradiation (Table 2), so was pEgr-IFN γ plus 20 Gy group compared with control and 20 Gy groups between 3 d and 15 d after irradiation (*P*<0.001).

RT-PCR analysis of IFN γ in tumor tissue

Melanoma-bearing mice were injected with plasmids, and the tumor received 20 Gy X-ray irradiation, 3 d later total RNA from tumor tissue was extracted for RT-PCR.

GAPDH bands were shown in all groups, but IFN γ cDNA bands were shown only in pEgr-IFN γ and pEgr-IFN γ +20 Gy groups (Figure 8).

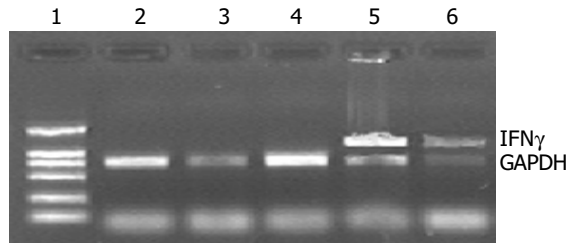


Figure 8 RT-PCR analysis of intratumor IFN γ . Lane 1: DL2000 Marker; Lane 2: control; Lane 3: 20 Gy; Lane 4: pcDNA3.1+20 Gy; Lane 5: pEgr-IFN γ ; Lane 6: pEgr-IFN γ +20 Gy.

DISCUSSION

In 1992 Weichselbaum put forward the new therapeutic strategy that took advantage of the dual tumor-killing effects of genetherapy and radiotherapy, namely, to choose certain exogenous genes that could be activated by irradiation and then transcript some cytotoxic proteins to kill the tumor cells. They also established the techniques that might be used for target gene therapy of carcinomas^[19-25].

It had been reported that Egr-1 was transcriptionally induced by exposure to irradiation, and its induction by irradiation was conferred by serum response or CC (A/T) rGG elements in its promoter region^[26-30]. Based on this finding, we firstly connected IFN γ cDNA with Egr-1 promoter to construct pEgr-IFN γ plasmid to investigate the expression properties in B16 melanoma cells. Furthermore, a melanoma model was established by subcutaneous injection of B16 cells, and then plasmids were injected to observe its antitumor effect *in vivo*.

Firstly, B16 cells transfected with pEgr-IFN γ received different doses of X-ray irradiation and the IFN γ expression was detected. The results showed that the IFN γ expression level in B16 cells post-transfection induced by irradiation was higher than that of sham-irradiation group ($P < 0.05-0.01$). Time-course studies revealed that IFN γ expression reached its peak at 6 h after 2Gy irradiation, and the maximal level was 1.8 times of that in control group ($P < 0.01$). Furthermore, after repeated irradiation the IFN γ expression in B16 cells post-transfection reached the peak level just after the first irradiation, and then decreased in time-dependent manner. All of these demonstrated that pEgr-IFN γ plasmid could enhance IFN γ expression.

Secondly, the results of *in vivo* experiments showed that the proliferation of melanoma was significantly inhibited in pEgr-IFN γ group in comparison with control group between 6 and 15 d after irradiation ($P < 0.001$). So was pEgr-IFN γ gene-radiotherapy group compared with control and 20 Gy groups between 3 and 15 d after irradiation ($P < 0.001$). IFN γ expression was detected in melanoma tissue having received injection of pEgr-IFN γ plasmid. These results demonstrated that injection of pEgr-IFN γ improved antitumor effect, and combined pEgr-IFN γ and irradiation showed the most optimal effect.

This study combined pEgr-IFN γ plasmid and irradiation, and demonstrated much more enhanced antitumor efficacy than either one in the melanoma model. It was very easy to administer directly the plasmid into melanoma tissue, and therapeutic dose could also be administered as required. The tumor could be effectively exposed to radiation with external beam or intratumoral

sources, or both, to enhance local IFN γ expression and boost local tumor control. Increased IFN γ levels might elicit systemic mediators, such as cytokines and matrix proteinases, which target occult distant metastases and thereby further enhance the therapeutic ratio. The absence of systemic toxicities with intratumoral administration of IFN γ supports the safe addition of pEgr-IFN γ gene radiotherapy to current antitumor protocols.

REFERENCES

- 1 Weichselbaum RR, Hallahan DE, Beckett MA, Mauceri HJ, Lee H, Sukhatme VP, Kufe DW. Gene therapy targeted by radiation preferentially radiosensitizes tumor cells. *Cancer Res* 1994; **54**: 4266-4269
- 2 Liu XF, Zou SQ, Qiu FZ. Construction of HCV-core gene vector and its expression in cholangiocarcinoma. *World J Gastroenterol* 2002; **8**: 135-138
- 3 Gou WJ, Yu EX, Liu LM, Li J, Chen Z, Lin JH, Meng ZQ, Feng Y. Comparison between chemoembolization combined with radiotherapy and chemoembolization alone for large hepatocellular carcinoma. *World J Gastroenterol* 2003; **9**: 1697-1701
- 4 Ido A, Uto H, Moriuchi A, Nagata K, Onaga Y, Onaga M, Hori T, Hirono S, Hayashi K, Tamaoki T, Tsubouchi H. Gene therapy targeting for hepatocellular carcinoma: selective and enhanced suicide gene expression regulated by a hypoxia-inducible enhancer linked to a human alpha-fetoprotein promoter. *Cancer Res* 2001; **61**: 3016-3021
- 5 Datta R, Rubin E, Sukhatme V, Qureshi S, Hallahan D, Weichselbaum RR, Kufe DW. Ionizing radiation activates transcription of the EGR1 gene via CAR elements. *Proc Natl Acad Sci U S A* 1992; **89**: 10149-10153
- 6 Tsai Morris CH, Cao XM, Sukhatme VP. 5' flanking sequence and genomic structure of Egr-1, a murine mitogen inducible zinc finger encoding gene. *Nucleic Acids Res* 1988; **16**: 8835-8846
- 7 Lokshin A, Mayotte JE, Levitt ML. Mechanism of interferon beta-induced squamous differentiation and programmed cell death in human non-small-cell lung cancer cell lines. *J Natl Cancer Inst* 1995; **87**: 206-212
- 8 Shiau AL, Lin CY, Tzai TS, Wu CL. Postoperative immunogene therapy of murine bladder tumor by *in vivo* administration of retroviruses expressing mouse interferon-gamma. *Cancer Gene Ther* 2001; **8**: 73-81
- 9 Siesjo P, Visse E, Sjogren HO. Cure of established, intracerebral rat gliomas induced by therapeutic immunizations with tumor cells and purified APC or adjuvant IFN-gamma treatment. *J Immunother Emphasis Tumor Immunol* 1996; **19**: 334-345
- 10 Saleh M, Jonas NK, Wiegman A, Stylli SS. The treatment of established intracranial tumors by *in situ* retroviral IFN-gamma transfer. *Gene Ther* 2000; **7**: 1715-1724
- 11 Li XM, Chopra RK, Chou TY, Schofield BH, Wills Karp M, Huang SK. Mucosal IFN-gamma gene transfer inhibits pulmonary allergic responses in mice. *J Immunol* 1996; **157**: 3216-3219
- 12 Fujinami K, Ikeda I, Miura T, Kondo I. Combination therapy with 5-fluorouracil (5-FU), cisplatin (CDDP) and interferon alpha-2B (IFN alpha-2B) for advanced renal cell carcinoma. *Gan To Kagaku Ryoho* 1996; **23**: 1689-1691
- 13 Yeow WS, Lawson CM, Beilharz MW. Antiviral activities of individual murine IFN-alpha subtypes *in vivo*: intramuscular injection of IFN expression constructs reduces cytomegalovirus replication. *J Immunol* 1998; **160**: 2932-2939
- 14 Ahn EY, Pan G, Vickers SM, McDonald JM. IFN-gamma upregulates apoptosis-related molecules and enhances Fas-mediated apoptosis in human cholangiocarcinoma. *Int J Cancer* 2002; **1**: 445-451
- 15 Blanck G. Components of the IFN-gamma signaling pathway in tumorigenesis. *Arch Immunol Ther Exp* 2002; **50**: 151-158
- 16 Nayak SK, McCallister T, Han LJ, Gangavalli R, Barber J, Dillman RO. Transduction of human renal carcinoma cells with human gamma-interferon gene via retroviral vector. *Cancer Gene Ther* 1996; **3**: 143-150
- 17 Tada H, Maron DJ, Choi EA, Barsoum J, Lei H, Xie Q, Liu W, Ellis L, Moscioni AD, Tazelaar J, Fawell S, Qin X, Propert KJ, Davis A, Fraker DL, Wilson JM, Spitz FR. Systemic IFN-beta

- gene therapy results in long-term survival in mice with established colorectal liver metastases. *J Clin Invest* 2001; **108**: 83-95
- 18 **Paradis TJ**, Floyd E, Burkhit J, Cole SH, Brunson B, Elliott E, Gilman S, Gladue RP. The anti-tumor activity of anti-CTLA-4 is mediated through its induction of IFN gamma. *Cancer Immunol Immunother* 2001; **50**: 125-133
- 19 **Weichselbaum RR**, Hallahan DE, Sukhatme VP, Kufe DW. Gene therapy targeted by ionizing radiation. *Int J Radiat Oncol Biol Phys* 1992; **24**: 565-567
- 20 **Weichselbaum RR**, Kufe DW, Advani SJ, Roizman B. Molecular targeting of gene therapy and radiotherapy. *Acta Oncol* 2001; **40**: 735-738
- 21 **Khodarev NN**, Park JO, Yu J, Gupta N, Nodzenski E, Roizman B, Weichselbaum RR. Dose-dependent and independent temporal patterns of gene responses to ionizing radiation in normal and tumor cells and tumor xenografts. *Proc Natl Acad Sci U S A* 2001; **98**: 12665-12670
- 22 **Gupta VK**, Park JO, Jaskowiak NT, Mauceri HJ, Seetharam S, Weichselbaum RR, Posner MC. Combined gene therapy and ionizing radiation is a novel approach to treat human esophageal adenocarcinoma. *Ann Surg Oncol* 2002; **9**: 500-504
- 23 **Hanna NN**, Seetharam S, Mauceri HJ, Beckett MA, Jaskowiak NT, Salloum RM, Hari D, Dhanabal M, Ramchandran R, Kalluri R, Sukhatme VP, Kufe DW, Weichselbaum RR. Antitumor interaction of short- course endostatin and ionizing radiation. *Cancer J* 2000; **6**: 287-293
- 24 **Takahashi T**, Namiki Y, Ohno T. Induction of the suicide HSV-TK gene by activation of the Egr-1 promoter with radioisotopes. *Hum Gene Ther* 1997; **8**: 827-833
- 25 **GrisCELLI F**, Li H, Cheong C, Opolon P, Bennaceur- Griscelli A, Vassal G, Soria J, Soria C, Lu H, Perricaudet M, Yeh P. Combined effects of radiotherapy and angiostatin gene therapy in glioma tumor model. *Proc Natl Acad Sci U S A* 2000; **97**: 6698-6703
- 26 **Christy B**, Nathans D. DNA binding site of the growth factor-inducible protein Zif268. *Proc Natl Acad Sci U S A* 1989; **86**: 8737-8741
- 27 **Seyfert VL**, Sukhatme VP, Monroe JG. Differential expression of a zinc finger-encoding gene in response to positive versus negative signaling through receptor immunoglobulin in murine B lymphocytes. *Mol Cell Biol* 1989; **9**: 2083-2088
- 28 **Joseph LJ**, Le-Beau MM, Jamieson GA Jr, Acharya S, Shows TB, Rowley JD, Sukhatme VP. Molecular cloning, sequencing, and mapping of EGR2, a human early growth response gene encoding a protein with "zinc-binding finger" structure. *Proc Natl Acad Sci U S A* 1988; **85**: 7164-7168
- 29 **Sukhatme VP**. Early transcriptional events in cell growth: the Egr family. *J Am Soc Nephrol* 1990; **1**: 859-866
- 30 **Cao XM**, Koski RA, Gashler A, McKiernan M, Morris, CF, Gaffney R, Hay RV, Sukhatme VP. Identification and characterization of the Egr-1 gene product, a DNA-binding zinc finger protein induced by differentiation and growth signals. *Mol Cell Biol* 1990; **10**: 1931-1939

Edited by Ren SY and Wang XL Proofread by Xu FM

Differentiation of rat marrow mesenchymal stem cells into pancreatic islet beta-cells

Li-Bo Chen, Xiao-Bing Jiang, Lian Yang

Li-Bo Chen, Xiao-Bing Jiang, Lian Yang, Department of Surgery, Union Hospital of Huazhong University of Science and Technology, Wuhan 430022, Hubei Province, China

Supported by the National Natural Science Foundation of China, No. 30170911

Correspondence to: Dr. Li-Bo Chen, Department of Surgery, Union Hospital of Huazhong University of Science and Technology, Wuhan 430022, Hubei Province, China. libo_chen@hotmail.com

Telephone: +86-27-85726301 **Fax:** +86-27-85776343

Received: 2003-12-10 **Accepted:** 2004-02-01

Abstract

AIM: To explore the possibility of marrow mesenchymal stem cells (MSC) *in vitro* differentiating into functional islet-like cells and to test the diabetes therapeutic potency of Islet-like cells.

METHODS: Rat MSCs were isolated from Wistar rats and cultured. Passaged MSCs were induced to differentiate into islet-like cells under following conditions: pre-induction with L-DMEM including 10 mmol/L nicotinamide+1 mmol/L β -mercaptoethanol+200 mL/L fetal calf serum (FCS) for 24 h, followed by induction with serum free H-DMEM solution including 10 mmol/L nicotinamide+1 mmol/L β -mercaptoethanol for 10 h. Differentiated cells were observed under inverse microscopy, insulin and nestin expressed in differentiated cells were detected with immunocytochemistry. Insulin excreted from differentiated cells was tested with radioimmunoassay. Rat diabetic models were made to test *in vivo* function of differentiated MSCs.

RESULTS: Typical islet-like clustered cells were observed. Insulin mRNA and protein expressions were positive in differentiated cells, and nestin could be detected in pre-differentiated cells. Insulin excreted from differentiated MSCs (446.93 \pm 102.28 IU/L) was much higher than that from pre-differentiated MSCs (2.45 \pm 0.81 IU/L (P <0.01)). Injected differentiated MSCs cells could down-regulate glucose level in diabetic rats.

CONCLUSION: Islet-like functional cells can be differentiated from marrow mesenchymal stem cells, which may be a new procedure for clinical diabetes stem-cell therapy, these cells can control blood glucose level in diabetic rats. MSCs may play an important role in diabetes therapy by islet differentiation and transplantation.

Chen LB, Jiang XB, Yang L. Differentiation of rat marrow mesenchymal stem cells into pancreatic islet beta-cells. *World J Gastroenterol* 2004; 10(20): 3016-3020
<http://www.wjgnet.com/1007-9327/10/3016.asp>

INTRODUCTION

Diabetic mellitus (DM), one of the leading causes of morbidity and mortality in many countries, is caused by an absolute insulin

deficiency due to the destruction of insulin secreting pancreatic cells (type 1 DM) or by a relative insulin deficiency due to decreased insulin sensitivity, usually observed in overweight individuals (type 2 DM). In both types of the disease, an inadequate mass of functional islet cells is the major determinant for the onset of hyperglycemia and the development of overt diabetes. Islet transplantation has recently been shown to restore normoglycemia in type 1 DM^[1]. However, a limited supply of human islet tissues prevents this therapy from being used in patients with type 1 DM. Alternatively, much effort has been made to increase β cell mass by stimulating endogenous regeneration of islets or *in vitro* differentiated islet-like cells^[2-5]. Multipotent stem cells have been described within pancreatic islets and in nonendocrine compartments of the pancreas^[6-12], and these cells have the capacity of differentiating into pancreatic islet-like structures. Furthermore, cells that do not reside within the pancreas, such as embryonic stem cells(ESC), hepatic oval cells, cells within spleen, have been differentiated into pancreatic endocrine hormone-producing cells *in vitro* and *in vivo*^[13-21]. However, despite their differentiating potency, differentiation of various stem cells into islet cells has two major obstacles preventing clinical application: One is that these stem cells do not originate from DM patients, transplanting them would unavoidably be rejected by DM recipients. The other is that the source is not enough to provide abundant stem cells. The current article reports a potential means to generate insulin-producing cells, islet differentiation from bone marrow-derived stem cells. We suggest that cells within the adult bone marrow (mesenchymal stem cells MSC) are capable of differentiating into functional pancreatic β cell phenotypes.

MATERIALS AND METHODS

Materials

Wistar rats were bought from Animal Center, Tongji Medical College. All procedure was accordant with animal experiment guideline of the university. Cell culture medium L-DMEM (4.5 mmol/L glucose), H-DMEM (23 mmol/L glucose) and fetal calf serum (FCS) were bought from GIBCO Co. Nicotinamide, β -mercaptoethanol, B27 were from Sigma Co. Anti-nestin, anti-insulin monoclonal antibodies were bought from Santa Cruz Co. RT-PCR kit and primers were purchased from GIBCO Co. Radioimmunoassay (RIA) kit was purchased from Beijing North Biotechnology Co.

Differentiation of rat marrow mesenchymal stem cells into functional islet β cells

Bone marrow was isolated from femoral bone under aseptic condition and dispersed into single cell suspension, L-DMEM cells were cultured in a density of $1 \times 10^6/L$ at 37 °C, 50 mL/L CO₂ for 48 h. Suspended cells were disposed and adherent cells were cultured in L-DMEM with 200 mL/L FCS for about 10 d, culture medium was changed at 3-d intervals. These cells were digested with 2.5 g/L trypsin and passed for 2-3 generations when the confluence reached 70-90%. Then, cells with 70-80% confluence were induced to differentiate into functional pancreatic cells. Cells were pre-induced with 10 mmol/L nicotinamide and 1 mmol/L

β -mercaptoethanol in L-DMEM for 24 h, and re-induced with 10 mmol/L nicotinamide and 1 mmol/L Mercaptoethanol in serum-free H-DMEM for another 10 h. Cells induced without nicotinamide or β -mercaptoethanol were used as controls.

Function assessment of differentiated cells

Cell morphology changes were investigated under converted microscope. Insulin-1 mRNA or protein expression was detected with immunocyto-chemical procedure and reverse transcription polymerase chain reaction (RT-PCR), and insulin level in culture suspension secreted from differentiated cells was detected with radio-immunological assay (RIA).

RT-PCR

Total RNA from 5×10^6 pre-treated or post-treated MSC cells was isolated according to a Qiagen protocol including DNase treatment. Reverse transcription was carried out using the Superscript protocol. Taq-man RT-PCR was performed using the Master Mix (Applied Biosystems). Insulin-1 primers were designed using the primer express program (Applied Biosystems) according to gene bank sequences. The following primers were used for Insulin-1: forward: 5'-GGGAACGTGGTTCCTTCTA-3', backward: 5'-TAGACGAGGGAGATGGTTGACC-3'. 35 cycles of 94 °C \times 30 s, 55 °C \times 30 s, 72 °C \times 30 s were performed and the PCR product for Insulin-1 was 187 bp. GAPDH was used as internal control with the following primers: forward: TGGTATCGTGGAAGGACTCATGA. backward: ATGCCAGTGAGCTTCCCCTTCAGC. Products were tested with 15 g/L gel electrophoresis.

Immunohistochemistry

Cells adherent to slides were fixed with 40 g/L para-formaldehyde. After washed, the slides were incubated with a biotin-goat anti-rat insulin or nestin monoclonal antibodies (Santa Cruz Co, USA) diluted 1:200 in 50 mL/L normal goat serum for 20 min at room temperature. Immuno-reactive cells were visualized using the Vectastain Elite ABC Kit (Vector Labs, USA) with 3'3 diaminobenzidine tetrachloride (DAB) (Boehringer-Mannheim) as the chromogen. All sections were counterstained with hematoxylin.

Radioimmunoassay

The amounts of immunoreactive insulin in supernatants secreted from differentiated cells 48 h after treatment and cells 24 h before treatment were determined by RIA using a commercially available RIA kit according to the manufacturer's instructions. Briefly, to each polypropylene RIA tube 100 μ L each of anti-Insulin, 125 I- insulin, and insulin or the samples were added. Immune complexes were precipitated 24 h later with 1 mL of 160 mL/L polyethylene glycol solution, and a gamma counter was used to determine the radioactivity in the precipitates. There was no nonspecific interference of the assay with the components of the samples. Determinations were carried out in triplicate and the means and standard deviations were obtained.

Primitive glucose controlling role of differentiated MSCs on STZ-diabetic rats

Diabetic animal models were made according to the standard procedure with modifications. Briefly, 10 Wistar rats (weighting about 200 grams) were intravenously injected with 50 mg/L streptozotocin (STZ) from caudal veins, and glucose levels were tested 1 week later with Roche ACCU-CHEK glucose tester. Two rats died and were excluded. After stable hyperglycemia level was achieved, 3 animals were subcutaneously injected with 5×10^6 differentiated cells, while 2 others received the same amount of un-differentiated cells, the remaining 1 did not receive any cells. One week after cell injection, animal glucose level

was recorded.

Statistical analysis

Data were analyzed with Student's *t* test, $P < 0.05$ was considered statistically significant.

RESULTS

Morphological changes of MSC differentiation

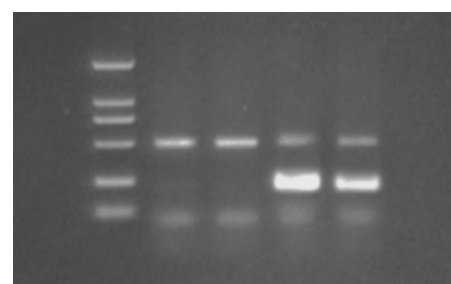
Under inverted microscope, undifferentiated MSCs were typical of adherent spindle and fibrocyte-like. However, under differentiation, these spindle-like cells changed rapidly into round or oval types with confluence. These cells were abundant in endocrinal granules, similar to those differentiated islet cells from ES cells. These grape-like cells lasted for at least 2 wk. Some cells changed into neuron-like cells with typical processes.



Figure 1 Islet-like grape-shaped cells isolated from marrow mesenchymal stem cells.

Insulin-1 transcription in differentiated cells

To assess insulin-1 mRNA expression in differentiated cells, RT-PCR was applied on MSCs shortly after bone marrow isolation (Neg), 24 h before nicotinamide and β -mercaptoethanol treatment (Pre), 48 h (Islet1) and 1 week after Nicotinamide and β -mercaptoethanol treatment (Islet2). There were no pre-differentiated MSCs (Figure 2). However, 48 h after treatment, insulin-1 mRNA transcription could be detected and continued for at least 1 wk. Since we did not observe any pancreatic islet-like cells in control group, RT-PCR was not performed on this group of cells.



Marker Neg Pre Islet1 Islet2

Figure 2 Insulin transcription in pre-differentiated MSCs shown in RT-PCR. Neg: MSCs undifferentiated; Pre: MSCs 24 h before differentiation; Islet1: cells 24 h after differentiation; Islet2: cells 1w after differentiation.

Insulin and nestin protein expression in different stages of MSCs

Immunocytochemistry was performed to test insulin or nestin protein expressions in MSCs. Insulin could be observed obviously in those grape-like cells (Islet-like), and in unchanged spindle-like cells not positively stained. Nestin was regarded

as an important pre-marker for islet cell differentiation, and its expression was tested. Immunocytochemistry showed nestin positivity in pre-differentiated spindle-like cells (Figure 4), while no nestin positivity in differentiated islet-like cells.

To further clarify the function of these differentiated cells, RIA was used to assess the insulin excretion from these cells in 6 independent cell cultures. As shown in Table 1, pre-differentiated MSCs seldom secreted insulin into their supernatant if any. However, 48 h after differentiation, these islet-like cells produced much insulin and secreted insulin in extra-cellular medium.



Figure 3 Insulin staining for islet-like cells. Strong brown staining indicates insulin positivity in differentially arranged grape shape cells.



Figure 4 Positive nestin in pre-differentiated MSCs.

Table 1 Insulin excretion changes in pre- and differentiated MSCs (RIA) (IU/L)

Group	Insulin excretion in pre-treated MSCs	Insulin excretion in treated islet-like cells
1	1.67	410.79
2	2.53	383.21
3	1.53	465.81
4	3.36	308.28
5	2.20	516.45
6	3.40	597.02

In supernatant of pre-differentiated MSC cells, there was no obvious insulin excretion (2.45 ± 0.81 IU/L). Forty-eight h after differentiation, cells excreted more insulin into supernatant, the insulin level was as high as 446.93 ± 102.28 IU/L ($t = 10.65$, $P < 0.01$).

To test if these MSC-differentiated islet-like cells could exert glucose-controlling function, 6 diabetic Wistar rat models were included. Each of 3 rats was administered subcutaneously 5×10^6 differentiated cells, 2 received similar un-differentiated MSCs injection, while the last one received none. Glucose levels of these 6 rats at different times are shown in Table 2. Although lack of statistical analysis, it could be suggested that MSC-

differentiated islet-like cells could change diabetic glucose level.

Table 2 Blood glucose level (mmol/L) changes in STZ-diabetic rats

Types of cells injected	Glucose level 24 h before injection	Glucose level 1 w after injection
Islet1	>33.3	25.4
Islet2	>33.3	21.4
Islet3	25.3	19.7
MSC1	>33.3	>33.3
MSC2	28.9	29.7
Non	>33.3	>33.3

Islet1, Islet1, Islet3: different STZ-diabetic rats received islet cell injection; MSC1, MSC2: STZ-diabetic rats received undifferentiated MSC injection; Non: STZ-diabetic rats did not receive cell injection.

DISCUSSION

Multipotent stem cells within pancreas and outside could develop into insulin-secreting islet cells^[7-21]. However, differentiation of various stem cells into islet cells has two major obstacles preventing clinical application. As these stem cells do not originate from DM patients, these cells transplanted would be rejected by DM recipients. The source is not enough to provide abundant stem cells.

Bone marrow mesenchymal cells (MSC) reside in bone marrow and are multipotent, and can differentiate into lineages of mesenchymal tissues, such as bone, cartilage, fat, tendon, muscle, adipocytes, chondrocytes, osteocytes^[22-24]. MSCs could differentiate into endodermal and epidermal cells, such as vascular endothelial cells, neurocytes, lung cells and hepatocytes^[25-27]. MSCs as differentiation donors are of advantages compared with other stem cells as ESC or stem cells from organs. MSCs are of great multiplication potency. Cell-doubling time is 48-72 h, and cells could be expanded in culture for more than 60 doublings^[28]. Functional cells differentiated from MSCs transplanted into MSC donors (autologous transplantation) would not cause any rejection.

Differentiation of MSCs into functional pancreatic islet cells is not yet reported. Ianus *et al.*^[29] reported, using a CRE-LoxP system, bone marrow from male mice with an enhanced green fluorescent protein (GFP) replacing insulin expression was transplanted into lethally irradiated recipient female mice. After 4-6 wk, recipient mice revealed both Y chromosome and GFP positivity in pancreatic islets. These GFP positive cells expressed insulin, glucose transporter-2 and other islet β cell related markers. Cells from bone marrow were able to differentiate into islet cells. MSCs could differentiate into hepatocytes^[25,27], precursor cells of hepatocytes could differentiate into pancreatic islet cells, adult hepatic stem cells could trans-differentiate into pancreatic endocrine hormone-producing cells^[19,20]. These reports indicated that, MSCs had the capacity of differentiating into pancreatic islet cells.

We found that MSCs could successfully differentiate into pancreatic islet β -like cells. These cells were morphologically similar to pancreatic islet cells. More importantly, they could also transcript, translate and excrete insulin. Cells were injected subcutaneously into NOD rat models, although lack of statistical data, these MSC-derived cells could regulate NOD blood glucose level. Nestin was regarded as a marker of precursors of pancreatic islet cells^[10,14]. In our study, nestin was also positive in pre-pancreatic islet MSCs, suggesting that MSCs could differentiate into islet cells. High glucose concentration was considered as a potent inducer for pancreatic islet differentiation. Nicotinamide was used to preserve islet viability and function through poly

(ADP-ribose) polymerase (PARP)^[30], β -mercaptoethanol was commonly used as a neurocyte inducer. In our primary experiment, high glucose alone could not effectively induce MSC to differentiate into islet-like cells. After nicotinamide was added, they could effectively transform MSCs into islet-like cells. This may imply that nicotinamide could be an effective inducer, or it could protect differentiated cells from dying or transforming into other cell types. β -mercaptoethanol increased the potency of nicotinamide in our experiment. Considering nestin expression in pre-differentiated MSCs, MSCs might differentiate into pancreatic islet-like cells through intermediate neurocyte stage. We did not test the insulin secretion based on the number of cells, the increased insulin in supernatant might be mainly from increased insulin excretion by islet-like cells.

Bone marrow stem cells are non-endodermal cells with no immediate relationship to putative pancreatic stem cells that are resident in tissues of endodermal origin or developmental neuro-endocrine stem cells derived from the endoderm. Alternatively, stem cells in bone marrow may be derived from sites of endodermal origin. Regardless of their germ layer of origin, these cells represent multi-potent cells mediated by circulating signals, and can be recruited to neuro-endocrine compartments of the pancreas. Once homing of these cells to pancreatic islets has occurred, local cell-cell interaction as well as paracrine factors may initiate differentiation.

There was an argument^[31] that Islet-like cells differentiated from ESC were falsely insulin positive from insulin-uptake. These insulin-positive cells which do not transcribe insulin mRNA, are TUNEL⁺. Bone marrow cells could also fuse with other cells and adopt the phenotypes of these cells^[32,33]. However, cell differentiation in our report was not the case. Islet cells expressed insulin at both mRNA and protein levels, the excreting insulin level was far more higher than that in culture media and that of pre-differentiated cells. Further more, these MSCs-derived cells could down-regulate glucose level in diabetic rats.

In conclusion, MSCs can differentiate into functional pancreatic islet-like cells *in vitro*. If human MSCs, especially MSCs from diabetes patients themselves can be isolated, proliferated, differentiated into functional pancreatic islet-like cells, and transplanted back into their donors (autologous transplantation), their high proliferation potency and rejection avoidance will provide one promising therapy for diabetes.

REFERENCES

- 1 Shapiro AM, Lakey JR, Ryan EA, Korbutt GS, Toth E, Warnock GL, Kneteman NM, Rajotte RV. Islet transplantation in seven patients with type 1 diabetes mellitus using a glucocorticoid-free immunosuppressive regimen. *N Engl J Med* 2000; **343**: 230–238
- 2 Bonner-Weir S, Taneja M, Weir GC, Tatarkiewicz K, Song KH, Sharma A, O'Neil JJ. *In vitro* cultivation of human islets from expanded ductal tissue. *Proc Natl Acad Sci U S A* 2000; **97**: 7999–8004
- 3 Abraham EJ, Leech CA, Lin JC, Zulewski H, Habener JF. Insulinotropic hormone glucagon-like peptide-1 differentiation of human pancreatic islet-derived progenitor cells into insulin-producing cells. *Endocrinology* 2002; **143**: 3152–3161
- 4 Schmied BM, Ulrich A, Matsuzaki H, Ding X, Ricordi C, Weide L, Moyer MP, Batra SK, Adrian TE, Pour PM. Transdifferentiation of human islet cells in a long-term culture. *Pancreas* 2001; **23**: 157–171
- 5 Lipsett M, Finegood DT. Beta-cell neogenesis during prolonged hyperglycemia in rats. *Diabetes* 2002; **51**: 1834–1841
- 6 Ramiya VK, Maraist M, Arfors KE, Schatz DA, Peck AB, Cornelius JG. Reversal of insulin-dependent diabetes using islets generated *in vitro* from pancreatic stem cells. *Nat Med* 2000; **6**: 278–282
- 7 Schwitzgebel VM, Scheel DW, Connors JR, Kalamaras J, Lee JE, Anderson DJ, Sussel L, Johnson JD, German MS. Expression of neurogenin3 reveals an islet cell precursor population in the pancreas. *Development* 2000; **127**: 3533–3542
- 8 Jensen J, Heller RS, Funder-Nielsen T, Pedersen EE, Lindsell C, Weinmaster G, Madsen OD, Serup P. Independent development of pancreatic alpha- and beta-cells from neurogenin3-expressing precursors: a role for the notch pathway in repression of premature differentiation. *Diabetes* 2000; **49**: 163–176
- 9 Guz Y, Nasir I, Teitelman G. Regeneration of pancreatic beta cells from intra-islet precursor cells in an experimental model of diabetes. *Endocrinology* 2001; **142**: 4956–4968
- 10 Zulewski H, Abraham EJ, Gerlach MJ, Daniel PB, Moritz W, Muller B, Vallejo M, Thomas MK, Habener JF. Multipotential nestin-positive stem cells isolated from adult pancreatic islets differentiate *ex vivo* into pancreatic endocrine, exocrine, and hepatic phenotypes. *Diabetes* 2001; **50**: 521–533
- 11 Gao R, Ustinov J, Pulkkinen MA, Lundin K, Korsgren O, Otonkoski T. Characterization of endocrine progenitor cells and critical factors for their differentiation in human adult pancreatic cell culture. *Diabetes* 2003; **52**: 2007–2015
- 12 Hardikar AA, Marcus-Samuels B, Geras-Raaka E, Raaka BM, Gershengorn MC. Human pancreatic precursor cells secrete GGF2 to stimulate clustering into hormone-expressing islet-like cell aggregates. *Proc Natl Acad Sci U S A* 2003; **100**: 7117–7122
- 13 Soria B, Roche E, Berna G, Leon-Quinto T, Reig JA, Martin F. Insulin-secreting cells derived from embryonic stem cells normalize glycemia in streptozotocin-induced diabetic mice. *Diabetes* 2000; **49**: 157–162
- 14 Lumelsky N, Blondel O, Laeng P, Velasco I, Ravin R, McKay R. Differentiation of embryonic stem cells to insulin-secreting structures similar to pancreatic islets. *Science* 2001; **292**: 1389–1394
- 15 Assady S, Maor G, Amit M, Itskovitz-Eldor J, Skorecki KL, Tzukerman M. Insulin production by human embryonic stem cells. *Diabetes* 2001; **50**: 1691–1697
- 16 Hori Y, Rulifson IC, Tsai BC, Heit JJ, Cahoy JD, Kim SK. Growth inhibitors promote differentiation of insulin-producing tissue from embryonic stem cells. *Proc Natl Acad Sci U S A* 2002; **99**: 16105–16110
- 17 Shiroy A, Yoshikawa M, Yokota H, Fukui H, Ishizaka S, Tatsumi K, Takahashi Y. Identification of insulin-producing cells derived from embryonic stem cells by zinc-chelating dithizone. *Stem Cells* 2002; **20**: 284–292
- 18 Kim D, Gu Y, Ishii M, Fujimiya M, Qi M, Nakamura N, Yoshikawa T, Sumi S, Inoue K. *In vivo* functioning and transplantable mature pancreatic islet-like cell clusters differentiated from embryonic stem cell. *Pancreas* 2003; **27**: E34–E41
- 19 Deutsch G, Jung J, Zheng M, Lora J, Zaret KS. A bipotential precursor population for pancreas and liver within the embryonic endoderm. *Development* 2001; **128**: 871–881
- 20 Yang L, Li S, Hatch H, Ahrens K, Cornelius JG, Petersen BE, Peck AB. *In vitro* trans-differentiation of adult hepatic stem cells into pancreatic endocrine hormone producing cells. *Proc Natl Acad Sci U S A* 2002; **99**: 8078–8083
- 21 Kodama S, Kuhlreiber W, Fujimura S, Dale EA, Faustman DL. Islet regeneration during the reversal of autoimmune diabetes in NOD mice. *Science* 2003; **302**: 1223–1227
- 22 Pittenger MF, Mackay AM, Beck SC, Jaiswal RK, Douglas R, Mosca JD, Moorman MA, Simonetti DW, Craig S, Marshak DR. Multilineage potential of adult human mesenchymal stem cells. *Science* 1999; **284**: 143–147
- 23 Krause DS, Theise ND, Collector MI, Henegariu O, Hwang S, Gardner R, Neutzel S, Sharkis SJ. Multi-organ, Multi-lineage engraftment by a single bone marrow-derived stem cells. *Cell* 2001; **105**: 369–377
- 24 Jiang Y, Jahagirdar BN, Reinhardt RL, Schwartz RE, Keene CD, Ortiz-Gonzalez XR, Reyes M, Lenvik T, Lund T, Blackstad M, Du J, Aldrich S, Lisberg A, Low WC, Largaespada DA, Verfaillie CM. Pluripotency of mesenchymal stem cells derived from adult marrow. *Nature* 2002; **418**: 41–49
- 25 Petersen BE, Bowen WC, Patrene KD, Mars WM, Sullivan

- AK, Murase N, Boggs SS, Greenberger JS, Goff JP. Bone marrow as a potential source of hepatic oval cells. *Science* 1999; **284**: 1168-1170
- 26 **Davani S**, Marandin A, Mersin N, Royer B, Kantelip B, Herve P, Etievent JP, Kantelip JP. Mesenchymal progenitor cells differentiate into an endothelial phenotype, enhance vascular density, and improve heart function in a rat cellular cardiomyoplasty model. *Circulation* 2003; **108**(Suppl 1): II253-258
- 27 **Schwartz RE**, Reyes M, Koodie L, Jiang Y, Blackstad M, Lund T, Lenvik T, Johnson S, Hu WS, Verfaillie CM. Multipotent adult progenitor cells from bone marrow differentiate into functional hepatocyte-like cells. *J Clin Invest* 2002; **109**: 1291-1302
- 28 **Reyes M**, Lund T, Lenvik T, Aguiar D, Koodie L, Verfaillie CM. Purification and *ex vivo* expansion of postnatal human marrow mesodermal progenitor cells. *Blood* 2001; **98**: 2615-2625
- 29 **Ianus A**, Holz GG, Theise ND, Hussain MA. *In vivo* derivation of glucose-competent pancreatic endocrine cells from bone marrow without evidence of cell fusion. *J Clin Invest* 2003; **111**: 843-850
- 30 **Kolb H**, Burkart V. Nicotinamide in type 1 diabetes. Mechanism of action revisited. *Diabetes Care* 1999; **22**(Suppl 2): B16-20
- 31 **Rajagopal J**, Anderson WJ, Kume S, Martinez OI, Melton DA. Insulin staining of ES cells progeny from insulin uptake. *Science* 2003; **299**: 363
- 32 **Terada N**, Hamazaki T, Oka M, Hoki M, Mastalerz DM, Nakano Y, Meyer EM, Morel L, Petersen BE, Scott EW. Bone marrow cells adopt the phenotype of other cells by spontaneous cell fusion. *Nature* 2000; **416**: 542-545
- 33 **Spees JL**, Olson SD, Ylostalo J, Lynch PJ, Smith J, Perry A, Peister A, Wang MY, Prockop DJ. Differentiation, cell fusion, and nuclear fusion during *ex vivo* repair of epithelium by human adult stem cells from bone marrow stroma. *Proc Natl Acad Sci U S A* 2003; **100**: 2397-2402

Edited by Wang XL and Ren SR Proofread by Xu FM

Adenoviral transfer of human interleukin-10 gene in lethal pancreatitis

Zi-Qian Chen, Yao-Qing Tang, Yi Zhang, Zhi-Hong Jiang, En-Qiang Mao, Wei-Guo Zou, Ruo-Qing Lei, Tian-Quan Han, Sheng-Dao Zhang

Zi-Qian Chen, Yao-Qing Tang, Yi Zhang, Zhi-Hong Jiang, En-Qiang Mao, Ruo-Qing Lei, Tian-Quan Han, Sheng-Dao Zhang. Department of Surgery, Ruijin Hospital, Shanghai Second Medical University, Shanghai 200025, China

Wei-Guo Zou. Institute of Biochemistry and Cell Biology, Shanghai Institute for Biological Sciences, Chinese Academy of Sciences, Shanghai 200031, China

Supported by Science and Technology Committee of Shanghai Municipal Government, No. 00419019

Correspondence to: Sheng-Dao Zhang, Department of Surgery, Affiliated Ruijin Hospital, Shanghai Second Medical University, Shanghai 200025, China. chenzyq@hotmail.com

Telephone: +86-21-64370045 Ext. 611002

Received: 2004-01-15 **Accepted:** 2004-02-24

Abstract

AIM: To evaluate the therapeutic effect of adenoviral-vector-delivered human interleukin-10 (hIL-10) gene on severe acute pancreatitis (SAP) rats.

METHODS: Healthy Sprague-Dawley (SD) rats were intraperitoneally injected with adenoviral IL-10 gene (AdvhIL-10), empty vector (Adv0) or PBS solution. Blood, liver, pancreas and lung were harvested on the second day to examine hIL-10 level by ELISA and serum amylase by enzymatic assay. A SAP model was induced by retrograde injection of sodium taurocholate through pancreatic duct. SAP rats were then administered with AdvhIL-10, Adv0 and PBS solution by a single intraperitoneal injection 20 min after SAP induction. In addition to serum amylase assay, levels of hIL-10 and tumor necrosis factor- α (TNF- α) were detected by RT-PCR, ELISA and histological study. The mortality rate was studied and analyzed by Kaplan-Meier and log rank analysis.

RESULTS: The levels of hIL-10 in the pancreas, liver and lung of healthy rats increased significantly after AdvhIL-10 injection (1.42 ng/g in liver, 0.91 ng/g in pancreas); while there was no significant change of hIL-10 in the other two control groups. The concentration of hIL-10 was increased significantly in the SAP rats after AdvhIL-10 injection (1.68 ng/g in liver, 1.12 ng/g in pancreas) compared to the other two SAP groups with blank vector or PBS treatment ($P < 0.05$). The serum amylase levels remained normal in the AdvhIL-10 transfected healthy rats. However, the serum amylase level was significantly elevated in the other two control SAP rats. In contrast, serum amylase was down-regulated in the AdvhIL-10 treated SAP groups. The TNF- α expression in the AdvhIL-10 treated SAP rats was significantly lower compared to the other two control SAP groups. The pathohistological changes in the AdvhIL-10 treated group were better than those in the other two control groups. Furthermore, the mortality of the AdvhIL-10 treated group was significantly reduced compared to the other two control groups ($P < 0.05$).

CONCLUSION: Adenoviral hIL-10 gene can significantly attenuate the severity of SAP rats, and can be used in the

treatment of acute inflammation process.

Chen ZQ, Tang YQ, Zhang Y, Jiang ZH, Mao EQ, Zou WG, Lei RQ, Han TQ, Zhang SD. Adenoviral transfer of human interleukin-10 gene in lethal pancreatitis. *World J Gastroenterol* 2004; 10(20): 3021-3025

<http://www.wjgnet.com/1007-9327/10/3021.asp>

INTRODUCTION

The pathogenesis of severe acute pancreatitis (SAP) is complicated. Studies have indicated that the explosive production and release of pro-inflammatory cytokines play an important role in its pathogenesis. There is evidence that TNF- α and interleukin-1 (IL-1) are very important inflammatory cytokines in this process^[1,2]. Although pro-inflammatory cytokines are necessary for protecting against inflammation in the early phase, uncontrolled and adverse inflammatory effects of the systemic cytokine response could also be harmful. Thus, inhibiting the synthesis of pro-inflammatory cytokines and altering the balance between pro- and anti-inflammatory cytokines might significantly affect the severity of pancreatitis and the survival rate^[3,4]. IL-10 is a major anti-inflammatory cytokine. It has been shown to be down-regulated the expression of TNF and other inflammatory cytokines from activated macrophages. IL-10 could block the release of oxygen free radicals and nitrogen oxide. In consequence^[5], it could decrease the mortality^[6-8]. These findings suggested that administration of IL-10 could be useful in blocking these pro-inflammatory cytokines during the initiation of acute pancreatitis.

Gene therapy as a novel drug delivery system to express proteins in individual tissues has been used in inflammatory diseases^[9]. The use of deficient adenovirus vectors might be a useful tool for this gene therapy due to its high infectious activity and high protein expression ability. Gene therapy has been proposed in many inflammation diseases to produce anti-inflammatory cytokines at local sites^[10,11]. However, transfection of SAP rats with an adenoviral vector has not been previously reported.

In this paper, we reported a successful gene therapy for SAP rats. Our experiments showed that human IL-10 expression in tissues could block the development of SAP and improve the survival rate. The results suggest a novel potential therapeutic approach for the treatment of patients with acute pancreatitis.

MATERIALS AND METHODS

Materials

Adenovirus expression system (Adenoviral Gateway Expression Kit, 293A Cell Line, Gateway LR Clonase Enzyme Mix, Lipofectamine 2000) and TRIzol reagent were provided by Invitrogen (San Diego, CA). pcDNA3IL-10 plasmid was generously donated by professor XY Liu (Shanghai Institute for Biological Sciences, Chinese Academy of Sciences, Shanghai, China). Restriction enzyme (*Hind*III, *Eco*RI, *Bam*HI, *Sal*I) was obtained from Promega (Madison, WI, USA). Sodium taurocholate was purchased from Sigma Chemical Company

(St Louis, MO). Amylase enzyme assay kits were obtained from Shanghai Kehua-Hualing Diagnosis Kit Co (Shanghai, China). An ELISA kit specific for human IL-10 was purchased from Diaclone Research International (BESANÇON Cedex, French).

Adenoviral vectors

Human IL-10 cDNA was cloned into the *Bam*HI and *Eco*RI sites of pEntr 1A vector. Then the IL-10 cDNA was moved into the adenoviral destination vector from pEntr 1A vector by Gateway LR Clonase. The recombinant E1 deleted type 5 adenoviral vector encode hIL-10 under the transcriptional control of the cytomegalovirus promoter and contained the bGHP(A) sequence. Adenovirus hIL-10 vector was transfected into 293A human embryonic kidney cell line with Lipofectamine 2000. After transfection, cells were fed with fresh DMEM solution until the onset of cytopathic effect. Viruses were propagated in the 293A and purified by ultra centrifugation through two caesium chloride gradients. The titer of adenoviral vectors was determined by plaque assay on 293A cells. Viral stocks were aliquoted and stored in 100 mL/L glycerol at -80 °C until use.

Adenovirus IL-10 gene transfection into healthy rats

Sprague-Dawley (SD) rats were purchased from Shanghai BK Experimental Animal Company (Shanghai, China) and maintained in filter-top cages under specific pathogen-free conditions. The Animal Study Ethics Committee of Shanghai Second Medical University approved all experiments. The experiments were conducted in 6-7 week-old male rats, weighing 170-180 g. Adult healthy male SD rats ($n = 20$) were given a single intraperitoneal injection of adenovirus PBS solution containing 10^{10} pfu of the AdvhIL-10. All injections were performed with a sterile 25-gauge needle in the left lower quadrant of the abdomen. Rats were anesthetized using sodium pentobarbital (40 mg/kg injection, intraperitoneal) and killed 24, 48, 96, and 168 h after transfection. Blood samples were obtained from the celiac artery. The samples were separated and stored at -70 °C for determination of amylase. Pancreas, liver and lung were immediately dissected from their attachments and divided for isolation of total RNA and total protein. Some samples were fixed in 40 g/L buffered formaldehyde for histopathological test. PBS control group ($n = 5$) received an intraperitoneal injection of PBS solution, and the empty vector control group ($n = 5$) was given a single intraperitoneal injection of empty vector (Adv0) containing 10^{10} pfu viruses. Tissues of both control groups were harvested 24 h later as previously described.

Adenovirus IL-10 gene therapy in SAP rats

SD rats ($n = 80$) were randomly divided into four groups: normal, AdvhIL-10, Adv0, and PBS groups. After laparotomy, SAP model was induced through injection of 0.5 mL of 30 g/L sodium taurocholate via the pancreatic duct. Twenty minutes after sodium taurocholate injection, AdvhIL-10 group received 0.5 mL single intraperitoneal injection of AdvhIL-10 containing 10^{10} pfu of AdvhIL-10. Two control groups received 0.5 mL single intraperitoneal injection of Adv0 (containing 10^{10} pfu viruses) or PBS solution, respectively. In each group, 5 rats were sacrificed by dislocation of the cervical vertebra 24 and 48 h after induction of SAP, respectively. Blood samples were obtained as previously described for determination of amylase. Pancreas, liver, and lungs were harvested as previously described and prepared for RT-PCR, ELISA, and histopathological test. Mortality was observed among the rats 7 d after the initiation of pancreatitis.

Assay

Serum amylase levels were measured at 37 °C by an enzymatic assay using a Beckman nucleic acid and protein analyzer DU

640 (BECKMAN, USA) standardized for these rat proteins. All serum samples were assayed in duplicate, and the results were averaged at the end of the experiment. Rat TNF- α , hIL-10 levels in the homogenates were determined using commercially available enzyme-linked immunosorbent assay (ELISA) kits from Diaclone Research International.

IL-10 and TNF- α mRNA expression

Total RNA was extracted from homogenized liver, pancreas, and lung with TRIzol reagent following the manufacturer's instructions. Aliquots of 5 μ g of total RNA were reverse-transcribed by using a first-strand cDNA synthesis kit (Promega A3500). The cDNA was then amplified by polymerase chain reaction using primers specific for hIL-10 or TNF- α with β -actin primers serving as controls. The primer sequences and sizes of amplification products were as follows: hIL-10 sense, 5'-GAGCG, GATCC, ATGAA, GTGGG, TAACC, TTTC-3'; antisense, 5'-ATACG, AATTC, CTGCA, GCGGC, CGCCA, CT-3' (540 base pairs); TNF sense, 5'-TGCCT, CAGCC, TCTTC, TCATT-3'; antisense, 5'-ACACC, CATT, CCTTC, ACAGA-3' (446 base pairs); β -actin sense, 5'-TTGTA, ACCAA, CCTGGG, ACGAT, ATGG-3'; antisense, 5'-TGGAA, GACTC, CTCCC, AGGTA-3' (515 base pairs). Following an initial denaturation at 94 °C for 5 min, the samples were amplified by 27 cycles of denaturation at 94 °C for 40 s, annealing at 58 °C for 50 s, extension at 72 °C for 90 s, and ended by extension at 72 °C for 15 min. The PCR reaction products were separated on 20 g/L agarose gels. Photo-micrographs of ethidium bromide stained gels were taken. Relative mRNA levels of hIL-10, TNF- α and β -actin were determined by computer-assisted densitometric scanning.

Histopathological analysis

Pancreas samples were fixed in 40 g/L buffered formaldehyde and embedded in paraffin. Then the samples were cut into 5 μ m thick sections, and stained with haematoxylin and eosin for light microscopic examination. Histological assessment was performed by an investigator blinded to the treatment group. The severity of pancreatitis was determined by the degree of edema, hemorrhage, inflammation and necrosis^[11].

Statistical analysis

Results were expressed as mean \pm SD. Differences between groups were compared by two-way ANOVA. $P < 0.05$ was considered statistically significant. Mortality was assessed by Kaplan-Meier and log rank analysis. All data processing was done with a statistical program, SPSS 11.0.

RESULTS

hIL-10 levels in pancreas, liver, and lung at 24 h post-transfection in healthy rats

Twenty-four h after transfection, The normal and two control groups did not show hIL-10 protein expression.

hIL-10 protein was effectively measured in healthy rats after AdvhIL-10 administration. The hIL-10 level in pancreas, liver, and lung increased and reached its peak at 24 h post-transfection, then decreased gradually 4 d after transfection. The hIL-10 level in the tissues was undetectable 7 d post-transfection, and was the highest in the liver among the three observed organs (Figure 1A).

Serum amylase levels and histological changes in healthy rats

There were no significant differences in serum amylase level among the rats effectively transfected with AdvhIL-10 and Adv0 and PBS treated rats in the duration of the experiment (Figure 6, $P > 0.05$). In addition, no detectable histology alternation of the pancreas, liver, and lungs was observed in the transfected rats.

Pancreatic edema, hyperemia, exudation and necrosis were not detected. These findings indicated that adenovirus gene transfer could be performed safely.

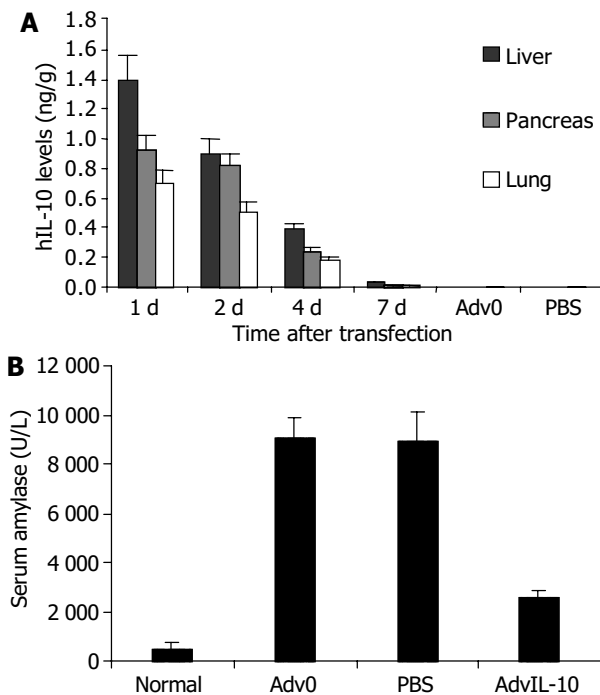


Figure 1 hIL-10 levels and serum amylase levels in pancreas, liver, and lung after administration of AdvIL-10, Adv0, and PBS in healthy and SAP rats. A: hIL-10 levels in pancreas, liver and lung after administration of AdvIL-10, Adv-0 and PBS in healthy rats. B: Serum amylase levels in pancreas, liver and lung after administration of AdvIL-10, Adv-0 and PBS in SAP rats.

Serum amylase in SAP rats

The SAP rats treated with Adv0 and PBS showed a significant increase in serum amylase level compared to normal rats ($P < 0.05$). Transfection with AdvhIL-10 after induction of pancreatitis decreased the severity of SAP, as evidenced by markedly attenuated amylase production compared to the two control SAP groups (Figure 1B, $P < 0.05$).

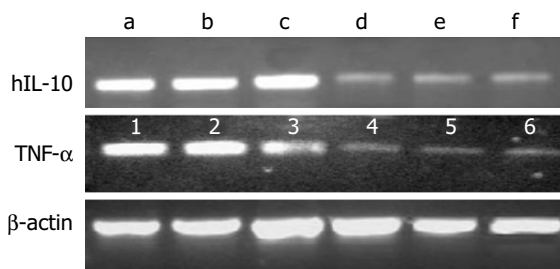


Figure 2 Expression of IL-10 and TNF- α in SAP rat tissues 24 h post-transfection with AdvhIL-10 and PBS. Lanes a, b and c: IL-10 expression in liver, pancreas, and lung, respectively, in AdvIL-10 treated SAP rats; Lanes d, e and f: IL-10 expression in liver, pancreas, and lung, respectively, in the PBS treated SAP rats; Lanes 1, 2, and 3: TNF- α expression in liver, pancreas, and lung, respectively, in AdvIL-10 treated SAP rats; Lanes 4, 5, and 6: TNF- α expression in liver, pancreas, and lung, respectively, in AdvIL-10 treated SAP rats. β -actin served as control.

IL-10 and TNF- α mRNA expression in SAP rats

hIL-10 mRNA was strongly expressed in the AdvhIL-10 treated pancreatitis rats 24 h post-transfection. The levels of hIL-10 in pancreas, liver, and lung did not show significant difference. A

weak expression of hIL-10 was observed in Adv0 and PBS treated pancreatitis rats 24 h post-transfection. TNF- α gene in the normal rats was not detected. The expression of TNF- α gene was significantly higher in the pancreatitis rats treated with Adv0 and PBS than that in those treated with AdvhIL-10 ($P < 0.05$, Figure 2). In the AdvhIL-10 group, the level of TNF- α gene was moderate in pancreas and weak in the liver and lung (Figure 3).

Levels of hIL-10 and TNF- α proteins in SAP rats

The levels of IL-10 in pancreas, liver and lung in the AdvhIL-10 group were markedly higher than those in the two control groups 24 and 48 h post-transfection ($P < 0.05$). No significant difference was observed between the two control groups (Figure 3A). In normal rats, TNF- α expression was undetectable. Twenty-four h after induction of pancreatitis, TNF- α level was significantly higher in Adv0 and PBS groups than that in AdvIL-10 group ($P < 0.05$, Figure 3B).

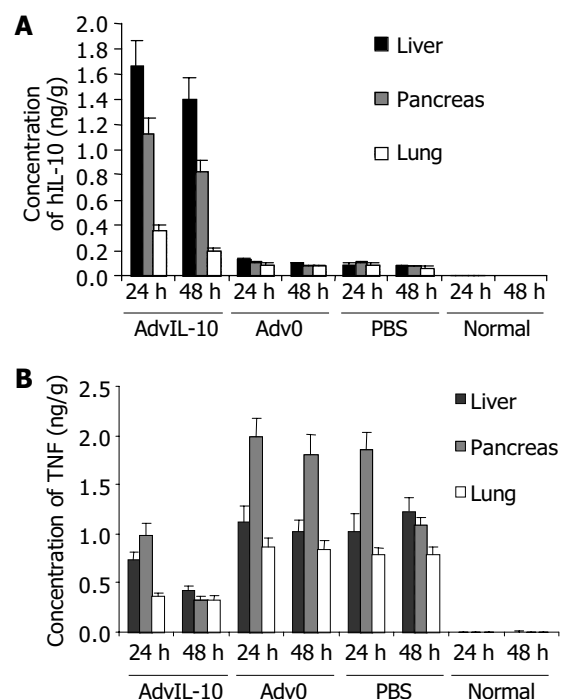


Figure 3 hIL-10 and TNF- α levels in liver, pancreas, and lungs of SAP rats after treatment with AdvIL-10, Adv0, and PBS. A: hIL-10 levels in liver, pancreas and lungs of SAP rats after treatment with AdvIL-10, Adv-0 and PBS. B: TNF- α levels in liver, pancreas and lungs of SAP rats after treatment with Adv-10, Adv-0 and PBS.

Histopathological changes

Hematoxylin and eosin-stained sections of pancreas from pancreatitis rats treated with Adv0 and PBS showed an increase in inflammation, hemorrhage, and necrosis after injection of sodium taurocholate. The histological changes in the AdvIL-10 treated pancreatitis rats were mild compared with the control groups. Most of the pathological parameters of pancreatic injury were significantly decreased in pancreatitis rats transfected with AdvIL-10 gene compared to the pancreatitis rats treated with Adv0 and PBS ($P < 0.05$, Table 1, Figure 4).

Mortality

No significant difference in mortality was observed between the two control SAP groups within 7 d after SAP induction, 90% of the rats were died in the Adv0 and PBS treated groups, while only 20% of the rats were died in the AdvIL-10 gene therapy group (Figure 5).

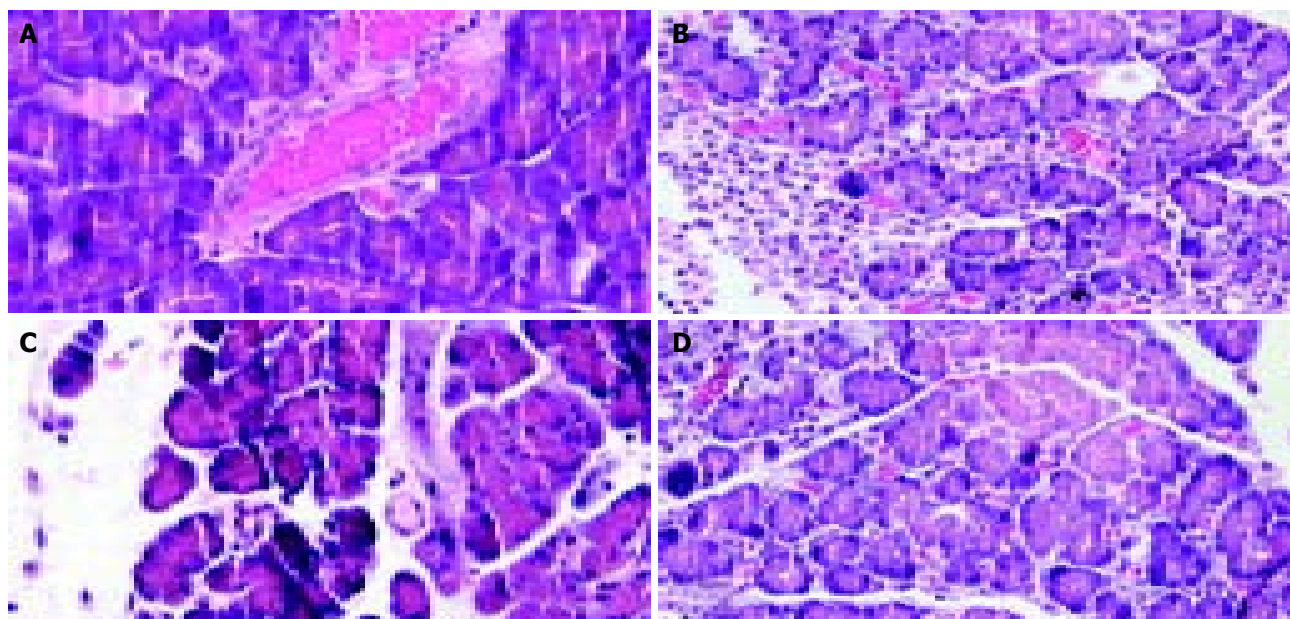


Figure 4 Histological sections of rat pancreas (HE, 200 \times). A: Normal rat pancreas; B: Severe necrotizing acute pancreatitis with hemorrhage and necrosis 24 h after induction with sodium taurocholate; C: Acute pancreatitis in rats treated with AdvhIL-10; D: Acute pancreatitis in rats treated with PBS (the pathology changes in the Adv0 group were completely the same as PBS group).

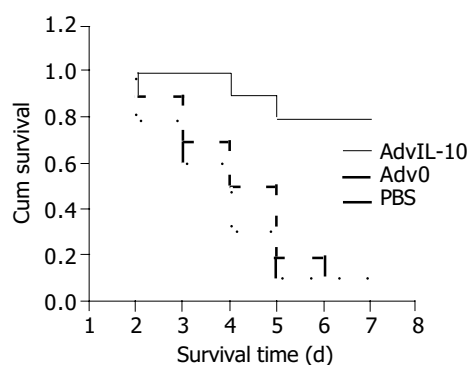


Figure 5 Survival rate of SAP rats after treatment.

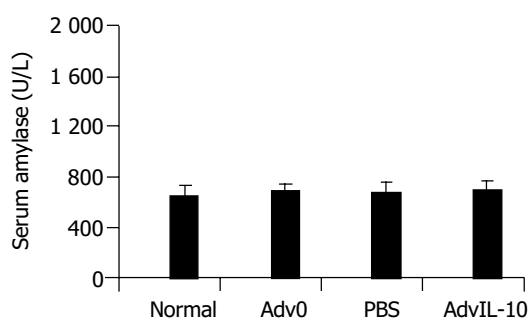


Figure 6 Serum amylase levels in healthy rats 24 h after transfection with Adv0, PBS and AdvIL-10.

Table 1 Histological scores of pancreas from rats with SAP (mean \pm SD)

	Normal	PBS (or Adv0)	hIL-10 transfected
Edema	0 \pm 0	2.26 \pm 0.13	1.74 \pm 0.13
Necrosis	0 \pm 0	2.56 \pm 0.21	0.51 \pm 0.13
Inflammation	0 \pm 0	3.43 \pm 0.14	0.46 \pm 0.14
Hemorrhage	0 \pm 0	2.31 \pm 0.17	0.13 \pm 0.11

DISCUSSION

IL-10 gene therapy has been widely explored for the treatment

of many diseases, including intestinal transplantation immune regulation, bronchiolitis, endotoxemia, and rheumatoid arthritis^[12-15]. In the present report, we explored the tissue levels, distribution, and biological responses of hIL-10 mediated by adenoviral vectors in healthy and pancreatitis rats. Adenovirus vector has many advantages. Adenovirus genomes did not integrate into the host cell chromosome and had a high efficiency state of tissues. Although the duration of gene expression was short, the level of therapeutic gene expression was much higher^[16]. Adenoviral vectors could bind to cell surface integrins and gain entry by receptor mediated endocytosis using receptors such as Coxsackie virus and adenovirus receptor^[17]. Thus, adenoviral vector could offer the opportunity to target specific tissues for highly local expression, owing to special tropism for pulmonary epithelial cells, hepatocytes, and pancreatic epithelial cells^[18-20]. Expression of adenoviral vector was rapid, protein appearance usually occurred within hours and peak concentration appeared within 1-2 d after adenoviral administration^[21]. Furthermore, adenovirus vectors could be prepared at a much higher titre.

Norman James^[22] reported that with very few exceptions, cytokines were not constitutively produced. The results of our experiment is consistent with Norman James's results. We explored the use of adenovirus based gene therapy to deliver hIL-10 gene intraperitoneally to healthy and pancreatitis rats. Tissue hIL-10 protein was highly produced 24, 48 h after AdvhIL-10 was injected into peritoneal cavity of healthy rats. The current study demonstrated that the current adenovirus delivery system could offer a highly efficient transfection and well-correlated tissue accumulation. We also found that highly efficient transfection with AdvhIL-10 did not result in an increase in amylase and lipase or any alteration in pancreatic histopathology. Therefore, adenoviral vector mediated hIL-10 gene delivery in healthy rats was well tolerable and safe. In SAP rats, AdvhIL-10 attenuated the release of serum amylase and decreased histologic injury significantly. In addition, the action of TNF- α could also be diminished by IL-10. The important factor of our experiment was the increase of survival rate resulted from adenoviral vector mediated hIL-10 gene delivery in rats with lethal acute pancreatitis. These results are consistent with several previous reports on adenoviral vector-mediated gene therapy in pancreatitis and acute lung inflammation^[9,23,24].

There is sufficient evidence (immunological, pathophysiological, and biochemical) that SAP is a systemic rather than a local critical condition. The severity of the process varied from a limited local inflammation of the pancreas to a systemic multi-organ failure. SAP was characterised by enzyme activation, interstitial edema, hemorrhage and necrosis^[25]. Many pro- and anti- inflammation cytokines are involved in the initiation of acute pancreatitis. IL-10, produced by TH2 cells, macrophages, stellate cells and hepatocytes, has been reported to play an important role in inflammatory diseases^[26]. It has been reported the deficiency of IL-10 gene could prompt colitis and fibrosis probably by its failure in inhibiting the overproduction of tumor growth factor- β , and TNF^[27,28]. The later is secreted by macrophages and can enhance inflammation in a local site. In animals, IL-10 is endogenously released during inflammatory diseases, and its blockade could result in higher elevations of TNF as well as more severe histologic injury^[10]. Production of large quantities of exogenous IL-10 in local sites of inflammation could change the balance of pro- and anti- inflammation cytokines and block the production and release of TNF and other pro-inflammation cytokines. IL-10 administration could improve of local and systemic conditions. In the current study, exogenous hIL-10 was found to be able to inhibit the progress of acute pancreatitis in rats. Similar results were also reported by previous studies^[10,11].

The time to administrate AdvIL-10 seems to be very important, since it takes time to transfect and express protein. Thus, early administration of AdvIL-10 might block the induction of TNF and IL-1^[5]. Kato *et al.* reported that the time to administrate hIL-10 should be in the early period of sepsis. In the current study, hIL-10 gene was administrated 20 min after the induction of SAP, and the highest level of IL-10 protein was observed 24 h after administration, which was very similar to a previous study by Denham *et al.*^[10].

In conclusion, human genes can be effectively transfected into rat pancreas, livers, and lungs using a adenoviral vector-mediated delivery system. Transfection of hIL-10 gene can decrease the severity of pancreatitis and improve the survival rate. As gene therapy is becoming a more acceptable method of treatment, it is anticipated that adenovirus-based gene therapy will become available as a drug delivery system. Cytokine modulating therapies, like IL-10, represent an attractive therapeutic approach for the treatment of acute pancreatitis patients in clinic.

REFERENCES

- Viedma JA, Perez-Mateo M, Dominguez JE, Carballo F. Role of C-reactive protein and phospholipase A. *Gut* 1992; **33**: 1264-1267
- Grewal HP, Mohey el Din A, Gaber L, Kotb M, Gaber AO. Amelioration of the physiologic and biochemical changes of acute pancreatitis using an anti-TNF alpha polyclonal antibody. *Am J Surg* 1994; **167**: 214-218
- Walley KR, Lukacs NW, Standiford TJ, Strieter RM, Kunkel SL. Balance of inflammatory cytokines related to severity and mortality of murine sepsis. *Infect Immun* 1996; **64**: 4733-4738
- Weiss YG, Deutschman CS. Modulation of gene expression in critical illness: a new millennium or a brave new world? *Crit Care Med* 2000; **28**: 3078-3079
- Rongione AJ, Kusske AM, Kwan K, Ashley SW, Reber HA, McFadden DW. Interleukin 10 reduces the severity of acute pancreatitis in rats. *Gastroenterology* 1997; **112**: 960-967
- Gazzinelli RT, Oswald IP, James SL, Sher A. IL-10 inhibits parasite killing and nitrogen oxide production by IFN-gamma-activated macrophages. *J Immunol* 1992; **148**: 1792-1796
- Pradier O, Gerard C, Delvaux A, Lybin M, Abramowicz D, Capel P, Velu T, Goldman M. Interleukin-10 inhibits the induction of monocyte procoagulant activity by bacterial lipopolysaccharide. *Eur J Immunol* 1993; **23**: 2700-2703
- Howard M, Muchamuel T, Andrade S, Menon S. Interleukin 10 protects mice from lethal endotoxemia. *J Exp Med* 1993; **177**: 1205-1208
- Minter RM, Ferry MA, Murday ME, Tannahill CL, Bahjat FR, Oberholzer C, Oberholzer A, LaFace D, Hutchins B, Wen S, Shinoda J, Copeland EM 3rd, Moldawer LL. Adenoviral delivery of human and viral IL-10 in murine sepsis. *J Immunol* 2001; **167**: 1053-1059
- Denham W, Denham D, Yang J, Carter G, MacKay S, Moldawer LL, Carey LC, Norman J. Transient human gene therapy: a novel cytokine regulatory strategy for experimental pancreatitis. *Ann Surg* 1998; **227**: 812-820
- Zou WG, Wang DS, Lang MF, Jin DY, Xu DH, Zheng ZC, Wu ZH, Liu XY. Human interleukin 10 gene therapy decreases the severity and mortality of lethal pancreatitis in rats. *J Surg Res* 2002; **103**: 121-126
- Zhu M, Wei MF, Liu F, Shi HF, Wang G. Interleukin-10 modified dendritic cells induce allo-hyporesponsiveness and prolong small intestine allograft survival. *World J Gastroenterol* 2003; **9**: 2509-2512
- Boehler A, Chamberlain D, Xing Z, Slutsky AS, Jordana M, Gauldie J, Liu M, Keshavjee S. Adenovirus-mediated interleukin-10 gene transfer inhibits post-transplant fibrous airway obliteration in an animal model of bronchiolitis obliterans. *Hum Gene Ther* 1998; **9**: 541-551
- Xing Z, Ohkawara Y, Jordana M, Graham FL, Gauldie J. Adenoviral vector-mediated interleukin-10 expression *in vivo*: intramuscular gene transfer inhibits cytokine responses in endotoxemia. *Gene Ther* 1997; **4**: 140-149
- Whalen JD, Lechman EL, Carlos CA, Weiss K, Kovacs I, Glorioso JC, Robbins PD, Evans CH. Adenoviral transfer of the viral IL-10 gene periarticularly to mouse paws suppresses development of collagen-induced arthritis in both injected and uninjected paws. *J Immunol* 1999; **162**: 3625-3632
- Wickham TJ. Targeting adenovirus. *Gene Therapy* 2000; **7**: 110-114
- Bergelson JM, Cunningham JA, Droguett G, Kurt-Jones EA, Krithivas A, Hong JS, Horwitz MS, Crowell RL, Finberg RW. Isolation of a common receptor for Coxsackie B viruses and adenoviruses 2 and 5. *Science* 1997; **275**: 1320-1323
- Crystal RG. The gene as the drug. *Nat Med* 1995; **1**: 15-17
- Worgall S, Wolff G, Falck-Pedersen E, Crystal RG. Innate immune mechanisms dominate elimination of adenoviral vectors following *in vivo* administration. *Hum Gene Ther* 1997; **8**: 37-44
- Weber M, Deng S, Kucher T, Shaked A, Ketchum RJ, Brayman KL. Adenoviral transfection of isolated pancreatic islets: a study of programmed cell death (apoptosis) and islet function. *J Surg Res* 1997; **69**: 23-32
- Minter RM, Rectenwald JE, Fukuzuka K, Tannahill CL, La Face D, Tsai V, Ahmed I, Hutchins E, Moyer R, Copeland EM 3rd, Moldawer LL. TNF-alpha receptor signaling and IL-10 gene therapy regulate the innate and humoral immune responses to recombinant adenovirus in the lung. *J Immunol* 2000; **164**: 443-451
- Norman J. The role of cytokines in the pathogenesis of acute pancreatitis. *Am J Surg* 1998; **175**: 76-83
- Van Laethem JL, Marchant A, Delvaux A, Goldman M, Robberecht P, Velu T, Deviere J. Interleukin 10 prevents necrosis in murine experimental acute pancreatitis. *Gastroenterology* 1995; **108**: 1917-1922
- Minter RM, Ferry MA, Rectenwald JE, Bahjat FR, Oberholzer A, Oberholzer C, La Face D, Tsai V, Ahmed CM, Hutchins B, Copeland EM 3rd, Ginsberg HS, Moldawer LL. Extended lung expression and increased tissue localization of viral IL-10 with adenoviral gene therapy. *Proc Natl Acad Sci U S A* 2001; **98**: 277-282
- Jungermann J, Lerch MM, Weidenbach H, Lutz MP, Kruger B, Adler G. Dissassembly of rat pancreatic acinar cytoskeleton during supramaximal secretagogue stimulation. *Am J Physiol* 1995; **G328**-338
- De Vries JE. Immunosuppressive and anti-inflammatory properties of interleukin 10. *Ann Med* 1995; **27**: 537-541
- Lindsay JO, Ciesielski CJ, Scheinin T, Hodgson HJ, Brennan FM. The prevention and treatment of murine colitis using gene therapy with adenoviral vectors encoding IL-10. *J Immunol* 2001; **166**: 7625-7633
- Thompson K, Maltby J, Fallowfield J, McAulay M, Millward-Sadler H, Sheron N. Interleukin-10 expression and function in experimental murine liver inflammation and fibrosis. *Hepatology* 1998; **28**: 1597-1606

Changes of inflammation-associated cytokine expressions during early phase of experimental endotoxic shock in macaques

Xiao-Hui Ji, Ke-Yi Sun, Yan-Hong Feng, Guo-Qing Yin

Xiao-Hui Ji, Ke-Yi Sun, Department of Microbiology and Immunology, Nanjing Medical University, Nanjing 210029, Jiangsu Province, China

Yan-Hong Feng, Guo-Qing Yin, Department of Infectious Diseases, Second Hospital of Medical College, Southeast University, Nanjing 210003, Jiangsu Province, China

Supported by the Foundation of the Municipal Government of Nanjing, No. ZKG9809 and Health Bureau of Jiangsu Province, No. TS9904

Correspondence to: Xiao-Hui Ji, Department of Microbiology and Immunology, Nanjing Medical University, 140 Hanzhong Road, Nanjing 210029, Jiangsu Province, China. immune@njmu.edu.cn

Telephone: +86-25-86862654 **Fax:** +86-25-86862655

Received: 2003-11-12 **Accepted:** 2003-12-22

Abstract

AIM: To study changes of inflammation-associated cytokine expressions during early phase of endotoxic shock in macaque.

METHODS: Experiments were performed in *Macaque mulatta* treated with LPS 2.8 mg/kg in shock model group or with normal saline in control group. Blood samples were collected before, or 60 min, or 120 min after LPS injection, respectively. Liver and spleen tissues were obtained at 120 min after LPS injection. The plasma levels of TNF- α , IL-1 β , IL-10 and IL-12P40 were determined by double-antibody sandwich ELISA with antibodies against human cytokines. The mRNA levels of TNF- α , IL-1 β , and IL-18 in peripheral blood mononuclear cells (PBMCs), liver and spleen were examined by real-time fluorescence semi-quantitative RT-PCR with the primers based on human genes.

RESULTS: Mean systemic arterial pressure (MAP), systemic vascular resistance index (SVRI) and left ventricular work index (LVWI) of macaques were significantly declined in shock model group on average 60 min after LPS injection. The plasma levels of TNF- α and IL-10 were significantly increased 60 min after LPS injection and then decreased. The plasma levels of IL-1 β and IL-12P40 were significantly increased at 120 min after LPS injection. The mRNA levels of TNF- α and IL-1 β were significantly increased 60 min after LPS stimulation in PBMCs and 120 min after LPS stimulation in livers. The mRNA level of IL-18 was significantly increased 120 min after LPS stimulation in PBMCs and livers. But in spleen, only TNF- α mRNA level in LPS group was significantly higher 120 min after LPS stimulation, compared with that in control group.

CONCLUSION: An endotoxic shock model of *Macaque mulatta* was successfully established. Both antibodies for ELISA and PCR primers based on human cytokine assays were successfully applied to detect macaque cytokines. In the model, inflammatory cytokines, such as TNF- α , IL-1 β , IL-12 and IL-18 as well as anti-inflammation cytokine IL-10, were released at very early phase of endotoxic shock within 120 min after LPS injection. PBMCs and liver cells might be the important sources of these cytokines.

Ji XH, Sun KY, Feng YH, Yin GQ. Changes of inflammation-associated cytokine expressions during early phase of experimental endotoxic shock in macaques. *World J Gastroenterol* 2004; 10(20): 3026-3033

<http://www.wjgnet.com/1007-9327/10/3026.asp>

INTRODUCTION

Endotoxin-induced shock mostly occurs during serious infection with Gram-negative bacteria. Lipopolysaccharide (LPS), residing in the outer membrane of all Gram-negative bacteria and being the major component of Gram-negative bacteria cell walls and the toxic component of endotoxin, is considered as an important initiating factor of the Gram-negative septic syndrome in human. Gram-negative sepsis has aroused great concern in clinic because of its high mortality. But LPS is not the direct causative factor. It is well known that LPS activates immunocytes, such as monocyte-macrophage and lymphocyte, and induces these cells to excessively release a series of potent inflammatory cytokines, including TNF- α , IL-1 β , IL-6, IL-8 and IL-18. It is the excessive cytokines, such as TNF- α , IL-1 β , IL-6 and IL-18, that result in high fever, hypotension, vascular endothelial cell damage and disseminated intravascular coagulation, blood capillary leak syndrome, and multiple organ failure. On the other hand, in patients with primary liver injury, such as viral hepatitis, LPS plays an important role in intestinal endotoxemia, which in turn induces secondary liver injury and liver failure^[1]. New therapeutic concepts for the treatment of endotoxic shock or endotoxemia with anti-inflammatory cytokines have been developed. Although knowledge about the changes of inflammation-associated cytokines during endotoxemia and endotoxic shock has been well addressed, the change pattern of inflammatory cytokines just during the early phase of endotoxemia and endotoxic shock is still not clear and worth working on, because it can help the selection of new therapeutic targets. The therapies in early phase are more effective.

The aim of the present study was to investigate the changes of TNF- α , IL-1 β , IL-10, IL-12 and IL-18 expressions during early phase (within 120 min) of endotoxic shock in macaques.

MATERIALS AND METHODS

Animals

Totally 25 macaques (*Macaca mulatta*) of 5-8 years old, weighing 4.8-9.2 kg (6.17 \pm 1.1 kg), were obtained from Shanghai Laboratory Animal Center, Chinese Academy of Sciences. All animal studies were carried out in accordance with the institutional regulations concerning animal experimentation of the Ministry of Health of China. The animals were housed at 10-25 °C with light, around 8-10 h per day for, at least, a week before experiment. One of 25 macaques was used in preliminary experiment for the optimal dose of LPS at which hypotension and shock should be induced. The other 24 macaques were divided into two groups: 19 in LPS group and 5 in normal saline (NS) group.

Agents

LPS, derived from *E. coli* O127: B8 and prepared by phenol

extraction, was purchased from Sigma Co. (Saint Louis, USA). ELISA kits for detecting human TNF- α , IL-1 β , IL-10 and IL-12 P40/ P70 were from Pharmingen (San Diego, USA). TriZol RNA extraction kit was from Gibco (Grand Island, USA). Moloney murine leukemia virus (M-MLV) reverse transcriptase, RNase inhibitor, PCR kit and PGEM-T vector were all from Promega (Shanghai, China). PCR product purification kit was from Boehringer Mannheim Co. (Mannheim, Germany). Plasmid DNA extraction kit was from Scientz Bio Co. (Shanghai, China).

PCR primers

In order to determine the mRNA expression levels of inflammatory cytokines by RT-PCR, some pairs of primers based on specific sequences published previously were used. These primers, synthesized in ShengGong Biotech Co. (Shanghai, China), are shown in Table 1.

Establishment of endotoxemic shock model

In the pilot experiment, one macaque was used to find out optimal dose of LPS. Intravenous injection of LPS of 2.8 mg/kg resulted in reduction of mean arterial pressure (MAP) from 17.55 to 10.80 kPa. This dosage was applied to establish macaque model of endotoxemic shock in this experiments. After being fasted overnight, macaques were anesthetized with ketamine (15 mg/kg, intramuscularly), then they were mechanically ventilated with a ventilator (SERVE900c, Siemens- Elama) through trachea intubator. Tidal volume was set at 12 mL/kg and the respiratory rate at 20 beat/min during experiment. A value of 5 cm H₂O (1 cm H₂O = 0.098 kPa) of positive end-expiratory pressure was applied to maintain end-expiratory lung volume. Anesthesia was maintained with repeated intravenous injection of sodium γ -hydroxybutyl acid (200 mg/kg·h) and intramuscular injection of fentanyl citras (a bolus of 6 μ g/kg·30 min). A pulmonary artery catheter was placed in the jugular vein for detecting hemodynamic parameters by thermodilution (Siemens,). After percutaneous puncture, the catheter was introduced into the femoral artery and forwarded into the abdominal aorta for measuring blood pressure. Nineteen animals in the shock group were given a dose of 2.8 mg/kg LPS i.v., while 5 animals in the control group were given 1 mL/kg normal saline. Occurrences of endotoxemic shock were confirmed by reduction of MAP by 30% and by other hemodynamic changes, such as the reduction of systemic vascular resistance index (SVRI) or left ventricular work index (LVWI), in LPS group. It took 60 min on average to establish shock after LPS injection. Venous blood of 18 animals in LPS group and 5 animals in NS control group were collected at 0, 60 and 120 min after LPS or NS injection for detection of inflammation-associated cytokines. Then, the macaques were sacrificed for detecting myocardial damages in another sub-study of this project. At the same time, a small portion of liver and spleen tissues were sliced and stored at -80 $^{\circ}$ C after being rapidly frozen in liquid nitrogen for mRNA assays.

Blood processing

Blood from the macaques, anticoagulated with EDTA-Na₂, were centrifuged, at 1 500 r/min \times 10 min, to separate plasma from cells. The plasma were stored at -20 $^{\circ}$ C for cytokines detection. The sedimentary cells were resuspended with Hanks' solution and the cell suspension was centrifuged with Ficoll-Hypaque lymphocyte separating medium, at 2 000 r/min \times 20 min, to get peripheral blood mononuclear cells (PBMCs). After being rapidly frozen in liquid nitrogen, PBMCs from the macaques were stored at -80 $^{\circ}$ C for mRNA assays.

Plasma cytokines detection

The levels of TNF- α , IL-1 β , IL-10 and IL-12P40/P70 in plasma were determined by double-antibodies sandwich ELISA using the kits. The assays were performed according to the kit protocol.

Test for intracellular cytokine mRNA

PBMCs of 10⁶ and liver or spleen tissue of 0.1 g were used to extract total cytoplasmic RNA according to the TriZol method. The total RNA was converted to complementary DNA (cDNA) by a reverse transcription step with M-MLV reverse transcriptase, OligodT primer, RNase inhibitor and dNTPs. Using the cDNA, specific primers, SYBR-Green I and PCR kit, a series of real-time semi-quantitative PCR were performed with a DNA amplifier (PE5700) to determine levels of mRNA coding for TNF- α , IL-1 β and IL-18, as well as β -actin which was used in the assay as an internal control, in PBMCs, liver and spleen. cDNA samples were amplified for 40 cycles: denaturation at 94 $^{\circ}$ C for 30 s, annealing at 60 $^{\circ}$ C for 60 s and extension at 68 $^{\circ}$ C for 120 s. The ratio of fluorescence intensity of cytokine-specific product to that of the internal control product represents relative levels of cytokine mRNA expression. After PCR, the products were cloned into PGEM-T vector, which was then used to transform JM109 *E. coli*. The plasmid DNAs of positive clones were extracted for sequencing.

Statistical analysis

All results were expressed as mean \pm SD. The significances of differences between LPS shock group and NS control group were evaluated by *t*-test. Testing standard was set at α = 0.05. *P*<0.05 indicates a significant difference, and *P*<0.01 indicates a remarkably significant difference.

RESULTS

Change of TNF- α within 120 min after LPS administration

Plasma concentration of TNF- α in LPS group increased earlier and was significantly higher than that in NS group at 60 min after LPS administration, then decreased to a level similar to that in NS group. This result is shown in Figure 1A. The dynamics for TNF- α mRNA expression by PBMCs in LPS group was similar to that for plasma TNF- α concentration. The result is shown in Figure 1B.

Table 1 PCR primer sequences for TNF- α , IL-1 β and IL-18 detection

Cytokine	Primer	Sequence	Reference
Human TNF- α	upstream	TCA CAG GGC AAT GAT CCC AAA GTA GAC CTG C	[2,3]
	downstream	ATG AGC ACT GAA AGC ATG ATC	
Human IL-1 β	upstream	TTA GGA AGA CAC AAA TTG CAT GGT GAA	[2,3]
	downstream	ATG GCA GAA GTA CCT GAG CTC	
Human IL-18	upstream	GCT TGA ATC TAA ATT ATC AGT C	[4]
	downstream	GAA GAT TCA AAT TGC ATC TTA T	
Human β -actin	upstream	TTC CAG CCT TCC TTC CTG G	[5]
	downstream	TTG CGC TCA GGA GGA GCA AT	

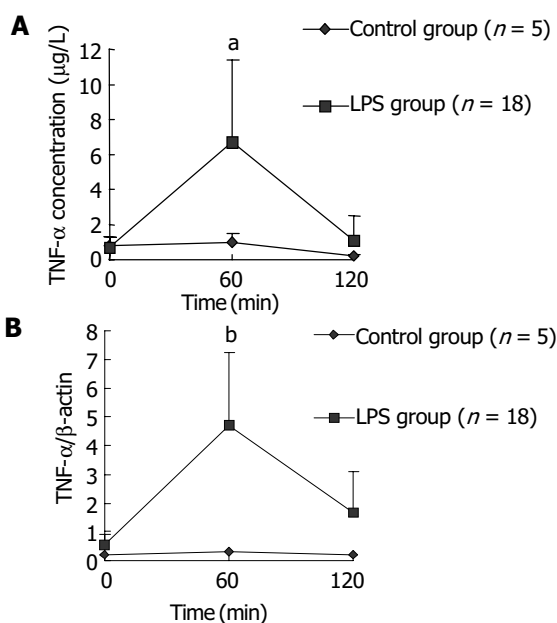


Figure 1 Kinetics curves for TNF- α expression in macaque plasma (A) and PBMCs (B) within 120 min after LPS administration. ^a $P < 0.05$ vs control group; ^b $P < 0.01$ vs control group.

The expression levels of TNF- α mRNA in liver and spleen in LPS group were remarkably higher than those in NS control group at 120 min after LPS challenge. The results were presented in Figure 2.

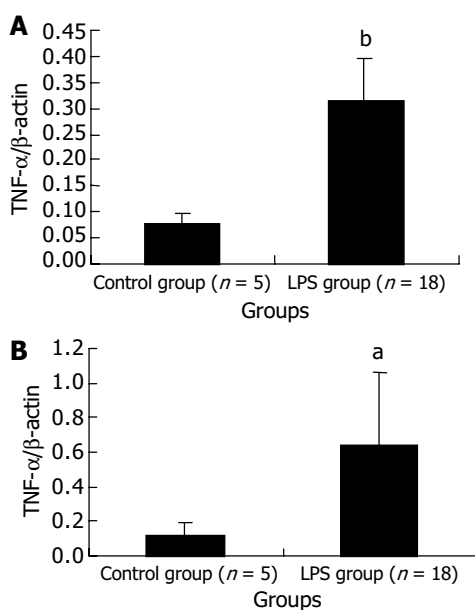


Figure 2 Transcript levels of TNF- α mRNA in liver (A) and spleen (B) at 120 min after LPS administration. ^a $P < 0.05$ vs control group, ^b $P < 0.01$ vs control group.

Change of IL-1 β within 120 min after LPS administration

The plasma IL-1 β level in LPS group began to rise at 60 min after LPS challenge and was significantly higher at 120 min after LPS challenge, compared with that in NS control group. Whereas the IL-1 β transcription level in PBMCs rose earlier than plasma IL-1 β level. The transcription level of IL-1 β in PBMCs of LPS group was significantly higher than that in control group at 60 min after LPS injection, and then dropped to a level similar to that in control group after another 60 min. Figure 3 shows the changes of plasma level and transcription

level of IL-1 β within 120 min after LPS injection.

The transcript level of IL-1 β mRNA in the liver of LPS group remarkably increased at 120 min after LPS administration. But the level in the spleen did not show a significant increase. These results are shown in Figure 4.

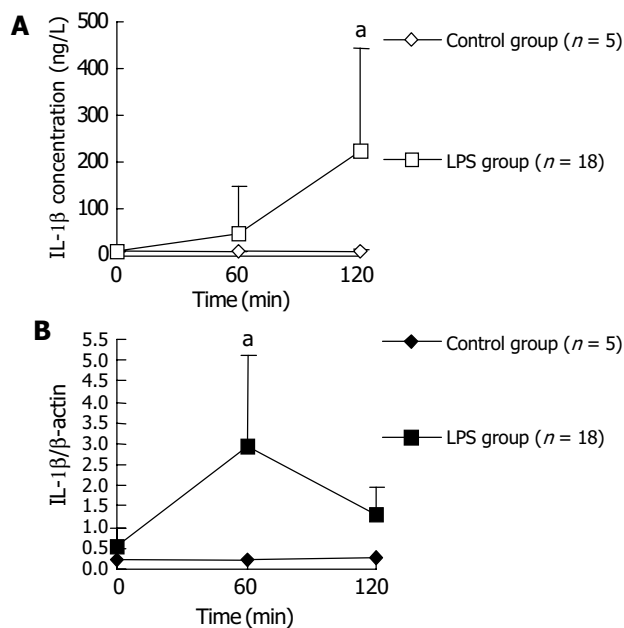


Figure 3 Dynamics of IL-1 β expression in macaque plasma (A) and PBMCs (B) within 120 min after LPS challenge. ^a $P < 0.05$ vs control group.

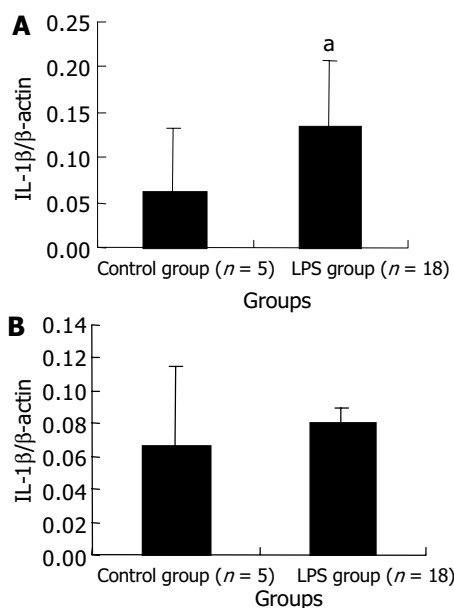


Figure 4 Transcript levels of IL-1 β mRNA in liver (A) and spleen (B) at 120 min after LPS administration. ^a $P < 0.05$ vs control group.

Changes of IL-18 mRNA expression in PBMCs, liver and spleen within 120 min after LPS administration

The expression level of IL-18 mRNA in PBMCs gradually increased with LPS challenge and a statistical significance could be found at 120 min after LPS challenge. The results are presented in Figure 5. Data in Figure 6 indicate at 120 min after LPS challenge, the expression levels of IL-18 mRNA in LPS group were significantly higher in liver cells, not in spleen cells, compared with those in control group after NS injection.

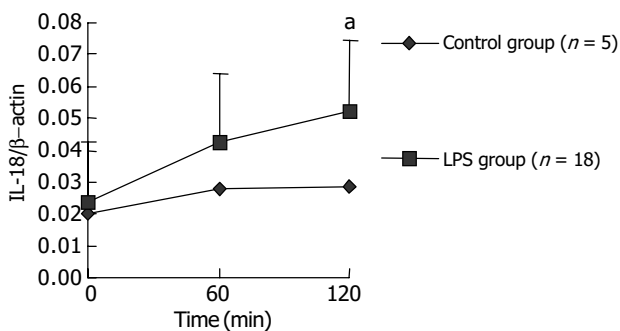


Figure 5 The change of IL-18 mRNA transcript level in PBMCs within 120 min after LPS challenge. ^a*P*<0.05 vs control group.

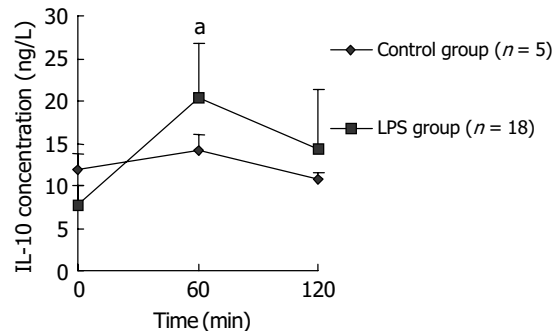


Figure 8 Change of plasma IL-10 level within 120 min after LPS injection. ^a*P*<0.05 vs control group.

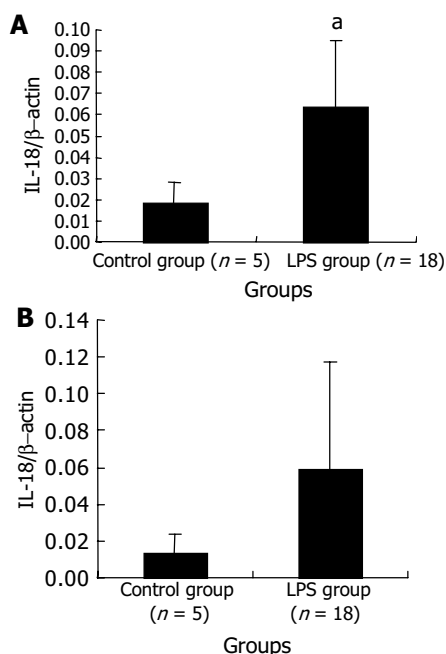


Figure 6 The levels of IL-18 mRNA transcript in liver (A) and spleen (B) at 120 min after LPS challenge. ^a*P*<0.05 vs control group.

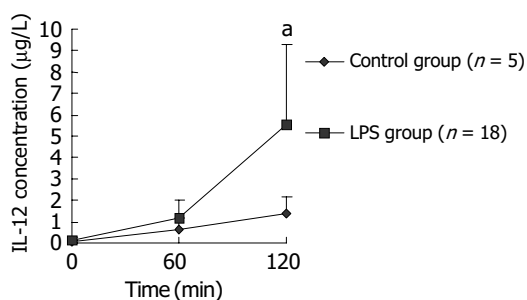


Figure 7 Change of plasma IL-12 levels within 120 min after LPS challenge. ^a*P*<0.05 vs control group.

Change of plasma IL-12 levels within 120 min after LPS challenge

Sixty minutes after LPS challenge, plasma IL-12P40/P70 level of macaques in LPS group gradually rose and was significantly higher than that in control group at 120 min after LPS challenge. Data are supplied in Figure 7.

Change of plasma IL-10 levels within 120 min after LPS administration

Immediately after LPS administration, plasma IL-10 level of macaques in LPS group increased slightly, and showed a statistically significant rise at 60 min after LPS injection, compared with control group. Thereafter the level gradually declined to normal level. The results are shown in Figure 8.

DISCUSSION

Endotoxic shock model

A series of endotoxic shock animal models have been established for studies. *Macaque Mulatta* belongs to primate animals. The physiological functions and anatomical features are similar among primates, including humans. Therefore, it is important to study primate model of endotoxic shock in order to understand septic shock in human. In the present study, an endotoxic shock model of macaque was established to study about changes of inflammation-associated cytokines during early phase of endotoxic shock.

In human volunteers, an intravenous injection with endotoxin bolus of 2-4 ng/kg caused pyrexia, cytokine release and mild decline of MAP^[6,7]. In non-human primate, however, LPS sensitivities were quite different: chimpanzee shared the sensitivity of human to LPS, while baboons and rhesus macaques were insensitive to LPS like rodents^[8,9]. Chimpanzee is too precious to be commonly used in research, baboon and macaque are used as primate model more commonly. The injection bolus of LPS of 10-20 mg/kg, or continuous infusion of LPS of 10 mg/(kg·h) was applied in several studies with rhesus macaques^[10,11]. A bolus injection of LPS 3.0 mg/kg for *Macaque mulatta* model had been reported previously by Hajek^[12]. In the present study, we successfully established an endotoxic shock model of *Macaque mulatta*, which was proved by the decline of MAP, SVRI and LVWI. The LPS dose we used was 2.8 mg/kg and consistent with the previous report in *Macaque mulatta* model^[12].

Methodology of detection for macaque cytokines

Unfortunately, no standard and commercial ELISA kits for detection of macaque cytokines are available. Nevertheless, it is reasonable to try application of human cytokine kits to detect macaque cytokines, because there is a high homology in genome between human and primate animals such as macaque^[2] and it was reported that IL-2 receptor on the surface of rhesus monkey cells reacted with antibody against human IL-2 receptor^[13] and IL-1, IL-2 and TNF-α from monkey cells could bind to antibodies against human IL-1, IL-2 and TNF-α in ELISA^[13,14]. In this experiment, we tried to use ELISA kits for detection human cytokines to determine the levels of TNF-α, IL-1 β, IL-12P40/P70 and IL-10 of *Macaque mulatta* and successfully obtained useful data.

Similarly, we used the primers based on human TNF-α, IL-1 β, IL-18 and β-actin genes to amplify the cDNA segments of macaque TNF-α, IL-1 β, IL-18 and β-actin by RT-PCR methods and successfully obtained the expected products such as 702-bp segment of TNF-α, 810-bp segment of IL-1 β, 341-bp segment of IL-18 and 225-bp segment of β-actin (Figure 9). The PCR products from one macaque were sequenced for homology comparison with human homologue. The results indicated that the identity of TNF-α or IL-18 gene segment between macaque and human was 97%, IL-1 β was 93% (Figure 10).

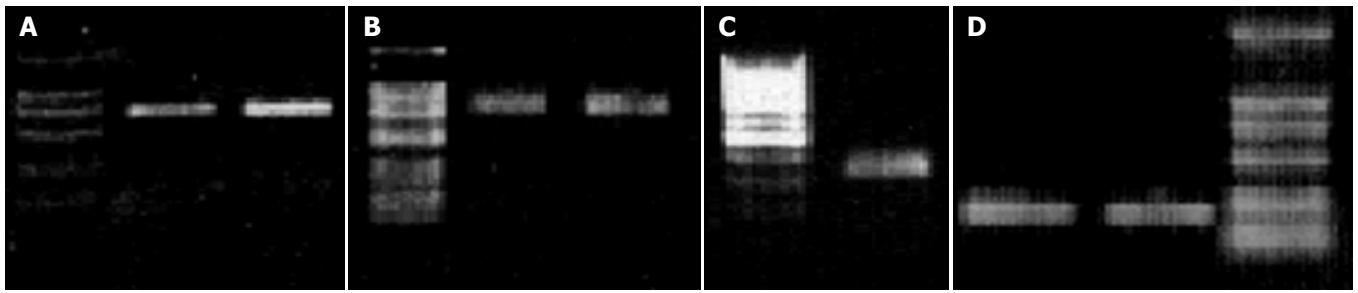


Figure 9 Identification of amplified products by RT-PCR with the method of agarose gel electrophoresis. A: 702 bp from TNF- α gene; B: 810 bp from IL-1 β gene; C: 341 bp from IL-18 gene; D: 225 bp from β -actin gene.

```

Query: 9   gggcaatgatcccaaagtagacctgccagactcggcaaaagtcgagatagtcgggcagat 68
          |||
Sbjct: 849 gggcaatgatcccaaagtagacctgccagactcggcaaaagtcgagatagtcgggcagat 790
Query: 69   tgatctcagcgtgagtcgatcacccttctccagctgaaagaccctctaggtagatgg 128
          |||
Sbjct: 789 tgatctcagcgtgagtcggtcacccttctccagctggaagaccctctccagatagatgg 730
Query: 129 gctcgtaccaggcttggcctcagccccctctggagctcctctggcagggctcttga 188
          |||
Sbjct: 729 gctcataccaggcttggcctcagccccctctggggctcctctggcagggctcttga 670
Query: 189 tggcagagaggaggttgaccttggctctggttaggagacggcgcgatgcggctgatggtgtggg 248
          |||
Sbjct: 669 tggcagagaggaggttgaccttggctctggttaggagacggcgcgatgcggctgatggtgtggg 610
Query: 249 tgaggagcacatggttggaggggcagccttggcccttgaagaggacctgggagtagatga 308
          |||
Sbjct: 609 tgaggagcacatggttggaggggcagccttggcccttgaagaggacctgggagtagatga 550
Query: 309 ggtacaggccttctgatggcaccaccagctggttatctgtcagctccacgccattggcca 368
          |||
Sbjct: 549 ggtacaggccttctgatggcaccaccagctggttatctgtcagctccacgccattggcca 490
Query: 369 ggagggcattggcccggcgggttcagccactggagctgcccctcagcttgagggtttgcta 428
          |||
Sbjct: 489 ggagggcattggcccggcgggttcagccactggagctgcccctcagcttgagggtttgcta 430
Query: 429 caacatgggcttacagcttgtcacttggggctcgagaagatgatctgactgcctgagcca 488
          |||
Sbjct: 429 caacatgggcttacagcttgtcacttggggctcgagaagatgatctgactgcctgagcca 370
Query: 489 gagggctgattagagaggggtccttggggaactcttccctctggggcccgatcactcaa 548
          |||
Sbjct: 369 gagggctgattagagagagggtccttggggaactcttccctctggggcccgatcactcaa 310
Query: 549 agtgcagcagacagaagagcgtggtggcgcctgccacgagcaggagaaggagaaggctga 608
          |||
Sbjct: 309 agtgcagcagcagaagagcgtggtggcgcctgccacgagcaggagaaggagaaggctga 250
Query: 609 ggaaccagcaccgcctggagccctggggccccgctgtcttctggggagcgcctcctcgg 668
          |||
Sbjct: 249 ggaacaagcaccgcctggagccctggggccccgctgtcttctggggagcgcctcctcgg 190
Query: 669 ccagctccagctcccgatcatgctttcagtgetcat 705
          |||
Sbjct: 189 ccagctccagctcccgatcatgctttcagtgetcat 153

Query: 33   tttaggaagacacaaattgcatggtgaagtcaagttatatactggccacctctggteccctc 92
          |||
Sbjct: 868 tttaggaagacacaaattgcatggtgaagtcaagttatatactggccacctctggteccctc 809
Query: 93   ccaagaagacgggcatgtttccgcttgagaggtgtgacgtaccagttggggaattggg 152
          |||
Sbjct: 808 ccaggaagacgggcatgtttctgcttgagaggtgtgacgtaccagttggggaactggg 749
Query: 153 cagactcgaattccagcttgttattgattctatcttgttgaagacaaatcgttttcca 212
          |||
Sbjct: 748 cagactcgaattccagcttgttattgattctatcttgttgaagacaaatcgttttcca 689
Query: 213 tcttctcttgggtagttttgggatctacactctccagctgtagcgtgggcttatacat 272
          |||
Sbjct: 688 tcttctcttgggtaattttgggatctacactctccagctgtagcgtgggcttatacat 629

```

```

Query: 273 ctttcaacacacaggacaggtacagattctttgcttgaggcccaaggccacaggtattt 332
      |||
Sbjct: 628 ctttcaacacgcaggacaggtacagattcttttcttgaggcccaaggccacaggtattt 569
Query: 333 tgtcattactttctctctgtacaaaggacatggagaacaccacttgttgcctccagat 392
      |||
Sbjct: 568 tgtcattactttctctctgtacaaaggacatggagaacaccacttgttgcctccat 509
Query: 393 cctgtccctggaggtggagagctttcagttcatatggaccagacatcaccaagcttttga 452
      |||
Sbjct: 508 cctgtccctggaggtggagagctttcagttcatatggaccagacatcaccaagctttttt 449
Query: 453 gctgtgcatcccggaatgtgcagtgatcgtacaggtgcatcgtcacaaaagcgt 512
      |||
Sbjct: 448 gctgtgagtcggagcgtgcagttcagtgatcgtacaggtgcatcgtgcacataagcct 389
Query: 513 cgttattgctgtgtcaggaaagacaggttcttcttcaaagatgaagggaatcaaggtgc 572
      |||
Sbjct: 388 cgttateccatgtgtcagaagaataggttcttcttcaaagatgaagggaatcaaggtgc 329
Query: 573 tcagtcatttctctggaagatctgtggcagggaaccageatcttcttagcttctcca 632
      |||
Sbjct: 328 tcagtcatttctctggaaggtctgtggcagggaaccageatcttcttagcttctcca 269
Query: 633 tggtacaacaaccgacagggcctgccggaagcctcgtttagtgctcgtgggagattt 692
      |||
Sbjct: 268 tgccacaacaactgacggcctgcctgaagccttgcctgtagtggtggcggagattc 209
Query: 693 gttagctggatgcccagccatccagagggcagaggtccaggtcctggaaggagcacttcact 752
      |||
Sbjct: 208 gttagctggatgcccagccatccagagggcagaggtccaggtcctggaaggagcacttcact 149
Query: 753 gtttagggccatcgactcaagaacaagtcatcctcgttgcctgtagtaagccatca 812
      |||
Sbjct: 148 gtttagggccatcgacttcaagaacaagtcatcctcattgccactgtaataagccatca 89
Query: 813 tttcactggcgagctcaggtacttctgceat 843
      |||
Sbjct: 88 tttcactggcgagctcaggtacttctgceat 58

Query: 34 gcttgaatctaaattatcagtcataaagaatttgaatgaccaagttctcttcatgacca 93
      |||
Sbjct: 117 gcttgaatctaaattatcagtcataaagaatttgaatgaccaagttctcttcatgacca 176
Query: 94 aggaaatcggccctatttgaagatagactgattctgactgtagagataatgcaccccg 153
      |||
Sbjct: 177 aggaaatcggccctatttgaagatagactgattctgactgtagagataatgcaccccg 236
Query: 154 gaccataattatataaataatgataaagatagccagcctagaggtatggctgtagccat 213
      |||
Sbjct: 237 gaccataattatataaagatgataaagatagccagcctagaggtatggctgtagccat 296
Query: 214 ctctgtgaaatgtgagaaaatttcaactctctctgtgagaacagaattatttctttaa 273
      |||
Sbjct: 297 ctctgtgaaatgtgagaaaatttcaactctctctgtgagaacagaattatttctttaa 356
Query: 274 ggaaatgaatcctctgataacatcaaggatacgaagtgacatcatattcttccagag 333
      |||
Sbjct: 357 ggaaatgaatcctctgataacatcaaggatacgaagtgacatcatattcttccagag 416
Query: 334 aagtgtcccaggacatgataataagatgcaatttgaatcttca 376
      |||
Sbjct: 417 aagtgtcccaggacatgataataagatgcaatttgaatcttca 459
    
```

Figure 10 Differences of cDNA fragments from TNF- α (A), IL-1 β (B) and IL-18 (C) gene between macaque and human according to GenBank.

Semi-quantitative analysis of mRNA based on RT-PCR can be completed by using β -actin mRNA as an internal standard and by densitometry of product electrophoresis band scanned or product dot hybridized with specific probe. The relative index (RI) of mRNA is calculated using a formula as $RI = \text{density scan value of specific product} / \text{density scan value of internal control}$. Here, RI may represent the relative level of specific mRNA. In the present study, we also used β -actin mRNA as an internal control. In order to increase detection sensitivity, we used SYBR-Green I, a kind of fluorescence stain for ds-DNA, in the

quantitative analysis. Moreover, a two step strategy of reverse transcription first and then PCR was applied to ensure the consistency of amplification efficiency between cytokine and control mRNA. On the other hand, a real-time PCR was performed to find the cycle number of exponential phase of target DNA. Because the cycle number of exponential phase of cellular target DNA is different from that of primer-dimer DNA, it is possible to exclude primer-dimer interference with target DNA quantitative analysis when the product of cellular target DNA is collected within its exponential phase. In our experiment,

the cycle numbers of exponential phase of cellular target DNA were all less than 40, while that of primer-dimer was far more than 40. So the PCR was carried out for 40 cycles.

Expression changes of inflammation-associated cytokines during early phase of endotoxic shock model of macaques

TNF- α is one of the most important inflammatory cytokines and has a lot of cellular origins such as monocyte-macrophages, lymphocytes and endotheliocytes. The present study demonstrated the level of plasma TNF- α peaked at 60 min after LPS injection and then gradually decreased. The change of mRNA expression level in PBMCs was nearly synchronous, which indicated PBMCs were one of main sources of plasma TNF- α . After LPS challenge, expression levels of TNF- α mRNA both in liver and in spleen increased, suggesting that liver and spleen were also the sources of plasma TNF- α . TNF- α releases firstly during infection or inflammatory reaction. In endotoxic shock models of rats, rabbits and monkeys, plasma TNF- α levels were reported to increase at 30 min after LPS injection and reach the peak about 60-120 min after LPS injection^[15], which was in great agreement with our results. Kupffer cells in liver were an important source of TNF- α . It was reported in endotoxin-induced liver injury model of mice, there were two expression peaks of TNF- α mRNA in liver, one happened within 2 h after LPS injection and the other happened 5 h after LPS injection. The first peak, during which TNF- α was derived from LPS-activated kupffer cells, was not as high as the second one. The second peak was induced by other inflammatory cytokines such as INF- γ and IL-18, and was the main factor inducing liver injury^[16]. In the present experiment, the increase of TNF- α mRNA in liver at 120 min after LPS injection should be the first peak. We found the expression level of TNF- α mRNA in spleen cells also increased after LPS injection. There are few studies on TNF- α production by spleen in endotoxic shock models, which needs more investigations.

IL-1 β , produced by activated monocyte-macrophages, is also an important inflammatory cytokine that is released early. Leturcq^[17] reported that the peak of plasma IL-1 β level in endotoxic shock model of cynomolgus monkeys appeared at 2 h after LPS stimulation which was slightly later than that of plasma TNF- α . This is similar to our result. We observed that IL-1 β plasma level increased in 2 h after LPS injection, but later than TNF- α level did. The fact that expression level of IL-1 β mRNA in PBMCs increased significantly at 60 min after LPS injection and quite earlier than plasma level suggested that PBMCs were the main source of circulating IL-1 β . PBMCs synthesized and released IL-1 β firstly and IL-1 β accumulated in plasma sequentially. The liver cells were also one of IL-1 β sources, but spleen cells the not.

IL-18, produced mainly by kupffer cells and other macrophages, is another important inflammatory factor. IL-18 activates cytokine network of liver and inflammatory reaction. By inducing INF- γ , IL-18 causes the second peak of TNF- α and sequential increase of FasL which induces apoptosis of liver cells^[16-18]. IL-18 was found to be expressed basically in fresh-separated human PBMCs and to increase significantly in 1 h after LPS stimulation^[4]. In LPS-induced acute liver injury model in Propionibacterium acnes-primed INF- γ -deficient mice, IL-18 was found to show a basic expression in liver followed by a remarkably increased expression within 2 h after stimulation with Propionibacterium acnes and LPS^[19]. In this study, we found in endotoxic shock model of macaques, IL-18 mRNA expression in PBMCs began to increase after LPS stimulation and showed a statistically significant increase 2 h later. We also demonstrated a significant increase of IL-18 transcription in liver cells after LPS stimulation. These discoveries in macaque models were not reported here before.

IL-12, produced mainly by macrophages, kupffer cells and dendritic cells, activates neutrophilic granulocytes and promotes release of inflammatory cytokines such as INF- γ , TNF- α etc.^[20,21], while inhibits the release of anti-inflammation cytokines such as IL-10^[22]. So, IL-12 is also closely related to inflammatory responses. Reports about the change of IL-12 expression in endotoxic shock was quite few except for Tsuji's work, in which plasma IL-12 level of acute liver injury model mice was reported to reach a peak within 3 h after LPS stimulation, following the first peak of TNF- α ^[19]. In Trinchieri's opinion, the observation of dynamics of inflammatory cytokines in above model mice suggested that the order of activation for these cytokines was: the first peak of TNF- α , IL-12, IL-18, INF- γ , the second peak of TNF- α and FasL^[23]. Our observation indicated in macaque mulatta, the plasma IL-12 concentration significantly increased in 120 min after LPS stimulation. To our knowledge, there were few reports about IL-12 dynamics in endotoxic shock primate model. Our results in macaque were compatible with Trinchieri's description.

IL-10, originated from Th1, Tr (regulator) or Th3 cells and B lymphocytes as well as monocyte-macrophages, is an anti-inflammation cytokine, inhibiting the release of inflammation cytokines such as TNF- α , IL-1 β , IL-6, IL-8, IL-12 and IL-18^[24,25]. It is one of the cytokines produced very early after LPS injection in mice model, like TNF- α . Dynamics curves showed two peaks of plasma IL-10 in mice model: plasma IL-10 level reached the first peak in 1-5 h after LPS injection and then declined; the second peak appeared in 8-12 h after LPS injection. Plasma IL-10 originated from kupffer cells in liver during the first peak, while it originated from peripheral blood lymphocytes during the second peak^[26]. The amount of IL-10 in the first peak during early phase of endotoxic shock was not enough to suppress the increases of inflammatory cytokines and hence effectively stop inflammation. So it is necessary to use exogenous recombinant IL-10 as a therapeutics in early phase of endotoxic shock to interrupt the chain release of inflammatory cytokines and to stop shock development^[27]. In the present study, we observed IL-10 level in shock model of macaques increased slightly, and significantly in 60 min after LPS injection and formed a smaller peak, and about 60 min later it returned nearly to the value of control group. Our result in macaque model was quite consistent with that in mouse model. The rise of IL-10 level we observed in early phase of endotoxic shock in macaque models should correspond to the first peak.

It is necessary to mention Kupffer cells for understanding the dynamics of inflammatory cytokine release induced by LPS. LPS is the main activator of Kupffer cells, while Kupffer cells are the major source of inflammatory cytokines, such as TNF- α , IL-12 and IL-18, which are produced in response to LPS. TNF- α is the key factor in systemic inflammation (for example, endotoxic shock and septic syndrome), and it is Kupffer cells that are the major source of TNF- α in the liver. So Kupffer cells play an important role in systemic inflammatory reaction caused by Gram-negative bacteria. On the other hand, Kupffer cells are the main scavengers of LPS and also play an important role in removing circulatory LPS and relieving the stimulation and injury caused by LPS^[28].

REFERENCES

- 1 **Han DW.** Intestinal endotoxemia as a pathogenetic mechanism in liver failure. *World J Gastroenterol* 2002; **8**: 961-965
- 2 **Villinger F, Brar SS, Mayne A, Chikkala N, Ansari AA.** Comparative sequence analysis of cytokine genes from human and nonhuman primates. *J Immunol* 1995; **155**: 3946-3954
- 3 **Benveniste O, Vaslin B, Villinger F, Le Grand R, Ansari AA, Dormont D.** Cytokine mRNA levels in unmanipulated and *in vitro* stimulated monkey PBMCs using a semi-quantitative RT-PCR and high sensitivity fluorescence-based detection

- strategy. *Cytokine* 1996; **8**: 32-41
- 4 **Puren AJ**, Fantuzzi G, Dinarello CA. Gene expression, synthesis, and secretion of interleukin-18 and interleukin-1 β are differentially regulated in human blood mononuclear cells and mouse spleen cells. *Proc Natl Acad Sci U S A* 1999; **96**: 2256-2261
- 5 **Takebe Y**, Seiki M, Fujisawa J, Hoy P, Yokota K, Arai K, Yoshida M, Arai N. SR alpha promoter: an efficient and versatile mammalian cDNA expression system composed of the simian virus 40 early promoter and the R-U5 segment of human T-cell leukemia virus type 1 long terminal repeat. *Mol Cell Biol* 1988; **8**: 466-472
- 6 **Pernerstorfer T**, Schmid R, Bieglmayer C, Eichler HG, Kapiotis S, Jilka B. Acetaminophen has greater antipyretic efficacy than aspirin in endotoxemia: a randomized, double-blind, placebo-controlled trial. *Clin Pharmacol Ther* 1999; **66**: 51-57
- 7 **Boujoukos AJ**, Martich GD, Supinski E, Suffredini AF. Compartmentalization of the acute cytokine response in humans after intravenous endotoxin administration. *J Appl Physiol* 1993; **74**: 3027-3033
- 8 **Redl H**, Bahrami S, Schlag G, Traber DL. Clinical detection of LPS and animal models of endotoxemia. *Immunobiology* 1993; **187**: 330-345
- 9 **Harper PL**, Taylor FB, DeLa Cadena RA, Courtney M, Colman RW, Carrell RW. Recombinant antitrypsin pittsburgh undergoes proteolytic cleavage during *E. coli* sepsis and fails to prevent the associated coagulopathy in a primate model. *Thromb Haemost* 1998; **80**: 816-821
- 10 **Richman AV**, Okulski EG, Balis JU. New Concepts in the pathogenesis of acute tubular necrosis associated with sepsis. *Ann Clin Lab Sci* 1981; **11**: 211-219
- 11 **Premaratne S**, May ML, Nakasone CK, McNamara JJ. Pharmacokinetics of endotoxin in a rhesus macaque septic shock model. *J Surg Res* 1995; **59**: 428-432
- 12 **Hajek M**, Trcka V, Vanecek M, Helfert I, Misak J. A model of experimental endotoxin shock in monkeys and its therapeutic control. *Z Exp Chir* 1978; **11**: 317-321
- 13 **Schmitt DA**. *In vitro* interleukin-1 and 2 production and interleukin 2 receptor expression in the rhesus monkey. *Life Sci* 1996; **59**: 931-937
- 14 **Verdier F**, Aujoulat M, Condevaux F, Descotes J. Determination of lymphocyte subsets and cytokine levels in cynomolgus monkeys. *Toxicology* 1995; **105**: 81-90
- 15 **Carvalho GL**, Wakabayashi G, Shimazu M, Karahashi T, Yoshida M, Yamamoto S, Matsushima K, Mukaida N, Clark BD, Takabayashi T, Brandt CT, Kitajima M. Anti-interleukin-8 monoclonal antibody reduces free radical production and improves hemodynamics and survival rate in endotoxemic shock in rabbits. *Surgery* 1997; **122**: 60-68
- 16 **Tsutsui H**, Matsui K, Kawada N, Hyodo Y, Hayashi N, Okamura H, Higashino K, Nakanishi K. IL-18 accounts for both TNF- α - and Fas ligand-mediated hepatotoxic pathways in endotoxin-induced liver injury in mice. *J Immunol* 1997; **159**: 3961-3967
- 17 **Leturcq DJ**, Moriarty AM, Talbott G, Winn RK, Martin TR, Ulevitch RJ. Antibodies against CD14 protect primates from endotoxin-induced shock. *J Clin Invest* 1996; **98**: 1533-1538
- 18 **Puren AJ**, Fantuzzi G, Gu Y, Su SM, Dinarello CA. Interleukin-18 (IFN- γ -inducing factor) induces IL-8 and IL-1 β via TNF- α production from non-CD14+ human blood mononuclear cells. *J Clin Invest* 1998; **101**: 711-721
- 19 **Tsuji H**, Mukaida N, Harada A, Kaneko S, Matsushita E, Nakanuma Y, Tsutsui H, Okamura H, Nakanishi K, Tagawa Y, Iwakura Y, Kobayashi K, Matsushima K. Alleviation of lipopolysaccharide-induced acute liver injury in *Propionibacterium acnes*-primed IFN- γ -deficient mice by a concomitant reduction of TNF- α , IL-12, and IL-18 production. *J Immunol* 1999; **162**: 1049-1055
- 20 **Trinchieri G**. Interleukin-12: a proinflammatory cytokine with immunoregulatory functions that bridge innate resistance and antigen-specific adaptive immunity. *Annu Rev Immunol* 1995; **13**: 251-276
- 21 **Carson WE**, Yu H, Dierksheide J, Pfeffer K, Bouchard P, Clark R, Durbin J, Baldwin AS, Peschon J, Johnson PR, Ku G, Baumann H, Caligiuri MA. A fatal cytokine-induced systemic inflammatory response reveals a critical role for NK cells. *J Immunol* 1999; **162**: 4943-4951
- 22 **Marshall JD**, Secrist H, Dekruyff RH, Wolf SF, Umetsu DT. IL-12 inhibits the production of IL-4 and IL-10 in allergen-specific human CD4+ T lymphocytes. *J Immunol* 1995; **155**: 111-117
- 23 **Trinchieri G**. Immunobiology of interleukin-12. *Immunol Res* 1998; **17**: 269-278
- 24 **Nemeth ZH**, Hasko G, Vizi ES. Pyrrolidine dithiocarbamate augments IL-10, inhibits TNF- α , MIP-1 α , IL-12, and nitric oxide production and protects from the lethal effect of endotoxin. *Shock* 1998; **10**: 49-53
- 25 **Marshall JD**, Aste-Amezaga M, Chehimi SS, Murphy M, Olsen H, Trinchieri G. Regulation of human IL-18 mRNA expression. *Clin Immunol* 1999; **90**: 15-21
- 26 **Barsig J**, Kusters S, Vogt K, Volk HD, Tiegs G, Wendel A. Lipopolysaccharide-induced interleukin-10 in mice: role of endogenous tumor necrosis factor- α . *Eur J Immunol* 1995; **25**: 2888-2893
- 27 **Howard M**, Muchamuel T, Andrade S, Menon S. Interleukin 10 protects mice from lethal endotoxemia. *J Exp Med* 1993; **177**: 1205-1208
- 28 **Terpstra V**, van Amersfoort ES, van Velzen AG, Kuiper J, van Berkel TJ. Hepatic and extrahepatic scavenger receptors: function in relation to disease. *Arterioscler Thromb Vasc Biol* 2000; **20**: 1860-1872

• CLINICAL RESEARCH •

Diagnostic role of secretin-enhanced MRCP in patients with unsuccessful ERCP

László Czakó, Tamás Takács, Zita Morvay, László Csernay, János Lonovics

László Czakó, Tamás Takács, János Lonovics, First Department of Medicine, University of Szeged, Szeged, Hungary
Zita Morvay, László Csernay, International Medical Center, Szeged, Hungary

Supported by the ETT 5K503 and the Hungarian Academy of Sciences, BÖ 5/2003

Correspondence to: Dr. László Czakó, First Department of Medicine, University of Szeged, Szeged, PO Box 469, H-6701, Hungary. czal@in1st.szote.u-szeged.hu

Telephone: +36-62-545201 Fax: +36-62-545185

Received: 2004-02-20 Accepted: 2004-04-06

Abstract

AIM: To evaluate the value of MR cholangiopancreatography (MRCP) in patients in whom endoscopic retrograde cholangiopancreatography (ERCP) was unsuccessfully performed by experts in a tertiary center.

METHODS: From January 2000 to June 2003, 22 patients fulfilled the inclusion criteria. The indications for ERCP were obstructive jaundice ($n = 9$), abnormal liver enzymes ($n = 8$), suspected chronic pancreatitis ($n = 2$), recurrent acute pancreatitis ($n = 2$), or suspected pancreatic cancer ($n = 1$). The reasons for the ERCP failure were the postsurgical anatomy ($n = 7$), duodenal stenosis ($n = 3$), duodenal diverticulum ($n = 2$), and technical failure ($n = 10$). MRCP images were evaluated before and 5 and 10 min after i.v. administration of 0.5 IU/kg secretin.

RESULTS: The MRCP images were diagnosed in all 21 patients. Five patients gave normal MR findings and required no further intervention. MRCP revealed abnormalities (primary sclerosing cholangitis, chronic pancreatitis, cholangitis, cholecystolithiasis or common bile duct dilation) in 10 patients, who were followed up clinically. Four patients subsequently underwent laparotomy (hepaticojejunostomy in consequence of common bile duct stenosis caused by unresectable pancreatic cancer; hepaticotomy+Kehr drainage because of insufficient biliary-enteric anastomosis; choledochojejunostomy, gastrojejunostomy and cysto-Wirsungo gastrostomy because of chronic pancreatitis, or choledochojejunostomy because of common bile duct stenosis caused by chronic pancreatitis). Three patients participated in therapeutic percutaneous transhepatic drainage. The indications were choledocholithiasis with choledochojejunostomy, insufficient biliary-enteric anastomosis, or cholangiocarcinoma.

CONCLUSION: MRCP can assist the diagnosis and management of patients in whom ERCP is not possible.

Czakó L, Takács T, Morvay Z, Csernay L, Lonovics J. Diagnostic role of secretin-enhanced MRCP in patients with unsuccessful ERCP. *World J Gastroenterol* 2004; 10(20): 3034-3038
<http://www.wjgnet.com/1007-9327/10/3034.asp>

INTRODUCTION

The most sensitive diagnostic modality in suspected biliopancreatic diseases is endoscopic retrograde cholangiopancreatography (ERCP)^[1-4]. However, the success rate of the examination mainly depends on the experience of the endoscopist, and does not exceed 95-98% even in the largest specialized centers. Previous operations (Billroth II, Roux-en-Y or biliary-enteric anatomy), duodenal stenosis, or duodenal diverticulum make cannulation of the ducts difficult or even impossible, and increase the risk of complications^[5-7]. If ERCP fails, intravenous (iv) or percutaneous transhepatic cholangiography (PTC) is the alternative method. Since the diagnostic accuracy of iv cholangiography is very low, it is no longer used. PTC is invasive, may be associated with severe complications, and can successfully be applied if the intrahepatic biliary tree is dilated. PTC and iv cholangiography are both unable to visualize the pancreatic duct^[8-10]. There is clearly a need for a noninvasive, sensitive and specific diagnostic modality for patients with suspected biliopancreatic disease if ERCP fails^[11]. Magnetic resonance cholangiopancreatography (MRCP) is a new noninvasive diagnostic modality capable of producing high-quality images of the pancreatobiliary tree. It has been emphasized that its sensitivity (81-100%), specificity (94-98%), positive (86-93%) and negative (94-98%) predictive values and diagnostic accuracy (94-97%) are as high as those of ERCP, which makes MRCP a promising alternative to diagnostic ERCP^[12-16]. Moreover, MRCP has the following advantages over ERCP. It is noninvasive, there are no complications, no radiation, no need for any contrast agent. It causes less discomfort for the patients, and can provide useful information on the parenchymatous organs in this region in combination with conventional cross-sectional MR sequences.

The aim of our study was to assess the value of MRCP in the management of patients with biliopancreatic diseases in whom ERCP was failed.

MATERIALS AND METHODS

Between January 2000 and June 2003 a prospective study was conducted. Twenty-two patients were enrolled, in whom ERCP performed by experts at our endoscopic unit failed to adequately visualize the clinically relevant duct(s). Failure meant two unsuccessful ERCP attempts by precut papillotomy with a needle knife when the ducts were not cannulated with the conventional approach. There were 10 males and 12 females, with a mean age of 51.2 years, range 24-82 years. The indications for ERCP were obstructive jaundice ($n = 9$), abnormal liver enzymes ($n = 8$), suspected chronic pancreatitis ($n = 2$), recurrent acute pancreatitis ($n = 2$), or suspected pancreatic cancer ($n = 1$). The reasons for the ERCP failure were the postsurgical anatomy ($n = 7$), duodenal stenosis ($n = 3$), duodenal diverticulum ($n = 2$), or technical failure ($n = 10$) (Table 1). All patients gave their informed consent after receiving a detailed explanation of the complete examination procedure.

MRCP

All patients underwent MR imaging (Signa Horizon LX 1.0 T-Scanner, General Electric, USA). T1-weighted and T2-weighted

axial plane fast spoiled gradient (FSPGR) images were acquired. These images were used to evaluate the liver and pancreas parenchyma and also to plan the MRCP data collection. The heavily T2-weighted MRCP images were taken in two sets. With a single shot technique, one 30.0–70.0-mm-thick slice was first acquired at TR 5 000 ms, TE 500 ms, with a 320×320 matrix and 40×36 FOV. In the second set, 9–13 thin (5.0 mm) slices with a 2-mm gap were taken from the same region. The breath-hold technique was used for all sequences. “Dualflex” flexible body coil was applied. MRCP images were evaluated before and 5 and 10 min after the iv administration of 0.5 IU/kg secretin (Secretolin, Hoechst, Frankfurt am Main, Germany)^[17]. The administration of secretin induced the secretion of bile and pancreatic juice. Consequently, the ductal filling was increased, and the visualization of the biliary and pancreatic ducts and the image quality were therefore improved^[18].

RESULTS

The MRCP images were of diagnostic quality in all but 1 patient. MRCP furnished normal findings in 5 cases and revealed abnormalities in 17 patients (Table 1). Conservative medical treatment was applied in 10 cases. MRCP demonstrated mild bile duct dilation caused by chronic pancreatitis in 3 patients. Since they were mainly asymptomatic, surgical intervention was not indicated. Primary sclerosing cholangitis was indicated by MRCP in 3 patients, the cholestasis was improved after treatment with ursodeoxycholic acid. Gallbladder stones were found in an 82-year-old female patient, operation was not recommended because of her age. In a 77-year-old female patient who had previously undergone choledochoduodenostomy, the extrahepatic biliary tree exhibited caliber changes. This finding was considered to correspond to cholangitis, the abnormal liver function was normalized by antibiotic therapy. In 2 patients with previous cholecystectomy and abnormal liver enzymes, MRCP revealed mild extrahepatic bile duct dilation (postcholecystectomy syndrome?). The liver function normalized without treatment in 1 patient, and in response to ursodeoxycholic acid treatment in the other (Table 1).

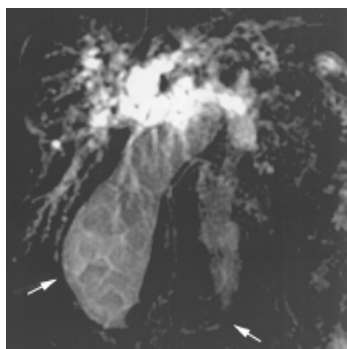


Figure 1 MRCP of a 78-year-old female patient. The common bile duct is dilated with a stricture at the level of the papilla of Vateri (open arrow), with multiple stones in the gallbladder (solid arrow). The Wirsung duct is not visible.

Seven patients required therapeutic interventions. Four of these 7 patients underwent surgery. The indication for operation was based on the MRCP findings, which were confirmed at surgery in 3 of the 4 cases. In 1 patient (No. 10, Figure 1), MRCP revealed only the site, but not the cause of the bile duct obstruction. This patient was referred to the endoscopy unit because of obstructive jaundice. MRCP demonstrated a preapillary common bile duct obstruction. The Wirsung duct was not visible. These findings, the clinical picture and the result of duodenoscopy led to a suspicion of pancreatic head carcinoma. The patient was operated

on, and the surgery confirmed the suspicion. Curative resection was not possible because of the local invasiveness of the tumor, bilio-enteric anastomosis was performed.

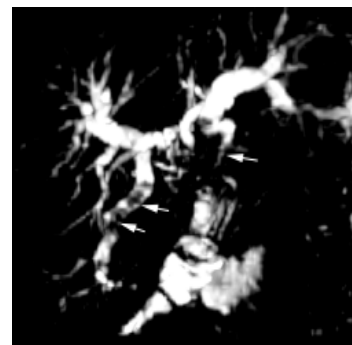


Figure 2 MRCP of a 58-year-old female patient in whom ERCP failed because of a previous Billroth II resection. The intrahepatic biliary tree is markedly dilated with stones (open arrows), and the choledochojejunostomy anastomosis is narrowed (solid arrow). The patient underwent hepaticotomy and Kehr drainage.

In 1 patient in whom ERCP was failed because of a previous Billroth II resection, MRCP demonstrated a stricture of the choledochojejunostomy anastomosis as the cause of a bile duct obstruction (No. 1, Figure 2). The intrahepatic biliary tree was markedly dilated and contained secondary stones. The patient subsequently underwent hepaticotomy and Kehr drainage.

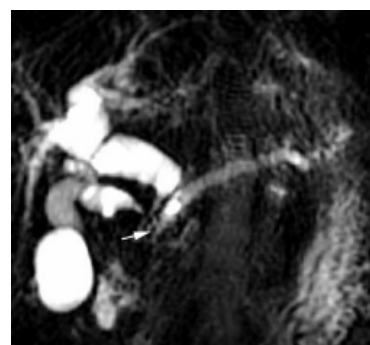


Figure 3 MRCP of a 63-year-old male patient in whom ERCP failed because of duodenal stenosis. The calcified pancreatic head obstructs the Wirsung duct and the common bile duct (arrow) with an upstream dilation, causing the “double duct sign”. The intrahepatic biliary tree and the cystic duct are also dilated. The patient underwent choledochojejunostomy, gastrojejunostomy and Wirsungogastrostomy.

In a patient with chronic pancreatitis, whose disease was not followed up regularly, ERCP was indicated because of obstructive jaundice, but it failed in consequence of duodenal stenosis. MRCP showed obstruction of the Wirsung duct and the common bile duct by the calcified pancreatic head, with an upstream dilation in both ducts, causing the “double duct sign” (No. 11, Figure 3). The intrahepatic biliary tree and the cystic duct were also dilated. The patient underwent choledochojejunostomy, gastrojejunostomy and Wirsungogastrostomy. Similarly, in a patient with chronic pancreatitis in whom a previous Billroth II resection precluded ERCP, MRCP demonstrated an intrapancreatic bile duct obstruction. Choledochoenterostomy was performed (No. 19).

In 3 patients of advanced age in a moribund physical status, the bile duct obstruction was treated with percutaneous transhepatic drainage (PTD). MRCP indicated common bile duct stones in a patient who had previously undergone choledochojejunostomy

Table 1 Indications for ERCP, reasons for ERCP failure, MRCP findings, and management of patients

Patient	Indication for ERCP	Reason for ERCP failure	MRCP findings	Management of patients
1	Obstructive jaundice	Billroth II anatomy (choledochojejunostomy anatomy)	stricture of choledochojejunostomy	hepaticotomy +Kehr drainage
2	Obstructive jaundice	Billroth II anatomy (choledochojejunostomy anatomy)	cholangitis	antibiotic treatment
3	Obstructive jaundice	choledochojejunostomy anatomy	choledocholithiasis	PTD
4	Obstructive jaundice	Roux and Y anatomy hepaticojejunostomy anatomy	stricture of hepaticojejunostomy	PTD
5	Cholestasis biliary pancreatitis	technical	cholecystolithiasis	follow-up
6	Cholestasis	technical	mild CBD dilatation	follow-up
7	Suspected pancreatic cancer	duodenal stenosis	chronic pancreatitis	follow-up
8	Obstructive jaundice	technical	cholangiocarcinoma	PTD
9	Cholestasis	technical	PSC	follow-up
10	Obstructive jaundice	technical	distal stricture of CBD	hepaticojejunostomy unresectable
11	Obstructive jaundice chronic pancreatitis	duodenal stenosis	"double duct sign"	pancreas carcinoma choledochojejunostomy gastrojejunostomy Wirsungogastrostomy
12	Obstructive jaundice chronic pancreatitis	technical	intrapancreatic stricture of CBD, chronic pancreatitis	follow-up
13	Cholestasis	technical (choledocho-duodenostomy anatomy)	normal	follow-up
14	Cholestasis	duodenal diverticulum	PSC	follow-up
15	Cholestasis	technical	PSC	follow-up
16	Obstructive jaundice	duodenal diverticulum	normal	follow-up
17	Recurrent pancreatitis	technical	normal	follow-up
18	Recurrent pancreatitis	technical	normal	follow-up
19	Obstructive jaundice	Billroth II anatomy	intrapancreatic stricture of CBD, chronic pancreatitis	choledochoenterostomy cholecystectomy
20	Cholestasis	technical	mild CBD dilation	follow-up
21	Obstructive jaundice	duodenal stenosis	intrapancreatic stricture of CBD, chronic pancreatitis	follow-up
22	Cholestasis	Billroth II anatomy	normal	follow-up

CBD: common bile duct; PSC: primary sclerosing cholangitis; PTD: percutan transhepatic drainage.

(No. 3), another with a hepaticojejunostomy anastomotic stricture (No. 4) and one with prepapillary cholangiocarcinoma (No. 8, Figure 4). These findings were confirmed by PTC and the patients subsequently underwent biliary drainage.

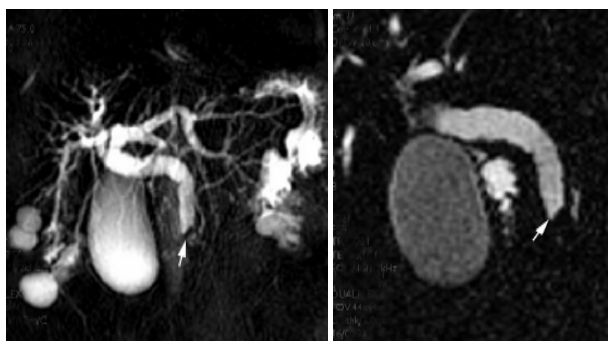


Figure 4 Normal Wirsung duct and bilateral renal cysts in an 81-year-old female patient. The intraluminal focus with low signal intensity in the distal common bile duct (arrow) proved to be cholangiocarcinoma. The biliary tree is dilated. With regard to her age and physical status, the patient underwent biliary stent implantation to ensure bile flow.

DISCUSSION

ERCP is the most sensitive and specific technique currently available for visualization of the biliary tree and pancreatic duct. Beside the establishment of a diagnosis, this examination at the same time offers therapeutic options. However, ERCP is invasive, and may be associated with complications, and patients who undergo ERCP need sedation. Another disadvantage is that it affords no information on extraductal lesions, and does not opacify the obstructed segment in the event of total duct obstruction. It was unsuccessful in 3-10% of the cases, even in the largest endoscopic centers^[5-7]. Inexperience of the endoscopist and anatomic factors such as previous gastroentero-anastomosis, duodenal stenosis, or periampullary diverticulum might lead to higher rates of unsuccessful ERCP^[19,20]. When the papilla of Vater is in the visual field of the duodenoscope, but conventional cannulation fail, precut papillotomy could be performed with a needle knife, and cannulation could subsequently be achieved. However, precut papillotomy could increase the frequency and severity of complications as compared with conventional ERCP (6-12% vs 1-5%)^[21,22]. Iv cholangiography or PTC examinations are the alternative choices for visualization of the biliary tree. However, iv cholangiography has been no longer used, because its

diagnostic accuracy was limited^[8]. PTC is a sensitive method of detecting biliary abnormalities, but it was invasive, might be associated with severe complications, and could successfully be applied if the intrahepatic biliary tree was dilated. In addition, neither PTC nor iv cholangiography was able to visualize the pancreatic duct^[9,10].

The need for a safe and noninvasive technique for examination of the biliary tree and pancreatic duct resulted in the development of MRCP. A number of studies have demonstrated that the sensitivity, specificity, positive and negative predictive values and diagnostic accuracy of MRCP in the detection of biliopancreatic diseases are as high as those of ERCP^[12-16]. Despite these data, the actual role of MRCP in the diagnostic work-up of patients with suspected biliopancreatic disease is not clear. Besides its advantages, MRCP has certain drawbacks. Most importantly, it does not allow simultaneous therapeutic intervention. While ERCP offers a therapeutic option in the same session after the diagnosis is made (papillotomy, removal of choledocholithiasis, stenting of a biliary stricture, *etc.*), MRCP yields only the diagnosis. Clips, stents, pneumobilia, hemobilia and ascites might result in artifacts and impede interpretation of the MRCP image. Despite the new technological advances in MR imaging, its resolution has remained behind that of ERCP^[23].

In the present study we assessed the value of MRCP in the management of patients in whom ERCP was unsuccessful. MRCP prevented an invasive procedure in 15 of 22 cases and guided therapy in the remaining 7. Ten patients were treated conservatively. They did not require further diagnostic examinations or therapeutic interventions; they were asymptomatic or responded well to the medical therapy during the follow-up. In 7 patients, therapeutic intervention was indicated by the MRCP findings. The information provided by MRCP was sufficient for the decision-making, and a further diagnostic work-up was required in only 1 patient. This patient (No. 10) was referred to the endoscopy unit because of obstructive jaundice. Duodenoscopy revealed an enlarged papilla of Vater with an irregular surface, which was suspicious of malignancy. Cannulation of the biliary or the pancreatic duct was impossible, even after precut papillotomy. The histological examination of the biopsy specimens taken from the papilla indicated no malignancy. MRCP demonstrated a dilated biliary tree with a severe prepapillary stricture (Figure 1). The pancreas was not separated well from its surroundings in the conventional axial plane MR images, because of the lack of peripancreatic fatty tissue. The Wirsung duct was not depicted or could not be identified among the fluid-filled bowels, despite the use of secretin. The evaluation of the MR images was hampered by the technical artifacts. These findings and the clinical picture together suggested pancreatic head carcinoma. The patient was operated on. The surgery confirmed the suspicion, but a curative resection was impossible as a result of the local invasiveness of the tumor. Biliary-enteric anastomosis was performed.

The sensitivity, specificity, positive and negative predictive values and diagnostic accuracy of MR imaging in the detection of pancreatic cancer were at least as high as those of computer tomography or ERCP^[24,25]. The combination of conventional MR imaging with MRCP and MR angiography could increase the accuracy in the diagnosis, the staging of pancreatic malignancies and the assessment of respectability^[26-29]. With this combined MR imaging technique, the biliary tree and pancreatic duct with the surrounding vessels and parenchymatous organs could be depicted in one examination, which makes it cost-effective. In our case, the poor quality of the MR imaging with significant amount of artifacts might explain why it was unable to diagnose the cause of the biliary obstruction.

Four patients underwent surgery without further diagnostic

examinations. In 3 cases the diagnosis made by MR was confirmed by the surgical findings. In 1 case (No. 10), the MR revealed only the site, but not the cause (i.e. pancreatic cancer) of the bile duct obstruction, which was diagnosed during the operation. In 3 patients, surgery was not recommended because of their moribund physical status. PTC was performed and in each case confirmed the results of MRCP. These patients subsequently underwent biliary drainage.

Seven out of 22 patients required intervention after MRCP. This points the major drawbacks of MRCP. It is unable to combine therapy with diagnosis. It could be argued that the 3 patients with obstructive jaundice who required PTC and PTD after MRCP might have better served by proceeding to this modality directly. However, the fact that MRCP is noninvasive is a powerful point in its favor. It can identify those patients where therapeutic intervention is needed.

Our results suggest that MRCP is a feasible and valuable diagnostic modality in patients in whom ERCP fails. MRCP facilitates the management of these patients. It differentiates patients who require invasive therapy from those who can be treated conservatively, and provides information necessary for the planning of surgical or radiological interventions.

REFERENCES

- 1 **Pasanen PA**, Partanen KP, Pikkariainen PH, Alhava EM, Janatuinen EK, Pirinen AE. A comparison of ultrasound, computed tomography and endoscopic retrograde cholangiopancreatography in the differential diagnosis of benign and malignant jaundice and cholestasis. *Eur J Surg* 1993; **159**: 23-29
- 2 **Ponchon T**, Pilleul F. Diagnostic ERCP. *Endoscopy* 2002; **34**: 29-42
- 3 **Baron TH**, Fleischer DE. Past, present, and future of endoscopic retrograde cholangiopancreatography: perspectives on the National Institutes of Health consensus conference. *Mayo Clin Proc* 2002; **77**: 407-412
- 4 NIH State of Science Conference on ERCP. 2002-01-14-16. Available from: URL: <http://consensus.nih.gov>
- 5 **Bilbao MK**, Dotter CT, Lee TG, Katon RM. Complications of endoscopic retrograde cholangiopancreatography (ERCP). A study of 10 000 cases. *Gastroenterology* 1976; **70**: 314-320
- 6 **Choudari CP**, Sherman S, Fogel EL, Phillips S, Kochell A, Flueckiger J, Lehman GA. Success of ERCP at a referral center after a previously unsuccessful attempt. *Gastrointest Endosc* 2000; **52**: 478-483
- 7 **Loperfido S**, Angelini G, Benedetti G, Chilovi F, Costan F, De Bernardinis F, De Bernardin M, Ederle A, Fina P, Fratton A. Major early complications from diagnostic and therapeutic ERCP: a prospective multicenter study. *Gastrointest Endosc* 1998; **48**: 1-10
- 8 **Tham TC**, Collins JS, Watson RG, Ellis PK, McIlrath EM. Diagnosis of common bile duct stones by intravenous cholangiography: prediction by ultrasound and liver function tests compared with endoscopic retrograde cholangiography. *Gastrointest Endosc* 1996; **44**: 158-163
- 9 **Ott DJ**, Gelfand DW. Complications of gastrointestinal radiologic procedures: II. Complications related to biliary tract studies. *Gastrointest Radiol* 1981; **6**: 47-56
- 10 **Harbin WP**, Mueller PR, Ferrucci JT Jr. Transhepatic cholangiography: complications and use patterns of the fine-needle technique: a multi-institutional survey. *Radiology* 1980; **135**: 15-22
- 11 **Soto JA**, Yucel EK, Barish MA, Chuttani R, Ferrucci JT. MR cholangiopancreatography after unsuccessful or incomplete ERCP. *Radiology* 1996; **199**: 91-98
- 12 **Lomanto D**, Pavone P, Laghi A, Panebianco V, Mazzocchi P, Fiocca F, Lezoche E, Passariello R, Speranza V. Magnetic resonance-cholangiopancreatography in the diagnosis of biliopancreatic diseases. *Am J Surg* 1997; **174**: 33-38
- 13 **Coakley FV**, Schwartz LH. Magnetic resonance cholangiopancreatography. *J Magn Reson Imaging* 1999; **9**: 157-162
- 14 **Takehara Y**. Can MRCP replace ERCP? *J Magn Reson Imaging*

- 1998; **8**: 517-534
- 15 **Soto JA**, Barish MA, Yucel EK, Siegenberg D, Ferrucci JT, Chuttani R. Magnetic resonance cholangiography: comparison with endoscopic retrograde cholangiopancreatography. *Gastroenterology* 1996; **110**: 589-597
- 16 **Sahai AV**, Devonshire D, Yeoh KG, Kay C, Feldman D, Willner I, Farber J, Patel R, Tamasky PR, Cunningham JT, Trus T, Hawes RH, Cotton PB. The decision-making value of magnetic resonance cholangiopancreatography in patients seen in a referral center for suspected biliary and pancreatic disease. *Am J Gastroenterol* 2001; **96**: 2074-2080
- 17 **Czako L**, Endes J, Takacs T, Boda K, Lonovics J. Evaluation of pancreatic exocrine function by secretin-enhanced magnetic resonance cholangiopancreatography. *Pancreas* 2001; **23**: 323-328
- 18 **Hellerhoff KJ**, Helmberger H 3rd, Rosch T, Settles MR, Link TM, Rummeny EJ. Dynamic MR pancreatography after secretin administration: image quality and diagnostic accuracy. *Am J Roentgenol* 2002; **179**: 121-129
- 19 **Nicaise N**, Pellet O, Metens T, Deviere J, Braude P, Struyven J, Matos C. Magnetic resonance cholangiopancreatography: interest of IV secretin administration in the evaluation of pancreatic ducts. *Eur Radiol* 1998; **8**: 16-22
- 20 **Mosca S**. How can we reduce complication rates and enhance success rates in Billroth II patients during endoscopic retrograde cholangiopancreatography? *Endoscopy* 2000; **32**: 589-590
- 21 **Rollhauser C**, Al-Kawas FH. Endoscopic access to the papilla of Vater for endoscopic retrograde cholangiopancreatography in patients with Billroth II or Roux-en-Y gastrojejunostomosis. *Gastrointest Endosc* 1997; **46**: 581-582
- 22 **Larkin CJ**, Huibregtse K. Precut sphincterotomy: indications, pitfalls, and complications. *Curr Gastroenterol Rep* 2001; **3**: 147-153
- 23 **Keogan MT**, Edelman RR. Technological advances in abdominal MR imaging. *Radiology* 2001; **220**: 310-320
- 24 **Adamek HE**, Albert J, Breer H, Weitz M, Schilling D, Riemann JF. Pancreatic cancer detection with magnetic resonance cholangiopancreatography and endoscopic retrograde cholangiopancreatography: a prospective controlled study. *Lancet* 2000; **356**: 190-193
- 25 **Ichikawa T**, Haradome H, Hachiya J, Nitatori T, Ohtomo K, Kinoshita T, Araki T. Pancreatic ductal adenocarcinoma: Preoperative assessment with helical CT versus dynamic MR imaging. *Radiology* 1997; **202**: 655-662
- 26 **Catalano C**, Pavone P, Laghi A, Panebianco V, Scipioni A, Fanelli F, Brillo R, Passariello R. Pancreatic adenocarcinoma: combination of MR imaging, MR angiography and MR cholangiopancreatography for the diagnosis and assessment of resectability. *Eur Radiol* 1998; **8**: 428-434
- 27 **Adamek HE**, Breer H, Karschkes T, Albert J, Riemann JF. Magnetic resonance imaging in gastroenterology: time to say goodbye to all that endoscopy? *Endoscopy* 2000; **32**: 406-410
- 28 **Mitchell RM**, Byrne MF, Baillie J. Pancreatitis. *Lancet* 2003; **361**: 1447-1455
- 29 **Kay CL**. Which test to replace diagnostic ERCP – MRCP or EUS? *Endoscopy* 2003; **35**: 426-428

Edited by Wang XL Proofread by Chen WW and Xu FM

Autonomic and sensory nerve dysfunction in primary biliary cirrhosis

Katalin Keresztes, Ildikó Istenes, Aniko Folhoffer, Peter L Lakatos, Andrea Horvath, Timea Csak, Peter Varga, Peter Kempler, Ferenc Szalay

Katalin Keresztes, Ildikó Istenes, Aniko Folhoffer, Peter L Lakatos, Andrea Horvath, Timea Csak, Peter Varga, Peter Kempler, Ferenc Szalay, 1st Department of Medicine, Semmelweis University, Budapest, Hungary

Correspondence to: Professor Ferenc Szalay, MD, PhD, 1st Department of Medicine, Semmelweis University, Koranyi S. 2/A, H-1083 Budapest, Hungary. szalay@bel1.sote.hu

Telephone: +36-1-210-1007 **Fax:** +36-1-210-1007

Received: 2004-01-10 **Accepted:** 2004-04-14

Abstract

AIM: Cardiovascular autonomic and peripheral sensory neuropathy is a known complication of chronic alcoholic and non-alcoholic liver diseases. We aimed to assess the prevalence and risk factors for peripheral sensory nerve and autonomic dysfunction using sensitive methods in patients with primary biliary cirrhosis (PBC).

METHODS: Twenty-four AMA M2 positive female patients with clinical, biochemical and histological evidence of PBC and 20 age matched healthy female subjects were studied. Five standard cardiovascular reflex tests and 24-h heart rate variability (HRV) analysis were performed to define autonomic function. Peripheral sensory nerve function on median and peroneal nerves was characterized by current perception threshold (CPT), measured by a neuroselective diagnostic stimulator (Neurotron, Baltimore, MD).

RESULTS: Fourteen of 24 patients (58%) had at least one abnormal cardiovascular reflex test and thirteen (54%) had peripheral sensory neuropathy. Lower heart rate response to deep breathing ($P = 0.001$), standing ($P = 0.03$) and Valsalva manoeuvre ($P = 0.01$), and more profound decrease of blood pressure after standing ($P = 0.03$) was found in PBC patients than in controls. As a novel finding we proved that both time domain and frequency domain parameters of 24-h HRV were significantly reduced in PBC patients compared to controls. Each patient had at least one abnormal parameter of HRV. Lower CPT values indicated hyperaesthesia as a characteristic feature at peroneal nerve testing at three frequencies (2000 Hz: $P = 0.005$; 250 Hz: $P = 0.002$; 5 Hz: $P = 0.004$) in PBC compared to controls. Correlation of autonomic dysfunction with the severity and duration of the disease was observed. Lower total power of HRV correlated with lower CPT values at median nerve testing at 250 Hz ($P = 0.0001$) and at 5 Hz ($P = 0.002$), as well as with those at peroneal nerve testing at 2000 Hz ($P = 0.01$).

CONCLUSION: Autonomic and sensory nerve dysfunctions are frequent in PBC. Twenty-four-hour HRV analysis is more sensitive than standard cardiovascular tests for detecting of both parasympathetic and sympathetic impairments. Our novel data suggest that hyperaesthesia is a characteristic feature of peripheral sensory neuropathy and might contribute to itching in PBC. Autonomic dysfunction is related to the duration and severity of PBC.

Keresztes K, Istenes I, Folhoffer A, Lakatos PL, Horvath A, Csak T, Varga P, Kempler P, Szalay F. Autonomic and sensory nerve dysfunction in primary biliary cirrhosis. *World J Gastroenterol* 2004; 10(20): 3039-3043

<http://www.wjgnet.com/1007-9327/10/3039.asp>

INTRODUCTION

Autonomic neuropathy (AN) is frequent complication of both alcoholic and non-alcoholic chronic liver diseases^[1]. Cardiovascular AN represents a serious complication as it carries a 5-fold risk of mortality in patients with chronic liver diseases^[2]. In a 10-mo long follow-up study in patients awaiting for liver transplantation the mortality was significantly higher in patients with AN (27%) compared to those without AN (0%), suggesting that AN should be taken into consideration for early liver transplantation in patients with advanced liver disease^[3]. Up to now the precise explanation of increased mortality associated with AN has not been identified. Beside the most severe complications of AN-silent myocardial ischaemia and infarction, cardiorespiratory arrest, major arrhythmias^[4] -the attenuation of circadian variation of blood pressure and heart rate may contribute to the higher death rate^[5,6]. Prolongation of the QT-interval is also involved in the poor prognosis of AN accompanying chronic liver disease^[7,8]. Autonomic neuropathy may also be regarded as a potential etiologic factor of hyperdynamic circulation and portal hypertension^[9].

Recently, attention has been focused on the importance of 24-h heart rate variability (HRV). It has been confirmed that HRV is a strong and independent predictor of mortality after an acute myocardial infarction^[10]. Time and frequency domain analysis of HRV proved to be a reliable, noninvasive tool to provide quantitative information on cardiovascular autonomic function differentiated into vagal and sympathetic components^[11]. Additionally, assessment of HRV is a sensitive method for early detection of autonomic neuropathy even if the standard cardiovascular reflex tests are normal^[12]. Depressed HRV has been described not only in cardiovascular disorders, but also in chronic liver diseases^[5,13-15]. Although autonomic and sensory neuropathy is known as a common extrahepatic manifestation in chronic liver diseases^[1,3,7,13], there are only few data on risk factors of neuropathy in PBC^[16,17].

The aim of our study was to assess the frequency and predisposing factors of autonomic and peripheral sensory neuropathy in PBC.

MATERIALS AND METHODS

Patients

Twenty-four female patients with PBC (mean age: 60.4±7.1 years; range: 45-73 years) from the Hepatological Outpatient Unit of Semmelweis University, Budapest and 20 age-matched healthy female controls (mean age: 59.3±6.8 years; range: 44-72 years) were recruited for this cross sectional study. The diagnosis of PBC was based on characteristic clinical and laboratory data, AMA M2 positivity and liver biopsy. The severity of liver disease was assessed by histologic classification. Stage I: 2, stage II: 5, stage III: 12 and stage IV: 5 patients. Full medical history was taken, followed by thorough physical and neurologic

examination in each patient and control. Patients were only included if they were normotensive, i.e. no history of hypertension, and at the time of inclusion visiting office blood pressure <140/90 mmHg calculated by the mean of three measurements using Korotkov's technique and no evidence of disease known to affect autonomic function (e.g. other hepatic disease, cardiovascular, kidney, endocrinologic, neurologic and psychiatric disorders including alcoholism). None was taking any antihypertensive drugs or other medications, apart from ursodeoxycholic acid, vitamin D and calcium supplementation^[18], and none had ascites. The healthy controls were recruited from the staff of our institution and their family members. Every participant was asked to refrain from consuming caffeine and alcoholic beverages, and tobacco products 12 h before autonomic testing.

Methods

The autonomic function was explored by the *five standard cardiovascular reflex tests*^[19]. Heart rate tests (heart rate responses to deep breathing, the 30/15 ratio and the Valsalva ratio) mainly reflect parasympathetic function while blood pressure responses to sustained handgrip and standing primarily allow the assessment of sympathetic integrity. Patients with at least one abnormal or two borderline cardiovascular tests were considered to have autonomic neuropathy. The same research assistant using a computerized ECG-recording-analyzing system developed by Innomed Inc, Budapest, Hungary, performed all reflex tests.

Two channel 24-h ECG recordings were done by CardioTens equipment (Meditech, Budapest, Hungary). This device complies with the requirements of the British Hypertension Society and the Association for the Advancement of Medical Instrumentation protocols. Automatic filters were used to continuously restore baseline and filter background and muscle noise. Analysis of stored data was done by Medibase software. The recording was also edited using visual control and manual corrections were made to omit ectopic beats, arrhythmic events and noise effects and only normal-to-normal beats (NN intervals) were used for further analysis. Ratio of normal beats to total number of beats was >95% in both groups.

To characterize 24-h HRV, time domain and frequency domain methods were used. Since there were several parameters cited in the literature to assess HRV, we selected a limited number of parameters according to the recommendations of the European Society of Cardiology and the North American Society of Pacing and Electrophysiology^[11]. Statistical time domain parameters could be calculated from either the direct measurements of NN intervals or from the differences between NN intervals. The following parameters were calculated from direct measurements of NN intervals: standard deviation of all NN (SDNN) intervals reflecting all the cyclic components responsible for variability and standard deviation of the averages of NN (SDANN) intervals in all 5-min segments of the entire recording, an estimate of the changes in heart rate due to cycles longer than 5 min.

Statistical time domain parameters deriving from NN interval differences are RMSSD and pNN50. RMSSD (the square root of the mean of the sum of the squares of differences between adjacent NN intervals) is an estimate of short-term components of HRV. PNN50 (the proportion of adjacent NN intervals differ by more than 50 ms) was considered to reflect the vagal tone of the heart.

A simple geometric time domain parameter, HRV triangular index (HRVTI) was also computed. HRVTI is the integral of the density distribution (the number of all NN intervals) divided by the maximum of the density distribution. HRVTI represents overall HRV.

In the frequency domain analysis (power spectral density analysis) of heart period oscillations low- (0.04-0.15 Hz) and high- (0.15-0.4 Hz) frequency bands of the power (i.e. variance)

spectrum (power distribution as function of frequency) was performed. The following frequency domain measures were computed: TP (total power: variance of all NN intervals), LF (power in the low frequency range) which is under both sympathetic and parasympathetic influences, HF (power in the high frequency range) which is an acknowledged measure of the parasympathetic (i.e. vagal) modulations.

Peripheral sensory function was characterized by the evaluation of the current perception threshold (CPT) with a neuroselective diagnostic stimulator (Neurotron, Baltimore, MD, USA), which permits transcutaneous testing at three sinusoidal frequencies (2000 Hz, 250 Hz and 5 Hz). The intensity of the stimulating current was changed within the range from 0.01 to 9.99 mA. The neurometer is the first instrument designed for the overall assessment of all types of sensory fibres. As demonstrated by the results of comparative trials conducted earlier^[20], CPT values measured during high frequency stimulation correlated best with tests of large fibre function and low frequency CPT values correlated with tests of small fibre function. Median and peroneal nerves (digital branches) were studied.

The Local Regional Committee of Science and Research Ethics approved the study. Written informed consent was obtained.

Statistical analysis

All analyses were performed using Statistica Software. Data are expressed as mean±SD and were compared between groups by Student's *t*-test. Correlations between variables were analysed by partial correlation coefficient calculation adjusted for age. $P < 0.05$ was regarded as statistically significant.

RESULTS

Autonomic function

Using standard cardiovascular tests^[18], 14 PBC patients (58%) had at least one abnormal autonomic function test. Among these patients parasympathetic neuropathy was found in 8 (57.1%) patients, sympathetic nerve dysfunction was observed in 2 patients, and 4 subjects had both parasympathetic and sympathetic damage.

As a novel finding we proved that both time domain and frequency domain parameters of HRV were significantly reduced in PBC patients compared to controls. Each patient had at least one abnormal parameter of HRV.

Results of cardiovascular reflex tests and HRV parameters are presented in Table 1. The heart rate response to deep breathing ($P = 0.001$), as well as to standing ($P = 0.03$) and Valsalva manoeuvre ($P = 0.01$) was significantly lower in PBC patients than in age matched control subjects. A more profound decrease of systolic blood pressure after standing ($P = 0.03$) was found in patients compared to healthy controls. By HRV analysis most of the time-domain indices were significantly lower in patients than in controls (PNN50: $P = 0.0008$; HRVTI: $P = 0.004$; RMSSD: $P = 0.006$ and SDNN: $P = 0.015$). PBC patients also showed significantly lower total power ($P = 0.0001$), power of LF band ($P = 0.00007$) and of HF band ($P = 0.004$).

Peripheral sensory nerve function

At least one abnormal sensory parameter was detected in 13 patients (54%), of whom 12 had hyperaesthetic type, and only one had hypoaesthetic type sensory nerve dysfunction. Among patients with sensory neuropathy the lower extremities were affected in all 13 patients, while 3 patients had abnormal CPT values at upper extremities testing. Lower CPT values, indicating hyperaesthesia, were found in PBC patients compared with age matched controls at peroneal nerve testing at all three frequencies ($P < 0.01$) as well as at median nerve testing at 250 Hz ($P = 0.03$). The CPT values of patients and controls are shown in Table 2.

Table 1 Results of cardiovascular reflex tests and 24-h heart rate variability (HRV) parameters in patients with PBC and age matched healthy controls

	Patients with PBC (n = 24)	Age-matched controls (n = 20)	P value
Cardiovascular reflex tests			
Deep breathing test (beats/min)	11.3 (4.4)	17.5 (6.6)	0.001
30/15 ratio	1.18 (0.1)	1.29 (0.2)	0.03
Valsalva ratio	1.32 (0.1)	1.48 (0.2)	0.01
Orthostatic test (mmHg)	-7.1 (8.6)	-1.5 (3.7)	0.03
Handgrip test (mmHg)	20.4 (8.1)	22.3 (4.4)	NS
Time domain parameters of HRV			
SDNN (ms)	119 (42)	151 (37)	0.015
SDANN (ms)	142 (102)	165 (66)	NS
RMSSD (ms)	23 (10)	38 (22)	0.006
PNN50 (%)	2.4 (4)	11 (10)	0.0008
HRVTI	28 (8)	38 (13)	0.004
Frequency domain parameters of HRV			
TP (ms ²)	1506 (701)	4032 (2787)	0.0001
LF (ms ²)	299 (176)	1213 (977)	0.00007
HF (ms ²)	150 (148)	525 (565)	0.004

Table 2 Current perception threshold (CPT) values in PBC patients and controls at median and peroneal nerve testing at three different frequencies

	Patients with PBC (n = 24)	Age-matched controls (n = 20)	P value
CPT (mA)-Median nerve			
2000 Hz	2.45 (0.75)	2.94 (0.87)	0.076
250 Hz	0.81 (0.33)	1.10 (0.46)	0.030
5 Hz	0.42 (0.23)	0.50 (0.17)	0.242
CPT (mA)-Peroneal nerve			
2000 Hz	2.91 (0.71)	3.61 (0.66)	0.005
250 Hz	1.01 (0.39)	1.40 (0.26)	0.002
5 Hz	0.68 (0.40)	1.06 (0.28)	0.004

Associations of autonomic function with clinical and biochemical characteristics

After adjustment for age, the longer duration of the disease was associated with less prominent increase of diastolic blood pressure during sustained handgrip test ($r = -0.52$, $P = 0.01$). Duration of the disease also correlated with reduced SDNN and SDANN ($r = 0.47$ and $r = -0.45$, $P < 0.05$, for both). The severity of PBC (stage) was found to negatively correlate with lower HRVTI ($r = -0.6$, $P = 0.01$) and lower SDANN ($r = -0.49$, $P = 0.04$) as well.

Partial correlation analysis revealed that lower prothrombin activity was associated with lower heart rate response to standing ($r = 0.79$, $P = 0.006$) as well as to deep breathing ($r = 0.63$, $P = 0.04$). The serum albumin positively correlated with SDNN and HRVTI ($r = 0.47$ and 0.57 , $P < 0.05$, for both). Serum AST and ALT levels negatively correlated with SDNN ($r = -0.54$, $P = 0.01$, for both). Positive correlations of SDNN ($r = 0.62$, $P = 0.004$) and Valsalva ratio ($r = 0.51$, $P = 0.02$) with serum triglyceride levels were found. These relationships remained significant after age adjustment.

Correlations of peripheral sensory nerve function with clinical and chemical characteristics

Negative correlations of serum ALT with CPT values at median nerve testing at 250 Hz ($r = -0.56$, $P = 0.005$) as well as with CPT at peroneal ($r = -0.48$, $P = 0.03$) and median nerve ($r = -0.45$, $P = 0.02$) at 5 Hz were revealed. AST and ALP levels were inversely related to CPT values at peroneal nerve testing at all three frequencies, as well as to those at median nerve testing at 250 Hz and 5 Hz. An inverse relationship was also found

between serum bilirubin levels and CPT values at median nerve testing at 5 Hz ($r = -0.43$, $P = 0.04$). None of these relationships was altered by adjustment for age.

Interestingly no correlation was found between peripheral sensory nerve function and duration and severity of PBC. Furthermore, no association was found between sensory nerve function and serum lipid levels, prothrombin activity and serum albumin levels.

Associations between autonomic and peripheral sensory nerve function

Reduced total power was associated with lower CPT values testing median nerve at 250 Hz ($r = 0.69$, $P = 0.0001$), and at 5 Hz ($r = 0.62$, $P = 0.002$), as well as with those testing peroneal nerve at 2000 Hz ($r = 0.53$, $P = 0.01$). HF-power was positively related to CPT values at peroneal nerve testing at 2000 Hz ($r = 0.51$, $P = 0.01$), LF-power correlated positively with CPT values testing median nerve at 250 ($r = 0.53$, $P = 0.01$), as well as at 5 Hz ($r = 0.47$, $P = 0.03$). A significant positive correlation was observed between the SDNN and the CPT values testing the median nerve at 2000 Hz ($r = 0.60$, $P = 0.003$), as well as at 250 Hz ($r = 0.53$, $P = 0.01$) and at 5 Hz ($r = 0.50$, $P = 0.02$). Lower SDANN values were associated with lower CPT values at the median nerve at 2000 Hz ($r = 0.52$, $P = 0.01$). The PNN50 values correlated positively with CPT values testing the peroneal nerve at 2000 Hz ($r = 0.50$, $P = 0.02$) and the beat-to-beat variation was also positively related to CPT values at the peroneal nerve at 250 Hz ($r = 0.47$, $P = 0.02$), even after adjustment for age.

DISCUSSION

Somatic neuropathy accompanying advanced stage primary biliary cirrhosis, was described as early as 1964 by Walker and Thomas^[21]. In the last two decades, autonomic neuropathy has been found as a common complication of this type of liver disease^[1,16,17,22]. The poor prognosis of neuropathy has been widely known even in chronic liver diseases, primarily as regards the impairment of autonomic functions^[2,3]. During the 4-year follow-up study of Hendrickse *et al.*, mortality was 30% among patients with autonomic neuropathy and 6% in those without AN^[2]. As suggested by the description of clinical features, the prognosis of sensory neuropathy was rather poor. In their 14-year follow-up study conducted on diabetic patients, Coppini *et al.* showed that sensory neuropathy was an independent predictor for mortality^[23].

There are only few studies on the prevalence of autonomic and sensory neuropathy in PBC, and the characteristics of the study population have a strong impact on prevalence data. Nevertheless, our data are consistent with previous findings showing that autonomic and sensory neuropathy were frequent complications in patients with PBC^[1,16,17].

Sensory neuropathy has also been found as a common complication in chronic liver diseases, yet there are no data on its prognostic importance.

Although many studies have been published on autonomic and sensory neuropathy in chronic liver diseases, some of the results were conflicting. To our knowledge this is the first study in PBC conducted on the evaluation of autonomic function assessed both by the standard cardiovascular reflex tests and by 24-h HRV analysis. HRV analysis could indicate the synchronic impairment of the parasympathetic and sympathetic systems in PBC. To date only one systematic study has assessed the factors that predispose to autonomic and sensory nerve dysfunction in PBC^[17], but in their study the autonomic function was only evaluated by the standard tests. We confirmed previous data showing that autonomic dysfunction was related to the severity of liver damage^[1,14,15,24], contrary to Oliver^[25] who did not show similar results. As a novel finding not only the severity, but also the duration of PBC was related to autonomic dysregulation. It would be worthy to investigate neuropathy in asymptomatic PBC population^[26]. We have also found a close correlation between decreased serum albumin and prothrombin activity with the autonomic dysfunction, which differed from the data of Lazzeri *et al.*^[5], but these results were consistent with two other studies^[3,15]. Moreover, in our study the serum AST and ALT levels were inversely related to the autonomic function. The markers of cholestasis did not correlate with the autonomic function, in keeping with the data of Coelho^[15]. An interesting finding in our study was that lower serum triglyceride level was associated with impaired autonomic function. This is of interest, since PBC related somatic neuropathy was originally attributed to lipid deposition^[21]. Later, however, no significant association of hyperlipidaemia with autonomic and sensory neuropathy was demonstrated^[17], which is consistent with our data regarding the serum cholesterol level.

Sensory impairment might involve both large myelinated fibres and small sensory fibres as demonstrated by Kempler^[16]. These data are consistent with the present results showing abnormal CPT values at all types of sensory fibres, testing both median and peroneal nerves. Abnormal CPT values were more frequent on the lower extremities, which were in accordance with previous observations that longer fibres were damaged earlier^[27]. The present data extended previous results by analysing which type of sensory nerve dysfunction was specific for PBC. Our data provide the first evidence that hyperaesthesia is a feature of peripheral sensory neuropathy in PBC. In this phase of neuropathy the degeneration and regeneration of non-myelinated small fibres occur concomitantly. These processes

were inaccessible to earlier methods for sensory testing, but the neurometer could permit the detection of this early phase of sensory nerve impairment^[28]. Evaluating the current perception threshold by neurometer seems a simple and comprehensive way of assessing even early abnormalities of peripheral sensory nerve function in patients with PBC. Recent studies have demonstrated that itching, a characteristic symptom in PBC, could be evoked by activation of peripheral unmyelinated C-fibers^[29,30]. In our study, patients with hyperaesthesia at 5 Hz had itching. Considering that 5 Hz CPT values demonstrate the unmyelinated C-fibre function, our results support the possible role for unmyelinated C-fibre damage in hyperaesthesia in the pathogenesis of pruritus in PBC.

Serum bilirubin and albumin were found to be associated with peripheral nerve function in the only one study published on correlation of sensory nerve dysfunction in PBC^[17]. Our results confirmed these data regarding serum bilirubin, but not serum albumin. Moreover, in our study not only elevated serum bilirubin, but higher serum AST, ALT and ALP were also related to lower CPT values.

Our results were consistent with those of Hendrickse^[17], showing that peripheral sensory nerve function correlates with cardiovascular autonomic function in patients with PBC. Prospective studies are required to evaluate the prognostic importance of sensory neuropathy in PBC.

In summary, autonomic and sensory nerve dysfunctions are frequent complications in patients with PBC and seem to be mutually related. The novel findings of reduced time and frequency domain parameters of 24-h HRV analysis indicate the synchronic impairment of parasympathetic and sympathetic systems. HRV analysis is more sensitive than standard cardiovascular tests for detecting autonomic neuropathy. This study provides the first evidence that hyperaesthesia involving all types of fibres is characteristic for sensory neuropathy in PBC. Hyperaesthesia of unmyelinated fibres might partly be responsible for itching, a characteristic symptom in PBC. Our data suggest that autonomic neuropathy is related to the severity and duration of liver disease as well as to the markers of hepatocellular dysfunction.

REFERENCES

- 1 Szalay F, Marton A, Keresztes K, Hermanyi ZS, Kempler P. Neuropathy as an extrahepatic manifestation of chronic liver diseases. *Scand J Gastroenterol* 1998; **228**(Suppl): 130-132
- 2 Hendrickse MT, Thuluvath PJ, Triger DR. The natural history of autonomic neuropathy in chronic liver disease. *Lancet* 1992; **339**: 1462-1464
- 3 Fleckenstein JF, Frank S, Thuluvath PJ. Presence of autonomic neuropathy is a poor prognostic indicator in patients with advanced liver disease. *Hepatology* 1996; **23**: 471-475
- 4 Valensi P. Diabetic autonomic neuropathy: what are the risks? *Diabetes Metab* 1998; **24**(Suppl 3): 66-72
- 5 Lazzeri C, La Villa G, Laffi G, Vecchiarino S, Gambilonghi F, Gentilini P, Franchi F. Autonomic regulation of heart rate and QT interval in nonalcoholic cirrhosis with ascites. *Digestion* 1997; **58**: 580-586
- 6 Moller S, Winberg N, Henriksen JH. Noninvasive 24-hour ambulatory arterial blood pressure monitoring in cirrhosis. *Hepatology* 1995; **22**: 88-95
- 7 Kempler P, Varadi A, Szalay F. Autonomic neuropathy and prolongation of QT-interval in liver disease. *Lancet* 1992; **340**: 318
- 8 Fischberger SB, Pittman NS, Rossi AF. Prolongation of the QT interval in children with liver failure. *Clin Cardiol* 1999; **22**: 658-660
- 9 Kempler P, Toth T, Szalay F. May autonomic neuropathy play a role in the development of hyperdynamic circulation and portal hypertension in chronic liver diseases? (Hypothesis). In: Aquino AV, Picdad FF, Sulit YQM (eds). *23rd Congress of the International Society of Internal Medicine Monduzzi Editore Bologna Italy* 1996: 251-254

- 10 **La Rovere MT**, Bigger JT, Marcus FI, Mortara A, Schwartz PJ. Baroreflex sensitivity and heart-rate variability in prediction of total cardiac mortality after myocardial infarction ATRAMI (Autonomic Tone and Reflexes After Myocardial Infarction) Investigators. *Lancet* 1998; **351**: 478-484
- 11 No author guideline: Heart rate variability: standards of measurement, physiological interpretation, and clinical use. Task Force of the European Society of Cardiology and the North American Society of Pacing and Electrophysiology. *Circulation* 1996; **93**: 1043-1065
- 12 **Barron SA**, Rogovski Z, Kanter Y, Hemli Y. Parasympathetic autonomic neuropathy in diabetes mellitus: the heart is denervated more often than the pupil. *Electromyogr Clin Neurophysiol* 1994; **34**: 467-469
- 13 **Dillon JF**, Plevris JN, Nolan J, Ewing DJ, Neilson JM, Bouchier IA, Hayes PC. Autonomic function in cirrhosis assessed by cardiovascular reflex tests and 24-hour heart rate variability. *Am J Gastroenterol* 1994; **89**: 1544-1547
- 14 **Fleisher LA**, Fleckenstein JF, Frand SM, Thuluvath PJ. Heart rate variability as a predictor of autonomic dysfunction in patients awaiting liver transplantation. *Dig Dis Sci* 2000; **45**: 340-344
- 15 **Coelho L**, Saraiva S, Guimaraes H, Freitas D, Providencia LA. Autonomic function in chronic liver disease assessed by Heart Rate Variability Study. *Rev Port Cardiol* 2001; **20**: 25-36
- 16 **Kempler P**, Varadi A, Kadar E, Szalay F. Autonomic and peripheral neuropathy in primary biliary cirrhosis: evidence of small sensory fibre damage and prolongation of the QT interval. *J Hepatol* 1994; **21**: 1150-1151
- 17 **Hendrickse MT**, Triger DR. Autonomic and peripheral neuropathy in primary biliary cirrhosis. *J Hepatol* 1993; **19**: 401-407
- 18 **Szalay F**. Treatment of primary biliary cirrhosis. *J Physiol Paris* 2001; **95**: 407-412
- 19 **Ewing DJ**, Martyn CN, Young RJ, Clarke BF. The value of cardiovascular autonomic function tests: 10 years experience in diabetes. *Diabetes Care* 1985; **8**: 491-498
- 20 **Pitei DL**, Watkins PJ, Stevens MJ, Edmonds ME. The value of the NEUROMETER® CPT in assessing diabetic neuropathy by measurement of the current perception threshold. *Diabetic Med* 1994; **11**: 872-876
- 21 **Walker JG**, Thomas PK. Xanthomatous neuropathy in primary biliary cirrhosis. *Tijdschr Gastroenterol* 1964; **48**: 84-86
- 22 **Thuluvath PJ**, Triger DR. Autonomic neuropathy and chronic liver disease. *Q J Med* 1989; **72**: 737-747
- 23 **Coppini DV**, Bowtell PA, Weng C, Young PJ, Sönksen PH. Showing neuropathy is related to increased mortality in diabetic patients – a survival analysis using an accelerated failure time model. *J Clin Epidemiol* 2000; **53**: 519-523
- 24 **Bajaj BK**, Agarwal MP, Ram BK. Autonomic neuropathy in patients with hepatic cirrhosis. *Postgrad Med J* 2003; **79**: 408-411
- 25 **Oliver MI**, Miralles R, Rubies-Prat J, Navarro X, Espadaler JM, Sola R, Andreu M. Autonomic dysfunction in patients with non-alcoholic chronic liver disease. *J Hepatol* 1997; **26**: 1242-1248
- 26 **Jiang XH**, Zhong RQ, Fan XY, Hu Y, An F, Sun JW, Kong XT. Characterization of M2 antibodies in asymptomatic Chinese population. *World J Gastroenterol* 2003; **9**: 2128-2131
- 27 **Oh SJ**. Clinical Electromyography: Nerve conduction studies. In: Oh SJ ed. Nerve conduction in polyneuropathies. *Baltimore William Wilkins* 1993: 579-591
- 28 **Kempler P**. Neurometer. In: Kempler P ed. Neuropathies. Pathomechanism, clinical presentation, diagnosis therapy. *Budapest Springer* 2002: 74-76
- 29 **Bergasa NV**. Pruritus and fatigue in primary biliary cirrhosis. *Clin Liver Dis* 2003; **7**: 879-900
- 30 **Stander S**, Steinhoff M, Schmelz M, Weisshaar E, Metzger D, Luger T. Neurophysiology of pruritus: cutaneous elicitation of itch. *Arch Dermatol* 2003; **139**: 1463-1470

Edited by Wang XL Proofread by Chen WW and Xu FM

Expression of mucins and E-cadherin in gastric carcinoma and their clinical significance

Hong-Kai Zhang, Qiu-Min Zhang, Tie-Hua Zhao, Yuan-Yuan Li, Yong-Fen Yi

Hong-Kai Zhang, Tie-Hua Zhao, Department of Pathology, Fuxing Hospital, Capital University of Medical Sciences, Beijing 100038, China

Qiu-Min Zhang, Shenzhen Nanling Hospital, Shenzhen 518123, Guangdong Province, China

Yuan-Yuan Li, Yong-Fen Yi, Department of Pathology, Chongqing Medical University, Chongqing 400016, China

Supported by the Science Research Foundation of the Health Bureau of Chongqing Municipality, No.2000-48

Correspondence to: Dr. Yong-Fen Yi, Department of Pathology, Chongqing Medical University, Chongqing 400016, China. yiyongfen1953@yahoo.com.cn

Telephone: +86-23-68485789

Received: 2004-01-02 **Accepted:** 2004-02-12

Abstract

AIM: To investigate the expression of three types of mucin (MUC1, MUC2, MUC5AC) and E-cadherin in human gastric carcinomas and their clinical significance.

METHODS: Ninety-four gastric cancer specimens were classified according to WHO criteria and detected by immunohistochemical assay of expression of mucins and E-cadherin.

RESULTS: The positive expression rates of MUC1, MUC2, MUC5AC and E-cadherin were 82% (77/94), 84% (79/94), 40% (38/94) and 56% (53/94) respectively. MUC1 expression was significantly correlated with the types of cancer (the positive rates of MUC1 in well and moderately differentiated tubular adenocarcinoma, poorly differentiated adenocarcinoma, signet-ring cell carcinoma and mucinous carcinoma were 91%, 87%, 71%, 71%, respectively, $P < 0.05$), age of patients (the positive rates of it among the people who are younger than 40 years, between 40-60 years and over 60 year were 74%, 81%, 89%, $P < 0.05$), lymph nodes involvement (the positive rates in the non-interfered group and the interfered group were 78%, 85%, $P < 0.05$) and tumor size (the positive rates in the tumors with the size less than 3 cm, 3-6 cm and larger than 6 cm were 69%, 92%, 69%, $P < 0.05$); MUC2 expression was significantly associated with types of cancers and had the strongest expression in mucinous carcinomas (the positive rates of MUC2 in well and moderately differentiated tubular adenocarcinoma, poorly differentiated adenocarcinoma, signet-ring cell carcinoma and mucinous carcinoma were 94%, 70%, 81%, 100%, $P < 0.05$), but it had no obvious relation to age, gender, tumor location, lymph nodes involvement, depth of invasion and metastasis to extra-gastric organs ($P > 0.05$); MUC5AC expression was not related to any of the characteristics investigated except that it had relation to gender, whereas MUC5AC showed the tendency to higher expression in less invasive lesions and lower expression in advanced stage cancers ($P > 0.05$); No significant difference was found for E-cadherin expression. There were strong positive relationships between the expression of MUC1 and E-cadherin, MUC2 and E-cadherin, MUC1 and MUC2 ($R = 0.33$, $R = 0.22$, $R = 0.32$, respectively, $P < 0.05$). According to the COX proportional hazards model, older patients,

involvement of lymph nodes, different types of gastric cancer and MUC2 expression were significantly associated with poorer outcome of gastric carcinoma patients ($\beta = 0.08$, $\beta = 3.94$, $\beta = 1.33$, $\beta = 0.75$, respectively, $P < 0.05$).

CONCLUSION: MUC1 and MUC2 are good markers of different types of gastric cancer. MUC2 is especially a good marker of mucinous carcinoma. MUC1, MUC2 may interfere with the function of E-cadherin in gastric carcinomas, and have synergic effect on progression of gastric cancers.

Zhang HK, Zhang QM, Zhao TH, Li YY, Yi YF. Expression of mucins and E-cadherin in gastric carcinoma and their clinical significance. *World J Gastroenterol* 2004; 10(20): 3044-3047 <http://www.wjgnet.com/1007-9327/10/3044.asp>

INTRODUCTION

Mucins, the high molecular weight glycoproteins that contain oligosaccharides, are the major components of the mucous gel covering the surface of epithelial tissue. Their main functions are thought to be lubrication and protection of the epithelial surface^[1,2]. To date, at least thirteen mucins have been found^[3].

MUC1, an epithelial mucin glycoprotein, is highly expressed in lactating mammary glands^[4]. Under pathological conditions, such as colon adenocarcinoma and pancreas adenocarcinoma or stomach adenocarcinoma, MUC1 would change its expression fashion and rate^[5]. MUC2, a gel-forming mucin, highly expresses in normal intestinal tissues and has no expression in normal gastric mucosa. However, it had *de novo* expression in stomach when the mucosa underwent metaplasia and carcinoma^[6]. MUC5AC, a gastric type mucin in gastric cardia and body mucosa, is decreased when the tissue has cancers^[7]. E-cadherin is a calcium-dependent cell-cell adhesion molecule and its expression decreases in the carcinoma tissues thus contributing to cancer progression and correlate with patients' prognosis^[8].

Despite many studies have been done in gastric carcinoma tissue, the results are still in contradiction. Some reported that MUC1 could well predict the patients' prognosis, while others thought not. MUC2 showed the same result^[9,10]. MUC5AC is a relatively less studied molecule, and its expression decreases in advanced cancers than in early cancers^[11]. Study on E-cadherin also remains contradictory^[12,13]. What's more, few studies have been done about their relationships, especially between E-cadherin and the mucins. The present study was designed to provide some useful information on these molecules.

MATERIALS AND METHODS

Materials

Ninety-four patients with gastric adenocarcinomas confirmed pathologically and underwent gastrectomy in our hospital from January 1989 to December 2000 were Systemically selected for the study. Patients' age, gender, tumor location, depth of invasion, local lymph nodes involvement, metastasis, tumor size were all obtained from the original records. Specimens were

histologically classified according to WHO criteria by two experienced pathologists. Among these subjects, there were 33 moderately and highly-differentiated tubular carcinomas, 23 poorly differentiated adenocarcinomas, 31 signet-ring cell carcinomas and 7 mucinous carcinomas. There were 64 male and 30 female patients with a mean age of 52.1 ± 12.1 years (range 25-75 years). The mean tumor size was 4.5 ± 2.0 cm in diameter (range 1-10 cm). A total of 48 patients provided full information during follow-up.

Reagents and methods

Antibodies against MUC1, MUC2 and MUC5AC were purchased from Shenzhen Jingmei Biotechnology, Inc., and the antibody against E-cadherin was from Fujian Maixin Co, Ltd. All the 94 formalin-fixed, paraffin-embedded specimens were sliced sequentially with a thickness of 4 μ m. According to the protocol, these tissue sections were dewaxed, rehydrated, incubated with 30 mL/L hydrogen peroxide in methanol for 30 min to block endogenous peroxidase, and then washed with PBS (phosphate buffered saline, pH 7.4). After that, they were incubated with non-immunized horse serum for 30 min at room temperature, washed again, and incubated with the specific antibodies overnight at 4 °C or 1 h at 37 °C. They were washed again, incubated with the secondary antibody (Biotin labeled goat anti-rabbit antibody) and streptavidin-biotin peroxidase for 30 min separately, visualized with 3,3'-diaminobenzidine tetra-hydrochloride and H₂O₂, counterstained with haematoxylin. Primary antibodies were replaced with PBS buffer as negative control.

In order to obtain a more precise relation between mucins and the clinical indicators, a semiquantitative analysis was performed to evaluate positively stained cells in carcinoma tissues as +++, ++, + or -. We examined 10 fields of each cancerous tissue at high magnification ($\times 400$) and scored the intensity of color as 0 for non-stained, 1 for the color of yellow, 2 for brown-yellow, 3 for brown; the rate of positive cell was judged as negative (0) if it was less than 5%, 1 for 5-25%, 2 for 26-50%, 3 for over 50%. The mean intensity scores were multiplied by the rate scores. Negative group (-) was defined when the result was 0, 1-3 was mild-positive (+), 4-5 was moderate-positive (++) and equal or greater than 6 was strong positive (+++).

Statistical analysis

χ^2 test, the hazards proportional analysis (COX) and the correlation analysis were used to determine differences between groups using SPSS 10.0 software. Statistical significance was established at $P < 0.05$.

RESULTS

Expression and distribution of MUC1, MUC2, MUC5AC and E-cadherin

The positivity rate of MUC1 was 82% in the cancerous tissues. It expressed in the cytoplasm diffusely or stained on the membrane of the cells. There were significant differences in its expression among different types of the cancer ($P < 0.05$) with the highest expression rate in well and moderately differentiated tubular

Table 1 protein expression in gastric carcinoma

	n	MUC1				MUC2				MUC5AC				E-cadherin			
		-	+	++	+++	-	+	++	+++	-	+	++	+++	-	+	++	+++
Types of cancer		$P = 0.005$				$P = 0.001$				NS				NS			
WMDTA	33	3	2	3	25	2	3	7	21	21	6	0	6	10	8	5	10
PDA	23	3	11	2	7	7	6	5	5	15	4	1	3	11	5	3	4
SRCC	31	9	10	2	10	6	9	10	6	14		5	8	15	8	4	4
MC	7	2	1	0	4	0	0	0	7	6	0	0	1	5	2	0	0
Age(yr)		$P = 0.03$				NS				NS				NS			
≤40	19	5	4	2	8	3	6	5	5	12	2	2	3	10	7	1	1
>40, ≤60	48	9	18	1	20	10	9	10	19	26	10	3	9	20	9	8	11
>60	27	3	2	4	18	3	2	7	15	18	2	1	6	11	7	3	6
Sex		NS				NS				$P = 0.02$				NS			
male	64	13	14	4	33	10	10	14	30	42	5	3	14	28	17	7	12
female	30	4	10	3	13	6	7	8	9	14	9	3	4	13	6	5	6
Location		NS				NS				NS				NS			
Upper 1/3	13	0	4	1	8	1	2	0	10	12	0	0	1	3	4	1	5
Middle 1/3	23	6	6	0	11	4	3	6	10	12	3	2	6	11	7	2	3
Lower 1/3	58	11	14	6	27	11	12	16	19	32	11	4	11	27	12	9	10
Invasion		NS				NS				NS				NS			
within mucosa & sub-mucosa	7	2	1	0	4	3	2	0	2	5	0	0	2	4	1	0	2
Muscular layer	19	5	7	1	6	5	4	6	4	9	1	3	6	9	3	5	2
Serosa	68	10	16	6	36	8	11	16	33	42	13	3	10	28	19	7	14
Metastasis to LN		$P = 0.031$				NS				NS				NS			
No	40	9	14	10	7	9	9	11	11	25	4	3	8	20	8	5	7
Yes	54	8	10	7	29	7	8	11	28	31	10	3	10	21	15	7	11
Metastasis to other organs		NS				NS				NS				NS			
No	70	14	19	7	30	13	12	18	27	42	7	5	16	32	19	8	11
Yes	24	3	5	0	16	3	5	4	12	14	7	1	2	9	4	4	7
Tumor size (cm)		$P = 0.044$				NS				NS				NS			
≤3	29	9	4	4	12	9	6	6	8	17	5	0	7	12	7	3	7
3-6	52	4	17	3	28	5	10	15	22	29	9	5	9	20	15	6	11
>6	13	4	3	0	6	2	1	1	9	10	0	1	2	9	1	3	0

NS: no significant difference; WMDTA: well and moderately differentiated tubular adenocarcinoma; PDA: Poorly differentiated adenocarcinoma; SRCC: Signet-ring cell; MC: mucinous carcinoma; LN: lymph node.

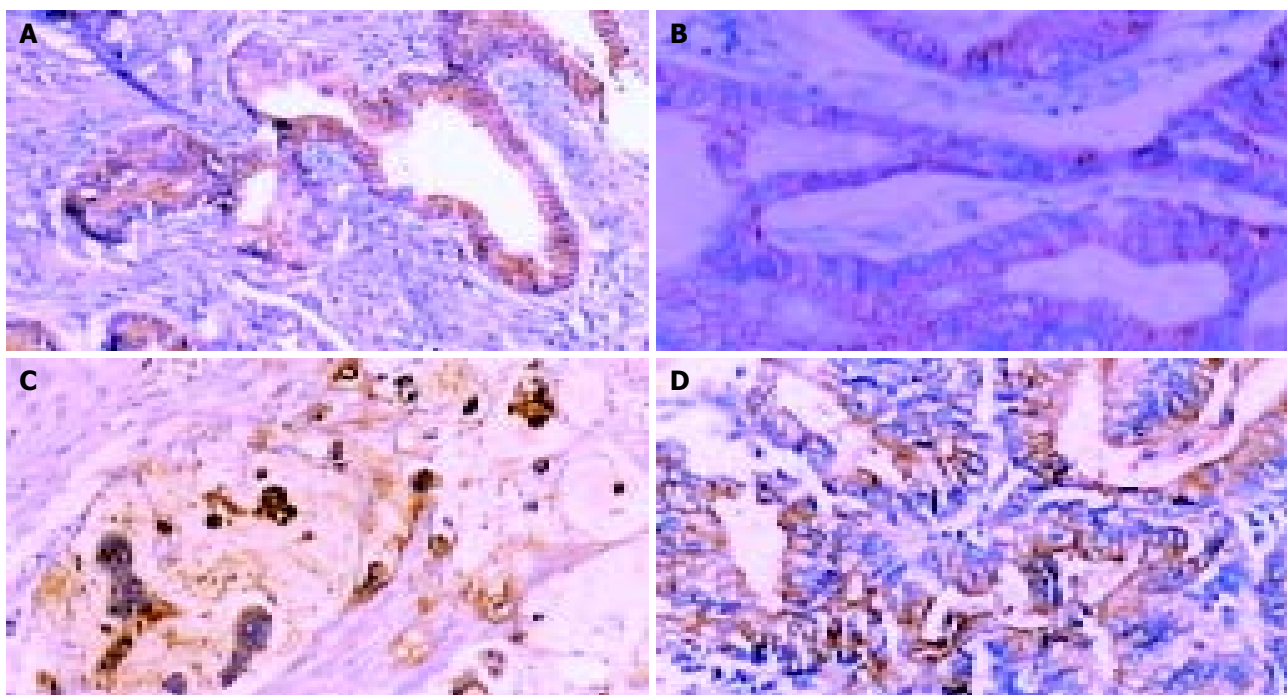


Figure 1 Results of immunohistochemical staining in gastric cancers (original magnification SP $\times 400$). A: MUC5AC expression; B: E-cadherin expression; C: MUC1 expression; D: MUC2 expression.

adenocarcinomas (91%). Moreover, its expression level had significant relationship with patients' age, local lymph nodes involvement and tumor size ($P < 0.05$). MUC2 had a positive expression rate of 84%, with the highest expression level in mucinous carcinomas (100%) and lowest expression level in signet-ring cell carcinoma (19%). Furthermore, it also showed significant differences in expression among different types of cancer ($P < 0.05$). MUC5AC had a positive expression rate of 40% and the lowest expression level in mucinous carcinoma (14%), but no significant differences in expression levels among different types of cancer were found ($P > 0.05$). It expressed mainly in the cytoplasm. E-cadherin had a positive expression rate of 56% with the highest expression in well and moderately differentiated cancers (70%) and the lowest in mucinous type (29%). There was no significant difference of expression level among different types of cancer ($P > 0.05$). Its positive expression was on the membrane and in the cytoplasm of cancerous cells. The expression of MUC2, MUC5AC, E-cadherin were not significantly different with regards to clinicopathological characteristics (Table 1, Figure 1).

Relationship between proteins' expression and prognostic factors

There were significantly positive relationships between MUC1 and MUC2, MUC1 and E-cadherin, MUC2 and E-cadherin ($P < 0.05$). According to COX analysis, patients' age, lymph node involvement, types of the cancer and the level of MUC2 expression were the factors related to patients' survival after operation (figures not shown).

DISCUSSION

We confirmed that mucin expression was associated with differentiation characteristics of gastric carcinoma. MUC1 was expressed in most of the studied gastric cancerous specimens (82%), being consistent with other studies^[10]. MUC1 expression related to clinical characteristics such as patients' age, tumor size and local lymph nodes involvement. MUC1 expressed higher in older patients with larger tumor or with more lymph nodes involvement. On the other hand, though the expression

of MUC1 was not significantly associated with the metastasis and depth of invasion ($P > 0.05$), it still had the tendency toward higher expression in advanced stage of cancer. However, we failed to find that MUC1 had the prognostic role in gastric cancer patients, which is different with Utsunomiya's conclusion^[9], but consistent with Reis's conclusion^[14]. These contradictory results might be due to our relatively small number of follow-up patients after operation.

MUC2, the intestinal mucin, expressed in most of the studied cases (86%), higher than that in other studies^[15]. However our result was in accordance with other results concerning its overwhelming expression in mucinous carcinomas^[15,16]. Contradictory to some reports that MUC2 indicated good prognosis^[9], our study found that MUC2 could predict poor outcome. Our *in vitro* study used anti-sense oligonucleotide of MUC2 to inhibit the growth of gastric cancer cells, while Sternberg used the anti-sense oligonucleotide of MUC2 in colon cells *in vitro* and *in vivo* and found that it decreased the adherence ability of cells to E-selectin and resulted in inhibition of liver metastasis^[17]. Both supported our conclusion that MUC2 might contribute to gastric cancer progress.

MUC5AC was thought to be gastric mucin and expressed higher in early stage of cancers than in the advanced stage^[18]. MUC5AC rarely expressed in mucinous carcinoma except in one case. Between different sex groups, MUC5AC had significant difference ($P < 0.05$).

E-cadherin is a calcium-dependent molecule, and acts as a tumor-inhibitory factor. Some studies have shown that the lower expression level it had, the faster the tumor progressed^[12]. But we could not draw a conclusion like this despite the tendency shown at present. While we noted its highest expression in the well and moderately differentiated tubular carcinoma which supported the view on its contribution to tubular structure formation^[19].

Although some studies showed that MUC1 expression in gastric cancers was negatively correlated with the expression of E-cadherin^[20], we found the positive relationships between them, what's more, the correlation of MUC1, MUC2 and E-cadherin were first studied by us. Both MUC1 and MUC2 might contribute to the progress of gastric cancer, and they might

restrain the role of E-cadherin.

In summary, MUC1 may contribute to gastric cancers progress, larger tumor size and metastasis to lymph nodes, at the same time, it may inhibit E-cadherin. MUC2 had the same role as MUC1, besides, it may be an indicator for prognosis of gastric cancer patients and good marker for mucinous cancers. E-cadherin could not be used a tangible marker to indicate gastric cancers progress but may play a role in the tubular formation. The role of MUC5AC in gastric cancers needs more investigation.

ACKNOWLEDGEMENTS

The authors express their gratitude to Dr. Jie Chen and Dr. Fu-Sheng Liu for their precious advice and suggestions. We thank Mr. Da-Hai Sun for his assistance in preparation of the manuscript.

REFERENCES

- 1 **Moniaux N**, Escande F, Porchet N, Aubert JP, Batra SK. Structural organization and classification of the human mucin genes. *Front Biosci* 2001; **6**: D1192-1206
- 2 **Corfield AP**, Myerscough N, Longman R, Sylvester P, Arul S, Pignatelli M. Mucins and mucosal protection in the gastrointestinal tract: new prospects for mucins in the pathology of gastrointestinal disease. *Gut* 2000; **47**: 589-594
- 3 **Williams SJ**, Wreschner DH, Tran M, Eyre HJ, Sutherland GR, McGuckin MA. Muc13: a novel human cell surface mucin expressed by epithelial and hemopoietic cells. *J Biol Chem* 2001; **276**: 18327-18336
- 4 **Gendler SJ**, Lancaster CA, Taylor-Papadimitriou J, Duhig T, Peat N, Burchell J, Pemberton L, Lalani EN, Wilson D. Molecular cloning and expression of human tumor-associated polymorphic epithelial mucin. *J Biol Chem* 1990; **265**: 15286-15293
- 5 **Seregini E**, Botti C, Massaron S, Lombardo C, Capobianco A, Bogni A, Bombardieri E. Structure, function and gene expression of epithelial mucins. *Tumori* 1997; **83**: 625-632
- 6 **Ho SB**, Shekels LL, Toribara NW, Kim YS, Lyftogt C, Cherwitz DL, Niehans GA. Mucin gene expression in normal, preneoplastic, and neoplastic human gastric epithelium. *Cancer Res* 1995; **55**: 2681-2690
- 7 **Guyonnet Duperat V**, Audie JP, Debailleul V, Laine A, Buisine MP, Galiegue-Zouitina S, Pigny P, Degand P, Aubert JP, Porchet N. Characterization of the human mucin gene MUC5AC: a consensus cysteine-rich domain for 11p15 mucin genes? *Biochem J* 1995; **305**(Pt 1): 211-219
- 8 **Berx G**, Staes K, van Hengel J, Molemans F, Bussemakers MJ, van Bokhoven A, van Roy F. Cloning and characterization of the human invasion suppressor gene E-cadherin(CDH1). *Genomics* 1995; **26**: 281-289
- 9 **Utsunomiya T**, Yonezawa S, Sakamoto H, Kitamura H, Hokita S, Aiko T, Tanaka S, Irimura T, Kim YS, Sato E. Expression of MUC1 and MUC2 mucins in gastric carcinomas: its relationship with the prognosis of the patients. *Clin Cancer Res* 1998; **4**: 2605-2614
- 10 **Baldus SE**, Zirbes TK, Engel S, Hanisch FG, Monig SP, Lorenzen J, Glossmann J, Fromm S, Thiele J, Pichlmaier H, Dienes HP. Correlation of the immunohistochemical reactivity of mucin peptide cores MUC1 and MUC2 with the histopathological subtype and prognosis of gastric carcinomas. *Int J Cancer* 1998; **79**: 133-138
- 11 **Reis CA**, David L, Carvalho F, Mandel U, de Bolos C, Mirgorodskaya E, Clausen H, Sobrinho-Simes M. Immunohistochemical study of the expression of MUC6 mucin and co-expression of other secreted mucins (MUC5AC and MUC2) in human gastric carcinomas. *J Histochem Cytochem* 2000; **48**: 377-388
- 12 **Gabbert HE**, Mueller W, Schneiders A, Meier S, Moll R, Birchmeier W, Hommel G. Prognostic value of E-cadherin expression in 413 gastric carcinomas. *Int J Cancer* 1996; **69**: 184-189
- 13 **Blok P**, Craanen ME, Dekker W, Tytgat GN. Loss of E-cadherin expression in early gastric cancer. *Histopathology* 1999; **34**: 410-415
- 14 **Reis CA**, David L, Seixas M, Burchell J, Sobrinho-Simoes M. Expression of fully and under-glycosylated forms of MUC1 mucin in gastric carcinoma. *Int J Cancer* 1998; **79**: 402-410
- 15 **Pinto-de-Sousa J**, David L, Reis CA, Gomes R, Silva L, Pimenta A. Mucins MUC1, MUC2, MUC5AC and MUC6 expression in the evaluation of differentiation and clinico-biological behaviour of gastric carcinoma. *Virchows Arch* 2002; **440**: 304-310
- 16 **Hanski C**, Hofmeier M, Schmitt-Graff A, Riede E, Hanski ML, Borchard F, Sieber E, Niedobitek F, Foss HD, Stein H, Riecken EO. Overexpression or ectopic expression of MUC2 is the common property of mucinous carcinomas of the colon, pancreas, breast, and ovary. *J Pathol* 1997; **182**: 385-391
- 17 **Sternberg LR**, Byrd JC, Yunker CK, Dudas S, Hoon VK, Bresalier RS. Liver colonization by human colon cancer cells is reduced by antisense inhibition of MUC2 mucin synthesis. *Gastroenterology* 1999; **116**: 363-371
- 18 **Reis CA**, David L, Nielsen PA, Clausen H, Mirgorodskaya K, Roepstorff P, Sobrinho-Simoes M. Immunohistochemical study of MUC5AC expression in human gastric carcinomas using a novel monoclonal antibody. *Int J Cancer* 1997; **74**: 112-121
- 19 **Correa P**, Shiao YH. Phenotypic and genotypic events in gastric carcinogenesis. *Cancer Res* 1994; **54**(7 Suppl): 1941s-1943s
- 20 **Tanaka M**, Kitajima Y, Sato S, Miyazaki K. Combined evaluation of mucin antigen and E-cadherin expression may help select patients with gastric cancer suitable for minimally invasive therapy. *Br J Surg* 2003; **90**: 95-101

Edited by Chen WW and Zhu LH Proofread by Xu FM

Effect of resveratrol and in combination with 5-FU on murine liver cancer

Sheng-Li Wu, Zhong-Jie Sun, Liang Yu, Ke-Wei Meng, Xing-Lei Qin, Cheng-En Pan

Sheng-Li Wu, Liang Yu, Ke-Wei Meng, Xing-Lei Qin, Cheng-En Pan, Department of Hepatobiliary Surgery, First Hospital of Xi'an Jiaotong University, Xi'an 710061, Shaanxi Province, China
Zhong-Jie Sun, Department of Hepatobiliary Surgery, People's Hospital of Shaanxi Province, Xi'an 710061, Shaanxi Province, China
Supported by Traditional Chinese Medicine Bureau Foundation of Shaanxi Province, No. 2001-035

Correspondence to: Dr. Sheng-Li Wu, Department of Hepatobiliary Surgery, First Hospital of Xi'an Jiaotong University, Xi'an 710061, Shaanxi Province, China. victorywu2000@163.com

Telephone: +86-29-5324009 **Fax:** +86-29-5323536

Received: 2004-01-15 **Accepted:** 2004-02-12

Abstract

AIM: To study the anti-tumor effect of resveratrol and in combination with 5-FU on murine liver cancer.

METHODS: Transplantable murine hepatoma₂₂ model was used to evaluate the anti-tumor activity of resveratrol (RES) alone or in combination with 5-FU *in vivo*. H₂₂ cell cycles were analyzed with flow cytometry.

RESULTS: Resveratrol could inhibit the growth of murine hepatoma₂₂, after the mice bearing H₂₂ tumor were treated with 10 mg/kg or 15 mg/kg resveratrol for ten days, and the inhibition rates were 36.3% ($n = 10$) and 49.3% ($n = 9$), respectively, which increased obviously compared with that in control group (85 ± 22 vs 68 ± 17 , $P < 0.01$). RES could induce the S phase arrest of H₂₂ cells, and increase the percentage of cells in S phase from 59.1% ($n = 9$) to 73.5% ($n = 9$) in a dose-dependent manner ($P < 0.05$). The enhanced inhibition of tumor growth by 5-FU was also observed in hepatoma₂₂ bearing mice when 5-FU was administered in combination with 10 mg/kg resveratrol. The inhibition rates for 20 mg/kg or 10 mg/kg 5-FU in combination with 10 mg/kg resveratrol were 77.4% and 72.4%, respectively, compared with the group of 20 mg/kg or 10 mg/kg 5-FU alone, in which the inhibition rates were 53.4% and 43.8%, respectively ($n = 8$). There was a statistical significance between the combination group and 5-FU group.

CONCLUSION: RES could induce the S phase arrest of H₂₂ cells and enhance the anti-tumor effect of 5-FU on murine hepatoma₂₂ and antagonize its toxicity markedly. These results suggest that resveratrol, as a biochemical modulator to enhance the therapeutic effects of 5-FU, may be potentially useful in cancer chemotherapy.

Wu SL, Sun ZJ, Yu L, Meng KW, Qin XL, Pan CE. Effect of resveratrol and in combination with 5-FU on murine liver cancer. *World J Gastroenterol* 2004; 10(20): 3048-3052
<http://www.wjgnet.com/1007-9327/10/3048.asp>

INTRODUCTION

Liver cancer is common in the world, especially in China^[1-10].

Since the introduction of 5-FU for the treatment of liver cancer, the prognosis of liver cancer patients has been greatly improved. However, the serious side effects of 5-FU restrict its extensive clinical application. Searching for some new types of drugs to substitute or combine with 5-FU is necessary. Recently, scientists have found that resveratrol (3,4,5-trihydroxy-trans-stilbene, RES), a kind of phytoalexin found in root extract of the weed *Polygonum cuaspdatum* and in grape skins as well as red wine, has comprehensive pharmacological effects. Studies demonstrated that RES could alter the synthesis and secretion of lipids and lipoproteins by liver cells, block human platelet aggregation and inhibit the synthesis of proaggregatory and proinflammatory eicosanoids by platelets and neutrophils^[11-15]. Some reports indicate that RES could prevent tumor growth and metastasis in human lung carcinoma, pancreatic cancer, prostate cancer, bronchial epithelium cancer and breast cancer models^[16-20]. The present investigation evaluated the potency of RES and in combination with 5-FU on tumor cell growth and proliferation and on cell cycle distribution in a transplantable murine hepatoma₂₂ model.

MATERIALS AND METHODS

Materials

Resveratrol was purchased from Sigma Co (USA), dissolved and sterilized in dimethyl sulfoxide (DMSO) first and then diluted to the required working concentrations in RPMI 1640 (Gibco, USA) containing 100 mL/L calf serum (Sijiqing Co, Hangzhou, China). Mouse hepatocellular carcinoma cell line H₂₂ was purchased from the Department of Pathology, Fourth Military Medical University. Male BALB/c mice, 6-8 wk old, weighing 20±2 g, were purchased from the Animal Center of Xi'an Jiaotong University.

Suppressive effect of RES on transplanted liver cancer

H₂₂ cells were first subcultured in RPMI 1640 containing 100 mL/L fetal bovine serum, and then washed twice and resuspended in RPMI 1640 culture medium (1×10^{11} /L). About 0.2 mL cell solution (including 2×10^7 cells) was taken and injected into the right groin of 5 Balb/c mice. After 14 d, when the tumors of 3-5 mm in diameter formed in the right groin of these mice, they were taken out and cut into small pieces of 1 mm³ under sterile condition. Fifty Balb/c mice were anesthetized using coeliotomy injection of pentobarbitone (70 mg/kg) and laparotomy was performed. Under sterile condition their middle lobes of liver were punctured to form a 3 mm-long sinus tract and a small piece of tumor tissue was put into each sinus tract. Then these mice were randomly divided into 5 groups: control group, 5-FU group and 3 experimental groups. The experimental groups were injected with RES (dissolved in DMSO and diluted to the working concentration of 25 mmol/L in RPMI 1640 containing 100 mL/L calf serum) at 5, 10 or 15 mg/kg body mass, respectively, while the control group was given the same volume of the solution as for the experimental group without RES and the 5-FU group was injected with 5-FU at 20 mg/kg body mass. Twenty-four hours following liver tumor transplantation, each mouse was injected a corresponding dosage of RES into its abdominal cavity once a day for 10 d. These mice were then

sacrificed on the following day after the last injection. After the maximum diameter and transverse length of tumor were measured, hepatocellular carcinoma tissues were sampled. The tumor volume was calculated by using the formula $V = 1/2$ (maximum diameter \times transverse length²). The suppressive rate of tumor growth was calculated as [(mean V of tumor in control group - mean V of tumor in experimental group)/mean V of tumor in control group] $\times 100\%$.

H₂₂ cell cycle in transplanted liver cancer

Fresh hepatocellular carcinoma tissues with a size of 0.5-0.7 cm³ were washed twice in saline and then single cells were isolated from sampled tissues using 21 g/L citric acid 5 g/L Tween 20 according to the method of Otto^[21]. After this, cells were first washed with PBS (pH 7.4) three times, then adjusted to the density of $1 \times 10^9/L$ in RPMI 1640, and 0.2 mL cell suspension was taken and stained with 0.2 mL PI compound dye for 20 min at room temperature. Then, cell suspension was centrifuged at 800 r/min for 10 min and washed twice in PBS at pH 7.4. Finally, the cells were added to 1 mL PBS followed by slight shaking at room temperature and cell cycle analysis was performed using flow cytometer (Coulter, Epice Elite, ESP, USA). By using the multicycle software program it was possible to calculate the proportion of H₂₂ cells in S and G₂/M phases in tumor.

Synergistic anti-tumor effects of RES and 5-FU

A total of 128 tumor-bearing BALB/c mice were randomly divided into 8 groups: control group, RES group, three 5-FU groups and three experimental groups. The RES group was injected with RES at 10 mg/kg body mass (this dosage was proven to have obvious anti-tumor effect in our preliminary study.) and the 5-FU groups were injected with 5-FU at 5, 10, or 20 mg/kg body mass, respectively, and 3 experimental groups were injected with RES at 10 mg/kg body mass+5-FU at 5, 10, or 20 mg/kg body mass, respectively. The control group was given the same volume of the solution as for the experimental group without RES and 5-FU. Twenty-four hours after liver tumor transplantation, each mouse was injected with a corresponding drug at respective dosage into its abdominal cavity once a day for 10 d. Half of the mice in each group were then sacrificed on the following day after the last injection and the maximum diameter and transverse length of tumor were measured. The tumor tissues of mice treated with various dosages of 5-FU alone or in combination with RES were observed and photographed with an Olympus BH-I microscope. The rest mice were kept on feeding and their survival time and changes of body mass were recorded and their tumor metastasis conditions in lung or abdominal cavity were observed.

Statistical analysis

Student's *t* test was used to evaluate the significance of the difference between experimental groups and control group, between combination groups and corresponding sole drug groups.

RESULTS

Suppressive effect of RES on transplanted liver cancer and distribution of H₂₂ cell cycles

Except 3 Balb/c mice (each in control group, 15 mg/kg RES group and 20.0 mg/kg 5-FU group), all the mice inoculated with hepatocarcinoma cell line H₂₂ were successively transplanted with liver cancer. After treatment of the tumour bearing mice with 5, 10 or 15 mg/kg RES for 10 d, the tumour size was reduced from 134 ± 40 mm³ in control group to 105 ± 14 mm³, 85 ± 22 mm³ and 68 ± 17 mm³ in three experimental groups, the inhibition rate of tumour growth was 21.6 %, 36.3 % and 49.3 %, respectively.

The inhibitory effect on the latter 2 therapeutic groups was significant higher than that on control group ($P < 0.01$). Though the inhibition rate of tumour growth of 5-FU was rather high (53.0%), its toxicity was serious and the concrete manifestations included poor ingestion, diarrhea, and decrease in body mass, while the mice in RES groups showed no evident toxicity and were alive at the end of treatment (Table 1).

The cell cycles were analysed using flow cytometer to calculate the number of H₂₂ cells in each phase in tumor under the action of various dosages of RES (5, 10, or 15 mg/kg body mass). The results showed that the number of H₂₂ cells in S phase increased from 0.60 in control group to 0.75 in 15.0 mg/kg RES group, while the number of H₂₂ cells in G₂ phase decreased from 0.11 to 0.00 and the effect was dose-dependent (Table 2, Figure 1).

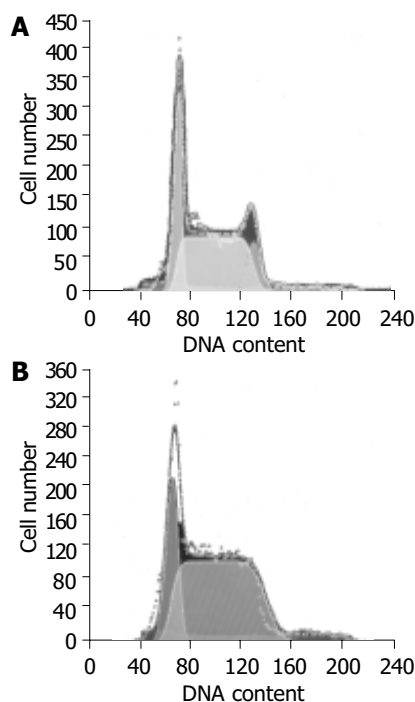


Figure 1 Number of H₂₂ cell cycles in transplanted liver cancer of mouse treated with RPMI-1640 (A) or 15.0 mg/kg (B).

Table 1 Suppressive effect of resveratrol on murine transplanted liver cancer (mean \pm SD)

Group	Dose (mg/kg)	n	Tumor size (mm ³)	Growth inhibitory rate (%)	t value
Control	0.0	9	134 \pm 40	-	
5-FU	20.0	9	63 \pm 29	53.0	4.36 ^b
RES	5.0	10	105 \pm 14	21.6	2.16 ^a
	10.0	10	85 \pm 22	36.6	3.36 ^b
	15.0	9	68 \pm 17	49.3	4.33 ^b

^a $P < 0.05$, ^b $P < 0.01$, vs control.

Table 2 Effect of RES on the number of H₂₂ cell cycles in transplanted liver cancer of mouse

Group	Dose (mg/kg)	n	Number of H ₂₂ cell cycles (%)		
			G0/G1	S	G2/M
Control	0	9	0.29	0.60	0.11
RES	5.0	10	0.30	0.60	0.09
	10.0	10	0.30	0.68 ^a	0.02 ^a
	15.0	9	0.25	0.75 ^a	0.00 ^a

^a $P < 0.05$, vs control.

Table 3 Suppressive effect of RES in combination with 5-FU on murine with transplanted liver cancer (mean±SD)

Group	Dose (mg/kg)	n	Tumor size (mm ³)		t value	Growth inhibitory rate (%)	
			Alone	With 5-FU		Alone	With 5-FU
Control	0	8	128±33				
RES	10.0	8	88±21			31.5	
5-FU	20.0	8	60±12	29±18	4.05 ^b	53.4	77.4
	10.0	8	72±17	35±13	4.89 ^b	43.8	72.4
	5.0	8	92±19	64±22	2.72 ^a	28.4	50.0

^a*P*<0.05, ^b*P*<0.01, vs control.

Table 4 Effect of RES in combination with 5-FU on survival time and body mass of tumor bearing mouse (mean±SD)

Group	Dose (mg/kg)	n	Last body mass(g)		t value	Survival time (d)		t value
			Alone	With 5-FU		Alone	With 5-FU	
Control	0	8	23.6±2.0			17.3±3.3		
RES	10.0	8	23.8±1.2			21.5±5.6		
5-FU	20.0	8	16.5±1.8	20.3±1.3	4.79 ^b	32.0±9.7	44.6±11.6	2.34 ^a
	10.0	8	19.6±1.8	23.2±2.5	3.25 ^b	23.6±5.4	36.3±9.4	3.22 ^b
	5.0	8	21.3±1.7	24.5±1.5	3.80 ^b	19.5±4.4	30.6±8.0	3.48 ^b

^a*P*<0.05, ^b*P*<0.01, vs control.

Suppressive effect of RES in combination with 5-FU on transplanted liver cancer

RES in combination with 5-FU had synergistic suppressive effects on transplanted liver cancer of mouse (Figure 2). When 10 mg/kg RES in combination with 5, 10 or 20 mg/kg 5-FU, the inhibition rate was 50.0%, 72.4%, and 77.4%, respectively. When the group administered 5, 10 or 20 mg/kg 5-FU alone, the inhibition rate was 28.4%, 43.8%, and 53.4%, respectively. There was a statistical significance between the combination group and the 5-FU alone group (Table 3). Morphologic observation showed that more cellular necrosis was found in the combination group than in control group (Figure 3).

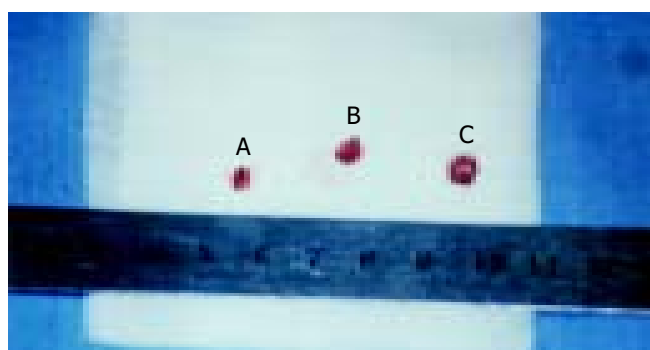


Figure 2 Tumor size of mice treated with 10.0 mg/kg RES+20.0 mg/kg 5-FU (tumor A: 3.5×3.1×2.6 mm) and RPMI-1640 (tumor B: 4.8×4.7×4.2 mm; tumor C: 5.3×5.2×4.8 mm).

Effect of RES in combination with 5-FU on survival time and tumor metastasis

When the mice were administered 10 mg/kg RES in combination with 5, 10 or 20 mg/kg 5-FU, the survival time of tumor bearing mouse was 30.6±8.0 d, 36.3±9.4 d, and 44.6±11.6 d, respectively. When group administered 5, 10 or 20 mg/kg 5-FU alone, the survival time was 19.4±4.4 d, 23.9±5.4 d, and 32.1±9.7 d, respectively (Figure 6). There was a statistical significance between the combination group and the 5-FU alone group. In

the beginning of the study, there was no statistical difference in the body mass of mouse among various groups. However, at the end of the investigation, the body mass of mouse in combination group was significantly heavier than that in sole drug group (*P*<0.01), showing that RES might antagonize the toxicity of 5-FU markedly (Table 4). Two Balb/c mice in control group had lung and celiac lymph node metastases, one in 5 mg/kg 5-FU therapeutic group had celiac lymph node metastasis. Except these 3 groups, all the mice inoculated with hepatocarcinoma cell line H₂₂ showed no signs of tumor metastasis.

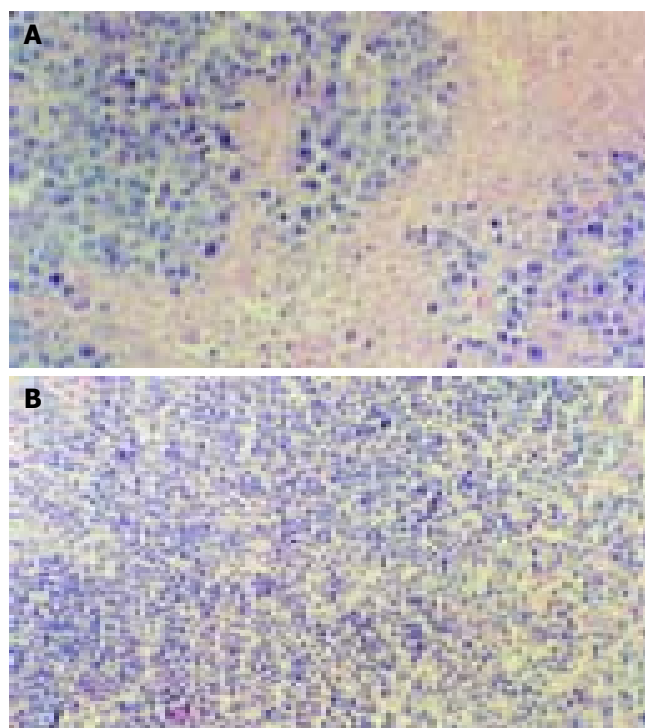


Figure 3 Morphologic observation of tumor tissues of mice treated with RPMI-1640 (A) or 10.0 mg/kg RES+20.0 mg/kg 5-FU(B).

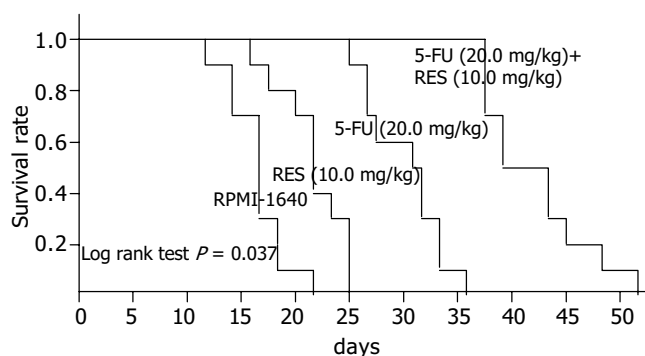


Figure 4 Kaplan-meier curves of survival rates of tumor bearing mice when administered RPMI-1640, 10 mg/kg RES, 20 mg/kg 5-FU, and 5-FU (20.0 mg/kg)+RES (10.0 mg/kg).

DISCUSSION

Great attention has been paid to the chemopreventive activities and low toxicities of dietary polyphenolic compounds like RES^[22]. The function of RES might be mediated via different mechanisms in different cells, and the ability of RES to inhibit cellular events associated with tumor initiation, promotion, and progression might be attributed to its anticyclooxygenase activity, inducing apoptosis of tumor cells, antagonism to mutation, antioxidation and anti-free radical activity and effect on cell cycles^[23-28]. Ahmad *et al.*^[29] proved that resveratrol treatment of human epidermoid carcinoma A431 cells caused an induction of WAF1/p21 inhibiting cyclin D1/D2-cdk6, cyclin D1/D2-cdk4, and cyclin E-cdk2 complexes, thereby imposing an artificial checkpoint at the G1-S transition of the cell cycle, which resulted in a G1 phase arrest of the cell cycle and subsequent apoptotic death of cancer cells. Our previous studies demonstrated that RES could suppress the growth of murine transplanted liver tumor H₂₂ and the anti-tumor mechanism of RES might prevent mitosis of tumor cells by suppressing the protein expression of cyclin B1 and p34cdc2, thus interfering with the process of tumor cells from S stage to G2/M stage^[30,31].

One main role of 5-fluorouracil is to affect the biosynthesis of nucleic acids. Inside cells, 5-FU is converted to 5-fluorouracil deoxynucleotide (5F-dUMP) and inhibits the function of deoxythymidylic acid synthetase, blocks the methylation of uracil deoxyribonucleotide into deoxythymidylic acid, thus affecting the synthesis of DNA. As a result, 5-FU can prevent the tumor cells from splitting and proliferating and its cardinal acting period is S phase. Besides that, after the conversion of 5-FU into 5-fluorouracil uridine (5-FUR) *in vivo*, it also can be added into RNA to interfere with the synthesis of proteins, so it can affect the cells in other phases. Therefore, RES can enhance the anti-tumor effect of 5-FU by inducing the S phase arrest of H₂₂ cells, a stage in which 5-FU can exert its max tumor cell killing function, and this synergism was proved in our *in vitro* experiments.

In the present investigation, RES was administered into murine abdomen, its potency on growth and proliferation of H₂₂-innoculated tumors and its synergism with 5-FU were evaluated by measuring the size of hepatoma and examining the distributions of H₂₂ cell cycles and observing the survival time of mice. The tumor size was reduced by each dosage of 5, 10 or 15 mg/kg of RES for 10 d. When the larger dosage of RES was applied, the tumor size was significantly reduced, the inhibition rate of tumor growth by 10 or 15 mg/kg reached to 36.3% and 49.3%, respectively ($P < 0.01$). It was also found that RES could induce the S phase arrest of H₂₂ cells. RES could increase the percentage of cells in S phase from 59.1% to 73.5% in a dose-dependent manner ($P < 0.05$). The enhanced inhibition

of tumor growth by 5-FU was also observed in hepatoma₂₂ bearing mice when 5-FU was administered in combination with 10 mg/kg RES. The inhibition rate of 10 mg/kg or 20 mg/kg 5-FU in combination with 10 mg/kg RES was 72.4% and 77.4%, respectively. The inhibition rate was 43.8% and 53.4%, when the group administered 10 mg/kg or 20 mg/kg 5-FU alone. There was a statistical significance between the combination group and the 5-FU alone group ($P < 0.01$). In addition to that, when RES was administered in combination with a smaller dosage of 5-FU, the therapeutic effect was similar to that of a larger dosage of 5-FU but without severe side effects of 5-FU, therefore the survival time of mice was elongated.

In short, the data suggest that RES can induce the S phase arrest of H₂₂ cells and enhance the anti-tumor effect of 5-FU on murine hepatoma₂₂ and antagonize its toxicity markedly. Resveratrol, a biochemical modulator to enhance the therapeutic effects of 5-FU, may be potentially useful in cancer chemotherapy.

REFERENCES

- 1 **Kuang SY**, Jackson PE, Wang JB, Lu PX, Munoz A, Qian GS, Kensler TW, Groopman JD. Specific mutations of hepatitis B virus in plasma predict liver cancer development. *Proc Natl Acad Sci U S A* 2004; **101**: 3575-3580
- 2 **Kew MC**. Synergistic interaction between aflatoxin B1 and hepatitis B virus in hepatocarcinogenesis. *Liver Int* 2003; **23**: 405-409
- 3 **Chen HB**, Huang Y, Dai DL, Zhang X, Huang ZW, Zhang QK, Wang HH, Zhang JS, Pan G. Therapeutic effect of transcatheter arterial chemoembolization and percutaneous injection of acetic acids on primary liver cancer. *Hepatobiliary Pancreat Dis Int* 2004; **3**: 55-57
- 4 **Luo W**, Birkett NJ, Ugnat AM, Mao Y. Cancer incidence patterns among Chinese immigrant populations in Alberta. *J Immigr Health* 2004; **6**: 41-48
- 5 **Chen JG**, Parkin DM, Chen QG, Lu JH, Shen QJ, Zhang BC, Zhu YR. Screening for liver cancer: results of a randomised controlled trial in Qidong, China. *J Med Screen* 2003; **10**: 204-209
- 6 **Zou CL**, Chen ZJ, Jin WY, Ni SC, Chen BF, Hu YL. Etiologic fraction and interaction of risk factors for primary hepatocellular carcinoma in Wenzhou, Zhejiang Province. *Zhonghua Yufang Yixue Zazhi* 2003; **37**: 355-357
- 7 **Tang B**, Kruger WD, Chen G, Shen F, Lin WY, Mboup S, London WT, Evans AA. Hepatitis B viremia is associated with increased risk of hepatocellular carcinoma in chronic carriers. *J Med Virol* 2004; **72**: 35-40
- 8 **Tang ZY**. Small hepatocellular carcinoma: current status and prospects. *Hepatobiliary Pancreat Dis Int* 2002; **1**: 349-353
- 9 **Lu W**, Li YH, He XF, Chen Y, Zhao JB. Changes of liver function after transcatheter arterial chemoembolization with use of different dose of anticancer drugs in hepatocellular carcinoma. *Shijie Huaren Xiaohua Zazhi* 2004; **12**: 38-41
- 10 **Shen BZ**, Liu Y, Li RF, Yang G, Yu YT, Dong BW, Liang P. Effects of intraarterial chemoembolization combined with percutaneous microwave coagulation on hepatocellular carcinoma: a clinical and experimental study. *Shijie Huaren Xiaohua Zazhi* 2003; **11**: 268-271
- 11 **Afaq F**, Adhmi VM, Ahmad N. Prevention of short-term ultraviolet B radiation-mediated damages by resveratrol in SKH-1 hairless mice. *Toxicol Appl Pharmacol* 2003; **186**: 28-37
- 12 **Fremont L**. Biological effects of resveratrol. *Life Sci* 2000; **66**: 663-673
- 13 **Sato M**, Ray PS, Maulik G, Maulik N, Engelman RM, Bertelli AA, Bertelli A, Das DK. Myocardial protection with red wine extract. *J Cardiovasc Pharmacol* 2000; **35**: 263-268
- 14 **Roemer K**, Mahyar-Roemer M. The basis for the chemopreventive action of resveratrol. *Drugs Today* 2002; **38**: 571-580
- 15 **Zou JG**, Wang ZR, Huang YZ, Cao KJ, Wu JM. Effect of red wine and wine polyphenol resveratrol on endothelial function in hypercholesterolemic rabbits. *Int J Mol Med* 2003; **11**: 317-320
- 16 **Kimura Y**, Okuda H. Resveratrol isolated from *Polygonum cuspidatum* root prevents tumor growth and metastasis to

- lung and tumor-induced neovascularization in Lewis lung carcinoma-bearing mice. *J Nutr* 2001; **131**: 1844-1849
- 17 **Narayanan BA**, Narayanan NK, Re GG, Nixon DW. Differential expression of genes induced by resveratrol in LNCaP cells: P53-mediated molecular targets. *Int J Cancer* 2003; **104**: 204-212
- 18 **Ding XZ**, Adrian TE. Resveratrol inhibits proliferation and induces apoptosis in human pancreatic cancer cells. *Pancreas* 2002; **25**: e71-76
- 19 **Kuo PL**, Chiang LC, Lin CC. Resveratrol-induced apoptosis is mediated by p53-dependent pathway in Hep G2 cells. *Life Sci* 2002; **72**: 23-34
- 20 **Banerjee S**, Bueso-Ramos C, Aggarwal BB. Suppression of 7, 12-dimethylbenz(a)anthracene-induced mammary carcinogenesis in rats by resveratrol: role of nuclear factor-kappaB, cyclooxygenase 2, and matrix metalloprotease 9. *Cancer Res* 2002; **62**: 4945-4954
- 21 **Otto FJ**. High-resolution analysis of nuclear DNA employing the fluorochrome DAPI. *Methods Cell Biol* 1994; **41**: 211-217
- 22 **Narayanan BA**, Narayanan NK, Stoner GD, Bullock BP. Interactive gene expression pattern in prostate cancer cells exposed to phenolic antioxidants. *Life Sci* 2002; **70**: 1821-1839
- 23 **Young J**, Barker M, Fraser L, Walsh MD, Spring K, Biden KG, Hopper JL, Leggett BA, Jass JR. Mutation searching in colorectal cancer studies: experience with a denaturing high-pressure liquid chromatography system for exon-by-exon scanning of tumour suppressor genes. *Pathology* 2002; **34**: 529-533
- 24 **Takahashi M**, Shimomoto T, Miyajima K, Iizuka S, Watanabe T, Yoshida M, Kurokawa Y, Maekawa A. Promotion, but not progression, effects of tamoxifen on uterine carcinogenesis in mice initiated with N-ethyl-N'-nitro-N-nitrosoguanidine. *Carcinogenesis* 2002; **23**: 1549-1555
- 25 **De la Fuente M**, Victor VM. Anti-oxidants as modulators of immune function. *Immunol Cell Biol* 2000; **78**: 49-54
- 26 **Falchetti R**, Fuggetta MP, Lanzilli G, Tricarico M, Ravagnan G. Effects of resveratrol on human immune cell function. *Life Sci* 2001; **70**: 81-96
- 27 **Schneider Y**, Durantou B, Gosse F, Schleiffer R, Seiler N, Raul F. Resveratrol inhibits intestinal tumorigenesis and modulates host-defense-related gene expression in an animal model of human familial adenomatous polyposis. *Nutr Cancer* 2001; **39**: 102-107
- 28 **Yu C**, Shin YG, Chow A, Li Y, Kosmeder JW, Lee YS, Hirschelman WH, Pezzuto JM, Mehta RG, van Breemen RB. Human, rat, and mouse metabolism of resveratrol. *Pharm Res* 2002; **19**: 1907-1914
- 29 **Ahmad N**, Adhami VM, Afaq F, Feyes DK, Mukhtar H. Resveratrol causes WAF-1/p21-mediated G(1)-phase arrest of cell cycle and induction of apoptosis in human epidermoid carcinoma A431 cells. *Clin Cancer Res* 2001; **7**: 1466-1473
- 30 **Holmes-McNary M**, Baldwin AS Jr. Chemopreventive properties of trans-resveratrol are associated with inhibition of activation of the I kappa B kinase. *Cancer Res* 2000; **60**: 3477-3483
- 31 **Nielsen M**, Ruch RJ, Vang O. Resveratrol reverses tumor-promoter-induced inhibition of gap-junctional intercellular communication. *Biochem Biophys Res Commun* 2000; **275**: 804-809

Edited by Wang XL and Ren SY Proofread by Xu FM

Sentinel lymph node concept in gastric cancer with solitary lymph node metastasis

Li-Yang Cheng, Shi-Zhen Zhong, Zong-Hai Huang

Li-Yang Cheng, Shi-Zhen Zhong, Institute of Clinical Anatomy, First Military Medical University, Guangzhou 510515, Guangdong Province, China

Zong-Hai Huang, Department of General Surgery, Zhujiang Hospital, First Military Medical University, Guangzhou 510282, Guangdong Province, China

Supported by the Natural Science Foundation of Guangdong Province, No. 032204

Correspondence to: Dr. Li-yang Cheng, Department of General Surgery, Guangzhou General Hospital of PLA, 111 Liuhua Road, Guangzhou 510010, Guangdong Province, China. chliyang2001@yahoo.com.cn

Telephone: +86-20-36653547 **Fax:** +86-20-36222275

Received: 2004-02-14 **Accepted:** 2004-02-24

Abstract

AIM: To study the localization of the solitary metastases in relation to the primary gastric cancers and the feasibility of sentinel lymph node (SLN) concept in gastric cancer.

METHODS: Eighty-six patients with gastric cancer, who had only one lymph node involved, were regarded retrospectively as patients with a possible sentinel node metastasis, and the distribution of these nodes were assessed. Thirteen cases with jumping metastases were further studied and followed up.

RESULTS: The single nodal metastasis was found in the nearest perigastric nodal area in 65.1% (56/86) of the cases and in 19.8% (17/86) of the cases in a fairly remote perigastric area. Out of 19 middle-third gastric cancers, 3 tumors at the lesser or greater curvatures had transverse metastases. There were also 15.1% (13/86) of patients with a jumping metastasis to N2-N3 nodes without N1 involved. Among them, the depth of invasion was mucosal (M) in 1 patient, submucosal (SM) in 2, proper-muscular (MP) in 4, subserosal (SS) in 5, and serosa-exposed (SE) in 1. Five of these patients died of gastric cancer recurrence at the time of this report within 3 years after surgery.

CONCLUSION: These results suggest that nodal metastases occur in a random and multidirectional process in gastric cancer and that not every first metastatic node is located in the perigastric region near the primary tumor. The rate of "jumping metastasis" in gastric cancer is much higher than expected, which suggests that the blind examination of the nodal area close to the primary tumor can not be a reliable method to detect the SLN and that a extended lymph node dissection (ELND) should be performed if the preoperative examination indicates submucosal invasion.

Cheng LY, Zhong SZ, Huang ZH. Sentinel lymph node concept in gastric cancer with solitary lymph node metastasis. *World J Gastroenterol* 2004; 10(20): 3053-3055

<http://www.wjgnet.com/1007-9327/10/3053.asp>

INTRODUCTION

The sentinel lymph node (SLN) which refers to the first lymph node to receive drainage from the primary tumor has been successfully introduced in the patients with breast cancer^[1] and malignant melanoma^[2] to assess tumor involvement in regional lymph nodes with less morbidity but equal accuracy to complete lymphadenectomy. But the feasibility of sentinel node mapping of gastric carcinoma is still unclear and controversial. To explore the applicability of sentinel node concept to gastric cancer and provide useful information for establishing a novel method to detect sentinel nodes during operation, we retrospectively investigated solitary lymph node metastases that hypothesized to represent sentinel lymph node.

MATERIALS AND METHODS

Patients

Between January 1997 and December 2003, 1 698 patients with gastric cancer underwent gastrectomy with lymph node dissection (more than D1) at the Department of General Surgery, Guangzhou General Hospital of PLA, Nanfang and Zhujiang Hospitals of First Military Medical University. Among them, 86 (5.1%) patients were rolled in this study by the following criteria: (1) the lesion was solitary and limited to one part of the stomach; (2) a curative gastrectomy with ELND was performed; and (3) the histological examination of all resected lymph nodes revealed only one lymph node involved. These patients were subdivided according to the primary site of gastric cancer: 16 upper-third (U) tumors; 19 middle-third (M) tumors; and 51 lower-third (L) tumors. According to the depth of wall invasion, mucosal (M) lesions, submucosal (SM) lesions, proper-muscular (MP) lesions, and subserosal (SS) lesions were observed in 2, 7, 47, and 30 patients, respectively. Regarding their histologic grades, 23 of high-differentiated cases, 55 of middle-differentiated cases, 7 of low-differentiated cases, and 1 of non-differentiated case were proven to have only one lymph node involved. Total gastrectomy, proximal subtotal gastrectomy and distal subtotal gastrectomy were carried out in 29, 6 and 51 cases, respectively.

Methods

The resected specimens and the lymph nodes were stained conventionally with hematoxylin and eosin (HE) and examined by pathologists. The clinicopathological data were evaluated according to the General Rules by the Japanese Research Society for Gastric Cancer^[3]. In the present study, to express the group and station number of each lymph node, No. and N were inserted in front of the number, i.e., No. 4 means group 4 lymph node and N1 means station 1 lymph node. If patients were histologically verified to have distant lymph nodes (N2 or N3) involved without perigastric node metastasis (N1), they were defined to have either jumping or skip metastases. If the tumors at the lesser or greater curvatures had metastasized to the lymph nodes located in the opposite curvatures, they were then defined to have transverse metastases. Ten of 13 patients with skip metastases were followed up for 1-5 years until December 2003.

RESULTS

Upper-third (U) tumors

In 13 out of 16 U tumors, the solitary node metastasis was found in perigastric area close to the tumor (N1). In 3 cases, the metastasis was found in N2 area. Among them, 2 nodes were along the left gastric artery (LGA) (No.7), the other 1 along common hepatic artery (CHA) (No.8a).

Middle-third (M) tumors

In 9 out of 19 M tumors, the single node metastasis was found either in the lesser (No.3) or greater curvature (No.4) perigastric area close to the primary tumor. Among them, 2 tumors at the lesser curvature and 1 tumor at the greater curvature had transverse metastases. In 6 cases, the metastasis was found in the remote perigastric area (No.1, 5 and 6), and another 4 cases in the N2 or N3 area (No.7, 8a and 12) were without N1 involvement.

Lower-third (L) tumors

Of 51 patients with L tumors, 34 had the single metastasis in the perigastric node close to the tumor (No.3 and 4), 11 had metastasized to the surrpyloric (No.5) or infrapyloric (No.6), both of which were N1 but somewhat remote from the primary tumor. In the other 6 cases, the metastasis was found in the N2 or N3 area (No.1, 4 s, 7 and 11 p) without N1 involvement.

Invasion and survival of patients with jumping metastasis

Among 13 cases with jumping metastasis, the depth of invasion was M in 1, SM in 2, MP in 4, SS in 5, and SE in 1. Among 6 out of 10 patients who received a follow-up, 5 died of tumor recurrence and 1 of other disease within 3 years after operation. The other 4 were alive at the time of this report for more than 3-5 years after surgery.

Metastasis of tumors

A total of 1376 lymph nodes were harvested in this group of 86 patients with D2-D3 lymphadenectomy. The average number of lymph nodes dissected was 16 in each case. The distribution of the single positive node is shown in Table 1 according to the location of the primary tumor. In total, the single nodal metastasis was found in 65.1% of cases in the nearest perigastric node area, in 19.8% of cases in a fairly remote perigastric area, and in 15.1% of cases in the N2 or N3 area without N1 involvement.

Table 1 Distribution of solitary lymph node metastasis

Location of positive node	Location of primary tumor		
	Upper	Middle	Lower
Right cardinal (No1)	2(N1)	1(N1)	1(N2)
Lesser curvature (No3)	7(N1)	7(N1)	20(N1)
Greater curvature (No4d)		2(N1)	14(N1)
Greater curvature (No4s)	2(N1)		1(N3)
Surrpyloric (No5)		2(N1)	5(N1)
Infrapyloric (No6)	2(N1)	3(N1)	6(N1)
Left gastric artery (No7)	2(N2)	2(N2)	3(N2)
Common hepatic artery (No8a)	1(N2)	1(N2)	
Splenic artery (No11p)			1(N2)
Proper hepatic artery (No12)		1(N3)	

No4d and 4 s represent nodes on right and left half of greater curvature respectively; No8a represents nodes on the anterior or upper of CHA; No11p represents nodes on proximal splenic artery.

DISCUSSION

Gastric cancer is generally thought to spread to N1 nodes first,

followed by involvement of distant nodes (N2-N3) just as other carcinomas. However, more recent studies have reported that lymph node involvement was noted not only in N1 but also in N2-N3 and that the rate of N2 lymph node metastases in patients with advanced gastric cancers was higher than expected^[4,5]. Lymphatic drainage route must be patient-specific and lesion-specific in gastric cancer due to complicated lymphatic streams from the stomach. Our results suggested that although most of the single nodal metastasis was found in the nearest perigastric node area, approximately one quarter of the patients had the first metastasis in a fairly remote perigastric area and up to 15% of patients demonstrated skip metastasis without N1 involvement. To date, to the authors knowledge, there are only 5 retrospective studies on gastric cancer patients with only one lymph node metastasis^[6-10]. In these studies, the single nodal metastases were distributed beyond the perigastric area in 12.6-29% of gastric cancer patients, which suggested that the conventional lymphatic routes in stomach that have long been generally accepted should be clarified further. Our present data confirm these results. Among 13 cases with skip metastasis in the current study, most (10/13) of the solitary node metastases were found in No.7, 8, or 12. This result seems to be comparable with other reports, where No.7, 8, 9 and 12 nodes were most commonly involved in patients with skip metastasis^[6-10], and suggests that No.7, 8, and 12 to be the most important stations as well as N1^[4,5]. In our study, 3 out of 19 mol/L tumors had transverse metastases, which indicates that gastric lymph channels are multidirectional and form complex networks. The survival and depth of invasion in gastric cancer patients with skip metastases presented in this report suggest that if the preoperative examination diagnosed submucosal invasion, then a ELND should be conducted.

Results from these retrospective studies not only demonstrated the feasibility of SLN concept to gastric cancer but also provided useful information for intraoperative sentinel node mapping. That the perigastric nodal area close to the primary tumor is the first site of metastasis in 65.1% of gastric cancers in the present study indicates that the so-called shine-through effect should be considered in sentinel node mapping by radioisotope (RI) method^[11]. The high incidence of skip metastasis to N2-N3 nodes suggests that blind examination of the nodal area close to the primary tumor can not be a reliable method to detect the first metastasis^[6]. Visualization of dye is useful for real-time observation of lymphatic vessels, but it is difficult to detect multiple sentinel nodes and SLNs in the second or third compartments because vital dye tends to diffuse rapidly from nodal tissue. A probe-guided approach is essential to cover the widespread distribution of SLNs in gastric cancer and is very useful to detect residual SLNs in unexpected areas^[12]. Therefore, a combination of the dye and radioguided methods for systemic lymphatic mapping of gastric cancers may be recommended to improve the detection rate and diagnostic accuracy^[13,14].

It remains unclear why jumping metastases occurred in these cases. The following reasons could all play some role: (1) N1 involved nodes and occult metastases to N1 nodes may have been missed during the dissection and the routine histopathologic examination, which result in a false skip metastasis. The possible sentinel nodes detected by conventional means might not always be primary portions of any metastasis and true skip metastasis in gastric cancer may be rare^[10]; (2) There may have been some aberrant lymphatic drainage patterns in patients with gastric cancer, through which metastasis bypasses lymphatic vessels^[7,8,15]; (3) Direct lymphatic flows to distant affected nodes from primary gastric lesions have been found in SLN mapping intraoperatively^[16]; (4) Lymphatic flows to the N1 nodes may have been blocked with cancer tissue; (5) The microenvironment in the N1 nodes is sometimes unfit for the

development of metastasis^[17]. Free cancer cells may diffuse through regional nodes to distant nodes. In addition, the risk factors associated with skip nodal metastasis may include the stage, depth of invasion, macroscopic classification and pathological type of gastric cancer.

Most surgeons are skeptical about the application of the SLN concept for gastric cancer because of the high incidence of skip metastases and the random process occurring in nodal metastases. However, Kitagawa *et al.*^[18,19] have pointed out that the sentinel node for gastrointestinal cancer is not the node necessarily located anatomically closest to the primary lesion and is not necessarily the only one. In those cases with a jumping metastasis to N2-N3 nodes, sentinel nodes in the second or third compartment are considered to be functionally first compartments. Bilchik *et al.*^[20] proposed the potential for universal application of sentinel node mapping in solid tumors. Cases with one or two lymph node metastasis examined in these retrospective studies only occupy a little part of patients with gastric carcinoma in which one or more SLNs can be detected in every case theoretically. Then the results from these studies can not represent the real characteristic as to the occurrence of SLN in all gastric cancers. Actual data from sentinel node mapping for gastric cancers, rather than a retrospective analysis of metastatic patterns, are needed to explore the feasibility and validity of sentinel node biopsy in gastric cancer.

REFERENCES

- 1 Nieweg OE, Bartelink H. Implications of lymphatic mapping for staging and adjuvant treatment of patients with breast cancer. *Eur J Cancer* 2004; **40**: 179-181
- 2 Kretschmer L, Hilgers R, Mohrle M, Balda BR, Breuninger H, Konz B, Kunte C, Marsch WC, Neumann C, Starz H. Patients with lymphatic metastasis of cutaneous malignant melanoma benefit from sentinel lymphonodectomy and early excision of their nodal disease. *Eur J Cancer* 2004; **40**: 212-218
- 3 Japanese Gastric Cancer Association. *Japanese Classification of Gastric carcinoma*. 13th ed. Tokyo: Kanehara 1999
- 4 Mishima Y, Hirayama R. The role of lymph node surgery in gastric cancer. *World J Surg* 1987; **11**: 406-411
- 5 Maruyama K, Gunven P, Okabayashi K, Sasako M, Kinoshita T. Lymph node metastases of gastric cancer. General pattern in 1931 patients. *Ann Surg* 1989; **210**: 596-602
- 6 Sano T, Katai H, Sasako M, Maruyama K. Gastric lymphography and detection of sentinel nodes. *Rec Res Cancer Res* 2000; **157**: 253-258
- 7 Kosaka T, Ueshige N, Sugaya J, Nakano Y, Akiyama T, Tomita F, Saito H, Kita I, Takashima S. Lymphatic routes of the stomach demonstrated by gastric carcinomas with solitary lymph node metastasis. *Surg Today* 1999; **29**: 695-700
- 8 Ichikura T, Morita D, Uchida T, Okura E, Majima T, Ogawa T, Mochizuki H. Sentinel node concept in gastric carcinoma. *World J Surg* 2002; **26**: 318-322
- 9 Tsuburaya A, Noguchi Y, Yoshikawa T, Kobayashi O, Sairenji M, Motohashi H. Solitary lymph node metastasis of gastric cancer as a basis for sentinel lymph node biopsy. *Hepatogastroenterology* 2002; **49**: 1449-1452
- 10 Arai K, Iwasaki Y, Takahashi T. Clinicopathological analysis of early gastric cancer with solitary lymph node metastasis. *Br J Surg* 2002; **89**: 1435-1437
- 11 Yasuda S, Shimada H, Ogoshi K, Tanaka H, Kise Y, Kenmochi T, Soeda J, Nakamura K, Kato Y, Kijima H, Suzuki Y, Fujii H, Tajima T, Makuuchi H. Preliminary study for sentinel lymph node identification with Tc-99m tin colloid in patients with esophageal or gastric cancer. *Tokai J Exp Clin Med* 2001; **26**: 15-18
- 12 Kitagawa Y, Ohgami M, Fujii H, Mukai M, Kubota T, Ando N, Watanabe M, Otani Y, Ozawa S, Hasegawa H, Furukawa T, Matsuda J, Kumai K, Ikeda T, Kubo A, Kitajima M. Laparoscopic detection of sentinel lymph nodes in gastrointestinal cancer: a novel and minimally invasive approach. *Ann Surg Oncol* 2001; **8**(9 Suppl): 86S-89S
- 13 Hayashi H, Ochiai T, Mori M, Karube T, Suzuki T, Gunji Y, Hori S, Akutsu N, Matsubara H, Shimada H. Sentinel lymph node mapping for gastric cancer using a dual procedure with dye-and gamma probe-guided techniques. *J Am Coll Surg* 2003; **196**: 68-74
- 14 Tokunaga A, Okuda T, Tajiri T, Onda M. Intraoperative lymphatic mapping by dye and/or radioactive tracer in early gastric cancer. *J Nippon Med Sch* 2002; **69**: 216-217
- 15 Bilchik AJ, Saha S, Tsioulis GJ, Wood TF, Morton DL. Aberrant drainage and missed micrometastases: the value of lymphatic mapping and focused analysis of sentinel lymph nodes in gastrointestinal neoplasms. *Ann Surg Oncol* 2001; **8**: 82-85
- 16 Miwa K, Kinami S, Taniguchi K, Fushida S, Fujimura T, Nonomura A. Mapping sentinel nodes in patients with early-stage gastric carcinoma. *Br J Surg* 2003; **90**: 178-182
- 17 Gervasoni JE Jr, Taneja C, Chung MA, Cady B. Biologic and clinical significance of lymphadenectomy. *Surg Clin North Am* 2000; **80**: 1632-1673
- 18 Kitagawa Y, Fujii H, Mukai M, Kubota T, Ando N, Watanabe M, Ohgami M, Otani Y, Ozawa S, Hasegawa H, Furukawa T, Kumai K, Ikeda T, Nakahara T, Kubo A, Kitajima M. The role of the sentinel lymph node in gastrointestinal cancer. *Surg Clin North Am* 2000; **80**: 1799-1809
- 19 Kitagawa Y, Kitajima M. Gastrointestinal cancer and sentinel node navigation surgery. *J Surg Oncol* 2002; **79**: 188-193
- 20 Bilchik AJ, Giuliano A, Essner R, Bostick P, Kelemen P, Foshag LJ, Sostrin S, Turner RR, Morton DL. Universal application of intraoperative lymphatic mapping and sentinel lymphadenectomy in solid neoplasms. *Cancer J Sci Am* 1998; **4**: 351-358

Edited by Kumar M Proofread by Chen WW and Xu FM

Cytotoxic T lymphocyte associated antigen-4 gene polymorphisms confer susceptibility to primary biliary cirrhosis and autoimmune hepatitis in Chinese population

Lie-Ying Fan, Xiao-Qing Tu, Qu-Bo Cheng, Ye Zhu, Ralph Feltens, Thomas Pfeiffer, Ren-Qian Zhong

Lie-Ying Fan, Xiao-Qing Tu, Ye Zhu, Ren-Qian Zhong, The center of Clinical Immunology, Changzheng Hospital, Second Military Medical University, Shanghai 200003, China

Qu-Bo Cheng, Department of Laboratory Diagnosis, Traditional Chinese Medicine Hospital, Guangzhou 501405, Guangdong Province, China
Ralph Feltens, Thomas Pfeiffer, Euroimmun, Medical Laboratory Diagnostic GmbH, Leubeck, Germany

Correspondence to: Lie-Ying Fan, M.D., The Center of Clinical Immunology, Changzheng Hospital, 415 Feng Yang Road, Shanghai 200003, China. flieying@hotmail.com

Telephone: +86-20-636310109 **Fax:** +86-20-33110236

Received: 2003-10-09 **Accepted:** 2003-12-08

Abstract

AIM: To investigate the association between Chinese patients with autoimmune hepatitis (AIH), primary biliary cirrhosis (PBC) and the polymorphisms of cytotoxic T lymphocyte-associated antigen-4 (CTLA-4) gene promoter (-318) and exon 1 (+49).

METHODS: CTLA-4 promoter (-318 T/C) and exon1 (+49A/G) polymorphisms were genotyped via restriction fragment length polymorphism methods in 62 Chinese AIH patients, 77 Chinese PBC patients and 160 healthy controls.

RESULTS: We found a significant association in CTLA-4 gene exon1 49 A/G polymorphism between PBC patients and controls ($P = 0.006$) and the frequency of G alleles was significantly increased in comparison with controls ($P = 0.0046$, OR = 1.8). We also found the frequency of C alleles in promoter -318 was significantly increased in AIH patients compared with controls ($P = 0.02$, OR = 0.41). Although the genotype distribution of the CTLA-4 exon 1-promoter gene was not significantly different between AIH and PBC patients and controls, the occurrence of GG-CC was increased in two groups of patients (AIH: 32.3%, PBC: 37.7%, control: 22.5%).

CONCLUSION: Polymorphisms of CTLA-4 gene probably confer susceptibility to AIH and PBC in Chinese population.

Fan LY, Tu XQ, Cheng QB, Zhu Y, Feltens R, Pfeiffer T, Zhong RQ. Cytotoxic T lymphocyte associated antigen-4 gene polymorphisms confer susceptibility to primary biliary cirrhosis and autoimmune hepatitis in Chinese population. *World J Gastroenterol* 2004; 10(20): 3056-3059

<http://www.wjgnet.com/1007-9327/10/3056.asp>

INTRODUCTION

Autoimmune hepatitis (AIH) is an immune-mediated chronic inflammation of liver tissue. It is characterized by elevated serum transaminase levels, hypergammaglobulinemia, serum autoantibodies, and a good response to immunosuppressive

therapy^[1,2]. Although its etiology is unknown, genetic factors have been implicated to be involved in its pathogenesis. In previous studies human HLA DRB1*0301, DRB*0401 (in Caucasian) and DRB1*0405 (in Chinese) have been identified as independent determinants of susceptibility to AIH^[3,4]. In addition, tumor necrosis factor α (TNF- α) and complement C4 alleles have been associated with AIH^[5].

Primary biliary cirrhosis (PBC) is also an immune-mediated chronic disease in which progressive destruction of the bile ducts leads to fibrosis and cirrhosis. It exhibits specific autoantibodies and disorder of liver function. Twin and family studies suggest that there is a genetic component in PBC^[6,7]. The genetic typing of HLA class II and III alleles revealed a highly significant increase of HLA DRw8 and C4A-Q0 alleles in patients with PBC compared with controls, and the HLA DRB1*0801-DQA1*0401-DQB1*0402 haplotype was considered to represent a marker of disease progression^[8]. Polymorphism of the interleukin 1 (IL-1) and vitamin D receptor genes have been reported to be associated with PBC^[8,9]. These genes, however, are neither necessary nor sufficient to cause AIH or PBC.

Cytotoxic T lymphocyte antigen-4 (CTLA-4) is involved in the regulation of T cells and is a member of the same family of cell surface molecules as CD28^[10]. CTLA-4 antigen is only expressed on activated T cells, which binds to B7 molecules on antigen-presenting cells. CTLA-4-B7 binding delivers negative signals to T cells affecting T cell proliferation, cytokine production, and immune responses. Breakdown in the B7-CD28/CTLA-4 pathway could alter T-cell response and lead to autoimmune diseases^[11]. Many studies have shown that specific CTLA-4 gene polymorphisms confer susceptibility to several autoimmune diseases, such as Graves' disease, insulin-dependent diabetes mellitus^[12,13]. However, studies on the polymorphisms within CTLA-4 exon 1 (+49) and promoter (-318) gene in rheumatoid arthritis, multiple sclerosis and AIH have shown conflicting results in different ethnicities^[14-20].

In this study, we investigated whether the polymorphisms of CTLA-4 exon 1 (+49) and promoter (-318) genes were associated with susceptibility to AIH and PBC in the Chinese population.

MATERIALS AND METHODS

Patients and controls

Blood samples were obtained from 62 patients with autoimmune hepatitis (40 females; mean age: 50 years with range 16-76 years) and 77 patients with PBC (68 females; mean age: 51.34 years, range 32-79 years). AIH cases included 44 patients with antinuclear antibodies (titer >1:100), 15 patients with antismooth muscle antibodies, 4 patients with antibodies against soluble liver antigen/liver pancreas antigen, and 2 patients with anti-liver/kidney microsomal antibodies. The diagnosis of AIH was based on the revised criteria defined by the International Autoimmune Hepatitis Group. Patients with PBC were positive for antimitochondrial antibody (titer >1:1000) and type M2 antimitochondrial antibody, and had abnormal liver function test, in which 10 patients had liver biopsy. Control group consisted of 160 healthy blood donors (100 females).

DNA preparation

Blood samples from all subjects were obtained for DNA extraction. Blood was collected in EDTA tubes and DNA was extracted using the method of proteinase K treatment and phenol/choroform extraction.

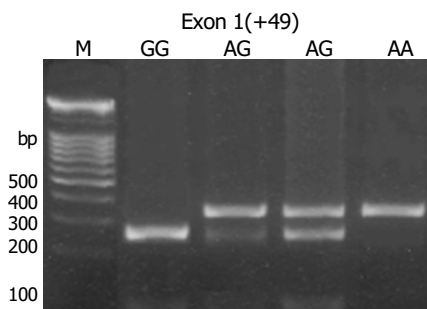


Figure 1 Gel electrophoresis of the products of BbvI restriction analysis.

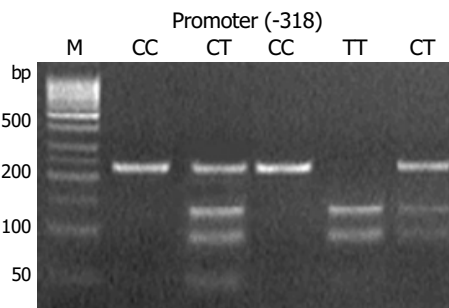


Figure 2 Gel electrophoresis of the products of Tru9 I restriction analysis.

Polymorphism typing of CTLA-4 exon 1 (+49) and promoter (-318)

CTLA-4 exon 1 +49 polymorphism was defined using a polymerase chain reaction-restriction fragment length polymorphism (PCR-RFLP) with BbvI restriction enzyme. PCR was carried out using a forward primer 5'-CCACGGCTTCCTTTCTCGTA-3' and a reverse primer 5'-AGTCTCACTCACCTTTGCAG-3'. Using a MJ PTC-200 Peltier thermal cycler samples were subjected to initial denaturation for 2 min at 95 °C, 40 cycles at 94 °C for 30 s, for denaturing, 45 s at 50 °C for annealing and 30 s at 72 °C for extension. A 327 bp fragment containing +49 A/G polymorphism in exon 1 of CTLA-4 was amplified. The substitution created a Bbv I restriction site in G allele. Amplified products were incubated at 65 °C for 2 h using 2 U of Bbv I per reaction. Digested products were electrophoresed on a 2.0% agarose

gel. Digested G allele yielded fragments of 244 bp and 84 bp, and an allele yielded a 327 bp fragment (Figure 1).

The CTLA-4 promoter polymorphism at position -318 was defined using PCR-RFLP and Tru9 I restriction enzyme. To amplify the target DNA in CTLA-4 promoter, PCR was performed with the forward primer 5'-AAATGAATTGGACTGGATGGT-3' and reverse primer 5'-TTACGAGAAAGGAAGCCGTG-3'. A247 bp fragment was amplified. The following conditions were applied: initial denaturation for 2 min at 95 °C, followed by 40 cycles (at 94 °C for 40 s, at 60 °C for 45 s, 60 °C, at 72 °C for 30 s), and a final extension for 2 min at 72 °C. PCR fragments with thymine at position -318 were cut into three fragments (21, 96 and 130 bp), whereas fragments with cytosine at the same position only had the restriction site at 21 bp (Figure 2).

Statistical analysis

Hardy-Weinberg equilibrium was tested by calculating the χ^2 for goodness of fit. Frequencies of the genotypes, alleles and phenotypes were analyzed by using chi-square test. Statistical significance was defined as $P < 0.05$. The odds ratio (OR) was calculated to measure the strength of the association observed. Calculation was made by using the Internet programs from www.myatt.demon.co.uk/epicalc.htm.

RESULTS

Samples from 62 cases of AIH, 77 cases of PBC and 160 control subjects were successfully genotyped for CTLA-4 exon 1 +49 and promoter -318 polymorphisms. Allelic variation at the +49 site of CTLA-4 exon 1 was significantly associated with PBC ($P = 0.006$). Compared with controls, the frequency of G alleles was increased in patients with PBC (PBC, 70.1%, controls, 56.6%, $P = 0.0046$, OR = 1.8). Although G allele was more frequent in AIH patients (62.9%), the distribution of alleles and phenotype at the +49 site were not associated with AIH (Table 1).

In CTLA-4 promoter (-318) polymorphisms between AIH, PBC patients and controls, CC genotypes occurred more frequently than TT genotypes was less frequently in patients than in controls, but the distribution of genotypes was not significantly different between AIH, PBC patients and controls ($P > 0.05$). Compared with controls, the frequency of C alleles was significantly increased (PBC, 93.6%, controls, 85.6%, $P = 0.02$, OR = 0.41) in patients with AIH (Table 2). The genotype distribution of CTLA-4 exon 1-promoter gene had no significant difference between PBC patients and controls ($\chi^2 = 13.02$, $P = 0.07$), but the frequency of GG-CC was increased in patients with PBC (PBC, 37.7%, controls, 22.5%). The frequency of GG-CC was also higher in AIH patients (32.3%), but the genotype distribution of CTLA-4 exon 1-promoter gene did not reach statistical

Table 1 CTLA-4 exon 1 +49 polymorphism in patients with AIH, PBC and controls

	Control (%)	AIH (%)	<i>P</i>	PBC (%)	<i>P</i>
Genotype frequencies			0.4		0.006
A/A	23 (14.4)	6 (9.7)		6 (7.8)	
A/G	93 (58.1)	34 (54.8)		34 (44.2)	
G/G	44 (27.5)	22 (35.5)		37 (48.0)	
Allele frequencies ⁽¹⁾			0.22		0.0046
A	139 (43.4)	46 (37.1)		46 (29.9)	
G	181 (56.6)	78 (62.9)		108 (70.1)	
Phenotype frequencies ⁽²⁾			0.32		0.035
A positive	116 (72.5)	40 (64.5)		40 (51.9)	
G positive	137 (85.6)	56 (90.3)		71 (92.2)	

¹Odds ratio for G allele (AIH) = 1.3, 95% CI = 0.85-1.99; Odds ratio for G allele (PBC) = 1, 95% CI = 1.20-2.72, ²Odds ratio for G phenotype (AIH) = 1.27, 95% CI = 0.79-2.05; Odds ratio for G phenotype (PBC) = 1.65, 95% CI = 1.03-2.63.

Table 2 CTLA-4 promoter -318 polymorphism in patients with AIH, PBC and controls

	Control (%)	AIH (%)	P	PBC (%)	P
Genotype frequencies			0.10		0.55
C/C	122 (76.3)	54 (87.1)		3 (81.8)	
C/T	30 (18.8)	8 (12.9)		12 (15.6)	
T/T	8 (5.0)	0 (0)		2 (2.6)	
Allele ⁽¹⁾			0.02		0.23
C	274 (85.6)	116 (93.6)		138 (89.6)	
T	46 (14.4)	8 (6.5)		16 (10.4)	
Phenotype frequencies ⁽²⁾			0.11		0.39
C positive	152 (95.0)	62 (100)		75 (97.4)	
T positive	38 (23.8)	8 (12.9)		14 (18.2)	

¹Odds ratio for C allele (AIH) = 0.41, 95% CI = 0.19-0.90; Odds ratio for C allele (PBC) = 0.69, 95% CI = 0.38-1.26, ²Odds ratio for C phenotype (AIH) = 0.52, 95% CI = 0.23-1.17; Odds ratio for C phenotype (PBC) = 0.75, 95% CI = 0.38-1.46.

difference between AIH patients and controls ($\chi^2 = 6.82$, $P = 0.45$) (Table 3).

Table 3 CTLA-4 exon 1- promoter genotypes in patients with AIH, PBC and controls

	Control	AIH ⁽¹⁾	PBC ⁽²⁾
AA-CC	12 (7.5)	4 (6.5)	4 (5.2)
AA-CT	7 (4.4)	2 (3.2)	1 (1.3)
AA-TT	4 (2.5)	0 (0)	1 (1.3)
AG-CC	70 (43.8)	30 (48.4)	30 (39.0)
AG-CT	19 (11.9)	4 (6.5)	3 (3.9)
AG-TT	4 (2.5)	0 (0)	1 (1.3)
GG-CC	36 (22.5)	20 (32.3)	29 (37.7)
GG-CT	8 (5.0)	2 (3.2)	8 (10.4)
Total	160 (100)	62 (100)	77 (100)

¹AIH vs controls: $\chi^2 = 6.82$, $P = 0.45$; ²PBC vs controls: $\chi^2 = 13.02$, $P = 0.07$.

DISCUSSION

CTLA-4 is essentially a costimulatory receptor that controls activation of T cells. In contrast to CD28, CTLA-4 delivers negative signals to T cells. CTLA-4 gene is located on chromosome 2q33 and three CTLA-4 gene polymorphisms in exon 1 (adenine or guanine at position) and in promoter -318, and a microsatellite (AT) n marker at position 642 of the 3'-untranslated region of exon 3^[21,22]. The polymorphism, A/G variation at position +49 (+49*A/G) in the first exon of the gene leads to the change of threonine to alanine in the leader peptide. Recently, several independent studies reported a reduced inhibitory function of CTLA-4 in individuals with certain CTLA-4 genotypes^[12,23]. Kouki studied the CTLA-4 expression and T cell proliferative responses in patients with Graves' disease and healthy controls genotyped for +49*A/G. They found a correlation of +49*G/G genotype with reduced inhibitory function of CTLA-4, and suggested that this particular polymorphism was the actual disease-associated allele^[24]. Maurer also got the same result^[25]. A similar effect on CTLA-4 function has been suggested for the second polymorphism^[26]. Wang showed that -318T allele was associated with a higher promoter activity than -318C alleles. The presence of -318T alleles may thus contribute to up regulation of the expression of CTLA-4, and consequently represents one mechanism to inhibit exaggerated immune activity.

Studies on the CTLA-4 polymorphisms in autoimmune liver diseases have shown conflicting results on the relations between the polymorphisms of CTLA-4 exon 1 +49 and AIH^[18,20,27].

Agarwal indicated that CTLA-4 G allele at exon 1 +49 was more common in European Caucasoid patients with type 1 AIH and represented a second susceptibility allele, and there might be synergy between HLA-DRB1*0301 and GG genotype in terms of disease risk. Djilali-Saiah found that the presence of +49GG predisposed to AIH type 1 in Canada children. However, Bittencourt found no associations between AIH (type 1 and type 2) and exon 1 CTLA-4 gene polymorphisms at position 49 in the Brazilian population.

In our study, we found that the frequency of -318C alleles was significantly increased in AIH patients compared with the control subjects, and GG-CC genotype occurred more frequently in CTLA-4 exon 1-promoter gene. It is therefore possible that the -318C allele and GG-CC genotype of CTLA-4 may contribute to susceptibility to Chinese patients with AIH. To our knowledge, this is the first report concerning an association of CTLA-4 promoter -318 polymorphism with AIH. In addition, we found a strong association between CTLA-4 exon 1 (+49) polymorphism and PBC, the GG genotype confers susceptibility to PBC in Chinese population. This result was coincident with Agarwal and colleague's conclusion^[19]. Likewise, the GG-CC genotype occurred more frequently compared with control subjects.

AIH and PBC are two autoimmune diseases of unknown pathogenesis. There is a general agreement that induction involves CD4⁺ T cells in the pathogenesis of AIH, but it is still not clear whether the liver damage was due to direct T cell cytotoxicity or involved autoantibodies, either through complement-mediated or antibody-dependent (ADCC) cytotoxic reactions^[28]. T cell responses would certainly participate in the pathogenesis of PBC, as judged by histochemical staining of tissue samples, and by analyzing T cell lines that proliferate in the presence of putative mitochondrial autoantigens^[29]. So we speculate that the single nucleotide polymorphism (SNP) of CTLA-4 (exon 1 +49 and promoter -318), and the interaction between these two SNPs may alter the inhibitory effect of CTLA-4 on T cells, and it may be an important factor in the pathogenesis of autoimmune hepatitis and primary biliary cirrhosis.

Besides CTLA-4 exon 1 (+49) and promoter (-318) polymorphisms, the CTLA-4 (AT) n microsatellite within the 3'-untranslated region of exon 3 was also a good candidate gene of autoimmune disease^[21]. Previous studies demonstrated that AT-rich tracks might contribute to mRNA instability^[30,31]. If the size of CTLA-4 AT tract limited the accumulation of CTLA-4 mRNA, down-regulation of CTLA-4 expression might account for the increase in the risk of an autoimmune disease. Several studies found that CTLA-4 (AT) n polymorphism was associated with Graves' disease and rheumatoid arthritis^[32,33]. Since it may be involved in mRNA stability, further studies are needed to determine the relations between CTLA-4 (AT) n polymorphism and autoimmune liver diseases.

In summary, this study showed a strong association between CTLA-4 exon 1 polymorphism (G-carrying genotypes) and PBC, and a significant association between CTLA-4 promoter -318C allele and AIH. In addition, we found that GG-CC genotype of CTLA-4 exon 1-promoter seemed to be susceptible to Chinese patients with AIH and PBC.

REFERENCES

- 1 **Krawitt EL**, Wiesner RH, Nishioka M. Autoimmune liver diseases. Second edition. The Netherlands: *Elsevier Science B.V* 1998: 343-360
- 2 **Krawitt EL**, Wiesner RH, Nishioka M. Autoimmune liver diseases. Second edition. The Netherlands: *Elsevier Science B.V* 1998: 361-380
- 3 **Czaja AJ**, Strettell MD, Thomson LJ, Santrach PJ, Moore SB, Donaldson PT, Williams R. Associations between alleles of the major histocompatibility complex and type 1 autoimmune hepatitis. *Hepatology* 1997; **25**: 317-323
- 4 **Qiu D**, Ma X. Relationship between type I autoimmune hepatitis and alleles of HLA-DRB1 in Chinese patients of Shanghai area. *Zhonghua Ganzangbing Zazhi* 2002; **10**: 347-349
- 5 **Czaja AJ**, Cookson S, Constantini PK, Clare M, Underhill JA, Donaldson PT. Cytokine polymorphisms associated with clinical features and treatment outcome in type 1 autoimmune hepatitis. *Gastroenterology* 1999; **117**: 645-652
- 6 **Jones DE**, Watt FE, Metcalf JV, Bassendine MF, James OF. Familial primary biliary cirrhosis reassessed: a geographically-based population study. *J Hepatol* 1999; **30**: 402-407
- 7 **Brind AM**, Bray GP, Portmann BC, Williams R. Prevalence and pattern of familial disease in primary biliary cirrhosis. *Gut* 1995; **36**: 615-617
- 8 **Donaldson P**, Agarwal K, Craggs A, Craig W, James O, Jones D. HLA and interleukin 1 gene polymorphisms in primary biliary cirrhosis: associations with disease progression and disease susceptibility. *Gut* 2001; **48**: 397-402
- 9 **Vogel A**, Strassburg CP, Manns MP. Genetic association of vitamin D receptor polymorphisms with primary biliary cirrhosis and autoimmune hepatitis. *Hepatology* 2002; **35**: 126-131
- 10 **Thompson CB**, Allison JP. The emerging role of CTLA-4 as an immune attenuator. *Immunity* 1997; **7**: 445-450
- 11 **Tivol EA**, Schweitzer AN, Sharpe AH. Costimulation and autoimmunity. *Curr Opin Immunol* 1996; **8**: 822-830
- 12 **Vaidya B**, Imrie H, Perros P, Young ET, Kelly WF, Carr D, Large DM, Toft AD, McCarthy MI, Kendall-Taylor P, Pearce SH. The cytotoxic T lymphocyte antigen-4 is a major Graves' disease locus. *Hum Mol Genet* 1999; **8**: 1195-1199
- 13 **Nistico L**, Buzzetti R, Pritchard LE, Van der Auwera B, Giovannini C, Bosi E, Larrad MT, Rios MS, Chow CC, Cockram CS, Jacobs K, Mijovic C, Bain SC, Barnett AH, Vandewalle CL, Schuit F, Gorus FK, Tosi R, Pozzilli P, Todd JA. The CTLA-4 gene region of chromosome 2q33 is linked to, and associated with, type I diabetes. Belgian Diabetes Registry. *Hum Mol Genet* 1996; **7**: 1075-1080
- 14 **Gonzalez-Escribano MF**, Rodriguez R, Valenzuela A, Garcia A, Garcia-Lozano JR, Nunez-Roldan A. CTLA4 polymorphisms in Spanish patients with rheumatoid arthritis. *Tissue Antigens* 1999; **53**: 296-300
- 15 **Lee YH**, Choi SJ, Ji JD, Song GG. No association of polymorphisms of the CTLA-4 exon 1 (+49) and promoter (-318) genes with rheumatoid arthritis in the Korean population. *Scand J Rheumatol* 2002; **31**: 266-270
- 16 **Bocko D**, Bilinska M, Dobosz T, Zoledziewska M, Suwalska K, Tutak A, Gruszka E, Frydecka I. Lack of association between an exon 1 CTLA-4 gene polymorphism A (49) G and multiple sclerosis in a Polish population of the Lower Silesia region. *Arch Immunol Ther Exp* 2003; **51**: 201-205
- 17 **Kantarci OH**, Hebrink DD, Achenbach SJ, Atkinson EJ, Waliszewska A, Buckle G, McMurray CT, de Andrade M, Hafler DA, Weinshenker BG. CTLA4 is associated with susceptibility to multiple sclerosis. *J Neuroimmunol* 2003; **134**: 133-141
- 18 **Agarwal K**, Czaja AJ, Jones DE, Donaldson PT. Cytotoxic T lymphocyte antigen-4 (CTLA-4) gene polymorphisms and susceptibility to type 1 autoimmune hepatitis. *Hepatology* 2000; **31**: 49-53
- 19 **Agarwal K**, Jones DE, Daly AK, James OF, Vaidya B, Pearce S, Bassendine MF. CTLA-4 gene polymorphism confers susceptibility to primary biliary cirrhosis. *J Hepatol* 2000; **32**: 538-541
- 20 **Bittencourt PL**, Palacios SA, Cancado EL, Porta G, Carrilho FJ, Laudanna AA, Kalil J, Goldberg AC. Cytotoxic T lymphocyte antigen-4 gene polymorphisms do not confer susceptibility to autoimmune hepatitis types 1 and 2 in Brazil. *Am J Gastroenterol* 2003; **98**: 1616-1620
- 21 **Deichmann K**, Heinzmann A, Bruggenolte E, Forster J, Kuehr J. An Mse I RFLP in the human CTLA4 promoter. *Biochem Biophys Res Commun* 1996; **225**: 817-818
- 22 **Polymeropoulos MH**, Xiao H, Rath DS, Merrill CR. Dinucleotide repeat polymorphism at the human CTLA4 gene. *Nucleic Acids Res* 1991; **19**: 4018
- 23 **Donner H**, Rau H, Walfish PG, Braun J, Siegmund T, Finke R, Herwig J, Usadel KH, Badenhop K. CTLA4 alanine-17 confers genetic susceptibility to Graves' disease and to type 1 diabetes mellitus. *J Clin Endocrinol Metab* 1997; **82**: 143-146
- 24 **Kouki T**, Sawai Y, Gardine CA, Fisfalen ME, Alegre ML, DeGroot LJ. CTLA-4 gene polymorphism at position 49 in exon 1 reduces the inhibitory function of CTLA-4 and contributes to the pathogenesis of Graves' disease. *J Immunol* 2000; **165**: 6606-6611
- 25 **Maurer M**, Loserth S, Kolb-Maurer A, Ponath A, Wiese S, Kruse N, Rieckmann P. A polymorphism in the human cytotoxic T-lymphocyte antigen 4 (CTLA4) gene (exon 1 +49) alters T-cell activation. *Immunogenetics* 2002; **54**: 1-8
- 26 **Wang XB**, Zhao X, Giscombe R, Lefvert AK. A CTLA-4 gene polymorphism at position -318 in the promoter region affects the expression of protein. *Genes Immun* 2002; **3**: 233-234
- 27 **Djilali-Saiah I**, Ouellette P, Caillat-Zucman S, Debray D, Kohn JI, Alvarez F. CTLA-4/CD 28 region polymorphisms in children from families with autoimmune hepatitis. *Hum Immunol* 2001; **62**: 1356-1362
- 28 **Krawitt EL**, Wiesner RH, Nishioka M. Autoimmune liver diseases. Second edition. The Netherlands: *Elsevier Science B.V* 1998: 35-48
- 29 **Krawitt EL**, Wiesner RH, Nishioka M. Autoimmune liver diseases. Second edition. *Amsterdam: Elsevier* 1998: 49-69
- 30 **Shaw G**, Kamen R. A conserved AU sequence from the 3' untranslated region of GM-CSF mRNA mediates selective mRNA degradation. *Cell* 1986; **46**: 659-667
- 31 **Jackson RJ**. Cytoplasmic regulation of mRNA function: the importance of the 3' untranslated region. *Cell* 1993; **74**: 9-14
- 32 **Hadj Kacem H**, Kaddour N, Adyel FZ, Bahloul Z, Ayadi H. HLA-DQB1 CAR1/CAR2, TNF α IR2/IR4 and CTLA-4 polymorphisms in Tunisian patients with rheumatoid arthritis and Sjögren's syndrome. *Rheumatology* 2001; **40**: 1370-1374
- 33 **Kotsa K**, Watson PF, Weetman AP. A CTLA-4 gene polymorphism is associated with both Graves disease and autoimmune hypothyroidism. *Clin Endocrinol* 1997; **46**: 551-554

Diagnostic and surgical therapeutic features of extrahepatic bile duct carcinoma without jaundice

Hui-Huan Tang, Shi Chang, Xian-Wei Wang, Yun Huang, Xue-Jun Gong, Jun Zhou

Hui-Huan Tang, Shi Chang, Xian-Wei Wang, Yun Huang, Xue-Jun Gong, Jun Zhou, Department of Surgery, Xiangya Hospital of Central South University, Changsha 410008, Hunan Province, China
Correspondence to: Shi Chang, Department of Surgery, Xiangya Hospital of Central South University, Changsha 410008, Hunan Province, China. changshi@medmail.com.cn

Telephone: +86-731-4327468

Received: 2003-11-12 **Accepted:** 2003-12-08

Abstract

AIM: To analyze the diagnostic and therapeutic features of extrahepatic bile duct carcinoma (EBDC) without jaundice.

METHODS: Between 1985 and 1999, 101 patients underwent surgery for EBDC in Xiangya Hospital. These patients were divided into two groups: 84 jaundiced patients and 17 non-jaundiced patients according to preoperative serum total bilirubin levels. The clinical manifestations, laboratory findings, location, pathology and surgical resectability of the tumors were compared between the two groups.

RESULTS: The laboratory parameters such as hemoglobin, serum albumin ALB, AKP, γ -GT, and sonography appearance were similar between the two groups, and there was no significant difference in tumor location, pathological type and resectability. However, the number of non-jaundiced patients associated with cholelithiasis was significantly greater than that of jaundiced patients ($P = 0.008$).

CONCLUSION: The presence of jaundice is not a reliable criterion for the prediction of the resectability and the extent of tumor progression in extrahepatic bile duct carcinoma. Decreased levels of blood hemoglobin and serum albumin, elevated levels of AKP and γ -GT, and /or abnormal sonography may be suggestive. Biopsy of a stenotic or thickened bile duct is strongly recommended for a correct diagnosis before the appearance of jaundice.

Tang HH, Chang S, Wang XW, Huang Y, Gong XJ, Zhou J. Diagnostic and surgical therapeutic features of extrahepatic bile duct carcinoma without jaundice. *World J Gastroenterol* 2004; 10(20): 3060-3061

<http://www.wjgnet.com/1007-9327/10/3060.asp>

INTRODUCTION

Primary carcinoma of the extrahepatic bile duct is an uncommon malignant tumor, with reported incidence rate of about 0.01-0.46%. About 2% of patients who died of cancer were autopsied to have this disease^[1-4]. Jaundice is generally thought to be the most important factor in the diagnosis of this disease, but there are still few cases seeking doctors' consultation before jaundice appears^[5-9]. Those patients could be underdiagnosed or misdiagnosed because of atypical clinical symptoms. In this study, the diagnostic and therapeutic features of bile duct carcinoma without jaundice were compared with those with jaundice.

MATERIALS AND METHODS

From January 1984 to December 1999, two hundred and thirty-nine patients who were diagnosed as extrahepatic bile duct carcinoma were admitted to Xiangya Hospital. One hundred and one were operated and the diagnosis was confirmed by pathology. Patients with carcinomas of gallbladder, intrahepatic bile duct and ampulla of Vater were excluded from the study. The patients under studies consisted of 58 males and 43 females, aged 27 to 76 years (an average age of 61.7 years).

According to the level of serum total bilirubin (STB), the patients were divided into non-jaundiced group (17 patients, $STB \leq 2.0$ mg/dL at the time of diagnosis) and jaundiced group (84 patients, $STB > 2.0$ mg/dL). Clinical data included symptoms, laboratory results, imaging findings, pathological results, treatments and resectabilities.

Statistical analysis

The difference between the two groups was compared using chi-square analysis and Student's *t* test. $P < 0.05$ was considered statistically significant.

RESULTS

Symptoms and signs

Fifteen (88.2%) patients in the non-jaundiced group had anorexia or/and vomiting, abdominal pain compared with 63 (75.0%) in the jaundiced group. Eight (47.1%) patients in the non-jaundiced group and fifty-seven (67.9%) patients in the jaundiced group were found to show positive signs in liver, spleen or gallbladder enlargement. (Table 1).

Laboratory examination

The patients showed no difference in the levels of abnormal serum albumin, alkaline phosphates (AKP), γ -glutamyltranspeptidase (γ -GT), except STB level (Table 2).

Image examination

All patients in the non-jaundiced group underwent sonography. The results showed segmental stenosis of extrahepatic bile duct, thickening of the bile duct wall, and dilatation of intra- or extra-hepatic bile duct proximal to the stenosis. Sixty-seven out of 78 patients showed stenosis or neoplastic space-occupying lesions within the extrahepatic bile duct.

Operation findings

During the operation, 59 patients had neoplasms located in the upper extrahepatic bile duct while 8 in the middle and 34 in the lower. There was no difference with regard to localization of the tumor between the two groups.

Pathological features

All patients were proved to have adenocarcinoma. The patients were categorized into three different grades by the degree of differentiation. The results showed that there was no difference between the patients with or without jaundice.

Treatment

Radical resection, biliary bypass, external drainage or biopsy

were performed according to the surgical findings. There was no difference in tumor resectability between the two groups ($P>0.05$, Table 3).

Table 1 Symptoms and signs

Symptom	Non-jaundiced		Jaundiced		P value
	No.	%	No.	%	
Abdominal discomfort	15	88.2	63	75.0	>0.05
Liver or gallbladder palpable	8	47.1	57	67.9	>0.05
Cholelithiasis	11	64.7	26	31.0	<0.05 ^a

No significant difference was found between the two groups in the clinical symptoms and signs. In the non-jaundice group, the rate of combined cholelithiasis was obviously higher than in the jaundice group.

Table 2 Laboratory data

	Non-jaundiced		Jaundiced		P value
	No.	%	No.	%	
Descending of HB	8	47.1	45	53.6	>0.05
Ascending of AKP	8	72.7	56	86.2	>0.05
Ascending of γ -GT	4	66.7	28	93.3	>0.05
Descending of ALB	4	23.5	39	47.0	>0.05

No significant difference was found between the two groups in laboratory data.

Table 3 Tumor location, pathological type, treatment

	Non-jaundiced		Jaundiced		P value
	No.	%	No.	%	
Location					
Upper	11	64.7	48	57.1	
middle	0	0.0	8	9.6	>0.05
Lower	6	35.3	28	33.3	
Differential					
Good	6	35.3	48	57.1	
mild	8	47.1	27	32.1	>0.05
Poor	3	17.7	9	10.8	
Biopsy	3	17.7	8	9.5	
Treatment					
drainage	9	52.9	43	51.2	>0.05
By pass	0	0.0	1	1.2	
Radical	5	29.4	32	38.1	

No significant difference was found between the two groups in tumor locations, pathological types and treatment methods.

DISCUSSION

Jaundice is the early and main manifestation of extrahepatic bile duct carcinoma. It has been reported to be the initial sign in 83-97% of patients^[5-9]. However, there are few patients coming to hospital before the appearance of jaundice. In the present study 16.8% of the patients with EBDC were diagnosed before the presence of jaundice. These patients were likely to be neglected during busy outpatient service. We found that, there were still some clues to the diagnosis of bile duct carcinoma for these patients without jaundice. Some laboratory parameters, such as hemoglobin, serum albumin, AKP and γ -GT may be suggestive.

Sonography is almost the first tool for the diagnosis of extrahepatic bile duct carcinoma because it is non-invasive and less expensive. Ninety-five of the patients underwent sonography in our study, of whom 84 (88.4%) had positive findings, such as duct stenosis, thickness of the bile duct wall or space-occupying lesions within the duct. The results were in accordance with those documented in the literature^[10-12].

The relationship between choledocholithiasis and bile duct carcinoma is still unclear. As reported, 6-37% of extrahepatic bile duct carcinomas were associated with bile duct stones^[13]. In the present study the number of patients who suffered from choledocholithiasis in the non-jaundiced group was significantly higher than that in the jaundiced group ($P<0.05$). Two factors may contribute to this finding. First, for patients with bile duct stones, the clinical manifestations were so typical that the doctor would pay more attention to the biliary system. Second, during the operation for choledocholithiasis, we usually took the whole layer of bile duct wall for biopsy whenever there was stenosis, sclerosis or nodular change in the bile duct. Eight patients were diagnosed by this means and radical resection was performed.

It was reported that extrahepatic bile duct carcinoma without jaundice occurred in the early stage of the disease. The tumor was well differentiated and the resection rate was usually high^[8]. However, there was no difference between the two groups in our study. The radical resection rate was 29.4% in the non-jaundiced group and 38.1% in the jaundiced group ($P>0.05$). Liver and/or intrabdominal lymph node metastases were found in 12 patients without jaundice. We suggest that the presence of jaundice cannot be taken as the major criterion to predict the tumor resectability or the extent of tumor progression.

ACKNOWLEDGEMENT

We are grateful to Professor Zhong-Shu Yan for his assistance in preparing this manuscript.

REFERENCES

- 1 **Helling TS.** Carcinoma of the proximal bile duct. *J Am Coll Surg* 1994; **178**: 97-106
- 2 **de Groen PC,** Gores GJ, LaRusso NF, Gunderson LL, Nagorney DM. Biliary tract cancers. *N Engl J Med* 1999; **341**: 1368-1378
- 3 **Chamberlain RS,** Blumgart LH. Hilar cholangiocarcinoma: a review and commentary. *Ann Surg Oncol* 2000; **7**: 55-66
- 4 **Tsujino K,** Landry JC, Smith RG, Keller JW, Williams WH, Davis LW. Definitive radiation therapy for extrahepatic bile duct carcinoma. *Radiology* 1995; **196**: 275-280
- 5 **Chung C,** Bautista N, O'Connell TX. Prognosis and treatment of bile duct carcinoma. *Am Surg* 1998; **64**: 921-925
- 6 **Miyazaki M,** Ito H, Nakagawa K, Ambiru S, Shimizu H, Shimizu Y, Kato A, Nakamura S, Omoto H, Nakajima N, Kimura F, Suwa T. Aggressive surgical approaches to hilar cholangiocarcinoma: hepatic or local resection? *Surgery* 1998; **123**: 131-136
- 7 **Suzuki M,** Takahashi T, Ouchi K, Matsuno S. The development and extension of hepatohilar bile duct carcinoma. A three-dimensional tumor mapping in the intrahepatic biliary tree visualized with the aid of a graphics computer system. *Cancer* 1989; **64**: 658-666
- 8 **Sugiyama M,** Atomi Y, Kuroda A, Muto T. Bile duct carcinoma without jaundice: clues to early diagnosis. *Hepatogastroenterology* 1997; **44**: 1477-1483
- 9 **Tamada K,** Sugano K. Diagnosis and non-surgical treatment of bile duct carcinoma: developments in the past decade. *J Gastroenterol* 2000; **35**: 319-325
- 10 **Choi BI,** Lee JH, Han MC, Kim SH, Yi JG, Kim CW. Hilar Cholangiocarcinoma: comparative study with sonography and CT. *Radiology* 1989; **172**: 689-692
- 11 **Chou FF,** Sheen-Chen SM, Chen YS, Chen CL. Surgical treatment of cholangiocarcinoma. *Hepatogastroenterology* 1997; **44**: 760-765
- 12 **Looser C,** Stain SC, Baer HU, Triller J, Blumgart LH. Staging of hilar cholangiocarcinoma by ultrasound and duplex sonography: a comparison with angiography and operative findings. *Br J Radiol* 1992; **65**: 871-877
- 13 **Schoenthaler R,** Phillips TL, Castro J, Efrid JT, Better A, Way LW. Carcinoma of the extrahepatic bile ducts. The university of california at san francisco experience. *Ann Surg* 1994; **219**: 267-274

Choledochal cysts in pregnancy: Case management and literature review

De-Quan Wu, Long-Xian Zheng, Qiu-Shi Wang, Wen-Hua Tan, Shuang-Jiu Hu, Pei-Ling Li

De-Quan Wu, Long-Xian Zheng, Qiu-Shi Wang, Department of Surgery, the Second Affiliated Hospital of Harbin Medical University, Harbin 150086, Heilongjiang Province, China

Wen-Hua Tan, Shuang-Jiu Hu, Pei-Ling Li, Department of Obstetrics and Gynecology, the Second Affiliated Hospital of Harbin Medical University, Harbin 150086, Heilongjiang Province, China

Correspondence to: Professor De-Quan Wu, Department of Surgery, the Second Affiliated Hospital of Harbin Medical University, 157 Baojian Road, City of Harbin, Harbin 150086, Heilongjiang Province, China. zhenglxhrbmu@hotmail.com

Telephone: +86-451-86605411

Received: 2004-02-14 **Accepted:** 2004-02-21

Abstract

AIM: To evaluate the diagnosis, management principles and long-term results of congenital choledochal cysts in pregnancy.

METHODS: Three adult patients were diagnosed as choledochal cysts in pregnancy from 1986 to 1989 and their long-term results were evaluated.

RESULTS: The first patient had a Roux-en-Y cysto-jejunosomy with T-tube external drainage and died of septic shock and multi-organ failure 25 d after operation. In the second patient, 4 wk after percutaneous trans-choledochal cyst was drained externally with a catheter under US guidance, four weeks later the patient delivered vaginally, and had a cysto-jejunosomy 3 mo after delivery, and lived well without any complications for 15 years after operation. The third patient received Roux-en-Y cysto-jejunosomy after a vertex delivery by induced labor at 28 wk gestation, and demonstrated repetitively intermittent retrograde cholangitis within 10 years, and then died of well-differentiated congenital cholangioadenocarcinoma one month after re-operation with exploratory biopsy at the age of 36.

CONCLUSION: More conservative approaches such as external drainage of choledochal cyst should be considered for pregnant patients with high risk, complete excision of choledochal cyst during hepaticojejunosomy or modified hepaticojejunosomy is highly recommended at the optimal time.

Wu DQ, Zheng LX, Wang QS, Tan WH, Hu SJ, Li PL. Choledochal cysts in pregnancy: Case management and literature review. *World J Gastroenterol* 2004; 10(20): 3065-3069
<http://www.wjgnet.com/1007-9327/10/3065.asp>

INTRODUCTION

Choledochal cysts in pregnant women represent a diagnostic and therapeutic challenge to a broad spectrum of the medical profession. Not only the rare association, but also the clinical signs and symptoms are obscured by physiological changes that occur during pregnancy. As a result, diagnosis is often delayed until patients present with life-threatening complications. We

reported our experiences in managing three cases of choledochal cyst in pregnant patients.

MATERIALS AND METHODS

Three adult patients were diagnosed as choledochal cyst in pregnancy from 1986 to 1989 and their long-term results were studied retrospectively (Tables 1, 2).

RESULTS

A 27-year-old primigravida (patient No.1) at 20-wk gestation presented with jaundice, dark urine, nausea, anorexia, vomiting, intermittent upper abdominal pain, fever and weight loss during the past three months and was admitted to our hospital in February, 1986. Physical examination demonstrated a palpable 12 cm×10 cm mass in the upper right quadrant of the abdomen, a tender protuberant abdomen due to her pregnant state, and fullness in the right upper quadrant. Laboratory evaluation data are shown in Table 2. Ultrasound examination showed a cystic lesion, 12 cm×9 cm×10 cm at the right upper quadrant with a connection to tubular structure, and dilated intrahepatic ducts in both lobes of liver. Impressive diagnosis was gestation with a type IV choledochal cyst. Perioperative fluid therapy and transfusion were administered. A Roux-en-Y cysto-jejunosomy was performed for the choledochal cyst with T-tube external drainage in the proximal part of the cyst. Five hundred milliliter bile was drained from T-tube post-surgery and documented everyday. The patient was afebrile with normal vital signs, flatus was released on d 3 and 10 postoperation. Progressive nausea, vomiting, anorexia, occurred with aggravated jaundice, hypokalemia (2.8 mEq/L), serum electrolyte disturbance and hypoalbuminemia, and then developed to retrograde bile duct infection. The primigravida lost, her consciousness on day 19 postoperation. She was diagnosed as incipient (threatened) abortion, and died of septic shock and multi-organ failure on the 25th d postoperation.

Patient No.2 was a 23-year-old primigravida at 36-wk G1P1 gestation with choledochal cyst. She had intermittent upper abdominal pain, progressive nausea, anorexia, vomiting and abdominal tenderness in the upper right quadrant and epigastric burning during the past several weeks. She was admitted to our hospital in February 1987. Physical examination demonstrated a nontender protuberant abdomen due to her pregnant state, and fullness in the right upper quadrant. Her skin and sclera were slightly jaundiced. Sonographic evaluation of the right upper quadrant demonstrated an oval-shaped, 15 cm×16 cm×3 cm cystic mass arising from the portal hepatic separated from the gallbladder, and diffuse dilatation of intrahepatic left ductal system. Clinical diagnosis was a type IV choledochal cyst with gestation (G1P1). Laboratory evaluation data are shown in Table 2. Percutaneous trans-choledochal cyst operation was performed on the patient with a catheter placed for external drainage under the abdominal ultrasonography guidance. About 3000 mL sap green bile was excreted from the cyst, and then about 600 mL sap green bile was excreted daily. Gradually, her clinical conditions were improved and remained stable and her pregnancy progressed without problems. She delivered vaginally 4 wk later without

Table 1 Information in 3 patients diagnosed as choledochal cysts in pregnancy

Patients No.	Age(yr)	Type	Size (cm)	Chief Complaints	Treatment		Complication		Survival time (postoperation)	Prognosis (postoperation)
					Initial operation	Final operation	Early	Late		
1	27	IV	12×9×10	Abdominal pain Jaundice Abdominal mass	Roux-en-Y cystojejunostomy with T-tube external drainage		Septic shock and multi-organ failure	25 d	died	
2	23	IV	15×16×3	Abdominal pain Jaundice	Plasement and fixation of a catheterization	Roux-en-Y cystojejunostomy		15 yr	survived	
3	26	I	20×20×20	Jaundice Abdominal mass	Roux-en-Y cystojejunostomy	Exploratory biopsy	Retrograde cholangitis Intermittent recurrence of Retrograde cholangitis Cholangioadenocarcinoma	10 yr	died	

Table 2 Analysis of pre-operation laboratory values for 3 patients

Parameters	Normal range	Patient No. 1	Patient No. 2	Patient No. 3
Total bilirubin (μmol/L)	1.6-20.6	59	57	26
Direct bilirubin (μmol/L)	0-6.4	8.0	8.7	8.1
Alkaline phosphatase (U/L)	35-150	171	63	110
r-GT (U/L)	0-60	51	58	26
Aspartate aminotranferase (U/L)	0-40	37	37	37
Alanine aminotranferase (U/L)	0-40	5	11	102
Total protein (g/L)	60-85	40	67	55
Albumin (g/L)	35-55	18	39	32
Globin (g/L)	-	22	25	23
Potassium (mmol/L)	3.5-5.5	1.9	4.2	4
Sodium (mmol/L)	135-145	134	128	139
Chloride (mmol/L)	101-111	89.3	96.9	105
Hemoglobin (g/L)	120-160	74	150	122
Erythrocyte (10 ¹² /L)	3.5-5.5	2.4	4.81	3.9
Hemoleukocyte (10 ⁹ /L)	3.5-10	5.8	4.4	9.7
Platelet (10 ⁹ /L)	100-300	92	177	128

complications. As choledochal cyst was extensively attached to the surrounding tissues, it was dissected using cystojejunostomy 3 mo after delivery. Choledochal cyst was histologically confirmed. The patient was discharged from hospital 40 d postoperation and was well without any complications for 15 years.

Patient No.3, a 26-year-old multiparous woman at 28-wk gestation with choledochal cyst was admitted to our hospital in July 1989. Her chief complaint was jaundice and she had a palpable mass in the upper right quadrant of the abdomen during the past 20 d. On examination, the patient was afebrile with normal vital signs with skin and her sclera slightly jaundiced. She had a soft palpable 8 cm×10 cm mass in the upper right quadrant of the abdomen without tenderness. Laboratory evaluation data are shown in Table 2. Ultrasound examination showed a large cyst of 20 cm×20 cm×20 cm at the right upper quadrant connected to tubular structure. The patient gave a vertex delivery by induced labor at 28-wk gestation on the second day of admission. Following treatment with prophylactic antibiotics, the patient received Roux-en-Y cystojejunostomy on d 8 after delivery. The patient had 4 or 5 times of recurrence of intermittent retrograde cholangitis annually for 10 years, lasting for about 20 d each time, and relieved after a few days of conservative antibiotics. However, the patient was not re-operated due to the extensive adherence with surrounding tissues, and died of well differentiated congenital mucinous cholangioadenocarcinoma proved at the age of 36 years.

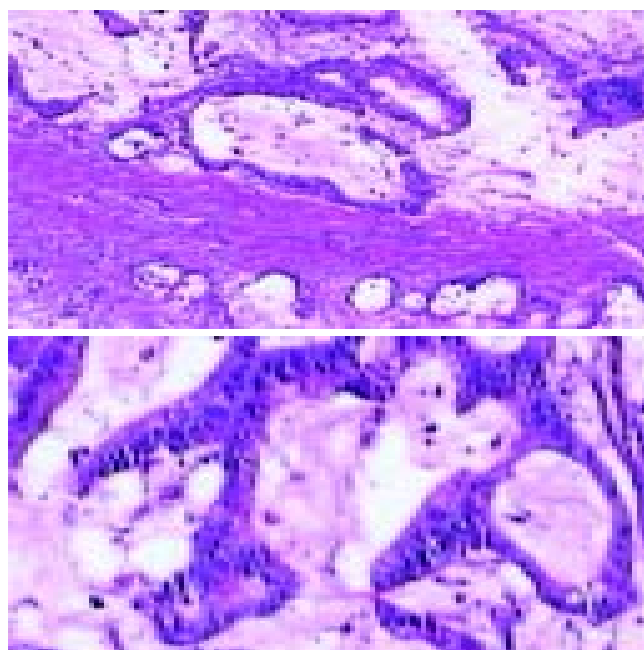


Figure 1 High-columnar or flat carcinoma cells with darkly stained nuclei and variation in size and shape arranged in irregular glandular pattern with intra- and extra-glandular mucin (hematoxylin and eosin, 40×10).

DISCUSSION

Choledochal cyst is a focal dilatation of the biliary tract. Although rare in adulthood, it is diagnosed more frequently with the advances in biliary imaging techniques^[1]. Of the numerous descriptions and classifications of choledochal cyst, the most practical is the classification proposed by Alonso-Lej 1 and modified by Todani^[1] in 1977 (Table 3). The major point of this classification is that the gallbladder is not usually distended and arises from a small cystic duct, not at the upper end of the cyst^[2].

Table 3 Todani modification of the Alonso-Lej, classification system of choledochal cyst

Type I	Fusiform dilation of the extrahepatic bile duct
Type II	Single saccular dilation or diverticulum of the extrahepatic bile duct
Type III	Dilation of the intraduodenal portion of the bile duct
Type IVa	Combined intra-and extrahepatic dilation of the bile duct
Type IVb	Multiple dilations of the extrahepatic bile duct
Type V	Isolated or diffuse intrahepatic biliary dilation (Caroli's disease when associated with hepatic fibrosis)

Since the first pathological description of a choledochal cyst by Vatero in 1723 and the first clinical report by Douglas in 1852, the aetiology of this abnormality has been controversial^[3]. It is unclear whether choledochal cyst is congenital, or acquired. In 1936 Yotsuyanagi^[3] suggested that choledochal cysts arose from inequality in the vacuolization of the biliary tract in early embryonic life. The common channel theory proposed by Babbitt^[3] in 1969 is most widely accepted, which was based on an abnormality of the pancreaticobiliary junction and the formation of an abnormally long common channel (greater than 15 mm) outside the control of the sphincters of Boyden. This configuration permits pancreatic enzymes to reflux into the common bile duct. The pancreatic enzymes then lead to persistent inflammation, epithelial denudation, thinning of the bile duct wall and distal obstruction, then eventually cyst formation. The incidence of choledochal cysts was reported as 1 in 13 000 to 1 in 2 million patients^[3,4]. It affects females 4 times as often as males, and more common in Asians and presents mainly in infancy and childhood (60%)^[1]. It is necessary to classify the type of cysts and to recognize the presence of an abnormal pancreaticobiliary duct junction, visualization of both the biliary tree and pancreatic duct. Thus, direct cholangiography, especially ERCP, is beneficial. But intraoperative cholangiography is not sensitive enough to detect the presence of an abnormal pancreaticobiliary duct junction. Radiographic visualization of both the biliary tree and pancreatic duct prior to surgery is helpful for surgical manipulation and complete excision of the cyst^[5-8]. Other pathologic features of choledochal cysts include acute and chronic mucosal inflammation, mucosal dysplasia, and absence of smooth or elastic fibers. A true mucosal lining may be hard to find, or it is usually cuboidal or columnar and frequently ulcerated if it is present. The cyst wall varies from 1 to 10 mm in thickness. Mucus-producing glands are rarely seen. There is usually a large amount of fibrosis, some of which may be involved in luminal stenoses. The bile is often very thick, and sometimes less pigmented than normal. Biliary calculi are uncommon. Pathologic complications include biliary obstruction, cholangitis, hepatic abscess, rupture, or development of cancer. Cholelithiasis due to choledochal cysts is unusual^[2,9].

Clinical manifestations are nonspecific and variable. The most common symptoms are abdominal pain and jaundice. If untreated, the condition may be fatal due to ascending cholangitis, biliary cirrhosis or diffuse peritonitis following

rupture of the cyst. Malignancy might also develop in the cyst and occur in pregnant women^[10]. Choledochal cyst in pregnancy is rare but poses a threat to both the mother and fetus. The maternal complications include cholangitis, pancreatitis, peritonitis and even malignancy. The fetal complications include fetal loss and preterm labor. Most reported cases were diagnosed when women presented with symptoms. It has been suggested that pregnancy may exacerbate the symptoms due to hormonal effect, compression by the gravid uterus and increase in intraabdominal pressure during pregnancy and postpartum. The cyst might be asymptomatic during the first pregnancy^[11,12], as demonstrated in our third patient. Asymptomatic cysts discovered on routine US could be observed with serial US examinations^[11].

Diagnosis of choledochal cysts during pregnancy is difficult. Radiologic imaging, ultrasound, computed tomography, cholangiography and biliary scintigraphy, could clinch the diagnosis^[1,12-15]. Although ultrasonography is a common useful investigation, difficulty may arise during pregnancy due to distortion of the normal abdominal anatomy and gravid uterus. Furthermore, ultrasound examination cannot demonstrate anatomic details of the biliary tree. Due to exposure of the fetus to ionizing radiation, contrast and ionizing imagings, such as CT or ERCP, should be avoided in pregnancy^[11,12,16]. Magnetic resonance imaging (MRI) could provide clear visualization of the relations between the choledochal cyst and biliary tree and of the extent and size of the choledochal cyst. Therefore, MRI is the investigation of choice in doubtful cases^[12,17]. To improve the management of this potentially serious condition in pregnancy, both clinicians and radiologists should be aware of this possibility in women with a right upper quadrant mass.

Concerning the optimal time of treatment, conservative management is commonly adopted during pregnancy. Once the diagnosis has been established, surgery is the only option for treatment^[11,12]. Surgical time is critical during pregnancy and the operative risk to the fetus and mother has to be balanced against the likelihood of cyst-related complications^[11,12]. Any patient who presents with a symptomatic or rapidly enlarging choledochal cyst or with cyst-related complications during pregnancy should undergo urgent treatment. Unfortunately, surgery during pregnancy has been associated with high fetal and maternal morbidity and mortality rate^[1,11,12,15]. Therefore, other more conservative approaches might have to be adopted until surgery could be performed under optimal conditions. Percutaneous cyst decompression might be done to relieve symptoms of pain and jaundice^[1,11,12,15,16]. In addition, antibiotics should be administered for treatment of cholangitis or for long-term prophylaxis, and the need for subsequent definitive cyst surgery should not be obviated^[11,12]. An operation should ideally be performed in the second trimester when the risk of surgery and anesthesia is lowest. When symptoms occur in the first trimester, surgery should be postponed unless the life of the mother is in danger, while in the third trimester, early cesarean section should be performed when amniocentesis indicates that the fetus is sufficiently mature. At the same time, a temporizing or definitive cyst operation could be undertaken as necessary^[1,11,12]. Definitive surgery depends on the cyst type and associated hepatobiliary pathology. Definitive surgical excision of the cyst can avoid postpartum complication and non-cyst excision may induce long-term complications.

Early reports suggested that internal or external drainage of a choledochal cyst by choledochocystojejunostomy or T-tube choledochocystostomy was a satisfactory treatment, but with a longer follow-up it has become clear that complications such as suppurative cholangitis, lithiasis, pancreatitis, secondary biliary cirrhosis, portal hypertension and intrahepatic abscess occurred in up to 40 percent of cases^[3,4,9,15]. This is similar as our results. The increased risk of bile duct carcinoma in

choledochal cysts has been well characterized^[3,4,9,10,14,15]. The reported incidence of biliary tract carcinoma in choledochal cysts varied from 2.5% to 17.5%, significantly higher than that found in the general population, which was from 0.01% to 0.05%^[3,4,9,10,14,15]. The incidence of cancer in patients with a choledochal cyst and in those undergone enteric drainage without cyst excision was much higher than that of carcinoma of the bile ducts in the general population. The age-related incidence of cyst-associated cancer has been shown to increase from 0.7 % in the first decade of life to 14.3 % after 20 years of age. It means the favorable outcome in congenital choledochal cyst patients was due to earlier diagnosis^[3,4,9,10,14,15].

Kasai *et al.*^[3] reported firstly the increased incidence of carcinoma in choledochal cysts and advocated primary cyst excision. The advances in diagnostic and therapeutic procedures and increased operative experience have lowered the mortality rate to 0-7%^[3,4,9,10,14,15]. Roux-en-Y choledochojejunostomy has replaced choledochoduodenostomy as the preferred operative procedure because of the high morbidity rate of cholangitis and the frequent need for reoperation later^[3,4,9,15].

Excision of types I, II and IV choledochal cysts is now widely accepted because of the lower incidence of postoperative complications. In contrast to cyst enterostomy, cyst excision with hepaticojejunostomy had satisfactory results. Although the occurrence of intrahepatic cholangiocarcinoma after the excision of a type I cyst has been reported^[18,19], but cyst excision is the primary choice of treatment for type I cysts. Type III cysts require adequate drainage and generally can be managed by endoscopic sphincterotomy and cannot be undertaken, operative sphincteroplasty with transduodenal cyst excision might be attempted^[5]. Sphincteroplasty either endoscopically or surgically has been found to be satisfactory^[20]. Treatment for type IV cysts is still controversial. Either excision of the extrahepatic cyst alone^[5] or total cyst excision including hepatectomy^[21] has been recommended. Concerning type V cysts, some authors recommended hepatic resection for unilobar Caroli's disease^[1].

Complete excision of the extrahepatic bile duct from the hepatic hilum to the pancreaticobiliary duct junction has become the choice of treatment for types I and IV cysts^[3-5,9,11,19,21-23]. However, it should be mentioned that since complete excision seems to be difficult in some patients, pancreaticoduodenectomy or hepatic resection should then be considered. In such cases, the distal choledochus is resected just above the pancreaticobiliary duct junction with the aid of preoperative ERCP and intraoperative US to avoid injuring the pancreatic duct. In the hepatic hilum, the hepatic duct must be resected at the hilum, and hepaticojejunostomy with a wide opening by plastic of both the hepatic ducts is necessary.

The reason why the three patients turned out quite different was their different clinical conditions. Our first Patient's situation was not quite good in peri-operation, she had a progressive nausea, vomiting, anorexia, fever, weight loss, and anemia with skin and her sclera slightly jaundiced, hypoalbuminemia, as well as disturbed blood electrolytes. Although the patient received fluid therapy and transfusion in peri-operation, the volume of blood was not enough to improve her clinical conditions within a short period of time, such as anemia, hypoalbuminemia. Gentamicin sulfate 240 000 iu one time per day could not prevent occurrence of retrograde bile duct infection, and the patient died of septic shock and multi-organ failure on day 25 postoperation.

Choledochal cyst in our No. 2 patient was drained externally with a catheter under the abdominal ultrasonography guidance, and she delivered safely. As the choledochal cyst was extensively infused with surrounding tissues, a cysto-jejunosomy was performed 3 mo after delivery. The patient's general condition was good. In our study, the No.3 patient developed a malignant tumor, because she did not receive re-operation for complete cyst excision, hepatojejunosomy or modified hepatojejunosomy

for treatment of repeated occurrence of intermittent retrograde cholangitis, which could be treated or avoided by early diagnosis and early complete cyst excision^[3,4,9,10,14,15], which are very important for the treatment of congenital choledochal cyst patients. Although cyst excision did not completely eliminate the risk of intrahepatic cholangiocarcinoma after the excision of a type I cyst^[3-5,9-11,14,15,18-22], but it significantly decreased the incidence of bile duct carcinoma. Thus, laparotomy during pregnancy should be avoided if possible and non-cyst excision cases should be explored to remove the cyst completely in the optimal surgical time.

Although choledochal cysts rarely occur in pregnancy, clinicians need to be aware of the condition. Inappropriate therapy may be catastrophic for both mother and child. This is why we recommend that patients should be admitted to a specialized hospital once the diagnosis is established. Complete excision of choledochal cyst with Roux-en-Y hepaticojejunostomy or modified Roux-en-Y hepaticojejunostomy is the choice of treatment for types I, II and IV choledochal cysts in non-pregnant adult patients; whereas in pregnancy, a more conservative approach should be adopted until the time when the surgical risk is lowest. Percutaneous external drainage of choledochal cyst under the abdominal ultrasonography guidance is indicated, if a complication of cystic rupture occurs. Complete excision of choledochal cyst with hepaticojejunostomy or modified hepaticojejunostomy is helpful in avoiding late complications such as retrograde cholangitis, biliary tract carcinoma, and is the most ideal choice of treatment for types I, II, IV choledochal cysts in pregnant adult patients, and is therefore highly recommended.

REFERENCES

- 1 Crittenden SL, McKinley MJ. Choledochal cyst- clinical features and classification. *Am J Gastroenterol* 1985; **80**: 643-647
- 2 Meyers WC, Jones RS. Textbook of liver and biliary surgery. *J B Lippincott Company* 1990: 312-318
- 3 Benhidjeb T, Munster B, Ridwelski K, Rudolph B, Mau H, Lippert H. Cystic dilatation of the common bile duct: surgical treatment and long-term results. *Br J Surg* 1994; **81**: 433-436
- 4 Chijiwa K, Koga A. Surgical management and long-term follow-up of patients with choledochal cysts. *Am J Surg* 1993; **165**: 238-242
- 5 Scudamore CH, Hemming AW, Teare JP, Fache JS, Erb SR, Watkinson AF. Surgical management of Choledochal cysts. *Am J Surg* 1994; **167**: 497-500
- 6 Sugiyama M, Atomi Y, Kuroda A. Pancreatic disorders associated with anomalous pancreaticobiliary junction. *Surgery* 1999; **126**: 492-497
- 7 Sugiyama M, Atomi Y. Anomalous pancreaticobiliary junction without congenital choledochal cyst. *Br J Surg* 1998; **85**: 911-916
- 8 Tagge EP, Tarnasky PR, Chandler J, Tagge DU, Smith C, Hebra A, Hawes RH, Cotton PB, Othersen HB Jr. Multidisciplinary approach to the treatment of pediatric pancreaticobiliary disorders. *J Pediatr Surg* 1997; **32**: 158-164
- 9 Yamataka A, Ohshiro K, Okada Y, Hosoda Y, Fujiwara T, Kohno S, Sunagawa M, Futagawa S, Sakakibara N, Miyano T. Complications after cyst excision with hepaticocenterostomy for choledochal cysts and their surgical management in children versus adults. *J Pediatr Surg* 1997; **32**: 1097-1102
- 10 Binstock M, Sondak VK, Herd J, Reimnitz C, Lindsay K, Brinkman C, Roslyn JJ. Adenocarcinoma in a choledochal cyst during pregnancy: A case report and guidelines for management. *Surgery* 1988; **103**: 588-592
- 11 Hewitt PM, Krige JEJ, Bornman PC, Terblanche J. Choledochal cyst in pregnancy: A therapeutic dilemma. *J Am Coll Surg* 1995; **181**: 237-240
- 12 Fok WY, Yip SK, Leung TN, Leung KF, Chui AKK. Large choledochal cyst present through 2 pregnancies. A case report. *J*

- Reprod Med* 2003; **48**: 482-484
- 13 **Beattie GJ**, Keay S, Muir BB, Boddy K. Acute pancreatitis with pseudocyst formation complicating pregnancy in a patient with a co-existent choledochal cyst. *Br J Obstet Gynaecol* 1993; **100**: 957-959
 - 14 **Bismuth H**, Krissat J. Choledochal cystic malignancies. *Ann Oncol* 1999; **10**(Suppl 4): S94-98
 - 15 **Hopkins NFG**, Benjamin IS, Thompson MH, Williamson RCN. Complications of choledochal cysts in adulthood. *Ann R Coll Surg Engl* 1990; **72**: 229-235
 - 16 **Russell JGB**, Taylor V, Torrance B. Ultrasonic diagnosis of choledochal cyst in pregnancy. *Br J Radiol* 1976; **49**: 425-426
 - 17 **Shanley DJ**, Gagliardi JA, Daum-Kowalski R. Choledochal cyst complicating pregnancy: antepartum diagnosis with MRI. *Abdom Imaging* 1994; **19**: 61-63
 - 18 **Kinoshita H**, Nagata E, Hirohashi K, Saki K, Kobayashi Y. Carcinoma of the gallbladder with an anomalous connection between the choledochus and the pancreatic duct. Report of 10 cases and review of the literature in Japan. *Cancer* 1984; **54**: 762-769
 - 19 **Todani T**, Watanabe Y, Toki A, Urushihara N, Sato Y. Reoperation for congenital choledochal cyst. *Ann Surg* 1988; **207**: 142-147
 - 20 **Venu RP**, Geenen JE, Hogan WJ, Dodds WJ, Wilson SW, Stewart ET, Soergel KH. Role of endoscopic retrograde cholangiopancreatography in the diagnosis and treatment of choledochoceles. *Gastroenterology* 1984; **87**: 1144-1149
 - 21 **Todani T**, Narusue M, Watanabe Y, Tabuchi K, Okajima K. Management of congenital choledochal cyst with intrahepatic involvement. *Ann Surg* 1978; **187**: 272-280
 - 22 **Hara H**, Morita S, Ishibashi T, Sako S, Otani M, Tanigawa N. Surgical treatment for congenital biliary dilatation, with or without intrahepatic bile duct dilatation. *Hepatogastroenterology* 2001; **48**: 638-641
 - 23 **Bose SM**, Lobo DN, Singh G, Wig JD. Bile duct cysts: presentation in adults. *Aust N Z J Surg* 1993; **63**: 853-857

Edited by Wang XL and Ren SY Proofread by Xu FM

Clinical significance of preoperative regional intra-arterial infusion chemotherapy for advanced gastric cancer

Cheng-Wu Zhang, Shou-Chun Zou, Dun Shi, Da-Jian Zhao

Cheng-Wu Zhang, Shou-Chun Zou, Dun Shi, Da-Jian Zhao,
Department of General Surgery, Zhejiang Provincial People's Hospital,
Hangzhou 310014, Zhejiang Province, China

Correspondence to: Cheng-Wu Zhang, Department of General
Surgery, Zhejiang Provincial People's Hospital, Hangzhou 310014,
Zhejiang Province, China. zcw1989@sina.com

Telephone: +86-571-85239988

Received: 2003-10-30 **Accepted:** 2003-12-16

Abstract

AIM: Preoperative intra-arterial infusion chemotherapy could increase the radical resection rate of advanced gastric cancer, but its effect on the long-term survival has not been assessed. This study was designed to evaluate the clinical significance of preoperative intra-arterial infusion chemotherapy for advanced gastric cancer.

METHODS: Clinicopathological data of 91 patients who underwent curative resection for advanced gastric cancer were collected. Among them, 37 patients undertaken preoperative intra-arterial infusion chemotherapy were used as the interventional chemotherapy group, and the remaining 54 patients as the control group. Eleven factors including clinicopathological variables, treatment procedures and molecular biological makers that might contribute to the long-term survival rate were analyzed using Cox multivariate regression analysis.

RESULTS: The 5-year survival rate was 52.5% and 39.8%, respectively, for the interventional group and the control group ($P < 0.05$). Cox multivariate regression analysis revealed that the TNM stage ($P < 0.001$), preoperative intra-arterial infusion chemotherapy ($P = 0.029$) and growth pattern ($P = 0.042$) were the independent factors for the long-term survival of patients with advanced gastric cancer.

CONCLUSION: Preoperative intra-arterial infusion chemotherapy plays an important role in improving the prognosis of advanced gastric cancer.

Zhang CW, Zou SC, Shi D, Zhao DJ. Clinical significance of preoperative regional intra-arterial infusion chemotherapy for advanced gastric cancer. *World J Gastroenterol* 2004; 10 (20): 3070-3072

<http://www.wjgnet.com/1007-9327/10/3070.asp>

INTRODUCTION

Gastric cancer is one of the most common cancers in China. Despite recent advances in experimental researches, early diagnosis and surgical techniques, the outcome of patients with gastric carcinoma is still far from satisfaction. Surgery remains the mainstay of potentially curative treatment, but the survival rates of patients with advanced gastric cancer are poor. A number of studies have investigated whether intravenous chemotherapy after a resection could improve the survival rate,

but the results were different and disputable^[1,2]. Preoperative regional intra-arterial infusion chemotherapy could increase the radical resection rate of advanced gastric cancer. However, there are few reports about the influence of preoperative intra-arterial chemotherapy on the long-term survival of patients with advanced gastric carcinomas after curative resections. In the current study, we analyzed retrospectively the clinicopathologic data of 91 patients with advanced gastric cancers undergone curative surgeries during recent years. To investigate the effect of preoperative intra-arterial chemotherapy on the prognosis of advanced gastric cancer, the Cox model of proportional hazards was utilized to identify the independent variables affecting the long-term survival of patients with gastric carcinomas.

MATERIALS AND METHODS

Clinicopathologic materials

The study comprised 91 patients who underwent curative resection for advanced gastric cancer from June 1984 to June 1992 at our hospital. All patients received follow-ups for 3 to 220 mo (mean time 57.1 ± 23.8 mo) and their clinicopathologic data were well-provided. There were 69 males and 22 females, their ages ranged from 25 to 73 years with a mean age of 54.9 ± 12.9 years. The tumor staging for each gastric cancer was evaluated according to the new TNM classification system of UICC^[3], and there were 27 patients with stage II, 49 with stage III and 15 with stage IV. Of the 91 cases, 2 had well-differentiated adenocarcinomas, 48 had moderately differentiated adenocarcinomas and 41 had poorly differentiated adenocarcinomas. Thirty-one were negative for lymphatic vessel invasions and 60 were positive for lymphatic vessel invasions. For venous vessel invasion of tumor, 78 cases were negative and 13 were positive. The tumor growth pattern was defined according to Ming classification. There were 40 patients with expansive types and 51 with infiltrative types. Expressions of CD44 splice variants v6(CD44V6) and E-cadherin(E-CD) and proliferating cell nuclear antigen(PCNA) in all the 91 resected gastric carcinomatous tissue specimens were detected by streptavidin-peroxidase immunohistochemistry. Of the patients, 37 patients undergone preoperative regional intra-arterial infusion chemotherapy were used as the interventional chemotherapy group and the remaining 54 patients as the control group. All the patients received systemic chemotherapy after surgeries. The clinicopathologic parameters of the two groups were analyzed and compared.

Preoperative intra-arterial infusion chemotherapy

Preoperative intra-arterial infusion chemotherapy was performed via transfemoral artery route using the Seldinger's approach before surgery. Celiac axis angiogram was initially carried out to document the visceral arterial anatomy and the arterial supply of tumor, and the digital subtraction technique was utilized in the study. According to the results of angiogram, the main blood supplying arteries of gastric cancer were detected and superselective catheterization of these arteries was performed. Then, chemotherapy drugs were administered via the placed catheter. Protocols of chemotherapy were FAP (5-FU 1.0 g+ADM 30-50 mg+DDP 40-60 mg) or FMP (5-FU 1.0 g+MMC 8-10 mg+DDP 40-60 mg). Preoperative interventional

chemotherapy was performed one or two times for each patient, and the interval time ranged from 10 to 14 d. Surgery was carried out two weeks after interventional chemotherapy. Of the 37 patients who underwent interventional chemotherapy, 31 received chemotherapy one time and 6 received two times.

Statistical analysis

The eleven variables observed including gender, age, preoperative intra-arterial infusion chemotherapy, TNM stage classification, differentiation grade, growth pattern, lymphatic vessel and venous vessel invasion, expressions of CD44V6 and E-CD, PCNA labeling index (PCNA LI), were stored in a computer, and analyses were performed using the SPSS 9.0 for Windows. Survival rates were calculated using life table method and the differences among the groups of patients were measured by Log rank test. Univariate analysis was performed first, and the variables found by univariate analysis significantly associated with survival rates were subjected to multivariate analyses using the Cox model of proportional hazards. $P < 0.05$ was considered statistically significant.

RESULTS

Comparison of pathological parameters between two groups

The differences of pathological parameters were not significant between two groups ($P > 0.05$, Table 1).

Comparison of immunohistochemistry results between two groups

The expressions of CD44V6 and E-CD and PCNA were not significantly different between two groups ($P > 0.05$, Table 2).

Comparison of postoperative complications and survival rates between two groups

No death occurred due to surgery in this study. One wound infection and 1 pneumonic infection were found in the interventional chemotherapy group, whereas 2 pneumonic infections and 1 abdominal cavity infection occurred in the control group after surgery. The incidence of postoperative complications was not significantly different between two groups ($P > 0.05$). The 5-year survival rate of the interventional chemotherapy group and the control group was 52.5% and 39.8%, respectively, and the difference between the two groups was significant ($P < 0.05$).

Univariate and multivariate analyses of prognostic factors

The results of univariate analysis demonstrated that the factors including gender, age and tumor cellular differentiation grade

were not associated with postoperative survival rate ($P > 0.05$). The variables significantly correlated with survival rates were TNM stage, growth pattern of tumor, lymphatic vessel and venous vessel invasion, intra-arterial infusion chemotherapy, expressions of CD44V6 and E-CD, PCNA LI ($P < 0.05$). These factors were subjected to multivariate analyses using the Cox model of proportional hazards. These analyses identified three independent prognostic variables which were TNM stage, preoperative interventional chemotherapy and growth pattern of tumor, according to influence strength (Table 3). The survival predicting equation ($\chi^2 = 37.63$, $P < 0.001$) was obtained, it suggested the foundation of the equation be reasonable.

Table 3 Independent prognostic variables identified by Cox proportional hazard model

Variables	SE	Wald	df	Sig	R	Exp(B)
TNM stage	0.1220	16.3113	1	0.0001	0.1753	1.6304
Interventional chemotherapy	0.2501	4.7491	1	0.0285	0.0681	1.6981
Growth pattern	0.2607	4.0105	1	0.0417	0.0711	1.6953

DISCUSSION

Preoperative chemotherapy was initiated in the 1980s as an auxiliary therapy for malignant neoplasms^[4]. It has been considered that preoperative chemotherapy could reduce activities of tumor cells, contract volumes of tumors, decrease iatrogenic diffusion of tumor cells during surgery, and improve curative resections for tumors. It was reported that serum concentration of chemotherapy drugs in abdominal organs by local intra-arterial infusion was nearly ten times as high as by systemic chemotherapy^[5]. Kosaka *et al.*^[6] investigated the therapeutic efficacy of intra-arterial infusion chemotherapy for advanced gastric cancer, and found that the response rate of tumors to intra-arterial infusion chemotherapy was significantly higher than that to systemic infusion chemotherapy. Liu^[7] reported that the overall response rate to preoperative interventional chemotherapy was 72.8% for gastric carcinomas, and it was revealed that preoperative intra-arterial infusion chemotherapy exerted its effect by introducing apoptosis of cancer cells, restraining tumor cell proliferation and promoting pathological necrosis of tumors^[8]. Tao *et al.* also demonstrated that preoperative regional artery chemotherapy showed inhibitory actions on growth of gastric cancer cells mainly through inhibiting proliferation and inducing the apoptosis of tumor cells^[9]. Our previous study also showed that preoperative intra-arterial infusion chemotherapy could dramatically improve the rate of radical resection for gastric cancer. However, the

Table 1 Comparison of pathological parameters between two groups

Groups	TNM stage			Differentiation grade			Growth pattern		Lymphatic vessel invasion		Venous vessel invasion	
	II	III	IV	Well	Moderately	Poorly	Expensiv	Infiltrative	Negative	Positive	Negative	Positive
Intervectional	11	12	6	1	19	17	15	22	14	23	32	5
Control	16	29	9	1	29	24	25	29	17	37	46	8
	$P > 0.05$			$P > 0.05$			$P > 0.05$		$P > 0.05$		$P > 0.05$	

Table 2 Comparison of immunohistochemistry results between two groups

Groups	Expression of CD44V6				Expression of E-CD				PCNA LI (%)
	-	+	++	+++	-	+	++	+++	
Interventional	8	14	5	10	11	13	9	4	63.8±17.6
Control	16	12	8	18	17	18	13	6	64.7±18.0
	$P > 0.05$				$P > 0.05$				$P > 0.05$

influence of preoperative intra-arterial infusion chemotherapy on the prognosis of patients with gastric cancer has been controversial. Masuyama *et al.*^[10] concluded that preoperative intra-arterial infusion chemotherapy might prevent local and lymph node metastases, but it could not improve the survival of gastric cancer patients. Whereas Shchepotin *et al.*^[11] reported superselective intra-arterial chemotherapy conferred a highly significant survival advantage compared to control or systemic intravenous chemotherapy for advanced nonresectable gastric cancer. This study demonstrated that the 5-year survival rate of preoperative interventional chemotherapy group was significantly higher than that of the control group, and there was no statistical difference between the incidences of postoperative complications of the two groups. It is suggested that preoperative intra-arterial infusion chemotherapy is both effective and safe for patients with advanced gastric cancer.

Among the prognostic factors of gastric cancer, the influence of clinical modalities on the prognosis of patients has been the focus of studies on gastric cancer. It has been proved that the most important prognostic variable for gastric cancer is curative resection of tumor^[12]. In the current study, all patients underwent curative resections of tumors. Furthermore, the clinicopathologic parameters of the two groups were not significantly different. This makes it possible to evaluate the effect of other therapeutic modalities on the prognosis of patients with advanced gastric cancers. As is shown in this article, among the seven variables significantly associated with the survival of patients with gastric cancer by univariate analysis, TNM stage was the most important independent prognostic factor by multivariate analyses using the Cox model of proportional hazards. It was consistent with previous reports^[13]. The results of our study also revealed that preoperative intra-arterial infusion chemotherapy and growth pattern of tumors were the independent prognostic variables affecting long-term survival of gastric cancer patients, suggesting that preoperative intra-arterial infusion chemotherapy is of great importance in improving the prognosis of patients with advanced gastric cancers after undergoing curative resections.

In summary, the results of the present study revealed that preoperative intra-arterial infusion chemotherapy was one of the independent prognostic variables of patients with advanced gastric cancer. Therefore, preoperative intra-arterial infusion chemotherapy in combination with curative resection would have important clinical values in improving the prognosis of patients with advanced gastric carcinoma.

REFERENCES

- 1 **Hermans J**, Bonenkamp JJ, Boon MC, Bunt AM, Ohyama S, Sasako M, Van de Velde CJ. Adjuvant therapy after curative resection for gastric cancer: meta-analysis of randomized trials. *J Clin Oncol* 1993; **11**: 1441-1447
- 2 **Janunger KG**, Hafstrom L, Nygren P, Glimelius B. A systematic overview of chemotherapy effects in gastric cancer. *Acta Oncol* 2001; **40**: 309-326
- 3 **Yoo CH**, Noh SH, Kim Y, Min JS. Comparison of prognostic significance of nodal staging between old (4th edition) and new (5th edition) UICC TNM classification for gastric carcinoma. *World J Surg* 1999; **23**: 492-497
- 4 **Leong T**, Michael M, Foo K, Thompson A, Lim Joon D, Weih L, Ngan S, Thomas R, Zalberg J. Adjuvant and neoadjuvant therapy for gastric cancer using epirubicin/cisplatin/5-fluorouracil (ECF) and alternative regimens before and after chemoradiation. *Br J Cancer* 2003; **89**: 1433-1438
- 5 **Tokairin Y**, Maruyama M, Baba H, Yoshida T, Kure N, Nagahama T, Ebuchi M. Pharmacokinetics of "subselective" arterial infusion chemotherapy. *Gan To Kagaku Ryoho* 2001; **28**: 1795-1798
- 6 **Kosaka T**, Ueshige N, Sugaya J, Nakano Y, Akiyama T, Tomita F, Saito H, Kita I, Takashima S. Evaluation of intra-arterial infusion chemotherapy for advanced gastric cancer. *Gan To Kagaku Ryoho* 1998; **25**: 1288-1291
- 7 **Liu FK**. The interventional therapy for advanced gastric cancer before and after operation. *Zhongguo Shiyong Waikexue* 2001; **21**: 403
- 8 **Dong XC**, Li B, Li YP. Effect of preoperative intra-arterial chemotherapy on apoptosis and p53 expression of gastric cancer. *Aizheng* 2002; **21**: 1078-1080
- 9 **Tao HQ**, Zou SC. Effect of preoperative regional artery chemotherapy on proliferation and apoptosis of gastric carcinoma cells. *World J Gastroenterol* 2002; **8**: 451-454
- 10 **Masuyama M**, Taniguchi H, Takeuchi K, Miyata K, Koyama H, Tanaka H, Higashida T, Koishi Y, Mugitani T, Yamaguchi T. Recurrence and survival rate of advanced gastric cancer after preoperative EAP-II intra-arterial infusion therapy. *Gan To Kagaku Ryoho* 1994; **21**: 2253-2255
- 11 **Shchepotin IB**, Chorny V, Hanfelt J, Evans SR. Palliative superselective intra-arterial chemotherapy for advanced nonresectable gastric cancer. *J Gastrointest Surg* 1999; **3**: 426-431
- 12 **Allgayer H**, Heiss MM, Schildberg FW. Prognostic factors in gastric cancer. *Br J Surg* 1997; **84**: 1651-1664
- 13 **Hermanek P**, Wittekind C. News of TNM and its use for classification of gastric cancer. *World J Surg* 1995; **19**: 491-495

Edited by Wang XL and Xu FM

Levels of plasma des- γ -carboxy protein C and prothrombin in patients with liver diseases

Xiao-Fan He, Zhi-Bin Wen, Min-Juan Liu, Hui Zhang, Qun Li, Shi-Lin He

Xiao-Fan He, Zhi-Bin Wen, Hui Zhang, Shi-Lin He, Haemostasis Physiology Laboratory, Department of Physiology, Xiangya Medical College, Central South University, Changsha 410078, Hunan Province, China

Min-Juan Liu, Second Affiliated Hospital of Guangzhou Medical College, Guangzhou 510260, Guangdong Province, China

Qun Li, Xiangya Hospital, Central South University, Changsha 410008, Hunan Province, China

Supported by the National Natural Science Foundation of China NO.C39600197, the Foundation of Education Ministry of China for Outstanding Youth Scholars, NO.2001:39

Correspondence to: Zhi-Bin Wen, Haemostasis Physiology Laboratory, Department of Physiology, Xiangya Medical College, Central South University, Changsha 410078, Hunan Province, China. wenzhibin2002@yahoo.com.cn

Telephone: +86-731-2355053 **Fax:** +86-731-2650668

Received: 2004-02-28 **Accepted:** 2004-04-29

Abstract

AIM: To study the plasma des- γ -carboxy protein C activity, antigen and prothrombin levels in patients with liver diseases and their clinical significance.

METHODS: Plasma protein C activity (PC:C) was detected by chromogenic assay and antigen (PC:Ag) and des- γ -carboxy protein C (DCPC) were detected by ELISA. Total prothrombin and unabsorbed prothrombin in plasma were detected by ecarin chromogenic assay.

RESULTS: Compared with the control, the levels of PC:C and PC:Ag in patients with hepatocellular carcinoma (HCC) and liver cirrhosis (LC) were lower (PC:C: 104.65 \pm 23.0%, 62.50 \pm 24.89%, 56.75 \pm 20.14%, PC:Ag: 5.31 \pm 1.63 μ g/mL, 2.28 \pm 1.15 μ g/mL, 2.43 \pm 0.79 μ g/mL, P <0.05). The levels of PC:Ag in patients with acute viral hepatitis (AVH) also was lower (2.98 \pm 0.91 μ g/mL, P <0.01), but PC:C was close to the control (93.76 \pm 30.49%, P >0.05). The levels of DCPC in patients with HCC were remarkably higher (0.69 \pm 0.29 μ g/mL, 1.18 \pm 0.63 μ g/mL, 0.45 \pm 0.21 μ g/mL, P <0.05) and its average was up to 50% of total PC:Ag. But those of DCPC in patients with AVH were not significantly different from the control. The levels of total prothrombin were lower in patients with LC, but higher in patients with HCC. The levels of unabsorbed prothrombin were predominantly higher than those of other groups.

CONCLUSION: PC:C and PC:Ag in patients with liver diseases (except PC:C in AVH) were lower. The total prothrombin was lower in patients with LC. The higher level of unabsorbed prothrombin may be used as a scanning marker for HCC. DCPC may be used as a complementary marker in the diagnosis of HCC.

He XF, Wen ZB, Liu MJ, Zhang H, Li Q, He SL. Levels of Plasma des- γ -carboxy protein C and prothrombin in patients with liver diseases. *World J Gastroenterol* 2004; 10(20): 3073-3075 <http://www.wjgnet.com/1007-9327/10/3073.asp>

INTRODUCTION

Protein C is a plasma glycoprotein of M_r 62 000 and is synthesized and degraded in the liver. There is 2-6 mg/L PC of plasma in healthy person, with about 72-139% biological activity. No difference in the content of protein C between males and females was found, but protein C shows an increased trend towards increasing age (with an average increase of 4% every 10 years). Thrombin formed during coagulation is responsible for conversion of protein C to activated protein C (APC). This activation takes place on the surface of endothelial cells and monocytes by compound thrombin with thrombomodulin^[1]. Because protein C is a vitamin K-dependent plasma protein, it is highly homologous in structure to factors X, IX, VII and prothrombin. Many studies have demonstrated that there are changes of factors X, IX, VII and prothrombin in patients with liver diseases, and des- γ -carboxy (abnormal) prothrombin is a useful tumor marker in the diagnosis of hepatocellular carcinoma^[2-4]. But up to now, few reports are available about the association between PC and liver diseases. Therefore, in the present study we not only reported the changes of PC and prothrombin in liver diseases, but also explored the relationship between des- γ -carboxy protein C (DCPC) and HCC.

MATERIALS AND METHODS

Clinical data

Fifty-three patients (33 males and 20 females, aged 20-81 years) were included in this study. Of them, 18 patients with hepatocellular carcinoma (HCC), 20 with liver cirrhosis (LC), 15 with acute viral hepatitis (AVH). They were from The Second Affiliated Hospital of Guangzhou Medical College and the Xiangya Hospital of Central South University. HCC and LC were diagnosed by clinical, pathological and ultrasonic examinations. AVH was diagnosed by clinical and immunological/RT-PCR examinations. Twenty healthy volunteers (10 males and 10 females, aged 25-65 years) were enrolled as the control group.

Materials

Blood sampling and preparation of plasma (for PC:C, PC:Ag assay) were as follows. Blood was drawn into 0.13 mol/L sodium citrate (9/1, v/v), plasma (for DCPC, prothrombin assay) was obtained by drawing blood (9vol) into 0.1 mol/L sodium oxalate (9/1, 1v/v), and centrifugation at 4 000 r/min for 10 min. All were snap frozen and stored at -40 °C.

PC activity (PC:C) and PC antigen (PC:Ag) kits were purchased from Shanghai Sun Biotech Company. Vials containing 50 U of ecarin were provided by Sigma Company. Chromogenic substance S2238 was obtained from American Diagnostica Inc. (ADI). BaCl₂, Tris, and others were of analytical grade and purchased from Shanghai Reagent Factory. ELX800 enzyme-linked immunosorbent detector was from America BIO-Tek Instruments Inc.

Methods

PC:C assay PC:C was detected by chromogenic assay (SH Sun Bio CO kits). Excessive activator was put into the diluted human plasma, PC was activate and convert it into activated protein C

(APC). Then chromozym APC was hydrolyzed, and PNA was released. PNA levels are determined by measuring the sample solution absorbances at 405 nm and comparing against those of standard curves generated using a PC:C. The assay procedures performed according to the instructions of the manufacturer.

PC:Ag assay PC:Ag was determined by ELISA (SH Sun Bio CO. kits). Murine PC antibody was used as capture antibody and an enzyme-linked antibody fragment that specifically recognizes bound hPC as detection antibody. After plasma PC bound to capture antibody and detection antibody, the substrate was hydrolyzed by enzyme and chromagenic reaction occurred. The sample absorbance at 492 nm was proportional to the concentrations of plasma PC. The assay procedures were performed according to the manufacturer's instructions.

DCPC assay A total of 40 μ L of 1 mol/L BaCl₂ was added into 500 μ L of normal reference plasma or pending measured plasma. The mixture was surged for 30 min at 4 °C. After centrifuged for 5 min, collect the supernatant was collected. Then the supernatant was absorbed by barium salt again and collected. The level of PC:Ag in the supernatant was measured by ELISA.

Prothrombin assay Ecarin could activate γ -carboxylated and des- γ -carboxylated prothrombin into thrombin and then thrombin amidolyse chromozym P. The absorbance at 405 nm was proportional to the concentration of γ -carboxylated and des- γ -carboxylated Prothrombin. Levels of prothrombin in plasma reflected the total prothrombin and those in plasma absorbed by BaCl₂ reflect the unabsorbed prothrombin.

Statistical analysis

Results were expressed as mean \pm SD. One way analysis of variance and Newman-keuls test were used for comparisons of the mean value in various groups. *P* values less than 0.05 was considered statistically significant.

RESULTS

PC:C and PC:Ag in liver diseases

Compared with the control, the levels of PC:C and PC:Ag in patients with hepatocellular carcinoma (HCC) and liver cirrhosis were lower (*P*<0.05). PC:Ag in acute viral hepatitis (AVH) also was lower, but PC:C was close to the control (*P*>0.05) (Table 1).

Table 1 The levels of PC:C and PC:Ag in patients with liver diseases (mean \pm SD)

	<i>n</i>	PC:C (%)	PC:Ag (μ g/mL)
Control	20	104.65 \pm 23.0	5.31 \pm 1.63
Hepatocellular carcinoma	18	62.50 \pm 24.89 ^a	2.28 \pm 1.15 ^b
Liver cirrhosis	20	56.75 \pm 20.14 ^a	2.43 \pm 0.79 ^b
Acute viral hepatitis	15	93.76 \pm 30.49	2.98 \pm 0.91 ^b

^a*P*<0.05, ^b*P*<0.01 vs control group.

DCPC in liver diseases

As shown in Table 2, the difference of DCPC between acute viral hepatitis group and control group was not statistically significant (*P*<0.01). But DCPC in patients with HCC was remarkably higher than those in patients with acute viral hepatitis and the control (*P*<0.01).

Prothrombin in liver diseases

In contrast to the control, the levels of total prothrombin was lower in patients with liver cirrhosis (*P*<0.05). There was no significant difference in plasma prothrombin between acute viral hepatitis and control groups (*P*>0.10). But the level of total prothrombin in patients with HCC was markedly higher than that in other groups (*P*<0.01). The levels of unabsorbed

prothrombin in patients with HCC were predominantly higher than those in the other groups (*P*<0.01).

Table 2 The levels of DCPC in patients with liver diseases (mean \pm SD)

	<i>n</i>	Total PC:Ag (μ g/mL)	DCPC:Ag (μ g/mL)	DCPC:Ag Total PC:Ag
Control	15	5.23 \pm 1.95	0.69 \pm 0.29	13.19%
Hepatocellular carcinoma	15	2.33 \pm 1.21	1.18 \pm 0.63 ^b	50.64% ^b
Acute viral hepatitis	15	2.98 \pm 0.91	0.45 \pm 0.21	15.10%

^b*P*<0.01 vs control and acute viral hepatitis groups.

Table 3 The levels of prothrombin in patients with liver diseases (mean \pm SD)

	<i>n</i>	Total prothrombin (%)	Unabsorbed prothrombin (%)
Control	20	101.99 \pm 12.29	0.30 \pm 0.18
Hepatocellular carcinoma	18	220.61 \pm 67.95 ^b	2.87 \pm 0.89 ^b
Liver cirrhosis	10	85.33 \pm 6.99 ^a	0.95 \pm 0.45 ^a
Acute viral hepatitis	15	99.05 \pm 14.97	1.09 \pm 0.36 ^a

^a*P*<0.05, ^b*P*<0.01 vs control groups.

DISCUSSION

Vitamin K-dependent zymogens, prothrombin, factor VII, IX, protein C and protein S are synthesized in the liver. It is understandable that the liver diseases are associated with thrombosis and/or hemorrhage. In the present investigation, we observed that the levels of total prothrombin decreased in patients with liver cirrhosis and increased in patients with HCC. The results are consistent with previous reports^[5].

Prior to secretion into plasma, all the vitamin K-dependent proteins undergo post-translational modifications by a vitamin K-dependent carboxylase that converts several specific glutamic acid residues to γ -carboxyglutamic acid (Gla). Gla residues are located in N-terminal of the mature proteins and contribute to the ability of these proteins to bind to Ca²⁺ and offer metal ions such as Ba²⁺, etc. Ca²⁺ binding induces conformational changes leading to expression of membrane-binding phospholipid, which is a key step to bring about biological activities. Therefore, des- γ -carboxylated proteins can not bind to divalent ions and lose their procoagulant or anticoagulant activities. Our data showed that after plasma was absorbed by barium salt, the levels of unabsorbed prothrombin from plasma of patients with HCC was very high and lower in patients with acute viral hepatitis and liver cirrhosis, and less in healthy volunteers. This fact further suggested that high levels of unabsorbed prothrombin in plasma could be used a scanning marker of HCC. It is due to unabsorbed prothrombin essentially reflecting des- γ -carboxy prothrombin(DCP). Recent studies demonstrated that DCP could not only differentiate HCC from nonmalignant chronic liver diseases, but also indicate prognosis for HCC^[3,4]. Because the assay of unabsorbed prothrombin is more economical and simpler than the determination of DCP, it maybe spread in clinic, especially in the developing countries.

The activation of protein C is catalyzed by a compound of α -thrombin and the endothelial cell surface protein thrombomodulin. In contrast to other vitamin K-dependent coagulation factors, activated protein C (APC) functions as an anticoagulant by proteolytic inactivation of factor Va and VIIIa. APC also promotes

fibrinolytic response by forming compounds with plasminogen activator inhibitor-1 and by diminishing the activation of thrombin-activatable fibrinolysis inhibitor via inhibition of thrombin generation. Thus the deficiency of protein C is associated with thrombosis^[6,7]. Previous reports demonstrated that the levels of protein C from plasma in patients with liver diseases were lower^[8,9]. Our data showed that PC:C in patients with hepatocellular carcinoma and liver cirrhosis was lower than control group, and the descendant degree was proportional to the damaged degree (unpublished data). Thus, the results provided further evidence for the association of protein C and liver diseases. However, PC:Ag in acute viral hepatitis (AVH) was also lower, but PC:C was close to the control, the reason is unknown. Protein C inhibitors synthesized in liver can specifically inactivate APC. Perhaps the decrease of protein C inhibitors in liver disease is one of the causes. In addition, the decrease of coagulation factors and some drugs may be partly responsible for it.

Because protein C is one of the vitamin K-dependent proteins synthesized in the liver, its biological functions are also dependent on complete Gla domain. Yashiikawa *et al.* reported that the impaired vitamin K-dependent γ -carboxylation in patients with HCC involved not only prothrombin, but also protein C^[10]. Our data showed that the levels of DCPC in patients with HCC were surprisingly high, almost up to 50% of total protein C. This fact shows that the high level of DCPC from plasma can be used as a complementary tumor marker of HCC. As surgical removal or reduction in tumor was with chemotherapy is associated with reduction or elimination of the abnormal prothrombin (des- γ -carboxy prothrombin, DCP), the tumor itself is responsible for the production of DCP. We believe that DCPC may have the same production process like DCP. Up to date, it is still unknown why tumor cells of HCC make so many DCP and DCPC as well as des- γ -carboxy proteins. Because vitamin therapy can not reduce the concentration of DCP and DCPC, the production of des- γ -carboxy protein is not due to vitamin K deficiency. Its specific mechanisms remain unclear.

It is becoming increasingly clear that there is an interaction network between coagulation and inflammation and natural anticoagulants have strong anti-inflammatory effects^[11,12]. Animal experiments indicated that protein C and activated protein C inhibits could inhibit DIC and improve survival rate^[11-13]. Clinical trials could demonstrated that recombinant human activated protein C (rhAPC) could attenuate systemic inflammatory response syndrome and reduces mortality in patients with severe sepsis^[14-16]. Therefore, it may be beneficial when an appropriate dose of protein C or rhAPC is given to the patients with liver diseases especially HCC to prevent and treat sepsis and DIC.

REFERENCES

- 1 **Esmon CT.** The protein C pathway. *Chest* 2003; **124**(3 Suppl): 26S-32S
- 2 **Liebman HA,** Furie BC, Tong MJ, Blanchard RA, Lo KJ, Lee SD, Coleman MS, Furie B. Des- γ -carboxy (abnormal) prothrombin as a serum marker of primary hepatocellular carcinoma. *N Engl J Med* 1984; **310**: 1427-1431
- 3 **Marrero JA,** Su GL, Wei W, Emick D, Conjeevaram HS, Fontana RJ, Lok AS. Des-gamma carboxyprothrombin can differentiate hepatocellular carcinoma from nonmalignant chronic liver disease in American patients. *Hepatology* 2003; **37**: 1114-1121
- 4 **Nagaoka S,** Yatsushashi H, Hamada H, Yano K, Matsumoto T, Daikoku M, Arisawa K, Ishibashi H, Koga M, Sata M, Yano M. The Des- γ -carboxy prothrombin index is a new prognostic indicator for hepatocellular carcinoma. *Cancer* 2003; **98**: 2671-2677
- 5 **Furie B,** Furie BC. The molecular basis of blood coagulation. *Cell* 1988; **53**: 505-518
- 6 **Castellino FJ.** Gene targeting in hemostasis: protein C. *Front Biosci* 2001; **6**: D807-819
- 7 **Esmon CT.** Protein C anticoagulant pathway and its role in controlling microvascular thrombosis and inflammation. *Crit Care Med* 2001; **29**(7 Suppl): S48-51
- 8 **Shimada M,** Matsumata T, Kamakura T, Suehiro T, Itasaka H, Sugimachi K. Changes in regulating blood coagulation in hepatic resection with special references to soluble thrombomodulin and protein C. *J Am Coll Surg* 1994; **178**: 65-68
- 9 **Kloczko J,** Mian M, Wojtukiewicz MZ, Babiuch L, Bielawiec M, Galar M. Plasma protein C as a marker of hepatocellular damage in alcoholic liver disease. *Haemostasis* 1992; **22**: 340-344
- 10 **Yoshikawa Y,** Sakata Y, Toda G, Oka H. The acquired vitamin K-dependent γ -carboxylation deficiency in hepatocellular carcinoma involves not only prothrombin, but also protein C. *Hepatology* 1988; **8**: 524-530
- 11 **He SL.** Coagulation-inflammatory network: anti-inflammatory effect of natural coagulation inhibitors. *Chin J Thromb Hemost* 2001; **7**: 147-149
- 12 **Esmon CT.** Role of coagulation inhibitors in inflammation. *Thromb Haemost* 2001; **86**: 51-56
- 13 **Taylor FB,** Chang A, Esmon CT, D'Angelo A, Viganò-D'Angelo SV, Blick KE. Protein C prevents the coagulopathic and lethal effects of *E.coli* infusion in the baboon. *J Clin Invest* 1987; **79**: 918-925
- 14 **Bernard GR,** Vincent JL, Laterre PF, LaRosa SP, Dhainaut JF, Lopez-Rodriguez A, Steingrub JS, Garber GE, Helterbrand JD, Ely EW, Fisher CJ Jr. Efficacy and safety of recombinant human activated protein C for severe sepsis. *N Engl J Med* 2001; **34**: 699-709
- 15 **Griffin JH,** Zlokovic B, Fernandez JA. Activated protein C: potential therapy for severe sepsis, thrombosis, and stroke. *Semin Hematol* 2002; **39**: 197-205
- 16 **Vincent JL,** Angus DC, Artigas A, Kalil A, Basson BR, Jamal HH, Johnson G, Bernard GR. Effects of drotrecogin alfa (activated) on organ dysfunction in the PROWESS trial. *Crit Care Med* 2003; **31**: 834-840

Edited by Chen WW and Wang XL Proofread by Xu FM

• CASE REPORT •

Fasciola hepatica infestation as a very rare cause of extrahepatic cholestasis

Ahmet Dobrucali, Rafet Yigitbasi, Yusuf Erzin, Oguzhan Sunamak, Erdal Polat, Hakan Yakar

Ahmet Dobrucali, Yusuf Erzin, Division of Gastroenterology, Cerrahpasa Medical Faculty, Istanbul University, Turkey
Rafet Yigitbasi, Oguzhan Sunamak, Division of General Surgery, Cerrahpasa Medical Faculty, Istanbul University, Turkey
Erdal Polat, Hakan Yakar, Division of Microbiology and Parasitology, Cerrahpasa Medical Faculty, Istanbul University, Turkey
Correspondence to: Dr. Yusuf Erzin, Hurriyet Cad. 9/1, 34 810 Florya-Istanbul, Turkey. dryusuf@doruk.net.tr
Telephone: +90-532-2655008 **Fax:** +90-212-5307440
Received: 2004-01-02 **Accepted:** 2004-01-17

Abstract

Fasciola hepatica, an endemic parasite in Turkey, is still a very rare cause of cholestasis worldwide. Through ingestion of contaminated water plants like watercress, humans can become the definitive host of this parasite. Cholestatic symptoms may be sudden but in some cases they may be preceded by a long period of fever, eosinophilia and vague gastrointestinal symptoms. We report a woman with cholangitis symptoms of sudden onset which was proved to be due to *Fasciola hepatica* infestation by an endoscopic retrograde cholangiography.

Dobrucali A, Yigitbasi R, Erzin Y, Sunamak O, Polat E, Yakar H. *Fasciola hepatica* infestation as a very rare cause of extrahepatic cholestasis. *World J Gastroenterol* 2004; 10(20): 3076-3077
<http://www.wjgnet.com/1007-9327/10/3076.asp>

CASE REPORT

A 40-year old woman with no prior complaints was admitted to our emergency unit due to fever, chills, nausea, vomiting and persistent right-upper quadrant pain for one week. She was born at the East of Turkey and in her medical history she had a cesarean section five years ago and was operated for inguinal hernia one year ago. She was a non-smoker and had no prior medication.

On her physical examination, she was pale but not jaundiced and had a body temperature of 36.8 °C. She was normotensive with a regular pulse of 92 per minute. She had a mild mid-systolic murmur on the aortic valve, but no additional pathologic heart sounds or murmurs on major arteries were noted. All peripheral pulses were palpable. Auscultation of the lungs revealed no pathology. She had a cesarean section incision and another right lower quadrant incision due to hernia repair. Her bowel sounds were hyperactive on auscultation of the abdomen and she had a prominent right subcostal tenderness, but no liver or spleen enlargements were noted on palpation.

Her complete blood count was: hematocrit 30%, mean corpuscular volume 75 fl (normal, 80-95 fl), white blood cells 8 700/mm³ (normal, 4 000-10 000) with 15% eosinophils on peripheral smear, platelets 169 000/mm³ (normal, 100 000-450 000). The erythrocyte sedimentation rate was 45 mm/h, C reactive protein (CRP) level was 75 mg/L (normal, 0-5). Her complete blood chemistry was normal but alanine aminotransferase (ALT) level was 74 U/L (normal, 5-37), aspartate aminotransferase (AST) level was 93 U/L (normal, 5-37), alkaline phosphatase

level (ALP) was 266 U/L (normal, 32-155), gamma glutamyl transferase (GGT) level was 319 U/L (normal, 7-49). Total bilirubin level and urinalysis were normal.

A chest x-ray and plain abdominal radiograph revealed no pathology. In suspicion of gallstone disease, an ultrasonographic examination was performed and it showed a normal liver parenchyma but two hyperechogen solid lesions measuring 9 mm×9 mm and 7 mm×8 mm in the 7th segment of the right lobe. The gallbladder wall was normal but besides sludge multiple, milimetric, intraluminal echogenic particles were noted. Intrahepatic bile ducts were normal but there was a slight enlargement of the common bile duct (11 mm).

Still in suspicion of cholangitis due to gallstone, ceftriaxone 2 g/d i.v. was empirically started and the patient was referred to our endoscopy unit for endoscopic retrograde cholangiopancreatography (ERCP). After its selective cannulation, the common bile duct was filled with contrast agent and a slight enlargement and multiple, mobile, oval shaped filling defects were noted. Intrahepatic bile ducts were proved to be normal (Figure 1). After sphincterotomy, balloon extraction was performed and five *Fasciola hepatica* worms were noted. All of them were captured and taken out via a dormia basket (Figure 2, 3). After this interesting finding the patient's stool examination disclosed the parasites' ova (Figure 4) and an indirect hemagglutination test proved to be positive in 1/1 320 titer.



Figure 1 Multiple oval shaped filling defects on cholangiogram.



Figure 2 *Fasciola hepatica* next to papilla of Vater after sphincterotomy and balloon extraction.

After extraction of the worms the patient's symptoms

rapidly regressed and her liver enzymes returned to normal levels, then she was put on bithionol treatment 30 mg/kg every other day for 15 doses.



Figure 3 Adult flukes measuring 2.5 cm×1.5 cm in diameter.



Figure 4 Ova of *Fasciola hepatica* (×40).

DISCUSSION

A variety of liver flukes, including *Fasciola hepatica* may colonize the biliary tree where they lay their eggs, which can give rise to the formation of gallstones by serving as nidus for them. Living or dead worms may occlude the bile ducts causing obstruction and sometimes cholangitis.

Fascioliasis is primarily a common disease of livestock animals as cattle and sheep with humans serving only occasionally as accidental hosts. This zoonotic disease is common in Africa, Western Europe and Latin America^[1]. In a recent study from the East of Turkey, its seroprevalance was reported to be 2.78% independent of age, educational and socioeconomical status^[2].

Two stages have been described in human *fascioliasis*, namely an acute phase which coincides with hepatic invasion and a chronic phase due to the presence of flukes in the bile ducts^[3]. The metacercariae for this parasite encyst on freshwater plants such as wild watercress and human consumption of aquatic plants harvested from contaminated areas lead to infection. Then developing larvae penetrate the gut wall and enter the peritoneal cavity. After a period of migration for 6 to 9 wk, the young flukes penetrate the capsule of the liver and they mature in the biliary tree and begin to pass their eggs. In the acute phase, the patient may have prolonged fevers, right upper quadrant pain, liver enlargement and eosinophilia which can be easily misdiagnosed. These symptoms abate with the

chronic phase. Once the flukes enter the bile ducts, they may cause symptoms due to cholestasis and cholangitis^[4].

Although the definitive diagnosis for *fascioliasis* can be made by detecting the parasite eggs in stool or duodenal aspirates, egg detection rate is not so high because of the low egg production rate of the parasite. Immunoserological tests become the cornerstone for the diagnosis of *fascioliasis* especially in early stage or ectopic infections^[5] but an ELISA test provides more rapid and reliable results^[6].

Although some parts of our country are endemic areas for human *fascioliasis*, this diagnosis was not suspected prior to give its full term (ERCP) as it is still a very rare cause of biliary obstruction. As usual^[7], sphincterotomy and balloon extraction rapidly alleviated symptoms in our patient.

Unlike other liver flukes, therapeutic failure was common in patients with *Fasciola hepatica* treated with piraziquantel so bithionol or triclabendazole has been the treatment of choice for this parasitic infection^[8]. The use of bithionol with the recommended dose of 30-50 mg/kg every other day for 10-15 doses or repeated doses has resulted in cure of acute and prolonged *fascioliasis*^[9]. Triclabendazole, another effective and safe drug for *fascioliasis*, has been found to be able to eradicate the parasite with a single oral dose of 10 mg/kg^[10]. Our patient was put on bithionol treatment 30 mg/kg every other day for 15 doses and no major side effects were noted.

We report this patient to draw attention to the latter that *fascioliasis* should be kept in mind in patients with cholestasis and preceding vague gastrointestinal symptoms especially in endemic areas of the world.

REFERENCES

- 1 **Mas-Coma MS**, Esteban JG, Bargues MD. Epidemiology of human fascioliasis: a review and proposed new classification. *Bull World Health Organ* 1999; **77**: 340-346
- 2 **Kaplan M**, Kuk S, Kalkan A, Demirdag K, Ozdarendeli A. Fasciola hepatica seroprevalence in the Elazig region. *Mikrobiyol Bul* 2002; **36**: 337-342
- 3 **Barrett-Conner E**. Fluke infections. In: Braude AI, editor. Infectious diseases and medical microbiology, 2nd ed. Philadelphia, PA: W. B Saunders 1986: 979-982
- 4 **King CH**, Mahmoud AAF. Schistosoma and other trematodes. In: Gorbach SL, Bartlett JG, Blacklow NR, editors. Infectious diseases. Philadelphia, PA: W.B. Saunders 1992: 2015-2021
- 5 **Harinasuta T**, Pungpak P, Keystone JS. Trematode infections. Opisthorchiasis, clonorchiasis, fascioliasis. *Infect Dis Clin North Am* 1993; **7**: 699-716
- 6 **Shaheen HI**, Kamal KA, Farid Z, Mansour N, Boctor FN, Woody JN. Dot-enzyme-linked immunosorbent assay (dot-ELISA) for the rapid diagnosis of human fascioliasis. *J Parasitol* 1989; **75**: 549-552
- 7 **el-Newihi HM**, Waked IA, Mihas AA. Biliary complications of Fasciola hepatica: the role of endoscopic retrograde cholangiography in management. *J Clin Gastroenterol* 1995; **21**: 309-311
- 8 **Pearson RD**. Parasitic diseases: Helminths. In: Yamada T, Alpers DH, Kaplowitz N, Laine L, Owyang C, Powell DW, editors. Textbook of gastroenterology, 4th ed. Philadelphia, PA: Lippincott Williams Wilkins 2003: 2608-2625
- 9 **Bacq Y**, Besnier JM, Duong TH, Pavie G, Metman EH, Choutet P. Successful treatment of acute fascioliasis with bithionol. *Hepatology* 1991; **14**: 1066-1069
- 10 **Loutan L**, Bouvier M, Rojanawisut B, Stalder H, Rouan MC, Buescher G, Poltera AA. Single treatment of invasive fascioliasis with triclabendazole. *Lancet* 1989; **2**: 383

Common bile duct obstruction due to fibrous pseudotumor of pancreas associated with retroperitoneal fibrosis: A case report

Mei-Fen Zhao, Yu Tian, Ke-Jian Guo, Zhi-Gang Ma, Hai-Hui Liao

Mei-Fen Zhao, Yu Tian, Ke-Jian Guo, Zhi-Gang Ma, Hai-Hui Liao, Department of General Surgery, First Affiliated Hospital, China Medical University, Shenyang 110001, Liaoning Province, China
Correspondence to: Dr. Mei-Fen Zhao, Department of General Surgery, First Affiliated Hospital, China Medical University, Shenyang 110001, Liaoning Province, China. zhaomeifen@medmail.com.cn
Telephone: +86-24-81677066 **Fax:** +86-24-81677066
Received: 2003-12-19 **Accepted:** 2004-01-12

Abstract

One 63-year-old woman, who presented with cholestatic jaundice due to common bile duct compression produced by primary retroperitoneal fibrosis, is studied. The patient was operated six years ago because of hydronephrosis, when the disease was first diagnosed. Magnetic resonance cholangiopancreatography (MRCP) revealed the presence of extrahepatic bile duct obstruction, which once was considered to be pathognomonic of pancreatic cancer. CT-scan demonstrated the change of retroperitoneal fibrosis around left kidney, atrophy of right kidney, and obstruction of extrahepatic bile duct (pancreatic head). An explorative laparotomy was performed, and the retroperitoneum and pancreas were grayish-white and hard, the fibrotic pancreatic head compressed the common bile duct. Bile duct stricture was managed by Rouxen-Y hepatocholangio-jejunostomy. To the best of our knowledge, few similar cases of retroperitoneal fibrosis have been reported.

Zhao MF, Tian Y, Guo KJ, Ma ZG, Liao HH. Common bile duct obstruction due to fibrous pseudotumor of pancreas associated with retroperitoneal fibrosis: A case report. *World J Gastroenterol* 2004; 10(20): 3078-3079
<http://www.wjgnet.com/1007-9327/10/3078.asp>

INTRODUCTION

Retroperitoneum is one of the most complex regions of human anatomy as it contains a variety of organs and structures from different systems, in particular those belonging to the urinary and digestive tracts and the vascular systems. Primary retroperitoneal fibrosis (Ormond's disease) is a rare disorder typically with an insidious clinical course, characterized by the presence of dense, grayish-white plaques centered around the abdominal aorta in this space. The peak incidence of this uncommon disease is between the ages of 40 and 60 years and mostly in men^[1]. Most commonly, it causes fibrous encasement of the ureters and subsequent obstructive hydronephrosis. Atypical sites of involvement include the duodenum, colon, urinary bladder, mesentery, small intestine and epidural space. Typically, mass effect from the enlarging fibrosis plaque leads to compromise of surrounding structures. For example, extrinsic compression can lead to small and large bowel obstruction, vena cava stasis, and arterial insufficiency in lower extremities.

In this report, we describe an unusual case of this rare disorder, which presented with obstructive jaundice caused by the compression of common bile duct due to the involved

diffusive pancreatic fibrosis. To the best of our knowledge, few similar cases of Ormond's disease have been reported.

CASE REPORT

One 63-year-old woman was sent to our hospital because of jaundice, slight loss of weight and anorexia in October 2003. The patient was operated six years ago because of hydronephrosis, when the Ormond's disease was first diagnosed. After operation, no corticosteroid was administrated and no reopening of the ureter was observed up to the admission to our hospital. Her antihypertensive medications included *Fufangluobuma* (TCM compound) and metoprolol.

The patient had been jaundiced for 9 d before sent to our hospital, and had no stigmata of chronic liver disease. Physical examination revealed a slight cachectic state. Abdominal examination was unremarkable without signs of ascites, and the liver edge was not palpable below the right costal margin. Patient had no fever and alcohol or drug abuse. Laboratory tests revealed a normal red and white blood cell counts. Erythrocyte sedimentation rate (ESR) was 120 mm/h in the first hour (normal 0-32), C-reactive protein (CRP) 0.4 mg/dL (normal <1 mg/dL). Blood urea nitrogen, creatinine level and amylase were normal. Total bilirubin was 278.3 $\mu\text{mol/L}$ (normal 2-20 $\mu\text{mol/L}$), direct bilirubin 237.1 $\mu\text{mol/L}$ (normal 0-3.4 $\mu\text{mol/L}$), alkaline phosphatase 326 U/L (normal 15-128 U/L), aspartate aminotransferase (AST) 27 U/L (normal 1-38 U/L), and alanine aminotransferase (ALT) 40 U/L (normal 1-41 U/L). Hepatitis and human immunodeficiency viruses were negative. Abdominal ultrasonography showed an enlarged pancreatic head and dilated intra- and extra- hepatic ducts. Additionally, cholecystolithiasis was detected. CT-scan demonstrated the change of retroperitoneal fibrosis around the left kidney, atrophy of right kidney, and obstruction of extra-hepatic bile duct (pancreatic head). The pancreatic head was slightly enlarged, but the enhanced scan showed that the density of the whole pancreas was homogeneous. Also gallbladder stones were found (Figure 1). Subsequent MRCP revealed the interruption of extrahepatic bile duct (Figure 2).



Figure 1 CT-scan demonstrated the change of retroperitoneal fibrosis around left kidney, atrophy of right kidney. The density of the whole pancreas was homogeneous.

A presumptive diagnosis of pancreatic cancer or cholangiocarcinoma was made and an explorative laparotomy was performed. We found that the retroperitoneum and pancreas

were grayish-white, and the consistency of them was hard (Figure 3). The fibrotic pancreatic head compressed the common bile duct. Then the gallbladder was resected and a Roux-en-Y hepatocholeangio-jejunostomy was constructed. Adjacent lymph nodes were not enlarged or malignant. The patient recovered fully after surgery.



Figure 2 MRCP revealed the interruption of extrahepatic bile duct.



Figure 3 Retroperitoneum and pancreas were grayish-white and hard.

DISCUSSION

Ormond's disease is a rare disorder characterized by transformation of normal fat tissue into a retractile fibrosis mass. Although the etiology of this chronic process is still unclear, the proposed mechanism is thought to be an autoimmune disorder secondary to the development of antibodies produced against ceroid, a polymer of oxidized lipid and protein^[2,3]. This hypothesis is based upon the finding of association between atherosclerotic plaques of the aorta and retroperitoneal fibrosis^[4,5]. It is thought that inflammatory antigens like ceroid pass through the adventitia into the periaortic fatty tissue and produce a periaortic and periarterial fibrosis^[6-8]. In addition, several pharmacological substances have been cited as possible causative agents of retroperitoneal fibrosis^[3]. Methysergide is the only drug that has been proved to cause retroperitoneal fibrosis^[2]. Other suspected causative drugs include β -adrenergic blockers, antihypertensives, analgesics^[3]. The medications of this patient included metoprolol, which is a kind of β -adrenergic blocker, but we were not able to identify the exact etiologic agent of this disease.

The presentation of retroperitoneal fibrosis in this patient was unique for two reasons. Ormond's disease often manifests clinically by constriction and compression of ureters, blood vessels and nerves. This patient had had an initial manifestation of Ormond's disease affecting left ureter before this admission. Uncommonly, upon this admission she presented with clinical manifestation of obstructive jaundice, which was due to the compression of portions of the common bile duct. There have

been only 9 reports of retroperitoneal fibrosis with cholestatic jaundice due to compression of the distal part of the common bile duct by fibrotic pancreatic head^[9-15]. A second distinctive feature of this Ormond's disease case was the direct involvement of the pancreas, which has not previously been highlighted and led to diagnostic difficulty. Obstructive jaundice due to the retroperitoneal fibrosis of pancreas head is easy to mimicking the carcinoma of pancreas. In some authors' opinion, sclerosing pancreatitis due to retroperitoneal fibrosis as this patient has been classified into the new clinical entity—"autoimmune related pancreatitis" or "autoimmune pancreatitis".

Management of retroperitoneal fibrosis includes surgical relief of extrinsically compressed or encased structures, deep tissue biopsies to confirm the diagnosis and to exclude the malignant variant, and the use of corticosteroids (and other immunosuppressants) to prevent further progression of the disease^[2]. There is no definitive duration or dosage of corticosteroids recommended for the therapy of this disease. This patient did not take corticosteroids.

In conclusion, this atypical retroperitoneal fibrosis illustrates that this disease involves the pancreas, and diffusive pancreatic fibrosis (sclerosing pancreatitis) can affect the common bile duct to manifest the initial symptom of cholestatic jaundice. Additionally, surgeons should pay attention to this condition mimicking pancreatic carcinoma or cholangiocarcinoma.

REFERENCES

- 1 Meier P, Gilabert C, Burnier M, Blanc E. Retroperitoneal fibrosis, an unrecognized inflammatory disease. Clinical observations and a review of the literature. *Nephrologie* 2003; **24**: 173-180
- 2 Kottra JJ, Dunnick NR. Retroperitoneal fibrosis. *Radiol Clin North Am* 1996; **34**: 1259-1275
- 3 Buff DD, Bogin MB, Faltz LL. Retroperitoneal fibrosis. A report of selected cases and a review of the literature. *N Y State J Med* 1989; **89**: 511-516
- 4 Mitchinson MJ. Retroperitoneal fibrosis revisited. *Arch Pathol Lab Med* 1986; **110**: 784-786
- 5 Martina B. Chronic periaortitis—a new interpretation of Ormond's disease. *Urol Res* 1990; **18**: 165-167
- 6 Amis ES Jr. Retroperitoneal fibrosis. *Am J Roentgenol* 1991; **157**: 321-329
- 7 Hughes D, Buckley PJ. Idiopathic retroperitoneal fibrosis is a macrophage-rich process. Implications for its pathogenesis and treatment. *Am J Surg Pathol* 1993; **17**: 482-490
- 8 Martina FB, Nuech R, Gasser TC. Retroperitoneal fibrosis and chronic periaortitis: a new hypothesis. *Eur Urol* 1993; **23**: 371-374
- 9 Renner IG, Ponto GC, Savage WT 3rd, Boswell WD. Idiopathic retroperitoneal fibrosis producing common bile duct and pancreatic duct obstruction. *Gastroenterology* 1980; **79**: 348-351
- 10 Remedios D, Coppen M, Bradbeer J, Theodossi A. Chronic periaortitis presenting as common bile duct obstruction. *Gut* 1991; **32**: 713-714
- 11 Laitt RD, Hubscher SG, Buckels JA, Darby S, Elias E. Sclerosing cholangitis associated with multifocal fibrosis: a case report. *Gut* 1992; **33**: 1430-1432
- 12 Cappell MS. Obstructive jaundice due to retroperitoneal fibrosis involving the head of the pancreas. *J Clin Gastroenterol* 1994; **18**: 53-56
- 13 Chutaputti A, Burrell MI, Boyer JL. Pseudotumor of the pancreas associated with retroperitoneal fibrosis: a dramatic response to corticosteroid therapy. *Am J Gastroenterol* 1995; **90**: 1155-1158
- 14 Pereira-Lima JC, Kromer MU, Adamek HE, Riemann JF. Cholestatic jaundice due to Ormond's disease (primary retroperitoneal fibrosis). *Hepatogastroenterology* 1996; **43**: 992-994
- 15 Dejacó C, Ferenci P, Schober E, Kaserer K, Fugger R, Novacek G, Gangl A. Stenosis of the common bile duct due to Ormond's disease: case report and review of the literature. *J Hepatol* 1999; **31**: 156-159

Maintaining cholesterol homeostasis: Sterol regulatory element-binding proteins

Lutz W. Weber, Meinrad Boll, Andreas Stampfl

Lutz W. Weber, 554 Mariner Point Drive, Clinton, TN 37716, USA
Meinrad Boll, Andreas Stampfl, Institute for Toxicology, GSF - National Research Center for Environment and Health, Munich, D-85758 Neuherberg, Germany

Correspondence to: Lutz W. Weber, Institute of Toxicology, GSF - National Research Center for Environment and Health, Munich, D-85758 Neuherberg, Germany. stampfl@gsf.de

Telephone: +49-89-3187-2625 **Fax:** +49-89-3187-3449

Received: 2003-10-15 **Accepted:** 2004-04-13

Abstract

The molecular mechanism of how hepatocytes maintain cholesterol homeostasis has become much more transparent with the discovery of sterol regulatory element binding proteins (SREBPs) in recent years. These membrane proteins are members of the basic helix-loop-helix-leucine zipper (bHLH-Zip) family of transcription factors. They activate the expression of at least 30 genes involved in the synthesis of cholesterol and lipids. SREBPs are synthesized as precursor proteins in the endoplasmic reticulum (ER), where they form a complex with another protein, SREBP cleavage activating protein (SCAP). The SCAP molecule contains a sterol sensory domain. In the presence of high cellular sterol concentrations SCAP confines SREBP to the ER. With low cellular concentrations, SCAP escorts SREBP to activation in the Golgi. There, SREBP undergoes two proteolytic cleavage steps to release the mature, biologically active transcription factor, nuclear SREBP (nSREBP). nSREBP translocates to the nucleus and binds to sterol response elements (SRE) in the promoter/enhancer regions of target genes. Additional transcription factors are required to activate transcription of these genes. Three different SREBPs are known, SREBPs-1a, -1c and -2. SREBP-1a and -1c are isoforms produced from a single gene by alternate splicing. SREBP-2 is encoded by a different gene and does not display any isoforms. It appears that SREBPs alone, in the sequence described above, can exert complete control over cholesterol synthesis, whereas many additional factors (hormones, cytokines, etc.) are required for complete control of lipid metabolism. Medicinal manipulation of the SREBP/SCAP system is expected to prove highly beneficial in the management of cholesterol-related disease.

Weber LW, Boll M, Stampfl A. Maintaining cholesterol homeostasis: Sterol regulatory element-binding proteins. *World J Gastroenterol* 2004; 10(21): 3081-3087

<http://www.wjgnet.com/1007-9327/10/3081.asp>

INTRODUCTION

The view of cholesterol as a nasty substance which clogs arteries and causes heart disease is wide-spread, but it does not do the molecule justice. Not only is it a vital component of cell membranes without which the cell cannot function, but it is also the precursor to all steroid hormones, bile acids, and oxysterols, which by themselves are important regulatory molecules in many metabolic pathways.

Cholesterol and fatty acids as building blocks of cell membranes are synthesized via regulated pathways. All cells must control these pathways in order to maintain levels within physiological boundaries. Excessive amounts of cholesterol in cells can destroy membrane function, precipitate as crystals which will kill the cell or result in atherosclerotic damage if spread to blood^[1]. However, the original view of random distribution of cholesterol and lipids in the cell membrane no longer holds: not only differs the lipid composition of the outer leaflet of the plasma membrane from the inner one, but the distribution of lipids and cholesterol in the outer leaflet is organized into domains, with so-called rafts^[2] and caveolae^[3] being rich in cholesterol and sphingomyelin. These structures play intricate roles in cholesterol trafficking to maintain cellular homeostasis, and they are also components of the cellular signalling system. The membranes of endoplasmic reticulum (ER) and Golgi, on the other hand, contain comparatively little cholesterol, a factor important in its own homeostasis, and one objective of this overview.

The understanding of cholesterol regulation has come a long way from the initial recognition of cholesterol feedback inhibition of its rate-limiting synthetic enzyme, 3-hydroxy-3-methylglutaryl coenzyme A (HMGCoA) reductase, through the role of lipoproteins in maintaining plasma cholesterol levels, to the recent discoveries of regulation of cholesterol synthesis via sterol-sensitive response elements (SREs), and degradation via liver X receptor (LXR) - or bile acid receptor (BAR) -regulated pathways.

Lipid homeostasis via SREs in animal cells is achieved by a family of transcription factors called SRE-binding proteins (SREBPs). SREBPs activate directly the expression of some 30-plus genes participating in the metabolism mostly of lipids, but also glucose. Activation of these originally membrane-bound transcription factors involves a proteolytic cascade through which the SREBP molecule is released from the membrane and obtains its mature form as a transcription factor. The active SREBP enters the nucleus and binds to those special DNA sequences, the SREs, in the promoter regions of many different genes.

In the health arena, SREBPs stand at a crucial point: they regulate expression of the LDL receptor, the molecule which enables the hepatocytes to remove cholesterol contained in LDL particles from the bloodstream. High (dietary) cholesterol prevents maturation of SREBPs and not only cuts off cholesterol synthesis, but also LDL receptor synthesis, resulting in high blood cholesterol and the imminent danger of atherosclerotic plaque formation. At this point in time the so-called statins, drugs which block HMGCoA reductase, another target of SREBP-mediated gene expression, are the most effective way to interrupt this vicious circle^[4].

This brief overview is concerned with the SREBP-mediated control of cholesterol and lipid synthesis. Lipid synthesis is subject to many other regulatory influences which cannot be addressed here, nor can the degradation of cholesterol via hormone or bile acid synthesis be covered, which again commands its own set of regulatory substances. The focus of this minireview is to present the latest data on the SREBP-induced mechanism. Recent in-depth reviews have been available^[5-9].

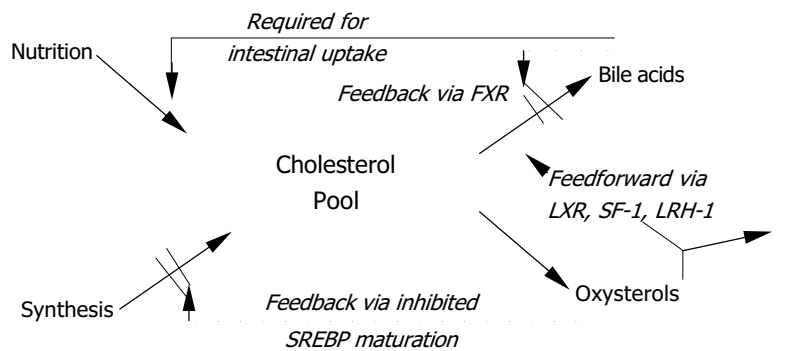


Figure 1 Feedforward and feedback effects of oxysterols FXR = farnesoid receptor; LRH-1 = liver receptor homologue-1; LXR = liver receptor; SF-1 = steroidogenic factor-1; SREBP = sterol responsive element binding protein.

OXYSTEROLS AS NEGATIVE AND POSITIVE REGULATORY MOLECULES

Cholesterol is not the only sterol inside the cell to act as a regulatory substance, many of its hydroxylated derivatives, the oxysterols, share these important functions. Oxysterols exert a feed-back effect and down-regulate cholesterol synthesis, to be detailed in the following sections of this overview, but they also up-regulate their own metabolism and elimination via a feed-forward effect which will be briefly described in this section.

Cholesterol directly affects two enzymes which are vital in its own removal. It activates acyl-CoA: cholesterol acyl transferase (ACAT), the enzyme required to synthesize cholesteryl esters, its major storage form, and it also activates cholesterol 7 α -hydroxylase (CYP7A1), the initial and rate-limiting enzyme of bile acid synthesis, the leading pathway of cholesterol elimination^[10].

The side chain-hydroxylated 27-hydroxycholesterol is presumed to function in cholesterol homeostasis by sustaining HDL-mediated reverse cholesterol transport, the process by which cholesterol is brought back to the liver from peripheral tissues^[11]. The most important action of oxysterols, however, is to serve as ligands for nuclear orphan receptors. This family of proteins has been recognized as nuclear hormone receptors based on their molecular properties, but since ligands were initially not known, they were named orphan receptors. Most important among these is liver X receptor (LXR), which controls expression of CYP7A1^[12] as the rate-limiting step of bile acid synthesis^[13,14], reverse cholesterol transport^[15], trafficking of cholesteryl esters, and aids in lipid metabolism^[16] and the intestinal absorption of cholesterol. This receptor displays specific requirements for the position of additional hydroxy group (s) on the cholesterol molecule, the most potent ligands being 20 (S)-OH-, 22 (R)-OH-, 20, 22-di-OH-, and 24-OH-cholesterol^[17,18]. An overview of oxysterol actions is shown in Figure 1.

Furthermore, oxysterols are ligands for steroidogenic factor-1 (SF-1) and liver receptor-homologue 1 (LRH-1), in which they regulate steroid hormone synthesis and sexual differentiation during prenatal development. SF-1 is limited to steroidogenic tissues, whereas LRH-1 occurs in liver and other tissues derived from the gut endoderm^[7]. Oxysterols also play a role in meiosis^[19]. Finally, these bile acids activate the farnesol X receptor (FXR)/retinoid X receptor (RXR)/receptor-interacting protein 14 (Rip14) system, FXR is also known as bile acid receptor (BAR). Binding of bile acids to FXR inhibits bile acids synthesis.

SREBPS, MEMBRANE-DERIVED TRANSCRIPTION FACTORS

SREBPs belong to the large family of basic helix-loop-helix-leucine zipper (bHLH-Zip) transcription factors. Three members of the SREBP family, SREBPs-1a, -1c, and -2, have been identified^[20,21]. They are synthesized as inactive precursors. Isoforms -1a and -1c are produced from a single gene on human chromosome 17p11.2 by use of alternate promoters and splicing,

resulting in different forms of exon-1^[21-23]. SREBP-2 is encoded by a separate gene on human chromosome 22q13^[20,24]. It has about 50% sequence identity with SREBP-1. Adipocyte determination differentiation factor (ADD)-1, a transcription factor which binds to E-boxes and promotes adipocyte differentiation in rats^[25] is the homologue of human SREBP-1c^[23].

Each nascent SREBP protein has a molecular size of about 125 ku and consists of about 1 150 amino acids (aa) in 3 functional domains. The first, NH₂-terminal domain of SREBP contains the bHLH-Zip and an acidic domain, located at the very NH₂ terminus. The acidic domain has to bind a transcription coactivator for function, it is shorter in SREBP-1c than in SREBP-1a, making SREBP-1c a weaker transcription activator^[26]. The acidic domain is essential for function. When removed, the bHLH-Zip portion of SREBP still binds to DNA, but no longer activates transcription, thus acting as an inhibitor^[27].

Adjacent to the acidic DNA-binding domain is a variable area rich in serine, proline, glutamine, and glycine. Next follows the bHLH-Zip sequence, whose basic region mediates DNA binding. The rest of the bHLH-Zip motif imparts the ability to dimerize. Other bHLH-Zips tend to homo-dimerize, whereas SREBP needs other transcription factors such as SP-1 or NF-Y for full function. The remainder of the SREBP molecule has no analogy with other bHLH-Zip transcription factors^[5].

SREBPs are embedded in membranes of the endoplasmic reticulum (ER) and the nuclear envelope, forming what has been called a hairpin shape^[28,29]. The NH₂-terminal portion of the SREBP molecule through the bHLH-Zip region protrudes into the cytosol. The following central portion of SREBP, the membrane anchoring region, is about 90 aa in length. It consists of two hydrophobic, membrane-spanning segments separated by a hydrophilic loop which extends into the lumen of the ER. The COOH terminal segment of about 590 aa again extends into the cytosol and serves as the regulatory domain for transformation into the mature, a transcriptionally active form also known as nuclear SREBP (nSREBP). Neither the membrane-spanning, nor the regulatory regions, are found in other bHLH-Zip transcription factors.

The NH₂-terminal domain of SREBP binds to a sterol binding element (SRE) which must contain a direct, or tandem, repeat of the recognition sequence^[30]. This is another evident difference to bHLH-Zip transcription factors, which will bind only to palindromic (i.e., tail-to-tail connected) repeats. SREBPs display no *in vivo* activity with palindromic sequences^[5,19].

SREBP CLEAVAGE ACTIVATION PROTEIN (SCAP), AN ESCORT AND STEROL SENSOR PROTEIN

SREBPs attain biological activity only after being transferred to the membrane of the Golgi complex, where they are cleaved at the luminal loop and the NH₂-end is released from the membrane. They are confined to the membranes of the ER unless they are

paired up with another protein which serves two functions: to sense the levels of sterols in the cell, and in response to low sterol levels, to escort SREBP to its place of activation. This is achieved by SREBP cleavage activating protein (SCAP), a protein originally cloned from a mutant cell line of Chinese hamster ovary cells which will not suppress SREBP cleavage even with very high sterol levels^[31]. The mutation affects one specific codon, 443, where a C (ytosine) to G (uanine) transition on the DNA side replaces an aspartic acid by an asparagine in the amino acid sequence, rendering SCAP unresponsive to sterols^[32].

SCAP has 1 276 amino acids^[31] in two domains^[33]: a membrane-spanning NH₂ terminal domain of 730 aa, and a COOH terminal domain of 546 aa, which extends into the cytosol. The NH₂-terminus contains eight hydrophobic sequences separated by short hydrophilic loops^[31], the hydrophobic sequences are thought to span the membrane with the hydrophilic loops protruding at either side. SCAP shares this feature with HMGCoA reductase^[34,35]. The membrane-spanning stretches comprise the sterol-sensing area, whereas the COOH-terminus contains all of the remaining biological activity^[31]. The COOH-terminus is organized in five repeat sequences characteristic of the WD family. Wherever this sequence occurs, it mediates protein-protein interactions^[36].

Newly synthesized SREBP forms a tight complex with the WD repeat domains of SCAP^[37], but in the presence of oxysterols this complex is confined to the ER, establishing a feedback loop to control cholesterol synthesis. With oxysterol depletion, the SCAP/SREBP complex appears in vesicles budding from ER membranes^[38] and translocates to another subcellular compartment, the Golgi^[39-43]. Transfer of SREBP and proteolytic cleavage to release nSREBP cannot occur unless this complex has formed^[42]. Oxysterols induce a change of the conformation of SCAP, and an additional protein has been postulated to retain SCAP in the ER once in its sterol-induced conformation^[44]. Not only cholesterol, but also several other oxysterols display

full activity in suppressing SCAP translocation into vesicles, but it has been suggested that cholesterol alone exerts the effect, while high levels of oxysterols simply force translocation of cholesterol from the plasma membrane to the ER^[44]. Complete understanding could be of immense benefit in the management of hyperlipidemias.

SREBP ACTIVATION VIA TWO-STEP PROTEOLYTIC CLEAVAGE

The SREBP/SCAP-containing vesicles from the ER also contain a membrane-anchored serine protease of the subtilisin family, Site-1 protease (S1P), in an inactive form which becomes activated only during its transport to the Golgi^[45]. The SREBP/SCAP complex and S1P now incorporate into the Golgi membrane. As the next step, the activated S1P attaches to the SCAP/SREBP complex and cuts the SREBP molecule right in the middle of its luminal hydrophilic loop^[29]. When active S1P is inserted into the ER, it will cleave SREBP without a need for SCAP^[43].

To release active SREBP, another enzyme is required, Site-2 protease (S2P, a trans-membrane zinc metalloprotease). The cellular location of this enzyme is as yet unclear, but likely resides in the Golgi. S2P cuts the still membrane-anchored SREBP in a rather unusual place, viz., three amino acids into the membrane-spanning portion on the cytoplasmic side^[46,47]. This process is known to regulate intra-membrane proteolysis (Rip)^[48], and typically produces proteins which are transcriptionally active and participate in the control of various cellular processes^[6]. S2P action is not directly affected by cellular oxysterol levels, since this enzyme cannot act unless S1P has separated the bHLH-Zip portion of SREBP from the regulatory COOH terminus^[49]. S2P action results in the release of a mature, 68 kDa nSREBP, consisting of the bHLH-zipper domain with the first three membrane-spanning amino acids attached, which now can migrate to the nucleus and bind to a sterol-responsive element (SRE). SCAP is recycled back to the ER to chaperone another 125 kDa SREBP molecule to the Golgi^[50], whereas the 68 kDa SREBP is degraded. Interestingly, the nuclear

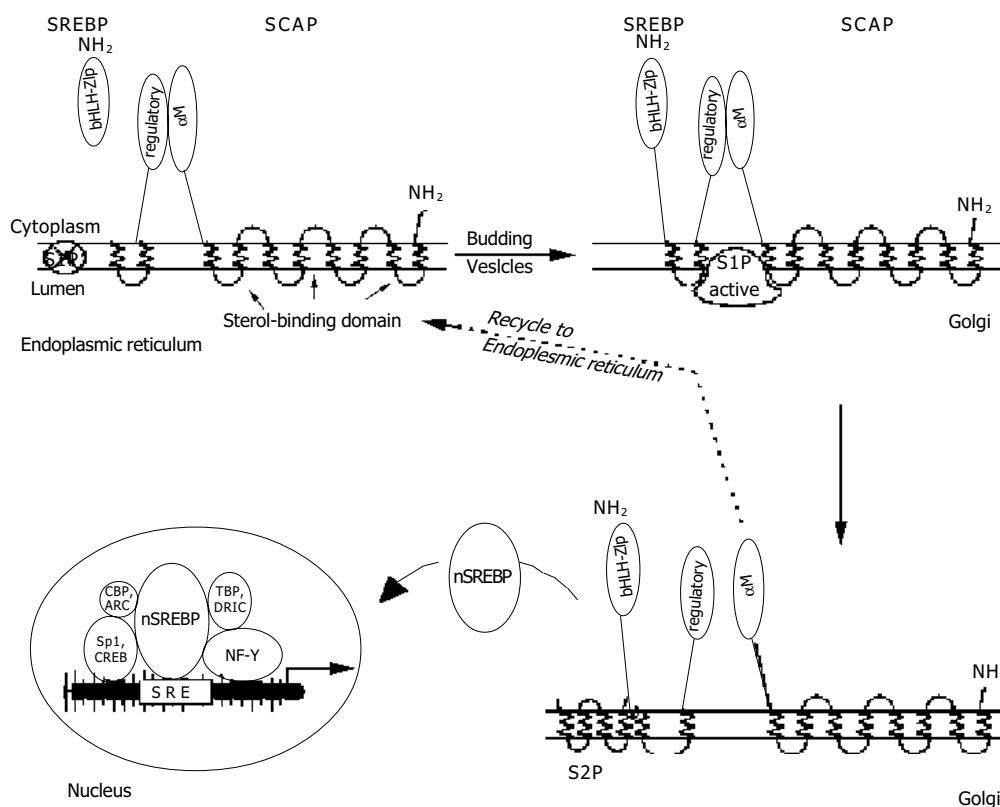


Figure 2 Maturation of SREBPs -NH₂ = amino-terminal ends of SREBP or SCAP. S1P = Site-1 protease (crossed-out = inactive); S2P = Site-2 protease. SRE = sterol-responsive element; nSREBP = nuclear SREBP. Arrangement of the additional transcription factors NF-Y, Sp1, CREB, ARC, CBP, TBP, and DRIC (see text) is tentative as their requirements are not exactly known.

action of nSREBP induces new SREBP mRNA synthesis by way of SREs located in the promoter regions of their own genes^[51]. A synopsis is shown in Figure 2.

The process of SREBP cleavage and activation thus comprises 4 components which, upon mutation, can result in loss of oxysterol-sensitive regulation of cholesterol homeostasis. As a matter of fact, much of the knowledge of the SREBP regulatory system stems from experimentally mutated cell lines and subsequent selection for oxysterol resistance or cholesterol auxotrophy^[8]. Oxysterol resistance has aided in cloning the genes for SREBP and SCAP, respectively. One type, class 1 mutation, produces an NH₂-terminal bHLH-Zip portion of SREBP which is truncated even before the S2P cleavage site^[52,53]. This molecule is therefore not membrane bound and can access the nucleus immediately after its synthesis, turning on the complete SREBP gene battery regardless of cellular oxysterol levels. Class 2 mutants contain a mutated SCAP molecule^[54] which holds the SREBP/SCAP/S1P complex in a permanently active configuration, no matter how high the oxysterol level in the cell, resulting in permanent release of nSREBP with concomitant overproduction of cholesterol^[31].

Cholesterol auxotrophy has been used as a selection criterion to clone the genes for S1P and S2P. With S1P^[55], S2P^[41,46,56] or SCAP^[57] rendered non-functional, cells become dependent on exogenous cholesterol because they cannot produce the enzymes necessary for its biosynthesis.

It is interesting to know that the proteolytic activation of SREBP-1 and SREBP-2, respectively, can be regulated individually. In rodents, treatment with cholesterol suppressing drugs (statins) or with cholesterol-sequestering agents results in up-regulation and increased activation of SREBP-2 while reducing activation of SREBP-1^[58]. Another interesting feature is that polyunsaturated fatty acids inhibit the proteolytic activation of SREBP-1, but contrary to the action of oxysterols, they have no effect on SREBP-2 maturation^[59]. In addition, glucose metabolites such as glucose-6-phosphate may serve to accelerate maturation of SREBP-1c only^[60], but mechanistic details have not been elucidated.

GENE ACTIVATION BY SREBPs, TARGET GENES

Immediately after the second cleavage of the SREBPs the now mature protein enters the nucleus where it binds to SREs in the promoters of the target genes and activates transcription. The SRE nucleotide sequence displays considerable variation among the promoters of the many genes activated by an SRE, a commonly found sequence is represented by 5'-nTCACnCCA Cn-3' (cf.^[6]). However, SREBP alone cannot activate transcription, but must act co-ordinately with additional transcription factors to obtain full activation of target genes.

Transcription factors known to activate SREs in conjunction with SREBP are Sp1, nuclear factor (NF)-Y, and cAMP response element binding protein (CREB)^[10,61-64]. NF-Y interacts directly with SREBP^[62], and Sp1 can stabilize the complex^[61]. It appears that the promoters of different SRE-activated genes respond to different combinations of these transcription factors. Once a stable complex has formed in a promoter region, additional factors such as CREB binding protein (CBP)^[65,66], activated recruited cofactor (ARC)^[67], vitamin D receptor interacting protein (DRIC)^[67], or TATA box-binding protein (TBP)-associated factors may be recruited to initiate transcription. Histone acetylation is also required for full transcriptional activity^[68]. Such complexes have been shown to exist with SREBP-1a and -2, but not with SREBP-1c. This may explain its rather weak potency to activate the SRE gene battery.

SREBP-activated genes predominantly belong to lipid metabolism pathways, viz, cholesterolgenesis, fatty acid synthesis, lipogenesis, triglyceride and phospholipid synthesis, but also glucose metabolism. Yet, the three SREBPs do not activate identical gene batteries. Using transgenic mice over-expressing just one

type of nSREBP it has been discovered that SREBPs-1a and -1c actions favour fatty acid synthesis, whereas SREBP-2 action favours cholesterol synthesis^[5,69-71], but *in vitro* both SREBPs-1a and -2 can trigger expression of the complete set of enzymes required for cholesterol synthesis with similar potency^[72]. While SREBPs-1a and -2 predominate in cultured cells, intact liver and most other tissues primarily express SREBP-1c and -2^[9]. An overview of SREBP pathways is given in Figure 3.

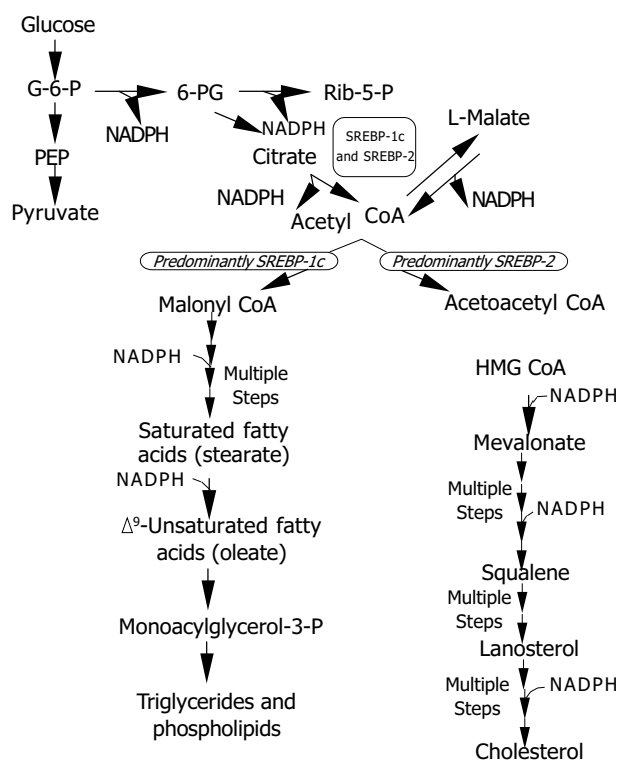


Figure 3 Metabolic pathways regulated by SREBPs G-6-P = glucose-6-phosphate; 6-PG = 6-phosphogluconate; Rib-5-P = ribulose-5-phosphate; PEP = phosphoenol pyruvate; CoA = coenzyme A; HMGCoA = 3-hydroxy-3-methylglutaryl coenzyme A. SREBP-1c and SREBP-2 activate genes for the generation of NADPH (ATP citrate lyase, malic enzyme, G-6-P dehydrogenase, 6-PG dehydrogenase) required in various steps of lipid synthesis.

SREBP-2 over-expression induces all 12 enzymes of the cholesterol biosynthetic pathway^[72], most notably the mRNA for HMGCoA reductase, which may increase as many as 75-fold^[73]. Overall cholesterol synthesis in such animals is up 28-fold, whereas fatty acid synthesis is increased only 4-fold. In contrast, expression of enzymes does not involve cholesterol synthesis but is related to cholesterol metabolism. Cholesterol 7 α -hydroxylase (rate-limiting enzyme for bile acid synthesis) and acyl-CoA:cholesterol acyltransferase (ACAT, catalyses cholesterol ester formation), are not activated^[72].

SREBP-1a appears to be constitutively expressed in most tissues, with as yet no known factor to stimulate its low expression^[26]. Over-expression in adult rats also resulted in over-stimulation of lipid synthesis, but in this case fatty acid synthesis was increased 26-fold, and cholesterol synthesis 5-fold. Since SREBP-1a and -1c (see below) also induce enzymes for fatty acid elongation and desaturation^[73,74], SREBP-1a over-expression resulted in elevated hepatic levels of oleate^[75].

SREBP-1c is predominantly involved in the regulation of adipogenesis and also in the regulation of insulin-responsive genes which control lipogenesis and glucose metabolism^[76,77], but *in vitro* it does not stimulate cholesterol synthesis^[75]. SREBP-1c mRNA synthesis responds to nutritional changes in

parallel to insulin levels^[78]. Insulin heightens the expression of SREBP-1c and its battery of genes involved in the synthesis of saturated and unsaturated fatty acids^[75,79] as well as glucose metabolism genes^[77,78]. The effect is opposed by glucagon and cyclic AMP. In short, available experimental data indicate that SREBP-1c mediates all effects of insulin on lipogenesis. In response to nutritional stimuli SREBP-1c also triggers expression of genes of enzymes required for fatty acid elongation^[74], and of glycerol 3-phosphate acyltransferase required for triglyceride and phospholipid synthesis^[6]. Last but not least SREBPs activate 3 genes necessary for the generation of NADPH, which is needed in fatty acid and cholesterol synthesis.

The promoter of the SREBP-1c gene contains response elements for insulin, glucagon, as well as liver X-activated receptors (LXR) α and LXR β , the latter is activated by sterols^[17,43]. This regulatory pathway, among others, results in increased synthesis of oleate^[75], the major fatty acid used for cholesterol esterification, to ensure its removal from the liver.

KNOCK-OUT ANIMALS AND HEALTH IMPLICATIONS OF SREBPS

Knock-out mice which lack all SREBPs, or S1P to activate them, die at an early stage of embryonic development^[80,81]. Specific knock-out of SREBP-2 also results in embryonic lethality. Deletion of SREBP-1a allows some fetuses to survive, whereas lack of SREBP-1c appears to be of no consequence. The survivors are found to compensate by higher SREBP-2 levels, and consequently, these animals have elevated hepatic cholesterol, but lower fatty acid levels^[9].

In order to study SREBP knock-outs in adulthood, a gene manipulation was used in Brown and Goldstein's laboratory which allows to turn specific genes off at will by stimulating interferon production. Disruption of the SCAP or S1P gene, respectively, almost abolished nSREBPs-1 and -2 in liver and diminished expression of all target genes of cholesterol and fatty acid synthesis. The result was a reduction in cholesterol and fatty acid levels in livers by 70-80%^[9].

The SREBP-related links between fatty acid and glucose metabolism draw immediate attention to the wide-spread disease, diabetes. It would appear that the fatty liver frequently observed in insulin-resistant diabetics is a result of high SREBP-1c levels caused by high insulin levels. Leptin, the organism's response to fat accumulation in adipocytes, opposes SREBP-1c action^[82], and consequently can heal the derailment of fat metabolism in diabetic animals^[83].

One of the genes activated by nSREBP-1c is that for the hepatic LDL receptor, an effect clearly targeting at maintaining plasma lipid homeostasis. At first sight this would appear beneficial for arteriosclerosis since it should reduce elevated LDL-cholesterol levels in blood. However, since nSREBP-1c also induces lipogenesis, its effect is ambiguous, and other factors will decide whether the net result fights arteriosclerosis, or rather exacerbates it^[7]. It is at this point where the HMGCoA reductase inhibitors or statins work, but they are effective only in one third of cases^[84].

It must be understood that fatty acid synthesis is not only subject to SREBP regulation, but a host of other factors, whereas cholesterol synthesis appears to be exclusively controlled by SREBPs. Additional unknowns are the exact regulation of system by which HDL via the scavenger receptor B-1 mediates efflux of cholesterol from the liver, and the ATP-binding cassette-1 (ABC-1) system which mediates transfer of cholesterol to HDL^[84]. Profound knowledge of these pathways will open a perspective beyond the statin drugs to specifically lower cholesterol levels in disease conditions.

REFERENCES

1 **Small DM**, Shipley GG. Physical-chemical basis of lipid depo-

- sition in atherosclerosis. *Science* 1974; **185**: 222-229
- 2 **Simons K**, Ikonen E. Functional rafts in cell membranes. *Nature* 1997; **387**: 569-572
- 3 **Anderson RG**. The caveolae membrane system. *Annu Rev Biochem* 1998; **67**: 199-225
- 4 **Goldstein JL**, Brown MS. Regulation of the mevalonate pathway. *Nature* 1990; **343**: 425-430
- 5 **Brown MS**, Goldstein JL. The SREBP pathway: Regulation of cholesterol metabolism by proteolysis of a membrane-bound transcription factor. *Cell* 1997; **89**: 331-340
- 6 **Edwards PA**, Tabor D, Kast HR, Venkateswaran A. Regulation of gene expression by SREBP and SCAP. *Biochim Biophys Acta* 2000; **1529**: 103-113
- 7 **Schoonjans K**, Brendel C, Mangelsdorf D, Auwerx J. Sterols and gene expression: control of affluence. *Biochim Biophys Acta* 2000; **1529**: 114-125
- 8 **Goldstein JL**, Rawson RB, Brown MS. Mutant mammalian cells as tools to delineate the sterol regulatory element-binding protein pathway for feedback regulation of lipid synthesis. *Arch Biochem Biophys* 2002; **329**: 139-148
- 9 **Horton JD**, Goldstein JL, Brown MS. SREBPs: activators of the complete program of cholesterol and fatty acid synthesis in the liver. *J Clin Invest* 2002; **109**: 1125-1131
- 10 **Jackson MS**, Ericsson J, Edwards PA. Signaling molecules derived from the cholesterol biosynthetic pathway. *Subcell Biochem* 1997; **28**: 1-21
- 11 **Björkhem I**, Andersson O, Diczfalusy U, Sevastik B, Xin RJ, Duan C, Lund E. Atherosclerosis and sterol 27-hydroxylase: Evidence for a role of this enzyme in elimination of cholesterol from human macrophages. *Proc Natl Acad Sci U S A* 1994; **91**: 8592-8596
- 12 **Lehmann JM**, Kliewer ST, Moore LB, Smith-Oliver TA, Oliver BB, Su JL, Sundseth SS, Winegar DA, Blanchard DE, Spencer TA, Willson TM. Activation of nuclear receptor LXR by oxysterols defines a new hormone pathway. *J Biol Chem* 1997; **272**: 3137-3140
- 13 **Schwarz M**, Lund EG, Russell DW. Two 7 alpha-hydroxylase enzymes in bile acid biosynthesis. *Curr Opin Lipidol* 1998; **9**: 113-118
- 14 **Russell DW**. The enzymes, regulation, and genetics of bile acid synthesis. *Annu Rev Biochem* 2003; **73**: 137-174
- 15 **Babiker A**, Anderson O, Lund E, Xiu RJ, Deeb S, Reshef A, Leitersdorf E, Diczfalusy U, Björkhem I. Elimination of cholesterol in macrophage and endothelial cells by the sterol 27-hydroxylase mechanism. Comparison with high density lipoprotein-mediated reverse cholesterol transport. *J Biol Chem* 1997; **272**: 26253-26261
- 16 **Ishibashi S**, Schwarz M, Frykman PK, Herz J, Russell DW. Disruption of cholesterol 7 α -hydroxylase gene in mice. I. Postnatal lethality reversed by bile acids and vitamin supplementation. *J Biol Chem* 1996; **271**: 18017-18023
- 17 **Janowski BA**, Willy PJ, Devi TR, Falck JR, Mangelsdorf DJ. An oxysterol signalling pathway mediated by the nuclear receptor LXR α . *Nature* 1996; **383**: 728-731
- 18 **Venkateswaran A**, Lefitte BA, Josyl SB, Mak PA, Wilpitz DC, Edwards PA, Tontonoz P. Control of cellular cholesterol efflux by the nuclear oxysterol receptor LXR α . *Proc Natl Acad Sci U S A* 2000; **97**: 12097-12102
- 19 **Edwards PA**, Ericsson J. Sterols and isoprenoids: Signaling molecules derived from the cholesterol biosynthetic pathway. *Annu Rev Biochem* 1999; **68**: 157-185
- 20 **Hua X**, Yokoyama C, Wu J, Briggs MR, Brown MS, Goldstein JL, Wang X. SREBP-2, a second basic-helix-loop-helix-leucine zipper protein that stimulates transcription by binding to sterol regulatory elements. *Proc Natl Acad Sci U S A* 1993; **90**: 11603-11607
- 21 **Yokoyama C**, Wang X, Briggs MR, Admon A, Wu J, Hua X, Goldstein JL, Brown MS. SREBP-1, a basic helix-loop-helix-leucine zipper protein that controls transcription of the LDL receptor gene. *Cell* 1993; **75**: 187-197
- 22 **Hua X**, Wu J, Goldstein JL, Brown MS, Hobbs HH. Structure of human gene encoding sterol regulatory element binding protein-1 (SREBF1) and localization of SREBF1 and SREBF2 to chromosomes 17p11.2 and 22q13. *Genomics* 1995; **25**: 667-673
- 23 **Shimomura I**, Shimano H, Horton JD, Goldstein JL, Brown

- MS. Differential expression of exons 1a and 1c in the mRNAs of sterol regulatory element binding protein-1 in human and mouse organs and cultured cells. *J Clin Invest* 1997; **99**: 838-845
- 24 **Miserez, AR**, Cao G, Probst L, Hobbs HH. Structure of the human gene encoding sterol regulatory element binding protein-2 (SREBP-2). *Genomics* 1997; **40**: 31-40
- 25 **Tontonoz P**, Kim JB, Graves RA, Spiegelman BM. ADD 1: a novel helix-loop-helix transcription factor associated with adipocyte determination and differentiation. *Mol Cell Biol* 1993; **13**: 4752-4759
- 26 **Shimano H**, Horton JD, Shimomura I, Hammer RE, Brown MS, Goldstein JL. Isoform-1c of sterol regulatory element-binding protein is less active than isoform 1a in livers of transgenic mice and in cultured cells. *J Clin Invest* 1997; **99**: 846-854
- 27 **Sato R**, Yang J, Wang X, Evans MJ, Ho YK, Goldstein JL, Brown MS. Assignment of the membrane attachment, DNA binding, and transcriptional activation domains of sterol regulatory element-binding protein-1 (SREBP-1). *J Biol Chem* 1994; **269**: 17267-17273
- 28 **Hua X**, Sakai J, Ho YK, Brown JL, Goldstein MS. Hairpin orientation of sterol regulatory element binding protein 2 in cell membranes as determined by protease protection. *J Biol Chem* 1995; **270**: 29422-29427
- 29 **Duncan EA**, Brown MS, Goldstein JL, Sakai J. Cleavage site for sterol regulatory protease localized to a Leu-Ser bond in luminal loop of sterol regulatory element binding protein-2. *J Biol Chem* 1997; **272**: 12778-12785
- 30 **Magaña MM**, Osborne TF. Two tandem binding sites for sterol regulatory element binding proteins are required for sterol regulation of fatty acid synthase promoter. *J Biol Chem* 1996; **271**: 32689-32694
- 31 **Hua X**, Nohturfft A, Goldstein JL, Brown MS. Sterol resistance in CHO cells traced to point mutations in SREBP cleavage activating protein (SCAP). *Cell* 1996; **87**: 415-426
- 32 **Nohturfft A**, Hua X, Brown MS, Goldstein JL. Recurrent G-to-A substitution in a single codon of SREBP cleavage-activating protein causes sterol resistance in three mutant CHO cell lines. *Proc Natl Acad Sci U S A* 1996; **93**: 13709-13714
- 33 **Nohturfft A**, Brown MS, Goldstein JL. Topology of SREBP cleavage activating protein, a polytopic membrane protein with a sterol sensing domain. *J Biol Chem* 1998; **273**: 17243-17250
- 34 **Liscum L**, Finer-Moore J, Stroud RM, Luskey KL, Brown MS, Goldstein JL. Domain structure of 3-hydroxy-3-methylglutaryl coenzyme A reductase, a glycoprotein of the endoplasmic reticulum. *J Biol Chem* 1985; **260**: 522-530
- 35 **Olender EH**, Simoni RD. The intracellular targeting and membrane topology of 3-hydroxy-3-methylglutaryl coenzyme A reductase. *J Biol Chem* 1992; **267**: 4223-4235
- 36 **Neer EJ**, Schmidt CJ, Nambudripad R, Smith TF. The ancient regulatory protein family of WD-repeat proteins. *Nature* 1994; **371**: 297-300
- 37 **Sakai J**, Nohturfft A, Cheng D, Ho YK, Brown MS, Goldstein JL. Identification of complexes between the COOH-terminal domain of sterol regulatory element binding protein (SREBPs) and SREBP cleavage-activating protein (SCAP). *J Biol Chem* 1997; **272**: 20213-20221
- 38 **Nohturfft A**, Jabe D, Goldstein JL, Brown MS, Espenshade PJ. Regulated step in cholesterol feed back localized to budding of SCAP from ER membranes. *Cell* 2000; **102**: 315-323
- 39 **Wang X**, Sato R, Brown MS, Hua X, Goldstein JL. SREBP-1, a membrane-bound transcription factor released by sterol-regulated proteolysis. *Cell* 1994; **77**: 53-62
- 40 **Hua X**, Sakai J, Brown MS, Goldstein JL. Regulated cleavage of sterol regulatory element binding proteins (SREBPs) requires sequences on both sides of the endoplasmic reticulum membrane. *J Biol Chem* 1996; **271**: 10379-10384
- 41 **Sakai J**, Duncan EA, Rawson RB, Hua X, Brown MS, Goldstein JL. Sterol regulated release of SREBP-2 from cell membranes require two sequential cleavages, one within a transmembrane segment. *Cell* 1996; **85**: 1037-1046
- 42 **Sakai J**, Nohturfft A, Goldstein JL, Brown MS. Cleavage of sterol regulatory element-binding proteins (SREBPs) at site-1 requires interaction with SREBP cleavage-activating protein. Evidence from *in vivo* competition studies. *J Biol Chem* 1998; **273**: 5785-5793
- 43 **DeBose-Boyd RA**, Brown MS, Li WP, Nohturfft A, Goldstein JL, Espenshade PJ. Transport dependent proteolysis of SREBP: relocation of site-1 protease protein from Golgi to ER. *Cell* 1999; **99**: 703-712
- 44 **Brown AJ**, Sun L, Feramisco JD, Brown MS, Goldstein JL. Cholesterol addition to ER membranes alters conformation of SCAP, the SREBP escort protein that regulates cholesterol metabolism. *Mol Cell* 2002; **10**: 237-245
- 45 **Espenshade PJ**, Cheng D, Goldstein JL, Brown MS. Autocatalytic processing of site-1 protease removes propeptide and permits cleavage of sterol regulatory element-binding proteins. *J Biol Chem* 1999; **274**: 22795-22804
- 46 **Rawson RB**, Zelenski NG, Nijhawan D, Ye J, Sakai J, Hasan MT, Chang TY, Brown MS, Goldstein JL. Complementation cloning of S2P, a gene encoding a putative metalloprotease required for intramembrane cleavage of SREBPs. *Mol Cell* 1997; **1**: 47-57
- 47 **Duncan EA**, Dave UP, Sakai J, Goldstein JL, Brown MS. Second-site cleavage in sterol regulatory element-binding protein occurs at transmembrane junction as determined by cysteine panning. *J Biol Chem* 1998; **273**: 17801-17809
- 48 **Brown MS**, Ye J, Rawson RB, Goldstein JL. Regulated intramembrane proteolysis: a control mechanism conserved from bacteria to humans. *Cell* 2000; **100**: 391-398
- 49 **Brown MS**, Goldstein JL. A proteolytic pathway that controls the cholesterol content of membranes, cells and blood. *Proc Natl Acad Sci U S A* 1999; **96**: 11041-11048
- 50 **Nohturfft A**, DeBose-Boyd RA, Scheek S, Goldstein JL, Brown MS. Sterols regulate cycling of SREBP cleavage activating protein (SCAP) between endoplasmic reticulum and Golgi. *Proc Natl Acad Sci U S A* 1999; **96**: 11235-11240
- 51 **Sato R**, Inoue J, Kawabe Y, Kodama T, Takano T, Maeda M. Sterol-dependent transcriptional regulation of sterol regulatory element-binding protein-2. *J Biol Chem* 1996; **271**: 26461-26464
- 52 **Metherall JE**, Ridgway ND, Dawson PA, Goldstein JL, Brown MS. A 25-hydroxycholesterol-resistant cell line deficient in acyl-CoA: cholesterol acyltransferase. *J Biol Chem* 1991; **266**: 12734-12740
- 53 **Yang J**, Sato R, Goldstein JL, Brown MS. Sterol-resistant transcription in CHO cells caused by gene rearrangement that truncates SREBP-2. *Genes Dev* 1994; **8**: 1910-1919
- 54 **Korn BS**, Shimomura I, Bashmakov Y, Hammer RE, Horton JD, Goldstein JL, Brown MS. Blunted feedback suppression of SREBP processing by dietary cholesterol in transgenic mice expressing sterol-resistant SCAP/D443N. *J Clin Invest* 1998; **102**: 2050-2060
- 55 **Rawson RB**, Cheng D, Brown MS, Goldstein JL. Isolation of cholesterol-requiring mutant Chinese hamster ovary cells with defects in cleavage of sterol regulatory element-binding proteins at site 1. *J Biol Chem* 1998; **273**: 28261-28269
- 56 **Hasan MT**, Chang CC, Chang TY. Somatic cell genetic and biochemical characterization of cell lines resulting from human genomic DNA transfections of Chinese hamster ovary cell mutants defective in sterol-dependent activation of sterol synthesis and LDL receptor expression. *Somat Cell Mol Genet* 1994; **20**: 183-194
- 57 **Rawson RB**, DeBose-Boyd R, Goldstein JL, Brown MS. Failure to cleave sterol regulatory element-binding proteins (SREBPs) causes cholesterol auxotrophy in Chinese hamster ovary cells with genetic absence of SREBP cleavage-activating protein. *J Biol Chem* 1999; **274**: 28549-28556
- 58 **Sheng Z**, Otani H, Brown MS, Goldstein JL. Independent regulation of sterol regulatory element-binding proteins 1 and 2 in hamster liver. *Proc Natl Acad Sci U S A* 1995; **92**: 935-938
- 59 **Yahagi N**, Shimano H, Hasty AH, Amemiya-Kudo M, Okazaki H, Tamura Y, Iizuka Y, Shionoiri F, Ohashi K, Osuga J, Harada K, Gotoda T, Nagai R, Ishibashi S, Yamada N. A crucial role of sterol regulatory element-binding protein-1 in the regulation of lipogenic gene expression by polyunsaturated fatty acids. *J Biol Chem* 1999; **274**: 35840-35844
- 60 **Mourrieras F**, Foufelle F, Foretz M, Morin J, Bouche S, Ferre P. Induction of fatty acid synthase and S14 gene expression by glucose, xylitol and dihydroxyacetone in cultured rat hepatocytes is closely correlated with glucose 6-phosphate concentrations. *Biochem J* 1997; **326**: 345-349
- 61 **Sanchez HB**, Yieh L, Osborne TF. Cooperation by sterol regu-

- latory element-binding protein and Sp1 in sterol regulation of low density lipoprotein receptor gene. *J Biol Chem* 1995; **270**: 1161-1169
- 62 **Dooley KA**, Millinder S, Osborne TF. Sterol regulation of 3-hydroxy-3-methylglutaryl-coenzyme A synthase gene through a direct interaction between sterol regulatory element binding protein and the trimeric CCAAT-binding factor/nuclear factor Y. *J Biol Chem* 1998; **273**: 1349-1356
- 63 **Dooley KA**, Bennett MK, Osborne TF. A critical role for cAMP response element-binding protein (CREB) as a coactivator in sterol-regulated transcription of 3-hydroxy-3-methylglutaryl coenzyme A synthase promoter. *J Biol Chem* 1999; **274**: 5285-5291
- 64 **Magaña MM**, Koo SH, Towle HC, Osborne TF. Different sterol regulatory element-binding protein-1 isoforms utilize distinct co-regulatory factors to activate the promoter of fatty acid synthetase. *J Biol Chem* 2000; **275**: 4762-4733
- 65 **Oliner JD**, Andresen JM, Hansen SK, Zhou S, Tjian R. SREBP transcriptional activity is mediated through an interaction with the CREB-binding protein. *Genes Dev* 1996; **10**: 2903-2911
- 66 **Ericsson J**, Edwards PA. CBP is required for sterol-regulated and sterol regulatory element-binding protein-regulated transcription. *J Biol Chem* 1998; **273**: 17865-17870
- 67 **Näär AM**, Beaurang PA, Zhou S, Abraham S, Solomon W, Tjian R. Composite co-activator ARC mediates chromatin-directed transcriptional activation. *Nature* 1999; **399**: 828-832
- 68 **Näär AM**, Beaurang PA, Robinson KM, Oliner JD, Avizonis D, Scheek S, Zwicker J, Kadonaga JT, Tjian R. Chromatin, TAFs, and a novel multiprotein coactivator are required for synergistic activation by Sp1 and SREBP-1a *in vitro*. *Genes Dev* 1998; **12**: 3020-3031
- 69 **Ericsson J**, Jackson SM, Kim JB, Spiegelman BM, Edwards PA. Identification of glycerol-3-phosphate acyltransferase as an adipocyte determination and differentiation factor 1- and sterol regulatory element-binding protein-responsive gene. *J Biol Chem* 1997; **272**: 7298-7305
- 70 **Guan G**, Dai PH, Osborne TF, Kim JB, Shechter I. Multiple sequence elements are involved in the transcriptional regulation of the human squalene synthase gene. *J Biol Chem* 1997; **272**: 10295-10302
- 71 **Guan G**, Dai PH, Shechter I. Differential transcriptional regulation of the human squalene synthase gene by sterol regulatory element-binding proteins (SREBP) 1a and 2 and involvement of 5' DNA sequence elements in the regulation. *J Biol Chem* 1998; **273**: 12526-12535
- 72 **Sakakura Y**, Shimano H, Sone H, Takahashi A, Inoue K, Toyoshima H, Suzuki S, Yamada N. Sterol regulatory element-binding proteins induce an entire pathway of cholesterol synthesis. *Biochem Biophys Res Commun* 2001; **286**: 176-183
- 73 **Horton JD**, Shimomura I, Brown MS, Hammer RE, Goldstein JL, Shimano H. Activation of cholesterol synthesis in preference to fatty acid synthesis in liver and adipose tissue of transgenic mice overproducing sterol regulatory element binding protein-2. *J Clin Invest* 1998; **101**: 2331-2339
- 74 **Moon YA**, Shah NA, Mohapatra S, Warrington JA, Horton JD. Identification of a mammalian long chain fatty acyl elongase regulated by sterol regulatory element-binding proteins. *J Biol Chem* 2001; **276**: 45358-45366
- 75 **Shimomura I**, Shimano H, Korn BS, Bashmakov Y, Horton JD. Nuclear sterol regulatory element-binding proteins activate genes responsible for the entire program of unsaturated fatty acid biosynthesis in transgenic mouse livers. *J Biol Chem* 1998; **273**: 35299-35306
- 76 **Flier JS**, Hollenberg AN. ADD-1 provides major new insight into the mechanism of insulin action. *Proc Natl Acad Sci U S A* 1999; **96**: 14191-14192
- 77 **Foretz M**, Guichard C, Ferre P, Foufelle F. Sterol regulatory element binding protein-1c is a major mediator of insulin action on the hepatic expression of gluco-kinase and lipogenesis-related genes. *Proc Natl Acad Sci U S A* 1999; **96**: 12737-12742
- 78 **Kim JB**, Sarraf P, Wright M, Yao KM, Mueller E, Solanes G, Lowell BB, Spiegelman BM. Nutritional and insulin regulation of fatty acid synthetase and leptin gene expression through ADD1/SREBP1. *J Clin Invest* 1998; **101**: 1-9
- 79 **Shimano H**, Yahagi N, Amemiya-Kudo M, Hasty AH, Osuga J, Tamura Y, Shionoiri F, Iizuka Y, Ohashi K, Harada K, Gotoda T, Ishibashi S, Yamada N. Sterol regulatory element-binding protein-1 as a key transcription factor for nutritional induction of lipogenic enzyme genes. *J Biol Chem* 1999; **274**: 35832-35839
- 80 **Mitchell KJ**, Pinson KI, Kelly OG, Brennan J, Zupicich J, Scherz P, Leighton PA, Goodrich LV, Lu X, Avery BJ, Tate P, Dill K, Pangilinan E, Wakenight P, Tessier-Lavigne M, Skarnes WC. Functional analysis of secreted and transmembrane proteins critical to mouse development. *Nat Genet* 2001; **28**: 241-249
- 81 **Yang J**, Goldstein JL, Hammer RE, Moon YA, Brown MS, Horton JD. Decreased lipid synthesis in livers of mice with disrupted site-1 protease gene. *Proc Natl Acad Sci U S A* 2001; **98**: 13607-13612
- 82 **Soukas A**, Cohen P, Succi ND, Friedman JM. Leptin-specific patterns of gene expression in white adipose tissue. *Genes Dev* 2000; **14**: 963-980
- 83 **Shimomura I**, Hammer RE, Ikemoto S, Brown MS, Goldstein JL. Leptin reverses insulin resistance and diabetes mellitus in mice with congenital lipodystrophy. *Nature* 1999; **401**: 73-76
- 84 **Libby P**, Aikawa M, Schönbeck U. Cholesterol and atherosclerosis. *Biochim Biophys Acta* 2000; **1529**: 299-309

CDH1 germline mutation in hereditary gastric carcinoma

Hai-Dan Wang, Jun Ren, Lian Zhang

Hai-Dan Wang, Center of Clinical Oncology and International Collaborative Group on Hereditary Gastric Carcinoma, Xijing Hospital, the Fourth Military Medical University, Xi'an 710032, Shaanxi Province, China

Jun Ren, Lian Zhang, Peking University School of Oncology, Beijing 100036, China

Supported by the Teaching and Research Award Program for Outstanding Young Teachers, Ministry of Education, P R China, No. TRAPOYT99-016

Correspondence to: Jun Ren, M.D., Ph.D, Professor and Chairman, Department of Medical Oncology, Peking University School of Oncology, Beijing 100036, China. renjun@fmmu.edu.cn

Telephone: +86-10-88123125 **Fax:** +86-10-88122437

Received: 2003-11-17 **Accepted:** 2004-01-15

Abstract

This paper provides a bird's-eye view both in preclinical and clinical aspects of E-cadherin germline gene (CDH1) in gastric cancer patients and their families. E-cadherin, a product of CDH1 gene, belonging to the functionally related trans-membrane glycoprotein family, is responsible for the Ca²⁺-dependent cell-cell adhesion mechanism and contributes to dissociation followed by acquisition of cell motility, which usually occurs in the first step of cancer invasion and metastasis. CDH1 gene germline mutation is common in many types of carcinoma, and occurs very frequent in hereditary gastric carcinoma (HGC) patients and their families. Recently, more and more researches support that E-cadherin plays an important role in the differentiation, growth and invasion of HGC. So it is of great value to clarify its mechanisms both for understanding HGC pathogenesis and for clinical therapy, especially in China, where there are a high risk population of gastric cancer and a high HGC incidence rate. In this paper, recent researches on CDH1 gene mutation, especially its role in tumor genesis and progress of HGC, are reviewed, and advances in evaluation of its mutation status for HGC diagnosis, therapy and prognosis, are also discussed briefly.

Wang HD, Ren J, Zhang L. CDH1 germline mutation in hereditary gastric carcinoma. *World J Gastroenterol* 2004; 10(21): 3088-3093

<http://www.wjgnet.com/1007-9327/10/3088.asp>

INTRODUCTION

CDH1 mutation in HGC

Gastric carcinoma is one of the leading causes of cancer mortality in many countries, especially in most Asian countries. It is also one of the leading malignant diseases in China. According to data, approximately one Chinese person died of gastric cancer every 2 to 3 min. In the past decades, the incidence tended to increase gradually. Some population based surveys revealed that about 10% gastric cancer patients demonstrated familial clustering. The identification of genes predisposing to HGC is an essential step towards understanding the molecular events underlying tumorigenesis and critical for the clinical

management. In 1998, a germline mutation in the CDH1 gene, which located on chromosome locus 16q22.1, was first recognized in Maori kindred from New Zealand with diffuse gastric carcinoma. The product of CDH1 gene, E-cadherin protein, a 120 ku transmembranous glycoprotein, is involved in Ca²⁺-dependent intercellular adhesion. More and more researches confirm that impaired expression of E-cadherin contributes to histogenesis, tumor growth, metastasis and poor survival of gastric cancer patients, especially HGC patients. So further analyses are needed to clarify the mechanism of gastric cancer and provide better strategies for treatment of HGC patients and prophylaxis of their families.

E-CADHERIN: STRUCTURE AND FUNCTION

The newly mutated gene discovered in HGC, CDH1, is composed of 16 exons and 15 introns encoding the E-cadherin protein. E-cadherin, also called epithelial cadherin or uvomorulin, is a member of the subclass of cadherins, which are Ca²⁺-dependent cell-cell adhesion receptors identified in vertebrates. The 120 ku E-cadherin molecule is made up of a 27 amino acid signal peptide (exons 1-2), a 154 amino acid precursor peptide (exons 2-4), and a 728 amino acid mature peptide. The mature protein consists of three major domains, five extracellular repeats (CAD repeats) (exons 4-13), a single membrane-spanning region (exons 13-14) and a cytoplasmic region (exons 14-16). The N-terminal CAD1 repeat is essential for the homophilic binding specificity that directs "like" E-cadherins with each other. The cytoplasmic domain is bound to the actin cytoskeleton *via* intracellular attachment proteins, the catenins, forming the E-cadherin/catenin complex (Figure 1).

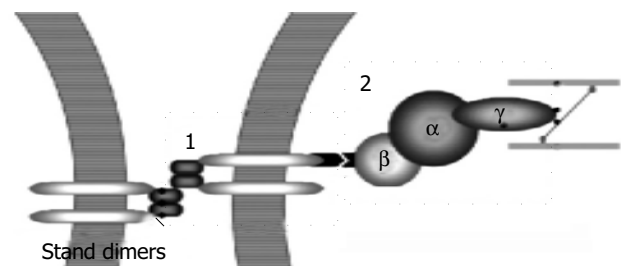


Figure 1 Formation of E-cadherin/catenin complex. Step1. E-cadherin stand dimers on the two adjacent cells' surface combine together and transfer the signals to catenin complex which is composed of β + α + γ subunits. Step2. The complex promotes actins to contract and enhance the intra-cellular adhesion.

Linkage between transmembranous cadherins and actin filament of the cytoskeleton is localized at the cell-cell adherent junction(AJ) and mediated by many associated undercoat proteins of the junction including catenins, vinculins, and actin^[1]. Catenins are a series of cadherin-associated cytoplasmic proteins that are co-immunoprecipitated with cadherin by nonionic detergent, and classified by their molecular mass as α -(102 ku), β -(88 ku), γ -(80 ku)^[2]. Furthermore, catenins connect cadherin to other integral membrane proteins, such as Na⁺-K⁺-ATPase, or to cytoplasmic structures, such as fodrin or ankyrin^[3]. All these form a transcellular network, mediating structural integrity, cellular polarity and epithelial morphogenesis^[4,5].

The CAD1 domain conformation of E-cadherin contains seven β strands (β A - β G) and two short α helices (α A, α B). The homophilic binding specificity appears to be governed by CAD1 domains through a surface including a HAV motif, which is found in or following β F. CAD1 also possesses the PEN (10-13), LDRE (66-69), DXND (100-104) motifs, while CAD2 possesses a DAD motif. These four Ca^{2+} -binding motifs can form a shared Ca^{2+} -binding pocket. The ligation of Ca^{2+} between tandem CAD domains explains the vulnerability of cadherins to proteolytic degradation when Ca^{2+} is depleted. Removal of Ca^{2+} would alter the junction between tandem CAD domains and likely expose the linkers to proteases. The binding of Ca^{2+} could provide the rigidity suggested by Ca^{2+} -induced changes of the entire extracellular region of E-cadherin from a globular to a rod-like structure observed by electronic microscopy^[2,6].

Full length E-cadherin has a cleavage site near the transmembrane domain and soluble E-cadherin (s-E-cadherin), a soluble 80-84 ku amino-terminal fragment, can be produced artificially in the culture medium digested by trypsin, so E-cadherin is also named as cell CAM120/80^[7]. s-E-cadherin can be detected in the protein extract of tissues, and in serum of peripheral blood or urine by means of immunoenzymometric assay (IEMA) and the volume did not depend on either age or sex^[8]. Research also found it could be released from some human carcinoma cell lines (for instance MCF-7) into the culture medium^[9].

E-CADHERIN ABNORMAL EXPRESSION IN CARCINOMA

E-cadherin is a crucial adhesion molecule which hampers tumor invasion and metastasis. Down-regulation of expression or impaired function would lead cells to poor intercellular adhesion through inhibiting homophilic binding. To normal epithelial tissues, it means poor differentiation, while to tumor, it means invasive growth pattern and easy to spread from the primary place. Disturbance of epithelial cell adhesion has been shown to be due to several mechanisms as shown in Figure1. The first is inefficiency of E-cadherin homophilic binding, the second is abnormality or deletion of catenins, the last is biochemical modification of catenins, such as tyrosine phosphorylation of β -catenin^[10,11]. Among the factors that lead to inefficient homophilic binding of E-cadherin, the most important and widely recognized is E-cadherin down regulation or dysfunction due to CDH1 mutations.

Down-regulation of E-cadherin expression or CDH1 mutations could cause a change towards a less epithelial morphology and also interfered with initial adhesion of cells. Moreover, changed E-cadherins could sharply increase cell motility and change the organization of actin cytoskeleton. Nagafuchi *et al.*^[12] showed that the enhanced expression of E-cadherin cDNA in fibroblastic cells could generate epithelial structures in their recent research. McNeill *et al.*^[13] found that E-cadherin could cause polarized distribution of Na^+ - K^+ -ATPase, an important factor in the establishment of cell polarities. Mutations have been also found at very early non-invasive stages, thus associating E-cadherin mutations with loss of growth control and defining CDH1 as a real tumor suppressor^[14,15]. All of these may contribute to the significant correlation between abnormal E-cadherin expression and degree of differentiation ($P = 0.0001$) or local tumor size ($P = 0.002$)^[16].

Immunohistochemical studies have shown that expression of E-cadherin is reduced or lost in more than 15 different human carcinomas^[17]. The frequency of reduced E-cadherin expression is higher in tumors with infiltrative growth than in those with expansive growth. These observations are supported by *in vitro* studies, which evaluated the influence of E-cadherin on cell behavior. Behrens *et al.*^[18] found MDCK cells could invade into collagen gels when their E-cadherins were inactivated with antibodies. Frixen *et al.*^[19] also observed the similar phenomenon

that the invasiveness of several human carcinoma lines was suppressed by mouse E-cadherin cDNA transfection. Down regulation of E-cadherin or its functional defects could change the construction of actin cytoskeleton, which can weaken intracellular adhesion, increase the activity of epithelial cells and lead to more invasions.

Extensive immunohistopathologic studies, including those of squamous cell carcinomas of the head, neck and prostate also support the possibility that loss of E-cadherin expression may promote tumor metastasis to lymph nodes. Reduced E-cadherin expression of breast cancer was also found to have a higher frequency of blood-borne distant metastasis (*e.g.* bone or lung) than preserved E-cadherin expression of other tumors. There was a significant correlation between the degree of E-cadherin expression and the degree of tumor differentiation, as well as histological type according to the Lauren or the WHO classifications. Similarly, the correlation between E-cadherin expression and prognostic parameters (depth of invasion, lymph node involvement and vascular invasion) could be demonstrated according to some researches. These findings are consistent with the previous hypothesis that inhibition of E-cadherin function could enhance the release of cancer cells from their primary sites.

CDH1 MUTATION IN HGC PATIENTS AND FAMILIES

Lauren's classification of gastric cancer includes the intestinal (glandular) and diffuse type, as well as the mixed type. It has been reported that two histologic types have differences in epidemiology, clinicopathologic profile and molecular genetics, while both originate from *Helicobacter pylori* positive gastritis. The intestinal (glandular) type is especially predominant in high-risk population and elderly patients, and related with environmental factors, and their incident rates are decreasing in developed countries, suggesting that the pathogenesis of intestinal-type gastric carcinoma has an environmental component. Diffuse gastric cancer is determined significantly by heredity and the criteria for familial gastric cancer worked out by some investigators^[20,21] are as follows. There should be at least 3 relatives with gastric cancer. One should be a first-degree relative of the other 2. At least 2 successive generations should be affected. At least 1 should be diagnosed before age 50. Other familial tumors should be excluded.

Several investigations outlined the role of lost or mutated junctional molecules (E-cadherin, catenins, integrins, *etc.*) in the pathogenesis of diffuse gastric cancer (DGC). In particular, more than 50% of advanced diffuse gastric cancer patients showed mutations of CDH1 gene^[22-25]. Germline mutations of the CDH1 gene have been recently reported in gastric cancer families with diffuse-type tumors but not in those with intestinal-type tumors^[26]. These families are characterized by a highly penetrant susceptibility to DGC with an autosomal dominant pattern of inheritance, predominantly in young persons. Familial aggregation of GC occurs in about 1% of gastric cancer patients. Although the genetic factors resulting in this aggregation have been unclear, the study indicates that germline mutations of CDH1 genes, do contribute to such a clustering. Mutations of the CDH1 gene has a high penetrance and confers a lifetime risk of gastric cancer of 75-80% for carriers^[27-30].

The International Gastric Cancer Linkage Consortium (IGCLC) predicted that up to 25% of families fulfilling the criteria for hereditary DGC would harbour CDH1 germline mutations^[29]. CDH1 is well known as a strong invasion suppressor in experimental tumor cell systems. Inactivated mutations have been identified for the CDH1 gene in HGC. To date, 69 somatic mutations have been reported comprising, in addition to few missense mutations, mainly splice site mutations and truncation mutations caused by insertions, deletions and nonsense mutations. Up to now,

27 germline mutations previously reported are distributed along with CDH1 gene in Table 1. While in sporadic gastric cancers, truncation mutations are uncommon and sequence changes usually result in either missense mutations (most commonly in exons 8 and 9) or exon skipping, especially in exons 6-9^[30]. From the 27 CDH1 mutations described to date, 24 are inactivated ones (splice-site, frame shift and nonsense) and the remaining 4 are missense^[31-37].

Table 1 CDH1 gene germline mutation patterns in HGC families

Ethnic background	Age at diagnosis	Mutation type	Mutation site
White	30-67	45insT	Exon 1
White	34-69	49-2A→G	Exon 2
-	-	53delC	Exon 2
White	27-50	59G→A	Exon 2
White	37-46	70G→T	Exon 2
Japanese	46-72	185G→T	Exon 3 ¹
White	33-69	187C→T	Exon 3
Maori	22-28	190C→T	Exon 3
White	41-47	283C→T	Exon 3
White	15-58	372-377del1	Exon 3
White	31-55	586G→T	Exon 5
Korean	30-63	731A→G	Exon 6 ¹
White	23-70	832 G→A	Exon 6
White	14-67	1008G→T	Exon 7
White	35-47	1018 A→G	Exon 8 ¹
African-American	29-58	1137+1G→A	Intron 8
Korean	42-49	1460T→C	Exon 10 ¹
White	32-40	1472insA	Exon 10
White	31	1487del7	Exon 10
-	-	1565+1 G→T	Intron 10
White	40-63	1588insC	Exon 11
-	-	1710delT	Exon 11
White	30-68	1711insG	Exon 11
White	23-43	1792C→T	Exon 12
Maori	30	2095C→T	Exon 13
-	-	2295+5 G→A	Intron 14
White	16-35	2381insC	Exon 15

¹Missence mutation; -No information obtained from the published paper.

Mutant E-cadherins are not localized in the lateral regions of cell-to-cell contact sites of adherin junctions (AJs) and show apical and perinuclear localization. It is explained by an inability of the cells to complete polarization^[38]. These may result in disassembly of AJs and consequently conversion to a spindled and more scattered cell morphology^[39]. Impaired processing of mutant E-cadherin, loss of the putative calcium binding sites or essential amino acid motives, may cause a transition from a rigid to a more globular molecular structure of the extracellular domain. In response to extracellular signals, cells react by dissolving their cell-to-cell contacts and by changing their shape and the strength of their attachment to the substrate, thus resulting in significant reduction or loss of its ability to bind in a homophilic fashion to neighboring cells^[40,41]. Cell motility is thought to be the result of the concerted action of all these individual events.

Mutant E-cadherin lacking the cytoplasmic domain or the β -catenin-binding site may tie up essential catenins, which influences its function to suppress cell motility. Actin filaments are drastically reduced^[42]. The actin belt characteristics of epithelial cells are lost^[43]. Because proper anchorage to the cytoskeleton is necessary for E-cadherin function, suppression of E-cadherin expression or of its functional activity, or a defect in any of the molecules involved in this system, may account for the ability of cancer cells to detach from the primary tumor and invade locally. Cells with initial calcium-dependent cell aggregation exhibits decreased aggregation and remarkably increase cell motility when E-cadherin is not expressed (Figure 2).

We can conclude that these E-cadherin mutations may not only affect cell adhesion but also play an important role in a trans-dominant-active manner, thus leading to increased cell motility. They are the cause of multiple morphological and functional disorders and could induce scattered morphology and invasive behavior of diffuse gastric cancer.

Tissue specific gene expression has been explained by the interaction of promoter sequences with their specific transcription factors. *In vivo*, foot printing analysis revealed that positive regulatory elements of the E-cadherin promoter were specifically bound to transcription factors in E-cadherin-expressing cells. Mapping of DNase type I hypersensitive sites showed that the chromatin structure in the promoter region was loosened in expressing cells but condensed in non-expressing cells. Furthermore, endogenous E-cadherin promoter was methylated at CpG island sites in undifferentiated cells. All these suggested that silencing of the promoter during epithelial mesenchymal transition and tumor progression was due to a loss of factor-binding *in vivo* and chromatin rearrangement in

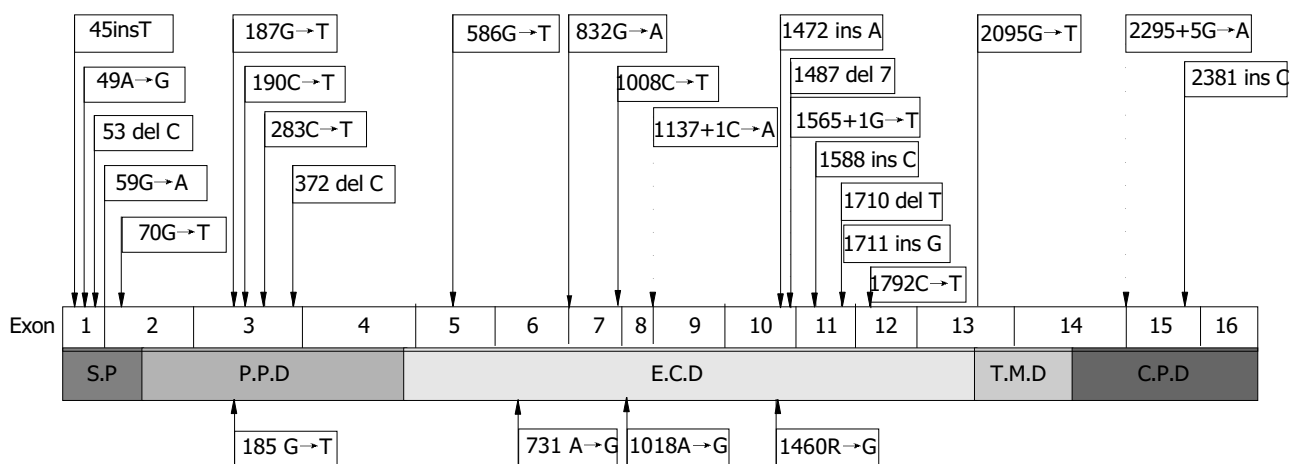


Figure 2 Schematic of CDH1 germline mutations in HGC. Truncating mutations are shown above the gene and missense mutations below. Arrowhead indicates the status in the dot frame refers to the alteration of intron pointed. S.P.: signal peptide, P.P.D: protein precursor domain, E.C.D: extracellular domain, T.M.D: transmembrane domain and C.P.D: cytoplasmic domain.

the regulatory region^[10,44]. Comijn *et al.*^[11] reported that multi-zinc finger protein, SIP1 (ZEB-2) and snail showing specific DNA binding activity could bind to partly overlapping promoter sequences and had similar silencing effects.

CDH1 MUTATION FOR HCG DIAGNOSIS AND THERAPY

Indicator for prophylactic total gastrectomy

HGC was associated with E-cadherin. Penetrance of the gene ranged from 70% to 80%, and the average age of gastric cancer patients was 37 years^[20,45,46]. These characteristics have led to the consideration of prophylactic total gastrectomy (PTG) in family members with CDH1 mutations. Lewis *et al.*^[45] performed this operation on 6 asymptomatic members in 2 families based on family pedigree and genetic analysis. The gastric specimens appeared normal and the results of routine pathologic examination were negative for cancer, but all the patients had microscopic foci of cancer, often at multiple sites, with overlying normal gastric mucosa. These results indicate that CDH1 gene mutations in association with familial gastric cancer are a new disease for PTG. Huntsman *et al.*^[28] also recommended genetic counseling and prophylactic gastrectomy in young people. The morbidity of this operation was much higher than that of other genetic diseases. The morbidity of prophylactic gastrectomy in the young, healthy population has been estimated as following: 1-2% mortality, 10-20% major acute morbidity, principally related to esophageal anastomotic procedure, and 100% long term morbidity related to weight loss, rapid intestinal transit, dumping syndrome, and diarrhoea. The high surgical risk of the procedure should be minimised by operations at centers with experience rich in gastric surgery. The decision to perform prophylactic gastrectomy should be balanced with age based risk and based on age specific penetrance data. Other factors, for example, the decision to operate on children, may affect the decision regarding the timing of prophylactic gastrectomy, and it is essential that patients carrying the gene have the opportunity extensive counseling and discussion with clinicians, geneticists, and counsellors before making the decision. The risk of other cancers (breast, colon) should also be targets of screening, as they may also be increased in this population, and patients should be counselled regarding these. However, germline mutations of E-cadherin could be used to identify individuals with a high risk^[47].

Target for radioimmunotherapy

Radiolabeled mAb used in radioimmunotherapy is limited because of lack of tumor specific antigens. In most cases reported thus far, tumor antigens serving as targets are not tumor-specific, being overexpressed in tumor cells and also at a lower level in normal cells. Only one tumor-specific mAb that recognizes a mutant form of the epidermal growth factor receptor (EGFRv III) has been found in different tumor types^[48]. Inframe deletions of exons 8 or 9 in the mRNA coding for E-cadherin are characteristic of DGC. So a rat mAb (d9mAb) was generated that specifically reacts with this mutation, and d9mAb was found to react with 13% of E-cadherin-expressing DGCs^[49]. Senekowitsch-Schmidtke *et al.*^[50] conjugated d9mAb with the α -emitting radionuclide ²¹³Bi, and tested for its binding specificity in sc and ip tumors expressing mutant E-cadherin. Seventy-eight percent of the total activity in ascites fluid was bound to free tumor cells, whereas in control cells expressing wild-type E-cadherin, the binding was only 18%. The selective binding of the ²¹³Bi-labeled, mutation-specific monoclonal antibody d9mAb raised its significant potential for the local radio-immunotherapy of disseminated, diffuse-type gastric carcinoma.

Markers for prognosis and evaluation

Gastric cancer remains a major cause of cancer mortality globally

but no good prognostic tumor markers are available. The most frequently used tumor markers in gastric cancer are carcinoembryonic antigen (CEA) and CA19-9^[51]. Gastric cancer antigen MG-7 may be a good marker for GC^[52], or even the detection of circulating DNA in serum reported recently^[53], but only a modest proportion of patients had elevated levels of these markers. Under-expression of E-cadherin molecules has been found in various malignancies and has a potential value as a prognostic marker^[54]. Serum soluble E-cadherin was found in the circulation of normal individuals but was particularly elevated in patients with malignancies. s-E-cadherin might derive from cancer tissues, though the expression of E-cadherin was decreased. With increased protease, the degradation products of tissue E-cadherin could accumulate and release into peripheral blood. However, its value in gastric cancer is controversial. Velikova *et al.*^[55] were unable to show a significant difference in serum soluble E-cadherin between patients with gastric cancer and normal subjects, while Gofuku *et al.*^[8] showed that concentrations were significantly elevated in 67% patients. Chan *et al.*^[56] confirmed its potential value as a prognostic marker. A high concentration could predict palliative/conservative treatment and T4 invasion. Gabbert *et al.*^[57] studied 413 gastric cancer patients, including all histological tumor types and stages. As shown by univariate and multivariate Cox regression analyses, patients with E-cadherin-positive tumors had significantly better 3 and 5 year survival rates than patients with E-cadherin-negative tumors. This prognostic effect remained present in a multivariate Cox regression analysis, including the prognostic parameters pT category, pN category and vascular invasion, suggesting that it is an independent prognostic marker.

In short, hereditary gastric cancer is still a challenge, especially its diagnosis and treatment^[58], although some progress has been achieved in recent years with the development of molecular biology and new methods.

ACKNOWLEDGEMENTS

We greatly thank Professor Bo-Rong Pan of the Fourth Military Medical University for his valuable comments on our study and Dr. Ying Lin, Department of Otolaryngology, Xijing Hospital, the Fourth Military Medical University for her helpful assistance on the manuscript.

REFERENCES

- 1 Nagafuchi A, Takeichi M, Tsukita S. The 102 kd cadherin-associated protein: similarity to vinculin and posttranscriptional regulation of expression. *Cell* 1991; **65**: 849-857
- 2 Ozawa M, Baribault H, Kemler R. The cytoplasmic domain of the cell adhesion molecule uvomorulin associates with three independent proteins structurally related in different species. *EMBO J* 1989; **8**: 1711-1717
- 3 Nathke IS, Hinck L, Swedlow JR, Papkoff J, Nelson WJ. Defining interactions and distributions of cadherin and catenin complexes in polarized epithelial cells. *J Cell Biol* 1994; **125**: 1341-1352
- 4 Overduin M, Harvey TS, Bagby S, Tong KI, Yau P, Takeichi M, Ikura M. Solution structure of the epithelial cadherin domain responsible for selective cell adhesion. *Science* 1995; **267**: 386-389
- 5 Shapiro L, Fannon AM, Kwong PD, Thompson A, Lehmann MS, Grubel G, Legrand JF, Als-Nielsen J, Colman DR, Hendrickson WA. Structural basis of cell-cell adhesion by cadherins. *Nature* 1995; **374**: 327-337
- 6 Nagar B, Overduin M, Ikura M, Rini JM. Structural basis of calcium-induced E-cadherin rigidification and dimerization. *Nature* 1996; **380**: 360-364
- 7 Matsuyoshi N, Tanaka T, Toda K, Okamoto H, Furukawa F, Imamura S. Soluble E-cadherin: a novel cutaneous disease marker. *Br J Dermatol* 1995; **132**: 745-749

- 8 **Gofuku J**, Shiozaki H, Doki Y, Inoue M, Hirao M, Fukuchi N, Monden M. Characterization of soluble E-cadherin as a disease marker in gastric cancer patients. *Br J Cancer* 1998; **78**: 1095-1101
- 9 **Damsky CH**, Richa J, Solter D, Knudsen K, Buck CA. Identification and purification of a cell surface glycoprotein mediating intercellular adhesion in embryonic and adult tissue. *Cell* 1983; **34**: 455-466
- 10 **Hennig G**, Behrens J, Truss M, Frisch S, Reichmann E, Birchmeier W. Progression of carcinoma cells is associated with alterations in chromatin structure and factor binding at the E-cadherin promoter *in vivo*. *Oncogene* 1995; **11**: 475-484
- 11 **Comijn J**, Berx G, Vermassen P, Verschueren K, van Grunsven L, Bruyneel E, Mareel M, Huylebroeck D, van Roy F. The two-handed E box binding zinc finger protein SIP1 downregulates E-cadherin and induces invasion. *Mol Cell* 2001; **7**: 1267-1278
- 12 **Nagafuchi A**, Shirayoshi Y, Okazaki K, Yasuda K, Takeichi M. Transformation of cell adhesion properties by exogenously introduced E-cadherin cDNA. *Nature* 1987; **329**: 341-343
- 13 **McNeill H**, Ozawa M, Kemler R, Nelson WJ. Novel function of the cell adhesion molecule uvomorulin as an inducer of cell surface polarity. *Cell* 1990; **62**: 309-316
- 14 **Blok P**, Craanen ME, Dekker W, Tytgat GN. Loss of E-cadherin expression in early gastric cancer. *Histopathology* 1999; **34**: 410-415
- 15 **Li YJ**, Ji XR. Relationship between expression of E-cadherin-catenin complex and clinicopathologic characteristics of pancreatic cancer. *World J Gastroenterol* 2003; **9**: 368-372
- 16 **Karayiannakis AJ**, Syrigos KN, Chatzigianni E, Papanikolaou S, Karatzas G. E-cadherin expression as a differentiation marker in gastric cancer. *Hepatogastroenterology* 1998; **45**: 2437-2442
- 17 **Potter E**, Bergwitz C, Brabant G. The cadherin-catenin system: implications for growth and differentiation of endocrine tissues. *Endocr Rev* 1999; **20**: 207-239
- 18 **Behrens J**, Vakaet L, Friis R, Winterhager E, Van Roy F, Mareel MM, Birchmeier W. Loss of epithelial differentiation and gain of invasiveness correlates with tyrosine phosphorylation of the E-cadherin/beta-catenin complex in cells transformed with a temperature-sensitive v-SRC gene. *J Cell Biol* 1993; **120**: 757-766
- 19 **Frixen UH**, Behrens J, Sachs M, Eberle G, Voss B, Warda A, Lochner D, Birchmeier W. E-cadherin-mediated cell-cell adhesion prevents invasiveness of human carcinoma cells. *J Cell Biol* 1991; **113**: 173-185
- 20 **Humar B**, Toro T, Graziano F, Muller H, Dobbie Z, Kwang-Yang H, Eng C, Hampel H, Gilbert D, Winship I, Parry S, Ward R, Findlay M, Christian A, Tucker M, Tucker K, Merriman T, Guilford P. Novel germline CDH1 mutations in hereditary diffuse gastric cancer families. *Hum Mutat* 2002; **19**: 518-525
- 21 **Caldas C**, Carneiro F, Lynch HT, Yokota J, Wiesner GL, Powell SM, Lewis FR, Huntsman DG, Pharoah PD, Jankowski JA, MacLeod P, Vogelsang H, Keller G, Park KG, Richards FM, Maher ER, Gayther SA, Oliveira C, Grehan N, Wight D, Seruca R, Roviello F, Ponder BA, Jackson CE. Familial gastric cancer: overview and guidelines for management. *J Med Genet* 1999; **36**: 873-880
- 22 **Becker KF**, Atkinson MJ, Reich U, Becker I, Nekarda H, Siewert JR, Hofler H. E-cadherin gene mutations provide clues to diffuse type gastric carcinomas. *Cancer Res* 1994; **54**: 3845-3852
- 23 **Mayer B**, Johnson JP, Leitl F, Jauch KW, Heiss MM, Schildberg FW, Birchmeier W, Funke I. E-cadherin expression in primary and metastatic gastric cancer: down-regulation correlates with cellular dedifferentiation and glandular disintegration. *Cancer Res* 1993; **53**: 1690-1695
- 24 **Graziano F**, Humar B, Guilford P. The role of the E-cadherin gene (CDH1) in diffuse gastric cancer susceptibility: from the laboratory to clinical practice. *Ann Oncol* 2003; **14**: 1705-1713
- 25 **Zhou YN**, Xu CP, Han B, Li M, Qiao L, Fang DC, Yang JM. Expression of E-cadherin and beta-catenin in gastric carcinoma and its correlation with the clinicopathological features and patient survival. *World J Gastroenterol* 2002; **8**: 987-993
- 26 **Zheng ZH**, Sun XJ, Qiu GR, Liu YH, Wang MX, Sun KL. E-cadherin gene mutation in precancerous condition' early and advanced stages of gastric cancer. *Shijie Huaren Xiaohua Zazhi* 2002; **10**: 153-156
- 27 **Giarelli E**. Prophylactic gastrectomy for CDH1 mutation carriers. *Clin J Oncol Nurs* 2002; **6**: 161-162
- 28 **Huntsman DG**, Carneiro F, Lewis FR, MacLeod PM, Hayashi A, Monaghan KG, Maung R, Seruca R, Jackson CE, Caldas C. Early gastric cancer in young, asymptomatic carriers of germ-line E-cadherin mutations. *N Engl J Med* 2001; **344**: 1904-1909
- 29 **Oliveira C**, Bordin MC, Grehan N, Huntsman D, Suriano G, Machado JC, Kiviluoto T, Aaltonen L, Jackson CE, Seruca R, Caldas C. Screening E-cadherin in gastric cancer families reveals germline mutations only in hereditary diffuse gastric cancer kindred. *Hum Mutat* 2002; **19**: 510-517
- 30 **Berx G**, Becker KF, Hofler H, van Roy F. Mutations of the human E-cadherin (CDH1) gene. *Hum Mutat* 1998; **12**: 226-237
- 31 **Richards FM**, McKee SA, Rajpar MH, Cole TR, Evans DG, Jankowski JA, McKeown C, Sanders DS, Maher ER. Germline E-cadherin gene (CDH1) mutations predispose to familial gastric cancer and colorectal cancer. *Hum Mol Genet* 1999; **8**: 607-610
- 32 **Guilford PJ**, Hopkins JB, Grady WM, Markowitz SD, Willis J, Lynch H, Rajput A, Wiesner GL, Lindor NM, Burgart LJ, Toro TT, Lee D, Limacher JM, Shaw DW, Findlay MP, Reeve AE. E-cadherin germline mutations define an inherited cancer syndrome dominated by diffuse gastric cancer. *Hum Mutat* 1999; **14**: 249-255
- 33 **Shinmura K**, Kohno T, Takahashi M, Sasaki A, Ochiai A, Guilford P, Hunter A, Reeve AE, Sugimura H, Yamaguchi N, Yokota J. Familial gastric cancer: clinicopathological characteristics, RER phenotype and germline p53 and E-cadherin mutations. *Carcinogenesis* 1999; **20**: 1127-1131
- 34 **Gayther SA**, Goringe KL, Ramus SJ, Huntsman D, Roviello F, Grehan N, Machado JC, Pinto E, Seruca R, Halling K, MacLeod P, Powell SM, Jackson CE, Ponder BA, Caldas C. Identification of germ-line E-cadherin mutations in gastric cancer families of European origin. *Cancer Res* 1998; **58**: 4086-4089
- 35 **Dussaulx-Garin L**, Blayau M, Pagenault M, Le Berre-Heresbach N, Raoul JL, Champion JP, David V, Bretagne JF. A new mutation of E-cadherin gene in familial gastric linitis plastica cancer with extra-digestive dissemination. *Eur J Gastroenterol Hepatol* 2001; **13**: 711-715
- 36 **Keller G**, Vogelsang H, Becker I, Hutter J, Ott K, Candidus S, Grundeit T, Becker KF, Mueller J, Siewert JR, Hofler H. Diffuse type gastric and lobular breast carcinoma in a familial gastric cancer patient with an E-cadherin germline mutation. *Am J Pathol* 1999; **155**: 337-342
- 37 **Yoon KA**, Ku JL, Yang HK, Kim WH, Park SY, Park JG. Germline mutations of E-cadherin gene in Korean familial gastric cancer patients. *J Hum Genet* 1999; **44**: 177-180
- 38 **Handschuh G**, Candidus S, Luber B, Reich U, Schott C, Oswald S, Becke H, Hutzler P, Birchmeier W, Hofler H, Becker KF. Tumour-associated E-cadherin mutations alter cellular morphology, decrease cellular adhesion and increase cellular motility. *Oncogene* 1999; **18**: 4301-4312
- 39 **Birchmeier W**, Hulsken J, Behrens J. Adherens junction proteins in tumour progression. *Cancer Surv* 1995; **24**: 129-140
- 40 **Lauffenburger DA**, Horwitz AF. Cell migration: a physically integrated molecular process. *Cell* 1996; **84**: 359-369
- 41 **Fukudome Y**, Yanagihara K, Takeichi M, Ito F, Shibamoto S. Characterization of a mutant E-cadherin protein encoded by a mutant gene frequently seen in diffuse-type human gastric carcinoma. *Int J Cancer* 2000; **88**: 579-583
- 42 **Mitchison TJ**, Cramer LP. Actin-based cell motility and cell locomotion. *Cell* 1996; **84**: 371-379
- 43 **Zhu AJ**, Watt FM. Expression of a dominant negative cadherin mutant inhibits proliferation and stimulates terminal differentiation of human epidermal keratinocytes. *J Cell Sci* 1996; **109** (Pt 13): 3013-3023
- 44 **Leung WK**, Yu J, Ng EK, To KF, Ma PK, Lee TL, Go MY, Chung SC, Sung JJ. Concurrent hypermethylation of multiple tumor-related genes in gastric carcinoma and adjacent normal tissues. *Cancer* 2001; **91**: 2294-2301
- 45 **Lewis FR**, Mellinger JD, Hayashi A, Lorelli D, Monaghan KG, Carneiro F, Huntsman DG, Jackson CE, Caldas C. Prophylac-

- tic total gastrectomy for familial gastric cancer. *Surgery* 2001; **130**: 612-617
- 46 **Chun YS**, Lindor NM, Smyrk TC, Petersen BT, Burgart LJ, Guilford PJ, Donohue JH. Germline E-cadherin gene mutations: is prophylactic total gastrectomy indicated? *Cancer* 2001; **92**: 181-187
- 47 **Becker KF**, Keller G, Hoefler H. The use of molecular biology in diagnosis and prognosis of gastric cancer. *Surg Oncol* 2000; **9**: 5-11
- 48 **Wikstrand CJ**, McLendon RE, Friedman AH, Bigner DD. Cell surface localization and density of the tumor-associated variant of the epidermal growth factor receptor, EGFRvIII. *Cancer Res* 1997; **57**: 4130-4140
- 49 **Becker KF**, Kremmer E, Eulitz M, Becker I, Handschuh G, Schuhmacher C, Muller W, Gabbert HE, Ochiai A, Hirohashi S, Hofler H. Analysis of E-cadherin in diffuse-type gastric cancer using a mutation-specific monoclonal antibody. *Am J Pathol* 1999; **155**: 1803-1809
- 50 **Senekowitsch-Schmidtke R**, Schuhmacher C, Becker KF, Nikula TK, Seidl C, Becker I, Miederer M, Apostolidis C, Adam C, Huber R, Kremmer E, Fischer K, Schwaiger M. Highly specific tumor binding of a ²¹³Bi-labeled monoclonal antibody against mutant E-cadherin suggests its usefulness for locoregional alpha-radioimmunotherapy of diffuse-type gastric cancer. *Cancer Res* 2001; **61**: 2804-2808
- 51 **Ren J**, Ge L, Li Y, Bai J, Liu WC, Si XM. Detection of circulating CEA molecules in human sera and leukopheresis of peripheral blood stem cells with *E. coli* expressed bispecific CEAScFv-streptavidin fusion protein-based immuno-PCR technique. *Ann N Y Acad Sci* 2001; **945**: 116-118
- 52 **Ren J**, Chen Z, Juan SJ, Yong XY, Pan BR, Fan DM. Detection of circulating gastric carcinoma-associated antigen MG7-Ag in human sera using an established single determinant immuno-polymerase chain reaction technique. *Cancer* 2000; **88**: 280-285
- 53 **Wang HD**, Ren J, Si XM, Zhang YJ, You XH, Liu WC, Fan L. Detection of circulating p53 gene mutation in HCC patients by DHPLC. *Int J Cancer* 2002; **13**: s112
- 54 **Takeichi M**. Cadherins in cancer: implications for invasion and metastasis. *Curr Opin Cell Biol* 1993; **5**: 806-811
- 55 **Velikova G**, Banks RE, Gearing A, Hemingway I, Forbes MA, Preston SR, Jones M, Wyatt J, Miller K, Ward U, Al-Maskatti J, Singh SM, Ambrose NS, Primrose JN, Selby PJ. Circulating soluble adhesion molecules E-cadherin, E-selectin, intercellular adhesion molecule-1 (ICAM-1) and vascular cell adhesion molecule-1 (VCAM-1) in patients with gastric cancer. *Br J Cancer* 1997; **76**: 1398-1404
- 56 **Chan AO**, Lam SK, Chu KM, Lam CM, Kwok E, Leung SY, Yuen ST, Law SY, Hui WM, Lai KC, Wong CY, Hu HC, Lai CL, Wong J. Soluble E-cadherin is a valid prognostic marker in gastric carcinoma. *Gut* 2001; **48**: 808-811
- 57 **Gabbert HE**, Mueller W, Schneiders A, Meier S, Moll R, Birchmeier W, Hommel G. Prognostic value of E-cadherin expression in 413 gastric carcinomas. *Int J Cancer* 1996; **69**: 184-189
- 58 **Medina-Franco H**. Hereditary gastric cancer. Genetics and clinical management. *Rev Gastroenterol Mex* 2003; **68**: 51-54

Edited by Zhu LH and Wang XL Proofread by Xu FM

Expression of survivin in primary and metastatic gastric cancer cells obtained by laser capture microdissection

Zhen-Ning Wang, Hui-Mian Xu, Li Jiang, Xin Zhou, Chong Lu, Xue Zhang

Zhen-Ning Wang, Li Jiang, Xue Zhang, The Research Center for Medical Genomics and MOH Key Laboratory of Cell Biology, China Medical University, Shenyang 110001, Liaoning Province, China

Zhen-Ning Wang, Hui-Mian Xu, Xin Zhou, Chong Lu, Department of Surgical Oncology, the First Affiliated Hospital of China Medical University, Shenyang 110001, Liaoning Province, China

Xue Zhang, Department of Medical Genetics and National Key Laboratory of Medical Molecular Biology, Chinese Academy of Medical Sciences and Peking Union Medical College, Beijing 100005, China

Supported by the National 1973 Program of China, No. G1998051203, the National Science Fund for Distinguished Young Scholars of China, No. 30125017, and the MOE TRAPOYT Program of China, No. 1999-96

Correspondence to: Dr. Xue Zhang, The Research Center for Medical Genomics, China Medical University, Shenyang 110001, Liaoning Province, China. xuezhang@pumc.edu.cn

Telephone: +86-10-86319731 **Fax:** +86-10-65124876

Received: 2003-09-06 **Accepted:** 2003-10-22

Abstract

AIM: Survivin, a recently identified member of the inhibitor of apoptosis protein family, is expressed during development and in various human cancers. However, its expression in normal tissues and clinical relevance in cancers are still debated. In the present study, we analyzed the expression of the survivin gene in human primary and metastatic gastric cancer cells as well as in paired epithelial cells from normal gastric mucosa by means of a novel laser capture microdissection (LCM) technique coupled with reverse transcription - polymerase chain reaction (RT-PCR).

METHODS: Thirty patients who had undergone gastrectomy with lymph node dissection for gastric cancer without preoperative treatments were included. Neoplastic tissue, metastatic lymph nodes, and apparently uninvolved normal tissue were collected from each patient. LCM-captured "pure" cell groups were respectively subjected to RT-PCR analysis with primers specific for the survivin gene.

RESULTS: Of the paired samples from 30 gastric cancer patients studied, 24 (80%) primary gastric cancer cell groups and 7 (23%) adjacent morphologically "normal" gastric epithelial cell groups were shown to have a detectable survivin expression. There was a statistically significant difference in survivin expression between these two groups ($P < 0.01$). Meanwhile, 95% (19/20) of the metastatic gastric cancer cell groups from lymph nodes had a clear expression of the survivin gene. However, no significant correlation between survivin expression and clinicopathological features of gastric cancer was observed in the present study.

CONCLUSION: Survivin expression is present in the majority of gastric cancer cell groups obtained by LCM techniques. The high expression rate in metastatic lesions suggests a possible role of survivin in cancer invasiveness and metastasis. It may contribute to the detection of gastric

cancer micrometastasis as a potential molecular marker. In addition, the high expression percentage renders survivin a potential target in the therapy for gastric cancer.

Wang ZN, Xu HM, Jiang L, Zhou X, Lu C, Zhang X. Expression of survivin in primary and metastatic gastric cancer cells obtained by laser capture microdissection. *World J Gastroenterol* 2004; 10(21): 3094-3098

<http://www.wjgnet.com/1007-9327/10/3094.asp>

INTRODUCTION

Alteration of the balance between apoptosis and cell proliferation could result in a disturbance of tissue homeostasis, and dysregulation of apoptosis is associated with various cancers^[1]. Considerable interest has focused on the identification of regulators of apoptosis, which may potentially contribute to the development of cancer. Recently, a novel member of the inhibitor of apoptosis (IAP) protein family, designated as survivin, has been identified. The surviving gene is located on chromosome 17 and spans 14.7 kb, encoding a protein of 142 amino acids. Unlike other IAP proteins, survivin contains a single baculovirus IAP repeat and lacks a C-terminal RING finger^[2]. Another significant feature of survivin is its unique expression pattern as one of the most tumor-specific human gene products^[3]. While embryonic and fetal organs contain abundant survivin mRNA and protein, most terminally differentiated normal tissues do not. By contrast, dramatically strong expression of survivin is detected in the vast majority of tumors^[4]. Moreover, the overexpression of survivin has been shown to be correlated with aggressive and histologically unfavorable neuroblastoma^[5], and associated with the poor prognostic outcome in colorectal cancer^[6], non-small-cell lung cancer^[7], breast cancer^[8], soft tissue sarcoma^[9] and B-cell lymphoma^[10].

However, since its identification five years ago, there have been some contradictory reports about the clinical relevance of survivin expression in cancer. Gianani *et al.*^[11] found the expression of survivin was not a specific marker of adenocarcinoma of the colon but showed characteristic patterns of expression in normal colonic mucosa. In gastric carcinoma which is the second most frequent cause of cancer death according to a worldwide estimation, Lu *et al.*^[12] showed that survivin could promote aberrantly tumor cell viability, whereas Okada *et al.*^[13] indicated that survivin expression in nuclei of tumor cells was predictive of favorable prognosis in patients. In the present study, we used laser capture microdissection (LCM), a novel technique that allows rapid, reliable and accurate procurement of cells from specific regions of tissue sections under direct visualization, to obtain the primary and metastatic gastric cancer cells as well as the matched normal epithelial cells from the same patient and analyzed mRNA expression of the survivin gene.

MATERIALS AND METHODS

Patients

Thirty patients (25 males and 5 females) underwent gastrectomy

with lymph node dissection for gastric carcinoma at China Medical University between March and September of 2 000 were included in the study. None of the patients received preoperative chemotherapy. The patients ranged in age from 33 to 78 years (median, 57 years). Routinely, the resected specimens were histologically examined by H&E staining according to the general rules of the classification of gastric carcinoma suggested by the Japanese Research Society of Gastric Cancer^[14]. Details of the Borrmann gross type, the Lauren histological classification, the Ming classification of growth patterns, grade of differentiation, and levels of lymph node metastasis were obtained from the operative records and the pathology reports. The pT classification representing the depth of wall invasion and the pN classification representing the extent of regional lymph node metastasis were performed using standard criteria of the 5th TNM staging system^[15]. The total lymph node number collected from the tissue was 15 or more for a reliable pN classification.

Tissue samples

Tumor tissues, lymph nodes, and apparently uninvolved normal tissues were collected from each patient immediately after surgical removal and snap-frozen in liquid nitrogen and kept at -80 °C until use. The tissues were then embedded in OCT for subsequent LCM harvest. Sections were cut at 8 µm with a cryostat and mounted on uncoated glass slides. The slides could be immediately stored at -80 °C for a few weeks. In order to exclude the areas of necrosis, tumor tissues from all patients were selected from the most viable areas of tumors. The lymph nodes were obtained according to the standard protocol. The number of removed and positive lymph nodes for various stations was documented by the pathologists. For the selection of matched uninvolved gastric mucosa, specimens were obtained from tissues at a distance of more than 10 cm from the tumor edge and confirmed histologically.

LCM

OCT embedded blocks of frozen tissue were serially cut. For each case, the first section was stained with H&E routinely for histological analysis and digitalized. The following serial sections stained with H&E according to the standard protocol recommended by NIH^[16] were subjected to LCM using a LM200 system (Olympus, Japan/Arcturus Engineering Inc, US). Areas of interest were selected under microscopic guidance, and covered with ethylene vinyl thermoplastic (EVA) film mounted on optically transparent cap. The infrared laser was activated by the push of a button, which melts the film directly above the target cells. This melt caused a binding to form between the cells and the transfer film that was stronger than the binding between the cells and the slide^[17]. The parameters used for LCM included a laser diameter of 7.5 µm, laser power of 50-60 mW. Five thousand laser pulse discharges per specimen were used to "capture" approximately 10 000 morphologically normal gastric epithelial cells, malignant primary gastric cancer cells and malignant metastatic (to a perigastric lymph node) gastric cancer cells from each case. Each population was estimated to be >95% "homogeneous" as determined by microscopic visualization of the captured cells. The caps with captured cells were then fitted onto 0.5 mL microcentrifuge tubes containing 200 µL TRIZOL Reagent. Caps briefly placed onto the section without laser activation were used as negative control.

RNA extraction from LCM-captured cells

Total RNA from each population of laser-captured cells was independently extracted using TRIZOL Reagent (Life Technologies, Inc) by means of a modification of the RNA microisolation protocol recommended by the manufacturer. Briefly, tubes containing collected cells and TRIZOL Reagent

were inverted and allowed to sit at room temperature for 30 min, then 0.5 µL glycogen (20 µg/µL) carrier and 40 µL chloroform were added to each tube. The tubes were vigorously shaken by hand for 15 s and incubated at room temperature for 2 min. The samples were centrifuged at 11 000 g for 15 min at 4 °C. The aqueous layer was transferred to a fresh 0.5 mL tube, 100 µL isopropanol was added and precipitated at -70 °C for 1 h. After centrifuged at 11 000 g for 10 min at 4 °C, the pellet was then washed in 200 µL of 750 mL/L ethanol and resuspended in 7 µL diethylpyrocarbonate-treated RNase free water.

Reverse transcription-polymerase chain reaction (RT-PCR)

For RT-PCR analysis of the LCM-captured cells, first strand cDNA was prepared from total RNA by using a first-strand synthesis kit (Life Technologies, Inc). Seven microliters of total RNA isolated from approximate 10 000 cells was mixed with 1 µL of oligo-(dT)₁₂₋₁₈ primer, 1 µL of random hexamers primer (N₆) and 1 µL of 10 mmol/L dNTPs in a total volume of 10 µL. They were heat denatured at 65 °C for 5 min, then chilled in ice. Four microliters of 5×first-strand reaction buffer, 2 µL of 0.1 mol/L DTT, 2 µL of 25 mmol/L MgCl₂, 1 µL of RNasin (40 U/µL) (Promega, Madison, WI, USA), and 1 µL of SUPERScript II RTase (200 U/µL) (Life Technologies, Inc) were added and incubated at 25 °C for 10 min, followed by incubation at 42 °C for 50 min for first-strand synthesis. The reverse transcriptase was inactivated at 70 °C for 15 min. PCR amplification with specific primers was performed in a final reaction volume of 50 µL containing 1×PCR buffer, 200 µmol/L each dNTP, 0.5 µmol/L each primer, 1.25 unit of Taq polymerase (TaKaRa Biotech, Dalian, China) and 2 µL of RT product. Programmable temperature cycling (UNO II, Biometra, Germany) was performed using the following profiles: an initial hot start at 95 °C for 2 min, followed by 38 cycles at 95 °C for 30 s, at 58 °C for 20 s and at 72 °C for 30 s. After the last cycle, an elongation step was extended at 72 °C for 5 min. For each set of PCR, parallel reactions with human genomic DNA from peripheral blood were performed to test for genomic DNA contamination, and double distilled water instead of cDNA template was also included as negative control to assure the quality of PCR. An 8 µL aliquot of the PCR product underwent electrophoresis on 15 g/L agarose gel stained with ethidium bromide and was visualized under UV trans-illuminator. The following primers were used: (A) survivin gene, forward primer 5'-CCCTGCCTGGCAGCCCTTTC-3', and reverse primer 5'-CTGGCTCCCAGCCTTCCA-3' (PCR product, 188 bp); (B) glyceraldehyde-3-phosphate dehydrogenase (G3PDH), forward primer 5'-AGGGGTCTACATGGCAACTG-3', and reverse primer 5'-CGACCACTTTGTCAAGCTCA-3' (PCR product, 227 bp).

Statistical analysis

Statistical comparisons for significance between nominal variables were evaluated by the chi-square test and the Fisher's exact probability test. All the statistical analyses were performed using SPSS10.0 computer software and *P* of 0.05 was used as significance criterion.

RESULTS

Survivin expression in microdissected gastric epithelial and cancer cells

As shown in Figure 1, LCM allowed us to precisely sample the targeted cells. In this manner, gastric normal epithelial or cancer cells were homogeneously obtained and bonded to the transfer film. When the cap together with the film was lifted from the tissue section, surrounding tissues remained attached to the glass slide. As a result, the morphology of the captured cells was well preserved and could be readily visualized under a microscope. To detect survivin gene mRNA expression by RT-PCR, a pair of specific primers located at 2 flanking exons was

designed and synthesized. The expected specific transcript of survivin gene represented by an 188 bp fragment was amplified (Figure 2). Of the paired samples from 30 gastric cancer patients studied, 24 (80%) primary gastric cancer cell groups and 7 (23%) adjacent morphologically "normal" gastric epithelial cell groups were shown to have a detectable survivin expression. There was a statistically significant difference in survivin expression between these two groups ($P < 0.01$). Furthermore, survivin mRNA was never detected in morphologically non-tumorous gastric epithelial cell groups when the paired cancer cell group was negative for survivin mRNA.

Strikingly, 95% (19/20) of the metastatic gastric cancer cell groups from lymph nodes had a clear expression of the survivin gene. Three cases showed positive results for the surviving-

specific RT-PCR assay in metastatic cancer cells while none of their paired primary cancer cells had a detectable expression of the survivin mRNA.

Relationship between survivin expression and clinicopathological characteristics in gastric cancer patients

We examined the relationship between survivin expression in microdissected primary cancer tissues and the clinicopathological features of gastric cancer (Table 1). There was no significant correlation between survivin expression and Borrmann gross type, depth of wall invasion, Lauren histological classification, Ming's classification of growth patterns, grade of differentiation, the presence and extent of lymph node metastasis.

We also analyzed the survivin gene expression pattern in

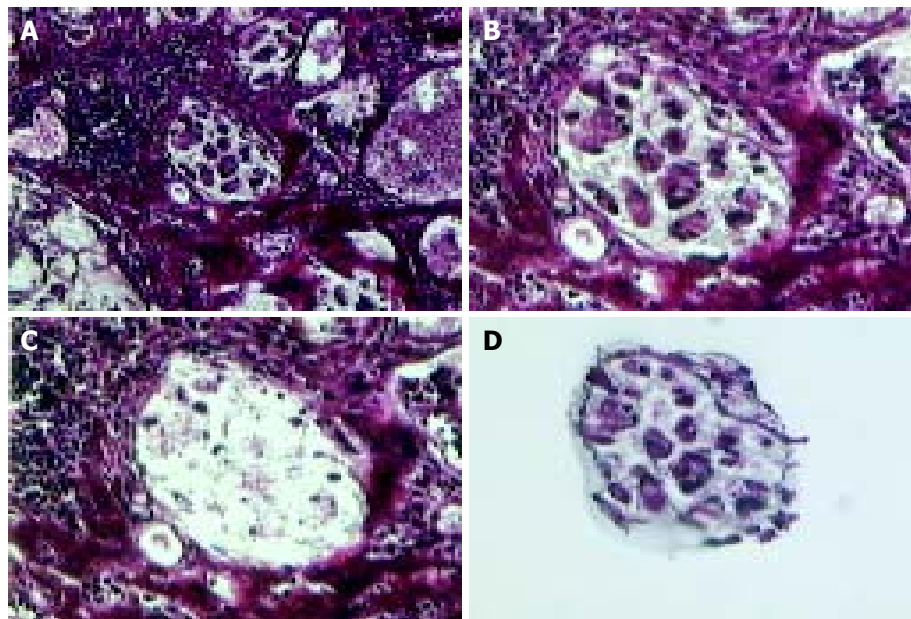


Figure 1 Laser capture microdissection of cells from gastric carcinoma. A: Morphology map view for pathological diagnosis ($\times 100$). B: Group of gastric carcinoma cells were selected for LCM ($\times 200$). C: The same section revealed where carcinoma cells were lifted from the section ($\times 200$). D: The carcinoma cells were removed on the plastic film to provide a template for PCR.

Table 1 Relationship between survivin expression and different histopathological features

Variant	Survivin expression in primary cancer		¹ P	Survivin expression pattern in cancer and normal tissues			P
	Positive	Negative		N(-)T(-)	N(-)T(+)	N(+)T(+)	
Gross type							
Borrmann I + II	7	1	² NS	1	4	3	NS
Borrmann III+IV	17	5		5	13	4	
Depth of invasion							
pT ₁ +pT ₂	9	1	NS	1	5	4	NS
pT ₃ +pT ₄	15	5		5	2	3	
Differentiation							
Well and medorate	7	1	NS	1	4	3	NS
Poor and undifferentiate	17	5		5	13	4	
Lauren classification							
Intestinal type	21	4	NS	4	16	5	NS
Diffuse type	3	2		2	1	2	
Ming growth pattern							
Expanding	9	3	NS	3	6	3	NS
Infiltrative	15	3		3	11	4	
Lymph node metastasis							
pN0	8	2	NS	2	5	3	NS
pN1	5	1		1	3	2	
pN2+pN3	11	3		3	9	2	

¹P was estimated by the ffsher's exact test ²NS, not significant.

both paired normal and primary cancer cells and its relationship with clinicopathological features. Thirty patients were divided into N (-) T (-), N (-) T (+) and N (+) T (+) groups. Still, no significant correlation between survivin expression pattern and the factors mentioned above was observed.

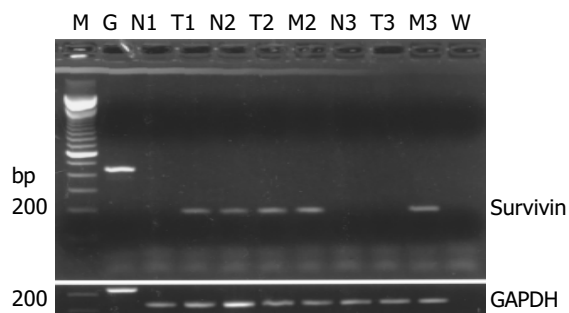


Figure 2 Representative RT-PCR results of survivin expression in normal (N), tumor (T) and metastatic carcinoma (M) cells obtained by LCM from 3 patients suffering gastric cancer. Case 1 was a patient without lymphatic metastasis, cases 2 and 3 were patients with lymphatic metastasis. G: Genomic DNA from human peripheral blood. W: Water as negative control.

DISCUSSION

Apoptosis plays an important role in organ homeostasis, by eliminating senescent or damaged cells. The suppression of apoptosis has been considered to contribute to carcinogenesis and cancer progression by aberrantly prolonging cell viability with accumulation of mutations^[18,19]. Survivin is a newly identified bifunctional protein that suppresses apoptosis and regulates cell division. Based on the previously published studies, its mRNA is abundantly expressed in fetal tissues, but not in normal adult tissues except placenta and thymus. Meanwhile, reactivation of survivin expression has been demonstrated in tumors of lung^[7], stomach^[20], breast^[8], colon^[21], esophagus^[22], liver^[23], pancreas^[24], bladder^[25], uterus^[26], ovary^[27], *etc.* This specific distribution pattern has aroused great interest in making the survivin gene as a potential cancer therapeutic target. However, the expression of the survivin gene in normal tissues is currently debated. Several recent studies have shown survivin expression in normal tissues including skin^[28], endometrium^[29], endothelial cells^[30], colonic mucosa^[11] and muscle^[9]. In the present studies, we sought to investigate whether survivin expression could be a specific marker during the development of gastric cancer.

It has been generally accepted that molecular analysis of neoplastic tissues *in vivo* is challenged by the heterogeneity of samples. Genetic alternations can be masked by contaminating bystander cells. Survivin mRNA was detected in normal tissue adjacent to soft tissue sarcoma cells^[9]. Therefore, it is necessary to obtain a pure population of cells to evaluate the possible role of the survivin gene in tumor progression. The recent development in LCM, a highly sophisticated technique for the transfer of isolated pure cells from the histological slide into a reaction tube, could afford the opportunity to overcome this obstacle^[31]. A few published studies and our previous data (unpublished data) have shown that LCM coupled with RT-PCR technique is a reliable method for the molecular analysis of gene profiles in specific tissues. We combined RT-PCR with LCM to determine the survivin expression in primary cancer cells, metastatic cancer cells, and paired normal epithelial cells.

Our results demonstrated that 23% of morphologically normal epithelial cells had a detectable survivin mRNA expression. By contrast, Lu *et al.*^[12] reported that no survivin expression was found in normal gastric mucosa neighboring the cancer cells in an immunohistochemical analysis. Meanwhile,

the rate of survivin expression was relatively lower in normal tissue we examined than in previous studies reporting 47.1% in normal esophageal epithelial tissues^[22] and 29.1% or 100% in normal colorectal tissues^[6,11]. One possible explanation for these results could be the different sensitivity of methods and the varied criteria for positivity determination. Further studies may be required to check out whether the expression of the survivin gene in normal tissues is caused by a high proportion of mitotically active cells.

In accordance with the recently published reports showing 88% positive survivin expression in gastric cancer tissues, we found a detectable expression of the survivin gene in 24 of 30 primary gastric cancer cell groups. The percentage was significantly higher than that in normal gastric epithelial cells. These results suggested that survivin expression in gastric cancer was a quite common event and might play an important role in the carcinogenesis of stomach. Several studies have consistently shown that survivin expression could inhibit cell death induced by various apoptotic stimuli^[4]. A role for survivin in blocking apoptosis has also been found *in vivo*^[32]. Like other proteins in the IAP family, survivin might bind specifically to caspase-3 or caspase-9, which are the effectors of apoptosis^[33]. On the other hand, survivin was expressed in the G2-M phase of the cell cycle and its overexpression might contribute to overcoming the G2-M phase checkpoint to enforce progression of cells through mitosis^[34]. Therefore, not surprisingly, survivin was shown to be present in the majority of gastric cancer cells.

Even though no significant correlation was observed between survivin expression in primary cancer or its distribution pattern in normal and cancer tissues and tumor invasiveness or the presence of lymph node metastasis, it is still striking to find that 95% of the metastatic cancer cells from lymph nodes had a clear expression of the survivin mRNA. In three cases, survivin expression was detected in metastatic lesions, but not in primary cancer cell groups. One possible explanation might be that survivin expression was upregulated in some metastatic cancer cells. By sensitive quantitative RT-PCR assay, significantly increased survivin expression levels were found in soft tissue sarcomas with more aggressive biological behavior^[9]. Alternatively, more survivin expressions detected in metastatic lesions could result from the presence of a higher proportion of survivin-expressing cells compared with that in primary sites. Immunohistochemical analysis revealed that the percentage of survivin-positive cells in primary gastric cancer was quite variable, ranging from 20-100%^[12]. It has been shown that failures in normal apoptosis pathways could contribute to cancer progression by supporting anchorage-independent survival during metastasis. Considering the anti-apoptotic function of survivin, it seems reasonable to deduce that survivin expression might facilitate the survival of cancer cells at distant sites^[35]. Also, survivin played a crucial role in angiogenesis^[30,36], which is considered as one of the critical steps for cancer cell spread and metastasis. Moreover, when analyzed retrospectively, cancer patients expressing survivin exhibited a shorter survival, correlated with unfavorable prognosis and accelerated rates of recurrences^[5-10]. These results together with ours suggested a possible role of survivin in cancer invasiveness and metastasis. Further analysis is necessary to assess the expression levels in metastatic lesions by accurately quantitative methods.

Furthermore, the extremely high survivin expression rate in metastatic lesions indicated a possible approach using survivin as a molecular diagnostic marker for micrometastasis in gastric cancer. Our parallel studies have shown that the detection of survivin expression in peritoneal lavaged fluid is a specific and sensitive assay for prediction of peritoneal micrometastasis in gastric cancer. Also, survivin was detected in the urine of all patients tested with new or recurrent bladder cancer, whereas normal volunteers and patients with non-neoplastic diseases were tested negative for urine survivin^[4]. However, a large scale

and long follow-up should be carried out to validate these results.

Recently, expression of a phosphorylation-defective survivin mutant (Thr34→Ala), which acted as a dominant-negative antagonist of survivin pathway and prevented phosphorylation of endogenous protein, has been reported to trigger apoptosis in several human melanoma cell lines *in vitro* and to prevent tumor formation or suppress the growth of existing tumors by 60-70% *in vivo*^[37]. Therefore, the role of survivin in cancer progression has made it an attractive therapeutic target against cancer development.

In summary, our data indicate survivin expression is present in the majority of gastric cancer cell groups obtained by LCM techniques. The high expression rate in metastatic lesions suggests a possible role of survivin in cancer invasiveness and metastasis. It might contribute to the detection of micrometastasis in gastric cancer as a potential molecular marker. In addition, the high expression percentage renders survivin a candidate target in the therapy for gastric cancer.

REFERENCES

- 1 **Hetts SW**. To die or not to die: an overview of apoptosis and its role in disease. *JAMA* 1998; **279**: 300-307
- 2 **Ambrosini G**, Adida C, Altieri DC. A novel anti-apoptosis gene, survivin, expressed in cancer and lymphoma. *Nat Med* 1997; **3**: 917-921
- 3 **Velculescu VE**, Madden SL, Zhang L, Lash AE, Yu J, Rago C, Lal A, Wang CJ, Beaudry GA, Ciriello KM, Cook BP, Dufault MR, Ferguson AT, Gao Y, He TC, Hermeking H, Hiraldo SK, Hwang PM, Lopez MA, Luderer HF, Mathews B, Petroziello JM, Polyak K, Zawel L, Kinzler KW, Zhang W, Zhang X, Zhou W, Haluska FG, Jen J, Sukumar S, Landes GM, Riggins GJ, Vogelstein B, Kinzler KW. Analysis of human transcriptomes. *Nat Genet* 1999; **23**: 387-388
- 4 **Altieri DC**. The molecular basis and potential role of survivin in cancer diagnosis and therapy. *Trends Mol Med* 2001; **7**: 542-547
- 5 **Adida C**, Berrebi D, Peuchmaur M, Reyes-Mugica M, Altieri DC. Anti-apoptosis gene, survivin, and prognosis of neuroblastoma. *Lancet* 1998; **351**: 882-883
- 6 **Sarela AI**, Macadam RC, Farmery SM, Markham AF, Guillou PJ. Expression of the antiapoptosis gene, survivin, predicts death from recurrent colorectal carcinoma. *Gut* 2000; **46**: 645-650
- 7 **Monzo M**, Rosell R, Felip E, Astudillo J, Sanchez JJ, Maestre J, Martin C, Font A, Barnadas A, Abad A. A novel anti-apoptosis gene: re-expression of survivin messenger RNA as a prognosis marker in non-small-cell lung cancers. *J Clin Oncol* 1999; **17**: 2100-2104
- 8 **Tanaka K**, Iwamoto S, Gon G, Nohara T, Iwamoto M, Tanigawa N. Expression of survivin and its relationship to loss of apoptosis in breast carcinomas. *Clin Cancer Res* 2000; **6**: 127-134
- 9 **Kappler M**, Kohler T, Kampf C, Diestelkötter P, Wurl P, Schmitz M, Bartel F, Lautenschlager C, Rieber EP, Schmidt H, Bache M, Taubert H, Meye A. Increased survivin transcript levels: an independent negative predictor of survival in soft tissue sarcoma patients. *Int J Cancer* 2001; **95**: 360-363
- 10 **Adida C**, Haioun C, Gaulard P, Lepage E, Morel P, Briere J, Dombret H, Reyes F, Diebold J, Gisselbrecht C, Salles G, Altieri DC, Molina TJ. Prognostic significance of survivin expression in diffuse large B-cell lymphomas. *Blood* 2000; **96**: 1921-1925
- 11 **Gianani R**, Jarboe E, Orlicky D, Frost M, Bobak J, Lehner R, Shroyer KR. Expression of survivin in normal, hyperplastic, and neoplastic colonic mucosa. *Hum Pathol* 2001; **32**: 119-125
- 12 **Lu CD**, Altieri DC, Tanigawa N. Expression of a novel antiapoptosis gene, survivin, correlated with tumor cell apoptosis and p53 accumulation in gastric carcinomas. *Cancer Res* 1998; **58**: 1808-1812
- 13 **Okada E**, Murai Y, Matsui K, Isizawa S, Cheng C, Masuda M, Takano Y. Survivin expression in tumor cell nuclei is predictive of a favorable prognosis in gastric cancer patients. *Cancer Lett* 2001; **163**: 109-116
- 14 **Hermanek P**. The second English edition of the Japanese Classification of Gastric Carcinoma. A Western commentary. *Gastric Cancer* 1999; **2**: 79-82
- 15 **Wang Z**, Xu H, Wang S, Chen J. Relationship between new TNM classification and the prognosis and biological behavior of gastric cancer. *Zhonghua Waikhe Zazhi* 2000; **38**: 493-495
- 16 <http://dir.niehs.nih.gov/dirlep/lcm/protocols.html>
- 17 **Bonner RF**, Emmert-Buck M, Cole K, Pohida T, Chuaqui R, Goldstein S, Liotta LA. Laser capture microdissection: molecular analysis of tissue. *Science* 1997; **278**: 1481-1483
- 18 **Ogawa N**, Dang H, Talal N. Apoptosis and autoimmunity. *J Autoimmun* 1995; **8**: 1-19
- 19 **Wyllie AH**. Apoptosis and carcinogenesis. *Eur J Cell Biol* 1997; **73**: 189-197
- 20 **Zhu XD**, Lin GJ, Qian LP, Chen ZQ. Expression of survivin in human gastric carcinoma and gastric carcinoma model of rats. *World J Gastroenterol* 2003; **9**: 1435-1438
- 21 **Lin LJ**, Zheng CQ, Jin Y, Ma Y, Jiang WG, Ma T. Expression of survivin protein in human colorectal carcinogenesis. *World J Gastroenterol* 2003; **9**: 974-977
- 22 **Kato J**, Kuwabara Y, Mitani M, Shinoda N, Sato A, Toyama T, Mitsui A, Nishiwaki T, Moriyama S, Kudo J, Fujii Y. Expression of survivin in esophageal cancer: correlation with the prognosis and response to chemotherapy. *Int J Cancer* 2001; **95**: 92-95
- 23 **Ikeguchi M**, Ueda T, Sakatani T, Hirooka Y, Kaibara N. Expression of survivin messenger RNA correlates with poor prognosis in patients with hepatocellular carcinoma. *Diagn Mol Pathol* 2002; **11**: 33-40
- 24 **Satoh K**, Kaneko K, Hirota M, Masamune A, Satoh A, Shimosegawa T. Expression of survivin is correlated with cancer cell apoptosis and is involved in the development of human pancreatic duct cell tumors. *Cancer* 2001; **92**: 271-278
- 25 **Swana HS**, Grossman D, Anthony JN, Weiss RM, Altieri DC. Tumor content of the antiapoptosis molecule survivin and recurrence of bladder cancer. *N Engl J Med* 1999; **341**: 452-453
- 26 **Saitoh Y**, Yaginuma Y, Ishikawa M. Analysis of Bcl-2, Bax and Survivin genes in uterine cancer. *Int J Oncol* 1999; **15**: 137-141
- 27 **Yoshida H**, Ishiko O, Sumi T, Matsumoto Y, Ogita S. Survivin, bcl-2 and matrix metalloproteinase-2 enhance progression of clear cell and serous-type ovarian carcinomas. *Int J Oncol* 2001; **19**: 537-542
- 28 **Chiodino C**, Cesinaro AM, Ottani D, Fantini F, Giannetti A, Trentini GP, Pincelli C. Communication: expression of the novel inhibitor of apoptosis survivin in normal and neoplastic skin. *J Invest Dermatol* 1999; **113**: 415-418
- 29 **Konno R**, Yamakawa H, Utsunomiya H, Ito K, Sato S, Yajima A. Expression of survivin and Bcl-2 in the normal human endometrium. *Mol Hum Reprod* 2000; **6**: 529-534
- 30 **O'Connor DS**, Schechner JS, Adida C, Mesri M, Rothermel AL, Li F, Nath AK, Pober JS, Altieri DC. Control of apoptosis during angiogenesis by survivin expression in endothelial cells. *Am J Pathol* 2000; **156**: 393-398
- 31 **Simone NL**, Bonner RF, Gillespie JW, Emmert-Buck MR, Liotta LA. Laser-capture microdissection: opening the microscopic frontier to molecular analysis. *Trends Genet* 1998; **14**: 272-276
- 32 **Grossman D**, Kim PJ, Blanc-Brude OP, Brash DE, Tognin S, Marchisio PC, Altieri DC. Transgenic expression of survivin in keratinocytes counteracts UVB-induced apoptosis and cooperates with loss of p53. *J Clin Invest* 2001; **108**: 991-999
- 33 **Tamm I**, Wang Y, Sausville E, Scudiero DA, Vigna N, Oltersdorf T, Reed JC. IAP-family protein survivin inhibits caspase activity and apoptosis induced by Fas (CD95), Bax, caspases, and anticancer drugs. *Cancer Res* 1998; **58**: 5315-5320
- 34 **Li F**, Ambrosini G, Chu EY, Plescia J, Tognin S, Marchisio PC, Altieri DC. Control of apoptosis and mitotic spindle checkpoint by survivin. *Nature* 1998; **396**: 580-584
- 35 **Reed JC**. Dysregulation of apoptosis in cancer. *J Clin Oncol* 1999; **17**: 2941-2953
- 36 **Tran J**, Rak J, Sheehan C, Saibil SD, LaCasse E, Korneluk RG, Kerbel RS. Marked induction of the IAP family antiapoptotic proteins survivin and XIAP by VEGF in vascular endothelial cells. *Biochem Biophys Res Commun* 1999; **264**: 781-788
- 37 **Grossman D**, Kim PJ, Schechner JS, Altieri DC. Inhibition of melanoma tumor growth *in vivo* by survivin targeting. *Proc Natl Acad Sci U S A* 2001; **98**: 635-640

Interferon plus ribavirin and interferon alone in preventing hepatocellular carcinoma: A prospective study on patients with HCV related cirrhosis

Azzaroli Francesco, Accogli Esterita, Nigro Giovanni, Trerè Davide, Giovanelli Silvia, Miracolo Anna, Lodato Francesca, Montagnani Marco, Tamé Mariarosa, Colecchia Antonio, Mwangemi Constance, Festi Davide, Roda Enrico, Derenzini Massimo, Mazzella Giuseppe

Francesco Azzaroli, Accogli Esterita, Nigro Giovanni, Giovanelli Silvia, Miracolo Anna, Lodato Francesca, Montagnani Marco, Tamé Mariarosa, Colecchia Antonio, Mwangemi Constance, Festi Davide, Roda Enrico, Mazzella Giuseppe, Department of Internal Medicine and Gastroenterology, University of Bologna
Trerè Davide, Derenzini Massimo, Department of Experimental Pathology, University of Bologna

Correspondence to: Azzaroli Francesco, M.D., Department of Internal Medicine and Gastroenterology, S.Orsola Hospital (Pad. 5), University of Bologna Via Massarenti 9, 40138 Bologna. azzaroli@med.unibo.it
Telephone: +39-338-5316190 **Fax:** +39-51-6363316
Received: 2003-11-04 **Accepted:** 2004-04-06

Abstract

AIM: To determine the role of interferon (IFN) with or without ribavirin in preventing or delaying hepatocellular carcinoma (HCC) development in patients with hepatitis C virus (HCV) related cirrhosis. Data on the preventive effect of IFN plus ribavirin treatment are lacking.

METHODS: A total of 101 patients (62 males and 39 females, mean age 55.1 ± 1.4 years) with histologically proven HCV related liver cirrhosis plus compatible biochemistry and ultrasonography were enrolled in the study. Biochemistry and ultrasonography were performed every 6 mo. Ultrasound guided liver biopsy was performed on all detected focal lesions. Follow-up lasted for 5 years. Cellular proliferation, evaluated by measuring Ag-NOR proteins in hepatocytes nuclei, was expressed as AgNOR-Proliferative index (AgNOR-PI) (cut-off = 2.5). Forty-one patients (27 males, 14 females) were only followed up after the end of an yearly treatment with IFN-alpha2b (old treatment control group = OTCG). Sixty naive patients were stratified according to sex and AgNOR-PI and then randomized in two groups: 30 were treated with IFN-alpha2b + ribavirin (treatment group = TG), the remaining were not treated (control group = CG). Nonresponders (NR) or relapsers in the TG received further IFN/ribavirin treatments after a 6 mo of withdrawal.

RESULTS: AgNOR-PI was significantly lowered by IFN ($P < 0.001$). HCC incidence was higher in patients with $\text{AgNOR-PI} > 2.5$ (26% vs 3%, $P < 0.01$). Two NR in the OTCG, none in the TG and 9 patients in the CG developed HCC during follow-up. The Kaplan-Mayer survival curves showed statistically significant differences both between OTCG and CG ($P < 0.004$) and between TG and CG ($P < 0.003$).

CONCLUSION: IFN/ribavirin treatment associated with re-treatment courses of NR seems to produce the best results in terms of HCC prevention. AgNOR-PI is a useful marker of possible HCC development.

Francesco A, Esterita A, Giovanni N, Davide T, Silvia G, Anna M, Francesca L, Marco M, Mariarosa T, Antonio C, Constance

M, Davide F, Enrico R, Massimo D, Giuseppe M. Interferon plus ribavirin and interferon alone in preventing hepatocellular carcinoma: A prospective study on patients with HCV related cirrhosis. *World J Gastroenterol* 2004; 10(21): 3099-3102
<http://www.wjgnet.com/1007-9327/10/3099.asp>

INTRODUCTION

A number of studies have reported that treatment of HCV related cirrhosis might have a preventive effect on hepatocellular carcinoma development^[1-15]. This has been recently confirmed by a meta-analysis concluding that "Interferon (IFN) prevents or delays the development of hepatocellular carcinoma (HCC) in patients with HCV-related cirrhosis, the magnitude of the overall effect is low and the benefit may be partly due to spurious associations. The preventive effect seems more evident among sustained responders to IFN^[16]". However, with old interferon schedules, sustained responders did not exceed 10-15% of treated patients^[1-15].

The response rate to IFN has changed since the introduction of ribavirin^[17], the induction protocols^[18] and, finally, the pegylated interferons^[19]. Data on the preventive effect on HCC of more powerful therapeutic schemes are lacking.

Our study was started in 1997 with the purpose of assessing the efficacy of interferon (given with an induction protocol) plus ribavirin (the gold standard treatment at that time) in the prevention of HCC development.

MATERIALS AND METHODS

Patients

A total of one hundred and one consecutive patients (62 males and 39 females, mean age 55.1 ± 1.4 years) with HCV related liver cirrhosis diagnosed by liver biopsy plus compatible biochemical parameters and ultrasonographic signs of portal hypertension were enrolled in the study. The baseline histologic activity of all patients was moderate to severe.

Study design (Figure 1)

Forty one subjects (27 males and 14 females, mean age 55.0 ± 1.1 years), who were ending a 12-mo IFN course were followed-up without any other treatment (old treatment control group = OTCG). All patients of OTCG underwent liver biopsy at the end of treatment, while still on IFN.

The other 60 untreated patients (35 males and 25 females, mean age 55.7 ± 1.7 years) were randomized in two groups of 30 subjects stratified according to sex and silver stained nucleolar organizer region - proliferative index (AgNOR-PI). Thirty were treated with IFN+ribavirin (treatment group = TG) and the remaining received no drugs (control group = CG). Nonresponders or relapsers to IFN/ribavirin received further courses of treatment after a 6 mo withdrawal. All patients were followed up for five years.

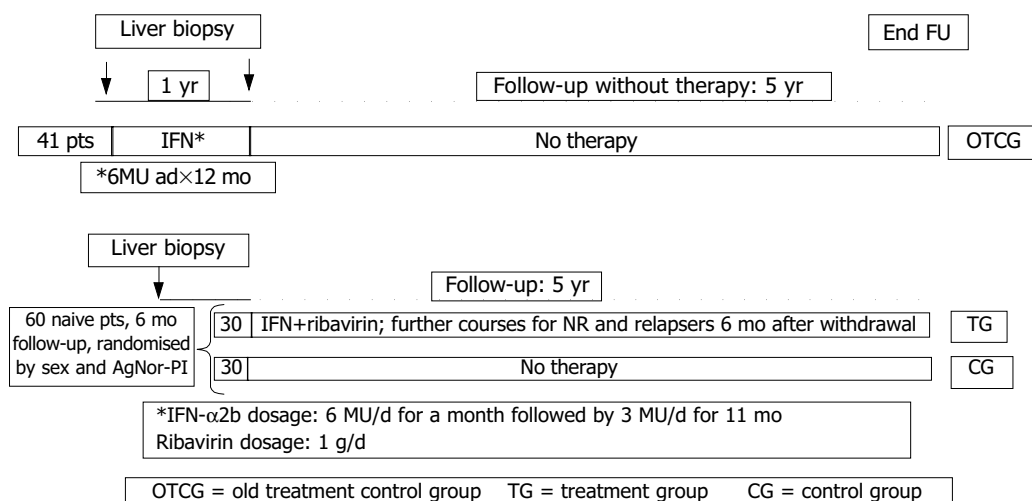


Figure 1 Study design.

The study was carried out according to the Helsinki protocol and all patients gave their written informed consent.

Ultrasonographies, blood cell count, α 1-fetoprotein, γ GT, transaminases, PT, total protein and their fractions were performed every 3 mo in all patients. Additional tests were performed in patients under active treatment: blood cell count every 10 d for two months and then monthly; transaminases, urea, creatinine and uric acid were tested monthly. When focal lesions were detected by ultrasound (US), US-guided liver biopsy was performed.

Protocol treatments

The 41 patients in OTCG were treated with IFN α -2b 6 MU/d for a month followed by 3 MU/d for 11 mo. The 30 patients in TG received the following α -2b schedule: 6 MU/d for a mo then 3 MU/d for 11 mo plus ribavirin 1 g/d for 12 mo. IFN and ribavirin dose reductions were made according to the biochemistry and tolerance of each patient. However, a total dose equal to or greater than 540 MU and 400 mg of ribavirin per day were considered suitable. Nonresponders and/or relapsers received further IFN treatment courses after a 6-mo withdrawal.

Liver histology and AgNOR-PI determination

Ultrasound guided liver biopsies were fixed in 40 g/L formaldehyde solution for 6 h and embedded in paraffin wax. Four 4 μ m thick sections were cut from routinely processed paraffin blocks. Hematoxylin-eosin, silver impregnation, Pearl's staining were performed to define the severity of parenchymal, portal and periportal inflammation and the stage of disease by evaluating fibrosis and the presence of stainable iron into the liver. Histology was evaluated by two blinded independent observers according to Scheuer score.

The AgNOR staining was performed on routine sections of liver tissue on poly-lysine pretreated slides after immersion in xylene and ethanol. After progressive re-hydration sections were covered with plastic resistant to high temperature, put in a sodium citrate (100 g/L, pH 6.0) solution and boiled in pressured ovens (120 $^{\circ}$ C for 20 min). Then, sections were stained by silver impregnation in a gelatine solution (formic acid 10 mL/L and silver nitrate 500 g/L, 100:2 v/v) according to Ploton^[20], for 10 min, at 37 $^{\circ}$ C. Quantitative analysis of Ag-NOR proteins was made by measuring silver-stained areas (μ m²) within nuclei present in 50 consecutive microscopic fields (40 \times magnification) using a specific computer-assisted imaging software on biopsy specimen sections (VIDAS, Kontron Elektronik, Germany). The percentage of hepatocytes with an AgNOR area >7 μ m² (indicative of a proliferative state) was expressed as proliferative

index (AgNOR-PI) (cut-off = 2.5%).

Statistical analysis

Results were expressed as mean \pm SE. The statistical analysis was carried out according to the intention to treat analysis. Wilcoxon test was used when appropriate and the Kaplan-Mayer model was applied to the evaluation of survival probability.

RESULTS

Biochemistry

Demographic and biochemical characteristics of the patients at enrollment are shown in Table 1. The three groups were comparable for age, sex, biochemical parameters, genotype distribution and AgNOR-PI.

Table 1 Baseline patient characteristics

	OTCG	TG	CG	P<
M:F ratio	27:14	17:13	18:12	NS
Age (yr)	55.3 \pm 1.8	54.6 \pm 2.1	57.2 \pm 2.0	NS
AST (U/L)	67.1 \pm 6.6	61.9 \pm 7.2	79.4 \pm 8.4	NS
ALT (U/L)	92.5 \pm 10.8	79.8 \pm 8.7	91.8 \pm 9.1	NS
γ GT (U/L)	56.5 \pm 7.2	52.1 \pm 7.3	65.2 \pm 9.4	NS
Albumin (g/dL)	4.2 \pm 0.07	4.2 \pm 0.07	4.1 \pm 0.06	NS
α 1feto (ng/mL)	6.8 \pm 1.25	8.4 \pm 2.36	6.3 \pm 1.0	NS
HCV1b	63%	67%	65%	NS
AgNOR-PI (%)	20.1 \pm 2.35	19.6 \pm 2.84	18.2 \pm 2.6	NS

OTCG = old treatment control group; TG = treatment group, CG = control group.

AgNOR PI

A significant reduction in AgNOR-PI was observed after IFN-treatment (Figure 2).

A significant difference in HCC development was observed according to AgNOR-PI: 9 out of 35 (26%) with basal AgNOR-PI >2.5% vs 2 out of 66 (3%) with basal AgNOR-PI <2.5% (P <0.01) (Figure 3).

Virological response

Six months after IFN withdrawal 8 out of 19 responders (24.5%) achieved sustained response (6 with genotype 2 or 3 and 2 with genotype 1) in the OTCG. Twenty one out of 30 patients in TG (70%) achieved a virological response that was sustained in 13 (43%) (9 genotype 2 and 4 genotype 1). None of the re-treated patients showed a sustained response.

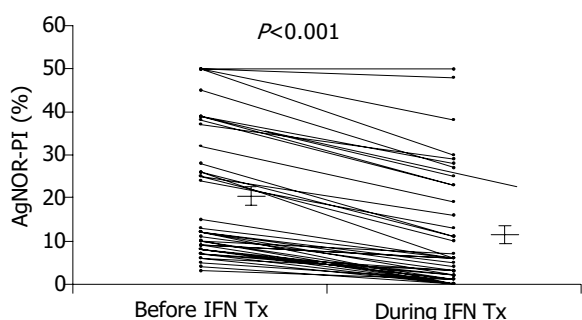


Figure 2 AgNOR-PI in OTCG before and after 1 year of IFN treatment.

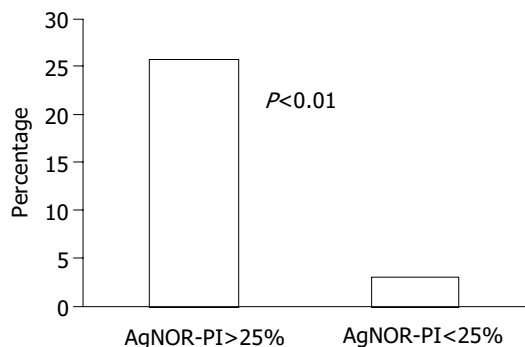


Figure 3 Incidence of HCC according to AgNOR-PI.

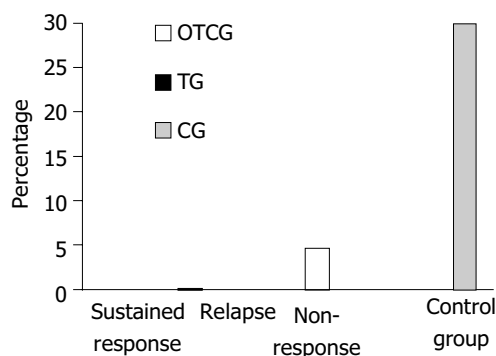


Figure 4 Percentage of HCC according to response to IFN.

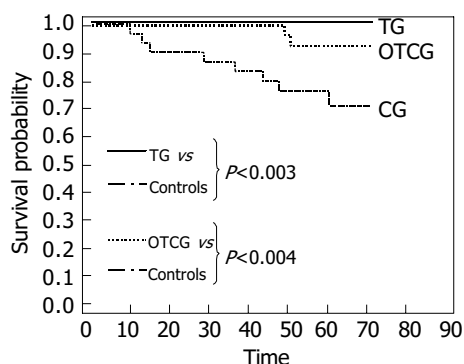


Figure 5 Survival probability evaluated by Kaplan-Mayer model.

HCC appearance

Two nonresponders in OTCG developed HCC during 5 years of follow-up after about 50 mo from interferon withdrawal. No subject in TG while 9 (30%) patients in CG developed HCC (Figure 4). The Kaplan-Mayer survival model showed statistically significant differences both between OTCG and CG ($P<0.004$) and between TG and CG ($P<0.003$) (Figure 5). The HCC annual

rate of incidence in the CG was 5%.

DISCUSSION

The present data add new evidence on the clinical efficacy of IFN re-treatment of cirrhotic patients and show the usefulness of AgNOR-PI. The ability of IFN to prevent HCC development is evident both alone and in combination with ribavirin.

Previous observations in patients with chronic hepatitis C^[21-24], with or without cirrhosis, reported that re-treatment with IFN was more effective than single courses in preventing HCC appearance. However, in these studies^[21-24], the vast majority of patients had chronic hepatitis and no conclusions could be drawn on cirrhotic patients. We extended those observations to patients with HCV related cirrhosis. In accordance with a previous study^[1], a single course of IFN did not seem to be protective toward HCC appearance in a long term follow-up. In fact, in the two nonresponder patients of OTCG, HCC developed after about 50 mo, suggesting that the protective effect of IFN may vanish over time. This hypothesis is strengthened by the observation that re-treatment of nonresponders in the TG prevented HCC development during the 5 years of follow-up.

It is interesting to note that no statistically significant difference was observed in survival between TG and OTCG. This may suggest that the addition of ribavirin to IFN did not add any significant benefit in cirrhotics. However, the number of patients was probably not sufficient to appreciate any possible difference coming from the higher rate of sustained response obtained with the combination treatment. However, it remains that the key to HCC prevention is treatment with interferon that might be helpful even after a curative resection of HCC^[25].

Our study also showed that AgNOR-PI was a useful marker of hepatocyte regeneration which is able to predict a possible evolution to HCC. Furthermore, the two patients who developed HCC in the OTCG were those with the highest AgNOR-PI without improvement after treatment. This underlines the relevance of the index in the clinical setting, particularly in nonresponders to IFN. In fact, it may restrict the need of a strict surveillance only to those patients with a higher risk of developing HCC.

Previous observations with different techniques^[26-29] have shown that high hepatocyte proliferation is associated with HCC development. A recent paper evaluating nucleolar hypertrophy in patients with HBV and HCV related cirrhosis reported the index was significantly predictive of HCC development only in patients with HBV related cirrhosis^[30]. In patients with HCV related cirrhosis the index was not significantly related with HCC development, although a trend could be appreciated. A much larger and more homogeneous population of patients with HCV related cirrhosis (only Child A) in our study could account for the different results between the two studies.

In conclusion, the preventive effect of IFN on HCC development in HCV related cirrhosis is confirmed. Furthermore, a more efficacious treatment associated with re-treatment courses of nonresponders seems to produce the best results in term of HCC prevention. AgNOR-PI is a useful marker of hepatocyte proliferation that identifies patients at higher risk of developing HCC.

REFERENCES

- 1 **Nishiguchi S**, Kuroki T, Nakatani S, Morimoto H, Takeda T, Nakajima S, Shiomi S, Seki S, Kobayashi K, Otani S. Randomised trial of effects of interferon-alpha on incidence of hepatocellular carcinoma in chronic active hepatitis C with cirrhosis. *Lancet* 1995; **346**: 1051-1055
- 2 **Mazzella G**, Accogli E, Sottili S, Festi D, Orsini M, Salzetta A, Novelli V, Cipolla A, Fabbri C, Pezzoli A, Roda E. Alpha inter-

- feron treatment may prevent hepatocellular carcinoma in HCV-related liver cirrhosis. *J Hepatol* 1996; **24**: 141-147
- 3 **Bruno S**, Silini E, Crosignani A, Borzio F, Leandro G, Bono F, Asti M, Rossi S, Larghi A, Cerino A, Podda M, Mondelli MU. Hepatitis C virus genotypes and risk of hepatocellular carcinoma in cirrhosis: a prospective study. *Hepatology* 1997; **25**: 754-758
 - 4 **Fattovich G**, Giustina G, Degos F, Tremolada F, Diodati G, Almasio P, Nevens F, Solinas A, Mura D, Brouwer JT, Thomas H, Njapoum C, Casarin C, Bonetti P, Fuschi P, Basho J, Tocco A, Bhalla A, Galassini R, Noventa F, Schalm SW, Realdi G. Morbidity and mortality in compensated cirrhosis type C: a retrospective follow-up study of 384 patients. *Gastroenterology* 1997; **112**: 463-472
 - 5 International Interferon-alpha Hepatocellular Carcinoma Study Group. Effect of interferon-alpha on progression of cirrhosis to hepatocellular carcinoma: a retrospective cohort study. *Lancet* 1998; **351**: 1535-1539
 - 6 **Imai Y**, Kawata S, Tamura S, Yabuuchi I, Noda S, Inada M, Maeda Y, Shirai Y, Fukuzaki T, Kaji I, Ishikawa H, Matsuda Y, Nishikawa M, Seki K, Matsuzawa Y. Relation of interferon therapy and hepatocellular carcinoma in patients with chronic hepatitis C. *Ann Intern Med* 1998; **129**: 94-99
 - 7 **Gramenzi A**, Andreone P, Fiorino S, Camma C, Giunta M, Magalotti D, Cursaro C, Calabrese C, Arienti V, Rossi C, Di Febo G, Zoli M, Craxi A, Gasbarrini G, Bernardi M. Impact of interferon therapy on the natural history of hepatitis C virus related cirrhosis. *Gut* 2001; **48**: 843-848
 - 8 **Serfaty L**, Aumaitre H, Chazouilleres O, Bonnand AM, Rosmorduc O, Poupon RE, Poupon R. Determinants of outcome of compensated hepatitis C virus-related cirrhosis. *Hepatology* 1998; **27**: 1435-1440
 - 9 **Sofia S**, Casali A, Buscarini E, Castagnetti E, Rapaccini GL, Levantesi L, Salmi A, Boccia S, Miglio F, Ricca Rossellini S, Bolondi L. Effect of lymphoblastoid IFN in the treatment of liver cirrhosis and prevention of HCC. *Ital J Gastroenterol Hepatol* 1998; **30**: A67
 - 10 **Benvengnu L**, Chemello L, Noventa F, Fattovich G, Pontisso P, Alberti A. Retrospective analysis of the effect of interferon therapy on the clinical outcome of patients with viral cirrhosis. *Cancer* 1998; **83**: 901-909
 - 11 **Shioda A**, Moriyama M, Kaneko M, Shimizu T, Gotou I, Tanaka N, Ookubo H, Arakawa Y. Long term prognosis of hepatocellular carcinoma developing after treatment of interferon in patients with chronic hepatitis C and liver cirrhosis. *Hepatology* 1999; **30**: A268
 - 12 **Yoshida H**, Shiratori Y, Moriyama M, Arakawa Y, Ide T, Sata M, Inoue O, Yano M, Tanaka M, Fujiyama S, Nishiguchi S, Kuroki T, Imazeki F, Yokosuka O, Kinoyama S, Yamada G, Omata M. Interferon therapy reduces the risk for hepatocellular carcinoma: national surveillance program of cirrhotic and noncirrhotic patients with chronic hepatitis C in Japan. IHIT Study Group. Inhibition of Hepatocarcinogenesis by Interferon Therapy. *Ann Intern Med* 1999; **131**: 174-181
 - 13 **Mura D**, Delliperi R, Fastame L, Carlini A, Cussu PA, Pisanu G, Dore MP, Realdi G. Five years follow-up after interferon therapy in HCV positive compensated cirrhosis. *Ital J Gastroenterol Hepatol* 1998; **30**: A114
 - 14 **Valla DC**, Chevallerier M, Marcellin P, Payen JL, Trepo C, Fonck M, Bourliere M, Boucher E, Miguet JP, Parlier D, Lemonnier C, Opolon P. Treatment of hepatitis C virus-related cirrhosis: a randomized, controlled trial of interferon alfa-2b versus no treatment. *Hepatology* 1999; **29**: 1870-1875
 - 15 **Ikeda K**, Saitoh S, Arase Y, Chayama K, Suzuki Y, Kobayashi M, Tsubota A, Nakamura I, Murashima N, Kumada H, Kawanishi M. Effect of interferon therapy on hepatocellular carcinogenesis in patients with chronic hepatitis type C: A long-term observation study of 1,643 patients using statistical bias correction with proportional hazard analysis. *Hepatology* 1999; **29**: 1124-1130
 - 16 **Camma C**, Giunta M, Andreone P, Craxi A. Interferon and prevention of hepatocellular carcinoma in viral cirrhosis: an evidence-based approach. *J Hepatol* 2001; **34**: 593-602
 - 17 **Davis GL**. Combination treatment with interferon and ribavirin for chronic hepatitis C. *Clin Liver Dis* 1999; **3**: 811-826
 - 18 **Vroljik JM**, Bekkering FC, Brouwer JT, Hansen BE, Schalm SW. High sustained virological response in chronic hepatitis C by combining induction and prolonged maintenance therapy. *J Viral Hepat* 2003; **10**: 205-209
 - 19 **McHutchison JG**, Fried MW. Current therapy for hepatitis C: pegylated interferon and ribavirin. *Clin Liver Dis* 2003; **7**: 149-161
 - 20 **Ploton D**, Menager M, Jeannesson P, Himber G, Pigeon F, Adnet JJ. Improvement in the staining and in the visualization of the argyrophilic proteins of the nucleolar organizer region at the optical level. *Histochem J* 1986; **18**: 5-14
 - 21 **Hino K**, Kitase A, Satoh Y, Fujiwara D, Yamaguchi Y, Korenaga M, Shingai Y, Konishi T, Yamashita S, Uchida K, Mori K, Hanada H, Kodama T, Nukui K, Okita K. Interferon retreatment reduces or delays the incidence of hepatocellular carcinoma in patients with chronic hepatitis C. *J Viral Hepat* 2002; **9**: 370-376
 - 22 **Tanaka H**, Tsukuma H, Kasahara A, Hayashi N, Yoshihara H, Masuzawa M, Kanda T, Kashiwagi T, Inoue A, Kato M, Oshima A, Kinoshita Y, Kamada T. Effect of interferon therapy on the incidence of hepatocellular carcinoma and mortality of patients with chronic hepatitis C: a retrospective cohort study of 738 patients. *Int J Cancer* 2000; **87**: 741-749
 - 23 **Toyoda H**, Kumada T, Nakano S, Takeda I, Sugiyama K, Kiriya S, Sone Y, Hisanaga Y. The effect of retreatment with interferon-alpha on the incidence of hepatocellular carcinoma in patients with chronic hepatitis C. *Cancer* 2000; **88**: 58-65
 - 24 **Takimoto M**, Ohkoshi S, Ichida T, Takeda Y, Nomoto M, Asakura H, Naito A, Mori S, Hata K, Igarashi K, Hara H, Ohta H, Soga K, Watanabe T, Kamimura T. Interferon inhibits progression of liver fibrosis and reduces the risk of hepatocarcinogenesis in patients with chronic hepatitis C: a retrospective multicenter analysis of 652 patients. *Dig Dis Sci* 2002; **47**: 170-176
 - 25 **Sun HC**, Tang ZY. Preventive treatments for recurrence after curative resection of hepatocellular carcinoma-A literature review of randomized control trials. *World J Gastroenterol* 2003; **9**: 635-640
 - 26 **Tarao K**, Ohkawa S, Shimizu A, Harada M, Nakamura Y, Ito Y, Tamai S, Hoshino H, Inoue T, Kanisawa M. Significance of hepatocellular proliferation in the development of hepatocellular carcinoma from anti-hepatitis C virus-positive cirrhotic patients. *Cancer* 1994; **73**: 1149-1154
 - 27 **Ballardini G**, Groff P, Zoli M, Bianchi G, Giostra F, Francesconi R, Lenzi M, Zauli D, Cassani F, Bianchi F. Increased risk of hepatocellular carcinoma development in patients with cirrhosis and with high hepatocellular proliferation. *J Hepatol* 1994; **20**: 218-222
 - 28 **Sangiovanni A**, Colombo E, Radaelli F, Bortoli A, Bovo G, Casiraghi MA, Ceriani R, Roffi L, Redaelli A, Rossini A, Spinzi G, Minoli G. Hepatocyte proliferation and risk of hepatocellular carcinoma in cirrhotic patients. *Am J Gastroenterol* 2001; **96**: 1575-1580
 - 29 **Donato MF**, Arosio E, Del Ninno E, Ronchi G, Lampertico P, Morabito A, Balestrieri MR, Colombo M. High rates of hepatocellular carcinoma in cirrhotic patients with high liver cell proliferative activity. *Hepatology* 2001; **34**: 523-528
 - 30 **Treà D**, Borzio M, Morabito A, Borzio F, Roncalli M, Derenzini M. Nucleolar hypertrophy correlates with hepatocellular carcinoma development in cirrhosis due to HBV infection. *Hepatology* 2003; **37**: 72-78

Transfection of p27^{kip1} enhances radiosensitivity induced by ⁶⁰Co γ -irradiation in hepatocellular carcinoma HepG₂ cell line

Xiao-Xiang Guan, Long-Bang Chen, Gui-Xia Ding, Wei De, Ai-Hua Zhang

Xiao-Xiang Guan, Long-Bang Chen, Department of Oncology, Jinling Hospital, Nanjing University School of Medicine, Nanjing 210002, Jiangsu Province, China

Gui-Xia Ding, Ai-Hua Zhang, Center of Pediatric Nephrology, Nanjing Medical University, Nanjing 210029, Jiangsu Province, China

Wei De, Institute of Molecular and Cellular Biology, Nanjing Medical University, Nanjing 210029, Jiangsu Province, China

Supported by the National Postdoctor Research Foundation of China, No. 2003034383

Co-correspondents: Ai-Hua Zhang

Correspondence to: Dr. Long-Bang Chen, Department of Oncology, Jinling Hospital, Nanjing University School of Medicine, Nanjing 210002, Jiangsu Province, China. xxguan@hotmail.com

Telephone: +86-25-86062033 **Fax:** +86-25-84801861

Received: 2004-03-27 **Accepted:** 2004-04-13

Abstract

AIM: To study the cell cycle alterations of human hepatoma cell line HepG₂ *in vitro* after ⁶⁰Co γ -irradiation and further to examine the mechanisms underlying the enhancement of radiosensitivity to γ -irradiation in HepG₂ transiently transfected with wild type p27^{kip1}.

METHODS: The proliferation of HepG₂ cells was evaluated with MTT assay, and the cell cycle profile and apoptosis were assessed by cell morphology, DNA fragmentation analysis and flow cytometry. HepG₂ cells were transfected with p27^{kip1} wild type by using Lipofectamine (LF2000), and the expression and subcellular localization of p27^{kip1} in HepG₂ were detected by immunocytochemistry.

RESULTS: ⁶⁰Co γ -irradiation inhibited the growth of HepG₂ cells in a dose-dependent manner. Apoptosis of HepG₂ cells was induced 48 h after γ ray exposure. Furthermore research was carried out to induce exogenous expression of p27^{kip1} in HepG₂. The expression of p27^{kip1} induced G₀/G₁ phase arrest in HepG₂ cells. The overexpression of p27^{kip1} enhanced ⁶⁰Co γ -irradiation-induced radiosensitivity in HepG₂ cells.

CONCLUSION: Overexpression of p27^{kip1} is a rational approach to improve conventional radiotherapy outcomes, which may be a possible strategy for human hepatoma therapy.

Guan XX, Chen LB, Ding GX, De W, Zhang AH. Transfection of p27^{kip1} enhances radiosensitivity induced by ⁶⁰Co γ -irradiation in hepatocellular carcinoma HepG₂ cell line. *World J Gastroenterol* 2004; 10(21): 3103-3106

<http://www.wjgnet.com/1007-9327/10/3103.asp>

INTRODUCTION

Hepatocellular carcinoma (HCC) is a relatively common malignancy, ranking fifth in frequency on a worldwide basis and causing more than one million deaths annually^[1,2] and there has been a progressive increase in the number of hepatoma cases over the past two decades^[3]. Unfortunately, most of the

cases of hepatoma are not curable because extensive resection is not possible. Though many approaches, such as transarterial chemoembolization (TACE), percutaneous ethanol injection (PEI), radiofrequency ablation (RFA), radiotherapy and liver transplantation have been developed to treat it, and the effective and survival rates are increased, a large number of patients would die from recurrence and metastasis^[4-8]. It is well known that improving the overall therapeutic effects of liver cancer depends on the combined therapies. The purpose of combined interventional therapies for HCC is to increase their therapeutic efficiencies and to reduce the side effects and complications.

Radiotherapy presents another interesting option for the treatment of HCC amidst the wide array of non-surgical modalities available^[11] and experimental and clinical studies have been reported that gene therapy is one of the more promising approaches for patients with advanced liver tumours^[9-12].

It is unknown about the combination of radiotherapy and gene therapy, especially the relationship between p27^{kip1} and radiosensitivity, although p27^{kip1} is a target for cancer therapeutics^[13]. p27^{kip1} is a key molecule in cell cycle control because of their specific and periodic expression during cell cycle progression. Knowledge of the function of cell cycle checkpoints in tumour cells may be important to develop treatment strategies for human cancers. Recent studies indicate that mutations in the p27^{kip1} gene have not been seen in many tumors including human hepatoma^[14]. Down-regulation and mislocalization expression of p27^{kip1} have recently been found to be associated with a poor prognosis in patients with hepatoma^[15]. However, the role of p27^{kip1} expression and gamma irradiation-induced apoptosis in human hepatoma cells has not been examined previously.

The purpose of this study was to investigate the function of p27^{kip1} and ⁶⁰Co γ -irradiation in the HepG₂ cell cycle progress and apoptosis, and then to examine the molecular mechanisms of radiosensitivity induced by p27^{kip1} and gamma irradiation in human hepatoma cells, focusing on the possibility that it might act, at least in part, by increasing the expression of p27^{kip1} in human hepatoma cells. This study may help us to understand radiosensitivity and develop a new treatment strategy.

MATERIALS AND METHODS

Reagents

RPMI-1640 medium and Lipofectamine (LF2000) were purchased from GIBCO. Anti-Flag (M2) was purchased from Sigma. FITC conjugated-IgG was purchased from Santa Cruz Biotechnology. The plasmid containing p27^{kip1} was kindly provided by Dr. Keiichi Nakayama at Kyushu University, Japan.

Cells and treatment with gamma-irradiation radiation treatment

Human hepatoma cell line, HepG₂, was routinely maintained in RPMI-1640 medium supplemented with 100 mL/L heat-inactivated fetal bovine serum at the 100 mL/L concentration and incubated in 100 U/mL penicillin-streptomycin in 50 mL/L CO₂ in air at 37 °C with 5 mL/L CO₂. Hepatoma cells were plated into 6-well culture plates (5×10⁴ cells/well) and exposed to 0, 1.0, 2.0, 3.0, 4.0, 5.0 and 6.0 Gy of γ -irradiation from a telecobalt therapy source at a dose rate of 5.0 cGy/minute.

Transient transfection of p27^{kip1}

Transfection of the cells with wild type p27^{kip1} cDNA constructs was performed using Lipofectamine (LF2000) reagent according to the manufacturer's instructions. Briefly, cells were plated in a 6-well plate at a density of 5×10^4 /well and incubated overnight in RPMI-1640 supplemented with 100 mL/L FCS. The cDNA constructs encoding p27^{kip1} were diluted in RPMI-1640 (100 μ L) and then mixed with the transfection solution for 15 min. After washed twice with phosphate-buffered saline (PBS) to remove serum, the cells were incubated with the transfection mixture at 37 °C for 4 h and then refreshed with RPMI-1640 medium.

Proliferation assays

Cell proliferation was measured by MTT assay. After HepG₂ cells were treated with different dose gamma-irradiation for indicated time and dose, then 10 μ L MTT (5 mg/mL) was added to each well and incubated for an additional 4 h, and then the liquid in the wells was evaporated. To dissolve the formazan, 200 μ L of DMSO was added. Control wells were treated with 1 g/L DMSO alone. The absorbance was detected in the microplate reader 550 model at 570 nm wavelength. Growth inhibition was equal to (1-absorbance of the treated wells)/(absorbance of the control wells) \times 100%.

Immunohistochemistry

Immunohistochemical staining was performed to determine the expression of Flag-P27^{kip1} fusion protein. HepG₂ cells transiently expressing p27^{kip1} were grown on a glass coverslip in a 6-well plate for 24 h after transfection. The cells on the coverslips were fixed in 20 g/L paraformaldehyde at room temperature for 5 min on the next day of transfection, and sequentially incubated for 60 min with anti-mouse Flag (M2) and then FITC-conjugated second antibody. The slides were lightly counterstained with Hoechst 33258, washed with water and then mounted. Finally coverslips were mounted with other glass slides, the cells were examined by immunofluorescence microscopy at the excitation/emission wavelengths of 488 nm and 520 nm alternatively.

Flow cytometry analysis

HepG₂ cells were plated onto a 6-well plate (5×10^4 cells/well) in RPMI-1640 containing 100 mL/L FBS and grown overnight to allow cell attachment. They were then treated with irradiation, harvested, fixed with 700 mL/L ethanol, centrifuged, resuspended in 400 μ L of PBS, and 2 mg/mL RNase was added to avoid double-stranded RNA staining, then stained with 400 μ L of 0.1 mg/mL propidium iodide (PI). The cell suspension was filtered through a 60- μ m Spectra/Mesh nylon filter. Samples of 20 000 cells were then analyzed for DNA histograms and cell cycle phase distributions by flow cytometer using a FACSCalibur instrument (Becton Dickinson), and the data were analyzed by a CELLQuest computer program.

DNA fragmentation assay

The integrity of DNA was assessed by agarose gel electrophoresis. Cells (1×10^6) were centrifuged for 5 min at 3 000 r/min, washed once with PBS, and cell pellets were resuspended in 100 μ L of lysis buffer (50 mmol/L Tris-HCl, pH 8.0, 10 mmol/L tetraacetic acid, 4 g/L SDS, 0.5 g/L proteinase K) and incubated for 8 h at 50 °C, then 10 μ L of 0.5 g/L RNase A was added. The samples were incubated for 1 h at 50 °C and heated to 70 °C for 5 min, then 100 μ L of phenol: chloroform:isopropanol (25:24:1) was added. After centrifugation, the supernatants were transferred to new tubes, and twice volume ethanol (ice cold) was added. After centrifugation, the pellets were solubilized in TE buffer and loaded on 18 g/L agarose gel for electrophoresis. The gel was stained with ethidium bromide, and photographed with UV illumination.

Hoechst 33258-propidium iodide counterstaining

Apoptosis and death cells were identified by Hoechst 33258-PI counterstaining^[16]. Briefly, cell pellets (1×10^9) were suspended by 100 μ L PBS containing Hoechst33258 at the concentration of 1 μ L/mL. The cells were incubated at 37 °C for 7 min, and then centrifuged. The cell pellets were resuspended in 100 μ L staining solution containing PI at the concentration of 5 μ g/mL. The stained cells were analyzed using a fluorescence microscope. Samples of 200 cells were then analysed.

Statistical analysis

Data were represented as mean \pm SD. Differences were evaluated by SPSS10.0 software. $P \leq 0.05$ was considered statistically significant.

RESULTS

Growth inhibition of HepG₂ cells by ⁶⁰Co γ -irradiation

The irradiation of HepG₂ cells caused a dose-dependent cell growth inhibition, and a maximum inhibitory effect was observed at 6 Gy. MTT assay showed that irradiation had anti-proliferative effects on HepG₂ cells in a dose-dependant manner. At the dose of 0, 1.0, 2.0, 3.0, 4.0, 5.0 and 6.0 Gy, the inhibitory rate was $2.62 \pm 0.18\%$, $26.85 \pm 0.21\%$, $54.11 \pm 0.47\%$, $57.19 \pm 0.54\%$, $60.26 \pm 0.53\%$ and $67.12 \pm 0.65\%$ respectively (Figure 1). The cell growth inhibitory effect was due to apoptosis or necrosis induced by excessively high dose irradiation. The counterstaining of PI and Hoechst 33258 proved to be an excellent probe to distinguish apoptotic cells from necrotic cells. Live and apoptotic cells were only probed by Hoechst 33258 (blue in color) and exclusion of propidium iodide due to plasma membrane integrity. The morphological features of apoptotic cells were cell shrinkage, nuclear condensation and genomic fragmentation down to the size of individual nucleosome units. On the contrary, necrotic cells were probed by PI (red in colors) (Figure 2). The apoptotic rate reached the top at the dose of 4.0 Gy, when irradiated by 6.0 Gy, most of HepG₂ cells were in necrotic state (Figure 3).

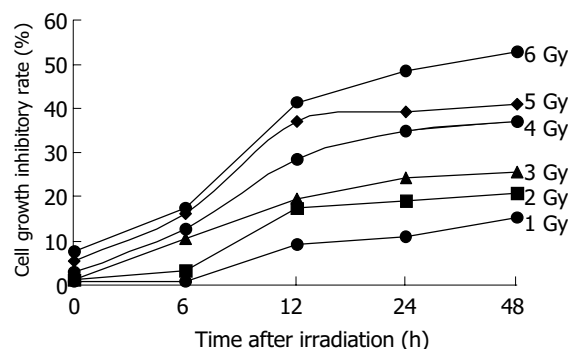


Figure 1 Effect of irradiation on proliferation of HepG₂ cells.

p27^{kip1} expression enhanced radiosensitivity induced by ⁶⁰Co γ -irradiation in HepG₂ cells

Overexpression of p27^{kip1} protein was observed in transfected cells (Figure 4). As a result, the proliferation of HepG₂ cells was greatly inhibited and cell cycle was arrested in G₁ phase after exogenous p27^{kip1} expression (Figure 5). Further results showed that overexpression of p27^{kip1} enhanced radiosensitivity in HepG₂ cells induced by ⁶⁰Co γ -irradiation, and 2.0 Gy irradiation induced maximum apoptotic rate by 40.6% in HepG₂ cells transfected with p27^{kip1}, whereas HepG₂ cells transfected empty vector, only 4.0 Gy reached the maximum apoptotic rate of 35.3% (Figure 6). Apoptosis of HepG₂ cells indicated by flow cytometry and Hoechst33258 staining was then confirmed by DNA fragmentation, which was visualized as the characteristic oligonucleosome-sized fragmentation in ethidium bromide after DNA agarose gel electrophoresis (date not shown).

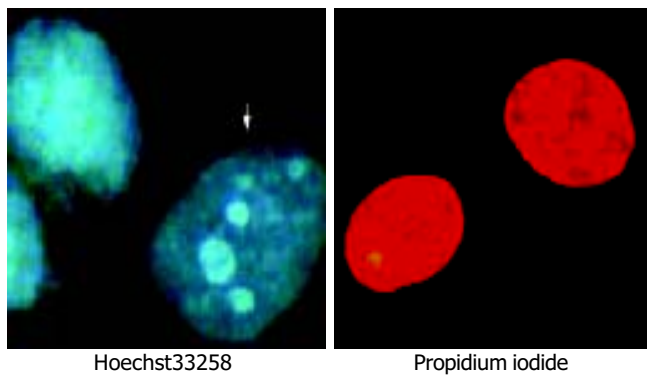


Figure 2 Counterstaining of Hoechst 33258 and propidium iodide to distinguish apoptotic from necrotic cells.

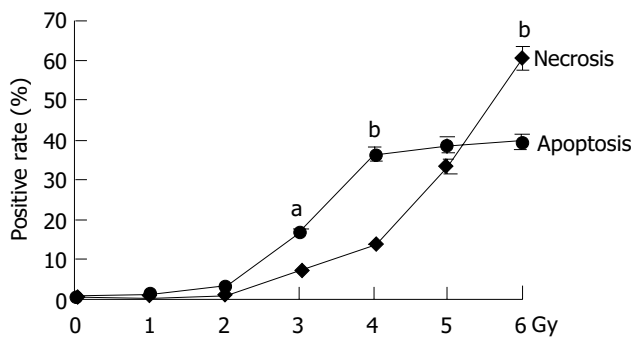


Figure 3 Comparison of apoptosis and necrosis rate of HepG₂ treated by ⁶⁰Co γ -irradiation. ^a $P < 0.05$, ^b $P < 0.01$ vs necrosis.

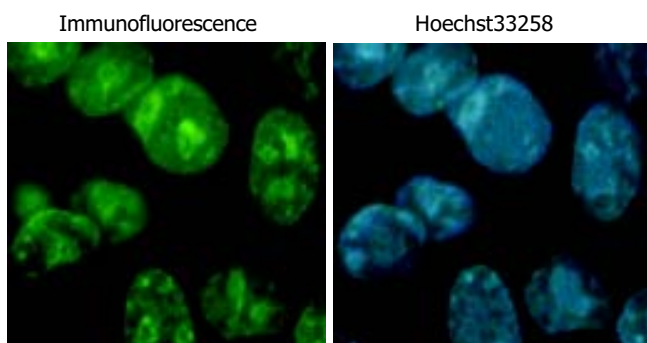


Figure 4 Subcellular localization and expression of p27^{kip1} in transfected HepG₂ cells.

DISCUSSION

HCC remains one of the most difficult tumors to treat. Primary HCC is the second most common cancer and the leading cause of cancer deaths behind gastric cancer in China. Surgical resection has been accepted as the only curative therapy for primary liver cancer. Unfortunately, most patients are surgically unresectable, and are sometimes recommended to receive non-surgical therapies, including radiotherapy, radiofrequency hyperthermia, gene therapy or combination of the above methods. Radiation therapy has been commonly used in the treatment of unamenable human hepatoma. Unfortunately, the cause of this radiosensitization has not met expectations fully. New approaches that may reduce side-effects and provide good quality of life are required. Thus, it is imperative to develop new and effective treatments, such as gene therapy, in order to treat this disease.

Gene therapy is one of the more promising approaches for patients with advanced liver tumour. Experimental and clinical studies have reported that gene therapy and molecular prevention are becoming a part of patient management and

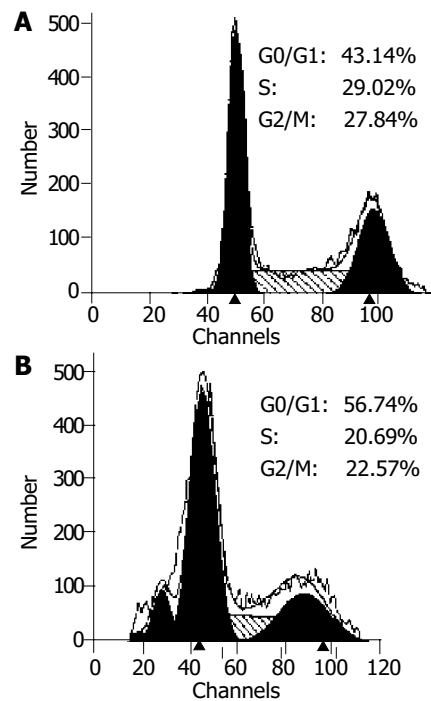


Figure 5 Flow cytometry analysis of cell cycle of nontransfected and transiently transfected HepG₂ cells. A: nontransfected HepG₂ cells. B: p27^{kip1} transiently transfected HepG₂ cells.

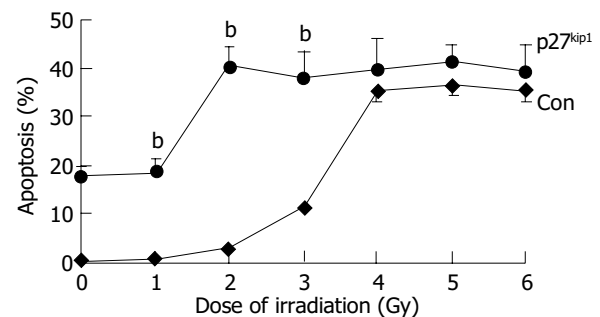


Figure 6 Apoptotic rates induced by γ -irradiation in nontransfected and transfected HepG₂ cells. ^b $P < 0.01$ vs control.

would eventually complement or in part replace the existing therapeutic and preventive strategies^[17]. Recent researches have indicated that p27^{kip1} is a new target for gene therapy and p27^{kip1} is a new suitable candidate for gene therapy^[9,18]. The protein p27^{kip1} is an important factor that regulates cell cycle progression and apoptosis. Mutations in p27^{kip1} gene have not been seen in many tumors including human hepatoma. Down-regulation and mislocalized expression have recently been found to be associated with poor prognosis in patients with hepatoma. Therefore, regulation of p27^{kip1} activity is a new strategy for hepatoma therapy.

Pretreatment of hepatocellular carcinoma cells with overexpression of p27^{kip1} protein before irradiation enhanced the cell-killing effect of irradiation. Interaction with moderate doses of radiation caused a substantial increase in tumor cell killing. The beneficial effect of this interaction was further evidenced by the significant increase in the number of apoptic cells. The HepG₂ cells treated with p27^{kip1} and exposed to 6.0 Gy showed a maximum apoptosis percentage when compared to the other irradiation doses or p27^{kip1} transfection. Our results showed that overexpression of p27^{kip1} could enhance the radiosensitivity in HepG₂ cells. Overexpression of p27^{kip1} in HepG₂ cells could sensitize cells to ionizing radiation. Recent advances have been made in the understanding of molecular

events following cell exposure to ionizing radiation. Our results suggest that p27^{kip1} protein could be used to modulate radio-induced cellular responses.

However, the molecular mechanism of p27^{kip1} in radiosensitivity induced by ⁶⁰Co γ -irradiation is still unclear, and further studies are needed to identify the molecular mechanisms for the radiosensitizing activity, with emphasis on the study of p27^{kip1} in cell cycle progress and radiosensitivity.

Our results here provide some experimental evidences that overexpression of p27^{kip1} increases the radiosensitivity of gamma irradiation. It may help us understand radiosensitivity and develop strategies for liver cancer.

REFERENCES

- 1 **Hao XS**, Chen KX, Wang PP, Rohan T. Changes in survival patterns in urban Chinese patients with liver cancer. *World J Gastroenterol* 2003; **9**: 1212-1215
- 2 **Bosch FX**, Ribes J, Borrás J. Epidemiology of primary liver cancer. *Semin Liver Dis* 1999; **19**: 271-285
- 3 **el-Serag HB**. Epidemiology of hepatocellular carcinoma. *Clin Liver Dis* 2001; **5**: 87-107
- 4 **Hanazaki K**, Kajikawa S, Shimozaawa N, Mihara M, Shimada K, Hiraguri M, Koide N, Adachi W, Amano J. Survival and recurrence after hepatic resection of 386 consecutive patients with hepatocellular carcinoma. *J Am Coll Surg* 2000; **191**: 381-388
- 5 **Takayama T**, Sekine T, Makuuchi M, Yamasaki S, Kosuge T, Yamamoto J, Shimada K, Sakamoto M, Hirohashi S, Ohashi Y, Kakizoe T. Adoptive immunotherapy to lower postsurgical recurrence rates of hepatocellular carcinoma: a randomised trial. *Lancet* 2000; **356**: 802-807
- 6 **Huang YH**, Wu JC, Lui WY, Chau GY, Tsay SH, Chiang JH, King KL, Huo TI, Chang FY, Lee SD. Prospective case-controlled trial of adjuvant chemotherapy after resection of hepatocellular carcinoma. *World J Surg* 2000; **24**: 551-555
- 7 **Tung-Ping Poon R**, Fan ST, Wong J. Risk factors, prevention, and management of postoperative recurrence after resection of hepatocellular carcinoma. *Ann Surg* 2000; **232**: 10-24
- 8 **Keng GH**, Sundram FX. Radionuclide therapy of hepatocellular carcinoma. *Ann Acad Med Singapore* 2003; **32**: 518-524
- 9 **Schmitz V**, Wang L, Barajas M, Gomar C, Prieto J, Qian C. Treatment of colorectal and hepatocellular carcinomas by adenoviral mediated gene transfer of endostatin and angiostatin-like molecule in mice. *Gut* 2004; **53**: 561-567
- 10 **Shiba H**, Okamoto T, Futagawa Y, Ohashi T, Eto Y. Efficient and cancer-selective gene transfer to hepatocellular carcinoma in a rat using adenovirus vector with iodized oil esters. *Cancer Gene Ther* 2001; **8**: 713-718
- 11 **Iwazawa T**, Chau GY, Mori T, Dookeran KA, Rubin JT, Watkins S, Robbins PD, Lotze MT, Tahara H. Potent antitumor effects of intra-arterial injection of fibroblasts genetically engineered to express IL-12 in liver metastasis model of rat: no additional benefit of using retroviral producer cell. *Cancer Gene Ther* 2001; **8**: 17-22
- 12 **Humphreys MJ**, Ghaneh P, Greenhalf W, Campbell F, Clayton TM, Everett P, Huber BE, Richards CA, Ford MJ, Neoptolemos JP. Hepatic intra-arterial delivery of a retroviral vector expressing the cytosine deaminase gene, controlled by the CEA promoter and intraperitoneal treatment with 5-fluorocytosine suppresses growth of colorectal liver metastases. *Gene Ther* 2001; **8**: 1241-1247
- 13 **Sasaki T**, Katayose Y, Suzuki M, Yamamoto K, Shiraso S, Mizuma M, Unno M, Takeuchi H, Lee CT, Matsuno S. Adenovirus expressing mutant p27^{kip1} enhanced apoptosis against cholangiocarcinoma than adenovirus-p27^{kip1} wild type. *Hepatogastroenterology* 2004; **51**: 68-75
- 14 **Ponce-Castaneda MV**, Lee MH, Latres E, Polyak K, Lacombe L, Montgomery K, Mathew S, Krauter K, Sheinfeld J, Massague J. p27^{Kip1}: chromosomal mapping to 12p12-12p13.1 and absence of mutations in human tumors. *Cancer Res* 1995; **55**: 1211-1214
- 15 **Fiorentino M**, Altamari A, Ravaioli M, Gruppioni E, Gabusi E, Corti B, Vivarelli M, Bringuier PP, Scoazec JY, Grigioni WF, D'Errico-Grigioni A. Predictive value of biological markers for hepatocellular carcinoma patients treated with orthotopic liver transplantation. *Clin Cancer Res* 2004; **10**: 1789-1795
- 16 **Darzynkiewicz Z**, Bruno S, Del Bino G, Gorczyca W, Hotz MA, Lassota P, Traganos F. Features of apoptotic cells measured by flow cytometry. *Cytometry* 1992; **13**: 795-808
- 17 **Blum HE**. Molecular therapy and prevention of hepatocellular carcinoma. *Hepatobiliary Pancreat Dis Int* 2003; **2**: 11-22
- 18 **Katner AL**, Gootam P, Hoang QB, Gnarr JR, Rayford W. A recombinant adenovirus expressing p7(Kip1) induces cell cycle arrest and apoptosis in human 786-0 renal carcinoma cells. *J Urol* 2002; **168**: 766-773

Edited by Zhang JZ and Wang XL Proofread by Xu FM

Nude mice model of human hepatocellular carcinoma via orthotopic implantation of histologically intact tissue

Yong-Shun Gao, Xiao-Ping Chen, Kai-Yan Li, Zai-De Wu

Yong-Shun Gao, Xiao-Ping Chen, Zai-De Wu, Hepatic Surgery Center, Tongji Hospital, Tongji Medical College, Huazhong University of Science and Technology, Wuhan 430030, Hubei Province, China
Kai-Yan Li, Department of Ultrasonography, Tongji Hospital, Tongji Medical College, Huazhong University of Science and Technology, Wuhan 430030, Hubei Province, China

Supported by the Science and Technology Special Fund of Ministry of Public Health, No. WKZ-2000-1-15; the Key Clinic Programs of Ministry of Public Health, No. 2001-2003

Correspondence to: Xiao-Ping Chen, M.D., Professor and Chairman, Department of Surgery, Tongji Hospital, Tongji Medical College, Huazhong University of Science and Technology, Wuhan 430030, Hubei Province, China. chenxp-53@sina.com

Telephone: +86-27-83662599 **Fax:** +86-27-83662851

Received: 2003-11-13 **Accepted:** 2003-12-16

Abstract

AIM: To establish a nude mice model of human hepatocellular carcinoma (HCC) via orthotopic implantation of histologically intact tissue, in order to study biologic features of HCC *in vivo* and to direct clinical treatment respectively.

METHODS: Histologically intact fresh specimens of HCC were orthotopically implanted in nude mice (BALB/c, nu/nu). Survival rate and growth curve were investigated with B-ultrasound. Morphological characteristics of pathology and spontaneous metastatic rates were detected with microscopy. Expression of multidrug resistance genes studied with immunohistochemical method and RT-PCR, and other biologic features of implanted tumor were observed and compared with human HCC specimens.

RESULTS: Out of the specimens from two patients with HCC, only one specimen survived in nude mice. The orthotopic implantation tumor survival rate, spontaneous intrahepatic metastatic rate, pulmonary metastatic rate and bone metastases rate were 100%, 75.0%, 37.5% and 37.5% respectively in the first passage. AFP was kept on secreting and increasing with the size of the tumor. The morphological characteristics and biologic features were similar to the donor's, the protein and mRNA of MDR1 and LRP were expressed in tumors of the model and the donor, and there was no significant difference between them ($P > 0.05$).

CONCLUSION: The model of nude mice with orthotopic implantation of histologically intact HCC tissue is an ideal model to study biologic features of HCC *in vivo* and to direct clinical treatment.

Gao YS, Chen XP, Li KY, Wu ZD. Nude mice model of human hepatocellular carcinoma via orthotopic implantation of histologically intact tissue. *World J Gastroenterol* 2004; 10 (21): 3107-3111

<http://www.wjgnet.com/1007-9327/10/3107.asp>

INTRODUCTION

Liver cancer is one of the most common carcinomas, the highest

age-standardised mortality rate in China, and accounts for 53% of all liver cancer deaths worldwide^[1,2]. Surgical resection has been accepted as the best treatment for hepatocellular carcinoma (HCC). However, recurrence and metastases and non-sensitivity to chemotherapy remain the major obstacles for further prolonging survival after resection^[3]. Study of HCC, therefore, has become an important issue. But the experiments can not be done on patients with HCC. So human HCC model in nude mice is needed for the study of HCC and its mechanism, chemotherapy, multidrug resistance (MDR), etc.

Shimosato *et al.*^[4,5] established a series of human tumors in nude mice including the human HCC nude mice model for study of alpha-fetoprotein (AFP) in relation to tumor growth in 1976. Liu *et al.*^[6] established a nude mice xenograft model from human HCC in 1995. Leveille-Webster *et al.*^[7] established an intrahepatic xenograft of human HCC in severe combined immunodeficiency mice for the study of multidrug resistance in 1996. Sun *et al.*^[8,9] reported a metastatic human HCC model in nude mice with 100% of spontaneous metastases to lung, lymph node and liver. Peng *et al.*^[10] established a human HCC model in nude mice using orthotopic implantation and observed malignant behavior. Tao *et al.*^[11] established a human HCC in nude mice model using SMMC-LTNM tumor transplanted into abdominal cavity and liver, the lung metastatic rate was 59%. Genda *et al.*^[12] reported the construction of metastatic models using orthotopic implantation of human HCC cell lines into livers of SCID mice, two of the 5 cell lines injected showed vascular tumor thrombi and intrahepatic metastases. Zheng *et al.*^[13] established an orthotopic implantation tumor model from the subcutaneous model of human HCC in nude mice, the spontaneous metastatic rate was 57.8%. Shi *et al.*^[14] established a human HCC model in nude mice with a high metastatic rate in lymph node.

Metastatic models constructed in nude mice by orthotopic implantation of histologically intact patient specimens have been used in Hoffman's group, and several such models including cancers of the lung, pancreas and ovarium, have been reported^[15-17]. However, patient-like human HCC model in nude mice with metastatic behaviors was not found. After the study on HCC cell lines and subcutaneous HCC model in nude mice, we established a patient-like human HCC model with spontaneous metastases in liver, lung and bones.

MATERIALS AND METHODS

Mice

There to four weeks BALB/c, nu/nu, nude mice (Experimental Animal Center, Tongji Medical College, Huazhong University of Science and Technology, Wuhan), weighting 10.1-16.0 g, were used in this study.

Surgical specimens of human HCC

Fresh surgical specimens were obtained from 2 patients with HCC who underwent surgery at the Hepatic Surgery Center, Tongji Hospital, Tongji Medical College, Huazhong University of Science and Technology. The specimens were rinsed and preserved in saline at 4-8 °C and sent to the Experimental Animal Center as soon as possible. After necrotic tissue and non-

cancerous tissue of the specimens were removed, the remaining cancerous tissues were cut into small pieces of about 1 mm³ in size.

Implantation procedure

Tumor pieces were implanted into the livers of nude mice. A left subcostal incision was made under anaesthesia with 200 g/L urethane. The left lobe of the liver was exposed and the liver capsule was mechanically injured with needle. Then one or two pieces of tumor tissue were filled into the liver tissue with forceps which could be seen as a white spot and abdominal wall was finally closed. Mice were kept in laminar-flow cabinets under specific-pathogen-free conditions.

Evaluation of growth and metastases

Nude mice were weighted and the size of tumors was weekly measured with B-ultrasound from 2 to 9 wk after orthotopic implantation. Tumor size (mm³) was evaluated by measurement of two diameters with B-ultrasound and using the formula $1/2 LW^2$, where L is the longest diameter and W is the shortest diameter. Bone metastases was detected with SPECT 8 wk after implantation and then other organ metastases was detected with autopsy and microscopy when the mice were killed. The liver, lymph node, lungs, and bone suspected of metastases were collected and processed for routine gross and microscopic examination. Metastases was diagnosed if at least one microscopic metastatic lesion was found in any resected organ.

Serum detection

AFP in serum from tail vein was detected every two weeks, and hepatitis virus-B surface antigen (HBsAg), antibody to hepatitis virus-B surface (HBsAb), hepatitis virus-B e antigen (HBeAg), antibody to hepatitis virus-B e (HBeAb) and antibody to hepatitis virus-B core (HBcAb) of serum from heart blood were detected after mice were killed (ELISA assay).

Immunohistochemical studies

Expression of MDR1 and LRP was studied by using mouse anti-human MDR1 C219 and LRP monoclonal antibodies (neomarkers) respectively. Tumor tissues from patients with HCC and mice carrying human HCC were fixed in formalin and embedded in paraffin. Sections of 5 μm were assayed for MDR1 and LRP expression by immunoperoxidase staining with the SP method (SP kit, Zhongshan Biocompany, China).

Table 1 Primers for MDR1 and LRP

Gene	Size (bp)	Quantification method	Sequence (5'-3')
B-actin	530	Forward primer	GTGCGTGACATTAAGGAG
		Reverse primer	CTAAGTCATAGTCCGCCT
MDR1	174	Forward primer	CATTGGTGTGGTGAGTCAGG
		Reverse primer	CTCTCTCTCCAACCAGGGTG
LRP	237	Forward primer	TAAGGGCTTCCAGCACCAAC
		Reverse primer	GGAGTTCTCGCTTCTCGTCC

Detection of MDR1 and LRP expression by RT-PCR

Total RNA was extracted from tumors of nude mice and patients using Trizol (Promega) according to the manufacturer's instructions. Reverse transcription (RT) was performed with random primers using a complementary DNA (cDNA) synthesis kit (promega). Following RT-reaction reagents were added: 2 μL MgCl₂ (50 mmol/L), 2 μL RT buffer (Tris-HCL pH 8.3), 2 μL deoxynucleotide mixture (100 mmol/L), 0.5 μL RNase (20 units), 1 μL M-MLV reverse transcriptase, 1 μL of random primers (500 μg/mL) and 5 μg substrate RNA. The final volume of RT-reaction (25 μL) was completed with RNase free water. First strand cDNA synthesis was carried out at 37 °C for 60 min in a

DNA thermal cycler. Afterwards, the tubes were incubated at 95 °C for 5 min to terminate the reaction. Then each tube was kept at -20 °C until PCR was performed. Primers of the target gene MDR1, LRP and endogenous reference GAPDH were designed using the Primer Express software (Applied Biosystems) (Table 1). The final volume of PCR reaction (50 μL) was completed including an initial phase at 94 °C for 4 min, and followed by 30 cycles at 94 °C for 1 min, and at 56 °C for 45 s, at 72 °C for 45 s, and finally at 72 °C for 10 min.

Statistical analysis

Data were presented as mean±SD and analyzed with SPSS11.0. $P < 0.05$ was considered statistically significant.

RUSULTS

Establishment of patient-like metastatic HCC model

Human HCC model of orthotopic implantation was successfully established in nude mice with histologically intact tissues. Out of the 2 specimens from 2 patients with HCC, only one specimen from a 39-year-old man with HCC was at Edmonson grade II-III, whose serum AFP (1 746 ng/mL), HBsAg, HBeAg, HBcAb were all positive, and he had extensive intrahepatic metastases but no hilus hepatis lymph node metastases during operation. Bone metastases were found in the patient one month after operation. Two weeks after implantation, all the livers of 8 nude mice gave rise to tumors and the size of tumors was observed every week with B-ultrasound or by autopsy after they were killed. (Figures 1-3).



Figure 1 Ultrasonic image of implanted tumors in nude mice liver.



Figure 2 Implanted tumors in nude mice liver by autopsy.

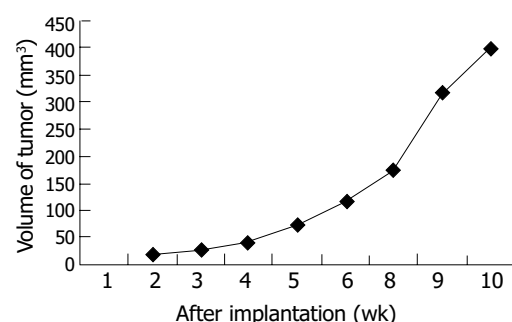


Figure 3 Relation between volume of implanted tumor and time after implantation.



Figure 4 Implanted tumor in nude mice liver metastases to lungs. The first passage just formed a few metastatic lesions A; The 4th passage formed multiple metastatic lesions B; and metastatic lesions in lungs were found under microscope C.

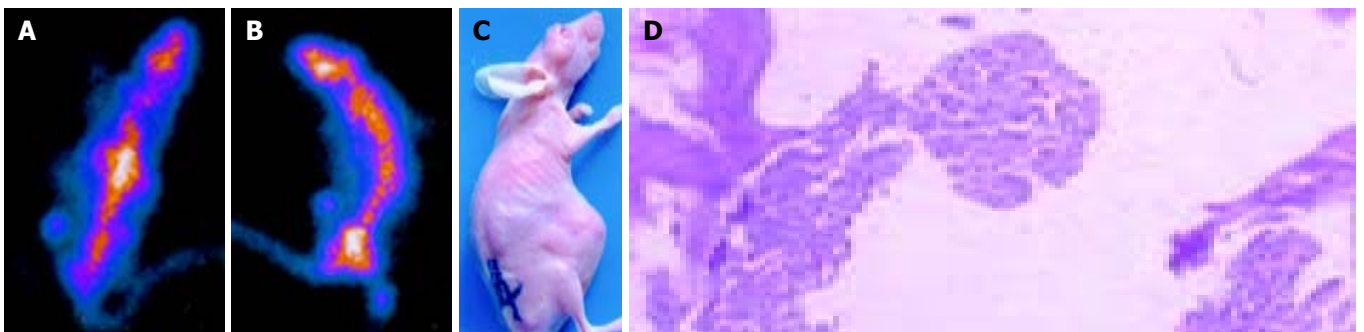


Figure 5 Implanted tumor in nude mice liver spontaneously metastasized to bone. The first passage metastasized to vertebra thoracica just as the donor A, and the 4th passage showed multiple bone metastases B, C. Metastatic lesions were shown in bones under microscope D.

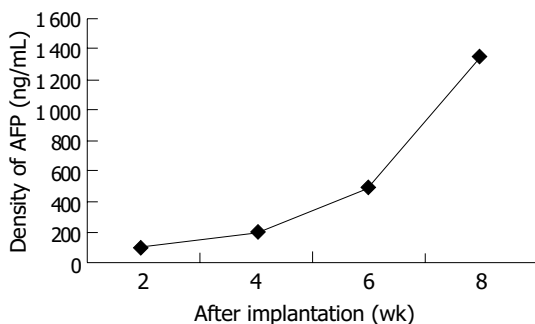


Figure 6 Relation between density of AFP in serum and time of tumor after implantation.

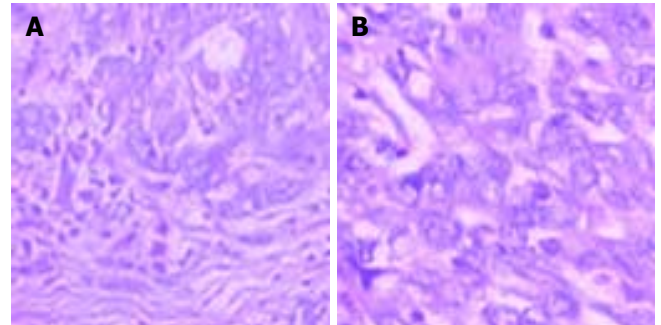


Figure 7 Edmonson grade II-III HCC specimen from patients A and in tumor tissue from nude mice model B.

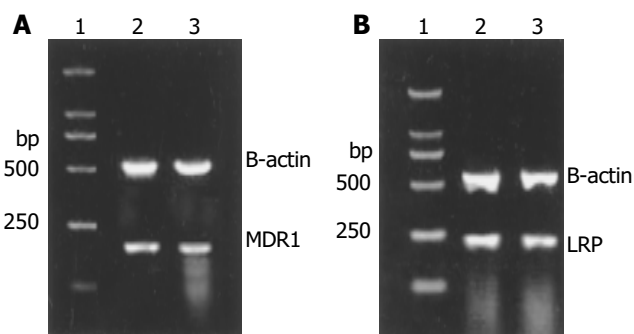


Figure 8 MDR1 and LRP expressed in tumors of the donor (2) and the nude mice model (3), and the expression had no significant difference between both. A: MDR1 expressed in tumors. B: LRP expressed in tumors.

The tumor behavior of this model was the same as the tumor in the patient who donated the specimen. Nine weeks after

implantation, the 8 nude mice with normal weight were killed by drawing blood from heart. According to autopsy and microscopic examination, implanted tumor survived in all nude mice (8/8), intrahepatic invasion was seen in all nude mice (8/8), intrahepatic metastases was seen 75% (6/8) (Figure 2), lung metastases was seen in 3 nude mice (35.5%) (Figure 4), the wound seeding was seen in all mice (8/8), and bone metastases occurred in 35.5% (3/8) (Figure 5), but lymph node metastases was not found.

Findings in serum

Serum AFP was detected from tail blood of nude mice (Figure 6), but all markers of hepatitis were negative.

Histological findings

Histological characteristics of the model tumor were similar to those of the donor's tumor (Figure 7).

Immunohistochemistry and RT-PCR results (Figure 8, Table 2)

Table 2 Expression of MDR1 and LRP in HCC from donor and nude mice

	Immunohistochemistry (%)		mRNA of RT-PCR (%)	
	MDR1	LRP	Mdr1	LRP
Donor	31.26	27.18	61.47	56.71
Nude mice	29.20±2.81	25.44±2.43	65.42±13.59	58.63±9.37
<i>t</i>	2.077	2.030	0.823	2.288
<i>P</i>	0.076	0.080	0.438	0.056

DISCUSSION

Subcutaneous tumor implantation has been used as a standard method to establish animal models of human cancer^[18,19]. Although such models help to understand the nature of human cancers and their therapeutic approaches, but many problems still remain unsolved. One major problem is that the tumor which was derived from a patient and implanted subcutaneous into an immunodeficient animal no longer behaves as it did in the patient. Although the tumor could sometimes grow subcutaneously, it was encapsulated and usually failed to metastasize either regionally or at distant site^[19].

Recently, a new strategy of "orthotopic implantation" has been used to develop rodent models of metastatic human cancer^[19,20]. In the first generation of these models, cell lines or disaggregated cells were injected into the organ of mice that corresponded to the organ from which human tumor was derived. This method allowed metastases to occur at least in certain cases^[19,21-23]. The cell line and disaggregated cells used for orthotopic implantation were obtained by disrupting the original structure of human tumor tissue, which might lead to a change in nature and biological behavior and could be the basis of the greatly reduced metastases rate^[24]. Holfman^[25] developed an orthotopic implantation model utilizing intact tissues obtained directly from surgery. This approach has yielded a high survive rate and frequent metastases in cancers of the colon^[26], bladder^[24], lung^[27], pancreas^[28], prostate^[29] and stomach^[30]. These models of human cancer in nude mice could show various manifestations similar to tumor behavior in patients.

However, it remains difficult to obtain satisfactory models for human cancers in nude mice, particularly with regard to spontaneous metastases and reduction of the latent period when cell suspension or histologically intact tissues were used for orthotopic implantation, which could not really reflect the nature of HCC of patients and preclude *in vivo* effective study of important events including spontaneous metastases and multidrug resistance. Therefore, our approach includes the selection of highly invasive and intrahepatic metastases of human HCC samples and orthotopic transplantation of histologically intact tissues into 3-4 wk old nude mice. In the first generation, the result demonstrated that the specimen from the 39-year-old patient with HCC gave rise to growth of tumor at the implantation site in all the 8 nude mice 2 wk after implantation. In the course of the study, lung and bone metastases were found in the patient donating specimens 1 mo after operation. So we began to pay attention to nude mice in terms of metastases. Fortunately, metastases occurred in all the mice 7-8 wk after implantation, 3 (3/8) had lung metastases, and 3 (3/8) had spontaneous bone metastases, and all had wound seeding and intrahepatic invasion. Lymph node metastases, however, was not found. Spontaneous metastases of human cancer xenografts in nude mice was rare^[9,11]. We believe the reasons of cancer growth and metastases in nude mice were that the specimen selected was highly metastatic and that the nude mice were younger (3-4 wk) than those used in other studies^[13,31]. But metastases was not found in all the mice. We believe the reasons might be that the time after implantation was not so

long that the metastases could not occur in each one, and that it was related to the methods detecting the metastases. So in the 2-4 passages, the nude mice carrying implantation tumor were not killed until they developed signs of distress so as to give full time to metastases and to observe the nature of the tumor. As a result, intrahepatic, lung and bone metastases and wound seeding and multiple metastatic sites in those organs were surprisingly observed in all nude mice over a period ranging 5-16 wk after implantation. Besides selection of the highly invasive and metastatic samples and age of the nude mice, we think there were two key factors, one was that we selected and isolated more higher metastatic subpopulation from the parent tumor, and the other was that a long time could give chance to implanted tumor to metastasize.

As shown in the results, the expression of AFP, MDR1, and LRP was well maintained in locally growing tumor tissues as well as in metastases. These results indicated that this nude mice model represented the majority of biological natures including local invasion, spontaneous lung, bone and intrahepatic metastases, MDR and secreted AFP, suggesting that our model indeed has some features resembling the natural biological behaviors of human HCC.

Although spontaneous metastases models of HCC have been established in nude mice, but bone metastases and MDR studies are not available. Our model well maintained the native structure of HCC and exhibited spontaneous lung metastases, especially spontaneous bone metastases and expression of MDR just as the patient donating the specimen. Thus, this model represents the features of patients with HCC, and could be an interesting tool for studying human HCC.

REFERENCES

- Zhang S, Li L, Lu F. Mortality of primary liver cancer in China from 1990 through 1992. *Zhonghua Zhongliu Zazhi* 1999; **21**: 245-249
- Pisani P, Parkin DM, Bray F, Ferlay J. Estimates of the world-wide mortality from 25 cancers in 1990. *Int J Cancer* 1999; **83**: 18-29
- Chen XP, Wu ZD, Qiu FZ. The history, present and prospect of the surgical treatment of primary liver cancer in China. *Zhongguo Puwai Jichu Yu Linchuang Zazhi* 2000; **4**: 257-258
- Shimosato Y, Kameya T, Nagai K, Hirohashi S, Koide T, Hayashi H, Nomura T. Transplantation of human tumors in nude mice. *J Natl Cancer Inst* 1976; **56**: 1251-1260
- Hirohashi S, Shimosato Y, Kameya T, Koide T, Mukojima T, Taguchi Y, Kageyama K. Production of alpha-fetoprotein and normal serum proteins by xenotransplanted human hepatomas in relation to their growth and morphology. *Cancer Res* 1979; **39**: 1819-1828
- Liu X, Hu J, Cui H, Yang X, Li S. Establishment and biological characteristics of the nude mice xenograft model from human hepatocellular carcinoma. *Zhongguo Yixue Kexueyuan Xuebao* 1995; **17**: 98-103
- Leveille-Webster CR, Arias IA. Establishment and serial quantification of intrahepatic xenografts of human hepatocellular carcinoma in severe combined immunodeficiency mice, and development of therapeutic strategies to overcome multidrug resistance. *Clin Cancer Res* 1996; **2**: 695-706
- Sun FU, Tang Z, Liu K. Growth pattern and metastatic behavior of orthotopically metastatic model of human hepatocellular carcinoma in nude mice. *Zhonghua Yixue Zazhi* 1995; **75**: 673-675
- Sun FX, Tang ZY, Lui KD, Ye SL, Xue Q, Gao DM, Ma ZC. Establishment of a metastatic model of human hepatocellular carcinoma in nude mice via orthotopic implantation of histologically intact tissues. *Int J Cancer* 1996; **66**: 239-243
- Peng BG, Ding J, Lü MD, Cheng LJ, Huang JF, Lu LJ. A model of transplantation of human hepatocellular carcinoma in mouse: its establishment and characterization. *Zhongshan Yike Daxue Xuebao* 1996; **17**(Suppl): 7-10

- 11 **Tao WZ**, Zheng WQ, Gong ZJ. The tumor invasion and metastasis in the transplantation of transplanted human hepatocellular carcinoma into nude mice abdominal cavity and orthotopic hepatic tissue. *Dier Junyi Daxue Xuebao* 1998; **19**: 54-56
- 12 **Genda T**, Sakamoto M, Ichida T, Asakura H, Kojiro M, Narumiya S, Hirohashi S. Cell motility mediated by rho and Rho-associated protein kinase plays a critical role in intrahepatic metastasis of human hepatocellular carcinoma. *Hepatology* 1999; **30**: 1027-1036
- 13 **Zheng JM**, Tao WZ, Zheng WQ, Bao JZ, Wang YL, Zhu MH. Establishment of the orthotopic transplantation tumor model from the subcutaneous model of human hepatocellular carcinoma in nude mice. *Dier Junyi Daxue Xuebao* 2000; **21**: 456-459
- 14 **Shi CH**, Wang XW, Wang WY, Shi XY, Zhu DS. Experimental study on a human hepatocellular carcinoma model using orthotopic transplantation. *Zhongguo Shiyen Dongwu Xuebao* 2001; **9**: 57-61
- 15 **Fu X**, Guadagni F, Hoffman RM. A metastatic nude-mouse model of human pancreatic cancer constructed orthotopically with histologically intact patient specimens. *Proc Natl Acad Sci U S A* 1992; **89**: 5645-5649
- 16 **Wang X**, Fu X, Hoffman RM. A patient-like metastasizing model of human lung adenocarcinoma constructed via thoracotomy in nude mice. *Anticancer Res* 1992; **12**: 1399-1401
- 17 **Fu X**, Hoffman RM. Human ovarian carcinoma metastatic models constructed in nude mice by orthotopic transplantation of histologically-intact patient specimens. *Anticancer Res* 1993; **13**: 283-286
- 18 **Fidler IJ**. Rationale and methods for the use of nude mice to study the biology and therapy of human cancer metastasis. *Cancer Metastasis Rev* 1986; **5**: 29-49
- 19 **Fidler IJ**. Critical factors in the biology of human cancer metastasis: twenty-eighth G.H.A. Clowes memorial award lecture. *Cancer Res* 1990; **50**: 6130-6138
- 20 **Manzotti C**, Audisio RA, Pratesi G. Importance of orthotopic implantation for human tumors as model systems: relevance to metastasis and invasion. *Clin Exp Metastasis* 1993; **11**: 5-14
- 21 **Giavazzi R**, Jessup JM, Campbell DE, Walker SM, Fidler IJ. Experimental nude mouse model of human colorectal cancer liver metastases. *J Natl Cancer Inst* 1986; **77**: 1303-1308
- 22 **Bresalier RS**, Raper SE, Hujanen ES, Kim YS. A new animal model for human colon cancer metastasis. *Int J Cancer* 1987; **39**: 625-630
- 23 **Morikawa K**, Walker SM, Nakajima M, Pathak S, Jessup JM, Fidler IJ. Influence of organ environment on the growth, selection, and metastasis of human colon carcinoma cells in nude mice. *Cancer Res* 1988; **48**: 6863-6871
- 24 **Fu XY**, Theodorescu D, Kerbel RS, Hoffman RM. Extensive multi-organ metastasis following orthotopic onplantation of histologically-intact human bladder carcinoma tissue in nude mice. *Int J Cancer* 1991; **49**: 938-939
- 25 **Hoffman RM**. Orthotopic is orthodox: why are orthotopic-transplant metastatic models different from all other models? *J Cell Biochem* 1994; **56**: 1-3
- 26 **Fu XY**, Besterman JM, Monosov A, Hoffman RM. Models of human metastatic colon cancer in nude mice orthotopically constructed by using histologically intact patient specimens. *Proc Natl Acad Sci U S A* 1991; **88**: 9345-9349
- 27 **Wang X**, Fu X, Hoffman RM. A new patient-like metastatic model of human lung cancer constructed orthotopically with intact tissue via thoracotomy in immunodeficient mice. *Int J Cancer* 1992; **51**: 992-995
- 28 **Fu X**, Guadagni F, Hoffman RM. A metastatic nude-mouse model of human pancreatic cancer constructed orthotopically with histologically intact patient specimens. *Proc Natl Acad Sci U S A* 1992; **89**: 5645-5649
- 29 **Fu X**, Herrera H, Hoffman RM. Orthotopic growth and metastasis of human prostate carcinoma in nude mice after transplantation of histologically intact tissue. *Int J Cancer* 1992; **52**:987-990
- 30 **Furukawa T**, Fu X, Kubota T, Watanabe M, Kitajima M, Hoffman RM. Nude mouse metastatic models of human stomach cancer constructed using orthotopic implantation of histologically intact tissue. *Cancer Res* 1993; **53**: 1204-1208
- 31 **Tang ZY**, Sun FX, Tian J, Ye SL, Liu YK, Liu KD, Xue Q, Chen J, Xia JL, Qin LX, Sun HC, Wang L, Zhou J, Li Y, Ma ZC, Zhou XD, Wu ZQ, Lin ZY, Yang BH. Metastatic human hepatocellular carcinoma models in nude mice and cell line with metastatic potential. *World J Gastroenterol* 2001; **7**: 597-601

Edited by Wang XL and Zhang JZ Proofread by Xu FM

Experimental and clinical assessment of percutaneous hepatic quantified ethanol injection in treatment of hepatic carcinoma

Li-Wu Lin, Xue-Ying Lin, Yi-Mi He, Shang-Da Gao, En-Sheng Xue, Xiao-Dong Lin, Li-Yun Yu

Li-Wu Lin, Xue-Ying Lin, Yi-Mi He, Shang-Da Gao, En-Sheng Xue, Xiao-Dong Lin, Li-Yun Yu, Fujian Provincial Ultrasonic Medicine Institute, Ultrasound Department, Union Hospital of Fujian Medical University, Fuzhou 350001, Fujian Province, China
Correspondence to: Li-Wu Lin, Ultrasound Department, Union Hospital of Fujian Medical University, Fuzhou 350001, Fujian Province, China. lxdghl@163.net
Telephone: +86-591-3357896 Ext. 8352 **Fax:** +86-591-3339732
Received: 2003-09-15 **Accepted:** 2003-10-22

Abstract

AIM: To detect the relationship between absolute ethanol injection quantity, the interval and formation of fibroboard, the curative effect in treatment of hepatocarcinoma and to evaluate the clinical application of percutaneous hepatic quantified ethanol injection (PHQEI) in treatment of hepatic carcinoma (HCC).

METHODS: (1) Experimental study: Twenty-four human hepatic carcinoma SMMC-7721 xenografted nude mice were randomly divided into three groups: group A injected with quantified ethanol at short intervals (QESI), group B with quantified ethanol at long intervals (QELI) and group C with a small quantity of ethanol at long intervals (SQLI). The tumor tissues were sent for patho-histology and electron microscopic examinations. The diameters of tumors were measured with high frequency ultrasound before and after therapies and tumor growth index (TGI) was calculated. (2) Clinical study: Tumors of 122 cases of pathologically proved HCC were injected with quantified ethanol guided by ultrasound every 3-5 d 4-10 times per period of treatment. The quantity of ethanol was calculated according to the regressive equations where $Y = 2.885X$ when the mass was ≤ 5 cm in diameter and $Y = 1.805X$ when the mass was > 5 cm in diameter (X is the maximal diameter of the mass with the unit cm, Y is the ethanol quantity with the unit mL). The survival rates of 1, 2, 3 and 4 years and recurrent rates *in situ* as well as dystopia in the liver were calculated.

RESULTS: (1) Experimental study: TGI of QESI group (0.072 ± 0.018) and QELI group (0.094 ± 0.028) was apparently lower than that of SQLI group (1.982 ± 0.482) ($P < 0.01$). TGI of QESI group seemed to be lower than that of QELI group, but it was not markedly different ($P > 0.05$) between two groups. Severe degeneration and necrosis could be seen in QESI group by patho-histology examination. Coagulative necrosis could be seen in most tumors of QESI group and there were no residual cancer cells under electronic microscope, while the residual cancer and inflammatory cells and fibre tissues could be seen around the tumors of QELI group. Infiltration of inflammatory cells could be seen and fibre tissues were formed. (2) Clinical study: B mode ultrasound showed that 62.5% of tumors shrank after PHQEI. The survival rates of 1, 2, 3 and 4 years of the group with tumors ≤ 3 cm in diameter

were higher than those of the group with tumors > 3 cm in diameter. The recurrent rates of tumors *in situ* of the former group were apparently lower than those of the latter group. The recurrent rates of tumors in dystopia in the liver of the former group were markedly lower than those of the latter group. The 122 cases underwent a total of 1221 PEI. There were no complications such as hemorrhage and severe heart, liver and kidney functional injuries except for 1 case of melena and 4 cases of jaundice who recovered after 1-2 wk under common therapies.

CONCLUSION: The experimental study shows quantified ethanol at intervals of 3-5 d could improve the curative effect of hepatocarcinoma. The clinical study shows PHQEI is an effective therapeutic method for HCC with few side-effects, and a low-cost. The treatment efficacy is more remarkable for tumors ≤ 3 cm in diameter.

Lin LW, Lin XY, He YM, Gao SD, Xue ES, Lin XD, Yu LY. Experimental and clinical assessment of percutaneous hepatic quantified ethanol injection in treatment of hepatic carcinoma. *World J Gastroenterol* 2004; 10(21): 3112-3117
<http://www.wjgnet.com/1007-9327/10/3112.asp>

INTRODUCTION

Because ultrasound-guided percutaneous ethanol injection (PEI) has the advantages of easy operation, definite curative effect, little damage and few side-effects, it has been widely used in clinical practice in recent years since the report by Japanese scholars in 1983^[1-10]. Though more ultrasound-guided methods have been applied since then^[11-20], PEI is still one of the most widely used non-operative methods in the treatment of hepatic carcinoma. Because there is no common standard for ethanol injection quantity and interval, the efficacy is affected apparently. In order to improve the efficacy, according to the pathological biological characteristics of HCC that there are capsula and tiny satellitic foci of cancer cells in the periphery of HCC, we once conducted the study of percutaneous hepatic quantified ethanol injection (PHQEI) in treatment of HCC (Ethanol was injected until the diffusing area was 1-2 cm more than the maximal diameter of tumor ≤ 5 cm in diameter. According to the endurance of patients the ethanol was injected from several directions and diffused throughout the nodules > 5 cm in diameter as fully as possible.) and we put forward the regressive equations^[21]: $Y = 2.885X$ ($X \leq 5$ cm), $Y = 1.805X$ ($X > 5$ cm) (X is the maximal diameter of the tumor with the unit cm, Y is the ethanol quantity with the unit mL). Recently, some scholars have reported that it could cause cancer cells to remain as the fibroboard in tumors affected the wide infiltration of ethanol^[22]. So we carried out experimental studies to prove the relationship between absolute ethanol injection quantity and the formation of fibroboard. We have followed up 122 cases of hepatocarcinoma treated by PHQEI for 1-4 years to assess its clinical application.

MATERIALS AND METHODS

Experimental studies

Experimental animals For the experiment, we used 24 BALB/CA nude mice, which were 5-8 wk old, provided by the Medical Experiment Animal Unit of Anti-cancer Center of Xiamen University, China. The average weight was 18 ± 2.1 grams. They were raised in the layer drift shelves under aseptic conditions. The cages, cushion, drinking water and standard forage provided by Shanghai Bikai Company were changed periodically.

Experimental methods Twenty-four nude mice with human HCC-transplanted hypodermically were randomly divided into three groups: group A injected with quantified ethanol (the ethanol diffused throughout the tumor) at short intervals (5 d) (QESI), group B with quantified ethanol at long intervals (10 d) (QELI) and group C with a small quantity of ethanol (half quantity of ethanol as used in QESI) at long intervals (SQLI). Each group contained 8 nude mice.

Three dimensional diameters of the tumors were measured by high frequency ultrasound (Aloka-5500 with 10 MHz probe) after 10 d of transplantation of HCC and the volume was calculated. Then ethanol was injected into the center of the tumor with No.5 needles. All the mice were injected twice. The three dimensional diameters of the tumors were measured again 5 d after the last injection and then the mice were killed. The center and peripheral tissues of tumors were sent for pathologic histology and electron microscopic examination. The experiment was carried out with double blind method.

Observation indexes Tumor growth index (TGI) was calculated by the formula: volume of the tumor (after treatment-before treatment)/volume of the tumor (before treatment). The degree of degeneration and necrosis, inflammatory response of tissues and fibre tissue were observed by pathologic histology examination. The microstructure of tumor tissues, inflammatory cells and fibre cells, fibreboard were observed under electron microscope.

Statistical methods

The data of each group were expressed as mean \pm SD. Necrosis area of each group was calculated and analyzed with ANOVA. $P < 0.05$ was considered statistically significant. All statistical analyses were performed using SPSS for windows version 8.0 software package.

Clinical studies

Patients One hundred and twenty-two cases of HCC, including 96 cases recurring after operation, consisted of 105 males and 17 females were enrolled in the study. The mean age was 54.8 years (range, 28-81). The diagnosis was established by pathocytology and/or histology. One hundred and twenty-two cases had 168 nodules including 62 cases with single nodules. The mean diameter of tumor was 3.8 cm (1.2-7.2 cm) and 122 cases comprised 64 cases with tumors < 3 cm in diameter and 58 cases with tumors > 3 cm in diameter (27 cases with tumor > 5 cm in diameter). Seventy-eight cases had AFP > 20 ng/mL.

Instruments Real-time ultrasonography (Aloka-650, 1700, Japan) was performed with a 3.5 MHz probe. The puncture needles were 22G PTC fine-needles and 15-20 cm in length. The platelet count of the patients was $> 50 \times 10^9/L$.

Injection methods The point of puncture was determined by ultrasonography. Under local anesthesia, the fine needle punctured from the point into the posterior of the axis of nodules. Then ethanol was injected into the nodule gradually and the needle was withdrawn slowly. The injection quantity was calculated according to the regressive equations: $Y = 2.885X$ ($X < 5$ cm), $Y = 1.805X$ ($X > 5$ cm) (X is the maximal diameter of the tumor with the unit cm, Y is the ethanol quantity with the unit mL).

All the cases were injected every 3-5 d 4-10 times per period of treatment. The tumor > 5 cm in diameter could also be injected 10-20 times per period of treatment.

Follow-up time The follow-up period lasted for 12-48 mo (mean period 34 mo). The survival rates of 1, 2, 3 and 4 years and recurrent rates *in situ* as well as dystopia in the liver of each group were calculated and compared using ANOVA. The 14 nodules of 9 cases were resected after quantified ethanol injection 2-4 times and sent for pathologic examination.

RESULTS

Experimental studies

Tumor growth index Table 1 shows that TGI of QESI and QELI groups was apparently smaller than that of SQLI group ($P < 0.01$). TGI of QESI group seemed to be smaller than that of QELI group, but not different markedly ($P > 0.05$).

Table 1 Comparison of TGI between groups (mean \pm SD)

Groups	Cases (n)	TGI	P
A: QESI	8	0.072 \pm 0.018	$> 0.05^1$
B: QELI	8	0.094 \pm 0.028	$< 0.01^b$
C: SELI	8	1.982 \pm 0.482	$< 0.01^d$

¹ $P > 0.05$ vs group B, ^b $P < 0.01$ vs group C, ^d $P < 0.01$ vs group A.

Table 2 Comparison of the percentage of tumor necrosis between groups

Necrosis area	QESI (A)	QELI (B)	SELI (C)	P
80%-	87.5 (7/8)	50 (4/8)	0	$< 0.01^b$ $< 0.01^d$
30%-	12.6 (1/8)	50 (4/8)	100 (8/8)	$< 0.01^f$

^b $P < 0.01$ between groups A and C, ^d $P < 0.01$ between groups A and B, ^f $P < 0.01$ between groups B and C.

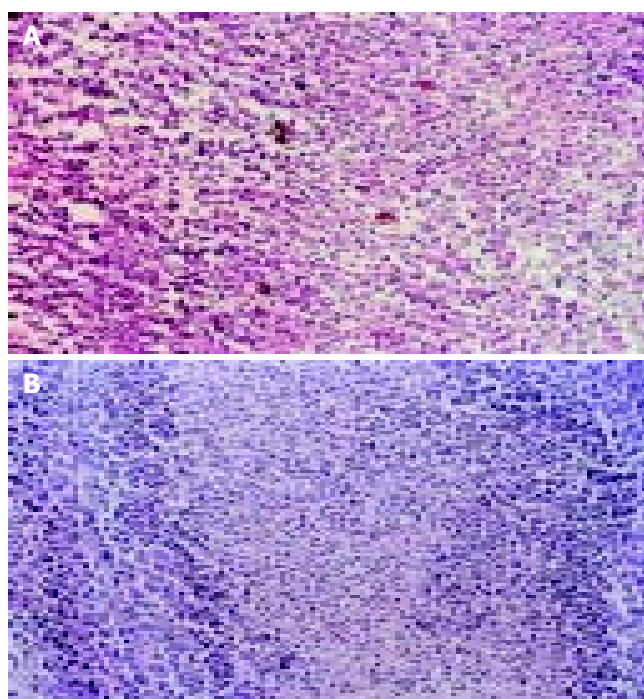


Figure 1 Coagulation necrosis in the center to periphery of the tumors of QESI after injection. (A, HE $\times 10$). The center of the tumor of SELI appeared coagulation necrosis, but in the periphery cancer cells grew luxuriantly after injection (B, HE $\times 10$).

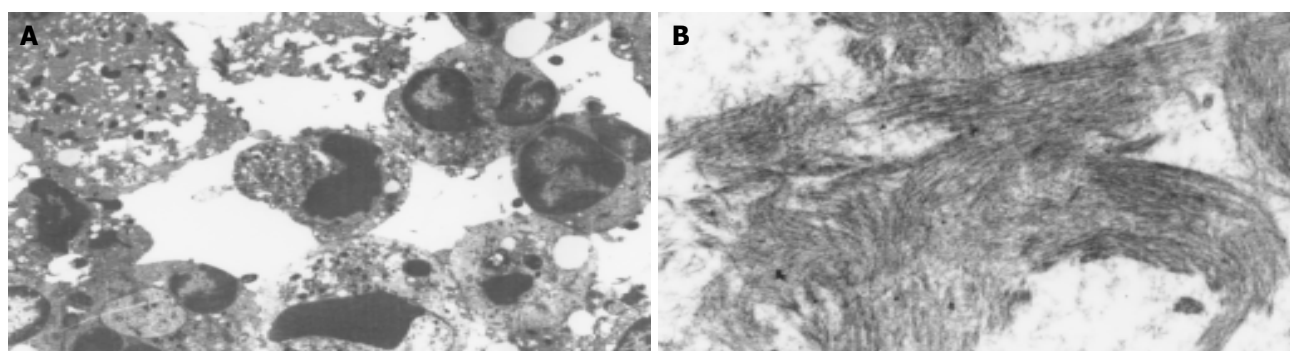


Figure 2 Inflammation cell infiltration (A) and faciculus (B) in the periphery of tumors of SQLI group. electron microscope examination.

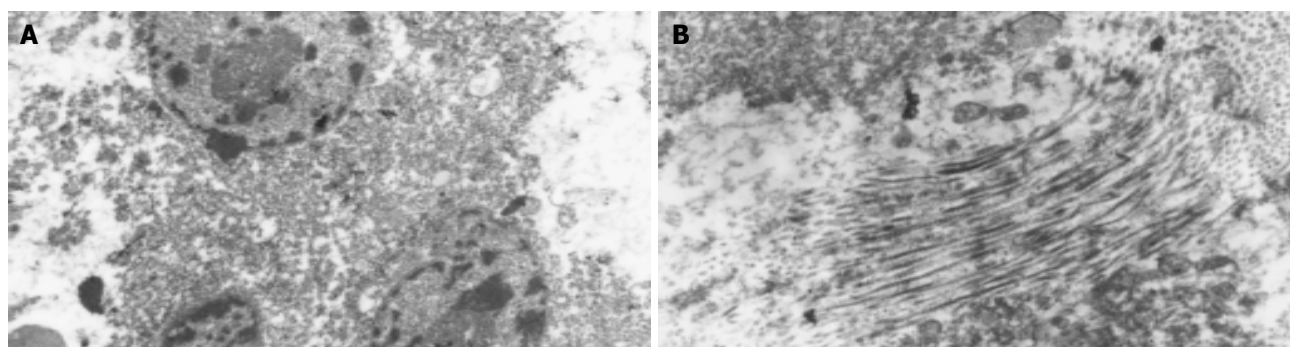


Figure 3 Degeneration cancer cells (A) and fasciculus (B) in the periphery of the tumors of QELI. Shown in electron microscope examination after injection.

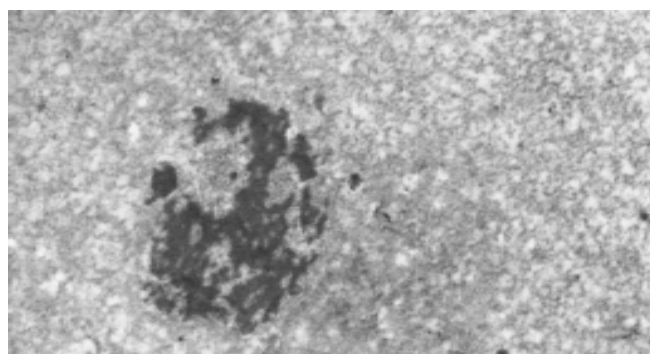


Figure 4 Necrosis changes such as karyolysis, karyorrhexis and cell membrane disappearance in the tumors of QESI after injection under election microscope.

Patho-histology examination Table 2 shows the percentage of tumor necrosis of each group. Necrosis of QESI group was most severe. Coagulative necrosis could be seen from center to periphery of the tumor of QESI group. Eighty-seven point five percent of QESI group showed necrosis area >80%, markedly higher than those of QELI and SELI groups. None of SELI group showed necrosis area >80%. The center of the tumor of SELI group showed necrosis but in the periphery cancer cells grew actively (Figure 1).

Electron microscopic observation (1) SELI group: Cancer cells showed coagulation necrosis in the center only and most cancer cells grew luxuriantly, especially in the periphery. Most cancer cells only showed orbicular karyotheca, nuclei in different size, abundant euchromatin, orbicular cytomembrane, many inflammatory cells, fibrocytes and fasciculus (Figure 2).

(2) QELI group: Coagulation necrosis was comparably severe, but in the periphery orbicular cancer cells, some degenerative cancer cells, inflammatory cells and fasciculus could be seen (Figure 3).

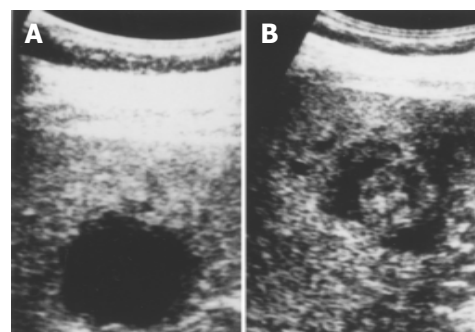


Figure 5 Reduction of the average diameter of HCC nodules from 3.6 cm (before injection, A) to 2.6 cm (two years after injection, B) and hyperechogenic rings in the periphery with haloes surrounding them after injection.

(3) QESI group: Necrotic changes, such as karyolysis, karyorrhexis and cell membrane disappearance could be seen in most cancer cells (6/8) (Figure 4). There were severe degenerative cancer cells in which heterochromatin agglutinated under the nuclear membrane. No fasciculus formed.

Clinical studies

Ultrasonography, CT or MRI showed that 168 nodules in 122 cases of HCC shrank 2-8 wk after the last PHQEI. The average diameter reduced from 3.8 cm to 2.9 cm. Ultrasound showed the echoes of tumor nodules enhanced after PEI therapy. Hyperechogenic rings could be seen in the periphery of 25% (42/168) cases of haloes surrounding them (Figure 5). The diameters of 62.5% (105/168) tumors shrank and the internal echo enhanced and facula or light dot formed (Figure 6). Tumor nodules disappeared in 12.5% cases. CT showed that the nodules showed homogeneous hypodensity or/and non-enhanced changes in 62 cases after PHQEI. MRI showed that 38 nodules of 26 cases showed low T1 and T2 signals. fine-needle or/and

thick-needle biopsies were taken 1-3 times in all the cases and no cancer cells appeared in 88.5% (108/122) cases and degenerative cancer cells appeared in 11.5% (14/122) cases with nodules >5 cm in diameter. After therapy AFP reduced in 78 cases with high AFP before therapy and 82.1% (64/78) cases turned negative.

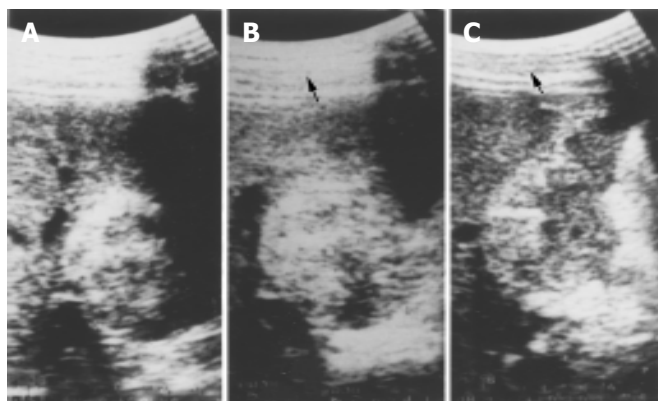


Figure 6 A: Average diameter of HCC nodule was 4.4 cm. B: It was 4.8 cm after 10 injections of absolute ethanol and the echogenic enhanced. C: After 42 mo of therapy the tumor shrank to 2.9 cm in diameter and formed facula.

Table 3 Efficacy of PEI reported in literature

Scholar	Time	Cases	Diameters of nodules (cm)	Survival rate (%)				
				1 yr	2 yr	3 yr	4 yr	5 yr
Ebara	1992	112	≤3	94	84	63	49	39
Castells	1992	162	<5	90	80	63		
Li Po	1996	188	4.6	85	44	19		
This article	2002	58	>3	84	64	58	52	
This article	2002	64	≤3	94	85	72	63	

Table 3 shows the survival rates of 1, 2, 3 and 4 years of each group with tumors <3 cm (64 cases) and >3cm in diameter (58 cases) and the treatment efficacy reported by different scholars.

Table 4 shows that the recurrent rate of tumors *in situ* and dystopia of the group with tumor ≤3 cm in diameter was apparently lower than that of the group with tumor >3 cm in diameter.

None of 9 cases with 14 nodules but 1 case showed cancer cells in pathologic examination of the resected specimens after 2-4PHQEIs.

The 122 cases underwent a total of 1 221 PHQEIs. There were no complications such as hemorrhage and severe heart, liver and kidney functional injuries except that 1 case of melona after the injection of 8 mL ethanol and 4 cases of jaundice after 2-3 PHQEIs recovered after 1-2 wk under common therapies. Different degrees of pains occurred in 33.6% (41/122) cases after 1-2 PHQEIs and disappeared in 30 min without any therapy. Low-fever appeared in 56.6% (69/122) cases and disappeared after 2-4 d. GPT increased in 16.4% (20/122) cases and reduced

to normal in 1 mo. There were no apparent changes of kidney function and ECG examination in all cases before and after therapy.

DISCUSSION

HCC is one of the most common cancers throughout the world. In order to surmount the obstinate disease scholars at home and abroad have conducted a great number of studies from many aspects, such as causa moli, pathology, diagnosis and therapy, and have acquired some accomplishments, especially in therapy^[23-35]. Operation is the most common method in early stage, while HCC has the biologic characteristics of early invasion to blood vessels and multiple origins, which cause low resection rate and high recurrent rate (90%) of 5 years. With the advantages of definite efficacy, low complication and easy operation, PEI is still one of the most appropriate non-operative methods for small HCC which is unsuitable for resection and recurrent hepatic carcinoma. The mechanism of PEI is to make cancer cells incur dehydration and coagulative necrosis by injecting ethanol into tumors. But there is not a unified standard for total injection quantity, quantity per time and injection interval. At present, some scholars have adopted the formula^[36]: $V = 4/3 \pi (r+0.5)^3$ (V is the total quantity, r is the radius of focus.) and others used the calculation^[37]: Injection quantity (mL) = diameter (cm) or quantity (mL) = diameter (cm) + 1 (tumor ≤5 cm in diameter) and quantity (mL) = diameter (cm) + 2 (tumor >5 cm in diameter). Liu *et al.*^[38] reported that 238 cases of HCC were given PEI with 1-20 mL ethanol per injection and 1-2 times per week. The injection area involved the center as well as periphery of tumor and the part adhering closely to the capsule. Excessive ethanol increases side-effects and unnecessary liver injury, while too little ethanol could not kill cancer thoroughly and cause tumors to recur and metastasize. We once conducted the study of percutaneous hepatic quantified ethanol injection in treatment of HCC and put forward the regressive equation based on tumor diameter and injection quantity of ethanol^[21]. The initial clinical application and following observation showed PHQEI had apparent efficacy. This experimental study was to further probe the pathologic basis of ethanol injection quantity, interval and the formation of fibreboard and to assess the clinical application value of PHQEI by follow-up observations.

Experimental study showed that tumor growth of QESI group (The ethanol diffused throughout the tumor and was injected every 5 d) was markedly inhibited after 2 injections. Extensive coagulative necrosis could be seen from the center to periphery of tumors and the necrosis area of 87.5% (7/8) cases reached more than 80% by pathologic histology. Electron microscopy showed the majority had coagulative necrosis and some had severe degenerative tumor cells. Though the growth of tumor of QELI group (The injection quantity was the same as that of QESI, but the interval was prolonged twice.) was also inhibited, the necrosis area of only 50% (4/8) cases was >80%. There were more residual cancer cells in the periphery of tumors and fibre tissue and inflammatory cells could be seen under electron microscope. Because ethanol injection was only half of that of QESI group and the injection interval was prolonged twice, growth inhibition and necrosis degree of tumors of Sqli group

Table 4 Comparison of the recurrent rates between groups

Group	Total Cases	Recurrent rate <i>in situ</i> (%)				Recurrent rate in dystopia (%)			
		1 yr	2 yr	3 yr	4 yr	1 yr	2 yr	3 yr	4 yr
>3 cm (A)	58	6.9 (4/58)	7.1 (3/42)	24.2 (8/33)	28.6 (6/21)	15.5 (9/58)	21.4 (9/42)	36.4 (12/33)	52.4 (11/21)
≤3 cm (B)	64	0 (0/64) ^a	2.1 (1/48)	5.1 (2/39) ^a	4.2 (1/24) ^a	9.0 (6/64)	10.4 (5/48)	12.8 (5/39) ^a	20.8 (5/24) ^a

^aP<0.05 vs group A.

were apparently slighter than those of the former two groups. Except for necrosis in the center, cancer cells grew luxuriantly, inflammatory response appeared and fasciculus formed in the periphery of the tumor.

Tumors in 122 cases of pathologically proved HCC, including 58 cases with tumors >3 cm in diameter and 64 cases with tumors ≤3 cm in diameter, were given PHQEL. We followed up the cases for 12-48 mo and proved that PHQEI had good efficacy, especially for tumors ≤3 cm in diameter. The 1-4 year survival rates of the group with tumors ≤3 cm in diameter were markedly higher than those of the group with tumors >3 cm in diameter and *in situ* tumor as well as dystopia recurrent rates were lower than those of the latter group. The reason might be that the ethanol quantity was not enough to meet the therapy standard for tumors >5 cm in diameter of 27/58 cases for the patients were weak and their liver function was bad. Giorgio *et al.*^[39] reported that 112 cases were given single-session percutaneous large dosage ethanol injection therapy with 16-120 mL ethanol per injection in panplegia. Five patients died after 7-10 h, and the 1, 2 and 3 year survival rates of the remaining 107 cases were 88%, 76% and 76%, respectively. The result showed that large amount ethanol injection could improve the treatment efficacy, while the side-effect also increased. So patients with advanced HCC of large tumors should be closely observed and an appropriate injection quantity should be chosen^[40].

Recently, some scholars have proposed that fibreboard also appeared in HCC of 3 cm in diameter and the infiltration capacity of absolute ethanol was bad. In order to improve the treatment efficacy, ethanol should be injected from different points repeatedly^[22]. Some scholars used drugs with a stronger infiltration capacity, for example, 50% acetic acid injection (PAAI)^[41]. Ohnishi *et al.*^[42] reported that the 1 and 2 year survival rates of PAAI were 100% and 92%, markedly higher than those of PEI which were 63% and 53%, respectively. The recurrent rate was 8%, lower than that of PEI which was 37%. But our study showed that the survival rate of HCC ≤3 cm in diameter was not lower and the recurrent rate was not higher than those of PAAI. The 4 year recurrent rate *in situ* was only 4.2% (1/24). Except for 1 case with a tumor of 5.1 cm in diameter none of the 9 cases with 14 nodules showed cancer cells in pathologic examination of resected specimens after 2-4 PHQEIs. Okuda *et al.* reported that about 90% of small HCCs had different degree of gross fibre pseudo-capsule and tumors <1 cm in diameter seldom had fibre capsule due to the gradually enhanced immune response of the body during the growth of tumor^[22]. Our experimental study showed that SQLI injection could stimulate strong immune response of organisms and cause inflammatory cell infiltration and fibreboard formation even if the tumor was less than 1 cm in diameter.

In conclusion, the experimental study shows that, in order to improve the efficacy of PEI adequate quantity must be adopted to maintain a strong diffusing capacity of ethanol in tumor and the interval must be short (The appropriate interval is 3-5 d) because small dosage and long interval will cause incomplete coagulated necrosis and formation of fibreboard and/or fasciculus which will influence the infiltration of ethanol and cause cancer cells to remain and metastasize.

The clinical study also shows that PHQEI has a high application value. So PEI is still the method with advantages of convenience, few side-effects and effectiveness. To further improve the treatment efficacy, studies on the quantity per injection and injection interval are needed.

REFERENCES

- 1 Kuriyama H, Okada S, Okusaka T, Ueno H, Ikeda M. Prognostic factors in patients with small hepatocellular carcinoma treated by percutaneous ethanol injection. *J Gastroenterol Hepatol* 2002; **17**: 1205-1210
- 2 Huo TI, Huang YH, Wu JC, Lee PC, Chang FY, Lee SD. Survival benefit of cirrhotic patients with hepatocellular carcinoma treated by percutaneous ethanol injection as a salvage therapy. *Scand J Gastroenterol* 2002; **37**: 350-355
- 3 Yamamoto J, Okada S, Shimada K, Okusaka T, Yamasaki S, Ueno H, Kosuge T. Treatment strategy for small hepatocellular carcinoma: comparison of long-term results after percutaneous ethanol injection therapy and surgical resection. *Hepatology* 2001; **34**(4 Pt 1): 707-713
- 4 Casella G, Cacopardo E, Rovere G, Buda CA, Cascinu S, Baldini V. Cutaneous seeding after ultrasound-guided percutaneous ethanol injection for treatment of hepatocellular carcinoma. *J Clin Ultrasound* 2001; **29**: 354-358
- 5 Giorgio A, Tarantino L, de Stefano G, Perrotta A, Aloisio V, del Viscovo L, Alaia A, Lettieri G. Ultrasound-guided percutaneous ethanol injection under general anesthesia for the treatment of hepatocellular carcinoma in cirrhosis: long-term results in 268 patients. *Eur J Ultrasound* 2000; **12**: 145-154
- 6 Fiore F, Vallone P, Ricchi P, Tambaro R, Daniele B, Sandomenico F, De Vivo R, Civiletti C, Izzo F, Pignata S, Ziviello M. Levovist-enhanced Doppler sonography versus spiral computed tomography to evaluate response to percutaneous ethanol injection in hepatocellular carcinoma. *J Clin Gastroenterol* 2000; **31**: 164-168
- 7 Caselitz M, Gebel M, Wagner S, Ockenga J, Lange P, Bleck JS, Ostertag H, Manns MP. Treatment of multilocular hepatocellular carcinoma (HCC) of 4.5 cm and 3.5 cm diameter using percutaneous ethanol injection in a patient with advanced liver cirrhosis. *Z Gastroenterol* 1999; **37**: 1175-1178
- 8 Lin SM, Lin DY, Lin CJ. Percutaneous ethanol injection therapy in 47 cirrhotic patients with hepatocellular carcinoma 5 cm or less: a long-term result. *Int J Clin Pract* 1999; **53**: 257-262
- 9 Hasegawa S, Yamasaki N, Hiwaki T, Sako K, Komorizono Y, Baba Y, Imamura Y, Kubozono O, Yoshida A, Arima T. Factors that predict intrahepatic recurrence of hepatocellular carcinoma in 81 patients initially treated by percutaneous ethanol injection. *Cancer* 1999; **86**: 1682-1690
- 10 Lin LW, He MY, Gao SD, Yu LY, Ye Z, Xue ES, Lin XD. Value of DNA analysis of ultrasound-guided fine-needle aspiration biopsy in assessment of therapeutic efficacy for hepatic carcinoma. *Zhongguo Chaosheng Yingxiangxue Zazhi* 2000; **10**: 538-541
- 11 Ahrar K, Gupta S. Hepatic artery embolization for hepatocellular carcinoma: technique, patient selection, and outcomes. *Surg Oncol Clin N Am* 2003; **12**: 105-126
- 12 Livraghi T, Lazzaroni S, Meloni F. Radiofrequency thermal ablation of hepatocellular carcinoma. *Eur J Ultrasound* 2001; **13**: 159-166
- 13 Llovet JM, Vilana R, Bru C, Bianchi L, Salmeron JM, Boix L, Ganau S, Sala M, Pages M, Ayuso C, Sole M, Rodes J, Bruix J. Increased risk of tumor seeding after percutaneous radiofrequency ablation for single hepatocellular carcinoma. *Hepatology* 2001; **33**: 1124-1129
- 14 Crucinio N, Palieri AP, Nacchiero MC, Cela EM, Muscatello N, Sgarro C, Faleo D. Radiofrequency ablation: a new approach in the treatment of hepatocellular carcinoma. *G Chir* 2001; **22**: 89-92
- 15 Cioni D, Lencioni R, Bartolozzi C. Therapeutic effect of transcatheter arterial chemoembolization on hepatocellular carcinoma: evaluation with contrast-enhanced harmonic power Doppler ultrasound. *Eur Radiol* 2000; **10**: 1570-1575
- 16 Levy I, Verstandig A, Sasson T, Wolf D, Krichon I, Libson E, Levensart P, Papo O, Yurim O, Id A, Shouval D. Transarterial oil chemoembolization for hepatocellular carcinoma, in 100 cases. *Harefuah* 2000; **138**: 89-93
- 17 Acunas B, Rozanes I. Hepatocellular carcinoma: treatment with transcatheter arterial chemoembolization. *Eur J Radiol* 1999; **32**: 86-89
- 18 Yamasaki T, Kurokawa F, Shirahashi H, Kusano N, Hironaka K, Okita K. Percutaneous radiofrequency ablation therapy for patients with hepatocellular carcinoma during occlusion of hepatic blood flow. Comparison with standard percutaneous radiofrequency ablation therapy. *Cancer* 2002; **95**: 2353-2360
- 19 Rui JA, Wang SB, Chen SG, Zhou L. Right trisectionectomy for

- primary liver cancer. *World J Gastroenterol* 2003; **9**: 706-709
- 20 **Lin LW**, Lin XY, He YM, Gao SD, Lin XD. Biological characteristics of HCC by ultrasound-guided aspiration biopsy and its clinical application. *World J Gastroenterol* 2003; **9**: 941-945
- 21 **Lin LW**, Ye Z, Xue ES, Gao SD, He YM. A study of percutaneous hepatic quantified ethanol injection in treatment of hepatocarcinoma. *Zhongguo Chaosheng Yixue Zazhi* 2000; **16**: 514-516
- 22 **Torimura T**, Ueno T, Inuzuka S, Tanaka M, Abe H, Tanikawa K. Mechanism of fibrous capsule formation surrounding hepatocellular carcinoma. Immunohistochemical study. *Arch Pathol Lab Med* 1991; **115**: 365-371
- 23 **Liao CS**, Yang KC, Yen MF, Teng LL, Duffy SW, Chen TH. Prognosis of small hepatocellular carcinoma treated by percutaneous ethanol injection and transcatheter arterial chemoembolization. *J Clin Epidemiol* 2002; **55**: 1095-1104
- 24 **Daniele B**, De Sio I, Izzo F, Capuano G, Andreana A, Mazzanti R, Aiello A, Vallone P, Fiore F, Gaeta GB, Perrone F, Pignata S, Gallo C. Hepatic resection and percutaneous ethanol injection as treatments of small hepatocellular carcinoma: a Cancer of the Liver Italian Program (CLIP 08) retrospective case-control study. *J Clin Gastroenterol* 2003; **36**: 63-67
- 25 **Chen X**, Luo P, Lin H, Shao P, Zhou Z, Fu L. Optimum mode of interventional treatment for hepatocellular carcinoma. *Zhonghua Zhongliu Zazhi* 2002; **24**: 501-503
- 26 **Kamada K**, Kitamoto M, Aikata H, Kawakami Y, Kono H, Imamura M, Nakanishi T, Chayama K. Combination of transcatheter arterial chemoembolization using cisplatin-lipiodol suspension and percutaneous ethanol injection for treatment of advanced small hepatocellular carcinoma. *Am J Surg* 2002; **184**: 284-290
- 27 **Kurokohchi K**, Watanabe S, Masaki T, Hosomi N, Funaki T, Arima K, Yoshida S, Miyauchi Y, Kuriyama S. Combined use of percutaneous ethanol injection and radiofrequency ablation for the effective treatment of hepatocellular carcinoma. *Int J Oncol* 2002; **21**: 841-846
- 28 **Kurokohchi K**, Watanabe S, Masaki T, Hosomi N, Funaki T, Arima K, Yoshida S, Nakai S, Murota M, Miyauchi Y, Kuriyama S. Combination therapy of percutaneous ethanol injection and radiofrequency ablation against hepatocellular carcinomas difficult to treat. *Int J Oncol* 2002; **21**: 611-615
- 29 **Arata S**, Tanaka K, Okazaki H, Kondo M, Morimoto M, Saito S, Numata K, Nakamura S, Sekihara H. Risk factors for recurrence of large HCC in patients treated by combined TAE and PEI. *Hepatogastroenterology* 2001; **48**: 480-485
- 30 **Liu Y**, Wu M, Qian G, Zhang B, Chen H, Fu J, Huang C. Changes and significance of circulating hepatocellular carcinoma cells in recurrent hepatocellular carcinoma patients after combined treatment. *Zhonghua Ganzhangbing Zazhi* 2001; **9**: 40-41
- 31 **Rust C**, Gores GJ. Locoregional management of hepatocellular carcinoma. Surgical and ablation therapies. *Clin Liver Dis* 2001; **5**: 161-173
- 32 **Puleo S**, Lombardo R, Li Destri G, Azzarello G, Rinziavillo C, Di Carlo I. Multimodal therapy of hepatocarcinoma: personal experience on 90 cases. *Hepatogastroenterology* 2000; **47**: 1379-1381
- 33 **Wu GX**, Lin YM, Zhou TH, Gao H, Pei G. Significant down-regulation of alpha-albumin in human hepatoma and its implication. *Cancer Lett* 2000; **160**: 229-236
- 34 **Allgaier HP**, Rossi S, Deibert P, Zuber I, Hering M, Blum HE. Hepatocellular carcinoma: percutaneous ethanol injection/transarterial chemoembolization/radiofrequency thermoablation. *Schweiz Rundsch Med Prax* 2000; **89**: 1056-1060
- 35 **Lin LW**, He YM, Gao SD, Yang FD, Ye Z, Xue ES, Yu LY, Lin XD. Value of ultrasound-guided fine-needle aspiration biopsy and ejection heavy needle biopsy in diagnosis and assessment of therapeutic effect for hepatic carcinoma. *Zhonghua Chaosheng Yixiangxue Zazhi* 2001; **10**: 608-610
- 36 **Livraghi T**, Salmi A, Bolondi L, Marin G, Arienti V, Monti F, Vettori C. Small hepatocellular carcinoma: percutaneous alcohol injection-results in 23 patients. *Radiology* 1988; **168**: 313-317
- 37 **Li B**, Chen H, Wu MC, Guo XH. Chao sheng yin dao gan zang chuan ci liu nei zhu she wu shui jiu jing zhi liao gan ai. *Zhongguo Shiyong Waike Zazhi* 1996; **16**: 84-85
- 38 **Liu LM**, Xu ZZ, Wang WP, Ding H. Percutaneous ethanol injection therapy for liver carcinoma. *Linchuang Yixue Yingxiang Zazhi* 1997; **8**: 101-104
- 39 **Giorgio A**, Tarantino L, Mariniello N, de Stefano G, Perrotta A, Aloisio V, Voza A, Finizia L, Alaia A, Del Viscovo L. Percutaneous ethanol injection under general anesthesia for hepatocellular carcinoma: 3 year survival in 112 patients. *Eur J Ultrasound* 1998; **8**: 201-206
- 40 **Meloni F**, Lazzaroni S, Livraghi T. Percutaneous ethanol injection: single session treatment. *Eur J Ultrasound* 2001; **13**: 107-115
- 41 **Ohnishi K**, Ohyama N, Ito S, Fujiwara K. Small hepatocellular carcinoma: treatment with US-guided intratumoral injection of acetic acid. *Radiology* 1994; **193**: 747-752
- 42 **Ohnishi k**, Ohyama N, Ito S, Fujiwara K. Comparison of percutaneous acetic acid injection and percutaneous ethanol injection for small hepatocellular carcinoma. *Hepatogastroenterology* 1998; **45**(Suppl 3): 1254-1258

Multi-phasic CT arterial portography and CT hepatic arteriography improving the accuracy of liver cancer detection

Li Li, Li-Zhi Liu, Zhuan-Miao Xie, Yun-Xian Mo, Lie Zheng, Chao-Mei Ruan, Lin Chen, Pei-Hong Wu

Li Li, Li-Zhi Liu, Zhuan-Miao Xie, Yun-Xian Mo, Lie Zheng, Chao-Mei Ruan, Lin Chen, Pei-Hong Wu, Imaging Diagnosis & Interventional Center, Cancer Center, Sun Yat-sen University, 651 Dongfeng Road East, Guangzhou 510060, Guangdong Province, China
Correspondence to: Dr. Pei-Hong Wu, Imaging Diagnosis & Interventional Center, Cancer Center, Sun Yat-sen University, 651 Dongfeng Road East, Guangzhou 510060, Guangdong Province, China. wupeihong@yahoo.com
Telephone: +86-20-87343270 **Fax:** +86-20-87343392
Received: 2004-02-23 **Accepted:** 2004-04-13

Abstract

AIM: To evaluate the value of multi-phasic CT arterial portography (CTAP) and CT hepatic arteriography (CTHA) in differential diagnosis of liver diseases, and to improve the specificity of CTAP and CTHA for liver cancer detection.

METHODS: From January 1999 to December 2002, multi-phasic CTAP and CTHA were performed in 20 patients with suspected liver disease. CT scanning was begun 25 s, 60 s and 120 s for the early-, late- and delayed-phase CTAP examinations, and 6sec, 40 s and 120 s for the early-, late- and delayed-phase CTHA examinations respectively, after a transcatheter arterial injection of non-ionic contrast material. If a lesion was diagnosed as a liver cancer, transcatheter hepatic arterial chemoembolization (TACE) treatment was performed, and the follow-up CT was performed three or four weeks later.

RESULTS: All eighteen HCCs in 12 cases were shown as nodular enhancement on early-phasic CTHA. The density of the whole tumor decreased rapidly on late and delayed phases, and the edge of 12 tumors (12/18) remained relatively hyperdense compared with the surrounding liver tissue, and demonstrated as rim enhancement. All HCCs were shown as perfusion defect nodules on multi-phasic CTAP. Five tumors (5/18) were shown as rim enhancement on delayed-phasic CTAP. Rim enhancement was shown as 1 to 2-mm-wide irregular, uneven and discontinuous circumferential enhancement at late-, and delayed-phase of CTHA or CTAP. Five pseudolesions and 4 hemoangiomas were found in multi-phasic CTAP and CTHA. No pseudolesions and hemoangiomas were shown as rim enhancement on late- or delayed-phasic CTHA and CTAP.

CONCLUSION: Multi-phasic CTAP and CTHA could help to recognize the false-positive findings in CTAP and CTHA images, and improve the accuracy of CTAP and CTHA of liver cancer detection.

Li L, Liu LZ, Xie ZM, Mo YX, Zheng L, Ruan CM, Chen L, Wu PH. Multi-phasic CT arterial portography and CT hepatic arteriography improving the accuracy of liver cancer detection. *World J Gastroenterol* 2004; 10(21): 3118-3121
<http://www.wjgnet.com/1007-9327/10/3118.asp>

INTRODUCTION

CT arterial portography (CTAP) and CT hepatic arteriography (CTHA) are considered as the most sensitive imaging methods of detecting small liver cancers^[1,2]. Micro liver cancer as small as 0.2 cm in diameter could be detected by CTAP and CTHA^[3]. However, the prevalence of tumor-mimicking benign perfusion abnormalities decreases the specificity of these examinations and the accuracy of tumor detection^[4,5]. In order to improve the specificity of CTAP and CTHA for liver cancer detection, multi-phasic helical CT arterial portography (CTAP) and multi-phasic helical CT hepatic arteriography (CTHA) are recommended^[6-8]. From January 1999 to December 2002, multi-phasic CTAP and multi-phasic CTHA examinations were performed for more accurate evaluation in 20 patients with suspected liver malignancy.

MATERIALS AND METHODS

Materials

From January 1999 to December 2002, 20 patients (10 men, 5 women) with suspected liver diseases underwent multi-phasic CTAP and CTHA including 12 cases of hepatocellular carcinomas (HCCs), 3 of cavernous hemangiomas, and 5 of pseudolesions. They aged from 25 to 64 years (mean age, 42.5 years). The serum level of α -fetoprotein (AFP) was elevated in all patients with small HCC, ranged from 410 ng/mL to 2540 ng/mL. Cirrhosis occurred in all 12 cases with HCC. Five patients with HCC were histologically proven by needle biopsy, and 7 were clinically diagnosed when tumors were demonstrated as lipiodol deposit foci on follow-up CT (lipiodol-CT, Lp-CT) images after transcatheter hepatic arterial chemoembolization (TACE), and the elevated AFP level returned to normal in all patients with HCC.

In this work, we decided a lesion was a pseudolesion when it was proved as normal hepatic tissue by needle liver biopsy, and did not change for at least 1 year. The diagnosis of a cavernous hemangioma was basic on typical findings on dynamic enhanced CT and MRI (very long T2) images, and when it did not enlarge for at least 1 year.

Methods

Multi-phasic CTAP examinations were performed with incremental scanning of liver in cranial-to-caudal direction with 2.7-mm to 5-mm collimation on an CT Twin Flash scanner (Philips Corp.). Data acquisition was started 25 s, 60 s and 120 s for the early-, late- and delayed-phase CTAP respectively, after a transcatheter superior mesenteric arterial injection of 40 mL of non-ionic contrast material at 3.0 mL/s, using an automatic power injector (Medrad, Pittsburgh). During the catheterization, contrast material administered before CT scanning was limited to 10 mL injected by hand to visualize aberrant vessels and to facilitate proper catheter placement.

Multi-phasic CTHA examinations were done 20 min after CTAP. Data acquisition was started 6 s, 40 s and 120 s for the early-, late- and delayed-phase CTHA respectively, after the initiation of a transcatheter common hepatic arterial injection of 15 mL of contrast material at 3.0 mL/s.

If serum AFP level exceeded 400 ng/mL, and a lesion was

highly suspected as an HCC on CTAP and CTHA images, TACE treatment was recommended to this patient, and plain CT scanning was performed 3 or 4 wk later (Lipiodol CT, Lp-CT).

RESULTS

The images of multi-phasic CTAP and CTHA in 20 cases were

carefully interpreted by two experienced radiologist. On early-phasic CTHA, all eighteen HCCs were shown as nodular enhancement. The density of the whole tumor decreased rapidly and became hypodense or isodense compared with the surrounding liver tissue on late and delayed phases. However, the edge of tumors (12/18) remained relatively hyperdensity compared with the surrounding liver tissue, and demonstrated as rim enhancement. Rim enhancement was demonstrated as



Figure 1 Images of multi-phasic CTAP and CTHA. A: A nodular perfusion defect of HCC on CTAP image. B: A small round enhancement nodule of HCC on early-phasic CTHA image. C: Rim enhancement of HCC on delayed-phasic CTHA image obtained 2 min later.



Figure 2 HCC on early-phasic CTAP and late-phasic CTHA. A: HCC shown as a well-fined hypodense nodule on early-phasic CTAP image. B: HCC demonstrated as rim enhancement on late-phasic CTHA image. C: HCC demonstrated as irregular enhancement on CTHA image.

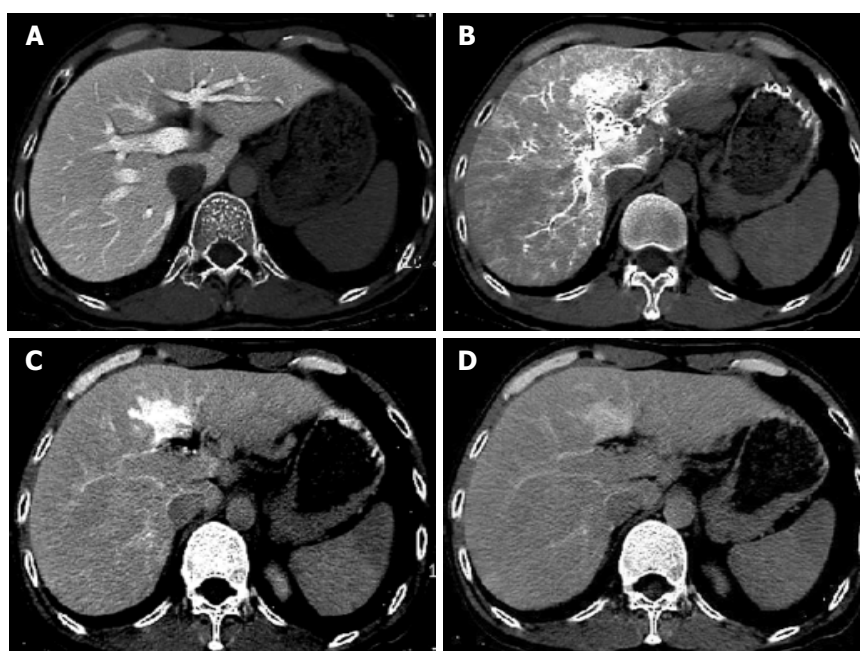


Figure 3 Pseudolesions on CTAP and CTHA. A: No lesion demonstrated on CTAP. B: Pseudolesion shown as an irregular enhancement focus on early-phasic CTHA. C: Change in shape and size of pseudolesion on late-phasic CTAP. D: Pseudolesion demonstrated as isodensity to liver tissue on delayed-CTHA.

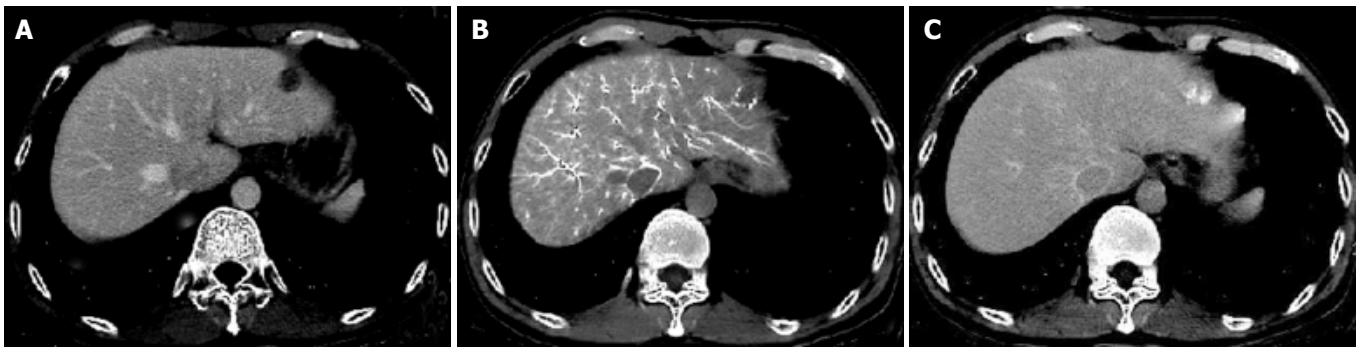


Figure 4 Hemangiomas on CTAP and CTHA. A: A small hemangioma in segment II of left lobe as a perfusion defect nodule on CTAP. B: Lesion demonstrated as a punctulate, peripheral enhancement focus on early-phasic CTHA. C: Hemangioma demonstrated as hyperdensity to liver tissue on delayed-CTHA.

distinct 1 to 2-mm-wide circumferential enhancement at late-, and delayed-phase of multi-phasic CTHA (Figure 1). The shape of enhancement might be irregular, uneven and discontinuous.

All HCCs were shown as perfusion defect nodules on multi-phasic CTAP. The edge of five HCCs (5/18) became relatively hyperdense compared with the surrounding liver tissue and demonstrated as rim enhancement during delayed CT scanning (Figure 2).

Four of 5 pseudolesions were found in the segment IV of left lobe, and one in the segment VI of right lobe. All pseudolesions were shown as isodense or hypodense compared with the surrounding liver tissue on CTAP images. On CTHA images, pseudolesions were demonstrated as oval, wedge or irregular enhancement. The shape and size of pseudolesions were changed during delayed CT scanning. All pseudolesions gradually became isodense compared with the surrounding liver tissue on delayed phase. No pseudolesions were demonstrated as rim enhancement on late- or delayed-phasic CTHA and CTAP (Figure 3).

Four hemangiomas of 3 cases were shown as well-defined nodular perfusion defects on multi-phasic CTAP images. On early-phasic CTHA, hemangiomas were demonstrated as peripheral enhancement or nodular enhancement foci. On delayed CT scanning, all hemangiomas became isodense compared with the surrounding liver tissue. There was no hemangioma demonstrated as rim enhancement on late- or delayed-phasic CTHA and CTAP images in our study (Figure 4).

DISCUSSION

CTAP and CTHA have a high sensitivity for detection of liver diseases^[3,9]. Especially, the use of helical CT technique has greatly improved the quality of images and accelerated the scanning^[1]. However, the false-positive findings on CTAP and CTHA images have greatly limited its further clinical application^[5,10]. Many methods were performed to improve the specificities of CTAP and CTHA for the detection of liver cancer, and combined CTHA and CTAP was recommended to interpret a malignant lesion^[9]. Inoue *et al.*^[8] and Matsuo *et al.*^[6] performed combined CTAP and biphasic CTHA in the pre-operative detection of liver neoplasms. Their results suggested that late-phasic CTHA was useful in differentiating a malignant hepatic tumor from a pseudolesion. Ueda *et al.* performed single-level dynamic CTHA in differentiating hypervascular pseudolesion from hypervascular HCC. They found that the stain of pseudolesion on CTHA was transient and could be divided into three phases: (1) inflow of contrast material into the portal vein within the lesion, (2) lesion staining, and (3) fading out of the staining. However, the staining of HCC might have four phases: (1) inflow of contrast material into tumor, (2) tumor staining, (3) inflow of contrast material into adjacent liver, and (4) "coronal staining"

of adjacent liver^[7,11].

Rim enhancement was demonstrated as distinct 1 to 2-mm-wide irregular coronal or circumferential enhancement at late-, and delayed-phase of multi-phasic CTHA or CTAP^[12,13]. According to our experience, the indistinct circumferential enhancement was only transiently demonstrated during multi-phasic of CTHA and CTAP. Delayed CT scanning 120 s after a transcatheter arterial injection of material might increase the detection of rim enhancement of liver malignancy.

Inoue *et al.* reported that 84% of hepatocellular carcinomas and 73% of hepatic metastases showed rim enhancement on late-phase CTHA, and all non-tumorous perfusions on CTHA images did not show rim enhancement^[8]. They concluded that biphasic CTHA was useful in differentiating hepatic malignancy from benign perfusion abnormalities. Similar findings were confirmed by Matsuo *et al.*^[6] and Ueda *et al.*^[7].

The reason why the malignant tumors showed delayed rim enhancement and pseudolesions did not at late-, or delayed-phase CTHA or CTAP is unclear^[14,13]. Ueda *et al.*^[7] suggested that rim enhancement in hepatocellular carcinoma was caused by inflow of contrast material from tumor into the adjacent liver. They studied the haemodynamics of hepatocellular carcinoma using single level dynamic CTHA, and demonstrated that arterial blood flowed into the tumor via the hepatic artery, filled the inner part of the tumor, penetrated the capsule, ran through the surrounding hepatic parenchyma and entered the portal branches. The haemodynamics can explain the change of homogeneous enhancement pattern on early-phasic CTHA to rim enhancement on late- or delayed-phasic CTHA. However, the contrast material inside pseudolesions faded out after lesion staining, just like liver tissue.

In our study, rim enhancement usually demonstrated on late-phasic CTHA images could be shown on late- and delayed-phase of CTAP in some cases. The reason of similar findings on CTAP might be that some HCCs could obtain blood supply from portal vein branches surrounding the tumor, especially, in the edge of tumor. This "double" blood supply usually occurred in liver tumors with less vascularity^[15]. The border of tumor could be enhanced as a rim of relatively high density during late- and delayed-phase CTAP.

There is a controversy that rim enhancement originates from the normal hepatic tissue surrounding the tumor or from the border of tumor (such as capsule or pseudo-capsule of tumor). Irie *et al.* had performed an CT-pathologic study of metastatic liver tumors, and suggested that rim enhancement of tumor on delayed-phasic CTAP or CTHA images was perilesional enhancement, and it could mainly be caused by an increased supply of arterial flow, a draining of tumorous blood, or an increased interstitial space in the hepatic parenchyma due to fibrotic and desmoplastic changes^[12]. However, Semelka *et al.* suggested that rim enhancement might be the enhancement of

histological tumor border that was defined as the histologically altered liver parenchyma surrounding the tumor, rather than the outer portion of the tumor^[14].

To our knowledge, it is difficult to distinguish tumor border from perilesional area on CT images. During growth, the tumor infiltrates and compresses surrounding hepatic tissue. The capsule or false-capsule of tumor is formed and contains rich blood flow. It might be difficult to distinguish perilesional enhancement of normal tissue from circumferential enhancement of tumor border on CT and MR images. Rim enhancement demonstrated on late- or delayed-phasic CTHA and CTAP might not be confined to the tumor border because it could extend into the surrounding normal liver tissue.

One of the commonest pseudolesions on CTAP and CTHA images was seen in the liver adjacent to gallbladder or in dorsum of segment IV^[4,16]. In our study, four of 5 pseudolesions were found in the left lobe, and one in segment VI of the right lobe. All five pseudolesions demonstrated as isodense lesions or perfusion defects on CTAP images. The shape of enhancement on early-phasic CTHA images might be oval, wedge or irregular. Pseudolesions were changed in shape and size on multi-phasic CTHA images, and gradually became isodense to normal on delayed phase. No pseudolesions were demonstrated as rim enhancement on late- or delayed-phasic CTHA.

Yamagami *et al.*^[4] investigated the haemodynamics of pseudolesions using a biphasic CTHA examination, and suggested that pseudolesions on segment IV were caused by direct blood inflow from cholecystic vein to the liver parenchyma, and concluded that later phase CTHA could clearly differentiate pseudolesions from tumors.

Multi-phasic CTAP and CTHA were valuable for differentiating benign lesions from malignancy^[10,17]. Hemangiomas were found on multi-phasic CTAP and CTHA images. Four hemangiomas of 3 cases were shown as well-defined perfusion defect nodules on CTAP images, and as nodular enhancement on early-phasic CTHA. On delayed CT scanning, all hemangiomas became isodense to the normal. No hemangioma was demonstrated as rim enhancement on late- or delayed-phasic CTHA images in our study. According to our experience, rim enhancement on multi-phasic CTHA could also be used as a characteristic finding to differentiate malignancy from benign lesions, such as hemangiomas.

In conclusion, multi-phasic CTAP and CTHA could raise the specificity for malignant hepatic tumor detection. Rim enhancement demonstrated on late- and delayed-phasic CTAP and CTHA images might help to differentiate a HCC from benign lesions.

REFERENCES

- 1 **Murakami T**, Oi H, Hori M, Kim T, Takahashi S, Tomoda K, Narumi Y, Nakamura H. Helical CT during arterial portography and hepatic arteriography for detecting hypervascular hepatocellular carcinoma. *Am J Roentgenol* 1997; **169**: 131-135
- 2 **Hori M**, Murakami T, Kim T, Takahashi S, Oi H, Tomoda K, Narumi Y, Nakamura H. Sensitivity of double-phase helical CT during arterial portography for detection of hypervascular hepatocellular carcinoma. *J Comput Assist Tomogr* 1998; **22**: 861-867
- 3 **Li L**, Wu PH, Mo YX, Lin HG, Zheng L, Li JQ, Lu LX, Ruan CM, Chen L. CT arterial portography and CT hepatic arteriography in detection of micro liver cancer. *World J Gastroenterol* 1999; **5**: 225-227
- 4 **Yamagami T**, Nakamura T, Kin Y, Nishimura T. Non-tumorous enhancement caused by cholecystic venous inflow shown on biphasic CT hepatic arteriography: comparison with hepatocellular carcinoma. *Br J Radiol* 2000; **73**: 1275-1281
- 5 **Li L**, Wu PH, Lin HG, Li JQ, Mo YX, Zheng L, Lu LX, Ruan CM, Chen L. Findings of non-pathologic perfusion defects by CT arterial portography and non-pathologic enhancement of CT hepatic arteriography. *World J Gastroenterol* 1998; **4**: 513-515
- 6 **Matsuo M**, Kanematsu M, Inaba Y, Matsueda K, Yamagami T, Kondo H, Arai Y, Hoshi H. Pre-operative detection of malignant hepatic tumours: value of combined helical CT during arterial portography and biphasic CT during hepatic arteriography. *Clin Radiol* 2001; **56**: 138-145
- 7 **Ueda K**, Matsui O, Kawamori Y, Nakanuma Y, Kadoya M, Yoshikawa J, Gabata T, Nonomura A, Takashima T. Hypervascular hepatocellular carcinoma: evaluation of hemodynamics with dynamic CT during hepatic arteriography. *Radiology* 1998; **206**: 161-166
- 8 **Inoue E**, Fujita M, Hosomi N, Sawai Y, Hashimoto T, Kuroda C, Nakano H, Sasaki Y, Ishiguro S. Double phase CT arteriography of the whole liver in the evaluation of hepatic tumors. *J Comput Assist Tomogr* 1998; **22**: 64-68
- 9 **Kim HC**, Kim TK, Sung KB, Yoon HK, Kim PN, Ha HK, Kim AY, Kim HJ, Lee MG. Preoperative evaluation of hepatocellular carcinoma: combined use of CT with arterial portography and hepatic arteriography. *Am J Roentgenol* 2003; **180**: 1593-1599
- 10 **Lim JH**, Kim EY, Lee WJ, Lim HK, Do YS, Choo IW, Park CK. Regenerative nodules in liver cirrhosis: findings at CT during arterial portography and CT hepatic arteriography with histopathologic correlation. *Radiology* 1999; **210**: 451-458
- 11 **Ueda K**, Matsui O, Kawamori Y, Kadoya M, Yoshikawa J, Gabata T, Nonomura A, Takashima T. Differentiation of hypervascular hepatic pseudolesions from hepatocellular carcinoma: value of single-level dynamic CT during hepatic arteriography. *J Comput Assist Tomogr* 1998; **22**: 703-708
- 12 **Irie T**, Tsushima Y, Terahata S, Hatsuse K, Kusano S. Rim enhancement in colorectal metastases at CT during infusion hepatic arteriography. Does it represent liver parenchyma or live tumor cell zone? *Acta Radiol* 1997; **38**: 416-421
- 13 **Terayama N**, Matsui O, Ueda K, Kobayashi S, Sanada J, Gabata T, Kawamori Y, Kadoya M. Peritumoral rim enhancement of liver metastasis: hemodynamics observed on single-level dynamic CT during hepatic arteriography and histopathologic correlation. *J Comput Assist Tomogr* 2002; **26**: 975-980
- 14 **Semelka RC**, Hussain SM, Marcos HB, Woosley JT. Perilesional enhancement of hepatic metastases: correlation between MR imaging and histopathologic findings-initial observations. *Radiology* 2000; **215**: 89-94
- 15 **Hayashi M**, Matsui O, Ueda K, Kawamori Y, Gabata T, Kadoya M. Progression to hypervascular hepatocellular carcinoma: correlation with intranodular blood supply evaluated with CT during intraarterial injection of contrast material. *Radiology* 2002; **225**: 143-149
- 16 **Yamagami T**, Takeuchi Y, Inaba Y, Matsueda K, Arai Y, Maeda T. Correlation of a defect of portal perfusion in the dorsal part of segment IV of the liver on CT arterial portography with inflow of the aberrant pancreaticoduodenal vein. *Br J Radiol* 1999; **72**: 552-555
- 17 **Onaya H**, Itai Y, Satake M, Luo T, Saida Y, Haruno M, Hasebe T, Moriyama N. Highly enhanced hepatic masses seen on CT during arterial portography: early hepatocellular carcinoma and adenomatous hyperplasia. *Jpn J Clin Oncol* 2000; **30**: 440-445

Induction of HSF1 expression is associated with sporadic colorectal cancer

Hui Cen, Shu Zheng, Yong-Ming Fang, Xiao-Ping Tang, Qi Dong

Cen Hui, Shu Zheng, Yong-Ming Fang, Qi Dong, Cancer Institute, The Second Affiliated Hospital of Medical School, Zhejiang University, Hangzhou 310009, Zhejiang Province, China

Hui Cen, Xiao-Ping Tang, Institute of Optic and Electronic Technologies, Chinese Academy of Sciences, Chengdu 610209, Sichuan Province, China
Supported by 100 Scholars Plan of Chinese Academy of Sciences

Correspondence to: Shu Zheng, Cancer Institute, The Second Affiliated Hospital of Medical School, Zhejiang University, Hanzhou 310009, Zhejiang Province, China. zhengshu@zju.edu.cn

Telephone: +86-571-87784501 **Fax:** +86-571-87214404

Received: 2003-06-21 **Accepted:** 2003-07-31

Abstract

AIM: To explore the activation of signal transduction pathways related with the carcinogenesis of sporadic colon cancers.

METHODS: A gene array monitoring the activation of 8 signal transduction pathways (PathwayFinder GEArray) was used to screen the differentially expressed genes between colorectal cancer and normal colon tissues. The differentially expressed genes were further analyzed by RT-PCR, using RNA derived from colorectal cancer and normal colon tissue of 35 patients.

RESULTS: The expression of HSF1, HSF27, HSP90 and iNOS was increased in colon cancer tissues compared to normal colon tissue using PathwayFinder GEArray. The RT-PCR results showed that the expression of HSF1 was increased in 86% (30/35) patients and the expression of iNOS was increased in 63% (22/35) patients.

CONCLUSION: The induction of HSF1 gene expression is associated with sporadic colon cancer. HSF1 induces heat shock stress signaling pathway, which might play a role in the carcinogenesis of sporadic colorectal cancer.

Cen H, Zheng S, Fang YM, Tang XP, Dong Q. Induction of HSF1 expression is associated with sporadic colorectal cancer. *World J Gastroenterol* 2004; 10(21): 3122-3126
<http://www.wjgnet.com/1007-9327/10/3122.asp>

INTRODUCTION

Colorectal cancer (CRC) is one of the most common cancers in China. The incidence of CRC has increased over the last years and the fourth or fifth most prevalent cancers in China. The incidence of CRC increases 3.7% in Chinese cities annually^[1] while the five-year survival rate has not improved significantly. Early detection and treatment remain a major factor for good survival rate of CRC. Therefore, exploration of early diagnostic markers and the mechanism study on CRC oncogenesis are in imminent need for early diagnostic and better treatments. Recently, mutation of APC tumor suppressor gene has been found to be responsible for initiating neoplastic process of familial adenomatous polyposis (FAP)^[2]. APC is a major regulator in the Wnt signal pathway that is activated due to

APC mutation in FAP. The Wnt signal pathway is the oncogenic pathway for FAP. Although APC mutation was found in 60% sporadic CRC, Wnt signal pathway has not been proved to be an oncogenic pathway for sporadic CRC or any specific type of CRC. The oncogenic pathway for sporadic CRC remains to be determined.

Potter^[3] has once summarized four signal pathways attributing to oncogenesis of hereditary CRC: APC-catenin-TCF-c-myc pathway (Wnt signal pathway) in FAP; microsatellite unstable pathway with mutation in hMLH1, hMSH2, hMSH6, hPMS1 or hPMS2 in HNPCC; p53 signal pathway with p53 mutation for CRC associated with chronic colon inflammation; estrogen receptor hypermethylation pathway for CRC associated with menopause. FAP and HNPCC are two hereditary CRCs. Other hereditary CRC also includes Peutz-Jeghers syndrome and juvenile polyposis whose genetic predisposition is currently under investigation. The hereditary CRCs makes up less than 1/3 of CRCs while more than 2/3 of CRCs are sporadic. Therefore, it is important to identify oncogenic pathways for sporadic CRC. As an open system, colon receives various chemical, physical and biological stimuli constantly. These stimuli vary among individuals according to their occupations, living environments and life styles. Some signal pathways that are activated by certain stimuli associated with particular occupations, environments and life styles may induce sporadic CRC. To explore the association between sporadic CRC and activation of signal pathways, we used PathwayFinder GEArray from SuperArray, a gene array capable of monitoring activation of 8 common signal transduction pathways to screen differential gene expression between colorectal cancer tissue and normal colon tissue. We found expressions of HSF1, HSF27, HSP90 and iNOS were increased in CRC tissue in comparison with normal colon tissue. RT-PCR was used for further confirmation. Our results suggest activation of heat shock stress signal pathway may attribute to oncogenesis of sporadic CRC.

MATERIALS AND METHODS

GEArray

PathwayFinder GEArray kit was obtained from SuperArray Bioscience Corp. (Frederick, MD, USA). It included reagents for probe generation and hybridization, and two identical gene arrays containing 23 marker genes for each array. The marker genes were used to monitor the activation of their associated pathways. The induction of marker genes suggested the activation of their associated pathways. The marker genes were transcriptional target genes of their associated pathways. These 8 signal transduction pathways and their associated marker genes are listed below.

Signal transduction pathways
Mitogenic signaling pathway
Stress signaling pathway

NFκB signaling pathway
NFAT signaling pathway
Anti-proliferation/TGFβ signaling pathway
Wnt signaling pathway
P53 signaling pathway
CREB signaling pathway

Marker genes
egr-1, c-fos, c-myc, ATF-2, c-fos, p53, hsf1, hsp90, hsp27, iNOS, NFκB, ikB, c-myc, IL-2, FasL, CD5, p19, p21^{waf1}, p57^{kip2}, c-myc, p21^{waf1}, pig7, pig8, mdm2, bax, cyp19, egr-1, c-fos

Tissue and RNA preparation

Specimens of colorectal cancer and normal colon tissues were obtained from 36 patients (age: 32-89 years) at the Second Affiliated Hospital of Zhejiang University. The membranes of cancer and normal tissues of each patient were separated and placed into liquid nitrogen immediately after the removal of cancer mass from the patients. Total RNA was prepared from each specimen using Trizol kit from GIBCO (San Diego, CA, USA) to derive total RNA from cancer tissue and normal tissue. One pair of specimens from a patient (patient 1) was used to perform gene array analysis and the rest of 35 pairs of specimens were used for RT-PCR analysis.

Probe preparation

Anneal Five μg total RNA was used to mix with 2 μL buffer A containing gene specific primers GEAprimers (SuperArray, Frederick, MD, USA) and water to bring up a volume to 20 μL . The annealing of GEAprimers to RNA was achieved at 72 $^{\circ}\text{C}$ for 2 min at 42 $^{\circ}\text{C}$ for 2 min in water bath.

Reverse transcription for probe labeling A cocktail containing the following components was assembled in a 0.5 mL centrifuge tube containing 16 μL of 5 \times GEAlabeling buffer, buffer B (SuperArray, Frederick, MD, USA), 10 μL of [α - ^{32}P]-dCTP (370 GBq/L), 2 μL of RNase inhibitor, 4 μL of MMLV reverse transcriptase (50 MU/L), 8 μL of RNase-free H_2O . The cocktail was placed in 42 $^{\circ}\text{C}$ water bath for 2 min followed by aliquoting 20 μL of the cocktail into the above primer annealed RNA from cancer tissue and 20 μL of the cocktail into above primer annealed RNA from normal tissue. After mixed, the mixture was placed in 42 $^{\circ}\text{C}$ water bath for 25 min for reverse transcription and labeling cDNA with α - ^{32}P .

Labeling termination A 5 μL of 10 \times stop solution, buffer C (SuperArray, Frederick, MD, USA) was added to each reaction mixture to stop reverse transcription.

Probe denaturation: The labeled probe was placed in 94 $^{\circ}\text{C}$ heat block for 5 min, then immediately placed on ice until use.

Hybridization

Two PathwayFinder GEArrays were prehybridized with 10 mL GEHyb solution (SuperArray, Frederick, MD, USA) for 2 h at 68 $^{\circ}\text{C}$. The denatured probes obtained from cancer and normal tissues of patient 1 were then added separately to two 5 mL GEHyb solution preheated to 68 $^{\circ}\text{C}$. Each of the probe-containing GEHyb solution was then used to hybridize with one PathwayFinder GEArray at 68 $^{\circ}\text{C}$ overnight. The GEArray was washed twice with 2 \times SSC, 10 g/L SDS for 20 min at 68 $^{\circ}\text{C}$ and twice with 0.1 \times SSC, 5 g/L SDS at 68 $^{\circ}\text{C}$. X-ray films were placed on GEArrays to capture array images at -70 $^{\circ}\text{C}$ overnight.

Density scan and analysis

The hybridization signals on the X-ray film were scanned by IS1000 system to obtain digital number for its density. The average signal was obtained from duplicates of each gene. The normalized value for each gene was calculated by the ratio of averaged value of each gene divided by the average value of β -actin or GAPDH.

RT-PCR

A 1 μg of total RNA obtained from each specimen was mixed with oligo (dT)₁₅ for reverse transcription using MMLV (Promega, Madison, WI, USA) to derive the first strand cDNA. A pair of gene specific PCR primers was designed for HSF1, iNOS, MDR1 and β -actin genes. HSF1: CCATCCTGCGGGAGAGTG AA for 5' end of the gene and GGCTCCGAGCCTGTGTCAG CA for 3' end of the gene. iNOS: CACATCCTGGTGGAACTCT for 5' end of the gene and TCTTGGGGCTTCAGGCT GTT for 3' end of the gene. MDR1: GCTCAAGTTAAAGGGGCTATA for 5' end of the gene and GCTCAAGTTAAAGGGGCTATA for

3' end of the gene. β -actin: GGCA TCCTCACCTGAAGTA for 5' end of the gene and GTCCAGACGCAGGATGGCA for 3' end of the gene. PCR reaction was carried out at 95 $^{\circ}\text{C}$ for 3 min for denaturing followed multiple cycles at 95 $^{\circ}\text{C}$ for 15 s, at 56 $^{\circ}\text{C}$ for 10 s, at 72 $^{\circ}\text{C}$ for 45 s. For HSF1, iNOS and MDR1, the cycle number was 35 and for β -actin, the cycle number was 25. The PCR products were separated by electrophoresis and their quantity was determined by Kodak 1D image analysis software.

RESULTS

Identification of differential gene expression between cancer and normal colorectal tissues

Two identical PathwayFinder gene arrays from SuperArray (Frederick, MD, USA), each of which contained 23 marker genes monitoring the activation of 8 signal transduction pathways, were used to hybridize with labeled probes obtained from total RNA of cancer and normal colorectal tissues of a patient separately. The hybridized signal detected for each gene was normalized to the signal obtained for β -actin or GAPDH on the same gene array to derive gene expression value for each gene. After comparing gene expression value of each gene between two gene arrays, we found increased expressions of HSF1, HSF27, HSF90 genes of stress signaling pathway and iNOS gene of NF κ B pathway in cancer tissue in comparison with normal tissue (Figure 1, Table 1).

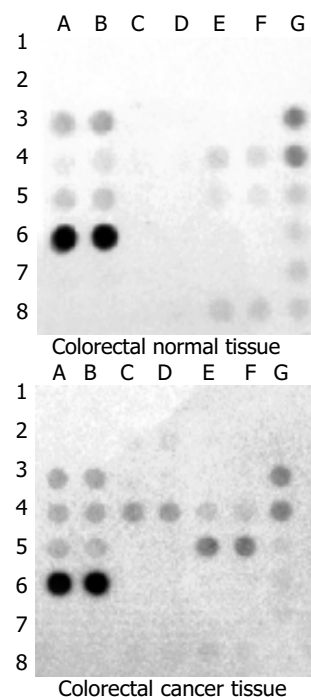


Figure 1 Comparison of hybridization results of gene arrays. Genes and their corresponding positions on gene arrays were as follows: ATF-2: 1A and 1B; Bax: 1C and 1D; CD5: 1E and 1F; c-fos: 2A and 2B; c-myc: 2C and 2D; Cyp19: 2E and 2F; egr-1: 3A and 3B; fas ligand: 3C and 3D; gadd45: 3E and 3F; hsp1: 4A and 4B; hsf27: 4C and 4D; hsp90: 4E and 4F; ikBa: 5A and 5B; Il-2 5C and 5D; iNOS: 5E and 5F; mdm2: 6A and 6B; NF κ B: 6C and 6D; p19: 6E and 6F; p21^{waf1}: 7A and 7B; p53: 7C and 7D; p57^{kip2}: 7E and 7F; Pig7: 8A and 8B; Pig8: 8C and 8D; β -actin: 3G and 4G; GAPDH: 5G, 6G, 7G, 8E, 8F and 8G; PUC18: 1G and 2G.

HSF1, HSF27 and HSP90 are marker genes for the stress signaling pathway. The induction of these genes in colorectal cancer tissue compared to its normal tissue indicated the activation of stress signaling pathway in cancer tissue. iNOS is a marker gene for NF κ B signaling pathway and its activation suggested that NF κ B might be activated. Since we did not detect

activation of other NF κ B pathways associated marker genes, the induction of iNOS expression might be due to the activation of other signal pathways other than NF κ B signal pathways.

Table 1 Analysis of scanned density on gene arrays

Gene	Ratio of cancer tissue vs normal tissue (β -actin) ¹	Ratio of cancer tissue vs normal tissue (GAPDH) ²
Egr-1	1.16	0.94
Hsf1	1.43	1.17
i κ B	1.23	1.00
Mdm2	0.98	0.80
Hsp27	1.58	1.28
Hsp90	1.31	1.06
iNOS	1.49	1.22

¹Ratio of cancer tissue versus normal tissue (β -actin): "Ratio to β -actin" from cancer/"Ratio to β -actin" from normal tissue;

²Ratio of cancer tissue versus normal tissue (GAPDH): "Ratio to GAPDH" from cancer/"Ratio to GAPDH" from normal tissue.

Table 2 Comparison of gene expression between normal and cancer tissue by RT-PCR

Patient	Dukes'	Ratio of cancer vs normal ¹		
		HSF1 ²	iNOS ²	MDR1 ²
1	C	0.87	0.78	2.71
2	B	2.13	2.57	0.64
15	B	1.34	1.17	0.23
21	A	1.68	0.81	1.71
29	A	1.96	1.32	1.02
33	C	1.71	0.72	0.64
34	B	3.44	1.04	2.08
38	B	1.78	1.17	0.87
40	B	2.25	0.35	0.25
45	B	2.07	0.44	1.50
48	A	1.96	0.60	0.81
52	B	1.75	1.83	0.35
71	D	0.91	3.55	1.31
79	C	1.11	0.39	0.99
82	C	0.79	2.33	0.29
84	C	1.53	1.07	1.04
85	C	2.25	6.49	0.70
95	C	1.64	0.88	0.40
99	C	1.28	3.79	0.61
100	A	1.70	0.62	0.16
104	A	57.47	2.77	0.47
105	B	1.54	4.53	0.55
106	C	4.52	4.97	0.25
113	C	2.08	0.17	0.97
117	C	1.84	2.49	0.87
118	B	1.43	4.45	2.08
122	C	1.78	0.57	0.25
125	C	4.14	12.24	1.73
128	B	0.79	1.31	0.08
130	C	1.07	0.73	0.73
131	B	2.11	2.66	1.61
132	C	0.73	1.55	1.20
142	C	2.44	6.00	0.52
151	B	2.16	1.06	4.31
153	C	1.20	0.62	0.37

¹Ratio of HSF1, iNOS or MDR1 to β -actin; ²[(HSF1, iNOS or MDR1)/ β -actin, Cancer]/[(HSF1, iNOS or MDR1)/ β -actin, Normal].

RT-PCR analysis for association of with sporadic colon cancer

A pair of gene specific PCR primers was designed for HSF1 and iNOS. RT-PCR was used to analyze the gene expression level of HSF1 and iNOS in both colon cancer and normal tissues of 35 patients. We confirmed increased HSF1 expression in 30 out of 35 patients in their cancer tissue in comparison to their normal tissue (Table 2). The average HSF1 expression value was 1.116 ± 0.849 for normal tissue and 1.823 ± 1.337 for cancer tissue. Using pair-wise *t* test analysis, the *t* value was 4.433 and *P* value was <0.001 (<0.05). Thus, it was statistically significant. The induction of HSF1 expression in tumor tissue was confirmed to be strongly associated with sporadic colorectal cancer. We also confirmed increased iNOS expression in 22 out of 35 patients in their cancer tissue in comparison to their normal tissue (Table 2). The average iNOS expression value was 0.867 ± 0.761 for normal tissue and 1.133 ± 0.843 for cancer tissue. Using pair-wise *t* test analysis, the *t* value was 1.803 and *P* value was 0.08 (>0.05). Thus, it was not statistically significant.

HSF1 was found to induce expression of MDR1. To explore whether HSF1 induction could increase expression of MDR1, we performed RT-PCR analysis on the same specimens from 35 patients. To our surprise, we found reduction of MDR1 expression in most (23/35) cancer tissues in comparison to normal tissues. The average MDR1 expression value was 1.099 ± 0.885 for normal tissue and 1.443 ± 1.096 for cancer tissue. Using pair-wise *t* test analysis, the *t* value was -2.329 and *P* value was 0.026 (<0.05). Thus, it was statistically significant.

Among sporadic CRCs from these 35 patients, 5 cases were at stage A, 12 at stage B, 17 at stage C and 1 at stage D. Five cases whose HSF1 expression did not increase in cancer tissue mainly belonged to late-stage patients (3 cases at stage C, 1 at stage D and 1 at stage B). However, statistical analysis could not be performed due to the limited number of cases.

DISCUSSION

Cellular signal transduction regulates almost all biological and physiological functions within cells. It is executed by a complex system where multiple signal transduction pathways interact together and are tightly controlled at different levels. The abnormality in cellular signal transduction can affect various cellular functions such as cell growth and proliferation, differentiation and metabolism and eventually lead to various diseases. Cancer is a typical disease resulting from abnormality in cellular signal transduction. Mutations of multiple genes in somatic cells are involved in the process of neoplastic formation. These mutations result in activation of oncogenes and inactivation of tumor suppressor genes, which lead to uncontrolled cell growth due to the loss of cellular differentiation and/or apoptosis ability. Further mutations in genes controlling cellular adherence and movement lead to tumor metastasis. Therefore, multiple signal transduction pathways in cell growth and proliferation, differentiation, apoptosis, adherence and movement are involved in initiation and progression of cancer.

There are four signal transduction pathways described by Potter^[3,4] to be involved in the oncogenesis of hereditary CRC: APC- β -catenin-TCF-myc (Wnt) pathway^[5], microsatellite unstable pathway^[6], p53 pathway and estrogen receptor hypermethylation pathway. However, the signal transduction pathways involved in sporadic CRC remain unclear. APC mutation responsible for FAP's oncogenesis was also found in 60-70% sporadic CRCs^[7,8]. Similarly, microsatellite instability was found in over 30% sporadic CRCs^[9] and p53 mutation was found in 50% sporadic CRCs^[10]. In addition, non-steroidal anti-inflammatory drugs (NSAIDs) were found to efficiently suppress tumorigenesis of CRC by inhibiting Cox-2 activity^[11-14]. It indicates Cox-2 pathway is involved in CRC oncogenesis as well. These results suggest multiple signal pathways are involved in the oncogenesis of

sporadic CRC. To efficiently identify signal pathways involved in sporadic CRC, we employed PathwayFinder gene arrays that utilize pathway target genes to monitor the activation of 8 important pathways related to cell growth, proliferation, survival, stress, apoptosis and inflammation. Monitoring induction of target genes by RT-PCR was found to be an effective way to identify the activation of Wnt signal pathway in adenomas of FAP compared to matched normal mucosa^[15,16]. The utilization of gene array to identify induction of target genes greatly increased its efficiency.

We found HSF1 gene expression was significantly increased (30/35) in cancer tissue compared to its normal tissue in 35 patients. HSF1 stands for heat shock transcription factor 1 and is a transcription factor with a molecular weight of 82KD. HSF1 could be induced by heat, chemicals and hypoxia^[17-19] and usually exists as a monomer in the cytoplasm. After heat stimulation, it became a trimer and could be translocated into nucleus^[20]. Its transcriptional activity was greatly increased by the phosphorylation of serine induced by stimuli. HSF1 could activate transcription of its target genes by binding to a heat shock element^[7]. The heat shock element was present in the promoter region of many genes such as HSP90, HSP27, HSP70 and drug resistant gene MDR1^[21]. Hoang^[22] recently reported HSF1 expression was increased in a prostate cancer cell line. Our study not only provided the first evidence to demonstrate the association of HSF1 gene expression and CRC, but also suggested that the induction of HSF1 gene expression might be associated with a broad range of cancer. The reduced HSF1 expression in the remaining 5 cancer tissues might be due to different oncogenic mechanisms occurring in these CRCs from HSF1 induction related sporadic CRCs.

In this study, the induction of HSF1 gene expression was accompanied with the induction of HSP27 and HSP90 which were two target genes of HSF1, suggesting that the induction of HSF1 gene expression could activate HSF1 heat shock stress signal pathway in sporadic CRC. Heat shock stress signal pathway is highly involved in carcinogenesis since heat shock proteins (HSP90, HSP70, *etc.*) are responsible for maintaining the conformation, stability and function of key oncogenic client proteins involved in signal transduction pathways leading to proliferation, cell cycle progression and apoptosis, as well as other features of the malignant phenotype such as invasion, angiogenesis and metastasis^[23-26]. HSP90 has currently served as an anti-cancer drug target for various drug development^[27-29]. Also, HSP70 was found to inhibit apoptosis^[30]. Our result suggested heat shock stress pathway contributed to carcinogenesis actively instead of passively as a bystander. Our hypothesis of heat shock stress pathway contributing to carcinogenesis of sporadic CRCs coincides with the fact that colon is an open system where it could retain and receive various kinds of "stress" substances for a long period of time. The "stress" substances might come from meat, alcohol, inflammatory tissue and others^[31]. The prolonged exposure of these "stress" substances could lead to activation of heat shock stress pathway, thus leading to carcinogenesis through enhancing function of oncogenic proteins occurring in cells. The heat shock stress pathway could be further activated by hypoxia occurring in the tumor which was found to increase HSF1 expression as well^[18,19]. Vegetables, nonsteroidal anti-inflammatory drugs (NSAIDs), hormone replacement therapy, and physical activity^[31] could reverse the activation of heat shock stress pathway and therefore suppress carcinogenesis.

Hoang *et al.*^[22] found HSF1 expression was increased in a prostate cancer cell line PC-3 derived PC-3M clone with metastatic ability compared to its parent cell line. By Western-blot and immunohistochemistry analysis of 18 prostate cancer and 4 normal prostate tissues, they confirmed the induction of HSF1 expression in prostate cancer tissues. However, since

Western-blot and immunohisto-chemistry analyses detect protein expression instead of gene expression, it remains to be confirmed that the induction of HSF1 is at gene expression level. Our gene array analysis and RT-PCR directly measured mRNA level. We clearly demonstrated the induction of HSF1 was on the gene expression level and its strong association with sporadic CRCs. Nevertheless, in our study, each cancer tissue was paired with its matched normal tissue from the same patient for comparison of gene expression eliminating differential gene expression caused by individual genetic background.

PathwayFinder gene array from SuperArray provided two spots for each gene. The variation between the two spots was below 5%. According to Table 1, if β -actin expression level was used for normalization, genes whose expression was increased in cancer tissue included HSP27 (1.58 fold), iNOS (1.49 fold), HSF1 (1.43 fold), HSP90 (1.31 fold), κ B (1.25 fold), *egr-1* (1.16 fold). However, if GAPDH expression level was used for normalization, genes whose expression was increased in cancer tissue only include HSP27 (1.28 fold), iNOS (1.22 fold), HSF1 (1.17 fold), HSP90 (1.06 fold). Therefore, it is important to use multiple housekeeping genes for normalization since expression of house keeping genes such as β -actin and GAPDH may fluctuate sometimes.

Vilaboa^[31] found HSF1 could bind to the promoter region of MDR1 to increase its expression transcriptionally. However, MDR1 was also a target gene for Wnt signal pathway and the expression of MDR1 was increased in precancerous lesion of FAP patients^[32]. We found reduced MDR1 gene expression in most (23/35) cancer tissues. Our result suggested MDR1 gene expression was not regulated under heat shock stress signal pathway in colon tissue, more likely under Wnt signal pathway. The reverse association of MDR1 expression with HSF1 and β -catenin (Wnt pathway) indicated that different signal pathways contributed to the carcinogenesis of FAP and sporadic CRC. The reduced MDR1 gene expression was also found in other cancers such as kidney cancer^[33] and brain cancer^[34].

Recently, a large number of studies have revealed the association of iNOS expression with various cancers^[35-39]. Yagihashi^[40] studied 22 cases of colorectal cancer tissues by immunohistochemistry and RT-PCR and found increased iNOS expression was associated with colorectal cancer. Bing *et al.*^[37] found increased expression of iNOS and production of prostanoids in colorectal cancer paralleled to the increase in COX-2, confirming the importance of this enzyme in colon cancer. Ropponen^[39] found iNOS expression in colorectal cancer might be used as a prognosis marker as well. Our study also confirmed induced iNOS expression in 22 out of 35 cancer tissues, indicating that the biological significance of MDR1 and iNOS expression in CRC needs to be further studied.

REFERENCES

- 1 Li LD, Rao KQ, Zhang SW, Lu FZ, Zhou XN. Statistical analysis of data from 12 cancer registries in China, 1993-1997. *Zhongguo Zhongliu* 2002; **11**: 497-507
- 2 Fearnhead NS, Britton MP, Bodmer WF. The ABC of APC. *Hum Mol Genet* 2001; **10**: 721-733
- 3 Potter JD. Colorectal cancer: molecules and populations. *J Natl Cancer Inst* 1999; **91**: 916-932
- 4 Tejpar S, Cassiman JJ, Van Cutsem E. The molecular basis of colorectal cancer. *Acta Gastroenterol Belg* 2001; **64**: 249-254
- 5 Wang HL, Wang J, Xiao SY, Haydon R, Stoiber D, He TC, Bissonnette M, Hart J. Elevated protein expression of cyclin D1 and Fra-1 but decreased expression of c-Myc in human colorectal adenocarcinomas overexpressing beta-catenin. *Int J Cancer* 2002; **101**: 301-310
- 6 Wijnen J, de Leeuw W, Vasen H, van der Klift H, Moller P, Stormorken A, Meijers-Heijboer H, Lindhout D, Menko F, Vossen S, Moslein G, Tops C, Brocker-Vriends A, Wu Y, Hofstra R, Sijmons R, Cornelisse C, Morreau H, Fodde R. Familial en-

- dometrial cancer in female carriers of MSH6 germline mutations. *Nat Genet* 1999; **23**: 142-144
- 7 **Chung DC**. The genetic basis of colorectal cancer: insights into critical pathways of tumorigenesis. *Gastroenterology* 2000; **119**: 854-865
- 8 **Bright-Thomas RM**, Hargest R. APC, beta-Catenin and hTCF-4; an unholy trinity in the genesis of colorectal cancer. *Eur J Surg Oncol* 2003; **29**: 107-117
- 9 **Goel A**, Arnold CN, Niedzwiecki D, Chang DK, Ricciardiello L, Carethers JM, Dowell JM, Wasserman L, Compton C, Mayer RJ, Bertagnolli MM, Boland CR. Characterization of sporadic colon cancer by patterns of genomic instability. *Cancer Res* 2003; **63**: 1608-1614
- 10 **Goh HS**, Elnatan J, Low CH, Smith DR. p53 point mutation and survival in colorectal cancer patients: effect of disease dissemination and tumour location. *Int J Oncol* 1999; **15**: 491-498
- 11 **Hasegawa K**, Ichikawa W, Fujita T, Ohno R, Okusa T, Yoshinaga K, Sugihara K. Expression of cyclooxygenase-2 (COX-2) mRNA in human colorectal adenomas. *Eur J Cancer* 2001; **37**: 1469-1474
- 12 **Ricchi P**, Zarrilli R, Di Palma A, Acquaviva AM. Nonsteroidal anti-inflammatory drugs in colorectal cancer: from prevention to therapy. *Br J Cancer* 2003; **88**: 803-807
- 13 **Nasir A**, Fernandez PM, Chughtai OR, Kaiser HE. COX-2, NSAIDs and human neoplasia. Part I: Colorectal neoplasms. *In Vivo* 2002; **16**: 501-509
- 14 **Reddy BS**, Rao CV. Novel approaches for colon cancer prevention by cyclooxygenase-2 inhibitors. *J Environ Pathol Toxicol Oncol* 2002; **21**: 155-164
- 15 **D'Orazio D**, Muller PY, Heinimann K, Albrecht C, Bendik I, Herzog U, Tondelli P, Bauerfeind P, Muller H, Dobbie Z. Overexpression of Wnt target genes in adenomas of familial adenomatous polyposis patients. *Anticancer Res* 2002; **22**: 3409-3414
- 16 **Kolligs FT**, Bommer G, Goke B. Wnt/beta-catenin/tcf signaling: a critical pathway in gastrointestinal tumorigenesis. *Digestion* 2002; **66**: 131-144
- 17 **Wu C**. Heat shock transcription factors: structure and regulation. *Annu Rev Cell Dev Biol* 1995; **11**: 441-469
- 18 **Eickelberg O**, Seebach F, Riordan M, Thulin G, Mann A, Reidy KH, Van Why SK, Kashgarian M, Siegel N. Functional activation of heat shock factor and hypoxia-inducible factor in the kidney. *J Am Soc Nephrol* 2002; **13**: 2094-2101
- 19 **Baek SH**, Lee UY, Park EM, Han MY, Lee YS, Park YM. Role of protein kinase Cdelta in transmitting hypoxia signal to HSF and HIF-1. *J Cell Physiol* 2001; **188**: 223-235
- 20 **Newton EM**, Knauf U, Green M, Kingston RE. The regulatory domain of human heat shock factor 1 is sufficient to sense heat stress. *Mol Cell Biol* 1996; **16**: 839-846
- 21 **Cotto JJ**, Kline M, Morimoto RI. Activation of heat shock factor 1 DNA binding precedes stress-induced serine phosphorylation. Evidence for a multistep pathway of regulation. *J Biol Chem* 1996; **271**: 3355-3358
- 22 **Hoang AT**, Huang J, Rudra-Ganguly N, Zheng J, Powell WC, Rabindran SK, Wu C, Roy-Burman P. A novel association between the human heat shock transcription factor 1 (HSF1) and prostate adenocarcinoma. *Am J Pathol* 2000; **156**: 857-864
- 23 **Ochel HJ**, Gademann G. Heat-shock protein 90: potential involvement in the pathogenesis of malignancy and pharmacological intervention. *Onkologie* 2002; **25**: 466-473
- 24 **Blagosklonny MV**. Hsp-90-associated oncoproteins: multiple targets of geldanamycin and its analogs. *Leukemia* 2002; **16**: 455-462
- 25 **Witkin SS**. Heat shock protein expression and immunity: relevance to gynecologic oncology. *Eur J Gynaecol Oncol* 2001; **22**: 249-256
- 26 **Sarto C**, Binz PA, Mocarelli P. Heat shock proteins in human cancer. *Electrophoresis* 2000; **21**: 1218-1226
- 27 **Neckers L**. Hsp90 inhibitors as novel cancer chemotherapeutic agents. *Trends Mol Med* 2002; **8**(4 Suppl): S55-61
- 28 **Manjili MH**, Wang XY, Park J, Facciponte JG, Repasky EA, Subjeck JR. Immunotherapy of cancer using heat shock proteins. *Front Biosci* 2002; **7**: d43-52
- 29 **Maloney A**, Workman P. HSP90 as a new therapeutic target for cancer therapy: the story unfolds. *Expert Opin Biol Ther* 2002; **2**: 3-24
- 30 **Beere HM**, Green DR. Stress management - heat shock protein-70 and the regulation of apoptosis. *Trends Cell Biol* 2001; **11**: 6-10
- 31 **Vilaboa NE**, Galan A, Troyano A, de Blas E, Aller P. Regulation of multidrug resistance 1 (MDR1)/P-glycoprotein gene expression and activity by heat-shock transcription factor 1 (HSF1). *J Biol Chem* 2000; **275**: 24970-24976
- 32 **Yamada T**, Takaoka AS, Naishiro Y, Hayashi R, Maruyama K, Maesawa C, Ochiai A, Hirohashi S. Transactivation of the multidrug resistance 1 gene by T-cell factor 4/beta-catenin complex in early colorectal carcinogenesis. *Cancer Res* 2000; **60**: 4761-4766
- 33 **Yan C**, Luo B, Chen WG. Expression of multidrug resistance genes and multidrug resistance-associated protein genes in renal cell carcinomas. *Qingdao Daxue Yixueyuan Xuebao* 2001; **37**: 103-105
- 34 **Demeule M**, Shedid D, Beaulieu E, Del Maestro RF, Moghrabi A, Ghosn PB, Moudmjan R, Berthelet F, Beliveau R. Expression of multidrug-resistance P-glycoprotein (MDR1) in human brain tumors. *Int J Cancer* 2001; **93**: 62-66
- 35 **Zhang SZ**, Peng JP, Ye F, Zheng S. Expression of inducible nitric oxide synthase in breast cancer and its relation to carcinogenesis. *Zhongguo Aizheng Zazhi* 2001; **20**: 762-765
- 36 **Wolf H**, Haeckel C, Roessner A. Inducible nitric oxide synthase expression in human urinary bladder cancer. *Virchows Arch* 2000; **437**: 662-666
- 37 **Bing RJ**, Miyataka M, Rich KA, Hanson N, Wang X, Slosser HD, Shi SR. Nitric oxide, prostanoids, cyclooxygenase, and angiogenesis in colon and breast cancer. *Clin Cancer Res* 2001; **7**: 3385-3392
- 38 **Brandao MM**, Soares E, Salles TS, Saad ST. Expression of inducible nitric oxide synthase is increased in acute myeloid leukaemia. *Acta Haematol* 2001; **106**: 95-99
- 39 **Ropponen KM**, Kellokoski JK, Lipponen PK, Eskelinen MJ, Alanne L, Alhava EM, Kosma VM. Expression of inducible nitric oxide synthase in colorectal cancer and its association with prognosis. *Scand J Gastroenterol* 2000; **35**: 1204-1211
- 40 **Yagihashi N**, Kasajima H, Sugai S, Matsumoto K, Ebina Y, Morita T, Murakami T, Yagihashi S. Increased in situ expression of nitric oxide synthase in human colorectal cancer. *Virchows Arch* 2000; **436**: 109-114

An integrated approach to the detection of colorectal cancer utilizing proteomics and bioinformatics

Jie-Kai Yu, Yi-Ding Chen, Shu Zheng

Jie-Kai Yu, Cancer Institute, the Second Affiliated Hospital of Zhejiang University Medical College, Hangzhou 310009, Zhejiang Province, China

Jie-Kai Yu, College of Life Science of Zhejiang University, Hangzhou 310029, Zhejiang Province, China

Jie-Kai Yu, Hangzhou Genomics Institute, Hangzhou 310008, Zhejiang Province, China

Yi-Ding Chen, Department of Oncology, the Second Affiliated Hospital of Zhejiang University Medical College, Hangzhou 310009, Zhejiang Province, China

Shu Zheng, Cancer Institute, Zhejiang University, Hangzhou 310009, Zhejiang Province, China

Supported by the Major State Basic Research Development Program of China 973 program, No. G1998051200

Correspondence to: Shu Zheng, Cancer Institute, Zhejiang University, Hangzhou 310009, Zhejiang Province, China. zhengshu@mail.hz.zj.cn

Telephone: +86-571-87783868 **Fax:** +86-571-87214404

Received: 2004-04-09 **Accepted:** 2004-05-09

Abstract

AIM: To find new potential biomarkers and to establish patterns for early detection of colorectal cancer.

METHODS: One hundred and eighty-two serum samples including 55 from colorectal cancer (CRC) patients, 35 from colorectal adenoma (CRA) patients and 92 from healthy persons (HP) were detected by surface-enhanced laser desorption/ionization mass spectrometry (SELDI-MS). The data of spectra were analyzed by bioinformatics tools like artificial neural network (ANN) and support vector machine (SVM).

RESULTS: The diagnostic pattern combined with 7 potential biomarkers could differentiate CRC patients from CRA patients with a specificity of 83%, sensitivity of 89% and positive predictive value of 89%. The diagnostic pattern combined with 4 potential biomarkers could differentiate CRC patients from HP with a specificity of 92%, sensitivity of 89% and positive predictive value of 86%.

CONCLUSION: The combination of SELDI with bioinformatics tools could help find new biomarkers and establish patterns with high sensitivity and specificity for the detection of CRC.

Yu JK, Chen YD, Zheng S. An integrated approach to the detection of colorectal cancer utilizing proteomics and bioinformatics. *World J Gastroenterol* 2004; 10(21): 3127-3131 <http://www.wjgnet.com/1007-9327/10/3127.asp>

INTRODUCTION

Colorectal cancer (CRC) is one of the most common malignant tumors that threaten people's health^[1-5]. At present, CRC is one of the three leading causes of worldwide cancer mortality and the second leading cause of cancer-related deaths in the Western world^[6,7]. The prognosis of CRC is strongly related to early diagnosis. CRC patients diagnosed in early stage have a

five-year survival post-operation of over 80%, but in the advanced stage the five-year survival is lower than 40%. So, early diagnosis is very important to improve the prognosis of CRC^[8].

Recently serum tumor markers, such as carcinoembryonic antigen (CEA), are commonly used to detect CRC for the advantages of less pain and accessibility. However all the existing biomarkers have a low diagnostic sensitivity in CRC (sensitivity of 23% with CEA^[9]). New biomarkers with a high sensitivity and specificity to detect CRC in early stage are urgently needed. A novel proteomic approach for the detection of cancer which is called surface enhanced laser desorption/ionization time-of-flight mass spectrometry (SELDI-TOF MS), and ProteinChip technology, have been developed. SELDI-TOF MS coupled with bioinformatics approach has successfully found new biomarkers and achieved high sensitivity and specificity for the diagnosis of cancers of bladder^[10], prostate^[11-14], ovary^[15,16], breast^[17,18], liver^[19], neck^[20], lung^[21,22], pancreas^[23].

The aim of this study was to find the potential biomarkers in CRC and to establish the patterns to diagnose CRC.

MATERIALS AND METHODS

Samples

A total of 182 serum samples were obtained from the serum banks of the Cancer Institute of the Second Affiliated Hospital of Zhejiang University Medical College. The cancer group consisted of 55 serum samples from CRC patients at different clinical stages: Dukes' A ($n = 8$), Dukes' B ($n = 22$), Dukes' C ($n = 13$), Dukes' D ($n = 12$). The median age of CRC patients was 57 years (range, 31-84 years). The two non-cancer control groups included 35 serum samples from patients with colorectal adenoma (CRA) and 92 serum samples from healthy persons (HP). They were age and sex matched with cancer group. Diagnoses were pathologically confirmed, and specimens were obtained before treatment. All samples were stored at -80°C .

Proteinchip array analysis

Serum samples were thawed in ice and centrifuged at 3 000 r/m for 5 min at 4°C , supernatants were retained. We added 90 μL of 5 g/L CHAPS (Sigma) (pH 7.4) in PBS to 10 μL of each serum sample, and vortex-mixed them. The diluted samples were added to 100 μL Cibacron Blue 3GA (Sigma) (previously equilibrated with 5 g/L CHAPS three times) in a 96-well cell culture plate and agitated on a platform shaker at 4°C for 60 min. After centrifuged at 1 000 r/m, 50 μL supernatant was sampled and further diluted by 150 μL 20 mmol/L HEPES (pH 7.4) and applied to each well of a bioprocessor (CIPHERGEN Biosystems) containing hydrophobic surface (H4) chips previously activated with 20 mmol/L HEPES. The bioprocessor was then sealed and agitated on a platform shaker for 60 min at 4°C . The excess serum mixtures were discarded, and the chips were washed three times with 20 mmol/L HEPES and 2 times with deionized water. The chips were then removed from the bioprocessor, air-dried. Before SELDI analysis, 0.5 μL of a saturated solution of α -cyano-4-hydroxycinnamic acid (CHCA) in 0.5 L/L acetonitrile and 5 mL/L trifluoroacetic acid was applied onto each chip twice, air-dried.

Chips were detected on the protein biological system II

(PBS-II) plus a mass spectrometer reader (CIPHERGEN Biosystems). Data were collected by averaging 65 laser shots with an intensity of 135, a detector sensitivity of 7, a highest mass of 30 000 Da and an optimized range of 2 000-20 000 Da. Mass accuracy was calibrated to less than 0.1% using the all-in-one peptide molecular mass standard (CIPHERGEN Biosystems).

Bioinformatics analysis

The spectra intensities of all samples were normalized to the total ion current of m/z between 2 000 and 30 000 Da. The noise of spectra was filtered and peaks were detected with an automatic peak detection pass using signal-to-noise ratio. Peak clusters were completed to cluster the peaks in different samples that had similar masses (defined by a mass window in 0.3% mass error). All these were performed using ProteinChip Software 3.1 (CIPHERGEN). The peak intensities were preprocessed by scaling all the data to the range[-1, 1].

The pattern recognition techniques were applied to diverse areas including prediction of cancer^[24], gene microarray^[25] and mass spectrometry^[26]. We utilized a multi-layer perception (MLP) ANN with a scaled conjugate gradient (SCG) optimized back propagation algorithm for discriminating CRC from HP, and a linear support vector machine (SVM) for discriminating CRC from CRA. They were powerful tools for analysis of the complex data^[14] derived from SELDI-MS.

Feature selection

We estimated the power of each peak in discriminating different group samples by integrating approaches such as *t*-test, receive option curve (ROC) and mean square error (MSE) of ANN.

The ANN used to calculate the MSE of each peak had 3 layers, with 1 node in input and output layer, 2 nodes in hidden. For each peak the ANN was trained with all the samples, performed 1 000 epochs to get the MSE respectively. The MSE was calculated as the difference between the target output and the ANN predictive value. The lower MSE value of the peak showed a higher relative importance value for their ability to accurately discriminate the different groups.

Integrated ANN classifier

The ANN established for discriminating different groups had 4 layers. Except output layer and input layer ANN also had 2 hidden layers each with 100 nodes. We randomly selected 1/3 of all the samples to be the blinded test set, and the remaining 2/3 samples for training, the procedure was repeated 10 times.

In the procedure of training ANN we used a cross-validation approach to reduce the risk of "over fit"^[27]. The samples for training were randomly divided into 2 sets: 2/3 samples for training set and 1/3 samples for validation set. The random shuffling was redone 100 times. Thus 100 different ANNs were established to predict the blinded test set samples. The predictive values of the blinded test set samples were the average of all the predicted outputs of 100 ANNs.

SVM classifier

SVM is a new machine learning approach originally proposed and developed by Vladimir Vapnik. SVM applications were actively pursued in various areas recently, from genomics to face recognition^[28,29]. SVM is powerful for small sample data. We used the linear SVM classifier and set the cost of the constrain violation (C) to 1. The 3-fold cross-validation approach was applied to estimate the accuracy of the classifier.

RESULTS

Bioinformatics analysis of CRC and HP data

After noise was filtered by CIPHERGEN ProteinChip Software 3.1,

there were 61 peaks detected for discriminating CRC from HP and 235 peaks for discriminating CRC from CRA. The peaks were between 2 k and 30 kDa. Peaks with an $m/z < 2$ kDa were mainly ion noise from the matrix and therefore excluded^[10].

The 61 qualified peaks detected from the two groups were ranked by the MSE values of ANN. We input the 61 peaks respectively. For each peak we trained the ANN with all the 147 healthy and CRC samples to give an MSE value. The top 15 peaks with lower MSE values were selected for further analysis (Figure 1). The *t*-test and ROC method confirmed the results with the same 15 peaks.

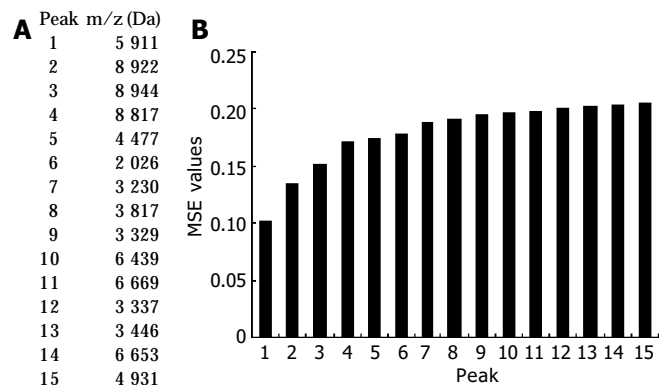


Figure 1 MSE values of the top 15 peaks. A: m/z of peaks. B: MSE values of peaks.

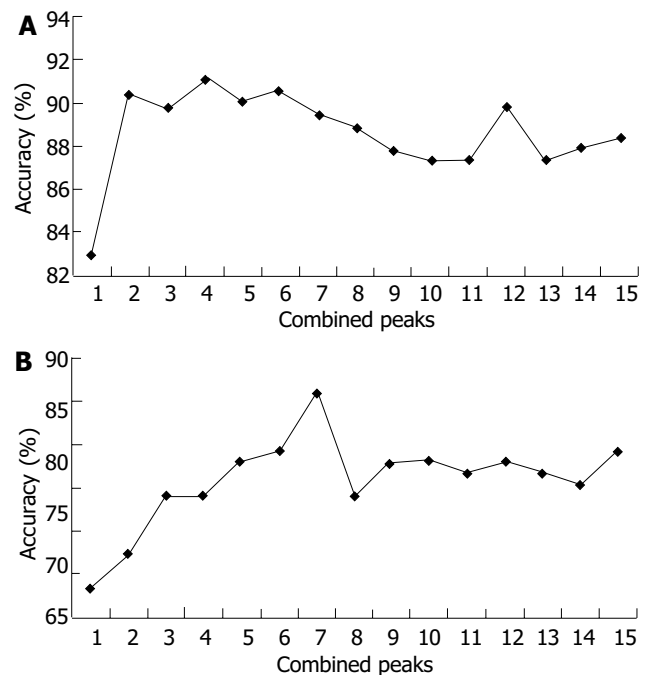


Figure 2 Accuracies of different combinations of peaks. A: Accuracies of different combinations of peaks in the pattern discriminating CRC patients from HP. B: Accuracies of different combinations of peaks in the pattern discriminating CRC patients from CRA patients.

To further select the set of candidate biomarkers, we used a stepwise approach in which many integrated ANNs were trained. The top 1 peak with the highest ability to predict the two groups (had the lowest MSE value) was selected as a single input to build the integrated ANN. We estimated the discriminating ability of this integrated ANN by the accuracy of blind test set. Next, the top 2 peaks were input to integrated ANN and the accuracy was calculated. The following peaks were added as

input stepwise to train integrated ANN and the accuracy was calculated. In this way, the 15 models combining different peaks were built. The peaks input to the model with the highest accuracy were selected as the set of potential biomarkers. The top 4 peaks were finally selected as potential biomarkers, an accuracy of 92% was achieved. The accuracies of these 15 models are plotted in Figure 2 (A).

The m/z of the 4 candidate biomarkers were 5 911, 8 922, 8 944, 8 817 Da. These 4 peaks all appeared to highly express in CRC and lowly express in healthy persons, as shown in Figure 3 (A, B). Between the two groups, the *P* value of *t*-test ($<10^{-9}$) and the area under the ROC curve (>8.0) showed statistical significance of all the 4 peaks. Table 1 shows the descriptive statistics of the 4 peaks.

Table 1 Descriptive data for the 4 potential biomarkers in the pattern discriminating CRC patients from HP (mean±SD)

M/Z (Da)	AUC	HP	CRC patients
5 911	0.908	0.824±0.504	2.763±1.720
8 922	0.872	1.254±0.724	2.767±1.445
8 944	0.828	0.999±0.626	2.651±1.851
8 817	0.811	0.878±0.607	1.744±0.940

AUC: area under the curve.

The 4 peaks were combined and evaluated by integrated ANN. We trained the integrated ANN with 89 samples and tested 49 samples. We randomly selected the test set 10 times, and each time 100 ANNs were built to predict the test set. So 1 000

ANNs were built up. Table 3 shows the results of this classifier. For the integrated ANN classifier, the estimated specificity in the blind test set was 92% with a 95% confidence interval of 89-95%, the estimated sensitivity was 89% (85-93%), the estimated positive predictive value was 86% (82-90%).

Table 2 Descriptive statistics for the 7 potential biomarkers in the pattern discriminating CRC patients from CRA patients (mean±SD)

M/Z (Da)	<i>P</i> value ($\times 10^{-5}$)	CRA patients	CRC patients
17 247	0.71	0.211±0.130	0.113±0.100
18 420	1.27	0.039±0.036	0.076±0.040
5 911	1.71	1.459±0.977	2.763±1.720
9 294	2.76	0.617±0.385	1.105±0.563
4 654	6.74	0.503±0.493	1.164±0.943
21 694	7.48	0.489±0.145	0.698±0.267
21 742	12.10	0.536±0.161	0.744±0.282

Table 3 Predicted results of classifier for discriminating CRC patients from HP

	Test set (49×10)		Training set (98×10)	
	HP	CRC	HP	CRC
HP (92×10)	287	25	599	9
CRC (55×10)	19	159	29	343
Specificity (%)	92(287/(287+25))		99(599/(599+9))	
Sensitivity (%)	89(159/(159+19))		92(343/(343+29))	
Positive value (%)	86(159/(159+25))		97(343/(343+9))	

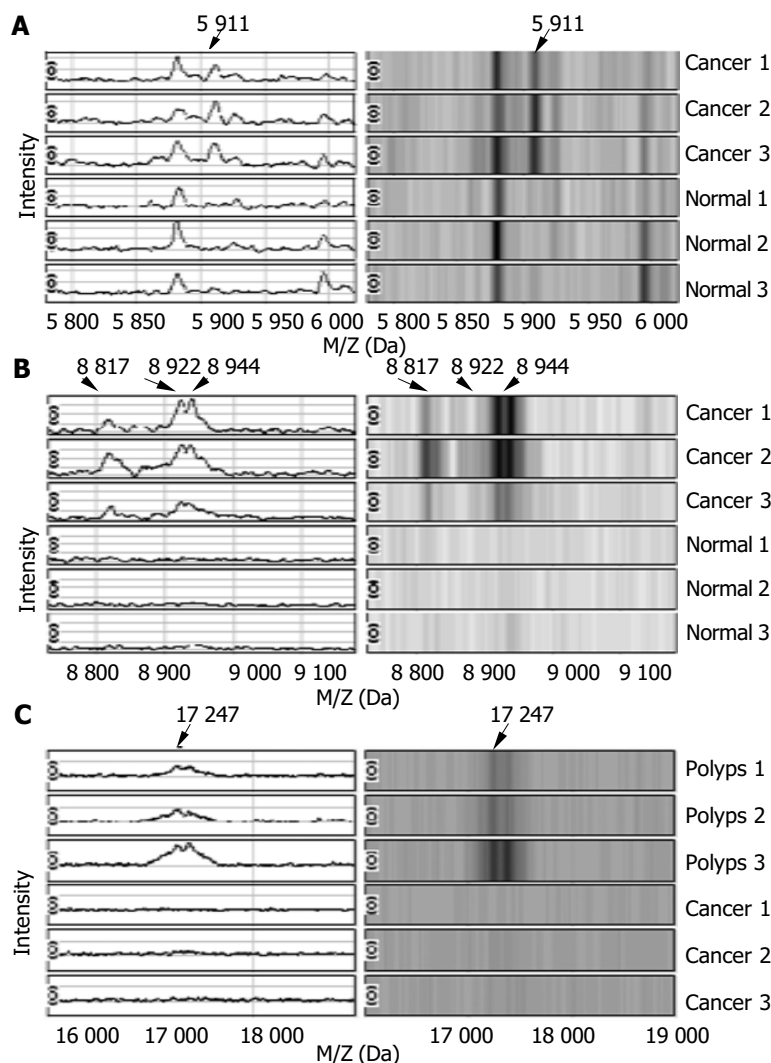


Figure 3 Spectra and gel maps of potential biomarkers. A: Spectra and gel maps of the peak with the m/z of 5 911 Da. B: Spectra and gel maps of the peak with the m/z of 8 922, 8 944, 8 817 Da. C: Spectra and gel maps of the peak with the m/z of 17 247 Da.

Bioinformatics analysis of CRC and CRA data

The 235 qualified peaks detected from the two groups were ranked by the *P* values of *t*-test. The top 15 peaks were selected for further analysis. For these data we utilized the 3-fold cross-validation SVM classifier to select the potential biomarkers to build the model to predict the test sets. This approach randomly selected 1/3 of samples to be the blinded test set, and the remaining 2/3 samples to be the training set and the procedure was repeated 3 times. We still used stepwise method to add the peaks in the rank of *P* value one by one to be the input of 3-cross-validation SVM. The top 7 peaks with the highest accuracy (86.7%) were selected as final potential biomarkers to separate the two groups. Table 2 shows the descriptive data of the 7 peaks. Between the two groups, the *P* values of *t*-test ($<10^{-4}$) and the area under the ROC curve (>7.0) showed the statistical significance of the 7 peaks. In the 7 peaks only the peak of 17 247 Da appeared to lowly express in CRC and highly express in CRA as shown in Figure 3C, others were highly expressed in CRC.

We used 3-fold cross-validation SVM to combine the 7 peaks, and trained it with 60 samples. For the 3-fold cross-validation SVM, the estimated specificity in the blind test set (30 samples) was 83% with a 95% confidence interval of 79-87%, the estimated sensitivity was 89% (86-92%), the estimated positive predictive value was 89% (86-92%). Table 4 shows our results for this classifier.

Table 4 Predicted results of classifier for discriminating CRC patients from CRA

	Test set (30×3)		Training set (60×3)	
	CRA	CRC	CRA	CRC
CRA (35×3)	29	6	56	14
CRC (55×3)	6	49	16	94
Specificity (%)	83(29/(29+6))		80(56/(56+14))	
Sensitivity (%)	89(49/(49+6))		85(94/(94+16))	
Positive value (%)	89(49/(49+6))		87(94/(94+14))	

DISCUSSION

CRC screening includes fecal occult blood test (FOBT), sigmoidoscopy, air-contrast barium enema examination, colonoscopy^[50]. But they have not been commonly accepted due to costs, bowel preparation, sedation and perforation risks. Detection of serum tumor markers (such as CEA) is an inexpensive and facile screening method compared to others. However, all the existing biomarkers in serum lack sufficient sensitivity for screening and diagnosis of CRC^[31-35]. In this study, we detected CEA values (cut-off value of CEA level of 5 ng/mL) of 182 serum samples (including 55 from CRC patients, 35 from CRA and 92 from HP which were also detected by SELDI), and a sensitivity of 47% was achieved in screening for CRC. The results also showed that CEA lacked sufficient sensitivity for screening and diagnosis of CRC.

Because of the multi-factorial nature of CRC, it is very clear that a combination of several markers would be necessary to effectively detect and diagnose CRC. SELDI-MS and the ProteinChip technology could provide the high-throughput proteomic profiling^[36]. Coupled with sophisticated bioinformatics tools for complex data analysis they could find the "fingerprints" of CRC and build the diagnosis model.

One hundred and forty-seven CRC patients and HP were detected by SELDI-TOF-MS and the complex data were analyzed by integrated ANN, we found 4 potential biomarkers and achieved a specificity of 92% (89-95%), sensitivity of 89% (85-93%), positive predictive value of 86% (82-90%). Ninety CRC and CRA patients were detected by SELDI-MS and analyzed by an SVM classifier. We found 7 potential biomarkers and achieved

a specificity of 83% (79-87%), sensitivity of 89% (86-92%), positive predictive value of 89% (86-92%).

Early detection remains one of the most urgent issues in CRC research^[37]. Our two patterns could recognize early Dukes samples as efficiently as other Dukes samples. The biomarkers used in the final selection were not sensitive to different Dukes, stages of cancer patients. In almost all the patients with CRC, preceding lesions were asymptomatic adenomas^[38]. So it is very important to discriminate the noncancer CRA patients from early CRC. We also achieved a high sensitivity and specificity model to recognize CRC and CRA patients.

We developed an integrated approach using bioinformatics and biostatics tools to analyze the large data of spectra. The ROC curve, *t*-test and MSE values were used to rank and select the peaks according to their contribution to the separation of two groups. To accurately estimate the sensitivity and specificity of the classifiers established by potential biomarkers, the test sets were randomly selected many times, independent of training sets each time.

The peak of 4 645 Da was identified as doubly charged forms of 9 294 Da by Ciphergen ProteinChip Software 3.1. The recognition of both the doubly charged and the singly charged forms of these peaks suggested their importance in discriminating the two diagnostic groups. The peak of 5 911 Da was selected as a potential biomarker in both the pattern discriminating CRC patients from HP and the pattern discriminating CRC from CRA patients. The expression of this biomarker increased step by step in HP, CRA and CRC patients as shown in Figure 3A. Therefore the peak of 5 911 Da may play an important role in the formation and progression of CRC.

In conclusion, SELDI-TOF-MS in combination with sophisticated bioinformatics tools could facilitate the discovery of new biomarkers and establish patterns with a high sensitivity and specificity for the detection of CRC.

REFERENCES

- Zhang YL, Zhang ZS, Wu BP, Zhou DY. Early diagnosis for colorectal cancer in China. *World J Gastroenterol* 2002; **8**: 21-25
- Thiis-Evensen E, Hoff GS, Sauar J, Majak BM, Vatn MH. Flexible sigmoidoscopy or colonoscopy as a screening modality for colorectal adenomas in older age groups? Findings in a cohort of the normal population aged 63-72 years. *Gut* 1999; **45**: 834-839
- Li S, Nie Z, Li N, Li J, Zhang P, Yang Z, Mu S, Du Y, Hu J, Yuan S, Qu H, Zhang T, Wang S, Dong E, Qi D. Colorectal cancer screening for the natural population of Beijing with sequential fecal occult blood test: a multicenter study. *Chin Med J* 2003; **116**: 200-202
- Repetto L, Venturino A, Fratino L, Serraino D, Troisi G, Gianni W, Pietropaolo M. Geriatric oncology: a clinical approach to the older patient with cancer. *Eur J Cancer* 2003; **39**: 870-880
- Gatta G, Faivre J, Capocaccia R, Ponz de Leon M. Survival of colorectal cancer patients in Europe during the period 1978-1989. *Eur J Cancer* 1998; **34**: 2176-2183
- Ries LA, Wingo PA, Miller DS, Howe HL, Weir HK, Rosenberg HM, Vernon SW, Cronin K, Edwards BK. The annual report to the nation on the status of cancer, 1973-1997, with a special section on colorectal cancer. *Cancer* 2000; **88**: 2398-2424
- Jemal A, Murray T, Samuels A, Ghafoor A, Ward E, Thun MJ. Cancer statistics, 2003. *CA Cancer J Clin* 2003; **53**: 5-26
- Dashwood RH. Early detection and prevention of colorectal cancer (review). *Oncol Rep* 1999; **6**: 277-281
- Mishaeli M, Klein B, Sadikov E, Bayer I, Koren R, Gal R, Rakowsky E, Levin I, Kfir B, Schachter J, Klein T. Initial TPS serum level as an indicator of relapse and survival in colorectal cancer. *Anticancer Res* 1998; **18**: 2101-2105
- Vlahou A, Schellhammer PF, Mendrinos S, Patel K, Kondylis FI, Gong L, Nasim S, Wright GL Jr. Development of a novel proteomic approach for the detection of transitional cell carcinoma of the bladder in urine. *Am J Pathol* 2001; **158**: 1491-1501
- Adam BL, Qu Y, Davis JW, Ward MD, Clements MA, Cazares

- LH, Semmes OJ, Schellhammer PF, Yasui Y, Feng Z, Wright GL Jr. Serum protein fingerprinting coupled with a pattern-matching algorithm distinguishes prostate cancer from benign prostate hyperplasia and healthy men. *Cancer Res* 2002; **62**: 3609-3614
- 12 **Qu YS**, Adam BL, Yasui Y, Ward MD, Cazares LH, Schellhammer PF, Feng Z, Semmes OJ, Wright GL Jr. Boosted decision tree analysis of surface-enhanced laser desorption/ionization mass spectral serum profiles discriminates prostate cancer from noncancer patients. *Clin Chem* 2002; **48**: 1835-1843
- 13 **Wagner M**, Naik DN, Pothan A, Kasukurti S, Devineni RR, Adam BL, Semmes OJ, Wright GL Jr. Computational protein biomarker prediction: a case study for prostate cancer. *BMC Bioinformatics* 2004; **5**: 26
- 14 **Jr GW**, Cazares LH, Leung SM, Nasim S, Adam BL, Yip TT, Schellhammer PF, Gong L, Vlahou A. Proteinchip (R) surface enhanced laser desorption/ionization (SELDI) mass spectrometry: a novel protein biochip technology for detection of prostate cancer biomarkers in complex protein mixtures. *Prostate Cancer Prostatic Dis* 1999; **2**: 264-276
- 15 **Petricoin EF**, Ardekani AM, Hitt BA, Levine PJ, Fusaro VA, Steinberg SM, Mills GB, Simone C, Fishman DA, Kohn EC, Liotta LA. Use of proteomic patterns in serum to identify ovarian cancer. *Lancet* 2002; **359**: 572-577
- 16 **Vlahou A**, Schorge JO, Gregory BW, Coleman RL. Diagnosis of ovarian cancer using decision tree classification of mass spectral data. *J Biomed Biotechnol* 2003; **2003**: 308-314
- 17 **Li J**, Zhang Z, Rosenzweig J, Wang YY, Chan DW. Proteomics and bioinformatics approaches for identification of serum biomarkers to detect breast cancer. *Clin Chem* 2002; **48**: 1296-1304
- 18 **Vlahou A**, Laronga C, Wilson L, Gregory B, Fournier K, McGaughey D, Perry RR, Wright GL Jr, Semmes OJ. A novel approach toward development of a rapid blood test for breast cancer. *Clin Breast Cancer* 2003; **4**: 203-209
- 19 **Poon TC**, Yip TT, Chan AT, Yip C, Yip V, Mok TS, Lee CC, Leung TW, Ho SK, Johnson PJ. Comprehensive proteomic profiling identifies serum proteomic signatures for detection of hepatocellular carcinoma and its subtypes. *Clin Chem* 2003; **49**: 752-760
- 20 **Wadsworth JT**, Somers KD, Stack BC Jr, Cazares L, Malik G, Adam BL, Wright GL Jr, Semmes OJ. Identification of patients with head and neck cancer using serum protein profiles. *Arch Otolaryngol Head Neck Surg* 2004; **130**: 98-104
- 21 **Xiao X**, Liu D, Tang Y, Guo F, Xia L, Liu J, He D. Development of proteomic patterns for detecting lung cancer. *Dis Markers* 2003; **19**: 33-39
- 22 **Zhukov TA**, Johanson RA, Cantor AB, Clark RA, Tockman MS. Discovery of distinct protein profiles specific for lung tumors and pre-malignant lung lesions by SELDI mass spectrometry. *Lung Cancer* 2003; **40**: 267-279
- 23 **Koopmann J**, Zhang Z, White N, Rosenzweig J, Fedarko N, Jagannath S, Canto MI, Yeo CJ, Chan DW, Goggins M. Serum diagnosis of pancreatic adenocarcinoma using surface-enhanced laser desorption and ionization mass spectrometry. *Clin Cancer Res* 2004; **10**: 860-868
- 24 **Bottaci L**, Drew PJ, Hartley JE, Hadfield MB, Farouk R, Lee PW, Macintyre IM, Duthie GS, Monson JR. Artificial neural networks applied to outcome prediction for colorectal cancer patients in separate institutions. *Lancet* 1997; **350**: 469-472
- 25 **Romualdi C**, Campanaro S, Campagna D, Celegato B, Cannata N, Toppo S, Valle G, Lanfranchi G. Pattern recognition in gene expression profiling using DNA array: a comparative study of different statistical methods applied to cancer classification. *Hum Mol Genet* 2003; **12**: 823-836
- 26 **Ball G**, Mian S, Holding F, Allibone RO, Lowe J, Ali S, Li G, McCauley S, Ellis IO, Creaser C, Rees RC. An integrated approach utilizing artificial neural networks and SELDI mass spectrometry for the classification of human tumours and rapid identification of potential biomarkers. *Bioinformatics* 2002; **18**: 395-404
- 27 **Khan J**, Wei JS, Ringner M, Saal LH, Ladanyi M, Westermann F, Berthold F, Schwab M, Antonescu CR, Peterson C, Meltzer PS. Classification and diagnostic prediction of cancers using gene expression profiling and artificial neural networks. *Nature* 2001; **7**: 658-659
- 28 **Peng S**, Xu Q, Ling XB, Peng X, Du W, Chen L. Molecular classification of cancer types from microarray data using the combination of genetic algorithms and support vector machines. *FEBS Lett* 2003; **555**: 358-362
- 29 **Koike A**, Takagi T. Prediction of protein-protein interaction sites using support vector machines. *Protein Eng Des Sel* 2004; **17**: 165-173
- 30 **Church TR**, Yeazel MW, Jones RM, Kochevar LK, Watt GD, Mongin SJ, Cordes JE, Engelhard D. A randomized trial of direct mailing of fecal occult blood tests to increase colorectal cancer screening. *J Natl Cancer Inst* 2004; **96**: 770-780
- 31 **Kornek GV**, Depisch D, Rosen HR, Temsch EM, Scheithauer W. Comparative analysis of CA72-4, CA195 and carcinoembryonic antigen in patients with gastrointestinal malignancies. *J Cancer Res Clin Oncol* 1992; **118**: 318-320
- 32 **Posner MR**, Mayer RJ. The use of serologic tumor markers in gastrointestinal malignancies. *Hematol Oncol Clin North Am* 1994; **8**: 533-553
- 33 **Ohuchi N**, Takahashi K, Matoba N, Sato T, Taira Y, Sakai N, Masuda M, Mori S. Comparison of serum assays for TAG-72, CA19-9 and CEA in gastrointestinal carcinoma patients. *Jpn J Clin Oncol* 1989; **19**: 242-250
- 34 **Ueda T**, Shimada E, Urakawa T. The clinicopathologic features of serum CA 19-9-positive colorectal cancers. *Surg Today* 1994; **24**: 518-525
- 35 **Nakagoe T**, Sawai T, Tsuji T, Jibiki MA, Nanashima A, Yamaguchi H, Yasutake T, Ayabe H, Arisawa K. Preoperative serum level of CA19-9 predicts recurrence after curative surgery in node-negative colorectal cancer patients. *Hepatogastroenterology* 2003; **50**: 696-699
- 36 **Srinivas PR**, Srivastava S, Hanash S, Wright GL Jr. Proteomics in early detection of cancer. *Clin Chem* 2001; **47**: 1901-1912
- 37 **Hurlstone DP**, Fujii T, Lobo AJ. Early detection of colorectal cancer using high-magnification chromoscopic colonoscopy. *Br J Surg* 2002; **89**: 272-282
- 38 **Vogelstein B**, Fearon ER, Hamilton SR, Kern SE, Preisinger AC, Leppert M, Nakamura Y, White R, Smits AM, Bos JL. Genetic alterations during colorectal-tumor development. *N Engl J Med* 1988; **319**: 525-532

• VIRAL HEPATITIS •

A novel hepatitis B virus genotyping system by using restriction fragment length polymorphism patterns of S gene amplicons

Guo-Bing Zeng, Shu-Juan Wen, Zhan-Hui Wang, Li Yan, Jian Sun, Jin-Lin Hou

Guo-Bing Zeng, Zhan-Hui Wang, Li Yan, Jian Sun, Jin-Lin Hou, Department of Infectious Diseases, Nanfang Hospital, Southern Medical University, Guangzhou 510515, Guangdong Province, China

Guo-Bing Zeng, Department of Infectious Diseases, 458 Hospital of PLA, Guangzhou 510602, Guangdong Province, China

Shu-Juan Wen, Genetic Laboratory, Nanfang Hospital, Southern Medical University, Guangzhou 510515, Guangdong Province, China

Supported by the Major State Basic Research Development Program of China. 973 Program, No.G1999054106; and the National Science Fund for Distinguished Young Scholars, No.30225042

Correspondence to: Dr. Jin-Lin Hou, Hepatology Unit and Department of Infectious Diseases, Nanfang Hospital, Southern Medical University, Guangzhou 510515, Guangdong Province, China. jlh@fimmu.edu.cn

Telephone: +86-20-85141941 **Fax:** +86-20-87714940

Received: 2003-08-03 **Accepted:** 2003-12-22

Abstract

AIM: Traditional hepatitis B virus (HBV) genotyping methods using restriction fragment length polymorphism (RFLP) can reliably identify genotypes A to F. As HBV genotypes G and H have been recently identified, this study was to establish an accurate and simple genotyping method for all eight HBV genotypes (A to H).

METHODS: Two hundred and forty HBV small S sequences obtained from GeneBank were analysed for restriction enzyme sites that would be genotype-specific. Restriction patterns following digestion with restriction enzymes BsrI, StyI, DpnI, HpaII, and EaeI, were determined to identify all eight HBV genotypes. Mixed genotype infections were confirmed by cloning and further RFLP analysis.

RESULTS: The new genotyping method could identify HBV genotypes A to H. Genotypes B and C could be determined by a single step digestion with BsrI and StyI in parallel. This was particularly useful in the Far East where genotypes B and C are predominant. Serum samples from 187 Chinese HBV carriers were analysed with this genotyping system, and the genotype distribution was 1.1% (2), 51.9% (97), 40.6% (76) and 4.8% (9) for genotypes A, B, C, and D, respectively. Mixed genotypes were found in only 3 patients (1.6%). Sequence data analysis confirmed the validity of this new method.

CONCLUSION: This HBV genotyping system can identify all eight HBV genotypes. It is accurate and simple, and can be widely used for studies on HBV genotyping.

Zeng GB, Wen SJ, Wang ZH, Yan L, Sun J, Hou JL. A novel hepatitis B virus genotyping system by using restriction fragment length polymorphism patterns of S gene amplicons. *World J Gastroenterol* 2004; 10(21): 3132-3136
<http://www.wjgnet.com/1007-9327/10/3132.asp>

INTRODUCTION

Hepatitis B virus (HBV) exhibits genetic variability which gives

rise to the well recognized subtypes and genotypes of the virus. In addition, virus variants arise during replication as a result of nucleotide misincorporations, in the absence of any proof-reading capacity by the viral polymerase. Based on an inter-group divergence of 8% or more in the complete genome nucleotide sequence, HBV has been classified into at least 8 different genotypes^[1-4]. Genotyping could also be accomplished based on partial sequences from the pre-S or S genes of the HBV genome^[5-7].

HBV genotypes have distinct geographical distributions. Genotypes A and D occur frequently in Africa and Europe^[5,8], while genotypes B and C are prevalent in Asia^[1]. Genotype E is almost entirely restricted to Africa, and F is found preferentially in Central and South America^[9]. Genotype G was reported in France and the United States^[3]. Recently, the eighth genotype H has been described in Central America^[4].

An increasing number of studies showed that HBV genotypes might influence HBeAg seroconversion rates^[10], mutation patterns in precore and core promoter regions^[11,12], severity of liver disease^[13-15] and response to antiviral treatment^[11,16]. In order to confirm and extend these observations, further studies are needed to be carried out, using reliable and simple methods for HBV genotyping. Though several HBV genotyping methods have been reported so far^[5-7,17,18], these could identify genotypes A to F, but not G or H.

The aim of this study was therefore to establish a simple and accurate HBV genotyping system using restriction fragment length polymorphism (RFLP) of the small S gene region, which could identify HBV genotypes A to H and would be applicable to large-scale studies.

MATERIALS AND METHODS

HBV sequences and computerized analyses

Two hundred and thirty-two complete and 8 S sequences of HBV were obtained from the DNA database (GenBank), comprising 24 sequences of genotype A, 35 of B, 97 of C, 38 of D, 5 of E, 30 of F, 8 of G and 3 of H. The small S gene regions of all these sequences were aligned and analysed to identify conserved regions and restriction enzyme sites that were genotype-specific. Five restriction enzymes were deemed to be appropriate for this purpose, and restriction patterns were determined by computerized analysis of each of the above mentioned sequences. The DNASIS software package (Hitachi Software Engineering, 1991) was used in this study.

Patient sera and HBV genotypes

Serum samples from 190 Chinese patients with chronic hepatitis B were collected from 2 liver units in mainland of China, and stored at -70 °C. All subjects (male/female = 161/29, mean age = 29.5 ± 9.16 years) were HBsAg-positive by commercially available immunoassays (Abbott Laboratories). Of them, 116 (61%) were HBeAg positive, and the mean alanine transaminase value (ALT) was 248.5 ± 342.8 IU/L. These samples were initially genotyped by RFLP analysis of pre-S amplicons as previously described^[6].

Genotyping PCR and restriction enzyme treatment

The S gene sequences were amplified by nested PCR. Based

on the most conserved regions, we designed PCR primers to amplify the sequence between nt 203 to nt 787, yielding an amplicon of 585 bp. The outer primers were PrsS2 (sense, nt 2820-2837, 5'-GGGACACCATATCTTGG) and S1R (antisense, nt 842-821, 5'-TTAGGGTTTAAATGTATACCCA). The inner primers were YS1 (sense, nt 203-221, 5'-GCGGGGTTTTTCTTGT TGA) and YS2 (antisense, nt 787-767, 5'-GGGACTCAAGATG TTGTACAG). DNA was extracted from the serum as previously described^[19]. A 5 µL of the resuspended DNA was added to an amplification mixture containing 5 µL of 10× Taq polymerase buffer, 5 µL of 25 mmol/L deoxyribonucleotide triphosphates, 1 µL (2U) of Taq polymerase (Promega, Beijing, China) and 10 pmol each of primers PrsS2 and S1R (total volume of 50 µL). The PCR profile was an initial 3 min denaturation at 94 °C, followed by 35 cycles of amplification including denaturation for 45 s at 94 °C, annealing for 60 s at 53 °C, and extension for 90 s at 72 °C. Strand synthesis was completed at 72 °C for 6 min. A 1 µL of the first-round PCR products was then used for the second-round PCR under the same conditions but with the primers YS1 and YS2.

A 10 µL of the second-round PCR products was mixed with 0.5 µL (5U) of the chosen restriction enzyme (New England Biolabs, Hong Kong, China), 1.5 µL of 10× buffer and 3.0 µL of water. After incubation at 37 °C for 4 h, the samples were electrophoresed on a 30 g/L agarose gel. A 10 µL of undigested second-round PCR products was run in parallel with the enzyme-digested samples. The restriction patterns were read visually under ultraviolet light.

Identification of mixed genotypes

When non-specific, atypical or mixed RFLP patterns were found, and the small S gene region was amplified with primers BS1 (sense, nt 56-76, 5'-CCTGCTGGTGGCGCCAGTTCC) and S1R, yielding an amplicon of 797-bp in length. These PCR products were purified and ligated into the pGEM-T vector using a commercial kit (Promega, Beijing, China). Ten positive clones were selected for further analysis. Extracted plasmid DNA was amplified with primers YS1 and YS2. PCR products were digested with restriction enzymes and analysed by electrophoresis. Samples that did not give clear results were then sequenced directly.

Sequencing and sequence data analysis

Three serum samples each of genotypes B, C and D, and 2

serum samples of genotype A by our method were randomly selected for sequencing. The small S gene region was amplified with primers BS1 and S1R and ligated into the pGEM-T vector as described above. Plasmid DNA was extracted from positive clones and sequenced using an ABI automatic DNA sequencer. Sequences were then edited, aligned and compared with reference sequences using the DNASIS software.

RESULTS

Predicted RFLP patterns

Following alignment of S gene sequences, five restriction enzymes, StyI, BsrI, DpnI, HpaII and EaeI were deemed to be suitable for yielding restriction patterns that would identify all eight HBV genotypes.

Genotype C had a StyI site at nt position 455, cutting the S gene into two fragments of 253- and 332-bp in length. This restriction pattern was found in 95 of 97 genotype C sequences examined. This restriction site was absent in all other genotypes. All genotype B sequences could be distinguished by the fact that the S gene had a unique BsrI site at nt position 328, which gave two characteristic bands of 126- and 459-bp in length. A BsrI site at nt position 502 was observed in 22 of 24 genotype A and all genotype E and G sequences. Moreover, genotype E PCR products could be digested at position 706 by HpaII, while genotype G had no EaeI site, which was present in all other genotypes. The BsrI site at nt position 502 was also found in 1 of 38 genotype D sequences, which could be mistaken as genotype A. Thus the sequences which still left unresolved were those of genotypes D, F and H. For genotype F, a DpnI site was found at nt positions 491 and 747, while genotypes D and H were cut at nt position 491 but not at 747. Finally, a HpaII site at nt position 292 in genotype H could be differentiated from genotype D. The sequences recognized by these enzymes are shown in Figure 1. The patterns created by these enzymes from the small S gene region are shown in Table 1.

Strategy for HBV genotyping using the new method

The optimal strategy, using the new method, which could be applied to a particular geographical region according to the most prevalent HBV genotype in that region, is summarized in Figure 2. For example, genotypes B and C were the most prevalent in the Far East. After parallel digestion by BsrI and

Table 1 Restriction digestion patterns that could identify HBV genotypes

Genotypes	Pattern	No. of sequences	Fragments obtained with				
			BsrI	StyI	DpnI	HpaII	EaeI
A	A1	12	300 285	585	85 204 296	585	100 485
	A2	10	300 285	585	289 296	585	100 485
	A3	1	585	585	85 204 296	585	100 485
	A4	1	585	585	289 296	585	100 485
B	B1	33	126 459	585	289 296	585	100 485
	B2	2	126 184 275	585	289 296	585	100 485
C	C1	95	585	253 332	585	585	100 485
	C2	2	585	585	585	585	100 485
D	D1	36	585	585	289 296	585	100 485
	D2	1	585	585	585	585	100 485
	D3	1	300 285	585	585	585	100 485
E	E1	4	300 285	585	289 296	504 81	100 485
	E2	1	126 174 285	585	289 296	504 81	100 485
F	F1	29	585	585	289 256 40	90 495	100 485
	F2	1	585	585	289 296	90 495	100 485
G	G1	8	300 285	585	289 296	585	585
H	H1	3	585	585	289 296	90 495	100 485

StyI, more than 90% of the serum samples from Chinese patients could be genotyped.

Comparison with genotyping by RFLP of PreS1 regions

Of the 190 serum samples, 3 were HBV DNA negative by nested PCR. Thus, 187 serum samples were analysed in this study, and compared to the results obtained by RFLP analysis of the

pre-S1 region. One hundred and eight-one of the 187 serum samples were classified as genotypes A (2), B (95), C (75) and D (9). These results were in full agreement with those obtained with our new method. Because of nonspecific amplification and atypical restriction patterns, 6 samples could not be classified by RFLP analysis of pre-S1 amplicons. However, these were resolved into either genotypes B (2), C (1) or mixed B+C (3) by

Genotype	GeneBank Access No.	*nt 287 DpnI	nt 292 HpaII	nt 302 EaeI	nt 328 BsrI	nt 455 StyI	nt 491 DpnI	nt 502 BsrI	nt 706 HpaII	nt 747 DpnI
A	X02763	GGATCT	CCGTGTG	TGGCCAA	CTCCAATC	ATCAAGGT	AGGATCAA	ACCAGTA	CGTAGGG	TGATGTG
B	D00329	GGAACA	CCGTGTG	TGGCCAA	CTCCAGTC	ATCAAGGT	AGGATCAT	ACCAGCA	CGTAGGG	TGATGTG
C	X001587	GGAGCA	CCACGTG	TGGCCAA	CTCCAATC	ACCAAGGT	AGGAACAT	ACCAGCA	CGTAGGG	TGATGTG
D	X59795	GGAACT	CCGTGTG	TGGCCAA	CTCCAATC	ATCAAGGT	AGGATCTT	ACCAGCA	CGTAGGG	TGATGTG
E	L24071	GGAGCA	CCGTGTG	TGGCCAA	CTCCAATC	ATCAAGGT	AGGATCAT	ACCAGTA	CGCCGGG	TGATGTG
F	X75658	GGAACA	CCGGGTG	TGGCCAA	CTCCAATC	ATCAAGGT	AGGATCTA	ACCAGCA	CGTAGGG	TGATCTG
G	AF160501	GGAGTG	CCGTGTG	TGGCCTA	CTCCAATC	ATCAAGGT	AGGATCCT	ACCAGTA	CGTAGGG	TGATGTG
H	AY090454	GTACCA	CCGGGTG	TGGCCAA	CTCCAATC	ATCAAGGT	AGGATCTA	ACCAGCA	CGTAGGG	TGATTTG

Figure 1 Genotype-specific sites recognized by restriction enzymes. GeneBank accession numbers and consensus sequences from HBV genotypes A to H are listed. The shaded letters indicate the sequences recognized by the relevant enzyme. StyI recognizes sequence C | C (A/T) (A/T) GG; BsrI, C | CAGT; DpnI, GA | TC; HpaII, C | CGG; EaeI, (C/T) | GGCC (A/G). *nt position number is from the unique EcoRI site according to the reference sequence x001587 (genotype C).

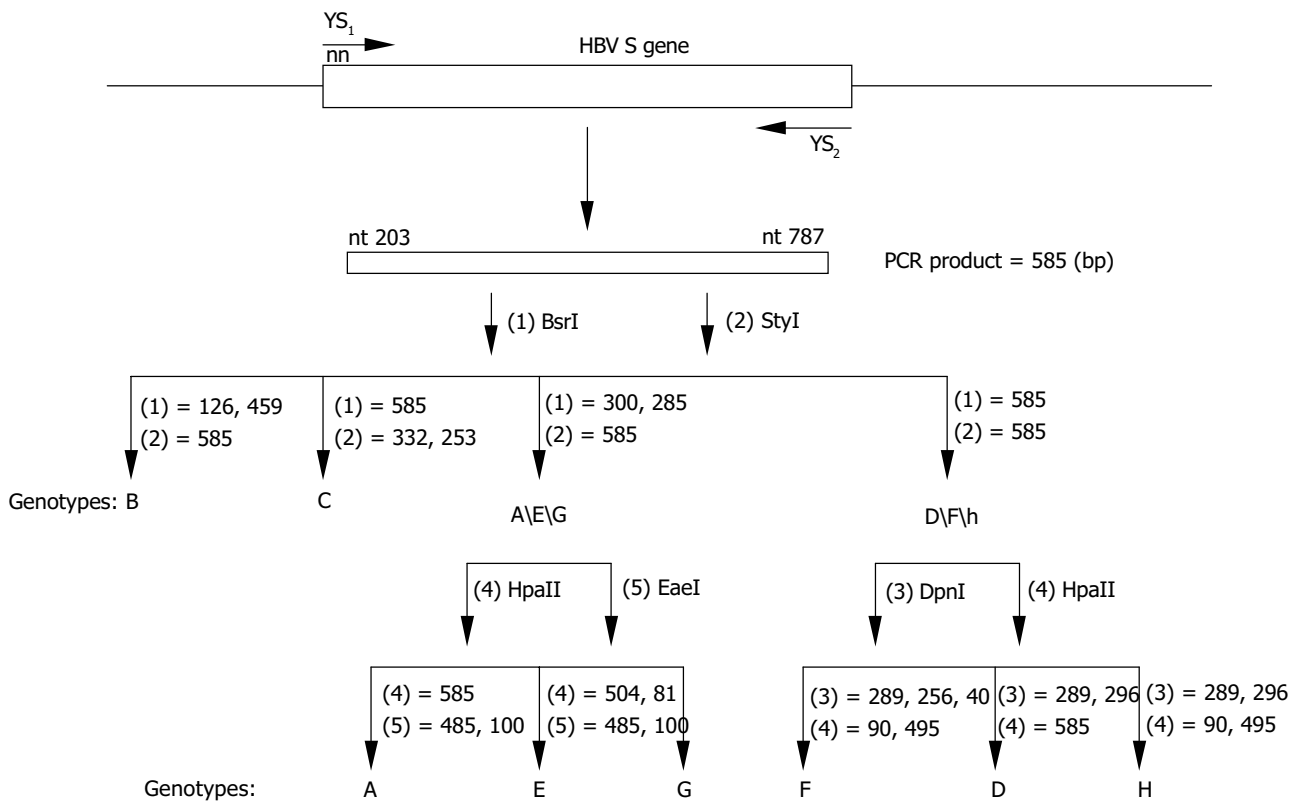


Figure 2 Diagrammatic representation of the position of PCR primers and RFLP analyses for HBV genotyping. The second round PCR products, which were 585 bp, were digested by (1) BsrI, (2) StyI, (3) DpnI, (4) HpaII and (5) EaeI. Genotypes B and C could be typed in one step using parallel digestion with BsrI and StyI.

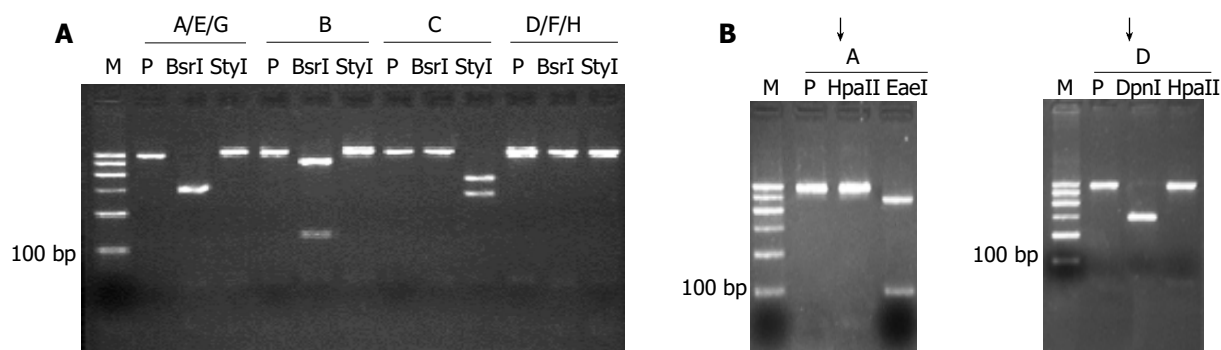


Figure 3 RFLP of S amplicon of HBV from 187 nested PCR-positive serum samples from Chinese carriers. Lane M: 100 bp ladder from 100-600 bp fragments, P: undigested PCR product. A: After the first step of parallel digestion with BsrI and StyI, the samples were divided into four groups: genotypes B, C, A/E/G and D/F/H; B: Groups A/E/G and D/F/H could be further resolved by the second parallel digestion. In this study, genotypes E, F, G and H were not observed, while genotypes B and C were the major ones.

our method after cloning and repeat RFLP analysis. These results were verified subsequently by direct sequencing of the S gene. Thus the final genotype distribution of the samples was A, 2 (1.1%); B, 97 (51.9%); C, 76 (40.6%); D, 9 (4.8%) and mixed (genotypes B and C), 3 (1.6%). Examples of RFLP analysis using the new method are shown in Figure 3.

Verification of reliability of the new method

Nucleotide sequences of 11 samples randomly selected were determined and then compared to reference sequences for genotypes A (X02763), B (D00329), C (X01587) and D (X59795). The homologies of the S gene region under investigation were 97.9-98.3%, 99.3-99.9%, 97.5-98.8% and 98.2-98.5%, respectively, which confirmed the validity of the new RFLP technique.

DISCUSSION

Great importance has been attached to the differences between HBV genotypes. In earlier studies^[20,21], a higher frequency of liver dysfunction was observed in patients with subtype adr (most often genotype C) compared to those with subtype adw (mainly genotype B). These findings concurred with those reported by Lindh *et al.*^[13] and Orito *et al.*^[15]. Mayerat *et al.*^[14] found that genotype A was more frequent in chronic hepatitis B patients than genotype D, while the opposite situation was true in acute hepatitis B patients. A study from Taiwan reported that genotype C was associated with more active liver disease compared to genotype B^[22], and this was supported by a more recent study^[23]. A retrospective study of 332 cases^[10] showed that patients with HBV genotype B had a lower prevalence and earlier seroconversion to anti-HBe than those with genotype C, which could explain the less active liver disease seen in patients with genotype B. Another study^[24] suggested that HBV genotype might influence HBV recurrence after liver transplantation as patients with genotype D appeared to have a higher risk for HBV recurrence and mortality. The correlation between HBV genotype and response to interferon therapy has also been reported. HBV genotype C was associated with a higher frequency of core promoter mutation and a lower response rate to interferon alfa therapy^[16]. Hou *et al.*^[11] studied 103 chronic hepatitis B patients from 16 European centers and found that HBV genotype A responded better to standard interferon treatment than other genotypes. This appeared to be related to its molecular characteristics, having a greater tendency to develop core promoter mutations and less variation in the nucleocapsid protein. A study reported that patients carrying the adw subtype were associated with a higher risk of lamivudine resistance than those with ayw subtype^[25], although Chan *et al.* found that HBeAg seroconversion after treatment by lamivudine was not influenced by the HBV genotype^[26]. To

interpret these differences between HBV genotypes, larger-scale investigations are needed. So, development of accurate, simple and inexpensive HBV genotyping methods would be very useful in this respect.

Several methods have been used for HBV genotyping including direct sequencing, RFLP, PCR with genotype-specific primers^[17], line probe assay^[18] and enzyme-linked immunoassay^[27]. Genotyping based on complete genome sequences is an ideal method, but sequencing is costly and cannot be easily carried out in clinical diagnostic laboratories for large-scale studies. Currently, PCR-RFLP is the most widely used method for HBV genotyping because it is simple and inexpensive. Norder *et al.*^[2] found that HBV genotyping could be accomplished based on the sequence of the S gene. After analyzing 73 HBV sequences from GeneBank, Lindh *et al.*^[5] developed a genotyping method based on RFLP patterns of a S gene amplicon, which first identified HBV genotypes A-F. They also reported another genotyping technique based on RFLP analysis of the pre-S region^[6]. However, pre-S gene was less suitable for genotyping than S gene because it was not so conserved as S gene^[28]. Mizokami *et al.*^[7] compared 68 complete and 106 small S HBV sequences and confirmed that S gene could be used to accurately identify the six HBV genotypes A to F. They also described a RFLP genotyping system using five enzymes, HphI, NciI, AlwI, EarI, and NlaIV. Because genotypes G and H were not discovered then, they could not be assessed by these methods.

Compared with previous methods, our new method has several relative advantages. Firstly, it can identify all eight HBV genotypes. Secondly, it is more accurate because it was based on analysing many of the sequences deposited in GeneBank. Thirdly, a simple and inexpensive strategy can be adopted according to the most prevalent HBV genotypes in a particular geographical region. For example, the strategy shown in Figure 2 was especially suitable for the Far East where genotypes B and C are mostly found (85-98.6%)^[21,29,30]. The RFLP patterns are simple, with one or two bands, and therefore easy to be recognized.

In this study, a new method for HBV genotyping based on RFLP analysis of S gene amplicons was established, and could identify all eight HBV genotypes. This HBV genotyping system is accurate, simple and can be expected to be widely used in studies of HBV genotyping.

REFERENCES

- 1 Okamoto H, Tsuda F, Sakugawa H, Sastrosoewignjo RI, Imai M, Miyakawa Y, Mayumi M. Typing hepatitis B virus by homology in nucleotide sequence: comparison of surface antigen subtype. *J Gen Virol* 1988; **69**(Pt 10): 2575-2583
- 2 Norder H, Courouce AM, Magnius LO. Complete genomes, phylogenetic relatedness, and structural proteins of six strains of the hepatitis B virus, four of which represent two new

- genotypes. *Virology* 1994; **198**: 489-503
- 3 **Stuyver L**, De Gendt S, Van Geyt C, Zoulim F, Fried M, Schinazi RF, Rossau R. A new genotype of hepatitis B virus: complete genome and phylogenetic relatedness. *J Gen Virol* 2000; **81**(Pt 1): 67-74
 - 4 **Arauz-Ruiz P**, Norder H, Robertson BH, Magnius LO. Genotype H: a new Amerindian genotype of hepatitis B virus revealed in Central America. *J Gen Virol* 2002; **83**(Pt 8): 2059-2073
 - 5 **Lindh M**, Andersson AS, Gusdal A. Genotypes, nt 1858 variants, and geographic origin of hepatitis B virus-large-scale analysis using a new genotyping method. *J Infect Dis* 1997; **175**: 1285-1293
 - 6 **Lindh M**, Gonzalez JE, Norkrans G, Horal P. Genotyping of hepatitis B virus by restriction pattern analysis of a pre-S amplicon. *J Virol Methods* 1998; **72**: 163-174
 - 7 **Mizokami M**, Nakano T, Orito E, Tanaka Y, Sakugawa H, Mukaide M, Robertson BH. Hepatitis B virus genotype assignment using restriction fragment length polymorphism patterns. *FEBS Lett* 1999; **450**: 66-71
 - 8 **Baptista M**, Kramvis A, Jammeh S, Naicker J, Galpin JS, Kew MC. Follow up of infection of chacma baboons with inoculum containing a and non-a genotypes of hepatitis B virus. *World J Gastroenterol* 2003; **9**: 731-735
 - 9 **Norder H**, Hammas B, Lee SD, Bile K, Courouce AM, Mushahwar IK, Magnius LO. Genetic relatedness of hepatitis B viral strains of diverse geographical origin and natural variations in the primary structure of the surface antigen. *J Gen Virol* 1993; **74**(Pt 7): 1341-1348
 - 10 **Chu CJ**, Hussain M, Lok AS. Hepatitis B virus genotype B is associated with earlier HBeAg seroconversion compared with hepatitis B virus genotype C. *Gastroenterology* 2002; **122**: 1756-1762
 - 11 **Hou J**, Schilling R, Janssen HLA, Heijtkink RA, Williams R, Schalm SW, Naoumov NV. Molecular characteristics of hepatitis B virus genotype A confer a higher response rate to interferon treatment. *J Hepatol* 2001; **34**(Suppl 1): 15-16
 - 12 **Hou J**, Lin Y, Waters J, Wang Z, Min J, Liao H, Jiang J, Chen J, Luo K, Karayiannis P. Detection and significance of a G1862T variant of hepatitis B virus in Chinese patients with fulminant hepatitis. *J Gen Virol* 2002; **83**(Pt 9): 2291-2298
 - 13 **Lindh M**, Hannoun C, Dhillon AP, Norkrans G, Horal P. Core promoter mutations and genotypes in relation to viral replication and liver damage in East Asian hepatitis B virus carriers. *J Infect Dis* 1999; **179**: 775-782
 - 14 **Mayerat C**, Mantegani A, Frei PC. Does hepatitis B virus (HBV) genotype influence the clinical outcome of HBV infection? *J Viral Hepat* 1999; **6**: 299-304
 - 15 **Orito E**, Mizokami M, Sakugawa H, Michitaka K, Ishikawa K, Ichida T, Okanoue T, Yotsuyanagi H, Iino S. A case-control study for clinical and molecular biological differences between hepatitis B viruses of genotypes B and C. Japan HBV genotype research group. *Hepatology* 2001; **33**: 218-223
 - 16 **Kao JH**, Wu NH, Chen PJ, Lai MY, Chen DS. Hepatitis B genotypes and the response to interferon therapy. *J Hepatol* 2000; **33**: 998-1002
 - 17 **Naito H**, Hayashi S, Abe K. Rapid and specific genotyping system for hepatitis B virus corresponding to six major genotypes by PCR using type-specific primers. *J Clin Microbiol* 2001; **39**: 362-364
 - 18 **Grandjacques C**, Pradat P, Stuyver L, Chevallier M, Chevallier P, Pichoud C, Maisonnas M, Trepo C, Zoulim F. Rapid detection of genotypes and mutations in the pre-core promoter and the pre-core region of hepatitis B virus genome: correlation with viral persistence and disease severity. *J Hepatol* 2000; **33**: 430-439
 - 19 **Hou J**, Karayiannis P, Waters J, Luo K, Liang C, Thomas HC. A unique insertion in the S gene of surface antigen-negative hepatitis B virus Chinese carriers. *Hepatology* 1995; **21**: 273-278
 - 20 **Shiina S**, Fujino H, Kawabe T, Tagawa K, Unuma T, Yoneyama M, Ohmori T, Suzuki S, Kurita M, Ohashi Y. Relationship of HBsAg subtypes with HBeAg/anti-HBe status and chronic liver disease. Part II: Evaluation of epidemiological factors and suspected risk factors of liver dysfunction. *Am J Gastroenterol* 1991; **86**: 872-875
 - 21 **Shiina S**, Fujino H, Uta Y, Tagawa K, Unuma T, Yoneyama M, Ohmori T, Suzuki S, Kurita M, Ohashi Y. Relationship of HBsAg subtypes with HBeAg/anti-HBe status and chronic liver disease. Part I: Analysis of 1744 HBsAg carriers. *Am J Gastroenterol* 1991; **86**: 866-871
 - 22 **Kao JH**, Chen PJ, Lai MY, Chen DS. Hepatitis B genotypes correlate with clinical outcomes in patients with chronic hepatitis B. *Gastroenterology* 2000; **118**: 554-559
 - 23 **Fang ZL**, Yang J, Ge X, Zhuang H, Gong J, Li R, Ling R, Harrison TJ. Core promoter mutations (A 1762 T and G 1764 A) and viral genotype in chronic hepatitis B and hepatocellular carcinoma in Guangxi, China. *J Med Virol* 2002; **68**: 33-40
 - 24 **Devarbhavi HC**, Cohen AJ, Patel R, Wiesner RH, Dickson RC, Ishitani MB. Preliminary results: outcome of liver transplantation for hepatitis B virus varies by hepatitis B virus genotype. *Liver Transpl* 2002; **8**: 550-555
 - 25 **Zollner B**, Petersen J, Schroter M, Laufs R, Schoder V, Feucht HH. 20-fold increase in risk of lamivudine resistance in hepatitis B virus subtype adw. *Lancet* 2001; **357**: 934-935
 - 26 **Chan HLY**, Wong ML, Hui AY, Chim AML, Tse AML, Hung LCT, Chan FKL, Sung JY. Hepatitis B virus genotype has no impact on hepatitis B e antigen seroconversion after lamivudine treatment. *World J Gastroenterol* 2003; **9**: 2695-2697
 - 27 **Usuda S**, Okamoto H, Iwanari H, Baba K, Tsuda F, Miyakawa Y, Mayumi M. Serological detection of hepatitis B virus genotypes by ELISA with monoclonal antibodies to type-specific epitopes in the preS2-region product. *J Virol Methods* 1999; **80**: 97-112
 - 28 **Mizokami M**, Orito E, Ohba K, Ikeo K, Lau JY, Gojobori T. Constrained evolution with respect to gene overlap of hepatitis B virus. *J Mol Evol* 1997; **44**(Suppl 1): S83-S90
 - 29 **Ding X**, Mizokami M, Yao G, Xu B, Orito E, Ueda R, Nakanishi M. Hepatitis B virus genotype distribution among chronic hepatitis B virus carriers in Shanghai, China. *Intervirol* 2001; **44**: 43-47
 - 30 **Orito E**, Ichida T, Sakugawa H, Sata M, Horiike N, Hino K, Okita K, Okanoue T, Iino S, Tanaka E, Suzuki K, Watanabe H, Hige S, Mizokami M. Geographic distribution of hepatitis B virus (HBV) genotype in patients with chronic HBV infection in Japan. *Hepatology* 2001; **34**: 590-594

• VIRAL HEPATITIS •

Antigenic and immunogenic changes due to mutation of *s* gene of HBV

Jun-Hui Ge, Hui-Min Liu, Jing Sun, Le-Zhi Zhang, Jin He, Yu-Li Li, Hong Liu, Yi Xu, Hong-Yu Yu, Yi-Ping Hu

Jun-Hui Ge, Hui-Min Liu, Jing Sun, Jin He, Yu-Li Li, Yi Xu, Hong-Yu Yu. Department of Pathology, Changzheng Hospital, Second Military Medical University, Shanghai 200003, China

Le-Zhi Zhang. Department of Experimental Diagnosis, Changhai Hospital, Second Military Medical University, Shanghai 200433, China
Hong Liu, Yi-Ping Hu. Department of Cell Biology, Second Military Medical University, Shanghai 200433, China

Supported by National Science Foundation of China, No. 396670669 and No.39970676; Keystone basic research program of STCM, No. 03DZ14023

Co-correspondents: Le-Zhi Zhang and Yi-Ping Hu

Correspondence to: Hong-Yu Yu, Department of Pathology, Changzheng Hospital, Second Military Medical University, Shanghai, 200003, China. yuhongyu795@hotmail.com

Telephone: +86-21-63610109-73703 **Fax:** +86-21-25070291

Received: 2004-01-09 **Accepted:** 2004-03-12

Abstract

AIM: To investigate the change of immunological characteristics of HBsAg caused by the mutation at codon 145 of HBsAg using DNA-based immunization.

METHODS: Plasmids expressing mutant and wild type envelope antigens were transfected into human hepatocellular carcinoma cells via electrotransformation. The antigenicity of HBsAg was studied with EIA and immunocytochemical staining. Then plasmids were used to immunize 5 C57BL/6 mice. Sera of mice were detected for anti-HBs and anti-preS2 with ELISA.

RESULTS: The mutant HBsAg could be detected by native antibody in EIA and immunocytochemical study. But the $A_{(450\text{ nm})}$ value of the mutant HBsAg in the supernatant was apparently lower than that of the wild-type. Both mutant and native HBsAg expression plasmid could stimulate a strong humoral immune response to HBsAg and preS2 antigen in mice. Protective antibodies against HBsAg elicited by the native HBsAg occurred earlier than that elicited by the mutant HBsAg about one to two weeks. The occurrence of protective antibodies against preS2 antigen was one to two weeks earlier than that of anti-HBs.

CONCLUSION: The amino acid substitution causes changes of the antigenicity and immunogenicity of HBsAg, but mutant HBsAg can still induce a protective humoral immune response in mice.

Ge JH, Liu HM, Sun J, Zhang LZ, He J, Li YL, Liu H, Xu Y, Yu HY, Hu YP. Antigenic and immunogenic changes due to mutation of *s* gene of HBV. *World J Gastroenterol* 2004; 10(21): 3137-3140

<http://www.wjgnet.com/1007-9327/10/3137.asp>

INTRODUCTION

Hepatitis B infection is a serious problem worldwide. HBV vaccine is effective in preventing HBV infection. Antibody responses to the common epitope of HBsAg, the "a" determinant,

are considered to confer protection against HBV infection regardless of viral subtypes. HBV infection still occurs in spite of the presence of anti-HBs^[1-3]. Some cases were infected with a variant of HBV. This variant has a point mutation from guanosine to adenosine at nucleotide position 587 of the *s* gene that results in an amino acid substitution of arginine for glycine at codon 145 of HBsAg^[4,5]. This mutation would greatly destroy the antigenicity of HBsAg, which directly impacts on the diagnosis and therapy of HBV^[6]. Also, this variant was found in patients who had liver transplantations for end-stage liver diseases associated with HBV infection and received human monoclonal anti-HBs antibody or HBIG in an attempt to prevent recurrent hepatitis B^[7-9]. This study was undertaken to determine whether the change from glycine to arginine at amino acid 145 of HBsAg could cause a loss of antigenicity and immunogenicity of HBsAg, thus allowing the mutant HBV to evade the humoral immune response.

MATERIALS AND METHODS

Reagents, plasmid, antibodies and animals

Restriction endonucleases and *T4* DNA ligase were obtained from Sangon Co. (Canada). Plasmid P II containing overlength HBV genomes was endowed by Dr. Jian-Wen He. Plasmid P II had a point mutation from guanosine to adenosine at the nucleotide position 587 of *s* gene and resulted in an amino acid substitution of arginine for glycine at codon 145 of HBsAg. Plasmid pCMV-S2.S was a generous gift of Dr. Heather Davis (Loeb Research Institute, Ottawa, Canada). This vector contained a cytomegalovirus promoter and respiratory syncytial virus enhancer element and encoded HBsAg and MHBs proteins. Plasmid SEAP expressing alkaline phosphatase was a generous gift of Dr. Jian-Wen He. HBsAg and HBsAb ELISA reagents were purchased from Abbott Laboratories and Sino-American Biotechnology Co., respectively. PreS2 antigen and preS2-specific antibodies were measured using ELISA kits from Hepatic Disease Institute of Beijing Medical University. The mouse monoclonal antibody against HBsAg was purchased from DAKO (USA). Sheep anti-mouse IgG-HRP was obtained from CALBIOCHEM (Germany). QIA quick gene gel kit and plasmid extraction kit were purchased from QIA gene. C57BL/6 mouse strain bought from Animal Center of Shanghai Birth Control Research Institute was kept under standard pathogen-free conditions in the animal facility and maintained on a 14:10 light-dark schedule (lights off at 10 pm, on at 8 am). Mice used were aged 6-8 wk.

Construction of DNA expression plasmid

Plasmid P II used as the source of mutant viral gene and plasmid pCMV-S2. S used as the source of the vector were digested with *Dra* III and *Xho* I, respectively. Then the segment of mutant *s* gene from plasmid P II was inserted into the vector from pCMV-S2.S by *T4* DNA ligase. Eukaryotic expression plasmid pCMV-S2.S+145R containing a point mutation from guanosine to adenosine was constructed. Plasmid pCMV-S2.S+145R was confirmed by restriction endonuclease digestion and HBV insert was sequenced by the dideoxy method using a commercial kit. The plasmid was grown in DH5 α and extracted by QIA quick gene kit. DNA was dissolved in double distilled water, adjusted to 1.6 mg/L, and then diluted to a final concentration of 1 mg/L

for *in vivo* studies. Concentration and purity of the DNA were confirmed by measuring the optical density at 260 nm and by agarose gel electrophoresis.

***In vitro* assays for HBV protein expression**

Human hepatocellular carcinoma cell lines (Hep G2) were transfected with the eukaryotic expression vectors pCMV-S2.S+145R, pCMV-S2.S or pcDNA3.0 via electrotransformation. The change of binding power of mutant antigens to anti-HBs was studied by EIA and immunocytochemical staining. To control transfection efficiency, cells were cotransfected with an alkaline-phosphatase-containing vector SEAP. Cells were lysed by freeze-thawing three times in phosphate-buffered saline (PBS), and the supernatants were collected at various time points after transfection for viral protein studies.

Analysis of viral proteins by ELISA

Concentrations of HBsAg and preS2 envelope proteins derived from culture supernatant or cell lysates of transfected cells were measured by enzyme-linked immunosorbent assay reagents according to the manufacturer's instructions. One hundred μL of culture supernatant or cell lysates was incubated with 100 μL of 2 \times SEAP buffer at 37 $^{\circ}\text{C}$ for 10 min. Twenty μL substrate buffer was added to the assay. $A_{(450\text{ nm})}$ value was determined after incubated at 37 $^{\circ}\text{C}$ for 30 min. All results were corrected according to the transfection efficiency using the SEAP assays.

Expression of viral proteins

Transfected cells were collected by centrifugation and spread on sterile glass slides, and then fixed with acetone at 4 $^{\circ}\text{C}$ for immunochemical staining. Slides were blocked with normal goat serum for 30 min at room temperature, then incubated either with monoclonal mouse anti-HBs at a dilution of 1:200 for detection of HBsAg or with monoclonal mouse anti-preS2 (1:500) for detection of preS2 antigen for 12 h at 4 $^{\circ}\text{C}$. After washed with PBS, a secondary antiserum consisting of biotin-conjugated goat anti-mouse immunoglobulin G was applied at a 1:100 dilution for 30 min at 37 $^{\circ}\text{C}$. The slides coated with antibody were washed with PBS, treated with streptavidin-horseradish peroxidase conjugates at a 1:600 dilution for 30 min at 37 $^{\circ}\text{C}$, stained with nitroblue tetrazolium chloride and 5-bromo-4-chloro-3-indolyl-phosphate (NBT/BCIP, MAXIN Co.), and counter-stained with Mayer's hematoxylin before mounted.

DNA immunization

Mice were injected on a single occasion with 100 μg of recombinant plasmid DNA pCMV-S2.S, pCMV-S2.S+145R or pcDNA3.0 in 100 μL of 0.9 g/L NaCl distributed into the anterior tibialis muscle of C57BL/6 mice 5 d after the injection of 100 μL bupivacaine (0.2-0.4%). Immunization with the empty plasmid pcDNA3.0 vector (mock) was used as a negative control. Mice were anesthetized with pentobarbitone prior to phlebotomy from the retro-orbital plexus 200 microliter using heparinized glass pipettes every week. Serum was isolated by centrifugation. Anti-HBs and anti-preS2 concentrations were analyzed by using ELISA kits according to the manufacturer's instructions.

Detection of serum anti-HBs and anti-preS2 titers

Standard anti-HBs at titres 80, 40, 20, 10 or 0 mIU/L was detected by ELISA at the time when serum samples were detected. The $A_{(450\text{ nm})}$ value was 0.872, 0.442, 0.225, 0.107 and 0.046, respectively. The data were analyzed by linear regression, and the equation between the $A_{(450\text{ nm})}$ value and the antibody titers was $y = 94.442x - 1.959$. According to the manufacturer's instructions, inhibition rate (%) = (A value of negative control - A value of sample) / (A value of negative control - A value of positive control) \times 100%.

Statistical analysis

The data were analyzed by SAS software.

RESULTS

Construction of recombinant eukaryotic expression plasmid pCMV-S2.S+145R

The results of endonuclease digestion and electrophoresis were in accordance to the graphic map of plasmids. The result of sequencing was same as the sequence in the other report^[10], except the point mutation from guanosine to adenosine at the nucleotide position 587 of *s* gene (Figure 1).

Secretion and expression of HBsAg and preS2 antigen

HepG2 cells were transfected with pCMV-S2.S+145R, pCMV-S2.S or pcDNA3.0 and culture supernatant was collected at various intervals of 3, 5, 7 d after transfection. pCMV-S2.S-transfected cells secreted a higher amount of HBsAg compared with the pCMV-S2.S+145R-transfected cells in the culture supernatant and the cell lysates of transfected cells (Figure 2). But preS2 antigen was not detected in the culture supernatant or in the cell lysates of pCMV-S2.S-transfected and pCMV-S2.S+145R-transfected cells. In contrast, immunocytochemical studies clearly showed a substantial cytoplasmic accumulation of HBsAg and preS2 antigen in both of the pCMV-S2.S-transfected and pCMV-S2.S+145R-transfected cells. Furthermore, there was no difference in the expression of HBsAg and preS2 antigen between the two plasmid transfected cells. No staining pattern was observed in mock-transfected cells (data not shown).

Humoral immune response to HBV proteins

Anti-HBs responses to pCMV-S2.S+145R were detectable 4 wk after the immunization in C57BL/6 mice. The titer of anti-HBs increased gradually by the end of observation. The highest titer was 95.60 mIU/L at the twelfth week after immunization. Most importantly, anti-HBs responses to pCMV-S2.S were detectable 2 wk after immunization in C57BL/6 mice. The titer of anti-HBs also increased gradually by the end of observation. The highest titer was 99.57 mIU/L at the twelfth week after immunization. The mice immunized with pCMV-S2.S+145R developed anti-HBs after a delay of approximately 2 wk compared with those injected with pCMV-S2.S (Figure 3). The occurrence of protective antibodies against HBsAg elicited by native HBsAg was one to two weeks earlier than that elicited by mutant HBsAg. Nevertheless, pCMV-S2.S+145R-immunized as well as pCMV-S2.S-immunized mice developed a strong humoral immune response against HBsAg at levels far above the known anti-HBs protection limit for humans (>10 mU/mL). Anti-HBs response was not detected in C57BL/6 mice immunized with pcDNA3.0.

Both pCMV-S2.S+145R-immunized and pCMV-S2.S-immunized mice developed a significant preS2-specific antibody response, whereas antibody responses to the preS2 antigen were detectable two weeks after immunization. There was a slight difference between the two groups with respect to the level of anti-preS2 antigen response (Figure 4A).

Standardization of anti-HBs titer

In order to analyze the difference in immune response induced by pCMV-S2.S+145R and pCMV-S2.S and the validity of immunization and the titer of Anti-HBs were corrected according to the inhibition rate of anti-preS2 which was little affected by the point mutation, because the structures of pCMV-S2.S+145R and pCMV-S2.S were exactly the same except for a point mutation from guanosine to adenosine at the nucleotide position 587 of *s* gene. Therefore, the ratio of HBsAg and preS2 antigen expressed by the two plasmids was similar. Then the difference between the two plasmids due to the mutation could be observed correctly (Figure 4B).

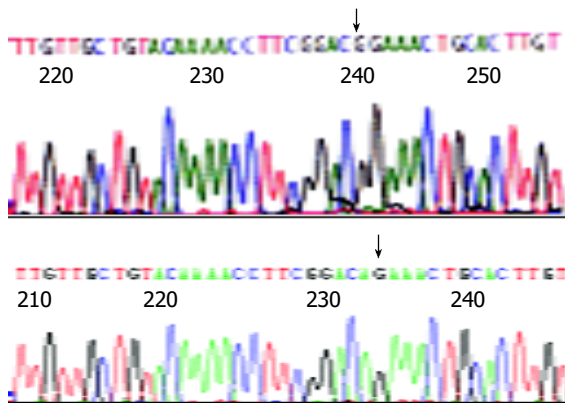


Figure 1 Partial sequences of plasmids pCMV-S.S2 and pCMV-S.S2+145R A: “↓”±stands for the “G” in gene sequences of pCMV-S.S2 B: “↓”±stands for the “A” in gene sequences of pCMV-S.S2+145R, namely mutant point.

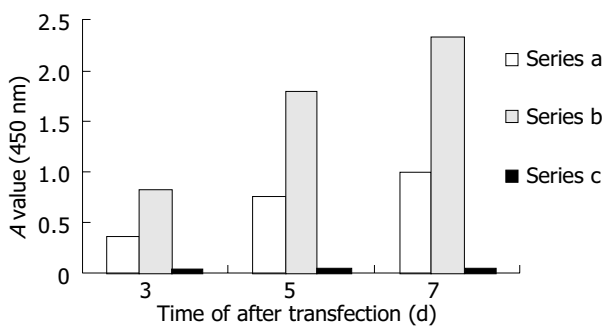


Figure 2 Secretion of HBsAg *in vitro*. Series A: HBsAg levels of supernatant collected from pCMV-S.S2+145R-transfected cells. Series B: HBsAg levels of supernatant collected from pCMV-S.S2-transfected cells. Series C: negative control.

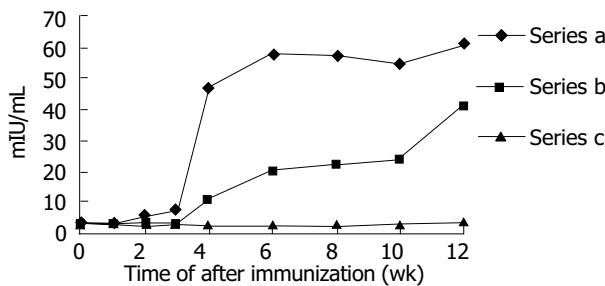


Figure 3 Humoral immune response induced by DNA-based immunization. Series A: anti-HBs level in pCMV-S.S2-immunized mice. Series B: anti-HBs level in pCMV-S.S2+145R-immunized mice. Series C: anti-HBs level in pcDNA3.0-immunized mice.

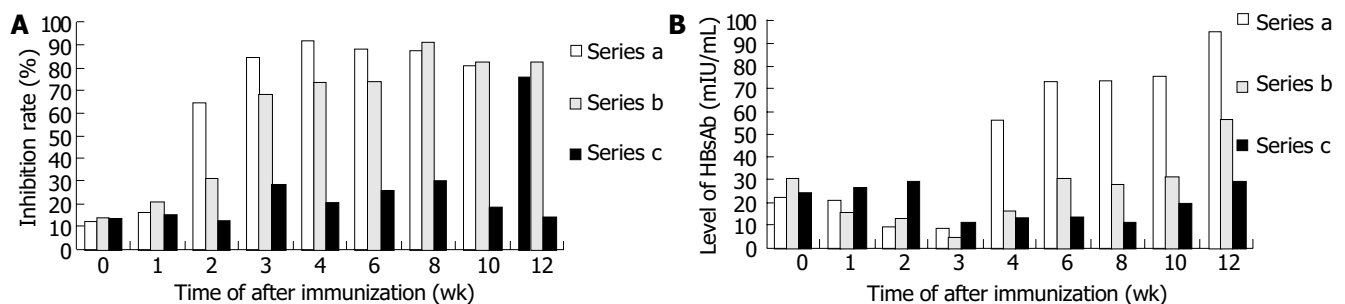


Figure 4 Comparison of humoral immune responses to preS2 antigen and HBsAg. A: Comparison of humoral immune responses to preS2 antigen. Series a: anti-preS2 level in pCMV-S.S2-immunized mice. Series b: anti-preS2 level in pCMV-S.S2+145R-immunized mice. Series c: negative control. B: Comparison of humoral immune responses to HBsAg. Series a: pCMV-S.S2-immunized mice. Series b: pCMV-S.S2+145R-immunized mice. Series c: negative control.

DISCUSSION

The antibody responses to the common “a” determinant of HBsAg confer protection against infection with HBV of all subtypes. Using monoclonal antibodies, this determinant is composed of a number of epitopes, and its tertiary structure is important for its antigenicity. The amino acid arginine, which is substituted for glycine, is a much larger residue and charged^[11]. As a result the hydrophobicity profiles of this region of the two antigens are quite different and would be expected to affect the secondary and tertiary structures of the antigen. This amino acid substitution lies within the “a” determinant and so potentially alters the epitopes recognized by the protective immune response.

The secondary and tertiary structures of HBsAg expressed by the eukaryotic expression vector were most similar to those of viruses, which could exclude possible alterations of the antigenic properties by purification procedures of the recombinant vaccine. In transfection and *in vitro* expression study, HBsAg secreted by pCMV-S2.S-transfected cells had a higher affinity to the anti-HBs compared with that secreted by pCMV-S2.S+145R-transfected cells in the culture supernatant and the cell lysates of transfected cells, although the transfection efficiency was corrected. The antigenicity of HBsAg was altered by this single amino acid substitution. The mutant antigen could not be totally recognized by anti-HBs induced by naive antigens. The point mutation could influence the affinity, but mutant antigen could still be detected by anti-HBs.

The immunogenicity of HBsAg was also altered by this point mutation. The anti-HBs titer to the native HBsAg induced by mutant HBsAg was significantly lower than that induced by native HBsAg, while there was no significant difference between the titers of anti-preS2 induced by the two antigens. These results support the suggestion that this mutation was the result of immune pressure^[12]. This variant could evade the immune response elicited after natural infection or after vaccination^[13,14].

Both HBsAg and preS2 antigens, expressed by these two plasmids, were able to induce a strong humoral immune response. Indeed, anti-HBs titers induced by both plasmids were far above 10 mIU/L. The level of anti-HBs was sufficient to protect humans against HBV infection after exposure to the virus. This DNA vaccine could also confer the protection against infection with prototype HBV.

The preS2 antigen was not detected in the culture supernatant or cell lysates of transfected cells, but a substantial cytoplasmic accumulation was detected in plasmid transfected cells by immunocytochemical study, and the anti-preS2 was also detected in mice after DNA immunization. It is likely that the preS2 antigen was a nonsecreted protein expressed by this vector in HepG2 cells. It could be a nonsecreted protein *in vivo*, but it was possible that bupivacaine followed by plasmid DNA injections caused early activation of nonspecific inflammatory mediators by recruiting professional APCs^[15,16], B cells, and T cells. In addition,

a specific immune response against muscle cells expressing viral peptides or proteins might subsequently lead to damage of muscle fibers and release of sequestered antigens. Such antigens might eventually reach lymph nodes or alternatively taken up locally by APCs. The occurrence of protective antibodies of anti-HBs2 was one to two weeks earlier than that of anti-HBs in the same group. This result was similar to other reports^[17,18]. There was little difference in occurrence, high titre and duration of anti-preS2 between the mutant and native viral protein expression plasmids. It indicated that this mutation had little impact on the antigenicity and immunogenicity of preS2 antigen. Therefore, the ingredient of preS2 antigen in hepatitis B vaccine would protect humans against this mutant HBV infection after exposure to the virus, and it also could shorten the occurrence of protective antibody and give an early stage protection. This would benefit the infants born by HBeAg positive mothers and persons exposed to HBV.

In conclusion, DNA immunization with the mutant HBsAg expression vector, produces a lower affinity than that elicited by the native HBsAg expression vector. The mutation changes the antigenicity and immunogenicity of HBsAg, and also induces a protective immune response.

REFERENCES

- 1 Lee KM, Kim YS, Ko YY, Yoo BM, Lee KJ, Kim JH, Hahm KB, Cho SW. Emergence of vaccine-induced escape mutant of hepatitis B virus with multiple surface gene mutations in a Korean child. *J Korean Med Sci* 2001; **16**: 359-362
- 2 Kidd-Ljunggren K, Miyakawa Y, Kidd AH. Genetic variability in hepatitis B viruses. *J Gen Virol* 2002; **83**(Pt 6): 1267-1280
- 3 Nainan OV, Khristova ML, Byun K, Xia G, Taylor PE, Stevens CE, Margolis HS. Genetic variation of hepatitis B surface antigen coding region among infants with chronic hepatitis B virus infection. *J Med Virol* 2002; **68**: 319-327
- 4 Cooreman MP, Leroux-Roels G, Paulij WP. Vaccine- and hepatitis B immune globulin-induced escape mutations of hepatitis B virus surface antigen. *J Biomed Sci* 2001; **8**: 237-247
- 5 Osioy C. Sensitive detection of HBsAg mutants by a gap ligase chain reaction assay. *J Clin Microbiol* 2002; **40**: 2566-2571
- 6 Fischer L, Kalinina T, Rogiers X, Will H, Sterneck M. GLY145ARG mutation emerging under HBIG treatment in patients with recurrent HBV after liver transplantation strongly reduces viral secretion. *Transplant Proc* 2001; **33**: 3633-3636
- 7 Kidd-Ljunggren K, Miyakawa Y, Kidd AH. Genetic variability in hepatitis B viruses. *J Gen Virol* 2002; **83**(Pt 6): 1267-1280
- 8 Rodriguez-Frias F, Buti M, Jardi R, Vargas V, Quer J, Cotrina M, Martell M, Esteban R, Guardia J. Genetic alterations in the S gene of hepatitis B virus in patients with acute hepatitis B, chronic hepatitis B and hepatitis B liver cirrhosis before and after liver transplantation. *Liver* 1999; **19**: 177-182
- 9 Grotola A, Buttafoco P, Del Buono MG, Cremonini C, Colantoni A, Gelmini R, Morelli C, Masetti M, Jovine E, Fruet F, Pinna A, Manenti F, Villa E. Pretransplantation pre-S2 and S protein heterogeneity predisposes to hepatitis B virus recurrence after liver transplantation. *Liver Transpl* 2002; **8**: 443-448
- 10 Gan RB, Chu MJ, Shen LP, Qian SW, Li ZP. The complete nucleotide sequence of the cloned DNA of hepatitis B virus subtype adr in pADR-1. *Sci Sin* 1987; **30**: 507-521
- 11 Waters JA, Kennedy M, Voet P, Hauser P, Petre J, Carman W, Thomas HC. Loss of the common "A" determinant of hepatitis B surface antigen by a vaccine-induced escape mutant. *J Clin Invest* 1992; **90**: 2543-2547
- 12 Oon CJ, Chen WN, Goo KS, Goh KT. Intra-familial evidence of horizontal transmission of hepatitis B virus surface antigen mutant G145R. *J Infect* 2000; **41**: 260-264
- 13 Hou J, Wang Z, Cheng J, Lin Y, Lau GK, Sun J, Zhou F, Waters J, Karayiannis P, Luo K. Prevalence of naturally occurring surface gene variants of hepatitis B virus in nonimmunized surface antigen-negative Chinese carriers. *Hepatology* 2001; **34**: 1027-1034
- 14 Chen WN, Oon CJ. Hepatitis B virus surface antigen (HBsAg) mutants in Singapore adults and vaccinated children with high anti-hepatitis B virus antibody levels but negative for HBsAg. *J Clin Microbiol* 2000; **38**: 2793-2794
- 15 Ulmer JB, Donnelly JJ, Parker SE, Rhodes GH, Felgner PL, Dwarki VJ, Gromkowski SH, Deck RR, DeWitt CM, Friedman A. Heterologous protection against influenza by injection of DNA encoding a viral protein. *Science* 1993; **259**: 1745-1749
- 16 Oka Y, Akbar SM, Horiike N, Joko K, Onji M. Mechanism and therapeutic potential of DNA-based immunization against the envelope proteins of hepatitis B virus in normal and transgenic mice. *Immunology* 2001; **103**: 90-97
- 17 Geissler M, Tokushige K, Chante CC, Zurawski VR Jr, Wands JR. Cellular and humoral immune response to hepatitis B virus structural proteins in mice after DNA-based immunization. *Gastroenterology* 1997; **112**: 1307-1320
- 18 Madalinski K, Sylvan SP, Hellstrom U, Mikolajewicz J, Zembrzaska-Sadkowska E, Piontek E. Antibody responses to preS components after immunization of children with low doses of BioHepB. *Vaccine* 2001; **20**: 92-97

Edited by Wang XL and Ren SY Proofread by Xu FM

• VIRAL HEPATITIS •

Replication and gene expression of mutant hepatitis B virus in a transgenic mouse containing the complete viral genome with mutant *s* gene

Jun-Hui Ge, Le-Zhi Zhang, Jian-Xiu Li, Hong Liu, Hui-Min Liu, Jin He, Yu-Cheng Yao, Yong-Ji Yang, Hong-Yu Yu, Yi-Ping Hu

Jun-Hui Ge, Hui-Min Liu, Jin He, Hong-Yu Yu, Department of Pathology, Changzheng Hospital, Second Military Medical University, Shanghai 200003, China

Le-Zhi Zhang, Department of Experimental Diagnosis, Changhai Hospital, Second Military Medical University, Shanghai 200433, China

Jian-Xiu Li, Hong Liu, Yu-Cheng Yao, Yong-Ji Yang, Yi-Ping Hu, Department of Cell Biology, Second Military Medical University, Shanghai 200433, China

Supported by National Science Foundation of China, No. 396670669 and No.39970676; Keystone basic research program of STCM, No. 03DZ14023

Co-correspondents: Le-Zhi Zhang and Yi-Ping Hu

Correspondence to: Hong-Yu Yu, Department of Pathology, Changzheng Hospital, Second Military Medical University, Shanghai, 200003, China. yuhongyu795@hotmail.com

Telephone: +86-21-63610109-73703 **Fax:** +86-21-25070291

Received: 2004-01-09 **Accepted:** 2004-03-12

Abstract

AIM: To establish the transgenic mouse line harbouring complete hepatitis B virus (HBV) genome with mutant *s* gene (*adr* subtype).

METHODS: Transgenic mice were generated by microinjecting HBV genome into fertilized eggs. Integration, expression, replication of HBV gene and histological changes in transgenic mice were estimated by genomic DNA PCR, serum DNA PCR, Southern blot, ELISA, HE staining, immunohistochemistry and transmission electron microscopy. Transgenic mice with HBsAg positive in serum were bred and analyzed.

RESULTS: A total of 288 eggs survived from microinjections were transplanted into the oviducts of 13 pseudopregnant mice and 49 pups were produced. Twenty-six mice were identified to have the integrated HBV gene. Serum HBsAg and HBeAg were detected in 2 of 43 mice. HBsAg and HBeAg in cytoplasm or nuclei of hepatocytes were detected in 10 mice. Founders with HBsAg in serum were named lineages G145R-15 and G145R-18. Of the 16 F1 offsprings generated by G145R-15 founder, 12 were positive for HBV genome with PCR, 10 were positive for HBsAg and HBeAg with immunohistochemistry and 7 were positive for HBsAg and HBeAg with ELISA. Only 1 of 8 F1 offsprings generated by G145R-18 founder was survived and it was detected positive for HBV genome, HBsAg, HBeAg and HBeAg. Both of the two lineages had some pathological characteristics of mild chronic hepatitis B in the liver, such as swelling of hepatocytes and focal hepatocellular necrosis and parenchymal lymphomononuclear cell infiltrate.

CONCLUSION: Transgenic mice harbouring HBV with mutant *s* gene can be generated. The HBV genes are integrated in the transgenic mice genome and can be expressed, replicated, packaged and excreted. HBV DNA can be stably transmitted in the transgenic mice.

Ge JH, Zhang LZ, Li JX, Liu H, Liu HM, He J, Yao YC, Yang YJ, Yu HY, Hu YP. Replication and gene expression of mutant hepatitis B virus in a transgenic mouse containing the complete viral genome with mutant *s* gene. *World J Gastroenterol* 2004; 10(21): 3141-3145

<http://www.wjgnet.com/1007-9327/10/3141.asp>

INTRODUCTION

Hepatitis B virus (HBV) is a major pathogen causing human acute and chronic hepatitis B^[1] and has a very close association with cirrhosis and human hepatocellular carcinoma (HCC)^[2-5]. Hepatitis B (HB) vaccine can protect human from infecting HBV. Many children born from HBeAg positive mothers would suffer from HBV after HB vaccination because of the mutation of HBV^[6-7]. Genetic mutation in viruses is usually associated with escape of host immune responses, development of drug resistance, modification of virulence and patterns of epidemiology of diseases. In addition, HBV has a limited host range, which impedes much of the study on its biological characteristics and human hepatitis B. Over the past several years, many transgenic lineages harbouring intact HBV gene^[8] or expressing the HBV envelope, core, precore and X proteins^[9] under the control of HBV or cellular liver-specific promoters have been generated, thereafter, the transgenic mouse system was applied in HBV studies^[10-12]. However, no reports of transgenic mouse harbouring mutant HBV are available.

HBV belongs to hepadnavirus family, containing a small (3.2-kb), circular, double-stranded DNA genome. The minus strand includes at least four open reading frames (ORF), of which, S-ORF is divided into pres1, pres2 and *s* gene. HBsAg encoded by the *s* gene is the major component of hepatitis B vaccine. It is also an important diagnostic evidence of HBV infection. Hepatitis B immunoglobulin could be used to protect the liver from reinfection after liver transplantation, but it depends on the interaction of HBsAg and anti-HBs. Therefore, the change of antigenicity of HBsAg has a direct impact on the diagnosis and therapy of HBV. It is most common to find the mutation at aa145 where glycine is substituted by arginine (G145R). This mutant could result in the failure of HB vaccination^[13] and failing to protect the liver from reinfection after liver transplantation^[14-16]. Recently, several lines of evidence of horizontal transmission have been found^[17-18]. It brings about many new problems to prophylaxis and therapy of HB. It is necessary to study further on the change of biological characteristics related with this point mutation. Transgenic mice harbouring G145R mutant are a good animal model in study of changes of antigenicity and immunogenicity as well as pathogenicity of HBV. Therefore, we generated transgenic mice harboring complete genome of HBV (*adr* subtype) G145R mutant by microinjection method, in which HBsAg and HBeAg could be expressed, and genomic DNA of HBV could be replicated and packed into complete virus particles. This model makes it possible to examine many aspects of HBV and its associated biomedical issues *in vivo*, and is an animal model for drug screen and therapy involved in this mutant.

MATERIALS AND METHODS

Reagents, Plasmid, antibodies and animals

Restriction endonucleases and T4 DNA ligase were obtained from Sangon Co. Canada. Plasmid P II was endowed by Dr. Jian-Wen He and contained overlenght HBV genomes, beginning at the middle of the X gene, terminating at nucleotides 1982, just downstream of the unique polyadenylation signal in the HBV genome at a unique *Bam*HI site. Plasmid P II contained a point mutation at the site of *s* gene nt 587(G→A). HBsAg and HBeAg ELISA reagents were purchased from Abbott Laboratories and Sino-American Biotechnology Co., respectively. Mouse monoclonal antibody against HBsAg and rabbit HBc/eAg primary anti-serum were purchased from DAKO, USA. Sheep anti mouse IgG-HRP was obtained from CALBIOCHEM, Germany. Serum DNA extraction kit was got from Sino-American Biotechnology. QIA quick gene gel kit and plasmid extraction kit were purchased from QIA-gene. C57BL/6 mice were SPF level and maintained on a 14:10 light-dark schedule (lights off at 10 pm, lights on at 8 am every day).

Microinjection and embryo manipulation of founder animals

HBV transgenic mice were produced by microinjection of the *Pvu* II fragment excised from plasmid P II into C57BL/6 embryos by conventional technology. In brief, the *Pvu* II fragment containing 1.2 copy HBV DNA was gel purified and dissolved in TE buffer (10 mmol/L Tris-HCl, 0.2 mmol/L EDTA, pH 7.5) at a final concentration of 1 mg/L (2000 copies/pL). After it was injected into male pronuclei obtained from C57BL/6 females, the eggs were implanted into oviducts of pseudopregnant recipients to enable further development before term. Founder animals were screened by analysis of serum for HBsAg and HBeAg. Animals positive for both antigens were expanded by repetitive backcrossing against the C57BL/6 strain and bred for analysis.

DNA isolation and PCR analysis of integrated transgenes

To isolate the total genomic DNA, approximately one third of the tail of 10-d-old mice was cut and placed into a 1.5 mL microcentrifuge tube containing 500 μ L of TB buffer. The tubes containing the tail fragments were incubated overnight at 55 °C. DNA was extracted once with 500 μ L of 1:1 (v/v) equilibrated phenol-chloroform, and precipitated with 2 volumes of ethanol. After centrifugation, precipitates were resuspended in 500 μ L water.

Total tail genomic DNA (1 mg) was analyzed by PCR using HBV-specific primers (5'-CCCAA CCTCC AATCA CTCAC CAACC-3' [sense, nt 2 139 to 2 153] and 5'-GGCCC CCAAT ACCAC ATCAT CCATA -3' [antisense, nt 2 583 to 2 556]). A 20 μ L of samples of the products from direct PCR amplifications was analyzed by electrophoresis on a 10 g/L agarose gel in the presence of 0.5 μ g of ethidium bromide per mL. DNA bands were visualized by UV fluorescence.

Southern blot analysis

Southern blot analysis was performed on the total genomic DNA by agarose gel electrophoresis of 20 μ g of restricted genomic DNA as previously described. Before electrophoresis, all DNA samples were digested with *Eco*R I at 10 U/ μ g for 4 h at 37 °C. Nylon filters were hybridized with HBV-specific digoxigeninlabeled DNA probes as previously described^[19].

PCR analysis of HBV DNA in serum

Total serum genomic DNA from transgenic mice was extracted according to the manufacturer's instructions, and analyzed by PCR using HBV-specific primers as described above.

Immunohistochemical analysis of the expression of HBV

In selected experiments, liver tissue derived from transgenic mouse lineages was also studied. In some experiments, mice

were anesthetized with pentobarbitone (Harvest Pharmaceutical Co. LTD) prior to phlebotomy from the retro-orbital plexus and before they were sacrificed by cervical dislocation. In the other experiments, mice were anesthetized with pentobarbitone prior to biopsy of the liver at the age of 3, 6, 9, 12, 15, 18 mo. Intracellular distributions of HBcAg and HBsAg were assessed by the labeled-avidin-biotin detection procedure^[20]. Briefly, paraffin-embedded sections in PBS, pH 7.4, were treated for 15 min at 37 °C with 30 mL/L hydrogen peroxide and washed with PBS. After the sections were blocked with normal goat serum for 30 min at room temperature, rabbit anti-HBc/eAg primary antiserum or mouse anti-HBsAg monoclonal antibody was applied at a 1:100 (HBcAg) or 1:500 (HBsAg) dilution for 12 h at 4 °C. After washed with PBS, a secondary antiserum consisting of biotin-conjugated goat anti-rabbit or goat anti-mouse immunoglobulin G was applied at a 1:100 dilution for 30 min at 37 °C. The antibody coated slides were washed with PBS, treated with streptavidin-horseradish peroxidase conjugates at a 1:600 dilution for 30 min at 37 °C, stained with nitroblue tetrazolium chloride and 5-bromo-4-chloro-3-indolylphosphate (NBT/BCIP, MAXIN Co.), and counterstained with Mayer's hematoxylin before mounted.

Serological analysis of the expression of HBV

Transgenic mice of lineages G145R-15 and G145R-18 were anesthetized with pentobarbitone prior to phlebotomy from the retro-orbital plexus 200 μ L every week. Serum was isolated by centrifugation. HBsAg and HBeAg concentrations were analyzed every month by using commercially available enzyme-linked immunosorbent assay reagents according to the manufacturer's instructions.

Serum antibody analysis of transgenic mice

Serum from transgenic mice was also assayed for anti-HBsAg, anti-HBeAg and anti-HBcAg every month by using commercially available enzyme-linked immunosorbent assay reagents according to the manufacturer's instructions.

Electron microscopy

Intracellular nucleocapsid particles were analyzed exactly as described elsewhere. Briefly, thin liver sections were fixed overnight at 4 °C in 40 g/L paraformaldehyde-1 g/L glutaraldehyde in PBS. Sections were then postfixed in 10 g/L OsO₄ in cacodylate buffer (pH 7.4) for 1 h at room temperature, dehydrated in gradient ethanol, and embedded in epoxy resin (TAAB 812; Emmer Green, Reading, England). Sections were cut on a LKB Ultratome III, mounted on copper grids, stained in uranyl acetate and lead citrate, and viewed with a Hitachi H-800 electron microscope.

Serum-derived virus particles were analyzed as follows. Five hundred microliters of transgenic-mouse serum was centrifuged (300 000 g) for 12-16 h at 4 °C through 2.4 mL of 100 g/L sucrose into 0.8 mL of 600 g/L sucrose. Fractions (100 μ L) were collected from the bottom, and the first fraction was incubated for 45 min at room temperature on MA18/7-coated (100 μ g/mL) Parlodion-carbon-coated nickel grids that were subsequently drained with a piece of filter paper and washed twice in PBS. The grids were then fixed in 15 g/L glutaraldehyde for 2 to 5 min, washed twice in H₂O, negatively stained with uranyl acetate, and viewed with a Hitachi H-800 electron microscope.

Histological analysis

Tissue samples were fixed in 40 g/L neutral buffered formaldehyde, embedded in paraffin, sectioned (4 μ m), and stained with hematoxylin and eosin as described^[8].

Biochemical evidence of hepatocellular and renal injury

Serum alanine aminotransferase (sALT), serum aspartate

aminotransferase (sAST), blood urea nitrogen (BUN), creatinine (Cr) and γ -glutamyl transpeptidase (γ -GT) were tested with an auto-biochemical analyzer.

RESULTS

Microinjection and production of transgenic mice

Hundreds of molecules of target fragments were microinjected into male pronuclei of fertilized eggs. A total of 288 eggs survived from microinjections were transplanted into the oviducts of 13 pseudopregnant mice and consequently, the mice were pregnant and gave birth to 49 pups. In addition, 43 were survived. HBsAg and HBcAg in cytoplasm or nuclei of hepatocytes were detected in 10 mice. Two of 43 founder animals whose sera were positive for both HBsAg and HBeAg were produced and named lineages G145R-15 and G145R-18. They were expanded by repetitive backcrossing against the C57BL/6 strain and studied in detail. Sixteen F1 offsprings of lineage G145R-15 founder mice were born. Twelve of them were identified as the integration of HBV gene by PCR and Southern blot hybridization analysis of tissues. HBsAg and HBcAg were detected in eight of them by immunohistochemistry. HBsAg and HBeAg were detected in seven of them by using ELISA. Only one of eight F1 offsprings generated by lineage G145R-18 founder was survived. In addition, all above methods detected it positive. F1 offsprings were positive for both HBsAg and HBeAg and expanded by repetitive backcrossing against the nontransgenic C57BL/6.

Analysis of integrated transgenes

Total DNA was isolated from tail tissues of lineages G145R-15 and G145R-18, digested with an enzyme (*Eco*R I) that was not cut within the transgene, and analyzed by Southern blot (Figure 1).

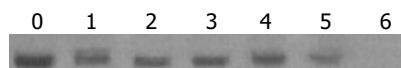


Figure 1 Southern blot analysis of 20 μ g of total DNA extracted from transgenic mouse tail tissues of lineages G145R-15 and G145R-18. Lane 0: Positive control; Lane 1: lineage G145R-15; Lane 2: lineage G145R-15; Lane 3: F₁ transgenic mice of lineage G145R-15; Lane 4: F₁ transgenic mice of lineage G145R-18; Lane 5: lineage of transgenic mice harbouring prototype HBV genome; Lane 6: non-transgenic mice as negative control. All DNA samples were RNase treated before gel electrophoresis. The filters were hybridized with a digoxigeninlabeled HBV specific DNA probe.

Expression of viral proteins

At the protein level, HBsAg (a product of the 2.1-kb mRNA)

and HBeAg (a product of the 3.5-kb mRNA) were easily detectable in the serum in both lineages (Table 1). As expected, HBcAg (also a product of the 3.5-kb mRNA) and HBsAg were easily detectable in the liver by immunohistochemical staining (Figures 2A, B).

Table 1 Serum HBV antigen levels

	4 wk	8 wk	12 wk	16 wk	72 wk
Normal mouse					
HBsAg ¹	0.056	0.052	0.056	0.055	0.053
HBe/cAg ²	0.052	0.059	0.053	0.052	0.055
G145R-15					
HBsAg	0.126	0.153	0.151	0.132	0.158
HBe/cAg	0.236	0.272	0.228	0.265	0.243
G145R-18					
HBsAg	0.133	0.143	0.155	0.129	0.128
HBe/cAg	0.256	0.236	0.268	0.257	0.261

¹Optical density (A) at 490 and 630 nm wavelength, cutoff value is 0.083. ²Optical density (A) at 405 nm wavelength, cutoff value is 0.106.



Figure 3 Ultrastructural analysis of HBcAg in the liver.

Distribution of HBcAg and HBsAg in liver

Both lineages displayed the same subcellular and architectural distribution of HBcAg in the liver. Figure 2A and 2B shows that HBcAg and HBsAg were present in the cytoplasm of almost all the hepatocytes distributed widely throughout the hepatic lobules from the centrilobular region around central veins to the periportal region around the portal tracts, but positive hepatocytes surrounding the central veins were much more than those around centrilobule. At the nucleic level, however, only HBcAg was detectable (Figure 2C). Typical 25-30 nm HBcAg particles (core particles and nucleocapsid particles) were detected in the nuclei (Figure 3). All indicated the existence of important host influences on viral gene expression in these animals.

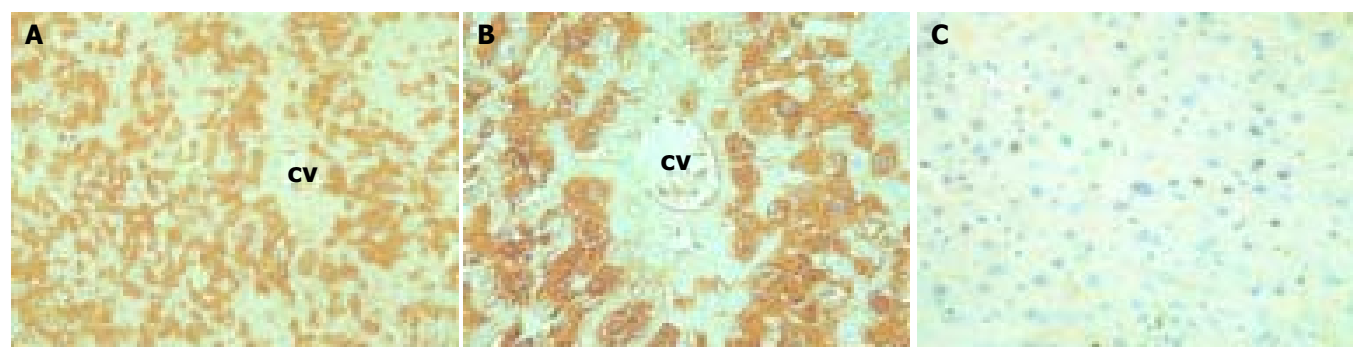


Figure 2 Immunohistochemical analysis of HBsAg and HBcAg in the liver. A: Presence of cytoplasmic HBsAg in almost all of hepatocytes in immunohistochemical analysis of the liver of an 6-week-old male mouse. Magnification, $\times 100$. B: Cytoplasmic HBcAg in centrilobular region hepatocytes surrounding the central veins. Magnification, $\times 200$. C: Nuclear HBcAg scattering widely throughout the hepatic lobule. Magnification, $\times 100$.

Circulating viral particles

To determine whether potentially infectious viral particles were formed and secreted into the blood of these mice, serum was analyzed for the presence of HBV DNA and sedimentable particles displaying the ultrastructural characteristics of complete virions (Dane particles). HBV DNA was detectable in the serum of an HBV transgenic-mouse lineage that replicated the viral genome.

Histopathological findings

Animals from lineages G145R-15 and G145R-18 were monitored histologically for over eighteen months without evidence of pathological changes in the kidney, brain, spleen, lung, testis, ovaries, skin, and muscle except for the liver. In some region of the liver, swollen hepatocytes, hydropic degeneration or ballooning degeneration was observed in hepatic lobules that were distributed in the centrilobular region around central veins (Figure 4A, B). In the other, focal or unicellular necrosis, together with predominantly lymphocyte infiltrate was present (Figure 4D). In the portal or periportal tract, mild or moderate inflammation was also observed, as illustrated in Figure 4C. Interface inflammation could be observed in some cases. However, fibrosis was absent. Acidophilic body was scarce.

Serum antibody in transgenic mice

The ELISA test indicated that there was no significant positive result of HBV antibodies in HBV transgenic mouse serum.

Biochemical evidence of hepatocellular and renal injury

Animals from lineages G145R-15 and G145R-18 were monitored to have biochemical changes for over eighteen months without evidence of hepatocellular and renal injury, although there were histopathological changes in the liver.

DISCUSSION

In the study of vaccinated children whose mothers were positive for HBeAg, about 15% of them became anti-HBc positive. A proportion of these would be HBsAg positive and

become the HBV carriers. About half of those were infected with variants of MHR, the most consistently observed to be G145R. Three population-based studies from Singapore, UK and USA had remarkably similar results. Mathematical modeling indicated it would be the dominant viral strain, although it could take a long time to emerge. Vaccination at birth is an ideal situation for selection of escape variants, being similar to liver transplantation, where high titer anti-HBs preparations are administered to prevent graft infection. Furthermore, naturally occurring G145R strains were reported.

To study the biological properties and pathologic conditions associated with this mutant, HBV transgenic mice whose hepatocytes expressed and replicated the virus and whose genome harbor HBV mutant G145R were produced with a terminally redundant, 1.2 genome length transgene that starts in the middle of the X gene and ends just downstream of the unique HBV polyadenylation site.

Only two of the forty-three founders were serum HBsAg-positive, and the expression level of the others was very low, which might be due to the different integrated sites of HBV DNA. In general, the exogenous gene would be integrated into multi-sites in transgenic mice. This is similar with other reports. Immunohistochemical assays of several tissues from transgenic mice revealed that HBV gene expressions were tissue-dependent, and the genes were only expressed in the liver and kidney, this is similar to HBV-infection in nature. The regulation of expression of a foreign gene in transgenic mice was subjected to different parameters, such as site of integration, influence of the mouse flanking sequences, cellular factors and structure of the integrated sequences. However, the general finding was that transgenes kept their developmental and tissue specific control of expression. Mouse genomic sequences might potentially have an influence on the level of transcription of tissue specificity. The important influence of cellular factors on expression was apparent since many hepatocytes, all the Kupffer cells, endothelial cells and bile duct epithelium in the tissue were antigen negative, although most cells in the liver probably contained integrated HBV DNA. It may be germane

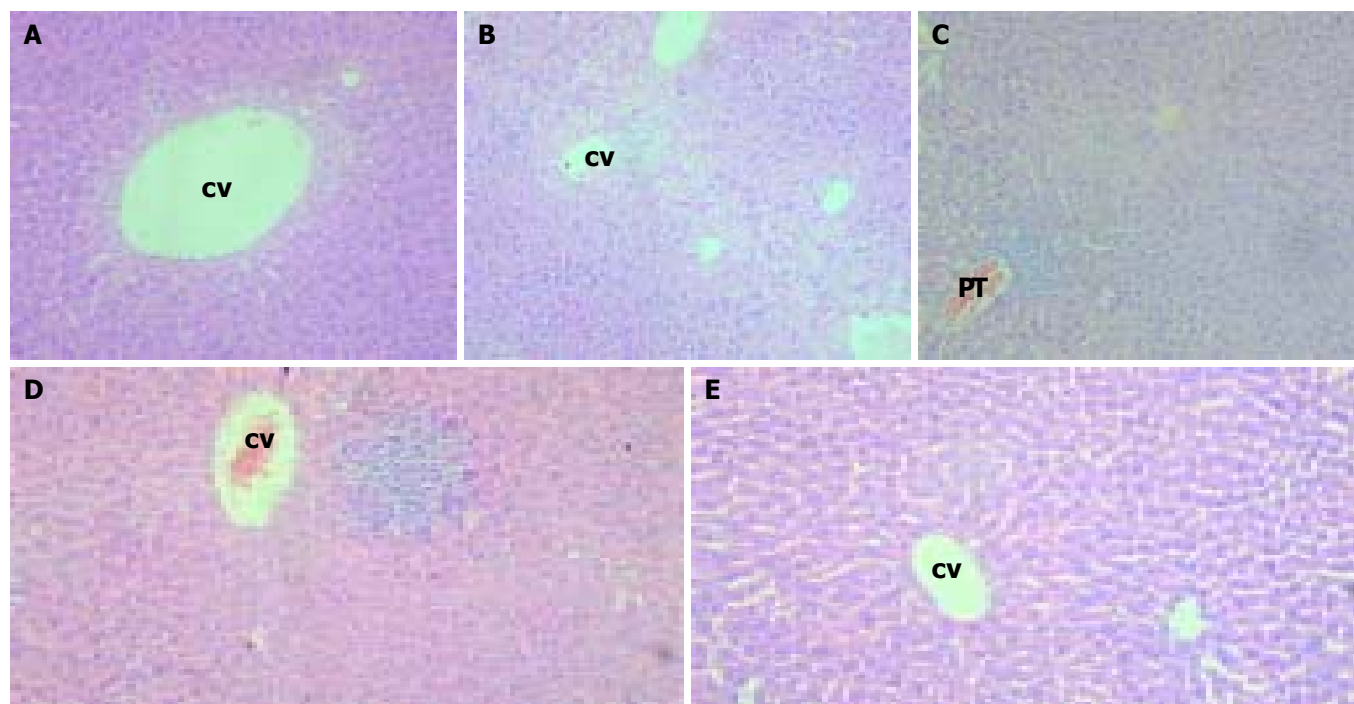


Figure 4 Analysis of pathological changes in the liver of transgenic mice by HE staining. Magnification $\times 100$. A: Mild swollen hepatocytes around the central veins (CV) in the centrilobular region. B: "Ballooning degeneration" around the central veins or between the two central veins in the liver. C: Predominantly lymphocytic cell infiltrates in portal tract area and hepatic lobules. D: Focal necrosis and predominantly lymphocytic cell infiltrates in hepatic lobule. E: Liver of normal mice.

that hepatocyte nuclear factor 1 alpha (HNF 1 a) and retinoic acid are known to be preferentially expressed in hepatocytes. Interestingly, the positive cells were clustered like clones of cells. This was described in infected humans, and it was proposed that the synthesis of viral antigens depended on the metabolic state of cells.

HBcAg was detected both in the nuclei and in the cytoplasm of hepatocytes. The presence of HBcAg in the nuclei of hepatocytes was found in most of HBV-infected humans. Cytoplasmic location of HBcAg was also observed in some cases with active viral replication. Capsid antigens of ground squirrel hepatitis virus, duck hepatitis B virus and woodduck hepatitis virus were found almost exclusively in the cytoplasm. This may be the consequence of the constantly high level of replication of these viruses. Pre-core RNA is only used as a mRNA for the production of HBeAg that is secreted into the serum. This polypeptide can be aggregated into unstable particles but its location is in cytoplasm. Therefore, it is likely that it is responsible for the cytoplasm structure.

HBV transgenic mice showed replication of HBV in hepatocytes and had evidence of pathological lesions in the liver, which are different from other reports. Although there were some pathological characteristics of mild chronic hepatitis B in the transgenic mice, the change was obviously different from that of human chronic hepatitis B. Cellular pathological changes, such as swelling of hepatocytes and focal hepatocellular necrosis and parenchymal lymphomononuclear cell infiltrate were the main lesions. While the histological changes, such as the change or destruction of structure of hepatic lobules caused by hyperplasia of fibers, were not observed in all transgenic mice. Even fibrocytes and fibrous tissue were difficult to be observed in the portal tract, it was likely due to the difference of species. In normal mice, the borderline of hepatic lobules is not clear as that of human being's.

Serum anti-HBs, anti-HBc and anti-HBe detected by ELISA were negative in all of the transgenic mice, suggesting that these mice were tolerant to HBsAg, HBcAg and HBeAg. This result is consistent with that of another report.

What caused the pathological changes of the liver? We supposed the immune response of transgenic mice caused the pathological lesions. Some of transgenic mice were partially immunological tolerant to viral antigens. In our and another study, HBsAb could be induced by injection of HB vaccine into muscles of the HBV transgenic mice. This indicated that the immunological tolerance was not complete. We assume that although the gene of virus was integrated in the genome of mice, the time of expression of exogenous gene in thymus was a little later than the formation of immunological tolerance. Some children whose mothers were HBeAg positive did also have pathological changes in their liver, but without HBsAb in the serum.

In conclusion, HBV genome introduced by microinjection can be integrated into the mouse genome, and HBV genes can be expressed, replicated and packaged. Therefore, these lineage mutant HBV transgenic mice may be used as animal models for the study on mutant HBV and its associated biomedical issues. It can also be applied in the selection of anti-mutant HBV drugs and vaccine.

REFERENCES

- 1 **Merican I**, Guan R, Amarapuka D, Alexander MJ, Chutaputti A, Chien RN, Hasnain SS, Leung N, Lesmana L, Phiet PH, Sjalfoellah Noer HM, Sollano J, Sun HS, Xu DZ. Chronic hepatitis B virus infection in Asian countries. *J Gastroenterol Hepatol* 2000; **15**: 1356-1361
- 2 **Birrer RB**, Birrer D, Klavins JV. Hepatocellular carcinoma and hepatitis virus. *Ann Clin Lab Sci* 2003; **33**: 39-54
- 3 **Rabe C**, Cheng B, Caselmann WH. Molecular mechanisms of hepatitis B virus-associated liver cancer. *Dig Dis* 2001; **19**: 279-287
- 4 **Arbuthnot P**, Kew M. Hepatitis B virus and hepatocellular carcinoma. *Int J Exp Pathol* 2001; **82**: 77-100
- 5 **Brechot C**, Gozuacik D, Murakami Y, Paterlini-Brechot P. Molecular bases for the development of hepatitis B virus (HBV)-related hepatocellular carcinoma (HCC). *Semin Cancer Biol* 2000; **10**: 211-231
- 6 **Lee KM**, Kim YS, Ko YY, Yoo BM, Lee KJ, Kim JH, Hahm KB, Cho SW. Emergence of vaccine-induced escape mutant of hepatitis B virus with multiple surface gene mutations in a Korean child. *J Korean Med Sci* 2001; **16**: 359-362
- 7 **Kidd-Ljunggren K**, Miyakawa Y, Kidd AH. Genetic variability in hepatitis B viruses. *J Gen Virol* 2002; **83**(Pt 6): 1267-1280
- 8 **Hu YP**, Hu WJ, Zheng WC, Li JX, Dai DS, Wang XM, Zhang SZ, Yu HY, Sun W, Hao GR. Establishment of transgenic mouse harboring hepatitis B virus (adr subtype) genomes. *World J Gastroenterol* 2001; **7**: 111-114
- 9 **Singh M**, Kumar V. Transgenic mouse models of hepatitis B virus-associated hepatocellular carcinoma. *Rev Med Virol* 2003; **13**: 243-253
- 10 **Kimura K**, Kakimi K, Wieland S, Guidotti LG, Chisari FV. Activated intrahepatic antigen-presenting cells inhibit hepatitis B virus replication in the liver of transgenic mice. *J Immunol* 2002; **169**: 5188-5195
- 11 **Sitia G**, Isogawa M, Kakimi K, Wieland SF, Chisari FV, Guidotti LG. Depletion of neutrophils blocks the recruitment of antigen-nonspecific cells into the liver without affecting the antiviral activity of hepatitis B virus-specific cytotoxic T lymphocytes. *Proc Natl Acad Sci U S A* 2002; **99**: 13717-13722
- 12 **Baron JL**, Gardiner L, Nishimura S, Shinkai K, Locksley R, Ganem D. Activation of a nonclassical NKT cell subset in a transgenic mouse model of hepatitis B virus infection. *Immunity* 2002; **16**: 583-594
- 13 **Cooreman MP**, Leroux-Roels G, Paulij WP. Vaccine- and hepatitis B immune globulin-induced escape mutations of hepatitis B virus surface antigen. *J Biomed Sci* 2001; **8**: 237-247
- 14 **Fischer L**, Kalinina T, Rogiers X, Will H, Sterneck M. GLY145ARG mutation emerging under HBIG treatment in patients with recurrent HBV after liver transplantation strongly reduces viral secretion. *Transplant Proc* 2001; **33**: 3633-3636
- 15 **Rodriguez-Frias F**, Buti M, Jardi R, Vargas V, Quer J, Cotrina M, Martell M, Esteban R, Guardia J. Genetic alterations in the S gene of hepatitis B virus in patients with acute hepatitis B, chronic hepatitis B and hepatitis B liver cirrhosis before and after liver transplantation. *Liver* 1999; **19**: 177-182
- 16 **Grottola A**, Buttafoco P, Del Buono MG, Cremonini C, Colantoni A, Gelmini R, Morelli C, Masetti M, Jovine E, Fruet F, Pinna A, Manenti F, Villa E. Pretransplantation pre-S2 and S protein heterogeneity predisposes to hepatitis B virus recurrence after liver transplantation. *Liver Transpl* 2002; **8**: 443-448
- 17 **Oon CJ**, Chen WN, Goo KS, Goh KT. Intra-familial evidence of horizontal transmission of hepatitis B virus surface antigen mutant G145R. *J Infect* 2000; **41**: 260-264
- 18 **Chakravarty R**, Neogi M, Roychowdhury S, Panda CK. Presence of hepatitis B surface antigen mutant G145R DNA in the peripheral blood leukocytes of the family members of an asymptomatic carrier and evidence of its horizontal transmission. *Virus Res* 2002; **90**: 133-141
- 19 **Wang Y**, Wu MC, Sham JS, Tai LS, Fang Y, Wu WQ, Xie D, Guan XY. Different expression of hepatitis B surface antigen between hepatocellular carcinoma and its surrounding liver tissue, studied using a tissue microarray. *J Pathol* 2002; **197**: 610-616
- 20 **Jin YM**, Yun C, Park C, Wang HJ, Cho H. Expression of hepatitis B virus X protein is closely correlated with the high periportal inflammatory activity of liver diseases. *J Viral Hepat* 2001; **8**: 322-330

Possibility of non-invasive diagnosis of gastric mucosal precancerous changes

Victor D. Pasechnikov, Sergey Z. Chukov, Sergey M. Kotelevets, Alexander N. Mostovov, Varvara P. Mernova, Maria B. Polyakova

Victor D. Pasechnikov, Sergey M. Kotelevets, Alexander N. Mostovov,
Department of Therapy, Medical Academy, Stavropol, Russian Federation

Sergey Z. Chukov, Varvara P. Mernova, Maria B. Polyakova,
Department of Pathology, Medical Academy, Stavropol, Russian Federation

Correspondence to: Professor Victor D. Pasechnikov, Aviationsnaya street, 21, Stavropol, 355017, Russian Federation. passetchnikov@mail.ru
Telephone: +7-8652-354700

Received: 2004-03-11 **Accepted:** 2004-04-09

Abstract

AIM: To assess the possibility of non-invasive screening of atrophic chronic gastritis for preventing further development of gastric cancer.

METHODS: One hundred and seventy-eight consecutive *Helicobacter pylori* (*H pylori*)-positive dyspeptic patients after detection of serum levels of pepsinogen-1 (PG-1) and gastrin-17 (G-17) by enzyme immunoassay were proposed for endoscopy and histology. The serologic and morphologic results were compared with estimating the sensitivity, specificity and prognostic values of the tests.

RESULTS: There was statistically significant reverse dependence between the grade of stomach mucosal antral or corpus atrophy and the proper decreasing of serum G17 or PG1 levels. The serologic method was quite sensitive in the diagnosis of non-atrophic and severe antral and corpus gastritis. Also, it was characterized by the high positive and negative prognostic values.

CONCLUSION: Detection of serum G-17 and PG1 levels can be offered as the screening tool for atrophic gastritis. The positive serologic results require further chromoendoscopy with mucosal biopsy, for revealing probable progressing of atrophic process with development of intestinal metaplasia, dysplasia or gastric cancer.

Pasechnikov VD, Chukov SZ, Kotelevets SM, Mostovov AN, Mernova VP, Polyakova MB. Possibility of non-invasive diagnosis of gastric mucosal precancerous changes. *World J Gastroenterol* 2004; 10(21): 3146-3150

<http://www.wjgnet.com/1007-9327/10/3146.asp>

INTRODUCTION

According to the modern representations about stages of gastric carcinogenesis, it is supposed that chronic *Helicobacter pylori* (*H pylori*) infection is the trigger mechanism in 60-90% of gastric cancer cases^[1,2]. In 1975, Correa proposed the consecutive line of events leading to gastric cancer development: normal mucosa - chronic active gastritis - chronic atrophic gastritis - intestinal metaplasia - dysplasia - carcinoma *in situ*. At present, this cascade of changes associates with a trigger role of *H pylori* and is called "Correa's gastric precancerous cascade"^[2,3]. The early detection of gastric precancerous changes, mainly atrophic

gastritis, may be helpful in prevention of gastric cancer or in diagnosis of cancer at curable stages. So, there is a critical need for valid diagnostic methods of stomach mucosal atrophy, that would be inexpensive and non-invasive, that is, suitable for screening of large groups of people.

Taking into account the known interrelations between the morphological status and functional activity of gastric corpus and antral mucosa and the secretion of, respectively, pepsinogen 1 and gastrin 17^[4,5], we carried out a prospective study with the aim to detect *H pylori*-induced gastric precancerous changes, that were leading to cancer formation, and to evaluate the possibility of non-invasive screening of dyspeptic patients.

MATERIALS AND METHODS

Materials

The study was carried out in a group of dyspeptic *H pylori*-infected patients.

Methods

H pylori antibodies (Hp-Ab), serum levels of pepsinogen I (PGI) and gastrin-17 (G-17) were analyzed by enzyme immunoassay with Biohit GastroPanel® (Biohit Plc, Helsinki, Finland). According to the instructions of its manufacturer, serum levels of PG1 <25 µg/L were estimated as markers of gastric corpus atrophy, serum levels of G17 <5 pmol/L were estimated as markers of gastric antral atrophy, serum levels of G17 <10 pmol/L in a combination with serum levels of PG1 <50 µg/L were estimated as markers of mild gastric corpus atrophy. HPAb IgG titers were estimated as follows: < 32 enzyme immunoassay unit (EIU) - negative result, 32 - 44 EIU - doubtful result, >44 EIU - positive result. The numerical meanings of researched parameters were analyzed by the program GastroSoft® (Biohit Plc, Helsinki, Finland) enclosed to test-system Biohit GastroPanel®. On the basis of inserted data, the program composed the diagnosis in a view of the presence or absence of *H pylori*-infection and mucosal atrophy, with the estimation of gastric cancer or peptic ulcer risk and with recommendations on the treatment according to Maastricht-2 consensus.

After getting the GastroSoft® diagnosis, we randomized 178 patients for the following study. The patients underwent the upper gastrointestinal endoscopy with subsequent biopsy of the antral and corpus mucosa. To increase the accuracy of endoscopic diagnosis, we carried out an additional chromoendoscopy with methylene blue staining allowing the detection of foci of intestinal metaplasia (IM) of gastric mucosa which were unrecognized by routine endoscopy. Biopsy specimens were stained with hematoxylin-eosin and PAS reaction in combination with alcian blue at pH 2.5. The grade of stomach mucosal atrophy was estimated from 0 to 3 according to Houston visual analogous scale.

Statistical analysis was used to calculate the statistical significance of received data (Mann-Whitney criterion). Spearman's correlation coefficient (r_s), positive predictive value (PPV) and negative predictive value (NPV) of diagnosis by Biohit GastroPanel®.

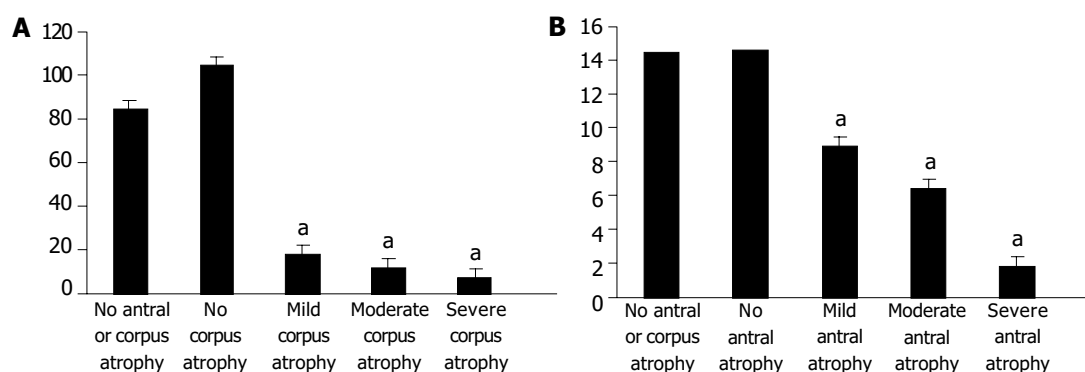


Figure 1 Comparison of serum PG1 (g/L) and G17 (pmol/L) levels and grade of gastric corpus and antral atrophy. A: Comparison of serum PG1 level and grade of gastric corpus atrophy. B: Comparison of serum G17 level and grade of gastric antral atrophy. ^a $P < 0.05$ vs non-atrophic state.

RESULTS

Of the 178 patients, non-atrophic chronic gastritis (no antral atrophy and no corpus atrophy) was detected only in 5 patients. The mean of serum PG-1, G-17 and anti-*H. pylori* IgG in this group was 85.28 ± 35.07 $\mu\text{g/L}$, 14.44 ± 1.90 pmol/L and 85.68 ± 17.81 EIU, respectively. In all these cases there was no IM or dysplasia in stomach mucosal epithelium.

The morphological status of gastric corpus mucosa was compared with serum PG-1 levels (Figure 1A). The non-atrophic corpus mucosa was detected in 99 (55.62%) of 178 patients, mild atrophy of corpus mucosa was detected in 17 (9.55%) patients, moderate atrophy of corpus mucosa was detected in 36 (20.22%) patients, severe atrophy of corpus mucosa was detected in 26 (14.61%) patients.

The statistical analysis revealed that there were marked differences between the levels of PG1 in non-atrophic and atrophic corpus gastritis. The levels of PG1 in mild, moderate and severe corpus atrophy were significantly lower ($P < 0.0001$) than those in non-atrophic state. In turn, the levels of PG1 in mild, moderate and severe corpus atrophy were significantly different from each other ($P < 0.0001$).

The morphological status of gastric antral mucosa was compared with serum G-17 levels (Figure 1B). The non-atrophic antral mucosa was detected in 12 (6.74%) of 178 patients. Mild atrophy of antral mucosa was detected in 31 (17.42%) patients. Moderate antral mucosa atrophy was detected in 69 (38.76%) patients. Severe antral mucosal atrophy was detected in 66 (37.08%) patients.

The statistical analysis revealed that there were marked differences between the levels of G17 in non-atrophic and atrophic antral gastritis. The latter was significantly lower ($P < 0.0001$). Moreover, the levels of G17 in mild, moderate and severe antral atrophy were significantly different from each other ($P < 0.0001$).

Table 1 Comparison of serum anti-*H. pylori* IgG titers (mean \pm SD) and grade of mucosal atrophy

	Anti- <i>H. pylori</i> IgG, EIU
No antral or corpus atrophy	85.68 ± 17.81
No antral atrophy	62.29 ± 12.02
Mild antral atrophy	78.25 ± 5.86
Moderate antral atrophy	74.08 ± 4.39
Severe antral atrophy	73.38 ± 5.38
No corpus atrophy	68.76 ± 8.35
Mild corpus atrophy	77.21 ± 6.13
Moderate corpus atrophy	76.47 ± 5.04
Severe corpus atrophy	72.61 ± 4.72

Both antral and corpus stomach mucosal atrophy were not accompanied with statistically significant changes in anti-*H. pylori* IgG serum titers (Table 1).

We detected intestinal metaplasia in 119 of 178 patients. The comparison of the grade of IM and the serum levels of PG-1 and G-17 showed the absence of invariables and statistically significant dependence between these parameters, except for the cases of moderate IM (Table 2).

Dysplasia of stomach mucosal epithelium was detected in 113 patients. We revealed the statistically significant dependence between the grade of dysplasia and the increased serum levels of PG-1, and the decreased levels of G-17 (Table 3), except the cases of severe dysplasia where the number of patients was not quite sufficient (6 subjects).

Table 2 Comparison of serum PG1 and G17 levels (mean \pm SD) and grade of IM

	No IM	Mild IM	Moderate IM	Severe IM
PG-1, $\mu\text{g/L}$	52.5 ± 7.74	66.07 ± 8.36	82.65 ± 10.72^a	53.08 ± 12.24
G-17, pmol/L	6.79 ± 0.55	5.48 ± 0.50	4.73 ± 0.67^a	5.11 ± 1.02

^a $P < 0.05$ vs non-metaplastic state.

Table 3 Comparison of serum PG1 and G17 levels (mean \pm SD) and the grade of dysplasia

	No dysplasia	Mild dysplasia	Moderate dysplasia	Severe dysplasia
PG-1, $\mu\text{g/L}$	33.6 ± 5.41	79.98 ± 7.92^a	84.41 ± 10.98^a	71.88 ± 27.25
G-17, pmol/L	7.37 ± 0.46	5.28 ± 0.50^a	3.73 ± 0.66^a	4.53 ± 1.95

^a $P < 0.05$ vs non-dysplastic state.

Among the 178 consecutive patients we detected 6 cases of gastric cancer: 2 early cancers and 4 progressed tumors. The mean of serum PG-1, G-17 and anti-*H. pylori* IgG in these cases was 46.73 ± 22.25 $\mu\text{g/L}$, 4.78 ± 2.086 pmol/L and 89.5 ± 11.7 EIU, respectively.

In general, our results showed that there was a statistically significant dependence between the presence and severity of stomach mucosal atrophy (antral or corpus) and the proper serologic markers (G17 or PG1) in *H. pylori*-associated chronic gastritis. On the other hand, the presence and degree of IM did not correspond to the serum level of G17 or PG1. Thus, the serologic screening by means of Biohit GastroPanel® was useful for the selection of patients with stomach mucosal atrophy by subsequent thorough endoscopic and histological examination for the possible development of precancerous or malignant changes in stomach mucosa.

Table 4 Correlations between results of different methods in diagnosis of gastric mucosal changes

Parameters	r_s
Detection of IM by endoscopy and histology	0.41
Detection of IM by chromoendoscopy and histology	0.92
Detection of antral atrophy by histology and serum levels of G-17	-0.75
Detection of corpus atrophy by histology and serum levels of PG-1	-0.71
Degree of stomach mucosal atrophy and IM	0.21
Degree of stomach mucosal atrophy and dysplasia	0.23
Degree of IM and dysplasia	0.41

Table 5 Sensitivity (Se) and specificity (Sp), PPV and NPV of Biohit GastroPanel® in diagnosis of antral mucosal atrophy

Degree of antral atrophy (by histology)	Se (%)	Sp (%)	PPV (%)	NPV (%)
No	83	95	53	99
Mild	61	84	45	91
Moderate	67	90	81	81
Severe	89	99	98	94

Table 6 Sensitivity (Se) and specificity (Sp), PPV and NPV of Biohit GastroPanel® in diagnosis of corpus mucosal atrophy

Degree of corpus atrophy (by histology)	Se (%)	Sp (%)	PPV (%)	NPV (%)
No	92	97	98	91
Mild	71	92	48	97
Moderate	72	96	81	93
Severe	88	97	82	98

Table 7 Sensitivity (Se) and specificity (Sp), PPV and NPV of routine endoscopy and chromoendoscopy in diagnosis of intestinal metaplasia (IM)

	Routine endoscopy				Chromoendoscopy			
	Se (%)	Sp (%)	PPV (%)	NPV (%)	Se (%)	Sp (%)	PPV (%)	NPV (%)
No	98	6	35	86	94	99	98	97
Mild	4	98	50	68	88	88	79	94
Moderate	no data	no data	no data	no data	71	95	80	92
Severe	6	99	33	89	82	98	82	98

Furthermore, we compared the results of the serology, endoscopy and histology by Spearman's correlation coefficient. As shown in Table 4, the correlation between the results of routine endoscopy and histology was positive, but obviously weaker than the correlation between the results of chromoendoscopy and histology. As it was expected, there was a strong reverse correlation between the presence and degree of stomach mucosal atrophy and the serum levels of proper markers of its functional activity. The correlation between the degree of stomach mucosal atrophy and the subsequent morphological changes of mucosa - IM and dysplasia, was positive but quite weak.

The levels of sensitivity and specificity, PPV and NPV of Biohit GastroPanel® in diagnosis of stomach mucosal atrophy are presented in Tables 5 and 6.

Thus, the investigated non-invasive method was quite sensitive in the diagnosis of non-atrophic and severe antral and corpus gastritis. Also, this method was characterized by the high PPV and NPV (except the cases of mild stomach

mucosal atrophy).

Finally, we carried out the comparison of sensitivity and specificity, PPV and NPV for routine endoscopy and chromoendoscopy in the diagnosis of IM (Table 7).

As a result, we established the obvious advantage of a method of chromoendoscopy in the diagnosis of IM, that had doubtless diagnostic importance in revealing precancerous changes of gastric mucosa.

DISCUSSION

Chronic *H pylori* gastritis eventually could lead in more than half of the affected subjects to a gradual loss of glandular structures with its specialized cells and a collapse of the reticulin skeleton of the mucosa, a condition of atrophic gastritis^[8]. As a result, the glandular layer of the mucosa became thinner, and glands were replaced by fibrosis and intestinal metaplasia. The major clinical importance of this condition was that it could significantly increase the risk for the intestinal type of gastric cancer. This risk might be elevated up to 90- fold in subjects with severe atrophic gastritis throughout the complete stomach^[9]. The annual incidence of gastric cancer among patients with atrophic gastritis varied in cohort studies between 0.3 and 1.0%^[10]. This could explain the interest in the diagnosis of atrophic gastritis. At present, there is a wide circle of questions related to the diagnosis of critical stages of gastric carcinogenesis - gastric epithelial atrophy, intestinal metaplasia and dysplasia. Therefore, it is extremely important to recognize dyspeptic patients who have very high risk of gastric malignant changes and require dynamic surveillance with the purpose of early revealing of the preneoplastic changes in stomach mucosa. Atrophic gastritis is a serious disease, which often does not receive much attention. The relationship between gastritis, atrophic gastritis and other diseases of the stomach is based on the fact that infection and atrophy could alter the physiological functions of the stomach^[11] and influence the growth and growth control of epithelial cells in the stomach. These consequences varied depending on whether the changes of the gastric mucosa caused by gastritis were located in the antrum or the corpus or both.

The most accurate diagnostic method of gastrointestinal tract diseases is endoscopy with subsequent biopsy, which should be made in all patients with the presence of clinical symptoms. However, because of patchy characteristics of atrophic changes in stomach mucosa, some histological researches could give false - negative results. Besides, biopsy was an expensive and labor-consuming method of research^[12], so it could not be carried out for all patients in succession. Contrarily, due to invasiveness of biopsy, it is expedient to make only for monitoring precancerous changes in stomach mucosa. For the selection of patients recommended to biopsy, the presence of a screening method is necessary. Such a method should be capable of reflecting objectively the functional condition of stomach mucosa and its morphological status.

It has been known for over two decades that atrophic gastritis of the corpus and fundus of the stomach can be determined reliably by measuring the serum level of pepsinogen I (PGI) or the PGI/PGII ratio from a blood sample^[13-15]. However, it has not been possible to determine from a blood sample the types of atrophic gastritis in which the atrophic changes are located solely in the antrum. The GastroPanel® serum test also enables the determination of atrophic gastritis of this antrum-limited subtype.

Group I pepsinogens are synthesized solely in the oxyntic glands and mucous neck cells of the gastric corpus. On the other hand, however, pepsinogens of group II are uniformly formed in the glands of the entire stomach and to some extent also in the Brunner glands in the first part of the duodenum.

The majority of pepsinogens are secreted into the lumen of the stomach where they are metabolized into an active pepsin. A small proportion of the pepsinogens leak for one reason or another into the blood circulation. In case of atrophic corpus gastritis, the level of serum pepsinogen I decreases whereas the level of pepsinogen II remains stable or decreases slightly. The level of serum pepsinogen I or the ratio of serum pepsinogen I to pepsinogen II could reflect with high reliability the number of cells and oxyntic glands in the corpus area of the stomach, i.e., they could reflect the degree of atrophy of the corpus mucosa^[14-16]. As the severity of atrophic corpus gastritis corpus increases, the level of serum pepsinogen I or the PGI/PGII ratio decreases.

Gastrin is synthesized in G-cells, which are found in the gastric antrum. The gastrin secreted by the antrum is over 90% of type G-17 whereas the gastrin secreted by the duodenum is primarily type G-34. The fasting serum gastrin is primarily in the form of G-34 but the proportion of type G-17 increases after the dietary stimulus. The secretion of gastrin-17 can be studied with a simple protein stimulation test. First, a blood sample is taken after fasting, after which the patient eats a protein-rich meal. The maximum increase in the level of gastrin-17 can be seen in the serum within 20 min. If the serum gastrin does not increase as a result of protein or other physiological stimulation it is an indication of the loss of gastrin secreting G cells, i.e., an indication of the atrophy of the antrum mucosa. It is possible to make indirect conclusions of the status of the antrum mucosa by simultaneously assaying the serum gastrin and acid output^[17]. In the cases with atrophic antral gastritis and loss of antral G cells, serum gastrin remains low although the stomach is achlorhydric or hypochlorhydric.

Several research groups have renewed the interest in serology for atrophic gastritis by combining gastrin and pepsinogens with *H pylori* serology. In this issue, Väänänen and colleagues presented a smart algorithm for the differentiation in both antrum and corpus between atrophic and non-atrophic gastritis^[18]. The algorithm was tested in a cross-sectional study correlating gastric mucosal histology with *H pylori* IgG serum antibodies, serum PGI levels, and fasting and postprandial serum gastrin-17 levels. It appeared that in roughly 80% of the 404 cases tested, histology and serology matched a similar diagnosis. Sixty (15%) of the 404 subjects had atrophic gastritis, 6 (1%) had previously undergone antral resection, and 340 (84%) had a non-atrophic gastric mucosa either with or without inflammation. In this population with a rather low prevalence of atrophic gastritis, the negative predictive value of the serology panel was 93-97% and the positive predictive value was 64-75%. For these calculations, the authors combined all subjects with atrophic gastritis of the antrum, the corpus, or both. The data, however, showed that the serology panel performed much better in diagnosing atrophic gastritis in the corpus than in the antrum. Only 19 (50%) of the 38 patients diagnosed by serology as having antrum atrophic gastritis had this condition confirmed by histology. This revival of interest in the serological testing of the condition of the gastric mucosa is of importance, given the fact that *H pylori* eradication may cure gastritis and help to prevent further progression of gland loss. It is likely that this might also reduce the risk for gastric cancer^[19], although many more data on this are needed. Screening and treatment of *H pylori* infection might in theory be cost-effective for the prevention of gastric cancer^[12].

Sipponen *et al.*^[20] have recently shown that simultaneous detection of serum concentrations of PGI and G17 and HPAb titers is an effective method for non-invasive screening and diagnosis of atrophic gastritis using blood samples of the patients.

In our present research, the use of the test - system GastroPanel® allowed to receive statistically significant differences between

the serum concentrations of PGI and G17 depending on a degree of stomach mucosal atrophy. We obtained the very satisfactory means of the PPV and NPV of GastroPanel® test in revealing the atrophic state of stomach mucosa. Moreover, this test was sufficiently sensitive and specific as it was proven by chromoendoscopy and histology.

Thus, our study confirmed the usefulness of the test - system GastroPanel® as a "serologic biopsy" for authentic and non-invasive diagnosis of atrophic changes of stomach mucosa in patients with dyspepsia associated with *H pylori* - infection. Besides, we managed to show the advantage of a chromoendoscopy method prior to routine endoscopy in the diagnosis of intestinal metaplasia. Now is the time, almost a decade after the conclusion of the World Health Organization (WHO) about *H pylori* as a class I carcinogen^[21], to use this serology for further studies in selected and general populations. This will allow evaluation of the feasibility of screening and treatment for gastritis and prevention of gastric cancer.

In conclusion, the noninvasive detection of gastric mucosal atrophy by means of enzyme immunoassay with assessment of G-17 and PGI levels can be offered as the screening tool for gastric precancerous conditions. On the other hand, this method does not allow to diagnose intestinal metaplasia and cancer development in stomach mucosa. Therefore, the results of serological screening indicating the stomach mucosal atrophy require carrying out the chromoendoscopy with subsequent mucosal biopsy, for revealing probable progressing of atrophic process with development of intestinal metaplasia, dysplasia or gastric cancer.

REFERENCES

- 1 **Malfertheiner P**, Megraud F, O'Morain C, Hungin AP, Jones R, Axon A, Graham DY, Tytgat G. Current concepts in the management of *Helicobacter pylori* infection - The Maastricht 2 Consensus Report. *Aliment Pharmacol Ther* 2002; **16**: 167-180
- 2 **Correa P**. Human gastric carcinogenesis: a multistep and multifactorial process. First american cancer society award lecture on cancer epidemiology and prevention. *Cancer Res* 1992; **52**: 6735-6740
- 3 **Correa P**. A human model of gastric carcinogenesis. *Cancer Res* 1988; **48**: 3554-3560
- 4 **Kiyohira K**, Yoshihara M, Iio M, Haruma K, Tanaka S, Chayama K. Serum pepsinogen concentration as a marker of *Helicobacter pylori* infection and the histologic grade of gastritis; evaluation of gastric mucosa by serum pepsinogen levels. *J Gastroenterol* 2003; **38**: 332-338
- 5 **Sipponen P**, Ranta P, Hëlse T, Kääriäinen I, Mäki T, Linnala A, Suovaniemi O, Alanko A, Härkönen M. Serum levels of amidated gastrin-17 and pepsinogen I in atrophic gastritis. An observational case-control study. *Scand J Gastroenterol* 2002; **37**: 785-791
- 6 **Murray CJ**, Lopez AD. Mortality by cause for eight regions of the world: global burden of disease study. *Lancet* 1997; **349**: 1269-1276
- 7 **Correa P**, Haenszel W, Cuello C, Tannenbaum S, Archer M. A model for gastric cancer epidemiology. *Lancet* 1975; **2**: 58-60
- 8 **Kuipers EJ**, Uytterlinde AM, Pena AS, Roosendaal R, Pals G, Nelis GF. Long term sequelae of *Helicobacter pylori* gastritis. *Lancet* 1995; **345**: 1525-1528
- 9 **Sipponen P**, Kekki M, Haapakoski J, Ihamäki T, Siurala M. Gastric cancer risk in chronic atrophic gastritis: statistical calculations of cross-sectional data. *Int J Cancer* 1985; **35**: 173-177
- 10 **Kuipers EJ**. Review article: relationship between *Helicobacter pylori*, atrophic gastritis and gastric cancer. *Aliment Pharmacol Ther* 1998; **12**(Suppl 1): S25-36
- 11 **Varis K**, Ihamäki T, Härkönen M, Samloff IM, Siurala M. Gastric morphology, function, and immunology in first-degree relatives of probands with pernicious anemia and controls. *Scand J Gastroenterol* 1979; **14**: 129-139
- 12 **Parsonnet J**, Harris RA, Hack HM, Owens DK. Modelling cost-

- effectiveness of *Helicobacter pylori* screening to prevent gastric cancer: a mandate for clinical trials. *Lancet* 1996; **348**: 150
- 13 **Miki K**, Ichinose M, Ishikawa KB. Clinical application of serum pepsinogen I and II levels for mass screening to detect gastric cancer. *Jpn J Cancer Res* 1993; **84**: 1086-1090
- 14 **Yoshihara M**, Sumii K, Haruma K, Kiyohira K, Hattori N, Kitadai Y, Komoto K, Tanaka S, Kajiyama G. Correlation of ratio of serum pepsinogen I and II with prevalence of gastric cancer and adenoma in Japanese subjects. *Am J Gastroenterol* 1998; **93**: 1090-1096
- 15 **Kekki M**, Samloff IM, Varis K, Ihamäki T. Serum pepsinogen serum and I gastrin in screening of severe atrophic corpus gastritis. *Scand J Gastroenterol* 1991; **186**: 109-116
- 16 **Varis K**, Sipponen P, Laxen F, Samloff IM, Huttunen JK, Taylor PR, Heinonen OP, Albanes D, Sande N, Virtamo J, Harkonen M. Implications of serum pepsinogen I in early endoscopic diagnosis of gastric cancer and dysplasia. Helsinki Gastritis Study Group. *Scand J Gastroenterol* 2000; **35**: 950-956
- 17 **Sipponen P**, Valle J, Varis K, Kekki M, Ihamäki T, Siurala M. Fasting levels of serum gastrin in different functional and morphological states of the antro-fundal mucosa. An analysis of 860 subjects. *Scand J Gastroenterol* 1990; **25**: 513-519
- 18 **Väänänen H**, Vauhkonen M, Helske T, Kääriäinen I, Rasmussen M, Tunturi-Hihnala H, Koskenpato J, Sotka M, Turunen M, Sandstrom R, Ristikankare M, Jussila A, Sipponen P. Non-endoscopic diagnosis of atrophic gastritis with a blood test. Correlation between gastric histology and serum levels of gastrin-17 and pepsinogen I: a multicentre study. *Eur J Gastroenterol Hepatol* 2003; **15**: 885-891
- 19 **Chun Y**, Wong B, Lam SK, Wong WM, Zheng T, Chen J, Chen B. Eradicating *Helicobacter pylori* infection in general population prevents gastric cancer: a 7-year prospective randomized placebo-controlled study. *Gastroenterology* 2002; **122** (Suppl 1): A588
- 20 **Suovaniemi O**, Harkonen M, Paloheimo L, Sipponen P. GastroPanel: diagnosing atrophic gastritis from serum - providing a tool for evidence-based medicine. *Business Briefing: Global Health Care* 2003: 1-4
- 21 International Agency for Research on Cancer. IARC monographs on the evaluation of carcinogenic risks to humans. Vol. 61: Schistosomes, liver flukes and *Helicobacter pylori*. Lyon: IARC 1994

Edited by Wang XL Proofread by Xu FM

Role of soluble Fas ligand in autoimmune diseases

Ning-Li Li, Hong Nie, Qi-Wen Yu, Ji-Ying Zhang, An-Lun Ma, Bai-Hua Shen, Li Wang, Jun Bai, Xue-Hua Chen, Tong Zhou, Dong-Qing Zhang

Ning-Li Li, Hong Nie, Qi-Wen Yu, Ji-Ying Zhang, An-Lun Ma, Bai-Hua Shen, Li Wang, Jun Bai, Dong-Qing Zhang, Department of Immunology, Shanghai Second Medical University, Shanghai Institute of Immunology, Shanghai 200025, China

Xue-Hua Chen, Department of Surgery, Shanghai Ruijin Hospital, Shanghai 200025, China

Tong Zhou, Department of Nephrology, Shanghai Ruijin Hospital, Shanghai 200025, China

Supported by Grant From Science and Technology Development Foundation of Shanghai High Education Committee, No. 98ZD35 (to Ning-Li Li), and No.S990202 (to Dong-Qing Zhang)

Correspondence to: Dong-Qing Zhang, Shanghai Second Medical University, Shanghai Institute of Immunology, Shanghai 200025, China. dqzhang13@sh163.net

Telephone: +86-21-64453149 **Fax:** +86-21-64453049

Received: 2003-12-23 **Accepted:** 2004-01-15

Abstract

AIM: To investigate the role of soluble Fas ligand in autoimmune diseases.

METHODS: RT-PCR was performed to amplify sFasL cDNA from the total RNA extracted from activated human peripheral blood lymphocytes. DNA fragments were cloned into PCR vector. After sequenced, sFasL gene fragments were inserted into pQE-31 vector and expressed in *E. Coli* M15 respectively. Proteins were purified through affinity chromatography column with ligand of 6×His tag and identified by SDS-PAGE and Western blot. Mice were immunized with sFasL protein and specific anti-serum was harvested 6 wk after immunization. Monoclonal anti-human FasL antibody was made from the immunized mice. Serum level of sFasL in different patients was detected using anti-FasL antibodies from the immunized mice.

RESULTS: The protein expressed was 24 ku by SDS-PAGE electrophoresis. The protein was specially bound to anti-human FasL antibody by Western blot analysis. The sFasL protein could induce Jurket cell apoptosis *in vitro*. The concentration of serum sFasL in patients with autoimmune diseases was higher than that in normal individuals. sFasL could reduce arthritis in collagen induced arthritis (CIA) mice model by subcutaneous injection.

CONCLUSION: sFasL may be involved in either induction of apoptosis or autoimmune diseases. Furthermore, sFasL may have potential application in treatment of autoimmune diseases.

Li NL, Nie H, Yu QW, Zhang JY, Ma AL, Shen BH, Wang L, Bai J, Chen XH, Zhou T, Zhang DQ. Role of soluble Fas ligand in autoimmune diseases. *World J Gastroenterol* 2004; 10 (21): 3151-3156

<http://www.wjgnet.com/1007-9327/10/3151.asp>

INTRODUCTION

Autoimmune diseases are a kind of diseases induced by auto-

reactive T or B cells. Most common autoimmune diseases include rheumatoid arthritis (RA), insulin-dependent diabetes mellitus (IDDM), multiple sclerosis (MS) and systemic lupus erythematosus (SLE). Among these diseases, RA, IDDM and MS are believed to be autoimmune diseases induced by Th1 cells which can recognize auto-antigens on special tissues. For example, RA is a common disease characterized by the chronic lesion of polyarthritides. Autoimmunity to cartilage antigens may play a significant role in the pathogenesis of chronic inflammatory polyarthritis. It has been commonly accepted that cell mediated immune responses are involved in chronic inflammation since T and B lymphocytes and antigen presenting cells are observed to be enriched in the synovium fluid of RA patients. *In vivo* studies showed that T cells infiltrating into the synovium could express IL-2 receptors, IL-10, IFN- γ and activated CD4 T cells could be detected in the synovial fluid of RA patients^[1,2]. It is believed that if auto-reactive T cells can be cleaned from circulation or RA can be located, the lesion induced by auto-reactive T cells may relieve. Actually, anti-TNF- α and anti-CD4 monoclonal antibodies have been used in treatment of RA patients.

In this study, we reported that sFasL proteins were expressed in *E. Coli* system. Anti-FasL antibodies were prepared in the mice using expressed FasL. Meanwhile, we set up a special ELISA method to identify sFasL molecules and its content in the serum of patients with RA, IDDM, MS and SLE. We also tried to use sFasL made in our lab oratory to treat collagen induced arthritis in this study.

MATERIALS AND METHODS

Blood samples and reagents

Fresh blood samples were supplied by healthy individuals. PHA was purchased from Sigma Com. San Diego, USA) IPTG and plasmid mini-prep Kit were products of Promega (Chicago, USA). DNA purification kit, Histidine resin, sequencing vector PCR2.1 and protein expression vector pQE-31 were purchased from QIAGEN (San Diego, USA). Rabbit anti-human FasL polyclonal antibody was purchased from Santa Cruz (Sweden). Goat anti-rabbit IgG/HRP was purchased from Huamei (Shanghai, China). Nitofible membrane was purchased from Amersham (London, England). Trizol, dNTP, restricted enzymes were purchased from Gibco BRL (San Diego, USA) and MBI Fermentans (Philadelphia, USA).

Activation of lymphocytes

Peripheral blood monocytes (PBMC) were isolated from blood from healthy individuals with Ficoll. PBMC were re-suspended in 100 mL/L fetal calf serum RPMI 1640 and incubated at 37 °C in bumidified atomosphere containing 5 mL/L CO₂ for 24 h. PHA (20 μ g/mL) was added into the culture and incubated for another 8 h.

Identification of sFasL expression

sFasL expression on the cell surface was detected by direct fluoroscense labeling with cytometry. Briefly, activated lymphocytes were collected and washed with PBS. FITC-labeled goat anti-human FasL (Oncogen Company, LA, USA) was added into the cells and incubated on ice for 30 min. The labeled

cells were washed with PBS and expression of FasL on the cell surface was detected by FACS. The percentage of expression of FasL was analyzed using system software II.

Amplification of gene fragments of sFasL

Total RNA was isolated from cells in which sFasL expression was enhanced and reversed into cDNA. sFasL gene fragments were amplified from cDNA template by special primers. sFasL: the sequence of forward primer was: 5'-ACG GAT CCG CAG CAG CCT TCA ATT A CC-3'; reverse primer: 5'-AAG CCG AAT ATA TTC GAG ATT AAG CTT CGC CG-3'. The size of sFasL fragments amplified from cDNA was 540 bp.

sFasL cloning and expression

PCR bands were cut and purified with gel extraction kit (QIAGEN). The purified PCR products were inserted into PCR 2.1 vector and DH 5 α (*E. Coli*) was transfected with TA cloning kit (Invitrogen) according to the manufacturers introductions. White clones were picked up on selected LB plates containing ampicillin and X-gel and expensed in 3 mL of LB medium overnight. Plasmids were prepared from the culture with mini-prep Kit (Promega). The positive clones were identified by *EcoR* I digested and sequenced by Shanghai South Gene Tech Ltd. The identified sFasL fragments were digested by *Bam*HIII and *Hind* III and purified by gel extraction kit. The purified sFasL fragments were ligated into the expression vector pQE-31 and M15 (*E. Coli*) was transfected. White clones were picked up on selected LB plates containing Kanamycin and expensed in 3 mL of LB medium overnight and inoculated in 200 mL of selected LB medium containing Kanamycin until A reached to 0.7. A 1 mol/L of IPTG was added to culture and shaken for another 4 h. Bacteria were collected by spinning at 6 000 r/min for 10 min and lyzed in lysis buffer. Protein expressed was purified by His Tag resin.

Identification of expressed sFasL

sFasL expressed was identified by SDS-PAGE electrophoresis and Western blot. sFasL showed a single band with M_r 24 000 respectively after running from SDS-PAGE (120 g/L concentrated gel and 40 g/L separated gel). The sFasL bands were transferred onto membranes and blocked with 50 mL/L of free fat milk for 2 h at room temperature. The membranes were washed 3 times with PBS. The rabbit anti-human sFasL polyclonal antibody was added and incubated for 1 h at room temperature. Goat anti-rabbit IgG-HRP was added and incubated for another 1 h at room temperature after washed with PBS. DAB and H₂O₂ were added and the reaction was stopped by washing the membranes with water when brown color was visible.

Detection of apoptosis

sFasL (25, 50 and 100 μ g/L) was added into 1×10^8 /L of Jurket cell lines respectively and incubated for 8 h at 37 °C in humidified atmosphere containing 5 mL/L CO₂. The cells were collected and fixed by 700 mL/L ethanol for 45 min at 4 °C. Ten μ L of RNase was added to the fixed cells after washed with PBS and incubated for 30 min at 37 °C. Then 10 μ L of PI (50 mg/mL) was added to the cells and detected by cytometry. The percentage of apoptotic cells was calculated by apoptotic peak (A₀) area.

Preparation of mouse anti-human sFasL antibody

Two Balb/C mice were immunized with 80 μ g of expressed sFasL mixed with complete Freund's adjuvent by injection with s.c on back. The mice were injected three times with sFasL, once every two weeks. Then blood was collected and anti-FasL titer was measured with ELISA.

Induction of collagen-induced arthritis in Wistar rats

Wistar rats were bred under pathogen-free conditions. Female

mice were used at 2-3 mo of age and allowed free access to standard laboratory diet and water. Collagen II (CII) emulsion was prepared in an equal volume of IFA. A 100 μ L (containing 300 μ g of CII) of CII/IFA emulsion was intradermally injected, using the loose skin at the base of the tail. Seven days later, the primary immunization was administered, a booster intradermal injection containing 100 μ g of CII in IFA. The rats were observed every day from the 4th wk after primary immunization. Arthritis was evaluated with standard 4 scores.

Administration of arthritis rats with sFasL

When arthritis occurred in rats immunized with CII/IFA, 1 μ g of sFasL expressed in 100 μ L of PBS was injected into one ankylosis side. Meanwhile 100 μ L of PBS was injected into another ankylosis side of same arthritis rats as control. The injection was given three times, once every two days.

Detection of serum sFasL concentration using prepared mouse anti-human FasL antibody

Serum level of soluble FasL in different patients was detected with indirect ELISA. The ELISA plate was coated with 100 μ L of serum and incubated overnight at 4 °C. The coated plate was completely washed with PBS and prepared mouse anti-human FasL antibody was added. Rabbit anti-mouse IgG-HRP was then added and incubated for another 1 h at room temperature after washed with PBS. DAB and H₂O₂ were added and the reaction was stopped by washing the membranes with water when brown color was visible.

RESULTS

Enhanced expression of FasL on PMBC after PHA activation

PBMC was isolated from healthy individuals FasL was expressed on the cell surface after activated with PHA. The expression of FasL in PBMC was significantly higher after activated. The percentage of FasL detected on the non-activated PBMC was very low (2.15 \pm 1.7%), while FasL expressed on the activated PBMC reached 17.98 \pm 1.8% using cytometry detection after cells were labeled with specific fluorescence anti-human FasL antibody (Figure 1).

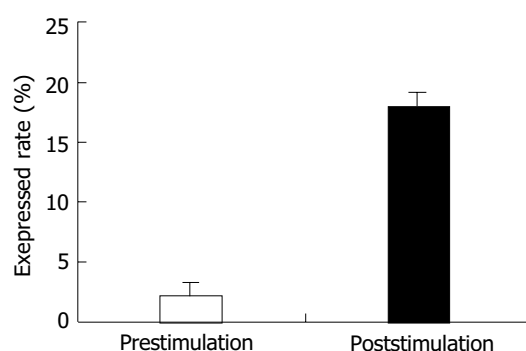


Figure 1 Peripheral blood mononuclear cells isolated from healthy individuals using Ficoll and co-cultured with PHA for 8 h at 37 °C in humidified atmosphere containing 50 mL/L CO₂. The expression of FasL on PBL before and after PHA stimulation was detected by special antibody using flow cytometer. Open bar indicates the percent of FasL on cells surface before PHA activation. Shadow bar shows the percent of FasL on cell surface after PHA stimulation.

Human sFasL cloning and expression

Human sFasL DNA fragments were amplified from activated PBMC using RT-PCR. The size of PCR product was 540 bp (Figure 2) which matched the size reported in the GenBank. The product was inserted into PCR2.1 vector and DH5 α was

successfully transfected. The insert was confirmed by digestion with *EcoR* I after plasmid was miniprepared. The fragments were separated with a 3.9 kb vector. This result showed that sFasL (Figure 3) fragments were successfully inserted into the vector. The sequences of the inserted fragments were same as reported by GenBank after sequenced with 377 Sequencer. Identified fragments were digested by both *Bam*HI and *Hind* III and ligated into the expression vector pQE-31. The ligated products were put on selected LB plates after M15 was transfected and incubated for 18 h at 37 °C. The expression was induced by IPTG for 4 h. The protein was purified by 6-histidine column. The molecular weight and purification of the protein were identified by SDS-PAGE. The result indicated that there was only one band in sFasL (24 000 dalton). Special mouse anti-human FasL antibody was used to confirm the bands transferred onto membranes with Western blotting. The result showed there was a sFasL positive band. This indicated that the protein expressed in M15 was human sFasL (Figure 4).

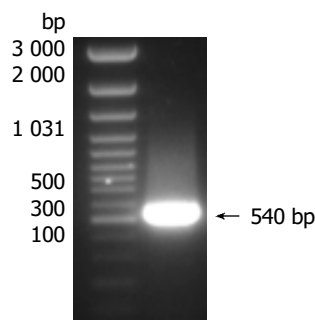


Figure 2 Reversion of total RNA isolated from PHA activated peripheral blood mononuclear cells to cDNA.

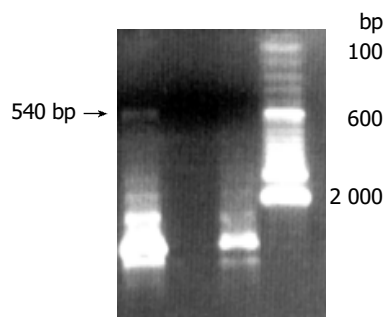


Figure 3 PCR bands and transfected DH 5a. Band1: inserted fragment of sFasL in pQE-31; Band 2: no inserted fragment.

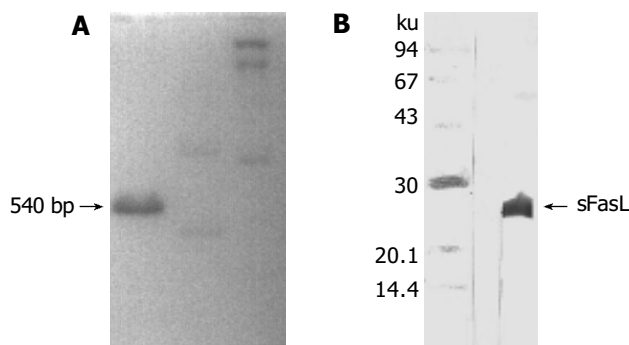


Figure 4 sFasL expression in SDS-gel (A) and hybridization with special anti-sFasL antibody (B).

Jurkat cell line apoptosis induced by sFasL expressed in M15
Different doses of expressed sFasL were added to log phase growing Jurkat cell line and cultured for another 18 h. The

percentage of apoptosis of tested cell line was determined by cytometry after stained with PI dye. Figure 5 shows the apoptosis of Jurkat cells after co-cultured with expressed sFasL. The percentage of apoptotic Jurkat cells was similar to that of apoptotic cells co-incubated with commercial human sFasL. This result indicated that sFasL was able to induce cell apoptosis (Figure 5).

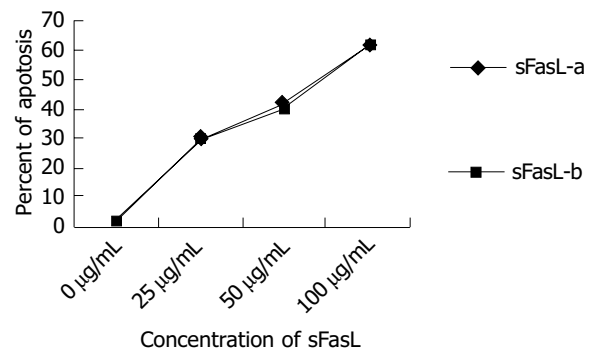


Figure 5 Cell apoptosis induced by different doses of sFasL (25, 50 and 100 µg/L).

Generation of anti-human sFasL antibody in mice immunized with expressed sFasL

Serum was isolated from two mice immunized with expressed human sFasL. We coated plates with this serum and detected anti-human FasL titer using special commercial standard sFasL protein by ELISA. The result showed that there was a high titer (>1:1 000) of anti-human sFasL special antibody in the serum of immunized mice. This indicated that expressed sFasL could specifically bind to standard human sFasL protein.

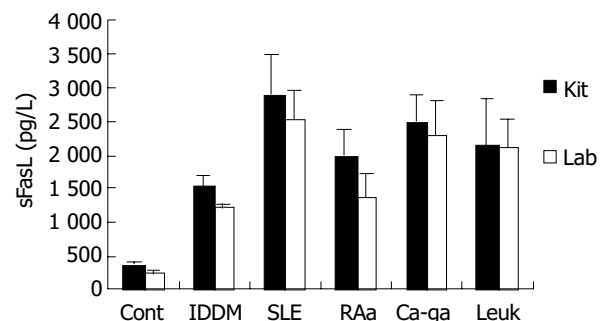


Figure 6 Levels of soluble FasL in serum from patients with different diseases. Cont: serum from healthy individuals; IDDM: serum from patients with IDDM; SLE: serum from IDDM; RAa: serum from RA patients with activated stage; Ca-ga: serum from patients with gastric cancer; Leuk: serum from patients with leukemia; Shadow bar: serum level detected by commercial sFasL kit. Open bar: serum level detected by anti-sFasL antibody.

Prepared special anti-humans sFasL antibody could be used to detect concentration of sFasL

We coated ELISA plates with special anti-human sFasL antibody generated from immunized mice to detect the concentration of sFasL in the serum of patients with tumor and autoimmune diseases. Twenty serum samples from healthy individuals, 95 serum samples from patients with different autoimmune diseases and 30 serum samples from patients with leukemia and cancer were detected by this way. As a parallel experiment, the concentration of sFasL in these serum samples was identified in duplicate using commercial Kit at the same time. The data showed that the concentration of sFasL was

significantly higher than that in healthy individuals ($P < 0.05$). The result determined with prepared sFasL antibody in our laboratory was same as that detected by commercial Kit (Figure 6).

Arthritis reduced by sFasL immunized rats

Arthritis occurred as early as 15 d after primary immunization with CII emulsified with IFA. The significant ankylosis was observed in rats. The joints of rats were red and swollen. The arthritis rats lost ability to move and showed difficult to reach food. The percentage of arthritis was 90% (Table 1). The mean score could reach the maximum 24 d after immunization began to decrease from d 30 (Figure 7).

Table 1 Incidence of chicken CII-induced arthritis in Wistar rats

Group	Immunized with	Incidence	Percentage of CIA (%)
Experimental	CII+CFA	18/20	90
Control	CII	0/5	0
	CFA	0/5	0

Wistar rats were intradermally injected with collagen II (CII) emulsion in an equal volume of IFA (100 μ L (containing 300 μ g of CII). Seven days later, a booster containing 100 μ g of CII in IFA intradermally administered. The rats were observed every day from 4 wk and evaluated with standard 4 scores.

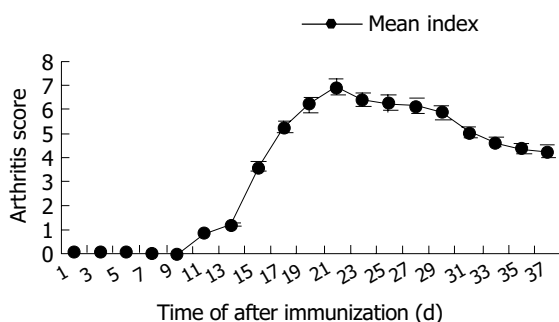


Figure 7 Mean arthritis score of rats with CIA.

When arthritis had a score of 7-8, 1 μ g of sFasL in 100 μ L of PBS was injected into one ankylosis side of rats. Meanwhile, 100 μ L of PBS was injected into another ankylosis side of the same arthritis rats as control. After the arthritis rats were injected 3 times with sFasL, the rats showed reducible arthritis (Figure 8A) while control rats which received an equal volume PBS suffered from a more serious ankylosis (Figure 8B).

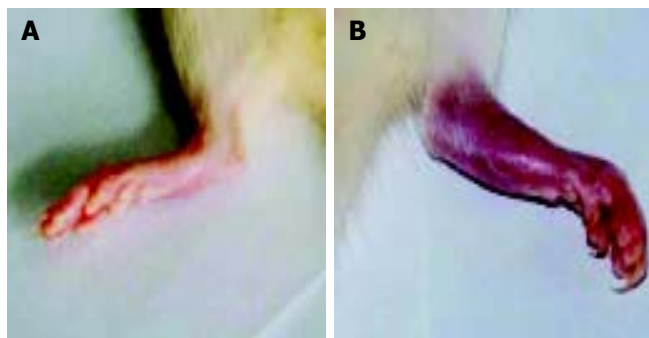


Figure 8 Ankylosis in arthritis rats. A: Ankylosis induced by sFasL in arthritis rats. B: Grade 4 inflammation in rat hind paw.

DISCUSSION

Human Fas ligand (CD95 ligand, FasL) was identified by

Nagata's laboratory in 1993. Human FasL is consisted of 281 amino acids and a member of TNF family. The N terminal of FasL was located in the cytoplasm and C terminal is on cell surface. The region of the molecules in cytoplasm is consisted of 80 amino acids. The region though the cell membrane of FasL is consisted of 22 amino acids. The region of FasL exposed to outside of the cells is consisted of 179 amino acids^[3]. Fas ligand molecules can be cut by matrix metalloproteinases (MMP) from membranes^[15] and become a soluble form which is called soluble FasL (sFasL). FasL could induce apoptosis of cells when it binds to Fas which expresses on cell surface and acts as a special receptor of FasL.

Fas is ubiquitously expressed on a number of different cells including tumor cells. Likewise, as a ligand of Fas, FasL has many important functions. The expression of FasL is not only restricted to activated T cells and NK cells, but also on immune privileged sites such as eyes and testis. FasL can be up-regulated when cells are responsive to UV irradiation or treated by cytotoxic drugs. Over expression of FasL can inhibit some autoimmune diseases by deleting auto-immune memory cells^[4,5]. Moreover, Fas-FasL interaction can protect allografts from immune attack and induce anti-tumor responses. Thus, myoblasts engineered to express FasL have been found to prolong the survival of co-transplanted islet allografts in diabetic mice. FasL expression on allogeneic fibroblasts was found to abolish tumor growth and induce specific protective immunity when mixed with neoplastic cells before implantation *in vivo*. Apoptosis induced by Fas-FasL interaction is believed to involve inflammation, anti-tumor and autoimmune reaction and aging^[6-8]. Apoptosis has been found in almost all processes of the life. For example, activation induced cell death (AICD) may play a very important role in T cell activation and differentiation.

As the out-membrane region of FasL, sFasL involves the deletion of potentially hazardous peripheral memory cells^[5]. Some studies suggested that change of sFasL in serum might be involved in many processes and progress of diseases. The serum level of sFasL was high in patients with large granule lymphocyte leukemia and NK like lymphoma, SLE, RA and EAE^[9-11]. sFasL was upregulated on the tumor surface upon drug incubation in chemosensitive tumor cells. Tumor cells could mediate autocrine or paracrine to release soluble FasL (sFasL) and induce apoptosis of peripheral normal cells, CTL and NK which could express Fas and promote local tumor invasion or metastases^[11-13]. Matsuno *et al.* reported that both sFas and sFasL were higher in the synovium fluid of RA patients compared with other arthritis^[14]. Serve RA showed a higher level of sFasL than mild RA^[13,21]. The concentration of Fas, receptors of FasL and sFasL, were changed in the process of diseases. Some investigators reported that sFas might block apoptosis by binding FasL or sFasL^[5,6]. Membrane-bound FasL induced apoptosis in cultured synovial cells from RA and OA patients, but naturally processed human sFasL did not^[23]. The role of sFasL still remains unclear.

T cells express both Fas and FasL on cell surface after stimulation. FasL exists in two forms: membrane-bound FasL and soluble FasL (sFasL). The out-membrane region of FasL is cleaved by a metalloproteinase (MP) and falls down from membrane to serum or body fluid^[14]. Inhibition of metalloproteinase cleavage could enhance the cytotoxicity of FasL^[15]. Activated T cells would die in a few minutes if no IL-2 was added after stimulation with antigens or mitogens. This process is called activated induced cell death (AICD). Because sFasL shows the same function of FasL but has smaller molecules. We expressed sFasL first in *E. Coli*. For preparing sFasL cDNA and stimulated T cells with PHA in this study. The expression of sFasL reached 20% after stimulation for 24 h compared with 3% expression on naïve T cells. We harvested sFasL expressed

T cells before they died and mRNA of sFasL was extracted. The fresh mRNA of sFasL was reversed into cDNA and successfully amplified. The sFasL was ligated into PCR2.1 vector. After the sFasL insert was confirmed by sequencing analysis, the fragment of sFasL was inserted into pQE-31 vector and expressed in M15 strain.

To identify whether sFasL expressed in this study had biological functions after purification, we chose Jucket cell line as a report cell because Fas molecules were expressed on Jucket cell line surface. When Fas expressed on cell surface bound to sFasL, the cells were activated and went to die after 48 h of binding. The results demonstrated that the expressed sFasL could induce Jucket cell line apoptosis. The percent of apoptosis increased with the increased concentration in the culture. This result indicated that sFasL had the same function membrane FasL.

Recently, some reports demonstrated that FasL and sFasL played a different role in apoptosis. Generally, membrane-bound FasL, or FasL is fully competent in transducing Fas-mediated signals for apoptosis and NF-kappaB nuclear translocation because membrane FasL could possess both Fas-focusing and signal transducing functions. While sFasL is known to be deficient in transducing signals upon engagement with membrane Fas^[4,14]. But in some cases, sFasL was found to be involved in the deletion of potentially hazardous peripheral memory cells^[10]. A more study suggested that change of sFasL in serum was involved in the process and progress of diseases^[9]. The report indicated there was a high serum level of sFasL in patients with large granular lymphocyte leukemia and NK-like lymphoma^[12]. sFasL increased significantly in the serum of patients with activated systemic lupus erythematosus (SLE) and rheumatoid arthritis (RA). In some autoimmune diseases the serum level of sFasL was dramatically decreased after treatment in some patients^[10,13]. We detected the serum level of sFasL in more than 90 samples from autoimmune disease in this study. Among these diseases, the serum levels were detected from 32 patients with IDDM, 31 patients with SLE, 16 RA patients in active stage and 16 RA patients in resting stage. This result indicated that the circulation level of sFasL was higher in these autoimmune diseases. The role of sFasL in the pathogenesis of these autoimmune diseases is still under investigation.

It has been commonly accepted that activated CD4 T cell mediated immune responses are involved in the pathogenesis of RA. Both CD4 and CD8 T cells were observed to be enriched in the synovial fluid of RA patients. It is possible that if auto-reactive T cells can be cleaned from circulation or RA can be located, the lesion caused by inflammation induced the auto-reactive T cells may relieve. Similar with RA, it is believed that Th1 is involved in the pathogenesis of CIA. Collagen induced arthritis (CIA) has become a common animal model in studying the pathogenesis of rheumatoid arthritis^[2,17]. Many potential factors involved in CIA^[2,18-20], Th1 cells are mainly involved in the CIA. If Th1 cells are deleted from joints, the evolvement of joints in CIA may be lighter. Mattsson *et al.*^[20] reported that the T cell marker O×40 was up-regulated in OVA-inhibited non-arthritis animals compared to control CIA animals. They found that the complete inhibition of CIA caused by addition of OVA to the collagen II inoculum was due to the presence of a TH2 environment resulting from an increased production of IL-4 mRNA and a parallel increase in O×40+ T cells^[20]. In this report, we used sFasL to treat CIA mice. The anklynosis was reduced after 3 times of sFasL injection in arthritis rats. This result indicated that sFasL might induce apoptosis of activated autoimmune Th1 cells which infiltrated in joints and synovium so that the inflammation induced by autoimmune T cells decreased, or the above process increased the Th2 switch. But how sFasL induces these changes is still under investigation.

In this study, human sFas ligand was engineered in *E. Coli*. The expressed sFasL could induce apoptosis of Jurkat cell line. Anti-human sFasL antibody could be generated in the mice immunized with expressed sFasL. Anti-human sFasL antibody could be used in detection of sFasL in the serum of patients with autoimmune diseases. The results demonstrated that the level of sFasL in sera of patients with IDDM, SLE and RA was much higher than that in healthy individuals. Meanwhile, the result showed that sFasL antibody revealed the same sensitivity as commercial sFasL antibody. Injection of sFasL with sc in CIA rats could reduce inflammation, which may indicate that sFasL can be used in treatment of autoimmune diseases.

ACKNOWLEDGEMENTS

We thank professors Kang-Yan Zhou and Shan-Qing Tong for their critical review of this paper and Dr. Zuo-Qing Li for his assistance in preparation of this manuscript.

REFERENCES

- 1 Li NL, Zhang DQ, Zhou KY, Cartman A, Leroux JY, Pode AR, Zhang YP. Isolation and characteristics of autoreactive T cells specific to aggrecan G1 domain from rheumatoid arthritis patients. *Cell Res* 2000; **10**: 39-49
- 2 Nandakumar KS, Andren M, Martinsson P, Bajtner E, Hellstrom S, Holmdahl R, Kleinau S. Induction of arthritis by single monoclonal IgG anti-collagen type II antibodies and enhancement of arthritis in mice lacking inhibitory FcγRIIB. *Eur J Immunol* 2003; **33**: 2269-2277
- 3 Takahashi T, Tanaka M, Inazawa J, Abe T, Suda T, Nagata S. Human Fas ligand: gene structure, chromosomal location and species specificity. *Int Immunol* 1994; **6**: 1567-1574
- 4 Ishimaru N, Yanagi K, Ogawa K, Suda T, Saito I, Hayashi Y. Possible role of organ-specific autoantigen for Fas ligand-mediated activation-induced cell death in murine sjogren's syndrome. *J Immunol* 2001; **167**: 6031-6037
- 5 Kim S, Kim KA, Hwang DY, Lee TH, Kayagaki N, Yagita H, Lee MS. Inhibition of autoimmune diabetes by Fas ligand: the paradox is solved. *J Immunol* 2000; **164**: 2931-2936
- 6 Hoffmann TK, Dworacki G, Tsukihito T, Meidenbauer N, Gooding W, Johnson JT, Whiteside TL. Spontaneous apoptosis of circulating T lymphocytes in patients with head and neck cancer and its clinical importance. *Clin Cancer Res* 2002; **8**: 2553-2562
- 7 Suzuki N, Ichino M, Mihara S, Kaneko S, Sakane T. Inhibition of Fas/Fas ligand-mediated apoptotic cell death of lymphocytes *in vitro* by circulating anti-Fas ligand autoantibodies in patients with systemic lupus erythematosus. *Arthritis Rheum* 1998; **41**: 344-353
- 8 French LE, Hahne M, Viard I, Radlgruber G, Zanone R, Becker K, Muller C, Tschopp J. Fas and Fas ligand in embryos and adult mice: ligand expression in several immune-privileged tissues and coexpression in adult tissues characterized by apoptotic cell turnover. *J Cell Biol* 1996; **133**: 335-343
- 9 Zhu B, Luo L, Chen Y, Paty DW, Cynader MS. Intrathecal Fas ligand infusion strengthens immunoprivilege of central nervous system and suppresses experimental autoimmune Encephalomyelitis. *J Immunol* 2002; **169**: 1561-1569
- 10 Christensson M, Pettersson E, Eneslatt K, Christensson B, Bratt J, Rantapaa-Dahlqvist S, Sundqvist KG. Serum sFAS levels are elevated in ANCA-positive vasculitis compared with other autoimmune diseases. *J Clin Immunol* 2002; **22**: 220-227
- 11 Kayagaki N, Kawasaki A, Ebata T, Ohmoto H, Ikeda S, Inoue S, Yoshino K, Okumura K, Yagita H. Metalloproteinase-mediated release of human Fas ligand. *J Exp Med* 1995; **182**: 1777-1783
- 12 Nagao M, Nakajima Y, Hisanaga M, Kayagaki N, Kanehiro H, Aomatsu Y, Ko S, Yagita H, Yamada T, Okumura K, Nakano H. The alteration of Fas receptor and ligand system in hepatocellular carcinomas: how do hepatoma cells escapem from the host immune surveillance *in vivo*? *Hepatology* 1999; **30**: 413-420

- 13 **Nozawa K**, Kayagaki N, Tokano Y, Yagita H, Okumura K, Hasimoto H. Soluble Fas (APO-1, CD95) and soluble Fas ligand in rheumatic diseases. *Arthritis Rheum* 1997; **40**: 1126-1129
- 14 **Matsuno H**, Yudoh K, Watanabe Y, Nakazawa F, Aono H, Kimura T. Stromelysin-1 (MMP-3) in synovial fluid of patients with rheumatoid arthritis has potential to cleave membrane bound Fas ligand. *J Rheumatol* 2001; **28**: 22-28
- 15 **Knox PG**, Milner AE, Green NK, Eliopoulos AG, Young LS. Inhibition of metalloproteinase cleavage enhances the cytotoxicity of Fas ligand. *J Immunol* 2003; **170**: 677-685
- 16 **Xiao S**, Jodo S, Sung SS, Marshak-Rothstein A, Ju ST. A novel signaling mechanism for soluble CD95 ligand. Synergy with anti-CD95 monoclonal antibodies for apoptosis and NF-kappaB nuclear translocation. *J Biol Chem* 2002; **277**: 50907-50913
- 17 **Vossenaar ER**, Nijenhuis S, Helsen MM, van der Heijden A, Senshu T, van den Berg WB, van Venrooij WJ, Joosten LA. Citrullination of synovial proteins in murine models of rheumatoid arthritis. *Arthritis Rheum* 2003; **48**: 2489-2500
- 18 **Banda NK**, Kraus DM, Muggli M, Bendele A, Holers VM, Arend WP. Prevention of collagen-induced arthritis in mice transgenic for the complement inhibitor complement receptor 1-related gene/protein. *J Immunol* 2003; **171**: 2109-2115
- 19 **Morgan ME**, Suttmuller RP, Witteveen HJ, van Duivenvoorde LM, Zanelli E, Melief CJ, Snijders A, Offringa R, de Vries RR, Toes RE. CD25+ cell depletion hastens the onset of severe disease in collagen-induced arthritis. *Arthritis Rheum* 2003; **48**: 1452-1460
- 20 **Mattsson L**, Lundberg K, Mussener E, Jansson A, Erlandsson Harris H, Larsson P. Antigen inhibition of collagen-induced arthritis is associated with up-regulation of IL-4 mRNA and induction of O×40 on T cells in draining lymph nodes. *Clin Exp Immunol* 2003; **131**: 241-247
- 21 **Hashimoto H**, Tanaka M, Suda T, Tomita T, Hayashida K, Takeuchi E, Kaneko M, Takano H, Nagata S, Ochi T. Soluble Fas ligand in the joints of patients with rheumatoid arthritis and osteoarthritis. *Arthritis Rheum* 1998; **41**: 657-662

Edited by Wang XL and Zhang JZ Proofread by Xu FM

Safe time to warm ischemia and posttransplant survival of liver graft from non-heart-beating donors

Xiao-Shun He, Yi Ma, Lin-Wei Wu, Wei-Qiang Ju, Jin-Lang Wu, Rui-De Hu, Gui-Hua Chen, Jie-Fu Huang

Xiao-Shun He, Yi Ma, Lin-Wei Wu, Wei-Qiang Ju, Gui-Hua Chen, Jie-Fu Huang, Organ Transplantation Center, First Hospital, Sun Yat-sen University, Guangzhou 510080, Guangdong Province, China
Jin-Lang Wu, Rui-De Hu, Department of Pathology, Sun Yat-Sen University, Guangzhou 510080, Guangdong Province, China

Supported by the Key Clinical Projects of Minister of Health, No 97040230 and the Scientific and Technological Committee of Guangdong Province, No. 99M4902G

Correspondence to: Xiao-Shun He, Organ Transplantation Center, First Hospital, Sun Yat-Sen University, Guangzhou 510080, Guangdong Province, China. xshe@gdvnnet.com

Telephone: +86-20-87335101

Received: 2004-01-09 **Accepted:** 2004-02-24

Abstract

AIM: To explore the dynamical changes of histology, histochemistry, energy metabolism, liver microcirculation, liver function and posttransplant survival of liver graft in rats under different warm ischemia times (WIT) and predict the maximum limitation of liver graft to warm ischemia.

METHODS: According to WIT, the rats were randomized into 7 groups, with WIT of 0, 10, 15, 20, 30, 45, 60 min, respectively. The recovery changes of above-mentioned indices were observed or measured after liver transplantation. The graft survival and postoperative complications in each subgroup were analyzed.

RESULTS: Liver graft injury was reversible and gradually resumed normal structure and function after reperfusion when WIT was less than 30 min. In terms of graft survival, there was no significant difference between subgroups within 30 min WIT. When WIT was prolonged to 45 min, the recipients' long-term survival was severely insulted, and both function and histological structure of liver graft developed irreversible damage when WIT was prolonged to 60 min.

CONCLUSION: The present study indicates that rat liver graft can be safely subjected to warm ischemia within 30 min. The levels of ATP, energy charge, activities of glycogen, enzyme-histochemistry of liver graft and its recovery potency after reperfusion may serve as the important criteria to evaluate the quality of liver graft.

He XS, Ma Y, Wu LW, Ju WQ, Wu JL, Hu RD, Chen GH, Huang JF. Safe time to warm ischemia and posttransplant survival of liver graft from non-heart-beating donors. *World J Gastroenterol* 2004; 10(21): 3157-3160

<http://www.wjgnet.com/1007-9327/10/3157.asp>

INTRODUCTION

Attributed to the widespread applications of effective immunosuppressants and the perfect perioperative management, liver transplantation has achieved a great success during the

past 40 years, but the shortage of liver donors has limited its clinical usage greatly. Quality of liver graft is a key factor for liver transplantation. Organs from NHBD (non-heart-beating donors) seem to be an option to alleviate the problem of liver donor shortage effectively^[1]. However, warm ischemia to the liver related to cardiac arrest remained a main obstacle to the use of livers from NHBD^[2-4]. Moreover, in liver transplantation, the allograft sustains inevitable cold ischemia in addition to rewarming injury during liver reperfusion^[5]. Therefore, warm ischemia-reperfusion injury of liver grafts has become a hot topic with theoretical and clinical significance, and it has drawn more and more attention^[1]. It is a main unfathomed problem of how to evaluate the quality of liver grafts and how to ascertain the safety time limit for warm ischemia of liver grafts. The outcomes of this research were rather different mainly because the previous researches focused on the relationship between warm ischemia time (WIT) and the short-time survival, neglecting the long-term survival and complications. We investigated the dynamical changes of histology, histochemistry, energy metabolism, microcirculation, especially focusing on liver function and posttransplant survival of liver graft, under different WIT to establish the predictive limitation of liver graft to warm ischemia injury, which might be helpful for the further research in similar clinical situation.

MATERIALS AND METHODS

Establishment of animal model

Adult healthy male Sprague-Dawley rats, weighing 250-300 g, supplied from Experimental Animal Center in Sun Yat-Sen University, were used for the models. Breeding conditions were in coincidence with SPF (specific pathogen free animal) standards. Mean weight of recipient rats was a little heavier than that of donor rats.

Animal model of warm ischemia A midline laparotomy was performed in supine position after an ether aspiration anesthesia, 0.2 mL of heparin sodium solution (1 250 U heparin sodium) was injected via dorsum of penis vein to heparinize the donor liver. Thereafter, we sheared diaphragm, clamped the basilar part of the heart and blocked the thoracic aorta. Thus, a donor liver warm ischemia model was established.

Animal model of liver transplantation After the predicted warm ischemia duration in each group, 20 mL of 0-4 °C lactic acid ringer's solution (50 U/mL heparin sodium) was infused into the abdominal aorta via a catheter. The liver graft turned fulvous when filling solution flowed out via the sheared right atria. All of the liver ligaments were dissected, the pyloric vein was ligated proximal to the portal vein after the hepatic proper artery and portal vein were freed, the infra-hepatic inferior vena cava was isolated and the right suprarenal vein and right renal vein were cut. The supra-hepatic inferior vena cava was cut in the position close to the diaphragm anulus, the hepatic artery was ligated and cut, the portal vein was cut in the confluence of portal vein and splenic vein, the infra-hepatic inferior vena cava was cut over the left renal vein. Specimens of donor liver were preserved in the 4 °C lactic acid ringer's solution. Anesthesia, position and incision were all the same in donors and recipients' operations. We modified the angio-anastomotic technique^[6] on the basis of cuff technique suggested by Kamada *et al.*^[7] and Sun *et al.*^[8].

Cold ischemia time (CIT) was 50 ± 3.5 min, anhepatic phase was 20 ± 2.5 min.

Group and observation index

Three hundred and seventy eight SD rats were used in our study. Forty two (6 in each group with WIT of 0, 10, 15, 20, 30, 45 and 60 min) were used for the observation of histology, histochemistry, ultrastructure and metabolism change after only warm ischemia injury; other 336 rats were performed with orthotopic liver transplantation according to the "modified cuff method"^[6]. Among the 336 rats, 168 were used for donors and 168 for receivers. The donor group was randomly divided into 2 subgroups: 84 for prolonged survival observation, including spirit, activity, complications, death diagnosis and mean survival; the other 84 rats for investigation of the dynamical changes of liver function, histology, histochemistry, microcirculation, energy metabolism and ultrastructure (transmission electron microscope and scanning electron microscope). Both groups were divided into 7 subgroups with WIT of 0, 10, 15, 20, 30, 45 and 60 min, each subgroup consisted of 12 rats. Liver transplantation and postoperative follow-up were performed respectively. Careful attention was paid to the fluid replacement after blood withdrawal.

Statistics analysis

Data were expressed as mean \pm SD. Analysis of variance (ANOVA including SNK-*q* test) was used to analyze the data. Enumeration data were analyzed by Chi-square test and Fisher test. The activity and distribution of succinic dehydrogenase (SDH), cytochrome oxidase (CO) and ATPase, were respectively observed under microscope in a semi-quantitative way. Kaplan-Meier analysis was applied for the relationship between WIT and survival, while correspondence analysis was applied for that between WIT and complication. All the statistical procedures were performed with SPSS package and $P < 0.05$ was considered statistically significant.

RESULTS

Survival situation

In groups with WIT of 0, 10, 15, 20, 30, 45 and 60 min, the median survival time was 140.5, 132.5, 76, 109, 58, 13.5 and 3 d, respectively (Figure 1). One week, 1-mo and 3-mo postoperation survivals of each group are shown in Table 1. There was no significant difference between groups with WIT less than 30 min. One week survival in WIT of 0 min and 60 min group was significantly different ($P < 0.05$). The difference was also significant between 45, 60 and 0 min in 1-mo and 3-mo survival ($P < 0.05$)^[9].

Dynamic histological and subcellular structure observation

The histological and subcellular structure change was a dynamic process^[10]. Histological structure changed slightly when WIT was less than 30 min. Cytoplasm loosening, cells edema and focal vacuole degeneration were noted when WIT was over 30 min, especially in the lobule center area, leukocytes infiltration was noted in the portal area, acidophilus was obvious in some hepatocytes. The above pathologic changes aggravated when WIT elongated to 60 min, cell degeneration was diffuse or extended to a focal area, and even lipid degeneration could be seen. The degree of degeneration was depending on the duration of WIT, but necrosis could hardly be observed under light microscope. Six hours and 24 h after reperfusion, injury to liver graft became severer; in WIT 30 min group, hepatic cells presented obvious edema and some ballooning degeneration; in WIT 45 min group, focal like necrosis could be noted, which was presented first in the lobule center area, the change aggravated with the elongation of WIT. Forty

eight hours after reperfusion, hepatic injury resumed gradually in groups with WIT less than 45 min, while in WIT 60 min group, hepatic cells presented plaque or diffuse necrosis and the pathologic change was irreversible^[11].

Electroscopically, swollen mitochondrion was noted and glycogen increased 24 h post liver transplantation in groups with WIT less than 30 min. When WIT was over 45 and 60 min, more swollen mitochondrion, vacuole degeneration, broken rough endoreticular, drop of nucleoprotein and hepatic apoptosis were observed, and cells necrosis could be noted with karyopyknosis, karyorrhexis and karyolysis. Thus, the subcellular structure then underwent irreversible injury. In addition, in WIT 45 min and 60 min groups, hepatic cells and endothelial cells presented apoptosis increasingly, and cells apoptosis and necrosis could be noted simultaneously^[12,13].

Table 1 One week, 1-mo and 3-mo survival rate under different WIT (n,%)

Warm ischemia time (min)	1-wk survival rate	1-mo survival rate	3-mo survival rate
0	91.7 (11/12)	83.3 (10/12)	83.3 (10/12)
10	83.3 (10/12)	66.7 (8/12)	66.7 (8/12)
15	83.3 (10/12)	58.3 (7/12)	50.0 (6/12)
20	75.0 (9/12)	58.3 (7/12)	58.3 (7/12)
30	83.3 (10/12)	58.3 (7/12)	50.0 (6/12)
45	66.7 (8/12)	33.3 (4/12) ^{a,c}	8.3 (1/12) ^{a,c}
60	8.3 (1/12) ^{a,c}	0.0 (0/12) ^a	0.0 (0/12) ^a

^a $P < 0.05$ vs WIT 0 min group (Fisher's exact test); ^c $P < 0.05$ vs groups WIT less than 45 min (Fisher's exact test).

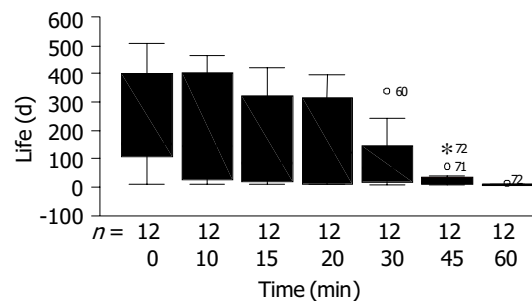


Figure 1 Statistical analysis of survival time.

Dynamic changes of histochemistry

The activities of SDH, CO, ATPase and content of glycogen decreased gradually after different WIT in a time-dependent manner, and especially significant over 30 min. The activities of SDH, CO, ATPase and content of glycogen of liver graft significantly decreased in 45 min and 60 min groups^[14].

Hepatic glycogen and enzyme activities were positively related to warm ischemia time in a time-dependent manner during the reperfusion period. In WIT 15 and 30 min groups, periodic acid-Schiff reaction (PAS reaction) and enzyme histochemical activities showed a recovery potency. While in WIT 45 and 60 min groups, the liver graft underwent an irreversible injury; therefore, no evident recovery potency was found 24 h after implantation.

Microcirculation change patterns of liver graft

The microcirculation changes of liver graft were measured by serum hyaluronic acid (HA) and ultrastructural observation. The microcirculation of liver graft injury could be gradually resumed normal after reperfusion when WIT was less than 30 min. In the WIT 45 min group, part of blood sinusoids were full of the cytoplasmic blebs stemming from the microvilli of

hepatocytes and hemocytes accumulated there; the level of serum HA of each group within 45 min of WIT would almost recover after reperfusion^[15].

Measurement of energy metabolism

ATP, TNA (Total adenine nucleotides) and EC in all groups were decreased dramatically after warm ischemia injury^[16,17]. ATP in WIT 10, 15, 20, 30, 60 min groups was decreased to 58.7%, 34.7%, 30.1%, 20.5%, 15.3%, and 9.3% of that in WIT 0 min group, respectively. Twenty-four hours after transplantation, ATP, TNA and EC showed a tendency of recovery potency. ATP, TNA and EC had no significant difference between groups with WIT less than 30 min and WIT 0 min group. But when WIT was over 45 min the observation showed significant difference, which also could be seen between the WIT 45 min and 60 min groups. Forty-eight hours after transplantation, the above mentioned indexes recovered close to the normal level, there was no difference between groups with WIT less than 45 min and WIT 0 min group, while the indexes in group with WIT 60 min were still different from those in WIT 0 min group and WIT 45 min group^[18].

Liver function

Twenty-four hours after transplantation, AST, ALT and LDH increased sharply with the elongation of WIT, the following recovering change showed a step-like pattern^[19,20]. AST and ALT in groups with WIT less than 30 min decreased close to the normal level 3 d after transplantation, and the recovering course took 5 d in WIT 45 min group. LDH in groups with WIT less than 45 min recovered to the normal level 3 d after transplantation, while enzymes in WIT 60 min group could hardly recovered to the normal^[21].

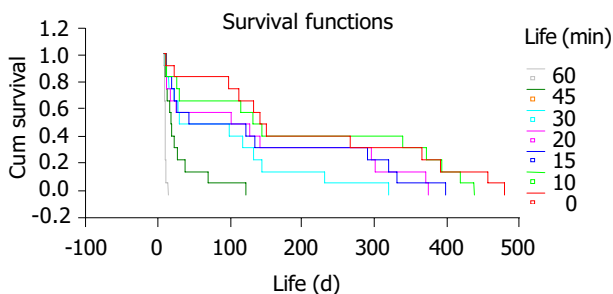


Figure 2 Survival curve (Kaplan-Meier method).

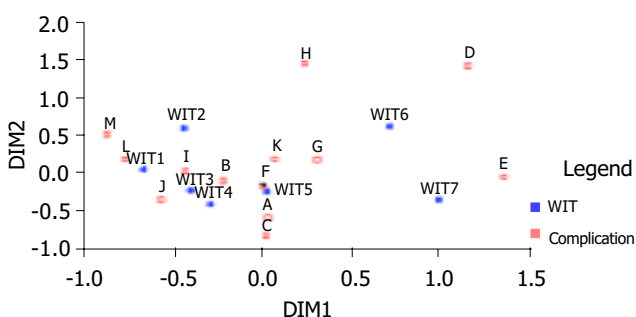


Figure 3 Relationship between WIT and complications (correspondence analysis). WIT 1, 2, 3, 4, 5, 6 and 7 represent WIT 0 min, 10 min, 15 min, 20 min, 30 min, 45 min and 60 min, respectively. A: Hemorrhage; B: SVC (superior vena cava) thrombosis; C: IVC (inferior vena cava) thrombosis; D: PV (portal vein) thrombosis; E: Liver dysfunction; F: Pulmonary infection; G: Abdominal infection; H: Bile leakage; I: Bile obstruction; J: Adhesive intestinal obstruction; K: Liver abscess; L: Unexplained; M: Natural death.

Relationship between WIT and survival

The survival curves are demonstrated in Figure 2. Survival time in groups with WIT less than 30 min had no statistical difference. Though short-term survival might be possible in WIT 45 min group, warm ischemia injury had insulted the long-term survival of liver graft. And in WIT 60 min group, the liver graft underwent irreversible injury.

Relationship between WIT and complication

The relationship between WIT and complications was illustrated by correspondence analysis (Figure 3). Complications in groups with WIT less than 30 min were similar, the incidence of liver graft dysfunction increased with the elongation of WIT and the incidence of biliary blockage was positively related to the survival time of recipient animals^[22-24].

DISCUSSION

In the past 40 years, liver transplantation has achieved a great success and become the most effective method to treat end-stage hepatic diseases. Nowadays, liver transplantation is developing rapidly as a result of the perfect perioperative treatments and widespread applications of some immunosuppressants. However, there is an obvious problem that recipients are greatly more than donors. The disparity between the increasing demand for liver donors and the limited supply of donor organs has led to a reconsideration of the use of marginal pools, such as NHBD^[25-27]. NHBD programs have been used successfully in kidney transplantation, and were able to increase donor pool of kidneys by 40%. In the field of liver transplantation the use of livers from NHBD shows a less favorable clinical results, because of the limited hepatic tolerance against warm ischemic damage compared with kidneys^[28-30]. Although several clinical and experimental studies have shown that liver can compensate 60 min of WIT during liver resection^[31,32], in transplantation settings, there were few studies about limit of the period of warm ischemia before transplantation. To evaluate the quality of liver grafts and to ascertain the safety time limit for warm ischemia of liver grafts, we should focus on the long-term survival of liver graft and the complications after transplantation^[33].

In present study, we found that the pathologic changes of hepatic cells undergoing only warm ischemia injury was irreversible when WIT was less than 60 min, only part of hepatic cells underwent irreversible injury. But the damage to liver graft would aggravate in the cold preservation, operative ischemia stage and the reperfusion process. Histological and subcellular structure changes were reversible in groups with WIT less than 30 min, especially at 48 h after transplantation. In WIT 45 min and 60 min groups, hepatocellular degeneration became severer, necrotic cells spread from the center lobule area to a sheet or foci-like area involved several hepatic lobules, the liver graft then underwent irreversible injury^[34].

The present study indicates that hepatic injury is reversible within 30 min of warm ischemia injury by cytochemical and histochemical dynamic observation. The glycogen and enzyme-histochemistry activities of liver graft and their recovery potency after reperfusion may serve as criteria to evaluate the quality of liver graft.

ATP, TAN and EC decreased after warm ischemia injury, especially in the first 30 min, the change was reversible within 30 min of warm ischemia injury. WIT and hepatic energy metabolism recovering potency were key factors to the postoperative survival. ATP, EC and their recovering potency of the liver graft may serve as criteria to evaluate the quality of liver graft.

Microcirculation of grafted liver could be gradually resumed normal after reperfusion when WIT was less than 30 min, which indicated that hepatic cells held the recovery potency and could regained normal microcirculatory structure after reperfusion if

the WIT was less than 30 min. After 45 min of warm ischemia, most hepatic sinus was unobstructed, but there were still some sinus filled with cytoplasm blebs, reticular fibrosis and hemocytes. So 45 min may be the deadline of hepatic warm ischemia. When WIT was more than 60 min, microcirculatory structure of liver graft presented irreversible injuries.

Besides the researches on the influence of warm ischemia time on energy metabolism, morphology and function, special attention was paid on the influence of warm ischemia on the postoperative long-term survival and complications. Correspondence analysis showed that complications in groups with WIT less than 30 min were similar; and the incidence of liver dysfunction increased gradually in a time-dependent manner; incidence of biliary obstruction increased with the elongation of survival time of the recipient rats. Kaplan-Meier analysis showed that survival time in groups with WIT less than 30 min had no significant difference. In WIT 45 min group, the animal might still survive early postoperative period, but the long-term survival was severely insulted, when WIT prolonged to 60 min, both function and histological structure of graft would develop irreversible damage and no recipients could survive.

REFERENCES

- Sato M, Ohkohchi N, Tsukamoto S, Koyamada N, Asakura T, Enomoto Y, Usuda M, Miyagi S, Okada A, Satomi S. Successful liver transplantation from agonal non-heart-beating donors in pigs. *Transpl Int* 2003; **16**: 100-107
- Fondevila C, Busuttil RW, Kupiec-Weglinski JW. Hepatic ischemia/reperfusion injury—a fresh look. *Exp Mol Pathol* 2003; **74**: 86-93
- Nowak G, Ungerstedt J, Wernerson A, Ungerstedt U, Ericzon BG. Hepatic cell membrane damage during cold preservation sensitizes liver grafts to rewarming injury. *J Hepatobiliary Pancreat Surg* 2003; **10**: 200-205
- Hines IN, Harada H, Wolf R, Grisham MB. Superoxide and post-ischemic liver injury: potential therapeutic target for liver transplantation. *Curr Med Chem* 2003; **10**: 2661-2667
- Totsuka E, Fung JJ, Urakami A, Moras N, Ishii T, Takahashi K, Narumi S, Hakamada K, Sasaki M. Influence of donor cardiopulmonary arrest in human liver transplantation: possible role of ischemic preconditioning. *Hepatology* 2000; **31**: 577-580
- Ma Y, He XS, Chen GH. Surgical technique of the model of orthotopic liver transplantation and prevention of operational complication in rat. *Zhonghua Xianwei Waike Zazhi* 2003; **26**: 45-47
- Kamada N, Calne RY. A surgical experience with five hundred thirty liver transplants in the rat. *Surgery* 1993; **93**: 64-68
- Sun JH, Zeng QH, Wu MC. Experience with orthotopic rat liver transplantation. *Chin Med J* 1990; **103**: 142-145
- He XS, Ma Y, Chen GH, Zhang JX, Wu JL, Liang YJ, Lin GY, Zhu ZY, Hu RD, Huang JF. The influence of warm ischemia injury on viability and posttransplantative outcome of liver graft from non-heart-beating donor in rats. *Zhonghua Yixue Zazhi* 2003; **83**: 1236-1240
- He XS, Ma Y, Chen GH, Wu JL, Hu RD, Liang YJ, Huang JF. Hepatic warm ischemia injury in rats: a dynamically histological and ultrastructural study. *Zhonghua Shiyian Waike Zazhi* 2002; **19**: 249-251
- Rudiger HA, Graf R, Clavien PA. Liver ischemia: apoptosis as a central mechanism of injury. *J Invest Surg* 2003; **16**: 149-159
- Kurokawa T, Takagi H. Mechanism and prevention of ischemia-reperfusion injury. *Transplant Proc* 1999; **31**: 1775-1776
- Belous A, Knox C, Nicoud IB, Pierce J, Anderson C, Pinson CW, Chari RS. Reversed activity of mitochondrial adenine nucleotide translocator in ischemia-reperfusion. *Transplantation* 2003; **75**: 1717-1723
- Ma Y, He XS, Chen GH, Liang YJ, Hu RD, Huang JF. Dynamical changes of glycogen and enzyme-histochemistry activities of liver graft following warm ischemia injury in rat. *Zhonghua Shiyian Waike Zazhi* 2003; **20**: 24-26
- Ma Y, He XS, Chen GH, Wu JL, Liang YJ, Hu RD, Huang JF. Dynamical changes of microcirculation of liver graft from non-heart-beating donor in rat. *Zhonghua Shiyian Waike Zazhi* 2003; **20**: 895-896
- Astarcioğlu H, Karademir S, Unek T, Ozer E, Menekay S, Coker A, Astarcioğlu I. Beneficial effects of pentoxifylline pretreatment in non-heart-beating donors in rats. *Transplantation* 2000; **69**: 93-98
- He X, Ma Y, Chen G, Lin G, Wu J, Zhu Z, Huang J. Influence of warm ischemia injury on energy metabolism and survival of liver graft in rats. *Zhonghua Waike Zazhi* 2002; **40**: 936-939
- Peralta C, Bartrons R, Serafin A, Blazquez C, Guzman M, Prats N, Xaus C, Cutillas B, Gelpi E, Rosello-Catafau J. Adenosine monophosphate-activated protein kinase mediates the protective effects of ischemic preconditioning on hepatic ischemia-reperfusion injury in the rat. *Hepatology* 2001; **34**: 1164-1173
- Ma Y, He XS, Chen GH, Hu RD, Huang JF. Effect of warm ischemia injury on hepatic functional status and survival of liver graft in rats. *Zhonghua Shiyian Waike Zazhi* 2003; **20**: 322-324
- Matsumoto K, Honda K, Kobayashi N. Protective effect of heat preconditioning of rat liver graft resulting in improved transplant survival. *Transplantation* 2001; **71**: 862-868
- He XS, Ma Y, Wu LW, Ju WQ, Chen GH, Hu RD, Huang JF. Influence of warm ischemia injury on hepatic functional status and survival of liver graft in rats. *Hepatobiliary Pancreat Dis Int* 2003; **2**: 504-508
- Moench C, Moench K, Lohse AW, Thies JC, Otto G. Arterial back table pressure perfusion prevents ischemic biliary lesions after orthotopic liver transplantation. *Chirurg* 2003; **74**: 570-574
- Steger U, Sawitzki B, Gassel AM, Gassel HJ, Wood KJ. Impact of hepatic rearterialization on reperfusion injury and outcome after mouse liver transplantation. *Transplantation* 2003; **76**: 327-332
- Abt P, Crawford M, Desai N, Markmann J, Olthoff K, Shaked A. Liver transplantation from controlled non-heart-beating donors: an increased incidence of biliary complications. *Transplantation* 2003; **75**: 1659-1663
- Takada Y, Taniguchi H, Fukunaga K, Yuzawa K, Otsuka M, Todoroki T, Iijima T, Fukao K. Hepatic allograft procurement from non-heart-beating donors: Limits of warm ischemia in porcine liver transplantation. *Transplantation* 1997; **63**: 369-373
- D'Alessandro AM, Hoffmann RM, Knechtle SJ, Eckhoff DE, Love RB, Kalayoglu M, Sollinger HW, Belzer FO. Controlled non-heart-beating donors: A potential source of extrarenal organs. *Transplant Proc* 1995; **27**: 707-709
- Imber CJ, St Peter SD, Lopez de Cenarruzabeitia I, Pigott D, James T, Taylor R, McGuire J, Hughes D, Butler A, Rees M, Friend PJ. Advantages of normothermic perfusion over cold storage in liver preservation. *Transplantation* 2002; **73**: 701-709
- Koti RS, Seifalian AM, Davidson BR. Protection of the liver by ischemic preconditioning: a review of mechanisms and clinical applications. *Dig Surg* 2003; **20**: 383-396
- Busuttil RW, Tanaka K. The utility of marginal donors in liver transplantation. *Liver Transpl* 2003; **9**: 651-663
- Regueira FM, Espi A, Nwose P, Diez-Caballero A, Baixauli J, Rotellar F, Olea J, Pardo F, Hernandez-Lizoain JL, Cienfuegos JA. Comparison between two warm ischemic models in experimental liver transplantation in pigs. *Transplant Proc* 2003; **35**: 1591-1593
- Schon MR, Pegg DE. The possibility of resuscitation livers after warm ischemia injury. *Transplant Proc* 1991; **23**: 2456-2458
- Jiang Y, Gu XP, Qiu YD, Sun XM, Chen LL, Zhang LH, Ding YT. Ischemic preconditioning decreases C-X-C chemokine expression and neutrophil accumulation early after liver transplantation in rats. *World J Gastroenterol* 2003; **9**: 2025-2029
- Selzner N, Rudiger H, Graf R, Clavien PA. Protective strategies against ischemic injury of the liver. *Gastroenterology* 2003; **125**: 917-936
- Donckier V, Loi P, Closset J, Nagy N, Quertinmont E, Le Moine O, Deviere J, Goldman M, Gelin M, Gianello P. Preconditioning of donors with interleukin-10 reduces hepatic ischemia-reperfusion injury after liver transplantation in pigs. *Transplantation* 2003; **75**: 902-904

Protective effects of tumor necrosis factor α antibody and ulinastatin on liver ischemic reperfusion in rats

Yan-Ling Yang, Ji-Peng Li, Xiao-Ping Xu, Ke-Feng Dou, Shu-Qiang Yue, Kai-Zong Li

Yan-Ling Yang, Ji-Peng Li, Ke-Feng Dou, Shu-Qiang Yue, Kai-Zong Li, Department of Hepatobiliary Surgery, Xijing Hospital, Fourth Military Medical University, Xi'an 710032, Shaanxi Province, China
Xiao-Ping Xu, Department of General Surgery, Zhujiang Hospital, First Military Medical University, Guangzhou 510282, Guangdong Province, China

Supported by the National Natural Science Foundation of China, No. 30070741

Correspondence to: Kai-Zong Li, Department of Hepatobiliary Surgery, Xijing Hospital, Fourth Military Medical University, Xi'an 710032, Shaanxi Province, China. gdwk@fmmu.edu.cn

Telephone: +86-29-83375259 **Fax:** +86-29-83375561

Received: 2003-08-26 **Accepted:** 2003-10-27

Abstract

AIM: To study the protective effects of tumor necrosis factor α (TNF α) antibody and ulinastatin on liver ischemic reperfusion in rats.

METHODS: One hundred and twenty male SD rats were randomly divided into four groups: normal control group, ischemic group, TNF α antibody group and TNF α antibody + ulinastatin group. The animals were killed at 0, 3, 6, 9, 12 h after ischemia for 60 min and followed by reperfusion. Serum alanine aminotransferase (ALT), malondialdehyde (MDA) and liver histopathology were observed.

RESULTS: After ischemic reperfusion, the serum ALT and MDA were remarkably increased, and the hepatic congestion was obvious. Treatment of TNF α antibody and ulinastatin could significantly decrease serum ALT and MDA levels, and relieve hepatic congestion.

CONCLUSION: Ulinastatin and TNF α antibody can suppress the inflammatory reaction induced by hepatic ischemic reperfusion, and have protective effects on rat hepatic ischemic reperfusion injury.

Yang YL, Li JP, Xu XP, Dou KF, Yue SQ, Li KZ. Protective effects of tumor necrosis factor α antibody and ulinastatin on liver ischemic reperfusion in rats. *World J Gastroenterol* 2004; 10(21): 3161-3164

<http://www.wjgnet.com/1007-9327/10/3161.asp>

INTRODUCTION

Liver ischemic reperfusion injury is induced when liver gets the retrieval of its blood perfusion or oxygen supply, and hepatic injury would aggravate due to ischemia and hypoxia injury^[1-4]. Hepatic insufficiency or primary liver graft non-function can be caused by liver ischemic reperfusion injury after portal blockage, hemorrhagic shock or liver transplantation. As liver ischemic reperfusion is hard to be avoided in hepatic surgical practice and the existing prevention and cure methods are not satisfactory, research of the mechanisms and therapy on liver ischemic reperfusion becomes one of the hotspots in hepatic surgery^[5,6].

Cytokines are polypeptides with extensive biological activities, and play important roles in the immunoregulation. They prevent body from diseases and accelerate tissue rehabilitation. But on the other hand, too many cytokines can also lead to or aggravate tissue damages^[7,8]. Recent researches have demonstrated that TNF α plays an important role in ischemic reperfusion injury of liver^[9-12]. At the same time, ulinastatin has been applied in the clinical treatment of pancreatitis, shock and extracorporeal circulation because of its significant inhibitory effect on inflammation^[13-15]. In the present study, we attempted to relieve ischemic reperfusion injury of liver by using TNF α antibody and ulinastatin, so as to provide experimental and theoretic bases for prevention and treatment of liver ischemic reperfusion injury.

MATERIALS AND METHODS

Animals

A total of 120 male Spargue-Dawfey (SD) rats weighing 230 \pm 20 g, were obtained from Animal Research Center of Shaanxi Chinese Medical Institute, and fed with standard rat chow.

Drugs

Ulinastatin (Tianpu Co. Ltd., Guangdong, China) was diluted to 50 U/L by saline prior to use. TNF α monoclonal antibody (Jingmei Co. Ltd., Guangdong, China) was diluted 100 times by saline prior to use.

Experimental grouping

The rats were randomly divided into four groups. Group I: the control group, sham operation was performed, hepatic lobes of the rats were exposed without any treatment. Group II: ischemic reperfusion injury group, in which blood stream of the rats' liver lobes were blocked and then recovered after 60 min. Group III: TNF α antibody treatment group, in which TNF α antibody (2.0 mg/kg) was injected into the rats through dorsum veins of penis 5 min prior to reperfusion. Group IV: TNF α antibody and ulinastatin treatment group, in which both TNF α antibody (2.0 mg/kg) and ulinastatin (500 000 U/L, 0.5 mL) were simultaneously injected into the rats through dorsum veins of penis 5 min prior to reperfusion. Blood samples (2 mL) of all animals in each group were taken from hepatic superior and inferior vena cava at 0, 3, 6, 9 and 12 h after reperfusion. Then the rats were killed and liver samples were obtained.

Operation

The animals were intraabdominally anesthetized by pentobarbital sodium (30 mg/kg, 0.1 mL/10 g), and incised through median incision of the abdomen. After the liver pedicel between left and middle lobes of liver was exposed, ligaments between liver and septum transversum and abdominal wall were cut. The scatheless vascular clamp was used to block blood stream of portal veins and hepatic arteries of left and middle lobes of liver. After 60 min, the vascular clamp was released and blood stream recovered. So approximately seventy percent of liver was hypoxia, thus severe congestion of the mesentery vein was prevented.

Table 1 Levels of serum ALT in rats (U/L)

Group	n	Time of after reperfusion (h)				
		0	3	6	9	12
I ^d	6	40.52±8.33	42.36±3.71	43.19±7.64	42.92±5.18	42.66±9.27
II	6	263.92±16.90	315.61±21.02	374.26±19.56	289.11±16.32	257.94±27.41
III	6	238.73±10.62	254.06±13.78	273.17±18.29	213.26±26.54	172.53±36.46
IV ^b	6	173.42±15.33	189.08±24.52	203.17±23.19	175.36±38.66	163.13±32.27

^b $P < 0.01$ vs other groups, ^d $P < 0.01$ vs group II and III.

Table 2 Levels of serum MDA of rats (mmol/L)

Group	n	Time of after reperfusion (h)				
		0	3	6	9	12
I ^d	6	7.82±0.17	7.91±0.08	8.11±0.13	8.04±0.67	7.93±0.41
II	6	13.81±4.19	38.65±4.73	46.36±2.54	35.09±5.12	24.09±3.20
III	6	10.71±2.52	18.23±3.58	23.31±4.49	16.83±2.29	11.26±3.16
IV ^b	6	9.12±3.41	12.29±6.83	15.18±3.22	11.72±4.15	9.42±5.28

^b $P < 0.01$ vs group II and III, ^d $P < 0.01$ vs other groups.

Determination of ALT and MDA in serum

The blood samples in each group were poured into centrifuge tubes and the placement lasted for 20 min without shaking. After centrifugation at 2 000 r/min for 10 min, the sample serum was extracted and stored at -80°C for determination.

ALT levels of sample serum were determined by an automatic biochemistry analyzer. MDA levels of sample serum were determined by the method introduced by Mourek *et al.*^[16], and the kit was purchased from Juli Biomedical Engineering Institute of Nanjing, China.

Pathological changes of liver

Fresh tissues of liver in each group were sampled. Haematoxylin-Eosin (HE) staining was performed on 100 g/L formaldehyde-fixed tissue sections. The histological patterns of the liver samples were observed under light microscope.

Statistical analysis

All the data were analyzed by Student's *t* test and expressed as mean±SD. $P < 0.05$ was considered statistically significant and $P < 0.01$ as very statistically significant.

RESULTS

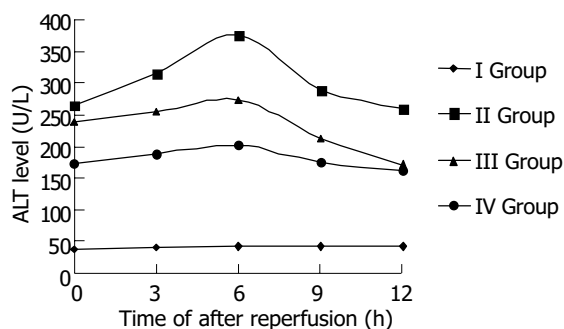
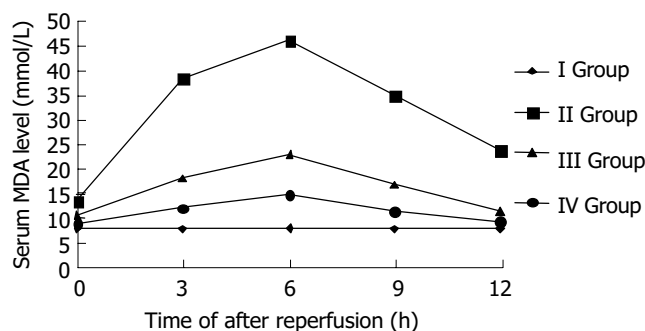
ALT levels of sample serum

ALT levels of sample serum in each group were determined to assess the liver function of rats. The levels of ALT in ischemic reperfusion injury group at different time points were significantly higher than those in control ($P < 0.01$). The levels of ALT increased gradually after reperfusion, reached the peak 6 h after reperfusion, and then decreased mildly. The levels of ALT in TNF α antibody treatment group were remarkably lower than those in ischemic reperfusion injury group ($P < 0.01$). The levels of ALT in TNF α antibody and ulinastatin treatment group were lower than those in ischemic reperfusion injury group and TNF α antibody treatment group ($P < 0.01$).

MDA levels of sample serum

The oxygen-derived free radicals induced lipid peroxidation reaction of polyvalent unsaturated fatty acid at plasmalemma, which developed lipid peroxidation products, such as MDA. So the MDA levels of sample serum showed the degree of lipid peroxidation injury of liver. The levels of MDA in ischemic reperfusion injury group at different time points were significantly

higher than those in control ($P < 0.01$). The levels of MDA increased gradually after reperfusion, reached the peak 6 h after reperfusion, and then decreased. The levels of MDA in TNF α antibody treatment group were remarkably lower than those in ischemic reperfusion injury group ($P < 0.01$). The levels of MDA in TNF α antibody and ulinastatin treatment group were lower than those in ischemic reperfusion injury group and TNF α antibody treatment group ($P < 0.01$).

**Figure 1** Serum ALT level after reperfusion in rats.**Figure 2** Serum MDA level after reperfusion in rats.

Histopathological observation

The blood stream in middle and left lobes of livers of rats was reperused 1 h after blocked for 60 min. In ischemic reperfusion injury group, the middle and left lobes of livers were found to be swollen and faint. HE staining showed disorganized hepatic

lobules and extensive hepatocytic edema with various degrees of vacuolation and lamellar necrosis. The liver tissues in TNF α antibody treatment group and in TNF α antibody + ulinastatin treatment group were found to insignificantly swollen and faint in appearance. HE staining showed a sprinkle of hepatocytic edema without vacuolation and lamellar necrosis.

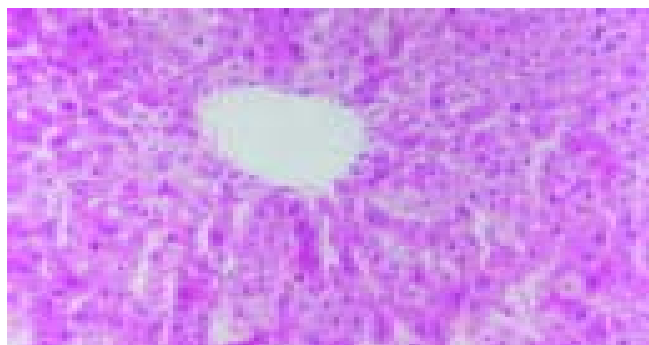


Figure 3 Disorganized hepatic lobules and extensive hepatocytic edema with various degrees of vacuolation and lamellar necrosis in ischemic reperfusion injury group.

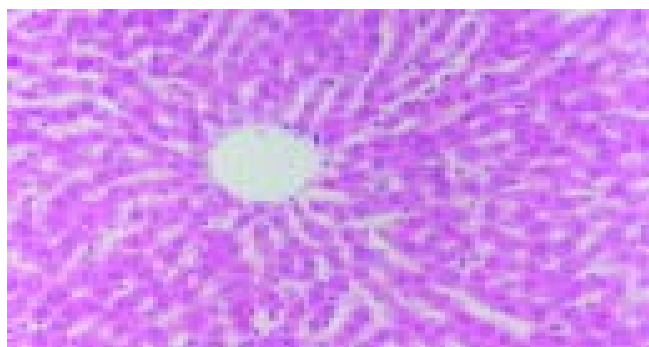


Figure 4 A sprinkle of hepatocytic edema without vacuolation and lamellar necrosis in TNF α antibody + ulinastatin treatment group.

DISCUSSION

Liver ischemic reperfusion injury can be frequently seen in surgical practice, and plays important roles in severe infection, trauma, shock, cardiorespiratory malfunction, organ transplantation, *etc.* Ischemic reperfusion can cause a series of injuries on metabolism, structure, and function in hepatic tissues and cells, and even liver function failure. So it is one of the major factors influencing the prognosis, operative success and survival of patients.

Cytokines, are the soluble polypeptides excreted by immunocytes, and play important roles in immunological activation and inflammatory reaction. The study of cytokine effects on ischemic reperfusion injury in liver has become highlights at present^[17-22]. TNF α is the polypeptide excreted by activated macrophages, endothelial cells, neutrophilic granulocytes and B lymphocytes, and plays an important role in inflammatory reaction. Liver possesses tremendous Kupffer cells (KC) that have the great potency to produce TNF α in human body. At the time of liver ischemia, for the blockage of ATP production, calcium pump of liver is in dysfunction, which causes intracellular calcium overload. Aggravated calcium overload can activate Kupffer cells. On the other hand, Kupffer cells have complement receptors, intracellular protein was released during ischemic reperfusion, thus activating complements, which can also activate Kupffer cells. The activated Kupffer cells excrete TNF α . Liver has plenty of TNF α receptors, and also is the major target organ of TNF α ^[23-26]. Some mechanisms were used to explain

the liver damage caused by TNF α ^[27-30]. Firstly, TNF α could directly injure hepatocytes. Secondly, TNF α could activate neutrophilic granulocytes and mononuclear macrophages to express IL-1 and IL-6, and phosphatidase A2 that can decompose arachidonic acids. Inflammatory media were produced such as platelet active factor, leukotriene, and thromboxane A2. So the inflammatory reaction was aggravated. Thirdly, the toxic effect of TNF α on endothelial cells could induce the circulatory disorder of hepatic sinusoid, and TNF α could activate complement system that aggravates tissue damage by cytotoxicity. Finally, the oxygen-derived free radicals induced by TNF α could facilitate oxidation explosion of neutrophilic granulocytes, which could also result in liver damage. Therefore, the way to block the production of TNF α in liver can be used to prevent liver from injury by TNF α .

Ulinastatin is one kind of glycoproteins containing 143 amino acids with molecular weight of 67 ku. It is the typical urine protease inhibitor isolated and purified from human urine. Ulinastatin has two active function domains which have a wide restrained zymogram with no overlapped region each other. So ulinastatin can inhibit many hydrolytic enzymes in one time, including trypsin, phospholipase A₂, aldase and elastase. Moreover, the components of low molecular mass decomposed from ulinastatin can also inhibit hydrolytic enzymes strongly. On the other hand, ulinastatin could ameliorate the shock situation by blocking the production of myocardial depressant factors and stabilizing the membrane of lysosome^[31-33]. Recent researches found that ulinastatin could block the release of inflammatory factors, prevent cascade reaction of cytokines, inhibit excessive activation of leukocytes and block vicious circles among cytokines, inflammatory factors and leukocytes. So when pancreatitis, shock or other severe infection occurred, the action of multiple hydrolytic enzymes necessitated the use of ulinastatin, which can inhibit many hydrolytic enzymes at the same time and alleviate the vicious effects of multiple proteases on tissues and organs^[34-36].

The present study was to verify the protective effect of TNF α antibody and ulinastatin on ischemic reperfusion injury of liver. The results showed that the levels of ALT and MDA in TNF α antibody and ulinastatin treatment group were remarkably decreased as compared with those in ischemic reperfusion injury group. Pathological changes of liver also demonstrated the significant protective effect of TNF α antibody and ulinastatin on ischemic reperfusion injury of liver. The present results suggest TNF α antibody and ulinastatin can effectively prevent ischemic reperfusion injury of liver. But further work is needed to make clear of their best concentrations, best ratio and their effect on immune system of the body.

REFERENCES

- 1 **Zhu X**, Qiu Y, Shi M, Ding Y. Matrine protects sinusoidal endothelial cells from cold ischemia and reperfusion injury in rat orthotopic liver transplantation. *Ann Clin Lab Sci* 2003; **33**: 216-225
- 2 **Zhou T**, Chen JL, Song W, Wang F, Zhang MJ, Ni PH, Geng JG. Effect of N-desulfated heparin on hepatic/renal ischemia reperfusion injury in rats. *World J Gastroenterol* 2002; **8**: 897-900
- 3 **Jawan B**, Goto S, Pan TL, Lai CY, Luk HN, Eng HL, Lin YC, Chen YS, Lan KM, Hsieh SW, Wang CC, Cheng YF, Chen CL. The protective mechanism of magnolol, a Chinese herb drug, against warm ischemia-reperfusion injury of rat liver. *J Surg Res* 2003; **110**: 378-382
- 4 **Teoh NC**, Farrell GC. Hepatic ischemia reperfusion injury: Pathogenic mechanisms and basis for hepatoprotection. *J Gastroenterol Hepatol* 2003; **18**: 891-902
- 5 **Fondevila C**, Busuttill RW, Kupiec-Weglinski JW. Hepatic ischemia/reperfusion injury-a fresh look. *Exp Mol Pathol* 2003; **74**: 86-93
- 6 **Donckier V**, Loi P, Closset J, Nagy N, Quertinmont E, Le Moine O, Deviere J, Goldman M, Gelin M, Gianello P. Precondi-

- tioning of donors with interleukin-10 reduces hepatic ischemia-reperfusion injury after liver transplantation in pigs. *Transplantation* 2003; **75**: 902-904
- 7 **Banks WA**, Farr SA, Morley JE. Entry of blood-borne cytokines into the central nervous system: effects on cognitive processes. *Neuroimmunomodulation* 2003; **10**: 319-327
- 8 **Trefzer U**, Hofmann M, Sterry W, Asadullah K. Cytokine and anticytokine therapy in dermatology. *Expert Opin Biol Ther* 2003; **3**: 733-743
- 9 **Tsuchihashi S**, Tamaki T, Tanaka M, Kawamura A, Kaizu T, Ikeda A, Kakita A. Pyrrolidine dithiocarbamate provides protection against hypothermic preservation and transplantation injury in the rat liver: the role of heme oxygenase-1. *Surgery* 2003; **133**: 556-567
- 10 **Dutkowski P**, Wahl W, Winkelbach V, Watzka M, Krysiak M, Junginger T. Calcium prevents loss of glutathione and reduces oxidative stress upon reperfusion in the perfused liver. *Int J Surg Investig* 2000; **2**: 1-7
- 11 **Langdale LA**, Kajikawa O, Frevert C, Liggitt HD. Sustained tolerance to lipopolysaccharide after liver ischemia-reperfusion injury. *Shock* 2003; **19**: 553-558
- 12 **Chimalakonda AP**, Mehvar R. Attenuation of Kupffer cell activation in cold-preserved livers after pretreatment of rats with methylprednisolone or its macromolecular prodrug. *Pharm Res* 2003; **20**: 1001-1008
- 13 **Masuda T**, Sato K, Noda C, Ikeda KM, Matsunaga A, Ogura MN, Shimizu K, Nagasawa H, Matsuyama N, Izumi T. Protective effect of urinary trypsin inhibitor on myocardial mitochondria during hemorrhagic shock and reperfusion. *Crit Care Med* 2003; **31**: 1987-1992
- 14 **Yano T**, Anraku S, Nakayama R, Ushijima K. Neuroprotective effect of urinary trypsin inhibitor against focal cerebral ischemia-reperfusion injury in rats. *Anesthesiology* 2003; **98**: 465-473
- 15 **Sato N**, Endo S, Kimura Y, Ikeda K, Aoki K, Iwaya T, Akiyama Y, Noda Y, Saito K. Influence of a human protease inhibitor on surgical stress induced immunosuppression. *Dig Surg* 2002; **19**: 300-305
- 16 **Mourek J**, Koudelova J. Adrenergic tocolytics-their effects on lipoperoxidation in the brain. *Ceska Gynekol* 1997; **62**: 15-18
- 17 **Kato A**, Gabay C, Okaya T, Lentsch AB. Specific role of interleukin-1 in hepatic neutrophil recruitment after ischemia/reperfusion. *Am J Pathol* 2002; **161**: 1797-1803
- 18 **Shinoda M**, Shimazu M, Matsuda S, Wakabayashi G, Tanabe M, Hoshino K, Kamei S, Koyasu S, Kitajima M. c-Jun N-terminal kinase activation during warm hepatic ischemia/reperfusion injuries in a rat model. *Wound Repair Regen* 2002; **10**: 314-319
- 19 **Cutrn JC**, Perrelli MG, Cavalieri B, Peralta C, Rosell Catafau J, Poli G. Microvascular dysfunction induced by reperfusion injury and protective effect of ischemic preconditioning. *Free Radic Biol Med* 2002; **33**: 1200-1208
- 20 **Iwasaki Y**, Tagaya N, Hattori Y, Yamaguchi K, Kubota K. Protective effect of ischemic preconditioning against intermittent warm-ischemia-induced liver injury. *J Surg Res* 2002; **107**: 82-92
- 21 **Takahashi Y**, Ganster RW, Gambotto A, Shao L, Kaizu T, Wu T, Yagnik GP, Nakao A, Tsoulfas G, Ishikawa T, Okuda T, Geller DA, Murase N. Role of NF-kappaB on liver cold ischemia-reperfusion injury. *Am J Physiol Gastrointest Liver Physiol* 2002; **283**: G1175-1184
- 22 **Zamora R**, Vodovotz Y, Aulak KS, Kim PK, Kane JM 3rd, Alarcon L, Stuehr DJ, Billiar TR. A DNA microarray study of nitric oxide-induced genes in mouse hepatocytes: implications for hepatic heme oxygenase-1 expression in ischemia/reperfusion. *Nitric Oxide* 2002; **7**: 165-186
- 23 **Hines IN**, Kawachi S, Harada H, Pavlick KP, Hoffman JM, Bharwani S, Wolf RE, Grisham MB. Role of nitric oxide in liver ischemia and reperfusion injury. *Mol Cell Biochem* 2002; **234**: 229-237
- 24 **Kim YI**, Song KE, Ryeon HK, Hwang YJ, Yun YK, Lee JW, Chun BY. Enhanced inflammatory cytokine production at ischemia/reperfusion in human liver resection. *Hepatogastroenterology* 2002; **49**: 1077-1082
- 25 **Ben-Ari Z**, Hochhauser E, Burstein I, Papo O, Kaganovsky E, Krasnov T, Vamichkim A, Vidne BA. Role of anti-tumor necrosis factor-alpha in ischemia/reperfusion injury in isolated rat liver in a blood-free environment. *Transplantation* 2002; **73**: 1875-1880
- 26 **Kim YI**, Hwang YJ, Song KE, Yun YK, Lee JW, Chun BY. Hepatocyte protection by a protease inhibitor against ischemia/reperfusion injury of human liver. *J Am Coll Surg* 2002; **195**: 41-50
- 27 **Kataoka M**, Shimizu H, Mitsuhashi N, Ohtsuka M, Wakabayashi Y, Ito H, Kimura F, Nakagawa K, Yoshidome H, Shimizu Y, Miyazaki M. Effect of cold-ischemia time on C-X-C chemokine expression and neutrophil accumulation in the graft liver after orthotopic liver transplantation in rats. *Transplantation* 2002; **73**: 1730-1735
- 28 **Kato A**, Edwards MJ, Lentsch AB. Gene deletion of NF-kappa B p50 does not alter the hepatic inflammatory response to ischemia/reperfusion. *J Hepatol* 2002; **37**: 48-55
- 29 **Peralta C**, Perales JC, Bartrons R, Mitchell C, Gilgenkrantz H, Xaus C, Prats N, Fernandez L, Gelpi E, Panes J, Rosello-Catafau J. The combination of ischemic preconditioning and liver Bcl-2 overexpression is a suitable strategy to prevent liver and lung damage after hepatic ischemia-reperfusion. *Am J Pathol* 2002; **160**: 2111-2122
- 30 **Harada N**, Okajima K, Uchiba M, Katsuragi T. Ischemia/reperfusion-induced increase in the hepatic level of prostacyclin is mainly mediated by activation of capsaicin-sensitive sensory neurons in rats. *J Lab Clin Med* 2002; **139**: 218-226
- 31 **Itabashi K**, Ito Y, Takahashi T, Ishii K, Sato K, Kakita A. Protective effects of urinary trypsin inhibitor (UTI) on hepatic microvasculature in hypotensive brain-dead rats. *Eur Surg Res* 2002; **34**: 330-338
- 32 **Lin SD**, Endo R, Sato A, Takikawa Y, Shirakawa K, Suzuki K. Plasma and urine levels of urinary trypsin inhibitor in patients with acute and fulminant hepatitis. *J Gastroenterol Hepatol* 2002; **17**: 140-147
- 33 **Saitoh Y**, Kaneda K, Murakawa M. The effect of ulinastatin pre-treatment on vecuronium-induced neuromuscular block in patients with hepatic cirrhosis. *Anaesthesia* 2002; **57**: 218-222
- 34 **Puglia MJ**, Takemura T, Kuwajima S, Suzuki M, Cast TK, Profit JA, Schulman LS, Ohta Y, Lott JA. Clinical utility of a rapid test for uristatin. *Clin Biochem* 2002; **35**: 105-110
- 35 **Furukawa K**, Kamimura T, Mahune Y, Ohta H, Yoshida T, Ishihara N, Tazaki K, Suzuki Y, Honda S, Ito K, Miki I, Suzuki K, Honma A. Two patients with severe alcoholic hepatitis accompanied by hypercytokinemia and granulocytic hyperelastemia, successfully treated by intravenous infusion of urinastatine Miracid. *J Gastroenterol Hepatol* 2001; **16**: 575-580
- 36 **Takada K**, Komori M, Notoya A, Tomizawa Y, Ozaki M. Effect of ulinastatin on microcirculation during excessive hemorrhage using fluid therapy. *In Vivo* 2003; **17**: 129-135

Oral and nasal administration of chicken type II collagen suppresses adjuvant arthritis in rats with intestinal lesions induced by meloxicam

Yong-Qiu Zheng, Wei Wei, Yu-Xian Shen, Min Dai, Li-Hua Liu

Yong-Qiu Zheng, Wei Wei, Yu-Xian Shen, Min Dai, Li-Hua Liu, Institute of Clinical Pharmacology, Anhui Medical University, Hefei 230032, Anhui Province, China

Correspondence to: Professor Wei Wei, Institute of Clinical Pharmacology, Anhui Medical University, Hefei 230032, Anhui Province, China. wwei@ahmu.edu.cn

Telephone: +86-551-5161208 **Fax:** +86-551-5161208

Received: 2004-03-23 **Accepted:** 2004-04-16

Abstract

AIM: To investigate the curative effects of oral and nasal administration of chicken type II collagen (CII) on adjuvant arthritis (AA) in rats with meloxicam-induced intestinal lesions.

METHODS: AA model in Sprague-Dawley (SD) rats with or without intestinal lesions induced by meloxicam was established and those rats were divided randomly into six groups which included AA model, AA model+meloxicam, AA model+oral CII, AA model+nasal CII, AA model+meloxicam+oral CII and AA model+meloxicam+nasal CII ($n = 12$). Rats were treated with meloxicam intragastrically for 7 d from d 14 after immunization with complete Freund's adjuvant (CFA), and then treated with chicken CII intragastrically or nasally for 7 d. Histological changes of right hind knees were examined. Hind paw secondary swelling and intestinal lesions were evaluated. Synovocyte proliferation was measured by 3-(4,5-dimethylthiazol-2-thiazolyl)-2,5-diphenyl-2H tetrazolium bromide (MTT) method. Activities of myeloperoxidase (MPO) and diamine oxidase (DAO) from supernatants of intestinal homogenates were assayed by spectrophotometric analysis.

RESULTS: Intragastrical administration of meloxicam (1.5 mg/kg) induced multiple intestinal lesions in AA rats. There was a significant decrease of intestinal DAO activities in AA+meloxicam group ($P < 0.01$) and AA model group ($P < 0.01$) compared with normal group. DAO activities of intestinal homogenates in AA+meloxicam group were significantly less than those in AA rats ($P < 0.01$). There was a significant increase of intestinal MPO activities in AA+meloxicam group compared with normal control ($P < 0.01$). Oral or nasal administration of CII (20 $\mu\text{g}/\text{kg}$) could suppress the secondary hind paw swelling ($P < 0.05$ for oral CII; $P < 0.01$ for nasal CII), synovocyte proliferation ($P < 0.01$) and histopathological degradation in AA rats, but they had no significant effects on DAO and MPO changes. However, oral administration of CII (20 $\mu\text{g}/\text{kg}$) showed the limited efficacy on arthritis in AA+meloxicam model and the curative effects of nasal CII (20 $\mu\text{g}/\text{kg}$) were shown to be more efficient than that of oral CII (20 $\mu\text{g}/\text{kg}$) both in AA model and in AA+meloxicam model ($P < 0.05$).

CONCLUSION: Oral administration of CII shows the limited efficacy on arthritis in AA rats with intestinal lesions, and nasal administration of CII is more efficient than oral administration of CII to induce mucosal tolerance in AA rats.

Zheng YQ, Wei W, Shen YX, Dai M, Liu LH. Oral and nasal administration of chicken type II collagen suppresses adjuvant arthritis in rats with intestinal lesions induced by meloxicam. *World J Gastroenterol* 2004; 10(21): 3165-3170

<http://www.wjgnet.com/1007-9327/10/3165.asp>

INTRODUCTION

Rheumatoid arthritis (RA) is a chronic autoimmune disease characterized by inflammation of the joints including proliferation of the synovium and progressive erosion of cartilages and bones^[1]. The goals of treatment include reduction of pain and inflammation, maintenance of functional ability, slowing of disease progression, and prevention of adverse effects of drugs^[2]. Administering antigens via a mucosal route has been recognized as a means to induce tolerance. The phenomenon of oral tolerance (OT) was first reported in 1911 by Wells^[3]. Further studies demonstrated that CII could suppress arthritis induced by adjuvant^[4], antigen^[5], pristane^[6] and collagen^[7] in mice and rats. Moreover, several clinical trials based on the results from those experimental animal systems, have been conducted to test the feasibility of using oral tolerance in the treatment of RA^[8,9]. However, it was reported that oral administration of CII in a low dose of 10 μg for 10 times demonstrated a doubtful effect on murine collagen-induced arthritis (CIA) model^[10]. In clinical trials, oral administration of CII showed no efficacy in human arthritis given along with existing treatment^[11] and moreover, the Peyer's patches (pp) in the gut-associated lymphoid tissue (GALT) were considered to mediate oral tolerance^[12]. As we know, nonsteroidal anti-inflammatory drugs (NSAIDs) including meloxicam, which have been usually considered as the main drugs in the management of RA, could induce digestive lesions^[13,14], and it might be an important reason for the invalidation of oral administration of CII. Therefore, nasal administration of CII should be considered as an alternative.

Adjuvant arthritis (AA) in rats is an experimental model that shares some features with human RA, such as swelling, cartilage degradation and loss of joint function^[15]. In the present study, therefore, AA rats with or without intragastrically administration of meloxicam were used to compare the curative effects of oral and nasal administration of CII in rats with or without intestinal lesions. Based on the results of our report that oral administration of CII suppressed pro-inflammatory mediator production by synovocytes in rats with adjuvant arthritis from 5 to 500 $\mu\text{g}/\text{kg}$ ^[12], we chose the single dose of 20 $\mu\text{g}/\text{kg}$ in the present study.

Diamine oxidase (DAO) is an intracellular enzyme with a high activity existing in intestinal villous cells and can catalyze the oxidation of diamines such as histamine, putrescine and cadaverine in both human beings and all other mammals. The activity of DAO in intestinal mucosa decreases when its cells are injured. Thus the determination of the DAO activity of intestinal mucosa can reflect the changes in its cellular integrity^[16]. Myeloperoxidase (MPO) plays a fundamental role in oxidant production by neutrophils and is considered to be a major effector in the tissue damage^[17]. In our studies, MPO and DAO were used as markers of intestinal dysfunction.

The purpose of the present study was to compare the curative effects of oral and nasal administration of CII in AA rats with or without intestinal lesions induced by meloxicam.

MATERIALS AND METHODS

Animals

Male Sprague-Dawley (SD) rats weighting 147 ± 25 g were purchased from Shanghai BK Experimental Animal Center (Grade II, Certificate No D-65). All rats were housed, five per cage and fed a standard laboratory chew and water and kept on a 12 h dark/12 h light cycle at a constant temperature of 20 ± 5 °C. All experimental protocols described in this study were approved by the Ethics Review Committee for Animal Experimentation of Institute of Clinical Pharmacology, Anhui Medical University.

Drugs and materials

Meloxicam (batch number 020401), nasal chicken CII (batch number 00031004) and oral chicken CII (batch number 00031002) were obtained from Shanghai Institute of Herb and Bio-medical Engineering and dissolved in sterile water containing 5 g/L carboxymethylcellulose (CMC-Na) solution. Dimethyl sulfoxide (batch number 000601) was obtained from Shanghai Vitriolic Factory. Bacillus Calmette Guerin (BCG) was obtained from Shanghai Biochemical Factory. Collagenase type II, trypsin, 3-(4,5-dimethylthiazol-2-thiazolyl)-2,5-diphenyl-2H tetrazolium bromide (MTT), RPMI 1640 medium, lipopolysaccharide (LPS), horseradish peroxidase, cadaverine dihydrochloride, diamine oxidase (DAO) and *O*-dianisidine were purchased from Sigma Chemical Co. (St. Louis, MO, USA).

Induction and evaluation of AA

Complete Freund's adjuvant (CFA) was prepared by suspending heat-killed BCG in liquid paraffin at 10 mg/mL. AA was induced by a single intradermal injection of 100 μ L of CFA into the left hind paw. On d 0, 14, 16, 20, 24 and 28 after immunization, the right hind paw volume was measured with a water replacement plethysmometer (Mukomachi Kiai CD, Japan). Paw swelling (mL) was calculated by taking away the paw volume on d 0 from the related one on d 14, 16, 20, 24 and 28.

Drug treatment

The rats with AA were divided randomly into six groups which included AA model, AA model+meloxicam, AA model+oral CII, AA model+nasal CII, AA model+meloxicam+oral CII and AA model+meloxicam+nasal CII. From d 14 after immunization, the rats were fasted for 12 h and then treated with meloxicam (1.5 mg/kg body weight) intragastrically for 7 d. The rats in normal group, AA group, AA model+oral CII group and AA+nasal CII group, were treated with an equal amount of vehicle. From d 21 after immunization, the rats were treated with oral or nasal administration of CII (20 μ g/kg body mass) for 7 d. The rats in normal group, AA group and AA+meloxicam group, were treated with an equal amount of vehicle.

Evaluation of intestinal lesions

Rats were sacrificed on day 29 after immunization. The small intestines were removed, spread out on filter paper and opened by a longitudinal incision along the antimesenteric side. The length and width of each lesion were observed and the extent of haemorrhage was also observed according to scale scores 0-2: 0, absence; 1, slight haemorrhage; 2, severe haemorrhage.

Synoviocyte proliferation

Synovial tissue from rat knees was excised and dispersed with sequential incubation of 4 g/L collagenase type II and 2.5 g/L trypsin and then synoviocytes were suspended in RPMI-1640

medium with 200 mL/L fetal bovine serum (FBS) at a concentration of 1×10^6 cells/mL. In 96-well plates, 100 μ L of synoviocyte suspension (1×10^5 cells/well) was cultured in triplicate with 100 μ L of LPS (10 mg/L) in RPMI-1640 medium (pH7.0) containing 200 mL/L heat-inactivated FBS, 100 U/mL penicillin, 100 g/L streptomycin, 2 mmol/L *L*-glutamine, 5×10^{-5} mol/L 2-mercaptoethanol and 25 mmol/L HEPES. After cultured for 48 h at 37 °C in humidified atmosphere containing 50 mL/L CO₂ in air, proliferation of synoviocytes was measured by the MTT colorimetric method^[18]. In brief, 48 h later, MTT was dissolved in phosphate buffered saline (PBS) at a dose of 5 mg/mL and added to all wells (10 μ L/well), then the plates were incubated at 37 °C in humidified atmosphere containing 50 mL/L CO₂ for an additional 4 h. After incubation, the cells were centrifuged at 1000 r/min for 10 min and all the supernatants were discarded. Then 200 μ L of dimethyl sulfoxide was added to each well, and the plates were read 30 sec later in an ELISA plate reader at a wavelength of 490 nm. The absorbance (*A*) of each well was regarded as the degree of synoviocyte proliferation.

Histological examination

The right legs and hind paws of rats were removed and fixed with 100 g/L paraformaldehyde in PBS, and then decalcified for 10 d with ethylene diamine tetraacetic acid (EDTA) and embedded in paraffin for histologic analysis. The paraffin sections were stained with hematoxylin and eosin. The slides were evaluated histologically by two independent observers, and the gradation of arthritis was scored from 0 to 4 according to the intensity of lining layer hyperplasia, mononuclear cell infiltration, and pannus formation, as described previously^[19]: 0, normal ankle joint; 1, normal synovium with occasional mononuclear cells; 2, definite arthritis, a few layers of flat to rounded synovial lining cells and scattered mononuclear cells and dense infiltration with mononuclear cells; 3, clear hyperplasia of the synovium with three or more layers of loosely arranged lining cells and dense infiltration with mononuclear cells; 4, severe synovitis with pannus and erosions of articular cartilages and subchondral bones.

MPO bioassay

Animals were sacrificed and their small intestines were flushed with 10 mL of sterile saline, followed by separation from bodies. After dried with filter paper, 0.5 g of intestinal specimens was weighed and placed in 5 mL of ice-cold potassium phosphate buffer (pH 6.0) with 5 g/L hexadecyl-trimethylammonium bromide. The specimens were homogenized for 20 s (2×10 s) and sonicated for 30 s (3×10 s) and centrifuged at 12000 g for 15 min at 4 °C. The supernatant was spectrophotometrically assayed for MPO activity by measuring the change in absorbance (at 460 nm) over time. The assay buffer consisted of 50 mmol/L potassium phosphate, pH 6.0 (50 mL), 0.83 mL of H₂O₂ (3 mL/L solution), and 8.34 mg of *O*-dianisidine hydrochloride. The supernatant was mixed at 1:80 (supernatant: assay buffer). MPO units were expressed as $\Delta A/(\text{min} \cdot \text{g})$.

DAO bioassay

Intestinal DAO activity was determined as follows. In brief, to 0.5 mL homogenate of intestinal specimens gained according to the above method or 0.5 mL diluted standard solution, 3 mL of PBS (0.2 mol/L, pH 7.2), 0.1 mL of horseradish peroxidase (4 μ g), 0.1 mL of DAO (500 μ g), and 0.1 mL of dianisidine were added. After mixed, the mixture was incubated in a water bath at 37 °C for 30 min, then the absorbance value at 436 nm (*A*₄₃₆) was recorded after rested for 5 min in the air. The DAO activities were calculated according to the standard curve. Protein activities of the tissue homogenates were determined with Lowry's method^[20]. DAO units were expressed as A/mg pro.

Statistical analysis

Results were expressed as mean±SD, and *t*-test was used to make comparisons between the groups. *P*<0.05 was considered statistically significant.

RESULTS

Intestinal lesions induced by meloxicam

As shown in Figure 1, intragastrical administration of meloxicam (1.5 mg/kg) for 7 d induced multiple intestinal lesions in AA rats. In normal control rats (Figure 1A), AA rats (Figure 1B), AA rats treated with oral CII (Figure 1D) and AA rats treated with nasal CII (Figure 1E), haemorrhage was not observed in antimesenteric side of small intestine (grade 0). In AA rats given meloxicam intragastrically (Figure 1C), AA+meloxicam rats treated with oral CII (Figure 1F) and AA+meloxicam rats treated with nasal CII (Figure 1G), severe haemorrhage was observed in antimesenteric side of small intestine (grade 2). After the animals were treated with oral or nasal administration of CII (20 µg/kg) for 7 d, development of these lesions was not prevented.

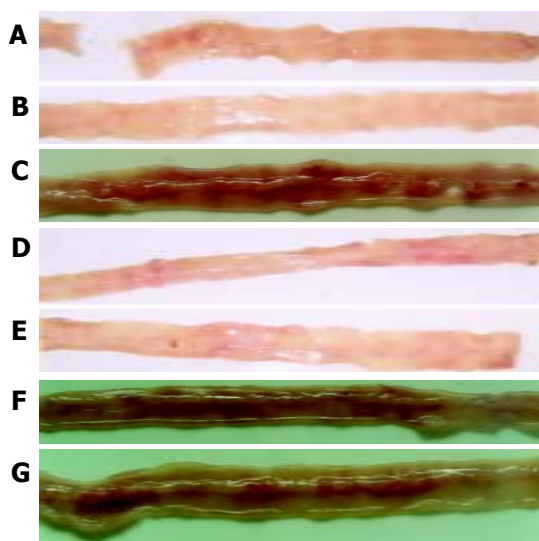


Figure 1 Intestinal lesions induced by meloxicam. A: Normal control rats; B: AA rats; C: AA rats given meloxicam intragastrically; D: AA rats treated with oral CII; E: AA rats treated with nasal CII; F: AA+meloxicam rats treated with oral CII; and G: AA+meloxicam rats treated with nasal CII.

DAO activities in intestinal homogenates

The levels of DAO in intestinal homogenates are shown in Table 1. There was a significant decrease of intestinal DAO activities in AA+meloxicam group (*P*<0.01) and AA model group (*P*<0.01) compared with normal group. DAO activities of intestinal

homogenates in AA+meloxicam group were significantly less than those in AA rats (*P*<0.01). Oral or nasal administration of CII had no significant effects on DAO changes.

MPO activities in intestinal homogenates

The levels of MPO in intestinal homogenates are shown in Table 1. There was a significant increase of intestinal MPO activities in AA+meloxicam group compared with normal control (*P*<0.01). Oral or nasal administration of CII had no significant effects on MPO changes.

Table 1 Effects of oral and nasal administration of CII on activities of intestinal MPO and DAO in AA rats with or without intragastrical administration of meloxicam (*n* = 12, mean±SD)

Groups	DAO (A/mg pro)	MPO (ΔA/(min·g))
Normal	0.37±0.065	99.47±22.54
AA model	0.26±0.031 ^b	139.80±25.14
AA model+meloxicam	0.15±0.032 ^{ab}	165.42±21.27 ^b
AA model+oral CII	0.27±0.051	137.15±26.32
AA model+nasal CII	0.28±0.029	132.17±23.18
AA model+meloxicam +oral CII	0.15±0.052 ^{ab}	159.25±33.36 ^b
AA model+meloxicam +nasal CII	0.16±0.029 ^{ab}	152.29±27.20 ^b

^a*P*<0.05 vs AA model; ^b*P*<0.01 vs normal control.

Effects of oral or nasal administration of CII on secondary arthritis in AA rats with or without intragastrical administration of meloxicam

As shown in Table 2, secondary arthritis appeared on d 14, and maintained to d 28 after immunization in AA rats (*P*<0.01). In AA+meloxicam rats, hind paw secondary swellings were suppressed on d 20 (*P*<0.05). The hind paw secondary swellings were suppressed on d 20 in AA model+meloxicam +oral CII group and AA model+meloxicam+nasal CII group (*P*<0.05). Oral treatment with CII (20 µg/kg body mass) significantly suppressed hind paw secondary swelling not only on d 24 and 28 in AA rats (*P*<0.05), but also on d 24 in AA rats with intestinal lesions induced by meloxicam (*P*<0.05). The effects of oral CII were more obvious in AA model than in AA model with intestinal lesions on d 28. While nasal treatment with CII at the same dose significantly suppressed hind paw secondary swelling on d 24 and 28 in both AA rats and AA rats with intestinal lesions (*P*<0.01). The effects of nasal CII in AA model were similar to those in AA+meloxicam model, and the effects of nasal CII were more efficient than those of oral CII both in AA model and in AA+meloxicam model (*P*<0.05).

Table 2 Effects of oral and nasal administration of CII on hind paw secondary swelling in AA rats with or without intragastrical administration of meloxicam (*n* = 12, mean±SD)

Groups	Dose (µg/kg)	d 14	d 16	d 20	d 24	d 28
Normal	---	0.07±0.05	0.12±0.04	0.19±0.04	0.23±0.03	0.26±0.03
AA model	---	0.41±0.31 ^d	0.63±0.16 ^d	0.99±0.21 ^d	1.22±0.27 ^d	1.16±0.21 ^d
AA model+meloxicam	---	0.29±0.32 ^a	0.45±0.27 ^a	0.68±0.18 ^{ad}	0.97±0.49 ^d	0.99±0.32 ^d
AA model+oral CII	20	0.39±0.12	0.59±0.27	0.97±0.15	0.81±0.17 ^a	0.79±0.21 ^a
AA model+nasal CII	20	0.38±0.12	0.63±0.13	1.03±0.10	0.69±0.07 ^b	0.48±0.09 ^{bc}
AA model+meloxicam+oral CII	20	0.31±0.09	0.46±0.26	0.70±0.12 ^a	0.79±0.31 ^a	0.95±0.25
AA model+meloxicam+nasal CII	20	0.32±0.16	0.43±0.19	0.73±0.22 ^a	0.61±0.21 ^b	0.57±0.17 ^{bc}

^a*P*<0.05 vs AA model; ^b*P*<0.01 vs AA model; ^c*P*<0.05 vs AA model + oral CII; ^d*P*<0.01 vs normal control; ^e*P*<0.05 vs AA model+meloxicam+oral CII.

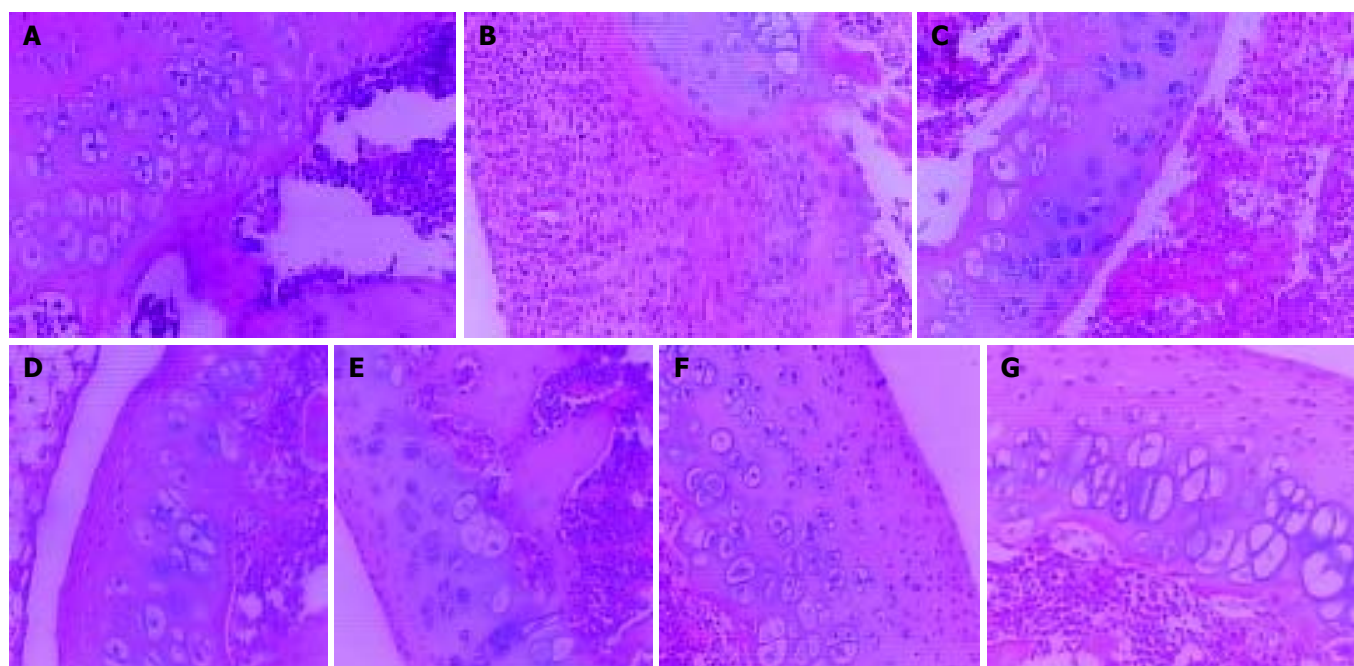


Figure 2 Effects of oral or nasal administration of CII on knee joint histopathology in AA rats with or without intragastrical administration of meloxicam (HE stain, $\times 100$). A: Normal control rats (grade 0); B: AA rats (grade 4); C: AA rats given meloxicam intragastrically (grade 4); D: AA rats treated with oral CII (grade 3); E: AA rats treated with nasal CII (grade 2); F: AA+meloxicam rats treated with oral CII (grade 3); and G: AA+meloxicam rats treated with nasal CII (grade 2).

Effects of oral or nasal administration of CII on synoviocyte proliferation in AA rats with or without intragastrical administration of meloxicam

As shown in Table 3, synoviocyte proliferation in AA rats and AA+meloxicam rats was increased ($P < 0.01$). Oral or nasal administration of CII (20 $\mu\text{g}/\text{kg}$) for 7 d significantly suppressed synoviocyte proliferation ($P < 0.01$) in AA rats. In AA rats with intestinal lesions, nasal administration of CII (20 $\mu\text{g}/\text{kg}$) could also significantly suppress synoviocyte proliferation ($P < 0.01$), while oral administration of CII at the same dosage suppressed synoviocyte proliferation at a lower degree ($P < 0.05$). There was a significant difference between degrees of synoviocyte proliferation in AA rats with intestinal lesions treated by oral CII and those in the same model treated by nasal CII ($P < 0.05$).

Table 3 Effects of oral and nasal administration of CII on synoviocytes proliferation in AA rats with or without intragastrical administration of meloxicam ($n = 12$, mean \pm SD)

Groups	Dose ($\mu\text{g}/\text{kg}$)	Synoviocytes proliferation (A_{490})
Nomal	-	0.27 \pm 0.024
AA model	-	0.32 \pm 0.045 ^d
AA model+meloxicam	-	0.31 \pm 0.025 ^d
AA model+oral CII	20	0.27 \pm 0.041 ^b
AA model+nasal CII	20	0.24 \pm 0.048 ^b
AA model I+meloxicam+oral CII	20	0.29 \pm 0.047 ^a
AA model+meloxicam+nasal CII	20	0.25 \pm 0.041 ^{bc}

^a $P < 0.05$ vs AA model; ^b $P < 0.01$ vs AA model; ^d $P < 0.01$ vs normal control; ^c $P < 0.05$ vs AA model+meloxicam+oral CII.

Effects of oral or nasal administration of CII on knee joint histopathology in AA rats with or without intragastrical administration of meloxicam

In normal rats, synoviocytes were monolayer (Figure 2A). In AA rats, synoviocytes proliferated three to eight layers and

became ovalis types, and articular cartilages were destructed and infiltrated with inflammatory cells. The hyperplastic synovial membranes in AA rats formed a large number of fibroblasts and new blood vessels. Proliferation of collagen fibrils was found under synovial membranes of AA rats (Figure 2B). In AA rats given meloxicam intragastrically, knee joint histopathology was similar to that in AA rats (Figure 2C). In AA rats treated with oral CII, hyperplastic synoviocytes decreased to two or three layers (Figure 2D). In AA rats treated with nasal CII, a few of hyperplastic fiber cells under synovial membranes could be found (Figure 2E). In AA+meloxicam rats treated with oral CII, synovial hyperplasia was observed and articular cartilages were destroyed and infiltrated with inflammatory cells (Figure 2F). In AA+meloxicam rats treated with nasal CII, a few of hyperplastic fiber cells under synovial membranes and partially reversed articular cartilage destruction could be found (Figure 2G).

Oral or nasal administration of CII could ameliorate the pathologic changes in AA rats or AA+meloxicam rats, but oral administration of CII showed limited efficacy on suppressing the histopathological degradation in AA model with intestinal lesions.

DISCUSSION

In this study, it was found that intragastric administration of meloxicam (1.5 mg/kg) could induce multiple intestinal lesions in AA rats. The activities of DAO in intestinal homogenates were decreased and the activities of MPO were increased. Oral or nasal administration of CII at a dose of 20 $\mu\text{g}/\text{kg}$ could suppress secondary hind paw swelling, synoviocyte proliferation and histopathological degradation in AA model and AA+meloxicam model. Moreover, oral administration of CII showed the limited efficacy on arthritis in AA+meloxicam model and curative effects of nasal CII were shown to be more efficient in comparison with oral CII both in AA model and AA+meloxicam model.

Just like RA, AA is a chronic disease and the ongoing disease can be blocked using antibodies to T cells. They are associated with major histocompatibility complex (MHC) and the primary inflammatory attack is directed to diarthrodial peripheral joints^[21].

Thus, development of mucosal tolerance methods for treatment of RA is suitable and could be found successfully both in humans^[22,23] and in animal models induced with various heterologous antigens^[4-6,24]. Histopathological study showed that oral administration of CII resulted in reduction of synovial hyperplasia, mononuclear infiltration, pannus formation and cartilage erosions^[6]. Results from the present study also showed that oral CII suppressed secondary paw swelling, synoviocyte proliferation and histopathological changes in AA rats. Furthermore, clinical studies with oral administration of heterologous CII in RA were carried out and had disputable results^[8,22]. Barnett *et al.*^[25] found that very low doses tended to give an overall ameliorative effect, whereas higher doses were negative. In addition, intranasal administration of CII could ameliorate ongoing arthritis in pristane-induced arthritis (PIA), collagen-induced arthritis (CIA) and AA^[26]. The use of nasal instead of oral administration of the autoantigens has been shown to be more efficient and to require lower tolerogen doses, as demonstrated in several models including CIA in mice^[27]. It was also demonstrated that nasal administration of CII in murine CIA model more efficiently inhibited the induction of CIA and CII-specific immune responses than oral administration^[10]. Our present study indicated that nasal CII could suppress secondary paw swelling, synoviocyte proliferation and histopathological changes in AA rats and was superior to oral CII.

Meloxicam is a NSAID belonging to the enolic acid group of the oxamic family^[28]. As a cyclooxygenase-2 inhibitor, meloxicam has been considered with a good gastric tolerance^[29,30]. But it was also reported that meloxicam could induce gastric lesions^[31]. Neutrophils, which secrete MPO, appear to be the main effector cells in meloxicam-induced small intestinal damage^[32]. On the other hand, there are two major mechanisms which have been put forward to explain the oral tolerance: active suppression or the antigen specific induction of regulatory cells and T cell clonal anergy/deletion^[33,34]. Cells from PP in GALT were reported to mediate the induction of active suppression^[35]. PP cell dysfunction induced by NSAIDs might be the main mechanism of the limited therapeutic effects of oral CII in the suppression of RA in clinical trials. So far, there are few reports to determine it.

In our study, we found that meloxicam (1.5 mg/kg) could induce multiple intestinal lesions in AA rats, and in this model, the activities of DAO were decreased and the activities of MPO were increased. We also found that meloxicam had little effect on AA rats from d 24. These results also indicated that there was a functional turbulence in intestinal systems of AA rats. Furthermore, we found that the effects of oral CII were more obvious in AA model than in AA model with intestinal lesion induced by meloxicam. However, the effects of nasal CII were not influenced by meloxicam in AA rats with intestinal lesions. The results suggested that nasal CII was more efficient than oral CII both in AA rats and in AA rats with intestinal lesions.

In conclusion, at the dose of 20 µg/kg, oral administration of CII has a limited efficacy on arthritis in AA+meloxicam model and the effects of nasal administration of CII on AA are more efficient than that of oral administration of CII both in AA rats and in AA rats with intestinal lesions induced by meloxicam.

REFERENCES

- 1 Strand V, Kavanaugh AF. The role of interleukin-1 in bone resorption in rheumatoid arthritis. *Rheumatology* 2004; **43** (Suppl 3): III10-16
- 2 Blake SM, Swift BA. What next for rheumatoid arthritis therapy? *Curr Opin Pharmacol* 2004; **4**: 276-280
- 3 Wells HG. Studies on the chemistry of anaphylaxis (III). Experiments with isolated proteins, especially those of the hen's egg. *J Infect Dis* 1911; **9**: 147-171
- 4 Hu Y, Zhao W, Qian X, Zhang L. Effects of oral administration of type II collagen on adjuvant arthritis in rats and its mechanisms. *Chin Med J* 2003; **116**: 284-287
- 5 Yoshino S, Quattrocchi E, Weiner HL. Suppression of antigen-induced arthritis in Lewis rats by oral administration of type II collagen. *Arthritis Rheum* 1995; **38**: 1092-1096
- 6 Thompson SJ, Thompson HS, Harper N, Day MJ, Coad AJ, Elson CJ, Staines NA. Prevention of pristane-induced arthritis by the oral administration of type II collagen. *Immunology* 1993; **79**: 152-157
- 7 Min SY, Hwang SY, Park KS, Lee JS, Lee KE, Kim KW, Jung YO, Koh HJ, Do JH, Kim H, Kim HY. Induction of IL-10-producing CD4+CD25+T cells in animal model of collagen-induced arthritis by oral administration of type II collagen. *Arthritis Res Ther* 2004; **6**: R213-219
- 8 Choy EH, Scott DL, Kingsley GH, Thomas S, Murphy AG, Staines N, Panayi GS. Control of rheumatoid arthritis by oral tolerance. *Arthritis Rheum* 2001; **44**: 1993-1997
- 9 Myers LK, Higgins GC, Finkel TH, Reed AM, Thompson JW, Walton RC, Hendrickson J, Kerr NC, Pandya-Lipman RK, Shlopov BV, Stastny P, Postlethwaite AE, Kang AH. Juvenile arthritis and autoimmunity to type II collagen. *Arthritis Rheum* 2001; **44**: 1775-1781
- 10 Higuchi K, Kweon MN, Fujihashi K, McGhee JR, Kiyono H. Comparison of nasal and oral tolerance for the prevention of collagen induced murine arthritis. *J Rheumatol* 2000; **27**: 1038-1044
- 11 Postlethwaite AE. Can we induce tolerance in rheumatoid arthritis? *Curr Rheumatol Rep* 2001; **3**: 64-69
- 12 Ding CH, Li Q, Xiong ZY, Zhou AW, Jones G, Xu SY. Oral administration of type II collagen suppresses pro-inflammatory mediator production by synoviocytes in rats with adjuvant arthritis. *Clin Exp Immunol* 2003; **132**: 416-423
- 13 Combe B, Flipo RM. What treatments can reduce the digestive complications of NSAIDs. *Presse Med* 2003; (37 Pt 2)**32**: S33-37
- 14 Hawkey CJ, Wilson I, Naesdal J, Langstrom G, Swannell AJ, Yeomans ND. Influence of sex and *Helicobacter pylori* on development and healing of gastroduodenal lesions in non-steroidal anti-inflammatory drug users. *Gut* 2002; **51**: 344-350
- 15 Jacobson PB, Morgan SJ, Wilcox DM, Nguyen P, Ratajczak CA, Carlson RP, Harris RR, Nuss M. A new spin on an old model: *in vivo* evaluation of disease progression by magnetic resonance imaging with respect to standard inflammatory parameters and histopathology in the adjuvant arthritic rat. *Arthritis Rheum* 1999; **42**: 2060-2073
- 16 Peng X, Yan H, You Z, Wang P, Wang S. Effects of enteral supplementation with glutamine granules on intestinal mucosal barrier function in severe burned patients. *Burns* 2004; **30**: 135-139
- 17 Takeuchi K, Tanaka A, Ohno R, Yokota A. Role of COX inhibition in pathogenesis of NSAID-induced small intestinal damage. *J Physiol Pharmacol* 2003; **54**(Suppl 4): 165-182
- 18 Russell CA, Vindelov LL. Optimization and comparison of the MTT assay and the 3H-TdR assay for the detection of IL-2 in helper T cell precursor assays. *J Immunol Methods* 1998; **217**: 165-175
- 19 Chen Q, Wei W. Effects and mechanisms of glucosides of *Chaenomeles speciosa* on collagen-induced arthritis in rats. *Int Immunopharmacol* 2003; **3**: 593-608
- 20 Tomazic-Jezic VJ, Truscott W. Identification of antigenic and allergenic natural rubber latex proteins by immunoblotting. *J Immunoassay Immunochem* 2002; **23**: 369-383
- 21 Mimran A, Mor F, Carmi P, Quintana FJ, Rotter V, Cohen IR. DNA vaccination with CD25 protects rats from adjuvant arthritis and induces an antiertotypic response. *J Clin Invest* 2004; **113**: 924-932
- 22 Choy EH, Scott DL, Kingsley GH, Thomas S, Murphy AG, Staines N, Panayi GS. Control of rheumatoid arthritis by oral tolerance. *Arthritis Rheum* 2001; **44**: 1993-1997
- 23 Cazzola M, Antivalle M, Sarzi-Puttini P, Dell'Acqua D, Panni B, Caruso I. Oral type II collagen in the treatment of rheumatoid arthritis. A six-month double blind placebo-controlled study. *Clin Exp Rheumatol* 2000; **18**: 571-577
- 24 Bardos T, Czipri M, Vermes C, Zhang J, Mikecz K, Glant TT. Continuous nasal administration of antigen is critical to main-

- tain tolerance in adoptively transferred autoimmune arthritis in SCID mice. *Clin Exp Immunol* 2002; **29**: 224-231
- 25 **Barnett ML**, Kremer JM, St Clair EW, Clegg DO, Furst D, Weisman M, Fletcher MJ, Chasan-Taber S, Finger E, Morales A, Le CH, Trentham DE. Treatment of rheumatoid arthritis with oral type II collagen. Results of a multicenter, double-blind, placebo-controlled trial. *Arthritis Rheum* 1998; **41**: 290-297
- 26 **Lu S**, Holmdahl R. Different therapeutic and bystander effects by intranasal administration of homologous type II and type IX collagens on the collagen-induced arthritis and pristane-induced arthritis in rats. *Clin Immunol* 1999; **90**: 119-127
- 27 **Garcia G**, Komagata Y, Slavin AJ, Maron R, Weiner HL. Suppression of collagen-induced arthritis by oral or nasal administration of type II collagen. *J Autoimmun* 1999; **13**: 315-324
- 28 **Albengres E**, Urien S, Barre J, Nguyen P, Bree F, Jolliet P, Tillement JP, Tsai RS, Carrupt PA, Testa B. Clinical pharmacology of oxicams: new insights into the mechanisms of their dose-dependent toxicity. *Int J Tissue React* 1993; **15**: 125-134
- 29 **Cryer B**, Dubois A. The advent of highly selective inhibitors of cyclooxygenase-a review. *Prostaglandins Other Lipid Mediat* 1998; **56**: 341-361
- 30 **Layton D**, Harris S, Shakir S. Reply: Re: Layton et al. Comparison of the incidence rates of selected gastrointestinal events reported for patients prescribed rofecoxib and meloxicam in general practice in England using prescription-event monitoring data. *Rheumatology* 2004; **43**: 681-682
- 31 **Laporte JR**, Ibanez L, Vidal X, Vendrell L, Leone R. Upper gastrointestinal bleeding associated with the use of NSAIDs: newer versus older agents. *Drug Saf* 2004; **27**: 411-420
- 32 **Villegas I**, Martin MJ, La Casa C, Motilva V, De La Lastra CA. Effects of oxicam inhibitors of cyclooxygenase on oxidative stress generation in rat gastric mucosa. A comparative study. *Free Radic Res* 2002; **36**: 769-777
- 33 **Song F**, Whitacre CC. The role of the gut lymphoid tissue in induction of oral tolerance. *Curr Opin Investig Drugs* 2001; **2**: 1382-1386
- 34 **Wu HY**, Weiner HL. Oral tolerance. *Immunol Res* 2003; **28**: 265-284
- 35 **Toussirot EA**. Oral tolerance in the treatment of rheumatoid arthritis. *Curr Drug Targets Inflamm Allergy* 2002; **1**: 45-52

Edited by Kumar M and Wang XL Proofread by Xu FM

• CLINICAL RESEARCH •

Expansion of endothelial surface by an increase of vessel diameter during tumor angiogenesis in experimental hepatocellular and pancreatic cancer

Eduard Ryschich, Eduard Schmidt, Sasa-Marcel Maksan, Ernst Klar, Jan Schmidt

Eduard Ryschich, Eduard Schmidt, Sasa-Marcel Maksan, Ernst Klar, Jan Schmidt, Department of Surgery, University of Heidelberg, Heidelberg, Germany

Correspondence to: Jan Schmidt, M.D., Department of Surgery, University of Heidelberg, Im Neuenheimer Feld 110, 69120 Heidelberg, Germany. jan_schmidt@med.uni-heidelberg.de

Telephone: +49-6221-562890 **Fax:** +49-6221-565331

Received: 2003-08-26 **Accepted:** 2004-01-20

Abstract

AIM: A low vessel density is a common feature of malignant tumors. We suggested that the expansion of vessel diameter might reconstitute the oxygen and nutrient's supply in this situation. The aim of the present study was to compare the number and diameter of blood vessels in pancreatic and liver carcinoma with normal tissue.

METHODS: Tumor induction of pancreatic (DSL6A) or hepatocellular (Morris-hepatoma) carcinoma was performed in male Lewis (pancreatic cancer) and ACI (hepatoma) rats by an orthotopic inoculation of solid tumor fragments (pancreatic cancer) or tumor cells (hepatoma). Six weeks (pancreatic cancer) or 12 d (hepatoma) after tumor implantation, the tumor microvasculature as well as normal pancreatic or liver blood vessels were investigated by intravital microscopy. The number of perfused blood vessels in tumor and healthy tissue was assessed by computer-assisted image analysis.

RESULTS: The vessel density in healthy pancreas (565 ± 89 n/mm²) was significantly higher compared to pancreatic cancer (116 ± 36 n/mm²) ($P < 0.001$). Healthy liver showed also a significantly higher vessel density (689 ± 36 n/mm²) compared to liver carcinoma (286 ± 32 n/mm²) ($P < 0.01$). The comparison of diameter frequency showed a significant increase of vessel diameter in both malignant tumors compared to normal tissue ($P < 0.05$).

CONCLUSION: The expansion of endothelial cells during tumor angiogenesis is accompanied to a large extent by an increase of vessel diameter rather than by formation of new blood vessels. This may be a possible adaptive mechanism by which experimental pancreatic and hepatocellular cancers expand their endothelial diffusion surface of endothelium to compensate for inadequate neoangiogenesis.

Ryschich E, Schmidt E, Maksan SM, Klar E, Schmidt J. Expansion of endothelial surface by an increase of vessel diameter during tumor angiogenesis in experimental hepatocellular and pancreatic cancer. *World J Gastroenterol* 2004; 10(21): 3171-3174
<http://www.wjgnet.com/1007-9327/10/3171.asp>

INTRODUCTION

Angiogenesis, defined as proliferation of endothelial cells and

subsequent formation of new blood vessels from pre-existing vessels, is a characteristic feature of numerous pathological processes, including cancer^[1,2]. Tumor growth depends on a continuous blood supply to cover increasing requirements for nutrients and oxygen. During tumor neovascularization, new capillaries are recruited from the existing microvasculature, a process that is controlled by positive and negative regulators of blood vessel growth^[3]. In contrast to the angiogenesis occurring in wound healing, the tumor angiogenesis is characterized by a discordance between pro- and anti-angiogenic factors. This discordant process of tumor angiogenesis leads to the formation of a microvascular system with a typically distorted vessel architecture^[4,5], and consequently irregular flow patterns and heterogeneous oxygen supply^[6,7] resulting in hypoxia^[8,9]. These parameters contribute to a unique tumor microenvironment which in turn modulates the therapeutic responsiveness of solid tumors, e.g., towards chemotherapeutic agents or radiation therapy^[10,11].

Our previous studies reported that the increased vessel diameter was an important feature of tumor microangiogenesis in pancreatic^[12] and hepatocellular^[13] cancer of the rat. This feature was not only specific for transplantable tumor models and was found in spontaneous pancreatic tumors in transgenic mice^[14]. We showed that the vessel dilation was the first detectable stage of ongoing angiogenesis during multistep tumorigenesis which preceded vessel sprouting^[14]. These observations encouraged us to start a detailed investigation of tumor blood vessels by a combination of different techniques including intravital microscopy and immunohistochemistry. We hypothesized that the vessel dilation indicated a possible adaptive process, which may help the tumor to expand their diffusion surface of endothelium and to compensate for the inadequate supply with oxygen and nutrients. In the present study, we used intravital microscopy and immunohistochemistry to investigate this phenomenon in normal and malignant pancreatic tissues as well as in hepatic tissue of rats. The present study demonstrated that the decrease of vessel density in experimental pancreatic and liver carcinoma was accompanied with an increase of vessel diameter.

MATERIALS AND METHODS

Tumor inoculation

Established cell lines of pancreatic duct-like (DSL6A)^[15] and hepatocellular carcinoma (Morris-hepatoma MH-3924A)^[13] of rats were used. Since the expression profile of tumor cells was strongly dependent on the site of growth, e.g. implantation^[16,17] we decided to inoculate the tumors orthotopically which ensured the appropriate microenvironment for tumor cell growth. Twelve male Lewis rats (160-180 g) were used for the inoculation of pancreatic carcinoma. Hepatocellular carcinomas were inoculated on 12 male ACI rats (220-250 g). Each animal was anesthetized with intramuscular injection of xylazine (10 mg/kg, Rompun®, Bayer, Leverkusen, Germany) and ketamine (40 mg/kg, Ketanest®, Parke Davis, Berlin, FRG).

Tumor implantation was performed as previously described

for pancreatic^[12] and hepatocellular^[13] carcinoma. For the inoculation of pancreatic cancer, two sterile polymethylmethacrylate (PMMA)-plates (Ø 11 mm, Glasflex, Stirling, NJ, USA) were applied in "sandwich-technique" on both sides of the pancreatic head. The tumor of approximately 1 mm³ was harvested from a subcutaneous parent tumor of a syngeneic rat and interposed intrapancreatically between the plates. Hepatocellular carcinomas were induced by a subcapsular injection of tumor cells (Morris hepatoma MH-3924A, 0.01 mL, 0.5×10⁶ cells) into the left upper liver lobe. Major steps of both models are summarized in Table 1.

Table 1 Summary of tumor models used in present study

	Pancreatic cancer	Hepatocellular cancer
Tumor cell line	DSL6A	Morris hepatoma 3924A
Syngeneic strain	Lewis	ACI
Tumor inoculation	Solid tumor fragment	Cell suspension
Time after inoculation	6 wk	12 d

Intravital microscopy

Intravital microscopy was performed 12 d after inoculation for hepatocellular carcinoma and 6 wk after inoculation for pancreatic cancer when tumors reached a diameter of 8-10 mm. All animals were re-anaesthetized as described above. A teflon catheter (I.D. 0.5 mm, B.Braun AG, Melsungen, FRG) was inserted into the right internal jugular vein for venous access. Another catheter was placed into the left carotid artery for blood sampling and monitoring of cardiovascular parameters. The abdomen was opened by midline incision. The animal was placed on a special stage automatically maintained at 37 °C. The tumor was macroscopically identified. The tumor bearing pancreatic head was immobilized in a temperature-controlled (37 °C) immersion chamber containing Ringer's solution. For the intravital microscopy of hepatocellular carcinoma, the tumor bearing liver lobe was placed on a rubber stage and superfused with Ringer's solution (37 °C).

For intravital microscopy, the entire preparation was placed under a fluorescence microscope (Leica GmbH, Wetzlar, FRG). The fluorescence filter with excitation 450-490 nm and emission 520 nm was used. After the preparation was completed, all animals received an intravenous injection of 50 mg/kg of FITC-labeled albumin (Sigma Chemicals Co., St. Louis, MO, USA) dissolved in 1 mL saline. This fluorescent plasma marker ensured the maximal contrast of blood vessels and was utilized for the measurement of vessel diameter and vessel density. The microcirculatory images were transmitted by a video camera (CF 8/1, Kappa GmbH, Gleichen, FRG) to a monitor (PVM-1440 M, Sony, Tokyo, Japan) and recorded on a videorecorder (sVHS, AG-7 350-E, Panasonic, Osaka, Japan) for subsequent off-line analysis. After the experiment, the tumors and a fragment of normal tissue were harvested and frozen immediately in liquid nitrogen. The evaluation of vessel diameter and density in tumor microcirculation and in normal tissue was performed using special software (Capimage®, Zeintl GmbH, Heidelberg, FRG). The number of blood vessels was calculated on 3-4 randomly chosen fields and expressed as per 1 mm² of tumor surface.

Immunohistochemistry

After intravital microscopy, the tumors were removed for further histological analysis. The tissue was snap frozen in liquid nitrogen. Five µm thick sections were cut, air-dried and fixed in acetone. Immunohistochemical staining of endothelium was performed using monoclonal antibodies recognising RECA-1 rat endothelial antigen (Clone HIS52, Serotec, Germany) and the LSAB-kit (Dako, Hamburg, Germany). In addition, the slides were counterstained with Mayer's acid hemalum (Fluka, Steinheim, Germany). Quantitative analysis of immunohistochemical staining was performed by computer-assisted image analysis. For this aim, three microscopic fields of 3.18 mm² were randomly chosen by light microscope (Leica DMRB, Leica GmbH, Germany),

digitalized by a colour video camera (CF 20/4DX, Kappa GmbH, Gleichen, Germany) to histological images and saved on a computer. The number of blood vessels was counted and expressed as per 1 mm² of surface.

Statistical analysis

All data were given as mean±SD. Mann-Whitney-U test was used to compare the differences between groups as appropriate. *P*<0.05 was considered statistically significant.

RESULTS

The intravital microscopy after injection of fluorescent plasma marker ensured the excellent contrast of all blood vessels in normal (Figure 1A, E) and in tumoral (Figure 1B, F) tissues. The microvascular system in healthy pancreas showed a capillary network of high density, the single afferent and efferent blood vessels were identified within normal pancreatic tissue (Figure 1A). Healthy liver showed a dense network of hepatic sinusoids which were drained by hepatic venules (Figure 1E). In contrast, the microangiarchitecture of both pancreatic and hepatocellular carcinomas was characterized by lost of normal vascular hierarchy "capillaries-arterioles (sinusoids)-venules", chaotic arrangement of blood vessels, irregular vessel diameters and formation of lacunar blood vessels (Figure 1B, F). In contrast to vascular systems of normal pancreatic and hepatic tissues, there were no specific features discriminating the microangiarchitecture of pancreatic cancer from that of hepatocellular carcinoma (Figure 1).

The measurement of vessel density either by intravital microscopy or by immunohistochemistry demonstrated different results (Tables 2, 3). The vessel density of all tissues measured by intravital microscopy was significantly higher than that measured by immunohistochemistry (*P*<0.05, Tables 2, 3). The vessel density in healthy pancreas was significantly higher compared to pancreatic cancer (*P*<0.001, Table 2). Healthy liver showed also a significantly higher vessel density compared to liver carcinoma (*P*<0.01, Table 3). The low vessel density of both pancreatic and hepatocellular carcinomas was accompanied with the development of tumor necrosis, which appeared frequently in the central area of the tumors and represented a characteristic feature of the tumors showing a cross-sectional diameter of more than 10 mm as opposed to smaller tumors.

Table 2 Vessel density in normal and malignant tissue

Vessel density (n/mm ²)	Healthy pancreas	Pancreatic cancer	<i>P</i>
Intravital microscopy	565±89	116±36	<0.001
Immunohistochemistry	91±22	35±10	<0.001

Table 3 Vessel density in normal and malignant liver tissue

Vessel density (n/mm ²)	Healthy liver	Liver carcinoma	<i>P</i>
Intravital microscopy	689±36	286±32	<0.01
Immunohistochemistry	196±30	49±13	<0.01

The frequency analysis of vessel diameters showed that the most frequent diameters in normal pancreas and liver were considerably smaller compared to the most frequent diameters in pancreatic and hepatocellular carcinomas (Figures 2, 3). Ninety-four percent of blood vessels in normal pancreas, 41% of blood vessels in pancreatic carcinoma and less than 9% of blood vessels in non-malignant and malignant hepatocellular tissues showed a diameter less than 10 µm. The most frequent diameter was between 10 and 20 µm (59%) in pancreatic carcinoma and more than 20 µm in hepatocellular carcinoma (59%).

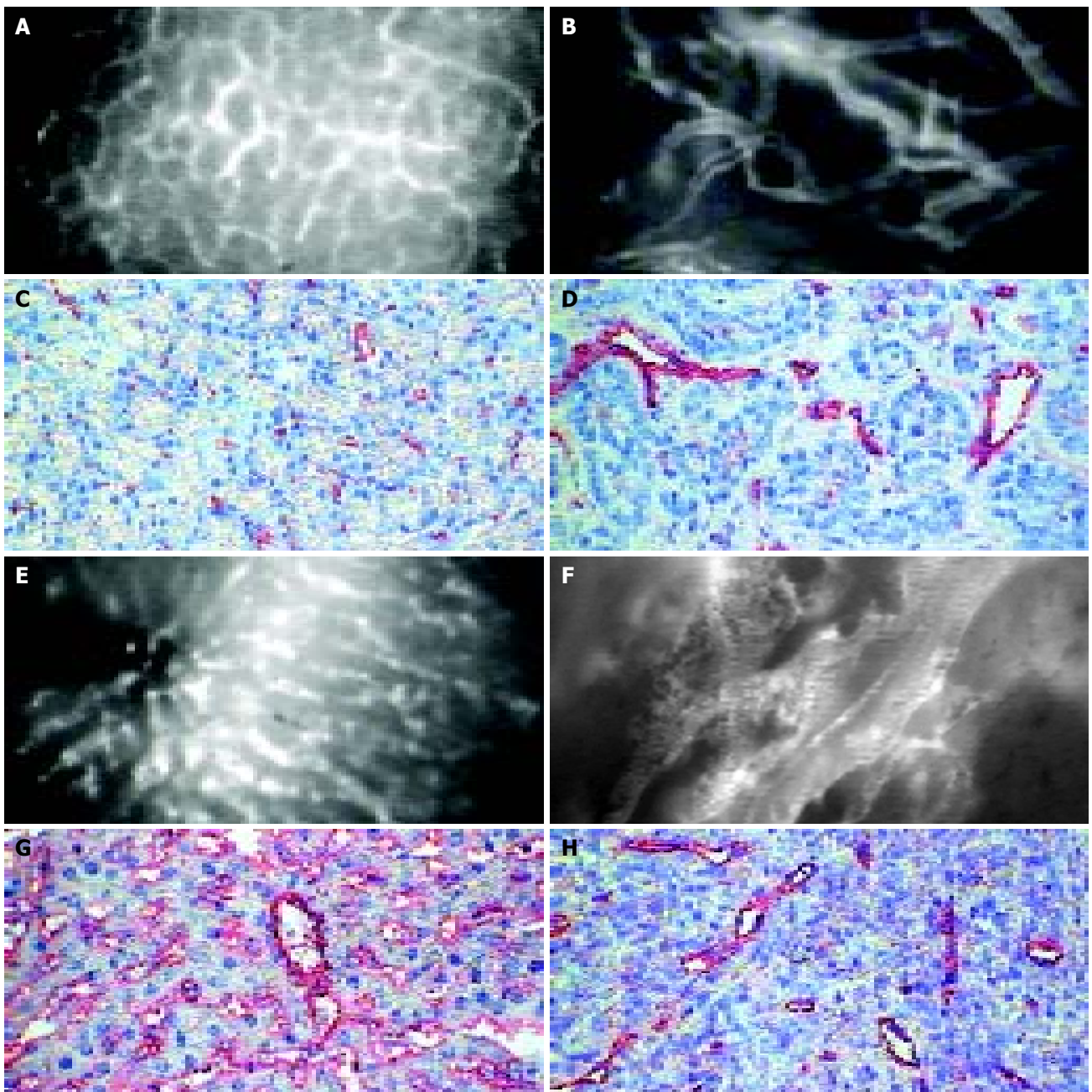


Figure 1 Microangiarchitecture investigated by intravital microscopy and immunohistochemical staining of endothelium of normal pancreas (A,B), liver (E,F), pancreatic (C,D) and hepatocellular (G,H) carcinoma: The microvascular system in healthy pancreas showed a dense network mainly consisting of capillaries in normal pancreas (A) and sinusoids in the liver (E). Both pancreatic (B) and hepatocellular (F) carcinomas showed a chaotic angioarchitecture with irregular diameter of blood vessels. Either intravital microscopy or immunohistochemical staining of endothelium turn up lower density and higher diameters of microvessels in both tumor types than in corresponding normal tissue (bar 50 μm).

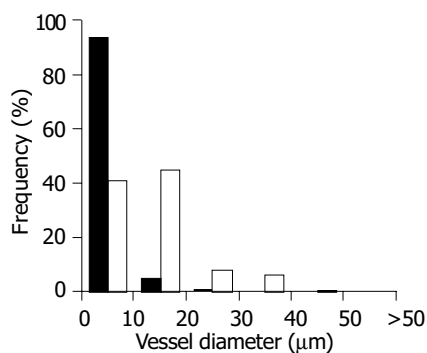


Figure 2 Frequency of vessel diameter in normal pancreas and experimental duct-like pancreatic carcinoma (DSL6A) ■-normal pancreas, □-pancreatic carcinoma.

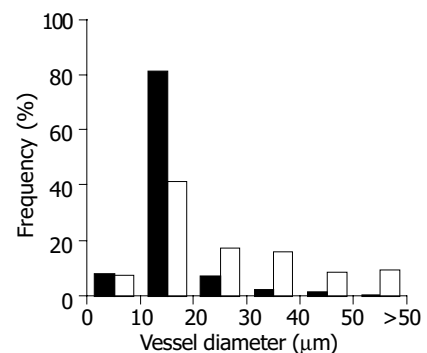


Figure 3 Frequency of vessel diameter in normal liver and experimental hepatocellular carcinoma (Morris-hepatoma) ■-normal liver, □-hepatocellular carcinoma.

DISCUSSION

Using intravital microscopy, we investigated the microvascular systems of pancreatic and liver carcinoma and performed a quantitative analysis of vessel density and vessel diameter. The present study demonstrated that the mean vessel density in both types of experimental malignant tumors was lower than that in the corresponding normal tissues. This hypovascularity was regarded as a main cause of hypoxia in tumor tissue which is responsible for the development of necrotic areas within solid tumors^[8,11] as it has been observed in the present models of pancreatic and hepatocellular carcinoma once diameters exceeded 10 mm. However, as it was shown in the present study, tumor angiogenesis could compensate in part for this insufficient vascularisation by other mechanisms than growth of new blood vessels. Although vessel sprouting has been accepted as the main mechanism of angiogenesis, some pathological processes might display an angiogenic phenotype characterized by an extensive vessel dilatation^[18,19]. Previous data demonstrated in a model of multistep tumorigenesis in mouse malignant insulinoma^[14] and in the model of thyroid hyperplasia^[18] that vessel dilatation was the first detectable stage of ongoing angiogenesis which preceded vessel sprouting and extended transformation of the cells. The results of the present study allowed to transfer these findings to solid murine tumors and demonstrated that the “non-sprouting” angiogenesis might accompany vessel sprouting during growth of solid pancreatic and hepatocellular cancer in rats. We suggested that the observed vessel dilatation during tumor development and growth could cause an increase of endothelial surface for the diffusion of oxygen and nutrition, representing a possible adaptive mechanism to compensate for the insufficient vascularisation.

In the present study, both tumor types were induced by an implantation of tumor cells and did not arise spontaneously. It is known that tumor blood vessels in transplantable tumor models develop from surrounding tissues^[20,21], whereas the growth of autochthonous blood vessels forms the vascular system in spontaneous tumors^[22,23]. However, the vessel dilatation as an initial step of the vascular transformation has been reported previously in spontaneous tumor model also and seems to be a feature which is likely to be a common feature in both transplanted and spontaneous tumors.

In a previous study we analysed the percentage of vascular surface of pancreatic cancer DSL6A which was performed on histological sections using intravascular perfusion with a fluorescent-labeled plasma marker^[12]. In the present study, the number of blood vessels per mm² was investigated by intravital microscopy and immunohistochemistry. The values of vessel density obtained by these analyses corresponded well and both showed a significantly lower microvascularity of malignant tumors compared to normal tissues. The vessel density investigated by intravital microscopy was higher than that by immunohistochemistry. Since the optical depth of tissue accessible for the intravital microscopy (30-50 μm) is considerably higher than the thickness of histological sections (5 μm), the difference between the results of intravital microscopy and immunohistochemistry finds its logical explanation.

In summary, we compared the vessel density and vessel diameter of two experimental tumors by intravital microscopy. The present study demonstrates that the vessel dilatation is an integral part of the angiogenic activity which represents a possible mechanism by which the tumors expand their diffusion surface of endothelium to compensate for the inadequate neoangiogenesis.

REFERENCES

1 Carmeliet P, Jain RK. Angiogenesis in cancer and other

diseases. *Nature* 2000; **407**: 249-257

- 2 Folkman J. Angiogenesis in cancer, vascular, rheumatoid and other disease. *Nat Med* 1995; **1**: 27-31
- 3 Hanahan D, Folkman J. Patterns and emerging mechanisms of the angiogenesis switch during tumorigenesis. *Cell* 1996; **86**: 353-364
- 4 Konerding MA, van Ackern C, Steinberg F, Streffer C. Combined morphological approaches in the study of network formation in tumor angiogenesis. Steiner R, Weisz PB, Langer R eds. *Angiogenesis: key principles-science-technology-medicine. Basel Birkhauser* 1992: 40-58
- 5 Steinberg F, Konerding MA, Sander A, Streffer C. Ultrastructural studies of tumour angiogenesis in human xenotransplanted tumours. *Int J Radiat Biol* 1991; **60**: 161-168
- 6 Vaupel P, Thews O, Kelleher DK, Hoeckel M. Oxygenation of human tumors: the Mainz experience. *Strahlenther Onkol* 1998; **174**(Suppl 4): 6-12
- 7 Dewhirst MW, Tso CY, Oliver R, Gustafson CS, Secomb TW, Gross JF. Morphologic and hemodynamic comparison of tumor and healing normal tissue microvasculature. *Int J Radiat Oncol Biol Phys* 1989; **17**: 91-99
- 8 West CM, Cooper RA, Loncaster JA, Wilks DP, Bromley M. Tumor vascularity: a histological measure of angiogenesis and hypoxia. *Cancer Res* 2001; **61**: 2907-2910
- 9 Koong AC, Mehta VK, Le QT, Fisher GA, Terris DJ, Brown JM, Bastidas AJ, Vierra M. Pancreatic tumors show high levels of hypoxia. *Int J Radiat Oncol Biol Phys* 2000; **48**: 919-922
- 10 Kerbel RS. Tumor angiogenesis: past, present and the near future. *Carcinogenesis* 2000; **21**: 505-515
- 11 Brown JM, Le QT. Tumor hypoxia is important in radiotherapy, but how should we measure it? *Int J Radiat Oncol Biol Phys* 2002; **54**: 1299-1301
- 12 Schmidt J, Ryschich E, Daniel V, Herzog L, Werner J, Herfarth CH, Longnecker DS, Gebhard MM, Klar E. Vascular structure and microcirculation of experimental pancreatic carcinoma in the rat. *Eur J Surg* 2000; **166**: 328-335
- 13 Maksan SM, Paulo H, Ryschich E, Kuntz C, Gebhard MM, Klar E, Schmidt J. *In vivo* assessment of angioarchitecture and microcirculation in experimental liver cancer: a new model in rats. *Dig Dis Sci* 2003; **48**: 279-290
- 14 Ryschich E, Schmidt J, Klar E, Haemmerling GJ, Ganss R. Transformation of the microvascular system during multistage tumorigenesis. *Int J Cancer* 2002; **97**: 719-725
- 15 Pettengill OS, Faris RA, Bell RHJ, Kuhlmann ET, Longnecker DS. Derivation of ductlike cell lines from a transplantable acinar cell carcinoma of the rat pancreas. *Am J Pathol* 1993; **143**: 292-303
- 16 Gullino PM. Microenvironment and angiogenic response. Steiner R, Weisz PB, Langer R eds. *Angiogenesis: key principles-science-technology-medicine. Basel Birkhauser* 1992: 125-128
- 17 Fukumura D, Yuan F, Monsky WL, Chen Y, Jain RK. Effect of host microenvironment on the microcirculation of human colon adenocarcinoma. *Am J Pathol* 1997; **151**: 679-688
- 18 Many MC, Denef JF, Haumont S. Precocity of the endothelial proliferation during a course of rapid goitrogenesis. *Acta Endocrinol Copenh* 1984; **105**: 487-491
- 19 Bull RH, Bates RO, Mortimer PS. Intravital capillaro-microscopy for the study of microcirculation in psoriasis. *Br J Dermatol* 1992; **126**: 436-445
- 20 Sckell A, Safabakhsh N, Dellian M, Jain RK. Primary tumor size-dependent inhibition of angiogenesis at a secondary site: an intravital microscopic study in mice. *Cancer Res* 1998; **58**: 5866-5869
- 21 Vajkoczy P, Thurnher A, Hirth KP, Schilling L, Schmiedek P, Ullrich A, Menger MD. Measuring VEGF-Flk-1 activity and consequences of VEGF-Flk-1 targeting *in vivo* using intravital microscopy: clinical applications. *Oncologist* 2000; **5**(Suppl 1): 16-19
- 22 Folkman J, Watson K, Ingber D, Hanahan D. Induction of angiogenesis during the transition from hyperplasia to neoplasia. *Nature* 1989; **339**: 58-61
- 23 Bergers G, Javaherian K, Lo KM, Folkman J, Hanahan D. Effects of angiogenesis inhibitors on multistage carcinogenesis in mice. *Science* 1999; **284**: 808-812

Biliary drainage after laparoscopic choledochotomy

Qi Wei, Hong-Jie Hu, Xiao-Yan Cai, Li-Bo Li, Guan-Yu Wang

Qi Wei, Xiao-Yan Cai, Li-Bo Li, Guan-Yu Wang, Department of General Surgery, Sir Run Run Shaw Hospital, Zhejiang University, Hangzhou 310016, Zhejiang Province, China

Hong-Jie Hu, Department of Radiology, Sir Run Run Shaw Hospital, Zhejiang University, Hangzhou 310016, Zhejiang Province, China

Correspondence to: Qi Wei, Department of General Surgery, Sir Run Run Shaw Hospital, Zhejiang University, Hangzhou 310016, Zhejiang Province, China. weiqi@hzcnc.com

Telephone: +86-571-86437761

Received: 2003-08-28 **Accepted:** 2003-09-25

Abstract

AIM: Transcystic biliary decompression (TCBD) has been proposed as an alternative to T-tube placement after laparoscopic choledochotomy (LCD). This permits safe primary closure of the choledochotomy and eliminates the complications associated with T-tubes. TCBD tube has been secured by Roeder knots and transfixation, and removed later than 3 wk after surgery. We presented a modified TCBD (mTCBD) method after LCD using the ureteral catheter and the Lapro-Clip (David and Geck, Danbury, Connecticut, USA), and compared it with T-tube drainage.

METHODS: Between October 2002 and June 2003, patients with choledocholithiasis undergoing LCD with mTCBD (mTCBD Group, $n = 30$) were retrospectively compared to those undergoing LCD with T-tube drainage (T-tube Group, $n = 52$) at a single institution.

RESULTS: There were no significant differences in operative time and retained stones between the two groups. Patients in mTCBD group had a significantly decreased average output of bile compared with those in T-tube group (306 ± 141 vs 409 ± 243 mL/24 h, $P = 0.000$). Removal of drain tubes in mTCBD group was done significantly earlier than that in T-tube group (median, 5 vs 29 d, $P = 0.000$). No complication related to drain tubes was found in mTCBD group, and morbidity rate with the T-tube was significantly higher (11.5%), and bile leakage following T-tube removal was 5.8%.

CONCLUSION: A modified TCBD after LCD is safe, effective and easy to perform. It may reduce postoperative complications, especially bile leakage.

Wei Q, Hu HJ, Cai XY, Li LB, Wang GY. Biliary drainage after laparoscopic choledochotomy. *World J Gastroenterol* 2004; 10(21): 3175-3178

<http://www.wjgnet.com/1007-9327/10/3175.asp>

INTRODUCTION

Laparoscopic choledochotomy (LCD) has been proposed as an efficacious, safe, and cost-effective method for the treatment of choledocholithiasis^[1-6]. However, it is associated with a relatively higher morbidity rate, mainly related to T-tube insertion^[7,8]. To eliminate the complications related to T-tubes, some authors have proposed transcystic biliary decompression (TCBD) after LCD, but the TCBD tube is still removed later

than 3 wk after surgery^[9,10], limiting the value of the procedure. We presented a modified TCBD (mTCBD) method using ureteral catheter and Lapro-Clip, and compared it with T-tube drainage.

MATERIALS AND METHODS

Patients

Eighty-two patients with choledocholithiasis undergoing LC plus laparoscopic choledochotomy were retrospectively reviewed at a single institution, between October 2002 and June 2003. mTCBD was performed for 30 patients (mTCBD group) and T-tube drainage for 52 patients (T-tube group). The clinical and demographic details are shown in Table 1. There were no significant differences between the groups. Preoperative investigations included liver function tests and external ultrasound. Six patients had ERCP or MRCP in the mTCBD group, and three in the T-tube group. The criteria for preoperative suspicion of CBD stones were serum alkaline phosphatase or bilirubin levels twice the upper normal limit, and an ultrasonic diameter of the CBD equal to or larger than 9 mm. Patients with acute cholecystitis underwent an operation within 48 h admission. Those with choledocholithiasis associated with acute pancreatitis were operated on after the acute bout of pancreatitis was subsided. The patients were restricted to the American Society of Anesthesiology class I and class II (ASA I and II). Cases were excluded if preoperative and intraoperative endoscopic sphincterotomy (ES) were performed. Two patients had previous biliary surgery in the mTCBD group, and three in the T-tube group.

Table 1 Clinical and demographic details of the patients

	mTCBD ¹	T-tube
<i>n</i>	30	52
Age range(yr)	28-77	26-82
Male:female	12:18	17:35
Jaundice	12	16
Acute cholecystitis	9	13
Acute pancreatitis	3	5
Known CBD stone (s)	16	37
Suspected CBD stone (s)	11	13
Dilated CBD (≥ 9 mm)	18	35
Biliary surgery	2	3

¹Modified transcystic biliary decompression.

Operative techniques

Laparoscopic cholecystectomy was performed by a standardized technique. One 10 mm port was inserted into the left upper quadrant. Intraoperative cholangiography (IOC) was mandatory. Choledochotomy was performed by a vertical incision. CBD stones were retrieved by instrumental exploration with forceps, flushing of CBD with saline, and use of a Dormia basket with a 5 mm chledochoscopy.

Modified transcystic biliary decompression (mTCBD) After complete clearance of the CBD, which was primarily closed with a running suture (3-0 vicryl). A 5Fr ureteral catheter was advanced into the CBD lumen 2 cm to 4 cm and a saline syringe was attached to the three-way stopcock external fitting of the catheter. If the position of the terminal segment of the ureteral

catheter inside CBD was correct, the catheter was fixed to the cystic duct by a 12 mm absorbable Lapro-Clip (Figure 1). Saline irrigation through the catheter was maintained during application of the Lapro-Clip to prevent overtightening the catheter. A loose loop of the catheter was left. A completion IOC was performed to confirm the correct position of the ureteral catheter, also to ensure the adequate closure of the CBD and free flow of contrast into the duodenal lumen. A postoperative cholangiogram was performed on d 3 to 7 after surgery. Under fluoroscopy, the catheter was removed.

T-tube drainage A latex rubber T-tube of appropriate size (12-16 Fr) was inserted completely into the abdomen. The T limbs were advanced with grasping forceps into the choledochotomy. After proper positioning, the choledochotomy was closed using interrupted sutures (3-0 vicryl). T-tube clamping was carried out 7-10 d postoperatively. A postoperative cholangiogram was performed 3 to 4 wk after surgery. If the examination was normal, the T-tube was removed. If retained stones were shown, the T-tube was left for another 3 to 4 wk. A No. 10 Jackson-Pratt drain was placed in the subhepatic space for all patients. The subhepatic drain tube was removed on the 3rd d for most of patients.

Five surgeons performed the 82 laparoscopic choledochotomies. In the mTCBD group, one senior author performed 25 of 30 procedures, whereas the remaining 5 procedures by one junior staff member. In the T-tube group, three senior staff performed 47 of 52 procedures, whereas 7 procedures by two junior members.

The output of bile was measured only during the hospital stay. The data recorded were insufficient in the case notes to compare the number and size of CBD stones, and postoperative liver function test.

A "drain complication" was defined as an event causing morbidity, requiring medical intervention, or resulting in a prolonged admission or requiring readmission. The complication had to be clearly related to the presence or removal of the drain.

Statistical analysis

Statistical analyses were performed using Student's *t* test, chi square test for likelihood ratio, and Mann-Whitney test for nonparametric data. Significance was set at the 5% level.

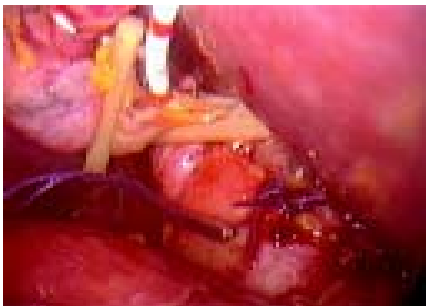


Figure 1 A 5 Fr ureteral catheter was placed for biliary decompression and secured with a 12 mm absorbable Lapro-Clip.

RESULTS

Outcome of mTCBD group

The average operative time was 178±34 min (Table 2). There were two conversions to open surgery (6.5%). One patient had large impacted stones, and the other had multiple stones. The modified transcystic biliary decompression (mTCBD) was also used in those patients. The average output of bile via the ureteral catheter was 306±141 mL/24 h. The median postoperative time of drain removal was 5 (range 4 to 5) d. Under fluoroscopy, the catheter could be pulled out easily from the cystic duct without any bile leakage or slippage of the Lapro-Clip (Figure 2). No patients developed complications from ureteral catheter occlusion. The median postoperative hospital stay was 5 (range 4 to 6) d.

Table 2 Comparison of clinical outcome between two groups

	mTCBD	T-tube	<i>t</i> or χ^2 (z)	<i>P</i>
Operative time (min)	178	173	-0.469	0.640 ²
Output of bile (mL/24 h)	306	409	2.118	0.037 ²
Postoperative stay(d)	5.4-6 ¹	4.4-6 ¹	(-2.060)	0.039 ⁴
Drain removal (d)	5.4-5 ¹	29.22-32 ¹	(-7.560)	0.000 ⁴
Complications (%)	0	11.5	5.736	0.017 ³
Retained stones (%)	3.3	13.5	2.574	0.109 ³
Convert to open (%)	6.5	3.8	0.315	0.575 ³

¹Median, 25-75% quartile rang; ²*t*-test; ³Chi square test with Likelihood Ratio; ⁴Mann-Whitney test.

One patient (3.3%) had unexpected retained stones, requiring endoscopic sphincterotomy (ES). Two patients had problems. The ureteral catheter was dislocated with the biliary tree not shown in the postoperative cholangiogram, but there was no bile leakage.

Outcome of T-tube group

The average operative time was 173±45 min (Table 2). There were two conversions to open surgery (6.5%). Two patients had large impacted stones. The average output of bile via T-tube was 409±243 mL/24 h. The median drain removal time was 29 (range 22 to 32) d. The median postoperative hospital stay was 4 (range 4 to 6) d.

Seven (13.5%) had retained stones (Table 4). There were intentionally retained stones in 5 patients (9.6%), 2 with intrahepatic duct stones, 1 with multiple common duct stones because of difficulty in removing them laparoscopically, and another 2 patients with temporary unavailability of the choledochoscope. There were unexpected residual stones in 2 patients (3.8%). All of the stones were successfully removed, 5 patients through the T-tube tract, using a choledochoscope, and a stone basket. The T-tube was taken out in two patients prior to planned removal, thereby requiring ES.

Table 3 Complications and problems of biliary drainage

	T-tube	mTCBD
Complications		
<i>n</i>	6 (11.5%)	0
Drain <i>in situ</i>		
Leak around drain	1	0
Stricture	1	0
Drain pulled out	1	0
Drain removed	3 (5.8%)	
Bile collection	2	0
Bile peritonitis	1	0
Problems		
<i>n</i>	3 (5.8%)	2 (6.7%)
Drain out	2	2
Dislocation	1	0

Table 4 Retained stones in T-tube group

	<i>n</i> (%)
Known stones	5 (9.6)
Instrument problems	2
Intrahepatic stones	2
Multiple stones	1
Unexpected stones	2 (3.8)
Total	7 (13.5)



Figure 2 A ureteral catheter was pulled out without bile leakage. The cystic duct was closed with the Lapro-Clip.

Postoperative complications occurred in 6 patients (11.5%) (Table 3). Following T-tube removal, three patients had significant bile leakage (5.8%). Two patients developed severe abdominal pain, sweating and tachycardia and were diagnosed as localized bile collection. They were treated with antibiotics, parental fluids, analgesia, and the drain tube was reinserted through T-tube sinus tract. Recovery was achieved with this management. The third patient developed biliary peritonitis and required open drainage.

One patient had a CBD stricture and T-tube stenting was necessary for 3 mo. In the other patient the T-tube was pulled out on the second day after surgery and the subhepatic suction drain provided biliary drainage for two weeks postoperatively.

Other related morbidity was found in one patient with a bile leak around the T-tube. In addition, the tip of the T-tube in one patient was dislocated from the bile duct, but caused no problem.

Comparison of clinical outcome between two groups

The statistical analyses comparing the mTCBD group with the T-tube group are presented in Table 2. There were no significant differences in operative time and retained stones. Patients in mTCBD group had a significantly decreased average output of bile compared with those in T-tube group ($P = 0.000$). The biliary drainage tube in the mTCBD group was removed significantly earlier than that in the T-tube group ($P = 0.000$). No morbidity was directly related to drain tube in the mTCBD group, and the morbidity rate in the T-tube group was significantly higher (11.5%, $P = 0.017$). However, the postoperative hospital stay in the mTCBD group was significantly longer compared with that in the T-tube group ($P = 0.039$).

There was no postoperative mortality or recurrence of choledocholithiasis in this study. The length of follow-up was 4 to 30 wk.

DISCUSSION

Previous studies have documented a temporary obstruction at the lower end of the CBD due to sludge, fibrin debris, or edema following manipulations to extract duct calculi or retained stones in the first few days after surgery^[9,11-16], thus temporary decompression is advisable in the prevention of postoperative bile leakage. A transcystic biliary decompression (TCBD) tube, like a T-tube, could achieve biliary decompression and has the advantage of avoiding the well-known complications of T-tubes. A TCBD tube was secured to the cystic duct with two Roeder knots or a transfixing suture. The biliary drainage tube must be kept in place for 2-4 wk^[9,10]. This might not be easy to manipulate, and could reduce the benefits of the minimal access approach.

In October 2002, a modified TCBD (mTCBD) was placed followed by primary closure of the CBD. The ureteral catheter was inserted down into the CBD and once in the correct position, the cystic duct was clipped by a 12 mm Lapro-Clip. The Lapro-Clip has a two-part compression closure mechanism, the inner flexible track piece could close around the cystic duct, and rigid

outer body could be then slide over the track piece to secure the cystic duct^[17]. The ureteral catheter was pulled out easily with no bile leakage and the cystic duct was closed automatically with the Lapro-Clip even if drain displacement occurred.

In mTCBD group, no bile leakage was related to drain tube removal, and median time for ureteral catheter removal was 5 (range 4 to 5) d. The ureteral catheter in two patients was dislocated, this also caused no bile leakage.

Complications related to T-tubes were reported to occur between 5-15.3%^[7,18,19]. Biliary leakage following removal was the most serious. Incidence of bile leak was 4.12-6.9%^[19,20]. There was no difference when laparoscopic cases were compared to open and converted cases for overall complications (13.8% vs 15.5%) or for bile leakage after planned tube removal (6.9% vs 6.9%)^[19].

In our study, postoperative complications in the T-tube group occurred in 6 patients (11.5%) (Table 3). Following T-tube removal, 3 patients developed bile leakage (5.8%). The T-tube was left in the three patients for three weeks postoperatively. Sinus tract formation of the T-tube might need a longer time because of the less reaction of laparoscopic approach^[21-23]. Bile leakage was inevitable with accidental T-tube dislocation^[7,18-20]. The median time for T-tube removed was 29 (range 22 to 32) d, even if cases of retained stones were excluded. The data suggest that placement of T-tube may require a longer time than 4 wk.

Biliary drainage with a TCBD tube and primary closure of the choledochotomy were indicated only for patients whose stones were completely extracted at the time of surgery. Routine intraoperative cholangiogram and chledochoscopy were used in the laparoscopic approach, and the occurrence of retained stones was decreased to accepted levels^[7,24,25]. Endoscopic sphincterotomy could be a back up procedure for retained stones^[25,26]. In the mTCBD group, one patient (3.3%) had unexpected retained stones retrieved by ES.

If there was any possibility of residual stones, T-tube placement was mandatory for postoperative choledochoscopy. Five patients (9.6%) in the T-tube group had intentionally retained stones (Table 4). T-tube placement may be needed for another 3-4 wk^[21-23], in order to form a mature tract. It was worthwhile without any injury to the sphincter of Oddi, and complete removal could be expected.

Although patients in the mTCBD group had a significantly decreased average output of bile compared with those in the T-tube group (306±141 vs 409±243 mL/24 h, $P = 0.000$), it was shown that enough output of bile led to a decrease in the biliary pressure. Consequently, this finding suggested that the output of bile from mTCBD was sufficient to decompress the biliary tract as T-tube. On the other hand, the T-tube drain mostly was clamped on d 7 to 10, which means that many patients were discharged with an open drain.

The postoperative hospital stay in mTCBD group was significantly longer compared with that in T-tube group (median, 5 vs 4 d, $P = 0.039$). It may relate to the drain removal during hospitalization because of our initial trial for the mTCBD.

A modified TCBD is not suitable for patients with abnormal anatomy of cystic duct, intrahepatic duct stones and stricture of duodenal papillary.

The chief concern of the Lapro-Clip is the occlusion of the catheter. Maintaining saline irrigation through the ureteral catheter prevents occluding. We also feel that the diameter of the ureteral catheter is an important factor for avoiding occlusion or dislocation, so a 5Fr ureteral catheter is most suitable. We used a 5Fr ureteral catheter in all mTCBD cases.

A 12 mm Lapro-Clip holds the cystic duct tightly to a 5Fr ureteral catheter while the spring of the Lapro-Clip closes the cystic duct when the ureteral catheter is removed. In this study, no slippage of the clip occurred. The short period of TCBD could reduce the risk of ureteral catheter occlusion. No patients

in the present study developed catheter occlusion.

Our results were similar to the use of exclusive C-tube and elastic thread described by some authors^[27-30]. Our initial experiences demonstrated that the modified transcystic biliary decompression (mTCBD) after laparoscopic choledochotomy (LCD) was useful for decreasing postoperative complications, especially bile leakage, and easy to perform. The patients were discharged without any drainage tube within a wk. If biliary drainage was used carefully with selected indications, patients with laparoscopic choledochotomy for CBD stones could achieve a better postoperative quality of life. We propose mTCBD as an option for patients with CBD stones.

ACKNOWLEDGMENTS

We thank Dr. C. Welch for editorial assistance and helpful suggestions.

REFERENCES

- Cuschieri A, Lezoche E, Morino M, Croce E, Lacy A, Toouli J, Faggioni A, Ribeiro VM, Jakimowicz J, Visa J, Hanna GB. E.A. E.S. multicenter prospective randomized trial comparing two-stage vs single-stage management of patients with gallstone disease and ductal calculi. *Surg Endosc* 1999; **13**: 952-957
- Heili MJ, Wintz NK, Fowler DL. Choledocholithiasis: endoscopic versus laparoscopic management. *Am Surg* 1999; **65**: 135-138
- Wei Q, Wang JG, Li LB, Li JD. Management of choledocholithiasis: Comparison between laparoscopic common bile duct exploration and intraoperative endoscopic sphincterotomy. *World J Gastroenterol* 2003; **9**: 2856-2858
- Memon MA, Hassaballa H, Memon MI. Laparoscopic common bile duct exploration: the past, the present, and the future. *Am J Surg* 2000; **179**: 309-315
- Patel AP, Lokey JS, Harris JB, Sticca RP, McGill ES, Arrillaga A, Miller RS, Kopelman TR. Current management of common bile duct stones in a teaching community hospital. *Am Surg* 2003; **69**: 555-560
- Petelin JB. Laparoscopic common bile duct exploration. *Surg Endosc* 2003; **17**: 1705-1715
- Martin IJ, Bailey IS, Rhodes M, O'Rourke N, Nathanson L, Fielding G. Towards T-tube free laparoscopic bile duct exploration: A methologic evaluation during 300 consecutive procedures. *Ann Surg* 1998; **228**: 29-34
- Thompson MH, Tranter SE. All-comers policy for laparoscopic exploration of the common bile duct. *Br J Surg* 2002; **89**: 1608-1612
- Hensman C, Crosthwaite G, Cuschieri A. Transcystic biliary decompression after direct laparoscopic exploration of the common bile duct. *Surg Endosc* 1997; **11**: 1106-1110
- Paganini AM, Feliciotti F, Guerrieri M, Tamburini A, DeSanctis A, Campagnacci R, Lezoche E. Laparoscopic common bile duct exploration. *J Laparoendosc Adv Surg Tech A* 2001; **11**: 391-400
- Holdsworth RJ, Sadek SA, Ambikar S, Cuschieri A. Dynamics of bile flow through the choledochal sphincter following exploration of the common bile duct. *World J Surg* 1989; **13**: 300-304
- DePaula AL, Hashiba K, Bafutto M, Machado C, Ferrari A, Machado MM. Results of the routine use of a modified endoprosthesis to drain the common bile duct after laparoscopic choledochotomy. *Surg Endosc* 1998; **12**: 933-935
- Gersin KS, Fanelli RD. Laparoscopic endobiliary stenting as an adjunct to common bile duct exploration. *Surg Endosc* 1998; **12**: 301-304
- Isla AM, Griniatsos J, Wan A. A technique for safe placement of a biliary endoprosthesis after laparoscopic choledochotomy. *J Laparoendosc Adv Surg Tech A* 2002; **12**: 207-211
- Chen XP, Peng SY, Peng CH, Liu YB, Shi LB, Jiang XC, Shen HW, Xu YL, Fang SB, Rui J, Xia XH, Zhao GH. A ten-year study on non-surgical treatment of postoperative bile leakage. *World J Gastroenterol* 2002; **8**: 937-942
- Yamaner S, Bilsel Y, Bulut T, Bugra D, Buyukuncu Y, Akyuz A, Sokucu N. Endoscopic diagnosis and management of complications following surgery for gallstones. *Surg Endosc* 2002; **16**: 1685-1690
- Darzi A, Soin B, Coleman J, Lirici NM, Angelini L. Initial experience with an absorbable laparoscopic ligation clip. *Br J Surg* 1997; **84**: 974-976
- Moreaux J. Traditional surgical management of common bile duct stones: a prospective study during a 20-year experience. *Am J Surg* 1995; **169**: 220-226
- Wills VL, Gibson K, Karihaloot C, Jorgensen JO. Complications of biliary T-tube after choledochotomy. *ANZ J Surg* 2002; **72**: 177-180
- Gharaibeh KI, Heiss HA. Biliary leakage following T-tube removal. *Int Surg* 2000; **85**: 57-63
- Schippers E, Tittel A, Ottinger A, Schumpelick V. Laparoscopy versus laparotomy: comparison of adhesion-formation after bowel resection in a canine model. *Dig Surg* 1998; **15**: 145-147
- Tittel A, Treutner KH, Titkova S, Ottinger A, Schumpelick V. Comparison of adhesion reformation after laparoscopic and conventional adhesiolysis in an animal model. *Langenbecks Arch Surg* 2001; **386**: 141-145
- Polymeneas G, Theodosopoulos T, Stamatiadis A, Kourias E. A comparative study of postoperative adhesion formation after laparoscopic vs open cholecystectomy. *Surg Endosc* 2001; **15**: 41-43
- Riciardi R, Islam S, Canete JJ, Arcand PL, Stoker ME. Effectiveness and long-term results of laparoscopic common bile duct. *Surg Endosc* 2003; **17**: 19-22
- Hawasli A, Lloyd L, Cacucci B. Management of choledocholithiasis in the era of laparoscopic surgery. *Am Surg* 2000; **66**: 425-430
- Yamakawa T, Sakai S, Mu ZB, Pineres G. Laparoscopic management of common bile duct stones. *J Hepatobiliary Pancreat Surg* 2000; **7**: 9-14
- Fujimura M, Hirano M, Sato I, Kinoshita T, Yamamoto I, Nishimura K, Takahara H, Yamamoto A. The C tube in biliary surgery -its development and clinical application. *Nippon Geka Hokan* 2000; **68**: 85-122
- Shimizu S, Yokohata K, Mizumoto K, Yamaguchi K, Chijiwa K, Tanaka M. Laparoscopic choledochotomy for bile duct stones. *J Hepatobiliary Pancreat Surg* 2002; **9**: 201-205
- Tokumura H, Umezawa A, Cao H, Sakamoto N, Imaoka Y, Ouchi A, Yamamoto K. Laparoscopic management of common bile duct stones: transcystic approach and choledochotomy. *J Hepatobiliary Pancreat Surg* 2002; **9**: 206-212
- Hotta T, Taniguchi K, Kobayashi Y, Johata K, Sahara M, Naka T, Maeda T, Tanimura H. Biliary drainage tube evaluation after common bile duct exploration for choledocholithiasis. *Hepato-gastroenterology* 2003; **50**: 315-321

Edited by Zhang JZ and Wang XL Proofread by Xu FM

Lack of association between seroprevalence of *Helicobacter pylori* infection and primary biliary cirrhosis

Marilena Durazzo, Floriano Rosina, Alberto Premoli, Enrico Morello, Sharmila Fagoonee, Rosaria Innarella, Enrico Solerio, Rinaldo Pellicano, Mario Rizzetto

Marilena Durazzo, Alberto Premoli, Enrico Morello, Department of Internal Medicine, University of Turin, Turin, Italy
Floriano Rosina, Rosaria Innarella, Enrico Solerio, Department of Gastroenterology, Gradenigo Hospital, Turin, Italy
Sharmila Fagoonee, Department of Biology, Biochemistry and Genetics, University of Turin, Turin, Italy
Rinaldo Pellicano, Mario Rizzetto, Department of Gastroenterology, Molinette Hospital, Turin, Italy
Supported by Grant from CNR 1999

Correspondence to: Professor Marilena Durazzo, Department of Internal Medicine, Corso A.M.Dogliotti 14, 10126 Turin, Italy. marilena.durazzo@unito.it

Telephone: +39-11-6336040 **Fax:** +39-11-6634751

Received: 2004-02-02 **Accepted:** 2004-04-07

Abstract

AIM: To determine the association between seroprevalence of *Helicobacter pylori* (*H. pylori*) infection and primary biliary cirrhosis (PBC).

METHODS: In this case-control study, 149 consecutive patients (10 males, 139 females, mean age 58.2±11 years, range 26-82 years) suffering from PBC and 619 consecutive healthy volunteer blood donors (523 males, 96 females, mean age 47±5.3 years, range 18-65 years) attending the Hospital Blood Bank and residing in the same area were recruited. A commercial enzyme linked immunosorbent assay was used to detect anti-*H. pylori* (IgG) antibodies in serum.

RESULTS: Antibodies to *H. pylori* were present in 78 (52.3%) out of 149 PBC-patients and in 291 (47%) out of 619 volunteers ($P = 0.24$, OR 1.24, 95% CI 0.85-1.80). In the subjects less than 60 years old, the prevalence of *H. pylori* infection among PBC-patients (40/79) was slightly higher than in controls (50.6% vs 46.2%) $P = 0.46$, OR = 1.19, 95% CI: 0.72-1.95). In those over 60 years, the prevalence of *H. pylori* infection was similar between PBC-patients and controls (54.2% vs 57.8%, $P = 0.7$, OR 0.86, 95% CI 0.36-2.07).

CONCLUSION: There is no association between seroprevalence of *H. pylori* infection and primary biliary cirrhosis.

Durazzo M, Rosina F, Premoli A, Morello E, Fagoonee S, Innarella R, Solerio E, Pellicano R, Rizzetto M. Lack of association between seroprevalence of *Helicobacter pylori* infection and primary biliary cirrhosis. *World J Gastroenterol* 2004; 10(21): 3179-3181
<http://www.wjgnet.com/1007-9327/10/3179.asp>

INTRODUCTION

Helicobacter pylori (*H. pylori*) infection is a chronic one. In most instances, it is acquired during childhood, and is often associated with low socio-economic class. The presence of

the bacterium has been established as the main cause of several gastroduodenal diseases, including peptic ulcer disease^[1,2], gastric carcinoma^[3], and gastric MALT lymphoma^[4].

Since the latest decade, several studies have reported on the link between chronic *H. pylori* or *Helicobacter species* (*H. species*) infections and a variety of extragastric manifestations. These include ischaemic heart disease (IHD), liver diseases, skin diseases, blood disorders and others^[5]. However, the hypothesis of an etiological role has not yet been fully investigated.

Epidemiological studies have frequently involved control selection bias, population of small sizes, and presence of confounders, like age and socio-economic conditions.

Non randomised, long-period and large studies on the follow-up of *H. pylori* eradication in extragastric diseases are lacking.

Several *H. species*, such as *H. bilis*, are capable of colonising different anatomical regions of the gastrointestinal tract in humans, including choledochus, gallbladder, intrahepatic bile ducts and liver^[6].

Primary biliary cirrhosis (PBC) is a chronic cholestatic liver disease in which intra-hepatic bile ducts are progressively destroyed. The etiology of PBC is unknown, but immunological mechanisms may play a part in the pathogenesis. A causal role of infectious agents has been proposed but the data are inconclusive. Recently, Bogdanos and coworkers have shown that microbial mimics, comprising that of *H. pylori*, are major targets of crossreactivity with human pyruvate dehydrogenase in PBC, strengthening the fact that microbial exposure may be instrumental to the appearance and/or maintenance of anti-mitochondrial antibody responses by a cross-reactive mechanism^[7]. These data indicate that a relationship between *H. species* and the biliary tract of humans might exist, where the bacteria could be potentially involved in inflammatory changes or other pathologic manifestations. However, these findings have not been confirmed in other studies^[8].

The prevalence of peptic ulcer is higher in cirrhotics than in control population and the risk is increased by the presence of *H. pylori* infection^[9]. However, in some groups of patients affected from liver disease, as in the case of PBC, the seroprevalence of *H. pylori* infection is still undetermined.

The present study attempted to highlight on the seroprevalence of antibodies against *H. pylori* in a cohort of patients suffering from PBC in comparison to a group of volunteers attending the Blood Bank of the San Giovanni Battista Hospital (Molinette) in Torino, Italy.

MATERIALS AND METHODS

The presence of anti-*H. pylori* antibodies was evaluated in 149 consecutive subjects (10 males, 139 females, mean age 58.2±11 years, range 26-82 years) suffering from PBC.

Patients were considered to have PBC if they fulfilled at least 2 of the following criteria: positive anti-mitochondrial antibody (AMA) at a titer higher than 1/40, abnormal liver function tests (alkaline phosphatase, gamma glutamyl transpeptidase, bilirubin, transaminase level) or liver histology diagnostic or consistent with PBC^[10].

AMA was evaluated by immunofluorescence using rat

stomach and kidney as substrate^[10].

Other causes of liver disease, such as viral (hepatitis B virus, hepatitis C virus), autoimmune (anti-nuclear, anti-smooth muscle and anti-microsome antibodies) or metabolic (serum iron, percentage of transferrin saturation, ferritin, ceruloplasmin, alpha-1 antitrypsin) hepatitis, were ruled out.

The controls were 619 consecutive volunteer blood donors (523 males, 96 females, mean age 47±5.3 years, range 18-65 years) attending the Hospital Blood Bank and residing in the same area^[11].

A commercial enzyme linked immunosorbent assay (ELISA, Helori-test® Eurospital, Trieste Italy) was used to detect anti-*H pylori* (IgG) antibodies in serum. The assay sensitivity and specificity versus histology were 70.6% and 90.5% respectively, positive predictive value was 87.2% and negative predictive value 77.0%^[12].

Briefly, calibrators, positive controls, negative controls and diluted (1:200) serum samples were added to wells coated with purified *H pylori* group-specific antigens. Plates were incubated for 60 min at 37 °C. The plate was then washed thrice and anti-IgG conjugate was pipetted into each well and the plate was incubated again for 60 min at 37 °C. The washing step was repeated, chromogenic substrate was added to each well, followed by incubation for 30 min at 37 °C. The reaction was then stopped. Reading was performed at 405 nm and the mean optical density was expressed as a percentage of the optical density of the positive control serum assayed on the same plate.

A commercial enzyme immunoassay (Helori®-CTX Eurospital, Trieste, Italy) was used to detect serum IgG antibodies against more virulent strains of the bacterium, expressing cytotoxin-associated gene product A (CagA). The manufacturer's instructions were followed. The assay sensitivity and specificity given by the manufacturer were 94.1% and 97.9% respectively.

The seroprevalence of *H pylori* infection in cases and controls was compared using the chi-square test (χ^2) by means of 2×2 contingency table. Fisher's exact test was used for small sample size. Results were considered statistically significant when $P < 0.05$.

RESULTS

Mean age between patients and controls was not statistically different.

The prevalence of antibodies to *H pylori* was 52.3% (78/149) in the patients with PBC compared to 47% (291/619) in the controls ($P = 0.24$, OR 1.24, 95% CI 0.85-1.80).

When the patients were subdivided into age-groups (<60 and ≥60 years), the difference was as follows. In the youngest age group (less than 60 years old), the prevalence of *H pylori* infection among CBP-patients (50.6%, 40/79) was higher than in controls (46.2%, 269/581), but this was not significant ($P = 0.46$, OR 1.19, 95% CI 0.72-1.95). In the group over 60 years, the prevalence of *H pylori* infection was lower in CBP-patients (38/70, 54.2%) than in controls (22/38, 57.8%) ($P = 0.7$, OR 0.86, 95% CI 0.36-2.07) (Table 1).

Table 1 Seroprevalence of anti-*Helicobacter pylori* antibodies among patients with primary biliary cirrhosis [PBC] and controls

Age (yr)	Patients with PBC Hp (+)/tot (%)		Controls Hp (+)/tot (%)		P
<60	(50.6)	40/79	269/581	(46.2)	0.46
≥60	(54.2)	38/70	22/38	(57.8)	0.7
Total	(52.3)	78/149	291/619	(47)	0.24

The anti-CagA antibodies were detected in 28.1% of patients with PBC (42/149) and in 44.8% of those with seropositivity for

anti-*H pylori* (35/78). In our population, anti-CagA antibodies were present in 61.8% of a general population admitted to the Emergency Care Unit, as published elsewhere^[13].

Out of the 10 patients with a past history of peptic ulcer, 7 had anti-*H pylori* antibodies in circulation. In 29 cases, the signs of portal hypertension [varices or congestive gastropathy] were shown by upper GI endoscopy while in 111 patients there were no abnormalities.

DISCUSSION

The prevalence of *H pylori* infection in patients with liver disease needed to be studied on the basis of clinical and experimental considerations.

From a clinical point of view, the medical history of cirrhotic patients was punctuated by frequent and recurrent hospitalisations due to high rate of complications. Among the most relevant of them, peptic ulcer and upper GI hemorrhage were of peculiar relevance, being life-threatening for the patient and of high cost for Health Care Services, requiring both emergency care and subsequent long hospital stay^[14]. By a multivariate analysis, Calvet *et al.* found that male sex and *H pylori* seropositivity (OR 1.7, 95% CI 1.02-2.81) were variables independently related to peptic ulcer in cirrhotics with different etiologies^[15]. Moreover, in the case of hemorrhage from peptic ulcer, the presence of cirrhosis was independently associated with increased mortality ($P < 0.001$)^[16]. Little information is available on the prevalence of peptic ulcer in subjects suffering from PBC or primary sclerosing cholangitis (PSC). The prevalence of duodenal ulcer (DU) in male cirrhotics was investigated by Rabinovitz *et al.* in 216 subjects. Occurrence of DU amounted to 7.8% in patients and 2.2% in controls ($P < 0.005$). When the patients were subdivided according to etiology, DU prevalence was observed in 9.4% of HBV-related chronic hepatitis patients, 12.2% of alcohol-related chronic hepatitis patients, 3.5% of cryptogenic, 6.6% of autoimmune cirrhosis, 9.5% of PSC and none of the patients with PBC. However, in the latter case only 9 patients were included^[17].

Since peptic ulcer is related to the presence of *H pylori* infection in non-cirrhotic patients, it is logical to suppose a similar role for the bacterium also in subjects with cirrhosis.

A high prevalence of anti-*H pylori* antibodies in HCV-infected cirrhotic patients has been reported in several North Italian towns^[18,19]. On the contrary, there was no increased seroprevalence in patients suffering from autoimmune hepatitis^[20]. Fan *et al.* demonstrated a higher seroprevalence of *H pylori* in Chinese patients with HBV-related chronic hepatitis than in controls matched for age and socio-economic status^[21]. In Taiwan, Chen *et al.* found no association between peptic ulcer and *H pylori* infection in cirrhotic patients^[22]. Selection biases and methods of diagnosis were possible sources of the heterogeneity of the studies. Contrasting results might arise from the choice of tests used for the diagnosis of *H pylori* infection. Indeed, when the diagnosis relies solely on histological examination of gastric biopsies, sampling error is the source of severe misdiagnosis. The European *H pylori* Study Group has recommended to search for IgG anti-*H pylori* when performing an epidemiological investigation^[23].

Regarding populations of subjects suffering from PBC, Floreani *et al.* showed that *H pylori* colonization was significantly more frequent in controls than in patients but IgG anti-*H pylori* were detected in the same percentage in the two groups^[24]. Thus, the latter finding is in agreement with those of our study. Dohmen and coworkers in Japan, have found that *H pylori* is a possible pathogenic factor in atrophic corpus gastritis in PBC-patients. Furthermore, a positive correlation between the titers of anti-pyruvate dehydrogenase antibody and anti-*H pylori* was confirmed^[25]. However, in this investigation,

no comparison with a control population has been made.

From an experimental point of view, infection of healthy A/JCr male mice with *H. hepaticus* could result in chronic hepatitis and liver cancer in a short time^[26]. Since this report, several other *H. species* have been subsequently found in the liver and biliary tract of cats and dogs suffering from hepatitis and hepatocellular carcinoma. *H. species* have been demonstrated both in the bile and in the gallbladder mucosa of Chilean patients with chronic gallbladder inflammation, raising the question as to whether the frequent finding of gallbladder cancer in Chile might arise from such an infection^[6]. By polymerase chain reaction, hybridisation and partial DNA sequencing in human liver of patients with PBC or PSC, Nilsson *et al.* found the positivity for *Helicobacter* genus-specific primers in 11 out of 12 samples of PBC-subjects and in 9 out of 12 samples of individuals suffering from PSC^[27].

In conclusion, we found that the seroprevalence of *H. pylori* in subjects suffering from primary biliary cirrhosis was not more frequent than in controls, suggesting that the putative role of *H. pylori* in triggering organ-specific autoimmunity does not hold true for PBC.

On the other hand, although these data do not provide proof for the association between *H. pylori* infection and PBC, a type II statistical error, i.e. the probability of accepting the *null hypothesis* when it is false, cannot be ruled out.

REFERENCES

- 1 **Bulent K**, Murat A, Esin A, Fatih K, MMMurat H, Hakan H, Melih K, Mehmet A, Bulent Y, Fatih H. Association of *CagA* and *VacA* presence with ulcer and non-ulcer dyspepsia in a Turkish population. *World J Gastroenterol* 2003; **9**: 1580-1583
- 2 **Testino G**, Cornaggia M, De Iaco F. *Helicobacter pylori* influence on gastric acid secretion in duodenal ulcer patients diagnosed for the first time. *Panminerva Med* 2002; **44**: 19-22
- 3 **Mladenova I**, Pellicano R. Infectious agents and gastric tumours. An increasing role for Epstein-Barr virus. *Panminerva Med* 2003; **45**: 183-188
- 4 **Wotherspoon AC**, Doglioni C, Diss TC, Pan L, Moschini A, de Boni M, Isaacson PG. Regression of primary low-grade B-cell gastric lymphoma of mucosa-associated lymphoid tissue type after eradication of *Helicobacter pylori*. *Lancet* 1993; **342**: 575-577
- 5 **Roussos A**, Philippou N, Gourgoulis KI. *Helicobacter pylori* infection and respiratory diseases: a review. *World J Gastroenterol* 2003; **9**: 5-8
- 6 **Fox JG**, Dewhirst FE, Shen Z, Feng Y, Taylor NS, Paster BJ, Ericson RL, Lau CN, Correa P, Araya JC, Roa I. Hepatic *Helicobacter* species identified in bile and gallbladder tissue from Chileans with chronic cholecystitis. *Gastroenterology* 1998; **114**: 755-763
- 7 **Bogdanos DP**, Baum H, Grasso A, Okamoto M, Butler P, Ma Y, Rigopoulou E, Montalto P, Davies ET, Burroughs AK, Vergani D. Microbial mimics are major targets of crossreactivity with human pyruvate dehydrogenase in primary biliary cirrhosis. *J Hepatol* 2004; **40**: 31-39
- 8 **Tanaka A**, Prindiville TP, Gish R, Solnick JV, Coppel RL, Keffe EB, Ansari A, Gershwin ME. Are infectious agents involved in primary biliary cirrhosis? A PCR approach. *J Hepatol* 1999; **31**: 664-671
- 9 **Vergara M**, Calvet X, Roque M. *Helicobacter pylori* is a risk factor for peptic ulcer disease in cirrhotic patients. A meta-analysis. *Eur J Gastroenterol Hepatol* 2002; **14**: 717-722
- 10 **Heathcote EJ**. Management of primary biliary cirrhosis. The American Association for the Study of Liver Diseases practice guidelines. *Hepatology* 2000; **31**: 1005-1013
- 11 **Ponzetto A**, Pellicano R, Morgando A, Cirillo D, Marchiaro G, Curti F, Rizzetto M. Seroprevalence of *Helicobacter pylori* infection among blood donors in Torino, Italy. *Minerva Gastroenterol Dietol* 2001; **47**: 3-7
- 12 **Palli D**, Vaira D, Menegatti M, Saieva C. A serologic survey of *Helicobacter pylori* infection in 3281 Italian patients endoscoped for upper gastrointestinal symptoms. The Italian *Helicobacter Pylori* Study Group. *Aliment Pharmacol Ther* 1997; **11**: 719-728
- 13 **Pellicano R**, Parravicini PP, Bigi R, Gandolfo N, Aruta E, Gai V, Figura N, Angelino P, Rizzetto M, Ponzetto A. Infection by *Helicobacter pylori* and acute myocardial infarction. Do cytotoxic strains make a difference? *New Microbiol* 2002; **25**: 315-321
- 14 **Rosina F**, Alaria P, Castelli S, Dirindin N, Rocca G, Actis GC, Borelli R, Ciancio AL, De Bernardi W, Fornasiero S, Lavezzo B, Lagget M, Martinotti R, Marzano A, Ottobrelli A, Sostegni R, Rizzetto M, Verme G. Effect of patient characteristics on hospital costs for cirrhosis: implications for the disease-related group [DRG] reimbursement system. *Ital J Gastroenterol* 1996; **28**: 401-405
- 15 **Calvet X**, Navarro M, Gil M, Lafont A, Sanfeliu I, Brullet E, Campo R, Dalmau B, Rivero E, Mas P. Epidemiology of peptic ulcer disease in cirrhotic patients: role of *Helicobacter pylori* infection. *Am J Gastroenterol* 1998; **93**: 2501-2507
- 16 **Douset B**, Suc B, Boudet MJ, Cherqui D, Rotman N, Julien M, Fagniez PL. Surgical treatment of severe ulcerous hemorrhages: predictive factors of operative mortality. *Gastroenterol Clin Biol* 1995; **19**: 259-265
- 17 **Rabinovitz M**, Schade RR, Dindzans V, Van Thiel DH, Gavaler JS. Prevalence of duodenal ulcer in cirrhotic males referred for liver transplantation. Does the etiology of cirrhosis make a difference? *Dig Dis Sci* 1990; **35**: 321-326
- 18 **Ponzetto A**, Pellicano R, Redaelli A, Rizzetto M, Roffi L. *Helicobacter pylori* infection in patients with Hepatitis C Virus positive chronic liver diseases. *New Microbiol* 2003; **26**: 321-328
- 19 **Leone N**, Pellicano R, Brunello F, Cutufia MA, Berrutti M, Fagoonee S, Rizzetto M, Ponzetto A. *Helicobacter pylori* seroprevalence in patients with cirrhosis of the liver and hepatocellular carcinoma. *Cancer Detect Prev* 2003; **27**: 494-497
- 20 **Durazzo M**, Pellicano R, Premoli A, Berrutti M, Leone N, Ponzetto A, Rizzetto M. *Helicobacter pylori* seroprevalence in patients with autoimmune hepatitis. *Dig Dis Sci* 2002; **47**: 380-383
- 21 **Fan XG**, Zou YY, Wu AH, Li TG, Hu GL, Zhang Z. Seroprevalence of *Helicobacter pylori* infection in patients with hepatitis B. *Br J Biomed Sci* 1998; **55**: 176-178
- 22 **Chen JJ**, Changchien CS, Tai DI, Chiou SS, Lee CM, Kuo CH. Role of *Helicobacter pylori* in cirrhotic patients with peptic ulcer. *Dig Dis Sci* 1994; **39**: 1565-1568
- 23 Guidelines for clinical trials in *Helicobacter pylori* infection. Working Party of the European *Helicobacter pylori* Study Group. *Gut* 1997; **41**(Suppl 2): S1-S9
- 24 **Floreani A**, Biagini MR, Zappala F, Farinati F, Plebani M, Rugge M, Surrenti C, Naccarato R. Chronic atrophic gastritis and *Helicobacter pylori* infection in primary biliary cirrhosis: a cross-sectional study with matching. *Ital J Gastroenterol Hepatol* 1997; **29**: 13-17
- 25 **Dohmen K**, Shigematsu H, Miyamoto Y, Yamasaki F, Irie K, Ishibashi H. Atrophic corpus gastritis and *Helicobacter pylori* infection in primary biliary cirrhosis. *Dig Dis Sci* 2002; **47**: 162-169
- 26 **Ward JM**, Fox JG, Anver MR, Haines DC, George CV, Collins MJ, Gorelick PL, Nagashima K, Gonda MA, Gilden RV, Tully JG, Russell RJ, Benveniste RE, Paster BJ, Dewhirst FE, Donovan JC, Anderson LM, Rice JM. Chronic active hepatitis and associated liver tumors in mice caused by a persistent bacterial infection with a novel *Helicobacter species*. *J Natl Cancer Inst* 1994; **86**: 1222-1227
- 27 **Nilsson H**, Taneera J, Castedal M, Glatz E, Olsson R, Wadstrom T. Identification of *Helicobacter pylori* and *Helicobacter* species by PCR, hybridization and partial DNA sequencing in human liver samples from patients with primary sclerosing cholangitis or primary biliary cirrhosis. *J Clin Microbiol* 2000; **38**: 1072-1076

Pathological characteristics of gastric leiomyoblastoma

Xiao-Feng Huang, Chun-Mei Wang, Bo-Rong Pan, Xiao-Wen Dai, Li Fang, Jia-Ji Yang, Hua Yu, Jun Ren

Xiao-Feng Huang, Chun-Mei Wang, Jia-Ji Yang, Hua Yu, Electron Microscope Center, Fourth Military Medical University, Xi'an 710032, Shaanxi Province, China

Bo-Rong Pan, Jun Ren, Department of Oncology, Xijing Hospital, Fourth Military Medical University, Xi'an 710032, Shaanxi Province, China

Xiao-Wen Dai, Li Fang, Department of Pathology, Chinese PLA 117 Hospital, Hangzhou 310013, Zhejiang Province, China

Supported by the Foundation of 117 Hospital, No.99008

Correspondence to: Chun-Mei Wang, Electron Microscope Center, Fourth Military Medical University, Xi'an 710032, Shaanxi Province, China. fmmuem@fmmu.edu.cn

Telephone: +86-29-83374572

Received: 2004-02-02 **Accepted:** 2004-03-24

Abstract

AIM: To determine the pathological characteristics of gastric leiomyoblastoma.

METHODS: All tissues were obtained during surgery or gastroscopy. Tissue specimens for examination by light microscope were 1 cm×1 cm×1 cm in size, fixed in 40 g/L neutral buffered formaldehyde, embedded in paraffin, and stained with hematoxylin and eosin. The fresh tissues obtained for electron microscopy were 1 mm×1 mm×1 mm in size, and fixed in phosphate buffered 30 g/L glutaraldehyde, postfixed in 10 g/L osmium tetroxide and dehydrated in graded alcohol, embedded in Epon 812. Ultrathin sections of 50 nm were stained with uranyl acetate and lead citrate and examined under a JEM-2000 EX transmission electron microscope.

RESULTS: The most important histopathological feature of leiomyoblastoma was the predominance of large, rounded or polygonal cells with characteristic perinuclear clear zone in cytoplasm. The tumor cells arranged in patch, cell junction or junctional complex could be found occasionally between cells under electron microscope. Most of the neoplastic cytoplasm were filled with myofilaments, dense bodies, and dense patches. Rough endoplasmic reticulum dilated as lakes, and large quantities of protein secretions of intermediate electron density were found in the dilated cisternae. Intracisternal segregation could also be found. The nuclei were round or oval, and anomalous nuclei were found in part of cells.

CONCLUSION: The diagnosis of gastric leiomyoblastoma can be confirmed by electron microscopy. The clear appearance of tumor cells is due to the dilation of rough endoplasmic reticulum, not fat droplets, glycogens or mucus in cytoplasm.

Huang XF, Wang CM, Pan BR, Dai XW, Fang L, Yang JJ, Yu H, Ren J. Pathological characteristics of gastric leiomyoblastoma. *World J Gastroenterol* 2004; 10(21): 3182-3184

<http://www.wjgnet.com/1007-9327/10/3182.asp>

INTRODUCTION

Gastric neoplasms are common in the world, specially in China^[1-8].

Gastrointestinal stromal tumor (GIST) is the most common mesenchymal tumor of gastrointestinal tract^[9], although GIST may arise from any portion of the foregut to hindgut, two thirds of stromal tumors originate from the stomach^[10]. Leiomyoblastoma, also called bizarre leiomyoma or epithelioid leiomyoma, is a rare smooth muscle tumor characterized by epithelioid cells with clear cytoplasm and an unknown biological behaviour. It is an unusual type of smooth muscle tumor which is biologically benign in most cases, but on rare occasions may behave in a malignant manner and metastasize^[11-15]. It is most frequently seen in the gastric wall but may occasionally be encountered in the uterus^[16,17], tongue^[18], round ligament^[19], omentum^[12], vulva^[20], urethra^[21], intestines, mesentery, retroperitoneum, mediastinum, and deep superficial soft tissues^[22,23]. Gastric leiomyoblastoma is a benign neoplasia, extremely uncommon and potentially malignant, arising from the muscular layer of the stomach^[24-26]. These neoplasms form solitary, well-defined, but not encapsulated, rounded or lobulated masses which, when small, tend to be localized intramurally. Multiple tumors are rare^[27-30]. The growth may take place towards the lumen, resulting in a polypoid mass and is covered by an attenuated mucosa.

MATERIALS AND METHODS

All the cases were obtained from the Chinese PLA 117 Hospital. Information of these cases is shown in Table 1. The patient population consisted of two men and three women. Their mean age was 51.4 years, ranging from 48 to 58 years at the time of diagnosis (Table 1). No relevant information of family history was found.

Table 1 Principal manifestations of gastric leiomyoblastoma

No	Sex	Age (yr)	Manifestations
1	Male	48	Abdominal dull pain, gasterorrhagia, dyspepsia
2	Male	56	Abdominal pain, abdominal mass, hemafecia
3	Female	42	Abdominal pain, nausea, vomiting
4	Female	53	Abdominal pain, vomiting, black stool
5	Female	58	Interrupted hematemesis, cupressus defecation

The cytologic samples were negative in all cases. The patients were explored surgically and neoplasms of stomach resected. All tissue specimens for examination by light microscope were 1 cm×1 cm×1 cm in size, fixed in 40 g/L neutral buffered formaldehyde, embedded in paraffin, and stained with hematoxylin and eosin. The fresh tissues obtained for electron microscopy were 1 mm×1 mm×1 mm in size, and fixed in phosphate buffered 30 g/L glutaraldehyde, postfixed in 10 g/L osmium tetroxide and dehydrated in graded alcohol, embedded in Epon 812. Ultrathin sections of 50 nm were stained with uranyl acetate and lead citrate and examined under a JEM-2000 EX transmission electron microscope.

RESULTS

Gross anatomy and gastroscopy

All resected tumors were well-circumscribed, and three tumors were located at the antro-pyloric region (cases 1, 3 and 4), one

at the body (case 2) and one at the gastric antrum (case 5). The size was measured between 2.5 cm and 13 cm, averaging 6.8 cm. The type of tumor growth was intraluminal (1/5) or extraluminal (2/5) or mixed (2/5). An ulcerated nodular tumor, located in the anterior wall and minor curvature of the gastric antrum (case 1), was found by gastroscopy.

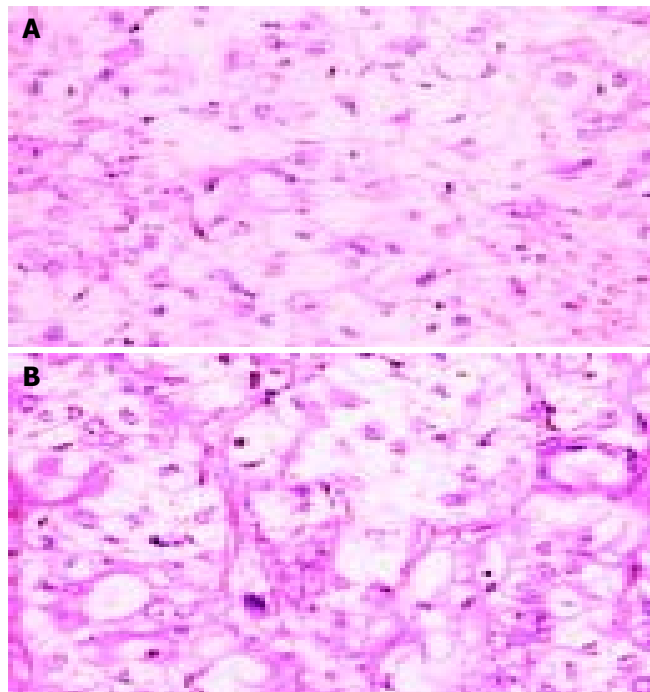


Figure 1 Round tumor cells, with clear cytoplasm, vary greatly in size and shape.

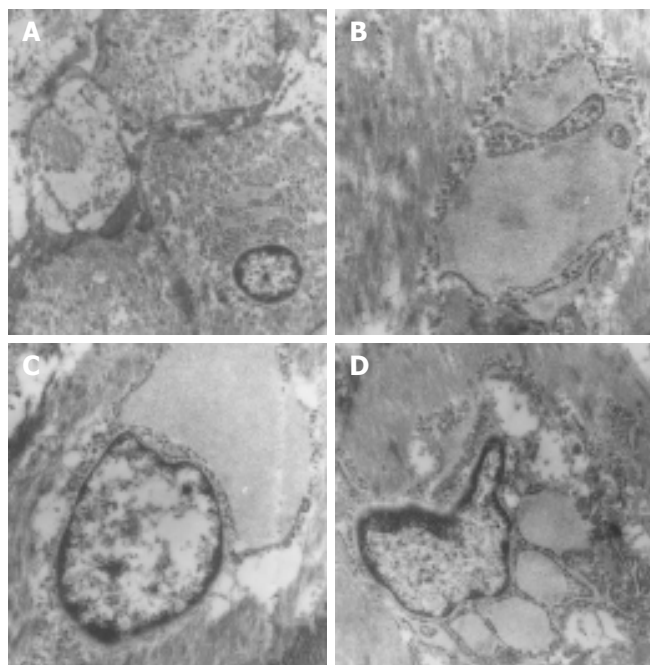


Figure 2 Ultrastructure of gastric leiomyblastoma. A: Tumor cells with many microfilaments, B: Intracisternal segregation could also be found, C: Rough endoplasmic reticulum dilatated as lakes, and protein secretion of intermediate electron density was found in the dilated cisternae, D: Distorted nuclei were found in tumor cells.

Histopathological appearances

Round tumor cells with clear cytoplasm, varied greatly in size

and shape in different parts of the same tumor (Figure 1). The cellular morphology of the muscle neoplasm was all homogenous and the frequency of mitosis was 2 mitoses in case 1 and 4 in case 5 in 10 HPFs, and some areas of fibrosis and degeneration were found in case 3. The most important feature of leiomyblastoma was the predominance of large, round or polygonal cells with characteristic perinuclear clear zone in cytoplasm (Figure 1). The nuclei might be pleomorphic with prominent nucleoli.

Ultrastructural characteristics

Ultrastructural studies confirmed that the origin of these tumors was smooth-muscle cells, and they were fusiform and round with many microfilaments. Tumor cells arranged in patch, and the cell junction or junctional complex could be found occasionally between cells. Most of the neoplastic cytoplasm were filled with myofilaments, dense bodies, and dense patches (Figure 2 A, B). Rough endoplasmic reticulum dilatated as lakes, and large quantities of protein secretions of intermediate electron density were found in the dilated cisternae (Figure 2C). Intracisternal segregation could also be found (Figure 2B). The nuclei were round or oval, and distorted nuclei were found in part of cells (Figure 2D).

DISCUSSION

The most important ultrastructural features of leiomyblastoma were myofilaments, dense bodies and dense patches present in most of the tumor cells. The perinuclear clear zone in cytoplasm was caused by dilation of rough endoplasmic reticulum. These characteristics proved that gastric leiomyblastoma arised from smooth muscle cells of the gastrointestinal (GI) tract. Leiomyblastoma was often previously diagnosed as GIST. Although the term GIST was first used in 1983 (by Mazur and Clark), the 1998 discovery by Hirota that GIST tumors could contain mutations in the c-kit gene and marked the beginning of a new understanding and reclassification of sarcomas of the GI tract. Prior to the year 2000, GISTs were classified as one of the types of soft tissue sarcoma (STS), including tumors of smooth-muscle origin (most commonly leiomyosarcoma, and also leiomyoma or leiomyblastoma) and of neural-crest origin (eg, Schwannoma, or nerve sheath tumour).

Most tumors previously diagnosed as gastrointestinal autonomic nerve tumors (GANTs) are also now classified as GISTs and contain essentially the identical KIT mutations as GIST. What establishes GIST as a separate diagnosis from these other soft tissue sarcomas is not just the description of where the tumor is located, but also the additional factor that it is KIT (CD117) positive. Most GIST patients are also CD34 positive and desmin negative. Well, one of the best ways to identify the cancer cell type (aside from just looking at the cells under a microscope) is to determine the proteins that the cells make. Specialized tests allow the pathologist to do this, usually by determining whether the cells will bind to antibodies against the protein of interest. So, “kit-positive” means that the cells make the protein “kit”, desmin-negative means that the cells do not make the protein “desmin”.

With the development of new effective therapies for GIST, it is vitally important that patients with soft tissue sarcomas of the GI tract have their tumor slides tested for KIT (CD117) by a pathologist experienced with GIST and KIT. Some (perhaps many) patients with pathology reports that were done prior to 2001 may think they have leiomyosarcoma, leiomyoma, leiomyblastoma, or GANT when in fact their pathology slides were never tested for KIT and they might have GIST. Once more, misdiagnosis can be a disaster. Pathology is critical. Fortunately, the pathology of GIST is now (2003) much better understood than it was in five years ago.

Another question is the origin of GIST. GISTs were previously thought to arise from smooth muscle cells of the GI tract. The discovery that GISTs could express KIT protein helps establish that GISTs do not originate from smooth muscles. The current thinking is that GIST tumors arise either from stem cells that differentiate towards interstitial cells of Cajal or directly from interstitial cells of Cajal (ICCs). The interstitial cells of Cajal are the pacemaker cells of the GI tract (they are named after a great Spanish biologist and microscopist named Cajal), they stimulate the movement (contractions) of the GI tract. These movements ("peristalsis") are the waves of contraction which force the digested food through the gut. GIST often spreads from the original (primary) site to distant locations. If this happens, these tumors are called metastases (or simply, "mets"). If GIST tumors metastasize they usually travel to the liver, or the peritoneum. Metastases to lymph-nodes and lungs are rare, but do occur. Metastasis is usually even worse than the growth of the primary one. Metastases can cripple a vital organ such as the liver. They are usually harder to treat than primary tumors. Metastases are the terrorist network of cancer, stealthily spreading to distant sites, where they can grow and do damage.

The results showed that gastric leiomyoblastoma cells did not differentiate to interstitial cells of Cajal, but differentiated to smooth muscle cells. Therefore, we think if definite smooth myocytes are found in this tumor, it should be diagnosed as leiomyoblastoma but not as GIST.

In summary, gastric leiomyoblastomas have a characteristic ultrastructure, electron microscopy may play a crucial role in diagnosis of gastric leiomyoblastoma.

REFERENCES

- 1 Lu JB, Sun XB, Dai DX, Zhu SK, Chang QL, Liu SZ, Duan WJ. Epidemiology of gastroenterologic cancer in Henan Province, China. *World J Gastroenterol* 2003; **9**: 2400-2403
- 2 Zhang JH, Li Y, Wang R, Gedder H, Guo W, Wen DG, Chen ZF, Wei LZ, Kuang G, He M, Zhang LW, Wu ML, Wang SJ. NQO1 C609T polymorphism associated with esophageal cancer and gastric cardiac carcinoma in North China. *World J Gastroenterol* 2003; **9**: 1390-1393
- 3 Wang KJ, Wang RT. Meta-analysis on the epidemiology of *Helicobacter pylori* infection in China. *Zhonghua Liuxingbingxue Zazhi* 2003; **24**: 443-446
- 4 Roder DM. The epidemiology of gastric cancer. *Gastric Cancer* 2002; **5**(Suppl 1): 5-11
- 5 Wu K, Crusius JB, Fan D, Pena AS. The immunogenetics and pathogenesis of gastric cancer. Highlights of the first Sino-European workshop on the immunogenetics and pathogenesis of gastric cancer. *Drugs Today* 2002; **38**: 391-417
- 6 Kasakura Y, Phan A, Ajani J. Adjuvant therapy for resected gastric carcinoma. *Surg Oncol Clin N Am* 2002; **11**: 431-444
- 7 Wang G, Hao C, Lai S. Endoscopic study on cancer of gastric cardia in the high incidence areas of China. *Zhonghua Zhongliu Zazhi* 2002; **24**: 381-383
- 8 Gao CM, Takezaki T, Wu JZ, Li ZY, Liu YT, Li SP, Ding JH, Su P, Hu X, Xu TL, Sugimura H, Tajima K. Glutathione-S-transferases M1 (GSTM1) and GSTT1 genotype, smoking, consumption of alcohol and tea and risk of esophageal and stomach cancers: a case-control study of a high-incidence area in Jiangsu Province, China. *Cancer Lett* 2002; **188**: 95-102
- 9 Trupiano JK, Stewart RE, Misick C, Appelman HD, Goldblum JR. Gastric stromal tumors: a clinicopathologic study of 77 cases with correlation of features with nonaggressive and aggressive clinical behaviors. *Am J Surg Pathol* 2002; **26**: 705-714
- 10 House MG, Guo M, Efron DT, Lillemoie KD, Cameron JL, Syphard JE, Hooker CM, Abraham SC, Montgomery EA, Herman JG, Brock MV. Tumor suppressor gene hypermethylation as a predictor of gastric stromal tumor behavior. *J Gastrointest Surg* 2003; **7**: 1004-1014
- 11 Shi HY, Yang XC, Zhang GZ. Malignant gastric leiomyoblastoma accompanied by metastasis in many sites: report of a case. *Xin Xiaohuabingxue Zazhi* 1994; **2**(Suppl 2): 39
- 12 Sun XL. The multiple leiomyoblastoma of omentum accompanied by metastasis of liver, spleen and colon transversum: report of a case. *Huaren Xiaohua Zazhi* 1998; **6**: 518
- 13 Diaz Plasencia J, Tantalean E, Guzman R, Pomatanta Plasencia J, Grados Mendez J, Vilela C. Malignant gastric leiomyoblastoma: case report. *Rev Gastroenterol Peru* 1997; **17**: 170-176
- 14 Kamiga M, Kimura W, Takasu N, Takeshita A, Ozawa K, Fuse A, Usuba O, Nagashima R. Successful resection of a liver metastasis from gastric leiomyoblastoma: report of a case. *Surg Today* 2000; **30**: 932-936
- 15 Ballarini C, Intra M, Ceretti AP, Prestipino F, Bianchi FM, Sparacio F, Berti E, Perrone S, Silva F. Gastrointestinal stromal tumors: a "benign" tumor with hepatic metastasis after 11 years. *Tumori* 1998; **84**: 78-81
- 16 Watanabe K, Ogura G, Suzuki T. Leiomyoblastoma of the uterus: an immunohistochemical and electron microscopic study of distinctive tumours with immature smooth muscle cell differentiation mimicking fetal uterine myocytes. *Histopathology* 2003; **42**: 379-386
- 17 Modafferi F. Epithelioid cell's uterine leiomyoma uteri. A case report with immunohistochemical study. *J Exp Clin Cancer Res* 2002; **21**: 295-298
- 18 Sancho Alvarez A, Poncela Blanco M, Morais Perez D, Martin Siguenza G, Peral Martinez JJ. Leiomyoblastoma of the tongue. *Acta Otorrinolaringol Esp* 2001; **52**: 70-73
- 19 Bakotic BW, Cabello-Inchausti B, Willis IH, Suster S. Clear-cell epithelioid leiomyoma of the round ligament. *Mod Pathol* 1999; **12**: 912-918
- 20 Hopkins-Luna AM, Chambers DC, Goodman MD. Epithelioid leiomyoma of the vulva. *J Natl Med Assoc* 1999; **91**: 171-173
- 21 Sakai Y, Yamada T, Fukuda H, Ichiyonagi N, Kamata S, Nagahama K, Tanizawa A, Watanabe T, Saitoh H, Itoyama S. A case of epithelioid leiomyoma (leiomyoblastoma) of the urethra. *Hinyokika Kyo* 2000; **46**: 41-43
- 22 Hou YY, Sun MH, Wei YK, Tan YS, Lu XY, Wang J, Zhu XZ, Zheng AH. Clinicopathological, immunohistochemical and molecular genetic study of intra-abdomen extra-gastrointestinal stromal tumors. *Zhonghua Binglixue Zazhi* 2003; **32**: 422-426
- 23 Abdulkader I, Cameselle-Teijeiro J, Gude F, Fraga M, Varela-Duran J, Barreiro F, Forteza J. Predictors of malignant behaviour in gastrointestinal stromal tumours: a clinicopathological study of 34 cases. *Eur J Surg* 2002; **168**: 288-296
- 24 Simeth C, Dellach C, Guarino G, Balani A. Gastric leiomyoblastoma. (Review of the literature in the light of a case). *Ann Ital Chir* 1999; **70**: 57-60
- 25 Mazzocconi G, Mantella F, Anselmi D, Nigita G, Terenzi A, Rossi Lemeni A, Sbaffi E. Gastric leiomyoblastomas: a clinical case report. *G Chir* 2000; **21**: 167-171
- 26 Barrier A, Huguier M, Levard H, Montariol T, Fagniez PL, Sauvanet A. Gastric stromal tumors. Results of a multicenter study. French Associations of Surgery Research. *Chirurgie* 1999; **124**: 494-502
- 27 Simeth C, Dellach C, Guarino G, Balani A. Gastric leiomyoblastoma. (Review of the literature in the light of a case). *Ann Ital Chir* 1999; **70**: 57-60
- 28 Medina Perez M, Reyes Lopez A, Garcia Ferris G. Epithelioid gastric leiomyosarcoma (malignant leiomyoblastoma) with intense expression of smooth muscle desmin and actin). *Rev Esp Enferm Dig* 1998; **90**: 595-596
- 29 Sofka CM, Semelka RC, Marcos HB, Calvo BF, Woosley JT. Metastatic gastric leiomyoblastoma: a case report. *Magn Reson Imaging* 1998; **16**: 343-346
- 30 Nozoe T, Nagamatsu A, Funahashi S, Kitamura M, Suehiro T, Matsumata T, Sugimachi K. Partial resection for leiomyoblastoma of stomach. *Hepatogastroenterology* 2001; **48**: 1806-1807

Changes of cytosolic $[Ca^{2+}]_i$ in neutrophils in pancreatic microcirculation of rats with caerulein-induced acute pancreatitis under fluid shear stress

Zong-Guang Zhou, You-Qin Chen, Xu-Bao Liu, Wei-Ming Hu, Bo-Le Tian, Huai-Qing Chen

Zong-Guang Zhou, You-Qin Chen, Xu-Bao Liu, Wei-Ming Hu, Bo-Le Tian, Department of General Surgery & Institute of Gastroenteric Surgery, West China Hospital, Sichuan University, Chengdu 610041, Sichuan Province, China

Huai-Qing Chen, Institute of Biomedical Engineering, West China Center of Medical Sciences, Sichuan University, Chengdu 610041, Sichuan Province, China

Supported by the National Natural Science Foundation of China, No. 39770722 and the Key Project of National Outstanding Youth Foundation of China, No. 39925032

Correspondence to: Professor Zong-Guang Zhou, Department of General Surgery & Institute of Gastroenteric Surgery, West China Hospital, Sichuan University, Chengdu 610041, Sichuan Province, China. zhou767@21cn.com

Telephone: +86-28-85422484 **Fax:** +86-28-85422484

Received: 2004-03-27 **Accepted:** 2004-04-05

Abstract

AIM: To investigate the fluid shear stress induced changes of $[Ca^{2+}]_i$ in neutrophils in pancreatic microcirculation of experimental acute pancreatitis (AP).

METHODS: Wistar rats ($n = 36$) were randomized into three groups. A model of AP was established by subcutaneous injection of caerulein. Low-shear 30 viscometer was used to provide steady fluid shear stress on separated neutrophils. The mean fluorescent intensity tested by flow cytometry was used as the indication of $[Ca^{2+}]_i$ quantity.

RESULTS: Under steady shear, cytosolic $[Ca^{2+}]_i$ showed biphasic changes. The shear rate changed from low to high, $[Ca^{2+}]_i$ in different groups decreased slightly and then increased gradually to a high level ($P < 0.05$). A close correlation was observed between the cytosolic $[Ca^{2+}]_i$ level and the alteration of fluid shear stress in regional microcirculation of AP.

CONCLUSION: The increase of $[Ca^{2+}]_i$ is highly related to the activation of neutrophils, which contributes to neutrophil adhesion to endothelium in the early phase of AP. The effect of fluid shear stress on $[Ca^{2+}]_i$ may play a crucial role in pancreatic microcirculatory failure of AP.

Zhou ZG, Chen YQ, Liu XB, Hu WM, Tian BL, Chen HQ. Changes of cytosolic $[Ca^{2+}]_i$ in neutrophils in pancreatic microcirculation of rats with caerulein-induced acute pancreatitis under fluid shear stress. *World J Gastroenterol* 2004; 10(21): 3185-3187

<http://www.wjgnet.com/1007-9327/10/3185.asp>

INTRODUCTION

Studies have confirmed the hypothesis that microcirculatory derangements play a pivotal role in the pathogenesis of acute pancreatitis (AP), including the process of conversion from edematous to necrotizing injury^[1-3]. Although several

pathophysiological sequences, such as protease activation, free radical generation, and inflammatory mediator release, have been described in acute pancreatitis, the precise mechanism by which acute pancreatitis is initiated is unknown^[4-7]. Cellular calcium, a key physiological signaling element in cell function and also a crucial pathological intracellular messenger in cell injury, appears to be involved in the initiation and development of acute pancreatitis^[8-12]. Previous studies have suggested that AP is frequently associated with sequestration of inflammatory cells, particularly neutrophils, within pancreas, and it is generally believed to be an early and important event in the evolution of pancreatitis^[13,14]. Recently, considerable attention has been directed at identifying the chemoattractant substances responsible for leukocyte sequestration within these tissues and the factors released from these inflammatory cells that contribute to progression of AP^[15-21]. Cytosolic free Ca^{2+} , a well-known second messenger, takes part in many cellular reaction processes and regulates the activity of many enzymes^[8]. Caerulein-induced AP has been shown to cause cytosolic free Ca^{2+} transient increase^[9-12]. Increase in leukocyte cytosolic $[Ca^{2+}]_i$ might be involved in intercellular adhesion by regulating the affinity of surface adhesion molecules or by facilitating transendothelial leukocyte migration, which might lead to increased leukocytic infiltration and tissue damage during AP^[9-12].

Previous studies mainly concentrated on the peripheral blood neutrophils during AP under static state due to limitation of experimental methodology. However, to the authors' knowledge, no reports are available about local pancreatic microcirculatory neutrophils during AP under flow state. Although the number of neutrophils in circulation is much less compared with the total mature neutrophils in the body, these circulating cells move with blood in the whole body, and execute disinfectant functions. The stored neutrophils replenish at a certain rate into the blood to maintain a dynamic balance between circulation pool and bone marrow storage pool^[22,23]. When it is necessary, bone marrow can release more neutrophils to enhance the defense efficacy. So blood flow is an important physiological environment for neutrophils^[22,23]. We first undertook to investigate the change of $[Ca^{2+}]_i$ in local pancreatic microcirculatory neutrophils during AP under fluid shear stress. The results of this study might provide a new insight into the pathogenesis of AP.

MATERIALS AND METHODS

Animals

Adult male Wistar rats weighting 250-350 g were purchased from Center of Experimental Animals, Sichuan University, Chengdu, China. All animals were starved for 24 h prior to experimentation. All animal experiments were conducted according to the guidelines of the Local Animal Use and Care Committees and the National Animal Welfare Law.

Induction of acute pancreatitis

All rats of the experimental groups were injected with 5.5 $\mu\text{g}/\text{kg}$ and 7.5 $\mu\text{g}/\text{kg}$ of caerulein (Sigma Co., USA) subcutaneously

at 0 and 1 h after the beginning of experiment respectively, while the rats of the control group were subcutaneously injected with normal saline solution.

Experimental protocol

Experimental animals were divided into three groups, with 12 rats each group. Group 1: normal control, group 2 (AP- I): rats at 2 h after the induction of AP, and group 3 (AP- II): rats at 4 h after the induction of AP. Rats in each experimental group were killed to obtain blood by splenic vein puncture at 2 and 4 h after first caerulein injection.

Preparation of neutrophils

Rat polymorphonuclear cells (PMNs) were isolated according to the technique described by Hjorth *et al.*^[24] for human PMNs. Blood was immediately mixed with heparin (50 U/mL) and centrifuged in a discontinuous Percoll gradient to yield a fraction of approximately 97% purity. Cell viability, as assessed by trypan blue exclusion, was above 96% under all experimental conditions.

Shear stress action on neutrophil suspension

Low-shear 30 viscometer (Switzerland) was used to provide low shear rate (5.96/s, 14.98/s, 51.2/s, 94.5/s and 128.5/s), then 37 g/L formaldehyde was added to fix neutrophils after sheared for 1 min.

Measurement of $[Ca^{2+}]_i$

Cells were loaded (5×10^6 /mL) with the Ca^{2+} -sensitive fluorescent dye fluo-3/AM (2 μ mol/L; Molecular probes, Eugene OR) at 37 °C for 30 min in 145 mmol/L NaCl, 5 mmol/L KCl, 1 mmol/L $MgCl_2$, 10 mmol/L glucose, 4 mmol/L probenecid, 10 mmol/L HEPES, pH 7.4. Fluorescence intensity was then measured with flow cytometry. The intensity of fluorescence correlated with the concentration of $[Ca^{2+}]_i$. Therefore, the mean fluorescence intensity (MFI) indicated the level of $[Ca^{2+}]_i$.

Statistical analysis

The results were expressed as mean \pm SD. The mean of MRI between groups was compared by a two-tailed Student's *t* tests. $P \leq 0.05$ was considered statistically significant.

RESULTS

Under steady shear, cytosolic $[Ca^{2+}]_i$ had biphasic changes. When the shear rate was very low, $[Ca^{2+}]_i$ decreased slightly. With the increase of shear rate, $[Ca^{2+}]_i$ increased gradually. When the shear rate was increased higher than 50/s, $[Ca^{2+}]_i$ in the experimental group was higher than that in the control group. With the shear rate changed from low to high, cytosolic $[Ca^{2+}]_i$ gradually increased to a significantly high level compared with the stationary control ($P < 0.05$). After treated with a shear rate of 128.5/s, the cytosolic $[Ca^{2+}]_i$ of AP-II group was significantly induced compared with AP-I group ($P < 0.05$) (Figure 1).

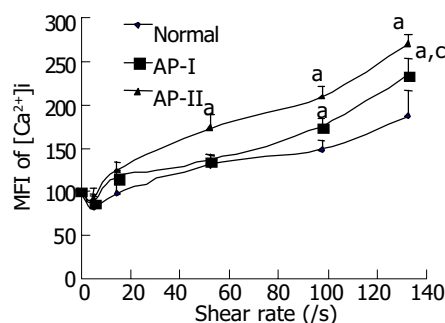


Figure 1 Effects of fluid shear stress on cytosolic $[Ca^{2+}]_i$ in neutrophils in pancreatic microcirculation of rats with AP. $^a P < 0.05$ vs normal; $^c P < 0.05$ vs AP- I.

DISCUSSION

Acute pancreatitis remains a clinical challenge because it is difficult to predict whether the disease is mild or runs a severe course with a possibly fatal outcome in a given patient^[25]. In recent years, researches on the morphology of pancreatic microcirculation have revealed that the blood supply of pancreatic lobules in most cases is provided by a single intralobular arteriole^[26]. This arteriole sends forth the tree-like branches when entering pancreatic lobule, and has no anastomosis with adjacent intralobular arterioles and their branches, and could be considered as an end-artery^[26]. This characteristic suggested pancreatic lobules were susceptible to ischemic injury due to spasm of intralobular arterioles, embolization of arterioles, formation of microthrombi or compression by interstitial edema^[1-3]. However, causative factors of early-stage ischemia and the precise triggering factors of local microcirculatory disturbance remain obscure^[3].

Cellular calcium, a key physiological signaling element in cell function and also a crucial pathological intracellular messenger in cell injury, appears to be involved in the initiation and development of acute pancreatitis^[7-12]. The present study provided several lines of evidence supporting this suggestion. We investigated whether calcium was involved in the priming response encountered during AP. We found that cytosolic $[Ca^{2+}]_i$ showed a biphasic changes when the neutrophil suspension was under a steady shear. When the shear rate changed from low to high, cytosolic $[Ca^{2+}]_i$ decreased slightly under a very low shear rate (5.96/s) and then increased gradually to a high level. From this study we could also infer that cytosolic $[Ca^{2+}]_i$ might be an identifying marker for AP.

Activation of neutrophils is one of the critical roles in pathologic process of AP, and cytosolic $[Ca^{2+}]_i$ has a close relation with neutrophil activation^[27,28]. Our study demonstrated the fluid shear stress induced changes of cytosolic $[Ca^{2+}]_i$ in neutrophils in pancreatic microcirculation of rats with caerulein-induced AP. These lines of evidence indicate that altered intracellular calcium might play an important role in the initiation and development of AP. In conclusion, cellular calcium may be an important factor in the pathogenesis of cerulein-induced acute pancreatitis.

REFERENCES

- Vollmar B, Menger MD. Microcirculatory dysfunction in acute pancreatitis. A new concept of pathogenesis involving vasomotion-associated arteriolar constriction and dilation. *Pancreatology* 2003; **3**: 181-190
- Chen HM, Sunamura M, Shibuya K, Yamauchi JI, Sakai Y, Fukuyama S, Mikami Y, Takeda K, Matsuno S. Early microcirculatory derangement in mild and severe pancreatitis models in mice. *Surg Today* 2001; **31**: 634-642
- Menger MD, Plusczyk T, Vollmar B. Microcirculatory derangements in acute pancreatitis. *J Hepatobiliary Pancreat Surg* 2001; **8**: 187-194
- Gomez-Cambronero LG, Sabater L, Pereda J, Cassinello N, Camps B, Vina J, Sastre J. Role of cytokines and oxidative stress in the pathophysiology of acute pancreatitis: therapeutic implications. *Curr Drug Targets Inflamm Allergy* 2002; **1**: 393-403
- Frossard JL. Pathophysiology of acute pancreatitis: a multi-step disease. *Acta Gastroenterol Belg* 2003; **66**: 166-173
- Makhija R, Kingsnorth AN. Cytokine storm in acute pancreatitis. *J Hepatobiliary Pancreat Surg* 2002; **9**: 401-410
- Weber CK, Adler G. From acinar cell damage to systemic inflammatory response: current concepts in pancreatitis. *Pancreatology* 2001; **1**: 356-362
- Sutton R, Criddle D, Raraty MG, Tepikin A, Neoptolemos JP, Petersen OH. Signal transduction, calcium and acute pancreatitis. *Pancreatology* 2003; **3**: 497-505
- Parekh AB. Calcium signaling and acute pancreatitis: specific

- response to a promiscuous messenger. *Proc Natl Acad Sci U S A* 2000; **97**: 12933-12934
- 10 **Raraty MG**, Petersen OH, Sutton R, Neoptolemos JP. Intracellular free ionized calcium in the pathogenesis of acute pancreatitis. *Baillieres Best Pract Res Clin Gastroenterol* 1999; **13**: 241-251
- 11 **Kruger B**, Albrecht E, Lerch MM. The role of intracellular calcium signaling in premature protease activation and the onset of pancreatitis. *Am J Pathol* 2000; **157**: 43-50
- 12 **Niederer C**, Luthen R, Klonowski-Stumpe H, Schreiber R, Soika I, Sata N, Bing H, Haussinger D. The role of calcium in pancreatitis. *Hepatogastroenterology* 1999; **46**: 2723-2730
- 13 **Acioli JM**, Isobe M, Kawasaki S. Early complement system activation and neutrophil priming in acute pancreatitis: participation of trypsin. *Surgery* 1997; **122**: 909-917
- 14 **Frossard JL**, Past CM. Experimental acute pancreatitis: new insights into the pathophysiology. *Front Biosci* 2002; **7**: d275-d287
- 15 **Bhatia M**, Mochhala S. Role of inflammatory mediators in the pathophysiology of acute respiratory distress syndrome. *J Pathol* 2004; **202**: 145-156
- 16 **de Dios I**, Perez M, de La Mano A, Sevillano S, Orfao A, Ramudo L, Manso MA. Contribution of circulating leukocytes to cytokine production in pancreatic duct obstruction-induced acute pancreatitis in rats. *Cytokine* 2002; **20**: 295-303
- 17 **Rau B**, Baumgart K, Kruger CM, Schilling M, Beger HG. CC-chemokine activation in acute pancreatitis: enhanced release of monocyte chemoattractant protein-1 in patients with local and systemic complications. *Intensive Care Med* 2003; **29**: 622-629
- 18 **Frossard JL**, Saluja AK, Mach N, Lee HS, Bhagat L, Hadenque A, Rubbia-Brandt L, Dranoff G, Steer ML. *In vivo* evidence for the role of GM-CSF as a mediator in acute pancreatitis-associated lung injury. *Am J Physiol Lung Cell Mol Physiol* 2002; **283**: L541-L548
- 19 **Bhatnagar A**, Wig JD, Majumdar S. Expression of activation, adhesion molecules and intracellular cytokines in acute pancreatitis. *Immunol Lett* 2001; **77**: 133-141
- 20 **Lundberg AH**, Granger N, Russell J, Callicutt S, Gaber LW, Kotb M, Sabek O, Gaber AO. Temporal correlation of tumor necrosis factor-alpha release, upregulation of pulmonary ICAM-1 and VCAM-1, neutrophil sequestration, and lung injury in diet-induced pancreatitis. *J Gastrointest Surg* 2000; **4**: 248-257
- 21 **Berney T**, Gasche Y, Robert J, Jenny A, Mensi N, Grau G, Vermeulen B, Morel P. Serum profiles of interleukin-6, interleukin-8, and interleukin-10 in patients with severe and mild acute pancreatitis. *Pancreas* 1999; **18**: 371-377
- 22 **Kantor AB**, Stall AM, Adams S, Watanabe K, Herzenberg LA. De novo development and self-replenishment of B cells. *Int Immunol* 1995; **7**: 55-68
- 23 **Suratt BT**, Young SK, Lieber J, Nick JA, Henson PM, Worthen GS. Neutrophil maturation and activation determine anatomic site of clearance from circulation. *Am J Physiol Lung Cell Mol Physiol* 2001; **281**: L913-L921
- 24 **Hjorth R**, Jonsson AK, Vretblad P. A rapid method for purification of human granulocytes using percoll. A comparison with dextran sedimentation. *J Immunol Methods* 1981; **43**: 95-101
- 25 **Beger HG**, Rau B, Isenmann R. Prevention of severe change in acute pancreatitis: prediction and prevention. *J Hepatobiliary Pancreat Surg* 2001; **8**: 140-147
- 26 **Zhou ZG**, Gao XH. Morphology of pancreatic microcirculation in the monkey: light and scanning electron microscopic study. *Clin Anat* 1995; **8**: 190-201
- 27 **Petty HR**. Neutrophil oscillations: temporal and spatiotemporal aspects of cell behavior. *Immunol Res* 2001; **23**: 85-94
- 28 **Davies EV**, Hallett MB. Cytosolic Ca²⁺ signalling in inflammatory neutrophils: implications for rheumatoid arthritis (Review). *Int J Mol Med* 1998; **1**: 485-490

Edited by Kumar M and Wang XL Proofread by Xu FM

Expression of human augmenter of liver regeneration in pichia pastoris yeast and its bioactivity *in vitro*

Qi Liu, Hui-Feng Yu, Hang Sun, Hua-Feng Ma

Qi Liu, Hui-Feng Yu, Hang Sun, Hua-Feng Ma, Institute for Viral Hepatitis, Chongqing University of Medical Sciences, Chongqing 400010, China

Supported by Excellent Youth Teacher Fund, Ministry of Education, No. 200065

Correspondence to: Professor Liu Qi, Institute for Viral Hepatitis, Chongqing University of Medical Science, Chongqing 400010, China. liuqiz@hotmail.com

Telephone: +86-23-63825854 Ext. 2225

Received: 2004-01-09 **Accepted:** 2004-02-26

Abstract

AIM: To construct a yeast expression system of human augmenter of liver regeneration (hALR) and to examine its bioactivity *in vitro*.

METHODS: With PCR and gene recombination techniques, cDNA of open reading frame of hALR was obtained from recombinant plasmid pcDNA3.1-hALR and inserted into plasmid pPIC9. The cDNA of hALR from recombinant plasmid pPIC9-hALR demonstrated by sequencing was subcloned into plasmid pPIC9K. The recombinant plasmid pPIC9K-hALR was transformed into GS115 with electroporation. hALR was expressed by GS115 under the induction of 5 mL/L methanol and purified with ultrafiltration after it was analyzed by 15% SDS-PAGE and Western blot. The effects of hALR on *in vitro* proliferation of QGY and HepG₂ cells were evaluated by ³H-TdR methods.

RESULTS: The correctness and integrity of recombinant plasmids pPIC9-hALR and pPIC9K-hALR were identified by restriction digestion, PCR and sequencing methods, respectively. hALR as a secretive protein was successfully expressed by GS115. Its molecular weight was about 15 ku and the target protein was about 60% of the total protein in the supernatant from GS115 with plasmid pPIC9K-hALR. The results of Western blot of hALR showed the specific band. The high qualitative hALR was obtained through ultrafiltration. hALR could stimulate *in vitro* proliferation of QGY and HepG₂ cells in a dose-dependent manner, but there was a difference in reactivity to hALR between QGY and HepG₂.

CONCLUSION: The hALR as a secretive protein can be successfully expressed by GS115. It may stimulate *in vitro* proliferation of QGY and HepG₂ cells at a dose-dependent manner. But QGY and HepG₂ cells have different reactivities to hALR.

Liu Q, Yu HF, Sun H, Ma HF. Expression of human augmenter of liver regeneration in pichia pastoris yeast and its bioactivity *in vitro*. *World J Gastroenterol* 2004; 10(21): 3188-3190
<http://www.wjgnet.com/1007-9327/10/3188.asp>

INTRODUCTION

Augmenter of liver regeneration (ALR) is an important cytokine

recently discovered and cloned from rat livers^[1,2]. It could stimulate DNA synthesis of liver cancer cells *in vitro* and enhance liver regeneration in rats after partial hepatectomy, but there is a debate whether it could directly stimulate DNA synthesis of hepatocytes *in vitro*^[1,3]. It has also been proved that ALR could partially reverse the liver fibrosis in experimental rats^[4] and enhance the success rate of fetal pancreas transplantation in rats^[5]. It seems to bring a bright future in the treatment of severe liver diseases. Although the recombinant human and rat ALR were successfully expressed in *E.coli* in our laboratory^[6-8], there are some defects that the target protein as an inclusion body expressed in *E.coli* could not often be refolded and modified correctly and that the procedure to purify ALR is very complicated. Because the pichia pastoris expressing system could overcome all these defects, it was selected to express ALR, which could be secreted into supernatants so that it was easy to purify ALR. It is possible for us to carry out further study with purified ALR.

MATERIALS AND METHODS

Reagents, plasmid, bacteria and cell strain

Escherichia coli JM109 and TOP10F⁺, plasmid pcDNA3.1-hALR, hepatocarcinoma HepG2 and QGY strains were preserved and monoclonal antibody against hALR was made in our laboratory^[9]. *Pichia pastoris* GS115, plasmids pPIC9 and pPIC9K were from Invitrogen Corporation, USA. DNA ladder marker, restriction endonuclease, and T4 DNA ligase were from Shanghai Sango, China. Peptone and YNB were from Amresco Co. USA. Yeast power was from Oxoid. 8200 cell filter, 5 kD and 30 kD membranes were from Millipore Co. USA. Gene pulser-II was from Bio-Rad Co. Ltd., USA.

Preparation of hALR gene

According to the maps of plasmids pcDNA3.1-hALR, pPIC9 and pPIC9K, the sequences of primers were designed as follows: forward: P₁5'-CACTCGAGAAAAGACGGACCCAGCAGAAG C-3'. reverse: P₂5'-CTGCGGCCGCTTAGTCACAGGAGCCGTC CTTC-3'. *Xho*I and *Not*I restriction sites were introduced and defined by the underline. Primers were synthesized by BoYa Co. Ltd. hALR sequence was amplified by polymerase chain reaction (PCR) for 30 cycles from pcDNA3.1-hALR containing the full-length open reading frame of hALR gene. Each cycle consisted of denaturation for 45 s at 94 °C, annealing for 45 s at 62 °C, and extension for 1 min at 72 °C. The PCR products were analyzed on 15 g/L agarose gel electrophoresis as specific band examination.

pPIC9-hALR and pPIC9K-hALR construction and identification

The PCR products of hALR from the gel extraction and pPIC9 were digested with *Xho* I and *Not* I and then purified, respectively. pPIC9 and hALR fragments were mixed with 3:1 mol/L and ligated by T4 DNA ligase overnight at 16 °C, then transformed into JM109 with CaCl₂ method. The positive clones were selected in LB plates with ampicillin and identified by PCR, restriction enzyme digestion and sequencing, respectively. After the correction and integrity of recombinant pPIC9-hALR were

proved, pPIC9-hALR and pPIC9K were digested with *SalI* and *SacI*. A 3.4 kb fragment containing hALR was obtained from pPIC9-hALR and 6.3 kb fragment from pPIC9K. Both fragments were mixed with 2:1 mol/L, ligated by T4 DNA ligase and transformed into TOP10F' with CaCl₂ method. The positive clones were selected in LB plates with ampicillin and karamycin and the plasmids from them were identified by PCR and restriction enzyme digestion on the next day.

Transformation and expression

Recombinant plasmids pPIC9K-hALR (8 μ L) and pPIC9K (8 μ L) were linearized, respectively, by digestion with *SalI*. Competent *pitch pastoris* GS115 was prepared according to the manual of Invitrogen Corporation. The linear plasmids pPIC9K (5-10 μ g) and pPIC9K-hALR (5-10 μ g) were mixed with competent GS115 (80 μ L), respectively. Under the conditions of 1500V, 25 μ F and 200 Ω , the competent GS115 was transformed by different mixtures using the Bio-Rad gene pulser, then planted and cultured in plates of minimal dextrose medium without histidine at 30 $^{\circ}$ C for 2 d for screening positive clones. The positive clones with pPIC9K-hALR or pPIC9K were respectively cultured in 3 mL buffered glycerol-complex medium (BMGY) overnight after identified by PCR. Then 15 μ L of GS115 was planted into 5 mL BMGY medium and cultured at 28 $^{\circ}$ C until the optical density at 600 nm (A_{600}) reached four. The GS115 with pPIC9K-hALR or pPIC9K were collected by centrifugation, resuspended by buffered methanol-complex medium to A_{600} reaching one and cultured continuously at 28 $^{\circ}$ C for 3 d. The 5 mL/L methanol in the medium was kept by methanol compensation at every 24 h. The expressed products at the different time points were analysed by 160 g/L SDS-PAGE and the expressed level was evaluated by computer scan.

Western blot analysis

Supernatants from GS115 with pPIC9K and pPIC9K-hALR were respectively loaded on 150 g/L SDS-PAGE for protein separation and transferred to polyvinylidene difluoride membrane by electrotransfer. After blocked with 50 mL/L milk in PBS, the membrane was incubated with monoclonal antibody (diluted 1:2 000) against hALR for 1 h at room temperature, washed three times with phosphate buffered saline, then mixed with goat anti-mouse IgG antibody coupled with horseradish peroxidase for 45 min, the bands were visualized by 3-3'-diaminobenzidine (DAB).

Purification and quantification

The ultrafiltration purification was selected according to the SDS-PAGE analysis of the supernatant from GS115 with pPIC9K-hALR there were no other bands except target one under 50 kD. The supernatant from GS115 induced by pPIC9K-hALR was centrifuged at 3 000 r/min for 10 min, and passed through 30 kD and 5 kD membranes and the filtrate between 30 kD and 5 kD was collected. As a control the supernatant from GS115 with pPIC9K was treated with same procedure as described above. The purified products were analyzed by 160 g/L SDS-PAGE and qualified by Lowary methods.

hALR bioactivity

Human hepatoma cell lines HepG₂ and QGY were planted at a concentration of 1×10^4 cell/well in 96-well plates supplemented with 80 mL/L fetal bovine serum, 5×10^5 mol/L penicillin, 80 μ g/mL streptomycin, and stimulated with different doses of hALR expressed by yeast and *E. coli* at 37 $^{\circ}$ C, 50 mL/L CO₂ for 8-9 h. The supernatant from GS115 with pPIC9K as negative control was also added. Three parallel wells were stimulated by the same concentration of hALR. The cells were harvested after 12 h of culture by adding 1 μ Ci/well ³H-TdR. The count per minute (cpm) value of cells from each well was measured by liquid

scintillation counter.

Statistical analysis

The data were expressed as mean \pm SD. Comparison was carried out using analysis of variance. *P* value less than 0.05 was considered statistically significant.

RESULTS

PCR result and identification of recombinant plasmid

The specific 400 bp fragment of hALR amplified by PCR from plasmid pcDNA3.1-hALR was analysed by 15 g/L agarose gel electrophoresis. The correctness and integrity of hALR fragments in recombinant plasmid pPIC9-hALR were proved by *XhoI*+*NotI* digestion and sequencing. The 3.4 kb fragment containing hALR was released from pPIC9K-hALR by digestion with *salI* and *sacI*. The 400 bp fragment was also obtained from pPIC9K-hALR by PCR (Figure 1).

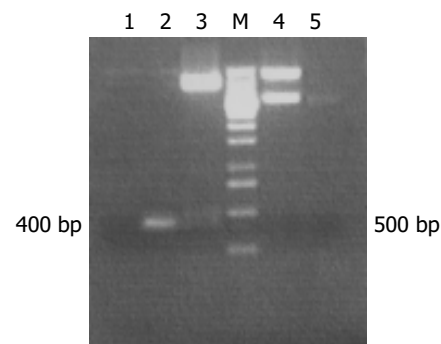


Figure 1 Identifications of recombination plasmid. Lane 1: amplified from pPIC9K; Lane 2: amplified from pPIC9K-hALR; Lane 3: pPIC9-hALR digested by *XhoI*+*NotI*; Lane M: 1 kb DNA ladder; Lane 4: pPIC9K-hALR digested by *SacI*+*SalI* (6.3 kb+3.4 kb); Lane 5: 3.4 kb fragment with hALR.

Expression and purification of hALR

Electrophoresis of supernatants from GS115 induced by pPIC9K-hALR showed that there was a specific band with 1.5×10^4 dalton molecular weight coinciding with the theoretical value and the target protein was about 60% of the total protein in the supernatant. There was no corresponding band in supernatant from GS115 transfected with pPIC9K. A single band of hALR was obtained through ultrafiltration purification (Figure 2).

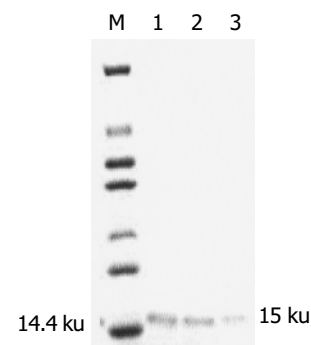


Figure 2 SDS-PAGE analysis of purified hALR. Lane M: protein marker; Lanes 1, 2, and 3: purified hALR.

Detection of protein expression by Western blot

Western blot result showed that the supernatant from GS115 with pPIC9K-hALR could specially bind to monoclonal antibody against hALR in 15 kD site, but the supernatant from GS115 with pPIC9K could not bind (Figure 3).

Table 1 Effect of different dosages of hALR on HepG₂ and QGY proliferation (mean±SD)

Cells	Control		Concentrations of hALR from yeast and <i>E.coli</i>				
			0.1 ng	10 ng	1 µg	8 µg	16 µg
HepG ₂	7 174±494	yeast	1 3779±1 431 ^a	13 679±1 205 ^a	15 279±1 802 ^a	22 670±1 402 ^{bc}	24 958±1 326 ^{bc}
		<i>E.coli</i>	1 0754±2 756 ^a	11 189±1 447 ^a	12 997±1 683 ^a	13 858±440 ^a	14 411±1 452 ^a
QGY	821±11	yeast	2 549±526 ^{bc}	2 298±203 ^{bc}	3 188±564 ^{bc}	11 825±841 ^{bc}	17 021±795 ^{bc}
		<i>E.coli</i>	934±50 ^a	883±106	1 222±168 ^a	1 362±171 ^a	6 209±225 ^b

^a*P*<0.05, ^b*P*<0.01 vs control; ^c*P*<0.05 vs hALR from *E.coli*.

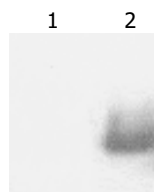


Figure 3 Western blot analysis of supernatants from GS115 treated with different plasmids. Lane 1: supernatant from GS115 with pPIC9K; Lane 2: supernatant from GS115 with pPIC9K-hALR.

Evaluation of hALR bioactivity

Results showed that hALR from GS115 with pPIC9K-hALR could stimulate the proliferation of HepG₂ and QGY on nanogram level in a dose-dependent manner. There was a marked difference in the reactivity to hALR between QGY and HepG₂ although both cells were from human liver cancer. In addition, hALR from yeast had stronger effect on the proliferation of HepG₂ and QGY than that from *E.coli* at same concentration (Table 1).

DISCUSSION

The *Pichia pastoris* system has been widely used in recent years due to its simple procedure, low expenditure and easy scaling up. It is more important that the foreign protein can be correctly refolded and modified, more than 200 proteins have been expressed by this system^[10]. Our results showed that hALR with 1.5×10⁴ dalton molecular weight as a secretive protein was successfully expressed by GS115 and about 60% of total protein was expressed in the supernatant. The ultrafiltration purification for hALR in the supernatant was applied because there were no other bands around the target protein, and a satisfactory purification effect was achieved. Our results demonstrated that not only the purification efficiency was greatly enhanced, but also the purification procedure was obviously simplified. Although it was reported that rat ALR could not directly stimulate liver cancer cells *in vitro*^[1], our data demonstrated that hALR could stimulate QGY and HepG₂ proliferation in a dose-dependent manner. Previously, we and others also obtained the similar results in rat ALR researches^[11,12]. These results suggested that ALR enhanced liver regeneration not only through indirect pathway i.e. immune regulation^[1,13-16], but also through direct one. Our result showed that at the same concentration, hALR expressed in yeast had a stronger effect on the proliferation of HepG₂ and QGY than that expressed in *E.coli*, although it was reported that there was no N-glycosylation site in its amino acid sequence^[1]. Our result suggests that there might exist some unknown modifications such as O-glycosylation site in hALR molecules expressed by yeast, and modification of protein after translation is very important for keeping higher bioactivity of target protein. Hence, the successful expression of ALR in *pichia pastoris* and its purification may provide a good tool for further research in this field.

REFERENCES

1 Hagiya M, Francavilla A, Polimeno L, Ihara I, Sakai H, Seki T,

Shimonishi M, Porter KA, Starzl TE. Cloning and sequence analysis of the rat augments of liver regeneration (ALR) gene: expression of biologically active recombinant ALR and demonstration of tissue distribution. *Proc Natl Acad Sci U S A* 1994; **91**: 8142-8146

2 Hagiya M, Francavilla A, Polimeno L, Ihara I, Sakai H, Seki T, Shimonishi M, Porter KA, Starzl TE. Cloning and sequence analysis of the rat augments of liver regeneration (ALR) gene: expression of biologically active recombinant ALR and demonstration of tissue distribution. *Proc Natl Acad Sci U S A* 1995; **92**: 3076

3 Yang XM, Xie L, Qiu ZH, Gong F, Wu ZZ, He FC. cDNA clone, expression and biological activity study of augments of liver regeneration. *Shengwu Huaxue Zazhi* 1997; **13**: 130-135

4 Wang AM, Yang XM, Guo RF, Zhang L, Li PJ, Wang QM, He FC. The recombinant augments of liver regeneration reverse fibrosis in experimental rat. *Zhonghua Ganzangbing Zazhi* 1999; **7**: 243

5 Adams GA, Maestri M, Squiers EC, Alfrey EJ, Starzl TE, Dafeo DC. Augments of liver regeneration enhances the success rate of fetal pancreas transplantation in rodents. *Transplantation* 1998; **65**: 32-36

6 Liu Q, Wang Z, Luo Y. The cDNA clone and sequence analysis of the coding region of human augments of liver regeneration (hALR) gene. *Zhonghua Ganzangbing Zazhi* 1999; **7**: 156-158

7 Liu Q, Shi XF, Luo Y, Zhang DF. Construction of prokaryotic expression vector of hALR and its expression in *E.coli*. *Zhonghua Ganzangbing Zazhi* 2000; **8**: 9-11

8 Ma HF, Liu Q. The cDNA clone of the coding region of rat augments of liver regeneration gene and its prokaryotic expression. *Chongqing Yikedaxue Xuebao* 2002; **27**: 9-11

9 Ma HF, Liu Q. Preparation of monoclonal antibody to human augments of liver regeneration: screening of hybridomas with unpurified antigen expressed by *E.coli*. *Zhongguo Mianyixue Zazhi* 2002; **18**: 671-673

10 Cregg JM, Cereghino JL, Shi J, Higgins DR. Recombinant protein expression in *Pichia pastoris*. *Mol Biotechnol* 2000; **16**: 23-53

11 Yu HF, Liu Q. Expression of rat augments of liver regeneration in *pichia pastoris* and evaluation of its bioactivity *in vitro*. *Zhonghua Ganzangbing Zazhi* 2003; **11**: 421-423

12 Yang XM, Hu ZY, Xie L, Wu ZZ, Wu CT, He FC. *In vitro* stimulation of HTC hepatoma cell growth by recombinant human augments of liver regeneration (ALR). *Shengli Xuebao* 1997; **49**: 557-561

13 Francavilla A, Vujanovic NL, Polimeno L, Azzarone A, Iacobellis A, Deleo A, Hagiya M, Whiteside TL, Starzl TE. The *in vivo* effect of hepatotrophic factors augments of liver regeneration, hepatocyte growth factor, and insulin-like growth factor-II on liver natural killer cell functions. *Hepatology* 1997; **25**: 411-415

14 Gandhi CR, Kuddus R, Subbotin VM, Prelich J, Murase N, Rao AS, Nalesnik MA, Watkins SC, DeLeo A, Trucco M, Starzl TE. A fresh look at augments of liver regeneration in rats. *Hepatology* 1999; **29**: 1435-1445

15 Polimeno L, Margiotta M, Marangi L, Lisowsky T, Azzarone A, Ierardi E, Frassanito MA, Francavilla R, Francavilla A. Molecular mechanisms of augments of liver regeneration as immunoregulator: its effect on interferon-gamma expression in rat liver. *Dig Liver Dis* 2000; **32**: 217-225

16 Tanigawa K, Sakaida I, Masuhara M, Hagiya M, Okita K. Augments of liver regeneration (ALR) may promote liver regeneration by reducing natural killer (NK) cell activity in human liver diseases. *J Gastroenterol* 2000; **35**: 112-119

Photocatalytic killing effect of TiO₂ nanoparticles on Ls-174-t human colon carcinoma cells

Ai-Ping Zhang, Yan-Ping Sun

Ai-Ping Zhang, Yan-Ping Sun, Chemical Engineering Department, Taiyuan University of Technology, Taiyuan 030024, Shanxi Province, China

Supported by the National Natural Science Foundation of China, No. 29776032 and the Natural Science Foundation of Shanxi Province, No.971013

Correspondence to: Yan-Ping Sun, Chemical Engineering Department, Taiyuan University of Technology, Taiyuan 030024, Shanxi Province, China. ypsun@tyut.edu.cn

Telephone: +86-351-6010070

Received: 2003-10-10 **Accepted:** 2003-12-29

Abstract

AIM: To investigate the photocatalytic killing effect of photoexcited TiO₂ nanoparticles on human colon carcinoma cell line (Ls-174-t) and to study the mechanism underlying the action of photoexcited TiO₂ nanoparticles on malignant cells.

METHODS: Ls-174-t human colon carcinoma cells were cultured in RPMI 1640 medium supplemented with 199 mL/L calf serum in a humidified incubator with an atmosphere of 50 mL/L CO₂ at 37 °C. Viable cells in the samples were measured by using the MTT method. A GGZ-300 W high pressure Hg lamp with a maximum ultraviolet-A (UVA, 320-400 nm) irradiation peak at 365 nm was used as light source in the photocatalytic killing test.

RESULTS: The photocatalytic killing of Ls-174-t cells was carried out *in vitro* with TiO₂ nanoparticles. The killing effect was weak by using UVA irradiation without TiO₂ nanoparticles. In our studies, the photocatalytic killing effect was correlated with the concentration of TiO₂ and illumination time. Once TiO₂ was added, Ls-174-t cells were killed at a much higher rate. In the presence of 1 000 µg/mL TiO₂, 44% of cells were killed after 10 min of UVA irradiation, and 88% of cells were killed after 30 min of UVA irradiation.

CONCLUSION: When the concentration of TiO₂ is below 200 µg/mL, the photocatalytic killing effect on human colon carcinoma cells is almost the same as that of UVA irradiation alone. When the concentration of TiO₂ is above 200 µg/mL, the remarkable killing effect of photoexcited TiO₂ nanoparticles can be found.

Zhang AP, Sun YP. Photocatalytic killing effect of TiO₂ nanoparticles on Ls-174-t human colon carcinoma cells. *World J Gastroenterol* 2004; 10(21): 3191-3193
<http://www.wjgnet.com/1007-9327/10/3191.asp>

INTRODUCTION

The application of TiO₂ photocatalysis has received increasing attention since the first report of microbiocidal effects by Matsunaga *et al.* in 1985^[1]. In recent years, in contrast to many studies using TiO₂ powder for photodecomposition of organic

pollutants^[2-9], few studies have investigated the application of TiO₂ in life science, especially in the field of cancer treatment^[10-12]. The incidence of colon cancer is rising in China. Despite that surgical operation is used currently, people have recognized its limitation. The way to treat cancer usually includes radiation therapy and chemical therapy, which may generate severe side effects in human body. Therefore, this study tried to investigate a new therapy for cancer. Ls-174-t cells were used as experiment objects in this study. The photocatalytic killing effect of TiO₂ nanoparticles on malignant cells and its killing mechanism were investigated.

MATERIALS AND METHODS

Reagent preparation

TiO₂ colloid solutions were prepared^[13,14] by hydrolysis of titanium isopropoxide, Ti [OCH(CH₃)₂]₄ (97%, Aldrich Chemical Co). In brief, 12.5 mL of Ti [OCH(CH₃)₂]₄ was added to 2 mL isopropanol, then the mixture was added to 150 mL of distilled deionized water containing 2 mL of 700 mL/L nitric acid and vigorously stirred for 6 h at 75 °C. Approximately 150 mL of TiO₂ colloid solution being stable for several months at 4 °C was obtained after the organic layer was removed. The average diameter determined by Zetasizer 3000HS_A (USA) was 21.2 nm.

The pH value of TiO₂ colloid solutions used in the subsequent experiment had to be adjusted from 1.8 to 5.5-6.5 in order not to damage the normal growth of cells. Therefore, 1 mol/L NaOH aqueous solution and 1.5 mL/L polyvinyl alcohol were added to the colloid solutions before the pH adjustment to prevent the TiO₂ from precipitation. The final TiO₂ colloid solutions were sterilized by autoclaving and then diluted to the required concentration. Other chemical reagents used were all of analytical purity from commercial sources.

Cell culture and treatment

Human colon carcinoma cell lines Ls-174-t were purchased from Shanghai Institute of Cell Biology, Chinese Academy of Sciences, Shanghai, China. The cell lines were cultured in RPMI 1640 (Gibco) medium supplemented with calf serum 100 mL/L, penicillin (100×10³ µ/L) and streptomycin (100 mg/L). pH was maintained at 7.2-7.4 by equilibration with 50 mL/L CO₂. Temperature was maintained at 37 °C. Cells were sub-cultured with a mixture of ethylenedinitrile tetraacetic acid (EDTA) and trypsin. All experiments were performed using cells during the exponential growth phase. Cell concentration was determined by using a hemocytometer and the cell density was adjusted to the required final concentration.

Ls-174-t cells were treated with TiO₂ diluted in RPMI 1640 medium for 2 h at 37 °C. Then the solutions were irradiated with a GGZ-300W high pressure Hg lamp (E_{max} = 365 nm) at room temperature. A UV pass filter was used to obtain a light wavelength between 300-400 nm. The light intensity at the liquid surface was measured by a VLX-3W radiometer-photometer (USA). The incident light intensity was 3.7 mW/cm². In our study, three groups of tests were carried out. One group was treated in the absence of TiO₂. Another group was treated in the absence of UVA. The third group was treated with different TiO₂ concentrations and irradiated by UVA.

Measurement of the viability of Ls-174-t cells

Viable cells in the samples were measured by using the MTT staining method^[15]. MTT [3-(4, 5-dimethylthiazol-2-yl)-2, 5-diphenyl tetrazolium bromide] was dissolved in phosphate-buffered saline (PBS, pH 7.4) at 5 mg/mL and filtered to be sterilized. Twenty microliters of stock MTT solution were added to all wells for an assay, and plates were incubated at 37 °C for 4 h. One hundred and fifty microliters of DMSO were added to all wells and mixed thoroughly to dissolve the blue-violet crystals. After a few minutes at room temperature to ensure that all crystals were dissolved, the plates were read on a Bio-Rad Novapath[™] microplate reader (Japan), using a test wavelength of 595 nm, taking the solution without MTT as control. Then optical absorptions [A] were obtained. Plates were normally read within 1 h after DMSO was added. The survival rate could be calculated according to $[A]/[A]_i$, where $[A]_i$ is the optical absorption of untreated cells.

RESULTS

Determination of the average diameter of TiO₂ particles

Zetasizer 3000HSA (USA) was used to determine the average diameter of TiO₂ nanoparticles. The result is shown in Figure 1. The average volume size of TiO₂ nanoparticles was 21.2 nm.

Cytotoxicity of TiO₂ nanoparticles

The cytotoxicity of TiO₂ nanoparticles (without UVA irradiation) was determined by exposing cells to various concentrations of TiO₂ in RPMI 1640 (Gibco) medium for 24 h. The surviving fraction of the cells was greater than 90% when the concentration of TiO₂ was in the range of 1 000 µg/mL, as shown in Figure 2. The result confirmed that nonirradiated TiO₂ nanoparticles were not toxic to the Ls-174-t cells. It was consistent with those in literatures^[16-17].

Effect of photoexcited TiO₂ nanoparticles on Ls-174-t cells

The fact that the surviving fraction was greater than 90% after 30 min as shown in Figure 3 (A) indicated that TiO₂ nanoparticles without UVA irradiation showed little toxicity to living cells. The killing effect of UVA without TiO₂ is shown in (B) with the surviving fraction of Ls-174-t cells given as a function of the UVA light irradiation time. About 20% cells were killed after 30 min exposure, whereas after 20 min exposure, more than 90% of the cells survived. Once TiO₂ was added, the Ls-174-t cells were killed at a much higher rate as shown in (C). For example, in the presence of 1 000 µg/mL of TiO₂, 44% of the cells were killed after 10 min of UVA irradiation, and after 30 min irradiation, 80% of the cells were killed. Therefore it was concluded that photoexcited TiO₂ nanoparticles had an active killing effect on Ls-174-cells.

Effect of TiO₂ concentration on Ls-174-t cells activity

The effect of the TiO₂ concentration ranging from 200 to 1 000 µg/mL on the rate of cell killing by UVA light is shown in Figure 4. The light intensity was 3.7 mW/cm² and kept constant. The experimental results demonstrated that cell viability decreased monotonically as TiO₂ concentration increased and cell viability decreased with time.

Although a higher concentration of TiO₂ could achieve a higher reaction rate, the difficulties in separation and measurement had to be considered. So the effect of a higher TiO₂ concentration ($C > 1\,029\ \mu\text{g/mL}$) on Ls-174-t cell activity was not investigated. The concentration of TiO₂ was set at $< 1\,029\ \mu\text{g/mL}$ with which the dark cytotoxicity was considered to be negligible. The range of TiO₂ concentrations was close to that used previously^[18].

Morphological changes of Ls-174-t cells

Untreated and TiO₂-treated cells were collected by centrifugation and resuspended in RPMI 1640 medium. The samples were pipetted into a 24-well plate, which was directly observed with

an inverted phase-contrast microscope. When treated by photoexcited TiO₂, the cellular shape was condensed and nuclei were dispersed in fragments.

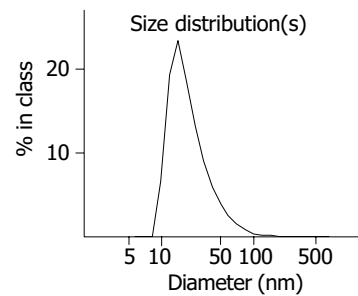


Figure 1 Volume size distribution of TiO₂.

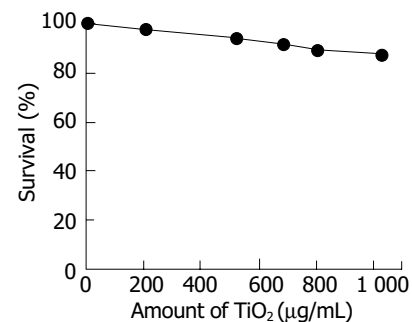


Figure 2 After Ls-174-t cells were incubated in RPMI 1640 medium for 24 h without irradiation, the survival of Ls-174-t cells was shown.

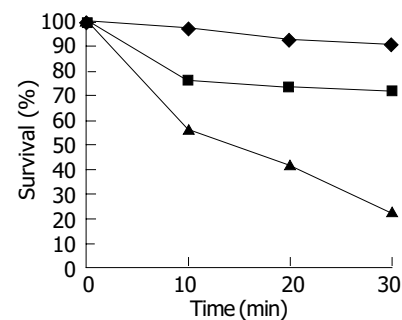


Figure 3 Effect of light and TiO₂ on viability of Ls-174-t cells. (A) TiO₂ (1 000 µg/mL) in the dark; (B) no TiO₂ in the light; (C) TiO₂ (1 000 µg/mL) in the light. Initial cell concentration: 5×10^5 cell/mL, light intensity: 3.7 mW/cm².

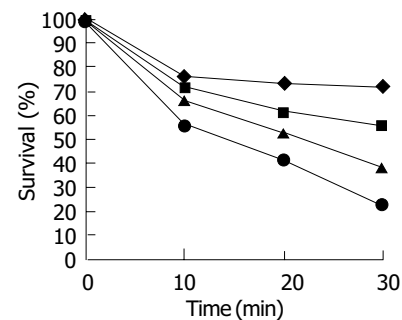


Figure 4 Influence of TiO₂ concentration on Ls-174-t cells activity. (A) 204 µg/mL, (B) 524 µg/mL, (C) 804 µg/mL, (D) 1 029 µg/mL.

DISCUSSION

In this experiment, the TiO₂ nanoparticle system was used, displaying its superiority. TiO₂ nanoparticles were easy to attach

to the cellular membranes and accumulate. They were also easy to enter into the cytoplasm via phagocytosis^[19]. It could lead to accumulation of ROS on the surface of cell membranes and in the cytoplasm. Hence under light irradiation, TiO₂ nanoparticles had more significant cell killing effect *in vitro*.

Human colon carcinoma cells treated with photoexcited TiO₂ nanoparticles (C>200 µg/mL) were effectively damaged, with cells contracted and a lot of cell fragments simultaneously observed by an inverted phase-contrast microscope^[18]. According to these characteristics, we assumed that the mechanism of photoexcited TiO₂ in killing human colon carcinoma cells might be through a series of oxidized chain reactions and in inducing cell death by reactive oxygen species^[20-25]. Human colon carcinoma cell damages occurred in two stages. The initial oxidative damage took place on the cell membranes, where the TiO₂ photocatalytic surface had its first contact with intact cells, the membranes became somewhat permeable. At this stage the cells did not lose their viability. Photocatalytic action made the cell membranes permeable, intracellular components began to leak from the cells and free TiO₂ nanoparticles might also diffuse into the damaged cells and directly attack intracellular components, eventually leading to cell death. It is different from the bactericidal effect of TiO₂ photocatalytic reaction. Bacteria are simple prokaryotic cells that do not contain the nucleus characteristics of eukaryotic cells. Whereas human colon carcinoma cells are eukaryotic cells and their structure is complex. Based on their structural differences, we assumed that killing cancer cells might be more difficult than killing bacteria by the photocatalytic reaction of TiO₂ nanoparticles.

In the present study, cultured human colon carcinoma cells were effectively killed by photoexcited TiO₂ nanoparticles *in vitro*. The concentration of TiO₂ affected the photocatalytic killing effect. When the concentration of TiO₂ was below 200 µg/mL, there was only a slight decrease in survival ratio after UVA irradiation for more than 30 min. It was almost the same as that of UVA irradiation alone. It indicated that minor cell membrane leakage might occur and the cell viability was not lost. When the concentration of TiO₂ was above 200 µg/mL, the survival ratio decreased rapidly with increasing TiO₂ concentration. It indicated that major rupture of cell membranes and decomposition of essential intracellular components might take place, thus accelerating cell death. It verified the mechanism of TiO₂ nanoparticles in killing human colon carcinoma cells.

The photocatalytic killing effect of TiO₂ nanoparticles on human colon carcinoma cells suggested the idea of cancer treatment using TiO₂ nanoparticles and light irradiation. Under these conditions, it could be adapted to an anticancer modality by the local or regional treatment of the tumor with TiO₂ nanoparticles, followed by light irradiation focusing on the tumor. Although UVA light (320-400 nm) cannot penetrate the human body deeply, it may be possible that the modality will be applied to several human tumors in the future.

REFERENCES

- 1 **Matsunaga T**, Tomoda R, Nakajima T, Wake H. Photoelectrochemical sterilization of microbial cells by semiconductor powders. *FEMS Microbiol Lett* 1985; **29**: 211-214
- 2 **Byrne JA**, Eggins BR, Brown NMD, Mckinney B, Rouse M. Immobilisation of TiO₂ powder for the treatment of polluted water. *Appl Catal B Environ* 1998; **17**: 25-36
- 3 **Wang KH**, Hsieh YH, Ko RC, Chang CY. Photocatalytic degradation of wastewater from manufactured fiber by titanium dioxide suspensions in aqueous solution. *Environ Int* 1999; **25**: 671-676
- 4 **Byrne JA**, Eggins BR, Byers W, Brown NMD. Photoelectrochemical cell for the combined photocatalytic oxidation of organic pollutants and the recovery of metals from waste waters. *Appl Catal B Environ* 1999; **2**: L85-L89
- 5 **Horikoshi S**, Satou Y, Hidaka H, Serpone N. Enhanced photocurrent generation and photooxidation of benzene sulfonate in a continuous flow reactor using hybrid TiO₂ thin films immobilized on OTE electrodes. *J Photochem Photobiol A* 2001; **146**: 109-119
- 6 **Molinari R**, Grande C, Drioli E, Palmisano L, Schiavello M. Photocatalytic membrane reactors for degradation of organic pollutants in water. *Catal Today* 2001; **67**: 273-279
- 7 **Shephard GS**, Stockenstrom S, de Villiers D, Engelbrecht WJ, Wessels GE. Degradation of microcystin toxins in a falling film photocatalytic reactor with immobilized titanium dioxide catalyst. *Water Res* 2002; **36**: 140-146
- 8 **Muneer M**, Singh HK, Bahnemann D. Semiconductor-mediated photocatalysed degradation of two selected priority organic pollutants, benzidine and 1, 2-diphenylhydrazine, in aqueous suspension. *Chemosphere* 2002; **49**: 193-203
- 9 **Alhakimi G**, Studnicki LH, Al-Ghazali M. Photocatalytic destruction of potassium hydrogen phthalate using TiO₂ and sunlight: application for the treatment of industrial wastewater. *J Photochem Photobiol A* 2003; **154**: 219-228
- 10 **Fujishima A**, Cai RX, Otsuki J, Hashimoto K, Itoh K, Yamashita T, Kubota Y. Biochemical application of photoelectrochemistry: photokilling of malignant cells with TiO₂ powder. *Electrochim Acta* 1993; **38**: 153-157
- 11 **Mills A**, Hunte SL. An overview of semiconductor photocatalysis. *J Photochem Photobiol A* 1997; **108**: 1-35
- 12 **Fujishima A**, Rao TN, Tryk DA. Titanium dioxide photocatalysis. *J Photochem Photobiol C* 2000; **1**: 1-21
- 13 **Kormann C**, Bahnemann DW, Hoffmann MR. Preparation and characterization of quantum-size titanium dioxide. *J Phys Chem* 1988; **92**: 5196-5201
- 14 **O'Regan B**, Moser J, Anderson M, Gratzel M. Vectorial electron injection into transparent semiconductor membranes and electric field effects on the dynamics of light-induced charge separation. *J Phys Chem* 1990; **94**: 8720-8726
- 15 **Mosmann T**. Rapid colorimetric assay for cellular growth and survival: application to proliferation and cytotoxicity assays. *J Immunol Methods* 1983; **65**: 55-63
- 16 **Bernard BK**, Osheroff MR, Hofmann A, Mennear JH. Toxicology and carcinogenesis studies of dietary titanium dioxide-coated mica in male and female Fischer 344 rats. *J Toxicol Environ Health* 1990; **29**: 417-429
- 17 **Linnainmaa K**, Kivipensas P, Vainio H. Toxicity and cytogenetic studies of ultrafine titanium dioxide in cultured rat liver epithelial cells. *Toxicol In Vitro* 1997; **11**: 329-335
- 18 **Xu MH**, Huang NP, Xiao ZD, Lu ZH. Photoexcited TiO₂ nanoparticles through ·OH- radicals induced malignant cells to necrosis. *Supramole Sci* 1998; **5**: 449-451
- 19 **Cai RX**, Hashimoto K, Itoh K, Kubota Y, Fujishima A. Photokilling of malignant cells with Ultrafine TiO₂ powder. *Bull Chem Soc Jpn* 1991; **64**: 1268-1273
- 20 **Jaeger CD**, Bard AJ. Spin trapping and electron spin resonance detection of radical intermediates in the photodecomposition of water at TiO₂ particulate systems. *J Phys Chem* 1979; **83**: 3146-3152
- 21 **Rao MV**, Rajeshwar K, Pal Verneker VR, DuBow J. Photosynthetic production of H₂ and H₂O₂ on semiconducting oxide grains in aqueous solutions. *J Phys Chem* 1980; **84**: 1987-1991
- 22 **Harbour JR**, Hair ML. Superoxide generation in the photolysis of aqueous cadmium sulfide dispersions. Detection by spin trapping. *J Phys Chem* 1977; **81**: 1791-1793
- 23 **Harbour JR**, Tromp J, Hair ML. Photogeneration of hydrogen peroxide in aqueous TiO₂ dispersions. *Can J Chem* 1985; **63**: 204-208
- 24 **Hong AP**, Bahnemann DW, Hoffmann MR. Cobalt (II) tetrasulfophthalocyanine on titanium dioxide: a new efficient electron relay for the photocatalytic formation and depletion of hydrogen peroxide in aqueous suspensions. *J Phys Chem* 1987; **91**: 2109-2117
- 25 **Hidaka H**, Horikoshi S, Serpone N, Knowland J. *In vitro* photochemical damage to DNA, RNA and their bases by an inorganic sunscreen agent on exposure to UVA and UVB radiation. *J Photochem Photobiol A* 1997; **111**: 205-213

Gene expression profiling in Barrett's esophagus and cardia intestinal metaplasia: A comparative analysis using cDNA microarray

Ying Chang, Jun Gong, Bin Liu, Jun Zhang, Fei Dai

Ying Chang, Jun Gong, Jun Zhang, Fei Dai, Department of Digestion, Second Hospital of Xi'an Jiaotong University, Xi'an 710004, Shaanxi Province, China

Bin Liu, Department of Emergence Surgery, Shaanxi Provincial People's Hospital, Xi'an 710068, Shaanxi Province, China

Supported by the Clinical Principal Discipline Foundation of Public Health Ministry of China, No.20012130

Correspondence to: Professor Jun Gong, Department of Digestion, Second Hospital of Xi'an Jiaotong University, Xi'an 710004, Shaanxi Province, China. emulan@126.com

Telephone: +86-29-85212945 **Fax:** +86-29-87678758

Received: 2004-04-22 **Accepted:** 2004-04-29

Abstract

AIM: To study the difference of gene expression profile changes in Barrett's esophagus (BE) and cardia intestinal metaplasia (CIM) and to screen the novel genes in the early stage by cDNA microarray.

METHODS: cDNA retrotranscribed from an equal amount of mRNA from BE and CIM epithelial tissues was labeled with Cy3 and Cy5 fluorescence as probes. The mixed probe was hybridized with three pieces of BiostarH-40 s double dot human whole gene chip. The chips were scanned with a ScanArray 4000. The acquired images were analyzed using GenePix Pro 3.0 software.

RESULTS: A total of 141 genes were screened out that exhibited different expression in all three chips. There were 74 upregulated and 67 downregulated genes in gene expression profiles of BE which were two times of that in CIM.

CONCLUSION: There is a difference in gene expression level between BE and CIM epithelia. These 141 genes probably relate to the occurrence and development of BE and the progression to adenocarcinoma.

Chang Y, Gong J, Liu B, Zhang J, Dai F. Gene expression profiling in Barrett's esophagus and cardia intestinal metaplasia: A comparative analysis using cDNA microarray. *World J Gastroenterol* 2004; 10(21): 3194-3196
<http://www.wjgnet.com/1007-9327/10/3194.asp>

INTRODUCTION

The incidence of adenocarcinoma in the esophagus and gastroesophageal junction (GEJ) has been increasing over the last two decades in North America and Europe^[1]. Barrett's esophagus (BE) is thought to be a premalignant condition for esophageal adenocarcinoma and most of adenocarcinomas at GEJ^[2]. Recently the presence of cardia intestinal metaplasia (CIM) in some normal GEJ has been described^[3]. The relation of this condition to BE has not yet been investigated.

Recently, cDNA microarray methods are applied to the study of gene expression. The differentially expressed genes in

different specimens may be detected with parallel analysis by gene chips which has greatly improved the traditional experiments in that only a single or several gene expression can be observed for each test, thereby speeding up the identification of differentially expressed genes and the construction of differential expression profiles.

This study was conducted on three 4096-chips, to analyse the gene expression profiles between BE and CIM epithelia, and to screen novel genes by cDNA microarray, which is helpful to understand the molecular mechanism of cell transformation and provides molecular markers and target genes for clinical diagnosis, prevention and treatment of BE and esophageal adenocarcinoma and adenocarcinoma at GEJ.

MATERIALS AND METHODS

Tissue specimens

Tissue specimens in this study were provided by the Second Hospital of Xi'an Jiaotong University, with the approval of hospital and personnel authorities. BE and CIM tissues from 13 operated or biopsy specimens (7 BE and 6 CIM) were proved pathologically. For each sample, one part was cut and frozen in liquid nitrogen immediately after resection, and the other part was used for histopathological examination. Standardized endoscopy was performed by experienced endoscopists. The appearance of sternoclavicular joint (SCJ) was carefully studied from both prograde and retrograde views. BE was defined as any columnar-lined mucosa above the GEJ, which was further confirmed by Alcian blue staining. CIM was defined by the presence of barrel-shaped goblet cells in normal GEJ.

Chip preparation

4 086 of target cDNA clones used in cDNA chips were provided by United Gene Ltd. and cooperative fellows. These genes were amplified with PCR using universal primers and then purified with standard method. The quality of PCR was monitored by agarose gel electrophoresis. The obtained genes were dissolved in 3×SSC spotting solution and then spotted on silylated slides (Telechem, Inc) by Cartesian 7 500 Spotting Robot (Cartesian, Inc). Each target gene was dotted twice. After spotting, the slides were hydrated for 2 h and dried for 0.5 h at room temperature. The samples were cross-linked with UV light and treated with 2 g/L SDS, H₂O and 2 g/L NaBH₄ for 10 min respectively. Then the slides were dried in cold condition and ready for use.

Probe preparation

Total sample RNA was extracted by single step method. Briefly, after taken out from liquid nitrogen, specimens were ground into tiny powder while liquid nitrogen was added in ceramic mortar and then homogenized in D solution plus 10 mL/L mercaptoethanol. After centrifugation, the supernatant was extracted with phenol: chloroform (1:1), NaAc and acidic phenol: chloroform (5:1) respectively. The aqueous phase was precipitated by an equal volume of isopropanol and centrifuged. The precipitates were dissolved with purified H₂O. After further purification by LiCl precipitating method, the obtained RNA sample was analyzed.

mRNAs were isolated and purified with Oligotex mRNA Midi Kit (Quagen, Inc.). The fluorescence-labeled cDNA probe was prepared through retrotranscription, referring to the method of Schena. The probes from CIM tissue were labeled with Cy3-dUTP, while those from BE tissue with Cy5-dUTP respectively. The probes were mixed and precipitated by ethanol, and then resolved in 20 mL hybridization solution (5×SSC + 2 g/L SDS).

Hybridization and washing

Probes and chips were denatured respectively in 95 °C bath for 5 min, then the probes were added on the chip. They were hybridized in a sealed chamber at 60 °C for 15-17 h and washed in turn with solutions of 2×SSC + 2 g/L SDS, 0.1×SSC + 2 g/L SDS and 0.1% SSC for 10 min each, then dried at room temperature.

Fluorescent scanning and result analysis

The chips were read by Scan Array 4000 Scanner (General Scanning Inc). The overall intensities of Cy3 and Cy5 were normalized and corrected by a coefficient according to the ratios of the 40 located housekeeping genes. The acquired image was further analyzed by GenePix Pro 3.0 software with a digital computer to obtain the intensities of fluorescent signals and the Cy3/Cy5 ratio. The data were taken on an average of the two repeated spots. The differentially expressed genes were defined as follows: The absolute value of the Cy5/Cy3 natural logarithm was more than 0.69 (the variation of gene expression was more than 2-fold). Either Cy3 or Cy5 signal value was required for more than 800. The PCR results were satisfactory.

RESULTS

Scatter plot of hybridization signals on gene chip

The scatter plots that were plotted with Cy3 and Cy5 fluorescent signal values displayed a quite disperses pattern in distribution. Most of the spots gathered around a 45° line, in which red spots represented the area where the signal intensities varied between 0.5 to 2-fold compared with those of the control. Some yellow spots distributed beyond or far from 45° line indicated the existence of abnormal gene expressions in BE and CIM epithelia. Their signal intensities were 2 times more than that of the control (Figure 1).

Table 1 Gene function classification between BE and CIM epithelia

Gene function	n	Ratio>2.0	Ratio<0.5
Proto-oncogene and tumor suppression genes	9	6	3
Cell signals and transducing proteins	5	2	3
Cell cycle proteins	8	6	2
Extra-pressure reaction proteins	1	1	0
Cell regulatory proteins	4	4	0
Cell apoptosis related proteins	3	2	1
DNA synthesis, repair and recombinant proteins	3	2	1
DNA binding, transcription and its factor	4	3	1
Cell receptors	1	0	1
Cell surface antigen and adhesion proteins	10	4	6
Ion-channel and transporters	11	6	5
Metabolism-related proteins	16	7	9
Protein synthesis-related genes	11	6	5
Development-related genes	0	0	0
Other genes	38	17	21
New genes	17	8	9
Total	141	74	67

Results and gene expression pattern

As shown in Figure 2, 141 genes were screened out that exhibited different expressions in all three chips, there were 74 up-regulated and 67 down-regulated genes in the gene expression profiles of BE which was 2 times of that in CIM. These genes might be divided into 16 groups (Table 1) according to their functions.

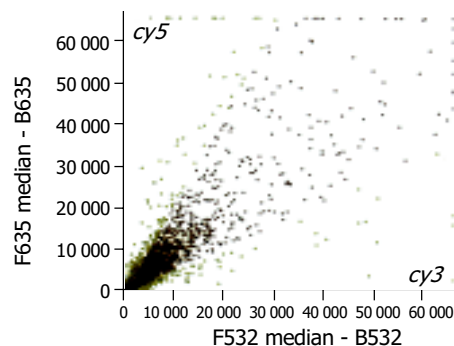


Figure 1 Scatter plot of hybridization signals on gene chip.



Figure 2 Fluorescence scanning of gene expressions on gene chip.

DISCUSSION

Over the last two decades, the incidence of adenocarcinoma of the esophagus and gastric cardia has been increasing rapidly. Barrett's metaplasia is recognized as a precancerous lesion of esophageal adenocarcinoma and most of the adenocarcinomas were found at the GEJ. Progression from metaplasia, dysplasia to adenocarcinoma has been well understood^[4]. Traditionally Barrett's esophagus (BE) is defined as a circumferential segment of columnar lined epithelium of 2 or 3 cm in length in the lower esophagus. Recently this macroscopic definition has been questioned, as it excludes shorter segments and "tongues" of columnar lined epithelium, which are frequently found in the distal esophagus, and endoscopic measurements may be imprecise. It has therefore been proposed that the diagnosis of BE be reserved for patients with intestinal metaplasia detected in biopsy specimens from the distal esophagus. Recently the presence of cardia intestinal metaplasia (CIM) in some normal GEJ has been described^[5-7]. Detection of intestinal metaplasia in the distal esophagus as well as within the gastric cardia was reported with increasing frequency^[8]. The prevalence of BE was reported to vary from 2% to 12% and that of CIM from 5% to 23% in patients undergoing routine upper endoscopy^[9]. The detection of intestinal metaplasia in the BE potentially committed patients to regular surveillance with biopsy. The incidence of adenocarcinoma in patients with BE was estimated to be 30-50 times that of the general population^[10,11]. However, the exact incidence of cancer in patients with BE is unknown, and the role of CIM as a premalignant lesion is still unclear. The relation of this condition to BE has not yet been investigated. It is, however, not clear whether intestinal metaplasia of the

cardia and esophageal mucosa origins has a common pathogenesis and identical risk factors. Despite the frequent occurrence of cardia intestinal metaplasia and its association with *H pylori* gastritis and multifocal gastric intestinal metaplasia, there is still no evidence that this finding could indicate an increased risk of malignancy in the cardia. The well known association of traditional BE with symptoms and endoscopic features of gastroesophageal reflux disease (GERD) has, however, not been confirmed in CIM^[12]. Future studies should differentiate BE from CIM in order to enhance our understanding of the pathophysiology and the malignant potential of each clinical entity. It is therefore necessary to explore new and efficacious diagnostic methods to discriminate BE from CIM.

cDNA microarray methods have been applied in the study of gene expression, DNA sequence, novel genes and gene mutants, DNA polymorphism, and in screening drugs, diagnosing diseases and mapping gene library^[13]. The differentially expressed genes in different specimens may be detected with parallel analysis by gene chips which has greatly improved the traditional experiments in that only a single or several gene expression can be observed for each test, thereby speeding up the identification of differentially expressed genes and the construction of different expression profiles. Profiling of differentially expressed genes of BE to each of the normal upper gastrointestinal (GI) mucosae, including gastric, duodenal, and squamous epithelia of the esophagus by cDNA expression array was also reported^[14]. It has been shown that there was a clear distinction among the expression profiles of gastric, duodenal, and squamous epithelia whereas the BE profiles showed a considerable overlap with normal tissues. Furthermore, the clusters of genes that are specific to each of the tissues from BE, and a cluster of genes distinct from squamous and non-squamous epithelia, were identified. However, no investigation on the difference in gene expression profiles between BE and CIM epithelia by gene chip has been reported yet.

In the present study, we performed an analysis on three 4096 chips in order to acquire the difference in gene expression profiles between BE and CIM epithelia. The results showed that a total of 141 genes were screened out that exhibited different expressions in all three chips. In the gene expression profiles of BE there were 74 upregulated and 67 downregulated genes which were two times of those of CIM. A comparison between these two gene profiles showed that the gene expression levels were different between BE and CIM epithelia. These 141 genes probably relate to the occurrence and development of BE and the promotion or progression in adenocarcinoma, which might be helpful to understand the molecular mechanism of cell transformation and provides molecular markers and target genes for clinical diagnosis, prevention, treatment of BE and esophageal adenocarcinoma and most of adenocarcinomas at GEJ. The gene expression difference between BE and CIM detected by gene chip might provide a new direction for diagnosis, therapy

and prevention of BE.

REFERENCES

- 1 **O'Connor JB**, Falk GW, Richter JE. The incidence of adenocarcinoma and dysplasia in Barrett's esophagus: report on the Cleveland Clinic Barrett's Esophagus Registry. *Am J Gastroenterol* 1999; **94**: 2037-2042
- 2 **Geboes K**. Barrett's esophagus: the metaplasia-dysplasia-carcinoma sequence: morphological aspects. *Acta Gastroenterol Belg* 2000; **63**: 13-17
- 3 **Morales TG**, Sampliner RE, Bhattacharyya A. Intestinal metaplasia of the cardia. *Am J Gastroenterol* 1997; **92**: 414-418
- 4 **Voutilainen M**, Farkkila M, Juhola M, Mecklin JP, Sipponen P. Complete and incomplete intestinal metaplasia at the oesophagogastric junction: prevalences and associations with endoscopic erosive oesophagitis and gastritis. *Gut* 1999; **45**: 644-648
- 5 **Spechler SJ**, Zeroogian JM, Antonioli DA, Wang HH, Goyal RK. Prevalence of metaplasia at the gastroesophageal junction. *Lancet* 1994; **344**: 1533-1536
- 6 **Goldstein NS**, Karim R. Gastric cardia inflammation and intestinal metaplasia: associations with reflux esophagitis and *Helicobacter pylori*. *Mod Pathol* 1999; **12**: 1017-1024
- 7 **Pereira AD**, Suspiro A, Chaves P, Saraiva A, Gloria L, de Almeida JC, Leitao CN, Soares J, Mira FC. Short segments of Barrett's epithelium and intestinal metaplasia in normal appearing oesophagogastric junctions: the same or two different entities? *Gut* 1998; **42**: 659-662
- 8 **Ruol A**, Parenti A, Zaninotto G, Merigliano S, Costantini M, Cagol M, Alfieri R, Bonavina L, Peracchia A, Ancona E. Intestinal metaplasia is the probable common precursor of adenocarcinoma in Barrett's esophagus and adenocarcinoma of the gastric cardia. *Cancer* 2000; **88**: 2520-2526
- 9 **Byrne JP**, Mathers JM, Parry JM, Attwood SE, Bancewicz J, Woodman CB. Site distribution of oesophagogastric cancer. *Clin Pathol* 2002; **55**: 191-194
- 10 **Hamilton SR**, Smith RL, Cameron JL. Prevalence and characters of Barrett's esophagus in patients with adenocarcinoma of the esophagogastric junction. *Hum Pathol* 1998; **19**: 942-948
- 11 **Dulai GS**, Guha S, Kahn KL, Gornbein J, Weinstein WM. Preoperative prevalence of Barrett's esophagus in esophageal adenocarcinoma: A systematic review. *Gastroenterology* 2002; **122**: 26-33
- 12 **Sharma P**, Weston AP, Morales T, Topalovski M, Mayo MS, Sampliner RE. Relative risk of dysplasia for patients with intestinal metaplasia in the distal esophagus and in the gastric cardia. *Gut* 2000; **46**: 9-13
- 13 **Xu SH**, Qian LJ, Mou HZ, Zhu CH, Zhou XM, Liu XL, Chen Y, Bao WY. Difference of gene expression profiles between esophageal carcinoma and its pericarcinoma epithelium by gene chip. *World J Gastroenterol* 2003; **9**: 417-422
- 14 **Barrett MT**, Yeung KY, Ruzzo WL, Hsu L, Blount PL, Sullivan R, Zarbl H, Delrow J, Rabinovitch PS, Reid BJ. Transcriptional analyses of Barrett's metaplasia and normal upper GI mucosa. *Neoplasia* 2002; **4**: 121-128

Edited by Wang XL and Chen WW Proofread by Xu FM

Antitumor immunity induced by DNA vaccine encoding alpha-fetoprotein/heat shock protein 70

Xiao-Ping Wang, Guo-Zhen Liu, Ai-Li Song, Hai-Yan Li, Yu Liu

Xiao-Ping Wang, Guo-Zhen Liu, Ai-Li Song, Hai-Yan Li, Yu Liu, Department of Pathology, Capital University of Medical Sciences, Beijing 100054, China

Supported by the Research Fund for Young Scholars of Beijing, No. 02120031

Correspondence to: Dr. Xiao-Ping Wang, Department of Pathology, Capital University of Medical Sciences, Beijing 100054, China. wxpphd@yahoo.com.cn

Telephone: +86-10-63051455

Received: 2004-03-18 **Accepted:** 2004-04-07

Abstract

AIM: To construct a DNA vaccine encoding human alpha-fetoprotein (hAFP)/heat shock protein 70 (HSP70), and to study its ability to induce specific CTL response and its protective effect against AFP-expressing tumor.

METHODS: A DNA vaccine was constructed by combining hAFP gene with HSP70 gene. SP2/0 cells were stably transfected with pBBS212-hAFP and pBBS212-hAFP/HSP70 eukaryotic expression vectors. Mice were primed and boosted with DNA vaccine hAFP/HSP70 by intramuscular injection, whereas plasmid with hAFP or HSP70 was used as controls. ELISPOT and ELISA were used to detect IFN- γ -producing splenocytes and the level of serum anti-AFP antibody from immunized mice respectively. *In vivo tumor challenge* was measured to assess the immune effect of the DNA vaccine.

RESULTS: By DNA vaccine immunization, the results of ELISPOT and ELISA showed that the number of IFN- γ -producing splenocytes and the level of serum anti-AFP antibody were significantly higher in rhAFP/HSP70 group than in hAFP and empty plasmid groups (95.50 ± 10.90 IFN- γ spots/ 10^6 cells vs 23.60 ± 11.80 IFN- γ spots/ 10^6 cells, 7.17 ± 4.24 IFN- γ spots/ 10^6 cells, $P < 0.01$; 126.50 ± 8.22 $\mu\text{g/mL}$ vs 51.72 ± 3.40 $\mu\text{g/mL}$, 5.83 ± 3.79 $\mu\text{g/mL}$, $P < 0.01$). The tumor volume in rhAFP/HSP70 group was significantly smaller than that in pBBS212-hAFP and empty plasmid groups (37.41 ± 7.34 mm^3 vs 381.13 ± 15.48 mm^3 , 817.51 ± 16.25 mm^3 , $P < 0.01$).

CONCLUSION: Sequential immunization with a recombinant DNA vaccine encoding AFP and heat shock protein 70 could generate effective AFP-specific T cell responses and induce definite antitumor effects on AFP-producing tumors, which may be suitable for some clinical testing as a vaccine for HCC.

Wang XP, Liu GZ, Song AL, Li HY, Liu Y. Antitumor immunity induced by DNA vaccine encoding alpha-fetoprotein/heat shock protein 70. *World J Gastroenterol* 2004; 10(21): 3197-3200 <http://www.wjgnet.com/1007-9327/10/3197.asp>

INTRODUCTION

The incidence of hepatocellular carcinoma (HCC) is increasing

worldwide and accounts for as many as 1.2 million deaths annually. It is also rising rapidly in China because of hepatitis B and C infections^[1,2]. Although surgery and liver transplantation are the effective therapy, most patients lost chance due to diagnosis at a late stage or underlying liver insufficiency in the setting of cirrhosis^[3]. Novel therapies for HCC should be developed. A combined therapy is likely to prolong patients' life and living quality.

Much attention has been paid to the induction of host immunity to tumor cells. 80% of HCCs have a high expression of alpha-fetoprotein (AFP), which could serve as a target for immunotherapy^[4-8]. AFP is an oncofetal protein during HCC development, which could generate weaker and less reproducible antitumor protection. A DNA-based vaccine may be a good method for enhancing host immunity^[9-12]. A number of groups have shown that high levels of T-cell immunity could be generated using a heterogeneous prime-boost protocol, in which animals were primed and boosted with a plasmid vector encoding the stimulating molecules and targeted peptides^[8-10]. In many of these vaccine models^[11-15], heat shock protein 70 could combine with certain antigen prime enhanced immunogenicity, presumably through processing and presenting the antigen to host APCs. In the present study, we investigated whether the immunogenicity of AFP could be improved by presenting to APCs through HSP70 molecules. We constructed a eukaryotic expression vector containing the molecular chaperon-HSP70 and AFP fragments. Then priming mice with the genetic vaccine, we elicited robust strong protective immunity.

MATERIALS AND METHODS

Mice and cell line

Balb/c mice were provided by Department of Experimental Animal Center at Capital University of Medical Sciences. SP2/0 mice myeloma cells were maintained in RPMI 1640 (Life Technologies, Inc.) supplemented with 100 mL/L fetal bovine serum (Hyclone Technologies, Inc.). The cells were transduced with pBBS212-hAFP or pBBS212-hAFP/HSP70 through calcium phosphate precipitation (Promega Technologies, Inc.). Positive cell clones were screened by conditioned medium and supernatants were detected by AFP radioimmunoassay (Institute of Nuclear Sciences, Beijing) following the manufacturer's instructions.

Construction of recombinant expression vector

RT-PCR primers were designed to contain the partial hAFP coding region, including the signal sequence. The upper primers were 5'-CCGCTCGAGATGAAGTGGGTGGAATCAA-3', while the down primers were 5'-CGCGGATCCTTATGGAGTGGGCTTTTGTGTG-3'. RT-PCR template total RNA was isolated from HepG2 hepatocarcinoma cells by TRIzol (Life Technologies, Inc.) reagent. Then the 400-bp hAFP cDNA PCR products were cloned into the pBBS212 empty vector and pBBS212-HSP70 eukaryotic expression vector (provided by Dr. Ye L of Zhongshan Medical University, Guangzhou, China). pBBS212-hAFP/HSP70 and pBBS212-hAFP were constructed using the pBBS212 herpes simplex virus expressing vector, in which the backbone

contained the hygromycin resistance gene, being suitable for screening cell clones. The recombinant vectors were identified by restriction enzyme analysis and sequencing. Different plasmid and recombinant expressing vectors were stored at $-80\text{ }^{\circ}\text{C}$ for intramuscular immunization^[16].

Mice immunized with recombinant expression vector

Forty female Balb/c mice were divided into rhAFP/HSP70 group, rhAFP group, HSP70 group and empty vector group, PBS group. Each group had 8 mice. Before injection, plasmid and recombinant expressing vectors were diluted in saline to 1 g/L. Various plasmids were injected into the left anterior tibialis muscle of mice. Priming and boosting with plasmid were performed with 100 μg rhAFP or rhAFP/HSP70 vector, whereas pBBS212-HSP70 and empty vectors were used as controls. A 25-gauge, 0.5-inch insulin syringe was used for intramuscular injection. Mice were intramuscularly boosted with above plasmids twice at intervals of two weeks after the first priming.

ELISPOT and ELISA assay

IFN- γ ELISPOT assay was used to measure the frequency of cells producing cytokine IFN- γ in splenocytes harvested from immunized mice. Two weeks after the last immunization, splenocytes were harvested and restimulated directly in anti-IFN- γ monoclonal antibody (PharMingen) coated ELISPOT plate wells *in vitro* with 5 $\mu\text{g}/\text{mL}$ of AFP containing 100 mL/L fetal bovine serum, 10 U/mL of human interleukin-2. The plates were incubated at $37\text{ }^{\circ}\text{C}$ for 24 h, then washed and incubated with a biotin-conjugated secondary antibody and developed. The color spots, representing cytokine producing cells, were counted under a dissecting microscope. To detect the level of anti-AFP antibody in mice, we examined the serum of mice tail vein after the last immunization by ELISA using AFP ELISA kits (Biotinge Biomedicine Co, LTD, Beijing) following the manufacturer's instructions.

In vivo tumor load

Another 40 female Balb/c mice were grouped and immunized as above. Tumor challenge was performed 2 wk after the last immunization with 1×10^5 AFP-transfected SP2/0 cells. SP2/0 AFP-transduced tumor cells for challenge were washed after enzymatic digestion and resuspended in 0.2 mL PBS per animal to be injected *s.c.* into the left flank, while empty plasmid and PBS were used as controls. The sizes of tumors were assessed 3 times a week using calipers. Tumor volume was approximated by the following calculation: $\frac{4}{3} \pi r^3$ (r = radius).

Statistical analysis

Results were expressed as mean \pm SD. The frequency of IFN- γ -producing splenic cells were valued using χ^2 test. The Student's *t* test was performed to analyze the significance of differences between the final tumor volumes of different groups. $P < 0.05$ was considered statistically significant.

RESULTS

Prime-boost vaccines induced T-cell responses and anti-AFP antibody in Balb/c mice

Immunization of Balb/c mice with recombinant hAFP/HSP70 vector elicited much more strong T-cell responses than rhAFP group (95.50 \pm 10.90 IFN- γ spots/ 10^6 cells vs 23.60 \pm 11.80 IFN- γ spots/ 10^6 cells, $P < 0.01$), whereas an intramuscular vaccination with plasmid-HSP70 and empty plasmid produced a weak response (95.50 \pm 10.90 IFN- γ spots/ 10^6 cells vs 9.25 \pm 5.44 IFN- γ spots/ 10^6 cells, 7.17 \pm 4.24 IFN- γ spots/ 10^6 cells, $P < 0.01$). Recombinant hAFP/HSP70 immunized mice also produced a higher level of anti-AFP antibody than rhAFP group (126.50 \pm 8.22 $\mu\text{g}/\text{mL}$ vs 51.72 \pm 3.40 $\mu\text{g}/\text{mL}$, $P < 0.01$), while plasmid-HSP70 and empty plasmid produced a lower level (126.50 \pm 8.22 $\mu\text{g}/\text{mL}$ vs 6.26 \pm 4.27 $\mu\text{g}/\text{mL}$, 5.83 \pm 3.79 $\mu\text{g}/\text{mL}$, $P < 0.01$) (Table 1).

Boost immunization protected mice from in vivo tumor challenge

Balb/c mice were primed and boosted with rhAFP/HSP70, rhAFP, HSP70 and empty plasmid. The mice were challenged with SP2/0 cells, which were transduced with hAFP. Tumor sizes were significantly smaller in rhAFP/HSP70-immunized mice than in HSP70 and empty plasmid immunized mice (37.41 \pm 7.34 mm^3 vs 785.83 \pm 13.87 mm^3 , 817.51 \pm 16.25 mm^3 , $P < 0.01$). Although rhAFP immunized group produced an obvious tumor, it was still significantly bigger than rhAFP/HSP70 group (37.41 \pm 7.34 mm^3 vs 381.13 \pm 15.48 mm^3 , $P < 0.01$) (Table 2).

DISCUSSION

Recent studies on the immunodominant epitopes of AFP have provided a solution to the obstacle of HCC immunotherapy. AFP is produced at low serum levels after birth throughout life^[2-5]. The majority of human HCCs could overexpress the oncofetal antigen AFP, M_r 70 000 glycoprotein^[4,5]. Despite being exposed to high plasma levels of this oncofetal protein during embryonic development, the body has a low immunity to it^[3]. Butterfield *et al.*^[17-19] recently found that four peptides of human AFP processed and presented in the context of HLA-A0201, could

Table 1 Spots of IFN- γ -producing splenic cells and level of anti-AFP antibody in mice (mean \pm SD)

Group	hAFP/HSP70	hAFP	HSP70	Empty	PBS
Spots (10^6 cells)	95.50 \pm 10.90 ^{bd}	23.60 \pm 11.80 ^f	9.25 \pm 5.44	7.17 \pm 4.24	5.54 \pm 2.16
Anti-AFP ($\mu\text{g}/\text{mL}$)	126.50 \pm 8.22 ^{bd}	51.72 \pm 3.40 ^f	6.26 \pm 4.27	5.83 \pm 3.79	3.42 \pm 2.35

^b $P < 0.01$, vs empty group; ^d $P < 0.01$, vs HSP70 group; ^f $P < 0.01$, vs empty group.

Table 2 Comparison of tumor growth in mice injected with hAFP-transduced SP2/0 tumor cells (mean \pm SD)

Group	No. of tumor-bearing/ No. of mice challenge	10 d after tumor challenge/ Size of tumor (mm^3)	20 d after tumor challenge/ Size of tumor (mm^3)
hAFP/HSP70	2/8	24.43 \pm 6.10 ^{bd}	37.41 \pm 7.34 ^{bd}
hAFP	5/8	73.64 \pm 8.53 ^f	381.13 \pm 15.48 ^f
HSP70	8/8	118.24 \pm 14.65	785.83 \pm 13.87
Empty	8/8	132.26 \pm 17.27	817.51 \pm 16.25
PBS	8/8	149.73 \pm 16.54	860.53 \pm 14.72

^b $P < 0.01$, vs empty group; ^d $P < 0.01$, vs HSP70 group; ^f $P < 0.01$, vs empty group.

be recognized by human T cell repertoire, and could be used to generate AFP-specific CTL in human T cell cultures. It was also found that murine immune system could generate T-cell responses to this oncofetal antigen^[8]. Therefore, it may be a better target for immunotherapy. But AFP immunization alone still resulted in lower levels of specific response and poorly reproducible protective immunity^[3-7].

How to enhance host's active immunity to AFP may be an interesting strategy for HCC therapy. Previous studies on AFP specific immunotherapy for HCC included AFP plasmid immunization, AFP-transduced DCs immunization and AFP plasmid prime-AFP adenovirus boost immunization^[20-22]. AFP plasmid immunization produced detectable but low levels of AFP specific T cell responses and poorly reproducible protective immunity^[7,20]. DCs engineered to express murine AFP demonstrated a powerful ability to generate tumor-specific immune responses^[21]. However, the need for costly cell culture procedures limited their wide availability for clinical use, and the unstable culture technique might yield tolerating vaccines^[8,21]. AFP plasmid prime-AFP adenovirus boost immunization could engender significant AFP specific T-cell responses and protective immunity in mice^[22]. But the miscellaneous procedures precluded their use. In the present study, we tested a novel strategy to induce antitumor immunity by a DNA vaccine encoding both AFP and HSP70 in mice. We found that the vaccine could elicit strong AFP-specific T-cell responses and produce a distinctively protective effect on AFP-expressing tumors compared with other immunized groups. We should point out that the DNA vaccine hAFP also produced a definite antitumor immunity, but the effect was not sufficient and satisfactory in comparison with that of recombinant vaccine AFP/HSP70. It is of interest to note that recombinant DNA vaccines provoked not only the considerable stability of immunoprotection, but also a detectable level of anti-AFP antibody, although humoral immunity alone had a minor effect on antitumor activity^[23,24].

In the study, we attributed the successful AFP specific T-cell responses in mice to the HSP70 molecules by mediating APCs to efficiently uptake and process of AFP. A number of investigations have shown that HSP70 itself has no antigenicity and its immunogenicity can be attributed to the peptide chaperones carried by itself^[25-29]. It has been verified that HSP70 is a better molecular chaperone and adjuvant, which could process and present weak tumor antigens to MHC-I of host APCs, eliciting specific T-cell responses and CTL reactions^[26-28]. Suzue *et al.*^[29] using a recombinant heat shock fusion protein containing a large fragment of ovalbumin linked to HSP70 injected without adjuvants into Balb/c mice, CTLs were produced that recognized an ovalbumin-derived peptide and the mice were also protected against challenge with ovalbumin-expressing melanoma tumor cells. Several studies have shown that HSP70-associated peptides could anchor antigens on the cell membrane and directly present them to nature killer cells or $\gamma\delta$ T cells as superantigens without dependence on the stimulation of MHC-I molecules^[30-32]. In this experiment, tumor rejection assay demonstrated that recombinant vaccine AFP/HSP70 elicited strong specific antitumor immunity against AFP-producing SP2/0 cells than AFP DNA vaccine. The results indicated that AFP immunogenicity was greatly improved by HSP70 molecules and vaccination with DNA encoding HSP70 could increase both humoral and T-cell proliferation responses to AFP.

In summary, sequential immunization with a recombinant DNA vaccine encoding AFP and heat shock protein70 could generate effective AFP-specific T cell responses and induce definite antitumor effects on AFP-producing tumors, which may be suitable for some clinical testing as a vaccine for HCC.

REFERENCES

- 1 Schafer DF, Sorrell MF. Hepatocellular carcinoma. *Lancet* 1999; **353**: 1253-1257
- 2 Qin LX, Tang ZY. Hepatocellular carcinoma with obstructive jaundice: diagnosis, treatment and prognosis. *World J Gastroenterol* 2003; **9**: 385-391
- 3 Tang ZY. Hepatocellular carcinoma-Cause, treatment and metastasis. *World J Gastroenterol* 2001; **7**: 445-454
- 4 Guo J, Cai M, Wei D, Qin L, Huang J, Wang X. Immune responses of dendritic cells after loaded with cytotoxicity T lymphocyte epitope based peptide of human alpha-fetoprotein (hAFP). *Zhonghua Ganzhangbing Zazhi* 2002; **10**: 178-180
- 5 Grimm CF, Ortman D, Mohr L, Michalak S, Krohne TU, Meckel S, Eisele S, Encke J, Blum HE, Geissler M. Mouse alpha-fetoprotein-specific DNA-based immunotherapy of hepatocellular carcinoma leads to tumor regression in mice. *Gastroenterology* 2000; **119**: 1104-1112
- 6 Hanke P, Rabe C, Serwe M, Bohm S, Pagenstecher C, Sauerbruch T, Caselmann WH. Cirrhotic patients with or without hepatocellular carcinoma harbour AFP-specific T-lymphocytes that can be activated *in vitro* by human alpha-fetoprotein. *Scand J Gastroenterol* 2002; **37**: 949-955
- 7 Hanke P, Serwe M, Dombrowski F, Sauerbruch T, Caselmann WH. DNA vaccination with AFP-encoding plasmid DNA prevents growth of subcutaneous AFP-expressing tumors and does not interfere with liver regeneration in mice. *Cancer Gene Ther* 2002; **9**: 346-355
- 8 Saeki A, Nakao K, Nagayama Y, Yanagi K, Matsumoto K, Hayashi T, Ishikawa H, Hamasaki K, Ishii N, Eguchi K. Diverse efficacy of vaccination therapy using the alpha-fetoprotein gene against mouse hepatocellular carcinoma. *Int J Mol Med* 2004; **13**: 111-116
- 9 Pancholi P, Liu Q, Tricoche N, Zhang P, Perkus ME, Prince AM. DNA prime-canarypox boost with polycistronic hepatitis C virus (HCV) genes generates potent immune responses to HCV structural and nonstructural proteins. *J Infect Dis* 2000; **182**: 18-27
- 10 Kumar V, Sercarz E. Genetic vaccination: the advantages of going naked. *Nat Med* 1996; **2**: 857-859
- 11 Leitner WW, Ying H, Restifo NP. DNA and RNA-based vaccines: principles, progress and prospects. *Vaccine* 1999; **18**: 765-777
- 12 Moelling K. DNA for genetic vaccination and therapy. *Cytokines Cell Mol Ther* 1997; **3**: 127-135
- 13 Srivastava PK, Udono H. Heat shock protein-peptide complexes in cancer immunotherapy. *Curr Opin Immunol* 1994; **6**: 728-732
- 14 Huang XF, Ren W, Rollins L, Pittman P, Shah M, Shen L, Gu Q, Strube R, Hu F, Chen SY. A broadly applicable, personalized heat shock protein-mediated oncolytic tumor vaccine. *Cancer Res* 2003; **63**: 7321-7329
- 15 Casey DG, Lysaght J, James T, Bateman A, Melcher AA, Todryk SM. Heat shock protein derived from a non-autologous tumour can be used as an anti-tumour vaccine. *Immunology* 2003; **110**: 105-111
- 16 Wang XP, Chen RF, Song AL, Liu YF. Construction and identification of pBBS212-AFP/HSP70 eukaryotic expression vector. *Zhongliu Yanjiu Yu Linchuang* 2002; **14**: 363-365
- 17 Butterfield LH, Koh A, Meng W, Vollmer CM, Ribas A, Dissette V, Lee E, Glaspy JA, McBride WH, Economou JS. Generation of human T-cell responses to an HLA-A2.1-restricted peptide epitope derived from alpha-fetoprotein. *Cancer Res* 1999; **59**: 3134-3142
- 18 Meng WS, Butterfield LH, Ribas A, Heller JB, Dissette VB, Glaspy JA, McBride WH, Economou JS. Fine specificity analysis of an HLA-A2.1-restricted immunodominant T cell epitope derived from human alpha-fetoprotein. *Mol Immunol* 2000; **37**: 943-950
- 19 Butterfield LH, Meng WS, Koh A, Vollmer CM, Ribas A, Dissette VB, Faull K, Glaspy JA, McBride WH, Economou JS. T cell responses to HLA-A*0201-restricted peptides derived from human alpha fetoprotein. *J Immunol* 2001; **166**: 5300-5308
- 20 Vollmer CM Jr, Eilber FC, Butterfield LH, Ribas A, Dissette VB, Koh A, Montejó LD, Lee MC, Andrews KJ, McBride WH, Glaspy JA, Economou JS. Alpha-fetoprotein-specific genetic immunotherapy for hepatocellular carcinoma. *Cancer Res* 1999; **59**: 3064-3067

- 21 **Banchereau J**, Steinman RM. Dendritic cells and the control of immunity. *Nature* 1998; **392**: 245-252
- 22 **Meng WS**, Butterfield LH, Ribas A, Dissette VB, Heller JB, Miranda GA, Glaspy JA, McBride WH, Economou JS. alpha-Fetoprotein-specific tumor immunity induced by plasmid prime-adenovirus boost genetic vaccination. *Cancer Res* 2001; **61**: 8782-8786
- 23 **Le Poole IC**, Gerberi MA, Kast WM. Emerging strategies in tumor vaccines. *Curr Opin Oncol* 2002; **14**: 641-648
- 24 **Reilly RT**, Emens LA, Jaffee EM. Humoral and cellular immune responses: independent forces or collaborators in the fight against cancer? *Curr Opin Investig Drugs* 2001; **2**: 133-135
- 25 **Milani V**, Noessner E, Ghose S, Kuppner M, Ahrens B, Scharner A, Gastpar R, Issels RD. Heat shock protein 70: role in antigen presentation and immune stimulation. *Int J Hyperthermia* 2002; **18**: 563-575
- 26 **Harmala LA**, Ingulli EG, Curtsinger JM, Lucido MM, Schmidt CS, Weigel BJ, Blazar BR, Mescher MF, Pennell CA. The adjuvant effects of Mycobacterium tuberculosis heat shock protein 70 result from the rapid and prolonged activation of antigen-specific CD8+ T cells *in vivo*. *J Immunol* 2002; **169**: 5622-5629
- 27 **Noessner E**, Gastpar R, Milani V, Brandl A, Hutzler PJ, Kuppner MC, Roos M, Kremmer E, Asea A, Calderwood SK, Issels RD. Tumor-derived heat shock protein 70 peptide complexes are cross-presented by human dendritic cells. *J Immunol* 2002; **169**: 5424-5432
- 28 **Feng H**, Zeng Y, Graner MW, Likhacheva A, Katsanis E. Exogenous stress proteins enhance the immunogenicity of apoptotic tumor cells and stimulate antitumor immunity. *Blood* 2003; **101**: 245-252
- 29 **Suzue K**, Zhou X, Eisen HN, Young RA. Heat shock fusion proteins as vehicles for antigen delivery into the major histocompatibility complex class I presentation pathway. *Proc Natl Acad Sci U S A* 1997; **94**: 13146-13151
- 30 **Wei Y**, Zhao X, Kariya Y, Fukata H, Teshigawara K, Uchida A. Induction of autologous tumor killing by heat treatment of fresh human tumor cells: involvement of gamma delta T cells and heat shock protein 70. *Cancer Res* 1996; **56**: 1104-1110
- 31 **Dressel R**, Grzeszik C, Kreiss M, Lindemann D, Herrmann T, Walter L, Gunther E. Differential effect of acute and permanent heat shock protein 70 overexpression in tumor cells on lysability by cytotoxic T lymphocytes. *Cancer Res* 2003; **63**: 8212-8220
- 32 **Cheng WF**, Hung CF, Lin KY, Ling M, Juang J, He L, Lin CT, Wu TC. CD8+ T cells, NK cells and IFN-gamma are important for control of tumor with downregulated MHC class I expression by DNA vaccination. *Gene Ther* 2003; **10**: 1311-1320

Edited by Wang XL and Chen WW Proofread by Xu FM

Apoptosis pathway of liver cells in chronic hepatitis

Nai-Ling Chen, Ling Bai, Lin Li, Pei-Lan Chen, Chang Zhang, Chao-Ying Liu, Tao Deng, Hao Chen, Ke-Ming Jia, Zhen-Qiu Zhou

Nai-Ling Chen, Lin Li, Pei-Lan Chen, Chao-Ying Liu, Tao Deng, Ke-Ming Jia, Institute of Liver Disease, General Hospital of Beijing Military Command Beijing 100700, China

Ling Bai, Chang Zhang, Hao Chen, Department of Pathology, First People's Hospital of Lianyungang, Lianyungang 222002, Jiangsu Province, China

Zhen-Qiu Zhou, First People's Hospital of Lianyungang, Lianyungang 222002, Jiangsu Province, China

Supported by the National Natural Science Foundation of China, No. 39770660 and the Beijing Military Command Foundation, No. 95B008 and the Social Development Program of Lianyungang City, No. SH 0210

Correspondence to: Ling Bai, Department of Pathology, First People's Hospital of Lianyungang, Lianyungang 222002, Jiangsu Province, China. bailing1968@hotmail.com

Telephone: +86-518-5467012 **Fax:** +86-518-5462047

Received: 2004-01-10 **Accepted:** 2004-03-02

Abstract

AIM: To study the pathway of apoptosis in chronic liver disease and the role of mitochondria in programmed cell death.

METHODS: Liver biopsy specimens from 72 cases of chronic hepatitis and 29 cases of post hepatitis cirrhosis were studied. The pro-apoptotic protein Fas, FasL, Bax and the anti-apoptotic protein Bcl-2, Bcl-x_L, Bcl-2 α were studied immunohistochemically by SP method. Specimens from 15 cases of chronic hepatitis and post hepatitis cirrhosis were examined for their ultramicrostructures with special attention to their mitochondrial changes. Specimens from 3 normal adults (demised in traffic accidents) were used as control.

RESULTS: The expression of proapoptotic proteins (Fas, FasL, Bax) in hepatocytes was significantly higher in the chronic hepatitis group than in the cirrhosis group ($P < 0.001$). In the study of ultramicrostructure 364 hepatocytes were examined, from 12 cases of chronic hepatitis (including 10 mild cases, 1 moderate case and 1 severe case). Out of 364 hepatocytes 40 (11.0%) hepatocytes were found with various kinds of destruction in their mitochondria. Rupture of the outer membrane of mitochondria and the leakage of matrix from the intermembrane space were definitely demonstrated. The ultramicrostructural changes of mitochondria in the chronic hepatitis group were statistically higher than that in normal adults control group ($\chi^2 = 4.32$, $P < 0.05$).

CONCLUSION: The result of the study was in support of the current view that the apoptotic process in chronic hepatitis patients were largely along the intrinsic pathway (mitochondrial pathway), given that the intrinsic and extrinsic pathways could interlinked (converged) at some point on their progression, also it is impossible at present to exclude the possibility that the two pathways could be chosen by hepatocytes in parallel simultaneously.

Chen NL, Bai L, Li L, Chen PL, Zhang C, Liu CY, Deng T, Chen

H, Jia KM, Zhou ZQ. Apoptosis pathway of liver cells in chronic hepatitis. *World J Gastroenterol* 2004; 10(21): 3201-3204
<http://www.wjgnet.com/1007-9327/10/3201.asp>

INTRODUCTION

Fas receptor induced hepatocellular apoptosis has long been implicated in the pathogenesis of viral hepatitis and potentially other liver diseases. The apoptosis is initiated by binding of the Fas ligand expressed on the surface of lymphocytes to the Fas receptor on the hepatocytes^[1-3]. After initiation the apoptotic process, the cascade reaction of caspases and eventually to the DNA fragmentation and cell death continued^[4,5]. In addition to the above extrinsic pathway it was recognized recently that apoptosis can occur independent of cell surface receptors. Apoptosis can occur through the activation of p53 by DNA damage. Activation of p53 leads to translocation of proapoptotic protein Bax to the mitochondria and form pores at the outer mitochondrial membranes. The formation of pores induces the release of cytochrome c and other proteins from the intermembrane space. The released cytochrome c and other protein then activated other caspases and eventually lead to apoptosis (intrinsic pathway)^[6-8]. In this study we tried to find out the apoptosis pathway in chronic hepatitis. We studied it by immunohistochemical method and ultramicrostructural examination of mitochondrial changes.

MATERIALS AND METHODS

Liver biopsy specimens from 72 cases of chronic hepatitis of more than one year and 29 cases of post-hepatitis cirrhosis were studied immunohistochemically, out of them 12 cases of chronic hepatitis, 3 cases post-hepatitis cirrhosis and 3 normal adults, were examined by electronmicroscopy for the ultramicrostructures of apoptotic hepatocytes. Criteria of clinical and histological diagnoses were carried out in accordance with the consensus protocols published by the 10th Congress of Viral Hepatitis of China. The histological activity of hepatitis was assessed by the histological activity index (HAI) of Knodell *et al.*^[9] The intensity of expression in immunohistochemical assay was divided into (-), (+), (++) and (+++) in this study^[10,11].

Serum markers of HBV infection and anti-HCV antibody were detected by ELISA. Liver biopsy specimens were examined after hematoxylin and eosin staining. The immunohistochemical examination was carried out by streptavidin peroxidase conjugation. Mouse anti-human Bcl-2, Bcl-X_L monoclonal antibody and rabbit anti-human Fas and rabbit anti-human FasL polyclonal antibodies were obtained from Santo Cruz (USA). Mouse anti-Bcl-2 α monoclonal antibody was obtained from Maixin Bio company. Ultramicrostructure of mitochondria was studied by EM of Hitachi H-600 (Japan). The ultramicrostructure changes of mitochondria in specimens from 15 cases of chronic hepatitis and post hepatitis cirrhosis were examined with special attention to their mitochondrial changes. Specimens from 3 normal adults (demised in traffic accidents) were used as control. At least 15 hepatocytes in each section were observed.

The statistics was carried out by χ^2 with MINITAB software.

RESULTS

Immunohistochemical findings

Both the expressions of proapoptotic proteins (Fas, FasL, Bax) and antiapoptotic proteins (Bcl-2, Bcl-2 α , Bcl-X_L) were found mainly in cytoplasm and membranes of hepatocytes. Some expressions could also be found in cytoplasm of epithelial cells of the biliary canaliculus. In 101 cases of chronic liver disease the proapoptotic protein expression was significant higher than the antiapoptotic protein expression. The proapoptotic proteins Fas, FasL, Bax were 87.5%, 94.4% and 91.7% respectively. the antiapoptotic proteins Bcl-2, Bcl-X_L, Bcl-2 α were 56.9%, 61.1% and 38.9% ($P < 0.001$) respectively in the chronic hepatitis group (Figures 1, 2, Tables 1-3).

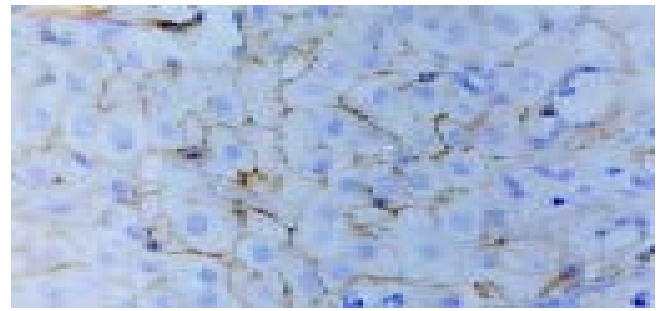


Figure 1 Expression of Fas in hepatocytes of chronic hepatitis (SP, original magnification: $\times 400$).

Table 1 Positive expression of apoptotic proteins in the liver specimens of chronic liver disease (%)

	<i>n</i>	Fas	FasL	Bax	Bcl-2	Bcl-X _L	Bcl-2 α
CH	72	63 (87.5)	68 (94.4)	66 (91.7)	41 (56.9)	44 (61.1)	28 (38.9)
LC	29	24 (82.8)	27 (93.1)	25 (86.2)	20 (69.0)	21 (72.4)	13 (44.8)

CH: Chronic hepatitis group. A: Fas: Bcl-2 $\chi^2 = 16.754$, B: Fas: Bcl-X_L $\chi^2 = 13.131$; C: Fas: Bcl-2 α $\chi^2 = 36.575$, D: FasL: Bcl-2 $\chi^2 = 27.517$; E: FasL: Bcl-X_L $\chi^2 = 23.143$, F: FasL: Bcl-2 α $\chi^2 = 50.00$; G: Bax: Bcl-2 $\chi^2 = 22.733$, H: Bax: Bcl-X_L $\chi^2 = 18.635$; I: Bax: Bcl-2 α $\chi^2 = 44.242$; J: Bcl-2: Bcl-2 α $\chi^2 = 8.472$, K: Bcl-X_L: Bcl-2 α $\chi^2 = 7.111$; J-K $P < 0.01$. LC: Liver Cirrhosis group. L: FasL: Bcl-2 α $\chi^2 = 15.789$; M: Bax: Bcl-2 α $\chi^2 = 10.898$; I-M: $P < 0.001$; N: Fas: Bcl-2 α $\chi^2 = 9.032$, $P < 0.01$; O: FasL: Bcl-2 $\chi^2 = 5.497$; P: FasL: Bcl-X_L $\chi^2 = 4.35$; O-P: $P < 0.05$.

Table 2 Degree of expression of proapoptotic proteins on the liver specimens of chronic liver disease (%)

<i>n</i>	Fas			FasL			Bax		
	(+)	(++)	(+++)	(+)	(++)	(+++)	(+)	(++)	(+++)
CH 72	32 (44.4)	29 (40.3)	2 (2.8)	29 (40.3)	34 (47.2)	5 (6.9)	26 (36.1)	24 (33.3)	16 (22.2)
LC 29	13 (44.8)	9 (31.0)	2 (6.9)	8 (27.6)	15 (51.7)	4 (13.8)	11 (37.9)	14 (48.3)	0

Table 3 Degree of expression of anti-apoptotic proteins on the liver specimens of chronic liver disease (%)

<i>n</i>	Bcl-2			Bcl-X _L			Bcl-2 α		
	(+)	(++)	(+++)	(+)	(++)	(+++)	(+)	(++)	(+++)
CH 72	21 (29.2)	13 (18.1)	7 (2.8)	27 (37.5)	10 (13.9)	7 (9.2)	25 (34.7)	3 (4.2)	0
LC 29	12 (41.4)	6 (20.7)	2 (6.9)	12 (41.4)	7 (24.1)	2 (6.9)	8 (27.6)	9 (10.4)	2 (6.9)

Table 4 Apoptosis and mitochondria of the liver specimens of chronic liver disease

Code No.		HAI Score			Fas	FasL	Bax	Bcl-2	Bcl-2 α	Bcl-X _L	A	B	A/B %
		G	S	HAI									
1	CH-mild	1	0	1	++	++	++	++	+	-	3	20	15.0
2	CH-mild	1	0	4	+	++	+++	+++	-	+	2	26	7.7
4	CH-mild	1	1	3	++	+	+	+	-	++	2	26	7.7
7	CH-mild	1	0	6	++	+++	++	++	-	++	4	36	11.2
9	CH-mild	1	0	2	+	+++	-	-	-	+++	6	25	24.0
10	CH-mild	1	0	1	++	+	-	-	-	++	5	41	12.2
11	CH-mild	2	0	3	+	++	-	-	+	-	2	37	5.4
13	CH-mild	1	0	2	-	+	-	-	-	+	1	31	3.2
14	CH-mild	1	0	1	++	-	-	-	-	-	1	15	6.7
15	CH-mild	1	0	3	++	+	-	-	-	+	4	31	12.9
3	CH-MOD	2	0	8	++	+	+	+	+	+	8	40	20.0
5	CH-SEV	4	15	15	++	+++	-	-	-	-	2	36	5.6
6	LC	3	12	12	+	+	+++	+++	-	++	0	15	
8	LC	4	15	15	-	-	+	+	-	+++	1	24	4.2
12	LC	4	8	8	+	+	-	-	-	++	5	34	14.7

MOD: Moderate; SEV: Severe; G: Grade; S: Stage. A: Number of hepatocytes with abnormal mitochondria; B: Total number of hepatocytes examined by EM.



Figure 2 Bcl-2 expression on cell membranes and cytoplasm of hepatocytes of chronic hepatitis (SP, original magnification: $\times 400$).

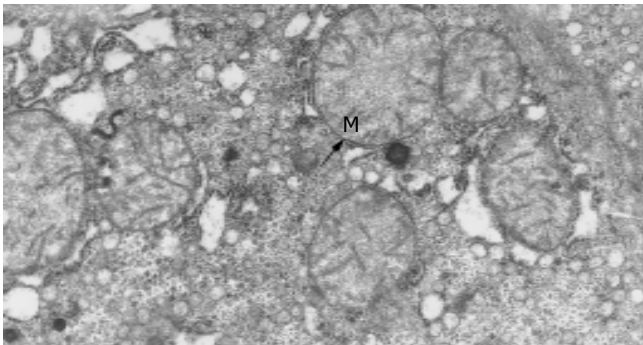


Figure 3 Normal mitochondria in normal adults (Trans-EM, original magnification: $\times 26\ 000$).

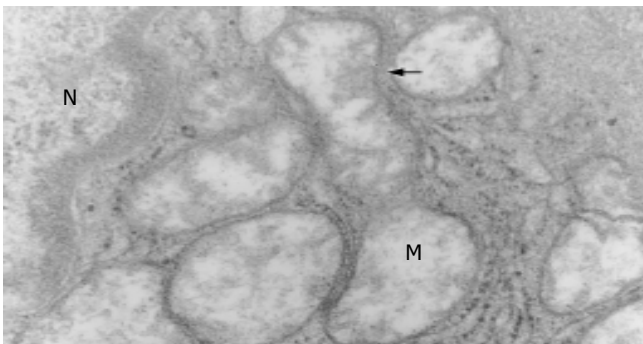


Figure 4 Membrane rupture, disappearance of crista due to apoptosis (Trans-EM, original magnification: $\times 25\ 000$).

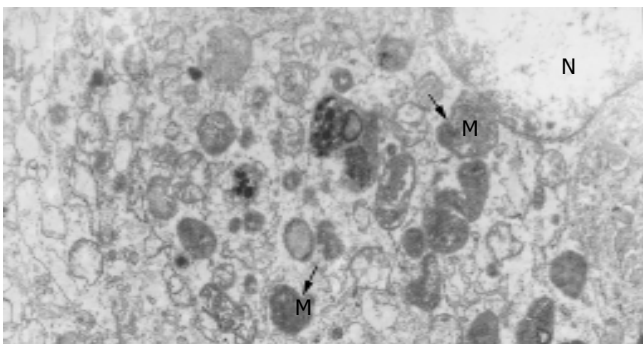


Figure 5 Herniation of matrix from ruptured membranes of apoptotic mitochondria (Trans-EM, original magnification: $\times 20\ 000$).

Untramicrostructure findings

The ultramicrostructures of mitochondria in 12 cases of chronic hepatitis (including 10 mild cases, 1 moderate case and 1 severe

case) were studied. Among the 364 hepatocytes examined, 40 hepatocytes (11.0%) were found with distinct abnormality in their mitochondria (Table 4). Changes of the mitochondria include disappearance of cristae, rupture of the outer membranes (Figures 3, 4), leakage of mitochondrial matrix, “herniation” of matrix from the ruptured membranes (Figures 5, 6).

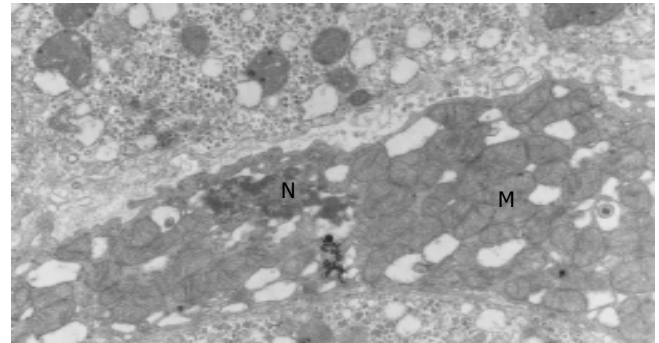


Figure 6 Degeneration and concentration of apoptotic mitochondria (Trans-EM, original magnification: $\times 15\ 000$).

DISCUSSION

This study demonstrated that the proapoptotic proteins in chronic hepatitis were significantly higher than the antiapoptotic proteins. This was in strong contrast to many tumor cells whose antiapoptotic proteins were higher than proapoptotic proteins. It was also noted that in the 12 cases of chronic hepatitis patients of more than one year the outer mitochondrial membrane damages or ruptures were also in strong contrast to the normal adults control. Recent investigations inclined to support the view that the apoptosis of hepatocytes may be taken the intrinsic pathway (or mitochondrial pathway)^[12-15]. In view of the prominent mitochondrial changes seen in this study the author was highly in favor of the current view that the apoptosis of hepatocytes in chronic hepatitis may begin from the injured DNA which activates the p53 protein to translocate the proapoptotic protein Bax to the mitochondrial and form pores at the outer mitochondrial membrane to release the cytochrome c to the cytosol. This beginning lead to the complete death of the hepatocytes^[16].

The result was considered consistent with the current view that the apoptosis in chronic hepatitis was a comparatively long persistent phenomenon which took place mainly along the intrinsic pathway (mitochondria pathway), although it was impossible at present to exclude the possibility that the intrinsic and extrinsic could take place in parallel simultaneously. Further study of the apoptotic pathway of chronic hepatitis would be helpful in finding out the effective methods of interrupting the progressive course of the disease.

ACKNOWLEDGEMENTS

We would like to express thanks to Professor Yao- Xuan Huang for directions.

REFERENCES

- 1 **Hengartner MO.** The biochemistry of apoptosis. *Nature* 2000; **407**: 770-776
- 2 **Ravi R, Bedi A.** Requirement of BAX for TRAIL/Apo2L-induced apoptosis of colorectal cancers: synergism with sulindac-mediated inhibition of Bcl-X_L. *Cancer Res* 2002; **62**: 1583-1587
- 3 **Zheng HC, Sun JM, Wei ZL, Yang XF, Zhang YC, Xin Y.** Expression of Fas ligand and Caspase-3 contributes to formation of immune escape in gastric cancer. *World J Gastroenterol* 2003;

- 9: 1415-1420
- 4 **Greenstein S**, Ghias K, Krett NL, Rosen ST. Mechanisms of glucocorticoid-mediated apoptosis in hematological malignancies. *Clin Cancer Res* 2002; **8**: 1684-1694
- 5 **Tsujimoto Y**. Bcl-2 family of proteins-Life-or-death. *Switch Clin Immunol* 2001; **36**: 266-273
- 6 **Adrain C**, Martin SJ. The mitochondrial apoptosome: a killer unleashed by the cytochrome seas. *Trends Biochem Sci* 2001; **26**: 390-397
- 7 **Capaldi RA**. The changing face of mitochondrial research. *Trends Biochem Sci* 2000; **25**: 212-214
- 8 **Feldmann G**, Haouzi D, Moreau A, Durand-Schneider AM, Bringuier A, Berson A, Mansouri A, Fau D, Pessayre D. Opening of the mitochondrial permeability transition pore causes matrix expansion and outer membrane rupture in Fas-mediated hepatic apoptosis in mice. *Hepatology* 2000; **31**: 674-683
- 9 **Knodell RG**, Ishak KG, Black WC, Chen TS, Craig R, Kaplowitz N, Kiernan TW, Wollman J. Formulation and application of a numerical scoring system for assessing histological activity in asymptomatic chronic active hepatitis. *Hepatology* 1981; **1**: 431-435
- 10 **Chen NL**, Bai L, Deng T, Zhang C, Chen H. Study on pathway of apoptosis in chronic liver disease. *Zhonghua Chuanranbing Zazhi* 2003; **21**: 122-124
- 11 **Chen NL**, Deng T, Chen PL, Li L. The regulation of apoptosis by Bcl-2, Bcl- χ_L , Bcl-2 α and Bax in chronic liver disease. *Zhonghua Neike Zazhi* 2000; **39**: 808-810
- 12 **Jaeschke H**, Bajt ML. Regulation of apoptotic signaling pathways in hepatocytes *in vivo*. *Hepatology* 2003; **37**: 942-945
- 13 **Fang DC**. Genetic instability in the development of gastric cancer. *Shijie Huaren Xiaohua Zazhi* 2003; **11**: 1-5
- 14 **Newmeyer DD**, Ferguson-Miller S. Mitochondria: releasing power for life and unleashing the machineries of death. *Cell* 2003; **112**: 481-490
- 15 **Green DR**. Overview: apoptotic signaling pathways in the immune system. *Immunol Rev* 2003; **193**: 5-9
- 16 **Rathmell JC**, Thompson CB. Pathways of apoptosis in lymphocyte development, homeostasis, and disease. *Cell* 2002; **109**: S97-S107

Edited by Wang XL Proofread by Chen WW and Xu FM

Cloning and sequence analysis of gene *oipA* encoding an outer membrane protein of human *Helicobacter pylori*

Dao-Rong Chen, Ai-Long Huang, Xiao-Hong Tao, Pi-Long Wang, Zheng Jiang

Dao-Rong Chen, Xiao-Hong Tao, Pi-Long Wang, Zheng Jiang, Department of Gastroenterology, the First Affiliated Hospital, Chongqing University of Medical Sciences, Chongqing 400016, China
Ai-Long Huang, Institute of Viral Hepatitis, Chongqing University of Medical Sciences, Chongqing 400010, China

Supported by Fund of Chongqing Health Bureau, No. 001110438
Correspondence to: Dr. Dao-Rong Chen, Department of Gastroenterology, the First Affiliated Hospital, Chongqing University of Medical Sciences, Chongqing 400016, China. cdrcdr@mail.china.com

Telephone: +86-23-68122549

Received: 2004-02-14 **Accepted:** 2004-03-06

Abstract

AIM: To construct a recombinant *E. coli* strain that would highly express the proinflammatory outer membrane protein of human *Helicobacter pylori* (*H pylori*).

METHODS: The *oipA* DNA was amplified by PCR, inserted into pET-32a, and transformed into Top10 *E. coli* strain. This recombinant plasmid of Top10 was sent out for nucleotide sequence analysis. Finally this sequence AF479754 was compared with HP0638 and JHP0581.

RESULTS: The sequence of the aim gene was obtained. It had 924 base pairs. The identity was 95.32% against HP0638, 95.02% against JHP0581, which was higher than the identity between HP0638 and JHP0581.

CONCLUSION: Although the aim gene was obtained, but it was different from the published sequence of GenBank. It is not clear what makes this difference. Maybe it is because different strain was used or because there were some variations. So more researches are required to prove it.

Chen DR, Huang AL, Tao XH, Wang PL, Jiang Z. Cloning and sequence analysis of gene *oipA* encoding an outer membrane protein of human *Helicobacter pylori*. *World J Gastroenterol* 2004; 10(21): 3205-3207

<http://www.wjgnet.com/1007-9327/10/3205.asp>

INTRODUCTION

In order to find a good vaccine to end the coexistence of human and *Helicobacter pylori* (*H pylori*), some scientists have focused on exploring some outer membrane proteins in these 10 years. Yamaoka *et al.* found six bands of the outer membrane proteins in *H pylori* on gels by immunoblot assay kits, 116 ku (CagA), 89 ku (VacA), 35 ku, 30 ku, 26.5 ku and 19.5 ku (Lpp20)^[1-5]. In which 35 ku band is broader than others. It always appears at 33-35 ku. Now a few scientists are studying the 35 ku protein including Yamaoka. They found that 33-35 ku protein was positive in 97.5% patients with peptic ulcer, 70% patients with chronic gastritis. The results showed that it was related to the presence of peptic ulcer. Yamaoka deduced that Hpo638 encoding outer membrane protein *oipA* had the most possibility, because it had great antigen characteristics, also could increase the

serum level of IL-8. Later studies have shown that *oipA* is the only index that can differ duodenum ulcer from gastritis, respond to high location of *H pylori*, serious mucosal infiltration with neutrophils cells, and high level of IL-8.

As so far, there is no study on the *oipA* in our country. We used PCR technology to amplify *oipA* gene, to construct the recombinant plasmid, and analyse the DNA sequence. We found that the target sequence AF479754 had some difference with HP0638 and JHP0581.

MATERIALS AND METHODS

Material

H pylori was afforded by the Department of Microbiology, Chongqing University of Medical Sciences. Top10 *E. coli* strain and pET32a(+) plasmid were presented by the Institute of Viral Hepatitis of Chongqing University of Medical Sciences. Endonucleases, T4 ligase and Pfu -Taq DNA polymerase were purchased from Promega. PCR marker was purchased from Shanghai Sangon. The kits for purification of plasmids and PCR products were obtained from Omega. Primers were synthesized in Shanghai Sangon.

Isolation and identification of *H pylori*

Each gastric biopsy specimen was inoculated on *H pylori* medium plates. The plates were incubated at 37 °C under microaerobic conditions (50 mL/L O₂, 100 mL/L CO₂ and 850 mL/L N₂) for 3 to 5 d. A bacterial isolate was identified as *H pylori* according to typical Gram staining morphology, biochemical tests positive for urease and oxidase, and agglutination with commercial rabbit antibody against whole cell of the microbe. All *H pylori* isolates were stored at -70 °C.

Preparation of DNA template

Genomic DNA of *H pylori* were extracted by the conventional phenol-chloroform method and DNase-free RNase treatment. The obtained DNA was dissolved in TE buffer, and its concentration and purity were determined by ultraviolet spectrophotometry.

Polymerase chain reaction

Oligonucleotide primers were designed to amplify the whole sequence of *oipA* gene from *H pylori* strain 26 695 based on the published corresponding genomic sequences. The sequence of *oipA* sense primer with an endonuclease site of *Bam*H I was 5'-CCGGATCCATGAAAAAGCTCTCTTACT-3'. The sequence of *oipA* antisense primer with an endonuclease site of *Xho*I was 5'-CGCGGCTCGAGTTAATGTTTGTGTTTAAAGTT-3'. The total volume per PCR was 100 L containing 2.5 mol/L each dNTP, 500 nmol/L each of the two primers, 15 mol/L MgCl₂, 3.0 U Pfu-Taq polymerase, 100 ng DNA template and 1×PCR buffer (pH8.8). The parameters for PCR were at 94 °C for 4 min, ×1; at 94 °C for 60 s, at 52 °C for 50 s, at 72 °C for 60 s, ×30; then at 72 °C for 7 min, ×1. The results of PCR were observed under UV light after electrophoresis in 10 g. l-1 agarose pre-stained with ethidium bromide.

Construction of *H pylori oipA* recombinant plasmid

PCR products were digested by endonucleases *Bam*H I and *Xho*I, meanwhile pET32a(+) plasmid was cut by *Bam*H I and *Xho*I. After purification by the kits for purification of PCR products, these two fragments were ligated with cohesive ends. Then the recombinant plasmid was transformed into *E. coli* line Top10. The *E. coli* Top10 containing the recombinant plasmid was amplified in LB medium containing AMP. Clones were picked out randomly through blue/white screening. Finally the plasmids were extracted with a plasmid extraction kit according to the manufacturer's instructions and identified by PCR and digestion endonucleases of *Bam*H I and *Xho*I.

Sequence analysis

Top10 *E. coli* strains containing recombinant plasmid were sent to Shanghai GeneCore Biotechnologies Co. for DNA sequence analysis.

RESULTS

PCR amplification of *oipA* encoding sequence

Target fragments of *oipA* genes with expected sizes amplified from DNA template of *H pylori* stains are shown in Figure 1.

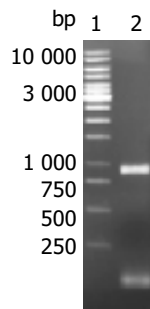


Figure 1 Amplification of human *H pylori oipA* gene by PCR. Lane 1: DNA markers (10 000, 8 000, 6 000, 5 000, 4 000, 3 500, 3 000, 2 500, 2 000, 1 500, 1 000, 750, 500, 250 bp from top to bottom); Lane 2. *oipA* gene fragment (924 bp).

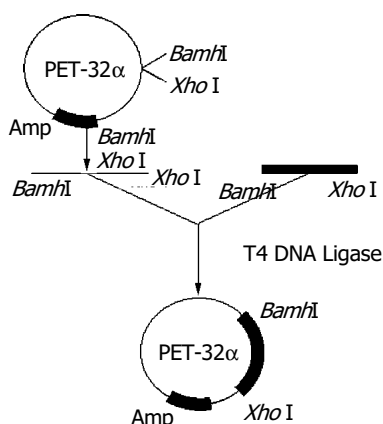


Figure 2 Construction technologic route of recombinant plasmids.

Construction and identification of recombinant plasmids

To construct the recombinant plasmid of *H pylori oipA*, purified PCR products were ligated with endonuclease-digested pET32a (+), and the recombinant was transformed into *E. coli* line Top10. White clones were picked out and confirmed by PCR and dual endonuclease digestion with *Bam*H I/*Xho*I. The technologic route is shown in Figure 2. Electrophoresis showed that a fragment of about 924 bp was released (Figure 3).

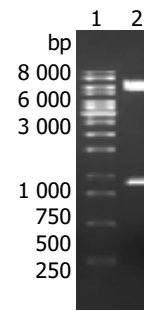


Figure 3 Dual endonuclease digestion identifications of recombinant plasmids. Lane 1: DNA markers (10 000, 8 000, 6 000, 5 000, 4 000, 3 500, 3 000, 2 500, 2 000, 1 500, 1 000, 750, 500, 250 bp from top to bottom). Lane 2: Digestion fragments of recombinant plasmids.

Sequence analysis

Samples were analyzed with an automatic sequence analyzer. Sequencing results are published in the GenBank. The accession number is AF479754. The identity was 95.32% against HP0638 and 95.02% against JHP0581, which was higher than the identity between HP0638 and JHP0581. HP0638 only was 918 bp while JHP0581 was 924 bp (6 bp TCTCTC at 37th site) and AF479754 also was 924 bp (6 bp CGAACA at 190th site).

DISCUSSION

How to prevent and eradicate *H pylori* infection is the core of the clinical therapy. The native immunity has little effect on it. Some experiments concluded that vaccine could decrease the infection, especial the incidence rate of peptic ulcer and gastric cancer. So an optimal vaccine can end the coexistence of human and *H pylori*. In recent 10 years, studies have gone deep in this wind of proteins, such as CagA, VacA, UreA, UreB, HSP, PldA, NAp.

Yamaoka deduced that Hp0638 encoding outer membrane protein *oipA* was the best candidate, because it had great antigen characteristics, and could increase the serum level of IL-8 also. Later studies showed that *oipA* was the only index that could differ duodenum ulcer from gastritis, respond to high location of *H pylori*, serious mucosal infiltration with neutrophil cells, and high level of IL-8. So far, there is no study on the *oipA* in our country. So we chose this subject. Our results showed that the identity was 95.32% against HP0638 and 95.02% against JHP0581, which was higher than the identity between HP0638 and JHP0581. The difference could be explained in two ways. One is that the strain we used was different from 26695 and J99. Different strains have different gene fragments, just as the difference between HP0638 and JHP0581. The other is that variation of the same strain induced the difference. Compared with JHP0581, AF479754 had the same base pairs. Only the insert site of 6 bp was different. It maybe one subtype of the same strain as 26695 or J99.

The value of the difference lay in three points. First, it contributes to the finding of new strains. Some surveys should be done in the whole country, to show the region characteristics of *H pylori*, and to confirm the main strains in our country. Second, it contributes to the analysis of the changes in pathogenicity and antigen activity, which are very important in elucidating the immune pathogeny. Third, it contributes to the development of new vaccines. The immunity study can provide some help to design the vaccine and optimal immune route. But a variety of strains would bring some difficulties to develop vaccines. So more work should be done to certify the pathogeny of *H pylori*, to develop effective vaccines for the eradication of *H pylori*.

ACKNOWLEDGEMENT

H pylori oipA sequence described in this paper was accepted by GenBank, GenBank accession number for it is AF479754.

REFERENCES

- 1 **Yamaoka Y**, Kodama T, Graham Y, Kashima K. Search for putative factors of *Helicobacter pylori*: the Low-Molecular-Weight (33-35K) antigen. *Dig Dis Sci* 1998; **43**: 1482-1487
- 2 **Shiesh SC**, Sheu BS, Yang HB, Tsao HJ, Lin XZ. Serologic response to lower-molecular-weight proteins of *H pylori* is related to clinical outcome of *H pylori* infection in Taiwan. *Dig Dis Sci* 2000; **45**: 781-788
- 3 **Yamaoka Y**, Kwon DH, Graham DY. A M(r) 34,000 proinflammatory outer membrane protein (oipA) of *Helicobacter pylori*. *Proc Natl Acad Sci U S A* 2000; **97**: 7533-7538
- 4 **Yamaoka Y**, Kikuchi S, el-Zimaity HM, Gutierrez O, Osato MS, Graham DY. Importance of *Helicobacter pylori* oipA in clinical presentation, gastric inflammation, and mucosal interleukin 8 production. *Gastroenterology* 2002; **123**: 414-424
- 5 **Ferreiro RL**, Labigne A. *Helicobacter pylori* vaccine development in the post-genomic era: can in silico translate to *in vivo*. *Scand J Immunol* 2001; **53**: 443-448

Edited by Wang XL and Xu FM

Effect of hepatic glucose production on acute insulin resistance induced by lipid-infusion in awake rats

Ling Li, Gang-Yi Yang

Ling Li, Department of Clinical Biochemistry, Chongqing Medical University, Chongqing 400016, China

Gang-Yi Yang, Department of Endocrinology, The Second Affiliated Hospital, Chongqing Medical University, Chongqing 400010, China

Supported by the National Natural Science Foundation of China, No. 30270631, No. 30370671, Science Foundation of Chongqing Health Bureau, No. 99-3002 and Applied Basic Research Foundation of Chongqing Science and Technology Committee, No. 02-34 and Science Foundation of China Education Ministry, No. 2003-406

Correspondence to: Dr. Gang-Yi Yang, Department of Endocrinology, The Second Affiliated Hospital, Chongqing Medical University, Chongqing 400010, China. yanggangyi@hotmail.com

Telephone: +86-23-68486115 **Fax:** +86-23-68486115

Received: 2003-11-18 **Accepted:** 2003-12-08

Abstract

AIM: To explore the influence of hepatic glucose production on acute insulin resistance induced by a lipid infusion in awake rats.

METHODS: A hyperinsulinaemic-euglycaemic clamp was established in awake chronically catheterized rats. Two groups of rats were studied either with a 4-h intraarterial infusion of lipid/heparin or saline. Insulin-mediated peripheral and hepatic glucose metabolism was assessed by hyperinsulinaemic-euglycaemic clamp combined with [$^3\text{-}^3\text{H}$]-glucose infusion.

RESULTS: During hyperinsulinaemic-euglycaemic clamp, there was a significant increase in plasma free fatty acid (FFA, from 741.9 ± 50.6 to 2346.4 ± 238.5 $\mu\text{mol/L}$, $P < 0.01$) in lipid-infused group. The glucose infusion rates (GIR) in the lipid infusion rats, compared to control rats, were significantly reduced (200-240 min average: lipid infusion; 12.6 ± 1.5 vs control; 34.0 ± 1.6 mg/kg.min, $P < 0.01$), declining to - 35% of the corresponding control values during the last time of the clamp (240 min: lipid infusion; 12.0 ± 1.9 vs control; 34.7 ± 1.7 mg/kg.min, $P < 0.0001$). At the end of clamp study, the hepatic glucose production (HGP) in control rats was significantly suppressed (88%) from 19.0 ± 4.5 (basal) to 2.3 ± 0.9 mg/kg.min ($P < 0.01$). The suppressive effect of insulin on HGP was significantly blunted in the lipid-infused rats (200-240 min: from 18.7 ± 3.0 to 23.2 ± 3.1 mg/kg.min ($P < 0.05$). The rate of glucose disappearance (GRd) was a slight decrease in the lipid-infused rats compared with controls during the clamp.

CONCLUSION: These data suggest that lipid infusion could induces suppression of hepatic glucose production, impairs the abilities of insulin to suppress lipolysis and mediate glucose utilization in peripheral tissue. Therefore, we conclude that lipid-infusion induces an acute insulin resistance *in vivo*.

Li L, Yang GY. Effect of hepatic glucose production on acute insulin resistance induced by lipid-infusion in awake rats. *World J Gastroenterol* 2004; 10(21): 3208-3211
<http://www.wjgnet.com/1007-9327/10/3208.asp>

INTRODUCTION

Insulin resistance plays a primary role in the development of type 2 diabetes and is a feature of other disorders including obesity, dyslipidemias, hypertension, and cardiovascular disease^[1]. The mechanism underlying the occurrence of insulin resistance is unknown but may be related to alterations in lipid metabolism^[2]. More than 30 years ago, Randle and colleagues demonstrated that free fatty acids (FFA) competed with glucose for substrate oxidation in isolated rat heart and diaphragm muscle preparations and speculated that increased fat oxidation might cause insulin resistance associated with diabetes and obesity^[3,4]. Subsequently, some studies have emphasized that, while an increase in circulating FFA during insulin clamp studies could promptly decrease the rate of carbohydrate oxidation, defective glucose uptake which could be detected 3-4 h after lipid infusion in humans^[5,6]. Roden and Dresner have revealed that lipid/heparin infusions could increase plasma FFA levels, inhibit whole-body glucose disposal during hyper- and euglycemic-hyperinsulinemia and insulin-dependent glucose uptake by human forearm tissues *in vivo*, and also found that acute elevations in plasma fatty acids in humans resulted in decreased glucose transport activity, as reflected by decreased concentrations of intracellular glucose 6-phosphate and glucose^[7,8]. Thus, it is possible that chronic elevation of endogenous FFAs contributes to insulin resistance in many pathophysiologic conditions in humans. Acute elevations in plasma FFA levels during a triglyceride emulsion infusion have also been shown to impair insulin-mediated glucose uptake and to inhibit hepatic glucose production (HGP) in rats^[9].

In the current study, we used a triglyceride and cholesterol ester emulsion infusion in combination with hyperinsulinemic-euglycemic clamps to assess the impact of elevated FFA levels on HPG and overall insulin action.

MATERIALS AND METHODS

Preparation of animals

A total of 24 Male Sprague-Dawley rats weighing 250-300 g were housed in individual cages and subjected to an environmentally controlled room with a 12-h light/dark cycle, where they had free access to standard rat chow and water. Five to 7 d before the *in vivo* study, rats were anesthetized with an intraperitoneal injection of pentobarbital (50 mg/kg body mass). A silastic catheter (I.D. = 0.02 in) was inserted into the right internal jugular vein and extended to the level of the right atrium. The catheter for carotid artery was constructed with a short (25 mm) segment of polyethylene tubing (PE-10), connected to a 10-cm length of PE-50 by heating in a flame. The smaller end was advanced through the left carotid artery until its tip reached the aortic arch. The free ends of the catheters were attached to the long segments of steel tubing and tunneled subcutaneously around the side to the back of the neck where they were exteriorized through a skin incision and then securely anchored to the skin by a standard wounded clip. At the end of the procedure, catheters were flushed with 300 μL isotonic saline containing heparin (20 U/mL) and ampicillin (5 mg/mL) and then filled with a viscous solution of heparin (300 U) and 800 g/L polyvinylpyrrolidone (PVP-10, Fisher, NJ) to prevent

refluxing of blood into the catheter lumen.

In vivo clamp studies

Animals were allowed at least five days to recover from the effects of surgery. All studies were conducted in the morning following a 12 to 14-h overnight fast. Throughout the study, the rats were allowed to move freely within the confines of a cage. One hour before clamping the venous and arterial lines were filled with a 9 g/L NaCl solution containing 10 IU/mL heparin. Three double lumen swivels, allowing separate fluid infusions, were connected to three peristaltic pumps. One arterial line was used for the infusion of a 250 g/L glucose solution at a variable rate and the other line was used for infusion of a mixture of (3-³H)-glucose (Amersham Inc, USA), insulin and 150 mL/L lipid emulsion/heparin (20 U/mL). The venous blood sampling tube allowed frequent sampling and repletion of blood loss by means of fresh whole blood obtained from littermates.

At the start of euglycaemic clamp, continuous infusions of isotonic saline (control group, $n = 12$) and lipid emulsion with heparin (lipid group, $n = 12$) were maintained for 4 h at a rate 1.5 mL/h during prolonged euglycemic-hyperinsulinemic clamp studies. At $t = 60$ min, a bolus (6 μ Ci) and continuous infusion (0.2 μ Ci/min) of (3-³H) glucose were initiated and continued throughout 3 h study. At $t = 120$ min, continuous infusions of insulin (4.8 mU/kg·min) and 250 g/L glucose were maintained for 2 h, 250 g/L glucose was adjusted every 5-10 min, maintaining basal plasma glucose concentrations (~ 5 mmol/L) during the insulin clamp studies. At $t = 0, 120, 200, 220, 230$ and 240 min, blood samples were collected for determination of plasma glucose, insulin, free fatty acid (FFA) and specific activity of tritiated glucose.

A separate set of 240 min lasting control clamp experiments without lipid infusion were performed to investigate the self-amplifying effect of long-term clamping on insulin-mediated glucose metabolism, since glucose metabolism was not constant during a 240 min study^[10]. The experimental procedure was identical to the lipid infusion clamps.

Analytical procedures

Plasma insulin was measured by radioimmunoassay (RIA) using rat insulin as standard (Linco Research, Inc. MO). Inter- and intra-assay variations of the insulin assay were 5.8% and 6.5%, respectively. Enzymatic colorimetric kits were used to determine plasma concentration of FFA (Wako Chemicals, Inc. VA). The inter- and intra-assay variations were 3.6% and 4.2%, respectively, during measurement of plasma FFA. Plasma for [3-³H]-glucose radioactivity (150 μ L) was deproteinized by barium hydroxide-zinc sulphate, the supernatant was evaporated to dryness at 60 °C to eliminate tritiated water and counted for 10 min in a beta scintillation counter.

Calculations

The rate of exogenous infused glucose to maintain euglycaemia during the steady-state period (from $t = 180$ -240 min) was used for the assessment of insulin action. All calculations were carried out in this period when the total amount of glucose taken up by all tissues of the body was equal to the input of glucose into the body. During this steady-state, when the rate of glucose appearance (GRa) was equal to the rate of glucose disappearance (GRd), the glucose turnover rate, which equaled to GRa and GRd in mg/min, was calculated by dividing the [3-³H]-glucose infusion rate (dpm/mg) by the steady-state value of glucose specific activity (dpm/mg). Under these conditions, the glucose turnover rate was equal to the sum of the rates of exogenous infused glucose and of hepatic glucose production (HGP). From this equation the rate of HGP was calculated. Since urinary glucose loss was not present, peripheral glucose uptake (PGU) was taken as glucose turnover rate which equaled to exogenous

glucose infusion rate plus rate of HGP.

Statistical analysis

Data were presented with mean \pm SD. Comparisons between groups were made by the two-tailed Student's *t* test. All statistical analyses were performed using SPSS.

RESULTS

General characteristics of animals

There were no differences in the mean body mass between control and lipid-infusion rats. Basic plasma concentrations of glucose, insulin, and free fatty acids (FFA) were similar in the two groups (Table 1).

Table 1 General characteristics of control and lipid-infusion rats ($n = 12$, mean \pm SE)

Group	Control	Lipid-infusion
Body mass (g)	279 \pm 19	286 \pm 17
Fasting blood glucose (mmol/L)	5.2 \pm 0.1	5.1 \pm 0.2
Fasting plasma insulin (mU/L)	30.3 \pm 2.4	27.9 \pm 2.2
Fasting free fatty acids (μ mol/L)	672.5 \pm 92.2	741.9 \pm 50.6

Effects of surgery

As expected, following surgery catheterized animals lost significant weight during the initial 24-h period, averaged 18 \pm 3 g. Following this catabolic stage they appeared well and normally active. Food intake was qualitatively normal, and average daily weight gain (~ 5 g) closely resembled that of normal littermates that did not undergo surgery.

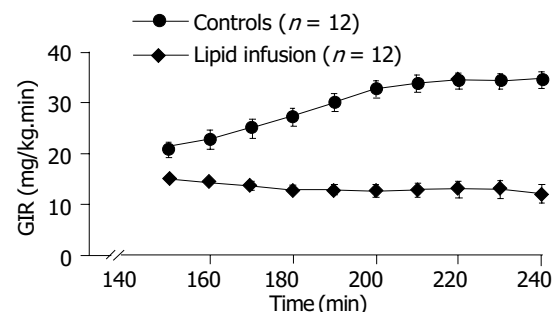


Figure 1 Time course of glucose infusion rate during hyperinsulinemic euglycemic clamping.

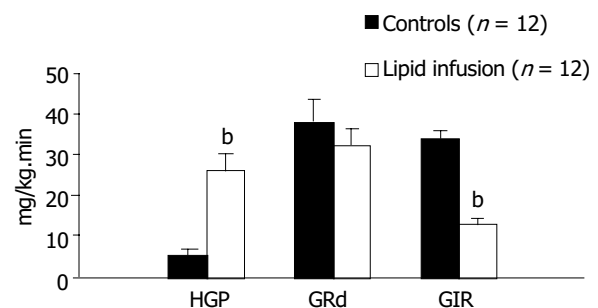


Figure 2 Steady-state hepatic glucose production, glucose disappearance rate, glucose infusion rate during hyperinsulinemic euglycemic clamp studies in control and lipid-infused rats. ^b $P < 0.01$, vs control.

Insulin clamp studies

A lipid infusion of 4 h at a rate of 1 mL/h was used to examine the effect on plasma insulin, FFA, peripheral glucose uptake

Table 2 Plasma parameters and glucose turnover data in control and lipid-infusion rats during euglycemic hyperinsulinemic clamping (mean±SE)

Group	Basal	Clamping time (min)				
		120	200	220	230	240
Glucose (mmol/L)						
Control (n = 12)	5.2±0.1	5.3±0.1	5.0±0.2	5.2±0.1	5.2±0.2	5.4±0.2
Lipid (n = 12)	5.1±0.2	5.3±0.2	5.2±0.2	5.3±0.2	5.5±0.2	5.5±0.2
FFA (μmol/L)						
Control (n = 12)	672.5±92.2	642.3±104.8	240.6±20.9	221.3±27.4	201.8±29.8	183.1±21.4
Lipid (n = 12)	741.9±50.6	2807.2±348.8 ^{bd}	3086.9±495.2 ^{bd}	2518.8±416.7 ^{bd}	2241.2±431.0 ^{bd}	2346.4±238.5 ^{bd}
Insulin (mU/L)						
Control (n = 12)	30.3±2.4	34.7±6.4	89.5±7.9	90.7±7.4	88.3±5.9	101.3±6.3
Lipid (n = 12)	27.9±2.2	31.4±3.3	84.2±6.7	93.3±8.9	103.5±16.3	104.5±14.8
GIR (mg/kg·min)						
Controls (n=12)	0		32.8±1.7	34.4±1.6	34.4±1.6	34.7±1.7
Lipid (n = 12)	0		12.7±1.3 ^b	12.9±1.6 ^b	12.9±1.8 ^b	12.0±1.9 ^b
GRd (mg/kg·min)						
Controls (n = 12)		19.0±4.5	43.1±6.1 ^d	40.1±6.7 ^d	35.5±6.8 ^d	33.2±3.2 ^d
Lipid (n = 12)		18.7±3.0	36.3±3.1 ^d	38.3±4.4 ^d	32.4±4.5 ^d	35.1±3.9 ^d
HGP (mg/kg·min)						
Controls (n = 12)		19.0±4.5	14.2±4.9 ^c	10.2±4.4 ^d	3.1±1.9 ^d	2.3±0.9 ^d
Lipid (n = 12)		18.7±3.0	23.4±4.3 ^{bc}	25.3±3.7 ^{bd}	21.5±3.5 ^b	23.2±3.1 ^{bd}

FFA: free fatty acids. GIR: glucose infusion rate. GRd: glucose disappearance rate. HGP: hepatic glucose production. ^a*P*<0.05; ^b*P*<0.01 vs control; ^c*P*<0.05; ^d*P*<0.01 vs Basal. The basal values of HGP were determined at 120 min.

and hepatic glucose production. During the euglycemic-hyperinsulinemic clamps blood glucose concentrations remained constant compared to the basal levels and were not different between control and lipid infusion studies. Plasma insulin concentrations increased similarly to ~100 mU/L in both studies (Table 2). The coefficients of variation in plasma glucose and insulin levels were 4.8 and 7.6%, respectively, in all studies. In the control study the plasma concentration of FFAs dropped by ~65% once the euglycemic clamp was started, but it increased approximately fourfold (from 741.9±50.6 to 2346.4±238.5 μmol/L, *P*<0.01) within 120 min of hyperinsulinemic clamp in the lipid-infused group (Table 2). The time course of the glucose infusion rate (GIR) during insulin clamp is shown in Figure 1. The GIR in lipid infusion rats, compared to control rats, was significantly reduced (200-240 min average; lipid infusion; 12.6±1.5 vs control; 34.0±1.6 mg/kg·min, *P*<0.01, Table 2 and Figure 2), declining to ~35% of the corresponding control values during the last time of the clamp (240 min: lipid infusion; 12.0±1.9 vs control; 34.7±1.7 mg/kg·min, *P*<0.0001, Figure 1). After a 14-h fast there was no significant difference in HGP between the two groups (19.0±4.5 vs 18.7±3.0 mg/kg·min in control and lipid-infused rats, respectively). At the end of hyperinsulinemic-euglycemic clamp study, the HGP in control rats was significantly suppressed (88%) from 19.0±4.5 (basal) to 2.3±0.9 mg/kg·min (*P*<0.01, Table 2). The suppressive effect of insulin on HGP was significantly blunted in lipid-infused rats (180-240 min: lipid infusion; from 18.7±3.0 to 23.2±3.1 mg/kg·min *P*<0.05, Table 2). The time courses of HGP for controls and lipid-infused rats are shown in Table 2. During the clamp, the GRd was significant increased compared with basal values. Although the GRd had no significant difference between the two groups, there was a slight decrease in lipid-infused rats compared with controls (Table 2). Figure 2 shows the average values of HGP, GRd and GIR during the clamp in control and lipid-infused rats.

DISCUSSION

Obesity is associated with insulin resistance and hyperinsulinemia, two important cardiovascular risk factors^[11]. What remains

uncertain is how obesity produces insulin resistance and hyperinsulinemia. It has recently become clear, however, that FFA plays a pivotal role in this process. Although there are a number of studies on this subject, the precise mechanisms of FFA effect on insulin action are not completely understood. In the present study we examined the effect of a 4-h lipid infusion on *in vivo* insulin action in conscious rats, by the hyperinsulinemic-euglycaemic clamp technique, in combination with a continuous infusion of [³H]-glucose. This method is considered to be the most suitable for the measurement of *in vivo* insulin. In our hyperinsulinemic clamping, insulin infusion increased plasma insulin levels to an approximate three-fold over basal insulin level, whereas blood glucose was clamped at approximately 5.3 mmol/L in the control and lipid infusion groups. Plasma FFA concentrations were suppressed by approximately ~65% during clamps in the control group. But in lipid infusion rats, the FFA levels had a rapid increase more than 3.8-fold over basal levels and the increase was maintained to the end of hyperinsulinemic clamp, suggesting that lipid infusion impaired the antilipolytic action of insulin and promoted the release of fatty acids from adipocytes or infused lipid. It is widely known that elevated FFA levels could exert a deleterious effect on insulin's overall actions, and this has been demonstrated in both animals and humans^[12]. The mechanisms underlying FFA-induced insulin resistance are not very clear, but elevated plasma levels of FFA produced at least two distinct biochemical defects: inhibition of insulin stimulated glucose transport and/or phosphorylation, and inhibition of muscle glycogen synthase activity^[13].

In the attempt to better our understanding of the pathophysiology of lipid-induced insulin resistance, we examined the effect of lipid infusions on HGP. We found that HGP was suppressed by ~88% in the controls during hyperinsulinemic-euglycaemic clamp, suggesting the impact of insulin on the suppression of endogenous glucose production. However, HGP was not significantly suppressed in lipid-infused rats. Thus, lipid infusion elevated the levels of circulating FFA and elevated FFA levels interfered with insulin's ability to inhibit hepatic glucose production. The increased hepatic glucose production in response to lipid infusion suggested that an experimental

elevation of circulating FFA levels could lead to hepatic insulin resistance. On the other hand, during insulin clamp glucose infusion rates (GIR), compared to control rats, were significantly reduced to -35% of the corresponding control values during the last time of the clamp. At clamping steady state, peripheral glucose uptake was equal to the sum of the rates of exogenous infused glucose (GIR) and hepatic glucose production (HGP). If HGP was completely suppressed, peripheral glucose uptake would equal to GIR (in controls). But, HGP was not significantly suppressed in lipid-infused rats, so peripheral glucose uptake was equal to GIR, which equaled to HGP plus GIR. Total glucose uptake is the sum of glucose removal by insulin-dependent as well as insulin-independent tissues. In the present study we found there was a slight decrease in GIR in lipid infusion groups, although the data did not reach statistical significance. Nonetheless, the trend is obvious since the brain and splanchnic tissues use glucose in an insulin-independent manner, roughly 750 g/L of total glucose utilization is considered to be insulin-independent in fasting condition. Thus, this might indicate that 4 h of lipid infusion induced a partial defect in insulin-stimulated peripheral glucose uptake, consistent with previous *in vivo* studies by Kim *et al.*^[14]. Considering the absence of HGP-suppressing effect of insulin under lipid infusion condition, we concluded that an experimental elevation of circulating FFA levels by lipid/heparin infusions could lead to peripheral and hepatic insulin resistance. The mechanism of lipid-induced insulin resistance remains poorly understood and may involve different IRS-1-associated PI3-kinase activation^[15], and the activity of I κ B kinase- β (I κ B- β , a known serine kinase)^[14,16].

In summary, the current studies showed that infusion of lipid emulsions with heparin to acutely raise plasma fatty acid concentrations could impair the ability of insulin to stimulate overall body glucose disposal and also interfered with insulin's ability to inhibit hepatic glucose production. Thus, we propose that a sustained increase in circulating FFA causes a hepatic insulin resistance, and may lead to a partial defect in insulin-stimulated peripheral glucose uptake, which can be attributed to lipotoxic effect on insulin action.

REFERENCES

- 1 **Reaven GM.** Role of insulin resistance in human disease. *Diabetes* 1988; **37**: 1595-1607
- 2 **Boden G.** Role of fatty acids in the pathogenesis of insulin resistance and NIDDM. *Diabetes* 1997; **46**: 3-10
- 3 **Randle PJ, Garland PB, Newsholme EA, Hales CN.** The glucose fatty acid cycle in obesity and maturity onset diabetes mellitus. *Ann N Y Acad Sci* 1965; **131**: 324-333
- 4 **Randle PJ, Garland PB, Hales CN, Newsholme EA.** The glucose fatty-acid cycle: its role in insulin sensitivity and the metabolic disturbances of diabetes mellitus. *Lancet* 1963; **1**: 785-789
- 5 **Boden G, Jadali F, White J, Liang Y, Mozzdi M, Chen X, Coleman E, Smith C.** Effects of fat on insulin-stimulated carbohydrate metabolism in normal men. *J Clin Invest* 1991; **88**: 960-966
- 6 **Kelley DE, Mokan M, Simoneau JA, Mandarino LJ.** Interaction between glucose and free fatty acid metabolism in human skeletal muscle. *J Clin Invest* 1993; **92**: 91-98
- 7 **Roden M, Price TB, Perseghin G, Petersen KF, Rothman DL, Cline GW, Shulman GI.** Mechanism of free fatty acid-induced insulin resistance in humans. *J Clin Invest* 1996; **97**: 2859-2865
- 8 **Dresner A, Laurent D, Marcucci M, Griffin ME, Dufour S, Cline GW, Slezak LA, Andersen DK, Hundal RS, Rothman DL, Petersen KF, Shulman GI.** Effects of free fatty acids on glucose transport and IRS-1-associated phosphatidylinositol 3-kinase activity. *J Clin Invest* 1999; **103**: 253-259
- 9 **Griffin ME, Marcucci MJ, Cline GW, Bell K, Barucci N, Lee D, Goodyear LJ, Kraegen EW, White MF, Shulman GI.** Free fatty acid-induced insulin resistance is associated with activation of protein kinase C θ and alterations in the insulin signaling cascade. *Diabetes* 1999; **48**: 1270-1274
- 10 **Koopmans SJ, van Mansfeld ADM, Jansz HS, Krans HMJ, Radder JK, Frolich M, de Boer SF, Kreutter DK, Andrews GC, Maassen JA.** Amylin-induced *in vivo* insulin resistance in conscious rats: the liver is more sensitive to amylin than peripheral tissues. *Diabetologia* 1991; **34**: 218-224
- 11 **Fontbonne AM, Eschwege EM.** Insulin and cardiovascular disease. Paris prospective study. *Diabetes Care* 1991; **14**: 461-469
- 12 **Hevener AL, Reichart D, Janez A, Olefsky J.** Thiazolidinedione treatment prevents free fatty acid-induced insulin resistance in male wistar rats. *Diabetes* 2001; **50**: 2316-2322
- 13 **Boden G.** Free fatty acids (FFA), a link between obesity and insulin resistance. *Front Biosci* 1998; **15**: d169-175
- 14 **Kim JK, Kim YJ, Fillmore JJ, Chen Y, Moore I, Lee J, Yuan M, Li ZW, Karin M, Perret P, Shoelson SE, Shulman GI.** Prevention of fat-induced insulin resistance by salicylate. *J Clin Invest* 2001; **108**: 437-446
- 15 **Yu C, Chen Y, Cline GW, Zhang DY, Zong HH, Wang YL, Bergeron R, Kim JK, Cushman SW, Cooney GJ, Atcheson B, White MF, Kraegen EW, Shulman GI.** Mechanism by which fatty acids inhibit insulin activation of insulin receptor substrate-1 (IRS-1)-associated phosphatidylinositol 3-kinase activity in muscle. *J Biol Chem* 2002; **277**: 50230-50236
- 16 **Yin MJ, Yamamoto Y, Gaynor RB.** The anti-inflammatory agents aspirin and salicylate inhibit the activity of I κ B kinase- β . *Nature* 1998; **396**: 77-80

Edited by Zhang JZ and Wang XL Proofread by Xu FM

Chronic gastritis rat model and role of inducing factors

Zun Xiang, Jian-Min Si, Huai-De Huang

Zun Xiang, Huai-De Huang, Department of Gastroenterology, First Affiliated Hospital, College of Medicine, Zhejiang University, Hangzhou 310003, Zhejiang Province, China

Jian-Min Si, Department of Gastroenterology, Sir Run Run Shaw Hospital, College of Medicine, Zhejiang University, Hangzhou 310016, Zhejiang Province, China

Correspondence to: Zun Xiang, Department of Gastroenterology, First Affiliated Hospital, College of Medicine, Zhejiang University, Hangzhou 310003, Zhejiang Province, China. xianghr@hotmail.com

Telephone: +86-571-87236863 **Fax:** +86-571-87236618

Received: 2003-12-28 **Accepted:** 2004-02-01

Abstract

AIM: To establish an experimental animal model of chronic gastritis in a short term and to investigate the effects of several potential inflammation-inducing factors on rat gastric mucosa.

METHODS: Twenty-four healthy, male SD rats were treated with intragastric administration of 600 mL/L alcohol, 20 mmol/L sodium deoxycholate and 0.5 g/L ammonia (factor A), forage containing low levels of vitamins (factor B), and/or indomethacin (factor C), according to an $L_8(2^7)$ orthogonal design. After 12 wk, gastric antral and body mucosae were pathologically examined.

RESULTS: Chronic gastritis model was successfully induced in rats treated with factor A for 12 wk. After the treatment of animals, the gastric mucosal inflammation was significantly different from that in controls, and the number of pyloric glands at antrum and parietal cells at body were obviously reduced ($P < 0.01$). Indomethacin induced gastritis but without atrophy, and short-term vitamin deficiency failed to induce chronic gastritis and gastric atrophy. In addition, indomethacin and vitamin deficiency had no synergistic effect in inducing gastritis with the factor A. No atypical hyperplasia and intestinal metaplasia in the gastric antrum and body were observed in all rats studied.

CONCLUSION: Combined intragastric administration of 600 mL/L alcohol, 20 mmol/L sodium deoxycholate and 0.5 g/L ammonia induces chronic gastritis and gastric atrophy in rats. Indomethacin induces chronic gastritis only. The long-term roles of these factors in gastric inflammation and carcinogenesis need to be further elucidated.

Xiang Z, Si JM, Huang HD. Chronic gastritis rat model and role of inducing factors. *World J Gastroenterol* 2004; 10 (21): 3212-3214

<http://www.wjgnet.com/1007-9327/10/3212.asp>

INTRODUCTION

Chronic gastritis including chronic atrophic gastritis (CAG) is common and CAG is a precancer lesion. It is very important to study the etiology of chronic gastritis, especially CAG. We established an experimental animal model of chronic gastritis and investigated the effects of inducing factors on gastric mucosa of rats.

MATERIALS AND METHODS

Animals

Twenty-four healthy, male SD rats weighing 270-290 g were involved in this study. Animals were housed in a controlled environment with a 12/12 h light /dark cycle. The care and handling of the animals were in accordance with the National Institutes of Health Guidelines for the Care and Use of Laboratory Animals.

Chemicals and experimental design

Pure ammonia (Wujin Chemicals Factory, Jiangsu, China) was used to be diluted to a 0.5 g/L solution. Pure alcohol (Yixing Nanxin Chemicals Factory, Jiangsu, China) was diluted to a 60% solution and sodium deoxycholate (DOC-Na) (SERVA Company) was dissolved into sterilized water to make a 20 mmol/L solution. A mixture of carboxymethyl cellulose containing 0.5 mg/mL indomethacin was dispensed.

In this study, an $L_8(2^7)$ orthogonal test was used and comprised 8 testing members, 3 treatment factors (A, B and C) and 2 levels (with or without treatment). Triple tests were conducted and 24 rats were used. Factor A: 0.5 g/L ammonia solution was used as drinking water everyday, intragastric administration of 2 mL of 600 mL/L alcohol was given twice in fasting per week and intragastric administration of 2 mL of 20 mmol/L DOC-Na without fasting everyday but intragastric administration twice in fasting per week was also given. Factor B: forage containing less vitamin was given. Factor C: intragastric administration with 1mg indomethacin was given everyday. All above doses were used for each rat, the testing period was 12 wk. The control rats had free access to normal rat chow and water.

Histology study

All rats were sacrificed with luxation of cervical vertebra and their stomachs were removed after 12 wk. Gastric mucosa for histological examinations was cut along the lesser curvature from the lower esophagus to the upper duodenum. Samples were immersed in buffered 40 g/L formaldehyde and embedded in paraffin. Paraffin sections were sliced, mounted on glass slides and stained with hematoxylin and eosin (H&E) for histological study. Inflammation grades of gastric antrum and body were based on semi-quantity. Four inflammation grades were classified in accordance with pathological diagnosis of chronic gastritis set up on Huston symposium in 1994^[1]. Four typical signs of inflammation grades were described: 0: no inflammation, the presence of few leukocytes infiltration in gastric mucosa; 1: mild inflammation, a few leukocytes infiltration in upper mucosa or at bottom of gastric glands; 2: moderate inflammation, a large number of leukocytes infiltration in total mucosa; 3: severe inflammation, leukocytes infiltration in heaps in total mucosa. Each inflammation grading result was based on an average of grades of 10 fields under microscope. Thickness of lamina propria mucosa of the stomach was measured at given points which was $150 \pm 10 \mu\text{m}$ away from the boundary of forestomach in body while $150 \pm 10 \mu\text{m}$ away from pyloric ring in antrum. Percentage ratio of pyloric gland area to total lamina propria area at gastric antrum was $100 \mu\text{m}$ to $200 \mu\text{m}$ away from pyloric ring. Also 10 intact oxyntic glands were observed at the above points in gastric body, parietal cell number in each gland and the median number were calculated.

Statistical analysis

All data were analyzed by using variance analysis of an $L_8(2^7)$ orthogonal test. $P < 0.05$ was considered statistically significant.

RESULTS

Effect of inflammation grades on gastric mucosa

At antrum, inflammation grade of gastric mucosa induced by a single factor A was 1.50, 1.67 and 1.75 respectively on three repeated tests. It was significantly higher than that of the control. The grade induced by factor C also was higher than that of the control ($P < 0.01$, Table 1, Figure 1). However, combined treatment of factors A+B+C, A+B, A+C had no effects on enhancing inflammation grades induced by a single factor A. In addition, a single factor B had no effect on inducing gastritis and inflammation grades induced by combined treatment of factors B+C had no difference from that induced by a single factor C (Table 1). The results were similar at gastric body (Table 1, Figure 2).



Figure 1 Severe infiltration of inflammatory cells, decreased thickness of lamina propria and lessened pyloric glands in gastric antrum of rats with gastritis induced by factor A. The results induced by factors A+B+C, A+C, A+B were similar. HE stain $\times 100$. Factor A: Combined intragastric treatments of 600 mL/L alcohol, 20 mmol/L sodium deoxycholate and 0.5 g/L ammonia; Factor B: Treatment of forage containing low levels of vitamins; Factor C: Treatment of indomethacin.



Figure 2 Severe infiltration of inflammatory cells, decreased parietal cells in oxyntic glands in gastric body of rats with gastritis induced by factor A with no changes in thickness of lamina propria. The results induced by factors A+B+C, A+C, A+B were similar. HE stain $\times 100$. Factor A: Combined intragastric treatments of 600 mL/L alcohol, 20 mmol/L sodium deoxycholate and 0.5 g/L ammonia; Factor B: Treatment of forage containing low levels of vitamins; Factor C: Treatment of indomethacin.

Effect of glandular atrophy on gastric mucosa

At antrum, the lamina propria mucosa of rats induced by single factor A was much thinner than that of the control ($P < 0.01$, Table 2) while the lamina propria of rats induced by single factor B or C had no difference from that of the control and there was no statistical difference between that of rats induced by factors A+B+C, A+B, A+C and that of rats induced by single factor A (Table 2). By calculating the percentage ratio of

pyloric gland area to total lamina propria area at antrum, we found the results were similar (Table 3, Figure 1). In addition, we found that although factors A, B or C had no effect on inducing the changes of lamina propria in gastric body, factor A induced a decrease of parietal cells in oxyntic glands. However, combined treatment of A+B+C, A+B, A+C had no synergistic effect with single factor A (Tables 2, 3 and Figure 2). Also no atypical hyperplasia and intestinal metaplasia in mucosa of gastric body and antrum in rats were observed in this study.

Table 1 $L_8(2^7)$ orthogonal test results of inflammation grades in stomachs of rats

Treatment factors	Triple orthogonal tests results					
	Antrum			Body		
A+B+C	2.10	1.83	2.00	1.67	1.60	1.64
A+B	1.67	1.50	1.63	1.30	1.40	1.38
A+C	2.10	2.10	1.83	1.67	1.64	1.67
A	1.50 ^b	1.67 ^b	1.75 ^b	1.29 ^b	1.25 ^b	1.40 ^b
B+C	1.17	1.25	1.00	1.00	1.08	0.90
B	0.75	0.75	0.83	0.60	0.67	0.63
C	1.25 ^d	1.17 ^d	1.00 ^d	0.88 ^d	1.00 ^d	1.10 ^d
Control	0.75	0.83	0.75	0.60	0.64	0.67

^b $P < 0.01$ vs the control, ^d $P < 0.01$ vs the control. Factor A: Combined intragastric treatments of 60% alcohol, 20 mmol/L sodium deoxycholate and 0.5 g/L ammonia; Factor B: Treatment of forage containing low levels of vitamins; Factor C: Treatment of indomethacin.

Table 2 $L_8(2^7)$ orthogonal test results of thickness of lamina propria in stomachs of rats

Treatment factors	Triple orthogonal tests results (μm)					
	Antrum			Body		
A+B+C	40.0	38.5	36.5	310.0	290.0	305.0
A+B	43.5	41.5	45.0	383.5	283.5	338.5
A+C	46.5	36.5	36.5	311.5	313.5	325.0
A	43.5 ^b	41.5 ^b	45.0 ^b	358.5	331.5	330.0
B+C	70.0	72.0	66.5	308.5	328.5	341.5
B	65.0	75.0	68.5	333.8	333.5	326.5
C	71.5	71.0	75.0	333.5	325.0	311.5
Control	66.5	71.5	75.0	300.0	310.0	313.5

^b $P < 0.01$ vs the control. Factor A: Combined intragastric treatments of 600 mL/L alcohol, 20 mmol/L sodium deoxycholate and 0.5 g/L ammonia; Factor B: Treatment of forage containing low levels of vitamins; Factor C: Treatment of indomethacin.

Table 3 $L_8(2^7)$ orthogonal test results of changes of glands in gastric lamina propria of rats

Treatment factors	Triple orthogonal tests results					
	Percentage ratio of pyloric gland area to total lamina propria at gastric antrum			Parietal cell number in observed oxyntic glands in gastric body		
A+B+C	0.2188	0.3750	0.3125	12	10	13
A+B	0.3750	0.3000	0.3750	14	12	14
A+C	0.3650	0.3125	0.3333	11	11	12
A	0.3438 ^b	0.3750 ^b	0.3230 ^b	14 ^b	12 ^b	15 ^b
B+C	0.5688	0.5150	0.5725	28	23	25
B	0.5385	0.5625	0.5313	25	26	23
C	0.5750	0.5840	0.6500	26	23	27
Control	0.5250	0.6050	0.5893	25	29	23

^b $P < 0.01$ vs the control. Factor A: Combined intragastric treatments of 600 mL/L alcohol, 20 mmol/L sodium deoxycholate and 0.5 g/L ammonia; Factor B: Treatment of forage containing low levels of vitamins; Factor C: Treatment of indomethacin.

DISCUSSION

CAG has been considered a precancerous disease^[2], it is essential to establish a stable, economic and effective experimental animal model of chronic gastritis including CAG for further study on gastritis. Previous studies showed that three methods were practicable to establish experimental models. (1) Biologically induced animal models. Animals such as rats, cats were infected with *Helicobacter pylori* (*H pylori*) and an experimental model was induced. However, just some of these animals could be induced and models were unstable and it was time-consuming. (2) Animal models induced by physiochemical injury. Models of chronic gastritis were induced by single factors such as alcohol or sodium deoxycholate or ammonia or X-ray irradiation, but the models were unstable and atypical. (3) Immunologically induced animal models. Models of CAG were induced by hypodermic injection with homogeneous, xenogenic or isogenic stomach antigens, but the procedure was complicated and expensive, the effects were unstable^[3-14].

The shortcomings of the above methods have limited further studies on etiology of CAG. However, according to previous studies, we concluded that factors such as infection of *H pylori*, excessive drinking, reflux of duodenal juice, long-term intake of nonsteroid drugs, malnutrition that could induce continuous gastritis, were considered to be the etiology of CAG^[15-25]. In our study we tried to administer 600 mL/L alcohol to injure gastric mucosa, 20 mmol/L sodium deoxycholate (DOC-Na) as a simulator to reflux of duodenal juice, 0.5 g/L indomethacin to interfere with synthesis of prostaglandin (PG) that was proved to be effective for preventing gastric mucosa from injury and 0.5 g/L ammonia as a simulator to *H pylori* to induce continuous gastritis in rats. Finally we found that combined administration of 600 mL/L alcohol, 20 mmol/L DOC-Na and 0.5 g/L ammonia for 12 wk could induce an animal model of chronic gastritis with some features of early CAG especially in antrum. Furthermore, our study showed that atrophy of gastric mucosa in rats also developed from gastric antrum to body. It proved once again that excessive drinking, reflux of bile and infection of *H pylori* played a vital role in inducing chronic gastric mucosal inflammation. It also suggests that the above factors may probably induce CAG. However, we found that indomethacin induced only chronic gastritis but not atrophy of glands in mucosa and had no effect on enhancing glandular atrophy induced by alcohol, ammonia and DOC-Na. In addition, single treatment of forage containing few vitamins in our study could not induce chronic gastritis and glandular atrophy, it is perhaps because the testing duration was too short. The long-term roles of these factors in gastric inflammation and atrophy need to be further elucidated.

In conclusion, an animal model of chronic gastritis can be established by combined intragastric administration with 60% alcohol, 20 mmol/L sodium deoxycholate and 0.5 g/L ammonia. These factors play a vital role in etiology of chronic atrophic gastritis.

REFERENCES

- Dixon MF, Genta RM, Yardley JH, Correa P. Classification and grading of gastritis. The updated sydney system. International workshop on the histopathology of gastritis, houston 1994. *Am J Surg Pathol* 1996; **20**: 1161-1181
- Kapadia CR. Gastric atrophy, metaplasia, and dysplasia: a clinical perspective. *J Clin Gastroenterol* 2003; **36**(5 Suppl): S29-36
- Hu PJ, Zeng ZR, Lin HL, Chen MH, Chen W, Peng XZ. Effect of eradication of *Helicobacter pylori* on development and reversion of atrophic gastritis in animal study. *Zhonghua Xiaohua Zazhi* 2000; **20**: 155-158
- Oda T, Marakami K, Nishizono A, Kodama M, Nasu M, Fujioka T. Long-term *Helicobacter pylori* infection in Japanese monkeys induces atrophic gastritis and accumulation of mutations in the

- p53 tumor suppressor gene. *Helicobacter* 2002; **7**: 143-151
- Kinoshita K, Watanabe H, Ando Y, Katayama M, Yamamoto H, Hirano N, Yoshikuni S, Yamamoto T. Effects of subtotal resection of the fundus on development of intestinal metaplasia induced by X-ray irradiation in Donryu rats. *Pathol Int* 2000; **50**: 879-883
- Kawano S, Tsujii M, Fusamoto H, Sato N, Kamada T. Chronic effect of intragastric ammonia on gastric mucosal structures in rats. *Dig Dis Sci* 1991; **36**: 33-38
- Watanabe H, Hirose F, Takizawa S, Terada Y, Fujii I. Morphological and biochemical changes in the gastric mucosa of A/HEJ mice injected with a xenogeneic stomach antigen. *Acta Pathol Jpn* 1977; **27**: 869-876
- Watanabe H, Uesaka T, Kido S, Ishimura Y, Shiraki K, Kuramoto K, Hirata S, Shoji S, Katoh O, Fujimoto N. Gastric tumor induction by 1, 2-dimethylhydrazine in Wistar rats with intestinal metaplasia caused by X-irradiation. *Jpn J Cancer Res* 1999; **90**: 1207-1211
- Eaton KA, Radin MJ, Krakowka S. An animal model of gastric ulcer due to bacterial gastritis in mice. *Vet Pathol* 1995; **32**: 489-497
- Lee A, Chen M, Coltro N, O'Rourke J, Hazell S, Hu P, Li Y. Long term infection of the gastric mucosa with *Helicobacter species* does induce atrophic gastritis in an animal model of *Helicobacter pylori* infection. *Zentralbl Bakteriol* 1993; **280**: 38-50
- Wang X, Willen R, Svensson M, Ljungh A, Wadstrom T. Two - year follow-up of *Helicobacter pylori* infection in C57BL/6 and Balb/cA mice. *APMIS* 2003; **111**: 514-522
- Ikeno T, Ota H, Sugiyama A, Ishida K, Katsuyama T, Genta RN, Kawasaki S. *Helicobacter pylori*-induced chronic active gastritis, intestinal metaplasia, and gastric ulcer in Mongolian gerbils. *Am J Pathol* 1999; **154**: 951-960
- Kim DH, Kim SW, Song YJ, Oh TY, Han SU, Kim YB, Joo HJ, Cho YK, Kim DY, Cho SW, Kim MW, Kim JH, Hahm KB. Long-term evaluation of mice model infected with *Helicobacter pylori*: focus on gastric pathology including gastric cancer. *Aliment Pharmacol Ther* 2003; **18**(Suppl 1): 14-23
- Bergin IL, Sheppard BJ, Fox JG. *Helicobacter pylori* infection and high dietary salt independently induce atrophic gastritis and intestinal metaplasia in commercially available outbred Mongolian gerbils. *Dig Dis Sci* 2003; **48**: 475-485
- Kamada T, Haruma K, Hata J, Kusunoki H, Sasaki A, Ito M, Tanaka S, Yoshihara M. The long-term effect of *Helicobacter pylori* eradication therapy on symptoms in dyspeptic patients with fundic atrophic gastritis. *Aliment Pharmacol Ther* 2003; **18**: 245-252
- Kearney DJ, Ritchie K, Peacock JS. Gastric-juice ammonia assay for diagnosis of *Helicobacter pylori* infection and the relationship of ammonia concentration to gastritis severity. *Am J Gastroenterol* 2000; **95**: 3399-3403
- Huizenga JR, Vissink A, Kuipers EJ, Gips CH. *Helicobacter pylori* and ammonia concentrations of whole, parotid and submandibular/sublingual saliva. *Clin Oral Investig* 1999; **3**: 84-87
- Bujanda L. The effects of alcohol consumption upon the gastrointestinal tract. *Am J Gastroenterol* 2000; **95**: 3374-3382
- Thuluvath P, Wojno KJ, Yardley JH, Mezey E. Effects of *Helicobacter pylori* infection and gastritis on gastric alcohol dehydrogenase activity. *Alcohol Clin Exp Res* 1994; **18**: 795-798
- Brown AS, Fiatarone JR, Wood P, Bennett MK, Kelly PJ, Rawlins MD, Day CP, James OF. The effect of gastritis on human gastric alcohol dehydrogenase activity and ethanol metabolism. *Aliment Pharmacol Ther* 1995; **9**: 57-61
- Bielecki K, Zawadzki JJ. Observations on gastric histology, endoscopy appearance and *Helicobacter pylori* after corrective surgery for bile reflux gastritis. *Mater Med Pol* 1994; **26**: 9-12
- Dixon MF, Mapstone NP, Neville PM, Moayyedi P, Axon AT. Bile reflux gastritis and intestinal metaplasia at the cardia. *Gut* 2002; **51**: 351-355
- Ito Y, Suzuki K, Ichino N, Imai H, Sakaguchi H, Hokama M, Nishii M, Nakano H. The risk of *Helicobacter pylori* infection and atrophic gastritis from food and drink intake: a cross-sectional study in Hokkaido, Japan. *Asian Pac J Cancer Prev* 2000; **1**: 147-156
- Kitahara F, Shimazaki R, Sato T, Kojima Y, Morozumi A, Fujino MA. Severe atrophic gastritis with *Helicobacter pylori* infection and gastric cancer. *Gastric Cancer* 1998; **1**: 118-124
- Ohkuma K, Okada M, Murayama H, Seo M, Maeda K, Kanda M, Okabe N. Association of *Helicobacter pylori* infection with atrophic gastritis and intestinal metaplasia. *J Gastroenterol Hepatol* 2000; **15**: 1105-1112

Effect of hepatitis B immunoglobulin on interruption of HBV intrauterine infection

Xiao-Mao Li, Min-Feng Shi, Yue-Bo Yang, Zhong-Jie Shi, Hong-Ying Hou, Hui-Min Shen, Ben-Qi Teng

Xiao-Mao Li, Yue-Bo Yang, Zhong-Jie Shi, Hong-Ying Hou, Hui-Min Shen, Ben-Qi Teng, Department of Obstetrics and Gynecology, Third Affiliated Hospital, Sun Yat-Sen University, Guangzhou 510630, Guangdong Province, China

Min-Feng Shi, Women's Hospital, School of Medicine, Zhejiang University, Hangzhou 310006, Zhejiang Province, China

Supported by the Science and Research Foundation of Guangzhou Science and Technology Committee, No.1999-J-005-01

Correspondence to: Professor Xiao-Mao Li, Department of Obstetrics and Gynecology, Third Affiliated Hospital, Sun Yat-Sen University, Guangzhou 510630, Guangdong Province, China. tigerlee777@163.net
Telephone: +86-20-85515609 **Fax:** +86-20-87565575

Received: 2004-02-06 **Accepted:** 2004-02-26

Abstract

AIM: To evaluate the efficacy of hepatitis B immunoglobulin (HBIG) in interrupting hepatitis B virus (HBV) intrauterine infection during late pregnancy.

METHODS: We allocated 112 HBsAg positive pregnant women into 2 groups randomly. Fifty seven cases in the HBIG group received 200 IU (unit) HBIG intramuscularly every 4 wk from the 28 wk of gestation to the time of delivery, while 55 cases in the control group received no special treatment. HBsAg, HBeAg, HBcAb, HBeAb, HBsAb and HBV DNA levels were tested in the peripheral blood specimens from all of the mothers at 28 wk of gestation, just before delivery, and in blood from their newborns within 24 h before administration of immune prophylaxis.

RESULTS: The intrauterine infection rate in HBIG group and control group were 10.5% and 27.3%, respectively, with significant difference ($P < 0.05$). It showed ascendant trend as HBV DNA levels in the peripheral blood increased before delivery.

CONCLUSION: HBIG is potent to cut down HBV intrauterine infection rate significantly when administered to pregnant women regularly during late pregnancy. The possibility of HBV intrauterine infection increases if maternal blood HBV DNA $\geq 10^8$ copies/mL.

Li XM, Shi MF, Yang YB, Shi ZJ, Hou HY, Shen HM, Teng BQ. Effect of hepatitis B immunoglobulin on interruption of HBV intrauterine infection. *World J Gastroenterol* 2004; 10(21): 3215-3217

<http://www.wjgnet.com/1007-9327/10/3215.asp>

INTRODUCTION

China is a high incidence area of hepatitis B virus (HBV) infection, with a mean HBsAg positive rate of about 10%. Forty to fifty percent of chronic HBV carriers are caused by vertical transmission, which ranks it among the important modes of HBV infection and an important reason of so many HBV carriers in the crowd. Also, it has close correlations with chronic hepatitis, liver

cirrhosis and liver cancer. Intrauterine transmission is one of the main resources of hepatitis B virus (HBV) vertical infection, but there is no definite prophylaxis up to now^[1-6]. Through HBV DNA quantitation by fluorogenic quantitative polymerase chain reaction (FQ-PCR), we evaluated the efficacy of HBIG in interrupting HBV intrauterine infection during late pregnancy and analyzed the relation between maternal HBV DNA level and the rate of intrauterine transmission.

MATERIALS AND METHODS

Patients

The subjects were drawn from pregnant women who had undergone regular prenatal check-up, and had been admitted for labor and followed up at the Obstetric Department of the Third Affiliated Hospital of Sun Yat-Sen University from December 1999 to October 2001.

The following eligible criteria should all be met: (1) single pregnancy; (2) gestational age ≤ 28 wk; (3) HBsAg positive in serum; (4) normal liver and kidney functions; (5) serial tests were negative for HAV, HCV, HDV and HEV; (6) exclusion of fetal anomalies by B-ultrasonography; (7) no receipt of other agents that were under research, anti-virus, immunomodulating, cytotoxic or steroid hormones during pregnancy; (8) their husbands were not HBV carriers or hepatitis B patients; and (9) ability to give written informed consent.

Methods

A total of 112 pregnant women according to the criteria set above and their newborns of 112 cases were chosen. The pregnant women were randomly divided into a HBIG group (57 cases) and a control group (55 cases). Each case in the HBIG group received 200 IU of HBIG (produced by Sichuan Shuyang Pharmaceutical Ltd.) intramuscularly (im) every four weeks from 28 wk of gestation till delivery, while patients in the control group were given no special treatment. Blood specimens were tested for HBsAg, HBeAg, HBsAb, HBeAb, and HBcAb by enzyme linked immunosorbent assay (ELISA, assay kits produced by Zhongshan Biological Products Ltd.), and HBV DNA quantitation by FQ-PCR (assay kits produced by Da'an Genetic Diagnosis Center of Sun Yat-Sen University) in all the subjects at 28 wk and on the day of delivery, and their newborns (blood from femoral vein) 24 h after birth before the administration of immune prophylaxis. All the subjects followed-up regularly during pregnancy.

HBV intrauterine infection was defined as follows: HBsAg and/or HBV DNA positive in peripheral blood of newborns in 24 h after birth before the administration of active or passive immune prophylaxis.

Statistics

The quantity of HBV DNA was transformed to the form of \log_{10} and then expressed as mean \pm SD. All data were analyzed as χ^2 (*chi-square*) test for positive difference and *t* test for comparisons of means between the 2 groups using SPSS 10.0 for windows. For all comparisons, $P < 0.05$ was considered statistically significant.

RESULTS

Clinical characteristics of pregnant women

There were no significant differences between the two groups as for age, nation, gravidity, abortive parity, gestational weeks, way of delivery, or pregnant complications ($P>0.1$, Table 1).

Table 1 Clinical characteristics of pregnant women of each group

Characteristics	HBIG group (n = 57)	Control group (n = 55)
Age (yr)	26.9±1.8	27.8±2.8
Nationality of Han	57	55
Gravidity	1.5±0.9	1.9±1.2
Abortive parity	0.6±0.7	0.7±1.0
Gestational weeks	39.5±1.9	39±1.3
Rate of cesarean section	27 (47.4%)	25 (45.5%)
Threatened abortion	7	5
Threatened premature labour	2	2
Premature rupture of membrane	0	0
Pregnancy induced hypertension syndrome	1	1
Premature delivery	0	1
Postmature labour	0	0
Elderly primipara	0	0
Medical and surgical associated diseases	2	2
HBeAg positive rate	36 (63.2%)	28 (50.9%)
HBV DNA level (log ₁₀)	5.75±2.98	5.54±3.09

Intrauterine transmission of HBV

There were 6 cases of intrauterine infection in HBIG group. The counterpart in control group was 15. HBV intrauterine infection rate in HBIG group and control group were 10.5% and 27.3%, respectively, with significant difference ($P<0.05$, Table 2).

Intrauterine transmission and the level of HBV DNA in maternal serum

The levels of HBV DNA were divided into 7 grades according to the fluorescent signals set by the operation manual, with grade 0 ($<10^5$ copies/mL), grade 1 ($<10^6$ copies/mL), grade 2 ($<10^7$ copies/mL), grade 3 ($<10^8$ copies/mL), grade 4 ($<10^9$ copies/mL), grade 5 ($<10^{10}$ copies/mL), and grade 6 ($<10^{11}$ copies/mL). The intrauterine infection rate increased with the increase in HBV DNA level in maternal blood, with odds ratio (OR) increasing. The results of rank correlation and *chi*-square test indicated that although it showed an ascendant trend, there were no significant differences in intrauterine infection rate between grade 2 and grade 1, grade 3 and grade 2, grade 5 and grade 4. But there was significant difference between grade 3 and grade 4 ($P<0.05$, Table 3).

Table 2 Characters of neonatal HBV intrauterine infection

	Neonates n	HBsAg	HBeAg	HBcAb	HBeAb	HBsAb	HBV DNA	n	Intrauterine infection n (%)
Control group	55	+	-	+	+	-	-	2	15 (27.27)
		-	-	-	-	-	+	3	
		-	-	-	+	-	+	3	
		-	+	+	-	-	+	3	
		-	-	+	+	-	+	4	
HBIG group	57	+	-	+	+	-	-	1	6 (10.53)
		+	+	+	-	-	-	1	
		-	-	+	-	-	+	4	

Table 3 HBV DNA levels in blood of mothers at delivery and HBV intrauterine infection

HBV DNA grade	Mothers (n)	Intrauterine infection		Value of OR
		n	Percentage (%)	
Grade 0 ($<10^5$ copies/mL)	26	0	0	...
Grade 1 ($<10^6$ copies/mL)	22	0	0	...
Grade 2 ($<10^7$ copies/mL)	15	2	13.33	1.00
Grade 3 ($<10^8$ copies/mL)	13	2	15.38	5.55
Grade 4 ($<10^9$ copies/mL)	32	15	46.88	26.91
Grade 5 ($<10^{10}$ copies/mL)	4	2	50.00	30.50

Safety

No adverse events such as fever, rigor, skin rash, inflammation and scleroma at local injected area, or impairment of renal function as well as other discomforts were found during the medication of HBIG. As to Apgar score and development reference such as weight and height of the newborns at delivery, there were no significant difference between the 2 groups ($P>0.1$, Table 4).

Table 4 Development indices of neonates and Apgar score (mean±SD)

	Weight (kg)	Height (cm)	1-minute Apgar score
HBIG group	3.05±0.25	48.0±1.4	10±0.0
Control group	3.04±0.45	48.1±1.5	9.9±0.3

DISCUSSION

Several studies have proved that maternal infectivity is the most important factor in intrauterine transmission of HBV^[7], in which HBV DNA shows directly the condition of replication and infectivity of the virus *in vivo*. The latter can be exactly reflected through HBV DNA quantitation by FQ-PCR test clinically^[8,9]. With the prominent sensitivity and specificity of the FQ-PCR test, our study indicated that the intrauterine infection rate had significant correlation with the level of HBV DNA in the maternal serum before delivery, which showed an ascendant trend; the intrauterine infection rate significantly increased at the level of HBV DNA $\geq 10^8$ copies/mL, which was consistent with the findings by Ngui *et al.*^[10]. Those findings suggest that the threshold of HBV DNA $\geq 10^8$ copies/mL is a potent index of HBV intrauterine infection. To those pregnant women whose serum levels of HBV DNA are high and have high infectivity, we propose to apply highly effective and safe anti-viral medicines to compress the replication of HBV and, therefore, rapidly and dramatically decrease HBV DNA level to interrupt intrauterine infection^[11].

In this study, the intrauterine infection rate in the HBIG group and control group were 10.5% and 27.3%, respectively,

which suggested that the intramuscular administration of HBIG regularly before delivery could effectively interrupt HBV intrauterine infection^[12]. HBIG is a kind of passive antibody. One of its components, HBsAb, can combine with HBsAg, activate the complements, clear HBV, lower the level of virus in maternal blood, and thereby prevent and decrease the infection of normal cells. It was reported that the interruptive effect of HBV intrauterine infection by HBIG might correlate with the acquisition of neonatal passive immune, because placenta could transmit the antibody of IgG actively from mother to fetus during late pregnancy^[13]. However, HBsAb was detected in none of the newborns in our study. The potential reason might be that the HBV level in maternal blood was so high (higher than the quantity that can be neutralized by the passive antibody) that the HBIG administered to mother might not be enough to enter fetal body through placenta. So, we consider to increase the quantity of HBIG in our further studies of HBV intrauterine interruption.

We found that some newborns were HBsAg and HBV DNA negative but HBeAg positive in their blood drawn from femoral vein within 24 h after birth. Whether HBeAg can pass placenta is still under hot debate. It has been suggested that HBeAg can be more easily transmitted via placenta than HBsAg in that it is smaller than the latter and is free from agglutination^[14]. HBeAg or the compound of HBeAg and α -HBeIgG can pass the barrier of placenta by means of active-transfer in human body^[15]. One study also showed that some babies of HBV infected mothers were HBeAg positive and HBsAg negative in femoral blood at birth, and HBsAg titres of the mothers were significantly higher than HBeAg titres (200 times or more). So the positive HBeAg in neonatal serum could not be interpreted as contamination or leakage from the placenta, but can only be explained by that HBeAg can indeed cross placenta^[16]. In our study, babies who were only HBeAg positive were born by mothers who were both HBsAg and HBeAg positive. Moreover, the sensitive and specific HBV-infection marker of HBV DNA quantitation were negative in neonatal peripheral blood, and HBeAg disappeared by 9-12 mo of age. So HBeAg in the neonatal peripheral blood is less likely to be an index of intrauterine infection, but transmitted passively from maternity.

REFERENCES

- 1 Hepatitis B vaccination-United States, 1982-2002. *Morb Mortal Wkly Rep* 2002; **51**: 549-552
- 2 **Kazim SN**, Wakil SM, Khan LA, Hasnain SE, Sarin SK. Vertical transmission of hepatitis B virus despite maternal lamivudine therapy. *Lancet* 2002; **359**: 1488-1489
- 3 **Gerdts V**, Babiuk LA, van Drunen Littel-van den Hurk, Griebel PJ. Fetal immunization by a DNA vaccine delivered into the oral cavity. *Nat Med* 2000; **6**: 929-932
- 4 **Chen DS**. Public health measures to control hepatitis B virus infection in the developing countries of the Asia-Pacific region. *J Gastroenterol Hepatol* 2000; **15**(Suppl): E7-10
- 5 **Mast EE**, Mahoney FJ, Alter MJ, Margolis HS. Progress toward elimination of hepatitis B virus transmission in the United States. *Vaccine* 1998; **16**(Suppl): S48-51
- 6 **Yu XL**, Chen CH, Zhong M. Reasons of failure in blocking mother-infant transmission of HBV by using vaccine and related strategies. *Zhonghua Huli Zazhi* 1997; **32**: 69-71
- 7 **Hamdani-Belghiti S**, Bouazzaou NL. Mother-child transmission of hepatitis B virus. State of the problem and prevention. *Arch Pediatr* 2000; **7**: 879-882
- 8 **Li XM**, Liu SL, Li X, Huang HJ, Lu JX, Gao ZL. The relative study of hepatitis B virus DNA in maternal blood, umbilical blood and breastmilk. *Acad J SUMS* 2000; **21**: 233-235
- 9 **Yang YB**, Teng BQ, Li XM, Lin CS, Hou HY, Shen HM. The application of PCR in the test of HBV DNA quantitation. *J Sun Yat Sen University* 2003; **24**: 20-23
- 10 **Ngui SL**, Andrews NJ, Underhill GS, Heptonstall J, Teo CG. Failed postnatal immunoprophylaxis for hepatitis B: characteristics of maternal hepatitis B virus as risk factors. *Clin Infect Dis* 1998; **27**: 100-106
- 11 **Li XM**, Yang YB, Hou HY, Shi ZJ, Shen HM, Teng BQ, Li AM, Shi MF, Zou L. Interruption of HBV intrauterine transmission: A clinical study. *World J Gastroenterol* 2003; **9**: 1501-1503
- 12 **Zhu Q**, Lu Q, Gu X, Xu H, Duan S. A preliminary study on interruption of HBV transmission in uterus. *Chin Med J* 1997; **110**: 145-147
- 13 **Yue YF**, Yang XI, Zhang SL, Han XB. Clinical study on the prevention of HBV transmission from mother to infant by injection of HBIG in pregnant women with HBsAg. *Chin J Practical Gynecol Obstet* 1999; **15**: 547-548
- 14 **Rumi MA**, Begum K, Hassan MS, Hasan SM, Azam MG, Hasan KN, Shirin M, Khan AK. Detection of hepatitis B surface antigen in pregnant women attending a public hospital for delivery: implication for vaccination strategy in Bangladesh. *Am J Trop Med Hyg* 1998; **59**: 318-322
- 15 **Suga M**, Shibata K, Kodama T, Arima K, Yamada S, Yachi A. A case of HBs antigen negative fulminant hepatitis with IgM antibody to hepatitis B core antigen persisting more than seven years. *Gastroenterol Jpn* 1991; **26**: 661-665
- 16 **Wang JS**, Zhu QR. Infection of the fetus with hepatitis B e antigen via the placenta. *Lancet* 2000; **355**: 989

Edited by Kumar M Proofread by Xu FM

Mad2 and p27 expression profiles in colorectal cancer and its clinical significance

Gang-Qiang Li, Hong-Fu Zhang

Gang-Qiang Li, Department of Pathology, Chinese PLA 455 Hospital, Shanghai 200052, China

Hong-Fu Zhang, Department of Pathology, Anhui Medical University, Hefei 230032, Anhui Province, China

Correspondence to: Gang-Qiang Li, Department of Pathology, Chinese PLA 455 Hospital, Shanghai 200052, China. lgqfm@163.com
Telephone: +86-21-62800157-41168

Received: 2004-02-02 **Accepted:** 2004-03-12

Abstract

AIM: To investigate the expression of tumor suppressor gene *p27* and spindle checkpoint gene *Mad2* and to demonstrate their expression difference in colorectal cancer and normal mucosa and to evaluate its clinical significance.

METHODS: Immunohistochemical staining was used for detection of expression of *Mad2* and *p27* in colorectal cancer and its corresponding normal mucosa.

RESULTS: *Mad2* was significantly overexpressed in colorectal cancer compared with corresponding normal mucosa ($P < 0.01$, $\chi^2 = 7.5$), and it was related to the differentiation of adenocarcinoma, lymph node metastasis and survival period after excision ($P < 0.05$, $\chi^2 = 7.72$, $\chi^2 = 4.302$, $\chi^2 = 6.234$). The rate of *p27* positive expression in adenocarcinomas and normal mucosa was 40% and 80% respectively. There was a significant difference in *p27* expression between adenocarcinomas and normal mucosa ($P < 0.001$, $\chi^2 = 13.333$), which was related to the differentiation degree of adenocarcinoma and lymph node metastasis ($P < 0.05$, $\chi^2 = 8.901$, $\chi^2 = 4$). The positive expression of *p27* was not correlated with survival period after excision.

CONCLUSION: Defect of spindle checkpoint gene *Mad2* and mutation of *p27* gene are involved mainly in colorectal carcinogenesis and associated with prognosis of colorectal cancer.

Li GQ, Zhang HF. Mad2 and p27 expression profiles in colorectal cancer and its clinical significance. *World J Gastroenterol* 2004; 10(21): 3218-3220

<http://www.wjgnet.com/1007-9327/10/3218.asp>

INTRODUCTION

Genomic instability is a hallmark of malignant cells and occurs either in the form of microsatellite instability or in the form of chromosomal instability (CIN)^[1]. Microsatellite instability is reflected by alteration in polymorphic, short, tandem repeats sequences and is associated with a small fraction of colorectal carcinomas with germ-line or somatic mutations of DNA mismatch repair genes^[2]. On the other hand, CIN, characterized by an alteration in chromosome number and commonly detected as aneuploidy, is likely to occur in most human malignancies. The fact suggests that CIN may contribute to tumorigenesis^[3-5]. In yeast, loss of mitotic checkpoint frequently leads to abnormal

chromosome number, resulting in aneuploidy or polyploidy^[6]. Two major groups of mitotic checkpoint genes, budding uninhibited by benomyl (BUB) 1-3 and mitotic arrest defect (MAD) 1-3, have been identified in budding yeast^[7]. Mammalian homologues of the yeast mitotic checkpoint protein have also been characterized^[8-10]. To date, little information is available in literature about the expression of *Mad2* in carcinoma tissue. In this study, we used immunohistochemical technique to examine the expression of *Mad2* and *p27* in colorectal cancer to elucidate the relation of *Mad2* and *p27* to carcinogenesis and clinical pathological factors.

MATERIALS AND METHODS

Specimens

Cancer tissues and corresponding normal tissues were obtained from Chinese PLA 455 Hospital from January 2001 to May 2003. No patient was treated with anti-neoplasm therapy before tumor removal. Forty patients (22 males, 18 females, aged 25 to 79 years, median age 52.5 years) were as follows: 21 cases of well differentiated adenocarcinoma, 11 cases of moderately differentiated adenocarcinoma, 8 cases of poorly differentiated adenocarcinoma. Twelve cases survived less than 18 mo, 28 cases survived more than 18 mo after excision. All the tissues were fixed in 40 g/L formaldehyde, embedded in paraffin, and cut into 4 μ m thick serial sections.

Reagents

Mad2 polyclonal rabbit antibodies directed against humans were provided by China Science and Technology University. *P27* and immunohistochemical kit were purchased from Beijing Zhongshan Biological Technology Ltd.

Immunohistochemistry

Immunohistochemical staining was performed following the manufacturer's instructions. Anti-*Mad2* antibody was diluted to 1:120. Anti-*p27* was ready to use reagent. For the negative control, the primary antibody was substituted by animal serum. *Mad2* positive expression was stained as brown-yellow mainly in cell plasma. *P27* positive expression was also stained in cell plasma. A semi-quantitative evaluation was used to determine positively expressed cells by viewing 10 vision fields at $\times 400$ magnification as follows^[11]: negative (-), <10% cells were stained; mild positive (+), 11-25% cells were stained; moderately positive (++) , 26-50% cells were stained; strong positive (+++) , >50% cells were stained. The last three grades were all regarded as positive.

Statistical analysis

The data were analyzed by SPSS version 10.0. χ^2 test was used for statistical analysis. $P < 0.05$ was considered statistically significant.

RESULTS

Expression of Mad2 protein

The positive signals of *Mad2* protein were stained brown-yellow mainly in cell plasma and strength of color was directly proportional to positive percentage (Figure 1A). Positive

expression of *Mad2* protein was detected in 30 of 40 (75%) colorectal cancers, and 18 of 40 (45%) normal tissues. There was a significant difference in *Mad2* expression between colorectal cancer and normal tissue ($P < 0.01$). Moreover, there were significant differences in *Mad2* expression among well, moderately, and poorly differentiated adenocarcinomas (Table 1). The expression of *Mad2* in colorectal cancer was related with lymph node metastasis and survival period after excision.

Table 1 Relationship between expression of *Mad2* protein and histological differentiation and lymph node metastasis

Groups	n	<i>Mad2</i>		Positive (%)	P
		+	-		
Normal tissue	40	18	22	45	
Adenocarcinoma	40	30	10	75	0.01
WD	21	12	9	61.9	
MD	11	10	1	99	
PD	8	8	0	100	0.041
Lymph node metastasis					
Absent	25	16	9	64	
Present	15	14	1	88	0.038
Survival period (months)					
<18	12	9	3	75	
≥18	28	9	19	32	0.013

WD: well differentiated adenocarcinoma; MD: moderately differentiated adenocarcinoma; PD: poorly differentiated adenocarcinoma.

p27 protein expression in colorectal cancer and normal tissue

The positive signals of *p27* protein were stained brown-yellow mainly in cell plasma, weak nuclear staining was also observed. Immunoreactivity for *p27* was found in both normal and neoplastic tissues (Figure 1B). High expression of *p27* was observed in 32 normal tissues, and low expression was observed in remaining 8 normal tissues. Of 40 colorectal cancer samples, 16 (40%) had low expression of *p27*, and 24 (60%) had high expression. There was a significant difference in *p27* expression between colorectal cancer and normal tissue ($P < 0.01$). Moreover, there were significant differences in *p27* expression among well, moderately, and poorly differentiated adenocarcinomas (Table 2). The expression of *p27* in colorectal cancer was related with lymph node metastasis. No relation of *p27* protein was found with survival period after excision.

Table 2 Relationship among expression of *p27* protein and histological differentiation and lymph node metastasis

Groups	n	<i>p27</i>		Positive (%)	P
		+	-		
Normal tissue	40	32	8	80	
Adenocarcinoma	40	16	24	40	0.001
WD	21	13	8	61.9	
MD	11	2	9	18.2	
PD	8	1	7	12.5	0.012
Lymph node metastasis					
Absent	25	13	12	52	
Present	15	3	12	20	0.046
Survival period after excision					
<18	12	4	8	33.3	
≥18	28	12	16	42.9	0.573

WD: well differentiated adenocarcinoma; MD: moderately differentiated adenocarcinoma; PD: poorly differentiated adenocarcinoma.

Correlation between *Mad2* protein and *p27*

We analyzed the correlation between *Mad2* and *p27* protein expressions by χ^2 test. There was no significantly positive correlation between the expressions of *Mad2* and *p27*.

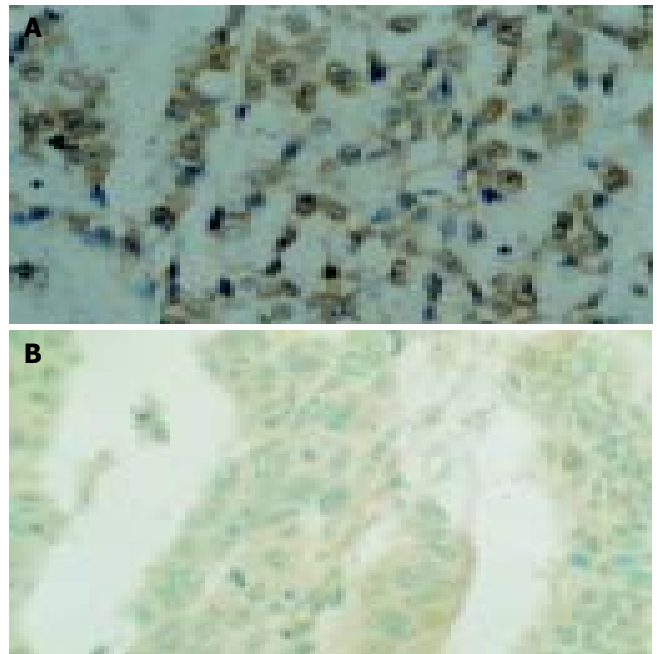


Figure 1 Strongly positive expression of *Mad2* and *p27* in poor differentiated and tubular adenocarcinomas. A: Strongly positive expression of *Mad2* in poor differentiated adenocarcinoma. B: Strongly positive expression of *p27* in tubular adenocarcinoma.

DISCUSSION

Mitotic checkpoints monitor the proper assembly of mitotic spindle and block the onset of anaphase unless all of the chromosomes are stably attached to a specialized region known as kinetochore^[12]. It has been proposed that the mitotic checkpoint proteins, especially *Mad2*, may be crucial for generating the “wait” signal to prevent the onset of anaphase after microtubule disruption^[13-15]. In the present study, the expressions of *Mad2* and *p27* proteins were examined in colorectal cancer and the corresponding normal tissue. *Mad2* expression in colorectal cancer was higher than that in the corresponding normal tissue. The expression of *Mad2* in colorectal cancer was related with histological differentiation, lymph node metastasis and survival period after excision. Our results regarding the expression of *Mad2* are not consistent with the finding that the reduced expression of *Mad2* in breast cancer cells reported by Li and Benezra^[7], but it was similar to the study by Tanaka *et al.*^[15]. The different expression might result from the surrounding in which cells lived. In an organ, cells could be influenced by nerves and endocrine hormones. Michel *et al.* showed that subtle differences in *Mad2* protein level markedly altered checkpoint function^[16]. Therefore, inactivation of *Mad2* would be sufficient to lead to a haplo-insufficient effect and loss of mitotic checkpoint control. The most convincing evidence of the role of mitotic checkpoint defect in CIN in mammalian cells came from two recent studies in *Mad2*^{-/-} mice, and in *Mad2*^{-/-} human and mouse cells, showing that disruption of *Mad2* expression resulted in CIN^[16,17]. It has been reported that CIN cells become aneuploidy, a hallmark of cancer that is associated with an aggressive tumor behavior and a poor prognosis^[18]. Recent studies reported that the *Mad2* protein interacted with estrogen receptor β or the cytoplasmic domain of insulin receptors, which are thought to be regulators

of cellular growth^[19-21]. Our study showed that *Mad2* protein overexpressed in cancer tissue was exclusively present in the cytoplasm of cancer cells. We speculate that cytoplasmic *Mad2* protein may enhance the positive regulatory action of estrogen receptor β and insulin receptor on cell proliferation.

p27 is a member of the Cip1/Kip1 family of cyclin-dependent kinase (CDK) inhibitors and a potential tumor suppressor gene^[22]. Recent studies have demonstrated that targeted inactivation of *p27* could lead to development of multiple organ hyperplasia and malignancy *in vivo*^[23,24]. In this study, we examined the expression of CDK inhibitor *p27* in colorectal adenocarcinomas and corresponding normal tissues. Low expression of *p27* was detected in cancer tissue compared with normal tissues. It was also related to histological differentiation and lymph node metastasis, but not related to survival period after excision. This evidence is similar to that previously reported in other tumors such as tumors of breast, stomach, prostate, lung, liver^[25-32].

Orr-Weaver *et al.* thought that aneuploidy might increase the rate at which tumor suppressors are lost through the loss of heterozygosity. Our study showed that there was no significantly positive correlation between the expressions of *Mad2* and *p27*.

In conclusion, expressions of *Mad2* and *p27* are related to histological differentiation and lymph node metastasis of colorectal cancer. *Mad2* and *p27* proteins might be good markers for predicting histological differentiation and prognosis of colorectal cancer.

REFERENCES

- Rooney PH, Murray GI, Stevenson DA, Haites NE, Cassidy J, Mcleod HL. Comparative genomic hybridization and chromosomal instability in solid tumours. *Br J Cancer* 1999; **80**: 862-873
- Lengauer C, Kinzler KW, Vogelstein B. Genetic instabilities in human cancers. *Nature* 1998; **396**: 643-649
- Lengauer C, Kinzler KW, Vogelstein B. Genetic instability in colorectal cancers. *Nature* 1997; **386**: 623-627
- Lengauer C, Kinzler KW, Vogelstein B. DNA methylation and genetic instability in colorectal cancer cells. *Proc Natl Acad Sci U S A* 1997; **94**: 2545-2550
- Li R, Murray AW. Feedback control of mitosis in budding yeast. *Cell* 1991; **66**: 519-531
- Hoyt MA, Totis L, Roberts BT. *S. cerevisiae* genes required for cell cycle arrest in response to loss of microtubule function. *Cell* 1991; **66**: 507-517
- Li Y, Benezra R. Identification of a human mitotic checkpoint gene: hsMAD2. *Science* 1996; **274**: 246-248
- Taylor SS, Mckeeon F. Kinetochores localization of murine Bub1 is required for normal mitotic timing and checkpoint response to spindle damage. *Cell* 1997; **89**: 727-735
- Jin DY, Spencer F, Jeang KT. Human T cell leukemia virus type 1 oncoprotein Tax targets the human mitotic checkpoint protein MAD1. *Cell* 1998; **93**: 81-91
- Barnes DM, Dublin EA, Fisher CJ, Levison DA, Millis RR. Immunohistochemical detection of p53 protein in mammary carcinoma: an important new independent indicator of prognosis? *Hum Pathol* 1993; **24**: 469-476
- Rudner AD, Murray AW. The spindle assembly checkpoint. *Curr Opin Cell Biol* 1996; **8**: 773-780
- Amon A. The spindle checkpoint. *Curr Opin Genet Dev* 1999; **9**: 69-75
- Waters JC, Chen RH, Murray AW, Salmon ED. Localization of Mad2 to kinetochores depends on microtubule attachment, not tension. *J Cell Biol* 1998; **141**: 1181-1191
- Sharp-Baker H, Chen RH. Spindle checkpoint protein Bub1 is required for kinetochores localization of Mad1, Mad2, Bub3, and CENP-E, independently of its kinase activity. *J Cell Biol* 2001; **153**: 1239-1250
- Tanaka K, Nishioka J, Kato K, Nakamura A, Mouri T, Miki C, Kusunoki M, Nobori T. Mitotic checkpoint protein hsMAD2 as a marker predicting liver metastasis of human gastric cancer. *Jpn J Cancer Res* 2001; **92**: 952-958
- Michel LS, Liberal V, Chatterjee A, Kirchweger R, Pasche B, Gerald W, Dobles M, Sorger PK, Murty VV, Benezra R. MAD2 haplo-insufficiency causes premature anaphase and chromosome instability in mammalian cells. *Nature* 2001; **409**: 355-359
- Dobles M, Liberal V, Scott ML, Benezra R, Sorger PK. Chromosome missegregation and apoptosis in mice lacking the mitotic checkpoint protein Mad2. *Cell* 2000; **101**: 635-645
- Pennisi E. Cell division gatekeepers identified. *Science* 1998; **279**: 477-478
- Poelzl G, Kasai Y, Mochizuki N, Shaul PW, Brown M, Mendelsohn ME. Specific association of estrogen receptor beta with the cell cycle spindle assembly checkpoint protein MAD2. *Proc Natl Acad Sci U S A* 2000; **97**: 2836-2839
- O'Neill TJ, Zhu Y, Gustafson TA. Interaction of MAD2 with the carboxyl terminus of the insulin receptor but not with the IGFIR. Evidence for release from the insulin receptor after activation. *J Biol Chem* 1997; **272**: 10035-10040
- Gliozzo B, Sung CK, Scalia P, Papa V, Frasca F, Sciacca L, Giorgino F, Milazzo G, Goldfine ID, Vigneri R, Pezzino V. Insulin-stimulated cell growth in insulin receptor substrate-1-deficient ZR-75-1 cells is mediated by a phosphatidylinositol-3-kinase-independent pathway. *J Cell Biochem* 1998; **70**: 268-280
- Masciullo V, Sgambato A, Pacilio C, Pucci B, Ferrandina G, Palazzo J, Carbone A, Cittadini A, Mancuso S, Scambia G, Giordano A. Frequent loss of expression of the cyclin-dependent kinase inhibitor p27 in epithelial ovarian cancer. *Cancer Res* 1999; **59**: 3790-3794
- Kiyokawa H, Kineman RD, Manova-Todorova KO, Soares VC, Hoffman ES, Ono M, Khanam D, Hayday AC, Frohman LA, Koff A. Enhanced growth of mice lacking the cyclin-dependent kinase inhibitor function of p27(kip1). *Cell* 1996; **85**: 721-732
- Fero ML, Rivkin M, Tasch M, Porter P, Carow CE, Firpo E, Polyak K, Tsai LH, Broudy V, Perlmutter RM, Kaushansky K, Roberts JM. A syndrome of multi organ hyperplasia with features of gigantism, tumorigenesis, and female sterility in p27(kip1)-deficient mice. *Cell* 1996; **85**: 733-744
- Kawamata N, Morosetti R, Miller CW, Park D, Spirin KS, Nakamaki T, Takeuchi S, Hatta Y, Simpson J, Wilczynski S, Lee Y, Bartram C, Koeffler H. Molecular analysis of the cyclin-dependent kinase inhibitor gene p27/Kip1 in human malignancies. *Cancer Res* 1995; **55**: 2266-2269
- Tan P, Cady B, Wanner M, Worland P, Cukor B, Magi-Galluzzi C, Lavin P, Draetta G, Pagano M, Loda M. The cell cycle inhibitor p27 is an independent prognostic marker in small (T1a, b) invasive breast carcinomas. *Cancer Res* 1997; **57**: 1259-1263
- Porter PL, Malone KE, Heagerty PJ, Alexander GM, Gatti LA, Firpo EJ, Daling JR, Roberts JM. Expression of cell-cycle regulators p27Kip1 and cyclin E, alone and in combination, correlate with survival in young breast cancer patients. *Nat Med* 1997; **3**: 222-225
- Catzavelos C, Bhattacharya N, Ung YC, Wilson JA, Roncari L, Sandhu C, Shaw P, Yeger H, Morava-Protzner I, Kapusta L, Franssen E, Pritchard KI, Slingerland JM. Decreased levels of the cell-cycle inhibitor p27Kip1 protein: prognostic implications in primary breast cancer. *Nat Med* 1997; **3**: 227-230
- Loda M, Cukor B, Tam SW, Lavin P, Fiorentino M, Draetta GF, Jessup JM, Pagano M. Increased proteasome-dependent degradation of the cyclin-dependent kinase inhibitor p27 in aggressive colorectal carcinomas. *Nat Med* 1997; **3**: 231-234
- Thomas GV, Szigei K, Murphy M, Draetta G, Pagano M, Loda M. Down-regulation of p27 is associated with development of colorectal adenocarcinoma metastases. *Am J Pathol* 1998; **153**: 681-687
- Ciaparrone M, Yamamoto H, Yao Y, Sgambato A, Cattoretti G, Tomita N, Monden T, Rotterdam H, Weinstein IB. Localization and expression of p27Kip1 in multistage colorectal carcinogenesis. *Cancer Res* 1998; **58**: 114-122
- Mori M, Mimori K, Shiraiishi T, Tanaka S, Ueo H, Sugimachi K, Akiyoshi T. p27 expression and gastric carcinoma. *Nat Med* 1997; **3**: 593-596

Effects of intestinal lymph on expression of neutrophil adhesion factors and lung injury after trauma-induced shock

Zuo-Bing Chen, Shu-Sen Zheng, Gao Yuan, Chen-Yan Ding, Yun Zhang, Xue-Hong Zhao, Lin-Mei Ni

Zuo-Bing Chen, Shu-Sen Zheng, Gao Yuan, Chen-Yan Ding, Yun Zhang, Xue-Hong Zhao, Lin-Mei Ni, Department of Emergency Surgery, First Affiliated Hospital, Zhejiang University School of Medicine, Hangzhou 310003, Zhejiang Province, China

Correspondence to: Zuo-Bing Chen, Department of Emergency Surgery, First Affiliated Hospital, Zhejiang University School of Medicine, 79 Qingchun Road, Hangzhou 310003, Zhejiang Province, China. chenzuoqing@hotmail.com

Telephone: +86-571-87236303

Received: 2004-02-03 **Accepted:** 2004-02-24

Abstract

AIM: To study how intestinal lymph after trauma-induced shock (TIS) interferes with expression of neutrophil adhesion factors (CD11b and CD18) and causes lung injury.

METHODS: Thirty-two adult healthy Sprague-Dawley rats were randomly divided into four experimental groups. Groups 1 and 2 included rats with TIS caused by hitting the mid-upper part of both side femoral bones with a 2 500 kg raw-iron, and with or without ligation of mesenteric lymph duct. Groups 3 and 4 included rats with sham-TIS and with or without ligation of mesenteric lymph duct. Expression of neutrophil CD18 and CD11b in at 1 and 3 h after a 90-min TIS/sham-TIS was evaluated. These rats were killed at 3 h after TIS/sham-TIS, and lungs were taken immediately. The main lung injury indexes (the MPO activity and lung injury score) were measured.

RESULTS: The expressions of CD18 and CD11b at 1 and 3 h after a 90-min TIS and the main lung injury indexes were significantly increased compared with those in the sham-TIS groups ($P < 0.05$). Moreover, at 1 and 3 h after TIS, the expressions of CD18 (32.12 ± 1.25 and 33.46 ± 0.98) and CD11b (29.56 ± 1.35 and 30.56 ± 1.85) were significantly decreased in rats with ligation of mesenteric lymph duct, compared with those (52.3 ± 1.12 and 50.21 ± 1.25 , and 42.24 ± 1.24 and 42.81 ± 1.12 , respectively) in those without the ligation (all $P < 0.05$). The main lung injury indexes in rats with TIS with ligation of mesenteric lymph duct (0.96 ± 0.12 and 6.54 ± 0.35) were also significantly decreased, compared with those (1.56 ± 0.21 and 9.56 ± 0.23) in rats with TIS without the ligation (both $P < 0.05$). However, there was no significant difference in expressions of CD18 and CD11b and the main lung injury indexes between the two sham-TIS groups.

CONCLUSION: Previous ligation of mesenteric lymph ducts prevents or alleviates the up-regulated expression of PMN CD18 and CD11b and the lung injury induced by TIS. Our findings also indicate that neutrophil adhesion molecule activation and lung injury during TIS appear to be caused by some factors that are released or produced by post-ischemic intestine through the mesenteric lymph pathway.

Chen ZB, Zheng SS, Yuan G, Ding CY, Zhang Y, Zhao XH, Ni LM. Effects of intestinal lymph on expression of neutrophil adhesion

factors and lung injury after trauma-induced shock. *World J Gastroenterol* 2004; 10(21): 3221-3224
<http://www.wjgnet.com/1007-9327/10/3221.asp>

INTRODUCTION

Trauma-induced-shock (TIS) could lead to splanchnic ischemia-reperfusion and gut barrier failure^[1]. These events could get the gut into an inflammatory cytokine-secreting organ, which contributes to the pathogenesis of shock-induced lung injury^[2,3]. Lung injury generally occurs when mediators released by systemic inflammatory processes up-regulate polymorphonuclear neutrophil (PMN) interactions with endothelial cells (ECs), thus favoring PMN sequestration and attack on the lung. Shock and trauma-induced neutrophil activation has been implicated in the pathogenesis of adult respiratory distress syndrome (ARDS) and also as a contributory factor in the development of multiple organ dysfunction syndrome (MODS)^[4,5]. Furthermore, enhanced endothelial-neutrophil interactions resulting in tissue injury appear to be the common pathways by which diverse initiating factors, such as bacterial infection, endotoxin, cytokines, shock, and ischemia can lead to organ injury and MODS^[6]. These events have been implicated in the pathogenesis of pulmonary microvascular injury after intestinal ischemia-reperfusion injuries^[7,8].

However, the exact mechanisms by which intestinal ischemia reperfusion subsequent to trauma and hemorrhage primes neutrophils remain uncertain. There are many discussions about this topic. Since Gonzalez *et al.* demonstrated that port vein blood did not contain such inflammatory mediators in patients with traumatic shock, such as endotoxin or bacteria, more and more people have attached importance to lymph pathway^[9]. Some study in a rat model of trauma-hemorrhagic shock (T/HS) has shown that ligation of the main mesenteric lymph draining the intestine could prevent lung injury^[10], and furthermore, it has been testified that mesenteric lymph from rats subjected to T/HS can prime neutrophils for an oxidative burst^[11]. TIS mesenteric lymph can activate PMNs and increase their ability to injure ECs, and on the other hand, PMN exposure to mesenteric lymph is both necessary and sufficient for the activation of rat PMN respiratory burst by TIS. From a mechanical point of view, respiratory burst activation in response to G-protein-coupled agonists is characterized by enhanced cell calcium $[Ca^{2+}]_i$ flux response to GPC agonists tested^[12,13]. In contrast, portal plasma from TIS rats lacks the potential to activate PMNs.

All these studies lead to the conclusion that lymph from the ischemic gut may be a crucial source of neutrophil priming factors after major hemorrhagic insults, such as lung injury, systemic inflammatory response syndrome (SIRS), MODS, and multiple system organ failure (MSOF). Therefore it has come to be accepted by more and more people that gut-induced lung injury is secondary to a shock-induced gut "inflammatory state", where gut-induced inflammatory factors enter the systemic circulation via mesenteric lymphatics rather than via portal bloodstream. To testify and further extend this concept that neutrophil priming activation was caused by release of factors

from gut into the mesenteric lymphatics, we performed this experiment to study whether TIS could up-regulate neutrophil adhesion molecule expression and cause lung injury, and whether such pathological changes could be prevented or alleviated by ligating mesenteric lymph ducts previously.

MATERIALS AND METHODS

Animals

Adult Sprague-Dawley rats (SD rats) weighing 300-350 g were used after a minimum acclimatization period of 7 d. The animals and their diet were provided by The Laboratory Animal Center, Zhejiang University, College of Medicine, China. The animals were had free access to food and water and were maintained in accordance with the guideline of the National Guide for the Care and Use of Laboratory Animals, and the experiment was approved by the Zhejiang University, College of Medicine.

Experimental design

The aim of this experiment was to assess how the lymph after TIS affected the expression of neutrophil adhesion molecules and caused lung injury in rats. Four groups were included. They were groups of rats subjected to TIS with or without mesenteric lymph duct ligation, and groups of rats subjected to sham TIS with or without mesenteric lymph duct ligation. Femoral artery blood samples were collected 1 and 3 h after a 90-min shock period for further evaluating the expression of PMN. Then these rats were killed immediately, lungs were removed for assessment of the severity of injuries, mainly by measuring myeloperoxidase (MPO) content and lung injury score.

TIS model

As previously described^[14], rats were anesthetized intraperitoneally using sodium pentobarbital (50 mg/kg), and a femoral artery catheter was placed for measuring the artery pressure and an other side femoral artery catheter for taking blood. Then a midline laparotomy was performed to expose the mesenteric lymph duct, which was either ligated with 2-0 silk or just left intact according to the experimental need. The incision was closed. A 2 500 kg raw-iron was used to hit the rat's mid-upper part of both side femoral bones from 30 cm height to cause TIS, then the rat artery pressure was maintained at about 30 mmHg for 90 min, by blood withdrawal or normal saline infusion through one side of the femoral artery catheter, the other side of femoral artery catheter was used to measure the artery pressure. The rats were subjected to TIS for 90 min and then their traumatic legs were tied up closely. The animal body temperature during the experiment was maintained at about 37 °C by using a heating pad.

Sham-TIS model

Except trauma treatment and being subjected to shock state, the sham-TIS model accepted the nearly same treatment as TIS model.

Assay of blood CD11b and CD18

Blood sample (1 mL) collected at 1 and 3 h after 90 min of TIS/sham-TIS state was collected and treated with anti-

coagulant EDTANa₂. A 100 μL blood sample was put into a 12 mm×75 mm tube and then 10 μL anti-rat CD11b or CD18 fluorescent labeled monoclonal antibody (BD Pharmingen) was added into the tube. The samples were gently vortexed for 10 min and then placed into a dark room for 40 min. Red blood cells of the sample were lysed and fixed with Coahem Q-PREP equipment (Couletr Company, USA) for 15 min on ice. After centrifuged and washed 3 times, PMN cells were analyzed for adhesion molecule expression using flow cytometer (ESPLL-XL, BECKMAN, USA) according to the recommendation of the manufacturer. The number of these neutrophils labelled with monoclonal antibody in 10 000 neutrophils was counted and the percentage was evaluated.

Assay of myeloperoxidase

Three hours later, rats were killed and the right lung was immediately taken and frozen. The frozen lung tissue was homogenized and processed for measuring myeloperoxidase (MPO) with the reagent kit (Jiancheng Bio-Technology Company, Nanjing, China) according to the manufacturer's instructions. One unit of MPO activity represented the amount of enzyme that reduced 1 μmol/L of peroxidase per minute.

Assay of lung injury score

The lung tissue was fixed in 40 g/L formaldehyde, cut into 4 μm sections and stained with HE. The lung injury score (LIS)^[15] was evaluated with OLMPUS optical microscope (Olympus, Japan). The severity of leukocyte sequestration in the lung tissue was classified as: 0=0%, 1=0-25%, 2=25-50%, 3=50-75%, 4=75-100%. The severity of leukocyte sequestration in lung alveoli was classified as: 0 = none, 1 = few, 2 = a lot, 3 = almost all, 4 = all. The severity of exudation (such as fibrin, transparent membrane and edema liquor) in lung alveoli was classified as: 0 = none, 1 = few, 2 = a lot, 3 = almost full, and 4 = absolute full.

Statistical analysis

Results were expressed as mean±SD. The data were analyzed with SPSS.11.0. The comparison among multiple groups was made with *t* test. Probabilities less than 0.05 were considered statistically significant.

RESULTS

The expressions of CD18 and CD11b in PMN were significantly increased after TIS with or without ligation of mesenteric lymph ducts compared with sham shock groups (*P*<0.05, Table 1). Both CD18 and CD11b expressions were up-regulated by the TIS pathological process. The expressions of CD18 and CD11b in sham shock with or without ligation of mesenteric lymph duct had no significant difference (*P*>0.05). It showed that ligation of mesenteric lymph duct itself had no effect on the expression of CD18 or CD11b. The results also showed that the expressions of CD18 and CD11b after TIS with ligation of mesenteric lymph duct were significantly decreased as compared with TIS without ligation of lymph duct (*P*<0.05). It was suggested that previous ligation of mesenteric lymph duct during TIS could down-regulate the expressions of CD18 and CD11b.

Table 1 Comparison of expressions of CD18 and CD11b in rats of all groups at 1 and 3 h after 90 min of TIS/sham-TIS state(%)

Group	CD18		CD11b	
	1st h	3rd h	1st h	3rd h
TIS with ligation of mesenteric lymph duct (8)	32.12±1.25	33.46±0.98	29.56±1.35	30.56±1.85
TIS without ligation of mesenteric lymph duct (8)	52.3±1.12	50.21±1.25	42.24±1.24	42.81±1.12
Sham TIS with ligation of mesenteric lymph duct (8)	17.02±0.95	15.68±0.98	14.02±1.23	13.63±1.23
Sham TIS without ligation of mesenteric lymph duct (8)	16.23±1.20	16.25±0.53	13.61±1.25	13.51±1.65

The main lung injury indexes (MPO activity and lung injury score) of TIS group were significantly increased compared with sham shock group ($P < 0.05$, Table 2). The results showed that the main lung injury indexes of sham shock groups with or without ligation of mesenteric lymph duct had no significant difference ($P > 0.05$). It seemed that ligation of mesenteric lymph duct itself could not cause lung injury. The results also showed that the MPO activity and lung injury score of TIS with previous ligation of mesenteric lymph duct were significantly decreased as compared with TIS without ligation of lymph duct ($P < 0.05$). It appeared that previous ligation of mesenteric lymph duct could alleviate lung injury effectively during TIS.

Table 2 Comparison of MPO activity and lung injury score in rats of all groups

Group (n = 8)	MPO activity (Ug ⁻¹ lung tissue)	LTS
TIS with ligation of mesenteric lymph duct	0.96±0.12	6.54±0.35
TIS without ligation of mesenteric lymph duct	1.56±0.21	9.56±0.23
Sham TIS with ligation of Mesenteric lymph duct	0.45±0.05	2.35±0.56
Sham TIS without ligation of Mesenteric lymph duct	0.50±0.08	2.53±0.41

DISCUSSION

It has been found that the phenomena of neutrophil activation is often accompanied by TIS, and that activated neutrophils may play a key role in the pathogenesis of lung injury or MODS, MSOF in TIS^[16]. But the mechanism of neutrophil activation, lung injury or MODS is still uncertain. Therefore, the soluble factors in neutrophil activation subjected to TIS and the cellular mechanisms for neutrophil activation are the hot topics. A lot of evidence showed that ischemia-reperfusion gut was an important source of factors that might cause neutrophil activation, lung injury or MODS after TIS^[17-19]. Post-ischemia gut has been shown to be a cytokine-generating organ, and the vascular bed of post-ischemia has been proven to be a priming bed for neutrophils by both clinical and experimental studies^[20]. It is usually believed that the loss of gut barrier function in shock states leads to bacterial translocation. Then such a bacterial translocation might cause sepsis and organ dysfunction in TIS patients. However, studies about TIS showed that neither bacteria nor endotoxin was found in portal blood of severely injured trauma patients. These findings have made people to doubt the theory of bacterial translocation during TIS.

It has been shown that the TIS induced increase in pulmonary capillary permeability could be prevented by ligation of mesenteric lymph ducts^[21], and mesenteric lymph from rats subjected to TIS, but not sham TIS could injure endothelial cells and increase their permeability^[22]. Shock-induced up-regulation of pulmonary endothelial P-selection expression could also be alleviated by mesenteric lymph duct ligation.

Based on these clinical and experimental findings, people come to hypothesize that lymphatics might be the primary route by which intestinal factors leave the gut and cause subsequent injury of lung or other organs instead of portal route. Neutrophil-endothelial interaction is involved in endothelial cell injury and endothelial cell adhesion molecule up-regulation. In order to investigate this hypothesis, we designed these experiments. To explore how TIS lymph affected PMN activation and lung injury, we compared TIS rats with or without ligation of the mesenteric lymph ducts. CD18 and CD11b were chosen as the indicators of PMN activation, and MPO and lung injury score

were chosen as the indicators of lung injury^[23,24].

The results of our study showed that the expressions of PMN CD18 and CD11b and the main lung injury indexes (the MPO activity and lung injury score) of TIS at 1 and 3 h after 90 min of TIS state were significantly increased compared with those of sham shock group, but had no significant difference between two sham shock groups with or without ligation of mesenteric lymph ducts. The results also showed that previous ligation of mesenteric lymph ducts could down-regulate the expressions of CD18 and CD11b and alleviate lung injury in rats subjected to TIS. These results are consistent with the studies of Harkin *et al.*^[25], who showed that mesenteric ligation prevented shock-induced CD11b up-regulation using a less severe shock model. The theory that the gut is a primary source of neutrophil-activating factors is consistent with our study and Adams *et al.*^[26], who found that the ability of plasma from rats subjected to TIS to prime neutrophils for an augment respiratory burst was lost after lymph duct ligation.

Generally, it seems that factors contained in TIS intestinal lymph are both necessary and sufficient to account for neutrophil activation and priming after TIS. The intestine could produce a wide range of inflammatory mediators, including cytokines, eicosanoids, oxidants, platelet-activating factors, complement fragments, and endotoxin^[27,28]. Many of these mediators can prime or activate neutrophils and endothelial cells directly or indirectly. It has been proven that primed and activated neutrophils are involved in the pathogenesis of posttraumatic inflammatory syndromes such as systemic inflammatory response syndrome (SIRS), adult respiratory distress syndrome (ARDS), MODS, and MSOF. It also has been testified that prevention of tissue neutrophil infiltration can reduce lung and other organ injury in the models of TIS^[29]. The results of our experiment also showed that pathologic neutrophil activation by gut lymph was critical to the pathogenesis of TIS.

Since no bacteria or endotoxin was found in mesenteric lymph subjected to TIS, further work is needed to study on the characterization and identification the neutrophil-activating factors in the TIS lymph. It has ever been thought that the lipid fraction of lymph was responsible for neutrophil activation^[30]. However, Daysl *et al.*^[31] pointed out that the respiratory burst of rat neutrophils was stimulated by the aqueous but not lipid fraction of the lymph samples. The exact explanation for these conflicting results is not known, but it may suggest that TIS lymph contains several factors which are capable of activating neutrophils. So, further study may still be needed to define the factors in TIS gut lymph which could activate neutrophils and cause injury of lung or other important organs.

In conclusion, mesenteric lymph after TIS contains multiple biologically active agents. These agents have the potential to modify both PMN and EC behaviors, which are probably involved in the pathogenesis of lung injury after TIS. The results showed that up-regulated expressions of PMN CD18 and CD11b and the lung injury induced by TIS could be prevented or alleviated by previous ligation of mesenteric lymph ducts. These findings may indicate that lung injury during TIS is caused by PMN adhesion molecule activation induced by some factors released or produced by postischemic intestine through mesenteric lymph pathway rather than traditionally believed portal vein.

REFERENCES

- 1 Deitch EA. Role of the gut lymphatic system in multiple organ failure. *Curr Opin Crit Care* 2001; 7: 92-98
- 2 Farber A, Connors JP, Friedlander RM, Wagner RJ, Powell RJ, Cronenwett JL. A specific inhibitor of apoptosis decreases tissue injury after intestinal ischemia-reperfusion in mice. *J Vasc Surg* 1999; 30: 752-760

- 3 **Ariceta J**, Ferrer JV, Guerrero D, Tellechea E, Balen E, Lera JM. Metabolism of the intestine with intermediate ischemia after intestinal ischemia-reperfusion injury: therapeutic effects of somatostatin. *Transplant Proc* 1999; **31**: 2572
- 4 **Deitch EA**, Adams C, Lu Q, Xu DZ. A time course study of the protective effect of mesenteric lymph duct ligation on hemorrhagic shock-induced pulmonary injury and the toxic effects of lymph from shocked rats on endothelial cell monolayer permeability. *Surgery* 2001; **129**: 39-47
- 5 **Sambol JT**, Xu DZ, Adams CA, Magnotti LJ, Deitch EA. Mesenteric lymph duct ligation provides long term protection against hemorrhagic shock-induced lung injury. *Shock* 2000; **14**: 416-419
- 6 **Hammerman C**, Goldschmidt D, Caplan MS, Kaplan M, Schimmel MS, Eidelman AI, Branski D, Hochman A. Amelioration of ischemia-reperfusion injury in rat intestine by pentoxifylline-mediated inhibition of xanthine oxidase. *J Pediatr Gastroenterol Nutr* 1999; **29**: 69-74
- 7 **Fekete Z**, Hauser CJ, Adams JM, Adams CA Jr, Forsythe RM, Hasko G, Xu DZ, Livingston DH, Deitch EA. Injury-enhanced calcium mobilization in circulating rat neutrophils models human PMN responses. *Shock* 2001; **16**: 15-20
- 8 **Miner TJ**, Tavaf-Motamen H, Stojadinovic A, Shea-Donohue T. Ischemia-reperfusion protects the rat small intestine against subsequent injury. *J Surg Res* 1999; **82**: 1-10
- 9 **Gonzalez RJ**, Moore EE, Biffi WL, Ciesla DJ, Silliman CC. The lipid fraction of post-hemorrhagic shock mesenteric lymph (PHSML) inhibits neutrophil apoptosis and enhances cytotoxic potential. *Shock* 2000; **14**: 404-408
- 10 **Johnson JL**, More EE, Hiester AA, Tamura DY, Zallen G, Silliman CC. Disparities in the respiratory burst between human and rat neutrophils. *J Leukoc Biol* 1999; **65**: 211-216
- 11 **Adams CA Jr**, Sambol JT, Xu DZ, Lu Q, Granger DN, Deitch EA. Hemorrhagic shock induced up-regulation of P-selectin expression is mediated by factors in mesenteric lymph and blunted by mesenteric lymph duct interruption. *J Trauma* 2001; **51**: 625-632
- 12 **Adams JM**, Hauser CJ, Adams CA Jr, Xu DZ, Livingston DH, Deitch EA. Entry of gut lymph into the circulation primes rat neutrophil respiratory burst in hemorrhagic shock. *Crit Care Med* 2001; **29**: 2194-2198
- 13 **Koltuksuz U**, Ozen S, Uz E, Aydin M, Karaman A, Gultek A, Akyol O, GURSOY MH, Aydin E. Caffeic acid phenethyl ester prevents intestinal reperfusion injury in rats. *J Pediatr Surg* 1999; **34**: 1458-1462
- 14 **Sun YG**, Huang ZH, Miao HF, Song HJ, Lei HY. Development of an experimental model of traumatic shock in rats. *Zhongguo Jiefangjun Yixue Zazhi* 2002; **12**: 1086-1087
- 15 **Holopainen R**, Aho H, Laine J, Halkola L, Kaapa P. Nitric oxide inhalation inhibits pulmonary apoptosis but not inflammatory injury in porcine meconium aspiration. *Acta Paediatr* 1999; **88**: 1147-1155
- 16 **Ustundag B**, Kazez A, Demirbag M, Canatan H, Halifeoglu I, Ozercan IH. Protective effect of melatonin on antioxidative system in experimental ischemia-reperfusion of rat small intestine. *Cell Physiol Biochem* 2000; **10**: 229-236
- 17 **Kazez A**, Demirbag M, Ustundag B, Ozercan IH, Saglam M. The role of melatonin in prevention of intestinal ischemia-reperfusion injury in rats. *J Pediatr Surg* 2000; **35**: 1444-1448
- 18 **Pockley AG**, Nakao M, Fairburn B, Wood RF. Effect of ischemia-reperfusion of the rat small bowel on peripheral blood neutrophil CD11b expression. *Transplant Proc* 2000; **32**: 1304
- 19 **Yoshida T**, Iwakiri R, Noda T, Okamoto K, Kojima M, Fukuyama K, Fujimoto K. Histaminergic effect on apoptosis of rat small intestinal mucosa after ischemia-reperfusion. *Dig Dis Sci* 2000; **45**: 1138-1144
- 20 **Vejjhapipat P**, Williams SR, Spitz L, Pierro A. Intestinal metabolism after ischemia-reperfusion. *J Pediatr Surg* 2000; **35**: 759-764
- 21 **Dayal SD**, Hauser CJ, Feketeova E, Fekete Z, Adams JM, Lu Q, Xu DZ, Zaets S, Deitch EA. Shock mesenteric lymph induced rat polymorphonuclear neutrophil activation and endothelial cell injury is mediated by aqueous factors *J Trauma* 2002; **52**: 1048-1055
- 22 **Yamamoto S**, Tanabe M, Wakabayashi G, Shimazu M, Matsumoto K, Kitajima M. The role of tumor necrosis factor-alpha and interleukin-1beta in ischemia-reperfusion injury of the rat small intestine. *J Surg Res* 2001; **99**: 134-141
- 23 **Kassirer M**, Zeltser D, Prochorov V, Schoenman G, Frimerman A, Keren G, Shapira I, Miller H, Roth A, Arber N, Eldor A, Berliner S. Increased expression of the CD11b/CD18 antigen on the surface of peripheral white blood cells in patients with ischemic heart disease: further evidence for smoldering inflammation in patients with atherosclerosis. *Am Heart J* 1999; **138**(3 Pt 1): 555-559
- 24 **Rizoli SB**, Kapus A, Parodo J, Rotstein OD. Hypertonicity prevents lipopolysaccharide-stimulated CD11b/CD18 expression in human neutrophils *in vitro*: role for p38 inhibition. *J Trauma* 1999; **46**: 794-798
- 25 **Harkin DW**, D'Sa AA, Yassin MM, Hoper M, Halliday MI. Gut mucosal injury is attenuated by recombinant bactericidal/permeability-increasing protein in hind limb ischemia-reperfusion injury. *Ann Vasc Surg* 2001; **15**: 326-331
- 26 **Adams CA Jr**, Xu DZ, Lu Q, Deitch EA. Factors larger than 100 kd in post-hemorrhagic shock mesenteric lymph are toxic for endothelial cells. *Surgery* 2001; **129**: 351-363
- 27 **Oberholzer A**, Oberholzer C, Moldawer LL. Sepsis syndromes: understanding the role of innate and acquired immunity. *Shock* 2001; **16**: 83-96
- 28 **Hauser CJ**, Fekete Z, Livingston DH, Adams J, Garced M, Deitch EA. Major trauma enhances store-operated calcium influx in human neutrophils. *J Trauma* 2000; **48**: 592-597
- 29 **Yaffe MB**, Xu J, Burke PA, Forse RA, Brown GE. Priming of the neutrophil respiratory burst is species-dependent and involves MAP kinase activation. *Surgery* 1999; **126**: 248-254
- 30 **Fukuyama K**, Iwakiri R, Noda T, Kojima M, Utsumi H, Tsunada S, Sakata H, Ootani A, Fujimoto K. Apoptosis induced by ischemia-reperfusion and fasting in gastric mucosa compared to small intestinal mucosa in rats. *Dig Dis Sci* 2001; **46**: 545-549
- 31 **Dayal SD**, Hasko G, Lu Q, Xu DZ, Caruso JM, Sambol JT, Deitch EA. Trauma/hemorrhagic shock mesenteric lymph upregulates adhesion molecule expression and IL-6 production in human umbilical vein endothelial cells. *Shock* 2002; **17**: 491-495

Inactivation of PTEN is associated with increased angiogenesis and VEGF overexpression in gastric cancer

Ye-Jiang Zhou, Yu-Xia Xiong, Xiao-Ting Wu, De Shi, Wei Fan, Tong Zhou, Yue-Chun Li, Xiong Huang

Ye-Jiang Zhou, Xiao-Ting Wu, Wei Fan, Tong Zhou, Yue-Chun Li, Xiong Huang, Department of General Surgery, West China Hospital, Sichuan University, Chengdu 610041, Sichuan Province, China

Yu-Xia Xiong, Department of Pharmacology, Luzhou Medical College, Luzhou 646000, Sichuan Province, China

De Shi, Department of General Surgery, the First Affiliated Hospital, Chongqing University of Medical Sciences, Chongqing 400016, China

Correspondence to: Xiao-Ting Wu, Department of General Surgery, West China Hospital, Sichuan University, Chengdu 610041, Sichuan Province, China. wx11@medmail.com.cn

Telephone: +86-28-88036679

Received: 2004-02-02 **Accepted:** 2004-02-24

CONCLUSION: Our results imply that inactivation of PTEN gene and over-expression of VEGF contribute to the neovascularization and progression of gastric cancer. PTEN-related angiogenesis might be attributed to its up-regulation of VEGF expression. PTEN and VEGF could be used as the markers reflecting the biologic behaviors of tumor and viable targets in therapeutic approaches to inhibit angiogenesis of gastric cancers.

Zhou YJ, Xiong YX, Wu XT, Shi D, Fan W, Zhou T, Li YC, Huang X. Inactivation of PTEN is associated with increased angiogenesis and VEGF overexpression in gastric cancer. *World J Gastroenterol* 2004; 10(21): 3225-3229

<http://www.wjgnet.com/1007-9327/10/3225.asp>

Abstract

AIM: To investigate the expression of PTEN/MMAC₁/TEP₁ and vascular endothelial growth factor (VEGF), their roles in biologic behavior and angiogenesis and their association in gastric cancer.

METHODS: Immunohistochemical staining was used to evaluate the expression of PTEN, VEGF and microvascular density (MVD) on paraffin-embedded sections in 70 patients with primary gastric cancer and 24 patients with chronic superficial gastritis (CSG). Expression of PTEN, VEGF and MVD were compared with clinicopathological features of gastric cancer. The relationship between expression of PTEN, VEGF and MVD as well as the relationship between PTEN and VEGF expression in cancer cells were investigated.

RESULTS: PTEN expression significantly decreased ($t = 3.98$, $P < 0.01$) whereas both VEGF expression and MVD significantly increased ($t = 4.29$ and 4.41 , respectively, both $P < 0.01$) in gastric cancer group compared with CSG group. PTEN expression was significantly down-regulated ($t = 1.95$, $P < 0.05$) whereas VEGF expression ($t = 2.37$, $P < 0.05$) and MVD ($t = 3.28$, $P < 0.01$) was significantly up-regulated in advanced gastric cancer compared with early-stage gastric cancer. PTEN expression in gastric cancer showed a negative association with lymph node metastasis ($t = 3.91$, $P < 0.01$), invasion depth ($t = 1.95$, $P < 0.05$) and age ($t = 4.69$, $P < 0.01$). MVD in PTEN-negative gastric cancer was significantly higher than that in PTEN-positive gastric cancer ($t = 3.69$, $P < 0.01$), and there was a negative correlation between PTEN expression and MVD ($\gamma = -0.363$, $P < 0.05$). VEGF expression was positively associated with invasion depth (especially with serosa invasion, $t = 4.69$, $P < 0.01$), lymph node metastasis ($t = 2.31$, $P < 0.05$) and TNM stage ($t = 3.04$, $P < 0.01$). MVD in VEGF-positive gastric cancer was significantly higher than that in VEGF-negative gastric cancer ($t = 4.62$, $P < 0.01$), and there was a positive correlation between VEGF expression and MVD ($\gamma = 0.512$, $P < 0.05$). VEGF expression in PTEN-negative gastric cancer was significantly stronger than that in PTEN-positive gastric cancer ($t = 2.61$, $P < 0.05$), and there was a significantly negative correlation between the expression of VEGF and PTEN ($\gamma = -0.403$, $P < 0.05$).

INTRODUCTION

Gastric cancer is one of the tumors with a relatively high incidence and mortality in the digestive system. Although many advanced measures have been taken to improve the outcome of patients suffering from gastric cancer, up to now, there has been no radical progress in reducing its incidence and mortality. This could be due to the fact that the underlying mechanism in tumorigenesis and progression of gastric cancer is still poorly understood. Many studies have demonstrated that tumor suppressor genes, such as *p53*, play an important role in oncogenesis and progression of various malignancies. Recently, many investigators have been interested in the role of PTEN/MMAC₁/TEP₁, a novel tumor suppressor gene, located on chromosome band 10q 23.3. Accumulated evidence has suggested that inactivation of PTEN/MMAC₁/TEP₁ gene was implicated in the carcinogenesis and progression of various tumors^[1-10]. Loss of PTEN expression was dominantly attributed to the inactive alteration of PTEN gene, including mutations, deletions, loss of heterozygosity (LOH) and promoter methylation in various malignancies^[11,12], meaning that the expressive intensity of PTEN could almost embody the status of *PTEN* gene.

Several studies have strongly implied that PTEN was associated with tumor-induced angiogenesis^[13-16]. However, less information regarding the role of PTEN in gastric cancer, to our knowledge, was available. The present study was designed to investigate the role of PTEN in tumorigenesis and progression of gastric cancer and its association with angiogenesis and VEGF expression.

MATERIALS AND METHODS

Subjects

Surgical specimens of 70 patients with histologically confirmed primary gastric adenocarcinoma and 24 patients with chronic superficial gastritis and duodenal ulcer were obtained from Department of General Surgery, Affiliated Hospital, Luzhou Medical College and Department of General Surgery, West China Hospital, Sichuan University in 1996-2000. There were 56 male and 14 female patients in gastric cancer group with age range from 31 to 66 (mean 45) years while there were 21 male and three female patients in chronic superficial gastritis group with age

range from 28 to 43 (mean 35) years. All patients with gastric cancer had received radical resection or palliative surgical treatments, but no one had ever accepted chemotherapy and radiotherapy as well as biotherapy before operation.

Evaluation of clinicopathological features

In gastric cancer group, 18 tumors were categorized histologically as well-differentiation and 52 poor-differentiations. Eight tumors were categorized as early-stage gastric cancer and 62 advanced gastric cancer. Thrifty two patients had serosa invasion, and 46 had lymph node metastasis. According to the criteria set out by the Union of International Cancer Commission (new TNM stage, UICC for gastric cancer, 1985), 20 tumors were categorized as stage I, 16 stage II, 30 stage III and four stage IV.

Antibodies and reagents

Rabbit anti-PTEN polyclonal antibody, rabbit anti-VEGF polyclonal antibody, mouse anti-CD34 monoclonal antibody and streptavidin-biotin-peroxidase (KIT-9710, UltraSensitive S-P for mouse or rabbit) as well as DAB reagents were all purchased from Maixin Corporation (Fuzhou, Fujian province, China).

Immunohistochemical staining

Five-micron paraffin-embedded sections were dewaxed in xylene, dehydrated in ethanol. Endogenous peroxidase activity was blocked by incubation of samples in a 3% solution of hydrogen peroxide in methanol and heated in pressure-cooker for 50 s to retrieve antigens. After washing with PBS, the samples were incubated for 60 min with primary antibody against CD34, PTEN or VEGF at 37 °C, for 60 min with the biotin-conjugated second antibody and for 10 min with the third antibody streptavidin-peroxidase at room temperature, and then the immunoreactive products were stained with DAB and counter-stained with methyl green subsequently. PBS was used instead of the primary antibodies for negative controls.

Evaluation of PTEN and VEGF immunostaining

PTEN and VEGF protein expression in benign and malignant gastric epithelium cells was assessed according to the score graded as the percentage of positive immunoreactive cells and the score graded as positive immunoreactive intensity, and the sum of both was used to reflect the level of PTEN and VEGF protein expression. The score graded as percentage of positive immunoreactive cells was defined as follows: <10% as 0, 10-25% as 1, 25-50% as 2, and $\geq 50\%$ as 3. The score graded as positive immunoreactive intensity was defined as follows: negative stain (equal to background) as 0, weak positive stain (weak yellow) as 1, positive stain (yellow) as 2, and strong positive stain (brown) as 3. The sum of scores less than or equal to 2 (≤ 2) was defined as negative PTEN (PTEN⁻) or VEGF (VEGF⁻) protein expression, and more than or equal to 3 (≥ 3) as positive PTEN (PTEN⁺) or VEGF (VEGF⁺) expression.

Microvascular density counting

Microvascular density (MVD) was determined according to the criterion introduced by Weidner^[17]: any separated single vascular endothelium cell or cluster of endothelium cells and microvascular tube with diameter less than 8 erythrocytes were counted. Briefly, the stained sections were screened at $\times 100$ magnifications under a light microscope (Olympus) to identify four regions with the highest number of microvessels, which were then counted at $\times 200$ magnifications, and the average was used to reflect MVD.

Statistical analysis

All results were expressed as mean \pm SD. Statistic software SPSS 11.5 for Windows was used to analyze the results using Student

t test and Pearson correlation analysis. The accepted level of significance was $P < 0.05$ (Two-tailed).

RESULTS

Characteristics and comparison of PTEN and VEGF expression and MVD in gastric cancer with those in chronic superficial gastritis

PTEN and VEGF expression were demonstrated to localize in cytoplasm of gastric glandular epithelium and tumor cells (Figures 1, 2). In gastric cancer, the positive immunoreactive signal in invasive front region was weaker for PTEN, but stronger for VEGF and microvessels (Figure 3) than that in the fundic region of tumor. There was a significant down-regulation of PTEN expression and a significant up-regulation of both VEGF and MVD in gastric cancer in comparison with those in chronic superficial gastritis (Table 1).

Table 1 Comparison in PTEN and VEGF expression and MVD between chronic superficial gastritis (CSG) group and gastric cancer (GC) group (mean \pm SD)

Groups	n	PTEN	VEGF	MVD
CSG	24	3.13 \pm 2.3	1.25 \pm 1.16	29.6 \pm 9.9
GC	70	1.34 \pm 1.75 ^b	2.94 \pm 1.80 ^b	48.3 \pm 19.9 ^b

^b $P < 0.01$ vs CSG group.

Association of PTEN and VEGF expression and MVD with clinicopathological profiles in gastric cancer

As showed in Table 2, The down-regulation of PTEN expression was closely associated with the older patients (>35 years), invasion depth and lymphatic metastasis of tumor, and a downtrend of PTEN expression was observed with the increase of invasion depth of tumor, especially in advanced stage of gastric cancer ($\geq T_2$) (Table 2). The up-regulation of both VEGF expression and MVD were significantly associated with the invasion depth, lymphatic metastasis and TNM stage, but none of them was associated with the histological differentiation of gastric cancer (Table 2).

Table 2 Association of PTEN and VEGF expression and MVD with clinicopathologic profiles in gastric cancer (mean \pm SD)

Variables	n	PTEN	VEGF	MVD
Age (yr)				
≤ 35	22	2.64 \pm 1.81	2.77 \pm 1.96	46.23 \pm 17.61
>35	48	0.83 \pm 1.33 ^b	3.02 \pm 1.76	49.20 \pm 20.05
Gender				
Male	56	1.32 \pm 1.69	3.00 \pm 1.91	48.45 \pm 20.39
Female	14	1.71 \pm 1.82	2.71 \pm 1.73	47.54 \pm 12.72
Differentiation				
Well	18	1.56 \pm 1.82	3.33 \pm 1.88	45.94 \pm 17.08
Poor	52	1.35 \pm 1.69	2.81 \pm 1.86	49.07 \pm 20.72
Invasion depth				
T ₁	8	2.50 \pm 1.73	1.5 \pm 1.91	27.94 \pm 12.1
$\geq T_2$	62	1.26 \pm 1.69 ^a	3.13 \pm 1.82 ^a	50.9 \pm 19.31 ^b
<T ₃	38	1.47 \pm 1.81	2.08 \pm 1.20	39.6 \pm 16.6
$\geq T_3$	32	1.31 \pm 1.66	3.97 \pm 1.15 ^a	58.6 \pm 18.9 ^b
LN metastasis				
Positive	46	0.87 \pm 1.36	3.57 \pm 1.77	53.9 \pm 18.2
Negative	24	2.42 \pm 1.93 ^b	1.74 \pm 2.07 ^a	37.5 \pm 19.3 ^b
TNM Stage				
I+II	36	1.83 \pm 1.81	2.51 \pm 1.29	39.6 \pm 18.3
III+IV	34	0.97 \pm 1.55	3.41 \pm 1.18 ^b	57.5 \pm 17.7 ^b

^a $P < 0.05$, ^b $P < 0.01$ vs different variables.

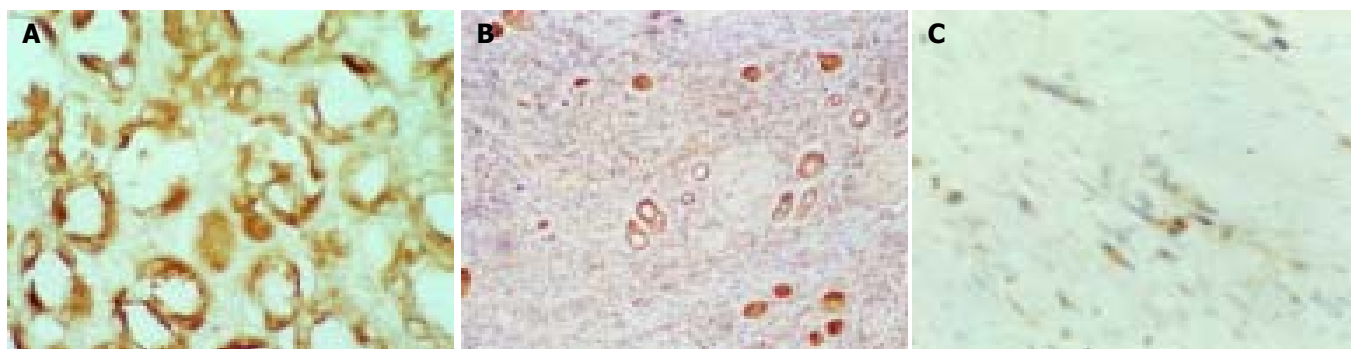


Figure 1 Expression of PTEN. A: Strongly positive expression in benign gastric glandular epithelium cells (Immunohistochemical staining, S-P \times 400). B: Positive expression in moderately differentiated cancer cells (Immunohistochemical staining, S-P \times 100). C: Weakly positive expression in poorly differentiated cancer cells. (Immunohistochemical staining, S-P \times 400).

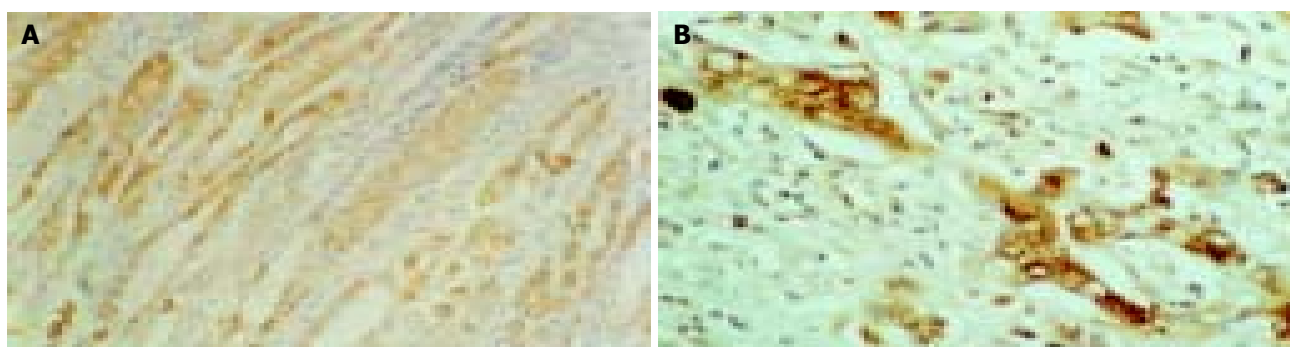


Figure 2 Expression of VEGF. A: Weakly positive expression in benign gastric glandular epithelium cells. B: Strongly positive expression in poorly differentiated cancer cells. (Immunohistochemical staining, S-P \times 400).

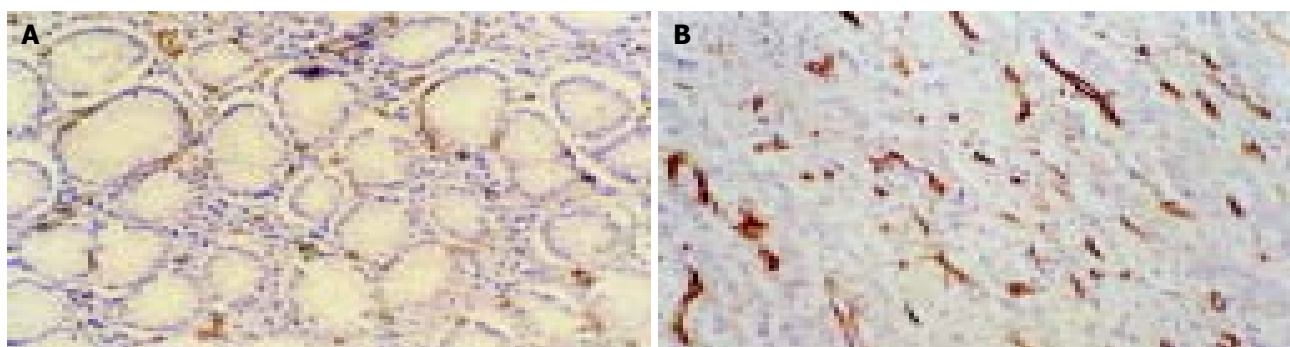


Figure 3 MVD in benign/malignant gastric tissues. A: Less and weakly stained microvessel labeled by CD34 was regularly distributed among the benign gastric epithelium gland (Immunohistochemical staining, S-P \times 400). B: Increased and strongly stained microvessel labeled by CD34 was irregularly infiltrated in poorly differentiated adenocarcinoma (Immunohistochemical staining, S-P \times 200).

Correlation of PTEN and VEGF expression with MVD in gastric cancer

MVD was significantly higher in PTEN negative ($n = 54$) than in PTEN positive gastric cancer ($n = 16$) (52.7 ± 19.6 vs 33.4 ± 13.2 , $t = 3.69$, $P < 0.01$), and significantly higher in VEGF positive ($n = 52$) than in VEGF negative gastric cancer ($n = 18$) (52.71 ± 19.59 vs 29.78 ± 12.9 , $t = 4.62$, $P < 0.001$). There was a significantly negative correlation between MVD and the intensity of PTEN expression ($\gamma = -0.363$, $P < 0.05$) and a positive correlation between MVD and the intensity of VEGF expression ($\gamma = 0.512$, $P < 0.01$).

Correlation between VEGF and PTEN expression

The intensity of VEGF expression was significantly higher in PTEN negative than in PTEN positive gastric cancer (3.18 ± 1.53 vs 2.15 ± 2.19 , $t = 2.61$, $P < 0.05$). Furthermore, there was a significantly negative correlation between VEGF and PTEN expression ($\gamma = -0.403$, $P < 0.05$).

DISCUSSION

PTEN/MMAC₁/TEP₁-encoding product, a dual-specificity protein-phospholipid phosphatase, which was involved in regulation of a variety of signal transduction pathways through dephosphorylation, including down-regulation of the activity of the focal adhesion kinase (FAK) to inhibit cell adhesion, invasion and metastasis^[18-20], disabling of phosphatidylinositol 3-kinase (PI3'k)/Akt signal pathway to accelerate cell apoptosis and inhibit cell proliferation and inhibition of MAPK signal pathway to restrain cell differentiation^[21-23]. Some studies^[18-20,24-27] have demonstrated that anti-sense or deletion of PTEN gene significantly up-regulates the ability of cell proliferation, adhesion and migration, accompanied by increased activity of FAK and PI3'k/Akt, whereas over-expression of PTEN protein in wild-type PTEN transfected cells is detected, with a resultant cell cycle arrest, increased cell apoptosis, decreased potential in cell mitosis, proliferation, adhesion and migration, and the

concomitant decrease of FAK and PI3'k/Akt activities, suggesting that PTEN regulates negatively the growth, invasion and metastasis of tumors, and then the inactivation of PTEN greatly contributes to the tumorigenesis and progression of tumors.

So far, little information on the expression and role of *PTEN* gene in gastric cancer is available. Recently, Byun *et al.*^[28] showed an abnormally low expression with only in 36% (20/55) gastric cancer tissues and 33% (5/15) cell lines while none of 71 cases with non-cancer tissues showed a decreased expression. The LOH of *PTEN* gene reached at 47% (14/30) and was closely linked to low expression of *PTEN* mRNA in gastric cancer. Furthermore, the rate of LOH was significantly higher in advanced gastric cancers (63%) than that in early-stage tumors (18%), and in poorly differentiated tumors (69%) than in well- or moderately differentiated tumors (29%). Fei *et al.*^[29] compared *PTEN* expression in 26 gastric cancer, 21 first-degree relatives of gastric cancer patients and 12 healthy individuals by RT-PCR and immunohistochemistry, and found that *PTEN* expression was significantly decreased in gastric cancer group and the first-degree relatives group compared with those in matched non-malignant gastric tissues and healthy control group. Kang *et al.*^[30] screened 310 cases with gastric carcinoma, and found that 62 cases lost *PTEN* expression, and the loss of *PTEN* expression was linked to the promoter methylation of *PTEN* gene, which was significantly associated with tumor depth and size, lymphatic invasion, advanced stage, pTNM stage, and patients' survival, implying that loss of *PTEN* expression is involved in the pathogenesis of gastric cancer. Nevertheless, there are some discrepant and conflict findings. One study from Japan did not find any mutation and promoter methylation of *PTEN* gene as well as the alteration of mRNA in gastric cancer cell lines and primary tumor tissues^[31]. Another study showed that the mutation rate of *PTEN* gene was not significantly increased in human advanced gastric cancer^[32], suggesting that *PTEN* does not participate in gastric carcinogenesis and progression as a tumor suppressor gene. In current study, *PTEN* expression was only slightly decreased in early gastric cancer cells but significantly decreased in advanced gastric cancer cells, compared with that in benign gastric epithelial cells. *PTEN* expression decreased as the invasion density increased, and lower *PTEN* expression was observed in gastric cancer with lymph node invasion and in TNM III/IV stage. Our results were very similar to those reported by Kang *et al.*^[30], suggesting that loss of *PTEN* expression is a relatively later molecule event in the pathogenesis of gastric cancer, and thus plays more important role in the progression than in oncogenesis of gastric cancer. The malignant gastric epithelial cells with loss of *PTEN* expression may hold the characteristics with a high aggressive and metastatic potential, and thus *PTEN* can be considered as an objective and reliable marker reflecting the pathobiological behaviors of gastric cancer. Moreover, Lee *et al.*^[33] showed that loss of *PTEN* expression was significantly associated with poor gastric carcinoma prognosis. In addition, we also observed a significantly decreased expression of *PTEN* protein in the older patients (>35 years) with gastric cancer compared with the younger patients, implying that *PTEN* may be more implicated in the gastric carcinogenesis in the elder. In other words, there might hold dissimilar tumorigenetic mechanisms between the older and younger patients with gastric cancer.

Angiogenesis is prerequisite for progressing tumor growth, invasion and metastasis. MVD in tumor tissue is unanimously considered as a better parameter to reflect the level of the neovascularization of tumor. VEGF, one of the most powerful pro-angiogenic factors, is dominantly involved in all the process including vascular endothelial cell mitosis, proliferation, adhesion and migration. VEGF expression is induced in a hypoxia-inducible factor alpha (HIF-1alpha)-dependent way through activation of the PI3 kinase signaling pathway^[34]. VEGF and MVD are all

involved in prognosis in various carcinomas^[35-38]. Our results revealed a significantly increase in MVD and VEGF expression in gastric cancer cells, and both the VEGF expression and MVD were significantly associated with the invasion depth, lymphatic metastasis and pTNM stage. Furthermore, MVD was significantly correlated with the intensity of VEGF expression. These results suggest VEGF is dominantly involved in the neovascularization of gastric cancer, and thus facilitates the tumor's growth, invasion and metastasis.

Several studies^[13-16] have suggested that *PTEN* is implicated in the regulation of tumor's angiogenesis, and loss of *PTEN* expression is closely associated with the increased neovascularization in various malignancies *in vitro* and *in vivo*. However, information on the relationship between *PTEN* protein expression and neovascularization in gastric cancer is scarce. Zheng *et al.* recently showed MVD was negatively related to *PTEN* expression in gastric cancer. In the present study, we also observed that MVD in *PTEN* negative gastric cancer was markedly higher than that in *PTEN* positive gastric cancer, and there was a significantly negative correlation between MVD and *PTEN* expression in gastric cancer tissue, implying that loss of *PTEN* expression is highly implicated in the neovascularization of tumor in gastric cancer.

The mechanism of *PTEN*-related angiogenesis is not well known. Recent *in vitro* studies^[39-41] have suggested that loss of *PTEN* expression significantly up-regulates VEGF expression via modulation of HIF-1alpha expression and VEGF-mediated pro-angiogenic signaling through PI3'K/Akt-dependent signaling transduction pathway to enhance the anti-apoptotic, proliferative, and chemotactic activity of endothelial cells and the ability of tube formation. Jiang *et al.* screened the expression of *PTEN* and *HIF-1alpha* mRNA and VEGF protein in human colorectal tumor tissues, and observed a negative correlation of *PTEN* expression with *HIF-1alpha* ($\gamma = -0.36, P < 0.05$) and VEGF ($\gamma = -0.48, P < 0.05$) and a positive correlation between VEGF and *HIF-1alpha* ($\gamma = 0.71, P < 0.01$). In this study, we also found a significantly increase in VEGF expression in *PTEN* negative gastric cancer compared with *PTEN* positive gastric cancer, and that the intensity of VEGF expression was negatively associated with *PTEN* expression. Taking all these findings together, we postulate that VEGF is a key downstream molecule for *PTEN* function in carcinogenesis and progression in a wide range of human carcinomas including gastric cancer. Therefore, inactivation of *PTEN* gene could contribute to gastric tumor progression by directly functioning on tumor cells to enhance the ability of growth, anti-apoptotic, invasion and metastasis through up-regulation of PI3'K/Akt signaling transduction pathway, by up-regulating VEGF expression in tumor cells, which enhances the activity of tumor-derived angiogenesis and functions on vascular endothelial cells to increase angiogenesis in tumor tissues. Based on these data, it is concluded that *PTEN* and VEGF are reliable targets in the therapeutic approach for the inhibition of angiogenesis in gastric cancer.

REFERENCES

- 1 Sato N, Tsunoda H, Nishida M, Morishita Y, Takimoto Y, Kubo T, Noguchi M. Loss of heterozygosity on 10q23.3 and mutation of the tumor suppressor gene *PTEN* in benign endometrial cyst of the ovary: possible sequence progression from benign endometrial cyst to endometrioid carcinoma and clear cell carcinoma of the ovary. *Cancer Res* 2000; **60**: 7052-7056
- 2 Kondo K, Yao M, Kobayashi K, Ota S, Yoshida M, Kaneko S, Baba M, Sakai N, Kishida T, Kawakami S, Uemura H, Nagashima Y, Nakatani Y, Hosaka M. *PTEN/MMAC1/TEP1* mutations in human primary renal-cell carcinomas and renal carcinoma cell lines. *Int J Cancer* 2001; **91**: 219-224
- 3 Mutter GL, Lin MC, Fitzgerald JT, Kum JB, Baak JP, Lees JA, Weng LP, Eng C. Altered *PTEN* expression as a diagnostic

- marker for the earliest endometrial precancers. *J Natl Cancer Inst* 2000; **92**: 924-930
- 4 **Davies MP**, Gibbs FE, Halliwell N, Joyce KA, Roebuck MM, Rossi ML, Salisbury J, Sibson DR, Tacconi L, Walker C. Mutation in the PTEN/MMAC1 gene in archival low grade and high grade gliomas. *Br J Cancer* 1999; **79**: 1542-1548
 - 5 **Rubin MA**, Gerstein A, Reid K, Bostwick DG, Cheng L, Parsons R, Papadopoulos N. 10q23.3 Loss of heterozygosity is higher in lymph node-positive (PT2-3, N+) versus lymph node-negative (PT2-3, NO) prostate cancer. *Hum Pathol* 2000; **31**: 504-508
 - 6 **Gianti G**, Resta N, Simone C, Cariola F, Demma I, Fiorente P, Gentile M. Involvement of PTEN mutations in the genetic pathways of colorectal cancerogenesis. *Hum Mol Genet* 2000; **9**: 283-287
 - 7 **Kimura F**, Watanabe J, Hata H, Fujisawa T, Kamata Y, Nishimura Y, Jobo T, Kuramoto H. PTEN immunohistochemical expression is suppressed in G1 endometrioid adenocarcinoma of the uterine corpus. *J Cancer Res Clin Oncol* 2003; **20**
 - 8 **Chung MJ**, Jung SH, Lee BJ, Kang MJ, Lee DG. Inactivation of the PTEN gene protein product is associated with the invasiveness and metastasis, but not angiogenesis, of breast cancer. *Pathol Int* 2004; **54**: 10-15
 - 9 **Kato H**, Fujimura M, Kumabe T, Ishioka C, Kanamaru R, Yoshimoto T. PTEN gene mutation and high MIB-1 labeling index may contribute to dissemination in patients with glioblastoma. *J Clin Neurosci* 2004; **11**: 37-41
 - 10 **Dicuozzo G**, Angeletti S, Garcia-Foncillas J, Brugarolas A, Okrouzhnov Y, Santini D, Tonini G, Lorino G, De Cesaris M, Baldi A. Colorectal carcinomas and PTEN/MMAC1 gene mutations. *Clin Cancer Res* 2001; **7**: 4049-4053
 - 11 **Sano T**, Lin H, Chen X, Langford LA, Koul D, Bondy ML, Hess KR, Myers JN, Hong YK, Yung WK, Steck PA. Differential expression of MMAC/PTEN in glioblastoma multiforme: Relationship to localization and prognosis. *Cancer Res* 1999; **59**: 1820-1824
 - 12 **Idoate MA**, Soria E, Lozano MD, Sola JJ, Panizo A, de Alava E, Manrique M, Pardo-Mindan FJ. PTEN protein expression correlates with PTEN gene molecular changes but not with VEGF expression in astrocytomas. *Diagn Mol Pathol* 2003; **12**: 160-165
 - 13 **Hsu SC**, Volpert OV, Steck PA, Mikkelsen T, Polverini PJ, Rao S, Chou P, Bouck NP. Inhibition of angiogenesis in human glioblastomas by chromosome 10 induction of thrombospondin-1. *Cancer Res* 1996; **56**: 5684-5691
 - 14 **Giri D**, Ittmann M. Inactivation of the PTEN tumor suppressor gene is associated with increased angiogenesis in clinically localized prostate carcinoma. *Hum Pathol* 1999; **30**: 419-424
 - 15 **Jiang BH**, Zheng JZ, Aoki M, Vogt PK. Phosphatidylinositol 3-kinase signaling mediates angiogenesis and expression of vascular endothelial growth factor in endothelial cells. *Proc Natl Acad Sci U S A* 2000; **97**: 1749-1753
 - 16 **Wen S**, Stolarov J, Myers MP, Su JD, Wigler MH, Tonks NK, Durden DL. PTEN controls tumor-induced angiogenesis. *Proc Natl Acad Sci U S A* 2001; **98**: 4622-4627
 - 17 **Weidner N**, Folkman J, Pozza F, Bevilacqua P, Allred EN, Moore DH, Meli S, Gasparini G. Tumor angiogenesis: a new significant and independent prognostic indicator in early-stage breast carcinoma. *J Natl Cancer Inst* 1992; **84**: 1875-1887
 - 18 **Tamura M**, Gu J, Matsumoto K, Aota S, Parsons R, Yamada KM. Inhibition of cell migration, spreading, and focal adhesions by tumor suppressor PTEN. *Science* 1998; **280**: 1614-1617
 - 19 **Cai T**, Lei QY, Wang LY, Zha XL. TGF- β_1 Modulated the expression of $\alpha 5$ beta 1 integrin and integrin-mediated signaling in human hepatocarcinoma cells. *Biochem Biophys Res Commun* 2000; **274**: 519-525
 - 20 **Zhang LN**, Yu Q, Wang LY, Jin JW, Zha XL. The effects of PTEN gene on migration and FAK phosphorylation of SMMC-7721 human hepatocarcinoma cell line. *Shengwu Huaxue Yu Shengwu Wuli Xuebao* 2003; **35**: 161-166
 - 21 **Maehama T**, Dixon JE. The tumor suppressor, PTEN/MMAC, dephosphorylates the lipid second messenger, phosphatidylinositol 3,4,5-trisphosphate. *J Biol Chem* 1998; **273**: 13375-13378
 - 22 **Besson A**, Robbins SM, Yong VW. PTEN/MMAC1/TEP1 in signal transduction and tumorigenesis. *Eur J Biochem* 1999; **263**: 605-611
 - 23 **Waite KA**, Eng C. Protean PTEN: form and function. *Am J Hum Genet* 2002; **70**: 829-844
 - 24 **Persad S**, Attwell S, Gray V, Delcommenne M, Troussard A, Sanghera J, Dedhar S. Inhibition of integrin-linked kinase (ILK) suppresses activation of protein kinase B/Akt and induces cell cycle arrest and apoptosis of PTEN-mutant prostate cancer cells. *Proc Natl Acad Sci U S A* 2000; **97**: 3207-3212
 - 25 **Sakurada A**, Hamada H, Fukushige S, Yokoyama T, Yoshinaga K, Furukawa T, Sato S, Yajima A, Sato M, Fujimura S, Horii A. Adenovirus-mediated delivery of the PTEN gene inhibits cell growth by induction of apoptosis in endometrial cancer. *Int J Oncol* 1999; **15**: 1069-1074
 - 26 **Ghosh AK**, Grigorieva I, Steele R, Hoover RG, Ray RB. PTEN transcriptionally modulates c-myc gene expression in human breast carcinoma cells and is involved in cell growth regulation. *Gene* 1999; **235**: 85-91
 - 27 **Saito Y**, Swanson X, Mhashilkar AM, Oida Y, Schrock R, Branch CD, Chada S, Zumstein L, Ramesh R. Adenovirus-mediated transfer of the PTEN gene inhibits human colorectal cancer growth *in vitro* and *in vivo*. *Gene Ther* 2003; **10**: 1961-1969
 - 28 **Byun DS**, Cho K, Ryu BK, Lee MG, Park JI, Chae KS, Kim HJ, Chi SG. Frequent monoallelic deletion of PTEN and its reciprocal association with PIK3CA amplification in gastric carcinoma. *Int J Cancer* 2003; **104**: 318-327
 - 29 **Fei G**, Ebert MP, Mawrin C, Leodolter A, Schmidt N, Dietzmann K, Malfertheiner P. Reduced PTEN expression in gastric cancer and in the gastric mucosa of gastric cancer relatives. *Eur J Gastroenterol Hepatol* 2002; **14**: 297-303
 - 30 **Kang YH**, Lee HS, Kim WH. Promoter methylation and silencing of PTEN in gastric carcinoma. *Lab Invest* 2002; **82**: 285-291
 - 31 **Sato K**, Tamura G, Tsuchiya T, Endoh Y, Sakata K, Motoyama T, Usuba O, Kimura W, Terashima M, Nishizuka S, Zou T, Meltzer SJ. Analysis of genetic and epigenetic alterations of the PTEN gene in gastric cancer. *Virchows Arch* 2002; **440**: 160-165
 - 32 **Wang JY**, Huang TJ, Chen FM, Hsieh MC, Lin SR, Hou MF, Hsieh JS. Mutation analysis of the putative tumor suppressor gene PTEN/MMAC1 in advanced gastric carcinomas. *Virchows Arch* 2003; **442**: 437-443
 - 33 **Lee HS**, Lee HK, Kim HS, Yang HK, Kim WH. Tumor suppressor gene expression correlates with gastric cancer prognosis. *J Pathol* 2003; **200**: 39-46
 - 34 **Sodhi A**, Montaner S, Miyazaki H, Gutkind JS. MAPK and Akt act cooperatively but independently on hypoxia inducible factor-1 α in rasV12 upregulation of VEGF. *Biochem Biophys Res Commun* 2001; **287**: 292-300
 - 35 **Zheng S**, Han MY, Xiao ZX, Peng JP, Dong Q. Clinical significance of vascular endothelial growth factor expression and neovascularization in colorectal carcinoma. *World J Gastroenterol* 2003; **9**: 1227-1230
 - 36 **Korkolopoulou P**, Konstantinidou AE, Kavantzias N, Patsouris E, Pavlopoulos PM, Christodoulou P, Thomas-Tsagli E, Davaris P. Morphometric microvascular characteristics predict prognosis in superficial and invasive bladder cancer. *Virchows Arch* 2001; **438**: 603-611
 - 37 **Terlikowski S**, Lenczewski A, Sulkowska M, Famulski W, Sulkowski S, Kulikowski M. Tissue expression of VEGF as a prognostic factor in early cervical squamous cell carcinoma. *Folia Histochem Cytobiol* 2001; **39**(Suppl 2): 112-113
 - 38 **Cianchi F**, Palomba A, Messerini L, Boddi V, Asirelli G, Perigli G, Bechi P, Taddei A, Pucciani F, Cortesini C. Tumor angiogenesis in lymph node-negative rectal cancer: correlation with clinicopathological parameters and prognosis. *Ann Surg Oncol* 2002; **9**: 20-26
 - 39 **Gomez-Manzano C**, Fueyo J, Jiang H, Glass TL, Lee HY, Hu M, Liu JL, Jasti SL, Liu TJ, Conrad CA, Yung WK. Mechanisms underlying PTEN regulation of vascular endothelial growth factor and angiogenesis. *Ann Neurol* 2003; **53**: 109-117
 - 40 **Koul D**, Shen R, Garyali A, Ke LD, Liu TJ, Yung WK. MMAC/PTEN tumor suppressor gene regulates vascular endothelial growth factor-mediated angiogenesis in prostate cancer. *Int J Oncol* 2002; **21**: 469-475
 - 41 **Huang J**, Kontos CD. PTEN modulates vascular endothelial growth factor-mediated signaling and angiogenic effects. *J Biol Chem* 2002; **277**: 10760-10766

Gallbladder motility in patients with hepatic cirrhosis before and after portal azygous disconnection

Hong-Xu Jin, Shuo-Dong Wu, Xue-Feng Zhang, Xian-Ying Chen, Guo-Xu Zhang

Hong-Xu Jin, Shuo-Dong Wu, Xue-Feng Zhang, Xian-Ying Chen, Guo-Xu Zhang, The Second Department of General Surgery, Second Hospital, China Medical University, Shenyang 110004, Liaoning Province, China

Xue-Feng Zhang, General Surgery, General Hospital of Shenyang Military Command, Shenyang 110016, Liaoning Province, China

Xian-Ying Chen, Guo-Xu Zhang, Department of Nuclear Medicine, General Hospital of Shenyang Military Command, Shenyang 110016, Liaoning Province, China

Correspondence to: Dr. Shuo-Dong Wu, The Second Department of General Surgery, Second Hospital, China Medical University, 36 Sanhao Street, Heping District, Shenyang 110004, Liaoning Province, China. hongxujin@tom.com

Telephone: +86-24-83955058

Received: 2004-02-06 **Accepted:** 2004-02-21

Abstract

AIM: To determine and compare the effect of vagus nerve on gallbladder motility in patients with hepatic cirrhosis before and after portal azygous disconnection (PAD).

METHODS: PAD operation (or Hassab's operation) was performed on 18 patients with portal hypertension, and anterior and posterior vagal trunks were cut. On d 3 before operation and d 10 after operation, ^{99m}Tc -EHIDA 185 MBq was administered intravenously to the patients, and scintigraphy was performed at 0.25 min/frame. A standard fat meal was administered 30 min after scintigraphy, and dynamic imaging was performed 60 min after the fat meal. Following appearance of the region of interest (ROI) in gallbladder, the time-activity curve of ROI was established. The following seven parameters were used: radioactivity at 30 min after injection of ^{99m}Tc -EHIDA (RC 30min), bile emptying fraction (EF), bile emptying period (EP), emptying rate (ER), latent period (LP), latent period radiocounting increment (LI), and latent period radiocounting increment rate (LR).

RESULTS: The RC 30 min decreased significantly after operation, compared with that before operation ($2\ 693.6 \pm 2\ 406.9$ vs $5\ 606.8 \pm 2\ 625.4$, $P < 0.05$). The radiocounting of gallbladder increased gradually during LP. LP after operation was significantly longer than that before operation (13.36 ± 5.92 vs 2.24 ± 1.48 , $P < 0.01$). LI and LR after operation were significantly higher than those before operation ($2\ 861.62 \pm 028.3$ vs 331.21 ± 421.02 , and 113.42 ± 49.52 vs 7.57 ± 10.75 , respectively, both $P < 0.01$). EP after operation was significantly shorter than that before operation (18.5 ± 6.3 vs 24.1 ± 6.4 , $P < 0.05$). EF and ER after operation were significantly lower than those before operation (13.1 ± 5.4 vs 32.3 ± 16.3 , and 0.7 ± 0.3 vs 1.4 ± 0.8 , respectively, both $P < 0.01$).

CONCLUSION: PAD operation is a good clinical model in studying the effect of vagus on gallbladder motility. The gallbladder tension after PAD operation decreases significantly

during the interdigestive phase. The latent period of gallbladder contraction prolongs and the motility weakens apparently after a standard fat meal. Human vagus influences the gallbladder motility, and cutting of the nerve inhibits the gallbladder motility.

Jin HX, Wu SD, Zhang XF, Chen XY, Zhang GX. Gallbladder motility in patients with hepatic cirrhosis before and after portal azygous disconnection. *World J Gastroenterol* 2004; 10(21): 3230-3233

<http://www.wjgnet.com/1007-9327/10/3230.asp>

INTRODUCTION

Cholecystolithiasis results from multi-factors^[1-5], of which gallbladder motor dysfunction is an important factor^[5,6]. Gallbladder motility is regulated by nerve system and body fluid^[7], especially the vagus^[8-10]. Because of the complicated interfering factor and its difficulty in control, there were few clinical studies on the gallbladder motility. In this study, vagus nerve effect on gallbladder motility was studied in patients with liver cirrhosis.

MATERIALS AND METHODS

Eighteen patients with portal hypertension (10 males and 8 females) with an average age of 50 years were included in this study. They had hypersplenotrophy and certain degree of hypersplenism. The esophagogastric varication was confirmed with gastroscop. No biliary abnormalities were found with ultrasonography. Hepatic function was classified as Child A level. Splenectomy (Hassab's operation) was performed, anterior and posterior trunks of vagus were cut off after inferior segment of esophagus was liberated. Aerofluxus was observed 48-96 h after operation. Hepatic function was recovered to Child A level 10 d postoperation.

With empty stomach on d 3 preoperation and d 10 postoperation, respectively, ^{99m}Tc -labeled diethyl acetyl acid anilide iminodiacetic acid scintigraphy (^{99m}Tc -EHIDA) 185 MBq was administered intravenously. American SPECT of GE Company was adopted to perform scintigraphy, 0.25 min/frame. Standard fat meals (ENSURE 250 mL standard solution containing caloric 1046.0 KJ, protein 14%, fattiness 31.5%, carbohydrate 54.5%) was provided for patients after 30 min of continuous displaying. The region of interest (ROI) in gallbladder and the time-activity curve of ROI were established (Figures 3A, B). Then, 7 parameters were used to analyze. the radiocounting of ^{99m}Tc -EHIDA injected 30 min later (RC 30 min), emptying fraction (EF, %), emptying period (EP min), emptying rate (ER, %/min): EF/EP, latent period (LP, min): the time from having fat meal to the initiation of contraction of gallbladder, latent period radiocounting increment (LI), latent period radiocounting increment rate (LR, %): the increased amount of radioactivity during LP/the initial radioactivity of LP \times 100. The results were expressed as mean \pm SD. SPSS11.0 software was used for analysis.

RESULTS

Each of the paired pre- and post-operative parameters was proved in normal distribution by normality test (Table 1).

Table 1 Comparison of gallbladder contractive function (mean±SD)

Parameters	Pre-surgery	Post-surgery
RC30 min	5 606.8±2 625.4	2 693.6±2 406.9 ^a
LP (min)	2.24±1.48	13.36±5.92 ^b
LI	331.21±421.02	2 861.6±2 028.3 ^b
LR (%)	7.57±10.75	113.42±49.52 ^b
EP (min)	24.1±6.4	18.5±6.3 ^a
EF (%)	32.3±16.3	13.1±5.4 ^b
ER (%/min)	1.4±0.8	0.7±0.3 ^b

^aP<0.05, ^bP<0.01, vs pre-operation.

Serum ^{99m}Tc-EHIDA in blood was rapidly taken by liver, egested to biliary system, stored and concentrated in gallbladder. Thirty min after injecting ^{99m}Tc-EHIDA, the radioactivity in gallbladder could reflect the bile quantity entered to gallbladder during interdigestive phase. The RC 30 min postoperation decreased obviously than that preoperation (2693.6±2406.9 vs

5606.8±2625.4, P<0.05)(Figure 1).

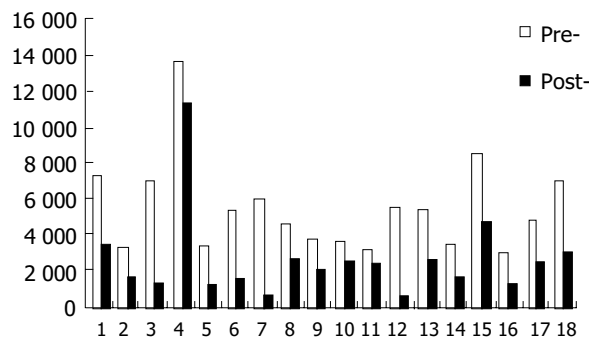


Figure 1 RC 30 min of gallbladder in pre-PAD and post-PAD.

LP in cirrhosis patients was very short preoperation, and LP prolonged significantly postoperation (13.36±5.92 vs 2.24±1.48, P<0.01). The radioactivity in gallbladder in LP increased gradually. LI and LR increased significantly postoperation (2861.6±2028.3 vs 331.21±421.02, 113.42±49.52 vs 7.57±10.75, P<0.01) (Figures 2A, B, C). EP in cirrhotic patients was shorter postoperation than that preoperation, EF and ER decreased significantly (13.1±5.4 vs 32.3±16.3, 0.7±0.3 vs 1.4±0.8, P<0.01) (Figures 2D, E, F).

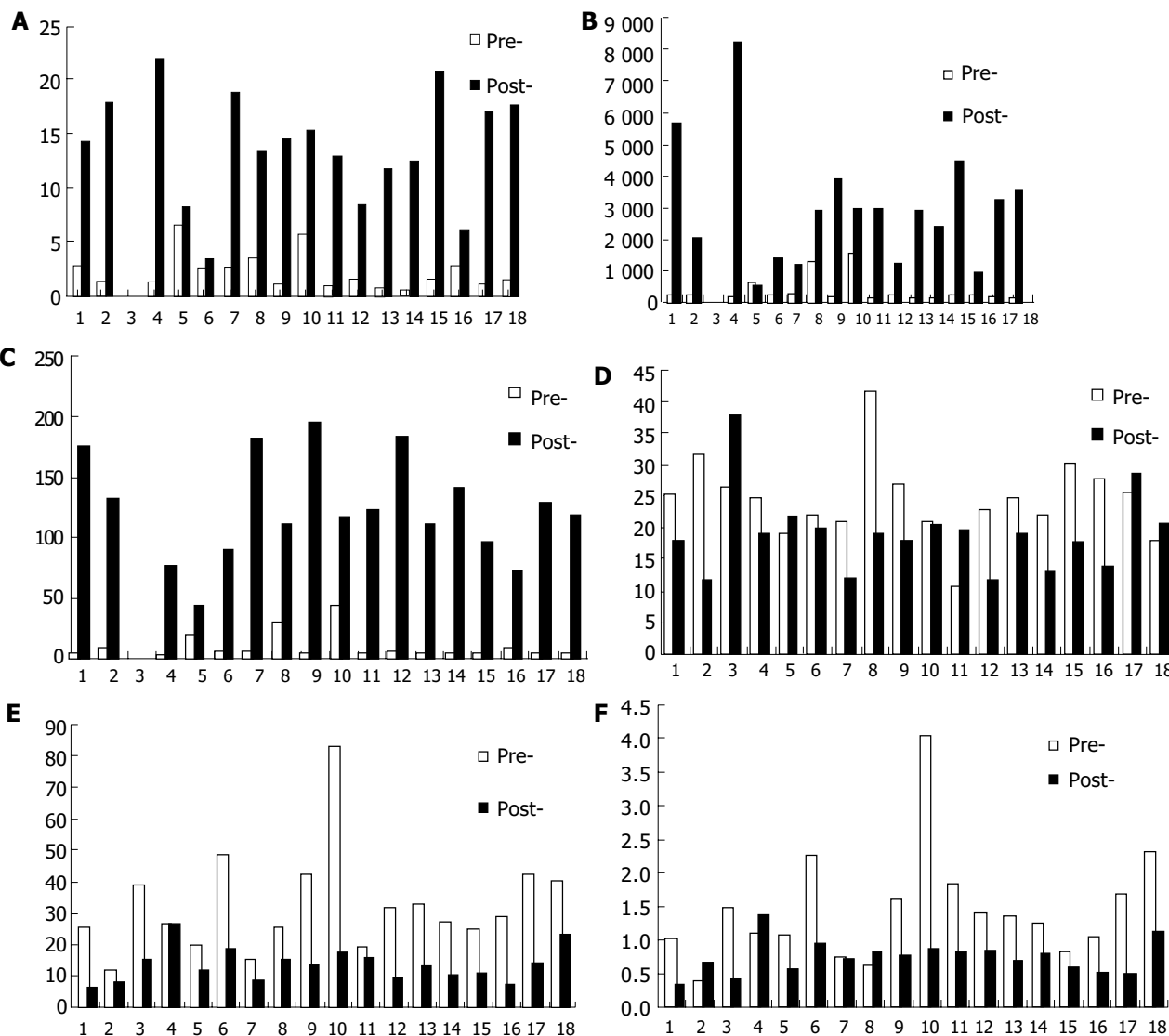


Figure 2 After administration of fat meal, changes in some parameters of gallbladder contraction. A: LP, B: LI, C: LR, D: EP, E: EF and F: ER.

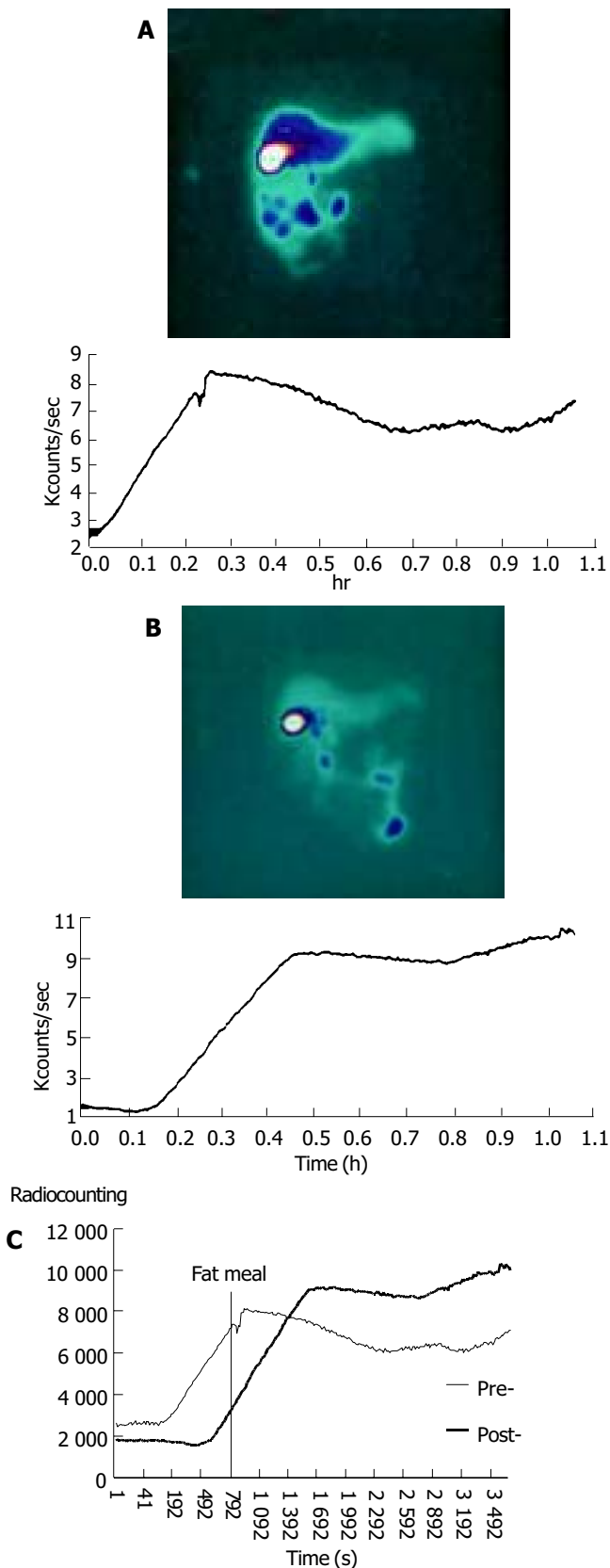


Figure 3 Time-activity curves of gallbladder in cirrhotic patients before (A) and after portal azygous disconnection (B) as well as their comparison (C).

DISCUSSION

The Portal azygous disconnection (PAD) is a clinical research model to study the function of human vagus. Most studies on vagus function in gallbladder motility were limited to animal experiments^[9-13]. Some scholars studied the gallbladder motility after gastrectomy and speculated that human vagus had an

important effect on gallbladder motility^[14-16]. In PAD anterior and posterior trunks of vagus were cut, while the integrality of alimentary canal was maintained. Therefore, PAD could eliminate many disturbing factors. Although the basic liver function of patients could disturb the research, we reduced the disturbance to the lowest degree by adjusting liver function of every patient to Child A level, and auto-control method was used on same patient pre- and post-operation.

Radioactive nuclide ^{99m}Tc-EHIDA can be specifically taken by liver cells, then egested with bile and discharged through biliary system to intestinal tract. Dynamic flowing of bile can be displayed accurately by SPECT scintigraphy with a clear picture and a high resolution. It has little radiation damage to the patients, and is a good way to study the motility of gallbladder and biliary system^[17-19].

Gallbladder motility is regulated by nerve system and body fluid factors. Gallbladder emptying after ingestion is affected by multiple factors. Vagus cholinergic fibers could cause gallbladder empty after ingestion, sham feeding could result in gallbladder emptying to 25-56%, and this function could be inhibited by cutting vagus or injection of atropine^[8-11,20,21]. Acetylcholine and other parasympathomimetic drugs could enhance the gallbladder tension and motility. Stimulating the vagus of dogs with electric current caused contraction of gallbladder, and gallbladder contracted slowly after both sides of the vagus were completely cut^[10]. In our study, vagus in patients with liver cirrhosis was cut off in PAD to study its effect on gallbladder motility. ^{99m}Tc-EHIDA scintigraphy was used. Gallbladder motility was compared between pre- and post-PAD. We found that EP was shortened post- PAD ($P < 0.05$), EF and ER were significantly reduced, and the motility of gallbladder was obviously weak after meal. Our study showed that human vagus had an important regulatory effect on gallbladder motility after meal.

Vagus is an important factor for maintaining gallbladder tension during interdigestive phase^[11,13,22], the gallbladder volume could increase two times if both sides of vagus were completely cut^[10]. Gallbladder was a weak in situation during interdigestive phase, and appeared rhythmic contraction and relaxation^[11]. Tenuity bile was continuously excreted by liver exchanges with condensed bile stored in gallbladder^[23-25]. Our study showed that RC 30 min post-operation was significantly decreased when fasting. The reason might be that cutting the vagus reduced the gallbladder tension during interdigestive phase, and then affected the exchange of bile.

Cholecystolithiasis patients did not contract at once after meal, but had a long latent period^[26]. In this study, LP post-operation after fat meal was prolonged ($P < 0.01$). The gallbladder lost the contractive stimulation in cephalic phase after vagus was cut. The result in our study was similar to that previously described^[27] (LI2861.6±2028.3, LR 113.42±49.52%). We conclude that bile containing nuclides entering into gallbladder more rapidly results from the heightened pressure of biliary tract. The motility of Oddi's sphincter is adjusted by vagus^[11], and the bile excreted by liver is mainly adjusted by body fluid^[28-31]. Fat meal may increase the bile excreted by liver through humoral regulation, and amputation of the vagus can weaken the contraction of Oddi's sphincter cephalic phase, so the pressure of biliary tract increases. Further study is required for clarifying the mechanism in detail.

REFERENCES

- Vitek L, Carey MC. Enterohepatic cycling of bilirubin as a cause of 'black' pigment gallstones in adult life. *Eur J Clin Invest* 2003; **33**: 799-810
- Wang DQ, Carey MC. Susceptibility to murine cholesterol gallstone formation is not affected by partial disruption of the HDL receptor SR-BI. *Biochim Biophys Acta* 2002; **1583**: 141-150

- 3 **Chuang CZ**, Martin LF, LeGardeur BY, Lopez A. Physical activity, biliary lipids, and gallstones in obese subjects. *Am J Gastroenterol* 2001; **96**: 1860-1865
- 4 **Behar J**. Clinical aspects of gallbladder motor function and dysfunction. *Curr Gastroenterol Rep* 1999; **1**: 91-94
- 5 **Rubin M**, Pakula R, Konikoff FM. Microstructural analysis of bile: relevance to cholesterol gallstone pathogenesis. *Histol Histopathol* 2000; **15**: 761-770
- 6 **Shi JS**, Ma JY, Zhu LH, Pan BR, Wang ZR, Ma LS. Studies on gallstone in China. *World J Gastroenterol* 2001; **7**: 593-596
- 7 **Wang J**, Luo J, Yu X. Study on biliary motility in cirrhotic patients with portal hypertension. *Zhonghua Ganzangbing Zazhi* 2000; **8**: 35-36
- 8 **Shaffer EA**. Review article: control of gall-bladder motor function. *Aliment Pharmacol Ther* 2000; **14**(Suppl 2): 2-8
- 9 **Axelsson HG**. Effects of gallstone-promoting diet and vagotomy on the mouse gallbladder epithelium. *Hepatogastroenterology* 1999; **46**: 2149-2152
- 10 **Muramatsu S**, Sonobe K, Tohara K, Tanaka T, Mizumoto A, Ibuki R, Suzuki H, Itoh Z. Effect of truncal vagotomy on gallbladder bile kinetics in conscious dogs. *Neurogastroenterol Motil* 1999; **11**: 357-364
- 11 **Liu CY**, Liu JZ, Li ZY, Liu KJ. The vagus nerve coordinates the motion of gallbladder and sphincter of Oddi in the interdigestive period in rabbits. *Zhongguo Yingyong Shenglixue Zazhi* 2000; **16**: 347-349
- 12 **Tsukamoto M**, Enjoji A, Ura K, Kanematsu T. Preserved extrinsic neural connection between gallbladder and residual stomach is essential to prevent dysmotility of gallbladder after distal gastrectomy. *Neurogastroenterol Motil* 2000; **12**: 23-31
- 13 **Xie YF**, Liu CY, Liu JZ. Nucleus raphe obscurus participates in regulation of gallbladder motility through vagus and sympathetic nerves in rabbits. *Chin J Physiol* 2002; **45**: 101-107
- 14 **Kinoshita H**, Imayama H, Hashino K, Aoyagi S. Study of cholelithiasis after gastrectomy. *Kurume Med J* 2000; **47**: 105-108
- 15 **Hagiwara A**, Imanishi T, Sakakura C, Otsuji E, Kitamura K, Itoi H, Yamagishi H. Subtotal gastrectomy for cancer located in the greater curvature of the middle stomach with prevention of the left gastric artery. *Am J Surg* 2002; **183**: 692-696
- 16 **Vassilakis JS**, Pechlivanides G, Fountos A, Zoras OJ, Xynos E. Roux-en-Y gastroenterostomy severely disturbs emptying of the gallbladder. *J Am Coll Surg* 1994; **179**: 313-317
- 17 **Madacsy L**, Velosy B, Szepes A, Szilvassy Z, Pavics L, Csernay L, Lonovics J. Effect of nitric oxide on gallbladder motility in patients with acalculous biliary pain: a cholescintigraphic study. *Dig Dis Sci* 2002; **47**: 1975-1981
- 18 **Chen SD**, Tsai SC, Shiau YC, Ho YJ, Kao CH. Evidence of gallbladder function changes in hepatoma after transcatheter arterial embolization by quantitative Tc-99m DISIDA cholescintigraphy. *Hepatogastroenterology* 2001; **48**: 393-396
- 19 **Kao CH**, Hsieh JF, Tsai SC, Ho YJ, Chen SD. Evidence of impaired gallbladder function in patients with liver cirrhosis by quantitative radionuclide cholescintigraphy. *Am J Gastroenterol* 2000; **95**: 1301-1304
- 20 **Robertson MD**, Mason AO, Frayn KN. Timing of vagal stimulation affects postprandial lipid metabolism in humans. *Am J Clin Nutr* 2002; **76**: 71-77
- 21 **Fisher RS**, Rock E, Malmud LS. Gallbladder emptying response to sham feeding in humans. *Gastroenterology* 1986; **90**: 1854-1857
- 22 **Parkman HP**, Pagano AP, Ryan JP. Investigation of endogenous neurotransmitters of guinea pig gallbladder using nicotinic agonist stimulation. *Dig Dis Sci* 1998; **43**: 2237-2243
- 23 **Woods CM**, Mawe GM, Shaffer EA, Toouli J, T P Saccone G. Effects of bioactive agents on biliary motor function. *Curr Gastroenterol Rep* 2003; **5**: 154-159
- 24 **von Kiedrowski R**, Huijghebaert S, Raedsch R. Mechanisms of von cisapride affecting gallbladder motility. *Dig Dis Sci* 2001; **46**:939-944
- 25 **Luiking YC**, Akkermans LM, Peeters TL, Cnossen PJ, Nieuwenhuijs VB, Vanberge-Henegouwen GP. Effects of motilin on human interdigestive gastrointestinal and gallbladder motility, and involvement of 5HT3 receptors. *Neurogastroenterol Motil* 2002; **14**: 151-159
- 26 **Xynos E**, Pechlivanides G, Zoras OJ, Chrysos E, Tzouvaras G, Fountos A, Vassilakis JS. Reproducibility of gallbladder emptying scintigraphic studies. *J Nucl Med* 1994; **35**: 835-839
- 27 **Pazzi P**, Petroni ML, Prandini N, Adam JA, Gullini S, Northfield TC, Jazrawi RP. Postprandial refilling and turnover: specific gallbladder motor function defects in patients with gallstone recurrence. *Eur J Gastroenterol Hepatol* 2000; **12**: 787-794
- 28 **Trauner M**, Boyer JL. Bile salt transporters: molecular characterization, function, and regulation. *Physiol Rev* 2003; **83**: 633-671
- 29 **Garcia F**, Kierbel A, Larocca MC, Gradilone SA, Splinter P, LaRusso NF, Marinelli RA. The water channel aquaporin-8 is mainly intracellular in rat hepatocytes, and its plasma membrane insertion is stimulated by cyclic AMP. *J Biol Chem* 2001; **276**: 12147-12152
- 30 **St-Pierre MV**, Kullak-Ublick GA, Hagenbuch B, Meier PJ. Transport of bile acids in hepatic and non-hepatic tissues. *J Exp Biol* 2001; **204**(Pt 10): 1673-1686
- 31 **Hooiveld GJ**, van Montfoort JE, Meijer DK, Muller M. Function and regulation of ATP-binding cassette transport proteins involved in hepatobiliary transport. *Eur J Pharm Sci* 2001; **12**: 525-543

Prognostic and clinicopathological features of E-cadherin, α -catenin, β -catenin, γ -catenin and cyclin D₁ expression in human esophageal squamous cell carcinoma

Ying-Cheng Lin, Ming-Yao Wu, De-Rui Li, Xian-Ying Wu, Rui-Ming Zheng

Ying-Cheng Lin, De-Rui Li, Department of Medical Oncology, Tumor Hospital, Shantou University Medical College, Shantou 515031, Guangdong Province, China

Ming-Yao Wu, Xian-Ying Wu, Rui-Ming Zheng, Department of Pathology, Shantou University Medical College, Shantou 515031, Guangdong Province, China

Supported by a grant of Shantou University Research & Development Fund, No. L03002

Correspondence to: Dr. Ying-Cheng Lin, Department of Medical Oncology, Tumor Hospital, Shantou University Medical College, Shantou 515031, Guangdong Province, China. linyingcheng@medmail.com.cn

Telephone: +86-754-8555844 Ext. 4042 **Fax:** +86-754-8560352

Received: 2004-01-20 **Accepted:** 2004-04-11

Abstract

AIM: To investigate the expression of E-cadherin, α -catenin, β -catenin, γ -catenin and cyclin D₁ in patients with esophageal squamous cell carcinoma (ESCC), and analyze their interrelationship with clinicopathological variables and their effects on prognosis.

METHODS: Expression of E-cadherin, α -catenin, β -catenin, γ -catenin and cyclin D₁ was determined by EnVision or SABC immunohistochemical technique in patients with ESCC consecutively, their correlation with clinical characteristics was evaluated and analyzed by univariate analysis.

RESULTS: The reduced expression rate of E-cadherin, α -catenin, β -catenin and γ -catenin was 88.7%, 69.4%, 35.5% and 53.2%, respectively. Cyclin D₁ positive expression rate was 56.5%. Expression of γ -catenin was inversely correlated with the degree of tumor differentiation and lymph node metastasis ($\chi^2 = 4.183$ and $\chi^2 = 5.035$, respectively, $P < 0.05$), whereas the expression of E-cadherin was correlated only with the degree of differentiation ($\chi^2 = 5.769$, $P < 0.05$). Reduced expression of E-cadherin and γ -catenin was associated with poor differentiation of tumor, reduced expression of γ -catenin was also associated with lymph node metastasis. There obviously existed an inverse correlation between level of E-cadherin and γ -catenin protein and survival. The 3-year survival rates were 100% and 56% in E-cadherin preserved expression group and in reduced expression one and were 78% and 48% in γ -catenin preserved expression group and in reduced expression one, respectively. The differences were both statistically significant. Correlation analysis showed the expression level of α -catenin correlated with that of E-cadherin and β -catenin ($P < 0.05$).

CONCLUSION: The reduced expression of E-cadherin and γ -catenin, but not α -catenin, β -catenin and cyclin D₁, implies more aggressive malignant behaviors of esophageal carcinoma cells and predicts the poor prognosis of patients.

Lin YC, Wu MY, Li DR, Wu XY, Zheng RM. Prognostic and

clinicopathological features of E-cadherin, α -catenin, β -catenin, γ -catenin and cyclin D₁ expression in human esophageal squamous cell carcinoma. *World J Gastroenterol* 2004; 10 (22): 3235-3239

<http://www.wjgnet.com/1007-9327/10/3235.asp>

INTRODUCTION

Esophageal squamous cell carcinoma (ESCC) is one of the most common malignant tumors in China^[1]. In recent years, the postoperative survival of patients with esophageal carcinoma has been improved. However, the overall prognosis for esophageal cancer patients remains poor, the 5-year survival rate of post operative advanced esophageal carcinoma patients was 20-35%. Although surgical techniques and preoperative management have progressed, early diagnosis and treatment are still important^[2-5]. The prognostic clinical characterization of esophageal carcinoma remains inadequate using conventional histological grading and staging systems. Recently, various attempts have been made to investigate the relationship between certain molecular markers and the clinical course of squamous cell carcinoma of esophagus. In fact, the biological factors that determine a different individual outcome (recurrent, survival) at an analogous stage of disease are obscure^[3-6].

E-cadherin and catenin are important adhesion molecules in normal epithelial tissue. Catenins, including α -catenin, β -catenin, γ -catenin, play an important role in the E-cadherin mediated intercellular signal transduction and cell adhesion. Loss of normal cellular adhesion plays a critical role in many aspects of tumor biology. For instance, alterations in cell-cell adhesion in cancer cells are reflected at the microscopic level in degree of cohesiveness and pattern of tumor growth. Detachment of cancer cells is an initial step in invasion of surrounding tissues and in spread to distant organs, and altered tumor cell adhesion is important in these processes. Several studies examined the role of the E-cadherin/catenin complex in growth mediation and maintenance of cell-cell adhesion in various tumors^[7-19]. The expression of adhesion molecules may reflect biological behaviors and characteristics of tumors and are conducive to predict and evaluate the risk of relapse and metastasis in patients with postoperative esophageal carcinoma, thus having practical significance in guiding individualized treatment^[3,18,20-23].

Cyclin D₁ encodes a cell-regulatory protein that is expressed at high level during the G₁ phase of the cell cycle. Cyclin D₁ binds to cyclin-dependent kinases and proliferating cell nuclear antigens. The formation of these complexes has been implicated in the control of cell proliferation^[24]. Cyclin D₁ is the target gene of beta-catenin, overexpression of the latter in the cytoplasm may promote malignant transformation by triggering cyclin D₁ expression in a number of cancers. It was regarded by several reports that cyclin D₁ could predict the prognosis in some cancers, including esophageal cancer^[25-28].

In this study, the expression of E-cadherin, α -catenin, β -catenin, γ -catenin and cyclin D₁ in 62 ESCC patients was

analyzed, concerning the histopathological and survival data, effects on progression of cancer and their prognostic value in ESCC. The results may provide some suggestions for clinical treatments.

MATERIALS AND METHODS

Materials

Specimens of cancer tissues were taken from 62 consecutive patients with squamous cell carcinoma of the thoracic esophagus who had undergone esophagectomy with regional lymph node dissected from January to December of 1996 at the Department of Thoracic Surgery, Cancer Hospital of Shantou University Medical College. None of them received irradiation or chemotherapy preoperatively. The patients included 49 men and 13 women with a mean age of 54 (range 35-79) years. Three tumors were located in the upper thorax, 36 in the middle thorax and 23 in the lower thorax (Table 1). The removed specimens were examined histological with hematoxylin and eosin staining, and then the clinicopathologic stage was determined according to TNM classification. Survival time was calculated from the date of operation to death or the date of last follow-up. Follow-up time ranged from 6 to 54 mo with an average of 36 mo.

Table 1 Background data of patients

Term	No. of cases (%)
Total	62
Age (yr)	
<50	22 (35.5)
≥50	40 (64.5)
Sex	
Male	49 (79.1)
Female	13 (20.9)
Location	
Upper thoracic	3 (4.8)
Middle thoracic	36 (56.5)
Lower thoracic	23 (37.1)
Histological grade	
I	16 (25.8)
II	35 (56.5)
III	11 (17.7)
Depth of invasion	
T1	2 (3.2)
T2	10 (16.1)
T3	32 (51.6)
T4	18 (29)
Lymph node metastasis	
Positive	35 (56.5)
Negative	27 (43.5)

Immunohistochemical staining

Immunohistochemical analysis was done retrospectively. Resected esophageal specimens, including both tumor and normal mucosae, were fixed in a 40 g/L formaldehyde solution and embedded in paraffin. The following antibodies were used in this study: mouse monoclonal anti-human cyclin D1 antibody (M-0024C, Antibody Company USA, diluted 1:50 in PBS), rabbit polyclonal anti-human E-cadherin antibody (BA0475, Antibody Company USA, diluted 1:100 in PBS), rabbit polyclonal anti-human α -catenin antibody (C-2081, Sigma Bioscience Company, USA, diluted 1:1 000 in PBS), rabbit polyclonal anti-human β -catenin antibody (C-2206, Sigma Chemical Company, USA, diluted 1:2 000 in PBS), goat polyclonal anti-human γ -catenin antibody (C-20 Santa Cruz Biot Co, USA, diluted 1:200 in PBS).

Four μ m thick sections of formalin-fixed paraffin-embedded tissue blocks of esophageal tumors were cut. The sections were deparaffinized, dehydrated and blocked to remove endogenous peroxidase activated by 3 mL/L H_2O_2 in methanol for 30 min. The sections were treated with microwave in 0.1 mol/L citrate buffer pH 6.0 at 750 W for 12 min. After incubation with 100 mL/L normal goat serum to block non-specific binding, they were then incubated with the primary antibodies overnight at 4 °C. After antibody was washed with PBS, the sections were incubated with the secondary antibody and immunostained by SABC method (γ -catenin, Boster Company, China) and EnVision method (E-cadherin, α -catenin, β -catenin and cyclin D1; EnVision, Cat. No. D-3001, 3002, Antibody Diagnostic Inc) according to the manufacturer's instructions, and finally DAB was visualized. Tissues were counterstained with hematoxylin. Negative control was designed by using PBS instead of primary antibody. Adjacent normal squamous epithelium served as an internal positive control of E-cadherin and catenin protein expression. Known immunostained-positive sections were used as positive control of cyclinD1 protein expression.

Positive criterion of immunohistochemical staining

Tumor sections were scored by light microscopy by 2 independent observers without knowledge of the stage and patient profiles. The percentage of positively stained cells was calculated after 100 cells were counted at more than 5 high-power (40 \times) fields. The following definitions were made: Cyclin D1: more than 10% positive staining in nuclei was defined as positive staining; E-cadherin and catenin: more than 10% positive staining in cell membrane was defined as positive staining; less than 50% positive staining in cell membrane was defined as reduced expression, more than 50% positive staining in cell membrane was defined as preserved expression.

Statistical analysis

χ^2 test or Fisher's exact probability test and Spearman rank correlation coefficient analysis were used to assess the association between immunohistochemical features and clinicopathological characteristics. The cumulative survival rate was calculated by the Kaplan-Meier method, and statistical significance was analyzed by the log-rank test. A *P* value less than 0.05 was considered statistically significant. All the statistical analyses were performed using the SPSS 10.0 V for Windows.

RESULTS

Expression of E-cadherin, α -catenin, β -catenin, γ -catenin and cyclin D1 in esophageal squamous cell carcinoma

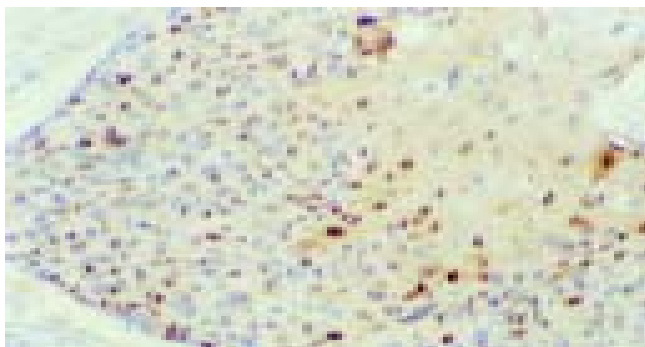
The positive expression rate of E-cadherin, α -catenin, β -catenin, γ -catenin and cyclin D1 in 62 esophageal cancer patients was 62.9% (39/62), 79% (49/62), 95.2% (59/62), 75.8% (47/62) and 56.5% (35/62), respectively. The reduced expression rate of E-cadherin, α -catenin, β -catenin and γ -catenin was 88.7%, 69.4%, 35.5%, 53.2%, respectively. Cyclin D1 positive expression showed brown stained signals in the nuclei (Figure 1), only a small number of expressions in cytoplasm or membrane of cells. E-cadherin, α -catenin, β -catenin and γ -catenin positive expression showed brown stained signals in membrane of cells and the intercellular junctions (Figure 2A-C).

Relationship between expressions of E-cadherin, α -catenin, β -catenin, γ -catenin and cyclin D1 in esophageal squamous cell carcinoma

Significant positive correlation was found between the intensity of α -catenin and β -catenin ($r = 0.274$, $P < 0.05$), E-cadherin and α -catenin ($r = 0.279$, $P < 0.05$). No significant differences were seen in other protein expressions.

Table 2 The relationship between clinicopathology and the expression of cyclin D₁, E-cad and catenins

Type	Cases	CyclinD ₁		P	E-cad		P	α-cat		P	β-cat		P	γ-cat		P
		Positive	Negative		Preserved	Reduced										
Histological grade																
I	16	6	10		5	11		7	9		10	6		8	8	
II	35	15	20	>0.05	5	30	<0.05	11	24	>0.05	24	11	>0.05	19	16	<0.05
III	11	6	5		0	11		1	10		6	5		3	8	
Depth of invasion																
T ₃	12	6	6	>0.05	4	8	>0.05	4	8	>0.05	6	6	>0.05	5	7	>0.05
T ₄	50	31	19		6	44		15	35		34	16		25	25	
Lymph node metastases																
Positive	35	14	21	>0.05	6	29	>0.05	9	26	>0.05	23	12	>0.05	12	23	<0.05
Negative	27	13	14		4	23		10	17		17	10		18	9	

**Figure 1** Positive expression of cyclinD1 protein in nuclei of esophageal squamous cell carcinoma. IHC×200.

Relationship between E-cadherin, α-catenin, β-catenin, γ-catenin and cyclin D1 expression and clinicopathologic variables in esophageal squamous cell carcinoma

Expression of E-cadherin correlated significantly only with histological grade. Poor differentiation was associated with reduced or loss of E-cadherin expression ($P < 0.05$). Significant inverse correlation existed between the intensity of γ -catenin expression and histological grade, and lymph node metastasis ($P < 0.05$). No significant correlation was found between abnormal expression of other proteins and histological grade, lymph node metastasis and depth of invasion (Table 2).

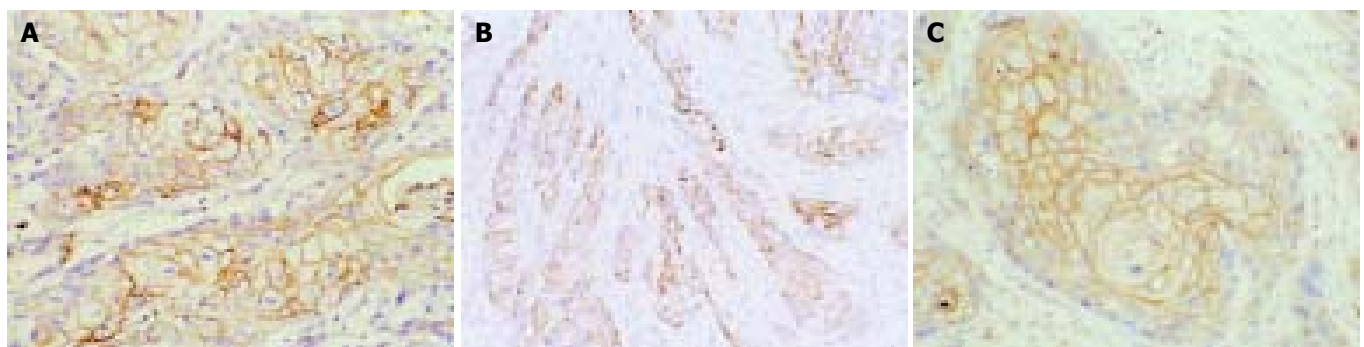
Relationship between E-cadherin, α-catenin, β-catenin, γ-catenin, and cyclin D1 expression and survival

Analysis of the 3-year survival after operation showed that the overall survival rate was 62% in 62 cases of esophageal cancer. Univariate analysis showed that the survival time was associated

with the histological grade, depth of invasion, lymph node metastasis, expression of E-cadherin and γ -catenin. Reduced E-cadherin or γ -catenin expression was correlated with poor prognosis. The mean survival time of grades I, II, III was 41, 45 and 12 mo ($P < 0.05$), respectively. The 3-year survival rate was 67.1% and 49.4% in T₃ and T₄ patients ($P < 0.05$), respectively, and was 47.8% and 80.3% in patients with positive and negative lymph node metastases ($P < 0.05$), respectively. The median survival time was 54 mo and 37 mo in patients with preserved and reduced or loss of E-cadherin expression, the 3-year survival rate was 100% and 56% ($P < 0.05$), respectively. The median survival time was 42 and 33 mo in patients with preserved and reduced or lost expression of γ -catenin, the 3-year survival rate was 78% and 48% ($P < 0.05$), respectively. No difference in survival curves was seen between reduced expression of α - and β -catenins compared with preserved expression. Similar results were found in the positive and negative expressions of cyclin D1. The median survival time was 39 and 38 mo in the patients with preserved and reduced or lost expression of α -catenin, the 3-year survival rate was 65%. The median survival time was 36 and 39 mo in the patients with preserved and reduced or loss expression of β -catenin, the 3-year survival rate was 65%. The median survival time was 40 and 34 mo in the patients with positive and negative expressions of cyclin D1, the 3-year survival rate was 68% and 58% ($P > 0.05$), respectively.

DISCUSSION

The main causes of treatment failure are recurrence and metastasis in resectable esophageal cancer. Modern molecular biology studies have demonstrated that invasion and metastasis of tumors as a continuous process, include three steps: a reduced cell-cell adhesion, alterations in the interaction of tumor cells with extracellular matrix, and invasion into surrounding

**Figure 2** Positive expression of E-cadherin and γ -catenin proteins in membrane of esophageal squamous cell carcinoma. A: Positive expression of E-cadherin protein in membrane of esophageal well differentiated squamous cell carcinoma. IHC ×200; B: Positive expression of γ -catenin protein in membrane of esophageal squamous cell carcinoma. IHC×200; C: Positive expression of γ -catenin protein in membrane of esophageal squamous cell carcinoma. IHC×400.

tissues including blood vessels and lymph duct. Thus the first and critical step is that the tumor cells could detach from primary foci and re-adhere to metastatic position^[12,29,30]. E-cadherin is a calcium-dependent cell-cell adhesion transmembrane glycoprotein, maintaining normal epithelial polarity, and intercellular adhesion, which are present in almost all normal epithelial cell surfaces. It is anchored to the cytoskeleton via cytoplasm proteins, including alpha and beta catenin^[13,14,31]. E-cadherin, therefore, is one of the most important adhesion molecules expressed by epithelial cells and is regarded as an invasion suppressor molecule^[13,14]. In this study, overall survival was inversely corrected with E-cadherin expression. Patients with preserved E-cadherin expressing tumor had a better prognosis than those with reduced expression of E-cadherin. This was in agreement with previous studies on a variety of cancers, such as cancer of head and neck^[15,16], breast^[17,18], stomach^[19,32,33], bladder^[27]. In all these studies, reduction or loss of E-cadherin expression was significantly associated with dedifferentiation, increased invasiveness, and high incidence of lymph node metastasis, hematogenous recurrence and poor prognosis in a number of human carcinomas, including esophageal cancer. But some other studies did not acquire the same results^[3]. There were different results of reduced E-cadherin protein expression in specimens from patients with ESCC in various researches^[21,23,32-35]. While in our investigation 88.7% of ESCC showed reduced expression of E-cadherin. It was postulated that selection of the patients entering into the study, immunohistochemical method, antibody origination, tumor heterogeneity and differences in staining evaluation might individually or in combination hold responsibility. As a marker associated with squamous cell differentiation^[36], the level of E-cadherin expression had an inverse correlation with histological grade. Reduced or loss of E-cadherin expression was correlated with poor differentiation, but not with lymphatic metastases and depth of tumor invasion, suggesting that the reduction of E-cadherin expression is associated with loss of the ability of adhesion and facilitate to blood vessel metastases, as previously reported^[21].

Catenins are a family of proteins including α -(102 ku), β -(88 ku), γ -(82 ku) catenins. The cytoplasmic domain of E-cadherin could bind directly to either β -catenin or γ -catenin, whereas α -catenin could link E-cadherin- (β , γ)-catenin complex to acting cytoskeleton. The integrity of the adhesion function of E-cadherin also depended on an intact catenin system^[15]. β -catenin could also play a role in intracellular signaling and function as an oncogene when it bound to T-cell factor 4 (Tcf4)-binding site in the promotor region of cyclin D1 and transactivated genes after translocation to the nuclei^[37-39]. Catenins had different clinicopathological roles in various cancers. In many epithelial carcinomas including carcinoma of the esophagus^[3,6,20,22,23,33], head and neck^[16], breast^[17-19,25], stomach^[19], colon^[24] and bladder^[27], catenins had a prognostic significance in survival. Some investigators reported that abnormal expression of α -catenin was associated with the prognosis of esophageal cancer. It also had predicative values for lymph node metastasis in esophageal carcinoma. Several reports suggested that abnormal expression of β -catenin could indicate poor prognosis in a number of tumors, including esophageal cancer^[17,20,25,33]. γ -catenin was found to be more important in nodal metastasis in tongue cancer. It was also predictive of the presence of subclinical nodal metastasis in clinically node-negative neck^[16]. The expression of α -catenin but not β - or γ -catenin was found to be correlated with the expression of E-cadherin in this study. The reduction or loss of γ -catenin expression was associated with more lymph node metastases than the preserved expression ($P < 0.05$). There was a correlation between poor differentiation of tumor and reduction or loss of γ -catenin expression. The reduction or loss of γ -catenin expression was in association

with shorter median survival time and lower 3-year survival rate. All these suggested that γ -catenin might be one of the prognostic factors in esophageal cancer. However, the expression of α -catenin and β -catenin was not related to the histological grade, depth of invasion, lymph node metastases and survival time.

The clinical significance of cyclin D1 expression was different in various tumors. It has shown that cyclin D1 gene amplification or enhanced expression was correlated with higher histological grade of tumor, lymphatic or hematogenous metastasis and poor prognosis^[40-43]. A controversial report, however, existed^[6]. Some investigators thought cyclin D1 was the target gene of β -catenin. Although a positive correlation between β -catenin activation and cyclin D1 expression was reported, our study did not show such a result. Furthermore, cyclin D1 expression was not associated with the extent of tumor infiltration, grade of differentiation, lymphatic metastases and survival time. These inconsistencies with other authors may be associated with location of tumor, pathologic classification, biologic behaviors, examination methods and evaluating criteria.

Our study showed that the main prognostic factors of postoperative survival time were histological grade, depth of tumor invasion and lymph node metastasis. The reduced expression of E-cadherin or γ -catenin was associated with poor differentiation of tumor cells. Reduced or loss of γ -catenin expression also had predictive values for nodal metastasis. The reduction or loss of E-cadherin and γ -catenin expression could predict the shorter survival time. Therefore we suggest that adjuvant radiation or chemotherapy should be considered in esophageal carcinoma patients with reduced expression of E-cadherin and γ -catenin in T4 stage, poor-differentiation in histopathology, and lymph node metastases in order to improve the survival rate.

REFERENCES

- 1 **Su M**, Lu SM, Tina DP, Zhao H, Li XY, Li DR, Zheng ZC. Relationship between ABO blood groups and carcinoma of esophagus and cardia in Chaoshan inhabitants of China. *World J Gastroenterol* 2001; **7**: 657-661
- 2 **Hofstetter W**, Swisher SG, Correa AM, Hess K, Putnam JB Jr, Ajani JA, Dolormente M, Francisco R, Komaki RR, Lara A, Martin F, Rice DC, Sarabia AJ, Smythe WR, Vaporciyan AA, Walsh GL, Roth JA. Treatment outcomes of resected esophageal cancer. *Ann Surg* 2002; **236**: 376-384
- 3 **Shiozaki H**, Doki Y, Kawanishi K, Shamma A, Yano M, Inoue M, Monden M. Clinical application of malignancy potential grading as a prognostic factor of human esophageal cancers. *Surgery* 2000; **127**: 552-561
- 4 **Shimada Y**, Imamura M, Watanabe G, Uchida S, Harada H, Makino T, Kano M. Prognostic factors of oesophageal squamous cell carcinoma from the perspective of molecular biology. *Br J Cancer* 1999; **80**: 1281-1288
- 5 **Goldberg RM**. Gastrointestinal tract cancer in: Casciato DA, Lowitz BB, eds. Manual of clinical oncology. 4th ed. *Lippincott Williams Wilkins Inc* 2000: 172-176
- 6 **Ikeda G**, Isaji S, Chandra B, Watanabe M, Kawarada Y. Prognostic significance of biologic factors in squamous cell carcinoma of the esophagus. *Cancer* 1999; **86**: 1396-1405
- 7 **Wijnhoven BP**, Dinjens WN, Pignatelli M. E-cadherin-catenin cell-cell adhesion complex and human cancer. *Br J Surg* 2000; **87**: 992-1005
- 8 **Yagi T**, Takeichi M. Cadherin superfamily genes: functions, genomic organization, and neurologic diversity. *Genes Dev* 2000; **14**: 1169-1180
- 9 **Ivanov DB**, Philippova MP, Tkachuk VA. Structure and Functions of classical cadherin. *Biochemistry* 2001; **66**: 1174-1186
- 10 **Van Aken E**, De Wever O, Correia da Rocha AS, Mareel M. Defective E-cadherin/catenin complexes in human cancer. *Virchows Arch* 2001; **439**: 725-751
- 11 **Behrens J**. Cadherins and catenins: role in signal transduction

- and tumor progression. *Cancer Metastasis Rev* 1999; **18**: 15-30
- 12 **Beavon IR.** The E-cadherin-catenin complex in tumour metastasis: structure, function and regulation. *Eur J Cancer* 2000; **36**: 1607-1620
- 13 **Hirohashi S.** Inactivation of the E-cadherin-mediated cell adhesion system in human cancers. *Am J Pathol* 1998; **153**: 333-339
- 14 **Christofori G, Semb H.** The role of the cell-adhesion molecule E-cadherin as a tumour-suppressor gene. *Trends Biochem Sci* 1999; **24**: 73-76
- 15 **Chow V, Yuen AP, Lam KY, Tsao GS, Ho WK, Wei WI.** A comparative study of the clinicopathological significance of E-cadherin and catenins (α , β , γ) expression in the surgical management of oral tongue carcinoma. *J Cancer Res Clin Oncol* 2001; **127**: 59-63
- 16 **Andrews NA, Jones AS, Helliwell TR, Kinsella AR.** Expression of the E-cadherin-catenin cell adhesion complex in primary squamous cell carcinomas of the head and neck and their nodal metastases. *Br J Cancer* 1997; **75**: 1474-1480
- 17 **Bukholm IK, Nesland JM, Borresen-Dale AL.** Re-expression of E-cadherin, α -catenin and β -catenin, but not of γ -catenin, in metastatic tissue from breast cancer patients. *J Pathol* 2000; **190**: 15-19
- 18 **Lim SC, Lee MS.** Significance of E-cadherin/beta-catenin complex and cyclin D1 in breast cancer. *Oncol Rep* 2002; **9**: 915-928
- 19 **Jawhari A, Jordan S, Poole S, Browne P, Pignatelli M, Farthing MJ.** Abnormal immunoreactivity of the E-cadherin-catenin complex in gastric carcinoma: relationship with patient survival. *Gastroenterology* 1997; **112**: 46-55
- 20 **Kadowaki T, Shiozaki H, Inoue M, Tamura S, Oka H, Doki Y, Iihara K, Matsui S, Iwazawa T, Nagafuchi A.** E-cadherin and α -catenin expression in human esophageal cancer. *Cancer Res* 1994; **54**: 291-296
- 21 **Tamura S, Shiozaki H, Miyata M, Kadowaki T, Inoue M, Matsui S, Iwazawa T, Takayama T, Takeichi M, Monden M.** Decreased E-cadherin expression is associated with haematogenous recurrence and poor prognosis in patients with squamous cell carcinoma of the oesophagus. *Br J Surg* 1996; **83**: 1608-1614
- 22 **Sanders DS, Bruton R, Darnton SJ, Casson AG, Hanson I, Williams HK, Jankowski J.** Sequential changes in cadherin-catenin expression associated with the progression and heterogeneity of primary oesophageal squamous carcinoma. *Int J Cancer* 1998; **79**: 573-579
- 23 **Nakanishi Y, Ochiai A, Akimoto S, Kato H, Watanabe H, Tachimori Y, Yamamoto S, Hirohashi S.** Expression of E-cadherin, alpha-catenin, beta-catenin and plakoglobin in esophageal carcinomas and its prognostic significance: immunohistochemical analysis of 96 lesions. *Oncology* 1997; **54**: 158-165
- 24 **Utsunomiya T, Doki Y, Takemoto H, Shiozaki H, Yano M, Sekimoto M, Tamura S, Yasuda T, Fujiwara Y, Monden M.** Correlation of beta-catenin and cyclin D1 expression in colon cancers. *Oncology* 2001; **61**: 226-233
- 25 **Lin SY, Xia W, Wang JC, Kwong KY, Spohn B, Wen Y, Pestell RG, Hung MC.** Beta-catenin, a novel prognostic marker for breast cancer: its roles in cyclin D1 expression and cancer progression. *Proc Natl Acad Sci U S A* 2000; **97**: 4262-4266
- 26 **Itami A, Shimada Y, Watanabe G, Imamura M.** Prognostic value of p27 (Kip1) and CyclinD1 expression in esophageal cancer. *Oncology* 1999; **57**: 311-317
- 27 **Shiina H, Igawa M, Shigeno K, Terashima M, Deguchi M, Yamanaka M, Ribeiro-Filho L, Kane CJ, Dahiya R.** Beta-catenin mutations correlate with over expression of C-myc and cyclin D1 genes in bladder cancer. *J Urol* 2002; **168**: 2220-2226
- 28 **Ueta T, Ikeguchi M, Hirooka Y, Kaibara N, Terada T.** Beta-catenin and cyclin D1 expression in human hepatocellular carcinoma. *Oncol Rep* 2002; **9**: 1197-1203
- 29 **Korn WM.** Moving toward an understanding of the metastatic process in hepatocellular carcinoma. *World J Gastroenterol* 2001; **7**: 777-778
- 30 **Stamenkovic I.** Matrix metalloproteinases in tumor invasion and metastasis. *Semin Cancer Biol* 2000; **10**: 415-433
- 31 **Bair EL, Massey CP, Tran NL, Borchers AH, Heimark RL, Cress AE, Bowden GT.** Integrin- and cadherin-mediated induction of the matrix metalloprotease matrilysin in cocultures of malignant oral squamous cell carcinoma cells and dermal fibroblasts. *Exp Cell Res* 2001; **270**: 259-267
- 32 **Debruyne P, Vermeulen S, Mareel M.** The role of the E-cadherin/catenin complex in gastrointestinal cancer. *Acta Gastroenterol Belg* 1999; **62**: 393-402
- 33 **de Castro J, Gamallo C, Palacios J, Moreno-Bueno G, Rodriguez N, Feliu J, Gonzatez-Baron M.** Beta-catenin expression pattern in primary oesophageal squamous cell carcinoma. Relationship with clinicopathologic features and clinical outcome. *Virchows Arch* 2000; **437**: 599-604
- 34 **Jian WG, Darnton SJ, Jenner K, Billingham LJ, Matthews HR.** Expression of E-cadherin in oesophageal carcinomas from the UK and China: disparities in prognostic significance. *J Clin Pathol* 1997; **50**: 640-644
- 35 **Pomp J, Blom J, van Krimpen C, Zwinderman AH, Immerzeel JJ.** E-cadherin expression in oesophageal carcinoma treated with high-dose radiotherapy; correlation with pretreatment parameters and treatment outcome. *J Cancer Res Clin Oncol* 1999; **125**: 641-645
- 36 **Wu H, Lotan R, Menter D, Lippman SM, Xu XC.** Expression of E-cadherin is associated with squamous differentiation in squamous cell carcinomas. *Anticancer Res* 2000; **20**: 1385-1390
- 37 **Peifer M.** β -catenin as oncogene: the smoking gun. *Science* 1997; **275**: 1752-1753
- 38 **Kolligs FT, Bommer G, Goke B.** Wnt/beta-catenin/tcf signaling: a critical pathway in gastrointestinal tumorigenesis. *Digestion* 2002; **66**: 131-144
- 39 **Gottardi CJ, Wong E, Gumbiner BM.** E-cadherin suppresses cellular transformation by inhibiting beta-catenin signaling in an adhesion-independent manner. *J Cell Biol* 2001; **153**: 1049-1060
- 40 **Kagawa Y, Yoshida K, Hirai T, Toge T.** Significance of the expression of p27Kip1 in esophageal squamous cell carcinomas. *Dis Esophagus* 2000; **13**: 179-184
- 41 **Matsumoto M, Natsugoe S, Nakashima S, Sakamoto F, Okumura H, Sakita H, Baba M, Takao S, Aikou T.** Clinical significance of lymph node micrometastasis of pN0 esophageal squamous cell carcinoma. *Cancer Lett* 2000; **153**: 189-197
- 42 **Itami A, Shimada Y, Watanabe G, Imamura M.** Prognostic value of p27 (Kip1) and CyclinD1 expression in esophageal cancer. *Oncology* 1999; **57**: 311-317
- 43 **Prognostic significance of CyclinD1 and E-Cadherin in patients with esophageal squamous cell carcinoma: multiinstitutional retrospective analysis. Research Committee on Malignancy of Esophageal Cancer, Japanese Society for Esophageal Diseases. J Am Coll Surg** 2001; **192**: 708-718

Elevated level of spindle checkpoint protein MAD2 correlates with cellular mitotic arrest, but not with aneuploidy and clinicopathological characteristics in gastric cancer

Chew-Wun Wu, Chin-Wen Chi, Tze-Sing Huang

Chew-Wun Wu, Department of Surgery, Taipei-Veterans General Hospital, Taipei, Taiwan

Chin-Wen Chi, Department of Medical Research and Education, Taipei-Veterans General Hospital and Institute of Pharmacology, National Yang-Ming University, Taipei, Taiwan

Tze-Sing Huang, Division of Cancer Research, National Health Research Institutes, Taipei, Taiwan

Correspondence to: Dr. Tze-Sing Huang, Cooperative Laboratory at VGH-Taipei, No. 201, Shih-Pai Road Sec. 2, Taipei 112, Taiwan. tshuang@nhri.org.tw

Telephone: +886-2-28712121 Ext. 2641 **Fax:** +886-2-28748307

Received: 2004-02-11 **Accepted:** 2004-02-26

Abstract

AIM: To study the relevance of spindle assembly checkpoint protein MAD2 to cellular mitotic status, aneuploidy and other clinicopathological characteristics in gastric cancer.

METHODS: Western blot analyses were performed to analyze the protein levels of MAD2 and cyclin B1 in the tumorous and adjacent nontumorous tissues of 34 gastric cancer patients. Cell cycle distribution and DNA ploidy of cancer tissues were also determined by flow cytometry. Conventional statistical methods were adopted to determine the relevance of abnormal MAD2 level to mitotic status, aneuploidy and clinicopathological parameters.

RESULTS: Out of 34 gastric cancer patients 25 (74%) exhibited elevated MAD2 levels in their tumorous tissues compared with the corresponding nontumorous tissues. Elevation of MAD2 levels significantly correlated with the increased levels of cyclin B1 expression and G₂/M-phase distribution ($P = 0.038$ and $P = 0.033$, respectively), but was not relevant to aneuploidy. The gastric cancer patients with elevated MAD2 levels showed a tendency toward better disease-free and overall survival ($P > 0.05$). However, no association was found between elevated MAD2 levels and patients' clinicopathological characteristics.

CONCLUSION: Elevation of MAD2 level is present in 74% of gastric cancer patients, and correlates with increased mitotic checkpoint activity. However, elevation of MAD2 level is not associated with patients' aneuploidy and any of the clinicopathological characteristics.

Wu CW, Chi CW, Huang TS. Elevated level of spindle checkpoint protein MAD2 correlates with cellular mitotic arrest, but not with aneuploidy and clinicopathological characteristics in gastric cancer. *World J Gastroenterol* 2004; 10(22): 3240-3244 <http://www.wjgnet.com/1007-9327/10/3240.asp>

INTRODUCTION

During the cell division cycle, the localization and segregation

of chromosomes are under the surveillance of one group of proteins, called spindle assembly checkpoint proteins^[1-3]. Mitotic arrest-deficient proteins (MADs) and budding uninhibited by benzimidazole proteins (BUBs) are the major members of spindle assembly checkpoint proteins^[4-6]. Among them, MAD2 is a key component of MAD/BUB complex that can censor mis-segregation of chromosomes by monitoring the microtubule attachment and tension^[4,7,8]. MAD2 is usually expressed at a high steady-state level and distributed at unattached kinetochores^[9,10]. Re-localization of MAD2 along microtubules to the spindle poles is achieved by minus-end-directed dynein-dynactin complex only when all kinetochores properly attach to microtubules^[10]. Once misaligned chromosomes or even a single unattached kinetochore is present, sufficient MAD2 molecules are kept in kinetochores to inhibit the onset of anaphase until all chromosomes exhibit proper bipolar attachment to the spindle. The kinetochore MAD2 can associate with and thus prevent the activation of anaphase-promoting complex (APC)^[7,11-14]. APC is a kinetochore-localizing, CDC27-based ubiquitin ligase responsible for cyclin B1 degradation and in turn down-regulation of cyclin B1-associated CDC2 kinase activity, which is required for metaphase-anaphase transition and for exit from mitosis^[7,11-14]. On the other hand, the microtubule-interfering agents, such as paclitaxel and nocodazole, can also elicit the spindle assembly checkpoint activity of MAD2^[4,15,16]. In paclitaxel-treated cells, MAD2 mediates inhibition of APC's ability to ubiquitinate cyclin B1, which avoids the degradation of cyclin B1 and thus leads the cyclin B1/CDC2 activity to sustain longer^[15]. This persistence of MAD2 and cyclin B1/CDC2 activation renders cells unable to exit from the metaphase and ultimately leads cells to apoptosis^[15].

As described above, the role of MAD2 in spindle checkpoint machinery has been evidenced in many cell line studies. Clinically, it was reported that MAD2 was rarely the target for genetic alterations in digestive tract cancers^[17,18]. Whatever from clinical investigation or animal models, the evidence demonstrating the relevance of MAD2 to cellular mitotic status or other histopathological characteristics is yet lacking. In this study, we investigated the level of MAD2 in 34 gastric cancer patients. The MAD2-related mitotic checkpoint activity was measured by cyclin B1 expression level and cell cycle G₂/M-phase fraction. Our data indicated that 25 out of 34 (74%) gastric cancer patients exhibited elevated MAD2 levels in their tumorous tissues rather than nontumorous tissues. Elevation of MAD2 level correlated with increased mitotic checkpoint activity but was not relevant to aneuploidy (chromosomal numerical alteration). Although the gastric cancer patients with elevated MAD2 levels exhibited a tendency toward better disease-free and overall survival, no correlation was found between abnormal MAD2 level and patients' clinicopathological characteristics.

MATERIALS AND METHODS

Patients and tumor specimens

Thirty-four primary gastric cancer tissues and their corresponding

normal mucosa were obtained from patients at Taipei Veterans General Hospital. The patients consisted of 25 men and 9 women (aged 43–80 years; mean: 63.8 years). Informed consent was obtained from each patient. All specimens were snap-frozen immediately after resection and stored at -80°C until use. Parts of the specimens were taken for protein extraction and DNA content determination, and the remaining tissues were fixed in 40 g/L buffered formaldehyde for histologic examination. Hematoxylin and eosin staining of tissue sections was adopted to categorize the tumors according to the classification of Lauren^[19].

Tissue lysate preparation and Western blot analysis

Tissue lysates were prepared by the method described previously^[20]. Briefly, tumor and non-tumor specimens were ground down into powder in the presence of liquid nitrogen. Around 0.5 g of tissue powder was resuspended in 1.5 mL of 10 mmol/L Tris-Cl, pH 7.8, 140 mmol/L NaCl, 5 g/L deoxycholate, 10 mL/L NP-40, 1 mmol/L phenylmethylsulfonyl fluoride, 10 $\mu\text{g}/\text{mL}$ aprotinin, 10 $\mu\text{g}/\text{mL}$ pepstatin A, and 10 $\mu\text{g}/\text{mL}$ leupeptin. The suspension was subjected to homogenization and further sonication on ice, and finally was ultracentrifuged at 100 000 g for 1 h at 4°C . The supernatant was saved and assayed for protein concentration (Bradford method). Aliquots (30 μg protein) of tissue lysates were separated on 100 g/L SDS-polyacrylamide gels, and electrotransferred onto polyvinylidene difluoride membranes. After blocked with PBST (phosphate-buffered saline plus 1 mL/L Tween-20) plus 50 g/L fat-free milk, the membranes were incubated with anti-MAD2, cyclin B1, and β -tubulin antibodies (Santa Cruz Biotechnology, Santa Cruz, CA, USA), respectively, in PBST plus 50 g/L milk at 4°C for 12 h. The membranes were then washed three times with PBST buffer, and incubated with horseradish peroxidase-conjugated secondary antibodies for 1 h at room temperature. After washed three times with PBST buffer, the protein bands were detected by enhanced chemiluminescence (Amersham Biosciences, Piscataway, NJ, USA).

Flow cytometric analysis of DNA content

The DNA ploidy and cell-cycle phase distribution of tissue specimens were measured by flow cytometric analysis^[21]. Frozen specimens were first minced into 2 to 5 mm^3 pieces and further digested into single cell suspensions^[22]. Cell suspensions were fixed with 800 mL/L ethanol at -20°C at least for 30 min before subsequent Triton X-100 permeabilization and propidium iodide staining^[16]. The cellular DNA content was analyzed using a FACStar flow cytometer with an argon laser tuned to the 488-nm line for excitation (BD Biosciences, San Jose, CA, USA).

Statistical analyses

Data were analyzed by χ^2 or *t* test. Survival rate was calculated by the Kaplan-Meier method. Statistical comparisons were made with Logrank test. The difference was considered to be significant when *P* value was less than 0.05.

RESULTS

Elevated MAD2 level occurs in human gastric cancer

Western blot analysis was performed to analyze the MAD2 expression level of the tumorous and adjacent nontumorous tissues of 34 gastric cancer patients. As shown in Figure 1, the MAD2 protein was detected in both tumorous and nontumorous tissue lysates. In most patients, MAD2 seemed labile in the nontumorous tissues rather than the tumorous tissues. The differential MAD2 level was confirmed by comparison with the

levels of β -tubulin in the same-paired tissue lysates. A patient with elevated MAD2 level was defined as one whose MAD2 level in the tumorous tissue was higher than that in the adjacent nontumorous tissue, and elevated MAD2 level could be found in 25 of 34 (74%) cases of human gastric cancer.

Elevated MAD2 level correlates with increased mitotic arrest but not aneuploidy

The MAD2-related mitotic arrest was measured by cyclin B1 level and cell cycle G₂/M-phase fraction. We found that 18 of 34 (53%) gastric cancer patients had elevated cyclin B1 expression level in their tumorous rather than nontumorous tissues (three examples shown in Figure 1). There was a statistically significant correlation between elevated MAD2 level and elevated cyclin B1 level (*P* = 0.038), as 16 of 25 (64%) gastric cancer patients who had elevated MAD2 levels also manifested higher levels of cyclin B1 in their tumorous tissues (Table 1). Moreover, the DNA contents of tumor specimens of 29 patients were successfully determined by flow cytometric analysis. The data presented by mean \pm SD (%) of phase fractions are shown in Table 2. We observed that the ratio of G₂/M-phase fraction in the tumor specimens exhibiting elevated MAD2 levels was statistically higher than that in the tumorous tissues with a normal MAD2 level ($10.6 \pm 4.9\%$ vs $6.4 \pm 4.0\%$, *P* = 0.033). No significant difference in the ratios of G₀/G₁ and S-phase fractions was found between the tumors with or without elevated MAD2 levels (Table 2). In addition, DNA ploidy was also determined from the tumor specimens of 32 patients. Although 18 of 32 (56%) patients were found to have aneuploid tumor cells, no correlation was observed between the occurrence of aneuploidy and elevated MAD2 level in cancer tissues (*P* = 1.000, Table 3).

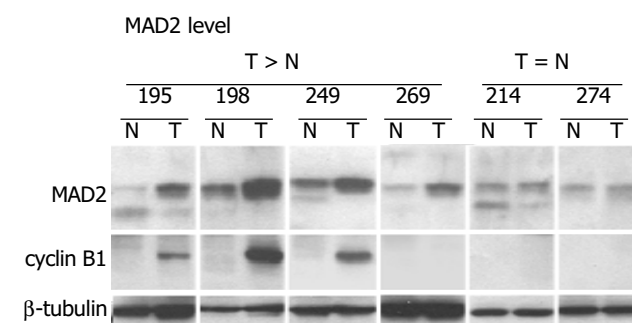


Figure 1 Examples of elevation of MAD2 and cyclin B1 levels in human gastric cancer. Western blot analyses were performed to analyze the protein levels of MAD2 and cyclin B1 in the lysates from non-tumorous tissues (N) and tumorous tissues (T) of gastric cancer patients, #195, #198, #249, #269, #214, and #274. The levels of β -tubulin in the same-paired tissue lysates were analyzed as internal control.

Table 1 Cyclin B1 expression status of 34 gastric cancer tissues with or without MAD2 overexpression

	Cyclin B1 level	
	T > N	T = N
MAD2 level		
T > N (<i>n</i> = 25)	16	9
T = N (<i>n</i> = 9)	2	7
	<i>P</i> = 0.038	

T: tumorous tissue; N: non-tumorous tissue.

Table 2 Cell cycle phase fractions of 29 gastric cancer tissues with or without MAD2 overexpression (mean±SD)

	Phase fraction (%)		
	G ₀ /G ₁	S	G ₂ /M
MAD2 level			
T > N (n = 20)	80.8±5.9	8.6±7.0	10.6±4.9
T = N (n = 9)	83.5±7.4	9.9±7.7	6.4±4.0
	P = 0.301	P = 0.657	P = 0.033

T: tumorous tissue; N: non-tumorous tissue.

Table 3 DNA ploidy status of 32 gastric cancer tissues with or without MAD2 overexpression

	Diploidy	Aneuploidy
MAD2 level		
T > N (n = 23)	10	13
T = N (n = 9)	4	5
	P = 1.000	

T: tumorous tissue; N: non-tumorous tissue.

Elevated MAD2 level does not correlate with clinicopathological characteristics

The relationship of elevated MAD2 level with clinicopathological characteristics was also investigated and summarized (Table 4). The evaluated parameters included age at diagnosis, tumor site and size, cell differentiation grade, stromal reaction, invasive and metastatic status, etc. For the 34 studied patients, age and gender did not associate with higher levels of MAD2 in cancer tissues (P>0.05). There was no association between elevated MAD2 levels and different tumor sites (upper, middle, lower or whole stomach), tumor sizes, and other histopathological characteristics including grade of cell differentiation, Borrmann type, stromal reaction (medullary, intermediate or schirrhous type), infiltration type (α, β or γ), Lauren histological classification (intestinal or diffuse type), and TNM staging (I-IV), either. In addition, elevation of MAD2 level in cancer tissues was not correlated with the invasion parameters, including the lymphatic duct or vessel invasion and depth of cancer invasion (mucosa, submucosa, propria muscle, subserosa, serosa, serosa exposed), and metastatic status such as peritoneal dissemination and lymph node or liver metastasis (Table 4). Finally, the patients with elevated MAD2 levels in tumor tissues exhibited higher five-year overall and disease-free survival rates in comparison with those without elevated MAD2 levels (48.0% vs 20.8% and 46.3% vs 11.1%, respectively), but the difference did not reach a significant level (P = 0.478 and 0.229, respectively; Table 4).

Table 4 Relationships between elevated MAD2 levels and clinicopathological characteristics (mean±SD)

	MAD2 level		
	T>N (n = 25)	T=N (n = 9)	P
Age (yr)	62.8±10.3	66.4±5.0	0.325
Sex (male/female)	19/6	6/3	0.586
Site of tumor			0.828
Upper stomach	4	2	
Middle stomach	6	2	
Lower stomach	14	4	
Whole stomach	1	1	
Size of tumor (cm)	7.3±2.3	8.0±2.9	0.470
Grade of cell differentiation			0.146

Well differentiated	1	0	
Moderately differentiated	13	8	
Poorly differentiated	11	1	
Borrmann type			0.664
0	2	0	
1 + 2	6	2	
3 + 4	17	7	
Stromal reaction			0.739
Medullary type	6	3	
Intermediate type	12	3	
Schirrhous type	7	3	
Infiltration type			0.475
α	4	2	
β	8	1	
γ	13	6	
Lauren histological classification			0.448
Intestinal type	13	3	
Diffuse type	12	6	
Lymph node metastasis (Yes/No)	15/10	6/3	1.000
Lymphatic duct invasion (Yes/No)	18/7	7/2	1.000
Vascular invasion (Yes/No)	2/23	1/8	1.000
Liver metastasis (Yes/No)	1/24	0/9	1.000
Peritoneal dissemination (Yes/No)	2/23	1/8	1.000
Depth of cancer invasion			0.738
Mucosa, submucosa	1	0	
Propria muscle, subserosa	5	1	
Serosa	18	8	
Serosa (infiltration) exposed	1	0	
TNM stage			0.932
I	3	1	
II	8	2	
III	8	3	
IV	6	3	
Five-yr overall survival rate	48.0%	20.8%	0.478
Five-yr disease-free survival rate	46.3%	11.1%	0.229

DISCUSSION

Spindle assembly checkpoint is one of the mechanisms to guard the fidelity of cell division cycle^[1-3]. MAD2 is a key component of spindle assembly checkpoint complex MAD/BUB that is responsible for monitoring the localization and segregation of chromosomes^[4,7,8]. MAD2 could induce mitotic arrest by associating with and thus inhibiting APC when microtubule-interfering agents were present in cancer cell cultures^[4,15]. However, the evidence demonstrating the clinical relevance of MAD2 to cancer cell mitotic status is yet lacking. In this study, we provided the clinical data to support the mitotic checkpoint role of MAD2 in cancer tissues. We found that 74% of our gastric cancer patients had elevated levels of MAD2 in their tumorous tissues. These patients also exhibited more cyclin B1 expression and G₂/M-phase distribution in their cancer cells. Because MAD2 can interfere with APC and APC is an ubiquitin ligase responsible for cyclin B1 degradation, elevation of both cyclin B1 expression and cellular G₂/M-phase ratio may be resulted from a higher mitotic checkpoint activity that is expected of elevated MAD2 level. Noteworthy, these patients had a tendency toward longer disease-free and overall survival. We speculate that the checkpoint activity of MAD2 exerted in these patients monitors the interaction of chromosomes with spindle fibers, which is finally linked with better disease-free and overall survival. Elevated level of MAD2 seems to be a possible target

for potential development of novel therapeutic or prognostic modalities in the future.

Our data indicate that elevated MAD2 levels did not prevent the occurrence of aneuploidy in gastric cancer. Aneuploidy is one of the hallmarks of cancer cells^[23-25]. Considering spindle assembly checkpoint proteins function as a monitor for the fidelity of chromosomal segregation, impairment of spindle assembly checkpoint is expected to associate with the development of cancer cell aneuploidy. However thus far, many aneuploid cancer cell lines did undergo mitotic arrest in response to spindle damage, indicating that not all cancer cells with aneuploidy had an impaired spindle checkpoint^[26-28]. Moreover, accumulating studies have demonstrated that the BUBs (BUB1, BUBR1 and BUB3) and MADs (MAD1 and MAD2) were rarely the targets for genetic alterations in a variety of human cancer types including head-and-neck squamous cell carcinoma^[29], non-small cell lung cancer^[29,30], thyroid follicular neoplasms^[28], hepatocellular carcinoma^[27], and digestive tract cancers^[17,18,30]. These data suggest that cancer cell aneuploidy may arise from the alternative defects yet to be discovered. Despite of the low frequency of gene mutation, a research of 43 gastric cancer patients concluded that overexpression of BUB1, BUBR1 or/and BUB3 was observed in >60% of cases^[31]. There was no statistically positive correlation between overexpression of BUBs and cancer aneuploidy. Instead, the overexpression was significantly correlated with Ki-67 expression of tumor cells, suggesting that BUBs are proliferation-associated proteins other than spindle checkpoint proteins in gastric cancer^[31].

The gastric cancer patients with different molecular alterations were shown to have distinct histopathological features. For example, simultaneous overexpression of hepatocyte growth factor receptor (c-Met), autocrine motility factor receptor (AMFR) and urokinase-type plasminogen activator receptor (uPAR) was correlated with positive lymphatic vessel invasion and infiltration^[32]. Estrogen receptor (ER) was more expressed in diffuse-type patients with regional lymph node metastasis^[33]. Additionally, positive expression of nm23 was detected in as high as 74% of gastric cancer patients and was related to patients' age, tumor size, Borrmann type, Lauren classification, and TNM stage^[34]. COX-2 overexpression significantly correlated with TNM staging; while abnormal expression of E-cadherin/ β -catenin complex occurred more significantly in Borrmann types III/IV than in types I/II. In our present study, no histopathological parameter was found to be associated with elevated MAD2 level in gastric cancer patients. It was reported consistently that MAD2 was significantly overexpressed in colorectal adenocarcinoma, but was not related to differentiation or other clinical parameters.

In conclusion, an elevation of spindle checkpoint protein MAD2 level was observed in 74% of our gastric cancer patients, and was significantly correlated with the increased levels of cyclin B1 expression and G₂/M-phase distribution in cancer tissues. However, an elevated MAD2 level was not associated with aneuploidy and other clinical factors, including demographic features and histopathological characteristics.

REFERENCES

- 1 Sorger PK, Dobles M, Tournébiz R, Hyman AA. Coupling cell division and cell death to microtubule dynamics. *Curr Opin Cell Biol* 1997; **9**: 807-814
- 2 Cleveland DW, Mao Y, Sullivan KF. Centromeres and kinetochores: from epigenetics to mitotic checkpoint signaling. *Cell* 2003; **112**: 407-421
- 3 Mollinedo F, Gajate C. Microtubules, microtubule-interfering agents and apoptosis. *Apoptosis* 2003; **8**: 413-450
- 4 Li Y, Benezra R. Identification of a human mitotic checkpoint gene: *hsMAD2*. *Science* 1996; **274**: 246-248
- 5 Taylor SS, Ha E, McKeon F. The human homologue of Bub3 is required for kinetochore localization of Bub1 and a Mad3/bub1-related protein kinase. *J Cell Biol* 1998; **142**: 1-11
- 6 Skoufias DA, Andreassen PR, Lacroix FB, Wilson L, Margolis RL. Mammalian mad2 and bub1/bubR1 recognize distinct spindle-attachment and kinetochore-tension checkpoints. *Proc Natl Acad Sci U S A* 2001; **98**: 4492-4497
- 7 Li Y, Gorbea C, Mahaffey D, Rechsteiner M, Benezra R. MAD2 associates with the cyclosome/anaphase-promoting complex and inhibits its activity. *Proc Natl Acad Sci U S A* 1997; **94**: 12431-12436
- 8 Dobles M, Liberal V, Scott ML, Benezra R, Sorger PK. Chromosomal missegregation and apoptosis in mice lacking the mitotic checkpoint protein Mad2. *Cell* 2000; **101**: 635-645
- 9 Howell BJ, Hoffman DB, Fang G, Murray AW, Salmon ED. Visualization of Mad2 dynamics at kinetochores, along spindle fibers, and at spindle poles in living cells. *J Cell Biol* 2000; **150**: 1233-1250
- 10 Howell BJ, McEwen BF, Canman JC, Hoffman DB, Farrar EM, Rieder CL, Salmon ED. Cytoplasmic dynein/dynactin drives kinetochore protein transport to the spindle poles and has a role in mitotic spindle checkpoint inactivation. *J Cell Biol* 2001; **155**: 1159-1172
- 11 Fang G, Yu H, Kirschner MW. The checkpoint protein MAD2 and the mitotic regulator CDC20 form a ternary complex with the anaphase-promoting complex to control anaphase initiation. *Genes Dev* 1998; **12**: 1871-1883
- 12 Gorbsky GJ, Chen RH, Murray AW. Microinjection of antibody to Mad2 protein into mammalian cells in mitosis induces premature anaphase. *J Cell Biol* 1998; **141**: 1193-1205
- 13 Kallio M, Weinstein J, Daum JR, Burke DJ, Gorbsky GJ. Mammalian p53CDC mediates association of the spindle checkpoint protein Mad2 with the cyclosome/anaphase-promoting complex, and is involved in regulating anaphase onset and late mitotic events. *J Cell Biol* 1998; **141**: 1393-1406
- 14 Wassmann K, Benezra R. Mad2 transiently associates with an APC/p53Cdc complex during mitosis. *Proc Natl Acad Sci U S A* 1998; **95**: 11193-11198
- 15 Huang TS, Shu CH, Chao Y, Chen SN, Chen LL. Activation of MAD 2 checkpoint protein and persistence of cyclin B1/CDC 2 activity associate with paclitaxel-induced apoptosis in human nasopharyngeal carcinoma cells. *Apoptosis* 2000; **5**: 235-241
- 16 Huang TS, Shu CH, Chao Y, Chen LT. Evaluation of GL331 in combination with paclitaxel: GL331's interference with paclitaxel-induced cell cycle perturbation and apoptosis. *Anti-Cancer Drug* 2001; **12**: 259-266
- 17 Imai Y, Shiratori Y, Kato N, Inoue T, Omata M. Mutational inactivation of mitotic checkpoint genes, *hsMAD2* and *hBUB1*, is rare in sporadic digestive tract cancers. *Jpn J Cancer Res* 1999; **90**: 837-840
- 18 Cahill DP, da Costa LT, Carson-Walter EB, Kinzler KW, Vogelstein B, Lengauer C. Characterization of MAD2B and other mitotic spindle checkpoint genes. *Genomics* 1999; **58**: 181-187
- 19 Lauren P. The two histological main types of gastric carcinoma. Diffuse and so-called intestinal type carcinoma: an attempt at a histoclinical classification. *Acta Pathol Microbiol Scand* 1965; **64**: 31-49
- 20 Chao Y, Shih YL, Chiu JH, Chau GY, Lui WY, Yang WK, Lee SD, Huang TS. Overexpression of cyclin A but not Skp 2 correlates with the tumor relapse of human hepatocellular carcinoma. *Cancer Res* 1998; **58**: 985-990
- 21 Chiu JH, Kao HL, Wu LH, Chang HM, Lui WY. Prediction of relapse or survival after resection in human hepatomas by DNA flow cytometry. *J Clin Invest* 1992; **89**: 539-545
- 22 Chen MH, Yang WK, Whang-Peng J, Lee LS, Huang TS. Differential inducibilities of GFAP expression, cytostasis and apoptosis in primary cultures of human astrocytic tumors. *Apoptosis* 1998; **3**: 171-182
- 23 Andreassen PR, Martineau SN, Margolis RL. Chemical induction of mitotic checkpoint override in mammalian cells results in aneuploidy following a transient tetraploid state. *Mutation Res* 1996; **372**: 181-194
- 24 Cahill DP, Lengauer C, Yu J, Riggins GJ, Willson JK, Markowitz SD, Kinzler KW, Vogelstein B. Mutations of mitotic checkpoint genes in human cancers. *Nature* 1998; **392**: 300-303

- 25 **Masuda A**, Takahashi T. Chromosome instability in human lung cancers: possible underlying mechanisms and potential consequences in the pathogenesis. *Oncogene* 2002; **21**: 6884-6897
- 26 **Tighe A**, Johnson VL, Albertella M, Taylor SS. Aneuploid colon cancer cells have a robust spindle checkpoint. *EMBO Rep* 2001; **2**: 609-614
- 27 **Saeki A**, Tamura S, Ito N, Kiso S, Matsuda Y, Yabuuchi I, Kawata S, Matsuzawa Y. Frequent impairment of the spindle assembly checkpoint in hepatocellular carcinoma. *Cancer* 2002, **94**: 2047-2054
- 28 **Ouyang B**, Knauf JA, Ain K, Nacev B, Fagin JA. Mechanisms of aneuploidy in thyroid cancer cell lines and tissues: evidence for mitotic checkpoint dysfunction without mutations in BUB1 and BUBR1. *Clin Endocrinol* 2002; **56**: 341-350
- 29 **Yamaguchi K**, Okami K, Hibi K, Wehage SL, Jen J, Sidransky D. Mutation analysis of hBUB1 in aneuploid HNSCC and lung cancer cell lines. *Cancer Lett* 1999; **139**: 183-187
- 30 **Jaffrey RG**, Pritchard SC, Clark C, Murray GI, Cassidy J, Kerr KM, Nicolson MC, McLeod HL. Genomic instability at the BUB1 locus in colorectal cancer, but not in non-small cell lung cancer. *Cancer Res* 2000; **60**: 4349-4352
- 31 **Grabsch H**, Takeno S, Parsons WJ, Pomjanski N, Boecking A, Gabbert HE, Mueller W. Overexpression of the mitotic checkpoint genes BUB1, BUBR1, and BUB3 in gastric cancer-association with tumor cell proliferation. *J Pathol* 2003; **200**: 16-22
- 32 **Taniguchi K**, Yonemura Y, Nojima N, Hirono Y, Fushida S, Fujimura T, Miwa K, Endo Y, Yamamoto H, Watanabe H. The relation between the growth patterns of gastric carcinoma and the expression of hepatocyte growth factor receptor (c-met), autocrine motility factor receptor, and urokinase-type plasminogen activator receptor. *Cancer* 1998; **82**: 2112-2122
- 33 **Zhao XH**, Gu SZ, Liu SX, Pan BR. Expression of estrogen receptor and estrogen receptor messenger RNA in gastric carcinoma tissues. *World J Gastroenterol* 2003; **9**: 665-669
- 34 **Lee KE**, Lee HJ, Kim YH, Yu HJ, Yang HK, Kim WH, Lee KU, Choe KJ, Kim JP. Prognostic significance of p53, nm23, PCNA and c-erbB-2 in gastric cancer. *Jpn J Clin Oncol* 2003; **33**: 173-179

Edited by Zhu LH and Xu FM

Expression level of wild-type survivin in gastric cancer is an independent predictor of survival

Hua Meng, Cai-De Lu, Yu-Lei Sun, De-Jian Dai, Sang-Wong Lee, Nobuhiko Tanigawa

Hua Meng, Department of General Surgery, First Affiliated Hospital of Dalian Medical University, Dalian 116011, Liaoning Province, China
De-Jian Dai, Department of Surgery, Second Affiliated Hospital of Zhejiang University School of Medicine, Hangzhou 310009, Zhejiang Province, China

Cai-De Lu, Department of Surgery, Lihuili Hospital of Ningbo University Medical School, Ningbo 315040, Zhejiang Province, China

Yu-Lei Sun, Department of Anaesthesiology, First Affiliated Hospital of Dalian Medical University, Dalian 116011, Liaoning Province, China

Sang-Wong Lee, **Nobuhiko Tanigawa**, Department of General and Gastroenterological Surgery, Osaka Medical College, 2-7 Daigakumachi, Takatsuki, Osaka 569-8686, Japan

Supported by the National Natural Science Foundation of China, No. 30271483 and Grant-in-Aid from the Japanese Ministry of Education, Culture, Sports, Science, and Technology of Japan, No.13470262

Correspondence to: Cai-De Lu, M.D., Department of Surgery, Lihuili Hospital of Ningbo University Medical School, Ningbo 315040, Zhejiang Province, China. lucd71@hotmail.com

Telephone: +86-574-87392290 Ext.7707 **Fax:** +86-574-87392232

Received: 2003-10-30 **Accepted:** 2003-12-16

Abstract

AIM: *Survivin* is a novel antiapoptotic gene in which three splicing variants have been recently cloned and characterized. *Survivin* has been found to be abundantly expressed in a wide variety of human malignancies, whereas it is undetectable in normal adult tissues. We aimed to study the expression of three *survivin* splicing variants in gastric cancer, and to evaluate the prognostic significance of the expression of *survivin* variants in gastric cancer.

METHODS: Real time quantitative RT-PCR was performed to analyze the expression of *survivin* variants in 79 paired tumors and normal gastric mucosa samples at the mRNA level. Proliferative and apoptotic activity was measured using Ki-67 immunohistochemical analysis and the TUNEL method, respectively.

RESULTS: All the cases tested expressed wild-type *survivin* mRNA, which was not only the dominant transcript, but also a poor prognostic biomarker ($P = 0.003$). Non-antiapoptotic *survivin*-2B mRNA was correlated with tumor stage ($P = 0.001$), histological type ($P = 0.004$), and depth of tumor invasion ($P = 0.041$), while *survivin*- Δ Ex3 mRNA showed a significant association with apoptosis ($P = 0.02$).

CONCLUSION: Wild-type *survivin* mRNA expression levels are of important prognostic value and significant participation of *survivin*-2B and *survivin*- Δ Ex3 is suggested in gastric cancer development.

Meng H, Lu CD, Sun YL, Dai DJ, Lee SW, Tanigawa N. Expression level of wild-type *survivin* in gastric cancer is an independent predictor of survival. *World J Gastroenterol* 2004; 10(22): 3245-3250

<http://www.wjgnet.com/1007-9327/10/3245.asp>

INTRODUCTION

Apoptosis, also called programmed cell death, plays an important

role in the development and homeostasis of tissues. Deregulation of apoptosis is involved in carcinogenesis by abnormally prolonged cell survival, facilitating the accumulation of transforming mutations and promoting resistance to immunosurveillance^[1]. Several studies have consistently shown that *survivin* could mediate suppression of apoptosis. Surprisingly, in a single copy of *survivin* gene, three alternatively splicing transcripts have been identified. In addition to wild-type *survivin*, two novel *survivin* variants (*survivin*-2B, *survivin*- Δ Ex3), which have different antiapoptotic properties, have been generated. *Survivin*-2B has lost its anti-apoptotic potential, whereas its anti-apoptotic potential is preserved in *survivin*- Δ Ex3^[2,3]. Their different functions in carcinogenesis are largely unknown.

Gastric carcinoma is one of the most frequent human malignancies^[4]. As shown by our group^[5], 34.5% of gastric cancers expressed *survivin* protein and a positive correlation between accumulated p53 and *survivin* expression in neoplasia was found. In this study, we investigated the distribution of *survivin* variants in paired tumors and normal gastric mucosa samples at the mRNA level and assessed the potential relationship between the expression of *survivin* variants and proliferative activity, apoptosis or prognostic significance.

MATERIALS AND METHODS

Patients and specimens

Matched pairs of tumors and normal gastric mucosa samples were obtained from 76 patients with gastric cancer and 1 patient with malignant lymphoma at the Department of General and Gastroenterological Surgery, Osaka Medical College Hospital during 2000-2002. The specimens resected at surgery were immediately frozen in liquid nitrogen and stored at -80°C until total RNA extraction. Clinicopathological parameters were assigned according to the principles outlined by Japanese Classification of Gastric Carcinoma^[6]. Samples included stage I cases ($n = 22$), stage II cases ($n = 11$), stage III cases ($n = 20$), stage IV cases ($n = 26$). There were 62 (78.5%) males and 17 (22.5%) females, and the mean age of the patients was 65.2 years (SD, 9.6 years; range, 40-87 years). No Patients received chemotherapy or radiation therapy either before or after surgery. The mean follow-up period was 19.7 mo (SD, 14.9 mo; range, 1.5-87 mo). Formalin-fixed paraffin-embedded blocks of primary tumors were taken from pathological archives. Two to four μm thick serial sections of 2-4 thickens were prepared from the cut surface of the blocks at the maximum cross-section of the tumors.

Total RNA extraction

Total RNA was extracted by an acid guanidinium-phenol-chloroform method using ISOGEN (Nippon Gene, Toyama, Japan) according to the manufacturer's instructions. Afterwards the total RNA was purified using DNase I (GIBCO-BRL, Gaithersburg, MD, USA). Extracted total RNA pellets were dissolved with RNase free diethyl pyrocarbonate (DEPC)-treated water.

Reverse transcription

Complementary DNA (cDNA) was synthesized with 5 μg of total RNA and 20 pmol oligo (dT)₁₈ primer using an Advantage

RNA-for-PCR kit (CLONTECH, Inc., Palo Alto, USA), with the exception of 200 U SurperScript™ II RNase H⁻ reverse transcriptase (Invitrogen, Inc., Carlsbad, USA) in a final 20 μ L reaction volume. RT reactions were performed at 50 °C for 120 min. Finally, cDNA solution was diluted to a total volume 100 μ L.

Quantitative real time RT-PCR

Quantitative real time RT-PCR was performed with a LightCycler (Roche Diagnostics, Mannheim, Germany). As an internal control, housekeeping gene G6PDH mRNA expression was measured at the same time. DEPC-treated H₂O was used as a negative control and MKN-74 was used as a positive control. Then, 1 μ L of cDNA mixture was subjected to amplification in 10 μ L reaction mixture. The PCR conditions were initial denaturation at 95 °C for 10 min, followed by 40 cycles of denaturation at 95 °C for 10 s, annealing at 62 °C for 10 s for survivin, survivin-2B and survivin- Δ Ex3 (or at 63 °C for G6PDH), extension at 72 °C for 10 s, respectively. A standard curve using fluorescent data was generated from serial tenfold dilution of specific plasmids from 10⁷ to 10² copies, respectively. The number of gene copies was calculated by the LightCycler Software Version 3.5.3 according to the Fit Points Above Threshold method. Primer pairs and hybridization probes for survivin, survivin-2B, survivin- Δ Ex3 and G6PDH mRNA were as follows. The sequence of the common forward primer for survivin variants was 5'-CCACCGCATCTC TACATTC A-3'. To distinguish the 3 splice variants of survivin, the sequences of reverse primers for survivin variants were designed to correspond to exon/exon borders of the complementary strand (5'-TATGTTCTCTATGGGGTCG-3' for survivin, 5'-AGTGCTGGTATTACAGGCGT-3' for survivin-2B, 5'-TTTCCT TTGCATGGGGTC-3' for survivin- Δ Ex3). The sequences of common hybridization probes for survivin variants were 5'-CAAGTCTGGCTCGTTCTCAGTGGG-3'-FITC and LCRed640-5'-CAGTGGATGAAGCCAGCCTCG-3'. The sequence of the forward primer for G6PDH was 5'-TGGACCTGACCTACGGCA ACAGATA-3'. The sequence of the reverse primer for G6PDH was 5'-GCCCTCATACTGGAAACCC-3'. The sequences of hybridization probes for G6PDH were 5'-TTTTCACCCCACTGC TGCACC-3'-FITC and LCRed640-5'-GATTGAGCTGGAGAAG CCCAAGC-3'.

PCR products were additionally checked by electrophoresis on 30 g/L agarose gels (BIO-RAD, Inc., Hercules, USA) containing ethidium bromide and visualized under UV transillumination.

Sequence analysis

To confirm the identity of the PCR products, their bands were excised from agarose gels and isolated by a QIAquick gel extraction kit (Qiagen, Tokyo, Japan), ligated into a pGEM-T-cloning vector (Promega), and cloned according to standard protocols. Plasmid DNA was recovered using a Plasmid Mini kit (Qiagen, Tokyo, Japan). Cycle was sequenced and analyzed in an ABI-PRISM310 (Applied Biosystems) using T7 or SP6-site specific primers. The sequences of the PCR products were compared with those in GenBank, which were found to be identical (Data not shown).

Ki-67 immunohistochemical staining and assessment of proliferative index

Immunohistochemical staining was performed by the standard avidin-biotin-peroxidase complex technique using L.V. Dako LSAB kit (DAKO, Copenhagen, Denmark) as described previously^[5,7,8]. The antibodies used were monoclonal mouse antibody Ki-67 (MIB-1, diluted 1:50; Immunotech, Marseilles, France). The labeling index (LI) of Ki-67 was determined in those tumor areas with positive stained nuclei. Five random areas within a section were chosen and counted under 200-fold magnification using a point counting technique. The average percentage of positivity was recorded as the Ki-67 LI for each case^[7].

Histochemical detection of apoptosis and determination of AI

Apoptotic cells in tissue sections were detected by terminal deoxynucleotidyl transferase-mediated dUTP-biotin nick end labeling (TUNEL), using an Apop Tag *in situ* detection kit (Oncor, Gaithersburg, MD). The staining procedures were based on a method described previously^[5,6,8]. The apoptotic index (AI) was expressed as the ratio of positively stained tumor cells and bodies to all tumor cells according to the criteria described elsewhere^[5,7]. Five areas were randomly selected for counting under 400-fold magnification.

Statistical methods

All statistical analyses were performed by the SPSS11.0 software package for Windows (SPSS Inc., Chicago, IL). Differences in the numerical data between the two groups were evaluated using the Mann-Whitney U test. The χ^2 test was further used to compare the distribution of individual variables and any correlation between AI or Ki-67 index and expression of survivin variants. The correlation between AI and expression of survivin variants for each case was also analyzed by Spearman's rank correlation test. Survival curves were calculated using the Kaplan-Meier method and analyzed by the log rank test. A two-tailed *P* value less than 0.05 was considered statistically significant.

RESULTS

Expression of survivin variants in clinical materials and cell lines

Among the 79 tumor samples, survivin expression was detected in all tumor samples (79/79), survivin-2B expression was demonstrated in 78.5% (62/79) of the samples and survivin- Δ Ex3 expression was detected in 64.6% (51/79) of the samples (Figure 1). In contrast, survivin expression was detectable in 46 (58.2%) of the normal mucosa samples, while survivin-2B expression and survivin- Δ Ex3 were detected in 23 (29.1%) and 12 (15.2%) of the mucosa samples respectively.

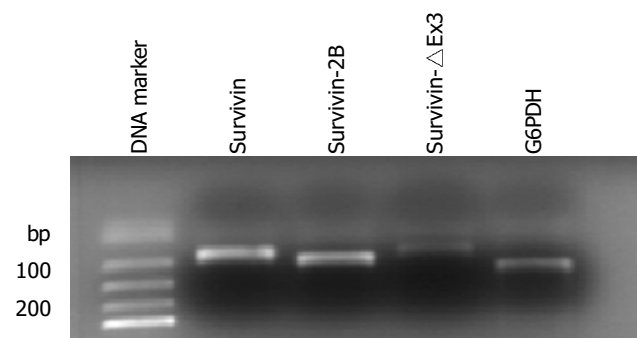


Figure 1 Amplification, separation and visualization of survivin (185 bp), survivin-2B (214 bp) survivin- Δ Ex3 (184 bp), and G6PDH (256 bp) mRNA (40 cycles) in a typical case.

The relative amounts of survivin variant mRNA were determined by dividing the amount of survivin variant mRNA by that of G6PDH mRNA for each sample. In tumor samples, the relative levels of survivin-2B and survivin- Δ Ex3 was further normalized by matched survivin. Because three alternatively spliced variants are derived from a common hnRNA precursor pool, these ratios seemed to be independent of any possible bias imposed by variations in housekeeping gene expression levels^[9,10]. Although there was a significant difference in G6PDH expression between normal tissues and cancer samples at the same amount of total RNA used ($P < 0.0001$, Mann-Whitney U test, Figure 2A), the survivin variant/G6PDH ratio in our cancer tissues were significantly higher than that in non-neoplastic tissues ($P < 0.0001$, Mann-Whitney U test, Figure 2B).

Table 1 Relationship among expression levels of survivin variants and clinicopathologic parameters, proliferative activity or apoptosis

Parameters	No. of patients (%)	Sur/G6PDH	Sur-2B/G6PDH	Sur- Δ Ex3/G6PDH	Sur-2B/sur	Sur- Δ Ex3/sur
Gender (median)						
Male	62 (78.5)	$P = 0.445$	$P = 0.598$	$P = 0.079$	$P = 0.125$	$P = 0.408$
Female	17 (22.5)					
Age yr (median)						
<64	39	$P = 0.462$	$P = 0.108$	$P = 0.177$	$P = 0.129$	$P = 0.262$
>64	40					
Histological type						
Differentiated	47	$P = 0.976$	$P = 0.004$	$P = 0.151$	$P = 0.053$	$P = 0.231$
Undifferentiated	32					
Depth of invade						
Not invasion	27	$P = 0.336$	$P = 0.042$	$P = 0.266$	$P = 0.354$	$P = 0.555$
Invasion	40					
Clinical stage						
Stage I+II	(22+11)	$P = 0.075$	$P = 0.001$	$P = 0.139$	$P = 0.018$	$P = 0.863$
Stage III+IV	(20+26)					
Ki67 (median)						
Low	39	$P = 0.791$	$P = 0.197$	$P = 0.567$	$P = 0.401$	$P = 0.512$
High	40					
Apop Tag (median)						
Low	39	$P = 0.421$	$P = 0.070$	$P = 0.0020$	$P = 0.408$	$P = 0.099$
High	40					

Two-tailed P values were calculated by the Mann-Whitney U test. Differentiated type: Papillary type, Tubular type. Undifferentiated type: Poorly differentiated type, Signet ring cell type, Mucinous type. Not invasion: No invasion of the serosa. Invasion: invasion of the serosa.

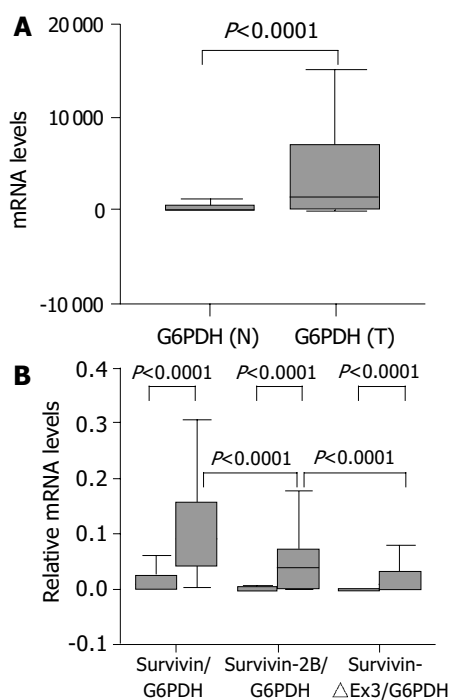


Figure 2 A: RT-PCR amplification of G6PDH in paired samples of normal gastric mucosa and gastric carcinoma. B: Relative (G6PDH-normalised) mRNA levels of survivin variants in paired samples of normal gastric mucosa and gastric carcinoma. Two-tailed P values were calculated by the Mann-Whitney U test.

Relationship between expression levels of survivin variants and clinicopathological parameters

The expression level of survivin-2B was significantly ($P = 0.001$, Table 1, $P < 0.0001$, χ^2 test, Figure 3A) decreased in advanced (III+IV) stage compared with early (I+II) tumor stage. Furthermore, the level of survivin-2B was inversely correlated with the grade of tumor differentiation ($P = 0.004$, Table 1, $P = 0.023$, χ^2 test, Figure 3B) and depth of tumor invasion ($P = 0.042$, Table 1, $P = 0.021$,

χ^2 test). A stage-dependent decrease of survivin-2B was also confirmed by the ratio of survivin-2B/survivin ($P = 0.018$, Table 1, $P = 0.022$, χ^2 test, Figure 3C).

None of the investigated clinicopathological parameters showed a statistically significant correlation with the expression of other types of survivin variants besides survivin-2B.

Correlation between expression levels of survivin variants and AI

Apoptotic cells and bodies were detected in all cases of gastric carcinoma tested (Table 1, Figure 4A). The mean AI was 1.07% (SD, 0.41%; range, 0.38-2.38%) with a median of 0.95%. The mean AI in survivin- Δ Ex3-low expression samples was significantly higher than that in survivin- Δ Ex3-high expression samples ($P = 0.02$, Table 1, $P = 0.028$, χ^2 test, Table 1). There was no correlation between apoptotic index and clinicopathological parameters described. Spearman's rank correlation test demonstrated a significant negative correlation between apoptotic index and expression level of survivin- Δ Ex3 ($\Gamma = -0.257$, $P = 0.022$).

Association of expression levels of survivin variants with PI

Proliferative cells were detected by intense nuclear immunoreactivity to the Ki-67 antigen, as illustrated in Figure 4B. The mean proliferative index (PI) in gastric tumors tested was 48.46% (SD, 9.54%; range, 28.49-82.98%) with a median of 46.87%. No significant relationship was identified between PI of tumor cells and clinicopathological parameters, as demonstrated in Table 1. In addition, no significant association was found between PI and any type of survivin variants.

Prognostic value of survivin mRNA expression

Postoperative survival of the 79 gastric cancer patients was analyzed according to the expression level of survivin variants. Results are shown in Figure 5. Each survivin variant value was divided by the median value. The survival curve of patients with high-survivin expression was significantly lower than that of those with low-survivin expression ($P = 0.003$, log-rank test). No prognostic significance for either survivin-2B or survivin- Δ Ex3, however, was found in the current study.

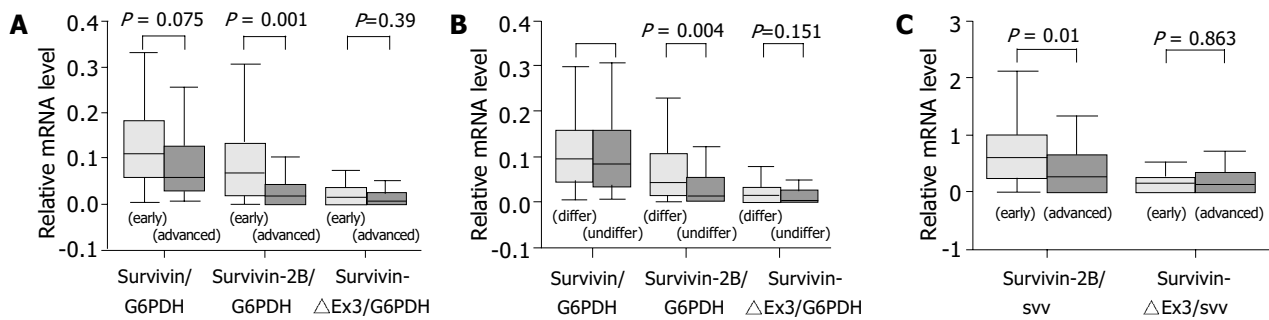


Figure 3 Relative mRNA levels of survivin variants. A: Significant decrease of relative (G6PDH-normalised) mRNA levels of survivin-2B in advanced stages ($P = 0.001$, Mann-Whitney U test). B: Significant decrease of relative (G6PDH-normalised) mRNA levels of survivin-2B in undifferentiated type ($P = 0.004$, Mann-Whitney U test). C: Significantly lower ratio of survivin-2B/survivin in advanced stages than that in early stages ($P = 0.018$, Mann-Whitney U test).

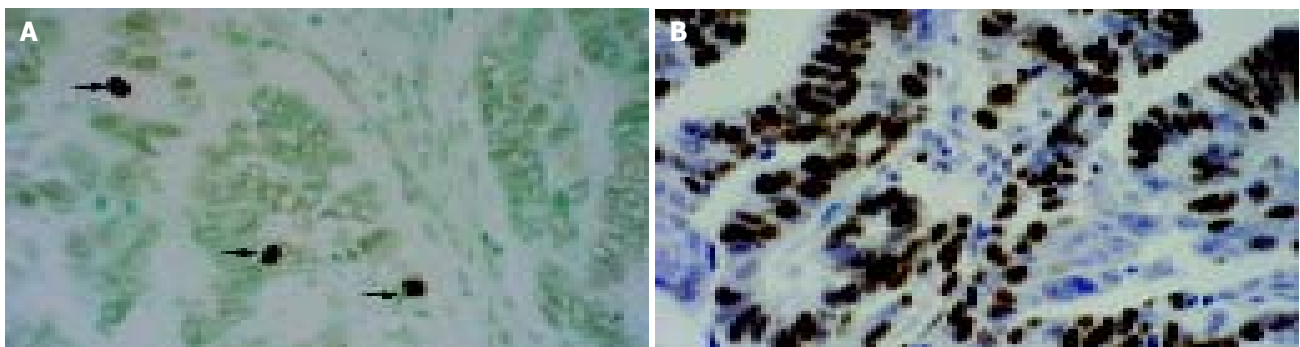


Figure 4 Histochemical staining for Ki-67 and apoptotic tumor cells. A: TUNEL *in situ* labeling for detecting apoptotic cells and bodies (arrows, magnification $\times 400$) in adenocarcinoma. B: Ki-67 nuclear immunohistochemical staining revealing proliferating tumor cells in adenocarcinoma (magnification $\times 400$).

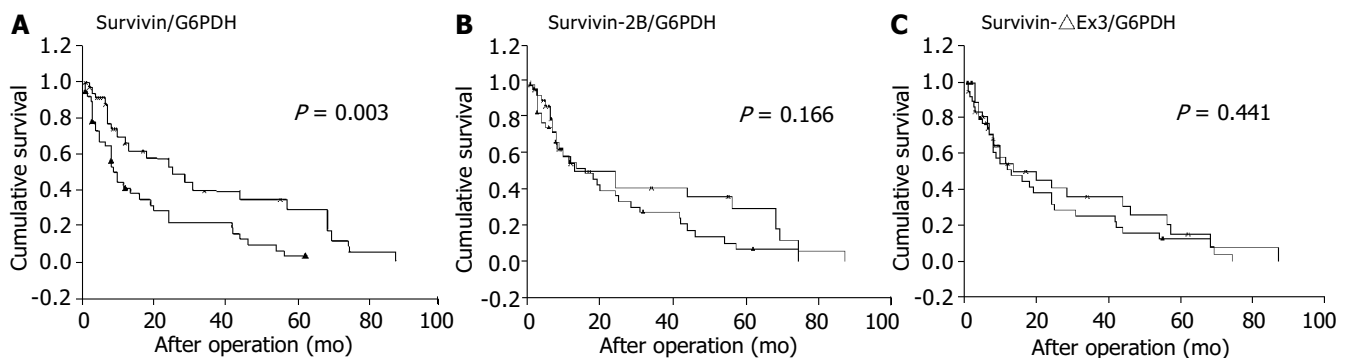


Figure 5 postoperative survivals of 79 gastric carcinoma patients. A: Shorter survival time of patients with high expression of wild-type survivin mRNA compared to patients with low expression of wild-type survivin expression ($P = 0.003$, log-rank test). B: No significance in expression of survivin-2B mRNA ($P = 0.166$, log-rank test). C: No significance in expression of survivin- Δ Ex3 mRNA ($P = 0.441$, log-rank test).

DISCUSSION

In this study, the prognostic significance of the expression of three survivin splicing variants in gastric carcinoma was examined for the first time. Interestingly, only increased wild-type survivin mRNA expression was prominently correlated with reduced survival time, whereas neither survivin-2B nor survivin- Δ Ex3 showed an association with prognosis. In accordance with recent studies, we did not find a correlation between mRNA expression levels of anti-apoptotic variants (survivin or survivin- Δ Ex3) and the investigated clinicopathological parameters^[9,10]. There is no doubt, however, survivin plays a role in enhancing the malignant behavior of tumors. In cell culture systems, over-

expression of survivin was consistently associated with inhibition of cell death^[2]. Strong survivin mRNA expression showed chemoradio resistance^[11-13] and a correlation with recurrence in patients^[14]. In retrospective trials, increased survivin mRNA or protein expression was reported to be a prognostic indicator of tumor progression in different types of human cancer^[15-19]. Our observations further confirmed that survivin mRNA was a poor prognostic biomarker. This suggests that a relatively straightforward detection of survivin protein or mRNA in clinical patients may provide an initial marker of aggressive diseases, potentially requiring in-depth follow-up protocols or alternative treatment regimens in the future.

The notion that survivin inhibits apoptosis has been established, but the mechanism (s) by which this occurs has not been conclusively determined. The actual molecular interaction partners of survivin variants, however, have remained elusive^[2]. Although there is a good agreement that deregulation of cell death/survival pathways contributes to malignant transformation, the potential predictive/prognostic impact of apoptosis regulatory molecules and AI has remained controversial^[8]. This study failed to show the relationship between apoptotic index and survivin expression in gastric carcinoma although it was shown in previous^[5,20] studies showed in gastric cancer that survivin expression was inversely correlated with apoptosis. These controversial findings were attributed in part to the dual function by which survivin regulates cell death and cell division. In recent studies, frameshift carboxyl terminus of survivin- Δ Ex3 was found to contain a bipartite localization signal, which mediates its strong nuclear accumulation and might interfere with degradation of survivin- Δ Ex3 protein by ubiquitin tagging. Survivin- Δ Ex3, therefore, could evade cell cycle-specific degradation by the ubiquitin-proteasome pathway, known for survivin. In contrast, cytoplasm has been found to be the most probable location of both survivin and survivin-2B^[21,22]. Other unique features in survivin- Δ Ex3 were also identified, including a mitochondrial localization signal and a BH2 domain, which might inhibit apoptosis by association with bcl-2, and suppress Caspase-3 activity by BIR-dependent pathway^[23]. Consequently, survivin- Δ Ex3 may play a more crucial role in the regulation of apoptosis.

Although mRNA levels of survivin-2B and survivin- Δ Ex3 have been found in different tumors^[3,10,24,25], little is known about the protein levels of endogenous survivin-2B and survivin- Δ Ex3, due to the lack of survivin variant-specific antibodies. Our results showed that a low mRNA expression level of survivin-2B was inversely correlated to the advanced (III+IV) stage, undifferentiated tumor histology and deep tumor invasion. There are at least two reasonable explanations for this finding. After losing its antiapoptotic potential, survivin-2B was hypothesized to be a naturally occurring antagonist of survivin from competitive binding to heterologous interaction partners, or from the formation of inactive survivin: survivin-2B heterodimers with respect to recently observed dimer formation of survivin^[21]. Downregulation of survivin-2B might weaken its functional antagonism, and moreover, could permit the generation of more survivin or survivin- Δ Ex3 because three survivin variants come from the same pool of a hnRNA precursor. Thus, the decrease in survivin-2B may result in the development, invasion and anaplasia of carcinomas.

In addition, our data showed that all gastric carcinoma samples expressed wild-type survivin at a significant level compared to the matched normal gastric mucosa samples. Similarly, the expression of survivin-2B or survivin- Δ Ex3 was significantly elevated in carcinoma tissue. Among three survivin variants, survivin was the dominant transcript. In this regard, our results were consistent with those of two recent TR-PCR studies^[10,26] on gastric cancer in which a few gastric mucosa samples (17-23%) of the first-degree relatives also expressed survivin mRNA, but the normal control subjects did not. All these findings may help explain why survivin variants played important roles in the early stage of carcinogenesis of gastric cancer.

In summary, survivin mRNA is a poor prognostic biomarker and that non-antiapoptotic survivin-2B was correlated to tumor stage, histological type and depth of tumor invasion. Even more striking is the observation for the first time that neither survivin nor survivin-2B show a close association with the apoptosis index, as observed in survivin- Δ Ex3, although further experimental work is necessary to elucidate

the functional properties of different splicing variants in more detail.

ACKNOWLEDGEMENTS

We thank Ms. Akiko Miyamoto and Drs. Takaharu Suga and Yoshiaki Tatsumi, Department of General and Gastroenterological Surgery, or Dr. Noda Naohiro, First Department of Pathology, Osaka Medical College for their excellent assistance throughout this investigation.

REFERENCES

- 1 **Rudin CM**, Thompson CB. Apoptosis and disease: regulation and clinical relevance of programmed cell death. *Annu Rev Med* 1997; **48**: 267-281
- 2 **Altieri DC**. Validating survivin as a cancer therapeutic target. *Nat Rev Cancer* 2003; **3**: 46-54
- 3 **Mahotka C**, Wenzel M, Springer E, Gabbert HE, Gerharz CD. Survivin-deltaEx3 and survivin-2B: two novel splice variants of the apoptosis inhibitor survivin with different antiapoptotic properties. *Cancer Res* 1999; **59**: 6097-6102
- 4 **Liu HF**, Liu WW, Fang DC, Men RP. Expression and significance of proapoptotic gene Bax in gastric carcinoma. *World J Gastroenterol* 1999; **5**: 15-17
- 5 **Lu CD**, Altieri DC, Tanigawa N. Expression of a novel antiapoptosis gene, survivin, correlated with tumor cell apoptosis and p53 accumulation in gastric carcinomas. *Cancer Res* 1998; **58**: 1808-1812
- 6 **Nishi M**, Omori Y, Miwa K. Japanese Classification of Gastric Carcinoma, First English edition. TOKYO: KANEHARA & CO., LTD 1995
- 7 **Kawasaki H**, Toyoda M, Shinohara H, Okuda J, Watanabe I, Yamamoto T, Tanaka K, Tenjo T, Tanigawa N. Expression of survivin correlates with apoptosis, proliferation, and angiogenesis during human colorectal tumorigenesis. *Cancer* 2001; **91**: 2026-2032
- 8 **Kawasaki H**, Altieri DC, Lu CD, Toyoda M, Tenjo T, Tanigawa N. Inhibition of apoptosis by survivin predicts shorter survival rates in colorectal cancer. *Cancer Res* 1998; **58**: 5071-5074
- 9 **Mahotka C**, Krieg T, Krieg A, Wenzel M, Suschek CV, Heydthausen M, Gabbert HE, Gerharz CD. Distinct *in vivo* expression patterns of survivin splice variants in renal cell carcinomas. *Int J Cancer* 2002; **100**: 30-36
- 10 **Krieg A**, Mahotka C, Krieg T, Grabsch H, Muller W, Takeno S, Suschek CV, Heydthausen M, Gabbert HE, Gerharz CD. Expression of different survivin variants in gastric carcinomas: first clues to a role of survivin-2B in tumour progression. *Br J Cancer* 2002; **86**: 737-743
- 11 **Asanuma K**, Moriai R, Yajima T, Yagihashi A, Yamada M, Kobayashi D, Watanabe N. Survivin as a radioresistance factor in pancreatic cancer. *Jpn J Cancer Res* 2000; **91**: 1204-1209
- 12 **Ikeguchi M**, Kaibara N. Changes in survivin messenger RNA level during cisplatin treatment in gastric cancer. *Int J Mol Med* 2001; **8**: 661-666
- 13 **Kato J**, Kuwabara Y, Mitani M, Shinoda N, Sato A, Toyama T, Mitsui A, Nishiwaki T, Moriyama S, Kudo J, Fujii Y. Expression of survivin in esophageal cancer: correlation with the prognosis and response to chemotherapy. *Int J Cancer* 2001; **95**: 92-95
- 14 **Azuhata T**, Scott D, Takamizawa S, Wen J, Davidoff A, Fukuzawa M, Sandler A. The inhibitor of apoptosis protein survivin is associated with high-risk behavior of neuroblastoma. *J Pediatr Surg* 2001; **36**: 1785-1791
- 15 **Ikeguchi M**, Kaibara N. Survivin messenger RNA expression is a good prognostic biomarker for oesophageal carcinoma. *Br J Cancer* 2002; **87**: 883-887
- 16 **Adida C**, Berrebi D, Peuchmaur M, Reyes-Mugica M, Altieri DC. Anti-apoptosis gene, survivin, and prognosis of neuroblastoma. *Lancet* 1998; **351**: 882-883
- 17 **Adida C**, Haiou C, Gaulard P, Lepage E, Morel P, Briere J, Dombret H, Reyes F, Diebold J, Gisselbrecht C, Salles G, Altieri DC, Molina TJ. Prognostic significance of survivin

- expression in diffuse large B-cell lymphomas. *Blood* 2000; **96**: 1921-1925
- 18 **Chakravarti A**, Noll E, Black PM, Finkelstein DF, Finkelstein DM, Dyson NJ, Loeffler JS. Quantitatively determined survivin expression levels are of prognostic value in human gliomas. *J Clin Oncol* 2002; **20**: 1063-1068
- 19 **Kamihira S**, Yamada Y, Hirakata Y, Tomonaga M, Sugahara K, Hayashi T, Dateki N, Harasawa H, Nakayama K. Aberrant expression of caspase cascade regulatory genes in adult T-cell leukaemia: survivin is an important determinant for prognosis. *Br J Haematol* 2001; **114**: 63-69
- 20 **Wakana Y**, Kasuya K, Katayanagi S, Tsuchida A, Aoki T, Koyanagi Y, Ishii H, Ebihara Y. Effect of survivin on cell proliferation and apoptosis in gastric cancer. *Oncol Rep* 2002; **9**: 1213-1218
- 21 **Mahotka C**, Liebmann J, Wenzel M, Suschek CV, Schmitt M, Gabbert HE, Gerharz CD. Differential subcellular localization of functionally divergent survivin splice variants. *Cell Death Differ* 2002; **9**: 1334-1342
- 22 **Rodriguez JA**, Span SW, Ferreira CG, Kruyt FA, Giaccone G. CRM1-mediated nuclear export determines the cytoplasmic localization of the antiapoptotic protein Survivin. *Exp Cell Res* 2002; **275**: 44-53
- 23 **Wang HW**, Sharp TV, Koumi A, Koentges G, Boshoff C. Characterization of an anti-apoptotic glycoprotein encoded by Kaposi's sarcoma-associated herpesvirus which resembles a spliced variant of human survivin. *EMBO J* 2002; **21**: 2602-2615
- 24 **Hirohashi Y**, Torigoe T, Maeda A, Nabeta Y, Kamiguchi K, Sato T, Yoda J, Ikeda H, Hirata K, Yamanaka N, Sato N. An HLA-A24-restricted cytotoxic T lymphocyte epitope of a tumor-associated protein, survivin. *Clin Cancer Res* 2002; **8**: 1731-1739
- 25 **Kappler M**, Kohler T, Kampf C, Diestelkötter P, Wurl P, Schmitz M, Bartel F, Lautenschlager C, Rieber EP, Schmidt H, Bache M, Taubert H, Meyer A. Increased survivin transcript levels: an independent negative predictor of survival in soft tissue sarcoma patients. *Int J Cancer* 2001; **95**: 360-363
- 26 **Yu J**, Leung WK, Ebert MP, Ng EK, Go MY, Wang HB, Chung SC, Malfertheiner P, Sung JJ. Increased expression of survivin in gastric cancer patients and in first degree relatives. *Br J Cancer* 2002; **87**: 91-97

Edited by Wang XL Proofread by Xu FM

Detection of bcl-2 and bax expression and bcl-2/JH fusion gene in intrahepatic cholangiocarcinoma

Lin-Lang Guo, Sha Xiao, Ying Guo

Lin-Lang Guo, Sha Xiao, Ying Guo, Department of Pathology, Zhujiang Hospital, Guangzhou 510282, Guangdong Province, China
Correspondence to: Dr. Lin-Lang Guo, Department of Pathology, Zhujiang Hospital, Guangzhou 510282, Guangdong Province, China. linlangg@yahoo.com

Telephone: +86-20-61643495 **Fax:** +86-20-84311872
Received: 2003-05-10 **Accepted:** 2003-06-04

Abstract

AIM: To investigate the relationship between bcl-2 gene and its related protein bax and intrahepatic cholangiocellular carcinoma (CCC).

METHODS: Semi-nested *in situ* PCR (SNISPCR) and immunohistochemistry were performed to detect bcl-2/JH fusion gene and bcl-2, bax protein expression in 29 cases of CCC.

RESULTS: No bcl-2/JH fusion gene was found in all cases of CCC, 72.4% of 29 cases expressed bcl-2 protein. Bcl-2 protein expression was related to histopathological grades ($P < 0.05$). There was no corresponding relationship between bcl-2/JH fusion gene formation and bcl-2 protein expression in CCC ($P < 0.05$). Bax was expressed in 10.3% of 29 cases. The ratio of bcl-2 to bax in normal liver tissues (3.5 to 1) was different from that in tumor tissues (7.0 to 1).

CONCLUSION: It is suggested that bcl-2/JH fusion gene formation is not a frequent event and may not play an important role in the pathogenesis of CCC. However, aberrant ratio of bcl-2 to bax protein expression may be involved in the course of tumorigenesis of CCC. Abnormal bcl-2 protein expression may not be solely resulted from bcl-2/JH fusion gene.

Guo LL, Xiao S, Guo Y. Detection of bcl-2 and bax expression and bcl-2/JH fusion gene in intrahepatic cholangiocarcinoma. *World J Gastroenterol* 2004; 10(22): 3251-3254
<http://www.wjgnet.com/1007-9327/10/3251.asp>

INTRODUCTION

Bcl-2 gene was first identified in B-cell leukemia and follicular lymphoma which conferred a survival advantage on B-cells by inhibiting apoptosis. Bcl-2 gene at chromosome 18 is juxtaposed with the immunoglobulin heavy chain gene (JH) on chromosome 14^[1]. The t(14; 18) chromosome translocation was present in 70% to 85% of follicular lymphoma and in 20% to 30% of diffuse large-cell lymphomas^[1-4]. While aberrant expression of bcl-2 protein was also found in follicular lymphoma. In the early study, bcl-2 gene was mainly investigated in lymphoid tissues. Recently, bcl-2 gene aberrant expression has been observed in a variety of tumors, such as adenocarcinoma of the prostate, bladder carcinoma, squamous cell carcinoma of the lung, nasopharyngeal carcinoma, breast carcinoma and cholangiocarcinoma^[5-17]. However, bcl-2/JH fusion gene and its relationship with bcl-2 protein expression have not been detected in

cholangiocellular carcinoma (CCC).

Bax, an important homologue of bcl-2, is a promoter of apoptosis. It has been proposed that the sensitivity of cells to apoptosis stimuli be closely related to the ratio of bcl-2/bax and other bcl-2 homology. When bcl-2 is in excess, cells are protected. However, when bax is in excess and bax homodimers dominate, cells are susceptible to apoptosis^[18]. Whether bcl-2/bax expression ratio is involved in the course of tumorigenesis of CCC remains unknown.

In this study, we demonstrated that bcl-2/JH fusion gene, bcl-2 and its related protein bax expression with semi-nested *in situ* PCR (SNISPCR) and immunohistochemistry in 29 cases of CCC to understand the relationship between bcl-2 gene and its related protein bax in CCC.

MATERIALS AND METHODS

Tissue preparation

A total of 29 samples were obtained by surgical resection in our department from 1995-06-01 to 1998-02-28. All samples were independently reviewed by two pathologists and graded as recommended by WHO. The cases of CCC were classified as follows: 6 cases of well differentiated, 14 cases of moderately differentiated and 9 cases of poorly differentiated carcinomas. Undamaged liver tissues from surgical resection specimens of young adults with minor liver injury who underwent partial hepatectomy were used as normal controls. All tissues were fixed in 40 g/L formaldehyde (pH 7.0) for 12-24 h and embedded in paraffin and then 4 μ m thick serial sections were cut and mounted on poly-L-lysine coated slides.

Immunohistochemical staining

The sections were deparaffinized and rehydrated routinely. Antigens were retrieved by heating the sections in a microwave oven at 700 W in 10 mmol/L citrate buffer (pH 6.0) for 10 min. After blocked with 3 mL/L H₂O₂ and swine serum, specimens were then incubated with the primary antibodies, directed against bcl-2 (Maxim Biotech Co., China) and bax (Santa Cruz). The staining was performed by streptavidin peroxidase enzyme conjugate method using a S-P kit (Zymed). Reaction products were visualized by DAB. Brown-yellow granules in cytoplasm were recognized as positive staining.

Semi-nested *in situ* PCR

Pretreatment: Sections were deparaffinized and dehydrated routinely, then washed in 0.1 mol/L HCl and PBS, digested with proteinase K (10 mg/L), and placed on the platform in a DNA thermal cycler at 98 °C for 2 min.

Amplification *in situ*: The final volume of 20 μ L (200 μ mol/L each of dATP, dCTP, dGTP and dTTP, 1.5 U Taq polymerase, 10 \times buffer). Two and half sets of primers specific for the two hot breakpoint regions on bcl-2 gene were synthesized according to the DNA sequences published by Gribben^[19]. The following oligonucleotides were used as primer pairs: A, 5'-CAGCCTTGA AACATTGATGG-3' for the mbr (in major breakpoint region); B, 5'-CGTGCTGGTACCACTCTG-3' for the mcr (in minor breakpoint region); C, 5'-TATGGTGGTTTGACCTTTAG-3' for the mbr (in major breakpoint region); D, 5'-GGACCTTCCTTGG

TGTGTTG-3' for mcr (in minor breakpoint region); Immunoglobulin heavy chain (JH), 5'-ACCTGAGGAGACGGTGACC-3'. At first, mbr-JH fusion gene was amplified by primer A and JH, and mcr-JH fusion gene was amplified by primer B and JH. The slides were covered after adding reaction mixture. The samples were subjected to 25 amplification cycles, each cycle consisting of denaturation at 94 °C for 1 min, annealing at 55 °C for 1 min and extension at 72 °C for 1 min. The final extension period was extended to 10 min. Reamplification was performed for 30 cycles using primer C, JH for mbr-JH fusion gene and D, JH for mcr-JH fusion gene. The conditions were the same as stated above.

In situ hybridization

The covers were removed and dehydrated routinely. The slides were incubated in 40 g/L poly formaldehyde for 10 min. Forty μ L hybridization solution (probe concentration 50 pmol/L) was added on slides overnight at 37 °C in a wet box. The oligonucleotide probe was labeled with biotin. Sequences of the probes were 5'-CCCTCCTGCCCTCCTCCG-3' for mcr and 5'-GGACCTTCCTTGGTGTGTTG-3' for mcr.

Non-specific antigen was blocked with 20 mL/L bovine serum and 3 g/L Triton X-100, followed by incubation with anti-biotin antibody alkaline phosphates mixture for 1 h. Slides were then visualized with BCIP/NBT. Purple-blue granules in nuclei were regarded as positive.

Controls

Follicular lymphoma was used as positive control. Negative controls included blank control with no primers, dNTP or Taq polymerase omission in PCR reaction solution, and probe omission in hybridization solution. To exclude false positive or negative results, each sample was analyzed at least twice. Non-corresponding tissues such as normal skin tissue were also treated to exclude the false positive possibility.

Statistical analysis

Statistical significance was calculated by χ^2 test, which was used to analyze the relation between bcl-2 and bax protein staining and positive bcl-2/JH fusion gene and histopathological grades. $P < 0.05$ was considered as statistically significant.

RESULTS

Expression of bcl-2 protein in CCC

Twenty-one of 29 cases expressed bcl-2 protein, including 5 well differentiated, 13 moderately differentiated and 3 poorly differentiated carcinomas. There was a statistically significant difference between moderately differentiated and poorly differentiated carcinomas in Bcl-2 expression ($P < 0.05$, $\chi^2 = 5.58$). Bcl-2 was also expressed in 87.5% (14/16) in normal liver tissues of small bile ducts (Figures 1, 3).

Detection of bcl-2/JH fusion gene in CCC

Bcl-2/JH fusion gene was not detected in any case of CCC and normal liver tissues.

Relationship between bcl-2 protein expression and bcl-2/JH fusion gene

No bcl-2/JH fusion gene was detected in bcl-2 protein positive and negative groups. There was no correlation between bcl-2 protein expression and bcl-2/JH fusion gene.

Expression of bax protein in CCC

Bax was expressed in 3 (10.3%) of 29 cases, in which 1/6 was well differentiated carcinoma, 2/14 were moderately differentiated carcinomas and none was poorly differentiated carcinoma. There was no statistically significant difference between bax expression

and histological grades. Four (25%) of 16 normal liver tissue samples expressed bax protein (Figures 2, 4).



Figure 1 Primary hepatic cholangiocarcinoma. Brown-yellow staining in cytoplasm of carcinoma cells for bcl-2 protein (arrowhead) Immunohistochemistry staining $\times 200$.



Figure 2 Primary hepatic cholangiocarcinoma. Brown-yellow staining in cytoplasm of carcinoma cells for bax protein (arrowhead) Immunohistochemistry staining $\times 200$.



Figure 3 Normal liver. Brown-yellow staining in cytoplasm of small bile duct epithelial cells for bcl-2 protein (arrowhead) Immunohistochemistry staining $\times 200$.

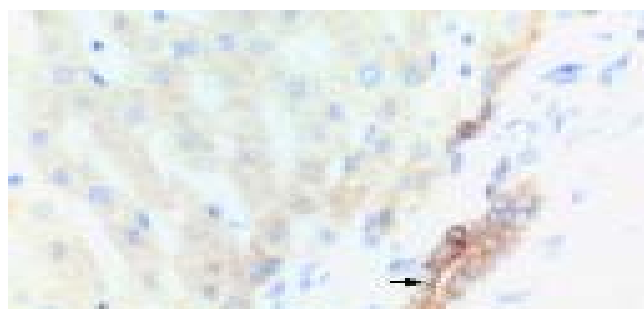


Figure 4 Normal liver. Brown-yellow staining in cytoplasm of small bile duct epithelial cells for bax protein (arrowhead) Immunohistochemistry staining $\times 200$.

Ratio of bcl-2 to bax in normal liver and CCC

In normal liver tissues, the expression rates of bcl-2 and bax

were 87.5% and 25%, while positive rates of bcl-2 and bax were 72.4% and 10.3% in CCC respectively. The ratio of bcl-2 to bax was 3.5 to 1 in normal liver tissues and 7.0 to 1 in CCC (Figure 5).



Figure 5 Non-Hodgkin's lymphoma. Purple-blue deposition in nuclear of lymphoma cells (positive for mbr, arrowhead). In situ PCR $\times 400$.

DISCUSSION

Varying results of bcl-2 protein expression in CCC were reported. Bcl-2 protein expression in normal and pathological human liver has been reported by Charlotte *et al.*^[11]. In the report, Charlotte *et al.* described that bcl-2 protein was expressed by small bile duct epithelia in normal liver, but not by hepatocytes or large bile duct epithelia. Eight of 11 CCCs were stained positively for bcl-2, whereas all 15 hepatocellular carcinomas were bcl-2 negative. So the authors suggested that bcl-2 protein appeared to be a diagnostic marker in distinguishing CCC from hepatocellular carcinoma^[11]. Skopelitou *et al.* found all ten samples of CCC were positive for bcl-2 protein staining^[12]. Ito *et al.* reported 31.7% (13/41) of CCCs were positive for bcl-2 protein^[13]. However, Terada *et al.* showed low or negative expression of bcl-2 protein in bile duct epithelia and CCC^[14-17]. In our report, 21 of 29 CCCs expressed bcl-2 protein (72.4%), which was similar to that reported by Charlotte *et al.* Significant differences of bcl-2 expression in CCC have not been known yet, probably because of the different methods used, and the difference of intrahepatic cholangiocarcinoma specimens from the liver^[13,16].

To clarify the role of bcl-2/JH in the pathogenesis of CCC, mbr-JH and mcr-JH which have been shown to be the important molecular event in the genesis of follicular lymphoma, were also studied in 29 cases of CCC. This is the first study to examine bcl-2/JH fusion gene in CCC by *in situ* PCR. Mbr-JH or mcr-JH was negative in all cases of CCC. It is suggested that bcl-2/JH fusion gene formation was not a common event and might not play an important role in the pathogenesis of CCC.

In the present study, bcl-2 protein expression did not correlate with bcl-2/JH in CCC. Similar results were also found in mucosa-associated lymphoma, large cell lymphoma, Hodgkin's disease and nasopharyngeal carcinoma^[20-25]. These findings suggested that abnormal bcl-2 protein expression might not be solely resulted from bcl-2/JH fusion sequences. Whether other types of bcl-2 gene aberrance such as mutation or methylation corresponding to bcl-2 protein expression are existed in CCC requires further investigation.

Compared to a high expression rate of bcl-2 in CCC (72.4%), only 10.3% (3/29) samples expressed bax. To understand the significance of the ratio of bcl-2 to bax in the regulation of apoptosis, Oltvai *et al.*^[18] found that over-expressed bcl-2 in two cell lines with high levels of bax and in cells with the lowest bcl-2 to bax ratio (0.55) was 73% viable at 24 h, but lost viability by d 7. When cells with high bcl-2 to bax ratios (2.04 and 1.65), they possessed viable cells over 2 wk following IL-3 deprivation. These data suggested a model in which the ratio of bcl-2 to bax could determine survival or death following an apoptotic stimulus. Similar results were also found by Lilling *et al.* and others^[26-29].

The alteration of Bcl-2 and Bax might be an important mechanism in the pathogenesis and progression of some tumors^[30-32]. Yue *et al.*^[30] showed that Bcl-2/Bax in acute myelogenous leukemia was significantly higher than that in normal control ($P < 0.001$). Madewell *et al.*^[31] found that the bax:bcl-2 ratio was lower in skin tumors than that in normal skin. But a lowered bcl-2/bax ratio and increased apoptosis were observed in oral squamous cell carcinomas, compared with normal oral epithelium^[32]. In this study, the ratio of bcl-2 to bax (7.0 to 1) in CCC was different from that in normal small bile ducts (3.5 to 1). We suppose that the changes of the ratio between bcl-2 and bax protein may influence the susceptibility of bile duct cells to apoptosis and would be involved in the tumorigenesis of CCC. Further evidence would be obtained from further investigations.

REFERENCES

- 1 Tsujimoto Y, Finger LR, Yunis J, Nowell PC, Croce CM. Cloning of the chromosome breakpoint of neoplastic B cells with the t (14; 18) chromosome translocation. *Science* 1984; **226**: 1097-1099
- 2 Weiss LM, Warnke RA, Sklar J, Cleary ML. Molecular analysis of the t (14; 18) chromosomal translocation in malignant lymphomas. *N Engl J Med* 1987; **317**: 1185-1189
- 3 Bskhshi A, Jensen JP, Goldman P, Wright JJ, McBride OW, Epstein AL, Korsmeyer SJ. Cloning the chromosomal breakpoint of t (14; 18) human lymphomas: clustering around JH on chromosome 14 and near a transcriptional unit on 18. *Cell* 1985; **41**: 899-906
- 4 Aisenberg AC, Wilkes BM, Jacobson JO. The bcl-2 gene is rearranged in many diffuse B-cell lymphomas. *Blood* 1988; **71**: 969-972
- 5 McDonnell TJ, Troncoso P, Brisbay SM, Logothetis C, Chung LW, Hsieh JT, Tu SM, Campbell ML. Expression of the protooncogene bcl-2 in the prostate and its association with emergence of androgen-independent prostate cancer. *Cancer Res* 1992; **52**: 6940-6944
- 6 Nakopoulou L, Vourlakou C, Zervas A, Tzonou A, Gakiopoulou H, Dimopoulos MA. The prevalence of bcl-2, p53, and Ki-67 immunoreactivity in transitional cell bladder carcinomas and their clinicopathologic correlates. *Hum Pathol* 1998; **29**: 146-154
- 7 Lu QL, Elia G, Lucas S, Thomas JA. Bcl-2 proto-oncogene expression in Epstein-Barr-virus-associated nasopharyngeal carcinoma. *Int J Cancer* 1993; **53**: 29-35
- 8 Pezzella F, Turley H, Kuzu I, Tungekar MF, Dunnill MS, Pierce CB, Harris A, Gatter KC, Mason DY. Bcl-2 protein in non-small-cell lung carcinoma. *N Engl J Med* 1993; **329**: 690-694
- 9 Papadimitriou CS, Costopoulos JS, Christoforidou BP, Kotsianti AJ, Karkavelas GS, Hytiroglou PM, Koufogiannis DJ, Nenopoulou HE. Expression of Bcl-2 protein in human primary breast carcinomas and its correlation with multifocality, histopathological types and prognosis. *Eur J Cancer* 1997; **33**: 1275-1280
- 10 Tjalma W, De Cuyper E, Weyler J, Van Marck E, De Pooter C, Albertyn G, van Dam P. Expression of bcl-2 in invasive and in situ carcinoma of the uterine cervix. *Am J Obstet Gynecol* 1998; **178**(1 Pt 1): 113-117
- 11 Charlotte F, L'Hermine A, Martin N, Geleyn Y, Nollet M, Gaulard P, Zafrani ES. Immunohistochemical detection of bcl-2 and protein in normal and pathological human liver. *Am J Pathol* 1994; **144**: 460-465
- 12 Skopelitou A, Hadjiyannakis M, Alexopoulou V, Krikoni O, Kamina S, Agnantis N. Topographical immunohistochemical expression of bcl-2 protein in human liver lesions. *Anticancer Res* 1996; **16**: 975-978
- 13 Ito Y, Takeda T, Sasaki Y, Sakon M, Monden M, Yamada T, Ishiguro S, Imaoka S, Tsujimoto M, Matsuura N. Bcl-2 expression in cholangiocellular carcinoma is inversely correlated with biologically aggressive phenotypes. *Oncology* 2000; **59**: 63-67
- 14 Terada T, Nakanuma Y. Utility of pancreatic digestive enzyme immunohistochemistry in the differential diagnosis of hepatocellular carcinoma, cholangiocarcinoma and metastatic adenocarcinoma of the liver. *Pathol Int* 1996; **46**: 183-188
- 15 Okaro AC, Deery AR, Hutchins RR, Davidson BR. The expres-

- sion of antiapoptotic proteins Bcl-2, Bcl-X(L), and Mcl-1 in benign, dysplastic, and malignant biliary epithelium. *J Clin Pathol* 2001; **54**: 927-932
- 16 **Arora DS**, Ramsdale J, Lodge JP, Wyatt JJ. p53 but not bcl-2 is expressed by most cholangiocarcinomas: a study of 28 cases. *Histopathology* 1999; **34**: 497-501
- 17 **Fiorentino M**, D'Errico A, Altimari A, Barozzi C, Grigioni WF. High levels of BCL-2 messenger RNA detected by *in situ* hybridization in human hepatocellular and cholangiocellular carcinomas. *Diagn Mol Pathol* 1999; **8**: 189-194
- 18 **Oltvai ZN**, Milliman CL, Korsmeyer SJ. Bcl-2 heterodimerizes *in vivo* with a conserved homolog, Bax, that accelerates programmed cell death. *Cell* 1993; **74**: 609-619
- 19 **Gribben JG**, Freedman A, Woo SD, Blake K, Shu RS, Freeman G, Longtine JA, Pinkus GS, Nadler LM. All advanced stage non-Hodgkin's lymphomas with a polymerase chain reaction amplifiable breakpoint of bcl-2 have residual cells containing the bcl-2 rearrangement at evaluation and after treatment. *Blood* 1991; **78**: 3275-3280
- 20 **Tang SC**, Visser L, Hepperle B, Hanson J, Poppema S. Clinical significance of bcl-2-MBR gene rearrangement and protein expression in diffuse large-cell non-Hodgkin's lymphoma: an analysis of 83 cases. *J Clin Oncol* 1994; **12**: 149-154
- 21 **Isaacson PG**, Wotherspoon AC, Diss TC, Pan LX. Bcl-2 expression in lymphomas. *Lancet* 1991; **337**: 175-176
- 22 **Huebner-Chan D**, Fernandes B, Yang G, Lim MS. An immunophenotypic and molecular study of primary large B-cell lymphoma of bone. *Mod Pathol* 2001; **14**: 1000-1007
- 23 **Kneba M**, Eick S, Herbst H, Pott C, Bolz I, Dallenbach F, Hiddemann W, Stein H. Low incidence of mbr bcl-2/JH fusion genes in Hodgkin's disease. *J Pathol* 1995; **175**: 381-389
- 24 **Nolte M**, Werner M, Spann W, Schnabel B, von Wasielewski R, Wilkens L, Hubner K, Fischer R, Georgii A. The bcl-2/JH gene rearrangement is undetectable in Hodgkin's lymphomas: results from the German Hodgkin trial. *Virchows Arch* 1995; **426**: 37-41
- 25 **Harn HJ**, HO LI, Liu CA, Liu GC, Lin FG, Lin JJ, Chang JY, Lee WH. Down regulation of bcl-2 by p53 in nasopharyngeal carcinoma and lack of detection of its specific t(14; 18) chromosomal translocation in fixed tissues. *Histopathology* 1996; **28**: 317-323
- 26 **Lilling G**, Hacoheh H, Nordenberg J, Livnat T, Rotter V, Sidi Y. Differential sensitivity of MCF-7 and LCC2 cells, to multiple growth inhibitory agents: possible relation to high bcl-2/bax ratio? *Cancer Lett* 2000; **161**: 27-34
- 27 **Chresta CM**, Masters JR, Hickman JA. Hypersensitivity of human testicular tumors to etoposide-induced apoptosis is associated with functional p53 and a high Bax: Bcl-2 ratio. *Cancer Res* 1996; **56**: 1834-1841
- 28 **Perlman H**, Zhang X, Chen MW, Walsh K, Buttyan R. An elevated bax/bcl-2 ratio corresponds with the onset of prostate epithelial cell apoptosis. *Cell Death Differ* 1999; **6**: 48-54
- 29 **Raisova M**, Hossini AM, Eberle J, Riebeling C, Wieder T, Sturm I, Daniel PT, Orfanos CE, Geilen CC. The Bax/Bcl-2 ratio determines the susceptibility of human melanoma cells to CD95/fas-mediated apoptosis. *J Invest Dermatol* 2001; **117**: 333-340
- 30 **Yue B**, Chen Y, Yu D, Xiang Z. Study on the relationship between the Bcl-2/Bax ratio and the growth types of leukemic cells and drug resistance in acute myelogenous leukemia. *J Tongji Med Univ* 1998; **18**: 101-104
- 31 **Madewell BR**, Gandour-Edwards R, Edwards BF, Matthews KR, Griffey SM. Bax/bcl-2: cellular modulator of apoptosis in feline skin and basal cell tumours. *J Comp Pathol* 2001; **124**: 115-121
- 32 **Loro LL**, Vintermyr OK, Liavaag PG, Jonsson R, Johannessen AC. Oral squamous cell carcinoma is associated with decreased bcl-2/bax expression ratio and increased apoptosis. *Hum Pathol* 1999; **30**: 1097-1105

Edited by Zhang JZ and Wang XL Proofread by Xu FM

Nuclear factor- κ B p65 (RelA) transcription factor is constitutively activated in human colorectal carcinoma tissue

Liang-Liang Yu, Hong-Gang Yu, Jie-Ping Yu, He-Sheng Luo, Xi-Ming Xu, Jun-Hua Li

Liang-Liang Yu, Jie-Ping Yu, He-Sheng Luo, Xi-Ming Xu, Jun-Hua Li, Department of Gastroenterology, Renmin Hospital, Wuhan University, Wuhan 430060, Hubei Province, China

Hong-Gang Yu, Laboratory for Experimental Gastroenterology, Department of Medicine I, St. Joseph Hospital, Ruhr-University Bochum, Bochum, Germany

Supported by Grants from National Natural Science Foundation of China No.39470330, and Natural Science Foundation of Hubei Province, China (SJ-97J083)

Correspondence to: Dr. Liang-Liang Yu, Department of Gastroenterology, Renmin Hospital, Wuhan University, Wuhan 430060, Hubei Province, China. yuliangliang@sina.com

Telephone: +86-27-88077184

Received: 2003-11-12 **Accepted:** 2003-12-16

Abstract

AIM: Activation of transcription factor nuclear factor- κ B (NF- κ B) has been shown to play a role in cell proliferation, apoptosis, cytokine production, and oncogenesis. The purpose of this study was to determine whether NF- κ B was constitutively activated in human colorectal tumor tissues and, if so, to determine the role of NF- κ B in colorectal tumorigenesis, and furthermore, to determine the association of RelA expression with tumor cell apoptosis and the expression of Bcl-2 and Bcl- x_L .

METHODS: Paraffin sections of normal epithelial, adenomatous and adenocarcinoma tissues were analysed immunohistochemically for expression of RelA, Bcl-2 and Bcl- x_L proteins. Electrophoretic mobility shift assay (EMSA) was used to confirm the increased nuclear translocation of RelA in colorectal tumor tissues. The mRNA expressions of Bcl-2 and Bcl- x_L were determined by reverse transcription polymerase chain reaction (RT-PCR) analysis. Apoptotic cells were detected by terminal deoxynucleotidyl transferase-mediated deoxyuridine triphosphate fluorescence nick end labeling (TUNEL) method.

RESULTS: The activity of NF- κ B was significantly higher in adenocarcinoma tissue in comparison with that in adenomatous and normal epithelial tissues. The apoptotic index (AI) significantly decreased in the transition from adenoma to adenocarcinoma. Meanwhile, the expressions of Bcl-2 and Bcl- x_L protein and their mRNAs were significantly higher in adenocarcinoma tissues than that in adenomatous and normal epithelial tissues.

CONCLUSION: NF- κ B may inhibit apoptosis via enhancing the expression of the apoptosis genes Bcl-2 and Bcl- x_L . And the increased expression of RelA/nuclear factor- κ B plays an important role in the pathogenesis of colorectal carcinoma.

Yu LL, Yu HG, Yu JP, Luo HS, Xu XM, Li JH. Nuclear factor- κ B p65 (RelA) transcription factor is constitutively activated in human colorectal carcinoma tissue. *World J Gastroenterol* 2004; 10(22): 3255-3260

<http://www.wjgnet.com/1007-9327/10/3255.asp>

INTRODUCTION

Rel/NF- κ B is a family of dimeric transcription factors that control the expression of numerous genes involved in cell growth, differentiation, regulation of apoptosis, cytokine production, and neoplastic transformation^[1,2]. The Rel/NF- κ B family comprises NF- κ B1 (p50), NF- κ B2 (p52), and the Rel proteins, RelA (p65), RelB, and c-Rel, which have a high level of sequence homology within their NH₂-terminal 300 amino acids, the Rel homology domain^[3]. The p50 and p52 can interact with the RelA proteins to form all possible homo- and heterodimer combinations. The most common dimer is the RelA (p65)/NF- κ B1 (p50) heterodimer, i.e., NF- κ B. In most unstimulated cells, Rel/NF- κ B proteins are sequestered in the cytoplasm and are complexed with specific inhibitor proteins called I κ B that render the Rel/NF- κ B proteins inactive^[3]. Stimulation of cells leads to phosphorylation and degradation of I κ B and allows translocation of Rel/NF- κ B to the nucleus, resulting in expression of target genes^[4]. A surprising variety of inducers have been found to activate Rel/NF- κ B^[3]. These pathways are involved in innate immune responses that involve cytokines such as tumor necrosis factor (TNF) - α and IL-1, responses to physical stresses such as UV light and ionizing radiation (χ and γ), and responses to oxidative stresses such as hydrogen peroxide and butyl peroxide^[5].

Several investigators have reported constitutive activation of NF- κ B in various types of human tumor cell lines, including those of lymphoid origin such as Hodgkin/Reed Sternberg cells^[6], T-cell lymphoma Hut 78 cells^[7], and multiple myeloma cells^[8]. In addition, nonlymphoid cell lines including ovarian cancer cells^[9], lung carcinoma cells^[10], breast cancer cells^[11], thyroid carcinoma cells^[12], melanomas^[13], and bladder cancer cells^[14] exhibited enhanced NF- κ B activity.

Recent studies also indicated that NF- κ B was constitutively activated in tumors such as pancreatic cancer and breast cancer^[15,16]. However, little information is available concerning NF- κ B activation in colorectal carcinoma, which is one of the most aggressive forms of cancer. The major objective of this study was to determine whether NF- κ B was constitutively activated in colorectal carcinoma tissues, to examine whether the expression of Bcl-2 and Bcl- x_L was regulated by NF- κ B activation, and to evaluate the correlation between NF- κ B activity and apoptosis in colorectal carcinoma.

MATERIALS AND METHODS

Materials

Ten normal colorectal mucosa, thirty colorectal adenoma (average age of the patients: 56.8 years), and thirty colorectal carcinoma (average age of the patients: 58 years) patients who gave informed consent before surgical treatment were entered into the present study. Specimens were obtained from the Department of Pathology, Renmin Hospital, Wuhan University (Wuhan, China). The patients had received neither chemotherapy nor radiation therapy before tumor resection. To justify comparisons, we excluded lesions from patients with familial colon carcinoma syndrome and suspected de novo cancers. Tissues were fixed with 40 g/L formaldehyde and embedded in paraffin for H & E staining and

immunohistochemistry. Tissue specimens were snap-frozen immediately in liquid N₂ and stored at -80 °C for EMSA assays and RT-PCR analysis. The study was approved by the Institutional Board of the Ethics Committee of Wuhan University under full consideration of the declaration on human rights of Helsinki.

Immunohistochemistry

Formalin-fixed, paraffin-embedded tissue blocks were cut into 5 µm thick and mounted onto glass slides. After that, they were kept in an oven at 4 °C overnight. Immunostaining was performed as previously described with a slight modification^[17]. Sections were deparaffinized in xylene and rehydrated. Endogenous peroxidase activity was blocked with 1% hydrogen peroxide for 20 min. To improve the quality of staining, microwave oven-based antigen retrieval was performed. Slides were probed with either anti-RelA (1:50, mouse monoclonal, Santa Cruz Biotechnology), anti-Bcl-2 (1:100, mouse monoclonal, Santa Cruz Biotechnology) or anti-Bcl-x_L (1:100, mouse monoclonal, Santa Cruz Biotechnology). Sections were washed three times with PBS for 10 min each and incubated with biotin-labeled anti-mouse IgG for 1 h at room temperature. After three washes with PBS for 10 min each, sections were stained with a streptavidin-peroxidase detection system. Incubation with PBS instead of the primary antibody served as a negative control. In specimens containing positive cells, the positive cells were counted in ten randomly selected fields under high power microscope (200-fold or 400-fold magnification) for each sample, and the average was expressed as the density of positive cells.

Determination of apoptosis

The TUNEL assay, originally described by Gavrieli *et al.*^[18], was used with minor modifications. Briefly, tissue sections of 5 µm were mounted onto glass slides, deparaffinized, hydrated, and treated for 15-30 min at 37 °C with proteinase-K (Roche Co.; 20 µg/mL in 10 mmol/L Tris-HCl buffer, pH 7.4). Slides were rinsed twice with PBS. Then, 50 µL of TUNEL reaction mixture (450 µL nucleotide mixture containing fluoresceinated dUTP in reaction buffer plus 50 µL enzyme TdT from calf thymus, Roche Co.) were added to the samples. To ensure homogeneous distribution of the TUNEL reaction mixture on tissue sections and to avoid evaporative loss, slides were covered with coverslips during incubation. Slides were incubated in a humidified chamber for 60 min at 37 °C. After rinsed, slides were incubated with anti-fluorescein antibody, with Fab fragment from sheep, conjugated with horse-radish peroxidase for 30 min at 37 °C. Slides were rinsed twice with PBS. Then, 50-100 µL of DAB substrate was added and incubated for 10 min at room temperature. Samples can be counterstained prior to analysis by light microscope. Positive signals were defined as presence of a distinct brown color nuclear staining of the neoplastic cells or morphologically defined apoptotic bodies. The apoptotic index (AI) was determined by counting a total of at least 1 000 neoplastic nuclei in 10 randomly chosen fields at 400-fold magnification. Apoptotic cells were identified using a TUNEL assay in conjunction with characteristic morphological changes such as cell shrinkage, membrane blebbing, and chromatin condensation, to distinguish apoptotic cells and apoptotic bodies from necrotic cells.

EMSA

Nuclear extracts were harvested according to protocols described previously.^[19] In brief, fresh samples were minced and homogenized in 400 µL of hypotonic lysis buffer A (10 mmol/L HEPES pH 7.9, 10 mmol/L KCl, 0.1 mmol/L EDTA, 0.1 mmol/L EGTA, 1 mmol/L DTT, and 1 mmol/L PMSF). Homogenized tissues were incubated on ice for 5 min, NP-40 was added to a

final concentration of 5 g/L, and samples were vigorously mixed and centrifuged. The cytoplasmic proteins were removed and the pellet nuclei were resuspended in 50 µL buffer C (20 mmol/L HEPES pH 7.9, 0.4 mol/L NaCl, 1 mmol/L EDTA, 1 mmol/L EGTA, 1 mmol/L DTT, and 1 mmol/L PMSF). After 30 min agitation at 4 °C, the samples were centrifuged and supernatants, containing nuclear proteins, were transferred to a fresh vial. The protein concentrations of nuclear extracts were determined by Bio-Rad protein assay. The nuclear extracts were stored at -80 °C until use. Nuclear protein extracts of carcinomas, adenomas, and normal tissues were analyzed by EMSA for NF-κB nuclear translocation as previously described^[20-22]. EMSA binding reaction mixture contained 8 µg protein of nuclear extracts, 2 µg of poly (deoxyinosinic- deoxycytidylic acid) (Sigma Co.), and [³²P]-labeled double-stranded oligonucleotide containing the binding motif of NF-κB probe (4 000 cpm) in binding buffer (10 mmol/L HEPES pH 7.9, 50 mmol/L NaCl, 1 mmol/L EDTA, 1 mmol/L DTT, 100 mL/L glycerol, and 0.2 g/L albumin). The sequence of the double-stranded oligomer used for EMSA was 5'-AGTTGAGGGGACTTTCCCAGGC-3'. The reaction was incubated for 30 min at room temperature before separation on a 50 g/L acrylamide gel, followed by autoradiography. For supershift experiments, 2 µg of mouse monoclonal antibodies against the p65 subunit (Santa Cruz Biotechnology) of NF-κB was incubated with the nuclear extracts 10 min before the addition of the [³²P]-labeled probe and then analyzed as described.

RT-PCR

The mRNA expressions of Bcl-2 and Bcl-x_L were assessed using RT-PCR standardized by coamplifying housekeeping gene β-actin, which served as an internal control. Total RNA was isolated from the normal epithelial, adenomatous and adenocarcinoma tissues by the single-step method^[23]. Total RNA was reversely transcribed into cDNA and used for PCR with human specific primers for Bcl-2, Bcl-x_L and β-actin. Sequences of Bcl-2 primers were 5'-CAGTGCACCTGACGCCCTT-3' (forward primer) and 5'-GCCTCCGTTATCCTGGATCC-3' (reverse primer), generating a 199 bp PCR product; for Bcl-x_L, the forward primer was 5'-AAGGATACAGCTGGAGTCAG-3' and the reverse primer was 5'-ATCAATGGCAACCCATCCTG-3', generating a 316 bp PCR product; for β-actin, the forward primer was 5'-AGCGGAAATCGTGCGTGAC-3' and the reverse primer was 5'-ACTCCTGCTTGCTGATCCACATC-3', producing a 471 bp PCR product^[24,25]. Briefly, the PCR was amplified by 32 repeat denaturation cycles at 95 °C for 30 s, annealing at 60 °C for 30 s, and extension at 72 °C for 30 s. During the first cycle, the denaturation was extended to 2 min, and in the final cycle the extension step was extended to 5 min. PCR products were separated on 15 g/L agarose gels containing 0.5 g/L of ethidium bromide and visualized by UV transillumination.

Statistical analysis

All statistical analyses were performed with SPSS10.0 statistical package for Microsoft Windows. Student's *t* test and one-way analysis of variance (ANOVA) were used to compare continuous variables among groups. Correlation coefficients between continuous variables were calculated by the method of Pearson's correlation coefficient. The χ² test was used to compare binomial proportions. A *P* value of <0.05 was considered significant.

RESULTS

RelA/NF-κB expression in colorectal carcinoma tissues

To investigate whether RelA/NF-κB-DNA binding activities were altered in human colorectal carcinoma tissues, we first carried out immunohistochemical analyses. The monoclonal antibodies used in this study detected only activated RelA

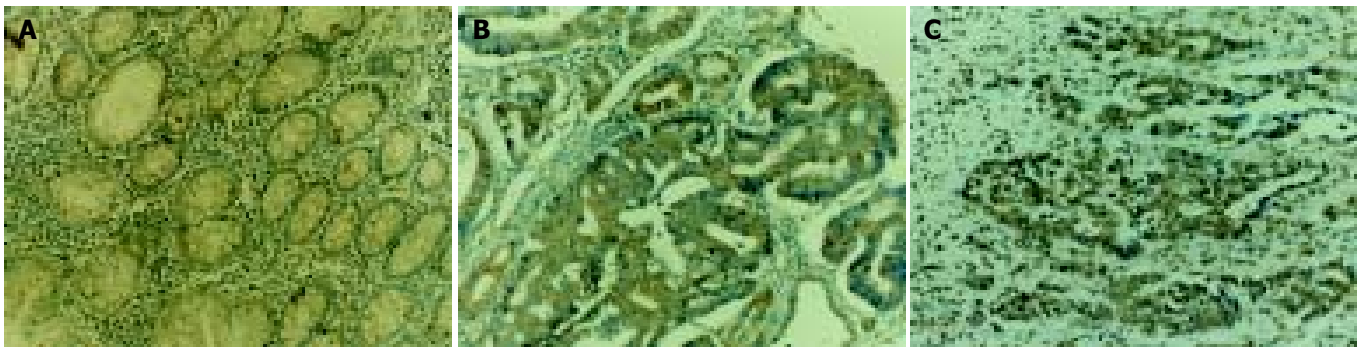


Figure 1 Immunohistochemical staining of RelA in tissue sections of colorectal adenoma (A) and adenocarcinoma (B, C). RelA protein is mainly expressed in the cytoplasm of tumor cells and nuclear accumulation of RelA is also detected. $\times 200$.

proteins^[17]. RelA staining was shown as brown color and detected in normal colorectal mucosa, colorectal adenoma and colorectal adenocarcinoma specimens. In colorectal adenoma and adenocarcinoma, positive staining of RelA was mainly observed in the cytoplasm, and nuclear staining for RelA was also detected (Figure 1). Tissues of colorectal adenocarcinoma showed more cells with nuclear staining for RelA than those in colorectal adenoma tissues. No nuclear staining for RelA was found in normal colorectal mucosa. As shown in Table 1, the density of RelA-positive cells was significantly increased ($P < 0.01$) in the transition from normal mucosa to adenoma and adenocarcinoma.

EMSA

To confirm the finding that RelA/NF- κ B-DNA binding activities were activated in human colorectal carcinoma tissues, we carried out EMSA analyses. Figure 2 shows increased NF- κ B DNA binding activity in adenocarcinoma tissues compared with that in adenoma and normal tissues. HPIAS-1000 SOFTWARE ANALYSIS took the image of electrophoresis. The absorbance of EMSA bands showed that the RelA/NF- κ B complexes were not presented in normal colorectal epithelium, 0.6587 ± 0.0021 in adenocarcinoma, and 0.2153 ± 0.0013 in adenoma. The RelA expressions were significantly increased ($P < 0.05$) in the transition from normal colorectal epithelium to colon tumor tissues. To confirm the specificity of NF- κ B DNA binding, we performed supershift analysis with antibodies specific for RelA (p65) and a competitive study with a 50-fold excess of unlabeled oligonucleotide. An antibody specific for RelA which recognizes RelA/NF- κ B heterodimer, unlabeled oligonucleotide diminished the intensity of RelA/NF- κ B complexes, indicating that complex was the NF- κ B binding-specific band. Our results showed that RelA was frequently activated in human colorectal tumor tissues but not in normal colon tissue.

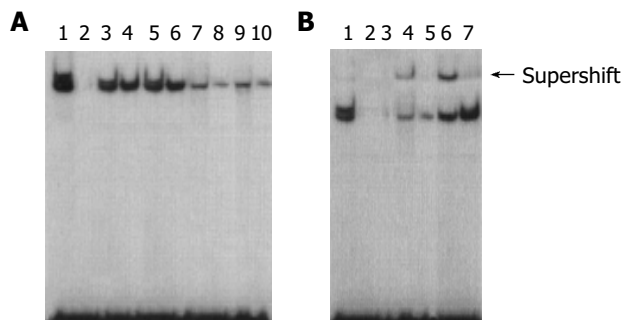


Figure 2 Electrophoretic mobility shift assay demonstrating increased nuclear translocation and DNA binding of NF- κ B. A: lane 1, positive control (using HeLa nuclear extract); lane 2, normal; lanes 3-6, adenocarcinoma; lanes 7-10, adenoma. B: lane 1, positive control (using HeLa nuclear extract); lanes 2-3, specific competitor (using excess of unlabeled oligonucleotide);

lanes 4-5, adenoma; lanes 6-7, adenocarcinoma; lane 4 and 6, supershift (addition of p65 antibodies to the nuclear extracts).

Bcl-2 and Bcl-x_L protein expression in colorectal carcinoma tissues

In the present study, the expressions of Bcl-2 and Bcl-x_L were also investigated using immunohistochemistry. Immunostaining specific for Bcl-2 and Bcl-x_L was cytoplasmic and shown as brown color (Figures 3, 4). The expressions of Bcl-2 and Bcl-x_L were significantly increased ($P < 0.01$) from normal mucosa to tumor tissue (Table 1). Expressions of Bcl-2 and Bcl-x_L were both significantly associated ($r = 0.95, 0.88$; $P < 0.05$) with RelA expression in adenoma and adenocarcinoma.

Table 1 Changes in expression of RelA, Bcl-2, Bcl-x_L and AI in transition from normal mucosa to tumor tissues

Group	n	RelA	Bcl-2	Bcl-x _L	AI
Normal	10	9.31 ± 0.56	15.62 ± 0.75	11.35 ± 0.71	13.09 ± 0.78
Adenoma	30	54.01 ± 4.53	55.64 ± 6.51	56.43 ± 6.14	105.91 ± 6.11
Adenocarcinoma	30	70.92 ± 7.23	78.23 ± 8.33	77.32 ± 6.51	31.53 ± 3.71

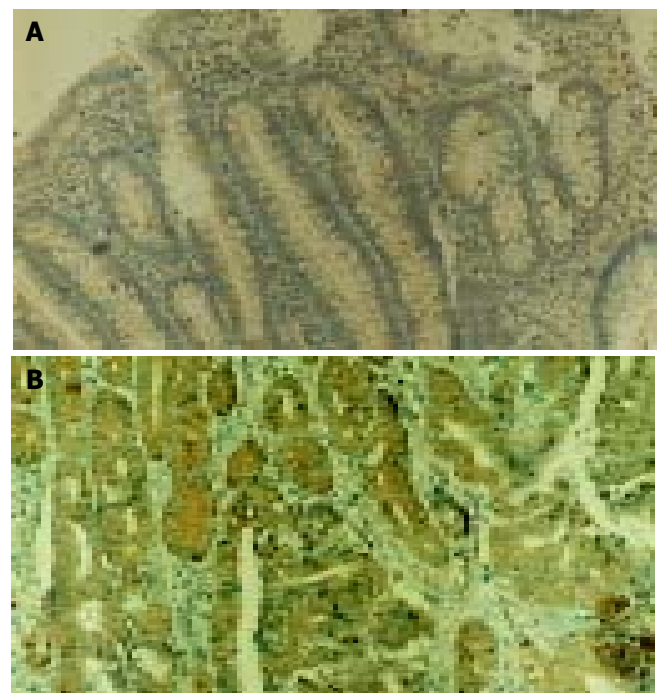


Figure 3 Immunohistochemical staining of Bcl-2 in tissue sections of colorectal adenoma (A) and adenocarcinoma (B). Bcl-2 expression is restricted to the cytoplasm of cancer cells. $\times 200$.

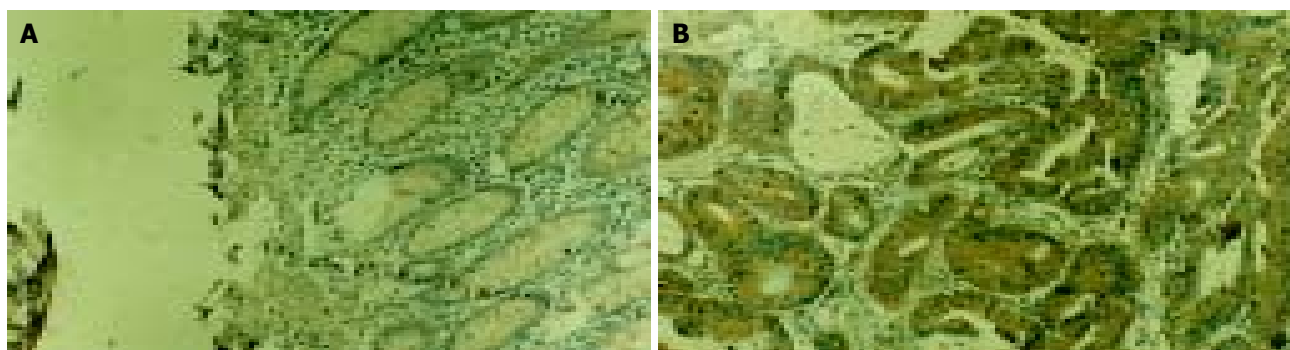


Figure 4 Immunohistochemical staining of Bcl-x_L in tissue sections of colorectal adenoma (A) and adenocarcinoma (B). Bcl-x_L expression is restricted to the cytoplasm of cancer cells. ×200.

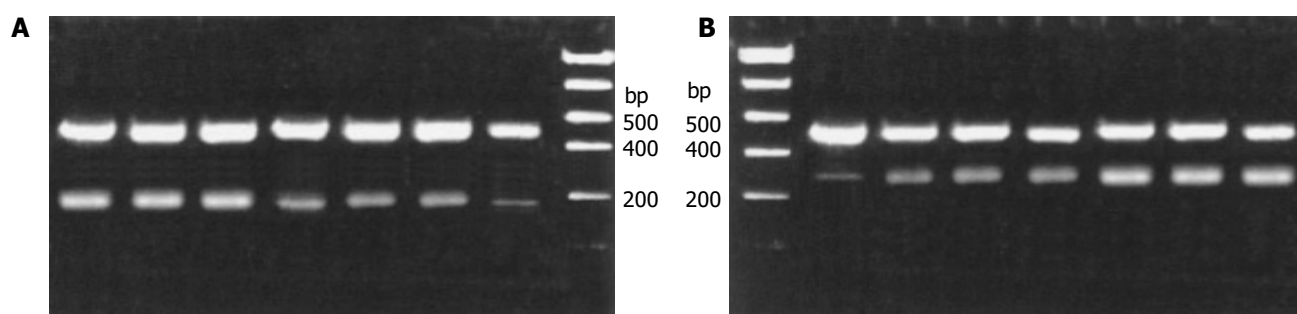


Figure 5 The mRNA expressions of Bcl-2 and Bcl-x_L were assessed using RT-PCR standardized by coamplifying the housekeeping gene β -actin. A: the mRNA expression of Bcl-2. lanes 1-3, adenocarcinoma; lanes 4-6, adenoma; lane 7, normal; lane 8, marker. B: the mRNA expression of Bcl-x_L. lane 1, marker; lane 2, normal; lanes 3-5, adenoma; lanes 6-8, adenocarcinoma.

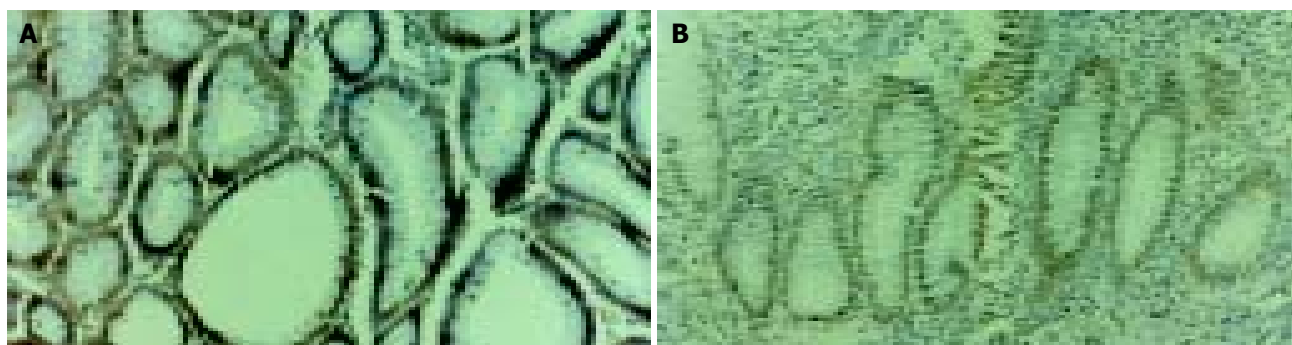


Figure 6 TUNEL staining in tissue sections of colorectal adenoma (A) and adenocarcinoma (B). TUNEL staining is restricted to the nucleus of apoptotic cells. ×200.

Bcl-2 and Bcl-x_L mRNA expression in colorectal carcinoma tissues

RT-PCR analysis of mRNA expressions of Bcl-2 and Bcl-x_L was standardized by co-amplifying these genes with the housekeeping gene β -actin. HPIAS-1000 SOFTWARE ANALYSIS took the image of electrophoresis with β -actin as internal standard. The relative absorbance of mRNA expression for Bcl-2: 2.43±0.27% in normal tissues, 17.96±1.51% in adenoma, and 36.71±2.17% in adenocarcinoma; for Bcl-x_L: 3.54±0.33% in normal tissues, 23.02±2.11% in adenoma, and 39.71±2.49% in adenocarcinoma (Figure 5). Our results showed that colon tumor tissue constitutively expressed Bcl-2 and Bcl-x_L. The mRNA expressions of Bcl-2 and Bcl-x_L were significantly increased ($P<0.05$) in the transition from normal colorectal epithelium to colon tumor tissue.

Cell apoptosis

In this study, TUNEL staining was restricted to the nucleus of apoptotic cells. TUNEL-positive staining cells were detected in normal colorectal mucosa, adenoma, and adenocarcinoma. The AI was significantly increased ($P<0.01$) in the transition

from normal colorectal mucosa to adenoma, but decreased from adenoma to adenocarcinoma (Figure 6). There was no association between the AI and the histological classification of adenoma and adenocarcinoma. The density of RelA-positive cells inversely correlated with the AI in the transition from adenoma to adenocarcinoma ($r = -0.89$; $P<0.001$).

DISCUSSION

We have demonstrated that RelA-DNA binding activity was constitutively activated in the majority of human colorectal carcinomas. Whereas the role for RelA/NF- κ B in tumorigenesis has not firmly established, recent work has suggested that it may play a role in this process. RelA/NF- κ B activation has been shown to be necessary for tumor formation in Hodgkin lymphoma cells^[26,27]. More recently, the inhibition of RelA/NF- κ B activity through the use of specific NF- κ B inhibitors (gliotoxin and MG132) resulted in spontaneous caspase-independent apoptosis in Hodgkin and Reed-Sternberg cells^[28]. Also, an increase in RelA/NF- κ B levels was identified in breast cancer

cell lines, primary human breast cancer, hepatocellular carcinoma, pancreatic adenocarcinoma, and gastric carcinoma when compared with nontransformed controls or normal tissues^[29-32]. In addition, NF- κ B transcriptional activity was required for oncogenic Ras-induced cellular transformation^[33], which likely occurred through the inhibition of transformation-associated apoptosis^[34]. However, the role of NF- κ B in colorectal tumorigenesis is unknown and currently under investigation.

We primarily used immunohistochemistry to detect NF- κ B activation in human colorectal carcinoma tissues. Its expression was significantly increased in the transition from normal colorectal mucosa to adenoma and adenocarcinoma. In our immunohistochemical analyses, we used monoclonal antibodies to detect RelA/NF- κ B-DNA binding activities, and their sensitivity and specificity have been characterized previously. They were useful in differentiating between activated and inactivated forms of RelA and facilitated the detection of the activated RelA proteins. In the current investigation, only 10-20% of RelA/NF- κ B protein was detectable in the nucleus, which was consistent with previous reports^[32]. And 80-90% of RelA still remained in the cytoplasm when RelA proteins were activated. It is unclear why the majority of RelA/NF- κ B proteins that were freed from I κ B remained in the cytoplasm. Possible explanations for this^[32] are: (1) I κ B was mutated and therefore could not bind to RelA and masked the nuclear translocation signal in RelA; (2) mutations in RelA prohibited I κ B binding to RelA, and (3) the RelA upstream signal transduction cascades were constitutively activated.

The Bcl-2 proto-oncogene is an apoptosis inhibitor originally described in association with the t(14; 18)(q32; q21) translocation in follicular B cell lymphoma, which places the Bcl-2 gene under the stimulatory control of the IgH promoter-enhancer at 14q32, resulting in increased Bcl-2 mRNA and protein^[35] and inhibition of apoptosis. The Bcl-x_L proto-oncogene, a member of Bcl-2 family, is a homologue of Bcl-2 and is an apoptosis inhibitor. The Bcl-2 and Bcl-x_L oncoproteins have been described in normal colonic mucosa^[35], where these were restricted to the epithelial regenerative compartment and the intestinal crypt bases. In our study, the expression of Bcl-2 and Bcl-x_L was increased in the transition from normal mucosa to adenoma and adenocarcinoma. These results also show that the increased RelA/NF- κ B expression occurred concomitantly with an increased expression of Bcl-2 and Bcl-x_L. To date, a number of gene products that inhibit apoptosis have been identified. These include Bcl-2 and Bcl-x_L genes. Indeed, Bcl-2 and Bcl-x_L have been identified as NF- κ B target genes^[36], but the exact role NF- κ B plays in its regulation remains controversial.

In recent years, increasing evidence indicates that activation of NF- κ B plays an important role in coordinating the control of apoptotic cell death. NF- κ B has been shown to prevent Fas-induced death in B cells through the upregulation of Bcl-2 and Bcl-x_L expression^[36], but has also been demonstrated to promote apoptosis in thymocytes by downregulating Bcl-2 and Bcl-x_L gene expression^[37]. However, the exact mechanism of NF- κ B in the regulation of apoptosis is not entirely clear. There are at least two distinct mechanisms by which NF- κ B blocks apoptosis^[38]: (1) induction of antiapoptosis factors including IEX-IL, TRAF1, TRAF2, c-IAP-1, c-IAP-2 *etc*; (2) interference of apoptotic pathway by protein-protein interaction. However, these two distinct mechanisms are not mutually exclusive since either mechanism alone cannot fully explain the antiapoptotic action of NF- κ B. In our study, apoptosis was significantly decreased in the transition from adenoma to adenocarcinoma, which was in contrast to the expressions of RelA, Bcl-2, and Bcl-x_L. We also observed an inverse relation between AI and the expression of RelA in the transition from adenoma to adenocarcinoma, implying that increased RelA protein expression to a certain level might be anti-apoptotic and thus promote tumorigenic

cell behavior. The anti-apoptotic role of NF- κ B has been well characterized and various down-stream targets of NF- κ B, including Bcl-2 and Bcl-x_L have been identified. In the present study, the statistical correlation between the increased expression of RelA, elevated Bcl-2 and Bcl-x_L expression implies that in colorectal tissue, activation of RelA might exhibit anti-apoptotic effects at least in part through upregulation of Bcl-2 and Bcl-x_L expression. This has been shown to decrease mitochondrial permeability changes and cytochrome C release and thus to block apoptosis^[39].

To date, NF- κ B has been believed to play an important role in coordinating the control of apoptotic cell death. However, the mechanism by which NF- κ B blocks apoptosis is still controversial. Some laboratories have reported that activation of NF- κ B is able to either promote or prevent apoptosis, depending on different stimuli and different cell types^[40-42]. For example, Grimm *et al.*^[43] reported that serum starvation activated NF- κ B and induced human embryonic kidney cells into apoptosis. Qin *et al.*^[44] found that NF- κ B activation contributed to the excitotoxin-induced death of striatal neurons. However, somewhat inconsistent results have also been presented by Beg and Baltimore^[45] that NF- κ B activation generally inhibited apoptosis in embryonic fibroblasts. A question arises: who is right on earth? We think the answer is expected by further studies.

In conclusion, our results demonstrate that the RelA/NF- κ B pathway is activated constitutively in colorectal carcinoma tissues, suggesting that activation of RelA/NF- κ B might play an important role in colorectal tumorigenesis. Further studies are required to elucidate the mechanisms of NF- κ B activation and to determine whether NF- κ B might serve as a therapeutic target in the anti-neoplastic treatment of colorectal cancer.

REFERENCES

- 1 **Zhu JW**, Yu BM, Ji YB, Zheng MH, Li DH. Upregulation of vascular endothelial growth factor by hydrogen peroxide in human colon cancer. *World J Gastroenterol* 2002; **8**: 153-157
- 2 **Loncar MB**, Al-Azzeh ED, Sommer PS, Marinovic M, Schmehl K, Kruschewski M, Blin N, Stohwasser R, Gott P, Kayademir T. Tumour necrosis factor alpha and nuclear factor kappaB inhibit transcription of human TFF3 encoding a gastrointestinal healing peptide. *Gut* 2003; **52**: 1297-1303
- 3 **Ghosh S**, May MJ, Kopp EB. NF- κ B and Rel proteins: evolutionarily conserved mediators of immune responses. *Annu Rev Immunol* 1998; **16**: 225-260
- 4 **Micheau O**, Tschopp J. Induction of TNF receptor I-mediated apoptosis via two sequential signaling complexes. *Cell* 2003; **114**: 181-190
- 5 **Siebenlist U**, Franzoso G, Brown K. Structure, regulation and function of NF- κ B. *Annu Rev Cell Biol* 1994; **10**: 405-455
- 6 **Bargou RC**, Leng C, Krappmann D, Emmerich F, Mapara MY, Bommert K, Royer HD, Scheidereit C, Dorken B. High-level nuclear NF- κ B and Oct-2 is a common feature of cultured Hodgkin/Reed-Sternberg cells. *Blood* 1996; **87**: 4340-4347
- 7 **Giri D K**, Aggarwal BB. Constitutive activation of NF- κ B causes resistance to apoptosis in human cutaneous T cell lymphoma HuT-78 cells. Autocrine role of tumor necrosis factor and reactive oxygen intermediates. *J Biol Chem* 1998; **273**: 14008-14014
- 8 **Feinman R**, Koury J, Thames M, Barlogie B, Epstein J, Siegel DS. Role of NF- κ B in the rescue of multiple myeloma cells from glucocorticoid-induced apoptosis by bcl-2. *Blood* 1999; **93**: 3044-3052
- 9 **Xiao CW**, Yan X, Li Y, Reddy SA, Tsang BK. Resistance of human ovarian cancer cells to tumor necrosis factor alpha is a consequence of nuclear factor kappaB-mediated induction of Fas-associated death domain-like interleukin-1beta-converting enzyme-like inhibitory protein. *Endocrinology* 2003; **144**: 623-630
- 10 **Mukhopadhyay T**, Roth JA, Maxwell SA. Altered expression of the p50 subunit of the NF- κ B transcription factor complex in non-small cell lung carcinoma. *Oncogene* 1995; **11**: 999-1003
- 11 **Nakshatri H**, Bhat-Nakshatri P, Martin DA, Goulet RJ Jr,

- Sledge GW Jr. Constitutive activation of NF- κ B during progression of breast cancer to hormone-independent growth. *Mol Cell Biol* 1997; **17**: 3629-3639
- 12 **Visconti R**, Cerutti J, Battista S, Fedele M, Trapasso F, Zeki K, Miano MP, de Nigris F, Casalino L, Curcio F, Santoro M, Fusco A. Expression of the neoplastic phenotype by human thyroid carcinoma cell lines requires NF- κ B p65 protein expression. *Oncogene* 1997; **15**: 1987-1994
- 13 **Ivanov VN**, Bhoomik A, Ronai Z. Death receptors and melanoma resistance to apoptosis. *Oncogene* 2003; **22**: 3152-3161
- 14 **Sumitomo M**, Tachibana M, Ozu C, Asakura H, Murai M, Hayakawa M, Nakamura H, Takayanagi A, Shimizu N. Induction of apoptosis of cytokine-producing bladder cancer cells by adenovirus-mediated I κ B overexpression. *Hum Gene Ther* 1999; **10**: 37-47
- 15 **Zelvyte I**, Ohlsson B, Axelson J, Janciauskiene S. Diverse responses between human pancreatic cancer cell lines to native alpha 1-antitrypsin and its C-terminal fragment. *Anticancer Res* 2003; **23**: 2267-2273
- 16 **Sovak MA**, Arsura M, Zanieski G, Kavanagh KT, Sonenshein GE. The inhibitory effects of transforming growth factor beta1 on breast cancer cell proliferation are mediated through regulation of aberrant nuclear factor-kappaB/Rel expression. *Cell Growth Differ* 1999; **10**: 537-544
- 17 **Zabel U**, Henkel T, Silva MS, Baeuerle PA. Nuclear uptake control of NF- κ B by MAD-3, an I κ B protein present in the nucleus. *EMBO J* 1993; **12**: 201-211
- 18 **Gavrieli Y**, Sherman Y, Ben-Sasson SA. Identification of programmed cell death in situ via specific labeling of nuclear DNA fragmentation. *J Cell Biol* 1992; **119**: 493-501
- 19 **Huang Y**, Johnson KR, Norris JS, Fan W. Nuclear factor- κ B/I κ B signaling pathway may contribute to the mediation of paclitaxel induced apoptosis in solid tumor cells. *Cancer Res* 2000; **60**: 4426-4432
- 20 **Wong BC**, Jiang X, Fan XM, Lin MC, Jiang SH, Lam SK, Kung HF. Suppression of RelA/p65 nuclear translocation independent of I κ Ba degradation by cyclooxygenase-2 inhibitor in gastric cancer. *Oncogene* 2003; **22**: 1189-1197
- 21 **Li-Weber M**, Laur O, Dern K, Krammer PH. T cell activation-induced and HIV tat-enhanced CD95(APO-1/Fas) ligand transcription involves NF- κ B. *Eur J Immunol* 2000; **30**: 661-670
- 22 **Sosic D**, Richardson JA, Yu K, Ornitz DM, Olson EN. Twist regulates cytokine gene expression through a negative feedback loop that represses NF- κ B activity. *Cell* 2003; **112**: 169-180
- 23 **Chomczynski P**, Sacchi N. Single-step method of RNA isolation by acid guanidine isothiocyanate-phenolchloroform extraction. *Anal Biochem* 1987; **162**: 156-159
- 24 **Kitamura S**, Kondo S, Shinomura Y, Kanayama S, Miyazaki Y, Kiyohara T, Hiraoka S, Matsuzawa Y. Met/HGF receptor modulates bcl-w expression and inhibits apoptosis in human colorectal cancers. *Br J Cancer* 2000; **83**: 668-673
- 25 **Nakajima-Iijima S**, Hamada H, Reddy P, Kakunaga T. Molecular structure of the human cytoplasmic β -actin gene: Interspecies homology of sequences in the introns. *Proc Natl Acad Sci U S A* 1985; **82**: 6133-6137
- 26 **Bargou RC**, Emmerich F, Krappmann D, Bommert K, Mapara MY, Arnold W, Royer HD, Grinstein E, Greiner A, Scheidereit C, Dorken B. Constitutive nuclear factor-kappaB-RelA activation is required for proliferation and survival of Hodgkin's disease tumor cells. *J Clin Invest* 1997; **100**: 2961-2969
- 27 **Schenkein D**. Proteasome inhibitors in the treatment of B-cell malignancies. *Clin Lymphoma* 2002; **3**: 49-55
- 28 **Izban KF**, Ergin M, Huang Q, Qin JZ, Martinez RL, Schnitzer B, Ni H, Nickoloff BJ, Alkan S. Characterization of NF-kappaB expression in Hodgkin's disease: Inhibition of constitutively expressed NF-kappaB results in spontaneous caspase-independent apoptosis in Hodgkin and Reed-Sternberg cells. *Mod Pathol* 2001; **14**: 297-310
- 29 **Sovak MA**, Bellas RE, Kin DW, Zanieski DJ, Rogers AE, Traish AM, Sonenshein GE. Aberrant nuclear factor-kappa B/Rel expression and the pathogenesis of breast cancer. *J Clin Invest* 1997; **100**: 2952-2960
- 30 **Tai DI**, Tsai SL, Chang YH, Huang SN, Chen TC, Chang KS, Liaw YF. Constitutive activation of nuclear factor kappaB in hepatocellular carcinoma. *Cancer* 2000; **89**: 2274-2281
- 31 **Sasaki N**, Morisaki T, Hashizume K, Yao T, Tsuneyoshi M, Noshiro H, Nakamura K, Yamanaka T, Uchiyama A, Tanaka M, Katano M. Nuclear factor-kappaB p65 (RelA) transcription factor is constitutively activated in human gastric carcinoma tissue. *Clin Cancer Res* 2001; **7**: 4136-4142
- 32 **Wang WX**, Abbruzzese JL, Evans DB, Larry L, Cleary KR, Chiao PJ. The nuclear factor- κ B relA transcription factor is constitutively activated in human pancreatic adenocarcinoma cells. *Clin Cancer Res* 1999; **5**: 119-127
- 33 **Finco TS**, Westwick JK, Norris JL, Beg AA, Der CJ, Baldwin AS Jr. Oncogenic Ha-Ras-induced signaling activates NF- κ B transcriptional activity, which is required for cellular transformation. *J Biol Chem* 1997; **272**: 24113-24116
- 34 **Mayo MW**, Wang CY, Cogswell PC, Rogers-Graham KS, Lowe SW, Der CJ, Baldwin AS Jr. Requirement for NF- κ B activation to suppress p53-independent apoptosis induced by oncogenic ras. *Science* 1997; **278**: 1812-1815
- 35 **Popescu RA**, Lohri A, de Kant E, Thiede C, Reuter J, Herrmann R, Rochlitz CF. Bcl-2 expression is reciprocal to p53 and c-myc expression in metastatic human colorectal cancer. *Eur J Cancer* 1998; **34**: 1268-1273
- 36 **Lee HH**, Dadgostar H, Cheng Q, Shu J, Cheng G. NF- κ B mediated up-regulation of Bcl-x and Bfl-1/A1 is required for CD40 survival signaling in B lymphocytes. *Proc Natl Acad Sci U S A* 1999; **96**: 9136-9141
- 37 **Hettmann T**, DiDonato J, Karin M, Leiden JM. An essential role for nuclear factor κ B in promoting double positive thymocyte apoptosis. *J Exp Med* 1999; **189**: 145-158
- 38 **Kajino S**, Suganuma M, Teranishi F, Takahashi N, Tetsuka T, Ohara H, Itoh M, Okamoto T. Evidence that *de novo* protein synthesis is dispensable for anti-apoptotic effects of NF- κ B. *Oncogene* 2000; **19**: 2233-2239
- 39 **Aams J**, Cory S. The Bcl-2 protein family arbiters of cell survival. *Science* 1998; **281**: 1322-1326
- 40 **Glasgow JN**, Wood T, Perez-Polo JR. Identification and characterization of nuclear factor- κ B binding sites in the murine Bcl-x promoter. *J Neurochem* 2000; **75**: 1377-1389
- 41 **O'Connor L**, Huang DC, O'Reilly LA, Strasser A. Apoptosis and cell division. *Curr Opin Cell Biol* 2000; **12**: 257-263
- 42 **Yoneda T**, Imaizumi K, Maeda M, Yui D, Manabe T, Katayama T, Sato N, Gomi F, Morihara T, Mori Y, Miyoshi K, Hitomi J, Ugawa S, Yamada S, Okabe M, Tohyama M. Regulatory mechanisms of TRAF2-mediated signal transduction by Bcl-10, a MALT lymphoma-associated protein. *J Biol Chem* 2000; **275**: 11114-11120
- 43 **Grimm S**, Bauer MK, Baeuerle PA, Schulze-Osthoff K. Bcl-2 down-regulates the activity of transcription factor NF- κ B induced upon apoptosis. *J Cell Biol* 1996; **134**: 13-23
- 44 **Qin ZH**, Wang Y, Nakai M, Chase TN. Nuclear Factor- κ B contributes to excitotoxin-induced apoptosis in rat striatum. *Mol Pharmacol* 1998; **53**: 33-42
- 45 **Beg AA**, Baltimore D. An essential role for NF- κ B in preventing TNF- α -induced cell death. *Science* 1996; **274**: 782-784

• COLORECTAL CANCER •

Expression of vascular endothelial growth factor-C and the relationship between lymphangiogenesis and lymphatic metastasis in colorectal cancer

Yi-Tao Jia, Zhong-Xin Li, Yu-Tong He, Wei Liang, Hui-Chai Yang, Hong-Jun Ma

Yi-Tao Jia, Wei Liang, Department of Oncology, the People's Hospital of Hebei Province, Shijiazhuang 050051, Hebei Province, China
Zhong-Xin Li, Yu-Tong He, Hui-Chai Yang, Department of Surgery, the Forth Hospital of Hebei Medical University, Shijiazhuang 050011, Hebei Province, China

Hong-Jun Ma, Experimental Centre of Electron Microscopy of Hebei Medical University, Shijiazhuang 050011, Hebei Province, China

Correspondence to: Dr. Zhong-Xin Li, Department of Surgery, the Forth Hospital of Hebei Medical University, Shijiazhuang 050011, Hebei Province, China

Telephone: +311-6033941-347

Received: 2003-12-23 **Accepted:** 2004-03-02

Abstract

AIM: To investigate the expression of vascular endothelial growth factor-C (VEGF-C) and the relationship between VEGF-C and lymphangiogenesis, lymph node metastasis in colorectal cancer.

METHODS: Fifty six cases of colorectal cancer were selected randomly. Expression of VEGF-C was detected by immunohistochemistry, and lymphatic vessels were stained by enzyme histochemical method.

RESULTS: VEGF-C expression was found in 66.7% (37/56) patients. In VEGF-C positive and negative patients, the lymphatic vessel density was 25.16 ± 7.52 and 17.14 ± 7.22 , respectively ($P < 0.05$). The rate of lymph node metastasis in VEGF-C positive patients (81.1%) was significantly higher than that in the negative group (42.1%).

CONCLUSION: VEGF-C expression may induce lymphangiogenesis in colorectal cancer, as a result, tumor cells can enter the lymphatic vessels easily. VEGF-C may serve as a useful prognostic factor in colorectal carcinoma.

Jia YT, Li ZX, He YT, Liang W, Yang HC, Ma HJ. Expression of vascular endothelial growth factor-C and the relationship between lymphangiogenesis and lymphatic metastasis in colorectal cancer. *World J Gastroenterol* 2004; 10(22): 3261-3263

<http://www.wjgnet.com/1007-9327/10/3261.asp>

INTRODUCTION

Colorectal cancer is a common cause of death throughout the world including China. The lymphatic system is the primary pathway of metastasis for gastrointestinal tract malignancies, and the extent of lymph node involvement is a key prognostic factor for the outcome of patients. However, the mechanism of lymphatic metastasis remains unclear.

Lymphangiogenesis, the development of new lymph vessels, is a relatively new area of clinical investigations. Recently, vascular endothelial growth factor C (VEGF-C) has been identified as a new member of the VEGF family^[1,2], and is believed

to be the only lymphangiogenic factor in the VEGF family. It activates both vascular endothelial growth factor receptor 2 (VEGFR-2) and VEGFR-3^[3,4]. VEGF-C induces the proliferation of lymphatic vessels in the stroma of gastric carcinoma by activating VEGFR-3 in lymphatic endothelial cells^[5]. But the precise role of VEGF-C in colorectal cancer has not been clearly understood. Therefore, in the current study, we used an enzyme-histochemical method for 5'-nucleotidase (5'-Nase) to distinguish lymph vessels in colorectal carcinoma, and immunohistochemistry to examine the correlation between the expression of VEGF-C, lymphangiogenesis and the clinicopathologic features.

MATERIALS AND METHODS

Patients

Fifty-six Chinese colorectal carcinoma patients were surgically treated in the Department of Surgery, the Forth Hospital of Hebei Medical University, China from 2001 to 2002. The patients included 34 males and 22 females, and ranged in age from 33 to 75 years (average age 58.5 years). The lesions included 13 colon cancers and 43 rectal cancers, two patients with stage I, 17 patients with stage II, 34 patients with stage III and three patients with stage IV.

Immunohistochemistry

Immunohistochemical staining for VEGF-C was performed using the streptavidin-peroxidase technique. Formalin fixed and paraffin embedded tissues were cut into 4 μ m thick sections and placed on saline coated slides. After deparaffinization in xylene and rehydration, endogenous peroxidase activity was blocked after incubated with 30 mL/L hydrogen peroxidase for 20 min. Tissue sections were then autoclaved at 121 °C in 10 mmol/L citrate buffer (pH 6.0) for 10 min for antigen retrieval and cooled at room temperature for 30 min, then incubated for 3 h with a 1:40 dilution of anti-VEGF-C rabbit polyclonal antibody (Santa Cruz Biotech, USA). Bound peroxidase was visualized using a solution of diaminobezidine as chromogen, and nuclei were counterstained with hematoxylin. Scoring was carried out by two independent observers who were blinded to the patient's status. Positive staining was defined as the presence of VEGF-C immunoreactivity in at least 10% of tumor cells.

Enzyme-histochemistry

Cryosections (7 μ m thick) of tissue were processed for 5'-nucleotide-alkaline phosphatase (5'-Nase-ALPase) double staining according to Ji *et al.*'s report^[6]. After rinsed in 0.1 mol/L cacodylate buffer (pH 7.2), specimens were incubated in the reaction medium for 5'-Nase for 50 min at 37 °C with 5'-adenosine monophosphate (AMP) (Sigma chemical, St. Louis, MO, USA) as a substrate, lead nitrate (Sigma, USA) as a capture agent, and 2 mmol/L L-tetramisole (Sigma, USA) as an inhibitor of nonspecific alkaline phosphatase. After washed with distilled water, the tissues were treated with 10 mg/L ammonium sulfide solution for 1 min at room temperature. Then, the sections were incubated in the reaction medium for ALPase for 30 min at 4 °C with fast blue BB, N,N-

dimethylformamide, naphthol AS-MX phosphate (Sigma, USA).

Lymphatic vessel density (LVD) counting

The stained sections were screened at $\times 40$ magnification to identify the regions of the highest vascular density within the tumor. Lymphatic vessels were counted in 3 regions of the highest vascular density at $\times 100$ magnification. The number of lymphatic vessels was the mean of vessels in these areas.

Statistical analysis

The data were analysed by *t* test and χ^2 test. All reported *P* values were two-sided, and $P < 0.05$ was considered statistically significant.

RESULTS

Immunohistochemistry

In specimens of normal colorectal mucosa, no VEGF-C protein was stained. Among the 56 examined tumors, 37 (66.7%) showed VEGF-C protein expression in the cytoplasm (Figure 1).



Figure 1 VEGF-C in cytoplasm of colorectal adenocarcinoma (SP $\times 200$).

Enzyme-histochemistry

Lymphatic vessels were 5'-Nase positive (brown) and blood vessels were ALPase positive (blue). The most lymphatic vessels were enlarged and dilated especially in peritumor areas. The walls of lymphatic vessels were thinner than that of blood vessels, and their profiles of lumens were more irregular. While the intratumoral lymphatic vessels were strip-like (Figure 2). The LVD of VEGF-C positive tumors (25.16 ± 7.52) was significantly higher than that of VEGF-C negative tumors (17.14 ± 7.22) ($P = 0.04$). No significant lymphangiogenesis was observed in normal and adenoma tissues.

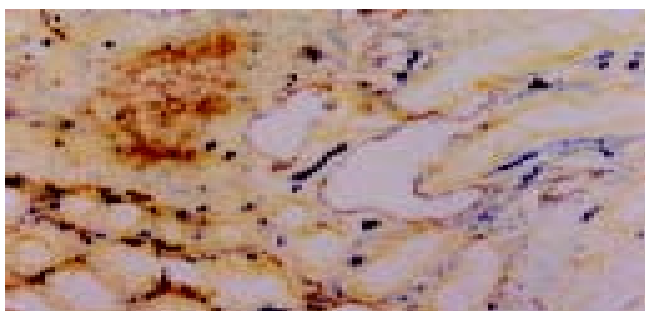


Figure 2 Positive 5'-Nase (brown) and ALPase (blue) in lymphatic and blood vessels ($\times 100$).

Correlation between VEGF-C and clinicopathologic factors

VEGF-C expression was observed frequently in patients with colorectal carcinoma. A positive association between VEGF-C expression and lymphatic metastasis was observed ($P < 0.05$, Table 1). However, no significant correlations with gender,

histologic differentiation, invasive depth, TNM stage were observed.

Table 1 Relationship between expression of VEGF-C and clinicopathologic features in colorectal carcinoma

Characteristic	<i>n</i>	VEGF-C		<i>P</i>
		(+)	(-)	
Gender	Male	34	25	0.143
	Female	22	12	
Lymph node metastasis	(+)	37	30	0.007
	(-)	9	8	
Differentiation	Well	40	25	0.372
	Poorly	16	12	
Invasion depth	Muscularis	17	10	0.499
	Adventitia	39	27	
Stage	I-II	19	13	0.790
	III-IV	37	24	

DISCUSSION

Clinical and pathological data pointed to the metastasis of solid tumors via the lymphatics as an important early event in metastatic diseases^[7]. However, little has been achieved in lymphangiogenesis and the role of lymphangiogenesis in promoting the metastasis of tumor cells via the lymphatic vessels. This might, in part, be due to difficulty in studying lymphatic vessels because of their morphology and lack of lymphatic-specific markers^[6,7]. Approximately 10 years ago, Kato *et al.*^[8] developed an enzyme-histochemical method for 5'-Nase-ALPase to distinguish lymphatic vessels from blood vessels. Many other markers such as LYVE1 and podoplanin were found later^[9,10]. Now, lymphangiogenesis or new lymphatic vessel growth has become an exciting area of research in cancer biology^[11]. So far, the occurrence and involvement of lymphangiogenesis have been demonstrated in some experimental mouse tumors, human head and neck cancers, oral squamous cell cancer by using these markers^[12-16]. Similarly, in our study, lymphangiogenesis was observed in primary colorectal carcinomas, and the vicinity of tumor was the dominant region. Most of lymphatic vessels were dilated, as a result, tumor cells could invade the lymphatics easily. On the other hand, most of the intratumoral lymphatic capillaries were strip-like. It is believed that tumor cells could utilize peritumoral lymphatics to spread, while intratumoral lymphatics should be regarded as an additional pathway rather than a necessity for metastasis^[17].

Vascular endothelial growth factor-C (VEGF-C) is the first lymphangiogenic factor identified. Moreover, there is ample evidence for the expression of VEGF-C in human tumors. But the precise role of VEGF-C in colorectal cancer is less well understood. With respect to VEGF-C expression, several authors have demonstrated associations between this growth factor expression and poor clinicopathologic outcome^[18-25]. Immunohistochemical detection of VEGF-C expression at the deepest invasive site of colorectal carcinoma was found in about 50% advanced tumors. Furudoi *et al.*^[26] suggested that the expression of VEGF-C was correlated with lymphatic and venous invasion, lymph node status, Dukes stage, liver metastasis, depth of invasion, poorer histological grade and microvessel density.

It is widely known that VEGF-C can bind to both VEGFR-2

and VEGFR-3. Activation of VEGFR-2 results in the mitogenesis of vascular endothelial cells. In contrast, VEGFR-3 activation by VEGF-C is considered to induce proliferation of lymphatic endothelial cells. Thus, angiogenic versus lymphangiogenic responses to VEGF-C have been found to depend on the expression of its receptors in blood versus lymphatic endothelial cells of the target tissue^[27]. In addition, the activation of lymphatics by VEGF-C is considered to induce secretion of chemokines and similar factors by the lymphatic endothelium, thus attracting tumor cells and facilitating their entry into lymphatics^[28]. Besides VEGF-C, another new member of VEGF family, VEGF-D, could also stimulate lymphangiogenesis by activating VEGFR-3 in human tumors^[29-32]. But the relationship between VEGF-C and VEGF-D expressions, as well as the role of VEGF-D in human tumors is still unclear.

In summary, our findings demonstrate a causal role of lymphangiogenesis in tumor metastasis, suggesting VEGF-C expression is related to the high incidence of metastasis in colorectal carcinoma. However, the mechanism of lymphangiogenesis is extremely complex, which is a subject of ongoing investigation.

REFERENCES

- 1 **Pepper MS.** Lymphangiogenesis and tumor metastasis: myth or reality? *Clin Cancer Res* 2001; **7**: 462-468
- 2 **Stacker SA,** Achen MG, Jussila L, Baldwin ME, Alitalo K. Lymphangiogenesis and cancer metastasis. *Nat Rev Cancer* 2002; **2**: 573-583
- 3 **Jussila L,** Alitalo K. Vascular growth factors and lymphangiogenesis. *Physiol Rev* 2002; **82**: 673-700
- 4 **Baldwin ME,** Stacker SA, Achen MG. Molecular control of lymphangiogenesis. *Bioessays* 2002; **24**: 1030-1040
- 5 **Yonemura Y,** Fushido S, Bando E, Kinoshita K, Miwa K, Endo Y, Sugiyama K, Partanen T, Yamamoto H, Sasaki T. Lymphangiogenesis and the vascular endothelial growth factor receptor (VEGFR)-3 in gastric cancer. *Eur J Cancer* 2001; **37**: 918-923
- 6 **Ji RC,** Kato S. Lymphatic network and lymphangiogenesis in the gastric wall. *J Histochem Cytochem* 2003; **51**: 331-338
- 7 **Stacker SA,** Baldwin ME, Achen MG. The role of tumor lymphangiogenesis in metastatic spread. *FASEB J* 2002; **16**: 922-934
- 8 **Kato S.** Intralobular lymphatic vessels and their relationship to blood vessels in the mouse thymus. Light- and electron-microscopic study. *Cell Tissue Res* 1988; **253**: 181-187
- 9 **Jackson DG.** The lymphatics Revisited New perspectives from the Hyaluronan Receptor LYVE-1. *Trends Cardiovasc Med* 2003; **13**: 1-7
- 10 **Reis-Filho JS,** Schmitt FC. Lymphangiogenesis in tumors: what do we know? *Microsc Res Tech* 2003; **60**: 171-180
- 11 **Duff SE,** Li C, Jeziorska M, Kumar S, Saunders MP, Sherlock D, O'Dwyer ST, Jayson GC. Vascular endothelial growth factors C and D and lymphangiogenesis in gastrointestinal tract malignancy. *Br J Cancer* 2003; **89**: 426-430
- 12 **Mattila MM,** Ruohola JK, Karpanen T, Jackson DG, Alitalo K, Harkonen PL. VEGF-C induced lymphangiogenesis is associated with lymph node metastasis in orthotopic MCF-7 tumors. *Int J Cancer* 2002; **98**: 946-951
- 13 **Krishnan J,** Kirkin V, Steffen A, Hegen M, Weih D, Tomarev S, Wilting J, Sleeman JP. Differential *in vivo* and *in vitro* expression of vascular endothelial growth factor (VEGF) -C and VEGF-D in tumors and its relationship to lymphatic metastasis in immunocompetent rats. *Cancer Res* 2003; **63**: 713-722
- 14 **He Y,** Kozaki K, Karpanen T, Koshikawa K, Yla-Herttuala S, Takahashi T, Alitalo K. Suppression of tumor lymphangiogenesis and lymph node metastasis by blocking vascular endothelial growth factor receptor 3 signaling. *J Natl Cancer Inst* 2002; **94**: 819-825
- 15 **Beasley NJ,** Prevo R, Banerji S, Leek RD, Moore J, van Trappen P, Cox G, Harris AL, Jackson DG. Intratumoral lymphangiogenesis and lymph node metastasis in head and neck cancer. *Cancer Res* 2002; **62**: 1315-1320
- 16 **Sedivy R,** Beck-Mannagetta J, Haverkamp C, Battistutti W, Honigschnabl S. Expression of vascular endothelial growth factor-C correlates with the lymphatic microvessel density and the nodal status in oral squamous cell cancer. *J Oral Pathol Med* 2003; **32**: 455-460
- 17 **Cassella M,** Skobe M. Lymphatic vessel activation in cancer. *Ann N Y Acad Sci* 2002; **979**: 120-130
- 18 **Tanaka K,** Sonoo H, Kurebayashi J, Nomura T, Ohkubo S, Yamamoto Y, Yamamoto S. Inhibition of infiltration and angiogenesis by thrombospondin-1 in papillary thyroid carcinoma. *Clin Cancer Res* 2002; **8**: 1125-1131
- 19 **Takahashi A,** Kono K, Itakura J, Amemiya H, Feng Tang R, Iizuka H, Fujii H, Matsumoto Y. Correlation of vascular endothelial growth factor-C expression with tumor-infiltrating dendritic cells in gastric cancer. *Oncology* 2002; **62**: 121-127
- 20 **Ichikura T,** Tomimatsu S, Ohkura E, Mochizuki H. Prognostic significance of the expression of vascular endothelial growth factor (VEGF) and VEGF-C in gastric carcinoma. *J Surg Oncol* 2001; **78**: 132-137
- 21 **Masood R,** Kundra A, Zhu S, Xia G, Scalia P, Smith DL, Gill PS. Malignant mesothelioma growth inhibition by agents that target the VEGF and VEGF-C autocrine loops. *Int J Cancer* 2003; **104**: 603-610
- 22 **Arinaga M,** Noguchi T, Takeno S, Chujo M, Miura T, Uchida Y. Clinical significance of vascular endothelial growth factor C and vascular endothelial growth factor receptor 3 in patients with non small cell lung carcinoma. *Cancer* 2003; **97**: 457-464
- 23 **Kaio E,** Tanaka S, Kitadai Y, Sumii M, Yoshihara M, Haruma K, Chayama K. Clinical significance of angiogenic factor expression at the deepest invasive site of advanced colorectal carcinoma. *Oncology* 2003; **64**: 61-73
- 24 **Tang RF,** Itakura J, Aikawa T, Matsuda K, Fuji H, Korc M, Matsumoto Y. Overexpression of lymphangiogenic growth factor VEGF-C in human pancreatic cancer. *Pancreas* 2001; **22**: 285-292
- 25 **Liu XE,** Sun XD, Wu JM. Expression and significance of VEGF-C and FLT-4 in gastric cancer. *World J Gastroenterol* 2004; **10**: 352-355
- 26 **Furudoi A,** Tanaka S, Haruma K, Kitadai Y, Yoshihara M, Chayama K, Shimamoto F. Clinical significance of vascular endothelial growth factor C expression and angiogenesis at the deepest invasive site of advanced colorectal carcinoma. *Oncology* 2002; **62**: 157-166
- 27 **Nisato RE,** Tille JC, Pepper MS. Lymphangiogenesis and tumor metastasis. *Thromb Haemost* 2003; **90**: 591-597
- 28 **Mandriota SJ,** Jussila L, Jeltsch M, Compagni A, Baetens D, Prevo R, Banerji S, Huarte J, Montesano R, Jackson DG, Orci L, Alitalo K, Christofori G, Pepper MS. Vascular endothelial growth factor-C-mediated lymphangiogenesis promotes tumour metastasis. *EMBO J* 2002; **20**: 672-682
- 29 **Nakamura Y,** Yasuoka H, Tsujimoto M, Yang Q, Imabun S, Nakahara M, Nakao K, Nakamura M, Mori I, Kakudo K. Flt-4-positive vessel density correlates with vascular endothelial growth factor-d expression, nodal status, and prognosis in breast cancer. *Clin Cancer Res* 2003; **9**: 5313-5317
- 30 **Stacker SA,** Hughes RA, Achen MG. Molecular targeting of lymphatics for therapy. *Curr Pharm Des* 2004; **10**: 65-74
- 31 **Onogawa S,** Kitadai Y, Tanaka S, Kuwai T, Kimura S, Chayama K. Expression of VEGF-C and VEGF-D at the invasive edge correlates with lymph node metastasis and prognosis of patients with colorectal carcinoma. *Cancer Sci* 2004; **95**: 32-39
- 32 **Koyama Y,** Kaneko K, Akazawa K, Kanbayashi C, Kanda T, Hatakeyama K. Vascular endothelial growth factor-C and vascular endothelial growth factor-d messenger RNA expression in breast cancer: association with lymph node metastasis. *Clin Breast Cancer* 2003; **4**: 354-360

• VIRAL HEPATITIS •

Hepatitis B virus genotypes, phylogeny and occult infection in a region with a high incidence of hepatocellular carcinoma in China

Zhong-Liao Fang, Hui Zhuang, Xue-Yan Wang, Xian-Min Ge, Tim J Harrison

Zhong-Liao Fang, Hui Zhuang, Department of Microbiology, School of Basic Medicine, Peking University Health Science Center, Beijing 100083, China

Xue-Yan Wang, Center for Disease Prevention and Control of Guangxi Zhuang Autonomous Region, Nanning 530021, Guangxi Zhuang Autonomous Region, China

Xian-Min Ge, Guangxi Worker Hospital, Nanning 530021, Guangxi Zhuang Autonomous Region, China

Tim J Harrison, Centre for Hepatology, Royal Free and University College Medical School, University College London, London, United Kingdom

Supported by Beijing Municipal Committee of Science and Technology, No. H020920020190

Correspondence to: Professor Hui Zhuang, Department of Microbiology, School of Basic Medicine, Peking University Health Science Center, Beijing 100083, China. zhuanghu@publica.chinfo.net

Telephone: +86-10-82802221 **Fax:** +86-10-82801617

Received: 2003-12-19 **Accepted:** 2004-03-02

Abstract

AIM: To determine the genotypes and phylogeny of hepatitis B viruses (HBVs) in asymptomatic HBV carriers, and the prevalence of occult HBV infection in Long An County, Guangxi Zhuang Autonomous Region, an area with a high incidence of hepatocellular carcinoma.

METHODS: A nested polymerase chain reaction (nPCR) was used for detection of HBV DNA in serum samples from 36 blood donors with asymptomatic HBV infection, and in serum samples from 52 HBsAg negative family members of the children who did not receive hepatitis B vaccination in Long An County. PCR products were sequenced, and the genotype of each HBV sequence was determined by comparison with sequences of known genotypes in the GenBank and EMBL nucleotide databases using the BLAST programme. Phylogenetic trees were constructed by the quartet maximum likelihood analysis using the TreePuzzle software.

RESULTS: Twenty (55.56%) of 36 HBV asymptomatic carriers were positive for HBV DNA. They were all genotype C by comparison with sequences of known genotypes in the GenBank and EMBL nucleotide databases. The full-length HBV DNA sequence isolated from the sample No. 624 contained 3 215 bases. No interesting mutations were found in this isolate. The homology analysis showed that this strain was closer to the Vietnamese HBV genotype C strain, with a homology of 97%, compared its relation to the same genotype of HBV isolated in Shanghai. Six (11.5%) of the 52 HBsAg negative family members were positive for HBV DNA. A point mutation was found in the sample No. 37, resulting in the substitution of amino acid glycine to arginine in the "a" determinant. Other samples with positive HBV DNA did not have any unusual amino acid substitutions in or around the "a" determinant, and were attributed to the wild-type HBV.

CONCLUSION: The HBVs isolated from asymptomatic

carriers of Long An County were all identified as genotype C, and the prevalence of occult HBV infection in the population of the county is as high as 11.5%. It is suggested that genotype C and persistent occult HBV infection may play an important role in the development of HCC in the county.

Fang ZL, Zhuang H, Wang XY, Ge XM, Harrison TJ. Hepatitis B virus genotypes, phylogeny and occult infection in a region with a high incidence of hepatocellular carcinoma in China. *World J Gastroenterol* 2004; 10(22): 3264-3268
<http://www.wjgnet.com/1007-9327/10/3264.asp>

INTRODUCTION

Infection with hepatitis B virus (HBV) may lead to a wide spectrum of liver diseases ranging from mild, self-limited to fulminant hepatitis in acute infection, and from an asymptomatic carrier state to severe chronic hepatitis, cirrhosis, and hepatocellular carcinoma (HCC) in chronic infection. Human HBV, a prototype member of the family hepadnaviridae, is a circular, partially double-stranded DNA virus of approximately 3200 nt^[1]. Traditionally, HBV was classified into 4 subtypes or serotypes (adr, adw, ayr, and ayw) based on antigenic determinants of hepatitis B surface antigen (HBsAg)^[2]. Epidemiological studies found that the prevalence of these serotypes varied in different parts of the world. In addition, antibody to the common determinant "a" confers protection against all serotypes. Advances in molecular biology techniques revealed significant diversities in sequences of HBV isolates, accounting for allelic differences among the 4 major HBV serotypes. Based on an intergroup divergence of 8% or more in the complete nucleotide sequence, HBV has been classified into eight genotypes, designated as A to H^[3-5]. Recent reports suggested that infections with HBV genotype C were associated with more severe liver diseases, including HCC, than infections with genotype B^[6-8]. However, HBV genotype B was suggested to be associated with the development of HCC in Taiwanese below the age of 50 years^[9].

Occult HBV infection is characterized by the presence of HBV infection with undetectable HBsAg. Undoubtedly, carriers of occult HBV may transmit the virus through blood transfusion or organ transplantation. Epidemiological and molecular studies performed since the 1980s indicate that persistent HBV infection might play a critical role in the development of HCC and in HBsAg-negative patients^[10,11].

The incidence rate of HCC in Long An County, southern Guangxi, China, is about 49.9/100 000, the highest in the world, and over 90% of HCC cases in the county are individuals with positive HBsAg in serum^[12,13]. In this study, HBV preC and basic core promoter from 36 HBV asymptomatic carriers in Long An County were amplified and sequenced. The whole genome of a strain from one of the carriers, and genotypes and phylogeny of all the isolates were also analyzed to clarify the difference among HBV strains from different areas. In addition, 52 serum samples from family members of children without hepatitis B vaccination, with negative HBsAg, from the county were

detected for HBV DNA to determine the prevalence of occult HBV infection in the population.

MATERIALS AND METHODS

Serum samples

A total of 36 sera were obtained from asymptomatic blood donors who were infected persistently with HBV in Long An County, southern Guangxi, China. Another 52 serum samples were collected from family members of children failed to have hepatitis B vaccination from the county. Sera were tested for HBsAg, anti-HBc, anti-HBs, HBeAg, and anti-HBe using HBV Marker ELISA kits (produced by Xiamen Xinchuang Scientific Technology Company, Limited, Fujian, China) (Tables 1, 2).

Table 1 Serological markers of 20 asymptomatic carriers with positive HBV DNA

No.	Age (yr)	Sex	HBsAg	Anti-HBs	Anti-HBc	HBeAg	Anti-HBe
601	18	Male	+	-	+	+	-
602	18	Male	+	-	+	+	-
603	28	Female	+	-	+	+	-
604	20	Male	+	-	+	+	-
605	27	Male	+	-	+	+	-
606	18	Male	+	-	+	+	-
607	31	Female	+	-	+	+	-
609	22	Female	+	-	+	+	-
610	19	Male	+	-	+	+	-
615	38	Male	+	-	+	+	-
618	22	Male	+	-	+	-	-
619	20	Male	+	-	+	+	-
621	24	Male	+	-	+	+	-
622	28	Male	+	-	+	+	-
623	30	Male	+	-	+	+	-
624	25	Male	+	-	+	+	-
629	28	Female	+	-	+	+	-
630	28	Female	+	-	+	+	-
633	18	Male	+	-	+	+	-
634	19	Male	+	-	+	+	-

Table 2 Serological markers of HBsAg-negative asymptomatic carriers with positive HBV DNA

Sample No.	HBsAg	Anti-HBs	Anti-HBs Titre (mIU/mL)	HBeAg	Anti-HBe	Anti-HBe
1	-	+	5.1	-	+	+
14	-	+	108.0	-	+	-
16	-	+	18.2	-	+	+
23	-	+	13.9	-	-	-
25	-	-	-	-	+	+
37	-	-	-	-	-	+

PCR amplification and sequence analysis

DNA was extracted from 85 μ L serum by phenol/chloroform extraction following digestion by pronase. For preC and basic core promoter amplification: the first round of PCR 35 cycles was carried out using primers B935 (nt 1240-1260, 5'-GCGCTGCAGAAGGTTTGTGGCTCCTCTG-3') and MDC1 (nt 2304-2324, 5'-TTGATAAGA TAGGGGCATTTG-3'). For each cycle, the samples was amplified at 94 $^{\circ}$ C for 30 s, at 50 $^{\circ}$ C for 30 s, and at 72 $^{\circ}$ C for 90 s in a 50 μ L reaction. The second

round of 30 PCR cycles was carried out on 5 μ L of the first round product using primers CPRF1 (nt 1678-1695, 5'-CAATGTCAACGACCG ACC-3') and CPRR1 (nt 1928-1948, 5'-GAGTAACTCCACAG TAGCTCC-3') and the same reaction conditions of the first round.

For the surface gene amplification: the first round of 35 cycles PCR was carried out using primers MD14 (5'-GCGCTGCAGCTATGCCTCATCTTC-3', nt 418-433) and HCO2 (5'-GCGAAGCTTGCTGTACAGACTTGG-3', nt 761-776). For each cycle, the samples was amplified at 94 $^{\circ}$ C for s, at 45 $^{\circ}$ C for 45 s, and at 72 $^{\circ}$ C for 2 min in a 50 μ L reaction. The second round of 30 PCR cycles was carried out on 5 μ L of the first round product using primers ME15 (5'-GCGCTGCAGCAAGGTATGTTG CCGG-3', nt 455-470) and HDO3 (5'-GCGAAGCTTCATCAT CCATATAGC-3', nt 734-748) and the same reaction conditions of the first round. PCR products from the second round were confirmed by 15 g/L agarose gels electrophoresis and then purified using the Wizard (PCR Preps DNA purification system (Promega, Madison, WI) according to the manufacturer's instructions. Cycle sequencing was carried out directly on 2 mL purified DNA using primers CPRF1 and 33P-dATP by the thermo sequenase radiolabeled terminator cycle sequencing kit (USB Corporation, Cleveland, OH) according to the manufacturer's instructions.

Sample NO. 624 was selected for whole genome sequencing. Its DNA was extracted from 170 μ L serum by phenol/chloroform extraction following digestion by pronase. The whole HBV genome was amplified in three fragments. Primers for fragment 1 for the first and second round PCR were LSOB1, BPOLEO1 and LSB11, and POLSEQ2. Primers for fragment 2 for the first and second round PCR were MDN5, BPOLEO1, BPOLBO2 and PSISEQ2. Primers for fragment 3 for the first and second round PCR were POLSEQ1, MDD2, POLSEQ6 and MDC1. The conditions of 30 PCR cycles were at 94 $^{\circ}$ C for 30 s, at 50 $^{\circ}$ C for 30 s, and at 72 $^{\circ}$ C for 90 s in a 50 μ L reaction. PCR products from the second round PCR for each fragment were cloned into the vector pCR2.1 (Invitrogen, Leek, The Netherlands) and mini preparations of DNA made from 1.5 mL of 15 mL cultures of individual colonies by phenol extraction and ethanol precipitation of the cell pellet. Plasmids with inserts were identified by digestion with *Eco*RI and remainder of the cultures used for extraction of DNA using a QIAprep spin kit (Qiagen, Crawley, UK). The purified DNA was sequenced as above. Sequencing primers for fragment 1 were LSB1, PSISEQ2, ds 2, ds, ADELN, MD14, ADELN, POLSEQ8, POLSEQ9, POLSEQ6, POLSEQ2. Primers for fragment 2 were BPOLBO2, POLSEQ4, LSOB1, POLSEQ5 and PSISEQ2. Primers for fragment 3 were POLSEQ6, B935, BPOLEO1, MDN5, B936 and MDC1 (Tables 3, 4).

Table 3 PCR Primers

Primers	Sequence	Position (nt)
LSOB1	5'-GGCATTATTTGCATACCCTTTGG-3'	2739-2762
BPOLEO1	5'-CTGAGAGTCCAAGAGTCCTCT-3'	1657-1677
LSB11	5'-TTGTGGGTACCCATATTCTT-3'	2809-2829
POLSEQ2	5'-AGCAAACACTTGGCATAGGC-3'	1168-1188
MDN5	5'-AGGAGGCTGTAGGCATAAAT-3'	1774-1794
BPOLEO1	5'-CTGAGAGTCCAAGAGTCCTCT-3'	1657-1677
BPOLBO2	5'-TCTTGTCTTACTTTTGGGAAGA-3'	2216-2236
PSISEQ2	5'-GCTGTTCCGGAATTGGAGCC-3'	65-84
POLSEQ1	5'-ACCAAGCGTTGGGGCTACTC-3'	847-866
MDD2	5'-GAAGAATAAAGCCCAGTAAA-3'	2481-2500
POLSEQ6	5'-TTTCACTTTCTCGCCAACTTA-3'	1089-1109
MDC1	5'-TTGATAAGATAGGGGCATTTG-3'	2304-2324

Table 4 Sequencing primers

Primers	Sequence	Position (nt)
LSB1	5'-TTGTGGGTCACCATATTCTT-3'	2809-2829
PSISEQ2	5'-GCTGTTCCGGAATTGGAGCC-3'	65-84
ds2	5'-AGTCCGGTACGTCACCTTG-3'	3198-1
ds	5'-TACCGAAAATGGAGAACAACA-3'	147-166
ADELN	5'-TAGTCCAGAAGAACCAACAAG-3'	432-453
MD14	5'-GCGCTGCAGCTATGCCTCATCTTC-3'	418-433
ADELP	5'-CCTGTATTCCCATCCCATCATC-3'	597-618
POLSEQ8	5'-TGTTTTCGAAAACCTCCTGT-3'	943-962
POLSEQ9	5'-ACAGGAAGTTTTCGAAAACA-3'	943-962
POLSEQ6	5'-TTTCACTTCTCGCCAACTTA-3'	1089-1109
POLSEQ2	5'-AGCAAACACTGGCATAGGC-3'	1168-1188
BPOLBO2	5'-TCTTGTCTACTTTTGGAGA-3'	2216-2236
POLSEQ4	5'-AAATGCCCTATCTTATCAA-3'	2305-2323
LSOB1	5'-GGCATTATTTGCATACCCTTTGG-3'	2739-2762
POLSEQ5	5'-GGGTCCTTGTGGGGTTGAAG-3'	2979-2999
B935	5'-GAAGGTTTGTGGCTCCTCTG-3'	1240-1260
BPOLEO1	5'-CTGAGAGTCCAAGAGTCTCT-3'	1657-1677
MDN5	5'-AGGAGGCTGTAGGCATAAAT-3'	1774-1794
B936	5'-TGGAGGCTTGAACAGTAGGACAT-3'	1851-1874
MDC1	5'-TTGATAAGATAGGGCATTG-3'	2304-2324

Database sequences

The following complete genomes (represented by their accession number) were used in phylogenetic tree analyses: genotype A: AJ344115; genotype B: AF282917, D00331; genotype C: AY040627, AF461357, M38454, AY057948, AF241410, AF241411, AF330110, AB048705, AB026812, D00329, AB014398, X75665, X14193, X52939, X59795; genotype D: AF280817, AJ344116; genotype E: X75664; genotype F: AB036908; genotype G: AF405706.

Genotype and phylogeny analysis

The genotype of each HBV sequence was determined by comparison with sequences of known genotypes in the GenBank and EMBL nucleotide databases using the programme BLAST^[14]. Phylogenetic trees were constructed by maximum likelihood analysis by quartet puzzling^[15]. TreePuzzle is available at <http://www.tree-puzzle.de>.

RESULTS

HBV genotypes

Compared with sequences of known genotypes in the GenBank and EMBL nucleotide databases using the programme BLAST, all genotypes of each HBV sequence from the 20 asymptomatic HBV carriers in Long An County were found to be genotype C viruses.

Characterization of HBV genome structure

The full-length HBV-DNA sequence of HBV isolated from sample No. 624 was determined by direct sequencing. This strain contained 3 215 bases. Its serotype is adw. There were 40 point mutations in polymerase gene resulting in changes of 11 amino acids. There were 11, 2, 3 point mutations in PreS1, PreS2 and S genes, leading to 3, 1, 1 amino acids changed in the respective regions. The amino acid mutation in PreS1 was TPP→PHQ at codes 68-70. Six point mutations including the double mutations were found in X gene causing changes of 4 amino acids. There were also 13 point mutations in C gene, leading to 2 amino acids changed. No mutation was found in "a" determinant and Pre C.

Phylogeny analysis

The homology with 23 HBV strains in GenBank was determined

by using the programme TreePuzzle. The HBV strain isolated from sample No. 624 in Long An County was closer to the Vietnamese HBV of genotype C, with 97% homology between them, as compared to the isolates of the same genotype from Shanghai, Beijing and Tibet in evolution (Figure 1).

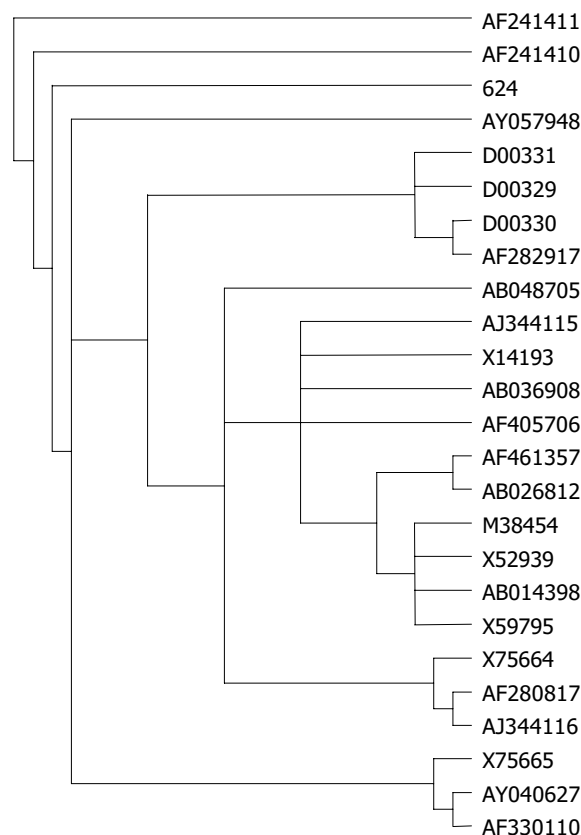


Figure 1 Phylogenetic trees based on comparison of the whole genome. The trees were created by maximum likelihood analysis using the TreePuzzle software with AF241411 as outgroup.

Prevalence of occult HBV infection

After nested PCR amplification, six samples of 52 family members of children without immunization of HBV vaccine were positive for HBV DNA, counting for 11.5% (6/52) (Table 2). The region of surface ORF of the samples with positive HBV DNA positive, including the "a" determinant of HBsAg, was sequenced. A point mutation from guanosine to adenosine at nucleotide position 587 resulted in an amino acid substitution from glycine to arginine in the highly antigenic "a" determinant of HbsAg, which was found in sample No. 37 only and was negative for both HBsAg and anti-HBs. The other samples with positive HBV DNA did not have unusual amino acid substitutions in or around the "a" determinant, and were attributed to the wild-type HBV of genotype C.

DISCUSSION

In 1988, Okamoto *et al.*^[3] established a method to classify HBV, and analyzed the complete HBV nucleotide sequences and classified them into four different HBV genotypes designated from A to D, according to an intergroup divergence of >8%, and an intragroup divergence of <5.6%. Today, HBV has been classified into eight different genotypes designated from A to H^[4,5,16,17] and HBV genotypes have a pattern of geographical distribution^[18,19]. Genotype A is prevalent in Northern and Central Europe, but is also common in North America and sub-Saharan Africa. Genotypes B and C are confined to Asia, genotype D is widespread but is the predominant genotype in

the Mediterranean region, while genotype E is found mainly in West Africa. Genotype F shows the highest divergence among the genotypes and is indigenous to aboriginal populations of the Americas^[20]. Genotype G was found in USA and France^[4], genotype H in the Central America^[5], and genotypes A, B, C and D in China. The predominant genotype in China is genotypes B and C^[21,22].

The incidence of HCC in Long An County is about 49.9/100 000 and the prevalence of HBsAg in the county is 16%^[13,23] and more than 90% of hepatocellular carcinoma (HCC) cases are individuals positive for HBsAg in serum^[12]. In Japan, HBV genotype C was found to be closely associated with severe liver diseases and the development of HCC^[7,24], although young HCC patients were found to be HBV genotype C in Taiwan^[25].

HBV infection is usually diagnosed when the circulating HBsAg is detected. However, advances in molecular biology techniques revealed that a low level of HBV DNA could be detected in serum and liver tissue in some individuals who were negative for HBsAg^[26,27]. Although there are some studies on occult HBV infection, the precise prevalence of this clinical entity is still unknown. Luo *et al.*^[28] found that the prevalence rate of occult HBV infection in Guangdong and Hainan Provinces was 2.0% (6/294) and 3.4% (68/1 995), respectively in the general population. Bower *et al.*^[29] reported that the prevalence was 4.3% (11/258) in subjects without liver disease in USA. In this study, we found that the prevalence of occult HBV infection in Long An County was higher (11.5%, 6/52). The mechanisms that HBV carriers have a low, but stable level of viral replication remain to be defined. HBV strains might have mutations in S region resulting in occult HBV infection^[30,31]. This kind of mutations was found in one of our samples. In addition, this type of carriers should be added to the typical HBsAg-positive carriers constituting about 16% of the general population, to estimate more precisely the proportion of asymptomatic HBV carriers in Long An County. It is clear that the prevalence of HBV infection in Long An County is in correspondence with its high incidence of HCC.

To extend the knowledge of molecular features of natural HBV isolates, sample No. 624 in this study was selected for whole genome sequencing. This strain contained 3 215 bases. HBsAg region sequence showed that it belonged to serotype adw. No special mutation which could change the expression function of viral proteins was found in the sequence of this isolate. By homology analysis with 23 HBV strains in GenBank, this isolate was found to be closer to the Vietnamese HBV genotype C strain^[32] than to the genotype C isolates from Shanghai in evolution^[33], with 97% homology with the Vietnamese isolate. At present, the only explanation about this is that Long An County is geographically close to Vietnam.

In summary, HBV infections in Long An County are attributable to HBV genotypes C. The prevalence of occult HBV infection in Long An County is higher.

ACKNOWLEDGMENTS

We are very grateful to the Beijing Municipal Committee of Science and Technology for the financial support in part and the Center for Disease Prevention and Control of Long An County for their help in collecting samples.

REFERENCES

- Magnius LO, Norder H. Subtypes, genotypes and molecular epidemiology of the hepatitis B virus as reacted by sequence variability of the S-gene. *Intervirology* 1995; **38**: 24-34
- Le Bouvier GL, McCollum RW, Hierholzer WJ Jr, Irwin GR, Krugman S, Giles JP. Subtypes of Australia antigen and hepatitis-B virus. *JAMA* 1972; **222**: 928-930
- Okamoto H, Tsuda F, Sakugawa H, Sastrosowignjo RI, Imai M, Miyakawa Y, Mayumi M. Typing hepatitis B virus by homology in nucleotide sequence: comparison of surface antigen subtypes. *J Gen Virol* 1988; **69**: 2575-2583
- Stuyver L, DeGendt S, VanGeyt C, Zoulim F, Fried M, Schinazi RF, Rossau R. A new genotype of hepatitis B virus: complete genome and phylogenetic relatedness. *J Gen Virol* 2000; **81**: 67-74
- Arauz-Ruiz P, Norder H, Robertson BH, Magnius LO. Genotype H: a new Amerindian genotype of hepatitis B virus revealed in Central America. *J Gen Virol* 2002; **83**: 2059-2073
- Ding X, Mizokami M, Yao GB, Xu B, Orito E, Ueda R, Nakanishi M. Hepatitis B virus genotype distribution among chronic hepatitis B virus carriers in Shanghai, China. *Intervirology* 2001; **44**: 43-47
- Fujie H, Moriya K, Shintani Y, Yotsuyanagi H, Iino S, Kimura S, Koike K. Hepatitis B virus genotypes and hepatocellular carcinoma in Japan. *Gastroenterology* 2001; **120**: 1564-1565
- Orito E, Ichida T, Sakugawa H, Sata M, Horiike N, Hino K, Okita K, Okanoue T, Iino S, Tanaka E, Suzuki K, Watanabe H, Hige S, Mizokami M. Geographic distribution of hepatitis B virus (HBV) genotype in patients with chronic HBV infection in Japan. *Hepatology* 2001; **34**: 590-594
- Kao JH, Chen PJ, Lai MY, Chen DS. Hepatitis B genotypes correlate with clinical outcomes in patients with chronic hepatitis B. *Gastroenterology* 2000; **118**: 554-559
- Paterlini P, Gerken G, Nakajima E, Terre S, D'Errico A, Grigioni W. Polymerase chain reaction to detect hepatitis B virus DNA and RNA sequences in primary liver cancers from patients negative for hepatitis B surface antigen. *N Engl J Med* 1990; **323**: 80-85
- Paterlini P, Poussin K, Kew M, Franco D, Brechot C. Selective accumulation of the X transcript of hepatitis B virus in patients negative for hepatitis B surface antigen with hepatocellular carcinoma. *Hepatology* 1995; **21**: 313-321
- Yeh FS, Yu MC, Mo CC, Luo S, Tong MJ, Henderson BE. Hepatitis B virus, aflatoxins, and hepatocellular carcinoma in southern Guangxi, China. *Cancer Research* 1989; **49**: 2506-2509
- Ding ZG. Epidemiological study on relationship between hepatitis B and liver cancer: a prospective study on development of liver cancer and distribution of HBsAg carriers and liver damage persons in Guangxi. *Zhonghua Liuxingbingxue Zazhi* 1988; **9**: 220-223
- Altschul SF, Gish W, Miller W, Myers EW, Lipman DJ. Basic local alignment search tool. *J Mol Biol* 1990; **215**: 403-410
- Strimmer K, Haeseler A. Quartet puzzling: a quartet maximum-likelihood method for reconstructing tree topologies. *Mol Biol Evolution* 1996; **13**: 964-969
- Norder H, Hammas B, Logfdahl S, Courouce AM, Magnius LO. Comparison of the amino acid sequences of nine different serotypes of hepatitis B surface antigen and genomic classification of the corresponding hepatitis B virus strains. *J Gen Virol* 1992; **73**: 1201-1208
- Norder H, Courouce AM, Magnius LO. Complete genomes, phylogenetic relatedness, and structural proteins of six strains of the hepatitis B virus, four of which represent two new genotypes. *Virology* 1994; **198**: 489-503
- Nakano T, Lu L, Hu X, Mizokami M, Orito E, Shapiro C, Hadler S, Robertson B. Characterization of hepatitis B virus genotype among Yuipa Indians in Venezuela. *J Gen Virol* 2001; **82**: 359-365
- Naumann H, Schaefer S, Yoshida CF, Gaspar AM, Repp R, Gerlich WH. Identification of a new hepatitis B virus genotype from Brazil that expresses HBV surface antigen subtype adw 4. *J Gen Virol* 1993; **74**: 1627-1632
- Norder H, Hammas B, Lee SD, Bile K, Courouce AM, Mushahwar IK, Magnius LO. Genetic relatedness of hepatitis B viral strains of diverse geographical origin and natural variations in the primary structure of the surface antigen. *J Gen Virol* 1993; **74**: 1341-1348
- Ding X, Mizokami M, Ge XM, Orito E, Iino S, Ueda R, Nakanishi M. Different hepatitis B virus genotype distributions among asymptomatic carriers and patients with liver diseases in Nanning, southern China. *Hepatology Research* 2002; **22**: 37-44
- Xia G, Nainan OV, Jia Z. Characterization and distribution of hepatitis B virus genotypes and subtypes in 4 provinces of

- China. *Zhonghua Liuxingbingxue Zazhi* 2001; **22**: 348-351
- 23 **Wang SS**, Xu ZY, Maynard JE, Prince AM, Beasley RP, Yang JY, Li YC, Nong YZ. Evaluation of the hepatitis B model immunization program in Long An county, China. *Guangxi Yufang Yixue Zazhi* 1995; **1**: 1-4
- 24 **Orito E**, Mizokami M, Sakugawa H, Michitaka K, Ishikawa K, Ichida T, Okanoue T, Yotsuyanagi H, Iino S. A case-control study for clinical and molecular biological differences between hepatitis B viruses of genotypes B and C. *Hepatology* 2001; **33**: 218-223
- 25 **Kao JH**, Chen DS. Hepatitis B virus genotypes and hepatocellular carcinoma in Japan: reply. *Gastroenterology* 2001; **120**: 1565
- 26 **Wang JT**, Wang TH, Sheu JC, Shih LN, Lin JT, Chen DS. Detection of hepatitis B virus DNA by polymerase chain reaction in plasma of volunteer blood donors negative for hepatitis B surface antigen. *J Infect Dis* 1991; **163**: 397-399
- 27 **Zhang YY**, Hansson BG, Kuo LS, Widell A, Nordenfelt E. Hepatitis B virus DNA in serum and liver is commonly found in Chinese patients with chronic liver disease despite the presence of antibodies to HBsAg. *Hepatology* 1993; **17**: 538-544
- 28 **Luo KX**, Zhou R, He C, Liang ZS, Jiang SB. Hepatitis B virus DNA in sera of virus carriers positive exclusively for antibodies to the hepatitis B core antigen. *J Med Virol* 1991; **35**: 55-59
- 29 **Bower WA**, Xia GL, Gao FX, Nainan OV, Kruszon-Moran D, Margolis HS. Isolated hepatitis B core antibody. *Antiviral Ther* 2000; **5**(Suppl 1): B22
- 30 **Blackberg J**, Kidd-Ljunggren K. Occult hepatitis B virus after acute self-limited infection persisting for 30 years without sequence variation. *J Hepatol* 2000; **33**: 992-997
- 31 **Yamamoto K**, Horikita M, Tsuda M, Itoh K, Akahane Y, Yotsumoto S, Okamoto H, Miyakawa Y, Mayumi M. Naturally occurring escape mutants of hepatitis B virus with various mutations in the S gene in carriers seropositive for antibodies to hepatitis B surface antigen. *J Virol* 1994; **68**: 2671-2676
- 32 **Hannoun C**, Norder H, Lindh M. An aberrant genotype revealed in recombinant hepatitis B virus strains from Vietnam. *J Gen Virol* 2000; **81**: 2267-2272
- 33 **Gan RB**, Chu MJ, Shen LP, Qian SW, Li ZP. The complete nucleotide sequence of the cloned DNA of hepatitis B virus subtype adr in pADR-1. *Sci Sin* 1987: 507-521

Edited by Ren SY and Wang XL Proofread by Xu FM

• VIRAL HEPATITIS •

Capsule oxymatrine in treatment of hepatic fibrosis due to chronic viral hepatitis: A randomized, double blind, placebo-controlled, multicenter clinical study

Yi-Min Mao, Min-De Zeng, Lun-Gen Lu, Mo-Bin Wan, Cheng-Zhong Li, Cheng-Wei Chen, Qing-Chuen Fu, Ji-Yao Wang, Wei-Min She, Xiong Cai, Jun Ye, Xia-Qiu Zhou, Hui Wang, Shan-Ming Wu, Mei-Fang Tang, Jin-Shui Zhu, Wei-Xiong Chen, Hui-Quan Zhang

Yi-Min Mao, Min-De Zeng, Lun-Gen Lu, Shanghai Institute of Digestive Disease, Renji Hospital, Shanghai Second Medical University, Shanghai 200001, China

Mo-Bin Wan, Cheng-Zhong Li, Changhai Hospital, Second Military Medical University, Shanghai 200433, China

Cheng-Wei Chen, Qing-Chuen Fu, Nanjing Military Command Liver Disease Research Center, Shanghai 200233, China

Ji-Yao Wang, Wei-Min She, Zhongshan Hospital, Fudan University, Shanghai 200032, China

Xiong Cai, Changzheng Hospital, Second Military Medical University, Shanghai 200003, China

Jun Ye, Shanghai Putuo District Central Hospital, Shanghai 200333, China

Xia-Qiu Zhou, Hui Wang, Ruijin Hospital, Shanghai Second Medical University, Shanghai 200025, China

Shan-Ming Wu, Mei-Fang Tang, Shanghai General Hospital of Infectious Diseases, Shanghai 200083, China

Jin-Shui Zhu, Wei-Xiong Chen, Shanghai No.6 People's Hospital, Shanghai 200230, China

Hui-Quan Zhang, Shanghai Shibe Hospital, Shanghai 200073, China

Supported by Grants From the Key Project of Shanghai Medical Development Foundation, NO:99ZDI001 and Grants From 1999 Youth Liver Diseases Foundation of Chinese Liver Diseases Association

Correspondence to: Yi-Min Mao, M.D., Shanghai Institute of Digestive Disease, Renji Hospital, Shanghai Second Medical University, Shanghai 200001, China. maoyimin1@sina.com

Telephone: +86-21-33070834 **Fax:** +86-21-63364118

Received: 2003-12-17 **Accepted:** 2004-02-24

Abstract

AIM: To evaluate the efficacy and safety of oxymatrine capsule in treatment of hepatic fibrosis in patients with chronic viral hepatitis.

METHODS: It was a randomized, double blind, placebo-controlled, multicenter clinical study. One hundred and forty-four patients were divided into oxymatrine capsule group (group A) and placebo group (group B). The course was 52 wk. Patients were visited once every 12 wk and the last visit was at 12 wk after cessation of the treatment. All patients had liver biopsy before treatment. part of them had a second biopsy at the end of therapy. Clinical symptoms, liver function test, serum markers of hepatic fibrosis were tested. Ultrasound evaluation was performed before, during and at the end of therapy.

RESULTS: One hundred and forty-four patients enrolled in the study. Of them 132 patients completed the study according to the protocol, 49 patients had liver biopsy twice (25 patients in group A and 24 in group B). At the end of therapy, significant improvements in hepatic fibrosis and inflammatory activity based on Semi-quantitative scoring system (SSS) were achieved in group A. The total effective rate of the treatment was 48.00%, much higher than that of 4.17% in group B ($P < 0.05$). Significant improvement in serum markers of hepatic fibrosis such as hyaluronic acid (HA) and type III procollagenic

peptide (P III P) in group A was seen ($P < 0.05$). The total effective rate of serum markers at the end of therapy in group A was 68.19%, much higher than that of 34.85% in group B ($P < 0.05$). The total effective rate of noninvasive markers at the end of therapy in group A was 66.67%, much higher than that of 30.30% in group B ($P < 0.05$). The rate of adverse events was similar in two groups.

CONCLUSION: Oxymatrine capsule is effective and safe in treatment of hepatic fibrosis due to chronic viral hepatitis.

Mao YM, Zeng MD, Lu LG, Wan MB, Li CZ, Chen CW, Fu QC, Wang JY, She WM, Cai X, Ye J, Zhou XQ, Wang H, Wu SM, Tang MF, Zhu JS, Chen WX, Zhang HQ. Capsule oxymatrine in treatment of hepatic fibrosis due to chronic viral hepatitis: A randomized, double blind, placebo-controlled, multicenter clinical study. *World J Gastroenterol* 2004; 10(22): 3269-3273
<http://www.wjgnet.com/1007-9327/10/3269.asp>

INTRODUCTION

Hepatic fibrosis is a kind of compensating and healing response in the liver to liver injury induced by a variety of causes and also a common pathological process of many chronic liver diseases characterized by hyperplasia and deposition of fibro-connective tissues. It is essential to block the genesis and progress of hepatic fibrosis^[1-5,30,31]. Oxymatrine is a kind of alkaloid extracted from a Chinese herb *Sophora alopecuroides* L. which has been proved to have antihepatic fibrosis effect^[6,7,18-20]. In this paper, we reported the clinical study data of oxymatrine capsule in treatment of hepatic fibrosis in patients with chronic viral hepatitis.

MATERIALS AND METHODS

Research design

This study was a clinical trial characterized by multicentre, randomization, double blinding, and placebo-control. Enrolled patients were randomly assigned into oxymatrine capsule group (group A) or vacant placebo control group (group B), with 72 cases in each group and a treatment course of 52 wk. This study was conformed to the Good Clinical Practice (GCP) of China. The research protocol was discussed and approved by the Ethic Committee of National Clinical Research Base of Drugs in the Institute of Digestive Disease of Renji Hospital. Informed consent was obtained from each patient.

Selection of subjects

Enrolled criteria were age: 18-65 years regardless of sex; positive serum markers of hepatitis B virus (HBV) and hepatitis C virus (HCV) for at least 6 mo before enrollment; abnormal serum value of alanine transaminase (ALT) twice or more within 6 mo before enrollment; liver biopsy examination during 1 mo before enrollment indicating the stage of hepatic fibrosis from 1 to 4 according to National Criteria of Grading and Staging for chronic

viral hepatitis amended in 1995 and the scores of stage equal or more than 1 assessed by the semi-quantitative scoring system (SSS) of hepatic fibrosis; total serum bilirubin level less than or equal to 85.5 $\mu\text{mol/L}$; no history of administering following drugs: antiviral drugs, immunoregulating drugs and other antifibrotic agents; promising not to receive other systemic antiviral agents, cytotoxic agents, immunoregulators, drugs capable of reducing serum enzyme activity and bilirubin level, and Chinese traditional medicines, *etc.* Following situations should be excluded: patients with positive laboratory test of HIV; uncompensable liver diseases; suggestive of autoimmune diseases with antinuclear antibody (ANA) titer greater than a 1:160 dilution; bone marrow inhibition; abnormality of serum creatinine with a value 1.5 times greater than normal; concurrence of other associated diseases which might affect the present treatment such as unstable diabetes, renal insufficiency, unstable angina pectoris, alcoholic liver disease, epilepsy, obvious manifestations of neurosis, drug abuser, psychosis, pancreatitis, disability of absorption and malignant disease, and so on; Having taken other drugs in clinical trial within 30 d before the first medication; hypersensitive to oxymatrine capsule; pregnancy and during breast-feeding period; female conceptive patients not adopting any contraceptives.

Treatment procedures and drugs

After completion of selection and assessment, qualified subjects were allocated into group A or B randomly. The patients in group A took 300 mg oxymatrine capsules orally 3 times a day, and 2 tablets of complex vitamins B and C at the same time for 52 wk. The patients in group B took 3 tablets of vacant capsules instead of oxymatrine capsules and complex vitamins B and C at the same frequency as described above for 52 wk. All patients received follow-up once every 12 wk during treatment and were followed up at out-patient department 12 wk after treatment. Oxymatrine capsule, vacant placebo capsule, complex vitamins B and C tablets were manufactured and provided by Ningxia Pharmaceutic Institute and Shanghai Green Valley Ecological Engineering Co.LTD.

Observation of indexes and assessment

Clinical manifestations Clinical symptoms and signs were divided into grades from 0 to 3 according to the symptomatic grading criteria, evaluated at each follow-up visit, and examined 24 and 52 wk after treatment and 12 wk after drug withdrawal.

Analysis of blood and urine routines and related liver function indexes These indexes were evaluated at each follow-up visit and examined 52 wk after treatment and 12 wk after drug withdrawal.

Analysis of serum markers of hepatic fibrosis Tests of serum hyaluronic acid (HA), laminin (LN), type III procollagenic peptide (p III p), type IV collagen-7S (IV-7S) were fulfilled by Military Clinical Immunologic Research Centre of Changzheng Hospital, Second Military Medical University. The above markers were evaluated before treatment, 24 and 52 wk after treatment, 12 wk after drug withdrawal respectively, and examined 24 and 52 wk after treatment, 12 wk after drug withdrawal, respectively.

Imaging examination (type B ultrasound) The detection included 5 indexes: maximal oblique radius of right liver lobe, main trunk diameter of portal vein and its blood flow parameters per minute; width of spleen at the hilus and the diameter of splenic vein. Ultrasound examination was performed on fixed machines and by fixed operators and the data were recorded and input in computers which were read by experts. All the indexes were evaluated before treatment and 52 wk after therapy, examined 52 wk after drug withdrawal.

Histopathological detection Histopathological specimens were independently observed and assessed based on National Criteria of Grading and Staging for chronic viral hepatitis amended in

1995 and SSS by 3 pathologists from Department of Pathology, Medical College, Fudan University. The observed results were checked by another 3 pathologists who did not anticipate in the study by Kappa test. The reciprocal consistence among the above pathologists was satisfactory. The observed results in all patients were evaluated before therapy and part of them were evaluated 52 wk after therapy. All data were examined 52 wk after therapy.

During treatment and after therapy was terminated, the following events were recorded: combined medication, adverse reactions and the compliance of patients.

Assessment of therapeutic effects

Indexes of histopathology The curative effect was evaluated based on SSS. Distinctly effective: the scores of hepatic fibrosis based on SSS from liver biopsy decreased at least 6 scores compared with that before treatment. Effective: the above scores decreased at least 2 scores. Ineffective: the effect did not meet the effective criteria.

Assessment of indexes of noninvasive tests These indexes were evaluated comprehensively in terms of clinical manifestations, serum liver fibrotic markers and ultrasound detection data. Distinctly effective: any two values among serum liver fibrotic indexes decreased by at least 80% compared with that before treatment, at least the main trunk diameter of portal vein and splenic width returned to normal after treatment, clinical symptoms and signs disappeared or their total scores decreased by at least 75% compared with that before treatment. Effective: any two values among serum liver fibrotic indexes decreased by at least 40% compared with that before treatment, the main trunk diameter of portal vein and splenic width reduced after treatment, clinical symptoms and signs disappeared basically or their total scores decreased by at least 25% compared with that before treatment. Ineffective: the effect did not meet the effective criteria.

Assessment of safety

Any abnormal clinical manifestations and laboratory tests occurred during treatment were recorded and divided into 4 grades according to the criteria published by WHO and the Ministry of Public Health of China in 1994.

Statistical analysis

Statistical analyses were performed by professor Su BH and He QB from Department of Statistics, Shanghai Second Medical University, and SAS 6.12 software kit was used.

RESULTS

Selected patients

A total of 144 patients satisfied the selection criteria. Of them, 12 cases withdrew or were excluded during treatment, 132 cases fulfilled the treatment course according to the required protocol (66 cases in group A and 66 cases in group B). Before treatment, the following general data between two groups were similar ($P>0.05$, respectively): sex, age, drinking history, duration of hepatitis, duration of abnormality of liver function and a more than 2-fold normal elevation of serum ALT, *etc.* Each qualified patient received liver biopsy before treatment. A total of 49 cases had a second liver biopsy (25 cases in group A and 24 cases in group B).

Analysis of observed indexes

Clinical symptoms and signs Clinical manifestations in group A were obviously improved 52 wk after therapy ($P<0.05$), except for epistaxis ($P = 1.0000$). Heptomegaly was also improved significantly after therapy ($P=0.0313$), symptoms of gum bleeding

and epistaxis were not improved obviously in group B ($P>0.05$). Signs of hepatomegaly, splenomegaly and liver palm were significantly improved in group B ($P<0.05$), improvement of anorexia in group A was greater than that in group B ($P=0.0263$).

Liver function Indexes of liver function in group A were significantly improved 52 wk after treatment ($P<0.05$) except for serum gamma glutamino transpeptidase (GGT) and TB ($P>0.05$). In group B, indexes such as serum ALT, AST, TB and alkaline phosphatase (ALP) had no obvious difference before and after therapy ($P>0.05$). Compared with group B, the improvement of ALT and AST in group A was much greater ($P=0.0007$ and 0.0025). Fifty-two wk after therapy, the normalization rate of ALT in group A was 70.77%, much higher than 39.68% in group B ($P=0.0003$). In groups A and B, 14 out of 46 cases (30.43%) and 12 out of 25 cases (48.00%) had their serum ALT levels returned to normal 52 wk after treatment, and their serum ALT levels became abnormal again after drug withdrawal.

Liver histologic examination Evaluation of hepatic fibrosis based on SSS: In group A, the scores of hepatic fibrosis after therapy were 4.72 ± 5.63 , much smaller than 6.76 ± 6.67 before therapy ($P=0.0001$), while the scores in group B after therapy increased significantly ($P=0.0009$). There was an obvious difference between two groups ($P=0$) (Table 1). Evaluation of histologic inflammatory activity based on SSS: In group A, the scores of histologic activity decreased from 46.08 ± 3.84 before treatment to 4.00 ± 2.97 after therapy ($P=0.0002$), while the scores in group B after therapy did not decrease obviously ($P=0.2344$). There was an obvious difference between two groups ($P=0.0008$) (Table 2).

Evaluation of serum markers of hepatic fibrosis In group A, serum levels of HA, LN, p III p and IV-7S decreased significantly 24 and 52 wk after treatment ($P<0.05$). In group B, serum levels of LN, p III p and IV-7S also decreased obviously after treatment ($P<0.05$). However, degrees of improvement in HA and p III p

between two groups were distinctly different ($P<0.05$). In group A, except for LN ($P=0.1493$), the other 3 liver fibrotic markers increased significantly 12 wk after drug withdrawal compared with that 52 wk after treatment ($P<0.05$). In group B, except for HA ($P=0.4212$), the other markers also increased obviously 12 wk after drug withdrawal compared with that 52 wk after treatment ($P<0.05$). The increase of HA in group A was more than that in group B ($P=0.0002$) and the increase of IV-7S in group B was more than that in group A ($P=0.0048$).

Imaging examination After treatment, the average values of main trunk diameters of portal vein and splenic width in group A obviously decreased ($P<0.05$). However, in group B, the above two parameters and the parameters of blood flow volume per minute of portal vein and diameters of splenic vein all increased significantly compared with those before therapy ($P<0.05$). The changes in main trunk diameters of portal vein and splenic width between two groups were statistically significant ($P<0.05$).

Analysis of therapeutic effect

Assessment of histopathology based on SSS After treatment, the rates of distinct effectiveness and effectiveness in group A were both 24.00%, and the total effective rate was 48.00%. In group B, none achieved distinct effectiveness and the effective rate was only 4.17%; Comparison of the rates of distinct effectiveness and effectiveness between two groups had a significant difference ($P=0.004$) (Table 3).

Assessment of serum markers of hepatic fibrosis The total effective rate of group A 24 and 52 wk after therapy was 57.43% and 68.19%, more than 24.24% and 34.85% of group B ($P=0.0002$ and 0.0004 , respectively). Twelve weeks after treatment, the total effective rate of group A was 50.00%, more than 15.16% of group B ($P=0.00$).

Assessment of noninvasive indexes of hepatic fibrosis After treatment, the rates of distinct effectiveness and effectiveness

Table 1 Liver fibrotic scores before and after therapy based on Semi-quantitative Scoring System

Group	Before	After	Before-after	Comparison before therapy		Comparison within group		Comparison between groups	
				Statistics	P	Statistics	P	Statistics	P
A (n = 25)	6.76±6.67	4.72±5.63	2.04±2.59	1.4098	0.1586	96.0	0.0001	4.8834	0
B (n = 24)	4.13±2.82	6.33±4.04	-2.21±3.72						

Table 2 Liver histologic activity scores before and after therapy based on Semi-quantitative Scoring System

Group	Before	After	Before-after	Comparison before therapy		Comparison within group		Comparison between groups	
				Statistics	P	Statistics	P	Statistics	P
A (n = 25)	6.08±3.84	4.00±2.97	2.08±2.71	0.0407	0.9675	69.5	0.0002	3.3543	0.0008
B (n = 24)	6.08±4.06	6.92±4.17	-0.83±3.38						

Table 3 Comparison of histopathology of hepatic fibrosis

Group	Distinctly effective	Effective	Ineffect-ive	Comparison between 2 groups	
				Statistics χ^2	P
A (n = 25)	6 (24.00%)	6 (24.00%)	13 (52.00%)	12.6970	0.0004
B (n = 24)	0 (0.00%)	1 (4.17%)	23 (95.83%)		

Table 4 Comparison of noninvasive markers of hepatic fibrosis

Group	Distinctly effective	Effective	Ineffect-ive	Comparison between 2 groups	
				Statistics χ^2	P
A (n = 66)	2 (3.03%)	42 (63.64%)	22 (33.33%)	16.2494	0.0001
B (n = 66)	0 (0.00%)	20 (30.30%)	46 (69.70%)		

in group A were respectively 3.03% and 63.64%, and the total effective rate was 66.67%. In group B, the rates of distinct effectiveness and effectiveness were respectively 0% and 30.30%, and the total effective rate was 30.30%. The comparison of the above statistics between two groups had a significant difference ($P = 0.0001$) (Table 4).

Adverse effects

In group A, there were 5 patients who suffered from adverse drug reactions and the incidence was 6.94%. The adverse drug reactions mainly included nausea, rash, chest discomfort, fever, epigastric comfort, diarrhea and poor taste, and most of them were mild or moderate. None of the patients withdrew because of adverse drug reactions. In group B, adverse effects occurred in 7 patients and the incidence was 9.72%. The manifestations were similar to those in group A and 1 patient withdrew because of weakness, anorexia, epigastric discomfort after taking drugs.

DISCUSSION

Hepatic fibrosis, a precursor of cirrhosis, is a consequence of sever liver damage that occurred in many patients with chronic liver disease, and involves the abnormal accumulation of extracellular matrix^[3,4,11,12]. Liver fibrosis represents a major worldwide healthcare burden. Current therapy is limited to removing the causal agent. This approach has been successful in some diseases, particularly in haemochromatosis and chronic viral hepatitis^[9,10,17,28]. However, for many patients treatment was not possible, while other patients presenting to medical attention were at an advanced stage of fibrosis^[8,9]. There is therefore a great need for novel therapies for liver fibrosis. Tremendous insights into the understanding of hepatic fibrosis have taken place over the past ten years. Foremost among these is the recognition that hepatic stellate cells (formerly known as lipocytes, Ito cells, or fat-storing cells) play a central role based on their ability to undergo activation following liver injury of any cause^[11,15,16,29]. Hepatic stellate cells have been recognised to be responsible for most of the excess extracellular matrix observed in chronic liver fibrosis. The detailed understanding of hepatic stellate cell biology has allowed the rational design of novel antifibrotic therapies^[29]. Effective therapy for hepatic fibrogenesis would probably also be multifactorial, based on the basic mechanisms underlying the fibrogenic process^[13,14,21-23].

At present, it is considered that treatment of hepatic fibrosis and antihepatic fibrosis are two different concepts and antifibrotic drugs should act on various parts of the genesis and development of hepatic fibrosis. Firstly, as for etiological treatment, oxymatrine could effectively treat chronic viral hepatitis and promote the serum markers of hepatitis B virus (HBV) and hepatitis C virus (HCV) in chronic hepatitis B and C to convert to negative and reduce serum level of ALT^[6,7]. Secondly, oxymatrine could inhibit the proliferation of hepatic stellate cells (HSC) at the concentrations of 0.5-16 $\mu\text{g}/\text{mL}$ *in vitro*. In addition, oxygen stress and lipid peroxidation are important mechanisms responsible for hepatic injury and hepatic stellate cell activation. Therefore, inhibition of lipid peroxidation is an essential strategy of antihepatic fibrosis^[12-16]. By establishing D-galactosamine-induced rat liver

fibrosis model, we observed the effect of oxymatrine on serum and tissue biochemical indexes, content of liver hydroxyline, expression of TGF β 1 mRNA and changes of tissue pathology, the results showed oxymatrine had prophylactic and therapeutic effects on D-galactosamine induced rat liver fibrosis. This was partly by protecting hepatocytes and suppressing fibrosis accumulation through anti-lipoperoxidation^[10]. In present study, We found that the scores of hepatic fibrosis after therapy in group A were 4.72 ± 5.63 , much smaller than 6.76 ± 6.67 before therapy, and the scores in group B after therapy increased significantly. There was an obvious difference between two groups. The scores of histological inflammatory activity in group A decreased from 46.08 ± 3.84 before treatment to 4.00 ± 2.97 after therapy, and the scores in group B after therapy did not decrease obviously. There was an obvious difference between two groups both in improvement of histopathology and in improvement of noninvasive indexes such as clinical manifestations, serum markers of hepatic fibrosis^[24-27]. Associated indexes of liver function and imaging detection indicated that oxymatrine was an ideal drug of antihepatic fibrosis. It is valuable to pay more attentions to the basic and clinical research of oxymatrine in order to explore the accurate mechanisms of its effect on antihepatic fibrosis.

REFERENCES

- 1 Arthur MJ. Pathogenesis, experimental manipulation and treatment of liver fibrosis. *Exp Nephrol* 1995; **3**: 90-95
- 2 Brenner DA, Waterboer T, Choi SK, Lindquist JN, Stefanovic B, Burchardt E, Yamauchi M, Gillan A, Rippe RA. New aspects of hepatic fibrosis. *J Hepatol* 2000; **32**(Suppl): 32-38
- 3 Albanis E, Friedman SL. Hepatic fibrosis. Pathogenesis and principles of therapy. *Clin Liver Dis* 2001; **5**: 315-334
- 4 Friedman SL. Molecular mechanisms of hepatic fibrosis and principles of therapy. *J Gastroenterol* 1997; **32**: 424-430
- 5 Rockey DC. The cell and molecular biology of hepatic fibrogenesis. Clinical and therapeutic implications. *Clin Liver Dis* 2000; **4**: 319-355
- 6 Li J, Li C, Zeng M. Preliminary study on therapeutic effect of oxymatrine in treating patients with chronic hepatitis C. *Zhongguo Zhongxiyi Jiehe Zazhi* 1998; **18**: 227-229
- 7 Yu YY, Wang QH, Zhu LM, Zhang QB, Xu DZ, Guo YB, Wang CQ, Guo SH, Zhou XQ, Zhang LX. A clinical research on oxymatrine for the treatment of chronic hepatitis B. *Zhonghua Ganzangbing Zazhi* 2002; **10**: 280-281
- 8 Chen Y, Li J, Zeng M, Lu L, Qu D, Mao Y, Fan Z, Hua J. The inhibitory effect of oxymatrine on hepatitis C virus *in vitro*. *Zhonghua Ganzangbing Zazhi* 2001; **9**(Suppl): 12-14
- 9 Yang W, Zeng M, Fan Z, Mao Y, Song Y, Jia Y, Lu L, Chen CW, Peng YS, Zhu HY. Prophylactic and therapeutic effect of oxymatrine on D-galactosamine-induced rat liver fibrosis. *Zhonghua Ganzangbing Zazhi* 2002; **10**: 193-196
- 10 Schuppan D, Porov Y. Hepatic fibrosis: From bench to bedside. *J Gastroenterol Hepatol* 2002; **17**(Suppl 3): S300-S305
- 11 Li D, Friedman SL. Liver fibrogenesis and the role of hepatic stellate cells: new insights and prospects for therapy. *J Gastroenterol Hepatol* 1999; **14**: 618-633
- 12 Poli G. Pathogenesis of liver fibrosis: role of oxidative stress. *Mol Aspects Med* 2000; **21**: 49-98

- 13 **Poli G**, Parola M. Oxidative damage and fibrogenesis. *Free Radic Biol Med* 1997; **22**: 287-305
- 14 **Bjorneboe A**, Bjorneboe GE. Antioxidant status and alcohol-related diseases. *Alcohol Alcohol* 1993; **28**: 111-116
- 15 **Tsukamoto H**, Rippe R, Niemela O, Lin M. Roles of oxidative stress in activation of Kupffer and Ito cells in liver fibrogenesis. *J Gastroenterol Hepatol* 1995; **10**(Suppl 1): S50-53
- 16 **Kim KY**, Choi I, Kim SS. Progression of hepatic stellate cell activation is associated with the level of oxidative stress rather than cytokines during CCl₄-induced fibrogenesis. *Mol Cells* 2000; **10**: 289-300
- 17 **Dong Y**, Xi H, Yu Y, Wang Q, Jiang K, Li L. Effects of oxymatrine on the serum levels of T helper cell 1 and 2 cytokines and the expression of the S gene in hepatitis B virus S gene transgenic mice: a study on the anti-hepatitis B virus mechanism of oxymatrine. *J Gastroenterol Hepatol* 2002; **17**: 1299-1306
- 18 **Xiang X**, Wang G, Cai X, Li Y. Effect of oxymatrine on murine fulminant hepatitis and hepatocyte apoptosis. *Chin Med J* 2002; **115**: 593-596
- 19 **Song J**, Wang LL, Zhu L, Zhong HM, Yao P. Effects of oxymatrine on procollagen metabolism and its gene expression in experimental fibrotic rats. *Zhonghua Ganzangbing Zazhi* 2003; **11**: 697
- 20 **Liu J**, Manheimer E, Tsutani K, Gluud C. Medicinal herbs for hepatitis C virus infection: a Cochrane hepatobiliary systematic review of randomized trials. *Am J Gastroenterol* 2003; **98**: 538-544
- 21 **Coutinho EM**, Barros AF, Barbosa A Jr, Oliveira SA, Silva LM, Araujo RE, Andrade ZA. Host nutritional status as a contributory factor to the remodeling of schistosomal hepatic fibrosis. *Mem Inst Oswaldo Cruz* 2003; **98**: 919-925
- 22 **Hui JM**, Sud A, Farrell GC, Bandara P, Byth K, Kench JG, McCaughan GW, George J. Insulin resistance is associated with chronic hepatitis C and virus infection fibrosis progression. *Gastroenterology* 2003; **125**: 1695-1704
- 23 **Perrillo RP**. Management of the patient with hepatitis B virus-related cirrhosis. *J Hepatol* 2003; **39**(Suppl 1): S177-180
- 24 **Kim CW**, Yoon SK, Jo BS, Shin JY, Jang JW, Choi JY, Han NI, Lee CD, Chung KW, Sun HS. Prediction of hepatic fibrosis using serum hyaluronic acid in patients with chronic liver disease. *Korean J Gastroenterol* 2003; **42**: 510-518
- 25 **Tang M**, Potter JJ, Mezey E. Activation of the human alpha1 (I) collagen promoter by leptin is not mediated by transforming growth factor beta responsive elements. *Biochem Biophys Res Commun* 2003; **312**: 629-633
- 26 **Xu GG**, Luo CY, Wu SM, Wang CL. The relationship between staging of hepatic fibrosis and the levels of serum biochemistry. *Hepatobiliary Pancreat Dis Int* 2002; **1**: 246-248
- 27 **Xie SB**, Yao JL, Zheng SS, Yao CL, Zheng RQ. The levels of serum fibrosis marks and morphometric quantitative measurement of hepatic fibrosis. *Hepatobiliary Pancreat Dis Int* 2002; **1**: 202-206
- 28 **Xie Y**, Zhao H, Dai WS, Xu DZ. HBV DNA level and antigen concentration in evaluating liver damage of patients with chronic hepatitis B. *Hepatobiliary Pancreat Dis Int* 2003; **2**: 418-422
- 29 **Oakley F**, Trim N, Constandinou CM, Ye W, Gray AM, Frantz G, Hillan K, Kendall T, Benyon RC, Mann DA, Iredale JP. Hepatocytes express nerve growth factor during liver injury: evidence for paracrine regulation of hepatic stellate cell apoptosis. *Am J Pathol* 2003; **163**: 1849-1858
- 30 **Kondou H**, Mushiake S, Etani Y, Miyoshi Y, Michigami T, Ozono K. A blocking peptide for transforming growth factor-beta1 activation prevents hepatic fibrosis *in vivo*. *J Hepatol* 2003; **39**: 742-748
- 31 **Dodig M**, Mullen KD. New mechanism of selective killing of activated hepatic stellate cells. *Hepatology* 2003; **38**: 1051-1053

Edited by Wang XL and Xu FM

Neither gastric topological distribution nor principle virulence genes of *Helicobacter pylori* contributes to clinical outcomes

Yan Wing Ho, Khek Yu Ho, Felipe Ascencio, Bow Ho

Yan Wing Ho, Bow Ho, Department of Microbiology, Faculty of Medicine, National University of Singapore, Singapore

Khek Yu Ho, Department of Medicine, Faculty of Medicine, National University of Singapore, Singapore

Felipe Ascencio, Departamento de Patologia Marina, Centro de Investigaciones Biologicas del Noroeste (CIBNOR), La Paz, Mexico

Yan Wing Ho, is a National University of Singapore Research Scholar Supported by NMRC Grant, No. 0415/2000, R-182-000-037-213

Correspondence to: Bow Ho, Department of Microbiology, Faculty of Medicine, National University of Singapore, 5 Science Drive 2, Singapore 117597, Republic of Singapore. michob@nus.edu.sg

Telephone: +65-68743672 **Fax:** +65-67766872

Received: 2004-02-27 **Accepted:** 2004-04-29

Abstract

AIM: Studies on *Helicobacter pylori* (*H pylori*) and gastroduodenal diseases have focused mainly on the distal sites of the stomach, but relationship with the gastric cardia is lacking. The aim of this study is to determine if the gastric topology and genotypic distribution of *H pylori* were associated with different upper gastrointestinal pathologies in a multi-ethnic Asian population.

METHODS: Gastric biopsies from the cardia, body/corpus and antrum were endoscoped from a total of 155 patients with dyspepsia and/or reflux symptoms, with informed consent. *H pylori* isolates obtained were tested for the presence of *26kDa*, *ureC*, *cagA*, *vacA*, *iceA1*, *iceA2* and *babA2* genes using PCR while DNA fingerprints were generated using random amplification polymorphic DNA (RAPD).

RESULTS: *H pylori* was present in 51/155 (33%) of patients studied. Of these, 16, 15 and 20 were isolated from patients with peptic ulcer diseases, gastroesophageal reflux diseases and non-ulcer dyspepsia, respectively. Of the *H pylori* positive patients, 75% (38/51) had *H pylori* in all three gastric sites. The prevalence of various genes in the *H pylori* isolates was shown to be similar irrespective of their colonization sites as well as among the same site of different patients. The RAPD profiles of *H pylori* isolates from different gastric sites were highly similar among intra-patients but varied greatly between different patients.

CONCLUSION: Topographic colonization of *H pylori* and the virulence genes harboured by these isolates have no direct bearing to the clinical state of the patients. In multi-ethnic Singapore, the stomach of each patient is colonized by a predominant strain of *H pylori*, irrespective of the clinical diagnosis.

Ho YW, Ho KY, Ascencio F, Ho B. Neither gastric topological distribution nor principle virulence genes of *Helicobacter pylori* contributes to clinical outcomes. *World J Gastroenterol* 2004; 10(22): 3274-3277

<http://www.wjgnet.com/1007-9327/10/3274.asp>

INTRODUCTION

Helicobacter pylori (*H pylori*) is a common gastric pathogen that has infected more than 50% of the world's population^[1]. It is the major aetiological agent of chronic active gastritis and is generally accepted as being the primary cause of peptic ulcer disease and a carcinogenic factor for gastric cancer (GC)^[2]. However, only a minority of *H pylori* infected subjects develops these diseases. This has led to the suggestion that clinical sequelae that develop may be dependent upon differentially expressed bacterial determinants, e.g., bacterial virulence genes: *cagA*, *vacA*, *iceA1*, *iceA2*, *babA2*^[3-5]. In many parts of Asia, the prevalence of *cagA* and *vacA* strains is high regardless of the presence or absence of disease states^[6]. This limits the usefulness of using these genes as markers to predict clinical outcome. Instead, other factors like host susceptibility as well as specific interactions between a particular strain and its host that occur during decades of coexistence might have contributed to an increased risk of developing certain clinical manifestations^[7].

Our current knowledge on the epidemiology of the organism is predominantly based on data obtained from serologic studies. It has also been reported that a single strain of *H pylori* predominates the gastric antrum and corpus of infected patients in Singapore^[8]. However, there is a need to study whether the topographic distribution of *H pylori* genotypes in various gastric sites in patients of different ethnic origins affects the disease state. Being an Asian country with a multi-ethnic population, Singapore is suitable for this investigation.

MATERIALS AND METHODS

Patients

Consecutive patients with dyspepsia and/or reflux symptoms presenting for upper gastrointestinal endoscopic examination to one of the authors (KYH) and who have not been exposed to antibiotics, proton pump inhibitors (PPI) or bismuth compounds within the past four weeks were invited to participate in the study. Patients who previously had been treated for *H pylori* infection, patients who refused gastric biopsies, patients who were unable to give consent because of age or mental illness and patients in whom gastric and oesophageal biopsies were contraindicated (e.g., coagulopathy, oesophageal varices and severe co-morbidity), subjects who were pregnant and those who were <18 years old, were excluded. Informed consent was obtained from each patient.

A total of 155 patients were included in the study. The patient population comprised 122 (79%) Chinese, 17 (11%) Indians, 8 (5%) Malays and 8 (5%) subjects of other ethnicities. Of these, 95 (61%) were males and 60 (39%) females. The mean age was 48.4±15.5 (range, 24-88) years. Based on clinical history and endoscopic examination, patients were classified into the following groups: gastroesophageal reflux disease (GERD) (*n* = 50), peptic ulcer disease (PUD) (*n* = 36) and non-ulcer dyspepsia (NUD) (*n* = 69). GERD was defined as the presence of predominant symptoms of reflux, e.g., heartburn, acid regurgitation and/or the presence of any length of mucosal break in the oesophagus due to gastroesophageal reflux. NUD was defined as patients with neither a history of GERD nor endoscopic evidence of organic pathologies. PUD refers to patients who were either

Table 1 Primer sequences of genes of interest

Region	Primer	Nucleotide sequence (5'→3')	PCR product (bp)	Reference
26kDa	26kDa-F	TGGCGTGTCTATTGACAGCGAGC	298	9
	26kDa-R	CCTGCTGGGCATACTTCACCAAG		
ureC	ureC-F	AAGCTTTTAGGGGTGTTAGGGGTTT	294	10
	ureC-R	AAGCTTACTTTCTAACACTAACGC		
cagA	cagA-F	AATACACCAACGCCTCCAAG	400	11
	cagA-R	TTGTTGCCGCTTTTGCTCTC		
vacA	vacA-F	GCTTCTCTTACCACCAATGC	1160	12
	vacA-R	TGTCAGGGTTGTTACCATG		
	m2-R	CATAACTAGCGCCTTGCCAC		
iceA1	iceA1-F	GTGTTTTTAACCAAAGTATC	246	5
	iceA1-R	CTATAGCCAGTCTCTTTGCA		5
iceA2	iceA2-F	GTTGGGTDTDTCACAATTTAT	229/334	5
	iceA2-R	TTGCCCTATTTTCTAGTAGGT		5
babA2	babA2-F	AATCCAAAAGGAGAAAAAGTATGAAA	831	4
	babA2-R	TGTTAGTGATTTCGGTGTAGGACA		4

F: forward primer R: reverse primer.

diagnosed upon endoscopy as suffering from gastric ulcers (ulcers at the corpus) or duodenal ulcers (ulcers at the antrum). A total of 465 biopsy specimens were obtained from the 155 patients.

Endoscopy

After an overnight or six hour fast, upper gastrointestinal endoscopy was performed according to standard technique. From each patient, one biopsy specimens was obtained using sterilized standard biopsy forceps from each of the three sites of the stomach: the cardia just below the z-line, the middle gastric corpus and the antrum within 2 cm of the pylorus, in that order. The biopsy forceps were thoroughly cleaned with alcohol swaps between biopsies to avoid contamination between specimens. The biopsies were transported in 0.85% sterile saline to the microbiological laboratory for processing within 6 h.

H pylori culture

Each biopsy specimen was homogenised aseptically in 500 µL of Brain Heart Infusion Broth (BHI, Oxoid Ltd., Basingstoke, UK) enriched with 4 g/L yeast extract (Oxoid Ltd., Basingstoke, UK). Approximately 100 µL homogenised specimens in BHI broth were inoculated onto *H pylori* selective chocolate blood agar plates and non-selective chocolate blood agar plates respectively. The selective blood chocolate agar was supplemented with 3 mg/mL vancomycin, 5 mg/mL trimethoprim, 10 mg/mL nalidixic acid and 2 mg/mL amphotericin B. All the antibiotics were from Sigma-Aldrich Chemie, Steinheim, Germany. The plates were incubated at 37 °C for up to 14 d in an incubator (Forma Scientific, USA) containing 50 mL/L CO₂.

Aliquots of 50 µL of BHI-biopsy suspension were each inoculated into catalase reagent, oxidase reagent and 20 g/L urea solution for their respective testing. An isolate was identified as *H pylori* if minute (-1 mm in diameter) rounded translucent colonies with gram-negative S-shaped motile cells that exhibited positive catalase, oxidase and urease activities. For this study, a patient was considered positive for *H pylori* if the organism was isolated from any of the three gastric sites.

Genotyping of *H pylori*

The DNA of each 3-d old *H pylori* culture was extracted according to the method as described by Hua *et al.*^[8]. A 50 ng working stock of DNA was used to amplify 26kDa^[9], ureC^[10], cagA^[11], vacA^[12], iceA1^[5], iceA2^[5] and babA2^[4] genes according to the protocol as described by Zheng *et al.*^[6] using the specific

forward and reverse primers for each of the corresponding genes (Table 1). The DNA fingerprint of the *H pylori* was obtained by PCR using the universal primer, 5'- AACGCGCAAC-3' and amplified according to protocol as described by Hua *et al.*^[13]. The PCR products obtained were electrophoresed and the ethidium bromide stained gels^[13] were then photographed with filtered UV illumination on Chemi Genius² (SynGene, Cambridge, UK).

Statistical Calculation

The significance of the results obtained was calculated using SPSS v.10 for Windows (SPSS, Chicago IL) to determine the Pearson chi-square whereby a *P* value <0.05 was considered to indicate statistical significance.

RESULTS

H pylori isolates in various clinical groups

Of the 155 patients studied, 51 (33%) were found to harbour *H pylori* in at least one of the 3 gastric biopsy sites. In all, 43, 47 and 44 isolates were obtained from gastric antrum, corpus and cardia respectively, giving a total of 134 isolates. *H pylori* was present in 16/36 (44%) PUD patients as compared with 15/50 (30%) GERD patients (*P* = 0.169) and 20/69 (29%) NUD patients (*P* = 0.113) (Table 2).

Table 2 Relationship between *H pylori* status and disease states

Groups	No. of patients	No. of biopsies	No. of <i>H pylori</i> (+)	<i>P</i>
PUD	36	108	16 (44%)	-
GERD	50	150	15 (30%)	0.169
NUD	69	207	20 (29%)	0.113

PUD, peptic ulcer disease; GERD, gastroesophageal reflux disease; NUD, non-ulcer dyspepsia. All test values were calculated with respect to PUD; *P*<0.05 indicates statistical significance.

Relationship between topographic distribution of *H pylori* isolates and clinical outcomes

Of the 51 *H pylori* positive patients, 38 (75%) showed the presence of *H pylori* in all the three gastric sites while 1 (1%), 2 (4%) and 4 (8%) had *H pylori* isolated from antrum & corpus, antrum & cardia, and corpus & cardia, respectively. *H pylori*

was isolated from a single site of the stomach in 6 (12%) patients, among which 2 isolates were from the antrum and 4 were from the corpus. This topographical pattern of *H pylori* colonization was observed in all the patients irrespective of the underlying clinical diagnosis.

Relationship between topographic distribution of *H pylori* genes of interest and clinical outcomes

All the *H pylori* isolates possessed the 26kDa gene and the ureC genes. The prevalence of virulence genes of interest were present in equal ratios in all the *H pylori* isolates obtained from all the 3 different gastric biopsy sites: 74-81% for cagA and 80-86% for vacA; 53-59% for iceA1 and 36-42% for baba2 regardless of the underlying clinical diagnosis. However, the iceA2 gene was present less frequently, at 20-26% of the *H pylori* isolates. It is noted that the difference in gene frequency between the various sites was also not statistically significant (Table 3).

Similar observation was noted with respect to the distribution of virulence genes of *H pylori* isolated from the same site among the different disease groups. The prevalence for each virulence gene within the same site was highly similar. No significant association of the virulence gene was found to be associated with a particular biopsied site, regardless of the disease state, with the exception of cagA in isolates from the corpus of the stomach of GERD patients (Table 4).

Table 3 Anatomical location of the 134 *H pylori* isolates and their virulence genes

	Antrum (%) n = 43	Body/Corpus (%) n = 47	Cardia (%) n = 44
Clinical Diagnosis			
PUD	12 (33)	15 (42)	12 (33)
GERD	13 (26)	15 (30)	14 (28)
NUD	18 (25)	17 (24)	18 (26)
Genotype			
26kDa	43 (100)	47 (100)	44 (100)
ureC	43 (100)	47 (100)	44 (100)
cagA	35 (81)	35 (74)	33 (75)
vacA	37 (86)	38 (81)	35 (80)
iceA1	25 (58)	25 (53)	26 (59)
iceA2	10 (23)	12 (26)	9 (20)
babA2	18 (42)	20 (38)	16 (36)

PUD, peptic ulcer disease; GERD, gastroesophageal reflux disease; NUD, non-ulcer dyspepsia. All test values were calculated with respect to gastric antrum and none were significant.

Table 4 Distribution of virulence genes of 134 *H pylori* isolates from the same anatomical site of different patient groups

	Isolates	26kDa (%)	ureC (%)	cagA (%)	vacA (%)	iceA1 (%)	iceA2 (%)	babA2 (%)
Antrum								
PUD	12	12 (100)	12 (100)	9 (75)	10 (83)	6 (50)	4 (33)	6 (50)
GERD	13	13 (100)	13 (100)	11 (85)	11 (85)	7 (54)	2 (15)	6 (46)
NUD	18	18 (100)	18 (100)	15 (83)	16 (89)	12 (67)	4 (22)	6 (33)
Body/Corpus								
PUD	15	15 (100)	15 (100)	9 (60)	10 (67)	6 (40)	5 (33)	7 (47)
GERD	15	15 (100)	15 (100)	14 (93) ¹	14 (93)	8 (53)	3 (20)	8 (53)
NUD	17	17 (100)	17 (100)	12 (71)	14 (82)	11 (65)	4 (24)	5 (29)
Cardia								
PUD	12	12 (100)	12 (100)	9 (75)	11 (92)	5 (42)	2 (17)	3 (25)
GERD	14	14 (100)	14 (100)	12 (86)	11 (79)	8 (57)	2 (14)	7 (50)
NUD	18	18 (100)	18 (100)	12 (67)	13 (72)	13 (72)	5 (28)	7 (39)

PUD, peptic ulcer disease; GERD, gastroesophageal reflux disease; NUD, non-ulcer dyspepsia. All test values were calculated with respect to PUD. ¹Indicates statistical significance ($P = 0.031$).

Relationship between topographic distribution of *H pylori* strain based on RAPD fingerprinting and clinical outcomes

For comparison, differences in 2 or more bands of the RAPD profile are considered different while variations in band intensity were not taken into account. On this basis, the RAPD profiles of all the *H pylori* strains isolated showed an overall similarity in profiles within individual patients, with minor differences such as the presence or absence of a single band. However, distinct differences in the DNA profiles were observed between patients (Figure 1). In this study, no comparison could be made in 6 patients since *H pylori* was isolated from only one site of the stomach in these patients.

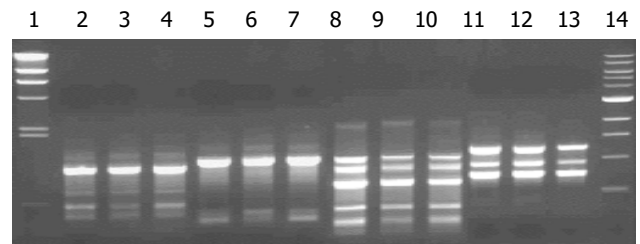


Figure 1 PCR-based RAPD patterns of *H pylori* isolated from 3 gastric sites of 4 individual patients. Lane 1: λ HindIII M marker, Lane 14: 1 kb M marker; Lane 2-4, 5-7, 8-10, 11-13 for patients 1, 2, 3 and 4 respectively. A: antrum; B: body; C: cardia.

DISCUSSION

It is noted that 50% of the world's population are infected with *H pylori* but only a small proportion manifest different gastroduodenal diseases^[14]. One of the factors contributing to this phenomenon could be the patchy distribution of *H pylori* in different gastric sites of the stomach. As most of the earlier studies focused on *H pylori* isolated from the distal sites of the stomach^[8,15], the present study shows that *H pylori* isolates obtained from all the 3 gastric sites, namely cardia, corpus and antrum, in 38/51 (75%) *H pylori* patients were similar genotypically. Care was taken in cleaning and disinfecting the biopsy forceps between biopsies to avoid contamination between specimens. The results imply that *H pylori* colonises the entire stomach instead of a predominant site in three quarters of our *H pylori* positive patients, irrespective of the underlying clinical diagnosis. The finding suggests that the site of *H pylori* colonization or topographic distribution does not contribute significantly to the outcome of the infection.

While studies in Europe suggested that virulence genes, e.g., *cagA* and *vacA* affect the clinical outcome of *H pylori* infection^[3,5], the present study confirms previous studies carried out in Asian countries^[6,15] that showed a high prevalence of *cagA* and *vacA* genes regardless of the clinical outcome. This study comprised Singapore patients of various ethnicities (Chinese, Malays, Indians and other races), also shows that each of the virulence genes, i.e., *cagA*, *vacA*, *iceA1*, *iceA2* and *babA2* were equally distributed in *H pylori* isolates obtained from all the three anatomical sites studied regardless of the disease states. Similarly, comparisons of these genes from the same anatomical site of different patients showed no significant presence, except for *cagA* in the corpus of GERD isolates. However, it is important to point out that the number of isolates obtained from each is relatively low ($n \leq 18$), regardless of the disease state. As such, the significant presence of *cagA* in the corpus of GERD patients needs further analysis with a larger pool of samples to confirm conclusively its contribution to the onset of GERD. The data therefore suggest that virulence genes and their topographic distribution do not contribute to the clinical status, at least in the Singapore population. This study supports the earlier reports^[15-17] that identifying such virulence genes in order to predict clinical outcome may be of limited value in Asian *H pylori* isolates.

The finding that RAPD profiles of the *H pylori* isolates were similar from 3 different anatomical sites (antrum, corpus & cardia) of each patient further strengthens our earlier study^[9] where isolates from 2 sites (antrum & corpus) were identical. This finding is complemented by the similar status of presence of various virulence genes in these isolates obtained from the respective patients. As such, the isolation of a strain from any gastric site in a single patient could be taken as representative of *H pylori* infection present in the *H pylori* infected gastric environment.

This study, which included consecutive patients with dyspepsia and/or reflux symptoms showed a lower frequency of PUD as compared with that of GERD. *H pylori* was found in only 44% of patients with PUD. This seems to run counter to the generally held view that *H pylori* occurs frequently in Asians patients with PUD^[13]. However, this finding is supported by an earlier study from the same unit^[18] showing the frequency of reflux oesophagitis was increasing while that of duodenal ulceration was decreasing in Singapore. The high frequency of patients with GERD in this study also relates to the fact that the endoscopist (KYH) sees most of the GERD patients in the hospital. The decreasing frequency of *H pylori* associated peptic ulcers was reported to be attributed to the increasing proportion of ulcers due to NSAID use^[19].

In summary, the present study shows that in Singapore, the topographic colonization of *H pylori* and their virulence genes within the host stomach do not play a significant role in the clinical manifestations of *H pylori* infection. This study also demonstrates that in Singapore, which has a multiethnic Asian population, the stomach of each patient with dyspeptic and/or reflux symptoms is colonized by a single predominant strain of *H pylori*, irrespective of the site of isolation and the clinical diagnosis of the patient. We suggest that the pathogenesis of *H pylori* induced gastroduodenal diseases is due to a more complex mechanism possibly involving host-pathogen interaction, environmental and dietary factors.

REFERENCES

- 1 Everhart JE. Recent developments in the epidemiology of *Helicobacter pylori*. *Gastroenterol Clin North Am* 2000; **29**: 559-578
- 2 Go MF. Review article: natural history and epidemiology of *Helicobacter pylori* infection. *Aliment Pharmacol Ther* 2002; **16**(Suppl 1): 3-15
- 3 Arents NLA, Van Zwet AA, Thijs JC, Kooistra-Samid AMD, van Slochteren R, Degener JE, Kleibeuker JH, van Doorn LJ. The importance of *vacA*, *cagA* and *iceA* genotypes of *Helicobacter pylori* infection in peptic ulcer disease and gastro-esophageal reflux disease. *Am J Gastroenterol* 2001; **96**: 2603-2608
- 4 Gerhard M, Lehn N, Neumayer N, Boren T, Rad R, Schepp W, Miehle S, Classen M, Prinz C. Clinical relevance of the *Helicobacter pylori* gene for blood-group antigen-binding adhesin. *Proc Natl Acad Sci U S A* 1999; **96**: 12778-12783
- 5 van Doorn LJ, Figueiredo C, Sanna R, Plaiser A, Schneeberger P, DeBoer W, Quint W. Clinical relevance of the *cagA*, *vacA* and *iceA* status of *Helicobacter pylori*. *Gastroenterology* 1998; **115**: 58-66
- 6 Zheng PY, Hua J, Yeoh KG, Ho B. Association of peptic ulcer with increased expression of Lewis antigen but not *cagA*, *iceA* and *vacA* in *Helicobacter pylori* isolates in an Asian population. *Gut* 2000; **47**: 18-22
- 7 Peek RM Jr. The biological impact of *Helicobacter pylori* colonization. *Semin Gastrointest Dis* 2001; **12**: 151-166
- 8 Hua J, Ling KL, Ng HS, Ho B. Isolation of a single strain of *Helicobacter pylori* from the antrum and body of individual patients. *Eur J Gastroenterol Hepatol* 2000; **12**: 1129-1134
- 9 Hammar M, Tyszkiewicz T, Wadstrom T, O'Toole PW. Rapid detection of *Helicobacter pylori* in gastric biopsy material by polymerase chain reaction. *J Clin Microbiol* 1992; **30**: 54-58
- 10 Labigne A, Cussac V, Courcoux P. Shuttle cloning and nucleotide sequence of *Helicobacter pylori* genes responsible for urease activity. *J Bacteriol* 1991; **173**: 1920-1931
- 11 Lage AP, Godfroid E, Fauconnier A, Burette A, Butzler JP, Bollen A, Glupczynski Y. Diagnosis of *Helicobacter pylori* infection by PCR: comparison with other invasive techniques and detection of *cagA* found in gastric biopsy specimens. *J Clin Microbiol* 1995; **33**: 2752-2756
- 12 Xiang Z, Censini S, Bayeli PF, Telford JL, Figura N, Rappuoli R, Covacci A. Analysis of expression of CagA and VacA virulence factors in 43 strains of *Helicobacter pylori* reveals that clinical isolates can be divided into 2 major types and that CagA is not necessary for expression of the vacuolating cytotoxin. *Infect Immun* 1995; **63**: 94-98
- 13 Hua J, Ho B. Is the coccoid form of *Helicobacter pylori* viable? *Microbios* 1996; **87**: 103-112
- 14 Hocker M, Hohenberger P. *Helicobacter pylori* virulence factors-1 part of a big picture. *Lancet* 2003; **362**: 1231-1233
- 15 Kim SY, Woo CW, Lee YM, Son BR, Kim JW, Chae HB, Youn SJ, Park SM. Genotyping *cagA*, *vacA* subtype, *iceA1*, *babA* of *Helicobacter pylori* isolates from Korean patients, and their association with gastroduodenal diseases. *J Korean Med Sci* 2001; **16**: 579-584
- 16 Kim JM, Kim JS, Jung HC, Song IS, Kim CY. Virulence factors of *Helicobacter pylori* in Korean isolates do not influence proinflammatory cytokine gene expression and apoptosis in human gastric epithelial cells, nor do these factors influence the clinical outcome. *J Gastroenterol* 2000; **35**: 898-906
- 17 Park SM, Park J, Kim JG, Cho HD, Cho JH, Lee DH, Cha YJ. Infection with *Helicobacter pylori* expressing the *cagA* gene is not associated with an increase risk of developing peptic ulcer disease in Korean patients. *Scand J Gastroenterol* 1998; **33**: 923-927
- 18 Ho KY, Gwee KA, Yeoh KG, Lim SG, Kang JY. Increasing frequency of reflux esophagitis in Asian patients. *Gastroenterology* 2000; **118**: A1246
- 19 Ong TZ, Ho KY. The increasing frequency of non-*Helicobacter pylori* peptic ulcer disease in an Asian country is related to NSAID use. *Gastrointestinal Endoscopy* 2003; **57**: AB153

A novel genetic polymorphism of inducible nitric oxide synthase is associated with an increased risk of gastric cancer

Jing Shen, Run-Tian Wang, Li-Wei Wang, Yao-Chu Xu, Xin-Ru Wang

Jing Shen, Yao-Chu Xu, Xin-Ru Wang, Department of Epidemiology & Biostatistics, School of Public Health, Nanjing Medical University, Nanjing 210029, Jiangsu Province, China

Run-Tian Wang, Health Science Center, Peking University, Beijing 100083, China

Li-Wei Wang, Yangzhong Cancer Research Institute, Yangzhong 212200, Jiangsu Province, China

Supported by Grants From the National Natural Science Foundation of China (30170827 to Jing. Shen and 30070671 to Run-Tian Wang)

Correspondence to: Jing Shen, Department of Environmental Health Sciences, Mailman School of Public Health, Columbia University, 701 West 168th St (Room 505), New York, NY 10032, USA. js2182@columbia.edu

Telephone: +212-305-8158 **Fax:** +212-305-5328

Received: 2003-07-12 **Accepted:** 2003-10-12

Abstract

AIM: Inducible nitric oxide synthase (iNOS) plays a central role in the pathway of reactive oxygen and nitrogen species metabolism when *Helicobacter pylori* (*H pylori*) infection occurs in humans. iNOS Ser⁶⁰⁸Leu allele, a novel genetic polymorphism (C/T) occurring within exon 16 of the iNOS reductase domain, may have a dramatic effect on the enzymatic activity. The aim of this study was to determine whether iNOS C/T polymorphism was associated with increased susceptibility to gastric cancer.

METHODS: We conducted a population based case-control study in a high gastric cancer incidence area, Yangzhong, China. Questionnaires from 93 patients with intestinal type gastric cancer (IGC), 50 with gastric cardia cancer (GCC) and 246 healthy controls were obtained between 1997 and 1998, and iNOS genotyping was carried out. Odds ratios (ORs), interaction index (γ), and 95% confidence intervals for the combined effects of iNOS genotype and *H pylori* infection, cigarette smoking or alcohol drinking were estimated.

RESULTS: The frequency of (CT+TT) genotypes was higher in cases than in control group (24.48% vs 23.17%), but the difference was not statistically significant. After adjusting for age and gender, past cigarette smokers with (CT+TT) genotypes had a significantly increased risk of IGC (OR = 3.62, 95% CI: 1.23-10.64), while past alcohol drinkers with (CT+TT) genotypes had a significantly increased risk of GCC (OR = 3.33, 95% CI: 1.14-9.67). *H pylori* CagA negative subjects with (CT+TT) genotypes had a significantly increased risk of both IGC and GCC (OR = 2.19 and 3.52, respectively).

CONCLUSION: iNOS Ser⁶⁰⁸Leu allele may be a potential determinant of susceptibility to cigarette -alcohol induced gastric cancer, but larger studies are needed to confirm the observations.

Shen J, Wang RT, Wang LW, Xu YC, Wang XR. A novel genetic polymorphism of inducible nitric oxide synthase is associated with an increased risk of gastric cancer. *World J Gastroenterol* 2004; 10(22): 3278-3283

<http://www.wjgnet.com/1007-9327/10/3278.asp>

INTRODUCTION

On a global scale, gastric cancer remains the world's second most common malignancy. There is a substantial international variation in gastric cancer incidence with the highest rates reported from China, Japan and other Eastern Asian countries^[1]. The discovery of *Helicobacter pylori* (*H pylori*) in the early 1980 s has been proven to be a turning point in understanding the pathogenesis of this malignancy. A major advance in this field came with the recognition that chronic *H pylori* infection could induce physiologic and morphologic changes within the gastric milieu, which increase the risk of neoplastic transformation^[2]. It has been widely accepted that chronic *H pylori* infection induces hypochlorhydria and gastric atrophy, both of which are precursors of gastric cancer^[2]. Epidemiological studies have also indicated that infection with *H pylori* is considered as a risk factor for gastric cancer^[3,4] and the WHO IARC has classified this bacterium as a definite biological carcinogen^[5]. However, while the majority of infected individuals develop no significant clinical disease, others develop two kinds of divergent clinical outcomes-peptic ulcer disease and gastric cancer^[2]. The reasons for developing these two extreme phenotypes, especially important in gastric cancer, have remained poorly understood, and are not explained by bacterial virulence factors alone^[2]. This highlights the need to explore potential candidate genes of the host in the pathways involved in the natural history of *H pylori* infection and its interactions with other risk factors in the development of gastric cancer in a high-risk population.

The inducible form of nitric oxide (NO) synthase (iNOS) is one of the most important enzymes involved in the pathway of reactive oxygen and nitrogen species metabolism in the presence of *H pylori* infection in humans. iNOS is a major source of NO production that is produced during inflammation by macrophages^[6,7]. Expression of iNOS in response to cytokines is part of the inflammatory response and contributes to tissue damage, suggesting its possible role in the processing of carcinogens^[7]. iNOS contains many sites for prosthetic groups and substrate binding^[8], which are all potentially important for the function of the enzyme. Furthermore, studies have indicated that even single amino acid changes may have dramatic effects on enzymatic activity^[8,9]. The human iNOS gene comprises 27 exons with the transcription start site in exon 2 (E2) and the stop codon in E27^[10]. E1-13 code for the oxygenase domain, and E14-27 encode for the reductase domain of the protein. Both of the domains represent different functional parts of the enzyme^[9]. Increased iNOS activities have been observed in patients with chronic gastritis caused by *H pylori* infection, and gastric cancer^[11,12]. A 13-21 years follow-up study showed that among the *H pylori* positive group, the expression of iNOS and nitro-tyrosine was significantly higher in the group that developed gastric cancer than the one that showed no evidence of gastric cancer, suggesting that *H pylori* positive subjects with high levels of reactive nitrogen species in gastric mucosa may be a high-risk group for gastric cancer^[13]. Furthermore, recent studies have revealed that *H pylori* infection may lead to a sustained production of reactive nitrogen species and the formation of nitro-tyrosine contributes to DNA damage and apoptosis in gastric mucosa^[12]. Infection with *H pylori* strains

possessing cytotoxin-associated gene (Cag) A, a molecular marker of *H pylori* virulence^[14,15], is particularly associated with an increased risk of developing adenocarcinoma of the stomach. It is suggested that iNOS may be a susceptible gene involved in the metabolic pathway of nitrogen and oxygen species of free radicals, and thus may be associated with both gastric cancer risk and *H pylori* infection.

Yangzhong city is one of the areas in China with the highest gastric cancer mortality and incidence rate. The crude mortality rate of gastric cancer was from 96.9 to 110.9/100 000 during 1991 and 1997, and the average adjusted incidence rate in the same period was over 115/100 000 (unadjusted rate was 155.46/100 000), which is over ten times higher than that in the United States^[16]. Based on the understanding of the physiology and pathogenesis of gastric cancer, and the genetic pathway related to *H pylori* infection, we hypothesized that higher frequency of iNOS Ser⁶⁰⁸Leu allele (i.e. C/T polymorphism)^[9,17] was responsible for the higher gastric cancer incidence in this area. We were especially interested in knowing whether the association between the polymorphism and gastric cancer was modified by infection with *H pylori* CagA strains and cigarette smoking reflecting high exposure to nitrogen and oxygen species of free radicals. Therefore, the aim of this study was to determine whether iNOS C/T polymorphism was associated with increased susceptibility to gastric cancer, and the effects of *H pylori* infection.

MATERIALS AND METHODS

Study subjects

All gastric cancer patients and "healthy" controls in this study were Han ethnic Chinese living in Yangzhong city for at least 25 years. Gastric cancer was diagnosed according to the International Classification of Diseases for Oncology IX, code = 151, and the criteria of Laurén^[18]. Because most diagnosed gastric cancer cases in Yangzhong were intestinal type gastric cancer (IGC) and gastric cardia cancer (GCC), we focused on these two kinds of cancers in the present study. A population based case-control design was used, and 165 gastric cancer cases (108 IGC, 57 GCC) and 295 controls were enrolled. The finally analyzed cases and controls were 143 (93 IGC, 50 GCC) and 246 cases, respectively, because of missing genotype data for some subjects. There were no significant differences comparing the finally analyzed subjects and those with missing data by age and sex. All cases were identified by endoscopic and pathological diagnosis in Yangzhong City Municipal Hospital from January 1997 to December 1998. To reduce misclassification of the histological types, two pathologists reviewed and confirmed all diagnosed cases. Controls were selected from cancer-free subjects living in the same community, who were either cases' siblings or their non-blood relatives (spouses and spouses' siblings with the same gender as cases). Both types of controls differed slightly in demographic features^[19]. Their results were combined to increase the sample size and to decrease type I error. This study was approved by the regional ethics committee, and all participants were given an explanation of the nature of the study, and informed consents both written and oral, were obtained. Study subjects completed a questionnaire administered by trained interviewers.

The questionnaire was designed to obtain detailed information on cigarette smoking, alcohol drinking, family history of cancers, and occupational and hazard exposures. Cigarette smokers were defined as subjects who reported ever smoking at least one cigarette per day for 12 mo or more, or whose accumulated cigarette consumption was over 18 packs per year. Past smokers were those who had stopped smoking 1 or more years before the interview. Alcohol drinkers were defined as subjects who reported to have an average of one drink or more per week for one or more years. Past alcohol drinkers were also defined as those

who had stopped drinking for 1 or more years before the interview.

Laboratory analysis

Blood was drawn from each participant by the designated coordinator according to the Guidelines of the National Heart, Lung, and Blood Institute Working Group on Blood Drawing, Processing, and Storage for Genetic Studies. Twenty milliliters of forearm venous blood was collected from each subject via venipuncture into two 10-mL vacutainer tubes containing EDTA. Puragene DNA isolation kits (Gentra Systems, Minneapolis MN) were used to isolate genomic DNA for genotyping. All blood samples were separated, and plasma was collected as soon as possible. The plasma was then stored at -20 °C in six 1.5-mL tubes for the detection of IgG antibody to *H pylori* CagA.

Denaturing high performance liquid chromatography (DHPLC) was used to scan the potential single nucleotide polymorphisms (SNPs) in all exons of iNOS, and then sequencing was performed to confirm the possible mutations. Finally, a new C/T polymorphism, which changes the coding amino acid from serine (TCG) to leucine (TTG), was identified^[17]. PCR-RFLP was carried out to identify the genotype of iNOS according to the features of SNP, which created a restriction enzyme recognition site of *Tsp 509 I*. Genomic DNA was amplified with primers F: 5'-TGTAACCAACTTCCGTGGTG-3' (T_m = 60.82 °C) and R: 5'-GTCTCTGCGGGTCTGAGAAG-3' (T_m = 60.14 °C). PCR was performed in a MJRESEARCH PCR system (PTC-225, USA), and in a 10 µL reaction volume containing 1 µL 10×PCR buffer, 1.6 µL dNTPs (1.25 µmol/L), 0.2 µL MgCl₂ (25 mmol/L), primers (20 µmol/L, Resgen Corp.) at 0.15 µL each, DMSO 0.5 µL, 6.34 µL dH₂O, 50 ng genomic DNA dried on the plate, and Hot Start Taq DNA polymerase 0.06 µL (5 U/µL, Promega Corp.). Touch down PCR procedure was used to amplify the target fragment. After an initial denaturation at 94 °C for 15 min, amplification was carried out for 10 cycles at 94 °C for 30 s, at 61 °C for 45 s, at 72 °C for 45 s and decreasing 0.5 °C per cycle. Then amplification was again carried out for 35 cycles at 94 °C for 30 s, at 56 °C for 45 s, and at 72 °C for 45 s, followed by a final elongation at 72 °C for 7 min. Then, 10 µL PCR products was digested with 0.2 µL *Tsp 509 I* (10 U/µL, NEB Corp.) in a 15 µL volume including 2 µL 10×buffer 1 (NEB Corp.), 0.15 µL BSA (100×) and 2.65 µL dH₂O. Digestion was performed for 15 h at 65 °C. The products were then electrophoresed on a 30 g/L agarose gel to allow unambiguous detection with ethidium bromide staining. Homozygous wide-type individuals (CC) showed 113 bp and 175 bp fragments, heterozygous individuals (CT) showed three bands: 113 bp, 142 bp and 175 bp, and homozygous rare allele individuals (TT) showed two bands: 113 bp and 142 bp^[17].

H pylori CagA IgG antibody in plasma was measured by an enzyme-linked immunosorbent assay (ELISA) kit offered by Jingying Biotech Limited Company, Shanghai, China (batch number 0052). The Absorbency at 450 nm was determined after terminating the enzyme reaction. The cutoff value equaled to the average *A* of the negative controls provided by the manufacturer plus 0.3 *A* units. A values of samples equaled to or higher than the cutoff point were considered positive.

Statistical analysis

All data were input double blinded into EPI-6 program by two persons separately. After modifying all errors and non-logical data, the differences in the relative associations between cases and controls were assessed by calculating crude odds ratios (OR) from contingency tables. The corresponding chi-square test on the cancer patients and controls was carried out, and 95% confidence intervals (95% CI) were determined using the Fisher exact test. A *P*-value <0.05 was considered statistically significant. Unconditional logistic regression analysis was performed in both univariate and multivariate models to assess the association between iNOS functional polymorphism and

gastric cancer susceptibility after adjusting for important confounding factors such as age and sex. Test of trend and interaction index (γ) that was determined by coefficient (β) in a multiple logistic regression model were calculated through logistic models based on dummy variables to examine the potential gene-environment interaction^[20]. All analyses were performed with the SAS package Genmod (SAS Institute, Cary, NC).

RESULTS

Table 1 compares the characteristics of study subjects. The mean age of cases was significantly greater than the controls (59.36 vs 51.89, $P < 0.01$). There was no significant difference in the male/female ratio between cases and controls. The proportions of past smokers and alcohol drinkers was significantly greater in the cancer group (36.97% and 30.30%) than in the control group (12.54% and 14.92%). However, there were more current smokers and drinkers in the control (47.12% and 30.85%) than in the case group (26.67% and 10.91%). Compared with controls, cases were significantly less likely to be positive for *H pylori* CagA antibody.

The frequency of iNOS genotypes in gastric cancer and control subjects showed no significant difference, although the

frequency of (CT+TT) genotypes was slightly higher in cases than in controls (24.48% versus 23.17%). A gene dose-response effect was not observed, i.e. the effect of heterozygote (CT) genotypes did not lie at or between the homozygotes (CC and TT).

For (CT+TT) the genotype frequency of iNOS in the past smoking subgroup, there were significant differences between the total cases and the controls and between GCC group and controls with an OR of 3.62 (95% CI: 1.23-10.64) and 4.63 (95% CI: 1.15-18.58), respectively. No significant difference was found between IGC cases and controls (Table 2). Although no gene dose-response effect was observed in heterozygote (CT) and homozygote (TT) individuals because of the small number in each cell, there was still a possible interaction between C/T polymorphism and past cigarette smoking in increasing the risk of GCC. In the past alcohol drinkers, there were significant differences in the C/T polymorphism between total cases and controls and between IGC group and controls with an OR of 3.33 (95% CI: 1.14-9.67) and 3.42 (95% CI: 1.03-11.35), respectively. No significant difference between GCC group and control group was found (Table 3). In *H pylori* CagA negative group, subjects with (CT+TT) genotypes had significantly increased risk of both IGC and GCC, with an OR of 2.19 (95% CI: 1.01-4.76) and 3.52 (95% CI: 1.44-8.61), respectively. *H pylori*

Table 1 Covariate distribution among study subjects and ORs for gastric cancer

Characteristics	No Cases (%) (n = 165)	No. Controls (%) (n = 295)	OR (95% CI)
Age (yr)			
Mean (yr±SD)	59.36±9.29 ^a	51.89±10.24	
Min. (yr)	34.72	30.77	
Max. (yr)	81.95	78.21	
Gender			
Male (%)	110 (66.67)	190 (64.41)	
Female (%)	55 (33.33)	105 (35.59)	
Ratio	2.00:1	1.81:1	
Smoking habit			
Never	60 (36.36)	119 (40.34)	1.00
Current	44 (26.67)	139 (47.12)	0.26 (0.15-0.46) ^b
Past	61 (36.97)	37 (12.54)	3.15 (1.77-5.61) ^b
Alcohol habits			
Never	97 (58.79)	160 (54.24)	1.00
Current	18 (10.91)	91 (30.85)	0.18 (0.10-0.35) ^b
Past	50 (30.30)	44 (14.92)	1.80 (1.06-3.08)
Plasma <i>H Pylori</i> CagA antibody			
Negative	136 (82.42)	107 (49.31)	1.00
Positive	29 (17.58)	110 (50.69)	0.18 (0.11-0.31) ^b
iNOS genotyping			
CC	108 (75.52)	189 (76.83)	1.00
CT	33 (23.08)	49 (19.92)	1.15 (0.68-1.96)
TT	2 (1.40)	8 (3.25)	0.42 (0.08-2.16)
CT+TT	35 (24.48)	57 (23.17)	1.03 (0.59-1.79)

^a $P < 0.05$ vs control group after adjusted for age and gender, ^b $P < 0.01$ vs control.

Table 2 Interaction between C/T polymorphism and past cigarette smoking for the risk of gastric cancer

C/T polymorphism	Past smoking	Total cases (n = 143)	Controls (n = 246)	OR ¹	95%CI	IGC (n = 93)	OR ²	95%CI	GCC (n = 50)	OR ³	95%CI
CC	No	67	162	1.00		46	1.00		21	1.00	
CT+TT	No	22	51	0.98	0.55-1.78	12	0.75	0.36-1.54	10	1.44	0.63-3.27
CC	Yes	41	27	2.92	1.53-5.57	27	2.47	1.19-5.09	14	3.65	1.42-9.38
CT+TT	Yes	13	6	3.62	1.23-10.64	8	3.06	0.91-10.35	5	4.63	1.15-18.58

¹Adjusted for age and gender, $\chi^2_{\text{trend}} = 26.26$, df = 1, $P = 0.00$, $\gamma = 1.29/1.07 = 1.21$ ²Adjusted for age and gender, $\chi^2_{\text{trend}} = 18.40$, df = 1, $P = 0.00$, $\gamma = 1.12/0.90 = 1.24$ ³Adjusted for age and gender, $\chi^2_{\text{trend}} = 17.53$, df = 1, $P = 0.00$, $\gamma = 1.53/1.29 = 1.19$.

Table 3 Interaction between C/T polymorphism and past alcohol drinking for the risk of gastric cancer

C/T polymorphism	Past alcohol drinking	Total cases (n = 143)	Controls (n = 246)	OR ¹	95%CI	IGC (n = 93)	OR ²	95%CI	GCC (n = 50)	OR ³	95%CI
CC	No	76	157	1.00		53	1.00		23	1.00	
CT+TT	No	24	51	0.83	0.46-1.50	13	0.62	0.30-1.28	11	1.22	0.55-2.70
CC	Yes	32	32	1.34	0.72-2.52	20	1.36	0.67-2.75	12	1.27	0.50-3.19
CT+TT	Yes	11	6	3.33	1.14-9.67	7	3.42	1.03-11.35	4	3.25	0.80-13.13

¹Adjusted for age and gender, $\chi^2_{\text{trend}} = 10.29$, $df = 1$, $P = 0.001$, $\gamma = 1.20/0.30 = 4.00$ ²Adjusted for age and gender, $\chi^2_{\text{trend}} = 5.65$, $df = 1$, $P = 0.017$, $\gamma = 1.23/0.31 = 3.97$ ³Adjusted for age and gender, $\chi^2_{\text{trend}} = 8.95$, $df = 1$, $P = 0.003$, $\gamma = 1.18/0.24 = 4.9$.

Table 4 Interaction between C/T polymorphism and *H pylori* CagA status for the risk of gastric cancer

C/T polymorphism	CagA antibody	Total cases (n = 143)	Controls (n = 178)	OR ¹	95%CI	IGC (n = 93)	OR ²	95%CI	GCC (n = 50)	OR ³	95%CI
CC	No	87	64	1.00		61	1.00		26	1.00	
CT+TT	No	28	19	2.53	1.29-4.98	17	2.19	1.01-4.76	11	3.52	1.44-8.61
CC	Yes	21	73	0.45	0.25-0.81	12	0.34	0.17-0.70	9	0.76	0.33-1.73
CT+TT	Yes	7	22	0.43	0.17-1.10	3	0.24	0.07-0.89	4	0.86	0.27-2.79

¹Adjusted for age and gender, $\chi^2_{\text{trend}} = 33.40$, $df = 1$, $P = 0.00$, $\gamma = -0.84/-0.79 = 1.06$ ²Adjusted for age and gender, $\chi^2_{\text{trend}} = 28.53$, $df = 1$, $P = 0.00$, $\gamma = -1.41/-1.08 = 1.31$ ³Adjusted for age and gender, $\chi^2_{\text{trend}} = 12.42$, $df = 1$, $P = 0.0004$, $\gamma = -0.15/-0.27 = 0.56$.

CagA positivity showed significant protective effects in IGC group in both on CC and CT+TT iNOS genotypes, with an OR of 0.24 (95% CI: 0.07-0.89) and 0.34 (95% CI: 0.17-0.70), respectively. However, no significant association was observed between iNOS genotypes and GCC (Table 4).

DISCUSSION

H pylori infection could produce a state of chronic immunostimulation in gastric epithelium^[21]. It could lead to changes in many factors that are important in the pathogenesis of gastric cancer, including reactive oxygen and nitrogen oxide species^[22]. NO, a potentially toxic gas with free radical properties is one of the most important bio-regulatory and signaling molecules produced in the process. It has been recently reported that NO, acting as a messenger molecule mediating various physiological functions^[23,24], may also play a role in the process of carcinogenesis.

It has been found that NO is synthesized enzymatically from L-arginine by NO synthase^[23,25]. Chronic infection and immunostimulation elevate endogenous synthesis of NO. High concentration of NO generated by macrophages after iNOS induction contributed to their cytotoxic and carcinogenic activity^[26]. There is now increasing evidence that NO produced by activated phagocytes may play a role in multistage carcinogenesis by mediating DNA damage^[27,28]. A T to C substitution in the iNOS gene, leads to more activated iNOS expression in the target cells, and finally elevates NO to a high level. Hence, it is reasonable to assume that human iNOS gene may be another important candidate gene for the development of gastric cancer by elevating NO production in target cells when functional polymorphisms occur. Nevertheless its genomic localization at chromosome 17q11.2^[29] was not the same as other gastric cancer susceptible genes related to the inflammatory response pathway, such as interleukin 1 β and interleukin 1RN, located at 2q14^[30]. The key question for gastric cancer agents is how *H pylori* infection could be associated with such totally divergent clinical outcomes as gastric cancer and peptic ulcer disease. A large number of previous studies have focused on the role of the bacterial virulence factors that contribute to the degree of tissue damage in the pathogenesis of these diseases. But these results still could not explain the different outcomes^[2,22,31]. With the development of a key concept about the interaction between

acid secretion and *H pylori*-induced gastritis during 1990 s, El-Omar proposed the idea for the first time that host genetic factors relevant to pro-inflammatory responses might be relevant to the development of gastric cancer. They explored a candidate IL-1 β gene in the context of *H pylori* related disease^[32,33]. Because IL-1 β can also induce the expression of many other genes, including pro-inflammatory mediator iNOS, by either regulating at the transcriptional level or initiating their mRNA^[8,9,34], it is easy to consider that functional polymorphisms occurring in the iNOS gene might also contribute to the increased risk of *H pylori* related gastric cancer.

We have previously reported a newly discovered C/T polymorphism in a Chinese population^[17] that had a high mutated allele frequency (24.4%). A report by Johannesen also showed that C/T polymorphism was one of the most frequent SNPs among 10 polymorphisms of human iNOS gene identified in a Danish population. They suggested that the amino acid change in exon 16 might be of functional interest^[9]. Our results showed no significant difference in the frequency of (CT+TT) genotypes between cases and controls, and no apparent gene dose-response effect was found. However, in past cigarette smokers and past alcohol drinkers, C/T polymorphism significantly increased the risk of gastric cancer despite the histological subtypes differed, i.e. past cigarette smokers with (CT+TT) genotypes had an increased risk of IGC, while past alcohol drinkers with (CT+TT) genotypes had increased risk of GCC. These findings suggest that C/T polymorphism in iNOS gene alone is not sufficient to show the increasing risk of gastric cancer. The importance of the interaction between C/T polymorphism and cigarette smoking or alcohol drinking varied depending on different histological subtypes of gastric cancer. Similar results were found by Machado for IL-1 genetic markers^[35]. Although these findings were not the major hypothesis we proposed, it is biologically plausible that oxidative stress due to carcinogenesis in cigarette might attribute to the increase of gastric cancer risk through interactions with iNOS C/T polymorphism. Larger and independent studies are needed to confirm these findings.

In the *H pylori* CagA positive group, regardless of whether subjects had CC or (CT+TT) genotypes, we always observed a significant protective effect when comparing IGC cases with controls. This suggests that plasma positive for *H pylori* CagA antibody in a highly infected area plays a protective role. This

is in concordance with the finding that *H pylori* density became progressively lower with progression from mild gastritis to severe gastritis, atrophy, intestinal metaplasia and finally gastric cancer^[29]. In *H pylori* CagA negative subjects with (CT+TT) genotypes, a high risk was found for gastric cancer group (OR = 2.53, 95% CI: 1.29-4.98) and both subgroups (IGC and GCC). No interaction was found between iNOS genotype and infection with *H pylori* CagA strains.

iNOS protein is a catalytic enzyme with two domains. In terms of functional importance, the deletion mutants retained maximal NO activity at lower concentrations of free Ca²⁺ compared with the wild-type^[36]. Identified C/T polymorphism in E16 of iNOS was located at the N-terminal of six amino acids from the deletion reported by Daff *et al.*, and the amino acid change in E16 might be of functional interest^[9]. To our knowledge, this study was the first one to examine the significance of iNOS polymorphism in gastric cancer. A research on other type of disease might support our observation^[9]. Gastric cancer patients having allele T polymorphism could have an increased expression of iNOS, resulting in higher levels of NO in gastric mucosa, mediating many pathological changes and finally leading to carcinogenesis in these patients. But specific functional tests of C/T shift need to be performed to substantiate the putative importance of the Ser⁶⁰⁸Leu locus in gastric cancer development.

Potential weaknesses in our study include possible recruitment bias in the selection of controls including cases' siblings. This kind of selection might create overmatching. Siblings were more likely to have the same genotypes as the cases than the non-blood related controls, thereby leading to some loss of statistical efficiency, i.e., larger sample sizes were required to attain the same statistical precision^[37]. Thus, our data may be more likely to underestimate the true effect of iNOS T alleles on the risk of gastric cancer. But others considered that the use of sibling controls could generally improve efficiency for gene-environment interactions^[38,39]. We could not rule out the potential influence of systematic differences between participants and non-participants.

In conclusion, the risk of gastric cancer is increased among past cigarette smoking or alcohol drinking individuals with a C/T polymorphism in E16 of iNOS gene in a Chinese population. But the findings need to be confirmed in other ethnic populations.

ACKNOWLEDGEMENTS

We thank Zhao-Xi Wang for his excellent technical assistance; and Professor Regina M. Santella and Dr. Yu-Jing Zhang for editing the manuscript. We also thank all the doctors for their kind help in collecting the biological samples and epidemiological data. We thank all participants for their co-operation.

REFERENCES

- 1 **Parkin DM**, Pisani P, Ferlay J. Estimates of the worldwide incidence of 25 major cancers in 1990. *Int J Cancer* 1999; **80**: 827-841
- 2 **El-Omar EM**, Chow WH, Rabkin CS. Gastric cancer and *H pylori*: Host genetics open the way. *Gastroenterology* 2001; **121**: 1002-1004
- 3 **Correa P**. Human gastric carcinogenesis: a multistep and multifactorial process—first American cancer society award lecture on cancer epidemiology and prevention. *Cancer Res* 1992; **52**: 6735-6740
- 4 **Komoto K**, Haruma K, Kamada T, Tanaka S, Yoshihara M, Sumii K, Kajiyama G, Talley NJ. *Helicobacter pylori* infection and gastric neoplasia: correlations with histological gastritis and tumor histology. *Am J Gastroenterol* 1998; **93**: 1271-1276
- 5 Schistosomes, liver flukes and *Helicobacter pylori*. IARC Working Group on the Evaluation of Carcinogenic Risks to Humans. Lyon, 7-14 June 1994. *IARC Monogr Eval Carcinog Risks Hum* 1994; **61**: 1-241
- 6 **Felley CP**, Pignatelli B, Van Melle GD, Crabtree JE, Stolte M, Diezi J, Corthesy-Theulaz I, Michetti P, Bancel B, Patricot LM, Ohshima H, Felley-Bosco E. Oxidative stress in gastric mucosa of asymptomatic humans infected with *Helicobacter pylori*: effect of bacterial eradication. *Helicobacter* 2002; **7**: 342-348
- 7 **Vallance P**, Collier J. Biology and clinical relevance of nitric oxide. *Br Med J* 1994; **309**: 453-457
- 8 **Stuehr DJ**. Mammalian nitric oxide synthases. *Biochim Biophys Acta* 1999; **1411**: 217-230
- 9 **Johannesen J**, Pie A, Paiot F, Kristiansen OP, Karlsen AE, Nerup J. Linkage of the human inducible nitric oxide synthase gene to type 1 diabetes. *J Clin Endocrinol Metab* 2001; **86**: 2792-2796
- 10 **Xu W**, Charles IG, Liu L, Moncada S, Emson P. Molecular cloning and structural organization of the human inducible nitric oxide synthase gene (NOS2). *Biochem Biophys Res Commun* 1996; **219**: 784-788
- 11 **Mannick EE**, Bravo LE, Zarama G, Realpe JL, Zhang XJ, Ruiz B, Fontham ET, Mera R, Miller MJ, Correa P. Inducible nitric oxide synthase, nitrotyrosine, and apoptosis in *Helicobacter pylori* gastritis: effect of antibiotics and antioxidants. *Cancer Res* 1996; **56**: 3238-3243
- 12 **Wee A**, Kang JY, Teh M. *Helicobacter pylori* and gastric cancer: correlation with gastritis, intestinal metaplasia, and tumour histology. *Gut* 1992; **33**: 1029-1032
- 13 **Rajnakova A**, Goh PM, Chan ST, Ngoi SS, Alponat A, Mochhala S. Expression of differential nitric oxide synthase isoforms in human normal gastric mucosa and gastric cancer tissue. *Carcinogenesis* 1997; **18**: 1841-1845
- 14 **Blaser MJ**, Perez-Perez GI, Kleanthous H, Cover TL, Peek RM, Chyou PH, Stemmermann GN, Nomura A. Infection with *Helicobacter pylori* strains possessing CagA is associated with an increased risk of developing adenocarcinoma of the stomach. *Cancer Res* 1995; **55**: 2111-2115
- 15 **Goto T**, Haruma K, Kitadai Y, Ito M, Yoshihara M, Sumii K, Hayakawa N, Kajiyama G. Enhanced expression of inducible nitric oxide synthase and nitrotyrosine in gastric mucosa of gastric cancer patients. *Clin Cancer Res* 1999; **5**: 1411-1415
- 16 **Stadtlander CT**, Waterbor JW. Molecular epidemiology, pathogenesis and prevention of gastric cancer. *Carcinogenesis* 1999; **20**: 2195-2208
- 17 **Shen J**, Wang RT, Wand LW, Wang ZX, Xing HX, Wang BY, Guo CH, Wang XR, Xu XP. Ser/Leu polymorphism of iNOS gene was found and identified in Chinese by denaturing high performance liquid chromatography. *Peking Daxue Xuebao* 2001; **33**: 486-492
- 18 **Laurén P**. The two histological main types of gastric carcinoma: diffuse and so-called intestinal-type carcinoma. An attempt at a histo-clinical classification. *Acta Pathol Microbiol Scand* 1965; **64**: 31-49
- 19 **Shen J**, Wang R, Wang Z, Xing H, Wang L, Wang B, Li M, Hua Z, Wang J, Guo C, Wang X, Xu X. The distributive features of three kinds of metabolic genes polymorphisms in population of Han nationality in south area of China. *Zhonghua Yixue Yichuanxue Zazhi* 2002; **19**: 302-307
- 20 **Taioli E**, Zocchetti C, Garte S. Models of interaction between metabolic genes and environmental exposure in cancer susceptibility. *Environ Health Perspect* 1998; **106**: 67-70
- 21 **Shapiro KB**, Hotchkiss JH. Induction of nitric oxide synthesis in murine macrophages by *Helicobacter pylori*. *Cancer Lett* 1996; **102**: 49-56
- 22 **El-Omar EM**. The importance of interleukin 1 beta in *Helicobacter pylori* associated disease. *Gut* 2001; **48**: 743-747
- 23 **Moncada S**, Palmer RM, Higgs EA. Nitric oxide: physiology, pathophysiology, and pharmacology. *Pharmacol Rev* 1991; **43**: 109-142
- 24 **Son HJ**, Rhee JC, Park DI, Kim YH, Rhee PL, Koh KC, Paik SW, Choi KW, Kim JJ. Inducible nitric oxide synthase expression in gastroduodenal diseases infected with *Helicobacter pylori*. *Helicobacter* 2001; **6**: 37-43
- 25 **Forstermann U**, Schmidt HH, Pollock JS, Sheng H, Mitchell JA, Warner TD, Nakane M, Murad F. Isoforms of nitric oxide synthase. Characterization and purification from different cell types. *Biochem Pharmacol* 1991; **42**: 1849-1857
- 26 **Grisham MB**, Ware K, Gilleland HE Jr, Gilleland LB, Abell CL, Yamada T. Neutrophil-mediated nitrosamine formation: role

- of nitric oxide in rats. *Gastroenterology* 1992; **103**: 1260-1266
- 27 **Esumi H**, Tannenbaum SR. US-Japan Cooperative Cancer Research Program: seminar on nitric oxide synthase and carcinogenesis. *Cancer Res* 1994; **54**: 297-301
- 28 **Ohshima H**, Bartsch H. Chronic infections and inflammatory processes as cancer risk factors: possible role of nitric oxide in carcinogenesis. *Mutat Res* 1994; **305**: 253-264
- 29 **Marsden PA**, Heng HH, Duff CL, Shi XM, Tsui LC, Hall AV. Localization of the human gene for inducible nitric oxide synthase (NOS2) to chromosome 17q11.2-q12. *Genomics* 1994; **19**: 183-185
- 30 **Patterson D**, Jones C, Hart I, Bleskan J, Berger R, Geyer D, Eisenberg SP, Smith MF Jr, Arend WP. The human interleukin-1 receptor antagonist (IL1RN) gene is located in the chromosome 2q14 region. *Genomics* 1993; **15**: 173-176
- 31 **Graham DY**, Yamaoka Y. Disease-specific *Helicobacter pylori* virulence factors: the unfulfilled promise. *Helicobacter* 2000; **5** (Suppl 1): S3-S9
- 32 **El-Omar EM**, Carrington M, Chow WH, McColl KE, Bream JH, Young HA, Herrera J, Lissowska J, Yuan CC, Rothman N, Lanyon G, Martin M, Fraumeni JF Jr, Rabkin CS. Interleukin-1 polymorphisms associated with increased risk of gastric cancer. *Nature* 2000; **404**: 398-402
- 33 **El-Omar EM**, Carrington M, Chow WH, McColl KE, Bream JH, Young HA, Herrera J, Lissowska J, Yuan CC, Rothman N, Lanyon G, Martin M, Fraumeni JF Jr, Rabkin CS. The role of interleukin-1 polymorphisms in the pathogenesis of gastric cancer. *Nature* 2001; **412**: 99
- 34 **Cho HJ**, Xie QW, Calaycay J, Mumford RA, Swiderek KM, Lee TD, Nathan C. Calmodulin is a subunit of nitric oxide synthase from macrophages. *J Exp Med* 1992; **176**: 599-604
- 35 **Machado JC**, Pharoah P, Sousa S, Carvalho R, Oliveira C, Figueiredo C, Amorim A, Seruca R, Caldas C, Carneiro F, Sobrinho-Simoes M. Interleukin 1B and interleukin 1RN polymorphisms are associated with increased risk of gastric carcinoma. *Gastroenterology* 2001; **121**: 823-829
- 36 **Daff S**, Sagami I, Shimizu T. The 42-amino acid insert in the FMN domain of neuronal nitric-oxide synthase exerts control over Ca(2+)/calmodulin-dependent electron transfer. *J Biol Chem* 1999; **274**: 30589-30595
- 37 **Thomas DC**, Witte JS. Point: population stratification: a problem for case-control studies of candidate-gene associations? *Cancer Epidemiol Biomark Prev* 2002; **11**: 505-512
- 38 **Gauderman WJ**, Witte JS, Thomas DC. Family-based association studies. *J Natl Cancer Inst Monogr* 1999; **26**: 31-37
- 39 **Witte JS**, Gauderman WJ, Thomas DC. Asymptotic bias and efficiency in case-control studies of candidate genes and gene-environment interactions: basic family designs. *Am J Epidemiol* 1999; **149**: 693-705

Edited by Xia HHX and Wang XL Proofread by Xu FM

A new subtype of 3' region of *cagA* gene in *Helicobacter pylori* strains isolated from Zhejiang Province in China

Ran Tao, Ping-Chu Fang, Hai-Yan Liu, Yun-Shui Jiang, Jing Chen

Ran Tao, Ping-Chu Fang, Hai-Yan Liu, Yun-Shui Jiang, Jing Chen, Department of Medical Microbiology and Parasitology, Zhejiang University School of Medicine, Hangzhou 310006, Zhejiang Province, China

Supported by China Medical Board, No. 96-628, and Natural Science Fund of Zhejiang Province, No. 302023

Correspondence to: Professor Ping-Chu Fang, Department of Medical Microbiology and Parasitology, Zhejiang University School of Medicine, 353 Yan'an Road, Hangzhou 310006, Zhejiang Province, China. fangpc@zju.edu.cn

Telephone: +86-571-87217403

Received: 2004-04-15 Accepted: 2004-05-09

Abstract

AIM: To isolate the subtypes of 3' region of *cagA* gene in *Helicobacter pylori* (*H pylori*) strains from Zhejiang Province in China and to investigate their relations to *H pylori*-associated gastroduodenal diseases.

METHODS: One hundred and thirty-seven *H pylori* clinical strains were isolated from the gastric mucosa specimens of 74 patients with chronic gastritis, 61 with peptic ulceration, and 2 with gastric cancer. Bacterial genomic DNA was extracted and 3' region of *cagA* gene was amplified by polymerase chain reaction (PCR). Subtypes of 3' region of *cagA* gene were determined by the size of PCR amplified segments. The sequences of the subtypes were analyzed by PCR-based sequencing.

RESULTS: Of the 137 *H pylori* isolates from Zhejiang Province, 132 (96.4%) yielded PCR products that could be classified into three groups of subtypes, named as subtypes I, II, and III according to their sizes. The sizes of subtypes I, II, and III were 648-650 bp, 705-707 bp, and 815 bp, respectively. Among the 132 *cagA*-positive *H pylori* strains, 123 (93.2%) belonged to the group of subtype I, 6 (4.5%) presented subtype II, 1 (0.8%) was subtype III, and 2 (1.5%) presented subtypes I and III both. The primary structure of subtype I was composed of 3 repeats of R1, 1 repeat of R2 and 1 repeat of R3. Subtype II possessing 4 repeats of R1, 2 repeats of R2 and 1 repeat of R3 was a newly found type of 3' region of *cagA* gene which had not been reported before. The primary structure of subtype III consisted of 4 repeats of R1, 1 repeat of R2 and 2 repeats of R3. Comparison of the sequences of subtype I strains with the corresponding sequences deposited in GenBank, showed a similarity of 95.0% (94.0-96.1%) for nucleotide sequences and 95.9% (94.9-97.4%) for deduced amino acid sequences. Comparison of the sequences of subtype III strains with the corresponding sequences deposited in GenBank, showed a similarity of 93.9% (90.8-96.9%) for nucleotide sequences and 93.2% (90.2-96.2%) for deduced amino acid sequences. Among subtype II strains, the nucleotide and deduced amino acid sequences showed a similarity of 95.2% (94.1-96.5%) and 96.4% (93.8-97.9%), respectively. There were no statistical differences in the

distribution of subtypes of 3' region of *cagA* gene among different *H pylori*-associated gastroduodenal diseases ($\chi^2 = 11.544$, $P > 0.05$).

CONCLUSION: There are three subtypes (I, II, and III) of 3' region of *cagA* gene in *H pylori* strains isolated from Zhejiang Province, and subtype II is predominant. Subtype II is a newly found subtype of 3' region of *cagA* gene. The result of this study does not support the view that the subtypes of 3' region of *cagA* gene in *H pylori* isolated from Zhejiang Province are correlated with the clinical outcomes of *H pylori* infection.

Tao R, Fang PC, Liu HY, Jiang YS, Chen J. A new subtype of 3' region of *cagA* gene in *Helicobacter pylori* strains isolated from Zhejiang Province in China. *World J Gastroenterol* 2004; 10(22): 3284-3288

<http://www.wjgnet.com/1007-9327/10/3284.asp>

INTRODUCTION

Although *Helicobacter pylori* (*H pylori*) is present in stomachs of at least half of the world's population^[1], only a small proportion of the carriers develop symptomatic diseases^[2]. The clinical spectrum of *H pylori* infection ranges from asymptomatic gastritis to peptic ulcer and gastric cancer^[3]. The causes of different outcomes of *H pylori* infection may include the virulence of infectious strains, the susceptibility of hosts, and environmental cofactors^[4-8]. The cytotoxin-associated gene A (*cagA*) is located at one end of a 40-kilobase DNA segment called *cag* pathogenicity island (*cag* PAI), which contains open reading frames encoding for a putative *H pylori* secretion system that may be associated with export of virulence factors to the extracellular compartment^[9,10]. The presence of *cagA* gene can be considered as a marker for *cag* PAI and is associated with more virulent *H pylori* strains^[11]. The structure of *cagA* gene contains a 5' highly conserved region and a variable 3' region, in which the presence of a variable number of repeat sequences results in a protein (CagA) with a molecular mass of 120 to 140 ku^[12]. Yamaoka *et al.*^[13] from Japan found that the structural organization of 3' region of *cagA* gene in Japanese *H pylori* isolates could be divided into four types (types A to D), and type C was associated with gastric atrophy and carcinoma. However, the genetic structure of 3' region of *cagA* gene in Chinese *H pylori* strains has been little exploited. In this study, we attempted to investigate the subtypes of 3' region of *cagA* gene in *H pylori* strains isolated from Zhejiang Province in China and their relations to *H pylori*-associated gastroduodenal diseases.

MATERIALS AND METHODS

H pylori isolates

A total of 137 *H pylori* isolates were obtained from *H pylori*-infected patients at the Second Affiliated Hospital of Zhejiang University and the Renmin Hospital of Daishan County in Zhejiang Province. The patients, consisting of 95 men and 42

women with a mean age of 42.6 years (ranging from 16 to 71 years), were classified into 3 groups including chronic gastritis ($n = 74$), peptic ulcer ($n = 61$), and gastric cancer ($n = 2$), according to the results of endoscopic and histological examination.

H pylori culture

Bacteria isolated from biopsy specimens were cultured on ECY selective solid medium^[14] at 37 °C for 5 d, under 100% humidity and microaerophilic conditions (50 mL/L O₂, 100 mL/L CO₂, and 850 mL/L N₂). *H pylori* strains were identified by the following criteria: Gram staining, colony morphology, rapid urease test, and catalase test. The cultured bacteria were defined to be *H pylori* if they formed typical colonies on the medium, were negative Gram stain with curved or spiral shape, and positive for urease and catalase production^[15].

Preparation of *H pylori* genomic DNA

The bacteria were harvested from the agar plates, then genomic DNA was extracted and purified from each *H pylori* isolate using cetyltrimethyl ammonium bromide (CTAB), phenol-chloroform-isoamyl alcohol, and ethanol precipitation^[16].

Amplification of 3' region of *cagA* gene by PCR

The primers 5'-ACCCTAGTCGGTAATGGGTTA-3' (CAG1) and 5'-GTAATTGTCTAGTTTCGC-3' (CAG2) described by Yamaoka *et al.*^[13] were used to amplify 3' region of *cagA* gene in this study. PCR was performed in a volume of 25 μ L containing 2.5 μ L of 10 \times PCR buffer, 2 μ L of 25 mmol/L MgCl₂, 2.5 μ L of 2 mmol/L dNTPs, 0.5 μ L of 20 μ mol/L primer sets, 0.2 μ L of Taq DNA polymerase, 1 μ L of bacterial genomic DNA, and 15.8 μ L of H₂O. PCR amplification was performed as following: an initial denaturation at 95 °C for 3 min, followed by 30 cycles, each consisting of denaturation at 94 °C for 30 s, annealing at 56 °C for 30 s, and extension at 72 °C for 45 s. The final cycle included a further extension at 72 °C for 7 min to ensure the full extension of PCR products. PCR products were analyzed by 20 g/L agarose gel electrophoresis with ethidium bromide staining.

Sequences analysis

PCR products were purified with the DNA purification kit (Shanghai Shenyong Biotechnology Co., Ltd.) according to the manufacturer's instructions. Purified PCR products were consigned to Shanghai BioAsia Biotechnology Co., Ltd. for sequencing. Biological software DNAssist (version 1.0) was used to analyze the sequences of 3' region of *cagA* gene and to compare them with the corresponding sequences deposited in GenBank.

Statistical analysis

The categorical data were analyzed using Chi-square (χ^2) test, and $P < 0.05$ was considered statistically significance.

RESULTS

PCR products of 3' region of *cagA* gene

PCR products of 3' region of *cagA* gene were electrophoresed on 20 g/L agarose gel (containing 0.5 μ g/mL ethidium bromide). Of the 137 *H pylori* strains isolated from Zhejiang Province, 132 (96.4%) strains yielded PCR products of three different sizes. The three different-size PCR-amplified segments were respectively named as subtype I (648-650 bp), subtype II (705-707 bp), and subtype III (815 bp) (Figure 1). Among the 132 *cagA*-positive strains, 123 (93.2%) presented subtype I, 6 (4.5%) presented subtype II, 1 (0.8%) presented subtype III, and 2 (1.5%) presented both subtypes I and III.

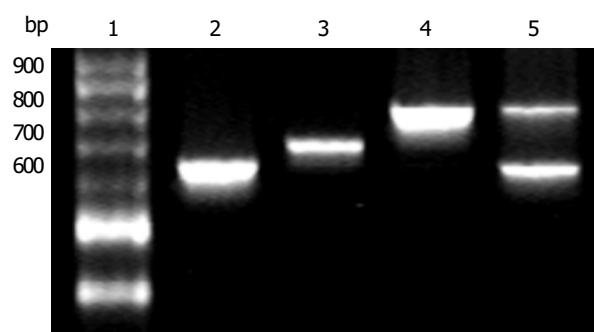


Figure 1 Amplified products of 3' region of *cagA* gene by PCR (20 g/L agarose gel electrophoresis) Lane 1: 100 bp DNA ladder; Lane 2: subtype I (648 bp); Lane 3: subtype II (705 bp); Lane 4: subtype III (815 bp); Lane 5: from a patient with both subtypes I and III.

Sequence analysis of subtypes of 3' region of *cagA* gene

The primary structure of 3' region of *cagA* gene was composed of a variable number of repeat regions, including R1 (15 bp), R2 (42 bp) and R3 (147 bp). The primary structures of the subtypes of 3' region of *cagA* gene in this study are illustrated in Figure 2. The primary structure of subtype I was composed of 3 repeats of R1, 1 repeat of R2 and 1 repeat of R3, so subtype I was equal to type A in Japanese *H pylori* strains reported by Yamaoka *et al.*^[13]. The primary structure of subtype III consisting of 4 repeats of R1, 1 repeat of R2 and 2 repeats of R3 was similar to that of type C reported by Yamaoka *et al.*^[13]. Subtype II possessing 4 repeats of R1, 2 repeats of R2 and 1 repeat of R3 had the primary structure not similar to any types reported by Yamaoka *et al.*^[13] and was regarded as a newly found subtype of 3' region of *cagA* gene in *H pylori*. Comparison of the sequences of 5 *H pylori* strains presented subtype I with the corresponding sequences of a Japanese type A strain JK25 deposited in GenBank (GenBank accession number AF043487), showed a similarity of 95.0% (94.0-96.1%) for nucleotide sequences and 95.9% (94.9-97.4%) for deduced amino acid sequences. Comparison of the sequences of 2 *H pylori* strains presented subtype III (including a strain presented both subtypes I and III) with the corresponding sequences of a Japanese type C strain Jk269 deposited in GenBank (GenBank accession number AF043489), showed a similarity of 93.9% (90.8-96.9%) for nucleotide sequences and 93.2% (90.2-96.2%) for deduced amino acid sequences. Among the 6 *H pylori* strains presented subtype II in this study, the nucleotide and deduced amino acid sequences showed a similarity of 95.2% (94.1-96.5%) and 96.4% (93.8-97.9%), respectively. Alignments of the deduced amino acid sequences of 5 strains presented subtype I and 2 strains presented subtype III with the corresponding sequences deposited in GenBank are illustrated in Figure 3 A, B. Alignments of the deduced amino acid sequences of 6 strains presented subtype II are also illustrated in Figure 3 C.

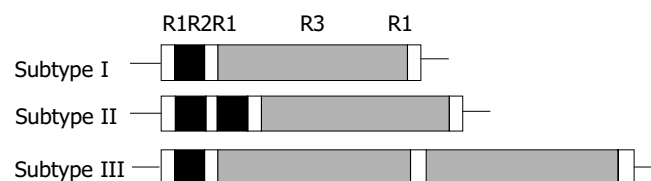


Figure 2 Primary structures of three subtypes of 3' region of *cagA* gene R1: 15 bp repeat region; R2: 42 bp repeat region; R3: 147 bp repeat region.

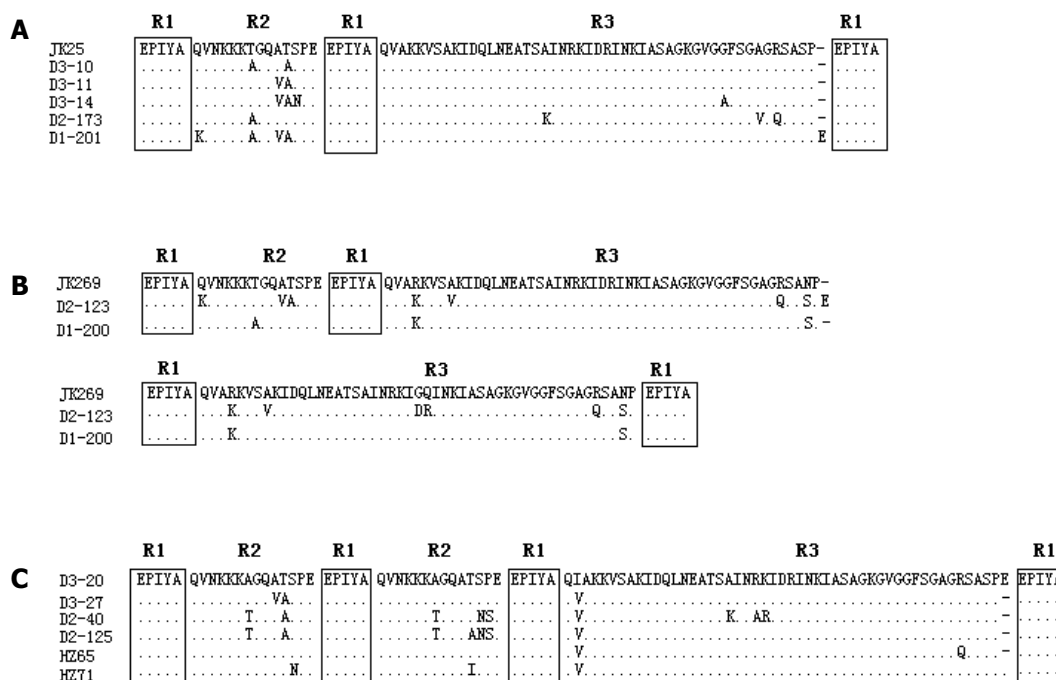


Figure 3 Alignment of amino acid sequences of subtypes of 3' region of *cagA* gene. A: Alignment of the deduced amino acid sequences of subtype I strains with the sequence of the corresponding region of a Japanese type A strain JK25 (GenBank accession number AF043487). Strain D2-173 was from a patient with chronic gastritis, and the remaining four strains were from patients with peptic ulcer. B: Alignment of the deduced amino acid sequences of subtype III strains with the sequence of the corresponding region of a Japanese type C strain JK269 (GenBank accession number AF043489). Strain D1-200 was from a patient with chronic gastritis, and strain D2-123 was from a patient with gastric ulcer. C: Alignment of the deduced amino acid sequences of six subtype II strains. Strain HZ65 and HZ71 were from patients with chronic gastritis, strain D2-40 was from a patient with gastric cancer, and the remaining three strains were from patients with peptic ulcer.

Relationship between subtypes of 3' region of *cagA* gene and gastroduodenal diseases

The distributions of the subtypes of 3' region of *cagA* gene in different groups of gastroduodenal diseases are demonstrated in Table 1. Statistical analysis showed that there were no significant differences among the subtypes of 3' region of *cagA* gene in different groups of gastroduodenal diseases ($\chi^2 = 11.544$).

Table 1 Relationship between subtypes of 3' region of *cagA* gene and different group of gastroduodenal diseases (n, %)

Group of diseases	Subtype I	Subtype II	Subtype III	Subtypes I and III	Total
Chronic gastritis	69 (95.8)	2 (2.8)	0 (0)	1 (1.4)	72
Peptic ulcer	53 (91.4)	3 (5.2)	1 (1.7)	1 (1.7)	58
Gastric cancer	1 (50.0)	1 (50.0)	0 (0)	0 (0)	2
Total	123 (93.2)	6 (4.5)	1 (0.8)	2 (1.5)	132

$\chi^2 = 11.544$, $P = 0.17 > 0.05$.

DISCUSSION

H pylori, a spiral shaped gastric organism, is the cause of chronic gastritis, and plays an important role in the pathogenesis of peptic ulceration, mucosa associated lymphoid tissue lymphoma, and gastric adenocarcinoma^[17-20]. It has been reported that 50-60% of *H pylori* strains contain *cagA* gene and consequently produce CagA protein^[21]. The CagA is a highly immunogenic outer membrane protein with a molecular weight of 120 to 140 ku. Variation in size of the protein has been correlated with the presence of a variable number of repeat sequences located in 3' region of the gene^[22,23]. The biological importance of the repeat sequences in 3' region of *cagA* gene remains unknown. Because CagA is strongly immunogenic, these repeat sequences have been supposed to alter immunogenicity

of the protein^[24]. This alteration in the gene and its protein seems to correlate with clinical outcomes *in vivo*. The proportion of *cagA*-positive *H pylori* isolates varies from one geographic region to another. Studies from Japan, Korea, and China have shown that more than 90% of *H pylori* strains are *cagA*-positive^[25-28], while in the United States of America, Canada, and Europe, these percentages are lower^[24,29,30]. Therefore, *cagA* gene cannot be used as a marker for the presence of severe gastroduodenal diseases in those regions where the prevalence of *cagA*-positive *H pylori* strains is uniformly high. Since allelic variation in *cagA* exists and distinct *H pylori* subtypes may circulate in different regions, differences in *cagA* subtype might provide a marker for differences in virulence among *cagA*-positive *H pylori* strains^[12].

Yamaoka *et al.*^[13] reported that 3' region of *cagA* gene in *H pylori* isolated from Japanese patients could be classified into four types (types A, B, C, and D) depending on the types and number of repeat regions including R1 (15 bp), R2 (42 bp) and R3 (147 bp). The PCR products of type A ranged from 642 to 651 bp, and possessed 1 repeat of R2 and 1 repeat of R3. The PCR products of type B and type D were all 756 bp, but type B possessed 3 repeats of R2 and 1 repeat of R3, while type D had 2 repeats of R3 and no repeat of R2. Type C having 1 repeat of R2 and 2 repeats of R3 yielded PCR products of 813-815 bp and was associated with high levels of CagA antibody and severe degrees of atrophy. The same authors have also found that the sequences of the second repeat regions of 3' region of *cagA* gene in *H pylori* strains from East Asia are completely different from those in strains from non-Asian countries^[31]. Non-Asian strains possess 102 bp second repeat regions, and East Asian strains possess 162 bp second repeat regions^[31,32].

In the present study, we used the same PCR primers as those described by Yamaoka *et al.*^[13] and found 132 (96.4%) of 137 strains yielded amplified products. The high prevalence of *cagA*-positive strains in Zhejiang Province was in accordance

with the result of our previous study^[13] and the findings in other Chinese areas^[11,27]. The PCR products could be classified into three subtypes according to their sizes and were named as subtype I, subtype II, and subtype III, respectively. The PCR products of subtype I ranged from 648 to 650 bp and possessed 1 repeat of R2 and 1 repeat of R3, so subtype I was equal to type A reported by Yamaoka *et al.*^[13]. The predominance of subtype I strains (93.2%) in this study was in agreement with that of type A strains (93.5%) in Japanese patients^[13]. The size and genetic structure of subtype III indicated that subtype III in this study was equal to type C in Japanese strains^[13]. Three (including 2 multiple subtypes strains) of 132 *cagA*-positive strains presented subtype III, and the prevalence of this subtype (2.3%) was close to that of type C (4.5%). In contradiction to the two above-mentioned subtypes, subtype II having the size of PCR product of 705-707 bp and the structure of 2 repeats of R2 and 1 repeat of R3 has not been reported before. Because sequence analysis showed that the structure of subtype II still accorded with the characteristics of 3' region of *cagA* gene in Asian strains, subtype II in this study was regarded as a new subtype of 3' region of *cagA* gene in Asian *H pylori* strains. The fact that we did not find type B and type D reported by Yamaoka *et al.*^[13], but discovered a new subtype revealed the diversity and randomness of the assembling mode of repeat regions located at 3' region of *cagA* gene and the possibility that this assembling mode varied in *H pylori* strains isolated from different areas. In addition, 2 strains presenting more than one subtype were observed in this study and thought to be from the patients with multiple *H pylori* infection. Sequence analysis revealed high similarities between the sequences of 3' region of *cagA* gene in *H pylori* isolated from Zhejiang Province and those in *H pylori* strains from Japanese patients and high similarities among the 6 subtype II strains, so we could draw a conclusion that despite of the genetic diversity of 3' region of *cagA* gene in *H pylori* strains isolated from Zhejiang Province, the sequences of the same subtype were still conservative. There were no significant differences among the subtypes of 3' region of *cagA* gene in different groups of gastroduodenal diseases, so the subtypes of 3' region of *cagA* gene in *H pylori* isolated from Zhejiang Province seemed not to be correlated with the clinical outcomes of *H pylori* infection.

In conclusion, there are three subtypes of 3' region of *cagA* gene in *H pylori* strains isolated from Zhejiang Province. Subtype I is a predominant one and subtype II is a newly found subtype of Asian *H pylori* strains. The result of this study does not support the view that the subtypes of 3' region of *cagA* gene in *H pylori* isolated from Zhejiang Province are correlated with the clinical outcomes of *H pylori* infection.

REFERENCES

- Blaser MJ. Ecology of *Helicobacter pylori* in the human stomach. *J Clin Invest* 1997; **100**: 759-762
- Perng CL, Lin HJ, Lo WC, Tseng GY, Sun IC, Ou YH. Genotypes of *Helicobacter pylori* in patients with peptic ulcer bleeding. *World J Gastroenterol* 2004; **10**: 602-605
- Dunn BE, Cohen H, Blaser MJ. *Helicobacter pylori*. *Clin Microbiol Rev* 1997; **10**: 720-741
- Kidd M, Lastovica AJ, Atherton JC, Louw JA. Heterogeneity in the *Helicobacter pylori vacA* and *cagA* genes: association with gastroduodenal disease in South Africa? *Gut* 1999; **45**: 499-502
- Gunn MC, Stephens JC, Stewart JA, Rathbone BJ, West KP. The significance of *cagA* and *vacA* subtypes of *Helicobacter pylori* in the pathogenesis of inflammation and peptic ulceration. *J Clin Pathol* 1998; **51**: 761-764
- Henriksson AE, Edman AC, Nilsson I, Bergqvist D, Wadstrom T. *Helicobacter pylori* and the relation to other risk factors in patients with acute bleeding peptic ulcer. *Scand J Gastroenterol* 1998; **33**: 1030-1033
- Olbe L, Fandriks L, Hamlet A, Svennerholm AM. Conceivable mechanisms by which *Helicobacter pylori* provokes duodenal ulcer disease. *Baillieres Best Pract Res Clin Gastroenterol* 2000; **14**: 1-12
- Dore MP, Graham DY. Pathogenesis of duodenal ulcer disease: the rest of the story. *Baillieres Best Pract Res Clin Gastroenterol* 2000; **14**: 97-107
- Censini S, Lange C, Xiang Z, Crabtree JE, Ghiara P, Borodovsky M, Rappuoli R, Covacci A. *Cag*, a pathogenicity island of *Helicobacter pylori*, encodes type I-specific and disease-associated virulence factors. *Proc Natl Acad Sci U S A* 1996; **93**: 14648-14653
- Akopyants NS, Clifton SW, Kersulyte D, Crabtree JE, Youree BE, Reece CA, Bukanov NO, Drazek ES, Roe BA, Berg DE. Analyses of the *cag* pathogenicity island of *Helicobacter pylori*. *Mol Microbiol* 1998; **28**: 37-53
- Qiao W, Hu JL, Xiao B, Wu KC, Peng DR, Atherton JC, Xue H. *cagA* and *vacA* genotype of *Helicobacter pylori* associated with gastric diseases in Xi'an area. *World J Gastroenterol* 2003; **9**: 1762-1766
- Rota CA, Pereira-Lima JC, Blaya C, Nardi NB. Consensus and variable region PCR analysis of *Helicobacter pylori* 3' region of *cagA* gene in isolates from individuals with or without peptic ulcer. *J Clin Microbiol* 2001; **39**: 606-612
- Yamaoka Y, Kodama T, Kashima K, Graham DY, Sepulveda AR. Variants of the 3' region of the *cagA* gene in *Helicobacter pylori* isolates from patients with different *H pylori*-associated diseases. *J Clin Microbiol* 1998; **36**: 2258-2263
- Fang PC, Zhu YL, Yin X, Wu QD, Lan MG, Wu PJ. Study on ECY blood-free medium for the isolation of *Helicobacter pylori*. *Zhonghua Yixue Jianyan Zazhi* 1993; **16**: 131-133
- Dore MP, Sepulveda AR, El-Zimaity H, Yamaoka Y, Osato MS, Mototsugu K, Nieddu AM, Realdi G, Graham DY. Isolation of *Helicobacter pylori* from sheep-implications for transmission to humans. *Am J Gastroenterol* 2001; **96**: 1396-1401
- Xu C, Li ZS, Tu ZX, Xu GM, Gong YF, Man XH. Distribution of *cagG* gene in *Helicobacter pylori* isolates from Chinese patients with different gastroduodenal diseases and its clinical and pathological significance. *World J Gastroenterol* 2003; **9**: 2258-2260
- Danesh J. *Helicobacter pylori* infection and gastric cancer: systematic review of the epidemiological studies. *Aliment Pharmacol Ther* 1999; **13**: 851-856
- Higashi H, Tsutsumi R, Fujita A, Yamazaki S, Asaka M, Azuma T, Hatakeyama M. Biological activity of the *Helicobacter pylori* virulence factor *cagA* is determined by variation in the tyrosine phosphorylation sites. *Proc Natl Acad Sci U S A* 2002; **99**: 14428-14433
- Watanabe T, Tada M, Nagai H, Sasaki S, Nakao M. *Helicobacter pylori* infection induces gastric cancer in mongolian gerbils. *Gastroenterology* 1998; **115**: 642-648
- Uemura N, Okamoto S, Yamamoto S, Matsumura N, Yamaguchi S, Yamakido M, Taniyama K, Sasaki N, Schlemper RJ. *Helicobacter pylori* infection and the development of gastric cancer. *N Engl J Med* 2001; **345**: 784-789
- Abasiyanik MF, Sander E, Salih BA. *Helicobacter pylori* anti-CagA antibodies: prevalence in symptomatic and asymptomatic subjects in Turkey. *Can J Gastroenterol* 2002; **16**: 527-532
- Covacci A, Censini S, Bugnoli M, Petracca R, Burroni D, Macchia G, Massone A, Papini E, Xiang Z, Figura N, Rappuoli R. Molecular characterization of the 128-kDa immunodominant antigen of *Helicobacter pylori* associated with cytotoxicity and duodenal ulcer. *Proc Natl Acad Sci U S A* 1993; **90**: 5791-5795
- Tummuru MK, Cover TL, Blaser MJ. Cloning and expression of a high-molecular-mass major antigen of *Helicobacter pylori*: evidence of linkage to cytotoxin production. *Infect Immun* 1993; **61**: 1799-1809
- Rudi J, Kolb C, Maiwald M, Kuck D, Sieg A, Galle PR, Stremmel W. Diversity of *Helicobacter pylori vacA* and *cagA* genes and relationship to *VacA* and *cagA* protein expression, cytotoxin production, and associated diseases. *J Clin Microbiol* 1998; **36**: 944-948
- Maeda S, Ogura K, Yoshida H, Kanai F, Ikenoue T, Kato N,

- Shiratori Y, Omata M. Major virulence factors, *VacA* and *cagA*, are commonly positive in *Helicobacter pylori* isolates in Japan. *Gut* 1998; **42**: 338-343
- 26 **Miehlke S**, Kibler K, Kim JG, Figura N, Small SM, Graham DY, Go MF. Allelic variation in the *cagA* gene of *Helicobacter pylori* obtained from Korea compared to the United States. *Am J Gastroenterol* 1996; **91**: 1322-1325
- 27 **Pan ZJ**, van der Hulst RW, Feller M, Xiao SD, Tytgat GN, Dankert J, van der Ende A. Equally high prevalences of infection with *cagA*-positive *Helicobacter pylori* in Chinese patients with peptic ulcer disease and those with chronic gastritis-associated dyspepsia. *J Clin Microbiol* 1997; **35**: 1344-1347
- 28 **Shimoyama T**, Fukuda S, Tanaka M, Mikami T, Saito Y, Munakata A. High prevalence of the *cagA*-positive *Helicobacter pylori* strains in Japanese asymptomatic patients and gastric cancer patients. *Scand J Gastroenterol* 1997; **32**: 465-468
- 29 **Peek RM Jr**, Miller GG, Tham KT, Perez-Perez GI, Cover TL, Atherton JC, Dunn GD, Blaser MJ. Detection of *Helicobacter pylori* gene expression in human gastric mucosa. *J Clin Microbiol* 1995; **33**: 28-32
- 30 **Perez-Perez GI**, Bhat N, Gaensbauer J, Fraser A, Taylor DN, Kuipers EJ, Zhang L, You WC, Blaser MJ. Country-specific constancy by age in *cagA*+ proportion of *Helicobacter pylori* infections. *Int J Cancer* 1997; **72**: 453-456
- 31 **Yamaoka Y**, Osato MS, Sepulveda AR, Gutierrez O, Figura N, Kim JG, Kodama T, Kashima K, Graham DY. Molecular epidemiology of *Helicobacter pylori*: separation of *H pylori* from East Asian and non-Asian countries. *Epidemiol Infect* 2000; **124**: 91-96
- 32 **Yamaoka Y**, Graham DY. Clarifications regarding the 3' repeat region of the *cagA* gene in *Helicobacter pylori* and clinical outcome. *J Clin Microbiol* 2001; **39**: 2369-2370
- 33 **You JF**, Fang PC, Ye SJ, Mao HY, Zhou LF, Qiu X. *Helicobacter pylori cagA, vacA* and *iceA* status of Zhejiang province and relationship to clinical outcomes. *Zhonghua Weishengwuxue He Mianyixue Zazhi* 2003; **23**: 111-112

Edited by Kumar M and Wang XL. Proofread by Xu FM

Pathogenicity and immune prophylaxis of cag pathogenicity island gene knockout homogenic mutants

Huan-Jian Lin, Jing Xue, Yang Bai, Ji-De Wang, Ya-Li Zhang, Dian-Yuan Zhou

Huan-Jian Lin, Jing Xue, Yang Bai, Ji-De Wang, Ya-Li Zhang, Dian-Yuan Zhou, PLA Institute of Digestive Medicine, Nan Fang Hospital, the First Military Medical University, Guangzhou 510515, Guangdong Province, China

Correspondence to: Dr. Huan-Jian Lin, Institute for Digestive Medicine, Nan Fang Hospital, the First Military Medical University, Guangzhou 510515, Guangdong Province, China. xj0302@fimmun.com

Received: 2003-06-16 **Accepted:** 2003-08-25

Abstract

AIM: To clarify the role of cag pathogenicity island (cagPAI) of *Helicobacter pylori* (*H pylori*) in the pathogenicity and immune prophylaxis of *H pylori* infection.

METHODS: Three pairs of *H pylori* including 3 strains of cagPAI positive wildtype bacteria and their cagPAI knockout homogenic mutants were utilized. *H pylori* binding to the gastric epithelial cells was analyzed by flow cytometry assays. Apoptosis of gastric epithelial cells induced by *H pylori* was determined by ELISA assay. Prophylaxis effect of the wildtype and mutant strains was compared by immunization with the sonicate of the bacteria into mice model.

RESULTS: No difference was found in the apoptosis between cagPAI positive and knockout *H pylori* strains in respective of the ability in the binding to gastric epithelial cells as well as the induction of apoptosis. Both types of the bacteria were able to protect the mice from the infection of *H pylori* after immunization, with no difference between them regarding to the protection rate as well as the stimulation of the proliferation of splenocytes of the mice.

CONCLUSION: The role of cagPAI in the pathogenicity and prophylaxis of *H pylori* infection remains to be cleared.

Lin HJ, Xue J, Bai Y, Wang JD, Zhang YL, Zhou DY. Pathogenicity and immune prophylaxis of cag pathogenicity island gene knockout homogenic mutants. *World J Gastroenterol* 2004; 10(22): 3289-3291

<http://www.wjgnet.com/1007-9327/10/3289.asp>

INTRODUCTION

Helicobacter pylori (*H pylori*) infected over half of human adults in the world, especially in Asian-Pacific countries. Only a small portion of patients display clinical symptoms such as peptic ulcer and gastric cancer^[1-14]. The difference between the infection and the outcomes is determined by both bacterial factors and host responses. Among the bacterial factors, cag pathogenicity island (PAI) had been studied widely, while the immune response to the infection is the overwhelming host factor that affects the outcome of infection. In respect of the bacterial factors, cytotoxin associated gene A (cag A) protein is usually considered as a toxic marker of the bacterium. A related gene cluster, PAI encodes several proteins with the similar biological activities. To define the relationship between cagPAI and the pathogenicity of *H pylori*, three pairs of *H pylori* harboured

cagPAI and their isogenic PAI knockout mutants were utilized. Their roles in the binding and apoptosis inducing activities as well as the immune protection were compared *in vivo* and *in vitro*.

MATERIALS AND METHODS

Materials

CT, PKH26, PMA and Ionomycin were obtained from Sigma Co, U.S.A; granulocyte-macrophage-colony-stimulating-faction (GM-CSF) enzyme linked immunosorbent assay (ELISA) kit was bought from Boehringer-Mannheim Co. German; Three pairs of *H pylori* harbouring cagPAI and their isogenic PAI knockout mutants were provided kindly by Professor Peter B Ernst from DyKesas University USA; *H pylori* strains and gastric epithelial cells (Kato-III) were from the Research Institute of Digestive Disease, Nanfang Hospital, First Military Medical University in Guangzhou, China. *H pylori* strains are showed in Table 1.

Table 1 cagA positive wildtype bacteria and their cagA knockout homogenic mutants

<i>H pylori</i>	cagPAI
LC11	+ wildtype
AH244	knockou cagPAI knockout of LC11
84183	+ wildtype
2-1	knockou cagPAI knockout of 84183
26695	+ wildtype
8-1	knockou cagPAI knockout of 26695

Methods

***H pylori* culture and *H pylori* sonicate (SON) preparation were performed by standard procedures** There was no difference between the groups of wildtype and knockout bacteria in the rate of growing (Figure 1).

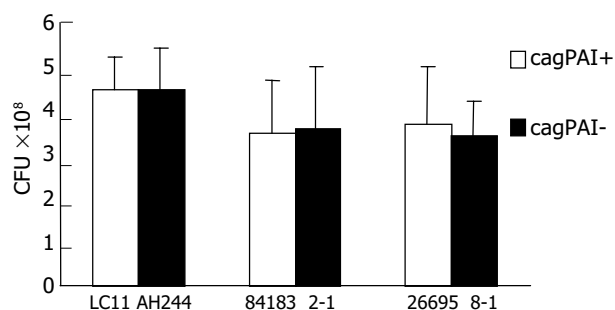


Figure 1 Equivalent growth of wildtype and knockout strains after 2 d culture.

Flow cytometry was used to detect adhesion of *H pylori* binding to gastric epithelial cells *H pylori* strain (ATCC26695) was marked by 10 mL/L PKH-26 and washed three times. The liquid after the third washing was used in the control groups, then bound to gastric epithelial cells (KatoIII) (bacteria/cells = 300:1), and incubated at 37 °C for 60 min. After washed, the sample was detected by FACs.

ELISA was used to detect apoptosis of gastric epithelial cells induced by *H pylori* The basic mechanism was to detect the release of DNA combined histone. According to the recommended procedures, cracked Kato-III cells with anti-histone monoclonal antibody were incubated and color was developed after adding substrate. Absorbency at the 405 nm level was measured in the enzyme-tagging instrument. Then, the apoptotic index (AI) was calculated in comparison with control group.

Mice were divided into 4 groups, five mice each group, except for the natural death. PBS Group: 200 μ L PBS /one mouse was fed once via mouth as negative control; CT Group: CT (10 μ g) 200 μ L/per mouse was fed once via mouth as adjuvant control Group; CagPAI positive Group: ultrasonic smashed *H pylori* 26695 (100 μ L) and CT (10 μ g) was fed at a time via mouth; CagPAI negative Group: ultrasonic smashed *H pylori* 8-1 (100 μ L) and CT (10 μ g) were fed once via mouth.

Immunity procedures

Before immunization and inoculation of *H pylori*, the mice were prohibited from water and food for over 12 h. Thirty min before inoculation, the mouse was fed with 200 μ L (0.01 mol/L) NaHCO_3 solution to neutralize gastric acid. The experimental group and the control group were inoculated with antigens and adjuvants, immunized on d 0, 7, and 14. They were allowed to drink water 1 h after immunization. Each group was attacked with *H pylori* 10^8 CFU once every other day, 3 wk after the latest immunization. The mice were killed 8 wk after the latest attack.

Evaluation of bacterial implantation

The spleen and stomach were removed immediately after the mouse neck was broke. The spleen was kept in the axenic cell culture media temporarily and dealt with it for 4 h. The stomach was cut along the greater curvature, washed with axenic fluid, then some tissues were sampled for rapid urea enzyme test and histological examination. Histological examination was graded semi-quantitatively according to the standard as follows: 0 point: no *H pylori*; 1 point: 1-2 *H pylori* in some gastric pits; 2 points: 3-10 *H pylori* in majority of gastric pits and 3 points: over 10 *H pylori* in majority of gastric pits.

Spleen cell proliferation text

Spleen tissue was triturated into homogenates at aseptis environment. The spleen cells were counted and implanted in the 96 well plate (2×10^5 cells/well) containing 500 ng/mL PMA and 10 ng/ml ionomycin RPMI1640 (including cow blood serum, mycillin, Hepes *ect*), *H pylori* ultrasonic smashed antigen was added into them in terms of 2.5, 5, 10 mg/mL, cultured for 24 h, then H^3 -thymidine was added, and cultured for 8 h, then the cell were collected and degraded. Each control group was compared with the blank control group in the count, and the proliferation quotiety was calculated. Differential proliferation quotiety equals each group's proliferation quotiety/PBS group's proliferation quotiety $\times 100\%$.

Statistical analysis

Data and their variance were analyzed using EXCEL software. $P < 0.05$ was considered statistically significant.

RESULTS

Adherence of CagPAI and *H pylori*

CagPAI positive culture and mutant strains showed a different bacteria/cell ratio, and were, marked with PKH26, then they were incubated with stomach cell Kato-III, the adherence ability was measured with flow cytometry positive cells and mean fluorescence intensity (MFI) were calculated. No difference was found between wild strain and mutant strain. The result was displayed in Figure 2.

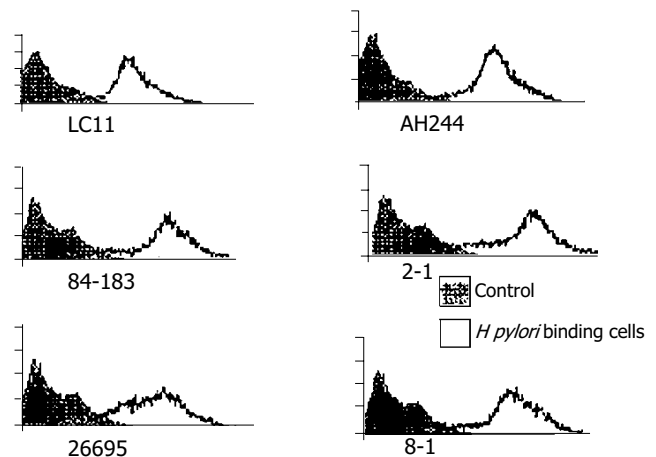


Figure 2 Binding of cag PAI wildtype *H pylori* and their mutant to gastric epithelial cell Kato-III.

Apoptosis-induced ability of cagPAI and *H pylori*

CagPAI and mutant strain were cultured with gastric epithelia cells at the ratio 300:1 for 24 h. The cells were deaged, the cell apoptosis was detected by ELISA. We found that the apoptosis-induced ability of 26 695 was slightly higher than that of 8-1 strain, and no difference was found in other couples. The result is displayed in Figure 3.

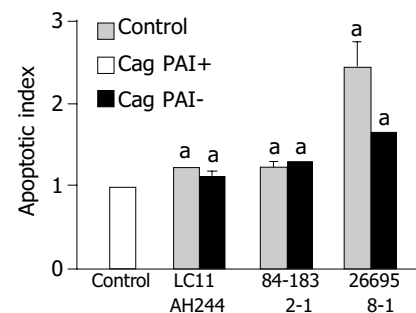


Figure 3 Apoptosis of gastric epithelial cells induced by positive cagPAI and knockout *H pylori* strains (determined by ELISA $^a P < 0.05$ vs the control).

Immune prevention to the cagPAI and *H pylori*

The protection rate of groups PBS, CT, 26695 and 8-1 was 0%, 0%, 40%, 60% (Table 2). CagPAI positive strain ATCC26695 and mutant strain 8-1 accompanied with mucous membrane adjuvant cholera toxin prevented *H pylori* from growing in the stomach of mice. There was no difference between the CagPAI positive strain and CagPAI negative strain. We found that full-protect rate of the two *H pylori* immune group was only 20% or so. It was found that immune was apparently decrease in semi-quantitative counting. No obvious difference was found between groups, and CT group had no prevention effect. The result is displayed in Figure 4.

Table 2 Ultrasonic smashed substance's protection against mice *H pylori* (result of urease test)

Immune project	Urease test (+)/number of animals (piece)	Protecting ratio (%)
PBS	5/5	0
CT	5/5	0
26695 SON+CT	3/5	40 ^a
8-1 SON+CT	2/5	60

^a $P < 0.05$, vs control groups.

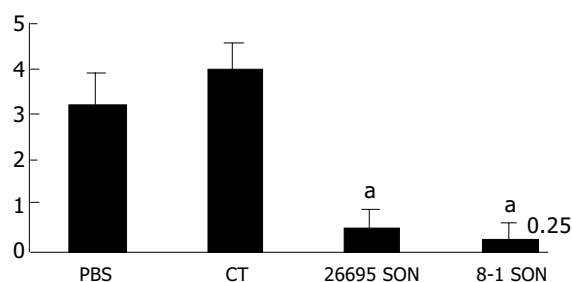


Figure 4 Semi-quantitative results of bacteria by histological examination. ^a $P < 0.05$ vs PBS control.

cagPAI and cell immune of mice *H pylori*

Comparing with PBS control, the CT control number of spleen cells was slightly increased, but that of two *H pylori* antigen-immune groups was greatly increased. The number of CagPAI mutant strains was more obvious. Compared with the two groups, no difference was found, ($P < 0.05$, Figure 5).

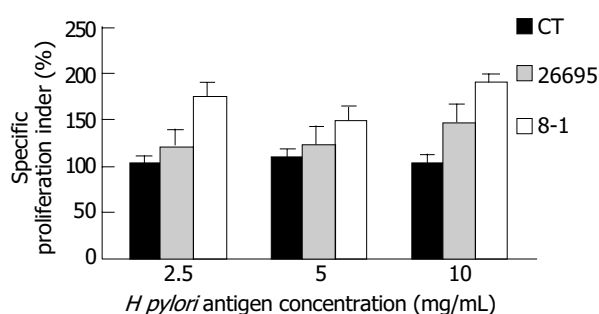


Figure 5 Specific proliferation index of immunized mice (compared to PBS group).

DISCUSSION

CagA is cytotoxin correlative protein, which is one of *H pylori* nosogenetic factors. The PAI is regarded as one of the signs of *H pylori* infection. Early researches found that this positive sign was higher in peptic ulcer and gastric carcinoma than in gastritis. For example, foreign researchers found that anti-CagPAI in serum was positive in 93% of the gastric carcinoma patients^[2], it is different in Asian-Pacific area, the positive ratio of the bacterial strain was much higher. A large number of reports approved that the pathogenicity of CagA (+) was stronger than that of CagA (-), inducing the production of IL-8 and GRO- α , ENA78 could produce and activated related nucleic transcription factors^[3]. Few reports about comparison of wildtype strain isogenic mutant strain *in vitro* were available. We studied three pairs of cagPAI wildtype strain and cagPAI gene-knockout mutant strain constructed by Dr. Bery. No difference was found between the growing speed and activity of the two strains.

There were many gene products concerned with *H pylori* adherence, including NLBH, porins, BabA *etc*^[4-9]. Our study showed that there was no difference in adherence to the epithelia of stomach between cagPAI (+) strain and cagPAI (-) strain.

CagPAI (+) strain could cause apoptosis and proliferation in stomach epithelia^[10]. However, it was proved by ELISA in our research that *in vitro* cagPAI was not concerned with apoptosis-induced ability, which did agree with the result of Le'Negrate. They found that cagE in cagPAI participated in the process of Fas-induced *H pylori* causing stomach epithelial apoptosis due to different the strain. we chose two stains in three pairs of strains, so the result was probably accurate.

In the immune prevention of *H pylori* infection, it was reported that cagA could prevent infection of the cagPAI (+). In our research,

SS1 strain which was used to infect animals was cag (+) strain, but we found that there was no difference in preventive effect between cagPAI (+) strain and mutant strain. Although there was no statistical difference, mutant stain had a higher protective trend. It showed that the immune prevention was not caused by protein coded by cagPAI. We do not support regarding cagPAI gene product is immune antigen of *H pylori* bacterin.

Cellular immunity, especially CD4⁺T cellular immunity is a very important mechanism, which can help B cells produce sIgA. We selected the spleen cell proliferation test as the target in immune. Because B cells could not live *in vitro*, the proliferation cells were mainly T cells. Both cagPAI (+) and cagPAI (-) strain were stimulated to proliferate T cells, indicating that some special T cells clones are existed in spleen cells. The number of cagPAI mutant strains is more than that of cagPAI (+) strains, agreeing with the histology.

The effect of cagPAI on *H pylori* immune and pathogenesis is very complex and needs further study.

REFERENCES

- Bai Y, Zhang YL, Wang JD, Zhang ZS, Zhou DY. Construction of the non-resistant attenuated *Salmonella typhimurium* strain expressing *Helicobacter pylori* catalase. *Diyi Junyi Daxue Xuebao* 2003; **23**: 101-105
- Vandenplas Y. *Helicobacter pylori* infection. *World J Gastroenterol* 2000; **6**: 20-31
- Blaser MJ. Hypothesis: the changing relationships of *Helicobacter pylori* and humans: implications for health and disease. *J Infect Dis* 1999; **179**: 1523-1530
- Covacci A, Censini S, Bugnoli M, Petracca R, Burroni D, Macchia G, Massone A, Papini E, Xiang Z, Figura N, Rappuoli R. Molecular characterization of the 128-kDa immunodominant antigen of *Helicobacter pylori* associated with cytotoxicity and duodenal ulcer. *Proc Natl Acad Sci U S A* 1993; **90**: 5791-5795
- Blaser MJ, Perez-Perez GI, Kleanthous H, Cover TL, Peek RM, Chyou PH, Stemmermann GN, Nomura A. Infection with *Helicobacter pylori* strains possessing CagA is associated with an increased risk of developing adenocarcinoma of the stomach. *Cancer Res* 1995; **55**: 2111-2115
- Odenbreit S, Puls J, Sedlmaier B, Gerland E, Fischer W, Haas R. Translocation of *Helicobacter pylori* CagA into gastric epithelial cells by type IV secretion. *Science* 2000; **287**: 1497-1500
- Bai Y, Dan HL, Wang JD, Zhang ZS, Odenbreit S, Zhou DY, Zhang YL. Cloning, expression, purification and identification of conservative region of four *Helicobacter pylori* adhesin genes in AlpA gene. *Prog Biochem Biophys* 2002; **29**: 922-926
- Bai Y, Zhany YL, Chen Y, Wang JD, Zhou DY. Study of Immunogenicity and safety and adherence of conservative region of four *Helicobacter pylori* adhesin *in vitro*. *Prog Biochem Biophys* 2003; **30**: 422-426
- Bai Y, Zhang YL, Wang JD, Zhang ZS, Zhou DY. Cloning and immunogenicity of conservative region of adhesin gene of *Helicobacter pylori*. *Zhonghua Yixue Zazhi* 2003; **83**: 736-739
- Bai Y, Wang JD, Zhang ZS, Zhang YL. Construction of the Attenuated *Salmonella typhimurium* strain expressing *Helicobacter pylori* conservative region of adhesin antigen. *Chin J Biotech* 2003; **19**: 77-82
- Bai Y, Chang SH, Wang JD, Chen Y, Zhang ZS, Zhang YL. Construction of the *E.coli* clone expressing adhesin BabA of *Helicobacter pylori* and evaluation of the adherence activity of BabA. *Diyi Junyi Daxue Xuebao* 2003; **23**: 293-295
- Bai Y, Zhang YL, Wang JD, Lin HJ, Zhang ZS, Zhou DY. Conservative region of the genes encoding four adhesins of *Helicobacter pylori*: cloning, sequence analysis and biological information analysis. *Diyi Junyi Daxue Xuebao* 2002; **22**: 869-871
- Rudnicka W, Covacci A, Wadstrom T, Chmiela M. A recombinant fragment of *Helicobacter pylori* CagA affects proliferation of human cells. *J Physiol Pharmacol* 1998; **49**: 111-119
- Wang RX, Zhang LY, Yin DL, Mufson RA, Shi Y. Protein kinase C regulates fas (CD95/APO-1) expression. *J Immunol* 1998; **161**: 2201-2207

Mechanisms mediating cholinergic antral circular smooth muscle contraction in rats

Helena F Wrzos, Tarun Tandon, Ann Ouyang

Helena F Wrzos, Tarun Tandon, Ann Ouyang, Division of Gastroenterology and Hepatology, Department of Medicine, College of Medicine, Pennsylvania State University, USA

Supported by NIH grant RO1-DK-34148

Correspondence to: Ann Ouyang, Division of Gastroenterology and Hepatology, Department of Medicine, College of Medicine, Pennsylvania State University, PO Box 850, Hershey, PA 17033, USA. aouyang@psu.edu

Telephone: +717-531-8741 Fax: +717-531-6770

Received: 2004-01-15 Accepted: 2004-02-13

Abstract

AIM: To investigate the pathway (s) mediating rat antral circular smooth muscle contractile responses to the cholinomimetic agent, bethanechol and the subtypes of muscarinic receptors mediating the cholinergic contraction.

METHODS: Circular smooth muscle strips from the antrum of Sprague-Dawley rats were mounted in muscle baths in Krebs buffer. Isometric tension was recorded. Cumulative concentration-response curves were obtained for (+)-cis-dioxolane (cD), a nonspecific muscarinic agonist, at 10^{-8} - 10^{-4} mol/L, in the presence of tetrodotoxin (TTX, 10^{-7} mol/L). Results were normalized to cross sectional area. A repeat concentration-response curve was obtained after incubation of the muscle for 90 min with antagonists for M1 (pirenzepine), M2 (methocramine) and M3 (darifenacin) muscarinic receptor subtypes. The sensitivity to PTX was tested by the ip injection of 100 mg/kg of PTX 5 d before the experiment. The antral circular smooth muscles were removed from PTX-treated and non-treated rats as strips and dispersed smooth muscle cells to identify whether PTX-linked pathway mediated the contractility to bethanechol.

RESULTS: A dose-dependent contractile response observed with bethanechol, was not affected by TTX. The pretreatment of rats with pertussis toxin decreased the contraction induced by bethanechol. Lack of calcium as well as the presence of the L-type calcium channel blocker, nifedipine, also inhibited the cholinergic contraction, with a reduction in response from 2.5 ± 0.4 g/mm² to 1.2 ± 0.4 g/mm² ($P < 0.05$). The dose-response curves were shifted to the right by muscarinic antagonists in the following order of affinity: darifenacin (M₃) > methocramine (M₂) > pirenzepine (M₁).

CONCLUSION: The muscarinic receptors-dependent contraction of rat antral circular smooth muscles was linked to the signal transduction pathway(s) involving pertussis-toxin sensitive GTP-binding proteins and to extracellular calcium via L-type voltage gated calcium channels. The presence of the residual contractile response after the treatment with nifedipine, suggests that an additional pathway could mediate the cholinergic contraction. The involvement of more than one muscarinic receptor (functionally predominant type 3 over type 2) also suggests more than one pathway mediating the cholinergic contraction in rat antrum.

Wrzos HF, Tandon T, Ouyang A. Mechanisms mediating

cholinergic antral circular smooth muscle contraction in rats. *World J Gastroenterol* 2004; 10(22): 3292-3298
<http://www.wjgnet.com/1007-9327/10/3292.asp>

INTRODUCTION

The mechanisms involved in the regulation of cholinergic contraction of intestinal smooth muscle are complex and not fully understood, despite the important role of the cholinergic system in the physiology of gastric emptying, and pathophysiology of several motility disorders. Cholinergic agonists activate muscarinic receptors which transduce cholinergic signals by activating G proteins^[1,2]. Different signal transduction pathways in different species, as well as different pathways for the circular and longitudinal layers of intestinal smooth muscle have been reported^[3-15].

Specific muscarinic receptors are abundantly present in the smooth muscles of gastrointestinal tract^[16-22]. Muscarinic receptor subtypes have shown a G-protein coupling specificity, however the published data are inconsistent. In some studies M₁, M₃, M₅ receptor subtypes were preferentially coupled to the Gq/11 protein class, the M₂ and M₄ receptors were linked to the PTX-sensitive Gi/Go proteins^[23-25]. Whereas in other studies muscarinic M₂ receptors were insensitive to pertussis toxin^[26].

Relatively few references are published characterizing rat stomach muscarinic receptor subtypes, again with conflicting results. Prevalence of M₃^[13,22,27], or of M₁^[28], or M₂ receptors^[29-33] has been reported. Which muscarinic receptor is more functionally important in the cholinergic contraction of antral circular muscle has not been determined.

The aim of this study was to examine the signal transduction pathway (s) mediating rat antral smooth muscle cholinergic contraction to fill the existing knowledge gaps: (1) what type of calcium channel was involved and was there a dependence on extracellular Ca²⁺ influx; (2) whether PTX-sensitive- or PTX-insensitive-G proteins coupled to muscarinic receptors were involved; and (3) what subtypes of specific muscarinic receptors were functionally involved. Determining the physiology of the pathway (s) mediating cholinergic contraction of the antrum should be helpful in understanding the functional motility changes described in models of disease conditions, such as diabetes^[34-36]. Preliminary accounts of some of these observations have been published in abstract form^[37,38].

MATERIALS AND METHODS

Animals

Young adult male Sprague-Dawley rats (Charles River Breeding Laboratories), weighing 200-450 g were used. Animals were anesthetized by ip injection of sodium pentobarbital (30-65 mg/kg). Anesthesia was given immediately before the tissue removal to avoid the effect of anesthesia on the contractile properties of the tissue. The abdomen was explored through midline incision and the stomach was removed. After the tissue was removed, animals were euthanized by injection of an overdose of pentobarbital. All our studies were approved by the Institutional Animal Care and Use Committee of the PSU College of Medicine.

Smooth muscle strip bath preparation^[39]

The antrum tissue was pinned in a dissecting dish in oxygenated Krebs solution, mucosa was gently removed by scraping, and strips were cut in the circular muscle orientation. The muscle was oxygenated in Krebs physiological buffer containing (in mmol/L) 130 Na, 4.7 K, 2.5 Ca, 1.0 Mg₂, 140.7 Cl, 19 HCO₃, 1.0 PO₄ and 10 glucose at 37 °C. The strips were sutured at one end to a glass rod and at the other end to an inelastic wire. The tissue, the rod and a wire were placed in a 10-mL double walled glass chamber with a constant temperature 37 °C. Glass surfaces were silicone coated with Sigmacote to prevent binding of the peptides. The chambers were filled with 5 mL of Krebs buffer and gassed with 95:5 mixture of O₂/CO₂. The free end of wire was attached to an isometric force transducer (Grass Instrument Co) and recordings were made on a multichannel rectilinear dynograph recorder (Beckman Instruments). The strips were allowed to equilibrate for 1 h. Tissues were stretched to an initial length (L_i) from which any additional stretch resulted in an increase in tension. The isometric tension response to bethanechol (10⁻⁴ mol/L) was noted. The strips were rinsed and the length increased by 1 mm increment until the maximum response to bethanechol (10⁻⁴ mol/L) was recorded. This length was labeled L₀. All subsequent studies were conducted at this length. Drugs were added to the tissue bath and the peak response within 8 min was compared with the maximum tension recorded during 5 min before addition of drugs. Antagonists were added 1 min before the addition of agonist. The peptidase inhibitors bestatin and phosphoramidon (both at 10⁻⁶ mol/L) were added at least 5 min before the agonist addition. The response was calculated as the change in the maximal force of contraction in g of tension normalized to the cross sectional area which was calculated as: cross section (mm²) = weight (g)/specific density × length (mm), where the specific density of muscle tissue = 1.056 (g/mm³).

Dispersed single muscle cell preparation^[40,41]

Smooth muscle cells were isolated from the circular muscle layer of the antrum. The mucosa was removed by dissection and the longitudinal muscle layer (with enteric plexus ganglia) was removed in strips using a Stadie-Riggs tissue slicer (Thomas TM). The circular muscle layer was minced and incubated for 45 min twice in Hepes buffer containing collagenase (CLS type II, Worthington) and 0.1 g/L soybean trypsin inhibitor at 31 °C. Partially digested strips were washed with enzyme-free Hanks' medium. Muscle cells were allowed to disperse spontaneously under the gentle force of bubbling 950 mL/L O₂+50 mL/L CO₂ for 30 min (no agitation), and then filtered through 500 µmol/L Nitinol mesh, to the culture media. Viability was checked by trypan blue exclusion test. Aliquots of cells were added to solutions containing the agonists at room temperature. The reaction was stopped after 30 min, by addition of acrolein to the final concentration of 1%. Aliquots were sealed under coverslips. Computerized image analysis (NIH Image 1.62) was used for quantification. A scale slide was used for reference. The length of single muscle cells was measured (at least 50 cells per concentration).

Contractile response of antrum smooth muscle strips to cholinergic agonist

To determine the effect of bethanechol on antrum circular smooth muscle contraction, muscle strips were exposed to the increasing doses of muscarinic agonist, bethanechol, at the concentrations of 10⁻⁴ to 10⁻⁷ mol/L in an organ bath.

Characteristics of effect of extracellular Ca²⁺ and type of calcium channel involved

To determine whether cholinergic contraction depended on the influx of extracellular Ca²⁺, the response to bethanechol chloride in the physiological Krebs buffer was tested, then the buffer was changed into Ca-free buffer (in mmol/L: NaCl 132.5; KCl 4.

7; MgCl₂ 1.0; NaH₂PO₄ 1.2; NaHCO₃ 20.0; D-glucose 10; EGTA (50 µmol/L), and contraction was subsequently recorded after 5 and 10 min.

To characterize the type of calcium channel involved in the cholinergic contraction, nifedipine (an L-type calcium channel antagonist) was used. Nifedipine was dissolved in ethanol and added to the physiological Krebs buffer at the concentration of 10⁻⁵ mol/L^[42] and contraction was recorded. Statistical significance of the difference between contraction in the presence and absence of nifedipine was calculated by paired *t*-test, the results were considered statistically significant at *P* ≤ 0.05.

Treatment with pertussis toxin (PTX)

In order to determine whether PTX-sensitive pathway was involved in cholinergic contraction, strips and dispersed muscle cells (myocytes) isolated from the antrum of PTX-pretreated and non-pretreated animals were compared.

Rats were injected with 100 mg/kg of PTX (dissolved in saline) intraperitoneally 5 d before the study^[43]. Muscle strips from PTX-treated and control rats in the tissue bath were exposed to cholinergic agonist, bethanechol, at the concentration of 10⁻⁴ to 10⁻⁶ mol/L. Statistical significance of the difference between the contraction of the muscle from PTX-pretreated and non-treated rats was defined by non-paired *t*-test, the results were considered statistically significant at *P* ≤ 0.05.

The changes in the pattern of contraction of muscle cells in dispersed cell suspension were also measured (detailed description in the "dispersed muscle cell preparation" section of Materials & Methods). Two concentrations of bethanechol (10⁻⁷ and 10⁻⁸ mol/L) were added to the cell suspensions in the tubes in the physiological buffer. Their contractions were measured as the percentage of the control cell diastolic length^[44]. The mean lengths of cells from control rats were compared to those of the cells from PTX-treated animals. Results were presented as mean ± SE. Statistical significance of the difference was calculated by the paired *t*-test, the results were considered statistically significant at *P* ≤ 0.05.

Characterization of muscarinic receptor subtypes involved

For the characterization of muscarinic receptor subtypes involved in cholinergic contraction we used a non-selective muscarinic agonist, (+)-cis-Dioxolane^[45,46] and relatively specific receptor subtype antagonists.

The conditions of organ bath were described above in the "Smooth muscle strip bath preparation" section of Materials and Methods. At the start of the experimental protocol, the viability of each tissue was assessed by determining the contractile response to bethanechol (10⁻⁴ mol/L). After washed, tissues were re-equilibrated for 10 min and allowed to regain baseline tension. Cumulative concentration-effect curves of (+)-cis-Dioxolane, (10⁻⁸ to 3 × 10⁻⁵ mol/L) were constructed for each tissue. Tissues were then equilibrated in either the absence (control) or presence of the antagonist for 90 min. Subsequently, a second concentration-effect curve to (+)-cis-Dioxolane was constructed. Smooth muscle strips were incubated with increasing concentrations of antagonists demonstrating a relative specificity for M₁, M₂ or M₃ muscarinic receptor subtypes (pirenzepine, methoctramine and darifenacin, respectively). Each antral smooth muscle strip was exposed to only one concentration of antagonists and incubated for 90 min at 37 °C, with a fresh antagonist added to the medium every 30 min^[47,48].

The EC₅₀ values for muscarinic antagonists were obtained (i.e. antagonist concentration resulting in 50% of inhibition of the contraction induced by cholinergic agonist, (+)-cis-Dioxolane (10⁻⁶ mol/L).

Drugs

Tetrodotoxin (TTX), sigmacote, neurokinin A (NKA), nifedipine,

papain, peptidase inhibitors bestatin and phosphoramidon, soybean trypsin inhibitor, acrolein and pirenzepine (predominantly M_1 muscarinic receptor antagonist), were from Sigma, St. Louis, MO.

(+)-cis-dioxolane (cholinergic agonist) and methocramine (predominantly M_2 muscarinic receptor antagonist) were purchased from RBI Inc., Natick, MA. PTX was purchased from List Biological Labs, Inc., Campbell, CA. Bethanechol chloride was purchased from Merck, West Point, PA and collagenase (CLS type II) from Worthington, PA. Darifenacin (predominantly M_3 muscarinic receptor antagonist) was a generous gift from Pfizer Ltd, Sandwich, Kent, GB.

RESULTS

Dose-response curve to cholinergic agonist

A contractile dose-response was observed, when the antral circular smooth muscle strips were exposed to the increasing doses of muscarinic agonist, bethanechol, at the concentrations of 10^{-4} to 10^{-7} mol/L in an organ bath. A significant increase of the tension over the baseline was observed at the bethanechol concentrations of 10^{-4} to 10^{-6} mol/L (Figure 1, $n = 4$).

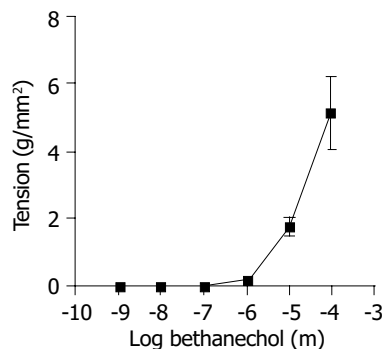


Figure 1 Effect of bethanechol on smooth muscle contraction. Antrum circular smooth muscle strips were incubated with increasing concentrations of bethanechol (10^{-4} mol/L to 10^{-7} mol/L). The vertical axis represents the developed tension (in grams per mm^2). Bethanechol significantly increased circular muscle tension ($P < 0.05$; paired t -test). Each data point represents mean \pm SE, $n = 4$.

Effect of tetrodotoxin (TTX)

Antrum circular smooth muscle strips were exposed to bethanechol at the concentration of 10^{-5} mol/L, in a buffer containing tetrodotoxin (10^{-5} mol/L), added prior to bethanechol to the organ bath. The cholinergic contraction was not affected by tetrodotoxin, neuronal toxin, with the contraction at $94.9 \pm 3.2\%$ of control.

The lack of inhibition of the contraction by TTX confirmed that a cholinergic agonist could induce contraction via muscarinic receptors present at the smooth muscle, without participation of neuronal factor.

Effect of calcium depletion on cholinergic contraction and characterization of a calcium channel subtype involved

Calcium-free buffer Incubation in calcium-free buffer diminished the antral contractile response to bethanechol (10^{-4} mol/L), with a reduction in response from 2.5 ± 0.4 g/ mm^2 to 1.2 ± 0.4 g/ mm^2 ($P < 0.05$) after 5 min of incubation in calcium-free buffer. After 10 min of incubation in Ca^{2+} -free buffer contractile activity was almost abolished (Figure 2).

Full recovery of the contraction was seen after return of the Ca^{2+} to the tissue bath medium, indicating that there was no damage to the cell resulting in a decreased contraction. These results showed that cholinergic contraction was dependent on the presence of extracellular calcium, a receptor-operated Ca^{2+} or voltage-sensitive Ca^{2+} channels.

Effect of calcium channel blocker The L-type calcium channel blocker, nifedipine at a concentration of 10^{-5} mol/L inhibited the cholinergic contraction response of antrum to the bethanechol, at the concentration of 10^{-4} mol/L from 4.02 ± 0.9 to 0.49 ± 0.18 g/ mm^2 ($P < 0.05$), indicating that the L-calcium channel could mediate this contraction.

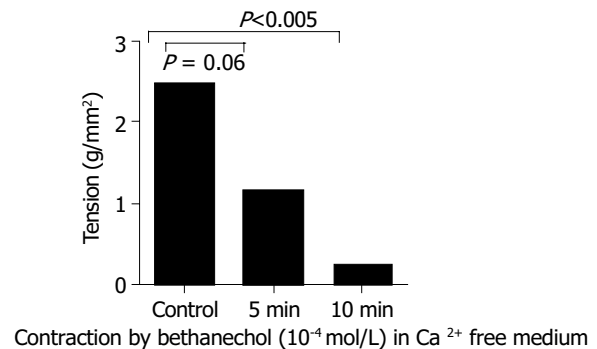


Figure 2 Effect of depletion of Ca^{2+} from medium on the contraction of antral circular smooth muscle strips to bethanechol (10^{-4} mol/L). Ca^{2+} depletion caused a significant decrease in the muscle tension; after 5 min incubation ($P < 0.06$, paired t -test); and after 10 min incubation ($P < 0.005$, paired t -test) compared to the base contraction induced by bethanechol before Ca^{2+} depletion. Each data point represents mean \pm SE, $n = 3$.

Identification of G-protein-linked signal transduction pathway by PTX

The response to bethanechol of antral circular muscle strips and dispersed smooth muscle cells from PTX-pretreated and control rats was compared (see Methods).

Smooth muscle strips The contractile response to bethanechol of the muscle strips from the PTX-pretreated animals was significantly lower than that of the muscle strip from the non-treated control rats at all concentrations, 10^{-6} to 10^{-4} mol/L (Figure 3, $P \leq 0.01$).

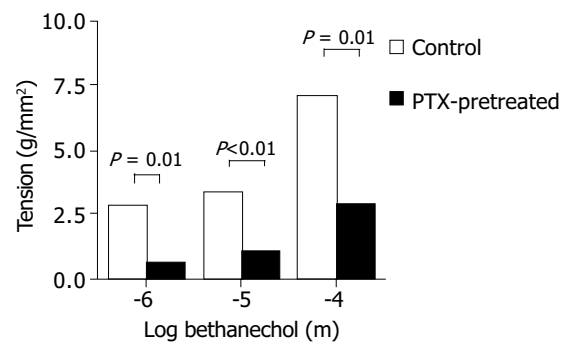


Figure 3 Effect of PTX on antrum circular smooth muscle strips contraction to bethanechol (10^{-4} mol/L to 10^{-6} mol/L). PTX significantly inhibited the contractile activity of the smooth muscle ($P \leq 0.01$; paired t -test) compared to control rats. Each point represents mean \pm SE, $n = 7$; dotted bars represent control animals; solid bars-PTX-pretreated animals.

The inhibiting effect of PTX on the contraction implied that cholinergic agonist was activating a PTX-sensitive pathway.

A low level of residual contractile activity was observed in the contraction of PTX-treated muscle strips suggesting either that there was a small PTX-insensitive fraction involved, or that the dose of PTX used was insufficient to completely inhibit PTX-sensitive pathways.

Dispersed antral smooth muscle cells When dispersed myocytes from PTX-treated rats and controls were compared, cells from PTX-pretreated rats showed significantly less contraction to

bethanechol than the cells isolated from the rats non-treated with PTX, at both bethanechol concentrations, 10^{-8} and 10^{-7} mol/L (Figure 4, $P \leq 0.005$). The inhibiting effect of PTX on the dispersed myocytes contraction, confirmed the smooth muscle strip data and suggested that the cholinergic agonist involved an occupation of specific muscarinic receptors coupled to PTX-sensitive mediated pathway.

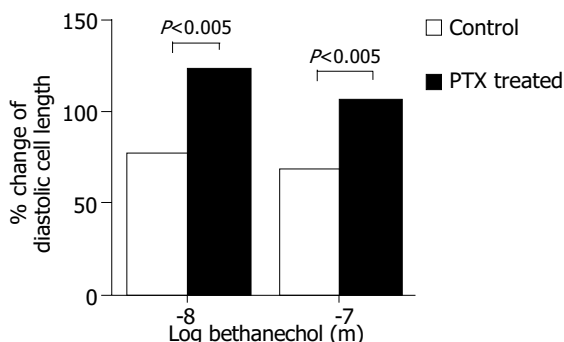


Figure 4 Effect of PTX on dispersed antral circular smooth muscle myocytes from PTX-pretreated rats contraction to bethanechol (10^{-7} mol/L and 10^{-8} mol/L). Myocytes from PTX-treated rats contracted less than myocytes from control rats. Each point represents mean \pm SE; of the percentage of the control cells diastolic length (no bethanechol). At least 50 myocytes per point were calculated, $P < 0.005$; $n = 7$ and 11. Dotted bars represent control animals; solid bars PTX-pretreated animals.

Characterization of the type of muscarinic receptor subtypes involved in contraction to cholinergic agonist To define pharmacologically the muscarinic receptors involved in the cholinergic contraction, specific muscarinic receptor antagonists were used in the presence of tetrodotoxin (10^{-7} mol/L).

For this functional muscarinic receptor study we chose a non-selective cholinergic agonist, (+)-cis-Dioxolane (see Methods), instead of bethanechol, which has been reported to selectively stimulate M_3 receptor^[45,46,49].

Pirenzepine, the M_1 muscarinic receptor antagonist, was used at the concentrations from 3×10^{-5} to 10^{-8} mol/L. Pirenzepine caused a significant inhibition of the of the contractile muscle response to the (+)-cis-dioxolane (Figure 5).

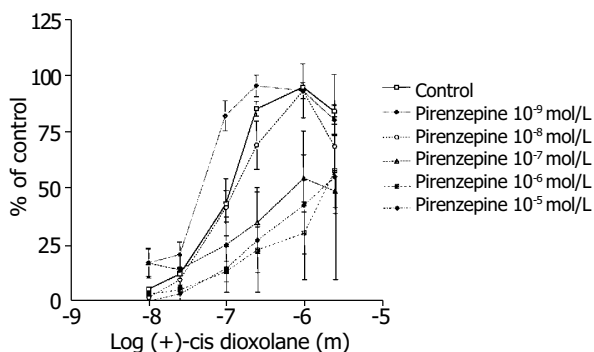


Figure 5 Concentration-response curves for the contractile effect of (+)-cis-Dioxolane alone and in combination with different concentrations of M_1 antagonist, pirenzepine (10^{-8} mol/L to 10^{-5} mol/L) on the rat antral circular smooth muscle strips. Each point represents the mean \pm SE, $n = 6, 6, 7$ and 8 strips. Cumulative concentration-effect curve was constructed for each strip for (+)-cis-Dioxolane, (10^{-8} to 3×10^{-5} mol/L). After washing, strips were equilibrated in either the absence (control) or presence of pirenzepine for 90 min. Subsequently, the second concentration-effect curve for (+)-cis-Dioxolane was constructed for each strip. Pirenzepine caused a significant inhibition of the contractile muscle response to (+)-cis-dioxolane.

Methocramine- M_2 muscarinic receptor antagonist was used at the concentration range between 3×10^{-5} and 10^{-8} mol/L. Methocramine caused a significant inhibition of the of the contractile muscle response to the (+)-cis-dioxolane (Figure 6).

Darifenacin was used at the concentration range from 3×10^{-5} to 10^{-9} mol/L (Figure 7). Darifenacin caused a significant inhibition of the contractile muscle response to the (+)-cis-dioxolane.

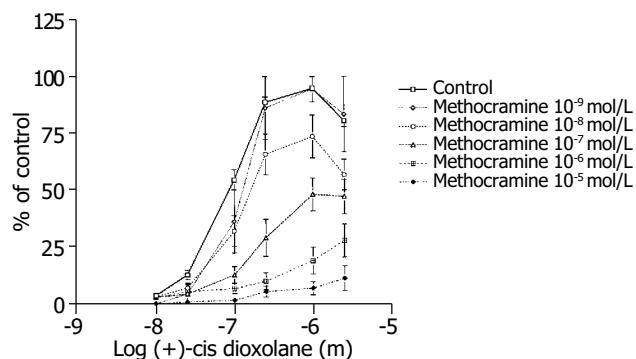


Figure 6 Concentration-response curves for the contractile effect of (+)-cis-Dioxolane alone and in combination with different concentrations of M_2 antagonist, methocramine (from 10^{-8} mol/L to 10^{-5} mol/L) on the rat antral circular smooth muscle strips. Each point represents the mean \pm SE; $n = 4, 9, 10$ and 11 strips. First, cumulative concentration-effect curve was constructed for each strip for (+)-cis-Dioxolane, (10^{-8} to 3×10^{-5} mol/L). After washing, tissues were equilibrated in either the absence (control) or presence of methocramine for a 90 min. Subsequently, the second concentration-effect curve for (+)-cis-Dioxolane was constructed for each strip. Methocramine caused a significant inhibition of the contractile muscle response to (+)-cis-Dioxolane.

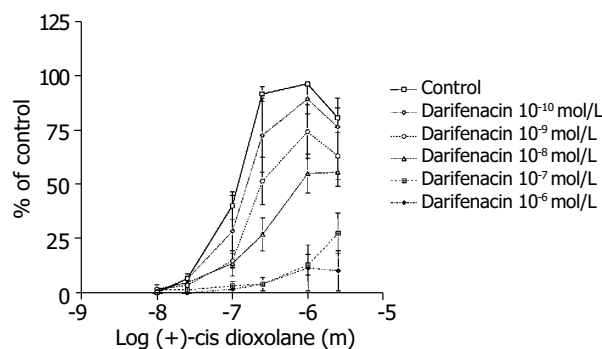


Figure 7 Concentration-response curves for the contractile effect of (+)-cis-Dioxolane alone and in combination with different concentrations of M_3 antagonist, darifenacin (from 10^{-10} mol/L to 10^{-6} mol/L) on the rat antral circular smooth muscle strips. Each point represents the mean \pm SE; $n = 4, 7, 11, 10$ strips. First, cumulative concentration-effect curve was constructed for each strip for (+)-cis-Dioxolane, (10^{-8} to 3×10^{-5} mol/L). After wash, tissues were equilibrated in either the absence (control) or presence of darifenacin for a 90 min. Subsequently, the second concentration-effect curve for (+)-cis-Dioxolane was constructed for each strip. Darifenacin caused a significant inhibition of the contractile muscle response to (+)-cis-Dioxolane.

Comparison the muscarinic M_1 , M_2 and M_3 receptor antagonists mediating the rat antral circular smooth muscle contraction

All three receptors (M_1 , M_2 and M_3) subtype antagonists inhibited the antral circular muscle contraction to cholinergic agonist (+)-cis-dioxolane. Darifenacin (M_3) was most potent in inhibiting rat antral smooth muscle cholinergic contraction. The dose-response curves were shifted to the right by muscarinic antagonists in the following order of affinity: darifenacin (M_3)

>methocramine (M_2) >pirenzepine (M_1). The EC_{50} for each antagonist was as follows: darifenacin 7.9, methocramine 7.2 and pirenzepine 6.8 (Figure 8).

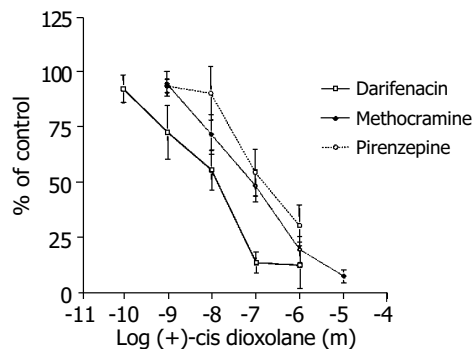


Figure 8 Comparison of the inhibition of the contractile response to cis-Dioxolane by 3 muscarinic receptor antagonists: M_3 - darifenacin, M_2 - methocramine, and M_1 - pirenzepine. The M_3 antagonist, darifenacin, was the most potent inhibitor of the contraction induced by (+)-cis Dioxolane (10^{-6} mol/L). The EC_{50} values for each were: for darifenacin (M_3) -7.9; for methocramine (M_2) -7.2; and for pirenzepine (M_1) -6.8.

DISCUSSION

It is well established that cholinergic agonists are of major importance for the stimulation of antral smooth muscle contraction and that their effect is mediated by muscarinic receptors. In various smooth muscle cells, the action of cholinergic agonists involved the occupation of specific receptors, activation of receptor-coupled G-proteins and subsequent activation of the second messenger systems, which would lead to the mobilization of Ca^{2+} from intracellular storage pools^[10]. Certain steps of the signaling pathway (s) for the cholinergic contraction of antral circular smooth muscle in rats are still not understood, for example, the second messenger system or the functional characteristics of the muscarinic receptor subtypes involved. In our study the cholinergic rat antral circular muscle contraction *in vitro* was sensitive to the depletion from the extracellular Ca^{2+} that significantly diminished the cholinergic contraction. This finding along with the inhibitory effect of nifedipine indicated a dependence on extracellular Ca^{2+} influx via L-type calcium channels^[50].

It is still not clear whether cholinergic contractile pathways of antral circular smooth muscle are mediated by PTX-sensitive GTP-binding protein through an increased inflow of extracellular calcium, or mediated via PTX-insensitive, inositol triphosphate (IP_3)-dependent pathway. The circular muscle of cat esophagus and the lower esophageal sphincter (LES) were reported to be linked to different pathways. LES circular muscle cholinergic contraction was shown to be linked to the PTX-insensitive pathway, whereas esophageal circular muscle cholinergic contraction has been reported to be linked to the PTX-sensitive pathway^[11-14].

In the present study, pretreatment with PTX significantly inhibited the contractile response to bethanechol of the antral smooth muscle strips in the organ bath and of the dissociated myocytes.

More than one muscarinic receptor may be responsible for cholinergically mediated contractility at a particular area^[6,22,51-56]. A major role for M_3 and a minor role for M_2 receptors in cholinergic-induced smooth muscle contraction have been shown at the tissue of various species and organs^[57-59], but it is still not clear how different receptors may interact to mediate a specific function. For example, M_2 receptor might serve as an inhibitory presynaptic autoreceptor^[60], or M_2 receptor could act by gating cation channels that were subsequently modulated by M_3 receptors^[61].

The functional characteristics of muscarinic receptor subtypes regulating antrum circular muscle cholinergic contraction have not been previously reported. In our functional studies, cholinergic contraction in response to cis-dioxolane in rat antral circular muscles was mediated mostly through M_3 , less by M_2 , and the least by M_1 muscarinic receptor subtypes.

The involvement of PTX-sensitive GTP-binding proteins in mediating the contractile response to muscarinic agonists has been reported to be linked to muscarinic M_2 receptor in many studies, such as in cat esophageal circular muscle^[11,12]. In contrast, our experiments in rat antral circular muscles indicated that the M_3 muscarinic receptor was functionally prevalent, and yet, PTX-sensitive pathways were shown to be activated in the process of antral cholinergic contraction. A few published reports were in agreement with our results^[13,22,26].

Possible explanations of the reported differences include: (1) Different experimental systems were used to compare the homogenous suspension of smooth muscle cells was compared with smooth muscle strips. (2) M_3 and M_2 receptors were expressed together at the shared site of the signaling pathways^[22,54,57,60,62]. (3) The cholinergic agonist (+/- cis-Dioxolane) was used in our studies. Although, it has been reported to be non-selective^[46,48,52], +/- cis-Dioxolane might be more selective for M_3 muscarinic receptor than it was originally described^[63]. (4) It has been suggested that seven transmembrane spanning receptors including muscarinic are promiscuous in that they could form interactions with multiple G-proteins^[64] or activate many different transduction pathways at the same time^[65]. (5) M_2 receptor might be masked by M_3 receptor, thus detectable when M_3 receptor was inhibited. Separating out these possibilities would require more specific antagonists than the currently available.

In conclusion, the rat antral circular smooth muscle contracts to cholinergic agonists (bethanechol chloride and (+)-cis-Dioxolane) in a dose-dependent fashion through activation of muscarinic receptors at the smooth muscle. The contractile responses to cholinergic agonists are dependent on the increase in intracellular calcium induced by the influx of extracellular calcium via L-type voltage gated calcium channels. Bethanechol activates M_3 and M_2 muscarinic receptors coupled to pertussis-toxin sensitive GTP-binding protein (s). The presence of a residual contractile cholinergic response after 5 and 10 min in calcium-free buffer, as well as a residual contractile response after the treatment with nifedipine, suggests a role for an additional pathway (s). M_3 receptor is predominant out of three functionally tested M_1 , M_2 , and M_3 muscarinic receptors regulating cholinergic contraction. The involvement of more than one muscarinic receptor indicates more than one pathway (s) regulating the cholinergic contraction of rat antrum circular smooth muscle.

The results of these studies have important clinical implications for possible treatment of gastric dysfunction with muscarinic subtype-selective agents.

ACKNOWLEDGEMENTS

Authors would like to thank John Ellis, Ph.D, for helpful discussions. An excellent technical assistance of Rohini Polavarapu is acknowledged.

REFERENCES

- Berridge MJ. Inositol trisphosphate and calcium signaling. *Nature* 1993; **361**: 315-325
- Bygrave FL, Roberts HR. Regulation of cellular calcium through signaling cross talk involves an intricate interplay between the actions of receptors, G-proteins, and second messengers. *FASEB J* 1995; **9**: 1297-1303
- Akbulut H, Goren Z, Iskender E, Eraslan A, Ozdemir O, Oktay S. Subtypes of muscarinic receptors in rat duodenum: a comparison with rabbit vas deferens, rat atria, guinea-pig ileum

- and gallbladder by using imperialine. *Gen Pharmacol* 1999; **32**: 505-511
- 4 **Grider JR**, Makhlof GM. Contraction mediated by Ca⁺⁺ release in circular and Ca⁺⁺ influx in longitudinal muscles cells. *J Pharmacol Exper Ther* 1988; **244**: 432-437
 - 5 **Murthy KS**, Grider JR, Makhlof GM. InsP₃-dependent Ca²⁺ mobilization in circular but not longitudinal muscle cells of intestine. *Am J Physiol* 1991; **261**(6 Pt 1): G937-G944
 - 6 **Li Z**, Ruan Y, Guo ZD, Cong H, Zhang KY, Takemura H. Function and localization of high and low affinity binding sites to muscarinic receptors in longitudinal and circular smooth muscles of human stomach. *Res Comm Chem Pathol Pharmacol* 1990; **67**: 31-42
 - 7 **Kerr PM**, Hillier K, Wallis RM, Garland CJ. Characterization of muscarinic receptors mediating contractions of circular and longitudinal muscle of human isolated colon. *Br J Pharmacol* 1995; **115**: 1518-1524
 - 8 **Lucchesi PA**, Romano FD, Scheid CR, Yamaguchi H, Honeyman TW. Interaction of agonists and selective antagonists with gastric smooth muscle muscarinic receptors. *Naunyn Schmiedebergs Arch Pharmacol* 1989; **339**: 145-151
 - 9 **Miyazaki H**, Koyama I, Nakamura H, Taneike T, Ohga A. Regional differences in cholinergic innervation and drug sensitivity in the smooth muscles of pig stomach. *J Autonomic Pharmacol* 1991; **11**: 255-265
 - 10 **Makhlof GM**, Murthy KS. Signal transduction in gastrointestinal smooth muscle. *Cell Signal* 1997; **9**: 269-276
 - 11 **Sohn UD**, Harnett KM, De Petris G, Behar J, Biancani P. Distinct muscarinic receptors G proteins, and phospholipases in esophageal and lower esophageal sphincter (LES) circular muscle. *J Pharmacol Exp Ther* 1993; **267**: 1205-1214
 - 12 **Sohn UD**, Han B, Tashjian AH, Behar J, Biancani P. Agonist-dependent, muscle-type-specific signal transduction pathways in cat esophageal and lower esophageal sphincter circular smooth muscle. *J Pharmacol Exp Ther* 1995; **273**: 482-491
 - 13 **Lin S**, Kajimura M, Takeuchi K, Kodaira M, Hanai H, Kaneko E. Expression of muscarinic receptor subtypes in rat gastric smooth muscle: effect of M₃ selective antagonist on gastric motility and emptying. *Dig Dis Sci* 1997; **42**: 907-914
 - 14 **Cao W**, Chen Q, Sohn UD, Kim N, Kirber MT, Harnett KM, Behar J, Biancani P. Ca²⁺-induced contraction of cat esophageal circular smooth muscle cells. *Am J Physiol* 2001; **280**: C980-C992
 - 15 **Bitar KN**, Saffouri B, Makhlof GM. Cholinergic and peptidergic receptors on isolated human antral smooth muscle cells. *Gastroenterology* 1982; **82**: 832-837
 - 16 **Konturek SJ**, Jaworek J, Tasler J, Cieszkowski M, Yanaihara N. Subtypes of muscarinic receptors in canine pancreatic secretion *in vivo* and *in vitro*. *Int J Pancreatol* 1987; **2**: 11-22
 - 17 **Liebmann C**, Nawrath S, Schnittler M, Schubert H, Jakobs KH. Binding characteristics and functional G protein coupling of muscarinic acetylcholine receptors in rat duodenum smooth muscle membranes. *Naunyn Schmiedebergs Arch Pharmacol* 1992; **345**: 7-15
 - 18 **Brann MR**, Ellis J, Jorgensen H, Hill-Eubanks H, Jones SVP. Muscarinic acetylcholine receptor subtypes: localization and structure/function. *Prog Brain Res* 1993; **98**: 121-127
 - 19 **Preiksaitis HG**, Krysiak PS, Chrones T, Rajgopal V, Laurier LG. Pharmacological and molecular characterization of muscarinic receptor subtypes in human esophageal smooth muscle. *J Pharmacol Exp Ther* 2000; **295**: 879-888
 - 20 **Eglen RM**. Muscarinic receptors and gastrointestinal tract smooth muscle function. *Life Sci* 2001; **68**: 2573-2578
 - 21 **Li M**, Bullock CM, Knauer DJ, Ehlert FJ, Zhou QY. Identification of Two Prokineticin cDNAs: Recombinant Proteins Potently contract gastrointestinal smooth muscle. *Mol Pharmacol* 2001; **59**: 692-698
 - 22 **Stengel PW**, Yamada M, Wess J, Cohen ML. M₃-receptor knockout mice: muscarinic receptor function in atria, stomach fundus, urinary bladder, and trachea. *Am J Physiol* 2002; **282**: R1443-R1449
 - 23 **Migeon JC**, Thomas SL, Nathanson NM. Differential coupling of m₂ and m₄ muscarinic receptors to inhibition of adenylyl cyclase by Gi alpha and G (o) alpha subunits. *J Biol Chem* 1995; **270**: 16070-16074
 - 24 **Murthy KS**, Makhlof GM. Differential coupling of muscarinic m₂ and m₃ receptors to adenylyl cyclases V/VI in smooth muscle. Concurrent M₂ - mediated inhibition via Galphai3 and m₃-mediated stimulation via Gbetagammaq. *J Biol Chem* 1997; **272**: 21317-21324
 - 25 **Kostenis E**, Zeng FY, Wess J. Structure-function analysis of muscarinic receptors and their associated G proteins. *Life Sci* 1999; **64**: 355-362
 - 26 **Yokotani K**, Osumi Y. Cholinergic M₂ muscarinic receptor-mediated inhibition of endogenous noradrenaline release from the isolated vascularly perfused rat stomach. *J Pharmacol Exp Ther* 1993; **264**: 54-60
 - 27 **Milovanovic DR**, Jankovic SM. Pharmacologic characterization of muscarinic receptor subtypes in rat gastric fundus mediating contractile responses. *Indian J Med Res* 1997; **105**: 239-245
 - 28 **Nelson DK**, Pieramico O, Dahmen G, Dominguez-Munoz JE, Malfertheiner P, Alder G. M₁-muscarinic mechanisms regulate interdigestive cycling of motor and secretory activity in human upper gut. *Dig Dis Sci* 1996; **41**: 206-215
 - 29 **Hammer R**. Muscarinic receptors in the stomach. *Scandinavian J Gastroenterol Suppl* 1980; **66**: 5-11
 - 30 **Herawi M**, Lambrecht G, Mutschler E, Moser U, Pfeiffer A. Different binding properties of muscarinic M₂-receptor subtypes for agonists and antagonists in porcine gastric smooth muscle and mucosa. *Gastroenterology* 1988; **94**: 630-637
 - 31 **Moumimi C**, Magous R, Strosberg D, Bali JP. Muscarinic receptors in isolated smooth muscle cells from gastric antrum. *Bioch Pharmacol* 1988; **37**: 1363-1369
 - 32 **Hasler WL**, Heldsinger A, Owyang C. Cisapride acts on muscarinic (glandular M₂) receptors to induce contraction of isolated gastric myocytes: mediation via a calcium-phosphoinositide pathway. *J Pharmacol Exp Ther* 1991; **259**: 1294-1300
 - 33 **Rhee JC**, Rhee PL, Park MK, So I, Uhm DY, Kim KW, Kang TM. Muscarinic receptors controlling the carbachol-activated nonselective cationic current in guinea pig gastric smooth muscle cells. *Jap J Pharmacol* 2000; **82**: 331-337
 - 34 **Takahashi T**, Kojima Y, Tsunoda Y, Beyer LA, Kamijo M, Sima AA, Owyang C. Impaired intracellular signal transduction in gastric smooth muscle of diabetic BB/W rats. *Am J Physiol* 1996; **270**(3 Pt 1): G411-G417
 - 35 **Xue L**, Suzuki H. Electrical responses of gastric smooth muscles in streptozotocin-induced diabetic rats. *Am J Physiol* 1997; **272** (1 Pt 1): G77-G83
 - 36 **Maruyama Y**, Sakai Y, Nobe K, Momose K. Subcellular distribution of protein kinase C isoforms in gastric antrum smooth muscle of STZ-induced diabetic rats. *Life Sci* 1999; **64**: 1933-1940
 - 37 **Wrzos HF**, Polavarapu R, Ouyang A. The signal transduction pathway involved in rat antral and colonic circular muscle response to muscarinic and neurokinin receptor agonists. Abstract. *Gastroenterology* 1997; **112**: A853
 - 38 **Wrzos HF**, Tandon T, Ouyang A. Functional significance of muscarinic receptor subtypes on rat antral circular muscle. Abstract. *Neurogastroenterol Motil* 1998
 - 39 **Bertiger G**, Reynolds JC, Ouyang A, Cohen S. Properties of the feline pyloric sphincter *in vitro*. *Gastroenterology* 1987; **92**: 1965-1972
 - 40 **Bitar KN**, Makhlof GM. Receptors on smooth muscle cells: characterization by contraction and specific antagonists. *Am J Physiol* 1982; **242**: G400-G407
 - 41 **Biancani P**, Hillemeier C, Bitar KN, Makhlof GM. Contraction mediated by Ca²⁺ influx in esophageal muscle and by Ca²⁺ release in LES. *Am J Physiol* 1987; **253**(6 Pt 1): G760-G766
 - 42 **Maggi CA**, Zagorodnyuk V, Giuliani S. Specialization of tachykinin NK1 and NK2 receptors in producing fast and slow atropine resistant neurotransmission to the circular muscle of the guinea-pig colon. *Neuroscience* 1994; **63**: 1137-1152
 - 43 **Thomas EA**, Ehlert FJ. Pertussis toxin blocks M₂ muscarinic receptor-mediated effects on contraction and cyclic AMP in the guinea pig ileum, but not M₃-mediated contractions and phosphoinositide hydrolysis. *J Pharmacol Exp Ther* 1994; **271**: 1042-1050
 - 44 **von Schrenck T**, Mackensen B, Mende U, Schmitz W, Sievers J, Mirau S, Raedler A, Greten H. Signal transduction pathway of the muscarinic receptors mediating gallbladder contraction.

- Naunyn Schmiedebergs Arch Pharmacol* 1994; **349**: 346-354
- 45 **Choppin A**, Eglén RM. Pharmacological characterization of muscarinic receptors in dog isolated ciliary and urinary bladder smooth muscle. *Br J Pharmacol* 2001; **132**: 835-842
- 46 **Hegde SS**, Choppin A, Bonhaus D, Briaud S, Loeb M, Moy TM, Loury D, Eglén RM. Functional role of M₂ and M₃ muscarinic receptors in the urinary bladder of rats *in vitro* and *in vivo*. *Br J Pharmacol* 1997; **120**: 1409-1418
- 47 **Smith CM**, Wallis RM. Characterisation of [3H]-darifenacin as a novel radioligand for the study of muscarinic M₃ receptors. *J Rec Sign Transduction Res* 1997; **17**: 177-184
- 48 **Choppin A**, Eglén RM, Hegde SS. Pharmacological characterization of muscarinic receptors in rabbit isolated iris sphincter muscle and urinary bladder smooth muscle. *Br J Pharmacol* 1998; **124**: 883-888
- 49 **Barocelli E**, Morini G, Ballabeni V, Lavezzo A, Impicciatore M. Effects of two new pirenzepine analogs on the contractile response of the guinea-pig oesophageal muscularis mucosae to acetylcholine, bethanechol, histamine and high potassium. *European J Pharmacol* 1990; **179**: 89-96
- 50 **Okamoto H**, Inoue K, Kamisaki T, Takahashi K, Sato M. Regional differences in calcium sensitivity in the guinea-pig intestine. *J Pharm Pharmacol* 1997; **49**: 981-984
- 51 **Dietrich C**, Kilbinger H. Prejunctional M₁ and postjunctional M₃ muscarinic receptors in the circular muscle of the guinea-pig ileum. *Naunyn Schmiedebergs Arch Pharmacol* 1995; **351**: 237-243
- 52 **Eglén RM**, Harris GC. Selective inactivation of muscarinic M₂ and M₃ receptors in guinea-pig ileum and atria *in vitro*. *Br J Pharmacol* 1993; **109**: 946-952
- 53 **Ehlert FJ**, Sawyer GW, Esqueda EE. Contractile role of M₂ and M₃ muscarinic receptors in gastrointestinal smooth muscle. *Life Sci* 1999; **64**: 387-394
- 54 **Sawyer GW**, Ehlert FJ. Muscarinic M₃ Receptor inactivation reveals a pertussis toxin-sensitive contractile response in the guinea pig colon: evidence for M₂/M₃ receptor interactions. *J Pharmacol Exp Ther* 1999; **289**: 464-467
- 55 **Wang J**, Krysiak PS, Laurier LG, Sims SM, Preiksaitis HG. Human esophageal smooth muscle cells express muscarinic receptor subtypes M₁ through M₅. *Am J Physiol* 2000; **279**: G1059-G1069
- 56 **Ren J**, Harty RF. Presynaptic muscarinic receptors modulate acetylcholine release from rat antral mucosal/submucosal nerves. *Dig Dis Sci* 1994; **39**: 1099-1106
- 57 **Chen Q**, Yu P, de Petris G, Biancani P, Behar J. Distinct muscarinic receptors and signal transduction pathways in gallbladder muscle. *J Pharmacol Exp Ther* 1995; **273**: 650-655
- 58 **Bellido I**, Fernandez JL, Gomez A, Sanchez de la Cuesta F. Otenzepad shows two populations of binding sites in human gastric smooth muscle. *Can J Physiol Pharmacol* 1995; **73**: 124-129
- 59 **Hanack C**, Pfeiffer A. Upper gastrointestinal porcine smooth muscle expresses M₂- and M₃- receptors. *Digestion* 1990; **45**: 196-201
- 60 **Parkman HP**, Pagano AP, Ryan JP. Subtypes of muscarinic receptors regulating gallbladder cholinergic contractions. *Am J Physiol* 1999; **276**(5 Pt 1): G1243-G1250
- 61 **Bolton TB**, Zholos AV. Activation of M₂ muscarinic receptors in guinea-pig ileum opens cationic channels modulated by M₃ muscarinic receptors. *Life Sci* 1997; **60**: 1121-1128
- 62 **Braverman AS**, Tallarida RJ, Ruggieri MR Jr. Interaction between muscarinic receptor subtype signal transduction pathways mediating bladder contraction. *Am J Physiol Regul Integr Comp Physiol* 2002; **283**: R663- R668
- 63 **Lanzafame A**, Christopoulos A, Mitchelson F. Interactions of agonists with an allosteric antagonist at muscarinic acetylcholine M₂ receptors. *Eur J Pharmacol* 1996; **316**: 27-32
- 64 **Nahorski SR**, Tobin AB, Willars GB. Muscarinic M₃ receptor coupling and regulation. *Life Sci* 1997; **60**: 1039-1045
- 65 **Parekh AB**, Brading AF. The M₃ muscarinic receptor links to three different transduction mechanisms with different efficacies in circular muscle of guinea-pig stomach. *Br J Pharmacol* 1992; **106**: 639-643

Edited by Chen WW and Wang XL. Proofread by Xu FM

Coxsackievirus B₃ infection and its mutation in Keshan disease

Li-Qun Ren, Xiang-Jun Li, Guang-Sheng Li, Zhi-Tao Zhao, Bo Sun, Fei Sun

Li-Qun Ren, Xiang-Jun Li, Guang-Sheng Li, Zhi-Tao Zhao, Bo Sun, Department of Pathology, Institute of Frontier Medical Science, Jilin University, Changchun 130021, Jilin Province, China
Fei Sun, Department of Cellular Biology, Institute of Frontier Medical Science, Jilin University, Changchun 130021, Jilin Province, China
Supported by National Natural Science Foundation of China, No. 39870668

Correspondence to: to Professor Guang-Sheng Li, Department of Pathology, Institute of Frontier Medical Science, Jilin University, Changchun 130021, Jilin Province, China. ligs@public.cc.jl.cn

Telephone: +86-431-5619287

Received: 2003-12-28 **Accepted:** 2004-02-10

Abstract

AIM: To investigate coxsackievirus B₃ infection and its gene mutation in Keshan disease.

METHODS: The expression of Coxsackievirus B₃ RNA was detected in autopsy specimens of acute (12 cases), sub-acute (27 cases) and chronic (15 cases) Keshan disease by *in situ* hybridization. In sub-acute Keshan disease specimens, 3 cases with positive result by *in situ* hybridization were selected RT-PCR analysis. The DNA segments were then sequenced.

RESULTS: Coxsackievirus B₃ RNA was detected in the cytoplasm of myocardiocyte. The positive rate was 83% in acute, 67% in sub-acute and 80% in chronic Keshan disease. In the conservative region of Coxsackievirus B₃ genome, there was a mutation in 234 (C-T) compared to the non-cardiovirulent strain, CVB_{3/0}.

CONCLUSION: Coxsackievirus B₃ RNA can survive and replicate in heart muscle of Keshan disease, which may play an important role in the occurrence of Keshan disease. The possible mechanism of occurrence of Keshan disease is associated with point a mutation in Coxsackievirus B₃ genome.

Ren LQ, Li XJ, Li GS, Zhao ZT, Sun B, Sun F. Coxsackievirus B₃ infection and its mutation in Keshan disease. *World J Gastroenterol* 2004; 10(22): 3299-3302
<http://www.wjgnet.com/1007-9327/10/3299.asp>

INTRODUCTION

Enteroviruses, particularly Coxsackie B viruses (CVB), are the most common cause of human viral myocarditis and are associated with dilated cardiomyopathy (DCM)^[1-3]. In general, neonates and children suffer more severe clinical syndromes due to CVB infection, often severe or life threatening, because of inflammation and necrosis of heart muscle^[4]. Many diseases are considered to have relationship with CVB₃ infect, but the mechanism is still not well understood. Although the immune response of the host undoubtedly plays an important role in the pathogenesis of viral heart disease^[5], direct viral cytotoxicity has been found to be crucial for organ pathology both during acute and persistent heart muscle infection. Coxsackievirus B₃ (CVB₃), one of six CVB serotypes, is a member of the genus *enterovirus* within the family *Picornaviridae* and its structure is well understood^[6,7].

Some studies suggest that the 5'NTR of enteroviruses maybe play an important role in producing or sustaining the myocardial virulence^[8-14].

Keshan disease is endemic exclusively in selenium-deficient rural areas of China, including 14 provinces and autonomous regions^[15]. Its clinical features are low body selenium content and acute or chronic episodes of heart disorder characterized by cardiogenic shock, arrhythmia, ECG changes (for example, right branch block), and/or congestive heart failure, with an enlarged heart. Four types of the disease are seen: acute, subacute, chronic, and latent or compensated. The basic pathological change is multifocal myocardial necrosis and fibrous replacement throughout the myocardium, with various degrees of cellular infiltration and calcification, depending upon the type of disease^[16,17]. Research suggests that not a single but several more factors may have a relationship with the occurrence of Keshan disease. The reasons are often considered as global, biological chemical factors (selenium deficiency), dietary nutritional factors (vitamin E deficiency) and infection (virus, especially enteroviruses). This hypothesis can explain both endemic and seasonal features of Keshan disease. Recent studies have also demonstrated a possible etiological role of enterovirus infection in a particular form of heart muscle disease, selenium deficiency-related endemic cardiomyopathy (Keshan disease), seen in China^[18,19]. Presently, patients of Keshan disease are rare and there is no ideal animal model, research of viral etiology of Keshan disease is relatively few. In this study, we detected all the four types of Keshan disease using *in situ* hybridization and sequenced the 5'NTR of CVB₃ from subacute Keshan disease in order to investigate the relationship between Keshan disease and CVB₃ infection.

MATERIALS AND METHODS

Case selected

All the samples were cardiac tissue isolated at post mortem and fixed in formaldehyde and embedded in paraffin wax and preserved in Institute of Keshan Disease, Jilin University from 1959-1985. The samples included 12 acute patients (7 males, 5 females, average age 16.3 years), 27 subacute patients (12 males, 15 females, average age 4.3 years) and 15 chronic patients (9 males, 6 females, average age 23.8 years). We used three non-Keshan disease patients as controls, including two normal and one perinatal period cardiomyopathy. The cultured human amniotic cell containing a cardiovirulent strain of CVB₃ served as positive control and by RT-PCR.

In situ Hybridization

An oblong nucleotide probe was purchased from Shanghai Sangon Biological Engineering Company. This probe, labeled with biotin, was designed to detect coxsackievirus B₃, whose sequence was 5'-GTC CGC AAT GGC GGG CGG TGG TGG TGT CTC-3'.

All slides were treated by APES solution (1:50 acetone) in order to prevent the section slipping from the slide. The 5 μm thick section was baked 3-4 h at 80 °C and overnight at 60 °C.

The paraffin wax was removed by immersing the slide in xylene. The slides were then rehydrated, treated with 0.1 g/L Triton X-100 for 2 min, digested with proteinase K (0.25 mg/mL) in PBS for 5 min at room temperature, then sealed with histidine (2 mg/mL) for 2 min, and then dehydrated in graded concentrated

ethyl alcohol. The tissue sections were denatured on heating block for 2 min at 80 °C and then cooled on ice immediately. They were pre-hybridized for 3-4 h at 42 °C by covering them with pre-hybridization liquid (6×SSC, 5×Denhardt, 5 g/L SDS, 100 µg/mL herring sperm DNA, 500 g/L deionized formamide) in a wet chamber. After removal of the pre-hybridization liquid, the sections were allowed to hybridize overnight under the same conditions as described above.

Following the hybridization, the slides were rinsed twice with 2×SSC containing 500 g/L deionized formamide, twice with 2×SSC, treated with 1 g/L Triton X-100 for 2 min and washed twice with buffer I (1 mol/L NaCl, 0.1 mol/L Tris, pH 7.5). Buffer II (3 g bovine serum albumin dissolved in buffer I) was added to each section and incubated for 1 h. After pouring off buffer II, the SA-AP (streptavidin-alkaline phosphatase conjugation) was added onto the tissue sections, and allowed to react in this mixture for 20 min, rinsed with buffer I and then with buffer III (0.1 mol/L NaCl, 0.1 mol/L Tris-Cl, 50 mmol/L MgCl₂, pH 9.5). Finally, freshly prepared developer solution (BCIP/NBT) was applied to the slides and incubated for 30 min to 4 h. A brownish blue color reaction was produced. Following routine dehydration, the sections were cleared and mounted.

To assess the specificity of the hybridization signal, the culture cell infected by CVB₃ were alternatively hybridized with the labeled oblong nucleotide probe encoding CVB₃ before and after digestion by Rnase, and hybridization solution without containing the labeled oblong nucleotide probe encoding CVB₃ was also used as negative control.

RT-PCR

Total RNA was extracted from paraffin-embedded heart tissue of patients with Keshan disease according to the following procedures. Several section slices (5-10 µm) were put into a 1.5 mL Eppendorf tube in which approximately 1 mL xylene was added in order to exclude paraffin. The xylene was changed every 2 h and the last time it was kept overnight at room temperature. After being centrifuged at 5 000 r/min for 5 min, the tissue was washed with non-water ethanol and then baked at 55 °C. The total RNA from the dried tissue was then extracted using Trizol reagent (GIBCO). Positive controls were the cultured human amniotic cells containing CVB₃. The RNA precipitate was dissolved in 10 µL of diethyl pyrocarbonate-treated H₂O.

The enterovirus specific primers used for RT-PCR and sequencing of the 5'NTR were purchased from Sigma Genosys Australia Pty. Ltd. The sequence of the primers was 3P: 5'-TCA ATTGTC ACCATA AGCAGCAGCCA-3' and 5P: 5'-CGG TAC CTTTGT GCCCCT GTT TT-3'.

RT was carried out following the manufacturer's instructions. A 2 µL of specific primer 3P and 1 µL of 10 mmol/L dNTPs were mixed with 8 µL of RNA template. The mixture was immediately put on ice after incubated at 65 °C for 5 min. Then the mixture of 4 µL of 5×first strand buffer, 1 µL of Rnase inhibitor, 1 µL Superscript II Rnase H-free reverse transcriptase and 3 µL of diethyl pyrocarbonate-treated H₂O was added to the reaction tube, followed by incubation at 42 °C for 5 min, and at 70 °C for 15 min in order to inactivate the reverse transcriptase.

PCR was carried out with a 25 µL mixture containing 10 pmol deoxynucleotide triphosphates, 15 pmol forward primer (5P), 15 pmol reverse primer (3P), 1×reaction buffer (Dingguo Biocompany), and 3 µL of the RT reaction product. The PCR reaction mixture was pre-denatured at 95 °C for 2 min, and then amplified through 30 cycles, each cycle consisting of denaturation at 95 °C for 45 s, annealing at 55 °C for 45 s, and extension at 72 °C for 45 s. Finally, an additional extension was carried out at 72 °C for 10 min. A negative control containing 22 µL of the reaction mixture plus 3 µL of autoclaved H₂O and a positive control containing 22 µL of the reaction mixture plus 3 µL of the RT reaction product from cells infected with the virulent laboratory strain

of CVB₃ were included in each set of PCR.

The amplification products of PCR were analyzed on 17 g/L agarose gel by electrophoresis and stained with ethidium bromide. To assess the specificity of RT-PCR, the extracted total RNA were digested by Rnase then used for PCR as template. The distilled water was also used as template in PCR reaction as negative control.

DNA sequencing

The sequencing reaction cycle was carried out using 4 µL of DNA polymerase FS-terminator mix (PE-ABI), 3.2 mmol/L primer, and 5 ng of PCR product per 100 bp length of template DNA with the volume made up to 10 µL with H₂O. Reactions were run for 25 cycles as follows: 96 °C for 30 s, 50 °C for 15 s, and 60 °C for 4 min. DNA was precipitated, dissolved in loading buffer (167 g/L formamide, 733 g/L dextran), and separated on 41 g/L denaturing polyacrylamide gel on an ABI model 377 DNA sequencer. This procedure was performed by Shanghai Sangon Biological Engineering Company.

RESULTS

In situ Hybridization

According to the feature of positive signal of the culture cell, the positive hybridization signals of the Coxsackievirus RNA appeared as deep brownish blue mass or granules (Figure 1). This criterion was applied to the tissue sample. In longitudinal sections, they were seen to adhere to myofibrils in one or several strings of beads (Figure 2A). They varied in size and, in cross section, were usually localized in the sarcoplasm in proximity to myocyte nuclei, but no signals were found in the nuclei themselves. The color of signal was the darkest in the myocardium of papillary muscles, trabeculae carneae and subendocardial muscle. It was lighter and less intense in the cells of the outer layers than those in the middle layers of ventricular walls. The myocardial cells surviving in fresh lesions and surrounding old necrotic foci often showed the hybridization signal. No signal was found in necrotic foci, and there were slight differences in the distribution and manifestation of positive hybrid signals in several types of Keshan disease. In most acute and subacute

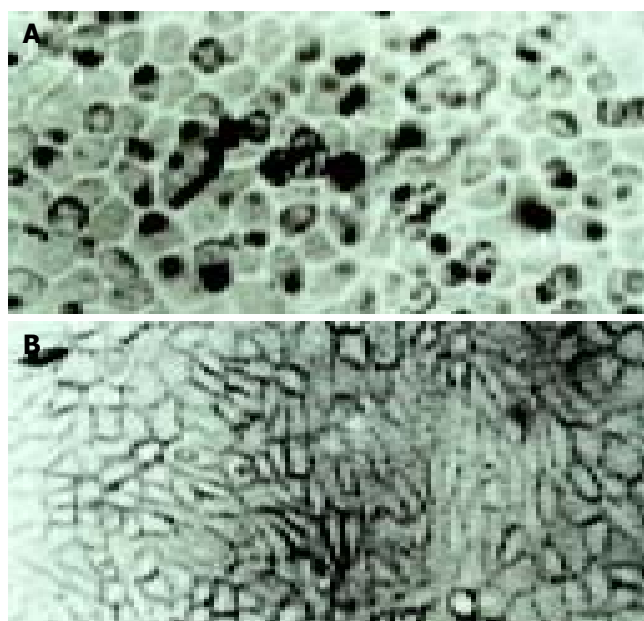


Figure 1 Positive signal in cultured cell A: the positive hybridization signals of the Coxsackievirus RNA appeared as deep brownish blue mass or granules (arrow) B: control, only hybridization solution was applied.

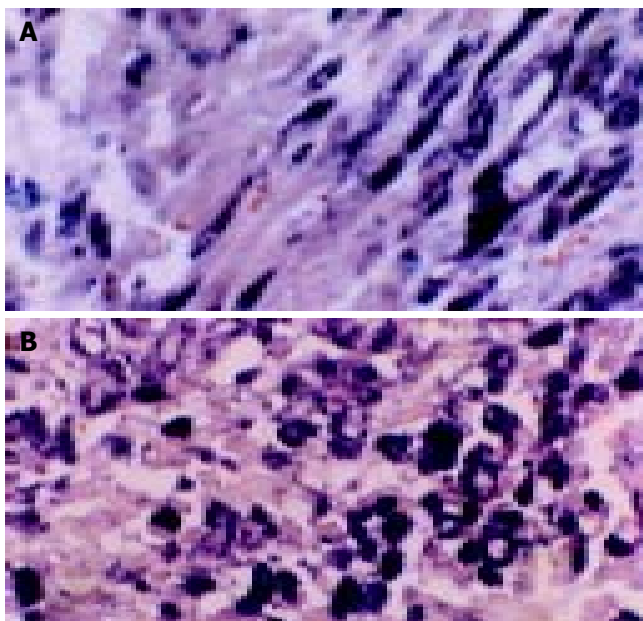


Figure 2 Positive signal of *in situ* hybridization in subacute myocardial tissue A: Feature positive signal of *in situ* hybridization with cardiac tissue is seen as deep brownish blue and seems to adhere onto myofibril, linked together in one or several strings of beads, when observed longitudinally ($\times 400$). B: The granules of positive signal were thick and with clear border in varying size and localized in the sarcoplasm.

cases, the signal appeared predominantly in the myocyte surrounding foci and surviving in fresh foci as well as cells beneath the endocardium and of papillary muscles. The hybridization-positive granules were thick, and had clear border. The sarcoplasm appeared dark, and sometimes, homogeneously blue (Figure 2B). In most of the chronic cases, the granules were usually distributed in all parts of the myocardium, and were small and without clear borders, like dirt. The detection rate in subacute specimens was the highest, and the rate in acute specimens was higher than that in chronic specimens, but there were no significant differences among the three types of Keshan disease.

The positive rate of hybridization in the three type of Keshan disease was 83% (10/12) in acute, 67% (18/27) in sub-acute and 80% (12/15) in chronic Keshan disease. No positive signals were found in any negative controls.

Results of 3 myocardial control specimens investigated with *in situ* hybridization were negative.

RT-PCR

RT-PCR revealed that the RNA extracted from the myocardial tissue with positive control of *in situ* hybridization amplified a DNA fragment about 541 bp, while the three negative controls did not amplify (Figure 3). The RNA extracted from cultured cell infected by CVB₃ were also amplified the DNA fragment about 541 bp.

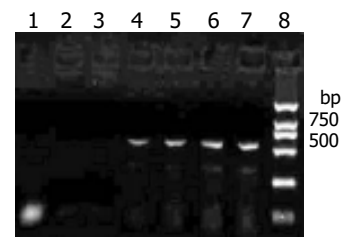


Figure 3 Agarose gel electrophoresis results Lanes 1, 2, 3: negative control; Lanes 4-6: subacute Keshan disease; Lanes 7: positive control; Lane 8: DL-2000 DNA Marker. A 541 bp DNA segment can be seen in lanes 4-7.

Sequence analysis

The DNA segments from RT-PCR were sequenced and compared to the non-cardiovirulent control, CVB_{3/0}, and the cardiovirulent strain, CVB_{3/Nancy} and CVB_{3/20}. We found that the sequence of the amplified segment had one nucleotide different compared to that of CVB_{3/0}. The 234th nucleotide in the genome of CVB_{3/0} was C while ours was T. But the sequence of our segment was similar that of CVB_{3/Nancy}, CVB_{3/20} and the positive control (Figure 4).

DISCUSSION

Keshan disease has been studied for over 60 years in China. One of the key issues is the complex etiology of this endemic disease, with a focus on environmental nutritional factors and infectious agents. Selenium deficiency in the food chain has been recognized as a major but not exclusive environmental-nutritional factor, and increasing evidence supports an etiological role of enteroviruses in Keshan disease. Recently, Peng *et al.*^[20] determined the sequences of the 5'NTR and the 3' end of the VP1 coding region from six enteroviruses isolate from cases of Keshan disease or outbreak myocarditis. From their results, they drew a conclusion that the sequence data confirm that coxsackievirus group B serotypes are predominant in the region where Keshan disease is endemic, and may be the etiological factors in outbreaks of myocarditis, and VP1 genotyping of enteroviruses is accurate and reliable. Animal experiments indicate that isolates may differ in pathogenicity. Virus infection combined with selenium deficiency in environments and vitamin E deficiency in dietary can illustrate both endemic and seasonal features of Keshan disease. The hypothesis of virus infection was accepted once it appeared, but the methods used in virology limited the development of a virus infection hypothesis of Keshan disease. The rapid development in molecular biology brings vitality to virology.

In situ hybridization is a method to detect the nucleic acids in a tissue or cell using a labeled oblong nucleotide chain as probe. This technique has already been widely used in biology and medicine because of its high specificity, sensitivity and location precision. Using a cloned cDNA probe obtained from CVB₄ infected cells and labeled by biotin-11-dUTP, Easton *et al.*^[21] found that 46% (6/13) patients who had been diagnosed coxsackievirus myocarditis can be found enterovirus infection in their myocardial tissue. Archard *et al.*^[22] examined enteroviruses

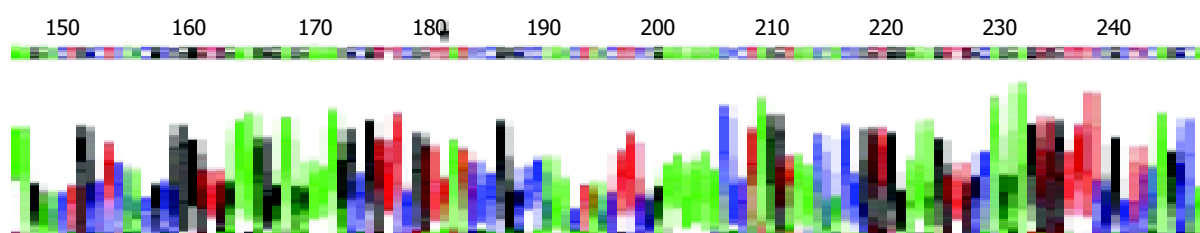


Figure 4 Sequence of segment of RT-PCR Compared to the nonvirulent strain of CVB_{3/0}, there was one nucleotide different (arrow). The nonvirulent strain of CVB_{3/0} was C while ours was T.

infection in human myocardial tissue using an enterovirus specific probe, and found that the rate of enterovirus infection was 45% (21/47) in myocarditis patients and 43% (35/82) in cured myocarditis and DMC patients. In our research, the specific oblong nucleotide probe of CVB₃ was labeled by biotin on 5' end, and the specimen was paraffin-embedded myocardial tissue from autopsy patients of Keshan disease. The object was to detect the coxsackievirus B₃ RNA by *in situ* hybridization. Among the three types of Keshan disease patients, we found the positive rate was 83%, 67%, and 80% in acute, sub-acute and chronic Keshan disease patients, respectively. Our results provide a new support to the hypothesis that enterovirus, especially CVB₃, might play an important role in pathogenesis of Keshan disease. Moreover, the area, range and the distribution of the positive signal of CVB₃ were associated with the development of Keshan disease. The positive signals in acute and sub-acute Keshan disease were located in the surviving cardiocyte in or around the necrosis foci while they were dispersed in almost all the cardiocyte in chronic Keshan disease. The results of *in situ* hybridization suggested that enterovirus could lead to heart muscle lesion when they involved in the myocardial tissue, and they can dispersed to the normal heart muscle with increase of time.

Though there was a high enterovirus infection rate in myocardial tissue of Keshan disease patients^[23,24], it is well known that the enterovirus could also be detected in many patients who had no heart muscle lesion. The change of viral cardiovirulence can undoubtedly play an important role. Some research has demonstrated that under some conditions, such as selenium deficiency, vitamin deficiency, the phenotype of enterovirus can be changed, that is, a non-cardiovirulent strain can change into a cardiovirulent strain, or the cardiovirulence can be increased in these conditions^[25-27]. Beck *et al.*^[28] sequenced the mutated strain, CVB_{30Se}, which was extracted from the heart muscle of selenium deficient mice, and found that there were six mutation points in CVB_{30Se}- and compared to the two-cardiovirulent strains, CVB₃₂₀, CVB_{3MI}, all mutated points were turned into that of a cardiovirulent strain. Can the same episodes also happen in Keshan disease patients? In our research, we found an about 541 bp DNA segment by RT-PCR. Compared to CVB_{3/0}, a non-cardiovirulent strain, the sequence of our segment had only one nucleotide different, which was 234 T. But the segment had the same sequence as that of CVB_{3/Nancy} and CVB_{3/20}, cardiovirulent strain. This result can give us some indications that the mutation of virus genome might play an important role in the pathogeny of Keshan disease. But this needs to further investigation.

As we know that RNA is degraded easily, so its detection is difficult, especially in paraffin-embedded tissue^[29,30]. But the paraffin-embedded myocardial tissue we select have been kept in our institute for a long time (10-50 years), and are generally thought not to be optimal for RNA research, but our results displayed that results of both *in situ* hybridization and RT-PCR were satisfactory.

REFERENCES

- Woodruff JF. Viral myocarditis. A review. *Am J Pathol* 1980; **101**: 425-484
- Bowles NE, Richardson PJ, Olsen EG, Archard LC. Detection of Coxsackie-B-virus-specific RNA sequences in myocardial biopsy samples from patients with myocarditis and dilated cardiomyopathy. *Lancet* 1986; **1**: 1120-1123
- Martino TA, Liu P, Sole MJ. Viral infection and the pathogenesis of dilated cardiomyopathy. *Circ Res* 1994; **74**: 182-188
- Kaplan MH, Klein SW, McPhee J, Harper RG. Group B coxsackievirus infections in infants younger than three months of age: a serious childhood illness. *Rev Infect Dis* 1983; **5**: 1019-1032
- Knowlton KU, Badorff C. The immune system in viral myocarditis: maintaining the balance. *Circ Res* 1999; **85**: 559-561
- Muckelbauer JK, Kremer M, Minor I, Diana G, Dutko FJ, Groarke J, Pevear DC, Rossmann MG. The structure of coxsackievirus B₃ at 3.5 Å resolution. *Structure* 1995; **3**: 653-667
- Wimmer E, Hellen CU, Cao X. Genetics of poliovirus. *Annu Rev Genet* 1993; **27**: 353-436
- Agol VI. The 5'-untranslated region of picornaviral genomes. *Adv Virus Res* 1991; **40**: 103-180
- Minor PD. The molecular biology of poliovaccines. *J Gen Virol* 1992; **73**(Pt 12): 3065-3077
- Rohll JB, Percy N, Ley R, Evans DJ, Almond JW, Barclay WS. The 5'-untranslated regions of picornavirus RNAs contain independent functional domains essential for RNA replication and translation. *J Virol* 1994; **68**: 4384-4391
- Le SY, Siddiqui A, Maizel JV Jr. A common structural core in the internal ribosome entry sites of picornavirus, hepatitis C virus, and pestivirus. *Virus Genes* 1996; **12**: 135-147
- Rinehart JE, Gomez RM, Roos RP. Molecular determinants for virulence in coxsackievirus B1 infection. *J Virol* 1997; **71**: 3986-3991
- Dunn JJ, Chapman NM, Tracy S, Romero JR. Genomic determinants of cardiovirulence in coxsackievirus B₃ clinical isolates: localization to the 5' non translated region. *J Virol* 2000; **74**: 4787-4794
- Tu Z, Chapman NM, Hufnagel G, Tracy S, Romero JR, Barry WH, Zhao L, Currey K, Shapiro B. The cardiovirulent phenotype of coxsackievirus B₃ is determined at a single site in the genomic 5' non translated region. *J Virol* 1995; **69**: 4607-4618
- Ge K, Yang G. The epidemiology of selenium deficiency in the etiological study of endemic diseases in China. *Am J Clin Nutr* 1993; **57**(2 Suppl): 259S-263S
- Li GS, Wang F, Kang D, Li C. Keshan disease: an endemic cardiomyopathy in China. *Hum Pathol* 1985; **16**: 602-609
- Gu BQ. Pathology of Keshan disease. A comprehensive review. *Chin Med J* 1983; **96**: 251-261
- Li Y, Peng T, Yang Y, Niu C, Archard LC, Zhang H. High prevalence of enteroviral genomic sequences in myocardium from cases of endemic cardiomyopathy (Keshan disease) in China. *Heart* 2000; **83**: 696-701
- Li Y, Yang Y, Chen H. Detection of enteroviral RNA in paraffin-embedded myocardial tissue from patients with Keshan by nested PCR. *Zhonghua Yixue Zazhi* 1995; **75**: 344-345
- Peng T, Li Y, Yang Y, Niu C, Morgan-Capner P, Archard LC, Zhang H. Characterization of enterovirus isolates from patients with heart muscle disease in a selenium-deficient area of china. *J Clin Microbiol* 2000; **38**: 3538-3543
- Easton AJ, Eglin RP. The detection of coxsackievirus RNA in cardiac tissue by *in situ* hybridization. *J Gen Virol* 1988; **69**(Pt 21): 285-291
- Archard LC, Bowles NE, Cunningham L, Freeke CA, Olsen EG, Rose ML, Meany B, Why HJ, Richardson PJ. Molecular probes for detection of persisting enterovirus infection of human heart and their prognostic value. *Eur Heart J* 1991; **12**(Suppl D): 56-59
- Huang Z, Xia Y, Jin Q, Wu H. Coxsackievirus B3 infection and Keshan disease. *Weisheng Yanjiu* 2002; **31**: 261-263
- Guanqing H. On the etiology of Keshan disease: two hypotheses. *Chin Med J* 1979; **92**: 416-422
- Levander OA, Beck MA. Interacting nutritional and infectious etiologies of Keshan disease. Insights from coxsackie virus B-induced myocarditis in mice deficient in selenium or vitamin E. *Biol Trace Elem Res* 1997; **56**: 5-21
- Beck MA, Kolbeck PC, Rohr LH, Shi Q, Morris VC, Levander OA. Benign human enterovirus becomes virulent in selenium-deficient mice. *J Med Virol* 1994; **43**: 166-170
- Beck MA, Kolbeck PC, Rohr LH, Shi Q, Morris VC, Levander OA. Vitamin E deficiency intensifies the myocardial injury of coxsackievirus B₃ infection of mice. *J Nutr* 1994; **124**: 345-358
- Beck MA, Shi Q, Morris VC, Levander OA. Rapid genomic evolution of a non-virulent coxsackievirus B3 in selenium-deficient mice results in selection of identical virulent isolates. *Nat Med* 1995; **1**: 433-436
- Jackson DP, Quirke P, Lewis F, Boylston AW, Sloan JM, Robertson D, Taylor GR. Detection of measles virus RNA in paraffin-embedded tissue. *Lancet* 1989; **1**: 1391
- Sariol CA, Pelegrino JL, Martinez A, Arteaga E, Kouri G, Guzman MG. Detection and genetic relationship of dengue virus sequences in seventeen-year-old paraffin-embedded samples from Cuba. *Am J Trop Med Hyg* 1999; **61**: 994-1000

Effect of actin microfilament on potassium current in guinea pig gastric myocytes

Xiang-Lan Li, Hai-Feng Zheng, Zheng-Yuan Jin, Meng Yang, Zai-Liu Li, Wen-Xie Xu

Xiang-Lan Li, Hai-Feng Zheng, Zheng-Yuan Jin, Meng Yang, Zai-Liu Li, Department of Physiology, Yanbian University College of Medicine, Yanji 133000, Jilin Province, China

Wen-Xie Xu, Department of Physiology, Shanghai Jiaotong University School of Medicine, 1954 Huashan Rd, Shanghai 200030, China

Supported by the National Natural Science Foundation of China, No. 30160028

Correspondence to: Professor Wen-Xie Xu, Department of Physiology, Shanghai Jiaotong University School of Medicine, 1954 Huashan Rd, Shanghai 200030, China. wenxiexu@sjtu.edu.cn

Telephone: +86-21-62932910 **Fax:** +86-21-62932528

Received: 2004-02-11 **Accepted:** 2004-03-18

Abstract

AIM: To investigate the effect of actin microfilament on potassium current and hyposmotic membrane stretch-induced increase of potassium current in gastric antral circular myocytes of guinea pig.

METHODS: Whole-cell patch clamp technique was used to record potassium current in isolated gastric myocytes.

RESULTS: When the membrane potential was clamped at -60 mV, an actin microfilament disruptor, cytochalasin-B (Cyt-B, 20 $\mu\text{mol/L}$ in pipette) increased calcium-activated potassium current ($I_{K(\text{Ca})}$) and delayed rectifier potassium current ($I_{K(\text{V})}$) to $138.4 \pm 14.3\%$ and $142.1 \pm 13.1\%$ respectively at +60 mV. In the same condition, an actin microfilament stabilizer phalloidin (20 $\mu\text{mol/L}$ in pipette) inhibited $I_{K(\text{Ca})}$ and $I_{K(\text{V})}$ to $74.2 \pm 7.1\%$ and $75.4 \pm 9.9\%$ respectively. At the holding potential of -60 mV, hyposmotic membrane stretch increased $I_{K(\text{Ca})}$ and $I_{K(\text{V})}$ by $50.6 \pm 9.7\%$ and $24.9 \pm 3.3\%$ at +60 mV respectively. In the presence of cytochalasin-B and phalloidin (20 $\mu\text{mol/L}$, in the pipette) condition, hyposmotic membrane stretch also increased $I_{K(\text{Ca})}$ by $44.5 \pm 7.9\%$ and $55.7 \pm 9.8\%$ at +60 mV respectively. In the same condition, cytochalasin-B and phalloidin also increased $I_{K(\text{V})}$ by $23.0 \pm 5.5\%$ and $30.3 \pm 4.5\%$ respectively. However, Cyt-B and phalloidin did not affect the amplitude of hyposmotic membrane stretch-induced increase of $I_{K(\text{Ca})}$ and $I_{K(\text{V})}$.

CONCLUSION: Actin microfilaments regulate the activities of potassium channels, but they are not involved in the process of hyposmotic membrane stretch-induced increase of potassium currents in gastric antral circular myocytes of guinea pig.

Li XL, Zheng HF, Jin ZY, Yang M, Li ZL, Xu WX. Effect of actin microfilament on potassium current in guinea pig gastric myocytes. *World J Gastroenterol* 2004; 10(22): 3303-3307 <http://www.wjgnet.com/1007-9327/10/3303.asp>

INTRODUCTION

Cytoskeleton is an intracellular superstructure that consists of microfilaments of actin and associated proteins, microtubules,

and intermediate filaments. Actin microfilaments of the cytoskeleton form a complex network, providing the structural basis for simultaneous interactions between multiple cellular structures. It is well established that many ion channels and transporters are anchored in the membrane by either direct or indirect association with the cytoskeleton. In addition, there is growing evidence that altering the integrity of cytoskeletal elements, in particular actin microfilaments, could modulate the activity of a variety of ion channels^[1] and receptors^[2]. Many previous studies have demonstrated that actin microfilament could mediate different types of potassium channels of a variety of cells such as those in rat collecting duct^[3], smooth muscle cell line DDT1 MF-2^[4], cardiac myocytes of guinea pig^[5], human meningioma cells^[6], rat hippocampal CA1 pyramidal neurons^[7], rat ventricular myocytes^[8] and xenopus oocytes^[9]. Wang *et al.*^[10] reported that neither the microfilaments nor the microtubules were involved in the enhancement of $I_{K(\text{V})}$ induced by cell distension in ventricular muscle cells of guinea pig. However, Ribeiro *et al.*^[11] showed that microtubule was involved in the cell volume-induced changes in K^+ transport across the rat colon epithelial cells. Our previous study demonstrated that main outward current was carried by calcium-activated potassium channel and delayed rectifier potassium channel in gastric antral circular myocytes of guinea pig and hyposmotic cell swelling enhanced the activity of that two kinds of potassium channel^[12,13]. In order to investigate the mechanism of hyposmotic membrane stretch-induced increase of potassium current, in the present study, the effect of actin microfilament on potassium currents was observed and the possibility whether actin microfilament was involved in the process of hyposmotic membrane stretch-induced increase of potassium currents was examined.

MATERIALS AND METHODS

Single cell preparation and electrophysiological recording

Fresh, single smooth muscle cells (SMCs) were isolated enzymatically from the circular layer of guinea pig antrum as previously described^[14]. Isolated SMCs were stored at 4 °C KBS until the time of use. All experiments were performed within 12 h after cell dispersion. The isolated cells were transferred to a small chamber (0.1 mL) on the stage of an inverted microscope (IX-70 Olympus, Japan) for 10-15 min to settle down. Solution was perfused at a speed of 0.9-1.0 mL/min through the chamber by gravity from the 8-channel perfusion system (L/M-sps-8; list electronics, Germany). Glass pipette with a resistance of 3-5 M Ω was used to make a giga seal of 5-10 G Ω the whole-cell currents were recorded with an Axopatch 1-D patch-clamp amplifier (Axon Instrument, USA).

Drugs and solution

Tyrode solution containing (mmol/L) NaCl 147, KCl 4, $\text{MgCl}_2 \cdot 6\text{H}_2\text{O}$ 1.05, $\text{CaCl}_2 \cdot 2\text{H}_2\text{O}$ 0.42, $\text{Na}_2\text{PO}_4 \cdot 2\text{H}_2\text{O}$ 1.81, and 5.5 mmol/L glucose was used. Ca^{2+} -free PSS containing (mmol/L) NaCl 134.8, KCl 4.5, glucose 5, and N-[2-hydroxyethyl] piperazine- N-[2-ethanesulphonic acid] (HEPES) 10 was adjusted to pH 7.4 with Tris [hydroxymethyl] aminomethane (TRIZMA). Modified K-B solution containing (mmol/L) L-glutamate 50, KCl 50, taurine 20, KH_2PO_4 20, $\text{MgCl}_2 \cdot 6\text{H}_2\text{O}$ 3, glucose 10, HEPES 10 and egtazic

acid 0.5 was adjusted to pH 7.40 with KOH. Isosmotic solution (290 mOsm/L) containing (mmol/L) NaCl 80, KCl 4.5, HEPES 10, MgCl₂·6H₂O 1, CaCl₂·2H₂O 2, Glucose 5, Sucrose 110, was adjusted to pH 7.4 with Tris. Hypoosmotic solution (200 mOsm/L) contained (in mmol/L) sucrose 30, and other ingredients was the same as the isosmotic solution. Pipette solution recording $I_{K(Ca)}$ contained (mmol/L) potassium-aspartic acid 110, Mg-ATP 5, HEPES 5, MgCl₂·6H₂O 1.0, KCl 20, egtazic acid 0.1, di-tris-creatine phosphate 2.5, disodium-creatine phosphate 2.5 and its pH was adjusted to 7.3 with KOH. Pipette solution recording $I_{K(V)}$ contained (mmol/L) EGTA 10, and other ingredients was the same as the pipette solution recording $I_{K(Ca)}$. Cytochalasin-B was dissolved in dimethyl sulphoxide (DMSO, 20 mmol/L) and phalloidin was dissolved in alcohol (1 mmol/L). The same amount of DMSO or alcohol as the final experimental solution was added to the pipette solution. All the chemicals in this experiment were purchased from Sigma (USA).

Data analysis

All data were expressed as mean±SD. Statistical significance was evaluated by a *t*-test. Differences were considered to be

significant when *P* value was less than 0.05.

RESULTS

Effect of Cyt-B and phalloidin on $I_{K(Ca)}$

Under the whole cell configuration, the membrane potential was clamped at -60 mV, $I_{K(Ca)}$ was elicited by step voltage command pulse from -40 mV to +100 mV for 440 ms with a 20 mV increment at 10 s intervals. An actin microfilament disruptor, Cyt-B (20 μmol/L in pipette) markedly increased $I_{K(Ca)}$ to 138.4±14.3% at +60 mV (*n* = 15, Figures 1B, C). In the same condition, an actin microfilament stabilizer, phalloidin (20 μmol/L in pipette) inhibited $I_{K(Ca)}$ to 74.2±7.1% at +60 mV (*n* = 15, Figures 2B, C).

Effect of Cyt-B and phalloidin on $I_{K(V)}$

Under the whole cell configuration, the membrane potential was clamped at -60 mV, $I_{K(V)}$ was elicited by step voltage command pulse from -40 mV to +80 mV for 440 ms with a 20 mV increment at 10 s intervals. Cyt-B (20 μmol/L in pipette) markedly increased $I_{K(V)}$ to 142.1±13.1% at +60 mV (*n* = 12, Figures 3B, C). In the same condition, phalloidin (20 μmol/L in pipette) inhibited $I_{K(V)}$ to 75.4±9.9% at +60 mV (*n* = 12, Figures 4B, C).

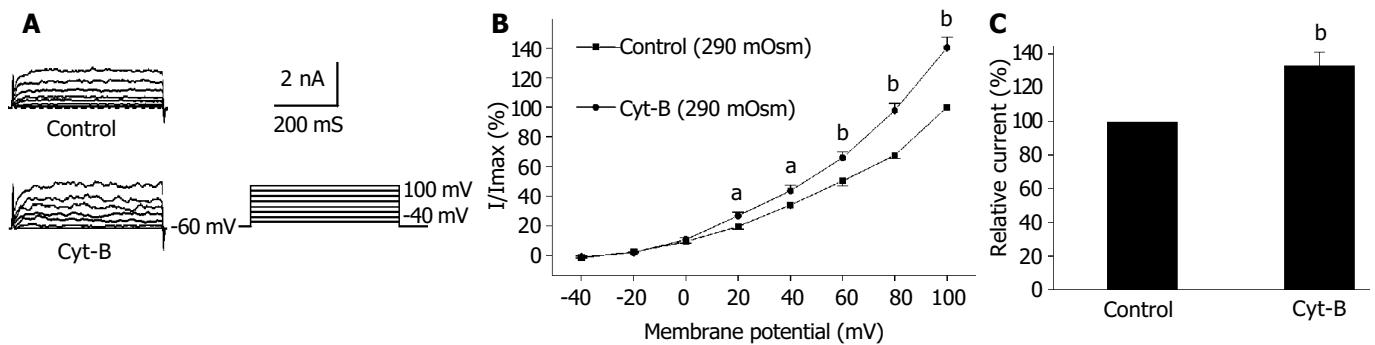


Figure 1 Effect of Cyt-B on $I_{K(Ca)}$. A: Representative current trace of $I_{K(Ca)}$. B: I/V relationship of $I_{K(Ca)}$. C: Cyt-B enhanced $I_{K(Ca)}$. In isosmotic condition. (*n* = 15, ^a*P*<0.05, ^b*P*<0.01 vs control).

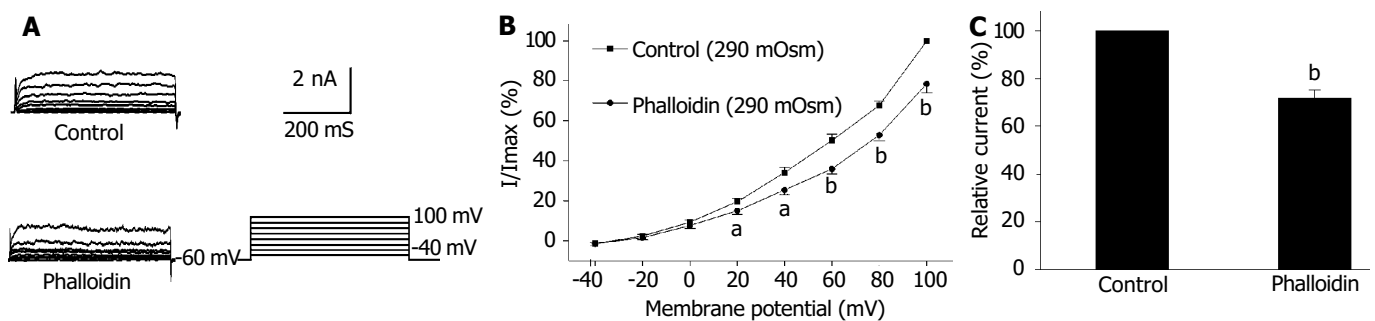


Figure 2 Effect of phalloidin on $I_{K(Ca)}$. A: Representative current trace of $I_{K(Ca)}$. B: I/V relationship of $I_{K(Ca)}$. C: Phalloidin inhibited $I_{K(Ca)}$ in isosmotic condition. (*n* = 15, ^a*P*<0.05, ^b*P*<0.01 vs control).

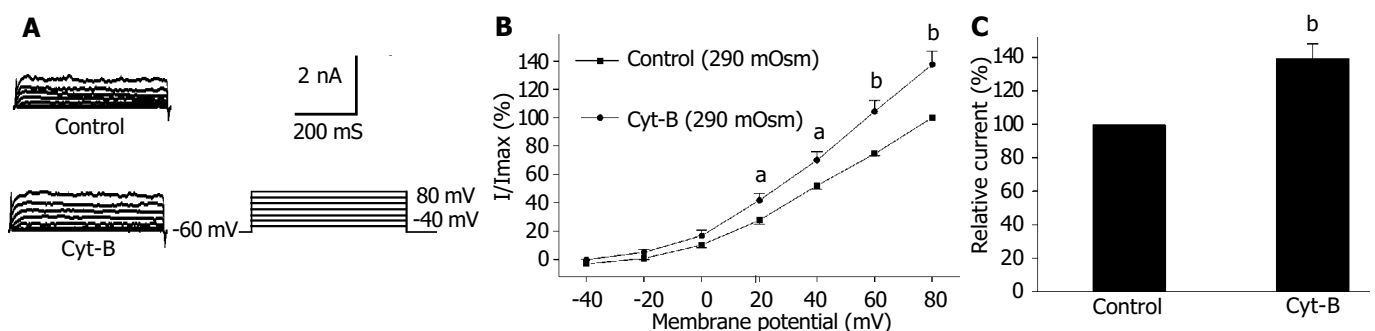


Figure 3 Effect of Cyt-B on $I_{K(V)}$. A: Representative current trace of $I_{K(V)}$. B: I/V relationship of $I_{K(V)}$. C: Cyt-B enhanced $I_{K(V)}$ in isosmotic condition. (*n* = 15, ^a*P*<0.05, ^b*P*<0.01 vs control).

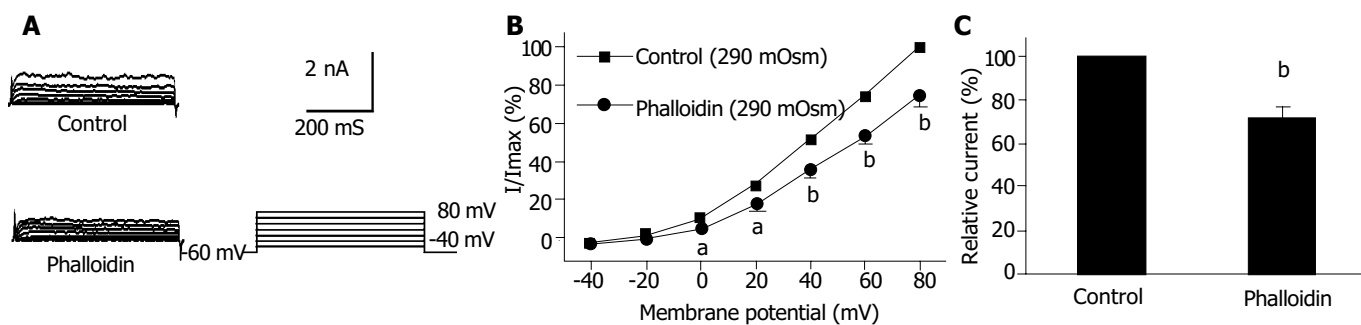


Figure 4 Effect of phalloidin on $I_{K(Ca)}$. A: Representative current trace of $I_{K(Ca)}$. B: I/V relationship of $I_{K(Ca)}$. C: Phalloidin inhibited $I_{K(Ca)}$ in isosmotic condition. ($n = 15$, $^aP < 0.05$, $^bP < 0.01$ vs control).

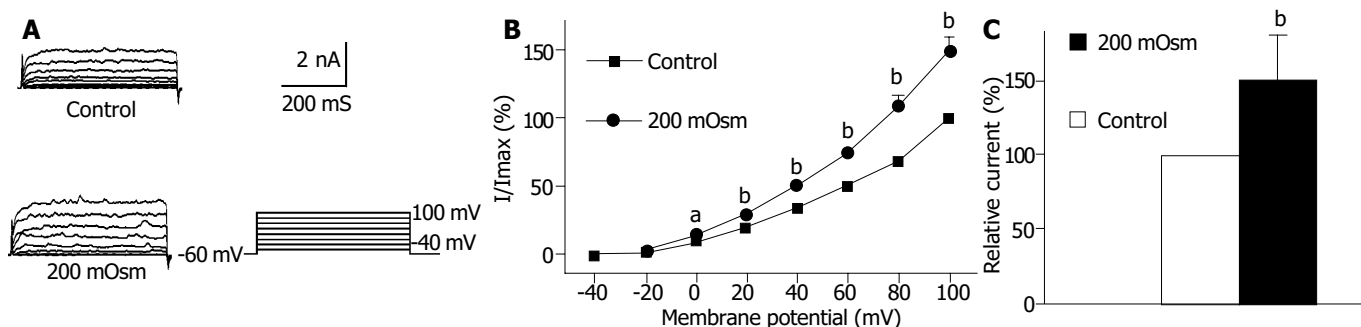


Figure 5 Effect of hyposmotic membrane stretch on $I_{K(Ca)}$. A: Representative current trace of $I_{K(Ca)}$. B: I/V relationship of $I_{K(Ca)}$. C: Hyposmotic membrane stretch increased $I_{K(Ca)}$. ($n = 15$, $^aP < 0.05$, $^bP < 0.01$ vs control).

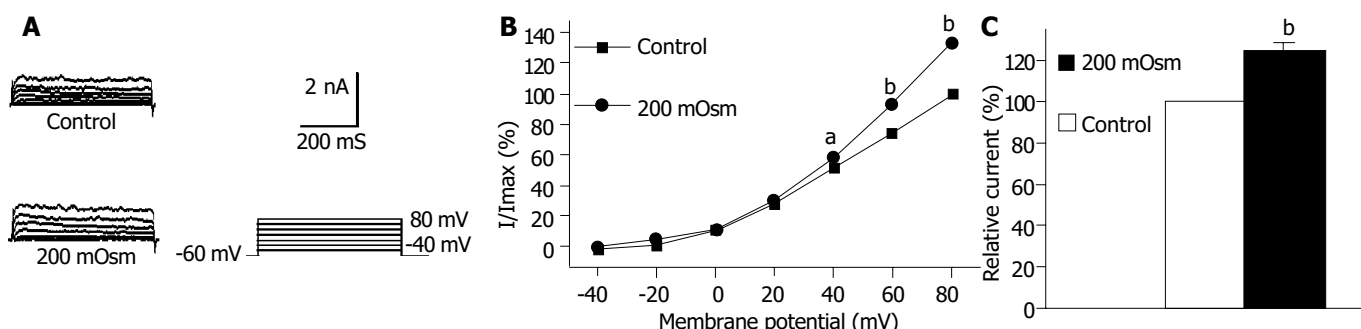


Figure 6 Effect of hyposmotic membrane stretch on $I_{K(V)}$. A: Representative current trace of $I_{K(V)}$. B: I/V relationship of $I_{K(V)}$. C: Hyposmotic membrane stretch increased $I_{K(V)}$. ($n = 15$, $^aP < 0.05$, $^bP < 0.01$ vs control).

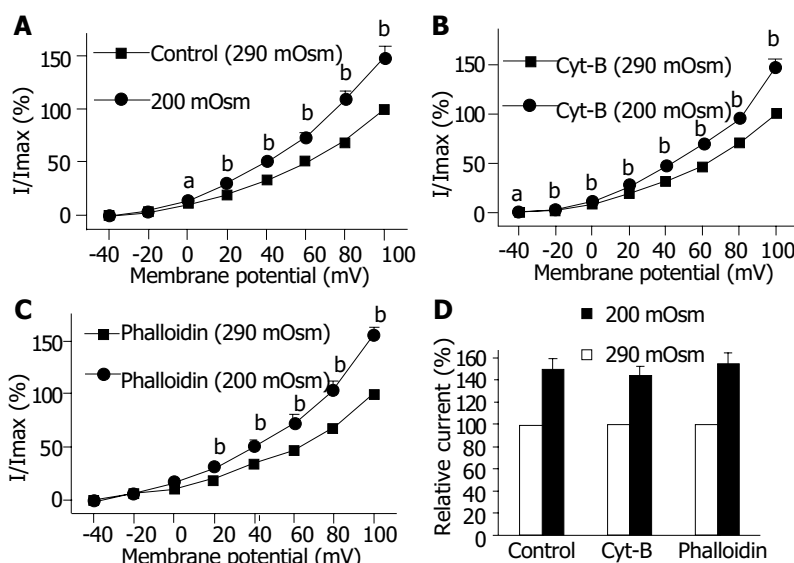


Figure 7 Effect of Cyt-B and phalloidin on hyposmotic membrane stretch-increase of $I_{K(Ca)}$. A, B and C: I/V relationship of $I_{K(Ca)}$. ($n = 15$, $^aP < 0.05$, $^bP < 0.01$ vs 290 mOsm). D: No effect of Cyt-B and phalloidin on the increased of $I_{K(Ca)}$ induced by hyposmotic membrane stretch ($n = 15$).

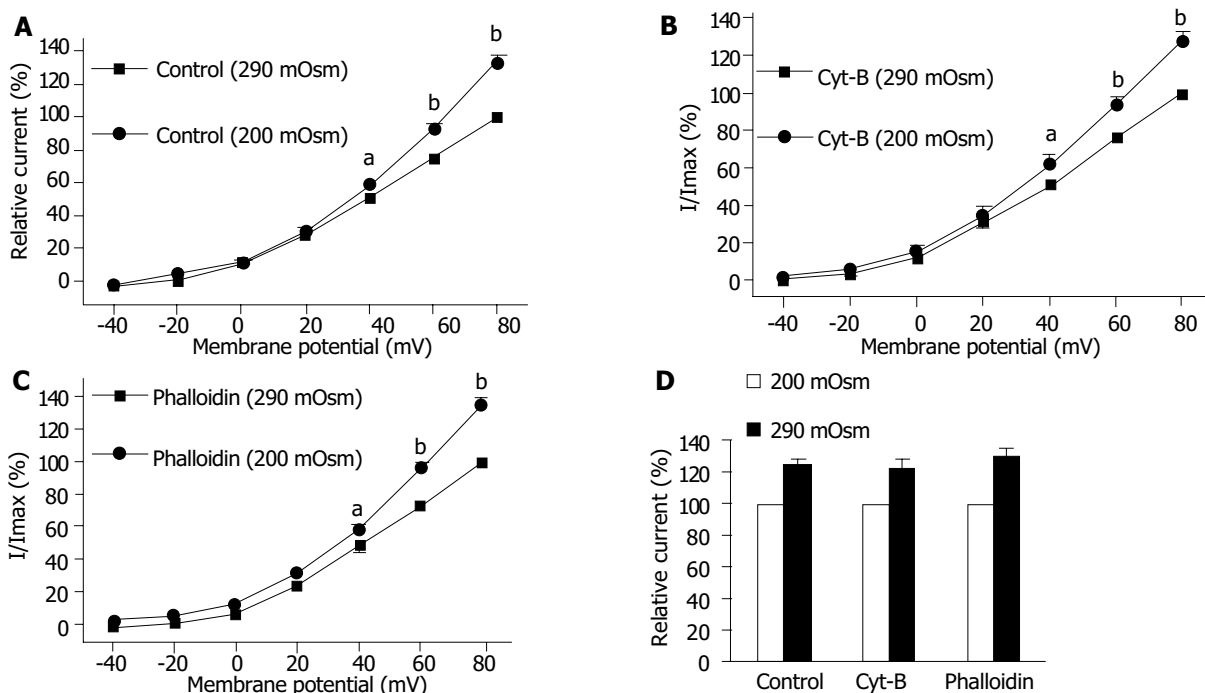


Figure 8 Effect of Cyt-B and phalloidin on hyposmotic membrane stretch-increase of $I_{K(V)}$. A, B and C: I/V relationship of $I_{K(V)}$. (n = 12, ^aP<0.05, ^bP<0.01 vs 290 mOsm). D: No effect of Cyt-B and phalloidin on the increased of $I_{K(V)}$ induced by hyposmotic membrane stretch (n = 12).

Effect of hyposmotic membrane stretch on $I_{K(Ca)}$ and $I_{K(V)}$

Using the same pulse protocol, the effect of hyposmotic membrane stretch on $I_{K(Ca)}$ and $I_{K(V)}$ was observed. When the cells were superfused with hyposmotic solution (200 mOsmol/L), step command pulse-induced $I_{K(Ca)}$ increased from 0 mV (Figure 5B) and the increasing amplitude was $50.6 \pm 9.7\%$ at +60 mV (n = 15, Figure 5C). In the same condition, hyposmotic superfusing increased step command pulse-induced $I_{K(V)}$ from +40 mV (Figure 6B) and the increasing amplitude was $24.9 \pm 3.3\%$ at +60 mV (n = 12, Figure 6C).

Effect of Cyt-B and phalloidin on hyposmotic membrane stretch-induced increase of $I_{K(Ca)}$

To determine the possibility of actin microfilament involved in hyposmotic membrane stretch-induced increase of $I_{K(Ca)}$, the effects of Cyt-B and phalloidin on $I_{K(Ca)}$ in which cells were perfused with isosmotic and hypoosmotic solutions were observed respectively. Hyposmotic membrane stretch increased $I_{K(Ca)}$ from 0 mV (Figure 7A) and the increasing amplitude was $50.6 \pm 9.7\%$ at 60 mV in the control group (n = 15, Figures 7A, 8D). In the presence of Cyt-B and phalloidin (20 μ mol/L in pipette) hyposmotic membrane stretch also increased $I_{K(Ca)}$ by $44.5 \pm 7.9\%$ (n = 15, Figures 7B, D) and $55.7 \pm 9.8\%$ (n = 15, Figures 7C, D) at +60 mV respectively. There was no significant difference between control group and Cyt-B group or phalloidin group.

Effect of Cyt-B and phalloidin on hyposmotic membrane stretch-induced increase of $I_{K(V)}$

Hyposmotic membrane stretch increased $I_{K(V)}$ by $24.9 \pm 3.3\%$ at +60 mV in the control group (n = 12, Figures 8A, D). In the presence of Cyt-B and phalloidin (20 μ mol/L in pipette) hyposmotic membrane stretch also increased $I_{K(V)}$ by $22.9 \pm 5.5\%$ (n = 12, Figures 8B, D) and $30.3 \pm 4.5\%$ (n = 12, Figures 8C, D) at +60 mV respectively. There was no significant difference between control group and Cyt-B group or phalloidin group.

DISCUSSION

Cytoskeleton is an intracellular superstructure that consists of

microfilaments of actin and associated proteins, microtubules, and intermediate filaments. Actin microfilament, in particular, are involved in structural support and a functional role in cell motility^[15]. Recent evidence indicated, however, actin-based cytoskeleton was involved in the control of ion channel activity across the plasma membranes of different cell types. For example, actin microfilaments were implicated in the regulation of sodium channels in human jejunal circular smooth muscle cells^[16] and ATP-sensitive potassium channel in ventricular myocytes^[5, 17]. Actin microfilaments could also regulate voltage-dependent channels, for example, actin microfilaments could mediate voltage-dependent epithelial sodium channels in neuron cells^[18].

It was proposed that cell surface proteins and extra cellular matrix were linked to the cytoskeleton by transmembrane proteins and modulate ion channels and enzymes by mechanical deformation under physiological conditions. In the present study, we observed that an actin microfilament disruptor, Cyt-B increased $I_{K(Ca)}$ and $I_{K(V)}$ significantly (Figures 1B, C, Figures 3B, C). However, an actin microfilament stabilizer, phalloidin inhibited $I_{K(Ca)}$ and $I_{K(V)}$ markedly (Figures 2B, C, Figures 4B, C) in gastric myocytes. These results suggested that when actin microfilaments were disrupted, $I_{K(Ca)}$ or $I_{K(V)}$ could be activated; while, when actin microfilaments were stabilized, $I_{K(Ca)}$ or $I_{K(V)}$ could be inhibited in gastric myocytes. Many previous studies also supported our experiment. For example, Cyt-D activated calcium-activated potassium channel in human meningioma cells^[6], Cyt-B activated K (ATP) channels in cardiac^[5].

Stretch is a physiological stimulation in gut smooth muscles. There are two kinds of potassium current, calcium-activated potassium current and delayed rectifier potassium current. In the present study, the two kinds of potassium current were activated by hyposmotic swelling in gastric antral smooth muscle cells of guinea pigs (Figures 5-6). In order to investigate the mechanism of hyposmotic membrane stretch-induced increase of $I_{K(Ca)}$ and $I_{K(V)}$, the relationship between potassium channel activity and actin microfilaments was observed. When actin microfilaments were disrupted by Cyt-B or stabilized by phalloidin, hyposmotic membrane stretch-induced increase of

$I_{K(Ca)}$ and $I_{K(V)}$ was not affected (Figures 7-8). These results indicated that actin microfilaments were not involved in the increase of potassium current induced by hyposmotic cell swelling in gastric circular myocytes of guinea pig. Previous studies supported our results. For example, Wang *et al.*^[10] observed that neither the microfilaments nor the microtubules were involved in the enhancement of $I_{K(V)}$ induced by cell distension in ventricular myocytes of guinea pig. We also observed that unsaturated fatty acids, exogenous and endogenous, were involved in the increase of calcium-activated potassium current induced by hyposmotic membrane stretch (data not shown). So that hyposmotic membrane stretch-induced increase of potassium currents may be related to unsaturated fatty acids in cell membranes.

Our previous study demonstrated that actin microfilaments played an important role in the modulation of membrane stretch-induced calcium influx and hyposmotic membrane stretch-induced increase of muscarinic current in guinea-pig gastric myocytes^[19,20]. It is obvious that cytoskeleton plays a different role in different types of cells and different kinds of ion channels. In gastric smooth muscle actin microfilaments may be involved in the process of hyposmotic membrane stretch-induced depolarization of membrane potential. However, actin microfilaments would not be involved in the process of cell swelling-induced hyperpolarization of membrane potential.

In summary, actin microfilaments regulate potassium channel activities in normal condition. However, actin microfilaments are not involved in hyposmotic cell swelling-induced increase of potassium currents.

REFERENCES

- 1 **Janmey PA.** The cytoskeleton and cell signaling: component localization and mechanical coupling. *Physiol Rev* 1998; **78**: 763-781
- 2 **Wang H,** Bedford FK, Brandon NJ, Moss SJ, Olsen RW. GABA_A-receptor-associated proteins link GABA_A receptors and the cytoskeleton. *Nature* 1999; **397**: 69-72
- 3 **Wang WH,** Cassola A, Giebisch G. Involvement of actin cytoskeleton in modulation of apical K channel activity in rat collecting duct. *Am J Physiol* 1994; **267**(4 Pt 2): F592-598
- 4 **Ehrhardt AG,** Frankish N, Isenberg G. A large-conductance K⁺ channel that is inhibited by the cytoskeleton in the smooth muscle cell line DDT1 MF-2. *J Physiol* 1996; **496**(Pt 3): 663-676
- 5 **Jovanovic S,** Jovanovic A. Diadenosine tetraphosphate-gating of cardiac K (ATP) channels requires intact actin cytoskeleton. *Naunyn Schmiedebergs Arch Pharmacol* 2001; **364**: 276-280
- 6 **Kraft R,** Benndorf K, Patt S. Large conductance Ca²⁺-activated K⁺ channels in human meningioma cells. *J Membr Biol* 2000; **175**: 25-33
- 7 **Huang H,** Rao Y, Sun P, Gong LW. Involvement of actin cytoskeleton in modulation of Ca (2+)-activated K (+) channels from rat hippocampal CA1 pyramidal neurons. *Neurosci Lett* 2002; **332**: 141-145
- 8 **Shimoni Y,** Ewart HS, Severson D. Insulin stimulation of rat ventricular K⁺ currents depends on the integrity of the cytoskeleton. *J Physiol* 1999; **514**(Pt 3): 735-745
- 9 **Song DK,** Ashcroft FM. ATP modulation of ATP-sensitive potassium channel ATP sensitivity varies with the type of SUR subunit. *J Biol Chem* 2001; **276**: 7143-7149
- 10 **Wang Z,** Mitsuiye T, Noma A. Cell distension-induced increase of the delayed rectifier K⁺ current in guinea pig ventricular myocytes. *Circ Res* 1996; **78**: 466-474
- 11 **Ribeiro R,** Heinke B, Diener M. Cell volume-induced changes in K⁺ transport across the rat colon. *Acta Physiol Scand* 2001; **171**: 445-458
- 12 **Li Y,** Xu WX, Li ZL. Effects of nitroprusside, 3-morpholino-sydnonimine, and spermine on calcium-sensitive potassium currents in gastric antral circular myocytes of guinea pig. *Acta Pharmacol Sin* 2000; **21**: 571-576
- 13 **Piao L,** Li Y, Li L, Xu WX. Increment of calcium-activated and delayed rectifier potassium current by hyposmotic swelling in gastric antral circular myocytes of guinea pig. *Acta Pharmacol Sin* 2001; **22**: 566-572
- 14 **Yu YC,** Guo HS, Li Y, Piao L, Li L, Li ZL, Xu WX. Role of calcium mobilization in sodium nitroprusside-induced increase of calcium-activated potassium currents in gastric antral circular myocytes of guinea pig. *Acta Pharmacol Sin* 2003; **24**: 819-825
- 15 **Stossel TP.** On the crawling of animal cells. *Science* 1993; **260**: 1086-1094
- 16 **Strege PR,** Holm AN, Rich A, Miller SM, Ou Y, Sarr MG, Farrugia G. Cytoskeletal modulation of sodium current in human jejunal circular smooth muscle cells. *Am J Physiol Cell Physiol* 2003; **284**: C60-66
- 17 **Terzic A,** Kurachi Y. Actin microfilament disrupters enhance K (ATP) channel opening in patches from guinea-pig cardiomyocytes. *J Physiol* 1996; **492**(Pt 2): 395-404
- 18 **Srinivasan Y,** Elmer L, Davis J, Bennett V, Angelides K. Ankyrin and spectrin associate with voltage-dependent sodium channels in brain. *Nature* 1988; **333**: 177-180
- 19 **Xu WX,** Kim SJ, So I, Kim KW. Role of actin microfilament in osmotic stretch-induced increase of voltage-operated calcium channel current in guinea-pig gastric myocytes. *Pflugers Arch* 1997; **434**: 502-504
- 20 **Wang ZY,** Yu YC, Cui YF, Li L, Guo HS, Li ZL, Xu WX. Role of actin microfilament in hyposmotic membrane stretch-induced increase in muscarinic current of guinea-pig gastric myocytes. *Shengli Xuebao* 2003; **55**: 77-182

Edited by Wang XL Proofread by Xu FM

Selection, proliferation and differentiation of bone marrow-derived liver stem cells with a culture system containing cholestatic serum *in vitro*

Yun-Feng Cai, Zuo-Jun Zhen, Jun Min, Tian-Ling Fang, Zhong-Hua Chu, Ji-Sheng Chen

Yun-Feng Cai, Department of Liver-biliary Surgery, the First Hospital of Foshan City, Foshan 528000, and Department of Hepatic-biliary Surgery, the 2nd Affiliated Hospital of Sun Yat-Sen University, Guangzhou 510120, Guangdong Province, China

Zuo-Jun Zhen, Department of Liver-biliary Surgery, the First Hospital of Foshan City, Foshan 528000, Guangdong Province, China

Jun Min, Department of Hepatic-biliary Surgery, Stem Cell Research Center, Research Center of Medicine, the 2nd Affiliated Hospital of Sun Yat-Sen University, Guangzhou 510120, Guangdong Province, China

Tian-Ling Fang, Zhong-Hua Chu, Ji-Sheng Chen, Department of Hepatic-biliary Surgery, the 2nd Affiliated Hospital of Sun Yat-Sen University, Guangzhou 510120, Guangdong Province, China

Supported by the National Natural Science Foundation of China, No. 30271277 and Natural Science Foundation of Guangdong Province, No.021851

Correspondence to: Dr. Yun-Feng Cai, Department of Liver-biliary Surgery, the First Hospital of Foshan City, 1 Dafu Nanlu, Foshan 528000, Guangdong Province, China. yfcai70@yahoo.com.cn

Telephone: +86-757-83833633-1119 **Fax:** +86-757-83835218

Received: 2003-10-20 **Accepted:** 2003-12-16

Abstract

AIM: To explore the feasibility of direct separation, selective proliferation and differentiation of the bone marrow-derived liver stem cells (BDLSC) from bone marrow cells with a culture system containing cholestatic serum *in vitro*.

METHODS: Whole bone marrow cells of rats cultured in routine medium were replaced with conditioning selection media containing 20 mL/L, 50 mL/L, 70 mL/L, and 100 mL/L cholestatic sera, respectively, after they attached to the plates. The optimal concentration of cholestatic serum was determined according to the outcome of the selected cultures. Then the selected BDLSC were induced to proliferate and differentiate with the addition of hepatocyte growth factor (HGF). The morphology and phenotypic markers of BDLSC were characterized using immunohistochemistry, RT-PCR and electron microscopy. The metabolic functions of differentiated cells were also determined by glycogen staining and urea assay.

RESULTS: Bone marrow cells formed fibroblast-like but not hepatocyte-like colonies in the presence of 20 mL/L cholestatic serum. In 70 mL/L cholestatic serum, BDLSC colonies could be selected but could not maintain good growth status. In 100 mL/L cholestatic serum, all of the bone marrow cells were unable to survive. A 50 mL/L cholestatic serum was the optimal concentration for the selection of BDLSC at which BDLSC could survive while the other populations of the bone marrow cells could not. The selected BDLSC proliferated and differentiated after HGF was added. Hepatocyte-like colony-forming units (H-CFU) then were formed. H-CFU expressed markers of embryonic hepatocytes (AFP, albumin and cytokeratin 8/18), biliary cells (cytokeratin 19), hepatocyte functional proteins (transthyretin and cytochrome P450-2b1), and hepatocyte nuclear factors (HNF-1 α and HNF-3 β). They

also had glycogen storage and urea synthesis functions, two of the critical features of hepatocytes.

CONCLUSION: The selected medium containing cholestatic serum can select BDLSC from whole bone marrow cells. It will be a new way to provide a readily available alternate source of cells for clinical hepatocyte therapy.

Cai YF, Zhen ZJ, Min J, Fang TL, Chu ZH, Chen JS. Selection, proliferation and differentiation of bone marrow-derived liver stem cells with a culture system containing cholestatic serum *in vitro*. *World J Gastroenterol* 2004; 10(22): 3308-3312
<http://www.wjgnet.com/1007-9327/10/3308.asp>

INTRODUCTION

Several recent reports have highlighted the broad developmental potential of bone marrow-derived stem cells and the term "stem cell plasticity" has been coined^[1]. Bone marrow-derived stem cells have been reported to produce not only all of the blood lineages, but also skeletal muscle^[2,3], neurons^[4,5], cardiac muscle^[6,7], pulmonary epithelium^[8], and liver epithelium^[9]. The transdifferentiation of bone marrow-derived cells into hepatic cells was described in rats^[9], mice^[10] and humans^[11,12]. This has brought a new hope for cell therapy using autologous bone marrow cells which have few ethical problems and applied to severe liver disease^[13]. However, bone marrow contains hematopoietic^[14,15], mesenchymal stem cells^[16,17] and multipotent adult progenitor cells^[18]. The characteristic surface markers of these specific bone marrow-derived liver stem cells (BDLSC) are still obscure. It is difficult to identify and sort these particular cells by immunological methods, such as fluorescent activated cell sorting (FACS)^[14] and magnetic activated cell sorting (MACS)^[19]. Although various bone marrow stem cells were found to proliferate injured liver cells, previous attempts at isolation of liver stem cells resulted in a mixture of hematopoietic cells and potential hepatocyte progenitors because they all shared common cell surface receptors and antigens, including hematopoietic stem cell markers CD34, Thy-1, c-Kit, and flt-3^[20-22]. It is necessary to find a new way to isolate and purify BDLSC. According to the principle that cells in culture can survive only when they accommodate to the existing environment, we assumed to develop a culture system that can select BDLSC from whole bone marrow cells directly. Within such a system, only BDLSC can survive while the other bone marrow cells cannot. This particular culture system must contain factors that can activate the proliferation of liver stem cells and ingredients inhibiting the growth of other cells. Studies of the relative mechanisms of liver regeneration and liver stem cells corresponding to liver injury^[23-26] indicated that the pathological serum after severe liver injury might provide the above conditions. We developed the culture system using cholestatic serum obtained after ligation of common bile duct to induce liver lesions, to select and proliferate BDLSC from whole bone marrow cells *in vitro*. We named this medium system as "pathological microenvironment" selecting medium.

MATERIALS AND METHODS

Preparation of conditional selection medium

Preparation of cholestatic serum Sprague-Dawley (SD) rats weighing 200-250 g were performed common bile duct ligation and transection under general (ether) anesthesia to induce cholestasis. After 10 d, whole blood of each rat was collected and serum was separated. The serum was then subjected to liver function test, and inactivated and aseptitized for culture use.

Ingredients of conditional selection medium Twenty mL/L, 50 mL/L, 70 mL/L, and 100 mL/L cholestatic serum were added into DMEM (Gibco) containing 20 mmol/L HEPES (Sigma), 10^{-7} mol/L dexamethasone (Sigma), and antibiotics to act as the conditional selection medium.

Selection, proliferation and differentiation of BDLSC

Culture of whole bone marrow cells Rat bone marrow cells were obtained by flushing femurs. The femurs were accessed through laparotomy to avoid contamination and to increase the cell yield. Bone marrow cells were suspended in DMEM and plated at the density of 1×10^9 cells/L onto culture dishes. DMEM enriched with 100 mL/L fetal bovine serum (FBS, Hyclone), 20 mmol/L HEPES, 10^{-7} mol/L dexamethasone, and antibiotics was used. Dishes were placed in a humidified incubator containing 50 mL/L CO₂-950 mL/L O₂ at 37 °C.

Selection, proliferation and differentiation of liver stem cells Three days after the culture, the medium and suspended cells were discarded and replaced by conditional selection medium with various concentrations of cholestatic serum. Cells cultured in medium containing FBS were used as control. After 4 d, the media were enriched with 25 µg/L hepatocyte growth factor (HGF, Peprotech EC). Medium was replaced every 3 d and the cultures were maintained for about 2 wk.

Morphological and phenotypic markers of differentiated cells

Immunohistochemistry Bone marrow cells were cultured and selected with the conditional selection medium on 6-well dishes with cover glasses. Twelve days after replacement of the conditional selection medium, cover glasses and the above differentiated BDLSC were taken out and fixed with 40 g/L paraformaldehyde (Sigma) for 30 min at room temperature. The primary antibodies were goat anti-rat albumin, alpha-fetoprotein (AFP), and cytokeratin -8/18 (CK8/18) polyclonal antibodies. The slides were incubated with various primary antibodies at room temperature for 2 h in a humidified chamber. Blocking serum and biotinylated

secondary antibody were matched with the primary antibody. Immunoperoxidase was stained and counterstained with DAB and Gill-I hematoxylin.

Electron microscopy Culture dishes were washed with PBS (pH 7.4), and fixed in cold 25 g/L glutaraldehyde in 0.1 mol/L sodium cacodylate buffer (pH 7.4) for 48 h. After fixation, cells were curretted and centrifuged to form aggregates. After postfixed in 10 g/L osmium tetroxide in 0.1 mol/L sodium cacodylate (pH7.4), cells were dehydrated in graded alcohols and embedded in low viscosity epoxy resin. Ultrathin sections were stained with uranyl acetate and lead citrate and viewed under electron microscope.

Total RNA isolation and reverse transcriptase-polymerase chain reaction (RT-PCR) Total RNA was extracted from 1×10^6 differentiated cells by using Trizol (Promega). cDNA was prepared from 2 µg of total RNA in a buffer containing MMLV reverse transcriptase (Promega) and 0.5 µg random primer (Takara). The RNA was incubated at 70 °C for 5 min, at 37 °C for 1 h, and at 95 °C for 5 min. Samples of cDNA corresponding to the input RNA were amplified in PCR reaction buffers containing primers and LA Taq DNA polymerase (Takara). Primers used for amplification were hepatocyte nuclear factor-1α (HNF-1α), hepatocyte nuclear factor-3β (HNF-3β), CK18, CK19, albumin, AFP, transthyretin (TTR), and cytochrome P450-2b1 (CYP2b1). The sequences are listed in Table 1. After initial denaturation (at 94 °C for 5 min), 30 cycles of PCR were performed (at 94 °C for 30 s, annealing at the optimal temperature for each pair of primers for 30 s, at 72 °C for 30 s), and extension at 72 °C for 7 min. Amplified products were subjected to electrophoresis in 20 g/L agarose gels and stained with ethidium bromide. All the procedures were performed according to the manufacturer's instructions.

Function tests of differentiated cells

Periodic acid-Schiff staining for glycogen Differentiated cells were fixed in 950 mL/L ethanol for 10 min, rinsed in dH₂O. Afterwards, cells were oxidized in 10 g/L periodic acid for 15 min and rinsed three times in dH₂O, then treated with Schiff's reagent for 30 min and rinsed in dH₂O for 10 min, stained with Mayer's hematoxylin for 1 min and rinsed in dH₂O.

Urea assay Urea concentrations were determined by colorimetric assay (640-A, Sigma). Differentiated cells were plated on 6-well dishes. Each well contained 1×10^6 cells. Urea concentrations were detected every day for 4 d according to the manufacturer's instructions. Culture medium and blank tube were used as negative controls.

Table 1 Sequence of primers and length of fragments

Gene	Primer	Fragment (bp)
HNF-1α	S:5'-AGCTGCTCCTCCATCATCAGA-3'	138
	A:5'-TGTTCCAAGCATTAAAGTTTTCTATTCTAA-3'	
HNF-3β	S:5'-CCTACTCGTACATCTCGTCATCA-3'	68
	A:5'-CGCTCAGCGTCAGCATCTT-3'	
CK-18	S:5'-GCCCTGGACTCCAGCAACT-3'	70
	A:5'-ACTTTGCCATCCACGACCTT-3'	
CK-19	S:5'-ACCATGCAGAACCTGAACGAT-3'	83
	A:5'-CACCTCCAGCTCGCCATTAG-3'	
Albumin	S:5'-CTGGGAGTGTGCAGATATCAGAGT-3'	141
	A:5'-GAGAAGGTCACCAAGTGCTGTAGT-3'	
AFP	S:5'-GTCCTTTCTTCCTCCTGGAGAT-3'	145
	A:5'-CTGTCACTGCTGATTTCTCTGG-3'	
TTR	S:5'-CAGCAGTGGTGTGCTGAGGAGTA-3'	152
	A:5'-GGGTAGAAGTGGACACCAAATC-3'	
CYP2b1	S:5'-ACTTTCCTGGTGCCACA-3'	157
	A:5'-TCCTTCTCCATGCGCAGA-3'	

RESULTS

Preparation of the conditioning selection medium

Ten days after the ligation of common bile duct, TBIL of the cholestatic rats was $107 \pm 48.2 \mu\text{mol/L}$. The conditional selection media containing 20 mL/L, 50 mL/L, 70 mL/L, and 10 mL/L cholestatic sera had TBIL concentrations of 2.1 $\mu\text{mol/L}$, 5.3 $\mu\text{mol/L}$, 7.4 $\mu\text{mol/L}$ and 10.8 $\mu\text{mol/L}$ accordingly.

Bone marrow cells cultured in different concentrations of cholestatic serum

In routine culture condition, part of the bone marrow cells attached to the plate in about 3 d, and then became elongated and fibroblast-like, conforming to the mesodermal characteristics of their origin. After replaced by the conditional selection medium containing 20 mL/L cholestatic serum, the attached cells still survived while the rapid growth was hindered. Seven days after cultured in the medium, colonies were mainly composed of fibroblast-like cells. Only a few colonies acquired hepatocyte-like morphology, although HGF was added. In the presence of 50 mL/L cholestatic serum, a large number of the attached cells exfoliated within 3 d, while many small colonies appeared (Figure 1). These colonies were composed of small, undifferentiated cells in the center, and epithelioid cells at the periphery. The cells enriched with HGF proliferated rapidly. In 70 mL/L cholestatic serum condition, most of the cells exfoliated, fewer colonies appeared, and HGF could not stimulate their proliferation. When the concentration increased to 100 mL/L, all of the cells exfoliated and became apoptosis.

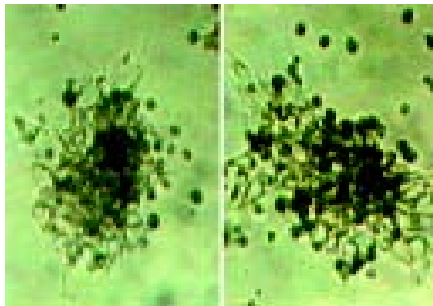


Figure 1 Cell colonies 3 d after selection. Polygonal surrounding cells could be seen.

Morphological evidence of BDLSC differentiation

During the first 3 d many colonies appeared in conditional selection culture containing 50 mL/L cholestatic serum. After enriched with HGF, the colonies enlarged, and the cells proliferated rapidly. Large hepatocyte-like colony-forming units (H-CFU) came into being in about 12 d. The H-CFU were composed of small, undifferentiated cells in the center, and large cells with regular multilateral contours, low nuclear-to-cytoplasmic ratio, and single round nuclei at the periphery. The differentiated cells formed cords or trabeculae resembling the hepatocyte cords in hepatic lobules (Figure 2). The largest colonies contained 1×10^6 cells and could be observed macroscopically, whereas the small colonies were about 30-50 cells. The central undifferentiated cells could still form H-CFU when they were picked out and cultured in the selection medium containing 50 mL/L cholestatic serum and HGF in about 1 wk.

Ultrastructurally, the differentiated cells were rich in endoplasmic reticulum and ribosomes and contained abundant ellipsoid mitochondria (Figure 3), which were different to the control cells. These ultrastructural features are typical of adult hepatocytes.

Phenotypic markers of differentiated cells

The identification of hepatocyte-like cells in 12-day-old selection

medium cultures prompted us to analyze these cells for biochemical evidence of hepatocytic differentiation. Immunohistochemistry was performed in cells grown on the cover glasses for the existence of albumin (Figure 4), AFP and CK8/18, the characteristic proteins expressed during hepatocyte development. Immunoperoxidase staining for these proteins revealed diffuse cytoplasmic staining of hepatocyte-like cells. In contrast, the fibroblast-like cells grew in the routine cultures did not express these proteins. RT-PCR further convinced the hepatocytic characteristics of differentiated cells as the results showed that there were mRNA transcripts of HNF-1 α , HNF-3 β , albumin, AFP, CK-18, CK-19, TTR, and CYP2b1, all of which were hepatic specific (Figure 5).

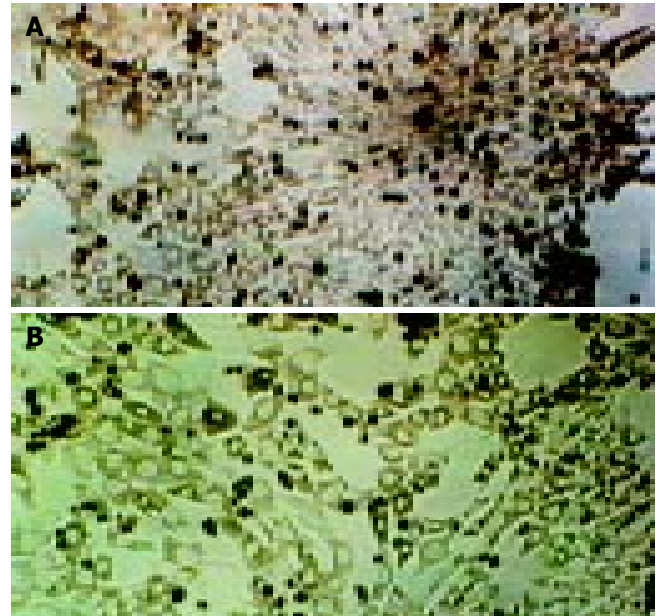


Figure 2 Appearance of hepatocyte-like colony forming units (H-CFU) 12 d after selection A: H-CFU, undifferentiated round cells in the center, surrounded by polygonal hepatocyte-like cells B: Regular arrangement of surrounding hepatocyte-like cells similar to the cords of hepatocytes.

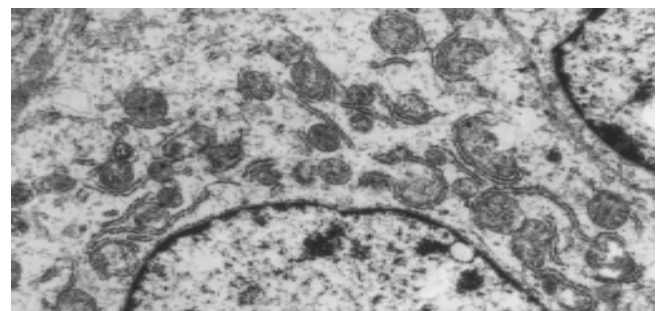


Figure 3 Ultrastructure of hepatocyte-like cells. 9 000 \times .



Figure 4 Positive staining of albumin immunohistochemistry 12 d after selection. ABC staining 200 \times .

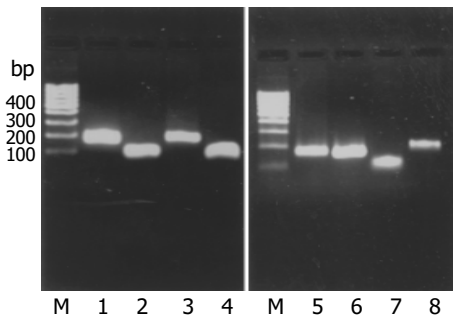


Figure 5 RT-PCR results M: marker, 1: AFP, 2: CK-18, 3: CYP2b1, 4: HNF-3 β , 5: Albumin, 6: TTR, 7: CK-19, 8: HNF-1 α .

Function tests of differentiated cells

We analyzed the levels of glycogen storage by periodic acid-Schiff (PAS) staining. Glycogen storage was seen as accumulation of magenta staining in the cytoplasm of hepatocyte-like differentiated cells (Figure 6). The control cells did not show similar staining. Urea production and secretion by hepatocyte-like cells were measured at various time points after the differentiated morphology appeared. Bone marrow cells and fibroblast-like cells did not produce urea. Urea assay revealed that urea concentration in the medium increased in a time-dependent manner (Figure 7).

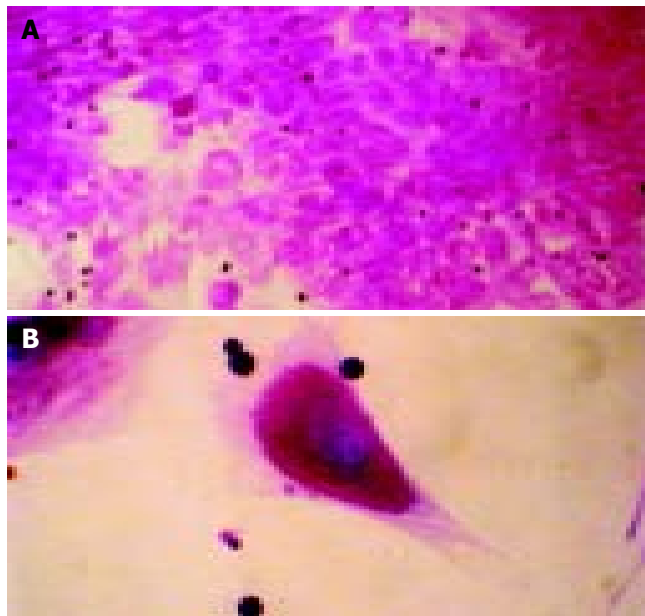


Figure 6 PAS staining of hepatocyte-like differentiated cells. The cells were positive in the cytoplasm (A) 200 \times , (B) 400 \times .

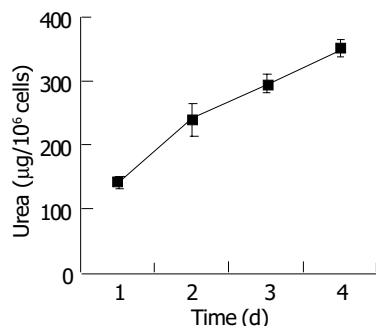


Figure 7 Urea synthetic function of bone marrow-derived liver stem cells (mean \pm SD, $n = 4$).

DISCUSSION

Since the results of cross-sex and cross-strain bone marrow and whole liver transplantation experiments indicated that the bone marrow might be a source of hepatocyte progenitors, great interests have been aroused in identification and isolation of liver stem cells from bone marrow cells. Until recently, several subsets of bone marrow cells have been found to have the potential to differentiate into hepatocytes, such as KTLS cells (c-kit^{high}Thy^{low}Lin^{Sca-1}⁺)^[20], β_2 -m⁻Thy-1⁺ cells^[27,28], multipotent adult progenitor cells (MAPC, CD44⁻CD45⁻HLA⁻c-kit⁺)^[18], and C1qR_p⁺ Lin⁻CD45⁺CD38⁻CD34^{+/+} cells^[29]. These stem cells could express different surface markers, and might represent different stages or different branches along the differentiation and developmental processes of bone marrow stem cells. So far, the characteristic surface markers of BDLSC and their pedigrees in the derivation of bone marrow stem cells remain obscure. Any subset sorting methods based on phenotypes would certainly lose other stem cells that have the ability to differentiate into hepatocytes. Furthermore, the sorting manipulations of the above stem cells with complicated surface markers are very difficult.

Studies on liver regeneration showed that liver stem cells could correspond to and repair liver injury only under certain severe pathological circumstances such as extensive liver necrosis due to chemical injury or hepatocytes treated with chemicals that could block their proliferation^[24]. Based on this mechanism, we assumed to imitate the *in vivo* pathological microenvironment of liver injury in culture of whole bone marrow cells, in order to provide specific proliferation signals for BDLSC, and to avoid resource loss of liver stem cells and complicated manipulation due to subset sorting. The key of this method is to develop an optimal "pathological microenvironment". Olynyk *et al.* demonstrated that in the cholestatic model of common bile duct ligation, intrahepatic liver stem cells showed great proliferation^[25]. Avital *et al.* recently reported that β_2 -m⁻Thy-1⁺ cells in bone marrow could differentiate into cells with hepatocyte-like phenotypes when co-cultured with adult hepatocytes in a medium containing cholestatic serum^[27], suggesting that there are stimulating factors in cholestatic serum. In our experiments, we used pathologically conditional selection medium containing cholestatic serum to culture whole bone marrow cells. Results showed that in the selection medium, a large number of the bone marrow cells exfoliated, only part of the remaining cells presented colonial growth during the first 3 d. When enriched with HGF on d 4, rapid proliferation and differentiation emerged, and H-CFU with various size appeared in 2 wk. The morphology and phenotypic markers manifested that the cells of H-CFU were similar to embryonic hepatoblasts. They expressed markers of embryonic hepatocytes (AFP, albumin and CK18), biliary cells (CK19), hepatocyte functional proteins (TTR and CYP2b1), and hepatocyte nuclear factors (HNF-1 α and HNF-3 β). HNF-1 α is a transcription factor required for subsequent hepatocyte differentiation, and transcription factor HNF-3 β was known to be important in endoderm specification. These results proved that H-CFU were colonies of liver stem cells.

In the culture system containing cholestatic serum, the concentration of "pathological microenvironment" needs to be considered. We found that 100 mL/L cholestatic serum was fatal to all of the bone marrow cells, 70 mL/L cholestatic serum prevented the colonies from growth and proliferation, 20 mL/L cholestatic serum could not inhibit the growth of other cells, while only 50 mL/L cholestatic serum acquired pure H-CFU. The differences can be explained by the toxic contents of cholestatic serum, which are the metabolic products cumulated under the circumstances of common bile duct obstruction and hepatic insufficiency, including bilirubin, bile acid, endotoxin, and ammonia, *etc.* When cholestatic serum was confined to the optimal concentration, BDLSC, possessing functions of bilirubin conjugation and detoxification^[30], could metabolize these toxic

products and survive, and selectively proliferate responding to the signal of liver injury. On the other hand, non-BDLSC could not adapt to the environment and resulted in apoptosis. To confirm that if the H-CFU had functional characteristics of hepatocytes, we tested the glycogen and urea synthesis functions of the cells and proved that the selected cells possessed hepatocyte-like functions. Therefore, the "pathological microenvironment" selecting medium based on cholestatic serum can select BDLSC in two ways, providing selective proliferation signals for BDLSC and eliminating non-BDLSC, so as to purify BDLSC.

We demonstrated that a "pathological microenvironment" selecting medium could select, proliferate and differentiate BDLSC from whole bone marrow cells *in vitro*. This method can not only provide a new and effective way for the isolation and purification of extrahepatic liver stem cells, but also supply a clue to obtain a readily available alternate source of cells for clinical hepatocyte therapy.

ACKNOWLEDGEMENTS

The authors thank Xiao-Dong Zhou, Jing Wei, Yu-Ru Fu, and Yu-Shen Lin, Clinical Research Center of Medicine, the 2nd Affiliated Hospital and the Center of Electron Microscopy, Sun Yat-Sen University for their technical support.

REFERENCES

- Krause DS. Plasticity of marrow-derived stem cells. *Gene Ther* 2002; **9**: 754-758
- Ferrari G, Cusella-De Angelis G, Coletta M, Paolucci E, Stornaiuolo A, Cossu G, Mavilio F. Muscle regeneration by bone marrow-derived myogenic progenitors. *Science* 1998; **279**: 1528-1530
- Gussoni E, Soneoka Y, Strickland CD, Buzney EA, Khan MK, Flint AF, Kunkel LM, Mulligan RC. Dystrophin expression in the mdx mouse restored by stem cell transplantation. *Nature* 1999; **401**: 390-394
- Brazelton TR, Rossi FM, Keshet GI, Blau HM. From marrow to brain: expression of neuronal phenotypes in adult mice. *Science* 2000; **290**: 1775-1779
- Mezey E, Chandross KJ, Harta G, Maki RA, McKercher SR. Turning blood into brain: cells bearing neuronal antigens generated *in vivo* from bone marrow. *Science* 2000; **290**: 1779-1782
- Orlic D, Kajstura J, Chimenti S, Limana F, Jakoniuk I, Quaini F, Nadal-Ginard B, Bodine DM, Leri A, Anversa P. Mobilized bone marrow cells repair the infarcted heart, improving function and survival. *Proc Natl Acad Sci U S A* 2001; **98**: 10344-10349
- Orlic D, Kajstura J, Chimenti S, Jakoniuk I, Anderson SM, Li B, Pickel J, McKay R, Nadal-Ginard B, Bodine DM, Leri A, Anversa P. Bone marrow cells regenerate infarcted myocardium. *Nature* 2001; **410**: 701-705
- Krause DS, Theise ND, Collector MI, Henegariu O, Hwang S, Gardner R, Neutzel S, Sharkis SJ. Multi-organ, multi-lineage engraftment by a single bone marrow-derived stem cell. *Cell* 2001; **105**: 369-377
- Petersen BE, Bowen WC, Patrene KD, Mars WM, Sullivan AK, Murase N, Boggs SS, Greenberger JS, Goff JP. Bone marrow as a potential source of hepatic oval cells. *Science* 1999; **284**: 1168-1170
- Theise ND, Badve S, Saxena R, Henegariu O, Sell S, Crawford JM, Krause DS. Derivation of hepatocytes from bone marrow cells in mice after radiation-induced myeloablation. *Hepatology* 2000; **31**: 235-240
- Alison MR, Poulson R, Jeffery R, Dhillon AP, Quaglia A, Jacob J, Novelli M, Prentice G, Williamson J, Wright NA. Hepatocytes from non-hepatic adult stem cells. *Nature* 2000; **406**: 257
- Theise ND, Nimmakayalu M, Gardner R, Illei PB, Morgan G, Teperman L, Henegariu O, Krause DS. Liver from bone marrow in humans. *Hepatology* 2000; **32**: 11-16
- Zhang Y, Bai XF, Huang CX. Hepatic stem cells: Existence and origin. *World J Gastroenterol* 2003; **9**: 201-204
- Spangrude GJ, Heimfeld S, Weissman IL. Purification and characterization of mouse hematopoietic stem cells. *Science* 1988; **241**: 58-62
- Baum CM, Weissman IL, Tsukamoto AS, Buckle AM, Peault B. Isolation of a candidate human hematopoietic stem-cell population. *Proc Natl Acad Sci U S A* 1992; **89**: 2804-2808
- Pereira RF, Halford KW, O'Hara MD, Leeper DB, Sokolov BP, Pollard MD, Bagasra O, Prockop DJ. Cultured adherent cells from marrow can serve as long-lasting precursor cells for bone, cartilage, and lung in irradiated mice. *Proc Natl Acad Sci U S A* 1995; **92**: 4857-4861
- Prockop DJ. Marrow stromal cells as stem cells for nonhematopoietic tissues. *Science* 1997; **276**: 71-74
- Schwartz RE, Reyes M, Koodie L, Jiang Y, Blackstad M, Lund T, Lenvik T, Johnson S, Hu WS, Verfaillie CM. Multipotent adult progenitor cells from bone marrow differentiate into functional hepatocyte-like cells. *J Clin Invest* 2002; **109**: 1291-1302
- Wong LS, Bateman WJ, Morris AG, Fraser IA. Detection of circulating tumour cells with the magnetic activated cell sorter. *Br J Surg* 1995; **82**: 1333-1337
- Lagasse E, Connors H, Al-Dhalimy M, Reitsma M, Dohse M, Osborne L, Wang X, Finegold M, Weissman IL, Grompe M. Purified hematopoietic stem cells can differentiate into hepatocytes *in vivo*. *Nat Med* 2000; **6**: 1229-1234
- Petersen BE, Goff JP, Greenberger JS, Michalopoulos GK. Hepatic oval cells express the hematopoietic stem cell marker Thy-1 in the rat. *Hepatology* 1998; **27**: 433-445
- Omori M, Omori N, Everts RP, Teramoto T, Thorgeirsson SS. Coexpression of flt-3 ligand/flt-3 and SCF/c-kit signal transduction system in bile-duct-ligated SI and W mice. *Am J Pathol* 1997; **150**: 1179-1187
- Hoffman AL, Rosen HR, Ljubimova JU, Sher L, Podesta LG, Demetriou AA, Makowka L. Hepatic regeneration: current concepts and clinical implication. *Semin Liver Dis* 1994; **14**: 190-210
- Sell S. Heterogeneity and plasticity of hepatocyte lineage cells. *Hepatology* 2001; **33**: 738-750
- Olynyk JK, Yeoh GC, Ramm GA, Clarke SL, Hall PM, Britton RS, Bacon BR, Tracy TF. Gadolinium chloride suppresses hepatic oval cell proliferation in rats with biliary obstruction. *Am J Pathol* 1998; **152**: 347-352
- Fausto N. Liver regeneration: from laboratory to clinic. *Liver Transpl* 2001; **7**: 835-844
- Avital I, Inderbitzin D, Aoki T, Tyan DB, Cohen AH, Ferrareso C, Rozga J, Arnaout WS, Demetriou AA. Isolation, characterization, and transplantation of bone marrow-derived hepatocyte stem cells. *Biochem Biophys Res Commun* 2001; **288**: 156-164
- Avital I, Ferrareso C, Aoki T, Hui T, Rozga J, Demetriou A, Muraca M. Bone marrow-derived liver stem cell and mature hepatocyte engraftment in livers undergoing rejection. *Surgery* 2002; **132**: 384-390
- Danet GH, Luongo JL, Butler G, Lu MM, Tenner AJ, Simon MC, Bonnet DA. C1qRp defines a new human stem cell population with hematopoietic and hepatic potential. *Proc Natl Acad Sci U S A* 2002; **99**: 10441-10445
- Vilei MT, Granato A, Ferrareso C, Neri D, Carraro P, Gerunda G, Muraca M. Comparison of pig, human and rat hepatocytes as a source of liver specific metabolic functions in culture systems-implications for use in bioartificial liver devices. *Int J Artif Organs* 2001; **24**: 392-396

• CLINICAL RESEARCH •

Upper gastrointestinal endoscopy: Are preparatory interventions or conscious sedation effective? A randomized trial

Lucio Trevisani, Sergio Sartori, Piergiorgio Gaudenzi, Giuseppe Gilli, Giancarlo Matarese, Sergio Gullini, Vincenzo Abbasciano

Lucio Trevisani, Sergio Sartori, Piergiorgio Gaudenzi, Giancarlo Matarese, Sergio Gullini, Vincenzo Abbasciano, Digestive Endoscopy Service, Department of Internal Medicine, S. Anna Hospital, Ferrara, Italy

Giuseppe Gilli, Health Physics Department, S. Anna Hospital, Ferrara, Italy

Correspondence to: Dr. Lucio Trevisani, Centro di Endoscopia Digestiva, Azienda Ospedaliera "Arcispedale S. Anna", C.so Giovecca 203, 44100 Ferrara, Italy. tvl@unife.it

Telephone: +1139-532-237558 **Fax:** +1139-532-236932

Received: 2004-02-20 **Accepted:** 2004-04-09

Abstract

AIM: The fears and concerns are associated with gastroscopy (EGD) decrease patient compliance. Conscious sedation (CS) and non-pharmacological interventions have been proposed to reduce anxiety and allow better execution of EGD. The aim of this study was to assess whether CS, supplementary information with a videotape, or presence of a relative during the examination could improve the tolerance to EGD.

METHODS: Two hundred and twenty-six outpatients (pts), scheduled for a first-time non-emergency EGD were randomly assigned to 4 groups: Co-group (62 pts): throat anaesthesia only; Mi-group (52 pts): CS with i.v. midazolam; Re-group (58 pts): presence of a relative throughout the procedure; Vi-group (54 pts): additional information with a videotape. Anxiety was measured using the "Spielberger State and Trait Anxiety Scales". The patients assessed the overall discomfort during the procedure on an 100-mm visual analogue scale, and their tolerance to EGD answering a questionnaire. The endoscopist evaluated the technical difficulty of the examination and the tolerance of the patients on an 100-mm visual analogue scale and answering a questionnaire.

RESULTS: Pre-endoscopy anxiety levels were higher in the Mi-group than in the other groups ($P < 0.001$). On the basis of the patients' evaluation, EGD was well tolerated by 80.7% of patients in Mi-group, 43.5% in Co-group, 58.6% in Re-group, and 50% in Vi-group ($P < 0.01$). The discomfort caused by EGD, evaluated by either the endoscopist or the patients, was lower in Mi-group than in the other groups. The discomfort was correlated with "age" ($P < 0.001$) and "groups of patients" ($P < 0.05$) in the patients' evaluation, and with "gender" (females tolerated better than males, $P < 0.001$) and "groups of patients" ($P < 0.05$) in the endoscopist's evaluation.

CONCLUSION: Conscious sedation can improve the tolerance to EGD. Male gender and young age are predictive factors of bad tolerance to the procedure.

Trevisani L, Sartori S, Gaudenzi P, Gilli G, Matarese G, Gullini S, Abbasciano V. Upper gastrointestinal endoscopy: Are preparatory interventions or conscious sedation effective? A randomized trial. *World J Gastroenterol* 2004; 10(22): 3313-3317
<http://www.wjgnet.com/1007-9327/10/3313.asp>

INTRODUCTION

Esophagogastroduodenoscopy (EGD) is a safe and quick procedure, and can be carried out without sedation^[1]. However, it can evoke anxiety, feelings of vulnerability, embarrassment and discomfort^[2], and the fears and concerns associated with endoscopic procedure decrease patient compliance^[2-4]. Indeed, anxiety, discomfort, and pain are interrelated, and each may increase the others^[5], making EGD execution more difficult. Several methods can be used to reduce patient pre-procedural worries, such as psychological interventions using relaxation and coping techniques^[6,7], hypnosis^[8], relaxation music^[9], acupuncture^[10], educational materials including videotapes^[11], and presence of a family member during EGD^[12]. However, conscious sedation with benzodiazepines is the method most widely employed^[5]. Although usually safe, such medications are not free of adverse effects^[13-15], and the likelihood of sedative-related complications increases in the presence of high anxiety levels, requiring higher doses of drugs^[2]. It follows that the role of conscious sedation is not well defined, and its use varies from country to country: up to 98% in USA, less frequently in European countries, and quite rarely in Asia and South America^[16]. The use of conscious sedation is also declining in the United Kingdom^[17], and many patients who receive detailed information about the advantages and risks of sedation choose to undergo EGD with pharyngeal anesthesia alone^[18,19]. In our endoscopy service, a standardized information sheet about EGD is given to all patients, and the examination is routinely performed with pharyngeal anesthesia alone.

This randomized prospective study was to evaluate if conscious sedation, additional information with a videotape, or the presence of a family member during the procedure could improve the tolerance to EGD and make the execution of EGD easier. In addition, particular emphasis was put on psychologic and procedure-related factors having a potential impact on the patient perception of tolerance.

MATERIALS AND METHODS

Study population

For six consecutive months, the first two outpatients daily referred for diagnostic EGD, fulfilling the eligibility criteria, were asked to enter the study. Inclusion criteria were age between 18 and 65 years, no prior experience of endoscopic examinations, and capability (evaluated by the endoscopist) of fully understanding and filling up the questionnaires of the study. Exclusion criteria were prior gastrectomy, psychiatric diseases or long-term psychiatric drug addiction, presence of neoplastic or other serious concomitant diseases, history of intolerance to benzodiazepines. On the whole, two hundred and eighty patients were asked to enter the study, and 228 of them were accepted. The patients were randomly assigned to four groups by a computer procedure. In the control group (Co-group), EGD was performed with topical pharyngeal anesthesia alone (100 g/L lidocaine spray). In the other three groups the following methods were used in addition to pharyngeal anesthesia: conscious sedation with i.v. midazolam 35 µg/kg (Mi-group); presence of a relative in the endoscopy room throughout the procedure (Re-group); additional information about the procedure using a videotape lasting for

about 10 min (Vi-group).

The study protocol was approved by the ethical committee of our hospital, and all patients gave their written consent to participate in the study.

Patients' assessments

Anxiety Since the anxiety experienced by patients undergoing EGD was hypothesized to be a factor related to potential discomfort, anxiety was measured by the Spielberger State-Trait Anxiety Inventory (STAI)^[20] in the validated Italian language version^[21]. Patients were asked to complete STAI before EGD. STAI is a 40-item questionnaire designed to measure state anxiety and trait anxiety. State anxiety is a temporary and situational anxiety, and trait anxiety is the tendency to awaken state anxiety under stress. Both kinds of anxiety were scored in the range of 20 to 80 points, a higher score indicated a greater anxiety. Before EGD, the patients had also to specify what they dreaded more about endoscopic examination, choosing among five items: fear of pain, fear of stifling, fear of complications, fear of endoscopic findings, and other.

Tolerance

Patients' assessment of tolerance to EGD was carried out at least 2 h after the end of the procedure. This interval was chosen to minimize the risk of persisting anterograde amnesia, which could potentially influence patient judgment. Patients assessed their tolerance answering the question: "how did you tolerate EGD?" ("well", "rather badly", "badly"), and rated the overall discomfort during EGD on an 100-mm visual analogue scale (0: no discomfort; 100: unbearable).

Endoscopist's assessment

All EGDs were carried out by the same endoscopist, using video endoscopes with a diameter of 9.8 mm (Fujinon video endoscopic system-Fujinon, Tokyo, Japan). Immediately after endoscopy, the operator recorded if EGD was completed, or it had to be interrupted, or it could be completed only after administration of sedatives (for Mi-group, after further sedatives in addition to midazolam previously administered). Moreover, he evaluated the ease of introduction of the instrument ("easy": no failed attempt of introduction; or "difficult": one or more failed attempts of introduction). Finally, he rated the discomfort caused to patients during EGD on an 100-mm visual analogue scale (0: no discomfort; 100: unbearable), and assessed the tolerance of the

patients grading it into three steps: "good", "poor", "very bad".

Parameters monitored

Blood oxygen saturation (SaO₂) and heart rate were continuously monitored during EGD. Desaturation was defined as a decrease in oxygen saturation below 90% for over 30 s. The occurrence of complications was recorded after each procedure. The duration of endoscopic examination was timed in all groups of patients. In Mi-group, the degree of sedation was evaluated using the Ramsay's scale^[22].

Statistical analysis

Characteristics of patients in the four groups were analyzed using one-way ANOVA and chi-square test. Endoscopic findings, tachycardia, motives of fear, answers of patients to the questions about their tolerance to EGD, ease of introduction of the instrument, and endoscopist's evaluation of tolerance of patients to EGD were compared in the four groups by using chi-square-test.

State and trait pre-endoscopic anxiety levels, and the discomfort rated by the patients and endoscopist on the 100-mm visual analogue scale were analyzed using one-way and two-way ANOVA. Two-way ANOVA was also used to evaluate the influence of sex, age, and anxiety levels on the discomfort caused by EGD. Linear-regression analysis was used to assess the relationship between the state and trait anxiety scores, as well as the correlation between patients' and endoscopist's evaluation of the discomfort caused by EGD. A general linear model (GLM) procedure was used to analyze the influence of sex, age, groups of patients, state anxiety, duration of EGD, and endoscopic findings on the degree of discomfort caused by EGD, assessed by either the endoscopist or the patients.

Results were considered statistically significant if *P* values were <0.05 (two-tailed test).

RESULTS

Two patients (1 in Co-group and 1 in Mi-group) were excluded from the study, as EGD was not completed. Two hundred and twenty-six patients (90 males and 136 females, mean age 38±10.62 years, range 19-63 years) could be evaluated. The four groups did not differ in age, endoscopic findings, and duration of the examination. The male: female ratio was lower in Mi-group than in the other groups (*P*<0.05) (Table 1).

Fourteen point five percent of patients in Co-group (6/62), 21.1% in Mi-group (11/52), 20.6% in Re-group (12/58), 16.6% in

Table 1 Demographic and clinical data of the patients

	Co-group	Mi-group	Re-group	Vi-group
Patients (n)	62	52	58	54
Gender (m/f)	25/37	9/43 ^a	28/30	28/26
Age (yr; mean±SD)	37.85±10.44	40.13±10.55	35.20±10.57	39.24±10.57
State anxiety (mean±SD)	46.66±10.73	54.19±10.89 ^b	46.03±11.42	39.62±9.05
Trait anxiety (mean±SD)	38.30±7.16	44.26±9.43 ^b	37.22±8.21	38.05±9.63
Duration of EGD (seconds; mean ± SD)	145.88±45.18	157.40±48.09	140.60±35.56	142.96±39.11
Endoscopic findings (No cases):				
Normal findings	30	25	26	22
Esophagitis	1	3	6	10
Hiatus Hernia	3	1	2	3
Gastritis or Duodenitis	24	19	19	14
Gastric or duodenal ulcer	2	2	3	3
Cancer	-	-	-	1
Other findings	2	2	2	1

^a*P*<0.05, ^b*P*<0.001 vs the other three groups.

Table 2 Tolerance to EGD and patients' and endoscopist's assessment

	Patients' assesment ^b				Endoscopist's assessment			
	Co-G (n)	Mi-G (n)	Re-G (n)	Vi-G (n)	Co-G (n)	Mi-G (n)	Re-G (n)	Vi-G (n)
Good	27	42 ^b	34	27	45	44 ^b	54	42
Poor	31	10 ^b	23	23	12	7 ^b	4	7
Very bad	4	0 ^b	1	4	5	1 ^b	0	5

Mi-G: ^b $P < 0.01$ vs the other three groups.

Table 3 Discomfort caused to patients during EGD and patients' and endoscopist's assessment (visual analogue scale)

	Co-G (mean±SD)	Mi-G (mean±SD)	Re-G (mean±SD)	Vi-G (mean±SD)
Patient evaluation	33.01±22.12	21.98±21.60	29.17±22.95	26.12±21.94
Endoscopist evaluation	23.51±22.99	14.17±18.07 ^a	16.43±14.42	20.81±24.04

^a $P < 0.05$ vs Co-G.

Table 4 Influence of some parameters on degree of discomfort caused by EGD (GLM procedure)

Parameter	Patient's assessment			Endoscopist's assessment		
	Coefficient	SE	P	Coefficient	SE	P
Gender	-0.251	3.153	0.937	-10.094	2.901	0.001
Age (yr)	-0.621	0.140	0.000	-0.159	0.129	0.219
Groups of patients	-1.138	1.325	0.391	-1.012	1.219	0.407
State anxiety	0.104	0.136	0.445	0.237	0.126	0.060
Time for EGD	0.046	0.039	0.237	-0.057	0.036	0.112
Endoscopic findings	-0.813	1.774	0.647	3.158	1.632	0.054

Vi-group (9/54) had a heart rate higher than 100 beats/min before starting EGD. During EGD, the heart rate exceeded 130 beats/min for at least 30 seconds in 5, 2, 3, and 2 patients in the four groups, respectively. No complication occurred, and no case of oxygen desaturation was observed. According to Ramsay's scale, in Mi-group grade 2 sedation was reached in 50 patients, and grade 3 in 2 patients.

State anxiety scores before EGD were significantly higher in Mi-group than in the other groups ($P < 0.001$), as well as trait anxiety scores ($P < 0.001$) (Table 1). State and trait anxiety scores were strongly correlated ($P < 0.001$).

In all groups the most frequent cause of fear before EGD was the fear of stifling (70 cases on the whole). The ease of introduction of gastroscope did not differ among the four groups, and the introduction resulted in difficulty just in one patient of Co-group and in 3 of Vi-group.

On the basis of patients' assessment, the tolerance to EGD was more frequently good when sedation was given: 80.7% of patients in Mi-group tolerated well gastroscopy, vs 43.5% in Co-group, 58.6% in Re-group, and 50% in Vi-group ($P < 0.01$) (Table 2). Conversely, no significant difference among the four groups was observed in the evaluation of the endoscopist, who nevertheless found that the discomfort caused by EGD was lower in Mi-group than in Co-group ($P < 0.05$) (Table 3). The degree of discomfort was lower in patients of Mi-group than in those of Co-group, but the difference was just close to threshold of significance, but did not reach it ($P = 0.059$) (Table 3). The other comparisons among the groups did not show any difference in the degree of discomfort caused by EGD. The evaluations of the patients and those of the endoscopist were strongly correlated ($P < 0.001$, $m = 0.45$), even though the endoscopist underestimated the degree of discomfort (Figure 1).

Two-way ANOVA performed on the degree of discomfort assessed by the patients, evaluated for factors "gender" and

"groups of patients" corrected for age, trait anxiety and state anxiety, showed an inverse influence of the age (i.e. better tolerance for older individuals, $P < 0.001$) and the factor "groups of patients" ($P < 0.05$). Conversely, the degree of discomfort assessed by the endoscopist was significantly influenced by the factors "gender" and "groups of patients" ($P < 0.001$ and $P < 0.05$, respectively). The factors "gender" and "groups of patients" showed a true and constant interaction (interaction factor $P < 0.01$), reflecting behaviors significantly different between males and females within the four groups, in particular in Co-group (Figures 2A, B).

Also the GLM procedure showed that age exerted the greatest influence on the discomfort caused by EGD in opinion of the patients (inverse correlation, $P < 0.001$), whereas in opinion of the endoscopist the discomfort was mainly influenced by the gender (females tolerated EGD better than males, $P < 0.001$) (Table 4).

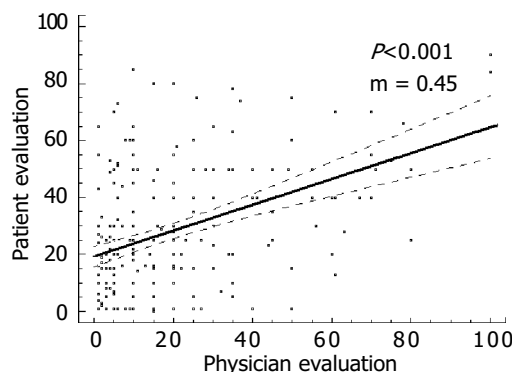


Figure 1 Linear regression of discomfort assessed by patients and endoscopist.

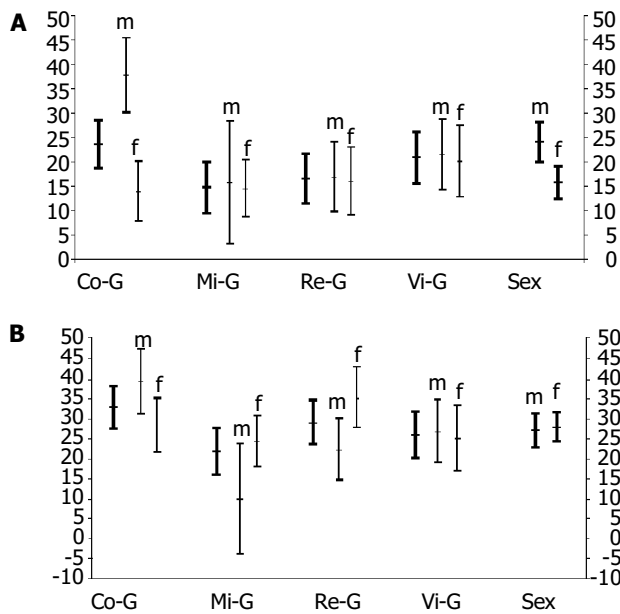


Figure 2 Discomfort assessed by patients and endoscopist, and mean values for factors "groups of patients" and "gender" with 95% c.l. Thick lines: m = males; f = females. Co-G: control group Mi-G: midazolam group Re-G: relatives group Vi-G: video group A: Discomfort assessed by patients B: Discomfort assessed by endoscopist.

DISCUSSION

Although conscious sedation is the method most widely used to reduce anxiety in patients undergoing EGD, its actual role is still an unresolved problem. Very large differences in sedation practice existed among different countries, and sometimes among different units within the same country^[5]. To our knowledge, this is the first randomized trial comparing the efficacy in improving the tolerance to EGD of conscious sedation, the presence of a relative in the endoscopy room throughout the procedure, and additional information by using a videotape. Abuksis *et al.* demonstrated that previous endoscopy experience could reduce anxiety level and influence patients' compliance^[23], and other authors identified endoscope size as a significant variable in determining tolerance to the procedure^[24,25]. For these reasons, in our study all patients enrolled had no prior endoscopy experience, and all EGDs were carried out using gastroscopes with the same diameter.

Our results suggested that low-dose conscious sedation with midazolam could improve the tolerance to EGD, according to a previous trial reporting a lower discomfort in sedated patients than in controls^[26]. Conversely, the presence of a relative attending the procedure and the use of informative videotape did not seem to give the patients significant advantages over the controls. However, better tolerance and lower discomfort were found in Re-group and Vi-group than in Co-group by either the patients or the endoscopist. Although these findings did not reach the significance level, in our opinion they suggested that the method used in controls (pharyngeal anesthesia only) was the worst approach to perform EGD. Indeed, the multivariate analysis showed constant differences among the groups of patients in concern of the discomfort caused by endoscopy, highlighting the usefulness of preparatory interventions in improving the tolerance to EGD.

The presence of relatives has been proved helpful in several medical fields, such as to children during hospitalization and to women during childbirth^[27], but it is not a standard procedure in digestive endoscopy. At present, just one randomized study was published on this topic, and the results suggested that the

presence of a family member throughout endoscopy could represent a promising approach^[12]. Conversely, the usefulness of additional information to reduce the anxiety and to improve the compliance of patients has been widely investigated, but with conflicting results. Detailed information before endoscopy has been reported to reduce anxiety levels^[11,28], but other studies failed in demonstrating any usefulness of this approach^[29], and some authors found that the over-information about endoscopy could even increase anxiety levels^[30,31].

The evaluation of the discomfort expressed by the patients and the endoscopist showed a strong correlation in our study (Figure 1). However, the endoscopist rated the patient degree of discomfort as lower than the patients themselves. According to the observation of Watson *et al.* that both endoscopists and nurses underestimated the discomfort felt by the patients^[32]. Besides anxiety, in our experience age and gender also influenced significantly the tolerance to endoscopy. Indeed, high levels of discomfort during EGD have been recently reported to be associated with younger age and high levels of pre-endoscopic anxiety^[24]. Older patients were likely to tolerate endoscopy better than their younger counterparts as they had a decreased pharyngeal sensitivity^[33,34]. Unlike several studies reporting better tolerance in men^[26,35], we found that female gender was associated with better tolerance. However, this gender-specific finding has been disputed by other authors^[3,24,33].

Despite the effectiveness of conscious sedation shown in our study, we think it should be avoided whenever possible in clinical practice. The extensive use of sedation would require several extra-charges, including the cost of drugs, prolongation of the procedure time, need of monitoring cardiopulmonary functions, need of recovery room for post-procedure observation, and the impossibility for patients to return to work immediately after endoscopic examination^[36]. Furthermore, sedative drugs are not free of adverse effects. In our series, no complications and oxygen desaturation were observed, and low-dose midazolam induced just rarely significant alterations in cardiorespiratory parameters^[26]. Nevertheless, conscious sedation could cause hypoxemia, which may induce cardiopulmonary complications, and most complications associated with endoscopy were attributable to the medications given for the procedure rather than the procedure itself^[13-15]. For these reasons, we think that further studies incorporating cut-off points are necessary to identify the patients who are likely to tolerate diagnostic gastroscopy without sedation. Some other preparatory interventions might also be effective to reduce endoscopy-related anxiety^[37]. The intervention techniques we used might be incorporated into our endoscopic practice, as they are simple, quick, easy to reproduce, and their extensive use does not require additional extra-charges, and expose the patients to the risk of complications.

REFERENCES

- 1 **Al-Atrakchi HA.** Upper gastrointestinal endoscopy without sedation: a prospective study of 2000 examinations. *Gastrointest Endosc* 1989; **35**: 79-81
- 2 **Brandt LJ.** Patients' attitudes and apprehensions about endoscopy: how to calm troubled waters. *Am J Gastroenterol* 2001; **96**: 280-284
- 3 **Campo R, Brullet E, Montserrat A, Calvet X, Moix J, Rue M, Roque Donoso L, Bordas JM.** Identification of factors that influence tolerance of upper gastrointestinal endoscopy. *Eur J Gastroenterol Hepatol* 1999; **11**: 201-204
- 4 **Dominitz JA, Provenzale D.** Patient preferences and quality of life associated with colorectal cancer screening. *Am J Gastroenterol* 1997; **92**: 2171-2178
- 5 **Bell GD.** Premedication, preparation, and surveillance. *Endoscopy* 2002; **34**: 2-12
- 6 **Gattuso SM, Litt MD, Fitzgerald TE.** Coping with gastrointestinal endoscopy: self-efficacy enhancement and coping style. *J*

- Consult Clin Psychol* 1992; **60**: 133-139
- 7 **Woloshynowych M**, Oakley DA, Saunders BP, Williams CB. Psychological aspects of gastrointestinal endoscopy: a review. *Endoscopy* 1996; **28**: 763-767
 - 8 **Conlong P**, Rees W. The use of hypnosis in gastroscopy: a comparison with intravenous sedation. *Postgrad Med J* 1999; **75**: 223-225
 - 9 **Bampton P**, Draper B. Effect of relaxation music on patient tolerance of gastrointestinal endoscopic procedures. *J Clin Gastroenterol* 1997; **25**: 343-345
 - 10 **Li CK**, Nauck M, Loser C, Folsch UR, Creutzfeldt W. Acupuncture to alleviate pain during colonoscopy. *Dtsch Med Wochenschr* 1991; **116**: 367-370
 - 11 **Luck A**, Pearson S, Maddem G, Hewett P. Effects of video information on precolonoscopy anxiety and knowledge: a randomised trial. *Lancet* 1999; **354**: 2032-2035
 - 12 **Shapira M**, Tamir A. Presence of family member during upper endoscopy: what do patients and escorts think? *J Clin Gastroenterol* 1996; **22**: 272-274
 - 13 **Herman LL**, Kurtz RC, McKee KJ, Sun M, Thaler HT, Winawer SJ. Risk factors associated with vasovagal reactions during colonoscopy. *Gastrointest Endosc* 1993; **39**: 388-391
 - 14 **Iber FL**, Sutberry M, Gupta R, Kruss D. Evaluation of complications during and after conscious sedation for endoscopy using pulse oximetry. *Gastrointest Endosc* 1993; **39**: 620-625
 - 15 **Mokhashi MS**, Hawes RH. Struggling toward easier endoscopy. *Gastrointest Endosc* 1998; **48**: 432-440
 - 16 **Lazzaroni M**, Bianchi Porro G. Preparation, premedication and surveillance. *Endoscopy* 1998; **30**: 53-60
 - 17 **Mulcahy HE**, Hennessy E, Connor P, Rhodes B, Patchett SE, Farthing MJ, Fairclough PD. Changing patterns of sedation use for routine out-patient diagnostic gastroscopy between 1989 and 1998. *Aliment Pharmacol Ther* 2001; **15**: 217-220
 - 18 **Hedenbro JL**, Lindblom A. Patient attitudes to sedation for diagnostic upper endoscopy. *Scand J Gastroenterol* 1991; **26**: 1115-1120
 - 19 **Pereira S**, Hussaini SH, Hanson PJ, Wilkinson ML, Sladen GE. Endoscopy: throat spray or sedation? *J R Coll Physicians Lond* 1994; **28**: 411-414
 - 20 **Spielberger CD**, Gorsuch RL, Lushene RE. Manual for the State-Trait Anxiety Inventory. *Palo-Alto: Consulting Psychologists Press* 1970
 - 21 **Spielberger CD**, Gorsuch RL, Lushene RE. Questionario di autovalutazione per l'ansia di stato e di tratto. Manuale di istruzioni. Traduzione di Lazzari R, Pancheri P. *Firenze: Organizzazioni Speciali* 1989
 - 22 **Ramsay MA**, Savege TM, Simpson BR, Goodwin R. Controlled sedation with alphaxalone-alphadolone. *Br Med J* 1974; **2**: 656-659
 - 23 **Abuksis G**, Mor M, Segal N, Shemesh I, Morad I, Plaut S, Weiss E, Sulkes J, Fraser G, Niv Y. A patient education program is cost-effective for preventing failure of endoscopic procedures in a gastroenterology department. *Am J Gastroenterol* 2001; **96**: 1786-1790
 - 24 **Mulcahy HE**, Kelly P, Banks MR, Connor P, Patchett SE, Farthing MJ, Fairclough PD, Kumar PJ. Factors associated with tolerance to, and discomfort with, unsedated diagnostic gastroscopy. *Scand J Gastroenterol* 2001; **36**: 1352-1357
 - 25 **Mulcahy HE**, Riches A, Kiely M, Farthing MJ, Fairclough PD. A Prospective controlled trial of an ultrathin versus a conventional endoscope in unsedated upper gastrointestinal endoscopy. *Endoscopy* 2001; **33**: 311-316
 - 26 **Froehlich F**, Schwizer W, Thorens J, Kohler M, Gonvers JJ, Fried M. Conscious sedation for gastroscopy: patient tolerance and cardiorespiratory parameters. *Gastroenterology* 1995; **108**: 697-704
 - 27 **Gjerdingen DK**, Froberg DG, Fontaine P. The effects of social support of women's health during pregnancy, labor and delivery, and the postpartum period. *Fam Med* 1991; **23**: 370-375
 - 28 **Leibo T**, Fitzgerald L, Matin K, Woo K, Mayer EA, Nalidoff BD. Audio and visual stimulation reduces patient discomfort during screening flexible sigmoidoscopy. *Am J Gastroenterol* 1998; **93**: 1113-1116
 - 29 **Levy N**, Landmann L, Stermer E, Erdreich M, Beny A, Meisels R. Does a detailed explanation prior to gastroscopy reduce the patient's anxiety? *Endoscopy* 1989; **21**: 263-265
 - 30 **Dawes PJ**, Davison P. Informed consent: what do patients want to know? *J R Soc Med* 1994; **87**: 149-152
 - 31 **Tobias JS**, Souhami RL. Fully informed consent can be needlessly cruel. *B M J* 1993; **307**: 1199-1201
 - 32 **Watson JP**, Goss C, Phelps G. Audit of sedated versus unsedated gastroscopy: do patients notice a difference? *J Qual Clin Pract* 2001; **21**: 26-29
 - 33 **Abraham N**, Barkun A, Larocque M, Fallone C, Mayrand S, Baffis V, Cohen A, Daly D, Daoud H, Joseph L. Predicting which patients can undergo upper endoscopy comfortably without conscious sedation. *Gastrointest Endosc* 2002; **56**: 180-189
 - 34 **Davies AE**, Kidd D, Stone SP, MacMahon J. Pharyngeal sensation and gag reflex in healthy subjects. *Lancet* 1995; **345**: 487-488
 - 35 **Tan CC**, Freeman JG. Throat spray for upper gastrointestinal endoscopy is quite acceptable to patients. *Endoscopy* 1996; **28**: 277-282
 - 36 **Schmitt CM**. Preparation for upper gastrointestinal endoscopy: opportunity or inconvenience? *Gastrointest Endosc* 1998; **48**: 430-432
 - 37 **Hackett ML**, Lane MR, McCarthy DC. Upper gastrointestinal endoscopy: are preparatory interventions effective? *Gastrointest Endosc* 1998; **48**: 341-347

• CLINICAL RESEARCH •

Opisthorchiasis-associated biliary stones: Light and scanning electron microscopic study

Banchob Sripa, Pipatphong Kanla, Poonsiri Sinawat, Melissa R. Haswell-Elkins

Banchob Sripa, Department of Pathology, Faculty of Medicine, Khon Kaen University, Khon Kaen 40002, Thailand

Pipatphong Kanla, Department of Anatomy, Faculty of Medicine, Khon Kaen University, Khon Kaen 40002, Thailand

Poonsiri Sinawat, Division of Anatomical Pathology, Khon Kaen Regional Hospital, Khon Kaen, Thailand and Department of Pathology, Faculty of Medicine, Khon Kaen University, Khon Kaen 40002, Thailand

Melissa R. Haswell-Elkins, Australia Centre for International and Tropical Health and Nutrition, University of Queensland, Brisbane, Australia

Supported by in part by the Tropical Health Program and NHMRC, Commonwealth Government, Australia

Correspondence to: Dr. Banchob Sripa, Department of Pathology, Faculty of Medicine, Khon Kaen University, Khon Kaen, 40002, Thailand. banchob@kku.ac.th

Telephone: +66-43-202024 **Fax:** +66-43-348375

Received: 2004-04-07 **Accepted:** 2004-05-25

Abstract

AIM: Biliary stones are frequently encountered in areas endemic for opisthorchiasis in Thailand. The present study was to describe the prevalence and pathogenesis of these stones.

METHODS: Gallstones and/or common bile duct stones and bile specimens from 113 consecutive cholecystectomies were included. Bile samples, including sludge and/or microcalculi, were examined for *Opisthorchis viverrini* eggs, calcium and bilirubin. The stones were also processed for scanning electron microscopic (SEM) study.

RESULTS: Of the 113 cases, 82 had pigment stones, while one had cholesterol stones. The other 30 cases had no stones. Most of the stone cases (76%, 63/83) had multiple stones, while the remainder had a single stone. Stones were more frequently observed in females. Bile examination was positive for *O. viverrini* eggs in 50% of the cases studied. Aggregates of calcium bilirubinate precipitates were observed in all cases with sludge. Deposition of calcium bilirubinate on the eggshell was visualized by special staining. A SEM study demonstrated the presence of the parasite eggs in the stones. Numerous crystals, morphologically consistent with calcium derivatives and cholesterol precipitates, were seen.

CONCLUSION: Northeast Thailand has a high prevalence of pigment stones, as observed at the cholecystectomy, and liver fluke infestation seems involved in the pathogenesis of stone formation.

Sripa B, Kanla P, Sinawat P, Haswell-Elkins MR. Opisthorchiasis-associated biliary stones: Light and scanning electron microscopic study. *World J Gastroenterol* 2004; 10(22): 3318-3321
<http://www.wjgnet.com/1007-9327/10/3318.asp>

INTRODUCTION

Liver fluke infestation caused by *Opisthorchis viverrini* remains

a major public health concern in Southeast Asia^[1], particularly in Thailand where an estimated 6 million people are infected^[2]. This infection is associated with a number of benign hepatobiliary diseases, including cholangitis, obstructive jaundice, hepatomegaly, cholecystitis and biliary lithiasis^[3]. Both experimental and epidemiological evidence implicate liver fluke infestation in the etiology of bile duct cancer, i.e. cholangiocarcinoma^[1,4,5].

An association between liver fluke infection and biliary lithiasis is well-recognized. *Opisthorchis* worm and/or eggs have been observed in the stones of infected or previously treated individuals^[6], just as *Clonorchis sinensis* eggs were found in the stones of those with Chinese liver fluke infection^[7,8]. Several community-based studies in Northeast Thailand have shown a significant increase in the frequency of biliary sludge in people with a heavy infection^[9-11]. Since biliary sludge is a precursor of stone formation^[12-14], opisthorchiasis likely plays a role in the development of biliary stones in certain individuals. However, the mechanism of liver-fluke-associated stone development is unclear.

We report the incidence of stone types, its relationship with *O. viverrini* infection and bile/stone examinations. The potential pathogenesis of opisthorchiasis-associated stones, in patients from endemic areas of Thailand, is proposed.

MATERIALS AND METHODS

Patients

This study was carried out in Northeast Thailand, an area endemic for opisthorchiasis. The study population included 113 consecutive patients scheduled for cholecystectomy at Khon Kaen Regional Hospital from whom bile was obtained between 1990 and 1991. The gallbladder diseases associated with the cholecystectomies included cholelithiasis ($n = 71$), cholecystitis with cholangiocarcinoma ($n = 29$) and cholecystitis with other miscellaneous diseases ($n = 13$). None of the patients had any history of hemolytic anemia or severe thalassemia.

Patients ranged between 17 and 94 years of age (mean, 54.97 ± 14.65) (45 females, 68 males). The study was carried out in accordance with the principles embodied in the 1975 Helsinki Declaration. A signed informed consent was obtained from each patient.

Specimen collection and laboratory investigations

Gallstones and/or common bile duct stones and bile specimens were collected from each individual. Bile samples aspirated from the gallbladder were centrifuged at 3 000 r/min for 10 min, then examined for the presence of *O. viverrini* eggs. At least four pellet-smears per individual were examined before the specimen was considered negative for eggs.

For a demonstration of calcium and bilirubin, the bile smears were air-dried and fixed in 40 g/L formaldehyde. Calcium and bilirubin staining were performed using histochemical methods^[15]. Calcium was stained black, bilirubin deep green.

Five stones from each group with *Opisthorchis* egg-negative and -positive bile underwent scanning electron microscopic (SEM) study. Briefly, the stones were thoroughly washed in distilled water and dried. After mechanical breaking, the stones

were sputter-coated with gold (agar aids-PS3, UK) and observed under a Hitachi (Model S-3200N, Japan) scanning electron microscope and photographed.

Statistical analysis

The χ^2 -test was used to analyze the association between the frequency of gallstones and sex, disease association, parasite egg status and age groups. A *P* value <0.05 was considered statistically significant.

RESULTS

Cholesterol or pigment stones were classified by visual inspection. Cholesterol stones were white or yellow and crystalline in composition, pigment stones were black or black-brown and amorphous.

Of the 113 cases, 83 had stones while 30 had none. Most of the stone cases (98.8%, 82/83) had pigment stones, while only one had cholesterol stone(s). In addition, 63 of the 83 cases (75.9%) contained multiple stones, while the remainder had a single stone. Of the 29 cases with cholangiocarcinoma, 9 (31.0%) contained stones while the others with miscellaneous diseases had stones in 3 out of 13 (23.1%) cases. The prevalence of

stones in all of the sample groups was significantly higher in females (χ^2 -test, *P* = 0.028). No association between stones and age groups (stratified as < 40, 40-49, 50-59 and > 60 years) was found (χ^2 -test, *P* = >0.05).

Bile examination was positive for *O. viverrini* eggs in 57 of the 113 cases (49.6%) studied. The presence of parasite eggs was not associated with the frequency of stones or disease association (χ^2 -test, *P* = >0.05). Most of the eggs were embedded in mucous gel. Aggregates of calcium bilirubinate precipitates were observed in all cases with sludge. Three cases had clear deposits of calcium bilirubinate on the eggshell, seen by special staining. Specifically, calcium was stained immediately adjacent to the eggshell, while bilirubin was observed in the outer layer (Figure 1 A, B). Examples of parasite egg-associated microcalculi aggregation and stone development are shown in Figures 2A-D.

A SEM study demonstrated the presence of parasite eggs in the center of stones from all of the *Opisthorchis* egg-positive cases. Interestingly, 3 of the 5 egg-negative cases contained the parasite eggs in the stones. Numerous crystals, morphologically consistent with calcium derivatives and cholesterol precipitates, were observed. Typical SEM pictures of the stones are shown in Figures 3A, B.

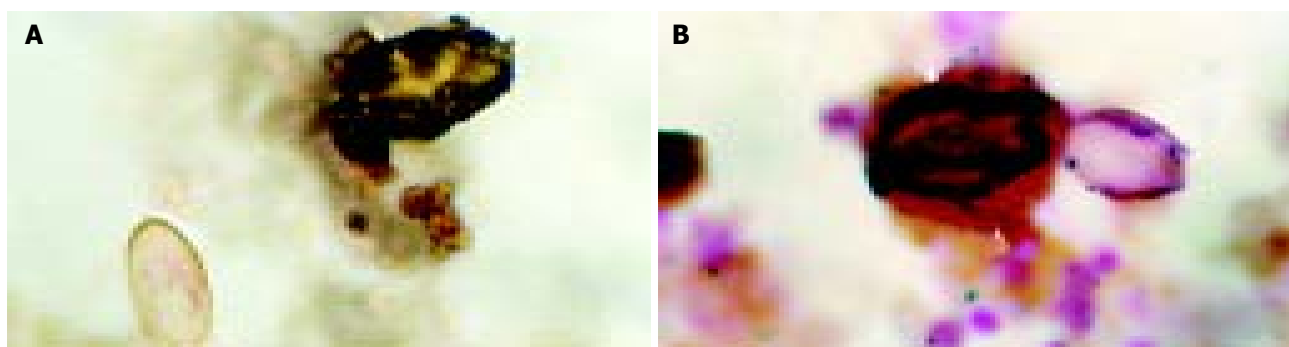


Figure 1 Histochemical staining of biliary sludge for bilirubin (A) and calcium (B). Calcium appears as dark deposits on the *Opisthorchis* eggshell (arrow) and bilirubin precipitates are demonstrated in the outer layer (arrowhead). Normal parasite eggs without deposition are shown in the same field. (A = Fouchet stain, B = von Kossa stain).

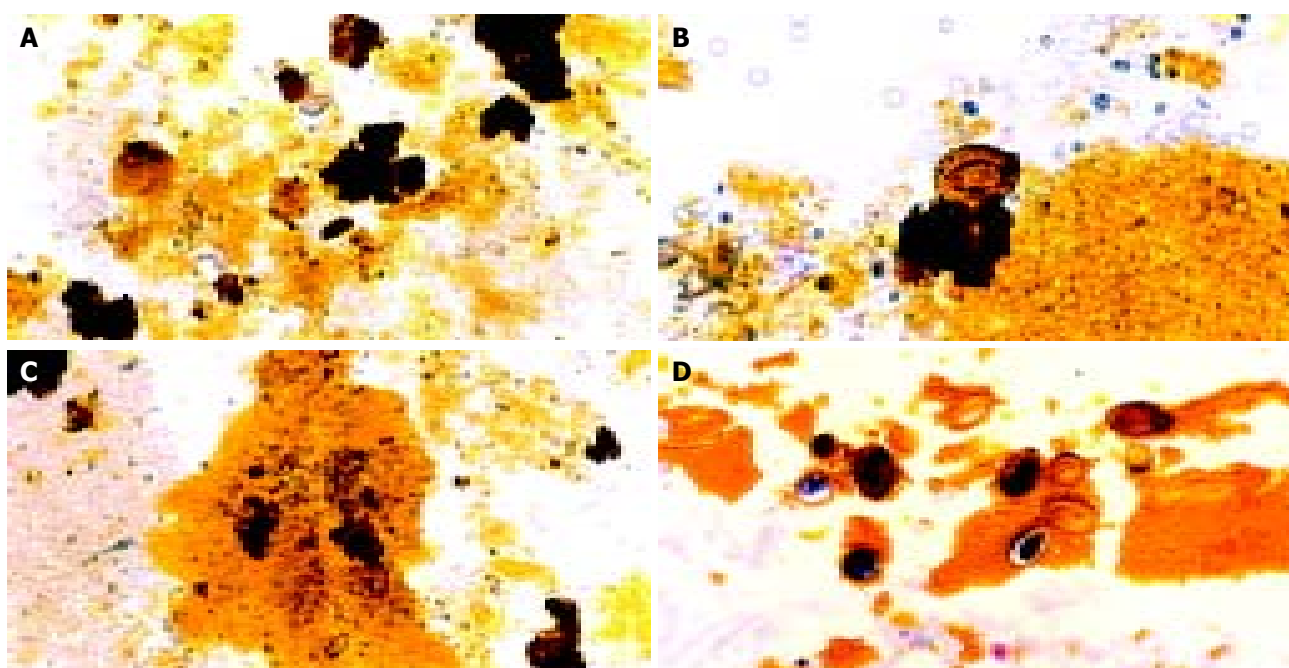


Figure 2 Typical pictures showing the cascades of *Opisthorchis* egg-associated stone formation starting from aggregation of the eggs admixed with mucin (A), deposition of calcium bilirubinate on the eggshells (B), and formation of tiny stones (C & D). Original magnification, x100 (A & C) and x200 (B & D).

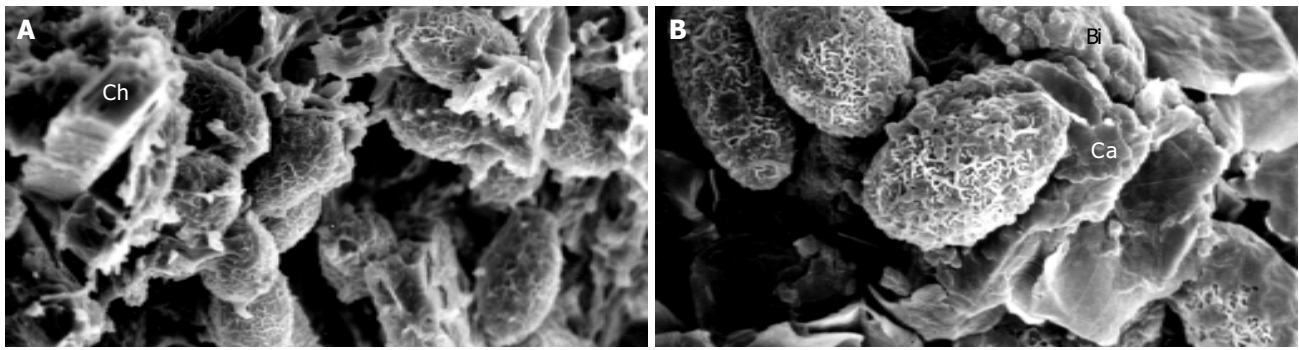


Figure 3 SEM micrographs of gallstones showing *Opisthorchis* eggs with typical musk-melon-eggshell surface in the nidi of the stones. Several crystalline structures consistent with calcium (Ca), bilirubin derivatives (Bi) and cholesterol (Ch) could be noted (AB). Higher magnification with highlighting calcium bilirubinate deposition on *Opisthorchis* eggshell and mucus is shown in Figure 3B.

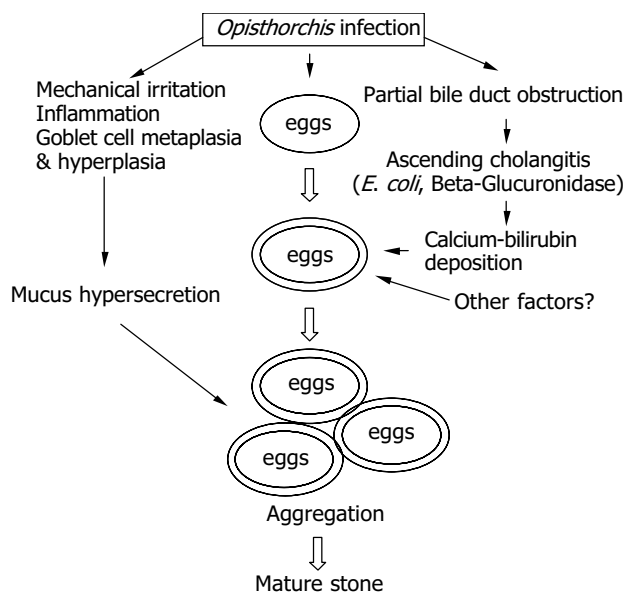


Figure 4 Diagram showing the proposed pathogenesis of *Opisthorchis*-associated biliary stone.

DISCUSSION

Biliary lithiasis is a common indication for cholecystectomy in most parts of the world. However, the prevalence and types of stones differ geographically^[16-18]. Pigment stones, mostly containing calcium bilirubinate, generally constitute 10 to 27 percent of all gallstones in America and Europe, the predominant type was cholesterol stones^[19-21]. In contrast, the prevalence of pigment stones is high in Asia, accounting for $\leq 90\%$ of all stones in some parts of China^[22]. In our study, almost all the cases (98.8%) of biliary lithiasis involved pigment stones. This is probably the highest reported relative frequency of pigment stones found during cholecystectomy. It exceeds a report from Bangkok, Central Thailand, where pure cholesterol stones represent $\leq 32\%$ of stones^[23]. Stones in our study of Northeast Thailand, however, occurred more frequently in females than in males as in other countries^[19-20].

The association between certain parasitic infections and biliary stone formation is well documented^[7,24-27]. Our study demonstrated *Opisthorchis* eggs in the sludge from the gallbladder bile confirmed the sludge seen in other ultrasound studies performed in Northeast Thailand^[12-14]. However, our study failed to demonstrate the association between *O. viverrini* infection and the presence of stones, perhaps because of previous self-treatment with praziquantel, an anthelmintic widely used in Northeast Thailand^[2]. We collected the treatment data,

but they were not reliable as patients did not record when or how many times they took the medication before cholecystectomy. Moreover, re-infection is common in people in endemic areas.

SEM data from egg-negative patients revealed parasite eggs in the nidi of the stones, indicating these patients were previously infected. Budget constraints meant that only a limited number of cases were confirmed by SEM. More stones should be studied to test the validity of the findings.

The mechanism by which parasite infection enhances pigment stone formation is not clearly understood. The present study demonstrated *O. viverrini* eggs in the biliary sludge and gallstones in both bile smears and the SEM, while Riganti *et al.*^[6] observed both adult worms and eggs in the nidi of gallstones from two patients. Riganti *et al.* also demonstrated calcium bilirubinate in pigment stones, as previously reported in stones associated with *C. sinensis*^[7,8] and ascariasis^[8,27,28]. These observations have led investigators to conclude that parasite eggs and/or worms may directly stimulate stone formation^[6,8]. Our histochemical findings on the calcium and bilirubin coatings on the *O. viverrini* eggs support this hypothesis. The presence of calcium coating on the outer surface of the parasite eggshell suggests that the eggs may act as a nucleus for stone formation. This may be similar to peripheral calcification of existing cholesterol stones^[29]. Since calcium is an active element, and can precipitate several bile constituents including bilirubin, carbonate and phosphate - major components of pigment stones^[30]. The parasite eggs precipitated with calcium bilirubinate and admixed with mucin, which is abundant in a liver fluke infection^[3,25]. Mucin secreted by biliary epithelial cells has been recognized as an important local factor in gallstone pathogenesis^[31]. This orchestrated process can eventually produce mature pigment stones as generally described^[32].

Additionally, liver flukes that inhabit the bile ducts can partially obstruct the lumen leading to bile stasis and ascending cholangitis^[3]. *E. coli*, a common bacterial species infecting the biliary system^[23,33], releases β -glucuronidases, which can hydrolyze the glucuronic acid from the conjugated bilirubin^[34-36]. The resulting unconjugated bilirubin precipitates as calcium salts, which is the first step in pigment stone formation^[32,34]. Bile stasis is not only a condition for ascending infection but also induces stagnation of the bile components leading to stone formation^[37]. Heavy *Opisthorchis* infection can induce poor emptying of the gallbladder^[9-11]. In addition, our recent report has shown that severe fibrosis of the gallbladder wall is the main histopathology of chronic opisthorchiasis^[38]. These altogether support the role of this liver fluke in gallbladder stasis, ascending cholangitis and enhanced stone formation. From previous data and our own observations, a proposed pathogenesis of *Opisthorchis*-associated pigment stone formation

is presented in Figure 4.

In conclusion, Northeast Thailand has a high incidence of pigment stones compared to cholesterol stones at cholecystectomy. Our study clearly demonstrates that calcium bilirubinate precipitates on parasite eggshells both in light and SEM studies. This supports the role of *O. viverrini* infection in the pathogenesis of pigment stone formation.

ACKNOWLEDGMENTS

The authors thank Mr. Bryan Roderick Hamman for helping with the English-language presentation.

REFERENCES

- 1 Infection with liver flukes (*Opisthorchis viverrini*, *Opisthorchis felineus* and *Clonorchis sinensis*). *IARC Monogr Eval Carcinog Risks Hum* 1994; **61**: 121-175
- 2 Jongsuksuntigul P, Imsomboon T. Opisthorchiasis control in Thailand. *Acta Trop* 2003; **88**: 229-321
- 3 Harinasuta T, Riganti M, Bunnag D. *Opisthorchis viverrini* infection: pathogenesis and clinical features. *Arzneimittelforschung* 1984; **34**: 1167-1169
- 4 Sithithaworn P, Haswell-Elkins MR, Mairiang P, Satarug S, Mairiang E, Vatanasapt V, Elkins DB. Parasite-associated morbidity: liver fluke infection and bile duct cancer in northeast Thailand. *Int J Parasitol* 1994; **24**: 833-843
- 5 Vatanasapt V, Sripa B, Sithithaworn P, Mairiang P. Liver flukes and liver cancer. *Cancer Surv* 1999; **33**: 313-343
- 6 Riganti M, Pungpak S, Sachakul V, Bunnag D, Harinasuta T. *Opisthorchis viverrini* eggs and adult flukes as nidus and composition of gallstones. *Southeast Asian J Trop Med Public Health* 1988; **19**: 633-636
- 7 Teoh TB. A study of gall-stones and included worms in recurrent pyogenic cholangitis. *J Pathol Bacteriol* 1963; **86**: 123-129
- 8 Ker CG, Huang TJ, Sheen PC, Chen ER. A study of structure and pathogenesis of *Ascaris* and *Clonorchis* stones. *Kaohsiung J Med Sci* 1988; **4**: 231-237
- 9 Elkins DB, Haswell-Elkins MR, Mairiang E, Mairiang P, Sithithaworn P, Kaewkes S, Bhudhisawasdi V, Uttaravichien T. A high frequency of hepatobiliary disease and cholangiocarcinoma associated with heavy *Opisthorchis viverrini* infection in a small community in Northeast Thailand. *Trans R Soc Trop Med Hyg* 1990; **84**: 715-719
- 10 Mairiang E, Elkins DB, Mairiang P, Chaikakum J, Chamadol N, Loapaiboon V, Posri S, Sithithaworn P, Haswell-Elkins MR. Relationship between intensity of *Opisthorchis viverrini* infection and hepatobiliary disease detected by ultrasonography. *J Gastroenterol Hepatol* 1992; **7**: 17-21
- 11 Mairiang E, Haswell-Elkins MR, Mairiang P, Sithithaworn P, Elkins DB. Reversal of biliary tract abnormalities associated with *Opisthorchis viverrini* infection following praziquantel treatment. *Trans R Soc Trop Med Hyg* 1993; **87**: 194-197
- 12 Lee SP, Nicholls JF. Nature and composition of biliary sludge. *Gastroenterology* 1986; **90**: 677-686
- 13 Lee SP, Maher K, Nicholls JF. Origin and fate of biliary sludge. *Gastroenterology* 1988; **94**: 170-176
- 14 Terada T, Nakanuma Y, Saito K, Kono N. Biliary sludge and microcalculi in intrahepatic bile ducts: Morphologic and X-ray microanalytical observations in 18 among 1 179 consecutively autopsied livers. *Acta Pathol Jpn* 1990; **40**: 894-901
- 15 Luna LG. Manual of histologic staining methods of the Armed Forces Institute of Pathology. 3rd ed. New York: McGraw-Hill 1968: 258
- 16 Weedon D. Pathology of the Gallbladder. New York: Masson 1984: 290
- 17 Kim WR, Brown RS Jr, Terrault NA, El-Serag H. Burden of liver disease in the United States: summary of a workshop. *Hepatology* 2002; **36**: 227-242
- 18 Shi JS, Ma JY, Zhu LH, Pan BR, Wang ZR, Ma LS. Studies on gallstone in China. *World J Gastroenterol* 2001; **7**: 593-596
- 19 Friedman GD, Kannel WB, Dawler TR. The epidemiology of gallstone disease: observation in the Framingham study. *J Chronic Dis* 1966; **19**: 273-292
- 20 Trotman BW, Soloway RD. Pigment vs cholesterol cholelithiasis: clinical and epidemiological aspects. *Am J Dig Dis* 1975; **20**: 735-740
- 21 Johnston DE, Kaplan MM. Pathogenesis and treatment of gallstones. *New Eng J Med* 1993; **11**: 411-421
- 22 Crowther RS, Soloway RD. Pigment gallstone pathogenesis: from man to molecules. *Semin Liver Dis* 1990; **10**: 171-180
- 23 Teparut V, Limsuvan B, Pitchayangura C, Vatanachote D, Banchuin C, Jenvatanavit T, Athiphanumpai A, Pokawatana C, Tancharoen S. Correlation among biliary stones, gallbladder pathology and aerobic biliary infections. *Bull Dept Med Serv* 1986; **11**: 523-532
- 24 Cook J, Hou PC, Ho HC, McFadzean AJS. Recurrent pyogenic cholangitis. *Br J Surg* 1954; **42**: 188-203
- 25 Hou PC. The pathology of *Clonorchis sinensis* infestation of the liver. *J Pathol Bacteriol* 1955; **70**: 53-64
- 26 Cobo A, Hall RC, Torres E, Cuello CJ. Intrahepatic calculi. *Arch Surg* 1964; **89**: 936-941
- 27 Yellin AE, Donovan AJ. Biliary lithiasis and helminthiasis. *Am J Surg* 1981; **142**: 128-136
- 28 Maki T. Cholelithiasis in Japanese. *Arch Surg* 1961; **82**: 599-612
- 29 Moore EW. Biliary calcium and gallstone formation. *Hepatology* 1990; **12**(3 Pt 2): 206S-214S
- 30 Rege RV. The role of biliary calcium in gallstone pathogenesis. *Front Biosci* 2002 **7**: E315-325
- 31 Ko CW, Lee SP. Gallstone formation. Local factors. *Gastroenterol Clin North Am* 1999; **28**: 99-115
- 32 Cahalane MJ, Neubrand MW, Carey MC. Physical-chemical pathogenesis of pigment gallstones. *Semin Liver Dis* 1988; **8**: 317-328
- 33 Truedson H, Elmros T, Holm S. The incidence of bacteria in gallbladder bile at acute and elective cholecystectomy. *Acta Chir Scand* 1983; **149**: 307-313
- 34 Maki T. Pathogenesis of calcium bilirubinate gallstone: Role of *E. coli*- β -glucuronidase and coagulation by inorganic ions, poly-electrolytes and agitation. *Ann Surg* 1966; **164**: 90-100
- 35 Swidsinski A, Lee SP. The role of bacteria in gallstone pathogenesis. *Front Biosci* 2001; **6**: E93-103
- 36 Nakai K, Tazuma S, Nishioka T, Chayama K. Inhibition of cholesterol crystallization under bilirubin deconjugation: partial characterization of mechanisms whereby infected bile accelerates pigment stone formation. *Biochim Biophys Acta* 2003; **1632**: 48-54
- 37 Pauletzki J, Paumgartner G. Review article: defects in gallbladder motor function-role in gallstone formation and recurrence. *Aliment Pharmacol Ther* 2000; **14**(Suppl 2): 32-34
- 38 Sripa B, Haswell-Elkins MR, Sinawat P. Histological analysis of cholecystitis in relation to opisthorchiasis in endemic areas of Thailand. *Acta Trop* 2003; **88**: 239-246

Edited by Wang XL Proofread by Zhu LH and Xu FM

• CLINICAL RESEARCH •

Long-term results of graded pneumatic dilatation under endoscopic guidance in patients with primary esophageal achalasia

Ahmet Dobrucali, Yusuf Erzin, Murat Tuncer, Ahmet Dirican

Ahmet Dobrucali, Yusuf Erzin, Murat Tuncer, Department of Gastroenterology, Cerrahpasa Medical Faculty, Istanbul University, Istanbul, Turkey

Ahmet Dirican, Department of Biostatistics, Cerrahpasa Medical Faculty, Istanbul University, Istanbul, Turkey

Correspondence to: Dr. Ahmet Dobrucali, Istanbul Universitesi, Cerrahpasa Tıp Fakültesi, İç Hastalıkları A.B.D., Gastroenteroloji B. D., Kocamustafapasa - Fatih, 34 300 Istanbul-Turkey. adobrucali@yahoo.com

Telephone: +90-532-4425551 **Fax:** +90-212-5307440

Received: 2004-02-27 **Accepted:** 2004-04-20

Abstract

AIM: Achalasia is the best known primary motor disorder of the esophagus in which the lower esophageal sphincter (LES) has abnormally high resting pressure and incomplete relaxation with swallowing. Pneumatic dilatation remains the first choice of treatment. The aims of this study were to determine the long term clinical outcome of treating achalasia initially with pneumatic dilatation and usefulness of pneumatic dilatation technique under endoscopic observation without fluoroscopy.

METHODS: A total of 65 dilatations were performed in 43 patients with achalasia [23 males and 20 females, the mean age was 43 years (range, 19-73)]. All patients underwent an initial dilatation by inflating a 30 mm balloon to 15 psi under endoscopic control. The need for subsequent dilatation was based on symptom assessment. A 3.5 cm balloon was used for repeat procedures.

RESULTS: The 30 mm balloon achieved a satisfactory result in 24 patients (54%) and the 35 mm balloon in 78% of the remainder (14/18). Esophageal perforation as a short-term complication was observed in one patient (2.3%). The only late complication encountered was gastroesophageal reflux in 2 (4%) patients with a good response to dilatation. The mean follow-up period was 2.4 years (6 mo - 5 years). Of the patients studied, 38 (88%) were relieved of their symptoms after only one or two sessions. Five patients were referred for surgery (one for esophageal perforation and four for persistent or recurrent symptoms). Among the patients whose follow up information was available, the percentage of patients in remission was 79% (19/24) at 1 year and 54% (7/13) at 5 years.

CONCLUSION: Performing balloon dilatation under endoscopic observation as an outpatient procedure is simple, safe and efficacious for treating patients with achalasia and referral of surgical myotomy should be considered for patients who do not respond to medical therapy or individuals that do not desire pneumatic dilatations.

Dobrucali A, Erzin Y, Tuncer M, Dirican A. Long-term results of graded pneumatic dilatation under endoscopic guidance in patients with primary esophageal achalasia. *World J Gastroenterol* 2004; 10(22): 3322-3327

<http://www.wjgnet.com/1007-9327/10/3322.asp>

INTRODUCTION

Achalasia is an uncommon disorder of the esophagus characterized by clinical, radiologic and manometric findings. Dysphagia, regurgitation, weight loss and chest pain are among the most recognized clinical features of the disease. Manometrically it is distinguished by esophageal aperistalsis and incomplete relaxation of the lower esophageal sphincter (LES). Esophageal dilatation and a tapered deformity of the distal esophagus are presumably late radiological manifestations of the disease^[1,2]. The pathogenesis of achalasia remains unknown. Available data suggest hereditary, degenerative, autoimmune and infectious factors as possible causes for achalasia, the latter two are the most commonly accepted possible etiologies. The mean age of onset varies between 30 and 60 years with a peak incidence in the fifth decade. The incidence is 1.1 per 100 000 with a prevalence of 7.9 to 12.6 per 100 000^[2,3].

Although there is no definite cure for achalasia, the goals of treatment should be: 1) relieving the patient's symptoms, 2) improving esophageal emptying and 3) preventing development of a megaesophagus. The optimal treatment of achalasia includes several options and presents a challenge for most gastroenterologists. It can be treated by botulinum toxin injection, pneumatic dilatation or esophagomyotomy, but the most effective treatment options are graded pneumatic dilatation and surgical myotomy. All of these therapeutic modalities are aimed at removing the functional barrier at the lower esophageal sphincter level. Although high success rates have been reported for these therapeutic modalities, the fact remains that the esophageal propulsive force is not usually restored and therefore it is conceivable that a normal esophageal function can never be expected among these patients^[2,4,5].

The aim of our study was to evaluate the safety and efficacy of graded pneumatic dilation using two different size (3.0 and 3.5 cm) balloon dilators (Rigiflex) in patients with primary esophageal achalasia. We hereby report our experience, which indicates that pneumatic dilatation can be safely performed under direct endoscopic observation without fluoroscopic guidance and with only a short-term clinical monitoring in an outpatient setting prior to discharge.

MATERIALS AND METHODS

Patients

Forty-three consecutive patients (23 males and 20 females) were evaluated. The ages ranged from 19 to 73 years with a mean age of 43 years. All patients were referred because of typical symptoms of achalasia. All had dysphagia, but some also had regurgitation or pulmonary aspiration (Table 1). The diagnosis of achalasia was made on the basis of clinical, radiologic and manometric criteria. Barium esophagogram showed a distal narrowing of the esophagus (bird beak deformity) and variable degrees of dilation of the esophagus in most patients (93%). Mean esophagus diameter was 3.8 cm (range, 2-6.3 cm). Upper endoscopy was done in all patients to exclude secondary causes of achalasia. Computerized tomography of the chest was done in 12 patients over age 40 with significant weight loss over a short period (six months or less) to exclude mediastinal malignancy

causing pseudoachalasia.

Eligibility criteria for entry into the study required: a diagnosis of achalasia by manometry as defined above, absence of obstructive intrinsic or extrinsic esophageal lesions by X-ray and endoscopy, and Absence of esophageal or gastric carcinoma, a peptic stricture or a prior surgical fundoplication.

Symptoms of the patients were scored using a questionnaire requesting information regarding the presence and severity of their difficulty in swallowing solids and liquids on a 5 point subjective visual scale: 0 = no symptoms, 1 = mild, 2 = moderate, 3 = severe, 4 = very severe.

Table 1 Clinical characteristics and demographic data of patients [mean±SD, (min-max)]

Age (yr)	44±16 (19-73)
Gender (M/F)	23/20
Dysphagia	43 (100%)
Chest pain	5 (11%)
Regurgitation	34 (79%)
Pulmonary aspiration	9 (21%)
Mean duration of symptoms (mo)	35±21 (6-72)
Mean weight loss (kg)	7.7±2 (4-11)
LES pressure (mmHg)	
Before dilation	38.6±12 (19-66)
After dilation	11.8±8 (0-16)
Vigorous achalasia	1 (2.3%)
Esophagus diameter (cm)	3.8 (2-6.5)

Esophageal manometry

Esophageal manometry was performed in all patients with a four lumen polyvinyl catheter with Dent sleeve working with a pneumohydraulic capillary perfusion system (Synectic PC polygraph- Gastrosoft Inc. Upper GI edition, version 6.0). Manometric examinations were performed by the same author. LES was localised using the station pull-through technique. Other three orifices, located 5 cm apart and also oriented at 90° angles, for determination of the peristalsis and pressures, by placing the distal orifice 5 cm above the LES. The peristalsis was measured with 10 wet swallows of 5 mL of water, each at intervals of 60 s or more. Aperistalsis was the absolute manometric criterion required for the diagnosis of achalasia with increased LES pressure and incomplete/absent relaxation were the complementary findings^[7]. Incomplete relaxation was defined as the failure of LES pressure to drop to gastric baseline during a dry and/or wet swallow (Figure 1).

Technique of pneumatic dilation

All dilations were performed on outpatients. Dilations were

done by the same authors using the Rigiflex achalasia balloon dilators (Microvasive) in a graded manner. A 3.0 cm dilator was always used first. If there was still no symptomatic response, a 3.5 cm dilator was used after 6-8 wk. After clear liquid diet for 24 h and an overnight fast, an endoscope (Pentax EG-2940) was passed after application of a local anesthetic to the pharynx under conscious sedation (Midazolam 0.04 mg/kg iv) to evacuate the residual liquid from the esophagus and to insert a guide wire. The guide wire was placed into the duodenum via stomach under endoscopic guidance and endoscope was removed. A Rigiflex balloon dilator, which was marked with a thick coloured marker at the mid section of the balloon was passed over the guidewire to stomach and slightly inflated (less than 5 psi) to get a soft tube shaped form. Endoscope was reinserted and positioned proximally to adjust and control the position of the balloon in the esophagus. Balloon was withdrawn to esophagus and marked part of the balloon was located within the gastroesophageal junction under endoscopic control (Figure 2). The balloon was then inflated until 15 psi, and inflation was maintained for 60 s. Ischemic ring at the lower esophageal sphincter level was seen during dilatation through the transparent balloon. After repeating of the same inflation procedure one more time at the same session endoscopic dilatation was terminated and endoscope, balloon and guidewire were removed. Balloon dilator surface was checked to see if there was blood on it. The procedure was well tolerated by all patients.

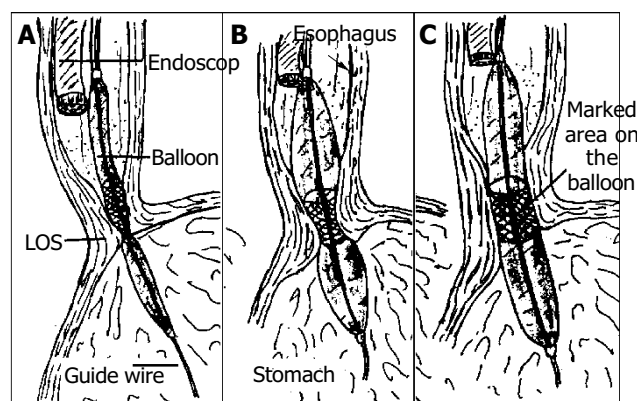


Figure 2 Technique for pneumatic dilatation under endoscopic control without fluoroscopy. The balloon was positioned so that its midsection was at the high pressure level (A). The balloon was inflated and the endoscopist observes with endoscope proximally to balloon (B). With successful dilatation the ischemic ring of dilated segment was diminished or disappeared (C).

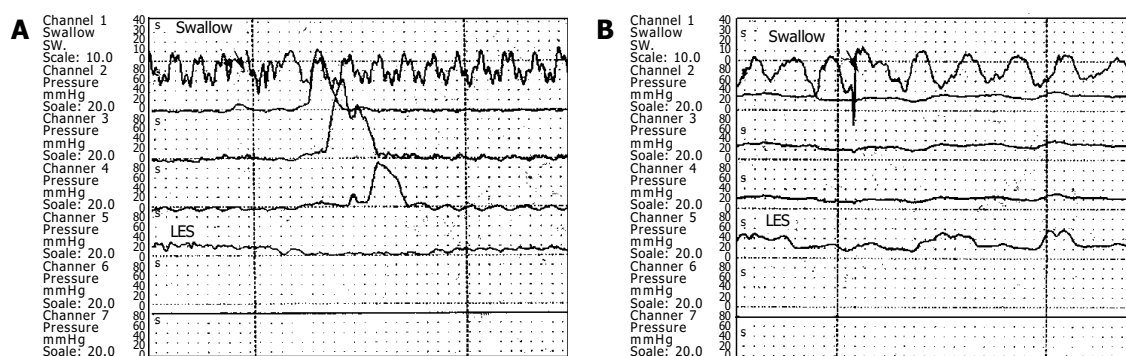


Figure 1 Manometric samples from a normal individual (A) and a patient with achalasia (B). Figure A illustrates the normal peristaltic activity forwarding at cranio-caudal direction whereas figure B shows typical manometric findings of achalasia. Note the aperistalsis, weak and simultaneous contractions (mirror sign), and incomplete LES relaxation after swallow. Basal LES pressure is high (40 mmHg).

The severity of chest pain in patients was scored after the balloon dilation on a scale of 0-10 (0, absence of pain; 10 severest pain). Gastrografin swallow was done few hours after dilation to exclude esophageal perforation. After an observation period of 6 h, patients were discharged and permitted to eat the next morning.

Second esophageal manometry and symptom scoring were performed in all patients with therapeutic response six weeks after pneumatic dilation to evaluate the efficacy of endoscopic balloon dilation.

The response to balloon dilation was considered excellent if there was no or very rare mild dysphagia, good if there was intermittent mild dysphagia, or poor if there was persistent daily mealtime dysphagia. The balloon therapy was considered successful if the patients had a good or excellent response.

Statistical analysis

Results were expressed as either percentages or mean±SD. Statistical analysis was performed using Chi-square test, Kendall's tau-b coefficient and Mann-Whitney U test as appropriate. $P < 0.05$ was considered statistically significant. The cumulative remission rates of the patients treated with balloon dilation were estimated by the Kaplan-Meier method and the difference between treatment groups was tested by the log rank test.

RESULTS

The clinical characteristics and demographic data of patients are shown in Table 1. The mean LES pressure was 37.6 ± 12 mmHg. Relaxation failure of LES and aperistalsis with low amplitude simultaneous uniform waves were present in all patients. Only one of the 5 patients with retrosternal pain was diagnosed as a vigorous achalasia (2.3%) at esophageal manometry. The LES pressures and symptom scores of successfully dilated patients were decreased significantly one month after dilation, (37.6 ± 12 vs 9.5 ± 3) and (2.9 ± 0.6 vs 0.8 ± 0.6) respectively ($P < 0.01$) (Figure 3). There was no significant correlation between the parameters of age, sex, initial LES pressure, symptom score and barium study findings.

Chest pain was reported by all patients during the initial dilation, with a mean pain score of 7.2 ± 2.3 (range, 4-10). Chest pain score was 8.1 ± 1.8 in patients who were successfully dilated at the first session although score was 4.8 ± 2.1 in patients with a poor response to initial balloon dilation ($P < 0.05$). Chest pain after the procedure usually lasted for 30-60 min and was substernal in nature, diminishing gradually over time and resolved completely within 2 to 6 h.

The results of balloon dilation are summarized in Table 2. A total of 65 dilations were performed in 43 patients for an average of 1.7 dilations per patient. The 3 cm balloon was always used first. Twenty-four patients (56%) were successfully dilated

with a 3 cm balloon only. Fourteen patients had an excellent response (32.5%) and 10 patients had a good response (23%) to 3.0 cm balloon dilation. Old age at the time of initial pneumatic dilation was significantly associated with a better clinical response to treatment as assessed by the need for subsequent treatments (Kendall's tau-b = 0.414, $P = 0.016$) (Table 3).

Table 2 Results of rigiflex balloon dilation under endoscopic control

Inflation pressure (psi)	15
Dilation time per session (s)	2×60
Success with 3.0 cm balloon	24/42(56%)
Success with 3.5 cm balloon	14/18(78%)
Overall success rate at first year ¹	19/24(80%)
Overall success rate at 5 years ¹	7/13(54%)
Complications	
Perforation	1(2.3%)
Bleeding	-
Mortality	-

¹Among the patients whose long term follow up information was available.

Table 3 Effect of age, LES pressure and esophageal diameter on the clinical benefit of the initial pneumatic dilation. ¹With 3 cm balloon

	Patients with successful initial pneumatic dilation (n = 24)	Patients with successful initial pneumatic dilation (%)	P
Age (yr)			
<35	4/14	28	<0.01
35-55	11/17	65	
>55	9/11	82	
LES pressure (mmHg)			
<30	6/12	50	NS
30-45	13/21	62	
>45	5/9	55	
Esophageal diameter (cm)			
<3	4/7	57	NS
3-4	11/21	52	
>4	9/14	64	

NS: Non significant.

Eighteen patients (42%) with a poor response to 3.0 cm balloon were dilated with a 3.5 cm balloon at intervals of 6-8 wk. Nine patients had excellent, five had good and four patients had poor response to the second dilation with a 3.5 cm balloon.

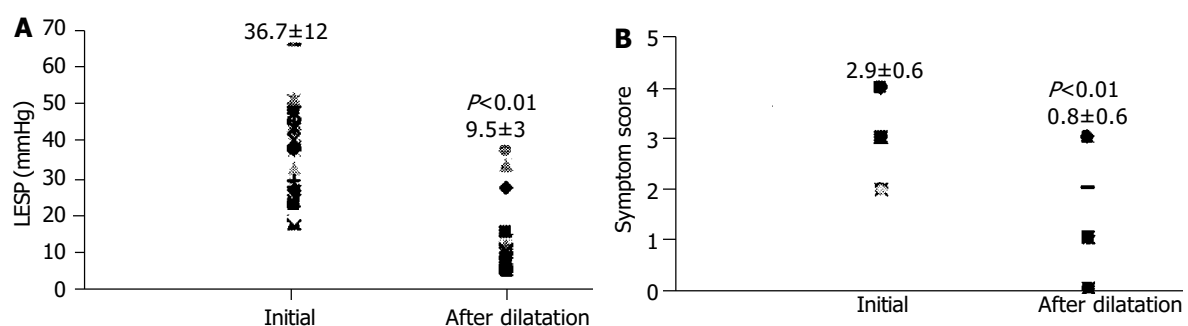


Figure 3 Lower esophageal sphincter pressures (LESP) (A) and symptom scores (B) of patients with therapeutic response initially and at one month after pneumatic dilatation.

Patients with a poor response to the second dilation with a 3.5 cm balloon were dilated with a 3.5 cm balloon at the third time but all of them were symptomatic after a while and these patients were no longer treated with a larger balloon (4 cm), instead, surgical treatment was suggested. One patient who refused surgery had repeated dilation every 6 to 12 mo with a 3.5 cm balloon due to symptom recurrence.

The mean follow-up period in the entire group was 2.4 years (range, 6 mo -5 years). Among the 38 patients whose long term follow up information was available, 33 (87%) at six months were asymptomatic [Among them 23 (70%) required once and 10 (30%) required twice dilation]. At the end of the first year, 16 of 24 patients (66%) whose follow up information was available were asymptomatic. Among the 24 patients, 3 (12.5%) complained of mild intermittent dysphagia and 5 (21%) had intermittent severe dysphagia. The total number of asymptomatic patients and patients with mild dysphagia was 19 (79%) at the end of the first year. Among these, 10 patients (52%) required a second dilation.

Among patients whose follow up information was available at 3 years the 19, 13 were in remission (68%) (5 asymptomatic and 8 with intermittent mild dysphagia). Among patients whose follow up information was available at 5 years the 13, 7 were in remission (54%) (3 were asymptomatic and 4 with mild intermittent dysphagia). Among the total, 3 patients (44%) required once and 4 (56%) required twice dilation (Figure 4). Figure 5 shows the Kaplan-Meier plot for the two treatment groups of patients who were dilated once or twice. The cumulative one, three and five year remission rates were higher in patients dilated twice but this difference was not statistically significant (Log rank $\chi^2 = 2.10, P = 0.1471$).

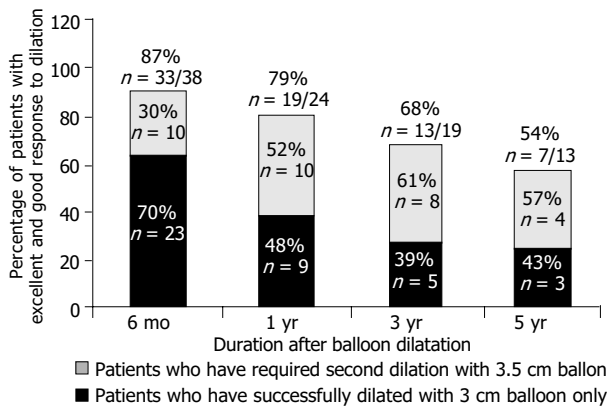


Figure 4 Percentage of patients with excellent and good response to dilatation at 6 mo, 1, 3 and 5 years.

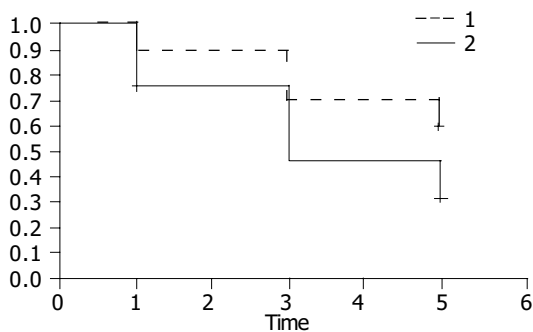


Figure 5 Kaplan-Meier plot for the two treatment groups of patients who were dilated once² or twice¹. The cumulative one, three and five year remission rates were higher in patients dilated twice but this difference was not statistically significant (Log rank $\chi^2 = 2.10, P = 0.1471$).

Gastrograffin swallow done immediately after balloon dilation revealed esophageal perforation in one patient (2.3%) (a 60 years old female) with persistent chest pain and surgical therapy was required. There were no other immediate complications. Reflux esophagitis as a late complication was observed in two of the patients who had a good response to dilatation during the follow up period (4%).

Blood on the balloon after dilatation was a common finding. There was no statistically significant correlation between bloody dilator and dilatation success ($P > 0.05$).

DISCUSSION

This study analysed the effectiveness of pneumatic balloon dilation and the clinical outcome in patients with achalasia. Our results showed that once or twice pneumatic dilatation provided good results in the majority of patients with achalasia and long term results were 79% at 1 year and 54% at 5 years. Of the patients studied, 38 (88%) were relieved of their symptoms after one or two sessions. An initial pneumatic dilation was an effective single treatment with no further treatment needed in 57% of patients in a short term period. The remaining 43% of patients treated initially with pneumatic dilation needed additional treatments due to persistent or recurrent symptoms and only 11% of patients failing pneumatic dilatation were referred for surgery (4 with poor response to repeated dilations and 1 with perforation due to dilation). Four patients with a poor response to the second dilation with a 3.5 cm balloon were dilated with a 3.5 cm balloon the third time but all of them were symptomatic after a while and these patients were not treated with a larger balloon. Some studies have reported using a 3.5 cm balloon instead of a 3 cm balloons one as the initial balloon but others have used 3 cm for the initial dilatation^[8,9,11]. In our series application of the second pneumatic dilation increased the long term clinical benefit of pneumatic dilation from 30% at six months to 57% at 5 years, but this difference was not statistically significant ($P > 0.05$) (Figure 4). To some extent, our results about the clinical benefit of a single pneumatic dilatation and the use of the second dilatation for patients with persistent symptoms are in agreement with other studies. It has been shown that the overall efficacy of endoscopic balloon dilation was approximately 85%, with an excellent to good response for 3, 3.5 and 4 cm dilators being 70%, 87% and 93% respectively (9 studies; four prospective, five retrospective, 261 patients, a mean follow up of 1.9 years (range; 0.3 to 6 years)^[10-17] (Table 4). Approximately 50% (range, 17% to 75%) of all patients required repeat dilations, equaling to 1.2 to 2 dilations per patient. About one half of patients responded to a repeat dilation, with the remainder either proceeding to surgical management or deciding to live with their persistent symptoms. The reported overall long-term efficacy of pneumatic dilatation was 50-90% at 1 year and 60% at 5 years^[1]. The major adverse event with pneumatic dilatation was esophageal perforation with a 2% cumulative rate. The American Society for Gastrointestinal Endoscopy has recommended that if a single dilation session (size of the balloon dilator unspecified) does not produce satisfactory relief, a second attempt may be warranted and if this fails, surgery usually is indicated^[15].

The patient population undergoing initial dilation in this study was not large enough to compare the effect of age on the dilation success, but our results indicate that initial pneumatic dilation was more effective in older patients (χ^2 value: 8.215^a, $P = 0.016$, Kendall's tau-b 0.414, $P = 0.001$). This increased clinical benefit of pneumatic dilation in old patients has also been described by other investigators^[19,21,22]. There was no significant difference between the mean ages of the patients with and without remission at the end of 1 and 5 years although

Table 4 Cumulative effectiveness of graded pneumatic dilators for achalasia

Author	Pt. #	Study design	Dilator % (size/cm)	Decrease of LESP	% Improvement Excellent/Good	Follow-up (yr) Mean (range)	Perforation (%)
Barkin ⁽¹¹⁾	50	Prospec.	3.5	-	90	1.3 (1-3.4)	0
Levine ⁽¹²⁾	62	Retrospec.	3-3.5	-	85-88	-	0
Wehrmann ⁽¹⁵⁾	40	Retrospec.	3-3.5	42	89	2-5	2.5
Lee ⁽⁹⁾	28	Prospec.	3-3.5-4	-	-	-	7
Gelfand ⁽¹⁰⁾	24	Prospec.	3-4	60-68	70-93	-	0
Kadakia ⁽¹³⁾	29	Prospec.	3-3.5-4	67	62-79-93	4 (3-6)	0
Abid ⁽¹⁴⁾	36	Retrospec.	3.5-4	-	88-89	2.3 (1-4)	6.6
Lambroza ⁽¹⁶⁾	27	Retrospec.	3	-	67	1.8 (0.1-4.8)	0
Bhatnagar ⁽¹⁷⁾	15	Prospec.	3-3.5	-	73-93	1.2 (0.3-3)	0

the patients in remission at 5 years were older, [43±16 ($n = 19$) vs 48±16 ($n = 5$) ($P > 0.05$) at 1 year and 53±17 ($n = 7$) vs 37±14 ($n = 6$) ($P > 0.05$), at 5 years respectively]. The efficacy of pneumatic dilatation was not influenced by initial LES pressure and esophageal diameter (Table 3).

After balloon dilation, the mean LES pressure was 11.8±4 mmHg (range, 0-16 mmHg) and it represented 75% decrease of basal LES pressure. It has been shown that basal LES pressure decreased from 39% to 68% after dilation but these changes did not allways indicate a dilation success. In general, a decrement in LES pressure of more than 50% or an absolute end-expiratory LES pressure of less than 10 mmHg were more indicative of clinical success^[2]. Timed barium esophagogram or scintigraphy may correlate with symptomatic improvement in up to 72% of patients. In spite of this similarity, approximately one third of patients who noted complete relief showed less than 50% improvement in barium column height and esophageal diameter^[21].

Only one of 43 patients in our series had an esophageal perforation during treatment with pneumatic dilatation (2.3%). This complication rate is similar to those reported by other experienced groups^[9,19,20]. Gradual increase in dilator size based on symptomatic response and the use of inflation pressure between 10 to 15 psi can minimize the risk of perforation. Esophageal perforation may occur in up to 5% of all reported cases, with a possible increased risk if hiatal hernia is present. In our study gastrograffin swallow was performed in all patients. Using immediate contrast studies to exclude perforation became routine in the late 1970's, and using this approach has been recommended in several studies and text books. Some authors suggested that contrast studies were indicated only when there was clinical suspicion of perforation. It has been reported that an immediate contrast study may not always exclude a perforation which may become clinically evident several hours later^[5].

Less commonly, intramural hematoma, diverticula at gastric cardia, mucosal tears, reflux esophagitis, prolonged post-procedure chest pain, fever, hematemesis without changes in hematocrit and angina may occur after pneumatic dilatation. Objective assessment of gastroesophageal reflux after pneumatic dilation rarely has been studied. Abnormal 24 h pH scores have been documented in approximately 20% to 33% of patients after dilation. In spite of these abnormal scores, very few of these patients were symptomatic or developed endoscopic or clinical evidence of GERD related complications. It has been shown that postdilatation LES pressures and gastric emptying were similar between reflux and non-reflux groups^[2]. Since GERD related symptoms correlated poorly in achalasia patients, 24 h pH monitoring has been recommended for patients that developed frequent heartburn, reflux or chest pain in spite of an otherwise good clinical response to dilation. One of the important points of this study was the dilatation technique which did not require fluoroscopic control (see materials and methods). Our experience

shows that Rigiflex balloon can be successfully positioned across the gastroesophageal junction and inflated under direct endoscopic observation. This technique is as effective as conventional fluoroscopic technique and has an advantage to prevent patients and endoscopists from an additional X-ray. Furthermore we have seen that patient tolerability was very good and success rates were reasonable and comparable with others. Safety and efficacy of pneumatic dilation for achalasia without fluoroscopic control also have been shown by Lambroza and Levine^[16,18].

In a recently published interesting study, Cheng *et al.* evaluated the usefulness of temporarily placing of covered stents for 3-7 d versus pneumatic dilatation and found that the early and late (at one and three years respectively) relapse rates were quite low in the stent treated group versus the pneumatic dilatation treated one^[23]. The success of this method was suggested to be due to chronic tearing of the cardia muscularis which resulted in a diminished amount of fibrosis and so restenosis after the stent was withdrawn.

The results of our study suggest that pneumatic dilatation for achalasia without fluoroscopic guidance is a safe and effective treatment modality. A gradual increase in dilator size based on symptomatic response minimizes complications. Symptomatic patients with achalasia who are good surgical candidates should be given an option of graded pneumatic dilatation before surgery. Although surgical myotomy, once with a high mortality and long hospital stay, can now be performed laparoscopically with a similar efficacy to the open surgical approach, reduced morbidity and hospitalization time, referral of myotomy should be considered for patients who do not respond to medical therapy or individuals that do not desire pneumatic dilatations. The advantages of pneumatic dilatation over surgical myotomy are a brief period of discomfort, a very short hospital stay and consequently low exposure.

REFERENCES

- 1 Clouse RE, Diamant NE. Esophageal motor and sensory function and motor disorders of the esophagus. In: Sleisenger MH, Friedman LS, Feldman M. Eds: *Gastrointestinal and Liver Disease. Philadelphia Saunders* 2002: 561-598
- 2 Dunaway PM, Wong RK. Achalasia. *Curr Treat Opt Gastroenterol* 2001; **4**: 89-100
- 3 Howard PJ, Maher L, Pryde A, Cameron EW, Heading RC. Five year prospective study of the incidence, clinical features and diagnosis of achalasia in Edinburgh. *Gut* 1992; **33**: 1011-1015
- 4 Csendes A, Braghetto I, Henriquez A, Cortes C. Late results of a prospective randomised study comparing forceful dilatation and oesophagomyotomy in patients with achalasia. *Gut* 1989; **30**: 299-304
- 5 Ciarolla DA, Traube M. Achalasia. Short-term clinical monitoring after pneumatic dilation. *Dig Dis Sci* 1993; **38**: 1905-1908
- 6 Prakash C, Clouse RE. Esophageal motor disorders. *Curr Op Gastroenterol* 1999; **15**: 339-346
- 7 Nair LA, Reynolds JC, Parkman HP, Ouyang A, Strom BL,

- Rosato I, Cohen S. Complications during pneumatic dilation for achalasia or diffuse esophageal spasm. Analysis of risk factors, early clinical characteristics, and outcome. *Dig Dis Sci* 1993; **38**: 1893-1904
- 8 **Stark GA**, Castell DO, Richter JE, Wu WC. Prospective randomized comparison of Brown-McHardy and microvasive balloon dilators in treatment of achalasia. *Am J Gastroenterol* 1990; **85**: 1322-1326
- 9 **Richter JE**, Lightdale CJ. Management of achalasia. AGA Postgraduate Course, May 19-20. 2001: 303-308
- 10 **Gelfand MD**, Kozarek RA. An experience with polyethylene balloons for pneumatic dilation in achalasia. *Am J Gastroenterol* 1989; **84**: 924-927
- 11 **Barkin JS**, Guelrud M, Reiner DK, Goldberg RI, Phillips RS. Forceful balloon dilation: an outpatient procedure for achalasia. *Gastrointest Endosc* 1990; **36**: 123-126
- 12 **Levine ML**, Moskowitz GW, Dorf BS, Bank S. Pneumatic dilation in patients with achalasia with a modified Gruntzing dilator (Levine) under direct endoscopic control: results after 5 years. *Am J Gastroenterol* 1991; **86**: 1581-1584
- 13 **Kadakia SC**, Wong RK. Graded pneumatic dilation using Rigiflex achalasia dilators in patients with primary esophageal achalasia. *Am J Gastroenterol* 1993; **88**: 34-38
- 14 **Abid S**, Champion G, Richter JE, McElvein R, Slaughter RL, Koehler RE. Treatment of achalasia: the best of both worlds. *Am J Gastroenterol* 1994; **89**: 979-985
- 15 **Wehrmann T**, Jacobi V, Jung M, Lembcke B, Caspary WF. Pneumatic dilation in achalasia with a low-compliance balloon: results of a 5-year prospective evaluation. *Gastrointest Endosc* 1995; **42**: 31-36
- 16 **Lambroza A**, Schuman RW. Pneumatic dilation for achalasia without fluoroscopic guidance: safety and efficacy. *Am J Gastroenterol* 1995; **90**: 1226-1229
- 17 **Bhatnagar MS**, Nanivadekar SA, Sawant P, Rathi PM. Achalasia cardia dilatation using polyethylene balloon (rigiflex) dilators. *Indian J Gastroenterol* 1996; **15**: 49-51
- 18 **Levine ML**, Dorf BS, Moskowitz G, Bank S. Pneumatic dilatation in achalasia under endoscopic guidance: correlation pre- and postdilatation by radionuclide scintiscan. *Am J Gastroenterol* 1987; **82**: 311-314
- 19 **Parkman HP**, Reynolds JC, Ouyang A, Rosato EF, Eisenberg JM, Cohen S. Pneumatic dilatation or esophagomyotomy treatment for idiopathic achalasia: clinical outcomes and cost analysis. *Dig Dis Sci* 1993; **38**: 75-85
- 20 **Robertson CS**, Fellows IW, Mayberry JF, Atkinson M. Choice of therapy for achalasia in relation to age. *Digestion* 1988; **40**: 244-250
- 21 **Vaezi MF**, Richter JE, Wilcox CM, Schroeder PL, Birgisson S, Slaug RL, Koehler RE, Baker ME. Botulinum toxin versus pneumatic dilatation in the treatment of achalasia: a randomised trial. *Gut* 1999; **44**: 231-239
- 22 **Fellows IW**, Ogilvie AL, Atkinson M. Pneumatic dilatation in achalasia. *Gut* 1983; **24**: 1020-1023
- 23 **Cheng YS**, Li MH, Chen WX, Chen NW, Zhuang QX, Shang KZ. Selection and evaluation of three interventional procedures for achalasia based on long-term follow-up. *World J Gastroenterol* 2003; **9**: 2370-2373

Edited by Zhu LH and Wang XL Proofread by Xu FM

• CLINICAL RESEARCH •

Seasonal variation in the onset of acute pancreatitis

Massimo Gallerani, Benedetta Boari, Raffaella Salmi, Roberto Manfredini

Massimo Gallerani, Benedetta Boari, Roberto Manfredini, Section of Internal Medicine, Department of Clinical and Experimental Medicine, University of Ferrara, via Savonarola 9, I-44100 Ferrara, Italy

Raffaella Salmi, Department of Internal Medicine, St Anna Hospital, corso Giovecca 203, I-44100 Ferrara, Italy

Supported by a Research Grant "ex-60%" From the University of Ferrara
Correspondence to: Roberto Manfredini, Section of Internal Medicine, Department of Clinical and Experimental Medicine, University of Ferrara, via Savonarola 9, I-44100 Ferrara, Italy. mfr@unife.it

Telephone: +39-532-236817 **Fax:** +39-532-210884

Received: 2003-11-12 **Accepted:** 2004-02-24

Abstract

AIM: A circannual variation in the onset of several acute diseases, mostly dealing with cardiovascular system, has been reported. The present study was to verify the possible existence of a seasonal variability in the onset of acute pancreatitis.

METHODS: All patients consecutively admitted to the Hospital of Ferrara, Italy, between January 1998 to December 2002, whose discharge diagnosis was acute pancreatitis, were considered. According to the time of admission, cases were categorized into twelve 1-mo intervals and in four periods by season. χ^2 test for goodness of fit and partial Fourier series were used for statistical analysis.

RESULTS: During the study period, 549 cases of acute pancreatitis were observed. A significant peak of higher incidence was found in March-May, both for total population, males and subgroups with and without cholelithiasis or alcoholism. Fourier analysis showed the existence of a circannual rhythmic pattern with its main peak in March (95% C.L.: February-April, $P = 0.005$), and a secondary one in September. Death occurred more frequently in December-February, compared to the other periods ($P = 0.029$), and chronobiologic analysis yielded a seasonal peak in November-December ($P < 0.001$).

CONCLUSION: This study shows the existence of a circannual variation in the onset of acute pancreatitis, with a significantly higher frequency of events in the spring, especially for patients with cholelithiasis or alcoholism. Moreover, events occurring during the colder months seem to be characterized by a higher mortality rate.

Gallerani M, Boari B, Salmi R, Manfredini R. Seasonal variation in the onset of acute pancreatitis. *World J Gastroenterol* 2004; 10(22): 3328-3331

<http://www.wjgnet.com/1007-9327/10/3328.asp>

INTRODUCTION

Many studies have shown a circannual variation in the onset of several diseases mostly dealing with cardiovascular system, characterized by an abrupt onset, e.g., fatal pulmonary embolism^[1,2], ischemic and hemorrhagic stroke^[3,4] and rupture of aortic aneurysms^[5,6]. Seasonal specific patterns have also been reported

for a series of miscellaneous diseases characterized by an acute onset, treated by the Emergency Department, including paralysis of cranial nerves^[7], microcrystalline arthritis^[8], herpes zoster infection^[9], epistaxis^[10], urinary retention^[11]. In the last few years several studies have investigated gastroenterologic diseases, and seasonal etiological patterns have been reported for the onset of peptic ulcer^[12-15] and exacerbation of inflammatory bowel diseases^[16-18]. The aim of the present study was to determine by means of a validated chronobiological analysis, whether acute pancreatitis, a common but potentially harmful entity, might show a rhythmic seasonal variation as well.

MATERIALS AND METHODS

All cases of acute pancreatitis (International Classification of Diseases, 9th Revision, Clinical Modification, ICD9-CM code: 577.0-8) consecutively observed from 1 January 1998 to 31 December 2002 at the St. Anna Hospital of Ferrara, Italy, were considered for the study. Ferrara is a small town in northern Italy particularly well suited for epidemiological studies. It has a stable population of approximately 150 000 inhabitants, almost exclusively white. The only available hospital in this community is St Anna Hospital, which also serves as the sole teaching center for the School of Medicine. The day and month of each event were categorized both into four 3-mo periods (according to seasons) and into twelve 1-mo intervals. Diagnosis was always made on the basis of clinical features, physical examination, laboratory data (serum amylase, isoamylase, lipase, and urinary amylase), and instrumental examinations, when necessary. For all subjects with acute pancreatitis the presence or absence of the two leading specific risk factors (alcoholism and biliary tract disease), was carefully investigated.

For statistical analysis, two different methods were used: χ^2 test for goodness of fit and partial Fourier series. To investigate possible differences in frequency peaks, χ^2 test for goodness of fit was applied to the total sample population and subgroups by gender, comparing observed against expected events during the four intervals season^[19]. On the other hand, to verify the possible existence of a reproducible rhythmic pattern, cosinor analysis and partial Fourier series were applied to the time series, using specific commercially available software written for the Apple Macintosh computer^[20]. The program allows, among all the possible combinations of the periods chosen by the user, the selection of the harmonic or the combination of harmonics that best explain the variance of data. The percentage of rhythms (PR: percentage of overall variability of data about the arithmetic mean attributable to the fitted rhythmic function) and the probability value resulting from the F statistic used to test the hypothesis of zero amplitude, were chosen to be reported in the results as representative parameters of goodness of fit and statistical significance of each fitted function, respectively. The program was used to calculate the midline estimating statistic of rhythm (MESOR: the rhythm-adjusted mean over the time period analyzed) and the amplitude (half the distance between the absolute maximum and minimum of the function) of the best-fitting-curve. The program was also used to calculate peak (ortophase) and trough (bathypase) times of the fitted curves (times of occurrence of the absolute maximum and minimum) and the acrophase of each single harmonic change, together with the 95% confidence limits (CL). Significance

levels were always assumed for $P < 0.05$. Conventional statistical analysis was performed using Student's *t* test for unpaired data. Significance levels were always set at $P < 0.05$.

RESULTS

From January 1998 to December 2002, 549 consecutive cases of

acute pancreatitis were observed, 285 cases were males (51.9%) and 264 were females (48.1%), their mean age was 65 ± 17 years (difference between sexes $t = 2.7$, $P = 0.007$). Two hundred and eighty-six had cholelithiasis (52.1%) and 48 had chronic alcoholism (8.7%).

Deaths from acute pancreatitis were 18 (14 males and 5 females), accounting for 3.2%. Their mean age was 56 ± 16 years,

Table 1 Monthly distribution of acute pancreatitis by gender and risk factors

Month	Total (<i>n</i> = 549)	Males (<i>n</i> = 285)	Females (<i>n</i> = 264)	Biliary tract disease (<i>n</i> = 286, 52.1%)	No bil. tract disease (<i>n</i> = 263, 48.9%)	Alcoholism (<i>n</i> = 48, 8.7%)	Fatal cases (<i>n</i> = 18, 3.2%)
January	34	18	16	17	17	1	3
February	46	19	27	22	24	2	2
March	62	35	27	28	34	8	1
April	61	33	28	31	30	7	0
May	56	32	24	35	21	5	0
June	44	23	21	19	25	3	0
July	40	20	20	23	17	2	1
August	45	25	20	30	15	4	1
September	39	20	19	22	17	4	1
October	40	20	20	19	21	2	2
November	46	25	21	22	24	6	3
December	36	15	21	17	19	3	4

Table 2 Seasonal distribution of acute pancreatitis (χ^2 test for goodness of fit)

	<i>n</i> (%)	December-February <i>n</i> (%)	March-May <i>n</i> (%)	June-August <i>n</i> (%)	September-November <i>n</i> (%)	χ^2	<i>P</i>
Total	549	116 (21.1)	179 (32.6)	129 (23.5)	125 (22.8)	17.5	0.001
Males	285 (51.9)	52 (18.2)	100 (35.1)	68 (23.9)	65 (22.8)	17.05	0.001
Females	264 (48.1)	64 (24.2)	79 (29.9)	61 (23.1)	60 (22.7)	3.55	0.316
Biliary tract disease	286 (52.1)	56 (19.5)	94 (32.8)	73 (25.4)	64 (22.3)	11.02	0.011
No bil. tract disease	263 (47.9)	60 (22.9)	85 (32.4)	56 (21.4)	61 (23.3)	7.93	0.049
Chronic alcoholism	48 (8.7)	6 (12.5)	20 (41.7)	10 (20.8)	12 (25)	8.67	0.035
Fatal cases	18 (3.2)	9 (50)	1 (5.6)	2 (11.1)	6 (33.3)	9.11	0.029

Table 3 Seasonal variation of acute pancreatitis (chronobiologic parameters by Fourier analysis)

	<i>n</i>	Period (h)	PR (%)	MESOR	Amplitude	Peak	95% CL	<i>P</i>
Total	549	8766	51.1			March	February-April	0.006
		4383	33.7			September	August-October	0.017
		Overall	84.8	45.68	3.28	March	February-April	0.005
Males	285	8766	42.6			March	February-April	0.030
		4383	32.7			September	NS	0.052
		Overall	75.4	23.71	9.06	March	February-April	0.027
Females	264	8766	50.9			March	February-April	0.024
		4383	22.3			September	NS	0.121
		Overall	73.3	21.97	4.52	March	February-April	0.035
Biliary tract disease	286	8766	42.2			March	NS	0.074
		4383	19.5			August	NS	0.234
		Overall	61.8	23.72	7.60	March	NS	0.108
No bil. tract disease	263	8766	44.8			March	February-April	0.041
		4383	25.1			October	NS	0.119
		Overall	69.9	21.96	7.66	March	NS	0.052
Chronic alcoholism	48	8766	13.2			March	NS	0.415
		4383	40.7			September	NS	0.109
		Overall	53.9	3.91	2.51	March	NS	0.192
Fatal cases	18	8766	86.2			November	November-December	<0.001
		4383	10.9			June	May-July	0.004
		Overall	97.1	1.50	1.90	November	November-December	<0.001

PR = percentage of rhythm (percentage of overall variability of data about arithmetic mean attributable to the rhythmic fitted function MESOR = midline estimated statistics of rhythm, the rhythm-adjusted mean over the time period analysed amplitude: half the distance between the absolute maximum and minimum of the function of the best-fitting curve 95% CL = 95% confidence limits NS = not significant, (when acrophase did not reach the significance level, 95% CL could not be given).

significantly lower than that of survived subjects (65 ± 17 years, $t = 2.20$, $P = 0.028$). Among the subgroups of fatal events, 3 had gallstones (16.6%, $\chi^2 = 1.91$, $P = 0.178$), and 4 had chronic alcoholism (22.2%, $\chi^2 = 3.78$, $P = 0.075$). Table 1 shows the monthly distribution by gender, and subgroups by risk factors. A peak of higher frequency of events was found in the period March-May for the total samples and in particular for males and subgroups of subjects with and without gallstones and chronic alcoholism (Table 2). The percentage of fatal events was significantly higher in December-February ($n = 9$, 17.3% of acute pancreatitis observed in that period, 50% of total deaths, $\chi^2 = 9.11$, $P = 0.029$, compared to the other periods).

Chronobiologic analysis (Table 3) showed the existence of a circannual rhythmic variation characterized by a main peak in March (PR 84.8, 95% CL: February-April, $P = 0.005$), and a secondary peak in September. This pattern was confirmed also for subgroups by gender (men: PR 75.4, 95% CL: February-April, $P = 0.027$), and (women: PR 73.3, 95% CL: February-April, $P = 0.035$). Moreover, a highly significant peak was noticed for fatal cases in late November (PR 97.1, 95% CL: October-December, $P < 0.001$). NO statistically significant trend for a peak in March was found for subgroups of subjects with or without cholelithiasis (respectively: PR 61.8, 95% CL: February-April, $P = 0.109$; and PR 69.9, 95% CL: February-April, $P = 0.052$).

DISCUSSION

Identification of patients with acute pancreatitis is important due to the increased risk of death.

To our knowledge, there was only one recent study in medical literature, which aimed to evaluate the seasonal variation in the onset of acute pancreatitis^[20]. In a total of 263 cases observed for a period of 9 years in a German hospital, no correlation between admissions and a specific month or season was found, other earlier reports were mostly hypotheses^[21,22]. Our study instead showed a clear seasonal variation in the onset of acute pancreatitis characterized by a higher frequency in the spring, with a maximum in March-May. This pattern was particularly evident for patients with cholelithiasis and chronic alcoholism. It is difficult to give an exhaustive explanation for such a temporal pattern. Seasonal and circannual patterns have been reported for the prevalence of *Helicobacter pylori* infection^[14], or for relapses of inflammatory bowel disease for hospital admissions^[15,23].

As for circadian aspects, some acute dramatic clinical events, e.g., variceal and gastrointestinal bleeding^[24-26] showed obvious circadian patterns. Daily variations of some biologic functions have also been found as possible co-factors in several gastrointestinal diseases, e.g., fibrinolysis in liver cirrhosis and esophageal varices^[27], electrical uncoupling and ectopic pacemaker activity in intestinal motor dysfunction^[28], melatonin and duodenal ulcer^[29,30], colonic motility in diverticular disease^[31] and rectal motor activity in constipation^[32].

At present we do not know enough about seasonal biological changes potentially affecting onset of acute pancreatitis, e.g., secretion of pancreatic enzymes, biliary acids. However, it is possible that variations in physiological functions with seasonal change may be associated with an increased risk of pancreatitis. Oxygen free radicals, for example, were known to be a meaningful index for the severity of pancreatitis^[33], but possible variations in free radical generation have not been investigated yet. Our results seemed to be able to identify a higher mortality for colder months (November-December). This is particularly interesting when considering that both the mean age of subjects and the incidence of risk factors (gallstones, alcoholism) in the subgroup of fatal cases were significantly lower compared with those in the subgroup of non fatal events. Thus, it seems that acute events of pancreatitis occurring in the colder months

may be more at risk in terms of severity and mortality. Further studies conducted on larger samples and addressed to other countries of different latitudes would be needed.

ACKNOWLEDGEMENTS

The authors thank Mr. Franco Guerzoni, from the Statistical Service of Ferrara St Anna Hospital, for his helpful assistance in collection of cases and analysis of data.

REFERENCES

- 1 **Gallerani M**, Manfredini R, Ricci L, Grandi E, Cappato R, Calo G, Pareschi PL, Fersini C. Sudden death from pulmonary thromboembolism: chronobiological aspects. *Eur Heart J* 1992; **13**: 661-665
- 2 **Manfredini R**, Gallerani M, Salmi R, Zamboni P, Fersini C. Fatal pulmonary embolism in hospitalized patient: evidence for a winter peak. *J Int Med Res* 1994; **22**: 85-89
- 3 **Gallerani M**, Trappella G, Manfredini R, Pasin M, Napolitano M, Migliore A. Acute intracerebral haemorrhage: circadian and circannual patterns of onset. *Acta Neurol Scand* 1994; **89**: 280-286
- 4 **Gallerani M**, Portaluppi F, Maida G, Chierigato A, Calzolari F, Trappella G, Manfredini R. Circadian and circannual rhythmicity in the occurrence of subarachnoid hemorrhage. *Stroke* 1996; **27**: 1793-1797
- 5 **Manfredini R**, Portaluppi F, Salmi R, Zamboni P, la Cecilia O, Kuwornu Afi H, Regoli F, Bigoni M, Gallerani M. Seasonal variation in the occurrence of nontraumatic rupture of thoracic aorta. *Am J Emerg Med* 1999; **17**: 672-674
- 6 **Mehta HR**, Manfredini R, Hassan F, Sechtem U, Bossone E, Oh JK, Cooper JV, Smith DE, Portaluppi F, Penn M, Hutchison S, Nienaber CA, Isselbacher EM, Eagle KA. Chronobiological patterns of acute aortic dissection. *Circulation* 2002; **106**: 1110-1115
- 7 **Gallerani M**, Delli Gatti C, Salmi R, Kuwornu Afi H, la Cecilia O, Manfredini R. Seasonal variations in the incidence of cranial nerve paralysis. *J Int Med Res* 1999; **27**: 130-133
- 8 **Gallerani M**, Govoni M, Mucinelli M, Bigoni M, Trotta F, Manfredini R. Seasonal variation in the onset of acute microcrystalline arthritis. *Rheumatology* 1999; **38**: 1003-1006
- 9 **Gallerani M**, Manfredini R. Seasonal variation in herpes zoster infection. *Br J Dermatol* 2000; **142**: 588-589
- 10 **Manfredini R**, Gallerani M, Portaluppi F. Seasonal variation in the occurrence of epistaxis. *Am J Med* 2000; **108**: 759-760
- 11 **Braverman DZ**, Morali GA, Patz JK, Jacobsohn WZ. Is duodenal ulcer a seasonal disease? A retrospective endoscopic study of 3105 patients. *Am J Gastroenterol* 1992; **87**: 1591-1593
- 12 **Tivon K**, Cohen P. Seasonality in duodenal ulcer disease: possible relationship with circannually cycling neurons enclosed in the biological clock. *Am J Gastroenterol* 1995; **90**: 1189-1190
- 13 **Thomopoulos KC**, Katsakoulis EC, Margaritis VG, Mimidis KP, Vagianos CE, Nikolopoulou VN. Seasonality in the prevalence of acute upper gastrointestinal bleeding. *J Clin Gastroenterol* 1997; **25**: 576-579
- 14 **Raschka C**, Schorr W, Koch HJ. Is there seasonal periodicity in the prevalence of *Helicobacter pylori*? *Chronobiol Int* 1999; **16**: 811-819
- 15 **Sonnenberg A**, Jacobsen SJ, Wasserman IH. Periodicity of hospital admissions for inflammatory bowel disease. *Am J Gastroenterol* 1994; **89**: 847-851
- 16 **Moum B**, Aadland E, Ekbohm A, Vatn MH. Seasonal variations in the onset of ulcerative colitis. *Gut* 1996; **38**: 376-378
- 17 **Zeng L**, Anderson FH. Seasonal change in the exacerbations of Crohn's disease. *Scand J Gastroenterol* 1996; **31**: 79-82
- 18 **Ott L**, Memdenhall W, Larson R. Statistical test of hypotheses: the one sample case. In: Statistics. Boston, MA: Duxbury Press 1978: 242-246
- 19 **Mojon A**, Fernandez JR, Hermida RC. Chronolab: an interactive software package for chronobiologic time series analysis written for the Macintosh computer. *Chronobiol Int* 1992; **9**: 403-412
- 20 **Lankisch PG**, Assmus C, Pflichthofer D. The calendar and acute pancreatitis. *Pancreas* 1998; **16**: 465-467
- 21 **Poikolainen K**. Seasonality of alcohol-related hospital admis-

- sions has implications for prevention. *Drug Alcohol Depend* 1982; **10**: 65-69
- 22 **Reimann HA**. Letter: Three periodic diseases as causes of recurrent abdominal pain in childhood. *Arch Dis Child* 1976; **51**: 244
- 23 **Minoli G**, Imperiali G, Colombo E, De Franchis R, Mortara G, Prada A, Rocca F. Biphasic annual periodicity in relapses of inflammatory bowel diseases. Gruppo di studio per le malattie infiammatorie intestinale. *J Clin Gastroenterol* 1995; **21**: 27-29
- 24 **Manfredini R**, Gallerani M, Salmi R, Calo G, Pasin M, Bigoni M, Fersini C. Circadian variation in the time of onset of acute gastrointestinal bleeding. *J Emerg Med* 1994; **12**: 5-9
- 25 **Siringo S**, Bolondi L, Sofia S, Hermida RC, Gramantieri L, Gaiani S, Piscaglia F, Carbone C, Misitano B, Corinaldesi R. Circadian occurrence of variceal bleeding in patients with liver cirrhosis. *J Gastroenterol Hepatol* 1996; **11**: 1115-1120
- 26 **Mann NS**, Hillis A, Mann SK, Buerk CA, Prasad VM. In cirrhotic patients variceal bleeding is more frequent in the evening and correlates with severity of liver disease. *Hepatogastroenterology* 1999; **46**: 391-394
- 27 **Piscaglia F**, Siringo S, Hermida RC, Legnani C, Valgimigli M, Donati G, Palareti G, Gramantieri L, Gaiani S, Burroughs AK, Bolondi L. Diurnal changes of fibrinolysis in patients with liver cirrhosis and esophageal varices. *Hepatology* 2000; **31**: 349-357
- 28 **Der T**, Bercik P, Donnelly G, Jackson T, Berezin I, Collins SM, Huizinga JD. Interstitial cells of cajal and inflammation-induced motor dysfunction in the mouse small intestine. *Gastroenterology* 2000; **119**: 1590-1599
- 29 **Malinovskaya N**, Komarov FI, Rapoport SI, Voznesenskaya LA, Wetterberg L. Melatonin production in patients with duodenal ulcer. *Neuroendocrinol Lett* 2001; **22**: 109-117
- 30 **Kato K**, Murai I, Asai S, Takahashi Y, Nagata T, Komuro S, Mizuno S, Iwasaki A, Ishikawa K, Arakawa Y. Circadian rhythm of melatonin and prostaglandin in modulation of stress-induced gastric mucosal lesions in rats. *Aliment Pharmacol Ther* 2002; **16**(Suppl 2): 29-34
- 31 **Bassotti G**, Battaglia E, Spinuzzi F, Pelli MA, Tonini M. Twenty-four hour recordings of colonic motility in patients with diverticular disease: evidence for abnormal motility and propulsive activity. *Dis Colon Rectum* 2001; **44**: 1814-1820
- 32 **Rao SS**, Sadeghi P, Batterson K, Beaty J. Altered periodic rectal motor activity: a mechanism for slow transit constipation. *Neurogastroenterol Motil* 2001; **13**: 591-598
- 33 **Park BK**, Chung JB, Lee JH, Suh JH, Park SW, Song SY, Kim H, Kim KH, Kang JK. Role of oxygen free radicals in patients with acute pancreatitis. *World J Gastroenterol* 2003; **9**: 2266-2269

Edited by Wang XL Proofread by Xu FM

• CLINICAL RESEARCH •

Composite score of reflux symptoms in diagnosis of gastroesophageal reflux disease

Jin-Hai Wang, Jin-Yan Luo, Lei Dong, Jun Gong, Ai-Li Zuo

Jin-Hai Wang, Jin-Yan Luo, Lei Dong, Jun Gong, Ai-Li Zuo,
Department of Gastroenterology, Second Hospital of Xi'an Jiaotong University, Xi'an 710004, Shaanxi Province, China

Supported by Janssen Research Foundation of China (2001)

Correspondence to: Dr. Jin-Hai Wang, Department of Gastroenterology, Second Hospital of Xi'an Jiaotong University, 710004, Shaanxi Province, China. jinhaiwang@hotmail.com

Telephone: +86-29-7679290 **Fax:** +86-29-7231758

Received: 2003-12-19 **Accepted:** 2004-02-01

Abstract

AIM: To evaluate the significance of the composite score of reflux symptoms in the diagnosis of gastroesophageal reflux disease (GERD), and to determine the relationship of the composite score with reflux esophagitis (RE) and pathological gastroesophageal reflux (PGER).

METHODS: Upper digestive endoscopy and /or 24-h esophageal pH monitoring were performed in 244 subjects. Of these, 54 were consecutive patients attending our clinic with symptoms suggestive of GERD, and 190 were randomly selected from 2532 respondents who participated in our previous general population-based study on GERD. A standardized questionnaire was used to classify both the frequency and severity of typical symptoms of GERD (heartburn, acid and food regurgitation) using a 4-score scale, and the composite score of main reflux symptoms (score index: SI, range from 0 to 18) were calculated for every subject. RE was diagnosed according to the Savary-Miller criteria. Subjects with abnormal pH-metry (DeMeester score more than 14.7) were considered to have PGER. GERD patients were defined as the subjects with RE and/or PGER.

RESULTS: The sensitivity of SI in the diagnosis of GERD was inversely associated with SI, but the specificity tended to increase with increased SI. With the cut-off of 8, the SI achieved the highest accuracy of 70.0%, with a sensitivity of 78.6% and a specificity of 69.2% in diagnosing GERD, followed by the cut-off of 3, which had an accuracy of 62.1%, a sensitivity of 96.4% and a specificity of 34.6%. The prevalence of RE, PGER and GERD was strongly associated with increased SI ($P < 0.01$), but there was no significant association between the severity of RE and SI ($P > 0.05$). Among patients with RE, 69.2% had PGER, and 30.8% were confirmed to have negative findings of pH monitoring. Among patients with PGER, 52.9% were identified to have RE and 47.1% had negative endoscopic findings in esophagus.

CONCLUSION: According to the composite score of main reflux symptoms, the diagnosis of GERD can be made without further tests in most cases. However, 24-h esophageal pH monitoring and upper digestive endoscopy are still indicated in patients with mild and atypical symptoms.

Wang JH, Luo JY, Dong L, Gong J, Zuo AL. Composite score

of reflux symptoms in diagnosis of gastroesophageal reflux disease. *World J Gastroenterol* 2004; 10(22): 3332-3335
<http://www.wjgnet.com/1007-9327/10/3332.asp>

INTRODUCTION

Gastroesophageal reflux disease (GERD) is a very common disorder both in China^[1-2] and Western countries^[3-8]. The disease results from the abnormal reflux of gastric contents into the distal esophagus causing symptoms in most patients and subsequent mucosal damage in some patients. It has been proved that chronic GERD tends to develop to Barrett's esophagus associated with an increased risk of esophageal adenocarcinoma^[9-13]. Heartburn and regurgitation are the typical symptoms of GERD, and 24-h esophagus pH monitoring and upper digestive endoscopy are the main methods to confirm the diagnosis. These examinations, however, are inconvenient and not universal in many hospitals of China, especially 24-h esophagus pH monitoring. Although the relationship between reflux symptoms and GRED were evaluated by some clinical studies, the results varied considerably because the symptoms were quantified by different criteria and methods^[3,14-16]. As far as we know, data about the relationship between the combination of main reflux symptoms and proven GERD are lacking. The aim of this study was to establish a standard system to quantify the severity and frequency of typical reflux symptoms, and to evaluate the role of the composite score of main reflux symptoms in the diagnosis of GERD, and to determine the association between the composite score and reflux esophagitis (RE), pathological gastroesophageal reflux (PGER), and GERD.

MATERIALS AND METHODS

Subjects

Two hundred and forty-four subjects were included in this study. Among these, 54 were consecutive patients (32 men and 22 women; mean age, 45.3±13.2 years) who attended our clinic with symptoms suggestive of GERD and underwent both 24-h esophageal pH monitoring and upper digestive endoscopy. The remaining 190 subjects were randomly selected from 2532 respondents who were previously enrolled in our general population-based study on GERD, according to the composite score (score index, SI) of main reflux symptoms (Table 1), and who underwent 24-h esophageal pH monitoring (50 subjects) or/and upper digestive endoscopy (140 subjects). Patients with previous foregut surgery and other systemic disorders affecting the gastrointestinal motility were excluded. Five selected respondents (3 in the normal group and 1 in the mild symptom group) refused to participate in this study, 1 (normal group) had intolerance to pH monitoring, and 1 (normal group) did not complete the evaluation. All of the 7 incomplete respondents were replaced by our clinic patients with same gender, SI, and similar age (±5 years). There were no appreciable differences in age or gender among these groups ($P > 0.05$).

Questionnaire

A standardized questionnaire based on our previous work was

Table 1 Gender and age distribution of 190 subjects in symptom severity groups

Severity of symptoms	Responders	Upper digestive endoscopy			24-h pH monitoring		
		Subjects	Men/Women	Mean age (yr)	Subjects	Men/Women	Mean age (yr)
Normal	2 102	40	17/23	45.5±9.9	15	8/7	45.3±10.4
Mild	332	40	20/20	46.1±14.4	15	6/9	46.5±13.3
Moderate	74	40	18/22	47.4±9.6	10	5/5	47.4±10.6
Severe	24	20	11/9	49.1±10.2	10	4/6	49.7±11.5
Total	2 532	140	66/74	47.0±11.0	50	23/27	47.2±11.5

Table 2 Relationship between SI and RE, PGER, GERD

Criteria of SI	Endoscopic examination		pH monitoring		Endoscopic or/and pH examination	
	Subjects	RE (%)	Subjects	PGER (%)	Subjects	GERD (%)
Normal (SI = 0-2)	40	0 (0.0)	15	0 (0.0)	55	0 (0.0)
Mild (SI = 3-7)	40	3 (7.5)	15	2 (13.3)	52	4 (7.69)
Moderate (SI = 8-12)	40	11 (27.5) ^b	10	4 (40.0) ^a	45	12 (26.7) ^b
Severe (SI ≥13)	20	13 (66.5) ^b	10	6 (60.0) ^b	24	13 (54.2) ^b

^a $P < 0.05$ and ^b $P < 0.01$ vs normal group.

used to classify both the frequency and severity of typical symptoms of GERD (heartburn, acid regurgitation and food regurgitation) for all subjects before pH monitoring and upper digestive endoscopy. Personal interviews were carried out in our clinic with patients and respondents.

Endoscopy

General upper digestive endoscopy was performed using a Pentax videoendoscope, and the same two gastrointestinal physicians made the diagnosis according to VHS videocassettes recorded.

Twenty-four hour esophageal pH monitoring

Twenty-four hour ambulatory esophageal pH monitoring was performed using a Synectic device. The pH electrode should be positioned 5 cm above the lower esophageal sphincter. Subjects were instructed to fill in diary cards regarding the time of meals, supine position and the time of symptoms experienced during the 24-h period. In addition, they were asked to press a button on the digital data logger at the beginning of each symptom episode. No restrictions were imposed on food and beverage intake or smoking.

Definitions

The following definitions for symptom categories and diseases were used. Only symptoms occurring in the past year before the interview were considered. Heartburn was defined as a burning pain or burning sensation behind the breastbone in the chest, acid regurgitation as a bitter or sour-tasting fluid coming into throat or mouth, food regurgitation as eaten foods coming into mouth. Heartburn, acid regurgitation and food regurgitation were considered to be the typical symptoms of GERD. Each of these symptoms was estimated according to its severity and frequency measured on a 4-score scale. Severity was assessed as follows: 0, none; 1, mild (could be ignored); 2, moderate (could not be ignored but did not affect lifestyle); 3, severe (affected lifestyle). The score of symptom frequency was estimated as follows: 0, none or less than one occasion per month on average; 1, several occasions (once to three times) a month; 2, several occasions (once to six times) a week; 3, one or more daily occasions. Based on the scores of severity and frequency of the main GERD symptoms, the composite score (SI: ranged from 0 to 18) of every subject was calculated. All subjects were grouped as follows: SI = 0-2, normal; SI = 3-7,

mild; SI = 8-12, moderate; SI ≥13, severe. Patients with symptomatic gastroesophageal reflux disease (SGERD) were defined as subjects with SI ≥3. Those with RE were defined as subjects whose endoscopic findings met Savary-Miller criteria, those with PGER as subjects with abnormal pH-metry (DeMeester score more than 14.7), those with GERD as subjects with RE and/or PGER.

Statistical analysis

Data were analyzed with descriptive statistics and expressed as mean±SD. Median values and ranges were used for nonparametric variables. Relative proportions were calculated for the analysis of prevalence and relative frequencies. The comparison between groups was performed by means of parametric tests such as the Student's *t* test for dimensional variables and χ^2 test for non-dimensional variables. The critical two-tailed value of alpha was set at 0.05.

RESULTS

Relationship between SI and its diagnostic accuracy for GERD

Among the 54 outpatients with symptoms suggestive of GERD, 28 patients (51.9%) were identified as GERD (16 patients with RE, 12 patients with PGER, 10 patients with RE and PGER), and 26 patients (48.1%) were normal, based on the findings of upper digestive endoscopy and 24-h esophageal pH monitoring. Figure 1 summarizes the relationship between criteria and its diagnostic accuracy for GERD compared with the diagnosis of endoscopy and pH monitoring. The sensitivity was inversely associated with increased SI, but the specificity tended to be higher with increased SI. The SI ≥8 had the highest accuracy (70.0%) for diagnosing GERD with a sensitivity of 78.6% and a specificity of 69.2%, followed by SI ≥3 with an accuracy of 62.1%, a sensitivity of 96.4% and a specificity of 34.6%.

Relationship between SI and RE, PGER, GERD

As shown in Table 2, the rate of RE was the highest in the severe group, followed by moderate, mild and normal groups, and the results were similar to both PGER and GERD. The rate of RE, PGER and GERD was strongly associated with increased SI. In the severe and moderate groups, the frequency of RE, PGER and GERD was significantly higher than that of the normal group ($P < 0.05$ or $P < 0.01$).

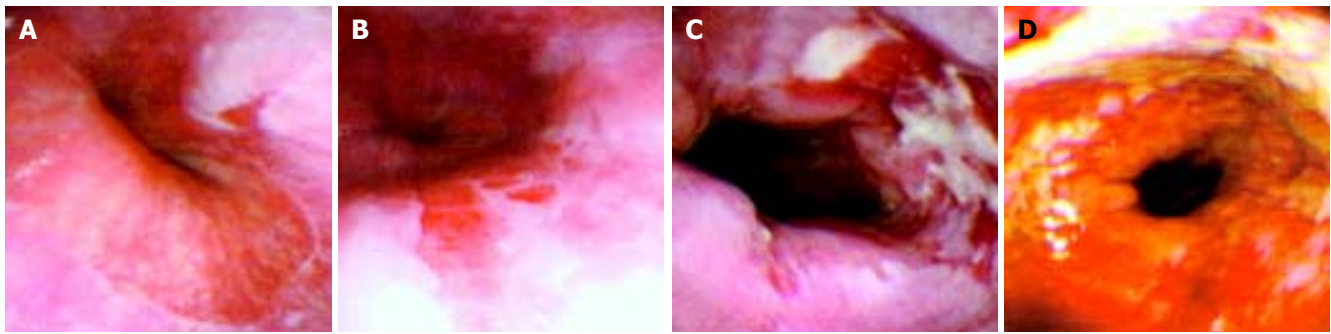


Figure 2 Endoscopic photographs of some patients with RE. A: Female, 46 years old, SI = 12, grade I RE; B: Male, 50 years old, SI = 16, grade II RE; C: Male, 42 years old, SI = 12, grade III RE; D: Male, 51 years old, SI = 13, grade IV RE.

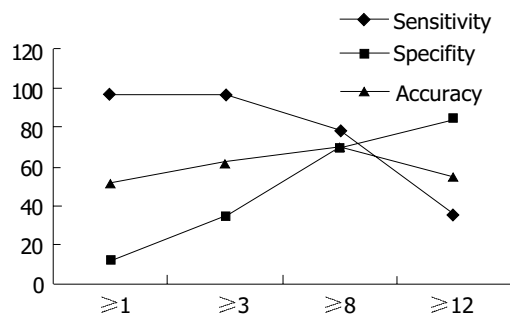


Figure 1 Relationship between SI and its diagnostic accuracy.

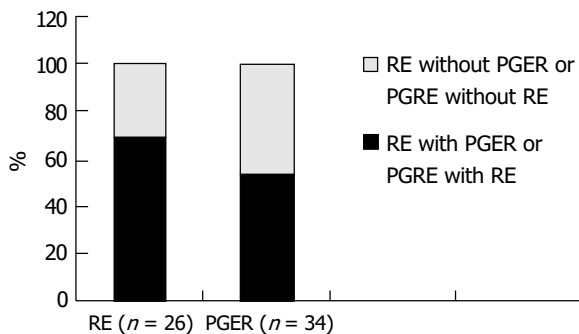


Figure 3 The relationship between RE and PGER.

Relationship between SI and degree of RE

RE was diagnosed in a total of 43 patients on the basis of endoscopic findings (16 cases were outpatients and 27 cases came from general subjects). Thirty patients were males and 13 were females. The mean age was 55.3 ± 6.8 years. Table 3 shows the relationship between SI and the severity of RE. The SI was similar among all groups (from grade I to grade IV, $P > 0.05$). Figure 2 illustrates endoscopic photographs of some patients with RE.

Table 3 Relationship between severity of symptoms and grade of RE

Severity of RE	Patients	SI (mean \pm SD)
Grade I	19	10.63 \pm 4.74
Grade II	13	11.32 \pm 5.26
Grade III	7	11.85 \pm 5.11
Grade IV	4	12.00 \pm 4.12

Relationship between RE and PGER

Of the 43 patients with RE, 26 patients underwent 24-h esophageal pH monitoring. Eighteen patients with RE (69.2%) complicated by PGER and 8 patients (30.8%) were confirmed to

have negative pH monitoring. Upper gastrointestinal tract endoscopy was performed in 34 patients with PGER, of them, 18 (52.9%) were identified to have RE, but the remaining 16 (47.1%) patients were proven to have a negative endoscopic finding in the esophagus. The results are summarized in Figure 3.

DISCUSSION

Gastroesophageal reflux disease is a common disease with many typical and atypical symptoms. A low pressure exerted by the lower esophageal sphincter (LES) and an increased frequency of transient LES relaxation might contribute to the development of GERD^[17-19]. Esophageal testing, particularly 24-h pH monitoring has become the key to make the diagnosis and to ensure adequate acid suppression or prior to surgical therapy^[20]. Although the test could yield accurate and reliable information, it is inconvenient for patients. The problem is whether all patients require 24-h esophageal pH monitoring to establish the diagnosis of GERD. If so, its use, however, is not popular and many hospitals in China are unable to perform this special testing. For these reasons, we are trying to develop a standard system to quantify the symptoms and to evaluate the accuracy of the combination of typical reflux symptoms in the diagnosis of GERD with the hope of eliminating the need for the monitoring.

Laboratory studies have demonstrated that there is a close relationship between classic reflux symptoms and esophageal acid exposure, but some clinical studies revealed that these symptoms were neither specific nor sensitive to the diagnosis of GERD^[15,21-23]. For example, Tefera and his colleagues^[21] reported that moderate or severe heartburn could be used to diagnose GERD with a sensitivity of 68.42% and a specificity of 62.96%, and moderate or severe regurgitation with a sensitivity of 56.76% and a specificity of 65.08%. There were some common grounds in these clinical studies. These symptoms were evaluated separately. The frequency of each symptom was quantified but the severity was not considered. In our study, every typical symptom was estimated by quantifying both the frequency and the severity, and a combination score (SI) of all symptoms was calculated for every subject to exclude those subjects with trivial symptoms and to improve the accuracy of SI in the diagnosis of GERD.

We found that the sensitivity of the composite score of main reflux symptoms in the diagnosis of GERD was inversely associated with increased SI, but the specificity tended to be higher with increased SI. $SI \geq 8$ had the highest accuracy of 70.0% for diagnosing GERD with a sensitivity of 78.6% and a specificity of 69.2%, followed by $SI \geq 3$ with an accuracy of 62.1%, a sensitivity of 96.4%, and a specificity of 34.6%. Because $SI \geq 3$ had the highest sensitivity, this criterion is the common choice in epidemiological studies. With the highest accuracy, $SI \geq 8$ is very useful for diagnosing GERD in clinical work. We, therefore, prompted to develop a criterion based on the main reflux symptoms. The standardized symptom questionnaire and the scoring techniques (system) are important for

gastroenterological doctors to estimate the patients with typical reflux symptoms, especially in hospitals or clinics without objective tests. We suggest that patients with $SI \geq 8$ may be treated pharmaceutically combined with life style counseling. If the symptoms have not improved after 6 to 12 wk, 24-h pH monitoring and/or endoscopic examination should be performed, and if necessary, barium radiographing and manometry should be done.

Our study showed that the prevalence of RE, PGER and GERD was strongly associated with increased SI, but no significant association was found between the severity of RE and SI, indicating that patients with more severe reflux symptoms tend to have GERD, but the grade of esophagitis could not be evaluated on the basis of the severity of typical symptoms.

The present study also revealed that almost one third of patients with RE (30.8%) were confirmed to have negative pH monitoring and half of patients with PGER (47.1%) had negative endoscopic findings in the esophagus, the results were similar to previous studies^[24-26]. Excessive bile exposure of esophageal mucosa was the main cause of RE with normal acid exposure^[27-29]. We suggest that endoscopy-negative reflux disease (ENRD) should be treated as endoscopy positive GERD because longterm acid exposure would rapidly damage esophageal mucosa.

Patients with atypical symptoms such as cough, asthma, hoarseness, chest pain, and ear, nose and throat symptoms were not included in this study because they always had their first visit at specialized services. According to some studies the prevalence of GERD in patients with atypical symptoms ranged from 25% to 80%. We suggest that diagnostic tests such as upper digestive endoscopy and 24-h pH monitoring are a necessity for patients with atypical symptoms.

In conclusion, developing a criterion based on the composite score of typical reflux symptoms is useful to the diagnosis of GERD. Symptom questionnaire and scoring techniques are an important step in this analysis. For patients with a moderate or severe composite score, the diagnosis of GERD can be made without further tests in most situations. However, 24-h esophageal pH monitoring is still needed in patients with mild and atypical symptoms.

REFERENCES

- 1 **Lim LG**, Ho KY. Gastroesophageal reflux disease at the turn of millennium. *World J Gastroenterol* 2003; **9**: 2135-2136
- 2 **Pan GZ**, Xu GM, Ke MY, Han SM, Guo HP, Li ZS, Fang XC, Zou DW, Lu SC, Liu J. Epidemiological study of symptomatic gastroesophageal reflux disease in China: Beijing and Shanghai. *Chin J Dig Dis* 2000; **1**: 2-8
- 3 **Kennedy T**, Jones R. The prevalence of gastro-oesophageal reflux symptoms in a UK population and the consultation behaviour of patients with these symptoms. *Aliment Pharmacol Ther* 2000; **14**: 1589-1594
- 4 **Locke GR III**, Talley NJ, Fett SL, Zinsmeister AR, Melton LJ III. Prevalence and clinical spectrum of gastroesophageal reflux: a population based study in Olmsted County. *Gastroenterology* 1997; **112**: 1448-1456
- 5 **Talley NJ**, Zinsmeister AR, Schleck CD, Melton LJ III. Dyspepsia and dyspepsia subgroups: a population-based study. *Gastroenterology* 1992; **102**: 1259-1268
- 6 **Talley NJ**, Boyce P, Jones M. Identification of distinct upper and lower gastrointestinal symptom groupings in an urban population. *Gut* 1998; **42**: 690-695
- 7 **Isolauri J**, Laippala P. Prevalence of symptoms suggestive of gastro-oesophageal reflux disease in an adult population. *Ann Med* 1995; **27**: 67-70
- 8 **Louis E**, DeLooze D, Deprez P, Hiele M, Urbain D, Pelckmans P, Deviere J, Deltenre M. Heartburn in Belgium: prevalence, impact on daily life, and utilization of medical resources. *Eur J Gastroenterol Hepatol* 2002; **14**: 279-284
- 9 **Bytzer P**, Christensen PB, Damkier P, Vinding K, Seersholm N. Adenocarcinoma of the esophagus and Barrett's esophagus: a population-based study. *Am J Gastroenterol* 1999; **94**: 86-91
- 10 **Falk GW**. Barrett's esophagus. *Gastroenterology* 2002; **122**: 1569-1591
- 11 **Buttar NS**, Wang KK, Leontovich O, Westcott JY, Pacifico RJ, Anderson MA, Krishnadath KK, Lutzke LS, Burgart LJ. Chemoprevention of esophageal adenocarcinoma by COX-2 inhibitors in an animal model of Barrett's esophagus. *Gastroenterology* 2002; **122**: 1101-1112
- 12 **Shirvani VN**, Ouatu-Lascar R, Kaur BS, Omary MB, Triadafilopoulos G. Cyclooxygenase 2 expression in Barrett's esophagus and adenocarcinoma: Ex vivo induction by bile salts and acid exposure. *Gastroenterology* 2000; **118**: 487-496
- 13 **Sampliner RE**. Practice guidelines on the diagnosis, surveillance, and therapy of Barrett's esophagus. *Am J Gastroenterol* 1998; **93**: 1028-1033
- 14 **Klauser AG**, Schindlbeck NE, Muller-Lissner SA. Symptoms in gastro-oesophageal reflux disease. *Lancet* 1990; **335**: 205-208
- 15 **Costantini M**, Crookes PF, Bremner RM, Hoeft SF, Ehsan A, Peters JH, Bremner CG, DeMeester TR, Calif LA. Value of physiologic assessment of foregut symptoms in a surgical practice. *Surgery* 1993; **114**: 780-787
- 16 **Ho KY**, Kang JY, Seow A. Prevalence of gastrointestinal symptoms in a multiracial Asian population, with particular reference to reflux-type symptoms. *Am J Gastroenterol* 1998; **93**: 1816-1822
- 17 **Grossi L**, Ciccaglione AF, Travaglini N, Marzio L. Transient lower esophageal sphincter relaxations and gastroesophageal reflux episodes in healthy subjects and GERD patients during 24 hours. *Dig Dis Sci* 2001; **46**: 815-821
- 18 **Kahrilas PJ**, Shi G, Manka M, Joehl RJ. Increased frequency of transient lower esophageal sphincter relaxation induced by gastric distention in reflux patients with hiatal hernia. *Gastroenterology* 2000; **118**: 688-695
- 19 **Cadiot G**, Bruhat A, Rigaud D, Coste T, Vuagnat A, Benyedder Y, Vallot T, Le Guludec D, Mignon M. Multivariate analysis of pathophysiological factors in reflux oesophagitis. *Gut* 1997; **40**: 167-174
- 20 **Ueno M**, Hongo M. Clinical significance of 24-hour intraesophageal pH monitoring in GERD patients. *Nippon Rinsho* 2000; **58**: 1818-1822
- 21 **Tefera L**, Fein M, Ritter MP, Bremner CG, Crookes PF, Peters JH, Hagen JA, DeMeester TR. Can the combination of symptoms and endoscopy confirm the presence of gastroesophageal reflux disease? *Am Surg* 1997; **63**: 933-936
- 22 **Colas-Atger E**, Bonaz B, Papillon E, Gueddah N, Rolachon A, Bost R, Fournet J. Relationship between acid reflux episodes and gastroesophageal reflux symptoms is very inconstant. *Dig Dis Sci* 2002; **47**: 645-651
- 23 **Ott DJ**, McManus CM, Ledbetter MS, Chen MY, Gelfand DW. Heartburn correlated to 24-hour pH monitoring and radiographic examination of the esophagus. *Am J Gastroenterol* 1997; **92**: 1827-1830
- 24 **Arango L**, Angel A, Molina RI, Marquez JR. Comparison between digestive endoscopy and 24-hour esophageal pH monitoring for the diagnosis of gastroesophageal reflux esophagitis: "presentation of 100 cases". *Hepatogastroenterology* 2000; **47**: 174-180
- 25 **Chan CC**, Lee CL, Wu CH. Twenty-four-hour ambulatory esophageal pH monitoring in patients with symptoms of gastroesophageal reflux. *J Formos Med Assoc* 1997; **96**: 874-878
- 26 **Quigley EM**. Non-erosive reflux disease: part of the spectrum of gastro-oesophageal reflux disease, a component of functional dyspepsia, or both? *Eur J Gastroenterol Hepatol* 2001; **13**(Suppl 1): S13-18
- 27 **Kauer WK**, Peters JH, DeMeester TR, Ireland AP, Bremner CG, Hagen JA. Mixed reflux of gastric and duodenal juices is more harmful to the esophagus than gastric juice alone. The need for surgical therapy re-emphasized. *Ann Surg* 1995; **222**: 525-531
- 28 **Lin KM**, Ueda RK, Hinder RA, Stein HJ, DeMeester TR. Etiology and importance of alkaline esophageal reflux. *Am J Surg* 1991; **162**: 553-557
- 29 **Vaezi MF**, Richter JE. Role of acid and duodenogastroesophageal reflux in gastroesophageal reflux disease. *Gastroenterology* 1996; **111**: 1192-1199

• CLINICAL RESEARCH •

Clinical characteristics and prognostic factors of severe acute pancreatitis

Lei Kong, Nn Santiago, Tian-Quan Han, Sheng-Dao Zhang

Lei Kong, Nn Santiago, Tian-Quan Han, Sheng-Dao Zhang, Shanghai Institute of Digestive Surgery, Department of Surgery, Ruijin Hospital, Shanghai Second Medical University, Shanghai 200025, China

Correspondence to: Dr. Tian-Quan Han, Department of Surgery, Ruijin Hospital, Shanghai Second Medical University, Shanghai Institute of Digestive Surgery, 197 Ruijin II Road, Shanghai 200025, China. digsurgeryrj@yahoo.com.cn

Telephone: +86-21-64373909 **Fax:** +86-21-64373909

Received: 2004-04-22 **Accepted:** 2004-04-29

Abstract

AIM: To investigate the clinical characteristics and prognostic factors of a consecutive series of patients with severe acute pancreatitis (SAP).

METHODS: Clinical data of SAP patients admitted to our hospital from January 2003 to January 2004 were retrospectively reviewed. Collected data included the age, gender, etiology, length of hospitalization, APACHE II score at admission, local and organ/systemic complications of the patients.

RESULTS: Of the 268 acute pancreatitis patients, 94 developed SAP. The mean age of SAP patients was 52 years, the commonest etiology was cholelithiasis (45.7%), the mean length of hospitalization was 70 d, the mean score of APACHE II was 7.7. Fifty-four percent of the patients developed necrosis, 25% abscess, 58% organ/systemic failure. A total of 23.4% (22/94) of the SAP patients died. Respiratory failure was the most common organ dysfunction (90.9%) in deceased SAP patients, followed by cardiovascular failure (86.4%), renal failure (50.0%). In the SAP patients, 90.9% (20/22) developed multiple organ/systemic failures. There were significant differences in age, length of hospitalization, APACHE II score and incidences of respiratory failure, renal failure, cardiovascular failure and hematological failure between deceased SAP patients and survived SAP patients. By multivariate logistic regression analysis, independent prognostic factors for mortality were respiratory failure, cardiovascular failure and renal failure.

CONCLUSION: SAP patients are characterized by advanced age, high APACHE II score, organ failure and their death is mainly due to multiple organ/systemic failures. In patients with SAP, respiratory, cardiovascular and renal failures can predict the fatal outcome and more attention should be paid to their clinical evaluation.

Kong L, Santiago N, Han TQ, Zhang SD. Clinical characteristics and prognostic factors of severe acute pancreatitis. *World J Gastroenterol* 2004; 10(22): 3336-3338
<http://www.wjgnet.com/1007-9327/10/3336.asp>

INTRODUCTION

Acute pancreatitis, as a relatively common pancreatic disease,

can be found in every part of the world with an incidence of 35-80 cases per 100 000 inhabitants per year^[1,2]. According to Atlanta Classification, acute pancreatitis is clinically classified into a mild or severe type depending on the presence of local and systemic complications^[3]. Severe acute pancreatitis (SAP) is characterized by high morbidity and mortality. The mortality of SAP patients varies from 7% to 47%^[4]. The factors most closely linked to a poor prognosis are pancreatic necrosis, infection and multiple organ/systemic failures, which are associated with a mortality of 50%^[4-7]; although in recent years this mortality rate has tended to decrease^[8]. Many attempts have been made to achieve an early prognosis of SAP. However, none seems to be reliable enough to justify its routine use.

In view of the high mortality associated with SAP, it is important to identify the cases that require close monitoring and aggressive resuscitation. The aim of this study was therefore to investigate the clinical characteristics and factors which could predict the outcome of patients with organ/systemic failure admitted to our hospital.

MATERIALS AND METHODS

Clinical data

From January 2003 to January 2004, the clinical histories of patients with acute pancreatitis (AP), admitted to the Department of Surgery, Ruijin Hospital of Shanghai Second Medical University, were retrospectively reviewed. The diagnosis of AP was established in cases with clinical presentations and biochemical findings when other causes were excluded. The severities of AP were assessed according to the Atlanta classification system^[3]. Etiology was divided into two groups: cholelithiasis and non-cholelithiasis. A biliary etiology was confirmed by ultrasonography, CT scan, ERCP, MRCP and operation. Pancreatic necrosis and abscess were defined by the findings on contrast-enhanced CT scan or in operation. The local and organ/systemic complications were defined according to the Atlanta classification system^[3,9].

The patients with SAP were divided according to their outcomes into two groups: deceased group and survived group. The data recorded for each patient included age, gender, etiology, length of hospitalization, APACHE II score at admission and the presence and type of local and organ/systemic complications. The relationship between clinical characteristics, specific single or multiple organ/systemic failures with mortality was evaluated in above-mentioned two groups.

Statistical analysis

Results were expressed as mean±SD. Statistical studies were made using SAS 6.12. Continuous data were evaluated by *t* test, and categorized data were analyzed by Chi-square test or Fisher's exact test. To identify the risk factors for SAP, multiple logistic regression analysis with backward elimination was used. *P*<0.05 was considered statistically significant.

RESULTS

Of the 268 patients with AP, 35.1% (94/268) developed SAP. Of the 94 SAP patients, 23.4% (22/94) died. The patients in the deceased group were significantly older and had a higher

APACHE II score than those in the survived group. The length of hospitalization was significantly shorter in those with a fatal outcome. There was no difference in etiology or gender (Table 1).

Regarding the local complications, the incidences of necrosis and abscess were significantly higher in the survived group than those in the deceased group. No patient in the deceased group developed pseudocysts (Table 2).

Table 1 Comparison of clinical characteristics (mean±SD)

Characteristics	Survival (n = 72)	Deceased (n = 22)	Total (n = 94)
Mean age (yr) (range)	49.7±14.9 ^b (15-82)	62.8±14.4 (42-83)	52.7±15.8 (15-83)
Gender (male/female)	45/27	10/12	55/39
Etiology (biliary/non-biliary)	31/41	12/10	43/51
Hospitalization (d) (range)	84.4±65.3 ^b (8-253)	26.2±28.2 (1-94)	70.8±63.7 (1-253)
APACHE II score (range)	6.3±3.5 ^b (0-14)	12.5±6.8 (1-33)	7.7±5.2 (0-33)

^bP<0.01 vs deceased group.

Table 2 Comparison of local complications

Local complications	Survival (n=72)	Deceased (n=22)	Total (n=94)
Necrosis, n (%)	47 (5.3) ^b	7 (31.8)	54 (57.4)
Abscess, n (%)	23 (31.4) ^a	2 (9.1)	25 (26.6)
Pseudocyst, n (%)	11 (15.3)	0 (0)	11 (11.7)

^aP<0.05, ^bP<0.01 vs deceased group.

A total of 61.7% (58/94) patients with SAP developed organ/systemic failures. In the deceased group, 90.9% (20/22) patients showed multiple organ/systemic failures (maximum 5 organ/systemic failures), only 18.1% (13/94) patients showed multiple organ/systemic failures in the survived group (Tables 3, 4). With regard to the organ/systemic complications, we found that the deceased group experienced a significantly greater incidence of episodes of respiratory failure, acute renal failure, cardiovascular failure and hematological failure than the survived group (Table 4).

Table 3 Comparison of the number of organ/systemic failure

Number of organ/systemic failure	Survival (n=72)	Deceased (n=22)	Total (n=94)
1, n (%)	23 (31.9) ^a	2 (9.1)	25 (26.6)
2, n (%)	10 (13.9)	6 (4.5)	16 (17.0)
3, n (%)	3 (4.2) ^a	4 (18.2)	7 (7.4)
4, n (%)	0 (0) ^b	7 (31.8)	7 (7.4)
5, n (%)	0 (0) ^a	3 (13.6)	3 (3.2)
Total, n (%)	36 (50.0) ^b	22 (100.0)	58 (61.7)

^aP<0.05, ^bP<0.01 vs deceased group.

As for the frequency of different specific single organ failures, pulmonary failure occurred in 35.1% (33/94) patients, cardiovascular failure in 22.3% (21/94) patients, gastrointestinal failure in 19.1% (18/94) patients, hepatic failure in 15.9% (15/94) and renal failure in 14.9% (14/94) patients. The incidences of neurologic and hematological failures were relatively lower, only in 8.5% (8/94) patients respectively (Table 5).

Logistic regression analysis was carried out for the independent prognostic factors including all the variables studied. Respiratory failure, cardiovascular failure and renal failure were found to be independent prognostic factors of the mortality in SAP patients (Table 6).

Table 4 Comparison of the features of organ/systemic failure

Organ/systemic failure	Survival (n=72)	Deceased (n=22)	Total (n=94)
Multiple organ/systemic failures n (%)	13 (18.1) ^b	20 (90.9)	33 (35.1)
Respiratory n (%)	13 (18.1) ^b	20 (90.9)	33 (35.1)
Renal n (%)	3 (4.2) ^b	11 (50.0)	14 (14.9)
Gastrointestinal n (%)	11 (15.3)	7 (31.8)	18 (19.1)
Hepatic n (%)	12 (16.7)	3 (13.6)	15 (15.9)
Neurologic n (%)	6 (8.3)	2 (9.1)	8 (8.5)
Cardiovascular n (%)	2 (2.8) ^b	19 (86.4)	21 (22.3)
Hematological n (%)	2 (2.8) ^b	6 (27.3)	8 (8.5)

^bP<0.01 vs deceased group.

Table 5 Frequency of organ/systemic failure

Organ/systemic	Number of organ/systemic failure	Frequency (%)
Respiratory	33	35.1
Renal	14	14.9
Gastrointestinal	18	19.1
Hepatic	15	15.9
Neurologic	8	8.5
Cardiovascular	21	22.3
Hematological	8	8.5

Table 6 Independent factors of the logistic regression model

Variable	OR	OR 95% confidence interval	P
Respiratory failure	186.5	9.942-999.0	0.006
Cardiovascular failure	29.9	2.243-999.0	0.021
Renal failure	118.7	3.784-999.0	0.029
Hospitalization, days	0.957	0.908-0.989	0.037

DISCUSSION

Most deaths of SAP patients were mainly related to multiple organ/systemic failures^[10]. Regarding the survival time, patients died more often of multiple organ/systemic failures in the first few days after admission^[5,11]. In the early phase of SAP, multiple organ/systemic failures seemed to be caused by cytokine and inflammatory mediators released due to systemic inflammatory response syndrome, and sterile pancreatic necrosis might even occur^[12]. Early deaths of SAP patients were commonly associated with multiple organ/systemic failure, accounting for 40-60% of mortality, and over the past decade this proportion has not declined^[13]. The present study showed that in the deceased group 90.9% (20/22) patients developed multiple organ/systemic failure and 50% (11/22) patients died within 2 wk after admission.

Previous studies^[14-16] showed that in SAP patients, organ/systemic failure occurred in 72-90.3%, single organ failure in 24.7-37%, multiple organ failure in 35-65.6%. Among the single organ failures, respiratory failure was the most common organ/systemic complications (39.1-63%), followed by cardiovascular failure (23-37.7%), hepatic failure (20.7%) and renal failure (8.5-13%). The present data showed that organ failure occurred in 61.7% (58/94) patients, single organ failure in 26.6% (25/94) patients, and multiple organ failure in 38.3% (36/94) patients. Respiratory failure was the most common single organ failure (35.1%, 33/94), followed by cardiovascular failure (22.3%, 21/94), gastrointestinal failure (19.1%, 18/94), hepatic failure (15.9%, 15/94) and renal failure (14.9%, 14/94). In a recent study, five independent prognostic factors for hospital mortality in SAP patients were the age and chronic health situation of the patients and organ failures (renal, respiratory and cardiovascular)^[4]. In our study, respiratory failure, cardiovascular failure and renal failure were shown to be the independent prognostic factors of

mortality by multivariate logistic analysis, which are consistent with the reports by Fernandez-Cruz *et al.* and Halonen *et al.*^[6, 17]. Apparently, the development of one of the above-mentioned complications is by far the worst prognostic factor in SAP, closely related to mortality.

Up to now, the development of pancreatic necrosis and infection has been considered as an important factor in the occurrence of multiple organ/systemic failure and subsequent death^[6, 18, 19]. There are even studies relating the site and extent of necrosis to the outcome and development of multiple organ failures^[18, 20]. In other studies, infected pancreatic necrosis and combined of organ/systemic failures were the most significant causes for hospital mortality of SAP patients^[1, 21]. The mortality rate of SAP patients was 7-47% (that of sterile necrotizing pancreatitis patients was 6-13% and SAP patients with infected necrosis was 14-80%)^[4, 22-26]. Conversely, there was a higher proportion of patients with necrosis and abscess in the survived group in our study. Using logistic regression analysis failed to identify necrosis and abscess as independent prognostic factors for mortality, although statistically significant difference was found between survived and deceased groups. This suggested that, rather than the development of necrosis or abscess itself, necrosis and abscess were not correlated with an increased mortality. The main factor indicating a poor prognosis in SAP was the development of multiple organ/systemic failures^[27, 28].

Although there was a higher incidence of pseudocysts in the survived group, no statistically significant difference was found compared with the deceased group. This observation must be made cautiously, because 50% (11/22) of the patients in deceased group died within 2 wk, which might be too short to develop a pseudocyst. In addition, in many patients the only complication was a pseudocyst, so they were classified as having SAP according to the Atlanta Criteria, although their clinical recovery was excellent^[3]. Patients with pseudocysts may develop complications, but since it takes at least 4 wk to develop a pseudocyst, it has no effect on early mortality.

Our results did not show that age was an independent poor prognosis factor in mortality, which was consistent with previous studies, but in contradiction to other investigators^[4, 6]. When deaths due to complications of acute pancreatitis were analyzed, the mortality rate was not significantly different between the young and elderly groups. Moreover, the complication rate and the proportion of patients with SAP (judged by the number of prognostic signs) were not higher in the elderly. Thus the severity of acute pancreatitis was not intrinsically due to advanced age when the influence of other secondary factors was not taken into consideration.

In conclusion, SAP patients are characterized by advanced age, high APACHE II score at admission, development of organ/systemic failure, and their death is mainly due to multiple organ/systemic failures. In SAP patients, respiratory, cardiovascular and renal failures can predict their fatal outcome and more attention should be paid to their clinical evaluation.

REFERENCES

- Steinberg W, Tenner S. Acute pancreatitis. *N Engl J Med* 1994; **330**: 1198-1210
- Company L, Saez J, Martinez J, Aparicio JR, Laveda R, Grino P, Perez-Mateo M. Factors predicting mortality in severe acute pancreatitis. *Pancreatol* 2003; **3**: 144-148
- Bradley EL. A clinically based classification system for acute pancreatitis, 3rd. Summary of the international symposium on acute pancreatitis, Atlanta, Ga, September 11 through 13, 1992. *Arch Surg* 1993; **128**: 586-590
- Halonen KI, Leppaniemi AK, Puolakkainen PA, Lundin JE, Kempainen EA, Hietaranta AJ, Haapiainen RK. Severe acute pancreatitis: prognostic factors in 270 consecutive patients. *Pancreas* 2000; **21**: 266-271
- Baron TH, Morgan DE. Acute necrotizing pancreatitis. *N Engl J Med* 1999; **340**: 1412-1417
- Fernandez-Cruz L, Navarro S, Valderrama R, Saenz A, Guarner L, Aparisi L, Espi A, Jaurieta E, Marruecos L, Gener J, De Las Heras G, Perez-Mateo M, Garcia Sabrido JL, Roig J, Carballo F. Acute necrotizing pancreatitis: a multicenter study. *Hepatogastroenterology* 1994; **41**: 185-189
- Banks PA. Predictors of severity in acute pancreatitis. *Pancreas* 1991; **6**: S7-12
- Talamini G, Bassi C, Falconi M, Sartori N, Frulloni L, Di Francesco V, Vesentini S, Pederzoli P, Cavallini G. Risk of death from acute pancreatitis. Role of early, simple "routine" data. *Int J Pancreatol* 1996; **19**: 15-24
- Gotzinger P, Wamser P, Exner R, Schwanzer E, Jakesz R, Fugger R, Sautner T. Surgical treatment of severe acute pancreatitis: timing of operation is crucial for survival. *Surg Infect* 2003; **4**: 205-211
- Miskovitz P. Acute pancreatitis: further insight into mechanisms. *Crit Care Med* 1998; **26**: 816-817
- Iseemann R, Rau B, Beger HG. Early severe acute pancreatitis: characteristics of a new subgroup. *Pancreas* 2001; **22**: 274-278
- Wilson PG, Manji M, Neoptolemos JP. Acute pancreatitis as a model of sepsis. *J Antimicrob Chemother* 1998; **41**: 51-63
- McKay CJ, Evans S, Sinclair M, Carter CR, Imrie CW. High early mortality rate from acute pancreatitis in Scotland, 1984-1995. *Br J Surg* 1999; **86**: 1302-1305
- Buchler MW, Gloor B, Muller CA, Friess H, Seiler CA, Uhl W. Acute necrotizing pancreatitis: treatment strategy according to the status of infection. *Ann Surg* 2000; **232**: 619-626
- Gotzinger P, Sautner T, Kriwanek S, Beckerhinn P, Barlan M, Armbruster C, Wamser P, Fugger R. Surgical treatment for severe acute pancreatitis: extent and surgical control of necrosis determine outcome. *World J Surg* 2002; **26**: 474-478
- Zhu AJ, Shi JS, Sun XJ. Organ failure associated with severe acute pancreatitis. *World J Gastroenterol* 2003; **9**: 2570-2573
- Halonen KI, Pettila V, Leppaniemi AK, Kempainen EA, Puolakkainen PA, Haapiainen RK. Multiple organ dysfunction associated with severe acute pancreatitis. *Crit Care Med* 2002; **30**: 1274-1279
- Iseemann R, Rau B, Beger HG. Bacterial infection and extent of necrosis are determinants of organ failure in patients with acute necrotizing pancreatitis. *Br J Surg* 1999; **86**: 1020-1024
- Raty S, Sand J, Nordback I. Difference in microbes contaminating pancreatic necrosis in biliary and alcoholic pancreatitis. *Int J Pancreatol* 1998; **24**: 187-191
- Kempainen E, Sainio V, Haapiainen R, Kivisaari L, Kivilaakso E, Puolakkainen P. Early localization of necrosis by contrast-enhanced computed tomography can predict outcome in severe acute pancreatitis. *Br J Surg* 1996; **83**: 924-929
- McFadden DW. Organ failure and multiple organ system failure in pancreatitis. *Pancreas* 1991; **6**(Suppl 1): S37-43
- de Beaux AC, Palmer KR, Carter DC. Factors influencing morbidity and mortality in acute pancreatitis: an analysis of 279 cases. *Gut* 1995; **37**: 121-126
- Karimani I, Porter KA, Langevin RE, Banks PA. Prognostic factors in sterile pancreatic necrosis. *Gastroenterology* 1992; **103**: 1636-1640
- Uomo G, Visconti M, Manes G, Calise F, Laccetti M, Rabitti PG. Nonsurgical treatment of acute necrotizing pancreatitis. *Pancreas* 1996; **12**: 142-148
- de Beaux AC, Goldie AS, Ross JA, Carter DC, Fearon KC. Serum concentrations of inflammatory mediators related to organ failure in patients with acute pancreatitis. *Br J Surg* 1996; **83**: 349-353
- Widdison AL, Karanjia ND. Pancreatic infection complicating acute pancreatitis. *Br J Surg* 1993; **8**: 148-154
- Tenner S, Sica G, Hughes M, Noordhoek E, Feng S, Zinner M, Banks PA. Relationship of necrosis to organ failure in severe acute pancreatitis. *Gastroenterology* 1997; **113**: 899-903
- Lankisch PG, Pflichthofer D, Lehnick D. No strict correlation between necrosis and organ failure in acute pancreatitis. *Pancreas* 2000; **20**: 319-322

A double stapled technique for oesophago-enteric anastomosis

A Kotru, A K John, E P Dewar

A Kotru, A K John, E P Dewar, Department of Surgery, Airedale General Hospital, Keighly BD20 6TD, UK

Correspondence to: A Kotru, 273-Spen Lane, West Park, Leeds LS16 5EJ, UK. ajokjohn@yahoo.com

Telephone: +44-1132288911

Received: 2004-02-11 Accepted: 2004-04-07

Abstract

AIM: Leakage from oesophageal anastomosis is associated with substantial morbidity and mortality. This study presented a novel, safe and effective double stapled technique for oesophago-enteric anastomosis.

METHODS: The data were obtained prospectively from hospital held clinical database. Thirty nine patients (26 males, 13 females) underwent upper-gastrointestinal resection between 1996 and 2000 for carcinoma ($n = 36$), gastric lymphoma ($n = 1$), and benign pathology ($n = 2$). Double stapled oesophago-enteric anastomosis was performed in all cases.

RESULTS: No anastomotic leak was reported. In cases of malignancy, the resected margins were free of neoplasm. Three deaths occurred, which were not related to anastomotic complications.

CONCLUSION: Even though the reported study is an uncontrolled one, the technique described is reliable, and effective for oesophago-enteric anastomosis.

Kotru A, John AK, Dewar EP. A double stapled technique for oesophago-enteric anastomosis. *World J Gastroenterol* 2004; 10(22): 3339-3341

<http://www.wjgnet.com/1007-9327/10/3339.asp>

INTRODUCTION

Leakage is a major problem associated with oesophago-enteric anastomosis. The anastomosis may be hand sewn or stapled^[1-4]. Even though there is no proven advantage between either techniques, basic principles of anastomosis surgery- tension free, good vascularity, and good mucosal apposition apply to both. A technique of double stapled anastomosis avoids stretch at oesophageal side of anastomosis and circumvents damage to vascularity.

MATERIALS AND METHODS

The double stapled oesophago-enteric reconstruction was performed as follows. The oesophagus was mobilized in the standard way to above the proposed level of division. A transverse incision was made in the anterior wall of the oesophagus at least 3 cm above the proximal extent of the tumour in those cases undergoing surgery for malignancy (Figure 1). An appropriately sized circular stapler (CA Ethicon) was selected based on the oesophageal diameter. A 2-0 polypropylene suture was placed through the 'eye-hole' situated in the plastic spike that fits the head of the circular stapler. The

polypropylene suture should be tied such that around 5 cm of suture with the attached needle remained attached to the spike attached to the circular stapler head. The transverse anterior oesophagotomy should be of sufficient size to allow insertion of the stapler head with attached spike - see step 7 (Figure 2). The circular stapler head with spike and attached needle were placed through the oesophagotomy into the proximal oesophagus (Figure 3). The suture needle was brought out through the anterior oesophageal wall 2 cm proximal to the oesophagotomy. The oesophagus was then cross-stapled and divided transversely below the site of needle puncture but above the oesophagotomy. The suture attached to the spike was used to pull the spike and axis of the circular stapler head through the anterior wall of the oesophagus, around 2 cm proximal to the transverse staple line (Figure 4). The spike was then removed from the stapler head. Resection of the gastric or oesophago-gastric specimen was then completed. The distal conduit (either distal stomach or jejunal limb) was prepared and mobilized to allow a tension free anastomosis. The body of the circular stapler was introduced into the lumen of the efferent conduit through an appropriately placed enterotomy (Figure 5). The circular stapler head was engaged with the body of the circular stapler gun. The gun was closed and fired creating a double stapled oesophago-enteric anastomosis (Figure 5). A naso-gastric tube was fed across the oesophago-enterostomy after completion of the anastomosis.

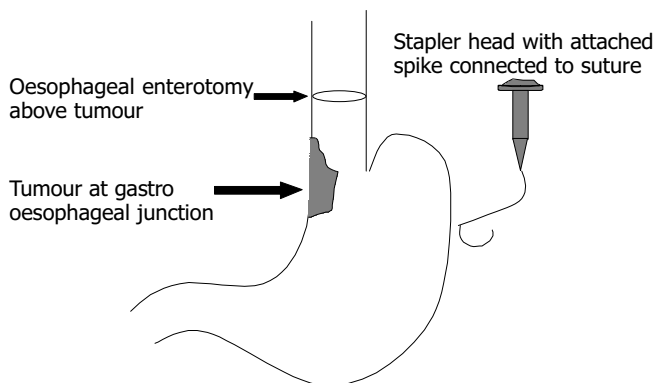


Figure 1 Transverse incision in anterior wall of oesophagus.

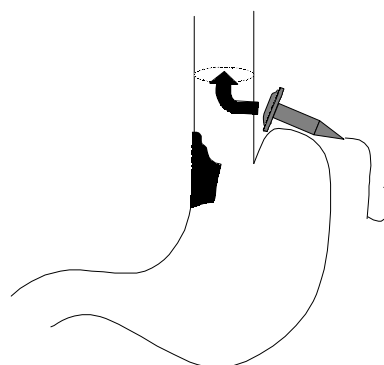


Figure 2 Transverse anterior oesophagotomy. Stapler head spike with attached needle inserted through oesophagotomy into proximal oesophagus.

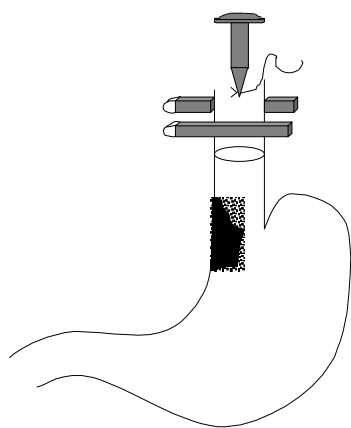


Figure 3 Placement of a circular stapler head with spike and attached needle. Needle was used to puncture anterior oesophagus -2 cm above the oesophagotomy. The oesophagus was then cross- stapled between the needle puncture site & the oesophagotomy.

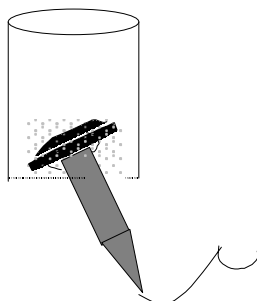


Figure 4 Suture used to drive head spike through oesophageal wall above transverse suture line.

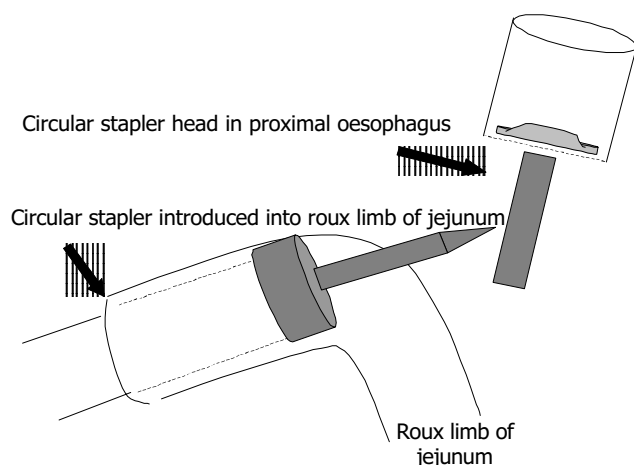


Figure 5 Introduction of the circular stapler body into the lumen of efferent conduit.

RESULTS

All patients were operated on by or under the direct supervision of a consultant surgeon with an upper gastrointestinal interest. Patients with malignancy underwent pre-operative staging with thoraco-abdominal computed tomography scan. Laparoscopy was used in selected instances. In elective cases, mechanical bowel preparation was employed. Thoracic epidural anaesthesia was employed for post-operative pain relief. Patients were kept nil by mouth for 5 d post-operatively. If the post-operative course was uneventful, fluids were introduced on d 5. Water

soluble contrast studies were not routinely used to assess anastomotic integrity unless there was clinical indication.

Data were obtained prospectively from the hospital-held clinical database.

Thirty-nine patients (26 males, 13 females) underwent upper gastrointestinal resection (total gastrectomy $n = 24$, Ivor-Lewis oesophago-gastrectomy $n = 15$) between 1996 and 2000. Indication for surgery was carcinoma ($n = 36$), gastric non-Hodgkin's lymphoma ($n = 1$), revision of a neo-gastric jejunal pouch ($n = 1$), gastric infarction secondary to volvulus ($n = 1$). The median age was 67 (36-82) years. Patient ASA grades were: ASA-1 $n = 12$, ASA- 2 $n = 14$, ASA- 3 $n = 9$, ASA- 4 $n = 3$, ASA- 5 $n = 1$. The median operative time for total gastrectomy was 175 (120-240) min and was 240 (180-360) min for Ivor-Lewis oesophago-gastrectomy. The median transfusion requirements were 2 (0-7) units for both procedures. The resection margins were free of tumour on histopathological examination in all cases of malignancy.

Morbidity and mortality rates are shown below (Tables 1-3). Risk adjusted morbidity and mortality rates were calculated using the physiological and operative scoring system for enumeration of morbidity and mortality (POSSUM) and Portsmouth POSSUM (P-POSSUM) models^[5,6].

Table 1 Morbidity and mortality of oesophago-gastrectomy (n , %)

	Total patients ($n = 15$)	POSSUM prediction	P-POSSUM prediction
Morbidity	5 (33)	63	-
Mortality	2 (14)	18	6

Table 2 Morbidity and mortality of total gastrectomy (n , %)

	Total patients ($n = 15$)	POSSUM prediction	P-POSSUM prediction
Morbidity	6 (25)	48	-
Mortality	1 (4)	16	9

Table 3 Analysis of morbidity

	Oesophagogastrectomy (n)	Total gastrectomy (n)
Chest infection	2	5
Chylothorax	1	-
DVT/PE	1	1
Anastomotic leak	-	-
Wound sepsis	1	-

Three deaths occurred, two post oesophago-gastrectomy and one post total gastrectomy. The deaths after oesophago-gastrectomy were shown at post-mortem to be due to left ventricular failure and myocardial infarction respectively. The patient who died after total gastrectomy deteriorated suddenly on the 10th post-operative day tolerated diet for three days. Symptoms, blood gases and electrocardiogram were compatible with a pulmonary embolus. Permission for a post-mortem was refused. No anastomotic leaks occurred on clinical grounds.

DISCUSSION

Anastomotic leakage following oesophago-enteric reconstruction may result in significant morbidity and mortality. The standard principles governing any gastro-intestinal anastomosis apply in dealing with the oesophagus. The anastomosis should be tension-free, well vascularized and there should be accurate mucosal apposition. Oesophageal anastomoses may be hand sewn (in one, two or even three layers) or stapled^[1-4]. There is no proven advantage to either the hand sewn or stapled technique.

Stapled anastomoses might be associated with a higher rate of subsequent benign stricture formation⁷¹. The stapled technique that is commonly used requires a purse string suture in the cut end of the proximal oesophagus to retain the head of the circular stapler. The anastomosis is completed by a single firing of the circular stapler.

It is the authors' contention that the oesophageal purse string may be a contributory factor to subsequent anastomotic related complications (leak and stricture). This is based on the observation that the distal oesophagus is stretched over the head of the circular stapler, and therefore possibly devascularized by the purse string suture. To avoid the use of a purse string, a double stapled oesophago-enteric anastomotic technique has been devised.

This paper described a novel technique of oesophago-enteric anastomosis using a double stapled technique. Whilst this was an uncontrolled study, the technique has proved reliable and to date has not resulted in any anastomotic leaks. Whilst this study cannot implicate the use of a proximal oesophageal purse string suture as a factor in anastomotic leakage, it is interesting to speculate whether the double stapled anastomosis does allow improved anastomotic healing through omission of

a purse string suture. The technique described merits further evaluation either in the setting of a larger uncontrolled study or more preferably in the context of a randomised trial.

REFERENCES

- 1 **Skinner DB.** Oesophageal reconstruction. *Am J Surg* 1980; **139**: 810-814
- 2 **Akiyama H.** Surgery for cancer of the oesophagus. Baltimore: *Williams Wilkins* 1990: 74-75
- 3 **Sweep RH.** Thoracic surgery. Philadelphia, London: *WB Saunders* 1950: 256-294
- 4 **Griffin SM, Raimes SA.** Upper gastrointestinal surgery. London, Philadelphia, Toronto, Sydney, Tokyo: *WB Saunders* 1997: 111-144
- 5 **Copeland GP, Jones D, Walters M.** POSSUM: A scoring system for surgical audit. *Br J Surg* 1991; **78**: 355- 360
- 6 **Prytherch DR, Whiteley MS, Higgins B, Weaver PC, Prout WG, Powell SJ.** POSSUM and Portsmouth POSSUM for predicting mortality. Physiological and Operative Severity Score for the enUmeration of Mortality and Morbidity. *Br J Surg* 1998; **85**: 1217-1220
- 7 **Bardini R, Asolati M, Ruol A, Bonavina L, Baseggio S, Peracchia A.** Anastomosis. *World J Surg* 1994; **18**: 373- 378

Edited by Wang XL Proofread by Xu FM

Helicobacter pylori seroprevalence in patients with lung cancer

Nikiphoros Philippou, Panagiotis Koursarakos, Evgenia Anastasakou, Vasiliki Krietsepi, Stavroula Mavrea, Anastasios Roussos, Dionissia Alepopoulou, Irineos Iliopoulos

Nikiphoros Philippou, Panagiotis Koursarakos, Vasiliki Krietsepi, Anastasios Roussos, Irineos Iliopoulos, 9th Department of Pulmonary Medicine, "SOTIRIA" Chest Diseases Hospital, Athens, Greece
Evgenia Anastasakou, Stavroula Mavrea, Dionissia Alepopoulou, Section of Immunology and Infectious Diseases, "SOTIRIA" Chest Diseases Hospital, Athens, Greece

Correspondence to: Dr. Nikiphoros Philippou, 9th Department of Pulmonary Medicine, "SOTIRIA" Chest Diseases Hospital, 152 Mesogion Street, PO Box 11527, Athens, Greece. roumar26@yahoo.com

Telephone: +301-210-8646215 **Fax:** +301-210-8646215

Received: 2003-08-02 **Accepted:** 2003-09-12

Abstract

AIM: To assess *Helicobacter pylori* (*H. pylori*) seroprevalence in a cohort of Greek patients with lung cancer.

METHODS: Seventy-two lung cancer patients (55 males and 17 females, aged 58.2±11.7 years) and 68, age and gender-matched, control subjects were enrolled. All subjects underwent an enzyme-linked immunosorbent assay IgG serologic test for *H. pylori* diagnosis.

RESULTS: A correlation between age and *H. pylori* IgG level was detected for both lung cancer patients ($r = 0.42$, $P = 0.004$) and controls ($r = 0.44$, $P = 0.004$). Seropositivity for *H. pylori* did not differ significantly between patients with lung cancer and controls (61.1% vs 55.9%, $P > 0.05$). Concerning the mean serum concentration of IgG antibodies against *H. pylori*, no significant difference between the two groups was detected (32.6±19.1 vs 27.4±18.3 U/mL, $P > 0.05$).

CONCLUSION: No significant association between *H. pylori* infection and lung cancer was found.

Philippou N, Koursarakos P, Anastasakou E, Krietsepi V, Mavrea S, Roussos A, Alepopoulou D, Iliopoulos I. *Helicobacter pylori* seroprevalence in patients with lung cancer. *World J Gastroenterol* 2004; 10(22): 3342-3344

<http://www.wjgnet.com/1007-9327/10/3342.asp>

INTRODUCTION

Helicobacter pylori (*H. pylori*) infection of the gastric mucosa affects approximately 50% of the world's population^[1]. It seems to be the main cause of chronic antral gastritis^[2] and is strongly associated with peptic ulcer disease^[3], gastric cancer^[4], and gastric MALT-lymphoma^[5]. In the past few years, a variety of extradigestive disorders, including cardiovascular, skin, rheumatic and liver diseases, have also been associated with *H. pylori* infection^[6,7]. As regards respiratory diseases, an increased *H. pylori* seroprevalence has been found in active bronchiectasis^[8], chronic bronchitis^[9,10] and active pulmonary tuberculosis^[11]. The activation of inflammatory mediators by *H. pylori* seems to be the common pathogenetic mechanism underlying the observed associations^[12].

It is well known that the prevalence of lung cancer in peptic ulcer patients is increased 2 to 3 fold compared with findings in ulcer-free controls^[13-18]. The major factor underlying this association seems to be the impact of cigarette smoking on both diseases. However, a recent pilot study, in a small number of patients, showed that *H. pylori* infection, *per se*, might be implicated in lung cancerogenesis^[19]. It suggested that the prolonged release of gastrin and cyclooxygenase (COX)-2 in *H. pylori* infected patients might account for the stimulation of lung cancer growth and tumor neoangiogenesis^[19]. However, insufficient information is available on the prevalence of *H. pylori* infection in lung cancer patients.

Therefore, in order to further investigate the relationship between *H. pylori* infection and lung cancer, we assessed *H. pylori* seroprevalence in a cohort of Greek patients with lung cancer and control subjects.

MATERIALS AND METHODS

Study subjects

The present study was conducted at the 9th Department of Pulmonary Medicine, "Sotiria" Chest Diseases Hospital (Athens, Greece). The local ethics committee approved the study and written informed consent was obtained from each participant. Following a predefined protocol, between March 1, 2002 and April 30, 2001, 104 consecutive patients with, histologically verified, primary lung cancer were recruited from our department. Exclusion criteria were: (1) prior *Helicobacter* eradication therapy, (2) consumption of acid suppressive drugs or antibiotics in the preceding 6 mo and (3) a history of vagotomy or operations of the upper gastrointestinal tract. A total of 32 patients were excluded. Therefore, 72 patients were eligible for analysis.

Controls were selected randomly from subjects who attended courses designed for public health education during the period of the study. Exclusion criteria for controls were: (1) a known history of lung cancer and (2) a known history of gastrointestinal tract pathology. Finally, we selected 68 controls out of 99 healthy subjects and we matched them with the patients for sex, age (within 2 years) and socioeconomic status.

Methods

All subjects enrolled (lung cancer patients and controls) underwent an enzyme-linked immunosorbent assay (ELISA) IgG serologic test for *H. pylori* diagnosis (HEL-P test, Park Co, Athens, Greece), in accordance with the manufacturer's guidelines. A positive, borderline or negative result was assigned when the concentration of IgG antibodies against *H. pylori* was greater than 25, between 20 and 25 and less than 20 U/mL respectively. The specificity and sensitivity of the serology test, validated in our local population, were 95% and 85% respectively.

Statistical analysis

Results are expressed as mean±SD. Significance of difference between groups was assessed by unpaired Student's *t*-test for continuous variables and χ^2 -test for proportions. Correlation coefficients between variables were determined using conventional

Pearson's correlation analysis. Statistical analysis was performed using SPSS program (SPSS Inc, IL, USA) and *P*-values were two-tailed analyzed. *P* less than 0.05 was considered statistically significant.

RESULTS

The demographic data of both patients and controls are shown in Table 1. There was no statistical difference in age or gender between the two groups. The majority of lung cancer patients were current cigarette smokers (60 patients, 83.3%) or ex-smokers (10 patients, 13.9%) and only 2 patients (2.8%) had never smoked. On the other hand, 40 out of 68 control subjects (58.8%) were never-smokers, 20 (29.4%) were current and 8 (11.8%) were previous smokers.

A correlation between age and *H pylori* IgG level was detected for both lung cancer patients ($r = 0.42$, $P = 0.004$) and controls ($r = 0.44$, $P = 0.004$). Among the lung cancer patients, 44 (61.1%) were anti-*H pylori* IgG positive, 2 (2.8%) had borderline values and 26 (36.1%) were seronegatives. Of the control subjects 38 (55.9%) were anti-*H pylori* IgG positive, 2 (2.9%) were borderline and 28 (41.2%) were seronegatives.

H pylori seropositivity did not differ significantly between patients with lung cancer and controls ($P > 0.05$) (Table 1). Concerning the mean serum concentration of IgG antibodies against *H pylori* no significant difference between the two groups was detected ($P > 0.05$).

Table 1 Demographic data and *H pylori* serologic parameters

Parameter	Control (n = 68)	Lung cancer (n = 72)	<i>P</i>
Age (yr)	54.8±12.1	58.2±11.7	0.79
Male gender (%)	73.5	76.3	0.88
<i>H pylori</i> IgG level (U/mL)	27.4±18.3	32.6±19.1	0.18
<i>H pylori</i> IgG seropositivity (%)	55.9	61.1	0.23

DISCUSSION

Data in literature on the relationship between *H pylori* infection and lung cancer are poor. Recently, Gocyk *et al.* carried out a pilot study in a sample of 50 Polish patients with lung cancer and showed an increased *H pylori* seroprevalence (89%). Moreover, they proposed that the seropositive patients might be considered for *H pylori* eradication in order to reduce the hypergastrinemia and COX-2 expression^[19], provoked by this bacterium. As both overexpression of COX-2 in lung tissue^[20-22] and increased serum levels of gastrin^[23] have been reported in lung cancer patients, a pathogenetic link between *H pylori* infection and lung cancer seems to exist.

Our study is the first one focusing on seroprevalence of *H pylori*, in a relatively large population of Greek patients with lung cancer. According to our results, *H pylori* seroprevalence in lung cancer patients did not differ significantly from that of the control subjects. The age-related pattern of infection, which in our study was detected for both lung cancer patients and controls, was common in developed countries and explained by the cohort effect^[24]. The socioeconomic status, which was related with both *H pylori* infection and risk of lung cancer, was similar between the two groups. Tobacco use could be another confounding factor. Cigarette smoking was the most important etiologic factor of lung cancer and seemed to fully account for the, observed in previous studies, association between peptic ulcer and lung cancer^[13-18]. However, data on the relationship between *H pylori* infection and smoking habits are controversial. The prevalence of *H pylori* infection in smokers has been variously reported as low^[25], normal^[26], and high^[27]. In the present study, we did not match patients with

control subjects in smoking habits. As the relation between smoking and *H pylori* infection has not been clarified yet, the possible impact of cigarette smoking on both lung cancer and *H pylori* infection should be regarded as a potential study limitation.

The present study did not focus on the potential pathogenetic mechanisms underlying a possible association between *H pylori* infection and chronic bronchitis. This association might reflect either susceptibility induced by common factors or a kind of causal relationship between these diseases. As far as we know, there are no common factors implicated in the susceptibility to both lung cancer and *H pylori* infection. However, we can not rule out this possibility, as the predisposing conditions to *H pylori* infection have not been clarified yet. With regard to the aetio-pathogenetic role of *H pylori* infection in lung cancer development, it has been suggested that the prolonged release of gastrin and cyclooxygenase (COX)-2 in *H pylori* infected patients might stimulate lung cancer growth and lead to tumor neoangiogenesis^[19]. The spilling or inhalation of *H pylori* or its exotoxins into the respiratory tract might also lead to their accumulation in lung tissue. However, as far as we know, neither identification of *H pylori* species in human bronchial tissue, nor isolation of *H pylori* from bronchoalveolar lavage (BAL) fluid has been achieved yet^[24]. Studies estimating the relative risk of developing lung cancer for *H pylori* infected patients and the effect of *H pylori* eradication on the natural history of chronic bronchitis are also needed to further investigate these hypotheses.

In conclusion, the present study suggests that *H pylori* seroprevalence in lung cancer patients did not differ significantly from that of control subjects. Our results should be confirmed in a larger number of patients. Further studies are needed to clarify the pathogenetic mechanisms, if those exist, underlying a possible association between these two diseases.

REFERENCES

- Mitchell H, Megraud F. Epidemiology and diagnosis of *Helicobacter pylori* infection. *Helicobacter* 2002; 7(Suppl 1): 8-16
- Cave DR. Chronic gastritis and *Helicobacter pylori*. *Semin Gastrointestinal Dis* 2001; 12: 196-202
- Cohen H. Peptic ulcer and *Helicobacter pylori*. *Gastroenterol Clin North Am* 2000; 29: 775-789
- Eslick GD, Lim LL, Byles JE, Xia HH, Taley NJ. Association of *Helicobacter pylori* infection with gastric carcinoma: a meta-analysis. *Am J Gastroenterol* 1999; 13: 1295-1302
- Parsonnet J, Hansen S, Rodriguez L, Gelb AB, Warnke RA, Jellum E, Orentreich N, Vogelmann JH, Friedman GD. *Helicobacter pylori* and gastric lymphoma. *N Engl J Med* 1994; 330: 1267-1271
- Realdi G, Dore MP, Fastame L. Extradigestive manifestations of *Helicobacter pylori* infection. Fact and fiction. *Dig Dis Sci* 1999; 44: 229-236
- Gasbarrini A, Franceschi F, Armuzzi A, Ojetti V, Candelli M, Sanz Torre E, Lorenzo AD, Anti M, Pretolani S, Gasbarrini G. Extradigestive manifestations of *Helicobacter pylori* gastric infection. *Gut* 1999; 45(Suppl 1): 9-12
- Tsang KW, Lam SK, Lam WK, Karlberg J, Wong BC, Yew WW, Ip MS. High seroprevalence of *Helicobacter pylori* in active bronchiectasis. *Am J Resp Crit Care Med* 1998; 158: 1047-1051
- Gaselli M, Zaffoni E, Ruina M, Sartori S, Trevisani L, Ciaccia A, Alvisi V, Fabbri L, Papi A. *Helicobacter pylori* and chronic bronchitis. *Scand J Gastroenterol* 1999; 34: 828-830
- Roussos A, Tsimpoukas F, Anastasakou E, Alepopoulou D, Paizis I, Philippou N. *Helicobacter pylori* seroprevalence in patients with chronic bronchitis. *J Gastroenterol* 2002; 37: 332-335
- Filippou N, Roussos A, Tsimboukas F, Tsimogianni A, Anastasakou E, Mavrea S. *Helicobacter pylori* seroprevalence in patients with pulmonary tuberculosis. *J Clin Gastroenterol* 2002; 34: 189

- 12 **Roussos A**, Philippou N, Gourgoulialis KI. *Helicobacter pylori* infection and respiratory diseases: a review. *World J Gastroenterol* 2003; **9**: 5-8
- 13 **Viskum K**. Peptic ulcer and pulmonary disease. *Scand J Respir Dis* 1974; **55**: 284-290
- 14 **Bonnevie O**. Causes of death in duodenal and gastric ulcer. *Gastroenterology* 1977; **73**: 1000-1004
- 15 **Hole DJ**, Quigley EM, Gillis CR, Watkinson G. Peptic ulcer and cancer. *Scand J Gastroenterol* 1987; **22**: 17-23
- 16 **Moller H**, Toftgaard C. Cancer occurrence in a cohort of patients surgically treated for peptic ulcer. *Gut* 1991; **32**: 740-744
- 17 **Caygill CP**, Knowles RL, Hall R. Increased risk of cancer mortality after vagotomy for peptic ulcer: a preliminary analysis. *Eur J Cancer Prev* 1991; **1**: 35-37
- 18 **Svanes C**, Lie SA, Lie RT, Soreide O, Svanes K. Causes of death in patients with peptic ulcer perforation: a long-term follow-up study. *Scand J Gastroenterol* 1999; **34**: 18-24
- 19 **Gocyk W**, Niklinski T, Olechnowicz H, Duda A, Bielanski W, Konturek PC, Konturek SJ. *Helicobacter pylori*, gastrin and cyclooxygenase-2 in lung cancer. *Med Sci Monit* 2000; **6**: 1085-1092
- 20 **Koki A**, Khan NK, Woerner BM. Cyclooxygenase-2 in human pathological disease. *Adv Exp Med Biol* 2002; **507**: 177-184
- 21 **Ermert L**, Dierkes C, Ermert M. Immunohistochemical expression of cyclooxygenase isoenzymes and downstream enzymes in human lung tumors. *Clin Cancer Res* 2003; **9**: 1604-1610
- 22 **Fang HY**, Lin TS, Lin JP, Wu YC, Chow KC, Wang LS. Cyclooxygenase-2 in human non-small cell lung cancer. *Eur J Surg Oncol* 2003; **29**: 171-177
- 23 **Zhou Q**, Zhang H, Pang X, Yang J, Tain Z, Wu Z, Yang Z. Pre- and postoperative sequential study on the serum gastrin level in patients with lung cancer. *J Surg Oncol* 1992; **51**: 22-25
- 24 **Peterson WL**, Graham DY. *Helicobacter pylori*. In: Feldman M, Scharschmidt BF, Sleisenger MH, eds. *Gastrointestinal and liver Disease. Pathophysiology, Diagnosis, Management*. 6th ed. Philadelphia: *WB Saunders* 1998: 604-619
- 25 **Ogihara A**, Kikuchi S, Hasegawa A, Kurosawa M, Miki K, Kaneko E. Relationship between *Helicobacter pylori* infection and smoking and drinking habits. *J Gastroenterol Hepatol* 2000; **15**: 271-276
- 26 **Brenner H**, Rothenbacher D, Bode G, Adler G. Relation of smoking and alcohol and coffee consumption to active *Helicobacter pylori* infection: cross sectional study. *BMJ* 1997; **315**: 1489-1492
- 27 **Parasher G**, Eastwood GL. Smoking and peptic ulcer in the *Helicobacter pylori* era. *Eur J Gastroenterol Hepatol* 2000; **12**: 843-853

Edited by Chen WW and Zhu LH Proofread by Xu FM

Patients with brain metastases from gastrointestinal tract cancer treated with whole brain radiation therapy: Prognostic factors and survival

Susanne Bartelt, Felix Momm, Christian Weissenberger, Johannes Lutterbach

Susanne Bartelt, Department of Radiation Oncology, University of Freiburg, Freiburg i. Br., Germany

Felix Momm, Department of Radiation Oncology, University of Freiburg, Freiburg i. Br., Germany

Christian Weissenberger, Department of Radiation Oncology, University of Freiburg, Freiburg i. Br., Germany

Johannes Lutterbach, Department of Radiation Oncology, University of Freiburg, Freiburg i. Br., Germany

Correspondence to: Susanne Bartelt, M.D., Radiologische Universitätsklinik, Abteilung Strahlenheilkunde, Robert-Koch Strasse 3, 79106 Freiburg, Germany. bartelt@mst1.ukl.uni-freiburg.de

Telephone: +49-761-270-9462 **Fax:** +49-761-270-9582

Received: 2004-02-27 **Accepted:** 2004-04-14

Abstract

AIM: To identify the prognostic factors with regard to survival for patients with brain metastasis from primary tumors of the gastrointestinal tract.

METHODS: Nine hundred and sixteen patients with brain metastases, treated with whole brain radiation therapy (WBRT) between January 1985 and December 2000 at the Department of Radiation Oncology, University Hospital Freiburg, were analyzed retrospectively.

RESULTS: Fifty-seven patients presented with a primary tumor of the gastrointestinal tract (esophagus: $n = 0$, stomach: $n = 10$, colorectal: $n = 47$). Twenty-six patients had a solitary brain metastasis, 31 patients presented with multiple brain metastases. Surgical resection was performed in 25 patients. WBRT was applied with daily fractions of 2 Gray (Gy) or 3 Gy to a total dose of 50 Gy or 30 Gy, respectively. The interval between diagnoses of the primary tumors and brain metastases was 22.6 mo vs 8.0 mo for patients with primary tumors of the colon/rectum vs other primary tumors, respectively ($P < 0.01$, log-rank). Median overall survival for all patients with brain metastases ($n = 916$) was 3.4 mo and 3.2 mo for patients with gastrointestinal neoplasms. Patients with gastrointestinal primary tumors presented significantly more often with a solitary brain metastasis than patients with other primary tumors ($P < 0.05$, log-rank). In patients with gastrointestinal neoplasms ($n = 57$), the median overall survival was 5.8 mo for patients with solitary brain metastasis vs 2.7 mo for patients with multiple brain metastases ($P < 0.01$, log-rank). The median overall survival for patients with a Karnofsky performance status (KPS) ≥ 70 was 5.5 mo vs 2.1 mo for patients with KPS < 70 ($P < 0.01$, log-rank). At multivariate analysis (Cox Model) the performance status and the number of brain metastases were identified as independent prognostic factors for overall survival.

CONCLUSION: Brain metastases occur late in the course of gastrointestinal tumors. Pretherapeutic variables like KPS and the number of brain metastases have a profound influence on treatment outcome.

Bartelt S, Momm F, Weissenberger C, Lutterbach J. Patients with brain metastases from gastrointestinal tract cancer treated with whole brain radiation therapy: Prognostic factors and survival. *World J Gastroenterol* 2004; 10(22): 3345-3348 <http://www.wjgnet.com/1007-9327/10/3345.asp>

INTRODUCTION

The metastatic dissemination of a solid tumor to the brain is generally associated with a poor prognosis^[1]. The most common primary tumors metastasizing to the brain are breast and lung cancer, whereas patients with other primary tumors, e.g. tumors of the gastrointestinal tract, rarely present with brain metastases^[2-4]. Furthermore, within the group of gastrointestinal tumors, the incidence of brain metastases shows notable differences. They are extremely rare in esophageal tumors^[5,6], but more common in rectal cancer. Few literatures concerning this group of patients are available and therefore prognosis and hence treatment strategies remain controversial.

We retrospectively evaluated patient-, tumor- and treatment-related variables in patients with brain metastases of primary tumors of the gastrointestinal tract (i.e. epithelial tumors of the esophagus, stomach, colon, sigma, and rectum) who were treated with whole brain radiation therapy (WBRT) at our institution. The aim of the study was to identify the prognostic factors with regard to the endpoint survival.

MATERIALS AND METHODS

The records of all patients with brain metastases, who were treated with WBRT at our institution between January 1985 and December 2000, were analyzed retrospectively. Brain metastases were detected by contrast-enhanced cerebral computed tomography (CT) ($n = 43$) or magnetic resonance imaging (MRI) ($n = 14$).

WBRT was performed in 16 patients with cobalt⁶⁰ gamma rays, and in 41 patients with 6 MV photons of a linear accelerator. During the study period two fractionation schemes were used: conventional fractionation with daily fractions of 2 Gray (Gy), five days per week to a planned total dose of 50 Gy ($n = 42$) and since 1997 hypofractionation with daily fractions of 3 Gy, five days per wk to a planned total dose of 30 Gy ($n = 15$). None of the patients underwent a chemotherapy during WBRT.

The recursive partitioning analysis (RPA) was used to classify the patients with brain metastases^[7]. Class I contained all patients with a Karnofsky performance status (KPS) ≥ 70 , age < 65 years, a controlled primary tumor and no extracerebral metastases), Class III contained all patients with a KPS < 70 , and Class II contained all other patients.

All patients alive at the time of analysis were censored with the date of last follow-up. The endpoint of the study was overall survival. Survival was calculated from the first day of radiotherapy using the method of Kaplan and Meier. Survival curves were compared using the log-rank test. All factors with a P -value ≤ 0.1 at univariate analysis were entered into a multivariate analysis using the proportional hazards model.

RESULTS

Patient characteristics

Fifty-seven (6.2%) of the 916 patients presented with brain metastases from a cancer of the gastrointestinal tract. The exact localization of the primary tumor is shown in Table 1. None of the patients had an esophageal tumor, the most common primary site was rectum ($n = 24$) and colon/sigma ($n = 23$). In all patients, histology obtained either from the primary tumor, brain metastases or from extracerebral metastases, was adenocarcinoma.

Table 1 Site of primary tumor within gastrointestinal tract¹

Site of primary tumor	n (%)
Esophagus	0 (0)
Stomach	10 (17.5)
Colon	17 (30)
Sigma	6 (10.5)
Rectum	24 (42)

¹Esophagus, stomach, colon, sigma, rectum.

Thirty patients were males, 27 females. Their median age at diagnosis was 65 years (range: 30-80 years). Twenty-nine patients (51%) had a KPS ≥ 70 . Twenty-six patients (46%) had a solitary brain metastasis, 31 (54%) had multiple lesions. Location of the metastases is shown in Table 2. Gross total resection was performed in 25 patients (19 patients with single metastasis, six patients with multiple metastases).

Table 2 Location of brain metastases

Location	n (%)
Single lesion	26 (100)
Frontal	4 (15)
Temporal	1 (4)
Parietal	6 (23)
Occipital	1 (4)
Cerebellum	14 (54)
Brainstem	0 (0)
Multiple lesions	31 (100)
Supratentorial	20 (64)
Infratentorial	3 (10)
Both	5 (16)
Unknown	3 (10)

All patients presented with extracerebral metastases, mostly of the lung and/or the liver. Grouped according to the RPA classes, none of the patients met the criteria for class I. Twenty-nine patients (51%) met the criteria for class II. Twenty-eight patients (49%) presented with a KPS < 70 , and therefore belonged to RPA class III.

Patients with a primary tumor of the gastrointestinal tract presented with a solitary brain metastasis significantly more often (46%) than patients with other primary tumors (30%) ($P < 0.05$, χ^2). In patients with a primary tumor of the gastrointestinal tract, 25% (14 of 43 patients) had a solitary metastasis localized in the cerebellum, whereas the localization of solitary metastases in the cerebellum in patients with other primary tumors was 5% (42 of 805 patients). This difference was statistically significant ($P < 0.01$). Other locations of brain metastases were not significantly different between these two groups.

The time from the diagnosis of primary tumors to the diagnosis of brain metastases was 16.3 mo, 27 mo, and 20 mo in patients with gastric carcinoma, colon carcinoma, and rectum carcinoma, respectively, and showed no statistically significant difference. Compared with patients with other primary tumors, patients

with primary tumors of the colon/rectum had a significant longer interval between the diagnoses of primary tumors and brain metastases (22.6 mo vs 8.0 mo, respectively, $P < 0.01$).

Survival data

The median overall survival (OS) time for patients with a primary tumor of the gastrointestinal system was 3.2 mo and showed no significant difference compared to the overall survival time of 3.5 mo for patients with brain metastases and other primary tumors (Figure 1). OS rate for patients with gastrointestinal tumors was 49%, 30%, and 7%, at 3, 6, and 12 mo, respectively. Within the group of gastrointestinal tumors, patients with a primary tumor of the stomach, colon/sigma, and rectum had a median OS time of 2.7, 5.2, and 3.2 mo, respectively. This was not a statistically significant difference.

Prognostic factors

The potential prognostic factors tested for significance in univariate analysis were sex, age ($\geq / < 65$ years), pretherapeutic performance status (KPS $\geq / < 70$), number (single vs multiple) and distribution of brain metastases (Table 2), extracerebral tumor activity (yes vs no), resection status (operation yes vs no), and fractionation scheme (conventional fractionation vs hypofractionation). The fractionation scheme (2 Gy daily, 50 Gy total dose vs 3 Gy daily, 30 Gy total dose) showed no statistical significance for OS.

Three factors had a P -value ≤ 0.1 in univariate analysis and were entered into multivariate analysis: pretherapeutic performance status, number of brain metastases, and resection status. Concerning the OS, patients with a KPS ≥ 70 had a median OS time of 5.5 mo vs 2.1 mo for patients with a KPS < 70 ($P < 0.01$) (Figure 2). The same values were found by comparing the patients in RPA class II vs RPA class III. The median OS time for patients with a solitary metastasis was 5.8 mo and 2.7 mo for patients with multiple metastases ($P < 0.01$) (Figure 3). The median OS time for patients with resection of brain metastasis was 6.6 mo and 2.7 mo for patients without resection ($P < 0.01$).

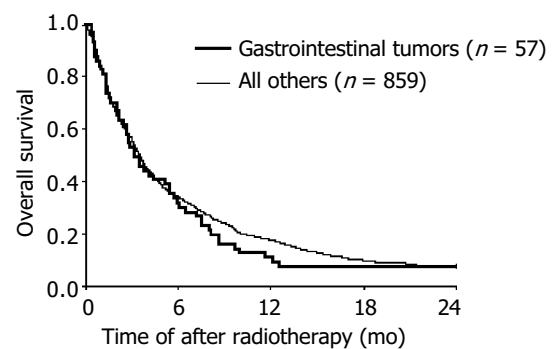


Figure 1 Overall survival according to primary tumor.

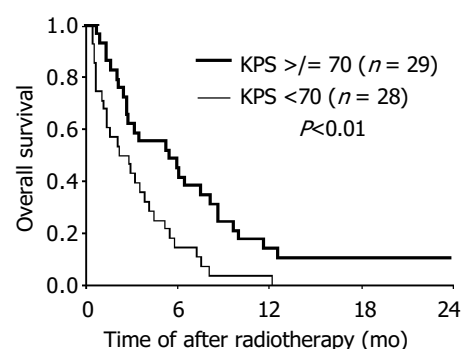


Figure 2 Overall survival according to KPS (≥ 70 vs < 70).

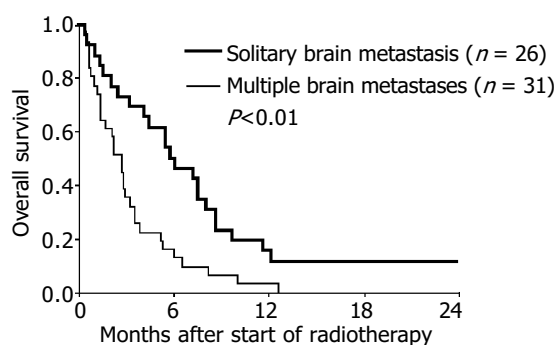


Figure 3 Overall survival according to the number of brain metastases (solitary vs multiple).

In the first multivariate model limited to pretherapeutic variables, the number of brain metastases (single *vs* multiple, relative risk [RR] 0.63, 95% confidence interval [KI] 0.45-0.88) and the KPS (≥ 70 *vs* < 70 , RR 0.59, 95% KI 0.42-0.82) turned out to be independent prognostic factors. In the second multivariate analysis we added the therapeutic variable 'resection'. The KPS and the number of brain metastases were still independent prognostic factors (RR 0.59, 95% KI 0.43-0.79, $P < 0.01$ and RR 0.65, 95% KI 0.45-0.90, $P < 0.05$ respectively), whereas resection status was not a prognostic factor.

DISCUSSION

In our series, 6.2 % of the patients treated with WBRT presented with a primary tumor located in the gastrointestinal tract. None of the 916 patients had a primary esophageal carcinoma. Brain metastases from esophageal carcinoma were extremely rare, with a reported incidences of approximately 1-5% in autopsy series^[8,9], and approximately 1-4% in clinical series^[5,6,10,11].

In ten patients the primary tumor was a gastric carcinoma. The majority of publications on brain metastases from gastric carcinoma were case reports^[12]. Two large studies found 0.7% of 3 320 patients, and 0.16% of 8 080 patients with gastric carcinoma to have brain metastases^[13,14]. In an autopsy series by Poser and Chernik, 5 of 46 patients (10.8%) with gastric carcinoma had brain metastases^[2]. The rarity of brain metastases both from esophageal and gastric cancer might result from the grim prognosis of these tumor entities^[15]. In esophageal cancer, brain metastases tended to occur in patients with large primary tumors^[5], usually implicating a short overall OS time. The low incidence in clinical trials might further result from an inadequate diagnostic evaluation, and symptoms indicating brain pressure like nausea and vomiting might be attributed to the primary tumor^[14]. The reason for the relatively high incidence of brain metastases from gastric cancer in our group is not clear. Gastric carcinoma is rare in Europe compared to Asian countries. In half of our patients gastric carcinoma was a gastric cardia carcinoma, and recent studies suggested, that they were distinct from adenocarcinomas of the esophagus and stomach regarding epidemiological and biological factors^[16-18]. These differences could possibly be associated with other pathways of metastatic spread, resulting in a relatively higher incidence of brain metastases.

Forty-seven patients had a primary colorectal carcinoma. The incidence of brain metastases in colorectal cancer ranged 2-10% in clinical studies^[19-21]. As observed in other studies^[14,21,22], the majority of primary tumors in our patients were located in the distal parts of the colon, i.e. sigma and rectum (64%). Significantly more patients with colorectal primary tumors presented with cerebellar metastases compared to patients with other primary tumors (25% *vs* 5%, respectively, $P < 0.01$). Studies by Wronski and Alden confirmed this finding, with a frequency for infratentorial location of 35% and 55%, respectively^[21,23]. The relative over-representation of cerebellar metastases in

colorectal carcinoma might be due to tumor spread by way of the vertebral system (i.e. Batson's plexus), bypassing the lungs^[24]. The two other possible routes of hematogenous dissemination of colorectal cancer to the brain were via the rectal vein plexus to the inferior vena cava, bypassing the liver, or via the portal veins to the liver and lung and then to the brain^[20,25]. The incidence of pulmonary metastases in our patients with colorectal cancer was 50% (23/46 patients), which was clearly higher than the approximately 30% for patients with metastatic colorectal cancer^[26], an observation also made in others^[19-21]. Presumably the rectal plexus of veins, draining into the inferior vena cava and subsequently the lung are also an important route for tumor spread to the brain.

The interval between the diagnosis of primary tumor and brain metastases in our study group for patients with gastric and colorectal carcinoma was significantly longer (22.6 mo) than that for patients with other primary tumors (8.0 mo). Although only few larger studies on patients with colorectal carcinoma and brain metastases are available to date, all reported a late onset of brain metastases, with a period ranging 21-36 mo between detection of primary tumors and diagnosis of brain metastases^[19-21,23,27-29] (the larger studies on gastric cancer did not give detailed information on this topic^[13,14,30]). Corresponding to the late onset of brain metastases in the clinical course of gastric and colorectal tumors, all of our patients had further extracerebral metastases (consequently none of our patients was qualified for RPA-class I). The high rate of extracerebral metastases was confirmed by most authors^[19-23,28,31,32] and even represented the most important prognostic factor in the study of Nieder *et al.*^[31].

Although the onset of brain metastases in our patients with gastrointestinal tumors was late, and the systemic disease was advanced, its median OS time was not statistically different from the median OS time of patients with brain metastases of other primary tumors (3.2 *vs* 3.5 mo, respectively). It was comparable to the median OS time for patients with brain metastases and colorectal carcinoma or gastric carcinoma treated with WBRT seen by others, which ranged from 2.0 to 3.6 mo for colorectal carcinoma^[20,22,23,32] and approximately 2 mo for gastric carcinoma^[13,14]. Hasegawa, in contrary, found a shorter survival time in a radiosurgically treated series of patients with gastrointestinal tumors compared to patients with other primary tumors^[27]. Several authors described a longer median OS time of approximately 9 mo for patients who underwent surgical resection of brain metastases as a sole treatment or followed by radiotherapy^[21,22,27,32,33]. Whereas resection of brain metastases seemed to be a favorable prognostic factor in our patients in univariate analysis, it was not statistically significant in multivariate analysis.

The independent factors correlated with a better prognosis in our multivariate analysis were a KPS ≥ 70 , and the presence of a solitary brain metastasis. It has been widely accepted that the pretherapeutic performance status is one of the most powerful predictive factors for the survival of patients with brain metastases^[7,34-38] which could be validated for patients with brain metastases from gastrointestinal tumors in our study group. The more favourable prognosis for patients with primary tumors of the gastrointestinal system presenting with a solitary brain metastasis was also found by Farnell *et al.*^[32], whereas others only found the surgical resection of brain metastases to be associated with a better survival^[19,23,27]. In our second multivariate analysis, including the therapeutic variable 'resection' status could not be identified as an independent prognostic factor, as mentioned above. In order to diagnose brain metastases in an early phase, in which a resection could still be possible, discrete symptoms hinting cerebral tumor spread should be taken seriously.

A basic problem concerning treatment recommendations for patients with brain metastases of gastrointestinal tumors is that to date only few retrospective studies with a relatively small

number of patients are available. Therefore, the results concerning the prognostic factors should be regarded with caution. The different prognostic factors from each study should be kept in mind when considering a therapeutic concept for individual patients.

In conclusion, brain metastasis is a late event in the course of gastrointestinal tumors, and it occurs later as in patients with other primary tumors. However, the overall survival time is comparable to patients with brain metastases from other primary tumors. Independent prognostic factors in our group were KPS and the number of brain metastases.

REFERENCES

- Nussbaum E, Djalilian H, Cho K, Hall W. Brain metastases. histology, multiplicity, surgery, and survival. *Cancer* 1996; **78**: 1781-1788
- Posner J, Chernik N. Intracranial metastases from systemic cancer. *Adv Neurol* 1978; **19**: 579-592
- Sadahiro S, Suzuki T, Ishikawa K, Nakamura T, Tanaka Y, Masuda T, Mukoyama S, Yasuda S, Tajima T, Makuuchi H, Murayama C. Recurrence patterns after curative resection of colorectal cancer in patients followed for a minimum of ten years. *Hepatogastroenterology* 2003; **50**: 1362-1366
- Weiss L, Grundmann E, Torhorst J, Hartveit F, Moberg I, Eder M, Fenoglio-Preiser C, Napier J, Horne C, Lopez M. Hematogenous metastatic patterns in colonic carcinoma: an analysis of 1 541 necropsies. *J Pathol* 1986; **150**: 195-203
- Ogawa K, Takafumi T, Sueyama H, Nobukazu F, Kakinohana Y, Kamata M, Adachi G, Saito A, Yoshii Y, Murayama S. Brain metastases from esophageal carcinoma. *Cancer* 2002; **94**: 759-764
- Quint L, Hepburn L, Francis I, Whyte R, Orringer M. Incidence and distribution of distant metastases from newly diagnosed esophageal carcinoma. *Cancer* 1995; **76**: 1120-1125
- Gaspar L, Scott C, Rotman M, Asbell S, Phillips T, Wasserman T, McKenna W, Byhardt R. Recursive partitioning analysis (RPA) of prognostic factors in three radiation therapy oncology group (RTOG) brain metastases trials. *Int J Radiat Oncol Biol Phys* 1997; **37**: 745-751
- Mandard A, Chasle J, Marnay J, Villedieu B, Bianco C, Roussel A, Elie H, Vernhes J. Autopsy findings in 111 cases of esophageal cancer. *Cancer* 1981; **48**: 329-335
- Bosch A, Frias Z, Caldwell W, Jaeschke W. Autopsy findings in carcinoma of the esophagus. *Acta Radiol Oncol Radiat Phys Biol* 1979; **18**: 103-112
- Gabrielsen T, Eldevik O, Orringer M, Marshall B. Esophageal carcinoma metastatic to the brain: clinical value and cost-effectiveness of routine enhanced head CT before esophagectomy. *Am J Neuroradiol* 1995; **16**: 1915-1921
- Weinberg J, Suki D, Hanbali F, Cohen Z, Lenzi R, Sawaya R. Metastasis of esophageal carcinoma to the brain. *Cancer* 2003; **98**: 1925-1933
- Perri F, Bisceglia M, Giannatempo G, Andriulli A. Cerebellar Metastasis as a unique presenting feature of gastric cancer. *J Clin Gastroenterol* 2001; **33**: 80-81
- York J, Stringer J, Ajani J, Wildrick D, Gokaslan Z. Gastric cancer and metastasis to the brain. *Ann Surg Oncol* 1999; **6**: 771-776
- Kim M. Intracranial involvement by metastatic advanced gastric carcinoma. *J Neurooncol* 1999; **43**: 59-62
- Brenner H. Long-term survival rates of cancer patients achieved by the end of the 20th century: a period analysis. *Lancet* 2002; **360**: 1131-1135
- Wang LD, Zheng S, Zheng ZY, Casson AG. Primary adenocarcinomas of lower esophagus, esophagogastric junction and gastric cardia: in special reference to China. *World J Gastroenterol* 2003; **9**: 1156-1164
- Powell J, McConkey C. Increasing incidence of adenocarcinoma of the gastric cardia and adjacent sites. *Br J Cancer* 1990; **62**: 440-443
- Blot W, Devesa S, Kneller R, Fraumeni F. Rising increase of adenocarcinoma of the esophagus and gastric cardia. *JAMA* 1991; **265**: 1287-1289
- Ko F, Lui J, Chen W, Chiang J, Lin T, Lin J. Risk and patterns of brain metastases in colorectal cancer: 27-year experience. *Dis Colon Rectum* 1999; **42**: 1467-1471
- Cascino T, Leavengood J, Kemeny N, Posner J. Brain metastases from colon cancer. *J Neurooncol* 1983; **1**: 203-209
- Wronski M, Arbit E. Resection of brain metastases from colorectal carcinoma in 73 patients. *Cancer* 1999; **85**: 1677-1685
- Hammoud M, McCutcheon I, Elsouki R, Schoppa D, Patt Y. Colorectal carcinoma and brain metastasis: distribution, treatment, and survival. *Ann Surg Oncol* 1996; **3**: 453-463
- Alden T, Gianino J, Saclarides T. Brain Metastases from colorectal cancer. *Dis Colon Rectum* 1996; **39**: 541-545
- Batson O. The role of the vertebral veins in metastatic processes. *Ann Intern Med* 1942; **16**: 38-45
- Burns F, Pfaff JJ. Vascular invasion in carcinoma of the colon and rectum. *Am J Surg* 1956; **92**: 704-710
- Copeland E, Miller L, Jones R. Prognostic factors in carcinoma of the rectum and colon. *Am J Surg* 1968; **116**: 875-881
- Hasegawa T, Kondziolka D, Flickinger J, Lunsford L. Stereotactic Radiosurgery for brain metastases from gastrointestinal tract cancer. *Surg Neurol* 2003; **60**: 506-515
- Zorrilla M, Alonso V, Herrero A, Corral M, Puertolas T, Trufero J, Artal A, Anton A. Brain metastases from colorectal carcinoma. *Tumori* 2001; **87**: 332-334
- Zulkowski K, Kath R, Liesenfeld S, Patt S, Hochstetter A, Behrendt W, Höffken K. Zerebrale metastasen bei kolorektalen karzinomen. *Med Klin* 2002; **97**: 327-334
- Kasakura Y, Fujii M, Mochizuki F, Suzuki T, Takahashi T. Clinicopathological study of brain metastasis in gastric cancer patients. *Surg Today* 2000; **30**: 485-490
- Nieder C, Niewald M, Schnabel K. Brain metastases of colon and rectum carcinomas. *Wien Klin Wochenschr* 1997; **109**: 239-243
- Farnell G, Buckner J, Cascino T, O'Connell M, Schomberg P, Suman V. Brain metastases from colorectal carcinoma. The long term survivors. *Cancer* 1996; **78**: 711-716
- D'Andrea G, Isidori A, Caroli E, Orlando E, Salvati M. Single cerebral metastasis from colorectal adenocarcinoma. *Neurosurg Rev* 2004; **27**: 55-57
- Lutterbach J, Bartelt S, Ostertag C. Long-term survival in patients with brain metastases. *J Cancer Res Clin Oncol* 2002; **128**: 417-425
- Lutterbach J, Cyron D, Henne K, Ostertag C. Radiosurgery followed by planned observation in patients with one to three brain metastases. *Neurosurgery* 2003; **52**: 1066-1073
- Nieder C, Nestle U, Motaref B, Walter K, Niewald M, Schnabel K. Prognostic factors in brain metastases: should patients be selected for aggressive treatment according to recursive partitioning analysis (RPA) classes? *Int J Radiat Oncol Biol Phys* 2000; **46**: 297-302
- Lohr F, Pirzkall A, Hof H, Fleckenstein K, Debus J. Adjuvant treatment of brain metastases. *Semin Surg Oncol* 2001; **20**: 50-56
- Schoeggel A, Kitz K, Reddy M, Zauner C. Stereotactic radiosurgery for brain metastases from colorectal cancer. *Int J Colorectal Dis* 2002; **17**: 150-155

Development and distribution of mast cells and neuropeptides in human fetus duodenum

Xiao-Yu Chen, Xue-Mei Jia, You-Su Jia, Xiao-Rong Chen, Hui-Zhu Wang, Wei-Qin Qi

Xiao-Yu Chen, Xue-Mei Jia, You-Su Jia, Xiao-Rong Chen, Hui-Zhu Wang, Wei-Qin Qi, Department of Histology and Embryology, Anhui Medical University, Hefei 230032, Anhui Province, China
Supported by Youth Teacher Science and Technology Educational Foundation of Anhui Province, No. 2003jq124; National Natural Science Foundation of Anhui Province, No. 2003kj187

Correspondence to: Dr. Xiao-Yu Chen, Department of Histology and Embryology, Anhui Medical University, Hefei 230032, Anhui Province, China. chenxiaoyuzlx@163.com

Telephone: +86-551-5161135

Received: 2003-06-04 **Accepted:** 2003-11-06

Abstract

AIM: To study the developmental regularities and heterogeneity of mast cells (MC) in human fetus duodenum and the distribution and developmental regularities of substance P(SP), calcitonin gene-related peptide (CGRP)-immunoreactive (IR) peptidergic nerves in fetus duodenum, as well as the relationship between MC, SP and CGRP-IR peptidergic nerves.

METHODS: Duodena from 21 cases of human fetus and one term infant were stained by hematoxylin-eosin (HE), toluidine blue (TB) and immunohistochemical avidin-biotinylated peroxidase complex (ABC) method.

RESULTS: Lobe-shape intestinal villi in duodenum were already developed at the twelfth week. At the 21st wk, muscular mucosa appeared gradually, and four layers were observed in the wall of duodenum. TB staining showed that the granules in the immature MC were pale violet, while the mature MC were strong violet in color by TB staining. Connective tissue MC (CTMC) appeared occasionally in submucosa and muscular layer of duodenum at the 16th wk. While the mucosa MC (MMC) appeared at the 18th wk. At the 22nd wk, both CTMC and MMC were activated, and distributed in the surrounding blood vessels and ganglions. The verge of some MC were unclear, and showed degranular phenomena. At the 14th wk, SP and CGRP-IR nerve fibers and cells appeared in the myenteric and submucous plexuses in small intestine, and the responses were turn strongly. Neurons were light to deep brown, and nerve fibers were present as varicose and liner profiles. On the corresponding site of serial sections, SP and CGRP immunohistochemical reactions were coexisted in one nerve fiber or cell. Some of MC showed SP and CGRP-IR positive staining.

CONCLUSION: There are two heterogeneous kinds of MC in duodenum, MMC and CTMC. MC might play an important role in regulating blood circulation and sensation.

Chen XY, Jia XM, Jia YS, Chen XR, Wang HZ, Qi WQ. Development and distribution of mast cells and neuropeptides in human fetus duodenum. *World J Gastroenterol* 2004; 10 (22): 3349-3352

<http://www.wjgnet.com/1007-9327/10/3349.asp>

INTRODUCTION

Previous microscopic anatomy studies have shown that somatic and visceral nerves are both widely approached to MC. MC and nerve cells interact with each other by connecting with a lemma or degranular style, so that they could regulate microenvironments. As far as organizations are concerned, the anatomic relation means interaction with function, but no studies are available about the development and distribution of MC and developmental regularities of SP, CGRP-IR nerves and cells in human fetus duodenum. BY investigating the relationship between MC and nerve- endocrine- immunological network^[1-3], we observed the histological changes in human fetus duodenum with HE staining, the developmental regularities and heterogeneity of MC with TB special staining, neuropeptide SP, CGRP by ABC methods, the relations between neuropeptide and MC. The study provided morphology data of the functional significance of mast cells in human fetus duodenum.

MATERIALS AND METHODS

Tissue specimens

Twenty-one fetuses of 3-9 mo old and one dead term infant were randomly collected within 1-5 h after birth, in which 10 were males and 11 were females. Duodena were taken out (near to bulbs), and fixed in 40 g/L formaldehyde for 12 h, cut into 10 mm×5 mm×3 mm, then embedded in paraffin and cut into 5µm thick serial section.

TB special staining

The paraffin embedded sections were deparaffined in serial xylene, dehydrated by alcohol solvents and mounted by xylene transparent neutral gum, then examined by microscopy and photographed.

Immunohistochemistry

The reactions were carried out according to the ABC method as previously reported^[4]. Briefly, the paraffin sections were deparaffined in xylene and graded alcohol. Sections were incubated at room temperature for 10 min with 30 mL/L H₂O₂ solution to block endogenous peroxidase activity. After washed with phosphate buffered saline (PBS) 3 times for 5 min each, slides were digested with trypsin, treated with 3 g/L Triton X-100, followed by incubation with antibodies SP (1:2 000, Sigma) or CGRP (1:1 000, Sigma) at 37 °C for 2 h and at 4 °C for 24 h. The sections were then incubated with biotin-conjugated IgG (diluted in PBS, 1:100) for 2.5 h at room temperature and washed with PBS 3 times for 5 min each, followed by incubation with the streptavidin-peroxidase complex for 1 h. At last, chromogen 3,3'-diaminobenzidine tetrahydrochloride (DAB) (1:50, Wuhan Boster) was added to visualize the reaction products of peroxidase.

The specific neuropeptide antibodies were replaced by PBS or normal rabbit serum for the negative controls. Adult duodenum tissue sections were used as positive controls, which showed immunoreactivity for SP and CGRP.

The results were judged as follows. Pale-yellow was

negative (-), shallow brown was weak positive (+), brown was moderately positive (++) and deep brown was strongly positive (+++).

RESULTS

HE staining

The histological differentiations were found in lobe-shape intestinal villi in duodenum at the 12nd wk. At the 15th wk, duodenal glands of mucous cells were formed in the submucosa. At the 21st wk, muscular mucosa appeared with 4 layers in the wall of duodenum gradually.

TB special staining

The experiments showed that CTMC in submucosa and muscular layer appeared by staining with 5 g/L toluidine blue with 500 mL/L alcohol dyeing for 5 min, but MMC in mucous layer appeared by staining with 5 g/L toluidine blue with one equivalent hydrochloric acid for 5 d. At the 16th wk, CTMC appeared occasionally in submucosa. But the time of MMC appearance was at the 18th wk. The granules in immature MC were pale violet, and strong violet in the mature MC as detected by TB special staining. CTMC in intermuscular appeared fusiform and cell bodies were small. MC in mucosa and submucosa layer were round or oval in shape and cell bodies were large (Figure 1A). With the increase of gestational age, the number of MC in duodenal wall increased gradually. At the 22nd wk, the two types of MC were activated and distributed in the surrounding blood vessels and ganglions. The verge of some MC was unclear, which might be a degranular phenomenon (Figure 1B). MC were closed together with connective tissue cells and there existed lemma connection in fetus duodenal mucous and submucous layer connective tissues.

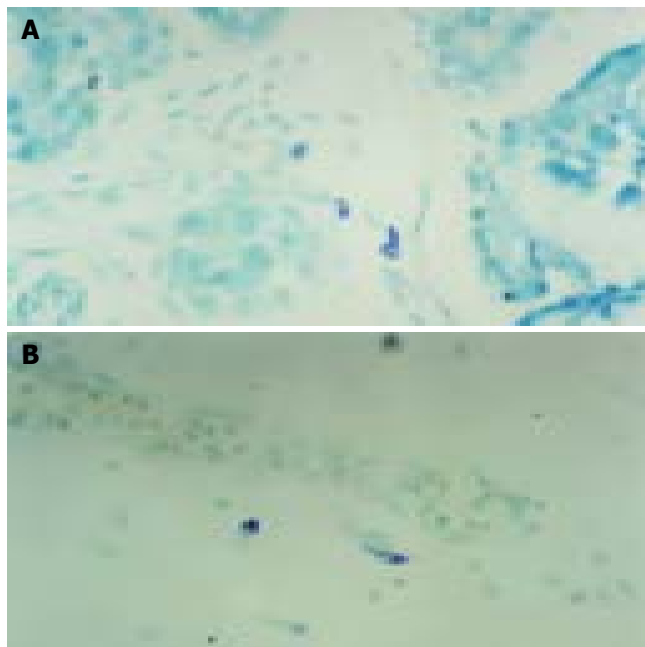


Figure 1 MC in submucous layer at the 21st wk (A) and in mucous layer at the 27th wk (B) of duodenum (TB×400).

Immune phenotype

The degree of positive SP-immunoreactivity (SP-IR) and CGRP-immunoreactivity (CGRP-IR) and their distribution in neurons and nerve fibers (NF) in fetus duodenum had no sex difference. At the 14th wk, SP-IR positive neurons appeared occasionally in the myenteric plexuses of duodenum and neuron cell bodies showed fusiform, few SP-IR-NF appeared

in submucosal layer. But nerve plexuses of CGRP-IR appeared at the 16th wk. Diffused SP and CGRP-IR neurons were appeared in submucous at the 21st wk, pale-brown neuron cell bodies were round or oval in shape and nuclei were negative (Figure 2B). SP-IR-NF response to reinforcement (+ to ++) was found in myenteric connective tissue, showing string pearls in shape. A few CGRP-IR-NF appeared in submucous (+), were showing point line in shape. With the growth of gestational age, nerve fibers were mainly distributed in connective tissue of mucous, submucous and myenteric layers. Nerve plexus density increased, and staining turned deep gradually. The dark black positive nerve plexuses were identified (+++) in fetus duodenum after 34th wk, showing network structures and obvious varicosity (Figure 2B). On the corresponding site of serial sections, SP-IR and CGRP-IR materials were partially coexisted in nerve fibers and neurons. In serial sections of TB histochemistry and ABC immunohistochemistry staining, about 10% MC were SP-IR positive, and less MC were CGRP-IR positive. Some of SP, CGRP-IR-NF positive cells were coexisted with MC, while some were closely contacted.

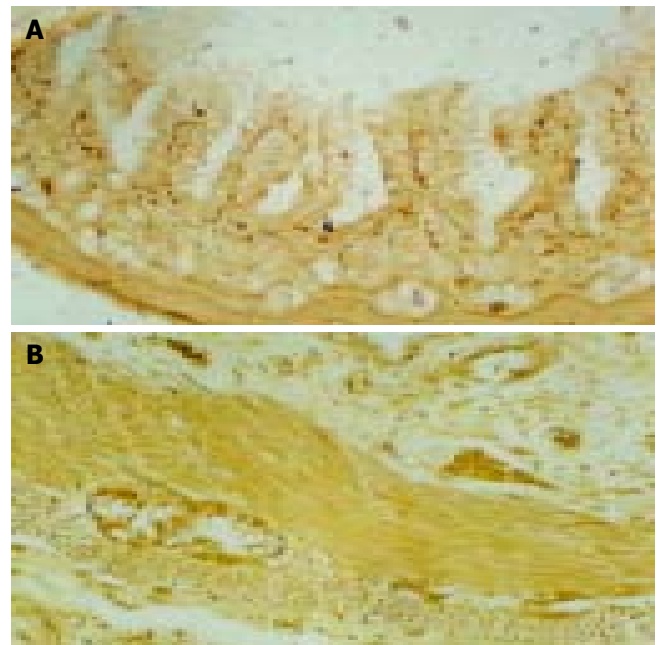


Figure 2 CGRP-IR (+) nerve fiber in duodenum submucous layer at the 21st wk (A) (ABC×100) and SP-IR (++) neuron in duodenum submucous layer and myenteric nerve plexuses at the 28th wk (B) (ABC×200).

DISCUSSION

The results of our experiment showed that there were two kinds of MC in connective tissue of fetus duodenum, namely MMC and CTMC, which possessed heterogeneity. Our results are consistent with Wang *et al.*^[5]. It might be related to many factors such as local microenvironment. The activated MC were localized around cells, small vessels and ganglions in submucosa, showing that MC were related with those cells and tissues. Surface of some MC boundary was not clear. MC showed degranulation, which means that the cells were releasing active media and affecting peripheral environments and cells, so we considered that MC might take part in allergic and other physiological activities during fetus development and maturation of its surrounding tissues and organs. With electron microscope, Li *et al.*^[6] observed MC cytoplasm in intestinal mucosa lamina propria had electron dense round granules and electron-lucent inequality of size vesicles, which

were phenotype of activated MC. MC were important effector cells. It conducted the signal of inflammation cells, and induce the occurrence of mucosa correlated diseases^[7-9]. Previous studies have shown the severity of gastrointestinal allergic diseases, such as *Hp* infection, stomach reflow in duodenum, neuro-psychical factor leading gastro-intestinal functional dyspepsia related with MC, and the more serious the disease, the more obviously increased the numbers of MC^[10,11]. MC could release inflammatory medium, secretory cytokines (IL-2, TNF- α), biologically active molecules through phospholipase A₂ pathway in earlier period of various kinds of enteritis, which could evoke physiological injuries in the intestinal^[12-14]. With the growth of gestational age, the number of MC in bowel wall connective tissue increases gradually, suggesting that MC play an important regulatory role in developing tissue cells in duodenum.

Our experiment showed that the SP-IR and CGRP-IR peptidergic nerves plexus appeared at different time. Owing to the difference of local microenvironments in gastrointestinal tract, various kinds of peptidergic nerves appeared in different time. This difference was decided by local microenvironments of neural crest cells on the way of migration or after its presence. The occurrence of peptidergic nerves was determined by interaction of microenvironmental factors and crest cells. Since different investigators used different specimen source, they adopted different methods and techniques, the detection rate of positive nerve fibers and neurons was different. For example, Larsson *et al.*^[15] reported that CGRP-IR-NF was not observed in fetus duodenum mucosa membrane. But Yang *et al.*^[16] reported that developing fetus from the 13th week showed mild CGRP-IR-NF in myenteric nerve plexus of duodenum. There were differences in the distribution of SP and CGRP peptidergic nerve plexus at the same gestational age. We found that the distribution and response of SP-IR-NF was slightly higher than those of CGRP-IR-NF in myenteric nerve plexus, but CGRP-IR-NF mainly existed in connective tissue of mucosa and submucosa layers, showing that there was a difference in distribution of peptidergic nerve fibers in the same individual organ. They were closely connected with the presence of digestive tract peptidergic nerve. SP peptidergic nerves exist mainly in duodenum myenteric connective tissue. It could activate cholinergic nerve of gastrointestinal tract, cause neurilemma depolarization in myenteric nerve plexus and increase the effect of acetylcholine, resulting in contraction of digestive tract smooth muscle and secretion of glands^[17]. CGRP peptidergic nerves exist mainly in mucous and submucous layers. It is probably related to differentiation of duodenal epithelium and excretion of duodenal gland. CGRP could expand blood vessels of gastrointestinal tract and increase capillary permeability. CGRP could inhibit smooth muscles of gastrointestinal tract and cause relaxation of circular and longitudinal muscles and decrease duodenum vermication^[18]. Previous studies have reported that decrease of the level of serum CGRP might be related to *Hp* infection, leading to occurrence of duodenal ampulla ulcer^[19]. By observing adjacent sections, we found there was partial concordance in localization of SP-IR and CGRP-IR positive neurons. Therefore it is possible that SP and CGRP neurotransmitters coexist in peptidergic nerves. In previous studies, besides the coexistence of CGRP, cells of SP, somatostatin, vasoactive intestinal peptide (VIP) and neuropeptide Y were also coexisted in thymus, sensory ganglion and other organs^[18,20,21]. Because SP, CGRP peptidergic nerve fibers project very extensive in central nervous system, it is possible that these neuropeptides together with nervous system produce an important effect on sensation, movement, endocrine and other aspects. Gastrointestine SP, CGRP could regulate stability of MC, which might play an important role in keeping homeostasis the occurrence and development of

many pathologic alternations.

There are a lot of MC in connective tissue of human duodenum. Meanwhile, there also existed a huge nervous system, including rich peptidergic neurotransmitters^[22,23]. Those made it possible to connect adequate information between MC and nervous system. Gastrointestinal mucous MC are next to gastrointestinal nervous system. It provides double directions of channel between center nervous system and intestinal tract. Thus nervous system can influence physiological functions of gastrointestinal tract. MC could also stimulate intestinal neurons and smooth muscle cells by releasing various kinds of media^[24,25]. By electron microscopy some researchers found lemma connection was existed between MC plasmalemma and axon of nonmyelinated nerve fibers in enteron mucosa, form "plywood structure" and synaptic connection^[6,26]. As far as organ is concerned, that MC closely contacted with nerves in anatomy means interaction of function by releasing certain active substances, such as histamine, nitrogen monoxide *etc.*, as transmitters; On the other hand, nerves could affect MC growth and development. Animal experiments confirmed that the number of MMC and CTMC could be increased by nerve growth factor (NGF), moreover, NGF receptors have been discovered on the surface of MC in rat belly^[27]. It has been confirmed that SP and VIP are coexisted in MC^[28]. Jia *et al.*^[29-31] observed MC in mouse submandibular glands or tongue, and found that most of the MC were SP-IR positive, and 14% MC were CGRP-IR positive. In our studies, we observed that about 10% MC in the wall of fetus duodenum were SP-IR positive, but fewer MC were CGRP-IR positive, indicating that MC in different species and organs contain different peptidergic activity substances. Thus, MC in fetus duodenum possess heterogeneity, whose physiological significance needs further research.

REFERENCES

- 1 Delgado M, Martinez C, Leceta J, Garrido E, Gomariz RP. Differential VIP and VIP1 receptor gene expression in rat thymocyte subsets. *Peptides* 1996; **17**: 803-807
- 2 Wang ZH, Chang XT, Fu XB. Relationship of small intestinal stem cells proliferation differentiation and development. *Shijie Huaren Xiaohua Zazhi* 2001; **9**: 1445-1448
- 3 Ward SM, Ordog T, Bayguinov JR, Horowitz B, Epperson A, Shen L, Westphal H, Sanders KM. Development of interstitial cells of Cajal and pacemaking in mice lacking enteric nerves. *Gastroenterology* 1999; **117**: 584-594
- 4 Nakajima S, Krishnan B, Ota H, Segura AM, Hattori T, Graham DY, Genta RM. Mast cell involvement in gastritis with or without *Helicobacter pylori* infection. *Gastroenterology* 1997; **113**: 746-754
- 5 Wang JX, Li JY, Zhang FJ, Zhang HW, Su JQ. Distribution of mast cells in adult porcine colon. *Zhongguo Shouyi Zazhi* 2001; **37**: 5-7
- 6 Li ZS, Dong WS, Zou DW, Zou XP, Zhang WJ. Enteromucosal mast cells in patients with irritable bowel syndrome. *Jiefangjun Yixue Zazhi* 2002; **27**: 628-630
- 7 Metcalfe DD, Baram D, Mekori YA. Mast cells. *Physiol Rev* 1997; **77**: 1033-1079
- 8 Drake-Lee AB, Price J. Ultrastructure of nasal mast cells in normal subjects and patients with perennial allergic rhinitis. *J Laryngol Otol* 1991; **105**: 1006-1013
- 9 Zhu LR, Li QX, Hou XH. Increase in the number of gastric mucosal mast cells in patients with functional dyspepsia. *Weichangbingxue* 2002; **7**: 27-29
- 10 Gu CM, Ke MY, Zhang SQ, Jiang YX, Liu YP. An tropyloroduodenal dyscoordination in functional dyspepsia studied by color Doppler flow imaging. *Zhonghua Neike Zazhi* 1998; **37**: 511-514
- 11 Li W, Zheng TZ, Qu SY. Effect of cholecystokinin and secretin on contractile activity of isolated gastric muscle strips in guinea pigs. *World J Gastroenterol* 2000; **6**: 93-95
- 12 Beil WJ, Schulz M, McEuen AR, Buckley MG, Walls AF. Number, fixation properties, dye-binding and protease expression of duodenal mast cells: comparisons between healthy subjects and

- patients with gastritis or Crohn's disease. *Histochem J* 1997; **29**: 759-773
- 13 **Pool V**, Braun MM, Kelso JM, Mootrey G, Chen RT, Yunginger JW, Jacobson RW, Gargiullo PM. Prevalence of anti-gelatin IgE antibodies in people with anaphylaxis after measles-mumps rubella vaccine in the United States. *Pediatrics* 2002; **110**: E71
- 14 **Gu CM**. Progress of study on gastrointestinal motility. *Shijie Yixue Zazhi* 1999; **3**: 82-85
- 15 **Larsson LT**, Helm G, Malmfors G, Sundler F. Ontogeny of peptide-containing neurons in human gut—an immunocytochemical study. *Regul Pept* 1987; **17**: 243-256
- 16 **Yang T**, Cai WQ. Ontogeny of 6 types of peptidergic nerves of small intestine in human fetuses. *Jiepu Xuebao* 1994; **25**: 84-87
- 17 **Lu CL**. Substance P. reference: Lu Changlin ed, Basic and clinical of neuropeptide. 1st ed. *Shanghai: Secondary Military Medicine University Press* 2000: 138-141
- 18 **Wang XQ**. Calcitonin gene related peptide. reference: Lu Changlin ed, Basic and clinical of neuropeptide. 1st ed. *Shanghai: Secondary Military Medicine University Press* 2000: 195-196
- 19 **Liu CQ**, Pu J, Li ZX. Changes of duodenal ulcer with peptide hormone in plasma. *Shijie Yixue Zazhi* 2000; **8**: 10-12
- 20 **Pan XF**, Sun PW, Zhu XH. An immunohistochemical study on neuropeptides in the thymus of adult BALB/c mice. *Beijing Yike Daxue Xuebao* 1998; **30**: 508-514
- 21 **Huang XQ**. Somatostatin—Probably the most widely effective gastrointestinal hormone in human body. *Huaren Xiaohua Zazhi* 1998; **6**: 93-96
- 22 **Ke MY**. Study on diseases of gastrointestinal motility. 1st ed. *Beijing: The Publishing Company of Science* 1996: 3-37
- 23 **Pan XZ**, Cai LM. Study on gastrointestinal hormones at the present stage. *Shijie Yixue Zazhi* 1999; **7**: 464-466
- 24 **Ruhl A**, Berezin I, Collins SM. Involvement of eicosanoids and macrophage-like cells in cytokine-mediated changes in rat myenteric nerves. *Gastroenterology* 1995; **109**: 1852-1862
- 25 **Suzuki R**, Furuno T, McKay DM, Wolvers D, Teshima R, Nakanishi M, Bienenstock J. Direct neurite-mast cell communication *in vitro* occurs via the neuropeptide substance P. *J Immunol* 1999; **163**: 2410-2415
- 26 **Zhai LP**, An W, Yan ML, Qiao CJ, Zhang Z. Ultrastructural features of human fetal mast cells in gastrointestinal tract. *Jiepu Xue Zazhi* 1997; **20**: 57-60
- 27 **Lan W**, Tang CW. Effects of gut peptides on the activation of mast cells from rat intestinal mucosa *in vitro*. *Zhongguo Mingyixue Zazhi* 2002; **18**: 847-851
- 28 **Feng Y**, Wu JL, Wang YN. Histochemical and immunohistochemical observations on heterogeneity in mast cells of rat. *Jiepu Xuebao* 1999; **20**: 90-94
- 29 **Jia XM**, Jia YS, Qi WQ, Wang HZ. The heterogeneity Of mast cells in mouse submandibular gland. *Jiepu Xue Zazhi* 1996; **19**: 344-347
- 30 **Jia XM**, Jia YS, Wang DB, Qi WQ. Localization study on substance P, vasoactive intestinal peptide and neuropeptide Y in rat tongue mast cells. *Jiepu Xue Zazhi* 1998; **21**: 242-245
- 31 **Jia YS**, Jiang Y, Qi WQ, Wang HZ. Study on distribution off VIP- and SP- immunoreactive nerves in human duodenum. *Zhangguo Zuzhi Huaxue Yu Xibao Huaxue Zazhi* 1999; **8**: 282-285

Edited by Kumar M and Wang XL Proofread by Xu FM

Protective effect of rhIL-1 β on pancreatic islets of alloxan-induced diabetic rats

Li-Ping Wu, Li-Hua Chen, Jin-Shan Zhang, Lan Sun, Yuan-Qiang Zhang

Li-Ping Wu, the Second Department of Geriatrics and Gerontology, Xijing Hospital, Fourth Military Medical University, Xi'an 710032, Shaanxi Province, China

Li-Hua Chen, Department of Immunology, the Fourth Military Medical University, Xi'an 710032, Shaanxi Province, China

Jin-Shan Zhang, Lan Sun, Yuan-Qiang Zhang, Department of Histology and Embryology, the Fourth Military Medical University, Xi'an 710032, Shaanxi Province, China

Supported by the National Natural Science Foundation of China, No. 39870109

Co-correspondents: Li-Hua Chen

Correspondence to: Professor Yuan-Qiang Zhang, Department of Histology and Embryology, the Fourth Military Medical University, 169 Changle West Road, Xi'an 710032, Shaanxi Province, China. zhangyq@fmmu.edu.cn

Telephone: +86-29-83374508 **Fax:** +86-29-83374508

Received: 2003-11-04 **Accepted:** 2003-12-08

Abstract

AIM: To observe the protective effect of rhIL-1 β on pancreatic islets of alloxan-induced diabetic rats.

METHODS: Protection of rhIL-1 β on pancreatic islets of alloxan-induced diabetic rats ($n = 5$) was demonstrated with methods of immunohistochemistry and stereology. The concentration of serum glucose was measured by GOD method and that of serum insulin by RIA.

RESULTS: The concentration of serum glucose increased but that of insulin decreased after administration of alloxan (150 mg/kg), and the volume density and numerical density of the islets were zero. In rhIL-1 β pretreated rats, although the concentration of serum insulin decreased (from 11.9 \pm 3.0 mIU/L to 6.1 \pm 1.6 mIU/L, $P < 0.05$), that of glucose was at normal level compared with the control group. As compared with alloxan group, the concentration of serum glucose in rhIL-1 β pretreated rats decreased (from 19.4 \pm 8.9 mmol/L to 12.0 \pm 4.0 mmol/L, $P < 0.05$) and the volume density increased (0/L to 1/L, $P < 0.05$).

CONCLUSION: rhIL-1 β pretreatment may have protective effect on the islets of alloxan-induced diabetic rats.

Wu LP, Chen LH, Zhang JS, Sun L, Zhang YQ. Protective effect of rhIL-1 β on pancreatic islets of alloxan-induced diabetic rats. *World J Gastroenterol* 2004; 10(22): 3353-3355
<http://www.wjgnet.com/1007-9327/10/3353.asp>

INTRODUCTION

The cytokine interleukin-1 β (IL-1 β) can not only promote immunological reaction but also regulate neuro-endocrine system^[1]. Previous studies found that IL-1 β could stimulate the central adrenergic system, promote production of PG, and downregulate glucose metabolism^[2].

Diabetes mellitus implicates many organs and tissues. It has been found that IL-1 β decreases serum glucose in experimental

animals and may potentially be therapeutic for diabetes mellitus^[3,4]. In this experiment, we observed changes in serum glucose and insulin in alloxan induced diabetic rats treated with IL-1 β . In addition, we detected the variation of volume density and numerical density of insulin positive pancreatic islets by ABC immunohistochemistry and stereology.

MATERIALS AND METHODS

Animals

Twenty male Sprague-Dawley rats weighing 200 to 300 g were housed in a temperature-controlled room (24 \pm 1 °C) with a 12-h light-dark cycle. The rats were provided with ordinary rat chow and water and divided into 4 groups ($n = 5$, every group): (1) Control group, each rat was injected with 2 mL saline every other day for 3 times, then injected with 2 mL saline on the 7th d; (2) rhIL-1 β group, each rat was injected with 1 \times 10⁴ U rhIL-1 β in 2 mL saline every other day for 3 times, then injected with 2 mL saline on the 7th d; (3) rhIL-1 β pretreated group, each rat was injected with 1 \times 10⁴ U rhIL-1 β in 2 mL saline every other day for 3 times, then was injected with 150 mg/kg alloxan in 2 mL saline on the 7th d; (4) Alloxan group, each rat was injected with 2 mL saline every other day for 3 times, then injected with 150 mg/kg alloxan in 2 mL saline on the 7th d.

Reagents

Guinea pig anti-rat insulin antibody and SPA-HRP were prepared by Professor Yun-Long Zhu (Department of Physiology) and Professor Cai-Fang Xue (Department of Parasitology) of our university respectively. DAB was purchased from Sigma.

Tissue preparation

Forty-eight hours after last injection of alloxan or saline, rats were anesthetized with ether and sacrificed by cervical dislocation. The blood was collected into heparinized tubes (50 kU/L) and centrifuged (3 000 g, 10 min, at room temperature). Plasma was aspirated and stored at -70 °C until assayed as described below. The pancreas was also removed and fixed in Bouin's solution overnight. Each piece was embedded in paraffin and 4- μ m sections were prepared.

Immunohistochemistry

Four-micrometer sections from rat pancreas were employed for immunohistochemical analysis. Several dilutions of the antibody were tested to find the optimal staining concentration before the entire series was processed. The staining procedure was carried out as previously reported, but without protease treatment. Briefly, (1) the sections were deparaffinized in xylene, hydrated in ethanol, and blocked with 3 mL/L H₂O₂ in methanol for 30 min to remove endogenous peroxides, then treated with 30 mL/L normal goat serum for 40 min and rinsed in 0.01 mol/L PBS. (2) The sections were incubated at 4 °C for 24 h with primary antibody, guinea pig anti-rat insulin antibody (1:1 000 dilution, final concentration 5 mg/L); (3) then with secondary antibody, SPA-HRP (1:200 dilution), at room temperature for 1 h. (4) Peroxidative reaction was performed using DAB as chromogen. The sections were washed three times for 10 min after incubation.

All slides were stained at the same time and under identical conditions. Primary antibodies were replaced by irrelevant antibodies and normal guinea pig serum as specific antibody control. Primary antibody was replaced by PBS as negative control. Primary antibody was omitted as blank control.

Detection of serum glucose and insulin

The concentration of serum glucose was measured by routine GOD method^[5] and the concentration of serum insulin was measured by RIA^[6,7]. Every sample was measured three times and the results were displayed as mean±SD.

Morphometry

Five specimens from each group were used for morphometric analysis of slides processed for light microscopy. Two sections from each specimen were then selected and five different regions of each section were chosen for the measurement of volume density and number density by double blind method.

Statistical analysis

The results were calculated by the following formula; $Nv = 2/3 \times \pi \times NA \times U (AT \times A)$; $Vv = A/AT$. Data were analyzed by χ^2 test. A *P* value of less than 0.05 was considered statistically significant.

RESULTS

Insulin expression in rat pancreas

There were more insulin immunoreactive cells in pancreas of control group and rhIL-1 β group than in alloxan group. Immunoreactive cells were mainly located in the central region

of the pancreas. Insulin immunopositive cells had dark-brown reaction products in the cytoplasm mostly and nuclei were not stained (Figure 1A, B). The number of insulin immunopositive cells in alloxan group decreased remarkably and there were only a few positive cells in each pancreatic islet (Figure 1C). The number of insulin immunopositive cells in rat pancreas of rhIL-1 β pretreated group decreased slightly compared with that of control group and rhIL-1 β group, whereas, the number of insulin immunopositive cells in rat pancreas of rhIL-1 β pretreated group increased remarkably compared with that of alloxan group (Figure 1D).

Destructive effect of alloxan on rat pancreatic B cells

The concentration of serum glucose increased significantly but that of insulin decreased remarkably after administration of alloxan (150 mg/kg) for 48 h compared with those of control rats. At the same time, the volume density and numerical density of the islets were zero (Table 1).

Stimulatory effect of rhIL-1 β on insulin secretion

Compared with control group rats, the concentration of serum insulin in rhIL-1 β group rats increased significantly whereas that of glucose was at normal level. Immunohistochemistry and stereology data showed that there were no significant differences in the number density and volume density of the pancreatic islets between rhIL-1 β group rats and control rats (Table 1).

Protective effect of rhIL-1 β on pancreatic islets of alloxan-induced diabetic rats

In rhIL-1 β pretreated group, when the rats were injected with

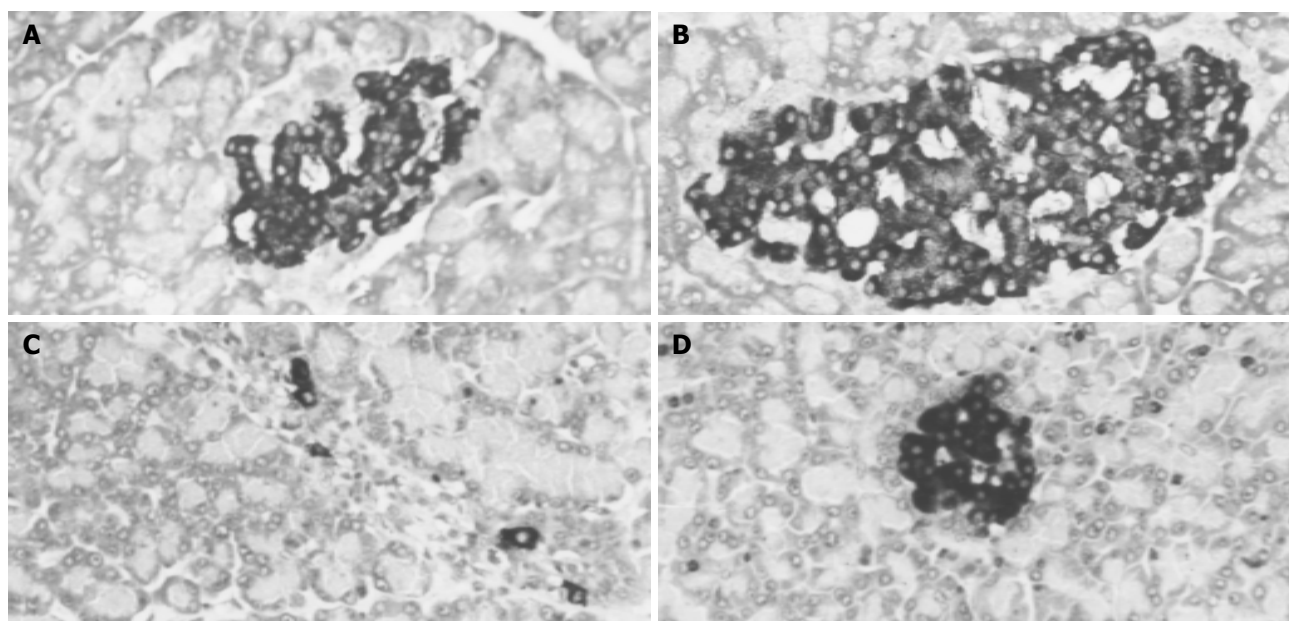


Figure 1 Insulin immunoreactive cells in pancreas. ABC method $\times 264$ A: control group. B: rhIL-1 β pretreated rat. C: alloxan-induced diabetic rat. D: rhIL-1 β pretreated alloxan-induced diabetic rat.

Table 1 Protective effect of rhIL-1 β on pancreatic islets of alloxan-induced diabetic rats

Group	Serum glucose (mmol/L, <i>n</i> = 5)	Serum insulin (mIU/L, <i>n</i> = 5)	Volume density (/L, <i>n</i> = 50)	Number density (/μm ² , <i>n</i> = 50)
Control	8.4±0.3	11.9±3.0	0.6±0.7	5.2±4.1
Alloxan	19.4±8.9 ^a	4.7±1.0 ^a	0 ^a	0 ^a
rhIL-1 β	8.0±1.3	20.0±6.6 ^a	0.6±0.5	5.6±5.3
rhIL-1 β pretreated	12.0±4.0	6.1±1.6 ^a	0.1±0.1 ^a	5.0±5.7

^a*P*<0.05 vs control.

alloxan for 48 h, although the concentration of serum insulin decreased significantly, that of glucose was at normal level compared with control group rats. Immunohistochemistry and stereology data showed that there were no significant differences in the number density of the pancreatic islets between rhIL-1 β pretreated rats and control rats, whereas the volume density decreased markedly in rhIL-1 β pretreated group (Table 1).

DISCUSSION

Interleukin 1 β (IL-1 β) is a multi-functional cytokine synthesized mainly by mononuclear/mo cells and is a key factor in the cytokine network^[8,9]. IL-1 β has many biological functions^[9-21]. Previous study showed that IL-1 β could decrease the serum glucose level and might be potentially a new drug for diabetes therapy^[2-4]. In our experiment, when the rats were injected with alloxan (150 mg/kg) for 48 h, the concentration of serum glucose increased significantly, and that of insulin decreased remarkably. At the same time immunohistochemistry and stereology data showed that the value of number density and volume density of the pancreatic islets were zero. In rhIL-1 β pretreated group, when the rats were injected with alloxan for 48 h, although the concentration of serum insulin decreased significantly, that of glucose was at normal level compared with control group rats. Immunohistochemistry and stereology data showed that there were no significant differences in the number density of the pancreatic islets between rhIL-1 β pretreated rats and control rats, whereas the volume density decreased remarkably in rhIL-1 β pretreated rats. Our results suggest that rhIL-1 β has protective effect on pancreatic islets of alloxan-induced diabetic rats and provide the experimental evidence that rhIL-1 β may be a new therapeutic drug for diabetes.

REFERENCES

- 1 **Song Y**, Shi Y, Ao LH, Harken AH, Meng XZ. TLR4 mediates LPS-induced HO-1 expression in mouse liver: Role of TNF-alpha and IL-1beta. *World J Gastroenterol* 2003; **9**: 1799-1803
- 2 **Lee SH**, Woo HG, Baik EJ, Moon CH. High glucose enhances IL-1beta-induced cyclooxygenase-2 expression in rat vascular smooth muscle cells. *Life Sci* 2000; **68**: 57-67
- 3 **Ikeda U**, Shimpo M, Murakami Y, Shimada K. Peroxisome proliferator-activated receptor-gamma ligands inhibit nitric oxide synthesis in vascular smooth muscle cells. *Hypertension* 2000; **35**: 1232-1236
- 4 **Doxey DL**, Cutler CW, Iacopino AM. Diabetes prevents periodontitis-induced increases in gingival platelet derived growth factor-B and interleukin 1-beta in a rat model. *J Periodontol* 1998; **69**: 113-119
- 5 **Nakashima E**, Nakamura J, Hamada Y, Koh N, Sakakibara F, Hotta N. Interference by gliclazide in the glucose oxidase/peroxidase method for glucose assay. *Diabetes Res Clin Pract* 1995; **30**: 149-152
- 6 **Li C**, Chen P, Vaughan J, Blount A, Chen A, Jamieson PM, Rivier J, Smith MS, Vale W. Urocortin III is expressed in pancreatic beta-cells and stimulates insulin and glucagon secretion. *Endocrinology* 2003; **144**: 3216-3224
- 7 **Durant S**, Alves V, Coulaud J, Homo-Delarche F. Nonobese diabetic (NOD) mouse dendritic cells stimulate insulin secretion by prediabetic islets. *Autoimmunity* 2002; **35**: 449-455
- 8 **Amel Kashipaz MR**, Swinden D, Todd I, Powell RJ. Normal production of inflammatory cytokines in chronic fatigue and fibromyalgia syndromes determined by intracellular cytokine staining in short-term cultured blood mononuclear cells. *Clin Exp Immunol* 2003; **132**: 360-365
- 9 **Musabak U**, Bolu E, Ozata M, Oktenli C, Sengul A, Inal A, Yesilova Z, Kilciler G, Ozdemir IC, Kocar IH. Gonadotropin treatment restores *in vitro* interleukin-1beta and tumour necrosis factor-alpha production by stimulated peripheral blood mononuclear cells from patients with idiopathic hypogonadotropic hypogonadism. *Clin Exp Immunol* 2003; **132**: 265-270
- 10 **Hasegawa K**, Ichiyama T, Isumi H, Nakata M, Sase M, Furukawa S. NF-kappaB activation in peripheral blood mononuclear cells in neonatal asphyxia. *Clin Exp Immunol* 2003; **132**: 261-264
- 11 **Tsirpanlis G**, Chatzipanagiotou S, Ioannidis A, Ifanti K, Bagos P, Lagouranis A, Pouloupoulou C, Nicolaou C. The effect of viable Chlamydia pneumoniae on serum cytokines and adhesion molecules in hemodialysis patients. *Kidney Int Suppl* 2003; **84**: S72-75
- 12 **Li L**, Jacinto R, Yoza B, McCall CE. Distinct post-receptor alterations generate gene- and signal-selective adaptation and cross-adaptation of TLR4 and TLR2 in human leukocytes. *J Endotoxin Res* 2003; **9**: 39-44
- 13 **Allan SM**, Pinteaux E. The interleukin-1 system: an attractive and viable therapeutic target in neurodegenerative disease. *Curr Drug Target CNS Neurol Disord* 2003; **2**: 293-302
- 14 **Boche D**, Cunningham C, Gaudie J, Perry VH. Transforming growth factor-beta 1-mediated neuroprotection against excitotoxic injury *in vivo*. *J Cereb Blood Flow Metab* 2003; **23**: 1174-1182
- 15 **Abe T**, Sugano E, Saigo Y, Tamai M. Interleukin-1beta and barrier function of retinal pigment epithelial cells (ARPE-19): aberrant expression of junctional complex molecules. *Invest Ophthalmol Vis Sci* 2003; **44**: 4097-4104
- 16 **Molina-Holgado F**, Pinteaux E, Moore JD, Molina-Holgado E, Guaza C, Gibson RM, Rothwell NJ. Endogenous interleukin-1 receptor antagonist mediates anti-inflammatory and neuroprotective actions of cannabinoids in neurons and glia. *J Neurosci* 2003; **23**: 6470-6474
- 17 **Boutin H**, Kimber I, Rothwell NJ, Pinteaux E. The expanding interleukin-1 family and its receptors: do alternative IL-1 receptor/signaling pathways exist in the brain? *Mol Neurobiol* 2003; **27**: 239-248
- 18 **Jeremy AH**, Holland DB, Roberts SG, Thomson KF, Cunliffe WJ. Inflammatory events are involved in acne lesion initiation. *J Invest Dermatol* 2003; **121**: 20-27
- 19 **Xie Z**, Morgan TE, Rozovsky I, Finch CE. Aging and glial responses to lipopolysaccharide *in vitro*: greater induction of IL-1 and IL-6, but smaller induction of neurotoxicity. *Exp Neurol* 2003; **182**: 135-141
- 20 **Lu M**, Zhang M, Kitchens RL, Fosmire S, Takashima A, Munford RS. Stimulus-dependent deacylation of bacterial lipopolysaccharide by dendritic cells. *J Exp Med* 2003; **197**: 1745-1754
- 21 **Wheeler RD**, Brough D, Le Feuvre RA, Takeda K, Iwakura Y, Luheshi GN, Rothwell NJ. Interleukin-18 induces expression and release of cytokines from murine glial cells: interactions with interleukin-1 beta. *J Neurochem* 2003; **85**: 1412-1420

Three new alternative splicing variants of human cytochrome P450 2D6 mRNA in human extratumoral liver tissue

Jian Zhuge, Ying-Nian Yu

Jian Zhuge, Ying-Nian Yu, Department of Pathophysiology, Environmental Genomics Center, School of Medicine, Zhejiang University, Hangzhou 310031, Zhejiang Province, China

Supported by the National Key Basic Research and Development Program of China, No. 2002CB512901, National Natural Science Foundation of China, No.39770868 and Natural Science Foundation of Zhejiang Province, No.397490

Correspondence to: Professor Ying-Nian Yu, Department of Pathophysiology, School of Medicine, Zhejiang University, Hangzhou 310031, Zhejiang Province, China. ynyu@hzcnc.com

Telephone: +86-571-87217149 **Fax:** +86-571-87217149

Received: 2004-01-10 **Accepted:** 2004-02-24

Abstract

AIM: To identify the new alternative splicing variants of human CYP2D6 in human extratumoral liver tissue with RT-PCR and sequencing.

METHODS: Full length of human *CYP2D6* cDNAs was amplified by reverse transcription-polymerase chain reaction (RT-PCR) from a human extratumoral liver tissue and cloned into pGEM-T vector. The cDNA was sequenced. Exons from 1 to 4 of human *CYP2D6* cDNAs were also amplified by RT-PCR from extratumoral liver tissues of 17 human hepatocellular carcinomas. Some RT-PCR products were sequenced. Exons 1 to 4 of *CYP2D6* gene were amplified by PCR from extratumoral liver tissue DNA. Two PCR products from extratumoral liver tissues expressing skipped mRNA were partially sequenced.

RESULTS: One of the *CYP2D6* cDNAs had 470 nucleotides from 79 to 548 (3' portion of exons 1 to 5' portion of exon 4), and was skipped. Exons 1 to 4 of *CYP2D6* cDNA were assayed with RT-PCR in 17 extratumoral liver tissues. Both wild type and skipped mRNAs were expressed in 4 samples, only wild type mRNA was expressed in 5 samples, and only skipped mRNA was expressed in 8 samples. Two more variants were identified by sequencing the RT-PCR products of exons 1 to 4 of *CYP2D6* cDNA. The second variant skipped 411 nucleotides from 175 to 585. This variant was identified in 4 different liver tissues by sequencing the RT-PCR products. We sequenced partially 2 of the PCR products amplified of *CYP2D6* exon 1 to exon 4 from extratumoral liver tissue genomic DNA that only expressed skipped mRNA by RT-PCR. No point mutations around exon 1, intron 1, and exon 4, and no deletion in *CYP2D6* gene were detected. The third variant was the skipped exon 3, and 153 bp was lost.

CONCLUSION: Three new alternative splicing variants of CYP2D6 mRNA have been identified. They may not be caused by gene mutation and may lose CYP2D6 activity and act as a down-regulator of CYP2D6.

Zhugue J, Yu YN. Three new alternative splicing variants of human cytochrome P450 2D6 mRNA in human extratumoral liver tissue. *World J Gastroenterol* 2004; 10(22): 3356-3360 <http://www.wjgnet.com/1007-9327/10/3356.asp>

INTRODUCTION

Over 90% medications are metabolized by cytochrome P450 (CYP) family of liver isoenzymes^[1]. The most important enzymes are CYP1A2, 3A4, 2C9/19, 2D6 and 2E1. Although CYP2D6 accounts for <2% of the total CYP liver enzyme, nevertheless it mediates metabolism in 25% of drugs in clinical use such as antipsychotics, antidepressants, beta-blockers, antiarrhythmic agents and opiates^[2]. CYP2D6 exhibits an extensive polymorphism^[3]. Over 40 *CYP2D6* allelic variants have been reported^[4].

Pre-mRNA splicing involves precise removal of introns from pre-mRNA, such that exons are spliced together to form mature RNAs with intact translation reading frames. Splicing requires exon recognition, followed by accurate cleavage and rejoining, which are determined by the invariant GU and AG intronic dinucleotides at the 5' (donor) and 3' (acceptor) exon-intron junctions, respectively^[5]. Human genes typically contain multiple introns, and in many cases the exons can be joined in more than one way to generate multiple mRNAs, encoding distinct protein isoforms. This process named alternative splicing is a major mechanism for modulating the expression of cellular and viral genes and enables a single gene to increase its coding capacity, allowing synthesis of several structurally and functionally distinct protein isoforms^[6-9].

CYP2D subfamily comprises *CYP2D6* gene and pseudogenes, i.e. *CYP2D7P* and *CYP2D8BP*. Six mRNA splice variants of *CYP2D* have been identified in human liver^[10], breast^[11], lung^[12], and brain tissues^[13]. Variants a and b retain intron 5 and 6, respectively; variant b' has missed the 3' 91 bp portion of exon 6; variant c has missed exon 6; variant d retains 57 bp portion of intron 6; variant e retains the 3' portion of intron 6 and has missed the 61 bp fragment at the 3' end of exon 6. Forms b' and c are variants of *CYP2D6*, and forms d, c, b, b' are variants of *CYP2D7P*^[10-13]. All of these *CYP2D* splice variant mRNAs disrupt open reading frames. If they are translated, they would not have CYP2D6 function.

Three new pre-mRNA alternative splicing variants of human *CYP2D6* in human extratumoral liver tissue were identified by RT-PCR and sequencing.

MATERIALS AND METHODS

Materials

Moloney murine leukemia virus (M-MuLV) reverse transcriptase was supplied by MBI Fermentas AB, Lithuania. Random hexamer primers, T4 DNA ligase and pGEM-T vector system were supplied by Promega Corp. PCR primers, DNA sequence primers, dNTPs and Taq DNA polymerase were synthesized or supplied by Shanghai Sangon Biotechnology Co. DNA sequencing kit was purchased from Perkin-Elmer Corp. Diethyl pyrocarbonate (DEPC) was from Sigma Chemical Co. DNA gel extraction kit was from Hangzhou V-gene Biotechnology Ltd. Other chemical reagents used were all of analytical purity from commercial sources. Extratumoral liver tissue samples were collected from patients undergoing hepatocellular carcinoma resection at affiliated hospitals of Zhejiang University School of Medicine and stored at -70 °C.

Cloning and sequencing of human CYP2D6 cDNA from a human extratumoral liver tissue

Total RNA was extracted from a human extratumoral liver tissue from a Han nationality Chinese with AGPC method^[14]. RT-PCR amplifications were described before^[15,16]. Two specific 28 mer oligonucleotide PCR primers were designed according to cDNA sequence of *CYP2D6* reported by Gonzalez *et al.*^[10] (GenBank accession no. NM_000106). The sequence of sense primer (*CYP2D6 F*) corresponds to base position of -39 to -12, i.e. 5'-AGGTGTGTCTCGAGGAGCCCATTTGGTA-3', with a restriction site of *XhoI* (underlined), and the antisense one (*CYP2D6 R*), corresponds to base position from 1 503 to 1 530, i.e. 5'-TGGCTAGGGATCCGGCTGGGGACTAGGT-3', with a restriction site of *BamHI* (underlined). The anticipated PCR products were 1.569 kb in length. PCR was performed at 94 °C for 5 min, then 35 cycles, each at 94 °C for 60 s, at 62 °C for 60 s, at 72 °C for 2 min, and a final extension at 72 °C for 10 min. An aliquot (10 µL) from PCR was subjected to electrophoresis in a 10 g/L agarose gel. The PCR products were ligated with pGEM-T vector, and transformed into *E. coli* DH5α. The *CYP2D6* cDNA cloned in pGEM-T was sequenced by dideoxy chain-termination method marked with BigDye with primers of T7 and SP6 promoters and a specific primer of 5'-ACCTCATGAATCACGGCAGT-3' (nt 1 069 to 1 088) on Perkin-Elmer-ABI Prism 310 automated DNA sequencer.

RT-PCR and sequencing analysis of liver transcripts of CYP2D6 exons 1 to 4

Transcripts of *CYP2D6* exons 1 to 4 were assayed with RT-PCR using 17 extratumoral liver tissues from Han nationality Chinese, with *CYP2D6 F* and *CYP2D6 4R* primer: 5'-GCAGAAAGCCCGACTCCTCCTTCA-3' (nt 638 to 661). Simultaneously the beta-actin (GenBank accession no. NM_001101) cDNA fragment was amplified in the same Eppendorf tube as an internal control^[17]. The sequences of sense and antisense primers used for amplification of beta-actin cDNA fragment were 5'-TCCCTGGAGAAGAGCTACGA-3' (nt 776 to 795) and 5'-CAAGAAAGGGTGTAACGCAAC-3' (nt 1 217 to 1 237) respectively. The anticipated PCR products of *CYP2D6* exons 1 to 4 were 700 bp in length, and those of beta-actin were 462 bp. PCR was performed at 94 °C for 3 min, then 35 cycles, each at 94 °C for 30 s, at 62 °C for 30 s, at 72 °C for 45 s, and a final extension at 72 °C for 7 min. An aliquot (10 µL) from PCR was subjected to electrophoresis in a 17 g/L agarose gel. Several RT-PCR products of *CYP2D6* exons 1 to exon 4 were shorter than the anticipated full length of 700 bp. The shorter RT-PCR products were separated by agarose gel electrophoresis and extracted using DNA gel extraction kit according to the manufacturer's instructions, and then sequenced by dideoxy chain-termination method marked with BigDye with primer of *CYP2D6 F* on Perkin-Elmer-ABI Prism 310 automated DNA sequencer.

Sequencing identification of exon 1 to exon 4 of CYP2D6 gene

Genomic DNA of human extratumoral liver tissues expressed full length of *CYP2D6* exons 1 to 4 only (3 samples), or only exons skipped (2 samples) or both of full length and skipped ones (3 samples) were extracted according to the methods reported by Gross-Bellard *et al.*^[18]. The segment of *CYP2D6* gene from exons 1 to 4 was amplified with *CYP2D6 F* and *CYP2D6 4R* primers. The anticipated PCR products were 2043 bp (from 1581 to 3623) in length. Two PCR products from extratumoral liver tissues that only expressed skipped mRNA were partially sequenced by RT-PCR.

RESULTS

Identification of a new alternative splicing variant from a cDNA clone

During cloning of *CYP2D6* cDNA, a 1.1 kb RT-PCR product was obtained, which was much shorter than anticipated 1.57 kb (Figure 1).

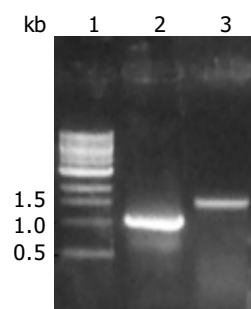


Figure 1 Electrophoresis of RT-PCR products of *CYP2D6* cDNA. Lane 1: 1 kb DNA marker, 2: Amplification of 1.1 kb in size, 3: Amplification of full length of 1.57 kb.

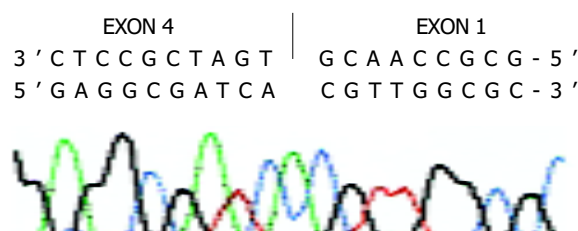


Figure 2 Partial sequences of the cloned human *CYP2D6* cDNA. The upper sequence represents the sense strand and the underside sequence represents the sequenced anti-sense strand.

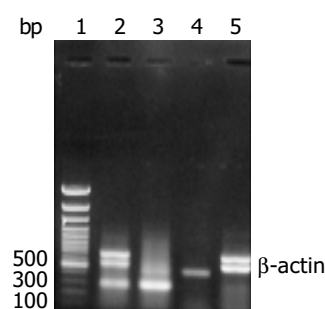


Figure 3 Representative electrophoresis of RT-PCR products of exons 1 to 4 of *CYP2D6* from human liver tissues and HepG2 cells with beta-actin as internal control (464 bp). Lane 1: 100 bp marker, lane 2: A sample having both full length of 700 bp and shorter 300 bp, lane 3: A sample having only shorter ones (300 bp), lane 4: HepG2 cells having no *CYP2D6* expressed, Lane 5: A sample having only full length 700 bp of exons 1 to 4 of *CYP2D6*.

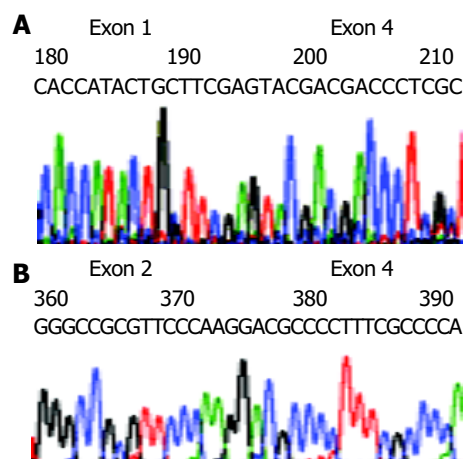


Figure 4 Partial sequences of two alternative splicing variants of *CYP2D6*. A: Part of skipped exon 1, exon 2, exon 3, and part of exon 4. B: Skipped exon 3.

<i>CYP2D6</i> cDNA	5'-AGGTGTGTCTCGAGGAGCCCATTTGGTA-3'	<i>CYP2D6F</i>	Primer
<i>CYP2D7</i> BP	AGGTGTGTCCAGAGGAGCCCATTTGGTAGTGAGGCAGGT		-1
<i>CYP2D6</i> variant f	AGGTGTGTCCAGAGGAGCCCATTTGGTAGTGAGGCAGGT		
<i>CYP2D6</i> variant g			
<i>CYP2D6</i> variant h			
Exon 1			
ATGGGGCTAGAAGCACTGGTGCCCTGGCCGTGATAGTGGCCATCTTCCTGCTCCTGGTG			60
ATGGGGCTAGAAGCACTGGTGCCCTGGCCGTGATAGTGGCCATCTTCCTGCTCCTGGTG			
GACCTGATGCACCGGCGCCAACGCTGGGCTGCACGCTACCCACCAGGCCCTGCCACTG			120
GACCTGATGCACCGGCGCCAACGCTGGGCTGCACGCTACCCACCAGGCCCTGCCACTG			
GACCTGATGCACCGGCGC-----			
GACCTGATGCACCGGCGCCAACGCTGGGCTGCACGCTACCCACCAGGCCCTGCCACTG			
GACCTGATGCACCGGCGCCAACGCTGGGCTGCACGCTACCCACCAGGCCCTGCCACTG			
CCCGGGCTGGGCAACCTGCTGCATGTGGACTTCCAGAACACACCATACTGCTTCGACCAG!			180
CCCGGGCTGGGCAACCTGCTGCATGTGGACTTCCAGAACACACCATACTGCTTCGACCAG!			
-----!			
CCCGGGCTGGGCAACCTGCTGCATGTGGACTTCCAGAACACACCATACTGCTTC-----!			
CCCGGGCTGGGCAACCTGCTGCATGTGGACTTCCAGAACACACCATACTGCTTCGACCAG!			
Exon 2			
TTGCGGCGCCGCTTCGCGGACGCTGTTTCAGCCTGCAGCTGGCCTGGACGCCGGTGGTCTGTG			240
TTGCGGCGCCGCTTCGCGGACGCTGTTTCAGCCTGCAGCTGGCCTGGACGCCGGTGGTCTGTG			
TTGCGGCGCCGCTTCGCGGACGCTGTTTCAGCCTGCAGCTGGCCTGGACGCCGGTGGTCTGTG			

CTCAATGGGCTGGCGGCCGTGCGCGAGGCGCTGGTGACCCACGGCGAGGACACCGCCGAC			300
CTCAATGGGCTGGCGGCCGTGCGCGAGGCGATGGTGACCCCGCGCGAGGACACCGCCGAC			

CTCAATGGGCTGGCGGCCGTGCGCGAGGCGCTGGTGACCCACGGCGAGGACACCGCCGAC			
CGCCCCCTGTGCCATCACCCAGATCCTGGGTTTCGGGCCGCGTTCCCAAG!GGGTGTTTC			360
CGCCCCCTGTGCCATC TAC CCAG G TCCTGGGCTTCGGGCCGCGTTCCCAAG!GGGTG A TC			
-----!			
CGCCCCCTGTGCCATCACCCAGATCCTGGGTTTGGGCCGCGTTCCCAAG!-----			
-----!			
CGCCCCCTGTGCCATCACCCAGATCCTGGGTTTGGGCCGCGTTCCCAAG!-----			
Exon 3			
CTGGCGGCTATGGGCCCGCTGGCGCGAGCAGAGGCGCTTCTCCGTGTCCACCTTGCGC			420
CTGTGCGCTATGGGCCCGCTGGCGCGAGCAGAGGCGCTTCTCCGTGTCCACCTTGCGC			

AACTTGGGCTGGGCAAGAAGTCGCTGGAGCAGTGGGTGACCGAGGAGGCCGCTGCCT			480
AACTTGGGCTGGGCAAGAAGTCGCTGGAGCAGTGGGTGACCGAGGAGGCCGCTGCCT			

TGTGCCGCTTCGCGACCAAGCCG!GACGCCCTTTCGCCCCAACGGTCTCTTGGACAAA			540
TGTGCCGCTTCGCGACCAAGCCG!GACGCCCTTTCGCCCCAACGGTCTCTTGGACAAA			
-----!			
-----!GACGCCCTTTCGCCCCAACGGTCTCTTGGACAAA			
Exon 4			
GCCGTGAGCAACGTGATCGCCTCCCTCACCTGCGGGCGCCGCTTCGAGTACGACGACCT			600
GCCGTGAGCAACGTGATCGCCTCCCTCACCTGCGGGCGCCGCTTCGAGTACGACGACCT			
-----CAACGTGATCGCCTCCCTCACCTGCGGGCGCCGCTTCGAGTACGACGACCT			
-----GAGTACGACGACCT			
GCCGTGAGCAACGTGATCGCCTCCCTCACCTGCGGGCGCCGCTTCGAGTACGACGACCT			
<i>CYP2D6</i> 4R Primer 3'-CTTCTCCTCAGCCGAAAGACG-5'			
CGCTTCCTCAGGCTGCTGGACCTAGCTCAGGAGGGATCGAAGGAGGAGTCCGGCTTCTG			660
CGCTTCCTCAGGCTGCTGGACCTAGCTCAGGAGGGATCGAAGGAGGAGTCCGGCTTCTG			
CGCGAG!GTGCTGAATGCTGTCCCGTCTCCTGCATATCCAGCGCTGGCTGGCAAGGTC			720
CGCGAG!GTGCTGAATGCTGTCCCGTCTCCTGCACATCCAGCGCTGGCTGGCAAGGTC			
CGCGAG!GTGCTGAATGCTGTCCCGTCTCCTGCATATCCAGCGCTGGCTGGCAAGGTC			
C//			
C//			

Figure 5 Comparison of sequences of *CYP2D6* cDNA, *CYP2D7* BP and 3 new *CYP2D6* alternative splicing variants, f, g, h. The different bases compared with wild type *CYP2D6* are indicated in boldface and “_”, and the border of exons is indicated by “!”. The skipped parts are indicated by “-”.

The cDNA obtained was then inserted into pGEM-T vector and sequenced. Compared with human wild type *CYP2D6* cDNA sequence reported by Kimura *et al.*^[19] (GenBank accession no.M33388), there were 470 nucleotides from 84 to 553, i.e., the 3' end portion 97 bp of exon 1 (180 bp), exon2, exon 3, and the 5' end portion 48 bp of exon 4 (161 bp) were skipped in the

cDNA shorter in length (Figures 2, 5). Substitution, insertion and deletion occurred in 13 base pairs, i.e. 620A→G, 712G→T, 1196T→G, 1401T→G, 1405C→G, 1408A→G, 1410T→C, 1432C→T, 1433A→C, 1435G→C, 1400 insG, 1442T→C, 1443T→A, 1449C del, 1457G→C. This cDNA had a premature stop codon at codon 96 and was named variant f.

RT-PCR analysis of transcripts of CYP2D6 exons 1 to 4 in 17 liver extratumoral tissues and HepG2 cells, two more new alternative splicing variants were identified by sequencing

In 17 liver tissues, 4 samples expressed both wild type and skipped mRNA, 5 samples expressed only wild-type mRNA, and 8 samples expressed only skipped mRNA. Representative electrophoresis of RT-PCR products of exons 1 to 4 of *CYP2D6* from human extratumoral liver tissues and HepG2 cells with beta-actin as internal control are shown in Figure 3.

The sequencing data of RT-PCR products demonstrated that the second variant lost 411 nucleotides (137 amino acid residues) from 177 to 587, i.e., the 3' end portion 4 bp of exon 1 (180 bp), exon 2, exon 3, and the 5' end portion 83 bp of exon 4 (161 bp) and gained a base substitution 100 C→T, resulting in one amino acid exchange P34S, as compared with the human wild type *CYP2D6* cDNA sequence reported by Kimura *et al.*^[19] (GenBank accession no.M33388) (Figure 4A, 5). This variant was identified in 4 different extratumoral liver tissues by sequencing RT-PCR products and was named variant g.

The third variant had skipped exon 3, losing 153 bp from nucleotides 353 to 505 or 51 amino acid residues from 117 to 167, and had 2 base substitutions 100 C→T and 336 T→C, resulting in one changed amino acid P34S and a samesense mutation 112F, respectively. This variant was named variant h (Figure 4B, 5).

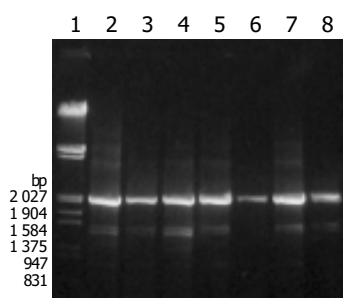


Figure 6 Electrophoresis of PCR products from genomic DNA amplified using *CYP2D6* F and *CYP2D6* 4R primers. Lane 1: λ /*EcoRI* and *Hind* III marker, lanes 2-4: PCR products from livers expressing full and short length RT-PCR products, Lanes 5, 6: PCR products from livers expressing full length RT-PCR products, Lanes 7, 8: PCR products from livers expressing only short length RT-PCR products.

No mutation events around splicing sites of exon 1 and exon 4 nor gene deletion from exon 1 to exon 4 of *CYP2D6* gene

The segment of *CYP2D6* gene at exons 1 to 4 was amplified with *CYP2D6*F and *CYP2D6*4R primers by PCR. All amplified products from 8 samples gave anticipated 2.04 kb in length but no 0.3 kb PCR products as predicted from the possibility that the shorter cDNA was originated from deleted mutations in *CYP2D6* gene rather than due to alternative splicing (Figure 6). Two PCR products from extratumoral liver tissues expressed only skipped exon were purified and partially sequenced. One showed 3 mutations, i.e., 1719 (nt 100) C→T in exon 1, resulting in P34S, 3280 (nt 408) G→C in exon 3, and samesense mutations 136 V, 3056 G→C in intron 2. Another one showed 3 mutations, i.e., 1719 (nt 100) C→T in exon 1, resulting in P34S, 1958 T→C in intron 1, and 3056 G→C in intron 2.

DISCUSSION

The mechanism of exon missed in cDNA may include gene deletion, alternative splicing, template sequence recombination present in PCR amplification^[20-22], and retroviral recombination^[23-25]. One or several exons missed entirely could ascribe to alternative splicing. The first mechanism of formation of recombinant molecules during PCR is mediated by premature termination of chain synthesis. Therefore, a short extension time or increased

dissociation of polymerases from the template may promote recombination. The optimum values to minimize recombinant molecule formation could prolong the extension time and could be achieved using 30 or 34 amplification cycles respectively. The second mechanism is template switching, it implicates that a fragment elongating on one template, can continue this elongation on another homologous template. The high template concentrations could facilitate template switching and *de novo* synthesize recombinant molecules. We performed PCR with lower template concentrations, 1 min/kb extension, and 32 to 35 amplification cycles to minimize the PCR recombination. During synthesis of the first DNA strand, reverse transcriptase could switch templates from one to other copy of RNA, a phenomenon known as copy-choice. The term 'template switching' implies that the nascent DNA strand is transferred from one RNA (the 'donor') to the other (the 'acceptor'). This process depends on a ribonuclease (RNase H) activity, carried by reverse transcriptase, which could degrade the RNA template once it has been copied^[26]. The RNA recombination is a very rare event. In this study, MMLV without RNase H activity was used and skipped mRNA was found in 12 out of 17 liver tissues by RT-PCR assay. Variant g was identified in 4 different extratumoral liver tissues by sequencing RT-PCR products. These facts indicated that the exon missed variant g did not come from PCR recombination or retroviral recombination. PCR amplification and sequencing identification of exon 1 to exon 4 of *CYP2D6* gene from genomic DNA indicated that the exon missed variant g came from neither gene mutation around splicing sites of exon 1 and exon 4 nor gene deletion.

Burset *et al.*^[27] analyzed canonical and non-canonical splice sites in mammalian genomes, and found that 99.24% contained canonical dinucleotides GT and AG for donor and acceptor sites, respectively, 0.69% contained GC-AG, 0.05% contained AT-AC and only 0.02% contained other types of non-canonical splice sites. Some non-canonical splice sites seemed to be involved in immunoglobulin gene expression and the others in alternative splicing events.

CYP2D6 gene has 9 exons and 8 introns. All alternative splicing *CYP2D* reported are located in exon 6 to exon 7. No alternative splicing in exon 1 to exon 4 has been reported. We identified 3 new alternative splicing *CYP2D6* cDNA in exon 1 to exon 4 in human extratumoral liver tissues. The skipped mRNA was not an unusually phenomenon, for 12 samples expressed skipped mRNA in 17 human liver tissue, whereas 9 samples expressed wild-type mRNA in this study.

We cloned a cDNA variant of human *CYP2D6*, the variant f with some exons skipped. The five nt 5'-CAACG-3', located at the boundary of partially skipped exons 1 and 4 (Figure 6). It looked as the 3' end portion of skipped exon 1 or the 5' end portion of exon 4. If we looked it as the 3' end portion of the skipped exon 1, then the splicing donor and acceptor sites would be CT-CG, which were not found as splice site pairs^[27]. If we looked it as the 5' end portion of exon 4, then there would be 470 nucleotides from 79 to 548, i.e., the 3' end portion 102 bp of exon 1 (180 bp), exon 2, exon 3, and the 5' end portion 43 bp of exon 4 (161 bp) were skipped. The splicing donor and acceptor sites would be the non-canonical splice sites: CA-AG^[27].

CYP2D gene exists in a number of structurally polymorphic haplotypes and also comprises several variants of *CYP2D7P* and *CYP2D8P* pseudogenes. *CYP2D6* is highly homologous to *CYP2D7* and *CYP2D8* pseudogenes. The characteristic base substitution, insertion and deletion of the variant f from 1401 to 1457 in exon 9 indicated that this exon was derived from *CYP2D7BP*^[28] (GenBank accession no.X58468). So this cDNA clone may be transcribed from *CYP2D6**36 (Trivial name: *CYP2D6Ch2* or *CYP2D6*10C*) gene, which has gene conversion to *CYP2D7* in exon 9^[29]. Johansson *et al.*^[29] using allele-specific polymerase chain reaction analysis of genomic DNA from 90 Chinese individuals revealed that *CYP2D6*10* (*CYP2D6Ch1*)

allele was the most common one, *CYP2D6**36 was not a common allele^[30] and so we got an alternative splicing variant from this allele only once.

Another alternative splicing *CYP2D6* cDNA, variant g, has 7 bp 5'-GCTTCGA-3', which locates at the boundary of partially skipped exons 1 and 4 (Figure 6). It can be regarded as the 3' end portion of skipped exon 1 or the 5' end portion of exon 4. The splicing donor and acceptor sites would be CC-GA or GC-CC which have not been found as splice site pairs^[27]. If we regarded it as the skipped nucleotides from 175 to 585, then 411 nucleotides (137 amino acid residues), i.e., the 3' end portion 6 bp of exon 1 (180 bp), exon 2, exon 3, and the 5' end portion 81 bp of exon 4 (161 bp) were skipped. The splicing donor and acceptor sites would be the non-canonical splice sites: GA-TC^[27]. As this variant has been identified in 4 different liver tissues by RT-PCR products sequencing, it could not be the RT-PCR artificial ones.

The third variant, variant h, having skipped the entire exon 3, would use the most common non-canonical GC-AG splice sites (Figure 6). It has an amino acid change of P34S which is a common polymorphism occurring in *CYP2D6**4, 10, 14, 36, 37. This variant might come from *CYP2D6**10, the most common allele in Chinese.

The cDNA sequence of *CYP2D6* is differed from that of *CYP2D7P* at nucleotides 629 to 639, *CYP2D6*^[19] was AGGAGGGACTG whereas *CYP2D7P*^[28] was AGGGAGGGATCG (Figure 6). All sequencing data of the alternative splicing cDNA and PCR products originated from related genomic DNA showed the characteristics of *CYP2D6*, so they were all derived from *CYP2D6* but not from *CYP2D7P*.

Variant f has premature stop codon at codon 96, which would cause loss of its enzyme activity. According to the homology modeling study of human CYP2 family enzyme reported by Lewis^[31], the substrate could recognize site (SRS) 1 of human *CYP2D6* located between amino acid residues 101 and 123 and the SRS2 located between amino acid residues 204 to 215. Variant g which lost 137 amino acid residues from 58 to 194, would lose SRS1, and might not have *CYP2D6* activity. Variant h having skipped the entire exon 3, would lose 51 amino acid residues from 117 to 167, where part of SRS1 located. It might not have *CYP2D6* activity.

All 3 *CYP2D6* splice variants might not have *CYP2D6* function. But the possibility of the expression of proteins with novel function(s) could not be excluded. The splice variants might have a role in the posttranscriptional down-regulation of the expression of *CYP2D6*. Formation of variant mRNAs at the expense of full-length mRNAs would ultimately result in a diminished expression of *CYP2D6* protein.

Three new *CYP2D6* pre-mRNA alternative splicing variants in human extratumoral liver tissues have been identified. Further work is needed to clarify if they are commonly existed in liver tissue or only in extratumoral liver tissue, and their relation with hepatocellular carcinoma as well.

REFERENCES

- Danielson PB. The cytochrome P450 superfamily: biochemistry, evolution and drug metabolism in humans. *Curr Drug Metab* 2002; **3**: 561-597
- Bertilsson L, Dahl ML, Dalen P, Al-Shurbaji A. Molecular genetics of *CYP2D6*: clinical relevance with focus on psychotropic drugs. *Br J Clin Pharmacol* 2002; **53**: 111-122
- Cascorbi I. Pharmacogenetics of cytochrome p4502D6: genetic background and clinical implication. *Eur J Clin Invest* 2003; **33**(Suppl 2): 17-22
- Bradford LD. *CYP2D6* allele frequency in European Caucasians, Asians, Africans and their descendants. *Pharmacogenomics* 2002; **3**: 229-243
- Nissim-Rafinia M, Kerem B. Splicing regulation as a potential genetic modifier. *Trends Genet* 2002; **18**: 123-127

- Graveley BR. Alternative splicing: increasing diversity in the proteomic world. *Trends Genet* 2001; **17**: 100-107
- Maniatis T, Tasic B. Alternative pre-mRNA splicing and proteome expansion in metazoans. *Nature* 2002; **418**: 236-243
- Kriventseva EV, Koch I, Apweiler R, Vingron M, Bork P, Gelfand MS, Sunyaev S. Increase of functional diversity by alternative splicing. *Trends Genet* 2003; **19**: 124-128
- Black DL. Mechanisms of alternative pre-messenger RNA splicing. *Annu Rev Biochem* 2003; **72**: 291-336
- Gonzalez FJ, Skoda RC, Kimura S, Umeno M, Zanger UM, Nebert DW, Gelboin HV, Hardwick JP, Meyer UA. Characterization of the common genetic defect in humans deficient in debrisoquine metabolism. *Nature* 1988; **331**: 442-446
- Huang Z, Fasco MJ, Kaminsky LS. Alternative splicing of *CYP2D* mRNA in human breast tissue. *Arch Biochem Biophys* 1997; **343**: 101-108
- Huang Z, Fasco MJ, Spivack S, Kaminsky LS. Comparisons of *CYP2D* messenger RNA splice variant profiles in human lung tumors and normal tissues. *Cancer Res* 1997; **57**: 2589-2592
- Woo SI, Hansen LA, Yu X, Mallory M, Masliah E. Alternative splicing patterns of *CYP2D* genes in human brain and neurodegenerative disorders. *Neurology* 1999; **53**: 1570-1572
- Chomczynski P, Sacchi N. Single-step method of RNA isolation by acid guanidinium thiocyanate-phenol-chloroform extraction. *Anal Biochem* 1987; **162**: 156-159
- Wu J, Dong H, Cai Z, Yu Y. Stable expression of human cytochrome *CYP2B6* and *CYP1A1* in Chinese hamster CHL cells: their use in micronucleus assays. *Chin Med Sci J* 1997; **12**: 148-155
- Qian Y, Yu Y, Cheng X, Luo J, Xie H, Shen B. Molecular events after antisense inhibition of *hMSH2* in a *Hela* cell line. *Mutat Res* 1998; **418**: 61-71
- Zhuge J, Luo Y, Yu YN. Heterologous expression of human cytochrome P450 2E1 in HepG2 cell line. *World J Gastroenterol* 2003; **9**: 2732-2736
- Gross-Bellard M, Oudet P, Chambon P. Isolation of high-molecular-weight DNA from mammalian cells. *Eur J Biochem* 1973; **36**: 32-38
- Kimura S, Umeno M, Skoda RC, Meyer UA, Gonzalez FJ. The human debrisoquine 4-hydroxylase (*CYP2D*) locus: sequence and identification of the polymorphic *CYP2D6* gene, a related gene, and a pseudogene. *Am J Hum Genet* 1989; **45**: 889-904
- Judo MS, Wedel AB, Wilson C. Stimulation and suppression of PCR-mediated recombination. *Nucleic Acids Res* 1998; **26**: 1819-1825
- Zaphiropoulos PG. Non-homologous recombination mediated by *Thermus aquaticus* DNA polymerase I. Evidence supporting a copy choice mechanism. *Nucleic Acids Res* 1998; **26**: 2843-2848
- Shammas FV, Heikkila R, Osland A. Fluorescence-based method for measuring and determining the mechanisms of recombination in quantitative PCR. *Clin Chim Acta* 2001; **304**: 19-28
- Negroni M, Buc H. Mechanisms of retroviral recombination. *Annu Rev Genet* 2001; **35**: 275-302
- Negroni M, Buc H. Retroviral recombination: what drives the switch? *Nat Rev Mol Cell Biol* 2001; **2**: 151-155
- Chetverin AB. The puzzle of RNA recombination. *FEBS Lett* 1999; **460**: 1-5
- Zhu S, Li W, Cao ZJ. Does MMLV-RT lacking RNase H activity have the capability of switching templates during reverse transcription? *FEBS Lett* 2002; **520**: 185
- Burset M, Seledtsov IA, Solovyev VV. Analysis of canonical and non-canonical splice sites in mammalian genomes. *Nucleic Acids Res* 2000; **28**: 4364-4375
- Heim MH, Meyer UA. Evolution of a highly polymorphic human cytochrome P450 gene cluster: *CYP2D6*. *Genomics* 1992; **14**: 49-58
- Johansson I, Oscarson M, Yue QY, Bertilsson L, Sjoqvist F, Ingelman-Sundberg M. Genetic analysis of the Chinese cytochrome P4502D locus: characterization of variant *CYP2D6* genes present in subjects with diminished capacity for debrisoquine hydroxylation. *Mol Pharmacol* 1994; **46**: 452-459
- Chida M, Ariyoshi N, Yokoi T, Nemoto N, Inaba M, Kinoshita M, Kamataki T. New allelic arrangement *CYP2D6**36 x 2 found in a Japanese poor metabolizer of debrisoquine. *Pharmacogenetics* 2002; **12**: 659-662

Effects of endostatin on expression of vascular endothelial growth factor and its receptors and neovascularization in colonic carcinoma implanted in nude mice

Yun-He Jia, Xin-Shu Dong, Xi-Shan Wang

Yun-He Jia, Xin-Shu Dong, Xi-Shan Wang, Department of Abdominal Surgery, Tumor Hospital of Harbin Medical University, Harbin 150040, Heilongjiang Province, China

Supported by the Key Technologies Research and Development Program of Heilongjiang Province During the 9th Five-Year Plan Period, No. G99C19-5

Correspondence to: Dr. Yun-He Jia, Department of General Surgery of Nanjing Jinling Hospital, Nanjing 210002, Jiangsu Province, China. jyhcuse@0451.com

Telephone: +86-25-80860034

Received: 2003-12-23 **Accepted:** 2004-02-01

Abstract

AIM: To investigate the antiangiogenic effects of endostatin on colonic carcinoma cell line implanted in nude mice and its mechanism.

METHODS: Nude mice underwent subcutaneous injection with LS-174t colonic carcinoma cell line to generate carcinoma and were randomly separated into two groups. Mice received injection of vehicle or endostatin every day for two weeks. After the tumor was harvested, the tumor volumes were determined, and the expressions of CD34, VEGF and Flk-1 were examined by immunohistochemical method.

RESULTS: Tumor volume was significantly inhibited in the endostatin group (84.17%) and tumor weight was significantly inhibited in the endostatin group (0.197 ± 0.049) compared to the control group (1.198 ± 0.105) ($F = 22.56$, $P = 0.001$), microvessel density (MVD) was significantly decreased in the treated group (31.857 ± 3.515) compared to the control group (100.143 ± 4.290) ($F = 151.62$, $P < 0.001$). Furthermore, the expression of Flk-1 was significantly inhibited in the treated group (34.29%) compared to the control group (8.57%) ($\chi^2 = 13.745$, $P = 0.001$). However no significant decrease was observed in the expression of vascular endothelial growth factor (VEGF) between these two groups ($\chi^2 = 0.119$, $P = 0.730$).

CONCLUSION: Endostatin can inhibit tumor growth and angiogenesis by blocking Vegf/Flk-1 pathway. This experiment provides the theory basis for developing a new anti-carcinoma drug through studying the properties of anti-angiogenesis inhibitors.

Jia YH, Dong XS, Wang XS. Effects of endostatin on expression of vascular endothelial growth factor and its receptors and neovascularization in colonic carcinoma implanted in nude mice. *World J Gastroenterol* 2004; 10(22): 3361-3364
<http://www.wjgnet.com/1007-9327/10/3361.asp>

INTRODUCTION

Angiogenesis is the process of sprouting of capillaries from

preexisting blood vessels. The overall process is a complex one that involves many biological functions and cell types. Previous researches since 1970s have demonstrated that tumor angiogenesis is required for the growth and metastasis of primary solid tumor. Endothelial cell activation, migration, and proliferation are major cellular events in this process. All of these processes are under the tight regulation of factors that either "promote" or "inhibit" angiogenesis. When the balance of these factors is disturbed, angiogenic factors can be released from tumor cells, such as vascular endothelial growth factor (VEGF)^[1] and basic fibroblast growth factor (bFGF), and migrate to the nearby blood vessel endothelia, signal the activation of the angiogenic response. Tumor cells also produce anti-angiogenic factors including angiostatin, endostatin. Administration of endostatin in tumor-bearing mice has been shown to keep the primary tumor in a dormant state^[2]. But the mechanisms are still unclear. One mechanism is that endostatin in combination with the endothelial cells to form a compound with tyrosine activity and thereby inducing apoptosis of endothelial cells. The other is that endostatin functions as a ligand for the integrin family of adhesion receptors on the surface of endothelial cells and is associated with MMP family^[3]. So, in order to explore the mechanism of endostatin, we provided data that endostatin showed a broad antitumor effect, which might be a result of its inhibitory mechanism on tumor angiogenesis.

MATERIALS AND METHODS

Materials

Endostatin donated from Hefei Sunny Biology-technology Institute, was a 20 ku C-terminal fragment of collagen X VIII. Human endostatin was cloned and expressed in *Escherichia coli* and purified by gene cloning technology by Gene Med Ltd.

Colon cancer cell line HL-174T was purchased from Shanghai Cellular Research Institute. The cells were cultured in 1640 medium supplemented with 100 mL/L fetal bovine serum at 37 °C in 50 mL/L CO₂ and the culture media were changed twice a week and observed in the invert microscope to assay the reproduction situation. All reagents and media for cell culture were obtained from GIBCO.

Methods

Subcutaneous xenograft models Tumor cells were implanted (0.5×10^6 cells/animal) subcutaneously using a 27-gauge needle in the back region of BALB/C-nu/nu female mice of 6-8 wk old. Tumor volume was measured every 3 d using a slide gauge. Tumor volumes were measured as the product of (length × width) × $\pi/6$. Mice were fed with a standard rodent diet for two weeks, and 14 of 20 mice with a similar tumor volume were selected and divided into two groups randomly. Animals of each group were treated once daily with a 0.1 mL (2 mg/mL) ip bolus injection of endostatin in saline or saline alone for 14 d. Upon termination of the efficacy portion of endostatin (3 d after drug withdrawal), the animals were euthanized, and the tumor was harvested from the animals and the volume was weighted. The tumors were submitted for immunohistochemical test.

Evaluation of MVD, VEGF and VEGFR/flk-1 expression in tumors Five- μ m paraffin embedded sections of the tumors were evaluated by immunohistochemistry. The sections were stained with anti-CD34 antibody (DAKO, 1:2 000) and polyclonal anti-VEGF antibody and polyclonal anti-Flk-1 antibody that could recognize VEGF isoforms and their receptors, following avidin-biotin complex methods.

Microvessel density was assessed by light microscopy in areas of invasive tumors containing the highest number of capillaries and small venules per area (neovascular "hot point"). Areas of the highest neovascularization were found by scanning the tumor sections at a low magnification ($\times 100$) and identified with the greatest number of distinct CD34 stained (brown) microvessels per area. Necrotic areas within tumors, where microvessels were sparse, were not included in the vessel counts. After the area of the highest neovascularization was identified, individual microvessels were counted under $\times 400$ field. A brown-stained endothelial cell or an endothelial cell cluster clearly separated from adjacent microvessels, tumor cells, and other connective-tissue elements, considered a single, countable microvessel. Vessel lumens were not necessary for a structure to be defined as a microvessel, and red cells were not used to define a vessel lumen. Results were expressed as the number of microvessels identified within 10 fields ($\times 400$).

VEGF was assessed by light microscopy ($\times 100$) in the areas of invasive tumor cells. VEGF expression was determined on adjacent serial visual fields and scored by a pathologic doctor. The number of positively and negatively stained cells was counted in 10 continuous visual fields. If more than 5% cells were brown stained, they were considered as positive, otherwise negative. The results were expressed as mean \pm SD.

Flk-1 was assessed by light microscopy ($\times 400$) in the areas of microvessel endothelial cells. The number of endothelial cells stained positively was counted in 10 continuous visual fields. Over 5% positively stained endothelial cells were determined as positive and else negative. The results were expressed as mean \pm SD.

Statistics

The analysis of variance test was used to compare the differences in tumor weight and MVD between the treated and control groups. The Chi-squared test was used to compare the differences in the expression of VEGF or VEGFR2/Flk-1 between the treated and control groups. The difference was considered statistically significant if the *P* value was less than 0.05. All the data were analyzed with SAS 6.22 by the statistical office of the Second Military Medical University.

RESULTS

Inhibition of tumor growth by endostatin

To determine the efficacy of endostatin on tumor growth, the volume of tumors were measured every three days after endostatin was used and tumors were weighed immediately after they were harvested. The tumor growth in the mice treated with endostatin was inhibited by 84.17% in volume. The growth of the tumors was stopped 3-5 d after using endostatin except two of them. The growth of primary colon tumor was significantly inhibited by endostatin (Figure 1). The tumor weight of the treated group was significantly less than that of the control group ($F = 22.56$; $P = 0.0005$) (Table 1).

Effects of endostatin on angiogenesis in primary tumors

Immunohistochemical analysis showed a significant inhibition of angiogenesis in the tumors treated with endostatin ($P < 0.05$) (Table 1). The MVD of tumors was significantly different ($F = 151.62$, $P = 0.001$) between the two groups, the treated group had a significant lower MVD.

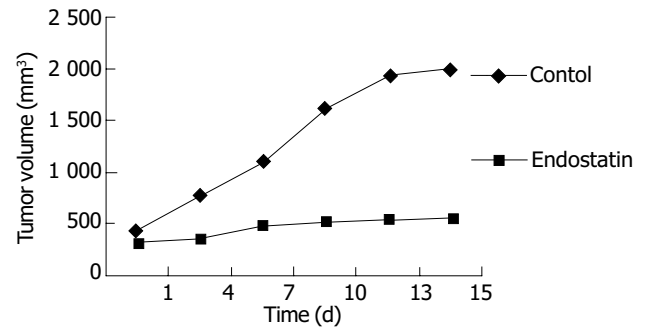


Figure 1 Changes in volume of tumors transplanted in dorsal skinfold chambers in nude mice.

Table 1 Reduction in tumor mass and MVD after endostatin treatment (mean \pm SD)

	Control	Endostatin	<i>F</i>	<i>P</i>
Mass	1.198 \pm 0.105	0.197 \pm 0.049	22.56	^a <i>P</i> = 0.0005
MVD	100.143 \pm 4.290	31.857 \pm 3.515	151.62	^b <i>P</i> = 0.0001

^a*P* = Mass difference between Control group and Endostatin group, ^b*P* = MVD difference between Control group and Endostatin group.

Table 2 Expression of VEGF and VEGFR2/Flk-1 in tumor after Endostatin treatment

	Positive	Negative		χ^2	<i>P</i>
Control-VEGF (1)	65	5	(1) vs (2)	0.119	0.730
Endostatin-VEGF (2)	66	4			
Control-Flk-1 (3)	64	6	(3) vs (4)	13.745	^a <i>P</i> = 0.001
Endostatin-Flk-1 (4)	46	24			

^a*P* = Flk-1 difference between Control group and Endostatin group.

Selectivity and potency of endostatin on VEGF and Flk-1

Immunohistochemical analysis showed that endostatin had a potent inhibition on Flk-1 expression ($\chi^2 = 13.745$, $P = 0.001$) but no inhibition on VEGF expression in tumor cells (Table 2). There was a significant difference in the tumors of treated mice and control mice after staining of endothelial cells with Flk-1 monoclonal antibody (Table 2) but no difference in the tumor tissue stained with VEGF between the two groups (Table 2).

DISCUSSION

Angiogenesis is a fundamental process by which new blood vessels are formed. It is essential in reproduction, development, and wound repair. Under these conditions, angiogenesis is highly regulated, turned on for brief periods and then completely inhibited. However some diseases are driven by persistently unregulated angiogenesis. Tumor growth is one of these kinds of diseases. Tumor growth and metastasis are angiogenesis-dependent. A tumor must continuously stimulate the growth of new capillary blood vessels for the tumor itself to grow. MVD was significantly high in colon cancer tissues compared with normal colon tissues^[4]. Tumor cells get oxygen and nutrition through angiogenesis. The Phenomena were also observed in other cancers, for example, breast carcinoma^[5] lung cancer^[6] prostate cancer^[7] and pancreatic tumor^[8], etc.

Endostatin, a 20-kD C-terminal cleavage product of collagen XVIII, was originally identified by O'Reilly *et al.*^[2] as a tumor-derived, highly active, and endothelial specific angiogenic inhibitor^[9]. Recombinant endostatin has been shown to inhibit

the growth of a wide variety of tumors in mice, with no toxic side effects observed. Importantly, tumors treated with several cycles of endostatin did not develop drug resistance and become dormant, which persisted even when the endostatin therapy was discontinued^[10]. In our experiment, we found that the tumor growth slowed down or even stopped three days after usage of endostatin, but when the treatment was stopped the tumor began to grow rapidly. So endostatin must be used continuously to prevent tumor growth. It is difficult for the patients to accept the treatment in their whole lifetime, so further research is necessary for the usage of endostatin. At present, the molecular mechanism of endostatin action remains unknown. There are some theories which are supported by various studies.

Our results showed that endostatin blocked the VEGF-VEGFR/Flk-1 pathway to inhibit the angiogenesis of colon tumor in nude mice. VEGF pathway is the only well-defined signaling pathway known to be required for the normal development of vasculature as well as for the pathologic angiogenesis that accompanies cancer and other disease states^[1,11,12]. The VEGF family of growth factors comprises at least five members, i.e., VEGF, placenta growth factor (PGF), VEGF-B, VEGF-C^[13], and VEGF-D. The VEGF pathway is initiated when VEGF binds to its receptors in endothelial cells. The three best characterized VEGF receptors are termed VEGF receptor 1 (VEGFR1/Flt-1) and VEGF receptor 2 (VEGFR2/Flk-1/KDR) and VEGF receptor 3 (VEGFR3/Flk-4). VEGFR1 and VEGFR2 are highly related transmembrane tyrosine kinases that use their ectodomains to bind to VEGF^[14,15]. These binding in turn, activate the intrinsic tyrosine kinase activity of their cytodomains, initiating intracellular signaling. VEGFR3 is expressed almost exclusively by the lymphatic endothelium, thus being considered as a major regulator of lymphangiogenesis^[16]. The blockade of VEGF by using a soluble VEGFR-3 extracellular domain could inhibit tumor lymphangiogenesis^[17]. While PlGF could bind selectively to VEGFR1, VEGF-C and VEGF-D could bind to both VEGFR3^[18,19] and VEGFR2. The corresponding receptor(s) for VEGF-B is VEGFR1. VEGF/VEGFR2 pathway is the most important for tumor angiogenesis, growth and metastasis. In our studies, we found VEGFR2 was obviously down-regulated in the endostatin group compared to the control group, but the expression of VEGF was not changed in both groups. So we think that endostatin can block the VEGF/VEGFR2 pathway by binding to VEGFR2, thus inhibiting the neovascularization.

Endostatin could function as a ligand for the integrin family of adhesion receptors on the surface of endothelial cells^[20]. Integrins are potential targets for endostatin function and they are important in endothelial cell biology and angiogenesis. The endostatin-integrin interaction is of functional significance *in vitro*, and the immobilized endostatin supports endothelial cell survival and migration in an integrin-dependent manner. Soluble endostatin in turn could inhibit integrin-dependent endothelial cell functions, such as cell migration^[20].

Matrix metalloproteinases (MMPs), a family of extracellular and membrane-associated endopeptidases, collectively digest almost all extracellular matrix and basement membrane components, thus playing an important role in tumor progression. Endostatin could prevent the fragmentation of pro-MMP-2 that is associated with reduction of catalytic activity. Endostatin had no effect on MMP-8 as shown by collagenase activity assays^[3]. Endostatin could block the activation and activities of certain tumor-associated pro-MMPs, such as pro-MMP-2, -9, and -13, which may explain at least in part, the antitumor effect of endostatin^[3,21].

Inhibition of angiogenesis has been shown to be an effective strategy in cancer therapy in mice. However, its widespread application has been hampered by difficulties in the large-scale production of antiangiogenic proteins. This limitation may be resolved by *in vivo* delivery and expression of antiangiogenic

genes. A recombinant adenovirus that could express murine endostatin that was biologically active *in vitro* as determined in endothelial cell proliferation assays, and *in vivo* by suppression of angiogenesis induced by VEGF has been constructed^[22]. Persistent high serum levels of endostatin were achieved after systemic administration of the vector to nude mice, which resulted in a significant reduction of the growth rates and the volumes of metastatic brain tumor^[23]. If the method can be used safely in clinic, it can effectively resolve the recurrence and overgrowth of tumors during the rest periods. Different targets have been found and effective results were achieved in gene therapy. An adenoviral vector carrying Tie2 gene, an endostatin-specific receptor tyrosine kinase, was constructed and tested in established primary tumor, a murine mammary carcinoma or a murine melanoma, which could significantly inhibit the growth rate of both murine mammary carcinoma and melanoma by 64% and 47%, respectively. So the potential of vector-mediated antiangiogenic gene therapy as a component is a very novel and effective strategy in cancer therapy^[24,25].

Synergy between endostatin and chemotherapy^[26] can be used to eradicate spontaneous tumor and metastases of colon cancer or other angiogenesis dependent diseases. Tumor necrosis was demonstrated only in animals receiving the combination therapy, but not when each agent was applied as monotherapy. The results suggested that these synergistic treatment modalities might provide a novel and effective tool for future therapies of metastatic cancer. Synergy between endostatin and interventional therapy is another way to inhibit the neovascularization. Endostatin can be sent directly to the microvessels around the tumor and destroy the tunica intima of vessels to starve the tumor to death. Other strategies also were used to block the VEGF/VEGFR pathway to inhibit the tumor growth. VEGF-trap is a potent blocker against the angiogenesis of the tumor and could result in stunted and almost completely avascular tumors. VEGF-Trap-mediated blockade may be a hopeful way for tumor treatment^[27]. More and more attention has been paid to the effectiveness and carrier and medication methods are paid more and more attention throughout the world. Endostatin may provide a novel and effective tool for future therapies of cancer^[28,29].

REFERENCES

- 1 Potti A, Moazzam N, Tendulkar K, Javed NA, Koch M, Kargas S. Immunohistochemical determination of vascular endothelial growth factor (VEGF) overexpression in malignant melanoma. *Anticancer Res* 2003; **23**: 4023-4026
- 2 O'Reilly MS, Boehm T, Shing Y, Fukai N, Vasios G, Lane WS, Flynn E, Birkhead JR, Olsen BR, Folkman J. Endostatin: an endogenous inhibitor of angiogenesis and tumor growth. *Cell* 1997; **24**: 277-285
- 3 Nyberg P, Heikkila P, Sorsa T, Luostarinen J, Heljasvaara R, Stenman UH, Pihlajaniemi T, Salo T. Endostatin inhibits human tongue carcinoma cell invasion and intravasation and blocks the activation of matrix metalloproteinase-2, -9, and -13. *J Biol Chem* 2003; **278**: 22404-22411
- 4 Dkhissi F, Lu H, Soria C, Opolon P, Griscelli F, Liu H, Khattar P, Mishal Z, Perricaudet M, Li H. Endostatin exhibits a direct antitumor effect in addition to its antiangiogenic activity in colon cancer cells. *Hum Gene Ther* 2003; **14**: 997-1008
- 5 Atiqur Rahman M, Toi M. Anti-angiogenic therapy in breast cancer. *Biomed Pharmacother* 2003; **57**: 463-470
- 6 Sridhar SS, Shepherd FA. Targeting angiogenesis: a review of angiogenesis inhibitors in the treatment of lung cancer. *Lung Cancer* 2003; **42**(2 Suppl): S81-S91
- 7 Uehara H. Angiogenesis of prostate cancer and antiangiogenic therapy. *J Med Invest* 2003; **50**: 146-153
- 8 Schuch G, Kisker O, Atala A, Soker S. Pancreatic tumor growth is regulated by the balance between positive and negative modulators of angiogenesis. *Angiogenesis* 2002; **5**: 181-190
- 9 Sim BK. Angiostatin and endostatin: endothelial cell-specific

- endogenous inhibitors of angiogenesis and tumor growth. *Angiogenesis* 1998; **2**: 37-48
- 10 **Kuroiwa M**, Takeuchi T, Lee JH, Yoshizawa J, Hirato J, Kaneko S, Choi SH, Suzuki N, Ikeda H, Tsuchida Y. Continuous versus intermittent administration of human endostatin in xenografted human neuroblastoma. *J Pediatr Surg* 2003; **38**: 1499-1505
- 11 **Zachary I**. VEGF signalling: integration and multi-tasking in endothelial cell biology. *Biochem Soc Trans* 2003; **31**(Pt 6): 1171-1177
- 12 **Qi L**, Robinson WA, Brady BM, Glode LM. Migration and invasion of human prostate cancer cells is related to expression of VEGF and its receptors. *Anticancer Res* 2003; **23**: 3917-3922
- 13 **Karkkainen MJ**, Haiko P, Sainio K, Partanen J, Taipale J, Petrova TV, Jeltsch M, Jackson DG, Talikka M, Rauvala H, Betsholtz C, Alitalo K. Vascular endothelial growth factor C is required for sprouting of the first lymphatic vessels from embryonic veins. *Nat Immunol* 2004; **5**: 74-80
- 14 **Dales JP**, Garcia S, Bonnier P, Duffaud F, Carpentier S, Djemli A, Ramuz O, Andrac L, Lavaut M, Allasia C, Charpin C. Prognostic significance of VEGF receptors, VEGFR-1 (Flt-1) and VEGFR-2 (KDR/Flk-1) in breast carcinoma. *Ann Pathol* 2003; **23**: 297-305
- 15 **Endo A**, Fukuhara S, Masuda M, Ohmori T, Mochizuki N. Selective inhibition of vascular endothelial growth factor receptor-2 (VEGFR-2) identifies a central role for VEGFR-2 in human aortic endothelial cell responses to VEGF. *J Recept Signal Transduct Res* 2003; **23**: 239-254
- 16 **Pimenta FJ**, Sa AR, Gomez RS. Lymphangiogenesis in human dental pulp. *Int Endod J* 2003; **36**: 853-856
- 17 **Kaipainen A**, Korhonen J, Mustonen T, van Hinsbergh VW, Fang GH, Dumont D, Breitman M, Alitalo K. Expression of the fms-like tyrosine kinase 4 gene becomes restricted to lymphatic endothelium during development PNAS. *Proc Natl Acad Sci U S A* 1995; **92**: 3566-3570
- 18 **Nakamura Y**, Yasuoka H, Tsujimoto M, Yang Q, Imabun S, Nakahara M, Nakao K, Nakamura M, Mori I, Kakudo K. Flt-4-positive vessel density correlates with vascular endothelial growth factor-d expression, nodal status, and prognosis in breast cancer. *Clin Cancer Res* 2003; **9**: 5313-5317
- 19 **Van Trappen PO**, Steele D, Lowe DG, Baithun S, Beasley N, Thiele W, Weich H, Krishnan J, Shepherd JH, Pepper MS, Jackson DG, Sleeman JP, Jacobs JJ. Expression of vascular endothelial growth factor (VEGF)-C and VEGF-D, and their receptor VEGFR-3, during different stages of cervical carcinogenesis. *J Pathol* 2003; **201**: 544-554
- 20 **Rehn M**, Veikkola T, Kukkk-Valdre E, Nakamura H, Ilmonen M, Lombardo CR, Pihlajaniemi T, Alitalo K, Vuori K. Interaction of endostatin with integrins implicated in angiogenesis. *Proc Natl Acad Sci U S A* 2001; **98**: 1024-1029
- 21 **Guan KP**, Ye HY, Yan Z, Wang Y, Hou SK. Serum levels of endostatin and matrix metalloproteinase-9 associated with high stage and grade primary transitional cell carcinoma of the bladder. *Urology* 2003; **61**: 719-723
- 22 **Sauter BV**, Martinet O, Zhang WJ, Mandeli J, Woo SLC. Adenovirus-mediated gene transfer of endostatin *in vivo* results in high level of transgene expression and inhibition of tumor growth and metastases PNAS. *Proc Natl Acad Sci U S A* 2000; **97**: 4802-4807
- 23 **Oga M**, Takenaga K, Sato Y, Nakajima H, Koshikawa N, Osato K, Sakiyama S. Inhibition of metastatic brain tumor growth by intramuscular administration of the endostatin gene. *Int J Oncol* 2003; **23**: 73-79
- 24 **Chen W**, Fu J, Liu Q, Ruan C, Xiao S. Retroviral endostatin gene transfer inhibits human colon cancer cell growth *in vivo*. *Chin Med J* 2003; **116**: 1582-1584
- 25 **Sridhar SS**, Shepherd FA. Targeting angiogenesis: a review of angiogenesis inhibitors in the treatment of lung cancer. *Lung Cancer* 2003; **42**(2 Suppl): S81-S91
- 26 **Plum SM**, Hanson AD, Volker KM, Vu HA, Sim BK, Fogler WE, Fortier AH. Synergistic activity of recombinant human endostatin in combination with adriamycin: analysis of *in vitro* activity on endothelial cells and *in vivo* tumor progression in an orthotopic murine mammary carcinoma model. *Clin Cancer Res* 2003; **9**: 4619-4626
- 27 **Byrne AT**, Ross L, Holash J, Nakanishi M, Hu L, Hofmann JJ, Yancopoulos GD, Jaffe RB. Vascular endothelial growth factor-trap decreases tumor burden, inhibits ascites, and causes dramatic vascular remodeling in an ovarian cancer model. *Clin Cancer Res* 2003; **9**: 5721-5728
- 28 **Shibuya M**. VEGF-receptor inhibitors for anti-angiogenesis. *Nippon Yakurigaku Zasshi* 2003; **122**: 498-503
- 29 **Tee D**, DiStefano J 3rd. Simulation of tumor-induced angiogenesis and its response to anti-angiogenic drug treatment: mode of drug delivery and clearance rate dependencies. *J Cancer Res Clin Oncol* 2004; **130**: 15-24

Proteomic analysis of blood level of proteins before and after operation in patients with esophageal squamous cell carcinoma at high-incidence area in Henan Province

Ji-Ye An, Zong-Min Fan, Ze-Hao Zhuang, Yan-Ru Qin, Shan-Shan Gao, Ji-Lin Li, Li-Dong Wang

Ji-Ye An, Laboratory for Cancer Research and the Third Teaching Hospital, College of Medicine, Zhengzhou University, Zhengzhou 450052, Henan Province, China

Zong-Min Fan, Ze-Hao Zhuang, Yan-Ru Qin, Shan-Shan Gao, Li-Dong Wang, Laboratory for Cancer Research, College of Medicine, Zhengzhou University, Zhengzhou 450052, Henan Province, China

Ji-Lin Li, Department of Pathology, Yaocun Esophageal Cancer Hospital, Linzhou 456592, Henan Province, China

Supported by National Science Fund for Outstanding Young Scholars of China, No.30025016; State Basic Research Development Program of China, No.G1998051206; Foundation of Henan Education Committee, No.1999125 and the US NIH Grant, No.CA65871

Correspondence to: Professor Li-Dong Wang, Laboratory for Cancer Research, College of Medicine, Zhengzhou University, Zhengzhou 450052, Henan Province, China. lidong0823@sina.com

Telephone: +86-11-371-6970165 **Fax:** +86-11-371-6970165

Received: 2004-02-02 **Accepted:** 2004-02-18

Abstract

AIM: To characterize the protein files in blood from same patients with esophageal squamous cell carcinoma (ESCC) before and after operation at the high-incidence area for ESCC in Henan Province, China.

METHODS: Two-dimensional electrophoresis, silver staining and ImageMaster 2-DE analysis software were applied to the determination of protein files in the blood obtained from normal controls and ESCC patients before and after operation.

RESULTS: A total of 655, 662 and 677 protein spots were identified, respectively, from the normal controls and ESCC patients before and after operation. No significant difference in the number of protein spots was observed between the normal group and ESCC patients. A total of seven protein spots were identified with a dramatic difference among the samples before and after operation. Six protein spots were up-regulated and one protein spot was down-regulated in the group after operation compared with those in normal and before operation. Three protein spots were further characterized by matrix-assisted laser desorption/ionization time of flying mass spectrometry (MALDI-TOF-MS). The proteins from these three spots were identified as serum amyloid A (SAA), amyloid related serum protein and haptoglobin.

CONCLUSION: Serum amyloid A, amyloid related serum protein and haptoglobin may be related with ESCC and/or surgery. The significance of these proteins needs to be further characterized. The present study provides informative data for the establishment of serum protein profiles related with ESCC.

An JY, Fan ZM, Zhuang ZH, Qin YR, Gao SS, Li JL, Wang LD. Proteomic analysis of blood level of proteins before and after operation in patients with esophageal squamous cell carcinoma at high-incidence area in Henan Province. *World J Gastroenterol* 2004; 10(22): 3365-3368

<http://www.wjgnet.com/1007-9327/10/3365.asp>

INTRODUCTION

Esophageal squamous cell carcinoma (ESCC) is one of the six most common malignant diseases in the world with a remarkable geographical distribution. The ratio between the high- and low-incidence areas could be as high as 500:1. The prognosis of ESCC is very poor, the five-year survival rate is only about 10% for the patients at late or advanced stage. China is a country with the highest incidence and mortality rate of ESCC in the world. There are about 300 000 new ESCC patients identified all over the world each year, half of them occur in China. Linzhou City (formerly Linxian County) and its neighbouring counties in Henan Province have been well-recognized as the highest incidence area in the world, the average incidence ratio of males and females is 161 and 103 per 100 000, respectively^[1]. ESCC remains the leading cause of cancer related-deaths in these areas. Unclear molecular mechanism, and lacking of sensitive and specific biomarkers for early diagnosis may be the reasons for the unchanged ESCC incidence pattern^[2].

Many studies have been focused on gene level for early diagnosis of ESCC. However, because alterations in DNA and RNA may or may not induce similar protein changes, genetic changes could not reflect the stage and progression of the disease directly and objectively^[3]. Proteomics based on two-dimensional electrophoresis and mass spectrometry is a new method for identification of cancer-specific protein markers^[4]. In this study, we analyzed the serum protein changes in ESCC patients before and after operation and compared them with normal controls by proteomic methods to find the specific ESCC-related proteins.

MATERIALS AND METHODS

Blood samples

Blood samples were collected from ESCC patients in Yaocun Esophageal Cancer Hospital of Linzhou, Henan Province. Of the ESCC patients, there were 4 males and 2 females with an average age of 63 years (range, 52-74 years). All the blood samples were collected two times from each patient, just before and one week after the operation. The control blood samples (10 mL/subject) were collected in our laboratory from the normal people with matched ages as the patients. There were not any abnormalities identified by physical and biochemical examinations in volunteers of the control group.

Reagents

Electrophoresis reagents, including 400 g/L acrylamide solution, *N, N*-methylenebisacryl amide, *N, N, N', N'*-tetramethylethylenediamine, urea, tris-base, glycine, glycerol, 3-[(3-cholannidopropyl)-dimethylammonio]-1-propanesulfonate (CHAPS), sodium dodecyl sulfate (SDS), dithiothreitol (DTT), ammonium persulfate, bromophenol blue, immobililine drystrips, immobilized pH gradient buffer and silver nitrate were from Amersham Pharmacia Biotechnology Inc. (Uppsala, Sweden). Iodoacetamide was from Acros (New Jersey, USA), sequence grade trypsin was from Washington Biochemical Corporation and trifluoroacetic acid (TFA) was from Fluka (Switzerland). All other reagents were of analytical grade.

Serum concentration detection

Serum samples were thawed and diluted by dH₂O as 1:5 (2 μ L serum was added to 8 μ L dH₂O), 1:10 (2 μ L diluent was added to 18 μ L dH₂O), 1:200 (4 μ L diluent was added to 796 μ L dH₂O) respectively, up to 1:10 000 dilution and then 800 μ L 1:10 000 diluent was added to 200 μ L protein assay reagent and absorbance was measured at 595 nm, finally the concentration of protein in serum was calculated.

First dimensional electrophoresis (Isoelectric focusing, IEF)

Precast IPG strips (pH 3-10 linear, 18 cm, Amersham Pharmacia Biotechnology Inc.) was used in the first dimension. A total amount of 250 μ g proteins was diluted to a total volume of 350 μ L with the buffer (8 mol/L urea, 20 g/L CHAPS, 5 g/L IPG buffer 3-10, 20 mol/L DTT and a trace of bromophenol blue). After being loaded on IPG strips, IEF was carried out according to the following protocol: rehydration for 6 h at 0 V, 10 h at 30 V, 1 h at 500 V, 1 h at 1 000 V and 7 h at 8 000 V. The current was limited to 50 μ A per gel.

Second dimensional electrophoresis (SDS-polyacrylamide gel electrophoresis, SDS-PAGE)

After IEF separation, the strips were immediately equilibrated for 2 \times 15 min with equilibration solution (50 mmol/L Tris-HCl, pH 6.8, 6 mol/L urea, 300 g/L glycerol and 20 g/L SDS). Then 20 mmol/L DTT was included in the first equilibration solution, and 20 g/L iodoacetamide was added in the second equilibration step to alkylate thiols. Thirteen percent SDS-PAGE gels were handled to become 1 mm thick. The strips were held in place with 5 g/L agarose dissolved in SDS/Tris running buffer and electrophoresis was carried out at constant power (2.5 W/gel for 40 min and 15 W/gel for 6 h) and temperature (20 $^{\circ}$ C) using Ettan Dalt II system (Amersham Pharmacia Biotechnology Inc.).

Silver staining

Gels were stained with silver nitrate according to the instructions of the silverstaining kit^[5] (Amersham Pharmacia Biotechnology Inc.).

Gel scanning and image analysis

Protein profiles were obtained in normal controls and ESCC patients before and after operation through correcting the background to detect, match and quantify the spots by ImageMasterTM two-dimensional Elite analysis software (Amersham Biosciences).

In-gel protein digestion

Individual protein spots were excised from the gel by Ettan spot picker (Amersham Pharmacia Biotechnology Inc.), destained with the solution (15 mmol/L potassium ferricyanide, 50 mmol/L sodium thiosulfate) and washed till opaque and colorless with 25 mmol/L ammonium bicarbonate/500 g/L acetonitrile. After being dried with vacuum concentrator (SpeedVac Plus, USA), the gel was rehydrated with 3-10 μ L of trypsin solution (10 ng/ μ L) at 4 $^{\circ}$ C for 30 min, followed by incubation at 37 $^{\circ}$ C overnight. Tryptic peptides were eluted and dried on SpeedVac vacuum concentrator.

Protein identification by MALDI mass spectrometry

The protein spots were analyzed by matrix-assisted laser desorption/ionization time of flying mass spectrometry (MALDI-TOF-MS) and SWISS-PROT database^[6].

RESULTS

A total of 655, 662 and 677 protein spots were identified, respectively, from the normal control and ESCC patients before and after operation. No significant difference in number of protein spots was observed between normal group and ESCC patients. A total of seven protein spots were identified with a dramatic difference among the samples before and after operation. Six protein

spots were up-regulated and one protein spot was down-regulated in the group after operation compared with those in normal and before operation. Of these six protein spots, three spots were further characterized by MALDI-TOF-MS. The proteins from these three spots were identified as serum amyloid A (SAA), amyloid related serum protein and haptoglobin (Figures 1, 2).

DISCUSSION

In the present study, we found that serum amyloid A (SAA) and its isoform amyloid related serum protein, and haptoglobin were significantly increased after operation in ESCC patients compared with those in normal and pre-operation by mass spectrum. It indicated that these proteins might be related with ESCC and/or surgery. Although the literatures have reported that these acute-phase proteins are associated with tumors, such as colon cancer, the changes of these proteins may be more concerned with stress response, for example, the trauma by operation. The significance for these proteins needs to be further characterized. Although two-dimensional electrophoresis coupled with mass spectrometry is a powerful tool for screening and identification of cancer-specific protein markers, it costs time and money. The present study provided informative data for the establishment of serum protein profiles related with ESCC.

SAA is an acute-phase protein existing as various isoforms in a molecular mass range of 11-14. It is derived mainly from two genes, SAA1 and SAA2^[7], mapped at chromosome 11p15.4-15.1^[8]. In normal individuals, SAA is produced by hepatocytes in the liver. After its production, it is secreted into serum and rapidly binds to high-density lipoproteins, 90% of the protein particles are bound to high-density lipoprotein. A review of the literature showed that only a low level of SAA could be found in the sera of healthy individuals^[9], but during the acute-phase response, its level in the blood could elevate 1 000-fold after various injuries, including trauma, infection, inflammation and neoplasia^[10,11].

Recently, many studies have shown that high SAA protein level is present in the serum of patients with disseminated cancer, reflecting the extent of malignant diseases, and inversely correlated with patient survival^[12]. The mechanism is not clear. The mode of involvement of SAA in metastatic processes has not been elucidated. Several proposed functions for SAA proteins are compatible with the mechanism of tumor cell invasion and metastasis. These include inhibition of malignant cell attachment to extracellular matrix (ECM) proteins^[13,14], induction of the expression of enzymes degrading the ECM^[15] and induction of adhesion, migration, and tissue infiltration of cells^[16-18]. Moreover, SAA contains functional arginine-glycine-aspartic acid (RGD)-like and tyrosine-isoleucine-glycine-serine-arginine (YIGSR)-like adhesion motifs^[19], and the peptides containing these motifs could inhibit tumor cell invasion, metastasis, and angiogenesis^[20,21]. Cumulatively, these findings, together with our observation of SAA alterations in blood after operation, imply that SAA may play a role in one or more steps of tumor progression or regression.

Glojnaric *et al.*^[22] indicated that although the presence of colorectal carcinoma caused an increase in serum levels of all the acute phase reactants studied, SAA protein showed the most powerful reaction in pre-operative disease stage, with the mean value of 330 mg/L as compared to the normal values of <1.2 mg/L obtained in 30 healthy adults. SAA protein concentration increased to 487 mg/L after surgery and declined during the post-operative clinical course until the sixth chemotherapy cycle, but never returned to the normal range. In the later chemotherapy cycles, the mean SAA protein increased to 163 mg/L, probably as a result of the disease relapse. According to the statistical relations among exact confidence intervals for proportions, SAA protein showed the best specificity for colorectal carcinoma of all the acute phase proteins studied (83-100%) and also a sensitivity of 100%. They concluded that SAA protein seems to be a

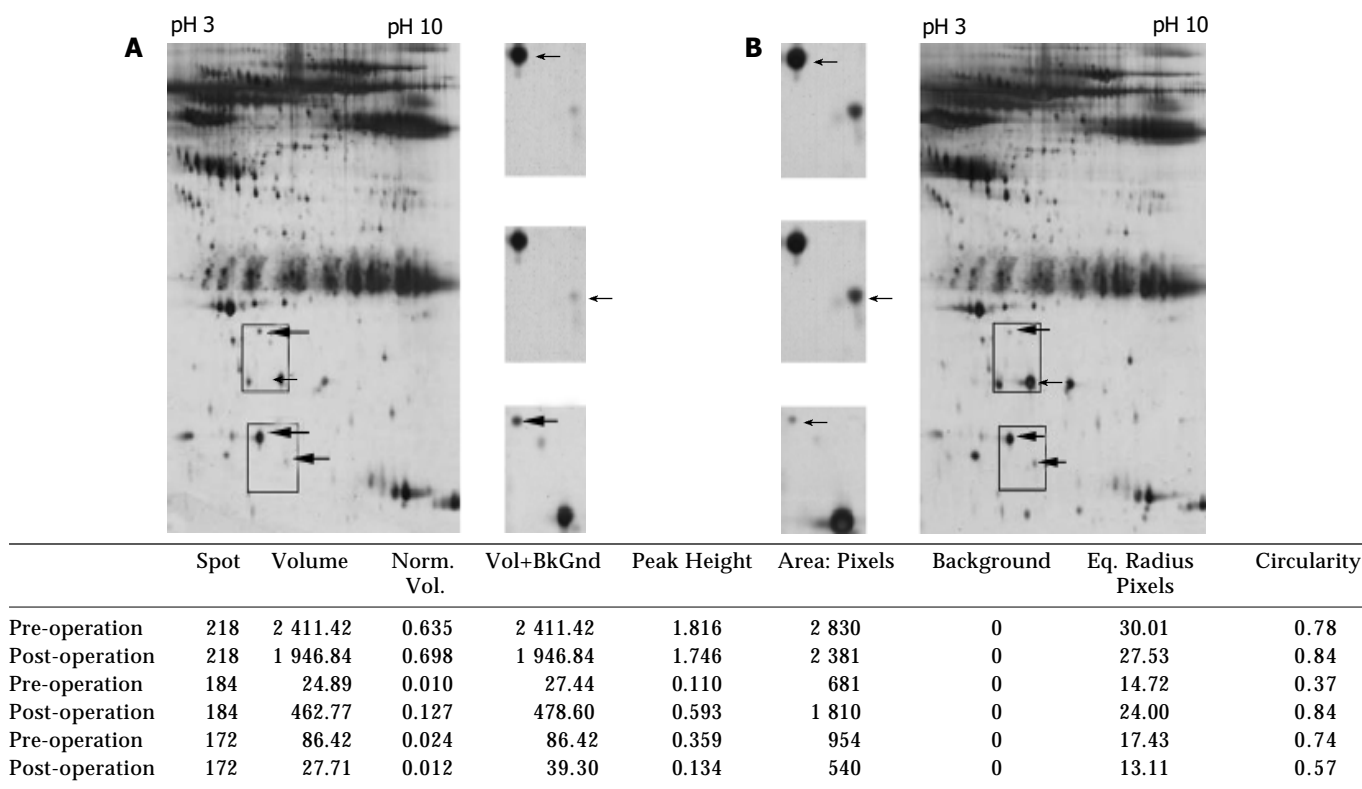


Figure 1 Representative of two-dimensional electrophoresis profiles and three-matched protein spots (arrows) analysis of the sera from esophageal squamous cell carcinoma patients before (A) and after (B) operation with different acidity from pH 3 to pH 10. Norm: normalization, Vol: volume, BkGnd: background, Eq: equality.

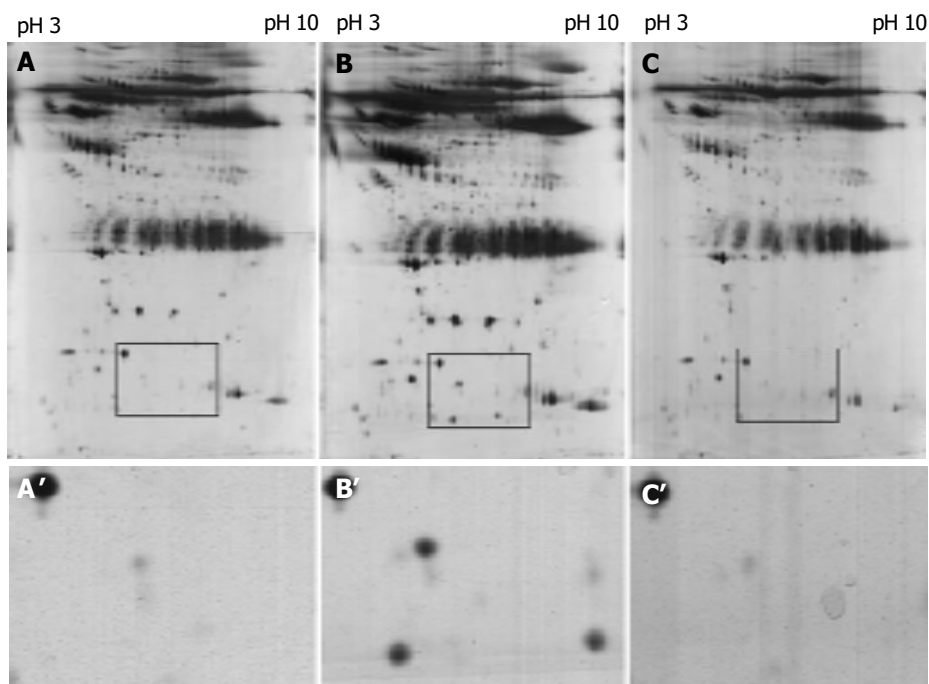


Figure 2 Representative of two-dimensional electrophoresis patterns of sera protein from the same esophageal squamous cell carcinoma patient before (A) and after (B) operation and the normal subject (C) with different acidity from pH 3 to pH 10. A', B' and C' are the magnification of A, B and C, respectively, for the sera protein with marked difference.

reliable parameter, which could be recommended for clinical routine as a non-specific tumor marker for colorectal carcinoma.

Haptoglobin is an acute phase protein capable of binding haemoglobin and may play a role in modulating many aspects of the acute phase response^[23]. The complex of haptoglobin with haemoglobin is metabolized in the hepatic reticuloendothelial system^[24]. Biosynthesis of haptoglobin occurs not only in the

liver, but also in adipose tissue and in lung, providing antioxidant and antimicrobial activity^[25]. Changes in the measured concentrations of haptoglobin in serum may help to assess the disease status of patients with inflammations, infections, malignancy, *etc*^[26]. Dynamic detection of haptoglobin in leukemia patient plasmas showed that haptoglobin level increased obviously in leukemia patients than that in normal persons and

dropped gradually with the improvement of diseases.

In conclusion, serum amyloid A, amyloid related serum protein and haptoglobin may be related with ESCC. The significance of these proteins needs to be further characterized. The present study provides informative data for the establishment of serum protein profiles related with ESCC.

REFERENCES

- 1 **Wang LD**, Zheng S. The mechanism of esophageal and gastric cardia carcinogenesis from the subjects at high-incidence area for esophageal cancer in Henan. *Zhengzhou Daxue Xuebao* 2002; **37**: 717-729
- 2 **Wang LD**, Zhou Q, Feng CW, Liu B, Qi YJ, Zhang YR, Gao SS, Fan ZM, Zhou Y, Yang CS, Wei JP, Zheng S. Intervention and follow-up on human esophageal precancerous lesions in Henan, northern China, a high-incidence area for esophageal cancer. *Gan To Kagaku Ryoho* 2002; **29**(Suppl 1): 159-172
- 3 **Hanash SM**, Bobek MP, Rickman DS, Williams T, Rouillard JM, Quick R, Puravs E. Integrating cancer genomics and proteomics in the post-genome era. *Proteomics* 2002; **2**: 69-75
- 4 **Anderson NL**, Anderson NG. The human plasma proteome: history, character, and diagnostic prospects. *Mol Cell Proteomics* 2002; **1**: 845-867
- 5 **Simpson RJ**. Proteins and Proteomics. A Laboratory Manual. 1st. *New York Cold Spring Harbor Laboratory Press* 2003: 75-76
- 6 **Bini L**, Magi B, Marzocchi B, Arcuri F, Tripodi S, Cintorino M, Sanchez JC, Frutiger S, Hughes G, Pallini V, Hochstrasser DF, Tosi P. Protein expression profiles in human breast ductal carcinoma and histologically normal tissue. *Electrophoresis* 1997; **18**: 2832-2841
- 7 **Yamada T**. Serum amyloid A (SAA): a concise review of biology, assay methods and clinical usefulness. *Clin Chem Lab Med* 1999; **37**: 381-388
- 8 **Watson G**, See CG, Woo P. Use of somatic cell hybrids and fluorescence in situ hybridization to localize the functional serum amyloid A (SAA) genes to chromosome 11p15.4-p15.1 and the entire SAA superfamily to chromosome 11p15. *Genomics* 1994; **23**: 694-696
- 9 **d'Eril GM**, Anesi A, Maggiore M, Leoni V. Biological variation of serum amyloid A in healthy subjects. *Clin Chem* 2001; **47**: 1498-1499
- 10 **Cho WC**, Yip TT, Yip C, Yip V, Thulasiraman V, Ngan RK, Yip TT, Lau WH, Au JS, Law SC, Cheng WW, Ma VW, Lim CK. Identification of serum amyloid A protein as a potentially useful biomarker to monitor relapse of nasopharyngeal cancer by serum proteomic profiling. *Clin Cancer Res* 2004; **10**(1 Pt 1): 43-52
- 11 **Urieli-Shoval S**, Linke RP, Matzner Y. Expression and function of serum amyloid A, a major acute-phase protein, in normal and disease states. *Curr Opin Hematol* 2000; **7**: 64-69
- 12 **Kimura M**, Tomita Y, Imai T, Saito T, Katagiri A, Ohara-Mikami Y, Matsudo T, Takahashi K. Significance of serum amyloid A on the prognosis in patients with renal cell carcinoma. *Cancer* 2001; **92**: 2072-2075
- 13 **Jensen LE**, Whitehead AS. Regulation of serum amyloid A protein expression during the acute-phase response. *Biochem J* 1998; **334**(Pt 3): 489-503
- 14 **Hershkovitz R**, Preciado-Patt L, Lider O, Fridkin M, Dastyh J, Metcalfe DD, Mekori YA. Extracellular matrix-anchored serum amyloid A preferentially induces mast cell adhesion. *Am J Physiol* 1997; **273**(1 Pt 1): C179-187
- 15 **Preciado-Patt L**, Levartowsky D, Prass M, Hershkovitz R, Lider O, Fridkin M. Inhibition of cell adhesion to glycoproteins of the extracellular matrix by peptides corresponding to serum amyloid A. Toward understanding the physiological role of an enigmatic protein. *Eur J Biochem* 1994; **223**: 35-42
- 16 **Migita K**, Kawabe Y, Tominaga M, Origuchi T, Aoyagi T, Eguchi K. Serum amyloid A protein induces production of matrix metalloproteinases by human synovial fibroblasts. *Lab Invest* 1998; **78**: 535-539
- 17 **Urieli-Shoval S**, Shubinsky G, Linke RP, Fridkin M, Tabi I, Matzner Y. Adhesion of human platelets to serum amyloid A. *Blood* 2002; **99**: 1224-1229
- 18 **Badolato R**, Wang JM, Murphy WJ, Lloyd AR, Michiel DF, Bausserman LL, Kelvin DJ, Oppenheim JJ. Serum amyloid A is a chemoattractant: induction of migration, adhesion, and tissue infiltration of monocytes and polymorphonuclear leukocytes. *J Exp Med* 1994; **180**: 203-209
- 19 **Iwamoto Y**, Nomizu M, Yamada Y, Ito Y, Tanaka K, Sugioka Y. Inhibition of angiogenesis, tumour growth and experimental metastasis of human fibrosarcoma cells HT1080 by a multimeric form of the laminin sequence Tyr-Iie-Gly-Ser-Arg (YIGSR). *Br J Cancer* 1996; **73**: 589-595
- 20 **Ruoslahti E**, Pierschbacher MD. New perspectives in cell adhesion: RGD and integrins. *Science* 1987; **238**: 491-497
- 21 **Thorn CF**, Lu ZY, Whitehead AS. Regulation of the human acute phase serum amyloid A genes by tumour necrosis factor-alpha, interleukin-6 and glucocorticoids in hepatic and epithelial cell lines. *Scand J Immunol* 2004; **59**: 152-158
- 22 **Glojnaric I**, Casl MT, Simic D, Lukac J. Serum amyloid A protein (SAA) in colorectal carcinoma. *Clin Chem Lab Med* 2001; **39**: 129-133
- 23 **Wassell J**. Haptoglobin: function and polymorphism. *Clin Lab* 2000; **46**: 547-552
- 24 **Kurash JK**, Shen CN, Tosh D. Induction and regulation of acute phase proteins in transdifferentiated hepatocytes. *Exp Cell Res* 2004; **292**: 342-358
- 25 **Bernard D**, Christophe A, Delanghe J, Langlois M, De Buyzere M, Comhaire F. The effect of supplementation with an antioxidant preparation on LDL-oxidation is determined by haptoglobin polymorphism. *Redox Rep* 2003; **8**: 41-46
- 26 **Dobryszczyka W**. Biological functions of haptoglobin-new pieces to an old puzzle. *Eur J Clin Chem Clin Biochem* 1997; **35**: 647-654

Edited by Kumar M and Wang XL. Proofread by Xu FM

Tumor micrometastases in mesorectal lymph nodes and their clinical significance in patients with rectal cancer

Yang-Chun Zheng, Yu-Ying Tang, Zong-Guang Zhou, Li Li, Tian-Cai Wang, Yi-Ling Deng, Dai-Yun Chen, Wei-Ping Liu

Yang-Chun Zheng, Zong-Guang Zhou, Li Li, Tian-Cai Wang. Department of Gastroenterological Surgery, West China Hospital, Sichuan University, Chengdu 610041, Sichuan Province, China

Yu-Ying Tang. Department of Anesthesiology, West China Hospital, Sichuan University, Chengdu 610041, Sichuan Province, China

Yi-Ling Deng, Dai-Yun Chen, Wei-Ping Liu. Department of Pathology, West China Hospital, Sichuan University, Chengdu 610041, Sichuan Province, China

Supported by the National Natural Science Foundation of China, No. 39925032

Correspondence to: Dr. Zong-Guang Zhou, Department of Gastroenterological Surgery, West China Hospital, Sichuan University, 37 Guo Xue Xiang, Chengdu 610041, Sichuan Province, China. zhou767@21cn.com

Telephone: +86-28-85422484 **Fax:** +86-28-85422484

Received: 2004-03-09 **Accepted:** 2004-04-05

Abstract

AIM: To investigate the number, size, and status of lymph nodes within the mesorectum and to explore the prognostic significance of lymph node micrometastases in patients with rectal cancer.

METHODS: Thirty-one patients with rectal cancer undergone total mesorectal excision between October 2001 and October 2002 were included. Mesorectal nodes retrieved from the resected specimens were detected with a combination of haematoxylin and eosin (HE) staining and immunohistochemistry (IHC). The relations between lymph node metastases, micrometastases and postoperative recurrence were analyzed.

RESULTS: A total of 548 lymph nodes were harvested, with 17.7 ± 8.2 nodes per case. The average number of metastatic nodes in HE-positive patients and micrometastatic nodes in IHC-positive patients was 5.2 ± 5.1 per case and 2.2 ± 1.3 per case, respectively. The mean size of all nodes and metastatic nodes was 4.1 ± 1.8 mm and 5.2 ± 1.7 mm in diameter, respectively. The mean size of micrometastatic nodes was 3.9 ± 1.4 mm in diameter. The size of the majority of mesorectal nodes (66.8%), metastatic nodes (52.6%), and micrometastatic nodes (79.5%) was less than 5 mm in diameter. During a median follow-up period of 24.6 ± 4.7 mo, 5 patients (16.7%) had recurrence, of them 2 died and 3 survived. Another case died of tumor unrelated cause and was excluded. All 5 recurrent cases had 3 or more nodes involved, and one of them developed only lymph node micrometastases. The mean number of both metastatic and micrometastatic nodes per case differed significantly between the recurrent and non-recurrent groups ($P < 0.01$ and $P = 0.01$, respectively).

CONCLUSION: The majority of lymph nodes, metastatic, and micrometastatic lymph nodes within the mesorectum are smaller than 5 mm in diameter. The nodal status and the number of lymph nodes involved with tumor metastases and micrometastases are related to the rapid postoperative recurrence.

Zheng YC, Tang YY, Zhou ZG, Li L, Wang TC, Deng YL,

Chen DY, Liu WP. Tumor micrometastases in mesorectal lymph nodes and their clinical significance in patients with rectal cancer. *World J Gastroenterol* 2004; 10(22): 3369-3373
<http://www.wjgnet.com/1007-9327/10/3369.asp>

INTRODUCTION

Lymph node involvement is one of the most important factors in determining the prognosis of patients with rectal cancer^[1-6]. Patients with lymph node involvement were found to suffer from more advanced diseases according to the tumor-node-metastasis (TNM) classification system^[6], and up to 30% of them eventually developed recurrences after a potentially curative resection^[7,8]. In contrast, some patients without positive lymph nodes also had postoperative recurrences or developed metastatic diseases, which were reported to be associated with lymph node micrometastases missed by conventional pathological examination^[9-13].

Lymph node spread of rectal cancer generally follows an anatomical route from the proximity to distance along the main supplying vessels of the rectum^[14,15]. Lymph nodes contained in the mesorectum are thereby the earliest and most frequent ones that might be involved when tumor spread occurs^[14-16]. Although reports have emphasized the importance of regional lymph nodes in the prognosis of rectal cancer^[11,2,17-21], few studies available have investigated the number and size of lymph nodes within the rectal mesentery^[22,23]. The clinical significance of mesorectal lymph node metastases and micrometastases remains to be fully acknowledged^[22,23]. This study was conducted to examine the number, size, and status of lymph nodes within the mesorectum, and to investigate the prognostic value of lymph node metastases, especially lymph node micrometastases, in patients with rectal cancer.

MATERIALS AND METHODS

Patients

From October 2001 to October 2002, 31 patients with rectal cancer undergone total mesorectal excision (TME) at the Department of Gastroenterological Surgery of West China Hospital were included. There were 18 males and 13 females, with an average age of 55 (32-72) years. Of them, 7 cases were patients with high rectal cancer (above the peritoneal reflection) and 24 cases were patients with lower rectal cancer (below the peritoneal reflection). Three tumors were highly differentiated, 20 moderately differentiated, and 8 poorly differentiated. All patients received standard preoperative examination and the diagnosis of rectal adenocarcinoma was made by fibrocolonoscopy and confirmed by pathological biopsy before surgery. All operations were carefully performed by skillful surgeons following the principle of TME^[24], and the rectal specimens resected were collected prospectively.

Specimen processing

After removal, the specimens were routinely processed with neutral buffered 100 mL/L formalin solution for 24 h, and immersed in lymph node revealing solution (LNRS) for 6 h or more^[25]. Later, they were washed thoroughly with running

water. Fat tissues in the specimens were dissected carefully at intervals of 2-3 mm from upward down to the level of distant transaction along the runway of the superior rectal artery (SRA). Lymph nodes stood out as white, and chalky nodules against the background of yellow fat were harvested and recorded.

Pathological examination

After retrieval, each lymph node was embedded separately in paraffin. The block was then sectioned serially at intervals of 20-40 μm , with each section of 4 μm in thickness. Two sections sampled randomly from 10 representative levels were subjected to haematoxylin and eosin (HE) staining. For nodes diagnosed negatively by HE staining, another 3 sections were further singled out, one for HE re-examination, the other two for immunohistochemistry (IHC).

Immunohistochemistry was performed using labelled streptavidin biotin method (LsAB). Briefly, all sections were deparaffinized and rehydrated. Then, they were immersed in 30 mL/L H_2O_2 for 20 min to block the endogenous peroxidase activity. Sections were then incubated with 100 mL/L normal goat serum for 20 min, followed by incubation with mouse monoclonal anti-human cytokeratin (CK) 20 antibody (Neomarkers, Lab Vision Corporation, CA, USA) (1:50) at 4 $^\circ\text{C}$ overnight. After that, the sections were washed with phosphate buffered solution (PBS) (0.01 mol/L, pH 7.2) and sequentially incubated with biotinylated goat anti-mouse IgG, and streptavidin biotin horseradish peroxidase complex following the manufacturer's instructions (HistostainTM-SP Kits, Zymed laboratories Inc., San Francisco, CA, USA). Staining was developed by immersing slides in 0.5 g/L 3,3'-diaminobenzidizing tetrahydrochloride (DAB) with 3.3 mol/L H_2O_2 . All slides were counterstained with haematoxylin, dehydrated and mounted. Yellowish staining of the tumor cell cytoplasm was taken as positive. Previously confirmed rectal adenocarcinoma tissue served as positive control, and substitution of the primary monoclonal antibody with PBS was used as negative control. Tumor micrometastases were occult diseases generally missed by HE staining while detected by IHC, and were characterized as single cell or small cluster of cells showing malignant morphology.

Follow-up

All patients were regularly followed up to now. The follow-up

interval was every 3 mo after surgery during the first year and every 6 mo thereafter. The time of recurrence and the cause of death were inquired and recorded.

Statistical analysis

The *t* test for difference in mean values and χ^2 test for difference in frequencies were performed using SPSS 10.0 software package. $P < 0.05$ was considered statistically significant.

RESULTS

Micrometastases and number of lymph nodes

A total of 548 mesorectal lymph nodes were retrieved from the 31 specimens, with 17.7 ± 8.2 lymph nodes per case. HE staining detected 114 lymph nodes positive in 22 patients (71.0%). The average number of metastatic lymph nodes in HE-positive patients was 5.2 ± 5.1 per case. IHC re-examination of the remaining negative nodes revealed 39 lymph nodes (9.0%) positive with tumor micrometastases from 18 cases (58.1%). Among them, 5 cases (16.1%) with 10 nodes positive with IHC staining were previously assumed free of metastatic diseases. The average number of micrometastatic lymph nodes in IHC-positive patients was 2.2 ± 1.3 per case.

Micrometastases and size of lymph nodes

The average diameter of all the 548 lymph nodes was 4.1 ± 1.8 mm. The mean size of 114 metastatic lymph nodes (5.2 ± 1.7 mm in diameter) was significantly larger than that of 39 micrometastatic lymph nodes (3.9 ± 1.4 mm in diameter) ($P < 0.01$). Of all the lymph nodes, 92 (16.8%) were ≤ 2 mm in diameter, with 4 metastatic and 3 micrometastatic lymph nodes; 182 (33.2%) ≥ 5 mm, with 54 metastatic and 8 micrometastatic lymph nodes; and 274 (50.0%) with a size between 2 mm and 5 mm in diameter, with 56 metastatic and 28 micrometastatic lymph nodes (Table 1). It was noted that the majority of lymph nodes (66.8%) were < 5 mm in diameter, and 52.6% of the metastatic nodes and a higher proportion of the micrometastatic nodes (79.5%) were < 5 mm in diameter also.

Lymph node metastases and micrometastases and prognosis

All the 31 patients were successfully followed-up. Patients with lymph node metastases received regular chemotherapy after surgery. However, during a median follow-up period of 24.6 ± 4.7 mo, one

Table 1 Size of lymph nodes (LNs) and status of tumor metastases and micrometastases

Size of LNs (mm)	No. of LNs				Positive ratio (%)
	Total	HE-positive	IHC-positive	Sum of positive	
≤ 2	92	4	3	7	7.6 ^b
2-5	274	56	28	84	30.7
≥ 5	182	54	8	62	34.1 ^d
Total	548	114	39	153	27.9

^b $P < 0.01$, vs 2-5; ^d $P < 0.01$, vs ≤ 2 .

Table 2 Clinicopathological features of five recurrent patients with lower rectal cancer

Case No.	Sex	Age (yr)	Characteristics of tumor		No. of LNs			Site of recurrence	Outcome
			Differentiation	Invasion	Total	M	MM		
1	Female	35	Well	Muscle	15	3	2	Lung	Surviving
2	Female	65	Poor	Serosa	22	22	0	Pelvis+liver	Dead
3	Male	50	Moderate	Muscle	27	0	3	Pelvis	Surviving
4	Male	45	Poor	Serosa	30	17	4	Pelvis	Dead
5	Male	32	Poor	Muscle	21	5	5	Pelvis	Surviving

LNs: lymph nodes; M: metastatic; MM: micrometastatic.

Table 3 Comparison of recurrence between patients with different nodal status

Variables	HE-positive		HE-negative		Total
	IHC-positive	IHC-negative	IHC-positive	IHC-negative	
No. of case	13	8	5	4	30
Recurrence	3	1	1	0	5
Recurrence rate (%)	23.1	12.5	20	0	16.7

Table 4 Comparison of nodal status between recurrent and non-recurrent group

Grouping	LNs (mean±SD)				Positive ratio (%)
	Total	HE-positive	IHC-positive	Sum of positive	
Recurrent group	23.0±5.8	9.4±9.6	2.8±1.9	12.2±8.9	53.0
Non-recurrent group	17.0±8.2	2.6±2.5	1.0±1.2	3.6±3.0	21.4
<i>P</i>	0.135	0.003	0.01	0.000	0.000

patient died of tumor unrelated cardiovascular disturbance 24 mo post operation and was excluded from the analysis. Among the five cases (16.7%) with lower tumor recurrences, 3 cases were localized in the pelvic floor, one case spread to the lung, and one case with both pelvic and liver involvements. Two of them died and the other three remained alive. All the recurrent patients shared the characteristics of having 3 or more lymph nodes involved with tumor metastases and/or micrometastases. Of them, one case with mere lymph node micrometastases also developed local recurrence 17 mo after operation (Tables 2, 3). Comparison analysis showed that both the number of metastatic and micrometastatic lymph nodes between the recurrent and non-recurrent groups differed significantly ($P < 0.01$ and $P = 0.01$, respectively), although such a statistical difference was not found between them in reference to the total number identified per case (Table 4).

DISCUSSION

The nodal status is the single powerful predictor of survival in rectal cancer^[1,2,20,21]. Both the number and location of lymph nodes involved have significant impacts on the outcome of patients with rectal cancer^[6,15,21,26]. However, the nodal staging accuracy is not easy to make^[27-29]. Factors contributing to this dilemma include the amount of mesentery resected, diligence for search of nodes paid, number of histological slices investigated, and methods of pathological examination employed^[30-33]. There are still wide variations regarding the minimum number of lymph nodes to be examined for a reliable node-negative diagnosis, the reported recommendations were 6 to 17 lymph nodes^[34-36]. The non-uniform extent of lymph nodes collected for investigation made the results incomparable between authors, and the absence of consensus on the number of lymph nodes contained in the mesentery worsened the situation further^[36,37].

It was established that the lymphatic spread of rectal cancer followed an anatomical way along which the normal lymphatic fluid drains^[14,15]. As a consequence, lymph nodes contained in the mesorectum are the earliest and the most frequent ones that might be involved when the dissemination of tumor cells takes place^[14-16]. Focused examination of the mesorectal lymph nodes, thereby, could identify most metastases and micrometastases in the first place^[15], though skip metastases might exist in a few cases^[38,39]. However, available data have provided little information on the lymph nodes enveloped within the mesorectum^[22,23]. The number and size of lymph nodes, and their tumor status remain to be defined.

Recently, Canessa *et al.*^[22] recovered 168 mesorectal lymph nodes from 20 cadavers and found that the mean number was 8.4 per specimen. They searched the lymph nodes from the division

of the superior rectal artery which excluded the lymph nodes that lie above it, i.e., the lymph nodes along the main trunk of it, that should otherwise be referred to 'mesorectal' nodes by strict definition^[40]. Also in another study on cadavers, an average of 24.9 pelvic lymph nodes were identified from 7 fresh specimens, which included 13.6 mesorectal lymph nodes per case^[23]. Their study employed modified LNRS to facilitate the identification of lymph nodes in the mesorectum. Therefore, the lymph nodes they retrieved outnumbered those in previous study markedly^[23]. In the current study, the LNRS was also used to help identify lymph nodes embedded in the mesorectal fat. A mean number of 17.7 lymph nodes per case were dissected. The majority of them (82.2%) were located along the superior rectal artery. The sizes of 66.8% of the total lymph nodes, 59.8% of the metastatic lymph nodes and 79.5% of the micrometastatic lymph nodes were <5 mm in diameter. The minimal size of lymph nodes found was 0.7 mm in diameter. These lymph nodes, especially those with a diameter ≤ 2 mm, were at great risk of being missed in routine pathological sampling with only naked speculation and manual palpitation^[41-43]. By further examining the HE-negative nodes with IHC staining, we identified 39 nodes positive with tumor micrometastases from 18 cases (58.1%). Of interest, 10 nodes with micrometastatic diseases in 5 cases (16.1%) were previously assumed free of tumor spread by routine pathological examination. Thus this group of patients was upstaged.

The superior sensitivity of IHC to HE staining in detecting micrometastases in colorectal cancer has been well recognized^[44-47]. Although its sensitivity remained ten times lower compared to reverse transcriptase polymerase chain reaction (RT-PCR) techniques, IHC is probably more specific and reliable, in that it allows examining the morphology of stained cells and differentiating from that of non-specific background staining^[44-46]. There are still many controversies regarding the prognostic significance of micrometastases in colorectal cancer^[10,11,47-54]. It was argued that although the application of IHC technique had the added ability to identify overt diseases missed by HE staining, it offered little prognostic information on the postoperative recurrence and long year survival^[10,49-52]. On the contrary, authors favoring the detection of lymph node micrometastases stated that it was not only one of the major concerns for the proper staging of diseases, but also of prognostic relevance to the outcome of patients with rectal cancer, thus suggesting helpful in the early planning of a multimodality treatment protocol for indicated patients^[11,53,54].

Choi *et al.*^[50] retrospectively reviewed 1 808 lymph nodes from 93 Dukes' B colorectal tumors with IHC staining and found that 54 lymph nodes (3.0%) from 29 cases (31.2%) harbored micrometastatic diseases. However, the five-year survival analysis showed no significant difference between the micrometastatic group and non-micrometastatic group. Yasuda *et al.*^[11] employed

IHC method and examined a total of 1 013 lymph nodes from 12 recurrent and 30 non-recurrent patients with histologically determined Dukes' B colorectal cancer. Micrometastases were confirmed in 59 lymph nodes (16%) from 11 cases (92%) in the recurrent group, and 77 lymph nodes (12%) from 21 cases (70%) in the non-recurrent group. They further demonstrated that micrometastases in four or more lymph nodes occurred more frequently in the recurrent group than in the non-recurrent group (58% vs 20%, $P < 0.05$), and micrometastases to N2 or higher nodes occurred more frequently in the recurrent group also (92% vs 47%, $P < 0.01$). Afterwards they concluded that the number and level of positive micrometastatic lymph nodes were both significantly correlated with postoperative recurrence of histologically determined Dukes' B colorectal cancer^[11].

In the present study, 5 patients with rectal cancer developed recurrences. The rate of recurrence was 16.7% within two years after curative operation. All patients suffering from recurrent diseases had three or more mesorectal nodes involved with tumor metastases and/or micrometastases, one patient with lymph node micrometastases developed recurrence also. It was noted that both the number of metastatic and micrometastatic lymph nodes differed significantly between the recurrent and non-recurrent groups ($P < 0.01$ and $P = 0.01$, respectively), implying that lymph node micrometastases and the number of lymph nodes involved might also correlate with the outcome of patients with rectal cancer, while the prognostic value of lymph node metastases was confirmed.

In summary, by using the LNRS to facilitate identifying lymph nodes, and with a combination of HE and IHC to detect tumor metastases and micrometastases, we have provided a detailed description of both the number and size of lymph nodes involved in the mesorectum, as well as their tumor status with metastases and micrometastases in rectal cancer. The rapid recurrence of tumor after a cure-intended surgery is related to the tumor status of mesorectal lymph nodes. The presence of lymph node micrometastases and the number of lymph nodes involved might have some value for the prediction of tumor recurrence in rectal cancer^[11,47,48,53,54], now that the importance of lymph node metastases has been widely acknowledged^[1-6,19,21]. However, it is too cursory to draw a convincing conclusion, concerning the small samples included and only short-term outcome investigated in the current study. Future multi-central large-sample controlled studies are needed to clearly define the role of lymph node micrometastases in the prognosis of patients with rectal cancer.

REFERENCES

- 1 **Fujita S**, Shimoda T, Yoshimura K, Yamamoto S, Akasu T, Moriya Y. Prospective evaluation of prognostic factors in patients with colorectal cancer undergoing curative resection. *J Surg Oncol* 2003; **84**: 127-131
- 2 **Bannura G**, Cumsille MA, Contreras J, Melo C, Barrera A, Reinero M, Pardo L. Prognostic factors in colorectal neoplasm. Multivariate analysis in 224 patients. *Rev Med Chil* 2001; **129**: 237-246
- 3 **Bernick PE**, Wong WD. Staging: what makes sense? Can the pathologist help? *Surg Oncol Clin N Am* 2000; **9**: 703-720
- 4 **Gennari L**, Doci R, Rossetti C. Prognostic factors in colorectal cancer. *Hepatogastroenterology* 2000; **47**: 310-314
- 5 **Sobin LH**. TNM: evolution and relation to other prognostic factors. *Semin Surg Oncol* 2003; **21**: 3-7
- 6 **Compton C**, Fenoglio-Preiser CM, Pettigrew N, Fielding LP. American joint committee on cancer prognostic factors consensus conference: Colorectal working group. *Cancer* 2000; **88**: 1739-1757
- 7 **Demols A**, Van Laethem JL. Adjuvant chemotherapy for colorectal cancer. *Curr Gastroenterol Rep* 2002; **4**: 420-426
- 8 **Frizelle FA**, Emanuel JC, Keating JP, Dobbs BR. A multicentre retrospective audit of outcome of patients undergoing curative resection for rectal cancer. *N Z Med J* 2002; **115**: 284-286
- 9 **Shimoyama M**, Yamazaki T, Suda T, Hatakeyama K. Prognostic significance of lateral lymph node micrometastases in lower rectal cancer: an immunohistochemical study with CAM5.2. *Dis Colon Rectum* 2003; **46**: 333-339
- 10 **Noura S**, Yamamoto H, Ohnishi T, Masuda N, Matsumoto T, Takayama O, Fukunaga H, Miyake Y, Ikenaga M, Ikeda M, Sekimoto M, Matsuura N, Monden M. Comparative detection of lymph node micrometastases of stage II colorectal cancer by reverse transcriptase polymerase chain reaction and immunohistochemistry. *J Clin Oncol* 2002; **20**: 4232-4241
- 11 **Yasuda K**, Adachi Y, Shiraishi N, Yamaguchi K, Hirabayashi Y, Kitano S. Pattern of lymph node micrometastasis and prognosis of patients with colorectal cancer. *Ann Surg Oncol* 2001; **8**: 300-304
- 12 **Liefers GJ**, Cleton-Jansen AM, van de Velde CJ, Hermans J, van Krieken JH, Cornelisse CJ, Tollenaar RA. Micrometastases and survival in stage II colorectal cancer. *N Engl J Med* 1998; **339**: 223-228
- 13 **Isaka N**, Nozue M, Doy M, Fukao K. Prognostic significance of perirectal lymph node micrometastases in Dukes' B rectal carcinoma: an immunohistochemical study by CAM5.2. *Clin Cancer Res* 1999; **5**: 2065-2068
- 14 **Bartholdson L**, Hultborn A, Hulten L, Roos B, Rosencrantz M, Ahren C. Lymph drainage from the upper and middle third of the rectum as demonstrated by 198 Au. *Acta Radiol Ther Phys Biol* 1977; **16**: 352-360
- 15 **Cserni G**, Tarjan M, Bori R. Distance of lymph nodes from the tumor: an important feature in colorectal cancer specimens. *Arch Pathol Lab Med* 2001; **125**: 246-249
- 16 **Yamada H**, Katoh H, Kondo S, Okushiba S, Morikawa T. Mesenteric lymph nodes status influencing survival and recurrence pattern after hepatectomy for colorectal liver metastases. *Hepatogastroenterology* 2002; **49**: 1265-1268
- 17 **Mukai M**, Ito I, Mukoyama S, Tajima T, Saito Y, Nakasaki H, Sato S, Makuuchi H. Improvement of 10-year survival by Japanese radical lymph node dissection in patients with Dukes' B and C colorectal cancer: a 17-year retrospective study. *Oncol Rep* 2003; **10**: 927-934
- 18 **Cserni G**. Nodal staging of colorectal carcinomas and sentinel nodes. *J Clin Pathol* 2003; **56**: 327-335
- 19 **Ueno H**, Mochizuki H, Hashiguchi Y, Hase K. Prognostic determinants of patients with lateral nodal involvement by rectal cancer. *Ann Surg* 2001; **234**: 190-197
- 20 **Gervasoni JE Jr**, Taneja C, Chung MA, Cady B. Biologic and clinical significance of lymphadenectomy. *Surg Clin North Am* 2000; **80**: 1631-1673
- 21 **Takahashi K**, Mori T, Yasuno M. Histologic grade of metastatic lymph node and prognosis of rectal cancer. *Dis Colon Rectum* 2000; **43**(10 Suppl): S40-S46
- 22 **Canessa CE**, Badia F, Fierro S, Fiol V, Hayek G. Anatomic study of the lymph nodes of the mesorectum. *Dis Colon Rectum* 2001; **44**: 1333-1336
- 23 **Topor B**, Acland R, Kolodko V, Galandiuk S. Mesorectal lymph nodes: their location and distribution within the mesorectum. *Dis Colon Rectum* 2003; **46**: 779-785
- 24 **Heald RJ**, Husband EM, Ryall RD. The mesorectum in rectal cancer surgery-the clue to pelvic recurrence? *Br J Surg* 1982; **69**: 613-616
- 25 **Koren R**, Siegal A, Klein B, Halpern M, Kyzer S, Veltman V, Gal R. Lymph node-revealing solution: simple new method for detecting minute lymph nodes in colon carcinoma. *Dis Colon Rectum* 1997; **40**: 407-410
- 26 **Luna-Perez P**, Rodriguez-Ramirez S, Alvarado I, Gutierrez de la Barrera M, Labastida S. Prognostic significance of retrieved lymph nodes per specimen in resected rectal adenocarcinoma after preoperative chemoradiation therapy. *Arch Med Res* 2003; **34**: 281-286
- 27 **Turner RR**, Nora DT, Trocha SD, Bilchik AJ. Colorectal carcinoma nodal staging. Frequency and nature of cytokeratin-positive cells in sentinel and nonsentinel lymph nodes. *Arch Pathol Lab Med* 2003; **127**: 673-679
- 28 **Miyake Y**, Yamamoto H, Fujiwara Y, Ohue M, Sugita Y, Tomita N, Sekimoto M, Matsuura N, Shiozaki H, Monden M. Extensive micrometastases to lymph nodes as a marker for rapid recurrence of colorectal cancer: a study of lymphatic mapping.

- Clin Cancer Res* 2001; **7**: 1350-1357
- 29 **Joseph NE**, Sigurdson ER, Hanlon AL, Wang H, Mayer RJ, MacDonald JS, Catalano PJ, Haller DG. Accuracy of determining nodal negativity in colorectal cancer on the basis of the number of nodes retrieved on resection. *Ann Surg Oncol* 2003; **10**: 213-218
 - 30 **Poller DN**. Method of specimen fixation and pathological dissection of colorectal cancer influences retrieval of lymph nodes and tumour nodal stage. *Eur J Surg Oncol* 2000; **26**: 758-762
 - 31 **Rosenberg R**, Friederichs J, Gertler R, Hoos A, Mueller J, Nahrig J, Nekarada H, Siewert JR. Prognostic evaluation and review of immunohistochemically detected disseminated tumor cells in peritumoral lymph nodes of patients with pN0 colorectal cancer. *Int J Colorectal Dis* 2004; **19**: 430-437
 - 32 **Johnson PM**, Malatjalian D, Porter GA. Adequacy of nodal harvest in colorectal cancer: a consecutive cohort study. *J Gastrointest Surg* 2002; **6**: 883-888
 - 33 **Wong JH**, Steinemann S, Tom P, Morita S, Tauchi-Nishi P. Volume of lymphatic metastases does not independently influence prognosis in colorectal cancer. *J Clin Oncol* 2002; **20**: 1506-1511
 - 34 **Cserni G**, Vinh-Hung V, Burzykowski T. Is there a minimum number of lymph nodes that should be histologically assessed for a reliable nodal staging of T3N0M0 colorectal carcinomas? *J Surg Oncol* 2002; **81**: 63-69
 - 35 **Leibl S**, Tsybrovskyy O, Denk H. How many lymph nodes are necessary to stage early and advanced adenocarcinoma of the sigmoid colon and upper rectum? *Virchows Arch* 2003; **443**: 133-138
 - 36 **Cianchi F**, Palomba A, Boddi V, Messerini L, Pucciani F, Perigli G, Bechi P, Cortesini C. Lymph node recovery from colorectal tumor specimens: recommendation for a minimum number of lymph nodes to be examined. *World J Surg* 2002; **26**: 384-389
 - 37 **Ratto C**, Sofo L, Ippoliti M, Merico M, Bossola M, Vecchio FM, Doglietto GB, Crucitti F. Accurate lymph-node detection in colorectal specimens resected for cancer is of prognostic significance. *Dis Colon Rectum* 1999; **42**: 143-154
 - 38 **Prabhudesai AG**, Kumar D. The sentinel lymph node in colorectal cancer - of clinical value? *Colorectal Dis* 2002; **4**: 162-166
 - 39 **Vekic B**, Radovanovic D, Cvetanovic M, Zivanovic J, Pavlovic I. Skip metastases in rectosigmoid carcinoma. *Srp Arh Celok Lek* 2003; **131**: 48-51
 - 40 **Shafik A**. Mesorectal lymph nodes and their relation to the superior rectal artery: do they exist below or above the superior rectal artery division? *Dis Colon Rectum* 2002; **45**: 1122
 - 41 **Andreola S**, Leo E, Belli F, Gallino G, Sirizzotti G, Sampietro G. Adenocarcinoma of the lower third of the rectum: metastases in lymph nodes smaller than 5 mm and occult micrometastases; preliminary results on early tumor recurrence. *Ann Surg Oncol* 2001; **8**: 413-417
 - 42 **Cserni G**. The influence of nodal size on the staging of colorectal carcinomas. *J Clin Pathol* 2002; **55**: 386-390
 - 43 **Nagtegaal ID**, van Krieken JH. The role of pathologists in the quality control of diagnosis and treatment of rectal cancer-an overview. *Eur J Cancer* 2002; **38**: 964-972
 - 44 **Nordgard O**, Aloysius TA, Todnem K, Heikkila R, OGREID D. Detection of lymph node micrometastases in colorectal cancer. *Scand J Gastroenterol* 2003; **38**: 125-132
 - 45 **O'Dwyer ST**, Haboubi NY, Johnson JS, Gardy R. Detection of lymph node metastases in colorectal carcinoma. *Colorectal Dis* 2001; **3**: 288-294
 - 46 **van Wyk Q**, Hosie KB, Balsitis M. Histopathological detection of lymph node metastases from colorectal carcinoma. *J Clin Pathol* 2000; **53**: 685-687
 - 47 **Tsavellas G**, Patel H, Allen-Mersh TG. Detection and clinical significance of occult tumour cells in colorectal cancer. *Br J Surg* 2001; **88**: 1307-1320
 - 48 **Feezor RJ**, Copeland EM 3rd, Hochwald SN. Significance of micrometastases in colorectal cancer. *Ann Surg Oncol* 2002; **9**: 944-953
 - 49 **Fisher ER**, Colangelo L, Wieand S, Fisher B, Wolmark N. Lack of influence of cytokeratin-positive mini micrometastases in "Negative Node" patients with colorectal cancer: findings from the national surgical adjuvant breast and bowel projects protocols R-01 and C-01. *Dis Colon Rectum* 2003; **46**: 1021-1025
 - 50 **Choi HJ**, Choi YY, Hong SH. Incidence and prognostic implications of isolated tumor cells in lymph nodes from patients with Dukes B colorectal carcinoma. *Dis Colon Rectum* 2002; **45**: 750-755
 - 51 **Noura S**, Yamamoto H, Miyake Y, Kim B, Takayama O, Seshimo I, Ikenaga M, Ikeda M, Sekimoto M, Matsuura N, Monden M. Immunohistochemical assessment of localization and frequency of micrometastases in lymph nodes of colorectal cancer. *Clin Cancer Res* 2002; **8**: 759-767
 - 52 **Tschmelitsch J**, Klimstra DS, Cohen AM. Lymph node micrometastases do not predict relapse in stage II colon cancer. *Ann Surg Oncol* 2000; **7**: 601-608
 - 53 **Deng H**, Shu XJ, Zhen HY, Deng L, Chen Y, Liu LJ. Prognostic significance of lymph node micrometastasis in colorectal cancer. *Aizheng* 2003; **22**: 762-766
 - 54 **Clarke G**, Ryan E, O'Keane JC, Crowe J, MacMathuna P. The detection of cytokeratins in lymph nodes of Duke's B colorectal cancer subjects predicts a poor outcome. *Eur J Gastroenterol Hepatol* 2000; **12**: 549-552

Edited by Kumar M and Wang XL Proofread by Xu FM

Possible stem cell origin of human cholangiocarcinoma

Chao Liu, Jie Wang, Qing-Jia Ou

Chao Liu, Jie Wang, Qing-Jia Ou, Department of General Surgery, Sun Yat-Sen Memorial Hospital, Sun Yat-Sen University, Guangzhou 510120, Guangdong Province, China

Correspondence to: Dr. Chao Liu, Department of General Surgery and Transplantation, University Hospital Essen, Hufelandstr. 55, Essen D-45122, Germany. mdliuchao@hotmail.com

Telephone: +49-201-7231104 **Fax:** +49-201-7235946

Received: 2004-02-28 **Accepted:** 2004-04-29

Abstract

AIM: To investigate the expression of CD34 and c-kit (receptor of stem cell factor) in cholangiocarcinoma.

METHODS: Fifteen cases of intrahepatic cholangiocarcinoma and 17 cases of extrahepatic cholangiocarcinoma were studied in this experiment. Using Envision detection system, paraffin-embedded sections of the resected cholangiocarcinoma tissue were stained with antibodies against CD34 and c-kit, respectively. The sections were counterstained with hematoxylin, and the results were examined under light microscope. Normal tonsil and mammary tissues were used as positive controls for CD34 and c-kit, respectively.

RESULTS: CD34 was positive in all sections, but only in capillary endothelial cells of tumor tissue. No cholangiocarcinoma cells were positive for CD34. In one case of extrahepatic cholangiocarcinoma, a few tumor cells (about 5%) were immunoreactive with c-kit.

CONCLUSION: CD34 or c-kit positive cells in liver tissue may represent liver stem cells, as they can differentiate into mature biliary cells *in vitro*. The expression of c-kit by some cholangiocarcinoma cells suggests that cholangiocarcinoma might originate from liver stem cells. However, other mechanisms of hepatocarcinogenesis, such as de-differentiation of mature cholangiocytes, may also exist.

Liu C, Wang J, Ou QJ. Possible stem cell origin of human cholangiocarcinoma. *World J Gastroenterol* 2004; 10(22): 3374-3376

<http://www.wjgnet.com/1007-9327/10/3374.asp>

INTRODUCTION

Two theories are available to explain the process of hepatocarcinogenesis, one is de-differentiation of mature liver cells (hepatocytes and cholangiocytes), the other is maturation arrest of liver stem cells^[1]. In normal liver, putative liver stem cells may exist at terminal bile ductules (canal of Hering) and periductular area^[2,3]. In rodent animals, when damage and loss of hepatocytes and/or cholangiocytes are combined with impaired regeneration of the mature cells, liver stem cells may be activated. They proliferate and differentiate towards both hepatic and biliary lineages^[2,4-7]. Activation of liver stem cells has been observed in various human liver diseases, such as acute liver necrosis^[8], hemochromatosis^[9], chronic cholestatic diseases^[10], alcoholic liver diseases^[9] and chronic viral hepatitis^[9,11,12]. In human liver focal nodular hyperplasia^[13], hepatic adenoma^[14], hepatocellular

carcinoma^[15] and hepatoblastoma^[16], some tumor cells have also been detected to express the specific markers of liver stem cells, indicating their possible stem cell origin. In animals, cholangiocarcinoma can also originate from liver stem cells^[17].

CD34 and c-kit are two hemopoietic markers, but in periductular area and occasionally within bile ducts, CD34 and c-kit positive cells were also found^[18]. CD34 or c-kit positive cells in human liver can be isolated with immunomagnetic separation techniques, and these isolated cells are able to differentiate into biliary epithelial cells *in vitro*^[18]. Thus, CD34 and c-kit positive cells in human liver may represent liver stem cells. In this study, the expression of CD34 and c-kit in human cholangiocarcinoma was investigated.

MATERIALS AND METHODS

Specimens

Paraffin-embedded specimens from 32 cases of resected cholangiocarcinoma at Sun Yat-Sen Memorial Hospital were studied in this experiment. They included 18 male and 14 female patients, ranging from 24 to 80 years old (mean and medium 64 years old). Fifteen cases had the tumor located in intrahepatic bile duct (IBD), 4 cases in common hepatic bile duct (CHBD) and 13 cases in common bile duct (CBD). Some clinical characteristics of the patients are summarized in Table 1.

Immunohistochemistry

Each paraffin-embedded specimen was cut consecutively into 6 sections. Three sections of CD34 and 3 sections of c-kit were stained with Envision detection system (DAKO, Denmark). CD34 retrieval was performed by heating the sections in 10 mmol/L citrate buffer (pH 6.0). In brief, the tissue sections were incubated with peroxidase blocking reagent (DAKO) for 5 min, incubated with CD34 (monoclonal mouse anti-human, IgG₁, kappa, ready to use; DAKO) for 10 min or c-kit (polyclonal rabbit anti-human, 1:50; DAKO) for 30 min at room temperature. Then, the sections were incubated with peroxidase labelled polymer conjugated to goat anti-rabbit or goat anti-mouse immunoglobulin for 30 min at room temperature, incubated with diaminobezidine (DAB) chromogen for 5 min, counterstained with hematoxylin and mounted with coverslip. Between each of these steps, the sections were rinsed gently with Tris-HCl buffer. Normal human tonsil and mammary tissues were used as positive controls for CD34 and c-kit, respectively. Negative control was performed at the same conditions by omitting incubation with the first antibody. The stained tissue sections were examined under light microscope.

RESULTS

CD34 and c-kit were positive in the staining of capillary endothelial cells in tonsil and ductal cells in normal mammary tissues, respectively. Negative controls were all negative. Among the specimens of 32 cases of cholangiocarcinoma, CD34 was strongly positive in the staining of all capillary endothelial cells and negative in tumor cells (Figure 1). However, c-kit was positive in the staining of tumor cells in 1 case of cholangiocarcinoma originating from common bile duct (case 32, Table 1). This was an 80 years old patient with moderately differentiated cholangiocarcinoma, and about 5% of the tumor cells were positively stained at cell

membrane and cytoplasm (Figure 2). The positive result was repeatedly identified in several sections from the same specimen.

Table 1 Clinical characteristic of the patients with cholangiocarcinoma

No.	Sex	Age (yr)	Location of adenocarcinoma	Differentiation
1	F	78	CBD	moderately
2	F	68	CBD	moderately
3	M	63	CBD	moderately
4	M	67	IHBC	moderately
5	M	58	IHBC	well
6	M	49	CBD	poorly
7	M	80	IHBC	well
8	M	75	CBD	poorly
9	M	77	IHBC	well
10	F	74	CBD	well
11	M	50	CHBD	well
12	F	68	CBD	well
13	M	62	IHBC	well
14	F	69	IHBC	well
15	F	67	IHBC	well
16	M	52	IHBC	moderately
17	M	59	IHBC	moderately
18	F	74	CBD	poorly
19	M	64	CHBD	well
20	F	62	IHBC	moderately
21	F	68	IHBC	poorly
22	M	61	CHBD	poorly
23	F	46	CBD	moderately
24	F	73	CBD	moderately
25	F	62	IHBC	well
26	M	59	CHBD	well
27	M	64	CBD	poorly
28	M	76	IHBC	moderately
29	M	24	IHBC	well
30	M	56	IHBC	moderately
31	F	60	CBD	moderately
32	F	80	CBD	moderately

F: Female; M: Male; CBD: Common bile duct; CHBD: Common hepatic bile duct; IHBC: Intrahepatic bile duct.

Liver stem-like cells are small and oval in shape with relatively large oval nuclei. They are immunoreactive for OV-6 (rat oval cell marker), cytokeratin (CK) 8 and CK 18 (both are epithelial cell markers), CK 7 and CK 19 (both are biliary cell markers), CK 14, and chromogranin-A^[15,19]. Liver stem-like cells are heterogeneous, and could be classified into 3 types based on their differentiation characteristics. Type I represents the most undifferentiated cells, type II the progenitor cells differentiating towards biliary lineage, and type III the progenitor cells differentiating towards hepatic lineage^[19]. In human liver, these liver stem-like cells have been found in focal nodular hyperplasia, hepatic adenoma, hepatocellular carcinoma and hepatoblastoma^[13-16].

CD34 and c-kit are two markers of hemapoeitic stem cells. However, recently in normal human liver, c-kit was detected in canal of Hering where the putative liver stem cells may exist^[3]. In patients with fulminant hepatic failure, over expression of c-kit was detected in activated liver stem-like cells^[20]. CD34 was also identified in rat liver stem-like cells^[21]. Using immunomagnetic separation method, CD34 and c-kit positive cells were isolated from human liver. These cells were able to proliferate and differentiate into both biliary epithelial and endothelial cells *in vitro*^[18]. This suggested that CD34 and c-kit positive cells in

liver might represent biliary progenitor cells, biliary and endothelial cells might share the same progenitor cells. Among the 12 cases of hepatoblastoma, Ruck *et al.* reported that CD34 was found to be immunoreactive with both tumor cells and endothelial cells in 1 case of small cell hepatoblastoma, and this indicated the possible stem cell origin of hepatoblastoma^[22].

In this study, a few tumor cells in 1 of 32 cases of cholangiocarcinoma were immunoreactive with c-kit, and this suggested their possible origin of biliary stem cells.

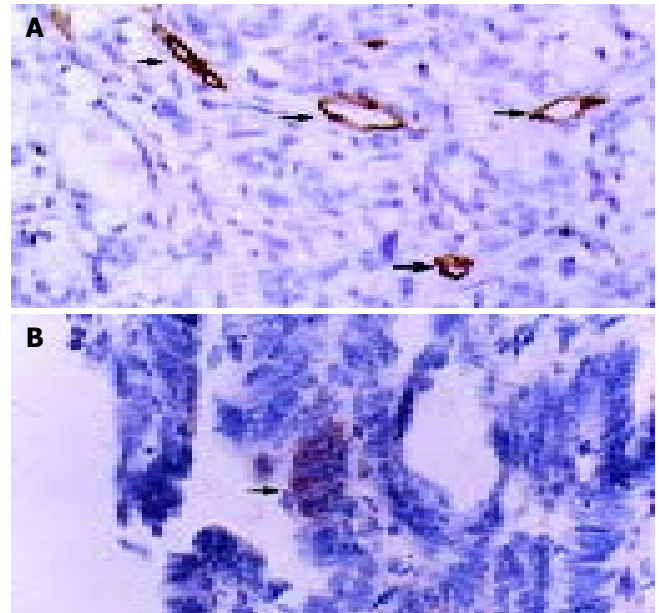


Figure 1 A: Immunohistochemical staining of cholangiocarcinoma with antibody against CD34. Arrowhead indicates strongly positive capillary endothelial cells. B: Immunohistochemical staining of cholangiocarcinoma with antibody against c-kit (Envision, original magnification: $\times 400$). Arrowhead indicates positive tumor cells.

As putative liver stem cells possibly exist in terminal bile ductules (canal of Hering), intrahepatic cholangiocarcinoma is supposed to originate from liver stem cells more likely than extrahepatic cholangiocarcinoma. However, the cells with stem cell characteristics may not only exist in intrahepatic bile ducts, but also in extrahepatic bile ducts. In embryonic development of rat liver, both intra- and extrahepatic bile ducts originated from AFP- and albumin-containing hepatoblasts^[23]. The remnant of embryo liver stem cells may also exist in extrahepatic bile ducts. In human, it was observed that hepatocellular carcinoma could also develop from extrahepatic bile ducts^[24-26]. These tumors might originate from liver stem cells in extrahepatic bile ducts by maturation arrest. Thus, extrahepatic cholangiocarcinoma that was immunoreactive with c-kit in this experiment might also originate from putative liver stem cells.

Based on animal experiments, different carcinogenic regimens might act on different level of cells in hepatic lineage and produce hepatic carcinoma by different mechanisms^[27]. Diethylnitrosamine acted on mature hepatocytes and induced hepatocellular carcinoma by de-differentiation. Furan injured bile duct progenitor cells and induced cholangiocarcinoma by maturation arrest. 2-acetylaminofluorene acted on ductular bipolar progenitor cells and induced hepatocellular carcinoma by maturation arrest. In choline deficiency models, the periductular stem cells could be activated to induce hepatocellular carcinoma by maturation arrest. The exact causes of human cholangiocarcinoma are still unclear, and there may be more than one mechanism of its carcinogenesis. In this study, only a few tumor cells in 1 case of cholangiocarcinoma were c-kit immunoreactive, and we could

not draw a sound conclusion. Tumor cells may lose their markers of stem cells during maturation arrest. Thus, further researches, such as increasing the number of cases and discovering new biliary progenitor cell markers, are needed to answer if human cholangiocarcinoma originates from stem cells.

ACKNOWLEDGEMENTS

The authors thank Professor Andrea Frilling at Department of General Surgery and Transplantation, University Hospital Essen, Germany, for the revision of the manuscript.

REFERENCES

- 1 Sell S. Cellular origin of cancer: dedifferentiation or stem cell maturation arrest? *Environ Health Perspect* 1993; **101**(Suppl 5): 15-26
- 2 Sell S. Is there a liver stem cell? *Cancer Res* 1990; **50**: 3811-3815
- 3 Theise ND, Saxena R, Portmann BC, Thung SN, Yee H, Chiriboga L, Kumar A, Crawford JM. The canals of hering and hepatic stem cells in humans. *Hepatology* 1999; **30**: 1425-1433
- 4 Zhang Y, Bai XF, Huang CX. Hepatic stem cells: existence and origin. *World J Gastroenterol* 2003; **9**: 201-204
- 5 Thorgeirsson SS. Hepatic stem cells. *Am J Pathol* 1993; **142**: 1331-1333
- 6 Sigal SH, Brill S, Fiorino AS, Reid LM. The liver as a stem cell and lineage system. *Am J Physiol* 1992; **263**(2 Pt 1): G139-G148
- 7 Alison M, Sarraf C. Hepatic stem cells. *J Hepatol* 1998; **29**: 676-682
- 8 Haque S, Haruna Y, Saito K, Nalesnik MA, Atillasoy E, Thung SN, Gerber MA. Identification of bipotential progenitor cells in human liver regeneration. *Lab Invest* 1996; **75**: 699-705
- 9 Lowes KN, Brennan BA, Yeoh GC, Olynyk JK. Oval cell numbers in human chronic liver diseases are directly related to disease severity. *Am J Pathol* 1999; **154**: 537-541
- 10 Crosby HA, Hubscher S, Fabris L, Joplin R, Sell S, Kelly D, Strain AJ. Immunolocalization of putative human liver progenitor cells in livers from patients with end-stage primary biliary cirrhosis and sclerosing cholangitis using the monoclonal antibody OV-6. *Am J Pathol* 1998; **152**: 771-779
- 11 Hsia CC, Everts RP, Nakatsukasa H, Marsden ER, Thorgeirsson SS. Occurrence of oval-type cells in hepatitis B virus-associated human hepatocarcinogenesis. *Hepatology* 1992; **16**: 1327-1333
- 12 Ma X, Qiu DK, Peng YS. Immunohistochemical study of hepatic oval cells in human chronic viral hepatitis. *World J Gastroenterol* 2001; **7**: 238-242
- 13 Roskams T, De Vos R, Desmet V. 'Undifferentiated progenitor cells' in focal nodular hyperplasia of the liver. *Histopathology* 1996; **28**: 291-299
- 14 Libbrecht L, De Vos R, Cassiman D, Desmet V, Aerts R, Roskams T. Hepatic progenitor cells in hepatocellular adenomas. *Am J Surg Pathol* 2001; **25**: 1388-1396
- 15 Wu PC, Lai VC, Fang JW, Gerber MA, Lai CL, Lau JY. Hepatocellular carcinoma expressing both hepatocellular and biliary markers also expresses cytokeratin 14, a marker of bipotential progenitor cells. *J Hepatol* 1999; **31**: 965-966
- 16 Ruck P, Xiao JC, Pietsch T, Von Schweinitz D, Kaiserling E. Hepatic stem-like cells in hepatoblastoma: expression of cytokeratin 7, albumin and oval cell associated antigens detected by OV-1 and OV-6. *Histopathology* 1997; **31**: 324-329
- 17 Lee JH, Rim HJ, Sell S. Heterogeneity of the "oval-cell" response in the hamster liver during cholangiocarcinogenesis following clonorchis sinensis infection and dimethylnitrosamine treatment. *J Hepatol* 1997; **26**: 1313-1323
- 18 Crosby HA, Kelly DA, Strain AJ. Human hepatic stem-like cells isolated using c-kit or CD34 can differentiate into biliary epithelium. *Gastroenterology* 2001; **120**: 534-544
- 19 Roskams T, De Vos R, Van Eyken P, Myazaki H, Van Damme B, Desmet V. Hepatic OV-6 expression in human liver disease and rat experiments: evidence for hepatic progenitor cells in man. *J Hepatol* 1998; **29**: 455-463
- 20 Baumann U, Crosby HA, Ramani P, Kelly DA, Strain AJ. Expression of the stem cell factor receptor c-kit in normal and diseased pediatric liver: identification of a human hepatic progenitor cell? *Hepatology* 1999; **30**: 112-117
- 21 Omori N, Omori M, Everts RP, Teramoto T, Miller MJ, Hoang TN, Thorgeirsson SS. Partial cloning of rat CD34 cDNA and expression during stem cell-dependent liver regeneration in the adult rat. *Hepatology* 1997; **26**: 720-727
- 22 Ruck P, Xiao JC, Kaiserling E. Immunoreactivity of sinusoids in hepatoblastoma: an immunohistochemical study using lectin UEA-1 and antibodies against endothelium-associated antigens, including CD34. *Histopathology* 1995; **26**: 451-455
- 23 Shiojiri N, Lemire JM, Fausto N. Cell lineages and oval cell progenitors in rat liver development. *Cancer Res* 1991; **51**: 2611-2620
- 24 Thomsen GH, Kruse A, Petersen A. Hepatocellular carcinoma presenting as a tumour of the hilar and extrahepatic bile ducts. *Eur J Gastroenterol Hepatol* 1998; **10**: 803-804
- 25 Cho HG, Chung JP, Lee KS, Chon CY, Kang JK, Park IS, Kim KW, Chi HS, Kim H. Extrahepatic bile duct hepatocellular carcinoma without primary hepatic parenchymal lesions-a case report. *Korean J Intern Med* 1996; **11**: 169-174
- 26 Park CM, Cha IH, Chung KB, Suh WH, Lee CH, Choi SY, Chae YS. Hepatocellular carcinoma in extrahepatic bile ducts. *Acta Radiol* 1991; **32**: 34-36
- 27 Sell S. Cellular origin of hepatocellular carcinomas. *Semin Cell Dev Biol* 2002; **13**: 419-424

Edited by Wang XL and Chen WW Proofread by Xu FM

Epidemiology of peptic ulcer disease in Wuhan area of China from 1997 to 2002

Wei-Guo Dong, Chun-Sheng Cheng, Shao-Ping Liu, Jie-Ping Yu

Wei-Guo Dong, Chun-Sheng Cheng, Jie-Ping Yu, Department of Gastroenterology, Renmin Hospital of Wuhan University, Wuhan 430060, Hubei Province, China

Shao-Ping Liu, Department of Gastroenterology, Huangshi Central Hospital, Huangshi 435000, Hubei Province, China

Co-first-authors: Wei-Guo Dong and Chun-Sheng Cheng

Correspondence to: Professor Wei-Guo Dong, Renmin Hospital of Wuhan University, 238 Jiefang Road, Wuhan 430060, Hubei Province, China. dongwg@public.wh.hb.cn

Telephone: +86-27-88041919 Ext. 6448

Received: 2004-01-15 **Accepted:** 2004-03-12

Abstract

AIM: To describe the epidemiological features of peptic ulcer disease in Wuhan area during 1997-2002, to analyze the sex, age and occupation characteristics, as well as the geographic distribution of peptic ulcer disease, and to determine the effective methods of preventing and controlling peptic ulcer disease.

METHODS: In the early 1980s, the peptic ulcer disease registry system was established to collect the data of peptic ulcer disease in Wuhan area. Here we performed a statistically detailed analysis of 4876 cases of peptic ulcer disease during 1997-2002.

RESULTS: The morbidity of peptic ulcer disease between males and females was significantly different ($\chi^2 = 337.9$, $P < 0.001$). The majority of peptic ulcer diseases were found at the age of 20 to 50 years. Because of different occupations, the incidence of peptic ulcer disease was different in different areas.

CONCLUSION: The incidence of peptic ulcer disease is highly associated with sex, age, occupation and geographic environmental factors. By analyzing the epidemiological features of peptic ulcer disease, we can provide the scientific data for prevention and control of peptic ulcer disease.

Dong WG, Cheng CS, Liu SP, Yu JP. Epidemiology of peptic ulcer disease in Wuhan area of China from 1997 to 2002. *World J Gastroenterol* 2004; 10(22): 3377-3379
<http://www.wjgnet.com/1007-9327/10/3377.asp>

INTRODUCTION

During 1997 to 2002, 21693 patients had a gastroscopy in Outpatient Department of the Renmin Hospital in Wuhan University, of them, 4876 were diagnosed as peptic ulcer disease. Factors that increased the risk of serious peptic ulcer disease included older age, history of peptic ulcer disease, gastrointestinal hemorrhage, dyspepsia and previous non-steroidal anti-inflammatory drug-associated (NSAID) intolerance, as well as poor living conditions^[1]. Furthermore, the epidemiological factors were important reasons leading to peptic ulcer disease. To explore the epidemiological features of peptic ulcer disease in

Wuhan area, we performed a statistical analysis of the data about sex, age, occupation and geographic environmental distribution.

MATERIALS AND METHODS

A total of 21 693 patients with gastrointestinal symptoms received a gastroscopy in Outpatient Department of the Renmin Hospital of Wuhan University, of them, 4 876 were diagnosed as peptic ulcer disease. The patients were classified according to gastric ulcer (GU), duodenal ulcer (DU), complex ulcer (CU), sex, age, occupation and geographic environment and a database was set up. All the data were checked and analyzed using the SPSS statistical software.

RESULTS AND DISCUSSION

Peptic ulcer disease mainly refers to the chronic ulcer which occurs in stomach and duodenum, because the formation of ulcer is linked to the digestive function of gastric acid-pepsin^[2]. Peptic ulcer disease is a worldwide common disease, but the incidence of peptic ulcer disease in different countries and regions is obviously different. The incidence of peptic ulcer disease has not been exactly investigated in China. Therefore, we performed a statistically detailed analysis of the data in Wuhan area from 1997 to 2002.

There were 4 876 cases of peptic ulcer disease out of 21 693 patients, and the incidence was 22.5%. Among the 4 876 cases diagnosed as peptic ulcer disease by gastroscopically, 3 899 males (79.9%) and 977 females (20.1%) had peptic ulcer disease. The sex ratio (males to females) was 3.95:1. Among the patients with peptic ulcer disease, 3 397 had duodenal ulcer disease, 1066 had gastric ulcer disease and 413 had complex ulcer disease. Duodenal ulcer diseases accounted for 69.6%, gastric ulcer diseases accounted for 21.9% and complex ulcer diseases accounted for 8.5%. The ratio of the three was 8.2:2.6:1. The data of the sex, age, occupation characteristics and geographic distribution of peptic ulcer disease are shown in Tables 1-4.

Table 1 Sex ratio of six different age groups in 4 876 cases of peptic ulcer disease

Age (yr) group	Duodenal ulcer	Gastric ulcer	Complex ulcer	Peptic ulcer
10-	3.66	5.00	10.00	3.96
20-	5.13	4.03	6.13	4.93
30-	4.12	4.63	7.53	4.39
40-	2.65	5.82	3.04	3.26
50-	2.53	5.56	2.86	3.37
60-	3.43	5.70	6.75	4.39
Mean	3.59	5.12	6.05	4.05

Sex difference

The incidence of peptic ulcer disease in males was always higher than that in females in different age groups. From Table 1, we could see that the sex ratio in duodenal ulcer disease was 2.53-5.13:1, the maximum ratio was 5.13, and the average ratio was 3.59. The sex ratio in gastric ulcer disease was 4.03-5.82:1, the maximum ratio was 2.53, and the average ratio was 5.12. The cases of complex ulcer disease were so few that they had no

statistic significance. After analyzing the trend of the mortality of peptic ulcer disease from 1952 to 1980 in Western Germany, we found that the general trend of mortality of males was descending but there was a fluctuating ascending, and the general trend of mortality of females was steadily ascending^[3]. Since the early 1960s in America, the incidence of the peptic ulcer disease in males has slightly decreased, but that of females has shown the increasing trend, and the difference of sex has gradually lessened^[4]. Mortality from non-perforated ulcer decreased markedly, while that from perforated ulcer decreased slightly, similar trends were observed in men and women^[5]. We carried out a statistical analysis of the data according to the different age groups ($\chi^2 = 337.9, P < 0.001$). From Table 2 and Figure 1, we could see that the incidence of peptic ulcer disease between males and females was significantly different.

Table 2 Comparison of sex among six different age groups in 4 876 cases of peptic ulcer disease

Gender	Age(yr) group					
	10-	20-	30-	40-	50-	60-
Male	190	858	1 340	880	576	282
Female	48	174	305	270	171	65

$\chi^2 = 337.9, P < 0.001$.

Table 3 Age distribution in 4 876 cases of peptic ulcer disease

Age (yr) group	Duodenal ulcer		Gastric ulcer		Complex ulcer	
	Male	Female	Male	Female	Male	Female
	10-	150	41	30	6	10
20-	656	128	153	38	49	8
30-	932	226	295	64	113	15
40-	519	196	285	49	76	25
50-	263	104	250	45	63	22
60-	141	41	114	20	27	4
Total	2 661	736	1 127	222	338	75

Table 4 Occupation distribution in six different age groups in 1 068 cases of peptic ulcer

Age (yr) group	Worker			Farmer			Cadre			Student		
	DU	GU	CU	DU	GU	CU	DU	GU	CU	DU	GU	CU
10-	2	1	0	0	1	0	2	0	0	24	6	6
20-	86	18	6	36	12	4	6	2	0	10	0	0
30-	168	22	8	96	44	8	32	20	2			
40-	26	6	6	66	38	14	34	14	4			
50-	28	10	2	32	26	8	16	16	2			
60-	18	8	2	14	28	2	12	12	2			
Total	328	65	24	244	149	36	102	64	10	34	6	6

Age distribution

People who suffered from peptic ulcer disease could be found out at whatsoever ages, but the majority of patients with peptic ulcer disease were adults. Our data indicated that the youngest patient was 9 years old, the oldest was 73 years old, 78.7% of the patients were between 20 and 50 years old, the peak age of incidence was between 30 and 40 years old in duodenal ulcer disease patients. In gastric ulcer disease patients, the youngest was 11 years old, and the oldest was 75 years old, 82.9% of the patients were between 20 and 50 years old, 92.2% of the patients were between 30 and 60 years old, and the peak age of incidence was between 30 and 40 years old. People with gastric ulcer disease were older than those suffering from duodenal ulcer

disease. The incidence of peptic ulcer disease in patients between 40 and 60 years old was obviously higher than that in patients between 10 and 30 years old. The actual number of peptic ulcers in the elderly decreased, however the percentage of elderly with peptic ulcer against total population increased^[6]. The age distribution of complicated ulcer disease was basically similar to that of gastric ulcer disease. The incidence of peptic ulcer disease was 22.5% in Wuhan area, the ratio of duodenal ulcer to gastric ulcer was 3.2:1, and the ratio of different age groups was 1.24-5.1:1. From Figure 2, we could see that the incidences of duodenal ulcer disease and gastric ulcer disease were not significantly different after 50 years old. Huang *et al.*^[7] found that peptic ulcer disease in children over 6 years old was mainly primary ulcer, the majority of them were duodenal ulcer, and the clinical symptoms of the peptic ulcer were similar to those in the adults. It was reported that 72-80% of peptic ulcer disease in Hunan and Guangdong provinces in China occurred in patients between 20 and 50 years old, which was similar to the results of the reports from India^[8]. The location of duodenal ulcer disease was on anterior wall and greater curvature of bulb, but in gastric ulcer disease was on gastric angle and antrum, and the peak age of incidence was 21 to 50 years^[9]. The results of our investigations were basically similar to them.

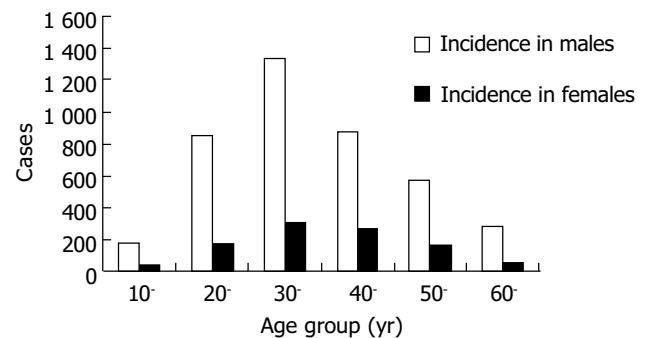


Figure 1 Age and sex distribution of peptic ulcer disease in Wuhan area, China.

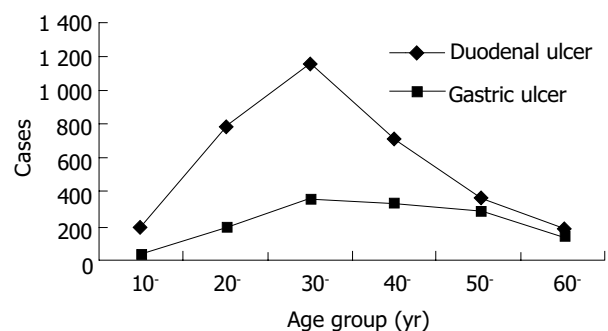


Figure 2 Age distribution of 4 876 cases of peptic ulcer disease in Wuhan area.

Social occupation factors

The sex difference and age distribution of peptic ulcer disease in different occupations were basically the same. The data of our study were divided into four parts, each from the workers, farmers, students and cadres, respectively, From Table 4, we know that the incidence of peptic ulcer disease among farmers was the highest, moderate in workers and the lowest in students. The incidence of duodenal ulcer disease was also very high among these special occupations such as drivers, firefighters and so on, which was similar to the report of Sonnenbeg *et al.*, who found the incidence of duodenal ulcer disease was very high among the firefighters, pilots and shift workers^[10,11]. The

study results from Western Germany indicated that the consumption of body's energy was a dangerous factor for the development of peptic ulcer disease^[11]. This may be related to social factors such as busy working, heavy mental stress and so on. It was reported that the occurrence, recurrence of peptic ulcer disease were closely associated with psychological contradiction, emotional-hindering and defective character. Depress, anxiety, fear, emotional irritability and cognitive disorganization were significantly increased in the integrated stress management program (ISMP) group in comparison with the progressive muscle relaxation (PMR) group, and the incidence of peptic ulcer disease was higher in the ISMP group than in the PMR group^[12]. In addition, irregular meal, over-eating, and fast-eating might cause injures to the digestive tract mucosa, leading to the occurrence of peptic ulcer disease^[13]. Peptic ulcer disease was more common in the working age groups. To any kind of occupation, age between 20 and 50 years was a period in which people were widely connected with society and participation in assorted social activities more frequently than ever. Heavy social psychological stress, frequent mobility and irregular working were extremely important factors in the formation of peptic ulcer disease. The increasing incidence of peptic ulcer disease in females was related to more and more social activities that females participated in gradually^[14].

Geographic and environment factors

Environmental factors played a role in peptic ulcer disease^[15]. The positive detectable rate of peptic ulcer disease in Han nationality was higher than that in Korea nationality at Yanbian area^[16]. Thors *et al.*^[17] demonstrated that peptic ulcer mortality and disease risk were particularly high in subjects born after the turn of the century and subsequent generations. Since 1945, a very rapid economic development has been achieved with the advent of electricity and refrigeration, clean water and food; The condition in Iceland changed from being anti-hygienic and poor to being rich and clean, the morbidity of peptic ulcer disease has decreased. The rise and fall in peptic ulcer during the 20th century might be caused by factors early in life in the generations born during these years with crowding and poor hygiene before living conditions and socio-economic status were improved. The incidence of peptic ulcer disease as reported was between 16% and 33% from different regions in China. The results from Hunan and Gansu Provinces indicated that the ratio of duodenal ulcer disease to peptic ulcer disease was 2.7-6.2:1 in the inpatient department during the same period. The peptic ulcer disease is very prevailing in all over China, but there is an increasing trend from the north to the south in region distribution. Furthermore, the morbidity of peptic ulcer disease is also different in different countries, and duodenal ulcer disease turns up more frequently than gastric ulcer disease in the majority of Western countries. The study report in Japan indicated that the incidence of gastric ulcer disease was higher than that of duodenal ulcer disease. The incidence of duodenal ulcer disease and gastric ulcer disease was almost equal to that in Norwegian. In respect to ethnicity, Bengali speaking Hindus showed high probability for gastric ulcers in both sexes^[18]. The detecting rates of peptic ulcer disease in Han and Hui nationalities were 13.42% and 10.66% respectively. Among peptic ulcer diseases 44.4% were duodenal ulcer disease, and 50.63% were gastric ulcer disease, the ratio being 0.88:1. The detecting rate of peptic ulcer in Han nationality was higher than that in Hui nationality, and gastric ulcer disease occurred

more often than duodenal ulcer disease in china. The regional difference in the type and level of peptic ulcer disease revealed that geographic and environmental factors probably played an important role in the development of peptic ulcer disease. Additionally, the incidence of peptic ulcer disease in the transition period between autumn and winter or between winter and spring was higher than that in other periods. The change of climate factors was also associated with occurrence of peptic ulcer disease; with the change of temperature and atmosphere, patients with peptic ulcer disease would appear gastroperiodynia.

In conclusion, the occurrence of peptic ulcer disease is highly associated with sex, age, occupation, geographic and environmental factors. By analyzing the epidemiological characteristics of peptic ulcer disease, we can provide the scientific data for prevention and control of peptic ulcer disease.

REFERENCES

- 1 **Griffin MR.** Epidemiology of Nonsteroidal Anti-inflammatory Drug-Associated Gastrointestinal Injury. *Am J Med* 1998; **104**: 23S-29S
- 2 **Xiao SD.** Peptic ulcer disease In: Ye RG eds. *MEDICINE fifth edition*. Beijing: *People Health Publishing House* 2002: 398
- 3 **Sonnenberg A, Fritsch A.** Changing mortality of peptic ulcer disease in Germany. *Gastroenterology* 1983; **84**: 1553-1557
- 4 **Wang YH, Wang HZ.** Epidemiology In: Wang HZ, Cao SZ, eds. *Xiandai Xiaohuaxing Kuifangbingxue 1st ed*. Beijing: *People's Military Medical Pub* 1999: 64-65
- 5 **Thors H, Svanes C, Thjodleifsson B.** Trends in peptic ulcer morbidity and mortality in Iceland. *J Clin Epidemiol* 2002; **55**: 681-686
- 6 **Kawano S, Fu HY.** Epidemiology of peptic ulcer disease in the aged in Japan. *Nippon Rinsho* 2002; **60**: 1490-1498
- 7 **Huang QY, Cao SZ, Wang HZ.** Peptic ulcer disease in children In: Wang HZ, Cao SZ, eds. *Xiandai Xiaohuaxing Kuifangbingxue 1st ed*. Beijing: *People's Military Medical Pub* 1999: 182-183
- 8 **Khuroo MS, Mahajan R, Zargar SA, Javid G, Munshi S.** Prevalence of peptic ulcer in India: an endoscopic and epidemiological study in urban Kashmir. *Gut* 1989; **30**: 930-934
- 9 **Huang BX, Wang GZ.** Clinical study of 2473 cases with peptic ulcer. *Zhonghua Xiaohua Neijing Zazhi* 2001; **18**: 27-29
- 10 **Segawa K, Nakazawa S, Tsukamoto Y, Kurita Y, Goto H, Fukui A, Takano K.** Peptic ulcer is prevalent among shift workers. *Dig Dis Sci* 1987; **32**: 449-453
- 11 **Sonnenberg A, Sonnenberg GS, Wirths W.** Historic changes of occupational work load and mortality from peptic ulcer in Germany. *J Occup Med* 1987; **29**: 756-761
- 12 **Han KS.** The effect of an integrated stress management program on the psychologic and physiologic stress reactions of peptic ulcer in Korea. *Int J Nurs Stud* 2002; **39**: 539-548
- 13 **Cai L, Zheng ZL, Zhang ZF.** Risk factors for the gastric cardia cancer: a case-control study in Fujian Province. *World J Gastroenterol* 2003; **9**: 214-218
- 14 **Chen SP.** Peptic ulcer disease In: Pan GZ, Cao SZ, eds. *Xiandai Weichangbingxue* Beijing: *Sic Pub* 1998: 899-900
- 15 **Chan FKL, Leung WK.** Peptic-ulcer disease. *Lancet* 2002; **360**: 933-941
- 16 **Pu FS, Cai HF, Jin HY, Gen M, Liang H.** Gastroscopic analysis of 4348 cases of peptic ulcer disease in Yanbian area. *Zhonghua Xiaohua Neijing Zazhi* 2001; **18**: 25-26
- 17 **Thors H, Svanes C, Thjodleifsson B.** Trends in peptic ulcer morbidity and mortality in Iceland. *J Clin Epidemiol* 2002; **55**: 681-686
- 18 **Hazra B, Hazra J.** Epidemiology of peptic ulcer in north Bengal, India. *Indian J Public health* 1998; **42**: 100-102

Effect of 2-(3-carboxy-1-oxopropyl) amino-2-deoxy-D-glucose on human esophageal cancer cell line

Jing Wu, Hong Lu, Yun Zhou, Liang Qiao, Rui Ji, Ai-Qing Wang, Wei-Min Liu, Qun-Ji Xue

Jing Wu, Ai-Qing Wang, Wei-Min Liu, Qun-Ji Xue, Lanzhou Institute of Chemical Physics, Chinese Academy of Sciences, Lanzhou 730000, Gansu Province, China

Jing Wu, Hong Lu, Yun Zhou, Rui Ji, Department of Gastroenterology and Hepatology, First Teaching Hospital of Lanzhou Medical College, Lanzhou 730000, Gansu Province, China

Liang Qiao, Storr Liver Unit, Westmead Millennium Institute, Department of Gastroenterology and Hepatology, Westmead Hospital, University of Sydney Westmead, NSW 2145, Australia

Correspondence to: Dr. Jing Wu, Department of Gastroenterology and Hepatology, First Teaching Hospital of Lanzhou Medical College, Lanzhou 730000, Gansu Province, China. wujing36@163.com

Telephone: +86-931-8619605

Received: 2004-04-22 **Accepted:** 2004-04-29

Abstract

AIM: To determine whether 2-(3-carboxy-1-oxopropyl) amino-2-deoxy-D-glucose (COPADG), a derivative of D-amino-glucose, inhibited the growth of human esophageal cancer cell line Eca-109.

METHODS: Effects of COPADG on Eca-109 cells cultured in RPMI 1640 medium were examined by a tetrazolium-based colorimetric assay (MTT assay).

RESULTS: COPADG inhibited the growth of Eca-109 cells in a dose- and time-dependent manner; the maximum inhibition rate was 83.75%.

CONCLUSION: COPADG can directly inhibit the proliferation of Eca-109 cells, which may serve as the experimental evidence for development of new drugs for esophageal cancer therapy.

Wu J, Lu H, Zhou Y, Qiao L, Ji R, Wang AQ, Liu WM, Xue QJ. Effect of 2-(3-carboxy-1-oxopropyl) amino-2-deoxy-D-glucose on human esophageal cancer cell line. *World J Gastroenterol* 2004; 10(22): 3380-3381

<http://www.wjgnet.com/1007-9327/10/3380.asp>

INTRODUCTION

2-(3-carboxy-1-oxopropyl) amino-2-deoxy-D-glucose (COPADG, structure is shown in Figure 1) is a derivative of D-glucose, a monose derivative of degraded chitosan. Previous researches have discovered that some amino-D-glucose derivatives are capable of inducing leukemia K562 cells to differentiate into macrophages^[1], but their efficacy in inducing apoptosis of tumor cells remains unclear. We conducted this study to determine whether COPADG could inhibit the proliferation of human esophageal cancer cell line Eca-109, to provide experimental evidence for new drug development for esophageal cancer therapy.

MATERIALS AND METHODS

Materials

COPADG, synthesized by the Lanzhou Institute of Chemical

Physics of Chinese Academy of Sciences, was dissolved in distilled water, filter-sterilized with 0.22 μm filter disc, and stored at 4 $^{\circ}\text{C}$ until use. Eca-109 cells were purchased from Shanghai Institute of Cell Biology of Chinese Academy of Sciences. RPMI 1640 medium, agarose, trypsin and fetal bovine serum (FBS) were obtained from Gibco BRL Company, and the reagents for MTT assay were purchased from Sigma Chemical Co. Ltd.

Cell culture

Eca-109 cells growing in logarithmic phase were cultured in RPMI 1640 medium supplemented with 100 mL/L heat-inactivated FBS, 100 $\mu\text{g}/\text{mL}$ penicillin and 100 $\mu\text{g}/\text{mL}$ streptomycin. The cells were maintained in a humidified atmosphere containing 50 mL/L CO_2 at 37 $^{\circ}\text{C}$. The medium was replaced every 48 h.

MTT colorimetric assay

MTT assay^[2] was based on the enzymatic reduction of the tetrazolium salt MTT in viable and metabolically active cells. Cells at 85% to 100% confluency were harvested with the mixture of 2.5 g/L trypsin and 0.2 g/L EDTA solution and seeded into a 96-well plate at a density of 4×10^3 /well, followed by incubation of the cells with COPADG at varied concentrations (0.01-0.09 mol/L) for different lengths of time (24-96 h, Table 1). The control cells were treated in the same way except that incubation was performed with sterile PBS instead of COPADG. After treatment, the medium was replaced by fresh medium and the cells were incubated for 4 h with 5 mg/mL MTT, which was dissolved in 150 μL of 100 g/L DMSO and kept for 1 h. The optical densities at 490 nm ($A_{490\text{nm}}$) in the 96-well plates were determined using a microplate reader. Cell growth inhibition was estimated with the following formula: Growth inhibition (%) = $1 - A_{490\text{nm}}(\text{treated cells}) / A_{490\text{nm}}(\text{control cells}) \times 100\%$.

Statistical analysis

Results were expressed as mean \pm SD. Each experiment was repeated at least three times. Statistical differences between each group were determined by single-factor analysis of variance and correlation analysis using SPSS 11.0 statistical software.

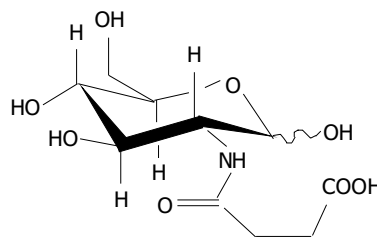


Figure 1 Chemical structure of 2-(3-carboxy-1-oxopropyl) amino-2-deoxy-D-glucose.

RESULTS

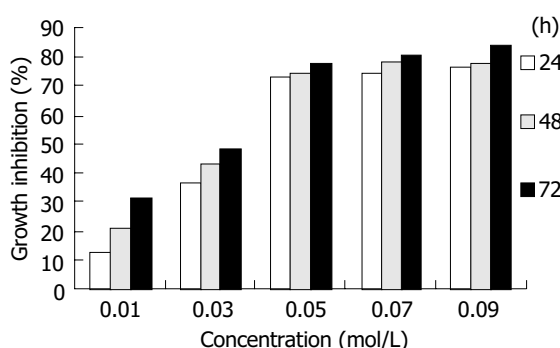
COPADG could effectively inhibit the growth of Eca-109 cells, the maximum inhibition rate was 83.75%. The inhibition exhibited

Table 1 Inhibitory effect of COPADG on the proliferation of esophageal cancer cell line Eca-109 (mean±SD)

Concentration (mol/L)	A_{490nm}			Inhibitory rate (%)		
	24 h	48 h	72 h	24 h	48 h	72 h
0 (Control)	1.505±0.090	1.686±0.067	1.745±0.077	12.76	20.81	31.29
0.01	1.313±0.053 ^b	1.336±0.057 ^b	1.199±0.083 ^b	12.76	20.81	31.29
0.03	0.958±0.028	0.966±0.086	0.900±0.056	36.35	42.68	48.42
0.05	0.400±0.064 ^{b,c}	0.429±0.065 ^{b,a}	0.384±0.050 ^{b,c}	73.42	74.57	77.99
0.07	0.383±0.045	0.360±0.039	0.342±0.037	74.55	78.66	80.44
0.09	0.355±0.046 ^c	0.362±0.053 ^c	0.280±0.039 ^a	76.41	78.54	83.75

At the same time point, $P < 0.01$ vs the control group; ^b $P < 0.01$ vs 0.03 mol/L; ^a $P < 0.05$, ^c $P > 0.05$ vs 0.07 mol/L.

an obvious time- and dose-dependent manner when the COPADG concentrations were below 0.05 mol/L, and higher concentrations tended to induce gradually stabilized inhibition, suggesting a saturation of the effects of COPADG (Table 1, Figure 2).

**Figure 2** Inhibition of Eca-109 cell growth by COPADG.

DISCUSSION

COPADG is a derivative of D-glucose, which is a low-molecular-weight compound with multiple biological activities and a monosaccharide derived from chitosan through release of an acetyl group followed by degradation of the residual group. D-glucose is the intermediate during the synthesis of protein-polysaccharide macromolecules, and distributed in almost every human tissue as a part of the structural components of cell membrane and tissues. From the biological standpoint, D-glucose not only is involved in hepatic and renal detoxification against toxic agents, but also acts to stimulate the anti-inflammatory response and enhance the synthesis of protein-polysaccharides. Studies^[3,4] have also shown that D-glucose could inhibit tumor cell growth, and partial derivatives of D-glucose could potentially induce differentiation of tumor cells. Some D-amine-glucose derivatives were able to induce leukemia K562 cells to differentiate into macrophages^[5], but this effect failed to be observed in human hepatocellular carcinoma cell line^[1]. Currently, COPADG has become a new focus of interest in cancer therapy.

By conducting this study, we aimed to test whether COPADG, the newest derivative of D-glucose, had any effect on the proliferation of human esophageal cancer cells. MTT assay showed that COPADG could effectively inhibit Eca-109 cell

proliferation, in a marked time- and dose-dependent manner below the concentration of 0.05 mol/L; the maximum inhibition rate was 83.75%. The inhibition, however, became stable when the concentrations were higher than 0.05 mol/L, indicating that the effects of the drug might be saturated at this concentration.

The development of cancer has been considered to be the combined results of unrestricted cell proliferation and impairment of normal cell apoptosis^[6]. These concepts provide a basis for the development of new strategies for cancer treatment. Agents with antiproliferative properties and proapoptotic effects have been widely investigated as potential chemotherapeutic options^[7,8].

Conclusion, COPADG has obvious time- and concentration-dependent inhibitory effects against the proliferation of human esophageal cancer cell line Eca-109 *in vitro*, but whether this effect can be achieved in other cell lines still awaits further examination, which may also be necessary to clarify the mechanism underlying this effect.

REFERENCES

- 1 Wang Z, Qiao Y, Huang GS, Wang AQ, Zhang YQ, Feng JL, Yang GR, Guo Y, Liang R. Glucosamine and glucosamine hydrochloride induced leukemia cell line K562 differentiation into macrophage. *Chin Pharmacological Bulletin* 2003; **19**: 290-293
- 2 Mosmann T. Rapid colorimetric assay for cellular growth and survival: application to proliferation and cytotoxicity assays. *J Immunol Methods* 1983; **65**: 55-63
- 3 McDonnell TJ, Meyn RE, Robertson LE. Implications of apoptotic cell death regulation in cancer therapy. *Semin Cancer Biol* 1995; **6**: 53-60
- 4 Xie QL, Dai Y, Sun FY, Lin J, Chen XY, Zhang MY, Chen XJ. The morphology of melanoma induced by glucosamine hydrochloride. *Anhui Zhongyixueyuan Xuebao* 2002; **21**: 42-44
- 5 Wang Z, Qiao Y, Huang GS, Wang AQ, Zhang YQ, Feng JL, Yang GR, Guo Y, Liang R. Induction of macrophagic differentiation of leukemia cell line K562 by N-acetyl-D glucosamine. *Disi Junyi Daxue Xuebao* 2003; **24**: 46-48
- 6 Oka Y, Naomoto Y, Yasuoka Y, Hatano H, Haisa M, Tanaka N, Orita K. Apoptosis in cultured human colon cancer cells induced by combined treatments with 5-fluorouracil tumor necrosis factor-alpha and interferon-alpha. *Jpn J Clin Oncol* 1997; **27**: 231-235
- 7 Kerr JF, Wyllie AH, Currie AR. Apoptosis: a basic biological phenomenon with wide-ranging implications in tissue kinetics. *Br J Cancer* 1972; **26**: 239-257
- 8 Kerr JF, Winterford CM, Harmon BV. Apoptosis. Its significance in cancer and cancer therapy. *Cancer* 1994; **73**: 2013-2026

A case of atypical caudate lobe hemangioma mimicking hepatocellular carcinoma: CT and angiographic manifestations

Hsin-Chi Chen, Chi-Ming Lee, Ching-Shyang Chen, Chih-Hsiung Wu

Hsin-Chi Chen, Chi-Ming Lee, Department of Radiology, Taipei Medical University Hospital, Taipei, Taiwan

Ching-Shyang Chen, Chih-Hsiung Wu, Department of Surgery, Taipei Medical University Hospital, Taipei, Taiwan

Correspondence to: Dr. Chi-Ming Lee, Department of Radiology, Taipei Medical University Hospital, No. 252 Wu-Hsing Street, Taipei 110, Taiwan. yayen0220@yahoo.com.tw

Telephone: +886-2-27372181 Ext. 1131 **Fax:** +886-2-23780943

Received: 2004-04-10 **Accepted:** 2003-05-13

Abstract

We report a case of caudate lobe hemangioma with an atypical CT enhancement pattern. In the present case, hemangioma exhibited a very subtle discontinuous peripheral rim enhancement at the post-enhanced arterial phase, and the peripheral enhanced zone had a moderately increased enhancement degree and with widened enhancement thickness during the portal-phase and delayed-phase. The slow enhancement rate for this caudate lobe hemangioma was due to sluggish perfusion by the small feeding arteries of caudate lobe branches as demonstrated by angiography.

Chen HC, Lee CM, Chen CS, Wu CH. A case of atypical caudate lobe hemangioma mimicking hepatocellular carcinoma: CT and angiographic manifestations. *World J Gastroenterol* 2004; 10 (22): 3382-3384

<http://www.wjgnet.com/1007-9327/10/3382.asp>

INTRODUCTION

Cavernous hemangioma is the most common benign hepatic tumor and usually presents with a typical enhancement pattern when studied by dynamic spiral computed tomography (CT). However, there are a small number of hemangiomas that exhibit atypical enhancement patterns due to the presence of intralesional non-enhanced or less-enhanced components^[1-4]. Herein, we report a case of hepatitis B and C with an atypical caudate lobe hemangioma that preoperatively was misdiagnosed as a hepatocellular carcinoma because the caudate lobe mass was supplied by small caudate lobe arteries with very sluggish perfusion, resulting in a slow enhancement rate and atypical enhancement patterns when studied by dynamic CT. CT imaging features and corresponding angiographic findings of the atypical caudate lobe hemangioma were provided.

CASE REPORT

An asymptomatic 58-year-old woman was found incidentally to have a hepatic mass in the caudate lobe by ultrasound study during a health examination. She was a known hepatitis B carrier (serum positive HBsAg) for 10 years and also known as a hepatitis C carrier (positive IgG anti-HCV) for 1 year. Laboratory evaluation demonstrated normal liver and renal function. The counts of red blood cells, white blood cells, and platelets, coagulation function test, urinalysis, and serum biochemistry profile analysis were normal. The serum alpha-

fetoprotein level was not elevated. Abdominal ultrasound detected a 4.0 cm×4.6 cm inhomogeneous hyperechoic mass situated at the caudate lobe.

Pre- and post-contrast triphasic spiral CT scans were subsequently performed with intravenous administration of a total of 100 mL of contrast material at an injection rate of 2 ml/s via a power injector. Hepatic arterial-phase, portal-phase and delayed-phase were obtained 35, 75 and 180 seconds, respectively, after the injection of contrast material. Pre-contrast CT revealed a well-circumscribed, low attenuation (attenuation value of 40 HU) ovoid mass (measuring approximately 4.0 cm×4.6 cm in dimension) occupying the caudate lobe. The mass exhibited a very faint discontinuous peripheral rim enhancement (attenuation value of 76 HU) at the arterial-phase (Figure 1A), with a moderately increased enhancement degree (attenuation value of 110 to 114 HU) and widened enhancement thickness for the enhanced peripheral zone during the portal-phase and delayed-phase (Figures 1B, C). Minimal enhancement (attenuation value of 61 HU) was also noted in the central portion of the mass during the delayed-phase.

The patient also received a conventional angiographic examination for further evaluation of the caudate lobe mass. Selective proper hepatic angiography showed two small, slightly tortuous, but not enlarged caudate lobe arteries deriving from the right and left hepatic arteries and supplying the caudate lobe mass. Very faint peripheral tumor stains were detected during the late arterial phase (Figure 2A) and parenchymal phase. However, there were no persistent, dense tumor stains at the late venous phase. During the angiographic study, 4 mL of lipiodol (iodized oil) was also slowly injected into the proper hepatic artery and showed several foci of spotty lipiodol retention in the peripheral and central portions of the caudate lobe mass (Figure 2B).

The patient underwent caudate lobe excision under the presumptive diagnosis of hepatocellular carcinoma based on the imaging findings. Pathological examination revealed a cavernous hemangioma occupying the caudate lobe. Only several small foci of organizing thrombi within the hemangioma were discovered.

DISCUSSION

Cavernous hemangioma is the most common benign hepatic tumor. The vast majority of hepatic hemangiomas present with a typically initial intense peripheral nodular enhancement with gradual central fill-in enhancement when studied by dynamic CT study, and it is easy to differentiate from other hepatic tumors. However a small number of hemangiomas could exhibit atypical enhancement patterns due to the presence of intralesional non-enhanced thrombosis, fibrotic, degenerated or calcified components^[1,4]. In addition, variable vascularity of hemangiomas could also influence the lesion's enhancement rate and result in atypical enhancement patterns^[2-4]. An atypical hemangioma may mimic a malignant hepatic tumor, causing diagnostic confusion, especially in patients at risk of malignancy.

Previous investigators^[2-4] have observed that atypical enhancing hemangiomas were more common for smaller lesions than for larger lesions. Approximately 15.6% to 22.2% of

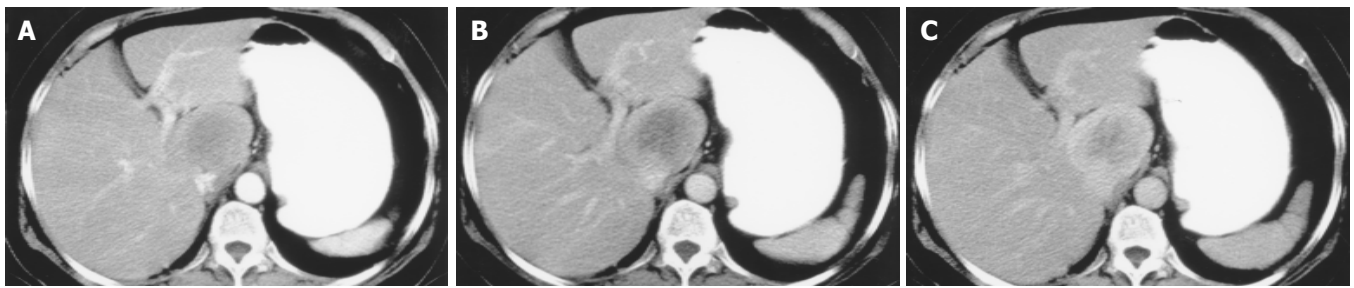


Figure 1 CT images were obtained from an asymptomatic 58-year-old woman with an atypical hepatic hemangioma. A: A 4.0 cm×4.6 cm caudate lobe mass, which exhibits a subtle, discontinuous peripheral thin-rim enhancement (attenuation value of 76 HU) shown by post-contrast triphasic CT scan at the arterial-phase. B and C: A moderately increased enhancement degree and a widened enhancement thickness for the enhanced peripheral zone (attenuation value of 110 to 114 HU) in the caudate lobe mass shown by post-contrast triphasic CT scans at the portal-phase and delayed-phase.

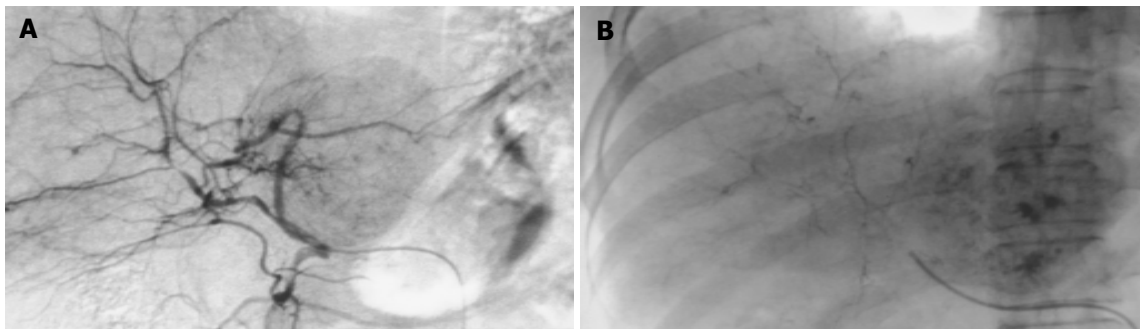


Figure 2 Peripheral tumor stains during the late arterial phase and foci of spotty lipiodol retention in the peripheral and central portions of the caudate lobe mass. A: Peripheral tumor stains during the late arterial phase. B: Foci of spotty lipiodol retention in the peripheral and central portions of the caudate lobe mass.

hemangiomas smaller than 2 cm in diameter might have an atypical enhancement pattern of low or iso-attenuation during the post-enhanced arterial and portal venous phases by dynamic CT^[2-4]. However, atypical enhancement patterns of large hemangiomas were very rare. Yun *et al.*^[2] reported that only 2.2% of hemangiomas larger than 2 cm in diameter presented with atypical enhancement patterns. These reports were correlated with the concept that the presence of typical peripheral nodular enhancement required larger blood supply vessels for hemangiomas and this was associated more with a larger lesion size. Thus, a hemangioma fed by small, not-enlarged supply arteries may fail to exhibit a typical enhancement pattern.

In this present case, although the caudate lobe hemangioma was larger than 4 cm in diameter, the angiograms showed that it was supplied by slightly tortuous, but un-enlarged feeding arteries due to its unique location on an independent hepatic segment of the caudate lobe that only receives the small diameter caudate arterial branches derived from the proximal portion of right and left hepatic arteries. So, this caudate lobe hemangioma failed to exhibit a typical initial peripheral nodular enhancement due to the absence of large feeding arteries. Moreover, the small caudate arteries with their sluggish perfusion also resulted in a slow enhancement rate for the caudate lobe hemangioma. On the post-enhanced arterial-phase, a very faint discontinuous peripheral rim enhancement was noted. During the portal-phase, there was a moderately increased enhancement degree for the enhanced peripheral zone, but the degree of enhancement was not as high as intra-hepatic vessels. At the delayed-phase, complete centripetal fill-in enhancement was not present in the hemangioma, but only a subtle enhancement of the intralesional central portion was noted. The enhancement pattern in the caudate lobe hemangioma thus simulated a well-differentiated hepatocellular carcinoma with delayed pseudocapsule

enhancement, because a well-differentiated hepatocellular carcinoma might usually only possess a slightly increased arterial supplement and is not fed by markedly enlarged vessels^[5]. Therefore, both a well-differentiated hepatocellular carcinoma and a hemangioma with small feeding arteries may exhibit a similar enhancement pattern on dynamic CT study. However, the thickness of pseudocapsules in a hepatocellular carcinoma was thinner than that of the enhanced peripheral rim in a hemangioma. Furthermore, the increased enhancement degree and the increased enhancement thickness of the intra-lesional peripheral rim also provided a diagnostic clue for the hemangioma with a slow progressive central fill-in enhancement. In contrast, a hepatocellular carcinoma usually exhibited contrast medium washout during the delayed-phase.

MR imaging is superior to CT study to improve diagnostic confidence for hepatic hemangiomas. CT has a sensitivity of 62-88% and a specificity of 84-100% (100% when enhancement is isoattenuating to the aorta) for detection of the typical globular enhancement in hemangiomas^[6]. However, MR imaging has a higher sensitivity of 98% and a specificity of 98% for detection of the hemangiomas^[7]. Some atypical hemangiomas can be diagnosed by MR imaging study. Nevertheless, some atypical hemangiomas will still remain uncertain at MR study due to the presence of intralesional thrombosis, calcified, hyalinized or cystic components that results in the loss of its characteristic appearance of markedly high signal intensity on heavy T2-weighted imaging and present with atypical enhancement patterns on post-enhanced study^[8]; and these cases will require biopsy and histopathologic examination.

Except that hemangiomas can exhibit peripheral rim enhancement, the presence of peripheral rim enhancement could also be observed in hepatic metastatic lesions^[9].

However, the peripheral rim enhancement in a metastatic lesion often has a serrated margin and not a lobular margin as seen in a hemangioma. Thus, in the present case, the caudate

lobe hemangioma had an enhanced peripheral rim with a lobular margin and not a serrated margin allowing it to be differentiated from a metastatic lesion.

As in the present case of a hepatitis carrier at risk for malignancy, CT and MR imaging were considered as complementary imaging study for detection of the malignant hepatic masses. Kang *et al.*^[10] reported that although MR imaging study had a higher sensitivity of 95% than that of CT study with a sensitivity of 88% for detection of the hepatocellular carcinomas. However, there was no significant difference in the diagnostic specificity between MR study (97%) and the CT study (98%).

Intra-arterial lipiodol injection has also been used to increase detection of small hepatic neoplasms. Lipiodol retention with a spotty and/or nodular type distribution in the peripheral or central portions of hepatic hemangiomas has been described by Moon *et al.*^[11]. However, the presence of spotty lipiodol retention has also been observed in other hepatic tumors, such as focal nodular hyperplasia, metastases and hepatocellular carcinoma. Hepatocellular carcinomas tended to exhibit a peripheral distribution of lipiodol accumulation, rather than a central distribution of lipiodol deposition as seen in hemangiomas. In this present case, conventional angiography failed to demonstrate the typical "cotton-wool" appearance of puddling of contrast material within the large vascular spaces and persisting into the venous phase of a caudate lobe hemangioma. The absence of persistent tumor stains in the hemangioma may be due to its unique location in the hepatic caudate lobe where there is a rapid venous drainage to the adjacent portal vein and inferior vena cava. In such a situation, it is difficult to distinguish a hemangioma from a hepatocellular carcinoma based only on conventional angiographic imaging findings. Whereas, intra-arterial lipiodol injection demonstrated spotty lipiodol retention at the intralesional peripheral and central portions, with a "cotton wool" appearance, and suggested a diagnosis of hemangioma. In addition, the number of lipiodol retention foci was also more pronounced than the number of contrast material stains as seen on conventional angiograms, because the lipiodol materials could be retained in the ectatic and tortuous vascular channels of the hemangioma, thus decreasing its venous washout degree via the portal vein and inferior vena cava. Therefore, intra-arterial lipiodol injection is able to help in the diagnosis of a hemangioma with a rapid venous drainage.

In conclusion, the presence of slow progressive peripheral rim enhancement persisting to the delayed phase, associated with the presence of central distributed spotty lipiodol retention in a caudate lobe mass should give rise to a suspicion of the possibility of hepatic hemangioma. This report emphasizes that a hepatic hemangioma in this unique caudate lobe location can

present with an atypical enhancement pattern and resembles a hepatocellular carcinoma. Thus, we recommend that when studying a caudate lobe lesion, a longer post-enhanced delayed time (more than 3 min) is required on CT, in order to reflect its actual vascularity characteristics. In addition, further evaluation by MR study with a long echo time of 150 to 180 ms is also necessary to confirm the diagnosis of a cavernous hemangioma in order to prevent inappropriate therapeutic decision making.

REFERENCES

- 1 **Mitsudo K**, Watanabe Y, Saga T, Dohke M, Sato N, Minani K, Shigeyasu M. Nonenhanced hepatic cavernous hemangioma with multiple calcifications: CT and pathologic correlation. *Abdom Imaging* 1995; **20**: 459-461
- 2 **Yun EJ**, Choi BI, Han JK, Jang HJ, Kim TK, Yeon KM, Han MC. Hepatic hemangioma: contrast-enhancement pattern during the arterial and portal venous phases of spiral CT. *Abdom Imaging* 1999; **24**: 262-266
- 3 **Hanafusa K**, Ohashi I, Himeno Y, Suzuki S, Shibuya H. Hepatic hemangioma: findings with two-phase CT. *Radiology* 1995; **196**: 465-469
- 4 **Leeuwen MS**, Noordzij J, Feldberg MAM, Hennipman AH, Doornwaard H. Focal liver lesions: characterization with triphasic spiral CT. *Radiology* 1996; **201**: 327-336
- 5 **Hwang GJ**, Kim MJ, Yoo HS, Lee JT. Nodular hepatocellular carcinomas: detection with arterial-, portal-, and delayed-phase images at spiral CT. *Radiology* 1997; **202**: 383-388
- 6 **Leslie DF**, Johnson CD, Johnson CM, Ilstrup DM, Harmsen WS. Distinction between cavernous hemangiomas of the liver and hepatic metastases on CT: value of contrast enhancement patterns. *Am J Roentgenol* 1995; **164**: 625-629
- 7 **Soyer P**, Gueye C, Somveille E, Laissy JP, Scherrer A. MR diagnosis of hepatic metastases from neuroendocrine tumors versus hemangiomas: relative merits of dynamic gadolinium chelate-enhanced gradient-recalled echo and unenhanced spin-echo images. *Am J Roentgenol* 1995; **165**: 1407-1413
- 8 **Vilgrain V**, Boulos L, Vullierme MP, Denys A, Terris B, Menu Y. Imaging of atypical hemangiomas of the liver with pathologic correlation. *Radiographics* 2000; **20**: 379-397
- 9 **Mitchell DG**, Saini S, Weinreb JW, De Lange EE, Runge VM, Kuhlman JE, Parisky Y, Johnson D, Brown JJ, Schnall M, Herfkens R, Davis PL, Gorczyca D, Sica G, Foster GS, Bernardino ME. Hepatic metastases and cavernous hemangiomas: distinction with standard- and triple-dose gadoteridol-enhanced MR imaging. *Radiology* 1994; **193**: 49-57
- 10 **Kang BK**, Lim JH, Kim SH, Choi D, Lim HK, Lee WJ, Lee SJ. Preoperative depiction of hepatocellular carcinoma: Ferumoxides-enhanced MR imaging versus triple-phase helical CT. *Radiology* 2003; **226**: 79-85
- 11 **Moon WK**, Han JK, Choi BI, Kim SH, Chung JW, Park JH, Han MC. Iodized-oil retention within hepatic hemangioma: characteristics on iodized-oil CT. *Abdom Imaging* 1996; **21**: 420-426

Edited by Wang XL Proofread by Zhu LH and Xu FM

• CASE REPORT •

Recurrence of hepatocellular carcinoma with rapid growth after spontaneous regression

Tomoki Nakajima, Michihisa Moriguchi, Tadashi Watanabe, Masao Noda, Nobuaki Fuji, Masahito Minami, Yoshito Itoh, Takeshi Okanoue

Tomoki Nakajima, Michihisa Moriguchi, Tadashi Watanabe, Masao Noda, Masahito Minami, Yoshito Itoh, Takeshi Okanoue, Molecular Gastroenterology and Hepatology, Kyoto Prefectural University of Medicine Graduate School of Medical Science, Kyoto, Japan
Nobuaki Fuji, Department of Surgery, Kyoto Prefectural Yosanomi Hospital, Kyoto, Japan

Correspondence to: Tomoki Nakajima M.D., Molecular Gastroenterology and Hepatology, Kyoto Prefectural University of Medicine Graduate School of Medical Science, Kawaramachi-Hirokoji, Kamigyo-ku, Kyoto 602-8566, Japan. tomnaka@silver.ocn.ne.jp

Telephone: +81-75-251-5519 **Fax:** +81-75-251-0710

Received: 2004-03-09 **Accepted:** 2004-04-16

Abstract

We report an 80-year-old man who presented with spontaneous regression of hepatocellular carcinoma (HCC). He complained of sudden right flank pain and low-grade fever. The level of protein induced by vitamin K antagonist (PIVKA)-II was 1 137 mAU/mL. A computed tomography scan in November 2000 demonstrated a low-density mass located in liver S4 with marginal enhancement and a cystic mass of 68 mm×55 mm in liver S6, with slightly high density content and without marginal enhancement. Angiography revealed that the tumor in S4 with a size of 25 mm×20 mm was a typical hypervascular HCC, and transarterial chemoembolization was performed. However, the tumor in S6 was hypovascular and atypical of HCC, and thus no therapy was given. In December 2000, the cystic mass regressed spontaneously to 57 mm×44 mm, and aspiration cytology revealed bloody fluid, and the mass was diagnosed cytologically as class I. The tumor in S4 was treated successfully with a 5 mm margin of safety around it. The PIVKA-II level normalized in February 2001. In July 2001, the tumor regressed further but presented with an enhanced area at the posterior margin. In November 2001, the enhanced area extended, and a biopsy revealed well-differentiated HCC, although the previous tumor in S4 disappeared. Angiography demonstrated two tumor stains, one was in S6, which was previously hypovascular, and the other was in S8. Subsequently, the PIVKA-II level started to rise with the doubling time of 2-3 wk, and the tumor grew rapidly despite repeated transarterial embolization with gel foam. In February 2003, the patient died of bleeding into the peritoneal cavity from the tumor that occupied almost the entire right lobe. Considering the acute onset of the symptoms, we speculate that local ischemia possibly due to rapid tumor growth, resulted in intratumoral bleeding and/or hemorrhagic necrosis, and finally spontaneous regression of the initial tumor in S6.

Nakajima T, Moriguchi M, Watanabe T, Noda M, Fuji N, Minami M, Itoh Y, Okanoue T. Recurrence of hepatocellular carcinoma with rapid growth after spontaneous regression. *World J Gastroenterol* 2004; 10(22): 3385-3387

<http://www.wjgnet.com/1007-9327/10/3385.asp>

INTRODUCTION

According to previous reports, spontaneous regression (SR)

of malignant tumors is estimated to occur once in 60 000-100 000 cancer patients^[1]. Neuroblastomas and urinary bladder cancers are well-known to regress spontaneously. However, in hepatocellular carcinoma (HCC) only 30 cases of SR have been reported in the English-language literature^[2-7]. Among them, there has been only 1 report of 2 cases of recurrent HCC after SR^[4]. In both cases, however, the new lesion developed at a different site in the liver while the preexisting HCC was regressing, suggesting that multicentric hepatocarcinogenesis was involved in the recurrence. In this paper, we present a case of spontaneously regressing HCC, which recurred locally during the course of 8 mo. Four months later, a new lesion developed at a different site in the liver, possibly through intrahepatic metastasis from the original tumor, and progressed rapidly. We discussed the possible mechanisms of SR in HCC.

CASE REPORT

An 80-year-old man was admitted to our hospital on November 14, 2000 due to right flank pain and low-grade fever, which continued for a day and worsened gradually. He drank 350 mL of beer every day but had no history of the use of herbal medicines.

His blood pressure was 170/104 mmHg and body temperature was 37.2 °C. There was no remarkable physical finding. The laboratory data on admission revealed that his white blood cell count and C-reactive protein (CRP) were elevated to 10 600/mm³ and 6.2 mg/dL, respectively. Aspartate aminotransferase (AST) and alanine aminotransferase (ALT) also were elevated to 201 IU/L and 234 IU/L, respectively. The level of alpha-fetoprotein (AFP) was within the normal limit, but protein induced by vitamin K antagonist (PIVKA)-II was 1 137 mAU/mL. His serum was negative for hepatitis B surface antigen and positive for hepatitis C antibody.

Enhanced computed tomography (CT) on admission demonstrated 2 hepatic tumors (Figure 1A). One was a low-density mass located in liver S4 with marginal enhancement. The other was a cystic mass of 68 mm×55 mm in S6 with slightly high density content but without marginal enhancement. Angiography demonstrated that the right hepatic lobe was supplied by the replaced right hepatic artery. A celiac arteriogram showed tumor stain in S4 with a size of 25 mm×20 mm, which was diagnosed as typical HCC (Figure 2A). Transarterial chemoembolization was performed using an emulsion of 3.2 mL Lipiodol (iodized oil manufactured by Andre Guerbert, Aulnay-sous-Bois, France) and 32 mg epirubicin^[8]. The super mesenteric arteriogram, on the other hand, demonstrated that the tumor in S6 was hypovascular (Figure 2B). Because this image was atypical of HCC, no therapy was given.

Low-grade fever disappeared on the second day of admission and the white blood cell count, CRP and transaminases became almost normal on the eighth day. Because the patient wanted to undergo an operation for gallbladder stones, preoperative evaluation for cholecystectomy was carried out. In December 2000, just before the operation, a CT scan showed that Lipiodol was accumulated in the tumor in S4 and that the cystic mass in S6 was decreased in size spontaneously, down to 57 mm×44 mm (Figure 1B). During the operation in December 2000, microwave coagulation was performed for HCC in S4. The surface of the cystic tumor in S6 was dark red and needle aspiration revealed bloody fluid, which was diagnosed cytologically as class I. Because there was no evidence of malignancy, we did not give any treatment for this lesion.

After the operation, the tumor in S6 continued to decrease in size (Figure 1C), whereas the tumor in S4 was treated successfully with a 5 mm margin of safety around it. The PIVKA-II level fell to the normal limit in February 2001. A CT scan in July 2001 revealed that the tumor was decreased further in size but demonstrated an enhanced area at the posterior margin of the tumor (Figure 1D). Furthermore, the PIVKA-II level increased slightly. In November 2001, a CT scan demonstrated that the enhanced area extended to the surrounding area of the cystic tumor (Figure 1E). Histological evaluation by tumor biopsy from the lesion in S6 revealed a well-differentiated HCC (Figure 1F). The celiac arteriogram in November 2001 showed that the previous tumor stain in S4 disappeared. The super mesenteric arteriogram demonstrated 2 tumor stains; one was in S6, which was previously hypovascular, and the other was in S8 (Figure 2D).

Subsequently, transarterial embolization with gel foam (TAE) was repeated but the tumor resisted therapy, with rapid invasion and intrahepatic metastasis. In February 2003, the

patient died of bleeding into the peritoneal cavity from the tumor that occupied almost the entire right lobe (Figure 3).

DISCUSSION

To our knowledge, there has been only 1 report of 2 cases of recurrence of HCCs after SR^[4]. In both cases, the recurrent HCCs developed at different sites in the liver before the preexisting HCC regressed completely, suggesting that multicentric hepatocarcinogenesis, rather than intrahepatic metastasis, was likely to have been involved in the recurrence. However, in our case, evidence of local recurrence in the regressing tumor was observed by CT scan before the newly developed lesion in S8 was found by angiography. In addition, when local recurrence was detected by CT scan, the serum PIVKA-II level started to rise again. This clinical course suggests that the new lesion in S8 might be due to intrahepatic metastasis from the locally recurrent tumor in S6, rather than multicentric hepatocarcinogenesis.

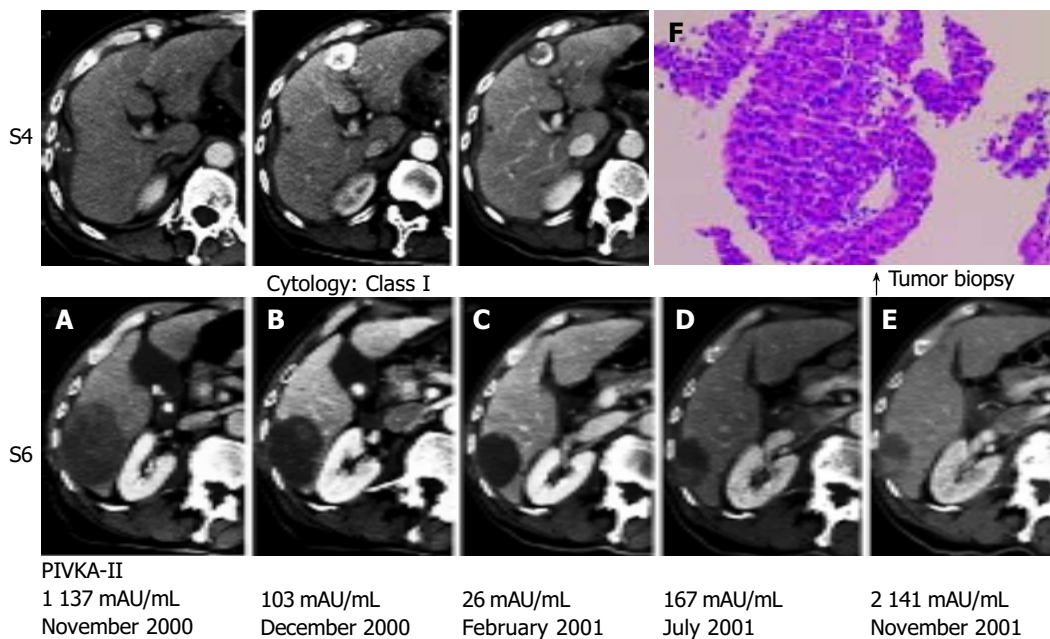


Figure 1 Enhanced computed tomography (CT). A: A low-density mass located in liver S4, with marginal enhancement and a cystic mass of 68 mm×55 mm in S6. B: Lipiodol accumulation in the tumor in S4 and the cystic mass in S6. C: Microwave coagulation performed for HCC in S4 during cholecystectomy. D: Further decrease in tumor size and enhanced area at the posterior cystic lumen of the tumor. E: Extension of the enhanced area to the surrounding area of cystic tumor. F: A well-differentiated HCC shown by histological evaluation.

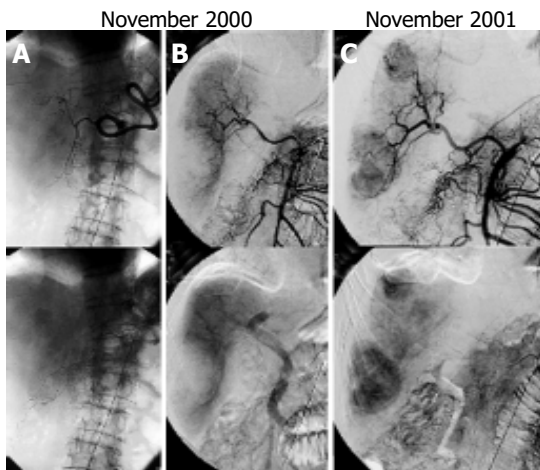


Figure 2 A: Celiac arteriogram showing tumor stain with a size of 25 mm×20 mm in S4. B: Blood supply of right hepatic lobe by the replaced right hepatic artery. C: Super mesenteric arteriogram demonstrating two tumor stains.

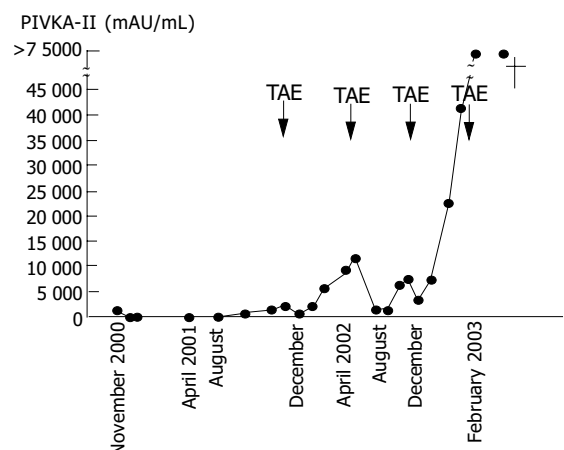


Figure 3 Clinical course of the patient. TAE: transarterial embolization with gel foam.

In previous reports, some authors made a definitive diagnosis by histological study after tumor resection but others suspected SR based on the following up radiological findings and the tumor markers^[2-7]. In this case, the PIVKA-II level was 1 137 mAU/mL on the first admission and decreased dramatically to 103 in 1 mo. However, at that point we were not certain whether this was due to SR of the HCC in S6 or to transarterial chemoembolization for a typical HCC in S4. In addition, a diagnosis of class I by tumor aspiration cytology in S6 prevented us from performing S6 segmentectomy, in view of evidence-based medicine. We could not make a definitive diagnosis of the tumor in S6 until it showed radiological signs of recurrence and was proven histologically to be HCC.

The precise mechanism of SR of HCC remains unclear, but various factors have been speculated to play a role, such as alcohol withdrawal^[9], androgen withdrawal^[10], and intake of herbal medicine^[2,11,12]. Secondary bacterial infection in the tumor has also been supposed to cause SR through the stimulation of cytokine production^[13,14] and fever^[15]. Because of the hypervascular nature of HCC, another important factor might be an insufficient blood supply to the tumor, possibly due to rapid natural tumor growth^[16,17], spontaneous arterial thrombosis^[18], or gastrointestinal bleeding^[19,20]. In our case, there was no history of alcohol or androgen withdrawal or the use of herbal medicines. The initial symptoms of right flank pain and fever suddenly appeared and lasted for only a day. Laboratory data showed that the levels of transaminases were elevated on admission but almost normalized in about a week. In addition, angiography clarified that the tumor in S6 was hypovascular. Furthermore, this tumor was cystic with slightly high density content, from which bloody fluid was obtained. These clinical manifestations suggest that the acute onset of the symptoms was due to local ischemia, leading to intratumoral bleeding or hemorrhagic necrosis, and as a result, causing SR.

In this case, the PIVKA-II level after recurrence showed a logarithmic increase throughout the entire clinical course, except that it stabilized for one month after each TAE. The doubling time of the PIVKA-II level, which is thought to reflect the tumor doubling time, was calculated to be 2-3 wk. This indicates that the recurrent tumor grew very rapidly, compared with the average natural growth rate of HCC reported previously^[21,22]. The PIVKA-II level was elevated to 1 137 mAU/mL on the first admission, decreased along with SR of the tumor in S6, and rose again after recurrence. It has been reported that HCCs with high PIVKA-II levels during the initial stage show aggressive behaviors and a poor prognosis. Therefore, we speculate that the initial tumor in S6 grew as fast as the recurrent tumor and this rapid growth itself might be the cause of insufficient blood supply to the tumor, finally inducing SR, as suggested in previous reports^[16,17].

REFERENCES

- 1 **Cole WH.** Efforts to explain spontaneous regression of cancer. *J Surg Oncol* 1981; **17**: 201-209
- 2 **Takeda Y, Togashi H, Shinzawa H, Miyano S, Ishii R, Karasawa T, Takeda Y, Saito T, Saito K, Haga H, Matsuo T, Aoki M, Mitsuhashi H, Watanabe H, Takahashi T.** Spontaneous regression of hepatocellular carcinoma and review of literature. *J Gastroenterol Hepatol* 2000; **15**: 1079-1086
- 3 **Izuishi K, Ryu M, Hasebe T, Kinoshita T, Konishi M, Inoue K.** Spontaneous total necrosis of hepatocellular carcinoma: report of a case. *Hepatogastroenterology* 2000; **47**: 1122-1124
- 4 **Lee HS, Lee JS, Woo GW, Yoon JH, Kim CY.** Recurrent hepatocellular carcinoma after spontaneous regression. *J Gastroenterol* 2000; **35**: 552-556
- 5 **Matsuo R, Ogata H, Tsuji H, Kitazono T, Shimada M, Taguchi K, Fujishima M.** Spontaneous regression of hepatocellular carcinoma - a case report. *Hepatogastroenterology* 2001; **48**: 1740-1742
- 6 **Ikeda M, Okada S, Ueno H, Okusawa T, Kuriyama H.** Spontaneous regression of hepatocellular carcinoma with multiple lung metastases: a case report. *Jpn J Clin Oncol* 2001; **31**: 454-458
- 7 **Morimoto Y, Tanaka Y, Itoh T, Yamamoto S, Mizuno H, Fushimi H.** Spontaneous necrosis of hepatocellular carcinoma: a case report. *Dig Surg* 2002; **19**: 413-418
- 8 **Fan J, Ten GJ, He SC, Guo JH, Yang DP, Wang GY.** Arterial chemoembolization for hepatocellular carcinoma. *World J Gastroenterol* 1998; **4**: 33-37
- 9 **Gottfried EB, Steller R, Paronetto F, Lieber CS.** Spontaneous regression of hepatocellular carcinoma. *Gastroenterology* 1982; **82**: 770-774
- 10 **McCaughan GW, Bilous MJ, Gallagher ND.** Long-term survival with tumor regression in androgen-induced liver tumors. *Cancer* 1985; **56**: 2622-2626
- 11 **Chien RN, Chen TJ, Liaw YF.** Spontaneous regression of hepatocellular carcinoma. *Am J Gastroenterol* 1992; **87**: 903-905
- 12 **Lam KC, Ho JC, Yeung RT.** Spontaneous regression of hepatocellular carcinoma: a case study. *Cancer* 1982; **50**: 332-336
- 13 **Watanabe N, Yamauchi N, Maeda M, Neda H, Tsuji Y, Okamoto T, Tsuji N, Akiyama S, Sasaki H, Niitsu Y.** Recombinant human tumor necrosis factor causes regression in patients with advanced malignancies. *Oncology* 1994; **51**: 360-365
- 14 **Nishimura T, Watanabe K, Yahata T, Ushaku L, Ando K, Kimura M, Saiki I, Uede T, Habu S.** Application of interleukin 12 to antitumor cytokine and gene therapy. *Cancer Chemother Pharmacol* 1996; **38**: S27-34
- 15 **Jansen PM, van der Pouw Kraan TC, de Jong IW, van Mierlo G, Wijdenes J, Chang AA, Aarden LA, Taylor FB Jr, Hack CE.** Release of interleukin-12 in experimental *Escherichia coli* septic shock in baboons: relation to plasma levels of interleukin-10 and interferon-gamma. *Blood* 1996; **87**: 5144-5151
- 16 **Suzuki M, Okazaki N, Yoshino M, Yoshida T.** Spontaneous regression of a hepatocellular carcinoma: a case report. *Hepatogastroenterology* 1989; **36**: 160-163
- 17 **Iwasaki M, Furuse J, Yoshino M, Moriyama N, Kanemoto H, Okumura H.** Spontaneous regression of hepatocellular carcinoma: a case report. *Jpn J Clin Oncol* 1997; **27**: 278-281
- 18 **Imaoka S, Sasaki Y, Masutani S, Ishikawa O, Furukawa H, Kabuto T, Kameyama M, Ishiguro S, Hasegawa Y, Koyama H.** Necrosis of hepatocellular carcinoma caused by spontaneously arising arterial thrombus. *Hepatogastroenterology* 1994; **41**: 359-362
- 19 **Gaffey MJ, Joyce JP, Carlson GS, Esteban JM.** Spontaneous regression of hepatocellular carcinoma. *Cancer* 1990; **65**: 2779-2783
- 20 **Tocci G, Conte A, Guarascio P, Visco G.** Spontaneous remission of hepatocellular carcinoma after massive gastrointestinal haemorrhage. *BMJ* 1990; **300**: 641-642
- 21 **Ebara M, Ohto M, Shinagawa T, Sugiura N, Kimura K, Matsutani S, Morita M, Saisho H, Tsuchiya Y, Okuda K.** Natural history of minute hepatocellular carcinoma smaller than three centimeters complicating cirrhosis. A study in 22 patients. *Gastroenterology* 1986; **90**: 289-298
- 22 **Nakajima T, Moriguchi M, Mitsumoto Y, Katagishi T, Kimura H, Shintani H, Deguchi T, Okanoue T, Kagawa K, Ashihara T.** Simple tumor profile chart based on cell kinetic parameters and histological grade is helpful for estimating the natural growth rate of hepatocellular carcinoma. *Hum Pathol* 2002; **33**: 92-99

• ESOPHAGEAL CANCER •

***GSTM1*, *GSTT1*, *GSTP1* and *CYP1A1* genetic polymorphisms and susceptibility to esophageal cancer in a French population: Different pattern of squamous cell carcinoma and adenocarcinoma**

Ahmed Abbas, Karine Delvinquière, Mathilde Lechevrel, Pierre Lebailly, Pascal Gauduchon, Guy Launoy, François Sichel

Ahmed Abbas, Karine Delvinquière, Mathilde Lechevrel, Pierre Lebailly, Pascal Gauduchon, François Sichel, GRECAN-EA1772, UFR des Sciences Pharmaceutiques, Université de Caen Basse-Normandie et Centre François Baclesse, Avenue du Général Harris, 14076 Caen cedex 05, France

Guy Launoy, GRECAN-EA1772, Université de Caen Basse-Normandie et Registre des Tumeurs Digestives du Calvados, UFR de Médecine, Avenue de la Côte de Nacre, 14032 Caen cedex, France

Supported by the Grants From Ligue Nationale Contre le Cancer, Comités Départementaux de la Manche, de l'Orne et du Calvados and from Université de Metz

Correspondence to: François Sichel, GRECAN-EA1772, UFR des Sciences Pharmaceutiques, Université de Caen Basse-Normandie et Centre François Baclesse, Avenue du Général Harris, 14076 Caen cedex 05, France. f.sichel@baclesse.fr

Telephone: +33-231-455070 **Fax:** +33-231-455172

Received: 2004-02-20 **Accepted:** 2004-04-27

Abstract

AIM: To evaluate the association between *CYP1A1* and *GSTs* genetic polymorphisms and susceptibility to esophageal squamous cell carcinoma (SCC) and esophageal adenocarcinoma (ADC) in a high risk area of northwest of France.

METHODS: A case-control study was conducted to investigate the genetic polymorphisms of these enzymes (*CYP1A1**2C and *GSTP1* exon 7 Val alleles, *GSTM1**2/*2 and *GSTT1**2/*2 null genotypes). A total of 79 esophageal cancer cases and 130 controls were recruited.

RESULTS: *GSTM1**2/*2 and *CYP1A1**1A/*2C genotype frequencies were higher among squamous cell carcinomas at a level close to statistical significance (OR = 1.83, 95% CI 0.88-3.83, *P* = 0.11; OR = 3.03, 95% CI 0.93-9.90, *P* = 0.07, respectively). For *GSTP1* polymorphism, no difference was found between controls and cases, whatever their histological status. Lower frequency of *GSTT1* deletion was observed in ADC group compared to controls with a statistically significant difference (OR = 13.31, 95% CI 1.66-106.92, *P* < 0.01).

CONCLUSION: In SCC, our results are consistent with the strong association of this kind of tumour with tobacco exposure. In ADC, our results suggest 3 distinct hypotheses: (1) activation of exogenous procarcinogens, such as small halogenated compounds by *GSTT1*; (2) contribution of *GSTT1* to the inflammatory response of esophageal mucosa, which is known to be a strong risk factor for ADC, possibly through leukotriene synthesis; (3) higher sensitivity to the inflammatory process associated with intracellular depletion of glutathione.

Abbas A, Delvinquière K, Lechevrel M, Lebailly P, Gauduchon P, Launoy G, Sichel F. *GSTM1*, *GSTT1*, *GSTP1* and *CYP1A1* genetic polymorphisms and susceptibility to esophageal cancer in a French population: Different pattern of squamous cell

carcinoma and adenocarcinoma. *World J Gastroenterol* 2004; 10(23): 3389-3393

<http://www.wjgnet.com/1007-9327/10/3389.asp>

INTRODUCTION

One of the highest incidences of esophageal cancer in Europe is observed in the Northwest of France^[1-4]. There are two predominant histological forms of this cancer: squamous cell carcinoma (SCC) and adenocarcinoma (ADC)^[4,5]. Recent epidemiological observations showed an important decrease in the incidence of SCC whilst ADC was slightly increased^[2,4].

In Western countries, smoking tobacco and drinking alcohol are the main risk factors for SCC. For ADC, exogenous risk factors are not well known. A link was found between this pathology, esophageal reflux and Barret's esophagus^[5].

Tobacco smoke contains many carcinogens such as polycyclic aromatic hydrocarbons (PAH) and *N*-nitrosamines that can be activated or deactivated by phase I (cytochromes P-450) and phase II enzymes (glutathione S-transferases). Cytochromes P450 (CYP) are a widely expressed enzyme family, some members of which present genetic polymorphisms (e.g. *CYP1A1*, *2E1*, *2D6*). *CYP1A1* is expressed in esophageal mucosa, which means that activation of tobacco carcinogens can happen *in situ*^[6]. Benzo[a]pyrene is activated by *CYP1A1* to diol-epoxide, which is a reactive and carcinogenic product. Four main genetic polymorphisms are described for *CYP1A1*. One of the most studied is Ile/Val polymorphism in exon 7 (*CYP1A1**2C allele). One study reported that Val-type could be associated with a higher aryl hydrocarbon hydroxylase activity^[7].

Many studies have reported the association of *CYP1A1* polymorphisms with lung cancer^[8], particularly with SCC of the lung^[9,10]. The level of DNA adducts was found to be linked to *CYP1A1**2C polymorphism^[11]. All these results suggest that susceptibility to tobacco-related cancers could be modified by *CYP1A1* polymorphisms.

The glutathione S-transferases are a family of phase II enzymes, which catalyse the conjugation of many endogenous and exogenous electrophilic compounds to glutathione. *GSTM1* and *GSTP1* are able to detoxify benzopyrene diol-epoxide^[12], whereas *GSTT1* can conjugate oxidised lipids and halogenated compounds^[12]. Both *GSTM1*, *P1* and *T1* are expressed in esophageal mucosa^[13,14]. *GSTP1* is the mainly expressed GST in this tissue^[15]. *GSTP1* presents a substitution polymorphism in exon 7 that results in a substitution of Ile by Val at amino acid position 104^[16]. Val variants were found to have a lower activity towards 1-chloro-2, 4-dinitrobenzene^[17]. *GSTM1* and *GSTT1* present deletion polymorphisms (*GSTM1**2/*2 and *GSTT1**2/*2), which are currently at about 50% and 20% among Caucasians, respectively^[18,19]. *GSTM1**2/*2 polymorphism has been found to increase the frequency of chromosome aberrations after tobacco-specific *N*-nitrosamine exposure *in vitro*^[20]. Many studies have shown that this deletion increases the susceptibility conferred by the *CYP1A1**2C allele for tobacco-associated cancer^[21]. While *GSTT1**2/*2 genotypes have not been clearly

associated with susceptibility to tobacco-linked cancers, an interaction with *GSTM1**2/*2 has often been found^[22,23].

The aim of our work was to evaluate the susceptibility conferred by *CYP1A1* and *GSTs* genetic polymorphisms to SCC and ADC of esophagus in a high risk European area.

MATERIALS AND METHODS

Controls and cases were from the geographic area of Basse-Normandie, France. Patients were recruited after endoscopic and histologic diagnosis of primary esophageal cancer. All cases were newly diagnosed and previously untreated patients. Controls were required to be free of any chronic diseases, having no cancer history and living in Basse-Normandie. They were matched with cases in sex and age. Alcohol and tobacco consumption were also evaluated during the recruitment of cases and controls by means of a questionnaire.

The research protocol was approved by the Comité Consultatif pour la Protection des Personnes dans la Recherche Biomédical en Basse-Normandie. A 20 mL sample of venous blood was taken and DNA extraction was performed by phenol/chloroform method.

The primer sequences and product sizes of each gene amplification are shown in Table 1. *GSTM1* and *GSTT1* multiplex PCR was performed according to the Lin *et al.* method^[24], with some modifications. A final mixture volume of 25 μ L was prepared containing 0.100 μ g of DNA, 0.25 μ mol/L of dNTP, 0.4 μ mol/L of primer for *GSTM1*, 0.8 μ mol/L of primer *GSTT1*, 0.8 μ mol/L of primer albumin, 5 μ L of 10 \times buffer, 2 mmol/L of MgCl₂ and 0.5 U per sample of DNA Gold *Taq* polymerase (Applied Biosystem, Coutaboeuf, France). The first step was performed for 15 min at 95 $^{\circ}$ C followed by 35 cycles: at 94 $^{\circ}$ C for 1 min (denaturation), at 58 $^{\circ}$ C for 1 min (annealing), at 72 $^{\circ}$ C for 1 min (elongation). PCR ended a final extension for 10 min at 72 $^{\circ}$ C. PCR products were visualised on 20 g/L agarose gel with ethidium bromide staining.

Table 1 Primer sequences and length of PCR products

Gene	Primer sequence	Size of PCR product (bp)	Reference
<i>GSTM1</i>	5'-GAACTCCCTGAAAAGCTAAAGC-3'	219	Lin <i>et al.</i> 1998 ^[24]
	5'-GTTGGGCTCAAATATACGGTGG-3'		
<i>GSTT1</i>	5'-TTCCTTACTGGTCTCACATCTC-3'	459	
	5'-TCACCGGATCATGGCCAGCA-3'		
<i>Albumin</i>	5'-GCCCTCTGTAACAAGTCTAC-3'	350	
	5'-GCCCTAAAAAGAAAATCCCAATC-3'		
<i>GSTP1</i>	5'-ACCCAGGGCTCTATGGGAA-3'	176	Harries <i>et al.</i> 1997 ^[16]
	5'-TGAGGGCACAAGAAGCCCT-3'		
<i>CYP1A1</i>	5'-GGCTGAGCAATCTGACCCTA-3'	206	Casorbi <i>et al.</i> 1996 ^[8]
	5'-TTCCACCGTTGCAGCAGGATAGCC-3'		

GSTP1 PCR restriction fragment length polymorphism (rflp) was performed using a method adopted by Harries *et al.*^[16] with slight modifications. The final mixture (40 μ L) was prepared containing 0.100-0.500 μ g of DNA, 0.25 μ mol/L of dNTP, 0.25 μ mol/L of each of the primers, 1.25 μ mol/L of MgCl₂, 4 μ L of 10 \times buffer, 4 μ L of DMSO, 1.5 U of *Taq* polymerase (Eurobio, Les Ulis, France). Briefly, the samples were denatured at 94 $^{\circ}$ C for 5 min and submitted to 30 cycles of amplification as follows: for 30 s at 94 $^{\circ}$ C (denaturation), for 30 s at 55 $^{\circ}$ C (annealing), for 30 s at 72 $^{\circ}$ C (extension) and a final extension at 72 $^{\circ}$ C for 5 min. PCR product of 12 μ L was digested by 5 U Alw26 I restriction enzyme (Eurogentec, Seraing, Belgium) for 12 h at 37 $^{\circ}$ C. Migration was performed on low melting 40 g/L agarose gel (Eurobio, Les Ulis, France), stained with ethidium bromide, in order to separate the 85 and 91 bp fragments.

*CYP1A1**2C polymorphism was determined by PCR-RFLP

as previously described^[8].

Each PCR analysis was performed twice in double blind.

Statistical analysis

Chi-square test and *P* value estimation were performed using Stata software (STATA Corporation, college Station, TX). Odds ratio was also evaluated using Stata $\text{\textcircled{O}}$ software and adjusted for age, sex and histological type.

RESULTS

The populations of controls and cases are described in Table 2. The patient group consisted of 52 SCCs and 27 ADCs. The mean ages for cases and controls were 62 and 56 years respectively. Unfortunately, we obtained tobacco and alcohol exposure data for only 48 cases. This was insufficient to allow us to study interaction between exposure and polymorphisms. As it could be expected, the vast majority of SCCs were smokers (93%, all with more than 20 years of tobacco consumption) and heavy drinkers (86% drinking more than 229 g/wk). Fewer ADCs were smokers (78%, of which 67% with more than 20 years of tobacco consumption) and only 50% were heavy drinkers (Table 2).

Table 2 Description of control and case populations

	Control n (%)	Case n (%)	SCC n (%)	ADC n (%)
Male	87 (0.67)	69 (0.87)	44 (0.85)	25 (0.93)
Female	43 (0.33)	10 (0.13)	8 (0.15)	2 (0.07)
Mean age (yr)	56 [19; 87]	62 [40; 85]	60 [40; 78]	66 [51; 85]
Tobacco duration ^{1,2} (years of smoking)				
Non-smokers	66 (0.66)	6 (0.13)	2 (0.07)	4 (0.22)
1-19	13 (0.13)	2 (0.04)	0 (-)	2 (0.11)
+20	21 (0.21)	40 (0.83)	28 (0.93)	12 (0.67)
Alcohol consumption ^{3,4} (g of ethanol per week)				
0-228	11 (0.64)	13 (0.28)	4 (0.14)	9 (0.50)
228.5 -/+ 470	6 (0.36)	35 (0.72)	26 (0.86)	9 (0.50)

¹Tobacco duration (year); ²Data were available for 77% of controls, 61% of cases, including 58% of SCC and 67% of ADC; ³Alcohol consumption (gram of ethanol per week); ⁴Data for alcohol consumption were available for only 13% of controls, 61% of cases, including 58% of SCC and 67% of ADC.

Frequencies of the different genetic polymorphisms in the control group were 0.06 for *CYP1A1**A/*2C (no homozygous *2C/*2C subject was found), 0.45 and 0.07 for Ile/Val and Val/Val *GSTP1* genotypes, 0.49 for *GSTM1**2/*2 and 0.26 for *GSTT1**2/*2 (Tables 3, 4).

A high frequency of *CYP1A1**1A/*2C genotype was found in SCC cancer patients (Table 3). However, the difference did not reach statistical significance (with a *P* value of 0.06). The ADC patient group did not show any significant difference compared to the control group.

*GSTM1**2/*2 genotype (*GSTM1* null) was increased among the cases compared to the controls, particularly among SCC patients (Table 4), but this difference was not statistically significant (OR = 1.83; 95% CI = 0.88-3.83). The distribution of *GSTM1**2/*2 genotype among ADCs did not differ from the controls.

The frequency of *GSTT1**2/*2 genotype (*GSTT1* null) was not different between cases and controls (Table 5). However, the ADC group showed a greatly decreased frequency of *GSTT1**2/*2 genotype (4%) compared to the control population (26%) and SCCs (29%) (OR = 13.31, 95% CI = 1.66-106.92).

Distribution of the *GSTP1* genotype did not differ between SCC, ADC and control groups (Table 6).

Table 3 Repartition of *CYP1A1* genotypes among controls and cases

	n	CYP1A1*1A/*1A		CYP1A1*1A/*2C		OR ¹	95% CI
		n	(%)	n	(%)		
Controls	107	101	(94)	6	(6)		
Cases	70	61	(87)	9	(13)	All cases vs controls ²	2.63 [0.84-8.28]
SCC	47	40	(85)	7	(15)	SCC vs controls ³	3.03 [0.93-9.90] ⁵
ADC	23	21	(91)	2	(9)	ADC vs controls ⁴	2.06 [0.33-13.04]

¹Adjusted OR for age and sex; ²Comparison of *CYP1A1*1A/*2C* genotype repartition in controls vs all cases; ³Comparison of *CYP1A1*1A/*2C* genotype repartition in controls vs SCCs; ⁴Comparison of *CYP1A1*1A/*2C* genotype repartition in controls vs ADCs; ⁵*P* = 0.067.

Table 4 Repartition of *GSTM1* genotypes among controls and cases

	<i>GSTM1*2/*2</i>			OR ¹	95% CI
	n	n	(%)		
Controls	120	59	(49)		
Cases	68	39	(57)	All cases vs controls ²	1.43 [0.76-2.69]
SCC	43	27	(63)	SCC vs controls ³	1.83 [0.88-3.83] ⁵
ADC	25	12	(48)	ADC vs controls ⁴	0.95 [0.38-2.41]

¹Adjusted OR for age and sex; ²Comparison of *GSTM1*2/*2* genotype repartition in controls vs all cases; ³Comparison of *GSTM1*2/*2* genotype repartition in controls vs SCCs; ⁴Comparison of *GSTM1*2/*2* genotype repartition in controls vs ADCs; ⁵*P* = 0.108.

Table 5 Repartition of *GSTT1* genotypes among controls and cases

	<i>GSTT1*2/*2</i>			OR ¹	95% CI
	n	n	(%)		
Controls	115	30	(26)		
Cases	70	14	(20)	All cases vs controls ²	1.78 [0.84-3.80]
SCC	44	13	(29)	SCC vs controls ³	1.03 [0.46-2.27]
ADC	26	1	(4)	ADC vs controls ⁴	13.31 [1.66-106.92] ^a

¹Adjusted OR for age and sex; ²Comparison of *GSTT1*2/*2* genotype repartition in controls vs all cases; ³Comparison of *GSTT1*2/*2* genotype repartition in controls vs SCCs; ⁴Comparison of *GSTT1*2/*2* genotype repartition in controls vs ADCs; ^a*P* < 0.05.

Table 6 Repartition of *GSTP1* genotypes among controls and cases

	n	<i>GSTP1</i>						OR ^{1,2}	95% CI
		Ile/Ile		Ile/Val		Val/Val			
		n	(%)	n	(%)	n	(%)		
Controls	124	59	(48)	56	(45)	9	(7)		
Cases	70	31	(44)	33	(47)	6	(9)	All cases vs controls ³	1.02 [0.55-1.89]
SCC	45	21	(47)	21	(47)	3	(6)	SCC vs controls ⁴	0.95 [0.47-1.91]
ADC	25	10	(40)	12	(48)	3	(12)	ADC vs controls ⁵	1.17 [0.46-2.97]

¹Adjusted OR for age and sex; ²Ile/Val and Val/Val genotypes were compared to Ile/Ile genotype; ³Comparison of *GSTP1* Ile/Val and Val/Val genotype repartition in controls versus all cases; ⁴Comparison of *GSTP1* Ile/Val and Val/Val genotype repartition in controls vs SCCs; ⁵Comparison of *GSTP1* Ile/Val and Val/Val genotype repartition in controls vs ADCs.

DISCUSSION

Esophageal cancer presents a very variable incidence in different regions and ethnic groups. In France, different levels of environmental exposure to carcinogens could not fully explain this high variability^[25-27], a fact which suggests a genetic susceptibility. Many epidemiological studies have established that exposure to tobacco smoke and alcohol is a major risk factor for SCC in Western countries, whereas ADC is not strongly linked to exogenous factors. As far as we know, only one study concerning the genetic susceptibility to esophageal cancer was performed among Caucasians^[28]. Moreover, the cases for this study were recruited in a low risk area in Europe.

The repartition of different polymorphisms in our control group agrees with available data for a Caucasian population^[8,16,18,19,29]. Recently, frequencies of these polymorphisms among a healthy population were evaluated and published by International Collaborative Study on Genetic Susceptibility to Environmental Carcinogens (GSEC)^[18].

Among SCC cases, *CYP1A1*2A/*2C* frequency was increased when compared to controls and adjusted OR was 3.03 (95% CI 0.93-9.90), however this result was not statistically significant (*P* = 0.067). The deletion of *GSTM1* gene was also more frequent among SCC cases when compared to controls (63% and 49% respectively, OR = 1.83; 0.88-3.83). But this result was also not statistically significant (*P* = 0.108). *CYP1A1*2A/*2C* and *GSTM1*2/*2* genotypes were found to increase the risk of SCC in a previous study in an Asian population, particularly among cases with higher tobacco consumption. However, some studies did not find *CYP1A1* and *GSTM1* gene polymorphisms to be related to SCC. No association was found between other genetic polymorphisms studied (*GSTT1*, *GSTP1*) and esophageal SCC, which is in accordance with the data in literature^[24,30,31]. It should be emphasized that, concerning *GSTT1*, our study is the first report about a Caucasian population.

No differences were found among ADC cases regarding the

frequencies of *CYP1A1*, *GSTM1* and *GSTP1* polymorphisms when compared to controls. This observation is in accordance with the weak association of tobacco smoke, alcohol consumption and ADC. In the ADC group, an unexpected protective effect of *GSTT1* deletion was found (OR = 13.31; 95% CI 1.66-106.92). Such results have been previously described for other sites such as renal or prostate carcinoma^[32,33]. It is well known that the risk of renal carcinoma is increased by exposure to small halogenated compounds such as dichloromethane or trichloroethylene. Activation of these compounds in electrophilic species implies *GSTT1*^[29], which could explain these results. However, to our knowledge, no studies have demonstrated a role of small halogenated compounds in esophageal ADC carcinogenesis. Exposure to these compounds is possible through occupational factors, chlorinated tap water consumption or tobacco smoke. The latter, which is a weakly associated risk factor for ADC, contains methyl chloride^[34]. However, our present data did not allow us to estimate exposure to halogenated compounds in our population.

Another hypothesis is that GST could participate in chronic inflammation through leukotriene synthesis^[35]. In particular, leukotriene A4 to C4 (LTC4) conversion requires GST activity. Inflammation is a major etiologic factor for ADC and leukotrienes have been found to be mediators implicated in this process^[5]. Furthermore, leukotriene LTD4, which is biosynthesized from LTC4, was found to induce contraction of the oesophagus and lower esophageal sphincter in animal models^[35,36]. This phenomenon is likely to be involved in gastro-oesophageal reflux, which constitutes the strongest risk factor for ADC. However, though *GSTT1* is also expressed in esophageal mucosa^[14], it remains unclear whether this enzyme contributes to LTC4 synthesis in this tissue.

The association between susceptibility to cancer and *GSTT1* genotypes could be also explained by depletion in intracellular glutathione in the presence of *GSTT1* enzyme. In this case, cells would be more sensitive to radical species produced during the inflammatory process observed among adenocarcinoma patients.

In conclusion, our study shows a different pattern of susceptibility to SCC and ADC of esophagus in a European high risk population. Whereas a slight susceptibility to SCC could be conferred by *CYP1A1**1A/*2C and *GSTM1**2/*2 genotypes, a high frequency of *GSTT1**1/*1 genotype was found among ADC. These results are consistent with the association of SCC with tobacco exposure, as other tobacco-related cancers such as lung cancer were found to be moderately linked to *CYP1A1**2C allele and *GSTM1**2/*2 genotype. In ADC, our results suggest 3 distinct hypotheses. (1) The activation of exogenous procarcinogens, such as small halogenated compounds (to which ways of exposure remain to be identified), by *GSTT1*. Unlike tobacco, the evaluation of exposure to small halogenated compounds remains difficult because of the wide distribution of these compounds. (2) The contribution of *GSTT1* to the inflammatory response of esophageal mucosa, which is known to be a strong risk factor for ADC, possibly by way of leukotriene synthesis. (3) Higher sensitivity to the inflammatory process associated with intracellular depletion of glutathione. A new study focusing on esophageal ADC with a larger recruitment would allow us to investigate these issues.

ACKNOWLEDGEMENTS

We thank Dr Dominique Arsène and Pr Marc Gignoux (Services de Gastroentérologie et de Chirurgie Digestive, CHU de Caen) for assistance in case recruitment. We thank Jacques Marnay and Dr Jacques Chasles (Laboratoire d'Anatomie Pathologique, Centre François Baclesse, Caen) for help in the histological

diagnosis of tumors. We thank Marie Ingouf, Jocelyne Dannetot and Anne Leclerc for technical assistance.

REFERENCES

- 1 Cancer incidence in five continents. Volume VII. *IARC Sci Publ* 1997; 478-481
- 2 Desoubreaux N, Le Prieur A, Launoy G, Maurel J, Lefevre H, Guillois JM, Gignoux M. Recent time trends in cancer of the oesophagus and gastric cardia in the region of Calvados in France, 1978-1995: a population based study. *Eur J Cancer Prev* 1999; 8: 479-486
- 3 Tuyns AJ. Oesophageal cancer in non-smoking drinkers and in non-drinking smokers. *Int J Cancer* 1983; 32: 443-444
- 4 Gignoux M, Launoy G. Recent epidemiologic trends in cancer of the esophagus. *Rev Prat* 1999; 49: 1154-1158
- 5 Chen X, Yang CS. Esophageal adenocarcinoma: a review and perspectives on the mechanism of carcinogenesis and chemoprevention. *Carcinogenesis* 2001; 22: 1119-1129
- 6 Lechevrel M, Casson AG, Wolf CR, Hardie LJ, Flinterman MB, Montesano R, Wild CP. Characterization of cytochrome P450 expression in human oesophageal mucosa. *Carcinogenesis* 1999; 20: 243-248
- 7 Kawajiri K, Watanabe J, Hayashi S. Identification of allelic variants of the human CYP1A1 gene. *Methods Enzymol* 1996; 272: 226-232
- 8 Cascorbi I, Brockmoller J, Roots I. A C4887A polymorphism in exon 7 of human CYP1A1: population frequency, mutation linkages, and impact on lung cancer susceptibility. *Cancer Res* 1996; 56: 4965-4969
- 9 Song N, Tan W, Xing D, Lin D. CYP 1A1 polymorphism and risk of lung cancer in relation to tobacco smoking: a case-control study in China. *Carcinogenesis* 2001; 22: 11-16
- 10 Lin P, Wang SL, Wang HJ, Chen KW, Lee HS, Tsai KJ, Chen CY, Lee H. Association of CYP1A1 and microsomal epoxide hydrolase polymorphisms with lung squamous cell carcinoma. *Br J Cancer* 2000; 82: 852-857
- 11 Bartsch H, Nair U, Risch A, Rojas M, Wikman H, Alexandrov K. Genetic polymorphism of CYP genes, alone or in combination, as a risk modifier of tobacco-related cancers. *Cancer Epidemiol Biomarkers Prev* 2000; 9: 3-28
- 12 Seidegard J, Ekstrom G. The role of human glutathione transferases and epoxide hydrolases in the metabolism of xenobiotics. *Environ Health Perspect* 1997; 105(Suppl 4): 791-799
- 13 Chen YK, Lin LM. Immunohistochemical demonstration of epithelial glutathione S-transferase isoenzymes in normal, benign, premalignant and malignant human oral mucosa. *J Oral Pathol Med* 1995; 24: 316-321
- 14 de Bruin WC, Wagenmans MJ, Peters WH. Expression of glutathione S-transferase alpha, P1-1 and T1-1 in the human gastrointestinal tract. *Jpn J Cancer Res* 2000; 91: 310-316
- 15 van Lieshout EM, van Haelst UJ, Wobbes T, Peters WH. Immunohistochemical localization of glutathione S-transferase alpha and pi in human esophageal squamous epithelium, Barrett's epithelium and carcinoma. *Jpn J Cancer Res* 1999; 90: 530-535
- 16 Harries LW, Stubbins MJ, Forman D, Howard GC, Wolf CR. Identification of genetic polymorphisms at the glutathione S-transferase Pi locus and association with susceptibility to bladder, testicular and prostate cancer. *Carcinogenesis* 1997; 18:641-644
- 17 Zimniak P, Nanduri B, Pikula S, Bandorowicz-Pikula J, Singhal SS, Srivastava SK, Awasthi S, Awasthi YC. Naturally occurring human glutathione S-transferase GSTP1-1 isoforms with isoleucine and valine in position 104 differ in enzymic properties. *Eur J Biochem* 1994; 224: 893-899
- 18 Taioli E. International collaborative study on genetic susceptibility to environmental carcinogens. *Cancer Epidemiol Biomarkers Prev* 1999; 8: 727-728
- 19 Nelson HH, Wiencke JK, Christiani DC, Cheng TJ, Zuo ZF, Schwartz BS, Lee BK, Spitz MR, Wang M, Xu X. Ethnic differences in the prevalence of the homozygous deleted genotype of glutathione S-transferase theta. *Carcinogenesis* 1995; 16: 1243-1245
- 20 Salama SA, Abdel-Rahman SZ, Sierra-Torres CH, Hamada

- FA, Au WW. Role of polymorphic GSTM1 and GSTT1 genotypes on NNK-induced genotoxicity. *Pharmacogenetics* 1999; **9**: 735-743
- 21 **Lazarus P**, Sheikh SN, Ren Q, Schantz SP, Stern JC, Richie JP Jr, Park JY. p53, but not p16 mutations in oral squamous cell carcinomas are associated with specific CYP1A1 and GSTM1 polymorphic genotypes and patient tobacco use. *Carcinogenesis* 1998; **19**: 509-514
- 22 **Landi S**. Mammalian class theta GST and differential susceptibility to carcinogens: a review. *Mutat Res* 2000; **463**: 247-283
- 23 **Saarikoski ST**, Voho A, Reinikainen M, Anttila S, Karjalainen A, Malaveille C, Vainio H, Husgafvel-Pursiainen K, Hirvonen A. Combined effect of polymorphic GST genes on individual susceptibility to lung cancer. *Int J Cancer* 1998; **77**: 516-521
- 24 **Lin DX**, Tang YM, Peng Q, Lu SX, Ambrosone CB, Kadlubar FF. Susceptibility to esophageal cancer and genetic polymorphisms in glutathione S-transferases T1, P1, and M1 and cytochrome P450 2E1. *Cancer Epidemiol Biomarkers Prev* 1998; **7**: 1013-1018
- 25 **Launoy G**, Milan C, Day NE, Faivre J, Pienkowski P, Gignoux M. Oesophageal cancer in France: potential importance of hot alcoholic drinks. *Int J Cancer* 1997; **71**: 917-923
- 26 **Launoy G**, Milan C, Day NE, Pienkowski MP, Gignoux M, Faivre J. Diet and squamous-cell cancer of the oesophagus: a French multicentre case-control study. *Int J Cancer* 1998; **76**: 7-12
- 27 **Launoy G**, Milan CH, Faivre J, Pienkowski P, Milan CI, Gignoux M. Alcohol, tobacco and oesophageal cancer: effects of the duration of consumption, mean intake and current and former consumption. *Br J Cancer* 1997; **75**: 1389-1396
- 28 **van Lieshout EM**, Tiemessen DM, Witteman BJ, Jansen JB, Peters WH. Low glutathione and glutathione S-transferase levels in Barrett's esophagus as compared to normal esophageal epithelium. *Jpn J Cancer Res* 1999; **90**: 81-85
- 29 **Pemble S**, Schroeder KR, Spencer SR, Meyer DJ, Hallier E, Bolt HM, Ketterer B, Taylor JB. Human glutathione S-transferase theta (GSTT1): cDNA cloning and the characterization of a genetic polymorphism. *Biochem J* 1994; **300**(Pt 1): 271-276
- 30 **Roth MJ**, Dawsey SM, Wang G, Tangrea JA, Zhou B, Ratnasingham D, Woodson KG, Olivero OA, Poirier MC, Frye BL, Taylor PR, Weston A. Association between GSTM1*0 and squamous dysplasia of the esophagus in the high risk region of Linxian, China. *Cancer Lett* 2000; **156**: 73-81
- 31 **van Lieshout EM**, Roelofs HM, Dekker S, Mulder CJ, Wobbes T, Jansen JB, Peters WH. Polymorphic expression of the glutathione S-transferase P1 gene and its susceptibility to Barrett's esophagus and esophageal carcinoma. *Cancer Res* 1999; **59**: 586-589
- 32 **Longueaux S**, Delomenie C, Gallou C, Mejean A, Vincent-Viry M, Bouvier R, Droz D, Krishnamoorthy R, Galteau MM, Junien C, Beroud C, Dupret JM. Candidate genetic modifiers of individual susceptibility to renal cell carcinoma: a study of polymorphic human xenobiotic-metabolizing enzymes. *Cancer Res* 1999; **59**: 2903-2908
- 33 **Kelada SN**, Kardia SL, Walker AH, Wein AJ, Malkowicz SB, Rebbeck TR. The glutathione S-transferase-mu and -theta genotypes in the etiology of prostate cancer: genotype-environment interactions with smoking. *Cancer Epidemiol Biomarkers Prev* 2000; **9**: 1329-1334
- 34 **Guerin MR**, Jenkins RA, Tomkins BA. The Chemistry of Environmental Tobacco Smoke: composition and Measurement. Boca Raton, FL: *Lewis Publishers* 1992: 43-62
- 35 **Kim N**, Cao W, Song IS, Kim CY, Sohn UD, Harnett KM, Biancani P. Leukotriene D4-induced contraction of cat esophageal and lower esophageal sphincter circular smooth muscle. *Gastroenterology* 1998; **115**: 919-928
- 36 **Kim N**, Sohn UD, Mangannan V, Rich H, Jain MK, Behar J, Biancani P. Leukotrienes in acetylcholine-induced contraction of esophageal circular smooth muscle in experimental esophagitis. *Gastroenterology* 1997; **112**: 1548-1558

Edited by Chen WW, Zhu LH and Wang XL Proofread by Xu FM

Expression of Dnmt1, demethylase, MeCP2 and methylation of tumor-related genes in human gastric cancer

Jing-Yuan Fang, Zhong-Hua Cheng, Ying-Xuan Chen, Rong Lu, Li Yang, Hong-Yin Zhu, Lun-Gen Lu

Jing-Yuan Fang, Zhong-Hua Cheng, Ying-Xuan Chen, Rong Lu, Li Yang, Hong-Yin Zhu, Lun-Gen Lu, Shanghai Institute of Digestive Disease, Shanghai Second Medical University Renji Hospital, Shanghai 200001, China

Supported by National Natural Science Foundation of China, No. 30170413; Foundation for the Author of National Excellent Doctoral Dissertation of China, No.199946 and the Key Project Funds of Shanghai Education Committee

Correspondence to: Dr. Jing-Yuan Fang, Shanghai Institute of Digestive Disease, 145 Shandong Zhong Road, Shanghai 200001, China. jingyuanfang@yahoo.com

Telephone: +86-21-63200874 **Fax:** +86-21-63266027

Received: 2004-03-27 **Accepted:** 2004-04-16

Abstract

AIM: To explore the effect of DNA methyltransferase, demethylase and methyl-CpG binding protein MeCP2 on the expressions and methylation of hMSH2 and proto-oncogene in human gastric cancer.

METHODS: Paired samples of primary gastric cancer and corresponding para-cancerous, non-cancerous gastric mucosae were obtained from surgically resected specimens of 28 patients. Transcription levels of Dnmt1, mbd2, MeCP2, p16^{INK4A}, hMSH2 and c-myc were detected by using real-time PCR or RT-PCR. Promoter methylation of p16^{INK4A}, c-myc and hMSH2 genes was assayed by methylation-specific PCR (MSP) and sequencing (mapping). Their relationships were analyzed by Fisher's exact test using the software SPSS.

RESULTS: The average mRNA level of Dnmt1 gene from cancerous tissue was higher and that of mbd2 gene from cancerous tissue was lower than that from non-cancerous tissue, respectively. mbd2 was lower in cancerous tissue than in non-cancerous tissue in 14 (50.0%) of patients but higher in 3 cases (10.7%) of non-cancerous gastric tissue ($P < 0.001$). c-myc expression was up-regulated in cancer tissues ($P < 0.05$). The up-regulation of mbd2 was found in all patients with hypomethylated c-myc. The transcriptional levels of p16^{INK4A} and MeCP2 genes did not display any difference between gastric cancerous and matched non-cancerous tissues. There were down-regulation and hypermethylation of hMSH2 in cancer tissues, and the hypermethylation of hMSH2 coexisted with down-regulated transcription. However, the transcription level of the above genes was not associated with biological behaviours of gastric cancers.

CONCLUSION: The up-regulation of proto-oncogene may be the consequence of epigenetic control of gene expression by demethylase, and mbd2 is involved in the regulation of hMSH2 expression in human gastric cancer.

Fang JY, Cheng ZH, Chen YX, Lu R, Yang L, Zhu HY, Lu LG. Expression of Dnmt1, demethylase, MeCP2 and methylation of tumor-related genes in human gastric cancer. *World J Gastroenterol* 2004; 10(23): 3394-3398
<http://www.wjgnet.com/1007-9327/10/3394.asp>

INTRODUCTION

Methylation of gene regulatory elements, a well-known epigenetic change, acts as an important alternative to genetic alteration for gene inactivation. DNA methyltransferase (Dnmt) and DNA demethylase are the enzymes potentially affecting promoter methylation status. Human DNA demethylase has been cloned^[1]. The inactivity of demethylase may play a role in production and maintenance of regional DNA hypermethylation, which frequently results in reduced expression of tumor suppressor genes in human cancers.

Gastric cancer is the second most common malignant tumor in Asia, with a much higher incidence than in Western countries. During gastric carcinogenesis, hypomethylation of c-myc and c-Ha-ras proto-oncogenes was frequently seen^[2,3], however the average level of mRNA for Dnmt1 was significantly higher in gastric cancers than in corresponding non-cancerous mucosa^[4]. mbd2 has been proposed to be a DNA demethylase, and the average level of mbd2 mRNA was significantly lower in gastric cancer than in non-cancerous mucosa. But there was no significant association between DNA demethylase mRNA level and malignant potential in gastric cancers^[5]. The mRNA expression levels for pro-methylation of Dnmt1, Dnmt3a and Dnmt3b and mbd2 are not the critical determinant of tumor-specific promoter hypermethylation of hMLH1, p16^{INK4A} or CDH1 in gastric cancer^[6]. However, little is known about the relationship between mbd2 or Dnmt1 and the methylation status of proto-oncogene or hMSH2, another important mismatch repair (MMR) gene. Furthermore, up-to date, there has not been any report about methyl-CpG binding protein MeCP2 associated with tumor-related genes in gastric cancer.

In the present study, we examined the methylation and transcriptional level of tumor-related genes including p16^{INK4A}, hMSH2 and c-myc, and detected the expression of Dnmt1, mbd2 and MeCP2. We therefore analyzed their relationship in normal and cancerous stomach tissues.

MATERIALS AND METHODS

Patients

Paired samples of histologically verified primary gastric cancer and corresponding para-cancerous (3-5 cm from cancer margin) and non-cancerous gastric mucosae were obtained immediately from surgically resected specimens of 28 patients (C1-C28) treated at Renji Hospital, Shanghai, China. A complete written informed consent was obtained from all patients. They were all diagnosed pathologically by HE-stained sections and classified according to WHO's histological classifications of gastric carcinoma. The histological characteristics in para-cancerous area were chronic gastritis or intestinal metaplasia, and dysplasia was present in ten cases. The clinico-pathological features of each patient were reviewed and recorded (Table 1). The mean age of patients (19 men and 9 women) at resection was 58 (range 45-79) years. A portion of the tissues (approximately 1-3 g) was snap-frozen on dry ice and kept in liquid nitrogen until used for DNA or RNA extraction. Other portions were used for histological examination.

RNA extraction and reverse-transcription polymerase chain reaction (RT-PCR)

First, mRNA expression of tumor-related genes in cancerous, para-cancerous and non-cancerous tissues from each patient was detected by using RT-PCR and real-time PCR. Total RNA was extracted using a commercial kit (Trizol) according to the manufacturer's instructions (Gibco BRL). RT reactions using 5 µg of total RNA in 20 µL of reaction buffer were performed with Superscript II reverse transcriptase (Life Technologies, Inc). mRNA transcription levels of mbd2, MeCP2, p16^{INK4A} and c-myc genes were evaluated by using RT-PCR. The sequence and PCR reaction for each primer are shown in Table 2. For control of RT-PCR, a 612 bp fragment of β-actin cDNA was also amplified. At the end of 40 cycles, reaction products were separated electrophoretically on a 3% agarose gel and stained with ethidium bromide for visual confirmation of PCR products. The density of bands in RT-PCR in each lane was normalized to the amount of total RNA as determined by the density of the band in RT-PCR for β-actin^[7]. RT-PCR analysis

was repeated at least thrice.

Real-time quantitative PCR for Dnmt1 and hMSH2

mRNA levels of Dnmt1 and hMSH2 were measured using a real-time quantitative PCR system. Relative quantitation using the comparative Ct method with the data from ABI PRISM 7700 sequence detection system (version 1.6 software) was performed according to the manufacturer's protocol.

Real-time PCR was also performed with Taqman β-actin to normalize each of the extracts for amplifiable human DNA. The results were expressed as the ratio of copies of each gene to β-actin, respectively. The Ct values were measured, and the average Ct value of triplicate samples was calculated. Alteration of mRNA expression was defined as a 3-fold difference in the expression level^[8]. The primers and the Taqman fluorogenic probes for Dnmt1, hMSH2 and β-actin were provided by Jikang Company, Shanghai, China.

The sequences of all primers and probes, as well as PCR programs are shown in Table 3.

Table 1 Relationship between Dnmt1 and pathological change in patients with gastric cancer (case number, %)

	Subtotal	Dnmt1 transcription			P
		Up-regulated	Normal	Down-regulated	
Total or subtotal	28 (100.0)	9 (32.14)	9 (32.14)	10 (35.72)	
Age (yr)					0.30
>50	18 (64.30)	7 (38.89)	4 (22.22)	7 (38.89)	
<50	10 (35.70)	2 (20.00)	5 (50.00)	3 (30.00)	
Size of tumor					0.88
>5 cm	14 (50.00)	4 (28.57)	5 (35.71)	5 (35.71)	
<5 cm	14 (50.00)	4 (28.57)	5 (35.71)	5 (35.71)	
Borrmann					0.34
II	6 (21.43)	2 (33.33)	0 (0.00)	4 (66.67)	
III	15 (53.57)	5 (33.33)	6 (40.00)	4 (26.67)	
IV	7 (25.00)	2 (28.57)	3 (42.86)	2 (28.57)	
Lymph node invasion					0.49
Positive	21 (75.00)	6 (28.57)	8 (38.10)	7 (33.33)	
Negative	7 (25.00)	3 (42.86)	1 (14.29)	3 (42.86)	

Table 2 Primer sequences and PCR conditions for RT-PCR, MSP and sequencing

Primers	Sense (5'→3')	Antisense (5'→3')	Product size (bp) PCR program	GenBank accession number
β-Actin	GGA GTC CTG TGG CAT CCA CG	CTA GAA GCA TTT GCG GTG GA	322 bp 94 °C 30 s, 60 °C 1 min, 72 °C 1 min, 27 cycles	BC023204
p16 ^{INK4A} RT-PCR	CCC GCT TTC GTA GTT TTC AT	TTA TTT GAG CTT TGG TTC TG	355 bp 94 °C 1 min, 58 °C 1 min, 72 °C, 1 min, 35 cycles	L27211
c-myc RT-PCR	CCA ACA GGA GCT ATG ACC TC	CTC GGT CAC CAT CTC CAG CT	290 bp 94 °C 1 min, 52 °C 1 min, 72 °C 1 min, 35 cycles	V00568
MeCP2 RT-PCR	ACT CCT CAG AAT ACA CCT TGC TT	TGA GGC CCT GGA GGT CCT	112 bp 95 °C 1 min, 50 °C 1 min, 72 °C 1 min, 35 cycles	MCB, 2000; 20: 3316
mbd2 RT-PCR	AAC CCT GCT GTT TGC TTA AC	CGT ACT TGC TGT ACT CGC TCT TC	101 bp 94 °C 1 min, 60 °C 1 min, 72 °C 1 min, 40 cycles	AF072242
p16 ^{INK4A} M-MSP	TTA TTA GAG GGT GGG GCG GAT CGC	GAC CCC GAA CCG CGA CCG TAA	150 bp 95 °C 30 s, 65 °C 30 s, 72 °C 1 min, 40 cycles	X94154
p16 ^{INK4A} UM-MSP	TTA TTA GAG GGT GGG GTG GAT TGT	CAA CCC CAA ACC ACA ACC ATA A	151 bp 95 °C 30 s, 60 °C 30 s, 72 °C 1 min, 40 cycles	X94154
c-myc M-MSP	TAG AAT TGG ATC GGG GTA AA	CGA CCG AAA ATC AAC GCG AAT	131 bp 95 °C 30 s, 56 °C 30 s, 72 °C 1 min, 40 cycles	AF002859
c-myc UM-MSP	TAG AAT TGG ATT GGG GTA AA	CCA ACC AAA AAT CAA CAT GAA T	132 bp 95 °C 30 s, 56 °C 30 s, 72 °C 1 min, 40 cycles	AF002859
hMSH2 sequencing	TGT TTA GAA AGA AAA AGG GA	AAA CCT CCT CAC CTC CT	94 °C 1 min, 55 °C 1 min, 72 °C 1 min, 35 cycles	AB006445
hMSH2 sequencing	AAA TAT TGG GAG GAG GAG GA	ACC CAC TAA ACT ATT TCC CA	327 bp 94 °C 1 min, 55 °C 1 min, 72 °C 1 min, 35 cycles	AB006445

Table 3 Sequence of primers and probes for real-time PCR

Gene	Sense (5'→3')	Antisense (5'→3')	Probe	GenBank No
Dnmt1	GCA CCT CAT TTG CCG AAT ACA	TCT CCT GCA TCA GCC CAA ATA	AGT CCC GAG TAT GCG C	XM_017218
hMSH2	ATC CAA GGA GAA TGA TTG GTA TTT G	CAA AGA GAA TGT CTT CAA ACT GAG AGA	CAT ATA AGG CTT CTC CTG GC	HSU04045
β-actin	CTG GCA CCC AGC ACA ATG	GGA CAG CGA GGC CAG GAT	ATC ATT GCT CCT CCT GAG	BC016045

Methyl-specific PCR (MSP) for p16^{INK4A} and c-myc genes

To amplify the promoters of p16^{INK4A} and c-myc genes, we carried out bisulfite modification^[9] and MSP.

Bisulfite could convert unmethylated cytosine residues to uracil, but methylated cytosines remained non-reactive. PCR amplified uracil as thymine while methylated cytosines were only amplified as cytosines. Two micrograms of total genomic DNA (from at least two independent treatments corresponding to RT-PCR experiments) were isolated by using QIAamp DNA blood mini kit (QIAGEN Inc.), then denatured by NaOH and modified by sodium bisulfite solution (2.35 mol/L) containing hydroquinone (40 mmol/L) freshly prepared. The bisulfite-treated DNA was desalted using Wizard DNA clean up kit (Promega) and amplified by PCR using primers specific for methylated and unmethylated p16^{INK4A} and c-myc promoters. PCR reaction buffer contained 0.1 mmol/L dNTP, 2.0 mmol/L MgCl₂, and 0.5 μmol/L primers. PCR products were directly loaded onto 3% agarose gels and electrophoresed. The gel was stained with ethidium bromide and directly visualized under UV illumination. Furthermore, the primers for wild-type p16^{INK4A} and c-myc were used to monitor complete conversion of DNA obtained in the bisulfite reaction.

Bisulfite modification and sequencing (mapping) for hMSH2

Primers were designed in the region without CpG dinucleotides to amplify both methylated and unmethylated alleles in hMSH2. The PCR products were recovered using QIA quick gel extraction kit (Gibco). Direct sequencing was performed by using ABI PRISM BigDye terminator kit (PE Biosystems, Foster City, CA). The products of sequencing PCR included 22 CpG sites in promoter of hMSH2 gene.

The sequences of all primers and PCR programs are shown in Table 2.

Statistical analysis

Results were representative of at least three independent experiments performed in triplicate and presented as mean±SD. Comparisons between groups were made using Student's paired *t* test. Their relationship was analyzed by Fisher's exact test using the software SPSS.

RESULTS

Expressions of Dnmt1, mbd2 and MeCP2 genes in cancerous and non-cancerous gastric tissues

After quantitative PCR, the specific products visually confirmed on agarose gels were about 101- and 96 bp, and no non-specific products were obtained upon amplification of Dnmt1 and β-actin, respectively. In all cancerous, para-cancerous and non-cancerous tissues, their mRNA expressions were detected, and 32.2% (9/28) of cancerous tissues over-expressed Dnmt1, and the copies of Dnmt1 were higher than in non-cancerous tissues (5.08 vs 1).

mbd2 was expressed in all samples. However, mbd2 was down-regulated in 50% (14/28) of gastric cancer tissues, up-regulated in 10.7% (3/28) cases, and no significant change in 3.39% (11/28), respectively. Average value of mbd2 mRNA expression was lower in cancerous tissues than in non-cancerous tissue (Figures 1, 2). In 11 patients, mbd2 mRNA level in gastric cancer was particularly low, being reduced by 50% or more when compared with that in the corresponding non-cancerous mucosae. However, we did not find association between expressions of MeCP2 and Dnmt1 and mbd2.

In addition, we did not find the association of overall aberrant methylation and expressions of Dnmt1, MeCP2, mbd2 with the age of patients.

Examination of mRNA expression of tumor-related genes and status of promoter methylation in primary gastric cancers

Figure 1 shows the results from RT-PCR and real-time PCR,

and Figure 2 shows the relative mRNA levels of each gene after normalization with the signal of β-actin. These data demonstrated that the expressions of p16^{INK4A} and hMSH2 (data not shown) were down-regulated in cancerous tissues from 11 cases (39.3%) and 10 cases (35.7%) respectively, but there was no significant difference between cancerous and non-cancerous tissues. As shown in Figure 2, c-myc transcription level was up-regulated in 14 patients with gastric cancer, and the mean value of expression in cancerous tissues was greater than that in non-cancerous tissues (*P*<0.05).

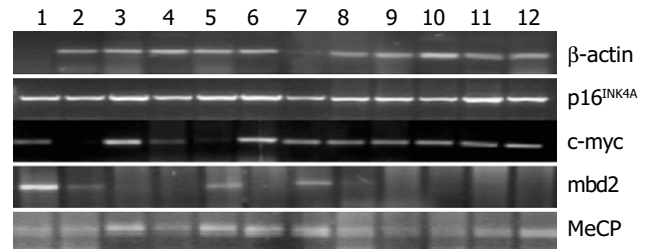


Figure 1 mRNA expression of p16^{INK4A}, c-myc, mbd2 and MeCP2 in cancerous (lanes 1, 4, 7 and 10), para-cancerous (lanes 2, 5, 8 and 11) and non-cancerous (lanes 3, 6, 9 and 12) tissues from patients with gastric cancer by using RT-PCR.

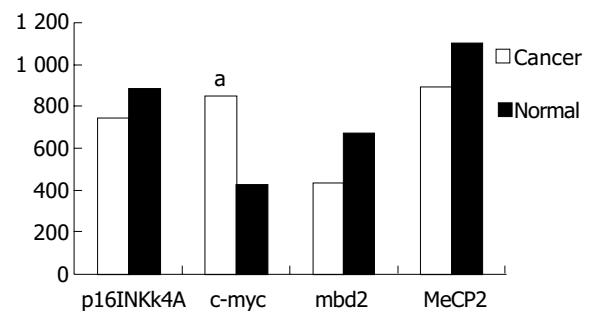


Figure 2 Density of bands from RT-PCR in each lane normalized to the total RNA as determined by the density of bands in RT-PCR for β-actin. Assuming β-actin was 4 562.39 units (pixels of brightness), the calculation [4 562.39/(density of actin)]×(density of each gene) equals each gene normalized to β-actin. Data shown are representative of three separate experiments. **P*<0.05.

To determine whether the expression of p16^{INK4A}, hMSH2 and c-myc genes in gastric cancer was associated with methylation, we selected the samples from cancerous, para-cancerous and non-cancerous tissues in ten patients for MSP or genomic bisulfite sequencing. Each tissue showed a positive 150 bp and a 151 bp band for methylated and unmethylated specific primer sets for p16^{INK4A}, indicating that the p16^{INK4A} gene was partially methylated in human gastric cancer. The methylated bands for the p16^{INK4A} gene in the cancerous and para-cancerous tissues were consistently stronger than the products of non-cancerous tissues (Figure 3A). Regarding c-myc gene, the methylated product (131 bp) was significantly lower and the unmethylated product (132 bp) was higher in cancerous and para-cancerous tissues than in non-cancerous tissues. Figure 3B displays representative examples of MSP products analyzed by electrophoresis on an agarose gel.

Bisulfite genomic sequencing of the representative PCR products of hMSH2 showed that all cytosines at non-CpG sites were converted to thymine. This excluded the possibility that successful amplification could be attributable to incomplete bisulfite conversion. Interestingly, methylation occurred at the -166 CpG site only (Figure 4).

Taken together, the results from MSP, sequencing, RT-PCR and real-time PCR indicated that hypermethylation of hMSH2

might be induced, inactivation and activation of c-myc were associated with its hypomethylation in human gastric cancer.

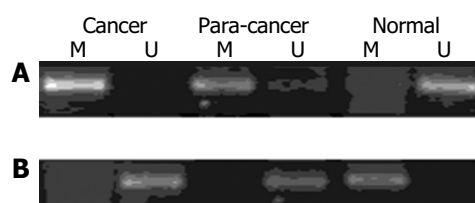


Figure 3 Hypermethylation of p16^{INK4A} promoter (A) and hypomethylation of proto-oncogene c-myc promoter (B) in gastric cancer tissue indicated by MSP. U: unmethylation-specific PCR; M: methylation-specific PCR.

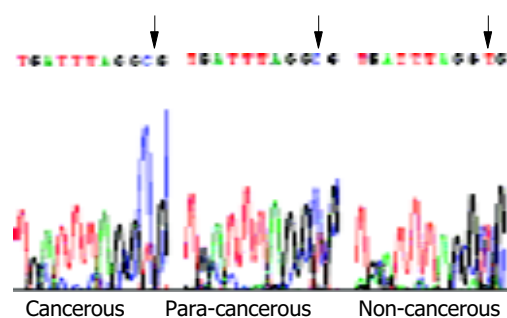


Figure 4 Methylation analysis of hMSH2 gene promoter by bisulfite sequencing. The arrows indicate the changes of CG to TG in promoters of non-cancerous and para-cancerous tissue, but CG remained in cancerous tissues.

Correlation between mRNA expression of Dnmt1, mbd2 and DNA methylation

Dnmt1 was not associated with the methylation status of p16^{INK4A} or c-myc gene.

Among Dnmt1 down-regulated cases, 6 (60%) had over-expression of c-myc in cancerous tissues. In the cancer cases with up-regulated mbd2, all 3 had an expression of c-myc. We also found that there was a positive correlation in the expression of c-myc and mbd2 ($r=0.59$, $P=0.026$), MeCP2 ($r=0.64$, $P=0.02$), but c-myc had no positive correlation with Dnmt1.

In contrast to cancer tissues, all normal tissues had a positive association of p16^{INK4A} with MeCP2 ($r=0.483$, $P=0.02$) or mbd2 ($r=0.483$, $P=0.027$).

Among the 10 cases with down-regulated hMSH2, 6 cases had a decreased mbd2 mRNA, but there was no significant association between expressions of Dnmt1 and hMSH2.

Association of Dnmt1, mbd2 and histological change

There was no significant association between Dnmt1, mbd2 mRNA level and clinico-pathological parameters of the tumors, such as histological differentiation, size of tumor and lymph node metastasis. These data failed to indicate their aberrant expression as an early event in gastric cancer.

DISCUSSION

Generally, the global DNA methylation level is lower in cancer cells than in normal cells, and some loci tend to show hypomethylation of proto-oncogene in human gastrointestinal cancers^[10]. Recent studies demonstrated that DNA methylation could contribute to inactivation of tumor suppressor genes, a key event in tumorigenesis of a wide spectrum of human tumors^[11,12].

Three enzymes are responsible for DNA methylation. The carboxy-terminal domain of Dnmt1 could catalyse the methylation of DNA containing hemi-methylated CpG dinucleotides more

efficiently than unmethylated DNA *in vitro*^[13]. DNA demethylase was first identified by Szyf's group, and they demethylated both fully methylated and hemimethylated DNA, showing dinucleotide specificity, and could demethylate mCpG in different sequence contexts^[5]. The shortest form of methyl-CpG binding domain (MBD)2, mbd2b, has been proposed to be a DNA demethylase which has been cloned and characterized^[14]. MeCP2 is the first true member of the family of proteins that could selectively recognize methylated CpG^[15]. It is a single polypeptide characterized by an MBD and a transcriptional repression domain^[16,17]. Aberrant methylation in tumor-related genes was frequently detected in gastric intestinal metaplasia of both cancer and non-cancer patients, suggesting their early involvement in the multi-step progression of gastric carcinogenesis^[18]. However, little is known about the relationship of Dnmt1, demethylase, MeCP2 with tumor-related genes.

We found that the average mRNA level of Dnmt1 gene in cancerous tissue was higher and that of mbd2 gene was lower than that in non-cancerous tissue. Regarding Dnmt1 expression, these results are consistent with a study by Kanai^[4]. On the other hand, Patra found that MBD2 protein expression was significantly higher in benign prostatic hyperplasia BPH-1 cells and deficient in prostate cancer cell lines and in BPH tissues^[19]. For mbd2, our result is consistent with another experiment of gastrointestinal cancer^[3]. They suggested that the average levels of demethylase mRNA expression normalized to GAPDH mRNA were significantly lower in colorectal (0.81 ± 0.55) and gastric (2.88 ± 0.23) cancers than in the non-cancerous mucosae (1.90 ± 0.16 and 5.11 ± 0.34 , respectively, $P<0.0001$). However, up to date, we have not found any report about the expression of MeCP2 in gastric cancer. Darwanto found that colonic mucinous adenocarcinomas showed a strong MeCP2 expression^[20], and Muller observed a higher expression level of MeCP2 mRNA in breast cancer tissues than in non-cancerous tissues^[21].

Previous studies indicated that the mRNA expression level for Dnmt1 and mbd2 was not a critical determinant of promoter hypermethylation of tumor-suppressor gene p16^{INK4A} in gastric cancer^[6,22]. Regarding the hMLH1, the result was different in different studies^[6,23]. During gastric carcinogenesis, hypomethylation of c-myc proto-oncogene is common, and it has not been linked to Dnmt1, mbd2 or MeCP2, or hMSH2. In the present study, we demonstrated that there was a positive association of mbd2 and c-myc proto-oncogene in gastric cancerous tissues. The up-regulation of mbd2 was found in all patients with hypomethylated c-myc. The correlation of mbd2 expression with unmethylation of c-myc promoter suggests that c-myc may be a target for demethylation by the enzymes.

Another interesting gene we tested was hMSH2. The second important finding in this study was the decrease of mbd2 mRNA in most patients with down-regulated hMSH2, but we did not find any correlation between hMSH2 and Dnmt1 or MeCP2. It suggests that mbd2 is also involved in the regulation of hMSH2 expression in human gastric cancer. We did not test the promoter region of hMLH1 gene, because the promoter was not associated with Dnmt1^[6,23] and mbd2^[6] in human gastric cancer.

In addition, the data from our study demonstrated that the transcription level of Dnmt1, mbd2 and MeCP2 might not be associated with biological behaviours in human gastric cancer. Kanai also suggested there was no significant association between DNA demethylase mRNA level and malignant potential in gastric cancers^[5]. Although the mbd2 expression was lower both in early and in advanced cancers, we could not demonstrate a definitive relationship between the histology and mbd2 expression due to the small number of patients studied.

In conclusion, the up-regulation of proto-oncogene may be the consequence of epigenetic control of gene expression by demethylase, and mbd2 is also involved in the regulation of hMSH2 expression in human gastric cancer.

ACKNOWLEDGEMENTS

Thanks are given to Dr. Yao Shi and Xiao-Yu Chen, Ms. Hong-Yin Zhu and Ms. Wei-Qi Gu for performing the diagnosis of pathology, MSP and real-time PCR.

REFERENCES

- 1 **Bhattacharya SK**, Ramchandani S, Cervoni N, Szyf M. A mammalian protein with specific demethylase activity for mCpG DNA. *Nature* 1999; **397**: 579-583
- 2 **Fang JY**, Zhu SS, Xiao SD, Jiang SJ, Shi Y, Chen XY, Zhou XM, Qian LF. Studies on the hypomethylation of c-myc, c-Ha-ras oncogenes and histopathological changes in human gastric carcinoma. *J Gastroenterol Hepatol* 1996; **11**: 1079-1082
- 3 **Fang J**, Zhu S, Xiao S, Shi Y, Jiang S, Zhou X, Qian L. Alterations of level of total genomic DNA methylation and pattern of c-Myc, c-Ha-ras oncogene methylation in human gastric carcinogenesis. *Chin Med J* 1996; **109**: 787-791
- 4 **Kanai Y**, Ushijima S, Kondo Y, Nakanishi Y, Hirohashi S. DNA methyltransferase expression and DNA methylation of CpG islands and peri-centromeric satellite regions in human colorectal and stomach cancers. *Int J Cancer* 2001; **91**: 205-212
- 5 **Kanai Y**, Ushijima S, Saito Y, Nakanishi Y, Sakamoto M, Hirohashi S. MRNA expression of genes altered by 5-azacytidine treatment in cancer cell lines is associated with clinicopathological parameters of human cancers. *J Cancer Res Clin Oncol* 2001; **127**: 697-706
- 6 **Oue N**, Shigeishi H, Kuniyasu H, Yokozaki H, Kuraoka K, Ito R, Yasui W. Promoter hypermethylation of MGMT is associated with protein loss in gastric carcinoma. *Int J Cancer* 2001; **93**: 805-809
- 7 **Fang JY**, Mikovits JA, Bagni R, Petrow-Sadowski CL, Ruscetti FW. Infection of lymphoid cells by integration-defective human immunodeficiency virus type 1 increases de novo methylation. *J Virol* 2001; **75**: 9753-9761
- 8 **Scanlan MJ**, Welt S, Gordon CM, Chen YT, Gure AO, Stockert E, Jungbluth AA, Ritter G, Jager D, Jager E, Knuth A, Old LJ. Cancer-related serological recognition of human colon cancer: identification of potential diagnostic and immunotherapeutic targets. *Cancer Res* 2002; **62**: 4041-4047
- 9 **Xiong Z**, Laird PW. COBRA: a sensitive and quantitative DNA methylation assay. *Nucleic Acids Res* 1997; **25**: 2532-2534
- 10 **Fang JY**, Xiao SD. Alteration of DNA methylation in gastrointestinal carcinogenesis. *J Gastroenterol Hepatol* 2001; **16**: 960-968
- 11 **Jones PA**, Takai D. The role of DNA methylation in mammalian epigenetics. *Science* 2001; **293**: 1068-1070
- 12 **Baylin SB**, Herman JG. DNA hypermethylation in tumorigenesis: epigenetics joins genetics. *Trends Genet* 2000; **16**: 168-174
- 13 **Bestor TH**. Activation of mammalian DNA methyltransferase by cleavage of a Zn binding regulatory domain. *EMBO J* 1992; **11**: 2611-2617
- 14 **Ramchandani S**, Bhattacharya SK, Cervoni N, Szyf M. DNA methylation is a reversible biological signal. *Proc Natl Acad Sci U S A* 1999; **96**: 6107-6112
- 15 **Nan X**, Meehan RR, Bird A. Dissection of the methyl-CpG binding domain from the chromosomal protein MeCP2. *Nucleic Acids Res* 1993; **21**: 4886-4892
- 16 **Ng HH**, Zhang Y, Hendrich B, Johnson CA, Turner BM, Erdjument-Bromage H, Tempst P, Reinberg D, Bird A. MBD2 is a transcriptional repressor belonging to the MeCP1 histone deacetylase complex. *Nat Genet* 1999; **23**: 58-61
- 17 **Nan X**, Campoy FJ, Bird A. MeCP2 is a transcriptional repressor with abundant binding sites in genomic chromatin. *Cell* 1997; **88**: 471-481
- 18 **To KF**, Leung WK, Lee TL, Yu J, Tong JH, Chan MW, Ng EK, Chung SC, Sung JJ. Promoter hypermethylation of tumor-related genes in gastric intestinal metaplasia of patients with and without gastric cancer. *Int J Cancer* 2002; **102**: 623-628
- 19 **Patra SK**, Patra A, Zhao H, Dahiya R. DNA methyltransferase and demethylase in human prostate cancer. *Mol Carcinog* 2002; **33**: 163-171
- 20 **Darwanto A**, Kitazawa R, Maeda S, Kitazawa S. MeCP2 and promoter methylation cooperatively regulate E-cadherin gene expression in colorectal carcinoma. *Cancer Sci* 2003; **94**: 442-447
- 21 **Muller HM**, Fiegl H, Goebel G, Hubalek MM, Widschwendter A, Muller-Holzner E, Marth C, Widschwendter M. MeCP2 and MBD2 expression in human neoplastic and non-neoplastic breast tissue and its association with oestrogen receptor status. *Br J Cancer* 2003; **89**: 1934-1939
- 22 **Sato M**, Horio Y, Sekido Y, Minna JD, Shimokata K, Hasegawa Y. The expression of DNA methyltransferases and methyl-CpG-binding proteins is not associated with the methylation status of p14(ARF), p16(INK4a) and RASSF1A in human lung cancer cell lines. *Oncogene* 2002; **21**: 4822-4829
- 23 **Etoh T**, Kanai Y, Ushijima S, Nakagawa T, Nakanishi Y, Sasako M, Kitano S, Hirohashi S. Increased DNA methyltransferase 1 (DNMT1) protein expression correlates significantly with poorer tumor differentiation and frequent DNA hypermethylation of multiple CpG islands in gastric cancers. *Am J Pathol* 2004; **164**: 689-699

Edited by Wang XL Proofread by Zhu LH and Xu FM

Transabdominal ultrasonography in preoperative staging of gastric cancer

Sheng-Ri Liao, Ying Dai, Ling Huo, Kun Yan, Lin Zhang, Hui Zhang, Wen Gao, Min-Hua Chen

Sheng-Ri Liao, Ying Dai, Ling Huo, Kun Yan, Lin Zhang, Hui Zhang, Wen Gao, Min-Hua Chen, Department of Ultrasonography, School of Oncology, Peking University, Beijing 10036, China
Supported by the Hospital Medicine Development Foundation, No. ZD 199909

Correspondence to: Min-Hua Chen, Department of Ultrasonography, School of Oncology, Peking University, Beijing 10036, China. shengri@sina.com

Telephone: +86-10-88121122 Ext. 2139

Received: 2004-02-28 **Accepted:** 2004-04-05

Abstract

AIM: To investigate the value of transabdominal ultrasonography (US) in the preoperative staging of gastric cancer.

METHODS: A total of 198 patients with gastric cancer underwent preoperatively transabdominal US, depth of tumor infiltration was assessed in 125 patients, and lymph node metastasis was assessed in 106 patients.

RESULTS: The staging accuracy of transabdominal US was 55.6%, 75.0%, 87.3% and 71.1% in T1, T2, T3 and T4 carcinomas, respectively. The overall accuracy was 77.6%. The detection rate for pancreatic invasion and liver invasion was 77.4%, 71.4%, respectively. The sensitivity, specificity, accuracy of transabdominal US in assessment of lymph node metastasis were 77.6%, 64.1%, 72.6%, respectively. Various shapes such as round, ovoid, spindle were encountered in benign and malignant lymph nodes. Majority of both benign and malignant lymph nodes were hyperechoic and had a distinct border. Benign lymph nodes were smaller than malignant lymph nodes in length and width ($P = 0.000, 0.005$). Irregular shape, fusional shape, infiltrative signs, inhomogenous echo were seen mainly in malignant lymph nodes ($P = 0.045, 0.006, 0.027, 0.006$).

CONCLUSION: Transabdominal US is useful for preoperative staging in gastric cancer, although it is difficult to differentiate benign from malignant lymph nodes.

Liao SR, Dai Y, Huo L, Yan K, Zhang L, Zhang H, Gao W, Chen MH. Transabdominal ultrasonography in preoperative staging of gastric cancer. *World J Gastroenterol* 2004; 10 (23): 3399-3404

<http://www.wjgnet.com/1007-9327/10/3399.asp>

INTRODUCTION

Gastric cancer is one of the most prevalent malignant tumors^[1,2]. An accurate preoperative staging is helpful for the prediction of prognosis and establishment of the individualized therapy. Although endoscopy and upper gastrointestinal series with double-contrast study have significantly improved the diagnostic accuracy in gastric cancer, they neither allow the assessment of the depth of tumor infiltration nor visualize perigastric lymph nodes^[3,4]. Currently, endoscopic ultrasonography (EUS) has

been considered as a useful modality for the preoperative staging of gastric cancer, and the accuracy of EUS in the assessment of the depth of tumor infiltration and lymph node metastasis is 67-92% and 63-78%^[5-11], respectively. However, EUS procedure is relatively complex, and can not be performed successfully in some patients, due to marked obstruction of gastric lumen caused by tumor or noticeable discomfort during examination.

Transabdominal ultrasonography (US) is applied widely in clinical practice. When condition of patients is suitable, transabdominal US can detect lymph nodes with a diameter of 5 mm, and the normal wall of fluid-filled stomach after the patients drank water can be described as a 5-layer structure^[12-14], which contributes to the assessment of the depth of tumor infiltration. Literature on the preoperative staging with transabdominal US is sparse^[15,16]. The aim of our study was to further assess the accuracy and limitations of transabdominal US in preoperative staging of the depth of tumor infiltration and lymph node metastasis.

MATERIALS AND METHODS

Between January 2000 to July 2003, 198 patients with gastric cancer confirmed by endoscopic biopsy underwent transabdominal US preoperatively. Patients with preoperative transabdominal US findings and detailed operative and pathological findings were included in this study. The depth of tumor infiltration was assessed in 125 patients (78 males, 47 females, ranged 27-78 years). Lymph node metastasis was assessed in 106 patients (66 males, 40 females, ranged 31-78 years).

All patients were required to drink water to fill stomach for the assessment of the depth of tumor infiltration. Transabdominal US was performed 3-5 min after 500-700 mL boiled water was drunk. Patients were examined usually in the supine position. Sitting position, left or right lateral decubitus position might be taken for visualization of lesions according to different locations of tumors.

The wall of fluid-filled stomach is described as a 5-layer structure^[12-14]. The innermost hyperechoic layer (the first layer) corresponds to the superficial mucosa, the second hypoechoic layer corresponds to the deep mucosa, the third hyperechoic layer corresponds to the submucosa plus the acoustic interface between the submucosa and muscularis propria, the fourth hypoechoic layer corresponds to the muscularis propria minus the acoustic interface between the submucosa and muscularis propria, the fifth hyperechoic layer corresponds to the subserosal fat and serosa.

According to the TNM (UICC) classification^[17], the depth of tumor infiltration was divided into 4 categories. T1 = tumor confined to mucosa or submucosa. For mucosal carcinoma, tumor located in the first and second layers, the third layers (submucosa) was intact; for submucosal carcinoma, layers 1 to 3 were interrupted or thickened and the fourth and fifth layers were normal sonographically (Figure 1A). T2 = tumor invading muscularis propria (the fourth layer) which became thickened, and the fifth layer was intact sonographically (Figure 1B). T3 = tumor invading serosa (the fifth layer), with interruption

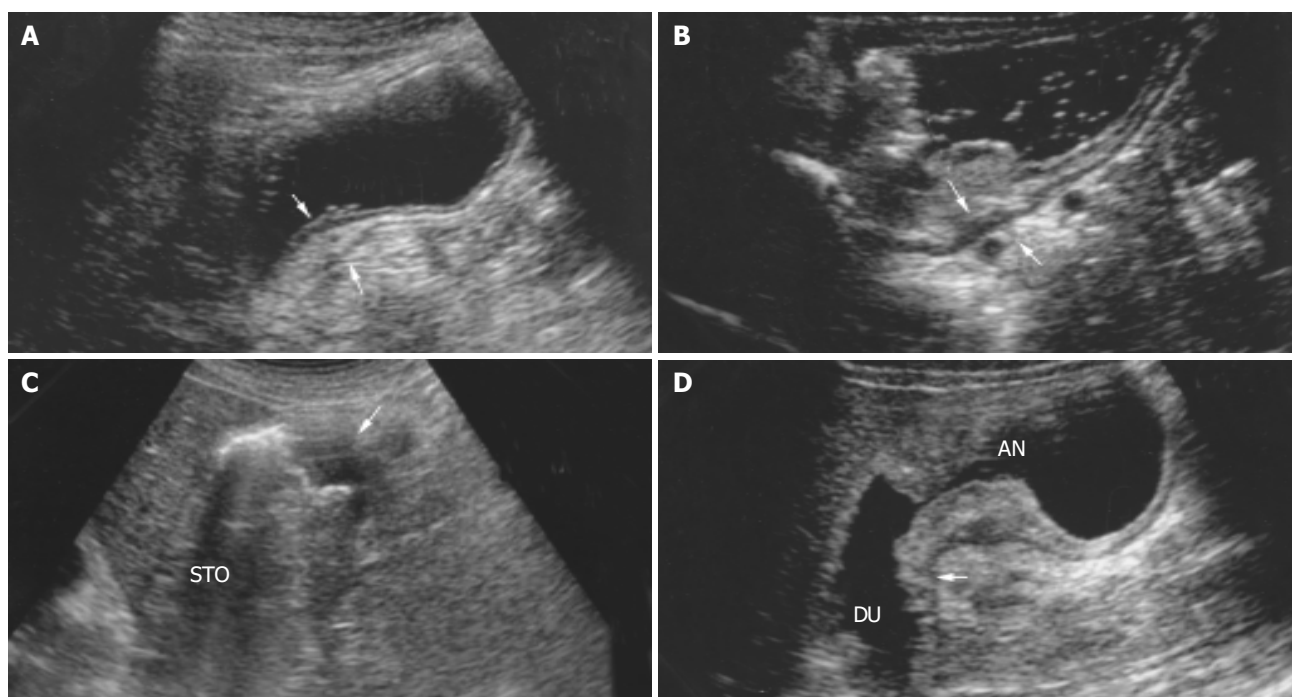


Figure 1 Sonograms of T1-T4 carcinoma. A: Submucosal carcinoma (T1) in gastric antrum. Arrow indicates segmental thickening of layers 1-3 of the posterior wall, triangle indicates normal layers 4-5. B: T2 carcinoma. The posterior wall of Gastric body is thickening. Arrow indicates the third hyperechoic layer is obliterated and the fourth hypoechoic layer is thickening, triangle indicates normal layer 5. C: T3 carcinoma. Tumor located in the greater curvature of stomach (STO) is hypoechoic with disappearance of wall all layer (arrow). D: T4 carcinoma. Sonogram shows tumor located in antrum (AN) infiltrating duodenum. Arrow indicates the segmental wall thickening of duodenal bulb.

or disappearance of all layers of wall sonographically (Figure 1C). T4 = tumor invading adjacent organs which had an indistinct border and was indistinguishable from involved organs sonographically (Figure 1D).

Assessment of regional lymph node metastasis was performed in a fasting state before water was drunk for evaluation of tumor infiltration. Regional lymph nodes around the following organs or structures were examined: stomach, liver, pancreas, gallbladder, aorta, hilum of spleen, comma hepatic aorta, superior mesenteric artery, celiac artery, and recorded number, size, shape, border, and echogenicity of lymph nodes.

Lymph nodes with a length of 5 mm or greater were considered metastatic. Regional lymph node staging was classified as N0 (no lymph node metastasis) and N+ (lymph node metastasis).

Lymph nodes detected with transabdominal US were divided into 3 groups according to their shapes: regular, irregular, fusional. Regular lymph nodes were classified into 3 categories of shape: spindle: width \leq half the length of the lymph node; ovoid: width \leq three quarters of the length of the lymph node; round: width $>$ three quarters of the length of the lymph node^[18].

The followings were considered as "infiltrative signs" of lymph nodes: ill-defined border, indistinguishable from the adjacent structures or loss of movement.

Sonographic examinations were performed with commercially available real time image units (Toshiba 6000, Aloka 2000, DU-6), and transducer frequency varied between 3.5-6.0 MHz.

Data were analyzed with SPSS10.0 software. $P < 0.05$ was considered statistically significant.

RESULTS

Assessment of depth of tumor infiltration

Table 1 summarizes the findings of transabdominal US and operative or pathological findings in 125 patients with gastric cancer. The accuracy of transabdominal US in staging of T1 carcinomas was 55.6%, 75.0% in T2 carcinomas, 87.3% in T3

carcinomas, and 71.1% in T4 carcinomas. The overall accuracy was 77.6%.

Tumors were overstaged in 8 patients. T1 carcinoma was overstaged as a T2 carcinoma in 3 patients and as a T3 carcinoma in 1 patient (Figure 2), and T2 carcinoma was overstaged as a T3 carcinoma in 4 patients. Tumors were understaged in 20 patients. T3 carcinoma was understaged as a T2 carcinoma in 7 patients. T4 carcinoma was understaged as a T2 carcinoma in 2 patients and as a T3 carcinoma in 11 patients.

Invasion of adjacent organs confirmed by operative or pathologic findings was as follows (Table 2): pancreas (31 patients), liver (7 patients), spleen and hilum of spleen (3 patients), transverse colon (3 patients), diaphragm (2 patients), and duodenum (9 patients). The detection rate for pancreas and liver invasion with transabdominal US was 77.4% and 71.4%, respectively, whereas the detection rate for the invasion of other organs was low.



Figure 2 Mucosal carcinoma (T1) was overstaged as a T3 carcinoma with transabdominal US. Sonogram of gastric body shows hypoechoic wall thickening with ulcer (arrow), loss of wall five-layer structure (triangle).

Table 1 Accuracy of transabdominal US in assessing the depth of tumor invasion in 125 patients

Stage	n	Staged by operative and pathological findings			
		T1	T2	T3	T4
T1	7	5	0	0	0
T2	34	3	12	7	2
T3	80	1	4	48	11
T4	38	0	0	0	32
Accuracy (%)		55.6 (5/9)	75.0 (12/16)	87.3 (48/55)	71.1 (32/45)

Table 2 Detection rate of tumor invasion with transabdominal US

Involved organs	n	Cases detected with transabdominal US	Detection rate (%)
Pancreas	31	24	77.4
Liver	7	5	71.4
Spleen and hilum of spleen	3	1	33.3
Transverse colon	3	1	33.3
Diaphragm	2	0	0
Duodenum	9	4	44.4

Assessment of regional lymph node metastasis

Accuracy of assessment of regional lymph metastasis Swollen lymph nodes were found pathologically in 106 patients. Lymph node metastasis was confirmed in 67 of 106 patients. Swollen lymph nodes were detected in 66 of 106 patients with transabdominal US. All lymph nodes detected sonographically had a length of 5 mm or greater, and were considered as metastatic. Of the 66 patients, lymph node metastasis was confirmed by pathological examination in 52 patients, and swollen lymph nodes were benign in the remaining 14 patients. No swollen lymph nodes were detected sonographically in 40 of 106 patients, and lymph node metastasis was confirmed in 15 of these 40 patients. The sensitivity of transabdominal US in the assessment of lymph node metastasis was 77.6% (52 of 67 patients). The specificity was 64.1% (25 of 39 patients). The accuracy was 72.6% (77 of 106 patients) (Table 3).

Table 3 Accuracy of transabdominal US in assessing lymph node metastasis in 106 patients

Diagnosis with transabdominal US	Pathological findings (n)	
	N+	N0
N+	52	14
N0	15	25

Sensitivity: 77.6% (52/67); Specificity: 64.1% (25/39); Accuracy: 72.6% (77/106).

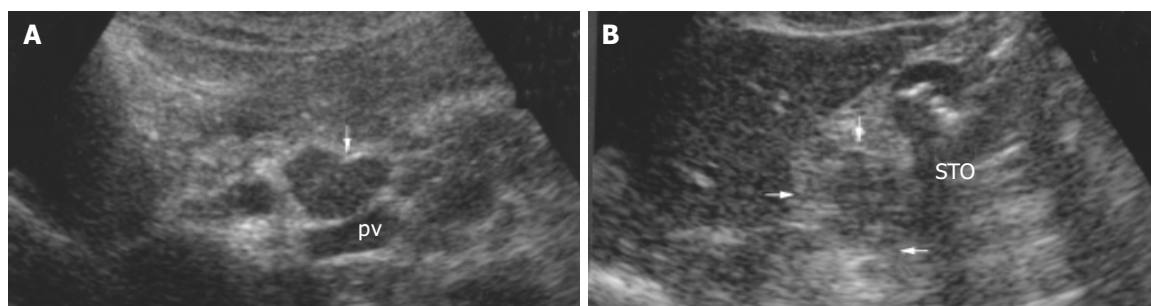
Sonographic features of benign and malignant lymph nodes

All lymph nodes in 14 of 66 patients with swollen lymph nodes detected with transabdominal US were confirmed benign (lymph

node without metastasis), and transabdominal US detected 46 lymph nodes in these patients. All lymph nodes in 11 of 52 patients with lymph node metastasis were confirmed malignant (metastatic), and transabdominal US detected 48 lymph nodes in these patients. Forty-six benign lymph nodes had a mean length of 1.26 cm and a mean width of 0.84 cm, 48 malignant lymph nodes had a mean length of 1.79 cm and a mean width of 1.25 cm. According to size, shape, echogenicity, and border, sonographic features of these benign and malignant lymph nodes were further analyzed (Table 4). The length and width of benign lymph nodes were significantly smaller than those of malignant lymph nodes ($P = 0.000, 0.005$). Sonographic features such as irregular or fusional shape, infiltrative signs, and inhomogenous echoes were found mainly in malignant lymph nodes (Figure 3). There was a significant difference between benign and malignant lymph nodes ($P = 0.045, 0.006, 0.027, 0.006$).

Table 4 Sonographic features of 46 benign and 48 malignant lymph nodes

Sonographic feature	Pathologic findings		P
	Benign lymph nodes (%)	Malignant lymph nodes (%)	
Length (cm)			0.000
<0.5	0	0	
0.5-1.0	26 (56.5)	9 (18.8)	
1.1-1.5	9 (19.6)	16 (33.3)	
1.6-2.0	9 (19.6)	8 (16.7)	
≥2.1	2 (4.3)	15 (31.2)	
Length (cm)			0.000
<0.5	0	0	
0.5-1.0	26 (56.5)	9 (18.8)	
1.1-1.5	9 (19.6)	16 (33.3)	
1.6-2.0	9 (19.6)	8 (16.7)	
≥2.1	2 (4.3)	15 (31.2)	
Width (cm)			0.005
<0.5	5 (10.9)	2 (4.2)	
0.5-1.0	34 (73.9)	22 (45.8)	
1.1-1.5	4 (8.7)	10 (20.8)	
1.6-2.0	3 (6.5)	11 (22.9)	
≥2.1	0 (0)	3 (6.3)	
Shape			
Spindle	9 (19.6)	5 (10.4)	
Ovoid	15 (32.6)	10 (20.8)	
Round	20 (43.5)	17 (35.4)	
Irregular	2 (4.3)	8 (16.7)	0.045
Fusional	0 (0)	8 (16.7)	0.006
Border			
Distinct	34 (73.9)	29 (60.4)	
Indistinct	12 (26.1)	13 (27.1)	
Infiltrative signs	0 (0)	6 (12.5)	0.027
Echogenicity			
Hypoechoic	40 (87.0)	38 (79.1)	
Slightly hyperechoic	6 (13.0)	2 (4.2)	
Inhomogenous	0	8 (16.6)	0.006

**Figure 3** Metastatic lymph node. A: Sonogram shows a irregular lymph node (arrow) adjacent to the portal vein (PV) with a distinct border and 2.1×1.7 cm in size. B: Sonogram shows fusional-shaped lymph node (arrow) (4×3 cm) adjacent to the stomach (STO), invading adjacent tissues and having an indistinct border.

DISCUSSION

Assessment of the depth of tumor invasion in gastric cancer

Compared with the operative and pathological findings, the accuracy of transabdominal US for T1, T2, T3, T4 was 55.6%, 75.0%, 87.3%, 71.1%, respectively, and the overall accuracy was 77.6% (Table 1).

Although the accuracy of transabdominal US in staging of T1 carcinoma was low (55.6%), T2, T3, and T4 staging results were compared favorably with those of EUS T staging. Lim *et al.*^[15] reported the accuracy of staging in early-stage carcinoma was 66.7% (10 of 15 patients) with transabdominal US. In the study of Segura *et al.*^[16], the accuracy of transabdominal US for T1, T2, T3, T4 was 100%, 50%, 87%, 81%, respectively. Due to the small number of patients with early stage carcinoma (2 patients), the results of T1 staging required further investigation.

In our study, the accuracy for T3 carcinomas was the highest (87.3%) among the four groups with different depths of infiltration. The normal serosal layer was a thin and smooth hyperechoic band sonographically. When tumor invaded into the serosal layer, this band was interrupted or disappeared, which could be assessed easily with transabdominal US.

In our study, the accuracy for T1 carcinomas was most unfavorable (55.6%) because of overstaging in 4 patients, of which 3 had ulcerative carcinoma. Similarly, misdiagnosis was made in 4 patients with T2 carcinoma due to overstaging as a T3 carcinoma, and these 4 patients also had ulcerative carcinoma. Previous studies showed that the hyperechoic submucosal layer became hypoechoic because of inflammation or edema around the tumor, which was similar to echogenicity of muscularis propria and tumor. It was difficult to differentiate 3 layers with transabdominal US^[19], so T1 carcinoma might be overstaged as T2 carcinoma (tumor invading muscularis propria). On the other hand, the ulcer in gastric cancer may cause gastric wall fibrosis and scar, which lead to wall thickening, loss of wall layers, and even interruption or disappearance of serosal layer, therefore, overstaging as T3 carcinoma may occur in T1 or T2 carcinoma (Figure 2). Difficulties in differentiation between tumors and peritumor inflammation or scar may be an important source of overstaging^[5,6,15,20-23].

As shown in Table 1, misdiagnosis was made in T1 and T2 carcinomas because of overstaging. On the contrary, misdiagnosis was made in T3 and T4 carcinomas because of understaging. The possible reasons for understaging were as follows: (1) The procedure did not practise adequately, because transabdominal US was technically difficult to perform and may fail to guarantee a correct diagnosis for tumors locating in gastric fundus, greater curvature or cardia^[15]. Tumors in 8 of 20 understaged patients located in the above locations, respectively. (2) Location of involved organs also affected the diagnosis, because it was difficult to clearly visualize hilum of spleen, diaphragm, and the tail of pancreas. Invasions of the tail of pancreas (4 patients), diaphragm (2 patients), spleen and hilum of spleen (2 patients) were not detected with transabdominal US. (3) Microscopic tumor invasion undetected with transabdominal US was another cause of understaging^[6], which occurred in 2 patients with T3 carcinoma.

Assessment of adjacent organ invasion with transabdominal US

The fact that gastric cancer invaded into adjacent organs would decrease surgical resectability, so it is important to assess preoperatively if organs are invaded by gastric cancer.

In our study, the followings were taken as the diagnostic criteria for gastric cancer invading into organs: interruption of the serosal layer of gastric wall, indistinguishable from adjacent organs, tumor and organs moving synchronously slow or no moving as breath changed.

Pancreas was the most common organ invaded by tumor, the detection rate in this study was 77.4%. In 3 of 7 patients undetected by transabdominal US, pancreas was invaded slightly, and the boundary between pancreas and tumor seemed to exist on sonogram, thus leading to understaging. In the remaining 4 patients, the tail of pancreas was invaded, which was not detected by transabdominal US due to interference of bowel gas and ribs.

The detection rate for liver invasion was higher (71.4%). Tumors invading liver located in anterior wall of stomach or lesser curvature and were close to the liver. The relationship between tumor and liver could be visualized clearly by using ultrasonographic beam through liver without interference of bowel gases.

Transverse colon was invaded in three patients, of them, correct diagnosis was made in 1 patient because complete circumference of transverse colon was invaded and marked tumor was detected. In two others undetected by transabdominal US, transverse colon was slightly invaded and bowel gases interfered severely. Correct diagnosis was made preoperatively in 1 of 3 patients with spleen and its hilum invasion. None was diagnosed preoperatively for diaphragm invasion. Spleen and its hilum, and diaphragm could not be observed completely with transabdominal US, leading to the low detection rate.

Correct diagnosis was made preoperatively in 4 of 9 patients with duodenum invasion. It was necessary to fill duodenum by drinking water for the assessment of duodenum. Because tumor caused gastric lumen obstruction, duodenum was not filled adequately and visualized clearly, leading to misdiagnosis of duodenum invasion.

Assessment of lymph node metastasis and differentiation between benign and malignant lymph nodes

The sensitivity of transabdominal US for lymph node metastasis was 77.6%, and the false positive rate was 13.2% (14 of 106 patients). The results showed transabdominal US did not permit the differentiation between benign and (metastatic) malignant lymph nodes in gastric cancer (Figures 4, 5).

Benign swollen lymph nodes due to immune reaction in patients with tumor are misdiagnosed easily as malignant lymph nodes. According to the analysis of sonographic features of lymph nodes (Table 4), benign lymph nodes were smaller than malignant lymph nodes in length and width ($P = 0.000, 0.005$). From Table 5, if the length ≥ 1.1 cm or 1.6 cm was defined as diagnostic criteria of malignant lymph nodes, the sensitivity was 81.3% and 47.9%, respectively, and the specificity was 56.5% and 76.1%, respectively. Hence the criteria could not differentiate benign from malignant lymph nodes. If the length ≥ 2.1 cm or the width ≥ 1.6 cm was defined as diagnostic criteria of malignant lymph nodes, the sensitivity was 33.3% and 29.2%, respectively, and the specificity was 95.7% and 93.5%, respectively. This result showed that lymph node with a length ≥ 2.1 cm or width ≥ 1.6 cm increased significantly the probability of metastasis. From the literature and our study, although benign lymph nodes were smaller than malignant lymph nodes, it is clear that there was a considerable overlap in size between benign and malignant lymph nodes; therefore, the value of lymph node size is limited for discriminating benign lymph nodes from malignant lymph node^[18,24,25].

In our study (Table 2), benign and malignant lymph nodes in round shape were encountered most commonly (Figures 4, 5) and spindle and ovoid lymph nodes were also seen, there was no significant difference between two kinds of lymph nodes. Malignant lymph nodes in irregular shape were mostly seen, and all fusional-shaped lymph nodes were malignant (Figure 3), there was a significant difference between benign and malignant lymph nodes ($P = 0.045, 0.006$). It was reported that

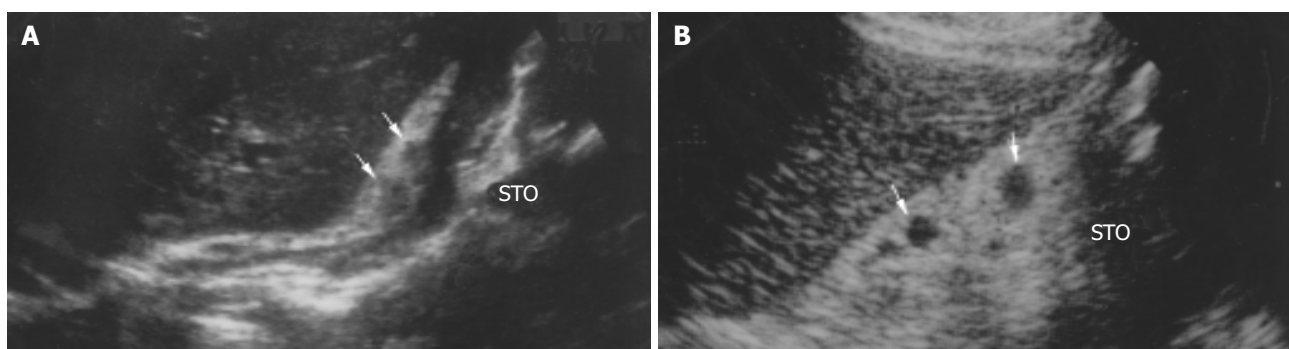


Figure 4 Differentiation between benign and metastatic lymph nodes. A: Benign lymph nodes. Sonogram shows multiple small lymph nodes (arrow) adjacent to the lesser curvature of stomach (STO). These hypoechoic lymph nodes are 5-8 mm, and misdiagnosed as metastatic with transabdominal US; Pathologic examination confirms that all these lymph nodes are reactive and noncancerous. B: Metastatic lymph nodes. Sonogram is similar to figure A. Multiple hypoechoic small lymph nodes (arrow) adjacent to the lesser curvature of stomach (STO) are 5-9 mm, and confirmed metastatic by pathologic examination.

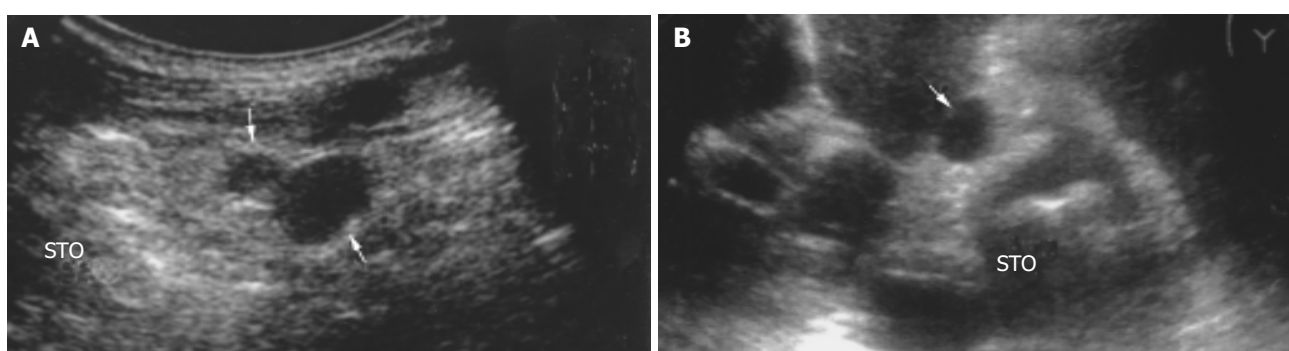


Figure 5 Differentiation between benign and metastatic lymph nodes. A: Benign lymph nodes. Sonogram shows multiple hypoechoic lymph nodes (arrow) adjacent to the greater curvature of stomach (STO). Of them, the largest is 1.8 cm with a distinct border. These lymph nodes are misdiagnosed as metastatic with transabdominal US. Pathologically, all these lymph nodes are reactive and noncancerous. B: Metastatic lymph node. Sonogram shows hypoechoic lymph node (arrow) adjacent to the lesser curvature of stomach (STO) with 1.6 cm in size and a distinct border. Pathologic examination confirms this lymph node is metastatic.

abdominal malignant lymph nodes were round or ovoid in shape, conversely, benign lymph nodes in people who were healthy or affected by benign disease were spindle or flat in shape^[9,18,24,26-30]. However in our study, both benign and malignant lymph nodes were mostly round in shape, and round shape did not allow the correct differentiation between benign and malignant lymph nodes. Immune reaction caused by tumor was different from that caused by benign diseases such as hepatitis or entities, which may be a cause for difficulties in differentiation between benign and malignant lymph nodes.

In our study the majority of benign and malignant lymph nodes had a distinct border (Figure 5), without statistical difference between them (Table 4). "Infiltrative signs" of lymph nodes were seen only in malignant lymph nodes ($P = 0.027$), which were typical and helpful for diagnosing malignant lymph nodes. Heintz *et al.*^[31] reported that both benign and malignant lymph nodes had an indistinct or distinct border by studying surgical resection specimens of patients with esophageal and gastric carcinomas. The study reported by Akahoshi *et al.*^[29,32] showed that malignant lymph nodes had a distinct border.

Table 4 shows that both benign and malignant lymph nodes were hypoechoic mostly (Figures 3-5), and the small number of lymph nodes was hyperechoic. There was no difference between benign and malignant lymph nodes. Inhomogenous echogenicity was seen only in malignant lymph nodes, there was a significant difference between benign and malignant lymph nodes ($P = 0.006$) and majority of inhomogenous lymph nodes were 2 cm greater in length. Contradictory data were published for echogenicity of lymph nodes. Heintz *et al.*^[31] stressed that echogenicity did not allow the correct differentiation

between benign and malignant lymph nodes. Other authors^[24,33] reported that most malignant lymph nodes were hypoechoic, and most benign lymph nodes were isoechoic or slightly hyperechoic. The different results might result from different patients studied.

In our study, the following 4 sonographic features were taken as the diagnostic criteria of malignant lymph nodes (Table 5): irregular shape, fusional shape, infiltrative signs, and inhomogenous echo. The sensitivity of the criteria was lower than 20 percent, and the specificity was higher than 90 percent. One of these 4 features was helpful to suggest malignant, however the similar sonographic features were observed in abdominal tuberculosis. Differential diagnosis was made on the basis of medical history.

Table 5 Diagnostic results of 46 benign and 48 malignant lymph nodes

Criterion	Sensitivity (%)	Specificity (%)
Length ≥ 1.1 cm	81.3 (39/48)	56.5 (26/46)
≥ 1.6 cm	47.9 (23/48)	76.1 (35/46)
≥ 2.1 cm	33.3 (15/48)	95.7 (44/46)
Width ≥ 1.1 cm	50.0 (24/48)	84.8 (39/46)
≥ 1.6 cm	29.2 (14/48)	93.5 (43/46)
Irregular	16.7 (8/48)	95.7 (44/46)
Fusional	16.7 (8/48)	100 (46/46)
Infiltrative signs	12.5 (6/48)	100 (46/46)
Inhomogenous	16.7 (8/48)	100 (46/46)

Swollen lymph nodes were found pathologically in 106 patients. But no swollen lymph nodes were detected with transabdominal US in 40 of 106 patients, and lymph nodes metastases were confirmed pathologically in 15 of these 40 patients. Missing lymph nodes were associated with the size of lymph nodes mainly. Lymph nodes less than 5 mm in size were usually undetectable with transabdominal US. In addition, obesity and bowel gas were unfavorable for detection of lymph nodes.

In conclusion, transabdominal US is useful for preoperative staging of gastric cancer, especially for assessment of advanced gastric cancer invasion. Although it is difficult to differentiate benign from malignant lymph nodes, typical sonographic features might contribute to diagnosis.

REFERENCES

- 1 **Sipponen P**, Jarvi O, Kekki M, Siurala M. Decreased incidences of intestinal and diffuse types of gastric carcinoma in Finland during a 20-year period. *Scand J Gastroenterol* 1987; **22**: 865-871
- 2 **Silverberg E**. Cancer statistics, 1980. *CA Cancer J Clin* 1980; **30**: 23-38
- 3 **Gelfand DW**, Ott DJ. Single-vs double-contrast gastrointestinal studies: critical analysis of reported statistics. *Am J Roentgenol* 1981; **137**: 523-528
- 4 **White RM**, Levine MS, Enterline HT, Laufer I. Early gastric cancer. Recent experience. *Radiology* 1985; **155**: 25-27
- 5 **Xi WD**, Zhao C, Ren GS. Endoscopic ultrasonography in preoperative staging of gastric cancer: determination of tumor invasion depth, nodal involvement and surgical resectability. *World J Gastroenterol* 2003; **9**: 254-257
- 6 **Wang JY**, Hsieh JS, Huang YS, Huang CJ, Hou MF, Huang TJ. Endoscopic ultrasonography for preoperative locoregional staging and assessment of resectability in gastric cancer. *Clin Imaging* 1998; **22**: 355-359
- 7 **Rosch T**. Endosonographic staging of gastric cancer .a review of literature results. *Gastrointest Endosc Clin N Am* 1995; **5**: 549-557
- 8 **Ohashi S**, Nakazawa S, Yoshino J. Endoscopic ultrasonography in the assessment of invasive gastric cancer. *Scand J Gastroenterol* 1989; **24**: 1039-1048
- 9 **Botet JF**, Lightdale CJ, Zaubler AG, Gerdes H, Winawer SJ, Urmacher C, Brennan MF. Preoperative staging of gastric cancer: comparison of endoscopic US and dynamic CT. *Radiology* 1991; **181**: 426-432
- 10 **Bolondi L**, Casanova P, Caletti GC, Grigioni W, Zani L, Barbara L. Primary gastric lymphoma versus gastric carcinoma: endoscopic US evaluation. *Radiology* 1987; **165**: 821-826
- 11 **Puylaert JB**. Acute appendicitis: US evaluation using graded compression. *Radiology* 1986; **158**: 355-360
- 12 **Kimmey MB**, Martin RW, Haggitt RC, Wang KY, Franklin DW, Silverstein FE. Histologic correlates of gastrointestinal Ultrasound images. *Gastroenterology* 1989; **96**(2 Pt 1): 433-441
- 13 **Wiersema MJ**, Wiersema LM. High-resolution 25-megahertz ultrasonography of the gastrointestinal wall: histologic correlates. *Gastrointest Endosc* 1993; **39**: 499-504
- 14 **Lim JH**, Jeong YM. Sonography of the stomach: an *in vitro* study to determine the anatomic cause of inner hyperechoic and hypoechoic layers of the gastric wall. *Am J Roentgenol* 1994; **162**: 335-338
- 15 **Lim JH**, Ko YT, Lee DH. Transabdominal US staging of gastric cancer. *Abdom Imaging* 1994; **19**: 527-531
- 16 **Segura JM**, Olveira A, Conde P, Erdozain JC, Suarez J. Hydrogastric sonography in the preoperative staging of gastric cancer. *J Clin Ultrasound* 1999; **27**: 499-504
- 17 **Sobin LH**, Hermanek P, Hutter RV. TNM classification of malignant tumors. A comparison between the new(1987) and the old editions. *Cancer* 1998; **61**: 2310-2314
- 18 **Smeets AJ**, Zonderland HM, van der Voorde F, Lameris JS. Evaluation of abdominal lymph nodes by ultrasound. *J Ultrasound Med* 1990; **9**: 325-331
- 19 **Tio TL**, Coene PP, Schouwink MH, Tytgat GN. Esophagogastric carcinoma: preoperative TNM classification with endosonography. *Radiology* 1989; **173**: 411-417
- 20 **Grimm H**, Binmoeller KF, Hamper K, Koch J, Henne-Bruns D, Soehendra N. Endosonography for preoperative locoregional staging of esophageal and gastric cancer. *Endoscopy* 1993; **25**: 224-230
- 21 **Dittler HJ**, Siewert JR. Role of endoscopic ultrasonography in gastric carcinoma. *Endoscopy* 1993; **25**: 162-166
- 22 **Tio TL**, Coene PP, Luiken GJ, Tytgat GN. Endosonography in the clinical staging of esophagogastric carcinoma. *Gastrointest Endosc* 1990; **36**(2 Suppl): S2-10
- 23 **Yanai H**, Matsumoto Y, Harada T, Nishiaki M, Tokiyama H, Shigemitsu T, Tada M, Okita K. Endoscopic ultrasonography and endoscopy for staging depth of invasion in early gastric cancer: a pilot study. *Gastrointest Endosc* 1997; **46**: 212-216
- 24 **Gimondo P**, Mirk P, Messina G, Pizzi C. Abdominal lymphadenopathy in benign diseases: sonographic detection and clinical significance. *J Ultrasound Med* 1996; **15**: 353-359
- 25 **Dorfman RE**, Alpern MB, Gross BH, Sandler MA. Upper abdominal lymph nodes: criteria for normal size determined with CT. *Radiology* 1991; **180**: 319-322
- 26 **Sutton RT**, Reading CC, Charboneau JW, James EM, Grant CS, Hay ID. US-guided biopsy of neck masses in postoperative management of patients with thyroid cancer. *Radiology* 1988; **168**: 769-772
- 27 **Sakai F**, Kiyono K, Sone S, Kondo Y, Oguchi M, Watanabe T, Sakai Y, Imai Y, Takeda S, Yamamoto K. Ultrasonic evaluation of cervical metastatic lymphadenopathy. *J Ultrasound Med* 1988; **7**: 305-310
- 28 **Vassallo P**, Wernecke K, Roos N, Peters PE. Differentiation of benign from malignant superficial lymphadenopathy: the role of high-resolution US. *Radiology* 1992; **183**: 215-220
- 29 **Akahoshi K**, Misawa T, Fujishima H, Chijiwa Y, Nawata H. Regional lymph node metastasis in gastric cancer: evaluation with endoscopic US. *Radiology* 1992; **182**: 559-564
- 30 **Subramanyam BR**, Balthazar EJ, Horii SC, Hilton S. Abdominal lymphadenopathy in intravenous drug addicts: sonographic features and clinical significance. *Am J Roentgenol* 1985; **144**: 917-920
- 31 **Heintz A**, Mildenerberger P, Georg M, Braunstein S, Junginger T. Endoscopic ultrasonography in the diagnosis of regional lymph nodes in esophageal and gastric cancer-results of studies *in vitro*. *Endoscopy* 1993; **25**: 231-235
- 32 **Francois E**, Peroux J, Mouroux J, Chazalle M, Hastier P, Ferrero J, Simon J, Bourry J. Preoperative endosonographic staging of cancer of the cardia. *Abdom Imaging* 1996; **21**: 483-487
- 33 **Metreweli C**, Ward SC. Ultrasound demonstration of lymph nodes in the hepatoduodenal ligament ('Daisy Chain nodes') in normal subjects. *Clin Radiol* 1995; **50**: 99-101

Surgical treatment and prognosis of gastric cancer in 2 613 patients

Xiang-Fu Zhang, Chang-Ming Huang, Hui-Shan Lu, Xing-Yuan Wu, Chuang Wang, Guo-Xian Guang, Jian-Zhong Zhang, Chao-Hui Zheng

Xiang-Fu Zhang, Chang-Ming Huang, Hui-Shan Lu, Xing-Yuan Wu, Chuang Wang, Guo-Xian Guang, Jian-Zhong Zhang, Chao-Hui Zheng, Department of Oncology, Affiliated Union Hospital of Fujian Medical University, Fuzhou 350001, Fujian Province, China
Correspondence to: Dr. Xiang-Fu Zhang, Department of Oncology, Affiliated Union Hospital, Fujian Medical University, Xingchun Road No.11, Fuzhou 350001, Fujian Province, China. zjzchina@vipsina.com

Telephone: +86-591-3320856 **Fax:** +86-591-3321970

Received: 2003-12-10 **Accepted:** 2004-01-08

Abstract

AIM: To analyze the factors influencing the prognosis of patients with gastric cancer after surgical treatment, in order to optimize the surgical procedures.

METHODS: A retrospective study of 2 613 consecutive patients with gastric cancer was performed. Of these patients, 2 301 (88.1%) received operations; 196 explorative laparotomy (EL), 130 by-pass procedure (BPP), and 1 975 surgical resection of the tumors (891 palliative resection and 1 084 curative resection). The survival rate was calculated by the actuarial life table method, and the prognostic factors were evaluated using the Cox regression proportional hazard model.

RESULTS: Of the patients, 2 450 (93.8%) were followed-up. The median survival period was 4.6 mo for patients without operation, 5.2 mo for EL, 6.4 mo for BPP, and 15.2 mo for palliative resection ($P = 0.0001$). Of the patients with surgical resection of the tumors, the overall 1, 3 and 5-year survival rates after were 82.7%, 46.3% and 31.1%, respectively, with the 5-year survival rate being 51.2% in patients with curative resection, and 7.8% for those with palliative resection. The 5-year survival rate was 32.5% for patients with total gastrectomy, and 28.3% for those with total gastrectomy plus resection of the adjacent organs. The factors that independently correlated with poor survival included advanced stage, upper third location, palliative resection, poor differentiation, type IV of Borrmann classification, tumor metastasis (N_3), tumor invasion into the serosa and contiguous structure, proximal subtotal gastrectomy for upper third carcinoma and D_1 lymphadenectomy after curative treatment.

CONCLUSION: The primary lesion should be resected as long as the local condition permitted for stage III and IV tumors, in order to prolong the patients' survival and improve their quality of life after operation. Total gastrectomy is indicated for carcinomas in the cardia and fundus, and gastric cancer involving the adjacent organs without distant metastasis requires gastrectomy with resection of the involved organs.

Zhang XF, Huang CM, Lu HS, Wu XY, Wang C, Guang GX, Zhang JZ, Zheng CH. Surgical treatment and prognosis of gastric cancer in 2 613 patients. *World J Gastroenterol* 2004; 10(23): 3405-3408

<http://www.wjgnet.com/1007-9327/10/3405.asp>

INTRODUCTION

Although the mortality rate of gastric cancer has been dramatically decreased in the western country since 1930^[1], cancer of the stomach remains the second most frequent malignancy in the world^[2,3], and an estimate of more than 1 million new cases were identified worldwide in 1997^[4]. From 1990 to 1992, the mortality rate of gastric cancer in China remained at a high level of 25.2/100 000, taking up 23.2% of the total cancer-related death, and claiming the largest death toll in cancer patients^[5]. As the generally acknowledged primary treatment modality for gastric cancer, surgical interventions^[6-9] give rise to many controversies concerning (1) the decision on palliative resection, by-pass procedure or avoidance of operation for advanced gastric cancer (including stage III_B or IV), (2) the optimal extent to be resected in patients with gastric cancer in the upper third, by total gastrectomy (TG) or proximal subtotal gastrectomy (PSTG), and (3) the optimal surgical resection for gastric cancer involving the neighboring organs. The aim of this retrospective study was to analyze the factors influencing the patients' prognosis after surgical treatment, curative or palliative, of gastric cancer, and find answers to above questions.

MATERIALS AND METHODS

Clinical data

This study included 2 613 patients with primary gastric cancer admitted in Department of Oncology, Affiliated Union Hospital of Fujian Medical University, during the period of June 1972 to June 2000. There were 2 059 male and 554 female patients whose ages ranged from 19 to 85 years with a mean of 55.6 ± 2.48 years. The tumors were found in the gastric cardia and fundus in 871 cases, in the gastric body in 544 cases, in the gastric antrum in 1 069 cases and involving the entire stomach in 129 cases. The dimension (maximum diameter) of the tumor was smaller than 3 cm in 254 cases, between 3.1 and 6 cm in 1 290 cases and more than 6 cm in 1 069 cases. The tumors were histologically classified according to WHO classification criteria, and staged according to the TNM system used since 1989 in China^[10], as listed in Table 1.

Table 1 Histological classification of the tumors in the 2 613 patients with gastric cancer

Histological classification	Number	Percentage (%)
Well differentiated adenocarcinoma	528	20.2
Moderately differentiated adenocarcinoma	1102	42.2
Mucinous adenocarcinoma	560	21.4
Poorly differentiated adenocarcinoma	277	10.6
Others	146	5.6
Borrmann's classification		
Type I	179	6.9
Type II	477	18.3
Type III	1683	64.4
Type IV	129	4.9
Early-stage cancer	145	5.6

Methods

Of all those patients, 312 had not received any previous surgical intervention, and 2 301 (88.1%) had undergone operations. Among the patients with a history of previous operations, 196 had explorative laparotomy (EL), 130 had by-pass procedure (BPP), 1 975 underwent surgical resection of the tumor, of whom 891 received palliative resection. The tumor resection was considered palliative on the basis of the presence of residual tumor or distant metastasis or both at the end of surgery. A total of 1 084 patients underwent curative resection, making up 54.9%. The surgical procedure was defined as curative when no grossly visible tumor tissue (metastasis or lymph node involvement) remained after the resection and the resection margins were histologically normal.

In all the 1 975 surgical patients, distal subtotal gastrectomy (DSTG) was performed in 894 patients, total gastrectomy (TG) in 615, and proximal subtotal gastrectomy (PSG) in 466. Among the patients undergoing curative resection, limited D₁ nodal dissection was performed in 159 patients (during the period of 1 972 to 1 979), extended D₂/D₂⁺ in 846 and extended D₃ in 79. The clinical data of the 1 975 patients with surgical tumor resection are shown in Table 2. Metastases involving such organs as the esophagus, spleen, pancreas, colon and the duodenum were identified in 439 patients.

Table 2 Clinical data of the 1 975 patients with surgical resection of the tumor

Characteristics	Number	Percentage (%)
Type of resection		
Radical resection	1 084	54.9
Palliative resection	891	45.1
Depth of invasion (T)		
Mucosa/submucosa (PT ₁)	145	7.3
Muscularis (PT ₂)	347	17.6
Serosa (PT ₃)	978	49.5
Serosa and contiguous structure (PT ₄)	505	25.6
Lymph node involvement (N)		
N ₀	207	10.5
N ₁	343	17.4
N ₂	936	47.4
N ₃	489	24.7
Stage		
I _A	125	6.3
I _B	131	6.6
II	251	12.7
III _A	404	20.5
III _B	442	22.4
IV	622	31.5
Type of nodal dissection (radical resection)		
D ₁	159	14.7
D ₂ /D ₂ ⁺	846	78.0
D ₃	79	7.3

The 5-year cumulative survival was calculated after both curative and palliative tumor resection by actuarial life-table method. Statistical analysis was carried out by using Chi-square test and Wilcoxon rank sum test. Multivariate analysis was applied using the Cox regression proportional hazard model. The SPSS 10.0 for Windows was used for all the statistical analyses.

RESULTS

Among the 2 613 patients with gastric cancer, 163 failed to be followed-up with the follow up rate of 93.8%. Postoperative complications arose in 189 cases with an incidence of 9.6%. Death within one month after operation occurred in 41 cases (2.1%).

The survival rate was calculated in 1 498 patients with surgical resection, curative and palliative, of the tumors. Univariate and multivariate analyses were used to evaluate 5-year survival rate with respect to the main clinicopathologic and treatment variables after both curative and palliative treatment. The overall 5-year survival after surgical resection (operative mortality excluded) was 31.6%, 51.2% for curative treatment, and 7.8% for palliative resection; 91.1% for stage I_A, 86.7% for stage I_B, 51.1% for stage II, 34.5% for stage III_A, 29.1% for stage III_B, and 5.9% for stage IV (Figure 1, Table 3). The median survival period was 4.6 mo after NO, 5.2 mo after EL, 6.4 mo after BPP, and 15.2 mo after palliative resection ($P = 0.0001$). The 5-year survival rate was 32.5% for patients with total gastrectomy, and 28.3% for those with total gastrectomy plus resection of the adjacent organs. Univariate and multivariate survival analyses showed that the variables independently correlated with poor survival included advanced stage, upper third location, palliative resection, poorly differentiated adenocarcinoma, type IV of Borrmann classification, tumor metastasis (N₃), tumor invasion into the serosa and contiguous structure, proximal subtotal gastrectomy for upper third carcinoma and D₁ lymphadenectomy after curative treatment (Table 4).

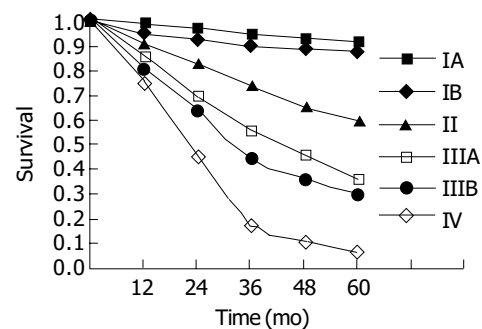


Figure 1 Survival curves of the 1 498 patients of different clinical stages undergoing surgical resection (radical and palliative) with operative death excluded.

Table 3 Univariate survival analysis of clinical and pathologic variables after surgical treatment in 1 498 cases with gastric carcinoma

Parameter	Number	5-yr survival rate (%)	P
Age (yr)			
≤30	19	21.0	0.05
30 to 60	926	29.2	
>60	553	36.2	
Tumor location			
C (upper third)	499	22.6	0.001
M (middle third)	312	35.3	
A (lower third)	613	40.9	
MCA (whole stomach)	74	2.7	
Tumor size (cm)			
<3	146	53.1	0.047
3 to 6	739	40.9	
>6	613	15.3	
Histological classification			
Well differentiated adenocarcinoma	303	38.3	0.001

Moderately differentiated adenocarcinoma	631	36.7	
Mucinous adenocarcinoma	321	28.3	
Poorly differentiated adenocarcinoma	159	15.7	
Others	84	13.1	
Type of operation			
DSTG	678	37.2	0.001
TG	466	32.4	
PSG	354	20.1	
Borrmann's classification			
Type I	103	61.1	0.001
Type II	274	45.2	
Type III	964	20.1	
Type IV	74	2.7	
Early cancer	83	90.0	
Type of resection			
Radical resection	822	51.2	0.001
Palliative resection	676	7.8	
Extent of nodal dissection			
D ₁	120	34.5	0.001
D ₂ to D ₂ ⁺	641	53.5	
D ₃	61	50.8	
Depth of cancer invasion			
T ₁	110	90.4	0.001
T ₂	263	55.2	
T ₃	742	25.9	
T ₄	383	10.0	
Lymph node involvement			
N ₀	157	86.1	0.001
N ₁	260	58.1	
N ₂	710	23.3	
N ₃	371	5.9	

Table 4 Multivariate analysis of prognostic variables for survival

Variables	Regression coefficient	P
Type of resection	0.45729	0.00081 ¹
Extent of nodal dissection	0.35851	0.00479 ¹
Borrmann's classification	0.42583	0.00295 ¹
Tumor location	0.25409	0.15204
Depth of cancer invasion	0.43839	0.00283 ¹
Lymph node involvement	0.26738	0.14962
Type of operation	0.25016	0.15978
Tumour size	0.00421	0.97279

¹Significant difference.

DISCUSSION

Surgical treatment of gastric cancer has been universally recognized as the most effective way of treatment, and the 5-year survival rate of curative resection in this study reached 51.2%. Although curative resection for gastric cancer is most effective, most cases are in stage III and IV on identification in China^[11-13], as seen from the high rate of 74.9% in this study, and many of them were ineligible for radical treatment. Ekbom *et al.*^[14] reported that BPP in advanced cases only resulted in the average survival period of 5.9 mo, and none of the patients survived for more than one year, similar to the results of without tumor resection^[15]. The average survival periods of patients without operation, with EL and BPP in China, as reported by

National Gastric Cancer Cooperation Organization, were 4.1, 4.7, and 5.5 mo, respectively^[11], comparable with our findings (4.6, 5.2, and 6.4 mo, respectively, $P>0.05$). In this study, the survival period after palliative resection was 15.2 mo with a 5-year survival rate reaching 7.8%, significantly higher than that in patients without operation or with EL and BPP ($P<0.01$). Therefore, for stage III and IV gastric cancer, resection of the primary focus should be performed as much as possible. After the resection, the patient's condition might be improved to tolerate postoperative chemotherapy, immunotherapy and comprehensive treatment by traditional Chinese medicine, and the survival period of the patients might consequently be prolonged and quality of life improved^[16-20].

There is still controversy over the impact of the extent of resection for tumors located in the upper third of the stomach (including cardia and fundus)^[21]. Some researchers^[22-25] advocate the performance of PSG so as to possibly retain the stomach even partially, and proper digestive function. It also enables patients to avoid the late stage complications following TG. However, Fujimaki and Lin discovered in their respective research that the rate of lymphatic metastasis of group 5 and 6 might reach up to 24.0% to 29.0% in some cases^[26,27]. It is difficult to eliminate all tumor tissues without performing TG. The incidence of postoperative regurgitant esophagitis is high and volume of residual stomach is small, and TG may overcome these defects to improve the 5-year survival rate^[28-31]. According to the review of our 28-year experience with the treatment of gastric cancer, two types of resection for cancer of the cardia (the upper 1/3 location) irrespective of the tumor stage contributed to a 5-year survival rate after TG of up to 32.5%, while the 5-year survival rate after PSG was only 20.1%, showing significant difference ($P<0.05$). Following great improvements in surgical techniques, postoperative care and measures of digestive tract reconstruction, postoperative complication and death rate have been remarkably decreased^[32-34]. The incidence of complication was only 12.7% and death rate 2.9% in the 615 patients receiving TG in this study. In recent years, we attempted routine TG for treating cancer of the upper 1/3 location as long as the patients' general condition permitted, and of all gastrectomy cases, 31.1% were received TG in the study.

In approximately 15.5-22.3% of patients with advanced gastric cancer, the malignancy had already invaded the neighboring organs when the diagnosis was established^[11,35,36], requiring critical decisions on the treatment for the best interests of the patients. In this study, 439 cases (22.9% of those with surgical resection) had combined resection of the involved organs, and the total 5-year survival rate was 28.3%. In these cases extensive radical resection of gastric cancer combined with resection of the spleen and the body and tail of pancreas was found to produce the best therapeutic effect, yielding a 5-year survival rate of 43.2%. For treatment of 28 cases of advanced gastric cancer involving multiple neighboring organs, left upper abdominal evisceration (LUAE) and resection of the total stomach, lower end of esophagus, left lobe of liver, spleen, body and tail of pancreas, transverse colon and partial suprarenal gland were performed, resulting in a 5-year survival rate of up to 16.7%. One of the patients has survived for 10 years. Pessimism toward gastric cancer invading nearby organs is not reasonable. For gastric cancer with metastasis to adjacent organs, but without incurable factors such as liver metastasis, peritoneal dissemination (P₂ and P₃) and widespread nodal involvement, complete excision of the invaded organs should be performed as much as possible, irrespective of the number or site of the invaded organs. Cure is possible in some cases of advanced gastric cancer. In cases with incurable factors, partial resection of the involved organs is not recommended, as it almost invariably fails to prolong the patients' survival in comparison with simple resection of the primary focus of gastric cancer, but increases the sufferings of the patient and prolongs the operation time.

Palliative operation to resect the primary focus might be a better alternative, for it not only relieves obstruction, hemorrhage and pain, but also prepares favorable condition for other postoperative treatments and at the same time, improves the quality of life and prolongs the survival period of the patient.

REFERENCES

- 1 **Abeloff MD**, Armitage JO, Lichter AS, Niederhuber JE. Clinical Oncology. Second edition. *China Science Press Harcourt Asia China* 2001: 1545-1585
- 2 **Price P**, Sikore K. Treatment of cancer. 4th edition London. *New York NewDeLHI Arnold press* 2002: 583-599
- 3 **Pisani P**, Parkin DM, Bray F, Ferlay J. Erratum: Estimates of the worldwide mortality from 25 cancers in 1990. *Int J Cancer* 1999; **83**: 870-873
- 4 World Health Organization, *the world health report*. Geneva WHO 1997
- 5 **Sun X**, Mu R, Zhou Y, Dai X, Qiao Y, Zhang S, Huangfu X, Sun J, Li L, Lu F. 1990-1992 mortality of stomach cancer in China. *Zhonghua Zhongliu Zazhi* 2002; **24**: 4-8
- 6 **Furukawa H**, Imamura H, Kodera Y. The role of surgery in the current treatment of gastric carcinoma. *Gastric Cancer* 2002; **5** (Suppl 1): 13-16
- 7 **Souhami RL**, Tannock I, Hohenberger P, Horiot JC. Oxford textbook of oncology. Second edition. *New York Oxford University Press* 2002: 1617-1635
- 8 **Wu CW**, Lo SS, Shen KH, Hsieh MC, Lui WY, P'eng FK. Surgical mortality, survival, and quality of life after resection for gastric cancer in the elderly. *World J Surg* 2000; **24**: 465-472
- 9 **Bland KJ**, Daly JM, Karakousis CP. Surgical oncology. *New York, San Francisco, AUCKland. McGRAN-Hill Medical Publishing Division* 2001: 623-625
- 10 **Zhang TZ, Xu GW**. Zhongliuxue. First edition, *Tianjing. Tianjing Science-Technology Publishing Division* 1996: 1421-1505
- 11 National gastric cancer cooperative groups, Surgical operation of gastric cancer (analyse of 11 734 cases). *Zhonghua Waik Zazhi* 1982; **20**: 577-580
- 12 **Zhang RG**, Fang DK, Zhang DW, Wang LJ, Zhang DC, Yang L, Cheng GY, Meng PJ, Sun KL, Liu XY, Li J, Li WX, Huang JF. Surgical treatment results for carcinoma of the gastric cardia in 1832 cases. *Zhonghua Zhongliu Zazhi* 1998; **40**: 140-142
- 13 **Wang QS**, Lin MB, Su BH, Gao SY, Cui TJ, Xie JQ, Lin ZW, Lin ZH, Ye SQ, Lin XY, Tong GQ. Studies on therapeutic efficacy of surgical treatment in 1629 cases of gastric cancer. *Zhongguo Zhongliu Linchuang* 1995; **22**: 17-20
- 14 **Ekbom GA**, Gleysteen II. Gastric malignancy: resection for palliation. *Surgery* 1980; **88**: 476-481
- 15 **Moreaux J**, Msika S. Carcinoma of the gastric cardia: surgical management and long-term survival. *World J Surg* 1988; **12**: 229-235
- 16 **Maehara Y**, Sugimachi K, Akagi M, Kakegawa T, Shimazu H, Tomita M. Early postoperative chemotherapy following noncurative resection for patients with advanced gastric cancer. *Br J Cancer* 1992; **65**: 413-416
- 17 **Zhang XF**, Lu HS, Yin FS, Feng YM, Zheng ZW, Wu XY, Huang CM, Wu JG. Clinical experience in the treatment of 1108 patients with gastric carcinoma. *Zhonghua Zhongliu Zazhi* 1990; **12**: 49-51
- 18 **Maehara Y**, Moriguchi S, Sakaguchi Y, Emi Y, Kohnoe S, Tsujitani S, Sugimachi K. Adjuvant chemotherapy enhances long-term survival of patients with advanced gastric cancer following curative resection. *J Surg Oncol* 1990; **45**: 169-172
- 19 **Kim JP**, Yu HJ, Lee JH. Results of immunochemo-surgery for gastric carcinoma. *Hepatogastroenterology* 2001; **48**: 1227-1230
- 20 **Tas F**, Aykan NF, Aydiner A, Uygun K, Basaran M, Camlica H, Topuz E. The roles of chemotherapy and surgery in gastric carcinoma and the influence of prognostic factors on survival. *Am J Clin Oncol* 2000; **23**: 53-57
- 21 **Hansson LE**, Ekstrom AM, Bergstrom R, Nyren O. Surgery for stomach cancer in a defined Swedish population: current practices and operative results. Swedish gastric cancer study group. *World J Surg* 2000; **166**: 787-795
- 22 **Zhang DW**, Cheng GY, Huang GJ, Zhang RG, Zhang DC, Wang LJ, Xu PZ, Yang L, Liu JS, Chen YH, Sun KL, Peng L, Fang DK, Liu XY, Yang LH, He J, Mao YS, Li J. Surgical management of adenocarcinoma of the gastric cardia experience in 937 patients. *Zhonghua Zhongliu Zazhi* 1988; **10**: 376-378
- 23 **Harrison LE**, Karpeh MS, Brennan MF. Total gastrectomy is not necessary for proximal gastric cancer. *Surgery* 1998; **123**: 127-130
- 24 **Jakl RJ**, Miholic J, Koller R, Markis E, Wolner E. Prognostic factors in adenocarcinoma of the cardia. *Am J Surg* 1995; **169**: 316-319
- 25 **McNeer G**, Bowden L, Booner RJ, McPeak CJ. Elective total gastrectomy for cancer of the stomach: end results. *Ann Surg* 1974; **180**: 252-256
- 26 **Fujimaki M**, Soga J, Wada K, Tani H, Aizawa O. Total gastrectomy for gastric cancer. Clinical considerations on 431 cases. *Cancer* 1972; **30**: 660-664
- 27 **Lin YZ**. Extended radical operation for gastric cancer. *Shiyong Waik Zazhi* 1985; **5**: 63-64
- 28 **Wang SB**. Thirty-seven-year clinical experience on gastric cancer-a report of 2326 cases. *Zhongguo Zhongliu Linchuang* 1999; **26**: 325-329
- 29 **Jackson JW**, Cooper DK, Guvendik L, Reece-Smith H. The surgical management of malignant tumours of the oesophagus and cardia: a review of the results in 292 patients treated over a 15-year period (1961-1975). *Br J Surg* 1979; **66**: 98-104
- 30 **Shao QS**, Chen XY, Zou SC. Biological behavior of cardiac cancer and its effect on surgical management. *Zhonghua Waik Zazhi* 2003; **41**: 738-740
- 31 **Huang CM**, Zhang XF, Lu HS, Zhang JZ, Wu XY, Guan GX, Wang C. Long-term therapeutic effects of total gastrectomy in cancer of the cardia and stomach fundus. *Zhonghua Waik Zazhi* 2003; **41**: 729-732
- 32 **Kishimoto H**, Koga S. Evaluation of gastrectomy combined with resection of other organs in the treatment of gastric cancer. *Jpn J Surg* 1979; **9**: 173-179
- 33 **Nagata T**, Ikeda M, Nakayama F. Changing state of gastric cancer in Japan. Histologic perspective of the past 76 years. *Am J Surg* 1983; **145**: 226-233
- 34 **Zhang JZ**, Lu HS, Huang CM, Wu XY, Guan GX, Wang C, Zheng CH, Zhang XF. Long-term effect of total gastrectomy on 615 cases with gastric cancer. *Zhonghua Weichang Waik Zazhi* 2002; **5**: 13-16
- 35 **Zhang XF**, Huang CM, Yin FS, Lu HS, Feng YM, Wu TG, Zheng ZW, Wu ZY, Guan GX. Evaluation of surgical resection for gastric cancer extending to adjacent organs. *Zhonghua Waik Zazhi* 1995; **33**: 603-605
- 36 **Korenaga D**, Okamura T, Bada H, Saito A, Sugimachi K. Results of resection of gastric cancer extending to adjacent organs. *Br J Surg* 1988; **75**: 12-15

Edited by Chen WW and Zhu LH Proofread by Xu FM

Epstein-Barr virus in hepatocellular carcinogenesis

Wei Li, Bao-An Wu, Yong-Ming Zeng, Guang-Can Chen, Xin-Xin Li, Jun-Tian Chen, Yu-Wen Guo, Man-Hong Li, Yi Zeng

Wei Li, Bao-An Wu, Yong-Ming Zeng, Guang-Can Chen, Xin-Xin Li, Jun-Tian Chen, Yu-Wen Guo, Department of General Surgery, the First Affiliated Hospital of Shantou University Medical College, Shantou 515041, Guangdong Province, China

Man-Hong Li, Department of Pathology, the First Affiliated Hospital of Shantou University Medical College, Shantou 515041, Guangdong Province, China

Yi Zeng, Oncogenic Virus Laboratory, Institute for Viral Disease Prevention and Control, Chinese Center for Disease Control and Prevention (China CDC), Beijing 100052, China

Supported by the Technology Program of Guangdong Province, China, No. 2KM04504s

Correspondence to: Wei Li, Department of General Surgery, the First Affiliated Hospital of Shantou University Medical College, No. 57, Changping Road, Shantou 515041, Guangdong Province, China. lwmail@medmail.com.cn

Telephone: +86-754-8258290-3256

Received: 2004-04-14 **Accepted:** 2004-05-09

Abstract

AIM: In recent years, studies have suggested that Epstein-Barr virus (EBV) is associated with HCC. The present study was to determine the prevalence of EBV in HCC patients, and whether EBV acted synergistically with hepatitis viruses in HCC carcinogenesis.

METHODS: Liver tissue 115 HCC patients and 26 non-carcinoma patients were studied. Polymerase chain reaction (PCR) was performed to detect EBV *Bam*HI W DNA, EBV LMP1 DNA, HBV X DNA, and HBV S DNA. Reverse transcription PCR (RT-PCR) was performed to detect HCV RNA and HDV RNA. Immunohistochemistry was performed to detect LMP1, HBsAg, HBeAg and HCV. The positive ratios were compared between HCC group and control group by χ^2 test.

RESULTS: Totally, 78 HCC samples whose β -globulin DNA was positively detected by amplified PCR were selected. PCR was performed in all cases for EBV DNA and HBV DNA. RT-PCR was performed in 18 cases for HCV RNA and HDV RNA. EBV *Bam*HI W and EBV LMP1 were positive in 18 and 6 cases, respectively. HBV X gene and HBV S gene were positive in 42 and 27 cases respectively. HCV was positive in one of the 18 cases, and none was positive for HDV. The positive rates were 28.2% (22 of 78) for EBV DNA (*Bam*HI W and/or LMP1) and 56.4% (44 of 78) for HBV DNA (X gene and/or S gene) respectively. In addition, 12 cases were positive for both EBV DNA and HBV DNA. Among the 26 cases in the control group, 2 cases were positive for EBV *Bam*HI W, 4 positive for HBV X gene and 3 positive for HBV S gene. The positive rates were 8.0% (2 of 26) and 23.1% (6 of 26), respectively, for EBV DNA and HBV DNA. The result of DNA sequencing of *Bam*HI W was 100% homologous with the corresponding sequence of B95-8. There was significant difference in EBV infection rate between HCC patients and controls ($\chi^2 = 4.622$, $P < 0.05$). The difference in HBV infection rate was also significant ($\chi^2 = 8.681$, $P < 0.05$). However, there was no obvious correlation between HBV and EBV in HCC patients ($\chi^2 = 0.835$, $P > 0.05$). LMP1, HBV (HBsAg, HBeAg) and HCV were detected positively in 25, 45 and 6 of 78

cases of HCC tissues respectively. In the 26 control cases, the corresponding positive cases were 2, 4 and 0. The difference in EBV infection rate between HCC patients and control cases was statistically significant ($\chi^2 = 6.02$, $P < 0.05$). The difference in HBV infection rate was also statistically significant ($\chi^2 = 10.03$, $P < 0.05$). In the 25 cases with positive LMP1 expression, 6 were in the nuclei of tumor cells, 9 in the cytoplasm of tumor cells and 10 in mesenchymal lymphocyte cytoplasm.

CONCLUSION: The existence of EBV infection in HCC tissues suggests that EBV may be involved in the hepatocellular carcinogenesis in China. HBV infection may be a major cause of HCC. There is no correlation between EBV and HBV in the development of HCC. The prevalence of HCV infection is low in our area, and HDV appears not to play a direct role in hepatocellular carcinogenesis.

Li W, Wu BA, Zeng YM, Chen GC, Li XX, Chen JT, Guo YW, Li MH, Zeng Y. Epstein-Barr virus in hepatocellular carcinogenesis. *World J Gastroenterol* 2004; 10(23): 3409-3413
<http://www.wjgnet.com/1007-9327/10/3409.asp>

INTRODUCTION

Hepatocellular carcinoma (HCC) is one of the most frequent malignant tumors. It possesses the characteristics of high malignancy, rapid progress and poor prognosis. In recent years, studies have suggested that Epstein-Barr virus (EBV) is associated with HCC although opposite results have been subsequently reported. The present study was to determine the prevalence of EBV in hepatocellular carcinoma (HCC) patients, and whether EBV acted synergistically with hepatitis viruses in HCC carcinogenesis.

MATERIALS AND METHODS

Patients and tissue samples

HCC samples from 115 patients, which were resected in the First Affiliated Hospital of Medical College, Shantou University and Shantou Central Hospital between October 1997 and October 2001, were fixed in 40 g/L neutral formaldehyde and embedded in paraffin. Of these, 78 samples satisfied the criteria that their β -globulin DNA presented positive. The patients consisted of 59 men and 19 women. Their ages ranged from 22 to 76 years (average 50.2 ± 2.4 years). According to the Edmondson (1956) HCC morphology standard, two, 34, 30 and 12 cases belonged to the levels I, II, III and IV, respectively. AFP was detected in 48 cases; the level was lower than 0.14 ng/mL in four cases, between 0.14 ng/mL and 5.6 ng/mL in 14 cases and higher than 5.6 ng/mL in 12 cases. Anti-hepatitis B virus (HBV) assay was performed by enzyme-linked immunosorbent assay (ELISA) in 62 cases, and 54 were positive. Anti-hepatitis C virus (HCV) assay was carried out in 58 cases and anti-EBV EA-IgA and VCA-IgA assays in 43 cases. The control group consisted of 20 cases with hepatolithiasis and lobectomy of liver, three cases with hepatic adenoma and three cases with hepatocyte focal nodular hyperplasia. HBV was positive in 10 cases. HCV and EBV were negative in all cases.

Reagents

Taq DNA polymerase, dNTP mixture, AMV reverse transcriptase XL, RNase inhibitor, random primer and DNA marker were purchased from TaKaRa® Biotechnology Co., Ltd (Dalian, China). The Trizol total RNA separating medium was purchased from Gibco® Co., Ltd (Grand Island, NY, USA). LMP1 monoclonal antibody (Clone CS1-4), HBsAg monoclonal antibody (Clone ZMHB5), HBcAg polyclonal antibody, the immediately-used-type of the second generation immunohistochemistry Elivision™ plus broad spectrum test kit were from Maixin Co., Ltd (Fuzhou, China). Rat-anti-human HCV monoclonal antibody (Clone TORJ1-22) was from Zhongshan Biotechnology Co. Ltd (Beijing, China).

PCR, DNA sequencing and RT-PCR

We downloaded the gene sequences of EBV, HBV, HCV and hepatitis D virus (HDV) from the GenBank. Each included four strains, and the homogeneity was compared among the strains by the Vector NTI suite7 software. The primers were designed by Oligo software (Table 1, LMP1^[1] and β -globulin^[2] primer sequences were adopted from literature) within the homogeneous gene regions, and synthesized in Shenggong Co., Ltd (Shanghai, China). The positive controls of EBV, HBV and HCV were, respectively, B95-8 cell line, PSDHBV-1 (HBV complete sequence plasmid, 7.8 k) and an HCV-positive serum. The HDV positive control could not be obtained. Fetal liver tissues served as the negative controls. Blank control was established. Primers flanking β -globulin gene were used as a positive control for DNA preservation. Full details of the sequences and genome coordinates of primers and amplification programs of PCR are given in Table 1. The PCR products were electrophoresed in 15 g/L agarose gel, stained with ethidium bromide (Et-Br), and photographed under a UV-transilluminator. After being retrieved and purified, PCR product was ligated with pMD 18-T vector, and then transfected *E. coli* competent cells. The clones were selected and identified. Sequencing of the positive clones was performed by Shenggong Co., Ltd. Bacteriophage M13 cloning vector was used to ligate the fragments. RNA extracts were prepared from paraffin sections. The tissue specimens were deparaffinized with xylene,

then washed with ethanol. RNA was extracted using TRIZOL total RNA separating medium. Reverse transcription was performed using AMV reverse transcriptase XL with cDNA synthesis performed for 1 h at 42 °C. Then nested PCR was carried out using the resulting cDNA as template. The detail is shown in Table 1.

Immunohistochemistry

We used a two-step method according to the instructions provided with the reagent kits. LMP1 located in nucleus or cytoplasm. HCV located in nucleus. HBsAg located in cytoplasm. HBcAg located in nucleus or cytoplasm. Positive cells were defined when there were clear small particles or granuloreticular reddening in cytoplasm or nucleus. The positive control was the positive tissue section provided by the company. Negative control was the sample of lobectomy of liver due to hepatolithiasis. Blank control was tissue section without addition of the first antibody.

Statistical analysis

The positive ratios were compared between HCC group and control group by means of χ^2 test. $P < 0.05$ was considered as statistically significant. The statistical software used was SPSS 10.0.

RESULTS

PCR and RT-PCR

Totally, 78 HCC samples whose β -globulin DNA was positively detected by amplified PCR were selected; PCR and RT-PCR were performed in all cases for EBV and HBV, and in 18 cases for HCV and HDV. EBV *BamHI* W and EBV LMP1 were positive in 18 and six cases, respectively. HBV X gene and HBV S gene were positive in 42 and 27 cases respectively. HCV was positive in 1 of the 18 cases, and none was positive for HDV. The positive rates were 28.2% (22 of 78) for EBV DNA (*BamHI* W and/or LMP1) and 56.4% (44 of 78) for HBV DNA (X gene and/or S gene) respectively. In addition, 12 cases were positive for both EBV DNA and HBV DNA. Among the 26 cases in the control group, 2 cases were positive for EBV *BamHI* W, four

Table 1 Primer sequences and amplification programs of PCR and RT-PCR detection

Transcript	Product size	Genomic coordinates in GenBank	Primer sequence (5'-3')	Amplification program
EBV	337 bp	B95-8	GAGTGTGTGCCAGTTAAGGT (168 056-16 8075 20 bp)	94 °C 3 min (94 °C 30 s 55 °C
LMP1 ^[1]		V01555	CTAGCGACTCTGCTGAAAT (168 373-16 8392 20 bp)	40 s 72 °C 1 min) × 40 72 °C 8 min
EBV	130 bp	B95-8	CATCACCGTCTGCTGACT (14 525-14 541 17 bp)	95 °C 3 min (94 °C 30 s 52 °C
<i>BamHI</i> W		V01555	GTTGGCTTAGCAGAAA (14 638-14 654 17 bp)	40 s 72 °C 45 s) × 40, 72 °C 7 min
HBV	198 bp	HBV	AGGTATGTTGCCGTTTGT (457-475 19 bp)	95 °C 5 min (94 °C 30 s 52 °C
S gene		AB073856	GAGGCCCACTCCCATAGG (637-654 18 bp)	40 s 72 °C 50s) × 35, 72 °C 7 min
HBV	232 bp	HBV	TGTGCTGCCAACTGGATCCT (1 387-1 406 20 bp)	95 °C 3 min (94 °C 30 s 55 °C
X gene		AB073856	GTGGTCTCCATGCGACGTG (1600-1618 19 bp)	40 s 72 °C 45 s) × 37 72 °C 7 min
HCV	165 bp	HCV	GCGGAACCGGTGAGTACAC (138-156 19 bp)	95 °C 5 min, (94 °C 30 s 55 °C
cDNA		NC_001433	GCACTCGCAAGCACCTATC (283-302 20 bp)	40 s 72 °C 50 s) × 40 72 °C 7 min
Outer				
HCV	142 bp	HCV	GGAATTGCCAGGACGACC (158-175 18 bp)	95 °C 5 min (94 °C 30 s, 55 °C
cDNA		NC_001433	CTCGCAAGCACCTATCAG (281-299 19 bp)	40 s 72 °C 50 s) × 40 72 °C 7 min
Inner				
HDV	216 bp	HDV	GCGGGTCCGTCGTTCCAT (653-670 18 bp)	95 °C 5 min (94 °C 30 s 55 °C
cDNA		AB037947	GTCCGACCTGGGCATCCGT (850-868 19 bp)	40 s 72 °C 50 s) × 35, 72 °C 7 min
Outer				
HDV	114 bp	HDV	TCGAGAATCGGCAAATG (752-768 17 bp)	95 °C 5 min (94 °C 30 s 52 °C
cDNA		AB037947	GACCTGGGCATCCGTAAG (847-864 18 bp)	40 s 72 °C 50 s) × 35, 72 °C 7 min
Inner				
β -globulin	210 bp	Beta-globin	ACACAAGTGTGTTCACTAGC (120-139 20 bp)	94 °C 5 min (94 °C 30 s 55 °C
(PCO3-PCO5) ^[2]		human	GAAACCCAAGAGTCTTCTCT (310-329,20bp)	40 s 72 °C 1 min) × 35 72 °C 8 min
		DNA	AY128650	

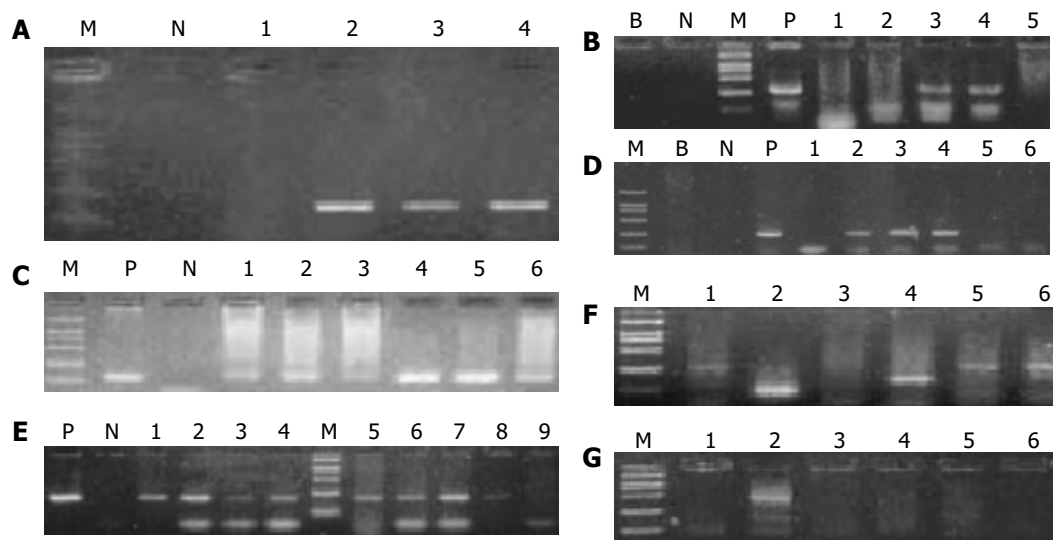


Figure 1 Results of PCR. P, positive control; N, negative control; B, blank control; M, marker of molecular mass. The sizes of the six bands of the marker are 2 000 bp, 1 000 bp, 750 bp, 500 bp, 250 bp, 100 bp, respectively. A: β -Globulin (Positive: Lanes 2-4, 210 bp), B: LMP 1 (Positive: Lanes 3 and 4, 337 bp), C: *Bam*HI W (Positive: Lanes 1-6, 130 bp), D: X gene (Positive: Lanes 2-4, 232 bp), E: S gene (Positive: Lanes 1-8, 198 bp), F: HCV (Positive: Lane 4, other lanes are nonspecific, 142bp), G: HDV (All are negative, Lane 5 is nonspecific).

positive for HBV X gene and three positive for HBV S gene. The positive rates were 8.0% (2 of 26) and 23.1% (6 of 26), respectively, for EBV DNA and HBV DNA (Figures 1A-G). The result of DNA sequencing of *Bam*HI W was 100% homologous with the corresponding sequence of B95-8 (Figure 2). There was significant difference in EBV infection rate between HCC patients and controls ($\chi^2 = 4.622, P < 0.05$). The difference in HBV infection rate was also significant ($\chi^2 = 8.681, P < 0.05$). However, there was no obvious correlation between HBV and EBV in HCC patients ($\chi^2 = 0.835$).

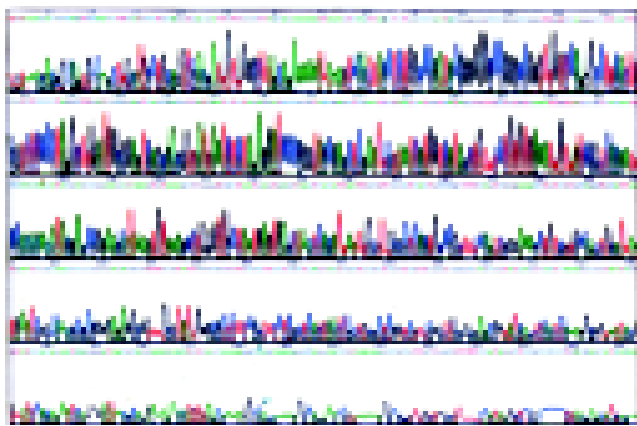


Figure 2 Sequencing results.

Immunohistochemistry

The immunohistochemical detection was performed for LMP1, HBV (HBsAg, HBcAg) and HCV in tissues of 78 cases of HCC, with 25, 45 and six cases positive, respectively. In the 26 control cases, the corresponding positive cases were two, four and zero. The difference in EBV infection rate between HCC patients and control cases was statistically significant ($\chi^2 = 6.02, P < 0.05$). The difference in HBV infection rate was also statistically significant ($\chi^2 = 10.03, P < 0.05$). In the 25 cases with positive LMP1 expression, six presented in the nuclei of tumor cells, nine in the cytoplasm of tumor cells and 10 in mesenchymal lymphocyte cytoplasm (Figures 3A-H).

DISCUSSION

EBV is considered as the first virus associated with human

malignancies including Burkitt's lymphoma^[3], T cell lymphoma^[4], parotid lymphoepithelioma^[5,6], nasopharyngeal carcinoma^[7], Hodgkin's disease^[8], gastric carcinoma^[9] and breast carcinoma^[10]. The virus proteins including EBNA1, 2, 3A, 3C, and LMP1 take part in the virus transformation and immortalization. Whether EBV has relation to HCC and whether it plays a role in the genesis of HCC has become the research focus of this field in recent years. However, the results so far are conflicting.

In Japan, Sugawara *et al.*^[11-13] found that the positive rate of EBNA1 in HCC was 37% and that cells infected by EBV could facilitate the replication of HCV. The positive rate of *Bam*HI W in HCC was 33% detected by PCR. Among patients with positive *Bam*HI W, anti-HCV positive rate was 40% and HBsAg positive rate was 14%, whereas the control subjects were all negative for anti-HCV and HBsAg. Moreover, EBV DNA load in HCC tissues was 1 000 times that in peripheral blood mononuclear cells of the healthy EBV-seropositive individuals. The authors concluded that EBV accelerates the onset of HCC and plays a role in oncogenesis of HCC, probably by promoting HCV replication, exacerbating inflammatory processes in liver tissue, promoting the proliferation of carcinoma cells or directly influencing tumorigenic potential. In China, Cheng *et al.*^[14] used EBV to transform the hepatitis C virus from an HCV positive patient to permanent lymphoblastoid cell lines. They found that HCV might exist and remain functional in a cultured cell line for a long period with the help of EBV. However, Chu *et al.*^[15] studied 41 cases of HCC from Los Angeles area in the United States, for evidence of EBV infection. Among these patients, one was positive for EBEB1 by *in situ* hybridization, and none was positive for LMP1 and EBNA4 by PCR. The authors concluded that there is no association between EBV and genesis of HCC. In addition, later studies carried out in Germany, United Kingdom and The Netherlands^[16-19] reported very low detection rates of EBV in HCC patients, further suggesting that EBV has little relation to hepatocellular carcinogenesis.

In our study, EBV DNA was detected in 28.2% of the HCC tissues by PCR while the positive rate of HBV DNA was 56.4%. HCV RNA was detected in 5.6% of the HCC tissues by RT-PCR while HDV RNA was not detected in all of 18 cases. The positive rate of LMP1 was 32.1% of the HCC tissues by immunohistochemistry. The positive signals of LMP1 were mainly localized in tumor cells. The infection rate of EBV was significantly higher in HCC patients than in control patients.

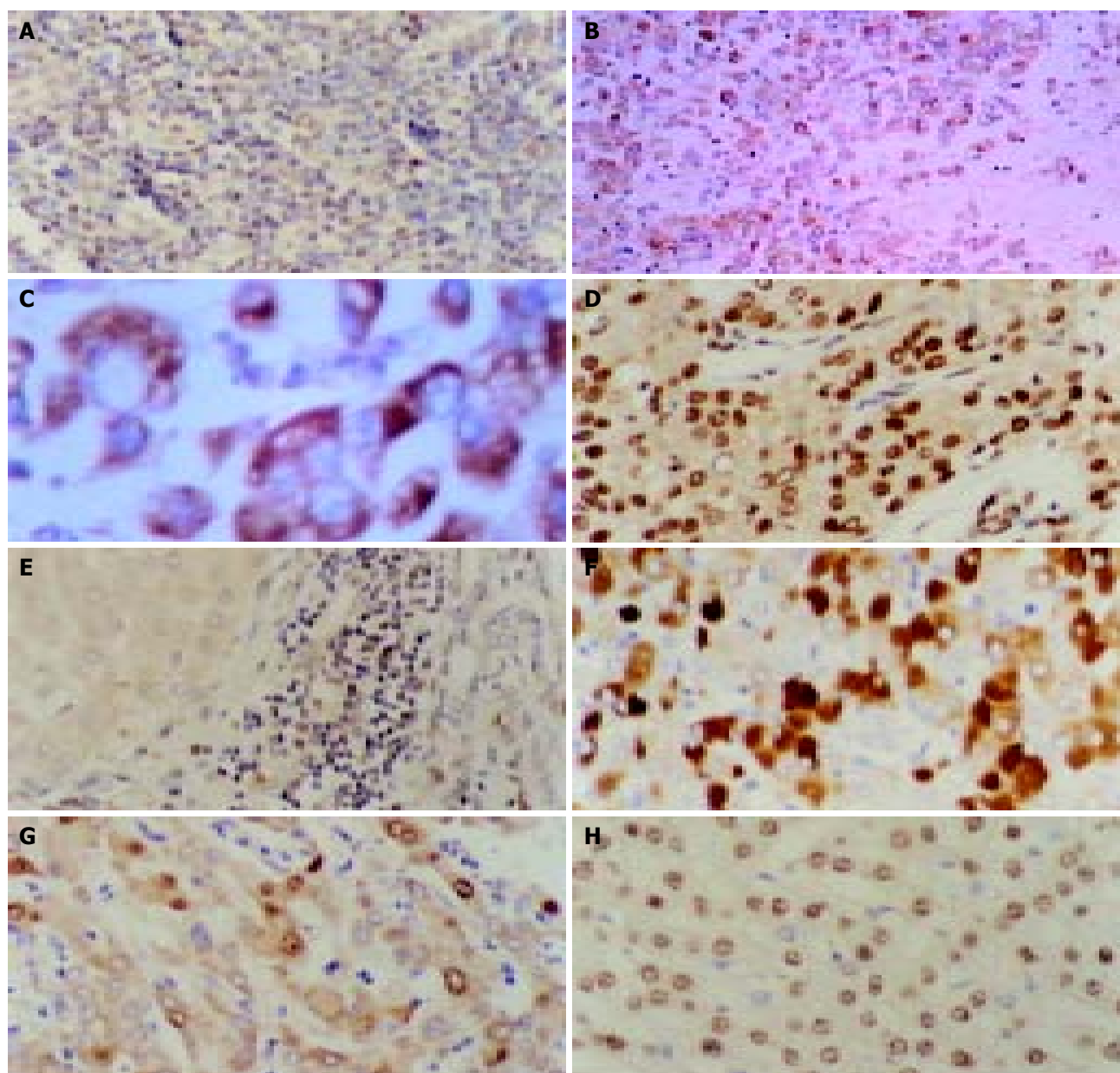


Figure 3 Results of immunohistochemistry. A: Positive-control of LMP1 from the tonsil tissue. The cytoplasm of lymphocytes showed positive signals. $\times 400$, B: Immunohistochemical staining with anti-LMP1 antibody of an HCC specimen. The positive signals were localized in the cytoplasm and membrane of neoplasm cells. $\times 100$, C: Immunohistochemical staining with anti-LMP1 antibody of an HCC specimen. The positive signals were localized in the cytoplasm and membrane of neoplasm cells. $\times 400$, D: Immunohistochemical staining with anti-LMP1 antibody of an HCC specimen. The positive signals were localized in the nuclei of neoplasm cells. $\times 400$, E: Immunohistochemical staining with anti-LMP1 antibody of an HCC specimen. The positive signals were localized in the interstitial lymphocytes but no clear positive signals were present in the adjacent neoplasm cells. $\times 400$, F: Immunohistochemical staining with anti-HBsAg antibody of an HCC specimen. The positive signals were localized in the cytoplasm of neoplasm cells. $\times 400$, G: Immunohistochemical staining with anti-HBsAg antibody of an HCC specimen. The positive signals were localized in the cytoplasm and nuclei of neoplasm cells. $\times 400$, H: Immunohistochemical staining with anti-HCV antibody of an HCC specimen. The positive signals were localized in the nuclei of neoplasm cells. $\times 400$.

These results are similar to those obtained by Sugawara *et al.* Moreover, we observed LMP1 expression in cytoplasm of interstitial lymphocytes in a large proportion of HCC tissues. Experiments *in vitro* have demonstrated that EBV can infect human B-lymphocytes, combine with C3d receptor on the surface of B lymphocyte and enter the cells, escape from the immune surveillance of the host, and then transform the cells. We postulate that EBV, which infects lymphocytes, can promote the genesis and development of HCC in an unidentified way.

Why the results of Sugawara *et al.* and ours are different from those of others? Previous studies produced controversial results on whether EBV played a role in the genesis and development of malignant tumors like breast cancer^[20-23],

esophageal cancer^[24,25], gastric cancer and colorectal cancer. It has been reported that the correlation between EBV and tumor incidence is stronger in Japan and Taiwan than in the western countries. Therefore, we assume that the significance of EBV in HCC may vary because of regional and racial differences. Further studies are required to reveal the underlying mechanism by which EBV contributes to hepatocellular carcinogenesis.

It has been confirmed that HBV and HCV play a certain part in hepatocellular carcinogenesis. Our study showed that EBV and HBV had no synergistic action in HCC, which is consistent with the report by Yuan *et al.*^[26]. Because the infection rate of HCV in our region is much lower than that in Japan, the issue whether HCV interacts with EBV in hepatocellular carcinogenesis

should be studied further. HDV is one kind of defective virus that can deteriorate the patient's condition if co-infected with HBV. It has been suggested that HDV also plays a role in hepatocellular carcinogenesis to some extent. But our study did not support such a point of view.

The method using paraffin-embedded samples for a retrospective molecular epidemiological study may be affected, to some extent, by sample processing and conservation. In this experiment, β -globulin gene was selected as an inner control in PCR amplification. Some cases in which DNA had been seriously degraded were excluded in order to reduce the false-negative rate. To increase the detectable rate, several indexes were used for each virus. *Bam*HI W is regarded as a sensitive index as it repeats 7 to 12 times in EBV genome. LMP1, as a major virus transform protein, is detected in tumors that are related to EBV such as nasopharyngeal carcinoma, Burkitt's lymphoma and other tumors. The primers and reaction conditions are also the important factors. We took advantage of the Internet and biology software to process sequence search, primer design and reaction condition simulation, and achieved a good performance.

The relationship between EBV and the malignant tumors including HCC is very complex and controversial. More studies with larger sample sizes are required to draw a scientific and precise conclusion. If the hypothesis that there is a relation between EBV and HCC comes into existence, then, research and development of EBV vaccines will become a more significant issue, and gene therapy aiming at EBV will be an important approach in the treatment of HCC.

ACKNOWLEDGEMENTS

The authors wish to acknowledge Professor Shu-Fang Tian from Heredity Laboratory, Institute for Viral Disease Prevention and Control, China CDC for kindly providing PSDHBV-1 plasmid. We also acknowledge Dr. Yi-Shu Yang, Dr. Shu-Hui Wang, and Dr. Hai-Jun Du from Oncogenic Virus Laboratory, Institute for Viral Disease Prevention and Control, China CDC for excellent assistance in the study.

REFERENCES

- Huang YP, Guo XC, He ZG, Zhao J, Zeng Y. Epstein-Barr virus induced thymus malignant T cell lymphoma. *Bindu Xuebao* 2001; **17**: 289-294
- Saiki RK, Scharf S, Faloona F, Mullis KB, Horn GT, Erlich HA, Arnheim N. Enzymatic amplification of beta-globin genomic sequences and restriction site analysis for diagnosis of sickle cell anemia. *Science* 1985; **230**: 1350-1354
- Bell A, Rickinson AB. Epstein-Barr virus, the TCL-1 oncogene and Burkitt's lymphoma. *Trends Microbiol* 2003; **11**: 495-497
- Yachie A, Kanegane H, Kasahara Y. Epstein-Barr virus-associated T-/natural killer cell lymphoproliferative diseases. *Semin Hematol* 2003; **40**: 124-132
- Kuo T, Hsueh C. Lymphoepithelioma-like salivary gland carcinoma in Taiwan: a clinicopathological study of nine cases demonstrating a strong association with Epstein-Barr virus. *Histopathology* 1997; **31**: 75-82
- Mok MY, Shek WH, Wong RW. Lymphoepithelioma-like carcinoma of the parotid gland in a patient with rheumatoid arthritis. *Clin Exp Rheumatol* 2002; **20**: 848-850
- Thorley-Lawson DA, Gross A. Persistence of the Epstein-Barr virus and the origins of associated lymphomas. *N Engl J Med* 2004; **350**: 1328-1337
- Gandhi MK, Tellam JT, Khanna R. Epstein-Barr virus-associated Hodgkin's lymphoma. *Br J Haematol* 2004; **125**: 267-281
- Mladenova I, Pellicano R. Infectious agents and gastric tumours. An increasing role for Epstein-Barr virus. *Panminerva Med* 2003; **45**: 183-188
- Wakiguchi H. Overview of Epstein-Barr virus-associated diseases in Japan. *Crit Rev Oncol Hematol* 2002; **44**: 193-202
- Sugawara Y, Mizugaki Y, Uchida T, Torii T, Imai S, Makuuchi M, Takada K. Detection of Epstein-Barr virus (EBV) in hepatocellular carcinoma tissue: a novel EBV latency characterized by the absence of EBV-encoded small RNA expression. *Virology* 1999; **256**: 196-202
- Sugawara Y, Makuuchi M, Kato N, Shimotohno K, Takada K. Enhancement of hepatitis C virus replication by Epstein-Barr virus-encoded nuclear antigen 1. *EMBO J* 1999; **18**: 5755-5760
- Sugawara Y, Makuuchi M, Takada K. Detection of Epstein-Barr virus DNA in hepatocellular carcinoma tissues from hepatitis C-positive patients. *Scand J Gastroenterol* 2000; **35**: 981-984
- Cheng JL, Liu BL, Zhang Y, Tong WB, Yan Z, Feng BF. Hepatitis C virus in human B lymphocytes transformed by Epstein-Barr virus *in vitro* by *in situ* reverse transcriptase-polymerase chain reaction. *World J Gastroenterol* 2001; **7**: 370-375
- Chu PG, Chen YY, Chen W, Weiss LM. No direct role for Epstein-Barr virus in American hepatocellular carcinoma. *Am J Pathol* 2001; **159**: 1287-1292
- Akhter S, Liu H, Prabhu R, DeLuca C, Bastian F, Garry RF, Schwartz M, Thung SN, Dash S. Epstein-Barr virus and human hepatocellular carcinoma. *Cancer Lett* 2003; **192**: 49-57
- Junying J, Herrmann K, Davies G, Lissauer D, Bell A, Timms J, Reynolds GM, Hubscher SG, Young LS, Niedobitek G, Murray PG. Absence of Epstein-Barr virus DNA in the tumor cells of European hepatocellular carcinoma. *Virology* 2003; **306**: 236-243
- Zur Hausen A, van Beek J, Bloemena E, ten Kate FJ, Meijer CJ, van den Brule AJ. No role for Epstein-Barr virus in Dutch hepatocellular carcinoma: a study at the DNA, RNA and protein levels. *J Gen Virol* 2003; **84**(Pt 7): 1863-1869
- Herrmann K, Niedobitek G. Epstein-Barr virus-associated carcinomas: facts and fiction. *J Pathol* 2003; **199**: 140-145
- Bonnet M, Guinebretiere JM, Kremmer E, Grunewald V, Benhamou E, Contesso G, Joab I. Detection of Epstein-Barr virus in invasive breast cancers. *J Natl Cancer Inst* 1999; **91**: 1376-1381
- Chu PG, Chang KL, Chen YY, Chen WG, Weiss LM. No significant association of Epstein-Barr virus infection with invasive breast carcinoma. *Am J Pathol* 2001; **159**: 571-578
- Touitou R, Bonnet-Duquenoy M, Joab I. Association of Epstein-Barr virus with human mammary carcinoma. Pros and cons. *Dis Markers* 2001; **17**: 163-165
- Preciado MV. Lack of evidence for an association of Epstein-Barr virus infection with breast carcinoma-another point of view. *Breast Cancer Res* 2003; **5**: E6
- Wang LS, Chow KC, Wu YC, Li WY, Huang MH. Detection of Epstein-Barr virus in esophageal squamous cell carcinoma in Taiwan. *Am J Gastroenterol* 1999; **94**: 2834-2839
- Kijima Y, Hokita S, Takao S, Baba M, Natsugoe S, Yoshinaka H, Aridome K, Otsuji T, Itoh T, Tokunaga M, Eizuru Y, Aikou T. Epstein-Barr virus involvement is mainly restricted to lymphoepithelial type of gastric carcinoma among various epithelial neoplasms. *J Med Virol* 2001; **64**: 513-518
- Yuan FP, Huang PS, Wang Y, Gong HS. Relationship between EBV infection in Fujian HCC and HBV and P53 protein expression. *Shijie Huaren Xiaohua Zazhi* 1999; **7**: 491-493

Expressions of cysteine-rich61, connective tissue growth factor and Nov genes in hepatocellular carcinoma and their clinical significance

Zhi-Jun Zeng, Lian-Yue Yang, Xiang Ding, Wei Wang

Zhi-Jun Zeng, Lian-Yue Yang, Xiang Ding, Wei Wang, Liver Cancer Laboratory, Department of Surgery, Xiangya Hospital, Central South University, Changsha 410008, Hunan Province, China

Supported by the National Key Technologies R and D Program, No. 2001BA703B04 and the National Natural Science Foundation of China, No.30371595

Correspondence to: Lian-Yue Yang, Liver Cancer Laboratory, Department of Surgery, Xiangya Hospital, Central South University, Changsha 410008, Hunan Province, China. lianyueyang@hotmail.com

Telephone: +86-731-4327326 **Fax:** +86-731-4327332

Received: 2004-02-28 **Accepted:** 2004-03-04

Abstract

AIM: To investigate the expression of cysteine-rich61 (Cyr61), connective tissue growth factor (CTGF) and nephroblastoma overexpressed gene (Nov) in hepatocellular carcinoma (HCC), and to evaluate the relationship between Cyr61, CTGF and Nov genes expression with invasion and metastasis of HCC.

METHODS: Thirty-one HCC specimens were divided into small hepatocellular carcinoma (SHCC), nodular hepatocellular carcinoma (NHCC), solitary large hepatocellular carcinoma (SLHCC) according to their diameter and number of nodes. Reverse transcription polymerase chain reaction (RT-PCR) was used to detect the mRNA expression levels of Cyr61, CTGF and Nov genes in 31 resected specimens of hepatocellular carcinoma and para-cancerous normal liver tissues semi-quantitatively and the relation between their expression levels and clinical pathological parameters were compared.

RESULTS: The expressions of Cyr61 and CTGF mRNA in carcinoma tissues were significantly higher than those in para-cancerous normal liver tissues ($P < 0.01$). The expressions of Cyr61 and CTGF mRNA in HCC with venous invasion were higher than those in HCC without venous invasion. CTGF expression in HCC Edmondson's grade III-IV was significantly higher than that in HCC Edmondson's grade I-II ($P = 0.022$). There was no obvious correlation between Nov mRNA and clinical-pathological features. Compared to NHCC, SLHCC had better cell differentiation, easier capsule formation, less microscopic venous invasion, milder liver cirrhosis. The expressions of Cyr61 and CTGF mRNA in NHCC were significantly higher than those in SLHCC and SHCC.

CONCLUSION: Cyr61 and CTGF genes may play an important role in hepatocellular carcinogenesis and correlate with recurrence and metastasis of hepatocellular carcinoma. SLHCC has better biological behaviors than NHCC.

Zeng ZJ, Yang LY, Ding X, Wang W. Expressions of cysteine-rich61, connective tissue growth factor and Nov genes in hepatocellular carcinoma and their clinical significance. *World J Gastroenterol* 2004; 10(23): 3414-3418
<http://www.wjgnet.com/1007-9327/10/3414.asp>

INTRODUCTION

Hepatocellular carcinoma (HCC) is one of the most common malignant cancers in the world, and the fourth most common cause of death from cancer, the second-leading cause of cancer death in China, which alone accounts for 53% of all liver cancer deaths worldwide. Although HCC resection plays an important role in improving HCC prognosis, it has been generally accepted that the high incidence of recurrence and metastasis is the most crucial prognostic factor in patients with HCC^[1]. The high recurrent rate in the liver with mainly intrahepatic metastatic spread remains a major obstacle to further improvement in the long-term survival after curative HCC resection^[2]. The mechanism of recurrence and metastasis of hepatocellular carcinoma is very complicated, and includes cell adhesion, matrix degradation, cell migration and angiogenesis^[3-7].

CCN gene family is a group of growth factor-inducible immediate-early genes, including cysteine-rich61 (Cyr61), connective tissue growth factor (CTGF), nephroblastoma overexpressed gene (Nov), Wnt-1 induced secreted protein 1 (WISP-1), WISP-2, WISP-3^[8,9]. CCN proteins are secreted extracellular matrix (ECM)-associated proteins that regulate cellular processes, such as adhesion, migration, mitogenesis, differentiation and survival^[10]. They also regulate more complex biological processes such as angiogenesis, chondrogenesis, tumorigenesis, fibrotic and vascular diseases^[11-13]. Cyr61 gene was originally identified as an immediately-early gene of mouse 3T3 fibroblasts, and was also found to be expressed in developing mouse cartilaginous elements and placental tissues^[14]. CTGF was originally identified in the conditioned culture medium of human umbilical vein endothelial cells, and revealed to be induced by transforming growth factor in human skin fibroblasts. Nov gene was identified as an aberrantly expressed gene in avian nephroblastomas induced by myeloblastosis-associated viruses. The overexpression of Nov gene was reported relative to human Wilms' tumors.

Taking cues from clinical observations and results of our laboratory researches, we have hypothesized that solitary large hepatocellular carcinoma (SLHCC) possesses relatively better biological behaviors^[15]. Furthermore, we have preliminarily proved our hypothesis by a series of researches^[16]. The clinical pathological features of SLHCC were better than nodular hepatocellular carcinoma (NHCC) and the molecular biological study also suggested that SLHCC possessed better molecular pathological features.

Cyr61, CTGF and Nov gene may overexpress in HCCs. In this report, we studied the expressions of Cyr61, CTGF and Nov genes in HCCs and para-cancerous normal liver tissues, to clarify whether these genes might play an important role in the recurrence and metastasis of HCCs. Furthermore, we examined the expressions of Cyr61, CTGF and Nov genes in SLHCC, NHCC and SHCC and compared their differences.

MATERIALS AND METHODS

Patients and tissue preparation

Thirty-one fresh HCC specimens and corresponding para-cancerous liver tissues were obtained by surgical resection at

Xiangya Hospital between March 2002 and March 2003. The patients with HCC consisted of 26 men and 5 women and the age of them ranged from 21 to 69 years (mean, 48 years). The patients were classified as SHCC (tumor largest diameter \leq 5 cm for a single tumor nodule or the sum of diameters \leq 5 cm for two tumor nodules), SLHCC (a single tumor nodule and tumor largest diameter $>$ 5 cm), NHCC (the nodules of tumor \geq 2, only two tumor nodules and the sum of diameters \leq 5 cm were excluded). Furthermore, we divided 31 specimens into six groups: tumors $<$ 5 cm diameter and \geq 5 cm, grade I-II and grade III-IV, liver cirrhosis and no liver cirrhosis, capsule formation and no capsule formation, microscopic portal vein tumor thrombosis and no microscopic portal vein tumor thrombosis. All specimens were examined under a microscope after haematoxylin and eosin (HE) staining.

RNA extraction and RT-PCR

Total RNA was isolated using Trizol reagent (GIBCO BRL, USA) and cDNA was synthesized from RNA by M-MLV reverse transcriptase (Promega, USA) with oligo-dT primers (Sango Technology, China). The primer sequences of Cyr61, CTGF and Nov genes were as follows: Cyr61, upstream: 5'-ACTTCATGGTCCCAGTGCGC-3', downstream: 5'-AAATCCGGGTTTCTTTCACA-3'; CTGF, upstream: 5'-GCAGGCTAGAGAAGCAGAGC-3', downstream: 5'-ATGTCTTCATGCTGGTGCAG-3'; Nov, upstream: 5'-AGCATGCAGAGTGTGCAGAG-3', downstream: 5'-GGTGTGCCACTTACCTGTCC-3'; β -actin, upstream: 5'-CTGCAATCCGAAAGAAGCTG-3', downstream: 5'-ATCTTCAAACCTCCATGATG-3'. The conditions of PCR were as follows: after an initial denaturation at 94 °C for 2 min, 30 cycles of denaturation at 94 °C for 30 s, annealing at 54 °C for 1 min and extension at 72 °C for 1 min. The bands representing amplified products were analyzed by Stratagene Eagle-eye scanner. Expressions of Cyr61, CTGF and Nov genes were presented by the relative yield of the PCR products of the target sequence to that of the β -actin gene.

Statistical analysis

The results of RT-PCR were statistically analyzed using the Student's *t* test. Fisher's exact test was used to determine the relationship between the expressions of Cyr61, CTGF and Nov genes and clinicopathological characteristics of HCCs. SPSS11.0 software was used. $P < 0.05$ was considered statistically significant.

RESULTS

Expression of Cyr61, CTGF and Nov mRNA in HCC and para-cancerous liver tissues

The expressions of Cyr61 and CTGF mRNA in HCC tissues were significantly higher than those in para-cancerous normal liver tissues. The expression of Nov gene was higher than that in para-cancerous normal liver tissues (Table 1). The difference in Nov gene expression between these two groups did not reach statistical significance. The expressions of Cyr61, CTGF and Nov genes are shown in Figure 1.

Table 1 Expression of Cyr61, CTGF and Nov mRNA in HCC and para-cancerous liver tissues (mean \pm SD)

	<i>n</i>	Cyr61	CTGF	Nov
HCC	31	2.34 \pm 0.46 ^b	2.21 \pm 0.34 ^b	1.56 \pm 0.21
Para-cancerous	31	0.48 \pm 0.29	0.65 \pm 0.33	0.89 \pm 0.64

^b $P < 0.01$ vs para-cancerous tissues.

Between the groups with different pathological characteristics, the expressions of Cyr61, CTGF and Nov genes were significantly different. Especially, the differences between the two groups with and without microscopic portal vein tumor thrombosis were of great significance. Moreover, CTGF expression was significantly different between Edmondson's grades I-II and III-IV. The relationship between the expression of Cyr61, CTGF, Nov mRNA and clinicopathological features of HCC patients is shown in Table 2.

Clinical and pathological features of three types of HCC

Thirty-one HCC specimens were divided into SLHCC, SHCC and NHCC according to their diameter and number of nodules. Liver cirrhosis, microvascular invasion, capsule formation, Edmondson's classification of HCC were studied in each group. NHCC group had a higher incidence of microvascular invasion compared with SLHCC and SHCC ($P < 0.05$). Only 8.3% of NHCCs were classified as Edmondson's grade I-II, while 62.5% of SLHCC and 63.6% of SHCC were classified as Edmondson's grade I-II. The differentiation of NHCC was significantly poorer than that of SLHCC and SHCC ($P < 0.05$). The other three pathological features of SLHCC and SHCC were also better than NHCC but did not reach statistical significance. No statistical difference in the five pathological features was observed between SLHCC and SHCC (Table 3).

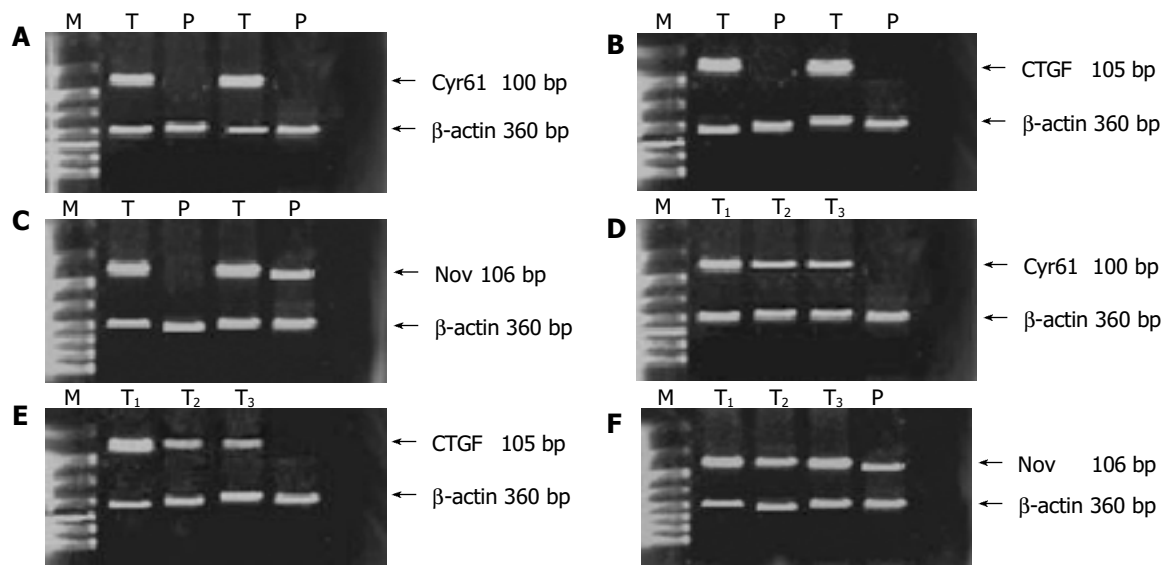


Figure 1 Expressions of Cyr61, CTGF and Nov mRNA in hepatocellular carcinoma A and D : Cyr61 mRNA expression, product size 100 bp; B and E : CTGF mRNA expression, product size 105 bp; C and F: Nov mRNA expression, product size 106 bp; M, DNA marker; T, tumor; P, para-cancerous normal liver tissues; T₁, NHCC; T₂, SLHCC; T₃, SHCC. PCR product of β -actin was 360 bp.

Table 2 Relationship between Cyr61, CTGF and Nov mRNA expressions and clinicopathological features (mean±SD)

	<i>n</i>	Cyr61	<i>P</i>	CTGF	<i>P</i>	Nov	<i>P</i>
PV thrombosis							
Present	16	2.59±0.41	0.024	2.41±0.39	0.031	1.45±0.56	0.147
Absent	15	2.08±0.65		2.10±0.58		1.56±0.45	
AFP level							
≤20 ng/mL	19	2.26±0.48	0.068	2.21±0.20	0.063	1.38±0.43	0.241
>20 ng/mL	12	2.36±0.71		2.23±0.84		1.66±0.71	
Tumor size (cm)							
≤ 5 cm	20	2.35±0.86	0.124	2.26±0.79	0.071	1.59±0.58	0.251
> 5 cm	11	2.32±0.41		2.09±0.53		1.55±0.31	
Capsule formation							
Positive	18	2.35±0.34	0.136	2.31±0.34	0.132	1.87±0.65	0.135
Negative	13	2.33±0.67		2.15±0.87		1.36±0.81	
Histological grade							
I-II	13	2.21±0.39	0.052	1.89±0.54	0.022	1.35±0.47	0.132
III-IV	18	2.51±0.41		2.51±0.61		1.58±0.68	

PV: portal vein.

Table 3 Pathological features of three types of HCC

Pathological features	<i>n</i>	SHCC (<i>n</i> =11)	NHCC (<i>n</i> =12)	SLHCC (<i>n</i> =8)
Microvascular invasion				
Present	16	3	10	3 ^a
Absent	15	8	2	5
Capsule formation				
Present	18	8	4	6
Absent	13	3	8	2
Edmondson's classification				
I-II	13	7	1	5 ^a
III-IV	18	4	11	3
Liver cirrhosis				
Present	9	4	9	2
Absent	22	7	3	6
AFP concentration				
≤20 ng/mL	19	6	9	4
>20 ng/mL	12	5	3	4

^a*P*<0.05 vs NHCC.

Expression of Cyr61, CTGF and Nov mRNA in three types of HCCs

The expression of Cyr61 mRNA in NHCC was significantly higher than that in SLHCC and SHCC (*P* = 0.024 and *P* = 0.031, respectively). The expression of CTGF mRNA in nodular HCC was also significantly higher than that in SLHCC and SHCC (*P* = 0.016 and *P* = 0.027, respectively). No statistical difference in the expression of Nov gene among NHCC, SLHCC and SHCC was observed (Table 4).

Table 4 Cyr61, CTGF and Nov mRNA expressions in three types of HCCs

HCC	<i>n</i>	Cyr61	<i>P</i>	CTGF	<i>P</i>	Nov	<i>P</i>
SLHCC	8	2.22±0.36		2.09±0.44		1.52±0.41	
NHCC	12	2.51±0.53	0.037 ^a	2.38±0.29	0.043 ^a	1.58±0.36	0.287
SHCC	11	2.18±0.42		2.03±0.31		1.46±0.19	

^a*P*<0.05 vs SLHCC.

DISCUSSION

All members of the CCN gene family possess a secretory signal peptide at the N terminus, indicating that they are secreted proteins. Several lines of evidence supported a role of CCN molecules in tumorigenesis^[8].

Cyr61 is a secreted, 40-kDa, cysteine-rich and heparin-binding protein coded by a growth factor-inducible immediate early gene^[14]. Recently, it has been reported as an angiogenic inducer that can promote tumor growth and vascularization^[17]. A mechanistic framework for the biological properties of Cyr61 has been provided by the finding that Cyr61 binds to integrin $\alpha_v\beta_3$, which represents the first molecularly defined receptor for any member of the CCN family^[18]. Interaction of $\alpha_v\beta_3$ with Cyr61 may account for its promotion of chemotaxis and growth factor-mediated DNA synthesis as well as cell adhesion since integrins have been known to modulate cell migration and growth factor signaling in other systems^[16,17]. In a direct interaction between the two molecules, Cyr61-mediated adhesion and migration of cultured endothelial cells were specifically inhibited by the peptide RGDS and/or antiintegrin $\alpha_v\beta_3$ ^[19-23]. In addition to its integrin-binding property, Cyr61 appears to be localized to its site of synthesis by associating with the ECM, possibly by binding to heparin-like molecules. This interaction could limit the extent of Cyr61 diffusion so that its site of action is in close proximity of its site of synthesis^[24]. In our study, the expression of Cyr61 gene in HCC tissue was markedly higher than that in para-cancerous normal liver tissues, indicating that Cyr61 may play an important role in hepatocellular carcinogenesis.

CTGF is a cysteine-rich mitogenic peptide that was originally identified as a growth factor secreted by vascular endothelial cells^[25]. It was selectively induced in fibroblasts after activation with TGF β ^[26]. A previous study demonstrated the coordinate expression of TGF1 and CTGF in granulation beds during wound

repair, and found that dermal fibroblasts in scleroderma lesions overexpressed CTGF^[27]. In addition to contributing to TGF- β -mediated AIG, CTGF could interact synergistically with EGF, PDGF, IGF-I, or bFGF, suggesting that it activates the receptors and/or signaling pathways used by other growth factors^[28,29]. Consistent with its profibrotic properties, CTGF has been found to be overexpressed in pancreatic cancers, mammary tumors, and melanomas^[30-32]. In our study, the expression of CTGF gene in HCC tissue was obviously higher than that in para-cancerous normal liver tissues, indicating that CTGF might play an important role in hepatocellular carcinogenesis.

Nov gene was first recognized as an overexpressed gene in nephroblastomas induced by myeloblastosis-associated virus type 1^[33]. Unlike the other members of this family, Nov gene expression was associated with quiescence and transcriptionally downregulated upon expression of p60 v-src in RSV-infected CEF^[34]. It has been reported that overexpression of normal Nov gene in CEF has an inhibitory effect on cell growth, whereas expression of an amino-terminal truncated form of Nov gene was able to induce morphological transformation^[35,36]. Therefore, Nov is a negative regulator of cell growth, the amino-truncation of which would result in oncogenic activation^[37,38]. Also, Koliopoulos *et al.*^[42] reported that Nov was a ligand of integrins $\alpha_v\beta_3$ and $\alpha_5\beta_1$, and acted directly upon endothelial cells to stimulate pro-angiogenic activities, thus inducing angiogenesis *in vivo*. While, in our study, the expression of Nov gene in HCC and para-cancerous normal liver tissues had no difference. The diagnostic significance of Nov gene expression in HCC needs to be further investigated with more samples.

Metastasis and invasion of HCC is a multistep process, the molecular and cellular mechanisms of which have not been fully understood^[39]. They may involve matrix degradation, cell motility, angiogenesis, *etc.* CCN proteins could regulate biological processes such as angiogenesis, chondrogenesis, tumorigenesis, fibrotic and vascular diseases^[4-6,40]. Numerous *in vitro* studies indicated that Cyr61 protein was related to angiogenesis^[41]. Overexpressions of Cyr61, CTGF and Nov genes have been found in metastatic lesions of esophageal cancer, breast cancer, colon tumors, lung cancer and osteosarcoma^[42-45]. In the present study, we statistically analyzed the clinical and pathological parameters. No significant correlation was found among the parameters of age, sex, cause of liver diseases. Cyr61 and CTGF mRNA levels in patients with portal vein tumor thrombosis were significantly higher compared to those in patients without portal vein invasion. Moreover, CTGF mRNA level in Edmondson's grade III-IV was significantly higher than that in Edmondson's grade I-II. These results indicated that Cyr61 and CTGF had a close relationship with invasion and metastasis of HCC.

Previous studies have shown that SLHCC is different from other types of HCC in pathological features and invasiveness^[16]. Coordinated with this, the relatively better pathological features of SHCC were found in this study. The differentiation of SLHCC was much better than that of NHCC, and microvascular invasion was observed more frequently in NHCC compared with SLHCC. No statistical difference in pathological features was observed between SHCC and SLHCC. In addition, the transcription level of Cyr61 and CTGF in NHCC was much higher than that in SLHCC and SHCC, while no statistical difference was observed between SLHCC and SHCC. The lower transcription of Cyr61 and CTGF mRNA in SLHCC was probably due to the relatively better molecular pathological features of SLHCC.

Our findings indicate that Cyr61 and CTGF genes are related to tumorigenesis of HCC, and may enhance the invasion and metastasis of HCC. Its molecular basis remains to be elucidated. What are the most important factors regulating the expression level of CCN family and how does CCN gene family regulate effector protein will be the subjects of our future studies. When

the upstream and downstream signaling pathways are understood, those findings will provide new potential tools for the prognosis or prevention of invasion and metastasis of HCC.

REFERENCES

- 1 **Zhou XD.** Recurrence and metastasis of hepatocellular carcinoma: progress and prospects. *Hepatobiliary Pancreat Dis Int* 2002; **1**: 35-41
- 2 **Nakashima Y,** Nakashima O, Tanaka M, Okuda K, Nakashima M, Kojiro M. Portal vein invasion and intrahepatic micrometastasis in small hepatocellular carcinoma by gross type. *Hepatol Res* 2003; **26**: 142-147
- 3 **Shiratori Y,** Yoshida H, Omata M. Management of hepatocellular carcinoma: advances in diagnosis, treatment and prevention. *Expert Rev Anticancer Ther* 2001; **1**: 277-290
- 4 **Arizumi S,** Takasaki K, Yamamoto M, Ohtsubo T, Katsuragawa H, Katagiri S. Histopathologic differentiation of the main nodule determines outcome after hepatic resection for synchronous multicentric hepatocellular carcinomas. *Hepatogastroenterology* 2004; **51**: 500-504
- 5 **McGlynn KA,** Edmonson MN, Michielli RA, London WT, Lin WY, Chen GC, Shen FM, Buetow KH. A phylogenetic analysis identifies heterogeneity among hepatocellular carcinomas. *Hepatology* 2002; **36**: 1341-1348
- 6 **Murawaki Y,** Ikuta Y, Okamoto K, Mimura K, Koda M, Kawasaki H. Plasma matrix metalloproteinase-9 (gelatinase B) in patients with hepatocellular carcinoma. *Res Commun Mol Pathol Pharmacol* 2000; **108**: 351-357
- 7 **Mukai M,** Nakamura H, Tatsuta M, Iwasaki T, Togawa A, Imamura F, Akedo H. Hepatoma cell migration through a mesothelial cell monolayer is inhibited by cyclic AMP-elevating agents via a Rho-dependent pathway. *FEBS Lett* 2000; **484**: 69-73
- 8 **Bork P.** The modular architecture of a new family of growth regulators related to connective tissue growth factor. *FEBS Lett* 1993; **327**: 125-130
- 9 **Brigstock DR,** Goldschmeding R, Katsube KI, Lam SC, Lau LF, Lyons K, Naus C, Perbal B, Riser B, Takigawa M, Yeger H. Proposal for a unified CCN nomenclature. *Mol Pathol* 2003; **56**: 127-128
- 10 **Kireeva ML,** MO FE, Yang GP, Lau LF. Cyr61, a product of a growth factor-inducible immediate-early gene, promotes cell proliferation, migration, and adhesion. *Mol Cell Biol* 1996; **16**: 1326-1334
- 11 **Hadjiargyrou M,** Ahrens W, Rubin CT. Temporal expression of the chondrogenic and angiogenic growth factor CYR61 during fracture repair. *J Bone Miner Res* 2000; **15**: 1014-1023
- 12 **Brigstock DR,** Steffen CL, Kim GY, Vegunta RK, Diehl JR, Harding PA. Purification and characterization of novel heparin-binding growth factors in uterine secretory fluids. Identification as heparin-regulated M_r 10000 forms of connective tissue growth factor. *J Biol Chem* 1997; **272**: 20275-20282
- 13 **Lake AC,** Bialik A, Walsh K, Castellot JJ Jr. CCN5 is a growth arrest-specific gene that regulates smooth muscle cell proliferation and motility. *Am J Pathol* 2003; **162**: 219-231
- 14 **O'Brien TP,** Lau LF. Expression of the growth factor-inducible immediate early gene *cyr61* correlates with chondrogenesis during mouse embryonic development. *Cell Growth Differ* 1992; **3**: 645-654
- 15 **Yang LY,** Huang GW. Surgical strategy of large hepatocellular carcinoma. *Linchuang Waikie Zazhi* 2001; **9**: 4-5
- 16 **Liu HL,** Yang LY, Huang GW, Yang JQ. The effect of integrin α_v subunit on the angiogenesis, invasiveness and metastasis of hepatocellular carcinoma. *Zhonghua Putong Waikie Zazhi* 2002; **9**: 542-543
- 17 **Inoki I,** Shiomi T, Hashimoto G, Enomoto H, Nakamura H, Makino K, Ikeda E, Takata S, Kobayashi K, Okada Y. Connective tissue growth factor binds vascular endothelial growth factor (VEGF) and inhibits VEGF-induced angiogenesis. *FASEB J* 2002; **16**: 219-221
- 18 **Leng E,** Malcolm T, Tai G, Estable M, Sadowski I. Organization and expression of the Cyr61 gene in normal human fibroblasts. *J Biomed Sci* 2002; **9**: 59-67
- 19 **Grzeszkiewicz TM,** Kirschling DJ, Chen N, Lau LF. CYR61

- stimulates human skin fibroblast migration through Integrin alpha vbeta 5 and enhances mitogenesis through integrin alpha vbeta 3, independent of its carboxyl-terminal domain. *J Biol Chem* 2001; **276**: 21943-21950
- 20 **Fataccioli V**, Abergel V, Wingertsman L, Neuville P, Spitz E, Adnot S, Calenda V, Teiger E. Stimulation of angiogenesis by Cyr61 gene: a new therapeutic candidate. *Hum Gene Ther* 2002; **13**: 1461-1470
 - 21 **Hilfiker A**, Hilfiker-Kleiner D, Fuchs M, Kaminski K, Lichtenberg A, Rothkotter HJ, Schieffer B, Drexler H. Expression of CYR61, an angiogenic immediate early gene, in arteriosclerosis and its regulation by angiotensin II. *Circulation* 2002; **106**: 254-260
 - 22 **Kothapalli D**, Grotendorst GR. CTGF modulates cell cycle progression in cAMP-arrested NRK fibroblasts. *J Cell Physiol* 2000; **182**: 119-126
 - 23 **Schober JM**, Chen N, Grzeszkiewicz TM, Jovanovic I, Emeson EE, Ugarova TP, Ye RD, Lau LF, Lam SC. Identification of integrin alpha (M) beta (2) as an adhesion receptor on peripheral blood monocytes for Cyr61 (CCN1) and connective tissue growth factor (CCN2): immediate-early gene products expressed in atherosclerotic lesions. *Blood* 2002; **99**: 4457-4465
 - 24 **Tamura I**, Rosenbloom J, Macarak E, Chaqour B. Regulation of Cyr61 gene expression by mechanical stretch through multiple signaling pathways. *Am J Physiol Cell Physiol* 2001; **281**: C1524-1532
 - 25 **Surveyor GA**, Wilson AK, Brigstock DR. Localization of connective tissue growth factor during the period of embryo implantation in the mouse. *Biol Reprod* 1998; **59**: 1207-1213
 - 26 **Wang JF**, Olson ME, Reno CR, Wright JB, Hart DA. The pig as a model for excisional skin wound healing: characterization of the molecular and cellular biology, and bacteriology of the healing process. *Comp Med* 2001; **51**: 341-348
 - 27 **Maquart FX**, Chastang F, Simeon A, Birembaut P, Gillery P, Wegrowski Y. Triterpenes from *Centella asiatica* stimulate extracellular matrix accumulation in rat experimental wounds. *Eur J Dermatol* 1999; **9**: 289-296
 - 28 **Denton CP**, Abraham DJ. Transforming growth factor-beta and connective tissue growth factor: key cytokines in scleroderma pathogenesis. *Curr Opin Rheumatol* 2001; **13**: 505-511
 - 29 **Ehrchen J**, Heuer H, Sigmund R, Schafer MK, Bauer K. Expression and regulation of osteopontin and connective tissue growth factor transcripts in rat anterior pituitary. *J Endocrinol* 2001; **169**: 87-96
 - 30 **Wenger C**, Ellenrieder V, Alber B, Lacher U, Menke A, Hameister H, Wilda M, Iwamura T, Beger HG, Adler G, Gress TM. Expression and differential regulation of connective tissue growth factor in pancreatic cancer cells. *Oncogene* 1999; **18**: 1073-1080
 - 31 **Frazier KS**, Grotendorst GR. Expression of connective tissue growth factor mRNA in the fibrous stroma of mammary tumors. *Int J Biochem Cell Biol* 1997; **29**: 153-161
 - 32 **Kubo M**, Kikuchi K, Nashiro K, Kakinuma T, Hayashi N, Nanko H, Tamaki K. Expression of fibrogenic cytokines in desmoplastic malignant melanoma. *Br J Dermatol* 1998; **139**: 192-197
 - 33 **Perbal B**. NOV (nephroblastoma overexpressed) and the CCN family of genes: structural and functional issues. *Mol Pathol* 2001; **54**: 57-79
 - 34 **Babic AM**, Kireeva ML, Kolesnikova TV, Lau LF. CYR61, a product of a growth factor-inducible immediate early gene, promotes angiogenesis and tumor growth. *Proc Natl Acad Sci U S A* 1998; **95**: 6355-6360
 - 35 **Xie D**, Nakachi K, Wang H, Elashoff R, Koeffler HP. Elevated levels of connective tissue growth factor, WISP-1, and CYR61 in primary breast cancers associated with more advanced features. *Cancer Res* 2001; **61**: 8917-8923
 - 36 **Sakamoto K**, Yamaguchi S, Ando R, Miyawaki A, Kabasawa Y, Takagi M, Li CL, Perbal B, Katsube K. The nephroblastoma overexpressed gene (NOV/ccn3) protein associates with Notch1 extracellular domain and inhibits myoblast differentiation via Notch signaling pathway. *J Biol Chem* 2002; **277**: 29399-29405
 - 37 **Kocialkowski S**, Yeger H, Kingdom J, Perbal B, Schofield PN. Expression of the human NOV gene in first trimester fetal tissues. *Anat Embryol* 2001; **203**: 417-427
 - 38 **Lin CG**, Leu SJ, Chen N, Tebeau CM, Lin SX, Yeung CY, Lau LF. CCN3 (NOV) is a novel angiogenic regulator of the CCN protein family. *J Biol Chem* 2003; **278**: 24200-24208
 - 39 **Zhao ZC**, Zheng SS, Wan YL, Jia CK, Xie HY. The molecular mechanism underlying angiogenesis in hepatocellular carcinoma: the imbalance activation of signaling pathways. *Hepatobiliary Pancreat Dis Int* 2003; **2**: 529-536
 - 40 **Chaqour B**, Whitbeck C, Han JS, Macarak E, Horan P, Chichester P, Levin R. Cyr61 and CTGF are molecular markers of bladder wall remodeling after outlet obstruction. *Am J Physiol Endocrinol Metab* 2002; **283**: E765-774
 - 41 **Wenger C**, Ellenrieder V, Alber B, Lacher U, Menke A, Hameister H, Wilda M, Iwamura T, Beger HG, Adler G, Gress TM. Expression and differential regulation of connective tissue growth factor in pancreatic cancer cells. *Oncogene* 1999; **18**: 1073-1080
 - 42 **Koliopoulos A**, Friess H, di Mola FF, Tang WH, Kubulus D, Brigstock D, Zimmermann A, Buchler MW. Connective tissue growth factor gene expression alters tumor progression in esophageal cancer. *World J Surg* 2002; **26**: 420-427
 - 43 **Pennica D**, Swanson TA, Welsh JW, Roy MA, Lawrence DA, Lee J, Brush J, Taneyhill LA, Deuel B, Lew M, Watanabe C, Cohen RL, Melhem MF, Finley GG, Quirke P, Goddard AD, Hillan KJ, Gurney AL, Botstein D, Levine AJ. WISP genes are members of the connective tissue growth factor family that are up-regulated in wnt-1- transformed cells and aberrantly expressed in human colon tumors. *Proc Natl Acad Sci U S A* 1998; **95**: 14717-14722
 - 44 **Astolfi A**, De Giovanni C, Landuzzi L, Nicoletti G, Ricci C, Croci S, Scopece L, Nanni P, Lollini PL. Identification of new genes related to the myogenic differentiation arrest of human rhabdomyosarcoma cells. *Gene* 2001; **274**: 139-149
 - 45 **Sampath D**, Winneker RC, Zhang Z. Cyr61, a member of the CCN family, is required for MCF-7 cell proliferation: regulation by 17beta-estradiol and overexpression in human breast cancer. *Endocrinology* 2001; **142**: 2540-2548

Peroxisome proliferator-activated receptor γ ligands suppress liver carcinogenesis induced by diethylnitrosamine in rats

Yan-Tong Guo, Xi-Sheng Leng, Tao Li, Jing-Ming Zhao, Xi-Hou Lin

Yan-Tong Guo, Jing-Ming Zhao, Xi-Hou Lin, Department of General Surgery, Beijing Jishuitan Hospital, the Forth Clinical Medical College of Peking University, Beijing 100035, China

Xi-Sheng Leng, Tao Li, Department of General Surgery, People's Hospital of Peking University, Beijing 100044, China

Supported by the National Natural Science Foundation of China, No. 30371387

Correspondence to: Yan-Tong Guo, PhD and M.D., Department of General Surgery, Beijing Jishuitan Hospital, the Forth Clinical Medical College of Peking University, Beijing 100035, China. guoyantong2002@sohu.com

Telephone: +86-10-86995076

Received: 2004-03-11 **Accepted:** 2004-04-13

Abstract

AIM: Peroxisome proliferator-activated receptor γ (PPAR γ) is known to regulate growth arrest and terminal differentiation of adipocytes and is used clinically as a new class of antidiabetic drugs. Recently, several studies have reported that treatment of cancer cells with PPAR γ ligands could induce cell differentiation and apoptosis, suggesting a potential application as chemopreventive agents against carcinogenesis. In the present study, 3 different kinds of PPAR γ ligands were subjected to the experiments to confirm their suppressive effects on liver carcinogenesis.

METHODS: Three PPAR γ ligands, pioglitazone (Pio) (200 ppm), rosiglitazone (Rosi) (200 ppm), and troglitazone (Tro) (1 000 ppm) were investigated on the induction of the placental form of rat glutathione S-transferase (rGST P) positive foci, a precancerous lesion of the liver, and liver cancer formation using a diethylnitrosamine-induced liver cancer model in Wistar rats, and dose dependency of a PPAR γ ligand was also examined.

RESULTS: PPAR γ ligands reduced the formation of rGST P-positive foci by diethylnitrosamine and induction of liver cancers was also markedly suppressed by a continuous feeding of Pio at 200 ppm.

CONCLUSION: PPAR γ ligands are potential chemopreventive agents for liver carcinogenesis.

Guo YT, Leng XS, Li T, Zhao JM, Lin XH. Peroxisome proliferator-activated receptor γ ligands suppress liver carcinogenesis induced by diethylnitrosamine in rats. *World J Gastroenterol* 2004; 10(23): 3419-3423

<http://www.wjgnet.com/1007-9327/10/3419.asp>

INTRODUCTION

Carcinogenesis is a complex process that has been divided into three stages: initiation, promotion and progression^[1]. These three stages of tumor formation have been characterized in many mammalian tissues, particularly in the liver^[2,3]. According to the concept of multistage carcinogenesis, clones of cells

arise with increasing autonomy from normal growth regulation at each stage of development, and from these selected populations of cells, neoplasms ultimately develop^[4]. The placental form of rat glutathione S-transferase (rGST P) positive foci is thought to be preneoplastic lesions of the liver^[5-12].

Peroxisome proliferator-activated receptor γ (PPAR γ), a nuclear hormone receptor, provides a strong link between lipid metabolism and regulation of gene transcription. PPAR γ is known to regulate growth arrest and terminal differentiation of adipocytes, and a group of PPAR γ activators are now widely prescribed and form a new class of antidiabetic drugs. Several specific ligands have been identified, such as the thiazolidinedione groups, including pioglitazone (Pio), rosiglitazone (Rosi), and troglitazone (Tro), 15-deoxy-prostaglandin J₂, and certain polyunsaturated fatty acids^[13]. PPAR γ is expressed in various organs including adipose tissue, breast epithelium, small intestine, lungs, and liver^[13]. Several studies have reported that treatment of cancer cells with PPAR γ ligands could induce cell differentiation and apoptosis, suggesting a potential application as chemopreventive agents against carcinogenesis^[14].

In present study, 3 different kinds of PPAR γ ligands were subjected to the experiments to confirm their suppressive effects on liver carcinogenesis in the rat model. In experiment 1, we investigated the effects of 3 PPAR γ ligands, Pio, Rosi, and Tro, on the development of rGST P-positive foci that were induced by diethylnitrosamine (DEN)^[6]. Dose dependency of the PPAR γ ligand was also examined. In experiment 2, a long-term carcinogenesis study of DEN was conducted^[15]. Our findings indicate that PPAR γ ligands are potential chemopreventive agents for liver carcinogenesis.

MATERIALS AND METHODS

Chemicals and animals

DEN was purchased from Beijing Chemical Reagents Company (Beijing, China). Three different PPAR γ ligands, Pio, Rosi, and Tro, were kindly provided by GlaxoSmithKline (BN, United Kingdom). To prepare experimental diets, each PPAR γ ligand was mixed with a powdered basal diet and stored at 4 °C until use. Fresh diets were provided to the rats once a week, and the dietary intake and body mass (bm) for each group of rats were measured every week. Concentrations of PPAR γ in experimental diets were 200 and 1 000 ppm for Pio and Tro, respectively. For Rosi, various concentrations in the diet, ranging from 0.88 to 500 ppm, were used to evaluate the dose-response effect of PPAR γ ligands on the formation of rGST P-positive foci. Fifteen-week-old male Wistar rats were purchased from Peking University Health Science Center (Beijing, China) and housed in a ventilated, temperature-controlled room (23±1 °C) with a 12-h light/dark cycle. After a period of 1-week acclimatization to the housing environment and the basal diet, groups of rats were fed either the basal diet or the experimental diet containing one of the PPAR γ ligands, from sixteen weeks of age until termination.

Induction of rGST P-positive foci (Experiment 1)

Rats were divided into 8 experimental groups, 4 DEN treated and

4 vehicle-treated. In DEN-treated cases (groups 1-4, Figure 1A), groups of 10 rats were fed diets without ligands (basal diet, group 1) or with a PPAR γ ligand (experimental diet, groups 2-4), beginning 1 wk prior to the subcutaneous injection of DEN as described below and continued until the end of the experiment. Starting at sixteen weeks of age (experimental wk 1), rats in each group were administered DEN subcutaneously twice, at 1-week intervals at a dose of 20 mg/kg bm in saline. In the vehicle-treated groups (groups 5-8, Figure 1A), groups of 5 rats were fed the basal diet (group 5) or experimental diet (groups 6-8) and given subcutaneous injections of an equal volume of saline without DEN. Four weeks after the first administration of DEN or saline, all rats were killed at experimental week 5. In a separate experiment, dose-dependent effect of Rosi, within the range of 0.67-500 ppm in diet, on formation of rGST P-positive foci was also examined. The entire liver was removed, and fixed in 40 g/L neutralized formaldehyde overnight at 4 °C. Then the liver sections were embedded in paraffin. Immunohistochemical staining was performed on sections by the peroxidase-antiperoxidase method, using the antibody against the rGST P. Sections were counterstained with haematoxylin. The number of rGST P-positive foci (consisting of single to several GST P positive cells, indicating preneoplastic lesions) was expressed as per cm² of liver sections^[16].

Induction of liver tumors (Experiment 2)

As in Experiment 1, rats were fed either the experimental diet or the basal diet, starting 1 wk prior to the injection of DEN or vehicle. A total of 80 rats were divided into 4 experimental groups, 2 DEN treated and 2 vehicle treated. For the former, groups of 30 rats were fed diets without ligands (basal diet) or with PPAR γ ligands (basal diet + pioglitazone 200 ppm), beginning 1 wk prior to the subcutaneous injection of DEN as described below and continued until the end of the experiment (Figure 1B). Starting at 16 wk of age (experimental week 1), rats in each group were administered DEN subcutaneously 6 times at 1-wk intervals at a dose of 20 mg/kg bm in saline. In the vehicle-treated groups, groups of 10 rats were fed the basal diet or experimental diet (basal diet + pioglitazone 200 ppm) and given subcutaneous injections of an equal volume of saline without DEN (Figure 1B). All surviving animals were killed 60 wk after the first injection of DEN. Livers were removed and fixed in 10% neutralized formalin as described above. The number, size, and location of liver tumors detected macroscopically or by stereomicroscopic observation were determined. Diameters were measured in 3 dimensions, and tumor size was calculated by (height + width + length)/3.

Histologic analysis of liver slices

Liver slices were embedded in paraffin blocks according to the standard procedures. In the case of liver tumors, lesions were resected, fixed in neutralized 40 g/L formaldehyde overnight at 4 °C, and embedded in paraffin blocks according to the standard procedures. Some of the tumors were bisected, and a half was frozen in liquid nitrogen and stocked at -80 °C until used for the frozen section preparation and RNA extraction. The other half was embedded in paraffin blocks as described above. Paraffin sections were prepared at 3.0- μ m thickness, stained with H & E, and subjected to histologic analysis.

Immunohistochemical analysis of liver tumors

Paraffin-embedded sections were deparaffinized and subjected to immunohistochemical staining using rabbit alpha fetoprotein polyclonal antibody (Novus Biologicals, Inc.) and rabbit PPAR γ polyclonal antibody (Santa Cruz Biotechnology, Inc.) following the manufacturer's instructions. The primary alpha fetoprotein (AFP) antibody was diluted at 1:200 and the PPAR γ antibody

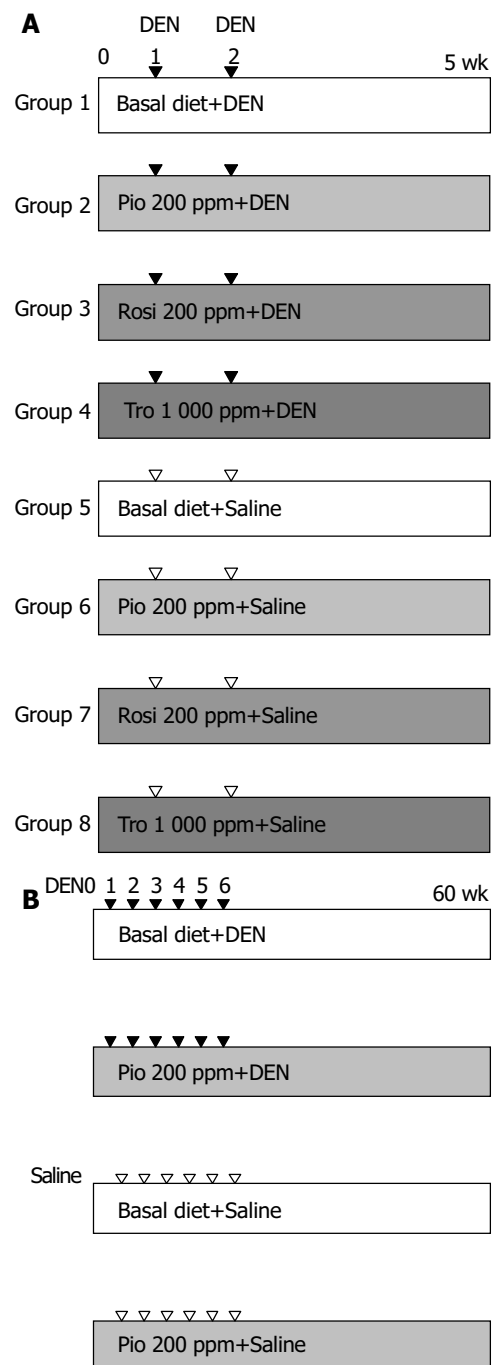


Figure 1 Experimental design for evaluation of chemoprevention efficacy of PPAR γ ligands against liver carcinogenesis. A: In the short-term study of rGST P-positive foci, groups of male Wistar rats were fed experimental diets containing 0 or 200 or 1 000 ppm of PPAR γ ligands from 1 wk prior to exposure to DEN at 20 mg/kg bm until the termination. B: For liver tumor study, groups of animals were given the basal diet or experimental diet containing 200-ppm Pio continuously from 1 wk prior to exposure of animals to DEN, IP, at 1 to 6 experimental weeks at 20 mg/kg bm until the termination.

to 1:400. To confirm the specificity of PPAR γ staining, addition of an excess amount of the N-terminal peptide of PPAR γ , used for immunization, was also carried out.

RT-PCR analysis for PPAR γ and β -actin expressions

RNA extraction from liver tumors and surrounding normal liver tissues was carried out as follows. Serial sections were prepared at 7- μ m thickness from frozen tissues, lesions were microdissected by scraping with a razor blade under microscopic observation,

and RNA was extracted using TRI reagent (Sigma). Extracted RNA was transcribed to cDNA using Oligo(dT)12-18 primer and SuperScript II RT (Invitrogen, Carlsbad, CA) and subjected to semiquantitative reverse-transcriptase (RT)-PCR analysis to quantify messenger RNA (mRNA) expression levels of the PPAR γ gene. PCR primers designed to amplify the 299-bp fragment of the PPAR γ gene were 5'-AGGATTCATGAC-CAGGGAGTT-3' (forward) and 5'-TCTGCCTGAGGTCT-GTCATCT-3' (reverse). For the internal control, expression of the β -actin gene for each sample was also quantified as above by amplifying the 138-bp fragment using a primer set: 5'-AGACTTCGAGCAGGAGATGGC-3' (forward) and 5'-AAGAAGGAAGGCTGGAAAAGA-3' (reverse). PCR amplification was carried out at 94 °C for 30 s, at 59 °C for 30 s, and at 72 °C for 45 s using MasterMix kit (tw-biotech, China) under the reaction conditions recommended by the manufacturer, and PCR cycles were set at 30 and 25 cycles for PPAR γ and β -actin, respectively. PCR products were run on 20 g/L agarose gels and visualized by ethidium bromide staining. In addition, the amount of PCR products was also quantified in real-time PCR using Taq RT-PCR kit (Ambion Inc.) and Smart cycler system (Cepheid, Sunny Vale, CA). Experiments were repeated at least twice, which gave similar results.

Statistical analysis

Statistical analysis for rGST P-positive foci and liver tumor multiplicity were conducted using the *t*-test (SPSS 10.0 for Windows). Other statistical analyses for liver tumor incidences and the distribution of tumor sizes were performed using the χ^2 -test (SPSS 10.0 for Windows). Differences were considered significant when *P* values were <0.05.

RESULTS

Effect of PPAR γ ligands on formation of rGST P-positive foci

One animal in the DEN+ 200-ppm Rosi-treated group and 4 in the DEN+1000-ppm Tro-treated group died within a few days after the injection of DEN, which were not included in the effective number of rats. Based on the diet consumption, the daily intake of PPAR γ ligands was estimated to be approximately 25 mg/kg bm (200 ppm in diet) for Pio and Rosi and 125 mg/kg bm (1 000 ppm in diet) for Tro. The mean body weight of rats given DEN was slightly decreased but stayed within 10% of the control value (data not shown). Administration of PPAR γ ligands alone did not significantly alter the body mass within the observation period of 5 wk (data not shown). After the administration of DEN, rats fed with the basal diet without a PPAR γ ligand developed 7.5 ± 3.1 rGST P-positive foci per cm² of liver sections by experimental wk 5. Treatment with 200-ppm Pio, 200-ppm Rosi, and 1000-ppm Tro significantly

reduced that to 2.5 ± 1.2 , 1.7 ± 1.1 , and 5.6 ± 2.3 , respectively (Table 1). This suppressive effect was observed in a dose-dependent manner within the range of 0.88 to 500 ppm of Rosi (Figure 2). Histologic analysis of a total of 40 liver sections of rGST P-positive foci (10 liver sections of rGST P-positive foci each from groups 1, 2, 3, and 4) revealed no significant histologic change. No rGST P-positive foci were induced by feeding experimental diet or basal diet alone without DEN administration.

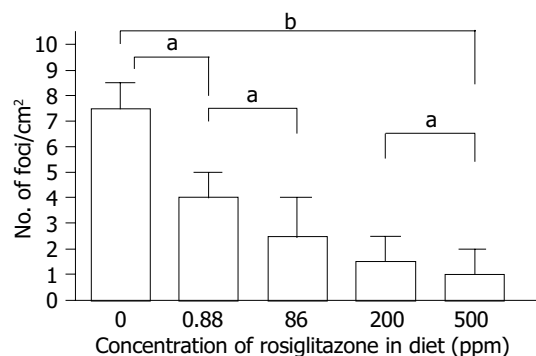


Figure 2 Dose-dependent suppression of the formation of rGST P-positive foci by rosiglitazone. As clearly demonstrated, Rosi suppressed the formation of rGST P-positive foci in a dose-dependent manner within the range of 0.88-500 ppm in diet (^a*P*<0.05, ^b*P*<0.01).

Effects of PPAR γ ligands on induction of liver tumors

Five animals treated with DEN+200 ppm Pio died before the termination without tumor development, which were not included in the effective number. With administration of DEN, body weight gradually decreased to approximately 90% of the vehicle-treated group by experimental wk 18, but the difference stayed within 10% of the control mass throughout the experimental period. Data for incidences, multiplicities (average numbers of tumors per animal), histologic features of liver tumors, and size distribution of tumors are summarized in Table 2. Administration of 200-ppm Pio almost halved the incidence of liver tumors, and the multiplicity was also significantly reduced by Pio treatment. As to the size, only 38% (3 of 8) of tumors observed in the Pio-treated group were more than 2 mm in diameter, and 38% (3 of 8) were less than 1 mm. In contrast, 76% (19 of 25) of those in rats without Pio treatment were more than 2 mm in diameter, and only 8% (2 of 25) were less than 1 mm (*P*<0.05). All of the lesions developed in both Pio-treated and untreated groups were diagnosed as hepatocellular carcinoma. No liver tumors were observed in the rats fed with the basal diet alone or diet with 200-ppm Pio (data not shown).

Table 1 Effect of PPAR γ ligands on the multiplicity of DEN-induced rGST P-positive foci in male Wistar rats (mean \pm SD)

Experimental group	DEN	Diet	No. of rats	No. of rGST P-positive foci/cm ² of liver sections
Group 1	+	Basal diet alone	10	7.5 \pm 3.1
Group 2	+	Basal diet+pioglitazone 200 ppm	10	2.5 \pm 1.2 ^a
Group 3	+	Basal diet+rosiglitazone 200 ppm	9	1.7 \pm 1.1 ^a
Group 4	+	Basal diet+troglitazone 1000 ppm	6	5.6 \pm 2.3 ^a
Group 5	-	Basal diet alone	5	0
Group 6	-	Basal diet+pioglitazone 200 ppm	5	0
Group 7	-	Basal diet+rosiglitazone 200 ppm	5	0
Group 8	-	Basal diet+troglitazone 1000 ppm	5	0

^a*P*<0.05 vs group 1.

Table 2 Effect of PPAR γ ligands on the incidence, multiplicity, and size of DEN-induced liver tumors in male Wistar rats (mean \pm SD)

Experimental group	Incidence(%) ¹	Histology		Tumor size(mm) ¹		
		Hepatocarcinoma	Multiplicity	0-1	1-2	>2
DEN+basal diet	13/30 (43)	25	0.83 \pm 1.22	2	4	19
DEN+pioglitazone 200 ppm	5/25 (20) ^a	8	0.32 \pm 0.75 ^a	3	2	3 ^a

¹Statistical analysis was conducted using χ^2 test. ^aP<0.05 vs DEN+basal diet group.

Histologic findings and immunohistochemical staining of liver tumors

Liver tumors in both Pio-treated and untreated rats demonstrated no appreciable histologic differences on H & E staining or AFP immunostaining. Furthermore, no variation was observed in PPAR γ expression levels in tumors developed in Pio-treated and untreated rats. Addition of an excessive antigenic PPAR γ N-terminal peptide used for immunization before incubation of the sections with the antibody blocked the staining completely (data not shown).

Expression of PPAR γ mRNA in liver tumors

RNA samples from 2 liver tumors and 1 normal liver sample from both Pio-treated and untreated groups were subjected to semiquantitative RT-PCR analysis. No products were amplified without reverse transcriptase (data not shown). Liver tumors and normal tissue from both Pio-treated and untreated animals expressed PPAR γ mRNA as shown in Figure 3, and the relative amounts, normalized to β -actin mRNA, were almost equivalent in liver tumors as compared with normal liver tissue in both groups. Real-time PCR analysis also gave similar results (data not shown).

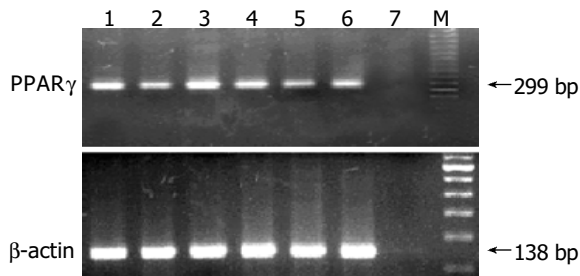


Figure 3 Expression of PPAR γ mRNA in liver tumors. Lanes 1 and 4: normal liver tissues; lanes 2, 3, 5, and 6: liver tumor tissues; lane 7: water.

DISCUSSION

In the present study of short- and long-term effects, clear evidence was obtained for preventive influence of the 3 different PPAR γ ligands, Pio, Rosi, and Tro, on rat liver carcinogenesis induced by DEN. In the short-term experiment, all 3 significantly suppressed the formation of rGST P-positive foci, the effect of the former 2 was particularly strong. Because this suppression was proved to be dose dependent, we considered the inhibitory effect of PPAR γ ligands on the formation of rGST P-positive foci to be due to pharmacologic actions rather than nonspecific toxicity. There were no significant differences in histopathologic features of rGST P-positive foci. In this context, the fact that the compounds reduced the formation of rGST P-positive foci without otherwise affecting their pathology is important. In the long-term carcinogenic experiment, the single PPAR γ ligand investigated also significantly suppressed the induction of liver tumors.

Our results are in good agreement with those from Rumi

et al.^[17], which demonstrated an inhibitory effect of PPAR γ on cell growth through PPAR γ activation. Our study has an advantage of the suppressive effect of rGST P-positive foci and liver tumors using 3 PPAR γ ligands in the rat model, including the dose-dependent experiments. In addition, PPAR γ could play roles in apoptosis, cell-cycle control through regulating p21^{waf/cipl}^[18]. Antiinflammatory activity of PPAR γ could also be involved in its suppression of liver carcinogenesis^[19]. However, the results of Hosokawa *et al.*^[20] and Kim *et al.*^[21], showing clofibrate, a peroxisome proliferator, enhanced liver carcinogenesis in their rat model in which GST-P-positive cells induced by DEN were changed to GST-P-negative cells on subsequent treatment with peroxisome proliferator, need to be taken into account. Now we have no reasonable explanation for the discrepancy.

In conclusion, PPAR γ ligands have substantial suppressive effects on liver carcinogenesis without affecting the histologic features of preneoplastic lesions or tumors. Although the molecular mechanisms underlying the inhibitory influence still remain largely unsolved, PPAR γ ligands may be potential chemopreventive agents against liver carcinogenesis.

REFERENCES

- 1 **Dragan YP**, Pitot HC. The role of the stages of initiation and promotion in phenotypic diversity during hepatocarcinogenesis in the rat. *Carcinogenesis* 1992; **13**: 739-750
- 2 **Farber E**, Solt D, Cameron R, Laishes B, Ogawa K, Medline A. Newer insights into the pathogenesis of liver cancer. *Am J Pathol* 1977; **89**: 477-482
- 3 **Pitot HC**, Barsness L, Goldsworthy T, Kitagawa T. Biochemical characterization of stages of hepatocarcinogenesis after a single dose of diethylnitrosamine. *Nature* 1978; **271**: 456-458
- 4 **Pitot HC**, Dragan Y, Sargent L, Xu YT. Biochemical markers associated with the stages of promotion and progression during hepatocarcinogenesis in the rat. *Environ Health Perspect* 1991; **93**: 181-189
- 5 **Satoh K**, Kitahara A, Soma Y, Inaba Y, Hatayama I, Sato K. Purification, induction, and distribution of placental glutathione transferase: a new marker enzyme for preneoplastic cells in the rat chemical hepatocarcinogenesis. *Proc Natl Acad Sci U S A* 1985; **82**: 3964-3968
- 6 **Ito N**, Tatematsu M, Hasegawa R, Tsuda H. Medium-term bioassay system for detection of carcinogens and modifiers of hepatocarcinogenesis utilizing the GST-P positive liver cell focus as an endpoint marker. *Toxicol Pathol* 1989; **17**(4 Pt 1): 630-641
- 7 **Reddy TV**, Daniel FB, Lin EL, Stober JA, Olson GR. Chloroform inhibits the development of diethylnitrosamine-initiated, phenobarbital-promoted gamma-glutamyltranspeptidase and placental form glutathione S-transferase-positive foci in rat liver. *Carcinogenesis* 1992; **13**: 1325-1330
- 8 **Zhu HZ**, Zhang XL, Chen YS. Expression of glutathione S-transferase placental mRNA in hepatic preneoplastic lesions in rats. *World J Gastroenterol* 1998; **4**: 38-40
- 9 **Denda A**, Kitayama W, Konishi Y, Yan Y, Fukamachi Y, Miura M, Gotoh S, Ikemura K, Abe T, Higashi T, Higashi K. Genetic properties for the suppression of development of putative preneoplastic glutathione S-transferase placental form-positive foci in the liver of carcinogen-resistant DRH strain rats.

- Cancer Lett* 1999; **140**: 59-67
- 10 **Sporn MB**, Suh N. Chemoprevention of cancer. *Carcinogenesis* 2000; **21**: 525-530
 - 11 **Nishikawa T**, Wanibuchi H, Ogawa M, Kinoshita A, Morimura K, Hiroi T, Funae Y, Kishida H, Nakae D, Fukushima S. Promoting effects of monomethylarsonic acid, dimethylarsinic acid and trimethylarsine oxide on induction of rat liver preneoplastic glutathione S-transferase placental form positive foci: a possible reactive oxygen species mechanism. *Int J Cancer* 2002; **100**: 136-139
 - 12 **Suzuki S**, Asamoto M, Tsujimura K, Shirai T. Specific differences in gene expression profile revealed by cDNA microarray analysis of glutathione S-transferase placental form (GST-P) immunohistochemically positive rat liver foci and surrounding tissue. *Carcinogenesis* 2004; **25**: 439-443
 - 13 **Lambe KG**, Tugwood JD. A human peroxisome-proliferator-activated receptor-gamma is activated by inducers of adipogenesis, including thiazolidinedione drugs. *Eur J Biochem* 1996; **239**: 1-7
 - 14 **Chang TH**, Szabo E. Induction of differentiation and apoptosis by ligands of peroxisome proliferator-activated receptor γ in non small cell lung cancer. *Cancer Res* 2000; **60**: 1129-1138
 - 15 **Dragan YP**, Hully J, Baker K, Crow R, Mass MJ, Pitot HC. Comparison of experimental and theoretical parameters of the Moolgavkar-Venzon-Knudson incidence function for the stages of initiation and promotion in rat hepatocarcinogenesis. *Toxicology* 1995; **102**: 161-175
 - 16 **Carter JH**, Richmond RE, Carter HW, Potter CL, Daniel FB, DeAngelo AB. Quantitative image cytometry of hepatocytes expressing gamma-glutamyl transpeptidase and glutathione S-transferase in diethylnitrosamine-initiated rats treated with Phenobarbital and/or phthalate esters. *J Histochem Cytochem* 1992; **40**: 1105-1115
 - 17 **Rumi MA**, Sato H, Ishihara S, Kawashima K, Hamamoto S, Kazumori H, Okuyama T, Fukuda R, Nagasue N, Kinoshita Y. Peroxisome proliferator-activated receptor gamma ligand-induced growth inhibition of human hepatocellular carcinoma. *Br J Cancer* 2001; **84**: 1640-1647
 - 18 **Kaga H**, Sakisaka S, Harada M, Takagi T, Hanada S, Taniguchi E, Kawaguchi T, Sasatomi K, Kimura R, Hashimoto O, Ueno T, Yano H, Kojiro M, Sata M. Involvement of p21(waf/cipl), p21 (kipl), and p18(INK4C) in troglitazone-induced cell-cycle arrest in human hepatoma cell lines. *Hepatology* 2001; **33**: 1087-1097
 - 19 **Chawla A**, Barak Y, Nagy L, Liao D, Tontonoz P, Evans RM. PPAR- γ dependent and independent effects on macrophage-gene expression in lipid metabolism and inflammation. *Nat Med* 2001; **7**: 48-52
 - 20 **Hosokawa S**, Tatematsu M, Aoki T, Nakanowatari J, Igarashi T, Ito N. Modulation of diethylnitrosamine-initiated placental glutathione S-transferase positive preneoplastic and neoplastic lesions by clofibrate, a hepatic peroxisome proliferator. *Carcinogenesis* 1989; **10**: 2237-2241
 - 21 **Kim DJ**, Lee KK, Hong JT. Differential effects of nongenotoxic and genotoxic carcinogens on the preneoplastic lesions in the rat liver. *Arch Pharm Res* 1998; **21**: 363-369

Edited by Zhang JZ and Wang XL Proofread by Xu FM

Preparation of human hepatocellular carcinoma-targeted liposome microbubbles and their immunological properties

Ai-Na Bian, Yun-Hua Gao, Kai-Bin Tan, Ping Liu, Gong-Jun Zeng, Xin Zhang, Zheng Liu

Ai-Na Bian, Yun-Hua Gao, Kai-Bin Tan, Ping Liu, Gong-Jun Zeng, Xin Zhang, Zheng Liu, Department of Ultrasonic Diagnosis, Xinqiao Hospital the Third Military Medical University, Chongqing 400037, China
Supported by the National Natural Science Foundation of China, No. 30270384

Correspondence to: Professor. Yun-Hua Gao, Director of Department of Ultrasonic Diagnosis, Xinqiao Hospital, the Third Military Medical University, Chongqing 400037, China. gyhxq@sina.com
Telephone: +86-23-68755631 **Fax:** +86-23-68755631
Received: 2003-12-23 **Accepted:** 2004-01-15

Abstract

AIM: To prepare the human hepatocellular carcinoma (HCC)-targeted liposome microbubbles and to investigate their immunological properties.

METHODS: Human hepatocarcinoma specific monoclonal antibody HAb18 was attached to the surface of home-made liposome microbubbles by static attraction to prepare the targeted liposome microbubbles. The combination of HAb18 with liposome microbubbles was confirmed by the slide agglutination test and immunofluorescent assay. Their immunological activity was measured by ELISA. Rosette formation test, rosette formation blocking test and immunofluorescent assay were used to identify the specific binding of targeted liposome microbubbles to SMMC-7721 hepatoma cells, and cytotoxicity assay was used to detect their effect on human hepatocytes.

RESULTS: The targeted liposome microbubbles were positive in the slide agglutination test and immunofluorescent assay. ELISA indicated that the immunological activity of HAb18 on the liposome microbubbles was similar to that of free HAb18. SMMC-7721 cells were surrounded by the targeting liposome microbubbles to form rosettes, while the control SGC-7901 gastric cancer cells were not. Proliferation of SMMC-7721 cells and normal human hepatocytes was not influenced by the targeted liposome microbubbles.

CONCLUSION: The targeted liposome microbubbles with a high specific biological activity have been successfully prepared, which specifically bind to human hepatocarcinoma cells, and are non-cytotoxic to hepatocytes. These results indicate that the liposome microbubbles can be used as a HCC-targeted ultrasound contrast agent that may enhance ultrasound images and thus improve the diagnosis of HCC, especially at the early stage.

Bian AN, Gao YH, Tan KB, Liu P, Zeng GJ, Zhang X, Liu Z. Preparation of human hepatocellular carcinoma-targeted liposome microbubbles and their immunological properties. *World J Gastroenterol* 2004; 10(23): 3424-3427
<http://www.wjgnet.com/1007-9327/10/3424.asp>

INTRODUCTION

Targeted ultrasound imaging is a promising method of imaging diagnosis^[1]. This technique can significantly improve the

sensitivity and specificity of ultrasonic diagnosis. At present, several targeted ultrasound contrast agents that can enhance imaging of specific tissues, such as thrombus-specific and inflammatory tissue-specific targeted ultrasound contrast agent, have successfully been developed abroad^[2-15], while study on hepatocellular carcinoma-targeted ultrasound contrast agent has not been reported.

In this study, liposome microbubbles containing fluorocarbon gases were prepared in our laboratory. Then human hepatocarcinoma specific monoclonal antibody HAb18 was attached to the surface of home-made liposome microbubbles to prepare targeted liposome microbubbles. Finally the immunological properties of targeted liposome microbubbles were investigated.

MATERIALS AND METHODS

Materials

Human hepatocarcinoma specific monoclonal antibody HAb18 was kindly provided by Research Centre of Cell Engineering, the Fourth Military Medical University. Rabbit anti-mouse serum was purchased from Beijing Zhongshan Biotechnology Co., Ltd, China. FITC conjugated sheep anti-mouse IgG and HRP conjugated sheep anti-mouse IgG were purchased from Huamei Bioengineering Company, China. MTT was purchased from Sigma. Human hepatoma cell line SMMC-7721 and human gastric carcinoma cell line SGC-7901 were maintained in our laboratory. Primary cultures of normal human hepatocytes were established from human liver tissue collected from person who died in accident.

Preparation of liposome microbubbles

The lipid film prepared previously in our laboratory and some mediators were mixed in proportion^[16]. Then the resulting mixture was sonicated, into which perfluoropropane gas was injected. The concentration and size of the microbubbles were measured under microscope. Zeta potential of the microbubbles was determined by the Chongqing Comed Nanopharma Co., Ltd, China.

Preparation of targeted liposome microbubbles

Human hepatocarcinoma specific monoclonal antibody HAb18 was added to the liposome microbubble suspension in proportion and mixed for 2 h at pH4.0, 4 °C^[17]. After the mixture was separated into 2 distinct layers, the lower layer was discarded and the upper layer was washed three times with phosphate-buffered saline (PBS) to elute the free HAb18.

Identification of targeted liposome microbubbles

Slide agglutination test A drop of rabbit anti-mouse serum or normal saline was mixed with a drop of targeted liposome microbubbles or liposome microbubbles respectively for about 5 min. The results were observed under a ×100 field of microscope.

Immunofluorescent assay A 100 μL of FITC conjugated sheep anti-mouse IgG was put into 200 μL of targeted liposome microbubbles and mixed for 30 min at 4 °C. After the mixture was separated into 2 distinct layers, the lower layer was discarded and the upper layer was washed three times with PBS to elute the free FITC conjugated sheep anti-mouse IgG. Then the microbubbles were observed under fluorescence microscope.

Assessment of immunological activity of targeted liposome microbubbles

SMMC-7721 cells (1×10^5) were placed in each well of a 96-well ELISA plate and cultured overnight. The cells were fixed in 0.25 g/L glutaraldehyde for 20 min. A 30 g/L of defatted milk powder was added and incubated for 1 h at 37 °C. Different concentrations of targeted liposome microbubbles or free HAb18 were added and incubated for 1.5 h at 37 °C. HRP conjugated sheep anti-mouse IgG was added and incubated for 1.5 h at 37 °C. O-phenylenediamine (OPD) and H_2O_2 were added and incubated for 10 min at 25 °C. A 2 mmol/L of H_2SO_4 was added to terminate the reaction. The optical absorbance (A) value at 490 nm was detected with ELISA.

Specific binding of targeted liposome microbubbles to SMMC-7721 cells

Rosette formation test^[18] Log phase SMMC-7721 cells and SGC-7901 cells were digested with 2.5 g/L trypsin. The isolated cells were adjusted to a concentration of 2×10^5 /mL in PBS respectively. One hundred μ L of targeted liposome microbubbles or liposome microbubbles was added to 200 μ L of SMMC-7721 or SGC-7901 cell suspension and mixed for 30 min at 25 °C. The resulting mixture was observed under microscope and the cells that formed rosette were counted.

Rosette formation blocking test SMMC-7721 cells were mixed with different concentrations of HAb18 for 30 min at 25 °C. The mixture was centrifuged and washed with PBS to elute free HAb18. Then targeted liposome microbubbles were added to cell suspension and mixed for 30 min at 25 °C. Cells forming rosette were counted under microscope.

Immunofluorescent assay one hundred μ L of targeted liposome microbubbles combined with FITC conjugated sheep anti-mouse IgG and 200 μ L of SMMC-7721 cells or SGC-7901 cells were mixed for 30 min at 25 °C. The suspension was observed under fluorescence microscope.

Cytotoxicity assay of targeted liposome microbubbles

SMMC-7721 cells or human hepatocytes (1×10^5 per well) were added into a 96-well culture plate. About three hours later different concentrations of targeted liposome microbubbles were added, while PBS was used as control. Three wells were used for each concentration. They were cultured in a CO_2 incubator at 37 °C for 48 h, then MTT (2 g/L, 50 μ L/well) was added and incubated at 37 °C for 6 h. The medium was discarded, and 100 μ L/well DMSO was added. The culture plate was shaken for 10 min and the optical absorbance (A) value at 570 nm was detected with ELISA.

RESULTS

Preparation of liposome microbubbles

The average diameter of liposome microbubbles ranged from 2 to 5 μ m, the concentration was 7×10^9 bubbles/mL (Figure 1). The mean zeta potential was -71.2 mV. Animal experiment demonstrated that the microbubbles could significantly enhance the ultrasound images of several tissues.



Figure 1 Light micrograph of liposome microbubbles under a $\times 200$ field of microscope.

Preparation and identification of targeted liposome microbubbles

The average diameter of targeted liposome microbubbles was similar to that of liposome microbubbles. HAb18 did not affect the size of microbubbles. The concentration was 5×10^8 bubbles/mL.

After rabbit anti-mouse serum was added, targeted liposome microbubbles agglutinated (Figure 2), but liposome microbubbles did not. While normal saline (NS) did not lead to agglutination of two kinds of microbubbles.

The surfaces of targeted liposome microbubbles gave out bright yellow-green fluorescence after they were stained with fluorescent agents (Figure 3), whereas liposome microbubbles did not give out any fluorescence.



Figure 2 Direct agglutination of targeted liposome microbubbles in the presence of rabbit anti-mouse serum.

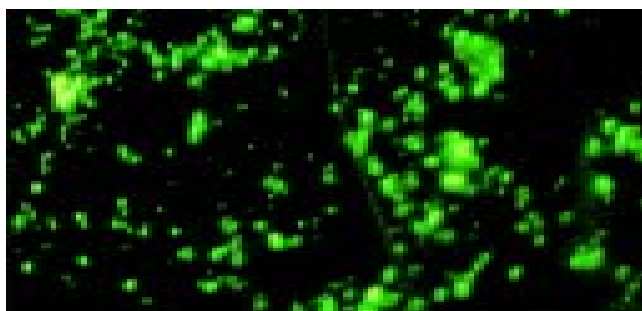


Figure 3 Immunofluorescence staining of targeted liposome microbubbles with FITC conjugated sheep anti-mouse IgG. Targeted liposome microbubbles were stained in yellow-green under a $\times 400$ field of fluorescence microscope.

Assessment of immunological activity of targeted liposome microbubbles

ELISA indicated that the immunological activity of HAb18 on liposome microbubbles was similar to that of free HAb18. There were no significant differences in optical absorbance (A) value between free HAb18 ground and conjugated HAb18 ground (Figure 4).

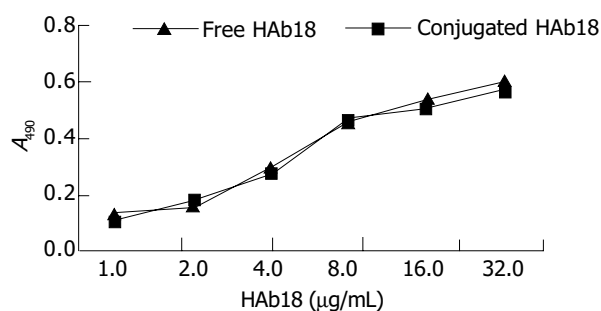


Figure 4 Activity assay of free HAb18 and conjugated HAb18 on microbubbles by ELISA.

Specific binding of targeted liposome microbubbles to SMMC-7721 cells

After targeted liposome microbubbles and SMMC-7721 cells or SGC-7901 cells were mixed for 30 min, SMMC-7721 cells were surrounded by targeted liposome microbubbles to form rosettes and the rate of rosettes reached 90% (Figure 5), while SGC-7901 cells were negative. Rosettes were not observed in the mixture of liposome microbubbles and SMMC-7721 cells under microscope. After SMMC-7721 cells were pretreated with different concentrations of HAb18, the rate of rosettes declined significantly, even dropped to 0. Immunofluorescent assay indicated that SMMC-7721 cells were surrounded by the microbubbles and gave out bright yellow-green fluorescence to form rosettes (Figure 6), whereas control cells were negative.



Figure 5 Light micrograph of the binding of targeted liposome microbubbles to SMMC-7721 cells under a $\times 400$ field of microscope. SMMC-7721 cells were surrounded by targeted liposome microbubbles to form rosettes.

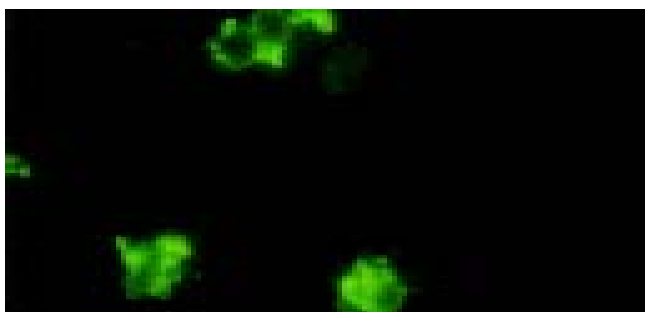


Figure 6 Immunofluorescent assay for identification of the binding of targeted liposome microbubbles to SMMC-7721 cells. SMMC-7721 cells were surrounded by the microbubbles and gave out bright yellow-green fluorescence.

Cytotoxicity assay of targeted liposome microbubbles

The result of MTT assay showed that the proliferation of human hepatocytes and SMMC-7721 cells were not influenced by targeted liposome microbubbles. There were no significant differences in average optical absorbance (A_{570}) value between experiment group and control group (Figure 7).

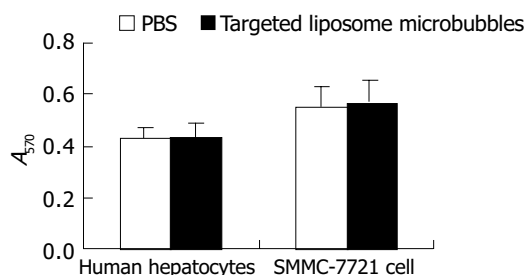


Figure 7 Effect of targeted liposome microbubbles on the proliferation of human hepatocytes and SMMC-7721 cells.

DISCUSSION

It has been nearly thirty years since the conception of ultrasound contrast imaging was suggested. Especially in recent years it has been developed rapidly and a number of ultrasound contrast agents have been described, but most of these are nontargeted. Now several targeted contrast agents that can bind to a specific acceptor have been developed^[2-15,19], and it has been demonstrated that such agents can enhance ultrasound images of chosen target tissues. Skyba *et al.*^[17,20-25] observed that ultrasound could induce intravascular microbubble destruction and bioeffects, and found that the application of ultrasound to thin-shelled microbubbles flowing through small microvessels ($<7 \mu\text{m}$ in diameter) could produce vessel wall ruptures and the microspheres in vessel could go out through the ruptured walls. Thus antibody-loaded ultrasound contrast microbubbles could also cross the ruptured microvessels and bind specifically to the target tissues.

At present, hepatocellular carcinoma (HCC) is one of the most common malignant tumors with a high incidence and mortality in the world^[26]. This cancer severely threatens our health and needs to be diagnosed as early as possible, but differential diagnosis of HCC at its early stage is still difficult. So it is important to find a specific and sensitive diadynamic method for it. Studies^[27] have demonstrated that human hepatocarcinoma specific monoclonal antibody HAb18 could specifically bind to hepatocellular carcinoma cells and can be used for site targeting. If the antibody was used as a target carrier to prepare targeted ultrasound contrast agent, the contrast agent could assemble in a higher concentration of hepatoma tissues and the aim of target imaging could be achieved.

In this study, we prepared and identified targeted liposome microbubbles and investigated their immunological properties. The results indicated that human hepatocarcinoma specific monoclonal antibody HAb18 was firmly attached to the surfaces of liposome microbubbles by static attraction and the immunological activity of HAb18 on liposome microbubbles was similar to that of free HAb18. These demonstrate that it is feasible to prepare targeted liposome microbubbles by static attraction. This method is simple and inexpensive. Moreover, the activity of the antibody can be retained completely. Besides, in order to investigate the properties of targeted liposome microbubbles bound specifically to target cells, rosette formation test and rosette formation blocking test as well as immunofluorescent assay were performed. These tests indicated that targeted liposome microbubbles could bind to human hepatocarcinoma cells specifically and effectively, and the binding was mediated by HAb18.

In order to evaluate the safety of targeted liposome microbubbles, we performed cytotoxicity assay. The result indicated that the microbubbles did not influence the proliferation of human hepatocytes and SMMC-7721 cells. These results lay a good foundation for further study.

REFERENCES

- 1 **Bian AN**, Gao YH. Research progress of targeted ultrasound contrast. *Zhonghua Chaosheng Yingxiangxue Zazhi* 2003; **12**: 558-559
- 2 **Unger E**, Metzger P 3rd, Krupinski E, Baker M, Hulett R, Gabaeff D, Mills J, Ihnat D, McCreery T. The use of a thrombus-specific ultrasound contrast agent to detect thrombus in arteriovenous fistulae. *Invest Radiol* 2000; **35**: 86-89
- 3 **Unger EC**, Matsunaga TO, McCreery TP, Sweitzer RH. Biomedical implications of a thrombus-specific US contrast agent. *Acad Radiol* 2002; **9**(Suppl 1): S56-57
- 4 **Hamilton A**, Huang SL, Warnick D, Stein A, Rabbat M, Madhav T, Kane B, Nagaraj A, Klegerman M, MacDonald R, McPherson D. Left ventricular thrombus enhancement after intravenous injection of echogenic immunoliposomes: studies in a new experimental model. *Circulation* 2002; **105**: 2772-2778

- 5 **Schumann PA**, Christiansen JP, Quigley RM, McCreery TP, Sweitzer RH, Unger EC, Lindner JR, Matsunaga TO. Targeted-microbubble binding selectively to GPIIb IIIa receptors of platelet thrombi. *Invest Radiol* 2002; **37**: 587-593
- 6 **Demos SM**, Onyuksek H, Gilbert J, Roth SI, Kane B, Jungblut P, Pinto JV, McPherson DD, Klegerman ME. *In vitro* targeting of antibody-conjugated echogenic liposomes for site-specific ultrasonic image enhancement. *J Pharm Sci* 1997; **86**: 167-171
- 7 **Unger EC**, McCreery TP, Sweitzer RH, Shen D, Wu G. *In vitro* studies of a new thrombus-specific ultrasound contrast agent. *Am J Cardiol* 1998; **81**: 58G-61G
- 8 **Takeuchi M**, Ogunyankin K, Pandian NG, McCreery TP, Sweitzer RH, Caldwell VE, Unger EC, Avelar E, Sheahan M, Connolly R. Enhanced visualization of intravascular and left atrial appendage thrombus with the use of a thrombus-targeting ultrasonographic contrast agent (MRX-408A1): *In vivo* experimental echocardiographic studies. *J Am Soc Echocardiogr* 1999; **12**: 1015-1021
- 9 **Demos SM**, Alkan-Onyuksek H, Kane BJ, Ramani K, Nagaraj A, Greene R, Klegerman M, McPherson DD. *In vivo* targeting of acoustically reflective liposomes for intravascular and transvascular ultrasonic enhancement. *J Am Coll Cardiol* 1999; **33**: 867-875
- 10 **Christiansen JP**, Leong-Poi H, Klibanov AL, Kaul S, Linder JR. Noninvasive imaging of myocardial reperfusion injury using leukocyte-targeted contrast echocardiography. *Circulation* 2002; **105**: 1764-1767
- 11 **Lindner JR**, Song J, Xu F, Klibanov AL, Singbartl K, Ley K, Kaul S. Noninvasive ultrasound imaging of inflammation using microbubbles targeted to activated leukocytes. *Circulation* 2000; **102**: 2745-2750
- 12 **Lindner JR**, Song J, Christiansen J, Klibanov AL, Xu F, Ley K. Ultrasound assessment of inflammation and renal tissue injury with microbubbles targeted to P-selectin. *Circulation* 2001; **104**: 2107-2112
- 13 **Klibanov AL**, Hughes MS, Villanueva FS, Jankowski RJ, Wagner WR, Wojdyla JK, Wible JH, Brandenburger GH. Targeting and ultrasound imaging of microbubble-based contrast agents. *MAGMA* 1999; **8**: 177-184
- 14 **Dayton PA**, Ferrara KW. Targeted imaging using ultrasound. *J Magn Reson Imaging* 2002; **16**: 362-377
- 15 **Hamilton A**, Rabbat M, Jain P, Belkind N, Huang SL, Nagaraj A, Klegerman M, Macdonald R, McPherson DD. A physiologic flow chamber model to define intravascular ultrasound enhancement of fibrin using echogenic liposomes. *Invest Radiol* 2002; **37**: 215-221
- 16 **Liu P**, Gao YH, Tan KB, Zuo S, Liu Z. Enhanced imaging of the rabbit liver using the self-made Liposome contrast agent: an earlier experimental study. *Zhongguo Chaosheng Yixue Zazhi* 2003; **19**: 4-6
- 17 **Shohet RV**, Chen S, Zhou YT, Wang Z, Meidell RS, Unger RH, Grayburn PA. Echocardiographic destruction of albumin microbubbles directs gene delivery to the myocardium. *Circulation* 2000; **101**: 2554-2556
- 18 **Kang JC**, Samten BK, Xie SS, Wei SL. Separation of human bladder cancer cells from bone marrow with a kind of immunomagnetic microspheres. *Yaoxue Xuebao* 1998; **33**: 52-56
- 19 **Leong-Poi H**, Christiansen J, Klibanov AL, Kaul S, Lindner JR. Noninvasive assessment of angiogenesis by ultrasound and microbubbles targeted to alpha (v) -integrins. *Circulation* 2003; **107**: 455-460
- 20 **Skyba DM**, Price RJ, Linka AZ, Skalak TC, Kaul S. Direct *in vivo* visualization of intravascular destruction of microbubbles by ultrasound and its local effects on tissue. *Circulation* 1998; **98**: 290-293
- 21 **Price RJ**, Skyba DM, Kaul S, Skalak TC. Delivery of colloidal particles and red blood cells to tissue through microvessel ruptures created by targeted microbubble destruction with ultrasound. *Circulation* 1998; **98**: 1264-1267
- 22 **Mukherjee D**, Wong J, Griffin B, Ellis SG, Porter T, Sen S, Thomas JD. Ten-fold augmentation of endothelial uptake of vascular endothelial growth factor with ultrasound after systemic administration. *J Am Coll Cardiol* 2000; **35**: 1678-1686
- 23 **Lawrie A**, Brisken AF, Francis SE, Cumberland DC, Crossman DC, Newman CM. Microbubble-enhanced ultrasound for vascular gene delivery. *Gene Ther* 2000; **7**: 2023-2027
- 24 **Price RJ**, Kaul S. Contrast ultrasound targeted drug and gene delivery: an update on a new therapeutic modality. *J Cardiovasc Pharmacol Ther* 2002; **7**: 171-180
- 25 **Zhang DZ**, Ren H, Wang ZG, Leng ZY, Ran HT, Zhang DF. Ultrasound enhancing the infection efficiency of adenoviral vector into the intact hepatocyte. *Linchuang Chaosheng Yixue Zazhi* 2002; **4**: 321-323
- 26 **Qian J**, Truebenbach J, Graepler F, Pereira P, Huppert P, Eul T, Wiemann G, Claussen C. Application of poly-lactide-co-glycolide-microspheres in the transarterial chemoembolization in an animal model of hepatocellular carcinoma. *World J Gastroenterol* 2003; **9**: 94-98
- 27 **Bian HJ**, Chen ZN, Lou C, Mi L, Wang J, Deng JL, Yu XL. ¹⁸⁸Re-labeled HAB18 F (ab')₂ for hepatoma radio-immunoimaging. *Zhongliu* 2000; **20**: 181-184

Edited by Zhang JZ and Wang XL Proofread by Xu FM

Effect of hepatoma H22 on lymphatic endothelium *in vitro*

Hua Yu, Hong-Zhi Zhou, Chun-Mei Wang, Xiao-Ming Gu, Bo-Rong Pan

Hua Yu, Chun-Mei Wang, Electron Microscopy Center, School of Basic Medicine, Fourth Military Medical University, Xi'an 710032, Shaanxi Province, China

Hong-Zhi Zhou, Xiao-Ming Gu, College of Stomatology, Fourth Military Medical University, Xi'an 710032, Shaanxi Province, China

Bo-Rong Pan, Department of Oncology, Xijing Hospital, Fourth Military Medical University, Xi'an 710032, Shaanxi Province, China

Co-first-authors: Hua Yu and Hong-Zhi Zhou

Correspondence to: Chun-Mei Wang, Electron Microscopy Center, School of Basic Medicine, Fourth Military Medical University, Xi'an 710032, Shaanxi Province, China. wangcm@fmmu.edu.cn

Telephone: +86-29-83374569 **Fax:** +86-29-83374467

Received: 2004-04-14 **Accepted:** 2004-05-09

Abstract

AIM: To determine the effect of metastatic hepatoma cells on lymphangioma-derived endothelium, and to establish *in vitro* model systems for assessing metastasis-related response of lymphatic endothelium.

METHODS: Benign lymphangioma, induced by intraperitoneal injection of the incomplete Freund's adjuvant in BALB/c mice, was embedded in fibrin gel or digested and then cultured in the conditioned medium derived from hepatoma H22. Light and electron microscopy, and the transwell migration assay were used to determine the effect of H22 on tissue or cell culture. Expressions of Flt-4, c-Fos, proliferating cell nuclear antigen (PCNA), and inducible nitric oxide synthase (iNOS) in cultured cells, and content of nitric oxide in culture medium were also examined.

RESULTS: The embedded lymphangioma pieces gave rise to array of capillaries, while separated cells from lymphangioma grew to a cobblestone-like monolayer. H22 activated growth and migration of the capillaries and cells, induced expressions of Flt-4, c-Fos, PCNA and iNOS in cultured cells, and significantly increased the content of NO in the culture medium.

CONCLUSION: Lymphangioma-derived cells keep the differentiated phenotypes of lymphatic endothelium, and the models established in this study are feasible for *in vitro* study of metastasis-related response of lymphatic endothelium.

Yu H, Zhou HZ, Wang CM, Gu XM, Pan BR. Effect of hepatoma H22 on lymphatic endothelium *in vitro*. *World J Gastroenterol* 2004; 10(23): 3428-3432

<http://www.wjgnet.com/1007-9327/10/3428.asp>

INTRODUCTION

Metastasis of most cancers occurs primarily through the lymphatic system, and is responsible for the majority of cancer deaths. But tumor-associated lymphatic system has been overshadowed by the greater emphasis placed on the blood vascular system^[1]. This scenario is changing rapidly after the identification of lymphangiogenic vascular endothelial growth factor C^[2]. The traditional view that lymphatic capillaries are passive participants in metastasis is currently being challenged, and recent studies indicate the importance of lymphatic vessel

activation in tumor dissemination^[3-5].

Better understanding of the lymphatic endothelial properties and their alteration in cancer may develop a new way to therapeutic intervention^[6,7]. *In vitro* experiments have been proven to be valuable, expeditious and easy of quantification in providing initial information on angiogenesis, a potentially important oncotherapy target^[8]. However such *in vitro* models have not been well established for revealing metastasis-related response of lymphatic endothelium. Therefore, the aim of our study was to determine the effect of metastatic hepatoma cells on lymphangioma-derived endothelium, and to establish *in vitro* model systems for assessing metastasis-related response of lymphatic endothelium.

MATERIALS AND METHODS

Animals and reagents

BALB/c mice of either gender, 2 mo old and weighing 22-25 g, were provided by Laboratory Animal Research Center, Fourth Military Medical University (FMMU, Xi'an, China). A mouse ascitic hepatoma cell line, H22, was obtained from Institute of Digestive Diseases, FMMU. Reagents for *in vitro* culture of lymphatic endothelium included incomplete Freund's adjuvant, Hanks' balanced salt solution (HBSS), M199 medium and fetal calf serum (FCS), which were purchased from Gibco Company (Carlsbad, California, USA), bovine fibrinogen, thrombin, gelatin, endothelial cell growth supplement (ECGS), heparin, collagenases I and II, which were products of Sigma Company (Saint Louis, Missouri, USA). The sABC and sABC-AP kits for immunohistochemical staining were purchased from Boster Company (Wuhan, China). Polyclonal anti-Flt-4 antibodies, monoclonal anti-iNOS antibody, anti-c-Fos antibody, and anti-PCNA antibody were products of Santa Cruz Company (Santa Cruz, California, USA). Nitric oxide (NO) detection kit was purchased from Nanjing Jiancheng Bioengineering Institute (Nanjing, China). Millicell culture plate inserts (12.0 µm) for transwell cell migration test were purchased from Millipore Corporation (Billerica, Massachusetts, USA).

Preparation of conditioned medium of H22

Hepatoma H22 cells were inoculated into abdominal cavity of 5 BALB/c mice for passage. To verify the capability of spontaneous lymphatic metastasis of H22, the generated carcinomatous ascites was transplanted into hindlimb claw pad of 10 healthy BALB/c mice and the lymph nodes in groin were harvested 10 d later for pathological examination. The conditioned medium of H22 (H22 CM) was prepared as a mixture of sterile ultra-filtrate of H22 ascites and M199 medium at the ratio of 1:5, supplemented with 150 mL/L FCS. The control medium was M199 medium supplemented with 150 mL/L FCS.

Induction of lymphangioma

Twenty healthy animals of BALB/c strain were intraperitoneally injected twice, with a 15-d interval, with 200 µL of the emulsified (1:1 with HBSS) incomplete Freund's adjuvant and killed one month later. Multicentric and clearly delimited white neoplasm on the abdominal surface of the diaphragm, varying in size from 3 to 15 mm², was collected for the following experiments. Histopathological examination of the tumors in our preparative experiment and other previous studies^[9] confirmed that this

neoplasm was benign lymphangioma.

Tri-dimensional lymphangioma culture

The lymphangioma masses were washed by HBSS, and cut into 1-mm² pieces. HBSS containing 3 g/L bovine fibrinogen was added into 48-well culture plates (0.5 mL/well), and fibrin gel clotting was induced by addition of 10 µL 50 kU/L thrombin. A piece of lymphangioma was then placed on gel surface, and additional 0.5 mL fibrinogen solution and 10 µL thrombin were added to embed the tissue. H22 CM was then added into 24 wells (as an experimental group), and the control medium into another 24 wells (as a control group). The gels were incubated, with culture medium changed every other day, at 37 °C with 50 mL/L CO₂ in air, and examined daily under an inverted microscope. To perform a quantitative analysis, images were taken every second day under same conditions (in brightness, contrast, and magnification), and measured by a computer-assisted image analysis system of Quantimet 570. For electron microscopy, six gels from each group were fixed two weeks later with 10 g/L glutaraldehyde in 0.1 mol/L sodium phosphate buffer, post-fixed with 10 g/L OsO₄ in s-collidine buffer, dehydrated in graded ethanol, and embedded in Epon. Ultrathin sections were cut and stained with lead citrate and examined with a JEM-200EX transmission electron microscope.

Primary cell culture

Lymphangioma masses were mechanically broken, and washed in M199 medium, supplemented with 100 kU/L penicillin. The tissues were then incubated for 30 min at 37 °C in HBSS containing 0.5 g/L collagenases (1:1 mixture of type I and II), and washed with a medium containing 150 mL/L FCS to stop digestion. Cells were centrifuged at 700 r/min, resuspended in M199 medium supplemented with 150 mL/L FCS, and equally seeded on 10 g/L gelatin-coated cover slips in a 24-well plate. To allow cell attachment, the plates were put still for one hour in an incubator at 37 °C with 50 mL/L CO₂ in air. Then the wells were gently washed to remove floating cells, and refilled with 2 mL H22 CM (24 wells) or 2 mL control medium (24 wells). Attached cells were cultured routinely, and examined daily under a phase-contrast microscope.

Immunocytochemical testing

Six days after primary cell seeding, the cover slips were fixed with 40 g/L formaldehyde in PBS for 20 min, with 2 g/L Triton X-100 in PBS, and incubated with 200 mL/L normal goat serum. Polyclonal anti-Flt-4 antibodies, monoclonal anti-iNOS antibody, anti-PCNA antibody and anti-c-Fos antibody were used as primary antibodies, and biotin-labeled goat anti-rabbit IgG antibodies as second antibodies. Streptavidin and biotinylated horseradish peroxidase complex (sABC) and DAB were used for anti-Flt-4 and anti-iNOS antibodies, and sABC-AP (alkaline phosphatase) and BCIP/NBT for anti-PCNA and anti-c-Fos antibodies.

Nitric oxide detection

The content of NO in fresh H22 CM and control medium was indicated by determining the total concentration of nitrite/nitrate by using the colorimetric method, according to the instructions provided with the NO detection kit. After primary cells were equally seeded and cultured with 2 mL H22 CM or control M199 medium for 48 h, the levels of NO in the two media were detected again. For an empty control, the two media were added into an empty plate, which was then incubated at 37 °C for 48 h before NO detection.

Transwell migration assay

Primary cells from lymphangioma were cultured to a confluent monolayer with a complete endothelium growth medium

(M199 supplemented with 100 mg/L heparin, 30 mg/L ECGS and 150 mL/L FCS), subjected to serum starvation for 4 h by switching the culture medium to M199 medium without growth factors or serum, trypsinized and suspended (1×10^8 cells/L) in serum-free M199 medium. Transwell migration assays were performed in Millicell inserts, with 1 g/L gelatin-coated 12 µm filter membrane, in a 24-well culture plate. H22 CM and the control medium were added, respectively, into 12 wells of the plate, and 0.5 mL of suspended cells was placed in chambers of the inserts. After 4-h incubation at 37 °C, the medium in the insert chamber was aspirated, and cells on the upper surface of the filter membrane were removed with a cotton swab. Cells on the lower surface were fixed, stained with hematoxylin and counted in 5 high-power fields per chamber under light microscope.

RESULTS

Basic feasibility of the assay

Spontaneous lymphatic metastasis of transplant H22 tumor was found in all 10 animals as demonstrated by pathological examination of the groin lymph nodes (Figure 1). H22 CM could be easily prepared, and stored for the entire experiments to ensure the continuity of the different parts of the assay. The induction of lymphangioma was also confirmed to be a simple and well duplicable procedure, and could provide adequate original tissues for the following experiments.



Figure 1 Metastatic H22 tumor in the groin lymph node ($\times 100$).

Effect of H22 CM on lymphangioma culture

Lymphangioma embedded in the fibrin gels gave rise to capillaries when cultured 3-4 d in both H22 CM and control M199 media. Neo-branches of the micro-vessels with obvious lumina were generated every day. Under the effect of H22 CM, rather straight capillaries stretching out to the fringe of the gel were generated, and the number of branching in micro-vessels increased more rapidly (Figure 2). Transmission electron microscopy revealed that the ultrastructure of the capillaries was plasmalemma invagination of a single cell, or formed by cytoplasmic flaps joined by overlapping contacts and specialized tight junction complexes (Figure 3). End-to-end intercellular contacts were rare. No typical Weibel-Palade body was distinguished in the cytoplasm.

Effect of H22 CM on primary cell activation

Primary cell culture was successfully established on gelatin-coated cover slips. When cultivated in H22 CM, the cells proliferated, albeit at a low rate with a doubling time of about 36-60 h, and reached sub-confluence in 6 d. At this stage, the lymphangioma cells showed appearance like cobblestone, the classical morphology of endothelial cells. In contrast, when cultured in the control M199 medium, the cells showed no obvious proliferation after attachment. Correspondingly, immunocytochemical staining for Flt-4, PCNA, and c-Fos were positive in cells cultured in H22 CM (Figure 4), but negative in cells cultured in the control medium.

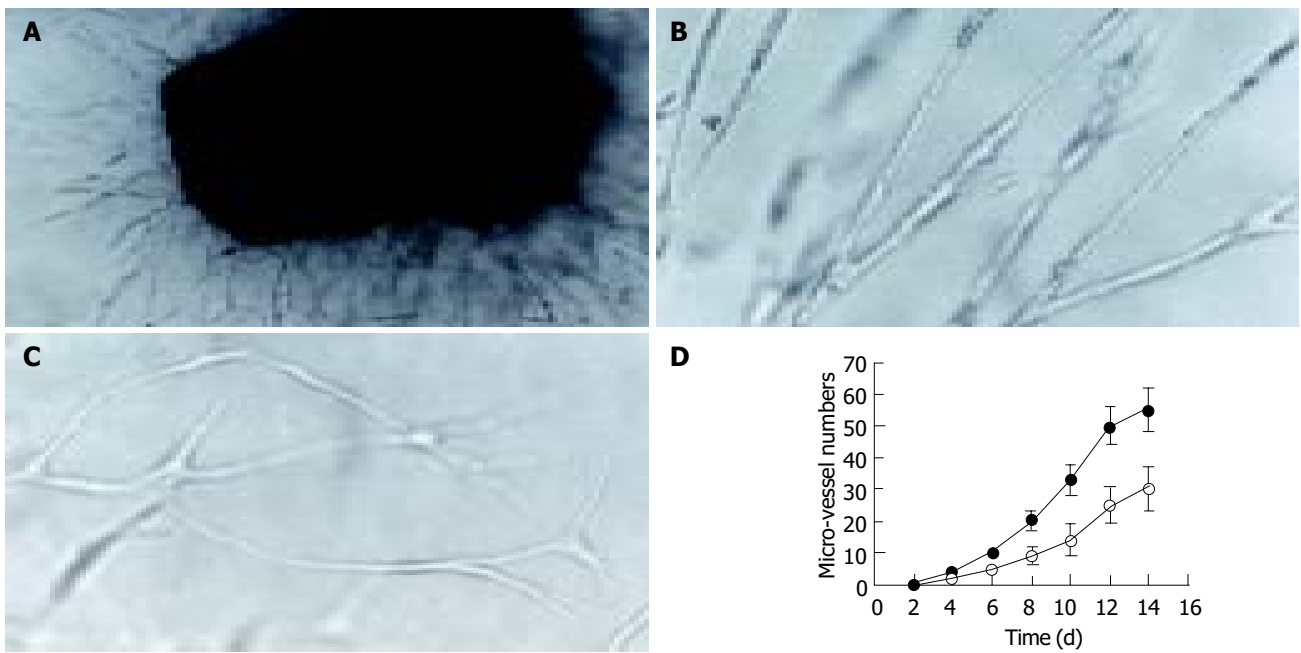


Figure 2 Tri-dimensional culture of lymphangioma. A: Microphotograph of the capillary network in the fibrin gel ($\times 100$); B: Straight micro-vessels in H22 CM ($\times 200$); C: Tortuous micro-vessels in the control medium ($\times 200$); D: Growth curves of micro-vessels in H22 CM (●) and the control medium (○). Data are expressed as means of 24 samples, and error bars represent SE.

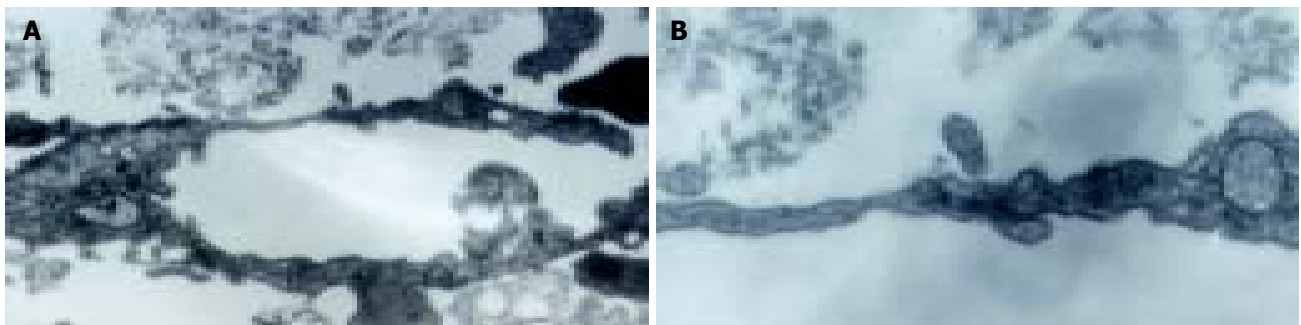


Figure 3 Electron transmission micrographs of the micro-vessel in fibrin gel. A: Lumen formed by cytoplasmic flaps joined by overlapping contacts ($\times 2\ 000$); B: Tight junction complexes between overlapping contacts ($\times 10\ 000$).

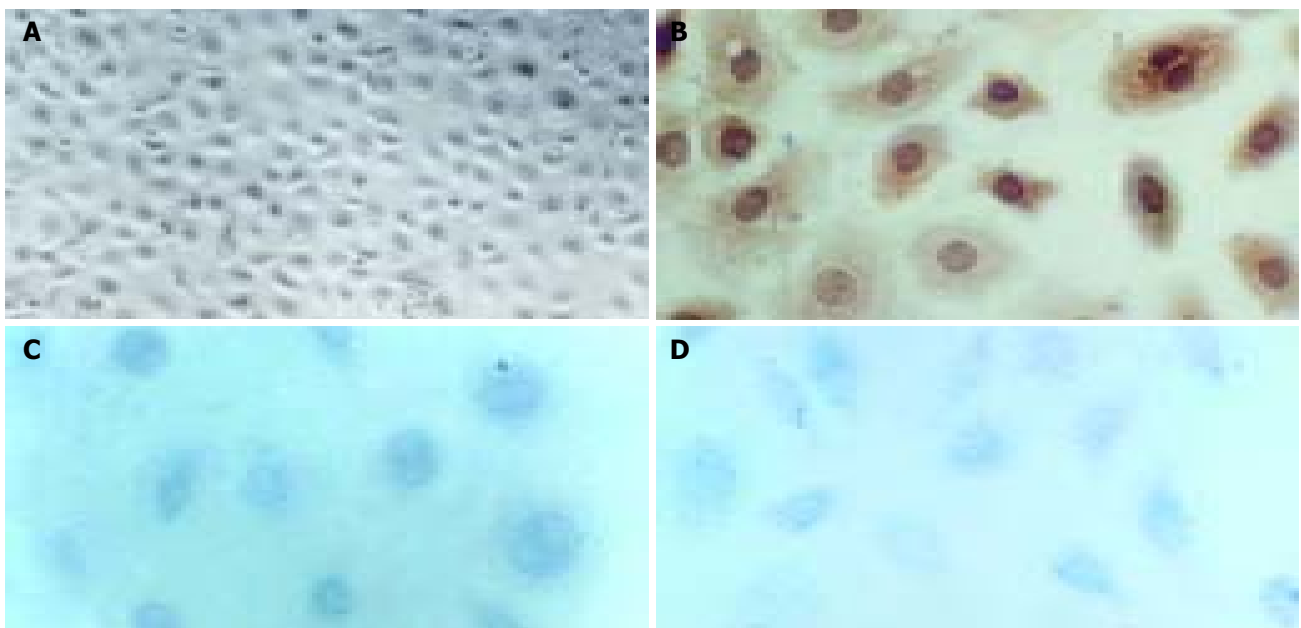


Figure 4 Primary cell culture with H22 CM and immunocytochemical staining. A: Microphotograph of the confluent cell monolayer ($\times 100$); B: Positive staining of Flt-4 (nucleus counterstained with hematoxylin, $\times 300$); C: Positive staining of PCNA ($\times 400$); D: Positive staining of c-Fos ($\times 400$).

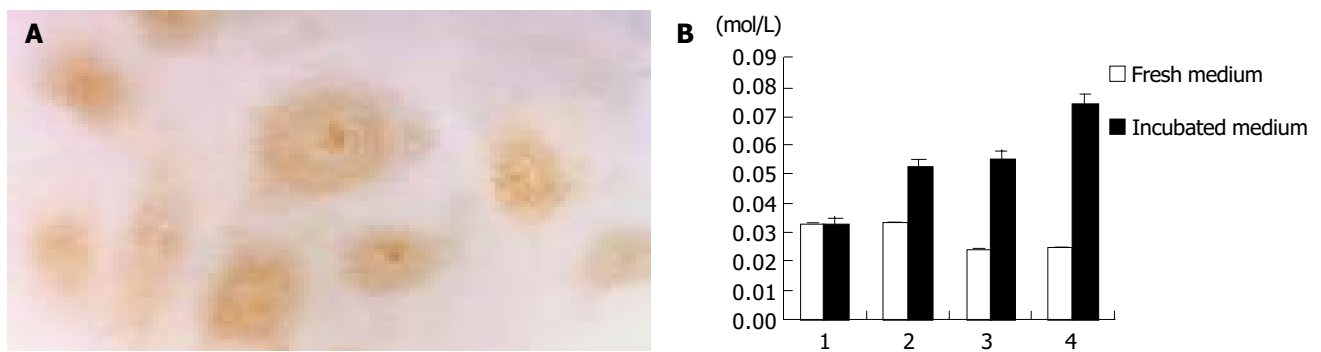


Figure 5 Expression of iNOS in lymphangioma cells and changes of NO level of the media after incubation. A: Positive staining of iNOS in cells cultured with H22 CM ($\times 400$); B: Changes of NO level of the control medium in empty plate (1) or primary culture plate (2), and H22 CM in empty plate (3) or primary culture plate (4).

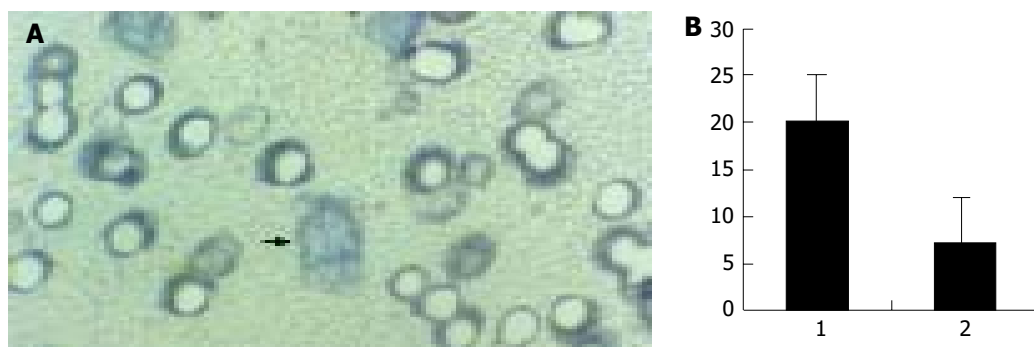


Figure 6 Transwell migration assay. A: Cells on lower surface of the filter membrane of the Millicell insert ($\times 400$); B: Migration cell number in H22 CM (1) and the control medium (2).

Effect of H22 CM on NO production

Immunostaining showed the expression of iNOS in lymphangioma cells after culture in H22 CM, and significantly increased content of NO in the culture medium (Figure 5). In contrast, cells cultured in the control M199 medium did not express iNOS, and the level of NO was rather low in the control medium.

Effect of H22 CM on cell migration

When cultured in the complete medium, the lymphangioma cells grew to a confluent monolayer in 8-10 d, and showed specialized cobblestone morphology, which further confirmed the nature of the cells. In transwell migration assay, the number of the cells on the lower surface of the filter membrane in H22 CM was significantly greater than in control medium (Figure 6).

DISCUSSION

The ascitic hepatoma H22 is a cell line with high potential of spontaneous lymphatic metastasis^[10], which was also verified in our experiments, and has been generally used in various experimental studies in oncology^[11-14]. It is proven to be a convenient and feasible tumor model for *in vitro* assessment on metastasis-related response of lymphatic endothelium.

The difficulty in isolation of lymphatic endothelium, especially from the animals commonly used in oncological experiments such as mice and rats, has limited studies on its reactions in tumorous environments. We used induced lymphangioma to solve this problem. When cultured in the fibrin gel, lymphangioma sprouts capillaries with ultrastructure similar to that of lymphatic vessels^[4,15]. Moreover, gelatin-anchorage dependent primary cell culture, and cobblestone morphology of confluent or subconfluent monolayer, are also specialized phenotype of lymphatic endothelium^[16,17]. Finally, positive expression of Flt-4 (also known as VEGFR-3), a marker of lymphatic endothelium in proliferation^[18,19], confirmed the

nature of the endothelium. These findings prove that lymphangioma is a proper original tissue for *in vitro* assay on lymphatic endothelium or lymphangiogenesis.

Despite the possible lymphangiogenic effect of fibrin^[20], H22 CM induced a faster formation of capillary network from lymphangioma in fibrin gels. Moreover, in primary cell culture, H22 CM showed similar capability to the complete growth medium in activating proliferation of lymphatic endothelial cells. Immunostaining for the common proliferating nuclear marker, PCNA^[21], and early-response gene signaling factor, c-Fos^[22], further confirmed the microscopic findings. Our results accord with the opinion on lymphatic vessel activation in cancer.

Endogenous NO is one of the key factors in the control of dilation of the lymphatic micro-vessels^[23,24]. The expression of iNOS in cancers is related to lymph node metastasis^[25,26]. iNOS is also evenly distributed throughout the cytoplasm of lymphatic endothelial cells^[27-29]. Our study demonstrates sustained expression of iNOS in cultured lymphatic endothelium and marked increase of NO levels in the culture medium under the effect of H22 CM, suggesting that dilation of lymphatics may be important for cancer invasion and metastasis.

There have been rare assays on lymphatic endothelial cell migration, which is an important event that initiates and coordinates lymphangiogenesis^[30]. Results from our study suggest that some soluble factors in H22 CM activate migration of lymphatic endothelial cells and tropistic lymphangiogenesis. The coadjuvant models established in our experiment are useful for further studies on migration inhibitors.

To our knowledge, this study is the first of its kind that bridges the gap between *in vivo* and *in vitro* studies on lymphatic endothelium and lymphangiogenesis. Both the culture medium and gel matrix in the experiment can be manipulated pharmacologically, which allows us to evaluate the activity of either soluble or solid-phase lymphangiogenesis inhibitors. Moreover, this spontaneous lymphatic metastasis

model of transplant H22 tumor will be helpful to determine whether inhibition of lymphangiogenesis is a realistic therapeutic strategy for inhibiting tumor dissemination and metastasis.

REFERENCES

- 1 **Pepper MS**. Lymphangiogenesis and tumor metastasis: myth or reality? *Clin Cancer Res* 2001; **7**: 462-468
- 2 **Joukov V**, Pajusola K, Kaipainen A, Chilov D, Lahtinen I, Kukk E, Saksela O, Kalkkinen N, Alitalo K. A novel vascular endothelial growth factor, VEGF-C, is a ligand for the Flt4 (VEGFR-3) and KDR (VEGFR-2) receptor tyrosine kinases. *EMBO J* 1996; **15**: 290-298
- 3 **Nathanson SD**. Insights into the mechanisms of lymph node metastasis. *Cancer* 2003; **98**: 413-423
- 4 **Pepper MS**, Skobe M. Lymphatic endothelium: morphological, molecular and functional properties. *J Cell Biol* 2003; **163**: 209-213
- 5 **Cassella M**, Skobe M. Lymphatic vessel activation in cancer. *Ann N Y Acad Sci* 2002; **979**: 120-130
- 6 **Stacker SA**, Hughes RA, Achen MG. Molecular targeting of lymphatics for therapy. *Curr Pharm Des* 2004; **10**: 65-74
- 7 **Mou JH**, Yan XC, Wang D, Wu XH, Li ZP, Xiang DB. Relationship between VEGF-C expression and lymph node metastasis and prognosis in large intestinal carcinoma. *Shijie Huaren Xiaohua Zazhi* 2004; **12**: 1061-1064
- 8 **Auerbach R**, Lewis R, Shinnars B, Kubai L, Akhtar N. Angiogenesis assays: a critical overview. *Clin Chem* 2003; **49**: 32-40
- 9 **Mancardi S**, Stanta G, Dusetti N, Bestagno M, Jussila L, Zweyer M, Lunazzi G, Dumont D, Alitalo K, Burrone OR. Lymphatic endothelial tumors induced by intraperitoneal injection of incomplete Freund's adjuvant. *Exp Cell Res* 1999; **246**: 368-375
- 10 **Jiang XP**, Tang ZY, Liu KD, Zhou XD, Lin ZY, Ling MY, Wu XF. mRNA levels of nm23 in murine ascites hepatoma (H22) clones with different lymphatic metastatic potential. *J Cancer Res Clin Oncol* 1996; **122**: 55-58
- 11 **Zhang J**, Zhang JK, Zhuo SH. A vaccine prepared by fusion of H₂₂ cells with the spleen-driven dendritic cells. *Shijie Huaren Xiaohua Zazhi* 2004; **12**: 276-279
- 12 **Yuan SF**, Wang L, Li KZ, Yan Z, Han W, Zhang YQ. Inhibitory effect of MUC1 gene immunization on H22 hepatocellular carcinoma growth. *Shijie Huaren Xiaohua Zazhi* 2003; **11**: 1322-1325
- 13 **Liang J**, Sun JY, Xie YH, Li Y, Yan L, Wang SW. Effect of monoclonal antibody 3A5 coupled with Chinese medicine compound Andi in targeted treatment of hepatocellular carcinoma. *Shijie Huaren Xiaohua Zazhi* 2003; **11**: 404-407
- 14 **Li ZS**, Zhu ZG, Yin HR, Chen SS, Lin YZ. Diversity of telomerase activity in human and murine tumor cells transfected with cytokine genes. *Shijie Huaren Xiaohua Zazhi* 1999; **7**: 194-196
- 15 **Azzali G**. The lymphatic vessels and the so-called "lymphatic stomata" of the diaphragm: a morphologic ultrastructural and three-dimensional study. *Microvasc Res* 1999; **57**: 30-43
- 16 **Mizuno R**, Yokoyama Y, Ono N, Ikomi F, Ohhashi T. Establishment of rat lymphatic endothelial cell line. *Microcirculation* 2003; **10**: 127-131
- 17 **Leak LV**, Jones M. Lymphatic endothelium isolation, characterization and long-term culture. *Anat Rec* 1993; **236**: 641-652
- 18 **Kaipainen A**, Korhonen J, Mustonen T, van Hinsbergh VW, Fang GH, Dumont D, Breitman M, Alitalo K. Expression of the fms-like tyrosine kinase 4 gene becomes restricted to lymphatic endothelium during development. *Proc Natl Acad Sci U S A* 1995; **92**: 3566-3570
- 19 **Karkkainen MJ**, Makinen T, Alitalo K. Lymphatic endothelium: a new frontier of metastasis research. *Nat Cell Biol* 2002; **4**: E2-5
- 20 **Palumbo JS**, Potter JM, Kaplan LS, Talmage K, Jackson DG, Degen JL. Spontaneous hematogenous and lymphatic metastasis, but not primary tumor growth or angiogenesis, is diminished in fibrinogen-deficient mice. *Cancer Res* 2002; **62**: 6966-6972
- 21 **Enholm B**, Karpanen T, Jeltsch M, Kubo H, Stenback F, Prevo R, Jackson DG, Yla-Herttuala S, Alitalo K. Adenoviral expression of vascular endothelial growth factor-C induces lymphangiogenesis in the skin. *Circ Res* 2001; **88**: 623-629
- 22 **Deed R**, Rooney P, Kumar P, Norton JD, Smith J, Freemont AJ, Kumar S. Early-response gene signalling is induced by angiogenic oligosaccharides of hyaluronan in endothelial cells. Inhibition by non-angiogenic, high-molecular-weight hyaluronan. *Int J Cancer* 1997; **71**: 251-256
- 23 **Nakaya K**, Mizuno R, Ohhashi T. B16-BL6 melanoma cells release inhibitory factor(s) of active pump activity in isolated lymph vessels. *Am J Physiol Cell Physiol* 2001; **281**: C1812-1818
- 24 **Mizuno R**, Koller A, Kaley G. Regulation of the vasomotor activity of lymph microvessels by nitric oxide and prostaglandins. *Am J Physiol* 1998; **274**(3pt 2): R790-796
- 25 **Niu XJ**, Wang ZR, Wu SL, Geng ZM, Zhang YF, Qing XL. Relationship between inducible nitric oxide synthase expression and angiogenesis in primary gallbladder carcinoma tissue. *World J Gastroenterol* 2004; **10**: 725-728
- 26 **Song ZJ**, Gong P, Wu YE. Relationship between the expression of iNOS, VEGF, tumor angiogenesis and gastric cancer. *World J Gastroenterol* 2002; **8**: 591-595
- 27 **Ji RC**, Kato S. Histochemical analysis of lymphatic endothelial cells in lymphostasis. *Microsc Res Tech* 2001; **55**: 70-80
- 28 **Marchetti C**, Casasco A, Di Nucci A, Reguzzoni M, Rosso S, Piovella F, Calligaro A, Polak JM. Endothelin and nitric oxide synthase in lymphatic endothelial cells: immunolocalization *in vivo* and *in vitro*. *Anat Rec* 1997; **248**: 490-497
- 29 **Marchetti C**, Casasco A, Di Nucci A, Cornaglia AI, Reguzzoni M, Rosso S, Piovella F, Calligaro A, Polak JM. Immunolocalization of endothelin and nitric oxide-synthase in lymphatic vessels and cultured lymphatic endothelial cells. *Microvasc Res* 1997; **53**: 282-285
- 30 **Boardman KC**, Swartz MA. Interstitial flow as a guide for lymphangiogenesis. *Circ Res* 2003; **92**: 801-808

Edited by Xia HHX Proofread by Zhu LH and Xu FM

Methylation profile of the promoter CpG islands of 14 "drug-resistance" genes in hepatocellular carcinoma

Sheng Ding, Bang-Dong Gong, Jian Yu, Jun Gu, Hong-Yu Zhang, Zu-Bin Shang, Qi Fei, Peng Wang, Jing-De Zhu

Sheng Ding, Bang-Dong Gong, Jian Yu, Jun Gu, Hong-Yu Zhang, Zu-Bin Shang, Qi Fei, Peng Wang, Jing-De Zhu, The State-Key Laboratory for Oncogenes and Related Genes, Shanghai Cancer Institute, Shanghai Jiaotong University, Shanghai 200032, China
Supported by the National High Technology Research and Development Program of China (863 program), No. 2002AA2Z3353 and the Science Foundation of Shanghai Municipal Government, No. 02DJ14056

Co-first-authors: Sheng Ding, Bang-Dong Gong and Jian Yu

Correspondence to: Dr. Jing-De Zhu, The State-key Laboratory for Oncogenes and Related Genes, Shanghai Cancer Institute, Shanghai Jiaotong University, LN 2200/25, Xie-Tu Road, Shanghai 200032, China. zhujingde@yahoo.com

Telephone: +86-21-64224285 **Fax:** +86-21-64224285

Received: 2003-04-14 **Accepted:** 2003-05-09

Abstract

AIM: To establish the DNA methylation patterns of the promoter CpG islands of 14 "drug-resistance" genes in hepatocellular carcinoma (HCC).

METHODS: The methylation specific polymerase chain reaction in conjunction with sequencing verification was used to establish the methylation patterns of the 14 genes in the liver tissues of four healthy liver donors, as well as tumor and the paired non-cancerous tissues of 30 HCC patients.

RESULTS: While 11 genes (ATP-binding cassette, sub-family G (WHITE), member 2 (*ABCG2*), activating transcription factor (*ATF2*), beta-2-microglobulin (*B2M*), deoxycytidine kinase (*DCK*), occludin (*OCLN*), v-raf-1 murine leukemia viral oncogene homolog (*RAF1*), ralA binding protein 1 (*RALBP1*), splicing factor (45 kD) (*SPF45*), S-phase kinase-associated protein 2 (p45) (*SKP2*), tumor protein p53 (Li-Fraumeni syndrome) (*TP53*) and topoisomerase (DNA) II beta (*TOP2B*) maintained the unmethylated patterns, three genes displayed to various extents the hypermethylation state in tumor tissues in comparison with the normal counterparts. The catalase (*CAT*) was hypermethylated in tumor and the neighboring non-cancerous tissue of one case (3.3%). Both glutathione S-transferase pi (*GSTpi*) (80%, 24/30 in tumor and 56.7%, 17/30 in the paired non-cancerous tissues) and cystic fibrosis transmembrane conductance regulator, ATP-binding cassette (sub-family C, member 7) (*CFTR*) (77%, 23/30 in tumor and 50%, 15/30 in the paired non-cancerous tissues) genes were prevalently hypermethylated in HCC as well as their neighboring non-cancerous tissues. No significant difference in the hypermethylation occurrence was observed between the HCC and its neighboring non-cancerous tissues.

CONCLUSION: Hypermethylation of promoter CpG islands of both *CFTR* and *GSTpi* genes occurs prevalently in HCC, which may correlate with the low expression of these two genes at the mRNA level and has the profound etiological and clinical implications. It is likely to be specific to the early phase of HCC carcinogenesis.

Ding S, Gong BD, Yu J, Gu J, Zhang HY, Shang ZB, Fei Q, Wang P, Zhu JD. Methylation profile of the promoter CpG islands of 14 "drug-resistance" genes in hepatocellular carcinoma. *World J Gastroenterol* 2004; 10(23): 3433-3440
<http://www.wjgnet.com/1007-9327/10/3433.asp>

INTRODUCTION

Hepatocellular carcinoma (HCC) is one of the most threatening malignancies, occurring prevalently in China^[1]. Its poor prognostic prospects have not only been attributed to the rapid advancing nature as well as the notorious metastasizing potential of the primary lesions, but also resulted from its refractoriness to the conventional chemotherapeutic practices^[2-4]. Altered expression of the crucial genes, even prior to the relevant treatment, is common in cancer cells, including HCC. The intrinsic drug resistance, reflected by the changes in the expression profile of the key genes in relevant pathways, including apoptosis, cell cycle progression, DNA repairs, *etc.*, is common in cancer cells, which certainly contributes to the more rapid growth ability of cancerous cells than the normal counterparts, in the adverse environments in particular. Furthermore, cancer cells can also acquire resistance to chemotherapeutic remedies during treatment. It has been regarded as the key mechanism for the post-remission return of the full-blown cancer of same origin. Therefore, a long-standing challenge in cancer field is the underlying mechanisms of the drug resistance nature of tumors. The genetic defects leading to the intrinsic drug resistance have been well-established, but the mechanisms at the epigenetic levels, DNA methylation in particular resulting in the changes in expression, have only gained the justified recognition recently^[5].

Over 50% of the protein coding genes are marked with the CpG rich segment at their 5' end, the methylation status of which profoundly affects the transcription status of the genes^[6]. Biochemically, the methylated CpG affects the sequence-specific DNA-protein interactions by eliminating the otherwise binding of the transcription factors to their cognate cis-elements, while unfolding the cascade of reactions leading to chromatin condensation initiated by the binding to the methylated CpG by members of the methyl CpG binding protein family (MBD). Hypermethylation of the promoter CpGs has been linked to the long-term transcription-silencing status of DNA segments, including genes as well as the transposon-like-repetitive sequences in cells^[7,8]. The genome-wide hypomethylation has been regarded contributive to activation of transcription of the otherwise silenced transposon like repetitive sequences (such as the Alu and LINE repeats in mammals) and instrumental to the transposition mediated loss of the genome stability during cell transformation^[9-11]. The CpG islands of several tumor suppressor genes, which are hypomethylated and express in normal cells, became frequently hypermethylated in almost all the cancers investigated, contributing to the loss of function of the tumor suppressor genes in cancer. On the other hand, the reverse processes, such as hypomethylation of CpG islands may also result in transcription activation of the otherwise inert genes^[12].

In our previous studies on HCC^[13], we have assessed a number of genes in the category of “drug-resistance” genes, including the O-6-methylguanine-DNA methyltransferase (*MGMT*) gene encoding an enzyme responsible for the cell’s resistance to the alkylating type of chemotherapeutic drugs, and mutL homolog 1, colon cancer, nonpolyposis type 2 (*hMLH1*), a mismatch repairing gene^[14]. The former is frequently methylated while the later maintains the unmethylated status in HCC tissues in comparison with the normal liver tissues. In this study, we extended our profiling efforts in the same group of HCC patients to other 14 “drug-resistance” genes, 13 of which were touched for the first time. This specifically oriented survey to “drug-resistance” should provide valuable insights into our understanding of the underlying mechanisms for the development of intrinsic resistance of HCC to chemotherapeutic drugs, and have important etiological implications to carcinogenesis of HCC.

MATERIALS AND METHODS

Tissue samples and DNA preparation

With the informed consent of all patients and approval of the ethics committee, the samples of tumors were collected from HCC patients ($n = 30$) during operation. The pathological classification of tumor tissues was carried out, and the stage of each case was graded according to the WHO classification^[15]. Total genomic DNA was extracted from frozen tissue specimens (50-100 mg) according to a standard protocol with some modifications^[16,17]. Frozen pulverized powders of the specimens were re-suspended with 2 mL lysis buffer containing 50 mmol/L Tris-HCl pH 8.0, 50 mmol/L EDTA, 10 g/L SDS, 10 mmol/L NaCl plus 100 μ g/mL boiling-treated RNase A (Sigma, USA). Following 1-h incubation at 37 °C, proteinase K (Roche, USA) was added to the cellular lysates for a final concentration of 100 μ g/mL, and the digestion was carried out at 55 °C for 2 h. Organic extractions with a half volume of phenol/chloroform/isoamyl alcohol (1:1:0.04) were repeatedly carried out until no visible interphase remained after centrifugation. DNA was precipitated from the aqueous phase in the presence of 0.3 mol/L NaOAc (pH 7.0) and two and a half volumes of ethanol, washed once in 700 mL/L ethanol, dissolved at 65 °C for 30 min with 0.2-0.4 mL TE (10 mmol/L Tris-HCl pH 7.4 and 1 mmol/L EDTA) and stored at 4 °C until use. The DNA concentrations were calculated according to the $A_{260\text{ nm}}$ readings.

Bioinformatics search for “drug-resistance” genes

We used “drug resistance” as the key word to search from the NCBI LocusLink database (<http://www.ncbi.nlm.nih.gov/LocusLink/list.cgi>). The sequence of the coding region (63 targets) plus 5 kb segments at each ends were downloaded, and subjected to search for the existence of the CpG island. The parameters were set as OBS/EXP (the minimum average observed to expected ratio of C plus G to CpG) = 0.6, MINPC (the minimum average percentage of G plus C) = 50, and LENGTH (the minimum length that a CpG island has to be) = 200 bp (<http://www.ebi.ac.uk/emboss/cpgplot/>). Thirty six genes were found containing the promoter CpG island (Table 1). Among this list 14 genes were selected for the methylation profiling, as they represent in different categories for the functions and properties (Table 2). The primer pairs (Table 3) for methylation specific polymerase chain reaction (MSP) in this report were designed according to the same principle with assistance of the web server for identification of the CpG islands (<http://www.ebi.ac.uk/emboss/cpgplot/index.html>) and the primer design software (http://micro-gen.ouhsc.edu/cgi-bin/primer3_www.cgi) (Table 3).

Table 1 The “drug-resistance” genes containing the promoter CpG island

Genes	Location relative to transcription start site	Genes	Location relative to transcription start site
ABCC4	-487 to +466	GSTP1	-391 to +91
ABCC1	-356 to +406	hMLH1	-72 to +393
ABCC13	+138 to +386	KIAA1337	-553 to +413
ABCC3	-96 to +358	MAPK14	-371 to +319
ABCB11	+1 255 to +1 565	OCLN	-9 to +967
ABCC5	-219 to +87	POLB	-209 to +34
ABCC6	-229 to +89	RAF1	-466 to +399
ABCC8	-185 to +531	RALBP1	-901 to +325
ABCG2	-741 to -17	RRM2	-718 to +426
ATF2	-418 to +545	SKP2	-663 to +182
B2M	-170 to +83	SLC19A1	-719 to +268
BCAR3	-328 to +126	SLC22A1L	-265 to +158
BCL2	-7 to +573	SPF45	-547 to +92
BIRC4	-527 to -235	SRI	-251 to +257
CAT	+35 to +395	SSA2	-195 to +152
CFTR	-515 to -55	TOP2A	-123 to +506
DCK	-267 to +155	TOP2B	-805 to +393
ERBB2	+173 to +534	TP53	+130 to +337

Bisulfite treatment of DNA and MSP

The methylation status of the promoter CpG islands of the 14 genes in all sample DNAs were analyzed by MSP on the sodium-bisulfite converted DNA^[16,17]. The primer pairs for MSP and the genes’ genome access on GenBank are detailed in Table 3. In detail, 2 μ g DNA in 50 μ L TE was incubated with 5.5 μ L of 3 mol/L NaOH at 37 °C for 10 min, followed by a 16 h treatment at 50 °C after adding 30 μ L of fresh-prepared 10 mmol/L hydroquinone and 520 μ L of freshly prepared 3.6 mol/L sodium-bisulfite at pH 5.0. The DNA was desalted using a home-made dialysis system with 10 g/L agarose. Then, the DNA (approximately 100 μ L) was denatured at 37 °C for 15 min with 5.5 μ L of 3 mol/L NaOH, followed by ethanol precipitation with 33 μ L 10 mol/L NH_4OAc and 300 μ L ethanol. After washing with 700 mL/L ethanol, the gently dried DNA pellet was dissolved with 30 μ L TE at 65 °C for 10 min. The DNA sample was finally stored at -20 °C until further use. PCR reaction was carried out in a volume of 15 μ L with 50 ng or less template DNA with JumpStart Taq polymerase (Sigma, USA). An initial denaturation step at 94 °C for 4 min was followed by 35 cycles of reaction at 94 °C for 20 s, variable annealing temperature (Table 3) for 20 s and 72 °C for 25 s, and a final extension at 72 °C for 5 min. The PCR products were separated by 12 g/L ethidium bromide containing agarose gel electrophoresis with 1 \times Tris Acetate EDTA (TAE) buffer and visualized under UV illumination. To verify the PCR results, representative bands from each target were gel-purified and cloned into T-vector (Buocai, Shanghai, China), followed by automatic DNA sequencing provided by Buocai. Only verified results are presented in this report.

The M. Sss I treated DNA from the normal liver tissue was used in the MSP procedure as the control template. The DNA from the liver tissue of the healthy liver donor^[14,16] was batch cleaved with *EcoRI*, followed by M. Sss I treatment overnight according to the manufacturer’s instruction (New England Biol., Boston, USA). The purified DNA was bisulphate treated as usual, and subjected to MSP with the primer pairs for 11 genes where no methylated alleles were detected in both cell lines and HCC tissues.

Cell culture and semi-quantitative reverse transcription^[18]

The established cell lines, BEL-7402 (human hepatocellular carcinoma cell line, No. TCHu68, Cell Bank in Shanghai),

Table 2 The “drug resistance” genes in this study

Resistance mechanism	Genes and ref.	Function
Plasma membrane transporters/pump decrease or increase to concentration	ABCG2	Belongs to the abc transporter family, appears to play a major role in the multidrug resistance phenotype of MCF-7 breast cancer cell line. When over-expressed, the transfected cells become resistant to mitoxantrone, daunorubicin and doxorubicin, display diminished intracellular accumulation reduce intracellular drug of daunorubicin, and manifest an ATP-dependent increase in the efflux of rhodamine
	CFTR	Belongs to the abc transporter family. MRP subfamily, involved in the transport of chloride ions
	RALBP1	Activates specifically hydrolysis of GTP bound to RAC1 and CDC42. Mediates ATP-dependent transport of S-(2,4-dinitrophenyl)-glutathione (DNP-SG) and doxorubicin(DOX) and is the major ATP-dependent transporter of glutathione conjugates of electrophiles (GS-E) and DOX in erythrocytes. Can catalyze transport of glutathione conjugates and xenobiotics, and may contribute to the multidrug resistance phenomenon
Transcription factor and/or tumor suppressor	ATF2	Belongs to the bZIP family, ATF subfamily, binding the cAMP response element (CRE) (consensus sequence: 5'GTGACGT(A/C)(A/G)-3') as a transcription activator
	TP53	Acts as a tumor suppressor in many tumor types, involved in cell cycle regulation as a transcription activator that acts to negatively regulate cell division by controlling a set of genes required for this process
The enzymes involved in drug activation or inactivation metabolism abnormality	CAT	Belonging to the catalase family, serves to protect cells from the toxic effects of hydrogen peroxide
	GSTP1	Belongs to the GST superfamily. Pi family; Conjugation of reduced glutathione to a wide number of exogenous and endogenous hydrophobic electrophiles
	TOP2B	Control of topological states of DNA by ATP-dependent breakage, passage and rejoining of double-stranded DNA
	DCK	Required for the phosphorylation of several deoxyribonucleosides and certain nucleoside analogs widely employed as antiviral and chemotherapeutic agents
Cell signaling alteration and cell cycle checkpoints alteration	RAF1	Belongs to the Ser/Thr family of protein kinases. RAF subfamily. Involved in the transduction of mitogenic signals from the cell membrane to the nucleus as a part of the Ras-dependent signaling pathway from receptors to the nucleus
	SKP2	Involved in regulation of G1/S transition as substrate recognition component of the SCF (SKP1-CUL1-F-box protein) E3 ubiquitin ligase complex which mediates the ubiquitination and subsequent proteasomal degradation of target proteins involved in cell cycle progression, signal transduction and transcription
Unclear mechanisms	B2M	Beta-2-microglobulin is the beta-chain of major histocompatibility complex class I molecules, Containing 1 immunoglobulin-like domain
	OCLN	May play a role in the formation and regulation of the tight junction (TJ) paracellular permeability barrier
	SPF45	Involved in nuclear mRNA splicing, via spliceosome

Note: All the information in this table was obtained from the web site of the OMIM section of the locus link (<http://www.ncbi.nlm.nih.gov/LocusLink/>) and GeneCards(<http://bioinfo.weizmann.ac.il/cards/>).

SMMC-7721 (human hepatocellular carcinoma cell line, No. TCHu13, Cell Bank in Shanghai), Hep3B (human hepatocellular carcinoma cell line, ATCC Number: HB-8064), HepG2 (human hepatocellular carcinoma cell line, ATCC Number: HB-8065), HCCLM3 (human hepatocellular carcinoma cell line, Cell Bank in Zhongshan Hospital, Shanghai), and L02 (immortalized normal liver cell line, No GNHu6, Cell Bank in Shanghai) were cultured in DEME medium plus 100 mL/L new born calf serum at 37 °C in a 50 mL/L CO₂ atmosphere.

Total RNA from various HCC cell lines was extracted using the TriPure isolation reagent kit (Roche, USA). Reverse transcription was subsequently carried out using the superscript II RNase H-reverse transcriptase kit. β -actin was used as an internal control in separate reaction. The *GSTpi* cDNA primers (sense: 5'-GGAGACCTCACCTGTACCA-3'; anti-sense: 5'-GGGCAGTGCCTTACATAGT-3') were the same as in a previously published paper^[19]. The primer sequences and reaction conditions are listed in Table 4. RT-PCR products were visualized under UV illumination after electrophoresis in 1.2% agarose, followed by the densitometric quantification.

Statistics

The methylation data were dichotomized as 1 for the co-existence of the methylated and unmethylated alleles; 2, for methylated allele only; and 0 for the unmethylated for both

alleles to facilitate statistical analysis using contingency tables. The statistic analyses for the association between the methylation profile of the gene and each of the clinical-pathological parameters were carried out with the statistics package (<http://www.R-project.org/>). Both Pearson's Chi-square test with Upton's adjustment and Fisher's exact test (<http://www.R-project.org/>) were used to deal with the sample cells with the low expected values. The relative frequency with a 95% confidence interval ($P < 0.05$) for a binomial distribution was calculated for the tumors and the paired non-cancerous tissues.

RESULTS

Our previous efforts^[14,16] provided an HCC specific altered pattern in DNA methylation of 11 among 44 genes by MSP in conjunction with sequencing verification. Among that list, there were several genes that might be classified as the drug resistance related genes, i.e., the *hMLH1* and *MGMT* genes. The former maintained the unmethylated status and the later displayed hypermethylation in liver cancer. Although the impact of the tumor specific changes in methylation pattern of the *MGMT* gene has not been fully evaluated experimentally, it remains desirable to establish the methylation profile of more genes in the category of “drug resistance”. Such efforts should provide new insights into the underlying mechanisms as well

Table 3 The primers for MSP analysis

GenBank No.	Gene symbol		Sense 5'-3'	Antisense 5'-3'	Position	Size(bp)
NT_016354	ABCG2	m	TGTCGCGTTGAGTCGTTA	AACGTCCTCCGATACTTCG	-698 to -464	235
		U	TGTGTTTTGTTGTTGAGTTGT	TCACTCTAATTCATTCCATTCAATC	-591 to -457	135
NT_005403	ATF2	m	GGGTCGGAATAACGAACG	ATCACCTCGAATACTCCTAACG	230 to 375	146
		U	GGAGGGGTTGGAATAATGAAT	CCCATTTCCTACCTCAA	220 to 379	160
NT_010194	B2M	m	ATTTGGTATTGCGTCGTTG	ACGAAACGAAACATCTCGAC	-128 to 23	151
		U	TTTTTAATTTGGTATTGTGTTGTTG	AACTCACACTAAATAACCTCCAAAC	-134 to 83	217
NT_009237	CAT	m	AGTAGCGGGTCGCGTAG	AACCACCCGAACCTATCG	118 to 372	255
		U	GGAAGGAGTAGTGGGTTGTGT	AACCACCCAAACCTATCACA	112 to 372	261
NT_007933	CFTR	m	AGAGGTGCGGATTGTCGTT	CGACTTTCTCCACCCACTACG	-316 to -114	203
		U	TTAAAGAGAGGTTGTGATTGTTGTT	TCCTTCACTCCCTACCA	-322 to -174	149
NT_006216	DCK	m	TATACGCGCGGTTTCGT	CGCCGACGAAATATCGAA	-168 to 27	195
		U	TTTTTTGTTATATGTGTGGTTTTGT	TACCCCTCAACCCTCACC	-176 to -75	102
NT_078018	OCLN	m	TGCGTTCGTTAGGTGAGC	CGAATCCCAACTCGAAAACG	538 to 753	216
		U	GTTAGGTGTGTTGTTAGGTGAGT	CACACCTCTCTAATTCACACA	532 to 772	241
NT_022517	RAF1	m	TCGGTCGTTTGGAAAGTC	CCCTAAAACGCGAAAACG	-72 to 180	252
		U	GGTTTGGTTGTTTTGGAAAGTT	CACCAAATATAACCACCTCCCACT	-2 to 183	185
NT_010859	RALBP1	m	GGGTAAGTCGTTTCGTTTTCG	CCTCTCCGCTCAAACGACT	-495 to -215	281
		U	GTTAGTATTATATTGGGGTAAAGTTGTTG	CCCTTCATCCCAAACTCA	-510 to -371	140
NT_006576	SKP2	m	GTCGTAGCGTCGTTTCGTT	CTACAACCCGCTCTACTTCG	-198 to 10	208
		U	TTTTTTAGTTAGTTGTTAGTTGTTGTTGTT	ACCCACTCTACTTCACAACCAC	-209 to 5	214
NT_077569	SPF45	m	AGTGTCTGTTCCGTTTCGTT	CCTCGAAAACCTCCGACTACG	-216 to -6	211
		U	GTGGAGTGTGTTGGTTTTGTT	AACTTACATCTAACACCTCCCAAA	-220 to -67	154
NT_022517	TOP2B	m	TGGGTTTCGTCGTTTCGT	CCGCGCTAAACCCGAAC	-241 to -66	176
		U	GGTTGTTGGGTTTTGTTGTTTT	TTCTCCTCAACCACCACACTAA	-254 to -60	195
NT_010718	TP53	m	CGGAGTCGAGAGTTCGTCG	CGAAAACACTTTTACGTTTCG	157 to 279	123
		U	GTTGAAAATATATGGAGTTGAGAGTTT	CTTTCCACAACAATAACACACTTC	190 to 291	102
NT_033903	GSTP1	m	GCGATTTCCGGGATTTTA	ACGACGACGAAAACCTCAA	-183 to 16	199
		U	GTTGGGGATTTGGGAAAG	TATAAAAATAATCCACCCCACT	-230 to -28	203

as the capability of predicting HCC patient's intrinsic profile of drug resistance, based upon the changes in DNA methylation pattern of the genes involved.

Bioinformatics search for the "drug-resistance" genes

Sixty three genes were revealed from NCBI LocusLink database from the searching with "drug-resistance" as the key words (<http://www.ncbi.nlm.nih.gov/LocusLink/list.cgi>). To identify the genes falling into the category of CpG island containing genes, the sequence of the coding region plus 5 kb each upstream and downstream was downloaded and subjected to the analysis with CpG island identification software (<http://www.ebi.ac.uk/emboss/cpgplot/>). Forty four genes were found containing one or more CpG islands, but only 36 genes really had the promoter embedded in a CpG island (Table 1). Hence, transcription of these 36 genes is likely to be subjected to the control of the DNA methylation status. From these genes, 14 genes representing different functions and mechanisms in "drug-resistance" (Table 2) were selected for methylation profiling; three genes encoding the various membrane transporters: *ABCG2*, *CFTR*, and *RALBP1*, two encoding the transcription factors, *ATF2*, and *TP53*, four encoding the enzymes mediating the drug activation or inactivation: *CAT*, *GSTpi*, *TOP2B* and *DCK*, two encoding the proteins involved in signaling or cell-cycle progression: *RAF1* and *SKP2*, and three with unknown underlying mechanisms: *B2M*, *OCLN* and *SPF45*.

Technological consideration

MSP is the most popular method for methylation profiling of any given targets in human cancers for both its easiness and sensitiveness. Based upon the distinguished difference in sensitivity of the methyl-cytosine from the cytosine to be

converted to uridine by bisulphate treatment: the later is amenable, but the former is resistant, the methylation status of the target fragments can be determined by parallel PCR reactions with one pair of the primers in which the CG in the wide-type sequence is maintained for detection of methylated allele, and the other in which the CG is replaced with TG for the unmethylated allele. However, inherent with the PCR-type assays, there are compelling reasons to eliminate both false positive and negative PCR reactions. As 13 genes in this list except for the *GSTpi* gene had not been subjected to MSP previously, we carried out optimization of the PCR reaction with a panel of five established cell lines. For those targets, only the unmethylated allele was detected, MSP with the DNA from the normal liver tissue was carried out, showing that all 14 genes were unmethylated. To ensure that failure to detect the methylated allele was not false negative artifact in PCR reaction, we *in vitro* methylated the DNA from the normal liver with *M. Sss I* methyl-transferase that was capable of transferring methyl to the fifth carbon atom of the cytosine in the CpG dinucleotides, followed by methylation profiling. As shown in Figure 1, while no methylated allele was detected with the methylation targeted primers with the liver DNA, the *M. Sss I* treated DNA led to the positive PCR reaction, indicating that the PCR condition used for the tumor samples was capable of detecting the methylated targets, including *ABCG2*, *ATF2*, *B2M*, *DCK*, *RAF1*, *RALBP1*, *SPF45*, *SKP2*, *TP53*, and *TOP2B* genes (panels 1-10, respectively). As the rest four genes were heterozygously methylated in some of liver cancer cell lines, it indicated that the PCR reactions specific to the methylated allele was acceptable (for instance, lane 11 for *OCLN*, Figure 1), the *in vitro* methylation by *M. Sss I* testing was exempted. To eliminate the false negative results, the representative PCR bands were subjected to T-cloning

and sequencing verification. Only the data, the bands of which had the correct identity in sequence, were regarded informative.

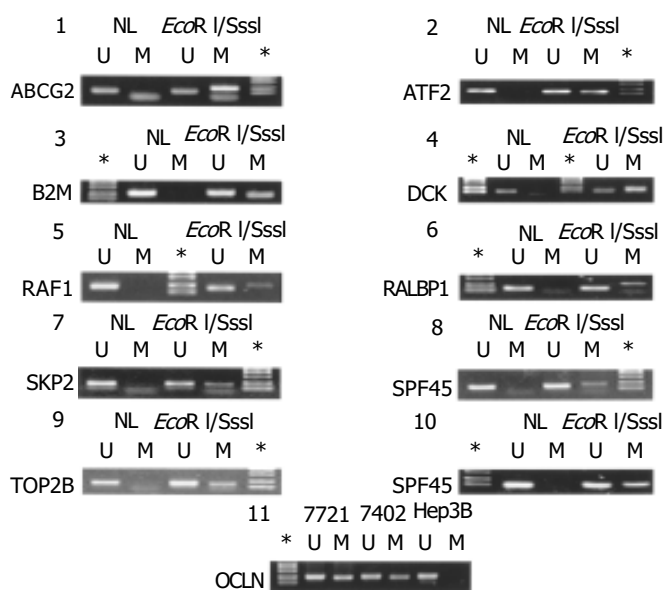


Figure 1 MSP testing with the M. Sss I treated normal liver tissue DNA. The *in vitro* methylated DNA from the normal liver tissue was used for MSP along with the untreated. Panels: 1, *ABCG2*; 2, *ATF2*; 3, *B2M*; 4, *DCK*; 5, *RAF1*; 6, *RALBP1*; 7, *SKP2*; 8, *SPF45*; 9, *TOP2b*; and 10, *TP53*. The PCR conditions for *OCN* gene were assessed by PCR in three liver cancer cell lines, 7721, 7402, and Hep3B (panel 11). U, unmethylated allele; M, methylated allele, NL, normal liver tissue; *the DNA size marker: DL-2000.

The methylation profiles of 14 genes in HCC

By MSP analysis, 13 genes displayed a uniform unmethylated status in the liver tissues from all four healthy donors, while the *RAF1* gene was heterozygous in one case, but fully unmethylated in the rest three cases. In all 30 cases of HCC, the following 11 genes: *ABCG2*, *ATF2*, *B2M*, *DCK*, *RAF1*, *RALBP1*, *SPF45*, *SKP2*, *TOP2B*, *OCN* and *TP53* maintained the same unmethylated status in both HCC tissues and the paired non-cancerous tissues (Figure 2), indicating no DNA methylation mediated changes in the control of the expression of these 11 genes in HCC. The remaining three genes displayed in varying degree hypermethylation in HCC tissues (Figure 2 and Table 4). Since hypermethylation of the *CAT* gene rarely occurred (3.3%) (Figure 2), its impacts on the HCC pathology might be rather trivial. Both *GSTpi* and *CFTR* genes were prevalently hypermethylated in HCC and their neighboring non-cancerous tissues (80% and 56.7%, and 77% and 50%, respectively, Table 4), highlighting the possibility that inactivation of transcription of these two genes may indeed occur in HCC, and have certain etiological significance.

It has been well recognized that the so-called non-cancerous cells pathologically defined may have already suffered from certain genetic lesions as the corresponding cancerous tissues. Inclusion of the neighboring non-cancerous tissues in this study made it possible to analyze our results from the stage-specific perspective of carcinogenesis. As shown in Table 5, no significant difference was detected in the occurrence of hypermethylated *GSTpi* and *CFTR* genes between HCC and the paired non-cancerous tissues ($P > 0.05$) (Table 4). If the neighboring non-cancerous tissues have indeed suffered from the early stage genetic and/or epigenetic lesions, the methylation changes of these two genes might occur at the early stage of HCC carcinogenesis.

To correlate the hypermethylated status with the transcription silencing of *GSTpi* gene, we carried out MSP analysis of this gene and semi-quantitative RT-PCR for its expression in five

established liver cancer cell lines. As shown in Figure 3, three liver cancer cell lines (i.e. HepG2, Hep3B and L-02) were fully methylated, and did not express *GSTpi*, while SMMC-7721 and HCCLM3 cell lines were heterozygously methylated, and expressed a detectable level of *GSTpi* mRNA. Therefore, the general notion stands correct in this case, that the hypermethylated status of the promoter CpG island is inversely correlated with the long-term transcription silencing state of the gene.

Glutathione-S-transferases (GSTs) are a family of phase II detoxification enzymes that catalyze the conjugation of glutathione to a wide variety of endogenous and exogenous electrophilic compounds, including subclasses of carcinogens and cytotoxic therapeutic drugs^[20,21], so that the cells are protected from DNA damages^[22]. Furthermore, the *GSTpi* isoform also regulates the mitogen-activated protein (MAP) kinase pathway that participates in cellular survival and death signals via protein: protein interactions with c-Jun N-terminal kinase 1 (JNK1) and apoptosis signal-regulating kinase (ASK1)^[23]. Therefore, GSTs serve two distinct roles in the development of drug resistance to both substrate-type and other types of chemotherapeutic drugs via direct detoxification as well as acting as inhibitors of the MAP kinase pathway^[24].

The cystic fibrosis trans-membrane conductance regulator (*CFTR*) belongs to the ABC transporter superfamily, and regulates the chloride permeability mainly in epithelial cells. Its defects may contribute to cystic fibrosis, a common autosomal recessive disorder among the Caucasian population, which affects multiple organs, including lung, pancreas, liver, sweat gland, reproductive system and intestine. *CFTR* gene has high expression level of transcripts in epithelial cells in pancreas and nasal polyps; low in lung, liver, and kidney; and undetectable in brain and fibroblasts^[25]. It functions as a cAMP-regulated chloride channel, a conductance regulator by an autocrine mechanism involving ATP and/or chloride efflux, and an inhibitor of epithelial Na⁺ channels when chlorides are released^[26]. The involvement of *CFTR* gene in drug resistance is implicated by observation that the forced over-expression of *CFTR* gene confers the multiple drug resistance to NIH 3T3 cells^[27], a similar behavior to the founding member of this family, multiple drug resistance 1 (MDR1), which was identified three decades ago, for its etiological role in the cellular resistance to the multiple chemotherapeutic drugs. The unmethylated status of *CFTR* gene in the normal liver tissues suggested that its expression may be necessary for the physiological activities of hepatocytes. Although whether this gene is expressed in HCC has not been tested, the possibility does remain for the functional loss of this gene in HCC, indicated by the prevalent hypermethylation of its promoter CpG islands.

Therefore, lacking of expression of these two genes, implicated by the hypermethylated state of the promoter CpG islands, may make the cells more susceptible to the carcinogenic insults, a feature associated with the proneness to the malignant state of cells. Hypermethylation of the promoter CpG islands may reflect the long-term silencing state of transcription of both *GSTpi* and *CFTR* genes in HCC, which may offer growth advantages of the malignant cells over their normal counterparts *in vivo*. Indeed, the hypermethylation of both genes was an early phase event, as no statistically significant difference in the hypermethylation frequency between the paired neighboring non-cancerous and HCC tissues was observed (Table 5). Nevertheless, the hypermethylated status of these two genes may not be all bad, as the HCC with the hypermethylated alleles of these two genes (if either or both genes did not express) may be more sensitive to the relevant chemotherapeutic drugs than their unmethylated counterparts. Indeed, in a recent report, a better response to chemotherapy was achieved in breast cancer patients lacking *GSTpi* expression than the expressing counterparts^[28].

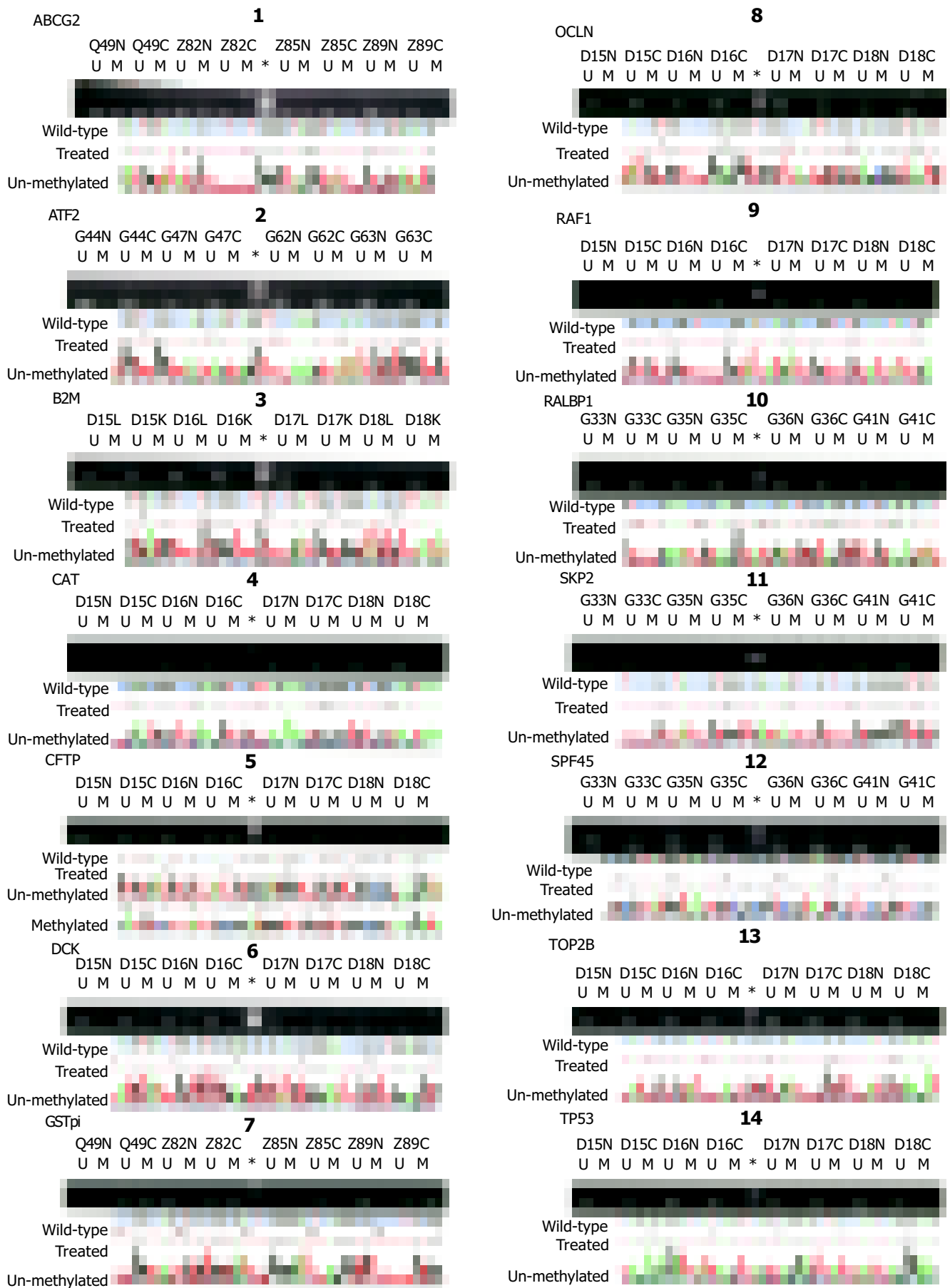


Figure 2 Methylation profiles of the promoter CpG islands of 24 genes in HCC. Both electrophoretic patterns of the representative PCR products of each of 14 targets and the sequencing verification of one representative PCR product were presented. To indicate the methylation status, the sequenced data are aligned with the wild-type sequence. *, size markers, the bands of 250 bp and 100 bp were shown. U, unmethylated; and M, the hypermethylated. Panels: 1, *ABCG2*; 2, *ATF2*; 3, *B2M*; 4, *CAT*; 5, *CFTP*; 6, *DCK*; 7, *GSTpi*; 8, *OCLN*; 9, *RAF1*; 10, *RALBP1*; 11, *SKP2*; 12, *SPF45*; 13, *TOP2B*; and 14, *TP53*.

Table 4 The hypermethylation for each gene in each of HCC patient samples

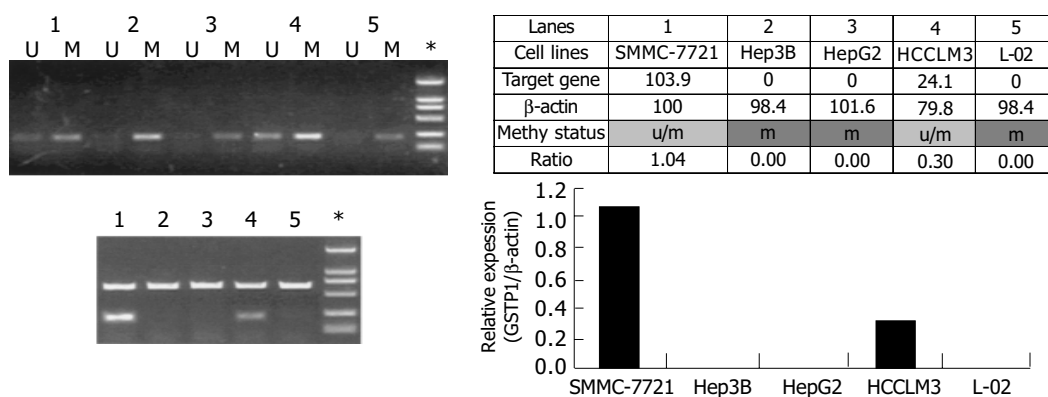
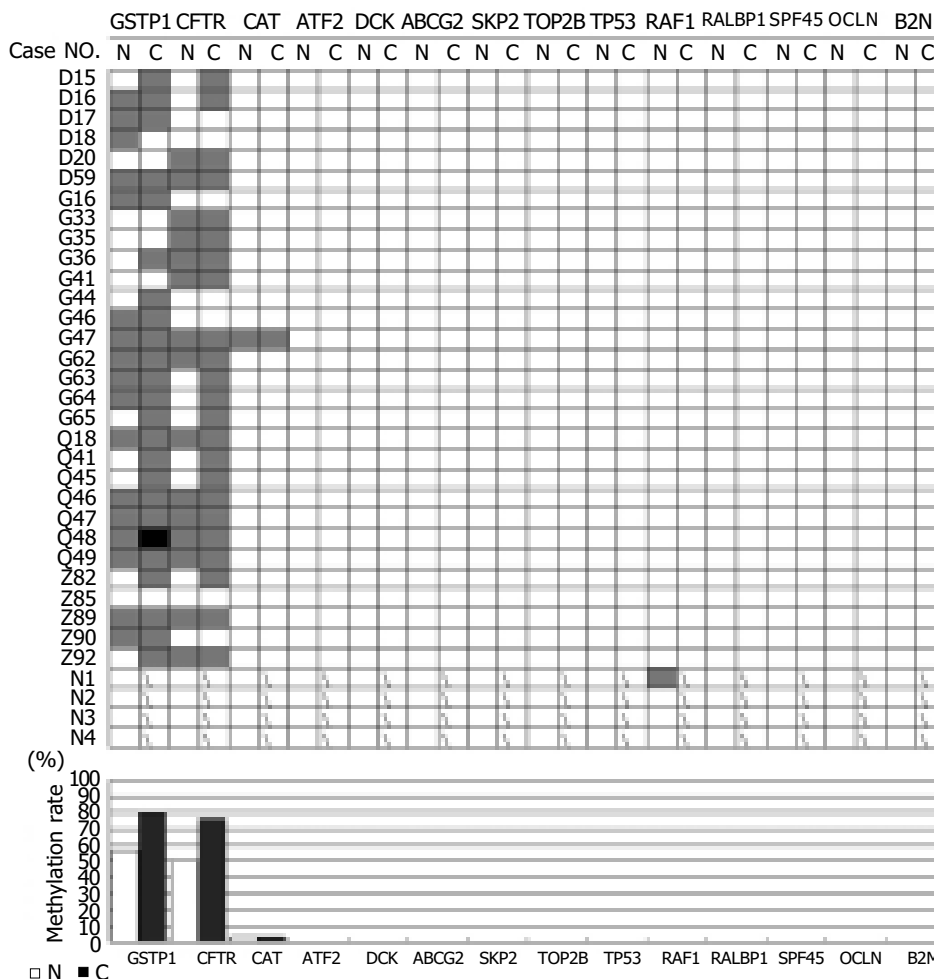


Figure 3 Methylation status of the promoter CpG Island correlated the expression state of the GSTpi gene in liver cancer cell lines. Both methylation status (panel 1) and mRNA level (panel 2) of the GSTpi gene in SMMC-7721 (lane 1), Hep3B (lane 2), HepG2 (Lane 3), HCCLM3 (lane 4) are determined and presented. *, size markers, the bands of 250 bp and 100 bp are shown. U, unmethylated; and M, the hypermethylated. The density of the bands (indicated in panel 3) for the internal control β-actin and the GSTpi gene were densitometrically recorded, where the density of the β-actin in SMMC-7721 cells was arbitrarily taken as 100%. The band-ratio of the GSTpi over the β-actin genes were calculated and summarized in the table and plot (panel 3).

Table 5 The early stage-specific change in methylation

Gene	C/M	N/M	P
GSTpi	24/30	17/30	0.052
CFTR	23/30	16/30	0.058

DISCUSSION

Drug resistance of cancers represents a formidable challenge in cancer management, and the underlying mechanisms of its

formation remain poorly defined. Both genetic and epigenetic defects can result in changes in expression of the “drug-resistance” genes in tumors. DNA methylation state of the promoter CpG islands has been demonstrated as a useful indicator for the transcriptional silencing state of the relevant genes. In this study, we determined the methylation profile of the genes at the focal point, classified as the drug-resistance type in DNA database in HCC, one of most devastating human cancers in Far East Asia, including China.

To identify suitable targets for such a study, we carried out

the search with key word "drug resistance" from the LocusLink part of the human genome database. Among 63 entries (<http://www.ncbi.nlm.nih.gov/LocusLink/list.cgi>), 44 (approximately 70%) fall into the category "the CpG island containing genes", of which, 36 genes have their promoter embedded in the CpG island (Tables 2, 3). Hence, the DNA methylation mediated mechanism likely exerts the important control of over expression of this type of genes, the key function of which is somehow linked to the drug-resistance of cancer cells. Finally, 14 genes were selected for the methylation profiling in HCC. Although 11 genes maintained the unmethylated state in all the tissue samples tested, including four cases of the liver tissues from the healthy liver donors, 30 HCC tissues and their neighboring non-cancerous tissues, three genes, *CAT*, *GSTpi* and *CFTR*, exhibited to various degrees the hypermethylation status in HCC. *CAT* was only hypermethylated in one (3.3%) case. Both *GSTpi* and *CFTR* genes were prevalently hypermethylated (Figure 2 and Table 4) in both HCC and the paired non-cancerous tissues. There was no significant difference in occurrence of the hypermethylated status between the HCC and the paired non-cancerous tissues, indicating that the hypermethylation of these two genes is likely to be the early rather than the late phase events behind the same rationale described previously^[14]. This observation would strengthen the notion that the DNA methylation mediated transcription silencing of these two genes may promote carcinogenesis of HCC, by failing to protect the cells from both intracellular and extracellular genotoxic insults. On the other hand, this may offer certain advantages from the angle of the chemotherapeutic treatment of HCC. It is probably true that the HCC with hypermethylated *GSTpi* and *CFTR* genes may respond to the relevant chemotherapies better than the unmethylated counterparts. To further evaluate this hypothesis, both retrospective and prospective clinical studies specifically addressing the association between the chemotherapeutic responses of the HCC and the methylation state of the promoter CpG islands of the drug resistance genes, including *GSTpi*, *CFTR* and *MGMT*^[14] genes with a larger cohort of HCC patients are underway.

ACKNOWLEDGEMENTS

Thanks are due to Jian-Guo Chen from Qidong Liver Cancer Institute, China, Li-Sheng Zhang from Guangxi Cancer Institute, Guangxi, China, Meng-Chao Wu from Eastern Hepatobiliary Surgery Hospital, Shanghai, China and Su-Shen Zhen, The First Affiliated Hospital, College of Medicine, Zhejiang University, Zhejiang, China for providing the patients' samples.

REFERENCES

- 1 **Parkin DM**, Pisani P, Ferlay J. Global cancer statistics. *CA Cancer J Clin* 1999; **49**: 33-64
- 2 **Bosch F**. Global epidemiology of hepatocellular carcinoma. *New York: Churchill Livingstone* 1997: 13-28
- 3 **Aflatoxins**. *IARC Monogr Eval Carcinog Risks Hum* 1993; **56**: 245-395
- 4 **Parkin DM**, Pisani P, Ferlay J. Estimates of the worldwide incidence of eighteen major cancers in 1985. *Int J Cancer* 1993; **54**: 594-606
- 5 **Kruh GD**. Introduction to resistance to anticancer agents. *Oncogene* 2003; **22**: 7262-7264
- 6 **Jaenisch R**, Bird A. Epigenetic regulation of gene expression: how the genome integrates intrinsic and environmental signals. *Nat Genet* 2003; **33**(Suppl): 245-254
- 7 **Jones PA**. Epigenetics in carcinogenesis and cancer prevention. *Ann N Y Acad Sci* 2003; **983**: 213-219

- 8 **Feninberg A**. Cancer epigenetics takes center stage. *Proc Natl Acad Sci U S A* 2001; **98**: 392-394
- 9 **Eden A**, Gaudet F, Waghmare A, Jaenisch R. Chromosomal instability and tumors promoted by DNA hypomethylation. *Science* 2003; **300**: 455
- 10 **Gaudet F**, Hodgson JG, Eden A, Jackson-Grusby L, Dausman J, Gray JW, Leonhardt H, Jaenisch R. Induction of tumors in mice by genomic hypomethylation. *Science* 2003; **300**: 489-492
- 11 **Chen RZ**, Pettersson U, Beard C, Jackson-Grusby L, Jaenisch R. DNA hypomethylation leads to elevated mutation rates. *Nature* 1998; **395**: 89-93
- 12 **Cho B**, Lee H, Jeong S, Bang YJ, Lee HJ, Hwang KS, Kim HY, Lee YS, Kang GH, Jeoung DI. Promoter hypomethylation of a novel cancer/testis antigen gene CAGE is correlated with its aberrant expression and is seen in premalignant stage of gastric carcinoma. *Biochem Biophys Res Commun* 2003; **307**: 52-63
- 13 **Cao L**, Owsianik G, Jaspers M, Janssens A, Cuppens H, Cassiman JJ, Nilius B. Functional analysis of CFTR chloride channel activity in cells with elevated MDR1 expression. *Biochem Biophys Res Commun* 2003; **304**: 248-252
- 14 **Yu J**, Zhang HY, Ma ZZ, Lu W, Wang YF, Zhu JD. Methylation profiling of twenty four genes and the concordant methylation behaviours of nineteen genes that may contribute to hepatocellular carcinogenesis. *Cell Res* 2003; **13**: 319-333
- 15 **Burger P**, Scheithauer B, Paulus W, Giannini C, Kleihues P. Astrocytic Tumours. In Pathology and Genetics of Tumours of the Nervous. *Lyon: IARC Press* 2000: 9-54
- 16 **Yu J**, Ni M, Xu J, Zhang H, Gao B, Gu J, Chen J, Zhang L, Wu M, Zhen S, Zhu J. Methylation profiling of twenty promoter-CpG islands of genes which may contribute to hepatocellular carcinogenesis. *BMC Cancer* 2002; **2**: 29
- 17 **Clark SJ**, Harrison J, Paul CL, Frommer M. High sensitivity mapping of methylated cytosines. *Nucleic Acids Res* 1994; **22**: 2990-2997
- 18 **Cai L**, Zhu JD. The tumor-selective over-expression of the human Hsp70 gene is attributed to the aberrant controls at both initiation and elongation levels of transcription. *Cell Res* 2003; **13**: 93-109
- 19 **Bakker J**, Lin X, Nelson WG. Methyl-CpG binding domain protein 2 represses transcription from hypermethylated pi-class glutathione S-transferase gene promoters in hepatocellular carcinoma cells. *J Biol Chem* 2002; **277**: 22573-22580
- 20 **Henderson CJ**, McLaren AW, Moffat GJ, Bacon EJ, Wolf CR. Pi-class glutathione S-transferase: regulation and function. *Chem Biol Interact* 1998; **111**: 69-82
- 21 **Zimniak P**, Nanduri B, Pikula S, Bandorowicz-Pikula J, Singhal SS, Srivastava SK, Awasthi S, Awasthi YC. Naturally occurring human glutathione S-transferase GSTP1-1 isoforms with isoleucine and valine in position 104 differ in enzymic properties. *Eur J Biochem* 1994; **224**: 893-899
- 22 **Ryberg D**, Skaug V, Hewer A, Phillips DH, Harries LW, Wolf CR, Ogreid D, Ulvik A, Vu P, Haugen A. Genotypes of glutathione transferase M1 and P1 and their significance for lung DNA adduct levels and cancer risk. *Carcinogenesis* 1997; **18**: 1285-1289
- 23 **Townsend DM**, Tew KD. The role of glutathione-S-transferase in anti-cancer drug resistance. *Oncogene* 2003; **22**: 7369-7375
- 24 **Tew KD**. Glutathione-associated enzymes in anticancer drug resistance. *Cancer Res* 1994; **54**: 4313-4320
- 25 **Bannykh SI**, Bannykh GI, Fish KN, Moyer BD, Riordan JR, Balch WE. Traffic pattern of cystic fibrosis transmembrane regulator through the early exocytic pathway. *Traffic* 2000; **1**: 852-870
- 26 **Morales MM**, Capella MA, Lopes AG. Structure and function of the cystic fibrosis transmembrane conductance regulator. *Braz J Med Biol Res* 1999; **32**: 1021-1028
- 27 **Wei LY**, Stutts MJ, Hoffman MM, Roepe PD. Overexpression of the cystic fibrosis transmembrane conductance regulator in NIH 3T3 cells lowers membrane potential and intracellular pH and confers a multidrug resistance phenotype. *Biophys J* 1995; **69**: 883-895
- 28 **Su F**, Hu X, Jia W, Gong C, Song E, Hamar P. Glutathione S transferase pi indicates chemotherapy resistance in breast cancer. *J Surg Res* 2003; **113**: 102-108

• COLORECTAL CANCER •

Methylation profile of the promoter CpG islands of 31 genes that may contribute to colorectal carcinogenesis

Xiao-Li Xu, Jian Yu, Hong-Yu Zhang, Meng-Hong Sun, Jun Gu, Xiang Du, Da-Ren Shi, Peng Wang, Zhen-Hua Yang, Jing-De Zhu

Xiao-Li Xu, Meng-Hong Sun, Xiang Du, Da-Ren Shi, Department of Pathology, Cancer Hospital, Fudan University, Shanghai 200032, China
Jian Yu, Hong-Yu Zhang, Jun Gu, Peng Wang, Jing-De Zhu, The State-Key Laboratory for Oncogenes and Related Genes, Cancer Institute of Shanghai Jiaotong University, Shanghai 200032, China
Zhen-Hua Yang, Institute of Respiratory Disease, Zhong Shan Hospital, Fudan University, Shanghai 200032, China

Supported by the National High Technology Research and Development Program of China (863 Program), No. 2002AA2Z3352, the Science Foundation of Shanghai Municipal Government, No. 02DJ14056, and the Special Fund set up by the State-Key Laboratory for Oncogenes and Related Genes, Shanghai Cancer Institute, Shanghai Jiaotong University. This work was also supported by the Science Foundation of Shanghai Municipal Government to Xiang Du, No. 024119010

Co-first-authors: Xiao-Li Xu, Jian Yu, Hong-Yu Zhang

Correspondence to: Jing-De Zhu, The State-Key Laboratory for Oncogenes and Related Genes, Cancer Institute of Shanghai Jiaotong University, LN2200/25, Xietu Road, Shanghai 200032, China. zhujingde@yahoo.com

Telephone: +86-21-64224285 **Fax:** +86-21-64224285

Received: 2004-04-22 **Accepted:** 2004-05-09

Abstract

AIM: To establish the methylation profile of the promoter CpG islands of 31 genes that might play etiological roles in colon carcinogenesis.

METHODS: The methylation specific PCR in conjunction of sequencing verification was used to establish the methylation-profile of the promoter CpG islands of 31 genes in colorectal cancer ($n = 65$), the neighboring non-cancerous tissues ($n = 5$), colorectal adenoma ($n = 8$), and normal mucosa ($n = 1$). Immunohistochemically, expression of 10 genes was assessed on the home-made tissue microarrays of tissues from 58 patients. The correlation of tumor specific changes with each of clinical-pathologic features was scrutinized with relevant statistic tools.

RESULTS: In comparison with the normal mucosa of the non-cancer patients, the following 14 genes displayed no tumor associated changes: breast cancer 1, early onset (*BRCA1*), cadherin 1, type 1, E-cadherin (epithelial) (*CDH1*), death-associated protein kinase 1 (*DAPK1*), DNA (cytosine-5)-methyltransferase 1 (*DNMT1*), melanoma antigen, family A, 1 (directs expression of antigen MZ2-E) (*MAGEA1*), tumor suppressor candidate 3 (*N33*), cyclin-dependent kinase inhibitor 1A (p21, Cip1) (*p21^{WAF1}*), cyclin-dependent kinase inhibitor 1B (p27, Kip1) (*p27^{KIP1}*), phosphatase and tensin homolog (mutated in multiple advanced cancers 1) (*PTEN*), retinoic acid receptor, beta (*RAR- β*), Ras association (RalGDS/AF-6) domain family 1 C (*RASSF1C*), secreted frizzled-related protein 1 (*SFRP1*), tissue inhibitor of metalloproteinase 3 (Sorsby fundus dystrophy, pseudoinflammatory) (*TIMP3*), and von Hippel-Lindau syndrome (*VHL*). The rest 17 targets exhibited to various extents the tumor associated changes. As changes in methylation of the following genes occurred marginally, their impact on the formation of colorectal cancer were trivial: adenomatous polyposis coli (*APC*) (8%, 5/65),

Ras association (RalGDS/AF-6) domain family 1A (*RASSF1A*) (3%, 2/65) and cyclin-dependent kinase inhibitor 2A, alternated reading frame (*p14^{ARF}*) (6%, 4/65). The following genes exhibited moderate changes in methylation: O-6-methylguanine-DNA methyltransferase (*MGMT*) (20%, 13/65), mutL homolog 1, colon cancer, nonpolyposis type 2 (E. coli) (*hMLH1*) (18%, 12/65), cyclin-dependent kinase inhibitor 2A (melanoma, p16, inhibits CDK4) (*p16^{INK4a}*) (10%, 10/65), methylated in tumor 1 (*MINT1*) (15%, 10/65), methylated in tumor 31 (*MINT31*) (11%, 7/65). The rest changed greatly in the methylation pattern in colorectal cancer (CRC): cyclin A1 (*cyclin a1*) (100%, 65/65), caudal type homeobox transcription factor 1 (*CDX1*) (100%, 65/65), *RAR-* (85%, 55/65), myogenic factor 3 (*MYOD1*) (69%, 45/65), cyclin-dependent kinase inhibitor 2B (p15, inhibits CDK4) (*p15^{INK4b}*) (68%, 44/65), prostaglandin-endoperoxide synthase 2 (prostaglandin G/H synthase and cyclooxygenase) (*COX2*) (72%, 47/65), cadherin 13, H-cadherin (heart) (*CDH13*) (65%, 42/65), CAAX box 1 (*CXX1*) (58%, 38/65), tumor protein p73 (*p73*) (63%, 41/65) and Wilms tumor 1 (*WT1*) (58%, 38/65). However, no significant correlation of changes in methylation with any given clinical-pathological features was detected. Furthermore, the frequent changes in methylation appeared to be an early phase event of colon carcinogenesis. The *in situ* expression of 10 genes was assessed by the immunohistochemical approach at the protein level: *CDH1*, *CDH13*, *COX2*, *cyclin A1*, *hMLH1*, *MGMT*, *p14^{ARF}*, *p73*, *RAR-*, and *TIMP3* genes in the context of the methylation status in colorectal cancer. No clear correlation between the hypermethylation of the promoter CpG islands and the negative expression of the genes was established.

CONCLUSION: The methylation profile of 31 genes was established in patients with colon cancer and colorectal adenomas, which provides new insights into the DNA methylation mediated mechanisms underlying the carcinogenesis of colorectal cancer and may be of prognostic values for colorectal cancer.

Xu XL, Yu J, Zhang HY, Sun MH, Gu J, Du X, Shi DR, Wang P, Yang ZH, Zhu JD. Methylation profile of the promoter CpG islands of 31 genes that may contribute to colorectal carcinogenesis. *World J Gastroenterol* 2004; 10(23): 3441-3454

<http://www.wjgnet.com/1007-9327/10/3441.asp>

INTRODUCTION

Colorectal carcinoma (CRC) is the third most common malignancy in the developed countries, with an annual incidence approximately 35-50/100 000^[1,2]. The risk factors of CRC include Western diet (low fiber, high fat diet), family history, smoking, obesity and inflammatory colorectal diseases. As a whole, China falls into the low incidence country in the world, with the relative incidence of CRC rates being the 4th-6th of the total malignances and the 2nd-3rd of those in the digestive system in China. However, CRC

occurrence exhibits an increasing trend, with an average 4.2% increase per year in the last two decades^[3]. CRC is the 3rd common malignancy in Shanghai and occurs more frequently in China (<http://www.caca.org.cn/zlyy/shanghai/index.asp>). Clinically and pathologically, CRC has been grouped as the sporadic (approximately 80% cases) and hereditary types of diseases (roughly 20% in the total).

Both activation of proto-oncogenes (e.g. the *CDH13* gene) and inactivation of tumor suppressor genes (e.g. the *APC*, *p53* and genes responsible for the mismatch repaired activity in cells) attributed to genetic defects have been proved instrumental to carcinogenesis of colorectal cancer. The well-known adenoma-carcinoma sequence of the genetic defects by Volgestein has gained both experimental supports and general recognition. However, the predicted accumulation of genetic events has not been substantiated in sporadic colorectal adenocarcinomas, and the expected increase in the number of genetic events in aging tissues has not materialized^[4]. Both observations are indeed at odds with the exponential increase in the incidence of colorectal cancer with age. Therefore, alternative mechanisms must be accounted for such a shortfall, which is associated with DNA methylation mediated control of the expression of critical genes overseeing cell growth, apoptosis, as well as cell cycle progression.

Addition of the methyl group at the fifth carbon of cytosine of CpGs is the only covalent DNA modification in vertebrate^[5]. Such epigenetic signatures in parental cells are passed to the daughter cells at high fidelity, by a similar semi-conserved mechanism during duplication of the genetic information. The hypermethylated status of CpGs can affect the DNA-protein interaction by eliminating the otherwise occurring DNA-protein interactions involved with the methylation-sensitive transcription factors, while unfolding a cascade of reactions toward the condensed chromatin that is initiated with binding to the methylated CpG by members of the methylated CpG binding protein family^[6]. Cancer specific changes in methylation occur widely in all the cancers tested^[7]. The global demethylation of DNA has been linked to the increased genome instability as the otherwise transcription-/ transposition-silenced repetitive sequences in normal cells are reactivated by DNA demethylation^[8,9]. Paradoxically, local hypermethylation (at the promoter CpG island) has been well established for inactivation of tumor suppressor genes and caught great attention. However, the local demethylation in human tumors has also been recently reported to be associated with transcription reactivation of the silenced genes in normal tissues, such as the *MAGEA1* gene in hepatocellular carcinoma^[10]. In view of the fact that the majority of the promoter CpG island containing genes (50% of the protein-coding genes fall into this category) have not been properly looked in the context of the tumor biology, methylation profiling remains valuable for new insights into the etiological mechanism.

CRC is one of the first few types of cancers for methylation profiling^[11,12]. Learnt from the rather extensive survey with more than 30 targets, a so called "CpG island methylation (CIM)" phenomenon has been reported, i.e., a clustering occurrence of multiple hypermethylated targets including upto a dozen of tumor suppressor genes^[11]. In this study, we recruited 65 CRC tissues, eight colorectal adenomatous tissues, five neighboring non-cancerous tissues and one normal mucosa tissue from Shanghai Cancer Hospital for a middle scale methylation profiling with the promoter CpG islands of 31 genes, aiming, to establish the methylation profile of CRC patients in China, and to assess the association between the methylation status and expression profile of the genes *in situ*. Our results presented in this report should provide some new insights into the role of the epigenetic mechanism in CRC carcinogenesis.

MATERIALS AND METHODS

Clinical-pathological profiles of CRC patients

With the informed consent of all patients and approval of the ethics committee, tumor tissues were obtained during surgery from 65 CRC patients at the Cancer Hospital of Fudan University in 1996-2003. They were 39 patients with sporadic colorectal cancer (SCRC), 10 with hereditary non-polyposis colorectal cancer (HNPPC) fulfilling Amsterdam criteria of IGC and Japanese criteria, and 16 in the category of Bethesda CRC. In addition, tissues were taken from the neighboring non-cancerous mucosa (at least 5-10 cm away from the tumorous lesions) of five patients. A cecum sample was obtained from a 68-year old female patient with inflammatory pseudotumor. In addition, Bethesda CRC concomitant adenomatous samples from six patients and sporadic colon adenomatous samples (one was cancer concomitant) from two patients were taken.

All samples were freshly obtained and cut into two parts. One was buried into an optimal cutting temperature compound (OCT, Miles Inc, USA), and put into fluid nitrogen for storage. The rest was fixed in formalin, embedded in paraffin and then cut into 4-5 μ m sections for routine pathological diagnosis.

Clinical-pathological features including the age and gender of patients, the tumor site histological type, Duke's stages, differentiation grades (only moderate and poor differentiation), lymph node metastasis status, and more than 3 years follow-up results (36 cases) are shown in Table 1. The clinical-pathologic data of the eight adenomas are shown in Table 2.

Table 1 Clinical-pathologic profiles of the CRC cases in this study

Clinical-pathologic features		Number of cases
Gender	Male	37
	Female	28
Age (yr)	Median	60
	Range	28-85
Tumor site	Left colon and rectum	43
	Right colon	22
Histological types	Adenocarcinoma	51
	Mucinous carcinoma	5
	Other types combined ¹	9
Differentiation	Moderate	51
	Poor	14
Follow-up (3 yr)	Survival	27
	Deceased	9
Duke's stage	A	6
	B	15
	C	30
	D	14

¹Other types combined included the mixed squamous cell carcinoma, carcinoid carcinoma, etc.

Table 2 Clinical-pathologic profiles of adenomas and neighboring tumor-free mucosae

Clinical-pathologic features		Adenoma	Mucosa
Gender	Male	4	2
	Female	4	4
Age (yr)	Median	60	68
	Range	34-83	47-76
Tumor site	Left colon	6	4
	Right colon	2	2
Histological type	Tubular	3	
	Tubulovillous	5	
Dysplasia	Light-moderate	8	

Table 3 Target CpG islands and the primers for MSP

Gene	GenBank No.	Primer		Location to transcription start	Size (bp)
		Sense (5'-3')	Anti-sense (5'-3')		
APC	U02509	(U) GTGTTTTATGTGGAGTGTGGGTT	CCAATCAACAAACTCCCAACAA	-17 147 to -17 050	108
		(M) TATGCGGAGTGCGGGTC	TCGACGAACTCCCGACGA	-17 153 to -17 046	97
BRCA1	L78833	(U) GGTAAATTTAGAGTTTGGAGAGATG	TCAACAAACTCACACCACACAATCA	-320 to -138	182
		(M) GGTAAATTTAGAGTTTCGAGAGACG	TCAACGAACTCACGCCGCGCAATCG	-320 to -138	182
CDH1	NM_004938	(U) GGTGGGTGGGTTGTTAGTTTTGT	AACTCACAAATCTTTACAATTCCAAC	-266 to -93	172
		(M) GTGGGCGGGTCGTTAGTTTC	CTCACAATACTTTACAATTCCGACG	-265 to -93	172
CDH13	AB001090	(U) TTGTGGGGTTGTTTTTTGT	AACTTTTCATTCATACACACA	-267 to -24	243
		(M) TCGCGGGTTCGTTTTTCGC	GACGTTTTTCATTCATACACGCG	-267 to -24	243
CDX1	NT_029289	(U) TGATTGGGTTGTGTTTATGG	TACCACCACCACCTCCAA	+290 to +522	233
		(M) CGATTGGGTCGTCGTTTA	CCGCATCCACTCGTAAAA	+290 to +491	202
COX2	NT_004487	(U) TTGTTTGTGTTGTGATGTTTG	TCCAAACTCTTTCCCAAATC	-119 to -324	206
		(M) GTTCGTCGTTGCGATGTT	CCAAACTCTTTCCCAAATCA	-121 to -323	203
CXX1	NT_011786	(U) TTAGGTTGGTTTTGTGGATATG	CACCCAACCATCCATCAC	-24 to +92	117
		(M) AGGTCGGTTTTCGTGGAT	GATCGATATCGCCGTCAA	-22 to +192	215
Cyclin1	AF124143	(U) GGGTAGTTTTGTGTGTTTTAGTTG	AACCACTAACAACCCCTCT	-762 to -565	199
		(M) TCGTCGCGTTTTAGTCGT	ACCCGTTCTCCCAACAAC	-755 to -550	206
DAPK1	NM_004938	(U) GGATAGTTGGATTGAGTTAATGTC	CAATCCCTCCCAAACACCAA	-332 to -229	103
		(M) GGATAGTCGGATCGAGTTAACGTC	CCCTCCCAAACGCCGA	-332 to -234	98
DNMT1	NT_011176	(U) GGGTGGTAGATGTTGTTTTGT	CACCCTACCTATCCCCTAA	-359 to -130	230
		(M) CGTCGTTTTCGTTTATCGTT	ATACCTACCGCTACGAACA	-320 to -140	181
hMLH1	AB017806	(U) TTTGATGTAGATGTTTATTAGGGTGT	ACCACCTCATCATAACTACCCACA	-526 to -654	118
		(M) ACGTAGACGTTTTATTAGGGTCGC	CCTCATCGTAACTACCCGCG	-531 to -655	124
MAGEA1	U82670	(U) GTTTGGTTGAAGGAATTTGA	ACCCACAACCCTCCCTCTTA	+24 to +347	324
		(M) GTTCGGTCAAGGAATTTGA	CCACAACCCTCCCTCTTAAA	+24 to +345	322
MGMT	AL355531	(U) TTTGTGTTTTGATGTTTGTAGGTTTTGT	AACTCCACACTTTCAAAAACAAAACA	-451 to -266	209
		(M) TTTGACGTTTCGTAGGTTTTGCG	GCACTTTCGGAAAACGAAAACG	-469 to -261	186
MINT1	AF135501	(U) TATTTTTGAAGTGTGTTTGGTGT	TCCCTCTCCCTCTAAACTTC	*	160
		(M) TTCGAAGCGTTTGTGTTG	CGCTAACCTAACGCACA	*	131
MINT31	AF135531	(U) GGGTGGGAATTGAGATGATT	CATCACCACCCTCACTTTA	*	176
		(M) GCGGGAATTGAGACGATT	ACGCTTACGCCACTACGA	*	213
MYOD1	NT_009307	(U) ATTTGATGGTTTTGATGGTTT	CACACACATACTCATCTCACA	+206 to +418	213
		(M) GACGGTTTTGACGGTTT	GCCCGAAAACCGAATACAC	+210 to +393	184
N33	NT_030737	(U) TTTGGTGAATTGGATGTTTTG	CACCCAACCTCCTACCACACAC	+20 to +169	150
		(M) TTTTCGGTGAATCGGATG	TACGCGCCCAACTCCTA	+18 to +173	156
p14 ^{ARF}	L41934	(U) TGAGTTGGTTTTGGAGGTGG	AACCACAACAACAACACCCCT	+97 to +262	165
		(M) GTCGAGTTCGGTTTTGGAGG	AAAACCACAACGACGAACG	+95 to +255	160
p15 ^{INK4b}	NM_004936	(U) TGTGATGTGTTGATTTTTGTGGTT	CCATACAATAACCAAACAACCAA	-318 to -164	154
		(M) GCGTTCGATTTTTGCGGTT	CGTACAATAACCGAACGACCGA	-312 to -165	147
p16 ^{INK4a}	NM_000077	(U) TTATTAGAGGGTGGGGTGGATTGT	CAACCCCAAAACCACAACCATAA	-80 to +71	151
		(M) TTATTAGAGGGTGGGGCGGATCGC	ACCCCGAACCGGACCGTAA	-80 to +69	149
p21 ^{WAF1}	NT_007592	(U) TTTTGTAGTATGTGAGTTTTGG	AACACAACCTCAACACAACCCTA	-200 to -1	200
		(M) TGTAGTACGCGAGGTTTCG	TCAACTAACGCAACTCAACG	-196 to +5	202
p27 ^{KIP1}	AB003688	(U) TGTGATTTGATGTTGGTAAGGT	CAAACCACAACCCAAACTCT	-363 to -141	223
		(M) CGACGTCGGTAAGGTTTG	AAACGCGCAAAAACACTACG	-355 to -163	193
p73	AB031234	(U) TGGGTGTTTGGTTGTAGGT	CCAACTCTCAACTCCCAAAA	-1 725 to -1 505	221
		(M) GCGTTCGGTTCGTAGGTT	CTCAACTCCCAAAAACCCAA	-1 722 to -1 511	212
PTEN	NM_000314	(U) TGGTTTTTTGAGGTGTTTG	TTCCATCATAACTACAACCTCCA	-979 to -812	167
		(M) GGTTTTTTCGAGGCGTTCG	CGCCTCACAACGACTCAACT	-978 to -786	192
RAR-β	NM_016152	(U) TTGAGAATGTGAGTGATTGA	AACCAATCCAACCAAAAACAA	-343 to -197	146
		(M) TCGAGAACGCGAGCGATTCCG	GACCAATCCAACCGAAACGA	-343 to -197	146
RASSF1A	NT_022517	(U) TTTGGTTGGAGTGTGTTAATGTG	CAAACCCCAAAACTAAAAACAA	+70 to +178	108
		(M) GTGTTAACGCGTTGCGTATC	AACCCCGGAACTAAAAACGA	+82 to +176	94
RASSF1C	NT_022517	(U) GGAGTTTGGATTGTTGGTTTTG	CACCCCAAAAATAACCTCAT	-370 to -137	187
		(M) AGTTTGGATTGTCGGTTTCG	TCACAAAACCCACCTACCAC	-370 to -137	187
SFRP1	NT_008251	(U) GTTTTGTGTTGTAAGTTGTTGTT	AAACCCCAACACTCCAA	-180 to +19	199
		(M) TCGCGGTCGTAAGTTGTT	CGCACTCCAACCTACAA	-177 to +11	188
TIMP3	NM_000362	(U) TTTTGTGTTGTTATTTTTGTTTTGGTTTT	CCCCAAAACCCCACTCA	-454 to -335	119
		(M) CGTTTCGTTATTTTTGTTTTCGGTTTC	CCGAAAACCCCGCTCG	-451 to -335	116
VHL	AF010238	(U) GTTGGAGGATTTTTGTGATGTT	CCCAAACCAAACACCACAAA	-185 to -20	165
		(M) TGGAGGATTTTTGCGTACGC	GAACCGAACGCCGCGAA	-183 to -25	158
WT1	X74840	(U) TGGGATTTGGGTGGTATTTG	CACCAACACCCACTACACCA	+295 to +510	216
		(M) GTTAGGCGTCGTCGAGGTTA	AAAACGCAAAATCCAACACC	+321 to +526	206

DNA preparation and methylation specific PCR analysis

Genomic DNA was extracted from frozen tissues by the protein precipitation method^[13]. Frozen tissue block was cut into 10-20 μm sections, put into a 1.5 mL Eppendorf tube, and then incubated at 37 °C in the cellular lysis buffer with proteinase K (SABC, Shanghai) for a final concentration of 100 $\mu\text{g}/\text{mL}$. The digestion was carried out at 55 °C for at least 2 h. After centrifuged, the upper liquid was collected and the protein precipitation mix was added. After centrifuged, 1:1 isopropanol was added. The deposition was washed with 750 mL/L ethanol, and naturally dried. The DNA pellet was washed once with 700 mL/L ethanol and dissolved with TE (10 mmol/L Tris HCl, pH 7.4 and 1 mmol/L EDTA), and stored at a concentration of 1 mg/mL at 4 °C.

The primers for methylation specific PCR (MSP) (Table 3) were adopted as the previously published works^[10,14] or designed with the assistance of the web server for the CpG islands identification (<http://www.ebi.ac.uk/emboss/cpgplot/index.html>) and the primer design software (http://micro-gen.ouhsc.edu/cgi-bin/primer3_www.cgi). DNA treatment and PCR reaction were carried out by the previously described method^[10,14,15]. In detail, 10 μg DNA in 50 μL TE was incubated with 5.5 μL of 3 mol/L NaOH at 37 °C for 10 min, followed by a 16 h treatment at 50 °C after 30 μL of freshly prepared 10 mmol/L hydroquinone and 520 μL of freshly prepared 3.6 mol/L sodium-bisulfite at pH 5.0 were added. The DNA was desalted using a home dialysis system with 10 g/L agarose. The DNA in the desalted sample (approximately 100 μL in volume) was denatured at 37 °C for 15 min with 5.5 μL of 3 mol/L NaOH followed by ethanol precipitation with 33 μL 10 mol/L NH₄OAc and 300 μL ethanol. After washed with 700 mL/L ethanol, the gently dried DNA pellet was dissolved with 30 μL TE at 65 °C for 10 min. DNA samples were finally stored at -20 °C until further use. The sample of 50 ng of DNA was reserved for PCR reaction. PCR reaction was carried out in a volume of 15 μL with 50 ng or less template DNA with FastStart Taq polymerase (Roche, Germany) as follows. After an initial denaturing step for 3 min at 94 °C, 35 cycles at 94 °C for 30 s, at varying temperatures with primer pairs for 30 s and at 72 °C for 30 s, were carried out. The PCR products were separated by 12 g/L ethidium bromide containing agarose gel electrophoresis with 1×TAE and visualized under UV illumination. To verify the PCR results, representative bands from each target were gel-purified. Then the PCR products were sequenced directly or cloned into T-vector (Promega, USA) followed by automatic DNA sequencing provided by Bioasia (Shanghai, China). Only verified results were presented in this report.

Immunohistochemistry analysis on a home made tissue microarray

The paraffin embedded tissues from 58 cancer cases were made into the tissue microarray paraffin blocks, followed by sectioning. For each sample, the H&E stained sections were first reviewed and marked for the picked point. At least 4 points of cancer tissue and 1 point of normal mucosa tissue were taken from the different positions on the paraffin block. The diameter of our tissue microarray punch was 1 mm. We put about 40-80 tissue dots in one array. To identify the tissue put into the array, all the made tissue microarray sections were stained with H&E and reviewed by two pathologists independently.

The immunostaining was performed with each of 10 commercially available antibodies (Table 4) using DAKO Envision system/3,3-diaminoben-aidine (DAB) staining. The result was scored by conjunction with both staining intensity and the percentage of positive staining cells. Each sample was given an intensity score (0-3) and a percentage of cell positive score (0=less than 5%, 1=5-25%, 2=25-50%, 3=50-75%, 4=more than 75%). An overall immunohistochemistry score was calculated by multiplying the intensity and percentage of cell

positive scores. Scores of 1-4 were recorded as +, 6-8 as ++, and 9-12 as +++.

Table 4 Antibodies for immunohistochemical analysis

Antibody name	Expression location	Company	Catalogue No.
CDH1	Membrane/Cytoplasm	Antibody Diagnostica INC.	M-0536
CDH13	Cytoplasm	Santa Cruz	sc-7940
COX2	Cytoplasm	Santa Cruz	sc-1746
Cyclin a1	Nuclear	Novocastra Lab.	NCL-CYCLINA
hMLH1	Nuclear	PharMingen	G168-15
MGMT	Cytoplasm	DAKO	M3610
p14 ^{ARF}	Nuclear/Cytoplasm	Santa Cruz	sc-8340
p73	Cytoplasm	Santa Cruz	sc-17823
RAR	Nuclear/ Cytoplasm	Santa Cruz	sc-552
TIMP3	Cytoplasm	Oncogene	IM43T

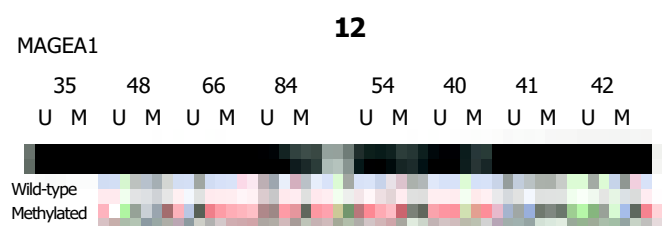
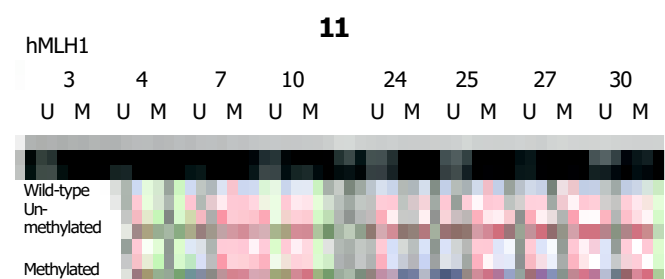
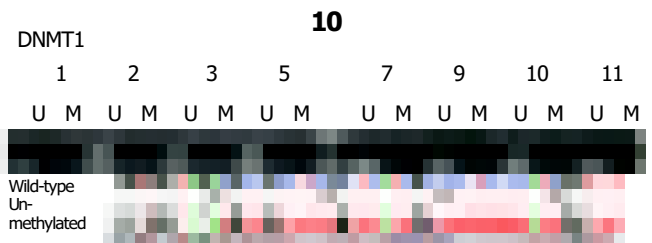
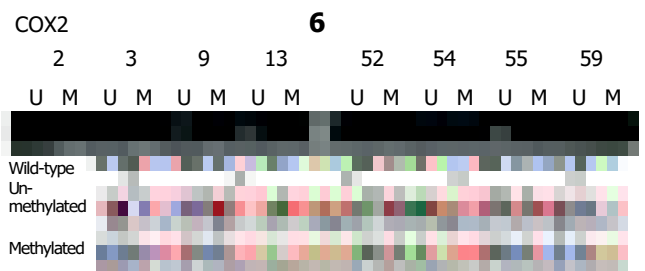
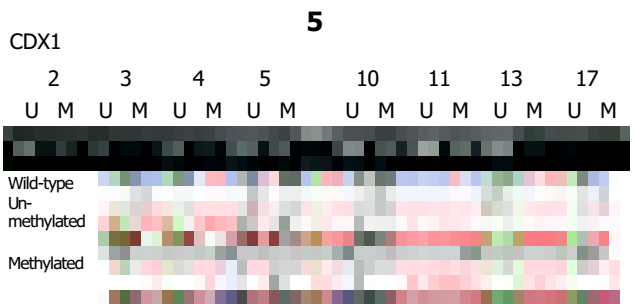
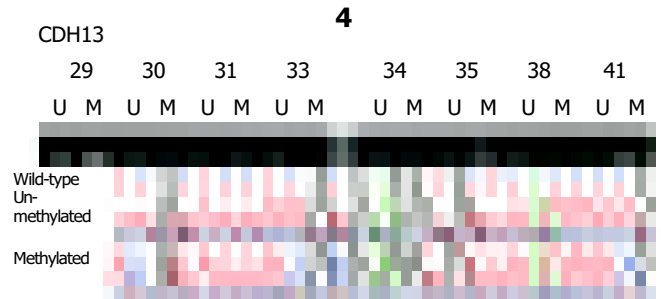
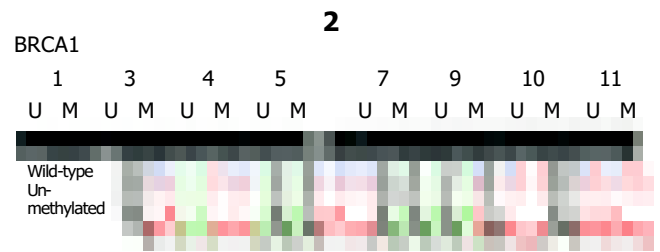
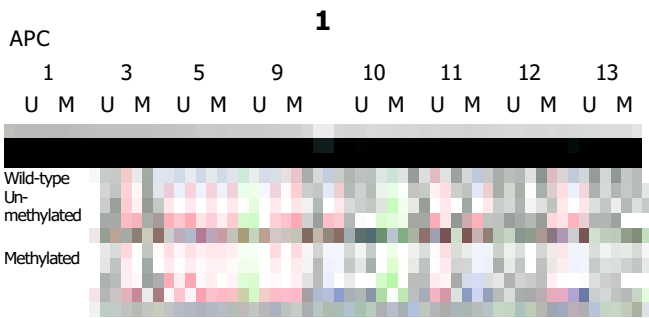
Statistical analysis

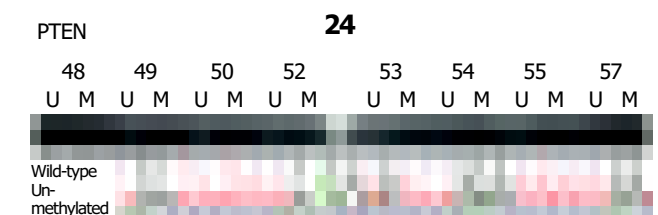
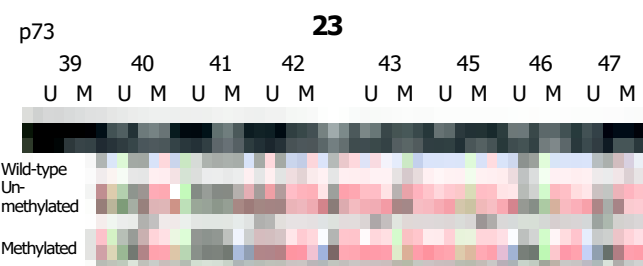
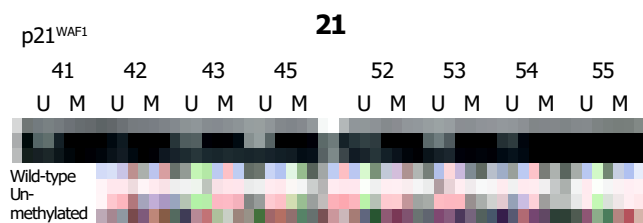
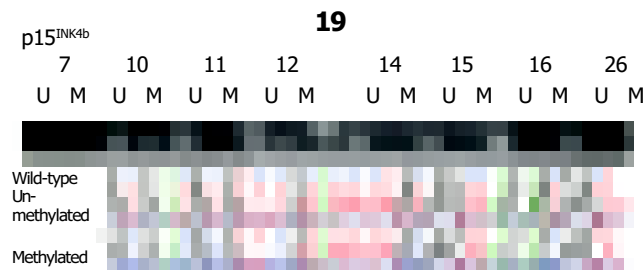
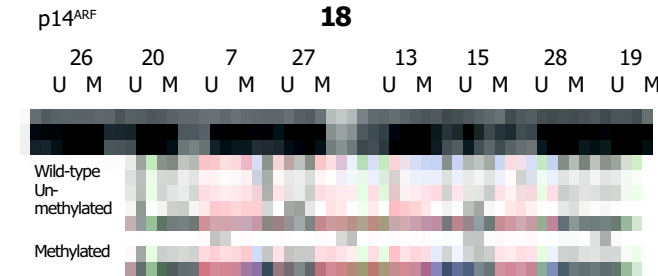
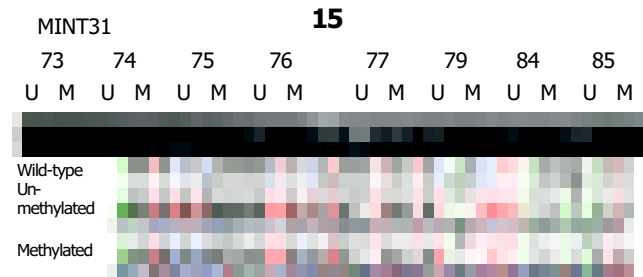
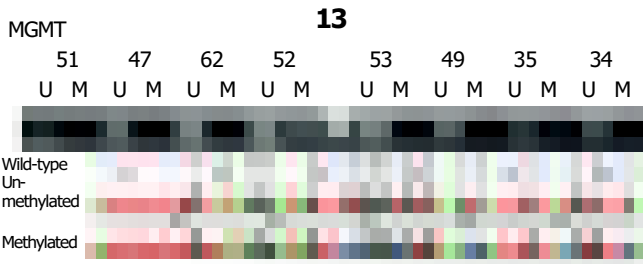
A comparison of the proportion was performed using Pearson ² test or the Fisher's exact method. Analysis of methylation status vs protein expression was performed using the contingency coefficient.

RESULTS

Among the 65 CRC patients, there were 39 SCRCs, 10 HNPCCs and 16 colorectal carcinoma in Bethesda category. In addition, eight colorectal adenomas, five non-cancerous mucosa tissues and one normal mucosa sample were also recruited for this study.

Twenty four genes among the 31 targets studied in this study were previously analyzed in liver cancer^[10] and astrocytoma (unpublished data) in this and other laboratories. They were *APC*, *BRCA1*, *CDH1*, *CDH13*, *DAPK1*, *hMLH1*, *p14^{ARF}*, *p15^{INK4b}*, *p16^{INK4a}*, *p27^{KIP1}*, *p73*, *PTEN*, *RAR-b*, *RASSF1A*, *RASSF1C*, *VHL* and *WT1*. The *CDX1*, *COX2*, *CXX1*, *MINT1*, *MINT31* and *TIMP3* genes have also been studied in colon cancer, the methylation pattern of which was found altered in CRC^[16] so that the relevant inter-study comparison of the methylation behaviors should be possible. In this list, there were genes with the proven roles in as well as those lacking any obvious association with the carcinogenesis of human tumors. For the later group, hypermethylation of the myogenetic lineage-specific transcription factor: MYOD1, occurs more frequently in aging tissues than its younger counterparts^[17]. In the category of cancer associated genes, the tumor suppressor genes made up the major part. There were proteins operating in the RB1/p16^{INK4a} pathway: p14^{ARF}, p15^{INK4b} and p16^{INK4a}, as well as the three cyclin-dependent kinase inhibitors: p21^{WAF1}, p27^{KIP1}^[18] and p57^{KIP2}^[19]. The rest in this subset were the p53 analogue, p73^[18,20], the two alternative forms of a tumor suppressors in the Ras mediated signal transduction pathway: RASSF1A and RASSF1C^[21], VHL^[22], APC^[23], PTEN^[6], N33 as well as the Wilms tumor 1 gene, WT1^[24]. Also included were the genes encoding the cell membrane proteins or nuclear receptors acting actively in intercellular interactions: e.g. melanoma specific antigen A1 (MAGEA1)^[25], and cadherins, CDH1^[26] and CDH13^[26]. One gene implicated in signal transduction was *cyclin A1*^[27]. The gene encoding O-6-methylguanine-DNA methyltransferase, *MGMT*^[28] was also included, which plays a key role in the cellular responses to alkylating agents and heavy metal stresses. The genes acting in DNA repair process were *hMLH1*^[29] and *BRCA1*^[30] as well as the gene acting in apoptosis, *DAPK1*^[31].





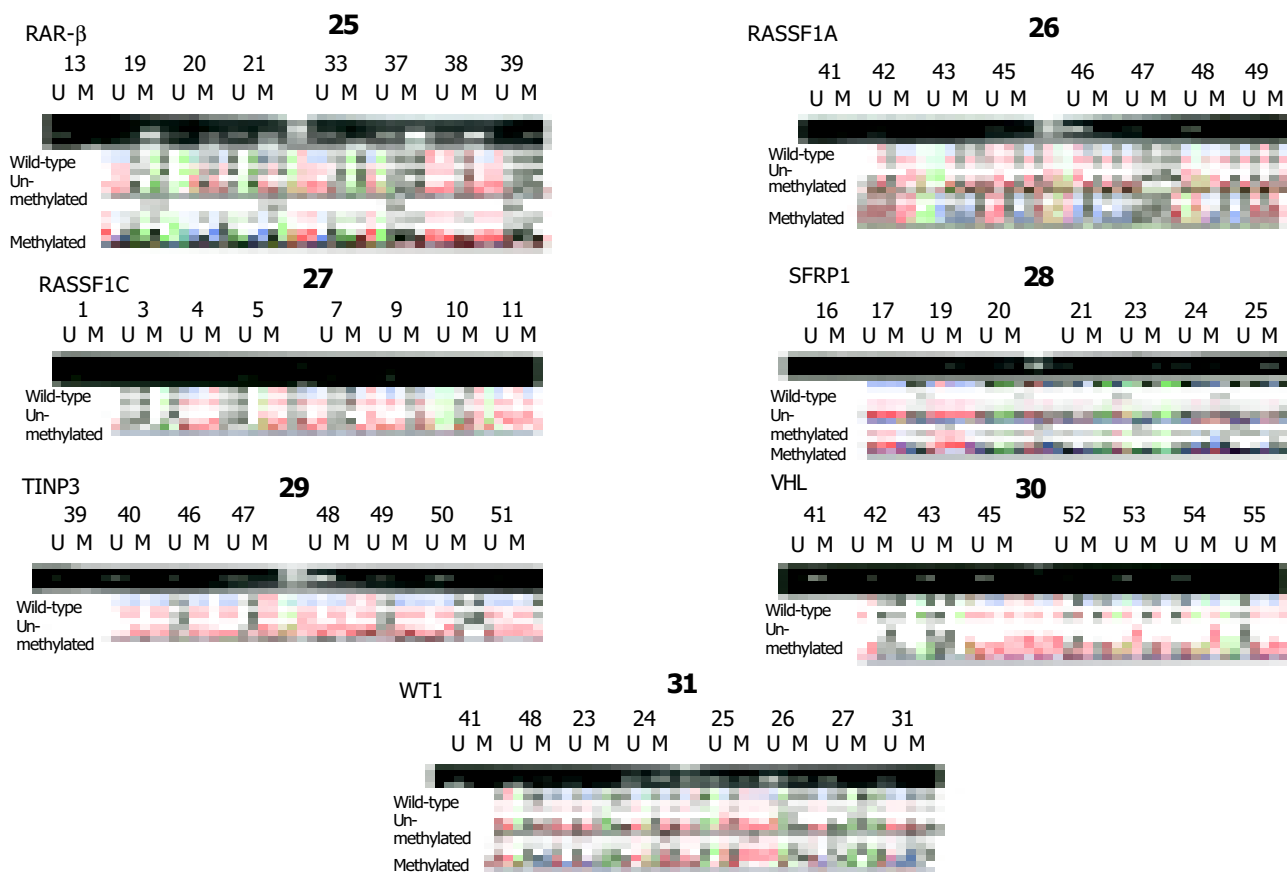


Figure 1 Methylation profiles of the promoter CpG islands of 31 genes in CRC. Both electrophoretic patterns of the representative PCR products of each of 31 targets (indicated respectively, at the top of figures) and the sequencing verification of the one representative PCR product are presented. To indicate the methylation status, the sequenced data are aligned with the wild-type sequence. ¹Size markers, the bands of 250 bp and 100 bp are shown. U, the unmethylated; M, hypermethylated. Panels: 1, *APC*, 2, *BRCA1*, 3, *CDH1*, 4, *CDH13*, 5, *CDX1*, 6, *COX2*, 7, *CXX1*, 8, *cyclin A1*, 9, *DPAK1*, 10, *DNMT1*, 11, *hMLH1*, 12, *MAGEA1*, 13, *MGMT*, 14, *MINT1*, 15, *MINT31*, 16, *MYOD1*, 17, *N33*, 18, *p14^{ARF}*, 19, *p15^{INK4b}*, 20, *p16^{INK4a}*, 21, *p21^{WAF1}*, 22, *p27^{KIP1}*, 23, *p73*, 24, *PTEN*, 25, *RAR-β*, 26, *RASSF1A*, 27, *RASSF1C*, 28, *SFRP1*, 29, *TIMP3*, 30, *VHL*, and 31, *WT1*.

Genes displayed no changes in methylation profile in tumor samples

As shown in Figure 1 and summarized in Figure 2, by comparing with the normal mucosa of non-cancerous samples, the following 14 genes did not display any tumor associated changes: *BRCA1* (panel 2), *CDH1* (panel 3), *DPAK1* (panel 9), *DNMT1* (panel 10), *MAGEA1* (panel 12), *N33* (panel 17), *p21^{WAF1}* (panel 21), *p27^{KIP1}* (panel 22), *PTEN* (panel 24), *RAR-* (panel 25), *RASSF1C* (panel 27), *SFRP1* (panel 28), *TIMP3* (panel 29) and *VHL* genes (panel 30). The *MAGEA1* gene was the only target that tends to be demethylated and transcription-activated in tumors, as we previously demonstrated in hepatocellular carcinoma (HCC)^[10]. But the hypermethylated state of its promoter CpG islands maintained in all the samples tested. The likely explanations for such no-change-type-observations were the following: no changes in expression of this set of genes occurred in CRC, and the changes in expression indeed occurred, but the DNA methylation mediated mechanisms was not involved.

It should be pointed out that our no change conclusion as to both *N33* and *TIMP3* genes was at odds with the previous report where both genes were hypermethylated rather frequently in CRC^[32]. Whether it was attributed to the inherent difference between patient groups in different studies remains to be clarified.

Genes displayed changes in methylation profile in tumor samples

To score the changes in each CRC case, the methylated status in the mucosa tissue of the non-cancerous patients was taken as the reference, any deviation from which was scored as positive (increasing methylation extent) or negative (decrease

in methylation extent).

Seventeen genes in this list displayed to various extents the tumor associated changes. As shown in Figures 1, 2, the changes of the following genes occurred marginally, and their impact on CRC looked trivial: *APC* (panel 1) (8%, 5/65), *RASSF1A* (3%, 2/65) (panel 26) and *p14^{ARF}* (6%, 4/65) (panel 18). It was surprising to see that the extremely low frequency in hypermethylation of the *RASSF1A* gene in CRC, which was hypermethylated in a wide range of the human tumors, including hepatocellular carcinoma^[10,14], astrocytoma (unpublished results) and other tumors^[33,34].

The following genes displayed significant alterations in methylation pattern deviated from that of the mucosa of the non-cancer tissues, including those with the moderate levels of changes: *MGMT* (20%, 13/65, panel 13), *hMLH1* (18%, 12/65, panel 11), *p16^{INK4a}* (10%, 10/65, panel 20), *MINT1* (15.4%, 10/65, panel 14), *MINT31* (11%, 7/65, panel 15); and with a great level of changes: *COX2* (72%, 47/65, (panel 6), *cyclin A1* (100%, 65/65, panel 8) and *CDX1* (100%, 65/65, panel 5), *RAR-* (85%, 55/65, panel 25), *MYOD1* (69%, 45/65, panel 16), *p15^{INK4b}* (68%, 44/65, panel 19), *CDH13* (66%, 43/65, panel 4), *CXX1* (58%, 38/65, panel 7), *p73* (63%, 41/65, panel 23) and *WT1* (58%, 38/65, panel 31, Figure 1). In this list, while changes in methylation pattern of the majority of targets, were compatible with the previously reported frequencies in CRC patients in the Western countries^[7,11,35,36], there was a noticeable difference. For instance, we have found the *p15^{INK4b}* was significantly methylated in CRC (68%, 44/65), while this gene was not methylated at all in a similar study in USA^[35].

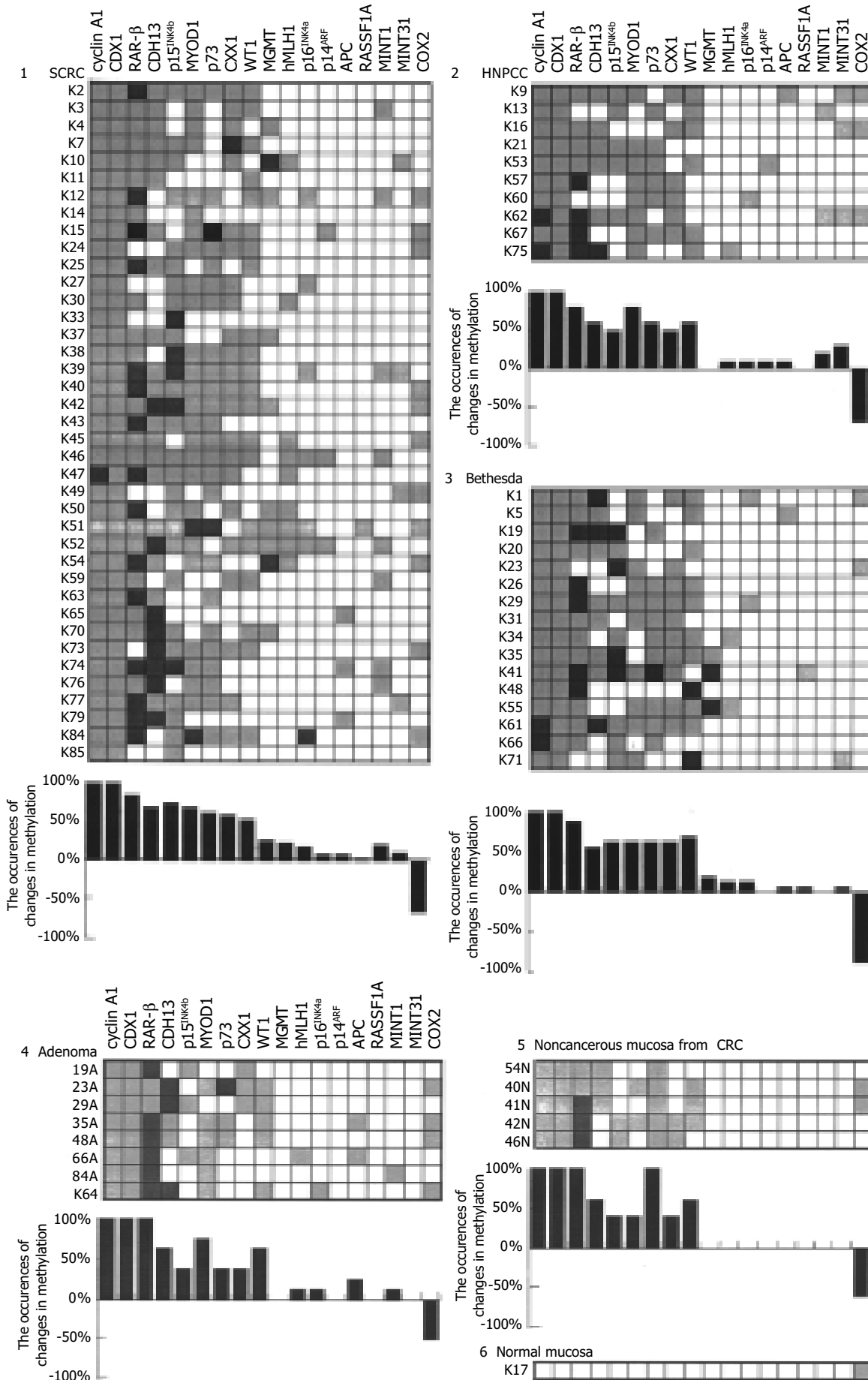


Figure 2 Changes in methylation pattern of genes in CRC and other relevant tissues. The frequency (%) of the hypermethylated targets among the total cases was calculated, and the frequency of the changes in the methylation pattern is presented in the plot as well as in the attached table. Panels: 1, SCRC, 2, HNPCC, 3, Bethesda, 4, Adenoma, 5, Non-cancerous mucosa from CRC patients and 6, the normal mucosa from a non-cancerous patient.

It was also our intention to correlate the methylation pattern with the clinical-pathological features of CRC patients. Subjected to the stringent statistic analysis ($P < 5\%$), none of the comparisons displayed any significant correlation. For instance, there was no statistic significance between the methylation changes of any given genes among different subgroups of CRC: SCRC and HNPCC as well as against other cohorts of tissues, such as colorectal adenoma and adjacent mucosa. This was likely to attribute to the small sample size. Although there was a decent number for SCRC ($n = 39$), the sample sizes for other subgroups were rather small: 10 HNPCCs, 16 Bethesda CRCs, eight adenomas, five non-cancerous mucosae and one normal mucosa.

It has been well recognized that the so-called non-cancerous cells pathologically defined may have already suffered some genetic lesions as the corresponding cancerous tissues, the outcome of the earlier events of carcinogenesis. The scenario of the genetic events from the normal mucosa to the full-blown CRC within the context of the well defined clinical and pathological parameters has been well characterized^[37]. In this study, we included samples of non-cancerous mucosa from five CRC patients, adenomatous samples from eight patients and tumorous tissues from 65 CRC cases including 39 SCRCs, 10 HNPCCs and 16 Bethesda CRCs, which enabled us to determine whether the changes in methylation pattern in CRC were specific to the early or late phases of carcinogenesis. Judged by the no difference in methylation pattern between the non-cancerous mucosa and adenoma and/or CRC (Figures 1, 2) (the same rationale used in our previous work on the hepatocellular carcinoma^[10]), we suggested that the high frequent changes in methylation pattern of the genes might be the early rather than the late phase events during carcinogenesis of CRC.

CRC was among the first few types of human cancers subjected to the rather intensive DNA methylation profiling, where changes in methylation in tumor samples were classified as the aging related as well as the cancer specific^[17,38,39]. For instance, the *MYOD1* was found also hypermethylated more frequently in the aged healthy epithelia tissues than their younger counterparts^[17]. Also from the studies of CRC, the concordant methylation profile of multiple genes was firstly reported, called "CpG island methylation phenotype (CIMP)", short for CpG island methylator phenotype^[11]. It implies that the unknown genetic mechanism (s) operating in CRC may contribute to the clustering profile of the DNA methylation of the multiple genes together. Among the 65 CRC cases, the distribution in occurrence of changes in the multiple genes was as following, 1, 3, 5, 7, 12, 11, 11, 7, 4, 1, and 3 cases, for assuming the methylation change of from 2, progressing step by step to 12 genes, respectively (Figure 3), with the 7 gene group as the peak.

In situ expression profile of 10 genes in CRC

Hypermethylation of the promoter CpG islands could reflect

the transcriptional silencing status of the gene. However, exceptions also were reported, suggesting the involvement of other mechanisms in the control of the gene transcription. To verify this notion, we immunostained 10 target proteins *in situ* on the home-made tumor tissue arrays, where the tissue blocks from 58 CRC samples along with several controls of the non-cancerous mucosa from the cancer patients were present. The results were scored from the negative (-), to positive: ranging from + to +++. With the expression level in the non-cancerous mucosa as reference, the relative level of expression of each protein in the context of the methylation state of the promoter CpG islands of the genes was assessed. As shown in Figure 4 and summarized in Table 5, the unmethylated states of the promoter CpG islands of the following genes were indeed positively correlated with the expression levels of the genes. Among the cases of the fully unmethylated targets, expression of each protein \geq one + level occurred very frequently: for the *CDH13*, 73% (16/22); *RAR-b*, 100% (8/8); *COX2*, 80% (35/44); *p73*, 60% (12/20); *hMLH1*, 75% (35/47); *p14^{ARF}*, 100% (51/51); *TIMP3*, 80% (46/58) and *CDH1*, 98% (57/58). The only exception was *MGMT*, only 25% (2/8) of the unmethylated cases expressed this protein, suggesting the mechanisms other than DNA hypermethylation being involved. For the CRC cases with the heterozygous methylated status (u/m), expression of each proteins was: *CDH13*, 50% (14/28); *cyclin A1*, 70% (37/53); *RAR-*, 79% (22/28); *COX2*, 100% (14/14); *p73*, 54% (19/35); *MGMT*, 24% (11/46); *hMLH1*, 36% (4/11) and *p14^{ARF}*, 100% (2/2), respectively. For the CRC cases with the fully methylated targets, the expression profile of the genes was as the following: *CDH13*, 38% (33/58), *cyclin A1*, 80% (4/5), *RAR-*, 85% (17/20) and *MGMT*, 50% (2/4). Except for the *CDH13*, which expressed less frequently in the methylated than the unmethylated containing cases, the expression frequency was not significantly less prevalently in the methylated cases, even higher as far as the *MGMT* was concerned. Therefore, the correlation between the methylation status and level of expression of these 10 genes was not in a good agreement with the conventional notion.

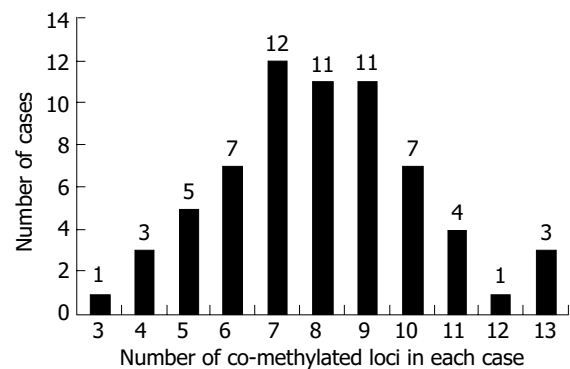
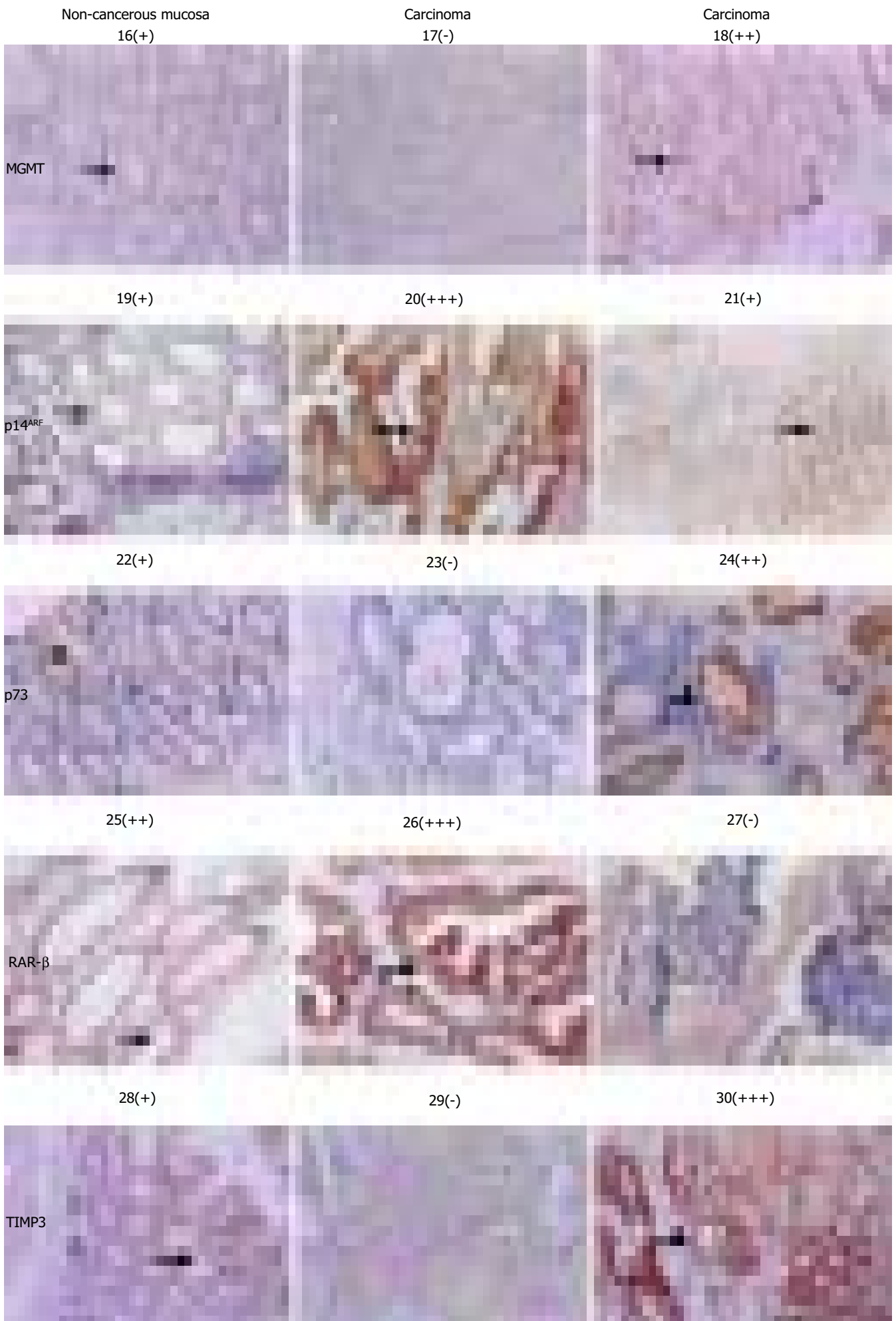


Figure 3 Concordant behavior of the multiple methylated loci in CRC.

Table 5 Expression profile of the genes in the context of DNA methylation status

Methylation status	Positive rate % (Positive cases/the total cases)									
	CDH13	Cyclin a1	RAR-	COX2	P73	MGMT	hMLH1	p14ARF	TIMP3	CDH1
U	73 (16/22)	/	100 (8/8)	81 (35/43)	60 (12/20)	24 (11/46)	74 (35/47)	100 (51/51)	80 (46/58)	98 (57/58)
U/M	50 (14/28)	70 (37/53)	79 (22/28)	93 (14/15)	54 (19/35)	25 (2/8)	36 (4/11)	100 (2/2)	/	/
M	38 (3/8)	80 (4/5)	85 (17/20)	/	/	50 (2/4)	/	/	/	/
Total	57 (33/58)	71 (41/58)	84 (47/56)	84 (49/58)	53 (31/58)	26 (15/58)	67 (39/58)	100 (53/53)	79 (46/58)	98 (57/58)
Non-cancerous mucosa	+	/	++	/	+	+	++	+	+	++



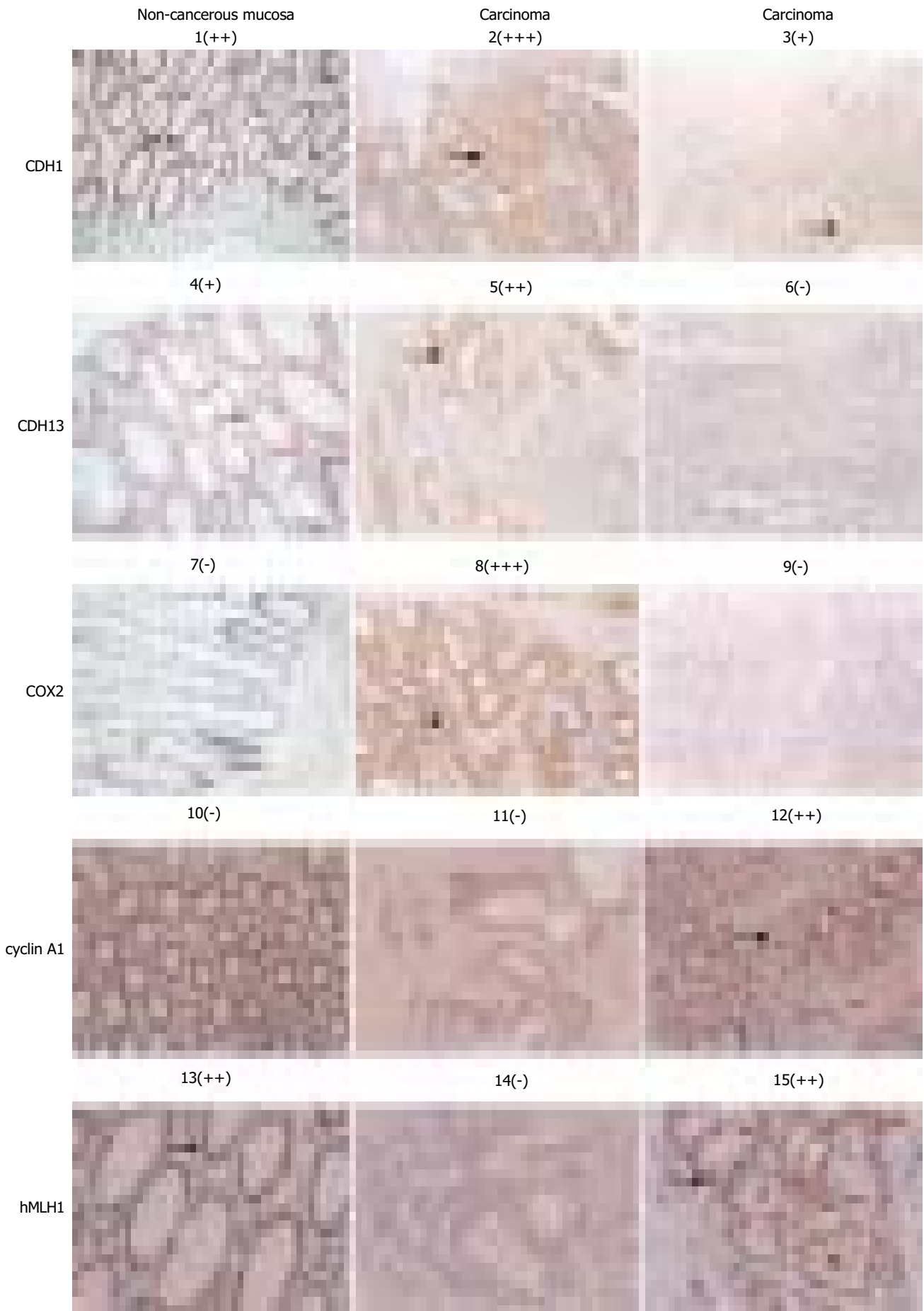


Figure 4 Immunohistochemical assessment of the expression level of each of 10 target genes. Both the protein targets (left site to) and sample identities (top down) of the immuno-chemical stained picture are indicated. The signs: -, +, ++, and +++ in bracket are used to provide the quantitative reference in pictures below. The areas pointed by the arrows are the regions showing the immunostaining data quantified.

DISCUSSION

In this study, 31 targets were selected to be studied, 65 cases of CRC, 8 cases of adenoma, five cases of non-cancerous mucosa from the cancer patients and one case mucosa from the non-cancerous patient. As far as the number of genes was concerned, this study is rather extensive, and it is the first of such a kind with CRC patients in China, and in Shanghai in particular.

Changes in methylation pattern of the promoter CpG islands are very common in CRC

By taking the methylation profile of the mucosa from the non-cancerous patient as the reference, CRC associated changes in methylation pattern were a very extensive event, 17 among of 31 targets assumed the altered patterns, the following 14 changed in more than 20% of CRC cases as a whole: *MGMT* (20%, 13/65), *hMLH1* (18%, 12/65), *p16^{INK4a}* (10%, 10/65), *MINT1* (15.4%, 10/65), *MINT31* (11%, 7/65), *COX2* (72%, 47/65), *cyclin A1* (100%, 65/65), *CDX1* (100%, 65/65), *RAR-* (85%, 55/65), *MYOD1* (69%, 45/65), *p15^{INK4b}* (68%, 44/65), *CDH13* (66%, 43/65), *CXX1* (58%, 38/65), *p73* (63%, 41/65) and *WT1* (58%, 38/65) genes. Furthermore, there was only one case assuming the methylation changes with three genes (Figure 3), no less than 76.3 % of cases assumed changes in methylation more than seven targets (49/65), 86% more than six targets (56/65), 93.8% more than five targets (61/65). This observation indeed supports the concept, "CpG island methylator phenotype", for that changes in methylation pattern in CRC indeed tend to be clustered. As a similar survey with the astrocytoma showed that less 26.4% patients assumed no more than two gene (among 31 targets being surveyed), and the occurrence of changes in methylation pattern for at least five, six and seven targets was 41.51%, 20.75 and 9.43% in a cohort of 56 astrocytoma patients (unpublished data). The high incidence of changes in CRC may be partly attributed to the fact that colorectal epithelial cells were much amenable to the environmental challenges.

Except for the genes that have been proved in the category of tumor associated genes, such as *p16^{INK4a}*, *p15^{CDKN4b}*, *p14^{ARF}*, *p27^{KIP1}*, *WT1*, *VHL*, *RB*, *p73*, *APC*, *N33*, *PTEN* and *BRCA1*, the *MAGEA1* and *RAR-* genes have not been studied in CRC. While the *MAGEA1* gene displayed the homozygously methylated state in all samples tested, the *RAR-* gene indeed changes its methylated state from the unmethylated in the normal mucosa toward the hypermethylated state at a significantly higher frequency in CRC, over 85% (55/65). The retinoic acid receptor (*RAR*) gene is a putative tumor suppressor gene on chromosome 3p24, where a high incidence of loss of heterozygosity (LOH) is detected in many types of tumors. Retinoic acid suppresses cancer cell growth through binding to *RARs*, especially *RAR-*, indicating a critical role in mediating anticancer effects. Selective loss or down-regulation of the *RAR* mRNA and protein has been reported in prostate cancers. The DNA methylation mediated silencing of this gene has been suggested as an etiological factor for carcinogenesis of prostate cancer^[40]. This result indicates that the *RAR-* hypermethylation may be the mechanism of expression silencing in these tumor cells^[41]. However, its etiological significance in carcinogenesis of CRC remains to be clarified.

The following genes: *CXX1*, *CDX1*, *SFRP1*, *MINT1* and *MINT31* were initially identified as the CRC associated hypomethylated genes by an approach at the genome level^[16]. Except for the *SERP1* gene that was not methylated with all the samples being tested, the rest targets were indeed hypermethylated to varying extents in CRC (Figures 1, 2). Tumor suppressor gene *RASSF1A* was inactivated predominantly by promoter methylation and rarely by somatic mutations. Wagner *et al.*^[34] investigated *RASSF1A* promoter methylation in colorectal

cancer and detected *RASSF1A* methylation in 80% (4/5) colorectal cancer cell lines and 45% (13/29) primary colorectal cancers. But we found that the frequency of *RASSF1A* methylation was extremely low in CRC although we previously found this gene was hypermethylated (100%) in HCC^[14].

Does the methylation profile of the promoter CpG islands of the genes correlate with the expression of the genes?

Although it has been generally accepted that the hypermethylated status of the promoter CpG islands represents the long-term transcription silencing state of the genes, its credential has not been thoroughly checked in clinical samples, due to various limiting factors, including availability and inherent diversity of the cell types in the actual samples. In this study, we immunostained the genes with antibodies to assess the expression of 10 genes in a home-made tissue array. For both homozygously and heterozygously unmethylated samples, nine of 10 targets (except for *MGMT*) expressed at a detectable level of more than 60% cases. It was generally fit with the expectation. For the fully methylated CRC, only four targets were involved, among which the profile of the *CDH13* gene met the expected profile. The expression frequency (38%, 3/8) in methylated samples was significantly lower than heterozygously methylated (50%, 14/28), and homozygously unmethylated (73%, 16/22). The profiles of the other three targets did not comply with the role at all. Both *cyclin A1* and *RAR-* genes expressed equally well as the CRC samples of m/u type. Furthermore, it was paradoxically found that the *MGMT* gene expressed more prevalently in the methylated CRC cases (50%, 2/4) than its counterparts (u/m: 25%, 2/8 and u: 25%, 11/46). As we have previously shown in astrocytoma cell lines, the methylated status of the promoter CpG islands inversely correlated with the expression of the *MGMT* gene (unpublished data), this rather unexpected observation should be looked into further. In conclusion, despite the general roles that have been followed as to the inverse correlation between the methylation state of the promoter CpG islands and expression, the exception is also distinguishingly noticeable. Therefore, it should be very cautious in correlating the methylated status with the expression profile of the genes.

Demethylation of the COX2 gene correlates with the increased frequency in its expression

Cyclo-oxygenase 2 (*COX2*), an inducible isoform of prostaglandin H synthase, which mediates prostaglandin synthesis during inflammation, and is selectively over-expressed in colon tumors, is thought to play an important role in colorectal carcinogenesis^[42]. Its expression in the normal epithelial cells is low, but can be induced by a variety of stressing agents, including tumor promoters and inflammatory cytokines. In the list of the genes displaying changes in methylation, it was noticed that the *COX2* gene was the only target that displayed CRC associated demethylation, i.e., from the heterozygous methylated state to fully demethylated in 47 among 65 cases being studied (72%) (Figures 1, 2). The *COX2* gene did not express in the control non-cancerous tissues, indicating that it seems less likely to have the physiological role in normal colon epithelial cells. Although there was no increase in the frequency of expression in CRC from the heterozygously to the fully unmethylated CRC cases (Figure 2), the fact that over 82% CRC cases expressed this gene was indeed supportive.

Tumor type specificity of the methylation profile

It has been well established that the methylation profile as an inheritable epigenetic signature in any given cells reflects both history of cell differentiation and the chronicle of aging, in addition to those closely associated with the biological profiles

of tumors^[6,43,44]. It is desirable to identify the changes, specific to one type of tumor from the others, otherwise our efforts to use the DNA methylation pattern, as the biomarkers for tumor diagnosis would be severely constrained. Therefore, we compared the methylation patterns in HCC^[10,14] with those in CRC. As shown in Figure 5, there were methylation changes common to both HCC and CRC i.e., the *p73* gene: 73% in HCC vs 62.5% in CRC and the *MYOD1* gene: 57.8% in HCC vs 69.23% in CRC. The following changes were more prevalent in CRC than in HCC: the *cyclin A1* gene: 100% in CRC vs 53.85% in HCC; the *WT1* gene: 58.46% in CRC vs 30.77% in HCC; and the *CDH13* gene: 64.62% in CRC vs 23.08% in HCC. The following two genes were more frequently hypermethylated in HCC than in CRC: the *RASSF1A* gene: 100% in HCC vs 3.08% in CRC; and the *p16^{INK4a}* gene: 53.85% in HCC vs 15.38% in CRC. Although little is known about the mechanisms underlying the tumor specific methylation profiles of CRC vs those of HCC, the distinct profiles of CRC vs HCC should have the profound implication in the future diagnostic tools to differentiate these two common human cancers.

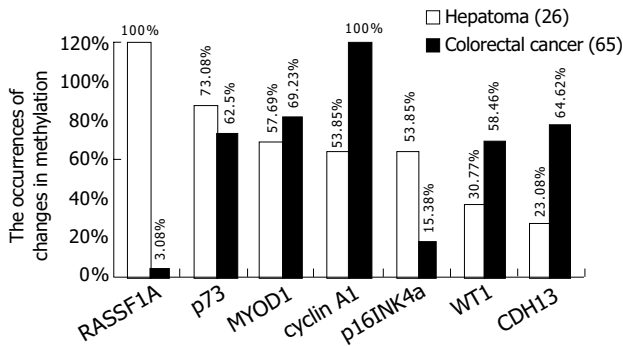


Figure 5 Tumor specific methylation pattern: CRC verse HCC.

In conclusion, the altered promoter CpG island methylation patterns of 17 genes are the common and distinguished hallmarks specific to the early phase of colon carcinogenesis, although no significant correlation has been detected between the changes in the methylation patterns with any given clinical-pathological features. The correlation between the methylated state of the promoter CpG islands and the expression of the corresponding genes has not been proved as close as previously suggested. Our observations from this rather extensive methylation-profiling maneuver would provide new insights into the role of the DNA methylation mediated control in the colon carcinogenesis as well as the clues for the development of robust diagnostic and prognostic tools for colorectal cancer.

REFERENCES

- 1 Du BR. COX-2 in large bowel cancer: a one-sided story. *Gut* 1999; **45**: 636-637
- 2 Kinzler KW, Vogelstein B. Landscaping the cancer terrain. *Science* 1998; **280**: 1036-1037
- 3 Parkin DM, Pisani P, Ferlay J. Global cancer statistics. *CA Cancer J Clin* 1999; **49**: 33-64
- 4 DePinho RA. The age of cancer. *Nature* 2000; **408**: 248-254
- 5 Bird AP. CpG-rich islands and the function of DNA methylation. *Nature* 1986; **321**: 209-213
- 6 Jaenisch R, Bird A. Epigenetic regulation of gene expression: how the genome integrates intrinsic and environmental signals. *Nat Genet* 2003; **33**(Suppl): 245-254
- 7 Feinberg AP. Cancer epigenetics takes center stage. *Proc Natl Acad Sci U S A* 2001; **98**: 392-394
- 8 Chen RZ, Pettersson U, Beard C, Jackson-Grusby L, Jaenisch R. DNA hypomethylation leads to elevated mutation rates. *Nature* 1998; **395**: 89-93
- 9 Gaudet F, Hodgson JG, Eden A, Jackson-Grusby L, Dausman

- J, Gray JW, Leonhardt H, Jaenisch R. Induction of tumors in mice by genomic hypomethylation. *Science* 2003; **300**: 489-492
- 10 Yu J, Zhang HY, Ma ZZ, Lu W, Wang YF, Zhu JD. Methylation profiling of twenty four genes and the concordant methylation behaviours of nineteen genes that may contribute to hepatocellular carcinogenesis. *Cell Res* 2003; **13**: 319-333
- 11 Toyota M, Ahuja N, Ohe-Toyota M, Herman JG, Baylin SB, Issa JP. CpG island methylator phenotype in colorectal cancer. *Proc Natl Acad Sci U S A* 1999; **96**: 8681-8686
- 12 van Rijnsoever M, Grieu F, Elsaleh H, Joseph D, Iacopetta B. Characterisation of colorectal cancers showing hypermethylation at multiple CpG islands. *Gut* 2002; **51**: 797-802
- 13 Cai Q. Molecular genetics research of HNPCC in China, Department of Pathology, Cancer Hospital of Fudan University, Fudan University, Shanghai 2002
- 14 Yu J, Ni M, Xu J, Zhang H, Gao B, Gu J, Chen J, Zhang L, Wu M, Zhen S, Zhu J. Methylation profiling of twenty promoter-CpG islands of genes which may contribute to hepatocellular carcinogenesis. *BMC Cancer* 2002; **2**: 29
- 15 Herman JG, Graff JR, Myohanen S, Nelkin BD, Baylin SB. Methylation-specific PCR: a novel PCR assay for methylation status of CpG islands. *Proc Natl Acad Sci U S A* 1996; **93**: 9821-9826
- 16 Suzuki H, Gabrielson E, Chen W, Anbazhagan R, van Engeland M, Weijnenberg MP, Herman JG, Baylin SB. A genomic screen for genes upregulated by demethylation and histone deacetylase inhibition in human colorectal cancer. *Nat Genet* 2002; **31**: 141-149
- 17 Ahuja N, Li Q, Mohan AL, Baylin SB, Issa JP. Aging and DNA methylation in colorectal mucosa and cancer. *Cancer Res* 1998; **58**: 5489-5494
- 18 Kibel AS, Christopher M, Faith DA, Bova GS, Goodfellow PJ, Isaacs WB. Methylation and mutational analysis of p27(kip1) in prostate carcinoma. *Prostate* 2001; **48**: 248-253
- 19 Li Y, Nagai H, Ohno T, Yuge M, Hatano S, Ito E, Mori N, Saito H, Kinoshita T. Aberrant DNA methylation of p57(KIP2) gene in the promoter region in lymphoid malignancies of B-cell phenotype. *Blood* 2002; **100**: 2572-2577
- 20 Watanabe T, Huang H, Nakamura M, Wischhusen J, Weller M, Kleihues P, Ohgaki H. Methylation of the p73 gene in gliomas. *Acta Neuropathol* 2002; **104**: 357-362
- 21 Agathangelou A, Honorio S, Macartney DP, Martinez A, Dallol A, Rader J, Fullwood P, Chauhan A, Walker R, Shaw JA, Hosoe S, Lerman MI, Minna JD, Maher ER, Latif F. Methylation associated inactivation of RASSF1A from region 3p21.3 in lung, breast and ovarian tumours. *Oncogene* 2001; **20**: 1509-1518
- 22 Linehan WM, Lerman MI, Zbar B. Identification of the von Hippel-Lindau (VHL) gene. Its role in renal cancer. *Jama* 1995; **273**: 564-570
- 23 Neiberghs HL, Hein DW, Spratt JS. Genetic profiling of colon cancer. *J Surg Oncol* 2002; **80**: 204-213
- 24 Laux DE, Curran EM, Welshons WV, Lubahn DB, Huang TH. Hypermethylation of the Wilms' tumor suppressor gene CpG island in human breast carcinomas. *Breast Cancer Res Treat* 1999; **56**: 35-43
- 25 De Smet C, De Backer O, Faraoni I, Lurquin C, Brasseur F, Boon T. The activation of human gene MAGE-1 in tumor cells is correlated with genome-wide demethylation. *Proc Natl Acad Sci U S A* 1996; **93**: 7149-7153
- 26 Toyooka S, Toyooka KO, Harada K, Miyajima K, Makarla P, Sathyanarayana UG, Yin J, Sato F, Shivapurkar N, Meltzer SJ, Gazdar AF. Aberrant methylation of the CDH13 (H-cadherin) promoter region in colorectal cancers and adenomas. *Cancer Res* 2002; **62**: 3382-3386
- 27 Muller C, Readhead C, Diederichs S, Idos G, Yang R, Tidow N, Serve H, Berdel WE, Koeffler HP. Methylation of the cyclin A1 promoter correlates with gene silencing in somatic cell lines, while tissue-specific expression of cyclin A1 is methylation independent. *Mol Cell Biol* 2000; **20**: 3316-3329
- 28 Esteller M, Corn PG, Baylin SB, Herman JG. A gene hypermethylation profile of human cancer. *Cancer Res* 2001; **61**: 3225-3229
- 29 Viswanathan M, Tsuchida N, Shanmugam G. Promoter hypermethylation profile of tumor-associated genes p16, p15, hMLH1, MGMT and E-cadherin in oral squamous cell carcinoma. *Int J Cancer* 2003; **105**: 41-46

- 30 **Fearon ER.** BRCA1 and E-cadherin promoter hypermethylation and gene inactivation in cancer-association or mechanism? *J Natl Cancer Inst* 2000; **92**: 515-517
- 31 **Zochbauer Muller S, Fong KM, Virmani AK, Geradts J, Gazdar AF, Minna JD.** Aberrant promoter methylation of multiple genes in non-small cell lung cancers. *Cancer Res* 2001; **61**: 249-255
- 32 **Issa J.** Genes Affected by Promoter CpG Island Methylation in Aging and/or Cancer, <http://www.mdanderson.org/departments/methylation/dIndex.cfm?pn = D02B3250-57D7-4F61-88358636A8073A08> 2001
- 33 **Maruyama R, Toyooka S, Toyooka KO, Harada K, Virmani AK, Zochbauer-Muller S, Farinas AJ, Vakar-Lopez F, Minna JD, Sagalowsky A, Czerniak B, Gazdar AF.** Aberrant promoter methylation profile of bladder cancer and its relationship to clinicopathological features. *Cancer Res* 2001; **61**: 8659-8663
- 34 **Wagner KJ, Cooper WN, Grundy RG, Caldwell G, Jones C, Wadey RB, Morton D, Schofield PN, Reik W, Latif F, Maher ER.** Frequent RASSF1A tumour suppressor gene promoter methylation in Wilms' tumour and colorectal cancer. *Oncogene* 2002; **21**: 7277-7282
- 35 **Esteller M, Fraga MF, Guo M, Garcia-Foncillas J, Hedenfalk I, Godwin AK, Trojan J, Vaur-Barriere C, Bignon YJ, Ramus S, Benitez J, Caldes T, Akiyama Y, Yuasa Y, Launonen V, Canal MJ, Rodriguez R, Capella G, Peinado MA, Borg A, Aaltonen LA, Ponder BA, Baylin SB, Herman JG.** DNA methylation patterns in hereditary human cancers mimic sporadic tumorigenesis. *Hum Mol Genet* 2001; **10**: 3001-3007
- 36 **Suh ER, Ha CS, Rankin EB, Toyota M, Traber PG.** DNA methylation down-regulates CDX1 gene expression in colorectal cancer cell lines. *J Biol Chem* 2002; **277**: 35795-35800
- 37 **Kinzler KW, Vogelstein B.** Lessons from hereditary colorectal cancer. *Cell* 1996; **87**: 159-170
- 38 **Jubb AM, Bell SM, Quirke P.** Methylation and colorectal cancer. *J Pathol* 2001; **195**: 111-134
- 39 **Rashid A, Shen L, Morris JS, Issa JP, Hamilton SR.** CpG island methylation in colorectal adenomas. *Am J Pathol* 2001; **159**: 1129-1135
- 40 **Nakayama T, Watanabe M, Yamanaka M, Hirokawa Y, Suzuki H, Ito H, Yatani R, Shiraishi T.** The role of epigenetic modifications in retinoic acid receptor beta2 gene expression in human prostate cancers. *Lab Invest* 2001; **81**: 1049-1057
- 41 **Cote S, Momparler RL.** Activation of the retinoic acid receptor beta gene by 5-aza-2'-deoxycytidine in human DLD-1 colon carcinoma cells. *Anticancer Drugs* 1997; **8**: 56-61
- 42 **Plummer SM, Holloway KA, Manson MM, Munks RJ, Kaptein A, Farrow S, Howells L.** Inhibition of cyclo-oxygenase 2 expression in colon cells by the chemopreventive agent curcumin involves inhibition of NF-kappaB activation via the NIK/IKK signalling complex. *Oncogene* 1999; **18**: 6013-6020
- 43 **Jones PA.** Epigenetics in carcinogenesis and cancer prevention. *Ann N Y Acad Sci* 2003; **983**: 213-219
- 44 **Jubb AM, Quirke P, Oates AJ.** DNA methylation, a biomarker for colorectal cancer: implications for screening and pathological utility. *Ann N Y Acad Sci* 2003; **983**: 251-267

Edited by Xia HHX and Wang XL Proofread by Xu FM

• COLORECTAL CANCER •

Effects of phosphorothioate anti-sense oligodeoxynucleotides on colorectal cancer cell growth and telomerase activity

Xi-Shan Wang, Kuan Wang, Xue Li, Song-Bin Fu

Xi-Shan Wang, Kuan Wang, Department of Abdominal Surgery, Tumour Hospital of Harbin Medical University, Harbin 150040, Heilongjiang Province, China

Xue Li, Song-Bin Fu, Department of Genetics, Harbin Medical University, Harbin 150086, Heilongjiang Province, China

Supported by the Youth Science Foundation of Heilongjiang Province, China, No.QC01C08, and Heilongjiang Provincial Technology Council Foundations, China, No.GC03C605-6

Correspondence to: Dr. Xi-Shan Wang, Department of Abdominal Surgery, Tumour Hospital of Harbin Medical University, Harbin 150040, Heilongjiang Province, China. 1966120808@sina.com

Telephone: +86-451-86677583 Ext. 2146 **Fax:** +86-451-86663760

Received: 2004-02-14 **Accepted:** 2004-02-24

Abstract

AIM: To investigate the inhibitory effect of phosphorothioate anti-sense oligodeoxynucleotides (PASODN) on colorectal cancer LS-174T cells *in vitro* and the mechanism of inhibition of telomerase activity in these cells.

METHODS: PASODN were used to infect LS-174T cells and block human telomerase RNA (hTR) through anti-sense technology. The inhibitory effect of PASODN was evaluated by colony-forming inhibition assay and growth curve. Changes of telomerase activity in LS-174T cells were detected by polymerase chain reaction-enzyme-linked immunosorbent assay (PCR-ELISA), and the level of apoptosis was analyzed by flow cytometry (FCM) assay.

RESULTS: PASODN showed a dose and time-dependent inhibition of cell proliferation. The optimal dosage of PASODN was 10 $\mu\text{mol/L}$. The colony-forming efficiency was 10.3% in PASODN group after 10 d, whereas that in phosphorothioate mis-sense oligodeoxynucleotides (PMSODN) group with the same concentration and in PBS group (blank control) was 49.1% and 50.7%, respectively. PCR-ELISA results indicated that telomerase activity in the PASODN group was obviously inhibited in comparison with in the control groups ($P < 0.01$, $t = 3.317$ and 3.241 , $t_{0.01(20)} = 2.845$). Meanwhile, before the number of cells was decreased, the morphological changes were observed in the cells of PASODN group. The cells in PASODN group showed the apoptotic peak at 72 h after infection, whereas the control group did not show.

CONCLUSION: Specific sequence oligonucleotides can inhibit telomerase activity and lead to cell apoptosis, suggesting a novel treatment strategy for malignant tumors induced by telomerase.

Wang XS, Wang K, Li X, Fu SB. Effects of phosphorothioate anti-sense oligodeoxynucleotides on colorectal cancer cell growth and telomerase activity. *World J Gastroenterol* 2004; 10(23): 3455-3458

<http://www.wjgnet.com/1007-9327/10/3455.asp>

INTRODUCTION

Telomerase, a ribonucleic acid-protein complex, adds hexameric

repeats of 5'-TTAGGG-3' to the ends of telomeres to compensate for the progressive loss in malignant tumor cells^[1,2]. Because of its preferential expression in malignant tumors and lack of expression in normal tissues^[3-5], the idea that telomerase is a potential target of cancer therapy has been widely accepted^[6,7]. From the theoretical point of view, telomerase-associated therapeutic approach to telomerase-positive tumors is the anti-telomerase cancer therapy that directly inhibits telomerase activity, resulting in apoptotic cell death or growth arrest. Two major components of the telomerase holoenzyme complex: human telomerase RNA (hTR) and catalytic subunit (human telomerase reverse transcriptase, hTERT), are considered as the therapeutic targets^[8]. Since the growth of majority, or even parts of malignant tumors depends on telomerase, the strategy of anti-telomerase cancer therapy is necessary and important. In this study, we investigated the inhibitory effect of PASODN on colorectal cancer cells.

MATERIALS AND METHODS

Human colorectal cancer cell line LS-174T was obtained from Shanghai Institute of Cell Biology (Shanghai, China). Oligonucleotides were synthesized in Shenggong Company (Shanghai, China). The sequences of oligonucleotides were as follows: PASODN: 5'-TTAGGG-3', and PMSODN: 5'-TGTGAG-3'. Telomerase PCR-ELISA kit (No. 1854666) was purchased from Roche Company.

Cell culture

Colorectal cancer LS-174T cells were cultured in RPMI 1640 (GIBCO, UK) supplemented with 100 mL/L charcoal-stripped FCS (GIBCO, UK), 500 units/mL penicillin and 0.1 $\mu\text{g/mL}$ streptomycin (SIGMA, USA) at 37 °C with a humidified atmosphere containing 50 mL/L CO₂. The medium was changed every 48 h. Cell cycle was 12 h approximately. Cells in logarithmic phase were used in all experiments.

Selection of optimal concentration of PASODN

The LS-174T cells (100 cells/mL in each well) were transferred to 24-well plates and cultured in 500 μL of RPMI 1640. Wells were divided into six groups with different final concentrations of PASODN: 0, 1, 2.5, 5, 10 and 20 $\mu\text{mol/L}$, respectively, the first one acted as a control. The medium was changed every other day. Ten days later, the cells in each well were stained with Giemsa and the colony-forming units were counted (consisting of more than 50 cells) under a phase contrast microscope. The optimal concentration of PASODN was screened according to the relative rate of inhibition of colony forming according to the formula: the relative rate of inhibition of colony-forming (%) = (1 - number of clone in experiment group / number of clones in control group) \times 100%.

Inhibition of colony formation

Logarithmic phase cells were digested, suspended and calculated, and then suspension was transferred to 6-well plates. Cell concentration was 400 cells/mL in each well. Wells were divided into: PASODN group, PMSODN group, and PBS group. The

later two groups acted as controls. Twenty hours after the cells were adhered, RPMI 1640 was removed and wells were washed with 2.5×PBS. Cells were incubated with 2 mL of RPMI 1640 culture medium containing 10 μmol/L PASODN, 10 μmol/L PMSODN and PBS (same volume). Medium was changed every other day. The incubation was terminated 10 d later. The colony-forming units were stained by Giemsa dye and counted. Colony-forming efficiency = (unit number / cell number) × 100%.

Inhibition of cell proliferation

LS-174T cells (10×10³ cells/mL in each well) were transferred to 24-well plates. Wells were divided into three groups and the cells were treated as mentioned above in 1 mL of RPMI1640 culture medium. Medium was changed every other day. The number of cells in each group was counted every day, and morphological changes were observed. The growth curve of the cells was obtained 13 d later.

Variation of telomerase activity detected by PCR-ELISA and silver staining assay

PCR-ELISA was performed following the manufacturer's instructions. All solutions were provided by the kit from Roche.

Briefly, the cells were digested, collected and centrifuged at 800 r/min for 10 min seven days after treatment with the reagents mentioned above. The supernatant was discarded. A total volume of 200 mL of the refrigerated lysis medium was added into a tube and placed on ice for 30 min. The cells were centrifuged at 16 000 g for 20 min at 4 °C. Then 100 mL of the supernatant was removed into a new tube. The telomere sequence was amplified in a 50 mL PCR system containing 25 mL of reaction solution, 2 mL of supernatant, 23 mL of triple-distilled water. PCR amplification was performed in the 9600 thermal cycler (PEPKIN ELMER): one cycle of primer extension at 25 °C for 30 min, 2 cycles of the inactivation at 94 °C for 5 min, 3-32 cycles of amplification at 94 °C for 30 s, at 50 °C for 30 s, at 72 for 90 s. The amplification products were stored at 4 °C.

The hybridization and ELISA were carried out as described below.

Denaturation solution and PCR products were incubated at room temperature for 10 min, 225 mL of hybridization solution was added and mixed thoroughly. Then 100 mL of the mixture was put in a 96-wells plate (provided by the kit), and the plate was vibrated (300 r/min) while it was incubated at 37 °C for 2 h. All the mixture was removed and the plate was rinsed 3 times. One hundred mL of anti-DIG peroxidase was added to each well, vibrated (300 r/min) and incubated at room temperature for 30 min. The solution was completely removed and each well was rinsed 5 times, 100 mL of substrate solution was added and incubated at room temperature for 15 min. Then the substrate solution was reserved, 100 mL stop solution was added into each well to terminate the discoloration development. The absorbance of the samples was measured (ΔSA value) at 450 nm and at 690 nm within 30 min after termination of the reaction. If the value of ΔSA of the sample was higher than '0.2 $\Delta SA_{450\text{nm}} - \Delta SA_{690\text{nm}}$ ', then the telomerase in the sample was regarded as positive. The final value was expressed as mean±SD, a statistical treatment was performed by using *t* test.

FCM analysis

Cells in logarithmic phase were incubated with 10 μmol/L PASODN for 72 h and subsequently harvested by trypsinization, beated upon with PRMI 1640 culture containing serum, and centrifuged at 1 000 r/min for 10 min. The supernatant was removed. The cells were fixed with 700 mL/L cold ethanol. FCM analysis of the DNA content was performed on a flow cytometer (FACS Calibur™ B.D USA).

Statistical analysis

The data were expressed as mean±SD. Analysis of data was performed using student's *t* test. *P*<0.01 was considered as statistically significant.

RESULTS

Optimal concentration of PASODN

Although colony formation in LS-174T cells was inhibited by PASODN at the lower concentrations (1, 2.5, 5 μmol/L) in a dose-dependent manner, 10 μmol/L seemed the best concentration and the relative rate of inhibition was 82.8% (slightly lower than that in 20 μmol/L group) (Table 1).

Table 1 Selection of optimal concentration of PASODN

Clones	Concentration of PASODN (μmol/L)					
	0	1	2.5	5	10	20
Mean	64.7	51.5	41.0	24.7	11.1	8.4
Inhibitive rate (%)	0	20.4	36.6	61.8	82.8	87.0

Effect of PASODN on colony formation

The colony-forming efficiency of cells treated with PASODN was 10.3%, which was significantly lower than that in PMSODN group (*P*<0.01, *t* = 3.174) and PBS group (*P*<0.01, *t* = 3.263). No significant difference was observed between PMSODN group and PBS group (Table 2).

Table 2 Colony-forming efficiency in each group (mean±SD)

	PASODN (10 μmol/L)	PMSODN (10 μmol/L)	PBS (same volume)
Mean±SD	41.2±5.5	196.3±13.5	202.8±8.5
Efficiency (%) vs PASODN	10.3	49.1	50.7
		<i>P</i> <0.01	<i>P</i> <0.01

Effect of PASODN on growth and morphology of LS-174T cells

No significant effect was observed during the initial 5 d, but a time-dependent effect was observed during the subsequent days (Table 3 and Figure 1). The growth inhibition was observed obviously from the 7th d, which reached the peak from the 11th to 13th d. But PMSODN had no evident effect on cell growth. Under microscopy, obvious morphological changes were observed in the cells of experiment group as follow. Cells turned round, cell membranes shrank, and nuclei were concentrated at the karyothecae. The number of cells was very small and cells did not compact with each other. On the other hand, cells in other groups grew bloomy and tightly (Figure 2).

Table 3 Variation of telomerase activity (mean±SD)

Group	SA	<i>P</i>
PASODN	0.18±0.12	
PMSODN	1.89±0.24	<0.01
PBS	1.98±0.25	<0.01

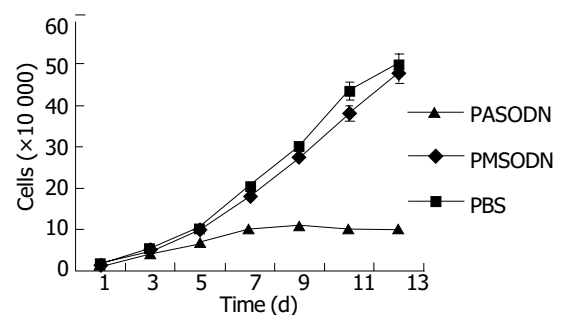


Figure 1 Curve of cell growth with time.

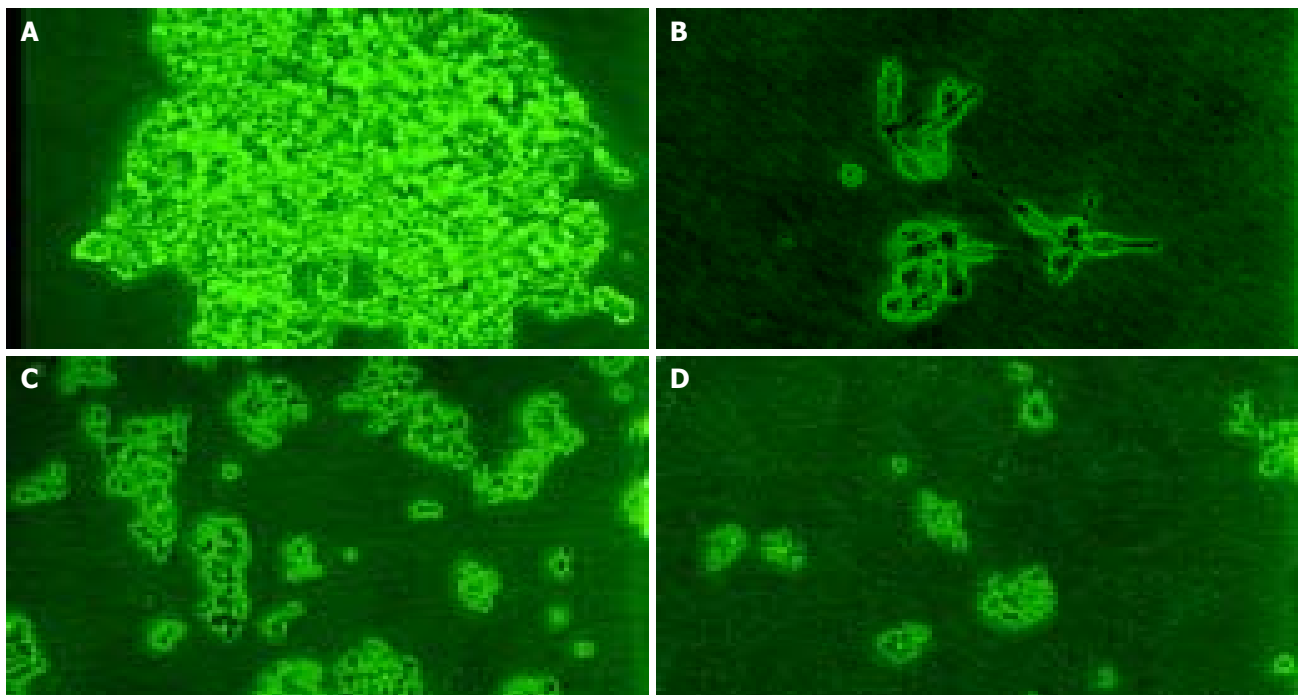


Figure 2 Changes in cell morphology and distribution. A: PMSODN group (10×40); B: PASODN group (10×40); C: PMSODN group (10×10); D: PASODN group (10×10).

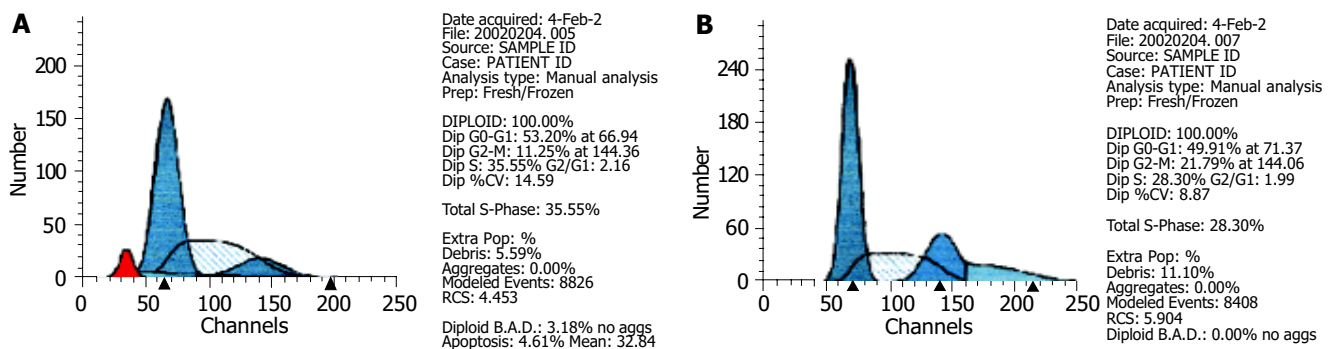


Figure 3 Cell cycle after 72 h of treatment with PASODN(A) and PMSODN(B) detected by FCM.

Variation of telomerase activity

Telomerase activity in PASODN group had no change. The ΔSA value of telomerase activity in PASODN group was significantly different from that in the other two control groups ($P < 0.01$, $t = 3.317$ and 3.241 , $t_{0.01(20)} = 2.845$) (Table 3).

Results of FCM

FCM analysis showed that the proportion of cells in G_0/G_1 and S phases increased appreciably 72 h after 10 $\mu\text{mol/L}$ PASODN treatment, but no difference was observed between experiment and control groups (Table 4). A hypo diploid apex representing the apoptotic cells, was found before the apex of G_0/G_1 in the experiment group (Figure 3A), but not in control group (Figure 3B).

Table 4 Effect of PASODN on LS-174T cell cycle

Groups	G_0/G_1	G_2/M	S
Control	49.91	21.79	28.30
PASODN	53.20	11.25	35.55

DISCUSSION

With the development of living conditions, the incidence of colorectal cancer has been going up year by year. Colorectal

cancer is not sensitive to traditional chemotherapy^[9]. So, it seems important to exploit potent and nontoxic drugs in this field. Telomerase activity has been reported to express in cancer but not in most normal somatic cells, suggesting that telomerase might be an important target for chemotherapy. Telomerase consists of an RNA component (hTR) that binds to telomere and a protein component (hTERT) that acts as a reverse transcriptase. In our opinion, targeting the template region of hTR with anti-sense reagents (such as oligonucleotides) may offer more advantages than targeting hTERT gene. It has been reported that the expression of telomerase activity depends on Watson-Crick base pair between hTR gene and telomere^[10]. This accessibility and indispensability make hTR an ideal and convincible target for oligonucleotides.

PASODN exerted its inhibitory effect on LS-174T cells both at the cellular and molecular levels, whereas no such effects were observed in the control groups. Moreover, the inhibitory effect was time and dose-dependent. The inhibitory effect of PASODN on the cells had a certain latent phase. The growth curve showed that the inhibitory effect of PASODN on the growth of LS-174T cells was obvious on the seventh day, and reached the greatest value from the 11th to 13th d. Besides, the growth curve combined with the result of telomerase activity showed that after telomerase activity turned negative (on the 7th d), the cells could still continue to cleavage a certain number

of times, and the phenomenon might be the “retarded effect” of telomerase inhibitor treatment.

In conclusion, specific oligonucleotide sequences can inhibit telomerase activity and lead to apoptotic cell death. The intrinsic existence of hTR in malignant tumors makes telomerase an ideal target for anti-sense reagent attack. But, we must pay attention to the fact that hTR also exists in normal somatic cells^[11,12]. How to improve the tumor-affinity to oligonucleotids is still a problem. The lag phase^[13] indicated that anti-telomerase inhibitors were unlikely to produce acute anti-proliferative effects. However, with researches going on in the field of telomerase and the advanced experiences of oligonucleotides in other molecular fields^[14-16], the trial in animals and humans will be taken in near future.

REFERENCES

- 1 **Morin GB.** The human telomere terminal transferase enzyme is a ribonucleoprotein that synthesizes TTAGGG repeats. *Cell* 1989; **59**: 521-529
- 2 **Meyerson M,** Counter CM, Eaton EN, Ellisen LW, Steiner P, Caddle SD, Ziaugra L, Beijersbergen RL, Davidoff MJ, Liu Q, Bacchetti S, Haber DA, Weinberg RA. hEST2, the putative human telomerase catalytic subunit gene, is up-regulated in tumor cells and during immortalization. *Cell* 1997; **90**: 785-795
- 3 **Kim NW.** Clinical implications of telomerase in cancer. *Eur J Cancer* 1997; **33**: 781-786
- 4 **Wang XS,** Wang K, Zhang QF, Chen F, Zhang DZ, Fu SB. Clinical significance of determination of telomerase activity in gastric cancer. *Zhongguo Zhongliu Linchuang Zazhi* 2001; **28**: 450-453
- 5 **Shong SH,** Dong XS, Wang XS, Gao DQ, Fu SB, Li Y. Study on telomerase activity in human colorectal carcinoma and metastatic lymph nodes. *Haerbin Yike Daxue Xuebao* 2002; **36**: 29-31
- 6 **Kim NW,** Piatyszek MA, Prowse KR, Harley CB, West MD, Ho PL, Coviello GM, Wright WE, Weinrich SL, Shay JW. Specific association of human telomerase activity with immortal cells and cancer. *Science* 1994; **266**: 2011-2015
- 7 **Zhang FX,** Zhang XY, Fan DM, Deng ZY, Yan Y, Wu HP, Fan JJ. Antisense telomerase RNA induced human gastric cancer cell apoptosis. *World J Gastroenterol* 2000; **6**: 430-432
- 8 **Kyo S,** Inoue M. Complex regulatory mechanisms of telomerase activity in normal and cancer cells: how can we apply them for cancer therapy? *Oncogene* 2002; **21**: 688-697
- 9 **Bearss DJ,** Subler MA, Hundley JE, Troyer DA, Salinas RA, Windle JJ. Genetic determinants of response to chemotherapy in transgenic mouse mammary and salivary tumors. *Oncogene* 2000; **19**: 1114-1122
- 10 **Egholm M,** Buchardt O, Christensen L, Behrens C, Freier SM, Driver DA, Berg RH, Kim SK, Norden B, Nielsen PE. PNA hybridizes to complementary oligonucleotides obeying the Watson-Crick hydrogen-bonding rules. *Nature* 1993; **365**: 566-568
- 11 **Hiyama E,** Hiyama K. Clinical utility of telomerase in cancer. *Oncogene* 2002; **21**: 643-649
- 12 **Nakamura TM,** Morin GB, Chapman KB, Weinrich SL, Andrews WH, Lingner J, Harley CB, Cech TR. Telomerase catalytic subunit homologs from fission yeast and human. *Science* 1997; **277**: 955-959
- 13 **Corey DR.** Telomerase inhibition, oligonucleotides, and clinical trials. *Oncogene* 2002; **21**: 631-637
- 14 **Crooke ST.** Potential roles of antisense technology in cancer chemotherapy. *Oncogene* 2000; **19**: 6651-6659
- 15 **Lebedeva I,** Stein CA. Antisense oligonucleotides: promise and reality. *Annu Rev Pharmacol Toxicol* 2001; **41**: 403-419
- 16 **Grillone LR,** Lanz R. Fomivirsen. *Drugs Today* 2001; **37**: 245-255

Edited by Wang XL and Kumar M Proofread by Xu FM

Honokiol: A potent chemotherapy candidate for human colorectal carcinoma

Fei Chen, Tao Wang, Yi-Feng Wu, Ying Gu, Xiao-Li Xu, Shu Zheng, Xun Hu

Fei Chen, Tao Wang, Ying Gu, Xiao-Li Xu, Shu Zheng, Xun Hu, Cancer Institute, Second Affiliated Hospital of Zhejiang University, Hangzhou 310009, Zhejiang Province, China

Yi-Feng Wu, Life Science College, Zhejiang University, Hangzhou 310027, Zhejiang Province, China

Supported by Cheung Kong Scholars Programme of National Ministry of Education, China, and Li Ka Shing Foundation, Hong Kong

Co-first-authors: Fei Chen and Tao Wang

Correspondence to: Professor Xun Hu, Cancer Institute, Second Affiliated Hospital of Zhejiang University, Hangzhou 310009, Zhejiang province, China. huxun@zju.edu.cn

Telephone: +86-571-87783868 **Fax:** +86-571-87214404

Received: 2004-02-14 **Accepted:** 2004-02-24

Abstract

AIM: To investigate the anticancer activity of Honokiol on RKO, a human colorectal carcinoma cell line *in vitro* and *in vivo*, and to evaluate its possible use in clinic.

METHODS: *In vitro* anticancer activity of honokiol was demonstrated by its induction of apoptosis in tumor cells. We analyzed cell proliferation with MTT assay, cell cycle with flow cytometer, DNA fragment with electrophoresis on agarose gels. To test the mechanism of honokiol-induced apoptosis, Western blotting was used to investigate the factors involved in this process. The pharmacokinetics study of honokiol was tested by high phase liquid chromatography. In *in vivo* study, Balb/c nude mice were incubated with RKO cells. Honokiol was injected intraperitoneally every other day into tumor bearing Balb/c nude mice.

RESULTS: Our results showed that honokiol induced apoptosis of RKO cells in a time- and dose-dependent manner. At 5-10 µg/mL for 48 h, honokiol induced apoptosis through activating Caspase cascades. Pharmacokinetics study demonstrated that, honokiol could be absorbed quickly by intraperitoneal injection, and maintained in plasma for more than 10 h. In nude mice bearing RKO-incubated tumor, honokiol displayed anticancer activity by inhibiting tumor growth and prolonging the lifespan of tumor bearing mice.

CONCLUSION: With its few toxicity to normal cells and potent anticancer activity *in vitro* and *in vivo*, honokiol might be a potential chemotherapy candidate in treating human colorectal carcinoma.

Chen F, Wang T, Wu YF, Gu Y, Xu XL, Zheng S, Hu X. Honokiol: A potent chemotherapy candidate for human colorectal carcinoma. *World J Gastroenterol* 2004; 10(23): 3459-3463 <http://www.wjgnet.com/1007-9327/10/3459.asp>

INTRODUCTION

In traditional Chinese medicine, Houpu (*Magnolia officinalis*) has long been one of the important herbs. It is widely used by Chinese people in treating thrombotic stroke, typhoid fever,

anxiety and nervous disturbance^[1] when used in combination with other herbs. With its major active constituent extracted from the bark of Houpu, honokiol has been found having a variety of pharmacological effects, such as anti-inflammatory^[2], antithrombotic^[3], anti-arrhythmic^[4], antioxidative^[5] and anxiolytic effects^[6]. Recently, honokiol has been reported to exhibit a potent cytotoxicity by inducing cell apoptosis in rat and human leukemia cells^[7,8], human fibrosarcoma cells^[9], human squamous lung cancer CH27 cells^[10] and human SVR angiosarcoma cells^[11], yet there has been no report on honokiol in the treatment of human colorectal carcinoma.

Previous studies have shown that honokiol can induce apoptosis with characteristic morphological changes and DNA fragments, involvement of Caspase family and Bcl-2 family^[10]. It could reduce tumor volume of SVR angiosarcoma in nude mice^[11]. However, it is still unclear whether honokiol can be used as a monomer in clinic. In this study, we chose colorectal carcinoma cells to investigate its possible application in clinical practice.

MATERIALS AND METHODS

Cell line and reagents

Human colorectal cell line RKO was provided by the Cancer Institute of Zhejiang University. Cells were maintained in RPMI-1640 medium (Gibco BRL) supplemented with 100 mL/L heat-inactivated fetal bovine serum (Si-Ji-Qing Biotechnology Co, Hangzhou, China), 100 U/mL penicillin and 100 µg/mL streptomycin at 37 °C in a 50 mL/L CO₂ atmosphere. Antibodies used in this study including Caspases-3, -9 and pan-actin were purchased from NeoMarkers, Fremont, CA, USA. Honokiol was obtained from the National Institute for Pharmaceutical and Biological Products, Beijing, China. The drug was dissolved in dimethyl sulfoxide (DMSO) at the stock concentration of 10 g/L. It was further diluted in culture medium at the final DMSO concentration <1%. 3-(4, 5-dimethylthiazol-2-yl)-2, 5-diphenyltetrazolium bromide (MTT) was purchased from Sigma Chemical Corporation, USA. Six weeks old female Balb/c mice and female BALB/c nude mice (weighing 20±2 g each) were provided by the Experimental Animal Center of Zhejiang University.

Cell proliferation assay

Cells (1×10⁴ in 100 µL) were seeded on 96-well plates in triplicate. Following a 24-h culture at 37 °C, the medium was replaced with fresh medium at various concentrations of honokiol in a final volume of 200 µL. Cells were incubated at 37 °C for 68 h^[12,13]. Then 50 µL of MTT (2 mg/mL in PBS) was added to each well, incubated for an additional 4 h, the plate was centrifuged at 1 000 r/min for 10 min, then the medium was removed. MTT formazan precipitate was dissolved in 100 µL of DMSO, shaken mechanically for 10 min and then read immediately at 570 nm in a plate reader (Opsys MR, Denex Technology, USA).

Morphological changes and detection of DNA fragmentation

RKO cells were exposed to a variety of concentrations of honokiol for 24 h, then examined under reverse microscope

(Olympus) and imaged with a digital camera. To detect DNA fragments, the cells were collected and lysed with lysis buffer containing 50 mmol/L Tris-HCL (pH 7.5), 20 mmol/L EDTA, and 10 g/L NP-40. Then 10 g/L SDS and RNase (5 $\mu\text{g}/\text{mL}$) were added to the supernatants, and incubated at 56 °C for 2 h, followed by incubation with proteinase K (2.5 $\mu\text{g}/\text{mL}$) at 37 °C for 2 h. After the DNA was precipitated by addition of both ammonium acetate (3.3 mol/L) and ethanol (99.5 %), it was dissolved in a loading buffer. DNA fragmentation was detected by electrophoresis on 15 g/L agarose gels and was visualized with ethidium bromide staining.

Cell cycle analysis by FCM

Honokiol-treated RKO cells and vehicles were fixed with 700 mL/L alcohol for 15 min at 4 °C, then stained with 1.0 $\mu\text{g}/\text{mL}$ propidium iodide (PI, Sigma, USA). The red fluorescence of DNA-bound PI in individual cells was measured at 488 nm with a FACSCalibur (Becton Dickinson, USA) and the results were analyzed using ModFit 3.0 software. Ten thousand events were analyzed for each sample.

Western blot assay

RKO cells (5×10^6) were lysed by 4 g/L trypsin containing 0.2 g/L EDTA, then collected after washed twice with phosphate-buffered saline (PBS, pH 7.4). Total protein extracts from the cells were prepared using cell lysis buffer [150 mmol/L NaCl, 0.5 mol/L Tris-HCL (pH 7.2), 0.25 mol/L EDTA (pH 8.0), 10 g/L Triton X-100, 50 mL/L glycerol, 12.5 g/L SDS]. The extract (30 μg) was electrophoresed on 120 g/L SDS-PAGE gel and electroblotted onto polyvinylidene difluoride membrane (PVDF, Millipore Corp., Bedford, MA) for 2 h in a buffer containing 25 mmol/L Tris-HCL (pH 8.3), 192 mmol/L glycine and 200 mL/L methanol. The blots were blocked with 50 g/L nonfat milk in TBST washing buffer for 2 h at room temperature and then incubated at 4 °C overnight with anti-caspase-3 and -9 antibodies (NeoMarkers), all of which were diluted 1:400 in TBST. After washed at room temperature with washing buffer, they were labeled with peroxidase-conjugated secondary antibodies.

Cell toxicity on primary cells

Primary human fibroblast cells were derived from fresh skin^[13]. Human monocytes were isolated from umbilical blood by Ficoll-Hyaque separation method while seeded in 96-well microplates at the concentration of 5 $\mu\text{g}/\text{mL}$ phytohemagglutinin (PHA)^[14]. HUVECs isolated from fresh human umbilical cords were inoculated into 96-well microplates at 5 000 cells/well^[15]. Following treatment with the concentrations of 5, 10, 20, 40 $\mu\text{g}/\text{mL}$ of honokiol for 24 h, cell viability was estimated by trypan blue exclusion. Three wells were measured at each time point/concentration. Six wells were measured for each concentration of test compound. All toxicity experiments were at least repeated three times.

Pharmacokinetics study

For intraperitoneal (ip) pharmacokinetics study, honokiol was mixed with PEG400/dextrose by 7:3 in volume at a concentration of 20 g/L. Thirty Balb/c mice received honokiol by i.p. at a dose of 250 mg/kg. Blood samples were collected as described^[16]. The plasma concentrations were tested by the total fluorescence intensity at 290 nm with high phase liquid chromatograph (HPLC, HEWLETT PACKARD)^[17]. Chromatography was carried out using a Hypersil C18 column (5 mm \times 100 mm \times 2.1 mm) with a flow rate of 0.2 mL/min. Pharmacokinetic parameters were estimated by Modkine programs (Biosoft, UK).

In vivo efficacy evaluation

Effect of honokiol on ascites formation in Balb/c nude mice
Five Balb/c nude mice in each group were transplanted with

1×10^7 RKO cells by ip. Honokiol was dissolved in PEG400/Tween 20 (9:1 by volume). Honokiol-treated group was intragastrically administered 2 mg of honokiol per mice on d 0, 2, 4, 6, 8 and 10 after inoculation of RKO cells. While the control group was given the same volume of PEG400/Tween20. Animals were regularly monitored for the appearance of peritoneal bulge and body weight.

Effect of honokiol on solid tumor growth in Balb/c nude mice

RKO cells (5×10^6) were injected subcutaneously at the axilla of Balb/c nude mice. When tumors became visible about one week after implant, the animals were randomized into four groups: Adriamycin-treated, honokiol-treated, vehicle and control. All mice received ip injection on days 8-11, 14-17, 21-24 and 28-31. Each mouse of honokiol-treated group received 80 mg/(kg/d) of honokiol suspended in PEG400/dextrose (7:3 by volume) intraperitoneally, while vehicle given equivalent solvent of PEG400/dextrose. Adriamycin dissolved in saline was injected ip at a dose of 2 mg/kg. Mice of control group were given the same volume of saline. Tumor growth was monitored with calipers every other day, and tumor volume was calculated using the modified ellipsoid formula: $A/6 \times A \times B^2$, where A is the longer axis and B is the axis perpendicular to A (Figure 1)^[18].

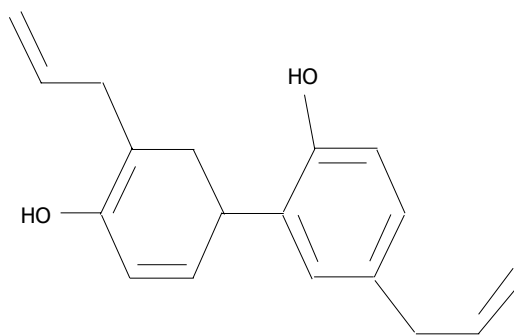


Figure 1 Chemical structure of honokiol ($\text{C}_{18}\text{H}_{18}\text{O}_2$, MW = 266.33).

Statistical analysis

Values were given as mean \pm SD. Statistical comparisons were made by Student's *t*-test, and $P < 0.05$ was taken as significant.

RESULTS

Inhibition of RKO cell proliferation

Cells treated with honokiol resulted in a dose- and time- dependent cytotoxicity in RKO cells. As shown in Figure 2A, honokiol-mediated cytotoxicity occurred at the concentration of 5 $\mu\text{g}/\text{mL}$ and above. A significant decrease in cell number was seen at 10 $\mu\text{g}/\text{mL}$. The concentration leading to a 50% decrease in cell number (IC50) was about 12.47 $\mu\text{g}/\text{mL}$. Moreover, treatment of RKO cells with 5 $\mu\text{g}/\text{mL}$ or 10 $\mu\text{g}/\text{mL}$ of honokiol resulted in a significant growth inhibition at various time points (Figure 2B).

Morphological changes and DNA fragmentation detection in RKO cells

According to MTT results, we chose 5, 10, 15 $\mu\text{g}/\text{mL}$ of honokiol to detect molecular changes. Under an inverted phase contrast microscope, honokiol-treated cells exhibited morphological features of apoptosis (Data not shown): rounded and granulated morphology, some vacuoles coming from cytoplasm, cell shrinkage and eventually detached from culture plates. In honokiol-treated cells, a degradation of chromosomal DNA into small internucleosomal fragments was evidenced by the formation of 180-200 bp DNA ladders on agarose gels (Figure 3), hallmark of cells undergoing apoptosis. No DNA ladders were detected in the samples isolated from control cultures. These results indicated that honokiol induced an apoptotic cell death in RKO cells.

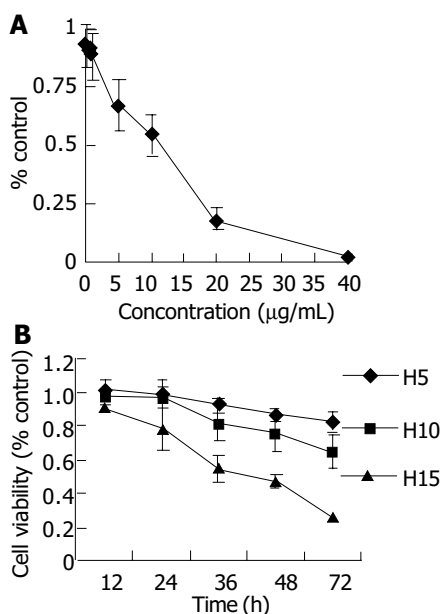


Figure 2 Concentration- and time-dependent inhibition of RKO cells exposed to honokiol shown by MTT assay. (A) RKO cells were plated in quadruplicate in 96-well plates and treated with increasing concentrations of honokiol for 68 h. (B) RKO cells treated with 5, 10 and 15 µg/mL of honokiol were tested at different time points.

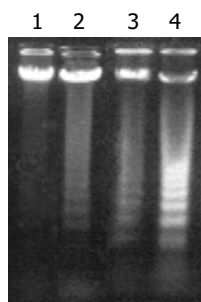


Figure 3 Differences in vehicle or honokiol induced apoptotic DNA laddering of RKO cells. lane 1: control; lane 2: 5 µg/mL; lane 3: 10 µg/mL; lane 4: 15 µg/mL.

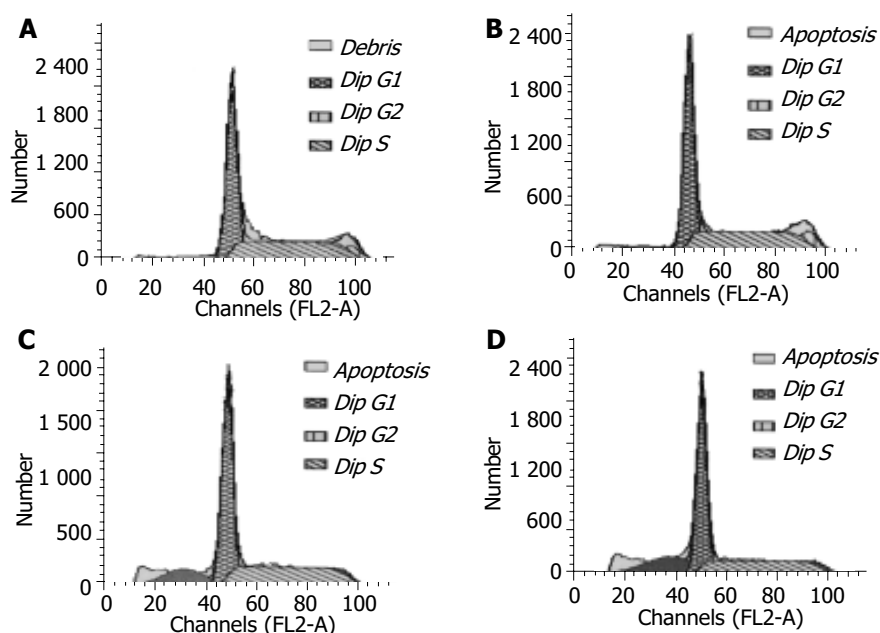


Figure 4 Apoptosis of RKO cells detected by FCM. (A) control; (B) 5 µg/mL; (C) 10 µg/mL; (D) 15 µg/mL.

Effect of honokiol on cell cycle analysis of RKO cells

RKO cells were exposed to increasing concentrations of honokiol (5-15 µg/mL) for 48 h, and the growth of cells was analyzed with flow cytometry. In the absence of honokiol, the cell populations were at G1, S, and G2/M phases (Figure 4), accompanied with increased concentrations of honokiol by a concomitant increase of the G1 phase (Table 1). From Figure 4, the peak areas of subdiploid were enlarged with increased concentrations of honokiol. This observation led to a suggestion of G1 arrest. DNA fragmentation was seen when the cells were exposed to honokiol at 10 µg/mL and above (14.10% and 20.31%, respectively).

Table 1 Effect of honokiol on cell cycle distribution and apoptosis of RKO cells

Groups	Cell cycle distribution (%)			Apoptosis (%)
	G0/G1	S	G2/M	
Control	44.45	45.10	10.14	0.27
5 µg/mL	48.03	42.37	9.60	4.51
10 µg/mL	54.04	40.30	5.66	14.10 ^a
15 µg/mL	58.94	39.36	1.70	20.31 ^b

^a $P < 0.05$, ^b $P < 0.01$ vs corresponding control group. Cell cycle distribution was determined after 48 h of treatment in each group. The tabulated percentages were an average calculated on the results of three separate experiments. The results were represented by mean \pm SD ($n = 3$).

Caspase -3 and -9 expression by Western blot

Since Caspases are the main factors in the apoptotic pathway, we investigated whether Caspases were involved in inducing apoptosis of RKO cells treated with honokiol. Cells induced for 48 h were analyzed for protein expression by Western blot. The results showed that Caspase-3 and -9 were up-regulated in a dose-dependent manner (Figure 5).

Effects of honokiol on primary cultured cells

As shown in Figure 6, honokiol had little cytotoxic effect on primary human fibroblast cells and human lymphocytes even up to 40 µg/mL. HUVEC cells after honokiol treatment resulted in a sharply dose-dependent cytotoxicity. These

results demonstrated that human fibroblast cells and lymphocytes were more resistant to the honokiol-mediated cytotoxicity than HUVECs.

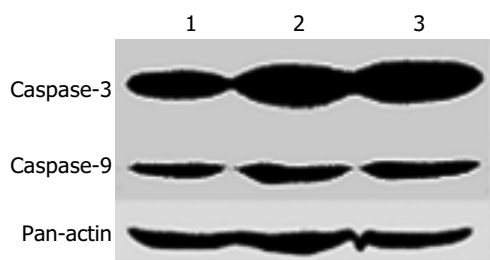


Figure 5 Western blot analysis for the expression of Caspase-3 and -9 in human colorectal carcinoma cell line RKO cells. Lane 1: vehicle; lane 2: 5 µg/mL; lane 3: 10 µg/mL.

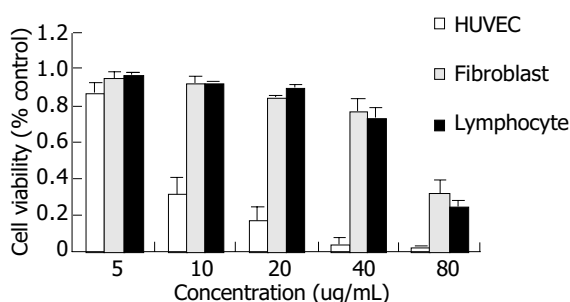


Figure 6 Cytocidal effect of honokiol on the growth of primary cultured human umbilical vein endothelial cells, primary human fibroblast cells and human lymphocytes.

Pharmacokinetics studies

The pharmacokinetics of honokiol was evaluated after intraperitoneal injection of 250 mg/kg to BALB/c mice. The maximum plasma concentration of honokiol was observed at 27.179±6.252 min after administration (Figure 7). The plasma disappearance curve could best be described by a first-order absorption one-compartment model, with an absorption half-life of 10.121±2.761 min, and an elimination half-life of 5.218±0.461 h (Figure 7).

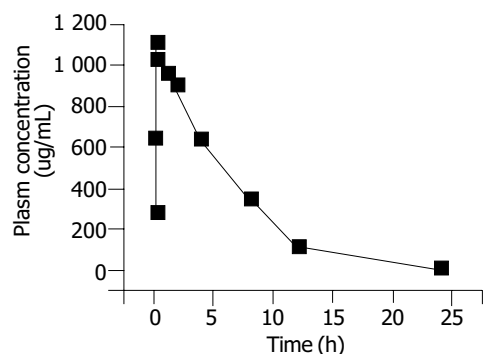


Figure 7 Honokiol concentration in plasma of BALB/c mice.

Inhibition of tumor growth in nude mice implanted with RKO cells

We studied the effect of honokiol on the growth of RKO tumor. There was significant inhibition of tumor growth by honokiol (Table 2). All the control mice developed peritoneal bulge and died by d 12. However, no peritoneal bulge was observed in 80% of the honokiol-treated animals and the mice survived for up to 30 d. These observations indicated the anti-tumor activity of honokiol *in vivo* (Table 2).

Table 2 Effect of honokiol on ascites growth of tumor in Balb/c nude mice

Group	Ascites	MST (d)	Dead (D)	Living (L)	Survival percentage (L/(D+L)×100%)
Control	5	10.7	5	0	0%
Honokiol	1	34.3	1	4	80%

MST: Mean survival time. RKO cells were transplanted intraperitoneally. Honokiol was administered 2 mg per mice on d 0, 2, 4, 6, 8, and 10 after tumor transplantation. The mice were monitored for peritoneal bulge and survived for up to 30 d. Control mice died by d 12 of RKO inoculation.

Inhibition of solid tumor growth in nude mice bearing RKO cells

From Figure 8, animals in control and vehicle groups showed a progressive increase in tumor volume, with a growth rate of 1627.6% and 1408.2% respectively on d 28. While in treated groups, tumor growth rate was increased to 968.9% in adriamycin group and 709.9% in honokiol-treated group. There was a significant difference between honokiol-treated group and its control (treated with PEG400/dextrose) ($P<0.05$). Similar results were found between adriamycin-treated group and its control ($P<0.05$). These data further confirmed that honokiol had an effective anticancer activity *in vivo*.

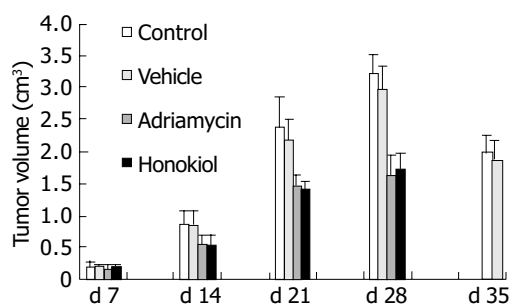


Figure 8 Effect of honokiol on the growth of xenografted RKO in Balb/c nude mice. The Y-axis represents tumor volume, X-axis represents time (day) after RKO cell inoculation.

Prolongation of life-span in nude mice bearing RKO solid tumor

The lifespan of mice in honokiol-treated group (80 mg/kg) was monitored and compared to the vehicle and adriamycin-treated group (Table 3). The mean survival time was 50.9 d in honokiol-treated group, with a significant prolongation compared to vehicle group (29.7 d, $P<0.05$). The survival rate in honokiol-treated group was 176.7%, much higher than that in vehicle group ($P<0.01$). There was no significant difference between control and vehicle groups and between adriamycin-treated and honokiol-treated groups. The results demonstrated that honokiol had a similar effect to adriamycin in prolongation of lifespan of tumor-bearing nude mice.

Table 3 Effect of honokiol on MST and T/C% in Balb/c nude mice bearing RKO-incubated tumor

Group	Number of mice	MST (d)	T/c (%)
Control	7	28.8	100
Vehicle	6	29.7	104.5
Adriamycin	7	46.2 ^a	160.4 ^b
Honokiol	7	50.9 ^a	176.7 ^b

MST, mean survival time. The survival rate (T/C%) was calculated according to the following equation: T/C (%) = [average survival period in the test group/average survival period in the control group]×100. ^a $P<0.05$; ^b $P<0.01$ vs vehicle or control.

DISCUSSION

Many anticancer drugs kill tumor cells by inducing apoptosis. Previous studies suggest that growth inhibition by honokiol resulted from the induction of apoptosis in several cell lines^[7-11]. A further study reported that in human squamous lung cancer cells, honokiol induced apoptosis by down-regulating Bcl-X_L and sequentially activating Caspase cascade^[10]. Our results confirmed this honokiol-mediated apoptotic progression in cultured RKO cells.

A variety of compounds with potent anticancer activity *in vitro* could not be used in clinic, one probable reason was due to their strong toxicities to normal cells^[17,18]. Therefore, we first investigated honokiol's effects on the toxicity of primary cultured human cells. Our data demonstrated that the IC50s were much higher in human fibroblasts and lymphocytes than in RKO cells, with the exception that HUVECs were more sensitive to honokiol. The safe doses for fibroblasts and lymphocytes could be up to 40 µg/mL (Figure 6), much greater than that for RKO and other tumor cells (data not shown). The phenomenon that primary cultured endothelial cells were more sensitive to honokiol might be related to the finding that honokiol had antiangiogenesis activity by inhibiting VEGF and its receptor 2 *in vitro*^[11]. In chemotherapy, antiangiogenesis is another important target besides apoptosis induction in tumor cells. Based on the fewer toxicity to normal fibroblasts and lymphocytes, we thus proposed that honokiol could be a safe and potent candidate of chemotherapy for colorectal cancer *in vivo*.

Another major obstacle was that many potent agents were poorly absorbed and quickly cleared *in vivo*, such as curcumin. Curcumin was difficult to absorb in the gastrointestinal tract and, even when systemically administered, it was rapidly cleared by hepatic metabolism^[11].

We then established two *in vivo* models with Balb/c nude mice bearing RKO cells, the ascitic tumor model and the solid tumor model. In RKO ascitic tumor model, honokiol exhibited a strong efficiency in prolonging the lifespan of ascitic tumor bearing mice and was highly effective on inhibiting intraperitoneal ascites in Balb/c nude mice. In our another model, honokiol also exhibited a potent efficiency in inhibiting solid tumor growth. In RKO incubated tumor bearing mice, honokiol at 80 mg/kg significantly inhibited the tumor growth and prolonged the lifespan compared to the vehicle ($P < 0.05$). The antitumor efficiency of honokiol was similar to that of the commonly used chemotherapy drug, adriamycin.

The results of the present study are encouraging because honokiol has shown significant inhibition of tumor growth *in vitro* and *in vivo*, as well as prolongation of lifespan in tumor-bearing mice *in vivo*. Together with its safety to human, honokiol might be a promising chemotherapy candidate in treating colorectal carcinoma or other cancers in clinic.

REFERENCES

- 1 Squires RF, Ai J, Witt MR, Kahnberg P, Saederup E, Sterner O, Nielsen M. Honokiol and magnolol increase the number of [3H] muscimol binding sites three-fold in rat forebrain membranes *in vitro* using a filtration assay, by allosterically increasing the affinities of low-affinity sites. *Neurochem Res* 1999; **24**: 1593-1602
- 2 Liou KT, Shen YC, Chen CF, Tsao CM, Tsai SK. The anti-inflammatory effect of honokiol on neutrophils: mechanisms in

- the inhibition of reactive oxygen species production. *Eur J Pharmacol* 2003; **475**: 19-27
- 3 Teng CM, Chen CC, Ko FN, Lee LG, Huang TF, Chen YP, Hsu HY. Two antiplatelet agents from *Magnolia officinalis*. *Thromb Res* 1988; **50**: 757-765
- 4 Liou KT, Lin SM, Huang SS, Chih CL, Tsai SK. Honokiol ameliorates cerebral infarction from ischemia-reperfusion injury in rats. *Planta Med* 2003; **69**: 130-134
- 5 Lo YC, Teng CM, Chen CF, Chen CC, Hong CY. Magnolol and honokiol isolated from *Magnolia officinalis* protect rat heart mitochondria against lipid peroxidation. *Biochem Pharmacol* 1994; **47**: 549-553
- 6 Kuribara H, Kishi E, Hattori N, Yuzurihara M, Maruyama Y. Application of the elevated plus-maze test in mice for evaluation of the content of honokiol in water extracts of magnolia. *Phytother Res* 1999; **13**: 593-596
- 7 Hirano T, Gotoh M, Oka K. Natural flavonoids and lignans are potent cytostatic agents against human leukemic HL-60 cells. *Life Sci* 1994; **55**: 1061-1069
- 8 Hibasami H, Achiwa Y, Katsuzaki H, Imai K, Yoshioka K, Nakanishi K, Ishii Y, Hasegawa M, Komiya T. Honokiol induces apoptosis in human lymphoid leukemia Molt 4B cells. *Int J Mol Med* 1998; **2**: 671-673
- 9 Nagase H, Ikeda K, Sakai Y. Inhibitory effect of magnolol and honokiol from *Magnolia obovata* on human fibrosarcoma HT-1080. Invasiveness *in vitro*. *Planta Med* 2001; **67**: 705-708
- 10 Yang SE, Hsieh MT, Tsai TH, Hsu SL. Down-modulation of Bcl-XL, release of cytochrome c and sequential activation of caspases during honokiol-induced apoptosis in human squamous lung cancer CH27 cells. *Biochem Pharmacol* 2002; **63**: 1641-1651
- 11 Bai X, Cerimele F, Ushio-Fukai M, Waqas M, Campbell PM, Govindarajan B, Der CJ, Battle T, Frank DA, Ye K, Murad E, Dubiel W, Soff G, Arbiser JL. Honokiol, a small molecular weight natural product, inhibits angiogenesis *in vitro* and tumor growth *in vivo*. *J Biol Chem* 2003; **278**: 35501-35507
- 12 Arbiser JL, Panigrathy D, Klauber N, Rupnick M, Flynn E, Udagawa T, D'Amato RJ. The antiangiogenic agents TNP-470 and 2-methoxyestradiol inhibit the growth of angiosarcoma in mice. *J Am Acad Dermatol* 1999; **40**(6pt 1): 925-929
- 13 LaMontagne KR Jr, Moses MA, Wiederschain D, Mahajan S, Holden J, Ghazizadeh H, Frank DA, Arbiser JL. Inhibition of MAP kinase kinase causes morphological reversion and dissociation between soft agar growth and *in vivo* tumorigenesis in angiosarcoma cells. *Am J Pathol* 2000; **157**: 1937-1945
- 14 Beddy D, Watson RW, Fitzpatrick JM, O'Connell PR. Increased vascular endothelial growth factor production in fibroblasts isolated from strictures in patients with Crohn's disease. *Br J Surg* 2004; **91**: 72-77
- 15 Goldrosen MH, Gannon PJ, Lutz M, Hloyoke ED. Isolation of human peripheral blood lymphocytes: modification of a double discontinuous density gradient of Ficoll-Hypaque. *J Immunol Methods* 1977; **14**: 15-17
- 16 Agrawal S, Jiang Z, Zhao Q, Shaw D, Cai Q, Roskey A, Channavajjala L, Saxinger C, Zhang R. Mixed-backbone oligonucleotides as second generation antisense oligonucleotides: *in vitro* and *in vivo* studies. *Proc Natl Acad Sci U S A* 1997; **94**: 2620-2625
- 17 Tsai TH, Chou CJ, Cheng FC, Chen CF. Pharmacokinetics of honokiol after intravenous administration in rats assessed using high-performance liquid chromatography. *J Chromatogr B Biomed Appl* 1994; **655**: 41-45
- 18 Eikesdal HP, Bjerkvig R, Dahl O. Vinblastine and hyperthermia target the neovasculature in BT (4) AN rat gliomas: therapeutic implications of the vascular phenotype. *Int J Radiat Oncol Biol Phys* 2001; **51**: 535-544

• *H pylori* •

Diagnosis of *Helicobacter pylori* infection and diseases associated with *Helicobacter pylori* by *Helicobacter pylori* outer membrane proteins

Zheng Jiang, Ai-Long Huang, Xiao-Hong Tao, Pi-Long Wang

Zheng Jiang, Xiao-Hong Tao, Pi-Long Wang, Department of Gastroenterology, the First Affiliated Hospital, Chongqing University of Medical Sciences, Chongqing 400016, China

Ai-Long Huang, Institute of Viral Hepatitis, Chongqing University of Medical Sciences, Chongqing 400010, China

Supported by the Basic Research Fund of Science and Technology Committee of Chongqing, [2002] 18-86; National Natural Science Foundation of China, No.30371318

Correspondence to: Dr. Zheng Jiang, Department of Gastroenterology, the First Affiliated Hospital, Chongqing University of Medical Sciences, Chongqing 400016, China. jianggooddoctor@mail.china.com

Telephone: +86-23-68891218

Received: 2003-10-15 **Accepted:** 2003-12-06

Abstract

AIM: To examine the serological response of patients with upper gastrointestinal diseases and *Helicobacter pylori* (*H pylori*) infection to two *H pylori* outer membrane proteins (OMPs) (M_r 18 000 and M_r 26 000) acquired by gene recombinant technique, and to determine the diagnostic significance of serological tests derived from these OMPs.

METHODS: Recombinant vectors encoding the two *H pylori* OMPs were used to transform and express in BL21 (DE3) *E. coli*. After purification with Ni^{2+} -NTA agarose resin, colloid gold kits were prepared with purified recombinant proteins to detect *H pylori* infection and *H pylori*-associated diseases by the immunity-marker technology. We selected 150 patients with *H pylori* infection and digestive symptoms without previous treatment, including chronic gastritis ($n = 60$), duodenal ulcer ($n = 30$), gastric ulcer ($n = 30$), and gastric cancer ($n = 30$). As controls, 33 *H pylori*-negative healthy volunteers were also recruited. Serum samples were collected from all subjects, and the antibodies to specific proteins of *H pylori* were tested with the colloid gold test kits. The sensitivity, specificity and accuracy of the colloid gold tests were evaluated, by using the combination of standard diagnostic methods (^{13}C urea breath test and bacteria culture) and classic enzyme-linked immunosorbent assay (ELISA) as reference.

RESULTS: After purification with Ni^{2+} -NTA agarose resin, the purity of recombinant fusion proteins was about 95%. The recombinant fusion proteins were recognized by the specific monoclonal antibodies against the two *H pylori* OMPs, as demonstrated by the ELISA. Of the 150 serum samples from patients infected with *H pylori* 141 (94.0%) responded positively to the recombinant protein with M_r 26 000, while the seropositive rates were 95.0%, 96.7%, 96.7% and 90.0% for patients with *H pylori*-associated chronic gastritis, duodenal ulcer, gastric ulcer, and gastric cancer respectively. The sensitivity, specificity, and accuracy of the colloid gold kit with M_r 26 000 protein were 94.0%, 97.0%, and 94.5%, respectively. Compared with the classic ELISA, bacteria culture and ^{13}C urea breath test results in detecting *H pylori*

infection, there was no significant difference ($P > 0.05$). For the colloid gold kit with M_r 18 000, the seropositive rates were 52.0%, 40.0%, 40.0%, 53.3% and 86.7%, respectively, in *H pylori*-infected patients, and those with *H pylori*-associated chronic gastritis, duodenal ulcer, gastric ulcer, and gastric cancer. There was a significant difference ($P < 0.05$) in seropositivity between patient with gastric cancer (86.7%) and those with other diseases (43.3%).

CONCLUSION: The two colloid gold kits derived from the recombinant OMPs are useful tools either for detecting *H pylori* infection, or for, predicting *H pylori*-associated gastric malignancy.

Jiang Z, Huang AL, Tao XH, Wang PL. Diagnosis of *Helicobacter pylori* infection and diseases associated with *Helicobacter pylori* by *Helicobacter pylori* outer membrane proteins. *World J Gastroenterol* 2004; 10(23): 3464-3469

<http://www.wjgnet.com/1007-9327/10/3464.asp>

INTRODUCTION

Since the initial report of an unidentified curved bacillus located on the gastric epithelium of patients with chronic active gastritis, the discovery of *Helicobacter pylori* (*H pylori*) and its association with a number of gastrointestinal diseases has revolutionized gastroenterology. It has attracted the interest of scholars in gastroenterology and microbiology. Infection of gastric mucosa with *H pylori* could be found in approximately 50% of the world population^[1], its association with peptic ulcer disease, chronic gastritis, mucosa-associated lymphoid tissue lymphoma, and gastric adenocarcinoma has been well documented over the past two decades^[2-19]. Moreover it was also found in some extradigestive diseases^[20-36]. The direct evidence of carcinogenesis was recently demonstrated in an animal model^[37,38], so this organism has been recently categorized as a class I carcinogenetic factor by the World Health Organization. It is obviously important to detect and eradicate *H pylori* infection.

The routine detecting methods including invasive and non-invasive tests have differences in sensitivity and specificity, each with their indication and characteristics in clinical practice^[39-48]. Because of great quantity of serum samples especially in epidemiological studies, enzyme linked immunosorbent assay (ELISA) is the widely used test^[49-52]. Antigens used in ELISA are divided into three kinds. The first is the total cell of microbacteria sonicated by ultrasonic wave, which is easy to be confused with *Helicobacter*, campylobacter, or a diverse range of other bacteria and incur to intercourse response with each other in detecting *H pylori* infection. The second is the partly purified antigens, with greatly increased specificity and decreased intercourse response, but *H pylori* could not be cultured in great quantity without special apparatus and conditions. The last is the recombinant purified antigen by gene recombinant technique. To date, many genes of OMP of *H pylori* have been amplified by scholars with polymerase chain

reaction from *H pylori* chromosomes and inserted into the compatible sites of expression vectors by using T₄ DNA ligase. Moreover recombinant vectors could be expressed in *E. coli*^[53-62], but a few reports are available on lower-molecular-mass OMP application to the detection of *H pylori* infection and diagnose *H pylori*-associated diseases. In order to acquire a great amount of purified 18 000, 26 000 OMP of *H pylori*, we constructed recombinant vectors containing genes encoding with M_r18 000, 26 000 OMP of *H pylori* expressed in *E. coli* respectively and identified the antigenicity of expressed products^[63]. So we prepared the colloid gold kits with purified recombinant proteins by antigen-antibody reaction and gold-marked technique to determine whether they were capable of detecting *H pylori* infection and *H pylori*-associated diseases.

MATERIALS AND METHODS

Material

Well-characterized strains of BL21/pET32a (+)/Omp₂₆, BL21/pET32a (+)/Omp₁₈ were constructed, expressed and identified by the Department of Microbiology. The expression fusion proteins were recognized by the corresponding monoclonal antibody with M_r18 000, 26 000 OMP of *H pylori* and the animal's serum immunized with recombinant fusion proteins respectively. After purification using Ni²⁺-NTA agarose resin columniation, the purity of recombinant fusion proteins was about 95%. ¹³C urea breath test was purchased from Headway Company, Ni²⁺-NTA agarose resin columniation was obtained from QIAGEN Company, ultrasonic liquid (50 mmol/L NaH₂PO₄, 300 mmol/L NaCl, PH 7.0), abluent (50 mmol/L phosphate, 300 mmol/L NaCl, 20 mmol/L imidazole, pH 7.80) and lavation (50 mmol/L phosphate, 300 mmol/L NaCl, 250 mmol/L imidazole, pH 7.80) were provided by the Institute of Viral Hepatitis of Chongqing University of Medical Sciences.

Sample collection

Sera were collected from 150 patients with gastrointestinal symptoms and *H pylori* infection in the Outpatient Clinic of the Gastroenterology Department of the University Hospital during Jan. 2002 to Dec. 2002 including 60 cases of gastritis, 30 cases of gastric ulcer, 30 cases of duodenal ulcer and 30 cases of gastric cancer diagnosed by gastroscopy. Sera from 31 healthy volunteers without *H pylori* infection were collected as control. All testee were forbidden to take H₂-antagonists, corticosteroids, proton pump inhibitors and antibiotics within 4 wk.

Expression of recombinant plasmid

Single bacterial colonies (BL21/pET32a (+)/Omp₁₈, BL21/pET32a (+)/Omp₂₆) were picked and cultured respectively in 2 mL LB broth containing 100 mg/L of ampicillin, at 300 r/min at 37 °C overnight. On the next day, BL21 *E. coli* strains containing recombinant plasmids were grown until mid-log phase (Absorbance at 600 nm = 0.5 to 1.0), and then induced to express recombinant fusion proteins in 100 mL LB by adding 1 mmol/L IPTG for 4 h. Following induction, bacteria were harvested by centrifugation at 12 000 r/min for 15 min, and stored at -20 °C for SDS-PAGE analysis.

Immunoblot analysis of recombinant fusion protein

Due to C end of recombinant fusion antigens with six histidines, recombinant fusion antigens were purified with Ni²⁺-NTA agarose resin. Briefly, 500 mL of cultivated bacteria suspension was prepared, centrifuged, resuspended with the buffer liquid (50 mmol/L phosphate, 300 mmol/L NaCl, pH 7.0), and sonicated by ultrasonic wave with the energy of 600 W×35% for 40 min, and ultracentrifuged for 15 min at 10 000 g at 4 °C. The sonicated recombinant fusion antigens were purified using Ni²⁺-NTA agarose

resin with abluent (50 mmol/L phosphate, 300 mmol/L NaCl, 20 mmol/L imidazole, pH 7.80) and lavation (50 mmol/L phosphate, 300 mmol/L NaCl, 250 mmol/L imidazole, pH 7.80), and quantified. The antigenicities of expressed recombinant fusion proteins were determined by immunoblotting. Following electrophoretic transfer of SDS-PAGE-separated (150 g/L acrylamide) recombinant fusion proteins to 0.45 µm pore size PVDF membrane, and after a 30-min wash in tris-saline blotting buffer, antigen-impregnated PVDF strips were incubated with the sera from patients infected with *H pylori* and anti-Omp₁₈ or anti-Omp₂₆ antibody for 2 h at RT. After washed, the proteins were detected by incubating the strips in alkaline phosphatase-conjugated goat anti-man IgG and alkaline phosphatase-conjugated goat anti-mice IgG antibody for 1 h at RT.

Colloid gold test of *H pylori* OMP

With gold marker and special antigen-antibody reaction technique, *H pylori* infection could be detected using the antigen-antibody-antigen method. The recombinant fusion proteins were impregnated in nitrocellulose membrane (NC) as a detecting strip, the recombinant fusion proteins were marked with gold as a colored reagent by which the special antibody of patient serum to *H pylori* could be detected in seconds. The criteria of the test were as follows: Negative (-): antigen-impregnated NC membrane was not recognized by patient serum, non-special antibody to *H pylori* in patient serum, so there was only an aubergine strip in mass-control district, and not in detecting district simultaneously. Positive (+): antigen-impregnated NC membrane was recognized by patient serum, special antibody to *H pylori* in patient serum. In mass-control and detecting district, there were aubergine strips. If there was no aubergine strip in mass-control district, errors might occur in experiment course. The colloid gold test paper is shown in Figure 1.

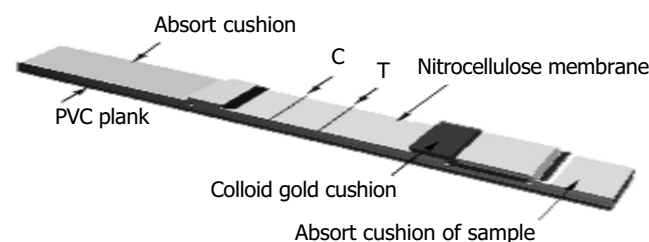


Figure 1 Colloid gold test paper.

Diagnostic criteria of the test

The sensitivity, specificity and accuracy of the colloid gold kits were evaluated on the basis of the serum ELISA results taken as reference with combined of standard diagnostic methods (¹³C urea breath test, bacteria culture as the gold standard). Patients were defined as *H pylori* infection if one out of two validated tests of ¹³C urea breath test and culture was positive, and as non-*H pylori* infection if two tests were negative. Patients infected with *H pylori* were determined as false negative if the colloid gold kits were negative; patients without *H pylori* infection were determined as false positive if the colloid gold kits were positive. Based on the above results, the applied value of the colloid gold kit in clinical practice was evaluated.

RESULTS

Analysis of recombinant fusion protein

After pET32a (+)/Omp₁₈ and pET32a (+)/Omp₂₆ were transfected into BL21 *E. coli* strains, the strains with high expressions of fusion proteins were selected and grown respectively until mid-log phase (Absorbance at 600 nm = 0.4 to 0.6), and then

induced to express recombinant fusion proteins by adding of 1 mmol/L IPTG for 4 h. Following induction, bacteria were harvested by centrifugation at 12 000 g for 5 min, resuspended in protein-buffer and seethed for 5 min. Their molecular mass was M_r 38 000 and 46 000 respectively by 150 g/L SDS-PAGE gel analysis. After the recombinant bacteria were sonicated by ultrasonic wave and ultracentrifuged (10 000 g, 15 min, 4 °C), the levels of soluble fusion proteins in the supernatant were about 18.96% and 26.38% of total cellular protein respectively. After purification by Ni^{2+} -NTA agarose resin columniation, the purity was about 95%. Recombinant fusion proteins were all recognized by the corresponding monoclonal antibody with M_r 18 000, 26 000 OMP of *H pylori* and the animal's serum immunized with recombinant fusion proteins respectively. The results showed recombinant fusion proteins could provide excellent antigenicity.

Detection of *H pylori* infection by colloid gold kit

Sera from 150 patients with gastrointestinal symptoms and *H pylori* infection including 60 cases of gastritis, 30 cases of gastric ulcer, 30 cases of duodenal ulcer and 30 cases of gastric cancer examined by gastroscopies, and sera from 33 healthy volunteers without *H pylori* infection were assayed using the colloid gold kits with M_r 18 000, 26 000 respectively (Table 1, Figure 2). The results were as follows. Ninety-four percent of patients infected with *H pylori* showed response to recombinant protein with M_r 26 000, while 95%, 96.7%, 96.7% and 90.0% of patients with *H pylori*-infected chronic gastritis, gastric ulcer, duodenal ulcer, and gastric cancer showed responses (Table 2). There was no significant difference between the conventional examined methods and the colloid gold kits ($P>0.05$), indicating that the prevalence of infection diagnosed by both methods was similar. To specific recombinant protein with M_r 18 000, 52.0% of patients showed response, while 40.0%, 40.0%, 53.3% and 86.7% of patients with *H pylori*-infected chronic gastritis, gastric ulcer, duodenal ulcer, and gastric cancer respectively showed responses (Table 3). Moreover there was a significant difference ($P<0.05$) in the detecting rates of *H pylori* infection between patients with gastric cancer (86.7 %) and those with other diseases (43.3%). Based on the classic ELISA, bacteria culture and ^{13}C urea breath test results, the sensitivity, specificity, and accuracy of the colloid gold kit with M_r 26 000 protein were 94.0%, 97.0%, and 94.5%, respectively.

Table 1 Detecting results of *H pylori* infection using colloid gold kit with M_r 18 000, 26 000 OMP

Methods	Testee	Positive	Negative	False positive	False negative
Routine methods	183	144	32	1	6
M_r 26 000 protein	183	141	32	1	9
M_r 18 000 protein	183	78	33	0	72

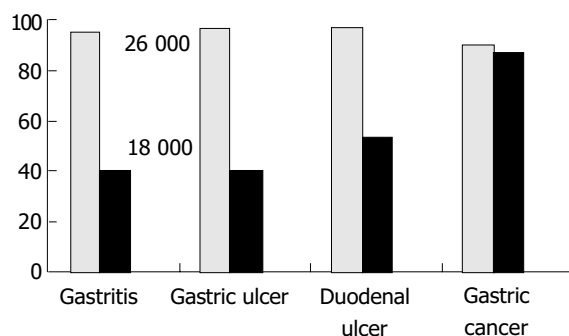


Figure 2 Detecting results of diseases infected with *H pylori* using colloid gold test kits with M_r 26 000, 18 000 OMP.

Table 2 Detecting results of diseases infected with *H pylori* using colloid gold kit with M_r 26 000 OMP

Disease	Patients	yr	Positive	Negative
Gastritis	60	50.3±15.9	57	3
Gastric ulcer	30	57.3±13.2	29	1
Duodenal ulcer	30	46.5±14.2	29	1
Gastric cancer	30	64.7±17.4	27	3

Table 3 Detecting results of diseases infected with *H pylori* using colloid gold kit with M_r 18 000 OMP

Disease	Patients	yr	Positive	Negative
Gastritis	60	50.3±15.9	24	36
Gastric ulcer	30	57.3±13.2	12	18
Duodenal ulcer	30	46.5±14.2	16	14
Gastric cancer	30	64.7±17.4	26	4

DISCUSSION

M_r 18 000, 26 000 OMP of *H pylori* are commonly expressed in all *H pylori* strains examined so far. Furthermore, no cross-reaction has been shown when antibodies (polyclonal and monoclonal) to low-molecular outer membrane proteins were used to screen closely related species of *Helicobacteria*, campylobacteria, or a diverse range of other bacteria^[64]. In our study, *H pylori* 18 000, 26 000 OMP were successfully expressed in *E.coli* with good antigenicity. With marked gold and special antigen-antibody reaction technique, *H pylori* infection could be detected by the antigen-antibody-antigen method. Recombinant fusion proteins were impregnated in NC membrane as a detecting strip, and marked with gold as a colored reagent by which the special antibody to *H pylori* could be determined in seconds. At first the recombinant proteins were prepared in large quantities, purified and regulated. Due to the diameter size of grained gold would affect directly the result of test, the diameter of grained gold was adjusted to 40-60 nm, at the same time the concentration of antibody was adjusted in order to acquire steady and reliable products marked with gold. A test detecting IgG antibodies to *H pylori* was thus constructed.

Sera were collected from 150 patients with gastrointestinal symptoms and *H pylori* infection and from 33 healthy volunteers without *H pylori* infection used as controls during one year. The detecting results using colloid gold kit were as follows. Ninety-four percent of patients infected with *H pylori* showed response to recombinant protein with M_r 26 000, 95.0%, 96.7%, 96.7% and 90.0% of patients with *H pylori*-infected chronic gastritis, gastric ulcer, duodenal ulcer, and gastric cancer, showed responses to specific proteins with M_r 26 000 respectively. There was no significant difference between the routine examined methods and colloid gold kits ($P>0.05$). 52.0% of patients infected with *H pylori* showed response to recombinant protein with M_r 18 000, while 40.0%, 40.0%, 53.3% and 86.7% of patients with *H pylori*-infected chronic gastritis, gastric ulcer, duodenal ulcer, and gastric cancer respectively, showed responses to specific proteins with M_r 18 000, moreover there was a significant difference ($P<0.05$) in the detecting rates of *H pylori* infection between gastric cancer (86.7 %) and other diseases (43.3%). The results showed that colloid gold kits with M_r 26 000 proteins of *H pylori* could be used as a conventional examination method. Based on the classic ELISA, bacteria culture and ^{13}C urea breath test results, the sensitivity, specificity, and accuracy of the rapid test kit with M_r 26 000 protein were 94.0%, 97.0%, and 94.5%, respectively, and a significant association was found between the serologic response to M_r 18 000 OMP antigen and malignant outcome of *H pylori* infection. The two colloid gold kits with

M_r 26 000, 18 000 proteins of *H pylori*, could be used to detect *H pylori* infection and *H pylori*-associated diseases, and to predict the risk of peptic ulcer or malignancy. The results mentioned above were consistent with those reported^[65-67].

All strains of *H pylori* could express low-molecular-mass OMP, which stimulates the body to produce corresponding antibodies, moreover the antibodies produced are related to the corresponding molecular size of antigens and immuno-status of the body. Decrease of the antibodies was associated with the corresponding molecular size of the antibodies. So the results showed that the responses of patients infected with *H pylori* to recombinant proteins with M_r 26 000 were stronger (94.0%) than that (52.0%) to recombinant proteins with M_r 18 000, while the growth of gastric cancer was associated with much more factors and stages. All pathogenic factors may act on the pre-carcinoma stage alone or together with each other in the model of chronic gastritis-atrophic gastritis-intestinal metaplasia-atypical hyperplasia-gastric cancer. Chua *et al.*^[68] compared the seroprevalence of antibodies with various *H pylori* antigens in Singaporeans with gastric adenocarcinoma and the normal Singaporean population using both conventional immunoglobulin (Ig) G ELISA and Western blot immunoassay, and found that strains of *H pylori* including antigens with M_r 19 500 and seronegative antigens with M_r 35 000 could provide their potential for carcinogenesis. Immunoreactive species-specific M_r 19 500 OMP of *H pylori* is actually Lpp20, while its actual molecular mass is 18 000 OMP. So *H pylori* strains based on carcinogenic potential could provide a basis for selective surveillance and eradication therapy. Low-molecular-mass OMP could lead to the 12th gene mutation of C-Ha-ras, and amplify p²¹ protein expressed by ras gene and c-met protein could also be overexpressed. Therefore the detecting rate of low-molecular-weight OMP of *H pylori* in gastric cancer is higher than other OMP. In our study, the detecting rate of M_r 26 000 OMP of *H pylori* in gastric cancer was similar to that of M_r 18 000 OMP. The results showed low-molecular-weight OMP could be used, not only in vaccine target candidates, but also in detection of gastric cancer in highly risk patients with *H pylori* infection. In a nutshell, the colloid gold kit constructed with M_r 18 000, 26 000 OMP of *H pylori* could detect anti-*H pylori* IgG-antibody. Compared with other methods, this method not only provides a rapid, simple and painless test, but also gives a reliable specificity, especially in diagnosis of gastrointestinal tumors. The colloid gold kit based on marked gold and special antigen-antibody reaction technique is a rapid diagnostic kit, only a few minutes are required to complete an assay, and no special instruments are needed. Compared with other immunoassay techniques, the colloid gold kit has following advantages. It is based on the antigen-antibody reaction on membranes, its detecting time is much shorter than ELISA, at the same time colloid gold is red in color, so there is no need to add other colored reagents, moreover, the products marked with gold are more stable than those marked with enzyme. The colloid gold kit evaluated in our study enables a simple, rapid, noninvasive, and accurate diagnosis of *H pylori* infection, and is an ideal test method for screening patients with gastrointestinal tumors.

REFERENCES

- 1 Michetti P, Kreiss C, Kotloff KL, Porta N, Blanco JL, Bachmann D, Herranz M, Saldinger PF, Corthesy-Theulaz I, Losonsky G, Nichols R, Simon J, Stolte M, Ackerman S, Monath TP, Blum AL. Oral immunization with urease and escherichia coli heat-labile enterotoxin is safe and immunogenic in *Helicobacter pylori*-infected adults. *Gastroenterology* 1999; **116**: 804-812
- 2 Hiyama T, Haruma K, Kitadai Y, Masuda H, Miyamoto M, Ito M, Kamada T, Tanaka S, Uemura N, Yoshihara M, Sumii K, Shimamoto F, Chayama K. Clinicopathological features of gastric mucosa-associated lymphoid tissue lymphoma: a comparison with diffuse large B-cell lymphoma without a mucosa-associated lymphoid tissue lymphoma component. *J Gastroenterol Hepatol* 2001; **16**: 734-739
- 3 Nakamura S, Matsumoto T, Suekane H, Takeshita M, Hizawa K, Kawasaki M, Yao T, Tsuneyoshi M, Iida M, Fujishima M. Predictive value of endoscopic ultrasonography for regression of gastric low grade and high grade MALT lymphomas after eradication of *Helicobacter pylori*. *Gut* 2001; **48**: 454-460
- 4 Uemura N, Okamoto S, Yamamoto S, Matsumura N, Yamaguchi S, Yamakido M, Taniyama K, Sasaki N, Schlemper RJ. *Helicobacter pylori* infection and the development of gastric cancer. *N Engl J Med* 2001; **345**: 784-789
- 5 Kate V, Ananthkrishnan N, Badrinath S. Effect of *Helicobacter pylori* eradication on the ulcer recurrence rate after simple closure of perforated duodenal ulcer: retrospective and prospective randomized controlled studies. *Br J Surg* 2001; **88**: 1054-1058
- 6 Xue FB, Xu YY, Wan Y, Pan BR, Ren J, Fan DM. Association of *H pylori* infection with gastric carcinoma: a Meta analysis. *World J Gastroenterol* 2001; **7**: 801-804
- 7 Peng ZS, Liang ZC, Liu MC, Ouang NT. Studies on gastric epithelial cell proliferation and apoptosis in *Hp* associated gastric ulcer. *Shijie Huaren Xiaohua Zazhi* 1999; **7**: 218-219
- 8 Xiao SD, Liu WZ. Current status in treatment of *Hp* infection. *Shijie Huaren Xiaohua Zazhi* 1999; **7**: 3-4
- 9 Meyer JM, Silliman NP, Dixon CA, Siepman NY, Sugg JE, Hopkins RJ. *Helicobacter pylori* and early duodenal ulcer status post-treatment: a review. *Helicobacter* 2001; **6**: 84-92
- 10 Casella G, Buda CA, Maisano R, Schiavo M, Peregò D, Baldini V. Complete regression of primary gastric MALT-lymphoma after double eradication *Helicobacter pylori* therapy: role and importance of endoscopic ultrasonography. *Anticancer Res* 2001; **21**: 1499-1502
- 11 Hurenkamp GJ, Grundmeijer HG, Van Der Ende A, Tytgat GN, Assendelft WJ, Van Der Hulst RW. Arrest of chronic acid suppressing drug use after successful *Helicobacter pylori* eradication in patients with peptic ulcer disease: a six-month follow-up study. *Aliment Pharmacol Ther* 2001; **15**: 1047-1054
- 12 Guo CQ, Wang YP, Liu GY, Ma SW, Ding GY, Li LC. Study on *Helicobacter pylori* infection and p53, *c-erbB-2* gene expression in carcinogenesis of gastric mucosa. *Shijie Huaren Xiaohua Zazhi* 1999; **7**: 313-315
- 13 Hiyama T, Haruma K, Kitadai Y, Masuda H, Miyamoto M, Ito M, Kamada T, Tanaka S, Uemura N, Yoshihara M, Sumii K, Shimamoto F, Chayama K. Clinicopathological features of gastric mucosa-associated lymphoid tissue lymphoma: a comparison with diffuse large B-cell lymphoma without a mucosa-associated lymphoid tissue lymphoma component. *J Gastroenterol Hepatol* 2001; **16**: 734-739
- 14 Hu PJ. *Hp* and gastric cancer: challenge in the research. *Shijie Huaren Xiaohua Zazhi* 1999; **7**: 1-2
- 15 Quan J, Fan XG. Progress in experimental research of *Helicobacter pylori* infection and gastric cancer. *Shijie Huaren Xiaohua Zazhi* 1999; **7**: 1068-1069
- 16 Delchier JC, Lamarque D, Levy M, Tkoub EM, Copie-Bergman C, Deforges L, Chaumette MT, Haioun C. *Helicobacter pylori* and gastric lymphoma: high seroprevalence of CagA in diffuse large B-cell lymphoma but not in low-grade lymphoma of mucosa-associated lymphoid tissue type. *Am J Gastroenterol* 2001; **96**: 2324-2328
- 17 Morgner A, Miehle S, Fischbach W, Schmitt W, Muller-Hermelink H, Greiner A, Thiede C, Schetelig J, Neubauer A, Stolte M, Ehninger G, Bayerdorffer E. Complete remission of primary high-grade B-cell gastric lymphoma after cure of *Helicobacter pylori* infection. *J Clin Oncol* 2001; **19**: 2041-2048
- 18 Zhang XQ, Lin SR. Progress in research on the relationship between *Hp* and stomach cancer. *Shijie Huaren Xiaohua Zazhi* 2000; **8**: 206-207
- 19 Hua JS. Effect of *Hp*: cell proliferation and apoptosis on stomach cancer. *Shijie Huaren Xiaohua Zazhi* 1999; **9**: 647-648
- 20 Armitage GC. Periodontal infections and cardiovascular disease-how strong is the association? *Oral Dis* 2000; **6**: 335-350
- 21 Tsai CJ, Huang TY. Relation of *Helicobacter pylori* infection and angiographically demonstrated coronary artery disease. *Dig Dis Sci* 2000; **45**: 1227-1232
- 22 Gocyk W, Niklinski T, Olechnowicz H, Duda A, Bielanski W,

- Konturek PC, Konturek SJ. *Helicobacter pylori*, gastrin and cyclooxygenase-2 in lung cancer. *Med Sci Monit* 2000; **6**: 1085-1092
- 23 **Baysoy G**, Ertem D, Ademoglu E, Kotiloglu E, Keskin S, Pehlivanoglu E. Gastric *Histopathology*, Iron status and iron deficiency anemia in children with *Helicobacter pylori* infection. *J Pediatric Gastroenterol Nutr* 2004; **38**: 146-151
- 24 **Caselli M**, Zaffoni E, Ruina M, Sartori S, Trevisani L, Ciaccia A, Alvisi V, Fabbri L, Papi A. *Helicobacter pylori* and chronic bronchitis. *Scand J Gastroenterol* 1999; **34**: 828-830
- 25 **Dauden E**, Jimenez Alonso I, Garcia Diez A. *Helicobacter pylori* and idiopathic chronic urticaria. *Int J Dermatol* 2000; **39**: 446-452
- 26 **Ojetti V**, Armuzzi A, De-Luca A, Nucera E, Franceschi F, Candelli M, Zannoni GF, Danese S, Di-Caro S, Vastola M, Schiavino D, Gasbarrini G, Patriarca G, Pola P, Gasbarrini A. *Helicobacter pylori* infection affects eosinophilic cationic protein in the gastric juice of patients with idiopathic chronic urticaria. *Int Arch Allergy Immunol* 2001; **125**: 66-72
- 27 **Vainio E**, Huovinen S, Liutu M, Uksila J, Leino R. Peptic ulcer and *Helicobacter pylori* in patients with lichen planus. *Acta Derm Venereol* 2000; **80**: 427-429
- 28 **Szlachcic A**, Sliwowski Z, Karczewska E, Bielanski W, Pytko-Polonczyk J, Konturek SJ. *Helicobacter pylori* and its eradication in rosacea. *J Physiol Pharmacol* 1999; **50**: 777-786
- 29 **Avcı O**, Ellidokuz E, Simsek I, Buyukgebiz B, Gunes AT. *Helicobacter pylori* and Behcet's disease. *Dermatology* 1999; **199**: 140-143
- 30 **Yazawa N**, Fujimoto M, Kikuchi K, Kubo M, Ihn H, Sato S, Tamaki T, Tamaki K. High seroprevalence of *Helicobacter pylori* infection in patients with systemic sclerosis: association with esophageal involvement. *J Rheumatol* 1998; **25**: 650-653
- 31 **Emilia G**, Longo G, Luppi M, Gandini G, Morselli M, Ferrara L, Amarri S, Cagossi K, Torelli G. *Helicobacter pylori* eradication can induce platelet recovery in idiopathic thrombocytopenic purpura. *Blood* 2001; **97**: 812-814
- 32 **Parkinson AJ**, Gold BD, Bulkow L, Wainwright RB, Swaminathan B, Khanna B, Petersen KM, Fitzgerald MA. High prevalence of *Helicobacter pylori* in the Alaska native population and association with low serum ferritin levels in young adults. *Clin Diagn Lab Immunol* 2000; **7**: 885-888
- 33 **Konno M**, Muraoka S, Takahashi M, Imai T. Iron-deficiency anemia associated with *Helicobacter pylori* gastritis. *J Pediatr Gastroenterol Nutr* 2000; **31**: 52-56
- 34 **Annibale B**, Lahner E, Bordi C, Martino G, Caruana P, Grossi C, Negrini R, Delle-Fave G. Role of *Helicobacter pylori* infection in pernicious anaemia. *Dig Liver Dis* 2000; **32**: 756-762
- 35 **Choe YH**, Kwon YS, Jung MK, Kang SK, Hwang TS, Hong YC. *Helicobacter pylori*-associated iron-deficiency anemia in adolescent female athletes. *J Pediatr* 2001; **139**: 100-104
- 36 **Kaplan K**, Beyan C, Ural AU, Cetin T, Avcu F, Gulsen M, Finci R, Yalcin A. *Helicobacter pylori*-is it a novel causative agent in Vitamin B12 deficiency? *Arch Intern Med* 2000; **160**: 1349-1353
- 37 **Nozaki K**, Shimizu N, Inada K, Tsukamoto T, Inoue M, Kumagai T, Sugiyama A, Mizoshita T, Kaminishi M, Tatematsu M. Synergistic promoting effects of *Helicobacter pylori* infection and high-salt diet on gastric carcinogenesis in mongolian gerbils. *Jpn J Cancer Res* 2002; **93**: 1083-1089
- 38 **Crabtree JE**, Court M, Aboshkiwa MA, Jeremy AH, Dixon MF, Robinson PA. Gastric mucosal cytokine and epithelial cell responses to *Helicobacter pylori* infection in mongolian gerbils. *J Pathol* 2004; **202**: 197-207
- 39 **Chua TS**, Fock KM, Teo EK, Ng TM. Validation of 13C-urea breath test for the diagnosis of *Helicobacter pylori* infection in the singapore population. *Singapore Med J* 2002; **43**: 408-411
- 40 **Kawai T**, Kawakami K, Kudo T, Ogiyama S, Handa Y, Moriyasu F. A new serum antibody test kit (E plate) for evaluation of *Helicobacter pylori* eradication. *Intern Med* 2002; **41**: 780-783
- 41 **Day AS**, Sherman PM. Accuracy of office-based immunoassays for the diagnosis of *Helicobacter pylori* infection in children. *Helicobacter* 2002; **7**: 205-209
- 42 **Oyedeji KS**, Smith SI, Arigbabu AO, Coker AO, Ndububa DA, Agbakwuru EA, Atoyebi OA. Use of direct Gram stain of stomach biopsy as a rapid screening method for detection of *Helicobacter pylori* from peptic ulcer and gastritis patients. *J Basic Microbiol* 2002; **42**: 121-125
- 43 **Wong WM**, Wong BC, Tang VS, Lai KC, Yuen ST, Leung SY, Hu WH, Lam SK. An evaluation of the pyloriTek test for the diagnosis of *Helicobacter pylori* infection in Chinese patients before and after eradication therapy. *J Gastroenterol Hepatol* 2001; **16**: 976-980
- 44 **Kakinoki K**, Takemori Y, Noda Y. Efficacy of the urine antibody test for detection of *Helicobacter pylori*: comparison with serum antibody tests. *Nippon Shokakibyo Gakkai Zasshi* 2001; **98**: 935-941
- 45 **Fujisawa T**, Kaneko T, Kumagai T, Akamatsu T, Katsuyama T, Kiyosawa K, Tachikawa T, Kosaka O, Machikawa F. Evaluation of urinary rapid test for *Helicobacter pylori* in general practice. *J Clin Lab Anal* 2001; **15**: 154-159
- 46 **Miwa H**, Akamatsu S, Tachikawa T, Sogabe T, Ohtaka K, Nagahara A, Sugiyama Y, Sato N. On-site diagnosis of *H pylori* infection by urine. *Diagn Microbiol Infect Dis* 2001; **39**: 95-97
- 47 **Yamamoto S**, Uemura N, Okamoto S, Yamaguchi S, Mashiba H, Tachikawa T. A new rapid test for detecting anti-*Helicobacter pylori* antibody excreted into urine. *Helicobacter* 2000; **5**: 160-164
- 48 **Ladas SD**, Malamou H, Giota G, Varzakakos I, Kitsanta P, Georgopoulos S, Spiliadi C, Raptis SA. Prospective evaluation of a whole-blood antibody test (FlexPack HP) for in-office diagnosis of *Helicobacter pylori* infection in untreated patients. *Eur J Gastroenterol Hepatol* 2000; **12**: 727-731
- 49 **Gisbert JP**, Cruzado AI, Cabrera MM, Carpio D, Benito LM, Perez Poveda JJ, Valbuena M, Cantero J, Pajares JM. "Rapid" serology for the diagnosis of *Helicobacter pylori* infection. Evaluation of its accuracy compared with a gold-standard and its concordance with "classic" serology. *Gastroenterol Hepatol* 2000; **23**: 159-164
- 50 **Xia HH**, Kalantar JS, Wyatt JM, Adams S, Cheung K, Eslick GD, Talley NJ. High sensitivity and specificity of a laboratory-based serological test, pylori DTect ELISA, for detection of *Helicobacter pylori* infection. *Diagn Microbiol Infect Dis* 2000; **36**: 69-74
- 51 **Miwa H**, Hirose M, Kikuchi S, Terai T, Iwazaki R, Kobayashi O, Takei Y, Ogiyama T, Sato N. How useful is the detection kit for antibody to *Helicobacter pylori* in urine (URINELISA) in clinical practice? *Am J Gastroenterol* 1999; **94**: 3460-3463
- 52 **Garcia Diaz E**, Castro Fernandez M, Romero Gomez M, Vargas-Romero J. The effectiveness of (IgG-ELISA) serology as an alternative diagnostic method for detecting *Helicobacter pylori* infection in patients with gastro-intestinal bleeding due to gastro-duodenal ulcer. *Rev Esp Enferm Dig* 2002; **94**: 725-736
- 53 **Liang SH**, Mao YF, Yan J. Cloning, expression and identification of flaB gene from a clinical isolate of *Helicobacter pylori*. *Zhejiang Daxue Xuebao Yixueban* 2003; **32**: 13-16
- 54 **Mao YF**, Yan J, Li LW. Cloning, expression and identification of hpaA gene from a clinical isolate of *Helicobacter pylori*. *Zhejiang Daxue Xuebao Yixueban* 2003; **32**: 9-12
- 55 **Liu X**, Hu J, Zhang X, Fan D. Oral immunization of mice with attenuated *Salmonella typhimurium* expressing *Helicobacter pylori* urease B subunit. *Chin Med J* 2002; **115**: 1513-1516
- 56 **Londono Arcila P**, Freeman D, Kleanthous H, O'Dowd AM, Lewis S, Turner AK, Rees EL, Tibbitts TJ, Greenwood J, Monath TP, Darsley MJ. Attenuated salmonella enterica serovar typhi expressing urease effectively immunizes mice against *Helicobacter pylori* challenge as part of a heterologous mucosal priming-parenteral boosting vaccination regimen. *Infect Immun* 2002; **70**: 5096-5106
- 57 **Reiche N**, Jung A, Brabletz T, Vater T, Kirchner T, Faller G. Generation and characterization of human monoclonal scFv antibodies against *Helicobacter pylori* antigens. *Infect Immun* 2002; **70**: 4158-4164
- 58 **Miyashita M**, Joh T, Watanabe K, Todoroki I, Seno K, Ohara H, Nomura T, Miyata M, Kasugai K, Tochikubo K, Itoh M, Nitta M. Immune responses in mice to intranasal and intracutaneous administration of a DNA vaccine encoding *Helicobacter pylori*-catalase. *Vaccine* 2002; **20**: 2336-2342
- 59 **Liao W**, Chen M, Zhu S. Construction of attenuated salmonella typhimurium vaccine strain expressing *Helicobacter pylori*

- catalase and observation on its protective immunity. *Natl Med J China* 2001; **81**: 613-616
- 60 **Koesling J**, Lucas B, Develioglou L, Aebischer T, Meyer TF. Vaccination of mice with live recombinant salmonella typhimurium aroA against *H pylori*: parameters associated with prophylactic and therapeutic vaccine efficacy. *Vaccine* 2001; **20**: 413-420
- 61 **Jiang Z**, Pu D, Huang AL, Tao XH, Wang PL. Construction, expression and antigenic study of bivalent vaccine candidate with 26000 OMP and hspA of human *H pylori*. *Zhonghua Yixue Zazhi* 2003; **83**: 862-867
- 62 **Bumann D**, Metzger WG, Mansouri E, Palme O, Wendland M, Hurwitz R, Haas G, Aebischer T, von Specht BU, Meyer TF. Safety and immunogenicity of live recombinant salmonella enterica serovar typhi Ty21a expressing urease A and B from *Helicobacter pylori* in human volunteers. *Vaccine* 2001; **20**: 845-852
- 63 **Jiang Z**, Huang A, Wang P. Gene cloning and expression of outer membrane protein of *Helicobacter pylori*. *Zhonghua Yixue Zazhi* 2001; **81**: 1416-1419
- 64 **Keenan J**, Oliaro J, Domigan N, Potter H, Aitken G, Allardyce K, Roake J. Immune response to an 18-kilodalton outer membrane antigen identifies lipoprotein 20 as a *Helicobacter pylori* vaccine candidate. *Infect Immun* 2000; **68**: 3337-3343
- 65 **Raymond J**, Sauvestre C, Kalach N, Bergeret M, Dupont C. Immunoblotting and serology for diagnosis of *Helicobacter pylori* infection in children. *Pediatr Infect Dis J* 2000; **19**: 118-121
- 66 **Todoroki I**, Joh T, Watanabe K, Miyashita M, Seno K, Nomura T, Ohara H, Yokoyama Y, Tochikubo K, Itoh M. Suppressive effects of DNA vaccines encoding heat shock protein on *Helicobacter pylori*-induced gastritis in mice. *Biochem Biophys Res Commun* 2000; **277**: 159-163
- 67 **Shiesh SC**, Sheu BS, Yang HB, Tsao HJ, Lin XZ. Serologic response to lower-molecular-weight proteins of *Helicobacter pylori* is related to, clinical outcome of *Helicobacter pylori* infection in Taiwan. *Dig Dis Sci* 2000; **45**: 781-788
- 68 **Chua TS**, Fock KM, Chan YH, Dhamodaran S, Sim CS, Ng TM, Teo EK. Seroreactivity to 19.5-kDa antigens in combination with absence of seroreactivity to 35-kDa antigens is associated with an increased risk of gastric adenocarcinoma. *Helicobacter* 2002; **7**: 257-264

Edited by Wang XL and Xu JY Proofread by Xu FM

Ethanol inhibits the motility of rabbit sphincter of Oddi *in vitro*

Réka Sári, Attila Pálvölgyi, Zoltán Rakonczay Jr, Tamás Takács, János Lonovics, László Czakó, Zoltán Szilvássy, Péter Hegyi

Réka Sári, Attila Pálvölgyi, Zoltán Rakonczay Jr, Tamás Takács, János Lonovics, László Czakó, Péter Hegyi, First Department of Medicine, Faculty of Medicine, University of Szeged H-6720, Koranyi fasor 10, Hungary

Zoltán Szilvássy, Department of Pharmacology, Medical University of Debrecen H-4032, Nagyerdei krt, 98, Hungary

Supported by The Wellcome Trust (Grant No. 022618), and by the Hungarian Scientific Research Fund (D42188, T43066 and T042589)

Correspondence to: Péter Hegyi, M.D., Ph.D., First Department of Medicine, University of Szeged, H-6701, PO Box 469, Hungary. hep@in1st.szote.u-szeged.hu

Telephone: +36-62-545200 **Fax:** +36-62-545185

Received: 2004-04-10 **Accepted:** 2004-05-25

Abstract

AIM: The role of the sphincter of Oddi (SO) in ethanol (ETOH)-induced pancreatitis is controversial. Our aim was to characterise the effect of ETOH on basal and stimulated SO motility.

METHODS: SOs removed from white rabbits were placed in an organ bath (Krebs solution, pH7.4, 37 °C). The effects of 2 mL/L, 4 mL/L, 6 mL/L and 8 mL/L of ETOH on the contractile responses of the sphincter were determined. SOs were stimulated with either 0.1 µmol/L carbachol, 1 µmol/L erythromycin or 0.1 µmol/L cholecystokinin (CCK).

RESULTS: ETOH at a dose of 4 mL/L significantly decreased the baseline contractile amplitude from 11.98±0.05 mN to 11.19±0.07 mN. However, no significant changes in the contractile frequency were observed. ETOH (0.6%) significantly decreased both the baseline amplitude and the frequency compared to the control group (10.50±0.01 mN, 12.13±0.10 mN and 3.53±0.13 c/min, 5.5±0.13 cycles(c)/min, respectively). Moreover, 0.8% of ETOH resulted in complete relaxation of the SO. Carbachol (0.1 µmol/L) or erythromycin (1 µmol/L) stimulated the baseline amplitudes (by 82% and 75%, respectively) and the contractile frequencies (by 150% and 106%, respectively). In the carbachol or erythromycin-stimulated groups 2-6 mL/L of ETOH significantly inhibited both the amplitude and the frequency. Interestingly, a 4-5 min administration of 6 mL/L ETOH suddenly and completely relaxed the SO. CCK (0.1 µmol/L) stimulated the baseline amplitude from 12.37±0.05 mN to 27.40±1.82 mN within 1.60±0.24 min. After this peak, the amplitude decreased to 17.17±0.22 mN and remained constant during the experiment. The frequency peaked at 12.8±0.2 c/min, after which the constant frequency was 9.43±0.24 c/min throughout the rest of the experiment. ETOH at a dose of 4 mL/L significantly decreased the amplitude from 16.13±0.23 mN to 14.93±0.19 mN. However, no significant changes in the contractile frequency were observed. ETOH at a dose of 6 mL/L inhibited both the amplitudes and the frequencies in the CCK-stimulated group, while 8 mL/L of ETOH completely relaxed the SO.

CONCLUSION: ETOH strongly inhibits the basal, carbachol, erythromycin, and CCK-stimulated rabbit SO motility. Therefore, it is possible that during alcohol-intake the

relaxed SO opens the way for pancreatic fluid to flow out into the duodenum in rabbits. This relaxation of the SO may protect the pancreas against alcohol-induced damage.

Sári R, Pálvölgyi A, Rakonczay Z Jr, Takács T, Lonovics J, Czakó L, Szilvássy Z, Hegyi P. Ethanol inhibits the motility of rabbit sphincter of Oddi *in vitro*. *World J Gastroenterol* 2004; 10(23): 3470-3474

<http://www.wjgnet.com/1007-9327/10/3470.asp>

INTRODUCTION

It is well documented that ethanol (ETOH) can cause acute pancreatitis^[1,2], but the mechanisms by which alcohol causes this severe pancreatic injury are not clear. Two main hypotheses have been put forward to explain the role of the sphincter of Oddi (SO) in ETOH induced pancreatitis. One is the obstruction-hypersecretion theory which holds that ETOH induces spasm of the SO and can increase the pressure in the pancreatic ductal system, which may lead to the disruption of small pancreatic ducts. Therefore, pancreatic juice can enter the parenchyma evoking acute pancreatitis^[3,4]. The other is the duodenopancreatic reflux theory which believes that ETOH reduces the SO motility, thus, the reflux of bile, activated enzymes, or other substances into the pancreatic ducts may cause pancreatitis after alcohol ingestion^[5,6]. Despite these contradictory theories, no data are available concerning the effect of alcohol on physiologically (postprandial)-stimulated SO motility.

Cholecystokinin (CCK) is generally regarded as the major hormone regulating postprandial SO motility. This regulatory effect of CCK is rather complex. CCK could directly stimulate SO motility in guinea pigs^[7], opossum^[8], rabbits^[9-11] and dogs^[12]. On the other hand, CCK could induce acetylcholine (Ach) and vasoactive intestinal peptide release from pre- and postjunctional sites in the enteric nervous system via CCK_A and CCK_B receptors in the canine gastrointestinal tract, which suggests an indirect effect of CCK^[13]. Others have also demonstrated that the contractile response of the guinea pig SO to CCK consists of a direct effect and an indirect effect mediated by Ach release from postganglionic parasympathetic neurons^[7,14].

Motilin is also a key peptide regulating phasic contractile activity of the stomach, duodenum, SO, and gallbladder^[15]. This regulation is mediated by the migrating myoelectric complex of the gastrointestinal tract^[16]. Motilin provoked an increase of the SO spike activity in a dose-dependent manner in rabbits^[17]. Erythromycin, a motilin agonist, has been found to stimulate interdigestive motility of the duodenum and SO in dogs^[18], Australian opossum^[19] and also in humans^[20]. However, there are no available data concerning the effect of erythromycin on rabbit SO motility.

The parasympathetic nervous system plays an important role in the stimulation of gastrointestinal motility after a meal. The parasympathetic neurotransmitter Ach and its analogues have been shown to stimulate SO motility in different species^[21]. Furthermore, Ach can be released from postganglionic parasympathetic neurons after hormonal stimuli, as described above.

In this study our aim was to characterise the effects of ETOH on the basal and differently stimulated SO motility in rabbits.

MATERIALS AND METHODS

Ethics

The present experiments conformed to the European Guiding Principles for Care and Use of Experimental Animals. In addition, the experimental protocol applied was approved by the local ethical boards of the Universities of Szeged and Debrecen, Hungary.

Isometric tension measurements

Isometric tension measurements were described in detail previously^[22]. Biliary SO muscle rings of approximately 6 mm long from adult male New Zealand white rabbits weighing 2–2.5 kg were prepared. The papilla Vateri was eliminated and the ampullary part of the muscle rings of approximately 3 mm long were mounted horizontally on two small L-shaped glass hooks, of which one was connected to a force transducer (SG-O2, Experimetria, Budapest, Hungary) attached to a six channel polygraph (R61 6CH, Mikromed, Budapest, Hungary) for measurement and recording of isometric tension as described^[22]. One muscle ring was prepared from one animal. The experiments were carried out in an organ bath (5 mL) containing Krebs bicarbonate buffer (in mmol/L: NaCl 118.1, KCl 4.7, MgSO₄ 1.0, KH₂PO₄ 1.0, CaCl₂ 2.5, NaHCO₃ 25.0, glucose 11.1) which was maintained at 37 °C and aerated continuously with carbogen (50 mL/L CO₂/950 mL/L O₂).

Experimental protocol

The muscle rings underwent brief experimental protocols as follows. Phasic activity of SO: contractile frequencies and their amplitudes were measured over 50 min in each experiment. The initial tension was set at 10 milliNewtons (mN) and the rings were allowed to equilibrate for over 30 min. After that amplitudes and frequencies were recorded for 60 min. In the first 10 min, baseline phasic activity was measured. From the second 10 min, phasic activities were stimulated with 0.1 μmol/L carbachol, 1 μmol/L erythromycin or 0.1 μmol/L CCK. During the last 40 min, ETOH was administered at the doses of 2 mL/L, 4 mL/L, 6 mL/L and 8 mL/L for equal periods (4 times, 10 min). The control SOs received no treatments.

Drugs and chemicals

All laboratory chemicals (including ions, carbachol, erythromycin, CCK and ETOH) were obtained from Sigma Chemical Company (Budapest, Hungary). CCK and carbachol were dissolved in Krebs solution, while erythromycin was dissolved in dimethyl sulfoxide.

Data and statistical analysis

Parameters producing the data for evaluation were as follows. The *amplitude of contractions* (mN) was referred to as the difference between peak contractions and relaxations. The average of the amplitudes was calculated every minute (results were expressed as mean±SE, *n* = number of frequencies in a minute). The *frequencies of contractions* (c/min) were calculated every minute. Statistical analysis was performed for 10 min of each of the experiments using either Student's *t*-test (when the data consisted of two groups) or ANOVA (when three or more data groups were compared). Results were expressed as mean±SE, *n* = 5, *P*<0.05 was considered statistically significant.

RESULTS

Effect of ETOH on basal SO motility

The amplitudes and frequencies of the basal SO motility were stable during the control experiments (11.98±0.04 mN and 5.37±0.07 c/min, respectively). ETOH (2 mL/L) had no effects on the baseline amplitudes and frequencies. When ETOH was administered at a dose of 4 mL/L, the baseline amplitude was significantly decreased *vs* the control (11.19±0.07 mN and 11.98±0.05 mN, respectively) (Figure 1A, B). However, no significant changes in the contractile frequency were observed *vs* the control (Figure 1C, D). ETOH (6 mL/L) significantly decreased both the baseline amplitude and frequency *vs* control (10.50±0.01 mN, 12.13±0.10 mN and 3.53±0.13 c/min, 5.50±0.17 c/min, respectively). ETOH (8 mL/L) completely relaxed the SO within 10 s. Therefore, neither the frequencies nor the amplitudes could be detected during the last 10 min of the experiments.

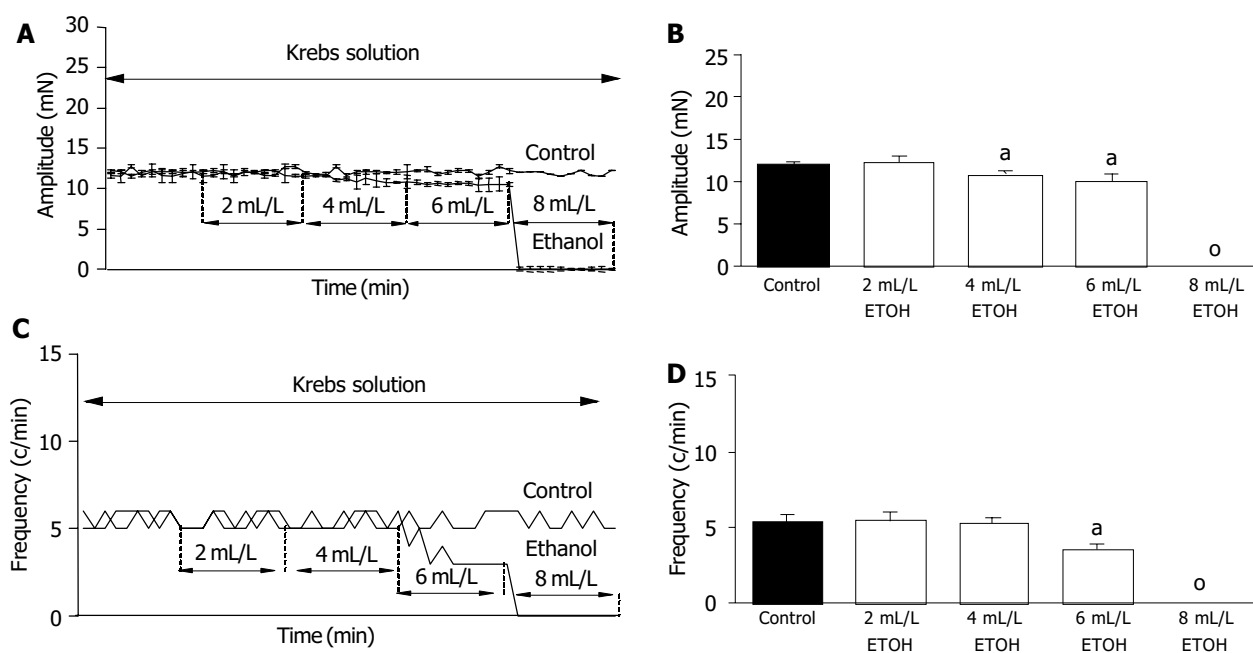


Figure 1 Basal SO motility inhibited by ETOH. Sphincter of Oddi (SO) was exposed to increasing doses of ethanol (ETOH; 2 mL/L, 4 mL/L, 6 mL/L and 8 mL/L). Each concentration of ETOH was administered for 10 min. A: Effect of ETOH on the baseline amplitude. Representative experiments of the control and the ETOH-treated groups are shown. B: Summary of the effect of ETOH on the baseline amplitude. mean±SE, *n* = 5, ^a*P*<0.05 *vs* the control; ^o: no contractile activity. C: Effect of ETOH on the contractile frequency. Representative experiments of the control and the ETOH-treated groups are shown. D: Summary of the effect of ETOH on the contractile frequency. mean±SE, *n* = 5, ^a*P*<0.05 *vs* the control; ^o: no contractile activity.

Effect of ETOH on carbachol-stimulated SO motility

Carbachol (0.1 $\mu\text{mol/L}$) stimulated the baseline amplitude by 82% and the contractile frequency by 150%. This carbachol-stimulated SO motility was stable during the experiment (Figure 2A-C). ETOH (2 mL/L) significantly inhibited both the amplitude and frequency vs the carbachol-stimulated group (19.42 \pm 1.16 mN, 20.81 \pm 0.49 mN and 12.32 \pm 0.16 c/min, 12.91 \pm 0.10 c/min, respectively) (Figure 2A-D). ETOH (4 mL/L) further reduced the amplitude (13.92 \pm 0.49 mN) and the frequency (9.24 \pm 0.21 c/min) of the SO motility. ETOH (6 mL/L) decreased the contractile frequency of the SO by 50% (4.61 \pm 0.46 c/min). However, it did not modify the amplitude frequency (12.23 \pm 0.22 mN). Interestingly, a 4.20 \pm 1.47 min administration of 6 mL/L ETOH suddenly and completely relaxed the SO.

Effect of ETOH on erythromycin-stimulated SO motility

Erythromycin (1 $\mu\text{mol/L}$) stimulated the baseline amplitude by 75% and the contractile frequency by 106%. This erythromycin-stimulated SO motility was constant over the experiment. ETOH (2 mL/L) significantly inhibited both the amplitude and the frequency vs the carbachol-stimulated group (19.10 \pm 0.25 mN, 19.65 \pm 0.45 mN and 9.66 \pm 0.29 c/min, 10.45 \pm 0.20 c/min, respectively). ETOH (4 mL/L) significantly decreased both the amplitude (16.27 \pm 0.33 mN) and the frequency (8.32 \pm 0.22 c/min), (Figure 2E-H). Administration of 6 mL/L ETOH caused a further decrease in the amplitude and frequency (11.85 \pm 0.41 mN and 4.10 \pm 0.37 c/min, respectively). Similar to that seen in the carbachol-stimulated group, a 4.10 \pm 0.55 min administration of 6 mL/L ETOH suddenly and completely relaxed the SO.

Effect of ETOH on CCK-stimulated SO motility

CCK (0.1 $\mu\text{mol/L}$) stimulated the baseline amplitude from 12.37 \pm 0.05 mN to 27.4 \pm 1.82 mN within 1.60 \pm 0.24 min. After this peak, the amplitude decreased to 17.17 \pm 0.22 mN and was constant during the experiment. The frequency peaked at 12.8 \pm 0.2 c/min, after which the constant frequency was 9.43 \pm 0.24 c/min throughout the rest of the experiment. ETOH (2 mL/L) mildly decreased the amplitude frequency (16.13 \pm 0.23 mN and 17.05 \pm 0.14 mN), but had no effect on the contractile frequency of the SO (9.32 \pm 0.15 mN and 9.50 \pm 0.31 mN). ETOH (4 mL/L) further decreased the amplitude frequency from 16.13 \pm 0.23 mN to 14.93 \pm 0.19 mN, but still had no effect on the contractile frequency of the SO (9.82 \pm 0.23 c/min). ETOH (6 mL/L) further decreased the amplitude and frequency of the SO to 12.13 \pm 0.11 mN and 7.26 \pm 0.27 c/min, respectively. ETOH (8 mL/L) resulted in complete relaxation of the SO within 10 s (Figure 2 I-L). After this time neither frequencies nor amplitudes could be detected during the remaining part of the experiments.

DISCUSSION

It has been widely known for a long time that ETOH may evoke acute pancreatitis^[23]. The role of SO in the pathogenesis of alcohol-induced acute pancreatitis has also been suggested^[3,6]. However, the effect of ETOH on SO is controversial. On the one hand, it has been demonstrated that ETOH reduces the SO pressure^[3,6]. On the other hand, alcohol was found to induce spasm of the SO^[24,25]. These contradictory results indicate that much more information is needed to clarify the effect of ETOH on SO motility.

To investigate these issues, we tested the effect of four different concentrations of ETOH on the resting SO motility. ETOH (2 mL/L) had no effect on the basal SO motility. This result is in accordance with the findings of Cullen *et al.*^[26]. They reported that ETOH at a dose of 2 mL/L had no significant effect on the baseline amplitude and the contractile frequency of SO in opossum. ETOH (4 mL/L) mildly decreased the baseline amplitude of the spontaneously contracting SO, but had no effect on the contractile frequency. When ETOH concentration

was elevated to 6 mL/L, both the baseline SO contractile amplitude and the frequency were decreased (13%, 34% respectively), while 8 mL/L of ETOH completely relaxed the SO.

Next we tested the effect of different doses of ETOH on physiologically stimulated SO motility (carbachol, erythromycin and CCK). We tested 3 different stimuli at the ED₅₀ doses. Carbachol was used to mimic the activity of parasympathetic nervous system, while CCK and a motilin receptor agonist erythromycin were administered to mimic neurohumoral stimuli.

Carbachol (0.1 $\mu\text{mol/L}$) stimulated the frequency (150%) and the amplitude (82%) of SO contractions. ETOH (2 mL/L) decreased the baseline amplitude and frequency of the carbachol-stimulated SO by the same rate (12%). ETOH (4 mL/L) decreased the amplitude of SO motility to the basal level, but the frequency still remained elevated. A 4-5 min administration of 6 mL/L ETOH completely relaxed the SO. These results demonstrate that ETOH may inhibit the activity of SO motility stimulated by the parasympathetic nervous system in a dose-dependent manner. Moreover, we can conclude that ETOH has a stronger effect on the contractile amplitude than on the frequency of SO.

The effect of ETOH was almost the same on erythromycin-stimulated as on carbachol-stimulated SO. ETOH (2 mL/L) mildly decreased the baseline amplitude and frequency by 10%. ETOH (4 mL/L) decreased both the amplitude and the frequency of erythromycin-stimulated SO. A 4-5 min administration of 6 mL/L ETOH completely relaxed the SO, as it was found during carbachol-stimulation.

Finally, the effect of ETOH was tested on CCK-stimulated SO motility. CCK stimulated the baseline amplitude and the contractile frequency of SO by 39% and 74%, respectively. ETOH (2 mL/L) mildly decreased the baseline amplitude (6 mL/L), but had no effect on the frequency of the SO. ETOH (4 mL/L) further decreased the baseline amplitude. Interestingly, 4 mL/L ETOH still had no effect on the contractile frequency. When the concentration of ETOH was increased to 6 mL/L, both the baseline amplitude and the contractile frequency of SO were decreased (29% and 23% respectively). ETOH (8 mL/L) immediately and completely relaxed the SO as it was seen during the study of unstimulated SO.

Taken together, ETOH inhibited the basal and neurally (carbachol), humorally (erythromycin, a motilin agonist) and neurohumorally (CCK) stimulated SO motility in a dose-dependent manner. Viceconte *et al.*^[6] suggested that alcohol might cause a hormone-mediated relaxation, but they could not exclude a nervous or direct mechanism. Cullen *et al.*^[26] demonstrated that 2 mL/L ETOH could decrease the frequency of H₂O₂-stimulated SO motility. These findings suggest that the main effect of alcohol is direct, independent of a specific neural and/or humoral pathway. Interestingly, we have to note that the inhibitory effect of ETOH was more pronounced during carbachol or erythromycin stimulation than during CCK stimulation. Therefore, we could not totally exclude a marginal specific effect of ETOH. There is no data available concerning the effect of low doses of ETOH on the SO in human. However, gastric absorption accounted for 30% of ETOH administered with food^[27], therefore, during a low alcohol-concentrated-fluid (2-5%) intake, small doses of alcohol may be found around the SO. These findings need further investigation.

The inhibitory effect of ETOH on SO motility may have an important pathophysiological role. ETOH has been found to increase basal pancreatic flow rate and protein output^[28,29], thus, elevating the intraluminal pressure in the pancreatic ductal system. The relaxation of SO opens the way for pancreatic fluid to flow out into the duodenum, thus, preventing the pancreas from the damage by the elevated intraluminal pressure during acute ETOH administration. It is hard to believe, that a duodeno-pancreatic reflux against the high pancreatic-juice-flow could play a decisive role in the pathogenesis of alcohol-induced

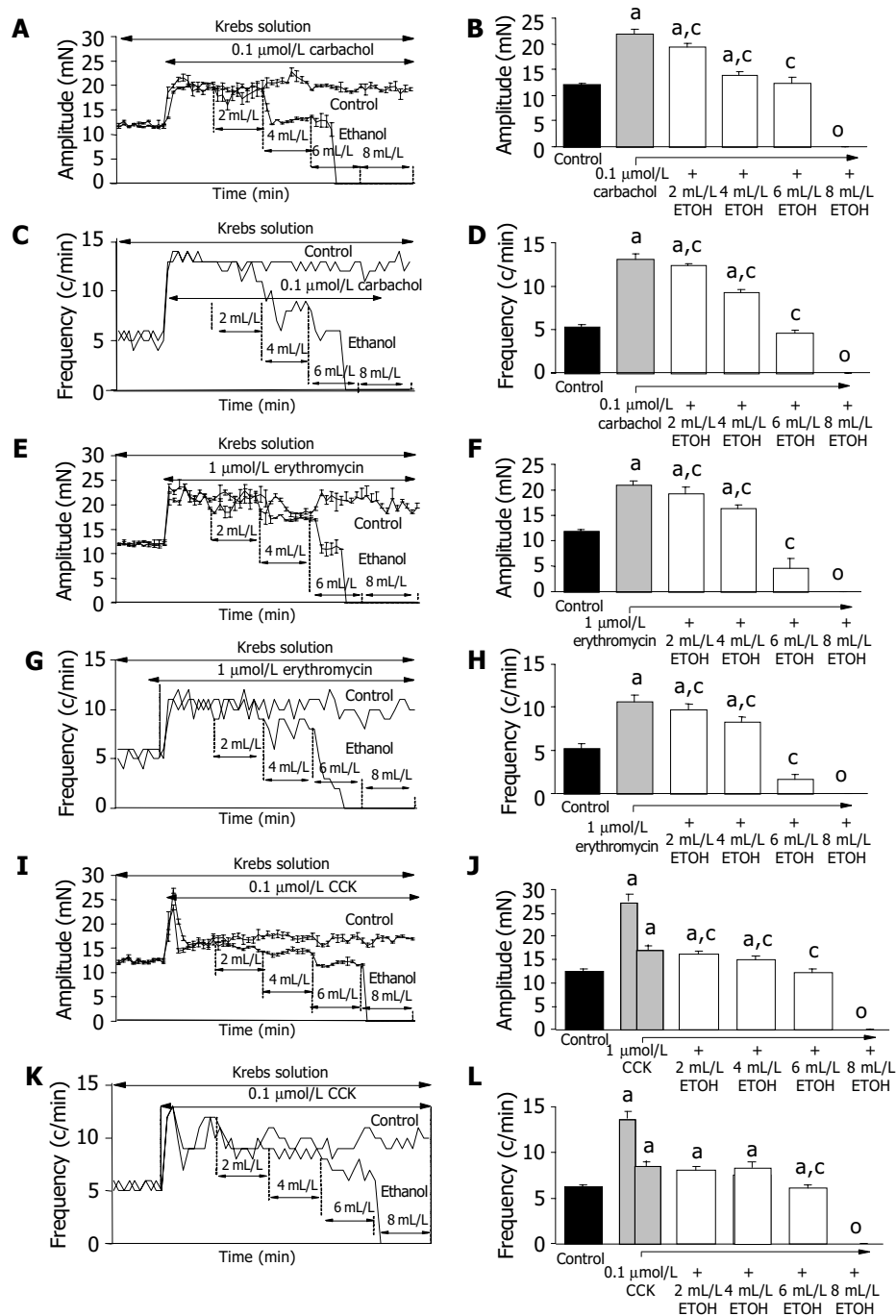


Figure 2 Effect of ETOH on carbachol, erythromycin, CCK stimulated SO motility. All of the SOs were stimulated by 0.1 μmol/L carbachol for 40 min. Different concentrations of ETOH were administered as described in Figure 1. A: Effect of ETOH on the carbachol-stimulated baseline amplitude. Representative experiments of the control (carbachol-treated) and the ETOH-carbachol-treated groups are shown. B: Summary of the effect of ETOH on the carbachol-stimulated baseline amplitude. mean±SE, $n = 5$, $^aP < 0.05$ vs control, $^cP < 0.05$ vs the carbachol-stimulated group, o: no contractile activity. C: Effect of ETOH on the contractile frequency. Representative experiments of the (carbachol-treated) and the ETOH-carbachol-treated groups are shown. D: Summary of the effect of ETOH on the carbachol-stimulated contractile frequency. mean±SE, $n = 5$, $^aP < 0.05$ vs control, $^cP < 0.05$ vs the carbachol-stimulated group, o: no contractile activity. E: Effect of ETOH on the erythromycin-stimulated baseline amplitude. Representative experiments of the control (erythromycin-treated) and the ETOH-erythromycin-treated groups are shown. F: Summary of the effect of ETOH on the erythromycin-stimulated baseline amplitude. mean±SE, $n = 5$, $^aP < 0.05$ vs the control, $^cP < 0.05$ vs the erythromycin-stimulated group, o: no contractile activity. G: Effect of ETOH on the contractile frequency. Representative experiments of the control (erythromycin-treated) and the ETOH-erythromycin-treated groups are shown. H: Summary of the effect of ETOH on the erythromycin-stimulated contractile frequency. mean±SE, $n = 5$, $^aP < 0.05$ vs the control, $^cP < 0.05$ vs the erythromycin-stimulated group, o: no contractile activity. I: Effect of ETOH on the carbachol-stimulated baseline amplitude. Representative experiments of the control (CCK-treated) and the ETOH-CCK-treated groups are shown. J: Summary of the effect of ETOH on the CCK-stimulated baseline amplitude. mean±SE, $n = 5$, $^aP < 0.05$ vs the control; o: no contractile activity. In the 0.1 μmol/L CCK-treated group, the first column represents the peak amplitude of contractile frequencies. The second column represents the constant amplitudes after the peak. $^aP < 0.05$ vs the constant amplitude of the CCK-treated group. K: Effect of ETOH on the contractile frequency. Representative experiments of the (CCK-treated) and ETOH-CCK-treated groups are shown. L: Summary of the effect of ETOH on the CCK-stimulated contractile frequency. mean±SE, $n = 5$, $^aP < 0.05$ vs the control; o: no contractile activity. In the 0.1 μmol/L CCK-treated group, the first column represents the peak of frequencies. The second column represents the constant frequencies after the peak. $^cP < 0.05$ vs the constant frequency of the CCK-treated group.

acute pancreatitis. Furthermore, it is also well documented that SO relaxants^[30-32] and endoscopic sphincterotomy^[33,34] have beneficial effects during acute pancreatitis, which argue against the duodeno-pancreatic reflux theory. All in all, we think that the response of SO motility to ETOH administration is protective against pancreatic injury rather than harmful to the pancreas.

In conclusion, ETOH can strongly inhibit the basal, carbachol, erythromycin, and CCK stimulated SO motility in rabbits, and it is possible that SO opens the way for the pancreatic fluid to flow out into the duodenum. This relaxation of the SO may prevent the pancreas against alcohol-induced damage.

REFERENCES

- 1 **Schneider A**, Whitcomb DC, Singer MV. Animal models in alcoholic pancreatitis-what can we learn? *Pancreatol* 2002; **2**: 189-203
- 2 **Dubagunta S**, Still CD, Komar MJ. Acute pancreatitis. *J Am Osteopath Assoc* 2001; **101**(4 Suppl Pt 1): S6-9
- 3 **Yamasaki K**, Okazaki K, Sakamoto Y, Yamamoto Y, Yamamoto Y, Okada T. Effects of ethanol on the motility of papillary sphincter and exocrine pancreas in the monkey. *Am J Gastroenterol* 1993; **88**: 2078-2083
- 4 **Becker JM**, Sharp SW. Effect of alcohol on cyclical myoelectric activity of the opossum sphincter of Oddi. *J Surg Res* 1985; **38**: 343-349
- 5 **Goff JS**. The effect of ethanol on the pancreatic duct sphincter of Oddi. *Am J Gastroenterol* 1993; **88**: 656-660
- 6 **Viceconte G**. Effects of ethanol on the sphincter of Oddi: an endoscopic manometric study. *Gut* 1983; **24**: 20-25
- 7 **Harada T**, Katsuragi T, Furukawa T. Release of acetylcholine mediated by cholecystokinin receptor from the guinea pig sphincter of Oddi. *J Pharmacol Exp Ther* 1986; **239**: 554-558
- 8 **Becker JM**, Moody FG. The dose/response effects of gastrointestinal hormones on the opossum biliary sphincter. *Curr Surg* 1980; **37**: 60-62
- 9 **Sarles JC**, Delecourt P, Castello H, Gaeta L, Nacchiero M, Amoros JP, Devaux MA, Awad R. Action of gastrointestinal hormones on the myoelectric activity of the sphincter of Oddi in living rabbit. *Regul Pept* 1981; **2**: 113-124
- 10 **Chiu JH**, Kuo YL, Lui WY, Wu CW, Hong CY. Somatic electrical nerve stimulation regulates the motility of sphincter of Oddi in rabbits and cats: evidence for a somatovisceral reflex mediated by cholecystokinin. *Dig Dis Sci* 1999; **44**: 1759-1767
- 11 **Elbrond H**, Ostergaard L, Huniche B, Larsen LS, Andersen MB. Rabbit sphincter of Oddi and duodenal pressure and slow-wave activity. Effects of cholecystokinin. *Scand J Gastroenterol* 1994; **29**: 537-544
- 12 **Muller EL**, Lewinski MA, Pitt HA. Action of cholecystokinin on sphincter of Oddi phasic wave activity in the prairie dog. *Curr Surg* 1985; **42**: 128-130
- 13 **Vergara P**, Woskowska Z, Cipris S, Fox-Threlkeld JE, Daniel EE. Mechanisms of action of cholecystokinin in the canine gastrointestinal tract: role of vasoactive intestinal peptide and nitric oxide. *J Pharmacol Exp Ther* 1996; **279**: 306-316
- 14 **Pozo MJ**, Salido GM, Madrid JA. Action of cholecystokinin on the dog sphincter of Oddi: influence of anti-cholinergic agents. *Arch Int Physiol Biochim* 1990; **98**: 353-360
- 15 **Chaussade S**, Michopoulos S, Sogni P, Guerre J, Couturier D. Motilin agonist erythromycin increases human lower esophageal sphincter pressure by stimulation of cholinergic nerves. *Dig Dis Sci* 1994; **39**: 381-384
- 16 **Bormans V**, Peeters TL, Janssens J, Pearce D, Vandeweerd M, Vantrappen G. In man, only activity fronts that originate in the stomach correlate with motilin peaks. *Scand J Gastroenterol* 1987; **22**: 781-784
- 17 **Sarles JC**, Delecourt P, Devaux MA, Amoros JP, Guichenev JC, Wunsch E. *In vivo* effect of 13 Leu motilin on the electric activity of the rabbit sphincter of Oddi. *Horm Metab Res* 1981; **13**: 340-342
- 18 **Kaufman HS**, Ahrendt SA, Pitt HA, Lillemoe KD. The effect of erythromycin on motility of the duodenum, sphincter of Oddi, and gallbladder in the prairie dog. *Surgery* 1993; **114**: 543-548
- 19 **Saccone GT**, Liu YF, Thune A, Harvey JR, Baker RA, Toouli J. Erythromycin and motilin stimulate sphincter of Oddi motility and inhibit trans-sphincteric flow in the Australian possum. *Naunyn Schmiedebergs Arch Pharmacol* 1992; **346**: 701-706
- 20 **Wehrmann T**, Pfeltzer C, Caspary WF. Effect of erythromycin on human biliary motility. *Aliment Pharmacol Ther* 1996; **10**: 421-426
- 21 **Konomi H**, Simula ME, Meedeniya AC, Toouli J, Saccone GT. Induction of duodenal motility activates the sphincter of Oddi (SO)-duodenal reflex in the Australian possum *in vitro*. *Auton Autacoid Pharmacol* 2002; **22**: 109-117
- 22 **Lonovics J**, Jakab I, Szilvassy J, Szilvassy Z. Regional differences in nitric oxide-mediated relaxation of the rabbit sphincter of Oddi. *Eur J Pharmacol* 1994; **255**: 117-122
- 23 **Sarles H**, Lebreuil G, Tasso F, Figarella C, Clemente F, Devaux MA, Fagonde B, Payan H. A comparison of alcoholic pancreatitis in rat and man. *Gut* 1971; **12**: 377-388
- 24 **Sarles JC**, Midejean A, Devaux MA. Electromyography of the sphincter of Oddi. Technic and experimental results in the rabbit: effect of certain drugs. *Am J Gastroenterol* 1975; **63**: 221-231
- 25 **Guelrud M**, Mendoza S, Rossiter G, Gelrud D, Rossiter A, Souney PF. Effect of local instillation of alcohol on sphincter of Oddi motor activity: combined ERCP and manometry study. *Gastrointest Endosc* 1991; **37**: 428-432
- 26 **Cullen JJ**, Ledlow A, Murray JA, Conklin JL. Effect of hydroxyl radical (OH.) on sphincter of Oddi motility. *Digestion* 1997; **58**: 452-457
- 27 **Levitt MD**, Li R, DeMaster EG, Elson M, Furne J, Levitt DG. Use of measurements of ethanol absorption from stomach and intestine to assess human ethanol metabolism. *Am J Physiol* 1997; **273**(Pt 1): G951-957
- 28 **Alonso RM**, Alvarez MC, San Roman JJ, Garcia LJ, Calvo JJ, Lopez MA. Effects of acute intravenous ethanol on basal exocrine pancreatic secretion in rat: cholinergic involvement. *Rev Esp Fisiol* 1994; **50**: 81-87
- 29 **Nakamura T**, Okabayashi Y, Fujii M, Tani S, Fujisawa T, Otsuki M. Effect of ethanol on pancreatic exocrine secretion in rats. *Pancreas* 1991; **6**: 571-577
- 30 **Lai KH**. Sphincter of Oddi and acute pancreatitis: a new treatment option. *JOP* 2002; **3**: 83-85
- 31 **Lai KH**, Lo GH, Cheng JS, Fu MT, Wang EM, Chan HH, Wang YY, Hsu PI, Lin CK. Effect of somatostatin on the sphincter of Oddi in patients with acute non-biliary pancreatitis. *Gut* 2001; **49**: 843-846
- 32 **Veloso B**, Madacsy L, Szepes A, Pavics L, Csernay L, Lonovics J. The effects of somatostatin and octreotide on the human sphincter of Oddi. *Eur J Gastroenterol Hepatol* 1999; **11**: 897-901
- 33 **Zhou MQ**, Li NP, Lu RD. Duodenoscopy in treatment of acute gallstone pancreatitis. *Hepatobiliary Pancreat Dis Int* 2002; **1**: 608-610
- 34 **Park SH**, Watkins JL, Fogel EL, Sherman S, Lazzell L, Bucksot L, Lehman GA. Long-term outcome of endoscopic dual pancreatobiliary sphincterotomy in patients with manometry-documented sphincter of Oddi dysfunction and normal pancreatogram. *Gastrointest Endosc* 2003; **57**: 483-491

DNA ploidy and *c-Kit* mutation in gastrointestinal stromal tumors

Ju Han Lee, Xianglan Zhang, Woon Yong Jung, Yang Seok Chae, Jong-Jae Park, Insun Kim

Ju Han Lee, Xianglan Zhang, Woon Yong Jung, Yang Seok Chae, Insun Kim, Department of Pathology, Medical College, Korea University, Seoul, Korea

Jong-Jae Park, Department of Internal Medicine, Medical College, Korea University, Seoul, Korea

Correspondence to: Dr. Insun Kim, Department of Pathology, Guro Hospital, 80, Guro-dong, Guro-Ku, Seoul, Korea

Telephone: +822-818-6233 **Fax:** +822-818-6239

Received: 2003-12-28 **Accepted:** 2004-01-30

Abstract

AIM: To investigate the prognostic significance of *c-Kit* gene mutation and DNA ploidy in gastrointestinal stromal tumors (GISTs).

METHODS: A total of 55 cases of GISTs were studied for the expression of *c-Kit* by immunohistochemistry, and the *c-Kit* gene mutations in exons 9, 11, 13, and 17 were detected by polymerase chain reaction-single strand confirmation polymorphism (PCR-SSCP) and denaturing high performance liquid chromatography (D-HPLC) techniques. DNA ploidy was determined by flow cytometry.

RESULTS: Of the 55 cases of GISTs, 53 cases (96.4%) expressed *c-Kit* protein. The *c-Kit* gene mutations of exons 11 and 9 were found in 30 (54.5%) and 7 cases (12.7%), respectively. No mutations were found in exons 13 and 17. DNA aneuploidy was seen in 10 cases (18.2%). The *c-Kit* mutation positive GISTs were larger in size than the negative GISTs. The aneuploidy tumors were statistically associated with large size, high mitotic counts, high risk groups, high cellularity and severe nuclear atypia, and epithelioid type. There was a tendency that *c-Kit* mutations were more frequently found in aneuploidy GISTs.

CONCLUSION: DNA aneuploidy and *c-Kit* mutations can be considered as prognostic factors in GISTs.

Lee JH, Zhang X, Jung WY, Chae YS, Park JJ, Kim I. DNA ploidy and *c-Kit* mutation in gastrointestinal stromal tumors. *World J Gastroenterol* 2004; 10(23): 3475-3479
<http://www.wjgnet.com/1007-9327/10/3475.asp>

INTRODUCTION

Gastrointestinal stromal tumors (GISTs) are the most common mesenchymal neoplasms of the gastrointestinal tract. The term, GIST, was first introduced in the 1980s to include a group of nonlymphomatous, nonepithelial tumors of the gut^[1]. With the advent of immunohistochemistry, CD117 (c-Kit) negative tumors, such as schwannomas, leiomyomas, and leiomyosarcomas, were excluded from the noncommittal term of "gastrointestinal stromal tumors". Recently, based on immunophenotypic and ultrastructural similarities, it is widely accepted that the precursor cells in GISTs are the interstitial cells of Cajal (ICCs)^[2]. Immunohistochemically, GISTs are typically positive for *c-Kit* and CD34, but negative for S-100 protein, desmin, and may express smooth muscle actin in 20% to 40% of cases^[3].

Yet despite their recognition as a distinct pathologic entity, because GISTs are widely diverse in terms of clinical presentation, morphology, and biologic behavior, the prediction of malignancy on the basis of pathologic features is often difficult. Many studies have analyzed the prognostic relevance of a variety of parameters such as anatomical location, mucosal invasion, tumor necrosis, and high cellularity, rather often leading to conflicting conclusions^[1,4-6]. However, two morphologic features have emerged as fairly reliable predictors of outcome: mitotic rate and tumor size^[4,7-12]. A consensus conference held at National Institutes of Health in April 2001 provided both an evidence-based definition and a practical scheme for assessing the risk (very low risk, low risk, intermediate risk, and high risk) of aggressive clinical behavior^[13]. Recently, a prognostic significance of *c-Kit* mutations was suggested by several clinicopathologic studies^[14-17]. The largest series has shown that *c-Kit* mutation in exon 11 was more common in large tumors, and that the presence of this mutation was an adverse prognostic factor^[14].

The conceptual evolution of GISTs and *c-Kit* mutation has been the subject of numerous previous articles. However, DNA ploidy studies in relation to *c-Kit* mutation are not well established. The purpose of this study was to examine the *c-Kit* mutations and DNA ploidy in GISTs to evaluate them as the prognostic factors.

MATERIALS AND METHODS

Histological review

The cases included in this study were retrieved from patients who were diagnosed as GISTs and treated at Korea University Hospitals between January 1997 and August 2003. The clinical history and postoperative courses were obtained from the review of clinical records. The tumor size in greatest dimension and the location were taken from the pathology reports. Histological slides were reviewed by two of the authors (Kim, I and Lee, JH) in all of the cases. The tumor cell type was determined by light microscopic study. The spindle cell type had a predominant fusiform morphology. Both cytoplasm and nuclei were elongated and aligned within the microscopic field. The epithelioid cell type had a predominantly spherical morphology. The nuclei were round and tended to be centrally placed within tumor cells. The number of mitosis was determined by counting the mitotic activity in 50 adjacent high-power fields (HPF) at a magnification of $\times 400$. The cytologic atypia of the tumor cells was determined to be mild, moderate, or severe. The cytologic atypia was assessed within the most proliferative area. Mild atypia indicated that the tumor cells were histologically benign or mildly atypical. Moderate atypia indicated that the tumor cells had moderately enlarged hyperchromatic or vesicular nuclei with or without prominent nucleoli and some nuclear irregularity. Severe atypia indicated that the tumor cells had enlarged irregular, hyperchromatic, or vesicular pleomorphic nuclei with prominent nucleoli. The cellularity was scored as low if the cell count was below 1 000/mm², intermediate for a range from 1 000 to 2 000 cells per mm², and high if exceeding 2 000 cells/mm². Tumor necrosis was determined to be present or absent. Tumor hemorrhage was determined to be present or absent. The growth pattern was determined to be expansive or invasive. GISTs were reclassified as very low, low, intermediate, and high risk groups for their estimated potential for aggressive clinical behavior as suggested by NIH consensus^[13].

Immunohistochemistry

Representative sections from each lesion were subjected to immunohistochemical staining by using the avidin-biotin-peroxidase complex (ABC) method. The target differentiation antigens visualized by the monoclonal and polyclonal antibodies were *c-Kit* (1:400; Dako, Glostrup, Denmark), CD34 (1:200; Neomarker, CA, USA), smooth muscle actin (SMA, 1:200; Dako, Glostrup, Denmark), and S-100 protein (1:400; Neomarker, CA, USA). The tumors were designated as positive when more than 10% of the tumor cells showed a positive reaction for CD34, SMA and S-100 protein. Positive reactions were classified by using the following criteria for *c-Kit*: (-) negative, if <10% cells were stained; (+), if 10-50% cells were immunoreactive; (++) if 51-100% cells were immunoreactive. The tumors which showed positive reaction for CD34 and/or *c-Kit* protein with or without SMA and S-100 protein were included in GISTs.

DNA extraction

DNA was extracted from the formaldehyde-fixed, paraffin-embedded tissue sections by using standard methods with proteinase K digestion and phenol/chloroform purification.

Polymerase - chain reaction - single strand confirmation polymorphism (PCR-SSCP)

PCR primers were designated to amplify exons 9, 11, 13, and 17 (Table 1). PCR was carried out with the following conditions: 50 μ L total reaction volume, with 5 μ L template, 5 μ L of each oligonucleotide primer, 10 μ L dNTP, 10 μ L ddH₂O, 2 μ L Taq polymerase, 8 μ L Mg²⁺ and 5 μ L 10 \times PCR buffer. Cycling conditions were as follows: an initial penetration at 95 $^{\circ}$ C for 4 min, 38 cycles each at 94 $^{\circ}$ C for 1 min, at 56 $^{\circ}$ C for 1 min, at 72 $^{\circ}$ C for 1 min, followed by one cycle at 72 $^{\circ}$ C for 10 min. PCR products were visualized by gel electrophoresis in 1.7 g/L agarose. Then the PCR products were subjected to 80 g/L non-denaturation polyacrylamide gel electrophoresis with 50 g/L glycerin and silver nitrate staining.

Table 1 Primer sequence for *c-Kit* exons 9, 11, 13, and 17 and the corresponding annealing temperature (T_A) and the size of expected PCR size products

<i>c-Kit</i> exon No.	Primers	Primer sequence 5'->3'	T _A ($^{\circ}$ C)	Product size (bp)
9	hEx9-F	TTCCTAGAGTAAGCCAGGG	53	298
	hEx9-R	AATCATGACTGATATGGT		
11	hEx11-F	CAGGTAACCATTTATTTGT	53	326
	hEx11-R	TCATTGTTTCAGGTGGAAC		
13	hEx13-F	ATCAGTTTGCCAGTTGTGCT	53	250
	hEx13-R	TTTATAATCTAGCATTGCC		
17	hEx17-F	GTTTCACTCTTTACAAGT	53	277
	hEx17-R	TTACATTATGAAAGTCACAGGAAAC		

Denaturing high performance liquid chromatography (D-HPLC)

To enhance heteroduplex formation, the untreated PCR products (5-7 μ L) were denaturated at 95 $^{\circ}$ C for 5 min followed by gradual reannealing to room temperature for over 30 min. Samples were analyzed in WAVE DHPLC. The gradient was formed by mixing buffer A (0.1 mmol/L TEAA) and buffer B (0.1 mol/L TEAA, 250 g/L acetonitrile). The analysis was carried out at a flow rate of 0.9 mL/min and buffer B gradient increase of 20 g/L per minute for 4 min. Oven temperature for optimal heteroduplex separation under partial DNA denaturation was determined for each amplified fragment by using WAVE Marker software. The most important criteria for assigning the presence of a sequence alteration in each DHPLC fragment were the numbers and the shape of elution peaks in comparison with a wild-type subject elution profile used as reference. To allow the detection of heteroduplex DNA molecules in homozygous patients, those

amplicons were pre-mixed with sequence-confirmed wild-type PCR controls. The mixed samples were then denatured at 94 $^{\circ}$ C for 5 min and cooled for over 45 min at room temperature, before D-HPLC analysis.

DNA ploidy

Nuclear suspensions from the selected tissue blocks, previously used in the immunohistochemical study, were prepared in each case. Three 50- μ m thick sections from the tissue block were dewaxed in xylene and rehydrated in a sequence of decreasing concentrations of alcohol. After being washed in Dulbecco's phosphate buffered saline (DPBS), the tissue was incubated in 2 g/L pepsin (Sigma Chemical Company, St. Louis, USA) at 37 $^{\circ}$ C water bath for 2.5 h. Then, the samples were neutralized by citrate buffer and treated with trypsin at 37 $^{\circ}$ C water bath for 10 min. After RNase treatment at 37 $^{\circ}$ C water bath for 30 min, the samples were stained with propidium iodide at 4 $^{\circ}$ C for 30 min. By using a FACS analyzer, the DNA histograms were obtained.

Statistical analysis

The data were analyzed with Chi-square and *t* tests by using SPSS 10.0 program.

RESULTS

Clinicopathologic characteristics

There were 25 males and 30 females. The mean age of the patients at the time of diagnosis was 60 (range: 29-80) years. The locations of tumors were as follows: one in the esophagus, 43 in the stomach, 10 in the small intestine (including duodenum), and one in the mesentery. The symptoms of patients were as follows: 24 cases of abdominal pain, 11 cases of gastrointestinal bleeding, 4 cases of palpable mass and 12 cases of nonspecific. The mean diameter of tumors was 5.29 (range: 0.4-17.0) cm. Three patients showed liver metastasis at the time of surgery. Two patients received re-operation due to recurrence. One patient had a local gastric recurrence after 17 mo and the other had a local duodenal recurrence after 33 mo.

Patients included in this study were diagnosed to have a GIST by a variety of histologic criteria. Spindle cell lesions occurred with or without an epithelioid component, the most common tumor lesions showed interlacing fascicles of spindle cells. Some lesions showed a palisaded morphology resembling peripheral neurilemmomas, but storiform, fascicular, or mixed growth patterns were seen. Some of them were composed of round and epithelioid cells appearing with perinuclear shrinkage of cytoplasm. In some tumors or parts of tumors, there was a mixture of epithelioid cells and spindle cells. Fifteen (27.3%) tumors were epithelioid cell type, whereas the remaining 40 (72.7%) were spindle cell type (Figure 1). The mitotic index ranged from 0 to 100 (mean: 11.4). The degree of cytologic atypia was mild in 27 (49.1%) patients, moderate in 21 (38.2%), and severe in 7 (12.7%). The degree of cellularity was low in 11 (20.0%) patients, intermediate in 37 (67.3%), and high in 7 (12.7%). Necrosis was present in 11 (20.0%), and hemorrhage was present in 17 (30.9%) tumors. Expansive growth was found in 30 (54.5%), and invasive growth in 25 (45.5%) tumors.

Correlation of risk groups and clinicopathologic parameters

Tumors were divided into very low (10/55, 18.2%), low (26/55, 47.3%), intermediate (4/55, 7.3%) and high risk (15/55, 27.3%) groups by NIH consensus^[13]. Correlation of risk groups and other clinicopathologic parameters is shown in Table 2. Higher risk (intermediate and high risk) groups showed more frequent necrosis, more severe nuclear atypia and higher cellularity than lower risk (very low and low risk) groups which were statistically significant. The epithelioid cell type was more frequent in higher risk group.

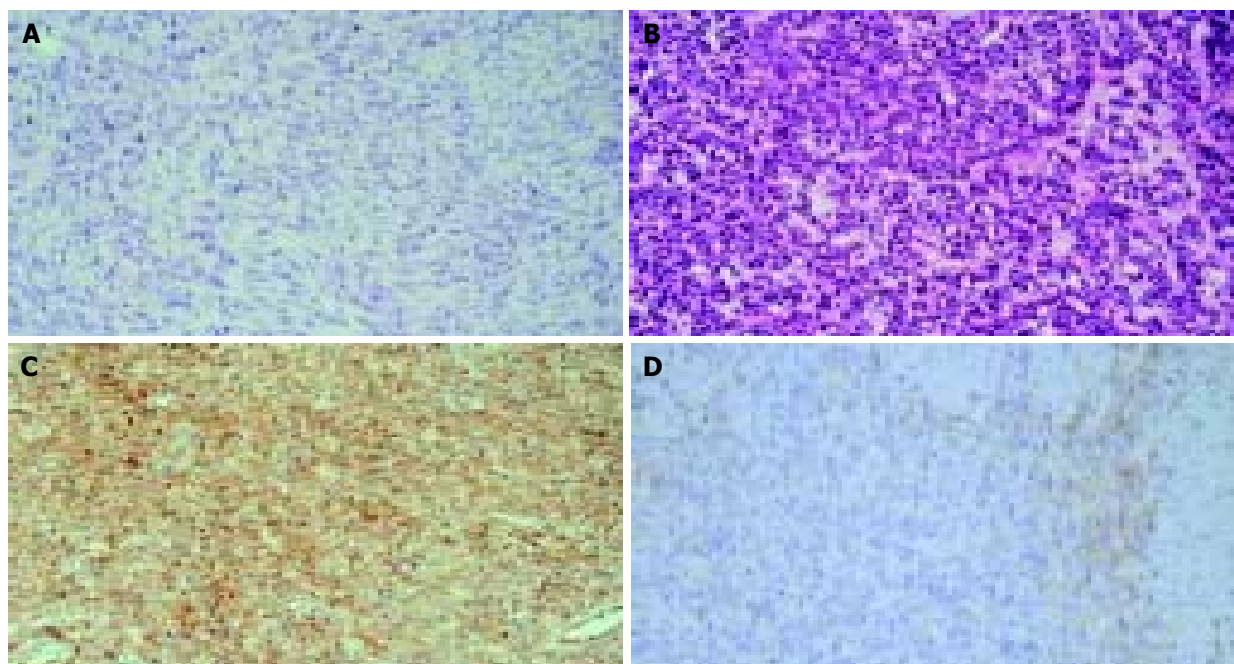


Figure 1 Histological features of various cell types of gastrointestinal stromal tumors and immunohistochemical staining for *c-Kit*. ×200. A: Spindle cell type; B: Epithelioid type; C: >50% tumor cells are positive for *c-Kit*; D: 10-50% tumor cells are positive for *c-Kit*.

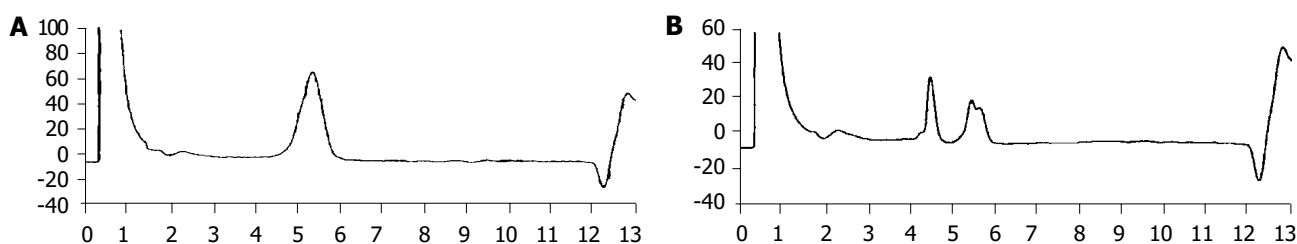


Figure 2 *c-Kit* mutations in exon 11 by denaturing high performance liquid chromatography. A: Normal; B: mutation.

Table 2 Comparison of clinicopathologic parameters according to the risk groups of gastrointestinal stromal tumors

Parameter	Risk group	Very low and low (n = 36)	Intermediate and high (n = 19)	P
Cellularity	Low	11	0	0.019
	Intermediate	22	15	
	High	3	4	
Nuclear atypia	Mild	22	5	0.019
	Moderate	12	9	
	Severe	2	5	
Necrosis	Absent	34	10	0.000
	Present	2	9	
Hemorrhage	Absent	28	10	0.055
	Present	8	9	
Infiltrative	Absent	22	8	0.178
Growth pattern	Present	14	11	
Tumor cell type	Spindle	29	11	0.001
	Epithelioid	7	8	

Results of immunohistochemistry

A positive reaction for *c-Kit* protein was obtained in 53 (96.4%), CD 34 in 53 (96.4%), SMA in 17 (30.9%), and S-100 protein in 3 (5.5%). Among 53 *c-Kit* positive cases, 10 cases (18.9%) were (+) and 43 cases (81.1%) were (++) (Figure 1).

Correlation of *c-kit* mutation with clinicopathologic parameters

Thirty cases (54.5%) showed mutations of *c-Kit* in exon 11 (Figure 2). Among 30 cases, 16 cases showed mutations by both PCR-SSCP and D-HPLC methods, 9 cases by PCR-SSCP, and 5 cases by D-HPLC method. Seven cases (12.7%) showed mutations of *c-Kit* in exon 9. Among them, 3 cases showed mutations by both

PCR-SSCP and D-HPLC methods, 3 cases by PCR-SSCP, and 1 case by D-HPLC method. Two cases showed mutations of both exons 9 and 11. No mutations were found in exons 13 and 17. The mutation-positive GISTs belonged to the large tumors (Table 3), but the association with the other parameters was not significant.

Table 3 Comparison of clinicopathologic parameters according to *c-Kit* mutations

Parameter	Mutations		P
	Negative (n = 20)	Positive (n = 35)	
Sex (M:F)	11:9	14:21	0.283
Age (mean, yr)	58.2	61.0	0.360
Mean tumor size (cm)	3.8	6.2	0.020
Mean mitoses counts	7.8	13.4	0.360
Risk group: Very low/low	14	22	0.592
Intermediate/high	6	13	
Cellularity: Low	5	6	
	Intermediate	13	0.741
	High	24	
	High	5	
Nuclear atypia	Mild	17	0.898
	Moderate	7	
	Severe	3	
Necrosis	Absent	18	0.161
	Present	2	
Hemorrhage	Absent	17	0.054
	Present	3	
Infiltrative growth	Absent	12	0.539
	Present	8	
Tumor cell type	Spindle	13	0.330
	Epithelioid	7	

Correlation of *c-kit* mutation with *c-kit* expression

Among 10 *c-Kit* (+) cases, 6 cases showed mutations of *c-Kit* in exon 9 or 11. Among 43 *c-Kit* (++) cases, 31 cases showed mutations of *c-Kit* in exon 9 or 11. The rate of *c-Kit* mutations was higher in *c-Kit* (++) group than that in *c-Kit* (+) group ($P=0.05$).

Correlation of DNA aneuploidy with clinicopathologic parameters

Ten cases (18.2%) were DNA aneuploidy (Figure 3). The tumors with aneuploidy were associated with the larger tumor size, high mitotic counts, higher risk groups, high cellularity, and severe nuclear atypia, and epithelioid cell type (Table 4).

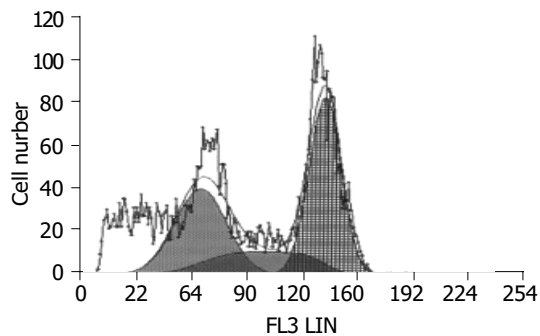


Figure 3 DNA aneuploidy in gastrointestinal stromal tumors.

Table 4 Comparison of clinicopathologic parameters according to DNA ploidy

Parameter	Diploid (n = 45)	Aneuploid (n = 10)	P
Sex (M:F)	21:24	4:6	0.702
Age(mean, yr)	60.8	56.1	0.225
Mean tumor size (cm)	4.1	10.5	0.007
Mean mitoses counts	5.0	40.0	0.022
Risk group: Very low/low	34	2	0.001
Intermediate/high	11	8	
Cellularity Low	11	0	0.008
Intermediate	31	6	
High	3	4	
Nuclear atypia Mild	24	3	0.016
Moderate	18	3	
Severe	3	4	
Necrosis Absent	38	6	0.080
Present	7	4	
Hemorrhage Absent	33	5	0.149
Present	12	5	
Infiltrative growth Absent	27	3	0.085
Present	18	7	
Tumor cell type Spindle	36	4	0.010
Epithelioid	9	6	

Correlations of *c-kit* mutation and DNA aneuploidy with metastasis or recurrence

Three metastatic GISTs showed *c-Kit* mutation. Among them, two cases showed mutations in exon 11, and the other one showed mutation in exon 9. Two of these 3 tumors had DNA aneuploidy. Among two recurrent GISTs, only one case showed mutation in exon 11, and the two cases were DNA diploidy.

Correlation of *c-kit* mutation with DNA aneuploidy

Correlation of *c-Kit* mutation with DNA ploidy state was analyzed (Table 5). There was a tendency that *c-Kit* mutations were more frequent in aneuploid tumors than in diploid ones, but not statistically significant ($P = 0.063$).

Table 5 Correlation of *c-Kit* mutation and DNA ploidy

DNA ploidy ¹	<i>c-Kit</i> mutation	
	Negative	Positive
Diploid	19	26
Aneuploid	1	9

¹ $P = 0.063$.

DISCUSSION

It has been reported that GISTs are strongly and nearly consistent *c-Kit* positive, and associated with the mutations of the *c-Kit* gene. Approximately 40% to 50% of GISTs, mostly the malignant variants, had mutations in the juxtamembrane domain (exon 11) of the *c-Kit* gene^[14-16], although some studies found mutations in only 15%^[18] or the others in as many as 80%^[19] of the analyzed cases. Lack of mutations in exon 11 in a significant portion of GISTs may suggest that mutations may occur in other domains of the *c-Kit* gene. However, no mutations were found in exon 17 (kinase domain) in a large group of GISTs studied^[14], which was the area where *c-Kit* mutations occur in mastocytoma^[20] and seminoma^[21]. Recently, new mutational hotspots were identified as a result of comprehensive sequencing of *c-Kit* cDNA obtained from 13 GISTs, which were negative for exon 11 mutations. Mutations in exon 9 and exon 13 were detected in 6 (46%) and 2 (15%) of them, suggesting that such mutations may be relatively common in GISTs^[19].

In this study, we analyzed 55 GISTs. Thirty cases (54.5%) showed mutations of *c-Kit* in exon 11 and 7 cases (12.7%) showed mutations in exon 9. No mutations were found in exon 13 and exon 17. The *c-Kit* mutation positive GISTs were large in size, and all three metastatic GISTs showed mutations, but the association with other clinicopathologic factors was not evident. The rate of *c-Kit* mutations was higher in *c-Kit* (++) group rather than in *c-Kit* (+) group.

The factors related to the tumor biology might usefully complement the clinical and morphological data. Thus, DNA aneuploidy has been claimed to allow a sensitive and specific discrimination between benign and malignant tumors of the gastrointestinal tract and to correlate with their prognosis^[22-28]. However, in other reports, aneuploidy could not be used as a diagnostic criterion of malignancy, but was associated with a mere tendency to an adverse outcome^[29,30]. In our study, 10 cases (18.2%) showed DNA aneuploidy. The aneuploid GISTs were associated with large tumor size, high mitotic counts, higher risk groups, high cellularity, severe nuclear atypia and epithelioid type. These results suggest that DNA aneuploidy represents high risk groups of GISTs suggested by NIH consensus^[13].

In conclusion, there is a tendency that *c-Kit* mutations are more frequent in aneuploid GISTs. Therefore, DNA ploidy and *c-Kit* mutations might be closely related.

REFERENCES

- 1 Appelman HD. Smooth muscle tumors of the gastrointestinal tract. What we know now that Stout didn't know. *Am J Surg Pathol* 1986; **10**: 83-99
- 2 Kindblom LG, Remotti HE, Aldenborg F, Meis-Kindblom JM. Gastrointestinal pacemaker cell tumor (GIPACT): gastrointestinal stromal tumors show phenotypic characteristics of the interstitial cells of Cajal. *Am J Pathol* 1998; **152**: 1259-1269
- 3 Miettinen M, Sarlomo-Rikala M, Lasota J. Gastrointestinal stromal tumors - recent advances in understanding of their biology. *Hum Pathol* 1999; **30**: 1213-1220
- 4 Appelman HD. Mesenchymal tumors of the gut: historical perspectives, new approaches, new results and dose it make any difference? *Monogr Pathol* 1990; **31**: 220-246

- 5 **Emory TS**, Sobin LH, Lukes L, Lee DH, O'Leary TJ. Prognosis of gastrointestinal smooth muscle (stromal) tumors. Dependence on anatomic site. *Am J Surg Pathol* 1999; **23**: 82-87
- 6 **Miettinen M**, Sarlomo-Rikala M, Sobin LH, Lasota J. Esophageal stromal tumors. A clinicopathologic, immunohistochemical and molecular genetic study of 17 cases and comparison with esophageal leiomyomas and leiomyosarcomas. *Am J Surg Pathol* 2000; **24**: 211-222
- 7 **Dematteo RP**, Lewis JJ, Leung D, Mudan SS, Woodruff JM, Brennan MF. Two hundred gastrointestinal stromal tumors. Recurrence patterns and prognostic factors for survival. *Ann Surg* 2000; **231**: 51-58
- 8 **Evans HL**. Smooth muscle tumors of the gastrointestinal tract. A study of 56 cases followed for a minimum of 10 years. *Cancer* 1985; **56**: 2242-2250
- 9 **Franquemont DW**. Differentiation and risk assessment of gastrointestinal stromal tumors. *Am J Clin Pathol* 1995; **103**: 41-47
- 10 **Miettinen M**, Lasota J. Gastrointestinal stromal tumors: definition, clinical, histological, immunohistochemical and molecular genetic features and differential diagnosis. *Virchows Arch* 2001; **438**: 1-12
- 11 **Ranchod M**, Kempson RL. Smooth muscle tumors of the gastrointestinal tract and retroperitoneum. A pathologic analysis of 100 cases. *Cancer* 1977; **39**: 255-262
- 12 **Reith JD**, Goldblum JR, Lytes RH, Weiss SW. Extra-gastrointestinal (soft tissue) stromal tumors: an analysis of 48 cases with emphasis on histological predictors of outcome. *Mod Pathol* 2000; **13**: 577-585
- 13 **Fletcher CDM**, Berman JJ, Corless C, Gorstein F, Lasota J, Longley BJ, Miettinen M, O'Leary TJ, Remotti H, Rubin BP, Shmookler B, Sobin LH, Weiss SW. Diagnosis of gastrointestinal stromal tumors: a consensus approach. *Hum Pathol* 2002; **33**: 459-465
- 14 **Taniguchi M**, Nishida T, Hirota S, Isozaki K, Ito T, Nomura T, Matsuda H, Kitamura Y. Effect of *c-kit* mutation on prognosis of gastrointestinal stromal tumors. *Cancer Res* 1999; **59**: 4297-4300
- 15 **Ernst SI**, Hubbs AE, Przygodzki RM, Emory TS, Sobin LH, O'Leary TJ. KIT mutation portends poor prognosis in gastrointestinal stromal/smooth muscle tumors. *Lab Invest* 1998; **78**: 1633-1636
- 16 **Lasota J**, Jasinski M, Sarlomo-Rikala M, Miettinen M. Mutations in exon 11 of *c-kit* occur preferentially in malignant versus benign gastrointestinal stromal tumors and do not occur in leiomyomas or leiomyosarcomas. *Am J Pathol* 1999; **154**: 53-60
- 17 **Lasota J**, Wozniak A, Sarlomo-Rikala M, Rys J, Kordek R, Nassar A, Sobin LH, Miettinen M. Mutations in exons 9 and 13 of KIT gene are rare events in gastrointestinal stromal tumors. A study of 200 cases. *Am J Pathol* 2000; **157**: 1091-1095
- 18 **Moskaluk CA**, Tian Q, Marshall CR, Rumpel CA, Franquemont DW, Frierson HF Jr. Mutations of c-kit JM domain are found in a minority of human gastrointestinal stromal tumors. *Oncogene* 1999; **18**: 1897-1902
- 19 **Lux ML**, Rubin BP, Biase TL, Chen CJ, Maclure T, Demetri G, Xiao S, Singer S, Fletcher CDM, Fletcher JA. KIT extracellular and kinase domain mutations in gastrointestinal stromal tumors. *Am J Pathol* 2000; **156**: 791-795
- 20 **Nagata H**, Worobec AS, Oh CK, Chowdhury BA, Tannenbaum S, Suzuki Y, Metcalfe DD. Identification of a point mutation in the catalytic domain of the protooncogene *c-kit* in peripheral blood mononuclear cells of patients who have mastocytosis with an associated hematologic disorder. *Proc Natl Acad Sci U S A* 1995; **92**: 10560-10564
- 21 **Tian Q**, Frierson HF, Krystal GW, Moskaluk CA. Activating c-kit mutations in human germ cell tumors. *Am J Pathol* 1999; **154**: 1643-1647
- 22 **Federspiel BH**, Sobin LH, Helwig EB, Mikel UV, Bahr GF. Morphometry and cytophotometric assessment of DNA in smooth-muscle tumors (leiomyomas and leiomyosarcomas) of the gastrointestinal tract. *Anal Quant Cytol Histol* 1987; **9**: 105-114
- 23 **Cooper PN**, Quirke P, Hardy GJ, Dixon MF. A flow cytometric, clinical and histological study of stromal neoplasm of the gastrointestinal tract. *Am J Surg Pathol* 1992; **16**: 163-170
- 23 **Carrillo R**, Candia A, Rodriguez-Peralto JL, Caz V. Prognostic significance of DNA ploidy and proliferative index (MIB-1 index) in gastrointestinal stromal tumors. *Hum Pathol* 1997; **28**: 160-165
- 24 **Kiyabu MT**, Bishop PC, Parker JW, Turner RR, Fitzgibbons PL. Smooth muscle tumors of the gastrointestinal tract: flow cytometric quantitation of DNA and nuclear antigen content and correlation with histologic grade. *Ann J Surg Pathol* 1988; **12**: 954-960
- 25 **Suzuki H**, Sugihira N. Prognostic value of DNA ploidy in primary gastric leiomyosarcoma. *Br J Surg* 1993; **80**: 1549-1550
- 26 **Shimamoto T**, Haruma K, Sumii K, Kajiyama G, Tahara E. Flow cytometric DNA analysis of gastric smooth muscle tumors. *Cancer* 1992; **70**: 2031-2034
- 27 **Cunningham RE**, Federspiel BH, McCarthy WF, Sobin LH, O'Leary TJ. Predicting prognosis of gastrointestinal smooth muscle tumors: role of clinical and histologic evaluation, flow cytometry, and image cytometry. *Am J Surg Pathol* 1993; **17**: 588-594
- 28 **Tsushima K**, Rainwater LM, Goellner JR, van Heerden JA, Lieber MM. Leiomyosarcomas and benign smooth muscle tumors of the stomach: Nuclear DNA patterns studied by flow cytometry. *Mayo Clin Proc* 1987; **62**: 275-280
- 29 **Lerma E**, Oliva E, Tugues D, Prat J. Stromal tumors of the gastrointestinal tract: a clinicopathologic and ploidy analysis of 33 cases. *Virchows Arch* 1994; **424**: 19-24
- 30 **Lerma E**, Lee SJ, Tugues D, Oliva E, Gich I, Prat J. Ploidy of 36 stromal tumors of the gastrointestinal tract: a comparative study with flow cytometry and image analysis. *Anal Quant Cyto Histol* 1994; **16**: 435-440

Edited by Wang XL and Xu CT Proofread by Pan BR and Xu FM

Genomic determination of CR1 CD35 density polymorphism on erythrocytes of patients with gallbladder carcinoma

Xing-Yuan Jiao, Ming-De Lü, Jie-Fu Huang, Li-Jian Liang, Jing-Sen Shi

Xing-Yuan Jiao, Ming-De Lü, Jie-Fu Huang, Li-Jian Liang, Department of Hepatobiliary Surgery, First Affiliated Hospital, Sun Yat-Sen University, Guangzhou 510080, Guangdong Province, China
Jing-Sen Shi, Hepatobiliary Research Laboratory, First Affiliated Hospital, Xi'an Jiaotong University, Xi'an 710061, Shaanxi Province, China

Supported by National Postdoctor Natural Science Foundation of China, No. 2001-14

Correspondence to: Xing-Yuan Jiao, Department of Hepatobiliary Surgery, First Affiliated Hospital, Sun Yat-Sen University, Guangzhou 510080, Guangdong Province, China. jiaoxingyuan@hotmail.com.cn
Telephone: +86-20-34152243 **Fax:** +86-20-34152456

Received: 2004-01-09 **Accepted:** 2004-03-16

Abstract

AIM: To study the changes of quantitative expression, adhering activity and genomic density polymorphism of complement types in erythrocytes (CR1) of patients with gallbladder carcinoma and the related clinical significance.

METHODS: Polymerase chain reaction (PCR), *Hind*III restriction enzyme digestion, quantitative assay of CR1 and adhering activity assay of CR1 in erythrocytes were used.

RESULTS: The number and adhering activity of CR1 in patients with gallbladder carcinoma (0.738 ± 0.23 , 45.9 ± 5.7) were significantly lower than those in chronic cholecystitis and cholelithiasis (1.078 ± 0.21 , 55.1 ± 5.9) and healthy controls (1.252 ± 0.31 , 64.2 ± 7.4) ($P < 0.01$). The number and adhering activity of CR1 in patients with chronic cholecystitis and cholelithiasis (1.078 ± 0.21 , 55.1 ± 5.9) were significantly lower than those in healthy controls (1.252 ± 0.31 , 64.2 ± 7.4) ($P < 0.05$). There was a positive correlation between quantitative expression and adhering activity of CR1 ($r = 0.79$, $P < 0.01$). Compared with those on preoperative day (0.738 ± 0.23 , 45.4 ± 4.9), the number and adhering activity of CR1 in patients with gallbladder carcinoma decreased greatly on the third postoperative day (0.310 ± 0.25 , 31.8 ± 5.1) ($P < 0.01$), and on the first postoperative week (0.480 ± 0.25 , 38.9 ± 5.2) ($P < 0.01$), but they were increased slightly than those on the preoperative day ($P > 0.05$). The number and adhering activity of CR1 recovered in the second postoperative week (0.740 ± 0.24 , 46.8 ± 5.9) ($P < 0.01$) and increased greatly in the third postoperative week (0.858 ± 0.35 , 52.7 ± 5.8) ($P < 0.01$) in comparison with those on the preoperative day and in the first postoperative week. The number and adhering activity of CR1 of gallbladder carcinoma patients with infiltrating, adjacent lymphogenous and distant organ metastases were significantly lower than those of gallbladder carcinoma patients without them ($P < 0.01$). No difference was observed between the patients with gallbladder carcinoma and healthy individuals in the spot mutation rate of CR1 density gene ($\chi^2 = 0.521$, $P > 0.05$). The distribution of expression was 67.8% in high expression genomic type, 24.8% in moderate expression genomic type, and 7.4% in low expression genomic type. The number and adhering activity of CR1 high expression genomic type

gallbladder carcinomas (0.749 ± 0.22 , 42.1 ± 6.2) were significantly lower than those of healthy individuals (1.240 ± 0.29 , 63.9 ± 7.2), and were also significantly lower than those of healthy individuals (0.921 ± 0.23 , 54.8 ± 7.1), but no difference was observed between the number and adhering activity of CR1 lower expression genomic type gallbladder carcinomas (0.582 ± 0.18 , 44.3 ± 5.5) and those of healthy individuals (0.610 ± 0.20 , 45.8 ± 5.7) ($P > 0.05$).

CONCLUSION: Defective expression of CR1 in gallbladder carcinoma is mostly acquired through central peripheral mechanisms. The changes in CR1 quantitative expression and adhering activity are consanguineously related to the development and metastasis in gallbladder carcinoma.

Jiao XY, Lü MD, Huang JF, Liang LJ, Shi JS. Genomic determination of CR1 CD35 density polymorphism on erythrocytes of patients with gallbladder carcinoma. *World J Gastroenterol* 2004; 10(23): 3480-3484

<http://www.wjgnet.com/1007-9327/10/3480.asp>

INTRODUCTION

Carcinoma of the gallbladder is the most common neoplasm in biliary tract, and its incidence has been rising in recent years^[1-4]. The C3b receptors (CR1, Cd35) on erythrocytes serve as the primary transport system for immune complexes from peripheral blood of the liver^[5-8], and CR1 plays an important role in this system, the rate of clearance of immune complexes from the circulation is directly related to the number of CR1 molecules expressed on erythrocytes^[9-11]. However, there are few reports on the changes of genomic density polymorphism of complement types in erythrocytes of patients with gallbladder carcinoma. We previously demonstrated the altered levels of cellular immunity and humoral immunity in patients with gallbladder carcinoma, and the effects of radical cholecystectomy on nutritional and immune status in patients with gallbladder carcinoma^[12-15]. In this study, we reported the changes in quantitative expression, adhering activity and genomic density polymorphism of complement types in erythrocytes (CR1) of patients with gallbladder carcinoma.

MATERIALS AND METHODS

Patients

A total of 33 patients with gallbladder carcinoma were admitted to the First Affiliated Hospital of Sun Yat-Sen University from August 2000 to August 2002. Those were 16 men and 17 women aged from 50 to 70 years (median, 52.7 years). Nineteen patients were preoperatively diagnosed as polypoid, cholelithiasis and chronic cholecystitis, and diagnosed as gallbladder carcinoma by frozen sections after surgery. Fourteen patients were diagnosed as gallbladder carcinoma preoperatively, of them, 4 patients had radical cholecystectomy, 7 patients had U-tube drainage operation, 3 patients cholecystectomy. Direct invasion or distant metastasis was found in 10 patients during operation, simple gallbladder carcinoma in 15 patients, both gallbladder carcinoma and cholelithiasis in 18 patients. The patients with gallbladder

carcinoma were grouped according to the staging system of Nevin^[16], the number of cases on stages I, II, III, IV and V was 7, 11, 5, 7 and 11, respectively. Tumor size ranged from 1.8 cm to 6 cm in diameter (median, 2 cm), 23 patients had tumors smaller than 2 cm in diameter, 10 patients had tumors larger 2 cm in diameter.

No therapy was administered to patients preoperatively. Meanwhile, 90 patients with cholecystitis or cholecystolithiasis had cholecystectomy, including 44 patients with cholecystitis and 46 patients with cholelithiasis. No severe systemic diseases were found, such as, myocardial infarction, cerebral vascular accidents, uncontrollable diabetes mellitus, Hypertension. Their disease was stable in a period of one month. All the surgical specimens were examined histologically, and classified into hyperplasia, atypical hyperplasia (mild, moderate and severe) according to Gong *et al.*^[17]. A total of 59 patients exhibited epithelial hyperplasia, 10 patients had mild dysplasia, 10 patients moderate dysplasia, 11 patients severe dysplasia. Normal controls were 30 healthy individuals (18 men and 12 women) aged from 56 years to 72 years (median 61.7 years).

Methods

Quantitative expression, adhering activity and genomic density polymorphism of complement types in erythrocytes (CR1) patients with gallbladder carcinoma were assessed preoperatively (1 wk before surgery), and on d 3, 7, 14 and 21 postoperatively.

Genomic determination of CR1 (Cd35) density polymorphism on erythrocytes^[18]

DNA samples DNA was extracted using the following simplified protocol. Following lysis of erythrocytes, nucleated cells from 10 mL of blood were incubated in 3.5 mL of 10 mmol/L Tris, 2 mmol/L EDTA buffer pH7.5, containing 0.4 mol/L NaCl, 7 g/L sodium dodecylsulfate and proteinase K (30 mg/L) for 16 h at 37 °C, 1 mL of 6 mol/L NaCl was added. After vortexed and ethanol-precipitated, the pellets were washed three times in 700 mL/L ethanol and solubilized in 10 mmol/L Tris, 1 mmol/L EDTA buffer pH7.5.

Sequencing

A construct in pUC-18 containing *Hind* III-kpn fragments from the introns located within the first and second exons of the short consensus repeat d2 from the long homologous repeat D of CR1 was sequenced. Sequencing was performed using the modified Sanger method with a commercial T₇ DNA polymerase kit.

Primers

Primers were designed based on the analysis of internal homologies within the CR1 gene and homologies with other human sequences obtained from the EMBL databank using the Bisanse software. The 5' primer was from base 4 415 to base 4 435 from the CR1 cDNA sequence. The 3' primer was 75 to 55 from the *Hind* III monomorphic restriction site in the introns. The latter primer was chosen due to the presence of five mismatches between the CR1 intron sequence and the consensus *Hind* III 1.9 ku repetitive sequence. Primers were synthesized on a 380 Applied Biosystem apparatus. Twenty base oligonucleotides were recovered from the solid phase by rinsing the column with 250 g/L ammonium. After incubation at 55 °C for 16 h, ammonium was expelled through evaporation using a Speed-Vac apparatus. Primers were used without further purification.

Amplification and agarose gel electrophoresis

PCR was performed using a Techne PHC-I apparatus with the Taq polymerase.

Amplified DNA was precipitated and then digested using the *Hind* III restriction enzyme, and separated by electrophoresis in 20 g/L agarose gels. Gels were analyzed under UV illumination. The genomic density polymorphism of complement type 1 (CR1)

in erythrocytes was classified into three types: high expression genomic type (1.8 Kb1), moderate expression type (1.8 kb, 1.3 Kb and 1.5 Kb) and low expression genomic type (1.3 Kb, 0.5 Kb).

Quantitative expression of CR1 in erythrocytes of patients with gallbladder carcinoma

EBC enzyme-linked immunosorbent assay This assay was based on the method of Cornillet *et al.*^[18]. All RBCs in the assay were routinely glutaraldehyde-fixed. Finally, 20 μL of S/BSA were added to each well, followed by 20 μL of substrate. The plates were incubated at 37 °C for 90 min with gentle agitation every 15-20 min to ensure the maximum contact of RBC with substrate. Subsequently, 100 μL of S/BSA was added to each well, the plate was centrifuged at 1 800 r/min for 90 s and 100 μL of supernatant was transferred to a clean microtitre plate for readings in a plate reader at 405 nm (Dynatech MR5000; DynatchmBillingshurst, Suaaex, UK). In each case, a mean of the readings obtained for the RBC without first antibody (the blank controls) was subtracted from the other readings obtained, in order to correct nonspecific phosphatase-like activity within RBC membranes. Duplicate values were obtained for each RBC sample with each antibody. Black control values were obtained for both the antimouse conjugates and for the anti-rabbit conjugates.

Adhering activity of CR1 in erythrocytes of patients with gallbladder carcinoma

A 50 μL of 1×10⁸/mL RBC suspensions was added to each well, then added and 50 μL of plasma itself and 100 μL of 1×10⁶/mL tumor cells, mixed completely, stained. Fields were examined (×640), 5 RBC combined each tumor cell were labeled as a flower, tumor cell flowers were assessed.

Statistical analysis

For each variable, muultiple analysis of variance for repeated measurements was used to compare the values measured before operation with those measured at four subsequent time points. The results were presented as mean±SE based on the mixed model of repeated measurement analysis. Statistical analysis was performed with SAS software. *P*<0.05 was considered statistically significant.

RESULTS

The number and adhering activity of CR1 in patients with gallbladder carcinoma, chronic cholecystitis and cholecystolithiasis and healthy individuals

As shown in Table 1, the number and adhering activity of CR1 in patients with gallbladder carcinoma (0.738±0.23, 45.9±5.7) were significantly lower than those in patients chronic cholecystitis and cholecystolithiasis (1.078±0.21, 55.1±5.9) and healthy individuals controls (1.252±0.31, 64.2±7.4) (*P*<0.01). In Table 2 the number and adhering activity of CR1 in patients with chronic cholecystitis and cholecystolithiasis were significantly lower than those in healthy controls (*P*<0.05). There was a positive correlation between quantitative expression and adhering activity of CR1 (*r* = 0.79, *P*<0.01).

In the series of epithelial pathologic changes including hyperplasia, atypical hyperplasia, carcinoma *in situ* or invasive carcinoma, the number and adhering activity of CR1 decreased gradually (Table 3), and there was a positive correlation between quantitative expression and adhering activity of CR1 (*r* = 0.77, *P*<0.01). In Table 4 compared with those on the preoperative day (0.738±0.23, 45.4±4.9), the number and adhering activity of CR1 in patients with gallbladder carcinoma decreased greatly on the third postoperative day (0.310±0.25, 31.8±5.1) (*P*<0.01) and in the first postoperative week (0.480±0.25, 38.9±5.2) (*P*<0.01), but they were increased slightly than those on the preoperative

day ($P>0.05$). In comparison with those on the preoperative day and in the first postoperative week, the number and adhering activity of CR1 recovered in the second postoperative week ($0.740\pm 0.24, 46.8\pm 5.9$) ($P<0.01$), and increased greatly in the third postoperative week ($0.858\pm 0.35, 52.7\pm 5.8$) ($P<0.01$).

The number and adhering activity of CR1 in gallbladder carcinoma patients with infiltrating, adjacent lymph node and distant organ metastases were significantly lower than those in gallbladder carcinoma patients without metastasis (Table 5, $P<0.01$).

Table 1 The number and adhering activity of CR1 in different groups before operation (mean \pm SE)

Group	Cases	CR1 (A_{405})	Adhering activity (%)
Healthy individuals	30	1.252 \pm 0.31	64.2 \pm 7.4
Chronic cholecystitis	90	1.078 \pm 0.21 ^a	55.1 \pm 5.9 ^a
Cholecystolithiasis			
Gallbladder carcinoma	33	0.738 \pm 0.23 ^{b,c}	45.9 \pm 5.7 ^{b,d}

^a $P<0.05$, ^b $P<0.01$ vs normal control; ^c $P<0.05$, ^d $P<0.01$ vs chronic cholecystitis and cholecystolithiasis.

Table 2 The number and adhering activity of CR1 in different groups before operation (mean \pm SE)

Group	Cases	CR1 (A_{405})	Adhering activity (%)
Healthy individuals	30	1.252 \pm 0.31	64.2 \pm 7.4
cholecystolithiasis	46	1.027 \pm 0.27 ^a	54.4 \pm 5.9 ^a
Gallbladder carcinoma	18	0.731 \pm 0.26 ^{b,c}	45.1 \pm 6.1 ^{b,d}
with cholecystolithiasis			
Simple gallbladder carcinoma	15	0.728 \pm 0.23 ^{b,c}	44.8 \pm 6.4 ^{b,d}

^a $P<0.05$, ^b $P<0.01$ vs normal control; ^c $P<0.05$, ^d $P<0.01$ vs chronic cholecystitis.

Table 3 The number and adhering activity of CR1 in different groups before operation (mean \pm SE)

Type	Cases	CR1 (A_{405})	Adhering activity (%)
Simple hyperplasia	59	1.175 \pm 0.22	61.1 \pm 6.2
Atypical hyperplasia	21	0.906 \pm 0.24 ^b	50.8 \pm 5.7 ^b
Gallbladder carcinoma (I-III stage)	23	0.761 \pm 0.23 ^b	41.6 \pm 6.1 ^b
Gallbladder carcinoma (IV-V stage)	10	0.602 \pm 0.31 ^b	30.4 \pm 6.5 ^b
F		6.4	11.5
P		<0.01	<0.01

^b $P<0.01$ vs each group.

Table 4 The number and adhering activity of CR1 on preoperative and postoperative day (mean \pm SE)

Group	Preoperative	3 rd d	1 st wk	2 nd wk	3 rd wk
CR1 (A_{405})	0.738 \pm 0.23	0.310 \pm 0.25 ^b	0.480 \pm 0.25 ^b	0.740 \pm 0.24	0.85 \pm 0.32 ^a
Adhering activity (%)	45.4 \pm 4.9	31.8 \pm 5.1 ^b	38.9 \pm 5.2 ^b	46.8 \pm 5.9	52.7 \pm 5.8 ^a

^a $P<0.05$, ^b $P<0.01$ vs normal control.

Table 5 The number and adhering activity of CR1 in gallbladder carcinoma with adjacent lymph nodes and metastasis (mean \pm SE)

Group	Healthy individuals	Infiltrating (-)	Infiltrating (+)	Adjacent lymph node (-)	Adjacent lymph node (+)	Metastasis (-)	Metastasis (+)
Cases	30	15	18	18	15	23	10
CR1 (A_{405})	1.252 \pm 0.31	0.95 \pm 0.22 ^a	0.81 \pm 0.29 ^{ab}	0.88 \pm 0.27 ^a	0.73 \pm 0.25 ^{ab}	0.78 \pm 0.26 ^a	0.44 \pm 0.29 ^{ad}
Adhering activity (%)	64.2 \pm 7.4	52.8 \pm 6.7 ^a	48.1 \pm 7.2 ^{ab}	47.6 \pm 7.0 ^a	41.1 \pm 7.1 ^{ab}	46.1 \pm 6.1 ^a	38.9 \pm 6.2 ^{ad}

^b $P<0.01$ vs normal control; ^a $P<0.05$, ^d $P<0.01$ vs negative.

Changes of genomic density polymorphism of CR1 in patients with gallbladder carcinoma

The distribution of genomic density polymorphism of CR1 in patients was 67.8% in high expression genomic type, 24.8% in moderate expression genomic type, 7.4% in low expression genomic type. Compared with healthy controls, no difference was observed between the patients with gallbladder carcinoma and healthy in the spot mutation rate of CR1 density gene ($\chi^2 = 0.521$, $P>0.05$). The number and adhering activity of CR1 high expression genomic type gallbladder carcinomas ($0.749\pm 0.22, 42.1\pm 6.2$) were significantly lower than those in healthy individuals ($1.240\pm 0.29, 63.9\pm 7.2$). The number and adhering activity of CR1 moderate expression genomic type gallbladder carcinomas ($0.641\pm 0.19, 34.2\pm 5.1$) were also significantly lower than those in healthy individuals ($0.921\pm 0.23, 54.8\pm 7.1$), but no difference was observed between the number and adhering activity of CR1 lower expression genomic type gallbladder carcinomas ($0.582\pm 0.18, 44.3\pm 5.5$) and those of healthy individuals ($0.610\pm 0.20, 45.8\pm 5.7$) ($P>0.05$).

DISCUSSION

The immune functions of erythrocytes have been studied at gene levels^[5-8]. RBCs are the major cellular component of the peripheral blood and occupy 50% of the total blood volume^[9]. Normal RBC cytosol contains the majority of natural killer enhancing factors and other factors, such as PIF. Damaged RBC could produce tumor necrosis factor inducing factor. RBCs appear to have an important regulating role in immune function, and RBC activity involves in regulating multiple cytokines such as IL-2, IL-3, CSF, IL-6, TNF-r, TNF. CD44 and CD58 expressed by RBC could serve as the center in controlling immune status, which can directly affect the development and progression of tumors^[8-11]. The changes of CR1 quantitative expression and adhering activity are consanguineously related to the development and metastasis of liver carcinoma.

In our study, the number and adhering activity of CR1 high expression genomic type gallbladder carcinomas were significantly lower than those in healthy individuals, indicating that defective expression of CR1 in gallbladder carcinoma is mostly acquired through central peripheral mechanisms.

Gallbladder carcinoma is often associated with cholecystolithiasis and cholecystitis in 40-100% of cases^[19-28]. Although no carcinogenic substance has so far been isolated from the bile or the stones in patients with cholecystolithiasis and cholecystitis, many scholars suggested that gallstone might play a role as a chronic injury factor to induce a series of epithelial pathologic changes^[29-38]. Gong *et al.*^[17] reported that in 150 consecutive cholecystectomy specimens for detection of cholelithiasis or cholecystitis, 76.68% exhibited epithelial hyperplasia, 16.89%

atypical hyperplasia, 1.32% carcinoma *in situ* and 2.11% invasive carcinoma. Simple epithelial hyperplasia was found in the mucus adjacent to invasive carcinoma. With the passage of time, a significant number of atypical hyperplasias presumably would progress to a higher grade lesion, becoming carcinoma. Toyonaga *et al.*^[39] reported that in 200 consecutive cholecystectomy specimens for detection of cholelithiasis or cholecystitis, 83% simple epithelial hyperplasias, 13.5% atypical hyperplasias and 3.5% carcinomas *in situ*. In general, a significant number of atypical hyperplasias presumably would progress to a higher grade lesion, 80% atypical hyperplasias could become pre-cancer lesions. Albores-Saavedra *et al.*^[11] results showed that cholelithiasis or cholecystitis produced a series of epithelial pathologic changes, such as simple epithelial hyperplasia, atypical hyperplasia and carcinoma *in situ*, which represented the precancer lesion of gallbladder carcinoma. The probable sequence of events appear to be as follows. Hyperplasia has been found to have atypical hyperplasia which in turn may progress to neoplasia. With the passage of time, a significant number of atypical hyperplasias presumably would progress to carcinoma *in situ* and invasive carcinoma^[24]. So almost all scholars have suggested that a small number of hyperplasias of the gallbladder would evolve toward *in situ* carcinoma which finally becomes invasive carcinoma^[40]. In our study, the number and adhering activity of CR1 in patients with gallbladder carcinoma were significantly lower than those in patients with chronic cholecystitis and cholelithiasis and healthy individuals ($P < 0.01$). The number and adhering activity of CR1 in patients with chronic cholecystitis and cholelithiasis were significantly lower than those in healthy individuals. There was a positive linear correlation between quantitative expression and the adhering activity of ECR1 ($r = 0.79$, $P < 0.01$). Compared with data the on preoperative day, the number and adhering activity of CR1 in patients with gallbladder carcinoma decreased greatly on the third postoperative day and in the first postoperative week, indicting that surgery plays an injurious role in the disorder of RBC and cytokine functions^[12,41,42]. The number and adhering activity of CR1 recovered in the second postoperative week, and increased greatly in the third postoperative week.

The number and the adhering activity of CR1 in gallbladder carcinoma patients with infiltrating, adjacent lymph node and distant organ metastases were significantly lower than those in patients without metastasis. This study demonstrates CR1 can be used as an immune therapy for gallbladder carcinoma.

REFERENCES

- Jiao XY, Lü MD, Huang JF. Current advances in the risk factors for gallbladder carcinoma. *Zhonghua Putong Waiké Zazhi* 2002; **17**: 117-119
- Lü MD, Jiao XY. Current status of research on tumor markers of biliary tumors. *Zhongguo Shiyong Waiké Zazhi* 2001; **9**: 522-523
- Jiao XY, Li DM, Lü MD, Huang JF, Liang LJ. Significance of nucleolar organizers regions associated proteins of T lymphocytes in diagnosis and monitoring of gallbladder carcinoma. *Zhonghua Putong Waiké Zazhi* 2002; **117**: 313-314
- Zou SQ, Zhang L. Relative risk factors analysis of 3922 cases of gallbladder cancer. *Zhonghua Waiké Zazhi* 2000; **38**: 800-805
- Birmingham DJ, Chen W, Liang G, Schmitt HC, Gavit K, Nagaraja HN. A CR1 polymorphism associated with constitutive erythrocyte CR1 levels affects binding to C4b but not C3b. *Immunology* 2003; **108**: 531-538
- Rowe JA, Raza A, Diallo DA, Baby M, Poudiougou B, Coulibaly D, Cockburn IA, Middleton J, Lyke KE, Plowe CV, Doumbo OK, Moulds JM. Erythrocyte CR1 expression level does not correlate with a Hind III restriction fragment length polymorphism in africans; implications for studies on malaria susceptibility. *Genes Immun* 2002; **3**: 497-500
- Zorzetto M, Bombieri C, Ferrarotti I, Medaglia S, Agostini C, Tinelli C, Malerba G, Carrabino N, Beretta A, Casali L, Pozzi E, Pignatti PF, Semenzato G, Cuccia MC, Luisetti M. Complement receptor 1 gene polymorphisms in sarcoidosis. *Am J Respir Cell Mol Biol* 2002; **27**: 17-23
- Nagayasu E, Ito M, Akaki M, Nakano Y, Kimura M, Looareesuwan S, Aikawa M. CR1 density polymorphism on erythrocytes of falciparum malaria patients in Thailand. *Am J Trop Med Hyg* 2001; **64**: 1-5
- Moulds JM, Zimmerman PA, Doumbo OK, Kassambara L, Sagara I, Diallo DA, Atkinson JP, Krych-Goldberg M, Hauhart RE, Hourcade DE, McNamara DT, Birmingham DJ, Rowe JA, Moulds JJ, Miller LH. Molecular identification of knobs blood group polymorphisms found in long homologous region D of complement receptor 1. *Blood* 2001; **97**: 2879-2885
- Wang HB, Qian BH, Niu F, Jiang AQ. Changes of genomic density polymorphism and quantitative expression of complement receptor type 1 in patients with liver diseases. *Zhonghua Ganzangbing Zazhi* 2000; **8**: 335-337
- Wang HB, Zhao XP, Guo F. Changes of quantitative expression, adhering activity and genomic density polymorphism of complement type1 in erythrocytes (CR1) of patients with liver cancer. *Zhonghua Jiannan Yixue Zazhi* 2000; **24**: 31-33
- Jiao XY, Shi JS, Wang JS, Yang JY, He P. Effects of radical cholecystectomy on nutritional and immune status in patients with gallbladder carcinoma. *World J Gastroenterol* 2000; **6**: 445-447
- Jiao XY, Shi JS, Gao JS, Zhou LS. Determination of levels of cellular immunity and humoral immunity in patients with gallbladder carcinoma. *Zhongguo Puwai Jichu Yu Linchuang Zazhi* 1999; **4**: 227-229
- Jiao XY, Shi JS, Gao JS, Zhou LS, Han WS, Liu G, Lu Y. Study on the serum IL-2, SIL-2r and CEA levels in patients with gallbladder carcinoma. *Zhonghua Gandan Waiké Zazhi* 1999; **5**: 342
- Shi JS, Wang JS, Liu G, Yu YL, Lu Y, Jiao XY, Yang YJ, Li GC, Han Y. Early diagnosis of primary gallbladder carcinoma. *Hepatobiliary Pancreat Dis Int* 2002; **1**: 273-275
- Nevin JE, Moran TJ, Kay S, King R. Carcinoma of the gallbladder: staging, treatment, and prognosis. *Cancer* 1976; **37**: 141-148
- Gong FQ, Gao ZY, Wang JB, Liu SG, Liu JQ. Pathologic study of precancerous lesion of the gallbladder. *Zhonghua Zhongliu Zazhi* 1989; **11**: 127-129
- Cornillet P, Philbert F, Kazatchkine MD, Cohen JHM. Genomic determination of the CR1 (CD35) density polymorphism on erythrocytes using polymerase chain reaction amplification and Hind III restriction enzyme digestion. *J Immunol Methods* 1991; **136**: 193-197
- Noshiro H, Chijiwa K, Yamaguchi K, Shimizu S, Sugitani A, Tanaka M. Factors affecting surgical outcome for gallbladder carcinoma. *Hepatogastroenterology* 2003; **50**: 939-944
- Wakai T, Shirai Y, Yokoyama N, Ajioka Y, Watanabe H, Hatakeyama K. Depth of subserosal invasion predicts long-term survival after resection in patients with T2 gallbladder carcinoma. *Ann Surg Oncol* 2003; **10**: 447-454
- Ishikawa T, Horimi T, Shima Y, Okabayashi T, Nishioka Y, Hamada M, Ichikawa J, Tsuji A, Takamatsu M, Morita S. Evaluation of aggressive surgical treatment for advanced carcinoma of the gallbladder. *J Hepatobiliary Pancreat Surg* 2003; **10**: 233-238
- Nakakubo Y, Miyamoto M, Cho Y, Hida Y, Oshikiri T, Suzuoki M, Hiraoka K, Itoh T, Kondo S, Katoh H. Clinical significance of immune cell infiltration within gallbladder cancer. *Br J Cancer* 2003; **89**: 1736-1742
- Enomoto T, Todoroki T, Koike N, Kawamoto T, Matsumoto H. Xanthogranulomatous cholecystitis mimicking stage IV gallbladder cancer. *Hepatogastroenterology* 2003; **50**: 1255-1258
- Jarnagin WR, Ruo L, Little SA, Klimstra D, D'Angelica M, DeMatteo RP, Wagman R, Blumgart LH, Fong Y. Patterns of initial disease recurrence after resection of gallbladder carcinoma and hilar cholangiocarcinoma: implications for adjuvant therapeutic strategies. *Cancer* 2003; **98**: 1689-1700
- Yanagisawa N, Mikami T, Yamashita K, Okayasu I. Microsatellite instability in chronic cholecystitis is indicative of an early stage in gallbladder carcinogenesis. *Am J Clin Pathol* 2003; **120**: 413-417
- Shukla VK, Adukia TK, Singh SP, Mishra CP, Mishra RN. Micronutrients, antioxidants, and carcinoma of the gallbladder. *J Surg Oncol* 2003; **84**: 31-35
- Kokudo N, Makuuchi M, Natori T, Sakamoto Y, Yamamoto J,

- Seki M, Noie T, Sugawara Y, Imamura H, Asahara S, Ikari T. Strategies for surgical treatment of gallbladder carcinoma based on information available before resection. *Arch Surg* 2003; **138**: 741-750
- 28 **Bani-Hani KE**, Yaghan RJ, Matalka II, Shatnawi NJ. Gallbladder cancer in northern Jordan. *J Gastroenterol Hepatol* 2003; **18**: 954-959
- 29 **Malik IA**. Clinicopathological features and management of gallbladder cancer in pakistan: A prospective study of 233 cases. *J Gastroenterol Hepatol* 2003; **18**: 950-953
- 30 **Andrea C**, Francesco C. Squamous-cell and non-squamous-cell carcinomas of the gallbladder have different risk factors. *Lancet Oncol* 2003; **4**: 393-394
- 31 **Hemminki K**, Li X. Familial liver and gall bladder cancer: a nationwide epidemiological study from Sweden. *Gut* 2003; **52**: 592-596
- 32 **Kondo S**, Nimura Y, Kamiya J, Nagino M, Kanai M, Uesaka K, Yuasa N, Sano T, Hayakawa N. Factors influencing postoperative hospital mortality and long-term survival after radical resection for stage IV gallbladder carcinoma. *World J Surg* 2003; **27**: 272-277
- 33 **Haratake J**, Kasai T, Makino H. Diffuse mucosal carcinoma of intrahepatic and extrahepatic bile ducts including gallbladder. *Pathol Int* 2002; **52**: 784-788
- 34 **Pandey M**. Risk factors for gallbladder cancer: a reappraisal. *Eur J Cancer Prev* 2003; **12**: 15-24
- 35 **Shi JS**, Zhou LS, Jiao XY, Lu Y, Hao XY, Han WS, Liu G. Clinical significance of detecting tumor necrosis factor and its receptor in serum and bile in patients with gallbladder cancer and gallstone. *Zhonghua Gandan Waik Zazhi* 2001; **7**: 82-83
- 36 **Misra S**, Chaturvedi A, Misra NC, Sharma ID. Carcinoma of the gallbladder. *Lancet Oncol* 2003; **4**: 167-176
- 37 **Parwani AV**, Geradts J, Caspers E, Offerhaus GJ, Yeo CJ, Cameron JL, Klimstra DS, Maitra A, Hruban RH, Argani P. Immunohistochemical and genetic analysis of non-small cell and small cell gallbladder carcinoma and their precursor lesions. *Mod Pathol* 2003; **16**: 299-308
- 38 **Rashid A**. Cellular and molecular biology of biliary tract cancers. *Surg Oncol Clin N Am* 2002; **11**: 995-1009
- 39 **Toyonaga T**, Chijiwa K, Nakano K, Noshiro H, Yamaguchi K, Sada M, Terasaka R, Konomi K, Nishikata F, Tanaka M. Completion radical surgery after cholecystectomy for accidentally undiagnosed gallbladder carcinoma. *World J Surg* 2003; **27**: 266-271
- 40 **Henson DE**, Albores-Saavedra J, Corle D. Carcinoma of the gallbladder carcinoma, histologic types, stage of disease, grade, and survival rates. *Cancer* 1992; **70**: 1493-1497
- 41 **Albores-Saavedra J**, Alcantra-Vazquez A, Cruz-Ortiz H, Herrera-Goepfert R. The precursor lesions, of invasive gallbladder carcinoma, hyperplasia, atypical hyperplasia and carcinoma *in situ*. *Cancer* 1980; **45**: 919-927
- 42 **Fan YZ**, Zhang JT, Yang HC, Yang YQ. Expression of MMP-2, TIMP-2 protein and the ratio of MMP-2/TIMP-2 in gallbladder carcinoma and their significance. *World J Gastroenterol* 2002; **8**: 1138-1143

Edited by Wang XL and Ren SY Proofread by Xu FM

Effects of dermatan sulfate derivatives on platelet surface P-selectin expression and protein C activity in blood of inflammatory bowel disease patients

Sheng-Li Ji, Hai-Yan Du, Yan-Qing Chi, Hui-Fei Cui, Ji-Chao Cao, Mei-Yu Geng, Hua-Shi Guan

Sheng-Li Ji, Mei-Yu Geng, Hua-Shi Guan, Key Laboratory of Marine Drugs, Marine Drug and Food Institute, Ocean University of China, Qingdao 266003, Shandong Province, China

Sheng-Li Ji, Hai-Yan Du, Hui-Fei Cui, Ji-Chao Cao, Institute of Biochemical and Biotech Drugs, School of Pharmacy, Shandong University, Jinan 250012, Shandong Province, China

Yan-Qing Chi, Department of Pharmacy, Shandong Provincial Hospital, Jinan 250021, Shandong Province, China

Supported by the National Natural Science Foundation of China, No. 30370613, and the Major State Basic Research Development Program of China, No. 2001CCA01600, and the Shandong Provincial Natural Science Foundation, No. Y2000C22

Co-correspondents: Hua-Shi Guan

Correspondence to: Sheng-Li Ji, Institute of Biochemical and Biotech drugs, School of Pharmacy, Shandong University, Jinan 250012, Shandong Province, China. shenglijj@sdu.edu.cn

Telephone: +86-531-8380288 **Fax:** +86-531-2929312

Received: 2004-03-31 **Accepted:** 2004-05-13

Abstract

AIM: To investigate the effect of dermatan sulfate (DS) derivatives on platelet surface P-selectin expression and blood activated protein C (APC) activity in patients with inflammatory bowel disease (IBD), and to clarify the anti-inflammatory mechanism of DS derivatives.

METHODS: Dermatan sulfate (DS) was sulfated with chlorosulfonic acid to prepare polysulfated dermatan sulfate (PSDS). The major disaccharides of DS and PSDS were determined by ^1H nuclear magnetic resonance spectroscopy ($^1\text{H-NMR}$) and $^{13}\text{C-NMR}$. Both DS and PSDS were depolymerized with hydrogen peroxide. The fragments were separated by gel filtration chromatography. The effects of DS derivatives on P-selectin expression were assayed by ELISA method, and blood APC activity was assayed by the synthetic chromogenic substrate method.

RESULTS: The major disaccharides of DS and PSDS were IdoA-1 \rightarrow 3-GalNAc-4-SO₃ and IdoA-2SO₃-1 \rightarrow 3-GalNAc4, 6-diSO₃, respectively. Compared with the adenosine diphosphate stimulated group and IBD control group, DS and its derivatives all had significant inhibitory effects on P-selectin expression ($P<0.01$), but there was no difference between DS-derived oligosaccharides (DSOSs) and PSDS-derived oligosaccharides (PSDSOSs). The experiments on APC activity showed that DS and its derivatives all enhanced APC activity. The most active DSOS was the one with a relative molecular weight (M_r) of 4 825, which enhanced the APC activity from 106.5 \pm 11.5% to 181.8 \pm 22.3% ($P<0.01$). With the decrease of M_r , the activity of DSOSs decreased gradually. The effect of PSDS on APC activity enhancement was more significant than that of DS, and the APC activity was raised to 205.2 \pm 22.1% ($P<0.01$). All the PSDSOSs were more active than DSOSs on the basis of comparable M_r . With the decrease of M_r , the activity of PSDSOSs increased gradually, and the

most active PSDSOS was PSDSOS₃ with M_r of 2 749, which enhanced the APC activity to 331.2 \pm 27.8% ($P<0.01$), then the activity of PSDSOSs decreased gradually.

CONCLUSION: DS and its derivatives can significantly inhibit P-selectin expression on platelet surface, but the effect has no correlation with DS molecular mass and sulfation. The effect of DS or its derivatives on APC activity at molecular level involves complex mechanisms that depend on the molecular mass, the degree of sulfation, and the heterogeneous composition of DS. On the same molecular size, the higher the degree of DS sulfation, the more significant the effect on enhancing APC activity.

Ji SL, Du HY, Chi YQ, Cui HF, Cao JC, Geng MY, Guan HS. Effects of dermatan sulfate derivatives on platelet surface P-selectin expression and protein C activity in blood of inflammatory bowel disease patients. *World J Gastroenterol* 2004; 10(23): 3485-3489

<http://www.wjgnet.com/1007-9327/10/3485.asp>

INTRODUCTION

Inflammatory bowel disease (IBD) is a chronic non-specific intestinal inflammation. Recent researches have revealed a number of links between inflammation and coagulation, patients with IBD may be at increased risk of having venous thromboembolism^[1-9]. Abnormal platelet activity has been reported in patients with ulcerative colitis (UC) and Crohn's disease (CD), and plays an important role in inflammation aggravation^[10-12]. P-selectin, a membrane glycoprotein expressed on activated platelets and endothelial cells, plays a crucial role in thrombosis and inflammatory response^[13]. P-selectin antagonism could decrease thrombosis and inflammation in animal models of venous thrombosis prophylaxis^[14]. The protein C anticoagulant pathway appears to be the major pathway involved in the cross link between inflammation and coagulation. Activated protein C (APC) contributes to systemic anticoagulant and anti-inflammatory activities^[15], and may reduce organ damage by inhibiting thrombin generation and leukocyte activation^[16]. To inhibit the release of P-selectin and enhance APC activities are helpful for the treatment of IBD and related thrombosis^[17].

Dermatan sulfate (DS) is a member of the family of structurally complex, sulfated and linear polysaccharides called glycosaminoglycans (GAGs). It is mainly composed of [4- α -L-IdoA-1 \rightarrow 3- β -D-GalNAc-1]_n and [4- α -L-GlcA-1 \rightarrow 3- β -D-GalNAc-1]_n, and their derivatives with sulfate groups at C-2 of L-IdoA, C-4 or/and C-6 of D-GalNAc (IdoA, iduronic acid, GalNAc, N-acetyl-galactosamine, GlcA, glucuronic acid). The relative molecular weight (M_r) of natural DS is within 15 ku to 45 ku^[18]. Polysulfated DS is the sulfated product of DS reacting with chlorosulfonic acids. DS-derived oligosaccharides (DS-Oligs) are the oligosaccharides from depolymerizing DS and PSDS. DS is an important glycosaminoglycan found in a wide variety of tissues

in animals. Recently, growing evidence has suggested that DS, like the better studied heparin and heparan sulfate, is an important cofactor in a variety of cell behaviors^[18]. Many of the biological activities of DS proteoglycans are associated with their glycosaminoglycan structure^[19]. In addition to its anticoagulant and antithrombotic activities^[20,21], DS has also been reported possessing anti-inflammatory activities^[22-24]. The mechanisms of anti-inflammation of DS are unknown. To the author's knowledge, the relationships between the molecular structure of DS-Oligs and their effects on P-selectin and APC activity have not been studied. The present study was designed to observe the effects of DS-Oligs with different M_r and structure on platelet surface P-selectin expression and blood APC activities in patients with IBD, and to clarify the anti-inflammatory mechanisms of DS in the treatment of IBD.

MATERIALS AND METHODS

Materials

Dermatan sulfate was donated by Dongying Tiandong Biochemical Industrial Co. Ltd and 300 mL/L hydrogen peroxide (H_2O_2) was purchased from Laiyang Fine Chemical Reagent Co. Ltd. Adenosine diphosphate (ADP) was purchased from Sigma Co., USA. Superdex-30 was purchased from Amersham Biosciences. Human P-selectin ELISA kit (96 tests) and protein C CSA were purchased from Shanghai Sun Diagnostics, China.

Preparation of DS-Oligs

PSDS was prepared by the reaction of DS with chlorosulfonic acids. DS and PSDS were degraded by oxidative depolymerization with hydrogen peroxide^[25] respectively. All DS-Oligs were obtained from the products separated by gel filtration chromatography with Superdex 30 column (26 mm×1 200 mm), and the DS-Oligs were eluted with 0.25 mol/L ammonium bicarbonate and dried with lyophilization.

Determination of the relative molecular weight of DS-Oligs

The relative molecular weight (M_r) of the Oligs was determined by high performance liquid chromatography (HPLC)^[26].

¹H-NMR and ¹³C-NMR analysis of DS and PSDS

¹H-NMR and ¹³C-NMR spectra of DS and PSDS were assayed using a 600 MHz instrument as previously described^[27].

Patients and controls

Ten healthy blood-donors served as a control group and blood samples from 10 IBD patients, including five patients with UC and five patients with CD were used for experiments.

Collection of blood samples

Blood used to prepare platelets was collected in silicone-coated tubes containing 32 g/L sodium citrate as anticoagulant just before preparation and analysis.

Preparation of isolated platelets (IP)

Nine milliliter of blood with sodium citrate as anticoagulant blood was centrifuged at 500 r/min for 20 min at room temperature to obtain platelet rich plasma (PRP). The upper PRP was taken out, and the remaining plasma was centrifuged at 3 000 r/min for 15 min again and the platelet poor plasma (PPP) was obtained. The PRP was diluted with PPP to the platelet density of 3.0×10^8 cells/mL for P-selectin test.

Preparation of P-selectin standard calibration curve

Standard P-selectin was diluted to 80, 40, 20, 10, 5 and 2.5 ng/mL with assay buffer, and then added to the standard wells. The

standard curve was tested according to the test kit manufacturer's instructions.

Measurement of P-selectin in IP by ELISA

A total of 225 μ L of afore mentioned PRP was added to tubes, 30 μ L of saline was added to the control group and adenosine diphosphate (ADP) control tubes, and then 30 μ L of 2.50 mg/mL DS, PSDS and DS-Oligs saline solution were added to the sample tubes. All the tubes were incubated for 10 min at 37 °C. Then 25 μ L of 4.68 μ mol/L ADP solution was added to the ADP and sample tubes and an equal volume of saline was added to the blank control tubes. Then all the tubes were incubated for 5 min at 37 °C, followed by centrifugation for 15 min at 3 000 r/min, and finally the P-selectin in the upper solution was tested by ELISA according to the test kit manufacturer's instructions.

Specimen collection and preparation for APC test

Five milliliter of venous blood, containing 32 g/L sodium citrate as an anticoagulant, was collected from ten patients with IBD and the sample was centrifuged immediately. The plasma was collected and stored at 2-8 °C until use.

Preparation of protein C activity standard calibration curve

Normal plasma was dissolved in 200 μ L of buffer and the APC activity was defined as 200%. The solution was diluted three times to make the activities 100%, 50% and 25%, respectively. The activity of buffer was 0% criterion. Twenty five microliters of the four standards was added to the standard wells of the test plate, then 50 μ L of activator at the concentration of 0.1 mg/mL was added to activate protein C. These points were determined according to the manufacturer's instructions at 405 nm. The absorbance (A_{405nm}) was plotted versus the known percentage of standard APC activity to give a standard curve.

Detection of APC activity

APC activity in the plasma pre-incubated with DS and its derivatives was determined according to test kit manufacturer's instructions with minor modifications. Fifty microliters of DS and its derivatives solution at the concentration of 0.20 g/L was used to produce 50 μ L of activator. The APC enhancement by 50 μ L of DS at the concentration of 0.20 g/L was defined as 100%. Fifty microliters of buffer served as a blank control without any activator. The APC activities of the DS-Oligs were calculated according to the calibration curve.

Statistical analysis

Data were expressed as mean \pm SD. Student's *t* test and one-way analysis of variance were used for statistical analysis according to the data obtained. *P* values less than 0.05 were considered statistically significant.

RESULTS

Analysis of ¹H-NMR and ¹³C-NMR spectra of DS and PSDS

The ¹H-NMR and ¹³C-NMR spectra of DS and PSDS and the main disaccharides in their structure are shown in Figure 1. The major disaccharide sequence in DS was IdoA-1 \rightarrow 3-GalNAc-4-SO₃. In the ¹H-NMR spectra of PSDS (Figures 1B, D), the chemical shift of all the protons was shifted downfield in PSDS with respect to the DS. Similar effects could also be seen in the ¹³C-NMR spectra (Figures 1 A, C). The chemical shift of C-6 in GalNAc was shifted downfield (from 63.89 ppm to 68.60 ppm), while that of C-5 in GalNAc was shifted upfield (from 74.63 ppm to 69.98 ppm). The same phenomenon occurred in IdoA. The spectra showed that the hydroxyl group of C-6 in GalNAc and C-2 in IdoA of PSDS was sulfated, and the major disaccharide sequence was IdoA-2SO₃-1 \rightarrow 3-GalNAc4, 6-diSO₃.

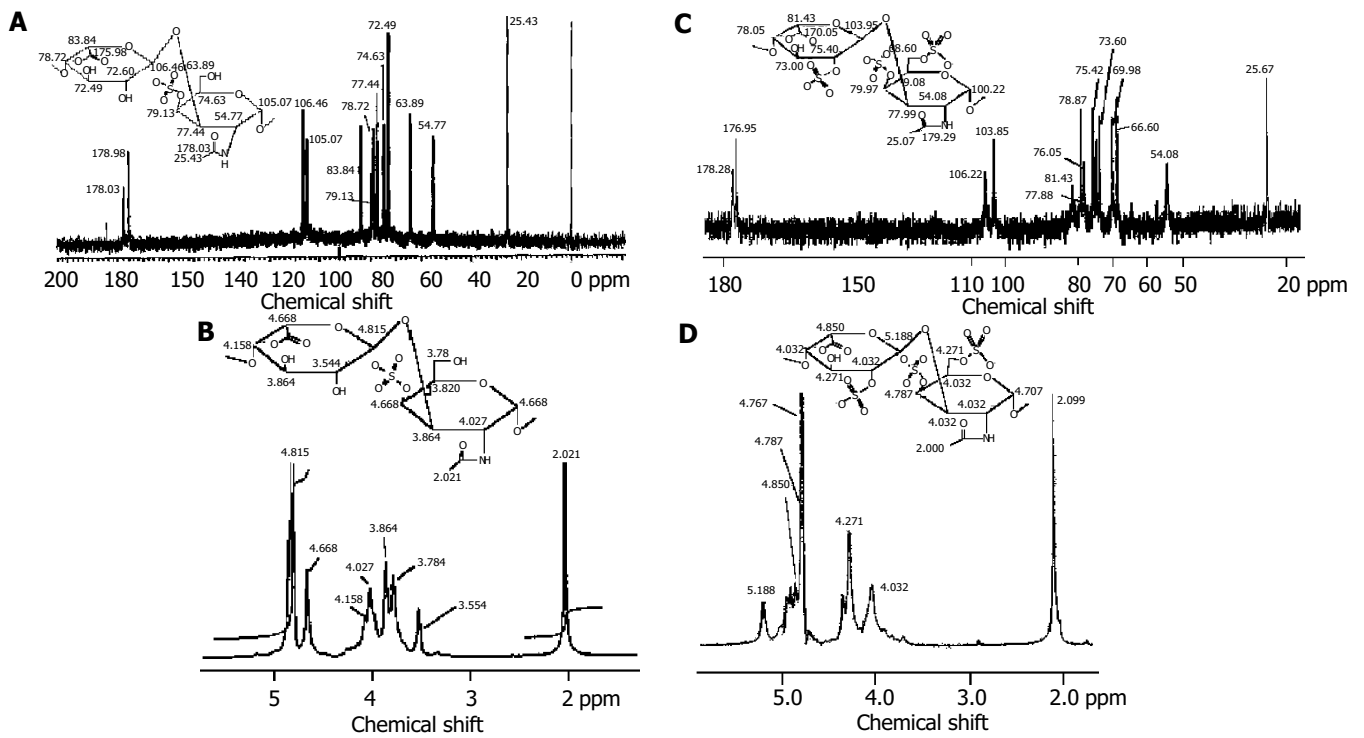


Figure 1 ¹H-NMR and ¹³C-MNR spectra of DS and PSDS. A and B: ¹³C-MNR and ¹H-NMR spectra of DS and the chemical shift of major disaccharides in DS; C and D: ¹³C-MNR and ¹H-NMR spectra of PSDS and the chemical shift of the major disaccharides in PSDS.

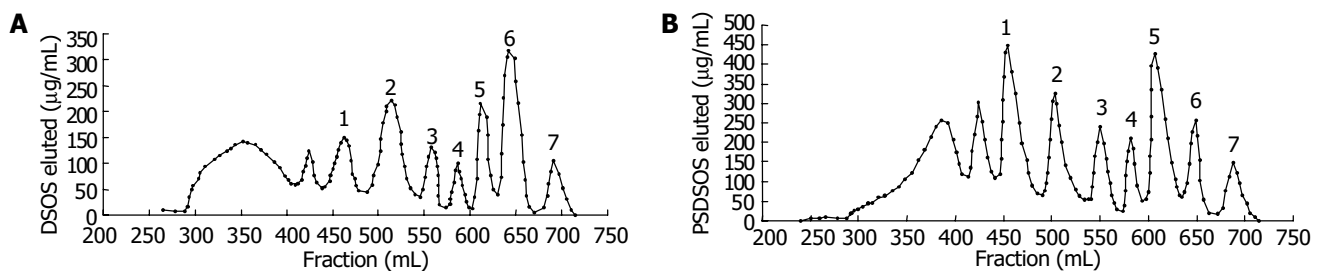


Figure 2 Fragment size separation of DS-Oligs. The products were separated on a Superdex 30 size exclusion column (26 mm×1 200 mm) at a flow rate of 0.5 mL/min in 0.25 mol/L ammonium bicarbonate. Elution profiles were monitored by carbazole assay. A and B: depolymerized products of DS and PSDS.

Fractionation of DS-Oligs

The DS-Oligs prepared from DS and PSDS degradation and separated by gel filtration chromatography are shown in Figure 2. The peaks numbered were DS-Oligs collected for the experiments on P-selectin and APC, and their *M_r* are listed in Table 1.

Table 1 *M_r* of DS-Oligs

DS oligosaccharides	<i>M_r</i>	PSDS oligosaccharides	<i>M_r</i>
DSOS ₁	4 825	PSDSOS ₁	4 959
DSOS ₂	3 926	PSDSOS ₂	4 280
DSOS ₃	2 254	PSDSOS ₃	2 749
DSOS ₄	1 696	PSDSOS ₄	2 107
DSOS ₅	1 309	PSDSOS ₅	1 594
DSOS ₆	1 038	PSDSOS ₆	1 021
DSOS ₇	709	PSDSOS ₇	785

Effects of DS derivatives on the expression of platelet surface P-selectin

Expression of platelet surface P-selectin on IP of IBD control group was significantly increased from 13.92±1.69 ng/mL (control group) to 23.95±2.51 ng/mL, and the ADP group showed a

significant increase in P-selectin expression after stimulation with ADP (*P*<0.01). All DS and its derivative groups showed a significant decrease in P-selectin expression compared with the ADP-stimulated group and IBD control group (*P*<0.01), but no significant differences could be seen as compared with the control group, and between DSOS and PSDSOS groups (Figure 3).

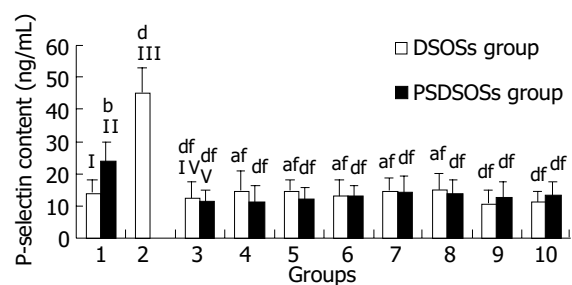


Figure 3 Effects of DS derivatives on expression of P-selectin on IP surface. Bars I, II, III, IV and V represent control group, IBD control group, ADP group, DS group and PSDS group, respectively. Groups 4 to 10 represent DS-Oligs from 1 to 7 listed in Table 1. ^b*P*<0.01 vs control group; ^a*P*<0.05, ^d*P*<0.01 vs IBD control group; [†]*P*<0.01 vs ADP group (*n* = 10 for each group).

Effects of DS derivatives on APC activity

The experimental results showed that all DS and its derivatives enhanced APC activity. The most active DSOS was DSOS₁ with M_r of 4 825, which enhanced the APC activity from 106.5±11.5% (DS group) to 181.8±22.3% ($P<0.01$). With the decrease of M_r , the activity of DSOSs decreased gradually. PSDS was more active than DS, which enhanced the APC activity from 106.5±11.5% (DS group) to 205.2±22.1% ($P<0.01$). On the same molecular size basis, PSDSOSs were more active than DSOSs. With the decrease of M_r , the activity of PSDSOSs increased, and the most active one was PSDSOS₃ with M_r of 2 749, which enhanced the APC activity to 331.2±27.8%, then decreased gradually (Figure 4).

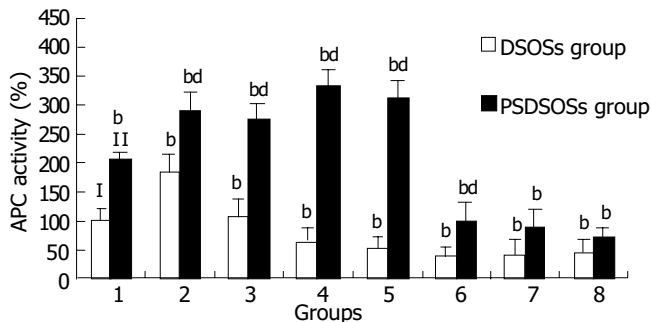


Figure 4 Effects of DS and its derivatives on APC activity. Bars I and II represent DS group and PSDS group, respectively. Groups 2 to 8 represent DS-Oligs from 1 to 7 listed in Table 1. ^b $P<0.01$ vs DS group, ^d $P<0.01$ vs PSDS group ($n = 10$ for each group).

DISCUSSION

IBD is a gastrointestinal disorder of unknown aetiology. Current research has paid attention to platelet dysfunction as a possible contributor to the disease, and the prevalence of IBD seems to be lower among patients with coagulation disorders^[28]. Platelets play a crucial role in hemostasis and inflammatory response. Normally, platelets circulate in a quiescent state, but after stimulation with agonists, such as thrombin, ADP and epinephrine, platelets begin to express P-selectin and release inflammatory mediators and factors, thereby promoting hemostasis^[29]. P-selectin acts as a cell-adhesion molecule in activated platelets and endothelial cells, and its main actions are to adhere to neutrophils and monocytes^[30] and to facilitate diapedesis. It has been reported that DS acts as a ligand to bind to P-selectin, and the sulfation plays an important role in the interactions between L- or P-selectin and DS^[31,32]. Our results showed that DS, PSDS and their derivatives significantly inhibited the P-selectin expression on IP surface, but there was no difference between DS and PSDS, and the effect seemed to be independent of molecular weight.

The increased risk of thrombosis in IBD patients has been attributed to a hypercoagulable state^[33-37]. Investigations of the hypercoagulation state and clinical risk factors in patients with IBD are of interest because thromboembolism is a significant and serious complication in IBD patients, with a high morbidity and mortality. The incidence of arterial and venous thromboembolic disease in patients with UC and CD is between 1% and 8%, and was 39% in some postmortem studies^[38]. Deficiencies and functional abnormalities of protein C, antithrombin III and protein S are the well-recognized causes of thrombotic disease^[8,39]. Blood coagulation is carefully controlled *in vivo* by several anticoagulant systems. Protein C pathway is one of these natural anticoagulant systems. It could regulate the coagulation process through proteolytic cleavage and inactivation of the two cofactors in the coagulation cascade,

the activated forms of factor V and VIII^[40-42]. The response of UC to heparin therapy^[43] and the low risk of IBD in patients with hemophilia and von Willebrand's disease^[29] also suggested that thrombosis and vascular occlusion might be important in the pathogenesis of IBD.

DS has been widely used as an antithrombotic drug. Its anticoagulant activity may involve multiple mechanisms. One of the mechanisms is that DS could promote the inhibition of thrombin activity by heparin cofactor II^[44]. The present experiments were designed to investigate the relationships between the APC activity enhancement and structures of DS or its derivatives *in vitro*. The results showed that DS and its derivatives all enhanced APC activity. Furthermore, a variety of experiments based on enhancement of APC activity compared the activity of various DS derivatives and defined the influences of DS molecular size and degree of sulfation on this activity. Two important variables of DS derivatives are the relative molecular weight and the degree of sulfation of the molecules. To assess the influence of molecular size, we studied different DS and PSDS fragments with M_r ranging from 0.7 ku to 5.0 ku. A clear correlation between the molecular size of DS and PSDS fragments and the degree of APC activity enhancement was observed by the synthetic chromogenic substrate method. With the decrease of molecular weight, the activity of DS-Oligs increased, and then decreased gradually. DSOS with M_r of 4 825, containing 16 to 24 monosaccharide residues, had more significant activity than undegraded DS. The same tendency was observed on PSDSOSs. But the most active PSDSOS was PSDSOS₃ with M_r of 2 749 containing about 8 to 10 monosaccharide residues.

To study the influence of the sulfate groups in DS molecules on APC enhancement, a chemically modified DS with a high degree of sulfation was prepared and compared with its parent DS. PSDSOSs were also compared with DSOSs with comparable M_r . The APC activity enhancement of PSDSOSs was much higher than that of DSOSs.

In conclusion interactions between APC and DS-Oligs at the molecular level involve complex mechanisms that depend on the M_r , the degree of sulfation, and the heterogeneous composition of DS, and are of great importance in the development of new anti-thrombotic DS-derived drugs.

REFERENCES

- Xia B, Han H, Zhang KJ, Li J, Guo GS, Gong LL, Zeng XC, Liu JY. Effects of low molecular weight heparin on platelet surface P-selectin expression and serum interleukin-8 production in rats with trinitrobenzene sulphonic acid-induced colitis. *World J Gastroenterol* 2004; **10**: 729-732
- Fichera A, Cicchiello LA, Mendelson DS, Greenstein AJ, Heimann TM. Superior mesenteric vein thrombosis after colectomy for inflammatory bowel disease: a not uncommon cause of postoperative acute abdominal pain. *Dis Colon Rectum* 2003; **46**: 643-648
- Saibeni S, Cattaneo M, Vecchi M, Zighetti ML, Lecchi A, Lombardi R, Meucci G, Spina L, de Franchis R. Low vitamin B (6) plasma levels, a risk factor for thrombosis, in inflammatory bowel disease: role of inflammation and correlation with acute phase reactants. *Am J Gastroenterol* 2003; **98**: 112-117
- Guedon C, Le Cam-Duchez V, Lalaude O, Menard JF, Lerebours E, Borg JY. Prothrombotic inherited abnormalities other than factor V Leiden mutation do not play a role in venous thrombosis in inflammatory bowel disease. *Am J Gastroenterol* 2001; **96**: 1448-1454
- Bernstein CN, Blanchard JF, Houston DS, Wajda A. The incidence of deep venous thrombosis and pulmonary embolism among patients with inflammatory bowel disease: a population-based cohort study. *Thromb Haemost* 2001; **85**: 430-434
- Grip O, Svensson PJ, Lindgren S. Inflammatory bowel disease promotes venous thrombosis earlier in life. *Scand J Gastroenterol* 2000; **35**: 619-623

- 7 **Jackson LM**, O'Gorman PJ, O'Connell J, Cronin CC, Cotter KP, Shanahan F. Thrombosis in inflammatory bowel disease: clinical setting, procoagulant profile and factor V Leiden. *QJM* 1997; **90**: 183-188
- 8 **Jorens PG**, Hermans CR, Haber I, Kockx MM, Vermylen J, Parizel GA. Acquired protein C and S deficiency, inflammatory bowel disease and cerebral arterial thrombosis. *Blut* 1990; **61**: 307-310
- 9 **Ghosh S**, Mackie MJ, McVerry BA, Galloway M, Ellis A, McKay J. Chronic inflammatory bowel disease, deep-venous thrombosis and antithrombin activity. *Acta Haematol* 1983; **70**: 50-53
- 10 **Mannaioni PF**, Di Bello MG, Masini E. Platelets and inflammation: role of platelet-derived growth factor, adhesion molecules and histamine. *Inflamm Res* 1997; **46**: 4-18
- 11 **Schaufelberger HD**, Uhr MR, McGuckin C, Logan RP, Misiewicz JJ, Gordon-Smith EC, Beglinger C. Platelets in ulcerative colitis and Crohn's disease express functional interleukin-1 and interleukin-8 receptors. *Eur J Clin Invest* 1994; **24**: 656-663
- 12 **Collins CE**, Rampton DS. Review article: platelets in inflammatory bowel disease-pathogenetic role and therapeutic implications. *Aliment Pharmacol Ther* 1997; **11**: 237-247
- 13 **Blann AD**, Noteboom WM, Rosendaal FR. Increased soluble P-selectin levels following deep venous thrombosis: cause or effect? *Br J Haematol* 2000; **108**: 191-193
- 14 **Myers D**, Wroblewski S, Londy F, Fex B, Hawley A, Schaub R, Greenfield L, Wakefield T. New and effective treatment of experimentally induced venous thrombosis with anti-inflammatory rPSGL-Ig. *Thromb Haemost* 2002; **87**: 374-382
- 15 **Esmon CT**. The anticoagulant and anti-inflammatory roles of the protein C anticoagulant pathway. *J Autoimmun* 2000; **15**: 113-116
- 16 **Shibata M**, Kumar SR, Amar A, Fernandez JA, Hofman F, Griffin JH, Zlokovic BV. Anti-inflammatory, antithrombotic, and neuroprotective effects of activated protein C in a murine model of focal ischemic stroke. *Circulation* 2001; **103**: 1799-1805
- 17 **Fagerstam JP**, Whiss PA, Strom M, Andersson RG. Expression of platelet P-selectin and detection of soluble P-selectin, NPY and RANTES in patients with inflammatory bowel disease. *Inflamm Res* 2000; **49**: 466-472
- 18 **Linhardt RJ**, Hileman RE. Dermatan sulfate as a potential therapeutic agent. *Gen Pharmacol* 1995; **26**: 443-451
- 19 **Whinna HC**, Choi HU, Rosenberg LC, Church FC. Interaction of heparin cofactor II with biglycan and decorin. *J Biol Chem* 1993; **268**: 3920-3924
- 20 **Linhardt RJ**, al-Hakim A, Liu JA, Hoppensteadt D, Mascellani G, Bianchini P, Fareed J. Structural features of dermatan sulfates and their relationship to anticoagulant and antithrombotic activities. *Biochem Pharmacol* 1991; **42**: 1609-1619
- 21 **Andrew M**, Mitchell L, Berry L, Paes B, Delorme M, Ofosu F, Burrows R, Khambalia B. An anticoagulant dermatan sulfate proteoglycan circulates in the pregnant woman and her fetus. *J Clin Invest* 1992; **89**: 321-326
- 22 **Kuschert GS**, Coulin F, Power CA, Proudfoot AE, Hubbard RE, Hoogewerf AJ, Wells TN. Glycosaminoglycans interact selectively with chemokines and modulate receptor binding and cellular responses. *Biochemistry* 1999; **38**: 12959-12968
- 23 **Kuwaba K**, Kobayashi M, Nomura Y, Irie S, Koyama Y. Elongated dermatan sulphate in post-inflammatory healing skin distributes among collagen fibrils separated by enlarged interfibrillar gaps. *Biochem J* 2001; **358**: 157-163
- 24 **Gozzo AJ**, Nunes VA, Carmona AK, Nader HB, von Dietrich CP, Silveira VL, Shimamoto K, Ura N, Sampaio MU, Sampaio CA, Araujo MS. Glycosaminoglycans affect the action of human plasma kallikrein on kininogen hydrolysis and inflammation. *Int Immunopharmacol* 2002; **2**: 1861-1865
- 25 **Fussi F**, inventors; Hepar Industries Inc., Assignee. Process for obtaining low molecular weight heparins endowed with elevated pharmacological properties, and product so obtained. US patent 4, 281, 108, 1981 July 28
- 26 **Kristensen HI**, Tromborg EM, Nielsen JR, Nielsen JI, Johansen KB, Ostergaard PB. Development and validation of a size exclusion chromatography method for determination of molecular masses and molecular mass distribution in low molecular weight heparin. *Thromb Res* 1991; **64**: 131-141
- 27 **Mascellani G**, Liverani L, Bianchini P, Parma B, Torri G, Bisio A, Guerrini M, Casu B. Structure and contribution to the heparin cofactor II-mediated inhibition of thrombin of naturally oversulphated sequences of dermatan sulphate. *Biochem J* 1993; **296**: 639-648
- 28 **Collins CE**, Rampton DS, Rogers J, Williams NS. Platelet aggregation and neutrophil sequestration in the mesenteric circulation in inflammatory bowel disease. *Eur J Gastroenterol Hepatol* 1997; **9**: 1213-1217
- 29 **Thompson NP**, Wakefield AJ, Pounder RE. Inherited disorders of coagulation appear to protect against inflammatory bowel disease. *Gastroenterology* 1995; **108**: 1011-1015
- 30 **de Bruijne-Admiraal LG**, Modderman PW, Von dem Borne AE, Sonnenberg A. P-selectin mediates Ca²⁺-dependent adhesion of activated platelets to many different types of leukocytes: detection by flow cytometry. *Blood* 1992; **80**: 134-142
- 31 **Kawashima H**, Hirose M, Hirose J, Nagakubo D, Plaas AH, Miyasaka M. Binding of a large chondroitin sulfate/dermatan sulfate proteoglycan, versican, to L-selectin, P-selectin, and CD44. *J Biol Chem* 2000; **275**: 35448-35456
- 32 **Kawashima H**, Atarashi K, Hirose M, Hirose J, Yamada S, Sugahara K, Miyasaka M. Oversulfated chondroitin/dermatan sulfates containing GlcA β 1/IdoA α 1-3GalNAc (4, 6-O-disulfate) interact with L- and P-selectin and chemokines. *J Biol Chem* 2002; **277**: 12921-12930
- 33 **Talbot RW**, Heppell J, Dozois RR, Beart RW Jr. Vascular complications of inflammatory bowel disease. *Mayo Clin Proc* 1986; **61**: 140-145
- 34 **Webberley MJ**, Hart MT, Melikian V. Thromboembolism in inflammatory bowel disease: role of platelets. *Gut* 1993; **34**: 247-251
- 35 **Lam A**, Borda IT, Inwood MJ, Thomson S. Coagulation studies in ulcerative colitis and Crohn's disease. *Gastroenterology* 1975; **68**: 245-251
- 36 **Hudson M**, Hutton RA, Wakefield AJ, Sawyerr AM, Pounder RE. Evidence for activation of coagulation in Crohn's disease. *Blood Coagul Fibrinolysis* 1992; **3**: 773-778
- 37 **Hudson M**, Chitolie A, Hutton RA, Smith MS, Pounder RE, Wakefield AJ. Thrombotic vascular risk factors in inflammatory bowel disease. *Gut* 1996; **38**: 733-737
- 38 **Koutroubakis IE**, Sfiridaki A, Mouzas IA, Maladaki A, Kapsoritakis A, Roussomoustakaki M, Kouroumalis EA, Manousos ON. Resistance to activated protein C and low levels of free protein S in Greek patients with inflammatory bowel disease. *Am J Gastroenterol* 2000; **95**: 190-194
- 39 **Aadland E**, Odegaard OR, Roseth A, Try K. Free protein S deficiency in patients with chronic inflammatory bowel disease. *Scand J Gastroenterol* 1992; **27**: 957-960
- 40 **Heneghan MA**, Cleary B, Murray M, O'Gorman TA, McCarthy CF. Activated protein C resistance, thrombophilia, and inflammatory bowel disease. *Dig Dis Sci* 1998; **43**: 1356-1361
- 41 **Griffin JH**, Evatt B, Wideman C, Fernandez JA. Anticoagulant protein C pathway defective in majority of thrombophilic patients. *Blood* 1993; **82**: 1989-1993
- 42 **Bertina RM**, Koeleman BP, Koster T, Rosendaal FR, Dirven RJ, de Ronde H, van der Velden PA, Reitsma PH. Mutation in blood coagulation factor V associated with resistance to activated protein C. *Nature* 1994; **369**: 64-67
- 43 **Gaffney PR**, Doyle CT, Gaffney A, Hogan J, Hayes DP, Annis P. Paradoxical response to heparin in 10 patients with ulcerative colitis. *Am J Gastroenterol* 1995; **90**: 220-223
- 44 **Maimone MM**, Tollefsen DM. Structure of a dermatan sulfate hexasaccharide that binds to heparin cofactor II with high affinity. *J Biol Chem* 1990; **265**: 18263-18271

Inhibitory effect of heparin-derived oligosaccharides on secretion of interleukin-4 and interleukin-5 from human peripheral blood T lymphocytes

Sheng-Li Ji, Hui-Fei Cui, Feng Shi, Yan-Qing Chi, Ji-Chao Cao, Mei-Yu Geng, Hua-Shi Guan

Sheng-Li Ji, Mei-Yu Geng, Hua-Shi Guan, Key Laboratory of Marine Drugs, Marine Drug and Food Institute, Ocean University of China, Qingdao 266003, Shandong Province, China

Sheng-Li Ji, Hui-Fei Cui, Feng Shi, Ji-Chao Cao, Institute of Biochemical and Biotech drugs, School of Pharmacy, Shandong University, Jinan 250012, Shandong Province, China

Yan-Qing Chi, Department of Pharmacy, Shandong Provincial Hospital, Jinan 250021, Shandong Province, China

Supported by the National Natural Science Foundation of China, No. 30370613 and the Major state Basic Research Development Program of China, 2001CCA01600

Correspondence to: Sheng-Li Ji, Institute of Biochemical and Biotech Drugs, School of Pharmacy, Shandong University, Jinan 250012, Shandong Province, China. shenglijj@sdu.edu.cn

Telephone: +86-531-8380288 **Fax:** +86-531-2929312

Received: 2004-03-19 **Accepted:** 2004-04-07

Abstract

AIM: To investigate the inhibitory effect of heparin-derived oligosaccharides (Oligs) on secretion of interleukin-4 (IL-4) and interleukin-5 (IL-5) from human peripheral blood T lymphocytes (PBTLs).

METHODS: Oligs were prepared by three different heparin depolymerization methods and separated by gel filtration chromatography. PBTLs from ten adult patients with allergic eosinophilic gastroenteritis were treated with phytohemagglutinin (PHA) and Oligs. The supernatants from the cell culture of PBTLs were harvested and subjected to the determination of IL-4 and IL-5 contents by ELISA method.

RESULTS: At the concentration of 5 $\mu\text{g/mL}$, Oligs with different M_r had different effects on the secretion of IL-4 and IL-5. The tetrasaccharide with M_r of 1 142, produced by depolymerizing heparin with hydrogen peroxide, had the strongest inhibitory effect on the secretion of IL-4. It decreased the IL-4 content from 375.6 ± 39.2 ng/L (PHA group) to 12.5 ± 5.7 ng/L ($P < 0.01$). The hexasaccharide with M_r of 1 806, produced by depolymerizing heparin with β -elimination method, had the strongest inhibitory effect on the secretion of IL-5. It decreased the IL-5 content from 289.2 ± 33.4 ng/L (PHA group) to 22.0 ± 5.2 ng/L ($P < 0.01$).

CONCLUSION: The inhibitory activity of Oligs on the secretion of IL-4 and IL-5 from human PBTLs closely depends on their molecular structure, and there may be an essential structure to act as an inhibitor. The most effective inhibitors of IL-4 and IL-5 secretion are tetrasaccharides and hexasaccharides, respectively.

Ji SL, Cui HF, Shi F, Chi YQ, Cao JC, Geng MY, Guan HS. Inhibitory effect of heparin-derived oligosaccharides on secretion of interleukin-4 and interleukin-5 from human peripheral blood T lymphocytes. *World J Gastroenterol* 2004; 10(23): 3490-3494
<http://www.wjgnet.com/1007-9327/10/3490.asp>

INTRODUCTION

Heparin is a highly sulfated, polyanionic glycosaminoglycan. It is composed of the trisulfated disaccharide unit [- L-iduronic acid-2-sulfate (IdoA2S) (1 \rightarrow 4)- α -D-glucosamine-N,6-disulfate (GlcNS6S)-], interrupted by irregular sequences containing undersulfated (or oversulfated) uronic acids and amino sugar residues, with an average relative molecular mass (M_r) of 12 000-15 000^[1]. In addition to its anticoagulatory effect, heparin has anti-inflammatory property, which has been used for treatment of ulcerative colitis and other inflammatory bowel diseases (IBD)^[2-15]. Although many studies have reported heparin's anti-inflammatory activities, there is little information available in literature about the specific oligosaccharide structures in heparin that inhibits the secretion of IL-4 and IL-5. IL-4 and IL-5 abnormalities have been reported to be consistent with the elevated IgE and eosinophilia in allergic eosinophilic gastroenteritis, suggesting that strategies targeting T lymphocytes may be efficacious in treatment of this kind of diseases^[16-19]. Here, we examined whether there was a relationship between the molecular weight of heparin-derived Oligs and their inhibitory effect on IL-4 and IL-5 secretion from PBTLs in allergic eosinophilic gastroenteritis.

MATERIALS AND METHODS

Drugs and reagents

Heparin sodium was donated by Dongying Tiandong Biochemical Industrial Co. Ltd, and 300 mL/L hydrogen peroxide (H_2O_2) was purchased from Laiyang Fine Chemical Regent Co, Ltd. Benzethonium chloride and (4-chloro)-benzyl chloride were purchased from Sigma Co., USA. Sodium nitrite was purchased from Jinan Chemical Reagents Co., Ltd. Superdex-30 was purchased from Amersham Biosciences. Human IL-4 and IL-5 ELISA kits (96 tests) were purchased from Bender Medsystems, USA. Phytohemagglutinin (PHA) was purchased from Shanghai Yihua Medical Science and Technology Co., Ltd. RPMI 1640 culture medium was purchased from Gibco, Paisley, UK.

Preparation of Oligs

Heparin was degraded by oxidative depolymerization with hydrogen peroxide^[20], deaminative cleavages with nitrous acid^[21] and β -eliminative cleavages with alkaline^[22], respectively. All Oligs were obtained from the products separated by gel filtration chromatography with Superdex-30 column (26 mm \times 1200 mm), and the oligosaccharides were eluted with 0.25 mol/L ammonium bicarbonate and dried with lyophilization.

Determination of the relative molecular weight of Oligs

The M_r of Oligs was determined by high performance size exclusion chromatography (HPSEC) on two Ultrahydrogel 250 (7.8 mm \times 300 mm) columns in series. The calibration was based on low molecular mass heparin for calibration CRS (Batch No 1A, European Pharmacopoeia) standards with number average molecular mass (M_n) of 3 700. A refractometer (RI) detector connected in series to an ultraviolet (UV) spectrophotometer

set at 234 nm was used for detection, and 28.4 g/L solution of sodium sulphate (pH 5.0) was used as the mobile phase at a flow rate of 0.5 mL/min^[23].

T cell separation and culture

Twenty-five milliliters of edetic acid anticoagulant peripheral blood was taken from ten adult patients with allergic eosinophilic gastroenteritis, and then mixed with 25 mL of PBS (pH 7.4, containing 50 mL/L fetal bovine serum). The diluted peripheral blood was then laid on 50 mL of lymphocyte separating solution carefully and centrifuged for 20 min at 2 000 r/min at room temperature. The peripheral blood lymphocytes (PBL) were collected and washed two times with PBS and suspended in RPMI 1640 solution (containing 200 mL/L fetal bovine serum). One millilitre of PBL suspending solution was added to the column of Nylon cotton (5 mm×16 mm). Then 0.2 mL of RPMI 1640 (containing 200 mL/L fetal bovine serum) was added on the Nylon cotton surface to close the column. The column was incubated for 30 min at 37 °C in an incubator. After that, PBTLs were eluted with RPMI 1640 (containing 200 mL/L fetal bovine serum) solution and then centrifuged for 10 min at 2 000 r/min. PBTLs were diluted to the cell density of 1.0×10^6 cells/mL, and 0.2 mL of the diluted cell suspending solution was added to a well of 96-well plate as a blank control. Another well was added into 0.2 mL of diluted cell suspending solution containing 20 µg of PHA as PHA control group. Other wells were added into 0.2 mL of diluted cell suspending solution containing 20 µg of PHA and 1 µL of 1.0 mg/mL heparin and Oligs. The cells were incubated for 48 h at 37 °C in a humidified atmosphere containing 50 mL/L CO₂ in air.

Detection of cytokines

The cells were harvested and centrifuged for 10 min at 1 000 r/min at room temperature. IL-4 and IL-5 in the cell culture solution were assayed by ELISA according to the manufacturer's instructions.

Statistical analysis

Data were expressed as mean±SD. Student's *t* test and one-way analysis of variance were used for statistical analysis. *P* values less than 0.05 were considered statistically significant.

RESULTS

Figure 1 shows the Oligs prepared from heparin degradation and separated by gel filtration chromatography. The peaks numbered were Oligs collected for inhibiting IL-4 and IL-5 experiments, and their *M_r* is listed in Table 1.

Table 1 Oligs obtained from chromatography eluted solution and their *M_r*

Oligs produced by H ₂ O ₂ oxidation		Oligs produced by β-elimination		Oligs produced by degradation with HNO ₂	
Samples	<i>M_r</i>	Samples	<i>M_r</i>	Samples	<i>M_r</i>
Olig H1	6 032	Olig B1	6 621	Olig N1	6 680
Olig H2	3 206	Olig B2	3 375	Olig N2	3 150
Olig H3	2 381	Olig B3	2 447	Olig N3	2 334
Olig H4	1 786	Olig B4	1 804	Olig N4	1 747
Olig H5	1 142	Olig B5	1 344	Olig N5	1 047
Olig H6	632	Olig B6	702	Olig N6	609

The effect of Oligs on secretion of IL-4 showed that all the Oligs had inhibitory activities and Oligs prepared from different methods or with different *M_r* had different effects. First, the Olig prepared from H₂O₂ depolymerizing method, was Olig H5 with *M_r* of 1 142 (tetrasaccharides), which had the strongest inhibitory effect and decreased the IL-4 content from 375.6±39.2 ng/L (PHA group) to 12.5±5.7 ng/L (*P*<0.01). Second, among the Oligs

from β-eliminative cleavage heparin, Olig B5 with *M_r* of 1 344 (tetrasaccharides) had the strongest inhibitory activity and decreased the IL-4 content to 54.4±6.3 ng/L (*P*<0.01). Third, the Olig from nitrous acid deaminative cleavage heparin, was Olig N5 with *M_r* of 1 107 (tetrasaccharides), which had the strongest inhibitory activity and decreased the IL-4 content to 47.4±5.8 ng/L (*P*<0.01). Although all these Oligs were tetrasaccharides, they had different *M_r*, because the amount of sulfate groups in their structure was different. The IL-4 content in the heparin group was 152.4±17.9 ng/L, and the difference in inhibitory activities between Oligs and heparin group was significant (*P*<0.01, Figures 2A, 3A).

The inhibitory effect of Oligs on secretion of IL-5 and IL-4 was similar. But there were some differences. Firstly, the Oligs prepared from H₂O₂ oxidation method, were Olig H4 with *M_r* of 1 786 and Olig H5 with *M_r* of 1 142, which had strongest inhibitory activities. They decreased the IL-5 content from 289.2±33.4 ng/L (PHA group) to 31.7±5.6 ng/L and 35.5±4.4 ng/L, respectively (*P*<0.01). Secondly, among the Oligs from β-eliminative cleavage heparin, Olig B4 with *M_r* of 1 804 (hexasaccharides) had the strongest inhibitory activity and decreased the IL-5 content to 22.0±5.2 ng/L (*P*<0.01). Thirdly, among the Oligs from nitrous acid deaminative cleavage heparin, Olig N4 with *M_r* of 1 747 (hexasaccharides) had the strongest inhibitory activity and decreased the IL-5 content to 69.2±6.3 ng/L (*P*<0.01). The inhibitory activities of these Oligs were stronger than those of unfractionated heparin (*P*<0.01, Figure 2B). The strongest inhibitor was Olig B4 (Figure 3B).

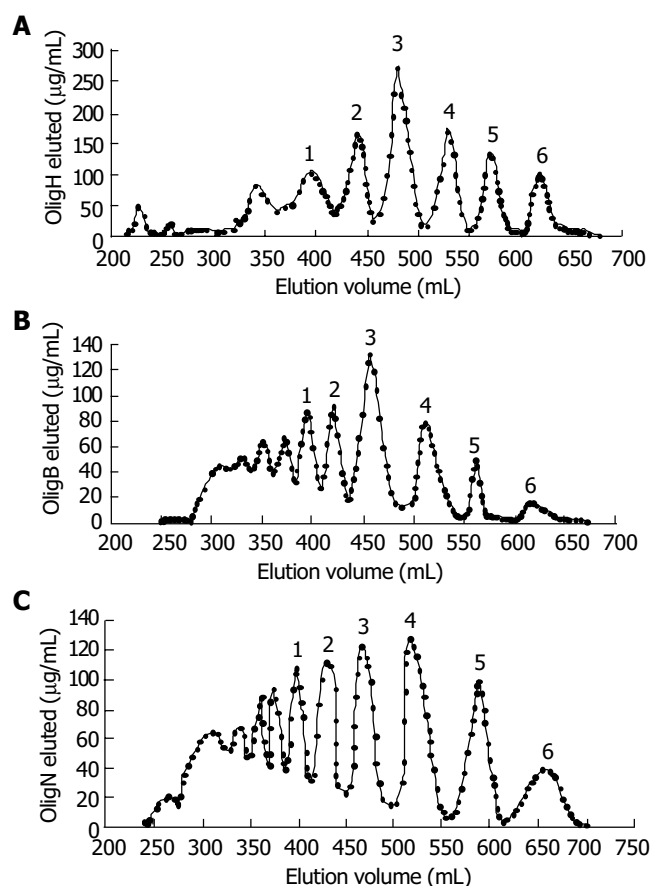


Figure 1 Size separation of heparin oligosaccharides. A: heparin degraded with hydrogen peroxide; B: heparin degraded with β-eliminative cleavage; C: heparin degraded with nitrous acids. The reaction products were separated on a Superdex 30 size exclusion column (26 mm×1 200 mm) at a flow rate of 0.5 mL/min in 0.25 mol/L ammonium bicarbonate. Elution profiles were monitored by carbazole assay.

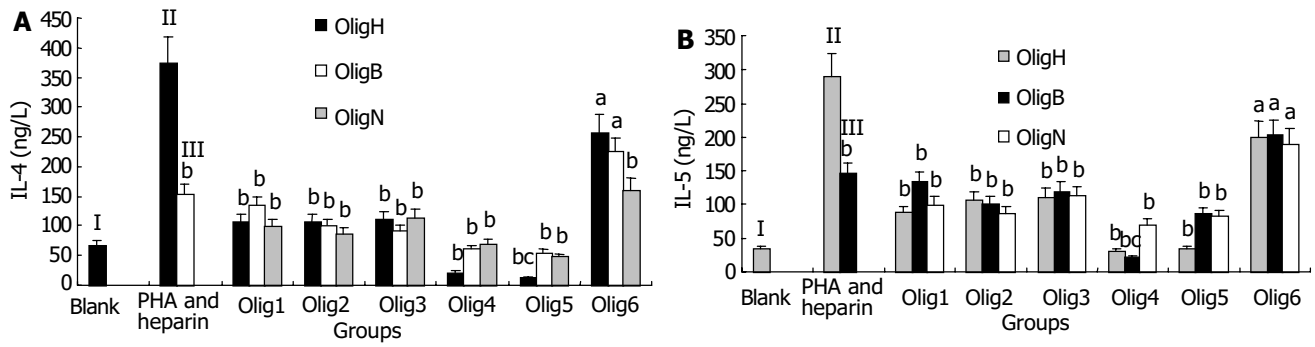


Figure 2 Content of IL-4 (A) and IL-5 (B) in PBTL culture solution of different groups. I, II and III represent blank control group, PHA control group and heparin group respectively. Olig1 to Olig 6 represent corresponding oligasaccharide samples described in Table 1 (from 1 to 6), respectively. ^a*P*<0.05, ^b*P*<0.01 vs PHA group; ^c*P*<0.05 vs Olig H4 group. (*n* = 10 for each group).

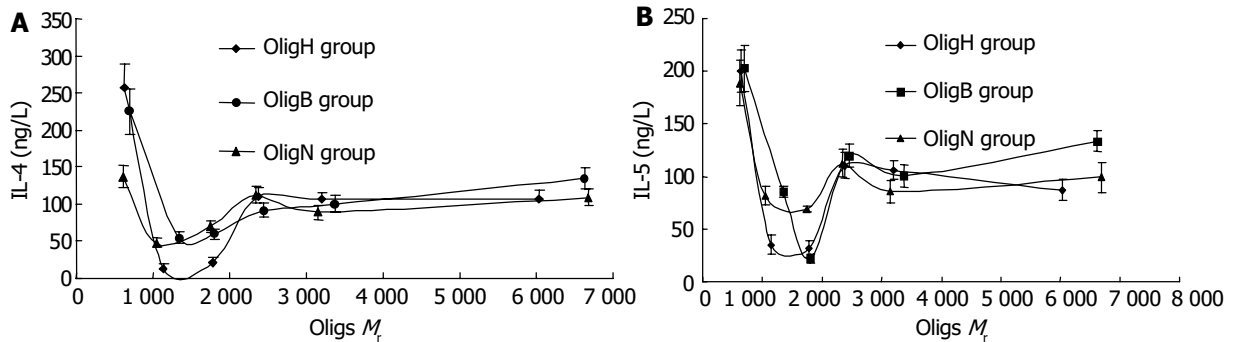


Figure 3 Relationship between *M_r* of Oligs and their activity on inhibiting IL-4 (A) and IL-5 (B) secretion. ^a*P*<0.05 vs Olig H4 group.

DISCUSSION

Allergic eosinophilic gastroenteritis is characterized by elevated total immunoglobulin E (IgE). IgE plays a significant role in allergic IBD by mediating the cross-linking of high-affinity Fc receptors (FcεRI) on mast cells, thus resulting in the release of a vast array of pro-inflammatory mediators including histamine, leukotrienes, and cytokines^[24] (Figure 4). In clinical studies, increased secretion of IL-4 and IL-5 by peripheral blood T cells has been reported in patients with eosinophilic gastroenteritis^[17]. Furthermore, T cells derived from the duodenum of patients with eosinophilic gastrointestinal disorder could preferentially secrete helper T cell 2 (Th2) cytokines that pre-dominantly include IL-4 and IL-5 when stimulated with milk proteins^[17]. IL-4 might play a critical role in mediating IgE-dependent allergic reactions, and regulation of IL-4 production or action might be useful for the prevention or therapy of immediate hypersensitivity disorders^[25-27]. IL-5, on the other hand, is most specific to the eosinophil lineage and responsible for the selective expansion of eosinophils and their release from bone marrow. Eosinophil granules contain a crystalloid core composed of major basic proteins (MBP) and a matrix composed of eosinophil cationic protein (ECP)^[28] (Figure 4). These cationic proteins share certain pro-inflammatory properties but differ in other aspects. MBP also triggers degranulation of mast cells and basophils. Triggering of eosinophils through engagement of receptors for cytokines could lead to the generation of a wide range of inflammatory cytokines, including IL-1, IL-3, IL-4, IL-5, IL-13, granulocyte-macrophage colony stimulating factor (GM-CSF), transforming growth factors (TGF), TNF-α, RANTES, macrophage inflammatory protein 1α, vascular endothelial cell growth factor, and eotaxin 1, indicating that they have the potential to modulate multiple aspects of the immune response^[29]. These findings imply that regulation of IL-5 production or action may also be useful for the prevention or therapy of allergy symptoms and inflammation.

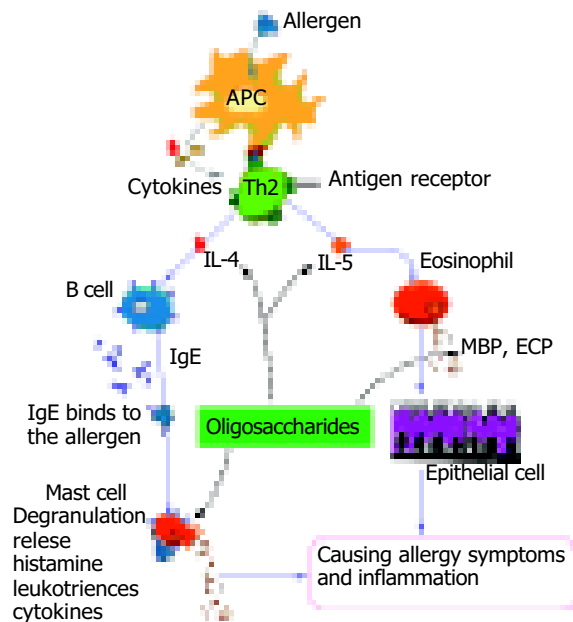


Figure 4 Interactions among inflammatory cells in pathogenesis of allergic eosinophilic gastroenteritis. Broken arrows denote the inhibitory effect of heparin-derived oligosaccharides on the various targets shown. MBP: major basic protein; and ECP: eosinophil cationic protein.

Heparin is a kind of polyanionic polysaccharides. In addition to its anticoagulant activity, heparin has a wide range of biological activities, including inhibition of complement activation^[30], regulation of cell proliferation^[31], inhibition of angiogenesis and tumor growth^[32,33], and antiviral activity^[34,35]. Over the last decade, heparin and low molecular mass heparin have been used to treat IBD in clinical practice^[36-50]. The mechanisms by

which heparin is able to treat IBD include its ability to inhibit the recruitment of neutrophils, reduce production of pro-inflammatory cytokines^[51] and restore the high-affinity receptor binding to antiulcerogenic growth factor^[12,13]. The ability of heparin to inhibit neutrophil activation, adhesion, and chemotaxis was also found in a mouse model of IBD^[14], suggesting that balanced interactions between mast cells and neutrophils might be important for the development of IBD. Furthermore, unfractionated heparin has potent immunomodulatory effects^[52-57]. Administration of unfractionated heparin may therefore be rational in patients with ulcerative colitis or Crohn's disease resistant to conventional forms of treatment^[39,40]. The anti-inflammatory effects of heparin can be most probably attributed to its physical binding to a variety of heparin-binding proteins such as TNF- α , IL-4, IL-5, RANTES, secretory leukocyte protease inhibitor, neutrophil-derived elastase and cathepsin G, eosinophil-derived major basic protein, and L- and P-selectins^[58-61]. Alternatively, heparin has been shown to specifically inhibit the inositol 1,4,5-triphosphate signal transduction pathway, which is important for a vast array of inflammatory cellular responses^[62,63].

If heparin is to be used as an anti-inflammatory drug, the risk of inducing bleeding must be abrogated. It has been reported that the anti-inflammatory effects of heparin were independent of its anticoagulant activity^[64-67], especially when it was used for treatment of allergic inflammation. Partial chemical modifications of heparin, such as depolymerization or partial desulfation, are the aim to develop heparin-derived anti-inflammatory drugs. We degraded heparin and separated the fragments by gel filtration chromatography. The oligosaccharides obtained were used as anti-inflammatory reagents and the results were promising. The hypothetical mechanisms for anti-inflammatory effects, such as inhibiting secretion of IL-4 and IL-5, were studied. Our results showed that Oligs with different M_r had different activities on inhibiting the secretion of IL-4 and IL-5. The Oligs, which had the strongest inhibitory activities on IL-4 secretion, were tetrasaccharides, but they had different M_r corresponding to the production methods. That was because different methods caused different desulfation during the process of degradation. The same phenomenon occurred in inhibiting the secretion of IL-5, but the strongest inhibitors were hexasaccharides other than tetrasaccharides. The mechanism needs further studies.

REFERENCES

- 1 **Casu B**. Heparin structure. *Haemostasis* 1990; **20**(Suppl 1): 62-73
- 2 **Gaffney PR**, Doyle CT, Gaffney A, Hogan J, Hayes DP, Annis P. Paradoxical response to heparin in 10 patients with ulcerative colitis. *Am J Gastroenterol* 1995; **90**: 220-223
- 3 **Evans RC**, Wong VS, Morris AI, Rhodes JM. Treatment of corticosteroid-resistant ulcerative colitis with heparin—a report of 16 cases. *Aliment Pharmacol Ther* 1997; **11**: 1037-1040
- 4 **Yoshikane H**, Sakakibara A, Ayakawa T, Taki N, Kawashima H, Arakawa D, Hidano H. Disseminated intravascular coagulation in an ulcerative colitis case not associated with surgery. *Hepato-gastroenterology* 2000; **47**: 1608-1610
- 5 **Cui HF**, Jiang XL. Treatment of corticosteroid-resistant ulcerative colitis with oral low molecular weight heparin. *World J Gastroenterol* 1999; **5**: 448-450
- 6 **Ang YS**, Mahmud N, White B, Byrne M, Kelly A, Lawler M, McDonald GS, Smith OP, Keeling PW. Randomized comparison of unfractionated heparin with corticosteroids in severe active inflammatory bowel disease. *Aliment Pharmacol Ther* 2000; **14**: 1015-1022
- 7 **Folwaczny C**, Wiebecke B, Loeschke K. Unfractionated heparin in the therapy of patients with highly active inflammatory bowel disease. *Am J Gastroenterol* 1999; **94**: 1551-1555
- 8 **Dotan I**, Hallak A, Arber N, Santo M, Alexandrowitz A, Knaani Y, Hershkovitz R, Brazowski E, Halpern Z. Low-dose low-molecular weight heparin (enoxaparin) is effective as adjuvant treatment in active ulcerative colitis: an open trial. *Dig Dis Sci* 2001; **46**: 2239-2244
- 9 **Vrij AA**, Jansen JM, Schoon EJ, de Bruine A, Hemker HC, Stockbrugger RW. Low molecular weight heparin treatment in steroid refractory ulcerative colitis: clinical outcome and influence on mucosal capillary thrombi. *Scand J Gastroenterol Suppl* 2001; **234**: 41-47
- 10 **Torkvist L**, Thorlacius H, Sjoqvist U, Bohman L, Lapidus A, Flood L, Agren B, Raud J, Lofberg R. Low molecular weight heparin as adjuvant therapy in active ulcerative colitis. *Aliment Pharmacol Ther* 1999; **13**: 1323-1328
- 11 **Papa A**, Danese S, Gasbarrini A, Gasbarrini G. Review article: potential therapeutic applications and mechanisms of action of heparin in inflammatory bowel disease. *Aliment Pharmacol Ther* 2000; **14**: 1403-1409
- 12 **Michell NP**, Lalor P, Langman MJ. Heparin therapy for ulcerative colitis? Effects and mechanisms. *Eur J Gastroenterol Hepatol* 2001; **13**: 449-456
- 13 **Day R**, Forbes A. Heparin, cell adhesion, and pathogenesis of inflammatory bowel disease. *Lancet* 1999; **354**: 62-65
- 14 **Wan MX**, Liu Q, Wang Y, Thorlacius H. Protective effect of low molecular weight heparin on experimental colitis: role of neutrophil recruitment and TNF-alpha production. *Inflamm Res* 2002; **51**: 182-187
- 15 **Fries W**, Pagiaro E, Canova E, Carraro P, Gasparini G, Pommeri F, Martin A, Carlotto C, Mazzon E, Sturniolo GC, Longo G. The effect of heparin on trinitrobenzene sulphonic acid-induced colitis in the rat. *Aliment Pharmacol Ther* 1998; **12**: 229-236
- 16 **Lalani T**, Simmons RK, Ahmed AR. Biology of IL-5 in health and disease. *Ann Allergy Asthma Immunol* 1999; **82**: 317-333
- 17 **Jaffe JS**, James SP, Mullins GE, Braun-Elwert L, Lubensky I, Metcalfe DD. Evidence for an abnormal profile of interleukin-4 (IL-4), IL-5, and gamma-interferon (gamma-IFN) in peripheral blood T cells from patients with allergic eosinophilic gastroenteritis. *J Clin Immunol* 1994; **14**: 299-309
- 18 **Lorentz A**, Schwengberg S, Mierke C, Manns MP, Bischoff SC. Human intestinal mast cells produce IL-5 *in vitro* upon IgE receptor cross-linking and *in vivo* in the course of intestinal inflammatory disease. *Eur J Immunol* 1999; **29**: 1496-1503
- 19 **Madden KB**, Whitman L, Sullivan C, Gause WC, Urban JF Jr, Katona IM, Finkelman FD, Shea-Donohue T. Role of STAT6 and mast cells in IL-4- and IL-13-induced alterations in murine intestinal epithelial cell function. *J Immunol* 2002; **169**: 4417-4422
- 20 **Fussi F**. Process for obtaining low molecular weight heparins endowed with elevated pharmacological properties, and product so obtained. *United States Patent* 1981; **4**: 108-281
- 21 **Lormeau JC**, Petitou M, Choay J, Choay SA. Oligosaccharides having anti-Xa activity and pharmaceutical compositions containing them. *United States Patent* 1998; **35**: 770
- 22 **Uzan A**, Rhone-Poulenc Rorer SA. Sulfated polysaccharides obtained from heparin, preparation process, pharmaceutical composition and use thereof. *United States Patent* 1998; **5**: 721-849
- 23 **Kristensen HI**, Tromborg EM, Nielsen JR, Nielsen JJ, Johansen KB, Ostergaard PB. Development and validation of a size exclusion chromatography method for determination of molecular masses and molecular mass distribution in low molecular weight heparin. *Thromb Res* 1991; **64**: 131-141
- 24 **Yamaguchi M**, Sayama K, Yano K, Lantz CS, Noben-Trauth N, Ra C, Costa JJ, Galli SJ. IgE enhances Fc epsilon receptor I expression and IgE-dependent release of histamine and lipid mediators from human umbilical cord blood-derived mast cells: synergistic effect of IL-4 and IgE on human mast cell Fc epsilon receptor I expression and mediator release. *J Immunol* 1999; **162**: 5455-5465
- 25 **Madden KB**, Urban JF Jr, Ziltener HJ, Schrader JW, Finkelman FD, Katona IM. Antibodies to IL-3 and IL-4 suppress helminth-induced intestinal mastocytosis. *J Immunol* 1991; **147**: 1387-1391
- 26 **Schreiber S**, Heinig T, Panzer U, Reinking R, Bouchard A, Stahl PD, Raedler A. Impaired response of activated mononuclear phagocytes to interleukin 4 in inflammatory bowel disease. *Gastroenterology* 1995; **108**: 21-33
- 27 **West GA**, Matsuura T, Levine AD, Klein JS, Fiocchi C. Interleukin 4 in inflammatory bowel disease and mucosal immune reactivity. *Gastroenterology* 1996; **110**: 1683-1695
- 28 **Gleich GJ**. Mechanisms of eosinophil-associated inflammation. *J Allergy Clin Immunol* 2000; **105**: 651-663

- 29 **Gharaee-Kermani M**, Phan SH. The role of eosinophils in pulmonary fibrosis (Review). *Int J Mol Med* 1998; **1**: 43-53
- 30 **Sharath MD**, Merchant ZM, Kim YS, Rice KG, Linhardt RJ, Weiler JM. Small heparin fragments regulate the amplification pathway of complement. *Immunopharmacology* 1985; **9**: 73-80
- 31 **Wright TC Jr**, Castellot JJ Jr, Petitou M, Lormeau JC, Choay J, Karnovsky MJ. Structural determinants of heparin's growth inhibitory activity. Interdependence of oligosaccharide size and charge. *J Biol Chem* 1989; **264**: 1534-1542
- 32 **Folkman J**, Langer R, Linhardt RJ, Haudenschild C, Taylor S. Angiogenesis inhibition and tumor regression caused by heparin or a heparin fragment in the presence of cortisone. *Science* 1983; **221**: 719-725
- 33 **Crum R**, Szabo S, Folkman J. A new class of steroids inhibits angiogenesis in the presence of heparin or a heparin fragment. *Science* 1985; **230**: 1375-1378
- 34 **Holodniy M**, Kim S, Katzenstein D, Konrad M, Groves E, Merigan TC. Inhibition of human immunodeficiency virus gene amplification by heparin. *J Clin Microbiol* 1991; **29**: 676-679
- 35 **Shieh MT**, Spear PG. Herpesvirus-induced cell fusion that is dependent on cell surface heparan sulfate or soluble heparin. *J Virol* 1994; **68**: 1224-1228
- 36 **Head KA**, Jurenka JS. Inflammatory bowel disease Part 1: ulcerative colitis-pathophysiology and conventional and alternative treatment options. *Altern Med Rev* 2003; **8**: 247-283
- 37 **Aiikhan R**, Cohen AT, Combe S, Samama MM, Desjardins L, Eldor A, Janbon C, Leizorovicz A, Olsson CG, Turpie AG. Prevention of venous thromboembolism in medical patients with enoxaparin: a subgroup analysis of the MEDENOX study. *Blood Coagul Fibrinolysis* 2003; **14**: 341-346
- 38 **Jani N**, Regueiro MD. Medical therapy for ulcerative colitis. *Gastroenterol Clin North Am* 2002; **31**: 147-166
- 39 **Prajapati DN**, Newcomer JR, Emmons J, Abu-Hajir M, Binion DG. Successful treatment of an acute flare of steroid-resistant Crohn's colitis during pregnancy with unfractionated heparin. *Inflamm Bowel Dis* 2002; **8**: 192-195
- 40 **Papa A**, Danese S, Gasbarrini A, Gasbarrini G. Review article: potential therapeutic applications and mechanisms of action of heparin in inflammatory bowel disease. *Aliment Pharmacol Ther* 2000; **14**: 1403-1409
- 41 **Kassis J**, Fugere F, Dube S. The safe use of epidural anesthesia after subcutaneous injection of low-dose heparin in general abdominal surgery. *Can J Surg* 2000; **43**: 289-294
- 42 **Ang YS**, Mahmud N, White B, Byrne M, Kelly A, Lawler M, McDonald GS, Smith OP, Keeling PW. Randomized comparison of unfractionated heparin with corticosteroids in severe active inflammatory bowel disease. *Aliment Pharmacol Ther* 2000; **14**: 1015-1022
- 43 **Katz S**. Update in medical therapy in inflammatory bowel disease: a clinician's view. *Dig Dis* 1999; **17**: 163-171
- 44 **Koutroubakis IE**, Sfiridaki A, Mouzas IA, Maladaki A, Kapsoritakis A, Roussomoustakaki M, Kouroumalis EA, Manousos ON. Resistance to activated protein C and low levels of free protein S in Greek patients with inflammatory bowel disease. *Am J Gastroenterol* 2000; **95**: 190-194
- 45 **Day R**, Ilyas M, Daszak P, Talbot I, Forbes A. Expression of syndecan-1 in inflammatory bowel disease and a possible mechanism of heparin therapy. *Dig Dis Sci* 1999; **44**: 2508-2515
- 46 **Haslam N**, Standen GR, Probert CS. An investigation of the association of the factor V Leiden mutation and inflammatory bowel disease. *Eur J Gastroenterol Hepatol* 1999; **11**: 1289-1291
- 47 **Torkvist L**, Thorlacius H, Sjoqvist U, Bohman L, Lapidus A, Flood L, Agren B, Raud J, Lofberg R. Low molecular weight heparin as adjuvant therapy in active ulcerative colitis. *Aliment Pharmacol Ther* 1999; **13**: 1323-1328
- 48 **Day R**, Forbes A. Heparin, cell adhesion, and pathogenesis of inflammatory bowel disease. *Lancet* 1999; **354**: 62-65
- 49 **McCarty MF**. Vascular heparan sulfates may limit the ability of leukocytes to penetrate the endothelial barrier-implications for use of glucosamine in inflammatory disorders. *Med Hypotheses* 1998; **51**: 11-15
- 50 **Korzenik JR**, Hsu A, Robert ME. Effect of heparin on dextran sulfate sodium-induced colitis. *Dig Dis Sci* 1998; **43**: 1800-1805
- 51 **Papa A**, Danese S, Gasbarrini A, Gasbarrini G. Review article: potential therapeutic applications and mechanisms of action of heparin in inflammatory bowel disease. *Aliment Pharmacol Ther* 2000; **14**: 1403-1409
- 52 **Ahmed T**, Abraham WM, D'Brot J. Effects of inhaled heparin on immunologic and nonimmunologic bronchoconstrictor responses in sheep. *Am Rev Respir Dis* 1992; **145**: 566-570
- 53 **Bowler SD**, Smith SM, Lavercombe PS. Heparin inhibits the immediate response to antigen in the skin and lungs of allergic subjects. *Am Rev Respir Dis* 1993; **147**: 160-163
- 54 **Chang NS**, Intrieri C, Mattison J, Armand G. Synthetic posu78-8Ifatd hyaluronic acid is a potent inhibitor for tumor necrosis factor production. *J Leukoc Biol* 1994; **55**: 74
- 55 **Lantz M**, Thysell H, Nilsson E, Olsson I. On the binding of tumor necrosis factor (TNF) to heparin and the release *in vivo* of the TNF-binding protein I by heparin. *J Clin Invest* 1991; **88**: 2026-2031
- 56 **Nelson RM**, Ceconi O, Roberts WG, Aruffo A, Linhardt RJ, Bevilacqua MP. Heparin oligosaccharides bind L- and P-selectin and inhibit acute inflammation. *Blood* 1993; **82**: 3253-3258
- 57 **Teixeira MM**, Hellewell PG. Suppression by intradermal administration of heparin of eosinophil accumulation but not oedema formation in inflammatory reactions in guinea-pig skin. *Br J Pharmacol* 1993; **110**: 1496-1500
- 58 **Lider O**, Mekori YA, Miller T, Bar-Tana R, Vlodavsky I, Baharav E, Cohen IR, Naparstek Y. Inhibition of T lymphocyte heparanase by heparin prevents T cell migration and T cell-mediated immunity. *Eur J Immunol* 1990; **20**: 493-499
- 59 **Fath MA**, Wu X, Hileman RE, Linhardt RJ, Kashem MA, Nelson RM, Wright CD, Abraham WM. Interaction of secretory leukocyte protease inhibitor with heparin inhibits proteases involved in asthma. *J Biol Chem* 1998; **273**: 13563-13569
- 60 **Tyrell DJ**, Kilfeather S, Page CP. Therapeutic uses of heparin beyond its traditional role as an anticoagulant. *Trends Pharmacol Sci* 1995; **16**: 198-204
- 61 **Jones CA**, Williams KA, Finlay-Jones JJ, Hart PH. Interleukin 4 production by human amnion epithelial cells and regulation of its activity by glycosaminoglycan binding. *Biol Reprod* 1995; **52**: 839-847
- 62 **Ghosh TK**, Eis PS, Mullaney JM, Ebert CL, Gill DL. Competitive, reversible, and potent antagonism of inositol 1,4,5-trisphosphate-activated calcium release by heparin. *J Biol Chem* 1988; **263**: 11075-11079
- 63 **Ahmed T**, Syryste T, Mendelssohn R, Sorace D, Mansour E, Lansing M, Abraham WM, Robinson MJ. Heparin prevents antigen-induced airway hyperresponsiveness: interference with IP3-mediated mast cell degranulation? *J Appl Physiol* 1994; **76**: 893-901
- 64 **Sy MS**, Schneeberger E, McCluskey R, Greene MI, Rosenberg RD, Benacerraf B. Inhibition of delayed-type hypersensitivity by heparin depleted of anticoagulant activity. *Cell Immunol* 1983; **82**: 23-32
- 65 **Xie X**, Rivier AS, Zakrzewicz A, Bernimoulin M, Zeng XL, Wessel HP, Schapira M, Spertini O. Inhibition of selectin-mediated cell adhesion and prevention of acute inflammation by nonanticoagulant sulfated saccharides. Studies with carboxyl-reduced and sulfated heparin and with trestatin a sulfate. *J Biol Chem* 2000; **275**: 34818-34825
- 66 **Fryer A**, Huang YC, Rao G, Jacoby D, Mancilla E, Whorton R, Piantadosi CA, Kennedy T, Hoidal J. Selective O-desulfation produces nonanticoagulant heparin that retains pharmacological activity in the lung. *J Pharmacol Exp Ther* 1997; **282**: 208-219
- 67 **Kariya Y**, Kyogashima M, Suzuki K, Isomura T, Sakamoto T, Horie K, Ishihara M, Takano R, Kamei K, Hara S. Preparation of completely 6-O-desulfated heparin and its ability to enhance activity of basic fibroblast growth factor. *J Biol Chem* 2000; **275**: 25949-25958

• CLINICAL RESEARCH •

Selection criteria for preoperative endoscopic retrograde cholangiopancreatography before laparoscopic cholecystectomy and endoscopic treatment of bile duct stones: Results of a retrospective, single center study between 1996-2002

Laszlo Lakatos, Gabor Mester, Gyorgy Reti, Attila Nagy, Peter Laszlo Lakatos

Laszlo Lakatos, Gabor Mester, 1st Department of Medicine, Csolnok F, Province Hospital, Veszprem, H-8200 Hungary
Gyorgy Reti, Attila Nagy, Department of Surgery, Csolnok F, Province Hospital, Veszprem, H-8200 Hungary
Peter Laszlo Lakatos, 1st Department of Medicine, Semmelweis University, Budapest, H-8200 Hungary
Correspondence to: Laszlo Lakatos, M.D., PhD, 1st Department of Medicine, Csolnok F, Province Hospital, Korhaz u.1, Veszprem, H-8200 Hungary. laklaci@hotmail.com
Telephone: +36-20-9119339 **Fax:** +36-1-3130250
Received: 2004-04-04 **Accepted:** 2004-05-25

Abstract

AIM: The optimal treatment for bile duct stones (in terms of cost, complications and accuracy) is unclear. The aim of our study was to determine the predictive factors for preoperative endoscopic retrograde cholangiopancreatography (ERCP).

METHODS: Patients undergoing preoperative ERCP (≤ 90 d before laparoscopic cholecystectomy) were evaluated in this retrospective study from the 1st of January 1996 to the 31st of December 2002. The indications for ERCP were elevated serum bilirubin, elevated liver function tests (LFT), dilated bile duct (≥ 8 mm) and/or stone at US examination, coexisting acute pancreatitis and/or acute pancreatitis or jaundice in patient's history. Suspected prognostic factors and the combination of factors were compared to the result of ERCP.

RESULTS: Two hundred and six preoperative ERCPs were performed during the observed period. The rate of successful cannulation for ERC was (97.1%). Bile duct stones were detected in 81 patients (39.3%), and successfully removed in 79 (97.5%). The number of prognostic factors correlated with the presence of bile duct stones. The positive predictive value for one prognostic factor was 1.2%, for two 43%, for three 72.5%, for four or more 91.4%.

CONCLUSION: Based on our data preoperative ERCP is highly recommended in patients with three or more positive factors (high risk patients). In contrast, ERCP is not indicated in patients with zero or one factor (low risk patients). Preoperative ERCP should be offered to patients with two positive factors (moderate risk patients), however the practice should also be based on the local conditions (*e.g.* skill of the endoscopist, other diagnostic tools).

Lakatos L, Mester G, Reti G, Nagy A, Lakatos PL. Selection criteria for preoperative endoscopic retrograde cholangiopancreatography before laparoscopic cholecystectomy and endoscopic treatment of bile duct stones: Results of a retrospective, single center study between 1996-2002. *World J Gastroenterol* 2004; 10 (23): 3495-3499
<http://www.wjgnet.com/1007-9327/10/3495.asp>

INTRODUCTION

The rate of coexisting common bile duct stones (CBDS) in patients undergoing cholecystectomy for cholelithiasis is approximately 7-20%^[1-3]. The dramatic shift from conventional to laparoscopic cholecystectomy (LC) in the last 15 years has opened a large debate over the optimal management of patients with CBDS undergoing cholecystectomy^[4,5]. It is generally accepted that bile duct stones should be removed (even if asymptomatic), because they may be associated with severe complications such as pancreatitis and cholangitis. The management of coexisting CBDS may be surgical or endoscopic followed by surgery. Gallbladder preservation has also been suggested, however it has not become universal^[6]. A group of surgeons have recommended laparoscopic management of coexisting CBDS by intraoperative cholangiography or intraoperative ERCP and surgical removal of the stones^[7-9]. However, manipulation of the bile duct during LC is not popular among laparoscopic surgeons. Recent studies suggest that it can be done safely and does not prolong hospitalisation^[10,11], but minimal invasiveness and cost-effectivity remain questionable^[12].

ERCP is the most popular peri-LC bile duct imaging method. It is readily available, safe, highly accurate and has therapeutic potential, even in old patients^[13]. Furthermore ERCP offers the possibility to study bile duct anatomy, identify abnormalities of the bile ducts as well as being useful in the differential diagnosis of questionable lesions (*e.g.* malignancy). The role of new, less invasive imaging techniques (*e.g.* endoscopic ultrasound - EUS, magnetic resonance cholangiopancreatography - MRCP) is less well characterized^[14-16].

Routine preoperative ERCP may not be recommended, due to the low percentage of coexisting cholecysto-choledocholithiasis, a large number of negative investigations, and a small but significant risk of associated morbidity and high additional costs. Postoperative ERCP could reduce the number of unnecessary interventions and the majority of retained stones and postoperative leakages can be treated, although a second operation is required in case of failure. The development of more reliable predictors of CBD stones, based on the patient's clinical, biochemical and ultrasound (US) presentations, could allow a more appropriate use of preoperative ERCP (or EUS, MRCP). However, there is still no consensus as to which particular indicator, or set of indicators should be used, or as to the threshold values of various indicators^[3,17-22].

The aim of this study was to determine a precise and easily applicable clinical, biochemical and US (selection) criteria for patients who should undergo further investigation (preoperative ERCP) prior to LC/surgery.

MATERIALS AND METHODS

Patients who underwent preoperative ERCP from the 1st January 1996 to the 1st January 2003 (≤ 90 d before laparoscopic cholecystectomy) were evaluated in this retrospective study.

The indications for ERCP were one or more of the following: elevated serum bilirubin ($\geq 2 \times$ upper limit of normal - ULN) concentration, elevated liver function tests [LFT, $\geq 1.5 \times$ ULN: either aspartate-aminotransferase (AST), alanine-aminotransferase (ALT), alkaline phosphatase (ALP) or γ -glutamyl transpeptidase (GGT) activities], dilated bile duct (≥ 8 mm) and/or stones at US examination, coexisting acute pancreatitis and/or acute pancreatitis or jaundice in patient's history. The predictive values of age, sex and colic were also investigated. The majority of the ERCPs were performed by two expert endoscopists. Suspected prognostic factors and combination of factors were compared to the results of the ERCP.

Serum bilirubin concentration, AST, ALT, ALP and GGT activities were measured by Olympus AU600 (Olympus Co. Ltd, Shizuoka, Japan) autoanalyser at 37 °C. The enzyme activities were expressed in U/L and serum bilirubin concentration was given in $\mu\text{mol/L}$.

Statistical analysis

Sensitivity, specificity, positive and negative predictive values were calculated for individual factors (compared to all other cases) and for combination of factors. Student *t*-test with separate variance estimates was performed to test the demographic differences. χ^2 test and Fisher exact test were performed to compare between patients with a different number of suggested factors. $P < 0.05$ was considered statistically significant. For the statistical analysis Statistica 6.1 (Statsoft Inc, OK, USA) was used.

RESULTS

A total of 2985 ERCPs and 1248 LCs were performed in the Csolnoky F. Province Hospital between 1st January 1996 and the 31st December 2002. Using our selection criteria (a minimum of one positive factor) preoperative ERCP was performed in 206 patients (16.5%, Table 1). Seventy-seven percent of the patients were women and 23% men. The mean age of women was significantly lower ($P = 0.02$, Table 2). The mean waiting time between ERCP and LC was 17.3 d. Thirty-nine percent of the patients were operated within 3 d, almost 60% within one week.

Table 1 Number of ERCP and/or LC cases per year in the Csolnoky Ferenc Hospital, Veszprém, Hungary

Year	ERCP	LC	ERCP-LC
1996	373	99	15
1997	393	164	28
1998	375	140	27
1999	490	189	33
2000	558	183	36
2001	378	246	42
2002	391	227	25
Total	2 258	1 248	206
Average	423/yr	178	29/yr

Table 2 Preoperative ERCP, age and gender of patients ($n=206$)

Gender	<i>n</i> (%)	Mean age
Male	48 (23)	57.4
Female	158 (77)	51.0
Total	206 (100)	52.5

A successful cannulation was done in 200 patients (97.1%,

Table 3). CBD stones were found in 81 patients (39.3%), the stone/stones were removed endoscopically in 79 cases (97.5%). There was a tendency of increased frequency of CBD stones in men (24/48 = 50.0%) compared to women (57/158 = 36.1%, $P = 0.06$ by Fisher exact test), but CBD stones were equally common in elder (≥ 60 years) and younger (< 60 years) patients (50/128 = 39.1% vs 31/78 = 39.7%).

The results for each individual criterion are shown in Tables 4, 5. With the exception of jaundice or pancreatitis in the patient's history the positive predictive value of each criterion was high (58-72%). Sensitivity and specificity were compared to patients lacking the specific factor.

Table 3 Results of preoperative ERCPs performed prior to LC ($n = 206$)

ERCP finding	<i>n</i>	%
Common bile duct (CBD) stone	81	39.3
Negative	119	57.8
CBD not filled	6	2.9
Successful EST and duct clearance	79/81	97.5
Complication	3	1.5
-bleeding	1	0.5
-pancreatitis	1	0.5
-stone impaction	1	0.5

Table 4 Common bile duct stones in cases of different positive prognostic factors (PPF)

Factor	Number	Stone	Negative	Unsuccessful	%
Hyperbilirubinaemia (> 2)	61	44	16	1	72
Elevated ASAT/ALAT ($> 50\%$)	116	74	39	3	64
Elevated GGT/ALP ($> 50\%$)	134	79	52	3	59
Acute pancreatitis (AP)	26	18	7	1	69
AP in the anamnesis	20	4	16	0	20
Jaundice in the anamnesis	29	1	26	2	3
US: CBD ≥ 8 mm	53	38	14	1	71
US: bile duct stone	7	4	3	0	57
Biliary colic	106	62	42	2	58

Table 5 Total predictive value of different positive predictive factors (PPF) for common bile duct stone

Factor	PPV %	NPV %	Sensitivity %	Specificity %
Hyperbilirubinaemia	73.3	73.6	54.3	86.6
Elevated ASAT/ALAT	65.4	91.9	91.3	67.2
Elevated GGT/ALP	60.3	97.1	97.5	56.3
Acute pancreatitis (AP)	72.0	73.5	22.2	96.2
AP in the anamnesis	20.0	57.2	4.9	86.5
Jaundice in the anamnesis	3.7	53.7	1.2	78.2
US: CBD ≥ 8 mm	73.1	70.9	46.9	88.2
US: bile duct stone	57.1	60.1	4.9	97.5

A more realistic approach was to compare the predictive value in association with other factors. Table 6 demonstrates that the positive predictive value of the investigated factor was high in cases with (at least) two concurrently positive factors. The positive predictive value of two positive markers was 41-55%, again with the exception of pancreatitis or jaundice in the anamnesis.

Table 6 Predictive value of positive predictive factors (PPF) for CBD stones and effect of associated other factors, *n* (%)

Factor	Alone	One further factor	Two or more further factors
Hyperbilirubinaemia	0/3	1/5 (20)	43/53 (81)
Elevated ASAT/ALAT	1/11 (9)	13/32 (41)	60/73 (82)
Elevated GGT/ALP	1/24 (4)	16/35 (46)	62/75 (83)
Acute pancreatitis (AP)	-	0/3	18/23 (78)
AP in the anamnesis	1/12 (8)	0/3	3/5 (60)
Jaundice in the anamnesis	0/27	1/2 (50)	-
US: CBD \geq 8 mm	0/7	6/11 (55)	32/35 (91)
US: bile duct stone	0/1	-	4/6 (67)

The association between the number of positive factors and the presence of CBD stones is shown in Tables 7, 8. One factor alone was associated with a very low risk of CBD stone (1.2%). In patients with two, three and four or more positive factors, CBD stones were detected in 43.1%, 72.5% and 91.4% respectively. If we omitted history of jaundice and pancreatitis from the factors the corresponding data were 2.7% (1/41), 1.9% (1/54), 45.6% (23/48) and 82.3% (56/69) for patients with zero, one, two and three or more positive factors.

Table 7 Association between the number of positive predictive factors and ERCP findings (*n* = 206)

Number of positive factors	Number	Stone	Negative	Unsuccessful	%
1	84	1	80	3	1.2
2	46	19	25	2	43.1
3	40	29	11	0	72.5
\geq 4	36	32	3	1	91.4

$P < 0.00001$ for the whole group, $P < 0.00001$, between group 1 and groups 2, 3, 4, group 2 and group 4, $P = 0.008$, between groups 2 and 3, $P = 0.035$, between groups 3 and 4.

Table 8 Predictive value of predictive factors according to the number of positive factors

Number of positive factors	Number	PPV %	NPV %	Sensitivity %	Specificity %
1	84	1.2	-	-	-
2	46	43.1	98.7	95.2	76.1
3	40	72.5	84.0	59.1	90.5
\geq 4	36	91.4	72.0	40.2	98.4

$P < 0.00001$ for the whole group, $P < 0.00001$, between group 1 and groups 2, 3, 4 and group 2 and group 4, $P = 0.008$, between groups 2 and 3, $P = 0.035$, between groups 3 and 4.

DISCUSSION

Although laparoscopic cholecystectomy has become the treatment of choice for cholelithiasis, the treatment of coexisting cholecysto-cholecho-lithiasis is still controversial^[1,3,8,10,15,17]. The surgical management of CBD stones requires a skilled laparoscopic surgeon and the options of management include conversion to open CBD exploration, intraoperative or postoperative ERC. In contrast, no single non-invasive method is sensitive and/or specific enough to predict the presence of CBD stones. Individual findings are less important than the overall clinical presentation.

A number of methods have been used for the diagnosis of CBDS, including new and improved radiological techniques. However some of them are invasive, more expensive and require special equipment. A major advantage of ERCP is that it could

also offer a therapeutic possibility. Approximately 90-95% of CBDS could be managed endoscopically^[1,23], but it is expensive, technically demanding and is associated with small but significant morbidity.

The question is whether preoperative ERCP should be routinely indicated or whether it should be kept for selected cases only. Most of the studies concluded that routine preoperative ERCP was not indicated^[1,20,24]. One of the earliest studies is the well-known study from Neuhaus *et al.*^[24]. They performed routine preoperative ERCP in 288 prospective patients prior to LC. The rate of successful cannulation was 91.7%, and normal anatomy was found in 86%. CBDS were proved in 29 patients (11%), the stone was asymptomatic in 9 patients. Endoscopic sphincterotomy was performed in all cases and the stones were extracted in all but three patients. One additional patient was operated due to complications. In concordance with the reported rate of 6-13.2% in other studies^[1,14,20], coexisting cholecysto-cholecho-lithiasis was found in 6.5% of our LC patients (81 cases by preoperative ERCP).

The aim of this and previous studies was to determine a precise and easily applicable selection of clinical, biochemical and US criteria, which would enable the identification of patients with low risk of CBD stones (without the necessity for invasive procedures), and with higher risk of CBD stones who should undergo further preoperative investigation. The selection of patients was difficult. CBD stones were more common in patients with symptoms (e.g. jaundice, cholangitis, pancreatitis) and laboratory alterations including elevated serum bilirubin and liver function test. However, 8-10% of gallstone patients might have asymptomatic ductal stones^[3,25,26].

The positive predictive value of laboratory data for CBD stones was found to be 60-87% in various studies^[26,27]. In our study it was 57.1-73.3% in univariate analysis. However in most of the cases they were not individual parameters. In concordance with previous studies we could not identify jaundice and pancreatitis in the anamnesis as a predictor variable.

Traditional abdominal US is a valuable diagnostic tool. Although it is less sensitive (20-30%) in the detection of ductal gallstones, it provides important additional information about the degree of dilation of the bile ducts. The sensitivity of iv. cholangiography is also relatively low, moreover, it is associated with a severe risk of side effects. However, due to new non-ionic radiocontrast agents and radiological techniques, more and more research groups have started to routinely apply this technique again with improving results^[3]. Laparoscopic intraoperative cholangiography is a useful and reliable method, although its indication remains debated^[10,28]. The sensitivity of traditional CT is similar to that of US, but 3D helical techniques could offer an accuracy comparable to that of MRCP^[29]. MRCP and endoscopic US could approach the diagnostic value of ERCP^[14,15,30].

None of the aforementioned and analyzed factors is fit for the prediction of bile duct stones with sufficient certainty by itself. A combination of the prognostic factors is routinely applied. Several authors have constructed complicated scoring systems^[16,23,27]. However, most of these systems require highly specific and sophisticated softwares, and no universally accepted system exists. More practical is the use of suggested clinical scores based on routine clinical data (jaundice, pancreatitis, liver function tests, ductal dilation and/or stones in the choledochus on US) in everyday practice^[17,20]. Some authors also included the presence of small gallstones, old age and gender.

In concordance with our study, in the different studies based on large patient populations, CBDS/ductal stones or other pathologic deviations were found in 40-60% of ERCP cases performed on selected/restricted indications^[1,16,18,20]. Based on the prognostic factors, patients were usually divided into low,

medium and high-risk CBD stone groups.

Peter Cotton^[31] has presented his guidelines in the American Journal of Surgery. In his opinion the main constituents of the indications of preoperative ERCP were the following: positive predictive factors for CBD stones, the expertise of the endoscopist, and the pressure for laparoscopic intervention as opposed to open surgery. In concordance with our suggestion, he identified low, medium and high-risk patients for CBD stones based on the anamnesis, liver function tests, and ductal dilation on US. According to his conclusions, preoperative ERCP was not indicated for low-risk patients, while it must absolutely be performed in the high-risk group. As for the medium risk group, seemingly paradoxically, preoperative ERCP was only indicated, if the local endoscopist was mediocre. With an experienced endoscopist, preoperative intervention should be avoided, ERCP is to be performed only after the surgery, if the need arises.

Rieger *et al.*^[26] found CBD stones in 56 patients (53%) of the 106 ERCP performed in combination with 1140 LC. More than two-fold elevation in any liver function test, multiple abnormal laboratory tests, stones in the biliary tract on US, a more than 7 mm, dilated ductus choledochus were taken as positive predicting factors for preoperative ERCP. The multicenter study of Welbourn *et al.*^[32] in England also aimed to identify the exact indications of selective preoperative ERCP. The retrospective analysis of 306 preoperative ERC and 1396 LC showed that the predictive value of jaundice was 75%, that of pancreatitis 56%, while the predictive value of pathologic US or liver function tests was 48%. In a prospective study of Sarli *et al.*^[3], 74 symptom-free, CBD stone patient data were evaluated. Positive US, biliary colic, elevated serum aminotransferase and alkaline phosphatase levels and the presence of multiple, smaller stones were associated with a higher risk, while acute cholecystitis and non-specific upper gastrointestinal complaints were associated with a lower risk. In our study jaundice, elevated LFTs and dilated choledochus or stones in the bile duct on US examination gave a similarly high positive predictive value in univariate analysis for bile duct stones.

In our opinion, the major shortcoming of the above studies is that they analyzed the effects of different predictive factors separately, which in accordance with our own findings, could easily result in misleading conclusions. Santucci *et al.*^[33] and Geron *et al.*^[7] came to the same conclusion, emphasizing the importance of the co-existence of several pathologic markers at the same time. Furthermore, the American Society for Gastrointestinal Endoscopy (ASGE) in its guideline^[29] favors the establishment of the aforementioned risk categories based on "simple clinical" data, such as clinical picture, laboratory findings and US. Interestingly, it recommends intraoperative (during the laparoscopic cholecystectomy) cholangiography to be performed even in low-risk/negative patients, followed by laparoscopic or endoscopic postoperative intervention, if required. In the medium-risk group endosonography or MRCP is recommended as the method of choice or, if these are not available, ERCP. According to the guideline, ERCP should be the first (therapeutic) intervention for high-risk patients.

In Hungary, ERCP is performed on a relatively high level and is generally available. Among the new imaging techniques, the availability of MRCP and endosonography is still limited. At the same time, due to financing reasons, ERCP turns out to be more cost-effective. The accessibility of intraoperative laparoscopic imaging techniques is also limited.

In summary, based on the literature and our own results, the following guideline can be established about the indications of preoperative ERCP.

The possibility of CBD stones should be considered after the evaluation of clinical, laboratory and US findings. Zero or one positive predictive factor indicates low risk, while the risk is high if three or more factors are present. Two positive

predictive factors suggest medium risk. In the low risk group preoperative ERCP is not recommended, LC is advisable without restrictions. In the high risk group the indication of preoperative ERCP is unambiguous. In the medium-risk population, preoperative ERCP is generally indicated. If available, MRCP can be a good alternative. In case of a highly qualified endoscopist, ERCP should be postponed until the surgery can be considered.

REFERENCES

- 1 Sarli L, Iusco DR, Roncoroni L. Preoperative endoscopic sphincterotomy and laparoscopic cholecystectomy for the management of cholecystocholedocholithiasis: 10-year experience. *World J Surg* 2003; **27**: 180-186
- 2 Miller RE, Kimmelstiel FM, Winkler WP. Management of common bile stones in the era of laparoscopic cholecystectomy. *Am J Surg* 1995; **169**: 272-276
- 3 Sarli L, Costi R, Gobbi S, Sansebastiani G, Roncoroni L. Asymptomatic bile duct stones: selection criteria for intravenous cholangiography and/or endoscopic retrograde cholangiography prior to laparoscopic cholecystectomy. *Eur J Gastroenterol Hepatol* 2000; **12**: 1175-1180
- 4 McEntee G, Grace PA, Bouchier-Hayes D. Laparoscopic cholecystectomy and the common bile duct. *Br J Surg* 1991; **78**: 385-386
- 5 Sahai AV, Mauldin PD, Marsi V, Hawes RH, Hoffman BJ. Bile duct stones and laparoscopic cholecystectomy: a decision analysis to assess the roles of intraoperative cholangiography, EUS, and ERCP. *Gastrointest Endosc* 1999; **49**: 334-343
- 6 Tian MG, Shi WJ, Wen XY, Yu HW, Huo JS, Zhou DF. Outcome of gallbladder preservation in surgical management of primary bile duct stones. *World J Gastroenterol* 2003; **9**: 1871-1873
- 7 Geron N, Reshef R, Shiller M. The role of endoscopic retrograde cholangiopancreatography in the laparoscopic era. *Surg Endosc* 1999; **13**: 452-456
- 8 Cuschieri A, Lezoche E, Morino M, Croce E, Lacy A, Toouli J, Faggioni A, Ribeiro VM, Jakimowicz J, Visa J, Hanna GB. E.A. E.S. multicenter prospective randomized trial comparing two-stage vs single-stage management of patients with gallstone disease and ductal calculi. *Surg Endosc* 1999; **13**: 952-957
- 9 Rhodes M, Sussman L, Cohen L, Lewis MP. Randomised trial of laparoscopic exploration of common bile duct versus postoperative endoscopic retrograde cholangiography for common bile duct stones. *Lancet* 1998; **351**: 159-161
- 10 Patel AP, Lokey JS, Harris JB, Sticca RP, McGill ES, Arrillaga A, Miller RS, Kopelman TR. Current management of common bile duct stones in a teaching community hospital. *Am Surg* 2003; **69**: 555-560
- 11 Enochsson L, Lindberg B, Swahn F, Arnelo U. Intraoperative endoscopic retrograde cholangiopancreatography (ERCP) to remove common bile duct stones during routine laparoscopic cholecystectomy does not prolong hospitalization: a 2-year experience. *Surg Endosc* 2004; **17**: 2
- 12 Urbach DR, Khajanchee YS, Jobe BA, Standage BA, Hansen PD, Swanstrom LL. Cost-effective management of common bile stones. *Surg Endosc* 2001; **15**: 4-13
- 13 Rodriguez-Gonzalez FJ, Naranjo-Rodriguez A, Mata-Tapia I, Chicano-Gallardo M, Puente-Gutierrez JJ, Lopez-Vallejos P, Hervás-Molina AJ, de Dios-Vega JF. ERCP in patients 90 years of age and older. *Gastrointest Endosc* 2003; **58**: 220-225
- 14 Napoleon B, Dumortier J, Keriven-Souquet O, Pujol B, Ponchon T, Souquet JC. Do normal findings at biliary endoscopic ultrasonography obviate the need for endoscopic retrograde cholangiography in patients with suspicion of common bile duct stone? A prospective follow-up study of 238 patients. *Endoscopy* 2003; **35**: 411-415
- 15 Kohut M, Nowak A, Nowakowska-Dulawa E, Marek T, Kaczor R. Endosonography with linear array instead of endoscopic retrograde cholangiography as the diagnostic tool in patients with moderate suspicion of common bile duct stones. *World J Gastroenterol* 2003; **9**: 612-614
- 16 Sharma SK, Larson KA, Adler Z, Goldfarb MA. Role of endo-

- scopic retrograde cholangiopancreatography in the management of suspected choledocholithiasis. *Surg Endosc* 2003; **17**: 868-871
- 17 **Rijna H**, Kemps WG, Eijssbouts Q, Meuwissen SG, Cuesta MA. Preoperative ERCP approach to common bile duct stones: results of a selective policy. *Dig Surg* 2000; **17**: 229-233
 - 18 **Masci E**, Fanti L, Mariani A, Guerini S, Zuliani W, Baccari P, Giacomelli M, Tittobello A. Selection criteria for pre-operative endoscopic retrograde cholangiography and endoscopic-laparoscopic treatment of biliary stones. *Eur J Gastroenterol Hepatol* 1999; **11**: 781-784
 - 19 **Hamy A**, Hennekinne S, Pessaux P, Lada P, Randriamananjo S, Lermite E, Boyer J, Arnaud JP. Endoscopic sphincterotomy prior to laparoscopic cholecystectomy for the treatment of cholelithiasis. *Surg Endosc* 2003; **17**: 872-875
 - 20 **Charfare H**, Cheslyn-Curtis S. Selective cholangiography in 600 patients undergoing cholecystectomy with 5-year follow-up for residual bile duct stones. *Ann R Coll Surg Engl* 2003; **85**: 167-173
 - 21 **Tanaka M**, Sada M, Eguchi T, Konomi H, Naritomi G, Takeda T, Ogawa Y, Chijiwa K, Deenitchin GP. Comparison of routine and selective endoscopic retrograd cholangiography before laparoscopic cholecystectomy. *World J Surg* 1996; **20**: 267-271
 - 22 **Abboud PA**, Malet PF, Berlin JA, Staroscik R, Cabana MD, Clarke JR, Shea JA, Schwartz JS, Williams SV. Predictors of common bile stones prior to cholecystectomy: a meta-analysis. *Gastrointest Endosc* 1996; **44**: 450-459
 - 23 **Sahai AV**, Mauldin PD, Marsi V, Hawes RH, Hoffman BJ. Bile duct stones and laparoscopic cholecystectomy: a decision analysis to assess the roles of intraoperative cholangiography, EUS, and ERCP. *Gastrointest Endosc* 1999; **49**: 334-343
 - 24 **Neuhaus H**, Feussner H, Ungeheuer A, Hoffmann W, Siewert JR, Classen M. Prospective evaluation of the use of endoscopic retrograde cholangiography prior to laparoscopic cholecystectomy. *Endoscopy* 1992; **24**: 745-749
 - 25 **Fussi F**, inventors; Hepar Industries Inc., Assignee. Process for obtaining low molecular weight heparins endowed with elevated pharmacological properties, and product so obtained. *United States Patent* 1981; **281**: 108
 - 26 **Rieger R**, Sulzbacher H, Woissetschlager R, Schrenk P, Wayand W. Selective use of ERCP in patients undergoing laparoscopic cholecystectomy. *World J Surg* 1994; **18**: 900-905
 - 27 **Onken JE**, Brazer SR, Eisen GM, Williams DM, Bouras EP, DeLong ER, Long TT 3rd, Pancotto FS, Rhodes DL, Cotton PB. Predicting the presence of choledocholithiasis in patients with symptomatic cholelithiasis. *Am J Gastroenterol* 1996; **91**: 762-767
 - 28 **van der Hul RL**, Plaisier PW, Hamming JF, Bruining HA. Detection and management of common bile duct stones in the era of laparoscopic cholecystectomy. *Scand J Gastroenterol* 1993; **28**: 929-933
 - 29 **Eisen GM**, Dominitz JA, Faigel DO, Goldstein JL, Kalloo AN, Petersen BT, Raddawi HM, Ryan ME, Vargo JJ 3rd, Young HS, Fanelli RD, Hyman NH, Wheeler-Harbaugh J. American Society for Gastrointestinal Endoscopy. Standards of Practice Committee. An annotated algorithm for the evaluation of choledocholithiasis. *Gastrointest Endosc* 2001; **53**: 864-866
 - 30 **Hintze RE**, Adler A, Veltzke W, Abou-Rebyeh H, Hammerstingl R, Vogl T, Felix R. Clinical significance of magnetic resonance cholangiopancreatography (MRCP) compared to endoscopic retrograde cholangiopancreatography (ERCP). *Endoscopy* 1997; **29**: 182-187
 - 31 **Cotton PB**. Endoscopic retrograde cholangiopancreatography and laparoscopic cholecystectomy. *Am J Surg* 1993; **165**: 474-478
 - 32 **Welbourn CR**, Mehta D, Armstrong CP, Gear MW, Eyre-Brook IA. Selective preoperative endoscopic retrograde cholangiography with sphincterotomy avoids bile duct exploration during laparoscopic cholecystectomy. *Gut* 1995; **37**: 576-579
 - 33 **Santucci L**, Natalini G, Sarpi L, Fiorucci S, Solinas A, Morelli A. Selective endoscopic retrograde cholangiography and pre-operative bile duct removal in patients scheduled for laparoscopic cholecystectomy: a prospective study. *Am J Gastroenterol* 1996; **91**: 1326-1330

Edited by Wang XL Proofread by Zhu LH and Xu FM

• CLINICAL RESEARCH •

Effect of integrated traditional Chinese and Western medicine on SARS: A review of clinical evidence

Ming-Ming Zhang, Xue-Mei Liu, Lin He

Ming-Ming Zhang, Chinese Evidence-Based Medicine Center, West China Hospital, Sichuan University, Chengdu 610041, Sichuan Province, China

Xue-Mei Liu, Editorial Department, Chinese Journal of Evidence-Based Medicine, Chinese Evidence-Based Medicine Center, West China Hospital, Sichuan University, Chengdu 610041, Sichuan Province, China

Lin He, Library of West China Hospital, Sichuan University, Chengdu 610041, Sichuan Province, China

Correspondence to: Mrs. Xue-Mei Liu, Editorial Department, Chinese Journal of Evidence-Based Medicine, Chinese Evidence-Based Medicine Center, West China Hospital, Sichuan University, Chengdu 610041, Sichuan Province, China. cochrane@mail.sc.cninfo.net

Telephone: +86-28-85422079 **Fax:** +86-28-85422253

Received: 2003-12-23 **Accepted:** 2004-02-08

Abstract

AIM: To assess the possible effect of integrated traditional Chinese and Western medicine on severe acute respiratory syndromes.

METHODS: The current available randomized controlled trials of integrated traditional Chinese and Western medicine on SARS were identified through systematically searching literature in any languages or any types of publications. Additional studies of gray literature were also collected. The quality of studies was evaluated by two investigators independently based largely on the quality criteria specified CONSORT. Statistical analysis of the results was performed using RevMan 4.2.0 software developed by the Cochrane Collaboration.

RESULTS: Six studies ($n = 366$) fulfilling the inclusion criteria were found, of which the quality of one study was graded as B, the remaining five were graded as C. Two studies were performed with meta-analysis, the other four studies existed some heterogeneity for which meta-analysis could not be performed, a significant effect on lung infiltrate absorption was found in the treatment groups of these two studies [RR 6.68, 95% CI (2.93, 15.24), $P < 0.01$], there was no significant differences between the mortality [RR 0.86, 95% CI (0.22, 3.29), $P = 0.82$] and the average dosage of corticosteroid [WMD -39.65, 95% CI (-116.84, 37.54), $P = 0.31$]. The other three studies also showed significant differences in infiltrate absorption, including national drug No. 2, 3, 4 in combination with Western medicine [RR 5.45, 95% CI (1.54, 19.26)], compound formulas NO. 1 combined with Western medicine [WMD 0.24, 95% CI (0.02, 0.46)], compound formulas combined with Western medicine [RR 8.06, 95% CI (0.40, 163.21)]. Kangfeidian No.4 in combination with Western medicine had no significant effect on symptom improvement such as loss of dyspnea and cough [RR 1.50, 95%CI (0.41, 5.43)] and [RR 1.29, 95%CI (0.30, 5.43)].

CONCLUSION: Integrated traditional Chinese and Western medicines has some positive effects on lung infiltrate absorption in SARS patients, and is recommended as an adjunct treatment

for SARS. However, its effect on SARS requires further careful study due to limited available randomized control trials.

Zhang MM, Liu XM, He L. Effect of integrated traditional Chinese and Western medicine on SARS: A review of clinical evidence. *World J Gastroenterol* 2004; 10(23): 3500-3505 <http://www.wjgnet.com/1007-9327/10/3500.asp>

INTRODUCTION

Severe acute respiratory syndromes (SARS) is a readily transmissible new disease emerged in the 21st century that imposes a threat to international health^[1-3]. SARS is caused by a novel coronavirus, first identified in Hong Kong, United States of American and Germany. It is due to an infection with SARS associated coronavirus (SARS-CoV). The genome of SARS-CoV is 29 727 nucleotides in length and has 11 open reading frames, and its genome organization is similar to that of other coronaviruses^[4-7], SARS is an acute respiratory illness with typical symptoms of fever, cough and difficult breathing. Besides, it may be associated with other symptoms, such as headache, muscular stiffness, myalgia, loss of appetite, malaise, chills, confusion, dizziness, rash, night sweat, nausea and diarrhea. SARS can be divided into 5 types and 4 stages. The 5 types are common type (typical type), mild type, severe type and more severe type. The four stages are potential stage (2-10 d), initial stage (1-7 d), developing stage (8-14 d), and recovery stage (1-14 d), which are classified based on the developing process of SARS patient conditions by the criteria of Western medicine. SARS can also be divided as initial stage (1-5 d), acute stage (3-10 d), critical stage (7-14 d) and recovery stage (10-18 d) based on the theory of traditional Chinese medicine^[8-11].

SARS demonstrates dramatically the global havoc that its epidemic had broken out worldwide including mainland China, Taiwan, Hong Kong, Vietnam, Singapore, Macao, North American and Europe when the first case was found in Foshan city, Guangdong Province, China on November 16, 2002. Airborne droplets from SARS patients are the main transmission routes. Based on the data from WHO. SARS epidemic appears to have peaked and is on the wane^[12,13]. A total of 916 SARS patients died in 8 422 cases and the mortality was about 11%. A total of 5 327 SARS patients occurred in mainland China and 349 of them died, the mortality was about 7%. A total of 1 755 SARS patients occurred in Hong Kong Special Administrative Region, China and 300 of them died, the mortality was about 17%. A total of 655 SARS patients occurred in Taiwan, China and 180 of them died, the mortality was 27%. The case fatality ratio was estimated to be less than 1% in persons aged 24 years or younger, 6% in persons aged 25 to 44 years, 15% in persons aged 45 to 64 years, and greater than 50% in persons aged 65 years and older^[14,15].

Western medicine for SARS

The treatment of SARS involves multiple disciplines, and current recommendations are mainly based on the methods of Western medicine including aliment therapy, respiratory

auxiliary ventilation, anti-infection and glucocorticoid therapy. The effectiveness for SARS was limited especially in the first and recovery stages. For example, in severe cases, corticosteroids and ribavirin (antiviral medication) were used, however there was no evidence to support their general or routine use at this stage and to confirm the risks and benefits of Western medicine in the treatment of SARS. Selective therapies included the use of antiviral agents, immunopotentiators and Chinese herbs^[8,9,11,15]

Chinese herbs in combination with western medicine for SARS

Traditional Chinese medicine (TCM) is a useful model for scientific therapies and has been practiced worldwide. Among the components of TCM, herbal agents possess complex biological activities. In the theory of TCM, herbs preparations might resolve toxin, eliminate pathological dampness, disperse the lung, invigorate the blood circulation and resolve the blood stasis, benefit Qi and nourish Yin^[16,17]. Based on this principle, Chinese practitioners suspected that SARS was caused by pestilential toxin, one of the important characteristics of SARS. Nine traditional Chinese patent medicines are optimized for controlling different symptoms of SARS. Compared with the simple treatment of Western medicine, Chinese medicine in combination with Western medicine for SARS may have better effects in that it may reduce the adverse events induced by anti-biotic and anti-virus treatments and other complications, shorten fever period and hospital stay, promote lung infiltrate absorption and decrease damage to the lung^[18-20]. The 5 kinds of herbs are Kangfeidian No.1,2,3^[29,34], compound formula No.1^[32], national drugs No.2,3,4^[31], compound herbs^[30], Kangfeidian No.4^[33]. Unfortunately, no strong evidence is available to demonstrate the benefits and risks of Chinese herbs in combination with Western medicine for SARS.

This review evaluated the possible effect of Chinese herbs in combination with Western medicine for SARS, summarized randomized controlled trials (RCT) and methods of integrated traditional Chinese and Western medicine for SARS, as well as a recommendation for future research.

MATERIALS AND METHODS

Data collection

A comprehensive searching strategy was used to identify all current relevant RCTs regardless of languages or types of publication (published, unpublished, in press, and in progress). We searched MEDLINE for relevant trials (1966 to 2003), EMBASE (1980 to 2003), CBM (Chinese Biomedical Database, 1981 to 2003), Chinese Cochrane Centre Controlled Trial Register (up to 2003), Cochrane Controlled Trial Register in Cochrane Library (issues 1 to 4, 2003), Current Controlled Trials and The National Research Register. The search terms were: "severe acute respiratory syndrome", "acute respiratory syndrome", "randomized-controlled-trial", "random allocation" "double blind method", "single blind method", "placebo", "herbs", "Chinese medicinal".

The references of relevant trials and reviews were identified and RCTs in the Database of Chinese Evidence-Based Medicine Center and in journals not included in this Database were manually searched. We also checked the citations of existing reviews and all studies identified by the above methods. The authors of identified literature and relevant specialists were contacted for additional information.

Types of studies and participants

Only randomized controlled trials of Chinese herbs in combination with Western medicine for SARS were included regardless of blinding, follow up, language or publication status. The followings were excluded such as clinical controlled trials of SARS patients that failed to allocate into either trial, control group, case study or animal experiments.

Only randomized controlled trials of Chinese herbs in combination with Western medicine for the diagnosis of SARS patients with standard criteria of WHO in 2003 were included. Moreover, those SARS patients complicated with other diseases such as diabetes, cardiovascular disease, hypertension, or cancers were also included. The suspected SARS patients and misdiagnosed patients were excluded.

Quality assessment

We screened the titles, abstracts, and keywords of every document retrieved to determine the quality of the papers. We retrieved the full articles for further assessment if the information given suggested that the study included diagnosed SARS patients; compared Chinese herbs in combination with Western medicine with placebo, Chinese herbs, Western medicine or any other active intervention; used random allocation to the comparison groups. Where differences in opinion existed, we would solve them through discussion. If we were unable to solve the disagreement through discussion, we would contact the authors for clarification.

The quality of each trial was assessed based largely on the quality criteria specified CONSORT^[21]. In particular, the following factors were assessed^[22,23] such as minimization of selection bias, minimization of performance bias, minimization of attrition bias, and minimization of detection bias. Based on these criteria, studies were subdivided into the following three categories^[23]: low risk of bias which met all quality criteria graded as A, moderate risk of bias which met one or more of the quality criteria graded as B, high risk of bias which did not meet one or more criteria graded as C.

Statistical analysis

Data were extracted independently by two investigators with a standardized form and analyzed using RevMan 4.2.0 software developed by the Cochrane Collaboration^[23,24]. Heterogeneity was tested using the *Z score* and the *Chi square*. Statistical significance was set at $P < 0.05$. We performed a meta-analysis for the data. The dichotomous data expressed as relative risk (RR). The continuous data expressed as weighted mean difference (WMD). We calculated the overall results based on the random effect model.

Hypothesis

When data were pooled, we hypothesized that all Western medicine interventions used in control and trial groups had the same effect on all the outcome measures indexed in this review.

RESULTS

Studies identified

The initial searching using the electronic search strategy listed above and manual searching yielded 650 studies. After scanned, 48 studies of Chinese herbs in combination with Western medicine for SARS were identified to meet the inclusion criteria. Most of the studies were published in Chinese. Of the 48 studies, one study of clinical report on the suspected SARS patients was excluded upon further scrutiny and the other 28 case reports and 9 case control studies were identified. There were 10 RCT studies identified. Because of some reasons, we did not obtain the complete report of studies. Further exclusion included one study identified as randomized sample, but not randomization allocation^[25], one study which compared Western medicine versus Western medicine for SARS^[26] and the other two studies which were duplicate publication^[27,28]. Finally, 6 RCT studies of Chinese herbs in combination with Western medicine fulfilling the inclusion criteria were identified^[29-34].

Six studies ($n = 366$) were included^[29-34]. The details of the designs of these studies are shown in Table 2. All six studies

were conducted in China. The median time of treatment was 17 d. Four studies reported the number of patients in common type and severe type^[29-31,34]; two studies performed a meta-analysis, the data were sufficient in quality, and similar^[29,34]. One study was Western medicine plus compound herbs^[32]; the other three studies were about Western medicine plus national drugs 2,3,4^[30-32] and Kangfeidian No.4^[33]. The constituents and dosage of Chinese herbs varied. Most of the studies with the heterogeneity of intervention prevented us from doing a meta-analysis and a meaningful subgroup analysis on Chinese herbs.

Study methodology

Most of the included studies had poor quality ('C')^[29-31,33,34] one study was graded as B^[32] (Table 1).

All of the studies claimed as randomization, but none of them described the method of randomization in details, and none of the studies referred allocation concealment. Of the six studies, one described its design in detailed randomization process and the baseline data were reported adequately^[32]. Two

studies were described as stratified randomization^[31,33] and the other three studies only mentioned 'randomization'^[29,30,34]. Withdrawals and loss of follow-up were not reported in six studies and none of the studies reported intention-to-treat analysis.

No adverse events of Chinese herbs were observed in the included studies. Only one study reported the quality of life as result index^[32]. The effect of integrated traditional Chinese medicine and Western medicine for SARS see Table 2.

Mortality

The mortality^[29-31,34] was reported in 4 studies.

National drugs No. 2. 3. 4 in combination with Western medicine did not show a significant difference on mortality compared to simple Western medicine (RR 0.41, 95% CI 0.04, 4.78).

Kangfeidian No. 1.2. 3 in combination with Western medicine was tested in two studies^[29,34] which used the same dosage and treatment time and had the same outcome. Compared to simple Western medicine, there was no significant effect on mortality [RR 0.86, 95% CI (0.22, 3.29), $P=0.82$, Table 3].

Table 1 Design of the RCTs of traditional Chinese medicine in combination with Western medicine for SARS

Study ID	Grade of method	Participants (case)				Trial interventions	Control interventions	Duration	Follow up	Main results
		Common type		Severe type						
Zhao CH 2003	C	51	26			Western medicine plus compound herbs of kangfeidian No.1,2,3.	Western medicine	14-21d	No	Mortality, lung infiltrate absorption, symptom improvement, dosage of glucocorticosteroids.
Wang BE 2003	C	Trial 13	Control 17	Trial 18	Control 12	Western medicine plus compound herbs.	Western medicine	10-20 d	No	Mortality, lung infiltrate absorption, Secondary infections, dosage of methyprednisolone, SO ₂ .
Wang RB 2003	C	Trial 5	Control 7	Trial 30	Control 23	Western medicine plus national drug No.2,3,4.	Western medicine	14 d	No	Mortality, lung infiltrate absorption, Secondary infections, symptom improvement
Jiang ZY 2003	B	40				Western medicine plus compound herbs No.1,2,3.	Western medicine	21 d or so	Yes	Lung infiltrate absorption, symptom improvement, quality of life
Zhang SN 2003	C	63				Western medicine plus kangfeidian No.4	Western medicine	7 d	No	Dose of glucocorticoid, lung infiltrate absorption, symptom improvement
Zhang XM 2003	C	Trial 7	Control 9	Trial 24	Control 23	Western medicine plus compound herbs of kangfeidian No.1,2,3.	Western medicine	21 d	No	Mortality, lung infiltrate absorption, symptom improvement, dose of glucocorticoid, length of fever

Table 2 Results of meta-analysis of integrated traditional Chinese and Western medicine for SARS at the end of treatment

Comparison or outcomes	Study	Participants			Statistical method	Effect estimate
		Total	Trial	Control		
National drugs No.2.3.4 combined with Western medicine versus Western medicine						
Mortality	Wang RB 2003	65	1/35	2/30	RR (fixed) 95%	0.41 (0.04, 4.78)
Lung infiltrate absorption		53	25/30	11/23		5.45 (1.54, 19.26)
The secondary infection		65	4/35	7/30		0.42 (0.11, 1.62)
Compound formulas No.1 combined with Western medicine versus Western medicine						
Symptom improvement integral	Jiang ZY 2003	40	7.90 (5.81)	6.50 (3.83)	WMD (fixed) 95%	1.40 (-1.65, 4.45)
Lung infiltrate absorption		40	0.65 (0.35)	0.38 (0.37)		0.24 (0.02, 0.46)
Quality of life integral		40	19.93 (3.69)	22.10 (4.90)		-2.17 (-4.86, 0.52)
Compound formulas combined with Western medicine versus Western medicine						
Lung infiltrate absorption	Wang BN 2003	59	30/30	26/29	RR (fixed) 95%	8.06 (0.40, 163.21)
Kangfeidian No.4 combined with Western medicine versus Western medicine						
Loss of dyspnea	Zhang SN 2003	38	12/20	9/18	RR (fixed) 95%	1.50 (0.41, 5.43)
Loss of cough		30	9/16	7/14		1.29 (0.30, 5.43)

Table 3 Effect of Kangfeidian No.1,2, 3 with Western medicine in SARS patients

Outcome measure	Kangfeidian No.1, 2, 3 combined with Western medicine	Western medicine alone	Relative risk (95% CI)	P	Reference
Mortality	(n/N)				
	4/31	4/32	1.04 (0.24, 4.57)		Zhang XM <i>et al.</i> (2003)
	0/37	1/39	0.34 (0.01, 8.67)		
Overall	4/68	5/71	0.86 (0.22, 3.29)	0.82	
Lung infiltrate	27/31	18/32	5.25 (1.49, 18.53)		Zhao CH <i>et al.</i> (2003)
Absorbing	22/37	6/39	8.07 (2.71, 23.98)		
Overall	49/68	24/71	6.68 (2.93, 15.24)	<0.00001	Zhao CH <i>et al.</i> (2003)
The average Dosage of	N (mean±SD)		WMD(95% CI)		
Glucocorticosteroids	31 (304.13±143.42)	32 (347.40±173.10)	-43.27 (-121.67, 35.13)		Zhang XM <i>et al.</i> (2003)
	15 (1 400.00±685.00)	20 (1 325.00±623.00)	75.00 (-366.27, 516.27)		Zhao CH <i>et al.</i> (2003)
Overall	46	52	-39.65 (-116.84, 37.54)	0.31	

Lung infiltrate absorption

Six studies reported the effect of Chinese herbs in combination with Western medicine on the lung infiltrate absorption^[29,34]. Of the six studies, three reported that Chinese herbs in combination with Western medicine had a better effect than simple Western medicine^[29,31,34].

National drugs No. 2. 3. 4 in combination with Western medicine^[31] showed a significant difference in lung infiltrate absorption [RR 5.45, 95% CI (1.54, 19.26)]. Kangfeidian No. 1. 2. 3 in combination with Western medicine^[29,34] showed a better positive effect on lung infiltrate absorption [RR 6.68, 95% CI (2.93, 15.24), $P < 0.01$] (Table 3). In the original study^[34], $n = 31$ in treatment group, $n = 32$ in control group, 21 d after treatment with Kangfeidian No. 1. 2. 3 in combination with Western medicine, symptoms were improved by 87% in treatment group, and 56% in control group. In the original study, $n = 77$ ^[29], it was reported that the lung infiltrate absorption was less two days in treatment group. In treatment group $n = 22$, the basic absorption time (16 ± 8.8 d) and in control group $n = 6$, the basic absorption time (18.4 ± 8.2 d).

Compound formulas No 1. in combination with Western medicine^[32] showed no significant difference in lung infiltrate absorption between treatment group and control group [WMD 0.24, 95% CI (0.02, 0.46)]. Compound formulas in combination with Western medicine^[31] showed a positive effect on lung

infiltrate absorption [RR 8.06, 95% CI (0.40, 163.21)].

Dosage of glucocorticosteroids

Kangfeidian No. 1. 2. 3 in combination with Western medicine versus Western medicine^[29,34] for SARS showed no significant effect on the treatment group [WMD -39.65, 95% CI (-116.84, 37.54) $P = 0.31$] (Table 3).

Additional results

Kangfeidian No 4 combined with Western medicine versus Western medicine^[33] showed no significant effects on loss of dyspnea [RR 1.50, 95% CI (0.41, 5.43)] and loss of cough [RR 1.29, 95% CI (0.30, 5.43)] (Table 3).

DISCUSSION

Standard treatment and outcome index

To assess accurately any potential benefits and risks in the treatment of SARS, treatment of Chinese herbs must be scientifically evaluated. Standard treatment and outcome index need to be developed, based on the principles used by the Chinese herb practitioners. For example, criteria for the dosage and components of compound herbs, duration of treatment, withdrawal and follow up, treatment protocols should be adjusted according to the conditions of patients^[35,36]. In the six

studies, none of them were standardized and one study described not any details on the dosage and components of compound herbs^[33]. Principal criteria for outcome index are another important issue to be taken into account, such as mortality, symptom improvement, lung infiltrate absorption, quality of life and adverse events. The six studies varied in outcome index.

Treatments to be tested should be selected and standardized so that potentially effective and important treatments are evaluated first. The best evidence should be systematically reviewed, summarized, and disseminated, which in turn would lead to evidence-based decision making in traditional Chinese medicine.

Long term studies

Most of the current studies had a short duration, ranging from 7 to 21 d and a small sample size. All studies did not report data on compliance and follow up. As a new kind of respiratory disease many unknown factors remain to be solved. SARS is likely to require a longer period of follow-up. Based on the current investigation, Chinese herbs may also be considered as an adjuvant treatment to improve the quality of life. Meanwhile, whether herbs have any toxic effects should also be considered and attention should be paid to their long-term adverse events. For example, adverse events should be monitored by a standardized effective reporting system in clinical trials and some severe adverse events should also be studied or observed by epidemiological studies.

Adequate randomization method

SARS is a sudden outbreak disease. It is somewhat difficulty for us to conduct RCT, particularly in acute or critical stage. The current six RCTs conducted suggest that it is a promising work. However, a well designed RCT requires a thorough understanding of randomization so that better research results could be achieved.

Randomization includes 3 important steps: namely sequence generation, allocation concealment and randomization implementation^[37]. Sequence generation is a method used to generate the random allocation sequence, including details of any restriction. Allocation concealment is to implement the random allocation sequence. Randomization implementation is to generate the allocation sequence. Well designed RCTs are required to evaluate Chinese herbs combined with Western medicine versus Western medicine.

REFERENCES

- 1 WHO. Severe acute respiratory syndrome (SARS): Status of the outbreak and lessons for the immediate future. *Geneva World Health Organization* 20 May 2003. Available from: URL: http://www.who.int/csr/media/en/sars_waha.pdf
- 2 Chan-Yeung M, Ooi GC, Hui DS, Ho PL, Tsang KW. Severe acute respiratory syndrome. *Int J Tuberc Lung Dis* 2003; **7**: 1117-1130
- 3 Marra MA, Jones SJ, Astell CR, Holt RA, Brooks-Wilson A, Butterfield YS, Khattra J, Asano JK, Barber SA, Chan SY, Cloutier A, Coughlin SM, Freeman D, Girn N, Griffith OL, Leach SR, Mayo M, McDonald H, Montgomery SB, Pandoh PK, Petrescu AS, Robertson AG, Schein JE, Siddiqui A, Smailus DE, Stott JM, Yang GS, Plummer F, Andonov A, Artsob H, Bastien N, Bernard K, Booth TF, Bowness D, Czub M, Drebot M, Fernando L, Flick R, Garbutt M, Gray M, Grolla A, Jones S, Feldmann H, Meyers A, Kabani A, Li Y, Normand S, Stroher U, Tipples GA, Tyler S, Vogrig R, Ward D, Watson B, Brunham RC, Kraiden M, Petric M, Skowronski DM, Upton C, Roper RL. The Genome sequence of the SARS-associated coronavirus. *Science* 2003; **300**: 1399-1404
- 4 Rota PA, Oberste MS, Monroe SS, Nix WA, Campagnoli R, Icenogle JP, Penaranda S, Bankamp B, Maher K, Chen MH, Tong S, Tamin A, Lowe L, Frace M, DeRisi JL, Chen Q, Wang D, Erdman DD, Peret TC, Burns C, Ksiazek TG, Rollin PE, Sanchez A, Liffick S, Holloway B, Limor J, McCaustland K, Olsen-Rasmussen M, Fouchier R, Gunther S, Osterhaus AD, Drosten C, Pallansch MA, Anderson LJ, Bellini WJ. Characterization of a novel coronavirus associated with severe acute respiratory syndrome. *Science* 2003; **300**: 1394-1399
- 5 Peiris JS, Lai ST, Poon LL, Guan Y, Yam LY, Lim W, Nicholls J, Yee WK, Yan WW, Cheung MT, Cheng VC, Chan KH, Tsang DN, Yung RW, Ng TK, Yuen KY. Coronavirus as a possible cause of severe acute respiratory syndrome. *Lancet* 2003; **361**: 1319-1325
- 6 Drosten C, Gunther S, Preiser W, van der Werf S, Brodt HR, Becker S, Rabenau H, Panning M, Kolesnikova L, Fouchier RA, Berger A, Burguiere AM, Cinatl J, Eickmann M, Escriu N, Grywna K, Kramme S, Manuguerra JC, Muller S, Rickerts V, Sturmer M, Vieth S, Klenk HD, Osterhaus AD, Schmitz H, Doerr HW. Identification of a novel coronavirus in patients with severe acute respiratory syndrome. *N Engl J Med* 2003; **348**: 1967-1976
- 7 Huang GH, Feng YL. SARS diagnosis and therapy. *Zhongguo Huxi Yu Weizhong Jianhu Zazhi* 2003; **2**: 153-158
- 8 Xu XY, Wang GF, Lu HY, Li HC, Huo N, Wang J, Nie LG, Que XL. The stage of SARS and the experience of SARS. *Beijing Daxue Xuebao* 2003; **5**(Suppl): 5-6
- 9 SARS preventive and treatment protocol by TCM. *Tianjin Zhongyiyao Feidian Zhuanji* 2003; **20**: 106-107
- 10 Zhong LS. Diagnosis and treatment protocol for SARS. *Zhonghua Yixue Zazhi* 2003; **83**: 1731-1752
- 11 Nie HQ, Luo XD, Zhang JZ, Su Q. Current status of severe acute respirator syndrome in China. *World J Gastroenterol* 2003; **9**: 1635-1645
- 12 Drazen JM. SARS-looking back over the first 100 days. *N Engl J Med* 2003; **349**: 319-320
- 13 WHO. Summary table of SARS cases by country, 1 November 2002-7August 2003. Available from: URL:http://www.who.int/csr/sars/country/en/country2003_08_15.pdf.
- 14 WHO. Cumulative number of reported probable cases of SARS. Available from: URL: http://www.who.int/csr/sars/country/2003_06_25/en/
- 15 Liu P, Cao Y, Qiao X. Clinical study on shenmai injection in promoting postoperative recovery in patients of breast cancer. *Zhongguo Zhongxiyi Jiehe Zazhi* 2000; **20**: 328-329
- 16 Cohen I, Tagliaferri M, Tripathy D. Traditional Chinese medicine in the treatment of breast cancer. *Semin Oncol* 2002; **29**: 563-574
- 17 Li XH, Zhang K, Hu JH, Guo XH, Hu ZJ, Yang Y, Liang LC. Clinical evaluation of the integrated traditional Chinese medicine with western medicine on treatment of severe acute respiratory syndrome (SARS). *Proceedings International Science Symposium SARS* 2003: 125-130
- 18 Hai X. Clinical experience of treating SARS in Guangdong hospital of TCM. *Tianjin Zhongyiyao Feidian Zhuanji* 2003; **20**: 24-25
- 19 Xiao PG, Wang YY, Cheng HS. Some research clues on Chinese herbal medicine for SARS prevention and treatment. *Zhongguo Zhongyao Zazhi* 2003; **28**: 481-483
- 20 Xiao XH, Wang JB, He CS. On the rational exertion for the prescriptions and drugs of TCM in prevention and treating SARS. *Zhongguo Zhongyao Zazhi* 2003; **28**: 664-668
- 21 Moher D, Schulz KF, Altman D. The CONSORT statement: revised recommendations for improving the quality of reports of parallel-group randomized trials. *JAMA* 2001; **285**: 1987-1991
- 22 Schulz KF, Chalmers I, Hayes RJ, Altman DG. Empirical evidence of bias. Dimensions of methodological quality associated with estimates of treatment effects in controlled trials. *JAMA* 1995; **273**: 408-412
- 23 Clarke M, Oxman AD, editors. *Cochrane Reviewers' Handbook 4.2 In: Review Manager (RevMan) [Computer program]. Version 4.2. Oxford, England: The Cochrane Collaboration, updated June 2000*
- 24 Egger M, Davey Smith G, Schneider M, Minder C. Bias in meta-analysis detected by a simple graphical test. *BMJ* 1997; **315**: 629-634
- 25 Kang J. The experience of treatment and preventing SARS by traditional Chinese integrated western medicine. Symposium on treating SARS by integrated traditional Chinese and western medicine from five provinces in north China and Guangdong

- province. Hosted by Chinese association for science & technology, Held by Chinese association of the integration of traditional and western medicine. *Beijing China* 2003: 39-41
- 26 **Zhao ZW**, Zhang FC, Xu M, Huang K, Zhong WL, Cai WP, Yin ZB, Huang SD, Deng ZB, Wei M. Clinical analysis of 190 cases of outbreak with atypical pneumonia in Guangzhou in spring 2003. *Zhonghua Yixue Zazhi* 2003; **83**: 713-719
- 27 **Wang RB**, Liu JM, Jian YY, Wu YZ, Wang XJ, Xu DZ. Traditional Chinese medicine treatment of 11 SARS cases. *Beijing Zhongyiyao Zazhi* 2003; **22**: 8-9
- 28 **Wang RB**, Liu JM, Wu YZ, Jiang YY, Wang XJ, Chi PP, Sun FX. Therapeutic effects of integrative traditional Chinese medicine and western medicine for SARS. *Proceedings international Sciences Symposium SARS* 2003: 293-297
- 29 **Zhao CH**, Li XH, Zhang K, Jing RH, Gou CY, Hu ZJ, Ye J, Yang Y, Guo XH, Liang LC, Hu JH, Li XM, Wu JS. Randomized control study of integrative traditional Chinese and western medicine in the treatment of 77 patients. *Zhongguo Zhongxiyi Jiehe Jijou Zazhi* 2003; **10**: 197-200
- 30 **Wang BE**, Zhang SW, Ren AM. Integrated traditional Chinese and western medicine for SARS. Symposium on treating SARS by integrated traditional Chinese and western medicine from five provinces in north China and Guangdong province. Hosted by Chinese association for science & technology, Held by Chinese association of the integration of traditional and western medicine. *Beijing China*: 2003: 50-52
- 31 **Wang RB**, Liu JM, Jiang YY, Wu YZ, Wang XJ, Chi PP, Sun FX. Preliminary study on clinical efficacy of integrative Chinese and western medicine in treating severe acute respiratory syndrome. *Zhongguo Zhongxiyi Jiehe Zazhi* 2003; **23**: 492-493
- 32 **Jiang ZY**, Tang XD, Qi WS, Bian YJ, Song QQ, Zhang ZZ, Li CX, Fu YL, Wang YH, Xiang XP, Wang RB, Chen YF, Liu BY, Xie YM. Clinical efficacy evaluation of TCM for convalescent patients with SARS Symposium on treating SARS by integrated traditional Chinese and western medicine from five provinces in north China and Guangdong province. Beijing China: Chinese association for science & technology, Chinese association of the integration of traditional and western medicine, June 2003: 41-54
- 33 **Zhang SL**. The clinical effect and character of traditional Chinese medicine integrated western medicine for lung fibrosis induced by SARS. *Chinese General Practice* 2003; **6**: 576-577
- 34 **Zhang XM**, Zhang YL, Yang ZF, Jin YW, Tang XH, Zhang Y, Feng GL, Ma YM, Yang YK, Wang MY, He YH, Zhang Y, Liu XS, Wang YL, Jin ZA, Lin Q, Liu WN. Clinical effective of serial SARS formula for SARS. *Zhongguo Yiyao Xuebao* 2003; **18**: 323-325
- 35 **Lin L**, Han Y, Yang ZM. Clinical observation on 103 patients of severe acute respiratory syndrome treated by integrative traditional Chinese and Western Medicine. *Zhongguo Zhongxiyi Jiehe Zazhi* 2003; **23**: 409-413
- 36 Integrative Chinese medicine and western medicine for SARS. *Zhongguo Zhongxiyi Jiehe Zazhi* 2003; **23**: 484-485
- 37 **Zheng SP**. Principle and method of clinical research design In: Wang JL. Clinical epidemiology-clinical research design and review. 2nd ed. Shanghai: *Shanghai Science Press* 2001: 47-59

Edited by Wang XL and Ren SY Proofread by Xu FM

• CLINICAL RESEARCH •

HDR-¹⁹²Ir intraluminal brachytherapy in treatment of malignant obstructive jaundice

Yi Chen, Xiao-Lin Wang, Zhi-Ping Yan, Jie-Min Cheng, Jian-Hua Wang, Gao-Quan Gong, Sheng Qian, Jian-Jun Luo, Qing-Xin Liu

Yi Chen, Xiao-Lin Wang, Zhi-Ping Yan, Jie-Min Cheng, Jian-Hua Wang, Gao-Quan Gong, Sheng Qian, Jian-Jun Luo, Qing-Xin Liu, Department of Radiology, Affiliated Zhongshan Hospital, Medical Center of Fudan University, Shanghai 200032, China

Correspondence to: Dr. Yi Chen, Department of Radiology, Affiliated Zhongshan Hospital, Medical Center of Fudan University, 180 Fenglin Road, Shanghai 200032, China

Telephone: +86-21-64041990 Ext. 2533

Received: 2004-01-10 **Accepted:** 2004-03-24

Abstract

AIM: To determine the feasibility and safety of intraluminal brachytherapy in treatment of malignant obstructive jaundice (MOJ) and to evaluate the clinical effect of intraluminal brachytherapy on stent patency and patient survival.

METHODS: Thirty-four patients with MOJ were included in this study. Having biliary stent placed, all patients were classified into intraluminal brachytherapy group (group A, $n = 14$) and control group (group B, $n = 20$) according to their own choice. Intraluminal brachytherapy regimen included: HDR-¹⁹²Ir was used in the therapy, fractional doses of 4-7 Gy were given every 3-6 d for 3-4 times, and standard points were established at 0.5-1.0 cm. Some patients of both groups received transcatheter arterial chemoembolization (TACE) after stent placement.

RESULTS: In group A, the success rate of intraluminal brachytherapy was 98.0%, RTOG grade 1 acute radiation morbidity occurred in 3 patients, RTOG/EORTC grade 1 late radiation morbidity occurred in 1 patient. Mean stent patency of group A (12.6 mo) was significantly longer than that of group B (8.3 mo) ($P < 0.05$). There was no significant difference in the mean survival (9.4 mo vs 6.0 mo) between the two groups.

CONCLUSION: HDR-¹⁹²Ir intraluminal brachytherapy is a safe palliative therapy in treating MOJ, and it may prolong stent patency and has the potentiality of extending survival of patients with MOJ.

Chen Y, Wang XL, Yan ZP, Cheng JM, Wang JH, Gong GQ, Qian S, Luo JJ, Liu QX. HDR-¹⁹²Ir intraluminal brachytherapy in treatment of malignant obstructive jaundice. *World J Gastroenterol* 2004; 10(23): 3506-3510

<http://www.wjgnet.com/1007-9327/10/3506.asp>

INTRODUCTION

Self-expanding metal stent, due to its minimal invasion, low risk of migration and efficient bile drainage, has been widely used for management of malignant obstructive jaundice (MOJ)^[1-11]. Although self-expanding metal stent seems to be the first choice in the palliation of MOJ, high rates of stent occlusion, which were mainly caused by tumor ingrowth or overgrowth, usually lead to jaundice recurrence^[12,13]. Therefore, treating underlying malignancy is critical to extend stent patency and patient

survival. Intraluminal brachytherapy is characterized by superiority in treatment of ductal or periductal tumor, thus preventing tumor from invading or compressing the duct. We designed a prospective study to evaluate the feasibility, safety of intraluminal brachytherapy in the treatment of MOJ and the clinical effect of intraluminal brachytherapy on stent patency and survival of patients.

MATERIALS AND METHODS

Study design

Patients were selected among those admitted to our department between November 2001 and September 2002 with the diagnosis of MOJ. Patients who had percutaneous transhepatic cholangiography and drainage (PTCD) followed by stent placement were included. Exclusion criteria were: (1) patients who were in end-stage MOJ; (2) serum total bilirubin concentration decreased to less than 100 $\mu\text{mol/L}$ or 50% of that before PTCD. After the nature of intraluminal brachytherapy was fully explained, patients were classified into two groups: group A with intraluminal brachytherapy and group B without intraluminal brachytherapy as control group, according to their own choice whether to receive the therapy. The study was performed with the approval of the institutional ethics committees. Written informed consent was obtained from all patients before treatment.

Methods of treatment

Venous blood samples were taken 1-3 d before PTCD for biochemical test. Intraluminal brachytherapy was routinely performed in group A within 1-3 wk after stent placement. Patients in group B did not receive the therapy. Some patients in both groups underwent transcatheter arterial chemoembolization (TACE).

Intraluminal brachytherapy: After stent placement, a 10 F external-internal drainage catheter or a 7 F long vascular sheath was placed, with its distal tip across the stricture. The applicator and sham source were placed through the drainage catheter or the sheath as a whole under fluoroscopic guidance. Irradiated volume was customized to extend 1 cm proximal and distal to the maximum length of the stricture as determined by cholangiography. Dwell positions were recorded, and therapy planning system (TPS) was connected to the remote afterloading microSelectron (Nucletron, Holland). After the sham source was manually removed, HDR-¹⁹²Ir (111-370 GBq) was driven by the remote afterloading system to the programmed locations (Figure 1). Fractional dose of 4-7 Gy was prescribed 0.5-1 cm from the source axis. The procedure was performed 3-4 times with an interval of 3-6 d. The drainage catheter or sheath was removed 1 wk later in case there were no complications related to the procedure.

Follow-up

The acute morbidity scoring criteria by Radiation Therapy Oncology Group (RTOG) and the late morbidity scoring criteria by Radiation Therapy Oncology Group/European Organization for Research and Treatment of Cancer (RTOG/EORTC) were used to evaluate the radiation toxicity^[14]. Follow-up of each patient was based on outpatient examinations, telephone interviews, and questionnaires.

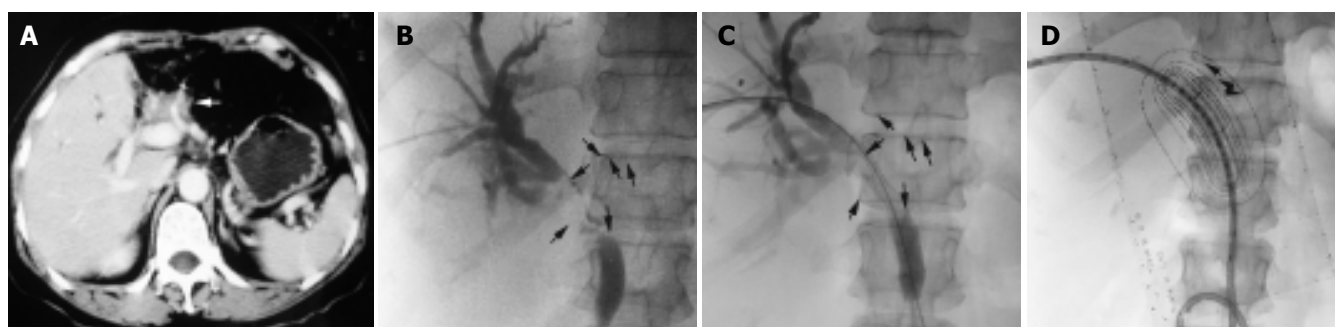


Figure 1 HDR-¹⁹²Ir (111-370 GBq) driven to the programmed locations. A: In the patient who had undergone left-lobe resection due to cholangiocarcinoma, hilar recurrence with bile duct dilation was shown by portal-phase CT scan (arrow). B: The stricture of bile duct was clearly shown by cholangiography during PTCd (arrow). C: An 8 mm×60 mm SMART stent was deployed across the stricture. D: The applicator and sham source were inserted through a 10 F internal-external drainage catheter. The dose distribution curves were obtained from the TPS (arrow).



Figure 2 Cholangiography, CT, or US before and after intraluminal brachytherapy. A: Bile duct dilation of left lobe caused by cholangiocarcinoma was shown by CT (arrow). B: Cholangiography showed hilar stricture (arrow). C: Intraluminal brachytherapy (fractional dose 7 Gy, total dose 21 Gy) was performed after an 8 mm×60 mm SMART stent insertion. D: CT follow-up 11 mo after intraluminal brachytherapy showed no progress of the tumor and no redilation of the bile duct (arrow).

In this study, stent patency period was defined as the interval between stent placement and obstructive jaundice recurrence. If occlusion did not occur during a patient's life time, the patency period was considered equal to the survival period but censored. Jaundice recurrence was defined as the symptom of jaundice recurred after it had subsided and met one of the followings: (1) cholangiography, CT or US demonstrated redilation of bile duct, (2) combined serum bilirubin concentration/total serum bilirubin concentration $\geq 35\%$ (Figure 2).

Statistical analysis

Comparisons between the two groups were performed with paired-samples *t* tests for metric data and χ^2 tests for frequencies. Stent patency and survival were evaluated according to the Kaplan-Meier method and compared with the log rank test. For all tests, a *P* value less than 0.05 was considered statistically significant.

RESULTS

Baseline data of patients

A total of 34 patients were enrolled in this study (18 male and 16 female; age range, 41-87 years; mean age, 62.0 years). Thirty-seven SMART stents (Cordis. Johnson & Johnson. USA) were placed and 28 TACE procedures were performed in these patients, 14 patients underwent intraluminal brachytherapy. In group A (*n* = 14), the causes of obstruction were cholangiocarcinoma (*n* = 7), gallbladder carcinoma (*n* = 2) and metastatic lymphadenopathy (*n* = 5, from stomach, colorectum or breast). In group B (*n* = 20), the causes of obstruction were cholangiocarcinoma (*n* = 9), gallbladder carcinoma (*n* = 2) and metastatic lymphadenopathy (*n* = 9, from stomach, colorectum or breast). The diagnosis was based on clinical, radiological findings or

histology. There were no differences between the two groups according to gender, mean age, preoperative serum bilirubin, alanine aminotransferase, alkaline phosphatase, albumin, hemoglobin concentration, obstructive duration, obstructive level, and times of TACE performed (Table 1).

Table 1 Baseline clinical characteristics of patients

Factor	Group A (<i>n</i> = 14)	Group B (<i>n</i> = 20)	<i>P</i>
Mean age (yr)	57.9±9.2	63.3±11.4	0.356
Gender			
Male	8	10	0.681
Female	6	10	
Mean total serum bilirubin concentration (μmol/L)	318±94	314±115	0.913
Mean alanine aminotransferase concentration (U/L)	71±52	106±107	0.261
Mean albumin concentration (g/L)	33.6±4.3	33.5±3.4	0.914
Mean alkaline phosphatase (U/L)	443±334	543±400	0.449
Mean hemoglobin concentration (g/L)	111±12	105±16	0.275
Mean obstructive duration (wk)	3.7±0.9	4.0±1.4	0.512
Obstructive level			
Hilar	8	12	0.868
Common bile duct	6	8	
TACE			
Performed	9	10	0.409
Not performed	5	10	

Intraluminal brachytherapy

A total of 52 procedures were programmed and 51 procedures were successfully performed, achieving the technical success rate of 98.0%. In 1 patient, a drainage catheter kink, which was caused by an acute angle on the drainage passage, resulted in the failure of driving HDR-¹⁹²Ir to scheduled position in the third procedure. The total dose of these 14 patients was 14-21 Gy. One patient developed nausea, one complained of abdominal upset, one developed diarrhea. One patient, who had undergone bilobectomy 4 mo before stent placement, developed hemobilia for a period of 4 d (Figure 3). The bleeding stopped soon after hemostatic was prescribed without transfusions. According to RTOG acute morbidity scoring criteria, 3 patients were classified into RTOG grade 1 acute morbidity, the others RTOG grade 0 acute morbidity. According to RTOG/EORTC late morbidity scoring criteria, 1 patient was classified into RTOG/EORTC grade 1 late morbidity, the others grade 0 late morbidity.

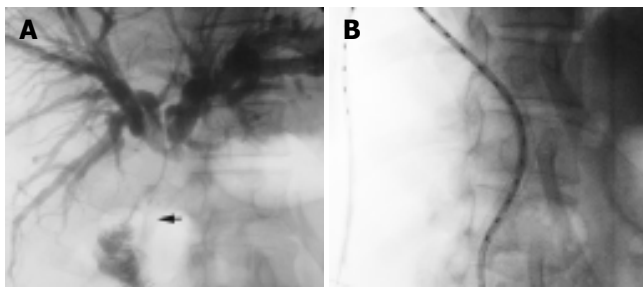


Figure 3 One patient undergoing bilenterostomy and ostomy, which was shown in irradiation region in intraluminal brachytherapy. A: Cholangiography indicated that jejunum was invaded by the malignancy (arrow). B: Jejunum and ostomy were in the irradiation region.

Stent patency and patient survival

The median follow-up time was 6.0 mo (range, 1-17 mo). In group B, 1 patient died 1 mo after stent placement of uncontrolled bleeding caused by tumor rupture, another one died 5 mo after stent placement due to cerebrovascular accident. The mean stent patency was 12.6 mo (median, 10.0 mo) with stent occlusion of 21.4% (3 of 14 patients) in group A, whereas the mean stent patency was 8.3 mo (median, 6.0 mo) with stent occlusion of 45.0% (9 of 20 patients) in group B. The stent patency of group A was significantly longer than that of group B ($P < 0.05$, Figure 4). The mean survival was 9.6 mo (median 7.0 mo) in group A and 6.4 mo (median 6.0 mo) in group B, showing no significant difference.

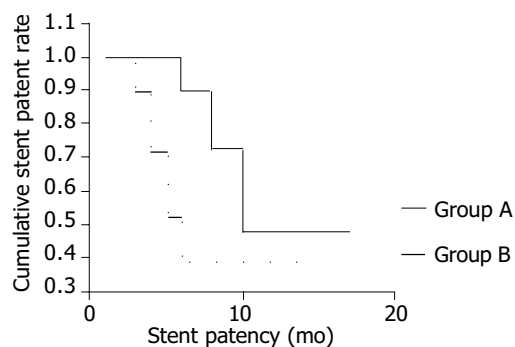


Figure 4 Stent patency of the two groups.

DISCUSSION

As a part of brachytherapies, intraluminal brachytherapy is defined as performing brachytherapy by inserting an applicator and radioactive source into a lumen (or cavity) such as

nasopharyngeal cavity, uterine cavity, esophagus, rectum and bile duct^[15]. The properties of this radiotherapeutic technique include^[16]: (1) Small source size enables itself to be very close to or contact with the target tissue. (2) The effective therapeutic range is 0.5-2.0 cm, which has little effect on normal tissue. (3) The absorbed dose is in inverse proportion to the square of the distance from radioactive source. With its irradiation extent confined to ductal wall and tissue adjacent to duct, intraluminal brachytherapy is a proper therapy for malignancy arising from a duct or adjacent to a duct. Because the absorbed dose falls off rapidly with increasing distance from the sources, intraluminal brachytherapy can deal with the malignancy without significantly affecting the adjacent normal tissues. To date, intraluminal brachytherapy not only has been the major therapeutics in treating the carcinoma of nasopharyngeal, uterine cervix, vagina, and endometrium^[17-20], but complementary to the treatment of carcinoma of esophagus, lung, and rectum^[21-23].

A number of isotopes were available for brachytherapy, including ²²⁶Ra, ⁶⁰Co, ¹³⁷Cs, ¹⁹²Ir and ⁹⁰Sr. With advantages of highly specific activity, relatively short half-life, easy to be shielded, and technical flexibility, ¹⁹²Ir is the most widely used brachytherapy source in clinical practice^[24]. According to the dose delivered per hour, brachytherapy can be classified into low dose rate (LDR, 0.4-2 Gy/h), median dose rate (MDR, 2-12 Gy/h) and high dose rate (HDR, >12 Gy/h). Among them, LDR and HDR are more frequently used. By comparison with LDR, HDR represents a technologic advance that offers the following advantages^[25]: (1) Improved physical dose delivery due to the short treatment time and negligible organ motion. (2) Improved radiation safety and protection with decreased exposure to personnel. (3) Reduced possibility of human error through computerized remote afterloading. (4) Increased efficiency because more patients can be treated with HDR per unit time. Additionally, while treating patients with MOJ by LDR, the applicator and radioactive source must be kept in the drainage catheter for several hours to several days, which may influence bile drainage and increase the risk of infection. The course of HDR therapy only needs several minutes, thus having no effect on bile drainage^[26]. For all the reasons mentioned above, we used HDR-¹⁹²Ir as the radioactive source in our study.

Intraluminal brachytherapy takes use of the drainage passage established during PTCD, making the procedure uncomplicated and inducing less damage. We only failed to complete the therapy in 1 patient in his third procedure. In this case we found an acute angle on the drainage passage. The narrow applicator lumen caused by the kink on the drainage catheter resulted in failure in radioactive source transmission. In patients who are scheduled to receive intraluminal brachytherapy, an acute angle should be avoided on the drainage passage during PTCD. Dose distribution of intraluminal brachytherapy is characterized by "inverse-square law" as we discussed before. In our study it was technically impossible to use instrument such as balloon-catheter to centralize the radioactive source in the bile duct, that is to say, the radioactive source usually located eccentrically in the lumen. The absorbed dose of bile duct wall close to the radioactive source is too high to be calculated by the "inverse-square law". Brambs^[27] investigated the bile duct tolerance in intraluminal brachytherapy in a swine model, and demonstrated that fractional dose of 7.5 Gy only caused slight fibrosis in the bile duct. Because the radiation damage in human is similar to that in swine, fractional dose of 7.5 Gy is deemed to be safe in clinical practice. As to other structures adjacent to bile duct such as hepatic artery, portal vein, duodenum, and pancreas, the distance between radioactive source and those structures makes the "inverse-square law" calculation possible. A tumor causing obstructive jaundice is thought to be at the advanced stage of the disease, the aim of the therapy is palliation rather than cure. Palliative

radiation therapy generally follows the regimen^[28]: the total dose of 20-30 Gy and the fractional dose of 5-10 Gy, with an intention to alleviate pain, maintain patency, stop bleeding, and reduce morbidity. In consideration of the poor clinical status of patients due to hyperbilirubinemia in our study, we prescribed fractional dose of 4-7 Gy with a total dose of 14-21 Gy, which was certainly tolerable. In this study, only 3 patients developed RTOG grade 1 acute morbidity, and 1 patient developed RTOG/EORTC grade 1 morbidity. One patient developed hemobilia for a period of 4 d without the need for transfusions. This patient had undergone bilioenterostomy and the ostomy, which was shown to be invaded by the malignancy, was in irradiation region in intraluminal brachytherapy. One of the reasons for hemobilia is tumor necrosis. On condition that block of tumor tissue necroses before the supplying arteriole could occlude, tumor bleeding will occur. The other one is ostomy hemorrhage. Jejunum and ostomy are dose-limiting tissues susceptible to irradiation.

MOJ is usually caused by cholangiocarcinoma, gallbladder carcinoma, metastatic lymphadenopathy (from stomach, colorectum, or breast), and pancreatic carcinoma. TACE has limited effect on these malignancies in most cases because of their character of relative avascularity^[29]. Cholangiocarcinoma, gallbladder carcinoma, and pancreatic carcinoma have the tendency of invading bile duct, so the rate of stent occlusion due to tumor ingrowth or overgrowth is inevitably high^[30-32]. There is an increasing demand for efficient therapy to palliate these malignancies, so to prolong stent patency and patient survival. External-beam irradiation has been used to treat abdominal tumors for nearly a hundred years. Major deterrents to improved results with MOJ are the limited tolerance of the structures (liver, duodenum, stomach, and kidney) around the lesion, lack of clear definition of the lesion's location, poor clinical status of the patients, and respiration interfering with the irradiation field^[33]. Fortunately, intraluminal brachytherapy, with special dosimetric characteristics and accurate location, overcome all the above shortcomings. Intraluminal brachytherapy in MOJ can efficiently palliate the underlying malignancies with fewer morbidities. Dvorak^[34,35] and cooperators reported their experiences of HDR-¹⁹²Ir intraluminal brachytherapy in treatment of 2 groups of patients with MOJ after bile drainage. The causes of MOJ were cholangiocarcinoma and gallbladder carcinoma in one group, cholangiocarcinoma and pancreas carcinoma in the other. The mean survival of both groups was 9 mo. After stent placement and subsequent jaundice subsidence, the underlying malignancy could be controlled by intraluminal brachytherapy, and invasion and compression of the bile duct avoided. Bruha *et al.*^[36] reported that patients with MOJ treated with intraluminal brachytherapy using HDR-¹⁹²Ir, the mean stent patency in patients with cholangiocarcinoma and gallbladder carcinoma were 418 and 220 d, respectively. The result of our study showed that the mean stent patency of intraluminal brachytherapy group (12.6 mo) was significantly longer than the control group (8.3 mo). We attribute the effect on prolonging stent patency to the followings: (1) Prohibit tumor from growing through the mesh of the stent (ingrowth) (2) Prohibit tumor from growing over the edge of the stent (overgrowth) (3) In cases with hilar obstruction, intraluminal brachytherapy in ipsilateral duct can prevent tumor tissue from invading contralateral duct. Although not statistically significant, it appeared that the mean survival in group A (9.6 mo) was longer than in group B (6.4 mo). We speculated that the advantage of intraluminal brachytherapy in extending survival be more prominent on condition that the cases were expanded or the follow-up was prolonged.

In conclusion, because the special dosimetric characteristics of HDR-¹⁹²Ir and the high dose tolerance of bile duct, HDR-¹⁹²Ir intraluminal brachytherapy is a safe and feasible method in the

treatment of MOJ. HDR-¹⁹²Ir intraluminal brachytherapy may prolong stent patency and has the potentiality of extending survival of patients with MOJ.

REFERENCES

- 1 **Freeman ML**, Overby C. Selective MRCP and CT-targeted drainage of malignant hilar biliary obstruction with self-expanding metallic stents. *Gastrointest Endosc* 2003; **58**: 41-49
- 2 **Mao AW**, Gao ZD, Xu JY, Yang RJ, Xiao XS, Jiang TH, Jiang WJ. Treatment of malignant digestive tract obstruction by combined intraluminal stent installation and intra-arterial drug infusion. *World J Gastroenterol* 2001; **7**: 587-592
- 3 **Inal M**, Akgul E, Aksungur E, Seydaoglu G. Percutaneous placement of biliary metallic stents in patients with malignant hilar obstruction: unilobar versus bilobar drainage. *J Vasc Interv Radiol* 2003; **14**: 1409-1416
- 4 **Inal M**, Aksungur E, Akgul E, Oguz M, Seydaoglu G. Percutaneous placement of metallic stents in malignant biliary obstruction: one-stage or two-stage procedure? Pre-dilate or not? *Cardiovasc Intervent Radiol* 2003; **26**: 40-45
- 5 **Shah RJ**, Howell DA, Desilets DJ, Sheth SG, Parsons WG, Okolo P 3rd, Lehman GA, Sherman S, Baillie J, Branch MS, Pleskow D, Chuttani R, Bosco JJ. Multicenter randomized trial of the spiral Z-stent compared with the Wallstent for malignant biliary obstruction. *Gastrointest Endosc* 2003; **57**: 830-836
- 6 **Pinol V**, Castells A, Bordas JM, Real MI, Llach J, Montana X, Feu F, Navarro S. Percutaneous self-expanding metal stents versus endoscopic polyethylene endoprotheses for treating malignant biliary obstruction: randomized clinical trial. *Radiology* 2002; **225**: 27-34
- 7 **Ahmad J**, Siqueira E, Martin J, Slivka A. Effectiveness of the Ultraflex Diamond stent for the palliation of malignant biliary obstruction. *Endoscopy* 2002; **34**: 793-796
- 8 **Nakamura T**, Hirai R, Kitagawa M, Takehira Y, Yamada M, Tamakoshi K, Kobayashi Y, Nakamura H, Kanamori M. Treatment of common bile duct obstruction by pancreatic cancer using various stents: single-center experience. *Cardiovasc Intervent Radiol* 2002; **25**: 373-380
- 9 **Hatzidakis AA**, Tsetis D, Chrysou E, Sanidas E, Petrakis J, Gourtsoyiannis NC. Nitinol stents for palliative treatment of malignant obstructive jaundice: should we stent the sphincter of Oddi in every case? *Cardiovasc Intervent Radiol* 2001; **24**: 245-248
- 10 **Ferlitsch A**, Oesterreicher C, Dumonceau JM, Deviere J, Leban T, Born P, Rosch T, Suter W, Binek J, Meyenberger C, Mullner M, Schneider B, Schofl R. Diamond stents for palliation of malignant bile duct obstruction: a prospective multicenter evaluation. *Endoscopy* 2001; **33**: 645-650
- 11 **Caldicott DG**, Ziprin P, Morgan R. Transhepatic insertion of a metallic stent for the relief of malignant afferent loop obstruction. *Cardiovasc Intervent Radiol* 2000; **23**: 138-140
- 12 **Kim HS**, Lee DK, Kim HG, Park JJ, Park SH, Kim JH, Yoo BM, Roe IH, Moon YS, Myung SJ. Features of malignant biliary obstruction affecting the patency of metallic stents: a multicenter study. *Gastrointest Endosc* 2002; **55**: 359-365
- 13 **Eschelmann DJ**, Shapiro MJ, Bonn J, Sullivan KL, Alden ME, Hovsepian DM, Gardiner GA Jr. Malignant biliary duct obstruction: long-term experience with Gianturco stents and combined-modality radiation therapy. *Radiology* 1996; **200**: 717-724
- 14 **Cox JD**, Stetz J, Pajak TF. Toxicity criteria of the radiation therapy oncology group (RTOG) and the european organization for research and treatment of cancer (EORTC). *Int J Radiat Oncol Biol Phys* 1995; **31**: 1341-1346
- 15 **Liu TF**. Xandai Fangshe Zhongliuxue. 1sted. Shanghai: Fudan University Pub 2001: 105-153
- 16 **Perez CA**, Brady LW. Principles and practice of radiation oncology. 3rded. Philadelphia: Lippincott Raven Pub 1997: 405-467
- 17 **Hareyama M**, Sakata K, Oouchi A, Nagakura H, Shido M, Someya M, Koito K. High-dose-rate versus low-dose-rate intracavitary therapy for carcinoma of the uterine cervix: a randomized trial. *Cancer* 2002; **94**: 117-124

- 18 **Alektiar KM**, McKee A, Venkatraman E, McKee B, Zelefsky MJ, Mychalczak BR, Hoskins WJ, Barakat RR. Intravaginal high-dose-rate brachytherapy for Stage IB (FIGO Grade 1, 2) endometrial cancer. *Int J Radiat Oncol Biol Phys* 2002; **53**: 707-713
- 19 **Kong W**, Sun J. Outcome with intracavitary high-dose-rate brachytherapy for primary vaginal cancer. *Zhonghua Fuchanke Zazhi* 2002; **37**: 94-96
- 20 **Syed AM**, Puthawala AA, Damore SJ, Cherlow JM, Austin PA, Spoto R, Ramsinghani NS. Brachytherapy for primary and recurrent nasopharyngeal carcinoma: 20 years' experience at Long Beach Memorial. *Int J Radiat Oncol Biol Phys* 2000; **47**: 1311-1321
- 21 **Sharma V**, Mahantshetty U, Dinshaw KA, Deshpande R, Sharma S. Palliation of advanced/recurrent esophageal carcinoma with high-dose-rate brachytherapy. *Int J Radiat Oncol Biol Phys* 2002; **52**: 310-315
- 22 **Aumock A**, Birnbaum EH, Fleshman JW, Fry RD, Gambacorta MA, Kodner IJ, Malyapa RS, Read TE, Walz BJ, Myerson RJ. Treatment of rectal adenocarcinoma with endocavitary and external beam radiotherapy: results for 199 patients with localized tumors. *Int J Radiat Oncol Biol Phys* 2001; **51**: 363-370
- 23 **Jain SK**, Dupuy DE, Cardarelli GA, Zheng Z, DiPetrillo TA. Percutaneous radiofrequency ablation of pulmonary malignancies: combined treatment with brachytherapy. *Am J Roentgenol* 2003; **181**: 711-715
- 24 **Hu YM**, Liu Z, She F, Xue WL. 1st ed. Beijing: *Atomic Energy Publishing House* 1999: 101-102
- 25 **Manning MA**, Arthur DW, Schmidt-Ullrich RK, Arnfield MR, Amir C, Zwicker RD. Interstitial high-dose-rate brachytherapy boost: the feasibility and cosmetic outcome of a fractionated outpatient delivery scheme. *Int J Radiat Oncol Biol Phys* 2000; **48**: 1301-1306
- 26 **Mohan DS**, Nori D. Intraluminal brachytherapy in the treatment of pancreas and bile duct carcinoma: regarding Montemaggi *et al.*, IJROBP 32:437; 1995. *Int J Radiat Oncol Biol Phys* 1995; **33**: 773-774
- 27 **Brambs HJ**, Freund U, Bruggmoser G, Laaff H, Kluger UW, Roth R, Wannemacher M. Radiation sensitivity of the normal bile duct during high dose rate afterloading irradiation with Iridium 192. Experimental studies in pigs. *Strahlenther Onkol* 1993; **169**: 721-728
- 28 **Xu BY**, Yu SC, Zeng DW, Chen GX. Modern Tumor Radiotherapy. 1st ed Beijing: *People's Military Publishing House* 2000: 190-199, 23-34
- 29 **Kawahara N**, Ono M, Taguchi K, Okamoto M, Shimada M, Takenaka K, Hayashi K, Mosher DF, Sugimachi K, Tsuneyoshi M, Kuwano M. Enhanced expression of thrombospondin-1 and hypovascularity in human cholangiocarcinoma. *Hepatology* 1998; **28**: 1512-1517
- 30 **Shirabe K**, Shimada M, Harimoto N, Sugimachi K, Yamashita Y, Tsujita E, Aishima S. Intrahepatic cholangiocarcinoma: its mode of spreading and therapeutic modalities. *Surgery* 2002; **131**(1 Suppl): S159-164
- 31 **Kim JH**, Kim TK, Eun HW, Kim BS, Lee MG, Kim PN, Ha HK. Preoperative evaluation of gallbladder carcinoma: efficacy of combined use of MR imaging, MR cholangiography, and contrast-enhanced dual-phase three-dimensional MR angiography. *J Magn Reson Imaging* 2002; **16**: 676-684
- 32 **Rieber A**, Brambs HJ. Metallic stents in malignant biliary obstruction. *Cardiovasc Intervent Radiol* 1997; **20**: 43-49
- 33 **Hayes JK Jr**, Sapozink MD, Miller FJ. Definitive radiation therapy in bile duct carcinoma. *Int J Radiat Oncol Biol Phys* 1988; **15**: 735-744
- 34 **Dvorak J**, Petera J, Papik Z, Melichar B, Vanasek T, Hulek P, Jandik P, Mergancova J, Zoul Z, Vacek Z. Transduodenal intraluminal high dose rate brachytherapy in the treatment of carcinomas of the subhepatic region. *Hepatogastroenterology* 2002; **49**: 1045-1047
- 35 **Dvorak J**, Jandik P, Melichar B, Jon B, Mergancova J, Zoul Z, Vacek Z, Petera J. Intraluminal high dose rate brachytherapy in the treatment of bile duct and gallbladder carcinomas. *Hepatogastroenterology* 2002; **49**: 916-917
- 36 **Bruha R**, Petryl J, Kubecova M, Marecek Z, Dufek V, Urbanek P, Kodadova J, Chodounsky Z. Intraluminal brachytherapy and selfexpandable stents in nonresectable biliary malignancies-the question of long-term palliation. *Hepatogastroenterology* 2001; **48**: 631-637

Edited by Chen WW and Zhu LH Proofread by Xu FM

Cloning and sequencing of *cagA* gene fragment of *Helicobacter pylori* with coccoid form

Ke-Xia Wang, Xue-Feng Wang

Ke-Xia Wang, Xue-Feng Wang, School of Medicine, Anhui University of Science & Technology Huainan 232001, Anhui Province, China

Supported by Natural Science Foundation of the Education Department of Anhui Province, China No.2003kj111

Correspondence to: Dr. Ke-Xia Wang, Department of Etiology and Immunology, School of Medicine, Anhui University of Science & Technology, Huainan 232001, Anhui Province, China. kexiawang2003@yahoo.com.cn

Telephone: +86-554-6658770 Fax: +86-554-6662469

Received: 2003-10-20 Accepted: 2003-12-08

Abstract

AIM: To clone and sequence the *cagA* gene fragment of *Helicobacter pylori* (*H pylori*) with coccoid form.

METHODS: *H pylori* strain NCTC11637 were transformed to coccoid form by exposure to antibiotics in subinhibitory concentrations. The coccoid *H pylori* was collected. *cagA* gene of the coccoid *H pylori* strain was amplified by PCR. After purified, the target fragment was cloned into plasmid pMD-18T. The recombinant plasmid pMD-18T-*cagA* was transformed into *E.coli* JM109. Positive clones were screened and identified by PCR and digestion with restriction endonucleases. The sequence of inserted fragment was then analysed.

RESULTS: *cagA* gene of 3 444 bp was obtained from the coccoid *H pylori* genome DNA. The recombinant plasmid pMD-18T-*cagA* was constructed, then it was digested by *Bam*H I + *Sac* I, and the product of digestion was identical with the predicted one. Sequence analysis showed that the homology of coccoid and the reported original sequence *H pylori* was 99.7%.

CONCLUSION: The recombinant plasmid containing *cagA* gene from coccoid *H pylori* has been constructed successfully. The coccoid *H pylori* contain completed *cagA* gene, which may be related to pathogenicity of them.

Wang KX, Wang XF. Cloning and sequencing of *cagA* gene fragment of *Helicobacter pylori* with coccoid form. *World J Gastroenterol* 2004; 10(23): 3511-3513

<http://www.wjgnet.com/1007-9327/10/3511.asp>

INTRODUCTION

Helicobacter pylori (*H pylori*) is one of the common bacteria causing chronic infection, which infects more than 50% of the human population, causes chronic gastritis and plays an important role in the pathogenesis of gastroduodenal ulceration. *H pylori* has also been suggested to be involved in the genesis of adenocarcinoma and MALT lymphoma of the stomach.^[1-5] *H pylori* cells growing actively *in vitro* are curved rods, which evolve into metabolically active but nonculturable coccoid cells after prolonged incubation^[6-8]. In the stomach mostly spiral-shaped bacteria are found, but coccoid cells have been observed

in the more severely damaged regions of the gastric mucosa^[9,10]. Many scholars believed that coccoid *H pylori* might lead to difficult recovery, easy relapse and epidemical transmission^[11]. But the pathogenicity of coccoid *H pylori* is unclear at present. The cytotoxin-associated protein encoded by *cagA* (cytotoxin-associated gene A) is important virulence determined by *H pylori*. *cagA*⁺ *H pylori* strains have been linked to more severe gastric inflammation, peptic ulcer disease, and gastric cancer in adults^[12-15]. *CagA* gene is a mono-replicon and locates 3' region of *cag*-PAI (*cag* pathogenity island), whose length varies from 3 400 bp to 4 000 bp. In order to probe into possible pathogenesis of coccoid *H pylori*, the recombinant plasmid encoding *cagA* gene of coccoid *H pylori* was constructed and detected for the sequence in this study.

MATERIALS AND METHODS

Materials

The strain NCTC11637 of *H pylori* was afforded by Chinese center for disease control and prevention. JM109 *E.coli* strains were preserved by our laboratory, pMD-18T (T-Vector), restriction endonuclease enzymes (*Bam*H I, *Sac* I), T₄ DNA ligase, LA Taq DNA polymerase, DNA Extraction Kit and DNA purification reagent kit were provided by TaKaRa Company.

Bacterial culture and induction of coccoid forms *H pylori* strains were grown on Columbia agar with 50 mL frozen-melting sheep blood, 100 mL/L fetal bovine serum, and Skirrow's antibiotic supplement in a microaerophilic atmosphere for 3 d at 37 °C, then the bacteria were suspended in brucella broth and supplemented with 0.02 mg/L of amphotericin, still were incubated at 37 °C for 3, 5, 7, and 10 d. Baterial morphology was determined by light microscopy after Gram staining. The coccoid forms were collected and stored at -20 °C.

Extraction of genomic DNA *H pylori* of coccoid form were added to a 1.5 mL microcentrifuge tube, rinsed once with phosphate-buffered saline (PH 7.2), and pelleted by centrifugation at 11 000 g. Genomic DNA was extracted by TaKaRa MiniBEST Bacterial Genomic DNA Extraction Kit, the DNA pellet was suspended in TE (10 mmol/L Tris-HCL, 1 mmol/L PH 8.0 EDTA), and stored at -20 °C.

Synthetic primers A single primer pair was used to amplify coccoid *H pylori* *cagA* gene based on GenBank. The primers had a *Bam*H I site incorporated into the 5' end and a *Sac* I site at the 3' end and their sequences as follows (5'-3'): AAGGATCC ACTAACGAAACCATTGACCA (forward) and AAGAGCTCA GATTTTTGGAAACCACCTT (reverse). The 5' region initiator and 3' end stop codon were banned.

PCR amplification PCR was performed in a 100 µL reaction mixture in 0.6-mL tube in an automatic thermal cycler (TP3000; TaKaRa BIO INC). The PCR mixture contained 10 µL of 10×PCR buffer, 1 µL of sample DNA, 10 µL of 2.5 mmol/L deoxynucleoside triphosphate, 4 µL of 10 µmol/L oligonucleotide primers, 0.5 µL of LA Taq polymerase, 74.5 µL of molecular-biology-grade distilled water. The mixtures were incubated for 1 min at 94 °C for initial denaturation of the target DNA and then subjected to 30 cycles of denaturation at 98 °C for 10 s, annealing at 55 °C for 30 s, and extension at 72 °C for 210 s. The amplified products (5 µL) were analyzed by electrophoresis on 10 g/L agarose gel

containing 0.1 µg of ethidium bromide per ml in TBE buffer. The PCR product was visualized under UV light and photographed. **Construction of recombinant plasmids** The PCR product was purified by TaKaRa PCR Fragment Recovery Kit. The purified product was cloned into the compatible sites of the T-vector pMD-18T by using T₄ DNA ligase at a molar ratio of 6:1 at 16 °C for 3 h. After the above product was transformed into *E. coli* JM109, pMD-18T/cagA was selected and identified by PCR and enzyme digestion.

Extraction of recombinant plasmid The single bacterial colony (JM109/pMD-18T/cagA) was picked, and cultivated in 3 mL LB broth containing 100 mg/L of ampicillin, at 300 r/min at 37 °C overnight, then recombinant plasmids were extracted according to manufacturer's instructions (TaKaRa MiniBest DNA Purification Kit), in the meantime, identified by PCR and restriction endonuclease enzyme digestion.

Sequence determination and homology analysis The sequence determination of cagA gene of recombinant plasmid was carried out by Takara Company, in the meantime, the sequence of gene and amino acid were analyzed by software sequence 3.0, and compared the homology based on the GenBank.

RESULTS

PCR amplification of coccoid *H pylori* cagA gene

H pylori with coccoid form cagA was amplified by PCR from the above primers and The PCR product was electrophoresed and visualized by 10 g/L agarose gel (Figure 1). It revealed that the size of cagA DNA fragment amplified by PCR was 3 444 bp, and was compatible with the expectant size.

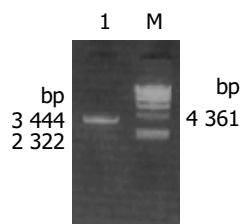


Figure 1 10 g/L agarose gel electrophoresis of cagA DNA fragment amplified by PCR from coccoid *H pylori*. Lane 1. PCR products, Lane M: λ -Hind III DNA marker.

Identification of recombinant vector by PCR

The plasmid was extracted from recombinant bacteria and conducted as template to amplify by PCR under the condition mentioned above. The PCR products were visualized by 10 g/L agarose gel electrophoresis (Figure 2). It indicated that recombinant plasmid contained the objective gene. At the same time, it was successful in transforming recombinant plasmid into JM109 *E. coli*.

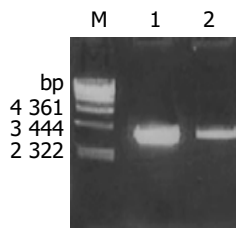


Figure 2 Identification of recombinant vector by PCR. Lane m: λ -Hind III DNA marker; Lane 1: amplification cagA gene from recombinant pMD-18T-cagA plasmid by PCR; Lane 2: Amplification cagA gene from coccoid *H pylori* genome DNA by PCR.

pMD-18T/cagA identification by restriction enzyme digestion

Recombinant plasmid pMD-18T/cagA was digested by bi-

enzyme digestion with *Bam*H I and *Sac* I, then digestive product was visualized on 10 g/L agarose gel (Figure 3). It demonstrated that recombinant plasmid was digested to 3 444 bp and 2 692 bp DNA fragment, which contained the objective gene.

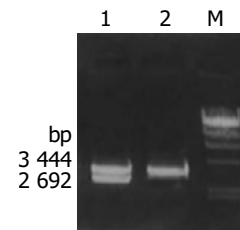


Figure 3 The identification of the pMD-18T-cagA by digestion with restriction endonucleases Lane1: Recombinant pMD-18T-cagA digested by *Bam*H I and *Sac* I; Lane 2: Amplification cagA gene from coccoid *H pylori* genome DNA by PCR; m: λ -Hind III DNA marker.

Sequence analysis of cloned cagA gene of coccoid

H pylori Sequence of inserted DNA was analyzed with BcaBEST Primer M13-47/BcaBEST Primer RV-M using automatic sequence analyzer by Sanger dideoxy chain termination method. The result of analysis showed that the size of inserted DNA was about 3 444 bp and 99.7% affinity in comparison with DNA sequence published on GenBank (locus: AB015416). The sequence of partial vacA gene was showed in Figure 4.

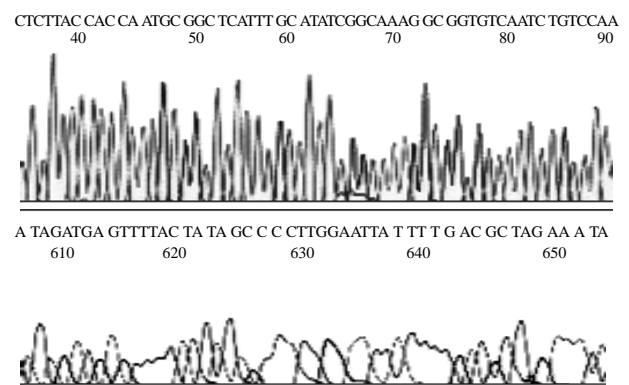


Figure 4 sequencing result of partial cagA gene.

DISCUSSION

Morphological conversion from spiral *H pylori* to coccoid forms has been described under several suboptimal conditions. These conditions include aerobiosis, alkaline pH, high temperature, extended incubation, or treatment with proton pump inhibitor or antibiotics^[16-18]. This coccoid form conversion phenomenon, which has been thought to result in a viable but nonculturable form of the bacterium, is not exclusive to *H pylori*, as it is common for other enteric pathogens. Controversy remains about the pathogenicity of coccoid *H pylori*. Many investigators have suggested that the coccoid form of *H pylori* represents a degenerative form with no infectious capability, but others believed that the coccoid form retains a weak metabolic activity, important structural components, and pathogenicity^[19-21]. Recently, successful infection with coccoid forms of *H pylori* in animal models has been reported^[22-24]. These findings have highlighted the possible role of the coccoid forms in transmission of infection and morphological conversion of coccoids to the spiral form. It is well known that cagA is an important virulence factor of *H pylori* and related to severe gastrointestinal diseases. However, the research of cagA gene of coccoid *H pylori* is few at present. In order to observe cagA and vacA expression

during conversion to the coccoid form, Sisto *et al.*^[25] analyzed the expression of ureA, cagA, vacA genes after prolonged incubation in a liquid medium in 2000, the results showed that although the coccoid forms had decreased DNA and RNA levels after 31 d, they were not degraded and still expressed the urease, cytotoxic island and vacuolating toxin genes. So in conclusion, coccoid forms are therefore viable and may act as a transmissible agent that plays a crucial role in disease relapses after antibiotic therapy. She *et al.* explored the virulence and the potential pathogenicity of coccoid *H pylori* transformed from spiral form by exposure to antibiotic in 2001, and found that the content of the protein with the molecular weight over M_r 74 000 decreased, but vacA, cagA, urea, ureB, hpaA gene remained to be preserved, so they concluded that the virulence and the proteins with molecular weight over M_r 74 000 in coccoid *H pylori* decrease, but no deletion exists in amplification fragments from ureA, ureB, hpaA, vacA and cagA genes, and suggested that coccoid *H pylori* may have potential pathogenicity. Furthermore, Monstein *et al.*^[26] confirmed that the transcription and translation of cagA and vacA gene might actively take place in coccoid *H pylori* cells.

In order to research the cagA gene existence, and explore the possible mechanism of pathogenicity in coccoid *H pylori*, we designed the specific primers based on cagA gene sequence reported in GenBank, and successfully amplified the cagA gene of coccoid *H pylori* by PCR, then inserted into pMD-18T vector. The recombinant plasmids were successfully identified containing cagA gene fragment by PCR and enzyme digestion, and sequence determination confirmed that cagA gene existed in coccoid *H pylori*, though existence of 0.3% difference with the reported sequence in GenBank. The reason for the discrepancy might be as follows: (1) the mutant base could come from the process of PCR amplification and sequencing, (2) *H pylori* provided have the transformation ability, which could lead to *H pylori* variation and genome reset. Our results also support the assumption that virulence-gene expression is differently regulated among *H pylori* strains.^[26]

In this study, the NCTC11637 strain with amphotericin for 3 d generated a high proportion of coccoid forms. Forms obtained after removal of bacterial clumps and amorphous debris by centrifugation at 600 r/min for 5 min were nearly 100% coccoid. Due to similar to the condition *in vivo* by antibiotic induction, the collected coccoid *H pylori* still remained complete cellular structure, and their genome DNA lost was less, so some important virulent gene, such as vacA, cagA and so on, could exist in their cells. Once coccoid *H pylori* live in suitable condition, they can recover their virulence and lead to the occurrence of diseases. Or coccoid *H pylori* may revert helical form, and result in the transmission and/or relapse of diseases with the complete cagA gene.

REFERENCES

- 1 Nguyen TN, Barkun AN, Fallone CA. Host determinants of *Helicobacter pylori* infection and its clinical outcome. *Helicobacter* 1999; **4**: 185-197
- 2 Vandenplas Y. *Helicobacter pylori* infection. *World J Gastroenterol* 2000; **6**: 20-31
- 3 Sakai T, Ogura Y, Narita J, Suto T, Kimura D, Aina S, Fujita H, Kamada M. Simultaneous early adenocarcinoma and mucosa-associated lymphoid tissue (MALT) lymphoma of the stomach associated with *Helicobacter pylori* infection. *Gastric Cancer* 2003; **6**: 191-196
- 4 Satoh K, Sugano K. Causal relationship between *Helicobacter pylori* infection and upper gastroduodenal diseases. *Nippon Rinsho* 2001; **59**: 239-245
- 5 Muller S, Seifert E, Stolte M. Simultaneous MALT-type lymphoma and early adenocarcinoma of the stomach associated with *Helicobacter pylori* gastritis. *Z Gastroenterol* 1999; **37**: 153-157
- 6 Ren Z, Pang G, Musicka M, Dunkley M, Batey R, Beagley K, Clancy R. Coccoid forms of *Helicobacter pylori* can be viable. *Microbios* 1999; **97**: 153-163
- 7 Willen R, Carlen B, Wang X, Papadogiannakis N, Odselius R, Wadstrom T. Morphologic conversion of *Helicobacter pylori* from spiral to coccoid form. Scanning (SEM) and transmission electron microscopy (TEM) suggest viability. *Ups J Med Sci* 2000; **105**: 31-40
- 8 Mizoguchi H, Fujioka T, Nasu M. Evidence for viability of coccoid forms of *Helicobacter pylori*. *J Gastroenterol* 1999; **11**(Suppl 11): 32-36
- 9 Saito N, Konishi K, Sato F, Kato M, Takeda H, Sugiyama T, Asaka M. Plural transformation-processes from spiral to coccoid *Helicobacter pylori* and its viability. *J Infect* 2003; **46**: 49-55
- 10 Janas B, Czkwianianc E, Bak-Romaniszyn L, Bartel H, Tosik D, Planeta-Malecka I. Electron microscopic study of association between coccoid forms of *Helicobacter pylori* and gastric epithelial cells. *Am J Gastroenterol* 1995; **90**: 1829-1833
- 11 Mizoguchi H, Fujioka T, Kishi K, Nishizono A, Kodama R, Nasu M. Diversity in protein synthesis and viability of *Helicobacter pylori* coccoid forms in response to various stimuli. *Infect Immun* 1998; **66**: 5555-5560
- 12 Mao HY, Fang PC, Ye SJ, You JF, Zhu YL, Yu JG. Analysis of babA2 cagA and vacA genotypes of *Helicobacter pylori* in chronic gastritis and peptic ulcer. *Zhejiang Daxue Xuebao Yixueban* 2003; **32**: 29-32
- 13 Oleastro M, Gerhard M, Lopes AI, Ramalho P, Cabral J, Sousa Guerreiro A, Monteiro L. *Helicobacter pylori* virulence genotypes in portuguese children and adults with gastroduodenal pathology. *Eur J Clin Microbiol Infect Dis* 2003; **22**: 85-91
- 14 Debets-Ossenkopp YJ, Reyes G, Mulder J, Aan De Stegge BM, Peters JT, Savelkoul PH, Tanca J, Pena AS, Vandenbroucke-Grauls CM. Characteristics of clinical *Helicobacter pylori* strains from Ecuador. *J Antimicrob Chemother* 2003; **51**: 141-145
- 15 Bravo LE, van Doorn LJ, Realpe JL, Correa P. Virulence-associated genotypes of *Helicobacter pylori*: do they explain the African enigma? *Am J Gastroenterol* 2002; **97**: 2839-2842
- 16 Kusters JG, Gerrits MM, Van Strip JA, Vandenbroucke-Grauls CM. Coccoid forms of *Helicobacter pylori* are the morphologic manifestation of cell death. *Infect Immun* 1997; **65**: 3672-3679
- 17 Narikawa S, Kawai S, Aoshima H, Kawamata O, Kawaguchi R, Hikiji K, Kato M, Iino S, Mizushima Y. Comparison of the nucleic acids of helical and coccoid forms of *Helicobacter pylori*. *Clin Diagn Lab Immunol* 1997; **4**: 285-290
- 18 Costa K, Bacher G, Allmaier G, Dominguez-Bello MG, Engstrand L, Falk P, de Pedro MA, Garcia-del Portillo F. The morphological transition of *Helicobacter pylori* cells from spiral to coccoid is preceded by a substantial modification of the cell wall. *J Bacteriol* 1999; **181**: 3710-3715
- 19 Sato F. *Helicobacter pylori* in culture: an ultrastructural study. *Hokkaido Igaku Zasshi* 2000; **75**: 187-196
- 20 Nakamura A, Park A, Nagata K, Sato EF, Kashiba M, Tamura T, Inoue M. Oxidative cellular damage associated with transformation of *Helicobacter pylori* from a bacillary to a coccoid form. *Free Radic Biol Med* 2000; **28**: 1611-1618
- 21 Monstein HJ, de la Cour CD, Jonasson J. Probing 23S ribosomal RNA cleavage sites in coccoid *Helicobacter pylori*. *Helicobacter* 2001; **6**: 100-109
- 22 Rabelo-Goncalves EM, Nishimura NF, Zeitune JM. Acute inflammatory response in the stomach of BALB/c mice challenged with coccoidal *Helicobacter pylori*. *Mem Inst Oswaldo Cruz* 2002; **97**: 1201-1206
- 23 Wang X, Sturegard E, Rupar R, Nilsson HO, Aleljung PA, Carlen B, Willen R, Wadstrom T. Infection of BALB/c A mice by spiral and coccoid forms of *Helicobacter pylori*. *J Med Microbiol* 1997; **46**: 657-663
- 24 Cao J, Li ZQ, Borch K, Petersson F, Mardh S. Detection of spiral and coccoid forms of *Helicobacter pylori* using a murine monoclonal antibody. *Clin Chim Acta* 1997; **267**: 183-196
- 25 Sisto F, Brenciaglia MI, Scaltrito MM, Dubini F. *Helicobacter pylori*: ureA, cagA and vacA expression during conversion to the coccoid form. *Int J Antimicrob Agents* 2000; **15**: 277-282
- 26 Monstein HJ, Jonasson J. Differential virulence-gene mRNA expression in coccoid forms of *Helicobacter pylori*. *Biochem Biophys Res Commun* 2001; **285**: 530-536

Real-time determination of human telomerase reverse transcriptase mRNA in gastric cancer

Li-Hua Hu, Feng-Hua Chen, Yi-Rong Li, Lin Wang

Li-Hua Hu, Feng-Hua Chen, Yi-Rong Li, Department of Transfusion, Union Hospital, Tongji Medical College, Huazhong University of Science and Technology, Wuhan 430022, Hubei Province, China
Lin Wang, Life Science College, Wuhan University, Wuhan 430070, Hubei Province, China

Supported by the Key Program of Science and Technology Foundation of Hubei Province, No. 2002AA304B10

Correspondence to: Dr. Li-Hua Hu, Department of Transfusion, Union Hospital, Tongji Medical College, Huazhong University of Science and Technology, Wuhan 430022, Hubei Province, China. xhllh@126.com

Telephone: +86-27-85726312

Received: 2004-01-15 **Accepted:** 2004-04-13

Abstract

AIM: To set up a real-time fluorescent quantitative reverse transcription-polymerase chain reaction (RT-PCR) assay, to detect human telomerase reverse transcriptase (hTERT) messenger RNA in gastric carcinomas, and to evaluate quantitative determination of hTERT mRNA in the diagnostic value of gastric carcinomas, and to analyze the correlation between the expression level of hTERT mRNA and clinicopathological parameters in patients with gastric cancer.

METHODS: A real-time quantitative RT-PCR (RQ-PCR) based on TaqMan fluorescence methodology and the LightCycler system was used to quantify the full range of hTERT mRNA copy numbers in 35 samples of gastric carcinomas and corresponding adjacent non-cancerous tissues. The normalized hTERT (NhTERT) was standardized by quantifying the number of GAPDH transcripts as internal control and expressed as $100 \times (\text{hTERT}/\text{GAPDH})$ ratio. Variables were analyzed by the Student's *t*-test, χ^2 test and Fisher's exact test.

RESULTS: NhTERT from gastric carcinomas and corresponding adjacent non-cancerous tissues was 6.27 ± 0.89 and 0.93 ± 0.18 , respectively ($t = 12.76$, $P < 0.001$). There was no significant association between gastric cancer hTERT mRNA expression level and patient's age, gender, tumor size, location and stage (p -TNM), but a significant correlation was found between hTERT mRNA expression level in gastric carcinomas and the degree of differentiation.

CONCLUSION: Quantitative determination of hTERT mRNA by RQ-PCR is a rapid and sensitive method. hTERT might be a potential biomarker for the early detection of gastric cancer.

Hu LH, Chen FH, Li YR, Wang L. Real-time determination of human telomerase reverse transcriptase mRNA in gastric cancer. *World J Gastroenterol* 2004; 10(23): 3514-3517
<http://www.wjgnet.com/1007-9327/10/3514.asp>

INTRODUCTION

Telomerase is a reverse transcriptase that adds telomeric repeats to chromosomal ends to compensate for sequence loss during

DNA replication. Telomerase activity has been detected in about 85% of human cancer samples and is associated with cell immortalization and the acquisition of malignancy, but most normal tissues have low or no telomerase activity^[1]. Telomerase is one of the most widespread tumor markers at present. To date, the main assay to detect telomerase activity is telomere repeat amplification protocol (TRAP). TRAP is a qualitative or semi-quantitative assay, and can not accurately exhibit telomerase expression level, and needs functional ribonucleoproteins, including both reverse transcriptase activity and undegraded RNA. The presence of telomerase inhibitors, Taq polymerase inhibitors, proteases, or RNases in tissue extract may influence its detection and subsequently lower its sensitivity. With the cloning of both genes coding for human telomerase RNA (hTR) and human telomerase reverse transcriptase (hTERT), hTERT becomes the catalytic subunit of telomerase and is a rate-limiting determinant of the enzymatic activity of human telomerase, and only the expression of hTERT is closely associated with telomerase activity^[2-5], whereas the expression of hTR is widespread. The close relationship between hTERT mRNA expression and telomerase activity suggests that quantification of the mRNA expression of the hTERT gene could be used as an alternative to measure telomerase activity. In this study, we used real-time quantitative reverse transcription-polymerase chain reaction (RQ-PCR) to detect and quantify hTERT mRNA in samples of gastric carcinoma and corresponding non-cancerous tissues, and to evaluate the quantitative determination of hTERT mRNA in the diagnostic value of gastric carcinomas, and to analyze the correlation between the expression level of hTERT mRNA and clinicopathological parameters in patients with gastric cancer.

MATERIALS AND METHODS

Patients and samples

We analyzed tissues (gastric cancer and corresponding non-cancerous tissues) from surgically removed primary gastric cancer in Union Hospital and Tongji Hospital of Tongji Medical College of Huazhong University of Science and Technology from October 2002 to May 2003. All patients (25 males and 10 females, mean age 55.2 years, range 34-73 years) were at initial presentation and had no radiotherapy or chemotherapy history before surgery. All samples were examined histopathologically to confirm the diagnosis. Control tissues were the corresponding non-cancerous mucosa from the stomach of cancer patients, and excised beyond 5 cm from neoplastic lesions. Samples were stored at -80°C until further analysis.

Reagents and instruments

TRIzol was the product of Omega. The reagents used for reverse transcription were purchased from Promega. The reagents used for PCR and PCR product purification, glyceraldehydes 3-phosphate dehydrogenase (GAPDH) quantification, and the primers and TaqMan probe of hTERT were all purchased from Shanghai Shenyong Company. Both T4 DNA ligase and PMD18-T vector were the products of TaKaRa. The other chemical reagents used in this study were ACS reagents of China. The fluorescent quantitative PCR instrumentation was the LightCycler system of Roche.

Real-time quantitative RT-PCR

We used a RQ-PCR assay based on TaqMan fluorescence methodology to quantify the full range of hTERT mRNA copy numbers^[6,7]. This method used a dual-labeled nonextendable oligonucleotide hydrolysis (TaqMan) probe in addition to the two amplification primers. The probe contained 6-carboxy-fluorescein (FAM) as a fluorescent reporter dye, and 6-carboxytetramethyl-rhodamine (TAMRA) as a quencher for its light emission spectrum. During the extension phase of PCR, the probe hybridized to the target sequence and was then cleaved due to the 5' to 3' exonuclease activity of *Taq* polymerase. The increase in the fluorescence signal of the reporter was proportional to the amount of specific PCR products, providing highly accurate and reproducible quantification. The number of PCR cycles to reach the fluorescence threshold was the cycle threshold (Ct). The Ct value for each sample was proportional to the log of the initial amount of input cDNA. By plotting the Ct value of an unknown sample on the standard curve, the amount of target sequences in the sample could be calculated.

To normalize the hTERT mRNA expression for sample-to-sample differences in RNA input, RNA quality, and reverse transcriptase efficiency, we amplified the housekeeping gene GAPDH. According to each standard curve, we got the copy numbers of GAPDH and hTERT, respectively. The ratio between copy numbers of hTERT and GAPDH represented the normalized hTERT (NhTERT) for each sample and could be compared with that of other samples^[8].

$$\text{NhTERT} = (\text{hTERT mRNA copies}_{\text{sample}} / \text{GAPDH mRNA copies}_{\text{sample}}) \times 100.$$

Primers and probes

According to GAPDH quantification reagents and the reference^[9], the nucleotide sequences of oligonucleotide TaqMan probes and primers are shown in Table 1.

RNA extraction and cDNA synthesis

According to the manufacturer's instructions, total RNA from frozen tumor and corresponding non-cancerous tissue specimens was isolated by disruption of 50-100 mg tissues in 1 mL of TRIzol. RNA was quantified spectrophotometrically, and its quality was determined by agarose gel electrophoresis and ethidium bromide staining. Only samples that were not degraded and showed clear 18 S and 28 S bands under ultraviolet light were used for real-time RT-PCR.

All samples were denatured for 10 min at 60 °C to melt secondary structure with the template and cooled immediately on ice for 5 min to prevent secondary structure from reforming. Total RNA (1-2 µg) was reverse transcribed in a total volume of 25 µL containing 1×RT buffer (Promega), 200 U of Moloney murine leukemia virus Reverse Transcriptase (M-MLV RT) (Promega), 20 U of RNasin (Promega), 0.2 µg random primer (Promega) and 1 mmol/L deoxynucleotides. The reaction was performed for

10 min at 25 °C, for 60 min at 42 °C and for 10 min at 70 °C. cDNA was stored at -20 °C until use.

Construction of recombinant plasmid calibrator

Pure hTERT fragments from classical RT-PCR were joined to PMD18-T vector by T4 DNA ligase, resulting in recombinant plasmid PMD18-hTERT. The recombinant plasmids were confirmed in including hTERT target fragments by sequencing, and extracted and purified. The recombinant plasmid DNAs at 10⁷ copies/mL were stored at -20 °C until use. GAPDH standard template was from the GAPDH quantification reagents.

LightCycler real-time PCR amplification

All PCR reactions were performed using the LightCycler System (Roche Diagnostics, Switzerland) in a total volume of 20 µL containing 1×*Taq* polymerase buffer, 4 mmol/L MgCl₂, 200 µmol/L deoxynucleotides, 300 nmol/L each primer, 150 nmol/L probe, 1 U *Taq* polymerase and 20 ng cDNA. Water instead of cDNA template was used for the negative controls. Both GAPDH and hTERT amplification were done in duplicate for each sample. The thermal cycling conditions were 5 min at 94 °C, followed by 40 cycles, each at 94 °C for 15 s and at 60 °C for 1 min for GAPDH or at 65 °C for 1 min for hTERT (two-step PCR). The number of GAPDH and hTERT transcripts in samples was calculated with the LightCycler software, using these standard curves.

Statistical analysis

Data were expressed as mean±SD. The Student *t*-test, χ^2 test and Fisher's exact test were used in this study. *P*<0.05 was considered statistically significant.

RESULTS

Standard curve construction

We used different concentrations of GAPDH and hTERT standard templates including 10⁴, 10⁵, 10⁶ and 10⁷ copies/mL to perform quantitative PCR and calculate the standard curves, respectively. The standard curves were: Ct_{GAPDH} = -3.86 log (GAPDH copies) +46.60; and Ct_{hTERT} = -3.42 log (hTERT copies) +37.31. The correlation coefficients were both -1.00 (Figure 1A, B).

hTERT mRNA expression levels in gastric cancer and corresponding adjacent non-cancerous tissues

The expression of hTERT mRNA in gastric carcinomas was analyzed by a highly sensitive RQ-PCR assay. hTERT mRNA expression was detectable not only in all 35 gastric carcinomas, but also in the corresponding non-cancerous gastric tissues (Figure 2). For each experimental sample, the amount of hTERT and GAPDH was determined from the appropriate standard curve. Then, hTERT amount was divided by the GAPDH amount to obtain NhTERT. NhTERT was significantly higher (*t* = 12.76, *P*<0.001) in tumor tissues (6.27±0.89) than in the corresponding non-cancerous tissues (0.93±0.18).

Table 1 Sequences of primers and probes used in this study

Gene and oligonucleotide	Sequence	PCR product size (bp)
GAPDH		
Upper primer	5'-GAAGGTGAAGGTCGGAGTC-3'	
Lower primer	5'-GAAGATGGTGATGGGATTTC-3'	226
Probe	5'-(FAM) CAAGCTTCCC GTTCTCAGCC (TAMRA)-3'	
hTERT		
Upper primer	5'-TGACACCTCACCTCACCCAC-3'	
Lower primer	5'-CACTGTCTTCCGCAAGTTTAC-3'	95
Probe	5'-(FAM) ACCCTGGTCCGAGGTGTGCCCTGA (TAMRA)-3'	

The primers placed in different exons, were tested to ensure that they did not amplify the contaminated genomic DNA.

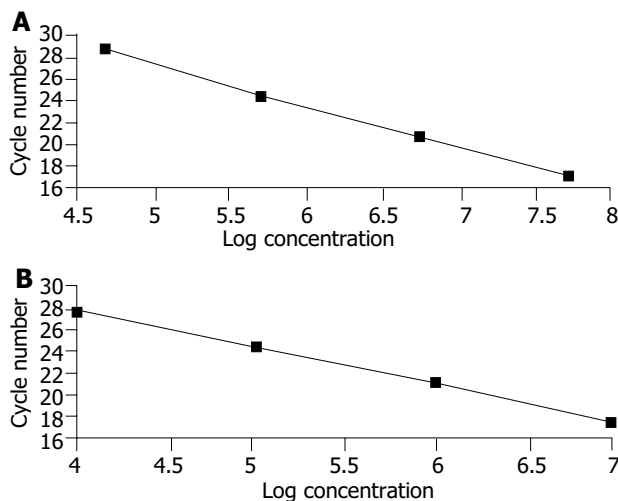


Figure 1 Standard curve of GAPDH and hTERT A: Standard curve of GAPDH: slope = -3.86, intercept = 46.60, $r = -1.00$. B: Standard curve of hTERT: slope = -3.42, intercept = 37.31, $r = -1.00$.

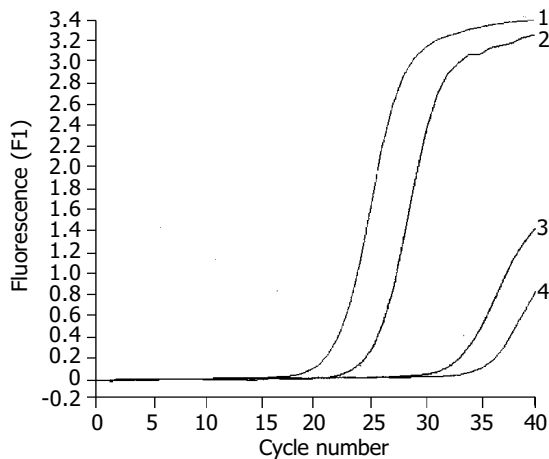


Figure 2 hTERT mRNA expression in samples of gastric cancer and corresponding non-cancerous tissues. Lanes 1, 2: Gastric cancer; Lanes 3, 4: Corresponding non-cancerous tissues.

Correlation between hTERT mRNA expression level and clinicopathological parameters

The data obtained by RQ-PCR were analyzed in relation to clinicopathological parameters of the patients. All 35 corresponding non-cancerous gastric tissue samples expressed low detectable NhTERT, ranging from 0.06 to 2.11. In the 35 gastric carcinomas, NhTERT varied greatly, ranging from 0.28 to 90.55. NhTERT was categorized as low or high, using a cutoff at 5.39, which was the value that represented the median value of the expression distribution. Thus, 17 tumors (48.6%) showed low hTERT expression, whereas 18 tumors (51.4%) had high hTERT expression. We observed the statistical links between hTERT mRNA expression levels and the degree of differentiation ($P = 0.007$). Seventy-three point six percent (14 of 19) of poorly differentiated and undifferentiated tumors showed high NhTERT expressions, whereas 75% (12 of 16) of well and moderately differentiated tumors exhibited low NhTERT expressions. Poorly differentiated and undifferentiated tumors had higher hTERT mRNA expression levels than well and moderately differentiated tumors. No relationship was found between hTERT mRNA expression level and patients' age, gender, tumor size, tumor location and stage (pTNM). The results obtained are shown in Table 2.

Table 2 Relationship between hTERT mRNA expression level and clinicopathological parameters in patients with gastric cancer

Parameter	n	NhTERT		P
		Low (n = 17)	High (n = 18)	
Age (yr)				
<50	13	7	6	0.73
≥50	22	10	12	
Gender				
Male	25	13	12	0.71
Female	10	4	6	
Size of diameter (cm)				
<5	19	11	8	0.31
≥5	16	6	10	
Location				
Cardia	14	8	6	0.50
Body and antrum	21	9	12	
Degree of differentiation				
Well and moderately differentiated	16	12	4	0.007
Poorly differentiated and undifferentiated	19	5	14	
Lymph node metastasis				
N ₀	8	4	4	0.40
N ₁	13	8	5	
N ₂	14	5	9	
Depth of invasion				
T ₁ and T ₂	24	13	11	0.43
T ₃ and T ₄	11	4	7	
Metastasis				
M ₀	20	12	8	0.17
M ₁	15	5	10	

DISCUSSION

We used RQ-PCR based on TaqMan methodology for the accurate quantification of hTERT mRNA expression in gastric carcinomas. This assay has several marked advantages over the TRAP assay for cancer detection. It needs only a 95-bp fragment of hTERT mRNA, making the assay less sensitive to RNase activity and insensitive to proteases and protein inhibitors. The assay output is numerical rather than qualitative, allowing appropriate diagnostic statistics to be applied. It uses endogenous controls (GAPDH in this study) which allow correction for parameters like RNA input, RNA degradation, or RT inhibitors. Real-time PCR makes RNA quantification much more precise and reproducible, based on Ct values established in the early exponential phase of the PCR reaction (when none of the reagents is rate-limiting) rather than end point quantification of the amount of accumulated PCR product. It does not require post-PCR sample handling and the closed-tube method minimizes the risk for cross-contamination. These suggest that quantitative determination of hTERT mRNA by RQ-PCR is a powerful method to investigate the telomerase status and superior in specificity and sensitivity to the evaluation of telomerase activity by the TRAP assay. In addition, we used recombinant hTERT plasmid DNA to calculate the external standard curves, and found it was better for the quantification of mRNA than the recombinant RNA calibrator or endogenous standards^[10,11]. Theoretically, the slope of the standard curve should be -3.3 if 10-fold dilutions are used, but in practice a slope between -3.0 and -3.9 is probably acceptable as long as the correlation coefficient is >0.95. The standard curves we obtained in this study had acceptable slopes and correlation coefficients.

In this study, the level of hTERT mRNA estimated with RQ-PCR procedure was the average amount of transcripts in a whole

tissue sample and mainly depended on the number of hTERT-positive cells present in the tissue. hTERT mRNA was detected in 100% of gastric carcinoma RNAs, and also in all the corresponding non-cancerous gastric mucosa RNAs. The highest NhTERT was detected in gastric cancer, whereas the lowest NhTERT was found in non-cancerous gastric tissues. However, NhTERT in samples of non-cancerous tissues was only approximately 14.8% of those found in the cancerous samples, and NhTERT was significantly higher ($t = 12.76$, $P < 0.001$) in tumor tissues (6.27 ± 0.89) than in the corresponding non-cancerous tissues (0.93 ± 0.18). We believed that these were not in contradiction to the findings using TRAP with which telomerase activity could not be detected in most non-malignant gastric tissues and the positive rate of hTERT mRNA expression by means of *in situ* hybridization or classical RT-PCR in gastric carcinoma^[12-15]. The difference could be explained by the increased sensitivity of the RQ-PCR assay and the presence of residual malignant cells, inflammatory lymphocytes or tumor infiltrating activated cells. Our results showed real-time measurement of hTERT expression could discriminate gastric carcinoma from nonmalignant gastric tumors. This discrimination would be more distinct if the percentage of tumor cells was higher in the selected tissues.

No relationship was found in our study between hTERT mRNA expression level and patients' age, gender, tumor size, location and tumor stage (pTNM) ($P > 0.05$) and there were statistical links between hTERT mRNA expression levels and the degree of differentiation ($P = 0.007$). These suggest that the up-regulation of hTERT appeared to be an early event in gastric carcinogenesis. hTERT may play a critical role in gastric carcinogenesis and have potential as a biomarker in the telomerase status for the early detection of gastric cancer. Real-time quantitative analysis of hTERT mRNA in tissues, cancer cells in the blood, and plasma or serum of the patients with cancer before and after surgery, radiotherapy or chemotherapy may be helpful for early detection and diagnosis of cancer, and find out therapeutic effect and estimate prognosis^[16-21]. hTERT may become a target in gene therapy of cancer and inaugurate a new approach for cancer therapy.

In conclusion, monitoring hTERT mRNA expression with RQ-PCR analysis appears to be a new effective and sensitive method to better differentiate gastric cancer from nonmalignant gastric tumors. hTERT mRNA expression status may be used as a molecular marker of gastric cancer. These findings must be confirmed in a larger series of gastric cancer patients.

REFERENCES

- 1 Shay JW, Bacchetti S. A survey of telomerase activity in human cancer. *Eur J Cancer* 1997; **33**: 787-791
- 2 Meyerson M, Counter CM, Eaton EN, Ellisen LW, Steiner P, Caddle SD, Ziaugra L, Beijersbergen RL, Davidoff MJ, Liu Q, Bacchetti S, Haber DA, Weinberg RA. hEST2, the putative human telomerase catalytic subunit gene, is up-regulated in tumor cells and during immortalization. *Cell* 1997; **90**: 785-795
- 3 Lingner J, Hughes TR, Shevchenko A, Mann M, Lundblad V, Cech TR. Reverse transcriptase motifs in the catalytic subunit of telomerase. *Science* 1997; **276**: 561-567
- 4 Feng J, Funk WD, Wang SS, Weinrich SL, Avilion AA, Chiu CP, Adams RR, Chang E, Allsopp RC, Yu J, Le S, West MD, Harley CB, Andrews WH, Greider CW, Villeponteau B. The RNA component of human telomerase. *Science* 1995; **269**: 1236-1241
- 5 Nakamura TM, Morin GB, Chapman KB, Weinrich SL, Andrews WH, Lingner J, Harley CB, Cech TR. Telomerase catalytic subunit homologs from fission yeast and human. *Science* 1997; **277**: 955-959
- 6 Bustin SA. Absolute quantification of mRNA using real-time reverse transcription polymerase chain reaction assays. *J Mol Endocrinol* 2000; **25**: 169-193
- 7 PE Biosystems. DNA/RNA real-time quantitative PCR. Available from: <http://www.wzw.tum.de/gene-quantification/pe-realttimeoverview-1.pdf>
- 8 ABI Prism 7700 Sequence detection System User Bulletin #2 (2001) Relative quantification of gene expression. Available from: <http://docs.appliedbiosystems.com/pebi/docs/04303859.pdf>
- 9 Bièche I, Noguès C, Paradis V, Olivi M, Bedossa P, Lidereau R, Vidaud M. Quantitation of hTERT gene expression in sporadic breast tumors with a real-time reverse transcription-polymerase chain reaction assay. *Clin Cancer Res* 2000; **6**: 452-459
- 10 Pfaffl MW, Hageleit M. Validities of mRNA quantification using recombinant RNA and recombinant DNA external calibration curves in real-time RT-PCR. *Biotechnol Lett* 2001; **23**: 275-282
- 11 Ke LD, Chen Z, Yung WK. A reliability test of standard-based quantitative PCR: exogenous vs endogenous standards. *Mol Cell Probes* 2000; **14**: 127-135
- 12 Yoo J, Park SY, Kang SJ, Kim BK, Shim SI, Kang CS. Expression of telomerase activity, human telomerase RNA, and telomerase reverse transcriptase in gastric adenocarcinomas. *Mod Pathol* 2003; **16**: 700-707
- 13 Miyachi K, Fujita M, Tanaka N, Sasaki K, Sunagawa M. Correlation between telomerase activity and telomeric-repeat binding factors in gastric cancer. *J Exp Clin Cancer Res* 2002; **21**: 269-275
- 14 Okusa Y, Ichikura T, Mochizuki H, Shinomiya N. Clinical significance of telomerase activity in biopsy specimens of gastric cancer. *J Clin Gastroenterol* 2000; **30**: 61-63
- 15 Yao XX, Yin L, Sun ZC. The expression of hTERT mRNA and cellular immunity in gastric cancer and precancerosis. *World J Gastroenterol* 2002; **8**: 586-590
- 16 Dasi F, Lledo S, Garcia-Granero E, Ripoll R, Marugan M, Tormo M, Garcia-Conde J, Alino SF. Real-time quantification in plasma of human telomerase reverse transcriptase (hTERT) mRNA: a simple blood test to monitor disease in cancer patients. *Lab Invest* 2001; **81**: 767-769
- 17 Buttitta F, Pellegrini C, Marchetti A, Gadducci A, Cosio S, Felicioni L, Barassi F, Salvatore S, Martella C, Coggi G, Bosari S. Human telomerase reverse transcriptase mRNA expression assessed by real-time reverse transcription polymerase chain reaction predicts chemosensitivity in patients with ovarian carcinoma. *J Clin Oncol* 2003; **21**: 1320-1325
- 18 Miura N, Shiota G, Nakagawa T, Maeda Y, Sano A, Marumoto A, Kishimoto Y, Murawaki Y, Hasegawa J. Sensitive detection of human telomerase reverse transcriptase mRNA in the serum of patients with hepatocellular carcinoma. *Oncology* 2003; **64**: 430-434
- 19 de Kok JB, Ruers TJM, van Muijen GNP, van Bokhoven A, Willems HL, Swinkels DW. Real-time quantification of human telomerase reverse transcriptase mRNA in tumors and healthy tissues. *Clin Chem* 2000; **46**: 313-318
- 20 Chen XQ, Bonnefoi H, Pelte MF, Lyautey J, Lederrey C, Movarekhi S, Schaeffer P, Mulcahy HE, Meyer P, Stroun M, Anker P. Telomerase RNA as a detection marker in the serum of breast cancer patients. *Clin Cancer Res* 2000; **6**: 3823-3826
- 21 Tchirkov A, Rolhion C, Kemeny JL, Irthum B, Puget S, Khalil T, Chinot O, Kwiatkowski F, Perissel B, Vago P, Verrelle P. Clinical implications of quantitative real-time RT-PCR analysis of hTERT gene expression in human gliomas. *Br J Cancer* 2003; **88**: 516-520

NDRG2 expression and mutation in human liver and pancreatic cancers

Xiao-Lan Hu, Xin-Ping Liu, Shu-Xin Lin, Yan-Chun Deng, Na Liu, Xia Li, Li-Bo Yao

Xiao-Lan Hu, Xin-Ping Liu, Yan-Chun Deng, Na Liu, Xia Li, Li-Bo Yao, Department of Biochemistry and Molecular Biology, Fourth Military Medical University, Xi'an 710032, Shaanxi Province, China

Shu-Xin Lin, Department of Pathophysiology, Fourth Military Medical University, Xi'an 710032, Shaanxi Province, China

Supported by the National Natural Science Foundation of China, No. 30370315, No. 30171044 and Medical and pharmaceutical Research Fund of PLA, No. 01MA185

Correspondence to: Li-Bo Yao, Department of Biochemistry and Molecular Biology, Fourth Military Medical University, 17 Changle West Road, Xi'an 710032, Shaanxi Province, China. bioyao@fmmu.edu.cn

Telephone: +86-29-83374513 **Fax:** +86-29-83374513

Received: 2004-03-18 **Accepted:** 2004-04-05

Abstract

AIM: To investigate the expression of NDRG2 and mutation of the entire coding region of NDRG2 in human liver and pancreatic cancers, and to further discuss the possible causes of NDRG2 distinct expression patterns.

METHODS: Reverse transcription-polymerase chain reaction (RT-PCR) was used to analyze the expression of NDRG2 mRNA in 37 fresh cancer specimens (including 8 cases of pancreatic cancer and 29 cases of liver cancer) and adjacent normal tissues collected from clinical operation. In addition, mutation analysis of the whole coding region of NDRG2 in these cancers was examined by polymerase chain reaction-single strand conformational polymorphism (PCR-SSCP).

RESULTS: Compared with adjacent normal tissues, the expression levels of NDRG2 mRNA in corresponding cancer tissues reduced significantly (pancreatic cancer: 0.680 ± 0.112 vs 2.089 ± 0.214 , $P < 0.01$) (liver cancer: 0.894 ± 0.098 vs 1.345 ± 0.177 , $P < 0.05$). Using PCR-SSCP, the mutation of the whole coding region of NDRG2 was not found in those cancer tissues where the expression of NDRG2 mRNA reduced markedly.

CONCLUSION: NDRG2 gene might express differently between normal tissues and cancer tissues, and might play an important role in the development of pancreatic cancer and liver cancer. Low expression of NDRG2 might be unrelated to the mutation of coding region of NDRG2.

Hu XL, Liu XP, Lin SX, Deng YC, Liu N, Li X, Yao LB. NDRG2 expression and mutation in human liver and pancreatic cancers. *World J Gastroenterol* 2004; 10(23): 3518-3521
<http://www.wjgnet.com/1007-9327/10/3518.asp>

INTRODUCTION

NDRG2, a new member of the N-Myc downstream-regulated gene (NDRG) family including NDRG1-4, was first discovered and cloned from normal human whole brain cDNA library by

subtractive hybridization in our laboratory^[1]. NDRG2 is located on chromosome 14q11.2, including 16 exons and 15 introns, and its cDNA is 2 024 bp in length^[2]. Studies from our laboratory and others have shown that NDRG2 was highly expressed in many normal tissues, especially in the brain, heart, skeletal muscle, and kidney, whereas low expressed or not detected in various tumors and tumor cell lines^[3,4]. This suggests that NDRG2 inactivation might play an important role in some tumor genesis or evolution, and NDRG2 might be a new cancer suppressor gene candidate. To date, no report on mutation analysis of NDRG2 in a variety of tumors has been presented. This study was conducted to determine whether the distinct expression of NDRG2 was related to gene mutation as most cancer suppressor genes. The expression of NDRG2 mRNA in 37 patients with liver cancer and pancreatic cancer was detected, and the mutation of the whole coding region of NDRG2 in normal and cancer specimens was analyzed by PCR-SSCP.

MATERIALS AND METHODS

Patients and tissue specimens

Thirty-seven fresh cancer specimens (including 8 cases of pancreatic cancer and 29 cases of liver cancer) and corresponding adjacent normal tissues were collected from patients who underwent surgery at First Affiliated Hospital of Xi'an Jiaotong University, Tangdu Hospital and Xijing Hospital between May 2003 and September 2003. All specimens were examined by microscope after haematoxylin and eosin (H&E) staining.

RNA isolation and RT-PCR

Total RNA was extracted from tissue specimens using TRIzol reagent (GIBCO BRL, USA) according to the manufacturer's instructions. Reverse transcription reaction was set up according to Promega's reverse transcription system protocol. cDNAs were then amplified by PCR using specific primers for human NDRG2: upstream primer 5'-GCGGA TCCATG GCG GAG CTG CAG GAG GTC -3'; and downstream primer 5'-GC GAA TTC AAC AAG GGC CAT TCA ACA GGA GAC -3', about 1 200 bp. The primer sequences of glyceraldehyde-3-phosphate dehydrogenase (GAPDH) which was used as an internal quantitative control for the amplification were as follows: upstream primer 5'-GCC TCA AGA TCA GCA AT -3'; downstream primer 5'-AGG TCC ACC ACT GAC ACG TT -3', 310 bp. Cycling condition for NDRG2 was at 94 °C for 5 min, followed by 32 cycles of 94 °C for 40 s, 59 °C for 50 s, and 72 °C for 60 s, and the cycling condition for GAPDH was at 94 °C for 5 min, followed by 30 cycles of 94 °C for 30 s, 57 °C for 30 s, and 72 °C for 30 s, and finally for 10 min at 72 °C. The PCR products were then analyzed and visualized on 12 g/L agarose gel containing 5 g/L ethidium bromides. Results were normalized by the ratio of band density of NDRG2 mRNA to GAPDH mRNA.

PCR-SSCP silver staining

According to cDNA sequence of NDRG2 gene, we designed by DNASTAR analysis software and synthesized 6 pairs of primers covering the whole coding region of NDRG2 gene, with length of each PCR product around 150 to 370 bp, and PCR reaction

Table 1 Primer sequence, annealing temperature and PCR product size for PCR-SSCP

	Primer	Sequence	Annealing temperature (°C)	PCR product size (bp)
A	Upstream	5'-ATGGCGGAGCTGCAGGAGGTC-3'	54	186
	Downstream	5'-ATTTATAGTTGAGTCCCACATC-3'		
B	Upstream	5'-CACCATACGGCTCTGTCACTTTCAC-3'	58	188
	Downstream	5'-CTCTTCCATTCCAGGGGCATCCAC-3'		
C	Upstream	5'-GCCAGCGATCCTTACCTACC-3'	58	365
	Downstream	5'-GGCTGCCCAATCCATCCAACC-3'		
D	Upstream	5'-CCGGACACTGTTGAAGGT-3'	55	364
	Downstream	5'-GGGTCCAGTTTGAGTTACATT-3'		
E	Upstream	5'-CTGTGATGCTGGTGGTAGGAGA-3'	58	286
	Downstream	5'-TGGGACAGGTGCGAGAG-3'		
F	Upstream	5'-GTCCGGTCTCGTACAGCCTCTC-3'	56	153
	Downstream	5'-AACAAGGGCCATTCAACAGGAGAC-3'		

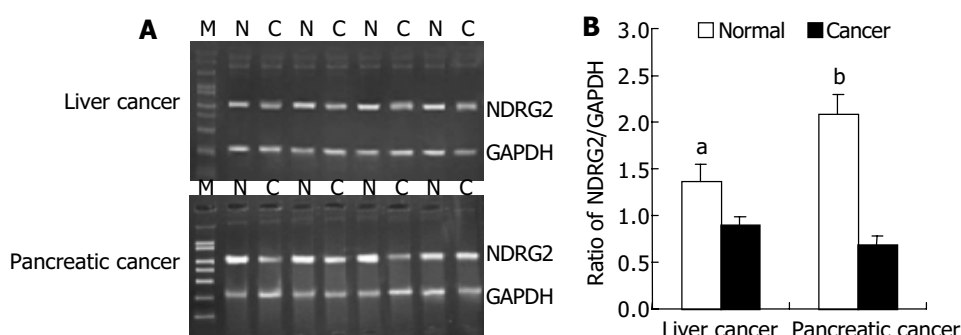


Figure 1 Expressions of NDRG2 mRNA in human liver cancer and pancreatic cancer. A: Representative agarose gels of RT-PCR-amplified NDRG2. M: DNA molecular weight marker; N: Normal tissue; C: Cancer tissue; B: Relative amount of NDRG2 mRNA was evaluated by the ratio of band optical density of NDRG2/GAPDH and the expression was significantly decreased in cancer ($n=29$ for liver cancer, and 8 for pancreatic cancer respectively) vs normal tissues. ^a $P<0.05$, ^b $P<0.01$ vs normal.

conditions are described in Table 1. The PCR products were separated by electrophoresis on 12 g/L agarose gel to check the specificity of each PCR reaction. The products were mixed with the same amount of formamide-loading buffer (950 g/L formamide, 10 mmol/L EDTA, and 0.5 g/L bromophenol blue, 0.5 g/L xylene cyanol) and heated at 100 °C for 5 min, and loaded on 80 g/L non-denaturing polyacrylamide gel in 1× TBE buffer for 8–12 h at 40 V. After electrophoresis, the gel was fixed, silver-stained, and finally developed, photographed and analyzed. The sample was considered normal if the band position was the same as that of the normal tissue. Otherwise, it was abnormal.

Statistical analysis

Statistical analysis was performed by SPSS version 10.0. Data were expressed as mean±SD, and analyzed by Student's *t* test. $P<0.05$ was considered statistically significant.

RESULTS

RT-PCR data

We investigated the expression patterns of NDRG2 mRNA by RT-PCR in 37 cases of human cancers including 29 liver cancers and 8 pancreatic cancers. Figure 1A shows PCR products of representative agarose gels for NDRG2 and GAPDH in human liver cancer and pancreatic cancer. The size of the RT-PCR products was as predicted, 1 200 bp for NDRG2 and 310 bp for GAPDH. The levels of NDRG2 mRNA expression were quantified by the ratio of band optical density of NDRG2/GAPDH (Figure 1B). Compared with adjacent normal tissues, there were marked decreases in NDRG2 mRNA expression in liver cancer (0.894 ± 0.098 vs 1.345 ± 0.177 , $P<0.05$) and pancreatic

cancer (0.680 ± 0.112 vs 2.089 ± 0.214 , $P<0.01$).

PCR-SSCP analysis

The PCR products, which were amplified by 6 pairs of primers covering the whole coding region of NDRG2 gene, were separated by electrophoresis on 12 g/L agarose gel to check the specificity of each PCR reaction (Figure 2). PCR products with only one specific band of right size in the gel can further be used for SSCP assay. Figure 3 shows representative results of SSCP silver staining of the PCR products amplified by 6 pairs of primers covering the whole coding region of NDRG2. By SSCP, all the PCR products from the cancer tissues of 27 patients of NDRG2 low-expression confirmed by RT-PCR, did not show any mutation.

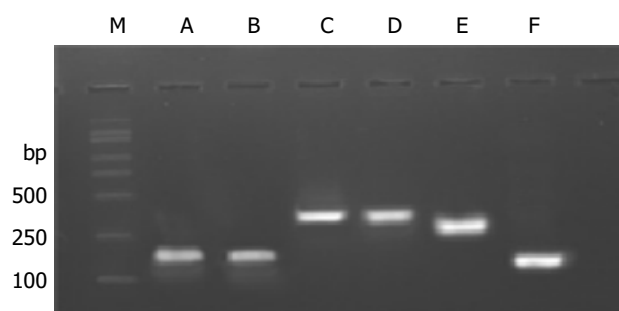


Figure 2 Agarose gel analysis of PCR products amplified by 6 pairs of primers covering the whole coding region of NDRG2. M: DNA molecular weight marker, PCR product size was 186 bp for A, 188 bp for B, 365 bp for C, 364 bp for D, 286 bp for E and 153 bp for F.

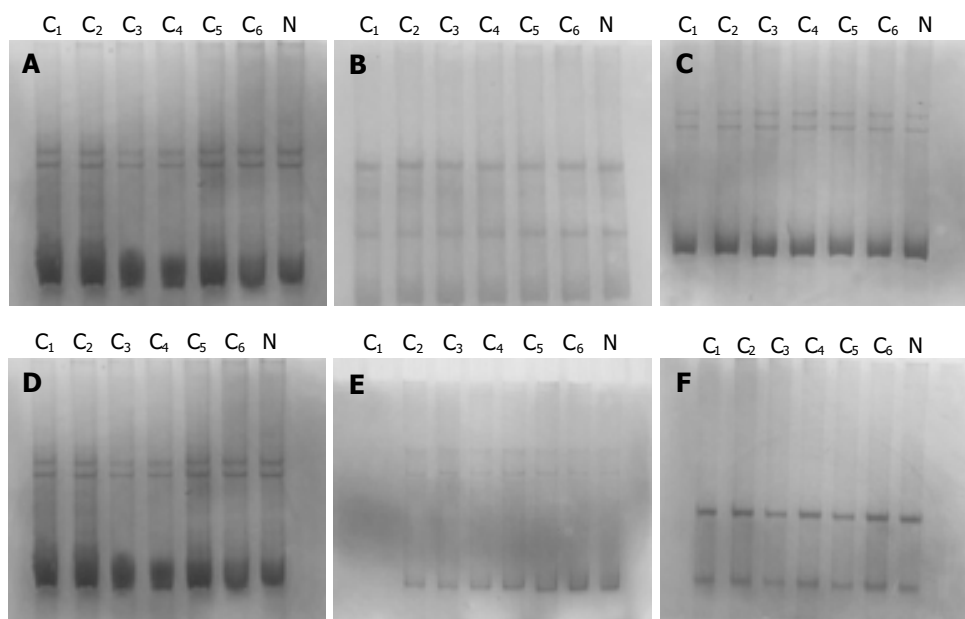


Figure 3 Representative results of SSCP silver staining of the PCR products (186 bp for A, 188 bp for B, 365 bp for C, 364 bp for D, 286 bp for E, and 153 bp for F) amplified by 6 pairs of primers covering the whole coding region of *NDRG2*. C: cancer tissue; N: normal tissue.

DISCUSSION

NDRG2, together with *NDRG1*, *NDRG3* and *NDRG4*, constitute *NDRG* gene family. The four members, which share 53-65% amino acid identity, belong to the alpha/beta hydrolase super family^[5]. Phylogenetic analysis of the family demonstrated that human *NDRG1* and *NDRG3* belong to a subfamily, and *NDRG2* and *NDRG4* to another. Expression of the fusion proteins showed that all of them were cytosolic proteins. Northern and dot blot analysis showed that *NDRG* gene family was evidently expressed in adult brain and almost not detected in some human cancer lines^[6-8]. In addition, *NDRG2* is highly expressed in adult skeletal muscle and brain, *NDRG3* remarkably expresses in brain and testis, and *NDRG4* evidently expresses in brain and heart, suggesting that they might display different specific functions in distinct tissues^[9,10]. Although *NDRG* gene family is believed to be involved in cell differentiation, the exact molecular and cellular function of members of this family is still unknown.

In 2000, our laboratory first discovered and successfully cloned human *NDRG2* cDNA from normal human whole brain cDNA library by subtractive hybridization. Our previous studies showed that the expression level of *NDRG2* mRNA was very high in brain, salivary gland, skeletal muscle and mammary gland, and low in bone marrow, testis, peripheral blood and placenta, and not detectable in leukocyte, colon and some tumor cell lines. Other studies have also shown similar result^[11,12], suggesting that *NDRG2* inactivation might play an important role in some cancer genesis or evolution, and *NDRG2* might be a new cancer suppressor gene candidate.

A recent study showed that over expression of *NDRG1* in tumor cells decreased the proliferation rate, enhanced differentiation, and suppressed metastasis potency of cancer cells. More interestingly, a nonsense mutation in *NDRG1* gene may be the cause of hereditary motor and sensory neuropathy-Lom (HMSNL)^[13].

The activation of oncogene and inactivation of cancer suppressor gene can lead to uncontrolled cell proliferation and occurrence of cancer. The inactivation of most cancer suppressor genes has been confirmed to relate to gene mutation such as *p53*, *p16* and *Rb* gene^[14]. To the authors' knowledge, we first investigated the expression patterns of *NDRG2* mRNA by RT-

PCR in 37 cases of human cancers including 29 liver cancers and 8 pancreatic cancers. The results showed that there was marked decrease in *NDRG2* mRNA expression in human liver cancer ($P < 0.05$) and pancreatic cancer ($P < 0.01$), compared with adjacent normal tissue. We speculated that different expression pattern of *NDRG2* might relate to gene mutation. The designed 6 pairs of primers covering the whole coding region of *NDRG2* gene to amplify the cancer tissue of 27 patients of *NDRG2* low-expression were confirmed by RT-PCR, but no mutation was found.

In conclusion, our results indicate that *NDRG2* gene expresses differently between normal tissues and cancer tissues, and it might play an important role in the development of pancreatic cancer and liver cancer. The low expression of *NDRG2* might be unrelated to mutation of the coding region of *NDRG2*. In addition, whether a mutation exists in the upstream sequence of transcription initial site of *NDRG2*, deserves further investigation.

ACKNOWLEDGEMENTS

We are grateful to Dai-Hua Yu, Bang-Yong Sun, Wei Lin, and Jiang-Wei Liu for the collection of tissue specimens and Jiang-Tian Yu, Li-Hu Wu, and Li-Feng Wang for digital photographs.

REFERENCES

- Deng YC, Yao LB, Liu XP, Nie XY, Wang JC, Zhang XG, Su CZ. Exploring a new gene containing ACP like domain in human brain and expression it in *E.coli*. *Prog Biochem Biophys* 2001; **28**: 72-76
- Okuda T, Kondoh H. Identification of new genes *ndr2* and *ndr3* which are related to *Ndr1/RTP/Drg1* but show distinct tissue specificity and response to N-myc. *Biochem Biophys Res Commun* 1999; **266**: 208-215
- Qu X, Zhai Y, Wei H, Zhang C, Xing G, Yu Y, He F. Characterization and expression of three novel differentiation-related genes belong to the human *NDRG* gene family. *Mol Cell Biochem* 2002; **229**: 35-44
- Deng Y, Yao L, Chau L, Ng SS, Peng Y, Liu X, Au WS, Wang J, Li F, Ji S, Han H, Nie X, Li Q, Kung HF, Leung SY, Lin MC. N-Myc downstream-regulated gene 2 (*NDRG2*) inhibits glioblastoma cell proliferation. *Int J Cancer* 2003;

- 106:** 342-347
- 5 **Shaw E**, McCue LA, Lawrence CE, Dordick JS. Identification of a novel class in the alpha/beta hydrolase fold superfamily: the N-myc differentiation-related proteins. *Proteins* 2002; **47**: 163-168
 - 6 **Zhou RH**, Kokame K, Tsukamoto Y, Yutani C, Kato H, Miyata T. Characterization of the human NDRG gene family: a newly identified member, NDRG4, is specifically expressed in brain and heart. *Genomics* 2001; **73**: 86-97
 - 7 **van Belzen N**, Dinjens WN, Diesveld MP, Groen NA, van der Made AC, Nozawa Y, Vlietstra R, Trapman J, Bosman FT. A novel gene which is up-regulated during colon epithelial cell differentiation and down-regulated in colorectal neoplasms. *Lab Invest* 1997; **77**: 85-92
 - 8 **Piquemal D**, Joulia D, Balaguer P, Basset A, Marti J, Commes T. Differential expression of the RTP/Drg1/Ndr1 gene product in proliferating and growth arrested cells. *Biochim Biophys Acta* 1999; **1450**: 364-373
 - 9 **Boulkroun S**, Fay M, Zennaro MC, Escoubet B, Jaisser F, Blot-Chabaud M, Farman N, Courtois-Coutry N. Characterization of rat NDRG2 (N-Myc downstream regulated gene 2), a novel early mineralocorticoid-specific induced gene. *J Biol Chem* 2002; **277**: 31506-31515
 - 10 **Zhao W**, Tang R, Huang Y, Wang W, Zhou Z, Gu S, Dai J, Ying K, Xie Y, Mao Y. Cloning and expression pattern of the human NDRG3 gene. *Biochim Biophys Acta* 2001; **28**: 134-138
 - 11 **Nichols NR**. Ndr2, a novel gene regulated by adrenal steroids and antidepressants, is highly expressed in astrocytes. *Ann N Y Acad Sci* 2003; **1007**: 349-356
 - 12 **Choi SC**, Kim KD, Kim JT, Kim JW, Yoon DY, Choe YK, Chang YS, Paik SG, Lim JS. Expression and regulation of NDRG2 (N-myc downstream regulated gene 2) during the differentiation of dendritic cells. *FEBS Lett* 2003; **553**: 413-418
 - 13 **Kalaydjieva L**, Gresham D, Gooding R, Heather L, Baas F, de Jonge R, Blechschmidt K, Angelicheva D, Chandler D, Worsley P, Rosenthal A, King RH, Thomas PK. N-myc downstream-regulated gene 1 is mutated in hereditary motor and sensory neuropathy-Lom. *Am J Hum Genet* 2000; **67**: 47-58
 - 14 **Wunderlich V**, Rajewsky MF. "Tumor suppressor gene" concept of carcinogenesis. *Lancet* 1995; **345**: 1570-1571

Edited by Chen WW Proofread by Zhu LH and Xu FM

Involvement of extracellular signal-regulated kinase/mitogen-activated protein kinase pathway in multidrug resistance induced by HBx in hepatoma cell line

Jian Guan, Xiao-Ping Chen, Hong Zhu, Shun-Feng Luo, Bin Cao, Lei Ding

Jian Guan, Xiao-Ping Chen, Hong Zhu, Shun-Feng Luo, Bin Cao, Lei Ding, Hepatic Surgery Center, Tongji Hospital, Tongji Medical College, Huazhong University of Science and Technology, Wuhan 430030, Hubei Province, China

Supported by the Key Clinic Programs of Ministry of Public Health, No. 2001-2003

Correspondence to: Xiao-Ping Chen, M.D., Professor and Chairman, Department of Surgery, Tongji Hospital, Tongji Medical College, Huazhong University of Science and Technology, Wuhan 430030, Hubei Province, China. chenxp_53@163.com

Telephone: +86-27-83662599 **Fax:** +86-27-83662851

Received: 2004-04-24 **Accepted:** 2004-05-13

Abstract

AIM: To investigate the molecular mechanism of the influence of HBx protein on multidrug resistance associated genes: multidrug resistance 1 (MDR-1), multidrug related protein (MRP-1), lung resistance related protein (LRP) in hepatoma cells and the potential role of extracellular signal-regulated kinase/mitogen-activated protein kinase (ERK/MAPK) pathway in this process.

METHODS: A cell model stably expressing the HBx protein was established by liposome-mediated transfection of HBx gene into HepG2 cell line. The expression of multidrug resistance associated genes and proteins was detected by RT-PCR and Western blot. AnnexinV-FITC/PI assay was used to confirm the multidrug resistance (MDR) phenotype of transfected cells by fluorescence cytometry (FACS). The ERK/MAPK pathway activation was measured by Western blot through comparing the ratio of phosphorylation of ERK/MAPK to total ERK/MAPK protein. After treated with the ERK/MAPK pathway inhibitor U0126, the HBx-expressing cells were harvested. Then RT-PCR, Western blot and FACS were used to analyze the alterations in the expression of multidrug resistance associated genes and the MDR phenotype after exposure.

RESULTS: Compared with the control group, the transfected cells showed a higher expression of MDR associated genes and proteins. Marked elevations in MDR-1 (64.3%), MRP-1 (87.5%) and LRP (90.8%) were observed in the transfected cells ($P < 0.05$). RT-PCR revealed that the over-expression of MDR associated proteins was due to amplification of such genes (MDR1 2.9 fold, MRP1 1.67 fold, LRP1.95 fold). Furthermore, we found that the ERK/MAPK activity was remarkably high in the HBx-expressing cells. The activation of ERK/MAPK, as measured by the ratio of phosphorylated ERK bands normalized to the total ERK bands, was increased by 2.3-fold in HBx-transfected cells compared with cells transfected with the empty vector. After treated with the ERK/MAPK pathway inhibitor, the level of MDR associated genes and proteins in the transfected cells decreased to some extent. Compared with controls, a significant decrease in MDR-1 mRNA (53.3%), MRP-1 mRNA (59.7%) as well

as LRP mRNA (56.4%) was observed in the U0126 treated transfected cells after 12 h. Western blot also demonstrated that the protein expression of these MDR associated genes slightly reduced after treated with U0126 for 12 h (MDR-1 40.1%, MRP-1 29.4%, LRP35.7%). This change was accompanied with the rise of cell apoptosis ratio confirmed by Annexin V-PI detection. The apoptosis index of U0126-treated cells increased by 1.28 fold, compared with that of transfected cells. Obviously, the MDR phenotype of these cells was obviously related with increased activities of the ERK/MAPK pathway.

CONCLUSION: HBx protein might be one of the causes for the occurrence of MDR in HCC, and ERK/MAPK pathway might be involved in this change.

Guan J, Chen XP, Zhu H, Luo SF, Cao B, Ding L. Involvement of extracellular signal-regulated kinase/mitogen-activated protein kinase pathway in multidrug resistance induced by HBx in hepatoma cell line. *World J Gastroenterol* 2004; 10(23): 3522-3527

<http://www.wjgnet.com/1007-9327/10/3522.asp>

INTRODUCTION

Hepatocellular carcinoma (HCC) is one of the most common cancers in China and approximately 90% of HCC cases in this region are associated with hepatitis B virus (HBV) infection^[1,2]. The mechanism underlying the development of HCC is still unclear. X gene, a unique open reading frame of HBV, codes for a 16.5 kd protein (X protein, HBx)^[3]. There is evidence that HBx is an essential viral protein with pleiotropic activity that might act directly or indirectly on development of hepatocellular carcinoma during chronic hepadnavirus infection^[4,5]. Over-expression of HBx induces transformation of some cell types^[6]. Additionally, it has been reported that HBx is involved in the arrest of cell cycle progression and the modulation of apoptosis^[7,8]. HBx protein also interacts with the tumor suppressor *p53*, resulting in a loss of its function^[9]. Due to its cytosolic localization, HBx has been shown to participate in a wide range of cellular signal transduction cascades, including Ras-Raf-mitogen-activated protein kinase, *c-Jun N-terminal kinase*, NF- κ B and Janus kinase (*JAK*) -signal transducer and activator transcription factor (*STAT*) pathway^[10-12]. It is well-known that tumor cells may avoid the death fate because apoptotic signals generated by the chemotherapeutic agents fail to activate the necessary pathways required to initiate apoptosis. Therefore, such survival signal pathways whose activation has been shown to play an anti-apoptotic role after treatment with various chemotherapeutic drugs have become the focus of recent researches. The mitogen-activated protein kinase (MAPK) family has emerged as one of such important membrane-to-nucleus signaling mechanisms of HBx, functioning as a mediator of cellular responses to a variety of cellular stimuli^[13]. The MAPK family has been classified into 3 distinct subfamilies: the extracellular signal-related protein

kinases (ERKs) including ERK1 and ERK2, the stress-activated *c-Jun* N-terminal protein kinase (JNKs) and *p38* kinase^[13]. Resistance to a broad spectrum of chemotherapeutic agents in cancer cells is called MDR^[15]. The MDR phenotype is associated with the increased drug efflux from cells that is mediated by an energy-dependent mechanism and the blockade of the apoptosis-inducing pathway, the latter is the highlight of research nowadays. The results of experiments aiming at exploring the role of HBx on apoptosis pathways, however, are controversial and hence disappointing^[15,16]. So we became more interested in determining whether these signal pathways were involved in the development of MDR, and investigated the potential role of MAPK pathways in multidrug resistance induced by HBx in hepatoma cells.

MATERIALS AND METHODS

Reagents

Dulbecco's modified Eagle's medium (DMEM), fetal bovine serum (FBS), lipofectamine 2 000 and G418 were purchased from Invitrogen Inc. ERK/MAPK pathway inhibitor U0126, was purchased from Alexis Inc. Anti-phospho-ERK₁/ERK₂ rabbit polyclonal antibody was purchased from RD systems. Anti-ERK₁/ERK₂ rabbit polyclonal antibody was purchased from Biovision Inc. Polyclonal antibody to multidrug related protein (MRP-1), was from Alexis Inc. Lung resistance-related protein (LRP) mouse antibody, multidrug resistance 1 (MDR-1) mouse antibody and pan actin antibody-5 were provided by Neomarker Inc. Dimethyl sulfoxide (DMSO) was purchased from Sigma.

Cell lines and cell culture

Human hepatocellular carcinoma cell line, HepG2 (GDC024) was purchased from the China Center for Type Culture Collection (Wuhan University, Hubei). Cells were maintained in DMEM supplemented with 100 mL/L heat-inactivated FBS at 37 °C in a humid atmosphere containing 50 mL/L CO₂.

Plasmids and stable transfection

The expression vector pcDNA3-HBx (a kindly gift from Lian-Rui Zhao, PhD; Thomas Jefferson University, USA) was constructed by inserting HBx DNA fragments between the *Hind*III and *Kpn*I cloning sites of the pcDNA3 vector. After amplification in *DH-5α*, we used the EZNA plasmid maxiprep kit (OMEGA, USA) to purify the plasmids. HepG2 cells at 70-80% confluence were transfected with plasmids, using lipofectamine 2 000 (Life Technologies, Inc.). Plasmid transfections were performed according to protocols supplied with the reagents. At 48 h post-transfection, cells were split at a 10:1 ratio and cultured in the presence of 800 g/L G418. After 21 d in selective medium, individual G418-resistant colonies were isolated. Expression of HBx in various cell lines was verified by RT-PCR and Western Blot. The control cell line (HepG2/pcDNA) was generated from cells transfected with the vector alone and selected using G418. After isolation of resistant clones, the concentration of G418 was changed to 400 µg/mL.

Reverse transcriptase-PCR

Total cellular RNA of the stably transfected HepG2 cells was extracted with Trizol (Life Technologies, Grand Island, NY) according to the manufacturer's instructions and reverse transcribed into cDNA with 2 units of Moloney murine leukemia virus reverse transcriptase (MMLV-RT; MBI Fermentas Inc., Amherst, New York, USA), 4 µL of 10 mmol/L dNTPs (Fermentas, Inc.), 2 µL of oligo (dT), 10 µL of 5X reaction buffer (Fermentas Inc.), 2 µL of ribonuclease inhibitor and 26 µL of deionized water for 90 min at 37 °C. PCR was performed with 100 ng of cDNA in a 50 mL reaction volume containing 20 mmol/L Tris, pH 8.0, 50 mmol/L KCl, 2 mmol/L MgCl₂, 10 mmol/L of each dNTP, 20 pmol of each primer, and 1.25 units of *Taq* DNA

polymerase (Fermentas, Inc.). The profile was 94 °C for 5 min before 25 cycles at 94 °C for 45 s, at Ta for 45 s, at 72 °C for 55 s, and a final extension at 72 °C for 10 min. All amplification products were separated on agarose gels and visualized by ethidium bromide staining under *uv* transillumination.

The primers used for semi-quantitative PCR were: sense 5'-TCT CCG TCT GCC GTT CCA -3' and antisense 5'-TCG GTC GTT GAC ATT GCT G-3' for HBx; sense 5'-TGA AGG ACT TCG TGT CAG CC-3 and antisense 5'-GTC CATGAT GGT GTT GAG CC-3' for MRP-1; sense 5'-CAT TGG TGT GGT GAG TCA GG-3' and antisense 5'-CTC TCT CTC CAA CCA GGG TG-3' for MDR-1; sense 5'-TAA GGG CTT CCA GCA CCA AC-3' and antisense 5'-GGA GTT CTC GCT TCT CGT CC -3' for LRP and sense 5'-GTG CGT GAC ATT AAG GAG-3' and antisense 5'-CTA AGT CAT AGT CCG CCT-3' for β-actin.

Protein preparation and Western blot analyses

Stably transfected HepG2 cells were rinsed with 0.01 mol/L PBS, and then lysed in a lysis buffer containing 50 mmol/L Tris-HCl (pH 8.5), 150 mmol/L NaCl, 0.2 g/L Na₃N, 0.1 g/L SDS, 100 µg/mL PMSF, 1 µg/mL aprotinin, 10 mL/L NP-40, 5 g/L sodium deoxycholate. The products were centrifuged at 14 000 g for 15 min to remove the cellular debris. Protein concentrations were determined by the Bradford methods. A total of 50-100 µg of protein was separated by electrophoresis using 60 g/L or 100 g/L sodium dodecyl sulfate-polyacrylamide gels (according to the molecular mass of target protein), transferred to a immunoblot NC membrane, blocked with degreased milk for 12 h and hybridized with polyclonal antibodies for MRP-1, LRP, MDR-1, p-ERK and ERK (each diluted to 1:1000) at 4 °C overnight. The membranes were then washed 4 times for 15 min incubation with TBST (10 mmol/L Tris-Cl, pH 7.4, 150 mmol/L NaCl, 10 mL/L Tween 20 and hybridized with peroxidase (HRP) -conjugated secondary antibodies corresponding to each primary antibody. Protein banding specifically to the antibodies was visualized by ECL-associated fluorography (Pierce Inc.).

Cell viability and apoptosis analysis by fluorescence cytometry (FACS)

Cells were plated and grown overnight until they reach 80% confluence, then the cells were treated with 20 µg/mL 5-Fu. Subsequently, detached cells in the medium were collected, and the remaining adherent cells were released by trypsinization. The cells were washed with phosphate-buffered saline (PBS) and resuspended in 250 µL binding buffer (annexinV-FITC kit; BD) containing 5 µL of annexin V-FITC stock and 10 µL of 20 µg/mL propidium iodide (PI) for the determination of phosphatidylserine (PS) exposure on the outer plasma membrane. After incubated for 10 min at room temperature in a light protected area, the samples were analyzed by a Becton Dickinson fluorescence cytometer using CellQuest software. We could discriminate intact cells (annexin⁻/PI⁻) from apoptotic cells (annexin⁺/PI⁻) and necrotic cells (annexin⁺/PI⁺) after treatment with 5-Fu.

Statistical analyses

The results were expressed as mean±SE. Student's *t* test was used to compare data. *P*<0.05 was considered statistically significant. All data were processed by SPSS10.0.

RESULTS

Isolation and identification of HBx-expressing cells

As shown in Figure 1, the restriction enzyme digestions demonstrated that the digestion products had exactly the expected size (about 500 bp). We also requested Shanghai Bioasia Biotechnology Inc to sequence the whole plasmid kindly gifted by Lian-Rui Zhao (Ph.D), and the result of sequencing was consistent with the sequence of V0866 in GeneBank.

After stable transfection, the cells of different groups were confirmed for the expression of HBx by using PCR and immunoprecipitation. The identification of the successful transfection at mRNA and protein levels is shown in Figure 2 and Figure 3, respectively. The expected bands could be seen in the HBx-expressing cells and the groups treated with ERK/MAPK signal pathway inhibitors. There was no detectable band in the control group. These results indicated that HBx was successfully transferred and expressed in HepG2 cells.

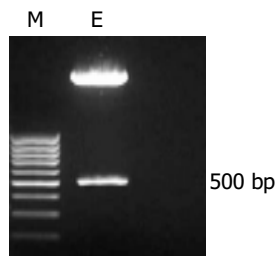


Figure 1 Restriction enzyme digestions of the plasmids. Lane M: markers (the brightest band of the marker presents the 500 bp); lane E: one of the split bands emerged at the exact position of 500 bp, and the other was the empty pcDNA3.0 vector as expected.

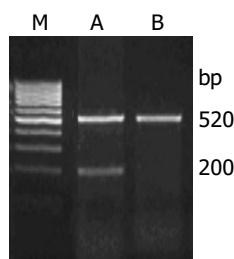


Figure 2 Confirmation of the successful transfection of HBx into HepG2 cells by RT-PCR. Lane M: markers (the brightest band of the marker presents the 500 bp); lane A: transfected cells; lane B: transfected cells treated with U0126; lane C: the control.

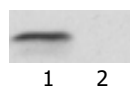


Figure 3 Western blot analysis of HBx protein in samples isolated from HepG2 cells with or without HBx transfection. Lane 1: the sample transfected with HBx; lane 2: the sample transfected with vector only.

Verification of MDR phenotype in HBx-expressing cells

To evaluate the effect of HBx introduction on the chemosensitivity of HepG2 cells, we initially used a FACS analysis of cells stained with PI and annexinV-FITC assay to compare the survival and apoptosis ratio of HepG2 cells transfected with empty pcDNA3.0 with HBx-transfected cells, i.e., HepG2/pcDNA and HepG2/pcDNA-HBx, after their exposure to 5-Fu (20 µg/mL) for 12 h and then cultured in normal medium for 6 h. Apoptosis index was quantified by a Becton Dickinson fluorescence cytometer. The apoptosis ratio in transfected cells ($9.83 \pm 1.5\%$) analyzed by CellQuest software after administration of 5-Fu was significantly lower than that of the control ($17.79 \pm 1.7\%$) (Figure 4). MTT assay also demonstrated that the inhibitory concentration 50% (IC_{50}) of adriamycin in the transfected cells was higher than that of the control (data not shown). The multidrug resistance transporter MDR-1, MRP-1, and LRP were associated with multidrug resistance. Western blot analysis was performed to examine whether the resistance to 5-Fu-induced apoptosis in HBx-expressing cells was due to the alterations of such proteins. Marked elevations in

MDR-1 protein (64.3%), MRP-1 (87.5%) and LRP (90.8%) proteins were observed in the transfected cells (Figure 5 and Tables 1-2), which were well correlated with the degree of resistance. Furthermore, semi-quantitative RT-PCR revealed that over-expression of MDR-associated proteins was due to amplification of such genes (1.9-fold MDR-1, 0.67-fold MRP-1, 0.95-fold LRP) (Figure 6). Taken together, these data suggested that reintroduction of HBx contributed to the development of MDR phenotype.

Table 1 Protein level of MDR associated genes (mean±SD)

Group	MDR-1	MRP-1	LRP
transfected	0.23±0.04	0.15±0.03	0.17±0.03
control	0.14±0.03	0.08±0.03	0.09±0.02
P	0.036	0.046	0.018

Table 2 mRNA level of MDR associated genes (mean±SD)

Group	MDR-1	MRP-1	LRP
Transfected	0.29±0.06	0.62±0.11	0.82±0.15
Control	0.10±0.03	0.37±0.09	0.42±0.07
P	0.038	0.012	0.014

ERK/MAPK pathway levels and activities in transfected cells

To assess the role of ERK/MAPK in HBx-induced activation of MDR1 expression, we measured the phosphorylation of ERK/MAPK in cells transfected with HBx. As shown in Figure 6, the phosphorylation of ERK/MAPK as measured by the ratio of the phosphorylated ERK bands (Figure 7A) normalized to the total ERK band (Figure 7B), was increased by 2.3-fold in HBx-transfected cells compared with control cells. These results suggested that the MDR phenotype induced by HBx was accompanied with the activation of ERK/MAPK pathways.

Effect of ERK/MAPK pathway inhibitors on MDR of HBx-expressing hepatoma cells

Based on the constitutive activation of ERK/MAPK, we determined whether U0126, a specific ERK inhibitor, could give rise to alterations in the expression of MDR associated genes and increase the transfected cell sensitivity to the cytotoxicity of 5-Fu. Treatment of transfected cells with U0126 decreased the levels of MDR-1 mRNA, as well as LRP and MRP-1 mRNA (Tables 3-4). Compared with controls, a significant decrease in MDR-1 mRNA (53.3%), MRP-1 mRNA (59.7%) as well as LRP mRNA (56.4%) was observed in U0126 treated transfected cells after 12 h. Western blot also demonstrated that the protein expression of these MDR associated genes was slightly reduced after treated with U0126 for 12 h (MDR-1 40.1%, MRP-1 29.4%, LRP 35.7%). The apoptosis index of U0126-treated cells increased by 1.28 fold, compared with that of transfected cells. All these observations proved that U0126 could impair the MDR phenotype induced by HBx and sensitize cells to the toxicity of 5-Fu.

Table 3 Changes of MDR related genes after treated with U0126 (mean±SD)

Group	MDR-1	MRP-1	LRP
Transfected	0.15±0.03	0.62±0.11	0.78±0.13
Treated with U0126	0.08±0.02	0.37±0.09	0.44±0.09
P	0.028	0.040	0.020

Table 4 Changes of MDR related proteins after treated with U0126 (mean±SD)

Group	MDR-1	MRP-1	LRP
Transfected	0.22±0.04	0.17±0.02	0.14±0.02
Treated with U0126	0.13±0.04	0.12±0.02	0.09±0.02
P	0.04	0.038	0.04

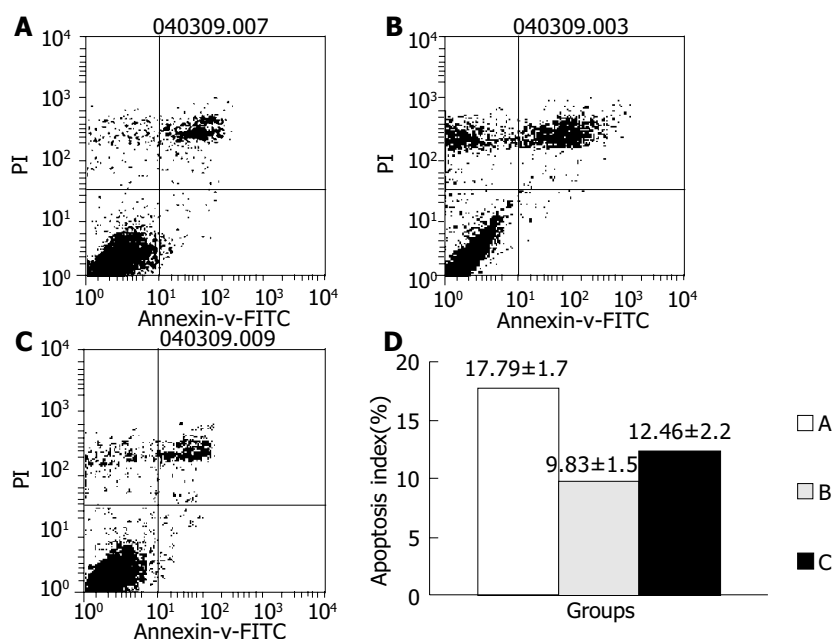


Figure 4 Apoptosis index of three different groups of cells after treatment with 5-Fu. A: HepG2/pcDNA3 cells; B: HepG2/pcDNA3-HBx cells; C: U0126 pretreated transfected cells. D: Apoptotic index quantitated by FACS.

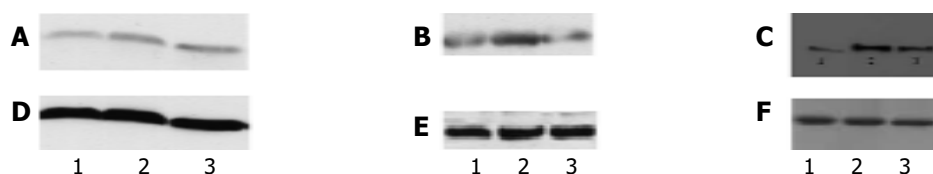


Figure 5 Protein levels of MDR associated genes in different groups of cells. Lane1: HepG2/pcDNA3 cells; lane2: HepG2/pcDNA3-HBx cells; lane3: transfected cells treated with U0126. The primary antibody for A, B, C, D was β -actin, MDR-1, MRP-1 and LRP respectively.

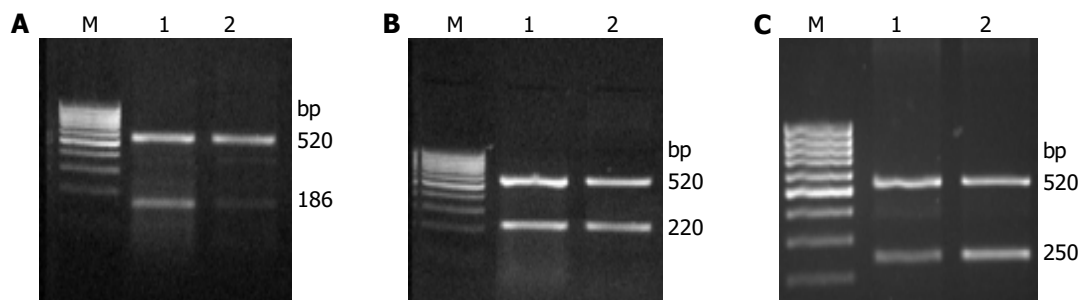


Figure 6 RT-PCR analysis of the expression of MDR associated genes in transfected and control cells. Lane 1: HBx-expressing cells; lane 2: control cells; lane M: markers. A: Specific primers to amplify MDR-1 gene; B: Specific primers to amplify MRP-1 gene; C: Specific primers to amplify LRP gene.

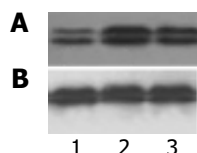


Figure 7 Increased phosphorylation of ERK induced by HBx in hepatoma cells analyzed by Western blot. Lane 1: transfected cells after treated with U0126; lane 2: HBx-expressing cells; lane 3: control cells. A: Specific antibody for phosphorylated-ERK; B: Specific antibody for total ERK.

DISCUSSION

MDR was the leading cause of failure to comprehensive therapy of HCC^[17]. Although the detailed molecular mechanisms of MDR remain to be explored, the disorder of anti-apoptotic and pro-

apoptotic signal pathways and the over-expression of certain efflux proteins are generally believed to be due to MDR phenotype^[18]. HBV infection is known as one of the most important risk factors in HCC development. Among the proteins coded by HBV genome, HBx has been proved to play a central role in virus duplication and carcinogenesis^[2]. According to previous study, HBx could participate in several pathological processes of the generation and growth of HCC^[2,4]. Apart from interfering with the suppressing function of *p53*, HBx could act as a multi-functional transcriptional transactivator to stimulate some important signal pathways. The effects of HBx on such signal pathways as ERK/MAPK, JNK, NF- κ B and Src have been well-documented, especially in the aspect of apoptotic signals^[16,19]. However, the pathological implications of these complex interactions in the evolvement of HCC malignant phenotypes have not been fully understood.

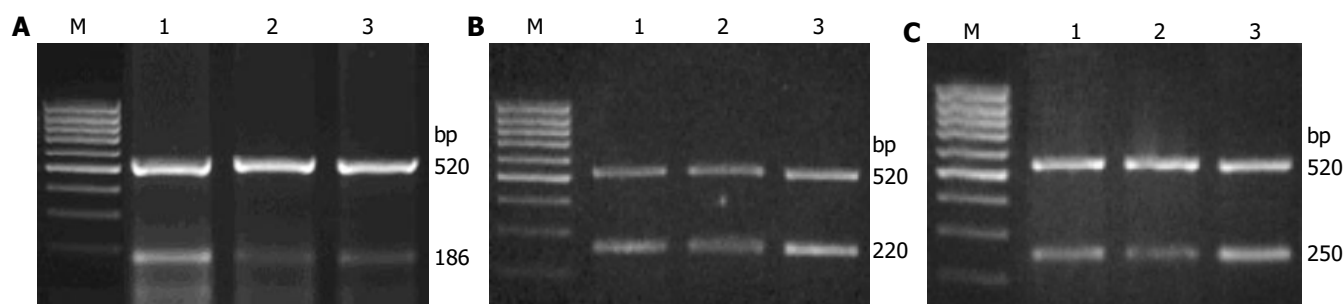


Figure 8 RT-PCR analysis of the expression of MDR associated genes in HBx-expressing cells in response to treatment of U0126. Lane 1: HBx-expressing cells; lane 2: control cells; lane 3: transfected cells treated with U0126; lane M: marker. A: Specific primers to amplify MDR-1 gene; B: Specific primers to amplify MRP-1 gene; C: Specific primers to amplify LRP gene.

In this study, we investigated the influence of HBx protein on MDR associated proteins and the potential role of ERK/MAPK pathways in this process. Our data provided the evidence that HBx up-regulated the expression of MDR associated genes. Similar changes were witnessed in protein level. Our results indicated that HBx protein was a survival factor that could protect transfected cells from death induced by anti-tumor drugs in a constitutive expression system. Subsequent studies showed that HBx protein contributed to the MDR phenotype which was confirmed by apoptosis detection through FCAS. Furthermore, we demonstrated that the ERK/MAPK pathway worked as a downstream effector of HBx, mediating the MDR phenotype in the ERK/MAPK signal transduction pathway which was activated in HBx-expressing cells. To further confirm our previous hypothesis that the MAPK signal pathway played an important role in the MDR phenotype induced by HBx protein, we examined whether MAPK inhibited by U0126 (20 $\mu\text{mol/L}$, 12 h) could alter the phenotype of MDR. The experimental results showed that P-glycoprotein (product of the *MDR-1* gene) mediated MDR of transfected cells is reduced by the treatment of such inhibitors, which supports corroborated our presumption.

Among the myriads of intracellular signaling molecules regulated by HBx, ERK/MAPK plays an important role in regulating several cellular processes, such as proliferation and differentiation^[20]. Several studies suggested that ERK/MAPK was involved in the acquired resistance of cancer cells to cytostatic drugs^[22,23]. Kisucka *et al.* reported that the effect of PD98059 and U0126 on vincristine resistance of L1210/VCR cells, suggesting that both substances were reversing agents of P-glycoprotein-mediated MDR, and the role of ERK-mediated phosphorylation cascades in the occurrence of MDR should be considered. Dent *et al.*^[25] also demonstrated that the activation of the ERK/MAPK pathway played a critical role in leukemia cell survival after treatment with chemotherapeutic drugs and ionizing radiation. As shown in our experiment, the up-regulation of P-glycoprotein expression might be one of the mechanisms by which HBx induces the MDR phenotype. This result was consistent with the data reported by Chen *et al.*^[26], who pointed out in his recent paper that inhibitors of the ERK/MAPK signal pathway could remarkably inhibited the expression of MDR-1. Barancik *et al.*^[27] also suggested that SB203580, a specific inhibitor of the *p38*/MAPK pathway, could reverse the resistance of L1210/VCR cells mainly via P-glycoprotein dependent mechanisms. However, we could not exclude the possibility that ERK/MAPK activated by HBx could enhance the activity of P-glycoprotein (product of the *MDR-1* gene) by phosphorylation. P-glycoprotein is a phosphorylation substrate for a number of protein kinases including protein kinase C (PKC), MAPK, phospholipase C (PLC) *etc.*^[28,29]. Therefore, phosphorylation of such MDR related proteins might be another function of ERK/MAPK pathway during MDR induced by

HBx protein. The influence of phosphorylation by such protein kinases as PKC or MAPK on the activity of MDR-1 protein and other MDR associated proteins is the target of our ensuing experiments in order to obtain a thorough understanding of the molecular mechanisms of interactions between HBx and MDR associated proteins.

In summary, MAPK pathway is involved in generation of MDR phenotype in hepatoma cells. The findings reported in this work might contribute to the understanding of pathogenic mechanisms involved in malignant phenotypes of HBV-associated hepatocellular carcinoma.

ACKNOWLEDGEMENTS

We thank Professor Lian-Rui Zhao (Ph.D, Thomas Jefferson University, USA) for his gift of plasmids and useful suggestions during the whole experiment. We are also grateful to Dr. Ji-Xiong Chen and Miss Shan-Shan Huang for their kind help and critical discussion.

REFERENCES

- Block TM, Mehta AS, Fimmel CJ, Jordan R. Molecular viral oncology of hepatocellular carcinoma. *Oncogene* 2003; **22**: 5093-5107
- Birrer RB, Birrer D, Klavins JV. Hepatocellular carcinoma and hepatitis virus. *Ann Clin Lab Sci* 2003; **33**: 39-54
- Koike K, Tsutsumi T, Fujie H, Shintani Y, Kyoji M. Molecular mechanism of viral hepatocarcinogenesis. *Oncology* 2002; **62** (Suppl 1): 29-37
- Murakami S. Hepatitis B virus X protein: a multifunctional viral regulator. *World J Gastroenterol* 2001; **36**: 651-660
- Wang T, Wang Y, Wu MC, Guan XY, Yin ZF. HBsAg and HBx knocked into the p21 locus causes hepatocellular carcinoma in mice. *Hepatology* 2004; **39**: 318-324
- Jung EY, Kang HK, Chang J, Yu DY, Jang KL. Cooperative transformation of murine fibroblast NIH3T3 cells by hepatitis C virus core protein and hepatitis B virus X protein. *Virus Res* 2003; **94**: 79-84
- Oh JC, Jeong DL, Kim IK, Oh SH. Activation of calcium signaling by hepatitis B virus-X protein in liver cells. *Exp Mol Med* 2003; **35**: 301-309
- Li D, Chen X, Zhang W. The inhibition of apoptosis of hepatoma cells induced by HBx is mediated by up-regulation of survivin expression. *J Huazhong Univ Sci Technol Med Sci* 2003; **23**: 383-386
- Wang XW. Microinjection technique used to study functional interaction between p53 and hepatitis B virus X gene in apoptosis. *Mol Biotechnol* 2001; **18**: 169-177
- Yun C, Cho H, Kim SJ, Lee JH, Park SY, Chan GK, Cho H. Mitotic aberration coupled with centrosome amplification is induced by hepatitis B virus X oncoprotein via the Ras-mitogen-activated protein/extracellular signal-regulated kinase-mitogen-activated protein pathway. *Mol Cancer Res* 2004; **2**: 159-169

- 11 **Diao J**, Khine AA, Sarangi F, Hsu E, Iorio C, Tibbles LA, Woodgett JR, Penninger J, Richardson CD. X protein of hepatitis B virus inhibits Fas-mediated apoptosis and is associated with up-regulation of the SAPK/JNK pathway. *J Biol Chem* 2001; **276**: 8328-8340
- 12 **Yoo YG**, Oh SH, Park ES, Cho H, Lee N, Park H, Kim DK, Yu DY, Seong JK, Lee MO. Hepatitis B virus X protein enhances transcriptional activity of hypoxia-inducible factor-1alpha through activation of mitogen-activated protein kinase pathway. *J Biol Chem* 2003; **278**: 39076-39084
- 13 **Nijhara R**, Jana SS, Goswami SK, Rana A, Majumdar SS, Kumar V, Sarkar DP. Sustained activation of mitogen-activated protein kinases and activator protein 1 by the hepatitis B virus X protein in mouse hepatocytes *in vivo*. *J Virol* 2001; **75**: 10348-10358
- 14 **Hilger RA**, Scheulen ME, Strumberg D. The Ras-Raf-MEK-ERK pathway in the treatment of cancer. *Onkologie* 2002; **25**: 511-518
- 15 **Fojo T**, Bates S. Strategies for reversing drug resistance. *Oncogene* 2003; **22**: 7512-7523
- 16 **Terradillos O**, de La Coste A, Pollicino T, Neuveut C, Sitterlin D, Lecoer H, Gougeon ML, Kahn A, Buendia MA. The hepatitis B virus X protein abrogates Bcl-2-mediated protection against Fas apoptosis in the liver. *Oncogene* 2002; **21**: 377-386
- 17 **Schuster R**, Hildt E, Chang SF, Terradillos O, Pollicino T, Lanford R, Gerlich WH, Will H, Schaefer S. Conserved transactivating and pro-apoptotic functions of hepadnaviral X protein in ortho- and avihepadnaviruses. *Oncogene* 2002; **21**: 6606-6613
- 18 **Huesker M**, Folmer Y, Schneider M, Fulda C, Blum HE, Hafkemeyer P. Reversal of drug resistance of hepatocellular carcinoma cells by adenoviral delivery of anti-MDR1 ribozymes. *Hepatology* 2002; **36**(4 Pt 1): 874-884
- 19 **Tsuruo T**. Molecular cancer therapeutics: recent progress and targets in drug resistance. *Intern Med* 2003; **42**: 237-243
- 20 **Shih WL**, Kuo ML, Chuang SE, Cheng AL, Doong SL. Hepatitis B virus X protein activates a survival signaling by linking SRC to phosphatidylinositol 3-kinase. *J Biol Chem* 2003; **278**: 31807-31813
- 21 **Chang F**, Steelman LS, Lee JT, Shelton JG, Navolanic PM, Blalock WL, Franklin RA, McCubrey JA. Signal transduction mediated by the Ras/Raf/MEK/ERK pathway from cytokine receptors to transcription factors: potential targeting for therapeutic intervention. *Leukemia* 2003; **17**: 1263-1293
- 22 **Ding S**, Chamberlain M, McLaren A, Goh L, Duncan I, Wolf CR. Cross-talk between signalling pathways and the multidrug resistant protein MDR-1. *Br J Cancer* 2001; **85**: 1175-1184
- 23 **Fan M**, Chambers TC. Role of mitogen-activated protein kinases in the response of tumor cells to chemotherapy. *Drug Resist Updat* 2001; **4**: 253-267
- 24 **Kisucka J**, Barancik M, Bohacova V, Breier A. Reversal effect of specific inhibitors of extracellular-signal regulated protein kinase pathway on P-glycoprotein mediated vincristine resistance of L1210 cells. *Gen Physiol Biophys* 2001; **20**: 439-444
- 25 **Dent P**, Jarvis WD, Birrer MJ, Fisher PB, Schmidt-Ullrich RK, Grant S. The roles of signaling by the p42/p44 mitogen-activated protein (MAP) kinase pathway; a potential route to radio- and chemo-sensitization of tumor cells resulting in the induction of apoptosis and loss of clonogenicity. *Leukemia* 1998; **12**: 1843-1850
- 26 **Chen B**, Jin F, Lu P, Lu XL, Wang PP, Liu YP, Yao F, Wang SB. Effect of mitogen-activated protein kinase signal transduction pathway on multidrug resistance induced by vincristine in gastric cancer cell line MGC803. *World J Gastroenterol* 2004; **10**: 795-799
- 27 **Barancik M**, Bohacova V, Kvacakajova J, Hudcova S, Krizanova O, Breier A. SB203580, a specific inhibitor of p38-MAPK pathway, is a new reversal agent of P-glycoprotein-mediated multidrug resistance. *Eur J Pharm Sci* 2001; **14**: 29-36
- 28 **Miao ZH**, Ding J. Transcription factor c-Jun activation represses mdr-1 gene expression. *Cancer Res* 2003; **63**: 4527-4532
- 29 **Ros JE**, Schuetz JD, Geuken M, Streetz K, Moshage H, Kuipers F, Manns MP, Jansen PL, Trautwein C, Muller M. Induction of Mdr1b expression by tumor necrosis factor-alpha in rat liver cells is independent of p53 but requires NF-kappaB signaling. *Hepatology* 2001; **33**: 1425-1431

Edited by Wang XL and Kumar M Proofread by Xu FM

Effect of environmental hyperthermia on gastrin, somatostatin and motilin in rat ulcerated antral mucosa

Feng-Peng Sun, Yu-Gang Song

Feng-Peng Sun, Yu-Gang Song, Department of Gastroenterology, Nanfang Hospital, First Military Medical University, Guangzhou 510515, Guangdong Province, China

Supported by Guangdong Provincial Natural Science Foundation, No.010578, Key Technological Program of Guangzhou, No.2002Z3-E0131 and Key Program in Social Development of Guangdong Province, No.2002C31210

Correspondence to: Dr. Feng-Peng Sun, Department of Gastroenterology, Nanfang Hospital, First Military medical University, Guangzhou 510515, Guangdong Province, China. phd@china.com

Telephone: +86-20-61648215 **Fax:** +86-20-61648216

Received: 2003-05-12 **Accepted:** 2003-06-07

Abstract

AIM: To study the effect of environmental hyperthermia on gastrin, somatostatin and motilin in rat ulcerated antral mucosa.

METHODS: Forty-two Wistar rats were equally divided into six groups, according to the room temperature (high and normal) and the treatment (acetic acid, normal saline and no treatment). Levels of gastrin, somatostatin and motilin in rat ulcerated antral mucosa were measured with a radioimmunoassay method.

RESULTS: The average temperature and humidity were 32.5 °C and 66.7% for the high temperature group, and 21.1 °C and 49.3% for the normal temperature group, respectively. Gastric ulcer model was successfully induced in rat injected with 0.05 mL acetic acid into the antrum. In rats with gastric ulcers, the levels of gastrin and motilin increased, whereas the somatostatin level declined in antral mucosa, compared with those in rats treated with normal saline and the controls. However, the change extent in the levels of gastrin, motilin and somatostatin in antral mucosa was less in the high temperature group than in the normal temperature group.

CONCLUSION: The levels of gastrin, somatostatin and motilin in rat ulcerated antral mucosal tissue remain relatively stable in a high temperature environment, which may relate to the equilibration of the dynamic system.

Sun FP, Song YG. Effect of environmental hyperthermia on gastrin, somatostatin and motilin in rat ulcerated antral mucosa. *World J Gastroenterol* 2004; 10(23): 3528-3530
<http://www.wjgnet.com/1007-9327/10/3528.asp>

INTRODUCTION

The abnormal secretion of gastrointestinal hormones such as gastrin, somatostatin, motilin may affect the function of alimentary tract^[1,2]. In a high temperature living environment, body could develop adaptation reaction to hyperthermia, meanwhile induces a series of compensatory regulations in the central nervous system and endocrine system^[3-8], the content

of gastrointestinal hormones could be changed accordingly. Our experiment investigated the influence of ambient temperature on gastrin, somatostatin, motilin in rat ulcerated antral mucosa and their biological significance.

MATERIALS AND METHODS

Animals and preparation

We used healthy adult male Wistar rats weighing 200-260 g (purchased from Experimental Animal Center, Sun Yat-Sen University of Medical Sciences). The rats were raised in our Experimental Animal Center and fed with standard rat chow. The rats were randomly divided into six groups of seven rats each, respectively. They were high temperature ulcer group, normal temperature ulcer group, high temperature saline group, normal temperature saline group, high temperature control group, normal temperature control group. The room temperature of the hyperthermia group was not interfered, but that of the normal group was controlled by airconditioning.

Radioimmunoassay kits of gastrin and motilin were purchased from Tianjin Qianye Biotech Co. Ltd, and the kits of somatostatin from Department of Neurobiology of Second Military Medical University.

The temperature of the animal houses was measured by catathermometer (produced by Shanghai Medical Instrument Factory) at 8:00 and 20:00 everyday, the relative humidity was converted through the scale at the base of the catathermometer, and average values of dry bulb temperature and relative humidity were recorded. The dry bulb temperature (°C) in houses on the d 0, 1, 2, 3 after model-making and the day of rat sacrifice was 31.7, 32.5, 33.0, 32.8, 32.4 (average 32.5±0.5) for the high temperature group, and 21.2, 21.1, 21.0, 21.3, 21.1 (average 21.1±0.1) for the normal temperature group, respectively. The relative humidity (%) was 58.0, 65.5, 69.0, 76.0, 65.0 (average 66.7±6.6) for the high temperature group and 46.5, 48.0, 51.5, 53.0, 47.5 (average 49.3±2.8) for normal temperature group, respectively.

Establishment of rat model and measurement of gastrin, somatostatin and motilin

The rats of high temperature ulcer group and normal temperature ulcer group were anesthetized with 30 g/L sodium pentobarbital intraperitoneally. The abdomen was opened and 0.05 mL acetic acid was injected into the antral tissues. Omentum majus and antral tissue of the injection site were stitched. The peritoneum, parietal abdomen and ventral muscle, and skin were stitched continually. The rats of high temperature saline group and normal temperature saline group were injected with 0.05 mL saline instead of acetic acid at the same site. The rats of control group did not receive any treatment. After operation, the model-making rats were raised separately, and fasted overnight with free access to water one day before sacrifice. No treatment was given to normal control group. The rat stomach was separated and split from the greater curvature, and mucosa of gastric antrum was scraped about 0.1 g to be boiled after weighed on electronic analytical balance. The boiled tissue was homogenized into homogenates in a homogenizer with 1 mL of 1 mol/L acetic acid and neutralized

with 1 mL of 1 mol/L NaOH, the liquid of homogenates was centrifuged at 3 500 r/min for 15 min to obtain supernatant, and the samples were then stored at -70 °C until assay. Gastrin, somatostatin and motilin were measured by using radioimmunoassay (RIA) method, measurement procedures were performed according to the instructions attached to the kits. The unit of result was transformed to ng/g.

Statistical analysis

Data among the groups were analyzed with factorial analysis of variance by SPSS 10.0 software. The comparison between the two means of different groups was analyzed by Student-Newman-Keuls. $P < 0.05$ was considered statistically significant.

RESULTS

Observation of gross specimens

Gastric contents of the rats in high temperature and normal temperature ulcer groups obviously increased, the diameter of round shape ulcers on the frontal wall of gastric antrum was about 0.5-0.7 cm, the center of the ulcer was pale covered with offwhite membrane, the base was flat with clear verge, and the mucosa around the ulcer had hyperemia and edema. Gastric contents of the rats in the other groups were suitable, mucosa plica of gastric antrum was obvious, and its color was pale red without hyperemia and edema. There was no ulcer on the surface.

Level of gastrin in rat antral mucosa of each group

The difference of gastrin level in antral mucosa between ulcer group and nonulcer group was significant ($F = 9.500$, $P = 0.000$), gastrin levels in ulcer group (average 5.99 ng/g) were higher than those in control group (3.68 ng/g) and saline group (3.98 ng/g). But the differences in gastrin levels among the groups were insignificant in high and normal temperature groups ($F = 1.465$, $P = 0.234$). There was no mutual effect between the two treatment factors of ulcer and temperature ($F = 0.980$, $P = 0.385$). The gastrin level in ulcerated antral mucosa increased significantly ($P < 0.01$). But the level of gastrin in antral mucosa in the high temperature ulcer group increased less than that in the normal temperature ulcer group ($P < 0.05$) (Table 1).

Table 1 Gastrin in rat antral mucosa ($n=7$, ng/g, mean±SD)

Group	Ulcer	Normal saline	Control
HT	5.24±1.65	3.91±1.31	3.64±1.15 ^b
NT	6.73±2.29 ^a	4.04±1.28	3.71±1.13

^a $P < 0.05$, vs high temperature ulcer group ^b $P < 0.01$ vs ulcer group.

Level of somatostatin in rat antral mucosa of each group

The difference of somatostatin level in antral mucosa between ulcer group and nonulcer group was significant ($F=15.087$, $P=0.000$), somatostatin levels in ulcer group (average 0.62 ng/g) were less than those in control group (1.37 ng/g) and saline group (1.24 ng/g). But the differences of somatostatin levels were insignificant in high and normal temperature groups ($F = 2.789$, $P = 0.104$). There was no mutual effect between the two treatment factors of ulcer and temperature ($F = 1.416$, $P = 0.256$). The level of somatostatin in gastric ulcerated antral mucosa declined significantly ($P < 0.01$). But the level of somatostatin in antral mucosa in the high temperature ulcer group declined less than that in the normal temperature ulcer group ($P < 0.05$) (Table 2).

Level of motilin in rat antral mucosa of each group

The difference of motilin level in antral mucosa between ulcer group and nonulcer group was significant ($F = 18.178$, $P = 0.000$), motilin levels in ulcer group (average 8.04 ng/g) were higher than

those in control group (4.27 ng/g) and saline group (4.58 ng/g). But the differences of motilin levels were insignificant in high and normal temperature groups ($F = 3.632$, $P = 0.065$). There was no mutual effect between the two treatment factors of ulcer and temperature ($F = 2.611$, $P = 0.087$). The level of motilin in gastric ulcerated antral mucosa increased significantly ($P < 0.01$). But the level of motilin in antral mucosa in the high temperature ulcer group increased less than that in the normal temperature ulcer group ($P < 0.05$) (Table 3).

Table 2 Somatostatin in rat antral mucosa ($n = 7$, ng/g, mean±SD)

Group	Ulcer	Normal saline	Control
HT	0.86±0.30	1.28±0.46	1.39±0.50 ^b
NT	0.37±0.15 ^a	1.19±0.41	1.36±0.41

^a $P < 0.05$, vs high temperature ulcer group ^b $P < 0.01$ vs ulcer group.

Table 3 Motilin in rat antral mucosa ($n = 7$, ng/g, mean ± SD)

Group	Ulcer	Salt	Cont
HT	6.58±2.04	4.46±1.30	4.22±1.24 ^b
NT	9.50±2.98 ^a	4.70±1.43	4.31±1.40

^a $P < 0.05$, vs high temperature ulcer group ^b $P < 0.01$ vs ulcer group.

DISCUSSION

Our experiment established the model of rat gastric ulcer. Gastrin, somatostatin and motilin were measured with the RIA method. The result revealed that gastrin and motilin in antral mucosa tissue increased, and somatostatin declined when the rats had gastric ulcer. Compensative changes of gastrointestinal tract and other organs took place to accommodate hyperthermia. Our experiment detected the level of gastrin, somatostatin and motilin in antral mucosa tissue of gastric ulcer rats in high and normal temperature environments. We discovered that the level of gastrin and motilin in antral mucosa in the high temperature ulcer group increased less than that in the normal temperature ulcer group, the level of somatostatin in the high temperature ulcer group declined less than that in the normal temperature ulcer group.

Complex changes of many cytokines in body occurred in heat stress environment^[9-15]. Hyperthermia could change heat stress proteins (HSP), atrial natriuretic factor (ANF), angiotensin, nerve growth factor (NGF), cortisol and plasma protein, blood sugar, serum lipoprotein, microelement as well as body immune system correspondingly^[16-20]. The system of neuroendocrine, cytokine and heat stress constituted an organic network, in which a chain in dynamic action could make internal milieu stable^[21,22]. The result of this experiment indicates that the levels of gastrin, somatostatin and motilin in antral mucosa tissue remain relatively stable in a high temperature environment. This may relate to the equilibration of the dynamic system.

REFERENCES

- 1 **Kaminska B**, Kozielska E, Korzon M, Czaja M, Banach P. Bleeding from alimentary tract in pseudo Zollinger-Ellison syndrome. *Med Sci Monit* 2000; **6**: 596-601
- 2 **Ku SK**, Lee HS, Lee JH. An immunohistochemical study of endocrine cells in the alimentary tract of the red-bellied frog, *Bombina orientalis*. *J Vet Med Sci* 2000; **62**: 589-594
- 3 **de Freitas MS**, Spohr TC, Benedito AB, Caetano MS, Margulis B, Lopes UG, Moura-Neto V. Neurite outgrowth is impaired on HSP70-positive astrocytes through a mechanism that requires NF-kappaB activation. *Brain Res* 2002; **958**: 359-370
- 4 **Pacheco-Lopez G**, Espinosa E, Zamorano-Rojas HM, Ramirez-Amaya V, Bermudez-Rattoni F. Peripheral protein immuniza-

- tion induces rapid activation of the CNS, as measured by c-Fos expression. *J Neuroimmunol* 2002; **131**: 50-59
- 5 **Deng X**, Jayanthi S, Ladenheim B, Krasnova IN, Cadet JL. Mice with partial deficiency of c-Jun show attenuation of methamphetamine-induced neuronal apoptosis. *Mol Pharmacol* 2002; **62**: 993-1000
- 6 **Fernandez F**, Aguerre S, Mormede P, Chaouloff F. Influences of the corticotropic axis and sympathetic activity on neurochemical consequences of 3,4-methylenedioxymethamphetamine (MDMA) administration in Fischer 344 rats. *Eur J Neurosci* 2002; **16**: 607-618
- 7 **Watanabe YG**. Immunohistochemical study on the fetal rat pituitary in hyperthermia-induced exencephaly. *Zoolog Sci* 2002; **19**: 689-694
- 8 **Khan VR**, Brown IR. The effect of hyperthermia on the induction of cell death in brain, testis, and thymus of the adult and developing rat. *Cell Stress Chaperones* 2002; **7**: 73-90
- 9 **Nelson EA**, Wong Y, Yu LM, Fok TF, Li K. Effects of hyperthermia and muramyl dipeptide on IL-1beta, IL-6, and mortality in a neonatal rat model. *Pediatr Res* 2002; **52**: 886-891
- 10 **Mearow KM**, Dodge ME, Rahimtula M, Yegappan C. Stress-mediated signaling in PC12 cells-the role of the small heat shock protein, Hsp27, and Akt in protecting cells from heat stress and nerve growth factor withdrawal. *J Neurochem* 2002; **83**: 452-462
- 11 **Henderson RF**, Barr EB, Blackwell WB, Clark CR, Conn CA, Kalra R, March TH, Sopori ML, Tesfaigzi Y, Menache MG, Mash DC. Response of rats to low levels of sarin. *Toxicol Appl Pharmacol* 2002; **184**: 67-76
- 12 **Suganuma T**, Irie K, Fujii E, Yoshioka T, Muraki T. Effect of heat stress on lipopolysaccharide-induced vascular permeability change in mice. *J Pharmacol Exp Ther* 2002; **303**: 656-663
- 13 **Nambiar MP**, Fisher CU, Enyedy EJ, Warke VG, Kumar A, Tsokos GC. Oxidative stress is involved in the heat stress-induced downregulation of TCR zeta chain expression and TCR/CD3-mediated [Ca(2+)](i) response in human T-lymphocytes. *Cell Immunol* 2002; **215**: 151-161
- 14 **Wang Y**, Li C, Wang X, Zhang J, Chang Z. Heat shock response inhibits IL-18 expression through the JNK pathway in murine peritoneal macrophages. *Biochem Biophys Res Commun* 2002; **296**: 742-748
- 15 **DuBose DA**, Balcius J, Morehouse D. Heat stress and/or endotoxin effects on cytokine expression by human whole blood. *Shock* 2002; **17**: 217-221
- 16 **Hildebrandt B**, Wust P, Ahlers O, Dieing A, Sreenivasa G, Kerner T, Felix R, Riess H. The cellular and molecular basis of hyperthermia. *Crit Rev Oncol Hematol* 2002; **43**: 33-56
- 17 **Roigas J**, Wallen ES, Loening SA, Moseley PL. Estramustine phosphate enhances the effects of hyperthermia and induces the small heat shock protein HSP27 in the human prostate carcinoma cell line PC-3. *Urol Res* 2002; **30**: 130-135
- 18 **van den Berg AP**, van den Berg-Blok AE, Kal HB, Reinhold HS. A moderate elevation of blood glucose level increases the effectiveness of thermoradiotherapy in a rat tumor model II. Improved tumor control at clinically achievable temperatures. *Int J Radiat Oncol Biol Phys* 2001; **50**: 793-801
- 19 **Afek A**, Keren G, Harats D, George J. Whole body hyperthermia accelerates atherogenesis in low-density lipoprotein receptor deficient mice. *Exp Mol Pathol* 2001; **71**: 63-72
- 20 **Ben-Hur T**, Cialic R, Itzik A, Barak O, Yirmiya R, Weidenfeld J. A novel permissive role for glucocorticoids in induction of febrile and behavioral signs of experimental herpes simplex virus encephalitis. *Neuroscience* 2001; **108**: 119-127
- 21 **Michael GJ**, Priestley JV. Differential expression of the mRNA for the vanilloid receptor subtype 1 in cells of the adult rat dorsal root and nodose ganglia and its downregulation by axotomy. *J Neurosci* 1999; **19**: 1844-1854
- 22 **Dux M**, Sann H, Schemann M, Jancso G. Changes in fibre populations of the rat hairy skin following selective chemodeneration by capsaicin. *Cell Tissue Res* 1999; **296**: 471-477

Edited by Ma JY and Wang XL Proofread by Xu FM

Effects of selenium on peripheral blood mononuclear cell membrane fluidity, interleukin-2 production and interleukin-2 receptor expression in patients with chronic hepatitis

Shui-Xiang He, Bing Wu, Xin-Ming Chang, Hong-Xia Li, Wen Qiao

Shui-Xiang He, Xin-Ming Chang, Hong-Xia Li, Wen Qiao, Department of Gastroenterology, First Hospital of Xi'an Jiaotong University, Xi'an 710061, Shaanxi Province, China

Bing Wu, Editorial Department of Journal of Xi'an Jiaotong University, Xi'an 710061, Shaanxi Province, China

Correspondence to: Dr. Shui-Xiang He, Department of Gastroenterology, First Hospital of Xi'an Jiaotong University, Xi'an 710061, Shaanxi Province, China. hesx123@163.net

Telephone: +86-29-5324001 **Fax:** +86-29-85221659

Received: 2003-12-19 **Accepted:** 2004-01-12

Abstract

AIM: To study the effect of selenium on peripheral blood mononuclear cell (PBMC) membrane fluidity and immune function in patients with chronic hepatitis.

METHODS: PBMCs were pretreated with selenium (1.156×10^{-7} mol/L) for 6 h *in vitro* or extracted directly from patients after administration of selenium-yeast continuously for 8-12 wk (200 µg/d), and then exposed to Con-A for 48 h. The membrane fluidity, interleukin-2 (IL-2) production and interleukin-2 receptor (IL-2R) expression in PBMCs and malondialdehyde (MDA) concentration in medium and lipid peroxide (LPO) in plasma were determined.

RESULTS: The PBMC membrane fluidity, IL-2 production and IL-2R expression in patients with chronic hepatitis were significantly lower than those in healthy blood donors (particle adhesive degree R, 0.17 ± 0.01 vs 0.14 ± 0.01 , $P < 0.01$; IL-2, 40.26 ± 9.55 vs 72.96 ± 11.36 , $P < 0.01$; IL-2R, 31.05 ± 5.09 vs 60.58 ± 10.56 , $P < 0.01$), and the MDA concentration in medium in patients with chronic hepatitis was significantly higher than that in healthy blood donors (1.44 ± 0.08 vs 0.93 ± 0.08 , $P < 0.01$). Both *in vitro* and *in vivo* administration of selenium could reverse the above parameters.

CONCLUSION: Supplement of selenium can suppress lipid peroxidation, and improve PBMC membrane fluidity and immune function in patients with chronic hepatitis.

He SX, Wu B, Chang XM, Li HX, Qiao W. Effects of selenium on peripheral blood mononuclear cell membrane fluidity, interleukin-2 production and interleukin-2 receptor expression in patients with chronic hepatitis. *World J Gastroenterol* 2004; 10(23): 3531-3533

<http://www.wjgnet.com/1007-9327/10/3531.asp>

INTRODUCTION

Hepatic viruses attack immune cells thus leading to cell immune functional disorders, which is one of the major mechanisms of chronic hepatitis^[1-4]. It is currently believed that the damage of immune cells caused by lack of the minor elements of selenium, proliferation of free particles and peroxidation of lipid are

probably associated with cell immune functional disorders in patients with chronic hepatitis^[5-9]. The use of anti-oxidants could contribute to improving the psychopathologic process of chronic hepatitis, suppress cell immune functional disorders and accelerate the recovery of liver functions^[10-12]. The minor elements of selenium have anti-oxidizing effects, and have been utilized in the immune regulation of many diseases, but the effect of selenium treatment on peripheral blood mononuclear cell (PBMC) functions in patients with chronic hepatitis is still unclear^[13-15]. We found during our early work that using selenium in the periphery could improve the interleukin-2 production of PBMCs and IL-2R expression in patients with chronic hepatitis^[16]. By examining the changes of PBMC membrane fluidity, interleukin-2 (IL-2) and its receptor system in patients with chronic hepatitis before and after using selenium, We further explored the effects and mechanism of selenium treatment on the cell immune functions in patients with chronic hepatitis.

MATERIALS AND METHODS

Patients

A total of 45 patients with chronic hepatitis were inpatients of our hospital from 1995 to 1997, among them 38 were males and 7 females, aged 21-52 years. The HBsAg of 30 patients with chronic hepatitis and 15 patients with cirrhosis was positive. The diagnosis was in accordance with the readjust standards of the National Academic Conference of Viral Hepatitis held in Shanghai in 1990. Besides, ten healthy blood donors were chosen as the control group.

Peripheral experiment

Elbow venous blood was taken from fasting healthy blood donors. Then PBMCs were routinely separated and floated in the RPMI-1640 culture medium. Then cell density was adjusted to 1×10^6 /L and 1 mL of cell suspension was added into each well of 24-well culture plates, and randomly divided into control group, tBHP damage inducing group, and selenium treatment group. In addition, PBMCs were taken and divided into 4 patient control group and 5 patient selenium group. NaSeO₂ (final density, 1.156×10^{-7} mol/L) was added into groups 3 and 5, each of the rest groups was added with the same amount of culture liquid followed by incubation for 6 h, and con A (5 mg/L) were added. Meanwhile, lipoperoxide inducing agents tBHP (20 µmol/L) were added into groups 2 and 3, and cultured at 37 °C for 48 h in a humidified atmosphere containing 50 mL/L CO₂.

Clinical treatment and survey

The patients were divided into two groups. The normal group was given bifendate pills and Fufangyiganling. Some individual patients were given compound ammonium glycyrrhetate injection and Qinkailing injection intravenously. Selenium treatment group, on the basis of the routine treatment, was given selenium yeast or selenium amylase (200-300 µg/d) orally for 8 to 12 wk. At the beginning of and after the treatment, blood was collected from the patients to separate PBMCs and to measure the blood plasma.

Measurement of induced IL-2 production and its activation

Each group of PBMCs was added with con-A (5 mg/L, Sigma) and cultured at 37 °C in a humidified atmosphere containing 50 mL/L CO₂. IL-2 activation expressed in 1×10³ U/L was measured.

Measurement of IL-2R expression

The cells of each group, after induction and production of IL-2, were collected to measure IL-2R expression by indirect immune fluorescence and the positive rate was expressed as percentage of positive cells.

Measurement of lipid peroxidation

The supernatant from each group or patients' blood plasma was subjected to the measurement of MDA or LPO content by using microfluorescence technique.

Measurement of membrane fluidity

The cells of each group were suspended in the RPMI-1640 culture medium to a cell density of 1×10⁶/L. The same amount of 2×10⁻⁶ mol/L fluorescence probing agents DPH (sigma product) was added and cultured at 25 °C for 30 min. The polarization deviation degree (P) was measured under the condition of 432 nm (transmitting light)/362 nm (irritating light) on MPF-4 polarization meter and the particle adhesive degree (R) was calculated. The value of R and membrane fluidity were in inverse proportion.

Statistical analysis

All the data were expressed as mean±SD, and analyzed by *t*-test and ANOVA analysis. *P*<0.05 was considered statistically significant.

RESULTS

Effects of selenium on IL-2 activation and IL-2R expression in human PBMCs

As shown in Table 1, after PBMCs in normal group were treated with tBHP, both IL-2R expression and IL-2 secreting activity were significantly declined, which was similar to those of the patient group. Six hours after addition of selenium, the above-mentioned changes in the cells of these two groups were obviously inhibited.

Table 1 Influence of selenium on IL-2 and IL-2R expression (mean±SD)

Groups	Cases	IL-2 activation (1×10 ³ U/L)	IL-2R expression (%)
Normal control group	10	72.96±11.36	60.58±10.56
+tBHP	10	42.12±12.06 ^b	37.05±8.06 ^b
+Selenium+tBHP	10	53.26±18.15 ^a	52.12±9.68 ^a
Patient control group	22	40.26±9.55 ^b	31.05±5.09 ^b
Patients+selenium	23	60.32±15.24 ^c	54.06±5.22 ^c

^b*P*<0.01 vs normal control group; ^a*P*<0.05 vs tBHP inducing damage group; ^c*P*<0.05 vs patient control group.

Influence of selenium on PBMC membrane fluidity

As shown in Table 2, after PBMCs in normal group were treated with tBHP, the amount of MDA increased and the membrane fluidity obviously lowered. The PBMC membrane fluidity of the patient group was also significantly lower than that of the normal control group. Six hours after addition of selenium, the above-mentioned changes could be obviously inhibited.

Changes in IL-2R expression and IL-2 secreting activity of PBMCs of patients before and after selenium treatment

As shown in Table 3, after treatment with selenium, both the

IL-2R expression and IL-2 secreting activity of PBMCs were significantly increased, while the content of MDA in the culture media was obviously decreased compared with the groups without selenium treatment (*P*<0.05).

Table 2 Influence of selenium on PBMC membrane fluidity (mean±SD)

Groups	Cases	R	MDA (μmol/L)
Normal control group	10	0.14±0.01	0.93±0.08
+tBHP	10	0.19±0.02 ^b	2.32±0.25 ^b
+Selenium+tBHP	10	0.16±0.02 ^a	1.36±0.09 ^a
Patient control group	22	0.17±0.01 ^b	1.44±0.08 ^b
Patients+selenium	23	0.15±0.01 ^c	1.21±0.09 ^c

^b*P*<0.01 vs normal control group; ^a*P*<0.05 vs tBHP inducing damage group; ^c*P*<0.05 vs patient control group.

Table 3 IL-2 and IL-2R expression in PBMCs of patients before and after selenium treatment (mean±SD)

Groups	Cases	IL-2 activation (1×10 ³ U/L)	IL-2R expression (%)
Before treatment			
Normal control group	22	43.22±9.25	31.24±5.20
Selenium treated group	23	42.26±9.55	31.05±5.09
After treatment			
Normal control group	18	49.45±15.25	35.12±6.49
Selenium treated group	17	60.32±13.28 ^a	46.05±4.46 ^b

^b*P*<0.01 vs before treatment.

Changes in PBMC membrane fluidity of patients before and after selenium treatment

As shown in Table 4, the PBMC membrane fluidity recovered remarkably and the content of MDA in blood plasma decreased strikingly, whereas no significant changes were observed in the control group. The result was similar to that *in vitro* experiment.

Table 4 Effect on PBMC membrane fluidity of patients before and after selenium treatment (mean±SD)

Groups	Cases	R	Lipid peroxide (nmol/L)
Before treatment			
Normal control group	22	0.17±0.01	7.36±4.15
Selenium treated group	23	0.17±0.01	7.36±4.08
After treatment			
Normal control group	18	0.16±0.01	6.15±3.85
Selenium treated group	17	0.15±0.01 ^b	5.02±2.50 ^b

^b*P*<0.01 vs before treatment.

DISCUSSION

Previous studies have shown that the activating oxidation or the organic peroxidation of the external chemical system could influence various functions of immune cells^[15,17-19]. Our previous study demonstrated that PBMCs from the patients with chronic hepatitis showed significantly increased production of IL-2 and expression of IL-2R after warmed with selenium for 6 h^[16]. In this experiment, our results showed that human PBMC producing IL-2 activation and IL-2R expression percentage obviously decreased after being induced by tertiary butyl peroxides. The content of lipoperoxide MDA in the culture liquid greatly increased, which was similar to the changes in PBMCs from chronic hepatitis B patients cultured *in vitro*. It was further reported that free particles and lipoperoxide receptor system probably associated with lipoperoxide reaction of

tertiary butyl peroxide could induce PBMC membranes, and thus resulting in changes of the normal structure and nature of PBMC membranes. Besides, some abnormal changes took place in receptors, enzymes and particle passages associated with the membranes, cell energy metabolism, signal transmission, proliferation, differentiation, *etc.*, thereby finally leading to the organic disorder of PBMCs^[20,21].

Fluidity, one of the basic characteristics of the membranes, is the basic precondition of cells showing various functions. In many pathologic cases, excessive free particles and initiating lipoperoxide could affect membrane fluidity and lead to disorder of cell immune functions^[22-25]. Our results showed that PBMC membrane fluidity in normal group obviously decreased after treated with peroxide, and was accompanied by MDA increase in the culture supernatant. Moreover, PBMC membrane fluidity decreased and its IL-2-producing activity as well as IL-2R expression percentage changed unanimously, which was identical with the result of the cultured PBMCs from patients with chronic hepatitis. Abnormally strengthened lipoperoxide reactions could lead to decrease of PBMC membrane fluidity, which might be one of the causes of immune function disorder of patients with chronic hepatitis.

Studies shown that selenium influences immune cell functions through two ways^[13-16,26]. On the one hand, selenium can affect the mRNA expression of some immune cell surface receptors, such as IL-2R, iron transporter protein receptor (TfR). On the other hand, it is associated with the functions of selenium anti-oxidization. Free particles can directly damage lymphocyte membranes and destroy their completeness and fluidity, thus restraining the expressions of their surface markers and immune functions. Selenium and enzymes in combination with selenium can inhibit cell membrane peroxidation damage and defend membrane fluidity as well as functional expression. In our experiment, the degree of membrane fluidity, IL-2 secretion and IL-2R expression of PBMCs caused by selenium still remained high. Meanwhile, the content of MDA in the culture supernatant was greatly decreased, suggesting that selenium might defend human PBMC membrane fluidity and its normal functional expression through lipoperoxidation damage induced by anti-tertiary butyl peroxide.

PBMCs and IL-2 system play an essential role in cell immune system of patients with chronic hepatitis, maintaining PBMC functions and correcting IL-2 system disorder, which is of great significance in treatment of chronic hepatitis^[1-3]. It has been found that internal or external selenium can improve PBMC functions and increase IL-2 secretion and IL-2R expression percentage in patients with chronic hepatitis. It has been initially proved that selenium treatment is helpful to correct dysfunction of PBMCs in patients with chronic hepatitis, which is of great significance in the complete recovery of hepatic functions of patients.

REFERENCES

- 1 Reshetnyak VI, Sharafanova TI, Ilchenko LU, Golovanova EV, Poroshenko GG. Peripheral blood lymphocytes DNA in patients with chronic liver diseases. *World J Gastroenterol* 2001; **7**: 235-237
- 2 Reshetnyak VI, Sharafanova TI, Ilchenko LY, Poroshenko GG. DNA structure in peripheral blood lymphocytes from patients with chronic viral liver damages. *Bull Exp Biol Med* 2002; **133**: 399-400
- 3 Wang JP, Li XH, Zhu Y, Wang AL, Lian JQ, Jia ZS, Xie YM. Detection of serum sIL-2R, IL-6, IL-8, TNF- α and lymphocytes subsets, mL-2R in patients with chronic hepatitis B. *Shijie Huaren Xiaohua Zazhi* 2000; **8**: 763-766
- 4 Tulek N, Saglam SK, Saglam M, Turkyilmaz R, Yildiz M. Soluble interleukin-2 receptor and interleukin-10 levels in patients with chronic hepatitis B infection. *Hepatogastroenterology* 2000; **47**: 828-831
- 5 Yu MW, Horng IS, Hsu KH, Chiang YC, Liaw YF, Chen CJ. Plasma selenium levels and risk of hepatocellular carcinoma among men with chronic hepatitis virus infection. *Am J Epidemiol* 1999; **150**: 367-374
- 6 Loguercio C, De Girolamo V, Federico A, Feng SL, Crafa E, Cataldi V, Gialanella G, Moro R, Del Vecchio Blanco C. Relationship of blood trace elements to liver damage, nutritional status, and oxidative stress in chronic nonalcoholic liver disease. *Biol Trace Elem Res* 2001; **81**: 245-254
- 7 Hatano R, Ebara M, Fukuda H, Yoshikawa M, Sugiura N, Kondo F, Yukawa M, Saisho H. Accumulation of copper in the liver and hepatic injury in chronic hepatitis C. *J Gastroenterol Hepatol* 2000; **15**: 786-791
- 8 Loguercio C, Federico A. Oxidative stress in viral and alcoholic hepatitis. *Free Radic Biol Med* 2003; **341**: 1-10
- 9 Hoek JB, Pastorino JG. Ethanol, oxidative stress, and cytokine-induced liver cell injury. *Alcohol* 2002; **27**: 63-68
- 10 Naghii MR. Sulfur mustard intoxication, oxidative stress, and antioxidants. *Mil Med* 2002; **167**: 573-575
- 11 Marotta F, Safran P, Tajiri H, Princess G, Anzulovic H, Ideo GM, Rouge A, Seal MG, Ideo G. Improvement of hemorheological abnormalities in alcoholics by an oral antioxidant. *Hepatogastroenterology* 2001; **48**: 511-517
- 12 Cui YH, Wang XL, Liu Q, Liu P. Influences of anti-oxidation of salvianolic acid B on proliferation of rat cultured hepatic stellate cells. *Shijie Huaren Xiaohua Zazhi* 2002; **10**: 317-319
- 13 Kiremidjian-Schumacher L, Roy M. Effect of selenium on the immunocompetence of patients with head and neck cancer and on adoptive immunotherapy of early and established lesions. *Biofactors* 2001; **14**: 161-168
- 14 Jahnova E, Horvathova M, Gazdik F, Weisssova S. Effects of selenium supplementation on expression of adhesion molecules in corticoid-dependent asthmatics. *Bratisl Lek Listy* 2002; **103**: 12-16
- 15 Lee CY, Wan JM. Immunoregulatory and antioxidant performance of alpha-tocopherol and selenium on human lymphocytes. *Biol Trace Elem Res* 2002; **86**: 123-136
- 16 He SX, Chang XM, Zhou QS, Li HX, Wu YE. Effects of selenium on the IL-2 production and IL-2R expression of PBMC from patients with chronic active hepatitis B. *Shijie Huaren Xiaohua Zazhi* 1999; **7**: 658
- 17 Lushpaeva IuA, Medvedeva IV, Fadienko GR. Changes in clinical and laboratory findings on oxidation metabolism in lymphocyte membranes of rheumatoid arthritis patients on synchronous programmed intensive therapy. *Klin Med* 2002; **80**: 39-42
- 18 Dey A, Parmar D, Dhawan A, Dash D, Seth PK. Cytochrome P450 2E1 dependent catalytic activity and lipid peroxidation in rat blood lymphocytes. *Life Sci* 2002; **71**: 2509-2519
- 19 Jobin N, Garrel DR, Champoux J, Bernier J. Improved immune functions with administration of a low-fat diet in a burn animal model. *Cell Immunol* 2000; **206**: 71-84
- 20 Maccarrone M, Manca-di-Villahermosa S, Meloni C, Massoud R, Mascali A, Guarina R, Finazzi-Agro A, Taccone-Gallucci M. Arachidonate cascade, apoptosis, and vitamin E in peripheral blood mononuclear cells from hemodialysis patients. *Am J Kidney Dis* 2002; **40**: 600-610
- 21 Azenabor AA, Hoffman-Goetz L. Effect of exhaustive exercise on membrane estradiol concentration, intracellular calcium, and oxidative damage in mouse thymic lymphocytes. *Free Radic Biol Med* 2000; **1**: 84-90
- 22 Gornicki A, Gutsze A. Erythrocyte membrane fluidity changes in psoriasis: an EPR study. *J Dermatol Sci* 2001; **27**: 27-30
- 23 Ferrante MC, Meli R, Mattace Raso G, Esposito E, Severino L, Di Carlo G, Lucisano A. Effect of fumonisin B1 on structure and function of macrophage plasma membrane. *Toxicol Lett* 2002; **129**: 181-187
- 24 Garcia JJ, Reiter RJ, Karbownik M, Calvo JR, Ortiz GG, Tan DX, Martinez-Ballarín E, Acuna-Castroviejo D. N-acetylserotonin suppresses hepatic microsomal membrane rigidity associated with lipid peroxidation. *Eur J Pharmacol* 2001; **428**: 169-175
- 25 Gornicki A, Gutsze A. *In vivo* and *in vitro* influence of etretinate on erythrocyte membrane fluidity. *Eur J Pharmacol* 2001; **423**: 127-134
- 26 Zhao R, Zhang GC, Yu BM, Zheng MH, Li DH, Zhu YM, Hu BY. Effect of selenium on T lymphocyte against colonic cancer cells. *Shijie Huaren Xiaohua Zazhi* 2000; **8**: 80-83

Successful management of a benign anastomotic colonic stricture with self-expanding metallic stents: A case report

Yong-Song Guan, Long Sun, Xiao Li, Xiao-Hua Zheng

Yong-Song Guan, Long Sun, Xiao Li, Xiao-Hua Zheng, Department of Radiology Huaxi Hospital, Sichuan University, Chengdu 610041, Sichuan Province, China

Correspondence to: Dr. Yong-Song Guan, Department of Radiology, Huaxi Hospital, Sichuan University, 37 Guoxuexiang, Chengdu 610041, Sichuan Province, China. yongsongguan@yahoo.com

Telephone: +86-28-85421008 **Fax:** +86-28-85421008

Received: 2004-02-11 **Accepted:** 2004-02-21

Abstract

AIM: To assess the effectiveness of and complications associated with metallic stent placement for treatment of anastomotic colonic strictures.

METHODS: A 46-year-old man undergoing two procedures of surgery for perforation of descending colon due to a traffic accident presented with pain, abdominal distention, and inability to defecate. Single-contrast barium enema radiograph showed a severe stenosis in the region of surgical anastomosis and the patient was too weak to accept another laparotomy. Under fluoroscopic and endoscopic guidance, we placed two metallic stents in the stenosis site of the anastomosis of the patient with anastomotic colonic strictures.

RESULTS: In this case of postsurgical stenosis, the first stent relieved the symptoms of obstruction, but stent migration happened on the next day so an additional stent was required to deal with the stricture and relieve the symptoms.

CONCLUSION: This case confirms that metallic stenting may represent an effective treatment for anastomotic colonic strictures in the absence of other therapeutic alternatives.

Guan YS, Sun L, Li X, Zheng XH. Successful management of a benign anastomotic colonic stricture with self-expanding metallic stents: A case report. *World J Gastroenterol* 2004; 10(23): 3534-3536

<http://www.wjgnet.com/1007-9327/10/3534.asp>

INTRODUCTION

Self-expandable metallic stent treatment for colorectal diseases was falling behind that for other organs. Recently, however, there have been many reports on the use of self-expanding metallic stents in colorectal diseases, mainly from the West. Self-expanding metallic stent is generally used as a palliative treatment for malignant strictures of the colon and rectum and before bridge as a surgery for obstructing colorectal cancers^[1-3]. Some investigators have reported on the usefulness of self-expanding metallic stents for strictures of benign diseases^[4,5]. Management of narrow (<5-mm) colonic anastomotic stricture mainly is performed endoscopically by repeated balloon dilation, often ineffectively^[6]. The use of metallic self-

expanding stents in malignant and benign strictures of the large bowel has been suggested only recently, and is still being debated^[7,8]. In this report we proposed a single-stage procedure that we developed to manage narrow anastomotic colonic strictures.

CASE REPORT

A 46-year-old man undergoing two procedures of surgery for perforation of descending colon due to a traffic accident presented with pain, abdominal distention, and inability to defecate. Single-contrast barium enema radiograph showed a severe stenosis in the region of surgical anastomosis. The patient was too weak to accept another laparotomy. He reached us with a significant stricture of the descending colon anastomoses (smaller than 5 mm in diameter).

With the patient in supine position and two knee joints flexing, a catheter was inserted over a hydrophilic guide-wire through the anus to the lesion targeted under fluoroscopic and endoscopic guidance. An 85-cm 6-F catheter (Cook) and a 180-cm 0.35-inch guide wire (Bard) were used. The guide wire was maneuvered passing the stricture and the catheter was advanced. This guide wire was then replaced with another guide wire (Amplatz super stiff Guide Wire) for stent delivery and insertion. The stent was then positioned precisely across the lesion and released. The symptoms were relieved immediately, but on the next day the patient manifested abdominal distention, and inability to defecate. Anteroposterior radiographs from a follow-up barium study showed the stent migrated and a second stent was needed. The second stent was deployed with the same stent placement techniques. Radiographs obtained after a water-soluble enema on the day after the second stent deployed showed that the stents expanded to provide an adequate lumen (Figures 1-4). The first coated stent (Nanjing MicroTech, China) was 12-cm in length, 32-mm in diameter. The second uncoated stent (Nanjing MicroTech, China) was 20-cm in length, 32-mm in diameter. At the time of this writing, ie, 18 mo of follow-up evaluation, the patient could defecate without any difficulty.

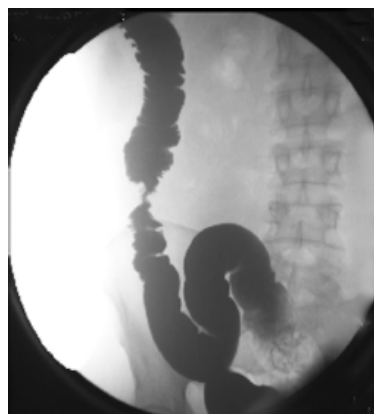


Figure 1 Stenosis at the segment of descending colon, less than 5 mm in diameter.

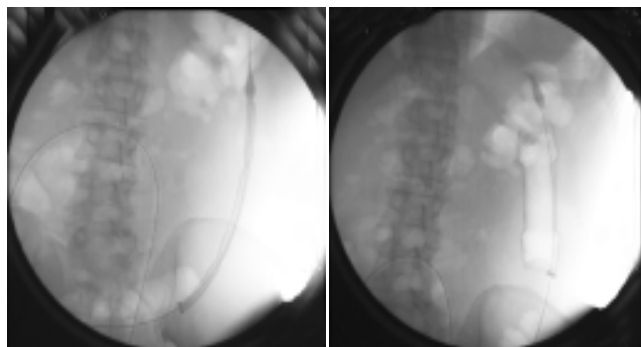


Figure 2 The first stent was appropriately positioned and deployed by withdrawing the enveloping membrane under fluoroscopic control to ensure that the lesion was adequately covered, thus relieving the obstruction.

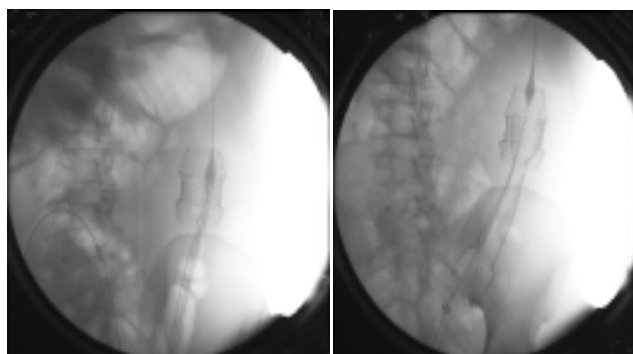


Figure 3 Clinical symptoms of obstruction recurred the next day. Anteroposterior radiographs showed the stent migrated above the lesion and a second stent was needed. Second stent was deployed with the same stent placement techniques through the lumen of the first stent.

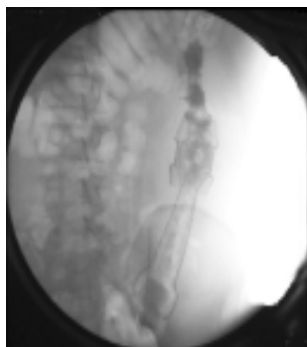


Figure 4 Radiograph obtained after a water-soluble enema on the day after the second stent was deployed shows that the stents expanded to provide an adequate lumen.

DISCUSSION

Benign postoperative anastomotic strictures are frequent^[9]. Several methods of treatment for benign anastomotic strictures after previous resection have been described, including microwave coagulation therapy, balloon and endoscopic bougie dilation, *etc*^[10-14]. Placement of self-expanding metallic stents across narrower anastomotic colonic strictures is a viable alternative to colostomy and, by avoiding emergent surgery, could potentially lower morbidity and mortality^[15-17]. The method of stent placement for treatment of benign colonic disorders is the same as that used in cases of malignant strictures, but few experiences with the placement of metallic stents for benign colonic disorders have been reported in the

literatures. The indications for stenting were failure to establish dilatation therapy and/or refusal of surgical treatment, in high-risk patients^[4-6].

In this case, the patient underwent two times of surgery and he was too weak to accept another surgery. Stenting might represent a therapeutic alternative, in cases of anastomotic strictures of esophageal carcinoma^[18,19]. Endoprotheses may have a more lasting dilating effectiveness than balloons or endoscopic bougies, and the ease of recovering the stent when it has fulfilled its purpose could make treatment of the stenosis last for months or years^[4-6].

Stent migration may be one of the most complications in treatment of anastomotic strictures. The stent tended to migrate once the stenosis was widened to a diameter at which it could no longer hold the prosthesis in place, and this phenomenon was followed by a recurrence of the clinical symptoms a few days later, which necessitated a series of interventions in these patients. The first stent migration happened and the second stent was needed to be placed in this case^[20-22].

We conclude that the application of self-expandable metallic stents in benign stenosis of the gastrointestinal tract may be a possible therapeutic tool in selected patients. Further trials with a greater number of patients dealing with the questions of duration of stay of self-expandable metallic stents and choice of stent type are needed.

REFERENCES

- 1 **Saida Y**, Sumiyama Y, Nagao J. Self-expandable metallic stent in the treatment of colorectal obstruction. *Nippon Geka Gakkai Zasshi* 2003; **104**: 554-557
- 2 **Mainar A**, De Gregorio Ariza MA, Tejero E, Tobio R, Alfonso E, Pinto I, Herrera M, Fernandez JA. Acute colorectal obstruction: treatment with self-expandable metallic stents before scheduled surgery-results of a multicenter study. *Radiology* 1999; **210**: 65-69
- 3 **Miyayama S**, Matsui O, Kifune K, Yamashiro M, Yamamoto T, Kitagawa K, Kasahara Y, Asada Y, Iida Y, Miura S. Malignant colonic obstruction due to extrinsic tumor: palliative treatment with a self-expanding nitinol stent. *Am J Roentgenol* 2000; **175**: 1631-1637
- 4 **Paul L**, Pinto I, Gomez H, Fernandez-Lobato R, Moyano E. Metallic stents in the treatment of benign diseases of the colon: preliminary experience in 10 cases. *Radiology* 2002; **223**: 715-722
- 5 **Dormann AJ**, Deppe H, Wigglinghaus B. Self-expanding metallic stents for continuous dilatation of benign stenoses in gastrointestinal tract-first results of long-term follow-up in interim stent application in pyloric and colonic obstructions. *Z Gastroenterol* 2001; **39**: 957-960
- 6 **Piccini G**, Nacchiero M. Management of narrower anastomotic colonic strictures. Case report and proposal technique. *Surg Endosc* 2001; **15**: 1227
- 7 **Morgan R**, Adam A. Use of metallic stents and balloons in the esophagus and gastrointestinal tract. *J Vasc Interv Radiol* 2001; **12**: 283-297
- 8 **Chevallier P**, Baque P, Benchimol D, Bernard J, Souci J, Chevallier A, Bourgeon A, Padovani B. Treatment of colorectal obstruction with self-expanding metallic stents under fluoroscopic guidance. *J Radiol* 2002; **83**(4 Pt 1): 473-477
- 9 **Schlegel RD**, Dehni N, Parc R, Caplin S, Tiret E. Results of reoperations in colorectal anastomotic strictures. *Dis Colon Rectum* 2001; **44**: 1464-1468
- 10 **Takeuchi K**, Tsuzuki Y, Ando T, Sekihara M, Hara T, Kori T, Nakajima H, Asao T, Kuwano H. Usefulness of flexible colonoscopic microwave coagulation therapy for a colorectal anastomotic stricture. *Dis Colon Rectum* 2003; **46**: 1430-1435
- 11 **Luck A**, Chapuis P, Sinclair G, Hood J. Endoscopic laser stricturotomy and balloon dilatation for benign colorectal strictures. *ANZ J Surg* 2001; **71**: 594-597
- 12 **Chia YW**, Ngoi SS, Tung KH. Use of the optical urethrotome

- knife in the treatment of a benign low rectal anastomotic stricture. *Dis Colon Rectum* 1991; **34**: 717-719
- 13 **Araki Y**, Kishimoto Y, Sato Y, Torigoe S, Kido K, Matono K, Shirouzu K. Transanal dilation using circular stapling for benign rectal stenosis: report of a case. *Kurume Med J* 2002; **49**: 149-151
- 14 **Brandimarte G**, Tursi A, Gasbarrini G. Endoscopic treatment of benign anastomotic colorectal stenosis with electrocautery. *Endoscopy* 2000; **32**: 461-463
- 15 **Wholey MH**, Levine EA, Ferral H, Castaneda-Zuniga W. Initial clinical experience with colonic stent placement. *Am J Surg* 1998; **175**: 194-197
- 16 **Mainar A**, Tejero E, Maynar M, Ferral H, Castaneda-Zuniga W. Colorectal obstruction: treatment with metallic stents. *Radiology* 1996; **198**: 761-764
- 17 **Kang SG**, Jung GS, Cho SG, Kim JG, Oh JH, Song HY, Kim ES. The efficacy of metallic stent placement in the treatment of colorectal obstruction. *Korean J Radiol* 2002; **3**: 79-86
- 18 **Wengrower D**, Fiorini A, Valero J, Waldbaum C, Chopita N, Landoni N, Judchack S, Goldin E. EsophaCoil: long-term results in 81 patients. *Gastrointest Endosc* 1998; **48**: 376-382
- 19 **Song HY**, Park SI, Do YS, Yoon HK, Sung KB, Sohn KH, Min YI. Expandable metallic stent placement in patients with benign esophageal strictures: results of long-term follow-up. *Radiology* 1997; **203**: 131-136
- 20 **Friedland S**, Hallenbeck J, Soetikno RM. Stenting the sigmoid colon in a terminally ill patient with prostate cancer. *J Palliat Med* 2001; **4**: 153-156
- 21 **Harris GJ**, Senagore AJ, Lavery IC, Fazio VW. The management of colorectal obstruction with colonicendolumenal stenting devices. *Am J Surg* 2001; **181**: 499-506
- 22 **Law WL**, Choi HK, Chu KW, Tung HM. Radiation stricture of rectosigmoid treated with self-expanding metallic stent. *Surg Endosc* 2002; **16**: 1106-1107

Edited by Wang XL Proofread by Zhu LH and Xu FM

Cyclooxygenase 2, pS2, inducible nitric oxide synthase and transforming growth factor alpha in gastric adaptation to stress

Shi-Nan Nie, Hai-Chen Sun, Xue-Hao Wu, Xiao-Ming Qian

Shi-Nan Nie, Hai-Chen Sun, Xue-Hao Wu, Xiao-Ming Qian, Emergency Department, Nanjing General Hospital of Nanjing PLA Command Area/Clinical School of Medical college of Nanjing University, Nanjing 210002, Jiangsu Province, China

Correspondence to: Shi-Nan Nie, M.D., Emergency Department, Nanjing General Hospital of Nanjing PLA Command Area, 305 Eastern Zhongshan Road, Nanjing 210002, Jiangsu Province, China. shnnie630504@sohu.com

Telephone: +86-25-80860143

Received: 2004-03-06 **Accepted:** 2004-04-16

Abstract

AIM: To determine the role of mucosal gene expression of cyclooxygenase 2 (COX-2), pS₂ (belongs to trefoil peptides), inducible nitric oxide synthase (iNOS) and transforming growth factor alpha (TGF α) in gastric adaptation to water immersion and restraint stress (WRS) in rats.

METHODS: Wistar rats were exposed to single or repeated WRS for 4 h every other day for up to 6 d. Gastric mucosal blood flow (GMBF) was measured by laser Doppler flowmeter-3. The extent of gastric mucosal lesions were evaluated grossly and histologically and expressions of COX-2, pS₂, iNOS and TGF α were determined by reverse transcriptase polymerase chain reaction (RT-PCR) and Western blot.

RESULTS: The damage to the surface of gastric epithelium with focal areas of deep haemorrhagic necrosis was induced by repeated WRS. The adaptive cytoprotection against stress was developed with activation of cell proliferation in the neck regions of gastric glands. The ulcer index (UI) in groups II, III and IV was markedly reduced as compared with group I (I: 47.23 \pm 1.20; IV: 10.39 \pm 1.18, P <0.01). GMBF significantly decreased after first exposure to WRS with an adaptive increasement of GMBF in experimental groups after repetitive challenges with WRS. After the 4th WRS, the value of GMBF almost restored to normal level (I: 321.87 \pm 8.85; IV: 455.95 \pm 11.81, P <0.01). First WRS significantly decreased the expression of pS₂ and significantly increased the expressions of COX-2, iNOS and TGF α . After repeated WRS, pS₂ and TGF α expressions gradually increased (pS₂: I: 0.37 \pm 0.02; IV: 0.77 \pm 0.01; TGF α : I: 0.86 \pm 0.01; IV: 0.93 \pm 0.03, P <0.05) with a decrease in the expressions of COX-2 and iNOS (COX-2: I: 0.45 \pm 0.02; IV: 0.22 \pm 0.01; iNOS: I: 0.93 \pm 0.01; IV: 0.56 \pm 0.01, P <0.01). Expressions of pS₂, COX-2, iNOS and TGF α showed regular changes with a good relationship among them.

CONCLUSION: Gastric adaptation to WRS injury involves enhanced cell proliferation, increased expression of pS₂ and TGF α , and reduced expression of COX-2 and iNOS. These changes play an important role in adaptation of gastric mucosa after repeated WRS.

Nie SN, Sun HC, Wu XH, Qian XM. Cyclooxygenase 2, pS₂, inducible nitric oxide synthase and transforming growth factor

alpha in gastric adaptation to stress. *World J Gastroenterol* 2004; 10(23): 3537-3541

<http://www.wjgnet.com/1007-9327/10/3537.asp>

INTRODUCTION

Gastric mucosa can enhance resistance to injury after exposure to repeated insults of noxious agents, such as aspirin, alcohol, stress or *H. pylori*-related gastrotoxins. This phenomenon is called gastric adaptation^[1]. It has been postulated that gastric adaptation involves enhancement of gastric blood flow and increased mucosal cell proliferation mediated by some growth factors, such as epidermal growth factor (EGF) or TGF α . The fact that the adaptation to stress is associated with increased cell proliferation let us to hypothesize that this process might be mediated by pS₂, COX-2, iNOS and TGF α .

It is now well established that trefoil peptides have cytoprotective functions in protecting the gastrointestinal tract against ongoing damage from agents as diverse as ethanol, non-steroidal anti-inflammatory drugs and restraint stress^[2]. The mechanism for this action is unclear. The pronounced and protracted increase in trefoil peptide expression in the inflamed and ulcerated stomach, intestine and colon implicates peptides in reparative processes of the injury gut. Studies reported that pS₂ took part in the protracted phase of glandular renewal (marked by proliferation, differentiation and migration)^[3]. TGF α , a 50 amino acid polypeptide produced in normal gastric mucosa, promotes cell proliferation, inhibits gastric acid secretion and exhibits gastroprotective activity against acute damage induced by topical irritants or stress^[4]. In addition, an increased TGF α mRNA expression has been detected during healing of chronic experimental ulcers and acute damage of gastric mucosa in rats, suggesting its important role in gastric mucosal repair. Previous studies showed that COX-2 was an inducible enzyme. Recently, studies have suggested that COX-2 is a constitutive enzyme expressed in gastrointestinal tract also, even plays a more important role than COX-1 for mucosal integrity^[5]. Gut epithelial COX-2 is rapidly induced by inflammatory stimuli, interleukin and TGF α . Suppression of COX-2 could result in exacerbation of inflammation-associated colonic injury, and impair the healing of gastric ulcer. It is generally accepted that nitric oxide (NO) plays an important role in gastric ulcer healing. NO production is highly increased by iNOS.

The aim of the present study was to determine the role of the expression of pS₂, COX-2, iNOS and TGF α , and the relationship among them in gastric adaptation to WRS in rats.

MATERIALS AND METHODS

Induction of gastric adaptation to WRS

Thirty male Wistar rats, weighing 210-250 g and fasted for 24 h with free access to water, were used. The animals were deprived of water 1 h before the experiment and divided into: normal control group ($n = 6$) and experimental control group ($n = 24$). After fasted for 24 h, the rats of normal control group were lightly anesthetized with ether and tied up on the rat board, the abdomen was opened, the stomach was exposed and GMBF

was measured in the oxyntic gland area, and then gastric mucosa was sampled. The rats of experimental control group were divided into four subgroups ($n = 6$ in each group) and exposed to repeated WRS^[3]. The rats of group I were lightly anesthetized with ether, tied up on the rat board and exposed to WRS for 4 h by placing in the water at 20-23 °C to the rat's xyphoid level at 10:00 am on the 1st d. Then the rats were anesthetized with pentobarbital (30 mg/kg ip), GMBF was measured and gastric mucosa was sampled. The rats of group II were treated similarly except that after WRS they were removed from the water, placed at room temperature, and refed with food and water until 10:00 am on the next day, at which time they were starved again for 24 h, and WRS was repeated. The rats of groups III and IV were exposed to the 3rd or 4th WRS as described above.

Measurement of GMBF

GMBF was measured by using laser Doppler flowmetry (LDF-3 flowmeter, Nankai University, Tianjin, China). In brief, the rats were anesthetized with pentobarbital (30 mg/kg ip), the abdomen was opened, the stomach was exposed and transected, and the gastric contents were gently evacuated to the exterior through the cut made in the stomach. Then, an optical probe was placed gently 0.5 mm above and perpendicular to the mucosal surface in the oxyntic gland area to monitor GMBF displayed in mV (value of Doppler signal voltage) on the digital panel of the flowmeter. After GMBF was stable, four points were selected for measurement (one point for 1 min) and the average value was calculated and expressed as U/mV .

Appreciation of UI

Mucosal lesions were evaluated by the score systems reported by Nie *et al.*^[3]. Briefly, after the measurement of GMBF, the stomach was dissected out and opened along the greater curvature, then examined with a 10× magnifier for the presence of erosions and scored as follows: 1 point for small round hemorrhagic erosions; 2 points when the length of hemorrhagic erosions was less than 1 mm; 3 points when the length was 1-2 mm; 4 points when the length was 2-3 mm; 5 points when the length was longer than 4 mm; and the score value multiplied 2 when the width of erosions was larger than 1 mm.

Detection of mRNA in pS2, COX-2, iNOS and TGF α by RT-PCR

The stomachs were removed from rats with intact gastric mucosa and from those exposed to a single stress or repeated stresses. Mucosal specimens (about 100 mg) were scraped off using a slide glass and immediately snap frozen in liquid nitrogen and stored at -80 °C until analysis. Total RNA was isolated from mucosal samples using a guanidium isothiocyanate/phenol chloroform single step extraction kit from Stratagene (Gibco BRL, USA). Following precipitation, the RNA was resuspended in RNase-free buffer and the concentration was estimated by absorbance at 260 nm wavelength. Furthermore, the quality of each RNA sample was determined by running the agarose formaldehyde electrophoresis. RNA samples were stored at -80 °C until analysis.

Single-stranded complementary DNA (cDNA) was generated from 5 μ g of total cellular RNA using StrataScript™ reverse transcriptase (Gibco BRL, USA) and oligo (dT) primers (Gibco BRL, USA). Briefly, 5 μ g of total RNA was used as the template to synthesize complementary DNA with 2.5 units of Maloney murine leukemia virus reverse transcriptase in 5 μ L of buffer containing 10 mmol/L Tris-HCl (pH 8.3), 50 mmol/L KCl, 5 mmol/L MgCl₂, 1 mmol/L of each deoxyribonucleoside triphosphate, 2.5 mmol/L of oligo (dt) primers and 1.4 U/ μ L RNase blocker. Reverse-transcription was performed at room temperature for 20 min, then at 37 °C for 15 min, at 90 °C for 5 min and at

5 °C for min. The resulting cDNA was used as a template for subsequent PCR.

A 124-base pair (bp) fragment of pS2 was amplified from single-stranded DNA by PCR using two oligonucleotide primers to pS2 sequence: sense primer, 5'-CCATGGAGCACAAGGTGA CCTG-3' and antisense primer, 5'-GGGAAGCCACAATTTAT TCT-3'. A 230-base pair (bp) fragment of COX-2 was amplified from single-stranded DNA by PCR using two oligonucleotide primers to COX-2 sequence: sense primer, 5'-GCCACCTCTGCG ATGCTCTT-3' and antisense primer, 5'-GTGTTTGGGGTGGGC TTCAG-3'. A 576-base pair (bp) fragment of iNOS was amplified from single-stranded DNA by PCR using two oligonucleotide primers to iNOS sequence: sense primer, 5'-GTGTTCCACCAGG AGATGTTG-3' and antisense primer, 5'-CTCCTGCCACTGA GTTCGTC-3'. A 246-base pair (bp) fragment of TGF α was amplified from single-stranded DNA by PCR using two oligonucleotide primers to TGF α sequence: sense primer, 5'-TCTGGGTACGTGGGTGTTTCG-3' and antisense primer, 5'-AGAGTGGCAGCAGGCAGTCC-3'. Concomitantly, amplification of the 521 bp fragment of rat β -actin was performed on the same RNA samples to assess RNA integrity using two oligonucleotide primers to β -actin sequence: sense primer, 5'-TGGGACGATATGGAGAAGAT-3' and antisense primer, 5'-ATTGCCGATAGTGATGACCT-3'. The nucleotide sequences of the primers for pS2, COX-2, iNOS and TGF α were based on the published cDNA sequences encoding pS2, COX-2, iNOS and TGF α ^[3,6,7]. The primers were synthesized by Bo-Ya Biotechnical Co. Ltd, Shanghai, China.

Reaction mixture for PCR contained cDNA template (2 μ L), 50 pmol of each primer, and 2.5 U of *Termus aquaticus* DNA (Promega) in 10 mmol/L Tris-HCl (pH 8.8), 50 mmol/L KCl, 1.5 mmol/L MgCl₂, 0.5 mmol/L dNTPs in a volume of 50 μ L. RT blanks (no RNA included) were incubated in each analysis. The mixture was overlaid with 25 μ L of mineral oil to prevent evaporation. Amplification was performed using a DNA thermal cycler for 35 cycles, each cycle consisting of denaturation for 2 min at 94 °C, annealing for 45 s at 55 °C (pS2), 52 °C (COX-2, iNOS) and 60 °C (TGF α), and extension for 1 min at 72 °C. The final cycle included an extension for 5 min at 72 °C to ensure a full extension of the product. The number of amplification cycles was previously determined to keep amplification in the linear to avoid the "plateau effect" associated with increased number of PCR cycles. Eight microliters of each PCR product was electrophoresed on 16 g/L agarose gel stained with ethidium bromide, and then visualized under *uv* light. Location of predicted PCR products was confirmed by using DNA digest phix 174/Hae III as a stained size marker. The gel was then photographed under *uv* transillumination. In addition to size analysis by agarose gel electrophoresis, specificity of the primer pairs for pS2, COX-2, iNOS and TGF α was assessed by sequencing PCR products. For quantification, we determined the intensity of PCR products on the negative film of gel photographs according to Morrissey *et al.*^[6]. Expression of the products was quantified using a video image analysis system (Tanon GIS-1000, Tanon Technical Co, Ltd, Shanghai, China). An index of mRNA expression was determined in each sample according to Konturek *et al.*^[8].

Western blot analysis of pS2, COX-2, iNOS and TGF α proteins

Gastric tissues for the analysis of protein expressions of pS2, COX-2, iNOS and TGF α were homogenized in a proteinase inhibitor buffer containing 50 mmol/L Tris HCl (pH 7.5), 150 mmol/L NaCl, 5 g/L β -cholate sodium, 1 g/L SDS, 2 mmol/L EDTA, 10 mL/L Triton X-100, 100 g/L glycerol, 1 mmol/L PMSF and aprotinin, and then centrifuged at 10 000 g for 15 min at 4 °C. The supernatant was collected and the protein content was determined with the dye-binding (Bio-Rad) method. Thirty micrograms of total protein was loaded onto SDS-polyacrylamide

gel and blotted onto hybrid C membranes (Amersham Life Science, Little Chalfont, Buckinghamshire, England) by electrophoresis. Pre-stained rainbow recombinant protein molecular mass markers (Amersham International plc, Little Chalfont, Buckinghamshire, England) were used for molecular mass determinations. Membranes were blocked with blocking buffer containing 50 g/L fat free milk powder, 10 mmol/L Tris-HCl (pH 7.5), 100 mmol/L NaCl and 1 mL/L Tween 20 for 1 h at room temperature. The blots were incubated overnight at 4 °C with 1:1 000 dilution of polyclonal antibodies against pS2 and TGF α (Stress-Gen, Victoria, Canada), monoclonal antibody against iNOS (Transduction Lab, Lexington, Kentucky, USA), polyclonal antibody against COX-2 (Santa Cruz Biotechnology INC, Santa Cruz, California, USA). After washed in washing buffer for 30 min, the membranes were treated with HRP conjugated secondary antibody (1:4 000 dilution) (Bio-Rad) for 1 h at room temperature, followed by another 30 min of washing. The ECL Western blotting system (Amersham Life Sciences) was used in accordance with the manufacturer's instructions for chemiluminescence of proteins, and the blots were then exposed to photographic films.

Statistical analysis

Results were expressed as mean \pm SD. Statistical comparisons were made by Student's *t* test. Linear correlation analysis was used to analyse the relationship between two variants. *P* values less than 0.05 were considered statistically significant.

RESULTS

Damage to the surface of gastric epithelium with focal areas of deep haemorrhagic necrosis was induced by repeated WRS. The adaptative cytoprotection against stress was developed

with activation of cell proliferation in the neck regions of gastric glands. The UI in groups II, III and IV was markedly reduced as compared with group I (I: 47.23 \pm 1.20; IV: 10.39 \pm 1.18, *P*<0.01). GMBF significantly decreased after the first exposure to WRS with a adaptive increasement of GMBF in experimental groups after repetitive challenges with WRS. After the 4th WRS, the value of GMBF almost restored to normal level (I: 321.87 \pm 8.85; IV: 455.95 \pm 11.81, *P*<0.01). The first WRS significantly decreased the expression of pS2 and significantly increased the expression of COX-2, iNOS and TGF α . After repeated WRS, pS2 and TGF α expressions gradually increased (pS2: I: 0.37 \pm 0.02; IV: 0.77 \pm 0.01; TGF α : I: 0.86 \pm 0.01; IV: 0.93 \pm 0.03, *P*<0.05) with a decrease in the expression of COX-2 and iNOS (COX-2: I: 0.45 \pm 0.02; IV: 0.22 \pm 0.01; iNOS: I: 0.93 \pm 0.01; IV: 0.56 \pm 0.01, *P*<0.01). The expressions of pS2, COX-2, iNOS and TGF α showed regular changes with a good relationship among them (decrease of COX-2 and iNOS was accompanied by an increased expression of pS2 and TGF α after 4 consecutive WRS). (Figure 1, Table 1).

DISCUSSION

The cytoprotective functions of pS2, COX-2, iNOS and TGF α in the gastrointestinal tract against ongoing damage may be accomplished in several ways, and there evidence is that these factors participate in both the early phase of epithelial repair known as restitution (marked by increased cell migration but no proliferation), and in the subsequent protracted phase of glandular renewal (marked by proliferation, differentiation and migration)^[9-11].

In this study, when WRS was applied once, it produced numerous gastric mucosal erosions, the adaptative cytoprotection against stress was developed after repeated stresses, and mucosal lesions were reduced markedly after the 2nd, 3rd and

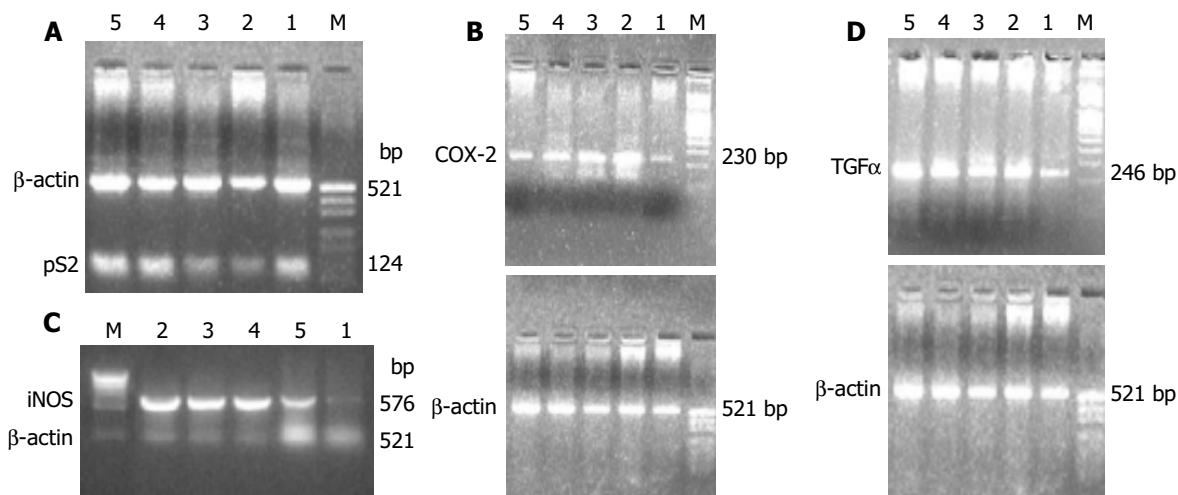


Figure 1 Expression of pS2 mRNA and β -actin (A), COX-2 mRNA and β -actin (B), iNOS mRNA and β -actin (C), TGF α mRNA and β -actin (D) in gastric mucosa of rats after repeated exposure to WRS and in control intact rats. Lane M: PCR size marker; Lane 1: control group; Lane 2-5: groups I-IV.

Table 1 Changes of gene expression of pS2, COX-2, iNOS, TGF α and GMBF, UI in gastric mucosa after repeated exposure to WRS

Group	GMBF (U/mV)	UI	iNOS	pS2	TGF α	COX-2
Control	484.01 \pm 10.97	0.00	0.16 \pm 0.01	0.63 \pm 0.01	0.26 \pm 0.01	0.10 \pm 0.01
Experimental						
I	321.87 \pm 8.85 ^b	47.23 \pm 1.20	0.93 \pm 0.01 ^b	0.37 \pm 0.02 ^b	0.86 \pm 0.01 ^a	0.45 \pm 0.02 ^b
II	418.35 \pm 7.94 ^{bd}	30.54 \pm 1.12 ^d	0.78 \pm 0.01 ^{bd}	0.42 \pm 0.01 ^{bd}	0.87 \pm 0.02 ^{ad}	0.38 \pm 0.02 ^{bd}
III	446.09 \pm 10.98 ^{bd}	20.75 \pm 1.54 ^d	0.67 \pm 0.02 ^{bd}	0.72 \pm 0.02 ^{bd}	0.88 \pm 0.01 ^{ad}	0.29 \pm 0.01 ^{bd}
IV	455.95 \pm 11.81 ^{bd}	10.39 \pm 1.18 ^d	0.56 \pm 0.01 ^{bd}	0.77 \pm 0.01 ^{bd}	0.93 \pm 0.03 ^{bc}	0.22 \pm 0.01 ^{bd}

^a*P*<0.05, ^b*P*<0.01 vs experimental control group; ^c*P*<0.05, ^d*P*<0.01 vs group I.

4th WRS. The expressions of COX-2, iNOS and TGF α were all up-regulated, but that of pS2 was down-regulated after the first stress in rats with WRS-induced ulcers. But the major finding of this study was the gastric adaptation to WRS involving a gradually decrease of overexpression of COX-2 and iNOS, and a gradually increase of expression of pS2 and TGF α , and an increased rate of cell proliferation in the gastric mucosa.

Members of the trefoil peptide family, including pS2, share a common structural feature, which is a motif of six cysteine residues termed a trefoil or a P domain. There is increasing evidence that trefoil peptides are important in maintaining the integrity of gastric mucosae and involved in the repair of ulcerated areas in the gastrointestinal tract^[12-16]. This is supported by an observation that an increased expression of trefoil peptides was found in the ulcer-associated cell lineage (UACL), which is a glandular structure adjacent to the ulcerated mucosa^[17], and by the findings from *in vitro* studies showing that trefoil peptides exhibited a mitogenic effect on different cell lines^[18,19]. It has also been reported that the trefoil peptide family could contribute to gastric mucosal defence and repair by affecting cell proliferation^[1,20].

It has been found that NO produced from inflammatory cells by the inducible isoforms of NOS has antimicrobial, antitumor and cytotoxic effects, but an excessive amount may lead to peroxynitrite formation, protein tyrosine nitration, hydroxyl radical production and tissue damage^[21]. The present study also demonstrated that overexpression of iNOS on d 1 after the first stress was accompanied with the enlargement of ulcer crater. The expression of iNOS protein was declined when the ulcer began to heal. High expression and enzymatic activity of COX at the late ulcer healing stage were observed in stress. The changes of COX activity might be mainly due to the changes of protein level and activity of COX-2. Since tissue remodeling including reepithelization of gastric mucosa, maturation of granulation tissue, and reconstruction of extracellular matrix mainly occurs at the late ulcer healing stage, COX-2 plays an essential role in these remodeling processes^[5,22-31].

There may be interactions among pS2, COX-2, iNOS and TGF α . In the present study, after the 4th WRS, GMBF almost restored to normal level, and during the process of tolerant cytoprotection, GMBF, UI and expressions of pS2, COX-2, iNOS and TGF α showed regular changes and a good relationship among them. A dramatic decrease of COX-2 and iNOS was accompanied with an increase expression of pS2 and TGF α after the 4th stress. This inverse relationship between COX-2, iNOS and pS2, TGF α expressions support the existence of a close interaction among these factors.

Trefoil peptides are a new class of regulatory peptides involving mucosal protection and repair in the gastrointestinal tract. NO and epithelium-associated mucin have important roles in sustaining mucosal integrity in the gastrointestinal tract, and trefoil peptide modulate epithelial NO production via the iNOS pathway^[32-35].

Treatment with COX-2 inhibitors and COX-2 antisense oligonucleotides could suppress these responses induced by TGF α , suggesting the involvement of COX-2 in proliferation of gastric mucosal epithelium, and the synergistic stimulation of COX-2 expression by TGF α . Gut epithelial COX-2 could be rapidly induced by inflammatory stimuli, interleukin and TGF α ^[4,36-40].

We confirmed that WRS-adapted mucosae exhibited an augment action of GMBF, but it is not clear whether COX-2, iNOS and pS2 could directly or indirectly account for the mucosal adaptation, or what is the mechanism of this mucosal hyperemia in the stomach. TGF α has been shown to increase GMBF^[41], while trefoil peptides could promote synthesis of TGF α ^[42-48]. Hence, we believe that hyperaemia observed during the development of adaptation might be mediated by the release of COX-2, iNOS and pS2.

In summary, different expressions of pS2, COX-2, iNOS and TGF α occur during gastric ulceration and healing. COX-2 and iNOS may contribute to tissue inflammation during ulcer formation, while pS2 and TGF α may promote ulcer healing by proliferation, since their expressions are correlated with the protracted phase of glandular renewal of ulcer tissues.

REFERENCES

- 1 **Konturek PC.** Physiological, immunohistochemical and molecular aspects of gastric adaptation to stress, aspirin and to *H pylori*-derived gastrotoxins. *J Physiol Pharmacol* 1997; **48**: 3-42
- 2 **Nie S, Li Z, Zhan X, Tu Z, Xu G, Gong Y, Man X.** Role of the pS2 (2) in gastric mucosa adaptative cytoprotection from stress. *Zhonghua Yixue Zazhi* 2002; **82**: 172-175
- 3 **Nie SN, Qian XM, Wu XH, Yang SY, Tang WJ, Xu BH, Huang F, Lin X, Sun DY, Sun HC, Li ZS.** Role of TFF in healing of stress-induced gastric lesions. *World J Gastroenterol* 2003; **9**: 1772-1776
- 4 **Konturek SJ, Brzozowski T, Majka J, Dembinski A, Slomiany A, Slomiany BL.** Transforming growth factor alpha and epidermal growth factor in protection and healing of gastric mucosal injury. *Scand J Gastroenterol* 1992; **27**: 649-655
- 5 **Franco L, Talamini G, Carra G, Doria D.** Expression of COX-1, COX-2, and inducible nitric oxide synthase protein in human gastric antrum with *Helicobacter pylori* infection. *Prostaglandins Other Lipid Mediat* 1999; **58**: 9-17
- 6 **Morrissey JJ, McCracken R, Kaneto H, Vehaskari M, Montani D, Klahr S.** Location of an inducible nitric oxide synthase mRNA in the normal kidney. *Kidney Int* 1994; **45**: 998-1005
- 7 **Brzozowski T, Konturek PC, Konturek SJ, Stachura J.** Gastric adaptation to aspirin and stress enhances gastric mucosal resistance against the damage by strong irritants. *Scand J Gastroenterol* 1996; **31**: 118-125
- 8 **Konturek PC, Brzozowski T, Pierzchalski P, Kwiecien S, Pajdo R, Hahn EG, Konturek SJ.** Activation of genes for spasmolytic peptide, transforming growth factor alpha and for cyclooxygenase (COX)-1 and COX-2 during gastric adaptation to aspirin damage in rats. *Aliment Pharmacol Ther* 1998; **12**: 767-777
- 9 **Podolsky DK.** Mucosal immunity and inflammation. V. Innate mechanisms of mucosal defense and repair: the best of defense is a good defense. *Am J Physiol* 1999; **277**(3 Pt 1): G495-499
- 10 **Wright NA.** Aspects of the biology of regeneration and repair in the human gastrointestinal tract. *Philos Trans R Soc Lond B Biol Sci* 1998; **353**: 925-933
- 11 **Podolsky DK.** Healing the epithelium: solving the problem from two sides. *J Gastroenterol* 1997; **32**: 122-126
- 12 **Farrell JJ, Taupin D, Koh TJ, Chen D, Zhao CM, Podolsky DK, Wang TC.** TFF2/SP-deficient mice show decreased gastric proliferation, increased acid secretion, and increased susceptibility to NSAID injury. *J Clin Invest* 2002; **109**: 193-204
- 13 **Ulaganathan M, Familari M, Yeomans ND, Giraud AS, Cook GA.** Spatio-temporal expression of trefoil peptide following severe gastric ulceration in the rat implicates it in late-stage repair processes. *J Gastroenterol Hepatol* 2001; **16**: 506-512
- 14 **Longman RJ, Douthwaite J, Sylvester PA, Poulosom R, Corfield AP, Thomas MG, Wright NA.** Coordinated localisation of mucins and trefoil peptides in the ulcer associated cell lineage and the gastrointestinal mucosa. *Gut* 2000; **47**: 792-800
- 15 **McKenzie C, Thim L, Parsons ME.** Topical and intravenous administration of trefoil factors protect the gastric mucosa from ethanol-induced injury in the rat. *Aliment Pharmacol Ther* 2000; **14**: 1033-1040
- 16 **Cook GA, Thim L, Yeomans ND, Giraud AS.** Oral human spasmolytic polypeptide protects against aspirin-induced gastric injury in rats. *J Gastroenterol Hepatol* 1998; **13**: 363-370
- 17 **Alison MR, Chinery R, Poulosom R, Ashwood P, Longcroft JM, Wright NA.** Experimental ulceration leads to sequential expression of spasmolytic polypeptide, intestinal trefoil factor, epidermal growth factor and transforming growth factor alpha mRNAs in rat stomach. *J Pathol* 1995; **175**: 405-414
- 18 **Chinery R, Coffey RJ.** Trefoil peptides: less clandestine in the intestine. *Science* 1996; **274**: 204

- 19 **Mashimo H**, Wu DC, Podolsky DK, Fishman MC. Impaired defense of intestinal mucosa in mice lacking intestinal trefoil factor. *Science* 1996; **274**: 262-265
- 20 **Modlin IM**, Poulson R. Trefoil peptides: mitogens, motogens, or mirages? *J Clin Gastroenterol* 1997; **25**(Suppl 1): S94-100
- 21 **Fischer H**, Huber V, Boknik P, Luess H, Neumann J, Schmitz W, Domschke W, Konturek JW. Effect of *Helicobacter pylori* eradication on cyclooxygenase 2 (COX-2) and inducible nitric oxide synthase (iNOS) expression during gastric adaptation to aspirin (ASA) in humans. *Microsc Res Tech* 2001; **53**: 336-342
- 22 **Brzozowski T**, Konturek PC, Moran AP, Kwiecien S, Pajdo R, Konturek SJ, Drozdowicz D, Ptak A, Pawlik W, Hahn EG. Enhanced resistance of gastric mucosa to damaging agents in the rat stomach adapted to *Helicobacter pylori* lipopolysaccharide. *Digestion* 2003; **67**: 195-208
- 23 **Helmer KS**, Cui Y, Chang L, Dewan A, Mercer DW. Effects of ketamine/xylazine on expression of tumor necrosis factor- α , inducible nitric oxide synthase, and cyclo-oxygenase-2 in rat gastric mucosa during endotoxemia. *Shock* 2003; **20**: 63-69
- 24 **Slomiany BL**, Slomiany A. Platelet-activating factor modulates gastric mucosal inflammatory responses to *Helicobacter pylori* lipopolysaccharide. *Biochem Biophys Res Commun* 2003; **306**: 261-266
- 25 **Slomiany BL**, Slomiany A. Suppression of gastric mucosal inflammatory responses to *Helicobacter pylori* lipopolysaccharide by peroxisome proliferator-activated receptor gamma activation. *IUBMB Life* 2002; **53**: 303-308
- 26 **Yang R**, Gallo DJ, Baust JJ, Watkins SK, Delude RL, Fink MP. Effect of hemorrhagic shock on gut barrier function and expression of stress-related genes in normal and gnotobiotic mice. *Am J Physiol Regul Integr Comp Physiol* 2002; **283**: R1263-1274
- 27 **van der Woude CJ**, Jansen PL, Tiebosch AT, Beuving A, Homan M, Kleibeuker JH, Moshage H. Expression of apoptosis-related proteins in Barrett's metaplasia-dysplasia-carcinoma sequence: a switch to a more resistant phenotype. *Hum Pathol* 2002; **33**: 686-692
- 28 **Shen X**. Effects of cyclooxygenase-2 on formation and healing of acetic acid-induced gastric ulcer in rats. *Zhonghua Yixue Zazhi* 2001; **81**: 1380-1383
- 29 **Yamamoto H**, Tanaka A, Kunikata T, Hirata T, Kato S, Takeuchi K. Inducible types of cyclooxygenase and nitric oxide synthase in adaptive cytoprotection in rat stomachs. *J Physiol Paris* 1999; **93**: 405-412
- 30 **Fu S**, Ramanujam KS, Wong A, Fantry GT, Drachenberg CB, James SP, Meltzer SJ, Wilson KT. Increased expression and cellular localization of inducible nitric oxide synthase and cyclooxygenase 2 in *Helicobacter pylori* gastritis. *Gastroenterology* 1999; **116**: 1319-1329
- 31 **Ferraz JG**, Sharkey KA, Reuter BK, Asfaha S, Tigley AW, Brown ML, McKnight W, Wallace JL. Induction of cyclooxygenase 1 and 2 in the rat stomach during endotoxemia: role in resistance to damage. *Gastroenterology* 1997; **113**: 195-204
- 32 **Zhang BH**, Yu HG, Sheng ZX, Luo HS, Yu JP. The therapeutic effect of recombinant human trefoil factor 3 on hypoxia-induced necrotizing enterocolitis in immature rat. *Regul Pept* 2003; **116**: 53-60
- 33 **Tan XD**, Liu QP, Hsueh W, Chen YH, Chang H, Gonzalez-Crussi F. Intestinal trefoil factor binds to intestinal epithelial cells and induces nitric oxide production: priming and enhancing effects of mucin. *Biochem J* 1999; **338**(Pt 3): 745-751
- 34 **Wolfe MM**. Future trends in the development of safer nonsteroidal anti-inflammatory drugs. *Am J Med* 1998; **105**: 444S-452S
- 35 **Modlin IM**, Hunt RH. Critical reappraisal of mucosal repair mechanisms. *Scand J Gastroenterol Suppl* 1995; **210**: 28-31
- 36 **Konturek PC**, Brzozowski T, Kwiecien S, Drozdowicz D, Harsch IA, Meixner H, Stachura J, Hahn EG, Konturek SJ. Effect of *Helicobacter pylori* on delay in ulcer healing induced by aspirin in rats. *Eur J Pharmacol* 2002; **451**: 191-202
- 37 **Akiba S**, Hatazawa R, Ono K, Kitatani K, Hayama M, Sato T. Secretory phospholipase A2 mediates cooperative prostaglandin generation by growth factor and cytokine independently of preceding cytosolic phospholipase A2 expression in rat gastric epithelial cells. *J Biol Chem* 2001; **276**: 21854-21862
- 38 **Sawaoka H**, Tsuji S, Tsujii M, Gunawan ES, Kawai N, Sasaki Y, Hori M, Kawano S. Involvement of cyclooxygenase-2 in proliferation and morphogenesis induced by transforming growth factor alpha in gastric epithelial cells. *Prostaglandins Leukot Essent Fatty Acids* 1999; **61**: 315-322
- 39 **Takahashi S**, Shigeta J, Ishikawa M, Kobayashi N, Okabe S. Role of thromboxane A2 in healing of gastric ulcers in rats. *Jpn J Pharmacol* 1999; **79**: 101-107
- 40 **Bamba H**, Ota S, Kato A, Matsuzaki F. Nonsteroidal anti-inflammatory drugs may delay the repair of gastric mucosa by suppressing prostaglandin-mediated increase of hepatocyte growth factor production. *Biochem Biophys Res Commun* 1998; **245**: 567-571
- 41 **Tepperman BL**, Soper BD. Effect of epidermal growth factor, transforming growth factor alpha and nerve growth factor on gastric mucosal integrity and microcirculation in the rat. *Regul Pept* 1994; **50**: 13-21
- 42 **Taupin D**, Pedersen J, Familiar M, Cook G, Yeomans N, Giraud AS. Augmented intestinal trefoil factor (TFF3) and loss of pS2 (TFF1) expression precedes metaplastic differentiation of gastric epithelium. *Lab Invest* 2001; **81**: 397-408
- 43 **Kato K**, Chen MC, Nguyen M, Lehmann FS, Podolsky DK, Soll AH. Effects of growth factors and trefoil peptides on migration and replication in primary oxyntic cultures. *Am J Physiol* 1999; **276**(5 Pt 1): G1105-1116
- 44 **Jones MK**, Tomikawa M, Mohajer B, Tarnawski AS. Gastrointestinal mucosal regeneration: role of growth factors. *Front Biosci* 1999; **4**: D303-309
- 45 **Cook GA**, Yeomans ND, Giraud AS. Temporal expression of trefoil peptides in the TGF-alpha knockout mouse after gastric ulceration. *Am J Physiol* 1997; **272**(6 Pt 1): G1540-1549
- 46 **Goldenring JR**, Poulson R, Ray GS, Wright N, Meise KS, Coffey RJ Jr. Expression of trefoil peptides in the gastric mucosa of transgenic mice overexpressing transforming growth factor-alpha. *Growth Factors* 1996; **13**: 111-119
- 47 **Sarraf CE**, Alison MR, Ansari TW, Wright NA. Subcellular distribution of peptides associated with gastric mucosal healing and neoplasia. *Microsc Res Tech* 1995; **31**: 234-247
- 48 **Poulson R**, Wright NA. Trefoil peptides: a newly recognized family of epithelial mucin-associated molecules. *Am J Physiol* 1993; **265**(2 Pt 1): G205-213

Hepatocellular carcinoma treated with interventional procedures: CT and MRI follow-up

Yong-Song Guan, Long Sun, Xiang-Ping Zhou, Xiao Li, Xiao-Hua Zheng

Yong-Song Guan, Long Sun, Xiang-Ping Zhou, Xiao Li, Xiao-Hua Zheng, Department of Radiology, Huaxi Hospital, Sichuan University, Chengdu 610041, Sichuan Province, China

Correspondence to: Dr. Yong-Song Guan, Department of Radiology, Huaxi Hospital, Sichuan University, 37 Guoxuexiang, Chengdu 610041, Sichuan Province, China. yongsongguan@yahoo.com

Telephone: +86-28-85421008 **Fax:** +86-28-85421008

Received: 2004-02-02 **Accepted:** 2004-02-21

Abstract

In the past decade, a variety of interventional procedures have been employed for local control of hepatocellular carcinoma (HCC). These include transcatheter arterial chemoembolization (TACE) and several tumour ablation techniques, such as percutaneous ethanol injection (PEI), radio-frequency ablation (RFA), or percutaneous microwave coagulation therapy (PMC), laser-induced interstitial thermotherapy (LITT), *etc.* For a definite assessment of the therapeutic efficacy of interventional procedures, histological examination using percutaneous needle biopsy may be the most definite assessment of the therapeutic efficacy of interventional therapy, however, it is invasive and the specimen retrieved does not always represent the entire lesion owing to sampling errors. Therefore, computed tomography (CT) and magnetic resonance imaging (MRI) play a crucial role in follow-up of HCC treated by interventional procedures, by which the local treatment efficacy, recurrent disease and some of therapy-induced complications are evaluated. Contrast enhanced axial imaging (CT or MR imaging) may be the most sensitive test for assessing the therapeutic efficacy. The goal of the review was to describe the value of CT and MRI in the evaluation of interventional treatments.

Guan YS, Sun L, Zhou XP, Li X, Zheng XH. Hepatocellular carcinoma treated with interventional procedures: CT and MRI follow-up. *World J Gastroenterol* 2004; 10(24): 3543-3548
<http://www.wjgnet.com/1007-9327/10/3543.asp>

INTRODUCTION

Hepatocellular carcinoma (HCC) is one of the most common cancers in the world^[1]. Its mortality is secondary to lung cancer in urban and gastric carcinoma in countryside in China^[2]. So far, surgical treatments including hepatic resection and liver transplantation are considered as the most effective treatment of HCC. However, less than 20% of HCC patients have been treated surgically, mainly because of multi-focal diseases, proximity of tumour to key vascular or biliary structures that precluded a margin-negative resection, potentially unfavorable biology with the presence of multiple liver metastases, or inadequate functional hepatic reserve related coexistent cirrhosis^[3]. Palliative treatment of patients with inoperable HCC, including transcatheter arterial chemoembolization (TACE)^[4], percutaneous ethanol injection (PEI)^[5], laser-induced interstitial thermotherapy (LITT)^[6,7], and local thermal ablation techniques

(such as percutaneous microwave coagulation therapy (PMC)^[8,9] and radio-frequency ablation (RFA)^[10]) have been tried. Despite initial remission of HCC, results of various therapeutic modalities in the treatment of HCC and the survival benefits of patients treated with them were not satisfactory because of frequent recurrences following the treatment. Therefore, to prevent recurrences following the initial excellent response may be crucial to improve the long-term outcomes of patients with HCC treated by these modalities^[11]. Early detection of a residual or locally recurrent tumour after interventional treatments is critical and can facilitate successful retreatment at early stage. Late diagnosis is associated with peripheral regrowth and makes retreatment difficult owing to unfavorable geometry^[12]. Histological examination using percutaneous needle biopsy may be the most definite assessment of the therapeutic efficacy of interventional therapy, however, it is invasive and the specimen retrieved does not always represent the entire lesion owing to sampling errors. Therefore, computed tomography (CT) and magnetic resonance imaging (MRI) play a crucial role in follow-up of HCC treated by interventional procedures.

MATERIALS AND METHODS

Resection or transplantation provides the potentially curative or survival-enhancing treatment. The aims of palliative treatment are to slow down tumour progression and provide palliation, and to improve survival. Which includes the use of TACE alone or in combination with other local treatments. Each treatment plan is tailored to the individual patients according to their tumour stage, symptomatology, age and overall health, needs and wishes^[13]. Most combined multimodal interventional therapies have enormous advantages as compared with any single therapeutic regimen alone, and play more important roles in treating unresectable HCC^[14]. Non-surgical palliative techniques include the following.

Radio-frequency ablation

Similar to other ablation techniques, RFA depends on several factors, such as clinical status, stage of liver cirrhosis and HCC of patients. RFA can be performed percutaneously, laparoscopically or after laparotomy^[15]. In comparison with PEI, RFA could achieve tumour necrosis in fewer sessions, and create large volumes of tumour necrosis in a shorter period of time than either laser or microwave therapy. RFA showed good control of tumors with necrosis in more than 90% of HCCs smaller than 5 cm in diameter^[16-19]. In HCCs larger than 5 cm in diameter, results were unsatisfactory with complete necrosis in less than 30%^[20].

The mechanism of RF is that a high-frequency alternating current (100 to 500 kHz), mostly 460 kHz, passes from an uninsulated electrode tip into the surrounding tissues and causes ionic vibrations as the ions attempt to follow the change in the direction of the rapidly alternating current. Such ionic vibrations cause frictional heating of the tissues surrounding the electrode, rather than the heat generated from the probe itself. The goal of RFA is to achieve local temperatures so that tissue destruction occurs. At the temperature above 60 °C, intracellular protein changes including collagen denaturation,

lipid bilayer melt and cell death are inevitable. Thermal coagulation begins at 70 °C and tissues desiccate at 100 °C, producing coagulation necrosis of tumor tissue and surrounding hepatic parenchyma. Tissue heating also drives extracellular and intracellular water out of the tissue and results in further destruction of the tissues due to coagulative necrosis^[21,22].

Andrea *et al.* reported that most frequent complications reported in literature were capsular necrosis, intraperitoneal hemorrhage (usually self-limiting), subcapsular hematoma, cholecystitis, hepatic abscesses. Needle track seeding after RFA was reported with a low incidence of complications (0.6-2.8%).

Frequency of major complications related to the procedure was low, ranging from 5% to 15%^[23,24]. Self-limiting intraperitoneal bleeding, liver abscess and right pleural effusions were the most frequently reported complications^[25]. Tumor seeding along the needle tract was also described, but its incidence from 0.6% to 12%, has been a matter of debate^[26-29]. Curley and Izzo^[30] suggested that RFA could be performed for unresectable hepatic malignancies less than 6.0 cm in diameter. In addition, equipments used for RFA were less expensive than either laser or microwave equipments. RFA could provide local control of advanced liver tumours with a low recurrence and an acceptable morbidity^[31].

Percutaneous ethanol injection

Livraghi *et al.* reported that in 746 HCCs with cirrhosis treated by PEI, the 5-year survival rate for a single HCC <5 cm was 47% for Child A, 29 % for Child B and 0 % for Child C, respectively^[32]. PEI was contraindicated in the presence of gross ascites, bleeding, or obstructive jaundice. PEI has been widely used with excellent results in patients with less than three HCCs^[33,34]. Ethanol in PEI acts by diffusing within the cells, which causes immediate dehydration of cytoplasmic proteins with consequent coagulation necrosis followed by fibrosis, and by entering the circulation, which induces necrosis of endothelial cells and platelet aggregation with consequent thrombosis of small vessels followed by ischemia of the neoplastic tissues. Advantages for using PEI include^[35,36]: no remarkable damage to the remaining parenchyma, relative safety, easy repetition when new lesions appear as in the majority of patients followed up for 5 years, application anywhere due to its low cost and easy operation, and fairly good long-term results.

Percutaneous microwave coagulation

It is well known that percutaneous microwave coagulation therapy (PMC) under local anesthesia is a palliative and effective therapy when carried out on a single occasion to treat HCC located near the liver surface, and it could be safely performed under direct visual guidance^[37]. MCT might be superior to PEI for the local control of moderately or poorly differentiated small HCC^[38], and for treating patients with HCC greater than or equal to 15 mm in diameter. In such patients with well-differentiated HCC, PEI was as effective as PMC^[39].

Laser-induced interstitial thermotherapy

Laser-induced interstitial thermotherapy (LITT) is another minimally invasive and attractive method for destroying relatively larger tumours within solid organs by causing carbonization and vaporization in tissues^[40]. MR-guided LITT is a local effective therapy with a low morbidity for malignant liver tumours with a maximum quantity of 5 and a size less than or equal to 5 cm in diameter^[41]. LITT may be also equivalent to limited hepatic resection and may influence the long-term survival comparable to that of segmentectomy, but local recurrence could occur even in small HCC, but infrequent^[42,45].

Transcatheter arterial chemoembolization

TACE uses combined agents to compromise the flow of hepatic

artery. The agents include gelatin (gelfoam), iodized oil (lipiodol), and a cytotoxic agent. Retreatment can be performed in 6-12 wk. The 5-year survival rate was reported to be 6-22%. TACE has been shown to reduce systemic toxicity and increase local effects thus improving the therapeutic results. However, its perceived benefit for survival has not been substantiated in randomized trials, presumably because its anticancer effect is offset by its adverse effects on liver functions. Its therapeutic effect is also limited due to lack of appropriate and reliable embolic agents and when the tumour is infiltrative in nature or is too large or too small.

LOCAL ABLATION THERAPY

Local ablation therapies fall into one or two categories: direct intratumoural injection of compounds such as absolute ethanol (PEI) or hot saline, and thermal ablation techniques such as laser-induced interstitial thermotherapy (LITT), percutaneous microwave coagulation therapy (PMC) and radiofrequency thermal ablation (RFA). These techniques produce coagulation necrosis of tumours with use of cytotoxic compounds or thermal energy. So the lesion should be avascular, if it has been treated successfully. For example, a typical RFA treatment producing a local tissue temperature over 100 °C could result in coagulative necrosis of the tumor tissue and surrounding hepatic parenchyma. The tissue microvasculature was completely destroyed, and thrombosis of hepatic arterial, portal venous or hepatic venous branches less than 3 mm in diameter occurred. For the assessment of therapeutic responses to these techniques, the same diagnostic criteria previously reported for lesions treated with TACE and PEI could be applied^[43-45]. The imaging appearances of the lesions after these treatments were very similar, regardless of which local ablation technique was used^[46].

IMAGING FOLLOW UP OF RADIO FREQUENCY ABLATION CT

Contrast-enhanced helical CT has been widely used in the evaluation of residual or recurrent tumours or of complications such as abscess, infarction, or hemorrhage in patients who have undergone percutaneous ablation therapy for a hepatic tumour^[47]. All successfully ablated lesions appeared as areas of low attenuation without contrast enhancements at follow up CT. This unenhanced low-attenuation area is believed to represent necrosis^[48,49]. Any focal enhancement in the treated region should be considered as an indicative of residual or recurrent lesions^[50].

All of the peripheral enhanced lesions at a short-term follow-up CT performed within 1 mo after treatment should not be regarded as a residual viable tumour^[51]. Reactive hyperemia surrounds the ablation lesions in tissue. It represents inflammatory reactions in the thermal injury frequently occurred during this period. Similar findings at CT have been reported in patients who underwent percutaneous ethanol injection therapy and microwave coagulation therapy^[52]. Peripheral rim enhancement resulting from reactive hyperemia was usually uniform in thickness and enveloped the ablated lesion, whereas a residual tumour showed focal and irregular peripheral enhancements. The other useful differentiating point between the two conditions was the peripheral rim enhancement, indicating that the reactive hyperemia had a high or isoattenuation during portal venous and equilibrium phases^[53]. The residual tumour usually became low in attenuation during the equilibrium phase. In addition to reactive hyperemia, nontumourous wedge like enhancement could occur at the periphery of the ablated lesion owing to iatrogenic arteriovenous shunt^[54,55].

It is well known that percutaneous needle biopsy and ethanol injection therapy could produce arteriovenous shunt along the needle tract^[56,57]. It was usually easy to differentiate residual

tumours from arteriovenous shunt at multiphase helical CT, because a residual tumour usually showed a high attenuation during the hepatic arterial phase and a low attenuation during the portal and equilibrium phases^[58]. If the finding of short-term follow-up CT was inconclusive, follow-up CT at 1-3-mo intervals could be helpful before invasive diagnostic procedures, such as percutaneous biopsy or retreatment were performed if the suspected lesion was small. Nontumourously enhanced lesions produced by reactive hyperemia and arteriovenous shunt were usually resolved by this time. During this period, even if one failed in detecting small residual tumours, they have seldom grown to a size for which successful retreatment was not feasible.

The absence of contrast enhancement in the ablated lesion at short-term follow-up CT within 3 mo after treatment could not always indicate successful treatment, as later follow up studies would demonstrate tumour regrowth at the periphery of the ablated lesion^[44,59]. Mitsuzaki *et al.*^[60] reported that 8 of 38 ablated lesions with the absence of contrast enhancement at 1-mo follow-up CT showed tumour recurrence at the margin of the treated lesions at subsequent follow-up CT performed 4-13 mo after treatment.

MRI

MR imaging may have an edge over CT in the early detection of local regrowth due to the high sensitivity of T2-weighted images. Two months after RF therapy, a uniform hypointensity on T2-weighted images, associated with lack of enhancement of RF-treated areas on contrast-enhanced T1-weighted images, always corresponded to complete efficient treatment^[61]. Most of the RF-treated areas were hyperintense on unenhanced T1-weighted images, which was probably due to hemorrhage or a proteinaceous material within the RF-treated area^[62]. Most of the RF-treated areas were hypointense on T2-weighted images, and this hypointensity could be explained by the dehydrating effect of RF-induced thermal damage resulting in coagulative necrosis. However, a marked hyperintensity on T2-weighted images, found in 14% of the successful treated areas, could signify bilomas or liquefactive necrosis, as an active tumour always displayed a less T2 signal intensity^[63].

The higher sensitivity of MR imaging over CT was mostly due to the T2 weighted images, which were the only imaging study capable of depicting tumours in two cases at two months^[64]. The superior sensitivity of T2-weighted images could be explained by an increase in contrast between the coagulated area, which had a low signal intensity and the viable residual tumour, which had high signal intensity. Moderately hyperintense areas on T2-weighted images corresponded to the presence of residual viable tumour in all cases. Therefore, T2-weighted imaging was demonstrated to be highly specific. Moreover, the moderately hyperintense areas on T2-weighted imaging associated with corresponding enhancement on contrast-enhanced T1-weighted imaging could offer an optimal specificity (100%) for residual viable tumours in all cases^[65].

Local regrowths were always depicted at the periphery of the treated area either as irregular thickening of one margin of the treated area or a new tumour nodule. These peripheral locations of treatment failures could be explained by lower energy deposition and reduced heating that was remote from the needle electrode^[66]. Furthermore, tissue perfusion could lower heat accumulation to cooling, and this phenomenon was even more marked in tissues in contact with large vessels. Indeed, regrowth close to large vessels arose in two of nine cases in their study and was described by others^[67].

Peripheral regrowth should not be diagnosed when a thin and regular (<1 mm) rim of progressive contrast enhancement was present at 2 mo in 32% of the entire RF-treated area and better seen at the later phase after contrast material administration.

It has been shown by comparison with histological findings that the thin ring is vascularized inflammatory reaction with granulation tissues surrounding the zone of coagulation necrosis^[68,69].

Similar findings were less frequently described in hepatocellular carcinoma treated with alcohol injection^[70] and in hepatic metastases treated with laser-induced thermotherapy^[71,72]. The peripheral rim disappeared with time and was present in only 8% of RF-treated areas at 4 mo^[73]. It could easily be differentiated from an active tumour whose area of contrast enhancement was thicker and irregular. Another RF-induced modification was the presence of wedge-shaped enhancement on arterial phase images in the liver parenchyma adjacent to the RF-treated area. This enhancement probably corresponded to peripheral arterioportal shunts caused by either needle punctures and/or thermal damage. These wedge-shaped areas should not be misinterpreted as tumour contrast material uptake^[74].

Although there are many similarities between the radiological aspect of RF-induced destruction and the necrosis induced by ethanol^[75], some differences need to be pointed out. First, T2-weighted MR imaging was demonstrated to be the best indicator of the efficacy of RF-treatment^[76]. In contrast, Sironi *et al.* and Fujita *et al.*^[75] described a limited value of T2-weighted signal intensity pattern of tumours injected with alcohol in ascertaining the viability of the tumour. This might be due either to differences in technical parameters (fast spin echo with respiratory monitoring versus standard spin echo with a higher rate of motion artifacts in their studies), or to histopathologic nature of the initial tumours, which was very different in their study from that of previous reports. Second, the area of RF-induced coagulation necrosis shrank more slowly than that of ethanol-induced necrosis. Indeed, in their study, 66% of the treated areas shrank, achieving a mean reduction of 15% at 6 mo, and 35% at 12 mo.

IMAGING FOLLOW UP OF TACE

Iodized oil is widely used with TACE. Because iodized oil shows a prolonged uptake in tumours and is readily identified with CT. The degree of uptake and the distribution within the tumour and the surrounding hepatic parenchyma could provide useful information on the degree of tumour necrosis and strategy for the subsequent TACE^[77]. Since it is difficult to completely kill the tumor cells once by TACE, the treatment efficacy of TACE is influenced by many factors, such as the size of tumors, blood supply and the ultra-selectivity of the catheter, *etc.* TACE is a liver-directed therapy that takes advantages of the relatively selective vascularization of hepatic arterial tumors. HCC could derive approximately 80% to 85% of their blood supply from the hepatic artery, whereas the portal vein as well as the hepatic artery supplied the normal hepatic parenchyma^[78]. Chemotherapeutic agents could thus be delivered angiographically with concomitant embolization to increase the local chemotherapeutic dwelling time and induce tumor ischemia. It is very important to objectively assess the viability and necrosis of the tumors after TACE in HCC, and to give further treatment to improve the general therapeutic effects and the survival rate.

After ablation therapy, contrast-enhanced CT is a reliable method for the assessment of therapeutic efficacy. On contrast-enhanced CT, necrotic tissues were unenhanced and viable tumours were enhanced. After TACE with iodized oil, however, retained iodized oil of high attenuation made it difficult to determine the presence of contrast enhanced within the tumour. It is generally agreed that the areas with retained iodized oil after a certain period (e.g. >4 wk) could be considered indicative of necrosis.

The complete disappearance of tumour was designated as complete remission, a 50% or more decrease in tumour as partial response, a less than 50% decrease or 25% increase in tumour as no response, and a 25% or more increase as progressive

disease. The focal defect in the mass with iodized oil or focal washout of iodized oil during follow-up suggested the presence of a viable tumour in the corresponding area, and further TACE was recommended. Sometimes, branches of hepatic arteries were totally obliterated and collateral vessels could feed the part of the tumour. Each collateral vessel supplies a specific area. The inferior phrenic artery supplies the right subphrenic location near the bare area, the internal mammary artery supplies the near falciform ligament, and the omental branches supply the anterolateral subcapsular location, *etc*^[74]. Focal washout of iodized oil from those areas suggests the presence of collateral vessels. Therefore, a careful search for the appropriate collateral vessel should be made during subsequent TACE.

Generally, the CT follow-up of patients treated with oily chemoembolization could be affected by artefacts produced by high concentrations of lipiodol, making it difficult to evaluate the characteristics of the lesion. On the other hand, the homogeneous and complete deposition of lipiodol within the lesions would indicate the high degree necrosis of the tumors, but it was difficult to judge the viability and necrosis of the tumors correctly due to the inhomogeneous deposition, because lipiodol negative areas could not actually represent the viability of the tumors^[79,80]. The necrosis within the lesions before TACE was also a lipiodol negative area.

Several authors considered that MR imaging was valuable in the evaluation of therapeutic efficiency of TACE, especially on spin echo (SE) T₂WI, most of viable tumors were hyperintense and the coagulative necrosis within the tumors considered as a positive response to TACE was hypointense^[81,82]. But a signal intensity of the tumors after TACE was variable on SE T₁WI and T₂WI, but all of viable tumors, hemorrhage, liquefied necrosis and inflammatory infiltration could also result in hyperintensity on the T₂WI. Therefore, it was difficult to assess the viable tumors of HCC after TACE by conventional SE imaging. However, it was reliable to judge coagulative necrosis on T₂WI, especially the changes during the process of intratumor hemorrhage after TACE presenting as a hyperintensity and then turned into coagulative necrosis presenting a hypointensity. It was significant to compare the signal intensity of HCC on T₂WI before and after TACE to evaluate the degree of coagulative necrosis. The original hyperintensity of HCC turned to hypointensity indicated the presence of coagulative necrosis after TACE.

Fast multiplanar spoiled gradient-recalled (FMPSGR) dynamic contrast scanning plays a very important role in the detection and characterization of HCC. It is possible to obtain high quality images of the whole liver during a single breath-hold with rapid acquisition. It could demonstrate accurately the blood supply of tumors and reveal the contrast enhancement patterns of HCC. HCC is hypervascular and enhanced rapidly and obviously at the dynamic early phase scanning and declined at the late phase^[83,84]. FMPSGR dynamic contrast scanning also has a great value in the evaluation of therapeutic efficacy of TACE. The residual viable tumors were shown as rapidly enhanced portions within the lesions, homogeneous or inhomogeneous, when necrotic portions had no enhancement at the contrast early phase scanning. At the late phase scanning, the enhancement of the most lesions became hypointense, and just a few lesions showed a persistent enhancement. Pathologically, both viable tumors and inflammatory infiltration could present such changes, so the contrast early phase scanning was more reliable in the evaluation of viable tumors combined with conventional SE sequence, and more accurate to assess the viability and necrosis of tumors and useful in the follow-up of HCC patients after TACE.

SUMMARY

In summary, CT and MRI have advantages and disadvantages

for evaluating the local treatment efficacy, recurrent disease and some of the therapy-induced complications. Surgeons and interventional radiologists have to choose the most suitable imaging means for patients who are treated by interventional procedures. Contrast enhanced CT or MR imaging may be the most sensitive test for assessing the therapeutic efficacy. For the later follow up, contrast-enhanced CT or MRI is then performed at 1 mo and every 3-mo thereafter. A short-term follow-up CT or MRI within 1 mo after treatment is not a reliable method for assessing the precise therapeutic effectiveness, because reactive hyperemia and/or arteriovenous shunt often make an accurate evaluation difficult. Knowledge of the serial changes at long-term follow-up CT and MRI is helpful in assessing the therapeutic response to HCC after interventional treatments.

REFERENCES

- 1 Schafer DF, Sorrell MF. Hepatocellular carcinoma. *Lancet* 1999; **353**: 1253-1257
- 2 Tang ZY. Hepatocellular carcinoma- cause, treatment and metastasis. *World J Gastroenterol* 2001; **7**: 445-454
- 3 Alsowmely AM, Hodgson HJ. Non-surgical treatment of hepatocellular carcinoma. *Aliment Pharmacol Ther* 2002; **16**: 1-15
- 4 Llovat JM, Real MI, Montana X, Planas R, Coll S, Aponte J, Ayuso C, Sala M, Muchart J, Sola R, Rodes J, Bruix J. Arterial embolisation or chemoembolisation versus symptomatic treatment in patients with unresectable hepatocellular carcinoma: a randomised controlled trial. *Lancet* 2002; **359**: 1734-1739
- 5 Livraghi T. Radiofrequency ablation, PEIT, and TACE for hepatocellular carcinoma. *J Hepatobiliary Pancreat Surg* 2003; **10**: 67-76
- 6 Vogl TJ, Straub R, Eichler K, Woitaschek D, Mack MG. Malignant liver tumors treated with MR imaging-guided laser-induced thermotherapy: experience with complications in 899 patients (2,520 lesions). *Radiology* 2002; **225**: 367-377
- 7 Pacella CM, Bizzarri G, Magnolfi F, Cecconi P, Caspani B, Anelli V, Bianchini A, Valle D, Pacella S, Manenti G, Rossi Z. Laser thermal ablation in the treatment of small hepatocellular carcinoma: results in 74 patients. *Radiology* 2001; **221**: 712-720
- 8 Seki T, Wakabayashi M, Nakagawa T, Imamura M, Tamai T, Nishimura A, Yamashiki N, Okamura A, Inoue K. Percutaneous microwave coagulation therapy for patients with small hepatocellular carcinoma: comparison with percutaneous ethanol injection therapy. *Cancer* 1999; **85**: 1694-1702
- 9 Itamoto T, Katayama K, Fukuda S, Fukuda T, Yano M, Nakahara H, Okamoto Y, Sugino K, Marubayashi S, Asahara T. Percutaneous microwave coagulation therapy for primary or recurrent hepatocellular carcinoma: long-term results. *Hepatogastroenterology* 2001; **48**: 1401-1405
- 10 Livraghi T, Goldberg SN, Lazzaroni S, Meloni F, Solbiati L, Gazelle GS. Small hepatocellular carcinoma: treatment with radio-frequency ablation versus ethanol injection. *Radiology* 1999; **210**: 655-661
- 11 Lee JK, Chung YH, Song BC, Shin JW, Choi WB, Yang SH, Yoon HK, Sung KB, Lee YS, Suh DJ. Recurrences of hepatocellular carcinoma following initial remission by transcatheter arterial chemoembolization. *J Gastroenterol Hepatol* 2002; **17**: 52-58
- 12 Vogl TJ, Eichler K, Zangos S, Mack M, Hammerstingl R. Hepatocellular carcinoma: Role of imaging diagnostics in detection, intervention and follow-up. *Rof Fortschr Geb Rontgenstr Neuen Bildgeb Verfahr* 2002; **174**: 1358-1368
- 13 Cao X, He N, Sun J, Wang S, Ji X, Fan H, Wang J, Zhang C, Yang J, Lu T, Li J, Zhang G. Interventional and synthetic therapy of advanced hepatocellular carcinoma. *Chin Med J* 2002; **115**: 1883-1885
- 14 Qian J, Feng GS, Vogl T. Combined interventional therapies of hepatocellular carcinoma. *World J Gastroenterol* 2003; **9**: 1885-1891
- 15 Allgaier HP, Galandi D, Zuber I, Blum HE. Radiofrequency thermal ablation of hepatocellular carcinoma. *Dig Dis* 2001; **19**: 301-310
- 16 Curley SA, Marra P, Beatty K, Ellis LM, Vauthey JN, Abdalla EK, Scaife C, Raut C, Wolff R, Choi H, Loyer E, Vallone P, Fiore F, Scordino F, De Rosa V, Orlando R, Pignata S, Daniele B, Izzo

- F. Early and late complications after radiofrequency ablation of malignant liver tumors in 608 patients. *Ann Surg* 2004; **239**: 450-458
- 17 **Horkan C**, Ahmed M, Liu Z, Gazelle GS, Solazzo SA, Kruskal JB, Goldberg SN. Radiofrequency ablation: Effect of pharmacologic modulation of hepatic and renal blood flow on coagulation diameter in a VX2 tumor model. *J Vasc Interv Radiol* 2004; **15**: 269-274
- 18 **Giovannini M**, Moutardier V, Danisi C, Bories E, Pesenti C, Delpero JR. Treatment of hepatocellular carcinoma using percutaneous radiofrequency thermoablation: results and outcomes in 56 patients. *J Gastrointest Surg* 2003; **7**: 791-796
- 19 **Shibata T**, Iimuro Y, Yamamoto Y, Maetani Y, Ametani F, Itoh K, Konishi J. Small hepatocellular carcinoma: comparison of radio-frequency ablation and percutaneous microwave coagulation therapy. *Radiology* 2002; **223**: 331-337
- 20 **Livraghi T**, Goldberg SN, Lazzaroni S. Hepatocellular carcinoma: radio-frequency ablation of medium and large lesions. *Radiology* 2000; **214**: 761-768
- 21 **Buscarini L**, Buscarini E, Di Stasi M, Vallisa D, Quaretti P, Rocca A. Percutaneous radiofrequency ablation of small hepatocellular carcinoma: long-term results. *Eur Radiol* 2001; **11**: 914-921
- 22 **Livraghi T**, Solbiati L, Meloni F, Ierace T, Goldberg SN, Gazelle GS. Percutaneous radiofrequency ablation of liver metastases in potential candidates for resection: the "test-of-time approach". *Cancer* 2003; **97**: 3027-3035
- 23 **Mulier S**, Mulier P, Ni Y, Miao Y, Dupas B, Marchal G, De Wever I, Michel L. Complications of radiofrequency coagulation of liver tumours. *Br J Surg* 2002; **89**: 1206-1222
- 24 **de Baere T**, Risse O, Kuoch V, Dromain C, Sengel C, Smayra T, Gamal El Din M, Letoublon C, Elias D. Adverse events during radiofrequency treatment of 582 hepatic tumors. *Am J Roentgenol* 2003; **181**: 695-700
- 25 **Galandi D**, Antes G. Radiofrequency thermal ablation versus other interventions for hepatocellular carcinoma. *Cochrane Database Syst Rev* 2004; **2**: CD003046
- 26 **Llovet JM**, Vilana R, Bru C, Bianchi L, Salmeron JM, Boix L, Ganau S, Sala M, Pages M, Ayuso C, Sole M, Rodes J, Bruix J. Increased risk of tumor seeding after percutaneous radiofrequency ablation for single hepatocellular carcinoma. *Hepatology* 2001; **33**: 1124-1129
- 27 **Bolondi L**, Gaiani S, Celli N, Piscaglia F. Tumor dissemination after radiofrequency ablation of hepatocellular carcinoma. *Hepatology* 2001; **34**: 608
- 28 **de Sio I**, Castellano L, De Girolamo V, di Santolo SS, Marone A, Del Vecchio Blanco C, Marone G. Tumor dissemination after radiofrequency ablation of hepatocellular carcinoma. *Hepatology* 2001; **34**: 609-610
- 29 **Goldberg SN**, Solbiati L. Tumor dissemination after radiofrequency ablation of hepatocellular carcinoma. *Hepatology* 2001; **34**: 609
- 30 **Curley SA**, Izzo F. Radiofrequency ablation of hepatocellular carcinoma. *Minerva Chir* 2002; **57**: 165-176
- 31 **Yamasaki T**, Kurokawa F, Shirahashi H, Kusano N, Hironaka K, Okita K. Percutaneous radiofrequency ablation therapy with combined angiography and computed tomography assistance for patients with hepatocellular carcinoma. *Cancer* 2001; **91**: 1342-1348
- 32 **Livraghi T**, Giorgio A, Marin G, Salmi A, de Sio I, Bolondi L, Pompili M, Brunello F, Lazzaroni S, Torzilli G. Hepatocellular carcinoma and cirrhosis in 746 patients: long-term results of percutaneous ethanol injection. *Radiology* 1995; **197**: 101-108
- 33 **Huo TI**, Huang YH, Wu JC, Lee PC, Chang FY, Lee SD. Survival benefit of cirrhotic patients with hepatocellular carcinoma treated by percutaneous ethanol injection as a salvage therapy. *Scand J Gastroenterol* 2002; **37**: 350-355
- 34 **Koda M**, Murawaki Y, Mitsuda A, Ohyama K, Horie Y, Suou T, Kawasaki H, Ikawa S. Predictive factors for intrahepatic recurrence after percutaneous ethanol injection therapy for small hepatocellular carcinoma. *Cancer* 2000; **88**: 529-537
- 35 **Livraghi T**. Role of percutaneous ethanol injection in the treatment of hepatocellular carcinoma. *Dig Dis* 2001; **19**: 292-300
- 36 **Livraghi T**. Percutaneous ethanol injection in the treatment of hepatocellular carcinoma in cirrhosis. *Hepatogastroenterology* 2001; **48**: 20-24
- 37 **Seki S**, Sakaguchi H, Kadoya H, Morikawa H, Habu D, Nishiguchi S, Shiomi S, Kitada T, Kuroki T. Laparoscopic microwave coagulation therapy for hepatocellular carcinoma. *Endoscopy* 2000; **32**: 591-597
- 38 **Seki T**, Wakabayashi M, Nakagawa T, Imamura M, Tamai T, Nishimura A, Yamashiki N, Okamura A, Inoue K. Percutaneous microwave coagulation therapy for patients with small hepatocellular carcinoma: comparison with percutaneous ethanol injection therapy. *Cancer* 1999; **85**: 1694-1702
- 39 **Horigome H**, Nomura T, Saso K, Itoh M. Standards for selecting percutaneous ethanol injection therapy or percutaneous microwave coagulation therapy for solitary small hepatocellular carcinoma: consideration of local recurrence. *Am J Gastroenterol* 1999; **94**: 1914-1917
- 40 **Pacella CM**, Bizzarri G, Cecconi P, Caspani B, Magnolfi F, Bianchini A, Anelli V, Pacella S, Rossi Z. Hepatocellular carcinoma: long-term results of combined treatment with laser thermal ablation and transcatheter arterial chemoembolization. *Radiology* 2001; **219**: 669-678
- 41 **Vogl TJ**, Straub R, Eichler K, Woitaschek D, Mack MG. Malignant liver tumors treated with MR imaging-guided laser-induced thermotherapy: experience with complications in 899 patients (2,520 lesions). *Radiology* 2002; **225**: 367-377
- 42 **Pacella CM**, Bizzarri G, Magnolfi F, Cecconi P, Caspani B, Anelli V, Bianchini A, Valle D, Pacella S, Manenti G, Rossi Z. Laser thermal ablation in the treatment of small hepatocellular carcinoma: results in 74 patients. *Radiology* 2001; **221**: 712-720
- 43 **Livraghi T**, Goldberg SN, Lazzaroni S, Meloni F, Ierace T, Solbiati L, Gazelle GS. Hepatocellular carcinoma: radio-frequency ablation of medium and large lesions. *Radiology* 2000; **214**: 716-718
- 44 **Li YH**, Wang CS, Liao LY, Wang CK, Shih LS, Chen RC, Chen PH. Long-term survival of Taiwanese patients with hepatocellular carcinoma after combination therapy with transcatheter arterial chemoembolization and percutaneous ethanol injection. *J Formos Med Assoc* 2003; **102**: 141-146
- 45 **Koda M**, Murawaki Y, Mitsuda A, Oyama K, Okamoto K, Idoe Y, Suou T, Kawasaki H. Combination therapy with transcatheter arterial chemoembolization and percutaneous ethanol injection compared with percutaneous ethanol injection alone for patients with small hepatocellular carcinoma: a randomized control study. *Cancer* 2001; **92**: 1516-1524
- 46 **Catalano O**, Esposito M, Nunziata A, Siani A. Multiphase helical CT findings after percutaneous ablation procedures for hepatocellular carcinoma. *Abdom Imaging* 2000; **25**: 607-614
- 47 **Solbiati L**, Goldberg SN, Ierace T, Dellanoce M, Livraghi T, Gazelle GS. Radio-frequency ablation of hepatic metastases: postprocedural assessment with a US microbubble contrast agent-early experience. *Radiology* 2000; **211**: 643-649
- 48 **Chen Y**, Chen H, Wu M, Zhou W, Wei G, Wang P, Li X. Curative effect of percutaneous microwave coagulation therapy for hepatocellular carcinoma. *Zhonghua Zhongliu Zazhi* 2002; **24**: 65-67
- 49 **Ohmoto K**, Tsuduki M, Kunieda T, Mitsui Y, Yamamoto S. CT appearance of hepatic parenchymal changes after percutaneous microwave coagulation therapy for hepatocellular carcinoma. *J Comput Assist Tomogr* 2000; **24**: 866-871
- 50 **Witzak-Malinowska K**, Zadrozny D, Studniarek M, Szurawska E, Michalska Z, Stalke P, Sikorska K, Lakomy EA. Preliminary assessment of utility of radiofrequency ablation technique in treatment of primary hepatocellular carcinoma (HCC) in patients with hepatic cirrhosis. *Med Sci Monit* 2003; **93**: 68-72
- 51 **Yamasaki T**, Kurokawa F, Shirahashi H, Kusano N, Hironaka K, Okita K. Percutaneous radiofrequency ablation therapy with combined angiography and computed tomography assistance for patients with hepatocellular carcinoma. *Cancer* 2001; **91**: 1342-1348
- 52 **Catalano O**, Esposito M, Lobianco R, Cusati B, Altei F, Siani A. Multiphase spiral computed tomography in hepatocarcinoma. An evaluation following different percutaneous ablative procedures. *Radiol Med* 1999; **98**: 500-508
- 53 **Ohmoto K**, Tsuduki M, Kunieda T, Mitsui Y, Yamamoto S. CT appearance of hepatic parenchymal changes after percutaneous microwave coagulation therapy for hepatocellular carcinoma. *J Comput Assist Tomogr* 2000; **24**: 866-871
- 54 **Lim HK**, Choi D, Lee WJ, Kim SH, Lee SJ, Jang HJ, Lee JH, Lim JH, Choo IW. Hepatocellular carcinoma treated with percutaneous evaluation with follow-up multiphase helical CT. *Radi-*

- ology 2001; **221**: 447-454
- 55 **Choi D**, Lim HK, Kim SH, Lee WJ, Jang HJ, Kim H, Lee SJ, Lim JH. Assessment of therapeutic response in hepatocellular carcinoma treated with percutaneous radio frequency ablation: comparison of multiphase helical computed tomography and power Doppler ultrasonography with a microbubble contrast agent. *J Ultrasound Med* 2002; **21**: 391-401
- 56 **Lee SJ**, Lim JH, Lee WJ, Lim HK, Choo SW, Choo IW. Transient subsegmental hepatic parenchymal enhanced on dynamic CT: a sign of postbiopsy arterioportal shunt. *J Comput Assist Tomogr* 1997; **21**: 355-360
- 57 **Lim JH**, Lee SJ, Lee WJ, Lim HK, Choo SW, Choo IW. Iodized oil retention due to postbiopsy arterioportal shunt: a false positive lesion in the investigation of hepatocellular carcinoma. *Abdom Imaging* 1999; **24**: 165-170
- 58 **Kim SK**, Lim HK, Kim YH, Lee WJ, Lee SJ, Kim SH, Lim JH, Kim SA. Hepatocellular carcinoma treated with radio-frequency ablation: spectrum of imaging findings. *Radiographics* 2003; **23**: 107-121
- 59 **Meloni MF**, Goldberg SN, Livraghi T, Calliada F, Ricci P, Rossi M, Pallavicini D, Campani R. Hepatocellular carcinoma treated with radiofrequency ablation: comparison of pulse inversion contrast-enhanced harmonic sonography, contrast-enhanced power Doppler sonography, and helical CT. *Am J Roentgenol* 2001; **177**: 375-380
- 60 **Mitsuzaki K**, Yamashita Y, Nishiharu T, Sumi S, Matsukawa T, Takahashi M, Beppu T, Ogawa M. CT appearance of hepatic tumors after microwave coagulation therapy. *Am J Roentgenol* 1998; **171**: 1397-1403
- 61 **Kettenbach J**, Blum M, Kilanowicz E, Schwaighofer SM, Lammer J. Percutaneous radiofrequency-ablation of liver cell carcinoma: a current overview. *Radiologe* 2004; **44**: 330-338
- 62 **Shibata T**, Iimuro Y, Yamamoto Y, Maetani Y, Ametani F, Itoh K, Konishi J. Small hepatocellular carcinoma: comparison of radio-frequency ablation and percutaneous microwave coagulation therapy. *Radiology* 2002; **223**: 331-337
- 63 **Dromain C**, de Baere T, Elias D, Kuoch V, Ducreux M, Boige V, Petrow P, Roche A, Sigal R. Hepatic tumors treated with percutaneous radio-frequency ablation: CT and MR imaging follow-up. *Radiology* 2002; **223**: 255-262
- 64 **Kang BK**, Lim JH, Kim SH, Choi D, Lim HK, Lee WJ, Lee SJ. Preoperative depiction of hepatocellular carcinoma: ferumoxides-enhanced MR imaging versus triple-phase helical CT. *Radiology* 2003; **226**: 79-85
- 65 **Sironi S**, Livraghi T, Meloni F, De Cobelli F, Ferrero C, Del Maschio A. Small hepatocellular carcinoma treated with percutaneous RF ablation: MR imaging follow-up. *Am J Roentgenol* 1999; **173**: 1225-1229
- 66 **Curley SA**, Izzo F, Delrio P, Ellis LM, Granchi J, Vallone P, Fiore F, Pignata S, Daniele B, Cremona F. Radiofrequency ablation of unresectable primary and metastatic hepatic malignancies: results in 123 patients. *Ann Surg* 1999; **230**: 1-8
- 67 **Solbiati L**, Ierace T, Goldberg SN, Sironi S, Livraghi T, FioCCA R, Servadio G, Rizzato G, Mueller PR, Del Maschio A, Gazelle GS. Percutaneous US-guided radio-frequency tissue ablation of liver metastases: treatment and follow-up in 16 patients. *Radiology* 1997; **202**: 195-203
- 68 **Rossi S**, Buscarini E, Garbagnati F, Stasi MD, Quaretti P, Rago M, Zangrandi A, Andreola S, Silverman D, Buscarini L. Percutaneous treatment of small hepatic tumors by an expandable RF needle electrode. *Am J Roentgenol* 1998; **170**: 1015-1022
- 69 **Bartolozzi C**, Crocetti L, Cioni D, Donati FM, Lencioni R. Assessment of therapeutic effect of liver tumor ablation procedures. *Hepatogastroenterology* 2001; **48**: 352-358
- 70 **Cioni D**, Lencioni R, Bartolozzi C. Percutaneous ablation of liver malignancies: imaging evaluation of treatment response. *Eur J Ultrasound* 2001; **13**: 73-93
- 71 **Vogl TJ**, Straub R, Eichler K, Sollner O, Mack MG. Colorectal carcinoma metastases in liver: laser-induced interstitial thermotherapy-local tumor control rate and survival data. *Radiology* 2004; **230**: 450-458
- 72 **Isbert C**, Ritz JP, Schilling A, Roggan A, Heiniche A, Wolf KJ, Muller G, Buhr HJ, Germer CT. Laser induced thermotherapy (LITT) of experimental liver metastasis-detection of residual tumors using Gd-DTPA enhanced MRI. *Lasers Surg Med* 2002; **30**: 280-289
- 73 **Arch-Ferrer JE**, Smith JK, Bynon S, Eckhoff DE, Sellers MT, Bland KI, Heslin MJ. Radio-frequency ablation in cirrhotic patients with hepatocellular carcinoma. *Am Surg* 2003; **69**: 1067-1071
- 74 **Dromain C**, de Baere T, Elias D, Kuoch V, Ducreux M, Boige V, Petrow P, Roche A, Sigal R. Hepatic tumors treated with percutaneous radio-frequency ablation: CT and MR imaging follow-up. *Radiology* 2002; **223**: 255-262
- 75 **Fujita T**, Honjo K, Ito K, Arita T, Koike S, Takano K, Tamura S, Matsumoto T, Matsunaga N. Fan-shaped hepatic parenchymal damage after ethanol injection therapy for hepatocellular carcinoma: MRI appearances. *Abdom Imaging* 1999; **24**: 56-60
- 76 **Kurokohchi K**, Masaki T, Miyauchi Y, Funaki T, Yoneyama H, Miyoshi H, Yoshida S, Himoto T, Morishita A, Uchida N, Watanabe S, Kuriyama S. Percutaneous ethanol and lipiodol injection therapy for hepatocellular carcinoma. *Int J Oncol* 2004; **24**: 381-387
- 77 **Takayasu K**, Arii S, Matsuo N, Yoshikawa M, Ryu M, Takasaki K, Sato M, Yamanka N, Shimamura Y, Ohto M. Comparison of CT findings with resected specimens after chemoembolization with iodized oil for hepatocellular carcinoma. *Am J Roentgenol* 2000; **175**: 699-704
- 78 **Uraki J**, Yamakado K, Nakatsuka A, Takeda K. Transcatheter hepatic arterial chemoembolization for hepatocellular carcinoma invading the portal veins: therapeutic effects and prognostic factors. *Eur J Radiol* 2004; **51**: 12-18
- 79 **Enomoto Y**, Itsubo M, Kawabe T, Koike K, Onoda H, Komuro O, Tsuno S, Toda G. Two cases of transcatheter therapy to hepatocellular carcinoma supplied by the right internal mammary artery. *Nippon Shokakibyo Gakkai Zasshi* 2000; **97**: 585-589
- 80 **Saccheri S**, Lovaria A, Sangiovanni A, Nicolini A, De Fazio C, Ronchi G, Fasani P, Del Ninno E, Colombo M. Segmental transcatheter arterial chemoembolization treatment in patients with cirrhosis and inoperable hepatocellular carcinomas. *J Vasc Interv Radiol* 2002; **13**: 995-999
- 81 **Kubota K**, Hisa N, Nishikawa T, Fujiwara Y, Murata Y, Itol S, Yoshida D, Yishida S. Evaluation of hepatocellular carcinoma after treatment with transcatheter arterial chemoembolization: comparison of Lipiodol-CT, power Doppler sonography, and dynamic MRI. *Abdom Imaging* 2001; **26**: 184-190
- 82 **Chan JH**, Tsui EY, Luk SH, Yuen MK, Cheung YK, Wong KP. Detection of hepatic tumor perfusion following transcatheter arterial chemoembolization with dynamic susceptibility contrast-enhanced echoplannar imaging. *Clin Imaging* 1999; **23**: 190-194
- 83 **Tsui EY**, Chan JH, Cheung YK, Cheung CC, Tsui WC, Szeto ML, Lau KW, Yuen MK, Luk SH. Evaluation of therapeutic effectiveness of transarterial chemoembolization for hepatocellular carcinoma: correlation of dynamic susceptibility contrast-enhanced echoplanar imaging and hepatic angiography. *Clin Imaging* 2000; **24**: 210-216
- 84 **Onaya H**, Itai Y. MR imaging of hepatocellular carcinoma. *Magn Reson Imaging Clin N Am* 2000; **8**: 757-768

Lymph node metastasis in early gastric cancer with submucosal invasion: Feasibility of minimally invasive surgery

Do-Joong Park, Hyeon-Kook Lee, Hyuk-Joon Lee, Hye-Seung Lee, Woo-Ho Kim, Han-Kwang Yang, Kuhn-Uk Lee, Kuk-Jin Choe

Do-Joong Park, Hyuk-Joon Lee, Han-Kwang Yang, Department of Surgery and Cancer Research Institute, Seoul National University College of Medicine, Seoul 110-744, Korea

Hyeon-Kook Lee, Department of Surgery, Ewha Woman's University College of Medicine, Seoul, Korea

Hye-Seung Lee, Woo-Ho Kim, Department of Pathology, Seoul National University College of Medicine, Seoul, Korea

Kuhn-Uk Lee, Kuk-Jin Choe, Department of Surgery, Seoul National University College of Medicine, Seoul, Korea

Correspondence to: Dr. Han-Kwang Yang, Department of Surgery and Cancer Research Institute, Seoul National University College of Medicine, 28 Yongon-Dong, Chongno-Gu, Seoul 110-744, Korea. hkyang@plaza.snu.ac.kr

Telephone: +82-2-7603797 **Fax:** +82-2-36720047

Received: 2004-01-02 **Accepted:** 2004-02-11

Abstract

AIM: To explore the feasibility of performing minimally invasive surgery (MIS) on subsets of submucosal gastric cancers that are unlikely to have regional lymph node metastasis.

METHODS: A total of 105 patients underwent radical gastrectomy with lymph node dissection for submucosal gastric cancer at our hospital from January 1995 to December 1995. Besides investigating many clinicopathological features such as tumor size, gross appearance, and differentiation, we measured the depth of invasion into submucosa minutely and analyzed the clinicopathologic features of these patients regarding lymph node metastasis.

RESULTS: The rate of lymph node metastasis in cases where the depth of invasion was $<500\ \mu\text{m}$, $500\text{--}2\ 000\ \mu\text{m}$, or $>2\ 000\ \mu\text{m}$ was 9% (2/23), 19% (7/36), and 33% (15/46), respectively ($P<0.05$). In univariate analysis, no significant correlation was found between lymph node metastasis and clinicopathological characteristics such as age, sex, tumor location, gross appearance, tumor differentiation, Lauren's classification, and lymphatic invasion. In multivariate analysis, tumor size ($>4\ \text{cm}$ vs $\leq 2\ \text{cm}$, odds ratio = 4.80, $P=0.04$) and depth of invasion ($>2\ 000\ \mu\text{m}$ vs $\leq 500\ \mu\text{m}$, odds ratio = 6.81, $P=0.02$) were significantly correlated with lymph node metastasis. Combining the depth and size in cases where the depth of invasion was less than $500\ \mu\text{m}$, we found that lymph node metastasis occurred where the tumor size was greater than $4\ \text{cm}$. In cases where the tumor size was less than $2\ \text{cm}$, lymph node metastasis was found only where the depth of tumor invasion was more than $2\ 000\ \mu\text{m}$.

CONCLUSION: MIS can be applied to submucosal gastric cancer that is less than $2\ \text{cm}$ in size and $500\ \mu\text{m}$ in depth.

Park DJ, Lee HK, Lee HJ, Lee HS, Kim WH, Yang HK, Lee KU, Choe KJ. Lymph node metastasis in early gastric cancer with submucosal invasion: Feasibility of minimally invasive surgery. *World J Gastroenterol* 2004; 10(24): 3549-3552
<http://www.wjgnet.com/1007-9327/10/3549.asp>

INTRODUCTION

Minimally invasive surgeries (MIS) such as endoscopic mucosal resection or laparoscopic surgery are performed as a treatment of early gastric cancer. This limited surgery should be conducted on strict indication in early gastric cancer which has a limited invasion in mucosa. Such a surgery can be attained without lymph node dissection. However, if the case is diagnosed as submucosal gastric cancer after MIS, the patient needs additional gastrectomy and lymph node dissection owing to the limitations of current diagnostic methods in assessing the depth of invasion and lymph node status.

Since the incidence of lymph node metastasis in submucosal gastric cancer is reported as less as about 20%, it can be expected that the chance of further operations will be reduced if we choose patients who have low risk of lymph node metastasis. Thus, we analyzed in our study the clinicopathological factors related to lymph node metastasis in submucosal gastric cancers retrospectively, in order to find out the subsets of submucosal gastric cancers to which MIS can be applied, and to establish the suitable treatment policy of submucosal gastric cancers.

MATERIALS AND METHODS

This study enrolled 105 submucosal gastric cancer cases that were pathologically proven after gastrectomy by lymph node dissection at Seoul National University Hospital from January 1995 to December 1995. The relationship between clinicopathological factors (sex, age, tumor location, gross appearance, tumor size, depth of invasion, tumor differentiation, Lauren's classification, and lymphatic invasion) and lymph node metastasis was investigated. Submucosal layer was divided into 3 layers (upper third = SM1, middle third = SM2, and lower third = SM3) and submucosal depth of invasion was directly measured from muscularis mucosae by a micrometer (Figure 1). χ^2 test and logistic regression analysis were used to evaluate risk factors for lymph node metastasis and $P<0.05$ was considered statistically significant.

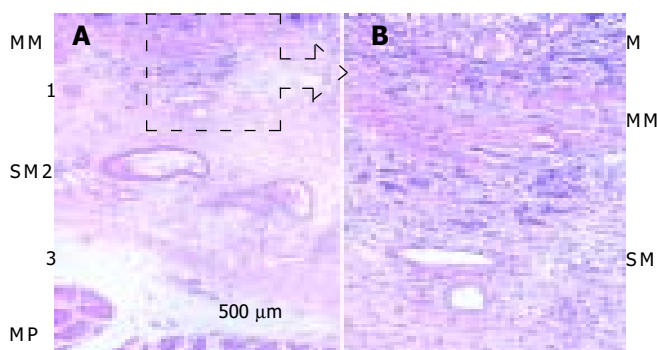


Figure 1 Depth of submucosal invasion of gastric cancer (arrow) in hematoxylin and eosin staining in A ($\times 10$) and B ($\times 100$). M: mucosa, MM: muscularis mucosae, SM: submucosa, MP: muscularis propria. This case was classified as SM1 or less than $500\ \mu\text{m}$ from muscularis mucosae.

RESULTS

Patient characteristics

A total of 105 patients with submucosal gastric cancer were included in the study. Of them, 74 were males and 31 were females. Their mean age was 54.9 years (18-80 years). The rate of lymph node metastasis was 22.9% (24/105 cases).

Depth of invasion (Table 1)

According to the SM category, SM1, SM2, and SM3 lesions were 28 (27%), 47 (45%), and 30 (28%) respectively. The depth of invasion measured directly from muscularis mucosae was less than 500 μm in 68% of SM1 gastric cancers, more than 1 000 μm (1 mm) in 75% of SM2 gastric cancers, and more than 2 000 μm in 84% of SM3 gastric cancers.

Table 1 Depth of submucosal invasion as compared with three SM category measurements

Depth (μm)	SM1 (%)	SM2 (%)	SM3 (%)
≤ 500 ($n = 23$)	19 (68)	4 (8)	0 (0)
500-1 000 ($n = 17$)	8 (28)	8 (17)	1 (3)
1 000-2 000 ($n = 19$)	1 (4)	14 (30)	4 (13)
$> 2 000$ ($n = 46$)	0 (0)	21 (45)	25 (84)
Total	28	47	30

Relationship between clinicopathological factors and lymph node metastasis (Table 2)

In univariate analysis, there was no significant factor related to lymph node metastasis among sex, age, tumor location, gross appearance, tumor differentiation, Lauren's classification, and lymphatic invasion.

Table 2 Relationship between clinicopathological factors and lymph node metastasis

	Total	Node-negative	Node-positive (n, %)	P
Sex				
M	74	57	17 (23.0)	0.965
F	31	24	7 (22.6)	
Age (yr)	105	54.8 \pm 12.5	55.4 \pm 12.2	0.822
Tumor location				
Upper	1	1	0 (0)	0.614
Middle	53	42	11 (20.8)	
Lower	48	35	13 (27.1)	
Entire	3	3	0 (0)	
Gross appearance				
Elevated	23	15	8 (34.8)	0.055
Flat	6	3	3 (50.0)	
Depressed	76	63	13 (17.1)	
Tumor differentiation				
Differentiated	47	35	12 (25.5)	0.557
Undifferentiated	58	46	12 (20.7)	
Lauren's classification				
Intestinal	44	35	9 (20.5)	0.572
Diffuse	53	41	12 (22.6)	
Mixed	8	5	3 (37.5)	
Depth of invasion				
SM1	28	24	4 (14.3)	0.448
SM2	47	35	12 (25.5)	
SM3	30	22	8 (26.7)	
Lymphatic invasion				
Absence	86	69	17 (19.8)	0.109
Presence	19	12	7 (36.8)	

Lymph node status in term of depth of invasion (Table 3)

The depth of invasion was significantly associated with lymph node metastasis. Especially, when the depth of invasion was more than 1 000 μm , three cases out of 65 (4.6%) were revealed to have more than 7 lymph node metastases (N2 stage).

Table 3 Lymph node status according to depth of invasion

Depth (μm)	Lymph node status (%)			
	pN0	pN+	pN1	pN2
≤ 500 ($n = 23$)	21 (91)	2 (9) ^a	2	0
500-1 000 ($n = 17$)	14 (82)	3 (18)	3	0
1 000-2 000 ($n = 19$)	15 (79)	4 (21)	3	1
$> 2 000$ ($n = 46$)	31 (67)	15 (33) ^a	13	2

^a $P < 0.05$.

Lymph node status in term of tumor size (Table 4)

Though there was no statistical significance in univariate analysis, the rate of lymph node metastasis was increased as the tumor size increased (≤ 2 cm, 11%; 2-4 cm, 26%; > 4 cm, 29%).

Table 4 Lymph node status according to tumor size

Size (cm)	Lymph node status (%)			
	pN0	pN+	pN1	pN2
≤ 2 ($n = 27$)	24 (89)	3 (11)	3	0
2-3 ($n = 30$)	22 (73)	8 (27)	7	1
3-4 ($n = 20$)	15 (75)	5 (25)	5	0
> 4 ($n = 28$)	20 (71)	8 (29)	6	2

$P = 0.403$.

Logistic regression analysis of factors associated with lymph node metastasis in submucosal gastric cancer (Table 5)

In multivariate analysis, the tumor size (> 4 cm in diameter vs ≤ 2 cm, odds ratio = 4.80, $P = 0.04$) and depth of invasion ($> 2 000$ μm of depth vs ≤ 500 μm , odds ratio = 6.81, $P = 0.02$) were significantly associated with lymph node metastasis.

Table 5 Logistic regression analysis for factors associated with lymph node metastasis in submucosal gastric cancer

Variables	Odds ratio	95% CI	P-value
Depth of invasion (μm)			
≤ 500	1		
500-1 000	2.02	0.30-13.86	0.473
1 000-2 000	3.14	0.49-20.24	0.228
$> 2 000$	6.81	1.36-34.17	0.020
Tumor size (cm)			
≤ 2	1		
2-3	4.35	0.95-19.96	0.059
3-4	4.05	0.78-20.97	0.096
> 4	4.80	1.05-22.06	0.044

CI: confidence interval.

Lymph node status in term of size and depth in submucosal gastric cancer (Table 6)

Lymph node status was analyzed in terms of tumor size and depth of invasion in submucosal gastric cancer. In cases where

the depth of invasion was less than 500 μm , lymph node metastasis was found only when the tumor size was greater than 4 cm. In cases where the tumor size was less than 2 cm, lymph node metastasis was found only when the depth of invasion was more than 2 000 μm .

Table 6 Lymph node status assessed by co-factor of size and depth in submucosal gastric cancer

Depth (μm)	Size (cm)			
	≤ 2	2-3	3-4	> 4
≤ 500 ($n = 23$)	0 ^a /4 ^b	0/6	0/6	2/7
500-1 000 ($n = 17$)	0/1	1/6	1/4	1/6
1 000-2 000 ($n = 19$)	0/5	2/8	1/2	1/4
$> 2 000$ ($n = 46$)	3/17	5/10	3/8	4/11

^aNumber of cases with lymph node metastasis; ^bNumber of total cases.

DISCUSSION

Gastric cancer is the most prevalent cancer in Korea, which accounted for 20.3% of the whole cancer cases^[1]. According to the report of Korea Gastric Cancer Association, the ratio of early gastric cancer was increased from 28.6% in 1995 to 32.8% in 1999^[2], while this tendency was more obvious in Japan, where the ratio of early gastric cancer in the last 20 years was increased from 18% to 57%^[3].

Lymph node metastasis was the most important prognostic factor in gastric cancer^[4,5]. Radical gastrectomy with D2 lymph node dissection, therefore, has been recognized as the standard surgical operation for early gastric cancer. But, as the five year survival rate of early gastric cancer patients has reached 93-98% recently, there arises more interest in preservation of body function and maintenance of quality of life rather than in radical treatment in order to reduce complications or sequelae, such as Dumping syndrome, reflux gastroesophagitis, nutritional deficit, and weight loss. Therefore, interest in MIS such as endoscopic mucosal resection and laparoscopic surgery or function-preserving surgery has been increased.

MIS with no or limited lymph node dissection should be applied to tumors that are unlikely to metastasize into lymph nodes. Endoscopic ultrasonography (EUS) has been introduced recently to diagnose the depth of invasion and lymph node status. An overall accuracy of EUS was reported over 80%^[6,7]. Yet, as the accuracy of EUS is not high enough to predict accurate lymph node status, it is important to know the prognostic factors related to lymph node metastasis. There have been already many reports on the prognostic factors associated with lymph node metastasis in early gastric cancer^[8-16], such as sex^[8], tumor size^[3,9,10,12], depth of invasion^[11], gross appearance of tumor^[8], tumor differentiation^[13] and lymphatic invasion^[14,15]. If we combine these prognostic factors successfully in the diagnosis of certain subtypes that have no lymph node metastasis, then they may become an indication of MIS. For example, the current indications of endoscopic mucosal resection of early gastric cancer are as follows, namely differentiated adenocarcinoma, mucosal cancer < 10 mm in diameter in IIb and IIc lesions without ulcer or ulcer scar, and mucosal cancer < 20 mm in diameter in IIa lesion^[17,18]. The reason why endoscopic mucosal resection can be applied to them is that these lesions are considered to have no lymph node metastasis.

When the depth of invasion reached mucosa in early gastric cancer, the rate of lymph node metastasis was reported as 1-3%, and submucosa as 11-20%^[19]. At present if endoscopic mucosal resection for early gastric cancer can detect the invasion of submucosal layer, additional gastrectomy and lymph node dissection are regarded necessary. However, as the incidence

of lymph node metastasis was about 20% in submucosal gastric cancer, lymph node dissection could be omitted if we chose cases with good selection of indications. In our study on submucosal gastric cancer, we found that sex, age, tumor location, tumor differentiation, Lauren's classification, gross appearance of tumor, were not associated with lymph node metastasis, but tumor size and depth of invasion were associated with lymph node metastasis. A recent study reported that there was a significant difference in the rate of lymph node metastasis according to submucosal depth of invasion, and the possibility of limited surgery for superficial submucosal gastric cancer was therefore suggested^[20]. We divided submucosal layer minutely into SM1, SM2, and SM3 on microscopic field and measured the depth of invasion by a micrometer directly from muscularis mucosae. Actually, because there was some difference between SM 1, 2, 3 categories and the directly measured depth associated with lymph node metastasis, it was considered more objective to use directly measured depth rather than SM category to describe submucosal tumor invasion. Ishigami *et al.*^[21] reported that patients with both slight invasion into submucosa and horizontal expansion that was < 5 mm were often negative in lymph node involvement. Kurihara *et al.*^[22] reported that when the pathological report revealed SM1 invasion after laparoscopic or endoscopic surgery, reoperation should be regarded unnecessary because SM1-carcinoma with its diameter less than 2 cm did not usually metastasize to lymph nodes. Moreover, Yasuda *et al.*^[23] showed that local resection could be applied when the depth of submucosal invasion was < 300 μm and tumor size was < 1 cm. Yamada *et al.*^[24] also showed that local resection might be possible when the depth of submucosal invasion was < 500 μm and tumor size was < 1.5 cm. Gotoda *et al.*^[25] proposed to expand the criteria for local treatment of submucosal gastric cancer by showing that none of the 145 differentiated adenocarcinomas, < 30 mm in diameter and without lymphatic or venous permeation, was associated with lymph node metastasis, provided the lesion invaded less than 500 μm into submucosa. In our study, the tumor size and depth of invasion as independent prognostic factors associated with lymph node metastasis were joined together. In cases where the depth of invasion was < 500 μm , lymph node metastasis was not found when the tumor size was < 4 cm. In cases where the tumor size was less than 2 cm, lymph node metastasis was not found when the depth of invasion was less than 2 000 μm . Therefore, the results suggest that additional operation is unnecessary when the depth of submucosal invasion is less than 500 μm and the tumor size is smaller than 2 cm after local excision. Moreover, in case that patients cannot endure general anesthesia because of old age or cardiopulmonary disability, in case that gastrectomy itself (with or without lymph node dissection) is considered to be dangerous to patients, or when patients refuse the operation, local excisions such as endoscopic mucosal resection, can be applied to submucosal gastric cancer.

In conclusion, the depth of invasion measured directly by a micrometer is more objective to describe cancer permeation into submucosal layer because it is associated more with lymph node metastasis than with SM category.

Our results suggest that additional operation is not necessary after MIS for submucosal gastric cancer when the depth of invasion is less than 500 μm and the tumor size is smaller than 2 cm.

REFERENCES

- 1 Korea Central Cancer Registry, Ministry of Health and Welfare Republic of Korea. *Annual Report of the Korea Central Cancer Registry 2003*
- 2 Nationwide gastric cancer report in Korea. Korea Gastric Cancer Association. *J Korean Gastric Cancer Assoc 2002*; 2: 105-114
- 3 Maehara Y, Orita H, Okuyama T, Moriguchi S, Tsujitani S, Korenaga D, Sugimachi K. Predictors of lymph node metasta-

- sis in early gastric cancer. *Br J Surg* 1992; **79**: 245-247
- 4 **Kunisaki C**, Shimada H, Takahashi M, Ookubo K, Moriwaki Y, Akiyama H, Nomura M. Prognostic factors in early gastric cancer. *Hepatogastroenterology* 2001; **48**: 294-298
 - 5 **Kim JP**, Kim YW, Yang HK, Noh DY. Significant prognostic factors by multivariate analysis of 3926 gastric cancer patients. *World J Surg* 1994; **18**: 872-877
 - 6 **Tio TL**, Schouwink MH, Cikot RJ, Tytgat GN. Preoperative TNM classification of gastric carcinoma by endosonography in comparison with the pathological TNM system: a prospective study of 72 cases. *Hepatogastroenterology* 1989; **36**: 51-56
 - 7 **Guo W**, Zhang YL, Li GX, Zhou DY, Zhang WD. Comparison of preoperative TN staging of gastric carcinoma by endoscopic ultrasonography with CT examination. *China Nati J New Gastroenterol* 1997; **3**: 242-245
 - 8 **Boku T**, Nakane Y, Okusa T, Hirozane N, Lmabayashi N, Hioki K, Yamamoto M. Strategy for lymphadenectomy of gastric cancer. *Surgery* 1989; **105**: 585-592
 - 9 **Kitamura K**, Yamaguchi T, Taniguchi H, Hagiwara A, Sawai K, Takahashi T. Analysis of lymph node metastasis in early gastric cancer: rationale of limited surgery. *J Surg Oncol* 1997; **64**: 42-47
 - 10 **Sano T**, Kobori O, Muto T. Lymph node metastasis from early gastric cancer: endoscopic resection of tumour. *Br J Surg* 1992; **79**: 241-244
 - 11 **Kwak CS**, Lee HK, Cho SJ, Yang HK, Lee KU, Choe KJ, Kim JP. Analysis of clinicopathological factors associated with lymph node metastasis in early gastric cancer review of 2.137 cases. *J Korean Cancer Assoc* 2000; **32**: 674-681
 - 12 **Yoshikawa T**, Tsuburaya A, Kobayashi O, Sairenji M, Motohashi H, Noguchi Y. Indications of limited surgery for gastric cancer with submucosal invasion - analysis of 715 cases with special reference to site of the tumor and level 2 lymph nodes. *Hepatogastroenterology* 2003; **50**: 1727-1730
 - 13 **Iriyama K**, Asakawa T, Koike H, Nishiwaki H, Suzuki H. Is extensive lymphadenectomy necessary for surgical treatment of intramucosal carcinoma of the stomach? *Arch Surg* 1989; **124**: 309-311
 - 14 **Ichikura T**, Uefuji K, Tomimatsu S, Okusa Y, Yahara T, Tamakuma S. Surgical strategy for patients with gastric carcinoma with submucosal invasion: A multivariate analysis. *Cancer* 1995; **76**: 935-940
 - 15 **Hyung WJ**, Cheong JH, Kim J, Chen J, Choi SH, Noh SH. Application of minimally invasive treatment for early gastric cancer. *J Surg Oncol* 2004; **85**: 181-185
 - 16 **Kitayama J**, Hatano K, Kaisaki S, Suzuki H, Fujii S, Nagawa H. Hyperlipidaemia is positively correlated with lymph node metastasis in men with early gastric cancer. *Br J Surg* 2004; **91**: 191-198
 - 17 **Takekoshi T**, Baba Y, Ota H, Kato Y, Yanagisawa A, Takagi K, Noguchi Y. Endoscopic resection of early gastric carcinoma: results of a retrospective analysis of 308 cases. *Endoscopy* 1994; **26**: 352-358
 - 18 **Korenaga D**, Orita H, Maekawa S, Maruoka A, Sakai K, Ikeda T, Sugimachi K. Pathological appearance of the stomach after endoscopic mucosal resection for early gastric cancer. *Br J Surg* 1997; **84**: 1563-1566
 - 19 **Adachi Y**, Shiraishi N, Kitano S. Modern treatment of early gastric cancer: review of the Japanese experience. *Dig Surg* 2002; **19**: 333-339
 - 20 **Amano Y**, Ishihara S, Amano K, Hirakawa K, Adachi K, Fukuda R, Watanabe M, Fukumoto S, Fujishiro H, Imaoka T. An assessment of local curability of endoscopic surgery in early gastric cancer without satisfaction of current therapeutic indications. *Endoscopy* 1998; **30**: 548-552
 - 21 **Ishigami S**, Hokita S, Natsugoe S, Tokushige M, Saihara T, Iwashige H, Aridome K, Aikou T. Carcinomatous infiltration into the submucosa as a predictor of lymph node involvement in early gastric cancer. *World J Surg* 1998; **22**: 1056-1059
 - 22 **Kurihara N**, Kubota T, Otani Y, Ohgami M, Kumai K, Sugiura H, Kitajima M. Lymph node metastasis of early gastric cancer with submucosal invasion. *Br J Surg* 1998; **85**: 835-839
 - 23 **Yasuda K**, Shiraishi N, Suematsu T, Yamaguchi K, Adachi Y, Kitano S. Rate of detection of lymph node metastasis is correlated with the depth of submucosal invasion in early stage gastric carcinoma. *Cancer* 1999; **85**: 2119-2123
 - 24 **Yamada H**, Nihei Z, Yamashita T, Shiota Y, Ichikawa W, Sugihara K. Is lymphadenectomy needed for all submucosal gastric cancers? *Eur J Surg* 2001; **167**: 199-203
 - 25 **Gotoda T**, Yanagisawa A, Sasako M, Ono H, Nakanishi Y, Shimoda T, Kato Y. Incidence of lymph node metastasis from early gastric cancer: estimation with a large number of cases at two large centers. *Gastric Cancer* 2000; **3**: 219-225

Microarray-based method for detecting methylation changes of p16^{Ink4a} gene 5'-CpG islands in gastric carcinomas

Peng Hou, Jia-Yao Shen, Mei-Ju Ji, Nong-Yue He, Zu-Hong Lu

Peng Hou, Jia-Yao Shen, Mei-Ju Ji, Nong-Yue He, Zu-Hong Lu, Chien-Shiung Wu Laboratory, Department of Biological Science and Medical Engineering, Southeast University, Nanjing 210096, Jiangsu Province, China

Supported by the National Natural Science Foundation of China, No. 60121101; and the National High Technology Research and Development Program of China, No. 2002AA2Z2004

Correspondence to: Professor Zu-Hong Lu, Chien-Shiung Wu Laboratory, Department of Biological Science and Medical Engineering, Southeast University, Nanjing 210096, Jiangsu Province, China. zhlu@seu.edu.cn

Telephone: +86-25-83792245 **Fax:** +86-25-83619983

Received: 2004-02-11 **Accepted:** 2004-03-18

Abstract

AIM: Aberrant DNA methylation of CpG site is among the earliest and most frequent alterations in cancer. Several studies suggest that aberrant methylation of the CpG sites of the tumor suppressor gene is closely associated with carcinogenesis. However, large-scale analysis of candidate genes has so far been hampered by the lack of high-throughput approach for analyzing DNA methylation. The aim of this study was to describe a microarray-based method for detecting changes of DNA methylation in cancer.

METHODS: This method used bisulfite-modified DNA as a template for PCR amplification, resulting in conversion of unmethylated cytosine, but not methylated cytosine, into thymine within CpG islands of interest. Therefore, the amplified product might contain a pool of DNA fragments with altered nucleotide sequences due to differential methylation status. Nine sets of oligonucleotide probes were designed to fabricate a DNA microarray to detect the methylation changes of p16 gene CpG islands in gastric carcinomas. The results were further validated by methylation-specific PCR (MSP).

RESULTS: The experimental results showed that the microarray assay could successfully detect methylation changes of p16 gene in 18 gastric tumor samples. Moreover, it could also potentially increase the frequency of detecting p16 methylation from tumor samples than MSP.

CONCLUSION: Microarray assay could be applied as a useful tool for mapping methylation changes in multiple CpG loci and for generating epigenetic profiles in cancer.

Hou P, Shen JY, Ji MJ, He NY, Lu ZH. Microarray-based method for detecting methylation changes of p16^{Ink4a} gene 5'-CpG islands in gastric carcinomas. *World J Gastroenterol* 2004; 10(24): 3553-3558

<http://www.wjgnet.com/1007-9327/10/3553.asp>

INTRODUCTION

The epigenetic event has been observed in GC-rich regions, called CpG islands, frequently located in the promoter and the

first exon regions of genes. CpG island hypermethylation is closely associated with transcriptional inactivation of tumor suppressor genes, which is a common feature in human carcinomas^[1]. Hypermethylated CpG islands therefore play a causal role in promoting tumor development and are useful molecular markers for cancer diagnosis and prognosis. p16, an inhibitor of the cyclin D-dependent protein kinases, is a classic tumor suppressor gene, and its inactivation is closely associated with carcinogenesis. Hypermethylation of the CpG islands of the p16 gene has been proposed as an alternative mechanism for the loss of p16 expression. p16 hypermethylation could be detected in each stage, which is consistent with the finding that aberrant methylation of p16 is a very early event in carcinogenesis^[2]. Detection of promoter hypermethylation of cancer-related genes may be useful for cancer diagnosis or the detection of recurrence^[3,4].

At present, several molecular biology methods are routinely used to determine the methylation status of a CpG island, such as Southern blot^[5], bisulfite genomic DNA sequencing^[6], restriction enzyme-PCR^[7], methylation-specific PCR (MSP)^[8], methylation-sensitive single nucleotide primer extension (MS-SNuPE)^[9], electrochemistry^[10], etc. Among these, bisulfite nucleotide sequencing is a standard technique for detailed mapping of methylated cytosine residues within a gene promoter. This meticulous method, developed by Frommer *et al.*^[6], relies on the ability of sodium bisulfite to deaminate cytosine residues into uracil in genomic DNA, whereas the methylated cytosine residues are resistant to this modification. The target DNA is then amplified by PCR with specific primers to yield fragments in which all uracil residues are converted to thymine, whereas methylated cytosine residues are amplified as cytosine. The PCR products are sequenced and the methylation status of individual CpG sites is then analyzed by comparing it with the unmodified sequences of a given promoter. Using this conventional method, many investigators have addressed the importance of promoter CpG hypermethylation in the regulation of specific gene transcription in cancer^[11-14]. The method, which requires cloning and sequencing of individual inserts, can be labor intensive and is restricted to the evaluation of DNA methylation on a gene-by-gene basis. Such an approach has given researchers a limited picture of complex epigenetic alterations in cancer. Clearly, it is of great importance to establish novel, reliable and high-throughput methods for the methylation detection of earlier cancer diagnosis.

For this purpose, considerable advances have been made in hybridization-based microarray technology for genome-wide analysis of gene mutations and single nucleotide polymorphisms^[15-17]. In this new approach, oligonucleotides are arrayed on solid supports known as probes, and the labeled complex DNA mixtures to be interrogated are known as targets^[18]. Recently, we developed an oligonucleotide microarray to analyze methylation patterns of several adjacent CpG sites^[19]. The DNA microarray can successfully map the methylation pattern of p16^{Ink4a} gene. However, it can not be used to quantify the methylation level of promoter region of gene. Gitan *et al.*^[20] have developed a methylation specific oligonucleotide (MSO) microarray to analyze methylation of human estrogen receptor (ER) α gene. The targets were derived from PCR products of bisulfite-modified DNA, whereas the probes used a series of

arrayed oligonucleotides that can discriminate between converted and unconverted nucleotides, that is, unmethylated and methylated cytosines, at CpG sites. The MSO microarray is a novel and powerful tool for determining the methylation level in multiple CpG island loci and for generating epigenetic profiles in cancer.

The aim of this study was to use oligonucleotides microarray method to analyze methylation changes of p16 gene CpG islands in gastric carcinomas. A 336 bp segment was selected in the 5' untranslated region and the first exon of the p16 gene, as the investigated target, which contain 32 CpG sites. Nine sets of oligonucleotide probes were designed to test 23 CpG sites within the island. Here, we described the oligonucleotide microarray procedure and its application for analyzing the methylation changes of p16 gene CpG islands in gastric tumor and corresponding normal tissues.

MATERIALS AND METHODS

Tissue samples

Eighteen gastric tumor and corresponding normal tissues were obtained from Gulou Hospital (Nanjing, China). Genomic DNA was isolated by standard methods using proteinase K digestion and phenol/chloroform extraction.

Bisulfite genomic sequencing

Bisulfite processing of DNA was performed as described by Frommer *et al.*^[6] and the modifications introduced by Clark *et al.*^[21]. Briefly, 1 µg of genomic DNA was digested by *EcoR* I and denatured in 0.35 mol/L NaOH at 37 °C for 20 min. Bisulfite reaction was carried out in 3.2 mol/L sodium bisulfite and 0.5 mmol/L hydroquinone (Sigma Chemical Co., USA) at 55 °C for 16-24 h. DNA was recovered by a desalting column (DNA Clean-Up System, Promega Inc., USA) and desulphonated in 0.2 mol/L NaOH at 37 °C for 15 min, neutralized by ammonium acetate, alcohol precipitated, dried and then dissolved in 30 µL of deionized water. After bisulfite processing, all unmethylated cytosine residues converted to uracil, whereas the methylated ones remained unchanged. For bisulfite genomic sequencing the sense strand of a 336 bp fragment of the p16 gene 5'-CpG island corresponding to nucleotides -128 to +208 relatively to the transcription start site^[22] was amplified with primers which did not contain cytosine in a CpG context and consequently annealed to the methylated status of the island. The sequence of forward primer is 5'-AAA GAG GAG GGG TTG GTT GGT TAT TA-3' and that of backward primer is 5'-TAC CTA ATT CCA ATT CCC CTA CAA ACT-3'. (Forward primer position 5-30 and reverse primer position 310-336 in GenBank accession number U12818). PCR-reaction was performed in a buffer containing 10 mmol/L Tris-HCl (pH 9.0), 50 mmol/L KCl, 1 g/L Triton X-100, 50 g/L DMSO, 1.75 mmol/L MgCl₂, 0.2 mmol/L of each dNTP and 1 µL bisulphite treated DNA. Amplification conditions were as follows: at 95 °C for 5 min; followed by 35 cycles, each at 95 °C for 1 min, at 62 °C for 1 min, and extension at 72 °C for 30 s, and ended with an extension at 72 °C for 7 min and quickly chilled to 4 °C on a PTC-225 thermocycler (MJ Research). PCR products were gel purified and cloned into the pMD18-T vector according to the manufacturer's instructions (TAKARA). Part of the same PCR products was fluorescently labeled later for MSO microarray analysis. Plasmid DNA from 30 positive recombinant clones was isolated, and inserts were sequenced on an automated sequence analyzer (ABI377A, Applied Biosystem Inc., USA).

Oligonucleotide microarray

Nine sets of paired oligonucleotides used in this study were designed to include two or three CpG sites of the p16 CpG island to be interrogated (Table 1). These oligonucleotides were specific to the bisulfite-modified sequence of portion of the p16 CpG island.

Each was synthesized with amino-linked C6 [NH₂(CH₂)₆] linker attached to its 5' end. These oligonucleotides were suspended in sodium carbonate buffer (0.1 mol/L, pH 9.0) to a final concentration of 80 µmol/L. Approximately, 1 nL (0.05-0.1 pmole) of each oligonucleotide was printed on the aldehyde-coated glass slides (DAKO) using a PixSys5500 microarrayer (Cartesian Technology Inc). After printed, the glass slides were incubated in a humid chamber at room temperature overnight, and then at 37 °C for 2 h. The slides were washed thoroughly in 1 g/L SDS to remove unbound oligonucleotides. After further treatment with a NaBH₄ solution for 15 min, the slides were ready for hybridization. For target labeling, PCR products of bisulfite-treated DNA were labeled with Cy3-dCTP (Amersham Pharmacia) by terminal transferase (TAKARA). The unincorporated dCTP was removed by passing the labeled target through a micro-Biospin column (Bio-Rad). The labeled products were resuspended in hybridization solution (1:3 dilution v/v). Then the mixture was denatured at 95 °C for 5 min, cooled to room temperature, and applied to the DNA microarray slides. Microarray hybridization was conducted in a moist hybridization chamber under a cover slip at 42 °C for 2 h. After hybridization, the slide was rinsed and washed at room temperature with 2×SSC-1 g/L SDS and 0.1×SSC-1 g/L SDS for a total of 15 min, respectively, and then dried by centrifugation at 600 rpm for 5 min.

Table 1 Nucleotide sequences of methylated and unmethylated probes analyzed in oligonucleotide microarray

p16 CpG sites	Oligonucleotide sequences	Tm (°C)
#4-6	M: 5'-NH ₂ -(T) ₁₀ -CAACCGCCGAACGCAC-3'	56
	U: 5'-NH ₂ -(T) ₁₀ -CAACCACCAAACACAC-3'	50
#8-10	M: 5'-NH ₂ -(T) ₁₀ -CAACCGCCGAACGCAC-3'	61
	U: 5'-NH ₂ -(T) ₁₀ -CCACCACCCACTACCTA-3'	53
#11-13	M: 5'-NH ₂ -(T) ₁₀ -CCGCGCCGACTCCAT-3'	61
	U: 5'-NH ₂ -(T) ₁₀ -CCACCACCAACTCCAT-3'	53
#15-17	M: 5'-NH ₂ -(T) ₁₀ -AACCGCGACCGTAACCAA-3'	58
	U: 5'-NH ₂ -(T) ₁₀ -AACCACAACCATAACCAA-3'	50
#18,19	M: 5'-NH ₂ -(T) ₁₀ -TCTACCCGACCCCGAACC-3'	60
	U: 5'-NH ₂ -(T) ₁₀ -TCTACCCAACCCCAAACC-3'	55
#20,21	M: 5'-NH ₂ -(T) ₁₀ -AACAACGCCCGCACCTC-3'	57
	U: 5'-NH ₂ -(T) ₁₀ -AACAACACCCACACCTC-3'	50
#22,23	M: 5'-NH ₂ -(T) ₁₀ -ACAACGCCCCCGCCTC-3'	59
	U: 5'-NH ₂ -(T) ₁₀ -ACAACACCCCCACCTC-3'	52
#24,25	M: 5'-NH ₂ -(T) ₁₀ -AACTATTCGATACGTTAAAC-3'	48
	U: 5'-NH ₂ -(T) ₁₀ -AACTATTCATACATTAAC-3'	39
#26-28	M: 5'-NH ₂ -(T) ₁₀ -ATCGACCTCCGACCGTAAC-3'	55
	U: 5'-NH ₂ -(T) ₁₀ -ATCAACCTCCAACCATAAC-3'	49

Image scanning and data processing

DNA microarray slide was scanned with ScanArray Lite microarray analysis systems (A Packard BioScience Company, USA) after the above treatment. Images acquired by the scanner were analyzed with software Genepix Pro 3.0. Each spot was defined by the positioning of a grid of circles over the array image. For each fluorescent image, the average pixel intensity within each circle was determined and a local background using mean pixel intensity was computed for each spot. The net signal was determined by subtraction of this local background from the mean average intensity for each spot. The data generated by the software were exported in a spreadsheet format and processed using Microsoft Excel. Statistical analyses were conducted using Origin 5.0 software.

Methylation-specific PCR (MSP)

The 5'-CpG island regions of the p16 gene were amplified with primers for methylated and unmethylated DNA, respectively. Primer pairs described in Table 2^[8] were synthesized and purified by Shengyou Inc (Shanghai, China). PCR amplification was performed in a buffer containing 10 mmol/L Tris-HCl (pH 9.0), 50 mmol/L KCl, 1 g/L Triton X-100, 50 g/L DMSO, 1.75 mmol/L

MgCl₂, 0.2 mmol/L of each dNTP and 1 μL bisulfite treated DNA in a final volume of 30 μL. The amplification was carried out for 35 cycles (30 s at 95 °C, 30 s at the annealing temperature listed in Table 2, and 30 s at 72 °C), followed by a final 4-min extension at 72 °C and quickly chilled to 4 °C on a PTC-225 thermocycler (MJ Research). Products amplified with both types of primers were examined on 10 g/L agarose gel.

Table 2 MSP primers used for amplification of p16 gene CpG island. MS and US represent methylated and unmethylated sense primers, respectively. MA1 and MA2, UA1 and UA2 represent methylated and unmethylated antisense primers, respectively

Primer sets	Sequences (5'→3')	Size bp	Annealing temp (°C)
MS	TTATTAGAGGGTGGGGCGGATCGC	234	65
MA1	CCACCTAAATCGACCTCCGACCG		
US	TTATTAGAGGGTGGGGTGGATTGT	234	60
UA1	CCACCTAAATCAACCTCCAACCA		
MS	TTATTAGAGGGTGGGGCGGATCGC	150	65
MA2	GACCCCGAACCGCGACCGTAA		
US	TTATTAGAGGGTGGGGTGGATTGT	151	60
UA2	CAACCCCAACCAACCAATAA		

RESULTS

Figure 1 outlines the MSO strategy for DNA methylation analysis. Test DNA samples were bisulfite-modified, PCR amplified products contained pools of DNA fragments with altered nucleotide sequences due to their differential methylation status. As shown, the unmethylated allele of a given DNA sequence was expected to have the unmethylated cytosine of the tested CpG sites converted to thymine, whereas these CpG sequences remained unchanged in the methylated allele. Target DNA was then hybridized to arrayed oligonucleotide probes specifically designed to discriminate between converted and unconverted nucleotides at these CpG sites.

A 336 bp segment was selected in the 5' untranslated region and the first exon of the p16 gene, as the investigated target, which contains 32 CpG sites (Figure 2). Nine sets of oligonucleotide probes were designed to test 23 CpG sites within the island, each set contained a pair of methylated and unmethylated oligonucleotides for interrogating 2 or 3 CpG sites in close proximity (Table 1). First, control DNA targets were used to test the accuracy and reproducibility of probes designed for microarray hybridization. We selected fully methylated and unmethylated ones as positive and negative controls from 36 positive recombinant clones. The positive control generated in this way remained 100% cytosine in the tested CpG sites, whereas the negative control had all cytosine residues converted into thymine in the tested CpG sites. Next, a series of microarray hybridization were performed with mixtures of Cy3 labeled positive and negative DNA targets at different proportions representing 0%, 25%, 50%, 75%, and 100% of DNA methylation

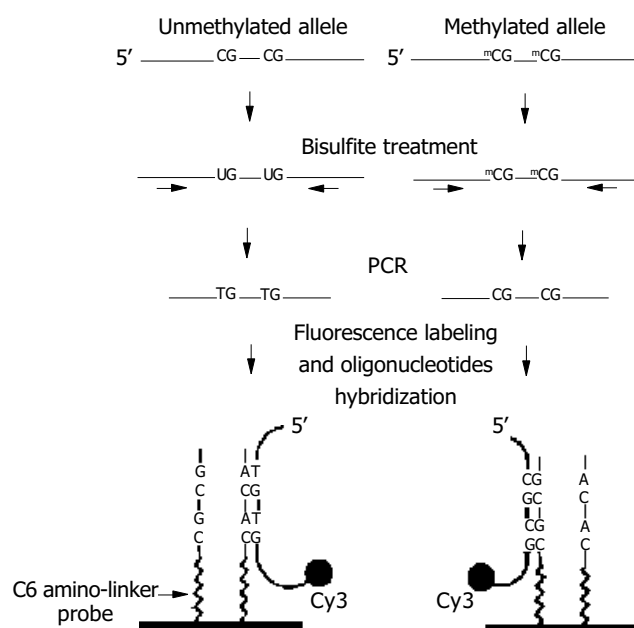


Figure 1 Schematic outline for analysis of DNA methylation based on oligonucleotide microarray^[20]. Genomic DNA was bisulfite treated and amplified by PCR for a specific CpG island region of interest. The amplified product was labeled with Cy3 fluorescence dye and hybridized to oligonucleotide probes attached to a glass surface. At left an oligonucleotide probe was designed to form a perfect match with a target DNA containing the unmethylated allele. At right a probe was designed to form a perfect match with the methylated DNA target.

to test the linearity of the protocol. An example of the microarray analysis for CpG#26-28 is shown in Figure 3A. The average intensity of hybridization signals from the four replicate spots for the methylated (M) and unmethylated (U) alleles was then derived and used to calculate the intensity ratio of M/(M+U). In this case, a linear relationship ($R_2 = 0.9882$) was established, showing that the increase in DNA methylation was proportional to the increase in intensity ratios in the control samples. The result suggested that this set of oligonucleotide probes was optimal for the detection of methylation changes at CpG#26-28. This approach was used to test other oligonucleotide probes and to generate a set of standards for the calibration of DNA methylation changes in the test samples (Figure 3B). We noticed that the regression line for CpG#24, 25 was much higher on the Y-axis than the rest of the CpG sites. Moreover, its slope was much lower than the others. This higher nonspecific hybridization was likely due to the lower melting temperature of the unmethylated probe. An oligonucleotide sequence such as this would result in the compression of the usable scale and make the assessment of methylation status a little more challenging.

Microarray assay was used to analyze the methylation status of 18 gastric tumor and corresponding normal tissues. Figure 4

GGCTGGCTGGTACCAGAGGGTGGGGCGGACCGCGTG⁴CGCT⁵CGG⁶CG
GCTGCGGAGAGGGGAGAGCAGGCAG⁸CGGG⁹CGG¹⁰CGGGAGCAGCA
TGGAGC¹¹CGG¹²CGG¹³CGGGGAGCAGCATGGAGCCTTCGGCTGACTGGC
TGGCCA¹⁵CGGC¹⁶CG¹⁷CGGCC¹⁸CGGGGT¹⁹CGGGTAGAGGAGGTG²⁰CGG
G²¹CGCTGCTGGAGG²²CGGGGG²³CGCTGCCAA²⁴CGCAC²⁵CGAATAGTT
A²⁶CGGT²⁷CGGAGGC²⁸CGATCCAGGTGGGTAGAGGGTCTGCAGCGGGAG
CAGGGGATGGCGGGCGACTCTGGAGGACGAAGTTTGCAGGGGAATTGG
AATCAGGTAGCGC

Figure 2 Nucleotide sequences of the 5' untranslated region and the first exon of the p16 gene (Genbank accession no.U12818.1 GI: 533724). The 23 CpG sites tested by oligonucleotide microarray are underlined and shown in bold.

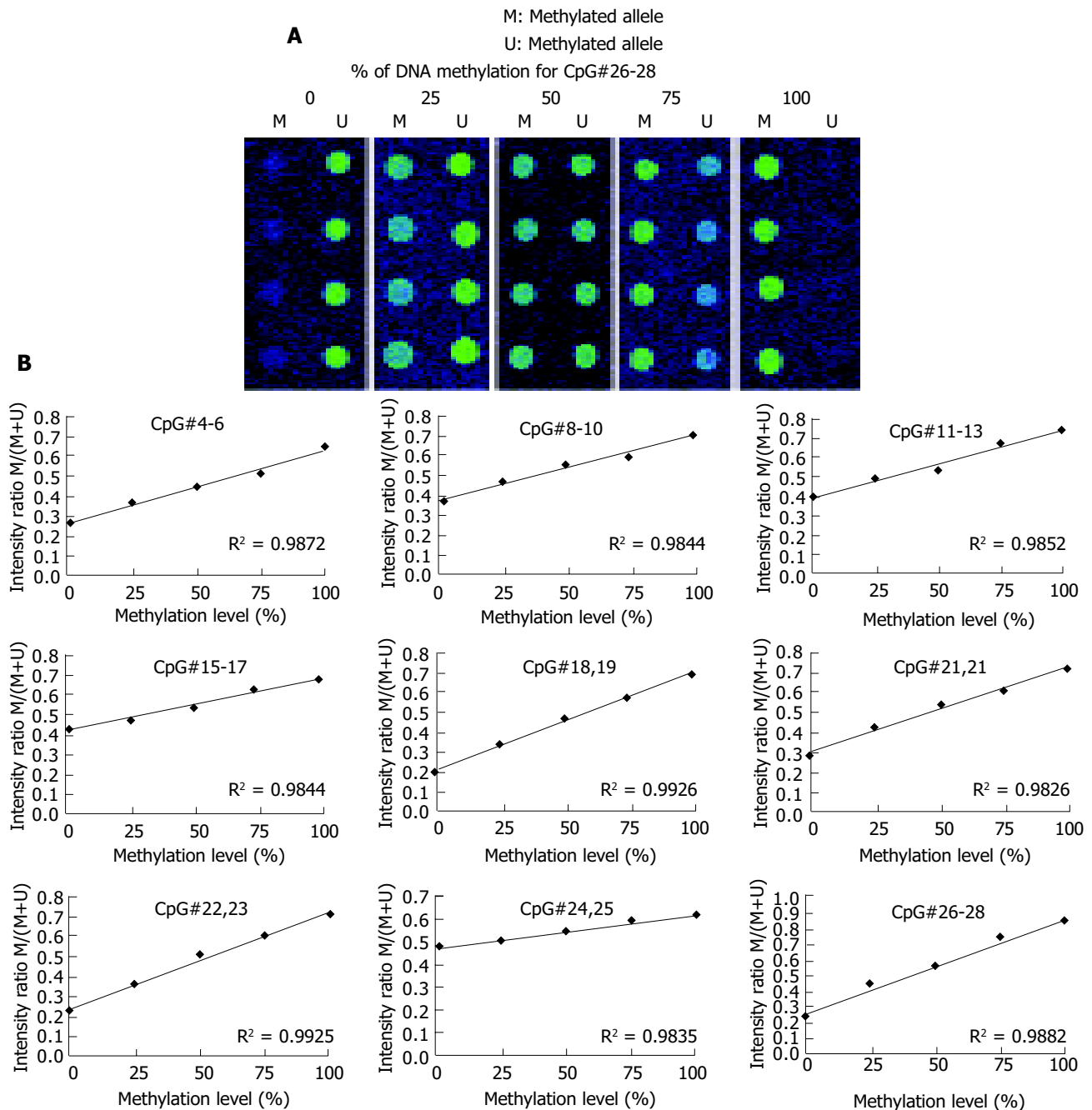


Figure 3 Standardization curve for microarray assays. A: Mixtures of fully methylated and unmethylated control DNA (from 36 positive recombinant clones) prepared and amplified by PCR using bisulfite primers for the p16 gene CpG island. B: A calibration curve for measuring methylation changes at the p16 gene CpG sites.

shows the representative examples of microarray results. By use of the standard curves derived from the aforementioned calibration controls, no methylation was detected in the normal tissues. Extensive methylation of the p16 CpG island was observed in 7 of 18 gastric tumor tissues (T1, T2, T3, T8, T9, T11, and T18), a modest degree of methylation was found in T10 and T15, whereas little or no methylation was seen in others (Figure 5).

To further validate the microarray findings in gastric tumors, methylaton-specific PCR (MSP) was conducted in 18 tumor and corresponding normal tissues. The primers MA1 and MA2 for MSP included CpG#16-19 and CpG#26-28 sites, respectively. Therefore, CpG#15-17 and CpG#26-28 sites were used for this conformation. A representation of the MSP analysis is shown in Figure 6. By use of this approach, two normal tissues were completely unmethylated (N4 and N8). MSP results of the 18 gastric tumor tissues completely matched with microarray results. Interestingly, the MSP results indicated that the methylation

was not detected in T1 when the amplification was performed with primers MS and MA2, whereas the methylation could be found in T1 when the amplification was performed with primers MS and MA1 (Figure 6). A most possible reason was that some CpG sites were not methylated in the region of primer MA2. Figure 5 indicates that CpG#15-17 sites had no methylation in T1, whereas CpG#26-28 sites had 47% methylation in T1, which were consistent with the MSP results.

The above results indicated that microarray assay could potentially increase the frequency of detecting p16 methylation from tumor samples than MSP. MSP was a simple, sensitive, and specific method for determining the methylation status of virtually any CpG-rich region. However, methylation could not be detected when some CpG sites were not methylated in region of MSP primers. The issue could be easily overcome using microarray assay. Furthermore, microarray assay could estimate which CpG sites (or CpG-rich region) were easily methylated in certain tumors.

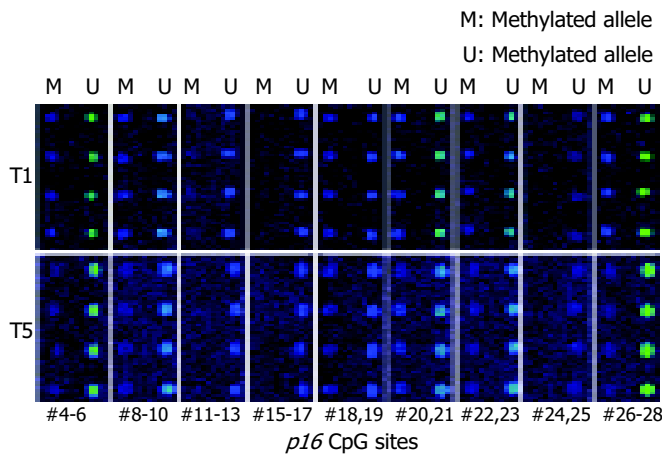


Figure 4 Methylation analysis of 23 CpG sites in p16 gene CpG island using oligonucleotide microarray.

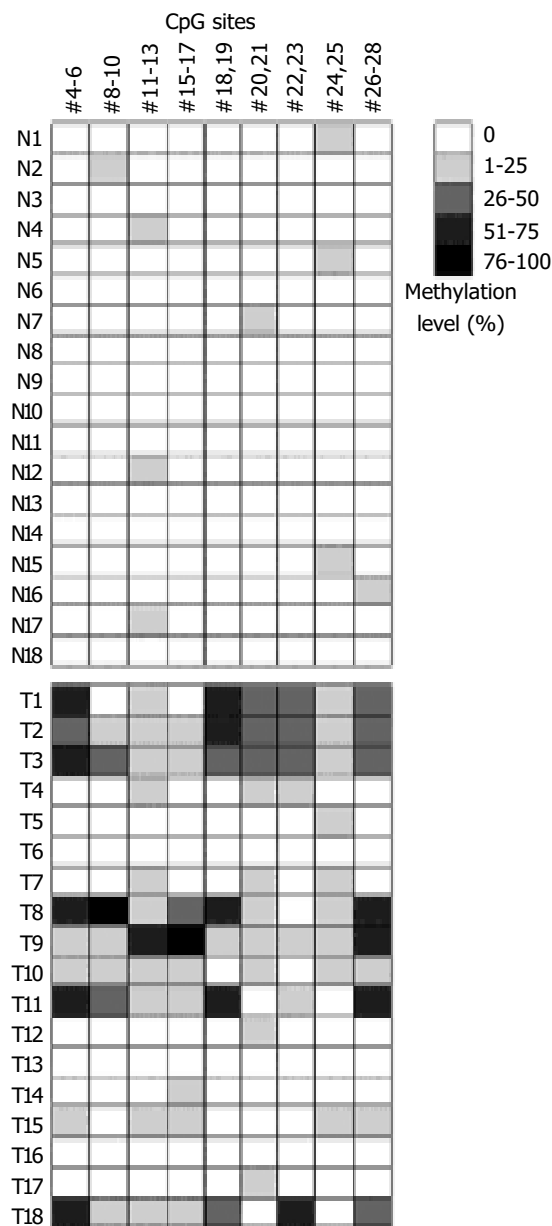


Figure 5 Methylation analysis of p16 gene CpG islands by oligonucleotide microarray. Summaries of the microarray results are shown for 18 gastric tumors and corresponding normal tissues. Gray scale shown at right represents the methylation levels in percentage determined from the calibration curve for the test CpG sites.



Figure 6 MSP analysis of the p16 gene CpG island in gastric tumor (T) and corresponding normal (N) tissues. M and U indicate amplification using methylated and unmethylated sequence-specific primers, respectively. DNA extracted from tumor and the corresponding normal tissues were amplified with primers MS and MA1 (A) and MS and MA2 (B), respectively. (Pos) Positive control; (Neg) negative control; (Mr.) DNA marker.

DISCUSSION

In this study, we have applied a microarray method to a comprehensive analysis of DNA methylation. The results indicated that the microarray was successfully used to map methylated CpG sites within the p16 gene CpG islands in clinical samples. The derived methylation information for gastric tumor and corresponding normal tissues was assessed quantitatively and independently validated by methylation-specific PCR.

This microarray-based analysis of DNA methylation is expected to provide new tools for research in this field. At present, most methylation assays have been limited to analyzing CpG islands of a few known genes and are restricted in throughput for a genome-wide analysis. Until recently, Gitan *et al.*^[20] have developed a novel technique called MSO microarray that combines bisulfite DNA assay and oligonucleotides microarray for analysis of DNA methylation. The MSO microarray potentially allows rapid screening of multiple CpG sites in many gene promoters. CpG island hypermethylation has been reported to be linked to the silencing of more than 100 cancer-related genes. A DNA microarray can be generated to contain hundreds of oligonucleotides designed to discriminate between methylated and unmethylated sequences in these gene promoters. Bisulfite-treated genomic DNA from each of these loci can be amplified from investigated samples in a 96-well format to generate multiple targets for oligonucleotides hybridization.

As with other oligonucleotide microarrays, cross-hybridization between imperfect-match probes and targets could be observed. In addition, some probes might inherently diminish hybridization signals, probably due to decreased duplex stability of targets and probes^[18]. Through careful data analysis, Gitan and his colleagues considered that cross-reactivity might also increase when oligonucleotide probes were designed to query methylation differences in one single CpG site. The issue is easily overcome by designing probes to include two or more CpG sites. This design consideration may limit the MSO assay's ability to detect methylation changes in single CpG sites. Adorjan *et al.*^[23] have developed a microarray-based assay that can analyze methylation changes of single CpG sites. Several hundred CpG sites were screened in 76 samples from four different human tumor types and corresponding healthy controls. The results demonstrated that the microarray could be applied as a powerful tool to the assessment of selected CpG dinucleotides and quantification of methylation at each site. As shown in this study, the use of a simple control system could test the accuracy and reproducibility of the probes designed for microarray hybridization. This control system can also be used to calibrate the levels of methylation changes detected in the investigated samples by microarray assay.

In summary, microarray assay can be readily used to high-throughput analysis of DNA methylation. It will contribute significant information to our understanding of CpG island methylation in cancer.

REFERENCES

- 1 **Baylin SB**, Herman JG, Graff JR, Vertino PM, Issa JP. Alteration in DNA methylation: a fundamental aspect of neoplasia. *Adv Cancer Res* 1998; **72**: 141-196
- 2 **Belinsky S**, Nikula KJ, Palmisano WA, Michels R, Saccomanno G, Gabrielson E, Baylin SB, Herman JG. Aberrant methylation of p16^{INK4a} is an early event in lung cancer and a potential biomarker for early diagnosis. *Proc Natl Acad Sci U S A* 1998; **95**: 11891-11896
- 3 **Valenzuela MT**, Galisteo R, Zuluaga A, Villalobos M, Nunez MI, Oliver FJ, Ruiz JM. Assessing the use of p16^{INK4a} promoter gene methylation in serum for detection of bladder cancer. *Eur Urol* 2002; **42**: 622-630
- 4 **Esteller M**, Sanchez-Cespedes M, Rosell R, Sidransky D, Baylin S, Herman JG. Detection of aberrant promoter hypermethylation of tumor suppressor genes in serum DNA from non-small cell lung cancer patients. *Cancer Res* 1999; **59**: 67-70
- 5 **Bickle TA**, Kruger DH. Biology of DNA restriction. *Microbiol Rev* 1993; **57**: 434-450
- 6 **Frommer M**, McDonald LE, Millar DS, Collis CM, Watt F, Grigg GW, Molloy PL, Paul CL. A genomic sequencing protocol that yields a positive display of 5-methylcytosine residues in individual DNA strands. *Proc Natl Acad Sci U S A* 1992; **89**: 1827-1831
- 7 **Kane MF**, Loda M, Gaida GM, Lipman J, Misbra R, Goldman H, Jessup JM, Kolodner R. Methylation of the hMLH1 promoter correlates with lack of expression of hMLH1 in sporadic colon tumors and mismatch repair-defective human tumor cell lines. *Cancer Res* 1997; **57**: 808-811
- 8 **Herman JG**, Graff JR, Myohanen S, Nelkin BD, Baylin SB. Methylation-specific PCR: a novel PCR assay for methylation status of CpG islands. *Proc Natl Acad Sci U S A* 1996; **93**: 9821-9826
- 9 **Kuppuswamy MN**, Hoffmann JW, Kasper CK, Spitzer SG, Groce SL, Bajaj SP. Single nucleotide primer extension to detect genetic diseases: experimental application to hemophilia B (factor IX) and cystic fibrosis genes. *Proc Natl Acad Sci U S A* 1991; **88**: 1143-1147
- 10 **Hou P**, Ji M, Ge C, Shen J, Li S, He N, Lu Z. Detection of methylation of human p16^{INK4a} gene 5'-CpG islands by electrochemical method coupled with linker-PCR. *Nucleic Acids Res* 2003; **31**: e92
- 11 **Hiltunen MO**, Alhonen L, Koistinaho J, Myohanen S, Paakkonen M, Marin S, Kosma VM, Janne J. Hypermethylation of the APC (adenomatous polyposis coli) gene promoter region in human colorectal carcinoma. *Int J Cancer* 1997; **70**: 644-648
- 12 **Stirzaker C**, Millar DS, Paul CL, Warnecke PM, Harrison J, Vincent PC, Frommer M, Clark SJ. Extensive DNA methylation spanning the Rb promoter in retinoblastoma tumors. *Cancer Res* 1997; **57**: 2229-2237
- 13 **Rice JC**, Massey-Brown KS, Futscher BW. Aberrant methylation of the BRCA1 CpG island promoter is associated with decreased BRCA1 mRNA in sporadic breast cancer cells. *Oncogene* 1998; **17**: 1807-1812
- 14 **Melki JR**, Vincent PC, Clark SJ. Concurrent DNA hypermethylation of multiple genes in acute myeloid leukemia. *Cancer Res* 1999; **59**: 3730-3740
- 15 **Ahrendt SA**, Halachmi S, Chow JT, Wu L, Halachmi N, Yang SC, Wehage S, Jen J, Sidransky D. Rapid p53 sequence analysis in primary lung cancer using an oligonucleotide probe array. *Proc Natl Acad Sci U S A* 1999; **96**: 7382-7387
- 16 **Favis R**, Barany F. Mutation detection in K-ras, BRCA1, BRCA2, and p53 using PCR/LDR and universal DNA microarray. *Ann N Y Acad Sci* 2000; **906**: 39-43
- 17 **Wen WH**, Bernstein L, Lescallett J, Beazer-Barclay Y, Sullivan-Halleyn J, White M, Press MF. Comparison of TP53 mutations identified by oligonucleotide microarray and conventional DNA sequence analysis. *Cancer Res* 2000; **60**: 2716-2722
- 18 **Hacia JG**. Resequencing and mutational analysis using oligonucleotide microarrays. *Nat Genet* 1999; **21**(Suppl): 42-47
- 19 **Hou P**, Ji M, Liu Z, Shen J, Cheng L, He N, Lu Z. A microarray to analyze methylation patterns of p16^{INK4a} gene 5'-CpG islands. *Clin Biochem* 2003; **36**: 197-202
- 20 **Gitan RS**, Shi H, Chen CM, Yan PS, Huang TH. Methylation-specific oligonucleotide microarray: a new potential for high-throughput methylation analysis. *Genome Res* 2002; **12**: 158-164
- 21 **Clark SJ**, Harrison J, Paul CL, Frommer M. High sensitivity mapping of methylated cytosines. *Nucleic Acids Res* 1994; **22**: 2990-2997
- 22 **Hara E**, Smith R, Parry D, Tahara H, Stone S, Peters G. Regulation of p16^{CDKN2} expression and its implications for cell immortalization and senescence. *Mol Cell Biol* 1996; **16**: 859-867
- 23 **Adorjan P**, Distler J, Lipscher E, Model F, Muller J, Pelet C, Braun A, Florl AR, Gütig D, Grabs G, Howe A, Kursar M, Lesche R, Leu E, Lewin A, Maier S, Müller V, Otto T, Scholz C, Schulz WA, Seifert HH, Schwöpe I, Ziebarth H, Berlin K, Pipenbrock C, Olek A. Tumour class prediction and discovery by microarray-based DNA methylation analysis. *Nucleic Acids Res* 2002; **30**: e21

Edited by Wang XL Proofread by Zhu LH and Xu FM

Alteration of *p53* and *p21* during hepatocarcinogenesis in tree shrews

Jian-Jia Su, Ke-Chen Ban, Yuan Li, Liu-Liang Qin, Hui-Yun Wang, Chun Yang, Chao Ou, Xiao-Xian Duan, Young-Lk Lee, Rui-Qi Yang

Jian-Jia Su, Yuan Li, Ke-Chen Ban, Liu-Liang Qin, Chun Yang, Chao Ou, Xiao-Xian Duan, Department of Experimental Pathology, Guangxi Cancer Institute, Nanning 530021, Guangxi Zhuang Autonomous Region, China

Hui-Yun Wang, Rui-Qi Yang, Cancer Center, Sun Yat-Sen University, Guangzhou 510080, Guangdong Province, China

Young-Lk Lee, Bioscience Research Division, Korea Research Institute of Bioscience and Biotechnology, South Korea

Supported by the National Natural Science Foundation of China, No. 39260033 and Natural Science Foundation of Guangxi, No. 0143058

Correspondence to: Professor Jian-Jia Su, Department of Experimental Pathology, Guangxi Cancer Institute, Nanning 530021, Guangxi Zhuang Autonomous Region, China. jianjiasu2002@yahoo.com

Telephone: +86-771-5331100 **Fax:** +86-771-5312000

Received: 2003-10-31 **Accepted:** 2004-01-12

development exists between HBV and AFB₁. *p53* mutation promotes the development of HCC. HBV and AFB₁ may synergistically induce *p53* gene mutation, and stimulate *ras* gene expression. *ras* gene is activated at the earlier stage during hepatocarcinogenesis. p21 protein may be an early marker, and the alterations of p53 may be a late event in the development of HCC.

Su JJ, Ban KC, Li Y, Qin LL, Wang HY, Yang C, Ou C, Duan XX, Lee YL, Yang RQ. Alteration of *p53* and *p21* during hepatocarcinogenesis in tree shrews. *World J Gastroenterol* 2004; 10(24): 3559-3563

<http://www.wjgnet.com/1007-9327/10/3559.asp>

Abstract

AIM: To investigate *p53* mutation and *p21* expression in hepatocarcinogenesis induced by hepatitis B virus (HBV) and aflatoxin B₁ (AFB₁) in tree shrews, and to reveal the role of these genes in hepatocarcinogenesis.

METHODS: Tree shrews were divided into four groups: group A, those infected with HBV and fed with AFB₁ ($n = 39$); group B, those infected with HBV alone ($n = 28$); group C, those fed with AFB₁ alone ($n = 29$); and group D, normal controls ($n = 20$). The tree shrews underwent liver biopsies once every 15 wk. Expression of p53 and p21 proteins and genes in the biopsies and tumor tissues of the experimental tree shrews was detected, respectively, by immunohistochemistry, and by Southern blotting and reverse transcription-polymerase chain reaction and sequencing.

RESULTS: The incidence of hepatocellular carcinomas (HCC) was higher in group A (66.7%) than that in group B (3.57%) and C (30%). The time of HCC occurrence was also earlier in group A than that in group C (120.0 ± 16.6 wk vs 153.3 ± 5.8 wk, respectively, $P < 0.01$). p53 protein was not detected by immunohistochemistry in all groups before the 75th wk of the experiment. At the 105th wk, the positive rates for p53 were 78.6%, 60% and 71.4% in groups A, B and C, respectively, which were significantly higher than that in group D (10%) (all $P < 0.05$). An abnormal band of *p53* gene was observed in groups A and C. The mutation points of *p53* gene in tree shrews with HCC were at codons 275, 78 and 13. The nucleotide sequence and amino acid sequence of tree shrew's wild-type p53 showed 91.7% and 93.4% homologies with those of human p53, respectively. The immunopositivity for p21 was found before HCC development. The incidence of HCC was significantly higher in tree shrews that were positive for p21 than those negative for p21 (80.0% vs 11.0%, $P < 0.001$). The incidence of HCC in p21 positive animals in group A was significantly higher than those positive for p21 in group C ($P < 0.05$).

CONCLUSION: A remarkable synergistic effect on HCC

INTRODUCTION

Hepatocellular carcinoma (HCC) is one of the world's most common cancers and is predominant in Africa and South-east Asia^[1]. Epidemiological studies indicated that contamination of food with aflatoxin B₁ (AFB₁) and chronic infection with hepatitis B virus (HBV) are the major risk factors for human HCC^[2,3].

p53, a tumor suppressor gene located on the short arm of chromosome 17, normally regulates the activity of the cell cycle machinery. Mutation of the *p53* gene has been observed with a high prevalence in diverse types of human cancer and frequently occurs with point mutation. The frequencies of *p53* mutation in HCC from different studies were varied from 18% to 67%^[4,5]. Mutation of G to T transversion at the third base of codon 249 of *p53* gene has been found in human HCC associated with high exposures to AFB₁ in Africa and Qidong, China^[6,7]. Where this mutation is absent from HCC in the area with negligible exposure to AFB₁. The *ras* gene coding for M_r 21 000 protein (p21) binds guanine nucleotides and possesses GTPase activity. Through this mechanism, the *ras* p21 participates in the control of cell proliferation, possibly as a signal transducer from cell surface receptors to the nucleus^[8]. *H-ras* oncogene could induce the metastatic phenotype of HCC cell *in vitro* to enhance its metastatic potential. The mutations of *ras* genes at codons 12, 13, and 61 leading to the increased expression of normal or mutant form of the p21 protein have been observed in human HCC and several other tumors^[9]. However, some report that *ras* proto-oncogene can enhance or inhibit the malignant phenotype *in vivo* in different systems^[10]. In the present study, using tree shrew (*Tupaia belangeri chinensis*) as an animal model for studying the development of HCC induced by human HBV and/or AFB₁, we investigated the alterations of p53 and p21 during hepatocarcinogenesis in tree shrews.

MATERIALS AND METHODS

Animals

Tree shrews were obtained from Kunming Medical Biology Institute, Chinese Academy of Sciences. One hundred and sixteen adult tree shrews weighed 127 ± 14.5 g. Animals were raised in stainless steel cage individually at room temperature of 25 ± 1 °C and fed with basic diet supplemented with fruits, milk, and eggs. Drinking water was given *ad libitum*.

HBV sera for infection

Sera positive for HBV surface antigen (HBsAg), e antigen (HBeAg) and antibody against c antigen (anti-HBc) were obtained from several blood donors. The titres of HBsAg and HBeAg were more than 1:1 024. The sera were preserved in a refrigerator at -40 °C and pooled before inoculation.

AFB₁

AFB₁ was purchased from Sigma Chemical Co., USA. It was dissolved into dimethylsulphoxide (DMSO) and mixed with milk to be sipped by tree shrews.

Reagents

Rabbit polyclonal antibody against human p53 protein (CM1) and avidin-biotin peroxidase complex kit were purchased from Vector Laboratories Inc., USA. RNase mini-kit was purchased from Qiagen Inc., Germany. PCR kit was the product of Stratagene Inc., USA. Rat antibody against human p21 (pan-ras) was purchased from Biosource Inc., USA.

Methods

Blood sample 1 mL was drawn through the femoral veins of each tree shrew before the experiment started. Some tree shrews were inoculated with 0.5 mL of human HBV-infected serum via the femoral vein. Three days later, another 0.5 mL of the same serum was injected peritoneally. After a week, the sera of these animals were checked weekly for HBV infection markers by enzyme-linked immunosorbent assay (ELISA). HBV-infected tree shrews confirmed by ELISA were randomly divided into group A (39 animals) and group B (28 animals). The un-inoculated tree shrews were randomly divided into group C (29 animals) and group D (20 animals). The animals of groups A and C were given AFB₁, 200-400 µg/kg·b.m. per day, while group D was used as control. Liver biopsies were performed in each group once every 15 wk. The samples of liver biopsy or HCC were cut into 2 pieces. One was fixed in 40 g/L buffered formaldehyde, and the other was kept at -80 °C after immersed in liquid nitrogen.

Southern blotting

Three samples of liver biopsy and 5 samples of HCC tissues stored at -80 °C were sent to Korea Research Institute of Bioscience and Biotechnology for Southern blotting to determine the p53 gene status.

Sequencing of p53

Total RNAs were extracted from 10 mg of frozen tumors or biopsied liver tissues. Exon 2-4 (415 bp) of the p53 gene was amplified using the forward primer CDF2: 5'-ATTGGCAGCCA GACTGCCTTCCGGG-3' and reverse primer CDR4: 5'-CGATT CTAGAGCAAACATCTTGTGAGGG-3'. Exon 5-11 (974 bp) of the p53 gene was amplified using the forward primer CDF5: 5'-CGATGAATTCTTGCATTCTGGGACAGCCAA-3', and reverse primer CDR11: 5'-CGATAAGCTTCTGACGCACACCT ATTGCAA-3'. The reactions containing 0.5 µg total RNA, 5 mmol/L MgCl₂, 1 mmol/L dNTP, 20 pmol of each primer, 40 units of RNase inhibitor, 5 units of AMV reverse transcriptase, 5 units of AMV Tag DNA polymerase in a final volume of 50 µL in mRNA selective PCR buffer were used. The mixture of reactants was incubated at 42 °C for 30 min followed by PCR amplification with 25 cycles of at 85 °C for 30 s and at 72 °C for 1 min. PCR products were analyzed on 15 g/L agarose gel containing ethidium bromide. The PCR product of p53 was purified and sequenced by an automatic DNA sequencer.

Immunohistochemistry for p53 and p21

p53 and p21 proteins were detected by immunohistochemical staining using the avidin-biotin complex (ABC) method on the

sections of liver tissues and tumors. In brief, formalin-fixed, paraffin-embedded sections were deparaffinized in xylene and were passed through ethanol series. After the endogenous peroxidase activity was blocked, the sections were rinsed in 0.01 mol/L PBS. Non-specific binding was blocked by treatment with 5% normal horse or goat serum for 20 min. Primary antibody was applied to the sections and incubated in a moist chamber overnight at 4 °C. After the sections were washed in 0.01 mol/L PBS, biotinylated horse or goat anti-mouse or rabbit immunoglobulin G was applied and sections were incubated for 50 min at room temperature. After washed, the sections were incubated with avidin-biotin-peroxidase complex for 50 min and then washed again. The chromogen, 3,3'-diaminobenzidine (DAB) was added for 5 to 10 min. Finally, the sections were washed and mounted. The section without primary antibody served as negative control.

Statistical analysis

Differences of HCC incidence and percentages of immunopositivity for p53 and p21 were analyzed by the Chi-square (χ^2) test. The difference of the average time for appearance of HCC was analyzed by the Student's *t* test.

RESULTS

The first case of HCC appeared at the 83rd wk of the experiment in group B. At that time the number of living animals in groups A, B, C and D were 39, 28, 29 and 20, respectively. After feeding of AFB₁ for 105 wk, the amount of AFB₁ in groups A and C was 11.6-15.5 mg and 11.4-16.09 mg, respectively. The difference was not statistically significant. The experimental period was 160 wk.

Incidence of HCC

HCC occurred only in groups A, B and C, and the rates of HCC in those groups were 58.9% (23/39), 3.57% (1/28) and 20.68% (6/29), respectively. No HCC was observed in group D. One tree shrew died at the 120th wk in group B had two proliferating pale nodules with 0.5 cm in diameter. They were large proliferating nodules of liver cells under the microscope. Not only was the HCC incidence higher but also the average time for HCC appearance was significantly shorter in group A than that in group C (120±16.6 wk vs 153±5.8 wk, *t* = 3.336, *P* < 0.01).

p53 gene

No p53 protein was detected by immunohistochemistry in each group at the 75th wk. The percentages of immunopositivity for p53 in group A (78.6%), B (60%) and C (71.4%) were significantly higher than that in group D (10.0%) at the 105th wk. The positive rates for p53 in HCC samples were not significantly different between groups A and C (52.17%, 12/23 vs 50%, 3/6, *P* > 0.05). Immunopositive signal of p53 was located in nucleus of cell (Figure 1). At the 105th wk, the extra bands of p53 were detected in 2 of 3 liver biopsy tissues from group C but none from other groups by Southern blotting. One case from group C appeared a new band with a size of 12.8 kb and lost a normal band of 1.6 kb at the same time. This tree shrew developed HCC at the 120th wk. A new band of 3.4 kb was found in another case from group C. Before the experiment started and during the 15th to 75th wk of the experiment, totally 12 biopsy liver tissues from 2 animals in group C were detected by Southern blotting and a light extra band of 3.8 kb was found in the tissues of 45th wk. Two of 8 HCCs from group A also appeared an extra band of 4.8 kb. The point mutation of p53 gene from 3 of 8 tumors was found by sequencing. The mutations were at codons 275, 78 and 13 (changing proline to serine, T→C transversion at the first nucleotide of codon 275; changing cysteine to arginine, A→G transversion at the third position of codon 78; C→T transversion

Table 1 Status of p53 gene from liver and tumor tissues of tree shrews

Animal (Groups)	Treatment		Tissues	Grade of tumors	Status of p53 gene	Change of nucleic acid
	HBV	AFB ₁				
5201 (C)	-	+	liver	-	wt	-
5207 (C)	-	+	tumor	I	wt	-
5063 (A)	+	+	tumor	II	mt (78)	GCA-GCG
5067 (A)	+	+	tumor	II	wt	-
5172 (A)	+	+	tumor	III	mt (13)	CCT-CTT
5173 (A)	+	+	tumor	II	mt (275)	TGT-CGT
1 (D)	-	-	liver	-	wt	-
2 (D)	-	-	liver	-	wt	-

Wt: wild type; mt: mutation.

Table 2 Expression of p21 in normal liver and liver tumor tissues of tree shrews

Group	No. of animals (n)	incidence of HCC (%)	p21+		p21-	
			Animal (n)	Incidence of HCC (%)	Animal (n)	Incidence of HCC (%)
A	39	23 (58.97) ^{bd}	16	16 (100.0) ^{af}	23	7 (30.43) ^{ij}
B	28	1 (3.57)	2	0	26	1 (3.84)
C	29	6 (20.68)	7	4 (54.14) ^h	22	2 (9.09)
D	20	0	0		20	0

^bP<0.01 vs Group C; ^dP<0.001 vs Group B; ^fP<0.001, p21+ vs p21- in Group A; ^hP<0.01, p21+ vs p21- in Group C; ^aP<0.05 vs Group C in p21+; ⁱP<0.01 vs Group B in p21-.

at the second position of codon 13; no amino acid change) (Table 1). The nucleotide sequence and amino acid sequence of tree shrew's wild-type p53 showed 91.7% and 93.4% homologies with those of human p53 sequence, and 77.2% and 73.4% homologies with mouse p53 sequence, respectively^[11].

**Figure 1** Expression of p53 protein located in nuclei of liver cancer cells (Original magnification: ×400).

p21 protein

p21 protein was located in plasma of liver cells (Figure 2) and overexpressed in totally 16 animals' liver tissues in group A during hepatocarcinogenesis. All those tree shrews developed HCC. However, only 7 of 23 tree shrews were p21-negative in liver tissues, and developed HCC in the same group at the end of experiment. The incidence of HCC was significantly higher in these p21-positive animals than in those negative ones. There were 2 animals positive for p21 protein in the liver tissues in group B, one of them died at the 120th wk and had 2 proliferating nodules with 0.5 cm in diameter. They were large proliferating nodules of liver cells under microscope. At the end of the experiment, 4 of 7 tree shrews that were positive for p21 developed HCC in Group C, whereas only 2 of 22 tree shrews that were negative for p21 developed HCC in this group. p21 overexpression was not found in group D (Table 2). Totally 25 animals were positive for p21 in liver tissues in all groups and

20 of them developed HCC (80%), while only 10 of totally 91 animals which were negative for p21 developed HCC (10.99%). Only 1 sample of HCC tissue was positive for p21 in all 30 samples of HCC tissues (Table 3).

Table 3 Relationship between p21 expression and HCC development

Group	Animal (n)	HCC (n)	Rate of HCC (%)
p21-positive	25	20	80.0 ^b
p21-negative	91	10	10.99

^bP< 0.001 vs p21-negative.

**Figure 2** p21 protein located in plasma of liver cells (Original magnification: ×200).

DISCUSSION

Animals in groups A and B were verified for infection with human HBV^[12]. In the present study, not only was the incidence of HCC significantly higher but also the average time for HCC development was shorter in the animals both infected with HBV and exposed to AFB₁ than those infected with HBV and exposed to AFB₁ alone. These results provided further support for the existence of the synergistic effect between HBV and AFB₁ in tree shrew's hepatocarcinogenesis^[13-15]. Even though

only one case of HCC developed in group B, which was infected with HBV alone, proliferation foci and/or nodules appeared quite early and frequently in this group. One tree shrew in group B which died at the 120th wk was found with 2 proliferating nodules with 0.5 cm in diameter in the liver. These results indicate that HBV has the capability of inducing liver cancer, but its capability is weak.

Wild type *p53* gene is the control gene at G₁ phase of cell cycle. It can inhibit DNA-damaged cell from entering G₁ phase and let the cell repair the damage^[16]. Mutated *p53* gene not only loses the functions that wild type *p53* has but also promotes malignant transformation of cells^[17]. All the liver tissues of tree shrews in all groups were negative for mutant *p53* protein by immunohistochemistry in early period of hepatocarcinogenesis. However, mutant *p53* proteins were detectable in the middle stage of hepatocarcinogenesis, before the appearance of HCC. This demonstrates that *p53* mutation occurs prior to the appearance of HCC. In the control group, no HCC developed and no mutant *p53* proteins and mutations of *p53* gene were detected, suggesting that the *p53* mutation is a crucial factor to initiate the malignant transformation of cell. The results of examining the status of *p53* gene by Southern blotting showed that 2 liver samples biopsied at the 45th wk in group C had an abnormal band of 3.8 kb. This indicates that the alteration of *p53* gene in the hepatocyte of tree shrew is dependent on a cumulative amount of AFB₁ and sufficient time, and also supports the finding that mutation of *p53* occurs before the appearance of HCC. The reason for loss expression of mutant *p53* in those 2 animals may be due to the low level of mutant *p53* protein. In the 8 samples sent to South Korea, *p53* mutation was not observed in 3 normal liver tissues, but 3 poorly-differentiated cases from the 5 HCC samples showed *p53* mutations. The rate of mutation was consistent with our previous report^[18]. It was also similar to the reports on human samples. The 3 tree shrews containing *p53* mutation gene were from group A treated by both HBV and AFB₁, implying that HBV and AFB₁ may play a synergistic role in *p53* mutation. This may be one of mechanisms that HBV synergies AFB₁ in hepatocarcinogenesis. *p53* mutations were located at codons 275, 78 and 13, respectively. No mutation was found at codon 249. It was differently from the mutation at codon 249 of the *p53* gene identified as a hotspot mutation in hepatocellular carcinomas occurring in populations exposed to AFB₁ and HBV^[4,5,19,20]. However, it was similar to the results of studies on non-human primate animal models^[21]. This discrepancy may be due to the different species, or too small amount of cases that were detected to find any mutation of *p53* at codon 249. Moreover, it also suggests that *p53* mutation, which is closely related to the development of HCC, does not merely occur at codon 249.

In HCC *ras* was first proved as one of the transforming genes, which belong to G-protein family gene. When it is converted to active oncogene by point mutation or gene amplification the signal transmission of cell membranes may change, which drives cell division, and results in abnormal differentiation and finally neoplasm formation. Oncogene *ras* directly takes part in human carcinogenesis, perhaps accounting for as many as 15-20% of all human tumors. It is well documented that the *ras* gene product, p21 protein, has GTPase activity and is involved in signal transduction. p21 is now well recognized for its essential function in transducing extracellular signals that regulate cell growth, survival, and differentiation. Overexpression and point mutations of *ras* gene were not only found in HCC^[22-23] but also found in liver cirrhosis and the correlation with liver cell dysplasia^[24]. We detected the p21 expression by immunohistochemistry in biopsied liver tissues of tree shrews at the 45th, 105th and 119th wk. The results showed that the accumulative total of positive rate for p21 in group A was 41.02%, which was significantly higher than that in group B (7.14%) and group C

(24.13%). This indicates that HBV and AFB₁ can synergistically activate *ras* gene in hepatocyte resulting in overexpression of p21^[25]. The p21 protein overexpression appeared before HCC development, indicating that the p21 protein overexpression is the early event during hepatocarcinogenesis and p21 protein may be an early marker in the development of HCC^[26]. In the present study, among the 25 animals that were positive for p21, 20 (80%) developed HCC whereas only 10 of 91 (10.99%) p21-negative animals developed HCC at the end of the experiment. This suggests that overexpression of p21 plays an important role in the development of HCC.

Comparison of the nucleotide and amino acid, sequences of human wild-type *p53* the structural homology was higher between tree shrews and human than between tree shrews and mouse^[11], indicating the tree shrew model is a useful animal model to study the etiology and pathogenesis of HCC in humans^[27].

REFERENCES

- 1 **Tang ZY**. Hepatocellular carcinoma-cause, treatment and metastasis. *World J Gastroenterol* 2001; **7**: 445-454
- 2 **Wang JS**, Huang T, Su J, Liang F, Wei Z, Liang Y, Luo H, Kuang SY, Qian GS, Sun G, He X, Kensler TW, Groopman JD. Hepatocellular carcinoma and aflatoxin exposure in Zhuqing village, Fusui County, People's Republic of China. *Cancer Epidemiol Biomarkers Prev* 2001; **10**: 143-146
- 3 **Smela ME**, Hamm ML, Henderson PT, Harris CM, Harris TM, Essigmann JM. The aflatoxin B (1) formamidopyrimidine adduct plays a major role in causing the types of mutations observed in human hepatocellular carcinoma. *Proc Natl Acad Sci U S A* 2002; **99**: 6655-6660
- 4 **Jackson PE**, Qian GS, Friesen MD, Zhu YR, Lu P, Wang JB, Wu Y, Kensler TW, Vogelstein B, Groopman JD. Specific *p53* mutations detected in plasma and tumors of hepatocellular carcinoma patients by electrospray ionization mass spectrometry. *Cancer Res* 2001; **61**: 33-35
- 5 **Shimizu Y**, Zhu JJ, Han F, Ishikawa T, Oda H. Different frequencies of *p53* codon-249 hot-spot mutations in hepatocellular carcinomas in Jiangsu province of China. *Int J Cancer* 1999; **82**: 187-190
- 6 **Hu W**, Feng Z, Eveleigh J, Iyer G, Pan J, Amin S, Chung FL, Tang MS. The major lipid peroxidation product, trans-4-hydroxy-2-nonenal, preferentially forms DNA adducts at codon 249 of human *p53* gene, a unique mutational hotspot in hepatocellular carcinoma. *Carcinogenesis* 2002; **23**: 1781-1789
- 7 **Bressac B**, Kew M, Wands J, Ozturk M. Selective G to T mutation of *p53* gene in hepatocellular carcinoma from southern Africa. *Nature* 1991; **350**: 429-431
- 8 **Wei S**, Kito K, Miyoshi A, Matsumoto S, Kauzi A, Aramoto T, Abe Y, Ueda N. Incidence of *p53* and *ras* gene mutations in DMBA-induced rat leukemias. *J Exp Clin Cancer Res* 2002; **21**: 389-396
- 9 **Basolo F**, Pinchera A, Fugazzola L, Fontanini G, Elisei R, Romei C, Pacini F. Expression of p21 *ras* protein as a prognostic factor in papillary thyroid cancer. *Eur J Cancer* 1994; **30**: 171-174
- 10 **Diaz R**, Lopez-Barcons L, Ahn D, Garcia-Espana A, Yoon A, Matthews J, Manges R, Perez-Soler R, Pellicer A. Complex effects of *Ras* proto-oncogenes in tumorigenesis. *Carcinogenesis* 2004; **25**: 535-539
- 11 **Park US**, Su JJ, Ban KC, Qin L, Lee EH, Lee YI. Mutations in the *p53* tumor suppressor gene in tree shrew hepatocellular carcinoma associated with hepatitis B virus infection and intake of aflatoxin B₁. *Gene* 2000; **251**: 73-80
- 12 **Yan RQ**, Su JJ, Huang DR, Gan YQ, Yang C, Huang GH. Human Hepatitis B virus and hepatocellular carcinoma. II. Experimental induction of hepatocellular carcinoma in tree shrews exposed to hepatitis B virus and aflatoxin B₁. *J Cancer Res Clin Oncol* 1996; **122**: 289-295
- 13 **Bannasch P**, Khoshkhou NI, Hacker HJ, Radaeva S, Mrozek M, Zillmann U, Kopp-Schneider A, Haberkorn U, Elgas M, Tolle T, Roggendorf M, Toshkov I. Synergistic hepatocarcinogenic effect of hepadnaviral infection and dietary aflatoxin B₁ in woodchucks. *Cancer Res* 1995; **55**: 3318-3330

- 14 **Kew MC.** Synergistic interaction between aflatoxin B1 and hepatitis B virus in hepatocarcinogenesis. *Liver Int* 2003; **23**: 405-409
- 15 **Li Y, Su JJ, Qin LL, Yang C, Ban KC, Yan RQ.** Synergistic effect of hepatitis B virus and aflatoxin B1 in hepatocarcinogenesis in tree shrews. *Ann Acad Med Singapore* 1999; **28**: 67-71
- 16 **Offer H, Erez N, Zurer I, Tang X, Milyavsky M, Goldfinger N, Rotter V.** The onset of p53-dependent DNA repair or apoptosis is determined by the level of accumulated damaged DNA. *Carcinogenesis* 2002; **23**: 1025-1032
- 17 **Balint EE, Vousden KH.** Activation and activities of the p53 tumor suppressor protein. *Br J Cancer* 2001; **85**: 1813-1823
- 18 **Su JJ, Qin GZ, Yan RQ, Huang DR, Yang C, Huang GH, Lotlikar PD.** Expression of p53 gene in hepatocellular carcinomas induced by aflatoxin B₁ with or without human hepatitis B virus in tree shrews. *Exp Mol Med* 1997; **29**: 177-182
- 19 **Zhu M, Dai Y, Zhan R.** HBxAg enhanced p53 protein accumulation in hepatoma cells. *Zhonghua Binglixue Zazhi* 1999; **28**: 31-34
- 20 **Lunn RM, Zhang YJ, Wang LY, Chen CJ, Lee PH, Lee CS, Tsai WY, Santella RM.** p53 mutations, chronic hepatitis B virus infection, and aflatoxin exposure in hepatocellular carcinoma in Taiwan. *Cancer Res* 1997; **57**: 3471-3477
- 21 **Rivkina MB, Cullen JM, Robinson WS, Marion PL.** State of the p53 gene in hepatocellular carcinomas of ground squirrels and woodchucks with past and ongoing infection with hepadnaviruses. *Cancer Res* 1994; **54**: 5430-5437
- 22 **Weihrauch M, Benicke M, Lehnert G, Wittekind C, Wrbitzky R, Tannapfel A.** Frequent k-ras -2 mutations and p16 (INK4A) methylation in hepatocellular carcinomas in workers exposed to vinyl chloride. *Br J Cancer* 2001; **84**: 982-989
- 23 **Parsons BL, Culp SJ, Manjanatha MG, Heflich RH.** Occurrence of H-ras codon 61 CAA to AAA mutation during mouse liver tumor progression. *Carcinogenesis* 2002; **23**: 943-948
- 24 **Feng Z, He R, Lu Z, Ling Y.** Expression of ras oncogene p21 product and proliferating cell nuclear antigen in liver cirrhosis and the correlation with liver cell dysplasia. *Zhonghua Ganzangbing Zazhi* 2000; **8**: 343-345
- 25 **Su JJ, Qin GZ, Yan RQ, Huang DR, Yang C, Lotlikar PD.** The expression of insulin-like growth factor II, hepatitis B virus X antigen and p21 in experimental hepatocarcinogenesis in tree shrews. *Ann Acad Med Singapore* 1999; **28**: 62-66
- 26 **Fearon ER.** K-Ras gene mutation as a pathogenetic and diagnostic marker in human cancer. *J Natl Cancer Inst* 1993; **85**: 1978-1980
- 27 **Cao J, Yang EB, Su JJ, Li Y, Chow P.** The tree shrews: adjuncts and alternatives to primates as models for biomedical research. *J Med Primatol* 2003; **32**: 123-130

Edited by Zhu LH and Chen WW Proofread by Xu FM

A novel, rapid strategy to form dendritomas from human dendritic cells and hepatocellular carcinoma cell line HCCLM3 cells using mature dendritic cells derived from human peripheral blood CD14+ monocytes within 48 hours of *in vitro* culture

Xin Guan, Ji-Run Peng, Lan Yuan, Hui Wang, Yu-Hua Wei, Xi-Sheng Leng

Xin Guan, Ji-Run Peng, Yu-Hua Wei, Xi-Sheng Leng, Center of Hepatobiliary Surgery, Peking University People's Hospital, 11 South Xizhimen Street, Beijing 100044, China

Hui Wang, Department of Hematology, Peking University People's Hospital, 11 South Xizhimen Street, Beijing 100044, China

Lan Yuan, Medical and Pharmaceutical Analysis Center, Peking University, 38 Xueyuan Street, Beijing 100083, China

Supported by the Key Program Foundation for Clinical Subject of the Ministry of Public Health, China (2001)

Co-first-authors: Xin Guan and Ji-Run Peng

Co-correspondents: Xin Guan

Correspondence to: Professor Xi-Sheng Leng, M.D., Ph.D., Center of Hepatobiliary Surgery, Peking University People's Hospital, 11 South Xizhimen Street, Beijing 100044, China. lengxs2003@yahoo.com.cn

Telephone: +86-10-68314422 Ext. 3500 **Fax:** +86-10-68318386

Received: 2004-02-27 **Accepted:** 2004-04-20

Abstract

AIM: Dendritomas formed by fusing cancer cells to dendritic cells have already been applied to clinical treatment trial of several types of cancers. Dendritic cells for the fusion in most trials and experiments were from blood monocytes in standard 7-d protocol culture, which requires 5-7 d of culture with granulocyte-macrophage-colony-stimulating factor (GM-CSF) and interleukin-4 (IL-4), followed by 2-3 d of activation with a combination of proinflammatory mediators such as tumor necrosis factor α (TNF α), interleukin-1 β (IL-1 β), interleukin-6 (IL-6) and prostaglandin E₂ (PGE₂). One study showed that mature monocyte-derived dendritic cells could be obtained within 48 h of *in vitro* culture with the same protocol as standard 7-d culture and referred to as FastDCs. Here we aimed to fuse human hepatocellular carcinoma cell line HCCLM3 cells with mature monocyte-derived dendritic cells within 48 h of *in vitro* culture (FastDC).

METHODS: HCCLM3 cells were cultured in RPMI 1640 with 150 mL/L fetal calf serum (FCS). CD14+ monocytes from healthy human peripheral blood were purified with MACS CD14 isolation kit and cultured in six-well plates in fresh complete DC medium containing RPMI-1640, 20 mL/L heat inactivated human AB serum, 2 mmol/L L-glutamine, 100 μ g/mL gentamicin, 1 000 U/mL GM-CSF and 500 U/mL IL-4 for 24 h, then proinflammatory mediators such as TNF α (1 000 U/mL), IL-1 β (10 ng/mL), IL-6 (10 ng/mL) and PGE₂ (1 μ g/mL) were supplemented for another 24 h, and thus mature FastDCs were generated. HCCLM3 cells and FastDCs were labeled with red fluorescent dye PKH26-GL and green fluorescent dye PKH67-GL respectively. After the red fluorescent-stained HCCLM3 cells were irradiated with 50 Gy, FastDCs and irradiated HCCLM3 cells were fused in 500 mL/L polyethylene glycol(PEG)+100 mL/L dimethyl sulfoxide (DMSO) to generate novel dendritomas. The FastDCs

and novel dendritomas were immunostained with anti-CD80, anti-CD86, anti-CD83, anti-HLA-DR mAbs and analyzed by fluorescence-activated cell sorting (FACS). Novel dendritomas were nucleus-stained with Hoechst 33258 and analyzed by confocal laser scanning microscopy.

RESULTS: Mature FastDCs with highly expressed surface markers CD80, CD86, CD83 and HLA-DR were generated within 48 h *in vitro*. Novel dendritomas with dual red-green fluorescence were constructed fast and successfully, and FACS analysis showed that the fusion efficiency was 24.27% and the novel dendritomas expressed the same activation markers as FastDCs. Confocal laser scanning microscopy analysis showed representative images of dendritomas.

CONCLUSION: Dendritomas can be formed fast with mature FastDCs from healthy human peripheral blood monocytes (PBMC) by incubation with GM-CSF and IL-4 for 24 h and by activation with proinflammatory mediators for an additional period of 24 h. Owing to shorter time required for *in vitro* DCs development, the generation of these novel dendritomas reduced labor and cost. This rapid method for formation of dendritomas may represent a new strategy for immunotherapy of hepatocellular carcinoma.

Guan X, Peng JR, Yuan L, Wang H, Wei YH, Leng XS. A novel, rapid strategy to form dendritomas from human dendritic cells and hepatocellular carcinoma cell line HCCLM3 cells using mature dendritic cells derived from human peripheral blood CD14+ monocytes within 48 hours of *in vitro* culture. *World J Gastroenterol* 2004; 10(24): 3564-3568

<http://www.wjgnet.com/1007-9327/10/3564.asp>

INTRODUCTION

Dendritic cells (DCs) are professional antigen-presenting cells (APCs) and play key roles in initiating and managing specific primary immune responses, including the activation of tumor-reactive cytotoxic T cells (CTLs)^[1,2]. The fusion of DCs with tumor cells among various tumor vaccination strategies focusing on DCs has become a promising approach^[3,4]. At present, most experimental and clinical studies rely on the *in vitro* development of DCs from CD34⁺ progenitor cells or blood monocytes^[5-7]. Commonly, according to standard 7-d protocol, blood monocytes were cultured for 5-7 d with GM-CSF and IL-4 to develop immature DCs which were activated for another 2-3 d with monocyte-conditioned media (MCM) or a combination of proinflammatory mediators such as TNF α , IL-1 β , IL-6 and PGE₂ so that mature DCs with full T stimulatory capacity were obtained^[8]. It was reported that mature DCs in 48 h *in vitro* culture with the same combination of proinflammatory mediators as standard 7-d protocol's were obtained and referred to as FastDCs^[8]. The report indicated that FastDCs were as effective as monocyte-

derived DCs from standard 7-d protocol culture in stimulating primary antigen-specific Th1-type immune responses⁽⁸⁾. Here we aimed to fuse human hepatocellular carcinoma cell line HCCLM3 cells with mature dendritic cells (FastDCs) within 48 h of *in vitro* culture.

MATERIALS AND METHODS

Materials

All reagents were obtained from the indicated sources. GM-CSF, TNF α , IL-1 β , IL-6 were purchased from R&D Systems (Minneapolis, USA), IL-4 from Promega (USA), PKH26-GL, PKH67-GL, 500 mL/L PEG+100 mL/L DMSO, gentamicin, Hoechst 33258 and PGE₂ from Sigma-Aldrich China Inc. (Shanghai, China), Fetal calf serum (FCS), RPMI-1640 medium, L-glutamine, penicillin and streptomycin from Invitrogen (USA). All mAbs (anti-HLA-DR, APC-conjugated; anti-CD80, Cy-Chrome-conjugated; anti-CD86, APC-conjugated; anti-CD83, APC-conjugated) were obtained from BD PharMingen (USA), and CD14 isolation kit from Miltenyi Biotec. (Bergisch-Gladbach, Germany), and Ficoll-Hypaque from Pharmacia (Sweden), Human AB serum from Chuanye Inc. (Tianjin, China). Human HCCLM3 cell line was a gift from Professor Zhao-You Tang in Liver Cancer Institute (Zhongshan Hospital, Fudan University).

Methods

Culture of hepatocellular carcinoma HCCLM3 cells Human HCCLM3 cells were grown in complete culture medium containing RPMI-1640, 150 mL/L heat-inactivated FCS, 2 mmol/L L-glutamine, 100 U/mL penicillin and 100 μ g/mL streptomycin.

Isolation and culture of CD14+ monocytes Peripheral blood mononuclear cells (PBMC) were isolated from peripheral blood of healthy donors by Ficoll-Hypaque (1.077 g) density gradient centrifugation. CD14+ cells of the PBMC were separated by performing positive selection with CD14+ micro magnetic beads according to the manufacturer's instructions and subsequently cultured in six-well plates (1×10^6 cells/mL) in fresh complete DC medium (RPMI-1640, 20 mL/L heat inactivated human AB serum, 2 mmol/L L-glutamine, 100 μ g/mL gentamicin, supplemented with 1000 U/mL GM-CSF and 500 U/mL IL-4) for 24 h, followed by incubation with a combination of proinflammatory mediators such as TNF- α (1 000 U/mL), IL-1 β (10 ng/mL), IL-6 (10 ng/mL) and PGE₂ (1 μ g/mL) for another 24 h to produce FastDCs.

Analysis of FastDCs by fluorescence-activated cell sorting FastDCs were immunostained with the following mAbs: anti-CD80, anti-CD86, anti-CD83, anti-HLA-DR. Surface marker analysis was performed by fluorescence-activated cell sorting (FACS).

Fluorescent labeling of dendritic cells and human HCCLM3 cells Commercial fluorescent cell linker kits PKH67-GL and PKH26-GL were used for membrane labeling of FastDCs and HCCLM3 cells. The FastDCs were labeled fluorescent green with PKH67-GL and HCCLM3 cells were labeled fluorescent red with PKH26-GL. The whole procedure was performed at 25 °C. The cells to be stained were washed with serum-free RPMI-1640. The cell suspension was centrifuged at 400 r/min for 5 min to produce a cell pellet. The supernatant was removed, leaving less than 25 μ L medium on the pellet. One milliliter of diluent C was added to resuspend the cells. Then 4×10^{-6} molar dyes ($\times 2$) were prepared with diluent C immediately before staining. The cells in diluent C were added rapidly to one milliliter of $2 \times$ dye. The cells and dye were mixed by gentle pipetting. The mixture was incubated at 25 °C for 5 min. The staining process was stopped by adding an equal volume of FCS and incubating for 1 min. The stained cells were diluted with an equal volume of complete culture medium and centrifuged at 400 r/min for 10 min and removed for at least three washes. Then the cells were

resuspended in fresh complete medium. The staining efficiency was monitored by fluorescent microscopy.

Fusion of dendritic cells and human HCCLM3 cells After the red fluorescent-stained HCCLM3 cells were irradiated with 50 Gy, the DCs and irradiated HCCLM3 cells were fused together by mixing two cell types at an 1:1 ratio in a 50 mL conical centrifugation tube. One milliliter of fusogen containing 500 mL/L PEG+ 100 mL/L DMSO was added to the mixture by dropping for 1-1.5 min. Nine milliliters of serum-free RPMI-1640 with 25 mmol/L Hepes was added to the mixture for over 5 min. Forty milliliters of serum-free RPMI-1640 was added to the cell mixture and the mixture was pelleted by centrifugation at 800 r/min for 10 min. After the supernatant was removed, the cells were resuspended in one milliliter of complete culture medium.

Sort and analysis of novel dendritomas The fused cells were resuspended in phosphate-buffered saline for detection of dual fluorescent dendritomas by FACS.

The novel dendritomas were sorted based on dual green and red fluorescence using a FACS caliber cell sorter (Becton Dickinson, USA). The cells were centrifuged at 800 r/min for 15 min. After the supernatant was removed, the cells were immunostained with the same mAbs as for FastDCs and activation markers were analyzed.

Analysis of novel dendritomas by confocal laser scanning microscopy The fused cells were resuspended in phosphate-buffered saline and centrifuged at 400 r/min for 10 min. After the supernatant was removed, Hoechst 33258 for nucleus staining was dropped in and the cells were resuspended in phosphate-buffered saline 5 min later and centrifuged at 400 r/min for 10 min again. After the cells were fixed with 10 g/L paraformaldehyde, nucleus-stained cells were resuspended in phosphate-buffered saline for analysis of dendritomas by confocal laser scanning microscopy.

RESULTS

Characteristics of DCs derived from human peripheral blood CD14+ monocytes within 48 h of *in vitro* culture

Monocytes were enriched from PBMC by CD14-positive selection with MACS and subsequently cultured with GM-CSF and IL-4 for 48 h. Proinflammatory mediators such as TNF α , IL-1 β , IL-6 and PGE₂ were added to accelerate DCs maturation after 24 h of culture with GM-CSF and IL-4. The cells displayed mature DC activation markers such as CD83⁺⁺, CD80⁺⁺, CD86⁺⁺ and HLA-DR⁺⁺ within 48 h (Figure 1A) and formed long cytoplasmic protrusions typical of mature DCs, while monocytes cultured with GM-CSF and IL-4 alone for 48 h displayed and maintained monocyte-like morphology. Using this two-step differentiation strategy, a large number of mature and viable DCs (about 30% of the initial population of monocytes) could be obtained.

Staining efficiency of dendritic cells and human HCCLM3 cells

After FastDCs and HCCLM3 cells were labeled with PKH67-GL and PKH26-GL respectively, the cells were examined under fluorescent microscopy and more than 95% of the cells were stained successfully.

Fusion efficiency indicated by FACS analysis

FastDCs were stained fluorescent green with PKH67-GL and HCCLM3 cells were stained fluorescent red with PKH26-GL. The stained two cell types were fused together by admixing them and dropping fusogen. The novel dendritomas would take on dual fluorescence. FACS analysis showed that the percentage of red and green dual fluorescent dendritomas in the fused cell mixture was 24.27%, which represented fusion efficiency (Figure 2) and the novel dendritomas expressed the same markers as FastDCs (Figure 1B).

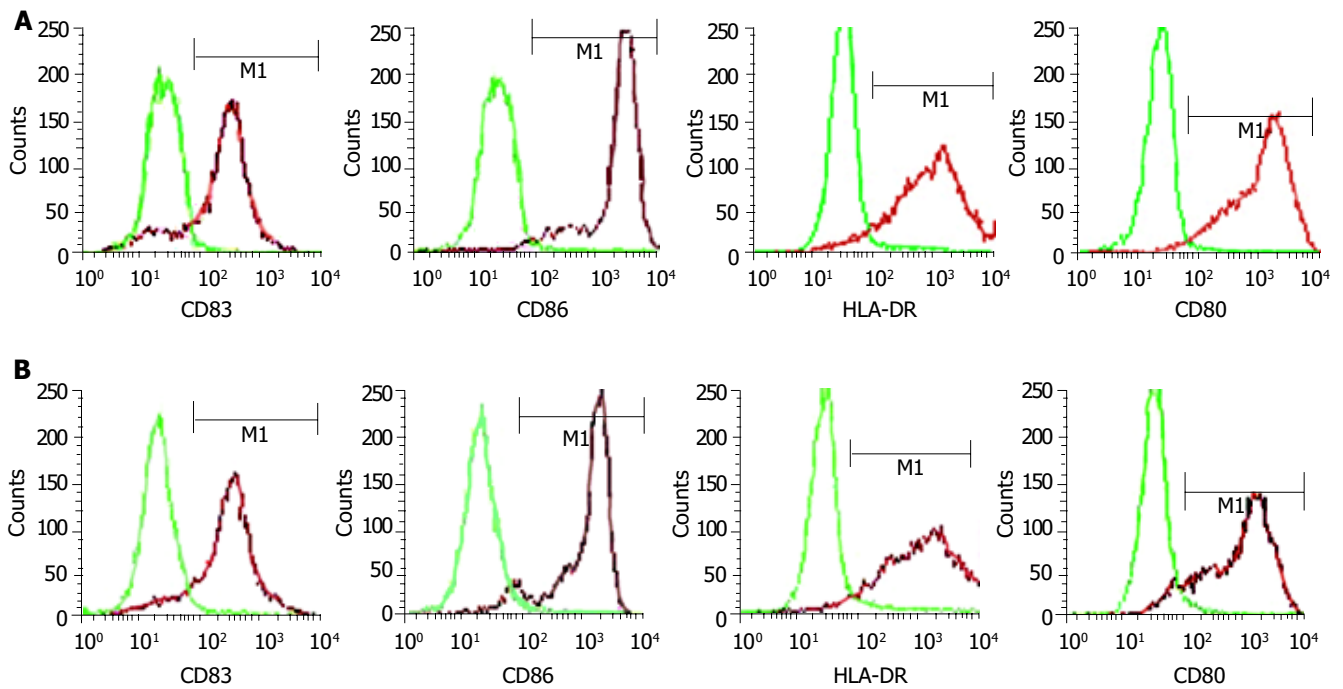


Figure 1 FACS analysis of activation markers on FastDCs and novel dendritomas. A: Expression of DCs activation markers on FastDCs determined by FACS. B: DCs activation markers expressing on novel dendritomas determined by FACS.

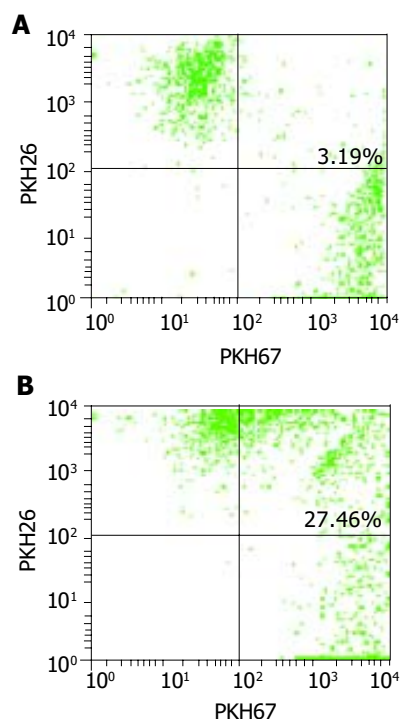


Figure 2 Fusion efficiency analysis by FACS. A: Control group (mixture): 3.19% dual-fluorescent cells. B: Fusion group: 27.46% dual-fluorescent cells.

Representative images of dendritomas under confocal laser scanning microscopy

FastDCs and HCCLM3 cells were stained with PKH67-GL and PKH26-GL respectively. After FastDCs and HCCLM3 cells were fused, nuclear counterstaining was performed using Hoechst 33258. Under confocal laser scanning microscopy, FastDCs were detected as green cells and HCCLM3 cells were detected as red and the representative image of a dendritoma was a dual fluorescent cell with two blue nuclei (Figure 3).

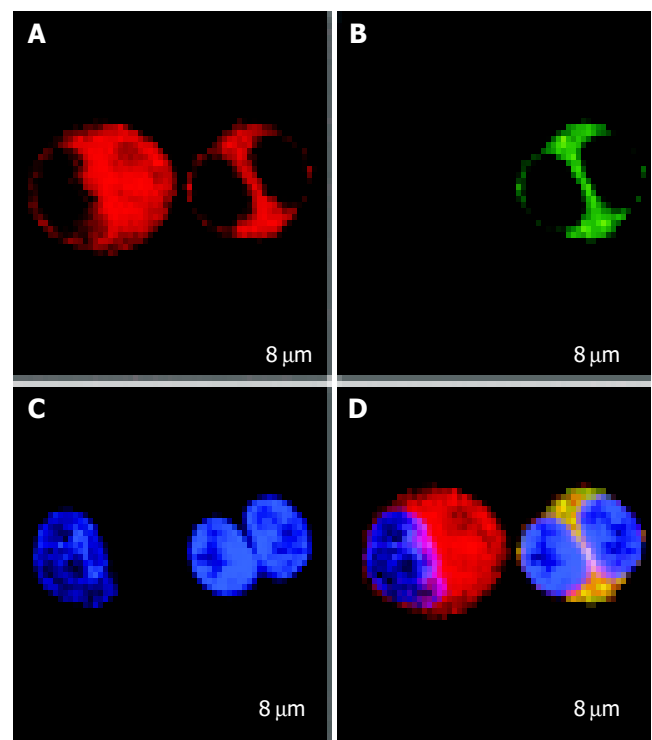


Figure 3 Images of novel dendritomas and HCCLM3 cells under confocal laser scanning microscopy. A: Red tumor and dendritoma cells. B: Green dendritoma cells. C: One dendritoma cell with two blue nuclei and one tumor cell with one nucleus. D: One dendritoma cell (right) characteristic of a dual-fluorescent cell with two blue nuclei while one red fluorescent tumor cell (left) with one nucleus.

DISCUSSION

As highly specialized antigen-presenting cells, DCs constitute a unique system of cells that induce and control immune responses. Owing to their unique ability to capture and present antigens, thereby inducing and managing immune responses,

DCs have become attractive vectors and targets for immunological intervention in numerous diseases and represent optimal candidates, especially for cancer immunotherapy. So far, various tumor vaccination strategies have been developed based on the loading of DCs with tumor-associated antigens (TAAs)^[9,10], including defined peptides of known sequences^[11-13], undefined acid-eluted peptides from autologous tumors^[14], whole tumor lysates^[15], tumor cell-derived RNA *et al.*^[16] Another promising alternative is the fusion of DCs with tumor cells^[3,4]. This approach is based on the idea that multiple TAAs are endogenously processed and presented by MHC class I molecules, thereby stimulating tumor-specific CTLs^[17].

In 1997, Gong *et al.*^[3] reported that they fused breast carcinoma cells with DCs to produce dendritomas which were capable of presenting antigens effectively and inducing antitumor-specific CTLs. Afterwards, a number of experimental and clinical trials with significant effects on several types of cancers such as melanoma, leukemia, glioma, gastric carcinoma, myeloma, renal cell carcinoma and ovarian carcinoma were reported^[18-31].

At present, DCs, for experimental and clinical fusion trial, were obtained mainly from *in vitro* standard 7-d protocol culture. In fact, the kinetics of DCs differentiation from blood monocytes under physiologic conditions might not be reflected by current standard protocols for the *in vitro* development of DCs^[8]. One research showed that a subpopulation of blood monocytes differentiated into DCs within 48 h in a model simulating transendothelial migration into lymphatic vessels^[31]. Dauer *et al.*^[8] reported that they cultured blood monocytes within 48 h *in vitro* with the same combination of proinflammatory mediators as standard 7-d protocol and obtained mature DCs with their ability similar to standard protocol DCs in stimulating primary antigen-specific Th1-type immune responses, and inducing the production of IFN γ and activating autologous naive T cells, and the DCs were referred to as FastDCs. We cultured and obtained FastDCs with activation markers using the same methods and successfully constructed dendritomas by fusing FastDCs with HCCLM3 cells. Our study showed that the fusion of the two cells was feasible and the novel dendritomas expressed the same surface markers as FastDCs. Compared with common standard protocol methods, this new strategy not only simplified the process and reduced labor, cost and time for the whole experiment procedure, but also may be less disrupted by microbial contamination.

In conclusion, our novel strategy may facilitate the use of dendritomas in clinical trials of cancer immunotherapy

ACKNOWLEDGMENTS

We express our gratitude to Professor Zhao-You Tang in Liver Cancer Institute of Zhongshan Hospital, Fudan University for his gift.

REFERENCES

- 1 **Banchereau J**, Steinman RM. Dendritic cells and the control of immunity. *Nature* 1998; **392**: 245-252
- 2 **Kurokawa T**, Oelke M, Mackensen A. Induction and clonal expansion of tumor-specific cytotoxic T lymphocytes from renal cell carcinoma patients after stimulation with autologous dendritic cells loaded with tumor cells. *Int J Cancer* 2001; **91**: 749-756
- 3 **Gong J**, Chen D, Kashiwaba M, Kufe D. Induction of antitumor activity by immunization with fusions of dendritic and carcinoma cells. *Nat Med* 1997; **3**: 558-561
- 4 **Soruri A**, Fayyazi A, Neumann C, Schlott T, Jung T, Matthes C, Zwirner J, Riggert J, Peters JH. Ex vivo generation of human antimelanoma autologous cytolytic T cells by dendritic cell/melanoma cell hybridomas. *Cancer Immunol Immunother* 2001; **50**: 307-314
- 5 **Caux C**, Dezutter-Dambuyant C, Schmitt D, Banchereau J. GM-CSF and TNF-alpha cooperate in the generation of dendritic Langerhans cells. *Nature* 1992; **360**: 258-261
- 6 **Romani N**, Gruner S, Brang D, Kampgen E, Lenz A, Trockenbacher B, Konwalinka G, Fritsch PO, Steinman RM, Schuler G. Proliferating dendritic cell progenitors in human blood. *J Exp Med* 1994; **180**: 83-93
- 7 **Sallusto F**, Lanzavecchia A. Efficient presentation of soluble antigen by cultured human dendritic cells is maintained by granulocyte/macrophage colony-stimulating factor plus interleukin 4 and downregulated by tumor necrosis factor alpha. *J Exp Med* 1994; **179**: 1109-1118
- 8 **Dauer M**, Obermaier B, Herten J, Haerle C, Pohl K, Rothenfusser S, Schnurr M, Endres S, Eigler A. Mature dendritic cells derived from human monocytes within 48 hours: a novel strategy for dendritic cell differentiation from blood precursors. *J Immunol* 2003; **170**: 4069-4076
- 9 **Thumer B**, Haendle I, Roder C, Dieckmann D, Keikavoussi P, Jonuleit H, Bender A, Maczek C, Schreiner D, von den Driesch P, Brocher EB, Steinman RM, Enk A, Kampgen E, Schuler G. Vaccination with mage-3A1 peptide-pulsed mature, monocyte-derived dendritic cells expands specific cytotoxic T cells and induces regression of some metastases in advanced stage IV melanoma. *J Exp Med* 1999; **190**: 1669-1678
- 10 **Mackensen A**, Herbst B, Chen JL, Kohler G, Noppen C, Herr W, Spagnoli GC, Cerundolo V, Lindemann A. Phase I study in melanoma patients of a vaccine with peptide-pulsed dendritic cells generated *in vitro* from CCD34 hematopoietic progenitor cells. *Int J Cancer* 2000; **86**: 385-392
- 11 **Mayordomo JI**, Zorina T, Storkus WJ, Zitvogel L, Celluzzi C, Falo LD, Melief CJ, Ildstad ST, Kast WM, Deleo AB. Bone marrow-derived dendritic cells pulsed with synthetic tumour peptides elicit protective and therapeutic antitumour immunity. *Nat Med* 1995; **1**: 1297-1302
- 12 **Porgador A**, Gilboa E. Bone marrow-generated dendritic cells pulsed with a class I-restricted peptide are potent inducers of cytotoxic T lymphocytes. *J Exp Med* 1995; **182**: 255-260
- 13 **Celluzzi CM**, Mayordomo JI, Storkus WJ, Lotze MT, Falo LD Jr. Peptide-pulsed dendritic cells induce antigen-specific CTL-mediated protective tumor immunity. *J Exp Med* 1996; **183**: 283-287
- 14 **Zitvogel L**, Mayordomo JI, Tjandrawan T, DeLeo AB, Clarke MR, Lotze MT, Storkus WJ. Therapy of murine tumors with tumor peptide-pulsed dendritic cells: dependence on T cells, B7 costimulation and T helper cell 1-associated cytokines. *J Exp Med* 1996; **183**: 87-97
- 15 **Fields RC**, Shimizu K, Mule JJ. Murine dendritic cells pulsed with whole tumor lysates mediate potent antitumor immune responses *in vitro* and *in vivo*. *Proc Natl Acad Sci U S A* 1998; **95**: 9482-9487
- 16 **Boczkowski D**, Nair SK, Snyder D, Gilboa E. Dendritic cells pulsed with RNA are potent antigen-presenting cells *in vitro* and *in vivo*. *J Exp Med* 1996; **184**: 465-472
- 17 **Der Bruggen P**, Zhang Y, Chau P, Stroobant V, Panichelli C, Schultz ES, Chapiro J, Van Den Eynde BJ, Brasseur F, Boon T. Tumor-specific shared antigenic peptides recognized by human T cells. *Immunol Rev* 2002; **188**: 51-64
- 18 **Trefzer U**, Weingart G, Chen Y, Herberth G, Adrian K, Winter H, Audring H, Guo Y, Sterry W, Walden P. Hybrid cell vaccination for cancer immune therapy: first clinical trial with metastatic melanoma. *Int J Cancer* 2000; **85**: 618-626
- 19 **Kugler A**, Stuhler G, Walden P, Zoller G, Zobywalski A, Brossart P, Trefzer U, Ullrich S, Muller CA, Becker V, Gross AJ, Hemmerlein B, Kanz L, Muller GA, Ringert RH. Regression of human metastatic renal cell carcinoma after vaccination with tumor cell-dendritic cell hybrids. *Nature Med* 2000; **6**: 332-336
- 20 **Gong J**, Nikrui N, Chen D, Koido S, Wu Z, Tanaka Y, Cannistra S, Avigan D, Kufe D. Fusions of human ovarian carcinoma cells with autologous or allogeneic dendritic cells induce anti-tumor immunity. *J Immunol* 2000; **10**: 1705-1711
- 21 **Galea-Lauri J**, Darling D, Mufti G, Harrison P, Farzaneh F. Eliciting cytotoxic T lymphocytes against acute myeloid leu-

- kemia-derived antigens: evaluation of dendritic cell-leukemia cell hybrids and other antigen-loading strategies for dendritic cell-based vaccination. *Cancer Immunol Immunother* 2002; **51**: 299-310
- 22 **Krause SW**, Neumann C, Soruri A, Mayer S, Peters JH, Andreessen R. The treatment of patients with disseminated malignant melanoma by vaccination with autologous cell hybrids of tumor cells and dendritic cells. *J Immunother* 2002; **25**: 421-428
- 23 **Kikuchi T**, Akasaki Y, Irie M, Homma S, Abe T, Ohno T. Results of a phase I clinical trial of vaccination of glioma patients with fusions of dendritic and glioma cells. *Cancer Immunol Immunother* 2001; **50**: 337-344
- 24 **Sloan AE**, Parajuli P. Human autologous dendritic cell-glioma fusions: feasibility and capacity to stimulate T cells with proliferative and cytolytic activity. *J Neurooncol* 2003; **64**: 177-183
- 25 **Gong J**, Koido S, Chen D, Tanaka Y, Huang L, Avigan D, Anderson K, Ohno T, Kufe D. Immunization against murine multiple myeloma with fusions of dendritic and plasmacytoma cells is potentiated by interleukin 12. *Blood* 2002; **99**: 2512-2517
- 26 **Homma S**, Matai K, Irie M, Ohno T, Kufe D, Toda G. Immunotherapy using fusions of autologous dendritic cells and tumor cells showed effective clinical response in a patient with advanced gastric carcinoma. *J Gastroenterol* 2003; **38**: 989-994
- 27 **Homma S**, Toda G, Gong J, Kufe D, Ohno T. Preventive antitumor activity against hepatocellular carcinoma (HCC) induced by immunization with fusions of dendritic cells and HCC cells in mice. *J Gastroenterol* 2001; **36**: 764-771
- 28 **Chen D**, Xia J, Tanaka Y, Chen H, Koido S, Wernet O, Mukherjee P, Gendler SJ, Kufe D, Gong J. Immunotherapy of spontaneous mammary carcinoma with fusions of dendritic cells and mucin 1-positive carcinoma cells. *Immunology* 2003; **109**: 300-307
- 29 **Zhang J**, Zhang JK, Zhuo SH, Chen HB. Effect of a cancer vaccine prepared by fusions of hepatocarcinoma cells with dendritic cells. *World J Gastroenterol* 2001; **7**: 690-694
- 30 **Akasaki Y**, Kikuchi T, Homma S, Abe T, Kufe D, Ohno T. Antitumor effect of immunizations with fusions of dendritic and glioma cells in a mouse brain tumor model. *J Immunother* 2001; **24**: 106-113
- 31 **Randolph GJ**, Beaulieu S, Lebecque S, Steinman RM, Muller WA. Differentiation of monocytes into dendritic cells in a model of transendothelial trafficking. *Science* 1998; **282**: 480-483

Edited by Kumar M and Wang XL Proofread by Xu FM

Differentially expressed genes between solitary large hepatocellular carcinoma and nodular hepatocellular carcinoma

Lian-Yue Yang, Wei Wang, Ji-Xiang Peng, Jie-Quan Yang, Gen-Wen Huang

Lian-Yue Yang, Wei Wang, Ji-Xiang Peng, Jie-Quan Yang, Gen-Wen Huang, Liver Cancer laboratory, Department of Surgery, Xiangya Hospital, Central South University, Changsha 410008, Hunan Province, China

Supported by National Key Technologies R and D Program of China during the 10th Five-year plan period, No. 2001BA703B04 and National Natural Science Foundation of China, No. 30371595 and Hunan Province Developing Planning Committee, No. 2001-907

Correspondence to: Professor Lian-Yue Yang, Department of Surgery, Xiangya Hospital, Changsha 410008, Hunan Province, China. lianyueyang@hotmail.com

Telephone: +86-731-4327326 **Fax:** +86-731-4327332

Received: 2003-12-19 **Accepted:** 2004-02-01

Abstract

AIM: To study the difference in gene expression between solitary large hepatocellular carcinoma (SLHCC) and nodular hepatocellular carcinoma (NHCC).

METHODS: Polymerase chain reaction (PCR) products of 8464 human genes were spotted on a chip in array. DNAs were then fixed on a glass plate. Total RNA was isolated from freshly excised human SLHCC ($n = 7$) and NHCC ($n = 15$) tissues, and was reversely transcribed to cDNAs with the incorporation of fluorescent dUTP for preparation of hybridization probes. The mixed probes were then hybridized to the cDNA microarray. After highly stringent washing, cDNA microarray was scanned for the fluorescent signals to display the difference between the two kinds of HCC. In addition, the expression of *RhoC* and *protocadherin LKC* was also detected with the reverse transcriptase polymerase chain reaction (RT-PCR) method.

RESULTS: Among the 8 464 human genes, 668 (7.89%) genes were expressed differentially at the mRNA levels between SLHCC and NHCC. Three hundred and fifty five (4.19%) genes, including *protocadherin LKC*, were up-regulated, whereas 313 (3.70%) genes, including *RhoC*, were down-regulated. The mRNA expression levels of *RhoC* and *protocadherin LKC* were confirmed by RT-PCR. Analysis of differentially expressed genes confirmed that our molecular data obtained by cDNA microarray were consistent with the published biochemical and clinical observations of SLHCC and NHCC.

CONCLUSION: cDNA microarray is an effective technique in screening the difference in gene expression between SLHCC and NHCC. Many of these differentially expressed genes are involved in the invasion and metastasis of HCC. Further analysis of these genes will help to understand the different molecular mechanisms of SLHCC and NHCC.

Yang LY, Wang W, Peng JX, Yang JQ, Huang GW. Differentially expressed genes between solitary large hepatocellular carcinoma and nodular hepatocellular carcinoma. *World J Gastroenterol* 2004; 10(24): 3569-3573

<http://www.wjgnet.com/1007-9327/10/3569.asp>

INTRODUCTION

Hepatocellular carcinoma (HCC) ranks one of the most common malignancies in the world. Although its morbidity and mortality have decreased recently in patients with surgically treated HCC, the long-term prognosis remains unsatisfactory because of the high recurrence and metastasis rate. It has been generally accepted that the invasive and metastatic potentials of HCC are mostly attributed to the individual clinical pathological and molecular biological characteristics. The diversity of biological characteristics determines the different invasive and metastatic potentials of HCC^[1]. In our institute, HCC was phenotypically divided into solitary large hepatocellular carcinoma (SLHCC, diameter >5 cm, and one node), nodular hepatocellular carcinoma (NHCC, node number ≥ 2) and small hepatocellular carcinoma (SHCC, diameter ≤ 5 cm). Our clinical observation implied different invasive and metastatic abilities between SLHCC and NHCC. To understand the mechanism of different invasive and metastatic potentials between SLHCC and NHCC, the changes in gene expression between SLHCC and NHCC need to be investigated.

Our previous investigations focused on the differentially expressed genes of integrin, matrix metalloproteinases-2 (MMP-2), vascular endothelial growth factor (VEGF), phosphatase and tensin homologue deleted on chromosome ten (PTEN), endoglin (CD105), survivin, which involved in invasion and metastasis, between SLHCC and NHCC^[2]. Given the complex molecular mechanisms of invasion and metastasis, however, it is not clear that expression of these specific genes alone can explain the diversity of molecular biological characteristics between SLHCC and NHCC. Therefore, a broad evaluation of difference in gene expression between SLHCC and NHCC is necessary.

cDNA microarray represents an important new tool to analyze human gene expression profiles. The technology enables investigators to measure the expression of several thousand mRNAs simultaneously in a biological specimen. It is technically possible to monitor almost the entire transcriptome, the collection of all mRNAs presented in a tumor specimen. cDNA microarray also enables us to study global gene profiles from various samples, thereby to speed up the identification of differentially expressed genes and the construction of different expression profiles. cDNA microarray analysis has become an increasingly popular tool to investigate the function of genes that are responsible for the phenotypes of diseases, to provide potential targets for treatment or prevention^[3-5].

Our study was designed to delineate the different expression gene profiles between SLHCC and NHCC from 22 patients to evaluate the difference in gene expression within the realm of 8 464 human genes for understanding the basement of the diversity of molecular biological characteristics between SLHCC and NHCC.

MATERIALS AND METHODS

Tissue specimens

The Ethics Committee of the Central South University approved the study protocol. Fresh surgical HCC was obtained from 22

(20 males and 2 females) patients, including 7 cases of SLHCC and 15 cases of NHCC with primary hepatocellular carcinoma who underwent hepatectomy at Xiangya Hospital of Central South University (CSU). The specimens were immediately freshly frozen in liquid nitrogen and stored at -80°C for RNA isolation. The median age of the patients was 52 year (range, 27-73 years). All specimens obtained from surgery resection were confirmed by pathological examination.

RNA isolation

Total RNA was extracted from frozen tissue specimens (30-100 mg) using TRIZOL (GIBCO BRL, Gaithersburg, USA) reagent according to the instructions provided by the manufacturer. The quality was checked on 10 g/L agarose gels and the concentration was measured using an ultraviolet spectrophotometer (Biochrom Ltd, Cambridge, England). The *uv* wavelength was adjusted at 260nm.

Construction of microarray

Microarray sequences included 8 464 full-length and partial complementary DNAs representing known, novel, and control genes were provided by United Gene Holdings, Ltd, Shanghai, China. The cDNA inserts were amplified by PCR using universal primers to plasmid vector sequences and then purified as described previously^[6]. The PCR products were then spotted onto silylated slides (CEL Associates, Houston, TX) using a Cartesian PixSys7500 motion control robot (Cartesian Technologies, Irvine, CA) fitted with Chipmaker micro-spotting technology (TeleChem International, Sunnyvale, CA). After spotting, the slide was exposed to ultraviolet light (65 mj/cm) and processed at room temperature by soaking in 2 g/L sodium dodecyl sulfate (SDS) for 10 min, distilled H_2O for 10 min, and 2 g/L sodium borohydride (NaBH_4) for 10 min. The slide was dried again and ready for use.

Probes of expression profile preparation

Individual RNA specimens from the same group of HCC were mixed equally to obtain 60 μg total RNA. Fluorescent cDNA probes were prepared through reverse transcription and then purified. RNA samples extracted from NHCC were labeled with Cy3-dUTP and those from SLHCC with Cy5-dUTP. The two color probes were then mixed, precipitated with ethanol and dissolved in 20 μL of hybridization solution containing 5 \times SSC (0.75 mol/L NaCl and 0.075 mol/L sodium citrate), 4 g/L SDS, 500 g/L formamide and 5 \times Denhardt's solution (1 g/L Ficoll, 1 g/L polyvinylpyrrolidone and 1 g/L bovine serum albumin).

Hybridization and washing

Microarrays was prehybridized with hybridization solution containing 5 g/L denatured salmon sperm DNA at 42°C for 6 h. Fluorescent probe mixtures were denatured at 95°C for 5 min, and the denatured probe mixtures were applied onto the prehybridized chip under a cover glass. Chips was hybridized at 42°C for 18 h. The hybridized chips was then washed at 60°C for 10 min each in solutions of 2 \times SSC and 2 g/L SDS, 0.1 \times SSC and 2 g/L SDS, and 0.1 \times SSC, then dried at room temperature.

Detection and analysis

The chip was scanned with Scan Array 4000 standard biochip scanning system (Packard Biochip Technologies, Virginia, USA). ImaGene 3.0 software (Bio Discovery, Los Angeles, USA) was used to analyze the intensity of spots. The intensities of each spot at the two wavelengths represented the quantity of Cy3-dUTP and Cy5-dUTP, respectively, hybridized to each spot. The ratio of Cy5 to Cy3 was computed for each location. Overall intensities were normalized with a correction coefficient obtained using the ratios of the housekeeping genes. Genes were identified as differentially expressed if the absolute value of the natural logarithm of the ratio was >0.69 . To minimize artifacts arising from low expression values, the genes with raw intensity values for Cy3 and Cy5 >800 counts were chosen for differential analysis.

RT-PCR

Total RNA (2 μg) was reversely transcribed in a final 25 μL reaction volume at 37°C for 1 h by using 200 U M-MULV reverse transcriptase (Promega, Madison, USA). PCR amplification was performed in a final volume of 50 μL containing 5 μL of first strand cDNA solution, 2 U of Taq polymerase (Sangon, Shanghai, China), 5 μL of 10 \times PCR reaction buffer, 10 $\mu\text{mol/L}$ of dNTP (Sangon, Shanghai, China) and 10 pmoL of each 3' and 5' sequence specific oligonucleotide primer (Sangon, Shanghai, China) for RhoC, protocadherin LKC and β_2 -microglobulin gene (positive control). The amplification was performed on a DNA thermal cycler (Perkin Elmer, Shelton, USA). The primer sequences and the annealing temperature are shown in Table 1. PCR products were electrophoresed on 17 g/L agarose gels. The bands representing amplified products were visualized using ethidium bromide during the exposure to a UV transilluminator. The density of the bands on the gel was quantified by densitometry analysis. The expression of the genes was presented by the relative intensity of the PCR product bands from target sequences to that from the β_2 -microglobulin gene^[7].

Statistical analysis

Statistical analysis was performed using the SPSS (version 11.0, Chicago, IL). The nonparametric Mann-Whitney test was performed to evaluate the differences in the expression of RhoC and protocadherin LKC between the groups. $P < 0.05$ was considered statistically significant.

RESULTS

Quality and examination of total RNA

Ethidium bromide-stained total RNA agarose gel of SLHCC and NHCC was performed (Figure 1). None of our analyzed samples had detectable RNA degradation present at the leading edge of the gel, which is critical for reproducible gene expression data. The productive rate of RNA from SLHCC and NHCC was 0.42-1.64 mg/g and 0.34-1.85 mg/g, respectively. The rate of A_{260}/A_{280} was 1.81-2.05. These results showed the high quality and purity of total RNA obtained.

Table 1 Primer sequences and annealing temperature for PCR

Gene		Primer sequences	Product size	Annealing temperature
RhoC	Up	5'-TCCTCATCGTCTTCAGCAAG-3'	183 bp	56 $^{\circ}\text{C}$
	Down	5'-CTGCAATCCGAAAGAAGCTG-3'		
protocadherin LKC	Up	5'-GAAGCTTCAAGCTATGAAAA-3	256 bp	52 $^{\circ}\text{C}$
	Down	5'-CCTTGATTTCTGACTGTTC-3'		
β_2 -MG	Up	5'-ACCCCACTGAAAAAGATGA-3'	120 bp	56 $^{\circ}\text{C}$
	Down	5'-ATCTCAAACCTCCATGATG-3'		

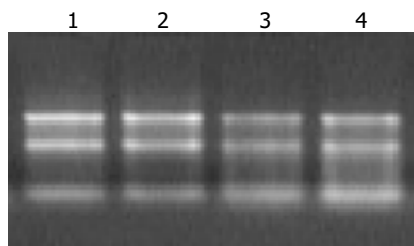


Figure 1 Ethidium bromide-stained 1% agarose gel of four RNA samples. There were sharp ribosomal bands and minimal degradation that was critical for expression analysis. Lanes 1 and 2 represent total RNA derived from SLHCC. Lanes 3 and 4 represent total RNA from NHCC.

Identification of genes differentially expressed between SLHCC and NHCC

By applying the threshold value of 2 (up-regulation) and 0.5 (down-regulation) for intensity ratio of SLHCC vs NHCC, 668 genes (7.89%) were selected as differentially expressed genes, including 355 up-regulated (4.19%) and 313 down-regulated (3.69%) genes (Figure 2). Consistent with the precision of the assay, scatter plots comparing SLHCC with NHCC showed a wide distribution of the ratio in which red or green spots represented differently expressed genes, while yellow spots were related to similarly expressed genes (Figure 3).

The result revealed that the activated and repressed genes represented a different subset of cellular genes with biochemical activities consistent with the physiology and pathology between SLHCC and NHCC. Collectively, the genes provided a quantitative view of the changes in gene expression that occurred at the level of the human genome between SLHCC and NHCC. Based on the function discrepancy of encoding proteins, these variably expressed genes were mainly divided into 15 classes (Table 2).

Detection mRNA expression of RhoC and protocadherin LKC in SLHCC and NHCC by RT-PCR

Expression of RhoC and protocadherin LKC mRNA was detected in all SLHCC and NHCC. SLHCC tissues revealed significantly higher levels of protocadherin LKC mRNA than NHCC ($P = 0.026$), and showed significantly lower levels of RhoC mRNA than NHCC ($P = 0.031$) (Figure 4). The results were consistent with the results of cDNA microarray.

Table 2 Numbers of variably expressed genes in SLHCC and NHCC

Class	No. of up-regulated genes	No. of down-regulated genes
Oncogenes and antioncogenes	6	5
Genes encoding proteins related to ionic channel and protein transportation	7	7
Genes encoding cellular cycle modulator	3	9
Genes associated with cellular stress	1	1
Genes associated with cellular skeleton and movement	5	7
Genes related to cellular apoptosis	2	2
Gene encoding proteins regulating synthesis, repair, and rearrangement of DNA	0	4
Genes encoding transcription factors and proteins binding with DNA	17	6
Cytokine receptor gene	4	3
Immunological protein gene	18	17
Genes associated with cellular metabolism	32	32
Genes encoding signal transductional factor	39	31
Genes encoding factors that regulated protein translation	11	37
Genes encoding proteins that were consistent with body growth and development	7	8
Other	203	144



Figure 2 cDNA microarray slide hybridized to SLHCC and NHCC shown before image analysis. The slide shown was spotted with 8 464 genes, hybridized to fluorescence-labeled cDNA, and exposed to scanArray 4000 for image capture. Red spots represent up-regulated genes, green spots represent down-regulated genes in SLHCC compared with NHCC. Yellow spots are related to genes of which gene expression was similar.

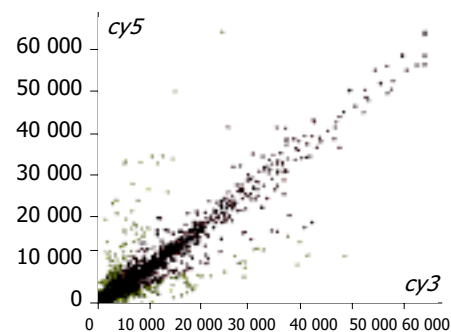


Figure 3 Scatter plot with ImaGene 3.0 software after hybridization of SLHCC (Cy5)/NHCC (Cy3) (8464 elements). Red spots represent similar expression genes. Yellow spots represent different expression genes.

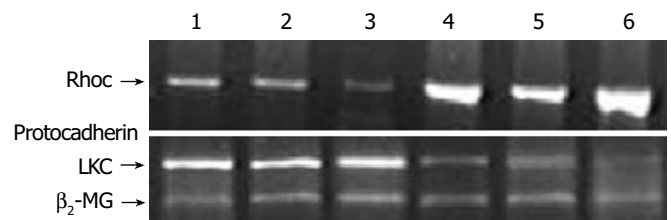


Figure 4 Expression of RhoC and protocadherin LKC mRNA in SLHCC (lanes 1-3) and NHCC (lanes 4-6) SLHCC tissues revealed significantly higher levels of protocadherin LKC mRNA than NHCC and showed significantly lower levels of RhoC mRNA than NHCC.

DISCUSSION

Traditional viewpoint insists that the classification and prognosis of HCC are determined by the size of HCC, large HCC is always considered as terminal HCC and unexcisable HCC. However, UICC has changed this opinion in the 6th TNM classification for HCC. The number of nodes, but not the size of HCC, is the crucial factor for classification and prognosis of HCC^[8]. It is generally accepted that different HCCs have individual clinical pathological and molecular biological characteristics, which determined the different invasive and metastatic potentials of HCC^[1]. Our clinical observation implied different invasive and metastatic abilities between SLHCC and NHCC. As the genomewide expression profile of tumor is a representation of the biology of the tumor, and the diversity in gene expression profile reflects molecular biological diversity, thus, the further investigation of different gene expression profiles between SLHCC and NHCC is anticipated.

In this study, systematic investigation of gene expression patterns between SLHCC and NHCC was performed by using cDNA microarray to understand the mechanism of the diversity of molecular biological characteristics of HCC. A total of 668 genes (7.89%) showed significant change in their expression level between SLHCC and NHCC. It is not surprising that some differentially expressed genes were associated with the progression of HCC and most of them were related to the invasion and metastasis of tumor. These findings lend support to the presence of various molecular characteristics between SLHCC and NHCC. The gene expression profiles also provided a quantitative view of the changes in gene expression that occurred at the level of HCC genome between SLHCC and NHCC. These genes include matrix-degraded gene, cellular skeleton and motion gene, cellular signal and transferring gene, apoptosis-associated gene and so on. Some genes which were propitious to invasion and metastasis were up-regulated and made against these were down-regulated. We focused on matrix-degraded genes, cellular skeleton and motion genes, which were closely related to invasion and metastasis, and selected some of them for further study.

Both cell-cell interaction and cell-stroma interaction play an important role during the invasion and metastasis. Connections through cell-adhesion molecules, integrins, and cadherins stabilize tissue integrity, whereas loss or alteration of these cell surface proteins is associated with increased metastatic potential. The results of our study indicated that cathepsinL (CTSL), integrin α_6 , (ITGA $_6$) were down-regulated in SLHCC compared with NHCC. We also found that protocadherin LKC gene and H-cadherin gene were overexpressed in SLHCC vs NHCC. CTSL could promote migration of HCC cells through degrading ECM^[9,10]. ITGA $_6$ could promote invasion and metastasis of HCC cells through activating MMPs^[11]. Loss of H-cadherin expression in invasive cutaneous squamous cell carcinoma suggested it was a potential invasive and metastatic suppressive gene^[12]. Protocadherins are a major subfamily of the cadherin superfamily. This gene is predominantly expressed in liver, kidney and colon tissues, thus designating protocadherin LKC. The expression of protocadherin LKC is markedly reduced in cancers arising from these tissues at both transcriptional and protein levels. When protocadherin LKC was introduced into colon cancer cell line HCT116, which does not express this gene, a significant inhibition of cell proliferation could be observed. Recently, researcher identified the status of protocadherin LKC as an invasion and metastasis suppressor or gene which could increase the coagulation of tumor cells^[13-16]. Our study showed that protocadherin LKC mRNA was down-regulated in NHCC, suggesting a more disperse degree of NHCC cells compared with SLHCC cells.

We also found that many genes associated with cellular skeleton and movement were differentially expressed between

SLHCC and NHCC, for instance, RAB34 and RhoC. We focussed on RhoC because it was recently reported to play a crucial role in tumorigenesis. RhoC was found overexpressed in pancreatic ductal adenocarcinomas^[7], and its up-regulation was associated with tumor progression in ovarian carcinomas^[17]. Our previous study also showed a significant higher level of RhoC in extrahepatic metastasis of HCC compared with intrahepatic HCC and overexpression of RhoC gene was correlated with vein invasion, number of tumor nodes and extrahepatic metastasis^[18]. The expression level of RhoC could reflect the mobility of HCC cells^[19-22]. The results of our study that RhoC was down-regulated in SLHCC compared with NHCC suggested that SLHCC cells had a lower invasive and metastatic potential than NHCC.

Apoptosis is thought to play an important role in the regulation of proliferation of HCC cells. Apoptosis is modulated by a number of gene products which act through protein-protein interactions either as inducers or inhibitors. In our study, the genes of DAP, PHLDA, ATF $_2$, p21 waf $_1$ /cip $_1$, and their products which could induce cellular apoptosis^[22-26], were obviously up-regulated in SLHCC compared with NHCC, whereas survivin, which inhibited cellular apoptosis^[27-31] was less in SLHCC than in NHCC. These data suggested that one of the mechanisms of SLHCC, which possesses a less invasive and metastatic potential than NHCC, might be a facility in apoptosis of HCC cells. Our study also showed many genes encoding proteins that were consistent with body growth and development were down-regulated in SLHCC compared with NHCC, for instance, SNRPN, NTRK3 and so on^[32,33]. These genes express usually in embryonic tissues and reflect the level of cell differentiation. These result suggested SLHCC cells has a better differentiation than NHCC cells.

In conclusion, the diversity of molecular biological characters between SLHCC and NHCC can be determined by differentially expressed gene profiles. SLHCC shares a better gene phenotype than NHCC, which is consistent with our previous clinical study.

ACKNOWLEDGEMENTS

We are grateful to Zhi-Li Yang, Wei-Qun Lu, Fa-Qing Tang, Jian-Qing Yang and He-Li Liu for their technical assistance.

REFERENCES

- 1 Okuda K. Hepatocellular carcinoma: clinicopathological aspects. *J Gastroenterol Hepatol* 1997; **12**: S314-318
- 2 Huang G, Yang L, Yang J, Liu H, Yang Z. Correlation between epidermal growth factor and overexpression of vascular endothelial growth factor in hepatocellular carcinoma. *Zhonghua Zhongliu Zazhi* 2002; **24**: 564-566
- 3 Golub TR, Slonim DK, Tamayo P, Huard C, Gaasenbeek M, Mesirov JP, Coller H, Loh ML, Downing JR, Caligiuri MA, Bloomfield CD, Lander ES. Molecular classification of cancer: class discovery and class prediction by gene expression monitoring. *Science* 1999; **286**: 531-537
- 4 Cherepinsky V, Feng J, Rejali M, Mishra B. Shrinkage-based similarity metric for cluster analysis of microarray data. *Proc Natl Acad Sci U S A* 2003; **100**: 9668-9673
- 5 King HC, Sinha AA. Gene expression profile analysis by DNA microarrays: promise and pitfalls. *JAMA* 2001; **286**: 2280-2288
- 6 Schena M. Genome analysis with gene expression microarrays. *Bioessays* 1996; **18**: 427-431
- 7 Suwa H, Ohshio G, Imamura T, Watanabe G, Arai S, Imamura M, Narumiya S, Hiai H, Fukumoto M. Overexpression of the rhoC gene correlates with progression of ductal adenocarcinoma of the pancreas. *Br J Cancer* 1998; **77**: 147-152
- 8 Poon RT, Fan ST. Evaluation of the new AJCC/UICC staging system for hepatocellular carcinoma after hepatic resection in Chinese patients. *Surg Oncol Clin N Am* 2003; **12**: 35-50
- 9 Atkins KB, Troen BR. Phorbol ester stimulated cathepsin L expression in U937 cells. *Cell Growth Differ* 1995; **6**: 713-718

- 10 **Niedergethmann M**, Hildenbrand R, Wolf G, Verbeke CS, Richter A, Post S. Angiogenesis and cathepsin expression are prognostic factors in pancreatic adenocarcinoma after curative resection. *Int J Pancreatol* 2000; **28**: 31-39
- 11 **Hourihan RN**, O'Sullivan GC, Morgan JG. Transcriptional gene expression profiles of oesophageal adenocarcinoma and normal oesophageal tissues. *Anticancer Res* 2003; **23**: 161-165
- 12 **Takeuchi T**, Liang SB, Matsuyoshi N, Zhou S, Miyachi Y, Sonobe H, Ohtsuki Y. Loss of T-cadherin (CDH13, H-cadherin) expression in cutaneous squamous cell carcinoma. *Lab Invest* 2002; **82**: 1023-1029
- 13 **Okazaki N**, Takahashi N, Kojima S, Masuho Y, Koga H. Protocadherin LKC, a new candidate for a tumor suppressor of colon and liver cancers, its association with contact inhibition of cell proliferation. *Carcinogenesis* 2002; **23**: 1139-1148
- 14 **Chen MW**, Vacherot F, De La Taille A, Gil-Diez-De-Medina S, Shen R, Friedman RA, Burchardt M, Chopin DK, Buttyan R. The emergence of protocadherin-PC expression during the acquisition of apoptosis-resistance by prostate cancer cells. *Oncogene* 2002; **21**: 7861-7871
- 15 **Wolverton T**, Lalande M. Identification and characterization of three members of a novel subclass of protocadherins. *Genomics* 2001; **76**: 66-72
- 16 **Suzuki ST**. Recent progress in protocadherin research. *Exp Cell Res* 2000; **261**: 13-18
- 17 **Horiuchi A**, Imai T, Wang C, Ohira S, Feng Y, Nikaido T, Konishi I. Up-regulation of small GTPases, RhoA and RhoC, is associated with tumor progression in ovarian carcinoma. *Lab Invest* 2003; **83**: 861-870
- 18 **Wang W**, Yang LY, Yang ZL, Huang GW, Lu WQ. Expression and significance of RhoC gene in hepatocellular carcinoma. *World J Gastroenterol* 2003; **9**: 1950-1953
- 19 **Donald CD**, Cooper CR, Harris-Hooker S, Emmett N, Scanlon M, Cooke DB 3rd. Cytoskeletal organization and cell motility correlates with metastatic potential and state of differentiation in prostate cancer. *Cell Mol Biol* 2001; **47**: 1033-1038
- 20 **Ridley AJ**. Rho GTPases and cell migration. *J Cell Sci* 2001; **114** (Pt 15): 2713-2722
- 21 **Clark EA**, Golub TR, Lander ES, Hynes RO. Genomic analysis of metastasis reveals an essential role for RhoC. *Nature* 2000; **406**: 532-535
- 22 **Zondag GC**, Evers EE, ten Klooster JP, Janssen L, van der Kammen RA, Collard JG. Oncogenic Ras downregulates Rac activity, which leads to increased Rho activity and epithelial-mesenchymal transition. *J Cell Biol* 2000; **149**: 775-782
- 23 **Matsumoto H**, Nagao M, Ogawa S, Kanehiro H, Hisanaga M, Ko S, Ikeda N, Fujii H, Koyama F, Mukogawa T, Nakajima Y. Prognostic significance of death-associated protein-kinase expression in hepatocellular carcinomas. *Anticancer Res* 2003; **23**: 1333-1341
- 24 **Neef R**, Kuske MA, Prols E, Johnson JP. Identification of the human PHLDA1/TDAG51 gene: down-regulation in metastatic melanoma contributes to apoptosis resistance and growth deregulation. *Cancer Res* 2002; **62**: 5920-5929
- 25 **Bhoumik A**, Huang TG, Ivanov V, Gangi L, Qiao RF, Woo SL, Chen SH, Ronai Z. An ATF2-derived peptide sensitizes melanomas to apoptosis and inhibits their growth and metastasis. *J Clin Invest* 2002; **110**: 643-650
- 26 **el-Deiry WS**, Tokino T, Velculescu VE, Levy DB, Parsons R, Trent JM, Lin D, Mercer WE, Kinzler KW, Vogelstein B. WAF1, a potential mediator of p53 tumor suppression. *Cell* 1993; **75**: 817-825
- 27 **Krysan K**, Merchant FH, Zhu L, Dohadwala M, Luo J, Lin Y, Heuze-Vourc'h N, Pold M, Seligson D, Chia D, Goodglick L, Wang H, Strieter R, Sharma S, Dubinett S. COX-2-dependent stabilization of survivin in non-small cell lung cancer. *FASEB J* 2004; **18**: 206-208
- 28 **Yamada Y**, Kuroiwa T, Nakagawa T, Kajimoto Y, Dohi T, Azuma H, Tsuji M, Kami K, Miyatake S. Transcriptional expression of survivin and its splice variants in brain tumors in humans. *J Neurosurg* 2003; **99**: 738-745
- 29 **Lo Muzio L**, Pannone G, Leonardi R, Staibano S, Mignogna MD, De Rosa G, Kudo Y, Takata T, Altieri DC. Survivin, a potential early predictor of tumor progression in the oral mucosa. *J Dent Res* 2003; **82**: 923-928
- 30 **Yang L**, Cao Z, Yan H, Wood WC. Coexistence of high levels of apoptotic signaling and inhibitor of apoptosis proteins in human tumor cells: implication for cancer specific therapy. *Cancer Res* 2003; **63**: 6815-6824
- 31 **Grabowski P**, Scherubl H. Survivin - an anti-apoptosis protein. *Med Sci Monit* 2003; **9**: LE25
- 32 **Bussey KJ**, Lawce HJ, Himoe E, Shu XO, Heerema NA, Perlman EJ, Olson SB, Magenis RE. SNRPN methylation patterns in germ cell tumors as a reflection of primordial germ cell development. *Genes Chromosomes Cancer* 2001; **32**: 342-352
- 33 **Hisaoka M**, Sheng WQ, Tanaka A, Hashimoto H. Gene expression of TrkC (NTRK3) in human soft tissue tumours. *J Pathol* 2002; **197**: 661-667

Edited by Kumar M and Wang XL Proofread by Xu FM

End-of-treatment virologic response does not predict relapse after lamivudine treatment for chronic hepatitis B

Chun-Jen Liu, Wen-Ling Huang, Pei-Jer Chen, Ming-Yang Lai, Jia-Horng Kao, Ding-Shinn Chen

Chun-Jen Liu, Pei-Jer Chen, Ming-Yang Lai, Jia-Horng Kao, Ding-Shinn Chen, Division of Gastroenterology, Department of Internal Medicine, National Taiwan University Hospital and National Taiwan University College of Medicine, Taipei 100, Taiwan, China
Wen-Ling Huang, Pei-Jer Chen, Ming-Yang Lai, Jia-Horng Kao, Ding-Shinn Chen, Graduate Institute of Clinical Medicine, National Taiwan University Hospital and National Taiwan University College of Medicine, Taipei 100, Taiwan, China

Jia-Horng Kao, Hepatitis Research Center, National Taiwan University Hospital and National Taiwan University College of Medicine, Taipei 100, Taiwan, China

Pei-Jer Chen, Ming-Yang Lai, Jia-Horng Kao, Department of Medical Research, National Taiwan University Hospital and National Taiwan University College of Medicine, Taipei 100, Taiwan, China

Supported by Grants From the Department of Health, the National Science Council, Executive Yuan, Taiwan; National Taiwan University Hospital (93S022); and Liver Disease Prevention and Treatment Research Foundation, Taipei, Taiwan

Correspondence to: Professor Jia-Horng Kao, Director, Hepatitis Research Center, National Taiwan University Hospital, 1 Chang-Te St., Taipei 100, Taiwan, China. kjh@ha.mc.ntu.edu.tw

Telephone: +886-2-23123456 Ext. 7307 **Fax:** +886-2-23317624

Received: 2004-02-06 **Accepted:** 2004-03-24

Abstract

AIM: Attaining hepatitis B e antigen (HBeAg) seroconversion during lamivudine treatment is associated with fewer relapses in HBeAg-positive patients. In HBeAg-negative patients, predictors for post-treatment relapse remain largely unknown. We therefore studied whether end-of-treatment virologic response correlated with relapse after lamivudine treatment.

METHODS: We prospectively analyzed 12 HBeAg-negative patients and 14 HBeAg-positive patients with chronic hepatitis B, who received at least 9 mo of lamivudine treatment and were followed up for 12 mo post-treatment. Relapse of hepatitis B activity was defined by an elevation of serum ALT level above twice the upper limit of normal as well as reappearance of serum HBV DNA by the branched DNA assay or HBeAg during the follow-up period. The serum viral loads during and at the end of treatment were further determined by a quantitative real-time polymerase chain reaction assay.

RESULTS: Relapse occurred in 6 (50.0%) HBeAg-negative patients within 12 mo post-treatment. Two relapsers had end-of-treatment serum viral load <1 000 copies/mL, the proportion was not significantly different from that in the 6 non-relapsers (33.3% vs 16.7%; $P = 1.00$). Hepatitis B virus (HBV) DNA levels did not correlate with post-treatment relapse in HBeAg-positive patients either. However, genotype C patients tended to have a lower relapse rate than genotype B patients (14.3% vs 57.9%, $P = 0.08$).

CONCLUSION: Our results suggest that end-of-treatment virologic response cannot predict post-treatment relapse in patients with HBeAg-negative or -positive chronic hepatitis B. The impact of HBV genotype on the response to lamivudine treatment awaits further studies.

Liu CJ, Huang WL, Chen PJ, Lai MY, Kao JH, Chen DS. End-of-treatment virologic response does not predict relapse after lamivudine treatment for chronic hepatitis B. *World J Gastroenterol* 2004; 10(24): 3574-3578

<http://www.wjgnet.com/1007-9327/10/3574.asp>

INTRODUCTION

Infection with hepatitis B virus (HBV) can cause a wide spectrum of liver diseases, such as fulminant or acute hepatitis, chronic hepatitis, liver cirrhosis, and hepatocellular carcinoma^[1]. About 350 million people throughout the world suffer from chronic HBV infection. Thus, active treatment of chronic hepatitis B to prevent progression into end-stage liver diseases is urgently needed.

Three drugs have been approved for the treatment of chronic hepatitis B: interferon (IFN) alpha, lamivudine and adefovir dipivoxil^[2-4]. IFN alpha is costly and has a narrow range of efficacy and tolerability. Adefovir is potent and has been approved for the treatment of chronic hepatitis B in the United States recently, but is nephrotoxic at doses higher than 10 mg per day and not available in other countries^[5]. Lamivudine is cheaper, better tolerated, and has been shown to be effective in patients with hepatitis B e antigen (HBeAg)-positive chronic hepatitis B^[6,7]. However, virologic response to lamivudine may not be as durable as that occurred spontaneously or induced by IFN treatment^[8,9]. Although Dienstag *et al.* reported that lamivudine-induced HBeAg seroconversion was durable after lamivudine treatment, conflicting data existed. It was reported that lamivudine-induced HBeAg seroconversion was not sustained and cumulative relapse rate within 12 mo was 38% in Korean patients^[9]. Thus, it is important to identify predictors for relapse after HBeAg seroconversion.

Lamivudine is also effective for HBeAg-negative chronic hepatitis B^[10-14]. The biochemical and virologic responses as well as the accumulated incidence of drug-resistant mutants were comparable to those in HBeAg-positive chronic hepatitis B^[11]. Nevertheless, in contrast to the HBeAg seroconversion as an unfavorable predictor for relapse in patients with HBeAg-positive chronic hepatitis B, predictors for post-treatment virologic response could be even more lacking in this special clinical setting, and thus the duration of lamivudine treatment is difficult to define^[2-4]. Recently, serum HBV DNA has been considered as a marker of efficacy during therapy for chronic HBV infection^[15]. The relationship between HBV DNA level and the post-treatment relapse in HBeAg-positive chronic hepatitis B has also been demonstrated^[16,17]. Whether similar situation holds true for patients with HBeAg-negative chronic hepatitis B remains to be clarified. In addition, HBV genotypes have been shown to correlate with the clinical outcomes of HBV infection, the response to IFN treatment, the rate of spontaneous HBeAg seroconversion, and the development of lamivudine resistance^[18-29]. It is therefore interesting to know the influence of HBV genotypes on the relapse after cessation of lamivudine treatment.

In this study, traditional polymerase chain reaction (PCR)-based assay was used to monitor and define the response to lamivudine treatment. In addition, we established a real-time PCR assay to quantify serum HBV DNA level in a wider dynamic

range, and compared the relapse rates between HBeAg-negative or -positive patients with detectable serum HBV DNA level and those with undetectable serum HBV DNA level at the end of lamivudine treatment. The impact of HBV genotype on the relapse rate was also analyzed.

MATERIALS AND METHODS

Patients

Between March 1998 and December 1999, 12 patients (10 men and 2 women, median age: 44 years, range: 19 to 61 years) with HBeAg-negative chronic hepatitis B (group I) and 14 patients (13 men and 1 woman, median age: 36 years, range: 20 to 55 years) with HBeAg-positive chronic hepatitis B (group II) who discontinued lamivudine treatment were prospectively enrolled for follow-up studies in the National Taiwan University Hospital. The diagnosis of HBeAg-negative chronic hepatitis B in group I patients was made upon elevated serum alanine aminotransferase (ALT) level at least twice the upper limit of normal (<40 IU/L) for more than 6 mo in the absence of HBeAg, but associated with active HBV replication as reflected by detectable serum HBV DNA by a commercial branched DNA assay (Bayer HBV DNA Assay, Bayer Corporation, Tarrytown, NY). All were positive for antibody to HBeAg (anti-HBe). The diagnosis of HBeAg-positive chronic hepatitis B in group II patients was made upon elevated serum alanine aminotransferase (ALT) level at least twice the upper limit of normal (<40 IU/L) for more than 6 mo in the presence of HBeAg and associated with active HBV replication. None had co-existing hepatitis C virus (HCV) or hepatitis delta virus infection. Other causes of hepatitis, such as alcoholic liver disease and autoimmune hepatitis were excluded. Patients with fulminant hepatitis accompanied with hepatic encephalopathy, concomitant human immunodeficiency virus infection, clinical evidence of pancreatitis, or in pregnancy were excluded.

All of the 12 group I patients received at least 9 mo of lamivudine treatment. During lamivudine therapy, liver biochemical tests were evaluated monthly. After the cessation of lamivudine treatment, liver biochemical tests were followed up monthly for 12 mo. Hepatitis B surface antigen (HBsAg), antibody to HBsAg (anti-HBs), HBeAg, and anti-HBe were examined every 3 mo. Relapse of hepatitis B activity was defined according to recommended criteria^[3,4,11], that was an elevation of serum ALT level above twice the upper limit of normal (<40 IU/L) as well as reappearance of serum HBV DNA by the bDNA assay or HBeAg during the follow-up period. Group II patients received the same regimen of lamivudine and follow-up schedule. In these patients, if HBeAg seroconversion (defined as loss of HBeAg and gain of anti-HBe) was attained, additional lamivudine treatment was given for at least 2 mo^[30]. For those not attaining HBeAg seroconversion after 9 mo of lamivudine treatment, to avoid the emergence of lamivudine-resistant mutants, the duration of therapy was determined arbitrarily by the attending physician^[30]. Again, post-treatment relapse of hepatitis B activity was defined according to recommended criteria^[3,4].

After written informed consent was obtained from each patient, serum samples were collected before treatment, at the 12th wk and at the end of lamivudine treatment, and at the time of relapse. Serum samples were stored at -70 °C until virologic assays.

Hepatitis virus markers

HBsAg, anti-HBs, HBeAg, anti-HBe, and anti-delta were assayed with commercial kits (AxSYM System®, Abbott Laboratories, North Chicago, IL). Anti-HCV was tested by a second-generation enzyme-linked immunoassay (Abbott Laboratories).

Quantification of HBV DNA level

In this study, we basically used the traditional PCR-based

method to monitor and define the response to lamivudine treatment both in HBeAg-positive and -negative patients. Serum HBV DNA levels at baseline, the 12th wk of treatment, the end of treatment, and at the time of post-treatment relapse were determined by a branched DNA assay (Bayer Corporation) according to the manufacturer's instructions. The detection limit of this quantitative assay was 2.5 pg/mL (or 700 000 genome equivalents/mL). The serum HBV DNA levels at the 12th wk and at the end of lamivudine treatment were further determined by the real-time PCR.

Development of real-time PCR assay

To further clarify whether HBV DNA levels in the low range correlated with the response to lamivudine treatment, we developed another real-time PCR assay to detect HBV DNA levels below 2.5 pg/mL.

Extraction of serum HBV DNA

Serum DNA was extracted using a commercially available kit (QIAamp DNA Blood Mini Kit, QIAGEN Inc, Valencia, CA, USA). **Preparation of quantitative standards** For preparation of an external standard of the real-time PCR detection assay, HBV DNA (3.2 kb) was cloned into vector pGEM-4Z (Promega, Madison, USA) and transformed into *Escherichia coli* DH5 α , and purified using a commercially available kit (GFX™ Micro Plasmid Prep Kit, Amersham Pharmacia Biotech Europe GmbH, Freiburg, Germany). The HBV copy number of the plasmid stock solution was determined by measuring the optical density at 260 nm. For each run, serial dilutions of the plasmid stock were prepared freshly from an aliquot stock solution.

Real-time PCR detection assay The real-time PCR assay including the design of primers and probes was performed as previously described^[31]. The number of HBV DNA copies was calculated relative to an HBV DNA plasmid 10-fold dilution series (1 pg/mL equals 280 000 copies/mL), which was included in each run. The input of this plasmid series ranged from 10 to 10¹⁰ copies per reaction mixture. Calibration curves were generated. The calculated r^2 was ≥ 0.99 in each run.

In our assay, less than 1 000 copies were not reliably detected by this assay, as judged by the varied detectable rate and the loss of linearity of the input copy number versus the cycle number at threshold crossing plot. For this reason, the lower limit for quantification was set at 1 000 copies/mL serum. In the range from 10³ to 10¹⁰ template molecules per reaction, the curves showed good linearity and only minimal run-to-run deviations (data not shown). In 20 HBsAg- and anti-HBs-negative EDTA-plasma samples, none showed positive reactions in duplicate. The HBV DNA levels of the serum samples were then extrapolated using these calibration curves.

Determination of HBV genotype and drug-resistant mutants

HBV genotype was identified by using PCR-restriction fragment length polymorphism^[21]. The mutation on tyrosine-methionine-aspartate-aspartate (YMDD) motif of the HBV polymerase gene was identified by PCR and direct sequencing^[32].

Ethical considerations

The study protocol conformed to the ethical guidelines of the 1975 Declaration of Helsinki, and was approved by the Ethical Committee of the National Taiwan University Hospital. The sera were sampled after written or oral informed consent was obtained from the patients.

Statistic analysis

mean \pm SD or median (range) was used to describe the distribution of continuous variables. Baseline characteristics between relapsers and non-relapsers were compared by Student's *t* test

for continuous variables and by Chi-square test with Yates' correction for categorical variables. Statistical significance of differences in the relapse rate among different subgroups was estimated by using 2×2 contingency table according to serum HBV DNA level. All tests were two-sided and a *P* value <0.05 was considered statistically significant.

RESULTS

Characteristics of patients

The baseline characteristics of group I and group II patients are shown in Table 1. There was no significant difference with regard to clinical and virologic features. The mean duration of lamivudine treatment in group II patients was 2 mo longer than group I patients, but with no statistical significance.

Seven group II patients attained seroconversion of HBeAg after a median treatment period of 7 mo (range: 4 to 16 mo). Lamivudine was continued for an additional 2 to 12 mo (median: 4 mo in the 7 HBeAg seroconverters. The other 7 non-seroconverters discontinued lamivudine treatment after a median treatment period of 12 mo (range: 9 to 27 mo). The baseline characteristics of the 7 seroconverters and the 7 non-seroconverters were similar (data not shown).

Table 1 Baseline characteristics of HBeAg-negative and -positive patients

	HBeAg-negative	HBeAg-positive	<i>P</i> value
Case number	12	14	-
Male-number (%)	10 (83)	13 (93)	0.58
Age (yr)	45.2±15.3	35.3±11.2	0.08
ALT (IU/L)	227 (80-2410)	281 (84-1298)	0.92
Serum total bilirubin (mg/dL)	2.9 (0.9-18.6)	1.1 (0.6-11.7)	0.24
Serum HBV DNA level (pg/mL)	272 (3-3121)	863 (7-3376)	0.65
HBV genotype B/C-number (%)	9/3 (75/25)	10/4 (71/29)	1.00
Duration of lamivudine treatment-mo	12.3±1.9	14.2±4.9	0.23

Continuous values are expressed as mean±SD or median (range). HBV DNA levels were determined by a branched DNA assay (Bayer Corporation).

Characteristics of relapsers

At the end of lamivudine treatment, all group I and group II patients had normal serum ALT and undetectable serum HBV DNA by the bDNA assay. None developed biochemical or virologic breakthrough during the treatment period. After the

end of the treatment, 10 patients relapsed within 6 mo, including 5 group I and 5 group II patients. Another 2 patients relapsed between 6 and 12 mo, including 1 group I and 1 group II patients. There was no significant difference with regard to clinical and virologic features among relapsers and non-relapsers in HBeAg-negative or -positive patients (Table 2, 3). The duration of lamivudine treatment did not differ between them. Only one of the 7 genotype C patients relapsed after the discontinuation of lamivudine treatment, the incidence was lower compared with that in the 19 genotype B patients (14% vs 58%, *P* = 0.08).

Among 14 group II patients, the 7 seroconverters tended to have a lower rate of relapse than the 7 non-seroconverters (29% vs 57%, *P* = 0.30) (Table 3). The duration of additional lamivudine treatment after attaining HBeAg seroconversion did not correlate with clinical relapse (Table 3). Two relapsers already received an additional 4 and 12 mo of lamivudine treatment, respectively, after HBeAg seroconversion.

Table 2 Characteristics of relapsers and non-relapsers in 12 patients negative for HBeAg before lamivudine treatment

	Relapsers	Non-relapsers	<i>P</i> value
Case number	6	6	-
Male-number (%)	6 (100)	4 (66.7)	0.13
Age (yr)	50.7±10.1	39.7±18.5	0.24
ALT (IU/L)	227 (80-452)	320 (98-2410)	0.24
Serum total bilirubin (mg/dL)	1.2 (0.8-6.5)	2.9 (0.6-18.6)	0.21
Serum HBV DNA level (pg/mL)	287 (16-2489)	117 (3-3121)	0.41
Duration of lamivudine treatment (mo)	12.5±2.6	12.2±1.2	0.78
HBV genotype B/C-number (%)	6/0 (100/0)	3/3 (50/50)	0.18

Values are expressed as mean±SD or median (range). HBV DNA levels were determined by a branched DNA assay (Bayer Corporation).

Relation between virologic response at the 12th wk of lamivudine treatment and relapse

At the 12th wk of lamivudine treatment, none of the group I patients had serum HBV DNA level ≥10⁵ copies/mL. Of the 12 group I patients, 8 (67%) had serum HBV DNA level ≥1 000 copies/mL. Relapse of hepatitis B activity occurred in 6 (50%) after cessation of lamivudine treatment. All relapsers remained HBeAg-negative and anti-HBe-positive. Three relapsers had serum HBV DNA level <1 000 copies/mL and the other three had serum HBV DNA level ≥1 000 copies/mL. The distribution of post-treatment relapse was similar between patients with detectable and undetectable serum HBV DNA by the real-time PCR.

Table 3 Characteristics of relapsers and non-relapsers in 14 patients positive for HBeAg before lamivudine treatment

	Relapsers	Non-relapsers	<i>P</i> value
Case number	6	8	-
Male-number (%)	5 (83.3)	8 (100)	0.43
Age (yr)	32.5±12.6	37.4±10.4	0.44
ALT (IU/L)	281 (84-1 298)	306 (97-868)	0.34
Serum total bilirubin (mg/dL)	1.1 (0.7-11.1)	1.2 (0.7-3.3)	0.28
Serum HBV DNA level at baseline (pg/mL)	310 (7-1 590)	280 (20-3376)	0.34
Duration of lamivudine treatment (mo)	15.5±6.5	13.3±3.5	0.47
HBeAg seroconversion-number (%)	2 (33.3)	5 (62.5)	0.30
Duration of additional lamivudine treatment after HBeAg seroconversion (mo)	12.4	6.0±4.7	0.75
HBV genotype B/C -number (%)	5/1 (83.3/16.7)	5/3 (62.5/37.5)	0.58

Values are expressed as mean±SD or median (range). HBV DNA levels were determined by a branched DNA assay (Bayer Corporation).

Table 4 Relation between virologic response and relapse after cessation of lamivudine treatment

HBV DNA level (copies/mL)	Total (<i>n</i> = 26)		HBeAg-positive				HBeAg-negative	
			HBeAg seroconverters		HBeAg non-seroconverters		Relapser <i>n</i> =6	Non-relapser <i>n</i> =6
	Relapser <i>n</i> = 12	Non-relapser <i>n</i> = 14	Relapser <i>n</i> = 2	Non-relapser <i>n</i> = 5	Relapser <i>n</i> = 4	Non-relapser <i>n</i> = 3		
<1 000 copies/mL -number (%)	4 (67)	2 (33)	1 (50)	1 (50)	2 (67)	1 (33)	2 (67)	1 (33)
≥1 000 copies/mL -number (%)	8 (40)	12 (60)	1 (20)	4 (80)	2 (50)	2 (50)	4 (44)	5 (56)
	<i>P</i> ¹ = 0.37		<i>P</i> = 1.00		<i>P</i> = 1.00		<i>P</i> = 1.00	

Virologic response was determined at the end of lamivudine treatment. HBV DNA levels were determined by the real-time PCR assay. ¹Two-sided.

Relation between virologic response at the end of lamivudine treatment and relapse

Likewise, none of the group I patients had serum HBV DNA level $\geq 10^5$ copies/mL at the end of lamivudine treatment. Of the 12 group I patients, 9 (75%) had serum HBV DNA level ≥ 1 000 copies/mL and 3 had serum HBV DNA level <1 000 copies/mL. Two of the 6 relapsers had serum HBV DNA level <1 000 copies/mL and the other 4 had serum HBV DNA level ≥ 1 000 copies/mL. When compared with the non-relapsers, the proportion of relapsers with undetectable serum HBV DNA by the real-time PCR was similar (*P* = 1.00, Table 4).

Similar findings were noted in group II patients. Relapse of hepatitis B activity was detected in 6 (43%) of the 14 patients post-treatment. Three of the 6 relapsers had serum HBV DNA level <1 000 copies/mL and the other 3 had serum HBV DNA level ≥ 1 000 copies/mL. When compared with non-relapsers, the proportion of relapsers with undetectable serum HBV DNA by the real-time PCR was also similar (50% *vs* 75%, *P* = 1.00, Table 4). When in-treatment occurrence of HBeAg seroconversion was taken into consideration, serum viral loads in the low range (<10⁵ copies/mL) did not correlate with clinical relapse during follow-up, either (Table 3).

At the end of lamivudine treatment, YMDD motif of the HBV polymerase gene was amplified in all patients. PCR products were detectable in 11 and variation at this motif was found in 2 of them, including methionine-to-valine substitution in one (viral load: 32 400 copies/mL; serum ALT: 24 U/L) and methionine-to-isoleucine substitution in the other (viral load: 22 344 copies/mL; serum ALT: 30 U/L). Both developed relapse with wild-type YMDD HBV strain during the follow-up period.

DISCUSSION

In this study, we found that the relapse rate after lamivudine treatment was high and comparable between HBeAg-negative (50%) and -positive (43%) patients, which did not correlate with serum viral load at the end of treatment.

Because we only evaluated relapsers whose serum ALT levels were greater than twice the upper limit of normal, the rate of post-treatment virologic relapse could be even higher. The high relapse rate in our series indicated a poor durability of virologic response to lamivudine treatment in Asian countries when compared with that in Western countries^[6,8,9,17,33], and an urgency of identifying an effective means to predict the durability of post-treatment virologic response. Lamivudine possesses potent inhibitory effect on viral replication, and previous studies have shown that after the reduction of viral load by lamivudine, a T cell response over viral replication could be restored^[21]. Because serum viral load under anti-viral treatment reflected the control from both drugs and hosts over viral replication, we thus assumed that keeping viral load in the lower range might confer an adequate control over viral replication and therein have a lower relapse rate. Previous studies indeed revealed that

viral load at the 12th wk and at the end of lamivudine treatment correlated with a higher HBeAg seroconversion rate and a lower post-treatment relapse rate, respectively^[16,17]. In addition, serum HBV DNA level less than 10 000 genomes/mL within 12 wk of starting treatment might predict HBeAg seroconversion^[16], and serum HBV DNA level less than 4 700 genomes/mL at the time of HBeAg seroconversion might be associated with a lower relapse rate^[17]. However, our results showed that there was no correlation between serum viral load <10⁵ copies/mL at the end of lamivudine treatment and post-treatment relapse. Consistently, one recent study demonstrated that the end-of-treatment viremic status by a qualitative PCR assay did not correlate with post-treatment relapse in HBeAg-negative patients receiving lamivudine treatment^[34]. This fact suggested that serum viral load might represent the susceptibility of viruses to lamivudine but not reflect the status of host immune control. When suppression pressure from anti-virals was removed, residual viruses within the hepatocytes might actively replicate again and lead to relapse. However, whether an extremely low level of serum viral load can predict a durable anti-viral response post-treatment awaits ultrasensitive HBV quantitative assays. Actually, one recent study demonstrated that in patients with end-of-treatment serum HBV DNA levels of <200 copies/mL, the post-treatment relapse rate was significantly lower than in those with end-of-treatment serum HBV DNA levels of >1 000 copies/mL^[35]. This finding supported our speculation.

In HBeAg-positive patients, the serum viral loads at the end of lamivudine treatment were comparable between seroconverters and non-seroconverters. From another aspect, the virologic response was more durable in the seroconverters than in the non-seroconverters during follow-up. Again, this implied that appearance of anti-HBeAg rather than the viremic levels could reflect the ability of host immune control over viral replication. Extended therapy has been suggested to ensure the durability of virologic responses after HBeAg seroconversion was attained^[9]. However, whether longer duration of therapy can further enhance the host immunity against HBV needs future immunological assays.

Our results showed that the viremic level at the end of lamivudine treatment could not guarantee a durable post-treatment anti-viral response. Of particular note, HBV genotype C tended to have a lower relapse rate compared with genotype B. Although the molecular virologic mechanisms accounting for clinical outcomes or response to anti-viral treatments remain largely unknown, pathogenic and therapeutic differences do exist among HBV genotypes^[18-29,36]. However, in the individualized setting of HBeAg-positive and -negative patients, HBV genotype was not a factor associated with post-treatment relapse (Tables 2, 3). In addition, conflicting data existed in recent reports^[34,37]. Since our case number is small, whether HBV genotype serves as a predictor for durability of virologic response to lamivudine treatment remains to be examined.

The major limitation in this pilot study was the relatively small case number in each group. However, our findings highlighted

that virologic response at the end of lamivudine treatment could not predict post-treatment relapse. Further large studies by using more sensitive quantitative assays are needed to address this important issue. Other genetic determinants of the virus and host should be clarified in the future. Since the relapse rate was high in both HBeAg-negative and HBeAg-positive patients in HBV endemic areas and such events were usually preceded by an upsurge of serum viral load^[32], frequent monitoring of liver biochemical tests and serum viral loads could be considered to detect early relapse. With the advent of novel anti-viral agents, patients without durable virologic response to current therapy may hopefully benefit from further treatments.

REFERENCES

- Kao JH**, Chen DS. Global control of hepatitis B virus infection. *Lancet Infect Dis* 2002; **2**: 395-403
- Leung N**. Treatment of chronic hepatitis B: case selection and duration of therapy. *J Gastroenterol Hepatol* 2002; **17**: 409-414
- Lok AS**, Heathcote EJ, Hoofnagle JH. Management of hepatitis B: 2000-summary of a workshop. *Gastroenterology* 2001; **120**: 1828-1853
- Lok AS**, McMahon BJ. Chronic hepatitis B. *Hepatology* 2001; **34**: 1225-1241
- Perrillo R**, Schiff E, Yoshida E, Statler A, Hirsch K, Wright T, Gutfreund K, Lamy P, Murray A. Adefovir dipivoxil for the treatment of lamivudine-resistant hepatitis B mutants. *Hepatology* 2000; **32**: 129-134
- Dienstag JL**, Schiff ER, Wright TJ, Perrillo RP, Hann HW, Goodman Z, Crowther L, Condreay LD, Woessner M, Rubin M, Brown NA. Lamivudine as initial treatment for chronic hepatitis B in the United States. *N Engl J Med* 1999; **341**: 1256-1263
- Lai CL**, Chien RN, Leung NW, Chang TT, Guan R, Tai DI, Ng KY, Wu PC, Dent JC, Barber J, Stephenson SL, Gray DF. A one-year trial of lamivudine for chronic hepatitis B. Asia Hepatitis Lamivudine Study Group. *N Engl J Med* 1998; **339**: 61-68
- Lee CM**, Ong GY, Lu SN, Wang JH, Liao CA, Tung HD, Chen TM, Changchien CS. Durability of lamivudine-induced HBeAg seroconversion for chronic hepatitis B patients with acute exacerbation. *J Hepatol* 2002; **37**: 669-674
- Song BC**, Suh DJ, Lee HC, Chung YH, Lee YS. Hepatitis B e antigen seroconversion after lamivudine therapy is not durable in patients with chronic hepatitis B in Korea. *Hepatology* 2000; **32**(4 Pt 1): 803-806
- Hadziyannis SJ**, Papatheodoridis GV, Dimou E, Laras A, Papaioannou C. Efficacy of long-term lamivudine monotherapy in patients with hepatitis B e antigen-negative chronic hepatitis B. *Hepatology* 2000; **32**(4 Pt 1): 847-851
- Hadziyannis SJ**, Vassilopoulos D. Hepatitis B e antigen-negative chronic hepatitis B. *Hepatology* 2001; **34**(4 Pt 1): 617-624
- Rizzetto M**. Efficacy of lamivudine in HBeAg-negative chronic hepatitis B. *J Med Virol* 2002; **66**: 435-451
- Santantonio T**, Mazzola M, Lacovazzi T, Miglietta A, Guastadisegni A, Pastore G. Long-term follow-up of patients with anti-HBe/ HBV DNA-positive chronic hepatitis B treated for 12 mo with lamivudine. *J Hepatol* 2000; **32**: 300-306
- Tassopoulos NC**, Volpes R, Pastore G, Heathcote J, Buti M, Goldin RD, Hawley S, Barber J, Condreay L, Gray DF. Efficacy of lamivudine in patients with hepatitis B e antigen-negative/ hepatitis B virus DNA-positive (precore mutant) chronic hepatitis B. Lamivudine Precore Mutant Study Group. *Hepatology* 1999; **29**: 889-896
- Mommeja-Marin H**, Mondou E, Blum MR, Rousseau F. Serum HBV DNA as a marker of efficacy during therapy for chronic HBV infection: analysis and review of the literature. *Hepatology* 2003; **37**: 1309-1319
- Gauthier J**, Bourne EJ, Lutz MW, Crowther LM, Dienstag JL, Brown NA, Condreay LD. Quantitation of hepatitis B viremia and emergence of YMDD variants in patients with chronic hepatitis B treated with lamivudine. *J Infect Dis* 1999; **180**: 1757-1762
- Lee KM**, Cho SW, Kim SW, Kim HJ, Hahm KB, Kim JH. Effect of virological response on post-treatment durability of lamivudine-induced HBeAg seroconversion. *J Viral Hepat* 2002; **9**: 208-212
- Chu CJ**, Lok AS. Clinical significance of hepatitis B virus genotypes. *Hepatology* 2002; **35**: 1274-1276
- Chu CJ**, Hussain M, Lok AS. Hepatitis B virus genotype B is associated with earlier HBeAg seroconversion compared with hepatitis C virus genotype C. *Gastroenterology* 2002; **122**: 1756-1762
- Kao JH**, Wu NH, Chen PJ, Lai MY, Chen DS. Hepatitis B genotypes and the response to interferon therapy. *J Hepatol* 2000; **33**: 998-1002
- Kao JH**, Chen PJ, Lai MY, Chen DS. Hepatitis B genotypes correlate with clinical outcomes in patients with chronic hepatitis B. *Gastroenterology* 2000; **118**: 554-559
- Kao JH**, Liu CJ, Chen DS. Hepatitis B viral genotypes and lamivudine resistance. *J Hepatol* 2002; **36**: 303-304
- Kao JH**. Hepatitis B viral genotypes: clinical relevance and molecular characteristics. *J Gastroenterol Hepatol* 2002; **17**: 643-650
- Kao JH**. Clinical relevance of hepatitis B viral genotypes: a case of deja vu? *J Gastroenterol Hepatol* 2002; **17**: 113-115
- Kao JH**, Chen PJ, Lai MY, Chen DS. Genotypes and clinical phenotypes of hepatitis B virus in patients with chronic hepatitis B virus infection. *J Clin Microbiol* 2002; **40**: 1207-1209
- Lin CL**, Liao LY, Liu CJ, Chen PJ, Lai MY, Kao JH, Chen DS. Hepatitis B genotypes and precore/basal core promoter mutants in HBeAg-negative chronic hepatitis B. *J Gastroenterol* 2002; **37**: 283-287
- Orito E**, Ichida T, Sakugawa H, Sata M, Horiike N, Hino K, Okita K, Okanoue T, Iino S, Tanaka E, Suzuki K, Watanabe H, Hige S, Mizokami M. Geographic distribution of hepatitis B virus (HBV) genotype in patients with chronic HBV infection in Japan. *Hepatology* 2001; **34**: 590-594
- Sanchez-Tapias JM**, Costa J, Mas A, Bruguera M, Rodes J. Influence of hepatitis B virus genotype on the long-term outcome of chronic hepatitis B in western patients. *Gastroenterology* 2002; **123**: 1848-1856
- Wai CT**, Chu CJ, Hussain M, Lok AS. HBV genotype B is associated with better response to interferon therapy in HBeAg(+) chronic hepatitis than genotype C. *Hepatology* 2002; **36**: 1425-1430
- Proceedings of the asia-pacific consensus meeting for the Diagnosis and treatment of hepatitis B and C. Kyoto, Japan, 6-7 September 1999. *J Gastroenterol Hepatol* 2000; **15**(Suppl): E1-193
- Chen RW**, Piiparinen H, Seppanen M, Koskela P, Sarna S, Lappalainen M. Real-time PCR for detection and quantitation of hepatitis B virus DNA. *J Med Virol* 2001; **65**: 250-256
- Liu CJ**, Chen PJ, Lai MY, Kao JH, Chen DS. Hepatitis B virus variants in patients receiving lamivudine treatment with breakthrough hepatitis evaluated by serial viral loads and full-length viral sequences. *Hepatology* 2001; **34**: 583-589
- Dienstag JL**, Schiff ER, Mitchell M, Casey DE Jr, Gitlin N, Lissos T, Gelb LD, Condreay L, Crowther L, Rubin M, Brown N. Extended lamivudine retreatment for chronic hepatitis B: maintenance of viral suppression after discontinuation of therapy. *Hepatology* 1999; **30**: 1082-1087
- Huang YH**, Wu JC, Chang TT, Sheen JJ, Lee PC, Huo TI, Su CW, Wang YJ, Chang FY, Lee SD. Analysis of clinical, biochemical and viral factors associated with early relapse after lamivudine treatment for hepatitis B e antigen-negative chronic hepatitis B patients in Taiwan. *J Viral Hepat* 2003; **10**: 277-284
- Lee HC**, Suh DJ, Ryu SH, Kim H, Shin JW, Lim YS, Chung YH, Lee YS. Quantitative polymerase chain reaction assay for serum hepatitis B virus DNA as a predictive factor for post-treatment relapse after lamivudine induced hepatitis B e antigen loss or seroconversion. *Gut* 2003; **52**: 1779-1783
- Kao JH**, Chen PJ, Lai MY, Chen DS. Basal core promoter mutations of hepatitis B virus increase the risk of hepatocellular carcinoma in hepatitis B carriers. *Gastroenterology* 2003; **124**: 327-334
- Chien RN**, Yeh CT, Tsai SL, Chu CM, Liaw YF. Determinants for sustained HBeAg response to lamivudine therapy. *Hepatology* 2003; **38**: 1267-1273

Forecasting model for the incidence of hepatitis A based on artificial neural network

Peng Guan, De-Sheng Huang, Bao-Sen Zhou

Peng Guan, Bao-Sen Zhou, Department of Epidemiology, School of Public Health, China Medical University, Shenyang 110001, Liaoning Province, China

De-Sheng Huang, Department of Mathematics, College of Basic Medical Sciences, China Medical University, Shenyang 110001, Liaoning Province, China

Supported by the National Natural Science Foundation of China, No. 30170833

Correspondence to: Dr. Bao-Sen Zhou, Department of Epidemiology, School of Public Health, China Medical University, Shenyang 110001, Liaoning Province, China. bszhou@mail.cmu.edu.cn

Telephone: +86-24-23256666 Ext. 5401

Received: 2004-04-06 **Accepted:** 2004-05-09

Abstract

AIM: To study the application of artificial neural network (ANN) in forecasting the incidence of hepatitis A, which had an autoregression phenomenon.

METHODS: The data of the incidence of hepatitis A in Liaoning Province from 1981 to 2001 were obtained from Liaoning Disease Control and Prevention Center. We used the autoregressive integrated moving average (ARIMA) model of time series analysis to determine whether there was any autoregression phenomenon in the data. Then the data of the incidence were switched into $[0,1]$ intervals as the network theoretical output. The data from 1981 to 1997 were used as the training and verifying sets and the data from 1998 to 2001 were made up into the test set. STATISTICA neural network (ST NN) was used to construct, train and simulate the artificial neural network.

RESULTS: Twenty-four networks were tested and seven were retained. The best network we found had excellent performance, its regression ratio was 0.73, and its correlation was 0.69. There were 2 input variables in the network, one was AR(1), and the other was time. The number of units in hidden layer was 3. In ARIMA time series analysis results, the best model was first order autoregression without difference and smoothness. The total sum square error of the ANN model was 9 090.21, the sum square error of the training set and testing set was 8 377.52 and 712.69, respectively, they were all less than that of ARIMA model. The corresponding value of ARIMA was 12 291.79, 8 944.95 and 3 346.84, respectively. The correlation coefficient of nonlinear regression (R_{NL}) of ANN was 0.71, while the R_{NL} of ARIMA linear autoregression model was 0.66.

CONCLUSION: ANN is superior to conventional methods in forecasting the incidence of hepatitis A which has an autoregression phenomenon.

Guan P, Huang DS, Zhou BS. Forecasting model for the incidence of hepatitis A based on artificial neural network. *World J Gastroenterol* 2004; 10(24): 3579-3582
<http://www.wjgnet.com/1007-9327/10/3579.asp>

INTRODUCTION

Hepatitis A is an important infectious disease in the world^[1-4]. Guidelines of vaccination *versus* hepatitis A call for correct estimation of the incidence of hepatitis A^[5-9]. The occurrence of infectious diseases has its rules, affected by the speed of pathogen variation, susceptible accumulation and environmental changes. Early recognition of the epidemic rules is significantly important for the prevention and control of hepatitis. Among the available models, time series analysis^[10,11] and regression analysis^[12-14] are poorly suited for discovering the epidemic rules. The reason for this lies in the complexity of their relationship.

However, artificial neural networks (ANN) can recognize the rules to make right prediction and provide assistance for decision-making because they have the characteristics of self-organizing and self-learning processes^[15-18]. Artificial neural networks are computation systems that process information in parallel, using a large number of simple units, and that excel in tasks involving pattern recognition. These intrinsic properties of the neural networks have been translated into higher performance accuracy in outcome prediction compared with expert opinion or conventional statistical methods^[19-22].

Recently, backpropagation (BP) artificial neural network has been widely applied to a variety of problems in the field of medicine^[23-26]. It is also called the front forward network because it is the front forward error propagation network without feedback. There is no mutual connection among the neurons in the same layer.

In the present work, we applied several artificial neural networks to the forecast of the incidence of hepatitis A. We also represented the basic principles and how to train the neural networks.

MATERIALS AND METHODS

Materials

The data of the incidence of hepatitis A in Liaoning Province from 1981 to 2001 were obtained from Liaoning Disease Control and Prevention Center. The highest incidence of hepatitis A during this period was 160.07 per one hundred thousand, and then the incidence descended progressively from 1981-1986 and rose from 1986 to 1989 (Figure 1). The low incidence could be seen from 1996. To switch these data into $[0,1]$ intervals, we applied the following transformation: the network theoretical output was equal to the incidence of hepatitis A / 200 by using $1/10^5$ as the unit of measurement.

Construction, training and simulation of the network

Automatic network designer The automatic network designer determined a suitable architecture, using a combination of heuristics and sophisticated optimization strategies. It conducted a large number of tests, which were used to determine the best architecture. It could automatically compare linear, probabilistic neural network (PNN), generalized regression neural network (GRNN), radial basis function and multilayer perceptron networks (Figure 2), and automatically choose the smoothing factor for PNN or GRNN, the smoothing factor and the number of units for radial basis function networks, and the number of

units for multilayer perceptrons. We could control the length and rigor of search iteration to be performed, and bias the search towards smaller networks using a unit penalty factor.

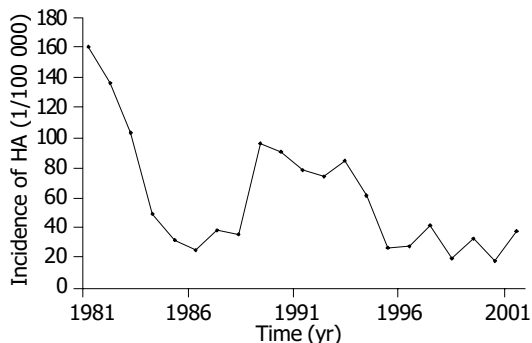


Figure 1 Incidence of hepatitis A in Liaoning Province, China.

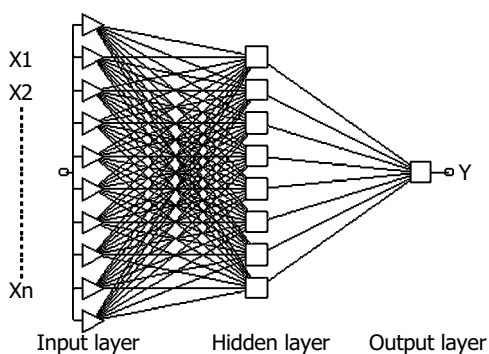


Figure 2 Topological structure of ANN.

Intelligent problem solver In ST NN, an intelligent problem solver was used to select the most excellent network. We chose the advanced version to customize the design process, the problem needed to be solved was a time series problem. Because many time series had a natural period, steps parameter equals to 1 was indicated here by ARIMA analysis. The output variables were transformed values of incidence of hepatitis A, and the input variables were time and AR (1) which meant former transforming values. The software could search for a useful subset of the specified variables. The cases in the data set were divided into three subsets, one for training the network, one for cross verification and the last one for testing. In practice, the data from 1981 to 1992 were used to train the network and the data from 1993 to 1997 were used as a verifying set. The performance of the network could be tested by estimating the data from 1998 to 2001.

Four types of networks, such as linear network, multilayer perceptron (3 layers), probability network or GRNN and radial basis function, needed to be considered. In the mean time, network complexity was determined automatically. A medium length of design procedure was selected, which conducted a fast search for an optimal network. The network saved would be one with balance performance against types and complexity. The best network found (taking account of diversity) was retained.

Choosing the number of hidden layers and units was the most critical problem. There were a few heuristics that could guide here. One hidden layer was sufficient for most problems when multilayer perceptrons were used. If the error could not be gotten down to an acceptable level even with a large number of hidden units, it might be worth trying two hidden layers.

A large number of hidden units could generally model a more complex problem, but required more training and were more prone to poor generalization. The changes in training and verification errors should be observed as the experiment was

being done. If the addition of more hidden units caused a decrease in both, then the network was probably too small. However, if the verification error was significantly larger than the training error and, in particular, if it deteriorated during iterative training, then the network was probably too large.

The number of weights and thresholds in the network should be less than or much less than the number of training cases. Ideally, there should be about two to five as many training cases as weights. If the number of training cases was small, the smaller networks should be used because of no enough data to model a complex function. If the cases were fewer than the product of the number of inputs and outputs, only a linear model should be used. Lack of sufficient data was one reason why it was sometimes good to remove input variables. Even if the variables had some genuine information, the reduction in network size consequent upon removing them might improve network performance.

Performance statistic index

One index to evaluate the performance of networks and ARIMA was sum square of error (SSE): $SSE = \sum (y_i - \hat{y}_i)^2$. The other was nonlinear determinant coefficient: $R_{NL} = 1 - \sqrt{\frac{\sum (y_i - \hat{y}_i)^2}{\sum y_i^2}}$, where y_i is the real value of case i and \hat{y}_i is the estimated value of case i.

RESULTS

Network structure and prediction

Finally 24 networks were tested, and 7 were retained. The best network we found was BP network, which had excellent performance, its regression ratio was 0.73, and its correlation was 0.69.

The structure of the network is shown in Figure 3. There were 2 input variables, one was AR(1), the other was time. The number of units in hidden layer was 3. The weight and threshold distribution of the best network is shown in Table 1.

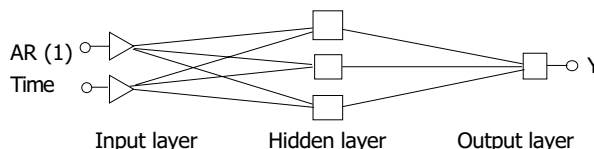


Figure 3 Topological structure of the best network.

Table 1 Weight and threshold distribution of the best network

	Unit 1	Unit 2	Unit 3	Y
Threshold	0.9607	1.0829	0.6224	0.4850
AR (1)	0.2390	0.7930	1.0584	
Time	0.4902	0.4344	0.4156	
Unit 1				0.5281
Unit 2				0.7572
Unit 3				1.0723

ARIMA model coefficient and its testing results

In ARIMA time series analysis results, the best model was first order autoregression without difference and smoothness. The coefficient of AR (1) and constant were 0.83 and 81.22, respectively (Table 2).

Table 2 ARIMA model coefficient and its testing results

Variables	Coefficient	SE of coefficient	t	P
AR (1)	0.83	0.12	6.88	5.27×10^{-6}
Constant	81.22	30.94	2.62	1.91

Comparison between BP network and ARIMA

The goal of training the network was to compare the performance with conventional methods by using inverse transforming predicted value obtained from the network. Predicted value and error are shown in Table 3, and its corresponding line graph is shown in Figure 4.

The total sum square error of the ANN model was 9 090.21, the sum square error of the training set and testing set was 8 377.52 and 712.69, respectively, while the corresponding value of ARIMA was 12 291.79, 8 944.95 and 3 346.84, respectively. The nonlinear determinant coefficient of ANN and the ARIMA linear autoregression model was 0.71 and 0.66, respectively.

Table 3 Comparison between BP network and ARIMA

Time (yr)	Incidence (1/100 000)	Predicted value from ANN	Error from ANN	Predicted value from ARIMA	Error from ARIMA
1981	160.07	-	-	-	-
1982	136.68	101.58	35.10	146.87	-10.19
1983	104.12	94.63	9.49	127.39	-23.27
1984	50.50	83.87	-33.37	100.29	-49.79
1985	32.99	62.34	-29.35	55.65	-22.66
1986	26.74	53.26	-26.52	41.07	-14.33
1987	39.94	49.11	-9.17	35.86	4.08
1988	36.75	53.72	-16.97	46.85	-10.10
1989	96.92	50.42	46.50	44.20	52.72
1990	91.33	73.84	17.49	94.29	-2.96
1991	79.52	70.90	8.62	89.64	-10.12
1992	75.31	64.60	10.71	79.81	-4.50
1993	85.57	61.39	24.18	76.30	9.27
1994	62.54	64.00	-1.46	84.84	-22.3
1995	28.23	52.11	-23.88	65.67	-37.44
1996	29.14	35.20	-6.06	37.11	-7.97
1997	42.90	34.36	8.54	37.86	5.04
1998	21.25	38.01	-16.76	49.32	-28.07
1999	34.36	27.27	7.09	54.66	-20.30
2000	19.31	30.87	-11.56	59.11	-39.80
2001	39.09	22.88	16.21	62.81	-23.72

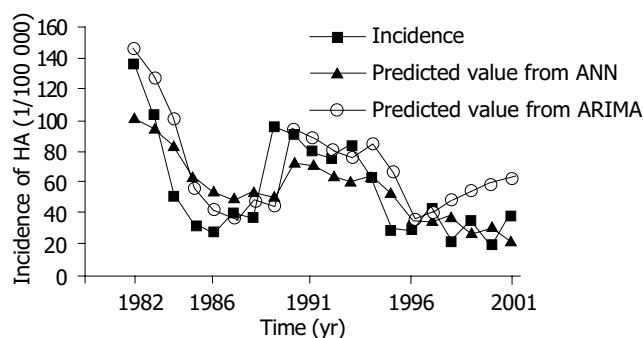


Figure 4 Incidence of hepatitis A and its predicted value.

DISCUSSION

From the above results, we can see that there was a first order autoregression phenomenon in the linear autoregression model. The nonlinear determinant coefficient of the ARIMA linear autoregression model was 0.66. The regression graph shows that there was an obvious linear tendency, but some values were still not perfectly fitted. Differences in the amount were great between values. The sum square error of the model was 12 291.79, the sum square error of the training set and testing set was 8 944.95 and 3 346.84, respectively. While in the model based on artificial neural networks, the nonlinear determinant

coefficient was 0.71, higher than that of linear autoregression model. The sum square error of the ANN model was 9 090.21, the sum square error of the training set and testing set was 8 377.52 and 712.69, respectively. In time series analysis, there was statistical significance in the test of coefficients, showing the existence of first order autoregression. Values from extrapolation forecasting based on ANN were mainly in concordance with the actual values, while values from ARIMA model forecasting were a little higher than the actual values of the incidence. These findings showed that ANN could recognize some rules by preliminary learning, but the effect of some special values over considering sum square error made the forecasting of low incidence inaccurate. Combined application of the traditional methods and artificial neural networks can make use of each other's merits and raise the right prediction level.

Forecasting the incidence of infectious diseases is very important for their prevention and control. Solving this problem calls for the ability to learn the unknown mapping or function only by the existing examples^[27,28]. However, after the mapping or a similar one is learned, artificial neural networks can be used to estimate the mapping when only several parts are known. Now artificial neural networks have been widely accepted as a potentially useful way in modeling complex nonlinear and dynamic systems^[29-31]. Neural networks could remove neither the need for knowledge nor prior information about the systems of interest^[32]. They just reduce the model's reliance on the prior information while totally removing the need for the model builders to correctly specify the precise functional forms of the relationship that the model seeks to represent^[33]. In addition, they offer real prospects for a cheaper, more flexible, less assumption-dependent and adaptive methodology.

Generally, there are two major ways to train the networks, one seeking high accuracy, and the other considering both the accuracy and performance. Through the former method, mapping was input from N-dimensional space and output to M-dimensional space. Thus, the phenomenon of overlearning occurred and the results of extrapolation were not perfect^[34]. In the present work, we divided the original data into three parts, one for training, one for verification, and one for extrapolation and prediction. Thus the problem of overlearning was solved effectively. Time series analysis showed that there was a first order autoregression phenomenon in the data without exponent smoothing. Autoregression phenomenon might often exist in the data of the incidence. Traditional method of solving this is time series analysis^[35]. However, it is difficult to practice because it requires to meet several conditions, such as white noise^[36]. There are no such limitations in artificial neural network, and the software could voluntarily choose appropriate order of autoregression to fit and predict. In addition, R_{NL} has shown that it is reasonable to employ artificial neural networks in modeling complex nonlinear data.

In conclusion, ANN is likely to be an effective tool in processing time series data. The construction and explanation of the model should be further explored.

REFERENCES

- 1 **Sitarska-Golebiowska J**, Bielak A. Hepatitis A in Poland in 2001. *Przegl Epidemiol* 2003; **57**: 129-134
- 2 **Lee MB**, Middleton D. Enteric illness in Ontario, Canada, from 1997 to 2001. *J Food Prot* 2003; **66**: 953-961
- 3 **Steinke DT**, Weston TL, Morris AD, MacDonald TM, Dillon JF. Epidemiology and economic burden of viral hepatitis: an observational population based study. *Gut* 2002; **50**: 100-105
- 4 **Mel'nichenko PI**, Muzychenko FV, Esaulenko NB, Demenev VI, Podlesnyi IV. Prophylaxis of viral hepatitis A in troops of the North-Caucasian Military District. *Voen Med Zh* 2001; **322**: 49-53, 96
- 5 **Wong KH**, Liu YM, Ng PS, Young BW, Lee SS. Epidemiology

- of hepatitis A and hepatitis E infection and their determinants in adult Chinese community in Hong Kong. *J Med Virol* 2004; **72**: 538-544
- 6 **Jenson HB**. The changing picture of hepatitis A in the United States. *Curr Opin Pediatr* 2004; **16**: 89-93
 - 7 **Lolekha S**, Pratuangtham S, Punpanich W, Bowonkiratikachorn P, Chimabuttra K, Weber F. Immunogenicity and safety of two doses of a paediatric hepatitis A vaccine in Thai children: comparison of three vaccination schedules. *J Trop Pediatr* 2003; **49**: 333-339
 - 8 **Pechevis M**, Khoshnood B, Buteau L, Durand I, Piquard Y, Lafuma A. Cost-effectiveness of hepatitis A vaccine in prevention of secondary hepatitis A infection. *Vaccine* 2003; **21**: 3556-3564
 - 9 **Averhoff F**, Shapiro CN, Bell BP, Hyams I, Burd L, Deladisma A, Simard EP, Nalin D, Kuter B, Ward C, Lundberg M, Smith N, Margolis HS. Control of hepatitis A through routine vaccination of children. *JAMA* 2001; **286**: 2968-2973
 - 10 **Fung KY**, Krewski D, Chen Y, Burnett R, Cakmak S. Comparison of time series and case-crossover analyses of air pollution and hospital admission data. *Int J Epidemiol* 2003; **32**: 1064-1070
 - 11 **Fuller JA**, Stanton JM, Fisher GG, Spitzmuller C, Russell SS, Smith PC. A lengthy look at the daily grind: time series analysis of events, mood, stress, and satisfaction. *J Appl Psychol* 2003; **88**: 1019-1033
 - 12 **Chan YH**. Biostatistics 201: linear regression analysis. *Singapore Med J* 2004; **45**: 55-61
 - 13 **Dinc E**. Linear regression analysis and its application to the multivariate spectral calibrations for the multiresolution of a ternary mixture of caffeine, paracetamol and metamizol in tablets. *J Pharm Biomed Anal* 2003; **33**: 605-615
 - 14 **Chen JJ**. Communicating complex information: the interpretation of statistical interaction in multiple logistic regression analysis. *Am J Public Health* 2003; **93**: 1376-1377
 - 15 **Mohamed EI**, Linder R, Perriello G, Di Daniele N, Poppl SJ, De Lorenzo A. Predicting Type 2 diabetes using an electronic nose-based artificial neural network analysis. *Diabetes Nutr Metab* 2002; **15**: 215-221
 - 16 **Becerikli Y**, Konar AF, Samad T. Intelligent optimal control with dynamic neural networks. *Neural Netw* 2003; **16**: 251-259
 - 17 **Kao JJ**, Huang SS. Forecasts using neural network versus Box-Jenkins methodology for ambient air quality monitoring data. *J Air Waste Manag Assoc* 2000; **50**: 219-226
 - 18 **Dassen WR**, Mulleneers RG, Den Dulk K, Smeets JR, Cruz F, Penn OC, Wellens HJ. An artificial neural network to localize atrioventricular accessory pathways in patients suffering from the Wolff-Parkinson-White syndrome. *Pacing Clin Electrophysiol* 1990; **13**(12 Pt 2): 1792-1796
 - 19 **Cimander C**, Bachinger T, Mandenius CF. Integration of distributed multi-analyzer monitoring and control in bioprocessing based on a real-time expert system. *J Biotechnol* 2003; **103**: 237-248
 - 20 **Augusteijn MF**, Shaw KA. Constructing a query-able radial basis function artificial neural network. *Int J Neural Syst* 2002; **12**: 159-175
 - 21 **Castellaro C**, Favaro G, Castellaro A, Casagrande A, Castellaro S, Puthenparampil DV, Salimbeni CF. An artificial intelligence approach to classify and analyse EEG traces. *Neurophysiol Clin* 2002; **32**: 193-214
 - 22 **Yen GG**, Meesad P. Constructing a fuzzy rule-based system using the ILFN network and Genetic Algorithm. *Int J Neural Syst* 2001; **11**: 427-443
 - 23 **Ignat'ev NA**, Adilova FT, Matlatipov GR, Chernysh PP. Knowledge discovering from clinical data based on classification tasks solving. *Medinfo* 2001; **10**(Pt 2): 1354-1358
 - 24 **Traeger M**, Eberhart A, Geldner G, Morin AM, Putzke C, Wulf H, Eberhart LH. Artificial neural networks. Theory and applications in anesthesia, intensive care and emergency medicine. *Anaesthetist* 2003; **52**: 1055-1061
 - 25 **Catto JW**, Linkens DA, Abbod MF, Chen M, Burton JL, Feeley KM, Hamdy FC. Artificial intelligence in predicting bladder cancer outcome: a comparison of neuro-fuzzy modeling and artificial neural networks. *Clin Cancer Res* 2003; **9**: 4172-4177
 - 26 **Ritchie MD**, White BC, Parker JS, Hahn LW, Moore JH. Optimization of neural network architecture using genetic programming improves detection and modeling of gene-gene interactions in studies of human diseases. *BMC Bioinformatics* 2003; **4**: 28
 - 27 **Hajmeer MN**, Basheer IA. A hybrid Bayesian-neural network approach for probabilistic modeling of bacterial growth/no-growth interface. *Int J Food Microbiol* 2003; **82**: 233-243
 - 28 **Casillas AM**, Clyman SG, Fan YV, Stevens RH. Exploring alternative models of complex patient management with artificial neural networks. *Adv Health Sci Educ Theory Pract* 2000; **5**: 23-41
 - 29 **Traeger M**, Eberhart A, Geldner G, Morin AM, Putzke C, Wulf H, Eberhart LH. Prediction of postoperative nausea and vomiting using an artificial neural network. *Anaesthetist* 2003; **52**: 1132-1138
 - 30 **Jerez-Aragones JM**, Gomez-Ruiz JA, Ramos-Jimenez G, Munoz-Perez J, Alba-Conejo E. A combined neural network and decision trees model for prognosis of breast cancer relapse. *Artif Intell Med* 2003; **27**: 45-63
 - 31 **Tambouratzis T**, Gazela M. The accurate estimation of meteorological profiles employing ANNs. *Int J Neural Syst* 2002; **12**: 319-337
 - 32 **Ma L**, Khorasani K. New training strategies for constructive neural networks with application to regression problems. *Neural Netw* 2004; **17**: 589-609
 - 33 **Callan DE**, Kent RD, Guenther FH, Vorperian HK. An auditory-feedback-based neural network model of speech production that is robust to developmental changes in the size and shape of the articulatory system. *J Speech Lang Hear Res* 2000; **43**: 721-736
 - 34 **Sasagawa F**, Tajima K. Prediction of protein secondary structures by a neural network. *Comput Appl Biosci* 1993; **9**: 147-152
 - 35 **Goodwin N**, Sunderland A. Intensive, time-series measurement of upper limb recovery in the subacute phase following stroke. *Clin Rehabil* 2003; **17**: 69-82
 - 36 **Haydon DT**, Shaw DJ, Cattadori IM, Hudson PJ, Thirgood SJ. Analysing noisy time-series: describing regional variation in the cyclic dynamics of red grouse. *Proc R Soc Lond B Biol Sci* 2002; **269**: 1609-1617

The effect of adenovirus expressing wild-type p53 on 5-fluorouracil chemosensitivity is related to p53 status in pancreatic cancer cell lines

Sven Eisold, Michael Linnebacher, Eduard Ryschich, Dalibor Antolovic, Ulf Hinz, Ernst Klar, Jan Schmidt

Sven Eisold, Ernst Klar, Department of General Surgery, Thoracic and Vascular Surgery, University of Rostock, Schillingallee 35, D-18057 Rostock, Germany

Eduard Ryschich, Dalibor Antolovic, Ulf Hinz, Jan Schmidt, Department of General Surgery, University of Heidelberg, INF, D-69120 Heidelberg, Germany

Michael Linnebacher, Molecular Pathology, University of Heidelberg, INF, D-68120 Heidelberg, Germany

Correspondence to: Sven Eisold, Department of General Surgery, Thoracic and Vascular Surgery, University of Rostock, Schillingallee 35, D-18057 Rostock, Germany. sven.eisold@med.uni-rostock.de

Telephone: +49-381-4946001 **Fax:** +49-381-4946002

Received: 2004-04-15 **Accepted:** 2004-06-07

Abstract

AIM: There are conflicting data about p53 function on cellular sensitivity to the cytotoxic action of 5-fluorouracil (5-FU). Therefore the objective of this study was to determine the combined effects of adenovirus-mediated wild-type (wt) p53 gene transfer and 5-FU chemotherapy on pancreatic cancer cells with different p53 gene status.

METHODS: Human pancreatic cancer cell lines Capan-1^{p53mut}, Capan-2^{p53wt}, FAMPAC^{p53mut}, PANC1^{p53mut}, and rat pancreatic cancer cell lines AS^{p53wt} and DSL6A^{p53null} were used for *in vitro* studies. Following infection with different ratios of Ad-p53-particles (MOI) in combination with 5-FU, proliferation of tumor cells and apoptosis were quantified by cell proliferation assay (WST-1) and FACS (PI-staining). In addition, DSL6A syngeneic pancreatic tumor cells were inoculated subcutaneously in to Lewis rats for *in vivo* studies. Tumor size, apoptosis (TUNEL) and survival were determined.

RESULTS: Ad-p53 gene transfer combined with 5-FU significantly inhibited tumor cell proliferation and substantially enhanced apoptosis in all four cell lines with an alteration in the p53 gene compared to those two cell lines containing wt-p53. *In vivo* experiments showed the most effective tumor regression in animals treated with Ad-p53 plus 5-FU. Both *in vitro* and *in vivo* analyses revealed that a sublethal dose of Ad-p53 augmented the apoptotic response induced by 5-FU.

CONCLUSION: Our results suggest that Ad-p53 may synergistically enhance 5-FU-chemosensitivity most strikingly in pancreatic cancer cells lacking p53 function. These findings illustrate that the anticancer efficacy of this combination treatment is dependent on the p53 gene status of the target tumor cells.

Eisold S, Linnebacher M, Ryschich E, Antolovic D, Hinz U, Klar E, Schmidt J. The effect of adenovirus expressing wild-type p53 on 5-fluorouracil chemosensitivity is related to p53 status in pancreatic cancer cell lines. *World J Gastroenterol* 2004; 10(24): 3583-3589

<http://www.wjgnet.com/1007-9327/10/3583.asp>

INTRODUCTION

Pancreatic cancer is a very aggressive tumor with a poor prognosis. Unfortunately, the majority of the patients are diagnosed at an advanced disease status and are not suitable for potentially curative resection. Intrinsic limitations of chemotherapy are the endogenous or acquired resistance of tumor cells to anti-cancer drugs and their toxicity to normal tissues, the latter being responsible for the occurrence of severe side effects. For these reasons, new approaches for the treatment of pancreatic cancer patients have to be developed.

The p53 tumor suppressor gene is functionally inactivated in about 50% of all human malignancies including up to 60% of pancreatic cancers^[1]. The tumor suppressor activity of p53 is mainly mediated through its ability to induce cell growth arrest or apoptosis in response to a variety of stress signals, whereas a lack of functional p53 usually leads to increased genomic instability, deregulated cell proliferation, accelerated tumor progression, and elevated cellular resistance to anticancer therapy^[2]. Expression of wt-p53 has been shown to be required for 5-FU-induced apoptosis and to greatly potentiate 5-FU-cytotoxicity^[3,4]. Several reports have suggested that the p53 status of the tumor cells may be an important response determinant to 5-FU-based chemotherapy^[5,6]. In contrast, other studies have failed to demonstrate any relationship between p53 expression and 5-FU chemotherapy^[7,8]. Gene therapy by adenovirus mediated introduction of the wild-type human p53 gene into tumors that are deficient in functional p53 has shown a significant tumor suppressing effect in preclinical studies and in clinical trials^[9-13]. Furthermore, these tumor suppressing activities of p53 reintroduction have been reported to be enhanced by combination with many chemotherapeutic drugs or ionizing radiation in various human tumors^[14,15]. However, the influence of the *de novo* expressed exogenous p53 on cellular sensitivity toward DNA-damaging agents is still not clear^[16-19].

The goal of the present study was to determine *in vitro* and *in vivo*, whether reintroduction of wt-p53 protein into pancreatic cancer cells could increase the sensitivity to 5-FU chemotherapy. Therefore, we tested pancreatic cancer cells with different p53 status. Our results demonstrate that wt-p53 gene transfer in pancreatic cancer cells with loss of p53 function has a significant impact on 5-FU-chemosensitivity leading to potential tumor regression both *in vitro* and in a pancreatic cancer model of immunocompetent rats.

MATERIALS AND METHODS

Cell lines and culture conditions

The human pancreatic cancer cell lines, Capan-1, Capan-2, PANC1 were provided by the Tumorbank, DKFZ, Heidelberg, Germany. FAMPAC was established in our laboratory from a 43 year old female with familial pancreatic cancer^[20]. The rodent pancreatic cancer cell lines, AS (BSp73AS) and DSL6A, were originally derived from a spontaneous pancreatic adenocarcinoma of a BDX rat^[21] and from a primary pancreatic carcinoma of an azaserine-treated Lewis rat^[22] respectively. All cells were grown

in Dulbecco's modified Eagle's medium (DMEM; Gibco BRL) supplemented with 100 mL/L heat inactivated fetal calf serum (FCS, Gibco BRL), 100 units/mL penicillin, 100 µg/mL streptomycin (Gibco BRL) and incubated at 37 °C in a humidified atmosphere with 50 mL/L CO₂.

Adenoviral vectors

The AdEasy system^[23] was used for construction and propagation of the human wt- p53 (Ad-p53) adenoviruses. The shuttle vector pAdTrack-CMV and the adenoviral backbone plasmid pAdEasy-1 were kindly provided by Bert Vogelstein (*Howard Hughes Medical Institute and Kimmel Cancer Center at Johns Hopkins University, Baltimore, MD 21 231*). The cDNA coding for human p53 was a gift from Martin Scheffner (*ATV, DKFZ, 69120 Heidelberg, Germany*). The control adenoviral vector expressing cytosine deaminase (Ad-CD) was kindly provided by Zhuangwu Li (*NIH/NCI Bldg.10/Rm. 12N226, 9000 Rockville Pike, Bethesda, MD 20 892*) and the AdlacZ vector was a gift from Petra Klein-Bauerschmitt (*ATV, DKFZ, 69120 Heidelberg, Germany*). Recombinant adenoviruses were propagated in 293 cells, harvested, aliquoted and stored as described^[24]. Adenovirus titer in plaque-forming units (p.f.u.) was determined by plaque formation assays on 293 cells. The multiplicity of infection (MOI) was defined as the ratio of p.f.u. per total number of cancer cells to be infected. Adenoviruses were administered in phosphate buffer (20 mmol/L NaH₂PO₄, pH 8.0, 130 mmol/L NaCl, 2 mmol/L MgCl₂, 20 g/L sucrose).

β-galactosidase expression

Pancreatic cancer cells were infected with AdlacZ in a variety of MOI ranging from 1 to 100, in 1 mL of medium in 25-cm³ tissue culture flasks under routine conditions. After 24 h infected cells were fixed in 960 mL/L ethanol and stained with X-gal solution. The percentage of positively blue stained cells was determined by scoring five random high power fields per 25-cm³ flask.

Western blotting

The expression of p53 protein was assayed in all six pancreatic cancer cell lines before and after Ad-p53- infection. Cells were transduced with 10² MOI Ad-p53 and harvested at 24h. The protein lysates were separated by electrophoresis on a 100 g/L SDS/acrylamide gel and transferred to a PVDF membrane. The membrane was blocked in 200 mL TTBS, 50 g/L skimmed milk, 1 g/L Tween-20 for 1 h, incubated with primary p53 DO7 antibody (DAKO, Cambridgeshire, UK) for 1 h. After washing in TTBS the membrane was incubated with horseradish peroxidase (HRP) conjugated anti-mouse IgG for 45 min. Signals were detected using the enhanced chemiluminescence system (ECL, Amersham Life Science Ltd, Bucks, UK).

WST-1 cell viability assay

Cells were seeded at a concentration of 5-10×10³ cells/well in 100 µL culture medium into 96-well microtiter plates. After a 12 h incubation period, cells were infected either with Ad-p53 in a variety of MOIs (10⁻²-10²) or treated as controls with Ad-CD. After 24 h cells were washed with PBS and treatment with 5-fluorouracil (5-FU, Medac, Hamburg, Germany) at the concentration of 5 µL/mL was started for a period of 48 h. All dilutions were performed in culture medium. Cells were washed with PBS and 10 µL/well of the cell proliferation reagent WST-1 (Boehringer Mannheim, Germany) was added in 100 µL cell culture medium for 4 h. Absorbance of the samples was analysed using a bichromatic ELISA reader at 450 nm and 690 nm. Relative proliferation (A/Ao) was defined as the ratio of absorption measured in Ad-p53- infected and/or 5-FU treated cells or Ad-CD- infected cells (A) compared with the absorption measured in untreated control cells (Ao). All experiments were performed in triplicate.

FACS analysis

Cells were plated at a density of 10⁵ per 25-cm³ flask and infected with viral vectors at an MOI of 1 for 24 h. After 24 h cells were washed with PBS and treatment with 5-fluorouracil (5-FU, Medac, Hamburg, Germany) at the concentration of 5 µL/mL was started for a period of 48 h. The cells were harvested and washed with PBS. The apoptotic fraction of treated or untreated cells was determined by FACS analysis (FACSCalibur, Becton Dickinson) following permeabilisation and propidium iodide (PI) staining of the cells. Briefly, 250 µL of PI staining solution (1 g/L TritonX-100, 50 µg/mL PI in PBS, pH 7.4) was added to 5×10⁵ cells and analysed within 1 h using the CellQuest software. The proportion of apoptotic cells was calculated for each group: mock infected, Ad-CD, 5-FU, Ad-p53 and Ad-p53+ 5FU. Cell debris and fixation artefacts were excluded by appropriate gating. All experiments were performed in triplicate.

Animal experiments

Male Lewis rats, purchased from Charles River WIGA Laboratories (Sulzfeld, Germany), were kept in isolators and received food and water ad libitum. Animal experiments were performed under NIH and institutional guidelines established for the Animal Care Facility at the University of Heidelberg. A total of 10⁶ DSL6A tumor cells were injected in 100 µL of PBS/animal subcutaneously (sc.) into the abdominal wall of 4 wk-old rats. Eight weeks after tumor cell inoculation, when the tumor nodules had an average size of 8 mm×8 mm, the treatment as indicated was started and repeated twice a week for 1 mo. 5-FU (5 mg/kg bm) was given intraperitoneally (ip.) and Ad-p53 or Ad-CD infections (10⁸ infective units) were injected intratumorally (it.). The animals were separated by randomisation into 5 groups of 8 rats each namely mock infected, Ad-CD (1×10⁸ infectious particles it.), 5-fluorouracil (5 mg/kg bm ip.), Ad-p53 (1×10⁸ infectious particles it.) and Ad-p53+5-FU. Tumor size (mm²) was determined by measuring the largest and smallest diameter as tumor length (mm)×tumor width (mm). When the tumor size reached >600 mm², animals were sacrificed. Tumor size and survival rate were documented weekly.

TUNEL assay

Tumor tissues were fixed in 40 g/L neutral formaldehyde or snap frozen in liquid nitrogen and stored at -80 °C. Sections (5 µm) were stained with hematoxylin and eosin using standard procedures. At least 6 representative tumors of each group of treated or untreated animals were analysed for apoptosis. Immunohistochemical detection and quantification of apoptosis in formalin fixed tumor tissue sections were performed using the 'In situ cell death detection kit, AP' (Roche Diagnostics, Mannheim, Germany). The sections were stained and analysed microscopically according to the manufacturer's instructions.

Reverse transcriptase-PCR analysis

From snap frozen tumor tissue total RNA was extracted using RNazol (Cinna/Biotech, Friendswood, TX). cDNA was then generated using the cDNA cycle kit for RT-PCR (Invitrogen, San Diego, CA, USA). To assay expression of the p53 transgene from Ad-p53 in infected tumors, the following primers were generated to amplify a 294 bp product which is specific for Ad-p53: forward primer: 5' GGTGCATTGGAACGCGGA TT 3', reverse primer: 5' GGGGACAGAACGTTGTTTTC 3'. PCR was performed by an initial heating step at 95 °C for 5 min, followed by 35 cycles at 95 °C for 1 min, at 58 °C for 1 min and at 72 °C for 1 min and a final extension step at 72 °C for 5 min. The PCR products were separated on 1% agarose gels and visualized by ethidium bromide staining and UV light.

Statistical analysis

Statistical analysis was performed using SPSS software (Release 11.0.1, SPSS Inc.). The rate of cell viability and the rate of

apoptotic cells were expressed as mean \pm SE and 95% confidence interval. The 95% confidence intervals of the means were used to analyse the rate of cell viability and the rate of apoptotic cells between two groups of each cell line. Differences between means without overlap of the confidence intervals were described as statistically significant. Tumor size in rats was given as mean \pm SD. Normal distribution of tumor size in different groups was judged by the Shapiro-Wilk test. ANOVA was performed to analyse the therapeutic effects after 4 cycles and at study end between the groups with respect to tumor size. Two-sided *P*-values were reported and an effect was considered statistically significant at *P*<0.05.

RESULTS

Adenovirus mediated gene transfer efficacy in pancreatic cancer cells

The efficacy of Ad-p53 gene transfer into pancreatic cancer cell lines was assessed as the percentage of X-gal stained positive cells 24 h after infection with AdlacZ. There was a variation in transduction efficacy as summarised in Table 1. An MOI of 50 resulted in 73-95% of cells stained blue in the tested cell lines.

Table 1 p53 status, transduction efficacy and IC₅₀ value of 5-FU in pancreatic cancer cell lines; mean \pm SD

Cell line	p53 status	β -gal ¹ %	5-FU-IC ₅₀ value ¹ μ g/mL
Human			
Capan-1	159 GCC \rightarrow GTC	92 (4.5)	8.25 (0.45)
Capan-2	wild type	95 (7.2)	5.75 (0.55)
FAMPAC	175 CGC \rightarrow CAT	82 (7.8)	8.00 (0.45)
PANCL	273 CGT \rightarrow CAT	82 (7.8)	9.50 (0.75)
Murine rat			
AS	wild type	73 (5.3)	6.55 (0.45)
DSL6A	Null	83 (6.2)	7.75 (0.55)

¹ β -gal was the percentage of X-gal positive cells 24 h after AdlacZ infection at a multiplicity of infection of 50. ²IC₅₀ values were defined for each cell line as the 5-FU concentration leading to 50% growth inhibition. Results are expressed as mean \pm SD from three independent experiments.

p53 status and p53 protein expression after Ad-p53 infection in vitro

To determine the p53 status of the tested cell lines, we reviewed the literature (Capan-1²⁵, Capan-2²⁵, PANC1²⁶) or analysed cell samples (FAMPAC²⁷) for mutations in exons 5-8 of p53. For the rat pancreatic cancer cell lines, DSL6A and AS, the p53 status was determined by PCR-SSCP analysis followed by direct sequencing^[28]. Despite repeated attempts, the DSL6A cell line failed to give rise to amplified products for tested exons 5-8 of p53, suggesting a homozygous deletion of the loci. All exons could be amplified from normal control DNA of AS cells. The mutation status of the pancreatic cancer cell lines is outlined in Table 1.

The expression of p53 protein was confirmed by Western blot analysis. The antibody used reacted with both wild type and mutant p53. This was done to confirm the expression after Ad-p53 infection and to establish the baseline protein expression patterns. These *in vitro* experiments demonstrated for all cell lines detectable amounts of p53 protein 24 h after infection with Ad-p53 indicating an efficient translation. As indicated in Figure 1 the quantity of p53 was increased following infection with Adp53, with the exception of Capan-1 and FAMPAC cell lines showing a strong baseline overexpression of mutated p53.

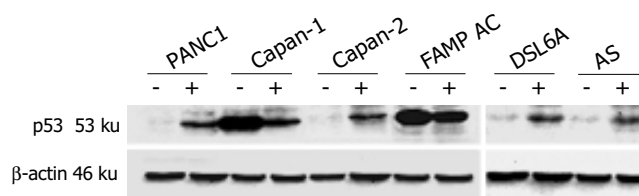


Figure 1 Expression of p53 protein before (-) and after infection with Ad-p53 (+) in pancreatic cancer cell lines.

Effect of p53 gene transduction on in vitro pancreatic tumor cell proliferation

To establish defined conditions for the *in vitro* experiments, all six pancreatic cancer cell lines were transduced with different multiplicity of infection (MOI = p.f.u./cell) of the Ad-p53 vector in the range from 10⁻² to 10². To test the effect of the p53 recombinant adenoviruses on tumor cell growth, we assayed the cell viability using a colorimetric cell proliferation test. Infection with the control vector Ad-CD had no significant effect on cell growth (data not shown). In contrast, we observed that Ad-p53 infection dose dependently resulted in significantly decreased cell viability. A significant inhibitory effect on tumor cell growth was achieved at MOI ³ 1 in all tested cell lines with an alteration of p53, whereas lower levels of Ad-p53 virus particles had no effect. Capan-2 cells containing wt-p53, were less sensitive and a similar inhibitory effect was only achieved with a higher MOI of 10. The rat pancreatic cancer cell line, AS containing wt-p53, revealed only a small effect on tumor growth (Figure 2).

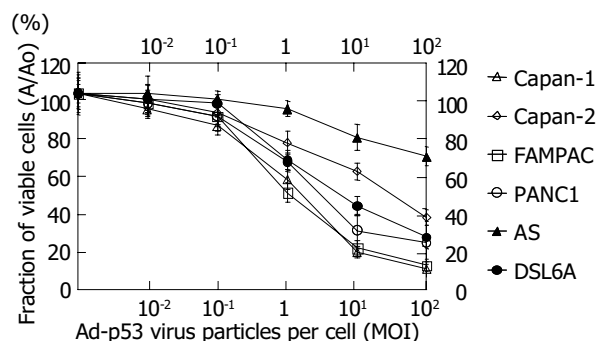


Figure 2 Decreased *in vitro* growth rate in pancreatic cancer cell lines 24 h after infection with Ad-p53. Data points represent means from 9 samples of viable cells in three independent experiments; bars, SD.

Efficacy of combined Ad-p53 and 5-FU therapy on tumor cell growth in vitro

To investigate whether the reintroduction of wt-p53 protein could enhance the tumor inhibitory effect of 5-FU treatment, all six pancreatic cancer cell lines were infected with Ad-p53 at MOI 1, which revealed an intrinsic antiproliferative activity by itself. 5-FU at the concentration of 5 μ g/mL was chosen for the combination experiments and was given 24 h after Ad-p53 infection. In preliminary dose escalation studies, the IC₅₀ values of each cell line were determined and listed in Table 1. Low dose FU (5 μ g/mL) given alone reduced cell viability most significantly to wt-p53 containing Capan-2 cells and AS cells compared to the other tested cell lines. The antiproliferative effects of the combination of Ad-p53 and 5-FU were next evaluated and non-functional p53 pancreatic cancer cell lines were most sensitive to the cytotoxic action of the combined treatment. This growth inhibitory effect was highly significant compared to either administration of p53 gene transduction or 5-FU treatment alone. For Capan-2 cells containing wt-p53, the combined antiproliferative effect of the two drugs was only 9%

Table 2 *In vitro* growth of different pancreatic cancer cell lines after indicated treatment ¹measured by WST-1 cell viability assay²; % mean (95% CI)

	Cell line	Control	Ad-CD-control	Ad-p53	5-FU	Ad-p53+5-FU
Human	Capan-1	97.8 (96.0-99.5)	91.9 (86.6-97.6)	55.0 (51.3-58.6)	72.9 (70.4-74.4)	30.7 (28.9-32.4)
	Capan-2	97.9 (95.7-100.0)	91.3 (88.2-94.5)	75.0 (71.3-78.6)	55.6 (53.1-58.0)	51.2 (48.0-54.4)
	FAMPAC	98.0 (95.9-100.1)	93.3 (90.5-96.2)	48.6 (44.7-52.4)	70.6 (68.0-73.1)	31.7 (29.6-33.8)
	PANCL	98.4 (97.1-99.8)	95.0 (92.2-97.8)	64.7 (59.8-69.5)	73.9 (71.6-76.2)	33.8 (31.5-36.0)
Murine rat	AS	99.0 (97.6-100.4)	97.9 (95.7-100.0)	92.3 (88.9-95.8)	56.8 (52.2-61.3)	53.1 (48.2-58.0)
	DSL6A	98.8 (97.5-100.0)	94.0 (90.8-97.2)	64.2 (60.5-67.9)	69.4 (66.0-72.9)	32.8 (29.3-36.2)

¹Cells were either infected with Ad-CD control or Ad-p53 (MOI 1) 24 h prior±5FU chemotherapy (5 µg/mL) given for 48 h. ²The data represents the ratio of the colorimetric values of viable cells treated as indicated (A) compared with the untreated control cells (Ao). Results are expressed as mean with 95% confidence interval (CI) from more than 9 samples in three independent experiments.

more than with 5-FU chemotherapy alone. In wt-p53 containing AS cells, Ad-p53 infection could not enhance the 5-FU antiproliferative action to a significant level (Table 2).

Effect of Ad-p53 gene transduction and 5-FU treatment on apoptotic cell death *in vitro*

To determine whether Ad-p53 mediated increase of 5-FU cytotoxic action was due to enhanced apoptosis, we analyzed DNA-fragmentation by fluorometric analysis of propidium iodide stained pancreatic cells. Cells treated with 5-FU (5 µg/mL) showed a percentage of dead cells between 8% and 16%, which was slightly above that of native cells or cells infected with the Ad-CD control vector. In cells transduced with the p53 gene (MOI 1), the percentage increased up to 25%. p53 gene transduction followed by 5-FU chemotherapy, caused a marked increase of apoptotic cell death. These findings were consistent showing the highest apoptotic rate for the pancreatic cancer cell lines with an altered p53 (47-58%), and the lowest apoptotic rate in wt-p53 containing cell lines (18-20%) as indicated in Figure 3.

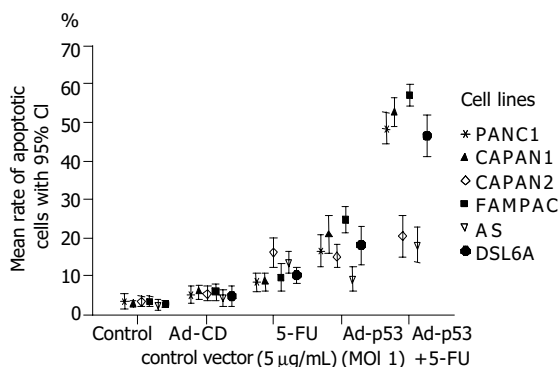


Figure 3 Percentage of apoptotic cells of human and rat pancreatic carcinoma cell lines either infected with Ad-CD control vector or Ad-p53 (MOI 1) 24 h prior±5-FU chemotherapy (5 µg/mL) given for 48 h. Points represent means from 9 samples in three independent experiments; bars, 95% CI.

In vivo effects of combined treatment on tumor growth in rat pancreatic cancer

Subcutaneous DSL6A tumors generated in 4-wk-old male Lewis rats were treated by intratumoral injection with adenoviral vectors and/or 5-FU chemotherapy given intraperitoneally twice a week for 1 mo. Details of the onset and cessation of treatment were indicated in the methods section. To determine if p53 recombinant adenoviruses could induce p53 mRNA expression, RT-PCR analysis was performed in the generated DSL6A tumors. Non-infected and Ad-p53 infected tumors were removed and p53 transgene expression was confirmed 24 h

after the last injection. As shown in Figure 4, a 294 bp band was detected only in Ad-p53 infected tumors.

Tumor growth was measured regularly during the 4 wk following treatment. Animals in both control groups showed an extensive tumor proliferation, and after 6 cycles of therapy tumor size was above 600 mm², so that treatment was stopped and animals were killed according to the protocol. During the first four cycles of treatment, in animals with 5-FU monotherapy tumor growth was significantly reduced compared to the controls (157±54 mm² vs 410±65 mm², *P*<0.0001). Ad-p53 treatment alone (72±19 mm², *P*<0.0001) or the combination Ad-p53 plus 5-FU (61±8 mm², *P*<0.0001) demonstrated local tumor growth control. However, within the following four cycles of therapy we observed an increasing tumor size in animals treated only with 5-FU (580±58 mm²) or Ad-p53 (347±52 mm²) alone compared to the combination of Ad-p53 plus 5-FU (67±14 mm², *P*<0.0001). As shown in Figure 5, the combination of Ad-p53 and 5-FU demonstrated the most potent inhibitory effect on tumor growth, but none out of the 8 animals was tumor free at the end of the treatment.

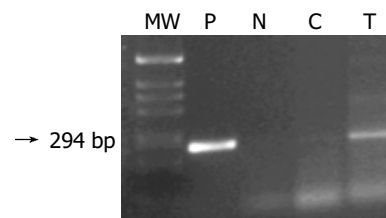


Figure 4 Gel electrophoresis for PCR products from DSL6A tumors removed from Lewis rats 24 h following the last treatment. (P) positive control, vector DNA; (N) negative control (RT minus control); (C) Ad-CD control virus treated tumor (Ad-CD); (T) Ad-p53 infected tumor.

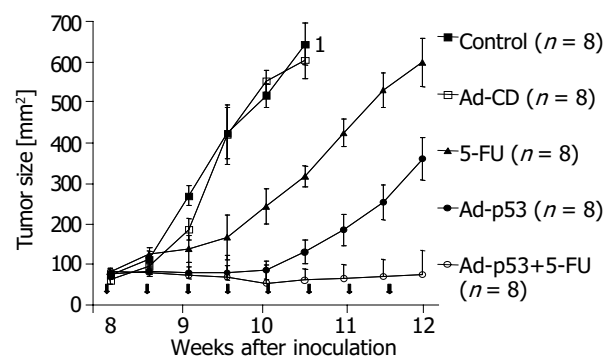


Figure 5 Efficacy of Ad-p53 infection and 5-FU as single agents vs the combination of both on tumor growth of Lewis rats challenged with DSL6A tumor cells. Arrowheads indicate treatment application. ¹All animals were killed after 6 cycles of therapy because the tumor size was above 600 mm².

Detection of apoptosis in tumor tissues after treatment

Since our *in vitro* data indicated that the tumor-inhibitory effects of the combined treatment of Ad-p53 plus 5-FU were significantly mediated by induction of apoptosis, we assessed the tumor tissue sections for DNA degradation using the TUNEL assay. Analyses of tumor sections of each group revealed a slight increase of apoptotic cells in rats treated with 5-FU compared to both control groups, mock or Ad-CD infected. Adenoviral p53 gene transduction significantly increased the number of apoptotic cells in comparison to single 5-FU chemotherapy. As shown in Figure 6, *in situ* quantification revealed the highest number of cells undergoing apoptosis in tumors treated with Ad-p53 plus 5-FU.

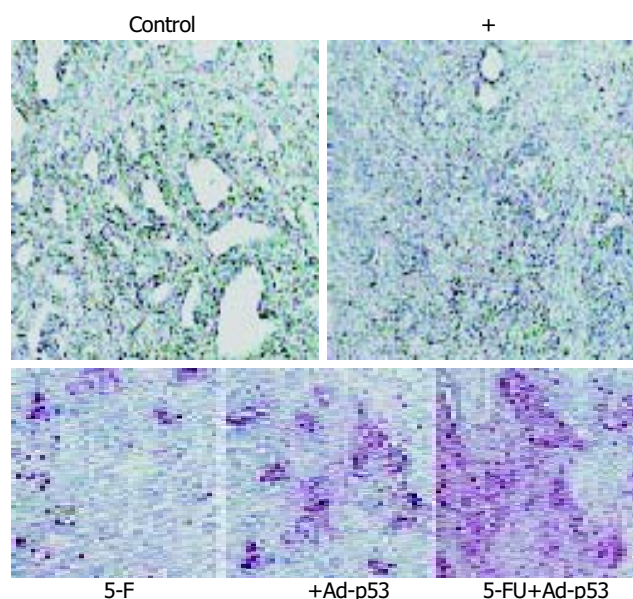


Figure 6 Ad-p53 mediated sensitisation of tumors to apoptosis in response to 5-FU *in vivo*. Formalin-fixed tissue sections were analyzed by TUNEL labelling. Original magnification $\times 200$.

DISCUSSION

A number of previous studies have shown that the restoration of wt-p53 may increase or decrease drug sensitivity, indicating that p53 status may influence the response of human cancers to chemotherapy in a cell- and drug specific manner^[3,16,17,29]. However, what is currently lacking is critical information on the cytotoxicity and target response to such a combined modality therapy. In this study we investigated a panel of human pancreatic cancer cell lines with well characterised defects in the p53 gene to identify differences following treatment with Ad-p53 vector and 5-FU chemotherapy. Because high concentrations of p53 were difficult to reach in patients by vectors available so far, and high doses of 5-FU could not be used *in vivo* due to their side effects, we evaluated the efficacy of low concentrations of p53 infection and low doses of 5-FU.

In our *in vitro* study infection with Ad-p53 alone produced tumor growth suppression in all pancreatic cancer cell lines ranging from highly significant to almost absent. The most prominent growth inhibitory effect was observed in the pancreatic cancer cell lines with an alteration of the p53 function. These findings may not only relate to the endogenous p53 status, but also to differences in transduction efficiency of cell lines to the expression of $\beta 3$ integrins and coxsackie virus and adenovirus receptors (CAR) on tumor cells^[30]. Ad-p53 infection at a low concentration (MOI 1) induced only a small number of apoptotic cells in the tested pancreatic cancer cell lines. These results are in agreement with those of other authors showing that levels of p53 expression that inhibited proliferation may

not be sufficient by themselves to induce cell death^[10,31-33]. The reduced cell proliferation observed after Ad-p53 infection might be rather attributed to a persistent S phase depletion and G0/G1 accumulation without induction of apoptosis.

However, the key question in our study was to correlate the exogenous p53 expression with the response to 5-FU based chemotherapy. Like a number of other studies the p53 replacement into tumor cell lines with altered p53, revealed the most effective tumor growth inhibition^[9-12]. Our data clearly support other *in vitro* studies, which have reported that loss of p53 function could reduce cellular sensitivity to 5-FU^[3,4,34]. These synergistic effects are less conclusive in cases of p53 transgene overexpression in wt-p53 tumors. Only a small, but not significant advantage of the combination regimen was achieved in the human Capan-2^{p53wt} cells, whereas the murine AS^{p53wt} cells failed to such a treatment. Since from the clinical point of view apoptotic death is the final outcome that can define the success of therapy, we screened for the induction of apoptosis in relation to the different treatment schedules. Our data demonstrated, that the combination regimen of Ad-p53 plus 5-FU was able to significantly increase the number of apoptotic cells in the pancreatic tumor cell lines with an altered p53 gene. Likewise to our findings some reports have shown, that high level expression of p53 could cause some cancer cells to undergo apoptosis, whereas others simply undergo prolonged cell cycle arrest^[10,31]. To overcome the resistance to p53 mediated apoptosis several reports have shown a significant advantage of Ad-p53 gene therapy in combination with DNA damaging agents^[10,14,15,32].

A foremost concern with such a strategy is whether sufficient chemosensitisation can be accomplished with relatively few supplemental gene therapy treatments during 5-FU based chemotherapy. Experimental studies reported a rate of gene transduction between 5% and 15% using immunohistochemical analysis^[9]. Therefore we used a subcutaneous pancreatic tumor model to allow assessment of the efficacy of this approach. In immunocompetent Lewis rats, combination of intratumoral Ad-p53 infection of implanted pancreatic DSL6A^{p53null} tumors with additional systemic 5-FU chemotherapy resulted in a significant retardation of tumor growth. These combined effects clearly exceeded those achieved by administration of either agent alone. In contrast to all other treatment modalities, the combination regimen Ad-p53 plus 5-FU revealed no further *in vivo* tumor growth during the time of treatment. The reason for incomplete tumor regression may be related to the low p53 transduction rate and limited spread within the tumor. Our *in vivo* data point to an enhancement of 5-FU mediated apoptosis in DSL6A tumors as a result of adenoviral mediated p53 gene transfer. This is in line with our *in vitro* findings, which strongly suggest that the sensitisation is mediated by enhancing the apoptotic response of neoplastic cells to 5-FU treatment. Similar anticancer therapy approaches using combined administration of adenovirus mediated p53 gene therapy and chemotherapeutic drugs have been evaluated. In some tumors, inactivation of p53 correlated with an increased resistance to radiation and several antineoplastic drugs and transduction of the wt-p53 gene increased the sensitivity^[3,16,17,32]. In contrast, in other tumors the expression of exogenous wt-p53 reduced sensitivity, while the disruption of p53 function increased sensitivity^[35-37]. A number of clinical studies have found that p53 overexpression, a surrogate marker for p53 mutations, correlated with resistance to 5-FU^[5,6,38,39], but other studies found no correlation^[40,41]. Such conflicting findings might in part, be due to the wide variation in immunohistochemical protocols, and the use of different antibodies to detect p53. Other techniques, such as DNA sequencing, might provide a more objective assessment of the p53 status. At present, despite the *in vitro* evidence for p53 involvement in downstream signalling in response to 5-FU, the clinical value of p53 as a

predictive marker for 5-FU based chemotherapy remains a matter for debate.

In conclusion, our results confirm the feasibility of sensitising pancreatic cancer cells to 5-FU chemotherapy *in vivo* using adenovirus mediated p53 gene therapy. In tumors, where sustained expression of wt-p53 cannot be achieved or the levels of expression are insufficient to significantly induce apoptosis, wt-p53 can be used as a therapeutic agent in combination with conventional antineoplastic drugs. Our results have confirmed that this enhanced cytotoxicity is mostly provided by driving significant numbers of neoplastic cells into apoptosis. Therefore, the assessment of endogenous p53 status by DNA sequencing, which may correlate with the response to 5-FU chemotherapy may have an important role in defining patients who are most likely to benefit from 5-FU chemotherapy or combination treatment in the future^[42].

REFERENCES

- 1 **Ghaneh P**, Kawesha A, Evans JD, Neoptolemos JP. Molecular prognostic markers in pancreatic cancer. *J Hepatobiliary Pancreat Surg* 2002; **9**: 1-11
- 2 **Levine AJ**. p53 the cellular gatekeeper for growth and division. *Cell* 1997; **88**: 323-331
- 3 **Lowe SW**, Ruley HE, Jacks T, Housman DE. p53-dependent apoptosis modulates the cytotoxicity of anticancer agents. *Cell* 1993; **74**: 957-967
- 4 **Bunz F**, Hwang PM, Torrance C, Waldman T, Zhang Y, Dillehay L, Williams J, Lengauer C, Kinzler KW, Vogelstein B. Disruption of p53 in human cancer cells alters the responses to therapeutic agents. *J Clin Invest* 1999; **104**: 263-269
- 5 **Lenz HJ**, Hayashi K, Salonga D, Danenberg KD, Danenberg PV, Metzger R, Banerjee D, Bertino JR, Groshen S, Leichman LP, Leichman CG. p53 point mutations and thymidylate synthase messenger RNA levels in disseminated colorectal cancer: an analysis of response and survival. *Clin Cancer Res* 1998; **4**: 1243-1250
- 6 **Ahnen DJ**, Feigl P, Quan G, Fenoglio-Preiser C, Lovato LC, Bunn PA Jr, Stemmerman G, Wells JD, Macdonald JS, Meyskens FL Jr. Ki-ras mutation and p53 overexpression predict the clinical behavior of colorectal cancer: a southwest oncology group study. *Cancer Res* 1998; **58**: 1149-1158
- 7 **Yeh KH**, Shun CT, Chen CL, Lin JT, Lee WJ, Lee PH, Chen YC, Cheng AL. Overexpression of p53 is not associated with drug resistance of gastric cancers to 5-fluorouracil-based systemic chemotherapy. *Hepatogastroenterology* 1999; **46**: 610-615
- 8 **Cascinu S**, Catalano V, Aschele C, Barni S, Debernardis D, Gallo L, Bandelloni R, Staccioli MP, Baldelli AM, Brenna A, Valenti A, Muretto P, Catalano G. Immunohistochemical determination of p53 protein does not predict clinical response in advanced colorectal cancer with low thymidylate synthase expression receiving a bolus 5-fluorouracil-leucovorin combination. *Ann Oncol* 2000; **11**: 1053-1116
- 9 **Ghaneh P**, Greenhalf W, Humphreys M, Wilson D, Zumstein L, Lemoine NR, Neoptolemos JP. Adenovirus-mediated transfer of p53 and p16 (INK4a) results in pancreatic cancer regression *in vitro* and *in vivo*. *Gene Ther* 2001; **8**: 199-208
- 10 **Sasaki Y**, Morimoto I, Ishida S, Yamashita T, Imai K, Tokino T. Adenovirus-mediated transfer of the p53 family genes, p73 and p51/p63 induces cell cycle arrest and apoptosis in colorectal cancer cell lines: potential application to gene therapy of colorectal cancer. *Gene Ther* 2001; **8**: 1401-1408
- 11 **Lang FF**, Bruner JM, Fuller GN, Aldape K, Prados MD, Chang S, Berger MS, McDermott MW, Kunwar SM, Junck LR, Chandler W, Zwiebel JA, Kaplan RS, Yung WK. Phase I trial of adenovirus-mediated p53 gene therapy for recurrent glioma: biological and clinical results. *J Clin Oncol* 2003; **21**: 2508-2518
- 12 **Shimada H**, Matsubara H, Ochiai T. p53 gene therapy for esophageal cancer. *J Gastroentero* 2002; **37**: 87-91
- 13 **Buller RE**, Shahin MS, Horowitz JA, Runnebaum IB, Mahavni V, Petrauskas S, Kreienberg R, Karlan B, Slamon D, Pegram M. Long term follow-up of patients with recurrent ovarian cancer after Ad p53 gene replacement with SCH 58500. *Cancer Gene Ther* 2002; **9**: 567-572
- 14 **Spitz FR**, Nguyen D, Skibber JM, Meyn RE, Cristiano RJ, Roth JA. Adenoviral-mediated wild-type p53 gene expression sensitizes colorectal cancer cells to ionizing radiation. *Clin Cancer Res* 1996; **2**: 1665-1671
- 15 **Nishizaki M**, Meyn RE, Levy LB, Atkinson EN, White RA, Roth JA, Ji L. Synergistic inhibition of human lung cancer cell growth by adenovirus-mediated wild-type p53 gene transfer in combination with docetaxel and radiation therapeutics *in vitro* and *in vivo*. *Clin Cancer Res* 2001; **7**: 2887-2897
- 16 **Gjerset RA**, Turla ST, Sobol RE, Scalise JJ, Mercola D, Collins H, Hopkins PJ. Use of wild-type p53 to achieve complete treatment sensitization of tumor cells expressing endogenous mutant p53. *Mol Carcinog* 1995; **14**: 275-285
- 17 **Blagosklonny MV**, el-Deiry WS. *In vitro* evaluation of a p53-expressing adenovirus as an anti-cancer drug. *Int J Cancer* 1996; **67**: 386-392
- 18 **Zeimet AG**, Marth C. Why did p53 gene therapy fail in ovarian cancer? *Lancet Oncol* 2003; **4**: 415-422
- 19 **Lain S**, Lane D. Improving cancer therapy by non-genotoxic activation of p53. *Eur J Cancer* 2003; **39**: 1053-1060
- 20 **Eisold S**, Ryschich E, Linnebacher M, Nauheimer D, Wild A, Bartsch DK, Büchler MW, Schmidt J. Characterisation of a new human pancreatic cancer cell line, FAMPAC, with a hereditary background. *Cancer* 2004; **100**: 1978-1986
- 21 **Matzku S**, Komitowski D, Mildenerberger M, Zoller M. Characterization of BSp73, a spontaneous rat tumor and its *in vivo* selected variants showing different metastasizing capacities. *Invasion Metastasis* 1983; **3**: 109-123
- 22 **Pettengill OS**, Faris RA, Bell RH Jr, Kuhlmann ET, Longnecker DS. Derivation of ductlike cell lines from a transplantable acinar cell carcinoma of the rat pancreas. *Am J Pathol* 1993; **143**: 292-303
- 23 **He TC**, Zhou S, da Costa LT, Yu J, Kinzler KW, Vogelstein B. A simplified system for generating recombinant adenoviruses. *Proc Natl Acad Sci U S A* 1998; **95**: 2509-2514
- 24 **Gerard R**, Meidell RS. Adenovirus vectors. In: Glover DM, Hames BD (eds). DNA cloning 4. A practical approach. *Oxford University press: Oxford* 1996: 285-306
- 25 **Berrozpe G**, Schaeffer J, Peinado MA, Real FX, Perucho M. Comparative analysis of mutations in the p53 and K-ras genes in pancreatic cancer. *Int J Cancer* 1994; **58**: 185-191
- 26 **Moore PS**, Sipos B, Orlandini S, Sorio C, Real FX, Lemoine NR, Gress T, Bassi C, Klöppel G, Kalthoff H, Ungefroren H, Lohr M, Scarpa A. Genetic profile of 22 pancreatic carcinoma cell lines. Analysis of K-ras, p53, p16 and DPC4/Smad4. *Virchows Arch* 2001; **439**: 798-802
- 27 **Erber R**, Conradt C, Homann N, Enders C, Finckh M, Dietz A, Weidauer H, Bosch FX. TP53 DNA contact mutations are selectively associated with allelic loss and have a strong clinical impact in head and neck cancer. *Oncogene* 1998; **16**: 1671-1679
- 28 **Hirayama Y**, Wakazono K, Yamamoto M, Kitano M, Tatematsu M, Nagao M, Sugimura T, Ushijima T. Rare mutations of p53, Ki-ras, and β -catenin genes and absence of K-sam and c-erbB-2 amplification in N-methyl-N'-nitro-N-nitrosoguanidine-induced rat stomach cancers. *Mo Carcinog* 1999; **25**: 42-47
- 29 **Mohiuddin M**, Chendil D, Dey S, Alcock RA, Regine W, Mohiuddin M, Ahmed MM. Influence of p53 status on radiation and 5-fluorouracil synergy in pancreatic cancer cells. *Anti-cancer Res* 2002; **22**: 825-830
- 30 **Pearson AS**, Koch PE, Atkinson N, Xiong M, Finberg RW, Roth JA, Fang B. Factors limiting adenovirus-mediated gene transfer into human lung and pancreatic cancer cell lines. *Clin Cancer Res* 1999; **5**: 4208-4213
- 31 **Kusumoto M**, Ogawa T, Mizumoto K, Ueno H, Niiyama H, Sato N, Nakamura M, Tanaka M. Adenovirus-mediated p53 gene transduction inhibits telomerase activity independent of its effects on cell cycle arrest and apoptosis in human pancreatic cancer cells. *Clin Cancer Res* 1999; **5**: 2140-2147
- 32 **Biroccio A**, Bufalo DD, Ricca A, D'Angelo C, D'Orazi G, Sacchi A, Soddu S, Zupi G. Increase of BCNU sensitivity by wt-p53 gene therapy in glioblastoma lines depends on the administration schedule. *Gene Ther* 1999; **6**: 1064-1072
- 33 **Longley DB**, Harkin DP, Johnston PG. 5-fluorouracil: mechanisms of action and clinical strategies. *Nat Rev Cancer* 2003; **3**: 330-338

- 34 **Longley DB**, Boyer J, Allen WL, Latif T, Ferguson PR, Maxwell PJ, McDermott U, Lynch M, Harkin DP, Johnston PG. The role of thymidylate synthase induction in modulating p53-regulated gene expression in response to 5-fluorouracil and antifolates. *Cancer Res* 2002; **62**: 2644-2649
- 35 **Parsels LA**, Zellars RC, Loney TL, Parsels JD, Clarke MF, Merchant AK, Lawrence TS, Maybaum J. Prevention of fluorodeoxyuridine-induced cytotoxicity and DNA damage in HT29 colon carcinoma cells by conditional expression of wild-type p53 phenotype. *Mol Pharmacol* 1997; **52**: 600-605
- 36 **Brachman DG**, Beckett M, Graves D, Haraf D, Vokes E, Weichselbaum RR. p53 mutation does not correlate with radiosensitivity in 24 head and neck cancer cell lines. *Cancer Res* 1993; **53**: 3667-3669
- 37 **Fan S**, Smith ML, Rivet DJ 2nd, Duba D, Zhan Q, Kohn KW, Fornace AJ Jr, O'Connor PM. Disruption of p53 function sensitizes breast cancer MCF-7 cells to cisplatin and pentoxifylline. *Cancer Res* 1995; **55**: 1649-1654
- 38 **Liang JT**, Huang KC, Cheng YM, Hsu HC, Cheng AL, Hsu CH, Yeh KH, Wang SM, Chang KJ. p53 overexpression predicts poor chemosensitivity to high-dose 5-fluorouracil plus leucovorin chemotherapy for stage IV colorectal cancers after palliative bowel resection. *Int J Cancer* 2002; **97**: 451-457
- 39 **Nio Y**, Dong M, Uegaki K, Hirahara N, Minari Y, Sasaki S, Takamura M, Iguchi C, Tamura K. p53 expression affects the efficacy of adjuvant chemotherapy after resection of invasive ductal carcinoma of the pancreas. *Anticancer Res* 1998; **18**: 3773-3779
- 40 **Paradiso A**, Ranieri G, Simone G, Silvestris N, Costa A, De Lena M, Leone A, Vallejo C, Lacava J. mdm2-p53 Interaction: lack of correlation with the response to 5-fluorouracil in advanced colorectal cancer. *Oncology* 2002; **62**: 278-285
- 41 **Elsaleh H**, Powell B, Soontrapornchai P, Joseph D, Gorla F, Spry N, Iacopetta B. p53 gene mutation, microsatellite instability and adjuvant chemotherapy: impact on survival of 388 patients with Dukes' C colon carcinoma. *Oncology* 2000; **58**: 52-59
- 42 **Barratt PL**, Seymour MT, Stenning SP, Georgiades I, Walker C, Birbeck K, Quirke P. UKCCCR AXIS trial collaborators. Adjuvant X-ray and fluorouracil infusion study. DNA markers predicting benefit from adjuvant fluorouracil in patients with colon cancer: a molecular study. *Lancet* 2002; **360**: 1381-1391

Edited by Wang XL. Proofread by Zhu LH and Xu FM

Enhanced anti-apoptosis and gut epithelium protection function of acidic fibroblast growth factor after cancelling of its mitogenic activity

Xiao-Bing Fu, Xiao-Kun Li, Tong Wang, Biao Cheng, Zhi-Yong Sheng

Xiao-Bing Fu, Biao Cheng, Zhi-Yong Sheng, Wound Healing and Cell Biology Laboratory, Burns Institute, 304 Medical Department, General Hospital of PLA, Trauma Centre of Postgraduate Medical College, Beijing 100037, China

Xiao-Kun Li, Tong Wang, Biopharmaceutical R&D Centre, Jinan University, Guangzhou 510632, Guangdong Province, China

Supported by the National Natural Science Foundation of China, No. 30170966, 30230370; National Basic Science and Development Program (973 Program), No.G1999054204; National High-Tech Development Program (863 Program), No.2001AA215131

Correspondence to: Professor Xiao-Bing Fu, M.D., Wound Healing and Cell Biology Laboratory, 304 Medical Department, General Hospital of PLA, Trauma Centre of Postgraduate Medical College, 51 Fucheng Road, Beijing 100037, China. fuxb@cgw.net.cn

Telephone: +86-10-66867396 **Fax:** +86-10-68480755

Received: 2004-04-04 **Accepted:** 2004-04-12

Abstract

AIM: Mitogenic and non-mitogenic activities of fibroblast growth factor (FGF) are coupled to a range of biological functions, from cell proliferation and differentiation to the onset of many diseases. Recent reports have shown that acidic fibroblast growth factor (aFGF) has a powerful anti-apoptosis function, which may have potentially therapeutical effect on gut ischemia and reperfusion injuries. However, whether this function depends on its mitogenic or non-mitogenic activity remains unclear. In this study, we identified the source of its anti-apoptosis function with a mutant, aFGF28-154 and observed its effect on reducing gut ischemia and reperfusion injury.

METHODS: aFGF28-154 was generated by amplification of appropriate DNA fragments followed by subcloning the products into pET-3c vectors, then they were expressed in BL21 (DE3) cells and purified on an M2 agarose affinity column. This mutant aFGF28-154 maintained its non-mitogenic activity and lost its mitogenic activity. With a dexamethasone (DEX)-induced mouse thymocyte apoptosis model *in vitro* and *in vivo*, we studied the anti-apoptotic function of aFGF28-154. Also, *in vivo* study was performed to further confirm whether aFGF28-154 could significantly reduce apoptosis in gut epithelium after gut ischemia-reperfusion injury in rats. Based on these studies, the possible signal transduction pathways involved were studied.

RESULTS: With a dexamethasone (DEX)-induced mouse thymocyte apoptosis model *in vitro* and *in vivo*, we found that the anti-apoptotic function of aFGF28-154 was significantly enhanced when compared with the wild type aFGF. *In vivo* study further confirmed that aFGF28-154 significantly reduced apoptosis in gut epithelium after gut ischemia-reperfusion injury in rats. The mechanisms of anti-apoptosis function of aFGF28-154 did not depend on its mitogenic activity and were mainly associated with its non-mitogenic activities, including the intracellular calcium ion balance protection, ERK1/2 activation sustaining and cell cycle balance.

CONCLUSION: These findings emphasize the importance of non-mitogenic effects of aFGF, and have implications for its therapeutic use in preventing apoptosis and other injuries in tissues and internal organs triggered by ischemia-reperfusion injury.

Fu XB, Li XK, Wang T, Cheng B, Sheng ZY. Enhanced anti-apoptosis and gut epithelium protection function of acidic fibroblast growth factor after cancelling of its mitogenic activity. *World J Gastroenterol* 2004; 10(24): 3590-3596

<http://www.wjgnet.com/1007-9327/10/3590.asp>

INTRODUCTION

Fibroblast growth factors (FGFs) are members of a family of polypeptides that are potent regulators of cell proliferation, differentiation, and function. They play very important roles in normal development, maintenance of tissues, wound healing and repair. They have also been implicated in a wide range of pathological conditions, including tumorigenesis and metastasis^[1-4]. Acidic and basic fibroblast growth factors (aFGF and bFGF), the important members of this family, were named for their different isoelectric points. They have similar molecular weights and spectra of biological activities, and show approximately 55% amino acid similarity. aFGF and bFGF stimulate the proliferation of all cells of mesodermal organ, and many cells of neuroectodermal, ectodermal, and endodermal origin. Also, both FGFs are chemotactic and mitogenic for endothelial cells *in vitro*, inducing production of many factors involved in regulation of many functions^[2-5]. Recent reports have shown that aFGF has a powerful anti-apoptotic function, which may have potentially therapeutical use in some diseases^[5-13]. However, whether this function depends on its mitogenic or non-mitogenic activity remains unclear, and clarification of this function may help to find its new mechanisms and active domains. In the present study, we modified the wild type of aFGF and acquired a mutant, aFGF28-154, which kept its non-mitogenic activity and lost its mitogenic activity. By using the dexamethasone (DEX)-induced apoptotic model, we found that the anti-apoptosis function of the modified aFGF28-154 was significantly enhanced when compared with the wild type of aFGF. The results indicated that the powerful anti-apoptosis function of aFGF28-154 was associated with the intracellular calcium ion balance protection and ERK1/2 activation sustaining, which did not depend on its mitogenic activity. Further studies showed that aFGF might have a surveillance function at the checkpoint of cell cycle, for determination of stagnation, division or apoptosis. Finally, *in vivo* study confirmed that aFGF28-154 could significantly reduce apoptosis in gut epithelium after gut ischemia-reperfusion injury in rats.

MATERIALS AND METHODS

Protein preparation

Plasmids encoding aFGF28-154 were generated by amplification of appropriate DNA fragments, followed by subcloning the

products into pET-3c vectors. aFGF28-154 protein was expressed in BL21 (DE3) cells and purified on an M2 agarose affinity column (Sigma). We carried out SDS-PAGE and Western blot analysis with aFGF monoclonal antibody (Sigma) to determine the accuracy of protein expression.

Mitogenic activity assay

MTT method was conducted to test the mitogenic activity of both aFGFs. NIH 3T3 fibroblasts and PC12 cell lines from Wuhan University were cultured in DMEM (Hyclone) with 150 mL/L fetal bovine serum (Gibico) plus 50 mL/L equine serum (Hyclone) for PC12 culture. These cells were stimulated with aFGF and aFGF28-154 at a final concentration of 0, 1, 2, 3, 4, 5, 6, 8, 10 ng/mL for 24 h before A value detection.

Apoptosis models in thymocytes and treatment methods in vitro

Twenty homogeneous Balb/c mice aged four weeks were randomised into 4 groups: control group (group 1); DEX group (group 2), DEX+aFGF (Biopharmaceutical R&D Centre) group (group 3) and DEX+aFGF28-154 (group 4). DEX, if applied, was taken at a final concentration of 1 μ mol. aFGF and aFGF28-154, if applied, were taken at a final concentration of 100 ng/mL. In order to explore the relationship between dosage and effects, different dosages of aFGF28-154 from 50 to 200 ng/mL were used in another experiment. After collected under sterile conditions, thymocytes were cultured in RPMI1640 medium (Hyclone) supplemented with 100 mL/L fetal bovine serum (Gibico) for 5 h.

In *in vivo* study, Group 1 was injected with saline, group 2 with DEX 10 mg/kg, group 3 with DEX 10 mg/kg and aFGF10 μ g/kg, and group 4 with DEX 10 mg/kg and aFGF28-154 10 μ g/kg. Animals were fed for 5 h before collection of thymocytes.

Flow cytometry

Flow cytometry was performed using an FACScaliber (Becton Dickinson). Phosphatidylserine (PS), a sign of early apoptosis, was stained with Annexin V-FITC (Baosai), while DNA fragments of the necrotic cells were evaluated with PI apoptosis.

Morphological observation and gel electrophoresis analysis of apoptosis

Transmission electron microscope was used to morphologically visualize apoptosis and agarose gel electrophoresis was performed to find the damage of nuclear chromatin DNA.

Analysis of intracellular Ca^{2+} concentration

Confocal microscope was used to analyse the changes of

intracellular Ca^{2+} concentration.

Apoptosis model in gut epithelium and treatment methods in vivo

Rat intestinal ischemia-reperfusion (I/R) injury was produced by clamping the superior mesenteric artery (SMA) for 45 min followed by reperfusion for 24 h. One hundred and fourteen Wistar rats were divided randomly into four groups, namely intestinal I/R plus saline treatment group (I/R+Saline), intestinal I/R plus wild type aFGF treatment group (I/R plus aFGF), intestinal I/R plus aFGF 28-154 group (I/R plus aFGF28-154) and normal control group (normal control). In groups 1, 2 and 3, SMA was separated and occluded for 45 min, then released for reperfusion for 24 h. At the onset of reperfusion, saline (0.5 mL) or aFGF (4 μ g/rat), or aFGF28-154 (4 μ g/rat) was injected through the jugular vein. In control group, SMA was separated without occlusion. After the animals were sacrificed, tissue biopsies were taken from the intestine at 30 min, 1, 2, 6, 12, and 24 h, respectively. Apoptosis in epithelium entericum was assayed with TUNEL technique and analyzed using light microscope. All animal experiments were carried out according to the Guidelines for Care and Use of Experimental Animals and approved by the internal ethical committees of the Trauma Centre of Postgraduate Medical College (Beijing).

Analysis of signal transduction in cells stimulated by DEX and both aFGFs in vitro

Cultured thymocytes were sampled to carry out Western blot analysis. Antibodies used were ERK1/2, p-ERK1/2, JNK1/2, p38 MAPK, c-Myc (Sigma), and Caspase-3 (Boster).

RESULTS

Protein preparation and mitogenic activation assay

Plasmids encoding aFGF28-154 were generated by amplification of appropriate DNA fragments, followed by subcloning the products into pET-3c vectors. aFGF28-154 protein was expressed in BL21 (DE3) cells and purified on an M2 agarose affinity column (Sigma). We carried out SDS-PAGE and Western blot analysis with aFGF monoclonal antibody (Sigma) to determine the accuracy of protein expression (Figure 1A, B). We tested both aFGF and aFGF28-154 for their effects on proliferation of NIH 3T3 fibroblasts and rat pheochromocytoma (PC12) cells. The results indicated that the latter significantly lost its mitogenic activity evidenced by MTT results (Figure 1C). Thus, we could perform a comparative research to clarify whether aFGF function depended on mitogenic activity.

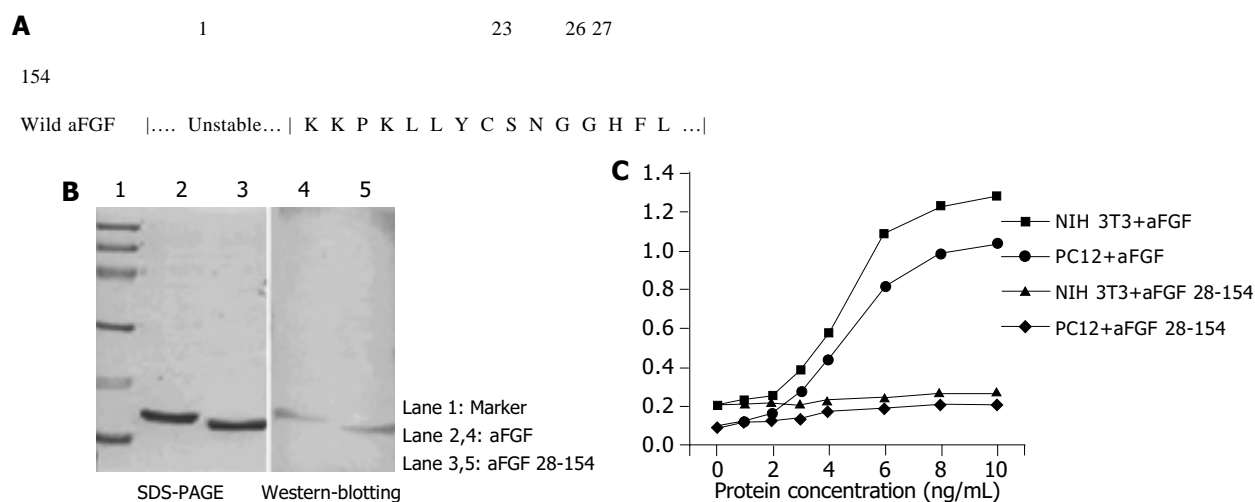


Figure 1 Loss of mitogenic activity in aFGF after modification. A: Sequence comparison between modified aFGF (aFGF28-154) and the wild type. B: Western blot analysis of purified aFGF and aFGF28-154. C: MTT assay of the mitogenic activity of both aFGFs.

Assay of anti-apoptotic activation of both aFGFs

We examined the anti-apoptotic effects of both aFGFs by a DEX-induced thymocyte apoptosis model in mouse, which was considered as one of the best characterized apoptosis research systems^[14-16]. First, a number of typical apoptotic thymocytes with apoptotic bodies from the DEX-induced group were visualized by transmission electron microscope (Figure 2A, B). Second, agarose gel electrophoresis results of this group also indicated characteristic ladder bands of oligonucleosomal fragments (180-200 bp) produced by extracted chromatin DNA, while few were found in blank group and the DNA damage in DEX-induced group was much more serious than that in both aFGFs treated groups (Figure 2C). Third, Annexin V-FITC/PI staining was used to distinguish apoptotic and necrotic cells from normal ones by flow cytometry (Figure 2D). Our test

indicated that under the stimulation of DEX, thymocytes showed apoptosis both *in vivo* and *in vitro* (44.40% and 20.07%, respectively) after 5-h culture. With the protection of aFGF, when exposed to DEX, the apoptosis rate was lower both *in vivo* and *in vitro* (33.71% and 18.31%, respectively). Under the same condition, however, the apoptosis rate was significantly lower in aFGF28-154 group than in DEX and aFGF groups both *in vivo* and *in vitro* (23.95% and 13.80%, respectively) (Figure 2D). The quantitative analysis of anti-apoptosis results and the dose-effect relationship of aFGF28-154 are summarized in Table 1. Fourth, we studied the changes of concentration of intracellular calcium ion (Ca²⁺) by confocal microscope to further confirm the anti-apoptotic effects of both aFGFs on mouse thymocytes. High concentration of intracellular Ca²⁺ caused by influx increase was involved in triggering protease and endonuclease

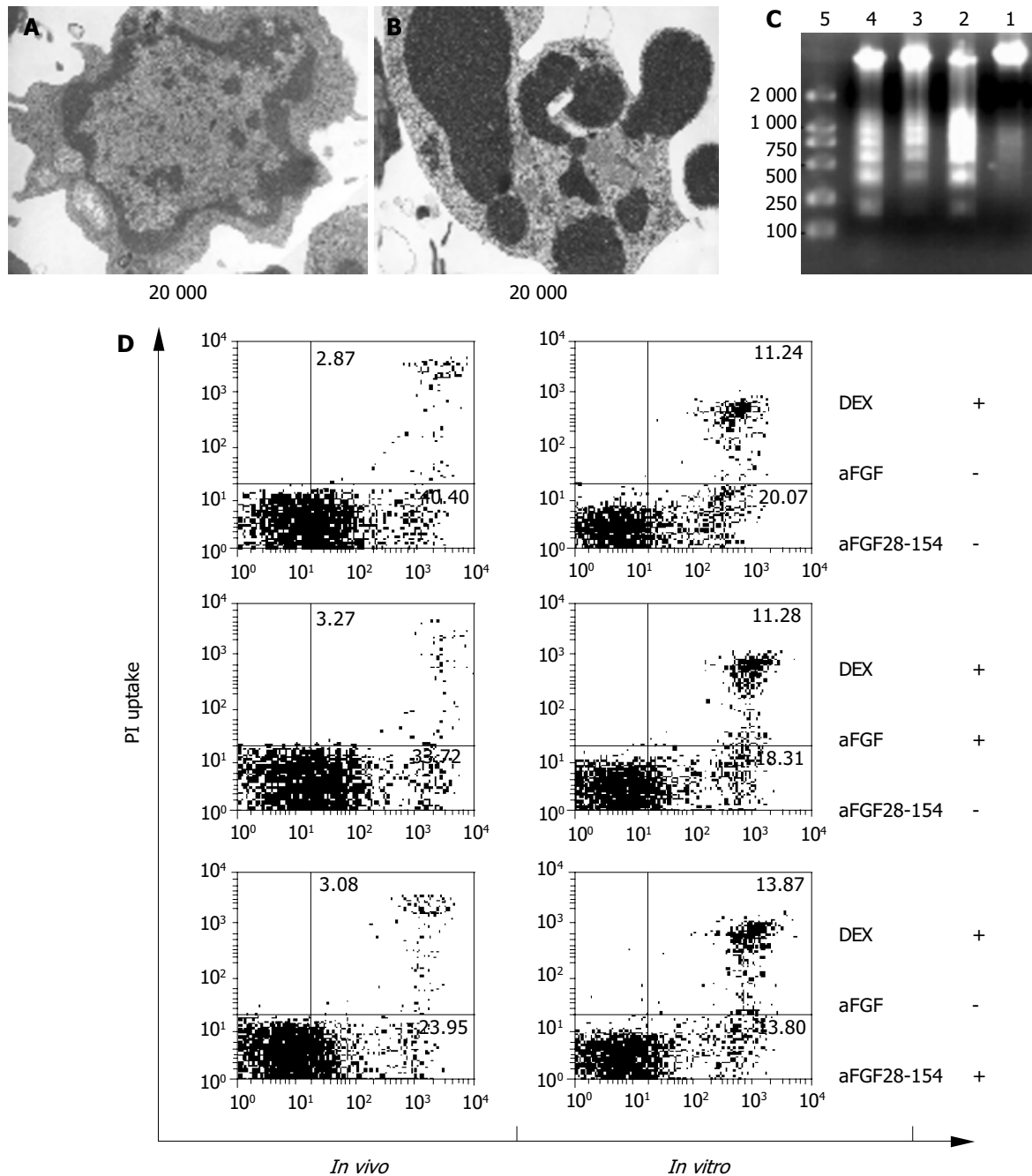


Figure 2 Comparative evaluation of the anti-apoptotic function of aFGF28-154 both *in vitro* and *in vivo*. A: TEM observation (×20 000) of DEX-induced apoptosis in mouse thymocytes. B: Typical apoptotic bodies in DEX-induced thymocytes. C: Damage of DNA analysis by agarose gel electrophoresis according to DNA ladder kit (Apoptosis DNA Laddering Kit-Ethidium Bromide, R&D Systems). Lane 1: DNA extracted from normal control group; lane 2: DNA from DEX only group; lane 3: DNA from DEX plus aFGF28-154 group; lane 4: DNA from DEX plus aFGF group; lane 5: DNA size markers (bp). D: Flow cytometry results.

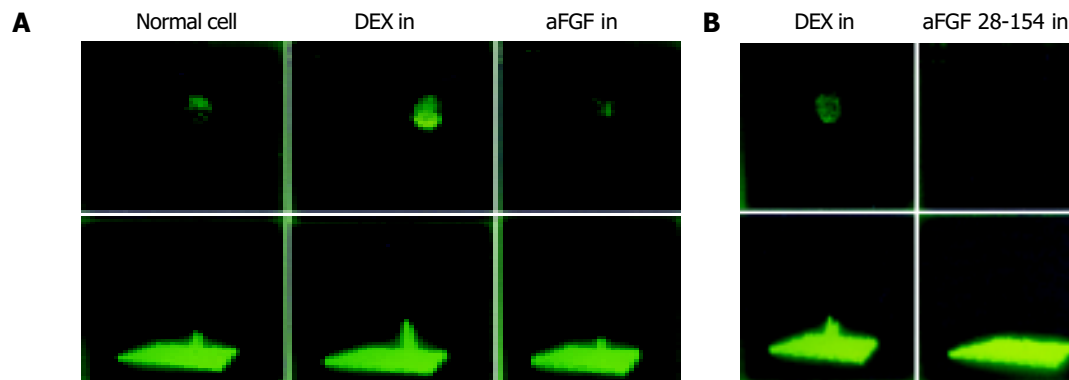


Figure 3 Balance of cytosolic calcium ion concentration protected by both aFGFs when stimulated by DEX. A: Mouse thymocytes from Ca^{2+} influx protected by wild type aFGF. B: Decrease of intracellular Ca^{2+} concentration caused by aFGF28-154.

activation and apoptosis. Hence, Ca^{2+} influx was considered as a sign of apoptosis occurrence^[17-19]. In this study, the intracellular Ca^{2+} concentration in thymocytes increased quickly when exposed to DEX. When administrated with aFGF, however, Ca^{2+} concentration decreased to a lower level (Figure 3A). However, the test for aFGF28-154 showed a marked reduction of Ca^{2+} influx (Figure 3B).

Table 1 *In vitro* quantitative analysis of anti-apoptotic effects and dose-effect relationship of aFGF28-154 on thymocytes induced by DEX (mean \pm SD)

Groups	Conc. (ng/mL)	Apoptosis (%)
Normal control		1.37 \pm 0.39
DEX only		18.99 \pm 0.52 ^a
DEX plus aFGF28-154	50	16.14 \pm 0.44 ^c
	100	12.35 \pm 0.36 ^b
	150	9.75 \pm 0.20 ^b
	200	11.23 \pm 0.71 ^b

^a $P < 0.05$ vs normal control; ^c $P < 0.05$, ^b $P < 0.01$ vs DEX only.

Gut epithelium apoptosis and treatment effects with both aFGFs *in vivo*

We investigated the therapeutic use of both aFGFs in gut ischemia-reperfusion injury in rats and found that the apoptosis rate of epithelium entericum was 5.83 \pm 1.47 in normal control rats, 46.16 \pm 4.06 in rats treated with saline, 39.66 \pm 3.56 in rats treated with wild type of aFGF and 40.66 \pm 2.73 in rats treated with aFGF28-154 2 h after ischemia-reperfusion injury (Table 2). The

Table 2 *In vivo* quantitative analysis of apoptosis in epithelium entericum in different groups (mean \pm SD)

Time	Normal control (n = 6)	I/R+Saline (n = 36)	I/R+aFGF (n = 36)	I/R+aFGF 28-154 (n = 36)
Before ischemia	5.83 \pm 1.47	5.83 \pm 1.47	5.83 \pm 1.47	5.83 \pm 1.47
I/R 30 min		29.83 \pm 3.43 ^b	23.83 \pm 2.78 ^c	25.50 \pm 1.87 ^c
I/R 60 min		39.33 \pm 4.32 ^b	30.33 \pm 3.07 ^c	33.44 \pm 5.60 ^c
I/R 2 h		46.16 \pm 4.60 ^b	39.66 \pm 3.56 ^c	40.66 \pm 2.73 ^c
I/R 6 h		31.33 \pm 3.72 ^b	25.5 \pm 2.16 ^c	26.00 \pm 2.61 ^c
I/R 12 h		62.5 \pm 3.08 ^b	48.50 \pm 2.74 ^c	50.16 \pm 3.71 ^c
I/R24 h		51.66 \pm 3.87 ^b	41.33 \pm 2.94 ^c	42.16 \pm 3.31 ^c

^b $P < 0.01$ vs normal control; ^c $P < 0.05$ vs I/R+Saline group. The percentage of positive apoptotic epithelium entericum was estimated after two hundred cells were counted in five different fields randomly chosen from preparation ($n = 5$). We did all analysis with SPSS. All data were presented as mean \pm SD. We used one-way analysis of variance and the t test where appropriate. Significance was defined as $P < 0.05$.

quantitative analysis of apoptosis in epithelium entericum in different groups of different time points is summarized in Table 2. The morphological examination with light microscope and immunohistochemical detection and quantification of apoptosis based on the labelling of DNA strand breaks confirmed that tissue edema, local necrosis (Figure 4A, C, E, G) and apoptosis in epithelium entericum were markedly reduced in both aFGFs treated rats (Figure 4B, D, F, H).

Analysis of possible signal transduction pathway

In vitro study, we analysed the changes of ERK1/2, p-ERK1/2, JNK1/2, p38 MAPK, c-Myc and Caspase-3. The results showed that only ERK1/2 pathway was activated in all of the three pathways during aFGF anti-apoptosis course (Figure 5A, B, C, D) and no phosphorylated JNK1/2 and p38 MAPK could be detected. In normal control thymocytes, steady ERK1/2 activation was observed, and such an activation was almost completely blocked when cells exposed to DEX. But both aFGFs attenuated this DEX-induced blockage, maintaining ERK1/2 activation, which is required for normal thymocyte cycle at a certain level (Figure 5A). P38 expression in control group was steady with time lapse (Figure 5B) and decreased gradually when cells exposed to DEX (Figure 5C). However, the total p38 MAPK expression decreased at 30 min and then a peak expression appeared at 60 min when the DEX-induced cells were protected with aFGF or aFGF28-154 (Figure 5D, E). The expression of c-Myc and Caspase-3 in thymocytes in the control group was kept at a stable level following the time course (Figure 5B). When stimulated merely by DEX, c-Myc was highly expressed in the first 30 min and the activated Caspase-3 increased following c-Myc (Figure 5C). These results indicated that DEX-induced thymocyte cell cycle turned out to be c-Myc-induced apoptosis. In the aFGF group, however, c-Myc was expressed only at 0 min, and then showed no significant change at other time points (Figure 5D). In the aFGF28-154 group, c-Myc showed a peak expression at 30 min, and then held at a relatively steady level (Figure 5E).

DISCUSSION

Currently, the anti-apoptotic effects of aFGFs have been established from the results of DNA ladder electrophoresis, Annexin V-FITC/PI staining, examination of Ca^{2+} concentration with confocal microscope, and *in vivo* study on gut ischemia-reperfusion injury in rats. But the results were far beyond our expectation. aFGF, especially the modified non-mitogenic aFGF28-154 with a powerful ability to reduce the apoptosis rate, made us to explore whether there were some special mechanisms involved in such an action.

To further investigate the mechanisms of the anti-apoptotic function of aFGF, we studied three protein kinases, including

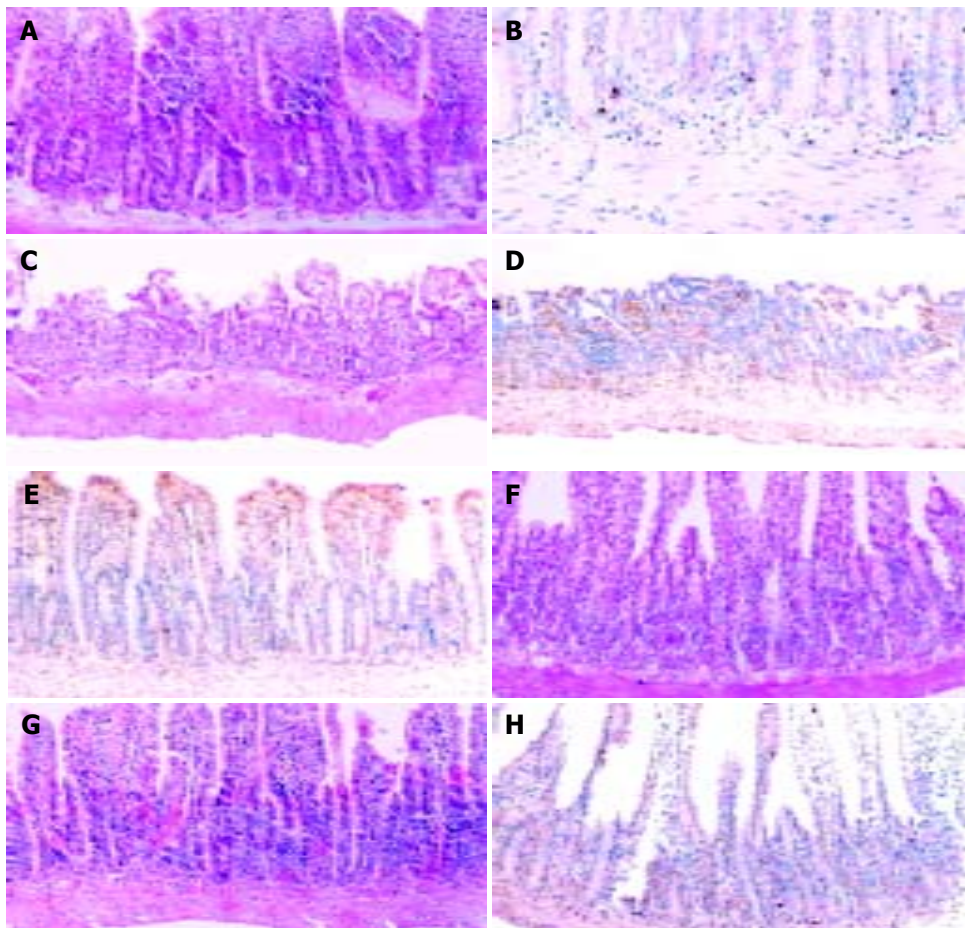


Figure 4 Morphological examination and immunohistochemical detection and quantification of apoptosis based on the labeling of DNA strand breaks (Roche Applied Science, Germany). A: Marked epithelial separation from the basement, subepithelial edema, haemorrhage, erosion. C: Necrosis in I/R plus saline control group. E and G: Tissue damage reduction in both aFGF and aFGF28-154 treated groups. B: Immunohistochemical detection and quantification of apoptosis in normal epithelium entericum. D: Increased number of apoptotic cells in epithelium entericum in rats treated with saline. F and H: Significant reduction of apoptotic cells in epithelium entericum in rats treated with both aFGF and aFGF28-154.

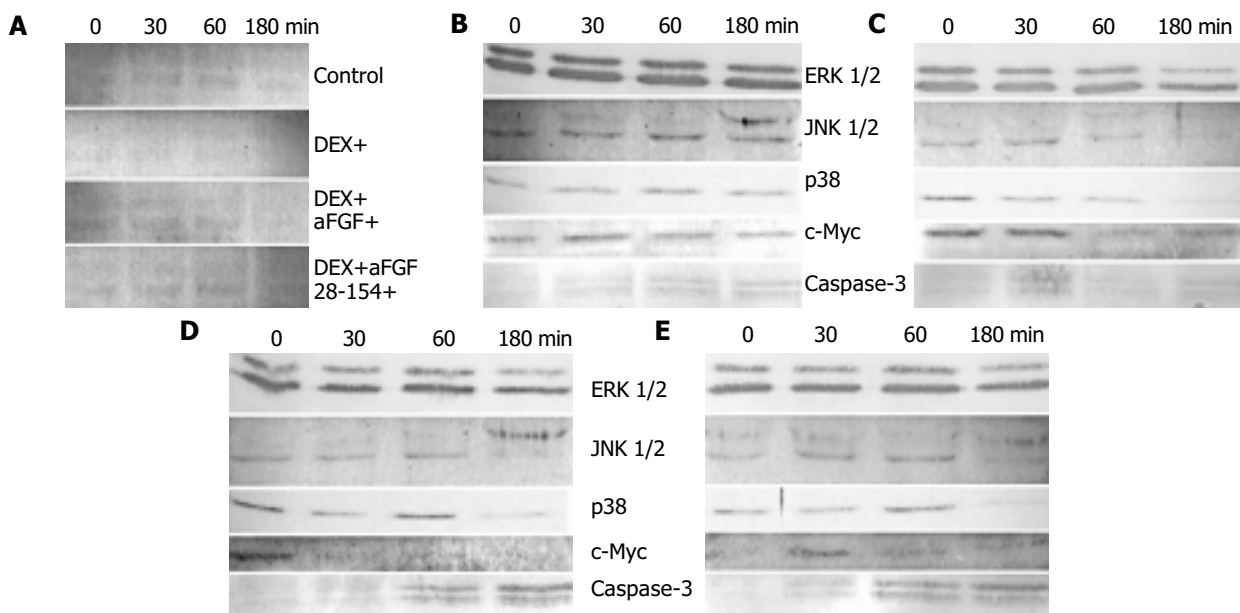


Figure 5 Function of aFGFs as a checker of cell cycle. A: Western blot analysis of the phosphorylation of ERK1/2. B: Western blot analysis of ERK1/2 MAPK, JNK1/2 and p38 MAPK, as well as c-Myc and Caspase-3 in control group. C: Analysis of thymocytes stimulated by DEX. D: Analysis of thymocytes under aFGF protection. E: Analysis of thymocytes under aFGF28-154 protection.

extracellular-signal-regulated kinase (ERK) 1/2, c-Jun-NH₂-terminal kinase (JNK) 1/2, and p38 mitogen associated protein kinase (MAPK). According to the Western blot analysis on

phosphorylation, we found that only ERK1/2 pathway was activated in all of the three pathways during aFGF anti-apoptosis course (Figure 5A) and no phosphorylated JNK1/2 and p38

MAPK could be detected. In normal control thymocytes, the steady ERK1/2 activation was observed, and such an activation was almost completely blocked when cells exposed to DEX. But both aFGFs attenuated this DEX-induced blockage, maintaining ERK1/2 activation, which is required for normal thymocyte cycle at a certain level (Figure 5A). ERK1/2 activation was crucial for aFGF to exert protective effects on many cell types^[20,21]. DEX could induce mitochondrial membrane potential collapse and promote Ca²⁺ release from intracellular pool and the subsequent stimulation of a Ca²⁺ influx from extracellular environment, which contributes to apoptosis^[16]. However, an ERK1/2 activation could protect mitochondrial membrane potential by downstreaming Bcl-X activation^[22]. The fact that only ERK1/2 pathway was activated in all of the three pathways and Ca²⁺ influx reduction in both aFGF groups strongly suggested that the anti-apoptotic activity of aFGF involved in maintaining ERK1/2 activation and regulation of intracellular Ca²⁺ concentration.

A very interesting finding from the results of total p38 MAPK expression attracted our great attention. p38 expression in control group was steady with time lapse (Figure 5B) and decreased gradually when cells exposed to DEX (Figure 5C). However, the total p38 MAPK expression decreased at 30 min and then a peak expression appeared at 60 min when the DEX-induced cells were protected with aFGF or aFGF28-154 (Figures 5D, E). Normally, the activation of p38 MAPK often follows stress induction^[23]. Although p38 MAPK was not markedly activated in all groups in our study, we noticed that according to a previous study by Lasa *et al.*, dexamethasone could cause sustained expression of MAPK phosphatase 1 and phosphatase-mediated inhibition of p38 MAPK^[24]. We also found p38 MAPK was constantly decomposed by DEX induction (Figure 5C). Because the cells in control group were not stressed and the other 3 groups were all exposed to DEX, we speculated that the peak expression of p38 MAPK at 60 min in both aFGF groups might reflect an unveiled stress, which was lagged in both aFGFs groups compared with the DEX group.

To investigate the anti-apoptotic function of aFGFs at protein level, we further examined the changes of c-Myc and Caspase-3. Thymocytes in control group were kept at a stable c-Myc level following the time course (Figure 5B). When stimulated merely by DEX, c-Myc was highly expressed in the first 30 min and the activated Caspase-3 increased following c-Myc (Figure 5C). These results indicated that DEX-induced thymocyte cell cycle turned out to be c-Myc-induced apoptosis. In aFGF group, however, c-Myc was expressed only at 0 min, and then showed no significant change at other time points (Figure 5D). In aFGF28-154 group, c-Myc showed a peak expression at 30 min, and then held at a relatively steady level (Figure 5E). c-Myc, in association with its partner Max, could function as a transcription factor to drive apoptosis when low quantities of survival factors such as IGF-1 and aFGF were present^[25,26]. These results indicated that cell cycle was stagnated in aFGF group, and balanced in aFGF28-154 group. In both aFGF groups, Caspase-3 activation remained nearly null during first 30-60 min and was suddenly enhanced at 60 min and still kept at a high level until 180 min (Figure 5D, E). This activation is cohort with the p38 reaction during stress stimulation and especially with c-Myc expression in normal and both aFGF groups.

The above signal transduction analysis suggested that aFGF might serve as a “checker” for cell cycle while exerting anti-apoptotic function. These functions, including stagnation determination, cell division or apoptosis induction may be similar to those of p53, a typical checker of G1, S and G2/M phases of cell cycle, which contribute both to the cell cycle arrest and apoptotic functions by preventing replication of cells from DNA damage^[27-30]. Our results illustrated that when exposed to apoptosis inducers, aFGF would also induce cell cycle arrest.

This action was reflected by the stagnation of c-Myc expression in our study (Figures 5D, E). At the time interval of null c-Myc expression, thorough check up and repair might be conducted, thereby, new c-Myc would be expressed by aFGF induction. We regarded that this procedure as a “sentence procedure”, reflected by p38 implied second stress, might be carried out by the combined effects of c-Myc and Caspase-3. C-Myc is a typical two-face protein, which is necessary not only for DNA-cleavage in G2 phase of cell cycle, but also for cell proliferation, when cells are protected by trophy factors^[31]. If cells can pass through the examination and undergo a thorough “overhaul”, they would be kept in normal cell cycle; whereas other non-recoverable cells would be “sentenced to death” with high activation of intracellular procaspase-3 by newly expressed c-Myc. Caspase-3 may finally cleave the damaged DNA and execute apoptosis.

Here we conclude that the anti-apoptotic function of aFGFs was enhanced after cancelling of its mitogenic activity and the anti-apoptotic function did not depend on its mitogenic activity. The action is associated with the protection of intracellular Ca²⁺ concentration balance, ERK1/2 pathway sustaining, and cell cycle balance. During the process of anti-apoptosis, aFGF may play a role as a “checker” for cell cycle. Furthermore, we speculate that there are two possible reasons for the anti-apoptotic function enhancement after aFGF modification. First, aFGF28-154 loses the ability of nuclear translocation, a typical aFGF characteristic^[8], causing a longer interaction period with FGF receptors and higher efficiency for aFGF28-154 than the wild one. Second, the structural change of aFGF28-154 may be better exposed with its active domain, which contributes to some anti-apoptosis related activities.

FGF has been widely used in the fields of wound repair and regeneration and some other fields^[32,33]. Because of its extensive distribution and broad mitogenic functions, the side-effects or potential tumour induction is of great concern for doctors. In this study, we demonstrate a genetically engineered method to abolish the mitogenic activity and maintain the non-mitogenic activity of aFGF. This may be helpful to reduce people’s worry about its tumour induction and to take as many preventive measures as possible clinically. In short, the powerful anti-apoptotic function of aFGF28-154 may play an important role in prophylaxis and treatment of some immune system diseases or as a protector in preventing apoptosis in tissues and organs triggered by ischemia and reperfusion injury.

ACKNOWLEDGEMENTS

We thank Professor Yao-Ying Zeng, Drs. Xiao-Ping Wu, Jing-Xian Zhao, Tong-Zhu Sun, Ping Zhang, Dan Sun and Dan Chen for their critical comment and great technical assistance.

REFERENCES

- 1 Galzie Z, Kinsella AR, Smith JA. Fibroblast growth factors and their receptors. *Biochem Cell Biol* 1997; **75**: 669-685
- 2 Nabel EG, Yang ZY, Plautz G, Forough R, Zhan X, Haudenschild CC, Maciag T, Nabel GJ. Recombinant fibroblast growth factor-1 promotes intimal hyperplasia and angiogenesis in arteries *in vivo*. *Nature* 1993; **362**: 844-846
- 3 Nurcombe V, Ford MD, Wildschut JA, Bartlett PF. Developmental regulation of neural response to FGF-1 and FGF-2 by heparan sulfate proteoglycan. *Science* 1993; **260**: 103-106
- 4 Fu X, Sheng Z, Wang Y, Ye Y, Xu M, Sun T, Zhou B. Basic fibroblast growth factor reduces the gut and liver morphologic and functional injuries after ischemia and reperfusion. *J Trauma* 1997; **42**: 1080-1085
- 5 Cuevas P, Reimers D, Carceller F, Martinez-Coso V, Redondo-Horcajo M, Saenz de Tejada I, Gimenez-Gallego G. Fibroblast growth factor-1 prevents myocardial apoptosis triggered by

- ischemia reperfusion injury. *Eur J Med Res* 1997; **2**: 465-468
- 6 **Cuevas P**, Carceller F, Reimers D, Gimenez-Gallego G. Fibroblast growth factor-1 inhibits medial smooth muscle cells apoptosis after balloon injury. *Neurol Res* 2000; **22**: 185-188
- 7 **Wan X**, Nass P, Duncan MD, Harmon JW. Acidic fibroblast growth factor overexpression partially protects 3T3 fibroblasts from apoptosis induced by synthetic retinoid CD437. *J Mol Med* 2001; **79**: 143-148
- 8 **Lozano RM**, Pineda-Lucena A, Gonzalez C, Angeles Jimenez M, Cuevas P, Redondo-Horcajo M, Sanz JM, Rico M, Gimenez-Gallego G. 1H NMR structural characterization of a nonmitogenic, vasodilatory, ischemia-protector and neuromodulatory acidic fibroblast growth factor. *Biochemistry* 2000; **39**: 4982-4993
- 9 **Yang YH**, Fu XB, Sun TZ, Jiang LX, Gu XM. bFGF and TGF β expression in rat kidneys after ischemic/reperfusional gut injury and its relationship with tissue repair. *World J Gastroenterol* 2000; **6**: 147-149
- 10 **Fu XB**, Yang YH, Sun XQ, Sun TZ, Gu XM, Sheng ZY. Protective effects of endogenous basic fibroblast growth factor activated by 2, 3 butanedion moncime on functional changes of ischemic intestine, liver and kidney in rats. *Zhongguo Weizhongbing Jijiu Yixue* 2000; **12**: 69-72
- 11 **Yang YH**, Fu XB, Sun TZ, Jiang LX, Gu XM. The effect of exogenous basic fibroblast growth factor on hepatic endogenous basic fibroblast growth factor and fibroblast growth factor receptor expression after intestinal ischemia-reperfusion injury. *Zhongguo Weizhongbing Jijiu Yixue* 1999; **11**: 734-736
- 12 **Fu XB**, Yang YH, Sun TZ, Sun XQ, Gu XM, Chang GY, Sheng ZY. Effects of inhibition or anti-endogenous basic fibroblast growth factor on functional changes in intestine, liver and kidneys in rats after gut ischemia-reperfusion injury. *Zhongguo Weizhongbing Jijiu Yixue* 2000; **12**: 465-468
- 13 **Sun XQ**, Fu XB, Zhang R, Lü Y, Deng Q, Jiang XG, Sheng ZY. Relationship between plasma D (-)lactate and intestinal damage after severe injuries in rats. *World J Gastroenterol* 2001; **7**: 555-558
- 14 **Wyllie AH**. Glucocorticoid-induced thymocyte apoptosis is associated with endogenous endonuclease activation. *Nature* 1980; **284**: 555-556
- 15 **Voris BP**, Young DA. Glucocorticoid-induced proteins in rat thymus cells. *J Biol Chem* 1981; **256**: 11319-11329
- 16 **McConkey DJ**, Nicotera P, Hartzell P, Bellomo G, Wyllie AH, Orrenius S. Glucocorticoids activate a suicide process in thymocytes through an elevation of cytosolic Ca²⁺ concentration. *Arch Biochem Biophys* 1989; **269**: 365-370
- 17 **McConkey DJ**, Zhivotovsky B, Orrenius S. Apoptosis-molecular mechanisms and biomedical implications. *Mol Aspects Med* 1996; **17**: 1-110
- 18 **Fernandez A**, Kiefer J, Fosdick L, McConkey DJ. Oxygen radical production and thiol depletion are required for Ca (2+)-mediated endogenous endonuclease activation in apoptotic thymocytes. *J Immunol* 1995; **155**: 5133-5139
- 19 **Helmberg A**, Auphan N, Caelles C, Karin M. Glucocorticoid-induced apoptosis of human leukemic cells is caused by the repressive function of the glucocorticoid receptor. *EMBO J* 1995; **14**: 452-460
- 20 **Udayakumar TS**, Stratton MS, Nagle RB, Bowden GT. Fibroblast growth factor-1 induced promatrilysin expression through the activation of extracellular-regulated kinases and STAT3. *Neoplasia* 2002; **4**: 60-67
- 21 **Buehler A**, Martire A, Strohm C, Wolfram S, Fernandez B, Palmén M, Wehrens XH, Doevendans PA, Franz WM, Schaper W, Zimmermann R. Angiogenesis-independent cardioprotection in FGF-1 transgenic mice. *Cardiovasc Res* 2002; **55**: 768-777
- 22 **Boucher MJ**, Morisset J, Vachon PH, Reed JC, Laine J, Rivard N. MEK/ERK signaling pathway regulates the expression of Bcl-2, Bcl-X (L), and Mcl-1 and promotes survival of human pancreatic cancer cells. *J Cell Biochem* 2000; **79**: 355-369
- 23 **Min do S**, Shin EY, Kim EG. The p38 mitogen-activated protein kinase is involved in stress-induced phospholipase D activation in vascular smooth muscle cells. *Exp Mol Med* 2002; **34**: 38-46
- 24 **Lasa M**, Abraham SM, Boucheron C, Saklatvala J, Clark AR. Dexamethasone causes sustained expression of mitogen-activated protein kinase (MAPK) phosphatase 1 and phosphatase-mediated inhibition of MAPK p38. *Mol Cell Biol* 2002; **22**: 7802-7811
- 25 **Harrington EA**, Bennett MR, Fanidi A, Evan GI. c-Myc-induced apoptosis in fibroblasts is inhibited by specific cytokines. *EMBO J* 1994; **13**: 3286-3295
- 26 **Amati B**, Littlewood TD, Evan GI, Land H. The c-Myc protein induces cell cycle progression and apoptosis through dimerization with Max. *EMBO J* 1993; **12**: 5083-5087
- 27 **Green DR**. A Myc-induced apoptosis pathway surfaces. *Science* 1997; **278**: 1246-1247
- 28 **Winters ZE**. P53 pathways involving G2 checkpoint regulators and the role of their subcellular localisation. *J R Coll Surg Edinb* 2002; **47**: 591-598
- 29 **Adachi S**, Obaya AJ, Han Z, Ramos-Desimone N, Wyche JH, Sedivy JM. c-Myc is necessary for DNA damage-induced apoptosis in the G (2) phase of the cell cycle. *Mol Cell Biol* 2001; **21**: 4929-4937
- 30 **Young M**, Oger J, Blanchard MH, Asdourian H, Amos H, Arnason BG. Secretion of a nerve growth factor by primary chick fibroblast cultures. *Science* 1975; **187**: 361-362
- 31 **Kumagai A**, Dunphy WG. Repeated phosphopeptide motifs in Claspin mediate the regulated binding of Chk1. *Nat Cell Biol* 2003; **5**: 161-165
- 32 **Fu X**, Sun X, Li X, Sheng Z. Dedifferentiation of epidermal cells to stem cells *in vivo*. *Lancet* 2001; **358**: 1067-1068
- 33 **Fu X**, Shen Z, Cheng Y, Xe J, Guo Z, Zhang M, Sheng Z. Randomised placebo-controlled trial of use of topical recombinant bovine basic fibroblast growth factor for second-degree burns. *Lancet* 1998; **352**: 1661-1664

Edited by Wang XL. Proofread by Zhu LH and Xu FM

Genetic alterations and reduced expression of tumor suppressor p33^{ING1b} in human exocrine pancreatic carcinoma

Guan-Zhen Yu, Ming-Hua Zhu, Zhi Zhu, Can-Rong Ni, Jian-Ming Zheng, Fang-Mei Li

Guan-Zhen Yu, Ming-Hua Zhu, Zhi Zhu, Can-Rong Ni, Jian-Ming Zheng, Fang-Mei Li, Department of Pathology, Changhai Hospital, Second Military Medical University, Shanghai 200433, China

Supported by the "258" Project Foundation of Changhai Hospital, Shanghai, China

Correspondence to: Ming-Hua Zhu, Department of Pathology, Changhai Hospital, Second Military Medical University, Shanghai 200433, China. mhzhu2000@hotmail.com

Telephone: +86-21-25074604 **Fax:** +86-21-25074604

Received: 2004-01-16 **Accepted:** 2004-02-24

Abstract

AIM: To detect the expression of p33^{ING1b} protein and the change of p33^{ING1b} gene in pancreatic carcinoma and to evaluate the significance of p33^{ING1b} in pancreatic cell carcinogenesis.

METHODS: Pathological specimens from pancreatic carcinoma and matched non-tumor pancreatic tissues were examined for p33^{ING1b} expression and mutation by immunohistochemistry, polymerase chain reaction single-strand conformation polymorphisms (PCR-SSCP) and loss of heterozygosity (LOH).

RESULTS: The rate of p33^{ING1b} protein expression was 85% (34/40). A single germline missense mutation was detected in 1 of 40 tumors located at codon 215:TGC-TCC (Cys-Ser). Fourteen (60.9%) of 23 tumor samples showed LOH in all of the informative markers tested, but no mutation was detected in these tumors and only two of the informative tumors lacked expressions of p33^{ING1b} protein.

CONCLUSION: Mutation and loss of expression are not the main reasons for the disfunction of p33^{ING1b} in pancreatic carcinoma, an abnormality at the level of chromosome and/or transcription may inhibit their normal functions, potentially contributing to pancreatic cell carcinogenesis.

Yu GZ, Zhu MH, Zhu Z, Ni CR, Zheng JM, Li FM. Genetic alterations and reduced expression of tumor suppressor p33^{ING1b} in human exocrine pancreatic carcinoma. *World J Gastroenterol* 2004; 10(24): 3597-3601

<http://www.wjgnet.com/1007-9327/10/3597.asp>

INTRODUCTION

A candidate tumor suppressor gene, ING1, has recently been cloned and mapped on human chromosome 13q34, encoding p33^{ING1b} mainly, a nuclear protein which physically interacts with p53^[1,2] and cooperates with it in many ways^[3,4]. Forced overexpression of the ING1 gene could lead to cell arrest in the G1 phase of the cell cycle and induce apoptosis in several cell types^[5,6]. Conversely, inhibition of ING1 expression by antisense constructs could promote the transformation of mouse breast epithelial cells and increase the frequency of focus formation

with NIH3T3 cells and protect cells from apoptosis. Recently, p33^{ING1b} protein has been found to contain many specific structures, such as plant homeodomain (PHD)-like finger, nuclear localization sequence (NLS), nucleolar targeting sequence (NTS), proliferating cell nuclear antigen (PCNA) interacting protein (PIP) domain, Sin3-associated polypeptide (SAP30) interaction region and bromodomain which implicate that the p33^{ING1b} protein might play a critical role with other genes in oncogenesis, apoptosis, DNA repair and cell cycle regulation^[7-9].

High rates of 13q loss of heterozygosity (LOH) have been detected in cancer of the esophagus, ovary, breast and head and neck^[10]. And several gene mutations and reduced protein expression of p33^{ING1b} were found in head and neck, esophageal, lung, bladder, ovary, kidney, breast, and liver cell cancers^[7]. Major sequence features and biological effects and genetic alterations of p33^{ING1b} indicate that p33^{ING1b} may be a tumor suppressor and that functional loss of p33^{ING1b} might contribute to tumorigenesis. To the author's knowledge, only one study showed that p33^{ING1b} expression was increased in pancreatic adenocarcinoma cell line Mia PaCa-2 after incubation with COX-2 inhibitors for specific times^[11]. But little is known about its role and changes in pancreatic cancer. Accordingly, we examined whether genetic alterations, such as allelic imbalance or mutations of p33^{ING1b} gene, as well as altered protein expression of p33^{ING1b}, might be responsible for the emergence and progression of human pancreatic carcinoma using immunohistochemical study, LOH analysis, and PCR-SSCP.

MATERIALS AND METHODS

Materials

Fourty tumor and 23 matched normal tissues were obtained from 40 patients with pancreatic carcinoma undergoing surgical resection as primary therapy for their disease after informed consent was obtained. All patients were from the Department of Pathology, Changhai Hospital. Another four pancreatitis and 5 normal samples were also from the department. Histological studies were performed and all tumors were confirmed as exocrine pancreatic carcinoma. Among these patients whose age ranged from 31 to 86 years, 24 were males and 16 were females, and the average age was 60.5 years. Four types of tumor were involved namely, adenocarcinoma, adeno-squamous cell carcinoma, cystadenocarcinoma, and acinar cell carcinoma. The number of cases was 36, 2, 1, and 1, respectively. Thirteen cases of adenocarcinoma were well differentiated, and the other 23 cases were moderately or poorly differentiated.

DNA Extraction

Genomic DNAs were isolated from formalin-fixed paraffin-embedded sections and frozen by proteinase K treatment (method D)^[12], phenol-choroform extraction, and ethanol precipitation following the manufacturer's instructions.

Immunohistochemistry

The expression of p33^{ING1b} protein in paraffin-embedded

histological sections was determined using the EnVision method. Histological sections (4 μ m thick) on 0.2 g/L poly-L-lysine-coated slides were deparaffinized and rehydrated, and the endogenous peroxidase activity was blocked by incubation with 20 mL/L H₂O₂ in phosphate buffer, followed by pre-treatment with proteinase K. Non-specific binding was blocked with normal goat serum, and sections were incubated with p33^{ING1b} antibody (supplied by Dr. Riabowol, Canada)^[1]. After washed with phosphate buffer, the sections were incubated with secondary antibody and enhanced labelled polymers for 3 h and washed with phosphate buffer, followed by incubation with DAB. Then the sections were washed and counterstained with methyl green. Sections of normal pancreas tissue were used as positive control for the expression of p33^{ING1b}, and the sections incubated with PBS instead of the corresponding primary antibody were used as negative controls. To quantitate the p33^{ING1b} expression in various samples, a scoring method was adopted^[13]. A mean percentage of positive tumor cells was determined in at least five areas at \times 400 magnification and assigned to one of the five following categories: 0, <5%; 1, 5-25%; 2, 25-50%; 3, 50-70%; and 4, >75%. The intensities of immunostaining were scored as follows: weak, 1+; moderate, 2+; and intense, 3+. For tumors showing heterogeneous staining, the predominant pattern was taken into account for scoring. The percentage of positive tumor cells and the staining intensity were multiplied to produce a weighted score for each case. Cases with weighted scores of less than 1 were defined as negative, otherwise as positive.

SSCP Analysis

The coding region of exon1 was amplified by PCR with primers on the flanking regions, primers S1 (5'-ATGTTGAGTCCTGCC AACGGGGA) and AS1 (5'-CTCTTGGTATTTCGCGTCCGAT), 138 bp; exon2 was amplified as four: overlapping fragments with four primer sets: (a) S2 (5'-ATCCTGAAG GAGCTAGACG AGTGC) and AS2 (5'-CTTGCCGCTGTTGCCCGCTG), 246 bp; (b) S3 (5'-TTCGAGGCGAGCAGGAGCT) and AS3 (5'-CTTGGCCTTCTCTCCTTGGG), 210 bp; (c) S4 (5'-CAGCAA CCACGACCACGACG) and AS4 (5'-TGAGCCCCACGCACGA GAAG), 240 bp; (d) S5 (5'-CCTCCCCATCGACCCCAACG) and AS5 (5'-CTACCTGTTGTAAGCCCTCTC), 235 bp. The PCR mixture contained 400 ng of DNA, 5 μ L of 25 mmol/L MgCl₂, 5 μ L of 10 \times PCR buffer, 5 μ L of 2.5 mmol/L each deoxynucleotide triphosphate, 25 pmol of each primer, and 1.25 unit of Taq DNA polymerase (Takara, Kyoto, Japan) in a 50- μ L volume. Initial denaturation at 94 $^{\circ}$ C for 4 min was followed by 35 amplification cycles, each consisting of a denaturation at 94 $^{\circ}$ C for 1 min, an annealing at 55 $^{\circ}$ C for 1 min, and an extension at 72 $^{\circ}$ C for 1 min. A final extension step at 72 $^{\circ}$ C for 10 min was carried out. Fifteen μ L of PCR products as mixed with 8 μ L of 3 \times loading dye (95% formamide, 20 mmol/L EDTA, 0.5 g/L bromphenol blue, and 0.5 g/L xylene cyanol), heat denatured, chilled on ice, applied onto an 400 g/L polyacrylamide gel with 50 g/L glycerol, and run at variable temperatures. The bands were detected by silver staining^[14]. Aberrantly migrating bands on the gels were excised, reamplified with the same sets of primers. Reproduction of the result was confirmed by sequencing the samples at least twice.

LOH analysis using a microsatellite marker on 13q

To study allelic deletion in pancreatic cancer, we examined DNA for LOH at D13S261, D13S1047, D13S1315 and DS42490^[15], which are located close to the ING1 locus. Primers sets were available through the Internet genome database. PCR was performed in 25- μ L reaction mixtures containing 200 ng of template genomic DNA, 5 pmol of each oligonucleotide primer, 0.75 unit of Taq DNA polymerase (Takara, Kyoto, Japan), 2.5 μ L

of 10 \times buffer, and 2.5 μ L of 2.5mmol/L deoxynucleotide triphosphate. After predenaturation for 3 min at 94 $^{\circ}$ C, PCR was carried out for 35 amplification cycles, each consisting of denaturation for 50 s at 94 $^{\circ}$ C, annealing for 50 s at 55 $^{\circ}$ C (D13S261, D13S1047, D13S1315) or at 60 $^{\circ}$ C (DS42490), and extension for 1 min at 72 $^{\circ}$ C. A final extension step at 72 $^{\circ}$ C for 10 min was performed. After amplification, 8 μ L of the reaction mixture was mixed with 8 μ L of 2 \times loading dye as described above, heat denatured, chilled on ice, and then electrophoresed on 80 g/L polyacrylamide gel containing 8 mol/L urea. DNA bands were visualized by silver staining. LOH was scored if one of the heterozygous alleles showed at least 50% reduced intensity in tumor DNA as compared with the corresponding normal DNA.

Statistical analysis

The SPSS 11.0 software package for Macintosh (SPSS Inc., Chicago, IL) was used for all statistical analyses. Variables associated with p33^{ING1b} expression were analyzed by χ^2 test. Differences in expression of p33^{ING1b} mRNA between groups were checked by independent *t* test. *P*<0.05 was considered statistically significant.

RESULTS

p33^{ING1b} protein expression detected by IHC

p33^{ING1b} protein expression was examined in paraffin-embedded specimens from 40 pancreatic cancer patients (Figure 1). Normal and benign lesion sections were examined for p33^{ING1b} expression as controls. All of the non-tumor tissues were weak positive for p33^{ING1b}, and reduced p33^{ING1b} protein expression was noted only in 6 tumor samples (15%). The positive staining in cancer tissues was significantly stronger than that in matched normal tissues and other non-tumor samples (Figure 1). Statistical analysis showed no obvious correlation in p33^{ING1b} expression between tumor and non-tumor tissues, and also no correlation between expression of p33^{ING1b} protein and clinicopathological factors of all the patients.

Detection of p33^{ING1b} gene mutation

To investigate whether the p33^{ING1b} gene was the target of functional loss in tumors, we searched for mutations in the coding regions of the gene in all the 40 samples of pancreatic carcinoma. Only one possible mutation was identified by SSCP and DNA sequencing (Figure 2). The sample showed a substitution of cysteine (TGC) with serine (TCC) at codon 215, which located in plant homeodomain (PHD) finger. This change might affect the PHD finger and break the three-dimensional structure of ING1 protein, leading to the loss of function. But this sample still showed p33^{ING1b} protein expression, implicating that the protein expressed in tumor could not exert its normal function.

LOH analysis

We examined DNA from 23 pairs of matched pancreatic carcinomas and normal tissues for losses at four microsatellite markers (D13S261, D13S1047, D13S1315 and DS42490) on the chromosome 13q33-34 region. Figure 3 shows the summary and representative examples. Fourteen of 23 informative tumors (60.9%) showed LOH of at least one marker. The rates of LOH at D13S261, D13S1047, D13S1315, and DS42490 loci was 8.7%, 21.5%, 13.0% and 26.1%, respectively. The most frequent loss was seen at marker DS42490, which was located in the ING1 region. These markers were less than 3 cM. Only two of these 23 pancreatic carcinomas showed no p33^{ING1b} protein expression and none had a single mutation.

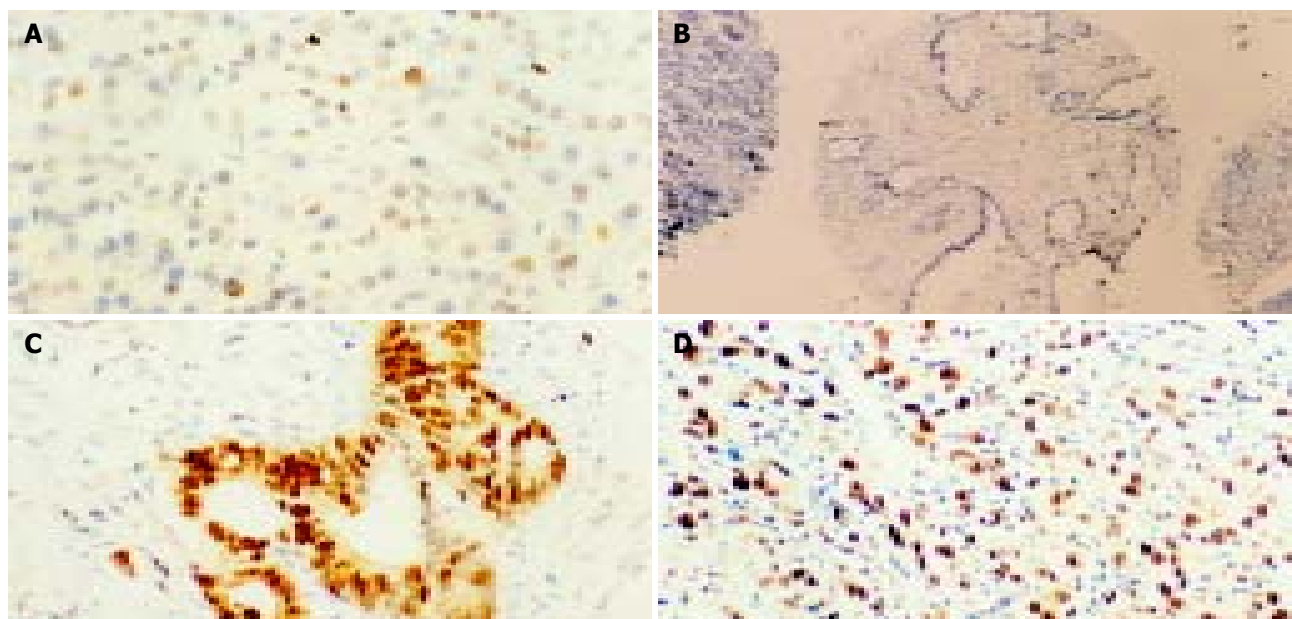


Figure 1 Representative examples of IHC staining for p33^{ING1b} (×200) on normal pancreatic tissues and cancer tissues. A: Weak positive pancreatic cells for p33^{ING1b}; B: No p33^{ING1b}; C and D: Extremely strong staining in pancreatic cancer samples.

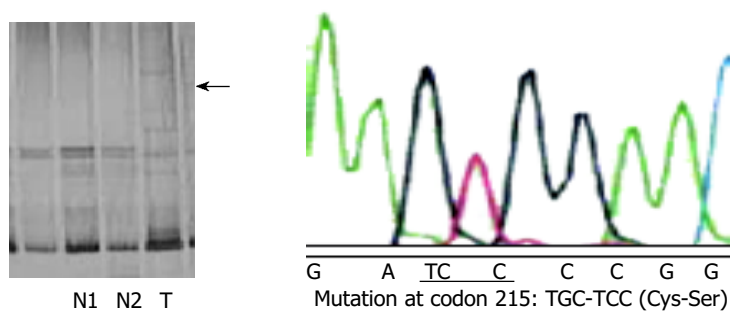


Figure 2 SSCP analysis of p33^{ING1b} gene in genomic DNA from pancreatic carcinomas. N: normal DNA; T: tumor DNA. Arrow point indicates the altered band in tumor DNA as compared with the corresponding normal DNA. The amino acid substitution of p33^{ING1b} are shown to the right.

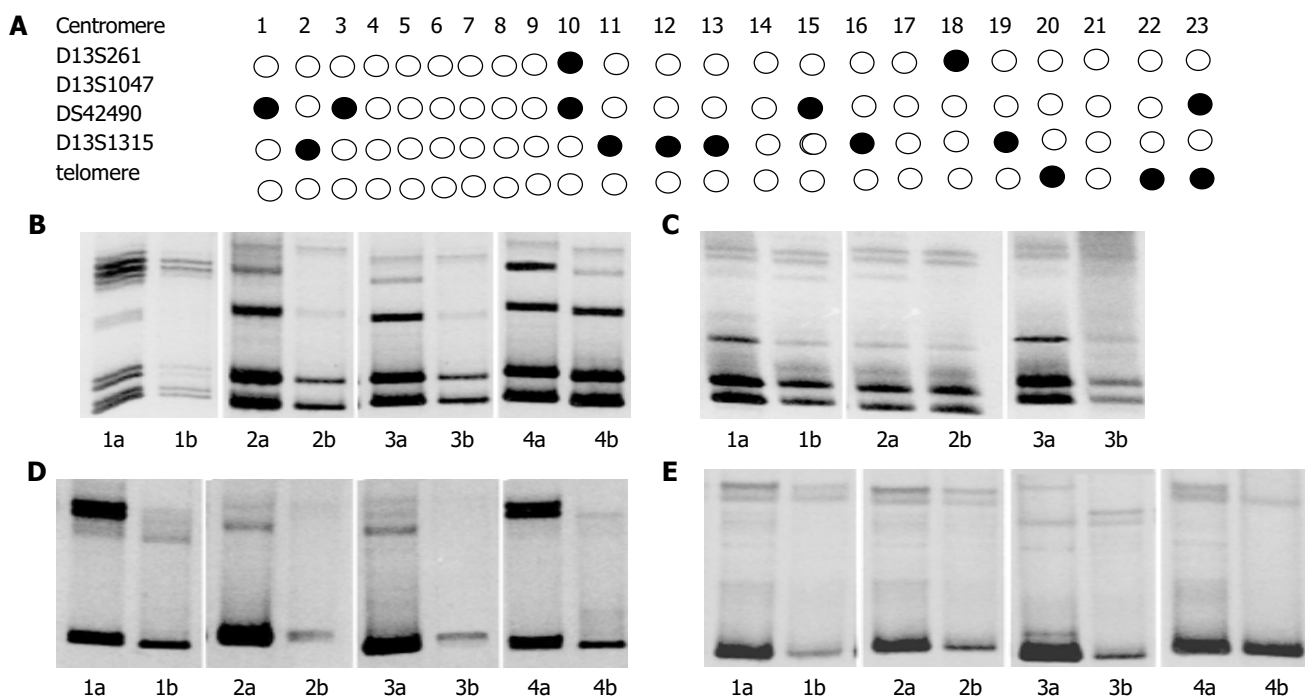


Figure 3 LOH analysis on chromosome 13q33-34 in PCs. A: Submatic representation of LOH distribution; ● LOH ○ without LOH; a: cancer; b: matched cancer; B: Analysis of D13S1315; C: LOH analysis of D13S261; D: LOH analysis of DS42490; E: LOH analysis of D13S1047.

DISCUSSION

Several studies showed that reduced p33^{ING1} expression was found in esophageal squamous cell cancer (100%)^[16] and hepatocellular carcinoma (66.3%)^[17]. In our study, positive p33^{ING1b} staining was present in 85.0% of the pancreatic carcinoma tissues. No significant difference was found between cancer and non-cancer tissues, indicating that loss of p33^{ING1b} protein expression was not a major cause of the cancerization of pancreatic cells. But p33^{ING1b} protein was overexpressed in tumors compared with matched normal tissues in the patients with positive p33^{ING1b} stainings. Our results are in agreement with two previous studies^[18,19]. The functions and states of these overexpressed p33^{ING1b} proteins still need further study.

Limited analysis of ING1 gene demonstrated rearrangement of the gene in one neuroblastoma cell line and reduced expression in primary breast cancers and cell lines^[1]. Then the following experiments found several missense mutations and silent changes in cancers of esophagus^[16], head and neck^[20], esophagogastric junction^[21], gastrointestinal^[22], skin^[18,19] and breast^[23]. These mutations were all located in PHD finger and/or nuclear localization signal (NLS) in the COOH-terminal half of ING1. The PHD finger was found in several proteins, including transcription factors and proteins that could regulate chromatin structure. Mutations in PHD finger may lead to loss of the functions of ING1 through inhibiting the transcriptional activity of the gene. Mutations in NLS might interfere with the accumulation of ING1 protein in nuclei^[7]. But the rate of mutations was very low and no missense mutations were found in oral squamous cell carcinoma^[24], lymphoid malignancies^[25], colorectal carcinoma^[26], and haematological malignancies^[27]. We only detected one missense mutation at codon 215: TGC-TCC (Cys-Ser) on PHD finger among 40 samples of pancreatic carcinomas. All of these results suggested that mutations in certain types of tumor could lead to loss of the functions of p33^{ING1b}, but they were not the main reason.

Several studies have been reported that high rates of LOH were found in human chromosome 13q33-34 region^[10,16,20]. The rate of LOH in esophageal/head and neck squamous cell cancers was 58.9% (20/34) and 68% (23/34), respectively^[16,20]. Another study found that the rate of LOH in head and neck squamous cell cancers was 48% (21/44)^[10]. But the range between every two markers was more than 1 cm, far from ING1 locus, and these markers could not reflect the particular information about ING1. So we selected four markers, D13S261, D13S1047, D13S1315, and DS42490, to detect LOH in 23 cancer tissues. D13S261 and D13S1047 located on the upstream of ING1, D13S1315 on the downstream, while DS42490 in the ING1 locus. The results were described as above. As compared with the LOH (60.9%), the loss of p33^{ING1b} protein expression (8.7%) was very low in pancreatic carcinomas and no missense mutation of p33^{ING1} gene was found. The lack of mutations suggests that the ING1 gene is not the suppressor gene target of tumors in which frequent LOH was observed at 13q. The high frequency of LOH at ING1 locus and the vicinity may affect the function of p33^{ING1b} but not the expression of p33^{ING1} protein. The reason is very complex. An alternative target of inactivation may be involved in this tumor type which can affect the function of p33^{ING1b} protein. In addition, alterations at the transcriptional or post-transcriptional level may be another reason for the abnormal expression of p33^{ING1b} protein, for several experiments also detected reduced expression of p33^{ING1b} mRNA in primary breast cancers and cell lines^[23,28], human gastric cancer^[22], myeloid leukaemia^[29], head and neck squamous cell carcinoma^[20] and human diploid fibroblast^[30]. More detailed studies are needed to elucidate this possibility.

REFERENCES

1 Garkavtsev I, Kazarov A, Gudkov A, Riabowol K. Suppres-

- sion of the novel growth inhibitor P33^{ING1} promotes neoplastic transformation. *Nat Genet* 1996; **14**: 415-420
- 2 Cheung KJ Jr, Li G. The tumor suppressor ING1: structure and function. *Exp Cell Res* 2001; **268**: 1-6
- 3 Garkavtsev I, Grigorian IA, Ossovskaya VS, Chernov MV, Chumakov PM, Gudkov AV. The candidate tumour suppressor p33ING1 cooperates with p53 in cell growth control. *Nature* 1998; **391**: 295-298
- 4 Leung KM, Po LS, Tsang FC, Siu WY, Lau A, Ho HT, Poon RY. The candidate tumor suppressor ING1b can stabilize p53 by disrupting the regulation of p53 by MDM2. *Cancer Res* 2002; **62**: 4890-4893
- 5 Helbing CC, Veillette C, Riabowol K, Johnston RN, Garkavtsev I. A novel candidate tumor suppressor, ING1, is involved in the regulation of apoptosis. *Cancer Res* 1997; **57**: 1255-1258
- 6 Shimada H, Liu TL, Ochiai T, Shimizu T, Haupt Y, Hamada H, Abe T, Oka M, Takiguchi M, Hiwasa T. Facilitation of adenoviral wild-type p53-induced apoptotic cell death by overexpression of p33(ING1) in T. Tn human esophageal carcinoma cells. *Oncogene* 2002; **21**: 1208-1216
- 7 Feng X, Hara Y, Riabowol K. Different HATS of the ING1 gene family. *Trends Cell Biol* 2002; **12**: 532-538
- 8 Scott M, Bonnefin P, Vieyra D, Boisvert FM, Young D, Bazett-Jones DP, Riabowol K. UV-induced binding of ING1 to PCNA regulates the induction of apoptosis. *J Cell Sci* 2001; **114**(Pt 19): 3455-3462
- 9 Aasland R, Gibson TJ, Stewart AF. The PHD finger: implications for chromatin-mediated transcriptional regulation. *Trends Biochem Sci* 1995; **20**: 56-59
- 10 Sanchez-Cespedes M, Okami K, Cairns P, Sidransky D. Molecular analysis of the candidate tumor suppressor gene ING1 in human head and neck tumors with 13q deletions. *Genes Chromosomes Cancer* 2000; **27**: 319-322
- 11 Tseng WW, Deganutti A, Chen MN, Saxton RE, Liu CD. Selective cyclooxygenase-2 inhibitor rofecoxib (Vioxx) induces expression of cell cycle arrest genes and slows tumor growth in human pancreatic cancer. *J Gastrointest Surg* 2002; **6**: 838-844
- 12 Frank TS, Svoboda-Newman SM, Hsi ED. Comparison of methods for extracting DNA from formalin-fixed paraffin sections for nonisotopic PCR. *Diagn Mol Pathol* 1996; **5**: 220-224
- 13 Lu CD, Altieri DC, Tanigawa N. Expression of a novel antiapoptosis gene, survivin, correlated with tumor cell apoptosis and p53 accumulation in gastric carcinomas. *Cancer Res* 1998; **58**: 1808-1812
- 14 Bassam BJ, Caetano-Anolles G, Gresshoff PM. Fast and sensitive silver staining of DNA in polyacrylamide gels. *Anal Biochem* 1991; **196**: 80-83
- 15 Borodina TA, Ivanov DV, Khusnutdinova EK, Spitsyn VA, Baranova AV, Iankovskii NK. A new pentanucleotide STR-marker, located in the intron of the ING1 tumor suppressor gene and its allelic polymorphism. *Genetika* 2001; **37**: 117-119
- 16 Chen L, Matsubara N, Yoshino T, Nagasaka T, Hoshizima N, Shirakawa Y, Naomoto Y, Isozaki H, Riabowol K, Tanaka N. Genetic alterations of candidate tumor suppressor ING1 in human esophageal squamous cell cancer. *Cancer Res* 2001; **61**: 4345-4349
- 17 Ohgi T, Masaki T, Nakai S, Morishita A, Yukimasa S, Nagai M, Miyauchi Y, Funaki T, Kurokohchi K, Watanabe S, Kuriyama S. Expression of p33 (ING1) in hepatocellular carcinoma: relationships to tumour differentiation and cyclin E kinase activity. *Scand J Gastroenterol* 2002; **37**: 1440-1448
- 18 Campos EI, Cheung KJ Jr, Murray A, Li S, Li G. The novel tumour suppressor gene ING1 is overexpressed in human melanoma cell lines. *Br J Dermatol* 2002; **146**: 574-580
- 19 Chen B, Campos EI, Crawford R, Martinka M, Li G. Analyses of the tumour suppressor ING1 expression and gene mutation in human basal cell carcinoma. *Int J Oncol* 2003; **22**: 927-931
- 20 Gunduz M, Ouchida M, Fukushima K, Hanafusa H, Etani T, Nishioka S, Nishizaki K, Shimizu K. Genomic structure of the human ING1 gene and tumor-specific mutations detected in head and neck squamous cell carcinomas. *Cancer Res* 2000; **60**: 3143-3146
- 21 Hara Y, Zheng Z, Evans SC, Malatjalian D, Riddell DC, Guernsey DL, Wang LD, Riabowol K, Casson AG. ING1 and p53

- tumor suppressor gene alterations in adenocarcinomas of the esophagogastric junction. *Cancer Lett* 2003; **192**: 109-116
- 22 **Oki E**, Maehara Y, Tokunaga E, Kakeji Y, Sugimachi K. Reduced expression of p33 (ING1) and the relationship with p53 expression in human gastric cancer. *Cancer Lett* 1999; **147**: 157-162
- 23 **Toyama T**, Iwase H, Watson P, Muzik H, Saettler E, Magliocco A, DiFrancesco L, Forsyth P, Garkavtsev I, Kobayashi S, Riabowol K. Suppression of ING1 expression in sporadic breast cancer. *Oncogene* 1999; **18**: 5187-5193
- 24 **Krishnamurthy J**, Kannan K, Feng J, Mohanprasad BK, Tsuchida N, Shanmugam G. Mutational analysis of the candidate tumor suppressor gene ING1 in Indian oral squamous cell carcinoma. *Oral Oncol* 2001; **37**: 222-224
- 25 **Ohmori M**, Nagai M, Tasaka T, Koeffler HP, Toyama T, Riabowol K, Takahara J. Decreased expression of p33ING1 mRNA in lymphoid malignancies. *Am J Hematol* 1999; **62**: 118-119
- 26 **Sarela AI**, Farmery SM, Markham AF, Guillou PJ. The candidate tumour suppressor gene, ING1, is retained in colorectal carcinomas. *Eur J Cancer* 1999; **35**: 1264-1267
- 27 **Bromidge T**, Lynas C. Relative levels of alternative transcripts of the ING1 gene and lack of mutations of p33/ING1 in haematological malignancies. *Leuk Res* 2002; **26**: 631-635
- 28 **Tokunaga E**, Maehara Y, Oki E, Kitamura K, Kakeji Y, Ohno S, Sugimachi K. Diminished expression of ING1 mRNA and the correlation with P53 expression in breast cancers. *Cancer Lett* 2000; **52**: 15-22
- 29 **Ito K**, Kinjo K, Nakazato T, Ikeda Y, Kizaki M. Expression and sequence analyses of p33 (ING1) gene in myeloid leukemia. *Am J Hematol* 2002; **69**: 141-143
- 30 **Garkavtsev I**, Riabowol K. Extension of the replicative life span of human diploid fibroblast by inhibition of the P33^{ING1}, candidate tumor suppressor. *Mol Cell Biol* 1997; **17**: 2014-2019

Edited by Kumar M and Wang XL Proofread by Xu FM

High-yield expression of recombinant SARS coronavirus nucleocapsid protein in methylotrophic yeast *Pichia pastoris*

Ru-Shi Liu, Kun-Yu Yang, Jian Lin, Yi-Wei Lin, Zhi-Hong Zhang, Jun Zhang, Ning-Shao Xia

Ru-Shi Liu, Kun-Yu Yang, Jian Lin, Yi-Wei Lin, Zhi-Hong Zhang, Jun Zhang, Ning-Shao Xia, The Key Laboratory for Cell Biology and Tumor Cell Engineering of the Ministry of Education; The Research Center for Medical Molecular Virology of Fujian Province, Xiamen University, Xiamen 361005, Fujian Province, China
Supported by the Excellent School Incubation Plan of Ministry of Education, China

Correspondence to: Professor Ning-Shao Xia, The Key Laboratory for Cell Biology and Tumor Cell Engineering of the Ministry of Education; The Research Center for Medical Molecular Virology of Fujian Province, Xiamen University, Xiamen 361005, Fujian Province, China. nsxia@jiangxian.xmu.edu.cn

Telephone: +86-592-2184110 **Fax:** +86-592-2184110

Received: 2004-04-22 **Accepted:** 2004-05-13

syndrome (SARS) coronavirus nucleocapsid (rSCoVN) protein can be successfully expressed in recombinant methylotrophic yeast *P.pastoris* GS115. The rSCoVN protein has a high specificity against SARS-CoVN-mAb and SARS positive sera, but has no cross-reaction with normal human serum. This provides a basis for further researches on the early diagnosis of SARS and the mechanism of SCoV.

Liu RS, Yang KY, Lin J, Lin YW, Zhang ZH, Zhang J, Xia NS. High-yield expression of recombinant SARS coronavirus nucleocapsid protein in methylotrophic yeast *Pichia pastoris*. *World J Gastroenterol* 2004; 10(24): 3602-3607
<http://www.wjgnet.com/1007-9327/10/3602.asp>

Abstract

AIM: Nucleocapsid (N) protein plays an important role in reproduction and pathological reaction of severe acute respiratory syndrome (SARS) coronavirus (SCoV), the antigenicity of the protein is better than spike (S) protein. This study was to find a highly specific and antigenic recombinant SCoV nucleocapsid (rSCoVN) protein, and to provide a basis for further researches on early diagnosis of SARS.

METHODS: Full length cDNA of SCoV nucleocapsid (SCoVN) protein was amplified through polymerase chain reaction (PCR) and cloned into yeast expression vector pPIC3.5K to construct plasmid of pPIC3.5K-SCoVN. The plasmid was linearized and then transformed into *Pichia pastoris* (*P.pastoris*) GS115 (*His Mut⁺*) by electroporation. *His⁺ Mut⁺* recombinant strains were identified by PCR and cultivated on MM/MD plates. The influence of different factors on biomass and rSCoVN protein production during induction phase, such as various induction media, dissolved oxygen (DO) and different final concentrations of methanol, was subsequently studied. The expression level and activation were detected by SDS-PAGE and Western-blot respectively.

RESULTS: All of the recombinants were *His⁺ Mut⁺* after transformation of *P.pastoris* with linearized plasmids. The BMMY medium was optimal for recombinant SCoV (rSCoVN) protein expression and growth of the recombinant strains. The final optimal concentration of methanol was 20 mL/L, the DO had a significant effect on rSCoVN protein expression and growth of recombinant strains. The rSCoVN protein expressed in recombinant strains was about 8% of the total cell protein, 520 mg/L of rSCoVN protein was achieved, and a maximum cell *A* at 600 nm of 62 was achieved in shake flask culture. The rSCoVN protein had a high specificity against mouse-anti-SARS-CoVN-mAb and SARS positive sera, but had no cross-reaction with normal human serum. The biological activity of rSCoVN expressed in *P.pastoris* was about 4-fold higher than that expressed in *E.coli* when the same rSCoVN protein quantity was used.

CONCLUSION: Active recombinant severe acute respiratory

INTRODUCTION

The etiologic agent of SARS has been recently identified as a novel coronavirus (SARS-CoV, SCoV) causing respiratory and enteric diseases in humans and other animals^[1-5]. The SCoV is a group of large, enveloped, positive single stranded RNA (ssRNA) viruses^[6]. Sequence analysis has revealed that the phylogeny of SCoV has most of the characteristic features of a coronavirus, but it belongs to a new group different from all known coronaviruses^[7]. The genome size is 29.725 kb in full-length, has 11 open reading frames (ORFs)^[8]. The SCoV is the largest virus found in any of the RNA viruses, encoding 23 putative proteins, including four major structural proteins, nucleocapsid (N), spike (S), membrane (M), and small envelope (E). The S, M, E and N mature proteins all contribute to generating the host immune response as seen in transmissible gastroenteritis coronavirus^[9], infectious bronchitis virus^[10,11], pig respiratory coronavirus^[12], and mouse hepatitis virus^[13].

SARS is an infectious disease with a high potential for transmission due to close contacts. The outbreak of SARS over 25 countries around the world, such as China, Singapore, Canada, threatened people's health throughout the world. Within a very short time, the disease became pandemic with new cases appearing in the rest of the world. However, it is not easy to differentiate SARS from other causes of pneumonia. Laboratory tests that can confirm a diagnosis of SCoV infection early in the course of the illness are therefore a critical clinical need^[14]. Serology is a sensitive and specific diagnostic approach in the early stage of the disease. N protein plays an important role in reproduction and pathology reaction of SCoV. Moreover, the antigenicity of N protein is better than S protein^[9,15,16]. To find an effective serologic diagnostic method, rSCoVN may be a perfect antigen.

Pichia pastoris (*P.pastoris*), a methylotrophic yeast, is an efficient host for recombinant protein production. The increasing popularity of this particular expression system can be attributed to several factors^[17-19], such as the simplicity of techniques needed for the molecular genetic manipulation of *P.pastoris*, the ability of *P.pastoris* to produce foreign proteins at high levels, many eukaryotic posttranslational modifications, and the commercially available expression system.

Up to now, rSCoVN has been expressed in *E.coli*. However, the biological activity of the rSCoVN protein expressed in *E.coli* is not perfectly understood. High-yield intracellular

expression in *P.pastoris* and activity analysis were investigated in this report. Western blot showed that the rSCoVN expressed in *P.pastoris* had a high specificity to mouse-anti-SCoVN-mAb and patient sera. The biological activity of rSCoVN expressed in *P.pastoris* was about 4-fold higher than that expressed in *E.coli* when the same rSCoVN protein quantity was used.

MATERIALS AND METHODS

Materials

E.coli strains used for cloning the gene were TOP10F⁺[proAB, lacI^q, lacZ Δ M15, Tn10 (Tet^R), and TG1 (supE hsd Δ 5 thi Δ (lac-proAB) F⁺[traD36 PROAB⁺ lacI^q, lacZ Δ M15]). These two strains were cultivated in LB medium (5 g/L yeast extract, 10 g/L peptone, 5 g/L NaCl). *P.pastoris* GS115 (*his mut*⁺) used as expression host was purchased from Invitrogen (California, USA). The following media were employed in cultivation of *P.pichia* cells under different conditions: YEPD (10 g/L yeast extract, 20 g/L peptone, 20 g/L dextrose), BMGY and BMMY (10 g/L yeast extract, 20 g/L peptone, 100 mmol/L potassium phosphate, 13.4 g/L YNB, 4 \times 10⁻⁵ biotin, 10 g/L glycerol, pH 6.0), for BMMY, 5 mL/L filtersterilized methanol was added instead of 10 g/L glycerol. BMG and BMM (100 mmol/L potassium phosphate, 13.4 g/L YNB, 4 \times 10⁻⁵ biotin, 10 g/L glycerol, pH 6.0), for BMM, 5 mL/L filtersterilized methanol was added instead of 10 g/L glycerol. MGY and MM (13.4 g/L YNB, 4 \times 10⁻⁵ biotin, 10 g/L glycerol), for MM, 5 mL/L filtersterilized methanol was added instead of 10 g/L glycerol. MD and MM agar plates (13.4 g/L YNB, 4 \times 10⁻⁵ biotin, 20 g/L dextrose, 15 g/L agar), for MM, 5 mL/L filtersterilized methanol was added instead of 20 g/L dextrose. RDB and RDHB (20 g/L dextrose, 13.4 g/L YNB, 4 \times 10⁻⁵ biotin, 0.05 g/L each of filtersterilized L-glutamic acid, L-lysine, L-leucine, L-isoleucine, L-methionine), for RDBH, 0.05 g/L filtersterilized histidine was added. RDB-G418 agar plates (RDB agar plates, 0.5-3 g/L G418 was added). T-vector was purchased from Takara (Dalian city, China), plasmid pPIC3.5K was purchased from Invitrogen (California, USA).

Methods

Construction of pPIC3.5K-SCoVN expression plasmid The standard recombinant DNA technologies^[20] were used. The coding sequence of SCoVN protein was amplified from the T-SCoVN plasmid using the upstream primer (SCoVNFp: 5'-GGATCCACCATGTCTGATAATGGACCCC-3') containing a *Bam*H I site, in addition to a Kozak consensus sequence, and the reverse primer (SCoVNRp: 5'-GAATTCCTTATGCCTGAGTTGAATCAG-3') contained an *Eco*R I site immediately downstream of an inframe stop codon. The primers facilitated the subcloning of SCoVN protein coding sequence into pPIC3.5K expression vector. The conditions for PCR were as follow: template was initially denatured at 94 °C, cultivated for 4 min, followed by 19 cycles, (each at 94 °C for 50 s, at 57 °C for 50 s, at 72 °C for 80 s), finally, a cycle was performed at 72 °C for 10 min. The PCR products were ligated to T-vector, then cut off by *Bam*H I and *Eco*R I and the fragments were ligated into the same enzymes digested multiple cloning sites of pPIC3.5K expression vector. Finally, the clone was sequenced by 5' *AOX* primer and 3' *AOX* primer in the kit, and the fragments were confirmed to be inserted into the correct sites.

Transformation of *P.pastoris* and selection of *his*⁺*Mut*⁺ transformants *P.pastoris* was transformed using electroporation protocol, competent cells were prepared as described^[21]. Transformed DNA was linearized using *Sac* I leading to targeting of recombinant plasmids to the chromosomal *his4* locus. Before transformation, the linearized DNA was desalted by gel extraction mini kit (Watson Biotechnologies, INC). Plasmid DNA (3-5 μ g) was mixed with 80 μ L of competent cells and stored on ice for 5 min. Cells transferred to an ice-cold 0.2 cm

electroporation cuvette. Transformation was performed using a BioRad GenePulser II. Parameters used were 7.5 KV/cm, 50 μ F and 400 Ω . After pushed, 1.0 mL of ice-cold RDB liquid media was immediately added to the cuvette, and then incubated at 29 °C for 60 min in a shaking incubator (250-300 rpm). Two aliquots of 400 μ L each were plated on RDB-geneticin agar plates, the plates were incubated at 29 °C for 3-4 d. Using sterile toothpicks, the *His*⁺ and geneticin resistant transformants were picked in a regular pattern on MM and MD plates and incubated at 29 °C for 2-3 d. The *His*⁺*Mut*⁻ (methanol utilization slow) transformants were differentiated from *his*⁺*Mut*⁺ (methanol utilization plus) via comparison of patch growth rate on MM and MD plates.

PCR analysis of *P.pastoris* recombinant transformants The primers used were as follows. 5' *AOX1*: 5'-GACTGGTTC CAAT TGACAAGC-3'; 3' *AOX1*: 5'-GCAAATGGCATTCTGACATCC-3'. The genomic DNA was isolated as described in multi-copy *Pichia* expression kit. PCR amplification was performed as follows: initial denaturation at 95 °C for 4 min, followed by 34 cycles, (each at 94 °C for 60 s, at 55 °C for 60 s, at 72 °C for 150 s) and a final extension at 72 °C for 10 min. The genomic DNAs isolated from recombinant *P.pastoris* transformed with parent plasmid and *P.pastoris* GS115 were used as control for PCR^[21].

Shake-flask cultivation of *P.pastoris* and intracellular expression of rSCoVN The recombinant *P.pastoris* strains judged by PCR analysis were grown in 15 mL BMGY medium at 29 °C, until the final cell OD at 600 nm reached 2-6 (log-phase growth). The cells were harvested by centrifuging at 1 500 r/min for 6 min at room temperature, cell pellets were resuspended to a cell A at 600 nm of 1.5 in BMMY medium and induced at 29 °C in a shaking incubator (250-300 rpm). A 100 mL/L of methanol was added to a final concentration 5 mL/L every 24 h to maintain induction. Induced *P.pastoris* transformed with the parent vector was used as a control for background intracellular expression. At each time (about 12-24 h), samples were withdrawn to analyse expression level, activity and to detect A at 600 nm.

Optimization of culture and induction protocol in shake flasks The highly expressed recombinant strains judged by BMGY/BMMY media firstly were grown in different media, and then induced in relevant media. At last, the A and the final methanol concentration were optimized during induction phase. At each time during induction, samples were withdrawn to analyse expression level and the biomass of the recombinant strains.

Lysis of cells and detection of proteins Yeast cells induced to express rSCoVN protein were harvested, the cells were washed with sterile water, and then harvested and stored at -80 °C. Frozen yeast cells were removed from storage and thawed for approximately 3 h at room temperature, breaking buffer (25 mmol/L sodium phosphate, 150 mmol/L sodium chloride, 1 mmol/L EDTA, 1 mmol/L DTT) was added, the cells (6 mL breaking buffer/g wet cells) were resuspended and then stirred for 15 min, followed by approximately 18 h at 4 °C, then disrupted by four passes through a sanitized APV Gaulin 30 CD homogenizer at chamber pressures of 12 000 to 14 000 psi, resulting in 95% cell disruption. About 10 μ L breaking sample mixed with 10 μ L ddH₂O and 10 μ L SDS-PAGE sample buffer^[22] were boiled for 5-10 min, then centrifuged at 12 000 g for 10 min at room temperature, and 10 μ L of the supernate was applied to SDS-PAGE, and separated on 100 g/L polyacrylamide gels with 50 g/L stacking gel. For protein estimations, Coomassie-stained SDS-gels were analyzed by densitometry using UVI.

Western blot analysis of rSCoVN protein After equilibration of gels and nitrocellulose membranes in transfer buffer (25 mmol/L Tris-HCl, 192 mmol/L glycine, 3.5 mmol/L SDS, 200 mL/L methanol), the protein was electroblotted onto a membrane (Amersham Pharmacia Biotech Hoefer TE 70 Series Semiphor Semi-Dry transfer Units, 0.8 mA/cm² 30 min)^[23]. After the membrane (50 g/L fat free milk/TN buffer (10 mmol/L Tris-HCl, 150 mmol/L NaCl, pH 8.0) was blocked, it was probed with a

mouse-anti-SCoVN-mAb (dilution 1:1 000, 50 g/L fat free milk/TN buffer or human serum (dilution 1:100 in 5% fat free milk/TN buffer; 20-25 °C, 1 h), followed by a sheep-anti-mouse or sheep-anti-human IgG coupled to alkaline phosphatase (dilution: 1:10 000 in 50 g/L fat-free milk/TN buffer; 20-25 °C, 1 h). Bound antibodies were detected using 5-bromo-4-chloro-3-indolyl-phosphate (BCIP) and nitro-blue tetrazolium (NBT) in 100 mmol/L NaCl, 5 mmol/L MgCl₂, 100 mmol/L Tris. HCl buffer, pH 9.5^[7] as substrates.

Quantitative activity analysis of rSCoVN proteins expressed in *P.pastoris* and *E.coli* The biological activity of rSCoVN proteins expressed in *P.pastoris* and *E.coli* was compared using Western blot. The purified protein expressed in *P.pastoris* and *E.coli* was diluted by 4-fold gradient, and 12, 3, 0.75, 0.18 µg proteins were added to each well of SDS-PAGE respectively, then probed with a mouse-anti-SCoVN-mAb.

RESULTS

Construction of pPIC3.5K-SCoVN expression plasmid

The coding sequences for SCoVN gene were amplified from T-SCoVN plasmid by PCR using primers (SCoVNFP and SCoVNRP) incorporating 5' *Bam*H I and 3' *Eco*R I, and subcloned into the *Bam*H I and *Eco*R I sites of the pPIC3.5K expression plasmid (Figure 1). Then the constructed expression plasmid was sequenced and proved to be correct. The SCoVN protein coding sequence was under the control of the AOX1 promoter.

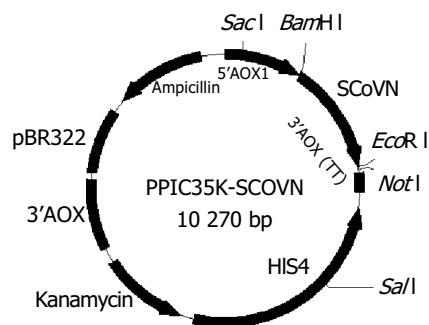


Figure 1 Construct of expression plasmid pPIC3.5K-SCoVN under the control of AOX1 promoter (5' AOX1: promoter fragment; 3' AOX1 (TT): transcription termination, HIS4 ORF: a select marker, SCoVN was inserted between 5' AOX1 and 3' AOX1 (TT), Kanamycin: multi-copy select marker).

Screening of transformant phenotype

pPIC3.5K-SCoVN or pPIC3.5K was digested with *Sac* I to linearize the plasmids, and then electroporated into *P.pastoris* GS115 (*his⁺mut⁺*) respectively. Twenty geneticin-resistant colonies were cultivated on MD and MM plates. They were all *His⁺Mut⁺*, because they all had the same growth rate. The geneticin-resistant colonies were grown in YPED for 24 h, then the genomic DNA was purified, PCR amplification of SCoVN gene was carried out with 5' *AOX1* primer and 3' *AOX1* primer. Twenty transformants each had the alcohol oxidase gene and SCoVN gene. The result demonstrated that all geneticin-resistant colonies were *His⁺Mut⁺*, identical to the result identified on MD and MM plates. The SCoVN protein coding sequence was correctly integrated into the *P.pastoris* genome in the positive recombinants via a single crossover (Figure 2: lanes 5 and 6).

Expression of rSCoVN protein in shake flasks and activity assay

A single recombinant colony (*His⁺Mut⁺*) was used for expression study in shake flask expression^[21]. After one day of cell growth on BMGY medium at 30 °C, 250 rpm, then the BMGY medium was changed to BMMY medium. The cells were fed with 100 mL/L methanol to 5 mL/L (final concentration) every day. The strains transformed by parent plasmid pPIC3.5K were taken as control.

Samples were withdrawn after 60 h. SDS-PAGE showed that heterologous rSCoVN protein was successfully expressed in *P.pastoris*, the rSCoVN protein expression level was about 6% of the total cell protein (Figure 3), a 45 ku protein band could be seen in the positive recombinant and there was no 45 ku protein band in control. To confirm the 45 ku protein was the SCoVN protein, 45 ku protein was detected by Western blot with mouse-anti-SCoVN protein mAb, SARS positive serum and negative serum. The results showed that a single positive reaction band at about 45 ku (Figure 4) could be seen in the nitrocellulose membrane. The band of the same molecular mass could not be detected in the induced recombinant strain transformed pPIC3.5K vector by Western blot analysis. The results showed that the recombinant protein was successfully expressed and had a high-specificity and good-antigenicity against SCoVN-Ab and SARS positive serum, but had no reaction with normal human serum.

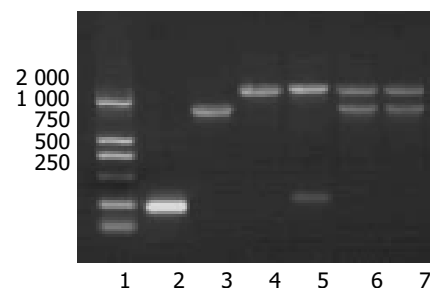


Figure 2 Integration of SCoVN gene into the *P.pastoris* GS115 confirmed by PCR using 5' *AOX1* primer and 3' *AOX1* primer (lane 1: DNA ladder, lane 2: PCR product of pPIC3.5K, lane 3: PCR product of pPIC3.5K-SCoVN, lane 4: PCR product of *P.pastoris* GS115 without transformation, lane 5: PCR product of control strains, lanes 6 and 7: PCR product of positive recombinants).

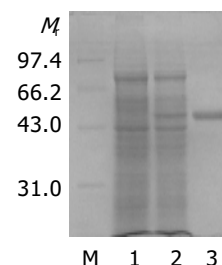


Figure 3 Expression analysis of intracellular SCoVN protein from recombinant yeasts on SDS-PAGE: lane M: protein molecular mass marker; lane 1: protein from control strain; lane 2: proteins from the best strain; lane 3: purified rSCoVN protein; Lane 4: purified SCoVN protein.

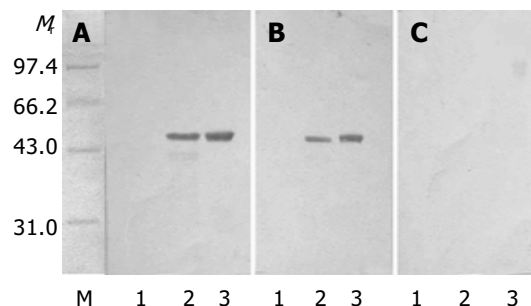


Figure 4 Western blot analysis of intracellular SCoVN protein from recombinant yeasts. A: Western blot analysis against mouse-anti-SCoVN-mAb; B: Western blot analysis against SARS positive serum; C: Western blot analysis against SARS negative serum: lane M: protein molecular-mass marker; lane 1: protein from control strain; lane 2: proteins from the best strain; lane 3: purified rSCoVN protein.

Comparison of biologic activity of rSCoVN in *P.pastoris* and *E.coli*

The biologic activities of rSCoVN protein expressed in *P.pastoris* and *E.coli* were compared using Western-blot. As shown in Figure 5, both rSCoV proteins were able to react with mouse-anti-SARS-mAb. However, the rSCoVN protein expressed in *P.pastoris* appeared to have a more potent activity than that in *E.coli*. Dose-response studies demonstrated that the biological activity of rSCoVN expressed in *P.pastoris* was approximately 4-fold higher than that in *E.coli* when the same rSCoVN protein quantity was used. But the Western blot and SDS-PAGE demonstrated that there was no glycosylation in the rSCoVN protein expressed in *P.pastoris*, because the rSCoVN protein expressed in *P.pastoris* had the same molecular weight as in *E.coli*. So rSCoVN protein expressed in *P.pastoris* had more application potential as a diagnostic agent.

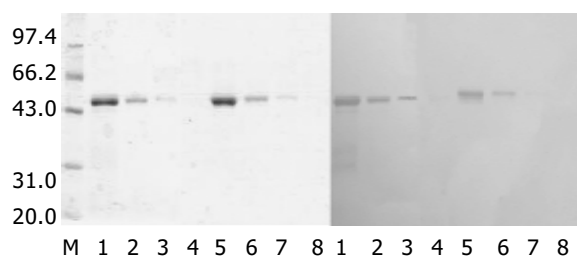


Figure 5 Determination of biological activity of rSCoVN protein expressed in *P.pastoris* and *E.coli*. SDS-PAGE (left) and Western blot (right). Lanes 1, 5: sample containing 12 μ g rSCoVN, lanes 2, 6: sample containing 3 μ g rSCoVN, lanes 3, 7: sample containing 0.75 μ g rSCoVN, lanes 4, 8: sample containing 0.18 μ g rSCoVN. Lanes 1, 2, 3, 4: sample expressed in *P.pastoris* and lanes 5, 6, 7, 8: sample expressed in *E.coli*.

Optimization of culture and expression condition

Comparison of the effect of various media on yeast growth and rSCoVN expression To investigate the effect of different media on rSCoVN expression level and the growth of recombinant strains, we compared the rSCoVN expression level and biomass in different induction media such as BMMY, BMM and MM

media in 20 mL scale. rSCoVN protein expression in *P.pastoris* was performed with a two-phase culture method: biomass production using glycerol as a solely carbon source and specific induction by methanol respectively in BMMY, BMM and MM media. Figure 6A, B show the biomass and rSCoVN protein expression level in each medium at different induction stages. The recombinant strains reached the stationary phase after 2 d of induction, and rSCoVN protein expression level also reached the maximum. A 2-fold difference in biomass and 3.5-fold difference in expression level were noticeable between BMMY and MM media. Difference in biomass and expression was also found between BMMY and BMM media. BMMY medium was optimal for induction expression.

Effect of DO on yeast growth and rSCoVN protein expression

The effect of DO in media on growth and rSCoVN protein expression of *P.pastoris* was also investigated. Different volume media (10, 20, 30, 40 and 50 mL) were loaded in 100 mL flasks. The different volume of the media loaded in flasks meant different DO. The more the medium was loaded, the less the DO was, and it should be noted that the shape was identical. Figure 6C, D show that the DO had an obvious effect on the yeast growth and expression of rSCoVN. The rSCoVN protein expression level was the same in the flask loaded 10 mL or 20 mL medium, because the DO was efficient for growth and rSCoVN protein expression of the recombinant strains in the flask, so the growth and rSCoVN expression level of the recombinant protein were very high, over 20% higher than others. When the volume of medium was increased (above 20 mL), the DO decreased, and the growth and expression level were decreased. So the DO was an important factor for the growth and rSCoV protein expression of the recombinants.

Effect of the final concentration of methanol during induction on yeast growth and rSCoVN protein expression

To find an optimum methanol feeding protocol, different volumes of 100% methanol were added to the media twice a day instead of once a day to decrease the resulting concentration shifts in the BMMY medium. Figure 6E, F show that when the

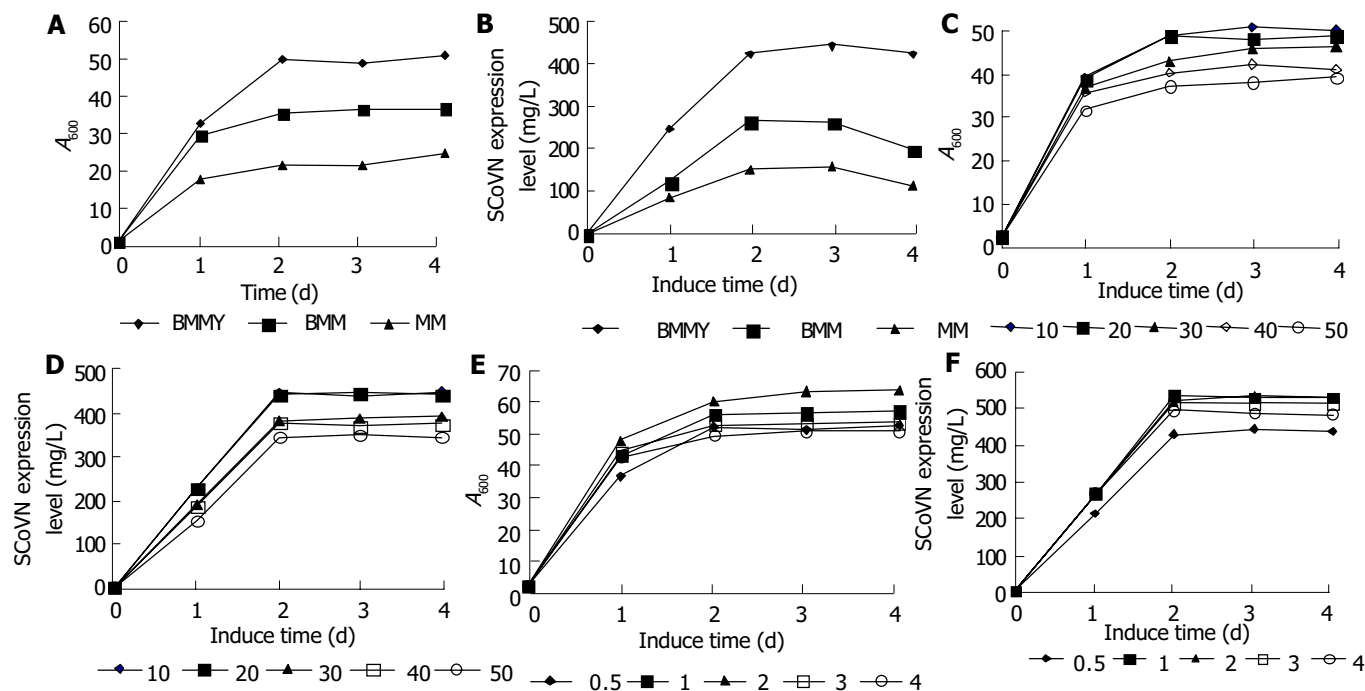


Figure 6 Effects of different media, DO (dissolved oxygen) and methanol amount on the growth and expression of rSCoVN. A, C, E: Growth curves during induction phase by different media, DO and methanol amount, B, D, F: rSCoVN expression and induction time by different media, DO and methanol amount.

methanol feeding was below 20 mL/L, and the concentration of methanol was increased, the biomass was also increased, while the rSCoVN protein expression level was the same at the methanol feeding of 10 mL/L and 20 mL/L, but was increased about 25% than that at the methanol feeding of 5 mL/L. Above the methanol feeding of 20 mL/L, the higher the methanol was fed, the lower the biomass and expression level were. So feeding with 20 mL/L methanol twice a day was considered an optimal feeding strategy.

Kinetics of biomass and rSCoVN protein expression of recombinant *P.pastoris*

After the optimal conditions for yeast growth and rSCoVN protein expression were found, the kinetics of the growth and expression were examined. The results are shown in Figure 7. The rSCoVN protein could be detected readily by SDS-PAGE after 12 h of induction (the inserted panel), rSCoVN protein expression was evident when cells entered the logarithmic growth state and peaked when cell growth reached a steady state and became more or less constant thereafter. The magnitude of expression level reached 526 mg/L. The rSCoVN protein expression was about 8% of the total cell protein, and the maximum cell OD at 600 nm of 62 was achieved. So the optimal harvesting time of cells was 48-60 h after induction. The insert in the panel showed the accumulation of rSCoVN protein by SDS-PAGE during the course of the 84 h experiment.

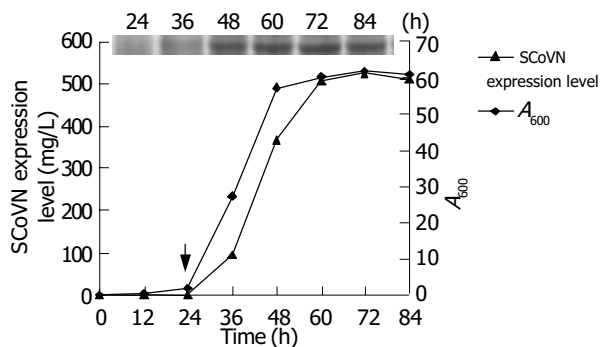


Figure 7 Kinetics of biomass and rSCoVN protein expression using SDS-PAGE over a span of 84 h. The insert shows rSCoVN protein expression level using SDS-PAGE during the course of experiment.

DISCUSSION

The *P.pastoris* expression system has gained acceptance as an important host organism for the production of foreign proteins as illustrated by the fact that a number of proteins synthesized in *P.pastoris* are tested for use as pharmaceuticals in clinic. IGF-1 as a treatment for amyotrophic lateral sclerosis and human serum albumin (HSA) in a serum replacement product have passed clinical trials. Another protein, hepatitis B surface antigen, has been currently available on the market as a subunit vaccine against hepatitis B virus^[24,25].

The etiologic agent of severe acute respiratory syndrome (SARS), has been recently identified as a novel coronavirus causing respiratory and enteric diseases in humans and other animals^[1-5]. SARS is an infectious disease with a high potential for transmission due to close contacts. So it is critical to find a perfect diagnostic agent. N protein plays an important role in reproduction and pathologic reaction of SCoV, and its antigenicity is better than spike protein. So N protein may be the perfect antigen.

In the present study, active rSCoVN was highly expressed in *P.pastoris*. Compared with various media, the BMMY medium

was optimal for rSCoVN expression. A 2-fold difference in biomass and 3.5-fold difference in expression level were noticeable between BMMY and MM media. Difference in biomass and expression was also presented between BMMY and BMM media. The result also revealed that peptone, yeast extracts and steady pH had prominent effects on the growth and expression of recombinant *P.pastoris*. The buffered medium could maintain a stable pH value, and benefit the absorption and use of the nutrients. Moreover, yeast extracts, peptone are rich in peptides, amino acids, vitamins and trace elements. These compounds could enhance the biomass and energy for foreign protein synthesis^[25].

The effect of DO on the growth and expression of rSCoVN revealed that DO was an important factor for yeast growth and expression of recombinant protein. While microorganisms growing on carbohydrates use molecular oxygen mainly for respiration. Oxygen availability could influence the production of proteins, both in prokaryotic cells^[26] and in yeast^[27]. Yeasts growing on methanol might also require a substantial amount of oxygen for the initial oxidation of methanol to formaldehyde^[28]. All methanol taken up by the cells is oxidized to formaldehyde in a coupled reaction involving alcohol oxidase (AOX) and catalase (CAT) in peroxisomes. These reactions use molecular oxygen as an ultimate electron acceptor. Foreign protein synthesis needs abundant energy, so it is important to maintain a relatively high DO for expressing foreign protein in *Pichia pastoris*.

For the expression of protein using AOX1 promoter, it is important to keep the methanol level within a relatively narrow range. In bioreactors it could be achieved by different methods^[29]. In shake flasks, a technique for online monitoring of methanol concentration was introduced^[30]. The ordinary methanol feeding protocol without any complicated devices, still has not been reported. So we established an empirically feeding protocol for our recombinant strains, which worked without any measuring devices. A methanol feeding of 20 mL/L, (final concentration) was optimal for yeast growth and expression of SCoVn protein. Slightly reduced growth and expression while methanol feeding below or above 20 mL/L was probably due to the limited carbon or the toxic effect of accumulated methanol^[30].

Western blot demonstrated that rSCoVN protein had a high-specificity and good-antigenicity against SCoVn-Ab and SARS positive serum, and no reaction with normal human serum. The biological activity of rSCoVN expressed in *P.pastoris* was about 4-fold higher than that expressed in *E.coli* when the same rSCoVN protein quantity was used. The preliminary results indicate that the conformation of rSCoVN protein expressed in *P.pastoris* is almost the same as the natural SCoVn protein, and the rSCoVN protein produced may be suitable for the detection of anti-SCoV in diagnostic assay.

REFERENCES

- 1 Poutanen SM, Low DE, Henry B, Finkelstein S, Rose D, Green K, Tellier R, Draker R, Adachi D, Ayers M, Chan AK, Skowronski DM, Salit I, Simor AE, Slutsky AS, Doyle PW, Krajden M, Petric M, Brunham RC, McGeer AJ. Identification of severe acute respiratory syndrome in Canada. *N Engl J Med* 2003; **348**: 1995-2005
- 2 Lee N, Hui D, Wu A, Chan P, Cameron P, Joynt GM, Ahuja A, Yung MY, Leung CB, To KF, Lui SF, Szeto CC, Chung S, Sung JJ. A major outbreak of severe acute respiratory syndrome in Hong Kong. *N Engl J Med* 2003; **348**: 1986-1994
- 3 Peiris JS, Lai S, Poon L, Guan Y, Yam LY, Lim W, Nicholls J, Yee WK, Yan WW, Cheung MT, Cheng VC, Chan KH, Tsang DN, Yung RW, Ng TK, Yuen KY. Coronavirus as a possible cause of severe acute respiratory syndrome. *Lancet* 2003; **361**: 1319-1325
- 4 Ksiazek TG, Erdman D, Goldsmith CS, Zaki SR, Peret T, Emery S, Tong S, Urbani C, Comer JA, Lim W, Rollin PE, Dowell SF, Ling AE, Humphrey CD, Shieh WJ, Guarner J, Paddock CD,

- Rota P, Fields B, DeRisi J, Yang JY, Cox N, Hughes JM, LeDuc JW, Bellini WJ, Anderson LJ. A novel coronavirus associated with severe acute respiratory syndrome. *N Engl J Med* 2003; **348**: 1953-1966
- 5 **Drosten C**, Gunther S, Preiser W, van der Werf S, Brodt HR, Becker S, Rabenau H, Panning M, Kolesnikova L, Fouchier RA, Berger A, Burguiere AM, Cinatl J, Eickmann M, Escriou N, Grywna K, Kramme S, Manuguerra JC, Muller S, Rickerts V, Sturmer M, Vieth S, Klenk HD, Osterhaus AD, Schmitz H, Doerr HM. Identification of a novel coronavirus in patients with severe acute respiratory syndrome. *N Engl J Med* 2003; **348**: 1967-1976
 - 6 **Anand K**, Ziebuhr J, Wadhvani P, Mesters JR, Hilgenfeld R. Coronavirus main mroteinase (3CL^{pro}) structure: basis for design of anti-SARS drugs. *Science* 2003; **300**: 11763-11767
 - 7 **Marra MA**, Jones SJM, Astell CR, Holt RA, Brooks-Wilson A, Butterfield YSN, Khattri J, Asano JK, Barber SA, Chan SY, Cloutier A, Coughlin SM, Freeman D, Girn N, Griffith OL, Leach SR, Mayo M, McDonald H, Montgomery SB, Pandoh PK, Petrescu AS, Robertson AG, Schein JE, Siddiqui A, Smailus DE, Stott JM, Yang GS, Plummer F, Andonov A, Artsob H, Bastien N, Bernard K, Booth TF, Bowness D, Czub M, Drebot M, Fernando L, Flick R, Garbutt M, Gray M, Grolla A, Jones S, Feldmann H, Meyers A, Kabani A, Li Y, Normand S, Stroher U, Tipples GA, Tyler S, Vogrig R, Ward D, Watson B, Brunham RC, Kraiden M, Petric M, Skowronski DM, Upton C, Roper RL. The genome sequence of the SARS-associated coronavirus. *Science* 2003; **300**: 1399-1345
 - 8 **Rota PA**, Oberste MS, Monroe SS, Nix WA, Campagnoli R, Lcenogle JP, Peñaranda S, Bankamp B, Maher K, Chen MH, Tong S, Tamin A, Lowe L, Frace M, DeRisi JL, Chen Q, Wang D, Erdman DD, Peret TCT, Burns C, Ksiazek TG, Rollin PE, Sanchez A, Liffick S, Holloway B, Limor J, McCaustland K, Olsen-Rasmussen M, Fouchier R, Gunther S, Osterhaus ADME, Drosten C, Pallansch MA, Anderson LJ, Bellini WJ. Characterization of a novel coronavirus associated with severe acute respiratory syndrome. *Science* 2003; **300**: 1394-1399
 - 9 **Gomez N**, Carrillo C, Salinas J, Parra F, Borca MV, Escribano JM. Expression of immunogenic glycoprotein S polypeptides from transmissible gastroenteritis coronavirus in transgenic plants. *Virology* 1998; **249**: 352-358
 - 10 **Jackwood MW**, Hilt DA. Production and immunogenicity of multiple antigenic peptide (MAP) constructs derived from the S1 glycoprotein of infectious bronchitis virus (IBV). *Adv Exp Med Biol* 1995; **308**: 213-219
 - 11 **Ndifuna A**, Waters AK, Zhou M, Collison EW. Recombinant nucleocapsid protein is potentially an inexpensive, effective serodiagnostic reagent for IBV. *J Virol Methods* 1998; **70**: 37-44
 - 12 **Callenbaut P**, Enjuanes L, Pensaert M. An adenovirus recombinant expression the spike glycoprotein of porcine respiratory coronavirus is immunogenic in swine. *J Gen Virol* 1996; **77**(Pt 2): 309-313
 - 13 **Homberger FR**. Nucleotide sequence comparison of the membrane protein genes of three enterotropic strains of mouse hepatitis virus. *Virus Res* 1994; **31**: 49-56
 - 14 **Riley S**, Fraser C, Donnelly CA, Ghani AC, Abu-Raddad LJ, Hedley AJ, Leung GM, Ho LM, Lam TH, Thach TQ, Chau P, Chan KP, Lo SV, Leung PY, Tsang T, Ho W, Lee KH, Lau EM, Ferguson NM, Anderson RM. Transmission dynamics of the etiological agent of SARS in Hong Kong: impact of public health interventions. *Science* 2003; **300**: 1961-1966
 - 15 **King B**, Brain DA. Bovine coronavirus structural proteins. *J Virol* 1982; **42**: 700-707
 - 16 **Daginakatte GC**, Chard-Bergstrom C, Andrews GA, Kapil S. Production, characterization, and uses of monoclonal antibodies against recombinant nucleoprotein of elk coronavirus. *Clin Diagn Lab Immunol* 1999; **6**: 341-344
 - 17 **Sreekrishna K**, Brankamp RG, Kropp KE, Blankenship DT, Tsay JT, Smith PL, Wiershke JD, Subramaniam A, Birkenberger LA. Strategies for optimal synthesis and secretion of heterologous protein in the methylotrophic yeast *Pichia pastoris*. *Gene* 1997; **190**: 55-62
 - 18 **Hasslacher M**, Schall M, Hayn M, Bona R, Rumbold K, Lückl J, Griengl H, Kohlwein SD, Schwab H. High-level intracellular expression of hydroxynitrile lyase from the tropical rubber tree *hevea brasiliensis* in microbial hosts. *Protein Expression Purification* 1997; **11**: 61-71
 - 19 **Hollenberg CP**, Gellissent G. Production of recombinant proteins by methylotrophic yeasts. *Curr Opin Biotechnol* 1997; **8**: 554-560
 - 20 **Sambrook J**. Molecular Cloning: A Laboratory manual, 2nd ed. cold spring harbor: cold spring harbor laboratory press, 1989
 - 21 **Invitrogen**. Instruction manual for multi-copy pichia expression kit-version F, 1999-2002
 - 22 **Laemmli UK**. Cleavage of structural proteins during the assembly of the head of bacteriophage T4. *Nature* 1970; **227**: 680-685
 - 23 **Amersham pharmacia biotech**. Hoef TE 70 Series semiphor semi-Dry Transfer Units User Manual, 1998
 - 24 **Cereghino JL**, Cregg JM. Heterologous protein expression in the methylotrophic yeast *Pichia pastoris*. *FEMS Microbiol Rev* 2000; **24**: 45-46
 - 25 **Cregg JM**, Vedvick TS, Raschke WC. Recent advances in the expression of foreign genes in *Pichia pastoris*. *Biotechnology* 1993; **11**: 905-910
 - 26 **Shioya S**, Morikawa M, Kajihara Y, Shimizu H. Optimization of agitation and aeration conditions for maximum virginiamycin production. *Appl Microbiol Biotechnol* 1999; **51**: 164-169
 - 27 **Hallborn J**, Gorwa MF, Meinander N, Penttila M, Keranen S, Hahn-Hagerdal B. The influence of cosubstrate and aeration on xylitol formation by recombinant *Saccharomyces cerevisiae* expressing the *XYL1* gene. *Appl Microbiol Biotechnol* 1994; **42**: 326-333
 - 28 **Veenhuis M**, Van Dijken JP, Harder W. The significance of peroxisomes in the metabolism of one-carbon compounds in yeasts. *Adv Microbiol Physiol* 1983; **24**: 1-82
 - 29 **Cereghino JL**, Cregg JM. Heterologous protein expression in the methylotrophic yeast *Pichia pastoris*. *FEMS Microbiol* 2000; **24**: 45-66
 - 30 **Boettner M**, Prinz B, Holz C, Stahl U, Lang C. High-throughput screening for expression of heterologous proteins in the yeast *Pichia pastoris*. *J Biotechnol* 2002; **99**: 51-62

Characteristic expression of γ -aminobutyric acid and glutamate decarboxylase in rat jejunum and its relation to differentiation of epithelial cells

Fang-Yu Wang, Masahito Watanabe, Ren-Min Zhu, Kentaro Maemura

Fang-Yu Wang, Ren-Min Zhu, Department of Gastroenterology, Nanjing General Hospital of Nanjing Military Command, Nanjing 210002, Jiangsu Province, China

Masahito Watanabe, Kentaro Maemura, Department of Anatomy, Osaka Medical College, Osaka 659-8686, Japan

Supported by Japan-China Sasagawa Medical Fellowship (1999-2000) and Osaka Medical Research Foundation for Incurable diseases (High-Tech Research Program of Osaka Medical College)

Correspondence to: Fang-Yu Wang, Department of Gastroenterology, Nanjing General Hospital of Nanjing Military Command, Nanjing 210002, Jiangsu Province, China. wangf65@yahoo.com

Telephone: +86-25-80860020 **Fax:** +86-25-80860119

Received: 2004-03-31 **Accepted:** 2004-05-13

Abstract

AIM: To investigate the expression between γ -aminobutyric acid (GABA) and glutamate decarboxylase and its relation with differentiation and maturation of jejunal epithelial cells in rat jejunum.

METHODS: Immunohistochemical expression of GABA and glutamate decarboxylase (GAD, including two isoforms, GAD65 and GAD67) was investigated in rat jejunum. Meanwhile, double staining was performed with GAD65 immunohistochemistry, followed by lectin histochemistry of fluorescent wheat germ agglutinin. Furthermore, evaluation of cell kinetics in jejunum was conducted by ^3H -thymidine autoradiography and immunohistochemistry using a monoclonal antibody to proliferating cell nuclear antigen (PCNA).

RESULTS: The cells showing positive immunoreactivity GABA and GAD65 were mainly distributed in the villi in rat jejunum, while jejunal epithelial cells were negative for GAD67. Positive GABA or GAD65 staining was mainly located in the cytoplasm and along the brush border of epithelial cells in the middle and upper portions. In addition, a few GABA and GAD65 strongly positive cells were scattered in the upper two thirds of jejunal villi. Double staining showed that GAD65 immunoreactivity was not found in goblet cells. ^3H -thymidine-labeled nuclei were found in the lower and middle portions of jejunal crypts, which was consistent with PCNA staining. Therefore, GABA and GAD65 were expressed in a maturation or functional zone.

CONCLUSION: The characteristic expression of GABA and GAD suggests that GABA might be involved in regulation of differentiation and maturation of epithelial cells in rat jejunum.

Wang FY, Watanabe M, Zhu RM, Maemura K. Characteristic expression of γ -aminobutyric acid and glutamate decarboxylase in rat jejunum and its relation to differentiation of epithelial cells. *World J Gastroenterol* 2004; 10(24): 3608-3611
<http://www.wjgnet.com/1007-9327/10/3608.asp>

INTRODUCTION

γ -aminobutyric acid (GABA), originally identified as the principal inhibitory neurotransmitter in the mammalian brain, has been demonstrated to be biologically active in different tissues throughout the body^[1-3]. In developing embryos, GABA was verified to play an important role in the morphogenesis and maturation of many tissues outside the nervous system^[4,5]. Our previous study indicated that GABA and glutamate decarboxylase (GAD, including two isoforms, GAD65 and GAD67) were expressed in chondrocytes on the epiphyseal growth plate of rats, and mainly localized in the maturation zone, rather than the reserve zone or proliferating zone^[6]. This suggests that GABA might play certain functional roles in the differentiation of chondrocytes during growth of the skeleton.

Recently, GABA and GAD have been proved to be increased in colorectal carcinoma tissues by both biochemical and immunohistochemical methods^[7,8]. However, the distribution patterns of GABA and GAD in growth zones of the intestinal epithelium have not been clarified. Therefore, the present study was designed to detect the expression of GABA and GAD in the growth zones of rat jejunum, with an attempt to elucidate the relationship between GABA expression and differentiation and maturation of intestinal epithelial cells.

MATERIALS AND METHODS

Reagents

Rabbit anti-GAD65 polyclonal antibody was purchased from Sigma (Sigma Co. St. Louis, MO, USA). Rabbit anti-GABA and anti-GAD67 polyclonal antibodies were acquired from Chemicon International Inc. (Temecula, CA, USA). Mouse anti-PCNA monoclonal antibody was obtained from Medical and Biological Laboratories Co. (Nagoya, Japan). Alexa FluorTM 488 goat anti-rabbit IgG (H+L) and Alexa FluorTM 594 wheat germ agglutinin (WGA) conjugates were acquired from Molecular Probes (Eugene, OR, USA). Biotin-conjugated anti-mouse immunoglobulin polyclonal antibody was purchased from Pharmingen International (San Diego, CA, USA). ^3H -thymidine was obtained from PerkinElmer Life Science Inc. ([^3H] - thymidine, specific activity: 528 GBq/mmol, Boston, MA, USA).

Animals and tissue preparation

Male Wistar rats (4-6 wk, Nihon Clea, Osaka, Japan), weighing 80-100 g, were caged under controlled conditions of light (lights on 06:00-18:00 h) and temperature (23 °C). The rats were given food and water *ad libitum*. The Ethics Review Committee for Animal Experimentation of Osaka Medical College approved the experimental protocol.

The animals ($n = 5$) were deeply anesthetized with pentobarbital (50 mg/kg body weight), and then fixed by transcardial perfusion with 40 g/L paraformaldehyde in Ringer's solution. After whole body fixation, segments of jejunum (2 cm from Treitz's ligament) were excised and immersed in cold 40 g/L paraformaldehyde in phosphate buffered saline (PBS, pH 7.2)

at 4 °C overnight. For light microscopy study, tissues were soaked overnight in 300 g/L sucrose in PBS, and longitudinal cryostat 5 µm thick sections were cut on a freezing microtome (Leica CM 3050, Nusloch, Germany).

Immunohistochemistry for GABA, GAD65 and GAD67

Immunohistochemical study was performed with polyclonal antibodies against GABA, GAD65, and GAD67. The final dilution for these antibodies was 1:800, 1:1 000, and 1:1 000, respectively. With all antibodies, a two-step indirect immunohistochemical method was used. Cryostat sections were fixed with ice-cold acetone, incubated with 100 mL/L normal goat serum at room temperature for 60 min, and then incubated with primary antibodies overnight at 4 °C. Incubation with primary antisera was followed by Alexa FluorTM488-labeled goat anti-rabbit immunoglobulins. The secondary antibodies were diluted to 1:250 in PBS prior to use, incubated for 60 min at room temperature in darkness, and washed three times with 0.01 mol/L PBS. Sections were finally mounted with MO2 Crystal/Mount (Cosmo Bio, Tokyo, Japan) and preserved at 4 °C in a dark refrigerator. Primary antibodies were replaced by PBS for the negative controls. None of the controls revealed any specific signal.

Double staining and lectin histochemistry

Sections were first applied to immunohistochemical staining for GAD65 as aforementioned. After reaction with the second antibody and a brief wash in PBS, sections were further incubated with Alexa Fluor^R 594 WGA at room temperature for 60 min in darkness, and washed with in 0.01 mol/L PBS three times and mounted with MO2 Crystal/Mount.

³H-thymidine autoradiography

Rats ($n = 2$) were injected intraperitoneally at 10:00 a.m with 100 µCi (3.7 MBq) ³H-thymidine. After 90 min, the rats were anesthetized and fixed by intracardial perfusion with 25 g/L glutaraldehyde. Samples of jejunum were taken as aforementioned, and 5 µm thick paraffin sections were prepared regularly. Autoradiography^[9] was performed as follows: Tissue sections were deparaffinized and dipped into NR-M2 emulsion (Konica Co. Tokyo, Japan) that was diluted with an equal volume of distilled water containing 10 g/L glycerin. After 10 d of exposure in a dark refrigerator, the sections were developed at 20 °C for 8 min in Kodak D-19 diluted with an equal volume of distilled water, terminated in 10 g/L acetic acid for 1 min, and fixed in 300 g/L sodium thiosulphate solution at 20 °C for 8 min. Finally, the sections were lightly counterstained with hematoxylin.

PCNA immunostaining

After three washes with PBS, endogenous peroxides were blocked in 10 g/L hydrogen peroxide in methanol for 30 min at room temperature. For antigen retrieval, the sections were treated with 1 g/L pepsin in 0.01 mol/L HCl. Non-specific binding sites were blocked with 40 g/L bovine serum albumin. Subsequently, anti-PCNA was diluted to 1:100 and reacted with tissue specimens at 4 °C overnight. The sections were then washed three times with PBS, and incubated with biotinylated secondary antibody at room temperature for 60 min. Finally, immunohistochemical staining was performed using the avidin-biotin-peroxidase complex (Vectastain ABC kit, Burlingame, CA, USA). Diaminobenzidine was used as a chromogen, and the sections were counterstained with hematoxylin.

Microscopic observation

For the convenience of description, the crypts of jejunum were divided into the lower, middle and upper portions, while the villi as the basal, middle and top portions. PCNA immunostaining

was observed with a Nikon light microscope equipped with a digital camera (PDMC Ie, Polaroid Co., MA, USA). Fluorescence observation was performed using a confocal laser scanning microscopy (Radiance 2000, Bio-Rad Laboratories, CA, USA) equipped with an argon laser. The laser scanning differential interference contrast (DIC) and confocal mode with an argon laser at 488 nm and/or 590 nm were used. ³H-thymidine autographs were observed with a confocal laser microscope (Carl Zeiss LS10, Germany)^[9]. ³H-thymidine labeling index or PCNA labeling index was calculated as the percentage of positive cells of the total cells by counting 10 different crypts^[10].

Statistical analysis

Welch's *t* test was used for the comparison of PCNA labeling index and ³H -thymidine labeling index.

RESULTS

³H-thymidine autoradiography

Radioactivity was located at the nuclei of cells at the lower and middle portions of the jejunal crypts, while the upper crypts and the whole villi were negative (Figure 1). The ³H -thymidine labeling index was 30±6%.



Figure 1 Autoradiograph of rat jejunum at 90 min after intraperitoneal injection of ³H-thymidine, observed by a confocal laser scanning microscope. A confocal image of reflectance from silver grains (red in color) was overlaid with the differential interference image (green in color). ×200.

PCNA immunostaining in rat jejunum

Strong PCNA staining was detected in the lower portion of the jejunal crypts, while epithelial cells in the villi were almost negative (Figure 2). PCNA labeling index was 57±8%, which was significantly higher than ³H -thymidine labeling index ($P < 0.01$, Welch's *t* test).

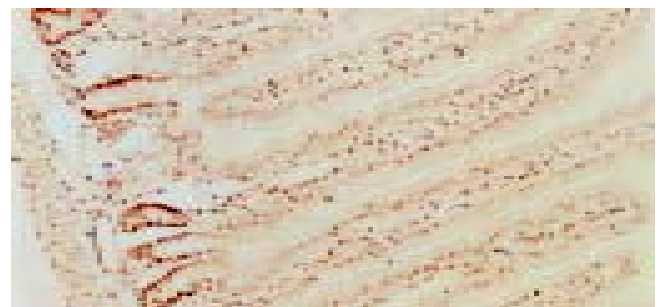


Figure 2 PCNA immunostaining in rat jejunum. ×100.

Expression of GABA in rat jejunum

GABA immunoreactive cells were distributed in the whole villi of rat jejunum. Strongly positive staining was mainly located in the cytoplasm and along the brush border of epithelial cells in the middle and upper portions (Figure 3).

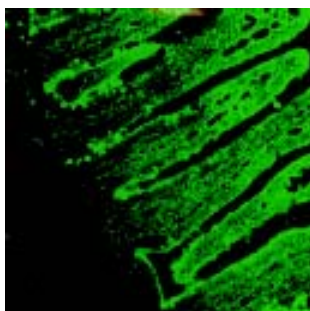


Figure 3 Confocal laser microscopic image of GABA immunoreactivity in rat jejunum. Note the strongly positive staining cells distributed in the middle and upper portions of the villi. $\times 1\ 000$.

Expression of GAD in rat jejunum

GAD65 immunopositive cells were distributed in the middle and upper portions of jejunal villi. Strongly positive staining of GAD65 was mainly localized along the brush border of enterocytes (Figure 4). In addition, a few strongly positive cells had no brush border, which were scattered in the middle or upper portion of jejunal villi. GAD67 was negative in jejunal epithelial cells.

The distribution of GABA and GAD65 immunopositive cells, in comparison with PCNA, is shown in Table 1. GABA and GAD65 were mainly localized in the place where PCNA was negative or weak positive. That is to say, GABA and GAD65 were distributed in the maturation zone and functional zone, rather than in the proliferating zone or stem cells of the jejunal epithelium.

Table 1 Immunoreactivity of GABA, GAD65 and PCNA in epithelium of rat jejunum

	Crypt			Villus		
	Lower	Middle	Upper	Basal	Middle	Top
PCNA	++	+++	±	±	±	-
GABA	±	-	+	+	++	++
GAD65	±	-	-	±	++	++

- negative, ± faint positive, + mild positive, ++ moderate positive, +++ strong positive.

Double staining of immunoreactive GAD65 and lectin histochemistry

Goblet cells were demonstrated by fluorescent WGA staining, while mature absorptive cells were characterized by a well-developed brush border that was positively stained for GAD65 in the jejunum. The GAD65 strongly positive cells in jejunal villi were negative for WGA (Figure 4). Pre-epithelial mucous layer was also stained by fluorescent WGA.

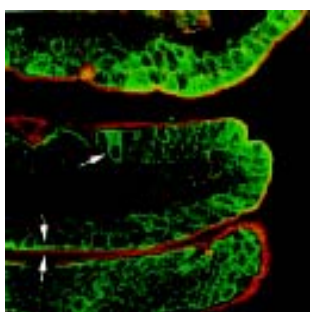


Figure 4 Double staining of immunofluorescent GAD65 (green in color) and fluorescent WGA (red in color) in rat jejunum. Arrow points to the GAD65 strongly positive cells showing WGA negative staining. Arrowhead indicates the strong line-like staining of GAD65 along the brush border, and the outer mucus layer stained by WGA. $\times 630$.

DISCUSSION

The replacement and cell kinetics in murine intestines have been established for decades. The proliferation sites are existed in the lower or middle portion of the small intestinal crypt and in the lower half crypt of the large intestine in rats^[11,12]. Bartkova *et al.*^[13] suggested that intestinal epithelium could be divided into four compartments, namely, stem cells at the base, proliferating zone, maturation zone, and functional zone near the luminal surface.

Cell kinetics has been examined traditionally by ³H-thymidine as a marker for S phase cells. PCNA is an evolutionarily highly conserved acidic nuclear protein, which can function as an auxiliary protein for DNA polymerase δ ^[14]. It has been proved that PCNA expression is maximal during S phase of the cell cycle, and PCNA mRNA normally accumulates only in proliferating cells^[15]. Consequently, PCNA has been found to be a useful marker in immunohistochemical analysis of cell kinetics^[16].

In this study, the growth zones of jejunum were demonstrated by PCNA immunohistochemistry and ³H-thymidine autoradiography. The proliferating zone was consisted of the lower and middle portions of the crypt in the jejunum. Our results also indicated that ³H-thymidine autoradiography was more specific for marking S-phase cells than PCNA immunohistochemistry, as PCNA labeling index was significantly higher than ³H-thymidine labeling index. Meanwhile, GABA and GAD65 immunoreactive cells were distributed in jejunal villi. In other words, GABA and GAD were found in maturation and function zones other than in proliferating zone in rat jejunum.

The characteristic distribution patterns of GABA and GAD in the intestinal epithelium remain unknown. Gilon *et al.*^[4] first reported their research about the possible role of GABA and cell differentiation. Their results documented the appearance of GABA in the developing pancreas and duodenum just prior to the termination of rapid growth and maturation of these tissues. These results are similar to the earlier findings in the developing brain^[17]. Our previous study also demonstrated that GABA and GAD were mainly localized in the hypertrophic zones rather than in the proliferating zone in rat epiphyseal growth plate chondrocytes^[6]. Recently, Kaita *et al.*^[18] reported that ciprofloxacin significantly increased the hepatic regenerative activity in animal models of alcohol-induced liver diseases. The results of PCNA staining showed an enhanced hepatic regeneration in the ciprofloxacin-treated group at 60 h (saline, 13.4 \pm 3.7%; ciprofloxacin, 47.4 \pm 7.3%; and putrescine, 8.4 \pm 2.8% positively stained hepatocytes). Our results also showed that the intensity of immunoreactive GABA and GAD65 on well-differentiated cells was stronger than that on proliferating cells. Based on these results, we presume that GABA should be involved in the regulation of differentiation and maturation of epithelial cells. On the other hand, the characteristic distribution of GABA and GAD65 also indicates that GABA might have some inhibitory effects on epithelial proliferation in rat jejunum.

The intestine has been recognized as a "diffuse endocrine" system, where a variety of endocrine cells produce different peptide hormones. A number of studies have demonstrated that GABA exists in endocrine cells in the gastrointestinal tract^[19-21]. This study showed that there were some strong GABA and GAD65 immunoreactive cells in jejunal villi. It is well known that stem cells in intestinal epithelium give rise to four different kinds of cells: enterocytes (absorptive cells), goblet cells, enteroendocrine cells, and Paneth cells. Mature enterocytes are characterized by the presence of a brush border at their apical surface, while Paneth cells are localized in the lower crypts^[22]. Goblet cells in rat jejunum were clearly demonstrated by lectin histochemistry, because of the specific binding of WGA to sugar residues in mucin within the cells^[23]. Double staining showed that GAD65 strongly positive cells were neither goblet cells nor mature absorptive cells. We believe that these cells are enteroendocrine cells that can synthesize GABA from glutamic

acid. Therefore, it seems reasonable to assume that GABA might be related to the endocrine function of the small intestine.

GABA is known to be synthesized principally from glutamic acid via single enzymatic catalysis of GAD. Two isoforms of mammalian GAD with a predicted molecular weight of 65 300 (GAD65) and 66 600 (GAD67) are highly conserved, but derived from separated genes^[24]. The phylogenetic tree study indicated that the multiplicity of mammalian GAD in central nervous system might have developed some 500 million years before, when the widespread of gene duplications occurred in vertebrates^[25]. Though these isoforms could catalyze the same biochemical reaction, they have been proved to have a different distribution and may have different functions in peripheral as well as the nervous system^[26]. Our result showed that GAD65 was positive, while GAD67 was negative in rat jejunum. This difference further supported the multiplicity of GAD in mammal non-neural tissues^[27].

It should be noted that the distribution of GABA in rat jejunum was not exactly parallel to that of GAD65. In the basal third of jejunal villi, GABA was found to be moderately positive, while GAD65 was weakly positive. GABA in these cells might not be synthesized from glutamic acid via GAD. That is to say, GABA in some intestinal epithelial cells might have other synthetic routes. Putrescine route is a well-known alternative pathway of GABA synthesis in gastrointestinal tract^[28]. Apart from GABA formation, putrescine can be utilized for the biosynthesis of polyamines, such as spermidine and spermine, which have been proved to be involved in the control of cell proliferation^[29,30]. Further research is necessary to elucidate the metabolic routes and functional roles of GABA-polyamine system in epithelial cells of the intestine.

In conclusion, GABA and GAD65 are mainly expressed in the maturation or functional zone in jejunal epithelium of rats. This characteristic expression suggests that GABA may be involved in the regulation of differentiation and maturation of epithelial cells.

REFERENCES

- 1 Watanabe M, Maemura K, Kanbara K, Tamayama T, Hayasaki H. GABA and GABA receptors in the central nervous system and other organs. *Int Rev Cytol* 2002; **213**: 1-47
- 2 Fujimura S, Shimakage H, Tanioka H, Yoshida M, Suzuki-Kusaba M, Hisa H, Satoh S. Effects of GABA on noradrenaline release and vasoconstriction induced by renal nerve stimulation in isolated perfused rat kidney. *Br J Pharmacol* 1999; **127**: 109-114
- 3 Azuma H, Inamoto T, Sakamoto T, Kiyama S, Ubai T, Shinohara Y, Maemura K, Tsuji M, Segawa N, Masuda H, Takahara K, Katsuoka Y, Watanabe M. Gamma-aminobutyric acid as a promoting factor of cancer metastasis; induction of matrix metalloproteinase production is potentially its underlying mechanism. *Cancer Res* 2003; **63**: 8090-8096
- 4 Gilon P, Reusens-Billen B, Remacle C, Janssens de Varebek P, Pauwels G, Hoet JJ. Localization of high-affinity GABA uptake and GABA content in the rat duodenum during development. *Cell Tissue Res* 1987; **249**: 593-600
- 5 Gilon P, Mallefet J, De Vriendt C, Pauwels S, Geffard M, Campistron G, Remacle C. Immunocytochemical and autoradiographic studies of the endocrine cells interacting with GABA in the rat stomach. *Histochemistry* 1990; **93**: 645-654
- 6 Tamayama T, Kanbara K, Maemura K, Kuno M, Watanabe M. Localization of GABA, GAD65 and GAD67 in rat epiphyseal growth plate chondrocytes. *Acta Histochem Cytochem* 2001; **34**: 201-206
- 7 Kleinrok Z, Matsuzek M, Jesipowicz J, Matsuzek B, Opolski A, Radzikowski C. GABA content and GAD activity in colon tumors taken from patients with colon cancer or from xenografted human colon cancer cells growing as s.c tumors in athymic nu/nu mice. *J Physiol Pharmacol* 1998; **49**: 303-310
- 8 Maemura K, Yamauchi H, Hayasaki H, Kanbara K, Tamayama T, Hirata I, Watanabe M. Gamma-amino-butyric acid immunoreactivity in intramucosal colonic tumors. *J Gastroenterol Hepatol* 2003; **18**: 1089-1094
- 9 Kuroda E, Watanabe M, Tamayama T, Shimata M. Autoradiographic distribution of radioactivity from ¹⁴C-GABA in the mouse. *Microsc Res Tech* 2000; **48**: 116-126
- 10 Yamada K, Yoshitake K, Sato M, Ahnen DJ. Proliferating cell nuclear antigen expression in normal, preneoplastic, and neoplastic colonic epithelium of the rat. *Gastroenterology* 1992; **103**: 160-167
- 11 Podolsky DK. Regulation of intestinal epithelial proliferation: a few answers, many questions. *Am J Physiol* 1993; **264**(2 Pt 1): G179-186
- 12 Thompson JS, Saxena SK, Sharp JG. Regulation of intestinal regeneration: new insights. *Microsc Res Tech* 2000; **51**: 129-137
- 13 Bartkova J, Thullberg M, Slezak P, Jaramillo C, Rubio C, Thomassen LH, Bartek J. Aberrant expression of G1-phase cell cycle regulators in flat and exophytic adenomas of the human colon. *Gastroenterology* 2001; **120**: 1680-1688
- 14 Bravo R, Frank R, Blundell PA, Macdonald-Bravo H. Cyclin/PCNA is the auxiliary protein of DNA polymerase-delta. *Nature* 1987; **326**: 515-517
- 15 Shpitz B, Bomstein Y, Mekori Y, Cohen R, Kaufman Z, Grankin M, Bernheim J. Proliferating cell nuclear antigen as a marker of cell kinetics in aberrant crypt foci, hyperplastic polyps, adenomas and adenocarcinomas of the human colon. *Am J Surg* 1997; **174**: 425-430
- 16 Chen H, Wang LD, Guo M, Gao SG, Guo HQ, Fan ZM, Li JL. Alterations of p53 and PCNA in cancer and adjacent tissues from concurrent carcinoma of the esophagus and gastric cardia in the same patient in Linzhou, a high incidence area for esophageal cancer in northern China. *World J Gastroenterol* 2003; **9**: 16-21
- 17 Watanabe M, Shimada M, Watanabe H, Nakanishi M. Amino acid content in several brain regions of the active and hibernating frog, *Rana esculenta*. *Comp Biochem Physiol B* 1990; **97**: 605-610
- 18 Kaita KD, Assy N, Gauthier T, Zhang M, Meyers AF, Minuk GY. The beneficial effects of ciprofloxacin on survival and hepatic regenerative activity in a rat model of fulminant hepatic failure. *Hepatology* 1998; **27**: 533-536
- 19 Krantis A, Tufts K, Nicholos K, Morris GP. [³H]GABA uptake and GABA localization in mucosal endocrine cells of the rat stomach and colon. *J Auton Nerv Syst* 1994; **47**: 225-232
- 20 Davanger S, Hjelle OP, Babaie E, Larsson LI, Hougaard D, Storm-Mathisen J, Ottersen OP. Colocalization of γ -aminobutyrate and gastrin in the rat antrum: an immunocytochemical and *in situ* hybridization study. *Gastroenterology* 1994; **107**: 137-148
- 21 Krantis A, Mattar K, Glasgow I. Rat gastroduodenal motility *in vivo*: interaction of GABA and VIP in control of spontaneous relaxations. *Am J Physiol* 1998; **275**(5 Pt 1): G897-903
- 22 Kong SE, Heel K, McCauley R, Hall J. The role of enterocytes in gut dysfunction. *Pathol Res Pract* 1998; **194**: 741-751
- 23 Bryk SG, Sgambati E, Gheri Bryk G. Lectin histochemistry of goblet cell sugar residues in the gut of the chick embryo and of the newborn. *Tissue Cell* 1999; **31**: 170-175
- 24 Ahman AK, Wagberg F, Mattsson MO. Two glutamate decarboxylase forms corresponding to the mammalian GAD65 and GAD67 are expressed during development of the chick telencephalon. *Eur J Neurosci* 1996; **8**: 2111-2117
- 25 Bosma PT, Blazquez M, Collins MA, Bishop JD, Drouin G, Priede IG, Docherty K, Trudeau VL. Multiplicity of glutamic acid decarboxylases (GAD) in vertebrates: molecular phylogeny and evidence for a new GAD paralog. *Mol Biol Evol* 1999; **16**: 397-404
- 26 Cram DS, Faulkner-Jones B, Kun J, Harrison LC. Glutamic acid decarboxylase-67 (GAD67): expression relative to GAD65 in human islets and mapping of autoantibody epitopes. *Endocrinology* 1995; **136**: 1111-1119
- 27 Katarova Z, Sekerkova G, Prodan S, Mugnaini E, Szabo G. Domain-restricted expression of two glutamic acid decarboxylase genes in midgestation mouse embryos. *J Comp Neurol* 2000; **424**: 607-627
- 28 Tillakaratne NJ, Medina-Kauwe L, Gibson KM. Gamma-aminobutyric acid (GABA) metabolism in mammalian neural and nonneural tissues. *Comp Biochem Physiol A Physiol* 1995; **112**: 247-263
- 29 Hardt J, Larsson LI, Hougaard DM. Immunocytochemical evidence suggesting that diamine oxidase catalyzes biosynthesis of gamma-aminobutyric acid in antropyloric gastrin cells. *J Histochem Cytochem* 2000; **48**: 839-846
- 30 Hopfner M, Berger A, Folsch UR, Loser C. Effects of insulin-like growth factor I on growth and polyamine metabolism in various organs in rats. *Digestion* 2002; **65**: 103-111

Inhibition of small-intestinal sugar absorption mediated by sodium orthovanadate Na_3VO_4 in rats and its mechanisms

Jing Ai, Jie Du, Ning Wang, Zhi-Min Du, Bao-Feng Yang

Jing Ai, Jie Du, Ning Wang, Bao-Feng Yang, Department of Pharmacology, Harbin Medical University, Bio-Pharmaceutical Key Laboratory of Heilongjiang Province-Incubator of State Key Laboratory, Harbin 150086, Heilongjiang Province, China
Zhi-Min Du, State Base for Drug Clinical Trial, Harbin Medical University, Harbin 150086, Heilongjiang Province, China
Supported by the Key Fund of the Technological Bureau of Heilongjiang Province, No.20010101001-00; the Fund of Educational Bureau of Heilongjiang Province, No.10531094

Co-correspondents: Jing Ai

Correspondence to: Professor Bao-Feng Yang, Department of Pharmacology, Harbin Medical University, Harbin 150086, Heilongjiang Province, China. yangbf@ems.hrbmu.edu.cn

Telephone: +86-451-86671354 **Fax:** +86-451-86669482

Received: 2004-02-27 **Accepted:** 2004-04-29

Abstract

AIM: To investigate the inhibitory effects of sodium orthovanadate on small-intestinal glucose and maltose absorption in rats and its mechanism.

METHODS: Normal Wistar rats were lavaged with sodium orthovanadate (16 mg/kg, 4 mg/kg and 1 mg/kg) for 6 d. Blood glucose values were measured after fasting and 0.5, 1, 1.5 and 2 h after glucose and maltose feeding with oxidation-enzyme method. α -glucosidase was abstracted from the upper small intestine, and its activity was examined. mRNA expression of α -glucosidase and glucose-transporter 2 (GLUT2) in epithelial cells of the small intestine was observed by *in situ* hybridization.

RESULTS: Sodium orthovanadate could delay the increase of plasma glucose concentration after glucose and maltose loading, area under curve (AUC) in these groups was lower than that in control group. Sodium orthovanadate at dosages of 10 $\mu\text{mol/L}$, 100 $\mu\text{mol/L}$ and 1000 $\mu\text{mol/L}$ could suppress the activity of α -glucosidase in the small intestine of normal rats, with an inhibition rate of 68.18%, 87.22% and 91.91%, respectively. Sodium orthovanadate reduced mRNA expression of α -glucosidase and GLUT2 in epithelial cells of small intestine.

CONCLUSION: Sodium orthovanadate can reduce and delay the absorption of glucose and maltose. The mechanism may be that it can inhibit the activity and mRNA expression of α -glucosidase, as well as mRNA expression of GLUT2 in small intestine.

Ai J, Du J, Wang N, Du ZM, Yang BF. Inhibition of small-intestinal sugar absorption mediated by sodium orthovanadate Na_3VO_4 in rats and its mechanisms. *World J Gastroenterol* 2004; 10(24): 3612-3615

<http://www.wjgnet.com/1007-9327/10/3612.asp>

INTRODUCTION

There is evidence that sodium orthovanadate could markedly

decrease the high blood sugar induced by alloxan and streptozotocin^[1,2]. Sodium orthovanadate acts on blood sugar by increasing the number of insulin-receptors and enhancing glucose transport via promoting the combination of insulin and insulin receptors^[3-7]. Besides, sodium orthovanadate can also inhibit glucose absorption from small intestines of rats by inhibiting the activity of Na^+/K^+ -ATPase and increasing contractility in the intestinal smooth muscles^[8,9]. Therefore we observed the effects of sodium orthovanadate on glucose and maltose absorption in the small intestine of Wistar rats and investigated the mechanisms in order to provide theoretical basis for its further development.

MATERIALS AND METHODS

Materials

Male and female Wistar rats weighing 180-220 g were obtained (Department of Animals, Harbin Medical University). Sodium orthovanadate was provided by Harbin Medical University. Acarbose was purchased from Bioer (Wuhan, China). Both α -amylase and p -nitrobenzene- α -D-malt pentose glycoside were supplied by Sigma (America). *In situ* hybridization kits of the small intestine GLUT2 and α -glucosidase were from BOSD Biotech (Wuhan, China).

Methods

Experimental schedule Normal Wistar rats were randomly divided into 5 groups (8 rats per group). Animals in group 1 were lavaged with saline, rats in groups 2-5 were lavaged with acarbose (30 mg/kg) and sodium orthovanadate (16 mg/kg, 4 mg/kg and 1 mg/kg) for 6 d at the dosage 1 mL/100 g. Blood glucose values 12 h after fasting and 0.5, 1, 1.5 and 2 h after feeding glucose (22 g/kg) were investigated using oxidation-enzyme method. The same method was used to determine the effects of sodium orthovanadate on maltose absorption. Small-intestine tissue was obtained after the blood glucose assay for *in situ* hybridization analysis.

α -glucosidase activity assay As described previously^[10,11], normal rats were killed 3 h after fasting. A 10 cm segment of the upper small intestine from the head of the dodecadactylon was washed twice with cool saline. Mucosae were homogenized after diluted at 1:10 in 0.5 mol/L NaCl-KCl buffer, then centrifuged at 2×10^4 g for 30 min (4 °C). Deposits were washed twice with cool saline, then 2×10^4 g centrifuged for 30 min (4 °C), diluted at 1:5 in saline again and 500 r/min centrifuged for 10 min (4 °C). Supernatant was collected and stored at -30 °C. After response architecture was dispensed, fluid samples were shaken and water-bathed for 10 min at 30 °C. Then samples were put into water bath at 85 °C to terminate the response. In the response architecture without enzymes and drugs, the control group was adjusted to zero absorption degree (A). In the response architecture without drugs, the standard group's enzyme activity was 100%. A was assayed at 405 nm wavelength. Then we calculated the percentage of inhibition of 10 $\mu\text{mol/L}$, 100 $\mu\text{mol/L}$ and 1 000 $\mu\text{mol/L}$ sodium orthovanadate on α -glucosidase activity.

In situ hybridization for α -glucosidase and GLUT2 expression

A 2 cm segment of the upper small intestine was obtained from

the head of dodecadactylon. *In situ* hybridization was carried out according to the manual of BOSD Biotech. Two microliters thick specimens sectioned from a paraffin-embedded block were dewaxed in xylene and rehydrated in serially graded ethanol (100%, 95%). The activity of endogenous enzymes was deactivated by hydrogen peroxide solution (30%) for 1 min. Specimens were ingested with pepsin for 15 min at 20–22 °C, force-hybridized for 3 h at 38 °C and hybridized for 12 h at 38 °C. Finally, the slides were washed 4 times with PBS, each time for 5 min. After trickled with biotin-rat antibodies to digoxin at 37 °C for 60 min, then streptavidin-biotin-enzyme complex (SABC) was added at 37 °C for 20 min and biotin-peroxidase was added at 37 °C for 20 min. At last the slides were washed 4 times with PBS, each time for 5 min, and stained with DAB for 2–4 min. The positive expression of α -glucosidase showed brown staining signals in villi of small intestine and GLUT2 in incisures between two villi of small intestine.

Statistical analysis

Data was tested using Student's *t*-test. The measurement results were expressed as mean \pm SD.

RESULTS

Effects of sodium orthovanadate on glucose absorption

Sodium orthovanadate at the dosage of 10 μ mol/L, 100 μ mol/L, 1 000 μ mol/L delayed the increase of blood glucose concentration induced by lavaged glucose (22 g/kg) after 1.5–2 h (Figure 1A), and decreased the AUC in these groups to that in control [17.03 \pm 0.60 mmol/(L·h)] (P <0.05), which was [8.24 \pm 0.63 mmol/(L·h)] (P <0.01), [9.69 \pm 0.38 mmol/(L·h)] (P <0.01), [13.76 \pm 0.39 mmol/(L·h)] (P <0.05), respectively.

Effects of sodium orthovanadate on maltose absorption

Blood glucose concentration increase in rats after maltose feeding (22 g/kg) was delayed by both sodium orthovanadate and acarbose, the peak values were shown 2 h after maltose loading, and high and moderate dosages of sodium orthovanadate also inhibited the increase of the blood glucose concentration peak value (P <0.05) (Figure 1B). The AUC of blood glucose concentration in sodium orthovanadate groups at the 3 dosages was markedly lower than that in the control group [18.40 \pm 1.46 mmol/(L·h)]. AUC at high and moderate dosages was [8.97 \pm 1.56 mmol/(L·h)], and [6.19 \pm 0.47 mmol/(L·h)], both were lower than that in acarbose group with AUC [13.10 \pm 0.43 mmol/(L·h)] (P <0.05).

Effects of sodium orthovanadate on α -glucosidase activity in small intestine

Sodium orthovanadate at the dosages of 10 μ mol/L, 100 μ mol/L, 1000 μ mol/L, could inhibit α -glucosidase activity in small intestine, the percentage of inhibition was 68.18%, 87.22% and

91.91%, respectively. The inhibiting action of sodium orthovanadate (100 μ mol/L) was stronger than that of the same dosage of acarbose (70.37%) (P <0.05, Table 1).

Table 1 Inhibitory effect of sodium orthovanadate on α -glucosidase activity in small intestine (mean \pm SD, n = 8)

Group	Dosage (μ mol/L)	A	Percentage of inhibition (%)
Control	-	0	100.00
Standard	-	0.594	0.00
Acarbose	100	0.176 \pm 0.076	70.37 \pm 6.43
Na ₃ VO ₄	10	0.189 \pm 0.034	68.18 \pm 3.46
	100	0.076 \pm 0.019	87.22 \pm 2.00 ^a
	1000	0.048 \pm 0.012	91.91 \pm 4.23 ^b

^a P <0.05, ^b P <0.01 vs positive control group.

Effects of sodium orthovanadate on α -glucosidase and GLUT2 mRNA expression in small intestine

Sodium orthovanadate at the dosages of 1 mg/kg, 4 mg/kg and 16 mg/kg, could depress α -glucosidase mRNA expression in epithelial cells of small-intestine, the positive expression number of α -glucosidase particles in each villus was 38 \pm 5, 34 \pm 5 and 33 \pm 4. They were fewer than that in control group (45 \pm 6), (P <0.05) (n = 16) (Figures 2 A, B). The inhibiting action of sodium orthovanadate showed no marked difference between high and moderate dosages. GLUT2 mRNA was diffusely expressed in the incisures between two villi of small intestine. Sodium orthovanadate could inhibit GLUT2 mRNA expression in a dose-dependent manner. In the vision field of 100 cm², the expression area of GLUT2 mRNA was decreased to 0.5 \pm 0.12 cm², 0.77 \pm 0.15 cm², 1.02 \pm 0.24 cm² after sodium orthovanadate loading at the 3 dosages from 2.5 \pm 0.5 cm² in control group (P <0.05) (n = 16) (Figures 2 C, D).

DISCUSSION

First, in this study, we observed the effects of sodium orthovanadate on glucose and maltose absorption. The result proved that sodium orthovanadate could delay the increase of blood glucose concentration after glucose or maltose feeding and decrease AUC.

Generally, sugar is divided into monosaccharide, disaccharide and polysaccharide. The absorption of monosaccharide is an active transport process with energy consumption. Na⁺-dependent transporters exist in the brush border of epithelial cells in intestinal mucosae, which can transport Na⁺ along its concentration gradient and monosaccharide counter to its concentration gradient into cells from intestinal lumen via the brush border, then both Na⁺ and monosaccharide diffuse into blood. In this process, the exchange activity of Na⁺/K⁺-ATPase plays an important role in maintaining the Na⁺ concentration

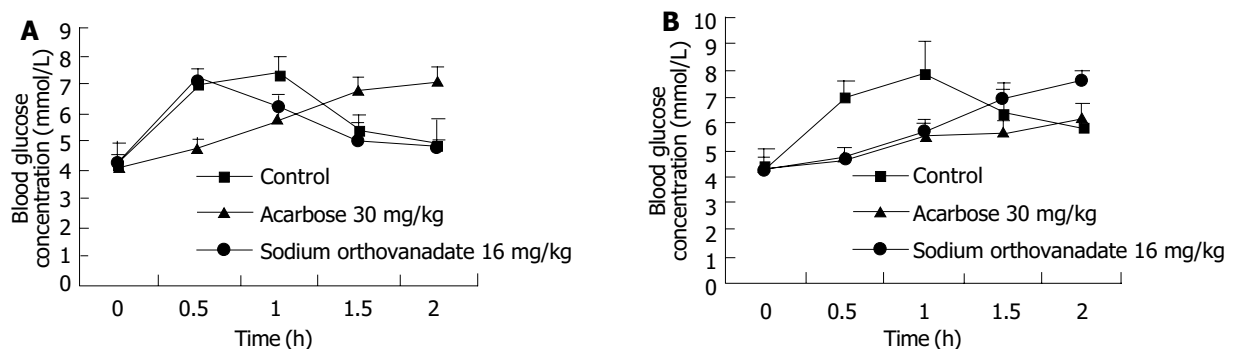


Figure 1 Effects of sodium orthovanadate on glucose absorption (A) and maltose absorption (B) in small intestine (n = 8).

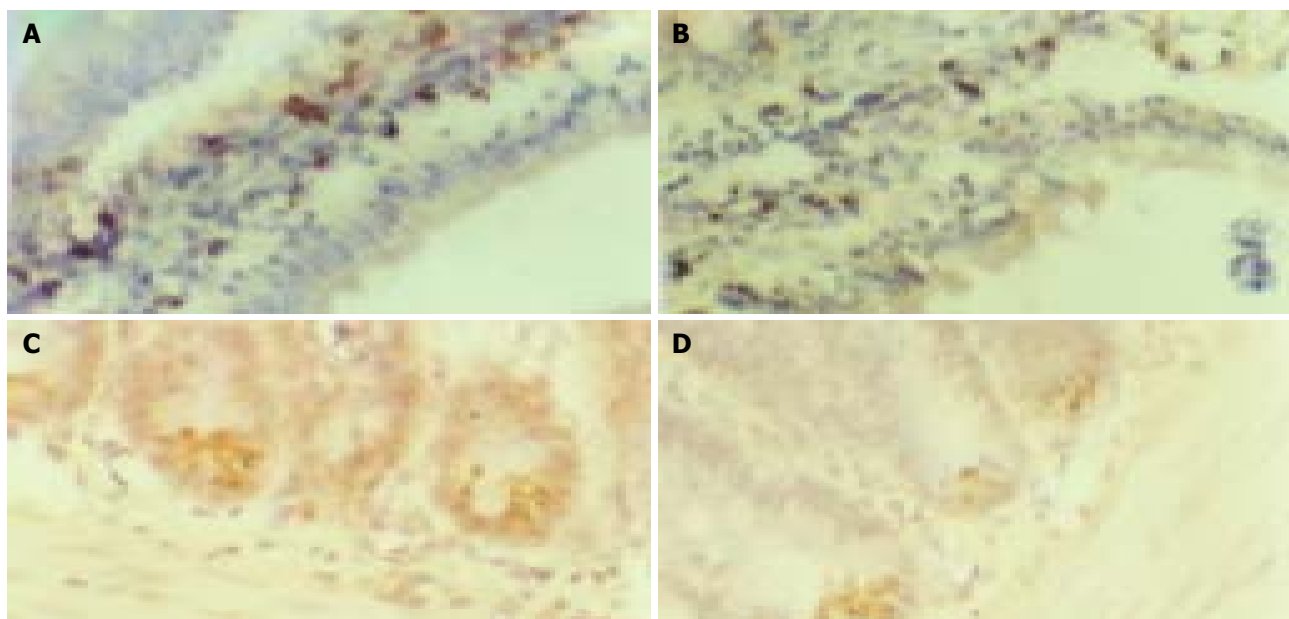


Figure 2 Effects of sodium orthovanadate on α -glucosidase and GLUT2 mRNA expression in small intestine A: Control group of α -glucosidase B: Sodium orthovanadate (4 mg/kg, 60 \times) on α -glucosidase C: Control group of GLUT2 D: Sodium orthovanadate (4 mg/kg, 60 \times) on GLUT2.

gradient. Decreased activity of Na^+/K^+ -ATPase can influence glucose transport and therefore decrease blood glucose concentration. In addition, GLUT2 existing in the epithelial cells of intestinal villi incisures can directly transport glucose into cells. Decreased expression and limited translocation process from cytoplasm to cell membranes of GLUT2 will decrease glucose absorption from the small intestine. In normal conditions, polysaccharides are the mainly existing pattern in foods, which can be absorbed into blood after degradation into oligosaccharides and disaccharides by amylase and further into monosaccharides by α -glucosidase existing in the brush border of epithelial cells in intestinal mucosae. So α -glucosidase is a very important factor, which can affect glucose absorption in small intestine. Acarbose, a kind of inhibitors of α -glucosidase used in clinic at present, can depress the absorption of polysaccharides by inhibiting α -glucosidase activity and effectively decrease postprandial blood glucose level of diabetes mellitus^[12,13], therefore Na^+/K^+ -ATPase, GLUT2 and α -glucosidase play the main role in increasing postprandial blood glucose concentration. Postprandial blood glucose concentration would change if any of them has dysfunction.

Sodium orthovanadate has antihyperglycemic actions by various means, such as increasing the protein expression of GLUT4 in skeletal muscles, accelerating hexose transport, increasing glycogen synthetase production by stimulating dextrose oxidan^[14,15], accelerating glycolysis and lipid synthesis, depressing Na^+ reabsorption via acting on $\text{Na}^+/\text{Ca}^{2+}$ exchanger^[16].

In the present study, we only investigated the effects of sodium orthovanadate on small-intestinal sugar absorption in rats. First, we observed the effects of sodium orthovanadate on glucose absorption. Glucose is a monosaccharide, which can be directly absorbed by the small-intestine without hydrolysis, so the function of both GLUT2 and Na^+/K^+ -ATPase can be reflected by its absorption state. The first body response after monosaccharide absorption is to induce insulin release by stimulating pancreatic islets to decrease blood glucose concentration. For this reason, blood sugar peak values show the tendency to elevate first and then decline, thus typical OGTT curve is formed. Studies have shown that acarbose, a kind of inhibitors of α -glucosidase, can inhibit the hydrolysis of disaccharides and polysaccharides, and then decrease postprandial blood glucose concentration and protect OGTT,

but it could not depress glucose absorption. Our results are similar to previous studies^[17-19]. In order to eliminate the lowering effect on blood sugar of insulin induced by pancreatic islets, sodium orthovanadate was orally administered into rats for 6 d to maintain a stabilizing effect on islet cells. Our results showed that sodium orthovanadate at all the 3 dosages could delay the absorption of glucose and blood sugar concentration peak value with decreased AUC in a dose-dependent manner. Compared with the control group, blood sugar concentration decrease at 0.5 h and 1 h after sodium orthovanadate feeding was due to decreased glucose absorption, but not due to insulin release, because AUC peak value was delayed but not extincted. The results imply that the activity and function of both Na^+/K^+ -ATP and GLUT2 may participate in this kind of actions of sodium orthovanadate. Studies have evidenced that sodium orthovanadate is a Na^+/K^+ -ATPase inhibitor, and has been used widely as a tool drug^[20]. So it is generally accepted that sodium orthovanadate can depress sugar absorption via inhibiting the activity of Na^+/K^+ -ATPase in the small intestine. The results in our study suggest that sodium orthovanadate can inhibit sugar absorption via affecting the function of GLUT2, because it could markedly inhibit the expression of GLUT2 mRNA in small-intestinal epithelia of normal rats.

But we still do not know if it is the whole mechanism of sodium orthovanadate underlying the inhibition of sugar absorption, and whether it also can affect the absorption of polysaccharides and disaccharides. Therefore we estimated the effect of sodium orthovanadate on maltose absorption.

Maltose is composed of two monosaccharides coupled with α -1,4 glycoside linkages, which can be absorbed only after it is hydrolyzed by α -glucosidase in the intestinal tract. The data reported here suggest that sodium orthovanadate can delay the absorption of maltose and the blood sugar concentration peak value in a dose-dependent manner. Moreover, the AUC of sodium orthovanadate in moderate and large dosage groups and acarbose group was definitely lower than that in the control group. The action of sodium orthovanadate was stronger than that of acarbose, because the AUC of sodium orthovanadate in moderate and high dosage groups was lower than that in the acarbose group. This phenomenon may be due to two reasons: One is the inhibition of sodium orthovanadate on the activity

of Na⁺/K⁺-ATPase and GLUT2 mRNA expression was stronger than that of acarbose on α-glucosidase, the other is that sodium orthovanadate might also inhibit the activity of α-glucosidase besides its action on Na⁺/K⁺-ATPase and GLUT2 mRNA expression. Its double action decreased blood sugar markedly. In order to further verify our tentative idea, we observed the influence of sodium orthovanadate on the activity of α-glucosidase; the results indicated that sodium orthovanadate could depress α-glucosidase activity in a dose-dependent manner.

There are two ways of sodium orthovanadate in decreasing the activity of α-glucosidase. One is that sodium orthovanadate could decrease α-glucosidase activity without enzyme protein content changes. The other is that it could reduce the expression of α-glucosidase. So we detected mRNA expression of α-glucosidase by *in situ* hybridization. The result demonstrated that sodium orthovanadate could depress the mRNA expression of α-glucosidase in a dose-dependent manner.

In conclusion, sodium orthovanadate has the ability to inhibit sugar absorption via versatile means which affect the function and activity of Na⁺/K⁺-ATPase, inhibit the activity and gene expression of α-glucosidase as well as depress gene expression of the glucose transporter.

REFERENCES

- 1 Meyerovitch J, Farfel Z, Sack J, Shechter Y. Oral administration of vanadate normalizes blood glucose levels in streptozotocin-treated rats. Characterization and mode of action. *J Biol Chem* 1987; **262**: 6658-6662
- 2 Meyerovitch J, Waner T, Sack J, Kopolovic J, Shemer J. Attempt to prevent the development of diabetes in non-obese diabetic mice by oral vanadate administration. *Isr Med Assoc J* 2000; **2**: 211-214
- 3 Shao J, Catalano PM, Yamashita H, Ishizuka T, Friedman JE. Vanadate enhances but does not normalize glucose transport and insulin receptor phosphorylation in skeletal muscle from obese women with gestational diabetes mellitus. *Am J Obstet Gynecol* 2000; **183**: 1263-1270
- 4 Marita AR, Anilkumar KL. Effect of vanadate on glycogen synthesis in dexamethasone-treated 3T3 adipocytes: evidence for a novel insulin sensitizing action. *Diabetes Obes Metab* 2001; **3**: 271-278
- 5 Pugazhenti S, Khandelwal RL, Angel JF. Insulin-like effect of vanadate on malic enzyme and glucose-6-phosphate dehydrogenase activities in streptozotocin-induced diabetic rat liver. *Biochim Biophys Acta* 1991; **1083**: 310-312
- 6 Madsen KL, Ariano D, Fedorak RN. Vanadate treatment rapidly improves glucose transport and activates 6-phosphofructo-1-kinase in diabetic rat intestine. *Diabetologia* 1995; **38**: 403-412
- 7 O'Connor JC, Freund GG. Vanadate and rapamycin synergistically enhance insulin-stimulated glucose uptake. *Metabolism* 2003; **52**: 666-674
- 8 Kellett GL, Barker ED. The effect of vanadate on glucose transport and metabolism in rat small intestine. *Biochim Biophys Acta* 1989; **979**: 311-315
- 9 Hudgins PM, Bond GH. Alteration by vanadate of contractility in vascular and intestinal smooth muscle preparations. *Pharmacology* 1981; **23**: 156-164
- 10 Zhang JT, Shen ZF, Qiao FX. α-glucosidase activity assay. Modern experimental methods in pharmacology (1). First edition. Peking. *Peking Medical University and Xie-he Medical University Publishing Company* 1998: 992
- 11 Yasuda K, Shimowada K, Uno M, Odaka H, Adachi T, Shihara N, Suzuki N, Tamon A, Nagashima K, Hosokawa M, Tsuda K, Seino Y. Long-term therapeutic effects of voglibose, a potent intestinal alpha-glucosidase inhibitor, in spontaneous diabetic GK rats. *Diabetes Res Clin Pract* 2003; **59**: 113-122
- 12 Wehmeier UF, Piepersberg W. Biotechnology and molecular biology of the alpha-glucosidase inhibitor acarbose. *Appl Microbiol Biotechnol* 2004; **63**: 613-625
- 13 Ron Y, Wainstein J, Leibovitz A, Monastirsky N, Habet B, Avni Y, Segal R. The effect of acarbose on the colonic transit time of elderly long-term care patients with type 2 diabetes mellitus. *J Gerontol A Biol Sci Med Sci* 2002; **57**: M111-M114
- 14 Gupta D, Raju J, Prakash J, Baquer NZ. Change in the lipid profile, lipogenic and related enzymes in the livers of experimental diabetic rats: effect of insulin and vanadate. *Diabetes Res Clin Pract* 1999; **46**: 1-7
- 15 Goldwaser I, Gefel D, Gershonov E, Fridkin M, Shechter Y. Insulin-like effects of vanadium: basic and clinical implications. *J Inorg Biochem* 2000; **80**: 21-25
- 16 Rowe WA, Tomicic TK, Hajjar JJ. Enhancement of rat intestinal calcium absorption by vanadate. *Proc Soc Exp Biol Med* 1991; **198**: 754-759
- 17 Bischoff H. Pharmacology of alpha-glucosidase inhibition. *Eur J Clin Invest* 1994; **24**(Suppl 3): 3-10
- 18 Ranganath L, Norris F, Morgan L, Wright J, Marks V. Delayed gastric emptying occurs following acarbose administration and is a further mechanism for its anti-hyperglycaemic effect. *Diabet Med* 1998; **15**: 120-124
- 19 Joubert PH, Venter HL, Foukaridis GN. The effect of miglitol and acarbose after an oral glucose load: a novel hypoglycaemic mechanism? *Br J Clin Pharmacol* 1990; **30**: 391-396
- 20 Scheiner-Bobis G, Hubschle T, Diener M. Action of palytoxin on apical H⁺/K⁺-ATPase in rat colon. *Eur J Biochem* 2002; **269**: 3905-3911

Edited by Wang XL and Zhu LH Proofread by Xu FM

Gastroprotective effect and mechanism of amtolmetin guacyl in mice

Yuan-Hai Li, Jun Li, Yan Huang, Xiong-Wen Lü, Yong Jin

Yuan-Hai Li, Jun Li, Yan Huang, Xiong-Wen Lü, Yong Jin, School of Pharmacy, Anhui Medical University, Hefei 230032, Anhui Province, China

Yuan-Hai Li, Department of Anesthesiology, the First Affiliated Hospital of Anhui Medical University, Hefei 230022, Anhui Province, China

Correspondence to: Professor. Jun Li, School of Pharmacy, Anhui Medical University, Institute of Clinical Pharmacology, Anhui Medical University, Tunxi West Road, Hefei 230032, Anhui Province, China. amuicplj@mail.hf.ah.cn

Telephone: +86-551-5161001 **Fax:** +86-551-5161001

Received: 2004-03-11 **Accepted:** 2004-04-16

Abstract

AIM: To investigate the gastroprotective effect and mechanism of amtolmetin guacyl (AMG, MED15) in mice.

METHODS: Male and female Kunming strain mice, weighing 18-22 g, were utilized in the experiment. Normal or ethanol-induced gastric mucosal damage models in mice were successfully established to investigate the gastroprotective effect and mechanism of AMG. In the experiment of gastric mucosal damage after repeated treatment with AMG, the mice were randomly divided into 5 groups: normal group, 3 AMG groups receiving (75, 150 and 300 mg/kg), and tolmetin group receiving 90 mg/kg. The mice were randomly divided into 6 groups as follows: normal group, model group, AMG groups with doses of 75, 150 and 300 mg/kg, respectively, and tolmetin group with a dose of 90 mg/kg in ethanol-induced gastric mucosal damage experiment. The severity of gastric mucosal lesions was scored from 0 to 5. Gastric tissue sections were stained with hematoxylin and eosin (HE) and examined under light microscopy. Also gastric tissue sections were stained with uranyl acetate and lead citrate, and examined under electron microscopy. In addition, nitric oxide (NO) and malondialdehyde (MDA) contents, and nitric oxide synthase (NOS) and superoxide dismutase (SOD) activities in the stomach tissue homogenates were measured by biochemical methods.

RESULTS: Repeated treatment with AMG (75, 150 and 300 mg/kg) for 7 d did not induce any appreciable mucosal damage, and the average score was not significantly different from that of normal mice. In contrast, tolmetin (90 mg/kg) produced significant gastric mucosal lesions compared with the normal group ($P < 0.01$). AMG (75, 150 and 300 mg/kg) significantly reduced the severity of gastric lesions induced by ethanol in a dose-dependent manner as compared with the model group ($P < 0.05$, AMG 75 and 150 mg/kg vs model; $P < 0.01$, AMG 300 mg/kg vs model). Light and electron microscopy revealed that AMG (150 and 300 mg/kg) induced minimal changes in the surface epithelium layer, without vascular congestion or leucocyte adherence. AMG (75, 150 and 300 mg/kg) demonstrated dose-dependent gastroprotective effects on mice in our

study. AMG (75, 150 and 300 mg/kg) could significantly increase NO content and NOS level in the stomach homogenates of mice compared with the model group ($P < 0.05$, AMG 75 mg/kg and 150 mg/kg groups vs model group; $P < 0.01$, AMG 300 mg/kg vs model group) respectively. Moreover, AMG (150 and 300 mg/kg) not only significantly increased SOD activities but also obviously decreased the MDA content in the stomach homogenates of mice.

CONCLUSION: AMG exerts significant gastroprotective actions on mice and the involved mechanisms may be its antioxidative effect and induction of NO production.

Li YH, Li J, Huang Y, Lü XW, Jin Y. Gastroprotective effect and mechanism of amtolmetin guacyl in mice. *World J Gastroenterol* 2004; 10(24): 3616-3620

<http://www.wjgnet.com/1007-9327/10/3616.asp>

INTRODUCTION

Nonsteroidal anti-inflammatory drugs (NSAIDs) are the extensively utilized medicines worldwide with antipyretic, analgesic and anti-inflammatory properties. Besides the direct stimulation, NSAIDs have some other adverse reactions to the gastrointestinal system, such as nausea, vomit, bellyache and even ulcer, perforation. All these effects are considered to be associated with the inhibition of prostaglandin (PG) synthesis in gastrointestinal system, and thereby limiting the clinical application of NSAIDs^[1-7].

Amtolmetin guacyl (AMG) is a novel NSAID, and its chemical name is 2-methoxyphenyl-1-methyl-5-p-methylbenzoyl-pyrrol-2-acetamido acetate, whose metabolites are MED5 (chemical name: 1-methyl-5-p-methylbenzoyl-pyrrol-2-acetamido acetic acid) and tolmetin (TOL)^[8-12]. As a novel NSAID, it has been reported that AMG possesses antipyretic, analgesic and anti-inflammatory effects in previous studies^[13-20]. At the same time, it can also enhance the NOS activity of gastric mucosae, which facilitates the synthesis and release of NO so as to reduce the gastrointestinal system damage^[21-23].

In this study, normal and ethanol-induced gastric mucosal lesion models in mice were established to investigate the gastroprotective effect and associated mechanisms, which could guide the rational use of medicine in clinical practice.

MATERIALS AND METHODS

Materials

Male and female Kunming strain mice, weighing 18-22 g, were purchased from Animal Center of Anhui Medical University. They were housed in plastic boxes, 5 mice in each box. All mice were allowed to take food and tap water *ad libitum*. AMG and TOL were provided by Anhui Kelong Medicine Company. The assay kits of MDA, SOD, NOS and Coomassie brilliant blue reagents were obtained from Nanjing Jiancheng Bioengineering Institute (Nanjing, China). All experimental protocols described

in this study were approved by the Ethics Review Committee for Animal Experimentation of Anhui Medical University.

Gastric mucosal damage after repeated treatment with AMG^[21]

The mice were equally divided into 5 groups randomly: normal group, 3 AMG groups (3 different doses) and TOL group. The mice in AMG groups intragastrically received 75, 150 or 300 mg/kg of AMG a day through an 18-gauge stainless steel animal feeding needle for 7 d prior to the experiment. Similarly, the mice in TOL group intragastrically received 90 mg/kg of TOL a day. In normal group, the mice were only fed with the same volume (0.5 mL/mouse) of carboxymethylcellulose (CMC). On the seventh day, all the mice were sacrificed by cervical dislocation and the stomachs were removed, opened along the great curvature and examined for the macroscopic evaluation of gastric mucosae. The severity of gastric mucosal lesions was examined by an experienced histologist who was unaware of the treatment conditions.

Establishment of ethanol-induced gastric mucosal damage model and drug treatment^[21,24]

The mice were randomly divided into six groups as follows: normal group, model group, 3 AMG groups receiving 75, 150 and 300 mg/kg, respectively, and TOL group receiving 90 mg/kg, ten mice in each group. The 5 groups were intragastrically administered AMG, TOL and CMC (model group) once. One hour later, the animals received 500 mL/L ethanol (0.5 mL/mouse) intragastrically except normal group mice. One hour later, the animals were killed and the stomachs were removed. The severity of gastric mucosal lesions and histological assessments were made by an experienced histologist who was unaware of the treatment conditions.

Grading criteria of gastric mucosal damage^[21]

The animals were killed, the stomachs were removed, rinsed with 5 mL of saline and immersed in 100 mL/L formalin. They were later opened along the greater curvature, for the macroscopic evaluation of gastric mucosae^[21,24]. The severity of lesions was scored from 0 to 5: 0, normal; 0.5, light local reddening; 1, general reddening or small hemorrhage (<1 mm); 2, large hemorrhage (>1 mm); 3, small ulcer (<2 mm); 4, large ulcer (>2 mm); and 5, perforated ulcer. One score was assigned to each lesion. A researcher who was unaware of the treatment conditions gave the scores of gastric mucosal injury.

Microscopic assessment of gastric lesions^[21]

Light microscopy At the end of the experiment, the stomach was immediately exposed and a small strip was excised from the glandular portion, 3 mm below and parallel to the limiting ridge, so that the greater curvature was approximately located in the middle of the strip. The tissue samples were fixed in 100 mL/L formalin, 5- μ m thick serial sections were taken from each block and stained with hematoxylin-eosin. The image of the sections to be examined was displayed on a color monitor by means of a videocamera attached to the microscope. An experienced histologist who was unaware of the treatment conditions made histological assessments.

Transmission electron microscopy After mice were killed, the stomachs were immediately removed, and a strip was excised in the same position as for light microscopy. Small specimens were fixed in 25 g/L glutaraldehyde liquid for 3 h at room temperature and post-fixed in 10 g/L OsO₄ in 0.1 mol/L phosphate buffer (pH 7.2) for 90 min at room temperature. After dehydration in a graded series of acetone and embedded in Araldite resin, semithin sections were cut for orientation. Thin sections (80 nm thick) were cut perpendicularly to the luminal

surface, stained with uranyl acetate and lead citrate, and examined with a Zeiss109 electron microscope. An experienced histologist who was unaware of the treatment conditions made histological assessments.

Tissue homogenization

Stomach tissue samples were weighed and homogenized in 9 g/L NaCl for the detection of SOD, MDA, NOS, NO₂⁻. Homogenates were centrifuged at 4 000 r/min for 10 min. Aliquots of the supernatants were used for studies. The assayed parameters were expressed as per mg protein, and the protein content of aliquots was determined by the method of Coomassie brilliant blue.

Measurement of MDA, SOD and NOS in stomach homogenates^[25]

SOD, MDA and NOS levels in stomach tissue homogenates were assayed by using assay kits (Nanjing Jiancheng Bioengineering Institute).

Examination of NO₂⁻

NO₂⁻ concentration in stomach tissue homogenates was measured as described by Prado *et al.*^[26].

Statistical analysis

The data were analyzed by SPSS 10.0 for windows. Results were expressed as mean \pm SD. Student's *t* test was used for statistical analysis. *P*<0.05 was considered statistically significant.

RESULTS

Repeated treatment with AMG on gastric mucosal damage in normal mice

Repeated treatment with AMG (75, 150 and 300 mg/kg) for 7 d did not induce any appreciable mucosal damage, and the average score was not significantly different from that of normal mice. In contrast, TOL, the prodrug of AMG, intragastrically administered at 90 mg/kg produced significant gastric mucosal lesions compared with the normal group (*P*<0.01) (Figure 1).

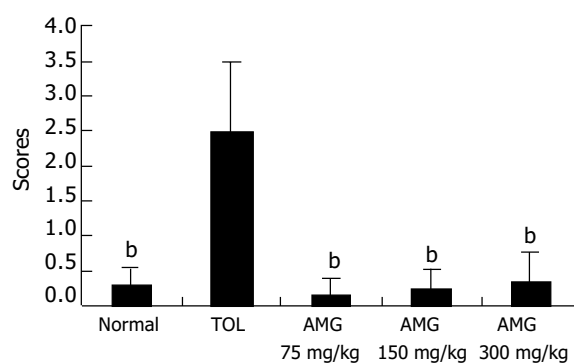


Figure 1 Repeated treatment with AMG on gastric mucosal damage in normal mice (*n* = 10). ^b*P*<0.01 vs TOL.

Effect of AMG on ethanol-induced gastric mucosal damage model

As showed in Figure 2, compared with that in the normal group, the average score of mice in the model group significantly increased (*P*<0.01). AMG (75, 150 and 300 mg/kg) significantly reduced the severity of gastric lesions induced by ethanol in a dose-dependent manner as compared with the model group (*P*<0.05, AMG 75 and 150 mg/kg vs model; *P*<0.01, AMG 300 mg/kg vs model). There was no obvious difference between TOL group and model group (Figure 2).

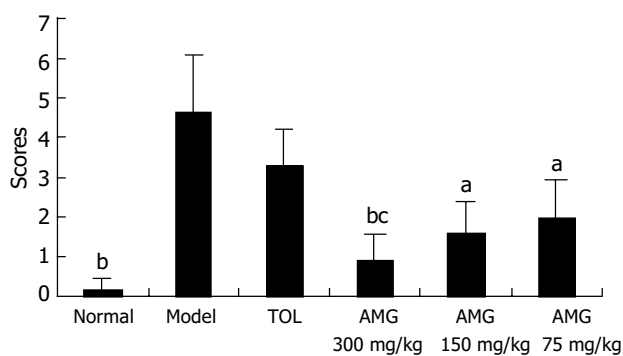


Figure 2 Effect of AMG on ethanol-induced gastric mucosal damage model ($n = 10$). ^a $P < 0.05$, ^b $P < 0.01$ vs model; ^c $P < 0.05$, AMG (300 mg/kg) vs TOL.

Microscopic assessment of AMG on ethanol-induced gastric lesion

Light microscopy As shown in Figure 3 for evaluation by light microscopy, the structure of gastric mucosae was normal in normal group. The cells were well stained by HE and there was no edema or exfoliation. In contrast, a visible hemorrhagic area was found in model group. In mice treated with AMG (300 mg/kg), the epithelial and parietal cells were slightly edematous with few epithelial cells exfoliated. In the group treated with AMG (150 mg/kg), severe edema was found with inflammatory cell infiltration. In the group administered AMG (75 mg/kg), edema was more severe in epithelial and parietal cells than that in AMG (300 mg/kg) group and many epithelial cells were deciduous. Conversely, in the TOL group, together with inflammatory cell infiltration, a hemorrhagic area was observed (Figure 3A).

Transmission electron microscopy As shown in Figure 4, gastric mucosal microvilli in normal group were well arranged with no deflection and shorting, while those in the model and TOL groups were mostly deciduous, broken and defective. The microvilli were almost integrated and well arranged with no deflection in mice treated with AMG (300 mg/kg). In mice administered AMG (150 mg/kg), the lesions were much smaller, while the microvilli were short and small and in a bad order with obvious deflection in mice treated with AMG (75 mg/kg) (Figure 3B).

Effects of AMG on NOS level and NO content in ethanol-induced stomach homogenates

Compared with those in the normal group, the NO content and NOS level were significantly decreased in the model group ($P < 0.01$). AMG (75, 150 and 300 mg/kg) could significantly increase the decreased NO content and NOS level compared with the model group ($P < 0.05$, AMG 75 mg/kg and 150 mg/kg groups vs model group; $P < 0.01$, AMG 300 mg/kg vs model group) respectively. The NO content and NOS level in TOL group where not evidently different from those in the model group (Table 1).

Table 1 Influence of AMG on NO and NOS contents in stomach homogenates in ethanol-induced gastric mucosal damage models ($n = 10$, mean \pm SD)

Group	n	Dose (mg/kg)	NO ₂ (μ mol/mgprot)	NOS (U/mgprot)
Normal	10	-	60.57 \pm 22.11 ^b	4.22 \pm 0.92 ^b
Model	10	-	33.08 \pm 12.85	2.41 \pm 0.56
TOL	10	90	46.46 \pm 12.69	3.27 \pm 0.68
AMG	10	300	70.37 \pm 27.97 ^b	5.25 \pm 1.62 ^b
	10	150	58.65 \pm 17.11 ^a	4.12 \pm 1.02 ^a
	10	75	30.98 \pm 11.97	3.47 \pm 1.17 ^a

^a $P < 0.05$, ^b $P < 0.01$, vs Model.

Effects of AMG on SOD activity and MDA content in ethanol-induced stomach homogenates

Results are shown in Table 2. Compared with that in the normal group, the SOD activity in the model group was significantly lower, but the MDA content in the model group was increased ($P < 0.01$). However, compared with model group, AMG (150 and 300 mg/kg) could significantly increase the SOD activity while evidently reduce the MDA level in stomach homogenates ($P < 0.01$, Table 2).

Table 2 Influence of AMG on SOD, MDA contents in stomach homogenates in ethanol-induced gastric mucosal damage models ($n = 10$, mean \pm SD)

Group	n	Dose (mg/kg)	SOD (U/mgprot)	MDA (nmol/mgprot)
Normal	10	-	702.61 \pm 144.77 ^b	2.85 \pm 1.32 ^b
Model	10	-	551.94 \pm 125.94	4.18 \pm 1.19
TOL	10	90	526.14 \pm 110.80	5.07 \pm 2.09
AMG	10	300	624.97 \pm 117.19 ^a	3.13 \pm 1.35 ^a
	10	150	612.06 \pm 101.90 ^a	3.46 \pm 1.21 ^a
	10	75	606.13 \pm 65.81	3.57 \pm 1.05

^a $P < 0.05$, ^b $P < 0.01$, vs Model.

DISCUSSION

Gastrointestinal system lesions are resulted from the major adverse reaction of NSAIDs, which limits the wide clinical application of NSAIDs. Though the mechanism of the lesion remains unclear, some documents have proposed that these effects are related with the inhibition of PGs releasing from the mucosal epithelial cells^[1,3,27]. It is known that vascular damage is considered to be the earliest process of gastric mucosal ulcer. Vasodilators, such as PGs and NO, play an important role in gastroprotection. At present, NO, gastroprotective NSAIDs, specific cyclooxygenase-2 (COX-2) inhibitors as well as COX and 5-lipoxygenase (5-LOX) double inhibitors are used in reducing the adverse reactions of NSAIDs^[28,29].

It has been demonstrated that AMG has gastroprotective properties^[21-23]. Tubaro *et al.*^[30] found that repeated treatment with AMG did not induce gastric mucosa damage. Another animal experiment indicated that AMG (50-300 mg/kg ig) did not induce stomach lesions in rats, while its metabolite TOL (15-60 mg/kg ig) did in a dose-dependent manner^[21]. Light and electron microscopic assessment suggested that AMG only caused very slight epithelial cell changes without vascular congestion and WBC adherence.

In our study, the 7-d treatment with AMG (75, 150 and 300 mg/kg ig) did not induce any appreciable mucosal damage, and the score was not different from that of normal group, while TOL (90 mg/kg ig) produced severe gastric mucosal lesions compared with normal group. Compared to its metabolite TOL, AMG had obvious gastroprotective effects. In ethanol-induced gastric mucosal damage model, the scores of AMG (75, 150 and 300 mg/kg ig) obviously decreased in a dose-dependent fashion. Compared to that in TOL group, the scores in AMG (300 mg/kg) group were greatly decreased. Furthermore, the scores had no obvious difference between TOL and model groups. Microscopic assessment of ethanol-induced gastric lesions showed that the degree of gastric damages in AMG (300 mg/kg) group was smaller than that in TOL and model groups, indicating the effect of AMG on gastric mucosa. Ultrastructural studies suggested that the microvilli were almost integrated and well arranged with no deflection in mice treated with AMG (300 mg/kg), but those in the model and TOL groups were mostly deciduous, broken and defective.

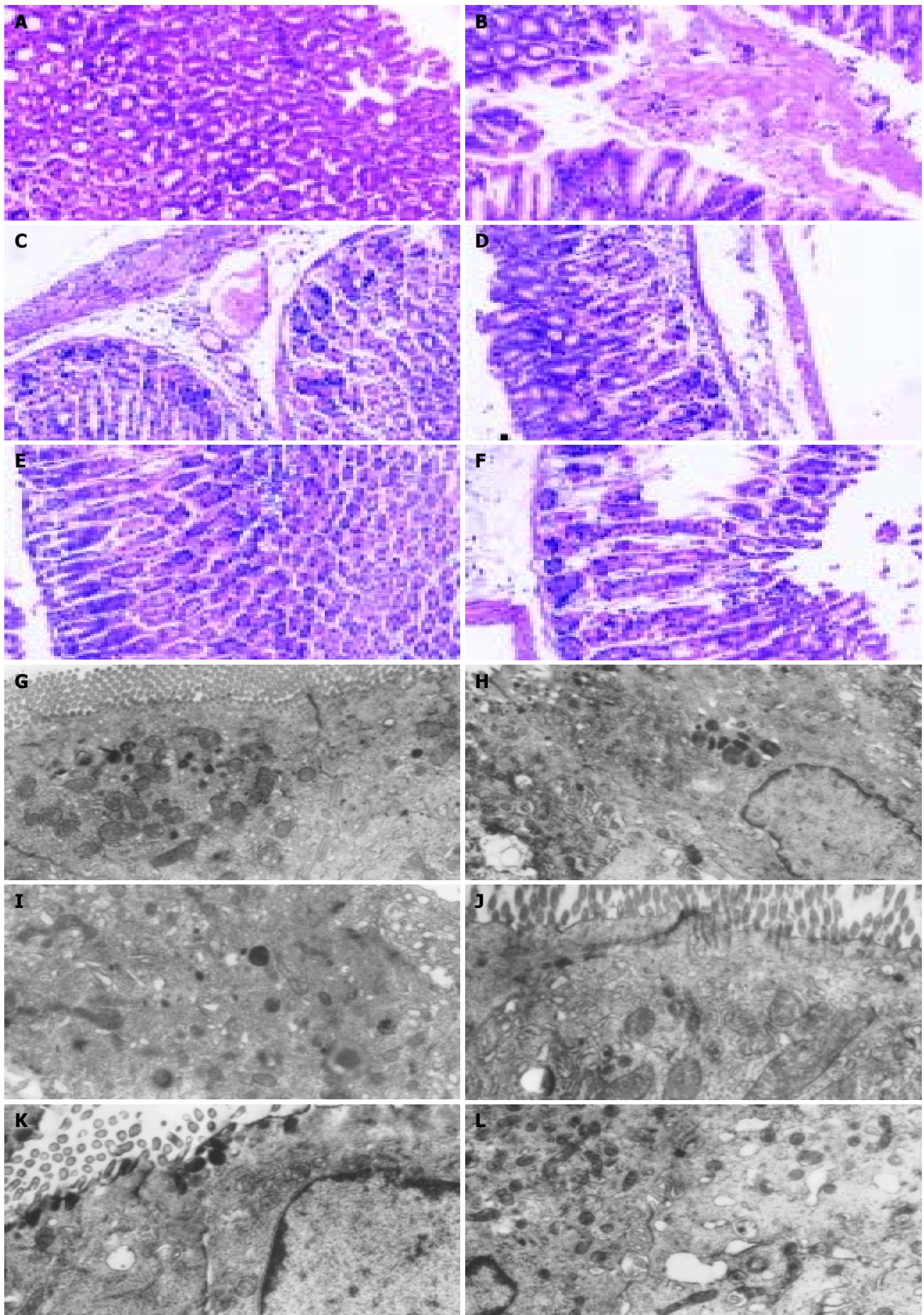


Figure 3 Light and electronic microscopy assessments of ethanol-induced gastric lesion. A: light microscopy assessment of ethanol-induced gastric lesion ($\times 100$). A: normal group, B: model group, C: ToL group, D: AMG (300 mg/kg) group E: AMG (150 mg/kg) group, F: AMG (75 mg/kg) group. B: Electronic microscopy assessment of ethanol-induced gastric lesion ($\times 6000$) G: normal group, H: model group, I: TOL group, J: AMG (300 mg/kg) group, K: AMG (150 mg/kg) group, L: AMG (75 mg/kg) group.

Tubaro *et al.*^[30] found that AMG could strongly inhibit the hydrochloric acid (HCl) excretion caused by histamine so as to exert gastroprotective effects. Compared with acetylsalicylic acid, AMG (50 mg/kg ig) caused no appreciable change in basal potential difference (PD) values in gastric mucosae. AMG (100 mg/kg ig) alleviated ethanol-induced damages, increased NOS activity and stimulated NO release, and thereby showing its gastric protective effect. A research showed that the nonspecific NOS inhibitor (L-NAME 10 mg/kg sc) could reverse the effect of AMG^[21]. Therefore, we concluded that the protective effect of AMG might be involved in NO release from gastric epithelial cells. In our study, AMG (75, 150 and 300 mg/kg) could significantly increase the NO content and NOS level in ethanol-induced gastric mucosal damage model group. These results suggested that the gastroprotective effect of AMG might be associated with promotion of NOS activity and induction of NO release, which is in agreement with previous reports^[21,31].

Moreover, it has been reported that ethanol is capable of generating oxygen radicals, inhibiting glutathione synthesis, producing glutathione loss from tissues, increasing MDA levels and impairing antioxidative defense systems in experimental animals. Our study also showed that AMG (150 and 300 mg/kg) could sharply decrease the increased MDA level while enhance the decreased SOD activity in the models of mice, suggesting that the gastroprotective effect of AMG could at least partly contribute to the antioxidative action, which has not been reported before.

In summary, AMG has significant gastroprotective effects in mice, and its mechanism may be associated with its antioxidative effect and promotion of NO release.

REFERENCES

- Wallace JL. NSAID gastroenteropathy: past, present and future. *Can J Gastroenterol* 1996; **10**: 451-459
- Yoshitani K, Kawaguchi M, Tatsumi K, Sasaoka N, Kurumatani N, Furuya H. Intravenous administration of flurbiprofen does not affect cerebral blood flow velocity and cerebral oxygenation under isoflurane and propofol anesthesia. *Anesth Analg* 2004; **98**: 471-476
- Garcia Rodriguez LA, Hernandez-Diaz S. Risk of uncomplicated peptic ulcer among users of aspirin and nonaspirin nonsteroidal antiinflammatory drugs. *Am J Epidemiol* 2004; **159**: 23-31
- Sinatra RS, Shen QJ, Halaszynski T, Luther MA, Shaheen Y. Preoperative rofecoxib oral suspension as an analgesic adjunct after lower abdominal surgery. *Anesth Analg* 2004; **98**: 135-140
- Kolesnikov YA, Wilson RS, Pasternak GW. The synergistic analgesic interactions between hydrocodone and ibuprofen. *Anesth Analg* 2003; **97**: 1721-1723
- Fries JF, Bruce B. Rates of serious gastrointestinal events from low dose use of acetylsalicylic acid, acetaminophen, and ibuprofen in patients with osteoarthritis and rheumatoid arthritis. *J Rheumatol* 2003; **30**: 2226-2233
- Dominick KL, Dudley TK, Grambow SC, Oddone EZ, Bosworth HB. Racial differences in health care utilization among patients with osteoarthritis. *J Rheumatol* 2003; **30**: 2201-2206
- Annuziato L, di Renzo G. A bioequivalence study in man of table and capsule formulations of the nonsteroidal anti-inflammatory compound 2-methoxyphenyl 1-methyl-5-(p-methylbenzoylpyrrol)-2-acetamidoacetate. *Clin Ter* 1993; **142**: 3-10
- Bianchi PG, Montrone F, Lazzaroni M, Manzionna G, Caruso I. Clinical and gastroscopic evaluation of amtolmetin guacyl versus diclofenac in patients with rheumatoid arthritis. *Ital J Gastroenterol Hepatol* 1999; **31**: 378-385
- Arrigoni-Martelli E. Profile of activity of a new anti-inflammatory agent, ST679 (MED15). *Drugs Exp Clin Res* 1990; **16**: 63-66
- Mancinelli A, Bruno G, Cardace G, Morabito E, Marzo A, Arrigoni Martelli E. High-performance liquid chromatographic evaluation of MED15 and its metabolites MED5 and tolmetin in rat plasma. *J Chromatogr* 1991; **553**: 81-86
- Annuziato L, di Renzo G. A bioequivalence study in man of tablet and capsule formulations of the nonsteroidal anti-inflammatory compound 2-methoxyphenyl 1-methyl-5-(p-methylbenzoylpyrrol)-2-acetamidoacetate. *Clin Ter* 1993; **142**: 3-10
- Coruzzi G, Bertaccini G. Gastric effects of the novel non-steroidal anti-inflammatory drug amtolmetin guacyl. *Nutrition* 1999; **15**: 325-326
- Nanni G, Sarro G, Antoci G, Bianchi P, Gossetti F, Catarci M, La Pinta M, Negro P, Nolf G. The drug treatment of postoperative pain. *Clin Ter* 1993; **142**: 41-46
- Nappi C, Nolf G, La Pinta M, Colace G, Ruotolo C, Affinito P. The treatment of postoperative pain in obstetrical-gynecologic surgery. A comparative study between ST-679 and paracetamol. *Clin Ter* 1993; **142**: 47-52
- De Santis E, La Pinta M, Nolf G. An evaluation of the analgesic activity and tolerance of ST-679 in patients with pain following orthopedic and traumatological interventions. *Clin Ter* 1993; **142**: 53-59
- Donati G, Spinazze R. A clinical study to determine the optimal dosage of st-679 in the treatment of rheumatic diseases. *Clin Ter* 1993; **142**: 19-28
- Lingetti M, Ciarimboli M, Porfido FA, Imperato L, Sorrentino GP, Garzya G, Saraceni G, Donati G, Nolf G. An evaluation of the therapeutic activity and tolerance of ST-679 in patients with osteoarthritis at different sites. A controlled double-blind study vs tolmetin. *Clin Ter* 1993; **142**: 29-40
- Meloni P, Demuro G, Cara L, Garau D, Uras G, Suddu L. Evaluation of the effectiveness and tolerability of MED15 vs piroxicam in patients with acute epicondylitis. *Clin Ter* 1995; **146**: 453-456
- Alicicco E, Delfino M, Kleszczynski D. Clinical trial comparing a new NSAID with 2 different dosages and diclofenac in patients with arthralgia in acute phase. *Clin Ter* 1995; **146**: 595-601
- Pisano C, Grandi D, Morini G, Coppelli G, Vesci L, Lo Giudice P, Pace S, Pacifici L, Longo A, Coruzzi G, Carminati P. Gastroprotective effect of new anti-inflammatory drug amtolmetin guacyl in the rat: involvement of nitric oxide. *Dig Dis Sci* 1999; **44**: 713-724
- Tubaro E, Belogi L, Mezzadri CM, Bettelli E. Impact on the bowel of amtolmetin guacyl, a new gastroprotective non-steroidal anti-inflammatory drug. *Eur J Pharmacol* 2003; **476**: 173-183
- Riezzo G, Chiloiro M, Montanaro S. Protective effects of amtolmetin guacyl versus placebo diclofenac and misoprostol in healthy volunteers evaluated as gastric electrical activity in alcohol-induced stomach damage. *Dig Dis Sci* 2001; **46**: 1797-1804
- Xia M, Tao JY. Pathogenesis of ethanol induced gastric mucosal lesion in mice. *Xin Xiaohuabingxue Zazhi* 1997; **5**: 211-212
- Yao HW, Li J, Jin Y, Zhang YF, Li CY, Xu SY. Effect of leflunomide on immunological liver injury in mice. *World J Gastroenterol* 2003; **9**: 320-323
- Prado WA, Schiavon VF, Cunha FQ. Dual effect of local application of nitric oxide donors in model of incision pain in rats. *Eur J Pharmacol* 2002; **441**: 57-65
- Villegas I, La Casa C, de la Lastra CA, Motilva V, Herreri;as JM, Martin MJ. Mucosal damage induced by preferential COX-1 and COX-2 inhibitors: Role of prostaglandins and inflammatory response. *Life Sci* 2004; **74**: 873-884
- Bonabello A, Galmozzi MR, Canaparo R, Isaia GC, Serpe L, Muntoni E, Zara GP. Dexibuprofen (S+-isomer ibuprofen) reduces gastric damage and improves analgesic and anti-inflammatory effects in rodents. *Anesth Analg* 2003; **97**: 402-408
- Morini G, Guaita E, Lazzaretti M, Grandi D, Coruzzi G. Morphological features of rat gastric mucosa after acute and chronic treatment with amtolmetin guacyl: comparison with non-selective and COX-2-selective NSAIDs. *Digestion* 2003; **68**: 124-132
- Tubaro E, Belogi L, Mezzadri CM. The mechanism of action of amtolmetin guacyl, a new gastroprotective nonsteroidal anti-inflammatory drug. *Eur J Pharmacol* 2000; **387**: 233-244
- Coruzzi G, Coppelli G, Spaggiari S, Cavestro GM, Okolicsanyi L, Lo Giudice P, Pisano C, Tepperman BL. Gastroprotective effects of amtolmetin guacyl: a new non-steroidal anti-inflammatory drug that activates inducible gastric nitric oxide synthase. *Dig Liver Dis* 2002; **34**: 403-410

Dynamic changes in the expression of matrix metalloproteinases and their inhibitors, TIMPs, during hepatic fibrosis induced by alcohol in rats

Guang-Fu Xu, Peng-Tao Li, Xin-Yue Wang, Xu Jia, De-Lu Tian, Liang-Duo Jiang, Jin-Xiang Yang

Guang-Fu Xu, Department of infectious Diseases, 1st Affiliated Dongzhimen Hospital, Beijing University of Traditional Chinese Medicine, Beijing 100700, China

Xin-Yue Wang, De-Lu Tian, Liang-Duo Jiang, Jin-Xiang Yang, Department of Digestive Diseases, 1st Affiliated Dongzhimen Hospital, Beijing University of Traditional Chinese Medicine, Beijing 100700, China

Peng-Tao Li, Xu Jia, Basic Medicine College of Beijing University of Traditional Chinese Medicine, Beijing 100029, China

Correspondence to: Director. Guang-Fu Xu, Department of Infectious Diseases, 1st Affiliated Dongzhimen Hospital, Beijing University of Traditional Chinese Medicine, Beijing 100700, China. guangfuxu@hotmail.com

Telephone: +86-10-84290755

Received: 2003-09-07 **Accepted:** 2003-11-06

Abstract

AIM: To determine the dynamic changes in the expression of matrix metalloproteinases (MMPs) and the endogenous tissue inhibitors of MMPs inhibitors (TIMPs) during hepatic fibrosis induced by alcohol.

METHODS: Male Sprague-Dawley rats were randomly divided into normal, 4 d, 2 wk, 4 wk, 9 wk and 11 wk groups, and the model rats were fed with a mixture of alcohol by gastric infusion at the designed time, respectively, then decollated and their livers were harvested for the examination of MMP-2, MMP-3, MMP-9, MMP-13, TIMP-1 and TIMP-2 by immunohistochemistry, zymography and Western blotting, respectively.

RESULTS: Normal rats had moderate expression of MMP-2, which was decreased in the model rats except in the 11 wk group, where MMP-2 expression slightly increased. MMP-3 had the similar changing pattern to MMP-2 despite weaker expression. MMP-9 expression decreased in the 4 d and 2 wk groups, rose in the 4 wk group, decreased again in the 9 wk group and returned to normal levels in the 11 wk group. MMP-13 expression decreased in the 4 d and 2 wk groups, and returned to normal levels in the 4 wk, 9 wk and 11 wk groups. TIMP-1 expression decreased in the 4 d and 2 wk groups, but sharply increased in the 4 wk group and sustained at a high level even after modeling was stopped for 2 wk. In normal rats TIMP-2 expression was strong. However, it decreased as soon as modeling began, and then gradually rose, but remained to a level lower than that in normal rats even after modeling was stopped for 2 wk.

CONCLUSION: MMP-2 may not always expresses at a high level during hepatic fibrosis. MMP-13 and MMP-3 are acutely affected by TIMP-1. In this model TIMP-1 is the most powerful factor imposed on capillarization and peri-sinusoidal fibrosis. TIMP-2 is the most effective regulator on the metabolism of type IV collagen located in the basement of sinus.

Xu GF, Li PT, Wang XY, Jia X, Tian DL, Jiang LD, Yang JX. Dynamic changes in the expression of matrix metalloproteinases and their inhibitors, TIMPs, during hepatic fibrosis induced by alcohol in rats. *World J Gastroenterol* 2004; 10(24): 3621-3627 <http://www.wjgnet.com/1007-9327/10/3621.asp>

INTRODUCTION

China's prosperity is accompanied with a dramatic rise in cases of alcoholic liver disease. Some scholars reported that hepatic pathological changes of alcoholic liver disease (ALD) included typical capillarization, peri-sinusoidal fibrosis, bridging fibrosis, and even cirrhosis which were often found in heavy drinkers who might have a drinking history over 10 to 20 years. In mild to moderate drinkers, however, the pathological changes which might be more popular at present were not thoroughly investigated. In order to probe into this field we improved a rat model of ALD induced by the gavage method, which is widely used among Chinese scholars to show the key mechanism of hepatic fibrosis. Liver fibrosis occurs as a consequence of net accumulation of matrix proteins (especially types I and III collagen) in response to liver injury. Liver fibrosis is underpinned by the activation of hepatic stellate cells (HSCs) to a myofibroblast like phenotype with a consequent increase in their synthesis of matrix proteins such as interstitial collagens that characterize fibrosis. The sinusoid and peri-sinusoidal space are the original site of fibrosis, which can badly affect the function of hepatocytes. The expression and ratio of matrix metalloproteinases/tissue inhibitor of matrix metalloproteinases (MMPs/TIMPs) are key factors to extra cellular matrix remodeling during hepatic fibrosis. The co-operation of urokinase and tissue plasminogen activator system is also very important. Considering that recent reports were almost all focused on MMPs/TIMPs, and that the dynamic changes of MMPs/TIMPs during ALD were not so clear, we decided to probe into such indexes. We have reported the early pathological changes of alcoholic liver disease located in sinusoid and peri-sinusoid (in another article), further elucidation of mechanism of such changes would depend on the investigation of the expression and ratio of MMPs/TIMPs during a dynamic course of fibrosis. So the dynamic changes of MMPs 2, 3, 9, 13, and TIMPs 1, 2 were worked out to show the mechanism of this new model.

MATERIALS AND METHODS

Materials

Male SD rats, weighing (150±5) g, were purchased from Beijing Vital River Company, corn oil from Carrefour Supermarket, xanthan gum and maltose from Beijing Chemical Agent Company, edible alcohol from Beijing General Alcohol Brewing Company, carbonyl iron and pirazole from Sigma, USA, First antibody for MMPs 2, 3, 9, 13 and TIMPs 1, 2 was purchased from Antibody Diagnostic Inc, ADI, USA with the help of its Chinese Dealer, Shanghai Long Island Antibody Company. PV-6 001 kits were from PowerVision, USA. ZLI-9 030 and ZLI9 001 were from Beijing Zhongshan Company.

Methods

Rats grouping: Normal (6), 4 d (8), 2 wk (8), 4 wk (10), 9 wk (12), 11 wk (12).

Modeling: The model of ALD was induced by intragastric infusion (gavage) of a mixture of alcohol (5g/d-kg), pirazole (30 mg/d-kg), corn oil (3 mL/d-kg), and carbonyl iron (35 mg/d-kg, decreased to 15 mg after 4 wk), a little xanthan gum and maltose, one time a day for 5 d consecutively, with 2 d off per week, until

the end of the ninth wk, and all rats were maintained on a standard diet with water *ad libitum*.

Liver tissue management: The rats were executed at the end of 4 d, 2 wk, 4 wk, 9 wk and 11 wk, respectively. Harvested livers were split and fixed for electron microscopy, hematoxylin and eosin and Masson complex staining, and a portion was snap frozen for biochemical and molecular analysis. Further sections were cut from each liver, deparaffinized, HE and Masson staining. Histological analysis of each liver was undertaken, then the sections subjected to amylopin antigen retrieval before stained with the two-step method for antigen MMPs 2, 3, 9, 13 and TIMPs 1 and 2. The semi-quantitative computations were conducted on the image analyzing system MIS-2000 from 3Y Company, USA. The activity of MMP-2 and MMP-9, Western blotting of TIMPs 1 and 2 were undertaken with Bio-Rad Electrophoresis System, pictures were taken and analyzed with

Image master VDS from Pharmacia Biotech Company.

Statistical analysis

All values were expressed as mean \pm SD. ANOVA was used to determine the significance of differences among the six groups. $P < 0.05$ was considered statistically significant.

RESULTS

The expression of MMP-2 in normal rats was at moderate level. However, during modeling it showed reducing curve changes and without recovery even after modeling was stopped for 2 wk. (Figure 1).

The expression of MMP-3 showed a similar pattern to that of MMP-2 but weaker, when modeling was stopped it recovered to normal level. (Figure 2).

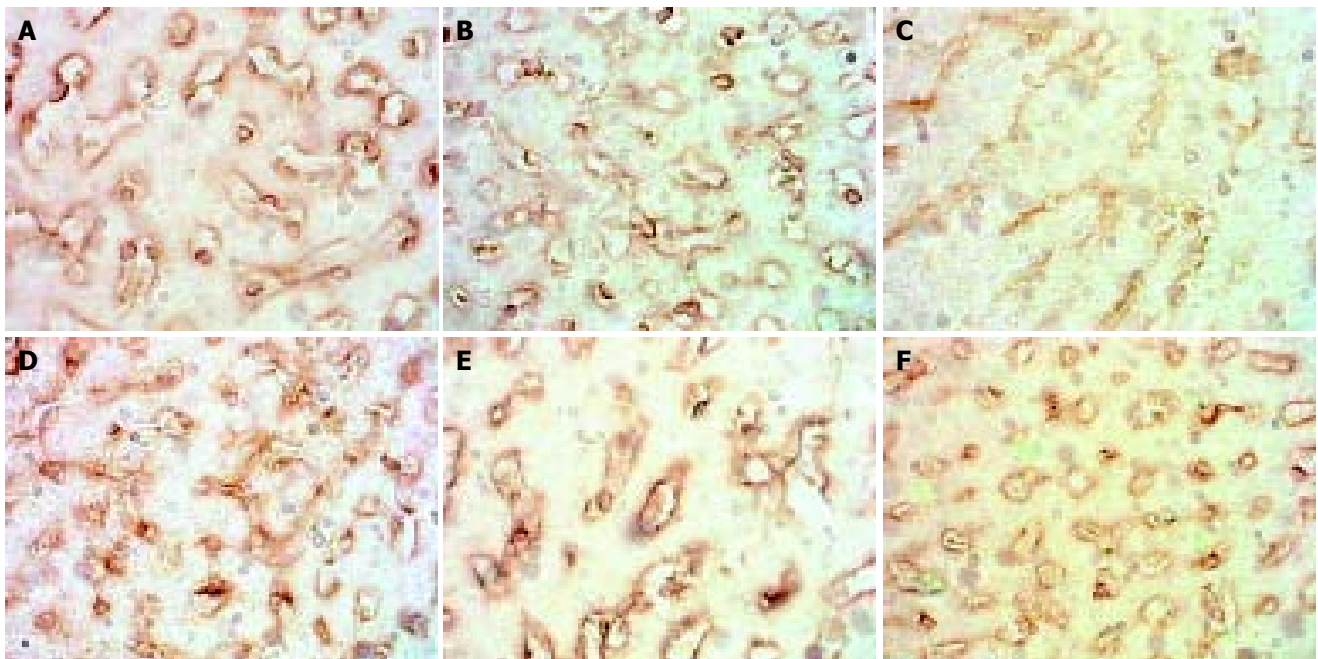


Figure 1 Dynamic changes of MMP-2. A: Normal rat, $\times 400$ B: 4 d group, $\times 400$ C: 2 wk group, $\times 400$ D: 4 wk group, $\times 400$. E: 9 wk group, $\times 400$ F: 11 wk group, $\times 400$.

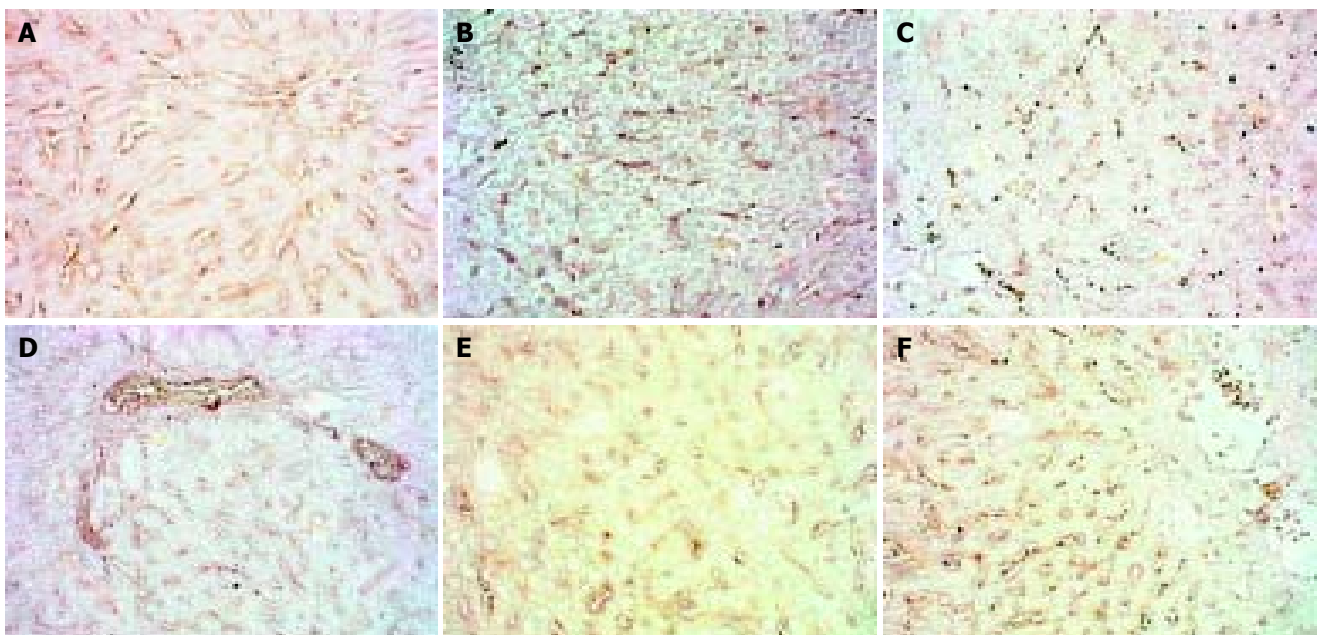


Figure 2 Dynamic changes of MMP-3. A: Normal rat, $\times 200$ B: 4 d group, $\times 200$ C: 2 wk group, $\times 200$ D: 4 wk group, $\times 200$. E: 9 wk group, $\times 200$ F: 11 wk group, $\times 200$.

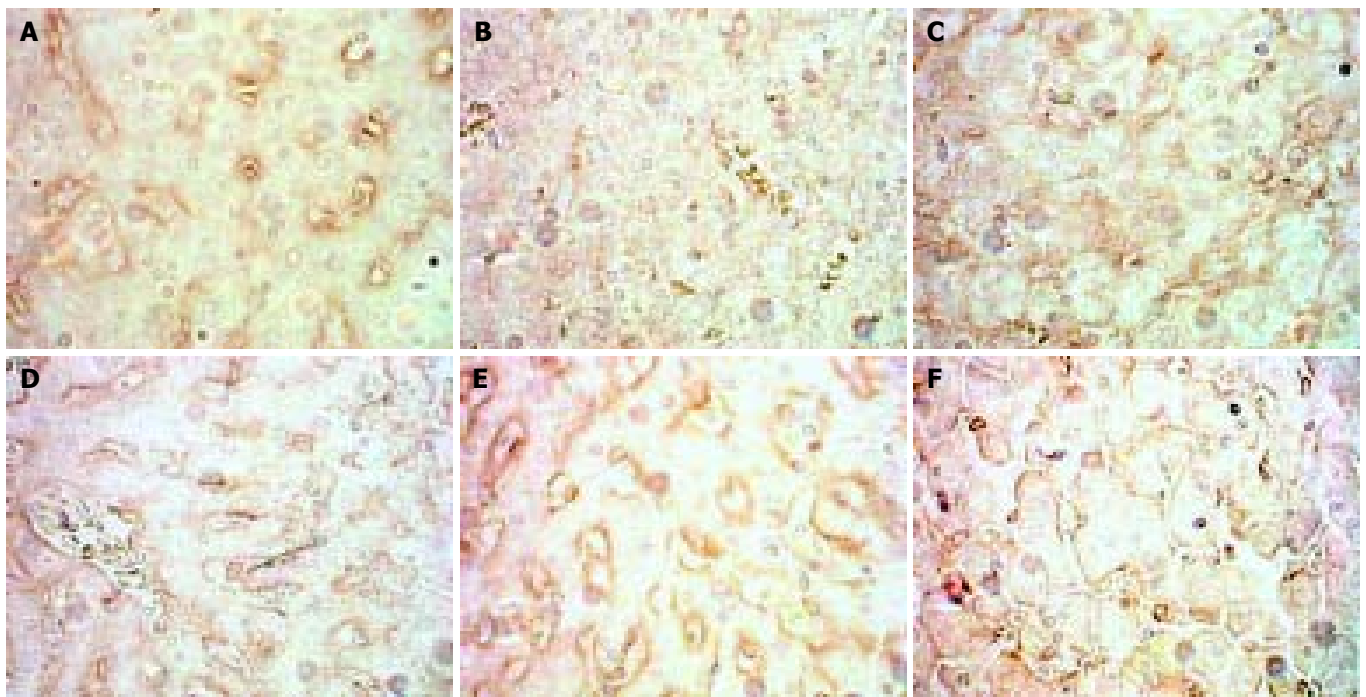


Figure 3 Dynamic changes of MMP-9. A: Normal rat, $\times 400$ B: 4 d group, $\times 400$ C: 2 wk group, $\times 400$ D: 4 wk group, $\times 400$ E: 9 wk group, $\times 400$ F: 11 wk group, $\times 400$.

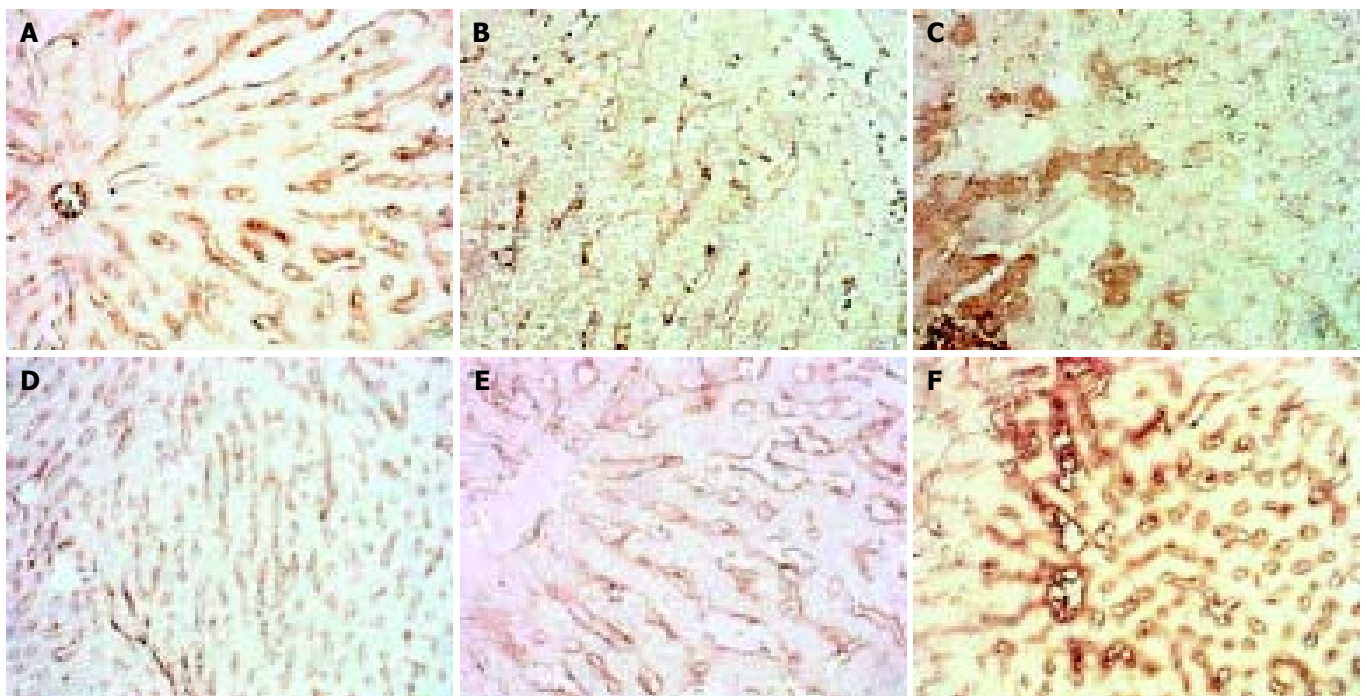


Figure 4 Dynamic changes of MMP-13. A: Normal rat, $\times 200$ B: 4 d group, $\times 200$ C: 2 wk group, $\times 200$ D: 4 wk group, $\times 200$ E: 9 wk group, $\times 200$ F: 11 wk group, $\times 200$.

The situation of MMP-9 was different from that of the two above. MMP-9 decreased in the 4 d and 2 wk groups, but in the 4 wk group and the following MMP-P showed higher expression than that of the normal rats with no significance. (Figure 3).

The expression of MMP-13 showed reduction in the 4 d and 2 wk groups, but recovered in the 4 wk group and then sustained, when modeling was stopped it showed higher expression than normal. (Figure 4).

The expression of TIMP-1 in the 4 d and 2 wk groups showed reduction, after then it gave distinct higher expression and did not recover to normal level even after modeling was stopped for 2 wk. (Figure 5).

The expression of TIMP-2 showed different type from that of TIMP-1. In normal rats it had a high level with some hepatocytes expressing, but as soon as modeling began it fell rapidly, then gradually ascended as modeling went on, but after modeling was stopped for 2 wk it was still lower than normal. (Figure 6).

We failed in this model to find any activities of MMP-2 and MMP-9 with zymography.

Western blotting tests showed that in the 4 wk and 9 wk groups there were strong expressions of TIMP-1, but in other groups there were not. As to TIMP-2 we did not find its expression. (Figures 7,8).

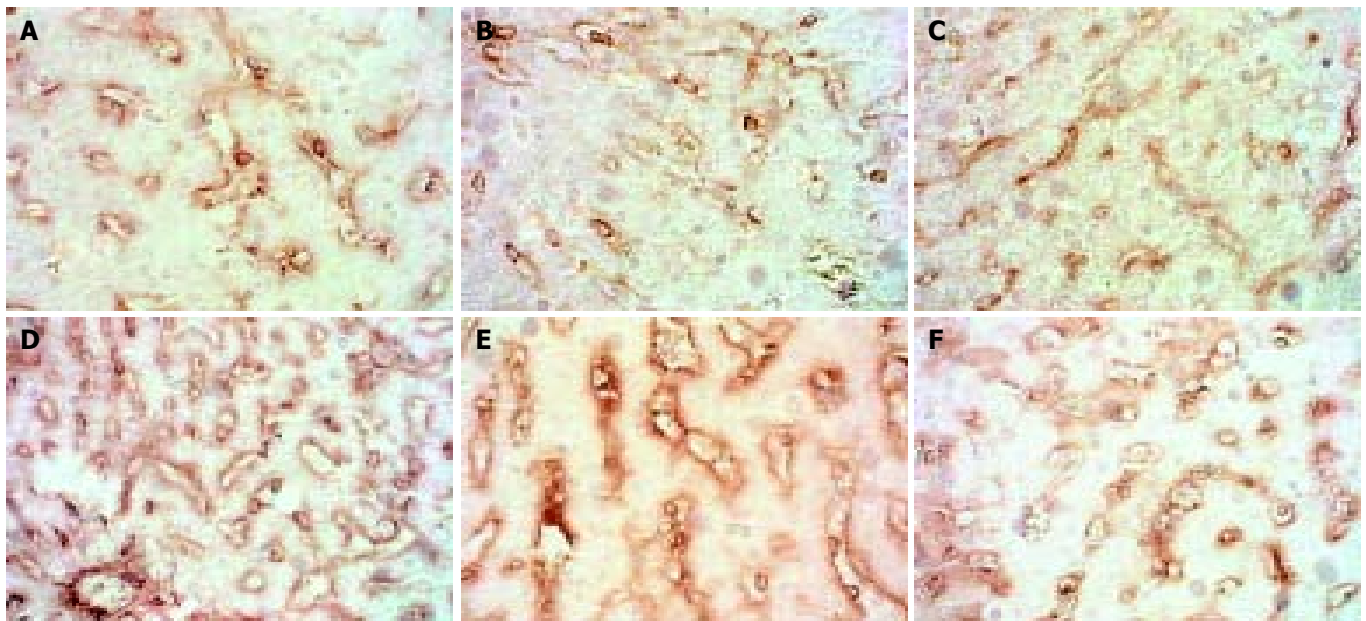


Figure 5 Dynamic changes of TIMP-1. A: Normal rat, $\times 400$ B: 4 d group, $\times 400$ C: 2 wk group, $\times 400$ D: 4 wk group, $\times 400$ E: 9 wk group, $\times 400$ F: 11 wk group, $\times 400$.

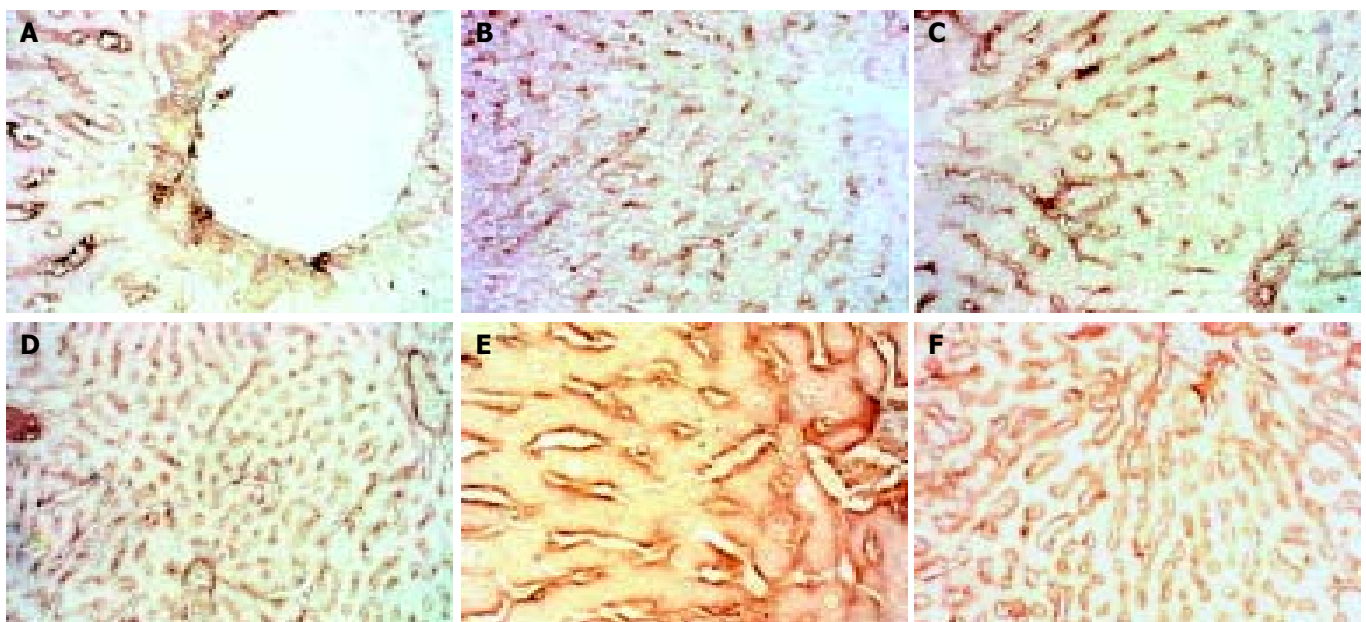


Figure 6 Dynamic changes of TIMP-2. A: Normal rat, $\times 200$ B: 4 d group, $\times 100$ C: 2 wk group, $\times 200$ D: 4 wk group, $\times 100$ E: 9 wk group, $\times 400$ F: 11 wk group, $\times 100$.

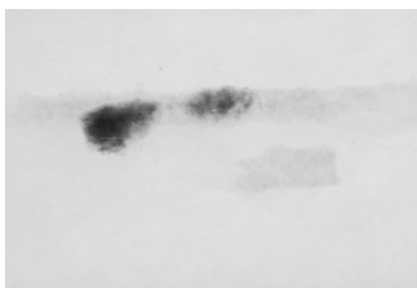


Figure 7 Expression of TIMP-1 in the 4 wk and 9 wk groups.

DISCUSSION

China's prosperity is accompanied with cases of alcoholic liver disease growing day by day. Alcohol can stimulate hepatic

stellate cells (HSCs) to proliferate and produce various fibrosis cytokines, which in turn result in hepatic fibrosis in the end. Abstinence itself can not reverse hepatic fibrosis, and more over, temperance is usually very difficult. So it is important to probe into the mechanism of hepatic fibrosis reversion in ALD research. Most of the recent reports^[1-11] reveal that the formation and prognosis of hepatic fibrosis were all related with MMPs/TIMPs, and this viewpoint has been accepted as a common sense. So we probed into the important factors among MMPs/TIMPs, and respective discussions were as follows.

Matrix Metalloproteinase-2 (MMP-2) is an important factor in the metabolism of type IV collagen in sinusoid basement. It has a peculiar activation course taking place on the membrane and forms a triple complex bridged with MT1-MMP by TIMP-2. Deactivation could be triggered by more competitive TIMP-2 to conjugate with MMP-2 to restrain the formation of triple complex. Because of local expression of TIMP-2 it is hypothesized

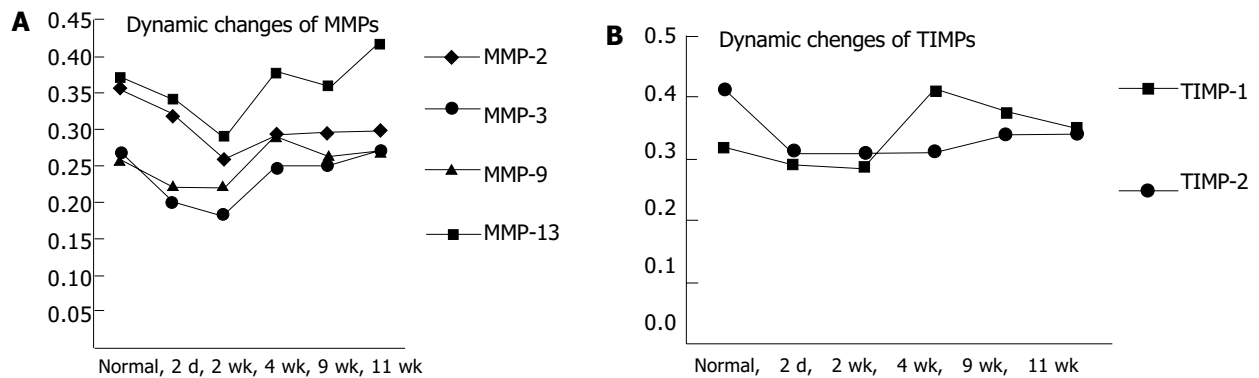


Figure 8 Dynamic changes of MMPs 2, 3, 9, 13 and TIMPs 1, 2. A: Dynamic changes of MMPs 2, 3, 9, 13. B: Dynamic changes of TIMPs 1, 2.

that MMP-2 could not be activated on a long trip, and it is only transient and local. Activated MMP-2 could decompose type IV collagen in the basement, resulting in broken micro circumstances of HSC and promoting HSC to activate, proliferate and migrate. Activated MMP-2 also could play an important role in reversion of hepatic fibrosis, metastasis of tumors, MOF induced by endotoxin, apoptosis of HSC, *etc*^[12-26]. MMP-2 is mainly composed and secreted by HSC in liver. Activation induced by various pathogens might need different time, and strong stimulation would result in rapid activation^[27]. It was reported that^[28] during reversion period activated MMP-2 was in favor of fibrosis reversion, so it was thought that MMP-2 played another role at this time because activated MMP-2 could activate HSC and promote fibrosis^[29,30].

The results of our experiment were different from those of others. MMP-2 showed moderate expression in SD rat liver slides along the sinus in normal, began to fall during modeling, instead of rising up as reported, meanwhile zymography tests did not show any activity of it. So we thought that it was peculiar that lowly expressed MMP-2 could also break down type IV collagen in sinus basement markedly. Capillarization of this model was not typical because of lower contents of type IV collagen than normal. This might imply lowly expressed MMP-2 not only decomposed parts of type IV collagen in sinus basement but also obstructed its accumulation, resulting in atypical capillarization in the end. It could not achieve success unless TIMP-2 markedly decreased its expression so as to alleviate MMP-2, and our experiment showed an authentic result just like this. This phenomenon may exclude the possibility that only high activity of MMP-2 could result in breakage of sinus basement and progression of fibrosis, and it also may imply that MMP-2 is not the most important factor imposed on the metabolism of type IV collagen in sinus basement. Our results also showed that the cooperation of MMP-2/TIMP-2 could make the contents of type IV collagen in sinus basement become normal after the modeling was stopped for 2 wk. This was not consistent with other scholar's report^[28] that apoptosis of HSC could decrease the expression of TIMP-2 and promote the activity of MMP-2. The differences between species, modeling, stages and types of pathology may be related with these diversities. The fast and accurate adjusting mechanism of MMP-2's function influenced heavily by TIMP-2, rather than TIMP-1, might be a commonfeature of different models.

MMP-3 also called stromelysin 1, originates from almost the same cells as MMP-1 but does not show synchronization in expression. MMP-3 has a wide range of substrates but important one may be laminin. It can also activate MMP-1, but there are not many reports about it. It has been reported that the measurement of serum MMP-3 was of little use for assessing fibrolysis in chronically diseased livers. However, because of the distinct pathological changes in sinusoid and peri-sinusoid in alcoholic

liver disease, the value of MMP-3 rose to some extent. We found that accumulation of laminin in basement was quite prominent during capillarization. It was evident that the sustained low expression during modeling of MMP-3 would be in favor of laminin's accumulation. The accumulated laminin in basement was still high after the modeling was stopped for 2 wk in spite of the normal expression of MMP-3, which might imply not only that the strong inhibiting effect of TIMP-1 on MMP-3 could result in delayed fashion of metabolism of laminin compared to that of type IV collagen, but also that sinusoid pathological changes were not entirely modulated by MMP-2/TIMP-2, and this is important.

MMP-9 is also called gelatinase B, the majority of which is secreted by kupffer cells in liver. MMP-9 could also decompose type IV collagen in basement, and this might happen a little earlier than that of MMP-2, implying MMP-9 might take part in the early events of fibrosis. In this model, however, MMP-9 had lower expression than MMP-2, and continued after the modeling began. It could be thought that MMP-9 did not play role in this model entirely. It was reported^[31] that widespread capillarization in cirrhosis suggested no MMP-2 activity but low MMP-9 activity, implying potent importance of MMP-9 in reversion of fibrosis. In this model in the 4 wk and 11 wk groups MMP-9 showed little higher expression than normal but still lower than that of MMP-2, actually it might not affect the accumulation of type IV collagen, so it was not an important factor. This result did not show any consistency with other reports^[29,30].

MMP-1, an interstitial collagenase (in rats it is MMP-13) is the most important enzyme secreted by kupffer cells and HSC in liver, and after secretion it is activated and the course may be related to plasminogen activator system. MMP-1/MMP-13 could be deactivated by forming a complex with TIMP-1 at a ratio 1:1. It was reported that kupffer cells in liver were one of the main originations of MMPs, including MMP-13. It was also reported recently that^[32] the rise of activity of MMP-13 would significantly improve cirrhosis, which could be realized by stimulating kupffer cells. This implied another way to reverse fibrosis. The activity of MMP-13 was also needed to ensure normal metabolism of hepatocytes^[33-35]. We found in our experiment that MMP-13 expressed themselves moderately mainly along sinusoid in normal rats which would support such a kind of viewpoints. MMP-13 decreased to some extent when the modeling began, in the 2 wk group some hepatocytes and kupffer cells showed active expression of MMP-13, then the expression along sinusoid again showed an ascending trend. In the 4 wk group when fibrosis was most severe the expression of MMP-13 was almost the same as normal, meaning that MMP-13 itself could not affect the course of peri-sinusoidal fibrosis. In the reversion phase the expression of MMP-13 was significantly higher than normal and the active stains implied that kupffer

cells might restart their expression, which would be helpful to fibrosis reversion, but the accumulation of type I collagen was not affected and became more severe with the modeling, evidently the inhibiting effect of TIMP-1 on MMP-13 should be the cause. The higher expression of MMP-13 in the reversion phase actually could not help reverse peri-sinusoidal fibrosis, demonstrating once more that TIMP-1 was the most important factor during hepatic fibrosis.

TIMP-1 is produced by kupffer cells, HSC and myofibroblasts in liver, but most of it is mainly produced by activated HSC, It could be induced by TGF beta, interferon or pentoxifylline. TIMP-1 could inhibit most of MMPs except MMP-14 and MMP-19 by integrating them at a ratio 1:1 to form a complex. Injured liver tissues showed more expression of TIMP-1, and in turn, this would help interstitial fibrils to accumulate^[33-36]. Serum TIMP-1 had a close relation to hepatic pathology, serum TIMP-1 could forecast hepatic pathological changes and prognosis, and could also be used as an index to evaluate the treatment. The transgenic model lacking TIMP-1 gene and anti-oligonucleotide treatment model aiming at TIMP-1 were established to find that without injury TIMP-1 itself could not result in fibrosis, but if there were injuries TIMP-1 would significantly accelerate the course in which fibrosis was formed. This might imply omni directional and all target treatment for hepatic fibrosis should be considered, nevertheless targeted and usual treatment still took TIMP-1 as a comprehensive index for evaluation^[37-41]. Overexpression of TIMP-1 could keep hepatic fibrosis by holding back the apoptosis of HSC, otherwise the down-regulation of TIMP-1 would promote MMPs to be activated, and in turn, fibrils decomposed, HSC apoptosis took place and fibrosis reversed. All this emphasized the importance of TIMP-1.

We found in this model that at the early phase TIMP-1 showed a relatively low expression, in the 4 wk and 9 wk groups TIMP-1 showed evident expression mainly along sinusoid, which might be attributed to the widely activated HSCs. The over-expression of TIMP-1 would inhibit MMP-13 and MMP-3, resulting in accumulation of type I collagen and laminin, which in turn would be in favor of the formation of capillarization and peri-fibrosis. This discovery supported the importance of TIMP-1. It was also underpinned by Western blotting tests which showed TIMP-1 expressed itself most evidently in the 4 wk and 9 wk groups. In this model after the stimulus was ceased for 2 wk TIMP-1 still showed high expression, which might imply that activated HSCs were difficult to start spontaneous apoptosis, and in turn, TIMP-1 would not cease its expression by itself, which again showed it was a key step to reduce the expression of TIMP-1 in order to reverse fibrosis. Our results demonstrated that even if MMP-13 expressed highly it still would be inhibited by TIMP-1 to result in accumulation of type I collagen. It was reasonable that normal-level MMP-3 was inhibited by over-expressed TIMP-1, resulting in high content of laminin in basement of sinusoid, and capillarization and peri-sinusoidal fibrosis were not drastically improved. So this should be attributed to the high expression of TIMP-1.

The ability of TIMP-2 to integrate MMP-2 is 7-9 fold higher than that of TIMP-1, so if it is true it is the most important factor imposed on the metabolism of type IV collagen in basement of sinus. MMP-2 itself could not affect the course of capillarization as found in this experiment. We also found in normal SD rat livers that TIMP-2 was highly expressed in hepatocytes and kupffer cells, but transformed to HSCs with few active stains along sinusoid as the modeling began, which might imply activated HSCs would be the main origin of TIMP-2. During the modeling decreased expression of TIMP-2 might weaken the inhibition on MMP-2 and result in the decomposition of type IV collagen in basement and could not accumulate to help form typical capillarization. This was a typical feature of our model. After the modeling was stopped for 2 wk, the expression

of TIMP-2 ascended but was little lower than normal, and the content of type IV collagen returned to normal level, which implied the gradually rising TIMP-2 could show its suppressing function on MMP-2, so that type IV collagen was protected and became normal. This demonstrated the significant effect of TIMP-2 and MMP-2 on the metabolism of type IV collagen in basement. However, TIMP-2 was apparently the more important.

In conclusion, the pathological changes of ALD model with fibrosis grades I-II can be controlled by TIMPs, especially the expression of TIMP-1 and TIMP-2 has significant effects on the prognosis of capillarization and peri-sinusoidal fibrosis, and MMPs are always dominated by TIMP-1 and TIMP-2. So the fatal step to reverse fibrosis might be to block or modulate the expression of TIMP-1 and TIMP-2.

ACKNOWLEDGEMENTS

The data of this article were obtained and analyzed with the help of Zhi-Gao Jin Professor and Ms. Hong Cai working in Academy of TCM. Many thanks to them!

REFERENCES

- 1 **Reeves HL**, Friedman SL. Activation of hepatic stellate cells-a key issue in liver fibrosis. *Front Biosci* 2002; **7**: d808-826
- 2 **Smart DE**, Vincent KJ, Arthur MJ, Eickelberg O, Castellazzi M, Mann J, Mann DA. JunD regulates transcription of the tissue inhibitor of metalloproteinases-1 and interleukin-6 genes in activated hepatic stellate cells. *J Biol Chem* 2001; **276**: 24414-24421
- 3 **Boeker KH**, Haberkorn CI, Michels D, Flemming P, Manns MP, Lichtinghagen R. Diagnostic potential of circulating TIMP-1 and MMP-2 as markers of liver fibrosis in patients with chronic hepatitis C. *Clin Chim Acta* 2002; **316**: 71-81
- 4 **Vaillant B**, Chiamonte MG, Cheever AW, Soloway PD, Wynn TA. Regulation of hepatic fibrosis and extracellular matrix genes by the th response: new insight into the role of tissue inhibitors of matrix metalloproteinases. *J Immunol* 2001; **167**: 7017-7026
- 5 **Watanabe T**, Niioka M, Ishikawa A, Hozawa S, Arai M, Maruyama K, Okada A, Okazaki I. Dynamic change of cells expressing MMP-2 mRNA and MT1-MMP mRNA in the recovery from liver fibrosis in the rat. *J Hepatol* 2001; **35**: 465-473
- 6 **Lichtinghagen R**, Michels D, Haberkorn CI, Arndt B, Bahr M, Flemming P, Manns MP, Boeker KH. Matrix metalloproteinase (MMP)-2, MMP-7, and tissue inhibitor of metalloproteinase-1 are closely related to the fibroproliferative process in the liver during chronic hepatitis C. *J Hepatol* 2001; **34**: 239-247
- 7 **Okazaki I**, Watanabe T, Hozawa S, Niioka M, Arai M, Maruyama K. Reversibility of hepatic fibrosis: from the first report of collagenase in the liver to the possibility of gene therapy for recovery. *Keio J Med* 2001; **50**: 58-65
- 8 **Ninomiya T**, Yoon S, Nagano H, Kumon Y, Seo Y, Kasuga M, Yano Y, Nakaji M, Hayashi Y. Significance of serum matrix metalloproteinases and their inhibitors on the antifibrogenetic effect of interferon-alfa in chronic hepatitis C patients. *Intervirology* 2001; **44**: 227-231
- 9 **Williams EJ**, Benyon RC, Trim N, Hadwin R, Grove BH, Arthur MJ, Unemori EN, Iredale JP. Relaxin inhibits effective collagen deposition by cultured hepatic stellate cells and decreases rat liver fibrosis *in vivo*. *Gut* 2001; **49**: 577-583
- 10 **Benyon RC**, Arthur MJ. Extracellular matrix degradation and the role of hepatic stellate cells. *Semin Liver Dis* 2001; **21**: 373-384
- 11 **Murphy FR**, Issa R, Zhou X, Ratnarajah S, Nagase H, Arthur MJ, Benyon C, Iredale JP. Inhibition of apoptosis of activated hepatic stellate cells by tissue inhibitor of metalloproteinase-1 is mediated via effects on matrix metalloproteinase inhibition: implications for reversibility of liver fibrosis. *J Biol Chem* 2002; **277**: 11069-11076
- 12 **Ueberham E**, Low R, Ueberham U, Schonig K, Bujard H. Conditional tetracycline-regulated expression of TGF-beta1 in liver of transgenic mice leads to reversible intermediary fibrosis. *Hepatology* 2003; **37**: 1067-1078
- 13 **Le Pabic H**, Bonnier D, Wewer UM, Coutand A, Musso O, Baffet G, Clement B, Theret N. ADAM12 in human liver cancers:

- TGF-beta-regulated expression in stellate cells is associated with matrix remodeling. *Hepatology* 2003; **37**: 1056-1066
- 14 **Yang C**, Zeisberg M, Mosterman B, Sudhakar A, Yerramalla U, Holthaus K, Xu L, Eng F, Afdhal N, Kalluri R. Liver fibrosis: insights into migration of hepatic stellate cells in response to extracellular matrix and growth factors. *Gastroenterology* 2003; **124**: 147-159
 - 15 **Gardi C**, Arezzini B, Fortino V, Comporti M. Effect of free iron on collagen synthesis, cell proliferation and MMP-2 expression in rat hepatic stellate cells. *Biochem Pharmacol* 2002; **64**: 1139-1145
 - 16 **Kobayashi H**, Li ZX, Yamataka A, Lane GJ, Miyano T. Clinical evaluation of serum levels of matrix metalloproteinases and tissue inhibitors of metalloproteinases as predictors of progressive fibrosis in postoperative biliary atresia patients. *J Pediatr Surg* 2002; **37**: 1030-1033
 - 17 **Giannelli G**, Bergamini C, Marinosci F, Fransvea E, Quaranta M, Lupo L, Schiraldi O, Antonaci S. Clinical role of MMP-2/TIMP-2 imbalance in hepatocellular carcinoma. *Int J Cancer* 2002; **97**: 425-431
 - 18 **Sawada S**, Murakami K, Murata J, Tsukada K, Saiki I. Accumulation of extracellular matrix in the liver induces high metastatic potential of hepatocellular carcinoma to the lung. *Int J Oncol* 2001; **19**: 65-70
 - 19 **Lee HS**, Huang GT, Miao LH, Chiou LL, Chen CH, Sheu JC. Expression of matrix metalloproteinases in spontaneous regression of liver fibrosis. *Hepatogastroenterology* 2001; **48**: 1114-1117
 - 20 **Chen PS**, Zhai WR, Zhou XM, Zhang JS, Zhang Y, Ling YQ. Effects of different causes on the expression of matrix metalloproteinase 2 in hepatic stellate cells. *Zhonghua Ganzangbing Zazhi* 2002; **10**: 279
 - 21 **Preaux AM**, D'ortho MP, Bralet MP, Laperche Y, Mavier P. Apoptosis of human hepatic myofibroblasts promotes activation of matrix metalloproteinase-2. *Hepatology* 2002; **36**: 615-622
 - 22 **Lv XH**, Wang BY, Xie YH, Liu CR, Fu BY. Dynamic change and expression of matrix metalloproteinase-2 and -9 in alcoholic liver disease in rats. *Zhonghua Ganzangbing Zazhi* 2001; **9**: 268
 - 23 **Xie YH**, Li L, Wang LE, Liu CR, Fu BY. Matrix metalloproteinase-2, -9 and hepatic fibrosis. *Chin J Med* 2002; **82**: 1172
 - 24 **Dudas J**, Kovalszky I, Gallai M, Nagy JO, Schaff Z, Knittel T, Mehde M, Neubauer K, Szalay F, Ramadori G. Expression of decorin, transforming growth factor-beta 1, tissue inhibitor metalloproteinase 1 and 2, and type IV collagenases in chronic hepatitis. *Am J Clin Pathol* 2001; **115**: 725-735
 - 25 **Sakaida I**, Hironaka K, Terai S, Okita K. Gadolinium chloride reverses dimethylnitrosamine (DMN)-induced rat liver fibrosis with increased matrix metalloproteinases (MMPs) of Kupffer cells. *Life Sci* 2003; **72**: 943-959
 - 26 **Lee HS**, Huang GT, Chen CH, Chiou LL, Lee CC, Yang PM, Chen DS, Sheu JC. Less reversal of liver fibrosis after prolonged carbon tetrachloride injection. *Hepatogastroenterology* 2001; **48**: 1312-1315
 - 27 **Woo SW**, Lee SH, Kang HC, Park EJ, Zhao YZ, Kim YC, Sohn DH. Butein suppresses myofibroblastic differentiation of rat hepatic stellate cells in primary culture. *J Pharm Pharmacol* 2003; **55**: 347-352
 - 28 **Gagliano N**, Arosio B, Grizzi F, Masson S, Tagliabue J, Dioguardi N, Vergani C, Annoni G. Reduced collagenolytic activity of matrix metalloproteinases and development of liver fibrosis in the aging rat. *Mech Ageing Dev* 2002; **123**: 413-425
 - 29 **Nie Q**, Zhou Y, Xie Y. Expression and significance of tissue inhibitors of metalloproteinases-1 and -2 in serum and liver tissue of patients with liver cirrhosis. *Zhonghua Yixue Zazhi* 2001; **81**: 805-807
 - 30 **Nie QH**, Cheng YQ, Xie YM, Zhou YX, Bai XG, Cao YZ. Methodologic research on TIMP-1, TIMP-2 detection as a new diagnostic index for hepatic fibrosis and its significance. *World J Gastroenterol* 2002; **8**: 282-287
 - 31 **Mastroianni CM**, Liuzzi GM, D'Ettorre G, Lichtner M, Forcina G, Di Campli NF, Riccio P, Vullo V. Matrix metalloproteinase-9 and tissue inhibitors of matrix metalloproteinase-1 in plasma of patients co-infected with HCV and HIV. *HIV Clin Trials* 2002; **3**: 310-315
 - 32 **Flisiak R**, Maxwell P, Prokopowicz D, Timms PM, Panasiuk A. Plasma tissue inhibitor of metalloproteinases-1 and transforming growth factor beta 1-possible non-invasive biomarkers of hepatic fibrosis in patients with chronic B and C hepatitis. *Hepatogastroenterology* 2002; **49**: 1369-1372
 - 33 **Yoshiji H**, Kuriyama S, Yoshii J, Ikenaka Y, Noguchi R, Nakatani T, Tsujinoue H, Yanase K, Namisaki T, Imazu H, Fukui H. Tissue inhibitor of metalloproteinases-1 attenuates spontaneous liver fibrosis resolution in the transgenic mouse. *Hepatology* 2002; **36**(4 Pt 1): 850-860
 - 34 **Melgert BN**, Olinga P, Van Der Laan JM, Weert B, Cho J, Schuppan D, Groothuis GM, Meijer DK, Poelstra K. Targeting dexamethasone to Kupffer cells: effects on liver inflammation and fibrosis in rats. *Hepatology* 2001; **34**(4 Pt 1): 719-728
 - 35 **Raetsch C**, Jia JD, Boigk G, Bauer M, Hahn EG, Riecken EO, Schuppan D. Pentoxifylline downregulates profibrogenic cytokines and procollagen I expression in rat secondary biliary fibrosis. *Gut* 2002; **50**: 241-247
 - 36 **Garcia L**, Hernandez I, Sandoval A, Salazar A, Garcia J, Vera J, Grijalva G, Muriel P, Margolin S, Armendariz-Borunda J. Pirfenidone effectively reverses experimental liver fibrosis. *J Hepatol* 2002; **37**: 797-805
 - 37 **Bruck R**, Genina O, Aeed H, Alexiev R, Nagler A, Avni Y, Pines M. Halofuginone to prevent and treat thioacetamide-induced liver fibrosis in rats. *Hepatology* 2001; **33**: 379-386
 - 38 **Jia JD**, Bauer M, Cho JJ, Ruehl M, Milani S, Boigk G, Riecken EO, Schuppan D. Antifibrotic effect of silymarin in rat secondary biliary fibrosis is mediated by downregulation of procollagen alpha1 (I) and TIMP-1. *J Hepatol* 2001; **35**: 392-398
 - 39 **Dubuisson L**, Desmouliere A, Decourt B, Evade L, Bedin C, Boussarie L, Barrier L, Vidaud M, Rosenbaum J. Inhibition of rat liver fibrogenesis through noradrenergic antagonism. *Hepatology* 2002; **35**: 325-331
 - 40 **Wang A**, Yang X, Wang W, Zuo F, Wang Q, He F. Effect of recombinant human augmenter of liver regeneration on gene expression of tissue inhibitor of metalloproteinase-1 in rat with experimental liver fibrosis. *Zhonghua Yixue Zazhi* 2002; **82**: 610-612
 - 41 **Spira G**, Mawasi N, Paizi M, Anbinder N, Genina O, Alexiev R, Pines M. Halofuginone, a collagen type I inhibitor improves liver regeneration in cirrhotic rats. *J Hepatol* 2002; **37**: 331-339

Scintigraphic detection of carcinoid tumors with a cost effectiveness analysis

Dimitris Dimitroulopoulos, Dimitris Xynopoulos, Klisthenis Tsamakidis, Emmanouel Paraskevas, Athanassios Zisimopoulos, Efthymios Andriotis, Ekaterini Fotopoulou, Marios Kontis, Ioannis Paraskevas

Dimitris Dimitroulopoulos, Dimitris Xynopoulos, Klisthenis Tsamakidis, Emmanouel Paraskevas, Gastroenterology Unit, Agios Savvas Cancer Hospital, Athens, Greece

Athanassios Zisimopoulos, Section of Nuclear Medicine, Agios Savvas Cancer Hospital, Athens, Greece

Efthymios Andriotis, CT Department, Agios Savvas Cancer Hospital, Athens, Greece

Ekaterini Fotopoulou, First Radiology-Oncology Department, Agios Savvas Cancer Hospital, Athens, Greece

Nikiforos Apostolikas, Pathology Department, Agios Savvas Cancer Hospital, Athens, Greece

Marios Kontis, Economics and Statistics Department, Agios Savvas Cancer Hospital, Athens, Greece

Ioannis Paraskevas, City University London, London, United Kingdom

Correspondence to: Dimitris Dimitroulopoulos, 35 Parnassou str., GR-152 34 Halandi-Athens, Greece. dimdim@otenet.gr

Telephone: +30210-6892460 **Fax:** +30210-6420146

Received: 2004-02-20 **Accepted:** 2004-03-13

Abstract

AIM: To evaluate the diagnostic sensitivity and accuracy and the cost-effectiveness of this technique in the detection of gastroenteropancreatic carcinoid tumors and their metastases in comparison with conventional imaging methods.

METHODS: Somatostatin receptor scintigraphy (SRS) was performed in 24 patients with confirmed carcinoids and 7 under investigation. The results were compared with those of conventional imaging methods (chest X-ray, upper abdominal ultrasound, chest CT, upper and lower abdominal CT). Also a cost-effectiveness analysis was performed comparing the cost in Euro of several combinations of SRS with conventional imaging modalities.

RESULTS: SRS visualized primary or metastatic sites in 71.0% of cases and 61.3% of conventional imagings. The diagnostic sensitivity of the method was higher in patients with suspected lesions (85.7% vs 57.1%). SRS was less sensitive in the detection of metastatic sites (78.9% vs 84.2%). The undetectable lesions by SRS metastatic sites were all in the liver. Between several imaging combinations, the combinations of chest X-ray/upper abdominal CT/SRS and chest CT/upper abdominal CT/SRS showed the highest sensitivity (88.75%) in terms of the number of detected lesions. The combinations of chest X-ray/upper abdominal US/SRS and chest CT/upper abdominal ultrasound /SRS yielded also a quite similar sensitivity (82%). Compared to the cost of the four sensitive combinations the combination of chest X-ray/upper abdominal ultrasound/SRS presented the lower cost, 1183.99 Euro vs 1251.75 Euro for chest CT/upper abdominal ultrasound/SRS, 1294.93 Euro for chest X-ray/upper abdominal CT/SRS and 1362.75 Euro for chest CT/upper abdominal CT/SRS.

CONCLUSION: SRS imaging is a very sensitive method for the detection of gastroenteropancreatic carcinoids but is

less sensitive than ultrasound and CT in the detection of liver metastases. Between several imaging combinations, the combination of chest X-ray/upper abdominal CT/SRS shows the highest sensitivity with a cost of 1294.93 Euro.

Dimitroulopoulos D, Xynopoulos D, Tsamakidis K, Paraskevas E, Zisimopoulos A, Andriotis E, Fotoopulou E, Kontis M, Paraskevas I. Scintigraphic detection of carcinoid tumors with a cost effectiveness analysis. *World J Gastroenterol* 2004; 10 (24): 3628-3633

<http://www.wjgnet.com/1007-9327/10/3628.asp>

INTRODUCTION

The carcinoid tumor, argentaffinoma, is a member of a very exclusive neoplastic family known as neuroendocrine or amine precursor uptake and decarboxylation (APUD) tumors.

Carcinoid tumor has been found to arise from almost every organ and system derived from the primitive entoderm, but most frequently originated from the gastrointestinal (GI) tract, accounting for approximately half of all GI endocrine tumors^[1].

Over 95 per cent of all GI carcinoids are located in only three sites: the appendix, rectum and small intestine.

Irrespectively to their location, carcinoids are capable of producing one or more of the following substances: 5-hydroxytryptamine (serotonin), gastrin kinin-peptide, histamine, catecholamine and glucagon. Some of them induce systemic manifestations known as the carcinoid syndrome characterized by flushing, diarrhea, right-sided heart disease and wheezing^[2,3].

Carcinoid tumors are rare (incidence: about 2/100 000 people)^[4], malignancy -that is mainly liver metastases, may be encountered in 10-60% of cases depending on the site of the primary tumor^[5,6]. Metastases are observed in less than 2% of carcinoids 1 cm or less in size. In contrast, nearly all carcinoids 2 cm or greater show evidence of metastatic spread^[1].

Tumor localization is essential since surgery remains the optimal treatment for most patients without metastases^[7,8].

Curative surgery is difficult since primary tumors are frequently very small (<1 cm) and potentially undetectable by conventional imaging. When liver metastases occur, staging of these patients is essential for therapeutic manipulation.

Tumor localization for accurate staging and therapeutic management justifies the use of sophisticated imaging techniques such as somatostatin receptor scintigraphy (SRS)^[9,10].

Since the introduction of somatostatin receptor imaging in 1989^[9], many reports on the usefulness and limitation of this technique have been published.

It has been shown by autoradiography using ¹²⁵I-labeled octreotide that endocrine tumors of GI tract and especially carcinoids possess somatostatin receptors^[11-13]. When octreotide is labeled with radionuclides such as ¹²³I^[14,15] or ¹¹¹In, the specific receptor binding can be exploited for the scintigraphic *in vivo* demonstration of receptor-expressing tumors^[9,10,16].

The radiolabeled analogue ¹¹¹In-DTPA-octreotide also known as octreoscan is cleared by renal than hepatobiliary route, thus causing less artifacts on hepatic and mesenteric imaging^[17,18].

MATERIALS AND METHODS

Materials

A total of 31 patients (18 males, 13 females, age ranged 27-73 years) under SRS ¹¹¹In-pentatreotide were enrolled between April 1997 and October 2003 at "Agios Savvas" Cancer Hospital (Section of Nuclear Medicine), Athens, Greece. Their data are listed in Table 1.

Inclusion criteria required histological or cytological confirmation of a presently or previously operated abdominal carcinoid, or for patients with suspected tumors, a history of carcinoid syndrome-related signs and symptoms with an additional elevation of urinary 5-HIAA. All patients gave informed consent to participation in the study, which was approved by the ethics committee of our hospital.

Seven of the patients were under investigation for suspected

carcinoids in different sites (caecum, appendix, small intestine, pancreas) while the remaining 24 had histologically/cytologically confirmed tumors, in 10 of them the primary lesion was excised. All gastric carcinoids were type II or "mixed cellular composition" gastric carcinoid tumors.

Seven patients were treated by octreotide prior to SRS, in all but 3 of them therapy was withdrawn 36 h prior to somatostatin receptor imaging in order to lift the blockade of SRS. In the rest 3 patients the 3-d withdrawal period was clinically impossible. The administration dose of octreotide in these patients was 0.5 mg daily.

A low-residue diet was started 3 d prior to SRS and stopped at the end of the imaging procedure. Twelve hours before the injection of the tracer a mild laxative was administered to minimize the false positive results, because a small quantity of the

Table 1 Characteristics of patients enrolled in study

Pt	Sex	Age (yr)	Primary tumor site	Metastases	Carcinoid syndrome related signs and symptoms	SRS primary metastases sites	Conventional imaging methods primary metastases sites
Patients with confirmed tumors							
1	F	69	Stomach			-	-
2	M	58	Stomach			+	-
3	M	55	Duodenum			-	-
4	M	55	Small intestine	Liver		+	+
5	F	69	Small intestine			+	-
6	M	33	Appendix	Lymph nodes		+	+
7	F	27	Appendix			-	-
8	M	39	Appendix	Liver-ribs	Diarrhoea	+	+
9	M	59	Caecum			-	-
10	F	64	Caecum			+	-
11	M	69	Rectum			+	-
12	F	57	Rectum			+	-
13	F	49	Pancreas	Liver-lung	Diarrhoea	+	+
14	M	58	Pancreas	Liver-lymph nodes	Diarrhoea flushes	+	+
Patients previously operated							
15	F	42	Stomach	Liver			+
16	M	34	Appendix	Liver			-
17	M	36	Appendix	Lymph nodes			+
18	F	40	Appendix	Liver-Lymph nodes			+
19	M	69	Small intestine	Lymph nodes			+
20	M	61	Small intestine	Liver			+
21	F	67	Caecum	Lymph nodes			+
22	F	56	Colon Liver				-
23	M	72	Rectum	Liver-lymph nodes			-
24	M	59	Pancreas	Liver			-
Patients with suspected carcinoid tumors							
25	M	34	Appendix		Flushes	-	-
26	F	33	Appendix		Diarrhoea	+	-
27	M	51	Small intestine	Liver	Diarrhoea flushes	-	+
28	M	62	Caecum		Diarrhoea	+	-
29	M	61	Caecum	Liver-lymph nodes	Diarrhoea flushes	+	+
30	F	71	Caecum	Liver	Diarrhoea flushes	+	+
31	F	73	Pancreas	Liver-lungs	Diarrhoea flushes	+	+

administrated dose underwent hepatobiliary excretion.

Patients were well hydrated prior to radioactive drug administration to increase renal clearance and to reduce radiation uptake to the thyroid, kidneys, bladder and other target organs. All individuals in our study had normal thyroid and renal function.

Methods

¹¹¹In-pentetreotide (Octreoscan, Mallinckrodt Medical BV, Petten, Holland) was supplied as two vial kits. The first contained ¹¹¹In as ¹¹¹InCl₃ diluted in 1.1 mL hydrochlorid acid and the other lyophilized pentetreotide. After reconstitution the pH of the final product was between 3.8 and 5. This product might be diluted with normal saline solution because the dilution would raise the pH slightly.

After an incubation period of 30 min at room temperature and before the administration, instant thin layer chromatography (ITLC) for quality control was performed. The dose for a planar investigation was 111 MBq (3.3 mCi) of octreoscan.

The radiolabeled somatostatin analogue was administered as an intravenous bolus and no side effects were observed after i.v. injection.

Imaging Whole body scanning and planar images were obtained with a large field of view gamma camera (Siemens) equipped with a medium-energy, parallel-hole collimator. The pulse-height analyser windows were centered over both ¹¹¹In peaks (172 keV and 245 keV) with a window width of 20%. Data from both windows were added to the acquisition frames. Images were obtained 24 and sometimes 48 h after tracer administration.

Scintigraphic results were compared with those obtained by other imaging methods such as chest X-ray performed, upper abdominal ultrasonography, chest CT scan performed, upper and lower abdominal CT scans.

Magnetic resonance imaging of the abdomen and digital abdominal angiography was performed in few cases, but because of the small number of patients these imaging techniques were not taken into account.

Statistical analysis

Statistical comparison between SRS and conventional imaging methods for the detection of primary and metastatic sites, globally and in each group of patients, was performed using McNemar's test based on discordant pairs. A *P* value ≤0.05 was considered statistically significant.

Cost analysis

A cost-effectiveness analysis was performed comparing the SRS with the conventional imaging methods (chest X-ray, upper abdominal ultrasonography, chest CT scan and upper and lower abdominal CT scan) in several combinations. The cost of each diagnostic procedure was calculated.

The personnel cost was calculated as the cost of a working hour for each person (physician, technician, nurse, assistant personnel).

The cost of materials was calculated including radiographs, injection systems, contrast liquids and kit material.

The equipment cost was calculated in working hours. A yearly payment on an annuity basis at 8% and a term of 5 and 8 years were used to calculate the cost of ultrasound equipment, scanners and gamma cameras. The prices of equipment were those of 2000. Maintenance cost was estimated at 8% of new value.

The housing and overhead costs based on the number of square meters required to investigate a patient, including the cost of furniture, cleaning, telephone and services of various overhead departments.

Costs were built up from a database of health care cost elements in Greece and from the currently applicable prices of octreoscan and contrast material.

RESULTS

SRS imaging visualized the primary tumor or metastatic sites in 22 (71.0%) out of 31 patients who had histologically-cytologically confirmed carcinoid tumors or were under investigation for highly suspected carcinoid (16/24-66.7% and 6/7-85.7% respectively) (Figure 1).

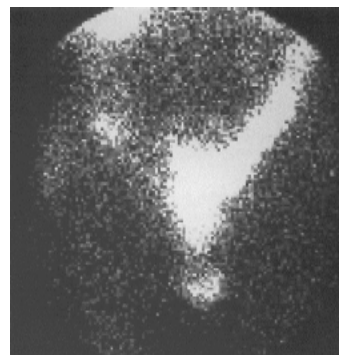


Figure 1 Carcinoid tumor of appendix (patient No 26).

Conventional imaging was positive in 19 (61.3%) patients (4/7- 57.1% with suspected carcinoids and 15/24-62.5% with known tumors). Thus, SRS provided additional detection sites compared with conventional imaging methods even if the global detection rate (71.0% vs 61.3%) was quite similar. Detection of primary sites was 33.3% higher with SRS than with conventional methods (71.4% vs 38.1% respectively, *P* = 0.039). The primary lesions were detected by SRS in 15 (71.4%) of 21 patients. Octreoscan scintigraphy failed to detect primary tumors in 6 patients (28.6%), 4 with known lesions (stomach, duodenum, appendix, caecum) and 2 under investigation (appendix, small intestine).

The 6 lesions (≤0.7 cm) that were not visualized after injection of ¹¹¹In-pentetreotide were detected by endoscopy (3) or surgery (3) and diagnosed by histology. Only 1 out of 6 lesions was visualized by conventional imaging methods (patient No 9). Further analysis of the results from each group of patients with residual primary tumors did not reveal any statistically significant difference between the two methods (*P*>0.05).

The positive detection rate in metastatic sites was similar by SRS and conventional imaging methods, which was 48.4% and 51.6% respectively (*P*>0.05).

In the 19 patients with metastatic disease, SRS detected metastatic lesions in 15 cases (78.9%) (Figures 2-5) and failed to visualize metastatic sites in 4 patients (21.1%), all in liver were subsequently detectable by ultrasonography and CT scans. On the other hand, conventional imaging visualized metastases in 16 (84.2%) patients with a detection rate of 5.3%, higher than that of SRS.

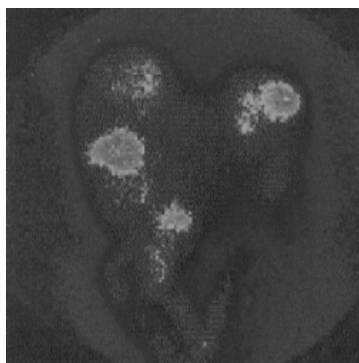


Figure 2 Increased accumulation of ¹¹¹In-octreotide in liver and abdominal lymph nodes (patient No 18).

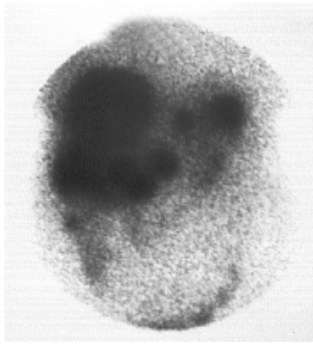


Figure 3 Metastatic sites in the abdominal lymph nodes from a previously operated carcinoid.

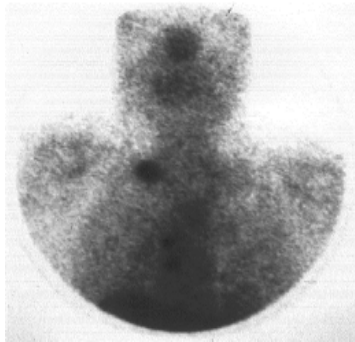


Figure 4 Increased accumulation of ¹¹¹In-octreotide in supraclavicular lymph node. Metastases from a carcinoid tumor located in appendix (patient No 8).

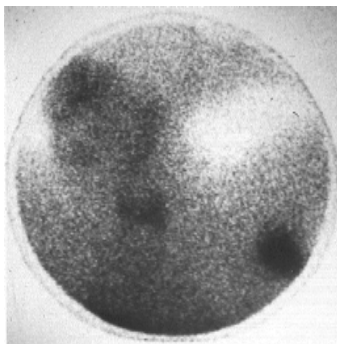


Figure 5 Metastatic sites in axillary lymph nodes (patient No 6).

False negative results of SRS and conventional imaging methods for primary and metastatic tumor sites in patients with known and suspected carcinoids are shown in Table 2, 3.

Table 2 False-negative results of SRS and conventional imaging methods for primary sites

Method	Detection of carcinoids		Patient No	False-negative (%)
SRS	Known carcinoids	4/14 patients	1, 3, 7, 9	28.57
	Suspected carcinoids	2/7 patients	25, 27	28.57
Conventional imaging methods	Known carcinoids	10/14 patients	1-7, 10-12	71.42
	Suspected carcinoids	3/7 patients	25, 26, 27	42.85

Table 3 False-negative results of SRS and conventional imaging methods for metastatic sites

Method	Detection of carcinoids		Patient No	False-negative (%)
SRS	Known carcinoids	4/24 patients	16, 22-24	16.66
	Suspected carcinoids	0/7 patients	-	0
Conventional imaging methods	Known carcinoids	1/24 patients	6	4.16
	Suspected carcinoids	2/7 patients	27, 29	28.6

Comparison of 8 imaging combinations showed that the combinations of chest X-ray/upper abdominal CT scan/SRS and chest CT scan/upper abdominal CT scan/SRS achieved the highest sensitivity in the detection of primary and metastatic lesions (88.75% for each one).

The combinations of chest X-ray/upper abdominal ultrasonography/SRS and chest CT/upper abdominal ultrasonography/SRS yielded also a similar sensitivity (82% for each one in terms of the number of detected lesions).

Cost-effectiveness analysis

Eight combinations of imaging techniques were evaluated for their sensitivity and cost. The cost of each imaging technique in Euro is shown in Table 4.

Table 4 Cost in Euro of used techniques

Chest X-ray	3.29
Upper abdominal ultrasonography	8.22
Chest CT-scan	71.11
Upper abdominal CT-scan	71.11
	48.11 • for the contrast liquid
Lower abdominal CT-scan	71.11
SRS	1 172.42

In the four most sensitive combinations, the combination of chest X-ray/upper abdominal ultrasonography/SRS presented the lower cost, 1183.93 Euro vs 1251.75 Euro for chest CT/upper abdominal ultrasonography/SRS, 1294.93 Euro for chest X-ray/upper abdominal CT/SRS and 1362.75 Euro for chest CT/upper abdominal CT/SRS. The related sensitivity rate/cost for the combinations reported above is shown in Figure 6.

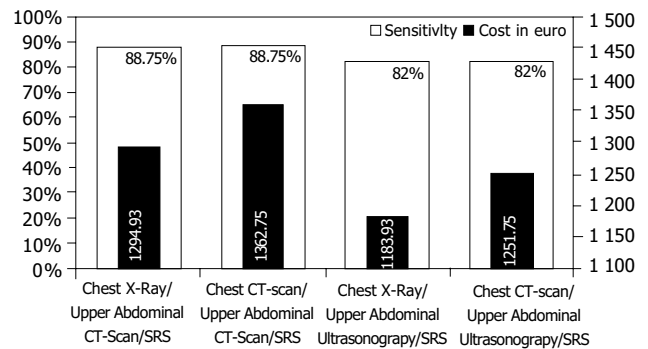


Figure 6 Relation between sensitivity rate and cost for combinations with the highest sensitivity.

DISCUSSION

Carcinoids were often indolent, asymptomatic, slow growing tumors and clinically silent for years^[31]. The vast majority would not cause symptoms until complications (e.g. intestinal obstruction) or symptoms and signs of the carcinoid syndrome occur. This syndrome occurred in less than 10% of cases and might be present in patients with midgut carcinoid tumors with liver metastases and also in some patients with foregut carcinoids. Patients with hindgut carcinoids did not exhibit the carcinoid syndrome.

The final diagnosis was not easy, unless bioptic material was examined for the secretory peptide chromogranin or the neuron-specific enolase^[19,20].

Due to their multiple localizations and their small size, images of carcinoid tumors were difficult to obtain even when the most sophisticated conventional imaging techniques were applied^[21-23]. MRI, CT scan and ultrasonography were very sensitive in the detection of liver metastases, but seemed to be less sensitive in the diagnosis of extrahepatic sites^[24-26].

It has been known that carcinoid tumors had a high expression of somatostatin receptors^[27,28]. More than 90% of patients with midgut carcinoids expressed somatostatin receptors detected by autoradiography with iodinated somatostatin analogues as ligands, while the somatostatin receptor expression in foregut carcinoid tumors was less frequent^[29].

Five different subtypes of somatostatin receptors have been cloned. Somatostatin receptor subtype 2 could bind to somatostatin analogues used in clinical practice with high affinity. Subtypes 3 and 5 had an intermediate affinity while subtypes 1 and 4 had low affinity for the available somatostatin analogues^[30].

SRS is a very sensitive method for the demonstration of receptor-positive tumors and their metastases and its diagnostic usefulness in patients with abdominal carcinoid tumors has already been reported^[31,32].

In our study SRS imaging visualized the primary or metastatic sites in 22 out of 31 patients with gastrointestinal and pancreatic carcinoid tumors (detection rate 71.0%) and the results were in concordance with other previously published reports^[31-33].

Conventional imaging was positive in 19 out of 31 patients (detection rate 61.3%).

Our results demonstrate that SRS, compared with conventional imaging, can provide major additional information.

More interestingly, SRS was positive in 71.4% of the primary tumor sites with a statistically significant difference ($P = 0.039$) compared with conventional imaging methods. Lebtahi *et al.* reported also similar results (75%) in a similar group of 38 patients^[34]. Conventional imaging modalities (ultrasonography and upper abdominal CT) are more sensitive in the detection of hepatic metastases. On the other hand SRS is more sensitive in the detection of extrahepatic metastatic sites and can provide additional information for previous unsuspected localizations. Schillaci *et al.*^[35] reported similar results in a group of 18 patients with abdominal carcinoid tumors.

Thus, it is clear that the combination of several conventional imaging techniques with SRS is the method of choice for a better evaluation of patients with carcinoid tumors. For individuals with carcinoid tumors of the digestive tract, gastrointestinal endoscopy is the first line diagnostic tool. Laparotomy can also provide useful information in some cases.

In our study, 2 (chest X-ray/upper abdominal CT scan/SRS and chest CT/upper abdominal CT scan/SRS) out of 8 combinations of imaging modalities yielded an overall sensitivity of 88.75% in the detection of primary and metastatic carcinoid sites. The cost was 1294.93 Euro for the combination of chest X-ray/upper abdominal CT scan/SRS and 1362.75 Euro for the combination of chest CT/upper abdominal CT scan/SRS. Thus, there was a benefit of 67.82 Euro using the first one.

In a similar cost-effectiveness analysis of patients with neuroendocrine tumors, Kwekkeboom *et al.* showed that the comb-

ination of SRS, chest radiography and upper abdominal ultrasound led to the detection of carcinoid lesions in all patients in whom carcinoid lesions could be demonstrated by any means, with a sensitivity of 100% in terms of the number of detected lesions, but the cost analysis was made between the proposed imaging strategy and the most sensitive combination of conventional imaging (chest and abdomen CT scans)^[36].

REFERENCES

- 1 **Wilson JD**, Braunwald E, Isselbacher KJ, Petersdorf RG, Martin JB, Fauci S, Root RK (eds). *Harrison's principles of internal medicine* (12th ed), New York: *McGraw Hill* 1991
- 2 **Pearse AG**, Polak JM, Heath CM. Polypeptide hormone production by "carcinoid" apudomas and their relevant cytochemistry. *Virchows Arch* 1974; **16**: 95-109
- 3 **Vinik AI**, McLeod MK, Fig LM, Shapiro B, Lloyd RV, Cho K. Clinical features, diagnosis and localization of carcinoid tumors and their management. *Gastroenterol Clin N Am* 1989; **18**: 865-896
- 4 **Janson ET**, Oberg K. Long-term management of the carcinoid syndrome. Treatment with octreotide alone and in combination with alpha-interferon. *Acta Oncol* 1993; **2**: 225-229
- 5 **Godwin JD**. Carcinoid tumors. An analysis of 2 837 cases. *Cancer* 1975; **36**: 560-569
- 6 **Moertel CG**. Karnofsky memorial lecture: An odyssey in the land of small tumors. *J Clin Oncol* 1987; **10**: 1502-1522
- 7 **Kvols LK**, Reubi JC. Metastatic carcinoid tumors and the malignant carcinoid syndrome. *Acta Oncol* 1993; **32**: 197-201
- 8 **Akerström G**, Makridis C, Johansson H. Abdominal surgery in patients with midgut carcinoid tumors. *Acta Oncol* 1991; **30**: 547-553
- 9 **Krenning EP**, Bakker WH, Breeman WA, Koper JW, Kooij PP, Ausoma L, Lameris JS, Reubi JC, Lamberts SW. Localization of endocrine-related tumors with radioiodinated analogue of somatostatin. *Lancet* 1989; **1**: 242-244
- 10 **Lamberts SW**, Bakker WH, Reubi JC, Krenning EP. Somatostatin receptor imaging in the localization of endocrine tumors. *N Engl J Med* 1990; **323**: 1246-1249
- 11 **Reubi JC**, Häcki WH, Lamberts SW. Hormone-producing gastro-intestinal tumors contain a high density of somatostatin receptors. *J Clin Endocrinol Metab* 1987; **65**: 1127-1134
- 12 **Reubi JC**, Laissue J, Krenning E, Lamberts SW. Somatostatin receptors in human cancer: incidence, characteristics, functional correlates and clinical implications. *J Steroid Biochem Mol Biol* 1992; **43**: 27-35
- 13 **Reubi JC**, Kvols L, Krenning E, Lamberts SW. Distribution of somatostatin receptors in normal and tumor tissue. *Metabolism* 1990; **39**(Suppl 2): 78-81
- 14 **Bakker WH**, Krenning EP, Breeman WA, Kooij PP, Reubi JC, Koper JW, de Jong M, Lameris JS, Visser TJ, Lamberts SW. *In vivo* use of a radioiodinated somatostatin analogue: dynamics, metabolism and binding to somatostatin receptor-positive tumors in man. *J Nucl Med* 1991; **32**: 1184-1189
- 15 **Bakker WH**, Krenning EP, Breeman WA, Koper JW, Kooij PP, Reubi JC, Klijn JG, Visser TJ, Docter R, Lamberts SW. Receptor scintigraphy with a radioiodinated somatostatin analogue: radiolabeling, purification, biologic activity and *in vivo* application in animals. *J Nucl Med* 1990; **31**: 1501-1509
- 16 **Joseph K**, Stapp J, Reinecke J, Hoffken H, Benning R, Neuhaus C, Trautmann ME, Schwerk WB, Arnold R. Rezeptorszintigraphie bei endokrinen gastroenteropankreatischen Tumoren. *Dtsch Med Wschr* 1992; **117**: 1025-1028
- 17 **Krenning E**, Kwekkeboom D, Bakker W, Breeman WA, Kooij PP, Oei HY, van Hagen M, Postema PP, de Jong M, Reubi JC. Somatostatin receptor scintigraphy with [¹¹¹In-DTPA-D-Phe¹] and [¹²³I-Tyr³]. *Eur J Nucl Med* 1993; **20**: 716-731
- 18 **Kvols L**. Somatostatin-receptor imaging of human malignancies: a new era in the localization, staging and treatment of tumors. *Gastroenterology* 1993; **105**: 1909-1914
- 19 **Nash SV**, Said JW. Gastroenteropancreatic neuroendocrine tumors: a histochemical and immunohistochemical study of epithelial (keratin proteins, carcinoembryonic antigen) and neuroendocrine (neuron-specific enolase, bombesin and

- chromogranin) markers in foregut, midgut and hindgut tumors. *Am J Clin Pathol* 1986; **86**: 415-422
- 20 **Simpson S**, Vinik AI, Marangos PJ, Lloyd RV. Immunohistochemical localization of neuron-specific enolase in gastroenteropancreatic neuroendocrine tumors. Correlation with tissue and serum level of neuron-specific enolase. *Cancer* 1984; **54**: 1364-1369
- 21 **Zimmer T**, Ziegler K, Bader M, Fett U, Hamm B, Riecken EO, Wiedenmann B. Localization of neuroendocrine tumors of the upper gastrointestinal tract. *Gut* 1994; **35**: 471-475
- 22 **Picus D**, Glazer HS, Levitt RG, Husband JE. Computed tomography of abdominal carcinoid tumors. *Am J Roentgenol* 1984; **143**: 581-584
- 23 **McCarthy SM**, Stark DD, Moss AA, Goldberg HI. Computed tomography of malignant carcinoid disease. *J Comput Assist Tomogr* 1984; **8**: 846-850
- 24 **Kressel HY**. Strategies for magnetic resonance imaging of focal liver disease. *Radiol Clin North Am* 1988; **26**: 607-617
- 25 **Kisker O**, Weinel RJ, Geks J, Zacara F, Joseph K, Rothmund M. Value of somatostatin receptor scintigraphy for preoperative localization of carcinoids. *World J Surg* 1996; **20**: 162-167
- 26 **Shi W**, Johnston CF, Buchanan KD, Ferguson WR, Laird JP, Crothers JG, McIlrath EM. Localization of neuroendocrine tumours with [¹¹¹In] DTPA-octreotide scintigraphy (Octreoscan): a comparative study with CT and MRI imaging. *QJM* 1998; **91**: 295-301
- 27 **de Herder WW**, Lamberts SW. Somatostatin and somatostatin analogues: diagnostic and therapeutic uses. *Curr Opin Oncol* 2002; **14**: 53-57
- 28 **Tomassetti P**, Migliori M, Lalli S, Campana D, Tomassetti V, Corinaldesi R. Epidemiology, clinical features and diagnosis of gastroenteropancreatic endocrine tumors. *Ann Oncol* 2001; **12**: s95-s99
- 29 **Reubi JC**, Kvols LK, Waser B, Nagorney DM, Heitz PU, Charboneau JW, Reading CC, Moertel C. Detection of somatostatin receptors in surgical and percutaneous needle biopsy samples of carcinoids and islet cell carcinomas. *Cancer Res* 1990; **50**: 5969-5977
- 30 **Reisine T**, Bell GI. Molecular biology of somatostatin receptors. *Endocr Rev* 1995; **16**: 427-442
- 31 **Kwekkeboom DJ**, Krenning EP, Bakker WH, Oei HY, Kooij PP, Lamberts SW. Somatostatin analogue scintigraphy in carcinoid tumors. *Eur J Nucl Med* 1993; **20**: 283-292
- 32 **Carnaille B**, Nocaudie M, Pattou F, Huglo D, Deveaux M, Marchandise X, Proge C. Scintiscans and carcinoid-tumors. *Surgery* 1994; **116**: 1118-1122
- 33 **Scherubl H**, Bader M, Fett U, Hamm B, Schmidt-Gayk H, Koppenhagen K, Dop FJ, Riecken EO, Wiedemann B. Somatostatin-receptor imaging of neuroendocrine gastroenteropancreatic tumors. *Gastroenterology* 1993; **105**: 1705-1709
- 34 **Lebtahi R**, Cadiot G, Sarda L, Daou D, Faraggi M, Petegnief Y, Mignon M, Le Guludec D. Clinical impact of Somatostatin receptor scintigraphy in the management of patients with neuroendocrine gastroenteropancreatic tumors. *J Nucl Med* 1997; **38**: 853-858
- 35 **Schillaci O**, Scopinaro F, Angeletti S, Tavolaro R, Danieli R, Annibale B, Gualdi G, Delle Fave G. SPECT improves accuracy of somatostatin receptor scintigraphy in abdominal carcinoid tumors. *J Nucl Med* 1996; **37**: 1452-1456
- 36 **Kwekkeboom DJ**, Lamberts SW, Habbema JD, Krenning EP. Cost-effectiveness analysis of somatostatin receptor scintigraphy. *J Nucl Med* 1996; **37**: 886-892

Edited by Wang XL and Chen WW Proofread by Xu FM

• CLINICAL RESEARCH •

Intra-tumor injection of H101, a recombinant adenovirus, in combination with chemotherapy in patients with advanced cancers: A pilot phase II clinical trial

Wei Lu, Shu Zheng, Xu-Feng Li, Jian-Jin Huang, Xiao Zheng, Zhen Li

Wei Lu, Shu Zheng, Xu-Feng Li, Jian-Jin Huang, Cancer Center, Second Affiliated Hospital, Medical College, Zhejiang University, Hangzhou 310009, Zhejiang Province, China

Xiao Zheng, Zhen Li, Zhejiang Cancer Hospital, Hangzhou 310022, Zhejiang Province, China

Supported by China "863" Hi-tech R&D Program, No. 2002AA2Z3304

Correspondence to: Dr. Shu Zheng, Cancer Center, Second Affiliated Hospital, Medical College, Zhejiang University, 88 Jiefang Road, Hangzhou 310009, Zhejiang Province, China. zhengshu@zju.edu.cn

Telephone: +86-571-87784501 Fax: +86-571-87784501

Received: 2004-04-15 Accepted: 2004-05-13

Abstract

AIM: H101, an E1B 55 kD gene deleted adenovirus, has been shown to possess oncolysis activity experimentally and proved to be safe in preliminary phase I study. The current study was designed to evaluate its anti-tumor activity and toxicity in combination with chemotherapy in patients with late stage cancers.

METHODS: H101 5.0×10^{11} virus particles were given by intra-tumor injection daily for five consecutive days at every three-week cycle, combined with routine chemotherapy, to one of the tumor lesions of 50 patients with different malignant tumors. Tumor lesions without H101 injection in the same individuals were used as controls. The efficacy and toxicity were recorded.

RESULTS: Forty-six patients were evaluable with a 30.4% response rate. H101 injection in combination with chemotherapy induced three complete response (CR) and 11 partial response (PR), giving an overall response rate of 28.0% (14/50) among intention-to-treat patients. The response rate for the control lesions was 13.0%, including one case with CR and five cases with PR, which was significantly lower than that for the injected lesions ($P < 0.05$). Main side effects were fever (30.2%) and pain at the injected sites (26.9%). Grade 1 hepatic dysfunction was found in four patients, grade 2 in one patient, and grade 4 in one patient. Hematological toxicity (grade 4) was found in four patients.

CONCLUSION: Intra-tumor injection of the genetically engineered adenovirus H101 exhibits potential anti-tumor activity to refractory malignant tumors in combination with chemotherapy. Low toxicity and good tolerance of patients to H101 were observed.

Lu W, Zheng S, Li XF, Huang JJ, Zheng X, Li Z. Intra-tumor injection of H101, a recombinant adenovirus, in combination with chemotherapy in patients with advanced cancers: A pilot phase II clinical trial. *World J Gastroenterol* 2004; 10(24): 3634-3638

<http://www.wjgnet.com/1007-9327/10/3634.asp>

INTRODUCTION

The fights against tumors are far from being finished. Biotherapy seems to be a potential anticancer weapon, but still needs strengthening. Engineered virus against cancer is one of the most hopeful therapeutic approaches. There are two different methods: (1) to use replication incompetent viruses as delivery agents for therapeutic genes to access to tumors, and (2) to destroy tumor by using replication-selective oncolytic viruses as therapeutic agents themselves^[1,2]. Multiple gene dysfunctions taking part in tumor formation have been known, single gene correction or modification can hardly reverse the malignancy. Viruses engineered for the purpose to replicate only in tumor cells and destroy the cells do not depend on the gene function they take on and have been shown to have great efficacy in both experimental and clinical studies^[3-5].

H101 is a recombinant human type-5 adenovirus (Ad5), in which E1B-55 kDs gene has been totally deleted. The H101 virus produced by Shanghai Sunway Biotech, also contains a deletion of 78.3-85.8 μ m gene segment in the E3 region. The E1B-55kD gene product is responsible for p53-binding and inactivation^[6]. If deleted, the virus would be unable to inactivate p53 for efficient replication in normal cells. However, cancer cells lacking functional p53 would hypothetically be sensitive to viral replication and subsequent cytopathic effects. p53 mutation is the most common genetic abnormality identified in human cancer^[7]. This characteristic can be utilized for H101 to identify the target. *In vitro* and *in vivo* studies have shown that H101 has anticancer activity, and has been proved to be safe through a five dosage of 5.0×10^7 - 1.5×10^{12} virus particles (VP)/d within 5 consecutive days in a clinical trial^[8]. We carried out this clinical trial to evaluate anti-tumor activity of H101 and its toxicity in combination with chemotherapy in patients with late stage cancers.

MATERIALS AND METHODS

Enrollment criteria

Histologically confirmed late stage cancer patients with more than two measurable lesions (at least one could be injected with H101), who had recurrent disease after surgery and/or radiotherapy for the primary tumor, or had progressed at or within 8 wk after completion of chemotherapy and/or radiotherapy, were recruited. Patients had to be ≥ 18 years old, with performance status above grade 2 according to The Eastern Cooperative Oncology Group (ECOG) standard, and life expectancy of ≥ 3 mo. Normal hematological and renal functions were also required. An informed consent was obtained from each patient or from the patient's legal guardian prior to enrollment. The p53 gene status was not critical for enrollment, because there were factors that inhibited p53 protein function including expression of the human papilloma virus E6 protein or *mdm-2* gene amplification^[9]. Institutional Review Board approval of the protocol and consent form were granted. This study was also approved by the State Food and Drug Administration of China.

Baseline assessment

Baseline assessments were made prior to treatment, but these

results were not used as enrollment criteria. Baseline blood tests such as complete blood counts, neutralizing antibody titers, electrolytes, blood urea nitrogen, creatinine, and liver function tests were performed. In addition, plain chest radiography, electrocardiogram and type B ultrasonography of upper abdomen were performed.

H101

H101 was formulated as a sterile viral solution in PBS buffer and kept at -20°C . Each vial contained 0.5 mL of virus solution with 5×10^{11} VP and titered $<1:60$ TCID₅₀. Sterile purified lots of virus were produced for human clinical use by Shanghai Sunway Biotech (Shanghai, China), and tested for the titer, sterility, and general safety by National Institute For the Control of Pharmaceutical and Biological Products (Beijing, China).

Treatment regimen

In each patient, the most symptomatic and/or largest tumor mass was injected with H101, and the patient was treated together with routine systemic chemotherapy simultaneously. The tumor for injection was mapped into five equally spaced sections. Local anesthesia was applied to the skin as needed. The tumor was injected with 5×10^{11} virus particles into one section per day for 5 consecutive days, and these injections were repeated every 3 wk as one treatment cycle. The suspension volume of saline used for H101 administration was normalized to 30% of the estimated volume of the tumor mass to be injected. Tumor volume was estimated as: $1/2$ (maximal transverse diameter \times maximal vertical diameter \times depth).

Tumor assessments and toxicity evaluation

Tumor masses were measured serially by either physical examination or radiographic scanning (computed tomography or magnetic resonance imaging), whichever the principal investigator deemed most accurate for the measurement of the injected tumor mass. In general, superficial lesions were measured by physical examination, and deep tumors were measured most accurately by radiographic scanning. The tumor mass injected with H101 (injected lesion) and non-injected lesion were evaluated independently. Tumor measurements were performed either every 3 wk (physical examination) while patients were on active study treatment. After treatment completion, patients' tumor (s) were assessed every 4 wk or sooner if signs/symptoms of progression became evident. Radiographic scanning was assessed by independent radiologists, who were not investigators on the study. The degree of response within injected tumors was categorized as follows: complete regression (CR), complete disappearance of measurable tumor; partial regression (PR), $\geq 50\%$ but $<100\%$ decrease in cross-sectional tumor area; minor response (MR), $<50\%$ but $\geq 25\%$ decrease in tumor area; stable disease (SD), $<25\%$ decrease or 25% increase in tumor area; and progressive disease (PD), $\geq 25\%$ increase in tumor area *versus* the baseline area. Toxicity was assessed using the National Cancer Institute Toxicity Criteria.

Additional follow-up after treatment initiation

Neutralizing antibody titers were repeated at the end of each cycle, and viral dissemination in blood was tested immediately after injection on d 5 and d 22 for each cycle. The routine blood tests were repeated every week. Fine-needle aspirate biopsies at the injected sites on day 22 of the first treatment cycle were optional, based on patients' consent because of ethical considerations. These biopsies were analyzed for type Ad5 coat protein by immunohistochemistry.

PCR detection of H101 viral genomes in plasma

The blood taken before and one day after injection were collected

for PCR detection of H101 genomes (the amplicon overlaps the E1B region deletion and does not detect wild-type adenovirus sequences). The left primer was 5'ctggcgcagaagtattccat3', at Tm 60.24 $^{\circ}\text{C}$ and the right primer was 5'gtcacatccagcatcacagg3', at Tm 60.12 $^{\circ}\text{C}$. Viral DNA was extracted from samples, using the Sangon DNA mini kit (Shanghai, China). The amplification procedure was: at 94 $^{\circ}\text{C}$ for 10 min, then 94 $^{\circ}\text{C}$ for 60 s, 55 $^{\circ}\text{C}$ for 45 s, 72 $^{\circ}\text{C}$ for 60 s for 35 cycles; then at 72 $^{\circ}\text{C}$, for 10 min. The products were analyzed by 10 g/L agarose electrophoresis. The lower limit of detection was 100 particles of H101 per microlitre plasma.

Detection of Ad-specific neutralizing antibodies by ELISA

Triplicate plasma (5 μL) taken before and on d 22 after injection were collected, and tested for Ad-specific antibodies according to the procedures provided by Jingmei Biotech (Shenzhen, China). The absorbance at 450 nm was read on a Bio-Rad Model 550 microplate reader. The positive results were those above or equal to the average of A_{450nm} negative control plus 0.10. Otherwise, the samples were defined as negative.

Immunohistochemistry for Ad5

Injection site fine-needle aspiration biopsies were formalin-fixed, paraffin-embedded and cut into sections. Sections were then deparaffinized and hydrated. Slides were subjected to antigen retrieval at 120 $^{\circ}\text{C}$ for 10 min in citrate buffer and incubated with an Ad5 monoclonal antibody (NeoMarker, America) for 90 min at room temperature. This was followed by incubation with a biotinylated goat anti-mouse secondary antibody, and the streptavidin/horseradish peroxidase conjugate, then mounted in DPX mounting medium (BDH Chemicals, America). The percentage of brown-stained cells (positive for Ad5) was determined by counting the cells under high-power magnification ($\times 40$) of microscope. The average percentage of three high-power field assessments was then calculated. Tumors that had greater than 10% of positively stained cells were considered to be Ad5 positive.

Statistical analysis

All patients enrolled were calculated under the ITT principle. The rates were compared by χ^2 test.

RESULTS

Patient characteristics

Totally, 50 patients were enrolled, including 18 with head and neck cancer, eight esophageal cancer, five gastric cancer, five lung cancer, three colorectal cancer, three breast cancer, three soft tissue sarcoma, two malignant melanoma, one ovarian cancer, one lymphoma and one chordoma. Most cancers were at end-stage. The head and neck cancer and esophageal cancer enrolled were all squamous carcinoma. Seventy percent of patients were males. The median age was 52 years. All patients had ECOG Performance Status of grade 0-2. Thirty-nine (78%) patients had received pretreatment before, and 31 (62%) had received more than two kinds of treatment. The tumor mass had a median cross-sectional area of 12.5 cm² (range, 1.43-360 cm²) (Table 1).

Tumor response

Overall, 46 patients were evaluable. The response rate (CR+PR) among these patients was 30.4% (14/46), and the overall response rate according to ITT principle was 28.0%. For the control lesions, the response rate was 13.0%, which was significantly lower than the H101 treated lesions ($\chi^2 = 4.08$, $P < 0.05$) (Table 2). In the 14 cases with effective H101 injection, there were one CR, three PRs, two MRs, three SDs, and five PDs for

the control lesions, respectively. In these patients, combination of H101 injection with chemotherapy was more effective than chemotherapy alone ($\chi^2 = 15.6, P < 0.001$). The response rates to H101 injection combined with chemotherapy were different, no effect for gastric cancer was found in this study (Table 3). Figure 1 shows regression of the injected lesion in a patient with head and neck cancer.

Table 1 Patients' demographics

Characteristic	
Age (yr)	
Median	52
Range	18-76
Sex	
Male (%)	35 (70%)
Female (%)	15 (30%)
ECOG Performance Status	
Grade 0	15 (30%)
Grade 1	21 (42%)
Grade 2	14 (28%)
Pretreatment	
Total	39 (78%)
Surgical	24 (48%)
Chemotherapy	37 (74%)
Radiotherapy	20 (40%)
Biotherapy	8 (16%)
Two or more treatment	31 (62%)
Tumor size (cm ²)	
Median	12.5
Range	1.43-360

Table 2 Response of H101 injected lesion and control lesion

Lesion	n	Median area (cm ²)	Efficacy					Response rate (%)
			CR	PR	MR	SD	PD	
H101 injection	46	12.5	3	11	11	13	8	30.4
Control	46	11.3	1	5	7	21	12	13.0

CR, complete regression; PR, partial regression; MR minor response; SD, stable disease; and PD, progressive disease. Response rate was calculated from cases with CR and PR over cases in each group.

Table 3 Efficacy of 46 evaluable patients treated with H101 and chemotherapy

Type of tumor	n	Response (CR+PR)
SCCHN ¹	15	4
Esophageal cancer	8	3
Gastric cancer	5	0/
Lung cancer	4	1
Colorectal cancer	3	1
Breast cancer	3	1
Soft tissue sarcoma	3	1
Malignant melanoma	2	1
Lymphoma	1	1
Chordoma	1	1
Ovarian cancer	1	0

¹SCCHN, squamous cell carcinoma of head and neck.

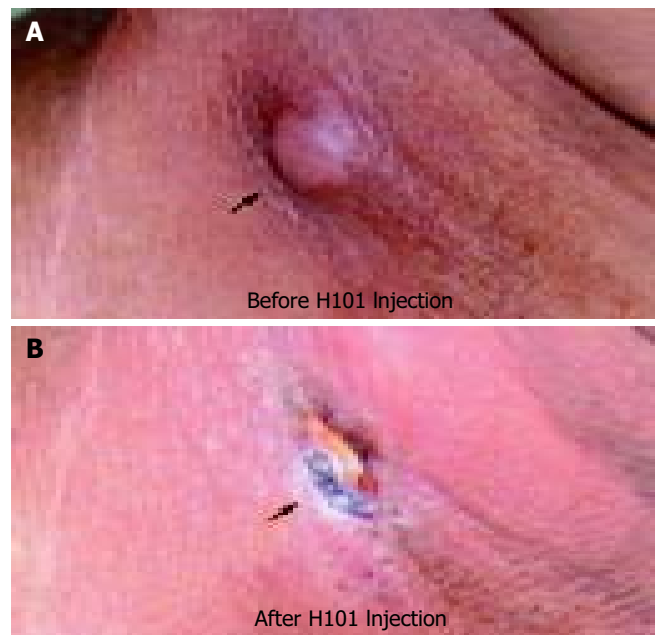


Figure 1 A 51 yr-old male patient with neck metastasis of soft palate squamous carcinoma. About 3 mo before enrollment, he had been treated with radiotherapy and Docetaxel plus DDP, but the metastatic tumor did not show any reaction to the treatment. Before the enrollment the tumor was about 2.2×1.5 cm² (A, arrow), then the tumor was injected with H101 5×10¹¹VP per day for 5 consecutive days with systemic administration of 5-Fu and DDP, after one cycle treatment the tumor regressed (B, arrow).

Adverse reaction

The most frequent adverse reaction was fever (30.2%), injection site pain (26.9%), flu-like symptoms (26.4%), nausea and vomiting (34.0%), leucopenia (49.1%), liver dysfunction (5.7%), alopecia (13.2%) (Table 4). Fever was moderate, which appeared at about 12 h post H101 injection, persisted for 2-4 h, and then returned to normal without treatment. There was a significant difference in the regression rate between patients with fever (69.2%, 9/13) and those without fever (21.2%, 7/33) ($\chi^2 = 9.48, P < 0.005$).

Table 4 Treatment-related toxicity

Adverse event	Grade				Total (%)
	I	II	III	IV	
Fever	10	5	1	0	16 (30.2)
Injection site pain	12	2	0	0	14 (26.4)
Nausea and vomiting	13	5	0	0	18 (34.0)
Leucopenia	12	7	3	4	26 (49.1)
Liver dysfunction	2	0	0	1	3 (5.7)
Flu-like symptom	13	2	0	0	15 (28.3)
Alopecia	3	3	1	0	7 (13.2)

Humoral immune response and plasma H101 viral genome

Fourteen patients were tested for the Ad-specific neutralizing antibody. Three (21.4%) of them were positive at baseline. Another six turned to be positive on day 22. Two patients positive at the baseline and two negative patients experienced tumor regression, and thus there was no correlation between baseline neutralizing antibody titers and induction of tumor response. Sixteen patients were tested for plasma H101 viral genome before injection and 30 min after. Only six cases were positive after injection (Table 5). All these patients were positive for blood Ad-specific neutralizing antibody on d 22.

Table 5 Humoral immune response and plasma H101 viral genome test

	Before injection		After injection	
	Negative	Positive	Negative	Positive
Ad neutralizing titer	11	3	5	9
Plasma H101 PCR	11	0	7	4

H101 immunohistochemistry detection

Totally, three fine-needle aspiration biopsies of tumor were obtained at the end of treatment on d 22 or d 44, and detected for Ad5 coat protein by immunohistochemistry for adenovirus presence. Two of them were positive (Figure 2).

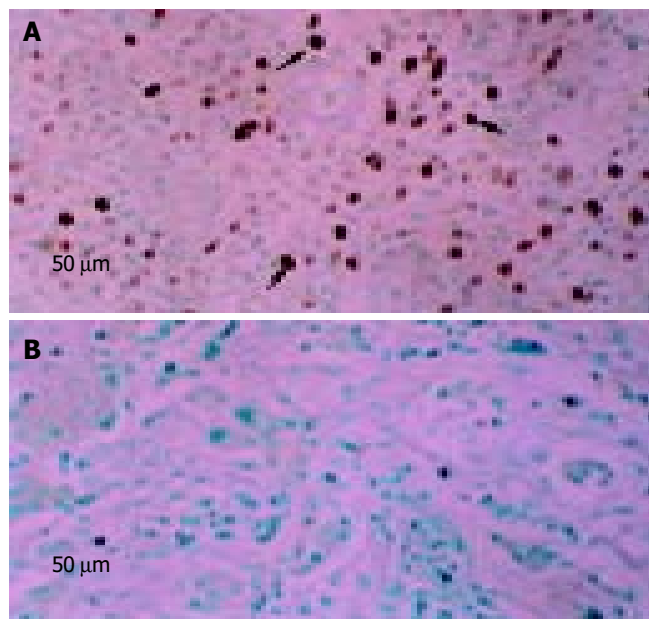


Figure 2 Immunohistochemical staining of Ad5 capsid from the fine-needle aspiration of the tumor tissue injected with H101 at the end of treatment cycle. The dark-brown stained granules (arrows in Figure A) represent a positive staining indicating adenovirus replication and package in the tumor cells. However negative staining was also obtained in one of the three samples (B).

DISCUSSION

Selective replication of E1B deleted adenovirus in the p53 dysfunctional human cancer for cancer therapy is one of promising treatment approaches. Its safety has been shown in a number of clinical trials^[5,10-12]. Although anticancer activity of the virus has been proved, the clinical efficacy is still not predominant. Therefore, the oncolytic ability needs to be enhanced. Current studies are focusing on arming these viruses with therapeutic genes to increase its potency.^[13-15]

But before that, the virus itself can be reinforced by augmentation or elimination of specific viral functions to enhance the anticancer efficacy. To enhance the virus-induced host anti-tumor immune response is one of the key points. However, the roles of the immune response to virotherapy are profound. Cutting down the functions of the virus to escape from immune surveillance can impede the spread of viral infection on the one hand, but augment tumor cell destruction through the recruitment of T cells “vaccinated” against tumor antigens on the other^[16]. The E3 region is related to the inhibition of host immunity, which enhances the virus replication and spread in tumor^[17]. But this is not necessary for intra-tumor injection of oncolytic viral. The virus replication and spread effect can be enhanced by

repeated injection. By sacrificing the spread ability, the virus may activate the host immune response to virus infected tumor cells and help the host immune system to recognize tumor cells themselves, and thus may benefit patients under such therapy. Metastasis is prevalent in malignant tumor patients, which is the main cause of treatment failure or even death. Moreover, patients may have more than one tumor lesion, and the lesion that cannot be injected could exist. Therefore, the ability of activating the host immune response seems crucial. So treatment with the E3 region deleted adenovirus, H101, may have additional benefit to patients.

The main purpose of this pilot study was to test the effect of H101 on a wide type of advanced cancers. Results showed that the total response rate was only 28.0% under the ITT principle, which was significantly higher than the lesions that received chemotherapy alone ($P < 0.05$). This indicates that H101 may have potential anticancer activity. The total regression rate observed is not salient for the treatment. This may be due to the late stage of the diseases, and most of the patients had been vigorously treated previously but failed at last. The other reason is the wide enrollment of the tumor types, some of which might not be sensitive to H101. For instance, gastric cancer showed no response.

However, some patients presented notable therapeutic efficacy without grievous adverse reactions. Moreover, in those who had fever during H101 injection, the efficacy was significantly higher than those who did not have fever ($P < 0.005$). Although there is not enough evidence to estimate the effect of H101 on host immunity to tumors, our results suggest that there is a relationship between the immune reaction to H101 and the efficacy, which was not well recognized in previous studies. In the beginning of last century, it was noticed that patients with various malignancies experienced spontaneous tumor regression after rabies vaccination, a viral illness or even bacterial infection^[18,19]. In these cases, virus infection may activate the host immune system, and elevated cell-mediated immunity may play a role in the tumor regression. But the mechanism is still unclear. On the basis of those results, immune modulation strategies should be further studied and developed.

Our study also shows that H101 intra-tumor injection is well tolerated. No severe toxicity was observed, and the main adverse reactions that related to H101 were injection site pain, nausea, fever and flu-like symptoms. Fever and flu-like symptoms were obviously caused by the virus injection and consequently transitory viraemia. H101 presence did not cause severe inflammation in peritumoral normal tissue, despite multiple directive injection. Thus, H101 may benefit the patient without adding severe affliction in clinical application.

Treatment for cancers with the recombinant oncolytic adenovirus is hopeful, but still immature. Experiences should be accumulated before it is applied in cancer therapy. Since patients enrolled in our clinical trial were in their end-stage of diseases, there were difficulties in patient selection and unifying the chemotherapy drugs due to ethical consideration, and immunosuppression was prevalent in those patients. The clinical benefit of intra-tumor injection with H101 should be further determined in randomized trials and, possibly, in earlier stage patients. The dosage, medication methods, treatment cycle and combined chemotherapy or immunotherapy should be explored in further studies as well. Genetically engineered and reinforced viruses may become a novel therapeutic platform for the treatment of cancers.

REFERENCES

- 1 Roth J, Cristiano RJ. Gene therapy for cancer: what have we done and where are we going? *J Natl Cancer Inst* 1997; **89**: 21-39

- 2 **Kirn D**, Martuza RL, Zwiebel J. Replication-selective virotherapy for cancer: biological principles, risk management and future directions. *Nat Med* 2001; **7**: 781-787
- 3 **Makower D**, Rozenblit A, Kaufman H, Edelman M, Lane ME, Zwiebel J, Haynes H, Wadler S. Phase II clinical trial of intralesional administration of the oncolytic adenovirus ONYX-015 in patients with hepatobiliary tumors with correlative p53 studies. *Clin Cancer Res* 2003; **9**: 693-702
- 4 **Habib NA**, Mitry RR, Sarraf CE, Jiao LR, Havlik R, Nicholls J, Jensen SL. Assessment of growth inhibition and morphological changes in *in vitro* and *in vivo* hepatocellular carcinoma models post treatment with dl1520 adenovirus. *Cancer Gene Ther* 2002; **9**: 414-420
- 5 **Hamid O**, Varterasian ML, Wadler S, Hecht JR, Benson A 3rd, Galanis E, Uprichard M, Omer C, Bycott P, Hackman RC, Shields AF. Phase II trial of intravenous CI-1042 in patients with metastatic colorectal cancer. *J Clin Oncol* 2003; **21**: 1498-1504
- 6 **Dobner T**, Horikoshi N, Rubenwolf S, Shenk T. Blockage by adenovirus E4orf6 of transcriptional activation by the p53 tumor suppressor. *Science* 1996; **272**: 1470-1473
- 7 **Hollstein M**, Sidransky D, Vogelstein B, Harris CC. p53 mutations in human cancer. *Science* 1991; **253**: 49-53
- 8 **Yuan ZY**, Zhang L, Li S, Qian XZ, Guan ZZ. Safety of an E1B deleted adenovirus administered intratumorally to patients with cancer. *Aizheng* 2003; **22**: 310-313
- 9 **Leach FS**, Tokino T, Meltzer P, Burrell M, Oliner JD, Smith S, Hill DE, Sidransky D, Kinzler KW, Vogelstein B. p53 mutation and MDM2 amplification in human soft tissue sarcomas. *Cancer Res* 1993; **53**: 2231-2234
- 10 **Kirn D**. Oncolytic virotherapy for cancer with the adenovirus dl1520 (Onyx-015): results of phase I and II trials. *Expert Opin Biol Ther* 2001; **1**: 525-538
- 11 **Nemunaitis J**, Khuri F, Ganly I, Arseneau J, Posner M, Vokes E, Kuhn J, McCarty T, Landers S, Blackburn A, Romel L, Randlev B, Kaye S, Kirn D. Phase II trial of intratumoral administration of ONYX-015, a replication-selective adenovirus, in patients with refractory head and neck cancer. *J Clin Oncol* 2001; **19**: 289-298
- 12 **Khuri FR**, Nemunaitis J, Ganly I, Arseneau J, Tannock IF, Romel L, Gore M, Ironside J, MacDougall RH, Heise C, Randlev B, Gillenwater AM, Bruso P, Kaye SB, Hong WK, Kirn DH. A controlled trial of intratumoral ONYX-015, a selectively-replicating adenovirus, in combination with cisplatin and 5-fluorouracil in patients with recurrent head and neck cancer. *Nat Med* 2000; **6**: 879-885
- 13 **Hermiston TW**, Kuhn I. Armed therapeutic viruses: strategies and challenges to arming oncolytic viruses with therapeutic genes. *Cancer Gene Ther* 2002; **9**: 1022-1035
- 14 **Stubdal H**, Perin N, Lemmon M, Holman P, Bauzon M, Potter PM, Danks MK, Fattaey A, Dubensky T, Johnson L. A prodrug strategy using ONYX-015-based replicating adenoviruses to deliver rabbit carboxylesterase to tumor cells for conversion of CPT-11 to SN-38. *Cancer Res* 2003; **63**: 6900-6908
- 15 **Bauzon M**, Castro D, Karr M, Hawkins LK, Hermiston TW. Multigene expression from a replicating adenovirus using native viral promoters. *Mol Ther* 2003; **7**: 526-534
- 16 **John TM**, Kenneth KT. Viral Oncolysis. *The Oncologist* 2002; **7**: 106-119
- 17 **Benedict CA**, Norris PS, Prigozy TI, Bodmer JL, Mahr JA, Garnett CT, Martinon F, Tschopp J, Gooding LR, Ware CF. Three adenovirus E3 proteins cooperate to evade apoptosis by tumor necrosis factor-related apoptosis-inducing ligand receptor-1 and -2. *J Biol Chem* 2001; **276**: 3270-3278
- 18 **Chabalgoity JA**, Dougan G, Mastroeni P. Live bacteria as the basis for immunotherapies against cancer. *Expert Rev Vaccines* 2002; **1**: 495-505
- 19 **Lamon EW**, Hale P, Whitten HD. Antibody-dependent, cell-mediated cytotoxicity with autochthonous lymphocytes and sera after infection with moloney sarcoma virus. *J Natl Cancer Inst* 1976; **56**: 349-355

Edited by Xia HHX and Zhu LH Proofread by Xu FM

Monocyte chemotactic protein-1 and soluble adhesion molecules as possible prognostic markers of the efficacy of antiviral treatment in chronic hepatitis C

Anatol Panasiuk, Danuta Prokopowicz, Bozena Panasiuk

Anatol Panasiuk, Danuta Prokopowicz, Bozena Panasiuk,
Department of Infectious Diseases, Medical University of Bialystok,
15-540 Bialystok, Zurawia Str., 14, Poland

Correspondence to: Dr. Anatol Panasiuk, Department of Infectious
Diseases, Medical University of Bialystok, 15-540 Bialystok, Zurawia
Str., 14, Poland. apanasiuk@wp.pl

Telephone: +4885-7416-921 **Fax:** +4885-7416-921

Received: 2004-02-20 **Accepted:** 2004-04-09

Abstract

AIM: To explain the role of Monocyte chemotactic protein-1 (MCP-1) and soluble adhesion molecules in chronic hepatitis C during the treatment of interferon alpha (IFN α) 2 b and ribavirin (RBV).

METHODS: Concentrations of MCP-1, soluble adhesion molecules intercellular adhesion molecule-1 (sICAM-1), sP-selectin, interleukin (IL) 6, and IL10 in serum were estimated in the group of 40 patients with chronic hepatitis C treated with IFN α 2 b and RBV in 0, 16, 32, 48 wk of the therapy.

RESULTS: In chronic hepatitis C, before and during the treatment, the serum levels of MCP-1 and sP-selectin in responders were similar to those of healthy subjects. In non-responders (NR), MCP-1 increased in the course of IFN α +RBV treatment, differences were statistically significant as compared to responders. MCP-1 correlated statistically with the activity of periportal inflammation ($r = 0.35$, $P < 0.05$) but not with staging of liver fibrosis. sICAM-1 positively correlated with inflammatory activity and fibrosis in NR. sP-selectin did not correlate with histological findings in the liver. The MCP-1 correlated with the soluble form of sP-selectin concentrations ($r = 6$, $P < 0.001$) and with IL-10 level in NR ($r = 0.4$, $P < 0.05$). There was no correlation observed between the concentration of MCP-1 and sICAM-1, IL-6 during the treatment.

CONCLUSION: MCP-1 concentration may be a prognostic marker of the efficacy of IFN+RBV therapy in patients with chronic hepatitis C.

Panasiuk A, Prokopowicz D, Panasiuk B. Monocyte chemotactic protein-1 and soluble adhesion molecules as possible prognostic markers of the efficacy of antiviral treatment in chronic hepatitis C. *World J Gastroenterol* 2004; 10(24): 3639-3642
<http://www.wjgnet.com/1007-9327/10/3639.asp>

INTRODUCTION

Alteration of the immune system in chronic hepatitis C patients may underlie their inadequate response to antiviral therapy. The factors responsible for the persistence of HCV infection and low response to interferon alpha treatment are poorly understood. Circulating monocytes/macrophages are important

for the host immune responses to HCV. HCV-RNA was detected in mononuclear cells of chronically infected patients^[1]. It seems that monocyte functioning impairment is a decisive factor of chronic HCV infection and lack of positive therapeutic response. Monocytes might be a reservoir of the virus and the source of re-infection after IFN treatment^[2]. In chronic hepatitis C, IFN-alpha mRNA was decreased in liver tissues and mononuclear cells significantly increased in peripheral blood. It might result in the inhibition of antiviral immune mechanisms in the liver and enable HCV infection persistence in monocytes^[3]. Some responders revealed, with negative HCV-RNA in blood serum, the presence of RNA virus in peripheral blood monocytes.

Hepatitis C virus chronic infection is associated with functional impairment of peripheral blood mononuclear cells. The application of IFN alpha could lead to HCV-RNA reduction in monocytes^[4]. Elimination of HCV in monocytes after 6-month treatment might be a coefficient of efficiency of the therapy^[5].

Chronic liver diseases are associated with increased hepatic and monocytic expression of monocyte chemotactic protein 1 (MCP-1). MCP-1 level was higher in hepatic veins than in peripheral blood and occurred in severe cases of liver diseases^[6]. Hepatic expression of MCP-1 is up-regulated during chronic HCV infection mainly in activated hepatic stellate cells (HSC). In chronic hepatitis C with advanced fibrosis and inflammation, hepatic MCP-1 mRNA levels were significantly higher^[7]. Peripheral blood monocytes and activated HSC are the source of MCP-1. Monocyte chemotactic protein-1 recruits monocytes and lymphocytes to damaged area in the liver tissue. Profibrinogenic properties of MCP-1 could be reflected by the induction of HSC chemotaxis and its transformation to myofibroblasts^[8].

Adhesion molecules are proteins expressed on a variety of cells, which mediate the interaction between endothelial cells with lymphocytes, monocytes and leukocytes^[9,10]. Intracellular adhesion molecule-1 (ICAM-1), a member of the immunoglobulin superfamily participates in the immunological system, cell-to-cell communication and in inflammatory responses. Many of proinflammatory proteins (IL-1, TNF α , GM-CSF) generated by leukocytes, monocytes, macrophages could enhance the expression of adhesion molecules on cells and in soluble form in circulation^[10]. Activated blood platelets which constitute inflammatory cells are the source of P-selectin^[11]. Soluble ICAM-1 and sP-selectin, secreted from activated cells or expressed on the microparticles, transmit signals from inflammation sites to peripheral circulating monocytes, lymphocytes and others cells. In viral hepatitis, cell-mediated responses could lead to accumulation of activated immunocompetent cells into the hepatic parenchyma. This phenomenon could cause viral elimination and/or focal liver damage^[12,13].

The aim of the study was to estimate the monocyte chemotactic protein-1 in correlation with adhesion molecules, such as sICAM-1, sP-selectin and with cytokine Th2 (IL-6, IL-10) in chronic hepatitis C during IFN alpha and ribavirin treatment. Correlation of the factors and histological staging and grading in liver tissue was also analyzed. The factor concentrations in responders (R) and non-responders (NR) were analyzed as well.

MATERIALS AND METHODS

Examinations were performed in 40 patients with chronic hepatitis C (16 women, 24 men), aged 36 ± 12 years. Chronic hepatitis was confirmed by HCV infection persisting for longer than 6 mo (HCV-RNA positive) and increased ALT values. Blind liver biopsies were done by means of the Hepafix System (Braun, Melsungen, Germany) before the treatment. Histopathological inflammatory activity (grading, 0-4 scale) and fibrosis grade (staging, 0-4 scale) were evaluated in accordance with the classification of chronic viral hepatitis according to Scheuer classification^[14]. Patients were divided into responders (R) and non-responders (NR) according to their sustained response to a course of interferon alpha 2 b (3 MU three times weekly for 48 wk, Rebetrone, Schering-Plough Corporation, USA) with ribavirin (1.2 g/d for 48 wk, Rebetrone, Schering-Plough Corporation, USA) treatment.

The levels of monocyte chemotactic protein-1, soluble intracellular adhesion molecule-1, soluble form of P-selectin, and cytokines IL-6 and IL-10 were determined by ELISA method in blood serum in 0-16-32-48 wk of the therapy. Moreover, routine biochemical examinations concerning the grade of liver damage were performed. Ethical approval for research was obtained from local Ethics Committee in Medical University.

Statistical analysis

The results were presented as mean \pm SD. The statistical analysis was performed using Student's *t*-test for pairs, and the correlation by using parametric Spearman's test.

RESULTS

MCP-1 in chronic hepatitis C

MCP-1 concentrations before and during the treatment in non-responders were higher than those in responders and increased during the treatment (Table 1). MCP-1 concentrations in R were comparable to the values observed in the controls. The second half of the treatment showed the statistically significant increase in MCP-1 in R as compared to the control group. However, it diminished to normal values at the end of the treatment (statistically significant difference to NR, $P < 0.05$). There was no correlation between MCP-1 and ALT level, prothrombin index, leukocyte and platelet count. There was a positive

correlation between MCP-1 and periportal inflammatory activity in R (Table 2). However, no correlation was observed between MCP-1 and the grade of fibrosis and periportal inflammatory activity. A positive correlation was observed between MCP-1 and sP-selectin and IL-10 in NR in the second half of the therapy (examinations III and IV; $r = 0.6$, $P < 0.001$, Spearman test). A correlation between MCP-1 level and ICAM concentration and IL-6 in chronic hepatitis C during treatment was not observed.

Table 2 Correlation of adhesion molecules, cytokines and MCP-1 levels with liver histopathology in responders (R) and non-responders (NR)

		Grading (inflammation)					
		Periportal		Intralobular		Staging (fibrosis)	
		R	NR	R	NR	R	NR
sICAM-1	<i>r</i>	<i>N</i>	0.36	0.38	0.56	<i>N</i>	0.32
	<i>P</i>	<i>N</i>	<0.05	<0.05	<0.01	<i>N</i>	<0.05
MCP-1	<i>r</i>	0.35	<i>N</i>	<i>N</i>	<i>N</i>	<i>N</i>	<i>N</i>
	<i>P</i>	<0.05	<i>N</i>	<i>N</i>	<i>N</i>	<i>N</i>	<i>N</i>
IL-6	<i>r</i>	<i>N</i>	<i>N</i>	0.53	<i>N</i>	<i>N</i>	0.38
	<i>P</i>	<i>N</i>	<i>N</i>	<0.01	<i>N</i>	<i>N</i>	<0.05
IL-10	<i>r</i>	<i>N</i>	<i>N</i>	<i>N</i>	<i>N</i>	<i>N</i>	<i>N</i>
	<i>P</i>	<i>N</i>	<i>N</i>	<i>N</i>	<i>N</i>	<i>N</i>	<i>N</i>
sP-selectin	<i>r</i>	<i>N</i>	<i>N</i>	<i>N</i>	<i>N</i>	<i>N</i>	<i>N</i>
	<i>P</i>	<i>N</i>	<i>N</i>	<i>N</i>	<i>N</i>	<i>N</i>	<i>N</i>

r -statistical correlation, Spearman test, $P < 0.05$ statistical significant.

sICAM-1 and sP-selectin in chronic hepatitis C

sICAM-1 concentrations were significantly higher in R than in NR and the controls. During IFNalpha+RBV treatment, sICAM-1 level decreased in both groups. Responders revealed its decrease, which was statistically significant ($P < 0.0001$) as compared to non-responders. However, there was a positive correlation between sICAM-1 concentrations and intralobular and periportal inflammatory activities and fibrosis in responders, which was not observed in non-responders. sICAM-1 and ALT levels, leukocytes, and platelet count showed a positive correlation.

Table 1 Levels of MCP-1, sICAM-1, sP-selectin, IL-6 and IL-10 in patients with chronic hepatitis C during IFN+RBV therapy in responders (R) and non-responders (NR)

		0-wk	16-wk	32-wk	48-wk	Control
sICAM-1 (pg/mL)	NR	434 \pm 104 ^{ab}	372 \pm 111 ^{ab}	404 \pm 87 ^b	389 \pm 77 ^b	230 \pm 29
	R	527 \pm 109 ^{ab}	433 \pm 87 ^{ab}	353 \pm 98 ^b	363 \pm 99	
sP-selectin (pg/mL)	NR	240 \pm 101 ^{ab}	137 \pm 47	145 \pm 33	147 \pm 41	144 \pm 75
	R	144 \pm 57 ^a	131 \pm 68	131 \pm 58	23 \pm 47	
MCP-1 (pg/mL)	NR	290 \pm 91	365 \pm 124 ^{ab}	315 \pm 61	325 \pm 50 ^a	268 \pm 109
	R	281 \pm 84	285 \pm 55 ^a	335 \pm 32 ^b	286 \pm 59 ^a	
IL10 (pg/mL)	NR	0.45 \pm 0.46 ^a	0.81 \pm 0.54	0.77 \pm 0.68	0.9 \pm 0.63	0.62 \pm 0.83
	R	0.88 \pm 0.78 ^a	0.89 \pm 0.74	0.69 \pm 0.73	1.01 \pm 0.77	
IL6 (pg/mL)	NR	0.65 \pm 0.61 ^{ab}	2.21 \pm 0.94 ^{ab}	1.07 \pm 1.68 ^b	1.56 \pm 1.32 ^b	0.22 \pm 0.49
	R	0.16 \pm 0.37 ^{ab}	0.76 \pm 0.69 ^{ab}	0.77 \pm 0.55 ^b	1.05 \pm 1.21 ^b	
ALT(IU/mL)	NR	82 \pm 40	26 \pm 17	23 \pm 10	61 \pm 91	32 \pm 6
	R	60 \pm 30	21 \pm 6	24 \pm 6	22 \pm 6	
Prothrombin index (%)	NR	96 \pm 23	97 \pm 6	98 \pm 11	99 \pm 10	98 \pm 6
	R	5 \pm 7	90 \pm 10	83 \pm 13	90 \pm 7	
Blood platelet (G/L)	NR	196 \pm 21	189 \pm 45	190 \pm 52	179 \pm 51	203 \pm 45
	R	196 \pm 21	189 \pm 45	190 \pm 52	17 \pm 51	

a-statistically significant differences between responders (R) and non-responders (NR), Student's *t* test, ^a $P < 0.05$, *b*-statistically significant differences compared to healthy, Student's *t* test, ^b $P < 0.01$.

The concentrations of sP-selectin were significantly higher in non-responders than in responders. During the treatment, sP-selectin concentrations decreased in both groups. Its concentrations in R were comparable to the control group and there was no correlation between histological changes in the liver and sP-selectin concentrations.

Serum Th2 interleukins (IL-6, IL-10) in chronic hepatitis C

The concentrations of IL-6 before and during the treatment were lower in R than in NR. Its levels in R were 8 times higher during the treatment while IL6 concentrations were significantly higher in NR than in R ($P < 0.02$) and during the treatment it increased twice. There was a positive statistical correlation between IL-6 concentrations and intralobular inflammatory activity in R, and fibrosis in NR. IL-6 level, leukocyte count, and prothrombin index showed a positive correlation.

IL-10 concentrations before the treatment were statistically higher in R than in NR ($P < 0.05$). Although IL-10 values increased during the therapy, there was a temporary decrease in IL-10 concentrations both in R and in NR during the second half of the treatment. There was no statistical correlation between IL-10 concentrations and histological changes in the liver.

DISCUSSION

The results confirmed that MCP-1 was a chemokine reflecting the inflammatory activity in the liver and might be a prognostic factor of the efficacy of the treatment with IFN α and RBV. Patients with a persisting long-lasting response to the treatment revealed MCP-1 concentrations statistically lower and during the treatment it did not undergo significant changes. Patients with negative effect of the therapy showed higher MCP-1 levels and increased significantly during IFN+RBV treatment.

Monocyte chemoattractant protein-1 is a potent chemokine secreted by monocytes and activated hepatic stellate cells undergoing up-regulation during chronic HCV infection. In normal liver, MCP-1 protein and gene expression detected by immunohistochemistry and *in situ* hybridization showed a modest expression in peri-sinusoidal cells and in bile duct epithelial cells^[15]. In chronic hepatitis, MCP-1 expression was directly correlated with the degree of inflammatory infiltrate in the portal tract, activated stellate cells and monocyte/macrophages. In active cirrhosis, MCP-1 expression was present in the portal tract, epithelial cells of regenerating bile ducts, and the active septa surrounding regenerating nodules^[15]. There was a direct relationship between MCP-1 expression and monocyte infiltration after acute liver injury. Monocytes stimulated by lipopolysaccharide, T lymphocytes and by IL-2 become mature macrophages and place themselves in the liver tissue. Antioxidants significantly reduced MCP-1 expression and the number of infiltrating monocytes in toxic liver injury^[16].

Hepatic tissues are damaged by activated monocytes, which secrete MCP-1, a chemoattractant and activator for circulating monocytes and T lymphocytes. Soo *et al.* in experiment on cultured monocytes infected with HCV showed that secreted proteins could influence the progress and outcome of liver injury^[17]. It was shown that HCV NS5A proteins could lead to monocyte activation with MCP-1 secretion^[17].

We did not observe any dependence between MCP-1 and Th2 lymphocyte stimulation during the treatment. IL-6 and IL-10 concentrations were higher in chronic hepatitis C than in healthy subjects and their levels increased in the course of IFN+RBV treatment. We showed significant differences in IL-6 and IL-10 concentrations between R and NR before the therapy. Masaki *et al.* noted that non-responders revealed a significantly higher Th1 and Th1/Th2 ratio than responders^[18]. The prognostic factors for favorable long-term virological responses were non-1b genotype, low HCV viremia (HCV viral load less than

500 kilocopies/mL), and low Th1/Th2 ratio^[18]. In hepatitis C, the predominance of Th2 cytokine IL-10 was observed. Monocytes secreting cytokines could enable cellular immune responses to activate, which decided the outcome of HCV infection^[19]. IL-10 and IL-12 secreted by monocytes were higher in asymptomatic HCV carriers than in chronic hepatitis C ones. After IFN+RBV therapy was completed, increased IL-12 was noted in responders and decreased in non-responders^[1]. It seemed to confirm that damage of monocyte function could decide chronic HCV infection and lack of positive therapeutic response^[1]. The use of IFN α had no influence on the production of IFN γ and IL-10 by monocytes^[4].

We presented a significant correlation of MCP-1 in chronic hepatitis C and soluble P-selectin concentration. The main sources of sP-selectin are activated blood platelets. Our previous studies showed that there was a positive correlation between platelet activation and a degree of histological change intensity in the liver^[20]. We also noted the inhibition of activated blood platelets by interferon alpha 2 b in chronic hepatitis C (data in press). It may reflect the cooperation of monocytes and platelets in the process of inflammation and fibrosis in chronic hepatitis C. Soluble P-selectin level was significantly lower in responders than in non-responders and its concentration was sustained lower during IFN α +RBV therapy. However, we did not observe any correlation between sP-selectin with histological changes in liver. These results suggest lack of priority of sP-selectin in efficacy of antiviral therapy. It reflects the intensity of inflammation and mobilization of blood platelets in chronic hepatitis C. Activated platelets have been found to play a crucial role in HSC transformation to myofibroblasts and in liver fibrosis^[21].

Activated monocytes could also lead to endothelial cell damage^[22]. Our studies did not show any correlation between activation of endothelial cells and monocytes. On the other hand, sICAM-1 concentrations correlated positively with periportal and intralobular inflammatory activity as well as staging of liver fibrosis, mainly in non-responders. Decreased sICAM-1 level during the treatment was common in all patients with chronic hepatitis C especially in responders. Our observations were similar to those of researchers who suggested that sICAM-1 might be used as a prognostic marker of efficacy of antiviral therapy in chronic hepatitis C^[10,23,24]. Decreased sICAM-1 level could reflect diminished inflammatory processes in the liver due to HCV elimination.

Studies conducted so far have ascribed an important role to monocytes in chronic hepatitis C pathogenesis. However, ways for effective elimination of HCV infection are still to be discovered. Monocytes are the cells that are damaged by HCV and the non-specific immunologic barrier which prevents or removes the infection. Thus, the question why most HCV infected patients were not able to eliminate HCV by their immune system is still to be answered.

REFERENCES

- 1 **Amaraa R**, Mareckova H, Urbanek P, Fucikova T. Production of interleukins 10 and 12 by activated peripheral blood monocytes/macrophages in patients suffering from chronic hepatitis C virus infection with respect to the response to interferon and ribavirin treatment. *Immunol Lett* 2002; **83**: 209-214
- 2 **Cribier B**, Uhl G, Schmitt C, Doffoel M, Vetter D, Kirn A, Stoll-Keller F. Follow-up of hepatitis C virus RNA in peripheral blood mononuclear cells during interferon therapy. *Arch Virol* 1999; **144**: 355-364
- 3 **Castelruiz Y**, Larrea E, Boya P, Civeira MP, Prieto J. Interferon alfa subtypes and levels of type I interferons in the liver and peripheral mononuclear cells in patients with chronic hepatitis C and controls. *Hepatology* 1999; **29**: 1900-1904
- 4 **Martin J**, Navas S, Fernandez M, Rico M, Pardo M, Quiroga JA, Zahm F, Carreno V. *In vitro* effect of amantadine and interferon alpha-2a on hepatitis C virus markers in cultured periph-

- eral blood mononuclear cells from hepatitis C virus-infected patients. *Antiviral Res* 1999; **42**: 59-70
- 5 **Gong GZ**, Lai LY, Jiang YF, He Y, Su XS. HCV replication in PBMC and its influence on interferon therapy. *World J Gastroenterol* 2003; **9**: 291-294
- 6 **Fisher NC**, Neil DA, Williams A, Adams DH. Serum concentrations and peripheral secretion of the beta chemokines monocyte chemoattractant protein 1 and macrophage inflammatory protein 1alpha in alcoholic liver disease. *Gut* 1999; **45**: 416-420
- 7 **Muhlbauer M**, Bosserhoff AK, Hartmann A, Thasler WE, Weiss TS, Herfarth H, Lock G, Scholmerich J, Hellerbrand C. A novel MCP-1 gene polymorphism is associated with hepatic MCP-1 expression and severity of HCV-related liver disease. *Gastroenterology* 2003; **125**: 1085-1093
- 8 **Marra F**, Romanelli RG, Giannini C, Failli P, Pastacaldi S, Arrighi MC, Pinzani M, Laffi G, Montalto P, Gentilini P. Monocyte chemotactic protein-1 as a chemoattractant for human hepatic stellate cells. *Hepatology* 1999; **29**: 140-148
- 9 **Marra F**, Pastacaldi S, Romanelli RG, Pinzani M, Ticali P, Carloni V, Laffi G, Gentilini P. Integrin-mediated stimulation of monocyte chemotactic protein-1 expression. *FEBS Lett* 1997; **414**: 221-225
- 10 **Taliani G**, Badolato MC, Bozza A, Poliandri G, Duca F, Pasquazzi C, Lecce R, Bruni R, De Bac C. HCV infection of peripheral blood mono nuclear cells and serum levels of soluble ICAM-1 in patients treated with interferon. *Arch Virol* 1997; **142**: 557-565
- 11 **Fijnheer R**, Frijns CJ, Korteweg J, Rommes H, Peters JH, Sixma JJ, Nieuwenhuis HK. The origin of P-selectin as a circulating plasma protein. *Thromb Haemost* 1997; **77**: 1081-1085
- 12 **McHutchison JG**, Fried MW. Current therapy for hepatitis C: pegylated interferon and ribavirin. *Clin Liver Dis* 2003; **7**: 149-161
- 13 **Woitas RP**, Petersen U, Moshage D, Brackmann HH, Matz B, Sauerbruch T, Spengler U. HCV-specific cytokine induction in monocytes of patients with different outcomes of hepatitis C. *World J Gastroenterol* 2002; **8**: 562-566
- 14 **Scheuer PJ**. Classification of chronic viral hepatitis: a need for reassessment. *J Hepatol* 1991; **13**: 372-374
- 15 **Marra F**, DeFranco R, Grappone C, Milani S, Pastacaldi S, Pinzani M, Romanelli RG, Laffi G, Gentilini P. Increased expression of monocyte chemotactic protein-1 during active hepatic fibrogenesis: correlation with monocyte infiltration. *Am J Pathol* 1998; **152**: 423-430
- 16 **Marra F**, DeFranco R, Grappone C, Parola M, Milani S, Leonarduzzi G, Pastacaldi S, Wenzel UO, Pinzani M, Dianzani MU, Laffi G, Gentilini P. Expression of monocyte chemotactic protein-1 precedes monocyte recruitment in a rat model of acute liver injury, and is modulated by vitamin E. *J Investig Med* 1999; **47**: 66-75
- 17 **Soo HM**, Garzino-Demo A, Hong W, Tan YH, Tan YJ, Goh PY, Lim SG, Lim SP. Expression of a full-length hepatitis C virus cDNA up-regulates the expression of CC chemokines MCP-1 and RANTES. *Virology* 2002; **303**: 253-277
- 18 **Masaki N**, Fukushima S, Hayashi S. Lower th-1/th-2 ratio before interferon therapy may favor long-term virological responses in patients with chronic hepatitis C. *Dig Dis Sci* 2002; **47**: 2163-2169
- 19 **Esquivel F**, Albillos A, Carrion F, Prieto A, Reyes E, Martinez-Martin B, Calleja JL, Cacho G, Alvarez-Mon M. Relationship between response to interferon-alpha and function of peripheral blood mononuclear cells in chronic hepatitis C patients. *Dig Dis Sci* 2002; **47**: 2154-2162
- 20 **Panasiuk A**, Prokopowicz D, Zak J, Matowicka-Karna J, Osada J, Wysocka J. Activation of blood platelets in chronic hepatitis and liver cirrhosis P-selectin expression on blood platelets and secretory activity of β -thromboglobulin and platelet factor-4. *Hepatogastroenterology* 2001; **48**: 818-822
- 21 **Li D**, Friedman SL. Liver fibrogenesis and the role of hepatic stellate cells: new insights and prospects for therapy. *J Gastroenterol Hepatol* 1999; **14**: 618-633
- 22 **Tang W**, Ziring D, Gershman G, French S. Role of macrophages and stellate cells in the pathogenesis of veno-occlusive disease: an electron microscopic case study. *Exp Mol Pathol* 2003; **75**: 201-209
- 23 **Capra F**, De Maria E, Lunardi C, Marchiori L, Mezzelani P, Beri R, Gabrielli GB. Serum level of soluble intercellular adhesion molecule 1 in patients with chronic liver disease related to hepatitis C virus: a prognostic marker for responses to interferon treatment. *J Infect Dis* 2000; **181**: 425-431
- 24 **Granot E**, Shouval D, Ashur Y. Cell adhesion molecules and hyaluronic acid as markers of inflammation, fibrosis and response to antiviral therapy in chronic hepatitis C patients. *Mediators Inflamm* 2001; **10**: 253-258

Edited by Wang XL Proofread by Chen WW and Xu FM

Interleukin (IL) 5 levels and eosinophilia in patients with intestinal parasitic diseases

Sebnem Ustun, Nevin Turgay, Songul Bayram Delibas, Hatice Ertabaklar

Sebnem Ustun, Department of Gastroenterology, School of Medicine, University of Ege, 35100 Bornova, Izmir, Turkey

Nevin Turgay, Department of Parasitology, School of Medicine, University of Ege, 35100 Bornova, Izmir, Turkey

Songul Bayram Delibas, Department of Parasitology, School of Medicine, University of Dokuz Eylul, Izmir, Turkey

Hatice Ertabaklar, Department of Microbiology, School of Medicine, University of Aydin Menderes, Aydin, Turkey

Correspondence to: Sebnem Ustun, M.D., Department of Gastroenterology, School of Medicine, University of Ege, 35100 Bornova, Izmir, Turkey. sustun@med.ege.edu.tr

Telephone: +90-232-3881969 Ext. 181

Received: 2004-03-03 **Accepted:** 2004-04-13

Abstract

AIM: Intestinal parasitic diseases are commonly accompanied with diarrhoeal symptoms and allergic reactions. Eosinophilia occurs as a result of IL-5 synthesized from Th2 cells during allergic reactions. IL-5 acts as a factor activating eosinophils. The aim of this study was to compare the IL-5 cytokine measurements in serum samples and cell cultures. And also to compare eosinophilia observed in helminth infections and protozoan infections accompanied with allergy.

METHODS: Twenty-three patients who presented with diarrhoeal symptoms and allergic complaints were tested positive for intestinal parasites, as well as 21 controls with allergic complaints who did not have any intestinal parasites were included in this study. IL-5 production in *in vitro* cell cultures prepared by using phytohemagglutinin (PHA) to stimulate peripheral blood mononuclear cells (PBMC) obtained from the blood samples taken from these patients were compared with the IL-5 level in serum. Furthermore, the IL-5 production in protozoan and helminth infections was also compared. Absolute eosinophil values in 1 mm³ of blood were calculated by means of peripheral smear in both groups within the scope of the study.

RESULTS: Parasites such as helminth detected in 15 (65.2%) and protozoan in 8 (34.8%) of the patients were included in this study. As regards the values of the sera in both patients with parasite infection and controls, the IL-5 production was found to be higher in the cell culture supernatant ($P < 0.001$ and $P < 0.05$). When the IL-5 level of the patients with helminth parasites was compared with that of those with protozoan, it was determined that the IL-5 level in serum was more significant in the patients with protozoan than in those with helminth ($P < 0.05$). In the study group, the patients were found to have parasites, the percentage of eosinophil was 7.0% compared to 6.5% in the control group. Thus, there was no significant difference between the eosinophil values ($P > 0.05$).

CONCLUSION: It was found that IL-5 cytokine levels in serum samples from the patients with helminth and protozoan displayed more measurable values as compared to the IL-5 levels after stimulation with mitogen. It is concluded that IL-5 acts as a triggering factor in the toxiallergic complaints

commonly seen in helminth and protozoan infections.

Ustun S, Turgay N, Delibas SB, Ertabaklar H. Interleukin (IL) 5 levels and eosinophilia in patients with intestinal parasitic diseases. *World J Gastroenterol* 2004; 10(24): 3643-3646 <http://www.wjgnet.com/1007-9327/10/3643.asp>

INTRODUCTION

Gastrointestinal (GI) parasites play an important role in the allergic and hypersensitive reactions. The prevalence of intestinal protozoans and helminths in stool samples of individuals with allergic symptoms was evaluated as a possible link between parasites and allergy^[1]. A wide variety of clinical findings related to the whole body are encountered in parasitic diseases. Hypersensitive reactions may start out in the host against the chemical substances excreted by the parasites. In addition, allergic reactions may occur^[2].

There has been an increase in the prevalence of allergic diseases in the past few decades. T helper 2 (Th2) responses associated with allergic diseases^[3]. Th2 cells elaborate cytokines such as IL-5 which works with toxic mediators of innate immune cells. Th2 cytokine involvement in allergy makes these cytokines attractive therapeutic targets, which protect against gastrointestinal worms^[4,5]. Immunological interventions could be designed to avoid induction of pathology while retaining protective responses^[6].

It has been shown that strong Th2 cytokine response occurs especially during the chronic phase of helminth infections. Allergic reactions triggered by this Th2 response are more commonly seen in helminth infections, and hypersensitive reactions against the chemical substances secreted by helminths may occur in some people^[7-9]. Long-lived parasites such as helminths, however, are more remarkable for their ability to downregulate host immunity, protecting themselves from elimination and minimizing severe pathology in the host^[10].

Allergic reactions may also be observed in protozoan diseases. Ameobiasis, giardiasis, Blastocystis were reported as the etiologic factors causing allergy in animals and human models in some publications^[1-11].

Eosinophilia is caused by the effect of IL-5 synthesized from the Th2 cells. IL-5 is the most important cytokine in the transformation and development of eosinophils, and acts as an "eosinophil activator". One of the significant causes of the increase in the amount of eosinophils in blood is parasitic diseases. Toxiallergic effects of certain parasites on the host's organism lead to an increase especially in eosinophil numbers. Eosinophils are effectors against parasitic targets. Both sets of diseases are associated with a polarized Th2-type immune response, typified by reactive cell types (eosinophils and mast cells)^[12,13].

It is suggested therefore that the function of IL-5 and eosinophils is to protect against repeated exposure to gastrointestinal parasites. On the other hand the eosinophilia observed may represent an immunopathological rather than a protective response and may merely be a consequence of the generalized inflammation induced by the Th2 response following infection with parasites. Th2 response is essential for the expulsion of GI helminths^[14].

Eosinophils are also responsible for considerable pathology

in mammals because they are inevitably present in large numbers in inflammatory lesions associated with helminth infections or allergic conditions^[15,16].

On the other hand current evidence shows a strong association between colonic infection and inflammation with development of inflammatory bowel disease (IBS)^[17]. It has been reported that mast cells and their inflammatory mediators are closely associated with a number of intestinal diseases including idiopathic IBD. Parasites induce mast cell degranulation, release histamine. Mast cells from healthy controls don't produce IL-5, but mast cells from patients with intestinal inflammatory disease could release a relatively large amount of IL-5^[18,19]. IL-5 induced by parasites may play a role in causing IBD.

The aim of this study was to compare the IL-5 cytokine measurements in the cell cultures of patients who presented with allergic complaints and diarrhea and were positive for parasites in stool examinations with the IL-5 syntheses determined in serum samples, and to investigate eosinophilia observed in helminth and protozoan infections accompanied with allergy and diarrhea.

MATERIALS AND METHODS

Twenty-three patients with intestinal parasites and 21 controls who had allergic complaints and not any intestinal parasite and diarrhea, were included in this study.

The study group included 12 females and 11 males, aged 18-45 and 25-53 years respectively. The control group included 9 females and 12 males, aged 20-45 and 28-50 years respectively.

IL-5 production in *in vitro* cell cultures prepared by using PHA to stimulate PBMC obtained from these patients was compared with the IL-5 level in serum. In addition, IL-5 production in protozoan and helminth infections was also compared.

Cells and sera

PBMC and serum samples separated from 5 mL of heparinized blood samples from the patients using the Ficoll hypaque density gradient centrifuge method were utilized in the study.

Mitogen and proliferation assay

PBMC (83×10^5 /mL) was incubated with PHA in RPMI 1640+10% HuS inside 96 well tissue culture plates containing 5 mL/L CO₂ for 48 h. Supernatants were taken at the end of 48 h and kept at -20 °C until cytokine analysis was carried out^[20].

IL-5 measurement

IL-5 levels in the supernatant and serum samples were evaluated using the double sandwich ELISA as previously described by Geiger *et al.*^[21].

Eosinophil count

Absolute values in 1 mm³ of blood were calculated by means of peripheral blood smear from the patients within the study as well as the controls.

Statistical analysis

Results were evaluated using the Student *t test*.

RESULTS

Helminths were detected in 15 (65.2%) and protozoans in 8 (34.8%) of the 23 patients (Table 1). All the patients had diarrheal symptoms.

A comparison between the sera of the treated group and the control group did not reveal any significant differences ($P > 0.05$ and $P > 0.05$). The nonspecific IL-5 synthesis determined after stimulation with PHA was higher as compared to the IL-5 values measured in the serum ($P < 0.05$) (Figure 1).

It was also established that the IL-5 cytokine measurements were higher in the group with protozoans than in the group with

helminths. These values were also higher as compared to the cytokine measurements in the cell cultures ($P < 0.05$) (Figure 2).

The eosinophil rate was 7.0% in the study group whereas the eosinophil rate was 6.5% in the control group. However, significant difference could not be found between these two groups ($P > 0.05$) (Table 2).

Table 1 Parasites, IL-5 levels and eosinophil values in patients group

Parasites	Those with parasite infection	Mean serum IL-5 (pg/mL)	Mean PHA-IL-5 (ng/mL)	Eosinophil %
<i>E. vermicularis</i>	9	15.5	383.4	8
<i>A. lumbricoides</i>	1	9.98	750	9
<i>H. nana</i>	1	13.61	620	8
<i>T. saginata</i>	4	12.9	652.5	6
<i>E. coli</i>	3	21.15	415	2.4
<i>I. butschlii</i>	2	15.61	297	8
<i>B. hominis</i>	1	17.27	NA	4.4
<i>G. intestinalis</i>	2	22.35	872.5	3

(NA: Not Available).

Table 2 Serum IL-5, *in-vitro* IL-5 and eosinophil values in patients with parasite infection and controls

	Serum IL-5 (pg/mL)	<i>In-vitro</i> IL-5 (pg/mL)	Eosinophil %
Patients with parasite infection	16.2	634	7.0
Control	32.4	885.4	6.5

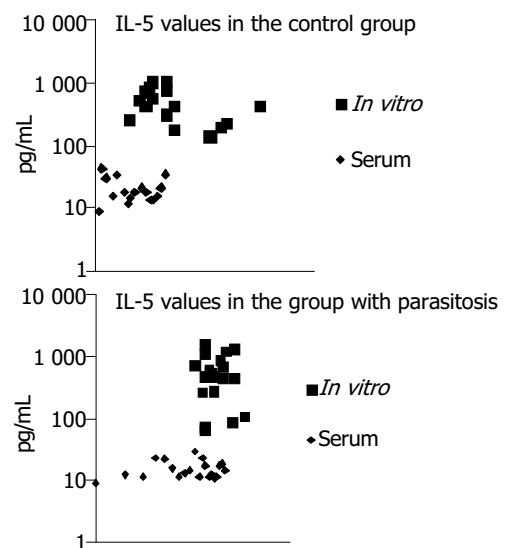


Figure 1 *In vitro* and serum IL-5 measurements in patients with parasite infection and control group.

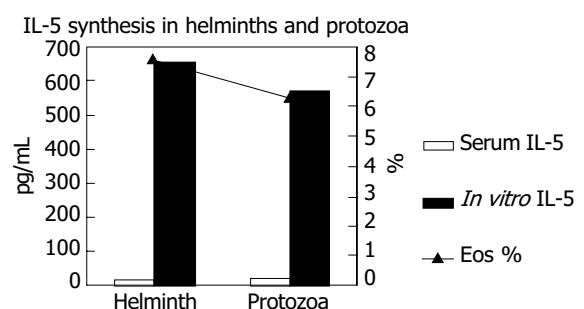


Figure 2 Comparison of IL-5 synthesis and eosinophil values in helminths and protozoans.

DISCUSSION

Th2 response is important in protection against and destroying the parasites. Especially in some tropical areas, helminths were the major immediate triggers of Th2 response^[22,23].

Pit *et al.* found that levels of IL-5 were induced by intestinal helminths^[24]. Protective immune responses to intestinal nematodes could be controlled by Th2 lymphocyte responses. Increased number of eosinophils in the GI mucosa and Th2 cell cytokine responsible for the generation of eosinophils, were prominent features of gastrointestinal nematode infections^[25]. Herrstom *et al.* found that *E. vermicularis* were more frequently found in children with allergic disease as defined by allergic symptoms^[26]. Sorci *et al.* suggested that there was an association between the pinworms (oxyuridae, nematoda) and eosinophil concentration^[27]. Varga *et al.* reported that patients infected with *A. lumbricoides*, had more severe allergic symptoms, and allergic symptoms were seen in patients infected with *G. intestinalis*^[28].

Previous studies, however, have shown that allergic complaints could precede other problems in protozoan infections. It was stated that allergic reactions also occurred in the disease caused by *G. intestinalis* that lives in the digestive tract. The relationship between allergy and giardiasis has been shown in various publications^[1-29]. In Moscow, during the clinical studies of children with *G. intestinalis* infection, allergic reactions were found in 15.7%^[30].

It was shown in some previous studies that IgG1, IgG3, IgM and IgA syntheses were important as resisting factors against the infection in intestinal protozoan infections such as giardiasis^[31]. The presence of anti-parasitic antibodies detected in the serum depended on the secretion of cytokines such as IL-4 which is also produced from Th2 cells. As high antibody levels triggered by IL-4 in the serum, high IL-5 levels coming from the same source of cells were found to be higher than those from, supernatants in patients with protozoan infection.

It was also reported that urticaria and eosinophilia were detected in people infected with *B. hominis*^[11]. Biedermann *et al.* reported that antigens from *B. hominis* caused urticaria^[32]. Hypersensitive (DTH) response to amebiosis delayed-type was evaluated in C3H/HeJ mice infected with *E. histolytica*^[33].

It is important to measure and assess IL-5 as a cytokine triggering eosinophilia in patients who present with allergic complaints and whose stool examinations reveal no parasites. It was established in this study that the IL-5 synthesis determined in the serum samples in the group with protozoa was more significant than that determined in the cell cultures in the group with helminths. Thus, eosinophilia was not only limited to helminth infection, but also in protozoan infection.

Eosinophils account was consisted of 2-3% of the total leukocytes in the blood and functioned as cytotoxic effector cells in allergic and parasitic disease, especially for the elimination of parasites^[34,35]. Eosinophilia occurred due to the IL-5 effect that reflects Th2 cell secretion^[36]. A number of studies have shown the presence of eosinophilia in parasitic infections. The blood eosinophils are associated with helminthic diseases. The primary function of the eosinophil is to protect against helminth parasites and eosinophils are responsible for a considerable amount of inflammatory pathology accompanying helminth infections^[16-37].

In the present study, the rate of eosinophilia was 7% in the study group and 6.5% in the control group. Because of the control group also had allergic complaints, no statistically significant difference could be found between the two groups ($P>0.05$).

It has also been shown that PBMC from healthy volunteers whose lymphocytes would not produce IL-5, failed to produce IL-5 after stimulation with PHA^[38]. Consistent with the results of Katial *et al.*^[38], IL-5 values obtained for 16 healthy volunteers

in the present study after stimulation with PHA were lower than those in the group with parasite infection and the control group.

Parasites induce IL-5 secretion. The effect of IL-5 on IBD should be investigated^[18]. Approximately 25% of patients with IBS had a history of infectious enteritis. Microbial agents including parasites could increase the number of mast cells within the colonic muscle wall, release pro-inflammatory substances, and increase the number of inflammatory cells that might cause IBS^[17].

REFERENCES

- 1 **Giacometti A**, Cirioni O, Antonicelli L, D'Amato G, Silvestri C, Del Prete MS, Scalise G. Prevalence of intestinal parasites among individuals with allergic skin diseases. *J Parasitol* 2003; **89**: 490-492
- 2 **Falcone FH**, Loukas A, Quinnell RJ, Pritchard DI. The innate allergenicity of helminth parasites. *Clin Rev Allergy Immunol* 2004; **26**: 61-72
- 3 **Black P**. Why is the prevalence of allergy and autoimmunity increasing? *Trends Immunol* 2001; **22**: 354-355
- 4 **Finkelman FD**, Urban JF Jr. The other side of the coin: the protective role of the TH2 cytokines. *J Allergy Clin Immunol* 2001; **107**: 772-780
- 5 **Fallon PG**, Jolin HE, Smith P, Emson CL, Townsend MJ, Fallon R, Smith P, McKenzie AN. IL-4 induces characteristic Th2 responses even in the combined absence of IL-5, IL-9 and IL-13. *Immunity* 2002; **17**: 7-17
- 6 **Garside P**, Kennedy MW, Wakelin D, Lawrence CE. Immunopathology of intestinal helminth infection. *Parasite Immunol* 2000; **22**: 605-612
- 7 **Holt PG**. Parasites, atopy, and the hygiene hypothesis: resolution of a paradox? *The Lancet* 2000; **18**: 1699-1700
- 8 **Bashir ME**, Andersen P, Fuss IJ, Shi HN, Nagler-Anderson C. An enteric helminth infection protects against an allergic response to dietary antigen. *J Immunol* 2002; **169**: 3284-3292
- 9 **Cribier B**, Noacco G. Chronic urticaria and infectious diseases. *Ann Dermatol Venereol* 2003; **130**: 43-52
- 10 **Maizels RM**, Yazdanbakhsh M. Immune regulation by helminth parasites: cellular and molecular mechanisms. *Nat Rev Immunol* 2003; **3**: 733-744
- 11 **Barahona Rondon L**, Maguina Vargas C, Naquira Velarde C, Terashima I A, Tello R. Human blastocystosis: prospective study symptomatology and associated epidemiological factors. *Rev Gastroenterol Peru* 2003; **23**: 29-35
- 12 **Yazdanbakhsh M**, van den Biggelaar A, Maizels RM. Th2 responses without atopy: immunoregulation in chronic helminth infections and reduced allergic disease. *Trends Immunol* 2001; **22**: 372-377
- 13 **Capron M**, Dombrowicz D. Eosinophils, parasites and allergy: from the biological to the clinical. *J Soc Biol* 2002; **196**: 23-28
- 14 **Lawrence CE**. Is there a common mechanism of gastrointestinal nematode expulsion? *Parasite Immunol* 2003; **25**: 271-281
- 15 **Behm CA**, Ovington KS. The role of eosinophils in parasitic helminth infections: insights from genetically modified mice. *Parasitol Today* 2000; **16**: 202-209
- 16 **Klion AD**, Nutman TB. The role of eosinophils in host defense against helminth parasites. *J Allergy Clin Immunol* 2004; **113**: 30-37
- 17 **Levy DA**. Parasites and Allergy: From IgE to Th1/Th2 and Beyond. *Clin Rev Allergy Immunol* 2004; **26**: 1-4
- 18 **He SH**. Key role of mast cells and their major secretory products in inflammatory bowel disease. *World J Gastroenterol* 2004; **10**: 309-318
- 19 **He SH**, Xie H, He YS. Induction of tryptase and histamine release from human colon mast cells by IgE-dependent or independent mechanisms. *World J Gastroenterol* 2004; **10**: 319-322
- 20 **Schierack P**, Lucius R, Sonnenburg B, Schilling K, Hartmann S. Parasite-specific immunomodulatory functions of filarial cystatin. *Infect Immun* 2003; **71**: 2422-2429
- 21 **Geiger SM**, Massara CL, Bethony J, Soboslay PT, Carvalho OS, Correa-Oliveira R. Cellular responses and cytokine profiles

- in *Ascaris lumbricoides* and *Trichuris trichiura* infected patients. *Parasite Immunol* 2002; **24**: 499-509
- 22 **Else KJ**, Finkelman FD. Intestinal nematode parasites, cytokines and effector mechanisms. *Int J Parasitol* 1998; **28**: 1145-1158
- 23 **Turner JD**, Faulkner H, Kamgno J, Cormont F, Van Snick J, Else KJ, Grecis RK, Behnke JM, Boussinesq M, Bradley JE. Th2 cytokines are associated with reduced worm burdens in a human intestinal helminth infection. *J Infect Dis* 2003; **188**: 1768-1775
- 24 **Pit DS**, Polderman AM, Schulz-Key H, Soboslay PT. Prenatal immune priming with helminth infections: parasite-specific cellular reactivity and Th1 and Th2 cytokine responses in neonates. *Allergy* 2000; **55**: 732-739
- 25 **Onah DN**, Nawa Y. Mucosal immunity against parasitic gastrointestinal nematodes. *The Korean J Parasitol* 2000; **38**: 209-236
- 26 **Herrstrom P**, Henricson KA, Raberg A, Karlsson A, Hogstedt B. Allergic disease and the infestation of *Enterobius vermicularis* in Swedish children 4-10 years of age. *J Investig Allergol Clin Immunol* 2001; **11**: 157-160
- 27 **Sorci G**, Skarstein F, Morand S, Hugot JP. Correlated evolution between host immunity and parasite life histories in primates and oxyurid parasites. *Proc R Soc Lond B Biol Sci* 2003; **270**: 2481-2484
- 28 **Varga M**, Dumitrascu D, Piloff L, Chioreanu E. Skin manifestations in parasite infection. *Roum Arch Microbiol Immunol* 2001; **60**: 359-369
- 29 **Di Prisco MC**, Hagel I, Lynch NR, Jimenez JC, Rojas R, Gil M, Mata E. Association between giardiasis and allergy. *Ann Allergy Asthma Immunol* 1998; **81**: 261-265
- 30 **Zalipaeva TL**. Clinical symptoms of giardia infection in children. *Med Parazitol* 2002; **3**: 29-32
- 31 **Soliman MM**, Taghi-Kilani R, Abou-Shady AF, El-Mageid SA, Handousa AA, Hegazi MM, Belosevic M. Comparison of serum antibody responses to *Giardia lamblia* of symptomatic and asymptomatic patients. *Am J Trop Med Hyg* 1998; **58**: 232-239
- 32 **Biedermann T**, Hartmann K, Sing A. Hypersensitivity to non-steroidal anti-inflammatory drugs and chronic urticaria cured by treatment of *Blastocystis hominis* infection. *Br J Dermatol* 2002; **146**: 1113
- 33 **Ghosh PK**, Gupta S, Ortiz-Ortiz L. Intestinal amoebiasis: delayed-type hypersensitivity response in mice. *J Health Popul Nutr* 2000; **18**: 109-114
- 34 **Meeusen EN**, Balic A. Do eosinophils have a role in the killing of helminth parasites? *Parasitol Today* 2000; **16**: 95-101
- 35 **Dombrowicz D**, Capron M. Eosinophils, allergy and parasites. *Curr Opin Immunol* 2001; **13**: 716-720
- 36 **Zacharia B**, Sherman P. Atopy, helminths, and cancer. *Med Hypotheses* 2003; **60**: 1-5
- 37 **Schneider M**, Hilgers RH, Sennekamp J. Allergy, total IgE and eosinophils in East and West - serious effects of different degrees of helminthiasis and smoking. *Eur J Med Res* 2002; **21**: 63-71
- 38 **Katial RK**, Sachanandani D, Pinney C, Lieberman MM. Cytokine production in cell culture by peripheral blood mononuclear cells from immunocompetent hosts. *Clin Diag Lab Immunol* 1998; **5**: 78-81

Edited by Wang XL Proofread by Chen WW and Xu FM

Diagnosis of abdominal tuberculosis: Experience from 11 cases and review of the literature

Ali Uzunkoy, Muge Harma, Mehmet Harma

Ali Uzunkoy, Department of Surgery, University of Harran, Faculty of Medicine, Sanliurfa, Turkey

Muge Harma, Mehmet Harma, Department of Gynecology and Obstetrics, Faculty of Medicine, Sanliurfa, Turkey

Correspondence to: Dr. Mehmet Harma, 6. Sokak, 2/9, Bahcelievler, 06500, Ankara, Turkey. mehmetharma@superonline.com

Telephone: +90-414-3163032 **Fax:** +90-414-3163032

Received: 2004-04-10 **Accepted:** 2004-05-13

Abstract

AIM: To analyze the experience within our hospital and to review the literature so as to establish the best means of diagnosis of abdominal tuberculosis.

METHODS: The records of 11 patients (4 males, 7 females, mean age 39 years, range 18-65 years) diagnosed with abdominal tuberculosis in Harran University Hospital between January 1996 and October 2003 were analyzed retrospectively and the literature was reviewed.

RESULTS: Ascites was present in all cases. Other common findings were weight loss (81%), weakness (81%), abdominal mass (72%), abdominal pain (72%), abdominal distension (63%), anorexia (45%) and night sweat (36%). The average hemoglobin was 8.2 g/dL and the average ESR was 50 mm/h (range 30-125). Elevated levels of cancer antigen CA-125 were determined in four patients. Abdominal ultrasound showed abnormalities in all cases: ascites in all, tuboovarian mass in five, omental thickening in 3, and enlarged lymph nodes (mesenteric, para-aortic) in 2. CT scans showed ascites in all, pelvic mass in 5, retroperitoneal lymphadenopathy in 4, mesenteric stranding in 4, omental stranding in 3, bowel wall thickening in 2 and mesenteric lymphadenopathy in 2. Only one patient had a chest radiograph suggestive of a new TB lesion. Two had a positive family history of pulmonary TB. None had acid-fast bacilli (AFB) in the sputum and the tuberculin test was positive in only two. Laparotomy was performed in 6 cases, laparoscopy in 4 and ultrasound-guided fine needle aspiration in 2. In those patients subjected to operation, the findings were multiple diffuse involvement of the visceral and parietal peritoneum, white 'miliary nodules' or plaques, enlarged lymph nodes, ascites, 'violin string' fibrinous strands, and omental thickening. Biopsy specimens showed granulomas, while ascitic fluid showed numerous lymphocytes. Both were negative for acid-fast bacilli by staining. PCR of ascitic fluid was positive for *Mycobacterium tuberculosis* (*M. tuberculosis*) in all cases.

CONCLUSION: Abdominal TB should be considered in all cases with ascites. Our experience suggests that PCR of ascitic fluid obtained by ultrasound-guided fine needle aspiration is a reliable method for its diagnosis and should at least be attempted before surgical intervention.

Uzunkoy A, Harma M, Harma M. Diagnosis of abdominal tuberculosis: Experience from 11 cases and review of the literature. *World J Gastroenterol* 2004; 10(24): 3647-3649 <http://www.wjgnet.com/1007-9327/10/3647.asp>

INTRODUCTION

Tuberculosis (TB) causes some 3 million deaths per year world wide and is increasing in incidence in developed, and developing countries. Abdominal TB, which may involve the gastrointestinal tract, peritoneum, lymph nodes or solid viscera, constitutes up to 12% of extrapulmonary TB and 1-3% of the total^[1,2]. The disease can mimic many conditions, including inflammatory bowel disease, malignancy and other infectious diseases^[3]. Diagnosis is therefore often delayed. This may not only result in mortality but also in unnecessary surgery. We therefore set out to establish the most useful diagnostic procedure(s) in the light of our experience and reports in the literature.

MATERIALS AND METHODS

A retrospective study of the files of patients admitted to Harran University Hospital from January 1996 to October 2003 was carried out. Cases of abdominal TB were identified and data on age, sex, clinical presentation, diagnostic investigations, treatment and outcome were abstracted.

RESULTS

Eleven patients, none of whom were immunocompromised, were diagnosed with abdominal TB during the period (Table 1). Nine cases had peritoneal TB, while the remaining two had TB of the colon. The median age was 39 years (range 18-65) and the ratio of males and females was 4:7.

The mean duration of symptoms was 14 wk (range 1-32 wk). Ascites was present in all cases, while 9 (81%) showed weight loss, 9 (81%) weakness, 8 (72%) abdominal mass, 8 (72%) abdominal pain, 7 (63%) abdominal distension, 5 (45%) anorexia and 4 (36%) night sweat.

The average hemoglobin was 8.2 g/dL and the average ESR was 50 mm/h (range 30-125). Levels of cancer antigen CA-125 were elevated in four patients.

Abdominal ultrasound (US) was carried out on all patients and abnormal findings were noted in all: ascites in all, tuboovarian mass in five, omental thickening in three, and enlarged lymph nodes (mesenteric, para-aortic) in two.

All patients also had computed tomography (CT) scans, with results consistent with US (Table 2).

At this stage, diagnoses of peritoneal carcinomatosis, colon cancer, Chron's disease and ovarian cancer were considered. Laparotomy was performed in the first six cases and the diagnosis of abdominal TB was made intraoperatively based on macroscopic findings, including multiple diffuse involvement of the visceral and parietal peritoneum, white 'miliary nodules' or plaques, enlarged lymph nodes, ascites, 'violin string' fibrinous strands and omental thickening, and confirmed by microscopic examination of biopsies of lymph nodes and peritoneal nodules and by positive polymerase chain reaction (PCR) for *Mycobacterium tuberculosis* (*M. tuberculosis*) on ascitic fluid taken during the procedure. Smears of ascitic fluid showed numerous lymphocytes but no acid-fast bacilli.

Laparoscopy was used in the examination of the next three cases. Biopsies were again taken and examined microscopically and confirmation of the diagnosis was made by PCR on ascitic fluid.

Table 1 Details of patients with abdominal tuberculosis

Case No.	Sex	Age (yr)	Clinical findings	Intervention	Diagnosis
1	M	38	Ascites, colonic obstruction, weight loss, weakness, abdominal distension, anorexia, retroperitoneal lymphadenopathy, bowel wall thickening	Laparotomy	Colon TB
2	F	26	Ascites, elevated CA-125 ($\times 4$), abdominal mass, weight loss, weakness, abdominal pain, anorexia	Laparotomy	Peritoneal TB
3	M	40	Ascites, abdominal mass, enlarged lymph nodes, weight loss, weakness, abdominal pain, abdominal distension, anorexia, bowel wall thickening	Laparotomy	Colon TB
4	F	54	Ascites, elevated CA-125 ($\times 3$), abdominal mass, weakness, abdominal pain, abdominal distension, night sweats	Laparotomy	Peritoneal TB
5	M	44	Ascites, omental thickening, enlarged lymph nodes, weakness, abdominal pain, anorexia	Laparotomy	Peritoneal TB
6	F	42	Ascites, tuboovarian mass, elevated CA-125 ($\times 4$), weight loss, weakness, abdominal pain, night sweats	Laparotomy	Peritoneal TB
7	M	65	Ascites, abdominal mass, weight loss, weakness, abdominal pain, abdominal distension	Laparoscopy	Peritoneal TB
8	F	51	Ascites, tuboovarian mass, positive family history of pulmonary TB, weight loss, weakness	Laparoscopy	Peritoneal TB
9	F	18	Ascites, elevated CA-125 ($\times 4$), tuboovarian mass, weight loss, weakness, abdominal distension	Laparoscopy	Peritoneal TB
10	F	20	Ascites, omental thickening, weight loss, abdominal pain, abdominal distension, anorexia, night sweats, retroperitoneal lymphadenopathy	Fine needle aspiration	Peritoneal TB
11	F	40	Ascites, abdominal mass, positive family history of pulmonary TB, omental thickening, weight loss, abdominal pain, abdominal distension, night sweats	Fine needle aspiration	Peritoneal TB

Table 2 CT scan characteristics of patients with abdominal tuberculosis

CT findings	No. of patients (%)
Ascites	11 (100)
Pelvic mass	5 (45)
Retroperitoneal lymphadenopathy	4 (36)
Mesenteric stranding	4 (36)
Omental stranding	3 (27)
Bowel wall thickening	2 (18)
Mesenteric lymphadenopathy	2 (18)

Because of this experience, the Radiology Department was alerted to the necessity of including abdominal TB in the differential diagnosis and the final two patients in the series were spared surgical intervention, the diagnosis was confirmed by PCR of ascitic fluid obtained by US-guided fine needle aspiration.

Only one patient had a chest radiograph suggestive of a new TB lesion. Two had a positive family history of pulmonary TB. None had acid-fast bacilli (AFB) in the sputum and the tuberculin test was positive in only two.

All patients were started on quadruple antituberculous therapy comprising rifampicin (10 mg/kg-d), isoniazid (5 mg/kg-d), ethambutol (15 mg/kg-d) and pyrazinamide (30 mg/kg-d) for two months and then maintained on rifampicin and isoniazid for 9-12 mo. Response was good in all patients. The mean follow-up time was 24 mo (range 19-38 mo).

DISCUSSION

In accord with other reports^[4,5], our 'typical' patient was a middle-aged female. Signs and symptoms observed were generally in line with those of other reports except that the percentage of our patients showing weight loss was the highest for any series. Fever was the most common finding (73%) in the series reported by Muneef *et al.*^[6], but our results agree with most other studies in reporting about half this incidence. The

most consistent finding, in our study and in the literature, was the presence of ascites, although Muneef *et al.*^[6] again differed in finding ascites present in only 61% of their patients.

Presence of TB at other sites or a patient with a family history of TB may be helpful in suggesting the diagnosis, but this occurs in somewhat less than 30% of patients. This may indicate that the majority of cases had primary lesions were acquired through the gastrointestinal tract. Given the preponderance of females affected, it may also be that some cases in females are acquired genitally (though not necessarily sexually). TB skin tests were positive in only about a quarter of patients in most reports but Demir *et al.*^[7] obtained a positive result in all their 26 patients.

Although US^[8] and CT scanning^[9] have been claimed to give definitive diagnoses, this was not the case in our series or in the other cases surveyed. Both US and CT were abnormal in all cases in most reports (though in only 80% of CT scans in the series reported by Muneef *et al.*^[6]) but findings were largely non-specific.

The great majority of reported cases were, like the first six cases in our series, diagnosed at laparotomy after they were initially misdiagnosed as tumors or carcinomas^[4-6,10-17]. In female patients, misdiagnosis was made even more likely by the raised levels of CA-125 that were apparently universally observed and the fact that an elevated level of CA-125 has been recognized as a marker of non-mucinous epithelial ovarian carcinomas^[13-17]. In the light of this finding, Thakur *et al.*^[13] went so far as to suggest that high serum CA-125 should always raise a suspicion of TB. However, the finding has not so far been validated in males.

Diagnosis at laparotomy was made largely by histology of frozen or paraffin-embedded sections, which typically revealed epithelioid granulomas with central caseous necrosis, although Muneef *et al.*^[6] reported 68% of peritoneal biopsies were positive by smear/culture. Zaidi and Conner^[12] performed PCR for *M. tuberculosis* on paraffin-embedded tissues.

With increasing experience, laparoscopy has become the diagnostic procedure of choice, both in our hospital and in the literature^[18-24]. Again, in most cases histology was the main confirmatory method, smear and culture were largely unhelpful.

PCR was used to confirm the diagnosis in two cases^[21,22].

Laparoscopy is, however, invasive and expensive, but was associated with an overall incidence of major complications in up to 5.7% of patients^[25]. Because of this, several investigators looked at abdominal paracentesis as a diagnostic method. Ascitic fluid in abdominal tuberculosis is exudative, usually containing 500 to 2000 cells. Lymphocytes typically predominate, although in some cases polymorphonuclear leukocytes were more abundant early in the process. Acid-fast stains were usually negative. Though culture might eventually be positive in up to a third of cases^[6], the time taken for growth (usually 6 wk) was too long to be useful in diagnosis.

The use of PCR to detect *M. tuberculosis* in abdominal tuberculosis was reported by Moatter *et al.*^[26]. In their study, as in most later ones^[12,21-23], DNA was extracted from tissues. They found that an IS6110 primer was detected in only 60% of specimens and another primer was necessary to detect the other 40%. Schwake *et al.*^[23] obtained a negative result in the two cases they tested, perhaps because they only used a single primer.

In all eleven patients presented here, PCR analyses for *M. tuberculosis* complex on ascitic fluid were positive. Protopoulos *et al.*^[24] (single case) and Tzoanopoulos^[27] (3 patients) also successfully used PCR of ascitic fluid to obtain a diagnosis.

In the light of our accumulated experience, we would suggest that PCR of ascitic fluid obtained by US-guided fine needle aspiration is now the investigation of choice for patients with the described clinical and radiological presentations and should at least be attempted before surgical intervention. Our final two patients were diagnosed by this means. If the result was negative, diagnostic laparoscopy or, if this was not feasible, laparotomy should be performed.

Ascitic fluid adenosine deaminase (ADA) activity has been proposed as a useful diagnostic test for abdominal TB. In countries with a high incidence of TB and in high risk patients, measurement of ADA in ascitic fluid might be a useful screening test^[28]. However, in populations with a low prevalence of TB and a high prevalence of cirrhosis, ascitic fluid ADA activity has been good in accuracy but poor in sensitivity and imperfect in specificity^[29].

In the reports reviewed, there was only one recorded death due to TB in patients with abdominal tuberculosis receiving anti-TB therapy (most commonly, a four drug regimen for several mo) and that was in a patient with extensive involvement of other organs^[6]. The prognosis was therefore good if the condition was promptly diagnosed and treated, though the emergence of multi-resistant strains might alter this picture.

In conclusion, abdominal TB should be considered in the differential diagnosis of abdominopelvic masses, ascites or elevated CA-125. PCR for *M. tuberculosis* complex is a non-invasive method which can provide the diagnosis in most cases. If this test is negative and a high index of clinical suspicion remains, laparoscopy or, if this is not feasible, laparotomy should be performed.

REFERENCES

- Farer LS, Lowell AM, Meador MP. Extrapulmonary tuberculosis in the United States. *Am J Epidemiol* 1979; **109**: 5-15
- Sheer TA, Coyle WJ. Gastrointestinal tuberculosis. *Curr Gastroenterol Rep* 2003; **5**: 273-278
- Jadvar H, Mindelzun RE, Olcott EW, Levitt DB. Still the great mimicker: abdominal tuberculosis. *Am J Roentgenol* 1997; **168**: 1455-1460
- Zhang Z, Shi X, Li J. Abdominal tuberculosis misdiagnosed as tumor. *Zhonghua Jiehe He Huxi Zazhi* 2001; **24**: 400-403
- Bilgin T, Karabay A, Dolar E, Develioglu OH. Peritoneal tuberculosis with pelvic abdominal mass, ascites and elevated CA 125 mimicking advanced ovarian carcinoma: a series of 10 cases. *Int J Gynecol Cancer* 2001; **11**: 290-294
- Muneef MA, Memish Z, Mahmoud SA, Sadoon SA, Bannatyne R, Khan Y. Tuberculosis in the belly: a review of forty-six cases involving the gastrointestinal tract and peritoneum. *Scand J Gastroenterol* 2001; **36**: 528-532
- Demir K, Okten A, Kaymakoglu S, Dincer D, Besisik F, Cevikbas U, Ozdil S, Bostas G, Mungan Z, Cakaloglu Y. Tuberculous peritonitis-reports of 26 cases, detailing diagnostic and therapeutic problems. *Eur J Gastroenterol Hepatol* 2001; **13**: 581-585
- Malik A, Saxena NC. Ultrasound in abdominal tuberculosis. *Abdom Imaging* 2003; **28**: 574-579
- Sinan T, Sheikh M, Ramadan S, Sahwney S, Behbehani A. CT features in abdominal tuberculosis: 20 years experience. *BMC Medical Imaging* 2002; **2**: 3-16
- Ozalp S, Yalcin OT, Tanir HM, Kabukcuoglu S, Akcay A. Pelvic tuberculosis mimicking signs of abdominopelvic malignancy. *Gynecol Obstet Invest* 2001; **52**: 71-72
- Mahdavi A, Malviya VK, Herschman BR. Peritoneal tuberculosis disguised as ovarian cancer: an emerging clinical challenge. *Gynecol Oncol* 2002; **84**: 167-170
- Zaidi SN, Conner M. Disseminated peritoneal tuberculosis mimicking metastatic ovarian cancer. *South Med J* 2001; **94**: 1212-1214
- Thakur V, Mukherjee U, Kumar K. Elevated serum cancer antigen 125 levels in advanced abdominal tuberculosis. *Med Oncol* 2001; **18**: 289-291
- Barutcu O, Erel HE, Saygili E, Yildirim T, Torun D. Abdominopelvic tuberculosis simulating disseminated ovarian carcinoma with elevated CA-125 level: report of two cases. *Abdom Imaging* 2002; **27**: 465-470
- Lantheaume S, Soler S, Issartel B, Isch JF, Lacassin F, Rougier Y, Tabaste JL. Peritoneal tuberculosis simulating advanced ovarian carcinoma: a case report. *Gynecol Obstet Fertil* 2003; **31**: 624-626
- Piura B, Rabinovich A, Leron E, Yanai-Inbar I, Mazor M. Peritoneal tuberculosis-an uncommon disease that may deceive the gynecologist. *Eur J Obstet Gynecol Reprod Biol* 2003; **110**: 230-234
- Panoskaltis TA, Moore DA, Haidopoulos DA, McIndoe AG. Tuberculous peritonitis: part of the differential diagnosis in ovarian cancer. *Am J Obstet Gynecol* 2000; **182**: 740-742
- Piura B, Rabinovich A, Leron E, Yanai-Inbar I, Mazor M. Peritoneal tuberculosis mimicking ovarian carcinoma with ascites and elevated serum CA-125: case report and review of literature. *Eur J Gynaecol Oncol* 2002; **23**: 120-122
- Rai S, Thomas WM. Diagnosis of abdominal tuberculosis: the importance of laparoscopy. *J R Soc Med* 2003; **96**: 586-588
- Wu JF, Li HJ, Ni YH, Yu SC, Chang MH. Tuberculous peritonitis mimicking peritonitis carcinomatosa: a case report. *Eur J Pediatr* 2003; **162**: 853-855
- Lal N, Soto-Wright V. Peritoneal tuberculosis: diagnostic options. *Infect Dis Obstet Gynecol* 1999; **7**: 244-247
- Bouma BJ, Tytgat KM, Schipper HG, Kager PA. Be aware of abdominal tuberculosis. *Neth J Med* 1997; **51**: 119-122
- Schwake L, von Herbay A, Junghanss T, Stremmel W, Mueller M. Peritoneal tuberculosis with negative polymerase chain reaction results: report of two cases. *Scand J Gastroenterol* 2003; **38**: 221-224
- Protopoulos A, Milingos S, Diakomanolis E, Elsheikh A, Protogerou A, Mavrommatis K, Michalas S. Miliary tuberculous peritonitis mimicking advanced ovarian cancer. *Gynecol Obstet Invest* 2003; **56**: 89-92
- Martin JR, Whitted R, Latchaw GA, Yebara S. Complications of operative and diagnostic laparoscopy: a retrospective study. *Obstet Gynecol* 2001; **97**: S20
- Moatter T, Mirza S, Siddiqui MS, Soomro IN. Detection of Mycobacterium tuberculosis in paraffin embedded intestinal tissue specimens by polymerase chain reaction: characterization of IS6110 element negative strains. *J Pak Med Assoc* 1998; **48**: 174-178
- Tzoanopoulos D, Mimidis K, Giaglis S, Ritis K, Kartalis G. The usefulness of PCR amplification of the IS6110 insertion element of *M. tuberculosis* complex in ascitic fluid of patients with peritoneal tuberculosis. *Eur J Intern Med* 2003; **14**: 367-371
- Voigt MD, Kalvaria I, Trey C, Berman P, Lombard C, Kirsch RE. Diagnostic value of ascites adenosine deaminase in tuberculous peritonitis. *Lancet* 1989; **1**: 751-754
- Hillebrand DJ, Runyon BA, Yasminah WG, Rynders GP. Ascitic fluid adenosine deaminase insensitivity in detecting tuberculous peritonitis in the United States. *Hepatology* 1996; **24**: 1408-1412

Serum concentration of sFas and sFasL in healthy HBsAg carriers, chronic viral hepatitis B and C patients

Tadeusz Wojciech Lapinski, Oksana Kowalczyk, Danuta Prokopowicz, Lech Chyczewski

Tadeusz Wojciech Lapinski, Danuta Prokopowicz, Department of Infectious Diseases, Medical University of Bialystok, Poland
Oksana Kowalczyk, Lech Chyczewski, Institute of Molecular Biology, Medical University of Bialystok, Poland

Correspondence to: Dr. Tadeusz Wojciech Lapinski, Department of Infectious Diseases, Medical University of Bialystok, 15-540 Bialystok, Zurawia str., 14, Poland. twlapinski@wp.pl

Telephone: +48-85-7416921

Received: 2004-02-20 **Accepted:** 2004-04-16

Abstract

AIM: To estimate the amount of apoptosis among healthy HBsAg carriers, patients with chronic HBV infection treated with lamivudine and patients with chronic HCV infection treated with interferon alpha and ribavirin. Activity of apoptosis was evaluated by serum sFas/sFasL concentration measurement. Moreover dependence between apoptosis and HBV-DNA or HCV-RNA levels was studied.

METHODS: Eighty-six persons were included into study: 34 healthy HBsAg carriers, 33 patients with chronic HBV infection and 19 patients with chronic HCV infection. Serum levels of sFas/sFasL were measured by ELISA assay. HBV-DNA and HCV-RNA were measured by RT-PCR assay. Levels of sFas/sFasL were determined before and 2 and 12 wk after therapy in patients with chronic hepatitis B and C infection. HBV-DNA or HCV-RNA was detected before treatment and 6 mo after treatment.

RESULTS: Twenty-four (71%) healthy HBsAg carriers showed HBV-DNA over 10^5 /mL, which was comparable to the patients with chronic hepatitis B. Independently from HBV-DNA levels, the concentration of sFas among healthy HBsAg carriers was comparable to healthy persons. Among patients with chronic hepatitis B and C, the concentration of sFas was significantly higher in comparison to healthy HBsAg carriers and healthy persons. In chronic hepatitis B patients the concentration of sFas was decreased during lamivudine treatment. Among chronic hepatitis C patients the concentration of sFas was increased during IFN alpha and ribavirin treatment. sFasL was not detected in control group. Furthermore sFasL occurred more frequently in chronic hepatitis C patients in comparison to chronic hepatitis B patients.

CONCLUSION: There are no correlations between apoptosis and HBV-DNA levels. However there is an association between apoptosis and activity of inflammation in patients with chronic HBV infection. Apoptosis can be increased in patients with chronic hepatitis C by effective treatment which may be a result of apoptosis stimulation by IFN- α .

Lapinski TW, Kowalczyk O, Prokopowicz D, Chyczewski L. Serum concentration of sFas and sFasL in healthy HBsAg carriers, chronic viral hepatitis B and C patients. *World J Gastroenterol* 2004; 10(24):3650-3653

<http://www.wjgnet.com/1007-9327/10/3650.asp>

INTRODUCTION

Apoptosis is one of the factors prolonging inflammation in chronic hepatitis B and C. Impaired apoptosis activity or its hyperactivity may induce unfavourable course of HBV and HCV infection. Fas and FasL are proteins that regulate activity of apoptosis^[1]. Fas is dominantly localized on liver cells. Activation of Fas is an after-effect of fusion with FasL lymphocyte receptors. These particles are recognised defining coefficient state of stimulation apoptosis^[2,3]. The concentration of Fas/FasL in serum patients with chronic hepatitis B and C can define the success of therapy.

The aim of this study was to define the activity of apoptosis among healthy HBsAg carriers and patients with chronic hepatitis B and C. Apoptosis was defined by use of sFas and sFasL serum concentration measurements. Moreover the apoptosis activity was compared with HBV-DNA or HCV-RNA serum levels. sFas and sFasL levels were monitored during antiviral therapy and afterwards depending on treatment effectiveness.

MATERIALS AND METHODS

The study included 86 persons divided into three groups: HBsAg carriers ($n = 34$, 15 women and 19 men, aged 20-43 years), chronic hepatitis B patients ($n = 33$, 10 women and 23 men, aged 18-76 years), and chronic hepatitis C patients ($n = 19$, 6 women and 13 men, aged 18 - 76 years). Criteria for inclusion of HBsAg carriers group were: HBsAg presence for at least 1 year; ALT, AST activity, concentration of bilirubin, albumin and PT in normal range in one-year period of observation (triple investigation); no changes in USG investigation of liver; absence of drug or alcohol abuse, autoimmune disease, HIV, delta virus or hepatitis C coinfection, and neoplastic and other serious diseases which might alter apoptosis activity. Criteria for inclusion of chronic hepatitis B patients were: HBsAg, HBeAg and HBV-DNA in serum for 6 mo; ALT activity over 80 IU; inflammatory changes in histological evaluation of liver tissue. All chronic hepatitis B patients were treated with nucleic analogue - lamivudine (Zeffix[®], GlaxoSmithKline, Great Britain) in a dose of 100 mg/24 h for 12 mo.

Criteria for inclusion of chronic hepatitis C patients were: presence of anti-HCV and HCV-RNA in serum for 6 mo, ALT activity over 80 IU and inflammatory changes in histological evaluation of liver tissue.

Patients with chronic HCV infection were treated with Rebetron[®] (IFN- α 2 b and ribavirin, Schering-Plough, USA): IFN- α 2 b in 9 M IU/wk and ribavirin 1 000-1 200 mg/24 h for 12 mo.

The standard concentration of sFas and sFasL in serum was evaluated in 12 healthy persons, 8 women and 4 men, aged 26-46 years. Individuals in control group were HBs and anti-HCV negative and ALT activity in serum was within normal range during 6 mo observation.

Methods

HBsAg and HBeAg in serum were detected by MEIA test (ABBOTT, USA).

Extraction of HBV DNA from sera of patients

HBV-DNA was extracted from 200 μ L of patients' sera the gene

elute mammalian genomic DNA Miniprep kit (Sigma, USA) for DNA isolation. Part of HBV-DNA was amplified by PCR system with pair of complement primer to conservative part of genome (sense 5'-AG GGG AGG AGA TTA GGT TAA-3' antisense 5'-AGG AGT GCG AAT CCA CACT C-3') in 20 μ L reaction mixture containing 200 μ mol/L dNTPs, 0.4 μ mol/L all primers, 1.5 mmol/L MgCl₂, 1.0 U Taq polymerase (Sigma) and 4 μ L DNA solution. Forty cycles of amplification were performed (at 96 °C for 30 s, at 57 °C for 60 s and at 72 °C for 60 s). The products of amplification were appointed in 20 g/L agar gel by electrophoresis, and stained by ethidium bromide. Electrophore was visualized in record system and computer analysis UVI-KS400i/Image PC (Syngen Biotech, USA). Part of solution from DNA was kept at temperature -20 °C for further stages of work.

In order to detect HBV-DNA sequences in sera of the patients, the conventional PCR method with primers to conserved pre-S/S region of the genome was used. Thermal cycling was performed using the following conditions: initial incubation at 96 °C for 120 s, and then 40 cycles at 94 °C for 30 s, at 50 °C for 30 s and at 72 °C for 60 s.

HBV-DNA concentration in sera was evaluated by real-time detection PCR based on TaqMan chemistry. Amplification was performed in 25 mL reaction mixture containing 2 \times TaqMan Universal Master Mix (Applied Biosystems, USA) with uracil N'-glycosylase, 30 pmol of forward primer, 30 pmol of reverse primer, 30 pmol TaqMan probe (5'-FAM) and 5 μ L of isolated DNA. After incubation for 2 min at 50 °C, which enabled uracil N'-glycosylase to inactivate possible contaminating amplicons, incubation for 10 min at 95 °C allowed AmpliTaq Gold polymerase to activate and inactivate the uracil N'-glycosylase. Next cycles of PCR were moved. Number of copies was counted by interpolation from definite standard curve.

Presence of anti-HCV antibodies in serum was detected by MEIA (ABBOTT, USA). Test consisted of recombinant core proteins for HCr43, structural proteins for c 200 (NS3 and NS4) and unstructured proteins for c 100-3 (NS4) and NS5.

Extraction of HCV-RNA from blood of patients

HCV-RNA was isolated from 50 μ L blood of patients. Parts of viral HCV-RNA were amplified in arrangement of RT nested PCR reaction with two peers nested primers, complementary to conservative part of genome virus (external primers: sense 5'-TCT AGC CAT GGC GTT AGT ATG AGT GT-3', antisense 5'-CACTCGCAAGCACCTATCAGGCA GT-3'; internal primers: sense 5'-GGC GAC ACT CCA CCA TAG AT-3', antisense 5'-GTG CAC GGT CTA CGA GAC CT-3'). Stages of reverse transcription as well as first PCR were executed in one test-glass in 20 μ L reaction mixture containing 200 mmol/L dNTPs, 1 mmol/L from each steam external primer, 1.5 mmol/L MgCl₂, 0.75 mmol/L MnSO₄, 2.0 At Tth of polymerase (EPICENTRE®, USA) as well as 8 mL RNA. After 30 min of incubation at 60 °C for 40 cycles of amplification were executed (at 94 °C for 30 s, at 55 °C for 60 s, at 72 °C for 60 s). A 1 mL product of first PCR was amplified with pair of internal primers in 20 mL reaction mixture containing 200 mmol/L dNTPs, 0.4 μ mol/L from each primer, 1.5 mmol/L MgCl₂, 1.0 U Taq of polymerase (Sigma, USA). Afterwards, 40 cycle of amplification were performed (at 94 °C for 30 s, at 55 °C for 60 s, at 72 °C for 60 s). The products of amplification were evaluated in 20 g/L of agar gel by electrophoresis and stained by brom etydyne. The electrophore was visualized in VI-KS400i / Image of PC system (Syngen Biotech, USA).

The minimum detectable dose of HCV was 50 copies per mL of serum.

Concentration of sFas and sFasL

The sFas/sFasL concentration in serum was measured twice by quantitative sandwich enzyme immunoassay (ELISA) technique (Bender Med Systems, Austria).

Informed consent was obtained from each patient and the Bioethics Committee at the Medical University of Bia³ystok approved the study protocol.

Statistical analysis

Statistical analysis was performed by use of non-parametric Mann-Whitney U, Wilcoxon rank and Pearson tests. $P < 0.05$ was considered statistically significant.

RESULTS

Twenty-four (71%) of 34 healthy HBsAg carriers showed active HBV replication. The HBV-DNA levels exceeding 10⁵/mL were observed in 22 (65%) HBsAg carriers. According to National Institutes of Health, such persons should be considered for antiviral treatment as chronic hepatitis B patients^[4,5]. All individuals in chronic hepatitis B group presented HBV-DNA levels exceeding 10⁵/mL.

Independently from HBV-DNA levels, the concentration of sFas among HBsAg carriers and healthy persons was comparable ($x = 15.4$ ng/mL, $x = 18.4$ ng/mL, $P < 0.05$). Among patients with chronic HBV or HCV infection, the concentration of sFas was significantly elevated in comparison to healthy persons and healthy HBsAg carriers ($x = 29.0$ ng/mL, $x = 28.0$ ng/mL, $P < 0.05$), (Figure 1A). There were no statistical differences between chronic hepatitis B and C patients (Table 1).

Table 1 Serum sFas concentration and frequency occurrence and concentration of sFasL in serum of patients

	n	sFas-medium ng/mL	patients with sFasL (%)	sFasL- medium ng/mL
Healthy	12	18.4	0	0
Total healthy HBsAg carriers	34	15.4	56	0.9
Healthy HBsAg carriers				
HBV-DNA <10 ⁴ /mL or 0	12	13.6	58	0.6
Healthy HBsAg carriers				
HBV-DNA >10 ⁵ /mL	22	16.3	55	1.0
Chronic hepatitis B	33	29	32	0.18
Chronic hepatitis C	19	28	68	1.0

sFasL was not detected in control group. This protein was identified more frequently in chronic hepatitis C patients than in chronic hepatitis B patients.

ALT activity reached normal values during the first three months of lamivudine treatment in all chronic hepatitis B patients (114 IU before treatment vs 32 IU after 3 mo of therapy, $P < 0.001$). In the same period the concentration of sFas was decreased in all patients (before treatment $x = 29.0$ ng/mL, after 14 d of therapy $x = 25.0$ ng/mL, after 3 mo of therapy $x = 22.0$ mg/mL). FasL expression in chronic hepatitis B group was decreased 14 d after an antiretroviral treatment and then returned to initial values.

The normalization of ALT was observed 2 wk after therapy in patients with chronic hepatitis C (102 IU before treatment vs 30 IU after 14 d of therapy). All of the chronic hepatitis C patients included in our study had undetectable HCV-RNA after 6 mo of treatment. The highest concentration of sFas was observed in chronic hepatitis C patients with virological response to antiretroviral treatment. The concentration of this protein kept increase during therapy (all HCV infected patients: before treatment $x = 28.0$ ng/mL, after 14 d $x = 31.0$ ng/mL, after 3 mo of therapy $x = 30.0$ mg/mL patients with HCV infection had good response: before treatment $x = 35.0$ ng/mL, after 14 d $x = 39.0$ ng/mL, after 3 mo of therapy $x = 39.0$ mg/mL), (Figure 1B). The number of patients with sFasL occurrence in serum was the highest before and 3 mo after treatment (83%) among all patients who were effectively treated.

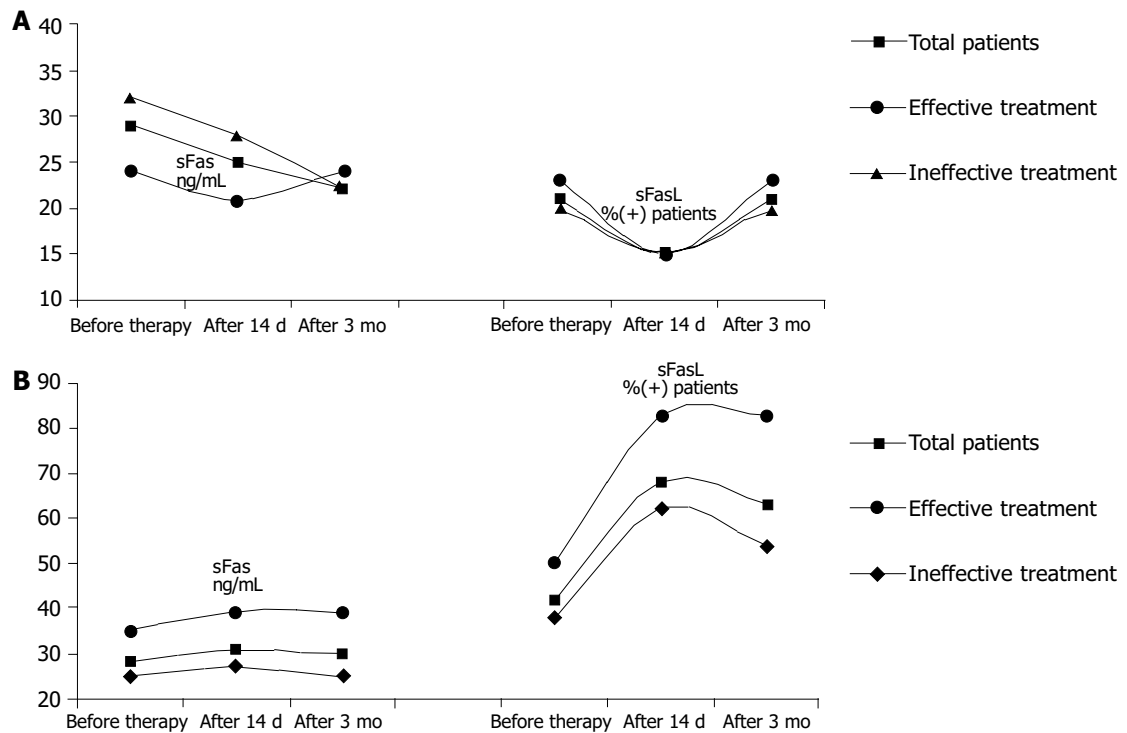


Figure 1 Concentration of sFas and sFasL in HBV infected patients and chronic hepatitis C patients. A: Concentration of sFas in HBV infected patients B: Concentration of sFasL in chronic hepatitis C patients.

DISCUSSION

Fas and FasL are “death domain”, proteins which regulate the process of apoptosis in patients with chronic inflammatory diseases, such as viral hepatitis^[6-9]. The Browicz-Kupffer cells participate in the process. It stimulates synthesis of cytokines regulating biosynthesis of Fas in hepatocytes. Recent studies indicated that it was dependent on the liver or serum sFas concentration and apoptosis activity as well as hepato-cytotoxic processes in viral chronic hepatitis patients^[10,11].

In this study we showed that the concentration of sFas in healthy persons and healthy HBsAg carriers was comparable and not dependant on the HBV-DNA levels. It was confirmed trough the lack of correlation between HBV-DNA levels and apoptosis. The concentration of sFas was significantly higher in patients with chronic hepatitis B infection than in healthy HBsAg carries, independent similar levels of HBV-DNA (>10⁵/mL).

Interestingly a large number of healthy HBsAg carriers presented sFasL in serum. The possible explanation of this fact is that HBV might stimulate expression of FasL on lymphocytes. The complex FasL and Fas could activate apoptosis and cytotoxic T lymphocytes. Activation of inflammation processes in the liver could influence FasL activity, associated with Fas and FasL complex formation. It could explain more uncommon occurrences of sFasL in patients with chronic hepatitis B than in healthy HBsAg carriers.

Hepatitis C virus core proteins could activate Fas particles expressed on hepatocytes through TNF-RI receptors stimulation. These receptors could enhance cysteine protease and subsequently interleukin-1 β -converting enzyme (ICE) and FADD like ICE (FLICE-Caspase 8) synthesis. Moreover ICE and FLICE could activate nuclear protein degradation, resulting in irreversible damage of cell DNA^[12-14].

However HCV could also inhibit apoptosis. HCV non-structural protein NS5A could suppress synthesis of Caspase 3, protein's kinase A and TNF- α stimulating polymerase^[15-17]. The protein's kinase A is known as an apoptosis initiating factor.

In patients with chronic hepatitis C, insufficient apoptosis activity could cause chronic inflammation^[18]. According to Di Martino *et al.*^[19] activity of apoptosis in chronic hepatitis C patients

was proportional to HCV-RNA levels. Ozaslan *et al.*^[20] suggested a positive dependence on chronic hepatitis C intensity and serum sFas concentration.

Our study showed a significant increase of sFas concentration in HCV infection patients compared to healthy persons, as well as a further raise in sFas serum levels during antiviral therapy. Moreover, we observed an association between high activity of apoptosis expressed as serum sFas concentration and sFasL occurrence, and antiviral treatment effectiveness.

Increased expression of FasL on peripheral blood mononuclear cells might be caused by IFN- α apoptosis stimulation^[21]. This fact is a probable explanation of the increased number of patients presenting sFasL during antiviral therapy. It may also confirm the beneficial influence of apoptosis in controlling chronic inflammation during HCV infection.

sFas serum concentration in chronic hepatitis B and C patients was comparable before treatment, but after antiviral therapy the concentration of this protein behaved in a different way. These differences underlined the diverse pathogenesis of an inflammation during chronic HBV and HCV infections. Our results indicated possible, new trends in antiviral therapy efficacy.

In conclusion, inflammation activity is associated with apoptosis in chronic hepatitis B, and there is no correlation between apoptosis and HBV-DNA concentrations. In HCV infection the effective therapy is accompanied with high activity of apoptosis, which can be a result of IFN- α activity.

REFERENCES

- 1 Wang XZ, Chen XC, Chen YX, Zhang LJ, Li D, Chen FL, Chen ZX, Chen HY, Tao QM. Overexpression of HBxAg in hepatocellular carcinoma and its relationship with Fas/FasL system. *World J Gastroenterol* 2003; **9**: 2671-2675
- 2 Mita E, Hayashi N. Apoptosis in human diseases: role of Fas system in liver cell injury by viral hepatitis. *Rinsho Byori* 1997; **45**: 477-482
- 3 Zhao J, Wang S, Xin S, Yi T, Liu P, Zhang L. Expression of CPP32, Fas and Fas ligand and the relationship between their expression and viral antigens in chronic hepatitis. *Zhonghua Ganzangbing Zazhi* 2000; **8**: 233-235

- 4 **Heo J**, Baik TH, Kim HH, Kim GH, Kang DH, Song GA, Cho M, Yang US. Serum hepatitis B virus (HBV) DNA levels at different stages of clinical course in patients with chronic HBV infection in an endemic area. *J Korean Med Sci* 2003; **18**: 686-690
- 5 **Mommeja-Marin H**, Mondou E, Blum MR, Rousseau F. Serum HBV DNA as a marker of efficacy during therapy for chronic HBV infection: analysis and review of the literature. *Hepatology* 2003; **37**: 1309-1319
- 6 **Yin XM**, Ding WX. Death receptor activation-induced hepatocyte apoptosis and liver injury. *Curr Mol Med* 2003; **3**: 491-508
- 7 **Canbay A**, Higuchi H, Bronk SF, Taniai M, Sebo TJ, Gores GJ. Fas enhances fibrogenesis in the bile duct ligated mouse: a link between apoptosis and fibrosis. *Gastroenterology* 2002; **123**: 1323-1330
- 8 **Ehrmann J Jr**, Galuszkova D, Ehrmann J, Krc I, Jezdinska V, Vojtesek B, Murray PG, Kolao Z. Apoptosis-related proteins, BCL-2, BAX, FAS, FAS-L and PCNA in liver biopsies of patients with chronic hepatitis B virus infection. *Pathol Oncol Res* 2000; **6**: 130-135
- 9 **Lee MO**, Kang HJ, Cho H, Shin EC, Park JH, Kim SJ. Hepatitis B virus X protein induced expression of the Nur77 gene. *Biochem Biophys Res Commun* 2001; **288**: 1162-1168
- 10 **Liaw YF**, Tsai SL, Chien RN, Yeh CT, Chu CM. Prednisolone priming enhances Th1 response and efficacy of subsequent lamivudine therapy in patients with chronic hepatitis B. *Hepatology* 2000; **32**: 604-609
- 11 **Xin S**, Zhao J, Wang L. Study on relationship between the apoptosis of hepatocytes and liver fibrosis of chronic viral hepatitis. *Zhonghua Shiyan He Linchuang Bingduxue Zazhi* 2000; **14**: 31-33
- 12 **Hahn CS**, Cho YG, Kang BS, Lester IM, Hahn YS. The HCV core protein acts as a positive regulator of fas-mediated apoptosis in a human lymphoblastoid T cell line. *Virology* 2000; **276**: 127-137
- 13 **Marusawa H**, Hijikata M, Chiba T, Shimotohno K. Hepatitis C virus core protein inhibits Fas- and tumor necrosis factor alpha-mediated apoptosis via NF-kappa B activation. *J Virol* 1999; **73**: 4713-4720
- 14 **Zhu N**, Ware CF, Lai MM. Hepatitis C virus core protein enhances FADD-mediated apoptosis and suppresses TRADD signaling of tumor necrosis factor receptor. *Virology* 2001; **283**: 178-187
- 15 **Ghosh AK**, Majumder M, Steele R, Meyer K, Ray R, Ray RB. Hepatitis C virus NS5A protein protects against TNF-alpha mediated apoptotic cell death. *Virus Res* 2000; **67**: 173-178
- 16 **Ezelle HJ**, Balachandran S, Sicheri F, Polyak SJ, Barber GN. Analyzing the mechanisms of interferon-induced apoptosis using CrmA and hepatitis C virus NS5A. *Virology* 2001; **281**: 124-137
- 17 **Satoh S**, Hirota M, Noguchi T, Hijikata M, Handa H, Shimotohno K. Cleavage of hepatitis C virus nonstructural protein 5A by a caspase-like protease (s) in mammalian cells. *Virology* 2000; **270**: 476-487
- 18 **Zuckerman E**, Zuckerman T, Sahar D, Streichman S, Attias D, Sabo E, Yeshurun D, Rowe J. Bcl-2 and immunoglobulin gene rearrangement in patients with hepatitis C virus infection. *Br J Haematol* 2001; **112**: 364-369
- 19 **Di Martino V**, Brenot C, Samuel D, Saurini F, Paradis V, Reynes M, Bismuth H, Feray C. Influence of liver hepatitis C virus RNA and hepatitis C virus genotype on Fas-mediated apoptosis after liver transplantation for hepatitis C. *Transplantation* 2000; **15**: 1390-1396
- 20 **Ozaslan E**, Kilicarslan A, Simsek H, Tatar G, Kirazli S. Elevated serum soluble Fas levels in the various stages of hepatitis C virus-induced liver disease. *J Int Med Res* 2003; **31**: 384-391
- 21 **Yoneyama K**, Goto T, Miura K, Mikami K, Ohshima S, Nakane K, Lin JG, Sugawara M, Nakamura N, Shirakawa K, Komatsu M, Watanabe S. The expression of Fas and Fas ligand, and the effects of interferon in chronic liver diseases with hepatitis C virus. *Hepatology* 2002; **24**: 327-337

Edited by Wang XL Proofread by Chen WW and Xu FM

***In vivo* suppressive effect of nuclear factor- κ B inhibitor on neutrophilic inflammation of grafts after orthotopic liver transplantation in rats**

Xiao-Ping Gu, Yu-Dong Qiu, Fu-Tao Xu, Yong Jiang, Yi-Tao Ding

Xiao-Ping Gu, Fu-Tao Xu, Department of Anesthesiology, Drum Tower Hospital, Medical Department of Nanjing University, Nanjing 210008, Jiangsu Province, China

Yong Jiang, Yu-Dong Qiu, Yi-Tao Ding, Department of Hepatobiliary Surgery, Drum Tower Hospital, Medical Department of Nanjing University, Nanjing 210008, Jiangsu Province, China

Supported by Education Foundation of Xuzhou Anesthesia Laboratory of Jiangsu Province, No.KJS02055

Correspondence to: Dr. Yi-Tao Ding, Department of Hepatobiliary Surgery, Drum Tower Hospital, Medical Department of Nanjing University, Nanjing 210008, Jiangsu Province, China. yys982002@yahoo.com.cn

Telephone: +86-25-83304616 **Fax:** +86-25-83317016

Received: 2004-04-04 **Accepted:** 2004-05-13

Abstract

AIM: To investigate the effect of pyrrolidine dithiocarbamate (PDTC), a novel nuclear factor- κ B (NF- κ B) inhibitor, on expression of multiple inflammatory mediators and neutrophilic inflammation of cold preserved grafts after rat liver transplantation and its significance.

METHODS: Orthotopic liver transplantation (OLT) was performed after 24 h of cold storage using University of Wisconsin solution with varied concentrations of PDTC. We determined the time course of NF- κ B activation and expression of multiple inflammatory signals, such as tumor necrosis factor- α (TNF- α), cytokine-inducible neutrophil chemoattractant (CINC), and intercellular adhesion molecule-1 (ICAM-1) by ELISA methods. Serum alanine aminotransferase (ALT), intrahepatic myeloperoxidase (MPO)/WBC (a measure of neutrophil accumulation) and Mac-1 expression (a measure of circulating neutrophil activity) were also evaluated.

RESULTS: PDTC decreased NF- κ B activation induced by prolonged cold preservation in a dose dependent manner (from 20 mmol/L to 60 mmol/L), diminished TNF- α , CINC, ICAM-1 proteins in the grafts, and reduced the expression of increases in plasma TNF- α levels induced by prolonged cold preservation. Neutrophilic inflammation of the graft was significantly suppressed after preservation with PDTC ($P < 0.05$). The total neutrophil accumulation in PDTC (40 mmol/L) group (7.04 ± 0.97) was markedly reduced compared to control group (14.07 ± 1.31) ($P < 0.05$). Mac-1 expression was significantly reduced in PDTC (40 mmol/L) group ($181 \pm 11.3\%$) compared with the control group ($281 \pm 13.2\%$) ($P < 0.05$) at 6 h after reperfusion. Furthermore, PDTC inhibited the increased serum ALT levels after liver transplantation.

CONCLUSION: PDTC can inhibit B NF- κ B activation and expression of the inflammatory mediators, which are associated with improved graft viability via inhibiting intrahepatic neutrophilic inflammation. Our study suggests that a therapeutic strategy directed at inhibition of NF- κ B activation in the transplanted liver might be effective in

reducing intrahepatic neutrophilic inflammation, and would be beneficial to cold preserved grafts.

Gu XP, Qiu YD, Xu FT, Jiang Y, Ding YT. *In vivo* suppressive effect of nuclear factor- κ B inhibitor on neutrophilic inflammation of grafts after orthotopic liver transplantation in rats. *World J Gastroenterol* 2004; 10(24): 3654-3658

<http://www.wjgnet.com/1007-9327/10/3654.asp>

INTRODUCTION

Poor graft viability is a frequent complication of liver transplantation, the incidence of primary graft nonfunction was reported to be 2-23%^[1]. Furukawa *et al.*^[2] reported that the primary nonfunction rate and retransplantation rate significantly rose as cold-ischemia time increased, especially beyond 20 h. It is currently accepted that sinusoidal endothelial cells (SECs) are the primary targets of cold ischemia-reperfusion injury^[3], however, parenchymal cell damage has direct effects on the deterioration of liver function. The functional impairment of the grafted liver, therefore, seems to be complex and multifactorial. Polymorphonuclear leukocytes (PMNs) have been implicated as a causal factor in the development of ischemia-reperfusion injury^[4,5]. In the previous study, we found the promoted neutrophil accumulation and activity in cold preserved grafts, and the evidence confirmed that cold preservation-reperfusion injury of liver allografts was a chain of cascades induced by activation of a variety of inflammatory mediators from early to late phase after reperfusion^[6]. Protective strategies were confused that inhibition of one mediator was always compensated by activation of other mediators from different pathways^[8]. Researchers are anxious to look for the core mediators that can trigger multiple proinflammatory genes. Recent studies have shown that transcription factor NF- κ B plays an essential role in regulation of these kinds of genes whose products take part in the pathogenesis of preservation-reperfusion injury in liver allografts^[6-11]. Hence, it is hypothesized that NF- κ B may be an appropriate target for treatment of reperfusion injury. NF- κ B appears to have both beneficial and harmful effects on liver transplantation^[12-16]. It was reported that NF- κ B could promote liver regeneration and prevent apoptosis^[14], and contribute to the inflammatory response of ischemia/reperfusion^[15]. In the present study, we determined the time course of NF- κ B activation after OLT in relation to the expression of tumor necrosis factor- α (TNF- α), intercellular adhesion molecule-1 (ICAM-1), and cytokine-induced neutrophil chemoattractant (CINC). The selectivity of pyrrolidine dithiocarbamate (PDTC) as an *in vivo* inhibitor of NF- κ B activation, the effects of PDTC on OLT-induced expression of these inflammatory gene products and the resultant hepatic neutrophilic inflammation, and the action of NF- κ B were studied.

MATERIALS AND METHODS

Reagents

Following reagent were purchased: Pyrrolidine dithiocarbamate (PDTC) from Sigma, nuclear extract kit and NF- κ B p65

Transcription factor assay kits from Active Motif, Pierce BCA protein assay reagent and MPO assay reagent from Jiancheng, Nanjing, ELISA assay kit for CINC, TNF- α and ICAM-1 from Amersham, Buckinghamshire, UK, FACS lysing solution from Becton Dickinson, San Jose, CA and FITC-labeled mouse anti-rat CD11b antibody from Camarillo, CA.

Animals

Male wistar rats, weighing 200 to 250 g, were purchased from Nanjing Medical Institute Animal Care Committee (Grade II, Certification No 2002-0017). Prior to the experiment, rats were fasted for 12 h and allowed free access to water.

Experimental protocol

Rats were allocated randomly into four groups (36 rats in each group): control group in which the grafts were harvested with injection of University of Wisconsin (UW) solution, PDTC20 group in which the grafts were harvested with the preservation solution added by 20 mmol/L PDTC, PDTC40 group in which the grafts were harvested with the preservation solution added by 40 mmol/L PDTC, and PDTC60 group in which the grafts were harvested with the preservation solution added by 60 mmol/L PDTC.

Liver harvesting and orthotopic transplantation were performed according to the methods described by Kamada and Calne^[17], with some minor modifications^[18], and the hepatic artery was not reconstructed. The graft liver was preserved with University of Wisconsin (UW) solution at 4 °C for 24 h. The portal vein clamping time in recipients varied from 18 to 20 min, implantation time was less than 50 min, all the procedures took about 60 min. No significant difference was seen in portal clamping time between groups. The recipients were sacrificed 0 h, 0.5 h, 1 h, 2 h, 4 h, and 6 h after reperfusion. Blood samples were collected from the hepatic vein draining the left lateral lobe as previously described to determine the serum levels of alanine aminotransferase (ALT) and neutrophil activity at indicated time points. The median lobe of the liver was carefully excised at the designated time point and stored at -80 °C for analysis.

Evaluation of NF- κ B activity

Preparation of nuclear extracts using a nuclear extract kit and determination of p65/relA subunits of NF- κ B using a TransAM NF- κ B p65 kit according to the manufacturer's instructions. The concentration of p65/relA subunits in liver tissue homogenates was standardized to the total nuclear protein content in each specimen as measured by the Pierce BCA protein assay reagent. NF- κ B activity was expressed as p65/relA subunits μ g/mg total nuclear protein.

Graft function test

Cellular function and damage were estimated by the peak serum ALT activity in six rats from each group at selected time points after reperfusion. Serum ALT was measured using the Opera clinical chemistry system.

Measurement of TNF- α , CINC and ICAM-1

Serum TNF- α and CINC were measured in duplicate by using the immunoassay kits according to the manufacturer's instructions.

Hepatic levels of TNF- α , CINC, and ICAM-1 were determined as previously described^[19]. In brief, the medial hepatic lobe was weighed and homogenized in 5 mL of 0.1 mol/L phosphate buffer (pH 7.4) containing 0.5 g/L of sodium azide at 4 °C. The homogenates were centrifuged at 2 000 r/min for 10 min to remove solid tissue debris. The supernatant was assayed using a rat ELISA system. The concentration of antigens in liver tissue

homogenates was standardized to the total protein content in each specimen as measured by the Pierce BCA protein assay reagent. The results were expressed as pictograms per gram of tissue (pg/g).

Intrahepatic neutrophil accumulation assessment

The activity of MPO, an enzyme in azurophilic granules of neutrophils, was used as a well-established marker to quantitate tissue neutrophil sequestration^[20]. Frozen livers were thawed and extracted for MPO, following the homogenization and sonication procedure as described in the manufacturer's protocol. One unit of MPO activity was defined as the amount of enzyme able to reduce 1 μ mol of peroxide/min. Results were expressed as units of MPO activity per gram of tissue. To control intravascular leukocytosis, we calculated the ratio of MPO activity in tissue to WBC count in peripheral blood, and expressed it as MPO/WBC.

Circulating neutrophil activity analysis

Blood samples collected from each animal at each time point were subjected to flow cytometric analysis^[21]. For CD11b and L-selectin determination, 50 μ L of samples were incubated with 10 μ L of PE-labeled mouse anti-rat L-selectin antibody and 10 μ L of FITC-labeled mouse anti-rat CD11b antibody for 15 min, then 1 mL of FACS lysing solution was added for 10 min, followed by centrifugation at 1 500 r/min for 5 min. Cell pellets were washed and then resuspended in 500 μ L of PBS. The cells were read on a Becton-Dickinson FACS calibur.

Statistical analysis

The data were expressed as mean \pm SE. Statistical analysis was performed using analysis of variance in SPSS software (version 11.0 for windows), followed by SNK multiple comparisons. *P* less than 0.05 were considered statistically significant.

RESULTS

PDTC inhibited NF- κ B activation in grafts of OLT rats

The time course of NF- κ B activity in liver tissue was established by evaluating p65/relA subunits in nuclear extracts from the whole liver obtained at various time points. In the control group, the activity of NF- κ B in preserved graft increased slightly 0.5 h after reperfusion, and markedly 1 h after reperfusion, peaked at 2 h of reperfusion and decreased 4 h after reperfusion (Figure 1). PDTC suppressed OLT-induced p65/relA subunit increase in a dose-dependent manner. PDTC administration did not affect the time course for maximal NF- κ B activation after OLT (Figure 1).

PDTC inhibited time course of expression of inflammatory mediators in grafts of OLT rats

We determined the time course of OLT-induced expression of TNF- α , CINC, and ICAM-1 in the same tissues as used for NF- κ B p65 transcription factor assay. We compared TNF- α , CINC, and ICAM-1 protein levels in tissue homogenates of livers treated by PDTC with those of livers untreated by PDTC. We observed different kinetics in the expression of inflammatory mediators. TNF- α expression was maximal 1 to 2 h after reperfusion, whereas CINC and ICAM-1 expression peaked 2 to 4 h after reperfusion (Figure 1). This was preceded by NF- κ B activation.

Pretreatment with 20, 40, and 60 mg/kg of PDTC suppressed the expression of these proteins, although the response was variable (Figure 1). Suppression by PDTC of OLT-induced expression of these proteins did not show a clear dose-dependency. Maximal inhibition of CINC and ICAM-1 expression was observed at a PDTC concentration of 40 mmol/L. Maximal inhibition of TNF- α expression was observed at a PDTC concentration of 60 mmol/L.

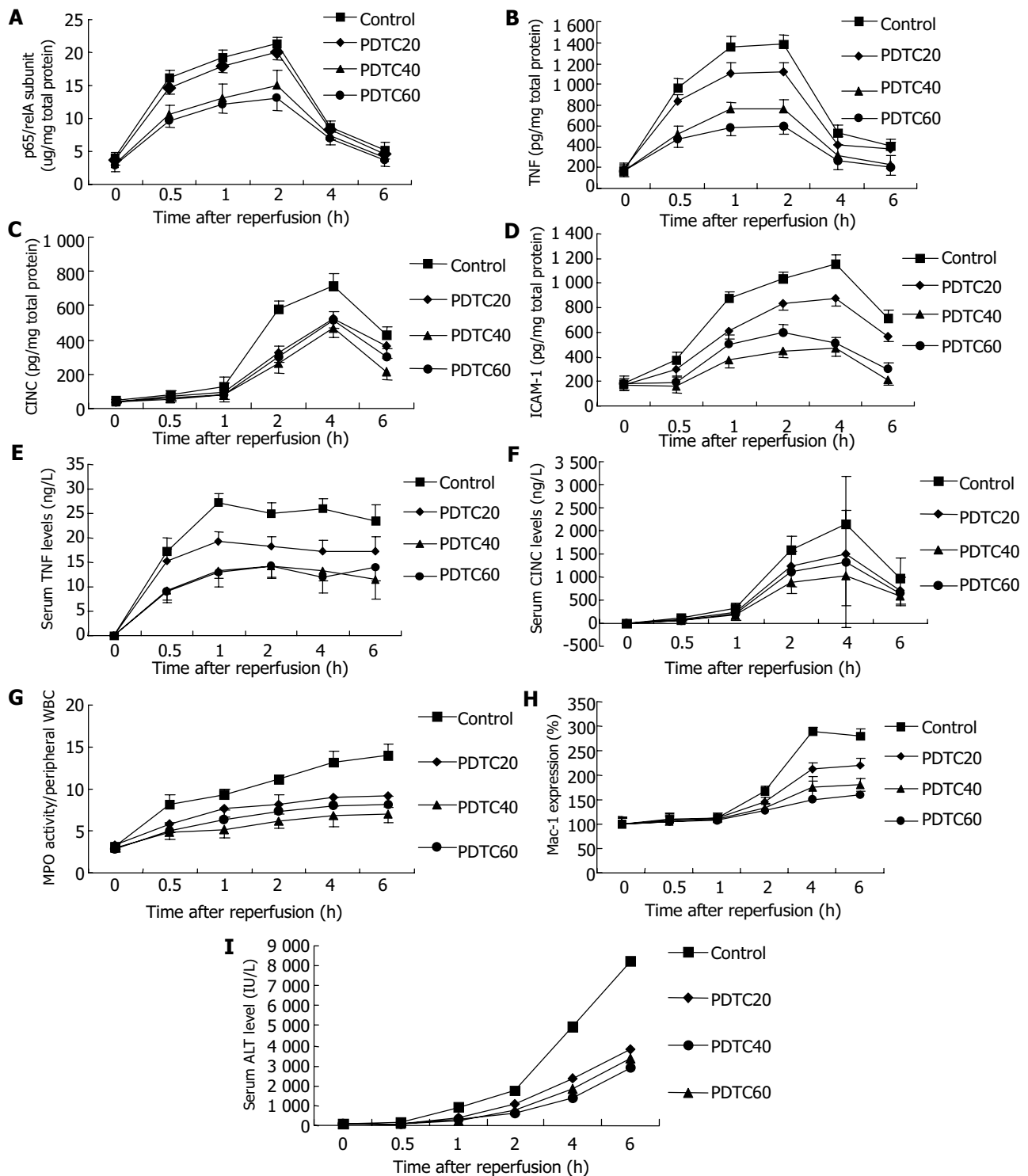


Figure 1 Effect of PDTC on NF- κ B (A), response of inflammatory mediators (B-D), systemic inflammatory recipients (E-F), intrahepatic neutrophil accumulation (G), Mac-1 expression (H), and serum ALT level (I) in OLT rats. Results are the mean \pm SD of six rats for each period in each group. A: Intrahepatic p65/reIA subunit levels were significantly inhibited in the PDTC cold-preserved group compared with the control group ($P < 0.05$). P65/reIA subunit was significantly different in three preserved groups ($P < 0.05$). Intrahepatic inflammatory mediator levels were significantly inhibited in the PDTC cold-preserved group compared with the control group ($P < 0.05$). B: TNF- α was significantly different in three-preserved groups within 0.5 h of reperfusion ($P < 0.05$), the maximal level reached at 1 h after reperfusion; C: CINC was significantly different in three preserved groups within 2 h after reperfusion ($P < 0.05$), the maximal level reached at 4 h after reperfusion; D: ICAM-1 was significantly different in three-preserved groups within 0.5 h of reperfusion ($P < 0.05$), the maximal level reached at 4 h after reperfusion. E: Serum TNF- α levels significantly inhibited in the PDTC cold-preserved group, compared with the control group since 0.5 h after reperfusion ($P < 0.05$). There is no significantly different in PDTC 40 and PDTC 60 groups ($P < 0.05$). F: Serum CINC levels significantly inhibited in the PDTC cold-preserved group, compared with the control group since 2 h after reperfusion ($P < 0.05$). Serum CINC was significantly different in three-preserved groups ($P < 0.05$). G: Intrahepatic neutrophil accumulation was significantly inhibited in the PDTC cold-preserved group, compared with the control group ($P < 0.05$). Intrahepatic neutrophil accumulation was significantly different in three-preserved groups ($P < 0.05$). H: Mac-1 expression in circulating neutrophil was significantly inhibited in the PDTC cold-preserved group, compared with the control group at 2 h after reperfusion ($P < 0.05$). There was no great different between Mac-1 expression in PDTC40 and PDTC60 ($P > 0.05$). I: Serum ALT was significantly inhibited in the PDTC cold-preserved group, compared with the control group ($P < 0.05$); which was significantly different in three-preserved groups ($P < 0.05$).

PDTC inhibited levels of systemic TNF- α and CINC response in OLT rats

The effects of PDTC on plasma TNF- α and CINC are shown in Figure 1. Pretreatment with PDTC at concentrations of 20, 40, and 60 mmol/L reduced the OLT-induced plasma TNF- α levels to 66%, 51%, 46% and plasma CINC levels to 70%, 48%, and 61% 4 h after reperfusion, respectively.

PDTC reduced neutrophil sequestration in grafts of OLT rats

We utilized the MPO biochemical assay to measure tissue neutrophil infiltration during the course of reperfusion. In control transplant livers, MPO/WBC was significantly elevated within 30 min of reperfusion than that in non-reperfusion liver tissue and remained significantly elevated throughout the 6 h of reperfusion. PDTC reduced the reperfusion-induced PMN accumulation (Figure 1). Maximal inhibition was observed at a PDTC concentration of 40 mmol/L that correlated with the inhibition of OLT-induced intrahepatic CINC and ICAM-1 expression.

PDTC inhibited circulating neutrophil activity in OLT rats

The CD11b content in circulating neutrophils was quantitatively evaluated by flow cytometric analysis at 0, 0.5, 1, 2, 4 and 6 h after the onset of reperfusion. In the control group, Mac-1 expression at the control time point (0 h) showed low levels of staining for CD11b [mean fluorescence intensity (MFI) = 76.75 \pm 19.15], which reached 167% of baseline levels at 2 h, and 289% of baseline levels at 4 h, respectively, and remained constantly elevated at 6 h (281%) after reperfusion in control group (Figure 1).

PDTC inhibited Mac-1 expression in circulating neutrophils in a dose-dependent manner (Figure 1). Maximal inhibition was observed at a PDTC concentration of 60 mmol/L that correlated with the inhibition of OLT-induced systemic TNF- α response but not systemic CINC response, indicating that TNF- α was a much more strong inflammatory mediator for neutrophil activation.

PDTC ameliorated posttransplant liver function

Serum ALT levels increased 0.5 h after reperfusion, remained greatly elevated throughout the 6 h reperfusion, and increased significantly in the 18 h and 24 h cold-preserved groups, compared with those in the 6 h group during the 6 h observation (Figure 1). PDTC ameliorated liver function after transplantation, the maximal increase was observed at a PDTC concentration of 40 mmol/L. PDTC administration did not affect the time course for maximal graft injury after OLT (Figure 1).

DISCUSSION

In this study, we extended our investigation on the pathogenesis of neutrophilic graft inflammation following rat orthotopic liver transplantation to assess the potential contribution of transcription factor after NF- κ B^[6]. Since transcription factors could determine cellular phenotypes by specifying protein production^[22], it is particularly interesting to relate changes in activation of transcription factors such as NF- κ B, to expression of a specific protein and evolution of biological relevant end points^[23-25]. We studied the expression of TNF- α , ICAM-1 and CINC because of their critical roles in the reperfusion-induced inflammatory responses. We demonstrated that reperfusion-induced NF- κ B activation *in vivo* preceded the expression of TNF- α , CINC and ICAM-1. In our rat model of orthotopic liver transplantation, we observed a link among NF- κ B activation, systemic and intrahepatic TNF- α and CINC responses, intrahepatic ICAM-1 expression, neutrophilic inflammation, and graft injury. In addition, we found that inhibition of NF- κ B activation with PDTC decrease local TNF- α ,

CINC and ICAM-1 expression, ameliorated neutrophilic inflammation, and improve graft function. These observations support the hypothesis that NF- κ B activation is critical for early graft injury in liver transplantation.

Dithiocarbamates, such as PDTC, represent a class of antioxidants reported to be potent inhibitors of NF- κ B and are capable of inhibiting the inflammatory process associated with the activation of NF- κ B^[26,27]. The most effective inhibitor of NF- κ B appears to be the pyrrolidine derivative of dithiocarbamate (PDTC) as a result of its ability to traverse the cell membrane and its prolonged stability in solution at physiological pH. PDTC, as well as other antioxidants, may inhibit NF- κ B by suppressing the production of intracellular reactive oxygen species^[26]. But it is well established that inhibition of NF- κ B is a major mechanism of the anti-inflammatory actions of PDTC^[27]. In our study, PDTC probably blocked neutrophilic inflammation in part by diminishing NF- κ B-dependent transcription of CINC and ICAM-1 expression. Blocking NF- κ B activation might also diminish the transcription of a variety of other genes involved in the production of inflammatory mediators.

It was interesting that PDTC at 60 mmol/L caused less inhibition of OLT-induced expression of CINC and ICAM-1 than PDTC at 40 mmol/L PDTC, although the higher concentration exerted greater inhibition of NF- κ B activation. This dissociation between inhibition of NF- κ B activation and ICAM-1, CINC expression might be explained by involvement of AP-1 in mediating the response^[14]. Thus, it is likely that 60 mmol/L PDTC inhibited the NF- κ B-mediated ICAM-1 and CINC expression, but augmented AP-1-mediated transcription of the ICAM-1 and CINC expression, the inhibitory effect of PDTC mediated through NF- κ B inhibition was consequently offset by the AP-1-mediated stimulatory effect, which needs further work to identify. In addition, PDTC at 60 mmol/L caused less neutrophil accumulation in the grafts, but the neutrophil activity correlated with less improvement of graft injury than 40 mmol/L PDTC, implying that local accumulation of activated neutrophils is the definitive factor of local neutrophilic inflammation.

The findings that PDTC administration ameliorated liver injury at 0.5 h and 1 h after reperfusion, as measured by serum ALT levels, were also noted to have some effects on neutrophil-independent phase of liver injury associated with OLT. In this study, neutrophil sequestration occurred quickly within 0.5 h after reperfusion, with no changes in Mac-1 and L-selectin expression at 0.5 h and 1 h time points. Previous studies demonstrated that increased expression of Mac-1^[28] and shedding of L-selectin^[29] were important to neutrophil-mediated injury. Hepatic injury at this time point was neutrophil-independent and was mediated by cytosolic xanthine oxidase and mitochondria in damaged hepatocytes^[30], the most relevant oxidant stress occurred initially in the vasculature and was produced by Kupffer cells^[31]. Our data suggested that there was a protective effect of PDTC in the liver at 0.5 h and 1 h after reperfusion, which might be mediated by antioxidants or Kupffer cells. In this study, the data showed that PDTC inhibited intrahepatic TNF- α expression in a dose-dependent manner. A study showed that TNF- α was probably from activated Kupffer cells in cold-preserved livers^[32], suggesting that the presence of primed Kupffer cells during extended cold preservation might result in overresponse and excessive production of TNF- α in the initial phase of reperfusion. The decreased expression of TNF- α in PDTC treatment group might in part reflect the inhibition of Kupffer cells.

In summary, the pathophysiological mechanisms of the protective effect of PDTC *in vivo*, appear to be pluripotent, comprising both antioxidative properties and inhibition of NF- κ B. Inhibiting early NF- κ B activity can protect against early graft injury in prolonged cold preservation after liver transplantation.

ACKNOWLEDGMENTS

We thank Dr. Jun-Bao Cheng, Li-Hua Zang from Drum Tower Hospital, Nanjing, for invaluable technical assistance.

REFERENCES

- 1 **Clavien PA**, Harvey PR, Strasberg SM. Preservation and reperfusion injuries in liver allografts. An overview and synthesis of current studies. *Transplantation* 1992; **53**: 957-978
- 2 **Furukawa H**, Todo S, Imventarza O, Casavilla A, Wu YM, Scotti-Foglieni C, Broznick B, Bryant J, Day R, Starzl TE. Effect of cold ischemia time on the early outcome of human hepatic allografts preserved with UW solution. *Transplantation* 1991; **51**: 1000-1004
- 3 **Natori S**, Selzner M, Valentino KL, Fritz LC, Srinivasan A, Clavien PA, Gores GJ. Apoptosis of sinusoidal endothelial cells occurs during liver preservation injury by a caspase-dependent mechanism. *Transplantation* 1999; **68**: 89-96
- 4 **Sakamoto N**, Sun Z, Bregman ML, Maemura K, Ozaki M, Bulkley GB, Klein AS. Hepatic reticuloendothelial system dysfunction after ischemia-reperfusion: role of P-selectin-mediated neutrophil accumulation. *Liver Transpl* 2003; **9**: 940-948
- 5 **Okaya T**, Lentsch AB. Cytokine cascades and the hepatic inflammatory response to ischemia and reperfusion. *J Invest Surg* 2003; **16**: 141-147
- 6 **Gu XP**, Jiang Y, Xu FT, Qiu YD, Ding YT. Effect of cold-ischemia time on nuclear factor- κ B activation and inflammatory response in graft after orthotopic liver transplantation in rats. *World J Gastroenterol* 2004; **10**: 1000-1004
- 7 **Kato A**, Yoshidome H, Edwards MJ, Lentsch AB. Regulation of liver inflammatory injury by signal transducer and activator of transcription-6. *Am J Pathol* 2000; **157**: 297-302
- 8 **Arii S**, Teramoto K, Kawamura T. Current progress in the understanding of and therapeutic strategies for ischemia and reperfusion injury of the liver. *J Hepatobiliary Pancreat Surg* 2003; **10**: 189-194
- 9 **Bradham CA**, Stachlewitz RF, Gao W, Qian T, Jayadev S, Jenkins G, Hannun Y, Lemasters JJ, Thurman RG, Brenner DA. Reperfusion after liver transplantation in rats differentially activates the mitogen-activated protein kinases. *Hepatology* 1997; **25**: 1128-1135
- 10 **Xu J**, Yang Z, Zeng J. Role of NF-kappa B in liver ischemia reperfusion injury of rats. *J Huazhong Univ Sci Technolog Med Sci* 2003; **23**: 158-160
- 11 **Takahashi Y**, Ganster RW, Ishikawa T, Okuda T, Gambotto A, Shao L, Murase N, Geller DA. Protective role of NF-kappaB in liver cold ischemia/reperfusion injury: effects of IkappaB gene therapy. *Transplant Proc* 2001; **33**: 602
- 12 **Tsoufias G**, Geller DA. NF-kappaB in transplantation: friend or foe? *Transpl Infect Dis* 2001; **3**: 212-219
- 13 **Bradham CA**, Schemmer P, Stachlewitz RF, Thurman RG, Brenner DA. Activation of nuclear factor-kappaB during orthotopic liver transplantation in rats is protective and does not require Kupffer cells. *Liver Transpl Surg* 1999; **5**: 282-293
- 14 **Takahashi Y**, Ganster RW, Gambotto A, Shao L, Kaizu T, Wu T, Yagnik GP, Nakao A, Tsoufias G, Ishikawa T, Okuda T, Geller DA, Murase N. Role of NF-kappaB on liver cold ischemia-reperfusion injury. *Am J Physiol Gastrointest Liver Physiol* 2002; **283**: G1175-1184
- 15 **Ricciardi R**, Kim RD, McDade TP, Perugini RA, Veal TM, Quarfordt SH, Callery MP, Chari RS, Meyers WC. NFkappaB expression during cold ischemia correlates with postreperfusion graft function. *J Surg Res* 2000; **93**: 35-40
- 16 **Bradham CA**, Schemmer P, Stachlewitz RF, Thurman RG, Brenner DA. Activation of nuclear factor-kappaB during orthotopic liver transplantation in rats is protective and does not require Kupffer cells. *Liver Transpl Surg* 1999; **5**: 282-293
- 17 **Kamada N**, Calne RY. Orthotopic liver transplantation in the rat. Technique using cuff for portal vein anastomosis and biliary drainage. *Transplantation* 1979; **28**: 47-50
- 18 **Jiang Y**, Gu XP, Qiu YD, Sun XM, Chen LL, Zhang LH, Ding YT. Ischemic preconditioning decreases C-X-C chemokine expression and neutrophil accumulation early after liver transplantation in rats. *World J Gastroenterol* 2003; **9**: 2025-2029
- 19 **Chandrasekar B**, Streitman JE, Colston JT, Freeman GL. Inhibition of nuclear factor kappa B attenuates proinflammatory cytokine and inducible nitric-oxide synthase expression in postischemic myocardium. *Biochim Biophys Acta* 1998; **27**: 91-106
- 20 **Schmekel B**, Karlsson SE, Linden M, Sundstrom C, Tegner H, Venge P. Myeloperoxidase in human lung lavage. I. A marker of local neutrophil activity. *Inflammation* 1990; **14**: 447-454
- 21 **Vuorte J**, Jansson SE, Repo H. Standardization of a flow cytometric assay for phagocyte respiratory burst activity. *Scand J Immunol* 1996; **43**: 329-334
- 22 **Lee JI**, Burckart GJ. Nuclear factor kappa B: important transcription factor and therapeutic target. *J Clin Pharmacol* 1998; **38**: 981-993
- 23 **Zwacka RM**, Zhang Y, Zhou W, Halldorson J, Engelhardt JF. Ischemia/reperfusion injury in the liver of BALB/c mice activates AP-1 and nuclear factor kappaB independently of IkappaB degradation. *Hepatology* 1998; **28**: 1022-1030
- 24 **Miyoshi H**, Rust C, Guicciardi ME, Gores GJ. NF-kappaB is activated in cholestasis and functions to reduce liver injury. *Am J Pathol* 2001; **158**: 967-975
- 25 **Kato A**, Edwards MJ, Lentsch AB. Gene deletion of NF-kappa B p50 does not alter the hepatic inflammatory response to ischemia/reperfusion. *J Hepatol* 2002; **37**: 48-55
- 26 **Hong HJ**, Wu CC, Yen MH. Pyrrolidine dithiocarbamate improves the septic shock syndromes in spontaneously hypertensive rats. *Clin Exp Pharmacol Physiol* 1998; **25**: 600-606
- 27 **Liu SF**, Ye X, Malik AB. Inhibition of NF-kappa B activation by Pyrrolidine dithiocarbamate prevents *in vivo* expression of proinflammatory genes. *Circulation* 1999; **100**: 1330-1337
- 28 **Vollmar B**, Menger MD, Glasz J, Leiderer R, Messmer K. Impact of leukocyte-endothelial cell interaction in hepatic ischemia-reperfusion injury. *Am J Physiol* 1994; **267**(Pt 1): G786-793
- 29 **Lawson JA**, Burns AR, Farhood A, Lynn Bajt M, Collins RG, Smith CW, Jaeschke H. Pathophysiologic importance of E- and L-selectin for neutrophil-induced liver injury during endotoxemia in mice. *Hepatology* 2000; **32**: 990-998
- 30 **Hines IN**, Harada H, Wolf R, Grisham MB. Superoxide and post-ischemic liver injury: potential therapeutic target for liver transplantation. *Curr Med Chem* 2003; **10**: 2661-2667
- 31 **Schauer RJ**, Bilzer M, Kalmuk S, Gerbes AL, Leiderer R, Schildberg FW, Messmer K. Microcirculatory failure after rat liver transplantation is related to Kupffer cell-derived oxidant stress but not involved in early graft dysfunction. *Transplantation* 2001; **72**: 1692-1699
- 32 **Arii S**, Monden K, Adachi Y, Zhang W, Higashitsuji H, Furutani M, Mise M, Fujita S, Nakamura T, Imamura M. Pathogenic role of Kupffer cell activation in the reperfusion injury of cold-preserved liver. *Transplantation* 1994; **58**: 1072-1077

Edited by Kumar M and Wang XL Proofread by Xu FM

Clinical analysis of eight kindreds of familial adenomatous polyposis

Yu-Long He, Chang-Hua Zhang, Mei-Jin Huang, Shi-Rong Cai, Wen-Hua Zhan, Jian-Ping Wang, Ji-Fu Wang

Yu-Long He, Chang-Hua Zhang, Mei-Jin Huang, Shi-Rong Cai, Wen-Hua Zhan, Jian-Ping Wang, Ji-Fu Wang, Department of Gastrointestinopancreatic Surgery, the First Affiliated Hospital, Sun Yat-Sen University, Guangzhou 510080, Guangdong Province, China
Supported by the Special Funds of Chinese Education Ministry for Returnees, No.03-5

Correspondence to: Professor Yu-Long He, Department of Gastrointestinopancreatic Surgery, the First Affiliated Hospital, Sun Yat-Sen University, Guangzhou 510080, Guangdong Province, China. ylh@medmail.com.cn

Telephone: +86-20-87755766 Ext. 8211 **Fax:** +86-20-87335945

Received: 2004-03-31 **Accepted:** 2004-05-13

Abstract

AIM: To study the early diagnosis and management of familial adenomatous polyposis (FAP).

METHODS: Eight pedigrees of FAP were collected and their pedigree trees were protracted. Clinical characteristics and treatment outcomes of FAP patients in these kindreds were analysed.

RESULTS: A total of 157 members were investigated in eight kindreds and 25 patients with FAP were diagnosed. The ratio of male patients and female patients was 16:9 and the average age at onset was 38 years. Among them, six patients died of cancer with a mortality rate of 28%, and 36% (9/25) FAP patients were diagnosed as synchronous colorectal cancer on the basis of FAP. A proband was diagnosed as synchronous colorectal cancer with liver metastasis and died 11 mo later after partial colectomy and hepatic metastatic lesion biopsy. The other seven probands received total abdominal colectomy and rectal mucosectomy with ileal pouch-anal anastomosis (IPAA), and one of them was diagnosed as synchronous colon cancer on the basis of FAP and was still alive after 7.5 years follow-up. Among the other seven patients with synchronous colorectal cancer on the basis of FAP underwent total abdominal colectomy with ileorectal anastomosis (IRA), one underwent total remnant rectum resection and ileostomy for recurrent carcinoma in the retained rectum 2.5 years later after the IRA and was still alive, while the others all died of recurrence with a median survival time of 4.6 years. Through close follow-up and termly endoscopic surveillance, three FAP patients were detected before presenting symptoms at the age of 18, 20 and 23 years, respectively. Prophylactic IPAA was performed and results were satisfactory after the patients were followed-up for 6, 1, and 8 years, respectively.

CONCLUSION: Pedigree investigation, close follow-up and termly endoscopic surveillance are very important for early detection of FAP. Prophylactic IPAA can give satisfactory results to FAP patients.

He YL, Zhang CH, Huang MJ, Cai SR, Zhan WH, Wang JP, Wang JF. Clinical analysis of eight kindreds of familial adenomatous polyposis. *World J Gastroenterol* 2004; 10(24): 3659-3661
<http://www.wjgnet.com/1007-9327/10/3659.asp>

INTRODUCTION

Familial adenomatous polyposis (FAP), which usually begins at a mean age of 16 years (range, 7-36 years), is an autosomal dominant hereditary colon cancer predisposition syndrome, in which hundreds to thousands of precancerous colonic polyps can develop. Without colectomy, colon cancer is inevitable. The mean age of developing colon cancer in untreated individuals is 39 years (range, 34-43 years)^[1]. Prophylactic colectomy has been considered to be the best treatment for familial adenomatous polyposis^[2]. In this paper, data of eight pedigrees of FAP were analysed retrospectively. The role of surveillance endoscopy and the effect of different surgical procedures were evaluated.

MATERIALS AND METHODS

We studied the patients with FAP and their families enrolled in our Familial Adenomatous Polyposis Registry from March 1991 to December 2003. Close follow-up and termly surveillance colonoscopy were performed and the results were analysed retrospectively. Pedigree trees were protracted according to their family history.

RESULTS

In our registry, eight probands had a family history. These eight pedigree trees were protracted (Figure 1). In these eight kindreds, a total of 157 members were investigated, among them 134 members were in the first to third generation with the age older than 14 years. As a result, 25 members (about 16%) were diagnosed as FAP with an average age of 38 years and the youngest patient was eighteen years old. The ratio of male patients and female patients was 16:9 and most of them were in the second and third generation. A total of 9 FAP patients (36%) were diagnosed as synchronous colorectal cancer, and six patients died of cancer with a mortality rate of 28%. Among 13 patients who had symptoms but no malignancy, 7 patients underwent total abdominal colectomy and rectal mucosectomy with ileal pouch-anal anastomosis (IPAA) and others received total abdominal colectomy with ileorectal anastomosis (IRA). All of them were still alive and no cancer was found after a median follow-up time of 4.2 years and 5.6 years, respectively.

In these eight kindreds, one proband was diagnosed as advanced colon cancer and died 11 mo later after partial colectomy and hepatic metastatic lesion biopsy, and the other probands underwent IPAA, among them one was diagnosed as synchronous colon cancer on the basis of FAP and was still alive after 7.5 years follow-up. Through endoscopic surveillance, three FAP patients were detected before presenting symptoms at the age of 18, 20 and 23 years, respectively. Prophylactic IPAA was performed and results were satisfactory after the patients were followed-up for 6, 1, and 8 years, respectively. Among the other seven patients with synchronous colorectal cancer on the basis of FAP, who received total abdominal colectomy with ileorectal anastomosis (IRA), one underwent total remnant rectum resection and ileostomy for recurrent carcinoma in the retained rectum 2.5 years later after the IRA and was still alive, while the others all died of cancer recurrence with a median survival time of 4.6 years. However, the other seven patients without colorectal cancer were still alive although one was given IPAA and the others received IRA.

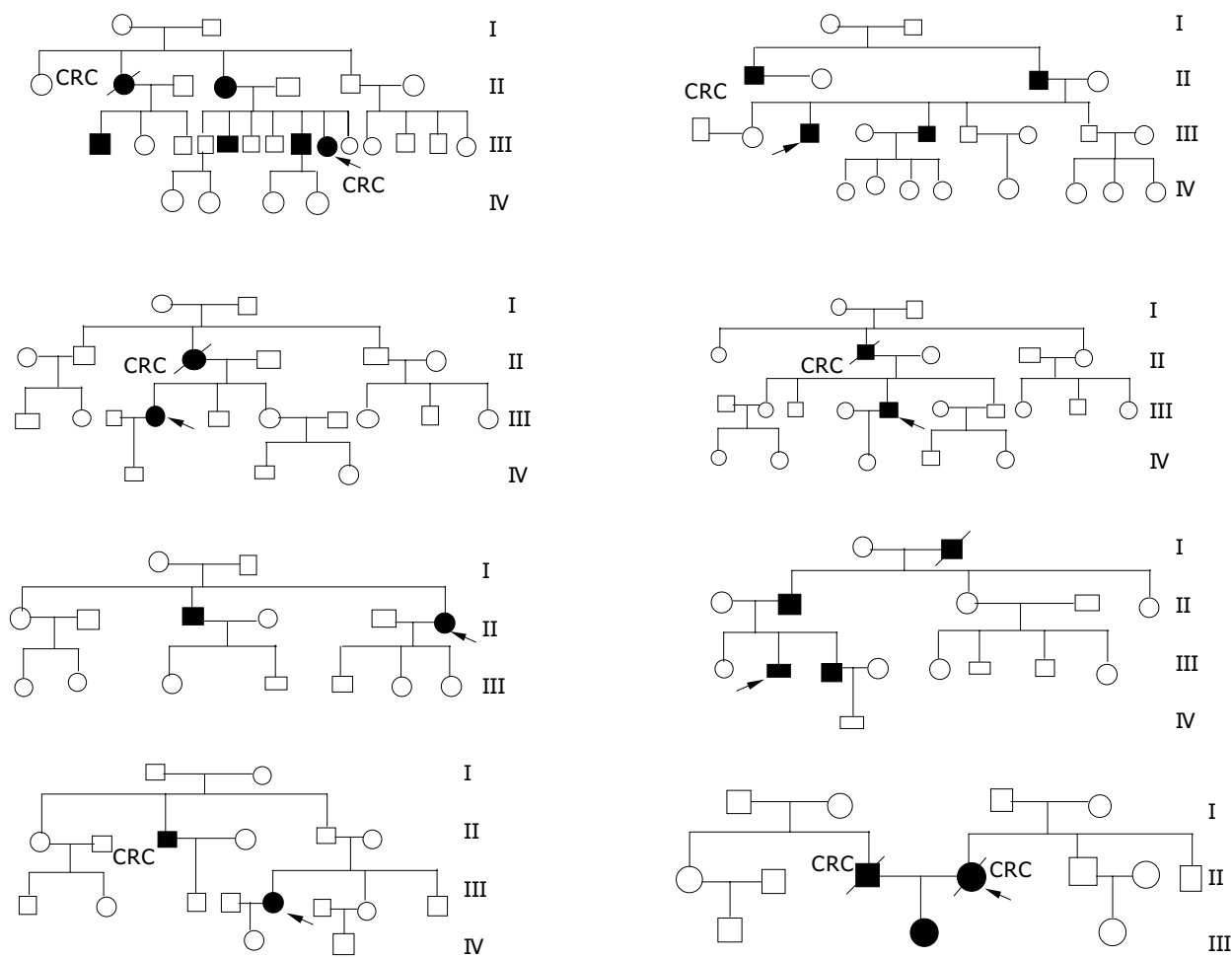


Figure 1 Pedigree trees of eight FAP kindreds. ○ woman □ man ■ Proband ● death ● patient. CRC: colorectal cancer.

DISCUSSION

FAP is an autosomal dominant hereditary disease. Approximately 80% of individuals with FAP had a family history^[3]. Offsprings of an affected individual had a 50% risk of the disease^[4]. The prevalence of FAP is 1 per 16 000 people to 1 per 8 000 people. Though FAP historically accounted for about 0.5% of all colorectal cancers, this figure has been declining as more family members at-risk underwent successful treatment following early polyp detection and prophylactic colectomy^[5-8]. In our study, the incidence rate of FAP in these eight kindreds was 16%, and most of the FAP patients were in the second and third generation without atavism. The average age of FAP patients was 38 years, and nine patients with FAP (36%) were in an advanced stage when they were diagnosed as colorectal cancer. Bulow^[5] reported that since the establishment of the Danish Polyposis Register, the prevalence of colorectal cancer had decreased considerably and the prognosis had improved substantially. They made a conclusion that the work of the Danish Polyposis Register was probably the main cause of this improvement. Other studies^[7-9] also showed that with pedigree investigation, close follow-up and termly endoscopic surveillance, more family members at-risk underwent successful treatment following early polyp detection and prophylactic colectomy, and the prevalence of colorectal cancer was considerably decreased and the prognosis was substantially improved. In our study, we established a FAP register in 1991, and then investigated all lineal and collateral relatives of FAP patients enrolled in our hospital and protracted their pedigree trees. Close follow-up and termly colonoscopy surveillance were performed to find early cases among the relatives at high risk. At the end, 3 FAP patients were detected before presenting symptoms at the age

18, 20 and 23 years, respectively. Prophylactic IPAA was performed and functional outcome and quality of life were satisfactory after the patients were followed-up for 6, 1 and 8 years, respectively. No patient was found with colorectal cancer or pouch adenoma or inflammation. Thus, we conclude that pedigree investigation, close follow-up and termly colonoscopy are feasible and effective methods for early diagnosis of FAP, although FAP has been found to be caused by mutations in adenomatous polyposis coli (APC) (chromosomal loci 5q21-q22) and molecular genetic testing and genetic counseling are clinically available in some developed countries^[6,10] while they are still in laboratories in China^[11].

For individuals with classic FAP, prophylactic colectomy is recommended when adenomas emerge. Colectomy includes total colectomy and rectal mucosectomy with IPAA and subtotal colectomy with IRA. Although IRA has fewer complications and comfortable defecation function, it is not generally accepted by patients because carcinoma may develop in 40% retained rectum^[12]. On the other hand, during IPAA all colorectal mucous membranes were removed to completely eliminate the risk of developing colonic carcinoma and a small reservoir was created to reduce the frequency of bowel movement. However, temporary ileostomy and creation of a reservoir might lead to more complications and increase the difficulty in operation^[2,8]. Parc *et al.*^[13] found that young patients had a good quality of life after IPAA, and suggested that this procedure was well suitable for the youth. In our study, three symptom-free patients underwent IPAA and all had satisfactory results. Among thirteen patients who had symptoms but no malignancy, although 7 patients underwent IPAA and 6 patients underwent IRA, no carcinoma developed after they were followed-up for 4.2 years and 5.6 years, respectively. But for those patients

with carcinoma, only one patient who underwent IPAA 7.5 years before was still alive, while the others who underwent IRA all died of cancer recurrence. Thus, we conclude that symptom-free patients should undergo prophylactic surgical procedure and IPAA should be preferred. Furthermore, IPAA should be the first choice for those patients with carcinoma.

REFERENCES

- 1 **de Vos tot Nederveen Cappel WH**, Jarvinen HJ, Bjork J, Berk T, Griffioen G, Vasen HF. Worldwide survey among polyposis registries of surgical management of severe duodenal adenomatosis in familial adenomatous polyposis. *Br J Surg* 2003; **90**: 705-710
- 2 **Delaney CP**, Fazio VW, Remzi FH, Hammel J, Church JM, Hull TL, Senagore AJ, Strong SA, Lavery IC. Prospective, age-related analysis of surgical results, functional outcome, and quality of life after ileal pouch-anal anastomosis. *Ann Surg* 2003; **238**: 221-228
- 3 **Iwama T**, Utsunomiya J. Anticipation phenomenon in familial adenomatous polyposis: an analysis of its origin. *World J Gastroenterol* 2000; **6**: 335-338
- 4 **Barrison AF**, Smith C, Oviedo J, Heeren T, Schroy PC 3rd. Colorectal cancer screening and familial risk: a survey of internal medicine residents' knowledge and practice patterns. *Am J Gastroenterol* 2003; **98**: 1410-1416
- 5 **Bulow S**. Results of national registration of familial adenomatous polyposis. *Gut* 2003; **52**: 742-746
- 6 **Grady WM**. Genetic testing for high-risk colon cancer patients. *Gastroenterology* 2003; **124**: 1574-1594
- 7 **Keating J**, Pater P, Lolohea S, Wickremesekera K. The epidemiology of colorectal cancer: what can we learn from the New Zealand Cancer Registry? *N Z Med J* 2003; **116**: U437
- 8 **Church J**, Kiringoda R, LaGuardia L. Inherited colorectal cancer registries in the United States. *Dis Colon Rectum* 2004; **47**: 674-678
- 9 **Church J**, Burke C, McGannon E, Pastean O, Clark B. Risk of rectal cancer in patients after colectomy and ileorectal anastomosis for familial adenomatous polyposis: a function of available surgical options. *Dis Colon Rectum* 2003; **46**: 1175-1181
- 10 **Bisgaard ML**, Ripa R, Knudsen AL, Bulow S. Familial adenomatous polyposis patients without an identified APC germline mutation have a severe phenotype. *Gut* 2004; **53**: 266-270
- 11 **Hu NP**, Zhan WH, Yan ZS, Ge MH, Lü XS. Protein truncation test of the APC gene in familial adenomatous polyposis. *Shijie Huaren Xiaohua Zazhi* 2001; **9**: 587-589
- 12 **Jang YS**, Steinhagen RM, Heimann TM. Colorectal cancer in familial adenomatous polyposis. *Dis Colon Rectum* 1997; **40**: 312-316
- 13 **Parc YR**, Moslein G, Dozois RR, Pemberton JH, Wolff BG, King JE. Familial adenomatous polyposis: results after ileal pouch-anal anastomosis in teenagers. *Dis Colon Rectum* 2000; **43**: 893-902

Edited by Kumar M and Wang XL Proofread by Xu FM

Effects of *c-myb* antisense RNA on TGF- β 1 and α 1-I collagen expression in cultured hepatic stellate cells

Hui-Hui Ma, Ji-Lu Yao, Gang Li, Chun-Lan Yao, Xue-Juan Chen, Shao-Ji Yang

Hui-Hui Ma, Ji-Lu Yao, Gang Li, Chun-Lan Yao, Xue-Juan Chen, Shao-Ji Yang, Department of Infectious Diseases, the 3rd Affiliated Hospital, Sun-Yat Sen University, Guangzhou 510630, Guangdong Province, China

Supported by the National Natural Science Foundation of China, No. 300243

Correspondence to: Dr. Hui-Hui Ma, Department of Infectious Diseases, the 3rd Affiliated Hospital, Sun-Yat Sen University, Guangzhou 510630, Guangdong Province, China. lucam@tom.com

Telephone: +86-20-85516867-2019

Received: 2004-03-23 **Accepted:** 2004-04-13

Abstract

AIM: To investigate the effects of *c-myb* antisense RNA on cell proliferation and the expression of *c-myb*, TGF- β 1 and α 1-I collagen in cultured hepatic stellate cells (HSC) from rats.

METHODS: Recombinant retroviral vector of *c-myb* antisense gene (pDOR-myb) was constructed, and then transfected into retroviral package cell line PA317 by means of DOTAP. The pseudoviruses produced from the resistant PA317 cells were selected with G418 to infect HSCs isolated from rat livers. The cell proliferation was measured by 3-[4, 5-Dimethylthiazolyl]-2, 5-diphenyl tetrazo-dium bromide (MTT) method. The expression of *c-myb*, α 1-I collagen and TGF- β 1 mRNA, and *c-myb* protein in HSCs was detected with semi-quantitative reverse transcription-polymerase chain reaction (RT-PCR) and Western-blot respectively.

RESULTS: HSCs from rats were isolated successfully with the viability >98%. In the pDOR-myb infected HSCs, the *c-myb* protein expression, cell proliferation, and α 1-I collagen and TGF- β 1 mRNA expression were repressed significantly compared with their corresponding control groups ($P < 0.01$).

CONCLUSION: *c-myb* plays a key role in activation and proliferation of HSC. *c-myb* antisense RNA can inhibit cell proliferation, α 1-I collagen and TGF- β 1 mRNA expression, suggesting that inhibition of *c-myb* gene expression might be a potential way for the treatment of liver fibrosis.

Ma HH, Yao JL, Li G, Yao CL, Chen XJ, Yang SJ. Effects of *c-myb* antisense RNA on TGF- β 1 and α 1-I collagen expression in cultured hepatic stellate cells. *World J Gastroenterol* 2004; 10(24): 3662-3665

<http://www.wjgnet.com/1007-9327/10/3662.asp>

INTRODUCTION

The activation and proliferation of hepatic stellate cells (HSC) have been regarded as the critical events in early hepatic fibrosis irrespective of the underlying etiology^[1-6]. *c-myb* oncogene encodes nuclear protein that functions as a transcriptional transactivator that regulates expression of genes critical for cell differentiation and proliferation^[7,8]. Several studies have indicated that *c-myb* expression is critical for HSC activation

and proliferation in rat and human livers affected by chronic viral hepatitis, and that the level of *c-myb* expression reflects the severity of disease activity^[9,10]. However, little information is available concerning the effects of *c-myb* expression on the pathogenesis of liver fibrosis.

It has been shown that α 1-I collagen is the main extracellular matrix (ECM) protein produced by HSCs during the pathogenesis of liver fibrosis, while TGF- β 1 has been identified as a potent cytokine in the regulation of the production, degradation and accumulation of ECM. In this study, retrovirus-mediated antisense *c-myb* RNA was transferred into cultured HSCs from rats to investigate its anti-proliferative and antifibrotic effects.

MATERIALS AND METHODS

Materials

PA317 and NIH3T3 cells were cultured in our laboratory. Anti-desmin and anti- α -SMA antibodies were purchased from DAKO Corporation, anti-*c-myb* antibody from Santa Cruz Biotechnology Corporation. G418, DMEM, and fetal bovine serum were from GibcoTM Invitrogen Corporation. Pronase E and collagenase IV were from Sigma-Aldrich Corporation. The retroviral vector pDOR was provided by Dr. Lin Yang (Department of Infectious Diseases, the 3rd Affiliated Hospital, Sun-Yat Sen University).

Cell isolation, culture and identification

Primary rat HSCs were isolated from 200-300 g male Sprague-Dawley rats by a two-step pronase-collagenase perfusion method^[11]. All cells were cultured in DMEM supplemented with 100-200 mL/L fetal bovine serum, 2 mmol/L glutamine and 1% antibiotic solution at 37 °C in a humidified atmosphere containing 50 mL/L CO₂. HSCs were identified by immunohistochemical staining for desmin and α -SMA with monoclonal mouse anti-desmin and anti- α -SMA antibodies, respectively.

Packaging of *c-myb* recombinant retroviral vector and its transfection into HSCs

The segment of *c-myb* gene amplified by RT-PCR from the spleen of a rat was cloned into pUC19 with TA cloning method, and then subcloned into retroviral vector pDOR after sequencing. The recombinant retroviral vector, named pDOR-myb, was transfected into retroviral package cell line PA317 by means of DOTAP. Stable retroviral vector-produced lines were generated by expanding the G418-resistant (600 μ g/mL) colonies. The supernatants containing the packaged retroviruses were harvested, filtered and titrated 9.0×10^4 - 2.2×10^5 CFU/mL determined in NIH3T3 cells^[12]. The fourth generation of HSCs was infected with the recombinant *c-myb* retrovirus (pDOR-myb) and controlled retrovirus (pDOR), while the untreated HSCs from the same generation were used as the control group. Infection was performed in suspension by a 30 min incubation of HSCs with 10 mL of virus supernatants, supplemented with 4 μ g/mL polybrene. The cultured medium was changed with DMEM containing G418 after 48 h, and repeated every 2-3 d.

Proliferation assay of infected HSCs

The cell proliferation was measured by 3-[4, 5-Dimethylthiazolyl]-2, 5-diphenyl tetrazo-dium bromide (MTT) method. HSCs of three

groups (pDOR-myb, pDOR and control groups) were seeded into 96-well plates (5×10^3 cells/well), respectively and incubated in a final volume of 200 μ L medium for 48 h. Fifty microliter of MTT (5 g/L) was subsequently added to each well. After the incubation was continued for 4 h, suspension was abandoned, and dimethyl sulphoxide (DMSO) 200 μ L was added to each well. Then absorbance at 570 nm ($A_{570\text{nm}}$) was measured using an automatic enzyme-linked immunosorbent assay plate reader.

Semi-quantitative reverse transcription-polymerase chain reaction (RT-PCR)

For reverse transcription PCR analysis, total RNA was extracted from cultured cells using a RNeasy Mini kit (QIAGEN). Complementary DNAs were prepared from 1 μ g of total RNA using a RT kit (MBI) with oligo (dt) primer according to the manufacturer's instructions. The resulting complementary DNA was amplified with the following sets of primers: GAPDH (420 bp), 5' ATGACTCTACCCACGGCAAG3' (forward) and 5' CCACAG TCTTCTGAGTGGCA3' (reverse); TGF- β 1 (143 bp), 5' GACCTG CTGGCAATAGCTTC3' (forward) and 5' GTTGAGGGAGAAA GCAGCAG3' (reverse); α_1 -collagen (269 bp), 5' GCGAGGACAT GAGGAGTAGC3' (forward) and 5' CCTGTGACCAGGGATGT CTT3' (reverse); *c-myb* (350 bp), 5' TCCTTCTCCTCCTCCTC CTC3' (forward) and 5' GTTCCACCAGCTTCTTAGC3' (reverse). *c-myb*, TGF- β 1 and α_1 -I collagen mRNA levels were determined by semi-quantitative RT-PCR followed by densitometry scanning. GAPDH served as an internal control. The following PCR program was performed for TGF- β 1 and α_1 -I collagen: at 94 $^{\circ}$ C for 2 min (initial denaturation), at 94 $^{\circ}$ C for 30 s, at 62 $^{\circ}$ C for 30 s, at 72 $^{\circ}$ C for 1 min, 35 cycles. For *c-myb*, except the primer annealing temperature was 65.5 $^{\circ}$ C, all other conditions were the same as above.

Western-blotting

c-myb proteins of the pDOR-myb group, pDOR group and control group were detected with Western-blotting. HSCs of the three groups were washed 2 times with PBS, and then 1 \times SDS loading buffer was added. After boiled for 5-10 min, 10 μ g of protein was electrophoresed on 100 g/L SDS-polyacrylamide gel. The protein was transferred to PVDF membrane, which was then blocked overnight at 4 $^{\circ}$ C with PBST (PBS containing 4 mL/L Tween 20)-30 g/LBSA. The blots were incubated with the primary polyclonal antibody against *c-myb* (1:100) at 4 $^{\circ}$ C overnight, and subsequently with HRP-labeled secondary antibody (1:100) at room temperature for 1 h. At last, the protein bands were visualized with 4-Cl-1-Naphenol- H_2O_2 .

Statistical analysis

Data were presented as mean \pm SE. The Student's *t* test was to

analyze the changes in different groups with SPSS10.0 software, and $P < 0.05$ was considered statistically significant.

RESULTS

HSCs identification

The number of isolated cells was $1-3 \times 10^7$ from a rat with the viability $> 98\%$. Immunohistochemical staining with desmin and α -SMA showed a selective cytoplasmic pattern with about 95% positive cells.

c-myb expression

Semi-quantitative RT-PCR and Western-blot were performed to determine *c-myb* expression in the recombinant *c-myb* virus infected HSCs. RT-PCR showed a 420 bp band corresponding to GAPDH in each sample. As expected, a 350 bp band of *c-myb* was detected in the pDOR group and the control group, but not in the pDOR-myb group, and the results of densitometry scanning showed that *c-myb* mRNA expression value in the pDOR-myb group was 4.63 ± 0.66 , significantly lower than that in the control (44.48 ± 2.79) and pDOR groups (46.91 ± 3.57) ($P < 0.01$). Western blot analysis demonstrated that *c-myb* protein was markedly reduced in the pDOR-myb group compared with the control group. (Figure 1).

HSC proliferation

Proliferation assay showed that $A_{570\text{nm}}$ values of the pDOR-myb group, pDOR group and control group were 0.40 ± 0.12 , 0.58 ± 0.10 and 0.59 ± 0.09 , respectively, indicating a marked decrease in the pDOR-myb group compared with the control groups ($P < 0.01$), but no difference between two control groups (Figure 2).

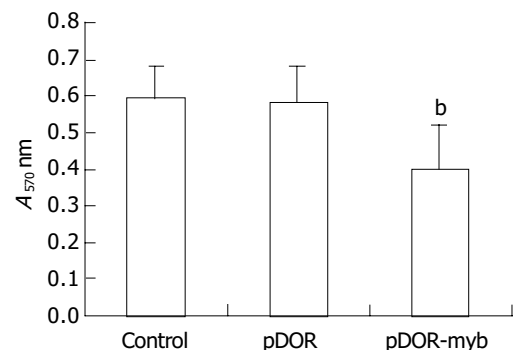


Figure 2 Measurements of cell proliferation with MTT method in three groups of HSCs. The results were expressed as mean \pm SE ($n = 6$). ^b $P < 0.01$ vs pDOR and control.

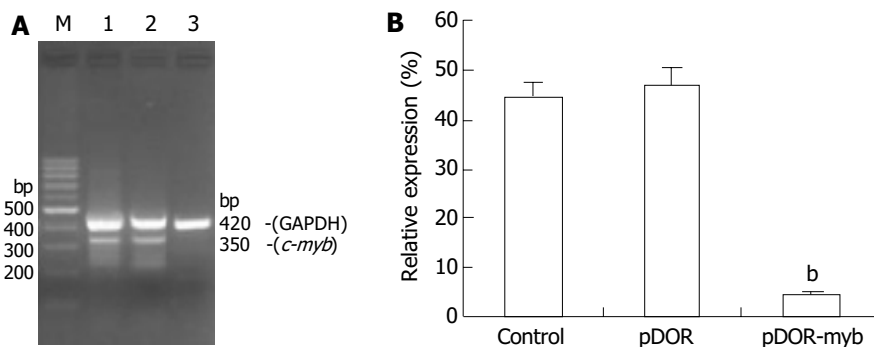


Figure 1 Expression of *c-myb* mRNA, internal control and *c-myb* protein by RT-PCR, density and Western blot. A: *c-myb* mRNA expression assayed by semi-quantitative RT-PCR analysis of total RNA. Co-amplification of GAPDH in all samples served as an internal standard. Lane 1: control HSC; Lane 2: pDOR treated HSC; Lane 3: pDOR-myb treated HSC; Lane M: 100 bp ladder. B: Relative expression levels are shown as percent of the internal control by densitometry scanning. The results were expressed as mean \pm SE ($n = 3$). ^b $P < 0.01$ vs pDOR and control. C: Western-blotting of *c-myb* protein expression. Fifty μ g of extracted cellular protein was loaded in each lane. Lane1: control HSC; Lane2: pDOR treated HSC; Lane3: pDOR-myb treated HSC.

TGF- β_1 and α_1 -I collagen mRNA expression

Semi-quantitative RT-PCR was used to analyze TGF- β_1 and α_1 -I collagen mRNA expression. The mRNA levels of α_1 -I collagen and TGF- β_1 were markedly reduced in the pDOR-myb group compared with the two control groups ($P < 0.01$). The results of densitometry scanning showed that α_1 -I collagen and TGF- β_1 mRNA expression values in the pDOR-myb group were 6.94 ± 1.58 and 10.09 ± 2.26 , respectively, which were markedly reduced compared with the control (44.10 ± 5.63 and 13.01 ± 0.94 , respectively) and pDOR groups (44.59 ± 2.54 and 12.47 ± 0.48 , respectively) ($P < 0.01$). But there was no difference between the two control groups (Figure 3).

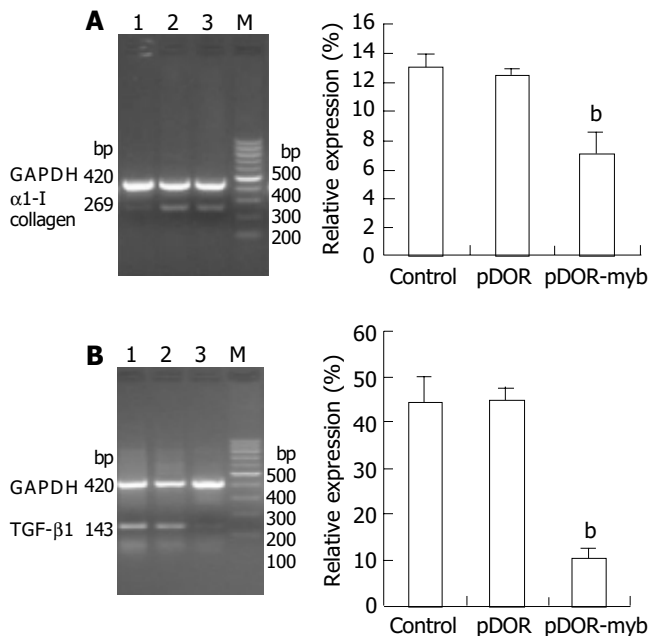


Figure 3 Expression of TGF- β_1 and α_1 -I collagen mRNA. A: α_1 -I collagen mRNA expression assayed by semi-quantitative RT-PCR analysis. Lane 1: pDOR-myb treated HSC; Lane 2: control HSC; Lane 3: pDOR treated HSC. B: TGF- β_1 mRNA expression assayed by semi-quantitative RT-PCR analysis. Lane 1: pDOR treated HSC; Lane 2: control HSC; Lane 3: pDOR-myb treated HSC. The relative expression levels were shown as percent of the internal control by densitometry scanning. The results were expressed as mean \pm SE ($n = 3$), ^b $P < 0.01$ vs pDOR and control. Co-amplification of GAPDH in all samples served as an internal standard.

DISCUSSION

HSC is regarded as one of the key cell types involved in progression of liver fibrosis, and as a therapeutic target for treatment of hepatic fibrosis^[1-6]. Several findings have implied that HSC activation status could be directly manipulated through controlled expression of *c-myb*. *c-myb* was reported to be involved in transcriptional regulation and cell proliferation, since high levels of *c-myb* DNA-binding activity were found in activated HSCs but not in quiescent HSCs^[13,14]. Transfection of *c-myb* stimulated α -SMA expression in quiescent HSCs, and transfection of *c-myb* antisense RNA inhibited the expression of α -SMA and the activation of HSCs^[14].

In this study, we found that the *c-myb* expression in HSCs could be successfully inhibited by *c-myb* antisense RNA transfection and this antisense *c-myb* RNA could dramatically inhibit HSC proliferation detected by MTT, suggesting that blockade of *c-myb* transcriptional signals in HSC might lead to the inhibition of HSC proliferation. However, little is known about how *c-myb* expression can influence HSC activation and proliferation. It has been reported that *c-myb* is an important

transcriptional factor that can regulate cell cycles and control plasma membrane Ca^{2+} -ATPase^[15,16], which may be involved in HSC proliferation.

TGF- β_1 is the most potent fibrogenic stimulant to HSCs. The activated HSCs respond to it by increasing production of collagen and decreasing its breakdown. Modifying the secretion or activity of TGF- β_1 could attenuate fibrosis, and recent studies of experimental liver fibrosis have shown the potential of this approach^[17-22]. Our study showed that TGF- β_1 mRNA expression was repressed significantly in the pDOR-*c-myb* infected group compared with their corresponding control groups. The mechanism might be partly related to the fact that *c-myb* antisense RNA could inhibit HSC proliferation and block TGF- β_1 autocrine loop. It is necessary to investigate HSC activation and its relationship with *c-myb* expression and TGF- β_1 secretion, since *c-myb* also plays an important role in HSCs activation^[1,14].

Hepatic fibrosis is characterized by accumulation of extracellular matrix (ECM), and collagen I is the main component of ECM while fibrosis occurs^[23-26]. Activated HSCs are known to be the major source of this fibrillar collagen. On the other hand, collagen I could further enhance HSC activation^[1]. Clearly, this feedback loop plays an important role in the progression of liver fibrosis. In our study, α_1 -I collagen mRNA expression in HSCs was inhibited significantly by transfection of *c-myb* antisense RNA. Considering *c-myb* antisense RNA could also inhibit HSC proliferation, which might influence α_1 -I collagen mRNA expression levels, the number of HSCs in each group was adjusted to the same count. Our results indicated that *c-myb* could influence α_1 -I collagen expression through some direct but yet unclear ways.

Liver fibrosis and its end stage, cirrhosis, represent worldwide healthcare problems. Current treatments for fibrosis and cirrhosis are limited to removing the underlying injurious stimuli, eradicating viruses using interferon, ribavirin, and lamivudine in viral hepatitis, and liver transplantation. To date, various new drugs have been attempted to prevent the progression of hepatic fibrosis, such as hepatocyte growth factor^[26,27], TGF- β_1 antagonist or truncated TGF- β_1 type II receptor^[21,28,29] and tissue inhibitors of metalloproteinases^[30]. Now that HSC activation and proliferation have been shown to be the critical events, and also to contribute to portal hypertension. Hence, the strategies to design some specific agents to inhibit HSC activation and proliferation are appealing. In conclusion, *c-myb* antisense RNA can inhibit *c-myb* gene expression, cell proliferation, α_1 -I collagen and TGF- β_1 mRNA expression in HSCs, suggesting that inhibition of *c-myb* gene expression might be a potential way for the treatment of liver fibrosis.

REFERENCES

- Friedman SL. Cytokines and fibrogenesis. *Semin Liver Dis* 1999; **19**: 129-140
- Wang JY, Zhang QS, Guo JS, Hu MY. Effects of glycyrrhetic acid on collagen metabolism of hepatic stellate cells at different stages of liver fibrosis in rats. *World J Gastroenterol* 2001; **7**: 115-119
- Pinzani M, Marra F, Carloni V. Signal transduction in hepatic stellate cells. *Liver* 1998; **18**: 2-13
- Marra F, Gentilini A, Pinzani M, Choudhury GG, Parola M, Herbst H, Dianzani MU, Laffi G, Abboud HE, Gentilini P. Phosphatidylinositol 3-kinase is required for platelet-derived growth factor's actions on hepatic stellate cells. *Gastroenterology* 1997; **112**: 1297-1306
- Li D, Friedman SL. Liver fibrogenesis and the role of hepatic stellate cell: new insights and prospects for therapy. *J Gastroenterol Hepatol* 1999; **14**: 618-633
- Burt AD. Pathobiology of hepatic stellate cells. *J Gastroenterol* 1999; **34**: 299-304
- Thompson CB, Challoner PB, Neiman PE, Groudine M. Expression of the *c-myb* proto-oncogene during cellular proliferation.

- Nature* 1986; **319**: 374-380
- 8 **Oh IH**, Reddy FP. The myb gene family in cell growth, differentiation and apoptosis. *Oncogene* 1999; **18**: 3017-3033
 - 9 **Kitada T**, Seki S, Nakatani K, Kawada N, Kuroki T, Monna T. Hepatic expression of c-myb in chronic human liver disease. *Hepatology* 1997; **26**: 1506-1512
 - 10 **Tappero G**, Farina M, Negro F, Anfossi G, Mattiello L, Giuli PD, Colombatto P, Brunetto MR, Angeli A, Bonino F. Intrahepatic expression of c-fos, c-myb and c-myc oncogenes: correlation with virus-induced chronic liver disease and response to interferon. *Ital J Gastroenterol Hepatol* 1997; **29**: 148-154
 - 11 **Xu LM**, Liu C, Liu P, Liu CH, Li FH, Gu HT, Cheng LZ. A steady and high-yield method of isolation hepatic fat-storing cells. *Xibaoshengwuxue Zazhi* 1995; **17**: 143-145
 - 12 **Ma HH**, Yao JI, Li G, Yao CL, Chen XJ, Yang SJ. Construction of c-myb antisense RNA recombinant retroviral vector and establishment of its packaging cell line PA317. *Acad J SUMS* 2001; **22**: 235-237
 - 13 **Lee KS**, Buck M, Houglum K, Chojkier M. Activation of hepatic stellate cells by TGF alpha and collagen type I is mediated by oxidative stress through c-myb expression. *J Clin Invest* 1995; **96**: 2461-2468
 - 14 **Buck M**, Kim DJ, Houglum K, Hassanein T, Chojkier M. c-Myb modulates transcription of the alpha-smooth muscle actin gene in activated hepatic stellate cells. *Am J Physiol Gastrointest Liver Physiol* 2000; **278**: G321-328
 - 15 **Husain M**, Jiang L, See V, Bein K, Simons M, Alper SL, Rosenberg RD. Regulation of vascular smooth muscle cell proliferation by plasma membrane Ca (2+)-ATPase. *Am J Physiol* 1997; **272**(6 Pt 1): C1947-1959
 - 16 **Afroze T**, Husain M. c-Myb-binding sites mediate G (1)/S-associated repression of the plasma membrane Ca (2+)-ATPase-1 promoter. *J Biol Chem* 2000; **275**: 9062-9069
 - 17 **Wrana JL**. Transforming growth factor- β signalling and cirrhosis. *Hepatology* 1999; **29**: 1909-1910
 - 18 **Roulot D**, Sevcsik AM, Coste J, Strosberg AD, Marullo S. Role of transforming growth factor beta type I receptor in hepatic fibrosis: studies of human chronic hepatitis C and experimental fibrosis in rats. *Hepatology* 1999; **29**: 1730-1738
 - 19 **George J**, Roulot D, Koteliensky VE, Bissell DM. *In vivo* inhibition of rat stellate cell activation by soluble transforming growth factor beta type II receptor: a potential new therapy for hepatic fibrosis. *Proc Natl Acad Sci U S A* 1999; **96**: 12719-12724
 - 20 **Qi Z**, Atsuchi N, Ooshima A, Takeshita A, Ueno H. Blockade of type β transforming growth factor signaling prevents liver fibrosis and dysfunction in the rat. *Proc Natl Acad Sci U S A* 1999; **96**: 2345-2349
 - 21 **Ueno H**, Sakamoto T, Nakamura T, Qi Z, Atsuchi N, Takeshita A, Shimizu K, Ohashi H. A soluble transforming growth factor β receptor expressed in muscle prevents liver fibrogenesis and dysfunction in rats. *Hum Gene Ther* 2000; **11**: 33-42
 - 22 **Friedman SL**, Roll FJ, Boyles J, Bissell DM. Hepatic lipocytes: the principal collagen-producing cells of normal rat liver. *Proc Natl Acad Sci U S A* 1985; **82**: 8681-8685
 - 23 **Theret N**, Lehti K, Musso O, Clement B. MMP2 activation by collagen I and concanavalin A in cultured human hepatic stellate cells. *Hepatology* 1999; **30**: 462-468
 - 24 **Senoo H**, Imai K, Matano Y, Sato M. Molecular mechanisms in the reversible regulation of morphology, proliferation and collagen metabolism in hepatic stellate cells by the three-dimensional structure of the extracellular matrix. *J Gastroenterol Hepatol* 1998; **13**(Suppl): S19-32
 - 25 **Arthur MJ**. Collagenases and liver fibrosis. *J Hepatol* 1995; **22** (2 Suppl): 43-48
 - 26 **Ueki T**, Kaneda Y, Tsutsui H, Nakanishi K, Sawa Y, Morishita R, Matsumoto K, Nakamura T, Takahashi H, Okamoto E, Fujimoto J. Hepatocyte growth factor gene therapy of liver cirrhosis in rats. *Nat Med* 1999; **5**: 226-230
 - 27 **Matsuno Y**, Iwata H, Umeda Y, Takagi H, Mori Y, Kosugi A, Matsumoto K, Nakamura T, Hirose H. Hepatocyte growth factor gene transfer into the liver via the portal vein using electroporation attenuates rat liver cirrhosis. *Gene Ther* 2003; **10**: 1559-1566
 - 28 **Roulot D**, Sevcsik A, Coste T, Strosberg D, Marullo S. Role of transforming growth factor beta type II receptor in hepatic fibrosis: studies of human chronic hepatitis C and experimental fibrosis in rats. *Hepatology* 1999; **29**: 1730-1738
 - 29 **Kondou H**, Mushiake S, Etani Y, Miyoshi Y, Michigami T, Ozono K. A blocking peptide for transforming growth factor-beta1 activation prevents hepatic fibrosis *in vivo*. *J Hepatol* 2003; **39**: 742-748
 - 30 **Sakaida I**, Hironaka K, Kimura T, Terai S, Yamasaki T, Okita K. Herbal medicine Sho-saiko-to (TJ-9) increases expression matrix metalloproteinases (MMPs) with reduced expression of tissue inhibitor of metalloproteinases (TIMPs) in rat stellate cell. *Life Sci* 2004; **74**: 2251-2263

Edited by Kumar M and Wang XL Proofread by Xu FM

Intravenous pantoprazole versus ranitidine for prevention of rebleeding after endoscopic hemostasis of bleeding peptic ulcers

Ping-I Hsu, Gin-Ho Lo, Ching-Chu Lo, Chiun-Ku Lin, Hoi-Hung Chan, Chung-Jen Wu, Chang-Bih Shie, Pei-Min Tsai, Deng-Chyang Wu, Wen-Ming Wang, Kwok-Hung Lai

Ping-I Hsu, Gin-Ho Lo, Ching-Chu Lo, Chiun-Ku Lin, Hoi-Hung Chan, Chung-Jen Wu, Chang-Bih Shie, Pei-Min Tsai, Kwok-Hung Lai, Division of Gastroenterology, Department of Internal Medicine, Kaohsiung Veterans General Hospital, National Yang-Ming University; Kaohsiung, Taiwan, China

Deng-Chyang Wu, Wen-Ming Wang, Division of Gastroenterology, Department of Internal Medicine, Kaohsiung Medical College, Kaohsiung, Taiwan, China

Supported by Grants From the Kaohsiung Veterans General Hospital (VGH93-01)

Co-first-authors: Ping-I Hsu

Co-correspondents: Kwok-Hung Lai

Correspondence to: Kwok-Hung Lai, M.D., Division of Gastroenterology, Department of Internal Medicine, Kaohsiung Veterans General Hospital, 386, Ta-Chung 1st Road, Kaohsiung 813, Taiwan, China. williamhsup@yahoo.com.tw

Telephone: +886-7-3422121 Ext. 2075 **Fax:** +886-7-3468237

Received: 2004-02-23 **Accepted:** 2004-05-13

Abstract

AIM: The role of intravenous pantoprazole in treatment of patients with high-risk bleeding peptic ulcers following endoscopic hemostasis remains uncertain. We therefore conducted the pilot prospective randomized study to assess whether intravenous pantoprazole could improve the efficacy of H₂-antagonist as an adjunct treatment following endoscopic injection therapy for bleeding ulcers.

METHODS: Patients with active bleeding ulcers or ulcers with major signs of recent bleeding were treated with distilled water injection. After hemostasis was achieved, they were randomly assigned to receive intravenous pantoprazole or ranitidine.

RESULTS: One hundred and two patients were enrolled in this prospective trial. Bleeding recurred in 2 patients (4%) in the pantoprazole group ($n = 52$), as compared with 8 (16%) in the ranitidine group ($n = 50$). The rebleeding rate was significantly lower in the pantoprazole group ($P = 0.04$). There were no statistically significant differences between the groups with regard to the need for emergency surgery (0% vs 2%), transfusion requirements (4.9 ± 5.9 vs 5.7 ± 6.8 units), hospital days (5.9 ± 3.2 vs 7.5 ± 5.0 d) or mortality (2% vs 2%).

CONCLUSION: Pantoprazole is superior to ranitidine as an adjunct treatment to endoscopic injection therapy in high-risk bleeding ulcers.

Hsu PI, Lo GH, Lo CC, Lin CK, Chan HH, Wu CJ, Shie CB, Tsai PM, Wu DC, Wang WM, Lai KH. Intravenous pantoprazole versus ranitidine for prevention of rebleeding after endoscopic hemostasis of bleeding peptic ulcers. *World J Gastroenterol* 2004; 10(24): 3666-3669
<http://www.wjgnet.com/1007-9327/10/3666.asp>

INTRODUCTION

Bleeding is a common and potential life threatening complication of peptic ulcer diseases. Recently, endoscopic hemostasis has been the treatment of first choice for bleeding peptic ulcer, providing better outcomes compared with both medical and surgical therapies^[1-4]. However, acute recurrent bleeding after initial hemostasis by therapeutic endoscopy has been reported to occur in 4% to 30% of cases, and the mortality rate in these patients is high^[5-10].

In vitro studies have shown that clotting proceeds more efficiently and the dissolution of clots by proteolytic enzymes occurs more slowly at high pH levels^[11-14]. Pepsin can digest blood clots overlying ulcer craters, and its activity is pH-related^[13]. Additionally, the function of platelets is severely impaired at low pH *in vitro*^[14]. A profound reduction of gastric acidity, therefore, could stabilize the clots over an ulcer and stop bleeding or prevent recurrent hemorrhage.

However, evidence of the effectiveness of H₂-receptor antagonists in bleeding peptic ulcers is conflicting. Collins *et al.*^[15] conducted a meta-analysis of 27 randomized studies and concluded that H₂-receptor antagonists reduced the rate of continued bleeding, the need for surgery, and the mortality rate among patients with gastric ulcers. Nonetheless, a subsequent large trial of 1 005 patients with bleeding peptic ulcers demonstrated that intravenous famotidine treatment did not affect the rebleeding rate, the operative rate, and the mortality^[16].

In vivo studies have shown that a regimen including a high dose of a proton pump inhibitor (PPI) can maintain intragastric pH at a nearly neutral level and inhibit acid production more effectively than does an infusion of an H₂-receptor antagonist^[17,18]. Thus, a high-dose PPI is theoretically better than an H₂-receptor antagonist as a treatment to prevent rebleeding of peptic ulcers. A recent meta-analysis^[19] disclosed that intravenous omeprazole was more effective than an H₂-antagonist in preventing persistent recurrent bleeding from peptic ulcer, but this advantage seemed to be restricted to those patients who did not have adjunct sclerotherapy. Nonetheless, the authors emphasized that the data were too scarce and heterogeneous to draw definitive conclusions, and further comparative trials were clearly warranted.

Currently, intravenous omeprazole is available in Europe and other countries, but it is not available in the United States of America. Although pantoprazole was the first intravenous PPI marketed in the United States of America, it does not have an indication for treatment of upper gastrointestinal bleeding, mainly due to the lack of published clinically relevant outcome data. We therefore conducted this pilot, prospective, randomized study to compare the efficacy of intravenous pantoprazole and ranitidine for prevention of rebleeding of peptic ulcers following initial endoscopic hemostasis.

MATERIALS AND METHODS

Patients

From October 2002 to September 2003, all patients with hematemesis, melena, or both, had emergent upper endoscopy

performed within 24 h of admission to the emergency units of Kaohsiung Veterans General Hospital. Patients with active bleeding ulcers or ulcers with major signs of recent bleeding were treated with distilled water injection. Patients with successful initial hemostasis and who gave their consents were enrolled in this study. Criteria for exclusion included: the presence of other possible bleeding sites (for example, esophageal varices, gastric cancer), coexistence of an acute significant illness (for example, sepsis, stroke, acute myocardial infarction, acute respiratory failure, acute surgical abdomen), the presence of a systemic bleeding tendency (for example, platelets $<50\,000/\text{mm}^3$, prolonged prothrombin time >3 s, or use of an anticoagulant).

Therapeutic endoscopy

Upper gastrointestinal endoscopy was performed within 24 h of hospital admission. The equipments used were the Olympus GIF XV10, GIF XQ 200, and GIF 1T20 (Olympus Corp., Tokyo, Japan). To improve the visual field, gastric lavage was carried out before endoscopy. Ulcers with stigmata were cleaned by water irrigation through the biopsy channel. We divided the ulcer lesions into six categories according to our previous study^[10]: clean base, red or black spot, adherent clot, nonbleeding visible vessel (NBVV), oozing visible vessel, and spurting visible vessel. An NBVV was defined as a raised red or bluish-red hemispheric lesion protruding from the ulcer base, without active bleeding. An adherent clot was defined as an overlying clot that was resistant to washing. If an adherent clot, NBVV or bleeding visible vessel was noted during the first examination, endoscopic local injection with distilled water was performed for hemostasis. Distilled water was injected in aliquots of 0.5-2 mL over and around the bleeding area, up to a total of 5.0-20.0 mL^[6,8]. Once hemostasis was achieved, the bleeding site was observed for at least 5 min. Initial hemostasis was defined as no endoscopic evidence of bleeding during 5 min of observation after therapy.

We did not check *H pylori* status for our patients during acute bleeding episodes since several studies^[20,21] disclosed that biopsy-based tests had decreased sensitivities for the detection of *H pylori* in bleeding peptic ulcers. Besides, it would increase operating time to take gastric specimens in critical patients who required therapeutic endoscopies.

Randomization

Patients with successful initial hemostasis were randomly assigned to two groups. Randomization of eligible patients was carried out by a neutral individual who opened sealed envelopes containing the treatment assignments, derived from a table of random numbers. One group was treated with intravenous pantoprazole, with an initial dose of 40 mg and subsequently with 40 mg every twelve hours during the first three days, followed by 40 mg a day orally. The other group was treated with intravenous ranitidine, with an initial dose of 50 mg and subsequently every eight hours during the first three days, followed by 150 mg of oral ranitidine every 12 h. We chose the dose of intravenous ranitidine because it was commonly used in clinical practice. Previous studies^[22] revealed that this dose of intravenous ranitidine could suppress gastric acid secretion by 83%. The study protocol was approved by the Medical Committee of Kaohsiung Veterans General Hospital.

Follow-up

During the stay in the hospital, patients received partial parenteral nutrition for 2 d. After a 48-h observation, patients were given soft diet for 48 h, and then a regular diet. The hemoglobin level was checked every day for 3 d, and a blood transfusion was given if the hemoglobin concentration fell below 8 gm/dL or if vital signs deteriorated.

A clinician independent of the endoscopist observed the patients for evidence of rebleeding. The definition of rebleeding

was recurrent hemorrhage during an 8-wk observation period. Evidence of rebleeding included fresh hematemesis, aspiration of fresh blood from NG tube, or continuous melena with a pulse rate greater than 100 beats/min, a fall in systolic blood pressure exceeding 30 mmHg, or a decrease in hemoglobin of at least 0.2 g/L. When rebleeding was suspected, a second therapeutic endoscopy was performed immediately. If hemostasis could not be achieved, surgical intervention of uncontrolled rebleeding was performed.

After discharge, patients assigned to the pantoprazole group were treated with pantoprazole 40 mg daily for up to 8 wk, and those in the ranitidine group were treated with ranitidine 150 mg twice daily. All patients were requested to return to the outpatient clinic 14 d, 4 wk and 8 wk after initial hemostasis.

Statistical analysis

The sample size was calculated according to previous experiences^[6-8,18,19]. The rebleeding rates following distilled water injection were 13% of patients treated with PPI^[7,18,19] and 29% of patients treated with H₂ receptor antagonist^[6,8]. A sample size of 46 was thus required for each group to achieve a statistical power of 80% at 10% type I error. The chi-square test with or without Yate's correction for continuity and Fisher's exact test were used when appropriate to compare the rates of rebleeding, emergency operation and mortality between groups. A *P* value less than 0.05 was considered statistically significant.

RESULTS

During the study period, 236 patients were admitted due to bleeding peptic ulcers. Endoscopic treatment was not required in 136 patients who had ulcers with clean bases or flat pigments. Nineteen patients were excluded from this study for the presence of other possible bleeding sites ($n = 5$), coexistence of an acute significant illness ($n = 9$), association with a systemic bleeding tendency ($n = 6$). One hundred and nine patients with high-risk bleeding ulcers received endoscopic injection therapy. Initial hemostasis was not achieved in 7 patients who had profuse bleeding, and they underwent surgical treatment or further endoscopic hemostasis with thermocoagulation or hemoclipping.

The other 102 patients with successful endoscopic hemostasis were randomly assigned to either pantoprazole ($n = 52$) or ranitidine ($n = 50$) therapies. Data regarding the clinical characteristics of patients at entry are summarized in Table 1. The two groups had comparable clinical features, site and size of ulcers, and bleeding severity. At index endoscopy, 40% of randomized patients had bleeding visible vessels (spurting: 6%; oozing: 34%), 38% had NBVVs and 22% had adherent clots in the ulcer craters.

All patients were followed up through the eight-week period after initial endoscopy. Treatment results are shown in Table 2. Rebleeding developed in 2 patients in the pantoprazole group. One of the rebleeding patients underwent a second endoscopy, and hemostasis was controlled by local injection of diluted epinephrine. The other died of profuse rebleeding. Neither second endoscopic therapy nor surgical intervention was performed for him because of rapid deterioration of clinical course. In the ranitidine group, 8 patients developed rebleeding. In 7 of the 8 treatment failure patients, endoscopic retreatment by local injection ($n = 5$), heater probe ($n = 1$) and hemoclipping ($n = 1$) stopped the bleeding. The other one patient underwent immediate surgery to control rebleeding after failure of second therapeutic endoscopy. None of the patients died of uncontrolled rebleeding, but one female patient died of heart attack.

The rebleeding rate of the pantoprazole group was significantly lower than that of the ranitidine group (3.8% vs 16.0%, $P = 0.04$). There were no statistically significant differences between the groups with regard to the need for emergency surgery (0% vs

2.0%), transfusion requirements (4.9±5.8 vs 5.7±6.8 units), the length of hospital stay (5.9±3.2 vs 7.5±5.0 d) or mortality (1.9% vs 2.0%).

Table 1 Base-line characteristics of the study patients with bleeding peptic ulcers *n* (%)

	Pantoprazole group (<i>n</i> = 52)	Ranitidine group (<i>n</i> = 50)	<i>P</i>
Age (yr) (SD)	63.2 (18.2)	64.7 (13.8)	0.64
Gender (M:F)	41:11	37:13	0.56
Smoking	17 (32.7)	16 (32.0)	0.94
Alcohol abuse	7 (13.5)	4 (8.0)	0.37
NSAID use	14 (26.9)	16 (32.0)	0.57
History of ulcer	32 (61.5)	28 (56.0)	0.57
History of ulcer bleeding	14 (26.9)	9 (18.0)	0.28
Hypovolemic shock	3 (5.8)	3 (6.0)	1.00
Hemoglobin (g/dL) (SD)	10.3 (3.0)	10.0 (2.8)	0.68
Endoscopic findings			
Ulcer size (cm) (SD)	1.2 (0.8)	1.2 (0.6)	0.79
Ulcer site			0.85
Stomach	25 (48.1)	25 (50.0)	
Duodenum	27 (51.9)	25 (50.0)	
Bleeding activity			
Spurting vessel	4 (7.7)	2 (4.0)	0.64
Oozing vessel	18 (34.6)	17 (34.0)	
Nonbleeding visible vessel	18 (34.6)	21 (42.0)	
Adherent clot	12 (23.1)	10 (20.0)	

Table 2 Clinical outcomes of pantoprazole and ranitidine groups *n* (%)

	Pantoprazole group (<i>n</i> = 52)	Ranitidine group (<i>n</i> = 50)	<i>P</i>
Rebleeding	2 (3.8)	8 (16.0)	0.04 ¹
Emergency operation	0 (0.0)	1 (2.0)	0.31
Hospital days (SD)	5.9 (3.2)	7.5 (5.0)	0.06
Units of Blood transfusion (SD)	4.9 (5.8)	5.7 (6.8)	0.42
Mortality	1 (1.9)	1 (2.0)	1.00

¹Significant difference.

DISCUSSION

The use of PPIs in patients with bleeding peptic ulcers has been evaluated in several studies. In a meta-analysis of 11 randomized trials^[19], Gisbert *et al.* showed that PPIs were more effective than H₂-receptor antagonists in preventing persistent or recurrent bleeding from peptic ulcers. However, meta-analysis had several limitations. For example, there was a marked variability between studies with respect to doses of PPIs and H₂-receptor antagonists, schemes of administration of the drugs, Forrest classification of bleeding ulcers and concomitant endoscopic therapies. The authors thus concluded that the data were too scarce and heterogeneous to draw definite conclusions. In addition, it is important to point out that all the trials^[23-26] analyzed by Gisbert *et al.* used omeprazole or lansoprazole as the test drug of PPIs.

To date, there are limited clinical outcome data on intravenous pantoprazole for the prevention of peptic ulcer rebleeding^[27]. Furthermore, all the published data concerning the effects of intravenous pantoprazole on bleeding peptic ulcers were in abstract form^[28], which has limited the ability to completely evaluate and generalize the suggested outcomes. We therefore designed the prospective randomized study to investigate the effects of intravenous pantoprazole on recurrent bleeding after endoscopic treatment of bleeding peptic ulcers. The rebleeding

rate of the pantoprazole and ranitidine groups in this study was 4% and 16%, respectively. The data suggest that pantoprazole is more effective than ranitidine for preventing rebleeding in high-risk bleeding ulcer patients.

However, it is important to note that continuous infusion of ranitidine was more effective to elevate intragastric pH than intermittent bolus injection^[22]. Additionally, the percentage of intragastric pH value equal to or above 7.0 was significantly greater during high dose ranitidine infusion (300-mg/24 h) compared with conventional dose infusion (150-mg/24 h)^[22]. Fired *et al.*^[28] revealed that the efficacy of infusion of high dose ranitidine to prevent recurrent ulcer bleeding was similar to that of pantoprazole infusion.

Data from *in vitro* studies suggest that both acid and pepsin can alter coagulation by interfering with the coagulation system, fibrinogen polymerization, and platelet aggregation^[12,13]. Therefore, profound acid suppression may improve the microenvironment at the bleeding point by keeping the gastric pH above the proteolytic range for pepsin to prevent clot lysis, and thus benefiting patients with bleeding peptic ulcers. Traditionally, pharmacological treatment for bleeding peptic ulcers has included H₂-receptor antagonists, but these drugs have shown no effect at all when compared with placebo^[16,29]. The lack of a clear beneficial effect of H₂-receptor antagonists could be due to the limited control of gastric pH. This is because at the conventional recommended doses of these drugs, gastric pH could not be maintained higher than 4.0 for a long period in patients with a bleeding peptic ulcer^[30]. On the other hand, intravenous PPIs could produce consistently high gastric pH values in patients with bleeding peptic ulcers^[25,31]. Pharmacokinetic studies with PPIs have shown that a bolus of 80 mg pantoprazole or omeprazole followed by immediate continuous infusion of 8 mg per hour could result in an intragastric pH of 7 within 20 min^[32]. Piseegna *et al.*^[33] also demonstrated that a single intravenous dose of pantoprazole 80 mg suppressed pentagastrin-induced acid output by 99% for approximately 24 h and had an onset of action in less than 1 h. Its acid inhibition effect was much stronger than that of intravenous famotidine. The loss of effectiveness of famotidine might be due to tolerance (tachyphylaxis), which is known to occur in response to repetitive doses of H₂-receptor antagonists^[34,35], but has never been found with PPIs. Therefore, parenteral PPIs seem to be more effective than H₂-antagonists in keeping the intragastric pH above the proteolytic range for pepsin to stabilize the clotting process.

In this study, there were no significant differences between the pantoprazole and ranitidine groups with regard to the need for emergency surgery, transfusion requirements, hospital stay or mortality. Several previous studies^[18,19] also reported that PPIs were not more effective than H₂-receptor antagonists for reducing surgery or mortality rates. However, the lack of differences in these parameters between study and control groups might be due to beta error since the numbers of cases in these studies were too small to draw definite conclusions to these parameters. In a large-scaled study of Lau *et al.*^[7], a high-dose infusion of omeprazole was reported to decrease the hospital stay of patients following endoscopic treatment of bleeding ulcers.

Recently, the combinations of injection and thermal coagulation therapies have been applied in the treatment of high-risk bleeding peptic ulcers^[36,37]. A meta-analysis by Calvet *et al.*^[37] demonstrated that combined therapies were superior to injection therapies alone. It merits further studies to investigate whether combined therapies for high-risk bleeding ulcers will effectively control bleeding ulcers and change the results in the current study.

In conclusion, after endoscopic injection treatment of bleeding peptic ulcers, intravenous pantoprazole is more effective than ranitidine for the prevention of rebleeding.

ACKNOWLEDGEMENTS

The authors express their deep appreciation to Dr. Lung-Chih Cheng, Chao-Ming Wu, Hsien-Chung Yu and Miss Yu-Shan Chen for their generous support.

REFERENCES

- 1 Laine L. Multipolar electrocoagulation vs injection therapy in the treatment of bleeding peptic ulcers. *Gastroenterology* 1990; **99**: 1303-1306
- 2 Cook DJ, Guyatt GH, Salena BJ, Laine LA. Endoscopic therapy for acute non-variceal upper gastrointestinal hemorrhage. A meta-analysis. *Gastroenterology* 1992; **102**: 139-148
- 3 Gralnek IM, Jensen DM, Gornbein J, Kovacs TO, Jutabha R, Freeman ML, King J, Jensen ME, Cheng S, Machado GA, Smith JA, Randall GM, Sue M. Clinical and economic outcomes of individuals with severe peptic ulcer hemorrhage and nonbleeding visible vessel: an analysis of two prospective clinical trials. *Am J Gastroenterol* 1998; **93**: 2047-2056
- 4 Laine L, Peterson WL. Bleeding peptic ulcer. *New Engl J Med* 1994; **331**: 717-727
- 5 Hsu PI, Lin XZ, Chan SH, Lin CY, Chang TT, Shin JS, Hsu LY, Yang CC, Chen KW. Bleeding peptic ulcer-risk factors for rebleeding and sequential changes in endoscopic findings. *Gut* 1994; **35**: 746-749
- 6 Lai KH, Peng SN, Guo WS, Lee FY, Chang FY, Malik U, Wang JY, Lo GH, Cheng JS, Lee SD. Endoscopic injection for the treatment of bleeding ulcers: local tamponade or drug effect? *Endoscopy* 1994; **26**: 338-341
- 7 Lau JY, Sung JJ, Lee KK, Yung MY, Wong SK, Wu JC, Charr FK, Ng EK, You JH, Lee CW, Chan AC, Chung SC. Effect of intravenous omeprazole on recurrent bleeding after endoscopic treatment of bleeding peptic ulcers. *N Engl J Med* 2000; **343**: 310-316
- 8 Chou YC, Hsu PI, Lai KH, Lo CC, Chan HH, Lin CP, Chen WC, Shie CB, Wang EM, Chou NH, Chen W, Lo GH. A prospective, randomized trial of endoscopic hemoclip placement and distilled water injection for treatment of high-risk bleeding ulcers. *Gastrointest Endosc* 2003; **57**: 324-328
- 9 Llach J, Bordas JM, Salmeron JM, Panes J, Garcia-Pagan JC, Feu F, Navasa M, Mondelo F, Pique JM, Mas A, Teres J, Rodes J. A prospective randomized trial of heater probe thermocoagulation versus injection therapy in peptic ulcer hemorrhage. *Gastrointest Endosc* 1996; **43**: 117-120
- 10 Hsu PI, Lai KH, Lin XZ, Yang YF, Lin M, Shin JS, Lo GH, Huang RL, Chang CF, Lin CK, Ger LP. When to discharge patients with bleeding peptic ulcers: a prospective study of residual risk of rebleeding. *Gastrointest Endosc* 1996; **44**: 381-387
- 11 Patchett SE, O'Donoghue DP. Pharmacological manipulation of gastric juice: thrombelastographic assessment and implications for treatment of gastrointestinal haemorrhage. *Gut* 1995; **36**: 358-362
- 12 Green FW Jr, Kaplan MM, Curtis LE, Levine PH. Effect of acid and pepsin on blood coagulation and platelet aggregation. A possible contributor to prolonged gastroduodenal mucosal hemorrhage. *Gastroenterology* 1978; **74**: 38-43
- 13 Patchett SE, Enright H, Afdhal N, O'Connell W, O'Donoghue DP. Clot lysis by gastric juice: an *in vitro* study. *Gut* 1989; **30**: 1704-1707
- 14 Chaimoff C, Creter D, Djaldetti M. The effect of pH on platelet and coagulation factor activities. *Am J Surg* 1978; **136**: 257-259
- 15 Collins R, Langman M. Treatment with histamine H₂ antagonists in acute upper gastrointestinal hemorrhage. *N Engl J Med* 1985; **313**: 660-666
- 16 Walt RP, Cottrell J, Mann SG, Freemantle NP, Langman MJ. Continuous intravenous famotidine for haemorrhage from peptic ulcer. *Lancet* 1992; **340**: 1058-1062
- 17 Netzer P, Gaia C, Sandoz M, Huluk T, Gut A, Halter F, Husler J, Inauen W. Effect of repeated injection and continuous infusion of omeprazole and ranitidine on intragastric pH over 72 hours. *Am J Gastroenterol* 1999; **94**: 351-357
- 18 Labenz J, Peitz U, Leusing C, Tillenburg B, Blum AL, Borsch G. Efficacy of primed infusions with high dose ranitidine and omeprazole to maintain high intragastric pH in patients with peptic ulcer bleeding: a prospective randomized controlled study. *Gut* 1997; **40**: 36-41
- 19 Gisbert JP, Gonzalez L, Calvet X, Roque M, Gabriel R, Pajares JM. Proton pump inhibitors versus H₂-antagonists: a meta-analysis of their efficacy in treating bleeding peptic ulcer. *Aliment Pharmacol Ther* 2001; **15**: 917-926
- 20 Lo CC, Lai KH, Peng NJ, Lo GH, Tseng HH, Lin CK, Shie CB, Wu CM, Chen YS, Huang WK, Chen A, Hsu PI. Polymerase chain reaction: a sensitive method for detecting *Helicobacter pylori* infection in bleeding peptic ulcers. *World J Gastroenterol* 2004 (in press)
- 21 Colin R, Bigard MA, Nottoghem B. Poor sensitivity of direct tests for detection of *Helicobacter pylori* on antral biopsies in bleeding ulcers. *Gastroenterology* 1997; **112**: A93
- 22 Ballesteros MA, Hogan DL, Koss MA, Isenberg JJ. Bolus or intravenous infusion of ranitidine: effects on gastric pH and acid secretion. *Ann Intern Med* 1990; **112**: 334-339
- 23 Michel P, Duhamel C, Bazin B, Raoul JL, Person B, Bigard MA, Legoux JL, Sallerin V, Colin R. Lansoprazole versus ranitidine in the prevention of early recurrences of digestive hemorrhages from gastroduodenal ulcers. Randomized double-blind multicenter study. *Gastroenterol Clin Biol* 1994; **18**: 1102-1105
- 24 Lanas A, Artal A, Blas JM, Arroyo MT, Lopez-Zaborras J, Sainz R. Effect of parenteral omeprazole and ranitidine on gastric pH and the outcome of bleeding peptic ulcer. *J Clin Gastroenterol* 1995; **21**: 103-106
- 25 Lin HJ, Lo WC, Lee FY, Perng CL, Tseng GY. A prospective randomized comparative trial showing that omeprazole prevents rebleeding in patients with bleeding peptic ulcer after successful endoscopic therapy. *Arch Intern Med* 1998; **158**: 54-58
- 26 Brunner G, Chang J. Intravenous therapy with high doses of ranitidine and omeprazole in critically ill patients with bleeding peptic ulcers of the upper intestinal tract: an open randomized controlled trial. *Digestion* 1990; **45**: 217-225
- 27 van Rensburg CJ, Hartmann M, Thorpe A, Venter L, Theron I, Luhmann R, Wurst W. Intragastric pH during continuous infusion with pantoprazole in patients with bleeding peptic ulcer. *Am J Gastroenterol* 2003; **98**: 2635-2641
- 28 Fried R, Beglinger C, Stumpf J, Adler G, Schepp W, Klein M, Schneider A, Fischer R. Comparison of intravenous pantoprazole with intravenous ranitidine in peptic ulcer bleeding (abstract). *Gastroenterology* 1999; **116**: A165
- 29 Falk A, Darle N, Haglund U, Tornqvist A. Histamine₂-receptor antagonists in gastroduodenal ulcer haemorrhage. *Scand J Gastroenterol* 1985; **110**(Suppl): 95-100
- 30 Reynolds JR, Walt RP, Clark AG, Hardcastle JD, Langman MJ. Intragastric pH monitoring in acute upper gastrointestinal bleeding and the effect of intravenous cimetidine and ranitidine. *Aliment Pharmacol Ther* 1987; **1**: 23-30
- 31 Huggins RM, Scates AC, Latour JK. Intravenous proton-pump inhibitors versus H₂-antagonists for treatment of GI bleeding. *Ann Pharmacother* 2003; **37**: 433-437
- 32 Brunner G, Luna P, Hartmann M, Wurst W. Optimizing the intragastric pH as supportive therapy in upper GI bleeding. *Yale J Biol Med* 1996; **69**: 225-231
- 33 Pisegna JR, Martin P, McKeand W, Ohning G, Walsh JH, Paul J. Inhibition of pentagastrin-induced gastric acid secretion by intravenous pantoprazole: a dose-response study. *Am J Gastroenterol* 1999; **94**: 2874-2880
- 34 Wilder-Smith CH, Merki HS. Tolerance during dosing with H₂-receptor antagonists. An-overview. *Scand J Gastroenterol* 1992; **193**(Suppl): 14-19
- 35 Merki HS, Wilder-Smith CH. Do continuous infusions of omeprazole and ranitidine retain their effect with prolonged dosing? *Gastroenterology* 1994; **106**: 60-64
- 36 Chung SS, Lau JY, Sung JJ, Chan AC, Lai CW, Ng EK, Chan FK, Yung MY, Li AK. Randomised comparison between adrenaline injection alone and adrenaline injection plus heat probe treatment for actively bleeding ulcers. *Br Med J* 1997; **314**: 1307-1311
- 37 Calvet X, Vergara M, Brullet E, Gisbert JP, Campo R. Addition of a second endoscopic treatment following epinephrine injection improves outcome in high-risk bleeding ulcers. *Gastroenterology* 2004; **126**: 441-450

Inhibition of transfected PTEN on human colon cancer

Shou-Shui Xu, Wen-Lu Shen, Song-Ying Ouyang

Shou-Shui Xu, Wen-Lu Shen, Second Affiliated Hospital, Shantou University Medical College, Shantou 515031, Guangdong Province, China

Song-Ying Ouyang, Faculty of Military Medicine, Quartermaster University of PLA, Changchun 130062, Jilin Province, China

Correspondence to: Postdoctor Shou-Shui Xu, Shantou University Medical College, Shantou 515031, Guangdong Province, China. smile4612003@yahoo.com.cn

Telephone: +86-754-8900466

Received: 2004-02-11 **Accepted:** 2004-03-04

Abstract

AIM: To study the inhibitory effect of transfected PTEN on LoVo cells.

METHODS: Human PTEN cDNA was transferred into LoVo cells via lipofectin and PTEN mRNA levels and its expression were analyzed by Western blot and flow cytometry. Before or after transfection, the effects of 5-Fu on inhibiting cell proliferation and inducing apoptosis were measured by flow cytometry, DNA bands and MTT.

RESULTS: PTEN transfection significantly up-regulated PTEN expression in LoVo cells. 5-Fu inhibited cell proliferation and induced apoptosis in transfected LoVo cells.

CONCLUSION: Transfected PTEN can remarkably up-regulate PTEN expression in LoVo cells and promote the apoptosis. PTEN transfection is associated with 5-Fu treatment effect and has a cooperatively cytotoxic effect.

Xu SS, Shen WL, Ouyang SY. Inhibition of transfected PTEN on human colon cancer. *World J Gastroenterol* 2004; 10 (24): 3670-3673

<http://www.wjgnet.com/1007-9327/10/3670.asp>

INTRODUCTION

Apoptosis and abnormal proliferation play a critical role in the development of carcinoma^[1-8]. 5-Fu is one of the most popular drugs in colon cancer treatment. *In vivo* 5-Fu converts into fluorouracil deoxynucleotide and inhibits thymidylate synthetase and consequently, hinders deoxyuridylic acid into deoxythymidylate catalyzed by the enzyme thus blocking DNA synthesis and inducing apoptosis in cancer cells. The effect of phosphatase and tensin homologue deleted on chromosome 10 (PTEN)^[9-21] transfection associated with 5-Fu on LoVo cells in human colon cancer was studied.

MATERIALS AND METHODS

Materials

Human LoVo cells and PTEN plasmid pcDNA-PTEN-WT, wild type-WT, plasmid DNA extraction kit were purchased from Hangzhou Weitejie BioTech Co. The samples of normal human tissue and highly malignant colon cancer tissues were obtained from 461 Hospital of PLA and immediately stored in liquid nitrogen. Plasmid pcDNA3.1 (+) of eukaryonal expression

vectors was from Invitrogen. *E. coli* DH5 α , LoVo were stored in our laboratory. Diethyl pyrocarbonate (DEPC) was from Sigma. Total RNA was extracted by Trizol (Gibco). Oligo dT, TaKaRa RNA PCR Kit (AMV) pMD 18-T, Ex TaqTM enzyme (including dNTPs and Mg²⁺), DNA Ligase Kit Ver.2, DNA marker were from TaKaRa. LipofectamineTM 2 000 transfection reagent was from Invitrogen. DNA sequence kit was ABI BigDye terminator kit. DNA fragment extraction and purification kit was from Beijing Dingguo Bio Corp. Rabbit-anti-human PTEN polyclonal antibody (rabbit anti-PTEN) was from Beijing Zhongshan Bio Corp. Horseradish enzyme labeled goat-anti-rabbit IgG (H+L) was obtained from Beijing Zhongshan Biotechnology Co., LTD. **Reagents and enzymes** Restriction enzymes *Bam* HI and *Hind* III, basic proteolytic enzyme, DNA kit, Lipofectin, G418 were used. **Primers** The primers were designed according to human PTEN sequence published in GenBank using Primer Premier 5.0 software. The upper stream primer was 5' AAG CTT ATG ACA GCC ATC ATC AAA GAG AT 3' with *Hind* III digestion site. The down stream primer was 5' -GGA TCC GGA ATA AAA CGG GAA AGT GCC-3' with *Bam*H I digestion site. The primers were synthesized by Beijing Baisheng Bio Corp.

Methods

RNA extraction One hundred milligrams of the samples in liquid nitrogen were taken. Total RNA was extracted by the protocol of Trizol.

RT-PCR amplification of PTEN gene It was carried out by TaKaRa RNA PCR kit. The reaction mixture was 20 μ L. Reaction condition was at 30 $^{\circ}$ C for 10 min, 45 $^{\circ}$ C for 40 min, 95 $^{\circ}$ C for 2 min, 5 $^{\circ}$ C for 5 min. The primer was designed as above. Amplification condition was at 94 $^{\circ}$ C for 5 min, 94 $^{\circ}$ C for 30 s, 53 $^{\circ}$ C for 30 s, 72 $^{\circ}$ C for 1 min, 72 $^{\circ}$ C for 10 min. After the reaction 5 μ L was taken for agarose gel electrophoresis.

PTEN clone and identification Fifty microliters of PCR product were used for 1% agarose gel electrophoresis to extract cDNA fragment and after extraction it was identified by agarose gel electrophoresis. cDNA fragment was inserted into pMD18-T vectors and ligated at 16 $^{\circ}$ C overnight to construct the recombinant plasmids pMD-PTEN-WT (wild type) and pMD-PTEN-MT (mutant type). The recombinant plasmids transfected competent DH5 α cells by CaCl₂. The transfected cells were cultivated in 50 mg/L ampicillin (Amp) LB agar plates at 37 $^{\circ}$ C for 14-16 h. Single colonies were inoculated in LB liquid medium with Amp at 37 $^{\circ}$ C overnight. The plasmids were extracted from cell culture. The positive clones were selected and doubly digested by *Hind* III and *Bam*H at 37 $^{\circ}$ C for 1 h. After digestion it was identified by electrophoresis and the sequences were verified by ABI 3 100 and the results were analysed by DNAsis software.

Construction and identification of eukaryonal expression vectors Recombinant plasmids with correct sequences were doubly digested by *Hind* III and *Bam*H I. The product was used for agarose gel electrophoresis to extract 1.4 kb PTEN fragments. pcDNA3.1 (+) was also doubly digested by *Hind* III and *Bam*H I and extracted. The linear vector fragments and extracted PTEN fragments were ligated by T4 DNA ligase at 16 $^{\circ}$ C overnight and the product was transferred into competent DH5 α cells. Single colonies were randomly selected and cultivated at 37 $^{\circ}$ C overnight. Plasmids were extracted and amplified by PCR and identified by digestion.

Transfection According to Lipofectamine™ 2000 transfection kit, pcDNA3.1 (+) vacant vector and none-transfected LoVo cells served as controls. After transfection the cells were grown at 37 °C with 50 mL/L CO₂ for 4-6 h and 2 mL of medium supplemented with 10% calf serum was changed and cultivated for 48 h. Four to ten cells were transferred and incubated. When the cells were 80% in confluence, 600 µg/mL G418 was added to select the positive clones.

Cell growth The cells were digested by 0.25% trypsin to get monocyte suspension and inoculated into 6 well plates at 1×10^4 /well. Seven wells were for each kind of cells. The medium was changed after 2 d. Cells were counted every day. The cell growth was observed for 7 d and cell growth curve was obtained.

Detection of PTEN gene expression Total RNA extracted was used as template for reverse transcription. The reaction system and condition were described as above. Western assay was performed according to the reports^[22-24], horseradish peroxidase-labeled rabbit-anti-human IgG was used as the second antibody.

Gene preparation Total RNA was extracted from tumor and normal tissues. PCR product was collected and ligated into pMD 18-T vectors and then transformed. The constructs were verified by DNA sequencing.

Cell culture Frozen cells were taken out of liquid nitrogen and rapidly melted at 37-40 °C for 1 min in water bath. The tube of cells stored was opened and the cell suspension was transferred into the culture plate. After the medium was added the cells were grown at 37 °C. The medium was changed after cell growing on the wall (around 4 h). After the cells were cultivated into a single layer, the next generation was grown. The restored cells were transferred onto the 35 mm plate and cultivated at 37 °C with 50 mL/L CO₂ for 18 h. The cells were digested by 0.25% pancreatin and cultured in 2 mL of DMEM supplemented with 10% fetal calf serum to stop digestion. The cells were cultured for 12 h. When the cells were in 30-50% confluence, they were transfected by plasmid DNA.

Western blot Total RNA was extracted with Trizol from transfected LoVo cells or non-transfected cells. Five microliters of samples were separated by electrophoresis, transblotted, prohybridized, hybridized and stained.

PTEN protein expression Before or after transfection PTEN protein expression was assayed by flow cytometry. The cells were resuspended in PBS, PTEN monoclonal IgG1 antibody was labeled and incubated at room temperature for 30 min and analyzed by flow cytometry.

DNA ladder bands assay 5-Fu at 20 µL/mL was added into PTEN cells transfected or non-transfected and incubated for 48 h and centrifuged. DNA was extracted from the cells and electrophoresis was performed in 2% agar gel in 0.5× TBS for 2 h. Photos were taken under UV light.

Inhibitory rates of 5-Fu on LoVo cells before or after transfection by MTT assay One hundred microliters of LoVo cells at 1×10^6 /mL was inoculated into 96 well plates and 100 µL of 5-Fu was added so the concentrations were 10, 20, 40, 100, 200, 400 µg/mL. After incubation for 48 h, 100 µL of dimethylsulfoxide was added. After 20 min, the absorbance in each well was measured by enzyme-labelled meter and the inhibition rate was calculated.

The inhibition rate = $[1 - (\text{the value of Abs in experiment} / \text{the value of Abs in the control})] \times 100\%$.

Flow cytometry The apoptosis of LoVo cells induced by 5-Fu was analyzed by flow cytometry. 5-Fu 10 µg/mL was added into LoVo cells transfected or non-transfected and incubated for 48 h, then centrifuged, and 20 µL of propidium iodide (PI) was added for half an hour in the dark and analyzed by flow cytometry.

Statistics analysis

The differences between groups were analyzed by *t* test.

RESULTS

The digested plasmid PTEN-pMD18-T is shown in Figure 1. After plasmid PTEN-pMD18-T was digested, two fragments were 5.3 kb and 1.4 kb, which were consistent with dl 2 000 marker.

Four cell growth curves are shown pcDNA-PTEN-WT cell growth was slower than other cells (Figure 2).

PTEN mRNA expression in LoVo cells was assayed by Western blot. The PTEN mRNA expression level was higher after transfection (Figure 3).

LoVo cells transfected with PTEN-WT gene were assayed by flow cytometry and it was mainly found in cell cycle blockage period G₀-G₁ (58.21%) (Figure 4).

The results of DNA-ladder bands showed that in transfected LoVo cells treated by 5-Fu there were typical DNA ladder bands, but in non-transfected LoVo cells there was no DNA ladder band.

After 5-Fu 10 µL/mL was added for 48 h, the apoptotic LoVo cells reached 71.75% and only 18.84% in the control (Figure 5).

The effect of same concentration of 5-Fu on PTEN transfected and non-transfected LoVo cells was detected using MTT. The inhibition rate on cell proliferation was higher in the former than that in the later, and there was a significant difference between them ($P < 0.01$).

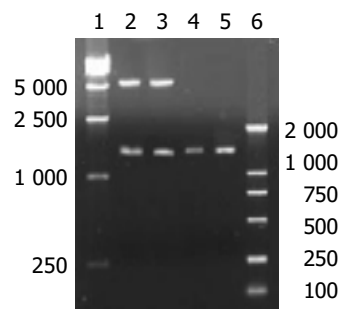


Figure 1 Digested plasmid PTEN-pMD18-T 1: DL15000 marker; 2: pcDNA-PTEN-WT doubly digested; 3: pcDNA-PTEN-MT doubly digested; 4: pcDNA-PTEN-WT PCR; 5: product of pcDNA-PTEN-MT PCR.

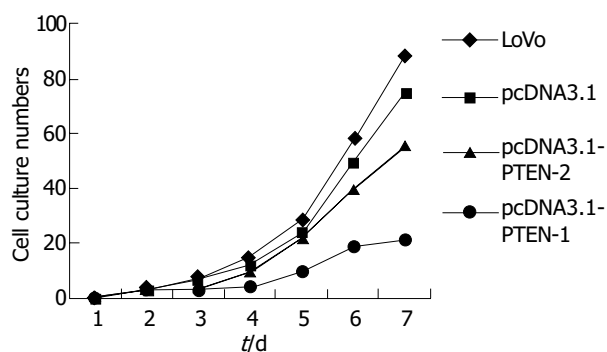


Figure 2 Growth curve of four cells. PTEN-1 (PTEN-wild type), PTEN-2 (PTEN-mutant type), PcDNA3.1 (vector).

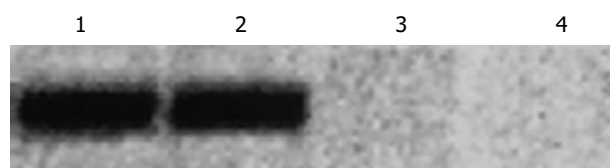


Figure 3 Detection of Western wild type and mutant type PTEN genes 1: transfected cell pcDNA-PTEN-WT; 2: transfected cell pcDNA-PTEN-MT; 3: transfected vacant vector cell pcDNA3.1(+); 4: nontransfected cells.

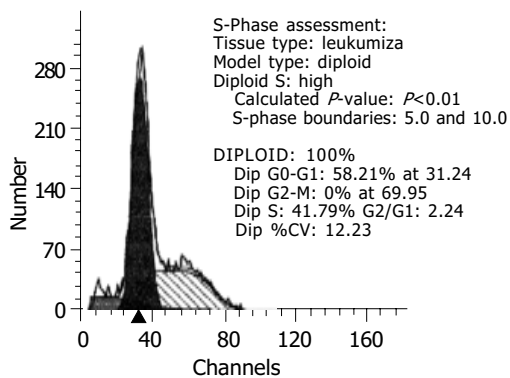


Figure 4 Result of LoVo cell cycle after transfection by flow cytometry.

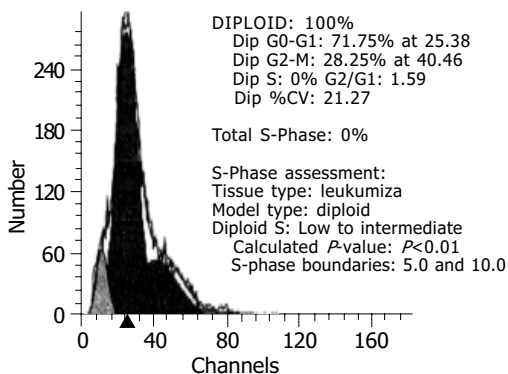


Figure 5 Result of apoptotic LoVo cells after transfection induced by 5-Fu.

DISCUSSION

Tumor formation is a process of multi-factors and multi-stages. The activation of cancer genes and inactivation and abnormality of anticancer genes are considered as important molecular mechanisms. Recently PTEN was found to be an anticancer gene^[25-28]. PTEN deletion and mutation were found in many malignant tumors including glioma, squamous carcinoma, prostate cancer, kidney cancer, endometrium cancer, breast cancer, colon cancer, etc.^[29-35]. The gene is on 10q23 chromosome in human and there are 9 exons at 5' terminal end and 804 nucleotides. The open reading frame is 1 209 bp encoding 403 amino acid residues of PTEN protein with a molecular weight 47.1 kD. Chromosome allele gene deletions mainly occurred in highly malignant tumors such as glioblastoma multiform (GBM) and malignant meningioma. PTEN mutation also occurred in GBM and was seldom found in low degree malignant glioma. Davies^[36] analyzed the DNA sequences in 46 glioma samples and found that PTEN mutation rate in an atlastic astrocytoma was 23% (3/13) and 36% (5/14) in GBM, but it was not found in 19 subjects with low degree malignant glioma. Such results indicated that PTEN might be related to the progress of glioma. Steck *et al.*^[37] discovered that 10q23 PTEN gene domain was frequently lost in GBM but was conserved in most low malignant tumors. The gene deletion was in 12q25-q26 domain and then PTEN gene loss appeared in the process of GBM. Dicuonzo *et al.*^[23] found that in colon cancer PTEN mutation, deletion and loss or replacement were all on chromosome 10 and the more malignant it was, the more evident the mutation and deletion were.

PTEN mutation rates in glioma cell lines and GBM were 41-63% and 17-44%, respectively. The literatures in Medline were reviewed for 674 malignant gliomas, the mutation rate of PTEN was 24%, including frame shift mutation, missense mutation, nonsense mutation and PTEN deletion. The point mutation rate was 41% and most of mutations were in core phosphorylase

domain of 5 exons. Davies *et al.*^[38] used adenovirus as vector and PTEN gene was transfected into glioma cell lines U251, pkb/akt, phosphorylation level was decreased and its activities were inhibited. The apoptosis rate was significantly higher than that in the control. It was reported that tumor cell growth was inhibited (60-70%) by transfected wild type PTEN with reverse transcription and PTEN mutation with U87MG and U178MG of glioma cell lines and cell growth stopped at G₁ stage by flow cytometry.

In our study, after transfection PTEN mRNA expression level in LoVo cells was higher than that before PTEN was transfected. After transfection PTEN protein expression level was higher by flow cytometry and the positive rate was increased from 21% to 47%, which indicated that PTEN gene was transferred into LoVo via lipofectin. Typical DNA ladder bands were found by 5-Fu in transfected LoVo cells and DNA ladder bands were not remarkable in non-transfected LoVo cells. The apoptosis rate was 71.75% after incubation of 5-Fu 10 μ L/mL in LoVo cells for 48 h and in the control it was only 18.84%. The effect of same concentration of 5-Fu on PTEN transfected LoVo cells and non-transfected LoVo cells was measured. The inhibition rate of cell proliferation was higher in the former than in the later and there was a significant difference between them, which demonstrated that PTEN gene expression promoted signaling in DNA damage by 5-Fu and induced apoptosis and inhibited cell proliferation in tumor.

PTEN protein is in cytoplasm of cells and homologous to tensin which is important in cell framework and in local adhesion. PTEN not only acts on the nuclei but also on membranes. PTEN protein could down-regulate the interaction of tumor cells and extracellular matrix (ECM) by inhibiting activities of focal adhesion kinase. (fak)^[39]. Malignant cells proliferate without local adhesion. Fak is an important signal mediated by integrin and its inhibition could induce apoptosis and its activation could induce non-dependent growth and tumor formation^[40]. Fak is over-expressed in many high degree malignant tumors. PTEN inhibits non-dependent cell growth by reducing Fak activities.

It was shown that apoptosis reached 71.75% when transfected LoVo cells were incubated with 5-Fu 10 μ L/mL for 48 h and it was 18.84% in the control. Maybe 5-Fu up-regulated the new protein synthesis on the surface of cells and promoted signaling in PTEN system in the cells or 5-Fu blocked some protective protein synthesis. The mechanism of cooperative effect of 5-Fu and PTEN gene transfection may be due to PTEN protein expression on the surface of cells and 5-Fu transmembrane transportation. 5-Fu can accumulate in cells and produce cytotoxin and induce cell apoptosis.

REFERENCES

- 1 Mayo LD, Dixon JE, Durden DL, Tonks NK, Donner DB. PTEN protects p53 from Mdm2 and sensitizes cancer cells to chemotherapy. *J Biol Chem* 2002; **277**: 5484-5489
- 2 Wu RC, Li X, Schonthal AH. Transcriptional activation of p21WAF1 by PTEN/MMAC1 tumor suppressor. *Mol Cell Biochem* 2000; **203**: 59-71
- 3 Tolkacheva T, Chan AM. Inhibition of H-Ras transformation by the PTEN/MMAC1/TEP1 tumor suppressor gene. *Oncogene* 2000; **19**: 680-689
- 4 Gu J, Tamura M, Yamada KM. Tumor suppressor PTEN inhibits integrin- and growth factor-mediated mitogen-activated protein (MAP) kinase signaling pathways. *J Cell Biol* 1998; **143**: 1375-1383
- 5 Xu B, Yao Q, Dai SZ. Detection of mutation and protein expression of PTEN gene in endometrial carcinoma. *Aizheng* 2004; **23**: 69-73
- 6 Mao JH, Wu D, Perez-Losada J, Nagase H, DelRosario R, Balmain A. Genetic interactions between Pten and p53 in radiation-induced lymphoma development. *Oncogene* 2003; **22**: 8379-8385

- 7 **Seminario MC**, Precht P, Wersto RP, Gorospe M, Wange RL. PTEN expression in PTEN-null leukaemic T cell lines leads to reduced proliferation via slowed cell cycle progression. *Oncogene* 2003; **22**: 8195-8204
- 8 **Shin Lee J**, Seok Kim H, Bok Kim Y, Cheol Lee M, Soo Park C. Expression of PTEN in renal cell carcinoma and its relation to tumor behavior and growth. *J Surg Oncol* 2003; **84**: 166-172
- 9 **Su JD**, Mayo LD, Donner DB, Durden DL. PTEN and phosphatidylinositol 3'-kinase inhibitors up-regulate p53 and block tumor-induced angiogenesis: evidence for an effect on the tumor and endothelial compartment. *Cancer Res* 2003; **63**: 3585-3592
- 10 **Choi Y**, Zhang J, Murga C, Yu H, Koller E, Monia BP, Gutkind JS, Li W. PTEN, but not SHIP and SHIP2, suppresses the PI3K/Akt pathway and induces growth inhibition and apoptosis of myeloma cells. *Oncogene* 2002; **21**: 5289-5300
- 11 **Malmer B**, Gronberg H, Andersson U, Jonsson BA, Henriksson R. Microsatellite instability, PTEN and p53 germline mutations in glioma families. *Acta Oncol* 2001; **40**: 633-637
- 12 **Lee JO**, Yang H, Georgescu MM, Di Cristofano A, Maehama T, Shi Y, Dixon JE, Pandolfi P, Pavletich NP. Crystal structure of the PTEN tumor suppressor: implications for its phosphoinositide phosphatase activity and membrane association. *Cell* 1999; **99**: 323-334
- 13 **Li J**, Simoson L, Takahashi M, Miliareis C, Myers MP, Tonks N, Parsons R. The PTEN/MMAC1 tumor suppressor induces cell death that is rescued by the AKT/protein kinase B oncogene. *Cancer Res* 1998; **58**: 5667-5672
- 14 **Nassif NT**, Lobo GP, Wu X, Henderson CJ, Morrison CD, Eng C, Jalaludin B, Segelov E. PTEN mutations are common in sporadic microsatellite stable colorectal cancer. *Oncogene* 2004; **23**: 617-628
- 15 **Saito Y**, Swanson X, Mhashilkar AM, Oida Y, Schrock R, Branch CD, Chada S, Zumstein L, Ramesh R. Adenovirus-mediated transfer of the PTEN gene inhibits human colorectal cancer growth *in vitro* and *in vivo*. *Gene Ther* 2003; **10**: 1961-1969
- 16 **Tanaka M**, Grossman HB. *In vivo* gene therapy of human bladder cancer with PTEN suppresses tumor growth, downregulates phosphorylated Akt, and increases sensitivity to doxorubicin. *Gene Ther* 2003; **10**: 1636-1642
- 17 **Han B**, Dong Z, Liu Y, Chen Q, Hashimoto K, Zhang JT. Regulation of constitutive expression of mouse PTEN by the 5'-untranslated region. *Oncogene* 2003; **22**: 5325-5337
- 18 **Radu A**, Neubauer V, Akagi T, Hanafusa H, Georgescu MM. PTEN induces cell cycle arrest by decreasing the level and nuclear localization of cyclin D1. *Mol Cell Biol* 2003; **23**: 6139-6149
- 19 **Ito K**, Kubokawa M, Harada N, Mibu R, Nawata H. p53 and PTEN/MMAC1 mutational analysis of the small-intestinal cancer. *Dig Liver Dis* 2003; **35**: 347-350
- 20 **Lin Q**, Zhuang YZ, Xu DP, Ye JX, Chen PQ. Expression of PTEN protein and its correlation with p27kip1 and cyclin D1 expression in primary breast cancer. *Zhonghua Zhongliu Zazhi* 2003; **25**: 246-249
- 21 **Marino M**, Acconcia F, Trentalance A. Biphasic estradiol-induced AKT phosphorylation is modulated by PTEN via MAP kinase in HepG2 cells. *Mol Biol Cell* 2003; **14**: 2583-2591
- 22 **Taniyama K**, Goodison S, Ito R, Bookstein R, Miyoshi N, Tahara E, Tarin D, Urquidí V. PTEN expression is maintained in sporadic colorectal tumours. *J Pathol* 2001; **194**: 341-348
- 23 **Dicuonzo G**, Angeletti S, Garcia-Foncillas J, Brugarolas A, Okrouzhnov Y, Santini D, Tonini G, Lorino G, De Cesaris M, Baldi A. Colorectal carcinomas and PTEN/MMAC1 gene mutations. *Clin Cancer Res* 2001; **7**: 4049-4053
- 24 **Lilja JF**, Wu D, Reynolds RK, Lin J. Growth suppression activity of the PTEN tumor suppressor gene in human endometrial cancer cells. *Anticancer Res* 2001; **21**: 1969-1974
- 25 **Li J**, Yen C, Liaw D, Podsypanina K, Bose S, Wang SL, Puc J, Miliareis C, Rodgers L, McCombie R, Pararsons R. PTEN a putative protein tyrosine phosphatase gene mutated in human brain, breast, and prostate cancer. *Science* 1997; **275**: 1943-1947
- 26 **Tashiro H**, Blazes MS, Wu R, Cho KR, Bose S, Wang SI, Li J, Parsons R, Ellenson LH. Mutations in PTEN are frequent in endometrial carcinoma but rare in other common gynecological malignancies. *Cancer Res* 1997; **57**: 3935-3940
- 27 **Steck PA**, Pershouse MA, Jasser SA, Yung WK, Lin H, Ligon AH, Langford LA, Baumgard ML, Hattier T, Davis T, Frye C, Hu R, Swedlund B, Teng DH, Tavtigian SV. Identification of a candidate tumour suppressor gene, MMAC1, at chromosome 10q23.3 that is mutated in multiple advanced cancers. *Nat Genet* 1997; **15**: 356-362
- 28 **Davies MA**, Koul D, Dhese H, Berman R, McDonnell TJ, McConkey D, Yung WK, Steck PA. Regulation of Akt/PKB activity, cellular growth, and apoptosis in prostate carcinoma cells by MMAC/PTEN. *Cancer Res* 1999; **59**: 2551-2556
- 29 **Li DM**, Sun H. PTEN/MMAC1/TEP1 suppresses the tumorigenicity and induces G1 cell cycle arrest in human glioblastoma cells. *Proc Natl Acad Sci U S A* 1998; **95**: 15406-15411
- 30 **Furnari FB**, Huang HJ, Cavenee WK. The phosphoinositid phosphatase activity of PTEN mediates a serum-sensitive G1 growth arrest in glioma cells. *Cancer Res* 1998; **58**: 5002-5008
- 31 **Zhao H**, Dupont J, Yakar S, Karas M, LeRoith D. PTEN inhibits cell proliferation and induces apoptosis by downregulating cell surface IGF-IR expression in prostate cancer cells. *Oncogene* 2004; **23**: 786-794
- 32 **Kato H**, Fujimura M, Kumabe T, Ishioka C, Kanamaru R, Yoshimoto T. PTEN gene mutation and high MIB-1 labeling index may contribute to dissemination in patients with glioblastoma. *J Clin Neurosci* 2004; **11**: 37-41
- 33 **Saito Y**, Gopalan B, Mhashilkar AM, Roth JA, Chada S, Zumstein L, Ramesh R. Adenovirus-mediated PTEN treatment combined with caffeine produces a synergistic therapeutic effect in colorectal cancer cells. *Cancer Gene Ther* 2003; **10**: 803-813
- 34 **Saga Y**, Mizukami H, Takei Y, Ozawa K, Suzuki M. Suppression of cell migration in ovarian cancer cells mediated by PTEN overexpression. *Int J Oncol* 2003; **23**: 1109-1113
- 35 **Nassif NT**, Lobo GP, Wu X, Henderson CJ, Morrison CD, Eng C, Jalaludin B, Segelov E. PTEN mutations are common in sporadic microsatellite stable colorectal cancer. *Oncogene* 2004; **23**: 617-628
- 36 **Davies MP**, Gibbs FE, Halliwell N, Joyce KA, Roebuck MM, Rossi ML, Salisbury J, Sibson DR, Tacconi L, Walker C. Mutation in the PTEN/MMAC1 gene in archival low grade and high grade gliomas. *Br J Cancer* 1999; **79**: 1542-1548
- 37 **Steck PA**, Lin H, Langford LA, Jasser SA, Koul D, Yung WK, Pershouse MA. Functional and molecular analyses of 10q deletions in human gliomas. *Genes Chromosomes Cancer* 1999; **24**: 135-143
- 38 **Davies MA**, Lu Y, Sano T, Fang X, Tang P, LaPushin R, Koul D, Bookstein R, Stokoe D, Yung WK, Mills GB, Steck PA. Adenoviral transgene expression of MMAC/PTEN in human glioma cells inhibits Akt activation and induces anoikis. *Cancer Res* 1998; **58**: 5285-5290
- 39 **Tamura M**, Gu J, Matsumoto K, Aota S, Parsons R, Yamada KM. Inhibition of cell migration, spreading, and focal adhesions by tumor suppressor PTEN. *Science* 1998; **280**: 1614-1617
- 40 **Tamura M**, Gu J, Danen EH, Takino T, Miyamoto S, Yamada KM. PTEN interactions with focal adhesion kinase and suppression of the extracellular matrix-dependent phosphatidylinositol 3-kinase/Akt cell survival pathway. *J Biol Chem* 1999; **274**: 20693-20703

Serum sIL-2R, TNF- α and IFN- γ in alveolar echinococcosis

Da-Zhong Shi, Fu-Rong Li, B Bartholomot, DA Vuitton, PS Craig

Da-Zhong Shi, Fu-Rong Li, Department of Parasitology, Lanzhou Medical College, Lanzhou 730000, Gansu Province, China

B Bartholomot, DA Vuitton, Department of Immunology, Besancon University, France

PS Craig, Department of Biological Sciences, Salford University, United Kingdom

Supported by the STD3 Programme of the EC, No. TS3-CT94-0270

Correspondence to: Professor Da-Zhong Shi, Department of Parasitology, Lanzhou Medical College, Lanzhou 730000, Gansu Province, China. shidz@public.lz.gs.cn

Telephone: +86-931-8616962 **Fax:** +86-931-8616962

Received: 2004-01-12 **Accepted:** 2004-06-21

Abstract

AIM: To approach the relationship between alveolar echinococcosis (AE) pathology and level of sIL-2R, TNF- α and IFN- γ in sera and the significance of cytokines in development of AE.

METHODS: After 23 patients with AE were confirmed by ELISA and ultrasound, their sera were collected and the concentrations of sIL-2R, TNF- α and IFN- γ were detected by double antibody sandwich. Twelve healthy adults served as controls. According to the status of livers of AE patients by ultrasound scanning, they were divided into 4 groups: P₂, P₃, P₄ groups and C group (control). Average of concentrations of sIL-2R, TNF- α and IFN- γ in homologous group was statistically analyzed by both ANOV and Newman-Keuls, respectively.

RESULTS: The mean of sIL-2R in P₂ group was 97±29, P₃: 226±80, P₄: 194±23 and control group (111±30)×10³ u/L (P <0.01). The mean of TNF- α in P₂ group was 1.12±0.20, P₃: 3.67±1.96, P₄: 1.30±0.25 and control group 0.40±0.19 μ g/L (P <0.01). The mean of IFN- γ in P₂ group was 360±20, P₃: 486±15, P₄: 259±19 and control group: 16±2 ng/L (P <0.01). Judged by ANOV and Newman-Keuls, the mean concentrations of sIL-2R, TNF- α and IFN- γ had a significant difference among groups. Except for P₂ group, the mean sIL-2R between other groups of AE patients had a significant difference (P <0.05). The mean of TNF- α concentration in P₃ group was the highest (P <0.01). The mean of IFN- γ concentration in all patients was higher than that in control group (P <0.01), but there was no difference between AE groups (P >0.05).

CONCLUSION: Low sIL-2R level indicates an early stage of AE or stable status, per contra, a progression stage. Higher level of TNF- α might be related to the lesion of liver. The role of single IFN- γ is limited in immunological defense against AE and it can not fully block pathological progression.

Shi DZ, Li FR, Bartholomot B, Vuitton DA, Craig PS. Serum sIL-2R, TNF- α and IFN- γ in alveolar echinococcosis. *World J Gastroenterol* 2004; 10(24): 3674-3676

<http://www.wjgnet.com/1007-9327/10/3674.asp>

INTRODUCTION

Alveolar echinococcosis (AE) is a rare and potentially fatal

parasitic disease^[1,2]. B ultrasound and immunological tests are the most useful diagnostic methods for AE. In keeping with the popularity of B-ultrasound in diagnosis and epidemiological survey of AE, it is of important clinical and theoretical significance to understand the relationship between AE clinical types or pathological process and cytokines from patients with AE. B ultrasound has the characteristics of rapidity, accurate location and direct viewing for AE diagnosis and could reflect the pathological process of AE.

Since the early 1990 s, the study on cell mediated immunity of AE has rapidly progressed^[3,4], but studies on AE clinical types coupled cytokines are rare. During the epidemiological survey in Gansu Province, China, cytokines in patients with AE were detected. According to the pathological lesions obtained by B-ultrasound, the patients were divided into different stages, and the relationship between clinical types and cytokines in sera was discussed.

MATERIALS AND METHODS

Twenty-three cases of AE were confirmed by ELISA and ultrasound and their sera were collected. Absorbency values of sIL-2R, TNF- α and IFN- γ were detected by double antibody sandwich. Twelve healthy adults served as controls. The standard curve was drawn and the concentrations of above cytokines were measured respectively. In reference to the standardization of TNM classification system for hepatocellular carcinomas, all subjects were divided into 4 groups: P₂, P₃, P₄ groups and C group (control group). The average of concentrations of sIL-2R, TNF- α and IFN- γ was statistically analyzed by both ANOV^[5] and Newman-Keuls^[6] respectively.

RESULTS

A total of 23 patients with AE were divided into P₂ group: 7 cases, P₃ group: 9 cases, P₄ group: 7 cases. The mean of sIL-2R in P₂ group was 97±29, 226±80 in P₃ group, 194±23 in P₄ group and (111±30)×10³ u/L in control group (F: 9.19; P <0.01). The mean of TNF- α in P₂ group was 1.12±0.2, 3.67±1.96 in P₃ group, 1.30±0.25 in P₄ group and (0.40±0.19) μ g/L in control group (F: 13.56; P <0.01). The mean of IFN- γ was 360±20 in P₂ group, 486±15 in P₃ group, 259±19 in P₄ group and (16±2) ng/L in control group (F: 17.25, P <0.01). This indicated that the mean concentrations of sIL-2R, TNF- α and IFN- γ had a significant difference between different groups (P <0.01). Except in P₂ group, the mean concentration of sIL-2R between other groups of AE patients and controls had a significant difference (P <0.05), so was between P₂ and other 2 groups of AE. The mean concentration of TNF- α in P₃ group was the highest and had a significant difference from the other 3 groups (P <0.01). The mean concentration of IFN- γ in all patients was higher than that in control group (P <0.01), but there was no difference between AE groups (P >0.05). Table 1 summaries the comparison of the Q value of mean sIL-2R, TNF- α , IFN- γ between each two groups.

DISCUSSION

Ninety-five percent of primary foci of AE locate in the liver. They proliferate through exogenous budding and metastasize from the primary location to distant sites. At the early stage of AE,

Table 1 Comparison of Q value of mean sIL-2R, TNF- α , IFN- γ between each two groups

	P ₂ and P ₃	P ₂ and P ₄	P ₃ and P ₄	P ₂ and C	P ₃ and C	P ₄ and C
sIL-2R	6.19 ^b	4.64 ^a	1.56	0.64	5.56 ^b	4.00 ^a
TNF- α	5.99 ^b	0.41	5.58 ^b	1.7	7.69 ^b	2.11
IFN- γ	0.28	1.72	2	7.98 ^b	8.26 ^b	6.26 ^b

^a $P < 0.05$, P₂ vs P₄, P₄ vs C for sIL-2R; ^b $P < 0.01$, P₂ vs P₃, P₃ vs C for sIL-2R; P₂ vs P₃, P₃ vs P₄, P₃ vs C for TNF- α ; P₂ vs C, P₃ vs C, P₄ vs C, for IFN- γ .

the main pathologic manifestation was limited to vesicles with a few millimeters in diameter, while hepatic ultrasound scanning showed limited nodes. Next AE lesions infiltrated, without well-defined limits, and tended to extend to a large area of the liver. The infiltration, which is similar to some malignant hepatic neoplasms, could bring about stenoses of intrahepatic bile ducts, the hepatic veins and portal branches. Following parasite reproduction, necrosis would occur and gave rise to a large central cavity containing gelatinous effusion with debris, bile and sometimes pus. Although TNM-system has some defect for the classification of liver cancers^[7], it is still considered authoritative, because it could reflect the size of tumor, growing pattern, encapsulation of tumor, daughter nodules (including microscopic nodules), vascular invasion, or biliary involvement and metastases^[8]. AE is similar to a malignant hepatic tumor in growth and pathologic process, however there has been no standard classification of AE by now. In reference to the standardization of liver cancer in the present study, AE was divided into 3 types, namely parasite location in the liver (type P), involvement of adjacent organs (type I), and metastasis (type M). Type P was further divided into 5 stages: P₀: no detectable tumor in the liver; P₁: single lesion involving <2 segments without intra-hepatic vascular or biliary involvement; P₂: single lesion involving 2 segments with intra-hepatic vascular or biliary involvement or single lesion involving 3 or 4 segments without intra-hepatic vascular or biliary involvement; P₃: single lesion involving 3 to 5 segments with intra-hepatic vascular or biliary involvement or multiple lesions without intra-hepatic vascular or biliary involvement; P₄: single lesion involving 6 to 8 segments or multiple lesions with intra-hepatic vascular or biliary involvement. Type I was also divided into 3 stages: I₀: no regional involvement; I₁: regional involvement of only one contiguous organ or tissue; I₂: regional involvement of several organs or tissues (> 1). There were a single lesion involving 2 segments in P₂ and P₁ groups with ultrasound image locating multiple nodule lesions, a single lesion involving 3-5 segments with heterogeneous hyper-reflective image in P₃ group; there were multiple lesions involving 3-5 segments and intra-hepatic vascular or biliary involvement with pseudocystic sonogram of central necrosis in P₄ group. Besides involvement of portal vein and gallbladder, the pathological process of liver involved 3-5 segments with pseudocystic sonogram of central necrosis in type I, which belonged to mid- and late stages of the disease. Since the late 1970 s, ultrasound has been used for detecting pathological lesions due to a number of parasitic infections including cystic echinococcosis. The manifestations of B ultrasound of AE were local multiple echogenic nodules in early stage and large non-heterogeneous hyperreflective lesion or pseudo-cystic image in mid- or late stage. B ultrasound could also reflect the pathological process of AE^[9].

In the early 1990 s, it was found that Th₁ cytokines had a role against AE infection and a relation with the slow growth stage of tumor or parasites. IL-2 secreted by CD₄⁺ T lymphocytes induced and activated by its antigens, reinforced host immunity and had anti-tumor activities or restrained growth of parasites^[10]. Its activity is dependent on expression of mL-2R (membrane

interleukin-2 receptor), which can block IL-2. Due to the action of protein lyase at special sites, mL-2R is partly incised and chopped off in blood, forming the so-called sIL-2R. It also has activity of blocking IL-2R and plays a negative regulation role in immune response of tumor and parasites, thus promoting the growth of tumor and parasites. Therefore sIL-2R level could also act as an index of tumor stage^[11]. As shown in Table 1 except for P₂ group, the mean of sIL-2R between other 2 groups of AE and controls had a significant difference ($P < 0.05$), so was the difference between P₂ and other 2 groups of AE ($P < 0.05$, $P < 0.01$). It could be rationally explained that IL-2 played a role in inhibiting worms in early stage or in stable status of AE, while low level of sIL-2R occurred in blood. Per contra, high-level of sIL-2R in blood means AE in progression stage.

TNF is secreted by macrophages and B lymphocytes and the former is called TNF- α and the latter TNF- β . Both have similar structures and functions, and act on the same acceptor. They could strengthen phagocytic ability of neutrophils. TNF could inhibit reproduction of some protozoa and decrease their density in blood. It could activate phagocytes, depending on nitric oxide that acts on parasites. However, the pathological process of brain tissue of patients with encephalic-malaria, omphalos lesion and vascular hemorrhagic necrosis, was related to the high level of TNF in blood^[12]. The mean concentration of TNF- α in P₃ group was the highest ($P < 0.01$) and had a significant difference from other 3 groups ($P < 0.01$). P₃ stage was the key time of AE from early stage to mid and late stages and the tissues appeared severe damage at this stage. It is obvious that TNF could participate in and exacerbate the pathological process of AE. But accompanying serious tissue necrosis, serum TNF concentration was also decreased in cases of P₄ group. This seems to be related with TNF location, in other words, it depends more on TNF concentration in local tissue. It was reported that TNF-mRNA was expressed in cells of the periparasitic granuloma in AE patients, and this particular expression was observed only in those patients with severe fertile lesions and associated with centro-granulomatous necrosis. No cytokine mRNA expression was observed in patients with an abortive disease^[13]. It was proved that TNF- α could inhibit growth of alveolar echinococcosis in experimental mice. In fact, TNF- α plays a complex role in patients with AE. But in cases of P₄ group, accompanying serious tissue necrosis, TNF value was also decreased and its mechanism still remains to be elucidated.

IFN- γ is induced by antigen and it could inhibit Th₂ cells to secrete in defence against parasites. It could fortify phagocytic function of macrophages and restrict multiplication of metacestodes in mice. In this study, the mean concentration of IFN- γ in any group of AE patients was higher than that in control group ($P < 0.01$), but there was no difference between AE groups ($P > 0.05$). This indicated the efficacy of IFN- γ was limited on inhibiting AE growth in humans. Even though IFN- γ inhibited metacestode growth in mice with AE at a low dose^[14], when it was used in combination with mebendazole or nitric oxide which plays a role in host defense mechanisms in human hydatidosis, it was effective for patients with AE^[15,16]. So IFN- γ depends on the synergism of chemical medicines or other factors to produce curative effects on AE.

REFERENCES

- 1 **Craig PS**, Giraudoux P, Shi D, Bartholomot B, Barnish G, Delattre P, Quere JP, Harraga S, Bao G, Wang Y, Lu F, Ito A, Vuitton DA. An epidemiological and ecological study of human alveolar echinococcosis transmission in south Gansu, China. *Acta Trop* 2000; **77**: 167-177
- 2 **Craig PS**, Deshan L, Macpherson CN, Dazhong S, Reynolds D, Barnish G, Gottstein B, Zhirong W. A large focus of alveolar

- echinococcosis in central China. *Lancet* 1992; **340**: 826-831
- 3 **Liance M**, Bresson-Hadni S, Meyer JP, Houin R, Vuitton DA. Cellular immunity in experimental *Echinococcus multilocularis* infection. I. Sequential and comparative study of specific *in vivo* delayed-type hypersensitivity against *E. multilocularis* antigens in resistant and sensitive mice. *Clin Exp Immunol* 1990; **82**: 373-377
 - 4 **Bresson-Hadni S**, Liance M, Meyer JP, Houin R, Vuitton DA. Cellular immunity in experimental *E. multilocularis* infection-II. *Clin Exp Immunol* 1990; **82**: 378-383
 - 5 **Yang SQ**. Hygienic statistics, 2nd ed. Beijing: *Chinese natural hygienic publishing house* 1990: 41
 - 6 **Yang SQ**. Hygienic statistics, 2nd ed. Beijing: *Chinese natural hygienic publishing house* 1990: 46
 - 7 **Chiappa A**, Zbar AP, Podda M, Audisio RA, Bertani E, Biella F, Paties C, Staudacher C. Prognostic value of the modified TNM (Izumi) classification of hepatocellular carcinoma in 53 cirrhotic patients undergoing resection. *Hepatogastroenterology* 2001; **48**: 229-234
 - 8 **Zhang Z**, Wu M, Shen F. Significance of TNM classification in prognostic evaluation of hepatocellular carcinoma following surgical resection. *Zhonghua Zhongliu Zazhi* 1999; **21**: 293-295
 - 9 **Shi DZ**, Li FR, Bartholomot B, Craig PS, Vuitton DA. The patterns of ultrasound of hepatic alveolar echinococcosis and relationship between pathology and sIL-2R in serum. *Shijie Huaren Xiaohua Zazhi* 2000; **8**: 821-822
 - 10 **Josimovic-Alasevic O**, Feldmeier H, Zwingenberger K, Harms G, Hahn H, Shrisuphanunt M, Diamantstein T. Interleukin 2 receptor in patients with localized and systemic parasitic diseases. *Clin Exp Immunol* 1988; **72**: 249-254
 - 11 **Murakami S**, Hirayama R, Satomi A, Okubo K, Matsuki M, Sakata H, Tsuji Y. Serum sIL-2R concentrations in patients with breast cancer. *Breast Cancer* 1997; **4**: 25-28
 - 12 **Grau GE**, Taylor TE, Molyneux ME, Wirima JJ, Vassalli P, Hommel M, Lambert PH. Tumor necrosis factor and disease severity in children with falciparum malaria. *N Engl J Med* 1989; **320**: 1586-1591
 - 13 **Bresson-Hadni S**, Petitjean O, Monnot-Jacquard B, Heyd B, Kantelip B, Deschaseaux M, Racadot E, Vuitton DA. Cellular localizations of interleukin-1 beta, interleukin-6 and tumor necrosis factor-alpha mRNA in a parasitic granulomatous disease of the liver, alveolar echinococcosis. *Eur Cytokine Netw* 1994; **5**: 461-468
 - 14 **Liance M**, Ricard-Blum S, Emery I, Houin R, Vuitton DA. *Echinococcus multilocularis* infection in mice: *in vivo* treatment with a low dose of IFN-gamma decreases metacestode growth and liver fibrogenesis. *Parasite* 1998; **5**: 231-237
 - 15 **Schmid M**, Samonigg H, Stoger H, Auer H, Sternthal MH, Wilders-Truschnig M, Reisinger EC. Use of interferon- γ and mebendazole to stop the progression of alveolar hydatid disease: case report. *Clin Infect Dis* 1995; **20**: 1543-1546
 - 16 **Touil-Boukoffa C**, Bauvois B, Sanceau J, Hamrioui B, Wietzerbin J. Production of nitric oxide (NO) in human hydatidosis: relationship between nitrite production and interferon-gamma levels. *Biochimie* 1998; **80**: 739-744

Edited by Wang XL and Zhu LH Proofread by Xu FM

Effect of arsenic trioxide on human hepatocarcinoma in nude mice

Hong-Yu Xu, You-Lin Yang, Shu-Mei Liu, Li Bi, Shu-Xiang Chen

Hong-Yu Xu, You-Lin Yang, Li Bi, Shu-Mei Liu, Shu-Xiang Chen,
Department of Gastroenterology, The First Hospital of Harbin Medical
University, Harbin 150001, Heilongjiang Province, China

Li Bi, Department of Laboratory, The First Hospital of Harbin
Medical University, Harbin 150001, Heilongjiang Province, China

Correspondence to: Dr. Hong-Yu Xu, Gastroenterology, Department,
The First Hospital of Harbin Medical University, Harbin 150001,
Heilongjiang Province, China. xuhrain@yahoo.com.cn

Telephone: +86-451-3643849-5263

Received: 2003-10-09 **Accepted:** 2003-11-19

Abstract

AIM: To study the effect of arsenic trioxide (As_2O_3) on human
hepatoma cell line BEL-7402 *in vivo*.

METHODS: Human hepatoma cell line BEL-7402 cultured
in vitro was inoculated into nude mice and arsenic trioxide,
5-Fu and saline were injected into abdominal cavity of the
nude mice respectively. The volumes of tumor and general
conditions of the nude mice and structural changes of the
liver and kidney were observed. Morphologic changes were
studied under electron microscope. Expression of AFP was
investigated by immunohistochemical method.

RESULTS: As_2O_3 could inhibit the growth of tumor. The tumor
growth inhibitory rate in mice treated with 2.5 mg/kg As_2O_3
was 53.42% on the tenth day. The tumor growth inhibitory
rate in mice treated with 5 mg/kg As_2O_3 was 79.28% on the
fifth day and 96.58% on the tenth day respectively. As_2O_3 did
not damage the liver and kidney of nude mice, or affect the
blood system. Typical apoptotic morphological changes
were found under electron microscope, and the change of
mitochondria was obvious. The expression rate of AFP
declined after treatment.

CONCLUSION: Arsenic trioxide can induce apoptosis of
human hepatoma cells, and inhibit proliferation of tumor
with no obvious side effects on liver and kidney.

Xu HY, Yang YL, Liu SM, Bi L, Chen SX. Effect of arsenic trioxide
on human hepatocarcinoma in nude mice. *World J Gastroenterol*
2004; 10(24): 3677-3679

<http://www.wjgnet.com/1007-9327/10/3677.asp>

INTRODUCTION

Liver cancer is one of the most aggressive malignancies and
the fourth leading cause of cancer death in China, and the vast
majority of patients die within the first year after diagnosis. There
is still no effective therapeutic modalities. Surgical resection is
the only potentially curative option, but it is not feasible in most
patients because of early spread of the disease. Since arsenic
trioxide (As_2O_3) has recently been recognized as an effective
treatment for patients suffering from acute promyelocytic
leukemia (APL)^[1-5], it has also been hypothesized to be effective
on some solid tumors^[6,7]. As_2O_3 has been shown to have dual
effects on human hepatocellular carcinoma (HCC) cell lines
in vitro^[8], including induction of apoptosis and inhibition of

proliferation^[9,10]. However it is not clear whether As_2O_3 has the
same effect *in vivo*. We established an HCC nude mice model to
evaluate anti-tumor effect of As_2O_3 *in vivo*, which might provide
an experimental basis for its clinical application to the treatment
of patients with HCC.

MATERIALS AND METHODS

Chemicals and reagents

As_2O_3 was purchased from Harbin Yida Medical Co (Harbin, China).
Murine monoclonal antibody and antimouse rabbit polyclonal
antibody were purchased from Maixin Co., Fuzhou, China.

Cell line and preparation

Human hepatoma BEL-7402 cells were purchased from the Cell
Institute of Chinese Academy of Sciences and maintained in
our laboratory. All media were supplemented with 100 mL/L
heat inactivated fetal bovine serum, penicillin G (100 IU/mL), and
streptomycin (100 μ g/mL). The cells were incubated at 37 °C in a
humidified atmosphere with 50 mL/L CO_2 and grown as monolayers
in RPMI 1640 medium supplemented with 80 mL/L calf serum.

Animals

Five-week-old male nude mice weighing 17-20 g were used for
subcutaneous implantation. All animals were housed in semisterile
microisolator cages with autoclaved bedding, maintained on a
12-h light/dark cycle and given food and water. The experimental
protocol was approved by the Experimental Animal Center of
Chinese Academy of Sciences (identification No. Scfk11-6A-
0006) in accordance with the national guidelines for animal care
and use of laboratory animals.

Tumor induction in nude mice

Human hepatoma BEL-7402 tumor cells were grown in
monolayer culture. The exponentially growing BEL-7402 cells
in culture flasks were harvested, and adjusted to the concentration
of 1×10^7 /mL. For subcutaneous tumor formation, 200 μ L of cells
was injected subcutaneously into the flanks of the animals
(donor mice). These mice were randomly divided into four
groups: negative control group (saline), and groups of As_2O_3
(2.5 mg/kg, 5 mg/kg), 5-Fu (2.5 g/L). Each group was injected
with the same volume of saline, As_2O_3 (2.5 mg/kg, 5 mg/kg), and
5-Fu (2.5 mg/mL) respectively, once a day for 10 d.

Tumor assessment

The tumor was measured with a caliper in all three perpendicular
dimensions on the 1st, 5th and 10th d of treatment, and tumor
volume was calculated using the following formula: volume =
length \times width \times depth/2. All animals were killed and underwent
complete examination of abdominal cavity after ten days. The
liver and kidney were resected and examined under microscope.
The tumor mass was isolated and weighed. The inhibitory rate
of tumor was evaluated using the following formula: inhibitory
rate of tumor (%) = (1-mean tumor weight in experiments / mean
tumor weight in controls) \times 100%.

Morphologic observation

Tumor specimens were fixed with 4 g/L formaldehyde and
wrapped with wax, then stained with HE.

Transmission electron microscopy

The samples were prefixed in 25 g/L glutaraldehyde, then in 10 g/L OsO₄, dehydrated in ethanol series, and replaced in propene oxide. The samples were examined with a JEM-1220 transmission electron microscope.

Immunohistochemistry

AFP protein was detected with SABC method. Tumor specimens were incubated with 3 mL/L hydrogen peroxide in methanol for 30 min to block endogenous peroxidase activity, then washed in PBS and incubated in 100 mL/L normal goat serum for 20 min to reduce nonspecific antibody binding. Specimens were then incubated with a 1:50 dilution of murine monoclonal antibody against human AFP oncoprotein overnight at 4 °C, followed by three washes with PBS, then incubated with biotinylated rabbit antimouse polyclonal antibody at a dilution of 1:100 for 30 min followed by 3 washes. Slides were then treated with streptavidin-peroxidase reagent for 30 min at a dilution of 1:100 and washed with PBS 3 times. Finally, slides were incubated in phosphate-buffered saline containing diaminobenzidine and 10 mL/L hydrogen peroxide for 10 min, counterstained with hematein, and mounted.

Blood routine test

Venous blood was taken from the orbital venous plexus of the mouse before the animal was killed. The blood routine test was done.

Statistical analysis

Data were presented as mean±SD, the differences between the rates of different groups were analyzed by χ^2 test.

RESULTS

General condition

The tumor node of the saline group was larger on the 5th and tenth days than on the first day. The appetite of mice was normal, as well as the body mass. The stool was normal. The tumor had no obvious increase after five days in 5-Fu group. The mice did not eat or drink, had a low spirit. The color of the skin turned red, and more weight was lost. The mice died gradually. The mice in As₂O₃ group was in better spirit and just the color turned red. Only two mice had diarrhea (Table 1).

Morphologic changes

The morphologic changes were observed by microscopy. Large areas of necrosis were seen under microscope. In saline group of mice BEL-7402 cells in areas of non-necrosis proliferated rapidly. The mitotic nuclei were more frequently seen. Large areas of necrosis could also be seen in the 5-Fu group, and also in the higher concentration As₂O₃ group. Nuclei appeared condensation. The liver system and kidney were normal in the low As₂O₃ group. A few vacuolar degeneration were found in the liver of the higher As₂O₃ group, but the kidney was normal. The nucleocytoplasmic ratio increased and microvilli were identified on the surface of cells in saline group. The distortion of the nuclei was frequent.

There were many endoplasmic reticula and mitochondria. In As₂O₃ group, the cell nuclei became round and smaller. The aberrant cells were fewer. The microvilli were much decreased. The intact cell membrane, nuclear condensation and apoptotic body formation were seen. The changes were more obvious in the high concentration As₂O₃ group.

Effect on blood system

White blood cells, hemoglobin, and blood platelets had no significant difference between saline group and As₂O₃ group (Table 2).

Table 2 Routine blood examination results (mean±SD)

Groups	Number	WBC (×10 ¹⁰ /L)	Hgb (g/L)	PLT) (×10 ⁹ /L)
Saline	10	1.05±0.12	140.24±13.21	221.65±70.34
As ₂ O ₃ (2.5 mg/kg)	10	1.13±0.16	138.67±13.17	231.75±68.48
As ₂ O ₃ (5 mg/kg)	10	1.21±0.16	142.58±15.29	246.38±60.45

Expression of AFP protein

The expression of AFP was significantly lower in As₂O₃ group than in saline group ($P<0.01$, Table 3).

Table 3 Expression of AFP protein (mean±SD)

Group	Number	AFP (%)
Saline	10	48.32±4.56
As ₂ O ₃ (2.5 mg/kg)	10	29.78±3.10 ^b
As ₂ O ₃ (5 mg/kg)	10	22.26±2.31 ^b

^b $P<0.01$ vs saline group.

DISCUSSION

Recent clinical studies in China have shown that arsenic trioxide is an effective and relatively safe drug in the treatment of acute promyelocytic leukemia^[1,2,11,12]. Chen^[8] found that arsenic trioxide could trigger apoptosis of APL cell line NB4 cells, associated with downregulation of Bcl-2 gene expressions and modulation of PML-RAR alpha chimeric protein.

Experimental studies on antitumor effect were carried out in solid tumor, cancers of the lung, esophagus, stomach, colon, pancreas, breast, cervix^[13,14]. It has been demonstrated that As₂O₃ could inhibit the proliferation of HCC cells and induce apoptosis of HCC *in vitro*^[8,15]. Antitumor function of As₂O₃ *in vivo* was limited. We studied the action and mechanism of As₂O₃ in human hepatocarcinoma of nude mice. Our results showed that tumor mass in As₂O₃ group was smaller than that in saline group after 5 d, but there was no significant difference between the two groups ($P>0.05$), the growth in As₂O₃ group became slower from the 6th d. The inhibitory rate of tumor was 53.42%. The tumor node of mice treated with 5 mg/kg As₂O₃ became smaller than that of saline group. There were obvious differences between the two groups. The inhibitory rate of

Table 1 Inhibitory action of arsenic trioxide on tumor mass (mean±SD)

Groups	Number	Volume d 1	Volume d 5	Volume d 10	Mouse mass (g)	Inhibitory rate (%) 5 th d	Inhibitory rate (%) 10 th d
Saline	10	0.123±0.052	0.234±0.072	0.415±0.084	23.07±3.14		
5-Fu	10	0.113±0.060	0.134±0.040	14.07±2.29		86.85	
As ₂ O ₃ (2.5 mg/kg)	10	0.102±0.041	0.218±0.099	0.238±0.043 ^b	20.50±1.95		53.42
As ₂ O ₃ (5 mg/kg)	10	0.098±0.030	0.121±0.038	0.103±0.042 ^b	20.28±1.63	79.28	96.58

^b $P<0.01$ vs saline group.

tumor was 79.28% on the 5th d and 96.58% on the 10th d. Our concern was the toxicity of As₂O₃. It has been proved that it was not so poisonous in experiments and clinic. The toxicity depended on its dosage and the time of its use. As₂O₃ could damage normal cells when treating APL or others^[2] at 0.1-0.2 μmol/L. Experiments showed that they had no effect on stem cells at this concentration. At 3.0 μmol/L As₂O₃ had teratogenic effect on mouse embryo. The results showed it had no effect on embryo growth, development and differentiation. Our study also showed that the mice were normal in higher As₂O₃ group. The weight of mice had no significant difference between As₂O₃ group and saline group. The number of WBC, RBC, PLT was not obviously different between the two groups. There was a higher inhibitory rate of tumor in 5-Fu group (86.8%), but the weight of nude mice was reduced. The mice died gradually in 5-Fu group. Although the inhibitory rate of tumor was higher in 5-Fu group, the mice did not eat or drink. The weight was lost, and dystrophy could inhibit the growth of tumor.

AFP is a specific marker of liver cancer. BEL-7402 cells could secrete AFP. The expression rate of AFP was decreased after treatment. It showed that the level of tumor cell differentiation could be raised and the number of tumor cells was reduced after treatment. The divisions of tumor cells were decreased and apoptotic cells could be found in the lower As₂O₃ group. Large areas of necrosis could be seen in 5-Fu group, but survival tumor cells grew vigorously. It showed that 5-Fu could inhibit tumor growth due to its cytotoxic function. As₂O₃ could induce apoptosis of tumor cells.

We observed the morphologic changes of apoptosis by TEM in As₂O₃ group, the nucleocytoplasmic ratio became smaller, nuclei appeared round, mitochondria became distended, cells wrinkled, nuclear condensation and apoptotic body formation occurred. Early and obvious changes occurred in mitochondria, suggesting that As₂O₃ is toxic to mitochondria. The change of mitochondria could induce apoptosis. Further studies on the mechanism of mitochondria denaturation in order to prove that As₂O₃ could treat HCC are needed.

In conclusion, arsenic trioxide can induce apoptosis of human hepatocarcinoma cells and inhibit their proliferation. It has no side effects on the liver, kidney and blood system.

REFERENCES

- 1 **Zhang P**, Wang SY, Hu LH, Shi FD, Qiu FQ, Hong LG, Han XY, Yang HF, Song YZ, Liu YP, Zhou J, Jing ZI. Treatment of acute promyelocytic leukemia with intravenous arsenic trioxide. *Zhonghua Xueyexue Zazhi* 1996; **17**: 58-60
- 2 **Andre C**, guillemin MC, Zhu J, Koken MH, Quignon F, Herve L, Chelbi Alix MK, Dhumeasx D, Wang ZY, Degos L, Chen Z, De The H. The PML and PML/RARalpha domains from autoimmunity to molecular oncology and from retinoic acid to arsenic. *Exp Cell Res* 1996; **229**: 253-260
- 3 **Wang ZY**. Development of arsenical clinical application and study of arsenical mechanism. *Zhonghua Xueyexue Zazhi* 1996; **17**: 57
- 4 **Shen ZX**, Chen GQ, NI JH, Li XS, Xiong SM, Qin QY, Zhu J, Tang W, Sun GL, Yang KQ, Chen Y, Zhou L, Fang ZW, Wang YT, Zhang P, Zhang TD, Chen SJ, Chen Z, Wang ZY. Use of arsenic trioxide in the treatment of Acute promyelocytic leukemia II. Clinical efficacy and pharmacokinetics in relapsed patients. *Blood* 1997; **89**: 3354-3360
- 5 **Konig A**, Wraze L, Warrell RP Jr, Rivi R, Pandolfi PP, Jakubowski A, Gabrilove JL. Comparative activity of melarsoprol and arsenic trioxide in chronic B-cell leukemia lines. *Blood* 1997; **90**: 562-570
- 6 **Tan LJ**, Chen XY, Zhang L, Tang XM, Shen ZY, Cai WJ. Study on the proliferative inhibition of human esophageal cancer cells with treatment of DMSO and As₂O₃. *Shanghai Dier Yikedaxue Xuebao* 1999; **19**: 5-8
- 7 **Tu SP**, Jiang SH, Tan JH, Jiang XH, Qiao MM, Zhang YP, Wu YL, Wu YX. Proliferation inhibition and apoptosis induction by arsenic trioxide on gastric cancer cell SGC-7901. *Shijie Huaren Xiaohua Zazhi* 1999; **7**: 18-21
- 8 **Chen HY**, Liu WH, Qin SK. Induction of arsenic trioxide on apoptosis of hepatocarcinoma cell lines. *Shijie Huaren Xiaohua Zazhi* 2000; **8**: 532-535
- 9 **Guo WJ**, Yu EX, Zheng SG, Shen ZZ, Luo JM, Wu GH, Xia SA. Study on the apoptosis and cell cycle arrest in human liver cancer SMMC7721 cells induced by Jianpiliqi herbs. *Shijie Huaren Xiaohua Zazhi* 2000; **8**: 52-55
- 10 **Shen YF**, Zhuang H, Shen JW, Chen SB. Cell apoptosis and neoplasms. *Shijie Huaren Xiaohua Zazhi* 1999; **7**: 267-268
- 11 **Feng CQ**, Ma WL, Zheng WL. Research advances on effect of arsenic trioxide on tumor. *Aizheng* 2002; **21**: 1386-1389
- 12 **Liu Q**, Hilsenbeck S, Gazitt Y. Arsenic trioxide-induced apoptosis in myeloma cells: p53-dependent G1 or G2/M cell cycle arrest, activation of caspase-8 or caspase-9, and synergy with APO2/TRAIL. *Blood* 2003; **101**: 4078-4087
- 13 **Kanzawa T**, Kondo Y, Ito H, Kondo S, Germano I. Induction of autophagic cell death in malignant glioma cells by arsenic trioxide. *Cancer Res* 2003; **63**: 2103-2108
- 14 **Huang SG**, Kong BH, Yang RF, Jiang S. Primary study of arsenic trioxide inhibits abdomino-metastatic tumor formation of human ovarian carcinoma in nude mice and its mechanisms. *Aizheng* 2002; **21**: 401-404
- 15 **Yu D**, Wang Z, Zhu L, Chew EC. Nuclear matrix associated protein PML: an arsenic trioxide apoptosis therapeutic target protein in HepG2 cells. *Chin Med J* 2003; **116**: 93-98

Edited by Wang XL and Zhu LH Proofread by Xu FM

Primary small cell carcinoma of esophagus: Report of 9 cases and review of literature

Zhu Wu, Jian-Yang Ma, Jun-Jie Yang, Yong-Fan Zhao, Shang-Fu Zhang

Zhu Wu, Jian-Yang Ma, Jun-Jie Yang, Yong-Fan Zhao, Department of Thoracic and Cardiovascular Surgery, West China Hospital, Sichuan University, Chengdu 610041, Sichuan Province, China

Shang-Fu Zhang, Department of Pathology, West China Hospital, Sichuan University, Chengdu 610041, Sichuan Province, China

Correspondence to: Dr. Zhu Wu, Department of Thoracic and Cardiovascular Surgery, West China Hospital, Sichuan University, Chengdu 610041, Sichuan Province, China. zhuwu36555@vip.sina.com
Telephone: +86-28-85130069

Received: 2004-01-15 **Accepted:** 2004-02-24

Abstract

AIM: To analyze the clinical manifestations, pathological features and treatment of primary small cell carcinoma (SCC) of the esophagus and to review the literature on this entity.

METHODS: The records of 9 patients with primary esophageal small cell carcinoma were examined and the demographic data, presenting symptoms, methods of tumor diagnosis, and types of treatment given, response to treatment, pathologic findings, and clinical outcome were reviewed. Features of mixed patterns of histological differentiation and lymph node metastases were specifically sought.

RESULTS: All the patients reported dysphagia, weight loss and chest pain as the initial symptoms. In 5 cases the tumors were located in the mid-esophagus, 3 cases in the lower third of the esophagus and 1 case in the upper third. The average length of esophageal involvement was 5 cm. They underwent radical resection, regional lymph node clearance and esophageal-stomach anastomosis in thorax or at neck. Two patients had a stage IIa disease, five had a stage IIb disease, and the other two had a stage III disease of International Union Contrele Cancer (UICC). All of them were histologically and immunohistochemically confirmed SCC of esophagus. Immunohistochemical staining for neuron-specific enolase (NSE), synaptophysin (Syn) and chromogranin A exhibited strong immunoreactivity in all specimens. Three of the nine resected specimens showed foci of squamous cell carcinoma *in situ*. Metastasis was present in 7 of 9 adjacent lymph nodes. All the patients survived the operations and made an uneventful postoperative recovery. They received adjuvant systemic chemotherapy and local radiation therapy after discharge. During follow-up, three patients developed multiple liver, brain, lung and bone metastases and died between 5 and 18 mo after the diagnosis. Three patients developed widespread metastasis disease and died between 18 and 37 mo after the diagnosis. There was no local tumor recurrence in these 6 patients. The other three patients were lost during follow-up.

CONCLUSION: Primary small cell carcinoma of the esophagus is a rare but very malignant tumor. Radical resection combined with chemotherapy and radiotherapy is helpful in limited stage cases.

Wu Z, Ma JY, Yang JJ, Zhao YF, Zhang SF. Primary small cell carcinoma of esophagus: Report of 9 cases and review of literature. *World J Gastroenterol* 2004; 10(24): 3680-3682
<http://www.wjgnet.com/1007-9327/10/3680.asp>

INTRODUCTION

Primary small cell carcinoma (SCC) of the esophagus is a rare tumor characterized by early dissemination and poor prognosis if untreated^[1]. To our knowledge the standard of treatment for esophageal SCC has not been defined yet due to the paucity of cases. Treatments such as operation alone^[2], local radiotherapy^[3], chemotherapy alone^[4], or operation with adjuvant therapy^[5] have been reported. Here we described the clinical manifestations, pathological feature and treatment of 9 patients with primary esophageal SCC treated at our institution between January 1985 and December 2000 and reviewed the available literature on this entity.

MATERIALS AND METHODS

Patients with a diagnosis of SCC of the esophagus were identified from clinical and pathologic records from a 16-year period. The clinical, radiographic, and pathologic findings were reviewed and all patients in which esophageal invasion by a primary bronchial SCC could not be ruled out were excluded from the study. A total of 9 patients identified from the records were considered to have a primary esophageal SCC.

The demographic data, presenting symptoms, methods of tumor diagnosis, staging procedures done, types of treatment given, response to treatment, pathologic findings, and clinical outcome were recorded. Histological sections were reviewed to confirm the diagnosis of SCC. Features of associated carcinoma, mixed patterns of histological differentiation, and lymph node metastases were specifically sought. Immunohistochemical staining was done in differential diagnosis.

RESULTS

The study group consisted of 9 consecutive patients. There were 6 men and 3 women, with a mean age of 56 years (range from 45 to 66). All the patients reported dysphagia, weight loss and chest pain as the initial symptoms. Barium swallow, flexible esophagoscopy and biopsy established their diagnosis. Preoperative work-up excluded distant metastasis diseases in all the patients. There was no evidence of a primary bronchogenic small-cell tumor on chest radiograph. Liver ultrasonography was done before resection to exclude liver metastases. Calcium, phosphate, and alkaline phosphatase levels were measured in an attempt to exclude occult bone metastases. In 5 cases the tumors were located in the midesophagus, 3 cases in the lower third of the esophagus, and 1 case in the upper third. The average length of esophageal involvement was 5 cm (range, 3 to 7 cm).

These patients underwent radical resection, regional lymph node clearance and esophageal-stomach anastomosis in thorax or at neck. During the curative operations, all the tumors were



Figure 1 Immunohistochemical staining in SCC of esophagus (LSAB×145). A: NSE staining; B: Syn staining; C: chromogranin A staining.

confirmed to be confined to the esophagus, and the adjacent lymph nodes were either uninvolved or less than 2 cm in the greatest dimension, discrete, and within the vicinity of the primary tumor. Based on the intraoperative findings and pathological assessment, two patients had a stage IIa disease, five had a stage IIb disease, and the other two had a stage III disease of UICC. All the patients were histologically and immunohistochemically confirmed to have a SCC of esophagus. The histological criteria for small cell lung carcinoma (SCLC) proposed by the World Health Organization were used. Immunohistochemical staining for neuron-specific enolase (NSE)^[6], synaptophysin (Syn)^[7] and chromogranin A^[8] exhibited strong immunoreactivity in the specimens, which indicated that neurosecretory granules were positive in the tumor cells (Figure 1). Three of the nine resected specimens showed foci of squamous carcinoma *in situ*. All the mucosal margins were negative for tumors. Metastasis was present in 7 of 9 adjacent lymph nodes.

All the patients survived the operation and made an uneventful postoperative recovery. They received adjuvant systemic chemotherapy and local radiation therapy after discharge. The regimen of the multi-drug chemotherapy was combined with cisplatin (DDP), fluorouracil (5-Fu) and bleomycin (BLM) of 4 cycles, alternating every 3 wk. They also received radiation of the tumor bed and regional lymph nodes with the doses of 5 000 cGy at a rate of 1 000 cGy/wk. During the follow-up, three patients developed multiple liver, brain, lung and bone metastases and died between 5 and 18 mo after the diagnosis. Three patients developed widespread metastasis diseases and died between 18 and 37 mo after the diagnosis. There was no local tumor recurrence in these 6 patients. The other three patients were lost during follow-up.

DISCUSSION

Undifferentiated SCC is an aggressive tumor most frequently described in the bronchial tree, which makes up approximately 15% of all lung cancers^[9]. The most common extrapulmonary sites of SCC are the salivary glands, pharynx and larynx, esophagus, stomach, pancreas, colon, rectum, skin and cervix^[4]. To our knowledge, more than 200 cases of esophageal SCC have been described in the medical literature^[10]. The incidence of esophageal SCC ranges between 0.4-7.6% of all esophageal malignancies in different regions^[11]. In our institution, these 9 patients represented about 1% of all patients with esophageal tumors between January 1985 and December 2000.

The cellular origins of esophageal SCC have been the subject of intense speculation and debate. Esophageal SCC was initially thought to arise from argyrophilic Kulchitsky cells in esophageal mucosa^[12]. These cells have the ability to synthesize and store amines and to decarboxylate some amino acids: a feat that gave rise to the term amine precursor uptake, decarboxylation

(APUD) cells. It would now appear that esophageal SCC is of endodermal origin derived from pluripotential basal epithelial cells served as the common precursor for adenocarcinoma, squamous cell carcinoma and SCC^[13]. The small cells retain their potential for further differentiation into either mucin-producing or keratin-forming cells. This explains the coexistence of small cells, squamous and glandular elements in the same lesion. The surgical resection specimens in our group showed mixed histologic types in three out of the nine cases, all of the mixed squamous and small cell carcinomas, showed this multiple differentiation. Our findings of a high incidence of histologic heterogeneity in esophageal SCC in association with squamous carcinoma *in situ* strongly support this unified hypothesis.

Esophageal SCC may show a variety of genetic changes, including mutation of tumor-suppressor gene and loss of heterogeneity involving the genetic loci for various tumor-suppressor genes. Recent studies have shown that microsatellite instability (MSI) may be more frequent in SCC of the esophagus than in squamous-cell carcinoma of the esophagus in the development of esophageal cancer^[14]. In a previous study, we used polymerase chain reaction-polyacrylamide gel-silver stain method to investigate the presence of MSI in 3 of the 9 cases in this series and MSI was observed in 3 out of 3 cases (100%), significantly higher than squamous cell carcinoma (40.3%)^[15]. This observation suggests that the incidence of MSI and DNA replication errors may play an important role in esophageal SCC and may be an early event in esophageal SCC carcinogenesis.

Grossly, esophageal SCC was not distinguishable from esophageal squamous carcinoma. Esophageal SCC might present as an ulcerating hard tumor mass on the mucosal surface of the esophagus or as a polypoid infiltrative process growing in the submucosal layer without obvious ulceration of the mucosal surface. Microscopically, in all of the cases, the tumor was described as having a histological appearance of SCLC, consisting of round to spindle-shaped cells with scanty cytoplasm, granular nuclei, inconspicuous nucleoli, and ultrastructural and immunohistochemical evidence of neuroendocrine differentiation^[16]. The cells might be argyrophil positive with neurosecretory granules seen on electron microscopy. Immunohistologically, these cells were immunoreactive with low-molecular-weight cytokeratins and epithelial membrane antigen. Although neurosecretory granules could be identified within esophageal SCC, and they could be stained immunohistochemically for various hormones, clinical manifestations of paraneoplastic syndromes were, however, infrequent, with only scattered reports. We have not encountered paraneoplastic syndromes in the current patients.

The mean age of patients with esophageal SCC at the time of presentation, the location of esophageal SCC and presenting symptoms of esophageal SCC are similar to those of esophageal squamous cell carcinomas. But esophageal SCC is a more aggressive tumor and associated with rapid growth, and

patients usually present with widespread metastasis disease. In our series, metastasis tumor was present in 7 of 9 (78%) adjacent lymph nodes. But preoperative work-up excluded distant metastasis diseases in all the patients and all the tumors were confined to the esophagus. The resectability of these 9 cases was significantly higher than that reported by other investigators. This might be due to the advance to the advantage of early diagnosis and treatment of esophageal carcinomas.

Prospective randomized trials of therapy for esophageal SCC were unlikely given the rarity of the disease. The management of primary esophageal SCC remains controversial. Yachida *et al.*^[17], described a patient with esophageal SCC with extensive lymph node metastases. Treatment comprised a subtotal esophagectomy and extended lymph node dissection, but no chemotherapy or radiation therapy. He has survived for more than 7 years with no evidence of recurrent disease. A recent work by Casas *et al.*^[18] suggests that multimodality therapy might improve resectability and overall outcome. To allow for the evaluation of prognostic factors that influenced survival, esophageal SCC patients were grouped according to limited stage (LS), which was defined as a disease confined to the esophagus, or extensive stage (ES), which was defined as a disease that had spread beyond locoregional boundaries. There was a significant difference in survival between patients with LS and those with ES ($P < 0.0001$)^[18]. The median survival time was 8 mo for patients with LS and 3 mo for those with ES. In LS, favorable prognostic factors were the tumor size (≤ 5 cm) and the association of chemotherapy with local treatment. The best prognostic factor for ES was the feasibility of any kind of active treatment. The longest survival in our series of esophageal SCC with multimodality was 37 mo. We conclude that patients with operable diseases should be offered resection with curative intent in combination with adjuvant chemotherapy and radiation therapy.

REFERENCES

- 1 **Pantvaidya GH**, Pramesh CS, Deshpande MS, Jambhekar NA, Sharma S, Deshpande RK. Small cell carcinoma of the esophagus: the Tata Memorial Hospital experience. *Ann Thorac Surg* 2002; **74**: 1924-1927
- 2 **Mitani M**, Kuwabara Y, Shinoda N, Sato A, Fujii Y. Long-term survivors after the resection of limited esophageal small cell carcinoma. *Dis Esophagus* 2000; **13**: 259-261
- 3 **Nemoto K**, Zhao HJ, Goto T, Ogawa Y, Takai Y, Matsushita H, Takeda K, Takahashi C, Saito H, Yamada S. Radiation therapy for limited-stage small-cell esophageal cancer. *Am J Clin Oncol* 2002; **25**: 404-407
- 4 **Shamelian SO**, Nortier JW. Extrapulmonary small-cell carcinoma: report of three cases and update of therapy and prognosis. *Neth J Med* 2000; **56**: 51-55
- 5 **Makino H**, Tajiri T, Onda M, Sasajima K, Miyashita M, Nomura T, Maruyama H, Nagasawa S, Tsuchiya Y, Hagiwara N, Yamashita K, Takubo K. Effectiveness of preoperative chemotherapy using carboplatin (CBDCA) and surgery against an esophageal small cell carcinoma. *Dis Esophagus* 2002; **15**: 237-241
- 6 **Koide N**, Hiraguri M, Kishimoto K, Nakamura T, Adachi W, Miyabayashi H, Terai N, Amano J. Small cell carcinoma of the esophagus with reference to alternating multiagent chemotherapy: report of two cases. *Surg Today* 2003; **33**: 294-298
- 7 **Suzuki H**, Takayanagi S, Otake T, Ishibashi R, Osawa S, Shirai T, Takashima M, Hanai H, Kaneko E. Primary small cell carcinoma of the esophagus with achalasia in a patient in whom pro-gastrin-releasing peptide and neuron-specific enolase levels reflected the clinical course during chemotherapy. *J Gastroenterol* 1999; **34**: 378-382
- 8 **Hatori S**, Imada T, Rino Y, Takahashi M, Amano T, Kondo J. Small cell carcinoma of the esophagus: a case report. *Hepatogastroenterology* 1999; **46**: 1788-1790
- 9 **Saijo N**. Progress in treatment of small-cell lung cancer: role of CPT-11. *Br J Cancer* 2003; **89**: 2178-2183
- 10 **Madroszyk A**, Egretreau J, Martin L, Queneau PE, Bosset JF, Merrouche Y. Small-cell carcinoma of the esophagus: report of three cases and review of the literature with emphasis on therapy. *Ann Oncol* 2001; **12**: 1321-1325
- 11 **Takubo K**, Nakamura K, Sawabe M, Arai T, Esaki Y, Miyashita M, Mafune K, Tanaka Y, Sasajima K. Primary undifferentiated small cell carcinoma of the esophagus. *Hum Pathol* 1999; **30**: 216-221
- 12 **Craig SR**, Carey FA, Walker WS, Cameron EW. Primary small-cell cancer of the esophagus. *J Thorac Cardiovasc Surg* 1995; **109**: 284-288
- 13 **Ugras S**, Akpolat N, Er M, Yalcynkaya I, Karaayvaz M. Primary composite tumour with bipartite differentiation of the esophagus. *Acta Chir Belg* 2000; **100**: 39-43
- 14 **Gonzalez LM**, Sanz-Esponera J, Saez C, Alvarez T, Sierra E, Sanz-Ortega J. Case report: esophageal collision tumor (oat cell carcinoma and adenocarcinoma) in Barrett's esophagus: immunohistochemical, electron microscopy and LOH analysis. *Histol Histopathol* 2003; **18**: 1-5
- 15 **Zhao YF**, Zhang JH, Chen GD, Xin JP. Study on the microsatellite DNA instability in Chinese esophageal carcinoma. *Zhongguo Xiongxinxueguan Waike Zazhi* 2000; **7**: 32-34
- 16 **Noguchi T**, Takeno S, Kato T, Wada S, Noguchi T, Uchida Y, Kashima K, Yokoyama S. Small cell carcinoma of the esophagus: clinicopathological and immunohistochemical analysis of six cases. *Dis Esophagus* 2003; **16**: 252-258
- 17 **Yachida S**, Matsushita K, Usuki H, Wanibuchi H, Maeba T, Maeta H. Long-term survival after resection for small cell carcinoma of the esophagus. *Ann Thorac Surg* 2001; **72**: 596-597
- 18 **Casas F**, Ferrer F, Farrus B, Casals J, Biete A. Primary small cell carcinoma of the esophagus: a review of the literature with emphasis on therapy and prognosis. *Cancer* 1997; **80**: 1366-1372

Edited by Zhang JZ and Wang XL Proofread by Xu FM

Integration of *E. coli aroG-pheA* tandem genes into *Corynebacterium glutamicum tyrA* locus and its effect on L-phenylalanine biosynthesis

Dong-Xin Liu, Chang-Sheng Fan, Ju-Hong Tao, Guo-Xin Liang, Shan-E Gao, Hai-Jiao Wang, Xin Li, Da-Xin Song

Dong-Xin Liu, Chang-Sheng Fan, Ju-Hong Tao, Guo-Xin Liang, Shan-E Gao, Hai-Jiao Wang, Xin Li, Da-Xin Song, Department of Microbiology, School of Life Sciences, Fudan University, Shanghai 200433, China

Supported by the National Natural Science Foundation of China, No. 30070020

Correspondence to: Chang-Sheng Fan, Department of Microbiology, School of Life Sciences, Fudan University, 220 Handan Road, Shanghai 200433, China. csfan@fudan.edu.cn

Telephone: +86-21-65642808 Fax: +86-21-65650149

Received: 2004-04-20 Accepted: 2004-05-13

Abstract

AIM: To study the effect of integration of tandem *aroG-pheA* genes into the *tyrA* locus of *Corynebacterium glutamicum* (*C. glutamicum*) on the production of L-phenylalanine.

METHODS: By nitrosoguanidine mutagenesis, five *p*-fluorophenylalanine (FP)-resistant mutants of *C. glutamicum* FP were selected. The *tyrA* gene encoding prephenate dehydrogenase (PDH) of *C. glutamicum* was amplified by polymerase chain reaction (PCR) and cloned on the plasmid pPR. Kanamycin resistance gene (Km) and the P_{BF} -*aroG-pheA*-T (GA) fragment of pGA were inserted into *tyrA* gene to form targeting vectors pTK and pTGAK, respectively. Then, they were transformed into *C. glutamicum* FP respectively by electroporation. Cultures were screened by a medium containing kanamycin and detected by PCR and phenotype analysis. The transformed strains were used for L-phenylalanine fermentation and enzyme assays.

RESULTS: Engineering strains of *C. glutamicum* (Tyr⁻) were obtained. Compared with the original strain, the transformed strain *C. glutamicum* GAK was observed to have the highest elevation of L-phenylalanine production by a 1.71-fold, and 2.9-, 3.36-, and 3.0-fold in enzyme activities of chorismate mutase, prephenate dehydratase and 3-deoxy-D-arabinoheptulosonate-7-phosphate synthase, respectively.

CONCLUSION: Integration of tandem *aroG-pheA* genes into *tyrA* locus of *C. glutamicum* chromosome can disrupt *tyrA* gene and increase the yield of L-phenylalanine production.

Liu DX, Fan CS, Tao JH, Liang GX, Gao SE, Wang HJ, Li X, Song DX. Integration of *E. coli aroG-pheA* tandem genes into *Corynebacterium glutamicum tyrA* locus and its effect on L-phenylalanine biosynthesis. *World J Gastroenterol* 2004; 10 (24): 3683-3687

<http://www.wjgnet.com/1007-9327/10/3683.asp>

INTRODUCTION

L-phenylalanine is one of the essential amino acids for humans. Its applications range from feed to food, and pharmaceutical products. Such as *p*-fluorophenylalanine are used as anti-tumour drugs. At present, L-phenylalanine biosynthesis genes have been well characterized and the enzymology of L-

phenylalanine biosynthesis has been extensively investigated^[1-10]. In bacteria, the biosynthesis of aromatic amino acids starts from condensation reaction of central carbon intermediates such as phosphoenol pyruvate (PEP) and erythrose-4-phosphate (E4P) to form 3-deoxy-D-arabino-heptulosonate-7-phosphate (DAHP), which is catalyzed by DAHP synthase (DS). DAHP is then converted to chorismate, the branch point of aromatic amino acid biosynthesis. L-phenylalanine is synthesized from chorismate by three continuous steps catalyzed by chorismate mutase (CM), prephenate dehydratase (PD) and aromatic-amino-acid transaminase (AT). *aroG*^[1-5] and *pheA*^[6-10] are two key genes in L-phenylalanine biosynthesis. In *E. coli*, they encode the 3-deoxy-D-arabinoheptulosonate-7-phosphate synthase (DS) and chorismate mutase/prephenate dehydratase (CM/PD), respectively. However, in *Corynebacterium glutamicum* (*C. glutamicum*), CM and PD are encoded by two different genes *pheB* and *pheA*^[10]. The over-expression of *aroG* and *pheA* can increase the yield of L-phenylalanine biosynthesis in *E. coli* or in *Corynebacteria* by shuttle vectors^[11-17]. *tyrA* encoding prephenate dehydrogenase (PDH) is a key gene in L-tyrosine biosynthesis branch pathway^[18]. DS and CM of *C. glutamicum* can be synergistically inhibited by L-tyrosine and L-phenylalanine. Every step from DAHP to chorismate is repressed weakly by L-tyrosine. In addition, PD is strongly inhibited by L-phenylalanine and L-tryptophan, L-tyrosine stimulates PD activity and restores the enzyme activity inhibition by L-phenylalanine and L-tryptophan^[19]. These regulations seem to result in balanced synthesis of L-tyrosine and L-phenylalanine (Figure 1). Therefore, elimination of feedback inhibition of L-phenylalanine on the key enzymes and deletion of *tyrA* gene can improve the yield of L-phenylalanine biosynthesis. There are successful examples by using homologous recombination technology to introduce genes into chromosome^[20-23].

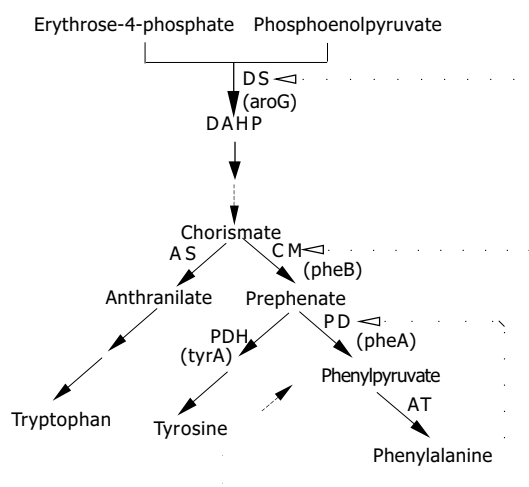


Figure 1 Pathway and primary regulations of phenylalanine biosynthesis in *C. glutamicum* ←--- indicates feedback inhibition, - - - ➔ indicates activation.

In this study, we used nitrosoguanidine (NTG) to treat *C. glutamicum*. Mutants resistant to FP were isolated in a

minimal medium plate with FP and named *C. glutamicum* FP. The tandem *aroG-pheA*^[15] genes obtained from *E. coli* resistant to FP were inserted into the chromosome of *C. glutamicum* FP by a double-exchange homologous recombination between the fragments of *tyrA* gene on targeting vectors and the *tyrA* gene on the chromosome of *C. glutamicum* FP. Enzyme activities and L-phenylalanine biosynthesis in the engineered strains of *C. glutamicum* KM and *C. glutamicum* GAK were analyzed.

MATERIALS AND METHODS

Bacterial strains, media, and culture conditions

The bacterial strains and plasmids used in this study are listed in Table 1. Minimal medium^[15] (MM) and NB (LB added with 10 g/L beef extract) were used for culture *C. glutamicum*. The medium for *C. glutamicum* fermentation was reported previously^[16]. LB was used for growth of *E. coli*. When required, appropriate antibiotics were added to the suitable concentrations. Solid media were made by the addition of agar at the concentration of 15 g/L.

Chemicals

T₄ DNA ligase, restriction enzymes, gel extract kit and DNA blunting kit were obtained from Takara Co. NTG and the reagents used in the enzyme assays were purchased from Sigma Co. They were used according to the instructions of their manufacturers.

Isolation of L-phenylalanine analogue resistant mutants

C. glutamicum cells were grown in NB supplemented with 20 mg/L nalidixic acid until log phase, and collected by centrifugation, followed by two washes with phosphate buffered saline (pH6.0). The cells were then resuspended in 500 µL of 9 g/L NaCl containing 5 mg of NTG and kept on shaking at 30 °C for another 30 min. The cells were collected by centrifugation followed by two washes before suspension in 9 g/L NaCl. Appropriate aliquots of the suspension were spread on the minimal agar plate containing different concentrations of *p*-fluorophenylalanine (*p*-FP) for mutant screening.

Preparation and manipulation of DNA

Chromosomal DNA of *C. glutamicum* was extracted as described previously^[10]. Manipulation of plasmid DNA was performed as described by Sambrook *et al.*^[24].

Construction of recombinant plasmids

Primers of *tyrA* and Km were designed according to the sequences in GenBank (NC_003450 and AF012346). Primer P1: 5'-G GCTGCAGCAGGCCATCCTCTTCAGTGTTC-3' and

primer P2: 5'-CCCAAGCTTCGAGGGTTTCAGCGTGGATG-3' were designed for amplifying *tyrA* gene carrying *Pst*I and *Hind*III restriction enzyme sites, respectively. Primer P3: 5'-GCGGAAT TCACCGGAATTGCCAGCTG-3' and primer P4: 5'-GCGGAAT TCTGCAGTTATCAGAAGAAGACTCGTCAA G-3' were designed for amplifying Km gene carrying *Eco*RI and *Pst*I sites, respectively. The primer P5 for PCR detection was 5'-CCCA AGCTTAGG AATCGCCTGAGAATCATCA-3'. Construction of recombinant plasmids was performed as shown in Figure 2.

Electroporation of linear DNA into C. glutamicum

Targeting vectors were digested by *Hind* III and the linear DNA was obtained by gel extraction. Then, they were denatured by 1 mol/L NaOH at 37 °C for 10 min, quickly placed on ice before the same volume of 1 mol/L HCl was added to neutralize the alkali. The method of Molenaar^[25] was used to introduce denatured targeting vectors into *C. glutamicum* FP.

Selection and identification of the recombinant strain

After electroporation, *C. glutamicum* was incubated in 1mL NB medium containing 0.5 mol/L sucrose at 30 °C by shaking (100 r/min) for 1 h, then the culture was plated on selective NB medium containing 0.5 mol/L sucrose, 10 µg/mL nalidixic acid and 15 µg/mL kanamycin for 96 h. The strains on resistant plates were singled out and inoculated on NB with 100 µg/mL ampicillin, 15 µg/mL kanamycin and NB with 15 µg/mL kanamycin, respectively; Clones (Ap^r Km^r) were detected by PCR using primers pair P3 and P5. PCR products were sequenced.

Detection of Tyr phenotype

The strain cultures were washed three times with sterile physiological saline and plated on MM plates containing 2 g/L glucose and 1 mol/L L-tyrosine or other amino acids to detect the Tyr⁻ auxotroph.

Enzymatic activities assay

Crude cell lysates used for enzymatic activity assays were prepared as described previously^[15]. Total protein level was determined according to the method of Bradford^[26]. DS activity was assayed as described previously^[15]. CM activity was determined as described by Xia *et al.*^[27]. PD activity was assayed as precisely described^[28].

Fermentation and analysis of phenylalanine

Transformants of *C. glutamicum* were obtained by PCR and phenotype analysis. L-phenylalanine fermentation of them was carried out in the shaking flask and the yields of L-phenylalanine biosynthesis were determined as described by Zeng *et al.*^[15].

Table 1 Strains and plasmids

Strains or plasmids	Relevant characteristics	Sources or references
<i>E. coli</i> JM110	Strain for vectors construction	Our laboratory
<i>C. glutamicum</i>	Nx ^r , original strain mutagenesis	ATCC
<i>C. glutamicum</i> FP	FP ^r , from <i>C. glutamicum</i> ATCC13032	This work
<i>C. glutamicum</i> KM	<i>C. glutamicum</i> FP inserted with Km gene	This work
<i>C. glutamicum</i> GAK	<i>C. glutamicum</i> FP inserted with GAK	This work
pBluscript SK (pSK)	Ap ^r , vector for gene cloning	Our laboratory
pPR	Ap ^r , pBR322 derivative, suicidal vector	Our laboratory
pGA	Km ^r , carrying P _{BF} - <i>aroG-pheA</i> -T fragment	Ref.15
pT	pPR carrying <i>tyrA</i> gene	This work
pTK	pT carrying Km gene(<i>tyrA</i> ::Km)	This work
pSKGAK	pSK carrying GAK fragment	This work
pTGAK	pT carrying GAK fragment (<i>tyrA</i> ::GAK)	This work

FP^r: resistance to *p*-fluorophenylalanine; Nx^r: resistance to nalidixic acid; Ap^r: resistance to ampicillin; Km^r: resistance to kanamycin; ATCC: American Type Culture Collection. P_{BF}: promoter from *C. glutamicum*; T: terminator of gene32 in T₄ phage. GAK: P_{BF}-*aroG-pheA*-T-Km fragment.

RESULTS

Isolation of *L*-phenylalanine analogue resistant mutants

Five mutants resistant to *p*-FP up to 3 mg/mL were picked out on MM plates after NTG mutagenesis. In those mutants, the feedback inhibition on the key enzymes in biosynthesis pathways was released from phenylalanine. The mutant with the highest yield of phenylalanine was named *C. glutamicum* FP and used as the recipient strain for electroporation (unpublished data). *C. glutamicum* FP was detected by PCR with primers P1 and P2. The sequence of PCR products was consistent with *tyrA* of *C. glutamicum* ATCC 13032.

Construction of recombinant plasmids

Km (950 bp) and *tyrA* (1067 bp) genes were amplified by PCR and they were verified by sequencing. pPR vector and *tyrA* gene were digested with *Pst*I and *Hind*III and ligated to form pT. pT was digested with *Bst*EII, and then blunted. Km gene and P_{BF}-*aroG*-*pheA*-T fragment from pGA plasmids were subcloned into pSK vector, then digested with *Pst*I and *Hind*III to get GAK fragment (P_{BF}-*aroG*-*pheA*-T-Km). This resulting fragment and the Km gene were inserted into the pT to form targeting vectors pTGAK and pTK, respectively. The detailed process refers to Figure 2.

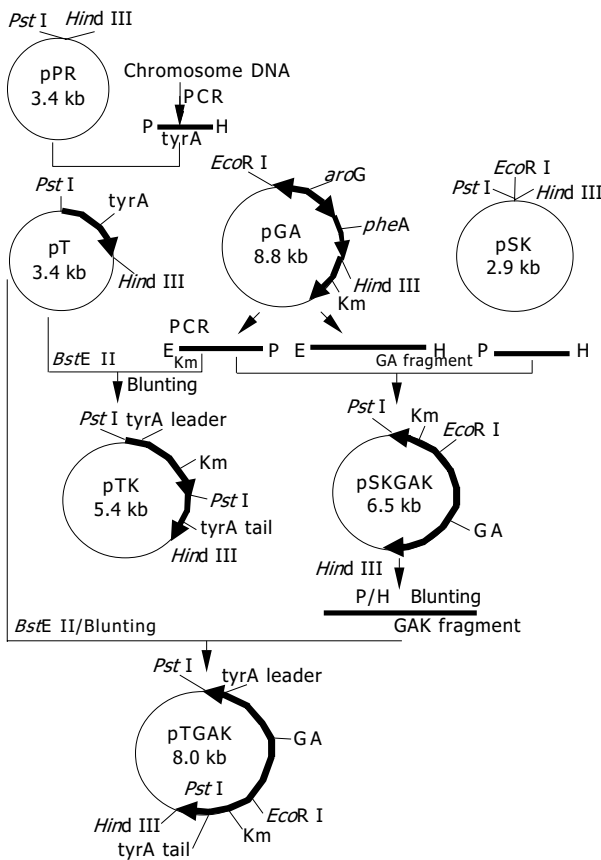


Figure 2 Construction of recombinant plasmids. E: *Eco*RI; P: *Pst*I; H: *Hind*III; GA: P_{BF}-*aroG*-*pheA*-T fragment; GAK: P_{BF}-*aroG*-*pheA*-T-Km fragment.

Identification of transformants

Because primer P5 was located at the end of *tyrA* gene, it only existed on the chromosome of *C. glutamicum*, but not on the targeting vector. Only when the Km gene was inserted into the chromosome of *C. glutamicum*, could the product be obtained by PCR using the primer pair P3 and P5 (Figure 3). The expected PCR products of 1570 bp are shown in Lane 3 and Lane 5 of Figure 4. Since a *Pst*I restriction site was introduced into Km

gene in fore side (Figure 2), the obtained PCR products could be digested by *Pst*I to produce two fragments whose sizes (950 bp and 620 bp) accorded to the sizes of Km gene and an expanded *tyrA* tail as shown in Lane 2 and Lane 4 of Figure 4. Sequencing of the 1570 bp fragment demonstrated it consisted of Km gene and a 620 bp fragment including *tyrA* tail (unpublished data). The strains obtained by PCR detection were named *C. glutamicum* KM (inserted with Km) and *C. glutamicum* GAK (inserted with GAK).

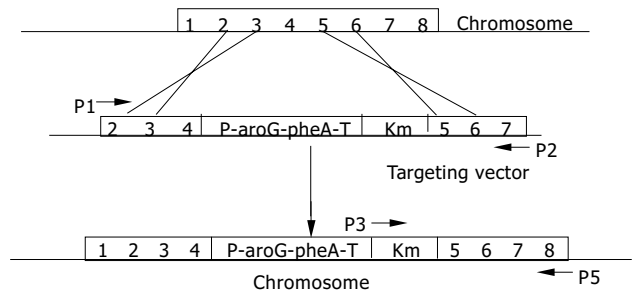


Figure 3 Insertion of P_{BF}-*aroG*-*pheA*-T-Km fragment of pTGAK into chromosome *tyrA* locus of *C. glutamicum* by double-exchange homologous recombination and detection of ligated DNA fragment Km-*tyrA* tail on chromosome by PCR amplification with P3 and P5.

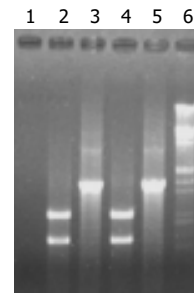


Figure 4 DNA detection of transformants by PCR amplification and *Pst*I digested PCR products. Lane 1: control for PCR; lane 2: *Pst*I digesting product of lane 3; lane 3: PCR detection of *C. glutamicum* KM; lane 4: *Pst*I digesting product of lane 5; lane 5: PCR detection of *C. glutamicum* GAK; lane 6: Markers, *Eco*RI/*Hind*III digesting λ phage DNA.

Detection of *Tyr* auxotroph

As shown in Figure 5, *C. glutamicum* GAK, in which *tyrA* was disrupted by inserting a GAK fragment, only grew on the MM with L-tyrosine, but not on MM and MM with L-tryptophan or L-phenylalanine plates. This result indicated that *C. glutamicum* GAK was an auxotroph requiring L-tyrosine for growth. Here, we demonstrated that the pathway of tyrosine biosynthesis at steps from prephenate to 4-hydroxyphenylpyruvate was disrupted, and the function of prephenate dehydrogenase was inactivated successfully.

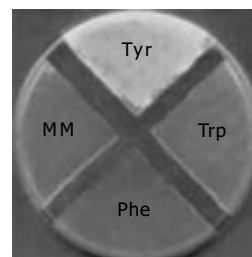


Figure 5 Auxanogram detection of *C. glutamicum* (Tyr). MM: *C. glutamicum* GAK on MM; Tyr: *C. glutamicum* GAK on MM+Tyr; Phe: *C. glutamicum* GAK on MM+Phe; Trp: *C. glutamicum* GAK on MM+Trp.

Enzyme assay

As shown in Figure 1, in the pathway of L-phenylalanine biosynthesis, there were three key enzymes, PD, CM and DS, encoded by *pheA*, *pheB* and *aroG*, respectively in *C. glutamicum*. The results of enzyme activity in *C. glutamicum* are listed in Table 2. The activity of the original strain was used as the control. Compared to the original strain, the relative activities of three enzymes (CM, PD and DS) in *C. glutamicum* FP were 1.73-, 2.37- and 1.93-fold higher and in *C. glutamicum* GAK were 2.9-, 3.36- and 3.0-fold higher respectively. The relative activities of these enzymes in *C. glutamicum* KM (Km^r FP^r) were similar to those in *C. glutamicum* FP (FP^r) respectively. The results indicated that the enzyme activities were increased differently by inhibiting the release of L-phenylalanine feedback using FP^r selection and the integration of tandem genes *aroG-pheA* into chromosome of *C. glutamicum*. At the same time, it also proved that the homologous recombination was successful.

Table 2 Relative activities of CM, PD and DS compared with the original strains

Strains	Enzymes		
	CM	PD	DS
<i>C. glutamicum</i>	1.0	1.0	1.0
<i>C. glutamicum</i> FP	1.73	2.37	1.93
<i>C. glutamicum</i> KM	1.74	2.30	1.95
<i>C. glutamicum</i> GAK	2.90	3.36	3.00

The enzyme activity of *C. glutamicum* was used as the standard, i.e. the relative activity of 1. CM: chorismate mutase; PD: prephenate dehydratase; DS: 3-deoxy-D-arabinoheptulosonate-7-phosphate synthase.

Measurement of phenylalanine yields

Recombinant strains were shaken in 25 mL of fermentation medium with 0.5 mol/L L-tyrosine in 250 mL flask at 30 °C for 72 h. The average yield of three measurements is shown in Table 3. From these data, we could find inhibition of the release of feedback contributed to increase the yield of L-phenylalanine obviously, the yield was increased 42%. On the other hand, interruption of the L-tyrosine branch pathway also increased 9% of the yield. Integration of the tandem genes *aroG-pheA* made 20% improvement. The total yield was increased 71%. The highest yield was added up to 3.97 g/L.

Table 3 Yields of L-phenylalanine biosynthesis in flask fermentation (mean±SD)

Strains	<i>C. glutamicum</i>	<i>C. glutamicum</i> FP	<i>C. glutamicum</i> KM	<i>C. glutamicum</i> GAK
Yields (g/L)	2.20±0.15	3.12±0.17	3.32±0.12	3.76±0.21
Relative yields	1	1.42	1.51	1.71

The phenylalanine yield of the original strain was used as the standard, i.e. the relative yield of 1.

DISCUSSION

The results of this study showed that interruption of the branch pathway of L-tyrosine biosynthesis could accumulate intermediates for L-phenylalanine synthesis and integration of the tandem *aroG-pheA* encoding DS, CM and PD from *E. coli* into the *C. glutamicum* chromosome was also favorable to L-phenylalanine synthesis due to the improvement of key enzyme activities in biosynthesis pathways. These two factors contributed to the increase of 30% yield in L-phenylalanine

biosynthesis. By increasing the precursors for phenylalanine synthesis, interruption of the tyrosine branch pathway could decrease L-tyrosine synthesis, and inhibit L-phenylalanine synthesis because L-tyrosine could stimulate prephenate dehydratase activity and restore the enzyme activity inhibited by L-phenylalanine and L-tryptophan. Ours results also indicated that mutagenesis by NTG was still an effective method for screening phenylalanine-producing strains. This method could effectively to improve the amino acid production in this study. The strains integrated with Km gene kept their resistance to kanamycin after cultured in medium without antibiotics for 96 h (unpublished data). Compared to the strains carrying plasmids^[15-17], strains integrated with heterologous genes had lower yields of L-phenylalanine but a higher stability. Further mutagenesis and application of strong promoters may be useful to increase the yield of L-phenylalanine of engineering strains. Further investigations are necessary to understand the mechanism of aromatic amino acid biosynthesis.

ACKNOWLEDGEMENTS

We thank professor Jiang Zhong, associate professor Han-Ying Yuan and De-Qiang Xu from Fudan University for their helps on this work.

REFERENCES

- Davies WD, Pittard J, Davidson BE. Cloning of *aroG*, the gene coding for phospho-2-keto-3-deoxy-heptonate aldolase (*phe*), in *Escherichia coli* K-12, and subcloning of the *aroG* promoter and operator in a promoter-detecting plasmid. *Gene* 1985; **33**: 323-331
- Kikuchi Y, Tsujimoto K, Kurahashi O. Mutational analysis of the feedback sites of phenylalanine-sensitive 3-deoxy-D-arabino-heptulosonate-7-phosphate synthase of *Escherichia coli*. *Appl Environ Microbiol* 1997; **63**: 761-772
- Ger YM, Chen SL, Chiang HJ, Shiu D. A single Ser-180 mutation desensitizes feedback inhibition of the phenylalanine-sensitive 3-deoxy-D-arabino-heptulosonate-7-phosphate (DAHP) synthase in *Escherichia coli*. *J Biochem* 1994; **116**: 986-990
- Jiang PH, Shi M, Qian ZK, Li NJ, Huang WD. Effect of F209S mutation of *Escherichia coli* *aroG* on resistance to phenylalanine feedback inhibition. *Shengwu Huaxue Yu Shengwuwuli Xuebao* 2000; **32**: 441-444
- Hu C, Jiang PH, Xu J, Wu Y, Huang W. Mutation analysis of the feedback inhibition site of phenylalanine-sensitive 3-deoxy-D-arabino-heptulosonate-7-phosphate synthase of *Escherichia coli*. *J Basic Microbiol* 2003; **43**: 399-406
- Zhang S, Wilson DB, Ganem B. Probing the catalytic mechanism of prephenate dehydratase by site-directed mutagenesis of the *Escherichia coli* P-protein dehydratase domain. *Biochemistry* 2000; **39**: 4722-4728
- Nelms J, Edwards RM, Warwick J, Fotheringham I. Novel mutations in the *pheA* gene of *Escherichia coli* K-12 which result in highly feedback inhibition-resistant variants of chorismate mutase/prephenate dehydratase. *Appl Environ Microbiol* 1992; **58**: 2592-2598
- Gavini N, Davidson BE. *pheA* mutants of *Escherichia coli* have a defective *pheA* attenuator. *J Biol Chem* 1990; **265**: 21532-21535
- Hsu SK, Lin LL, Lo HH, Hsu WH. Mutational analysis of feedback inhibition and catalytic sites of prephenate dehydratase from *Corynebacterium glutamicum*. *Arch Microbiol* 2004; **181**: 237-244
- Chan MS, Hsu WH. Cloning of m-fluorophenylalanine-resistant gene and mutational analysis of feedback-resistant prephenate dehydratase from *Corynebacterium glutamicum*. *Biochem Biophys Res Commun* 1996; **219**: 537-542
- Ozaki A, Katsumata R, Oka T, Furuya A. Functional expression of the genes of *Escherichia coli* in gram-positive *Corynebacterium glutamicum*. *Mol Gen Genet* 1984; **196**: 175-178
- Ikeda M, Ozaki A, Katsumata R. Phenylalanine production

- by metabolically engineered *Corynebacterium glutamicum* with the *pheA* gene of *Escherichia coli*. *Appl Microbiol Biotechnol* 1993; **39**: 318-323
- 13 **Jiang PH**, Liu AM, Ge HP, Zhang YY, Fan CS, Huang WD. Cloning and Expression of *aroG* Gene of *E. coli* and Its Co-expression with *pheA* and *tyrB* Genes. *Shengwu Huaxue Yushengwu Wuli Xuebao* 1998; **30**: 593-596
- 14 **Eikmanns BJ**, Kleinertz E, Liebl W, Sahn H. A family of *Corynebacterium glutamicum*/*Escherichia coli* shuttle vectors for cloning, controlled gene expression, and promoter probing. *Gene* 1991; **102**: 93-98
- 15 **Zeng XB**, Fan CS, Jiang PH, Chen YQ, Huang WD. Co-expression of heterologous genes *pheA*, *aroG* and *tyrB* for biosynthesis pathways of L-phenylalanine. *Chin J Biotechnol* 2000; **16**: 671-674
- 16 **Wu YQ**, Jiang PH, Fan CS, Wang JG, Shang L, Huang WD. Co-expression of five genes in *E coli* for L-phenylalanine in *Brevibacterium flavum*. *World J Gastroenterol* 2003; **9**: 342-346
- 17 **Fan C**, Zeng X, Chai Y, Jiang P, Huang W. Expression of genes *aroG* and *pheA* in phenylalanine biosynthesis. *Weishengwu Xuebao* 1999; **39**: 430-435
- 18 <http://www.ncbi.nlm.nih.gov/entrez/viewer.fcgi?db=nucleotide&val=23308765>
- 19 **Follettie MT**, Sinskey AJ. Molecular cloning and nucleotide sequence of the *Corynebacterium glutamicum pheA* gene. *J Bacteriol* 1986; **167**: 695-702
- 20 **Schafer A**, Tauch A, Jager W, Kalinowski J, Thierbach G, Puhler A. Small mobilizable multi-purpose cloning vectors derived from the *Escherichia coli* plasmids pK18 and pK19: selection of defined deletions in the chromosome of *Corynebacterium glutamicum*. *Gene* 1994; **145**: 69-73
- 21 **Fitzpatrick R**, O'Donohue M, Joy J, Heery DM, Dunican LK. Construction and characterization of *recA* mutant strains of *Corynebacterium glutamicum* and *Brevibacterium lactofermentum*. *Appl Microbiol Biotechnol* 1994; **42**: 575-580
- 22 **Ikeda M**, Katsumata R. A novel system with positive selection for the chromosomal integration of replicative plasmid DNA in *Corynebacterium glutamicum*. *Microbiology* 1998; **144**(Pt 7): 1863-1868
- 23 **Kirchner O**, Tauch A. Tools for genetic engineering in the amino acid-producing bacterium *Corynebacterium glutamicum*. *J Biotechnol* 2003; **140**: 287-299
- 24 **Sambrook J**, Russell DW. Molecular cloning: a laboratory Manual. 3thed. New York: Cold Spring Harbor Laboratory Press 2001: 48-51
- 25 **van der Rest ME**, Lange C, Molenaar D. A heat shock following electroporation induces highly efficient transformation of *Corynebacterium glutamicum* with xenogeneic plasmid DNA. *Appl Microbiol Biotechnol* 1999; **52**: 541-545
- 26 **Frederick M**, Ausubel, Roger Brent, Robert E, Kingston David D, Moore JG, Seidman John A, Smith Kevin Struhl. Short Protocols in Molecular Biology. 3thed. Beijing: Science Press 1998: 332
- 27 **Xia T**, Zhao G, Jensen RA. Loss of allosteric control but retention of the bifunctional catalytic competence of a fusion protein formed by excision of 260 base pairs from the 3' terminus of *pheA* from *Erwinia herbicola*. *Appl Environ Microbiol* 1992; **58**: 2792-2798
- 28 **Zhang S**, Wilson DB, Ganem B. Probing the catalytic mechanism of prephenate dehydratase by site-directed mutagenesis of the *Escherichia coli* P-protein dehydratase domain. *Biochemistry* 2000; **39**: 4722-4728

Edited by Kumar M and Wang XL Proofread by Xu FM

Co-mutation of p53, *K-ras* genes and accumulation of p53 protein and its correlation to clinicopathological features in rectal cancer

Zhi-Zhong Pan, De-Sen Wan, Gong Chen, Li-Ren Li, Zhen-Hai Lu, Bi-Jun Huang

Zhi-Zhong Pan, De-Sen Wan, Gong Chen, Li-Ren Li, Zhen-Hai Lu, Bi-Jun Huang, Department of Abdominal Surgery, Cancer Center, Sun Yat-Sen University, Guangzhou 510060, Guangdong Province, China

Correspondence to: Dr. Zhi-Zhong Pan, Department of Abdominal Surgery, Cancer Center, Sun Yat-Sen University, Guangzhou 510060, Guangdong Province, China. panzhizhong@medmail.com.cn

Telephone: +86-20-87343456 **Fax:** +86-20-87343392

Received: 2004-02-28 **Accepted:** 2004-04-05

Abstract

AIM: To determine the accuracy of p53 gene mutations predicted by overexpression of p53 protein immunohistochemically, and to investigate the co-mutation of p53 and *K-ras* genes in rectal cancer and its effect on promoting malignant biologic behaviors of tumors.

METHODS: Ninety-seven specimens of rectal cancer were surgically resected in our hospital from August 1996 to October 1997. The hot mutation areas of p53 gene (in exons 5-8) and *K-ras* gene (in codon 5/12 and 13) were detected with polymerase chain reaction-single strand conformation polymorphism (PCR-SSCP), and overexpression of p53 protein was detected with immunohistochemistry (IHC) in the 97 specimens of rectal cancer. Correlation between gene mutations and tumor clinicopathologic factors was studied, and survival analysis was performed as well.

RESULTS: There were 36 cases of p53 gene mutations in 61 p53 protein positive cases, and 21 cases of p53 gene non-mutation in 36 p53 protein negative cases respectively. The coincidence rate of p53 gene mutation by IHC method with PCR-SSCP method was 58.8% (57/97). The mutation rate of p53 gene was 52.6% (51/97), while *K-ras* gene mutation was observed in codons 12 and 13 in 61 cases with a mutation rate of 62.9% (61/97). Single gene mutation of p53 or *K-ras* was found in 32 cases. Both p53 and *K-ras* gene mutation were found in 48 cases. Statistical analysis showed that p53 and *K-ras* gene mutations were not related to the clinicopathologic factors, including tumor size, gross tumor type, histological classification, differentiation, invasion to intestinal veins, lymphatics and nerves, invasive depth to wall, lymph node metastasis, and Dukes' stages ($P > 0.05$). The survival in patients with no gene mutation, single gene mutation and both gene mutations were similar ($P > 0.05$).

CONCLUSION: IHC has a certain false positive and false negative rate in detecting p53 gene mutations. Malignant biological behaviours of rectal cancer are not enhanced by p53 and *K-ras* gene mutations. Co-mutation of p53 and *K-ras* gene has neither synergic carcinogenesis-promoting effect, nor prognostic effect on rectal cancer.

Pan ZZ, Wan DS, Chen G, Li LR, Lu ZH, Huang BJ. Co-mutation of p53, *K-ras* genes and accumulation of p53 protein and its correlation to clinicopathological features in rectal cancer. *World J Gastroenterol* 2004; 10(24): 3688-3690
<http://www.wjgnet.com/1007-9327/10/3688.asp>

INTRODUCTION

Carcinogenesis and development of colorectal cancer are a process with multiple steps, in which epithelial cells of colorectum go through small adenoma, large adenoma, and finally become adenocarcinoma^[1]. The changes of several genes involve this process, including the activation of *K-ras* oncogene and the mutation and deletion of p53 anti-oncogene^[2]. To date, the clinical significance of the change of these genes is still disputed. Some studies reported that simultaneous mutations of p53 and *K-ras* could promote the development of colorectal cancer directly or indirectly, and were related to lymphatic metastasis, and a poor prognosis, but others had opposite results^[3]. It is still unclear which one is the prognostic factor, the p53 cDNA mutation or the alteration of p53 protein expression or both^[4]. Moreover, 90% dot mutations of p53 happen in exons 5-8, the individual incident rate of p53 mutations in these exons is not known^[5]. Therefore, to explore the effect of simultaneous mutations of p53, *K-ras* gene on the promotion of malignant biologic behaviors of rectal cancer and its clinical significance, the mutation patterns of exons 5-8 of p53 gene and codons 12 and 13 of *K-ras* gene in rectal cancer were detected by PCR-SSCP.

MATERIALS AND METHODS

Patients

From August 1996 to October 1997, 97 patients with rectal cancer underwent surgical resection in our hospital, including 54 males and 43 females, aged from 21 to 84 years with an average age of 53 years. Gross classification of tumors consisted of 27 cases of protruding type, 63 cases of ulcerating type, and 7 cases of infiltrating type. Histological classification included 3 cases of adenoma with cancer, 17 cases of papillary adenocarcinoma, 69 cases of tubular adenocarcinoma, 1 case of mucinous adenocarcinoma, 7 cases of signet-ring cell carcinoma, with 20 cases of well differentiated, 51 moderately and 26 poorly differentiated. According to Dukes classification, patients were categorized into four stages: stage A ($n = 27$), stage B ($n = 22$), stage C ($n = 36$) and stage D ($n = 12$).

Methods

Serial paraffin sections were used for HE staining, anti-p53 immunohistological staining, and detection of p53 and *K-ras* gene mutation by PCR-SSCP.

Immunohistochemistry

The Labeling-streptavidin-biotin peroxidase complex (LSAB) method was used for IHC staining. The colorectal tissue positive for p53 was taken as positive control, normal tissue as negative control, PBS instead of first antibody as blank control. Background of IHC staining was clear.

Positive standards for IHC staining were the same as previously described. Cells with pale brown granules in nuclei were judged as positive. The sections with 10-25% positive cells were defined as +, 26-50% as ++, 51-70% as +++, more than 70% as +++++, less than 10% as -.

PCR-SSCP

DNA was abstracted from tissues of 5 μ m paraffin sections

with routine method, and then stored at -20 °C. Exons 5,6,7,8 of p53 gene and codons 12, 13 of K-ras gene were amplified by polymerase chain reaction (PCR, PCR amplifier produced by American PE Company) respectively. The primers were synthesized and provided by Genetics Department of Sun Yat-Sen University. The sequences of primers are shown in Table 1. The single DNA chain from denatured PCR products was treated by normal vertical plane electrophoresis and stained with silver. Increased, and decreased numbers and translocation of electrophoresis bands in tumor specimens compared with normal tissues suggested the existence of gene mutations.

Statistical analysis

Data were analyzed with SPSS statistical software (Version 8.0). The relationship between mutations of p53, *K-ras* genes and clinicopathological factors was analyzed by χ^2 test. Survival rates were calculated with life table and Wilcoxon-Gehan test.

RESULTS

Expression of p53 protein

p53 protein was detected in 61 cases (62.9%, 61/97) according to IHC staining, strong positive (++++), moderately positive (+++), (++) , weak positive (+) were found in 26/61, 22/61, 10/61, and 30/61, respectively.

Sensitivity of p53 IHC method to p53 gene mutation detection

p53 gene mutations (in exons 5-8, hot mutation area) were found in 51 cases of rectal cancer by PCR-SSCP, with a mutation rate of 52.6% (51/97). Among the cases with p53 positive IHC staining, 36 cases were positive for p53 gene mutations by PCR-SSCP, while no p53 gene mutation was found by PCR-SSCP in 21 cases negative for p53 IHC staining (Table 2). The accuracy of IHC method to detect p53 gene mutations was 58.8% (57/97), the sensitivity was 70.6% (36/51), and the specificity was 45.7% (21/46).

Table 2 Sensitivity of IHC to detect p53 gene mutation

p53 gene (PCR-SSCP)	p53 IHC staining (%)	
	Negative	Positive
No mutation	21(45.7)	25(54.3)
Mutation	15(29.4)	36(70.6)

Mutation of p53 and K-ras genes

In the present study, p53 gene mutations were located in exons 5,6 in one case, in exon 7 in 48 cases, in exons 5,6 and 7 in 2 cases, and no mutation was found in exon 8. The mutation rate of p53 gene was 52.6% (51/97). *K-ras* gene mutations were located in codons 12 and 13 in 61 cases with a rate of 62.9% (61/97). p53 or *K-ras* gene mutations were found in 32 cases, both p53 and *K-ras* gene co-mutations were found in 48 cases.

Correlation of gene mutation and clinicopathological factors

The differences between p53 and *K-ras* gene mutations and clinicopathological factors had no statistical significance ($P>0.05$), including tumor size, gross tumor type, histological classification and differentiation, invasion to intestinal veins, lymphatics and nerves, invasive depth to intestinal wall, lymph node metastasis, and Dukes' stages.

Correlation of gene mutation and prognosis

All cases were followed up to December 2002, ranging from 14 d to 2058 d with an average of 1107 d. One case died of cardiopulmonary disease 14 d after operation, 28 cases died of tumor metastasis or recurrence, 3 cases were lost for follow-up, 2 cases died of other diseases rather than tumor. Life table was used to assess survival rates. Results indicated that p53 and *K-ras* gene mutations had no effects on prognosis ($P>0.05$, Table 3).

Table 1 Sequences of primers used in the study

Gene	Extron/codon	Sequences of primers	Product size
p53	Exons5-6	5'TGTTCACTTGTGCCCTGACT3'	489bp
		5'GGAGGGCCACTGACAACCA3'	
	Exon 7	5'GGCGACAGAGCGAGATTCCA3'	286bp
		5'GGGTCAGCGGCAAGCAGAGG3'	
	Exon 8	5'GACAAGGGTGGTTGGGAGTAGATG3'	320bp
		5'GCAAGGAAAGGTGATAAAAAGTGAA3'	
<i>K-ras</i>	Codon 12-13	5'TCAAAGAATGGTCCTGCACC3'	178bp
		5'GCCTGCTGAAAATGACTGAA3'	

Table 3 Survival of 97 rectal cancer cases and its correlation to p53 and *K-ras* gene mutation

Survival (year)	p53 mutation		<i>K-ras</i> mutation		p53 and <i>K-ras</i> mutation		
	(-)	(+)	(-)	(+)	Neither	Either	Both
1 -	86.52	95.83	91.04	91.53	81.25	93.48	93.44
2 -	77.04	82.30	87.79	75.37	71.48	86.55	72.29
3 -	67.25	73.16	74.79	67.93	54.17	79.44	65.06
4 -	64.33	62.32	66.91	61.36	54.17	71.08	56.38
5 -	64.33	62.32	66.91	61.36	54.17	71.08	56.38
<i>P</i>	0.5672		0.4536		0.2030		

DISCUSSION

The methods normally used to detect p53 gene mutations include immunohistochemistry (IHC), PCR-SSCP, denaturing gradient gel electrophoresis (DGGE), and sequencing. According to literatures, the sensitivity of IHC was 75%, and its positive predictive value for detecting p53 gene mutations was 63%. More than 85% p53 gene mutations in exons 5-8 could be detected by PCR-SSCP with a sensitivity of 80-90%^[6,7]. In the present study, p53 gene mutations in rectal cancer were detected by IHC and PCR-SSCP respectively. The positive rate of IHC was 62.9% (61/97), while that of PCR-SSCP was 52.6% (51/97). The accuracy of IHC was 58.8%, and the sensitivity was 70.6%. However, its specificity was only 45.7%, implying that IHC had a rather high false positive and false negative rate in detecting p53 gene mutations.

It was reported that wild type p53 proteins could combine with viral oncoproteins or cellular oncoproteins to enhance their stability and prolong their half-life, leading to p53 protein accumulation in cells. In such cells, IHC staining was still positive even without p53 gene mutations, furthermore, about 10% p53 gene mutations could take place out side of exons 5-8. Therefore the positive rate of PCR-SSCP targeting only exons 5-8 was usually lower than that of IHC^[8-11]. The present study also had similar results. The variance in p53 gene mutations and p53 protein accumulation indicated that dysfunction of p53 gene might be caused by mechanisms other than mutations.

It is known that the oncogenesis and development of most colorectal cancers abide by the rule from normal epithelia to adenoma then to adenocarcinoma, and finally to metastasis. This complicated process has been found to involve several oncogene changes in a certain order, that is, from APC to *K-ras* to p53 to DCC^[12].

p53 and *ras* gene mutations could be observed in both adenoma and carcinoma of large intestine^[13]. Extent of p53 expression varies during different phases of tumor oncogenesis. p53 expression can be found extensively in villous adenoma, early stage of adenocarcinoma and well differentiated adenocarcinoma. The above lines of evidence support that p53 and *K-ras* gene mutation might happen before canceration and may be an early event in colorectal carcinogenesis and development. Participatin in the process from adenoma to adenocarcinoma, p53 and *ras* gene mutations may be used as the markers for early detection and diagnosis of colorectal cancer arising from adenoma.

Many studies indicated that the point mutation of p53 gene was related to lymph node metastasis in rectal cancer ($P < 0.001$), while the cross deletion was related to distal metastasis ($P = 0.0001$). The 5-year survival of colorectal cancer patients with chromosome 17p deletion was much poorer. p53 gene mutation was an important prognostic factor for colorectal cancer^[14]. On the contrary, some studies showed that intensity, distribution area and positive rate of p53 IHC staining were independent of the biological factors, such as tumor grade, histological type, tumor site, size, invasive depth to wall, invasion of local lymphatics and veins, lymph node metastasis, peritoneal seeding, and liver metastasis^[15]. Therefore, the clinical significance of p53 is still controversial.

In the present study, detected by PCR-SSCP, the p53 gene mutation rate in exons 5-8 was 52.6%. Most mutations (in 50 cases) took place in exon 7, 3 in exons 5-6, 2 in exon 7. No mutation was found in exon 8. The mutation rate of codons 12 and 13 of *K-ras* gene was 62.9%. Statistically p53 and *K-ras* gene mutations were independent of clinicopathological factors of rectal cancer, including tumor size, gross classification, histological type, differentiation, invasion of veins, lymphatics

and nerves, invasive depth to wall, lymph node metastasis and Dukes' stages. Co-mutation of *K-ras* and p53 gene had no correlation to clinicopathological factors or prognosis.

In conclusion, p53 and *K-ras* gene mutations have no effect on biological behaviours of tumor cells. The co-mutation of both genes has neither carcinogenesis-promoting effect, nor any effect on prognosis. Carcinogenesis and development of colorectal cancer involve changes of several genes, such as APC, *myc*, *K-ras*, *MMC* and p53. The accumulative effects of such genes may play a more important role during carcinogenesis than the order of change in these genes^[12,16]. So, genetic therapy for colorectal cancer should target multiple genes involved in the process of carcinogenesis.

REFERENCES

- 1 **Fearon ER**, Vogelstein B. A genetic model for colorectal tumorigenesis. *Cell* 1990; **61**: 759-767
- 2 **Jin W**, Gao MQ, Lin ZW, Yang DX. Multiple biomarkers of colorectal tumor in a differe diagnosis model: A quantitative study. *World J Gastroenterol* 2004; **10**: 439-442
- 3 **Klump B**, Nehls O, Okech T, Hsieh CJ, Gaco V, Gittinger FS, Sarbia M, Borchard F, Greschniok A, Gruenagel HH, Porschen R, Gregor M. Molecular lesions in colorectal cancer: impact on prognosis? Original data and review of the literature. *Int J Colorectal Dis* 2004; **19**: 23-42
- 4 **Galizia G**, Lieto E, Ferraraccio F, Orditura M, De Vita F, Castellano P, Imperatore V, Romano C, Ciardiello F, Agostini B, Pignatelli C. Determination of molecular marker expression can predict clinical outcome in colon carcinomas. *Clin Cancer Res* 2004; **10**: 3490-3499
- 5 **Soussi T**. The p53 tumor suppressor gene: from molecular biology to clinical investigation. *Ann N Y Acad Sci* 2000; **910**: 121-137
- 6 **Velculescu VE**, El-Deiry WS. Biological and clinical importance of the p53 tumor suppressor gene. *Clin Chem* 1996; **42** (6 Pt 1): 858-868
- 7 **Greenblatt MS**, Bennett WP, Hollstein M, Harris CC. Mutations in the p53 tumor suppressor gene: clues to cancer etiology and molecular pathogenesis. *Cancer Res* 1994; **54**: 4855-4878
- 8 **Fearon ER**, Hamilton SR, Vogelstein B. Clonal analysis of human colorectal tumors. *Science* 1987; **238**: 193-197
- 9 **Scott N**, Quirke P. Molecular biology of colorectal neoplasia. *Gut* 1993; **34**: 289-292
- 10 **Kastan MB**, Onyekwere O, Sidransky D, Vogelstein B, Craig RW. Participation of p53 protein in the cellular response to DNA damage. *Cancer Res* 1991; **51** (23 Pt 1): 6304-6411
- 11 **Hall PA**, McKee PH, Menage HD, Dover R, Lane DP. High levels of p53 protein in UV-irradiated normal human skin. *Oncogene* 1993; **8**: 203-207
- 12 **Wang Y**, Liu S, Hao D. Mutations of APC gene MCR region in sporadic colorectal adenomas and carcinomas. *Zhonghua Zhongliu Zazhi* 1998; **20**: 284-286
- 13 **Qian H**, Yu BM, Zhou XG, Wang RN, Huang W, Chen SJ, Chen Z. The significance of p53 gene mutations and expressions in human colorectal tumors. *Zhonghua Zhongliu Zazhi* 1995; **17**: 332
- 14 **Cunningham J**, Lust JA, Schaid DJ, Bren GD, Carpenter HA, Rizza E, Kovach JS, Thibodeau SN. Expression of p53 and 17p allelic loss in colorectal carcinoma. *Cancer Res* 1992; **52**: 1974-1980
- 15 **Kawasaki Y**, Monden T, Morimoto H, Murotani M, Miyoshi Y, Kobayashi T, Shimano T, Mori T. Immunohistochemical study of p53 expression in microwave-fixed, paraffin-embedded sections of colorectal carcinoma and adenoma. *Am J Clin Pathol* 1992; **97**: 244-249
- 16 **Bell SM**, Scott N, Cross D, Sagar P, Lewis FA, Blair GE, Taylor GR, Dixon MF, Quirke P. Prognostic value of p53 overexpression and c-Ki-ras gene mutations in colorectal cancer. *Gastroenterology* 1993; **104**: 57-64

Diagnostic evaluation of acute pancreatitis in two patients with hypertriglyceridemia

Yoshifumi Okura, Kozo Hayashi, Tetsuji Shingu, Goro Kajiyama, Yoshiyuki Nakashima, Keiji Saku

Yoshifumi Okura, Yoshiyuki Nakashima, Division of Internal Medicine, Fukuoka Dental College Hospital, Fukuoka, Japan

Kozo Hayashi, Tetsuji Shingu, Goro Kajiyama, First Department of Internal Medicine, Hiroshima University School of Medicine, Hiroshima, Japan

Keiji Saku, Division of Cardiology, Fukuoka University School of Medicine, Fukuoka, Japan

Correspondence to: Dr. Yoshifumi Okura, Division of Cardiology, Department of Internal Medicine, Fukuoka Dental College Hospital, 2-15-1, Tamura, Sawara-ku, Fukuoka 814-0193, Japan. okuray@college.fdcnet.ac.jp

Telephone: +81-92-801-0411 **Fax:** +81-92-801-0735

Received: 2004-01-02 **Accepted:** 2004-04-14

Abstract

We present two diagnostically challenging cases of acute pancreatitis with hypertriglyceridemia accompanied with chylomicronemia caused with a deficiency of lipoprotein lipase and with the presence of type V hyperlipidemia. Both cases suffered from acute abdomen following the ingestion of fatty food and revealed the increase in parameters of inflammation without significant elevation of serum amylase levels. The imaging examination of ultrasonography could not detect significant findings of acute pancreatitis and a computer tomography scan eventually confirmed the findings of acute pancreatitis. Both cases responded to a low fat diet and administration of a cholecystokinin receptor antagonist, exhibiting a relief of abdominal symptoms. As in the present cases with acute abdomen following the ingestion of fatty food, the identification of serum hypertriglyceridemia and an abdominal computer tomography scan might be useful in establishing the diagnosis of acute pancreatitis and in developing the therapeutic regimen, when hypertriglyceridemia interferes with the evaluation of pancreatic enzyme activities and ultrasound examination provides poor pancreatic visualization.

Okura Y, Hayashi K, Shingu T, Kajiyama G, Nakashima Y, Saku K. Diagnostic evaluation of acute pancreatitis in two patients with hypertriglyceridemia. *World J Gastroenterol* 2004; 10 (24): 3691-3695

<http://www.wjgnet.com/1007-9327/10/3691.asp>

INTRODUCTION

Secondary pancreatitis is caused by severe hypertriglyceridemia accompanied with chylomicronemia, and marked hypertriglyceridemia has been found in 12 to 22 percent of patients admitted to a hospital for acute pancreatitis^[1]. The diagnosis of acute pancreatitis is sometimes complicated, since the presence of hypertriglyceridemia may often produce multiple spurious laboratory data including serum and urinary amylase and serum lipase levels^[1-5]. Therefore, hypertriglyceridemia sometimes is underrecognized by admitting physicians as a possible cause of acute pancreatitis^[6]. Moreover, although the imaging examination of ultrasonogram is a relatively sensitive noninvasive test for the diagnosis of acute pancreatitis and can be performed rapidly and at the patient bedside, pancreatic visualization is limited by

intestinal gas or adipose tissue in 30- 40% of patients^[7]. In this report, we present two cases suffering from acute abdomen following the ingestion of fatty food in which the identification of hypertriglyceridemia proved to be useful in diagnosing acute pancreatitis.

CASE REPORT

Case 1

A 61-year-old Japanese woman was admitted to the emergency department of a local hospital for repeated episodes of vomiting and epigastric discomfort following the ingestion of fatty food. The white blood cell (WBC) count and serum amylase level were both mildly elevated. Although echosonogram could not detect pancreatic disorders such as hypoechoic change or fluid collections, the treatment with gabexate mesylate, an inhibitor of pancreatic serine proteinases, was initiated with a suspected diagnosis of acute pancreatitis and her epigastric discomfort and nausea improved. She was transferred next day for purposes of further examination of acute abdomen. She had midepigastric discomfort and tenderness that migrated to the back. Bowel sounds were normal to auscultation, and there was no hepatomegaly or splenomegaly. Arcus corneae, cutaneous eruptive xanthomas and the xanthomas of Achilles tendon were absent. A chest radiogram was normal. X-rays of the abdomen revealed no abnormal gas patterns, calcifications, or ascites.

Table 1 illustrates the laboratory data on admission. We observed an elevated WBC count and erythrocyte sedimentation rate (ESR) and a positive C-reactive protein (CRP), with moderate normocytic anemia. Although an elevated serum pancreatic secretory trypsin inhibitor (PSTI) level was revealed in the pancreatic enzymes, other pancreatic enzymes including serum and urinary amylase levels were normal. Marked hypertriglyceridemia and a low level of high density lipoprotein-cholesterol (HDL-C) were apparent. A layer of chylomicrons could be seen at the top of the plasma stored for 24 h in a refrigerator. Although an abdominal ultrasonogram showed no pancreas abnormality and no evidence of cholelithiasis or choledocholithiasis, a computer tomography (CT) scan of the abdomen could detect pancreatic edematous changes and enlargement with a score of 3 according to CT severity index by Balthazar^[8]. These findings were confirmed as an initial change of acute pancreatitis by two established radiologists and indicated a diagnosis of secondary pancreatitis with hypertriglyceridemia.

Figure 1 illustrates the patient's clinical course. Her epigastric discomfort improved after administration of loxiglumide, a cholecystokinin receptor antagonist 300 mg/d, and flomoxef, an antibiotic 2 g/d, and they disappeared after two days. The serum PSTI level returned to normal and there were no major changes in other serum pancreatic enzymes. The patient was started on a low fat diet on the third hospital day. We conducted a diagnostic investigation to exclude possible secondary causes for acute pancreatitis other than hypertriglyceridemia. Endoscopic retrograde cholangiopancreatography (ERCP) performed on the seventh hospital day revealed no apparent structural alterations in the common bile duct or pancreatic duct such as pancreas divisum. Despite the administration of a low fat diet for two weeks, hypertriglyceridemia and low serum

level of HDL-C failed to improve dramatically. The serum CRP level returned to normal on the eleventh hospital day.

Focusing on the hypertriglyceridemia, we evaluated the patient's glucose metabolism. The serum HbA1C level was 4.8 and 75 g oral glucose tolerance test (OGTT) performed on the twenty-third hospital day demonstrated an impaired glucose tolerance pattern, not that of diabetes mellitus (DM) as a cause of hypertriglyceridemia (Table 2). Excessive alcohol intake, and administration of estrogen, diuretics, and β -adrenergic blockers could be excluded as possible causes of hypertriglyceridemia according to her episode.

In terms of lipid metabolism, we observed high serum levels of apolipoprotein (Apo) B, CII, CIII and E, indicating the increase in triglyceride-rich lipoprotein (Table 2). Polyacrylamide gel electrophoresis (PAGE) demonstrated the presence of chylomicron fraction at base line and a decreased pre- β , β and α fraction, indicating the presence of chylomicron and low levels of very low density lipoprotein (VLDL), low density lipoprotein (LDL) and HDL, respectively (Figure 2a). The post-heparin plasma lipoprotein lipase (LPL) activity, which was obtained 15 min after 50 U/kg body weight intravenous injection of heparin, was markedly low and the immunoreactive LPL mass was below the level of detection (less than 20 ng/mL), confirming the diagnosis of LPL deficiency. These findings suggested that the fatty food ingestion led to acute pancreatitis in the patient with severe hypertriglyceridemia due to the LPL deficiency.

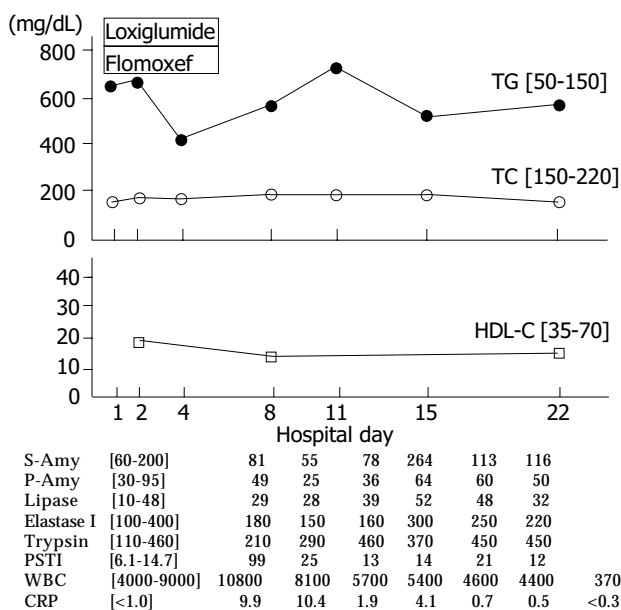


Figure 1 Clinical course of case 1. Normal range is shown in []. TG: triglycerides, TC: total cholesterol, HDL-C: high density lipoprotein-cholesterol, S-Amy: salivary amylase, P-Amy: pancreatic amylase, PSTI: pancreatic secretory trypsin inhibitor, WBC: white blood cell, CRP: C-reactive protein.

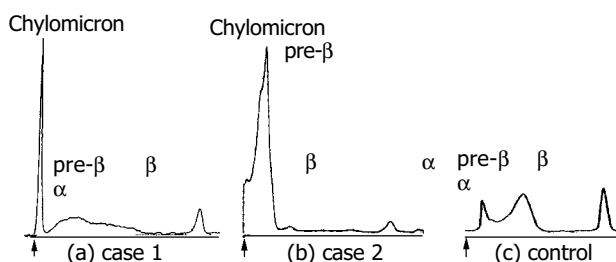


Figure 2 Polyacrylamide gel electrophoresis using the fasting plasma of (a) case 1, (b) case 2 and (c) control. The presence of chylomicrons is demonstrated at the base line indicated by arrows (\uparrow).

Table 1 Laboratory data on admission

	Case 1	Case 2	[Normal range]
Urinalysis			
pH	7.0	6.0	[4.8-7.5]
Sugar	(\pm)	(+)	[-]
Protein	(-)	(\pm)	[-]
Occult	(-)	(-)	[-]
Hematology			
WBC ($/\text{mm}^3$)	10 800	26 000	[4 000-9 000]
RBC ($/\text{mm}^3$)	387×10^4	474×10^4	[350×10^4 - 550×10^4]
Hemoglobin (g/dL)	10.1	20.8	[12-18]
Platelet ($/\text{mm}^3$)	18.2×10^4	32.1×10^4	[10×10^4 - 40×10^4]
ESR (mm/hr)	48	31	[<20]
Blood chemistry			
GOT (IU/L)	16	26	[8-40]
GPT (IU/L)	15	39	[6-35]
LDH (IU/L)	410	392	[100-450]
AI-P (IU/L)	158	198	[100-340]
LAP (IU/L)	33	58	[110-210]
γ GTP (IU/L)	71	71	[<70]
ChE (IU/L)	272	554	[186-406]
ZTT (U)	5	2	[4-12]
Total Bilirubin (mg/dL)	0.8	1	[0.3-1.0]
TC (mg/dL)	175	902	[150-220]
TG (mg/dL)	673	10 340	[50-150]
HDL-C (mg/dL)	18	16	[35-70]
Total Protein (g/dL)	6.1	7.6	[6.5-8.0]
Albumin (g/dL)	3.2	3.1	[3.5-5.0]
BUN (mg/dL)	8	13	[8-21]
Crea (mg/dL)	0.53	0.65	[0.6-1.2]
Uric acid (mg/dL)	3.2	4.6	[3.5-7.8]
Na^+ (mEq/L)	139	125	[135-145]
K^+ (mEq/L)	3.8	3.7	[3.5-5.0]
Cl^- (mEq/L)	107	88	[97-107]
Ca^{++} (mEq/L)	3.8	4.8	[4.3-5.8]
PO_3^- (mg/dL)	2.6	2.7	[2.6-3.8]
CRP (mg/dL)	9.9	13.9	[<1.0]
HbA1C (%)	4.8	9.0	[<5.5]
Pancreatic enzymes			
S-Amy (IU/L)	81	22	[60-200]
P-Amy (IU/L)	49	6	[30-95]
U-Amy (IU/h)	114	168	[160-960]
Lipase (IU/L)	29	54	[10-48]
Elastase I (ng/dL)	180	270	[100-400]
Trypsin (ng/dL)	210	234	[110-460]
PSTI (ng/dL)	99	19.5	[6.1-14.7]

ESR: erythrocyte sedimentation rate, TC: total cholesterol, TG: triglycerides, HDL-C: high density lipoprotein-cholesterol, CRP: C-reactive protein, HbA1c: hemoglobin A1c, S-Amy: salivary amylase, P-Amy: pancreatic amylase, U-Amy: urinary amylase, PSTI: pancreatic secretory trypsin inhibitor.

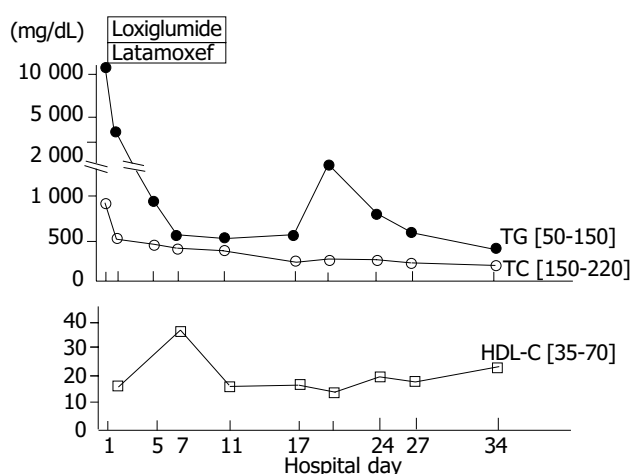
Case 2

This 30-year-old Japanese man was admitted with severe left hypochondralgia following the ingestion of fatty food. He had a history of moderate alcohol intake (more than 80 g/d) since the age of 20 and a history of repeated hospitalizations for acute abdomen following the ingestion of fatty food but the definite cause of acute abdomen was not determined. He was

obese, being 169 cm tall and weighing 78 kg, with a body mass index of 27.3 kg/m². He complained of abdominal pain that radiated to the left back. Abdominal auscultation revealed a decrease in bowel sounds. We observed eruptive xanthomas; small, yellow, papular, cutaneous lesions, localized over the buttocks, the femoral region and the extensor surface of the arms that had been present for the past two months. Chest X-rays showed no abnormalities. No abnormal gas patterns, calcifications, or ascites were noted on abdominal X-rays. An abdominal ultrasonogram provided poor pancreatic visualization due to the obesity. An abdominal CT scan revealed fatty changes in the liver and the presence of edematous and enlarged changes in the pancreas, suggesting acute pancreatitis, with a score of 3 according to CT severity index^[8]. These findings were confirmed as initial findings of acute pancreatitis by two established radiologists.

Laboratory data on admission (Table 1) revealed an elevated WBC count and ESR, positive CRP, elevated hemoglobin level and a low concentration of serum sodium. High serum levels of cholesterol and marked high triglyceride level of more than 10 000 mg/dL, compatible with type V hyperlipidemia according to the classification of Frederickson^[9], and a low serum level of HDL-C were present. Only an elevated serum PSTI level was revealed in pancreatic enzymes.

The patient's clinical course is illustrated in Figure 3. His pain in the left hypochondrium improved on fasting and administration of loxiglumide, 300 mg/d, and latamoxef, an antibiotic 2 g/d, and disappeared on the tenth hospital day. A low fat diet with 1 800 kcal/d was started on the tenth hospital day. Although there was no significant alteration in serum HDL-C levels after the diet was initiated, the markedly elevated serum triglyceride levels fell dramatically and serum cholesterol levels also decreased markedly, returning to normal limits. The WBC count, serum CRP level and serum PSTI level improved significantly. ERCP on the twenty seventh hospital day demonstrated no structural alterations and no stones in the pancreatobiliary ductal system.



S-Amy	[60-200]	22	16	16	31	32	43
P-Amy	[30-95]	6	5	8	8	19	-
Lipase	[10-48]	43	37	23	14	11	19
Elastase I	[100-400]	270	240	240	300	300	-
Trypsin	[110-460]	234	266	266	302	308	-
PSTI	[6.1-14.7]	19.5	-	-	6.2	7.3	-
WBC	[4000-9000]	26000	11400	11000	5200	8300	9300
CRP	[<1.0]	13.9	27.1	15.2	1.7	0.3	<0.3

Figure 3 Clinical course of case 2. Normal range is shown in []. TG: triglycerides, TC: total cholesterol, HDL-C: high density lipoprotein-cholesterol, S-Amy: salivary amylase, P-Amy: pancreatic amylase, PSTI: pancreatic secretory trypsin inhibitor, WBC: white blood cell, CRP: C-reactive protein.

In terms of the lipid metabolism, the presence of chylomicrons was identified from the development of a chylomicrons layer at the top of the patient's plasma taken on admission and placed overnight at 4 °C in a refrigerator. In addition, PAGE revealed the presence of chylomicrons fraction at base line and an increase in pre- β fraction, indicating an increase in VLDL (Figure 2b). On the thirty fourth hospital day after initiating a low fat diet, we performed a further investigation of the lipid metabolism and 75 g OGTT (Table 2). The 75 g OGTT demonstrated a pattern typical of DM and serum HbA1C was 9.0. Although the serum cholesterol level returned to normal and the serum triglyceride level fell to 251 mg/dL, we observed high serum levels of VLDL-triglyceride, Apo B and Apo CIII, indicating an increase in the hepatic VLDL-triglyceride synthesis. Post-heparin plasma LPL activity was within normal ranges. These findings suggested that ingestion of fatty food could lead to type V hyperlipidemia characterized by the presence of chylomicrons and an increase in VLDL. A low fat diet proved effective in managing this case of massive hypertriglyceridemia.

Table 2 75 g OGTT and serum lipid profile

		Case 1	Case 2	[Normal range]
75 g OGTT				
BS (mg/dL)	Before	82	113	<110
	30 min	148	198	<160
	60 min	176	274	<160
	120 min	159	262	<120
Insulin (μ U/mL)	Before	20.3	9.3	<20
	30 min	67.5	15.7	
	60 min	86.9	27.5	
	120 min	67.5	31.1	
Cholesterol fraction				
Total	(mg/dL)	161	199	[150-220]
VLDL	(mg/dL)		79.1	<38
LDL	(mg/dL)		97.5	[56-160]
HDL	(mg/dL)	15	22.4	[35-70]
Triglycerides fraction				
Total	(mg/dL)	571	382	[50-150]
VLDL	(mg/dL)		280.6	[6-84]
LDL	(mg/dL)		71.1	[10-35]
HDL	(mg/dL)		30.3	[11-28]
Apolipoproteins				
Apolipoprotein AI	(mg/dL)	71	78.9	[119-155]
Apolipoprotein AII	(mg/dL)	20	29.8	[25.9-35.7]
Apolipoprotein B	(mg/dL)	154	136.6	[73-109]
Apolipoprotein CII	(mg/dL)	11.1	7.0	[1.8-4.6]
Apolipoprotein CIII	(mg/dL)	22.4	21.9	[5.8-10.0]
Apolipoprotein E	(mg/dL)	20.6	6.4	[2.7-4.3]
Post-heparin plasma enzyme activities				
LPL activity	(μ mol FFA/mL/min)	0.048	0.181	[0.119-0.195]
LPL mass	(ng/mL)	<20		[136-321]

OGTT: oral glucose tolerance test, BS: blood sugar, VLDL: very low density lipoprotein, LDL: low density lipoprotein, HDL: high density lipoprotein, LPL: lipoprotein lipase, FFA: free fatty acid, HTGL: hepatic triglyceride lipase, LCAT: lecithin cholesterol acyl transferase.

DISCUSSION

Hypertriglyceridemia accompanied with chylomicronemia is clinically important because an elevated serum triglyceride level predisposes to the development of pancreatitis, occasionally

leading to total pancreatic necrosis and death^[1,10,11]. Both cases suffered from acute abdomen following the ingestion of fatty food and revealed high levels of inflammation parameters accompanied with hypertriglyceridemia. In pancreas enzymes, only serum PSTI revealed high levels and no elevation of serum and urinary amylase could be detected. On the imaging examination, an abdominal ultrasonogram could not detect pathological findings of acute pancreatitis and a CT scan eventually confirmed the findings of acute pancreatitis. Their symptoms improved after administration of a pancreatic serine proteinase inhibitor and fasting. The clinical courses supported the diagnostic evidence for acute pancreatitis with hypertriglyceridemia triggered by the ingestion of fatty food.

In the differential diagnosis of acute pancreatitis, the imaging examination detected no structural causes of acute pancreatitis such as gallstones, microlithiasis, pancreas divisum and sphincter of Oddi disease in both cases. Other etiologies of acute pancreatitis such as drug-induced pancreatitis, viral and bacterial infection could be deniable according to their clinical episodes.

Hypertriglyceridemia in case 1 was caused by a deficiency of LPL, a rate-limiting lipolytic enzyme that hydrolyzes triglyceride-rich lipoproteins in plasma. Brunzell *et al.* demonstrated that the appearance of chylomicrons was a marker for severely impaired triglyceride metabolism showing massive accumulation of triglyceride-rich lipoprotein in the serum^[1,12]. In case 1, the presence of chylomicrons might result from a severe reduction in the clearance of triglyceride-rich lipoproteins due to the LPL deficiency.

Marked hypertriglyceridemia has also been reported in other forms of impaired triglyceride metabolism besides LPL deficiency^[1,8,13,14]. Secondary causes of hypertriglyceridemia, such as a high fat diet or excessive alcohol intake, can lead to massive hypertriglyceridemia in patients with type IV hypertriglyceridemia. When an overproduction of VLDL-triglyceride was induced by secondary causes, extreme elevation of serum triglyceride levels, e.g. more than 10 000 mg/dL in case 2, might occur, since the LPL-related triglyceride removal system approached saturation at triglyceride concentrations of 700 to 1 000 mg/dL^[15]. In case 2, dietary fat restriction with a calorie control and alcohol prohibition had beneficial effects on serum lipids, and serum triglyceride level decreased dramatically.

Although the exact pathogenesis of pancreatitis caused by hypertriglyceridemia remains uncertain, hyperlipidemic pancreatitis is believed to result from chemical irritation to the pancreas from toxic fatty acids and lysolecithin^[16-19]. These compounds are liberated by pancreatic lipases from the core and surface of chylomicrons circulating at high concentrations in the capillaries of the exocrine pancreas. Moreover, there are some other hypotheses of the pathogenesis by which hypertriglyceridemia causes acute pancreatitis. Trypsinogen could be activated by acidosis due to the presence of free fatty acids, which may disturb the microcirculation of the pancreas by damaging the endothelium^[19,20]. Chylomicrons seem to be also involved in calcium-dependent agglutination by CRP, suggesting that non-traumatic fat embolism may be caused by agglutination of chylomicrons due to high levels of plasma CRP^[21]. Although hypertriglyceridemia with chylomicrons plays an important role in the occurrence of pancreatitis, hypertriglyceridemia sometimes was underrecognized in patients with acute pancreatitis^[6]. The measurement of serum triglyceride level or the identification of chylomicrons on the earliest available serum specimens may be important to increase the diagnostic yield and help prevent further occurrences of pancreatitis.

While pancreatitis is a major complication of hypertriglyceridemia, it is difficult to identify the onset of acute pancreatitis exactly from the clinical symptoms and laboratory data, since hypertriglyceridemia may often produce multiple spurious

laboratory results^[1-5]. Upon examination of patients with pain or discomfort in the abdomen of unknown origin, one should conduct tests to determine the lipid profile as well as the profile of pancreatic enzymes and imaging examination of the abdomen. If patients showed hypertriglyceridemia, it might be practical to measure serum amylase levels using diluted serum or plasma samples^[2]. Eruptive xanthomas, shown in case 2, caused by the phagocytosis of chylomicrons by macrophages in the skin^[22] may indicate the presence of chronic chylomicronemia. One of the simplest tests to detect plasma chylomicrons is the observation of a layer of chylomicrons at the top of the plasma stored overnight at 4 °C in a refrigerator, the so-called refrigerator test^[17]. However, this test can give false-negative results even in the presence of massive hypertriglyceridemia. PAGE remains one of the most useful methods for detecting and evaluating chylomicronemia, as demonstrated in this report (Figure 2). Measurement of serum remnant like particle-cholesterol levels^[23], a parameter of impaired triglyceride metabolism, could be useful to speculate on the presence of chylomicrons.

In conclusion, determination of serum triglyceride levels and identification of chylomicrons as well as measurement of pancreatic enzymes might be important in developing the therapeutic regimen. As in the present cases with acute abdomen following the fatty food ingestion, the identification of hypertriglyceridemia as well as an abdominal CT scan might be useful in establishing the diagnosis of acute pancreatitis and in preventing further progression of pancreatitis, when hypertriglyceridemia interferes with the evaluation of pancreatic enzyme activities and ultrasound examination provides poor pancreatic visualization.

ACKNOWLEDGMENTS

We thank Yuko Omura, Yurie Saito and Sayo Nakata for their invaluable assistance.

REFERENCES

- 1 Brunzell JD, Schrott HG. The interaction of familial and secondary causes of hypertriglyceridemia: role in pancreatitis. *Trans Assoc Am Physicians* 1973; **86**: 245-254
- 2 Lesser PB, Warshaw AL. Diagnosis of pancreatitis masked by hyperlipemia. *Ann Intern Med* 1975; **82**: 795-798
- 3 Cameron JL, Capuzzi DM, Zuidema GD, Margolis S. Acute pancreatitis with hyperlipemia: the incidence of lipid abnormalities in acute pancreatitis. *Ann Surg* 1973; **177**: 483-489
- 4 Fallat RW, Vester JW, Glueck CJ. Suppression of amylase activity by hypertriglyceridemia. *JAMA* 1973; **225**: 1331-1334
- 5 Mayan H, Gurevitz O, Mouallem M, Farfel Z. Multiple spurious laboratory results in a patient with hyperlipemic pancreatitis treated by plasmapheresis. *Isr J Med Sci* 1996; **32**: 762-766
- 6 Searles GE, Ooi TC. Underrecognition of chylomicronemia as a cause of acute pancreatitis. *CMAJ* 1992; **147**: 1806-1808
- 7 Agarwal N, Pitchumoni CS, Sivaprasad AV. Evaluating tests for acute pancreatitis. *Am J Gastroenterol* 1990; **85**: 356-366
- 8 Balthazar EJ, Robinson DL, Megibow AJ, Ranson JH. Acute pancreatitis: value of CT in establishing prognosis. *Radiology* 1990; **174**: 331-336
- 9 Beaumont JL, Carlson LA, Cooper GR, Fejfar Z, Fredrickson DS, Strasser T. Classification of hyperlipidaemias and hyperlipoproteinaemias. *Bull World Health Organ* 1970; **43**: 891-915
- 10 Fallat RW, Glueck CJ. Familial and acquired type V hyperlipoproteinemia. *Atherosclerosis* 1976; **23**: 41-62
- 11 Cox DW, Breckenridge WC, Little JA. Inheritance of apolipoprotein C-II deficiency with hypertriglyceridemia and pancreatitis. *N Engl J Med* 1978; **299**: 1421-1424
- 12 Brunzell JD, Bierman EL. Chylomicronemia syndrome. Interaction of genetic and acquired hypertriglyceridemia. *Med Clin North Am* 1982; **66**: 455-468

- 13 **Chait A**, Albers JJ, Brunzell JD. Very low density lipoprotein overproduction in genetic forms of hypertriglyceridaemia. *Eur J Clin Invest* 1980; **10**: 17-22
- 14 **Brunzell JD**, Albers JJ, Chait A, Grundy SM, Groszek E, McDonald GB. Plasma lipoproteins in familial combined hyperlipidemia and monogenic familial hypertriglyceridemia. *J Lipid Res* 1983; **24**: 147-155
- 15 **Brunzell JD**, Hazzard WR, Porte D Jr, Bierman EL. Evidence for a common, saturable, triglyceride removal mechanism for chylomicrons and very low density lipoproteins in man. *J Clin Invest* 1973; **52**: 1578-1585
- 16 **Morita Y**, Yoshikawa T, Takeda S, Matsuyama K, Takahashi S, Yoshida N, Clemens MG, Kondo M. Involvement of lipid peroxidation in free fatty acid-induced isolated rat pancreatic acinar cell injury. *Pancreas* 1998; **17**: 383-389
- 17 **Chait A**, Brunzell JD. Chylomicronemia syndrome. *Adv Intern Med* 1992; **37**: 249-273
- 18 **Toskes PP**. Hyperlipidemic pancreatitis. *Gastroenterol Clin North Am* 1990; **19**: 783-791
- 19 **Saharia P**, Margolis S, Zuidema GD, Cameron JL. Acute pancreatitis with hyperlipemia: studies with an isolated perfused canine pancreas. *Surgery* 1977; **82**: 60-67
- 20 **Niederer C**, Grendell JH. Intracellular vacuoles in experimental acute pancreatitis in rats and mice are an acidified compartment. *J Clin Invest* 1988; **81**: 229-236
- 21 **Hulman G**. Pathogenesis of non-traumatic fat embolism. *Lancet* 1988; **1**: 1366-1367
- 22 **Parker F**, Bagdade JD, Odland GF, Bierman EL. Evidence for the chylomicron origin of lipids accumulating in diabetic eruptive xanthomas: a correlative lipid biochemical, histochemical, and electron microscopic study. *J Clin Invest* 1970; **49**: 2172-2187
- 23 **Nakajima K**, Saito T, Tamura A. Cholesterol in remnant-like lipoproteins in human serum using monoclonal anti apo B-100 and anti apo A-I immunoaffinity mixed gels. *Clin Chim Acta* 1993; **223**: 53-71

Edited by Wang XL Proofread by Zhu LH and Xu FM